

FOURTH EDITION

BIOMATERIALS SCIENCE

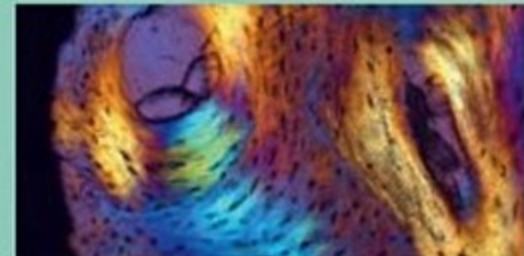
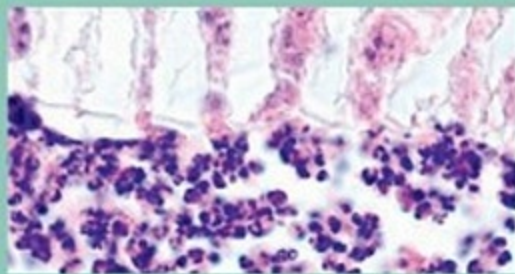
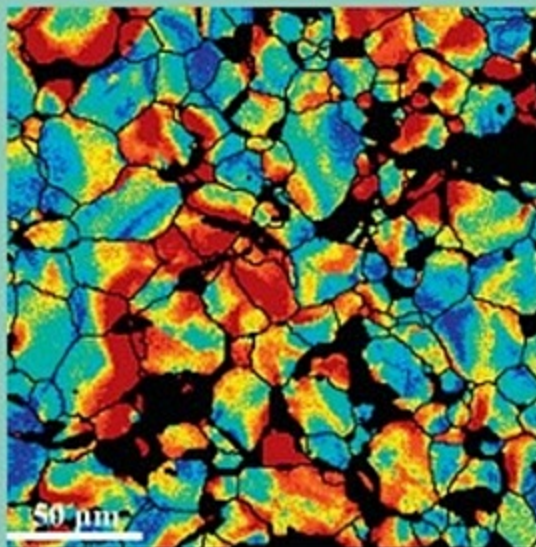
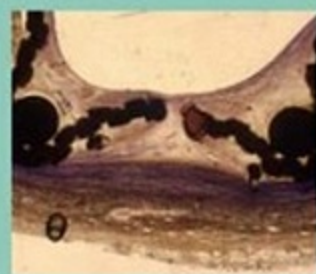
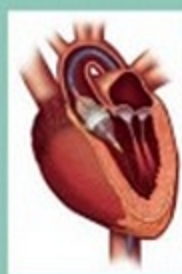
An Introduction to Materials in Medicine

EDITED BY

WILLIAM R. WAGNER, SHELLY E. SAKIYAMA-ELBERT
GUGEN ZHANG, MICHAEL J. YASZEMSKI

FOUNDING EDITORS

BUDDY D. RATNER, ALLAN S. HOFFMAN
FREDERICK J. SCHOEN, JACK E. LEMONS



Biomaterials Science

An Introduction to Materials in Medicine

Fourth Edition

Edited By

William R. Wagner

Distinguished Professor of Surgery
Bioengineering & Chemical Engineering
University of Pittsburgh
Director
McGowan Institute for Regenerative Medicine
Pittsburgh, PA, United States

Shelly E. Sakiyama-Elbert

Professor and Department Chair
Fletcher Stuckey Pratt Chair in Engineering
Department of Biomedical Engineering
The University of Texas at Austin
Austin, TX, United States

Guigen Zhang

Professor and F Joseph Halcomb III, M.D. Endowed
Chair, Chair of the F. Joseph Halcomb III, M.D.
Department of Biomedical Engineering
University of Kentucky
Lexington, KY, United States

Michael J. Yaszemski

Krehbiel Family Endowed Professor of Orthopedics
and Biomedical Engineering, Mayo Clinic
Rochester, MN, United States

Founding Editors

Buddy D. Ratner, Allan S. Hoffman

Frederick J. Schoen, Jack E. Lemons



ACADEMIC PRESS

An imprint of Elsevier

Academic Press is an imprint of Elsevier
125 London Wall, London EC2Y 5AS, United Kingdom
525 B Street, Suite 1650, San Diego, CA 92101, United States
50 Hampshire Street, 5th Floor, Cambridge, MA 02139, United States
The Boulevard, Langford Lane, Kidlington, Oxford OX5 1GB, United Kingdom

Copyright © 2020 Elsevier Inc. All rights reserved.

Chapter 11: Silicones: Copyright © 2020 DuPont, Published by Elsevier Inc. All Rights Reserved.

No part of this publication may be reproduced or transmitted in any form or by any means, electronic or mechanical, including photocopying, recording, or any information storage and retrieval system, without permission in writing from the publisher. Details on how to seek permission, further information about the Publisher's permissions policies and our arrangements with organizations such as the Copyright Clearance Center and the Copyright Licensing Agency, can be found at our website: www.elsevier.com/permissions.

This book and the individual contributions contained in it are protected under copyright by the Publisher (other than as may be noted herein).

Notices

Knowledge and best practice in this field are constantly changing. As new research and experience broaden our understanding, changes in research methods, professional practices, or medical treatment may become necessary.

Practitioners and researchers must always rely on their own experience and knowledge in evaluating and using any information, methods, compounds, or experiments described herein. In using such information or methods they should be mindful of their own safety and the safety of others, including parties for whom they have a professional responsibility.

To the fullest extent of the law, neither the Publisher nor the authors, contributors, or editors, assume any liability for any injury and/or damage to persons or property as a matter of products liability, negligence or otherwise, or from any use or operation of any methods, products, instructions, or ideas contained in the material herein.

Library of Congress Cataloging-in-Publication Data

A catalog record for this book is available from the Library of Congress

British Library Cataloguing-in-Publication Data

A catalogue record for this book is available from the British Library

ISBN: 978-0-12-816137-1

For information on all Academic Press publications visit our website at
<https://www.elsevier.com/books-and-journals>

Publisher: Matthew Deans

Acquisitions Editor: Sabrina Webber

Editorial Project Manager: Naomi Robertson

Production Project Manager: Surya Narayanan Jayachandran

Cover Designer: Alan Studholme

Typeset by TNQ Technologies



List of Contributors

Abhinav Acharya

School for Engineering of Matter, Transport and Energy, Biodesign Center for Immunotherapy, Vaccines and Virotherapy, Arizona State University, Tempe, AZ, United States

Marian A. Ackun-Farmer

Department of Biomedical Engineering, University of Rochester, Rochester, NY, United States; Department of Orthopaedics and Center for Musculoskeletal Research, University of Rochester, Rochester, NY, United States

John R. Aggas

Center for Bioelectronics, Biosensors and Biochips (C3B), Department of Biomedical Engineering, Texas A&M University, College Station, TX, United States; Department of Biomedical Engineering, Texas A&M University, College Station, TX, United States

Phillip J. Andersen

Andersen Metallurgical, LLC, Madison, WI, United States

James M. Anderson

Department of Pathology, Case Western Reserve University, Cleveland, OH, United States

Kristi Anseth

Department of Chemical and Biological Engineering, University of Colorado, Boulder, CO, United States; Biofrontiers Institute, University of Colorado, Boulder, CO, United States

Paul A. Archer

Parker H. Petit Institute for Bioengineering and Bioscience, Georgia Institute of Technology, Atlanta, GA, United States; School of Chemical and Biomolecular Engineering, Georgia Institute of Technology, Atlanta, GA, United States

Nureddin Ashammakhi

Center for Minimally Invasive Therapeutics (C-MIT), California NanoSystems Institute (CNSI), University of California-Los Angeles, Los Angeles, CA, United States

Jose D. Avila

W. M. Keck Biomedical Materials Research Laboratory, Washington State University, Pullman, WA, United States

Julia E. Babensee

Wallace H. Coulter Department of Biomedical Engineering, Georgia Institute of Technology and Emory University, Atlanta, GA, United States

Stephen f. Badylak

University of Pittsburgh, Pittsburgh, PA, United States

Kiheon Baek

Department of Biomedical Engineering, University of Rochester, Rochester, NY, United States; Center for Musculoskeletal Research, University of Rochester Medical Center, Rochester, NY, United States

Aaron B. Baker

Department of Biomedical Engineering, University of Texas at Austin, Austin, TX, United States

Syeda Mahwish Bakht

3B's Research Group, I3Bs—Research Institute on Biomaterials, Biodegradables and Biomimetics, University of Minho, Headquarters of the European Institute of Excellence on Tissue Engineering and Regenerative Medicine, Guimarães, Portugal; ICVS/3B's—PT Government Associate Laboratory, Braga/Guimarães, Portugal; The Discoveries Centre for Regenerative and Precision Medicine, Headquarters at University of Minho, Guimarães, Portugal

Amit Bandyopadhyay

W. M. Keck Biomedical Materials Research Laboratory, Washington State University, Pullman, WA, United States

Aaron Barchowsky

Department of Environmental and Occupational Health, University of Pittsburgh, Pittsburgh, PA, United States

Garrett Bass

Departments of Chemistry, Mechanical Engineering and Materials Science, Biomedical Engineering and Orthopaedic Surgery, Duke University, Durham, NC, United States

Matthew L. Becker

Departments of Chemistry, Mechanical Engineering and Materials Science, Biomedical Engineering and Orthopaedic Surgery, Duke University, Durham, NC, United States

Sarah Miho Van Belleghem

University of Maryland College Park; NIH/NIBIB Center for Engineering Complex Tissues

Danielle S.W. Benoit

Department of Biomedical Engineering, University of Rochester, Rochester, NY, United States; Department of Orthopaedics and Center for Musculoskeletal Research, University of Rochester, Rochester, NY, United States; Materials Science Program, University of Rochester, Rochester, NY, United States; Department of Chemical Engineering, University of Rochester, Rochester, NY, United States; Department of Biomedical Genetics and Center for Oral Biology, University of Rochester, Rochester, NY, United States; Translational Biomedical Science Program, University of Rochester, Rochester, NY, United States

Arne Biesiekierski

School of Engineering, RMIT University, Bundoora, VIC, Australia

Kristen L. Billiar

Biomedical Engineering Department, Worcester Polytechnic Institute, Worcester, MA, United States

Susmita Bose

W. M. Keck Biomedical Materials Research Laboratory, Washington State University, Pullman, WA, United States

Christopher Bowman

Department of Chemical and Biological Engineering, University of Colorado, Boulder, CO, United States

Steven Boyce

Department of Surgery, University of Cincinnati and Shriners Hospitals for Children – Cincinnati, Cincinnati, OH, United States

Bryan N. Brown

Department of Bioengineering, University of Pittsburgh, Pittsburgh, PA, United States; McGowan Institute for Regenerative Medicine, University of Pittsburgh, Pittsburgh, PA, United States

Justin L. Brown

Department of Biomedical Engineering, The Pennsylvania State University, University Park, PA, United States

Jeffrey R. Capadona

Department of Biomedical Engineering, Case Western Reserve University, Cleveland, OH, United States; Advanced Platform Technology Center, Rehabilitation Research and Development, Louis Stokes Cleveland VA Medical Center, Cleveland, OH, United States

David G. Castner

University of Washington, Seattle, WA, United States

Calvin Chang

Department of Biomedical Engineering, Johns Hopkins University, Baltimore, MD, United States; Translational Tissue Engineering Center, Johns Hopkins School of Medicine, Baltimore, MD, United States; Institute for NanoBio Technology, Johns Hopkins University, Baltimore, MD, United States

Philip Chang

Department of Surgery, University of Cincinnati and Shriners Hospitals for Children – Cincinnati, Cincinnati, OH, United States

Ashutosh Chilkoti

Department of Biomedical Engineering, Duke University, Durham, NC, United States

Karen L. Christman

Department of Bioengineering, Sanford Consortium of Regenerative Medicine, University of California San Diego, La Jolla, CA, United States

Sangwon Chung

Department of Textile Engineering, Chemistry & Science, North Carolina State University, Raleigh, NC, United States; Biomedical Engineering, Joint Department of Biomedical Engineering, North Carolina State University and University of North Carolina at Chapel Hill, Chapel Hill, NC, United States

Kelly P. Coleman

Medtronic, Physiological Research Laboratories, Minneapolis, MN, United States

Dan Conway

Department of Biomedical Engineering, Virginia Commonwealth University, Richmond, VA, United States

Keith E. Cook

Department of Biomedical Engineering, Carnegie Mellon University, Pittsburgh, PA, United States

Stuart L. Cooper

William G. Lowrie Department of Chemical and Biomolecular Engineering, The Ohio State University, Columbus, OH, United States

Elizabeth Cosgriff-Hernandez

The University of Texas at Austin, Austin, TX, United States

Arthur J. Coury

Northeastern University, Boston, MA, United States

Joseph D. Criscione

Department of Biomedical Engineering, University of Rochester, Rochester, NY, United States

Heidi Culver

Department of Chemical and Biological Engineering, University of Colorado, Boulder, CO, United States

Jim Curtis

DuPont Health Care Solutions, Midland, MI, United States

Feiyang Deng

Department of Biomedical Engineering, University of Rochester, Rochester, NY, United States

Prachi Dhavalikar

The University of Texas at Austin, Austin, TX, United States

Luis Diaz-Gomez

Department of Bioengineering, Rice University, Houston, TX, United States

Rui M.A. Domingues

3B's Research Group, I3Bs—Research Institute on Biomaterials, Biodegradables and Biomimetics, University of Minho, Headquarters of the European Institute of Excellence on Tissue Engineering and Regenerative Medicine, Guimarães, Portugal; ICVS/3B's—PT Government Associate Laboratory, Braga/Guimarães, Portugal; The Discoveries Centre for Regenerative and Precision Medicine, Headquarters at University of Minho, Guimarães, Portugal

Elaine Duncan

Paladin Medical, Inc., Stillwater, MN, United States; Joseph Halcomb III, MD. Department of Biomedical Engineering, College of Engineering, University of Kentucky, Lexington, KY, United States

Pamela Duran

Department of Bioengineering, Sanford Consortium of Regenerative Medicine, University of California San Diego, La Jolla, CA, United States

Pedro Esbrit

Chemical Department of Pharmaceutical Sciences, Faculty of Pharmacy, Universidad Complutense of Madrid, Spain

Suzanne G. Eskin

Wallace H. Coulter Department of Biomedical Engineering, Georgia Institute of Technology, Atlanta, GA, United States

Michael Y. Esmail

Tufts Comparative Medicine Services, Tufts University, Boston, MA, United States

Jack L. Ferracane

Department of Restorative Dentistry, Oregon Health & Science University, Portland, OR 97201

Claudia Fischbach

Nancy E. and Peter C. Meinig School of Biomedical Engineering, Cornell University, Ithaca, NY, United States; Kavli Institute at Cornell for Nanoscale Science, Cornell University, Ithaca, NY, United States

Gary Fischman, PhD

Future Strategy Solutions, LLC, Gambrills, MD, United States

John P. Fisher

University of Maryland College Park; NIH/NIBIB Center for Engineering Complex Tissues

Iolanda Francolini

Department of Chemistry, Sapienza University of Rome, Rome, Italy

Steven J. Frey

School of Chemical and Biomolecular Engineering, Georgia Institute of Technology, Atlanta, GA, United States

Akhilesh K. Gaharwar

Texas A&M University, College Station, TX, United States

Andrés J. García

George W. Woodruff School of Mechanical Engineering, Georgia Institute of Technology, Atlanta, GA, United States; Parker H. Petit Institute of Bioengineering and Biological Science, Georgia Institute of Technology, Atlanta, GA, United States

Iain R. Gibson

Institute of Medical Sciences, School of Medicine, Medical Sciences and Nutrition, University of Aberdeen, Aberdeen, United Kingdom

Jeremy L. Gilbert

Department of Bioengineering, Clemson University,
Charleston, SC, United States

Brian Ginn

Secant Group, Telford, PA, United States

Zachary E. Goldblatt

Biomedical Engineering Department,
Worcester Polytechnic Institute, Worcester,
MA, United States

Seth J. Goldenberg

Veeva Systems, Pleasanton, CA, United States

Manuela E. Gomes

3B's Research Group, I3Bs—Research Institute on
Biomaterials, Biodegradables and Biomimetics,
University of Minho, Headquarters of the European
Institute of Excellence on Tissue Engineering and
Regenerative Medicine, Guimarães, Portugal;
ICVS/3B's—PT Government Associate Laboratory,
Braga/Guimarães, Portugal; The Discoveries Centre for
Regenerative and Precision Medicine, Headquarters at
University of Minho, Guimarães, Portugal

Manuel Gómez-Florit

3B's Research Group, I3Bs—Research Institute on
Biomaterials, Biodegradables and Biomimetics,
University of Minho, Headquarters of the European
Institute of Excellence on Tissue Engineering and
Regenerative Medicine, Guimarães, Portugal;
ICVS/3B's—PT Government Associate Laboratory,
Braga/Guimarães, Portugal; The Discoveries
Centre for Regenerative and Precision Medicine,
Headquarters at University of Minho, Guimarães,
Portugal

Inês C. Gonçalves

i3S - Instituto de Inovação e Investigação em Saúde,
Universidade do Porto, Rua Alfredo Allen 208, Porto,
Portugal; INEB - Instituto de Engenharia Biomédica,
Universidade do Porto, Rua Alfredo Allen 208, Porto,
Portugal

Maud B. Gorbet

Department of Systems Design Engineering, University of
Waterloo, ON, Canada

David W. Grainger

Department of Biomedical Engineering, University
of Utah, Salt Lake City, UT, United States;
Department of Pharmaceutics and Pharmaceutical
Chemistry, University of Utah, Salt Lake City, UT,
United States

Miles Grody

Miles Grody Law, Potomac, MD, United States

Teja Guda

Department of Biomedical Engineering, University of
Texas at San Antonio, San Antonio, TX, United States

Scott A. Guelcher

Department of Chemical and Biomolecular Engineering,
Vanderbilt University, Nashville, TN, United States

Anthony Guiseppi-Elie

Center for Bioelectronics, Biosensors and Biochips
(C3B), Department of Biomedical Engineering,
Texas A&M University, College Station, TX, United
States; Department of Biomedical Engineering, Texas
A&M University, College Station, TX, United States;
ABTECH Scientific, Inc., Biotechnology Research Park,
Richmond, VA, United States

S. Adam Hacking

Laboratory for Musculoskeletal Research and Innovation,
Department of Orthopaedic Surgery, Massachusetts
General Hospital and Harvard Medical School, Boston,
MA, United States

Nadim James Hallab

Department of Orthopedic Surgery, Rush University
Medical Center, Chicago, IL, United States

Luanne Hall-Stoodley

Department of Microbial Infection and Immunity, The
Ohio State University, Columbus, OH, United States

Stephen R. Hanson

Division of Biomedical Engineering, School of Medicine,
Oregon Health & Science University, Portland, OR,
United States

Woojin M. Han

George W. Woodruff School of Mechanical Engineering,
Georgia Institute of Technology, Atlanta, GA, United
States; Parker H. Petit Institute of Bioengineering and
Biological Science, Georgia Institute of Technology,
Atlanta, GA, United States

Melinda K. Harman

Department of Bioengineering, Clemson University,
Clemson, SC, United States

Roger Harrington

Medical Products Development Director, Medtronic,
Boston, MA, United States

Martin J. Haschak

Department of Bioengineering, University of Pittsburgh, Pittsburgh, PA, United States; McGowan Institute for Regenerative Medicine, University of Pittsburgh, Pittsburgh, PA, United States

Daniel E. Heath

William G. Lowrie Department of Chemical and Biomolecular Engineering, The Ohio State University, Columbus, OH, United States

Emily Anne Hicks

Department of Chemical Engineering, McMaster University, Hamilton, ON, Canada

Ryan T. Hill

Center for Biologically Inspired Materials and Material Systems, Duke University, Durham, NC, United States

Allan S. Hoffman

Bioengineering and Chemical Engineering, University of Washington, Seattle, WA, United States

Thomas A. Horbett

Bioengineering and Chemical Engineering, University of Washington, Seattle, WA, United States

Jeffrey A. Hubbell

The University of Chicago, Chicago, IL, United States

Rasim Ipek

Department of Mechanical Engineering, Ege University, Izmir, Turkey

Joshua J. Jacobs

Department of Orthopedic Surgery, Rush University Medical Center, Chicago, IL, United States

Young C. Jang

School of Biological Sciences, Georgia Institute of Technology, Atlanta, GA, United States; Parker H. Petit Institute of Bioengineering and Biological Science, Georgia Institute of Technology, Atlanta, GA, United States

Shaoyi Jiang

Departments of Chemical Engineering and Bioengineering, Seattle, WA, United States

Richard J. Johnson

BioPhia Consulting, Lake Forest, IL, United States

Julian R. Jones

Department of Materials, Imperial College London, South Kensington Campus, London, United Kingdom

Vickie Y. Jo

Department of Pathology, Brigham and Women's Hospital and Harvard Medical School, Boston, MA, United States

Ravi S. Kane

School of Chemical and Biomolecular Engineering, Georgia Institute of Technology, Atlanta, GA, United States

David L. Kaplan

Department of Biomedical Engineering, Tufts University, Medford, MA, United States

Ronit Kar

The University of Texas at Austin, Austin, TX, United States

Benjamin George Keselowsky

Department of Biomedical Engineering, University of Florida, Gainesville, FL, United States

Ali Khademhosseini

Center for Minimally Invasive Therapeutics (C-MIT), California NanoSystems Institute (CNSI), University of California-Los Angeles, Los Angeles, CA, United States

Yu Seon Kim

Department of Bioengineering, Rice University, Houston, TX, United States

Martin W. King

Department of Textile Engineering, Chemistry & Science, North Carolina State University, Raleigh, NC, United States

Daniel S. Kohane

Laboratory for Biomaterials and Drug Delivery, Department of Anesthesiology, Division of Critical Care Medicine, Boston Children's Hospital, Harvard Medical School, Boston, MA, United States

David H. Kohn

Departments of Biologic and Materials Sciences, and Biomedical Engineering, The University of Michigan, Ann Arbor, MI, United States

Liisa T. Kuhn

Department of Biomedical Engineering, University of Connecticut Health Center, Farmington, CT, United States

Mangesh Kulkarni

Department of Bioengineering, University of Pittsburgh, Pittsburgh, PA, United States; McGowan Institute for Regenerative Medicine, University of Pittsburgh, Pittsburgh, PA, United States

Catherine K. Kuo

Department of Biomedical Engineering, University of Rochester, Rochester, NY, United States; Center for Musculoskeletal Research, University of Rochester Medical Center, Rochester, NY, United States; Department of Orthopaedics, University of Rochester Medical Center, Rochester, NY, United States

Angela Lai

Department of Biomedical Engineering, Carnegie Mellon University, Pittsburgh, PA, United States

Bryron Lambert

Sterilization Science, Abbott Vascular, Temecula, CA, United States

Ziyang Lan

The University of Texas at Austin, Austin, TX, United States

Robert A. Latour

Bioengineering Department, Clemson University, Clemson, SC, United States

Cato T. Laurencin

Department of Biomedical Engineering, The Pennsylvania State University, University Park, PA, United States

Bryan K. Lawson, M.D.

Department of Orthopaedic Surgery, Mike O'Callaghan Military Medical Center, Nellis AFB, NV, United States

Shannon Lee Layland

Department of Women's Health, Research Institute for Women's Health, Eberhard Karls University Tübingen, Tübingen, Germany

Jae Sung Lee

Department of Orthopedics and Rehabilitation, University of Wisconsin–Madison, Madison, WI, United States

David Lee-Parritz

Department of Environmental and Population Health, Tufts University Cummings School of Veterinary Medicine, North Grafton, MA, United States

Ying Lei

Biomedical Engineering Department, Worcester Polytechnic Institute, Worcester, MA, United States

Jack E. Lemons

Schools of Dentistry, Medicine and Engineering, University of Alabama at Birmingham, Birmingham, AL, United States

Robert J. Levy

Department of Pediatrics, The Children's Hospital of Philadelphia, The Perelman School of Medicine at the University of Pennsylvania, Philadelphia, PA, United States

Gregory M. Lewerenz

Medtronic, Physiological Research Laboratories, Minneapolis, MN, United States

Jamal S. Lewis

Biomedical Engineering, University of California Davis, CA, United States

Simone Liebscher

Department of Women's Health, Research Institute for Women's Health, Eberhard Karls University Tübingen, Tübingen, Germany

Chien-Chi Lin

Department of Biomedical Engineering, Indiana University-Purdue University Indianapolis, Indianapolis, IN, United States

Natalie K. Livingston

Department of Biomedical Engineering, Johns Hopkins University, Baltimore, MD, United States; Translational Tissue Engineering Center, Johns Hopkins School of Medicine, Baltimore, MD, United States; Institute for NanoBioTechnology, Johns Hopkins University, Baltimore, MD, United States

Yang Li

Laboratory for Biomaterials and Drug Delivery, Department of Anesthesiology, Division of Critical Care Medicine, Boston Children's Hospital, Harvard Medical School, Boston, MA, United States

Yuncang Li

School of Engineering, RMIT University, Bundoora, VIC, Australia

Helen Lu

Department of Biomedical Engineering, Columbia University, New York, NY, United States

Laura Macdougall

Department of Chemical and Biological Engineering, University of Colorado, Boulder, CO, United States; Biofrontiers Institute, University of Colorado, Boulder, CO, United States

Bhushan Mahadik

University of Maryland College Park; NIH/NIBIB Center for Engineering Complex Tissues

Sachin Mamidwar

Orthogen, LLC, Springfield, NJ, United States

Margaret P. Manspeaker

Parker H. Petit Institute for Bioengineering and Bioscience, Georgia Institute of Technology, Atlanta, GA, United States; School of Chemical and Biomolecular Engineering, Georgia Institute of Technology, Atlanta, GA, United States

Hai-Quan Mao

Department of Biomedical Engineering, Johns Hopkins University, Baltimore, MD, United States; Translational Tissue Engineering Center, Johns Hopkins School of Medicine, Baltimore, MD, United States; Institute for NanoBioTechnology, Johns Hopkins University, Baltimore, MD, United States; Department of Materials Science and Engineering, Johns Hopkins University, Baltimore, MD, United States

Peter X. Ma

Department of Biologic and Materials Science, School of Dentistry, University of Michigan, Ann Arbor, MI, United States

Tyler Marcet

Department of Biomedical Engineering, Tufts University, Medford, MA, United States

Jeffrey Martin

President and Principal Consultant, Sterilization and Quality System Consulting LLC, Dallas, TX, United States

M. Cristina L. Martins

INEB - Institute of Biomedical Engineering, University of Porto, Porto, Portugal

Sally L. McArthur

Bioengineering Research Group, Swinburne University of Technology, Melbourne, VIC, Australia; Biomedical Manufacturing, CSIRO Manufacturing, Melbourne, VIC, Australia

Meghan McGill

Department of Biomedical Engineering, Tufts University, Medford, MA, United States

Larry V. McIntire

Wallace H. Coulter Department of Biomedical Engineering, Georgia Institute of Technology, Atlanta, GA, United States

Lei Mei

Department of Biomedical Engineering, University of Texas at Austin, Austin, TX, United States

Bárbara B. Mendes

3B's Research Group, I3Bs—Research Institute on Biomaterials, Biodegradables and Biomimetics, University of Minho, Headquarters of the European Institute of Excellence on Tissue Engineering and Regenerative Medicine, Guimarães, Portugal; ICVS/3B's—PT Government Associate Laboratory, Braga/Guimarães, Portugal; The Discoveries Centre for Regenerative and Precision Medicine, Headquarters at University of Minho, Guimarães, Portugal

Antonios G. Mikos

Department of Bioengineering, Rice University, Houston, TX, United States

Richard N. Mitchell

Department of Pathology/Brigham and Women's Hospital and Harvard Medical School, Boston, MA, United States

Indranath Mitra

W. M. Keck Biomedical Materials Research Laboratory, Washington State University, Pullman, WA, United States

Ben Muirhead

Department of Chemical Engineering, McMaster University, Hamilton, ON, Canada

Khurram Munir

School of Engineering, RMIT University, Bundoora, VIC, Australia

William L. Murphy

Department of Orthopedics and Rehabilitation, University of Wisconsin—Madison, Madison, WI, United States; Department of Biomedical Engineering, University of Wisconsin—Madison, Madison, WI, United States

Phong K. Nguyen

Department of Biomedical Engineering, University of Rochester, Rochester, NY, United States; Center for Musculoskeletal Research, University of Rochester Medical Center, Rochester, NY, United States

Alexis L. Nolfi

Department of Bioengineering, University of Pittsburgh, Pittsburgh, PA, United States; McGowan Institute for Regenerative Medicine, University of Pittsburgh, Pittsburgh, PA, United States

Clyde Overby

Department of Biomedical Engineering, University of Rochester, Rochester, NY, United States; Department of Orthopaedics and Center for Musculoskeletal Research, University of Rochester, Rochester, NY, United States

Sertan Ozan

School of Engineering, RMIT University, Bundoora, VIC, Australia; Department of Mechanical Engineering, Yozgat Bozok University, Yozgat, Turkey

Robert F. Padera

Department of Pathology/Brigham and Women's Hospital and Harvard Medical School, Boston, MA, United States

Hannah A. Pearce

Department of Bioengineering, Rice University, Houston, TX, United States

Nicholas A. Peppas

Department of Chemical Engineering and Biomedical Engineering, Pediatrics, Surgery and Molecular Pharmaceutics and Drug Delivery, The University of Texas, Austin, TX, United States

Andreia T. Pereira

i3S - Instituto de Inovação e Investigação em Saúde, Universidade do Porto, Rua Alfredo Allen 208, Porto, Portugal; INEB - Instituto de Engenharia Biomédica, Universidade do Porto, Rua Alfredo Allen 208, Porto, Portugal; Graduate Program in Areas of Basic and Applied Biology, Instituto de Ciências Biomédicas Abel Salazar, Universidade do Porto, Rua Jorge de Viterbo Ferreira 228, Porto, Portugal

Carmem S. Pfeifer

Biomaterials and Biomechanics, Oregon Health & Science University, Portland, OR, 97201

Artur M. Pinto

LEPABE – Laboratory of Process Engineering, Environment, Biotechnology and Energy, Faculty of Engineering, University of Porto, Portugal

Nicole R. Raia

Department of Biomedical Engineering, Tufts University, Medford, MA, United States

Edward A. Rankin

Medtronic, Physiological Research Laboratories, Minneapolis, MN, United States

Buddy D. Ratner

Bioengineering and Chemical Engineering, Director of University of Washington Engineered Biomaterials (UWEB), Seattle, WA, United States

Maria Vallet Regi

Chemical Department of Pharmaceutical Sciences, Faculty of Pharmacy, Universidad Complutense of Madrid, Spain

Rui L. Reis

3B's Research Group, I3Bs—Research Institute on Biomaterials, Biodegradables and Biomimetics, University of Minho, Headquarters of the European Institute of Excellence on Tissue Engineering and Regenerative Medicine, Guimarães, Portugal; ICVS/3B's—PT Government Associate Laboratory, Braga/Guimarães, Portugal; The Discoveries Centre for Regenerative and Precision Medicine, Headquarters at University of Minho, Guimarães, Portugal

Alastair Campbell Ritchie

Department of Mechanical, Materials and Manufacturing Engineering, University of Nottingham, Nottingham, United Kingdom

Shelly E. Sakiyama-Elbert

Department of Biomedical Engineering, The University of Texas at Austin, Austin, TX, United States

Karim Salhadar

The University of Texas at Austin, Austin, TX, United States

Antonio J. Salinas

Chemical Department of Pharmaceutical Sciences, Faculty of Pharmacy, Universidad Complutense of Madrid, Spain

Katja Schenke-Layland

Department of Women's Health, Research Institute for Women's Health, Eberhard Karls University Tübingen, Tübingen, Germany; Natural and Medical Sciences Institute (NMI) at the University of Tübingen, Reutlingen, Germany; Cluster of Excellence iFIT (EXC 2180) "Image-Guided and Functionally Instructed Tumor Therapies", Eberhard Karls University Tübingen, Tübingen, Germany; Department of Medicine/Cardiology, Cardiovascular Research Laboratories (CVRL), University of California (UCLA), Los Angeles, CA, United States

Frederick J. Schoen

Department of Pathology/Brigham and Women's Hospital and Harvard Medical School, Boston, MA, United States

Brittany E. Schutrum

Nancy E. and Peter C. Meinig School of Biomedical Engineering, Cornell University, Ithaca, NY, United States

Michael V. Sefton

Department of Chemical Engineering and Applied Chemistry, Institute of Biomaterials and Biomedical Engineering, University of Toronto, ON, Canada

Michael A. Seidman

Department of Pathology/Brigham and Women's Hospital and Harvard Medical School, Boston, MA, United States

Darshan S. Shah, M.D.

Department of Orthopaedic Surgery, San Antonio Military Medical Center, Ft Sam Houston, TX, United States

Heather Sheardown

Department of Chemical Engineering, McMaster University, Hamilton, ON, Canada

Andrew J. Shoffstall

Department of Biomedical Engineering, Case Western Reserve University, Cleveland, OH, United States; Advanced Platform Technology Center, Rehabilitation Research and Development, Louis Stokes Cleveland VA Medical Center, Cleveland, OH, United States

Carl G. Simon, Jr.

Biosystems Biomaterials Division, National Institute of Standards & Technology, Gaithersburg, MD, United States

Josh Simon

Spiral Medical Development, Lansdale, PA, United States

Kenneth R. Sims Jr.

Department of Biomedical Engineering, University of Rochester, Rochester, NY, United States; Translational Biomedical Science Program, University of Rochester, Rochester, NY, United States

Steven M. Slack[†]**Benjamin Slavin**

Translational Tissue Engineering Center, Johns Hopkins School of Medicine, Baltimore, MD, United States; Department of Plastic and Reconstructive Surgery, Johns Hopkins School of Medicine, Baltimore, MD, United States

Kirstie Lane Snodderly

University of Maryland College Park; NIH/NIBIB Center for Engineering Complex Tissues

Patrick S. Stayton

Bioengineering, University of Washington, Seattle, WA, United States

Stephanie D. Steichen

DuPont Health Care Solutions, Midland, MI, United States

Paul Stoodley

Department of Microbial Infection and Immunity, The Ohio State University, Columbus, OH, United States; Departments of Orthopaedics and Microbiology, The Ohio State University, Columbus, OH, United States; Campus Imaging and Microscopy Facility, Office of Research, The Ohio State University, Columbus, OH, United States; National Centre for Advanced Tribology, Mechanical Engineering, University of Southampton, Southampton, United Kingdom

W. Benton Swanson

Department of Biologic and Materials Science, School of Dentistry, University of Michigan, Ann Arbor, MI, United States

Hobey Tam

Department of Bioengineering, Rhodes Engineering Research Center, Clemson University, Clemson, SC, United States

Aftab Tayab

Department of Chemical Engineering, McMaster University, Hamilton, ON, Canada

Susan N. Thomas

Parker H. Petit Institute for Bioengineering and Bioscience, Georgia Institute of Technology, Atlanta, GA, United States; George W. Woodruff School of Mechanical Engineering, Georgia Institute of Technology, Atlanta, GA, United States

Kellen D. Traxel

W. M. Keck Biomedical Materials Research Laboratory, Washington State University, Pullman, WA, United States

Rocky S. Tuan

Institute for Tissue Engineering and Regenerative Medicine, The Chinese University of Hong Kong, Hong Kong, SAR, China

Erik I. Tucker

Division of Biomedical Engineering, School of Medicine, Oregon Health & Science University, Portland, OR, United States

Rei Ukita

Department of Biomedical Engineering, Carnegie Mellon University, Pittsburgh, PA, United States

[†]Deceased.

Austin Veith

Department of Biomedical Engineering, University of Texas at Austin, Austin, TX, United States

Sarah E. Vidal Yucha

Department of Biomedical Engineering, Tufts University, Medford, MA, United States

Christopher Viney

School of Engineering, University of California at Merced, Merced, CA, United States

Naren Vyavahare

Department of Bioengineering, Rhodes Engineering Research Center, Clemson University, Clemson, SC, United States

William R. Wagner

Departments of Surgery, Bioengineering & Chemical Engineering, McGowan Institute for Regenerative Medicine, University of Pittsburgh, Pittsburgh, PA, United States

Min Wang

Department of Mechanical Engineering, The University of Hong Kong, Pok Fu Lam, Hong Kong, China

Raymond M. Wang

Department of Bioengineering, Sanford Consortium of Regenerative Medicine, University of California San Diego, La Jolla, CA, United States

Petra Warner

Department of Surgery, University of Cincinnati and Shriners Hospitals for Children – Cincinnati, Cincinnati, OH, United States

Cuie Wen

School of Engineering, RMIT University, Bundoora, VIC, Australia

Jennifer L. West

Duke University, Durham, NC, United States

Matthew A. Whitman

Nancy E. and Peter C. Meinig School of Biomedical Engineering, Cornell University, Ithaca, NY, United States

Frank Witte

Department of Prosthodontics, Geriatric Dentistry and Craniomandibular Disorders, Berlin, Germany

Michael F. Wolf

Medtronic, Corporate Science and Technology, Minneapolis, MN, United States

Zhicheng Yao

Translational Tissue Engineering Center, Johns Hopkins School of Medicine, Baltimore, MD, United States; Institute for NanoBioTechnology, Johns Hopkins University, Baltimore, MD, United States; Department of Materials Science and Engineering, Johns Hopkins University, Baltimore, MD, United States

Michael Yaszemski, M.D.

Department of Orthopaedic Surgery, Mayo Clinic, Rochester, MN, United States

Michael J. Yaszemski

Orthopaedic Surgery and Biomedical Engineering, Mayo Clinic College of Medicine, Rochester, MN, United States

Lichen Yin

Jiangsu Key Laboratory for Carbon-Based Functional Materials and Devices, Institute of Functional Nano and Soft Materials (FUNSOM), the Collaborative Innovation Center of Suzhou Nano Science and Technology, Soochow University, Suzhou, Jiangsu, China

Guigen Zhang

F Joseph Halcomb III, M.D. Department of Biomedical Engineering, University of Kentucky, Lexington, KY, United States

Peng Zhang

Department of Chemical Engineering, University of Washington, Seattle, WA, United States

Zhiyuan Zhong

Biomedical Polymers Laboratory and Jiangsu Key Laboratory of Advanced Functional Polymer Design and Application, College of Chemistry, Chemical Engineering and Materials Science, Soochow University, Suzhou, Jiangsu, China

Nicholas P. Ziats, Ph.D.

Pathology, Biomedical Engineering & Anatomy Vice Chair of Pathology for Academic Affairs Case Western Reserve University Department of Pathology Cleveland, Ohio

Preface

Biomaterials Science: An Introduction to Materials in Medicine was launched as an educational project to provide a nascent biomaterials community with an authoritative tool for training and education. Conceptual background material and a broad overview of applications were both envisioned as being integral to the textbook. In the late 1980s, biomaterials was in transition from an emerging field to a respected discipline embracing convergence (i.e., the merging of expertise from different “silos,” such as provided by engineers, biomedical scientists, and physicians)—the biomaterials community was in need of an integrated, comprehensive, and definitive educational resource. This rationale for launching the textbook has been validated by the success of the first three editions of *Biomaterials Science: An Introduction to Materials in Medicine*. With well over 33,000 print copies, numerous online readers through institutional subscriptions, and the thousands who have bought the e-book version, the text has made consequential contributions to the biomaterials education of students and researchers around the world. The previous editions have been widely adopted for classroom use and serve as a reference resource for thousands of biomaterials professionals.

Biomaterials Science: An Introduction to Materials in Medicine strives for a balanced view of the biomaterials field. When this project was first launched, monographs available at that time did articulately address biomaterials, but they tended to strongly emphasize the authors’ areas of expertise, while only superficially addressing other important subjects outside of their intellectual sphere. Balanced presentation means appropriate representation of:

- hard and soft biomaterials, with coverage of all major material classes both synthetic and biologically derived;
- the common application areas, including orthopedic, cardiovascular, ophthalmologic, dental, and emerging applications;
- a balance of fundamental biological and materials science concepts, contemporary medical/clinical concerns, and regulatory/commercial/societal issues that reflect the complex environment in which biomaterials are developed and used;
- coverage of the past, present, and future of biomaterials, their applications, and key challenges that lie ahead.

In this way, the reader can embrace the broad field, absorb the unifying principles common to all materials in contact with biological systems, and gain a solid appreciation for the special significance of the word *biomaterial*.

Biomaterials Science: An Introduction to Materials in Medicine, fourth edition, strives for curricular cohesion. By integrating the experience of many leaders in the biomaterials field, we endeavor to present a balanced yet comprehensive perspective on an exciting and rapidly evolving discipline—and present this information in a graphically attractive and readable format, intended to be useful as an educational resource to a broad array of students, teachers, and practicing professionals.

With this fourth edition a new set of four editors has taken on the challenge of moving the textbook forward. It is a humbling task to take over editor responsibilities from the four pioneers and visionaries in the field who launched the text and thoughtfully guided what became the quintessential biomaterials textbook through three editions. The new editor team recognized that the book could not physically grow any further than the size of the third edition (as any student who has carried that edition for a semester in a backpack would appreciate). Thus a balanced approach had to be implemented to both grow and cut back. Furthermore, with broad adoption of online access, the opportunity to place some supplementary content online was utilized (e.g., end-of-chapter questions and a further reading section).

First and foremost, the new editors wished to retain continuity with previous editions of the text and changed little where revision was not required. Moderate updates were made in many chapters, often keeping existing author teams and enlisting new coauthors. However, where a fresh direction seemed appropriate for a chapter given the state of the science, or the introduction of new chapters was indicated for where the field had expanded, new author teams were recruited. Overall there are 17 new chapters and 43 chapters with a new set of authors. To balance this growth, some topics were consolidated. A change the reader may notice in content is that the editors have elected to reduce the depth of emphasis on tissue engineering and some device topics, believing that there are now excellent texts devoted exclusively to the maturing tissue engineering field. With medical devices, the desire was not only to cover the critical application areas in overview and to include major new advances, but also to recognize that readers will be able to find field-specific, in-depth device coverage elsewhere. Finally, particular attention was given to the third section of the book, where guidance is provided that seeks to prepare the reader for the development pathway beyond the demonstration

of a proof-of-concept. Here our hope was that the disconnect between the vast biomaterials scientific literature and the reality of what devices are used clinically and how they are implemented can be appreciated. Such understanding is critical if scientific advances are to ultimately reach the target patient population.

The founding editors are still very much a part of this textbook. They have provided wise counsel as the new editors developed the plan for the fourth edition, but also authored revisions in several chapters from previous editions. Much of the excellent content and perspective that has made this text so useful to the community has come from the writings of the founding editors. We have sought to preserve and update this valued content.

Acknowledgments and thanks are in order. First, the Society for Biomaterials (SFB), sponsor and inspiration for this book, is a model of “multidisciplinary cultural diversity.” Composed of engineers, physicians, scientists, veterinarians, industrialists, inventors, regulators, attorneys, educators, ethicists, and others, the SFB provides the nidus for the intellectually exciting, humanistically relevant, and economically important biomaterials field. As was the case for all of the previous editions, the editors recognize the importance of the SFB by donating all royalties from sales of this volume to the Society, to directly support education and career development related to biomaterials. For information on the SFB, visit the SFB website at <http://www.biomaterials.org/>.

We offer special thanks to those who have generously invested time, energy, experience, and intelligence to author the chapters of this textbook. The over 100 scientists, physicians, engineers, and industry leaders who contributed their expertise and perspectives are clearly the backbone of

this work, and they deserve high praise—their efforts will strongly impact the education of the next generation of biomaterials scientists. It is only with such a distinguished group of authors that this text can provide the needed balance, scope, and perspective. We also pay respect and homage to biomaterials pioneers who have contributed to this or previous editions, but have since passed on; their contributions and collegiality are remembered and will be missed.

The organizational skills, experience, and encouragement of the staff at Elsevier Publishers have led this fourth edition from a broad and complex challenge to a valuable volume—a tangible resource for the community. Thank you, Elsevier, for this contribution to the field of biomaterials.

The biomaterials field, since its inception in the 1950s, has been ripe with opportunity, intellectual stimulation, compassion, creativity, and rich collaboration. In this field we look to the horizons where the new ideas from science, technology, and medicine arise. Importantly, we strive to improve the survival and quality of life for billions through biomaterials-based medical devices and treatments. We, the new editors, together with the founding editors hope that the biomaterials textbook you are now reading will stimulate you as much as it has us.

William R. Wagner
Shelly E. Sakiyama-Elbert
Guigen Zhang
Michael J. Yaszemski
Founding Editors:
Buddy D. Ratner
Allan S. Hoffman
Frederick J. Schoen
Jack E. Lemons
March, 2020

How to Use this Book

Biomaterials Science: An Introduction to Materials in Medicine, fourth edition, was conceived as a learning tool to “compatibilize” through common language and fundamental principles, a number of independent communities (basic sciences, engineering, medicine, dentistry, industry, regulatory, legal, etc.). Although the book has 98 chapters, 4 appendices, there is a logic of organization and curriculum that should make the book straightforward to use in an academic course or as a reference work.

A guiding principle in assembling this multiauthor, multidisciplinary textbook is that fundamental and translational progress in the field of biomaterials necessitates integration of concepts and tools from the full spectrum of the physical sciences, engineering, clinical medicine, biology, and life sciences. Indeed, the discipline of biomaterials utilizes a convergence of multidisciplinary elements to enable the development of specific diagnostic or therapeutic devices—i.e., using biomaterials science and technology to create and implement real medical devices and other products that solve clinical problems and improve patient outcomes. Nevertheless, the editors believe (and the book has been assembled so) that a physician should be able to pick up the textbook and glean a baseline knowledge of the science, engineering, and commercialization aspects of biomaterials. A chemist could use this book to appreciate the biology behind biomaterials, the physiology associated with medical devices, and the applications in medicine. An engineer hired by a medical device company might learn the basic science underlying the technological development and details on medical applications. Similarly, for other disciplines that interface with biomaterials, this book can guide the reader through diverse but related topics that are generally not found in one volume.

The textbook has well over 100 authors. The field of biomaterials is so diverse in subject matter that a guiding principle has been that no one author can write it all—let us use the experience and wisdom of acknowledged masters of each subject to communicate the best information to

the reader. But, to prevent this book from appearing to be simply a collection of review papers, considerable editorial effort has gone into ensuring logical curricular organization, continuity of ideas, and extensive cross-referencing between chapters.

Biomaterials Science: An Introduction to Materials in Medicine, fourth edition, is divided into three parts: Materials Science and Engineering, Biology and Medicine, and The Medical Product Life Cycle. Sections then serve to subdivide each of these three parts (for example, under the part called “Materials Science and Engineering” there are sections on properties of materials and classes of materials used in medicine). And finally, within these sections can be found chapters, for example, on the major types of materials that are used in medicine (hydrogels, polyurethanes, titanium alloys, etc.). Each section begins with an introduction by one of the editors that will guide the reader through the chapters, giving cohesion to the sections and highlighting key issues that are worthy of attention. Finally, there are appendices that tabulate useful data and information.

For most chapters, exercises are provided for classroom use and for self-testing. These can be accessed via the companion website at <https://www.elsevier.com/books-and-journals/book-companion/9780128161371>. This site makes it possible to update problems and add new ones, and provides other resource materials, including a full artwork catalog and downloadable images used in the text. For instructors, solutions to the end-of-chapter exercises are provided on an Instructor Site at <http://textbooks.elsevier.com/web/Manuals.aspx?isbn=9780128161371>.

We hope that the textbook organization, the extensive editorial effort, and the expertly authored chapters will serve their intended purpose—to guide the reader into and through this complex field of biomaterials science. The editors always appreciate feedback and commentary—contact information is provided for them.

And now it is time to delve into the rich world of biomaterials science.

1.1.1

Introduction to Biomaterials Science: An Evolving, Multidisciplinary Endeavor

BUDDY D. RATNER¹, ALLAN S. HOFFMAN², FREDERICK J. SCHOEN³,
JACK E. LEMONS⁴, WILLIAM R. WAGNER⁵, SHELLY E. SAKIYAMA-ELBERT⁶,
GUIGEN ZHANG⁷, MICHAEL J. YASZEMSKI⁸

¹Bioengineering and Chemical Engineering, Director of University of Washington Engineered Biomaterials (UWEB), Seattle, WA, United States

²Bioengineering and Chemical Engineering, University of Washington, Seattle, WA, United States

³Department of Pathology, Brigham and Women's Hospital and Harvard Medical School, Boston, MA, United States

⁴Schools of Dentistry, Medicine and Engineering, University of Alabama at Birmingham, Birmingham, AL, United States

⁵Departments of Surgery, Bioengineering & Chemical Engineering, McGowan Institute for Regenerative Medicine, University of Pittsburgh, Pittsburgh, PA, United States

⁶Department of Biomedical Engineering, The University of Texas at Austin, Austin, TX, United States

⁷F Joseph Halcomb III, M.D. Department of Biomedical Engineering, University of Kentucky, Lexington, KY, United States

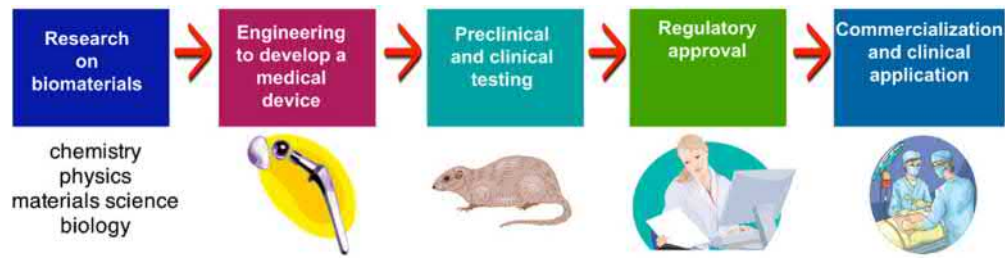
⁸Orthopaedic Surgery and Biomedical Engineering, Mayo Clinic College of Medicine, Rochester, MN, United States

Biomaterials and Biomaterials Science

Biomaterials Science: An Introduction to Materials in Medicine, fourth edition, addresses the design, fabrication, testing, applications, and performance as well as nontechnical considerations integral to the translation of synthetic and natural materials that are used in a wide variety of implants, devices, and process equipment that contact biological systems. These materials are referred to as biomaterials.

The compelling, human side to biomaterials is that millions of lives are saved, and the quality of life is improved for millions more.

The field of biomaterials is some 70–80 years old at the time of publication of this fourth edition. It significantly impacts human health, the economy, and many scientific fields. Biomaterials and the medical devices comprised of them are now commonly used as *prostheses* in cardiovascular, orthopedic, dental, ophthalmological, and reconstructive surgery, and in other interventions such as surgical sutures, bioadhesives, and controlled drug release devices. The compelling, human side to biomaterials is that millions of lives have been saved, and the quality of life improved for millions more, based on devices fabricated from biomaterials. The biomaterials field has seen accelerating growth since the



• **Figure 1.1.1.1** The path from the basic science of biomaterials, to a medical device, to clinical application.

first medical devices that were based on accepted medical and scientific principles made their way into human usage in the late 1940s and early 1950s. And the growth of the field is ensured, with the aging population, the increasing standard of living in developing countries, and the growing ability to address previously untreatable medical conditions.

Biomaterials science addresses both therapeutics and diagnostics. It encompasses basic sciences (biology, chemistry, physics) and engineering and medicine. The translation of biomaterials science to clinically important medical devices is dependent on: (1) sound engineering design; (2) testing in vitro, in animals and in humans; (3) clinical realities; and (4) the involvement of industry permitting product development and commercialization. Fig. 1.1.1.1 schematically illustrates the path from scientific development to the clinic.

Biomaterials science, in its modern incarnation, is an example of the emerging *convergence* paradigm that pushes multidisciplinary collaboration among experts and multidisciplinary integration of concepts and practice (Sharp and Langer, 2011). Not only biomaterials, but also bioinformatics, synthetic biology, computational biology, nanobiology, systems biology, molecular biology, and other forefront fields depend on convergence for their continued progress. This textbook aims to introduce these diverse multidisciplinary elements, particularly focusing on interrelationships rather than disciplinary boundaries, to systematize the biomaterials subject into a cohesive curriculum—a true convergence.

The title of this textbook, *Biomaterials Science: An Introduction to Materials in Medicine*, is accurate and descriptive. The intent of this work is: (1) to focus on the scientific and engineering fundamentals behind biomaterials and their applications; (2) to provide sufficient background knowledge to guide the reader to a clear understanding and appreciation of the clinical context where biomaterials are applied; and (3) to highlight the opportunities and challenges in the field. Every chapter in this text can serve as a portal to an extensive contemporary literature that expands on the basic ideas presented here. The magnitude of the biomaterials endeavor, its broadly integrated multidisciplinary scope, and examples of biomaterials applications will be revealed in this introductory chapter and throughout the book.

The common thread in biomaterials is the physical and chemical interactions between complex biological systems and synthetic or modified natural materials.

Although biomaterials are primarily used for medical applications (the focus of this text), they are also used to grow cells in culture, to assay for blood proteins in the clinical laboratory, in processing equipment for biotechnological applications, for implants to regulate fertility in cattle, in diagnostic gene arrays, in the aquaculture of oysters, and for investigational cell–silicon “neuronal computers.” How do we reconcile these diverse uses of materials into one field? The common thread is the physical and chemical interactions between complex biological systems and synthetic materials or modified natural materials.

In medical applications, biomaterials are rarely used as isolated materials, but are more commonly integrated into devices or implants, and complex devices may use multiple biomaterials, often selected from several classes (e.g., metal and polymer). Chemically pure titanium can be called a biomaterial, but shaped (machined) titanium in conjunction with ultrahigh molecular weight polyethylene becomes the device, a hip prosthesis. Although this is a text on biomaterials, it will quickly become apparent that the subject cannot be explored without also considering biomedical devices and the biological response to them. Indeed, both the material and the device impact the recipient (patient) and, as we will see, the patient’s host tissue impacts the device. These interactions can lead to device success or, where there is inappropriate choice of biomaterials or poor device design, device failure. Moreover, specific patient characteristics may influence the propensity to failure (e.g., obesity increasing the likelihood of fracture or excessive wear of a hip joint prosthesis, or clotting of a mechanical heart valve in a patient with a genetic mutation that causes hyper-coagulability).

Furthermore, a biomaterial must always be considered in the context of its final fabricated, sterilized form. For example, when a polyurethane elastomer is cast from a solvent onto a mold to form the pump bladder of a heart assist device, it can elicit different blood reactions compared to when injection molding is used to form the same device. A hemodialysis system serving as an artificial kidney requires materials that must function in contact with a patient’s blood, and also exhibit appropriate membrane permeability and mass transport characteristics. Much fabrication technology is applied to convert the biomaterials of the hemodialysis system (polysulfone, silicone rubber, polyethylene) into the complex apparatus that is used for blood purification.

Due to space limitations and the materials focus of this work, many aspects of medical device design are not addressed in this book. Consider the example of the hemodialysis system. This textbook will overview membrane materials and

their biocompatibility; there will be little coverage of mass transport through membranes, the burst strength of membranes, dialysate water purification, pumps, flow systems, and monitoring electronics. Other books and articles cover these topics in detail, and chapter authors provide references useful to learn more about topics not explicitly covered.

Key Definitions

The words “biomaterial” and “biocompatibility” have already been used in this introduction without formal definition. A few definitions and descriptions are in order, and will be expanded upon in this and subsequent chapters.

A definition of “biomaterial” endorsed by a consensus of experts in the field is:

A biomaterial is a nonviable material used in a medical device, intended to interact with biological systems.

WILLIAMS (1987).

A biomaterial is a nonviable material used in a medical device, intended to interact with biological systems.

Although biomaterials are most often applied to meet a therapeutic or diagnostic medical need, if the word “medical” is removed, this definition becomes broader and can encompass the wide range of applications already suggested. If the word “nonviable” is removed, the definition becomes even more general, and can address many new tissue-engineering and hybrid artificial organ applications where living cells are used.

“Biomaterials science” is the study (from the physical and/or biological perspective) of materials with special reference to their interaction with the biological environment. Traditionally, emphasis in the biomaterials field has been on synthesis, characterization, and the host–material interactions biology. Yet, most biomaterials (which meet the special criteria of biocompatibility—see Chapters 2.3.2 and 2.3.4) induce a nonspecific biological reaction that we refer to as

the foreign-body reaction (Chapter 2.2.2). This leads us to consider a widely used definition of biocompatibility:

“Biocompatibility” is the ability of a material to perform with an appropriate host response in a specific application.

WILLIAMS (1987).

“Biocompatibility” is the ability of a material to perform with an appropriate host response in a specific application.

Examples of “appropriate host responses” include resistance to blood clotting, resistance to bacterial colonization, and normal, uncomplicated healing. Examples of “specific applications” include a hemodialysis membrane, a urinary catheter, or a hip joint replacement prosthesis. Note that the hemodialysis membrane might be in contact with the patient’s blood for 5 h (and outside the body), the catheter may be inserted for a week (inside the body, and designed to be easily removed), and the hip joint may be in place for the life of the patient (deeply implanted and meant to be long-term). This general concept of biocompatibility has been extended to tissue engineering, in which in vitro and in vivo processes are harnessed by careful selection of cells, materials, and metabolic and biomechanical conditions to regenerate functional tissues. Ideas central to biocompatibility are elaborated upon in Ratner (2011) and Chapter 2.3.2.

In the discussion of these definitions, we are introduced to considerations that set biomaterials apart from most materials explored in materials science. Table 1.1.1.1 lists a few applications for biomaterials in the body. It includes many classes of materials used as biomaterials. Note that metals, ceramics, polymers, glasses, carbons, and natural and composite materials are listed. Such materials are used as molded or machined parts, coatings, fibers, films, membranes, foams, fabrics, and particulates. Table 1.1.1.1 also gives estimates of the specific device global market size and, where available, an estimate of the number of medical devices utilized annually. The human impact, and the size of the commercial market for biomaterials and the broad array of medical devices, is impressive (Tables 1.1.1.1 and 1.1.1.2).

TABLE
1.1.1.1

Key Applications of Synthetic Materials and Modified Natural Materials in Medicine

Application	Biomaterials Used	Number/Year—Global (or Global Market in US\$)
Skeletal System		
Joint replacements (hip, knee, and shoulder)	Titanium, CoCr, polyethylene, alumina, zirconia	4,000,000 (\$16B)
Trauma fixation devices (plates, screws, pins, and rods)	Titanium, stainless steel, CoCr, polyether ether ketone, poly(lactic acid) (PLA)	1,500,000 (\$5.5B)
Spine disks and fusion hardware	Nitinol, titanium, polyether ether ketone, stainless steel	1,100,000 (\$8.5B)
Bone defect repair	Calcium phosphates, human bone products	(\$4.5B)
Bone cement (fixation)	Polymethyl methacrylate (PMMA), glass polyalkenoate (ionomer), calcium phosphate cements	(\$1.1B)
Cartilage, tendon, or ligament repair and replacement	Decellularized porcine tissue, poly(lactide) and metallic fixation devices, collagen, hyaluronic acid lubricants	(\$8.6B)
Dental implant-tooth fixation	Titanium, zirconium	10,000,000 (\$4B)

(Continued)

TABLE
1.1.1.1

Key Applications of Synthetic Materials and Modified Natural Materials in Medicine—cont'd

Application	Biomaterials Used	Number/Year—Global (or Global Market in US\$)
Cardiovascular System		
Vascular grafts, patches, and endovascular devices (stent grafts)	Dacron, expanded poly(tetrafluoroethylene), Nitinol, CoCr, stainless steel, fixed tissue	(\$2.5B)
Heart valves: mechanical and bioprosthetic (transcatheter and traditional)	Dacron, carbon, CoCr, fixed bovine and porcine tissue, stainless steel, Nitinol	600,000 (\$5.5B)
Pacemakers	Titanium, polyurethane	1,000,000 (\$6.5B)
Implantable defibrillators	Titanium, polyurethane	300,000 (\$9.0B)
Stents: coronary, peripheral vasculature, and nonvascular	Stainless steel, Nitinol, CoCr, Pt, tantalum, Mg alloys, poly(styrene- <i>b</i> -isobutylene- <i>b</i> -styrene), poly(<i>n</i> -butyl methacrylate), polyethylene- <i>co</i> -vinyl acetate, phosphoryl choline containing block copolymers, poly(lactic- <i>co</i> -glycolic acid), PLA	5,000,000 (\$10.6B)
Catheters: cardiovascular, urologic, and others	Polytetrafluoroethylene (PTFE), poly(vinyl chloride), silicone, polyurethane	(\$28B)
Organs		
Cardiac assist devices (acute and chronic)	Titanium alloy, polycarbonate, PTFE, poly(ethylene terephthalate), stainless steel	(\$1.7B)
Hemodialysis	Polysulfone, modified cellulose, polyacrylonitrile, polycarbonate, silicone, polyvinylchloride	2,000,000 patients (\$12B)
Blood oxygenator	Polymethylpentene, polypropylene, polysiloxane, poly(vinyl chloride), polycarbonate	(\$300M)
Skin substitute (chronic wounds, burns)	Collagen, cadaver skin, alginate, polyurethane, carboxymethylcellulose, nylon, silicone	(\$1.3B)
Ophthalmologic		
Contact lens	PMMA, polyhydroxyethylmethacrylate (PHEMA), polyvinyl alcohol, polyvinyl pyrrolidone, silicone (polydimethyl siloxane [PDMS])	(\$7.5B)
Intraocular lens	PMMA, PDMS, polyacrylate-PMMA, PHEMA	25,000,000 (\$4.5B)
Glaucoma drains	Silicone, polypropylene, cross-linked collagen, stainless steel	(\$500M)
Other		
Cochlear prostheses	Platinum, platinum-iridium, PDMS, titanium, aluminum oxide	45,000 (\$2.7B)
Breast implants	PDMS	3,600,000 (\$1.2B)
Hernia and body wall repair meshes	Polypropylene, polyester, expanded PTFE, decellularized porcine/bovine tissue	(\$4.2B)
Sutures	Silk, nylon, poly(glycolic acid), PLA, polydioxanone, polyester copolymers, polypropylene, PTFE, processed bovine tissue	(\$3.9B)
Blood bags	Poly(vinyl chloride)	(\$170M)
Ear tubes (tympanostomy)	Silicone, PTFE	1,500,000 (\$70M)
Intrauterine device	Polyethylene, copper, stainless steel, PDMS	168,000,000 (\$2.9B)

Data compiled from multiple sources—these numbers should be considered rough estimates that are changing with growing markets and new technologies. Where only US numbers were available, world usage was estimated at approximately 2.5× US. *B*, Billion; *M*, million.

TABLE 1.1.1.2 The Medical Device Global Market by Segment With Projected Compound Annual Growth Rate (CAGR) (\$ Millions)

Segments	2016	2017	2022	CAGR 2017–2022 (%)
Drug delivery devices	200,072	207,814	243,367	3.2
Urology and renal	75,378	82,668	109,003	5.7
In vitro diagnostics	66,143	72,816	99,357	6.4
Orthopedics and spine	65,756	72,086	99,559	6.7
Imaging devices	41,194	45,816	64,282	7.0
Cardiovascular devices	25,384	29,658	45,260	8.8
Endoscopy	9,573	10,372	13,693	5.7
Total	483,500	521,230	674,521	5.3

Source: BCC Research.

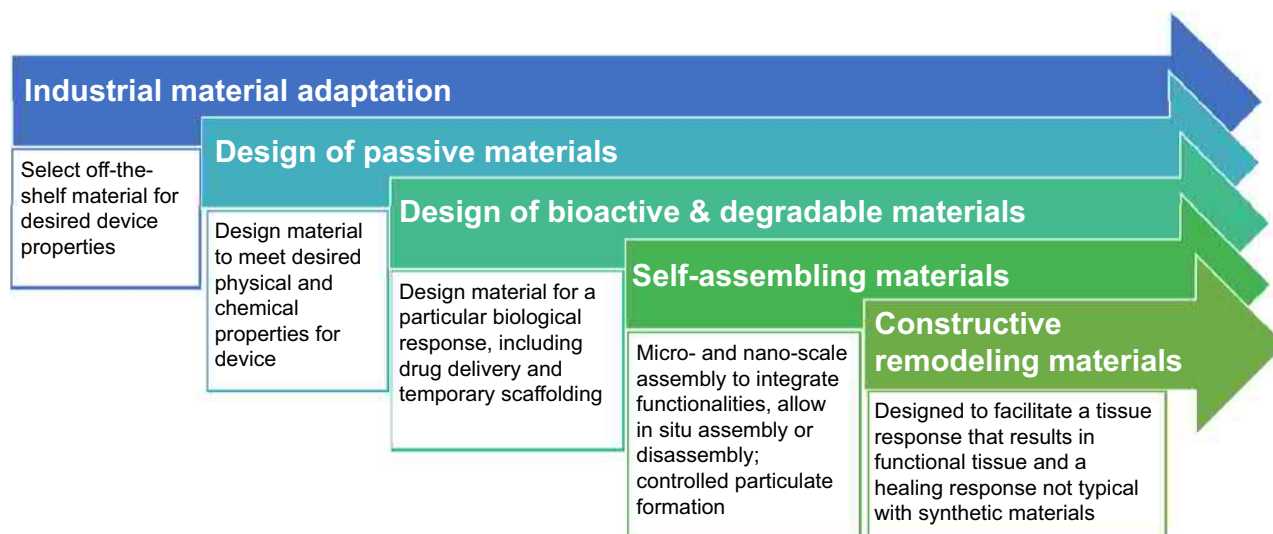
The Expansion of the Biomaterials Field

Biomaterials research and development have been stimulated and guided by advances in cell and molecular biology, pathology, clinical medicine and dentistry, chemistry, materials science, and engineering. The biomaterials community has been the major contributor to the understanding of the interactions of materials with the physiological environment (often referred to as the biointerface). The development of biomaterials for medical and dental applications has evolved with time, as new concepts and understandings are applied to offer a broadening repertoire of choices to meet device design objectives (Fig. 1.1.1.2).

Early applications of biomaterials sought to achieve a suitable combination of functional properties to adequately meet the design needs for the medical device under development.

Generally, this would involve the layering of biocompatibility concerns from host–material interactions on top of those more readily understood physical and chemical requirements. For instance, for a mechanical cardiac valve, materials could be selected and integrated to provide the functional response in an altering pressure flow field, resistance to cyclic mechanical wear, and suturability. In these early applications, industrial materials were typically taken off the shelf, i.e. “medical grade” biomaterials were not yet available. Nevertheless from the array of industrially available materials that might meet these requirements, considerations of blood and tissue compatibility would be included.

Pioneers in the device field effectively applied empirical approaches to arrive at materials that could meet both the traditional (nonbiological) design requirements and



• **Figure 1.1.1.2** The growing palette of biomaterials. Generally moving with time from the 1940s adaptation of industrially available materials for early medical devices to the present, the breadth of described biomaterials continues to grow. In device development a biomaterial may be selected to leverage recent progress. However, it is important to note that major advances in the medical device field continue to be made with materials that could be considered first generation. The growing palette provides the design engineer with more tools to optimize device functionality in concert with other concerns such as manufacturability, regulatory burden, and economic considerations.

exhibit adequate levels of biocompatibility. Materials would generally be selected because they were tolerable (i.e., they elicited minimal response from the host tissues), and this would be consistent with *biocompatibility* for many applications (see [Chapter 2.3.2](#)). While the understanding of biomaterials science has evolved substantially from these early days, it is important to recognize that industrially repurposed materials continue to be utilized in many widely used medical devices today, including poly(tetrafluoroethylene) and poly(ethylene terephthalate), from which virtually all synthetic vascular grafts are made, stainless steel, cobalt–chromium alloys and titanium alloys, from which many orthopedic devices are constructed, and the polyurethanes and polysiloxanes that are utilized in a broad array of catheters and medical tubing. Furthermore, industrially adapted materials continue to be the biomaterials of choice for many revolutionary *new* devices introduced in recent years such as many of the components related to neurostimulatory devices and structural heart repair.

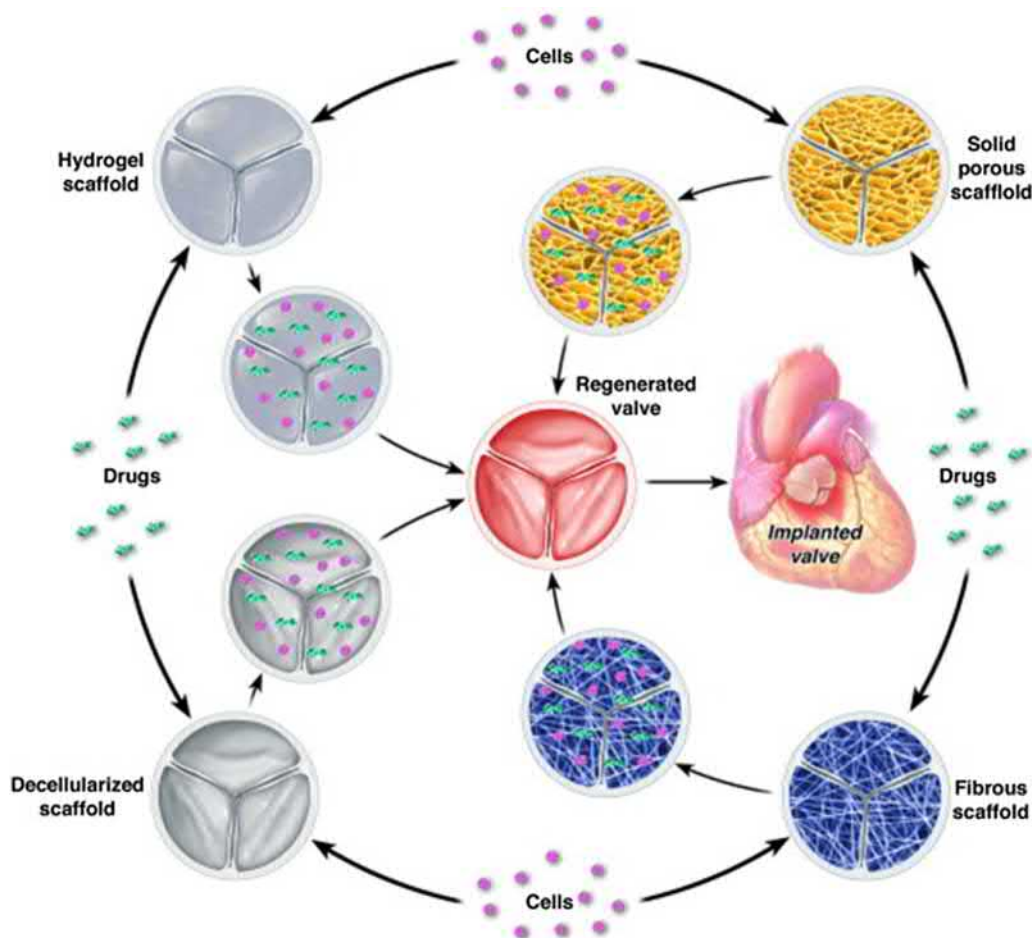
In this early period it would also occasionally be noted where an off-the-shelf material or class of materials might not fully achieve the target device design objectives and novel materials would be designed or refined specifically for a biomedical purpose. As highlighted in [Chapter 1.1.2](#), biomaterials scientists would, for instance, create polyurethanes with segments selected for the purpose of improving blood biocompatibility. Hydrogels would be synthesized for soft tissue applications. Pyrolytic carbon, originally developed in the 1960s as a coating material for nuclear fuel particles, was studied and tuned for what is now in wide use in modified compositions to coat components of mechanical cardiac valves. These designed materials broadened the biomaterials palette, but the materials were still designed to be passive in achieving biocompatibility. As with early adapted industrial materials, these types of biomaterials continue to play an important part in device design and active research continues to seek to develop materials that are better suited for specific device applications while still targeting a passive, bioinert posture. For instance, efforts to find more degradation-resistant polymers for challenging device applications are ongoing ([Chapter 2.4.2](#)).

As knowledge of biological interactions with materials evolved, new types of biomaterials were developed with the intention of eliciting a controlled reaction with the tissues they contacted to induce a desired therapeutic effect. In the 1980s, these *bioactive* materials were in clinical use in orthopedic and dental surgeries as various compositions of bioactive glasses and ceramics ([Hench and Pollak, 2002, Chapter 1.3.4](#)), in controlled localized drug release applications such as the Norplant hormone-loaded contraceptive formulation ([Meckstroth and Darney, 2001](#)), and in the attachment of the anticoagulant heparin to the surfaces of membrane oxygenators with various modification strategies ([Chapter 1.4.3B](#)). Vascular stents have also been profoundly impacted by the implementation of a bioactive approach, with the application of polymer coatings that release antiproliferative agents and markedly reduce a major failure mechanism of tissue overgrowth and vessel occlusion ([Chapter 2.5.2B](#)).

Bioactive biomaterial development has also included the synthesis of resorbable polymeric biomaterials, with rates of degradation that could be tailored to the requirements of a desired application ([Chapter 1.3.2F](#)). Thus the discrete interface between the implant site and the host tissue could be eliminated in the long term, because the foreign material would ultimately be degraded to soluble, nontoxic products by the host. Many groups continue to develop new biodegradable polymers designed with defined objectives in strength, flexibility, a chemical composition conducive to tissue development, and a degradation rate consistent with the specific application. Degradable materials have been integral to the tissue-engineering paradigm where a scaffold, alone or in combination with cells and drugs, may provide for the generation of functional tissue. This paradigm as applied to the engineering of a cardiac valve is presented in [Fig. 1.1.1.3](#) and is covered in the chapters of [Section 2.6](#). Tissue-engineering approaches often leverage degradable biomaterials scaffolds, drug-releasing biomaterials, and in some cases utilize specific cell receptor–ligand interactions or enzymatic degradability to build bioactivity into the biomaterials scaffold ([Chapters 1.4.4 and 1.4.5](#)).

A characteristic of bioactive biomaterials development over the past several decades has been the leverage of fundamental knowledge from molecular biology. As this knowledge base has grown, biomaterials scientists and engineers have translated the understanding of biomolecular interactions to engineer biological interactions with designed materials. An early example of this was the application of knowledge of the adhesion peptide sequences from proteins such as fibronectin (e.g., Arg-Glu-Asp-Val) to engineer peptide-modified surfaces that would support specific types of cell adhesion ([Hubbell et al., 1991](#)). Polymeric materials with other novel properties such as shape-memory and programmable and interactive surfaces that control the cellular microenvironment are areas of development ([Chapter 1.3.2G](#)). In addition to having implications for medical applications, such engineered smart biomaterials systems have been used to advance our understanding of molecular biology principles, for instance, in elucidating the roles of substrate stiffness, ligand density, and three-dimensional culture in mammalian cell behavior.

The need for maximally effective pharmacologic dosing regimens and minimization of systemic toxicities has stimulated development of innovative particulate systems for targeted drug delivery and gene therapy ([Chapter 1.3.8](#)). Such systems may also provide the basis for targeted imaging or the combination of targeted imaging and therapeutic delivery, representing the growing field of theranostics. This focus area is experiencing a great deal of research attention at present by the biomaterials community and many of the approaches involve the production of nano- and microscale particulates using the principles of self-assembling materials. Several factors are driving this effort to design better biomaterials-based approaches: advances in protein and nucleic acid-based drugs (which cannot be taken in classical pill form, have high cost, and are labile); a better understanding of transport mechanisms systemically, within

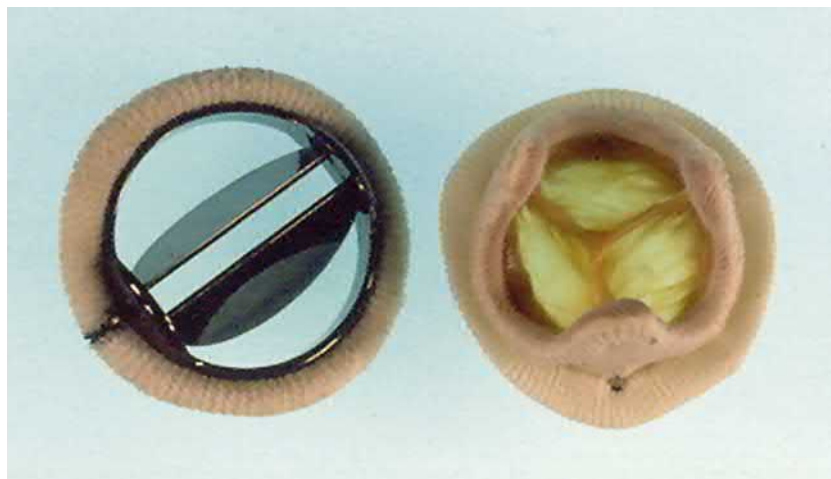


• **Figure 1.1.1.3** An example of various tissue-engineering paradigms applied to a cardiac valve. Current approaches for many tissues, including heart valves, may involve scaffolds, cells, and drugs. These components may be used alone or in combination. For each component, different material types, drugs, or cells may be used. Again, alone or in combination, bioreactors may be employed to allow some level of tissue construct maturation, or the body may serve as the bioreactor. (From Jana, S., Tefft, B.J., Spoon, D.B., Simari, R.D., 2014. Scaffolds for tissue engineering of cardiac valves. *Acta Biomater.* 10, 2877–2893.)

specific tissues or tumors, and intracellularly; and an increasing ability to create precise structures at macromolecular scales through controlled polymerization techniques and specific orthogonal reaction schemes.

Self-assembled biomaterials have allowed design at the nanoscale to protect drug payloads that are released with an appropriate signal (e.g., pH, radiation, intracellular environmental cues) upon delivery at the desired site through the surface presentation of targeting moieties and molecules that reduce fouling and improve pharmacokinetics. Self-assembled biomaterials have also found broad interest as injectable networks for the creation of scaffolds and depots in regenerative medicine, drug delivery, and immunoengineering (Sahoo et al., 2018). Here, by switching out functional groups on larger self-assembling molecules, the specific bioactivity and mechanical properties of an assembled network may be designed. Interest is also growing in the structural and functional tailoring of self-assembled two-dimensional organic biomaterials to open new opportunities by controlling biomaterials at the nanoscale for highly specific, spatially orchestrated biological interactions (Zhang et al., 2019).

A final category in the growing repertoire of biomaterials is what could be termed constructive remodeling materials. Such materials have been designed or processed to facilitate a healing response that does not follow the classic foreign-body response found with most synthetic tissues, but is characterized by remodeling of the tissue with minimal scarring. This response has been observed and well documented in biomaterials derived from animal-based tissues that have been decellularized to reduce immunogenicity, but which have not been chemically cross-linked. Chemical cross-linking is a critical part of maintaining structural viability for many biomaterials (e.g., bioprosthetic cardiac valves from bovine or porcine source tissues), but in this approach a tissue, such as porcine bladder or dermis, is meant to be degraded and remodeled at the implantation site, and in this remodeling process, be replaced with host tissue that is functional as opposed to fibrotic. These types of materials are described in Chapter 1.3.6, and the role of the immune response with these types of natural materials versus most synthetic materials or cross-linked natural materials is addressed in Chapter 2.2.2. As the biomaterials community better understands the mechanisms



• **Figure 1.1.1.4** Prosthetic heart valves. *Left*: A bileaflet tilting disk mechanical heart valve (St. Jude Medical Inc., St. Paul, MN). *Right*: A bioprosthetic (xenograft) tissue heart valve (Hancock valve, Medtronic Inc., MN).

by which constructive remodeling can be achieved, this knowledge is being applied in materials designed to orchestrate specific interactions with the immune system to moderate the host response. More broadly, biomaterials are being developed in the area of immunoengineering (Chapter 2.5.10) to impact the immune system in applications related to immunization, cancer, infection, and autoimmune diseases.

Examples of Today's Biomaterials Applications

Five examples of biomaterials applications now follow to illustrate important ideas. The specific devices discussed were chosen because they are widely used in humans with good success. However, key limitations with these biomaterial devices are also highlighted. Each of these examples is also discussed in detail in later chapters in this textbook.

Heart Valve Prostheses

Diseases and degeneration of the heart valves often make surgical repair or replacement necessary. The natural heart valve opens and closes over 40 million times per year, and can require replacement due to disease or wear. Approximately 4,500,000 replacement valves are implanted each year worldwide, because of acquired damage to the natural valve and congenital heart anomalies. There are many types of heart valve prostheses, and they are fabricated from carbons, metals, elastomers, plastics, fabrics, and animal or human tissues chemically pretreated to reduce their immunologic reactivity, and to enhance durability. Fig. 1.1.1.4 shows a bileaflet tilting disk mechanical heart valve and a bioprosthetic (porcine xenograft) tissue heart valve, two of the most widely used designs. Generally, as soon as the valve is implanted, cardiac function is restored to near normal levels, and the patient shows rapid improvement. In spite of the overall success seen with replacement heart valves, there are problems, many of them specific to a certain type of valve; they include

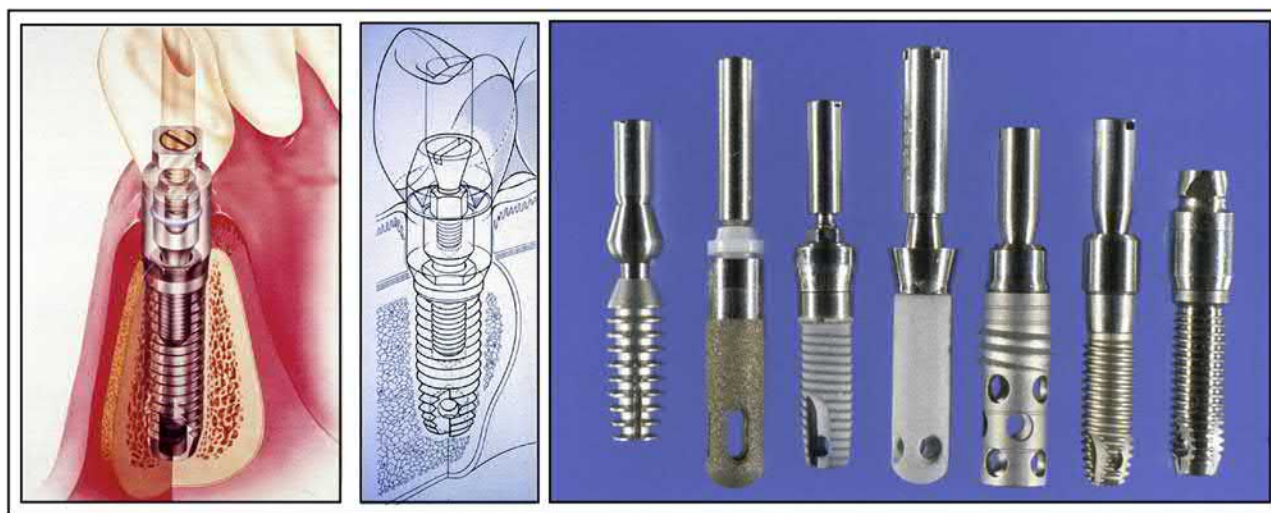


• **Figure 1.1.1.5** A hip prosthesis. Microplasty titanium alloy femoral stem, Biolox alumina–zirconia ceramic femoral head, and ultrahigh molecular weight polyethylene acetabular cup infused with vitamin E antioxidant. (Image courtesy of Biomet, Inc.)

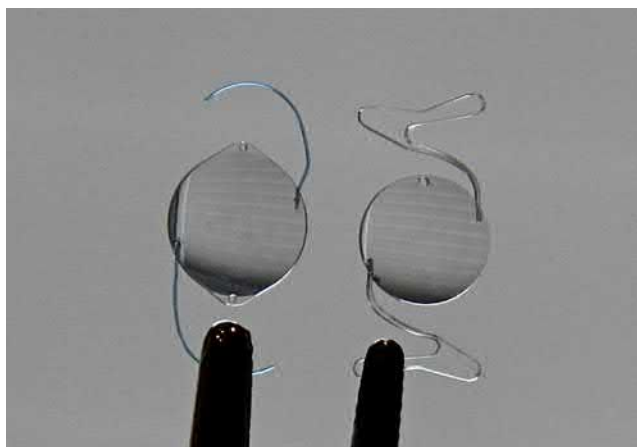
induction of blood clots, predominantly with mechanical valves (sometimes shed into the bloodstream as emboli and creating an ongoing risk for stroke, thus necessitating long-term therapy with potentially dangerous anticoagulant drugs), degeneration of valve tissue leaflets, mechanical failure, and infection. This biomaterial application continues to be an active area of innovation, most recently with growing clinical use of valve designs implanted through a catheter and in the advancement of tissue-engineering approaches for valve replacement (Zhang et al., 2019). Heart valve substitutes are discussed in Chapter 2.5.3A.

Total Hip Replacement Prostheses

The human hip joint is subjected to high levels of mechanical stress and receives considerable abuse in the course of normal and extraordinary activity. It is not surprising that after 50 or more years of cyclic mechanical stress or because of degenerative or rheumatoid disease, the natural joint wears out, leading to loss of mobility and sometimes confinement to a wheelchair. Hip joint prostheses are fabricated from a variety of materials, including titanium, stainless steel, special high-strength alloys, ceramics, composites, and ultrahigh molecular weight polyethylene. Replacement hip joints (Fig. 1.1.1.5) are implanted



• **Figure 1.1.1.6** Schematic images of early dental root form implants and a photograph of several designs used in clinical practice.



• **Figure 1.1.1.7** Two styles of multipiece intraocular lenses.

in more than 300,000 humans each year in the United States alone. With some types of replacement hip joints and surgical procedures that use a polymeric cement, ambulatory function is restored within days after surgery. For other types, a healing-in period is required for integration between bone and the implant before the joint can bear the full weight of the body. In most cases, good function is restored. Even athletic activities are possible, although those activities that subject the repaired joint to high stress are generally not advisable. After 10–15 years, many of these implants fail by loosening, which usually necessitates another operation (a revision procedure). Metal-on-metal implants also experience problems of corrosion and adverse responses to released metal ions. Artificial hip joint prostheses are discussed in [Chapter 2.5.4](#).

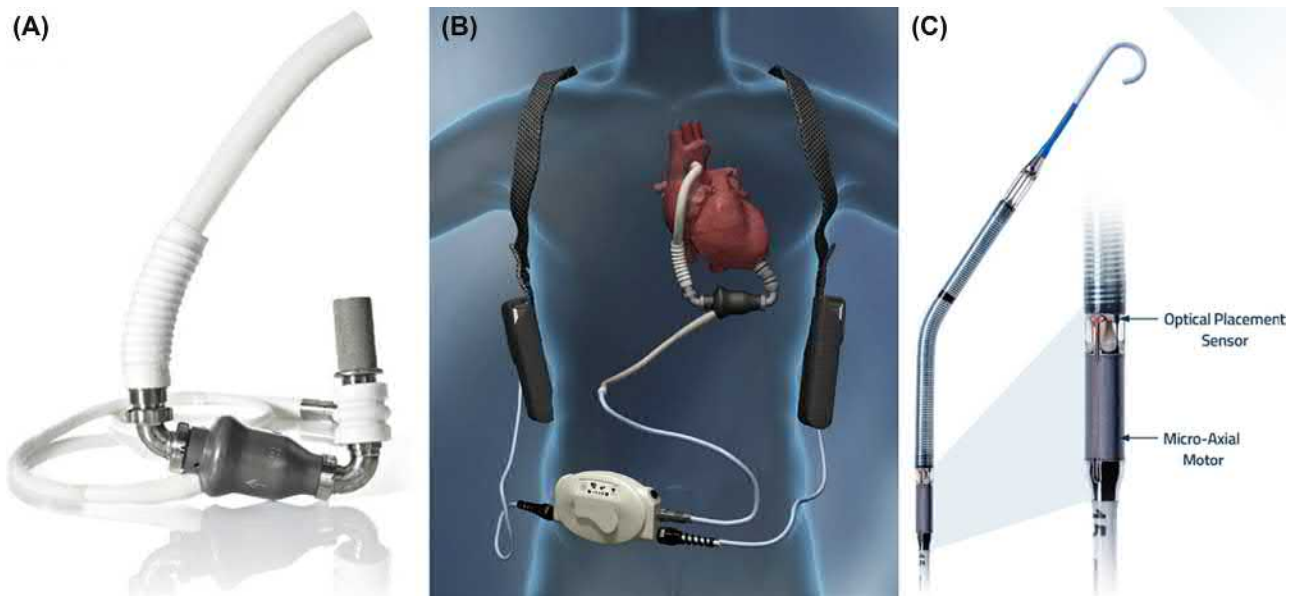
Dental Implants

The development of root form designs of titanium implants ([Fig. 1.1.1.6](#)) by Per-Ingvar Brånemark revolutionized dental implantology ([Carlsson et al., 1986](#)). These devices form

an implanted artificial tooth anchor upon which a crown is affixed and are implanted in 5,000,000 people each year in the United States alone, according to the American Dental Association. A special requirement of a material in this application is the ability to form a tight seal against bacterial invasion where the implant traverses the gingiva (gum). Other issues are associated with the rapidly growing junctional epithelium inhibiting regrowth of the slower growing bone. Also, in normal physiology, the tooth is connected to the jaw by the periodontal ligament and is not directly attached to the jawbone. One of the primary advantages originally cited for the titanium implant was its osseous integration with the bone of the jaw. In recent years, however, this attachment has been more accurately described as a tight apposition or mechanical fit, and not true bonding. Loss of tissue support leading to loosening remains an occasional problem, along with infection and issues associated with the mechanical properties of unalloyed titanium that is subjected to long-term cyclic loading. Dental implants are discussed in [Chapter 2.5.5](#).

Intraocular Lenses

Implants to replace lenses in the eye that have clouded due to cataracts are called intraocular lenses (IOLs). They have been fabricated from a variety of transparent materials, including poly(methyl methacrylate), silicone elastomer, soft acrylic polymers, and hydrogels ([Fig. 1.1.1.7](#)). By the age of 75, more than 50% of the population suffers from cataracts severe enough to warrant IOL implantation. This now translates to an estimated 25 million implants worldwide as cataract treatment is expanding rapidly in healthcare systems with growing economies and aging populations. Good vision is generally restored almost immediately after the lens is inserted, and the success rate with this device is high. IOL surgical procedures are well developed, and implantation is most often performed on an outpatient



• **Figure 1.1.1.8** A commonly utilized chronic ventricular assist device (VAD). (A) Continuous flow pump with associated inflow/outflow grafts and electrical drive line (Heartmate II device). (B) Schematic of VAD implanted as a left ventricular assist device with associated external power source. (C) A catheter-based rotary blood pump from Impella for acute cardiac support. The tip of the device is placed in the ventricle where openings allow blood flow into the lumen of the device. Blood is pumped with a microaxial rotary motor and expelled through catheter openings in the region of the device that rests in the aorta. (Images A and B obtained with permission from Thoratec Corporation. Image C obtained from https://mms.businesswire.com/media/20190831005001/en/740858/5/SmartAssist_Press_release_image.jpg?download=1.)

basis. Observations of implanted lenses through the cornea using a microscope to directly study the implants show that inflammatory cells such as macrophages migrate to the surface of the lenses after implantation. Thus the conventional healing pathway is seen with these devices, similar to that observed with materials implanted in other sites in the body. Outgrowth of cells onto the IOL from the posterior lens capsule, stimulated by the presence of the IOL, can cloud vision, and this is a significant complication. IOLs are discussed in [Chapter 2.5.6](#).

Ventricular Assist Devices

Nearly 5,000,000 Americans are living with seriously failing hearts (congestive heart failure), and 300,000 individuals will die each year from this disease. According to the American Heart Association, 50,000–100,000 of these individuals might benefit from cardiac transplantation or mechanical circulatory support. Since the available pool of donor hearts for transplantation is only ~3500 per year (United States), effective and safe mechanical cardiac assist or replacement seems like a desirable option. Ventricular assist devices (VADs) have evolved from a daring experimental concept, the mechanical total heart, to a life-prolonging tool (see [Chapter 2.5.2A](#)). A number of devices have received regulatory approval and designs have evolved from bulky pulsatile pumps with chambers and opposing valves (mimicking the human heart) to much smaller rotary devices compatible with a broader array of patients. VADs are now used in multiple ways: to maintain (“bridge”) a patient with a failing heart while awaiting a donor organ, as a permanent source of support for patients

not destined for a heart transplant, and as temporary support where cardiac function is at risk due to a procedure, or when a weakened heart is expected to recover in the short term and device support can be withdrawn. A commonly utilized rotary VAD for extended cardiac support and a catheter-based device used for temporary support are illustrated in [Fig. 1.1.1.8](#). Recipients of VADs designed for chronic support can have considerable mobility and freedom, with most being discharged from the hospital setting. Despite patients being supported in some cases for several years, there remains an elevated risk for device-related infection (particularly in the region where the control and power line crosses the skin) and stroke related to the embolization of clots formed within the device. Furthermore, although VAD therapy that sends a patient home with a device may be economically more efficient and provide better outcomes than an extended period in an intensive care unit, the therapy remains expensive and is not feasible for broad application in the health systems of many countries. Can so expensive an innovation be made available to the wide patient base that could benefit from them? Wider adoption and increased entries into the market are reducing costs, but the fact of profound global disparities in medical device adoption remains for VADs and other complex and new device technologies. Developing approaches for best practices in medical device management are an area of interest and study within the World Health Organization and the reader is referred to an ongoing series of publications and forums from this source that consider how to best translate medical device advances across disparate healthcare economies.

These five cases, only a small fraction of the important medical devices that could have been used as examples,

spotlight central ideas and themes relevant to most medical devices interfacing with the human biology. A few generalizations are:

- Implantation in hundreds of thousands of patients with good success is noted.
- A broad range of synthetic materials of varying properties are used.
- Most anatomical sites can be interfaced with a device.
- The normal response by which the body responds to foreign bodies is observed.
- Problems, concerns, unexplained observations, or unintended consequences may be noted for each device.
- Most device complications are related to biomaterials–tissue interactions.
- Companies are manufacturing devices and bringing value to shareholders (and patients).
- Regulatory agencies are carefully assessing device performance, and making policy decisions to monitor the device industry, ensure quality, and protect the patient.
- Ethical and societal issues are associated with each device.

These ideas are relevant to nearly all medical devices. As you work through this text, consider how these ideas impact the specific topic you are studying.

Characteristics of Biomaterials Science

Now that we have defined key terms and reviewed specific examples highlighting successes and also complications, we can examine core characteristics of the field of biomaterials.

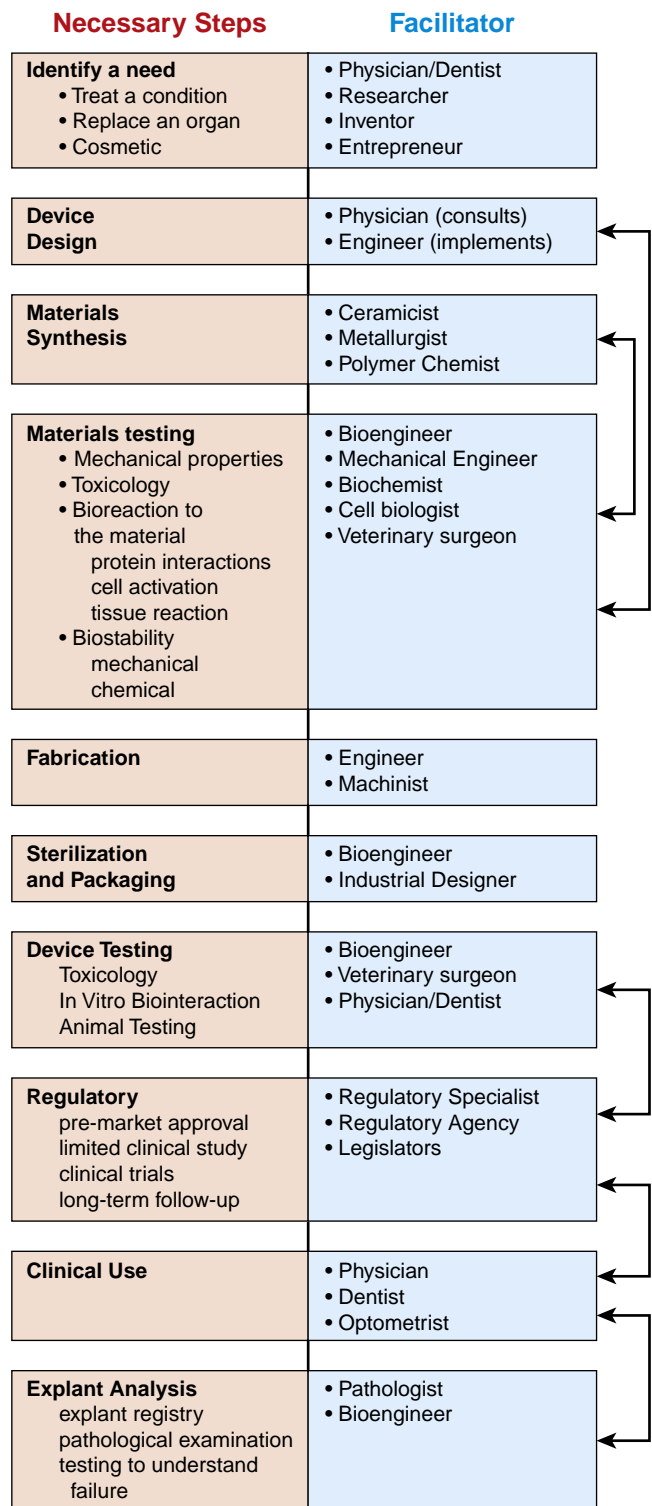
Multidisciplinary

More than any other field of contemporary technology, biomaterials science brings together teams of researchers from diverse academic and industrial backgrounds, who characteristically speak different “languages” yet must clearly communicate and integrate complex concepts and data. Fig. 1.1.1.9 lists some of the disciplines and key steps that are encountered in the progression from identifying the need for a biomaterial or device to its testing, regulation, manufacture, sale, and implantation.

Diverse Materials Are Used

The biomaterials scientist must have an appreciation of materials science, including polymers, metals, ceramics, glasses, composites, and biological materials. This may range from an impressive command of the theory and practice of the field demonstrated by the professional materials scientist to a general understanding of the properties of materials that should be possessed by the physician or biologist investigator involved in biomaterials-related research.

A wide range of materials is routinely used in medical devices (Table 1.1.1.1), and no one researcher will be comfortable synthesizing, processing, characterizing, designing, and fabricating with all these materials. Thus specialization is common and appropriate. However, a broad appreciation of the properties and applications of these materials,



• **Figure 1.1.1.9** The path from an identified need to a clinical product, and some of the disciplines that facilitate this developmental process.

the palette from which the biomaterials scientist “creates” medical devices, is a hallmark of professionals in the field.

There is a tendency to group biomaterials and researchers into the “hard tissue replacement” camp, typically represented by those involved in orthopedic and dental materials, and the “soft tissue replacement” camp, frequently associated with cardiovascular implants and general plastic surgery materials.

TABLE 1.1.1.3 Cardiovascular Device Market by Region and With Projected Compound Annual Growth Rate (CAGR) (\$ Millions)

Region	2016	2017	2020	CAGR 2017–2022 (%)
North America	9,811	11,329	16,543	7.9
Europe	7,293	8,458	12,084	7.4
Asia	5,610	6,709	11,406	11.2
Rest of World	2,670	3,162	5,218	10.6
Total	25,384	29,658	45,260	8.8

Source: BCC Research.

Hard tissue biomaterials researchers are thought to focus on metals and ceramics, while soft tissue biomaterials researchers are considered polymer experts. In practice, this division is artificial: a heart valve may be fabricated from polymers, metals, and carbons (and processed tissue). A hip joint will also be composed of metals and polymers (and sometimes ceramics), and may be interfaced with the body via a polymeric bone cement. There is a need for a general understanding of all classes of materials and the common conceptual theme of their interaction with the biological milieu. This text provides a background to the important classes of materials, hard and soft, and their interactions with the biological environment.

Biomaterials to Devices to Markets and Medicine

Thomas Edison once said that he would only invent things that people would buy. In an interesting way, this idea is central to biomaterials device development. The process of biomaterials/medical device innovation is driven by clinical need: an informed engineer, patient, or physician defines a need and then initiates an invention. However, someone must test and manufacture the device, and shepherd it through the complex and expensive development process, which includes rigorous regulatory requirements. This “someone” is generally a company, and a company exists (by law) to return value to its shareholders. Fig. 1.1.1.9 illustrates multidisciplinary interactions in biomaterials, and shows the progression in the development of a biomaterial or device. It provides a perspective on how different disciplines work together, starting from the identification of a need for a biomaterial through development, manufacture, implantation, and (possibly) removal from the patient. Note that the development process for medical devices is very different from that for drugs. There are insightful reference works available to help understand this specialized device commercialization process (Yock et al., 2015) and this pathway is the general focus of Part 3 of this text.

Magnitude of the Field

The magnitude of the medical device field expresses both the magnitude of the need and a sizable and growing commercial market (Table 1.1.1.2). Of particular note is how

various medical devices are seeing growth occurring in more recently expanding economies. This is exemplified by the cardiovascular device market (Table 1.1.1.3) and reflects economic growth, extending lifespans, and (unfortunately) increased cardiovascular disease burden in these regions.

Consider four commonly used biomaterial devices: a contact lens; a hip joint; a hydrocephalous drainage shunt; and a heart valve. Let us examine these devices in the contexts of human needs and commercial markets. The contact lens offers improved vision and, some will argue, a cosmetic enhancement. The hip joint offers mobility to the patient who would otherwise need a cane or crutch or be confined to a bed or wheelchair. The hydrocephalus shunt will allow an infant to survive without brain damage. The heart valve offers a longer life with improved quality of life. A disposable contact lens may sell for less than \$0.50, and the hip joint, hydrocephalus shunt, and heart valve may sell for \$1000–\$5000 each. Each year there will be hundreds of millions of contact lenses purchased worldwide, 4,500,000 heart valves, 160,000 hydrocephalus shunts, and 1,400,000 total artificial hip prostheses. Here are the issues for consideration: (1) the large number of devices (an expression of both human needs and commercial markets); (2) medical significance (cosmetic to life saving); and (3) commercial potential (who will manufacture it and why, for example, what is the market for the hydrocephalus shunt?). Always, human needs and economic issues color this field we call “biomaterials science.” Medical practice, market forces, and bioethics come into play almost every day.

Lysaght and O’Laughlin (2000) estimated the magnitude and economic scope of the contemporary organ replacement enterprise to be much larger than was generally recognized. In the year 2000, the lives of over 20 million patients were sustained, supported, or significantly improved by functional organ replacement. The impacted population grows at over 10% per year. Worldwide, first-year and follow-up costs of organ replacement and prostheses exceed US\$300 billion per year and represent between 7% and 8% of total worldwide healthcare spending. In the United States, the costs of therapies enabled by organ replacement technology exceed 2% of the gross national product. The costs are also impressive when reduced to the

needs of the individual patient. For example, the cost of an implanted heart valve is roughly \$5000. The surgery to implant the device entails a hospital bill and first-year follow-up costs upward of at least \$40,000. Reoperation for replacing a failed valve will have these same costs. Reoperations for failed valves now exceed 10% of all valve operations. Global expenditures on medical devices by category are summarized in [Table 1.1.1.2](#).

Success and Failure

Most biomaterials and medical devices perform satisfactorily, improving the quality of life for the recipient or saving lives. However, no artificial construct is perfect. All manufactured devices have a failure rate. Also, all humans are different, with differing ethnicities, ages, genetics, gender, body chemistries, living environments, and degrees of physical activity. Furthermore, physicians implant or use these devices with varying degrees of skill. The other side to the medical device success story is that there are problems, compromises, complications, and unintended consequences that often occur with medical devices. Central issues for the biomaterials scientist, manufacturer, patient, physician, and attorney are: (1) is the design competent and optimal; (2) who should be responsible when devices perform “with an inappropriate host response”; and (3) what are the risk/benefit or cost/benefit ratios for the implant or therapy?

Some examples may clarify these issues. Clearly, heart valve disease is a serious medical problem. Patients with diseased aortic heart valves have a 50% chance of dying within 3 years. Surgical replacement of the diseased valve leads to an expected survival of 10 years in 70% of the cases. However, of these patients whose longevity and quality of life have clearly been enhanced, approximately 60% will suffer a serious valve-related complication within 10 years after the operation. Another example involves VADs. A clinical trial called Randomized Evaluation of Mechanical Assistance for the Treatment of Congestive Heart Failure (REMATCH) led to the following important statistics ([Rose et al., 2001](#)). Patients with an implanted Heartmate VAD had a 52% chance of surviving for 1 year, compared with a 25% survival rate for patients who took medication. Survival for 2 years in patients with the Heartmate was 23% versus 8% in the medication group. Also, the VAD enhanced the quality of life for the patients—they felt better, were less depressed, and were mobile. Importantly, patients participating in the REMATCH trial were not eligible for a heart transplant. In the cases of the heart valve and the VAD, clinical complications possibly associated with less than stellar biomaterials performance do not preclude widespread clinical acceptance.

Biomaterials science:

- multidisciplinary;
- multibiomaterial;
- clinical need driven;
- substantial world market; and
- risk/benefit issues.

Thus, these five characteristics of biomaterials science:

- multidisciplinary
 - multibiomaterial
 - clinical need driven
 - substantial world market, and
 - risk/benefit issues
- color all aspects of the field.

In addition, there are certain unique subjects that are particularly prominent in our field and help delineate the biomaterials endeavor as a unique field of science and engineering. Let us review a few of these.

Subjects Integral to Biomaterials Science

Toxicology

A biomaterial should not be toxic, unless it is specifically engineered for such requirements (e.g., a “smart” drug delivery system that targets cancer cells with a toxic drug). Since the nontoxic requirement is the norm, toxicology for biomaterials has evolved into a sophisticated science. It deals with the substances that migrate out of biomaterials or result from their degradation. For example, for polymers, many low molecular weight “leachables” exhibit some level of physiologic activity and cell toxicity. It is reasonable to say that a biomaterial should not give off anything from its mass unless it is specifically designed to do so. Toxicology also deals with methods to evaluate how well this design criterion is met when a new biomaterial is under development. [Chapter 2.2.5](#) provides an overview of methods in biomaterials toxicology. Implications of toxicity are addressed in [Chapters 2.3.2–2.3.4](#).

Biocompatibility

The understanding and measurement of biocompatibility are unique to biomaterials science. Unfortunately, we do not have precise definitions or accurate measurements of biocompatibility. More often than not, biocompatibility is defined in terms of performance or success at a specific task. Thus for a patient who is doing well with an implanted large diameter Dacron fabric vascular prosthesis, few would argue that this prosthesis is not “biocompatible.” However, the prosthesis probably did not recellularize, and may also generate a small amount of surface-bound clot that may embolize, usually with little clinical consequence. This operational definition of biocompatible (“the patient is alive and not experiencing complications, so it must be biocompatible”) offers us little insight in designing new or improved vascular prostheses. It is probable that biocompatibility may have to be specifically defined for applications in soft tissue, hard tissue, and the cardiovascular system (blood compatibility, [Chapters 2.2.6 and 2.3.5](#)). In fact, biocompatibility may have to be uniquely defined for each application. The problems and meanings of biocompatibility will be explored and expanded upon throughout this textbook; in particular see [Chapters 2.3.1 and 2.3.2](#).

Inflammation and Healing

Specialized biological mechanisms are triggered when a material or device interfaces with the body. Injury to tissue will

stimulate the well-defined inflammatory reaction sequence that ultimately leads to healing. Healing can be normal (physiological) or abnormal (pathological). Where a foreign body (e.g., an implant) is present in the wound site (the surgical incision), the reaction sequence is referred to as the “foreign-body reaction” (Chapters 2.2.2 and 2.3.4). The normal response of the body will be modulated because of the solid implant. Furthermore, this reaction will differ in intensity and duration, depending upon the anatomical site involved. An understanding of how a foreign object shifts the normal inflammatory reaction sequence is an important concern for the biomaterials scientist, and how some classes of materials may avoid this reaction is an area of growing interest, as already noted.

Functional Tissue Structure and Pathobiology

Biomaterials-based medical devices are implanted into almost all tissues and organs. Tissues and organs vary widely in cell composition, morphological organization, vascularization, and innervation. Implantation of a biomaterial into bone, liver, or heart will have special physiological consequences. Therefore key principles governing the structure of normal (and abnormal) cells, tissues, and organs are important to biomaterials researchers. Also, techniques by which the structure and function of normal and abnormal tissue are studied must be mastered. In addition, fundamental mechanisms leading to abnormal cell, tissue, and organ structures (i.e., diseases and other pathologies) are critical considerations to biomaterials researchers (see Chapters 2.1.4 and 2.1.5).

Dependence on Specific Anatomical Sites of Implantation

Consideration of the anatomical site of an implant is essential. An intraocular lens may be implanted into the lens capsule or the anterior chamber of the eye. A hip joint will be implanted in bone across an articulating joint space. A prosthetic heart valve will be sutured into cardiac muscle and will contact both soft tissue and blood. A catheter may be placed in an artery, a vein, or the urinary tract. Each of these sites challenges the biomedical device designer with special requirements for anatomy, physiology, geometry, size, mechanical properties, and bioresponses.

Mechanical Requirements and Physical Performance Requirements

Each biomaterial and device has mechanical and performance requirements originating from the need to perform a physiological function. These requirements can be divided into three categories: mechanical performance, mechanical durability, and physical properties.

First, consider mechanical performance. A hip prosthesis must be strong and rigid. A tendon material must be strong and flexible. A tissue heart valve leaflet must be flexible and tough. A dialysis membrane must be strong and flexible, but not elastomeric. An articular cartilage substitute must be soft and elastomeric. One significant example of a controlled micromechanical interface is the contact zone between a synthetic biomaterial (titanium, tantalum, alumina, zirconia, and hydroxyapatites) and oral bones. Microstrain

magnitudes have been controlled through macro/micro/nanosurface topographies and construct designs to be within the microstrain limits of bone. The result has been decades of chemical stability, now called osseous integration.

Then, we must address mechanical durability. A catheter may only have to perform for 3 days. A bone plate may fulfill its function in 6 months or longer. A leaflet in a heart valve must flex 60 times per minute without tearing for the lifetime of the patient (realistically, at least for 10 or more years). A hip joint must not fail under heavy loads for 20 years or more.

Finally, the bulk physical properties impact other aspects of performance as they meet the physical and/or mechanical demands of the medical devices for which they are designed. In addition to mechanical durability, the dialysis membrane has a specified permeability, the acetabular cup of the hip joint must have high lubricity, and the intraocular lens has transparency and refraction requirements. To meet these requirements, design principles are borrowed from physics, chemistry, mechanical engineering, chemical engineering, and materials science.

Industrial Involvement

A significant basic research effort is now under way, primarily at universities, to understand how biomaterials function and how to optimize them. At the same time, companies are producing implants for use in humans and, appropriate to the mission of a company, earning profits on the sale of medical devices. Thus although we are now only learning about the fundamentals of biointeraction, we manufacture millions of devices for implantation in humans. How is this dichotomy explained? Basically, as a result of 50 or more years of experience we now have a set of materials that perform satisfactorily in the body. The medical practitioner can use them with reasonable confidence, and the performance in the patient is largely acceptable (generally considerably better than other alternatives). Though the devices and materials are far from perfect, the complications associated with the devices are fewer or of less impact than the complications of the original diseases.

Risk/Benefit and Corporate Realities

A risk/benefit analysis must be considered in developing new devices and improving existing devices. Central to biomaterials science is the desire to alleviate suffering and death, and also the desire to improve the quality of life for patients. These considerations are convoluted with the excitement of new scientific ideas, the corporate imperative to turn a profit, and the mandate of the regulatory agencies to protect the public. Indeed, although failure of biomaterials and medical devices is common, benefit to risk ratio in individual cases is often high, and despite a device complication, a patient may have had a markedly improved outcome (enhanced survival and/or quality of life) over the natural history of the disease.

The acceptable risk varies with different types of medical devices. Moreover, the acceptable risk of devices that sustain life (e.g., heart valve, defibrillator, cardiac assist device, hemodialysis device/access graft, hydrocephalus shunt) is greater than that of devices that alleviate pain/disability or enhance function (e.g., hip joint, drug delivery device, intraocular lens, intrauterine contraceptive device). Then consider the

acceptable risk for devices that have only cosmetic application (e.g., collagen injections, breast implants). Obviously, ethical concerns enter into the risk/benefit picture. Remember that companies have large investments in the development, manufacture, quality control, clinical testing, regulatory clearance, and distribution of medical devices. How much of an advantage (for the company and the patient) will be realized in introducing an improved device? The improved device may indeed work better for the patient. However, the company will incur a large expense (development and regulatory costs) that will be perceived by the stockholders as reduced profits. The development of a new or improved device, as well as offering benefits, entails risks that months or years after introduction some unforeseen complication will compromise the device. Product liability issues are a major concern to manufacturers. Consider questions about the ethics of withholding improved devices from people who could benefit from them because of development costs and regulatory hurdles, the market share advantages of having a better product, and the gargantuan costs (possibly nonrecoverable) of introducing a new product into the medical marketplace. If companies did not have the profit incentive, would there be any medical devices, let alone improved ones, available for clinical application?

From the biomaterials industry we see specialized, essential contributions to our field. Industry deals well with technologies such as packaging, sterilization, storage, distribution, quality control, and analysis. These subjects are grounded in specialized technologies, often ignored in academic communities, but having the potential to generate stimulating research questions. Also, many companies support in-house basic research laboratories, and contribute in important ways to the fundamental study of biomaterials science.

Ethics

A wide range of ethical considerations impact biomaterials science. Some key ethical questions in biomaterials science are summarized in Table 1.1.1.4. Typical of ethical questions, an absolute answer may be difficult to come by. Some articles have addressed ethical questions in biomaterials and debated the important points (Saha and Saha, 1987; Schiedermayer and Shapiro, 1989; Merryman, 2008). Chapter 3.1.11 introduces moral and ethical issues related to biomaterials and medical devices.

Regulation

The consumer (the patient) and the physician demand safe medical devices. To prevent inadequately tested devices and materials from coming on the market, and to screen out those clearly unqualified to produce biomaterials, the US government has evolved a complex regulatory system administered by the US Food and Drug Administration. In the United States, medical device regulatory requirements were introduced less than 50 years ago (with the 1976 Medical Device Amendments legislation). Most nations of the world have similar medical device regulatory bodies. The International Standards Organization has introduced international standards for the world community. Obviously, a substantial base of biomaterials knowledge went into establishing these standards. The costs to comply with the standards and to implement materials, biological, and

TABLE 1.1.1.4 Ethical Concerns Relevant to Biomaterials Science

Animals

Is the animal model relevant to human physiology? Specifically, is the experiment well designed and the outcome sufficiently important so that the data obtained will justify the suffering and sacrifice of the life of a living creature?

Human Subjects

How should human subject research be conducted to minimize negative outcomes to the patient and offer a reasonable risk/benefit ratio? How can we best ensure informed consent?

Industrial Involvement

Companies fund much biomaterials research and also own proprietary biomaterials. How can the needs of the patient be best balanced with the financial goals of a company? Consider that someone must manufacture devices—these would not be available if a company did not choose to manufacture them.

Researchers

Since researchers often stand to benefit financially from a successful biomedical device, and sometimes even have devices named after them, how can investigator bias be minimized in biomaterials research?

Patients

For life-sustaining devices, what is the trade-off between sustaining life and the quality of life with the device for the patient? Should the patient be permitted to “pull the plug” if the quality of life is not satisfactory?

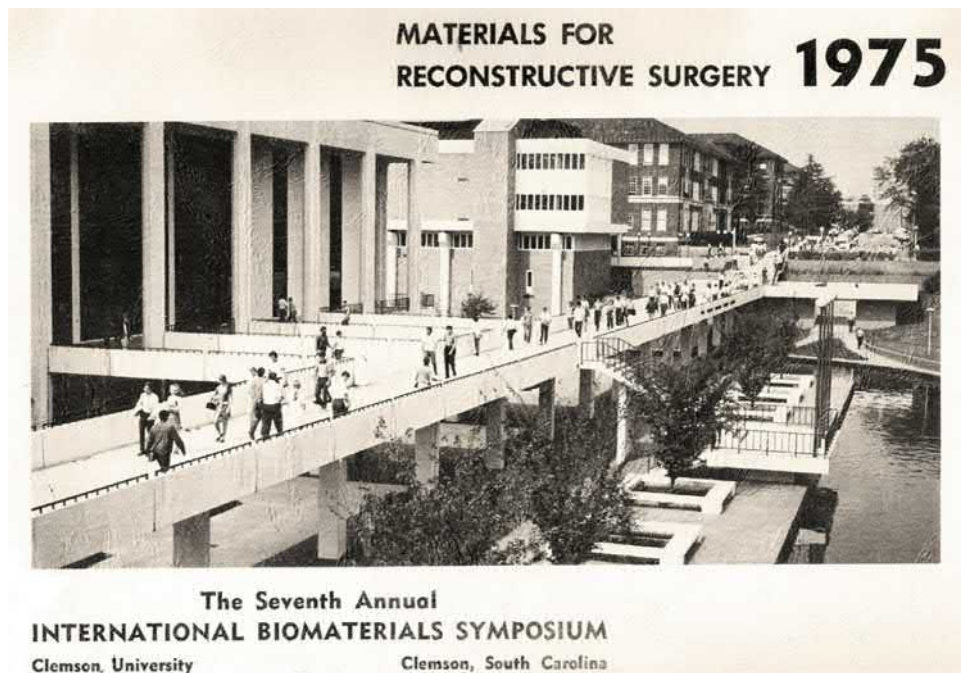
Regulatory Agencies

With so many unanswered questions about the basic science of biomaterials, do government regulatory agencies have sufficient information to define adequate tests for materials and devices and to properly regulate biomaterials?

clinical testing are enormous. Introducing a new biomedical device to the market requires a regulatory investment of tens of millions of dollars. Are the regulations and standards truly addressing the safety issues? Is the cost of regulation inflating the cost of healthcare and preventing improved devices from reaching those who need them? Under this regulation topic, we see the intersection of all the players in the biomaterials community: government, industry, scientists, physicians, and patients. The answers are not simple, but the problems must be addressed every day. Part 3 of this text contains several chapters that expand on standards and regulatory concerns to provide a whole-spectrum view, including issues related to device life cycle, safety and risk, sterilization and disinfection, verification and validation, commercialization, and legal concepts.

Biomaterials Literature

Over the past 70 years, the field of biomaterials has evolved from individual physicians innovating to save the lives of their patients to the science-grounded multidisciplinary endeavor we see today. In 1950, there were no biomaterials or medical device journals, and few books. Concurrent with the evolution



• **Figure 1.1.1.10** The cover of the program book for the 1975 International Biomaterials Symposium, Clemson, South Carolina.

of the discipline, a literature has also developed addressing basic science, applied science, engineering, medicine, and commercial issues. A bibliography is provided in [Appendix D](#) to highlight some of the key reference works and technical journals in the biomaterials field. As might be expected, these journals stem from many disciplines and technical societies.

Biomaterials Societies

The biomaterials field evolved from individual researchers and clinicians who intellectually associated their efforts with established disciplines such as medicine, chemistry, chemical engineering, materials science, or mechanical engineering, to a modern field called “biomaterials.” This evolution was paralleled by a growing sense of professionalism and the formation of biomaterials societies as homes for the profession to develop in. Probably the first biomaterials-related society was the American Society for Artificial Internal Organs. Founded in 1954, this group of visionaries established a platform to consider the development of devices such as the artificial kidney and the artificial heart. A Division of Interdisciplinary Studies, the administrative home of a nascent biomaterials effort, was established at Clemson University, Clemson, South Carolina, in 1969. Clemson began organizing annual International Biomaterials Symposia (IBS) in 1969. The first of these symposia was titled “Use of Ceramics in Surgical Implants.” About 100 scientists and physicians attended, and 17 papers were presented. Between 1969 and 1975, seven IBS were held at Clemson. The cover of the 1975 International Biomaterials Symposium program is shown in [Fig. 1.1.1.10](#).

The Society for Biomaterials (SFB) was chartered in San Antonio, Texas, in 1974 with 205 charter members from across the United States and nine other countries—a truly

international society. One unique feature of the SFB founding members was that they included clinicians, engineers, chemists, and biologists. Their common interest, biomaterials, was the engaging focus for the multidisciplinary participants. Because of the founding of the SFB in 1974, the seventh IBS in 1975 was also known as the world’s inaugural meeting of the SFB. [Table 1.1.1.5](#) lists the timeline of events leading to the start of the SFB annual meetings and the quadrennial World Biomaterials Congress (WBC), as well as the establishment of Clemson Awards and the honorary status of “Fellow, Biomaterials Science and Engineering.” The [Canadian Biomaterials Society/Société Canadienne des Biomatériaux](#) was established in 1973, a year earlier than the SFB. The European Society for Biomaterials was founded in 1975, and the Japanese Society for Biomaterials was formed in 1978. To promote international communication and cooperation, these four societies decided to establish an International Liaison Committee of Societies for Biomaterials (ILC) in 1980 to organize a WBC every 4 years and the first WBC was held in Baden, Vienna, Austria, that year. Six more international societies for biomaterials were established afterward: the [Society for Biomaterials & Artificial Organs \(India\)](#) in 1986, the [Australasian Society for Biomaterials and Tissue Engineering](#) in 1989, the [Korean Society for Biomaterials](#) in 1996, the [Chinese Taipei Society for Biomaterials and Controlled Release](#) in 1997, the [Latin American Society for Biomaterials and Artificial Organs](#) in 1998, and the [Chinese Society for Biomaterials](#) in 2011. In 1997, the constituent societies renamed the ILC to the International Union of Societies for Biomaterials Science and Engineering. Aside from these societies, there are other groups. For example, the Controlled Release Society is a group strongly rooted in biomaterials for drug delivery, and the Tissue Engineering and Regenerative Medicine International Society is also very active in biomaterials-related research.

TABLE 1.1.1.5 Timeline for Development of the Society for Biomaterials and Other International Biomaterials Organizations

1969	1st IBS Clemson, SC
1970	2nd IBS Clemson, SC
1971	3rd IBS Clemson, SC
1972	4th IBS Clemson, SC
1973	5th IBS Clemson, SC Clemson Awards Canadian Society
1974	6th SFB Clemson, SC Society For Biomaterials
1975	7th IBS / 1st SFB Meeting Clemson, SC European Society
1978	Japanese Society
1980	1st WBC Meeting Baden, Vienna, Austria ILC
1986	India Society
1989	Australasian Society
1992	4th WBC Meeting Berlin, Germany FBSE
1996	Korean Society
1997	Chinese Taipei Society ILC → IUSBSE
1998	Latin American Society
2011	Chinese Society
2020	11th WBC Meeting Glasgow, UK

FBSE, Fellow, Biomaterials Science and Engineering; IBS, International Biomaterials Symposia; ILC, International Liaison Committee of Societies for Biomaterials; IUSBSE, International Union of Societies for Biomaterials Science and Engineering; SC, South Carolina; SFB, Society for Biomaterials; WBC, World Biomaterials Congress.

The development of biomaterials professionalism and a sense of identity for the biomaterials field can be attributed to these societies and the researchers who organized and led them.

Summary

This chapter provides a broad overview of the biomaterials field. It offers a vantage point from which the reader can gain a perspective to see how the subthemes fit into the larger whole.

Biomaterials science may be the most multidisciplinary of all the sciences. Consequently, biomaterials scientists must

master certain key material from many fields of science, technology, engineering, and medicine to be competent and conversant in this profession. The reward for mastering this volume of material is immersion in an intellectually stimulating endeavor that advances a new basic science of biointeraction and contributes to reducing human suffering.

References

- Carlsson, L., Rostlund, T., Albrektsson, B., Albrektsson, T., Brånemark, P.I., 1986. Osseointegration of titanium implants. *Acta Orthop. Scand.* 57, 285–289.
- Hench, L.L., Pollak, J.M., 2002. Third-generation biomedical materials. *Science* 295, 1014–1017.
- Hubbell, J.A., Massia, S.P., Desai, N.P., Drumheller, P.D., 1991. Endothelial cell-selective materials for tissue engineering in the vascular graft via a new receptor. *Biotechnology* 9 (6), 568–572.
- Jana, S., Tefft, B.J., Spoon, D.B., Simari, R.D., 2014. Scaffolds for tissue engineering of cardiac valves. *Acta Biomater.* 10, 2877–2893.
- Lysaght, M.J., O’Laughlin, J., 2000. The demographic scope and economic magnitude of contemporary organ replacement therapies. *Am. Soc. Artif. Intern. Organs J.* 46, 515–521.
- Merryman, W.D., 2008. Development of a tissue engineered heart valve for pediatrics: a case study in bioengineering ethics. *Sci. Eng. Ethics* 14, 93–101.
- Meckstroth, K.R., Darney, P.D., 2001. Implant contraception. *Semin. Reprod. Med.* 19, 339.
- Ratner, B.D., 2011. The biocompatibility manifesto: biocompatibility for the twenty-first century. *J. Cardiovasc. Translat. Res.* 4 (5), 523–527.
- Rose, E.A., Gelijns, A.C., Moskowitz, A.J., Heitjan, D.F., Stevenson, L.W., Dembitsky, W., Long, J.W., Ascheim, D.D., Tierney, A.R., Levitan, R.G., Watson, J.T., Ronan, N.S., Shapiro, P.A., Lazar, R.M., Miller, L.W., Gupta, L., Frazier, O.H., Desvigne-Nickens, P., Oz, M.C., Poirier, V.L., Meier, P., 2001. Long-term use of a left ventricular assist device for end-stage heart failure. *N. Engl. J. Med.* 345, 1435–1443.
- Saha, S., Saha, P., 1987. Bioethics and applied biomaterials. *J. Biomed. Mater. Res. Appl. Biomater* 21, 181–190.
- Sahoo, J.K., VandenBerg, M.A., Webber, M.J., 2018. Injectable network biomaterials via molecular or colloidal self-assembly. *Adv. Drug Deliv. Rev.* 127, 185–207.
- Schiedermaier, D.L., Shapiro, R.S., 1989. The artificial heart as a bridge to transplant: ethical and legal issues at the bedside. *J. Heart Transplant.* 8, 471–473.
- Sharp, P.A., Langer, R., 2011. Promoting convergence in biomedical science. *Science* 333 (6042), 527.
- Williams, D.F., 1987. In: *Definitions in biomaterials. Proceedings of a Consensus Conference of the European Society for Biomaterials.* (Vol. 4). New York: Elsevier, Chester, England, March 3–5 1986.
- Yock, P.G., Zenios, S., Makower, J., Brinton, T.J., Kumar, U.N., Watkins, F.T.J., Denend, L., Krummel, T.M., Kurihara, C.Q. (Eds.), 2015. *Biodesign: The Process of Innovating Medical Technologies.* Cambridge: Cambridge University Press.
- Zhang, B.L., Bianco, R.W., Schoen, F.J., 2019. Preclinical assessment of cardiac valve substitutes: current status and considerations for engineered tissue heart valves. *Front. Cardiovasc. Med.* 6, 72.
- Zhang, X., Gong, C., Akakuru, O.U., Su, Z., Wu, A., Wei, G., 2019. The design and biomedical applications of self-assembled two-dimensional organic biomaterials. *Chem. Soc. Rev.* 48 (23), 5564–5595.

1.1.2

A History of Biomaterials

BUDDY D. RATNER¹, GUIGEN ZHANG²

¹Bioengineering and Chemical Engineering, Director of University of Washington Engineered Biomaterials (UWEB), Seattle, WA, United States

²F Joseph Halcomb III, M.D. Department of Biomedical Engineering, University of Kentucky, Lexington, KY, United States

History consists of a series of accumulated imaginative inventions.

Voltaire

At the turn of the third decade of the 21st century, biomaterials are still widely used throughout medicine, dentistry, and biotechnology. Just about 70 years ago, biomaterials as we think of them today did not exist. The word “biomaterial” was not used. There were no medical device manufacturers (except for external prosthetics such as limbs, fracture fixation devices, glass eyes, and dental fillings and devices), no formalized regulatory approval processes, no understanding of biocompatibility, and certainly no academic courses on biomaterials. Yet, crude biomaterials have been used, generally with poor to mixed results, throughout history. This chapter will broadly trace the history of biomaterials from the earliest days of human civilization to the third decade of the 21st century. It is convenient to organize the history of biomaterials into four eras: prehistory; the era of the surgeon-hero; designed biomaterials/engineered devices; and the contemporary era taking us into the new millennium. The emphasis of this chapter will be on the experiments and studies that set the foundation for the field we call biomaterials, largely between 1920 and 1980.

Biomaterials Before World War II

Before Civilization

The introduction of nonbiological materials into the human body took place throughout history. The remains of a human found near Kennewick, Washington, USA (often referred to as the “Kennewick Man”), were dated (with some controversy) to be 9000 years old. This individual, described by archeologists as a tall, healthy, active person, wandered through the region now known as southern Washington with a spear point embedded in his hip. It had apparently healed in and did not significantly impede

his activity. This unintended implant illustrates the body’s capacity to deal with implanted foreign materials. The spear point has little resemblance to modern biomaterials, but it was a “tolerated” foreign material implant. Another example of the introduction of foreign material into the skin, dated at over 5000 years ago, is the tattoo. The carbon particles and other substances probably elicited a classic foreign-body reaction. Moreover, one of the first surgical textbooks dated around 600 BC (Willyard, 2016) documented, arguably the first written record of skin-graft techniques, a method for repairing torn earlobes with skin from the cheek and the reconstruction of the nose from a flap of forehead skin.

Dental Implants in Early Civilizations

Unlike the spear point described earlier, dental implants were devised as implants and used early in history. The Mayan people fashioned nacre teeth from sea shells in roughly 600 AD, and apparently achieved what we now refer to as osseointegration (see Chapter 2.5.5), basically a seamless integration into the bone (Bobbio, 1972). Similarly, in France, a wrought iron dental implant in a corpse was dated to 200 AD (Crubezy et al., 1998). This implant, too, was described as properly osseointegrated. There was no materials science, biological understanding, or medicine behind these procedures. Still, their success (and longevity) is impressive and highlights two points: the adaptive nature of the human body and the pressing drive, even in prehistoric times, to restore the lost functions of physiologic/anatomic parts of the body with an implant.

Sutures Dating Back Thousands of Years

There is loose evidence that sutures may have been used even in the Neolithic period. Large wounds were closed early in history primarily by one of two methods—cautery or sutures. Linen sutures were used by the early Egyptians.

Catgut was used in the Middle Ages in Europe. In South Africa and India, the heads of large, biting ants clamped wound edges together.

Metallic sutures are first mentioned in early Greek literature. Galen of Pergamon (ca.130–200 AD) described ligatures of gold wire. In 1816, Philip Physick, University of Pennsylvania Professor of Surgery, suggested the use of lead wire sutures, noting little reaction. J. Marion Sims of Alabama had a jeweler fabricate sutures of silver wire, and in 1849 performed many successful operations with this metal.

Consider the problems that must have been experienced with sutures in times with no knowledge of sterilization, toxicology, immunological reaction to extraneous biological materials, inflammation, and biodegradation. Yet sutures were a relatively common fabricated or manufactured biomaterial for thousands of years.

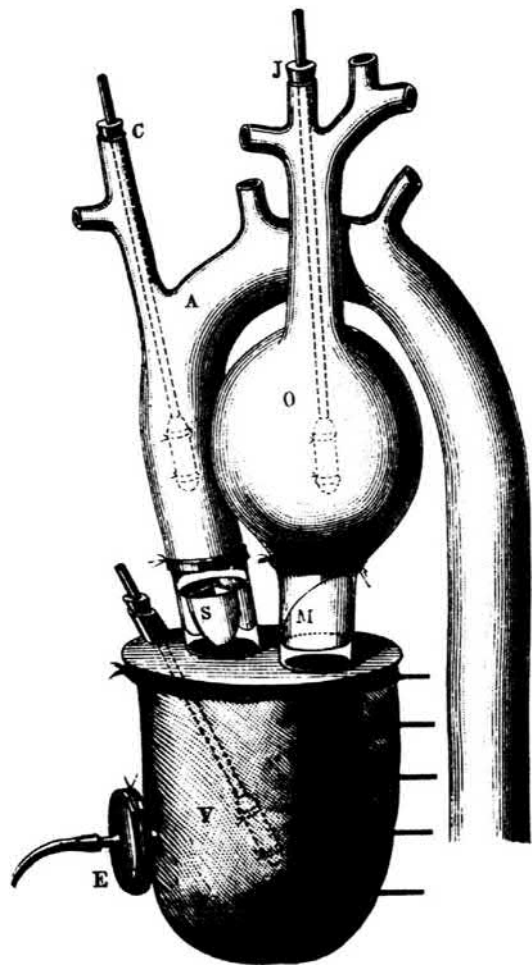
Artificial Hearts and Organ Perfusion

In the fourth century BC, Aristotle called the heart the most important organ in the body. Galen proposed that veins connected the liver to the heart to circulate “vital spirits throughout the body via the arteries.” English physician William Harvey in 1628 espoused a relatively modern view of heart function when he wrote “the heart’s one role is the transmission of the blood and its propulsion, by means of the arteries, to the extremities everywhere.” With the appreciation of the heart as a pump, it was a logical idea to think of replacing the heart with an artificial pump. In 1812, the French physiologist Le Gallois expressed his idea that organs could be kept alive by pumping blood through them. A number of experiments on organ perfusion with pumps were performed from 1828 to 1868. In 1881, Étienne-Jules Marey, a brilliant scientist and thinker who published and invented in photographic technology, motion studies, and physiology, described an artificial heart device (Fig. 1.1.2.1), primarily oriented to studying the beating of the heart.

In 1938, aviator (and engineer) Charles Lindbergh and surgeon (and Nobel Prize winner) Alexis Carrel wrote a visionary book, *The Culture of Organs*. They addressed issues of pump design (referred to as the Lindbergh pump), sterility, blood damage, nutritional needs of perfused organs, and mechanics. This book is a seminal document in the history of artificial organs. In the mid-1950s, Dr. Paul Winchell, better known as a ventriloquist, patented an artificial heart. In 1957, Dr. Willem Kolff and a team of scientists tested the artificial heart in animals. More modern conceptions of the artificial heart (and left ventricular assist device) are presented in the following sections and in [Chapter 2.5.2A](#) and [B](#).

Contact Lenses

Leonardo DaVinci, in the year 1508, developed the concept of contact lenses. Rene Descartes was credited with the idea of the corneal contact lens in 1632 and Sir John F.W. Herschel suggested in 1827 that a glass lens could protect the eye. Adolf Gaston Eugen Fick (nephew of Adolf Eugen Fick



• **Figure 1.1.2.1** An artificial heart by Étienne-Jules Marey, Paris, 1881.

of Fick’s law of diffusion fame) was an optometrist by profession. One of his inventions (roughly 1860) was a glass contact lens, possibly the first contact lens offering real success. He experimented on both animals and humans with contact lenses. In the period from 1936 to 1948, plastic contact lenses were developed, primarily of poly(methyl methacrylate).

Basic Concepts of Biocompatibility

Most implants prior to 1950 had a low probability of success, because of a poor understanding of biocompatibility and sterilization. As will be elaborated upon throughout this book, factors that contribute to biocompatibility include the chemistry of the implant, leachables, shape, mechanics, and design. Early studies, especially with metals, focused primarily on ideas from chemistry to explain the observed bioreaction.

Possibly the first study assessing the *in vivo* bioreactivity of implant materials was performed by H.S. Levert (1829). Gold, silver, lead, and platinum specimens were studied in dogs, and platinum, in particular, was found to be well tolerated. In 1886, bone fixation plates of nickel-plated sheet steel with nickel-plated screws were studied. In 1924, A. Zierold published a study on tissue reaction to various

materials in dogs. Iron and steel were found to corrode rapidly, leading to resorption of adjacent bone. Copper, magnesium, aluminum alloy, zinc, and nickel discolored the surrounding tissue. Gold, silver, lead, and aluminum were tolerated, but were inadequate mechanically. Stellite, a Co–Cr–Mo alloy, was well tolerated and strong. In 1926, M. Large noted inertness displayed by 18-8 stainless steel containing molybdenum. By 1929 Vitallium alloy (65% Co–30% Cr–5% Mo) was developed and used with success in dentistry. In 1947, J. Cotton of the United Kingdom discussed the possible use of titanium and alloys for medical implants.

The history of plastics as implantation materials does not extend as far back as metals, simply because there were few plastics prior to the 1940s. What is possibly the first paper on the implantation of a modern synthetic polymer, nylon, as a suture appeared in 1941. Papers on the implantation of cellophane, a polymer made from plant sources, were published as early as 1939, documenting it being used as a wrap for blood vessels. The response to this implant was described as a “marked fibrotic reaction.” In the early 1940s papers appeared discussing the reaction to implanted poly(methyl methacrylate) and nylon. The first paper on polyethylene as a synthetic implant material was published in 1947 (Ingraham et al.). The paper pointed out that polyethylene production using a new high-pressure polymerization technique began in 1936. This process enabled the production of polyethylene free of initiator fragments and other additives. Ingraham et al. demonstrated good results on implantation (i.e., a mild foreign-body reaction), and attributed these results to the high purity of the polymer they used. A 1949 paper commented on the fact that additives to many plastics had a tendency to “sweat out,” and this might be responsible for the strong biological reaction to those plastics (LeVeen and Barberio, 1949). They found a vigorous foreign-body reaction to cellophane, Lucite, and nylon, but an extremely mild reaction to “a new plastic,” Teflon. The authors incisively concluded: “Whether the tissue reaction is due to the dissolution of traces of the unpolymerized chemical used in plastics manufacture or actually to the solution of an infinitesimal amount of the plastic itself cannot be determined.” The possibility that cellulose might trigger the severe reaction by activating the complement system could not have been imagined, because the complement system had not yet been discovered.

World War II to the Modern Era: The Surgeon/Physician-Hero

During World War I, and particularly at the end of the war, newly developed high-performance metal, ceramic, and especially polymeric materials, transitioned from wartime restriction to peacetime availability. The possibilities for using these durable, inert materials immediately intrigued surgeons with needs to replace diseased or damaged body parts. Materials, originally manufactured for airplanes,

automobiles, clocks, and radios, were taken “off the shelf” by surgeons and applied to medical problems. These early biomaterials included silicones, polyurethanes, Teflon, nylon, methacrylates, titanium, and stainless steel.

A historical context helps us appreciate the contribution made primarily by medical and dental practitioners. Just after World War II, there was little precedent for surgeons to collaborate with scientists and engineers. Medical and dental practitioners of this era felt it was appropriate to invent (improvise) where the life or functionality of their patient was at stake. Also, there was minimal government regulatory activity, and human subject protections as we know them today were nonexistent (see [Chapters 3.1.7](#) and [3.1.11](#)). The physician was implicitly entrusted with the life and health of the patient and had much more freedom than is seen today to take heroic action when other options were exhausted. These medical practitioners had read about the post-World War II marvels of materials science. Looking at a patient open on the operating table, they could imagine replacements, bridges, conduits, and even organ systems based on such materials. Many materials were tried on the spur of the moment. Some fortuitously succeeded. These were high-risk trials, but usually they took place where other options were not available. The term “surgeon-hero” seems justified, since the surgeon often had a life (or a quality of life) at stake and was willing to take a huge technological and professional leap to repair the individual. This laissez faire biomaterials era quickly led to a new order characterized by scientific/engineering input, government quality controls, and a sharing of decisions prior to attempting high-risk, novel procedures. Still, a foundation of ideas and materials for the biomaterials field was built by courageous, fiercely committed, creative individuals, and it is important to look at this foundation to understand many of the attitudes, trends, and materials common today.

The regulatory climate in the United States in the 1950s was strikingly different from today. This can be appreciated in this recollection from Willem Kolff about a pump oxygenator he made and brought with him from Holland to the Cleveland Clinic (Kolff, 1998):

Before allowing Dr. Effler and Dr. Groves to apply the pump oxygenator clinically to human babies, I insisted they do 10 consecutive, successful operations in baby dogs. The chests were opened, the dogs were connected to a heart-lung machine to maintain the circulation, the right ventricles were opened, a cut was made in the interventricular septa, the septa holes were closed, the right ventricles were closed, the tubes were removed, and the chests were closed.

Intraocular Lenses

Sir Harold Ridley, MD (1906–2001) ([Fig. 1.1.2.2](#)), inventor of the plastic intraocular lens, made early, accurate observations of biological reaction to implants consistent with currently accepted ideas of biocompatibility. After World War II, he had the opportunity to examine aviators



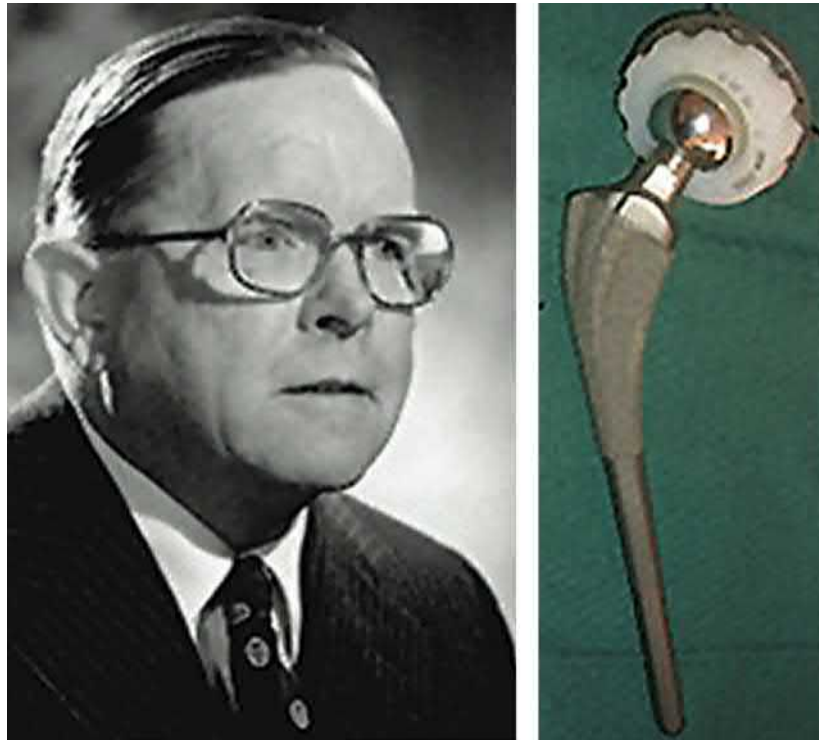
• **Figure 1.1.2.2** *Left:* Sir Harold Ridley, inventor of the intraocular lens, knighted by Queen Elizabeth II for his achievement. *Right:* Shards from the canopy of the Spitfire airplane were the inspiration leading to intraocular lenses. (Image by Bryan Fury75 at fr.wikipedia [GFDL (www.gnu.org/copyleft/fdl.html)], from Wikimedia Commons.)

who were unintentionally implanted in their eyes with shards of plastic from shattered canopies in Spitfire and Hurricane fighter planes (Fig. 1.1.2.2). Most of these flyers had plastic fragments years after the war. The conventional wisdom at that time was that the human body would not tolerate implanted foreign objects, especially in the eye—the body’s reaction to a splinter or a bullet was cited as examples of the difficulty of implanting materials in the body. The eye is an interesting implant site, because you can look in through a transparent window to observe the reaction. When Ridley did so, he noted that the shards had healed in place with no further reaction. They were, by his standard, tolerated by the eye. Today, we would describe this stable healing without significant ongoing inflammation or irritation as “biocompatible.” This is an early observation of “biocompatibility” in humans, perhaps the first, using criteria similar to those accepted today. Based on this observation, Ridley traced down the source of the plastic domes, ICI Perspex poly(methyl methacrylate). He used this material to fabricate implant lenses (intraocular lenses) that were found, after some experimentation, to function reasonably in humans as replacements for surgically removed natural lenses that had been clouded by cataracts. The first implantation in a human was on November 29, 1949. For many years, Ridley was the center of fierce controversy because he challenged the dogma that spoke against implanting foreign materials in eyes—it is hard to believe that the implantation of a biomaterial would provoke such an outcry. Because of this controversy, this industry did not instantly arise—it was the early 1980s before intraocular lenses became a major force in the biomedical device market. Ridley’s insightful observation, creativity, persistence, and surgical talent in the late 1940s evolved into an industry that presently puts more than 7,000,000 of these lenses annually in humans. Through all of human history, cataracts meant blindness or a surgical procedure that left the recipient needing thick, unaesthetic spectacle lenses that poorly corrected the vision. Ridley’s concept, using a plastic material found to be “biocompatible,” changed the course of history and substantially

improved the quality of life for millions of individuals with cataracts. Harold Ridley’s story is elaborated upon in an obituary (Apple and Trivedi, 2002).

Hip and Knee Prostheses

The first hip replacement was probably performed in 1891 by a German surgeon, Theodore Gluck, using a cemented ivory ball. This procedure was not successful. Numerous attempts were made between 1920 and 1950 to develop a hip replacement prosthesis. Surgeon M.N. Smith-Petersen, in 1925, explored the use of a glass hemisphere to fit over the ball of the hip joint. This failed due to poor durability. Chrome–cobalt alloys and stainless steel offered improvements in mechanical properties, and many variants of these were explored. In 1938, the Judet brothers of Paris, Robert and Jean, explored an acrylic surface for hip procedures, but it had a tendency to loosen. The idea of using fast-setting dental acrylics to glue prosthetics to bone was developed by Dr. Edward J. Haboush in 1953. In 1956, McKee and Watson-Farrar developed a “total” hip with an acetabular cup of metal that was cemented in place. Metal-on-metal wear products probably led to high complication rates. It was John Charnley (1911–82) (Fig. 1.1.2.3), working at an isolated tuberculosis sanatorium in Wrightington, Manchester, England, who invented the first really successful hip joint prosthesis. The femoral stem, ball head, and plastic acetabular cup proved to be a reasonable solution to the problem of damaged joint replacement. In 1958, Dr. Charnley used a Teflon acetabular cup with poor outcomes due to wear debris. By 1961 he was using a high molecular weight polyethylene cup, and was achieving much higher success rates. Interestingly, Charnley learned of high molecular weight polyethylene from a salesman selling novel plastic gears to one of his technicians. Dr. Dennis Smith contributed in an important way to the development of the hip prosthesis by introducing Dr. Charnley to poly(methyl methacrylate) cements, developed in the dental community, and optimizing those cements for hip replacement use. Total knee replacements borrowed elements of the hip



• **Figure 1.1.2.3** Left: Sir John Charnley. Right: The original Charnley hip prosthesis. (Hip prosthesis photo courtesy of the South Australian Medical Heritage Society, Inc.)

prosthesis technology, and successful results were obtained in the period 1968–72 with surgeons Frank Gunston and John Insall leading the way.

Dental Implants

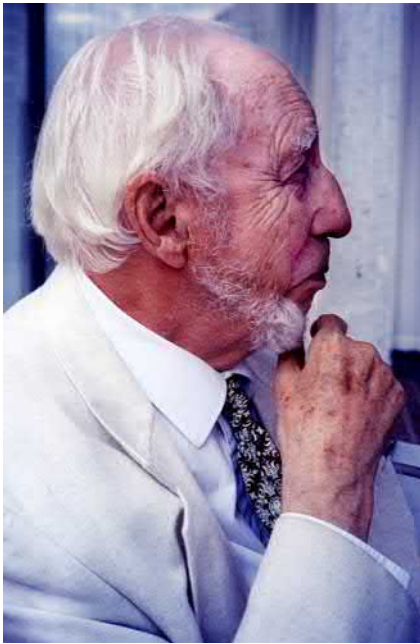
Some “prehistory” of dental implants has just been described. In 1809, Maggiolo implanted a gold post anchor into fresh extraction sockets. After allowing this to heal, he affixed to it a tooth. This has remarkable similarity to modern dental implant procedures. In 1887, this procedure was used with a platinum post. Gold and platinum gave poor long-term results, and so this procedure was never widely adopted. In 1937, Venable used surgical Vitallium and Co–Cr–Mo alloy for such implants. Also around 1937, Strock at Harvard used a screw-type implant of Vitallium, and this may be the first successful dental implant. A number of developments in surgical procedure and implant design (for example, the endosteal blade implant) then took place. In 1952, a fortuitous discovery was made. Per-Ingvar Brånemark, an orthopedic surgeon at the University of Lund, Sweden, was implanting an experimental cage device in rabbit bone for observing healing reactions. The cage was a titanium cylinder that screwed into the bone. After completing the experiment that lasted several months, he tried to remove the titanium device and found it tightly integrated in the bone (Brånemark et al., 1964). Dr. Brånemark named the phenomenon “osseointegration,” and explored the application of titanium implants to surgical and dental procedures. He also developed low-impact surgical protocols for tooth

implantation that reduced tissue necrosis and enhanced the probability of good outcomes. Most dental implants and many other orthopedic implants are now made of titanium and its alloys.

The Artificial Kidney

Kidney failure, through most of history, was a sentence to an unpleasant death lasting over a period of about a month. In 1910, at Johns Hopkins University, the first attempts to remove toxins from blood were made by John Jacob Abel. The experiments were with rabbit blood, and it was not possible to perform this procedure on humans. In 1943, in Nazi-occupied Holland, Willem Kolff (Fig. 1.1.2.4), a physician just beginning his career at that time, built a drum dialyzer system from a 100-L tank, wood slats, and 130 feet of cellulose sausage casing tubing as the dialysis membrane. Some successes were seen in saving lives where prior to this there was only one unpleasant outcome to kidney failure. Kolff took his ideas to the United States and in 1960, at the Cleveland Clinic, developed a “washing machine artificial kidney” (Fig. 1.1.2.5) taking advantage of Maytag washing machines purchased from Sears.

Major advances in kidney dialysis were made by Dr. Belding Scribner at the University of Washington (Fig. 1.1.2.6). Scribner devised a method to routinely access the bloodstream for dialysis treatments. Prior to this, after just a few treatments, access sites to the blood were used up and further dialysis was not possible. After seeing the potential of dialysis to help patients, but only acutely, Scribner tells the



• **Figure 1.1.2.4** Dr. Willem Kolff at age 92. (Photograph by B. Ratner.)



• **Figure 1.1.2.5** Willem Kolff (*center*) and the washing machine artificial kidney.

story of waking up in the middle of the night with an idea to gain easy access to the blood—a shunt implanted between an artery and vein that emerged through the skin as a “U.” Through the exposed portion of the shunt, blood access could be readily achieved. When Dr. Scribner heard about the new plastic, Teflon, he envisioned how to get the blood out of and into the blood vessels. His device, built with the assistance of Wayne Quinton (*Fig. 1.1.2.6*), used Teflon tubes to access the vessels, a Dacron sewing cuff through the skin, and a silicone rubber tube for blood flow. The Quinton–Scribner shunt made chronic dialysis possible,

and is said to be responsible for more than a million patients being alive today. Interestingly, Dr. Scribner refused to patent his invention because of its importance to medical care. Additional important contributions to the artificial kidney were made by chemical engineering Professor Les Babb (University of Washington) who, working with Scribner, improved dialysis performance and invented a proportioning mixer for the dialysate fluid. The first dialysis center was opened in Seattle making use of these important technological advances (*Fig. 1.1.2.6*). The early experience with dialyzing patients where there were not enough dialyzers to meet the demand also made important contributions to bioethics associated with medical devices (*Blagg, 1998*).

The Artificial Heart

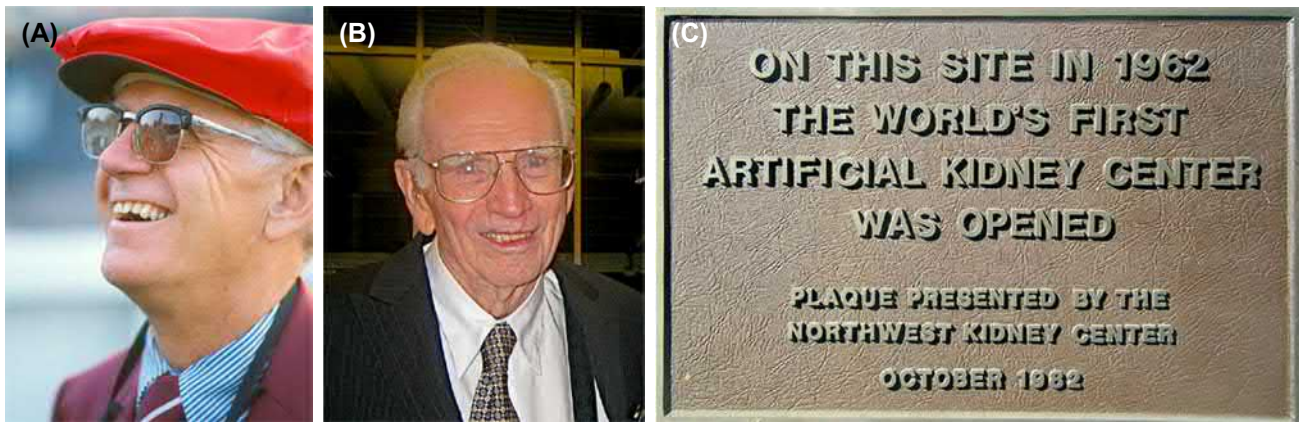
Willem Kolff was also a pioneer in the development of the artificial heart. He implanted the first artificial heart in the Western hemisphere in a dog in 1957 (a Russian artificial heart was implanted in a dog in the late 1930s). The Kolff artificial heart was made of a thermosetting poly(vinyl chloride) cast inside hollow molds to prevent seams. In 1953, the heart–lung machine was invented by John Gibbon, but this was useful only for acute treatment, such as during open heart surgery. In 1964, the National Heart and Lung Institute of the National Institutes of Health set a goal of a total artificial heart by 1970. Dr. Michael DeBakey implanted a left ventricular assist device in a human in 1966, and Dr. Denton Cooley and Dr. William Hall implanted a polyurethane total artificial heart in 1969. In the period 1982–85, Dr. William DeVries implanted a number of Jarvik hearts based upon designs originated by Drs. Clifford Kwan-Gett and Donald Lyman—patients lived up to 620 days on the Jarvik 7 device.

Breast Implants

The breast implant evolved to address the poor results achieved with direct injection of substances into the breast for augmentation. In fact, in the 1960s, California and Utah classified use of silicone injections as a criminal offense. In the 1950s, poly(vinyl alcohol) sponges were implanted as breast prostheses, but results with these were also poor. University of Texas plastic surgeons Thomas Cronin and Frank Gerow invented the first silicone breast implant in the early 1960s, a silicone shell filled with silicone gel. Many variations of this device have been tried over the years, including cladding the device with polyurethane foam (the Natural Y implant). This variant of the breast implant was fraught with problems. However, the basic silicone rubber–silicone gel breast implant was generally acceptable in performance (*Bondurant et al., 1999*).

Vascular Grafts

Surgeons have long needed methods and materials to repair damaged and diseased blood vessels. Early in the century,



• **Figure 1.1.2.6** (A) Belding Scribner; (B) Wayne Quinton; (C) plaque commemorating the original location in Seattle of the world's first artificial kidney center. ((A) Courtesy of Dr. Eli Friedman. (B) Photo by B. Ratner.)

Dr. Alexis Carrel developed methods to anastomose (suture) blood vessels, an achievement for which he won the Nobel Prize in medicine in 1912. In 1942 Blackmore used Vitalium metal tubes to bridge arterial defects in war-wounded soldiers. Columbia University surgical intern Arthur Voorhees (1922–92), in 1947, noticed during a postmortem that tissue had grown around a silk suture left inside a lab animal. This observation stimulated the idea that a cloth tube might also heal by being populated by the tissues of the body. Perhaps such a healing reaction in a tube could be used to replace an artery? His first experimental vascular grafts were sewn from a silk handkerchief and then parachute fabric (Vinyon N), using his wife's sewing machine. The first human implant of a prosthetic vascular graft was in 1952. The patient lived many years after this procedure, inspiring many surgeons to copy the procedure. By 1954, another paper was published establishing the clear benefit of a porous (fabric) tube over a solid polyethylene tube (Egdahl et al., 1954). In 1958, the following technique was described in a textbook on vascular surgery (Rob, 1958): "The Terylene, Orlon or nylon cloth is bought from a draper's shop and cut with pinking shears to the required shape. It is then sewn with thread of similar material into a tube and sterilized by autoclaving before use."

Stents

Partially occluded coronary arteries lead to angina, diminished heart functionality, and eventually, when the artery occludes (i.e., myocardial infarction), death of a localized portion of the heart muscle. Bypass operations take a section of vein from another part of the body and replace the occluded coronary artery with a clean conduit—this is major surgery, hard on the patient, and expensive. Synthetic vascular grafts in the 3 mm diameter size that is appropriate to the human coronary artery anatomy will thrombose, and thus cannot be used. Another option is percutaneous transluminal coronary angioplasty (PTCA). In this procedure, a balloon is threaded on a catheter into the coronary artery and then inflated to open the lumen of the occluding vessel.



• **Figure 1.1.2.7** Dr. Julio Palmaz, inventor of the coronary artery stent. (Photograph by B. Ratner.)

However, in many cases the coronary artery can spasm and close from the trauma of the procedure. The invention of the coronary artery stent, an expandable mesh structure that holds the lumen open after PTCA, was revolutionary in the treatment of coronary occlusive disease. In his own words, Dr. Julio Palmaz (Fig. 1.1.2.7) describes the origins and history of the cardiovascular stent:

I was at a meeting of the Society of Cardiovascular and Interventional Radiology in February 1978 when a visiting lecturer, Doctor Andreas Gruntzig from Switzerland, was presenting his preliminary experience with coronary balloon angioplasty. As you know, in 1978 the mainstay therapy of coronary heart disease was surgical bypass. Doctor Gruntzig showed his promising new technique to open up coronary atherosclerotic blockages without the need for open chest surgery, using his own plastic balloon catheters. During his

presentation, he made it clear that in a third of the cases, the treated vessel closed back after initial opening with the angioplasty balloon because of elastic recoil or delamination of the vessel wall layers. This required standby surgery facilities and personnel, in case acute closure after balloon angioplasty prompted emergency coronary bypass. Gruntzig's description of the problem of vessel reclosure elicited in my mind the idea of using some sort of support, such as used in mine tunnels or in oil well drilling. Since the coronary balloon goes in small (folded like an umbrella) and is inflated to about 3–4 times its initial diameter, my idealistic support device needed to go in small and expand at the site of blockage with the balloon. I thought one way to solve this was a malleable, tubular, crisscross mesh. I went back home in the Bay Area and started making crude prototypes with copper wire and lead solder, which I first tested in rubber tubes mimicking arteries. I called the device a BEIS or balloon-expandable intravascular graft. However, the reviewers of my first submitted paper wanted to call it a stent. When I looked the word up, I found out that it derives from Charles Stent, a British dentist who died at the turn of the century. Stent invented a wax material to make dental molds for dentures. This material was later used by plastic surgeons to keep tissues in place, while healing after surgery. The word "stent" was then generically used for any device intended to keep tissues in place while healing.

I made the early experimental device of stainless steel wire soldered with silver. These were materials I thought would be appropriate for initial laboratory animal testing. To carry on with my project I moved to the University of Texas Health Science Center in San Antonio (UTHSCSA). From 1983–1986 I performed mainly bench and animal testing that showed the promise of the technique and the potential applications it had in many areas of vascular surgery and cardiology. With a UTHSCSA pathologist, Doctor Fermin Tio, we observed our first microscopic specimen of implanted stents in awe. After weeks to months after implantation by catheterization under X-ray guidance, the stent had remained open, carrying blood flow. The metal mesh was covered with translucent, glistening tissue similar to the lining of a normal vessel. The question remained whether the same would happen in atherosclerotic vessels. We tested this question in the atherosclerotic rabbit model and to our surprise, the new tissue free of atherosclerotic plaque encapsulated the stent wires, despite the fact that the animals were still on a high cholesterol diet. Eventually, a large sponsor (Johnson & Johnson) adopted the project and clinical trials were instituted under the scrutiny of the Food and Drug Administration.

Coronary artery stenting is now performed in well over 1.5 million procedures per year.

Pacemakers

In London in 1788, Charles Kite wrote "An Essay Upon the Recovery of the Apparently Dead," where he discussed



• **Figure 1.1.2.8** The Albert Hyman Model II portable pacemaker, c. 1932–33. (Courtesy of the NASPE-Heart Rhythm Society History Project (www.Ep-History.org.)

electrical discharges to the chest for heart resuscitation. In the period 1820–80 it was already known that electric shocks could modulate the heartbeat (and, of course, consider the *Frankenstein* story from that era). The invention of the portable pacemaker, hardly portable by modern standards, may have taken place almost simultaneously in two groups in 1930–31—Dr. Albert S. Hyman (USA) (Fig. 1.1.2.8) and Dr. Mark C. Lidwill (working in Australia with physicist Major Edgar Booth).

Canadian electrical engineer, John Hopps, while conducting research on hypothermia in 1949, invented an early cardiac pacemaker. Hopps' discovery was if a cooled heart stopped beating, it could be electrically restarted. This led to Hopps' invention of a vacuum tube cardiac pacemaker in 1950. Paul M. Zoll developed a pacemaker in conjunction with the Electrodyne Company in 1952. The device was about the size of a small microwave oven, was powered with external current, and stimulated the heart using electrodes placed on the chest—this therapy caused pain and burns, although it could pace the heart.

In the period 1957–58, Earl E. Bakken, founder of Medtronic, Inc., developed the first wearable transistorized (external) pacemaker at the request of heart surgeon Dr. C. Walton Lillehei. Bakken quickly produced a prototype that Lillehei used on children with postsurgery heart block. Medtronic commercially produced this wearable, transistorized unit as the 5800 pacemaker.

In 1959 the first fully implantable pacemaker was developed by engineer Wilson Greatbatch and cardiologist W.M. Chardack. He used two Texas Instruments transistors, a technical innovation that permitted small size and low power drain. The pacemaker was encased in epoxy to inhibit body fluids from inactivating it.



• **Figure 1.1.2.9** The Hufnagel heart valve consisting of a poly(methyl methacrylate) tube and nylon ball. (United States Federal Government image in the public domain.)

Heart Valves

The development of the prosthetic heart valve paralleled developments in cardiac surgery. Until the heart could be stopped and blood flow diverted, the replacement of a valve would be challenging. Charles Hufnagel, in 1952, implanted a valve consisting of a poly(methyl methacrylate) tube and nylon ball in a beating heart (Fig. 1.1.2.9). This was a heroic operation and basically unsuccessful, but an operation that inspired cardiac surgeons to consider that valve prostheses might be possible. The 1953 development of the heart–lung machine by Gibbon allowed the next stage in the evolution of the prosthetic heart valve to take place. In 1960, a mitral valve replacement was performed in a human by surgeon Albert Starr, using a valve design consisting of a silicone ball and poly(methyl methacrylate) cage (later replaced by a stainless-steel cage). The valve was invented by engineer Lowell Edwards. The heart valve was based on a design for a bottle stopper invented in 1858. Starr was quoted as saying: “Let’s make a valve that works and not worry about its looks,” referring to its design that was radically different from the leaflet valve that nature evolved in mammals. Prior to the Starr–Edwards valve, no human had lived with a prosthetic heart valve longer than 3 months. The Starr–Edwards valve was found to permit good patient survival. The major issues in valve development in that era were thrombosis and durability. In 1969, Warren Hancock started the development of the first leaflet tissue heart valve based upon glutaraldehyde-treated pig valves, and his company and valve were acquired by Johnson & Johnson in 1979.

Pyrolytic Carbon

Pyrolytic carbon (PyC) is a manmade material not found in nature. The term “pyrolytic” is derived from “pyrolysis”—a thermal decomposition process. In other words, PyC is formed from the thermal decomposition of hydrocarbons such as propane, propylene, acetylene, and methane in the absence of oxygen. The use of PyC as leaflets for blood contact application was an accidental event, according to the story told by Professor Robert E. Baier of the University at Buffalo in 2016 (Baier, 2016). Here are his own words:

It was in late 1967, early 1968, that a strange finding emerged from the pioneering “Gott Ring” studies in canine vena cavae being done at Johns Hopkins Hospital, in Baltimore, Maryland. Classical inorganic materials scientist, Dr. Jack Bokros, of San Diego’s General Atomic Corp., had become “accidentally” a co-worker of Vincent Gott through Bill Ellis, who had read an abstract in Carbon by Gott et al.: “The Anticlot Properties of Graphite Coatings on Artificial Heart Valves” (Gott et al., 1964) and informed Bokros that colloidal graphite (carbon) coatings were being used as a “base” for blood anti-coagulant on Dr. Vincent Gott’s short-ring implants, to good effect. Ellis was a bit offended by the choice of a commercial product which was much less pure than what had recently been developed at General Atomic, and so samples of the newly developed PyC at General Atomic Corp. were sent to Dr. Gott as “positive” (clot-provoking) controls. I was one of the “boys in the back room,” providing surface analyses of all proposed new blood-contact materials. Early measurements predicted that these PyC rings would immediately cause both thrombosis and coagulation of slow-flowing dog blood. We were all surprised when the naked PyC rings stayed clean for 2-hours (most everything else had clotted solid by then), and then were amazed when the dogs were brought back after 2-weeks “at the farm!”

The rings were still clean, clearly violating all that we had considered ample predictive data to the contrary. Carrying the tests further, I was able to show that the PyC material uniquely bound one of the blood’s proteins in a configuration that expressed an outermost “Critical Surface Tension” in a zone prior identified as triggering the least thrombosis and coagulation. It was in that zone, and specifically for the PyC, that Surgeon Eugene Bernstein and Fred Schoen had shown that such PyC leaflets on a pioneering centrifugal blood pump least distorted attached blood platelets and thus did not trigger viscous metamorphosis and thrombus growth. Our colleague, Dr. Emery Nyilas, then working at AVCO-Everett Corporation near Boston, showed that the “heat of adsorption” was minimal during key blood protein trials (carried out in the middle of the night to avoid traffic vibrations) by micro-calorimetry. Drs. Andrade and Kim subsequently showed that the mode of protein adsorption and not the quantity of protein adsorbed on foreign surfaces was a key, consistent with Nyilas’ micro-calorimetric studies. PyC adsorbed a layer of blood proteins rapidly without the expected denaturing of proteins on blood contacting surfaces which generally triggered the clotting cascade.



• **Figure 1.1.2.10** An in vivo flow cell made of pyrolytic carbon, post-canine implantation.

Many others joined in, General Atomic became Gulf General Atomic which spun-off CarboMedics which inspired Medical Carbon Research Institute—and a large fraction of the world’s synthetic heart valves have since been rendered from those pioneering contributions between academia and industry. The recently announced sale of St. Jude Medical to Abbott Laboratories for \$25 Billion is predominantly owing to the initial success of St. Jude with these PyC heart valves, and subsequent copying of the technology. Fig. 1.1.2.10 is a contemporary photo of a PyC “flow cell” that had been implanted in a 27 kg dog by Dr. Gott, to establish the details of thromboresistance now shown in over 15 million successful valve implants.

Drug Delivery and Controlled Release

Throughout most of history drugs were administered orally or by hypodermic syringe. In general, there was no effort to modulate the rate of uptake of the drug into the body. In 1949, Dale Wurster invented what is now known as the Wurster process that permitted pills and tablets to be encapsulated and therefore slow their release rate. However, modern ideas of controlled release can be traced to a medical doctor, Judah Folkman. Dr. Folkman noted that dyes penetrated deeply into silicone rubber, and he surmised from this that drugs might do the same. He sealed isoproterenol (a drug used to treat heart block) into silicone tubes, and implanted these into the hearts of dogs (Folkman and Long, 1964). He noted the delayed release and later applied this same idea to delivering a birth control steroid. He donated this development, patent free, to the World Population Council. An entrepreneur and chemist, Alejandro Zaffaroni, heard of the Folkman work and launched a company in 1970, Alza (originally called Pharmetrics), to develop these ideas for the pharmaceutical industry. The company developed families of new polymers for controlled release, and also novel delivery strategies. Alza was a leader in launching this new field that is so important today; further details on the field of controlled release are provided in an excellent historical overview (Hoffman, 2008).

Designed Biomaterials

In contrast to the biomaterials of the surgeon-hero era, when largely off-the-shelf materials were used to fabricate medical devices, the 1960s saw the development of materials designed specifically for biomaterials applications. Here are some key classes of materials and their evolution from commodity materials to engineered/synthesized biomaterials.

Silicones

Although the class of polymers known as silicones has been explored for many years, it was not until the early 1940s that Eugene Rochow of General Electric pioneered the scale-up and manufacture of commercial silicones via the reaction of methyl chloride with silicone in the presence of catalysts. In Rochow’s 1946 book, *The Chemistry of Silicones* (John Wiley & Sons, Publishers), he comments anecdotally on the low toxicity of silicones, but did not propose medical applications. Possibly the first report of silicones for implantation was by Lahey (1946) (see also Chapter 1.3.2B). The potential for medical uses of these materials was realized shortly after this. In a 1954 book on silicones, McGregor has a whole chapter titled “Physiological Response to Silicones.” Toxicological studies were cited suggesting to McGregor that the quantities of silicones that humans might take into their bodies should be “entirely harmless.” He mentions, without citation, the application of silicone rubber in artificial kidneys. Silicone-coated rubber grids were also used to support a dialysis membrane (Skeggs and Leonards, 1948). Many other early applications of silicones in medicine are cited in Chapter 1.3.2B.

Polyurethanes

Polyurethane was invented by Otto Bayer and colleagues in Germany in 1937. The chemistry of polyurethanes intrinsically offered a wide range of synthetic options leading to hard plastics, flexible films, or elastomers (Chapter 1.3.2A). Interestingly, this was the first class of polymers to exhibit rubber elasticity without covalent cross-linking. As early as 1959, polyurethanes were explored for biomedical applications, specifically heart valves (Akutsu et al., 1959). In the mid-1960s a class of segmented polyurethanes was developed that showed both good biocompatibility and outstanding flex life in biological solutions at 37°C (Boretos and Pierce, 1967). Sold under the name Biomer by Ethicon and based upon DuPont Lycra, these segmented polyurethanes comprised the pump diaphragms of the Jarvik 7 hearts that were implanted in seven humans.

Teflon

DuPont chemist Roy Plunkett discovered a remarkably inert polymer, Teflon (polytetrafluoroethylene) (PTFE), in 1938. William L. Gore and his wife, Vieve, started a company in 1958 to apply Teflon for wire insulation. In 1969, their

son Bob found that Teflon, if heated and stretched, forms a porous membrane with attractive physical and chemical properties. Bill Gore tells the story that, on a chairlift at a ski resort, he pulled from his parka pocket a piece of porous Teflon tubing to show to his fellow ski lift passenger. The skier was a physician and asked for a specimen to try as a vascular prosthesis. Now, Goretex porous Teflon and similar expanded PTFEs are the leading synthetic vascular grafts, and are also used in numerous other applications in surgery and biotechnology (Chapters 1.3.2C and 2.5.2B).

Hydrogels

Hydrogels have been found in nature since life on earth evolved. Bacterial biofilms, hydrated extracellular matrix components, and plant structures are ubiquitous, water-swollen motifs in nature. Gelatin and agar were also known and used for various applications early in human history. But the modern history of hydrogels as a class of materials designed for medical applications can be accurately traced.

In 1936, DuPont scientists published a paper on recently synthesized methacrylic polymers. In this paper, poly(2-hydroxyethyl methacrylate) (polyHEMA) was mentioned. It was briefly described as a hard, brittle, glassy polymer, and clearly was not considered of importance. After that paper, polyHEMA was essentially forgotten until 1960. Wichterle and Lim published a paper in *Nature* describing the polymerization of HEMA monomer and a cross-linking agent in the presence of water and other solvents (Wichterle and Lim, 1960). Instead of a brittle polymer, they obtained a soft, water-swollen, elastic, clear gel. Wichterle went on

to develop an apparatus (built originally from a children's construction set; Fig. 1.1.2.11) for centrifugally casting the hydrogel into contact lenses of the appropriate refractive power. This innovation led to the soft contact lens industry, and to the modern field of biomedical hydrogels as we know them today.

Interest and applications for hydrogels have steadily grown over the years, and these are described in detail in Chapter 1.3.2E. Important early applications included acrylamide gels for electrophoresis, poly(vinyl alcohol) porous sponges (Ivalon) as implants, many hydrogel formulations as soft contact lenses, and alginate gels for cell encapsulation.

Poly(Ethylene Glycol)

Poly(ethylene glycol) (PEG), also called poly(ethylene oxide), in its high molecular weight form, can be categorized as a hydrogel, especially when the chains are cross-linked. However, PEG has many other applications and implementations. It is so widely used today that its history is best discussed in its own section.

The low reactivity of PEG with living organisms has been known since at least 1944, when it was examined as a possible vehicle for intravenously administering fat-soluble hormones (Friedman, 1944). In the mid-1970s, Frank Davis and colleagues (Abuchowski et al., 1977) discovered that if PEG chains were attached to enzymes and proteins, they would have a much longer functional residence time in vivo than biomolecules that were not PEGylated. Professor Edward Merrill of MIT, based upon what he called “various bits of evidence” from the literature, concluded



• **Figure 1.1.2.11** Left: Otto Wichterle (1913–98). (Wikipedia.) Right: The centrifugal casting apparatus Wichterle used to create the first soft, hydrogel contact lenses. (Photograph by Jan Suchy, Wikipedia public domain.)

that surface-immobilized PEG would resist protein and cell pickup. The experimental results from his research group in the early 1980s bore out this conclusion (Merrill, 1992). The application of PEGs to a wide range of biomedical problems was significantly accelerated by the synthetic chemistry developments of Dr. Milton Harris while at the University of Alabama, Huntsville.

Poly(Lactic-Glycolic Acid)

Although originally discovered in 1833, the anionic polymerization from the cyclic lactide monomer in the early 1960s made creating materials with mechanical properties comparable to Dacron possible. The first publication on the application of poly(lactic acid) in medicine may be by Kulkarni et al. (1966). This group demonstrated that the polymer degraded slowly after implantation in guinea pigs or rats, and was well tolerated by the organisms. Cutright et al. (1971) were the first to apply this polymer for orthopedic fixation. Poly(glycolic acid) and copolymers of lactic and glycolic acid were subsequently developed. Early clinical applications of polymers in this family were for sutures, based upon the work of Joe Frazza and Ed Schmitt at David & Geck, Inc (Frazza and Schmitt, 1971). The glycolic acid/lactic acid polymers have also been widely applied for controlled release of drugs and proteins. Professor Robert Langer's group at MIT was the leader in developing these polymers in the form of porous scaffolds for tissue engineering (Langer and Vacanti, 1993).

Hydroxyapatite

Hydroxyapatite is one of the most widely studied materials for healing in bone. It is a naturally occurring mineral, a component of bone, and a synthesized material with wide application in medicine. Hydroxyapatite can be easily made as a powder. One of the first papers to describe biomedical applications of this material was by Levitt et al. (1969), in which they hot pressed the hydroxyapatite powder into useful shapes for biological experimentation. From this early appreciation of the materials science aspect of a natural biomineral, a literature of thousands of papers has evolved. In fact, the nacre implant described in the prehistory section may owe its effectiveness to hydroxyapatite—it has been shown that the calcium carbonate of nacre can transform in phosphate solutions to hydroxyapatite (Ni and Ratner, 2003).

Titanium

In 1791, William Gregor, a Cornish amateur chemist, used a magnet to extract the ore that we now know as ilmenite from a local river. He then extracted the iron from this black powder with hydrochloric acid, and was left with a residue that was the impure oxide of titanium. After 1932, a process developed by William Kroll permitted the commercial extraction of titanium from mineral sources. At the

end of World War II, titanium metallurgy methods and titanium materials made their way from military application to peacetime uses. By 1940, satisfactory results had already been achieved with titanium implants (Bothe et al., 1940). The major breakthrough in the use of titanium for bony tissue implants was the Brånemark discovery of osseointegration, described earlier in the section on dental implants.

Bioglass

Bioglass is important to biomaterials as one of the first completely synthetic materials that seamlessly bonds to bone. It was developed by Professor Larry Hench and colleagues. In 1967 Hench was Assistant Professor at the University of Florida. At that time his work focused on glass materials and their interaction with nuclear radiation. In August of that year, he shared a bus ride to an Army Materials Conference in Sagamore, New York, with a US Army colonel who had just returned from Vietnam where he was in charge of supplies to 15 MASH units. This colonel was not particularly interested in the radiation resistance of glass. Rather, he challenged Hench with the following: hundreds of limbs a week in Vietnam were being amputated because the body was found to reject the metals and polymer materials used to repair the body. "If you can make a material that will resist gamma rays why not make a material the body won't resist?"

Hench returned from the conference and wrote a proposal to the US Army Medical R and D Command. In October 1969 the project was funded to test the hypothesis that silicate-based glasses and glass-ceramics containing critical amounts of Ca and P ions would not be rejected by bone. In November 1969 Hench made small rectangles of what he called 45S5 glass (44.5 wt% SiO₂), and Ted Greenlee, Assistant Professor of Orthopedic Surgery at the University of Florida, implanted them in rat femurs at the VA Hospital in Gainesville. Six weeks later Greenlee called: "Larry, what are those samples you gave me? They will not come out of the bone. I have pulled on them, I have pushed on them, I have cracked the bone and they are still bonded in place." Bioglass was born, and with the first composition studied! Later studies by Hench using surface analysis equipment showed that the surface of the bioglass, in biological fluids, transformed from a silicate-rich composition to a phosphate-rich structure, possibly hydroxyapatite (Clark et al., 1976).

The Contemporary Era (Modern Biology and Modern Materials)

It is probable that the modern era in the history of biomaterials, biomaterials engineered to control specific biological reactions, was ushered in by rapid developments in modern biology. As illustrated in Fig. 1.1.1.2, major advances in the medical device field continue to be made with materials that could be considered first generation with the incorporation of concepts and approaches from the later generations. In the 1960s, when the field of

biomaterials was laying down its foundational principles and ideas, concepts such as cell-surface receptors, growth factors, nuclear control of protein expression and phenotype, cell attachment proteins, stem cells, and gene delivery were either controversial observations or not yet discovered. Thus pioneers in the field could not have designed materials with these ideas in mind. It is to the credit of the biomaterials community that it has been quick to embrace and exploit new ideas from biology. Similarly, new ideas from materials science such as phase separation, anodization, self-assembly, surface modification, and surface analysis were quickly assimilated into the biomaterial scientists' toolbox and vocabulary. A few of the important ideas in biomaterials literature that set the stage for the biomaterials science we see today are useful to list:

- Protein adsorption
- Biospecific biomaterials
- Nonfouling materials
- Healing and the foreign-body reaction
- Controlled release (also, programmed release and release on demand)
- Tissue engineering
- Immunoengineering
- Regenerative materials
- Nanotechnology

Since these topics are addressed later in some detail in *Biomaterials Science: An Introduction to Materials in Medicine*, fourth edition, they will not be expanded upon in this history section. Still, it is important to appreciate the intellectual leadership of many researchers who promoted these ideas that comprise modern biomaterials—this is part of a recent history of biomaterials that will someday be completed. We practice biomaterials today immersed within an evolving history.

Conclusions

Biomaterials have progressed from adventurous practices by surgeon-heroes, sometimes working with engineers, to a field dominated by engineers, chemists, and physicists, to our modern era innovations with biologists and bioengineers as the key players. At the moment you are reading the fourth edition of *Biomaterials Science: An Introduction to Materials in Medicine*, many individuals who were biomaterials pioneers in the formative days of the field are well into their eighth or ninth decades of life. A number of leaders of biomaterials, pioneers who spearheaded the field with vision, creativity, and integrity, have passed away. Yet, since biomaterials is relatively a new field, the first-hand accounts of its roots are still available. We encourage readers of this book to document their conversations with pioneers of the field (many of whom still attend biomaterials conferences), so that the exciting stories and accidental discoveries that led to the successful and intellectually stimulating field we see today are not lost.

References

- Abuchowski, A., McCoy, J.R., Palczuk, N.C., van Es, T., Davis, F.F., 1977. Effect of covalent attachment of polyethylene glycol on immunogenicity and circulating life of bovine liver catalase. *J. Biol. Chem.* 252 (11), 3582–3586.
- Akutsu, T., Dreyer, B., Kolff, W.J., 1959. Polyurethane artificial heart valves in animals. *J. Appl. Physiol.* 14, 1045–1048.
- Apple, D.J., Trivedi, R.H., 2002. Sir Nicholas Harold Ridley, Kt, MD, FRCS, FRS. *Arch. Ophthalmol.* 120 (9), 1198–1202.
- Baier, R.E., 2016. Surprising blood Compatibility of pyrolytic carbon!. *Biomater. Forum* 38 (4), 4–5.
- Blagg, C., 1998. Development of ethical concepts in dialysis: Seattle in the 1960s. *Nephrology* 4 (4), 235–238.
- Bobbio, A., 1972. The first endosseous alloplastic implant in the history of man. *Bull. Hist. Dent.* 20, 1–6.
- Bondurant, S., Ernster, V., Herdman, R. (Eds.), 1999. *Safety of Silicone Breast Implants*. National Academies Press, Washington DC.
- Boretos, J.W., Pierce, W.S., 1967. Segmented polyurethane: a new elastomer for biomedical applications. *Science* 158, 1481–1482.
- Bothe, R.T., Beaton, L.E., Davenport, H.A., 1940. Reaction of bone to multiple metallic implants. *Surg. Gynecol. Obstet.* 71, 598–602.
- Branemark, P.I., Breine, U., Johansson, B., Roylance, P.J., Röckert, H., Yoffey, J.M., 1964. Regeneration of bone marrow. *Acta Anat.* 59, 1–46.
- Clark, A.E., Hench, L.L., Paschall, H.A., 1976. The influence of surface chemistry on implant interface histology: a theoretical basis for implant materials selection. *J. Biomed. Mater. Res.* 10, 161–177.
- Crubezy, E., Murail, P., Girard, L., Bernadou, J.-P., 1998. False teeth of the Roman world. *Nature* 391, 29.
- Cutright, D.E., Hunsuck, E.E., Beasley, J.D., 1971. Fracture reduction using a biodegradable material, polylactic acid. *J. Oral Surg.* 29, 393–397.
- Egdahl, R.H., Hume, D.M., Schlang, H.A., 1954. Plastic venous prostheses. *Surg. Forum* 5, 235–241.
- Folkman, J., Long, D.M., 1964. The use of silicone rubber as a carrier for prolonged drug therapy. *J. Surg. Res.* 4, 139–142.
- Frazza, E., Schmitt, E., 1971. A new absorbable suture. *J. Biomed. Mater. Res.* 5 (2), 43–58.
- Friedman, M., 1944. A vehicle for the intravenous administration of fat soluble hormones. *J. Lab. Clin. Med.* 29, 530–531.
- Gott, V.L., Whiffen, J.D., Dutton, R.C., Koepke, D.E., Daggett, R.L., Young, W.P., 1964. The ant clot properties of graphite coating on artificial heart valves. *Carbon* 1, 378.
- Hoffman, A., 2008. The origins and evolution of “controlled” drug delivery systems. *J. Control. Release* 132 (3), 153–163.
- Ingraham, F.D., Alexander Jr., E., Matson, D.D., 1947. Polyethylene, a new synthetic plastic for use in surgery. *J. Am. Med. Assoc.* 135 (2), 82–87.
- Kolff, W.J., 1998. Early years of artificial organs at the Cleveland Clinic Part II: open heart surgery and artificial hearts. *ASAIO J.* 44 (3), 123–128.
- Kulkarni, R.K., Pani, K.C., Neuman, C., Leonard, F., 1966. Polylactic acid for surgical implants. *Arch. Surg.* 93, 839–843.
- Lahey, F.H., 1946. Comments (discussion) made following the speech “Results from using Vitallium tubes in biliary surgery,” by Pearce H. E. before the American Surgical Association, Hot Springs, VA. *Ann. Surg.* 124, 1027.
- Langer, R., Vacanti, J., 1993. Tissue engineering. *Science* 260, 920–926.

- LeVeen, H.H., Barberio, J.R., 1949. Tissue reaction to plastics used in surgery with special reference to Teflon. *Ann. Surg.* 129 (1), 74–84.
- Levitt, S.R., Crayton, P.H., Monroe, E.A., Condrate, R.A., 1969. Forming methods for apatite prostheses. *J. Biomed. Mater. Res.* 3, 683–684.
- McGregor, R.R., 1954. *Silicones and Their Uses*. McGraw Hill Book Company, Inc., New York.
- Merrill, E.W., 1992. Poly(ethylene oxide) and blood contact. In: Harris, J.M. (Ed.), *Poly(ethylene Glycol) Chemistry: Biotechnical and Biomedical Applications*. Plenum Press, New York, pp. 199–220.
- Ni, M., Ratner, B.D., 2003. Nacre surface transformation to hydroxyapatite in a phosphate buffer solution. *Biomaterials* 24, 4323–4331.
- Rob, C., 1958. Vascular surgery. In: Gillis, L. (Ed.), *Modern Trends in Surgical Materials*. Butterworth & Co, London, pp. 175–185.
- Skeggs, L.T., Leonards, J.R., 1948. Studies on an artificial kidney: preliminary results with a new type of continuous dialyzer. *Science* 108, 212.
- Wichterle, O., Lim, D., 1960. Hydrophilic gels for biological use. *Nature* 185, 117–118.
- Willyard, C., 2016. Timeline: regrowing the body. *Nature* 540, S50.

1.2.1

Introduction: Properties of Materials— the Palette of the Biomaterials Engineer

JACK E. LEMONS¹, GUIGEN ZHANG²

¹Schools of Dentistry, Medicine and Engineering, University of Alabama at Birmingham, Birmingham, AL, United States

²F Joseph Halcomb III, M.D. Department of Biomedical Engineering, University of Kentucky, Lexington, KY, United States

The platform, or palette, upon which the biomaterials engineer arranges information into parts for subsequent blending has expanded and evolved significantly in content over the past several decades. The depth and breadth of what is now included on this palette go well beyond expectations expressed by the founding members of the Society for Biomaterials in the late 1960s and early 1970s. The *Science of Biomaterials* has expanded from dealing with the fundamental aspects of the physical, mechanical, chemical, electrical, electrochemical, thermal, optical, and biological (compatibility) properties of biomaterials of natural or synthetic origin, to the design principles of tissue/cell/molecule-synthesized or -engineered biomaterials and nanomaterials. Because of that, the methods for measuring and analyzing materials' properties have also evolved.

Following the recognition of the need by the pioneers of the biomaterials discipline in the 1960s, one focus of the science of biomaterials has been the fundamental structure versus property relationships leading to in vivo biocompatibility. These relationships, and the supporting scientific information, have changed with time and experience, especially as the biological and clinical disciplines have also expanded and evolved. For example, considerations for biocompatibility are very different for biomaterials listed within biotolerant, surface bioactive, and biodegradable categories. This shift of emphasis is reflected in the progression of content of the first four editions of this book. For

example, initial considerations focused on materials were based primarily on substances of the metallics, ceramics, and polymeric available within various biomedical applications. Thus the emphasis in the first edition was on materials of natural and synthetic origin, including metals, ceramics, polymers, and composites, and the underlying science leading to biomedical applications. The second and third editions represent the transitions from combination products to the new areas of bioactives and biodegradables and tissue-engineered constructs. As an integrated, comprehensive, and authoritative text, this fourth edition reflects a broader range of biomaterials as well as basic properties of new classes of biomaterials that possess more of a resemblance to complex biological constructs formed by nature and constantly remodeled by biology in response to biophysical demands and biomechanical environments.

Considering relationships between biomaterial and biological systems (the interface) and the dynamics of change from nanoseconds to years, we now better understand many mechanisms of interaction at the dimensions and concentrations used to describe interactions of atoms and molecules. It is also realized that all biomaterial and host-environment interactions play a role in the broader aspects of biocompatibility, especially the functionality and longevity of implant devices. In this regard, Part 1 on "Materials Science and Engineering" emphasizes the more basic information on the bulk and surface properties of synthetic and natural origin biomaterials. Critical aspects of constitution

(chemistry) and structure (nano-, micro-, and macrodimension) relationships are presented as related to properties of implant systems. These basic considerations include the nature of the matters (Chapter 1.2.2), bulk (Chapter 1.2.3), and surface (Chapter 1.2.4) properties, and the role of water in biomaterials (Chapter 1.2.5). The science of interactions of synthetic and natural substances with water is recognized as one of the key aspects of surgical implant biocompatibilities. This is especially important for the evolution of the

discipline to include new-generation biomaterials needed for future implant applications.

In short, the content of this Part 1 is broadly applicable to all parts of the fourth edition. Therefore students are advised to always consider the basic principles as provided in this section. This has been recognized as critical to the education of a specialist in biomaterials science leading to the selection of biomaterials for medical treatments utilizing all types of implant devices.

1.2.2

The Nature of Matter and Materials

BUDDY D. RATNER

Bioengineering and Chemical Engineering, Director of University of Washington Engineered Biomaterials (UWEB), Seattle, WA, United States

Introduction

Biomaterials are *materials*.

Biomaterials are *materials*. What are materials and how are they structured? This is the subject of this chapter, a lead into subsequent chapters with discussions of the bulk (including mechanical) properties of materials, surface properties, and the role of water (since biomaterials most commonly function in an aqueous environment, and that environment can alter both the nature of the material and the interactions that occur with the material). This chapter also considers fundamental atomic and molecular interactions that underlie subsequent chapters addressing specific classes of materials relevant to biomaterials (polymers, metals, ceramics, natural materials, and particulates).

Atoms and Molecules

The key to understanding matter is to understand attractive and interactive forces between atoms.

This “Nature of Matter” section aims to communicate an understanding of the basic structure of materials that will drive their properties—both the mechanical properties important for specific applications (strong, elastic, ductile, permeable, etc.), and the surface properties that will mediate reactions with the external biological environment.

The key to understanding matter is to understand attractive and interactive forces between atoms. Argon is a gas at room temperature—it must be cooled to extremely low temperatures to transition it into liquid form. An argon atom interacts (attracts) very, very weakly with another argon atom—so at room temperature, thermal fluctuations that randomly propel the atoms exceed attractive forces that might result in coalescence to a solid material.

A titanium atom strongly interacts with another titanium atom. Extremely high temperatures are required to vaporize titanium and liberate those atoms from each other. The understanding of matter is an appreciation of interactive forces between atoms.

What holds those atoms and molecules together to make a strong nylon fiber or a cell membrane, or a hard, brittle hydroxyapatite ceramic, or a sheet of gold, or a drop of water? Even in the early 18th century, Isaac Newton was pondering this issue: “There are therefore Agents in Nature able to make the Particles of Bodies stick together by very strong Attractions.”

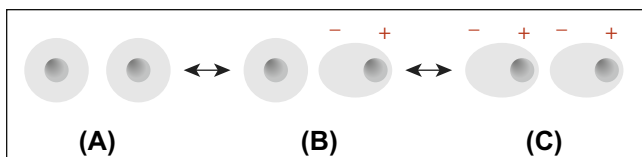
Entropy consideration would say these molecules and atoms should “fly apart” to increase randomness. However, there is an energy term contributing to the stability of the ensemble leading to a negative Gibbs free energy, which, according to the second law of thermodynamics, should make such solids energetically favorable (of course, we intuitively know this). Thus we must examine this energy term. We know of just four attractive forces in this universe:

- Gravitational
- Weak nuclear
- Strong nuclear
- Electromagnetic

Gravity holds us to the surface of the planet Earth (a massive body), but the gravitational potential energy of two argon atoms is only about 10^{-52} J, 30 orders of magnitude weaker than is observed for intermolecular forces. The weak nuclear force and the strong nuclear force are only significant over 10^{-4} nm—but molecular dimensions are 5×10^{-1} nm. So these forces do not explain what holds atoms together. This leaves, by default, electromagnetic forces (positive charge attracts negative charge). Electromagnetic forces have appropriate magnitudes and distance dependencies to justify why atoms interact. Interactions can be weak, leading to liquids, or stronger, leading to solids.

TABLE 1.2.2.1 Forces That Hold Atoms Together

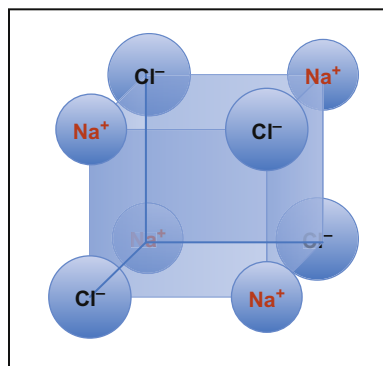
Interatomic Force	Explanation	Relative Strength	Examples
Van der Waals interactions	Transient fluctuations in the spatial localization of electron clouds surrounding atoms lead to transient positive and negative charges, and consequent interactive forces in molecules would seem to have no permanent polarity	Weak	Argon at cryogenic temperatures Polyethylene (the forces that hold the chains together to make a solid)
Ionic	Atoms with a permanent positive (+) charge attract atoms with a permanent negative (−) charge	Very strong	NaCl CaCl ₂
Hydrogen (H) bonding	The interaction of a covalently bound hydrogen with an electronegative atom, such as oxygen or fluorine	Medium	Water ice Nylon (the forces that hold the chains together to make a strong, high-melting point solid)
Metallic	The attractive force between a “sea” of positively charged atoms and delocalized electrons	Medium–strong	Gold Titanium metal
Covalent	A sharing of electrons between two atoms	Strong	The carbon–carbon bond Cross-links in a polyacrylamide hydrogel



• **Figure 1.2.2.1** (A) Consider the electron clouds (charge density in space) of two atoms or molecules, both without permanent dipole moments. (B) Electron clouds are continuously in motion and can shift to one side of the atom or molecule; therefore, at any moment, the atoms or molecules can create a “fluctuating instantaneous dipole.” (C) The “fluctuating instantaneous dipole” in one molecule electrostatically induces such an “instantaneous dipole” in the next molecule.

Electromagnetic forces manifest themselves in a number of ways. The types of interactions usually observed between atoms (all explained by electrostatics) are summarized in [Table 1.2.2.1](#). We consider here van der Waals forces (also called induction or dispersion forces), ionic forces, hydrogen bonding, metallic forces, and covalent interactions.

Van der Waals or dispersion forces rationalize the interaction of two atoms or molecules, each without a dipole (no plus or minus faces to the molecules). For example, argon atoms can be liquefied at low temperature. Why should this happen? Why should argon atoms want to interact with each other enough to form a liquid? [Fig. 1.2.2.1](#) explains the origin of dispersive forces. Such forces are important, as they dictate the properties of many materials (for example, some polymers such as polyethylene, which has no obvious dipole), but they also explain why the lipids in cell membranes assemble into the bilayer structure described later in this textbook. A typical van der Waals interactive force (for example,

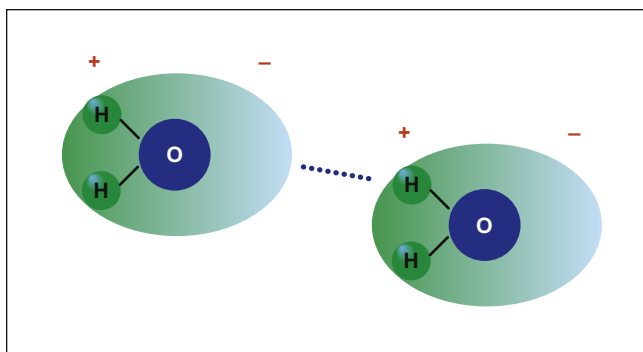


• **Figure 1.2.2.2** The unit cell of a sodium chloride crystal illustrating the plus–minus electrostatic interactions.

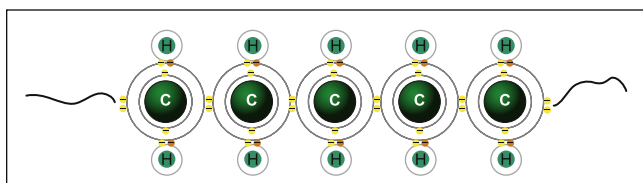
$\text{CH}_4 \cdots \text{CH}_4$) is about 9 kJ/mol. The $\text{Ar} \cdots \text{Ar}$ interactive force is approximately 1 kJ/mol.

Ionic forces are probably the easiest of the intermolecular forces to understand. [Fig. 1.2.2.2](#) illustrates a unit cell of a sodium chloride crystal. The + and − charges are arrayed to achieve the closest interaction of opposite charges and the furthest separation of similar charges. This unit cell can be repeated over and over in space, and the forces that hold it together are the electrostatic interaction of a permanent + charge and a permanent − charge. Typical ionic bond strengths (for example, NaCl) are about 770 kJ/mol.

Hydrogen bonding interactions are also straightforward to appreciate as electrostatic interactions. An electronegative element such as oxygen (it demands electrons) can distort the binding electron cloud from the hydrogen nucleus leaving the hydrogen (just a proton and electron) with less electron and thus more plus-charged proton.



• **Figure 1.2.2.3** A hydrogen bond between two water molecules.



• **Figure 1.2.2.5** Covalent bonding along a section of polyethylene chain. Carbons share pairs of electrons with each other, and each hydrogen shares an electron pair with carbon.

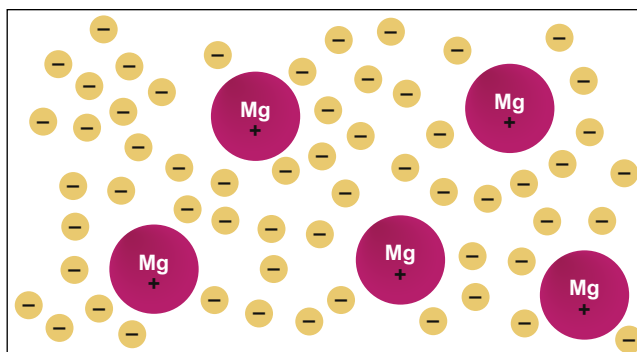
This somewhat positive charge will, in turn, then interact with an electronegative oxygen (Fig. 1.2.2.3). Typical hydrogen bond strengths (for example, $\text{O}-\text{H} \cdots \text{H}$) are about 20 kJ/mol.

Metallic bonding is explained by a delocalized “sea” of valence electrons with positively charged nuclear cores dispersed within it (Fig. 1.2.2.4). A single metallic bond is rarely discussed. The total interactive strength is realized through the multiplicity of the plus–minus interactions. The strength of this interaction can be expressed by heats of sublimation. For example, at 25°C, aluminum will have a heat of sublimation of 325 kJ/mol, while titanium will be about 475 kJ/mol.

Covalent bonds are relatively strong bonds associated with the sharing of pairs of electrons between atoms (Fig. 1.2.2.5). Typical covalent bond strengths (for example, C–C) are about 350 kJ/mol.

Molecular Assemblies

Atoms can combine in defined ratios to form molecules (usually they combine with covalent bonds), or they can form cohesive assemblies of atoms (think of gold and metallic interactive forces, for example). Thus materials can be made of atoms or of molecules (i.e., covalently joined atoms). The difference between the dense, lubricious plastics used in orthopedics, the soft, elastic materials of catheters, and the hard, strong metals of a hip joint is associated with how those atoms and molecules are organized (due to attractive and interactive forces) in materials. Metals used in biomaterials applications can be strong, rigid, and brittle, or flexible and ductile. Again, the difference is largely how the atoms making up the metal are organized, and how strongly their atoms interact.



• **Figure 1.2.2.4** Metallic bonding in magnesium. The 12 electrons from each Mg atom are shared among positively charged nuclear cores (the single + charge on each magnesium atom in the figure is simply intended to indicate there is some degree of positive charge on each magnesium nuclear core).

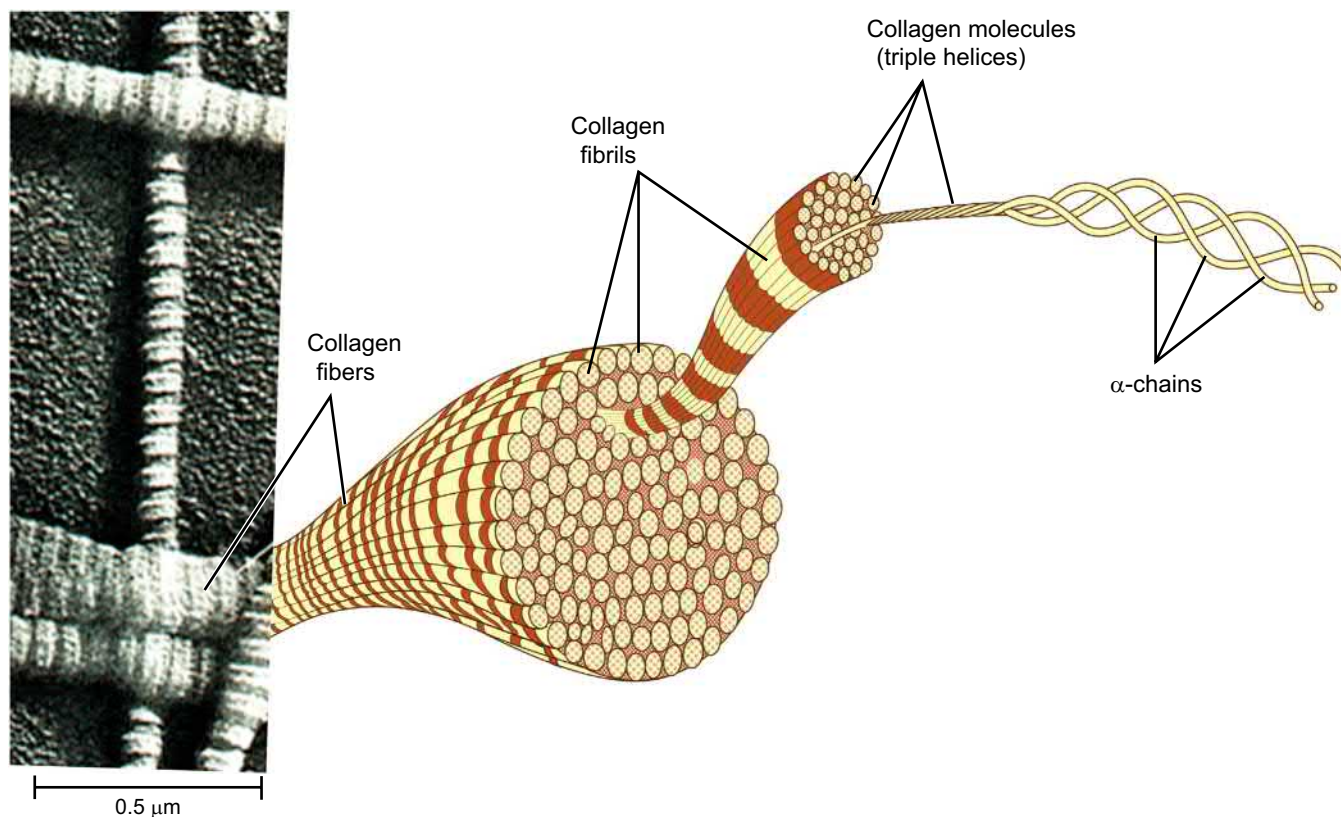
Molecules also organize or assemble. The widely varying properties of polymers are due to molecular organization. The assembly of lipid molecules to make a cell membrane or a microparticulate for drug delivery is another example of this organization.

A key concept in appreciating the properties of materials is hierarchical structures. The smallest size scale that we need consider here in materials is atoms, typically about 0.2 nm in diameter. Atoms combine to form molecules with dimensions ranging from 1 to 100 nm (some large macromolecules). Molecules may assemble or order to form supramolecular structures with dimensions up to 1000 nm or more. These supramolecular structures may themselves organize in bundles, fibers, or larger assemblies with dimensions reaching into the range visible to the human eye. This concept of hierarchical structure is illustrated in Fig. 1.2.2.6, using collagen protein as the example.

The single α -chains comprising the collagen triple helix would break under tension with an application of nanograms of force. On the other hand, the collagen fibers in a hierarchical structure such as a tendon can support many kilograms of force. Such hierarchical structures are noted frequently in both materials science and in biology.

Surfaces

As assemblies of atoms and/or molecules form, within the bulk of the material, each unit is uniformly “bathed” in a field of attractive forces of the types described in Table 1.2.2.1. However, those structural units that are at the surface are pulled upon asymmetrically by just the units beneath them. This asymmetric attraction distorts the electron distributions of the surface atoms or molecules, and gives rise to the phenomenon of surface energy, an excess energy associated with this imbalance. For this reason, surfaces always have unique reactivities and properties. This idea will be expanded upon in Chapter 1.2.4.



• **Figure 1.2.2.6** Collagen fibers make up many structures in the body (tendons, for example). Such anatomical structures as tendons are comprised of collagen fibrils, formed of aligned bundles of collagen triple helices that are themselves made up of single collagen protein chains (α -chains). The α -chains are constructed of joined amino acid units, and the amino acids are molecules of carbon, oxygen, nitrogen, and hydrogen atoms in defined ratios and orders. (Illustration from Becker, W., 2002. *The World of the Cell*. Reprinted with permission of Pearson Education, Inc.)

Conclusion

In this section we reviewed the transition from chemistry to matter. Interacting assemblies of atoms and molecules comprise matter. Without matter, we cannot have biomaterials. Matter exists because of electrostatic forces—positive and negative charges, in all cases, hold atoms together. The strength of those interactions, associated with the magnitude of the charge on each atom, and the environment the atoms are in (water, air, etc.) ultimately dictate the properties of matter (a soft gel, a hard metal, etc.). Now that we have a general idea what “matter” is, we can take these concepts from physics and chemistry and

bring them to a consideration of the mechanical properties of materials, the surface properties of materials, and then into the specifics of polymers, metals, ceramics, and other types of materials.

Further Reading

- Barton, A., 1997. *States of Matter, States of Mind*. Institute of Physics Publishing, Bristol, UK.
- Becker, W.M., 2003. *World of the cell*. In: Kleinsmith, L.J., Hardin, J. (Eds.), fifth ed. Pearson Education, Inc., Upper Saddle River, NJ.
- Holden, A., 1992. *The Nature of Solids*. Dover Publications Inc, New York, NY.

1.2.3

Bulk Properties of Materials

GUIGEN ZHANG¹, CHRISTOPHER VINEY²

¹F Joseph Halcomb III, M.D. Department of Biomedical Engineering, University of Kentucky, Lexington, KY, United States

²School of Engineering, University of California at Merced, Merced, CA, United States

Introduction

When describing a material, the term “bulk properties” is often used to differentiate, either intentionally or unintentionally, from the term “surface properties.” The importance of surfaces for biomaterials science is highlighted briefly in [Chapter 1.2.2](#) and in great detail in [Chapter 1.2.4](#). While it is important to know that the success or failure of many biomaterials depends on the physical and chemical characteristics of their surface because the surface properties dictate interactions between a material and its environment (thereby determining whether a permanently implanted material will be tolerated or rejected), it does not suggest that bulk properties of biomaterials are any less important. In fact, for almost all biomedical applications, either as short-term degradable applications or long-term structural or load-bearing applications, the bulk properties must meet the physical and/or mechanical demands of these applications over the desired time period, even if the surface properties are deemed to facilitate biocompatible material–tissue interactions. The requirements for biomaterials to exhibit certain *bulk* characteristics are multifaceted, including maintaining physical shapes, carrying mechanical loads, and possessing certain desirable electrochemical behavior, optic index, and/or thermal characteristics, among others.

As discussed in [Chapter 1.2.2](#), the differences in bulk properties of many materials such as metals, polymers, and ceramics are the results of different types of interatomic or intermolecular forces that hold atoms and molecules together. For example, metals and alloys are typically characterized by metallic bonds, ceramics are held together by ionic bonds, and polymers are predominately formed by covalent bonds. The differences in these bonding mechanisms and energies dictate the different bulk properties of these materials. This chapter provides an overview of some of the useful concepts related to the bulk properties of these materials, with an emphasis on mechanical properties. For more in-depth information, the reader is encouraged to consult books on materials science and strength of materials.

Mechanical Variables and Mechanical Properties

The mechanical properties of a material refer to the characteristic values of a material under various mechanical loading conditions. By characteristic values, we refer to quantitative measures of mechanical variables at which certain transitions in the material would occur. For example, stress and strain are two mechanical variables that are commonly referred to for a material, but they are not properties of the material. Only the stresses that cause certain structural changes, such as yielding or breaking, etc. will be regarded as properties. This can be likened to the fact that the temperature of water is a physical variable, but we do consider certain temperatures, at which transitions occur in the state of water, properties such as the freezing point or boiling point of water.

Taking a cylindrical rod with uniform cross-section area (often called prismatic rod) as an example of a material structure, stress (σ) is defined as force per unit area, obtainable by dividing the applied force (F) by the cross-section area (A) of the rod, $\sigma = F/A$.

Stress determined this way is commonly regarded as the *nominal stress* because the actual value of the area (cross-section) to which the load is applied will change as the sample deforms in response to the load. Nominal stress is often synonymously referred to as *engineering stress*.

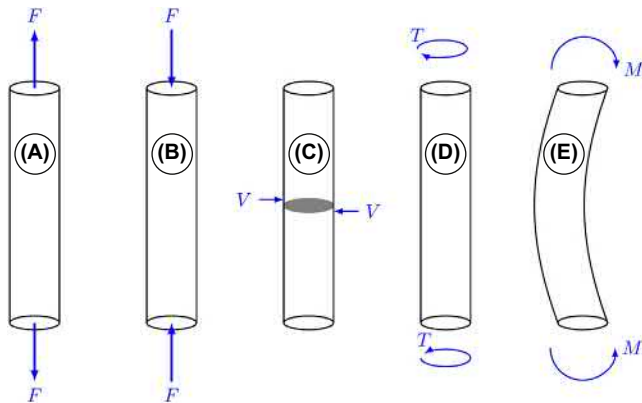
Strain (ϵ) is deformation per unit length, obtainable by dividing the deformation (δ) by the length of the rod (L), $\epsilon = \delta/L$.

By the same argument, strain determined this way is regarded as the *nominal strains or engineering strain* because the actual value of the length will change as the sample deforms in response to the load. Stresses and strains determined with reference to the actual cross-section area (A) and length (L) are initially known as true stresses and true strains, respectively. Unfortunately, because A and L change continuously during the course of a mechanical test, true stresses and strains can be difficult to measure in practice. Therefore, nominal stress and strain are commonly used instead of true stress and strain.

Stress (or strain) can be either normal or shear stress (or strain). Normal stress is determined by considering only the normal component of an arbitrary applied force, and shear stress by considering the tangent component of the force. The SI units of stress are newtons per square meter (N/m^2) or pascals (Pa), and strain is dimensionless.

Five Types of Mechanical Loading

A mechanical loading situation in a structure can be represented by a combination of several mechanical loads. In general, there are five basic types of loads as illustrated in Fig. 1.2.3.1 (Beer et al., 2014). When a pair of forces (F - F) with opposite directions is applied to a cylindrical rod along its axial direction, the situation is called axial loading. Under axial loading, we are more concerned with the deformations along the axial direction. If the axial load is making the rod longer, it is regarded as tensile loading, and if the axial load is making the rod shorter, it is compressive loading. When a pair of shear forces (V - V) with opposite directions



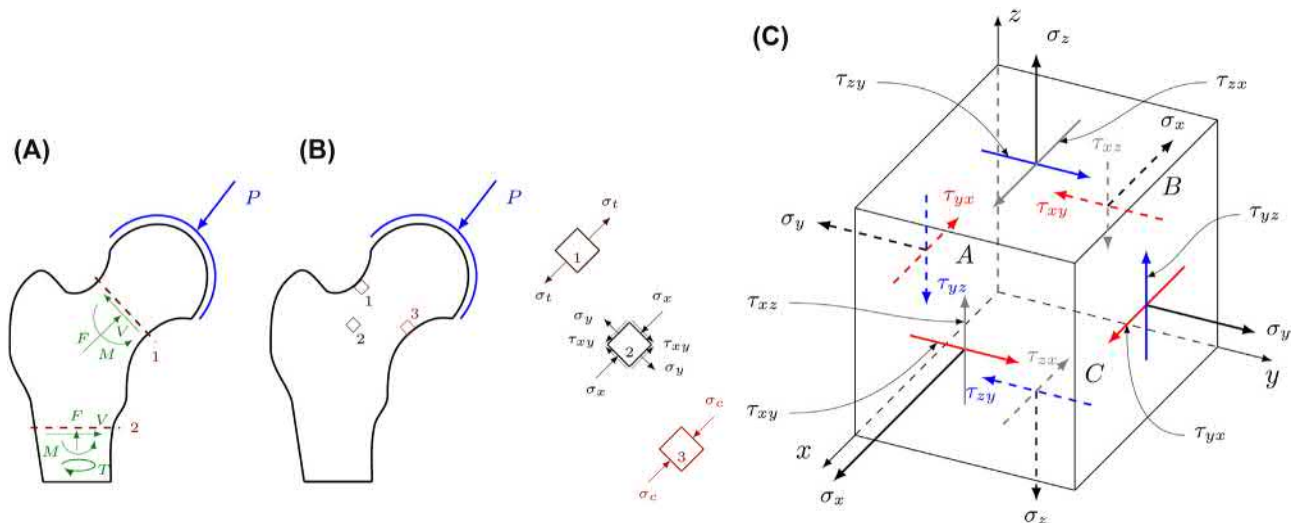
• **Figure 1.2.3.1** Five basic types of mechanical loading situations: (A) tension, (B) compression, (C) shearing, (D) torsion, and (E) bending.

is applied to the rod in a transverse direction, the loading condition is regarded as shearing loading with which we are mainly concerned about the transverse shear stress, strain, and deformation. When a pair of torques (T - T) with opposite directions is applied to the rod with respect to its axial orientation, the rod is regarded as under torsion loading in which we are concerned with twisting stress, strain, and angle. Finally, when a pair of moments (M - M) with opposite directions is applied to the rod, it is regarded as under bending. In a bending situation, we are more concerned about bending-induced tensile, compressive, and shear stresses and strains, as well as flexure deformation. Note that the term load is used here to represent all these forces, torques, and moments. Because of that, these loads will have different units, for instance, tensile, compressive, and shearing forces carry the units of newtons (N), and torque and moment have the units of newtons \times meter (Nm).

An actual structure is likely subjected to a combined loading situation consisting of several or all of these five types of basic loading. Very often, we impose certain mechanical constraints to the structure such that we can focus on stresses, strains, and deformations under the mechanical load and ignore other mechanical consequences such as translation and rotation, motion (linear and rotational velocity) and acceleration, among others.

From External Loads to Internal Loads and Stresses

In analyzing the mechanical properties of a material structure, the external loading condition (P) is first considered to determine the equivalent forces, torques, and moments at selected internal section planes. In a simplified two-dimensional (2D) view for example, in section plane 1 (Fig. 1.2.3.2A), the equivalent forces may consist of a compressive force (F), a shear force (V), and a bending moment



• **Figure 1.2.3.2** Two-dimensional illustration of how external mechanical loads are converted to equivalent internal forces, torques, and moments on different section planes (A), and internal stresses in a 2D (B) and 3D sense (C).

(M), but in section plane 2, an additional torque will have to be considered aside from the compressive and shear forces and moment. With these sectional forces, moments, and torques, the resulting internal stresses and strains as well as deformations can be obtained. As depicted by the three 2D stress elements shown in Fig. 1.2.3.2B, stress elements 1 and 3 are taken at the upper and lower surfaces of the neck region, where only tensile stress exists on stress element 1 and compressive stress on stress element 3. On a stress element isolated from an interior location (e.g., stress element 2), however, a much more complex stress state could exist. In a three-dimensional (3D) sense, we will have to deal with stress cubes on which six stress components would exist including σ_x , σ_y , σ_z , τ_{xy} , τ_{yz} , and τ_{xz} .

Linear and Nonlinear Relationship, Elastic and Plastic Behavior

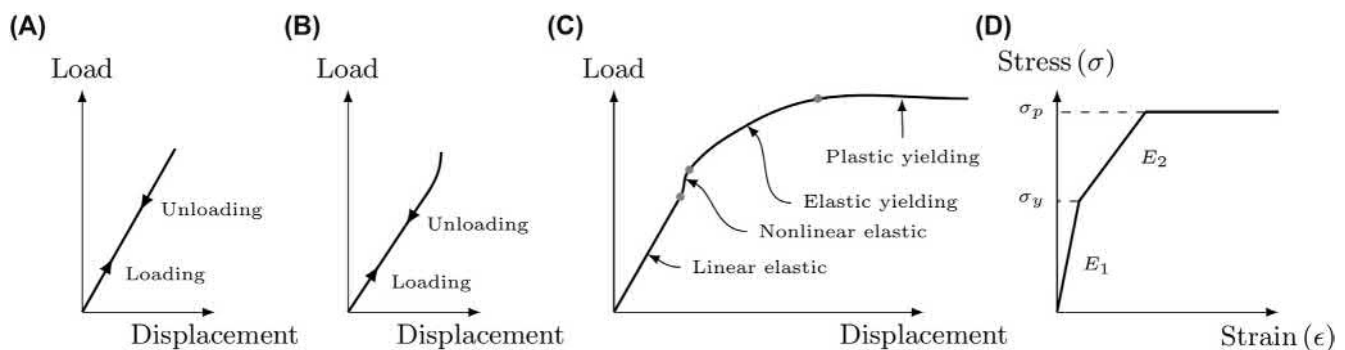
In dealing with materials' mechanical properties, we always encounter terms like linear and nonlinear relationship, and elastic and plastic behavior, and very often we tend to (wrongly) associate a linear relationship with elastic behavior and a nonlinear relationship with plastic behavior. The terms “linear” and “nonlinear” are often used to refer to a relationship between two variables such as in a load–displacement curve or in a stress–strain curve. When these relationships are straight lines, we call them linear, and when they are curved lines, we call them nonlinear. The terms “elastic” and “plastic,” however, refer to a material's deformational behavior, specifically the ability (or inability) to regain the original shape after the removal of loads. When a material structure regains its original shape (all deformations vanish) after the removal of loads, we consider it deforming with elastic behavior, and when it does not regain its original shape, we call it deforming with plastic behavior.

A linear relationship is not necessarily always associated with elastic behavior and a nonlinear relationship plastic behavior. In fact, these terms are often used in combinations to describe a certain mechanical property or behavior (Zhang, 2017). For example, a material structure can exhibit elastic behavior with either linear or nonlinear relationship between load and displacement. As illustrated in

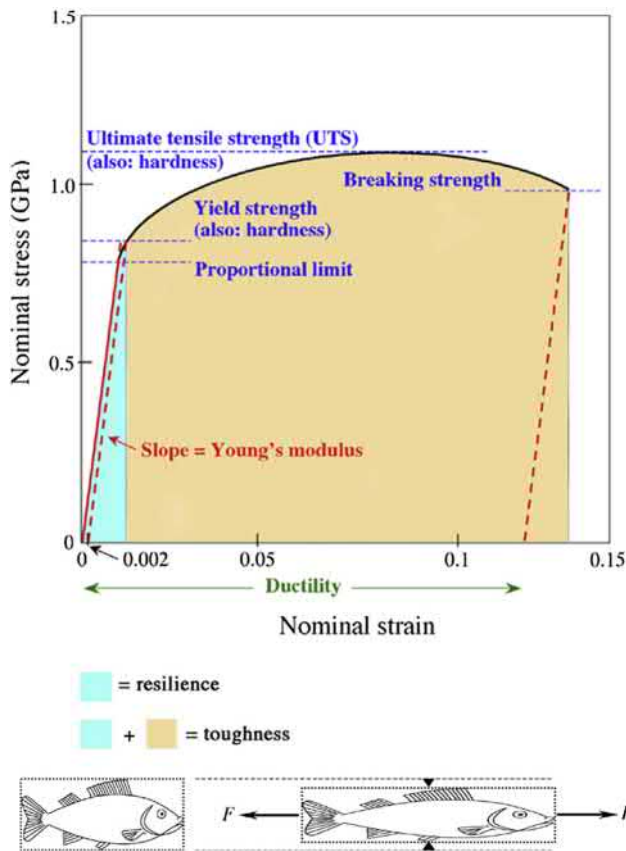
Fig. 1.2.3.3, linear elastic behavior (Fig. 1.2.3.3A) is one in which the load–displacement curve is a straight line (hence linear) and the loading and unloading curves follow the same trace such that the displacement will vanish (hence elastic) when the applied load is removed. Nonlinear elastic behavior (Fig. 1.2.3.3B) describes a curved load–displacement relationship, but the displacement induced by loading will vanish after the removal of the load.

As illustrated in Fig. 1.2.3.3C, the linear elastic behavior of a material typically occurs at the beginning of the loading stage when the induced displacement is extremely small. When the displacement increases slightly, the material may exhibit nonlinear but elastic behavior. This behavior is sometimes referred to as geometric nonlinearity. When the displacement increases further, the material will reach an elastic yielding zone where it still exhibits elastic behavior but with reduced rigidity. As the displacement continues to increase the material will enter a plastic yielding zone in which the displacement or deformation will keep increasing without needing any further increase in loads.

Fig. 1.2.3.3D shows the corresponding stress–strain curve derived conceptually from the load–displacement curve shown in Fig. 1.2.3.3C by dividing the load by the cross-section area and the displacement by the length. It presents a different look at the mechanical properties from a pure material's perspective by minimizing geometric-related influences. By convention, the stress is plotted vertically and the strain is plotted horizontally. When the material behaves elastically, in both a linear and nonlinear manner, the stress–strain curve typically exhibits a straight-line relationship with a constant slope E_1 (which is commonly known as the modulus of elasticity or Young's modulus; more discussion in the next section). When the stress in the material reaches its elastic yielding point σ_y it will start to exhibit reduced elastic property with decreased slope E_2 , where $E_2 < E_1$. As the strain in the material further increases, the material will reach its plastic yielding point σ_p after which full plastic deformation (i.e., deformation that keeps increasing without the need of increasing the applied loads) will occur and the stress in the material will remain the same until the material breaks.



• **Figure 1.2.3.3** Sketches of linear elastic (A) and nonlinear elastic (B) load–displacement curves. Sketches of a single load–displacement curve containing linear elastic, nonlinear elastic, elastic yielding, and plastic yielding behavior (C) and its corresponding stress–strain curve (D).



• **Figure 1.2.3.4** Schematic stress versus strain curve for a ductile metal, emphasizing the features that relate to specific mechanical properties and illustration of the Poisson ratio effect $\nu = -\frac{\epsilon_{\text{transverse}}}{\epsilon_{\text{longitudinal}}}$.

Pseudoelastic, Hyperelastic, and Viscoelastic Materials

Some materials, like shape memory alloys (SMAs), will undergo phase transition due to temperature changes, thereby exhibiting recoverable or reversible deformation behavior (hence elastic) as temperature changes back and forth. This type of “elastic” behavior is sometimes called pseudoelastic or superelastic. Superelasticity is an isotherm process in which phase transformation typically occurs from the austenite to martensite phase under an external load. Because the martensite phase is unstable, after removal of the external load the material will transform again to the austenite phase.

Other materials, like many polymeric materials and biological tissues, will undergo polymer-chain or collagen-fiber reorientation under stretching, leading to stiffening of the materials (i.e., an increase in the slope of the load–displacement curve). When the material is in its elastic nature, the observed nonlinear stiffening behavior is called hyperelastic.

Viscoelasticity is a term used to describe a material that possesses time- (or rate-) dependent behavior, meaning that the material may exhibit a different load–displacement or stress–strain curve when the loading rate is different. The main reason for this behavior is that viscoelastic materials are regarded as made of solid components that follow Hooke's law and fluidic components that follow Newton's

law. For viscoelastic materials, a combined Hookean and Newtonian method is often used to evaluate these combined solid/fluid-like characteristics with equivalent models made of springs (representing the elastic part) and dashpots (representing the viscous part). Load–displacement or stress–strain relationships of viscoelastic materials are always nonlinear with loading and unloading curves following two different paths, known as hysteresis. But after the removal of all loads, deformations in the material will vanish (hence elastic), albeit slowly, due to the viscous components. Common viscoelastic materials include paint, rubber, and many biological materials. For viscoelastic materials, the behavior stress relaxation (stress decays under a fixed constant strain condition) and creep (strain increases under a fixed constant stress condition) as well as the rate at which stress relaxes or strain creeps are common properties of interest.

Common Mechanical Properties of Isotropic Materials

Elastic Properties

Fig. 1.2.3.4 shows a typical stress–strain curve obtained from an isotropic ductile metallic slender rod subjected to tensile loading. An isotropic material is one that has properties considered to be independent of the direction one picks to examine the material. The linear segment of the curve reflects the simplified Hooke's law relationship in honor of Robert Hooke. The constant of proportionality (or slope) between stress and strain is known as the *Young's modulus*, E . The equivalent constant of proportionality in the case of a shear stress being applied is known as the *shear modulus*, G . The ratio of the resulting transverse strain (perpendicular to the direction of the applied load) and longitudinal strain (parallel to the direction of the applied load) is another elastic property of the material commonly known as the *Poisson's ratio*, which is defined as:

$$\nu = -\frac{\epsilon_{\text{transverse}}}{\epsilon_{\text{longitudinal}}}$$

The negative sign is used to obtain a convention in which the values of ν are positive for most materials. An illustration of such a Poisson ratio effect is given in Fig. 1.2.3.4, where a stretching force applied to a material causes it to become *narrower* as it gets longer. While most materials possess a positive Poisson ratio, a relatively small number of materials—known as auxetic materials—has a negative Poisson's ratio. Typically, these are low-density, cellular materials, with cell walls that are able to hinge or buckle when loads are applied. Pulling on a piece of auxetic material causes it to become *wider* as well as longer, while attempting to squash it will cause it to become thinner as well as shorter.

It can be shown that of the three elastic constants (E , G , ν) only two are independent, due to the following relationship among them:

$$G = \frac{E}{2(1 + \nu)}.$$

Yield Strength and Ductility

As the stress on the material increases, a point may be reached where the response is no longer linear, generating a permanent (irreversible) deformation, commonly known as *plastic* deformation. This occurs commonly in ductile metals and polymers, and rarely in brittle materials such as ceramics.

The amount of plastic deformation associated with a given stress can be found by drawing a line from the point of interest on the stress–strain curve, parallel to the initial linear segment of the curve, and marking the point where this constructed line intersects the horizontal (strain) axis. The horizontal distance from the origin to the point of intersection is a measure of the plastic strain. The value of plastic strain required to break the material defines the *ductility* (Fig. 1.2.3.4). The stress at which departure from a linear stress–strain relationship occurs is known as the *proportional limit* (Fig. 1.2.3.4).

It is not always easy to ascertain the proportional limit accurately, and so a more practical determination of the condition for plastic deformation is provided by the *yield strength* (Fig. 1.2.3.4), which is the stress at which *noticeable* plastic strain occurs. In this context, “noticeable” is often taken to be a value of 0.002 (0.2%) for metals—although it may be chosen to be much higher in polymers, where elastic behavior persists to strains that may be 10 or even 100 times higher, and where the transition from elastic to plastic behavior may be difficult to pinpoint.

A marked *yield drop* is often displayed in the stress versus strain plot when the yield stress of a polymer is exceeded. The yield drop occurs because the polymer chains become partially aligned during initial deformation, allowing easier relative motion of chains and reducing the stress needed to further deform the material. The chains then straighten and extend as deformation continues, requiring little increase in stress. Eventually, the opportunities for relative motion of chains are exhausted, along with the capacity for additional chain extension, and the stress versus strain plot then rises sharply.

Strength and Failure

Failure of a loadbearing material occurs when the material ceases to perform its loadbearing function. Different interpretations of “failure” are in common use, and so it is important to be clear about the intended meaning when we speak of materials failure. For materials that must not undergo in situ permanent deformation, failure is synonymous with the yield stress being exceeded, and so the yield stress represents an estimate of the strength of the material in those cases.

For materials in which permanent deformation is acceptable, failure may be deemed to occur when a noticeable “neck” (constriction) develops in the material. The effect of the neck is to concentrate the load on a smaller area; therefore, the load that can be supported by the sample is decreased. On a nominal stress versus nominal strain plot, where stresses are referred to the *original* loadbearing areas

of the sample, the stress required for additional deformation decreases. Therefore, the onset of necking corresponds to a maximum in the nominal stress versus nominal strain plot, defining the *ultimate tensile strength* (UTS) or simply the *tensile strength* of the material (Fig. 1.2.3.4). There is no corresponding maximum on a true stress versus true strain plot, because the stress continues to rise past the onset of necking as values of stress are obtained by dividing the applied load by the actual (small) cross-section of the neck.

On both nominal stress versus nominal strain and true stress versus true strain plots, a *breaking strength* can be defined at the point where the material actually breaks. However, to reach this point practically, at least in the case of most metals, the tensile strength of the material must first be reached, and it is tensile strength that represents the practically measurable maximum stress that a metal can survive. Ceramics, on the other hand, usually reach their breaking stress before they yield.

Thus, the perceived strength of a material depends in part on the definition of failure that is used (onset of plastic deformation, onset of necking, or actual occurrence of breaking). It also depends on the conditions that are used for testing. The *strain rate* used in a tensile test can affect the maximum stress that is reached, depending on the ability of the microstructure to undergo rearrangement to accommodate the imposed deformation.

Over long periods of time, even stresses that are below the conventionally measured yield strength of a material may be sufficient to cause gradual elongation and eventual failure via *creep*. Therefore, creep tests, in which a fixed load is applied while the strain is monitored until the sample breaks, are important for materials that are required to have a long projected service life—as is the case with many implants. Similarly, materials that will be subjected to cyclic loading patterns during service may undergo *fatigue* failure at loads that are smaller than those needed to trigger failure in a conventional stress versus strain test. Testing to determine the relationship between average load, maximum and minimum load, and the number of loading cycles that lead to failure is required in such cases. Finally, the catastrophic failure of a material can be triggered by preexisting flaws that locally concentrate the effect of an applied stress.

Hardness

The hardness of a material is measured by applying a known load to a small indenter of known geometry (typically pyramidal or spherical) in contact with the surface of the material, for a known period of time. The dimensions of the resulting indentation are measured, and this information, together with the experimental conditions, is used to rate the hardness of the material on a relative scale. Indents made in a soft material under a given set of conditions are larger than those made in a hard material. Therefore, hardness provides a measure of how successfully a material resists plastic deformation, which in turn is characterized by both yield strength and tensile strength. It is therefore possible to empirically develop calibration charts that can be used

to convert hardness measurements into both yield strength and tensile strength values. Hardness testing is popular for estimating the yield strength and tensile strength of materials because the equipment is relatively simple and inexpensive, and the tests are nondestructive.

Resilience

Resilience is a measure of the *elastic energy* that can be stored in a unit volume of stressed material. It corresponds to the area underneath a stress versus strain plot, extending from zero strain up to the strain at which the sample yields:

$$U_r = \int_0^{\epsilon_y} \sigma d\epsilon.$$

If the stress versus strain relationship is linear up to the yield strain (typical for ceramics, and approximate for many metals and polymers), the corresponding area under the stress versus strain plot is triangular, and the integral in the previous equation simplifies to:

$$U_r = \frac{1}{2} \sigma_y \epsilon_y = \frac{\sigma_y^2}{2E}.$$

Resilience is an important consideration for materials that need to be “springy,” i.e., that absorb and return significant amounts of energy. Examples include natural and replacement tendons and ligaments, and materials used in foot arch reconstruction or support.

Toughness

Toughness is a measure of the energy required to deform a unit volume of material to its breaking point. Therefore, the definition is similar to that used for resilience, except that we now take into account the entire area under the stress versus strain plot, extending from zero strain up to the strain at which the sample breaks:

$$U_{\text{break}} = \int_0^{\epsilon_{\text{break}}} \sigma d\epsilon.$$

Fracture Toughness and Fatigue Strength

Although fracture toughness and toughness sound superficially similar, they refer to quite different properties. Fracture toughness is a measure of the ability of a material to resist the propagation of a crack. It takes the form of critical stress intensity factor (K_{Ic}) of a sharp crack where propagation of the crack suddenly becomes rapid and unlimited.

When a material is subjected to repetitive, or cyclic loading, a process of fracture may result from the initiation and propagation of a crack. The process of initiation and propagation of a crack in response to cyclic stresses is called fatigue. The stresses required to induce a failure by fatigue are typically known as the fatigue strength. Typically, the fatigue strength is well below the yield strength or ultimate strength of the material, but the ultimate fracture of the material would require millions of cycles of loading, during which localized damage accumulates, leading to the crack initiation and propagation.

Fatigue strength is often assessed by subjecting a sample to a cyclic loading test, counting the number of cycles applied until failure and plotting the stress (S) versus the log of the number (N) of cycles to failure in so-called S–N curves. Detailed discussions on fracture toughness and fatigue strength of metallic materials can be found in [Chapter 1.3.3](#).

Generalized Hooke's Law and Anisotropy of Materials

As discussed in “[Common Mechanical Properties of Isotropic Materials](#),” in the simplest form, the stress and strain relationship of an isotropic elastic material can be expressed as $\sigma = E\epsilon$. While this equation captures well, conceptually, the stress–strain relationship governed by Hooke's Law, it is valid only for situations where uniaxial stress and strain in a one-dimensional structure are of concern. In a complex situation, one must deal with all six stress components (see “[From External Loads to Internal Loads and Stresses](#)”), in which case the generalized Hooke's law takes the following form:

$$\begin{Bmatrix} \sigma_x \\ \sigma_y \\ \sigma_z \\ \tau_{yz} \\ \tau_{xz} \\ \tau_{xy} \end{Bmatrix} = \begin{bmatrix} c_{11} & c_{12} & c_{13} & c_{14} & c_{15} & c_{16} \\ c_{12} & c_{22} & c_{23} & c_{24} & c_{25} & c_{26} \\ c_{13} & c_{23} & c_{33} & c_{34} & c_{35} & c_{36} \\ c_{14} & c_{24} & c_{34} & c_{44} & c_{45} & c_{46} \\ c_{15} & c_{25} & c_{35} & c_{45} & c_{55} & c_{56} \\ c_{16} & c_{26} & c_{36} & c_{46} & c_{56} & c_{66} \end{bmatrix} \begin{Bmatrix} \epsilon_x \\ \epsilon_y \\ \epsilon_z \\ \gamma_{yz} \\ \gamma_{xz} \\ \gamma_{xy} \end{Bmatrix}$$

in which the 6×6 square [c] matrix is sometimes called the modulus matrix. Since the [c] matrix is symmetric square matrix, the highest number of independent constants for an anisotropic material is 21. However, the actual number of independent constants can be much less due to certain symmetry in materials of different isotropy.

For instance, as shown in [Fig. 1.2.3.5A](#), for isotropic materials the [c] matrix has only two independent nonzero constants, c_{11} and c_{12} . These two constants are related to the three E , G , ν constants discussed earlier through the following relationships:

$$c_{11} = \frac{E(1-\nu)}{(1+\nu)(1-2\nu)} \quad \text{and} \quad c_{12} = \frac{E\nu}{(1+\nu)(1-2\nu)}$$

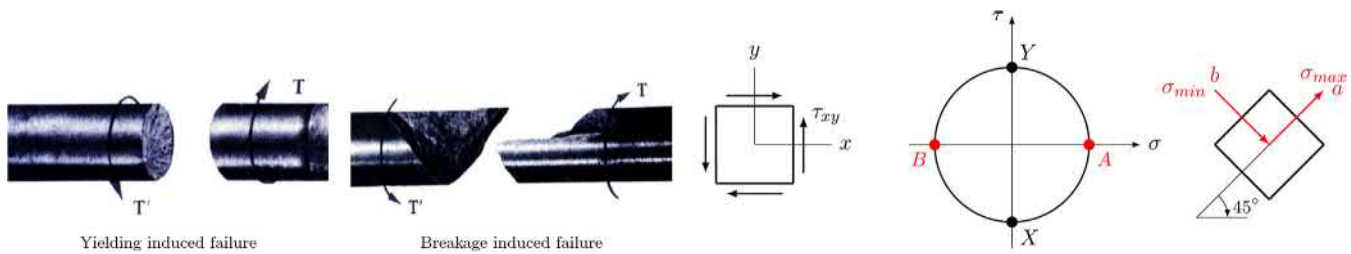
$$\frac{c_{11} - c_{12}}{2} = \frac{E}{2(1+\nu)} = G$$

Note that $\frac{c_{11} - c_{12}}{2} = \frac{E}{2(1+\nu)}$, confirming that of the three constants (E , G , ν), only two are independent.

Moreover, as also illustrated in [Fig. 1.2.3.5](#) ([Zhang, 2020](#)), materials with cubic (crystal) symmetry have three independent nonzero constants, c_{11} , c_{12} , and c_{44} ([Fig. 1.2.3.5B](#)); materials with hexagonal symmetry have five independent constants, c_{11} , c_{12} , c_{13} , c_{33} , and c_{44} ([Fig. 1.2.3.5C](#)); materials with tetragonal symmetry have seven independent constants, c_{11} , c_{12} , c_{13} , c_{16} , c_{33} , c_{44} , and c_{66} ([Fig. 1.2.3.5D](#)); materials with orthorhombic symmetry have nine independent constants, c_{11} , c_{12} , c_{13} , c_{22} , c_{23} , c_{33} , c_{44} , c_{55} , and c_{66} ([Fig. 1.2.3.5E](#)); and materials with monoclinic symmetry have 13 independent constants, c_{11} , c_{12} , c_{13} , c_{15} , c_{22} , c_{23} , c_{25} , c_{33} , c_{35} , c_{44} , c_{46} , c_{55} , and c_{66} ([Fig. 1.2.3.5F](#)). These

$$\begin{aligned}
 \text{(A)} \quad [c] &= \begin{bmatrix} c_{11} & c_{12} & c_{12} & 0 & 0 & 0 \\ c_{12} & c_{11} & c_{12} & 0 & 0 & 0 \\ c_{12} & c_{12} & c_{11} & 0 & 0 & 0 \\ 0 & 0 & 0 & \frac{c_{11} - c_{12}}{2} & 0 & 0 \\ 0 & 0 & 0 & 0 & \frac{c_{11} - c_{12}}{2} & 0 \\ 0 & 0 & 0 & 0 & 0 & \frac{c_{11} - c_{12}}{2} \end{bmatrix} & \text{(B)} \quad [c] &= \begin{bmatrix} c_{11} & c_{12} & c_{12} & 0 & 0 & 0 \\ c_{12} & c_{11} & c_{12} & 0 & 0 & 0 \\ c_{12} & c_{12} & c_{11} & 0 & 0 & 0 \\ 0 & 0 & 0 & c_{44} & 0 & 0 \\ 0 & 0 & 0 & 0 & c_{44} & 0 \\ 0 & 0 & 0 & 0 & 0 & c_{44} \end{bmatrix} & \text{(C)} \quad [c] &= \begin{bmatrix} c_{11} & c_{12} & c_{13} & 0 & 0 & 0 \\ c_{12} & c_{11} & c_{13} & 0 & 0 & 0 \\ c_{13} & c_{13} & c_{33} & 0 & 0 & 0 \\ 0 & 0 & 0 & c_{44} & 0 & 0 \\ 0 & 0 & 0 & 0 & c_{44} & 0 \\ 0 & 0 & 0 & 0 & 0 & \frac{c_{11} - c_{12}}{2} \end{bmatrix} \\
 \text{(D)} \quad [c] &= \begin{bmatrix} c_{11} & c_{12} & c_{13} & 0 & 0 & c_{16} \\ c_{12} & c_{11} & c_{13} & 0 & 0 & -c_{16} \\ c_{13} & c_{13} & c_{33} & 0 & 0 & 0 \\ 0 & 0 & 0 & c_{44} & 0 & 0 \\ 0 & 0 & 0 & 0 & c_{44} & 0 \\ c_{16} & -c_{16} & 0 & 0 & 0 & c_{66} \end{bmatrix} & \text{(E)} \quad [c] &= \begin{bmatrix} c_{11} & c_{12} & c_{13} & 0 & 0 & 0 \\ c_{12} & c_{22} & c_{23} & 0 & 0 & 0 \\ c_{13} & c_{23} & c_{33} & 0 & 0 & 0 \\ 0 & 0 & 0 & c_{44} & 0 & 0 \\ 0 & 0 & 0 & 0 & c_{55} & 0 \\ 0 & 0 & 0 & 0 & 0 & c_{66} \end{bmatrix} & \text{(F)} \quad [c] &= \begin{bmatrix} c_{11} & c_{12} & c_{13} & 0 & c_{15} & 0 \\ c_{12} & c_{22} & c_{23} & 0 & c_{25} & 0 \\ c_{13} & c_{23} & c_{33} & 0 & c_{35} & 0 \\ 0 & 0 & 0 & c_{44} & 0 & c_{46} \\ c_{15} & c_{25} & c_{35} & 0 & c_{55} & 0 \\ 0 & 0 & 0 & c_{46} & 0 & c_{66} \end{bmatrix}
 \end{aligned}$$

• **Figure 1.2.3.5** Independent, nonzero constants in the $[c]$ matrix for isotropic materials (A), and materials with cubic symmetry (B), hexagonal symmetry (C), tetragonal (D), orthorhombic symmetry (E), and monoclinic symmetry (F).



• **Figure 1.2.3.6** Two fractured rods after torsional tests. Mohr's circle for torsional rods and two important stress elements. (Reproduced with permission from McGraw Hill.)

types of crystal symmetry are commonly found in metals and ceramics.

Loading Modes, Stress States, and Mohr's Circle

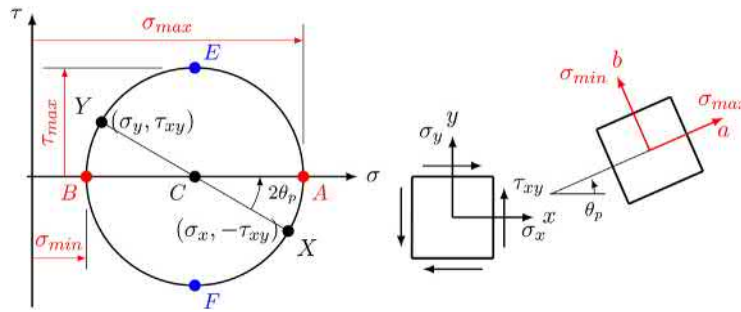
As we discussed in “From External Loads to Internal Loads and Stresses,” external loads dictate the resulting internal stresses. However, the external loading mode does not always reflect directly the failure mode of the material tested. For example, let us look at the two images in Fig. 1.2.3.6, in which two cylindrical rods failed in two different modes under the same type of torsional loading. The rod on the left has a fracture surface that resembles a perpendicular cross-section cut and the rod on the right has a fracture surface of a helical shape. The fact that these two rods, having the same geometric shape and subjected to the same type of loading, fail in two different modes confirms that the failure mode of a material does not always reflect directly its loading mode. To better understand the failure modes, it is necessary to consider the actual stress state induced in the material and its causal relationship with the breakage of the atomic bonds within the materials.

If we look closely at the fracture surfaces, we will note that the textures of the two fracture surfaces are also different. The one on the left shows the sign of material yielding and the one on the right sign of tensile breakage. So then, why do yielding and breakage failure modes cause the two rods to fracture in two different fracture surfaces? To answer

this question, we will need to know the stress states in these rods with the help of Mohr's circle.

Mohr's circle is a 2D graphical representation of the stress state of a given point in a material using a circle (for a 2D stress state; three circles will be needed for a 3D stress state) in a σ - τ coordinate system with a pair of opposite points on the circle representing the stress state of a stress element in a given direction. To visualize this, let us look at Fig. 1.2.3.7, where a Mohr's circle and two stress elements in a plane stress situation (see “Plane-Stress and Plane-Strain Simplification” for further discussion) are sketched. For the stress element shown in the middle, representing a viewing angle through the x - y orientation, we consider a normal stress σ_x and a shear stress τ_{xy} in the x -cut plane, and a normal stress σ_y and a shear stress τ_{xy} in the y -cut plane. By using these paired stress values as coordinates, we mark two points $X(\sigma_x, \tau_{xy})$ and $Y(\sigma_y, \tau_{xy})$ in the σ - τ coordinate system shown on the left with σ as the abscissa and τ as the ordinate. A sign convention is followed in this process in which tensile normal stresses (σ_x and σ_y) are considered positive and compressive normal stresses negative, and clockwise shear stresses (τ_{xy}) are positive and counterclockwise shear stresses negative. By linking the two points, X and Y , with a line we find an intersect with the abscissa at point C . Then using point C as the center point, we construct a circle passing through both points X and Y . This circle is the so-called Mohr's circle, honoring its creator Christian Otto Mohr.

On a Mohr's circle, any paired opposite points (with respect to the center point C), like the X - Y pair, represent



• **Figure 1.2.3.7** Mohr's circle and stress elements for depicting the stress state of a given point.

the stress state of the given point in a certain viewing orientation. This means that the stress state of the given point can be represented by countless different combinations of stress components depending on our viewing orientations. For the A–B pair, while still representing the same stress state of the point, because τ_{xy} is zero, it describes an orientation in which a stress element only has normal stresses acting on it. This orientation is called the principal directions and the corresponding stresses are called principal stresses.

From the Mohr's circle, we can see that a counterclockwise rotation by an angle of 2θ will transform the X–Y pair to the A–B pair. For the stress element, a counterclockwise rotation by θ (half of the rotation in the Mohr's circle) will transform the element in the x–y orientation to the one in the principal a–b orientation, as shown on the right in Fig. 1.2.3.7. With a further 90° counterclockwise rotation from the A–B orientation we will reach the E–F orientation where the shear stress reaches its maximum, τ_{max} . This means that a 45° counterclockwise rotation from the a–b stress element will obtain a stress element having maximum shear stresses.

Let us now return to the two torsional rods discussed earlier and analyze the cause for fracture by examining the stress states in them. Fig. 1.2.3.6 also shows the Mohr's circle for a surface point on a cylindrical rod undergoing pure torsional loading. From this Mohr's circle, we can see that in the x–y orientation (corresponding to the X,Y points on the circle) the stress element has only shear stresses acting on it with no normal stresses. This means that the x–y stress element experiences the maximum shear stresses. On the other hand, the principal stress element, the a–b stress element (corresponding to the A,B points on the circle), is a 45° counterclockwise rotation away, because the X–Y and A–B lines are 90° apart in the Mohr's circle. In the principal stress element, the maximum principal is maximum tension and the minimum principal stress is maximum compression. Taken together, when the two rods undergo a torsion loading test, the x-cut plane (as well as the y-cut plane) endures maximum shearing, the 45° -cut plane experiences the maximum tension and the 135° -cut plane the maximum compression.

Keep in mind that a ductile material tends to fail due to shear-induced material yielding and a brittle material due to tension-induced breakage. It becomes clear that the rod on the left failed in a shear mode due to its ductile material nature and the highest shear stress existing in the x-cut plane (incidentally this cut plane has the smallest cross-section

area). For the rod on the right, it failed in a tension mode due to its brittle nature and the highest tensile stress existing along a plane oriented at 45° . It is thus not surprising that the fracture surface caused by tension-induced breakage is oriented at a 135° angle from the x-cut plane, perpendicular to the direction of the maximum tension.

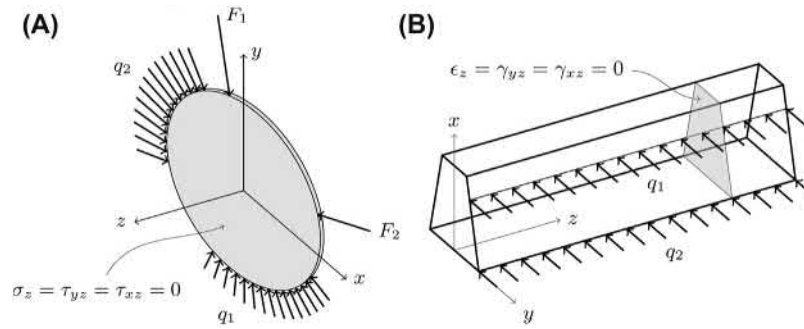
In short, the failure mode of a material is not determined by the loading mode but by the induced stress state (i.e., the maximum stresses and their orientations) and the type of materials. If the material is of the ductile type, shearing-induced yielding failure should be of concern and if the material is of the brittle type, tension-induced breakage should be avoided. To put this knowledge to use, the reader is encouraged to refer to Chapter 3.1.9 for case studies of some failure modes of various implant devices based on the observations made from implant retrieval analyses.

Plane-Stress and Plane-Strain Simplification

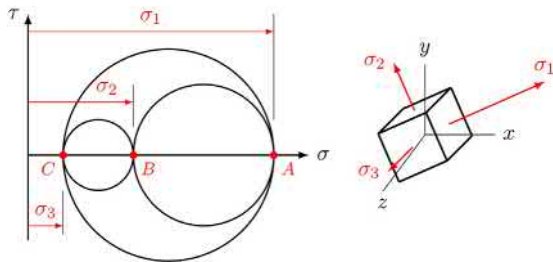
In real life we always encounter three-dimensional (3D) objects, yet we often use the terms two-dimensional (2D) and one-dimensional (1D) problems. Technically speaking, all problems are 3D in a geometry sense, but in certain circumstances they can be simplified through approximation into 2D and 1D problems. Due to the approximation nature, the conditions for making the simplification should be considered carefully. For example, when a material is thin in its third dimension (say, along the z axis) compared with the other two dimensions, and if the loading and deformations in the material occur only within the thin plane, the stresses in the third dimension, as illustrated in Fig. 1.2.3.8A, σ_z , τ_{yz} , and τ_{xz} are negligible. In this case, we can simplify the 3D problem into a 2D plane-stress problem. Another situation is when the material is very long in its longitudinal z direction as compared with the x, y dimensions and the loading, deformations, and cross-section area remain unchanged over the entire longitudinal length, as depicted in Fig. 1.2.3.8B. In this case, the strains in the third dimension, ϵ_z , γ_{yz} , and γ_{xz} are negligible, and we can simplify the 3D problem into a 2D plane-strain problem.

Trajectories of Tensile and Compressive Stress Lines

At any given point in a structure under mechanical loading we can identify the principal stresses and their directions by



• **Figure 1.2.3.8** 2D simplification of 3D solid mechanical problems: (A) plane-stress situation, and (B) plane-strain situation.



• **Figure 1.2.3.9** 3D Mohr's circles and the first, second, and third principal stresses.

constructing Mohr's circles and determining the orientation of the stress element that corresponds to the pairs of extrema with zero shear stresses, i.e., the A–B, B–C, or A–C pairs on the Mohr's circles in Fig. 1.2.3.9.

Let us now consider a plane stress situation. Referring to Fig. 1.2.3.10, we assume that the first principal stress (σ_1) is positive (tensile), the second one (σ_2) zero, and the third one (σ_3) negative (compressive). After identifying the directions of the first (tension) and third (compression) principal stresses at randomly selected points across the plane structure, we mark the two directions using perpendicular crosses at these points (note that these two principal stresses are always perpendicular to each other). To distinguish the two stresses, we use red to represent the tensile direction and blue the compressive direction. By connecting the red and blue lines together, respectively, we obtain two sets of lines representing the directions of maximum tensile stress (red lines) and maximum compressive stress (blue lines), which sometimes are also referred to as the stress trajectories. Fig. 1.2.3.10 shows the trajectories of tension and compression lines in a rectangular beam structure subjected to three-point bending. With a close inspection, we note that these two sets of lines are indeed orthogonal, indicating that, at each intersect, a red line is perpendicular to a blue line, as expected.

Assuming the beam structure is made of concrete, we should expect tension-induced breakage as the failure mode. Referring to the principal stress element shown in the figure, a fracture surface caused by tensile stresses should be perpendicular to the tensile stress, meaning that the breaking surface in the concrete should coincide with the compression lines. By examining the images of the actual fracture lines near the corner and at the bottom of the beam shown

in Fig. 1.2.3.10, one can see that these fracture lines follow exactly the compression lines in these regions.

Knowing the stress trajectories provides us with crucial insight into how to strengthen certain structural design. The structure of the human femoral head is an example that our body knows how to strengthen bone structure according to the stress trajectories as a result of constant bone remodeling. The architecture of the spongy bone is likely the result of the bone remodeling process with the purpose of meeting the strengthening needs of human growth and daily activities, guided by the stress trajectories inside the femoral head.

Other Bulk Properties

The bulk properties of a material are of course not limited to performance in mechanical tests. Other types of bulk properties that may have to be taken into account during the selection of a biomaterial include: thermal properties; optical properties; electrical properties; and magnetic properties. Even cost—financial and environmental—can be considered to be a bulk property, given the dependence of cost on: (1) the type and volume of material that is used; and (2) the complexity of microstructural rearrangement during processing.

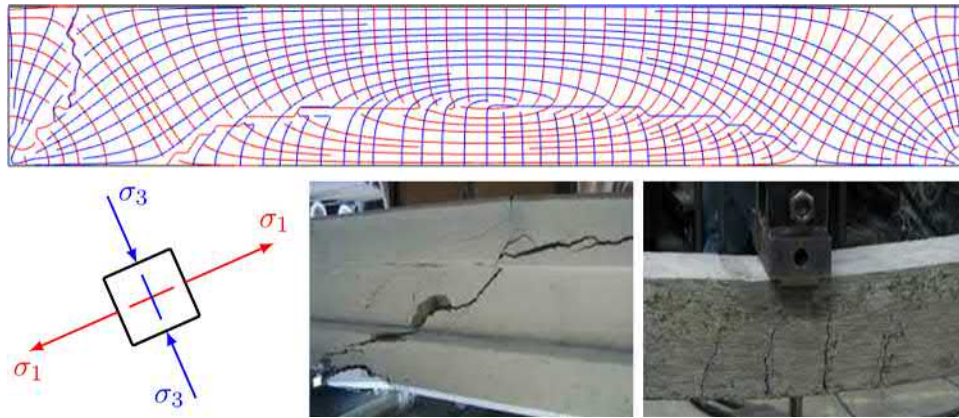
Thermal Properties

Thermal conductivity becomes a significant consideration if an implanted material contributes to an unnatural flow of heat through the surrounding tissue. For example, metal rods selected for their combination of stiffness, strength, fracture toughness, and biocompatibility can promote heat loss and cause the patient to feel colder than normal. Heat conduction through a metal dental filling can also be a source of discomfort and may therefore play a role in the choice between a metal or nonmetal filling.

Thermal expansion is a (nominal) strain that occurs when the temperature of a material is changed:

$$\epsilon_{\text{thermal}} = \alpha (T_{\text{final}} - T_{\text{initial}})$$

where α is the thermal expansion coefficient; its units are (degrees)⁻¹, with “degrees” measured on whatever standard scale is used to measure temperature T .



• **Figure 1.2.3.10** Trajectories of tension (red) and compression (blue) lines in a beam structure subjected to three-point bending along with a principal stress element and two images of fracture lines in concrete beams under the same type of loading.

Attempts to match the properties of a dental filling to those of the surrounding tissue must therefore extend beyond achieving compatible elastic constants to include consideration of thermal expansion, to avoid premature failure of the interface.

Optical Properties

In the context of biomaterials, the most significant bulk optical properties are color, refractive index, and transparency; all three are important in the selection of materials for intraocular lenses or fluids. The color of a transparent material is controlled by composition, and therefore demands a high degree of quality control to avoid impurities that could adversely affect color. Long-term stability of material composition is also important: components should not selectively diffuse into the surrounding tissue, and no chemical changes should occur—either by reactions between the components or in response to light.

The *refractive index* n of a material is defined as:

$$n = \frac{c_{\text{vacuum}}}{c_{\text{material}}}$$

where c denotes the speed of light in the subscripted medium. When light crosses the interface between two media (materials), it is deviated from its original path by an angle that is an increasing function of the difference between the refractive indices of the media. Therefore, the effectiveness of a material as a lens is directly related to its refractive index. Refractive index increases along with the content of electron-rich atoms, which is why lead “crystal” is so useful in both lenses and decorative glassware.

Transparency is a qualitative term that describes the ability of a material to transmit light without attenuating (absorbing or scattering) it. To minimize absorption, the primary bonds in the material must be strongly covalent or ionic (and definitely not metallic). Scattering is minimized if the material is free of internal interfaces (which could

reflect light) and compositional differences (which would be associated with refractive index differences that could deviate light from an uninterrupted path through the material). Thus, an optimally transparent material will either be a homogeneous single crystal or it will be completely and homogeneously amorphous.

There is no commonly accepted quantitative definition of transparency. Instead, it is usual to consider the complementary property, *opacity*. This is itself a colloquial term, but it lends itself to a more formal description by way of the *mass attenuation coefficient*. If light of a given frequency (color) and initial intensity I_0 travels a distance x through a material, then the intensity is decreased to:

$$I(x) = I_0 \exp(-\mu \rho x)$$

where μ is the mass attenuation coefficient of the material, and ρ is the density.

Piezoelectric Properties

Piezoelectricity deals with the coupled mechanical and electrical properties of a material that becomes electrically polarized when it is mechanically strained. There are two forms of piezoelectric effect. Direct piezoelectric effect describes the generation of electric dipoles and polarization as a result of displaced atoms and the associated redistribution of electrons inside a solid when it is mechanically strained. This polarization in turn generates an electric field. By contrast, reverse piezoelectric effect is a phenomenon in which a solid becomes strained when placed in an electric field. Piezoelectric effect was first discovered and demonstrated in its direct form by the brothers Pierre and Jacques Curie in 1880. Since then, the science of piezoelectricity has slowly moved from research laboratories to real-world applications such as sonars, devices for the production and detection of sound and for mechanical actuation, sensors for thickness and temperature measurements, even biosensors, among others. The theory of piezoelectricity allows us to deal with relationships between the generated electrical field and applied strains, or vice versa, within the material's elastic deformation limit.

Weibull Modulus and Nonbrittle Materials

The Weibull distribution of fracture probability for materials provides a statistical measure of brittleness, via the specification of a Weibull modulus m (Derby et al., 1992). The value of m can in theory range from zero (totally random fracture behavior, where the failure probability is the same at all stresses, equivalent to an ideally brittle material) to infinity (representing a precisely unique, reproducible fracture stress, equivalent to an ideally nonbrittle material).

This quantitative approach to defining nonbrittleness is more robust than a qualitative description, since there is no single antonym of “brittle.” Both “tough” and “ductile” are in particular senses the opposite of “brittle,” but we have seen that “tough” and “ductile” are not interchangeable, and their corresponding nouns are associated with very different features on a stress–strain curve (Fig. 1.2.3.4).

Weibull statistics were initially adopted to quantify failure in classically brittle materials (Kelly and Macmillan, 1986), where tensile strength is dominated by the size distribution of preexisting flaws, and the use of this method is rarely extended to materials that are regarded as nonbrittle. However, there is no a priori reason to restrict Weibull statistics to the analysis of failure in classically brittle materials. For example, although natural silks exhibit large extensions to failure, and many of them behave like an elastomer at least during the initial stages of deformation,

Weibull analysis has proved to be useful for characterizing and contextualizing the failure strength variability of these materials (Pérez-Rigueiro et al., 1998, 2001).

Why is a Weibull analysis appropriate for nonbrittle materials? A justification can be formulated simply on phenomenological grounds: after significant deformation, silk *develops* the statistical failure *characteristics* of a brittle material, even though it initially deserves classification as an elastomer. While the existence of strength-limiting defects can be inferred from this description, their nature has yet to be confirmed; it is not clear whether they are present in as-spun material, or whether they begin to develop during the earlier stages of deformation.

The appropriateness of Weibull analysis for a nonbrittle material can also be justified fundamentally (Viney, 2002), given the equation that is used as the basis for measuring m (see “Statistical Aspects of Failure”):

$$1 - F = \exp\left(-\frac{\sigma}{\sigma_0}\right)^m$$

If F is to be independent of σ , which is the hallmark of an ideally brittle material, this equation requires m to be equal to zero. However, practical Weibull analysis necessarily admits to nonzero values of m , so it is implicit that ductile contributions to failure can also be accommodated.

Under the conditions of constant stress and constant strain, the constitutive relation governing piezoelectricity can be expressed as

$$D = \epsilon E^e + dT \text{ and } D = \epsilon E^e + eS$$

respectively, where D is electric displacement vector, E^e electric field, T stress vector, S strain vector, ϵ permittivity constants, d piezoelectric strain constants, and e piezoelectric stress constants (Zhang, 2020). Of these seven terms, D , E^e , T , and S are physical variables, and d , e , and ϵ are piezoelectric properties. For an anisotropic piezoelectric material in a 3D space, D and E^e are 3×1 vectors, T and S are 6×1 vectors, d and e are 3×6 matrices, and ϵ is a 3×3 matrix. Very often, due to structural symmetry in the material, the actual numbers of constants in these matrices is much lower. For example, a cubic crystal with class 23 symmetry has only one independent nonzero constant in d , e , and ϵ matrices, respectively.

Electrochemical Properties

The electrochemical properties of a biomaterial (typically of metals and alloys) are the material's characteristics in an electrochemically corrosive environment, including electrochemical potentials, reaction constants, etc. These properties dictate the responses of such metallic biomaterials governed by corrosive oxidation and reduction reactions, where the oxidation processes take metal (zero valence) and increase its valence to make ions (cations) or oxides (or other solid oxidation products). On the reduction side, processes may include water and oxygen reduction to form hydroxide ions and/or reactive oxygen intermediates, aside from many other biologically based molecules that are susceptible to redox processes. The oxidation and reduction reactions are electrically connected through the metal and complete the circuit through the solution (commonly known as the

two half-cell reactions), resulting in currents (electronic and ionic) through both phases. All metallic biomaterials exhibit some form of corrosion process, whether passive dissolution of ions through the passive film, to more aggressive process caused by wear or crevice geometries. Fortunately, the common implantable metals and alloys (with the exception of noble metals such as gold or platinum) have protective oxide films to control corrosion of the material to acceptable levels. These oxides are commonly referred to as passive films, typically of only a few nanometers in thickness, and will limit transport of metallic ions to the implant surface. More detailed discussions on the electrochemical properties of many metallic biomaterials are given in Chapters 1.3.3 and 2.4.3.

References

- Beer, F.P., Johnston, E.R., Dewolf, J.T., Mazurek, D.F., 2014. Mechanics of Materials, seventh ed. McGraw-Hill Education.
- Derby, B., Hills, D.A., Ruiz, C., 1992. Materials for Engineering: A Fundamental Design Approach. Longman Scientific & Technical, Harlow, UK.
- Kelly, A., Macmillan, N.H., 1986. Strong Solids, third ed. Oxford University Press, Oxford, UK.
- Pérez-Rigueiro, J., Viney, C., Llorca, J., Elices, M., 1998. Silkworm silk as an engineering material. J. Appl. Polym. Sci. 70, 2439–2447.
- Pérez-Rigueiro, J., Elices, M., Llorca, J., Viney, C., 2001. Tensile properties of *Argiope trifasciata* drag line silk obtained from the spider's web. J. Appl. Polym. Sci. 82, 2245–2251.
- Viney, C., 2002. In: Elices, M., Llorca, J. (Eds.), Fibre Fracture. Elsevier Science Ltd, Oxford, UK, pp. 303–328.
- Zhang, G., 2017. Introduction to Integrative Engineering: A Computational Approach to Biomedical Problems. CRC Press.
- Zhang, G., 2020. Bulk and Surface Acoustic Waves and Applications, Notes (in preparation for publication).

Chapter Questions

1. A stainless-steel rod with a circular cross-section has a length of 100 mm and a diameter of 2.0 mm. It is deformed elastically in compression by a force of 500 N applied parallel to its length. The material has a Young's modulus of 200 GPa, a shear modulus of 77 GPa, and a yield strength of 0.3 GPa. Calculate (A) the amount by which the rod will decrease in length; and (B) the amount by which the rod will increase in diameter.

Solution:

- (A) Before we solve the problems, it is helpful to convert all units to the SI units. Doing so, we have the length of the rod $L = 0.1$ m and diameter $d = 0.002$ m. By the definition of stress, $\sigma = F/A$, we calculate the compressive stress as

$$\sigma = \frac{F}{A} = \frac{-500 \text{ (N)}}{\frac{\pi}{4}(0.002 \text{ m})^2} = -0.159 \text{ (GPa)}$$

Since the induced compressive stress is below the yield strength of 0.3 GPa, the rod is deforming elastically. Moreover, because we are dealing with a rod under uniaxial loading, we can use the simplified Hooke's Law to capture the linear relationship between stress and strain with:

$$\sigma = E\varepsilon$$

and find the induced strain in the rod

$$\varepsilon = \frac{\sigma}{E} = \frac{-0.159 \text{ (GPa)}}{200 \text{ (GPa)}} = -7.962 \times 10^{-4}$$

Knowing the strain value, the change in length of the rod can be determined by

$$\delta = L\varepsilon = 0.1 \text{ (m)} \times (-7.962) \times 10^{-4} = -7.962 \times 10^{-5} \text{ (m)} = -7.962 \times 10^{-2} \text{ (mm)}$$

The negative value suggests that the length of the rod is getting shorter due to a compressive force.

- (B) To determine the change in diameter, we will need to know the Poisson's ratio. From the known relationship between Young's modulus (E) and shear modulus (G), namely,

$$G = \frac{E}{2(1 + \nu)}$$

we have

$$\nu = \frac{E}{2G} - 1 = \frac{200 \text{ (GPa)}}{2 \times 77 \text{ (GPa)}} - 1 = 0.299$$

From the definition of the Poisson's ratio

$$\nu = - \frac{\varepsilon_{\text{transverse}}}{\varepsilon_{\text{longitudinal}}}$$

and with the longitudinal strain determined earlier, we calculate

$$\varepsilon_{\text{transverse}} = -\nu\varepsilon_{\text{longitudinal}} = -0.299 \times (-7.962) \times 10^{-4} = 2.378 \times 10^{-4}$$

With this, the change in diameter can be determined as

$$\delta = d\varepsilon_{\text{transverse}} = 0.002 \text{ (m)} \times 2.378 \times 10^{-4} = 4.757 \times 10^{-7} \text{ (m)}$$

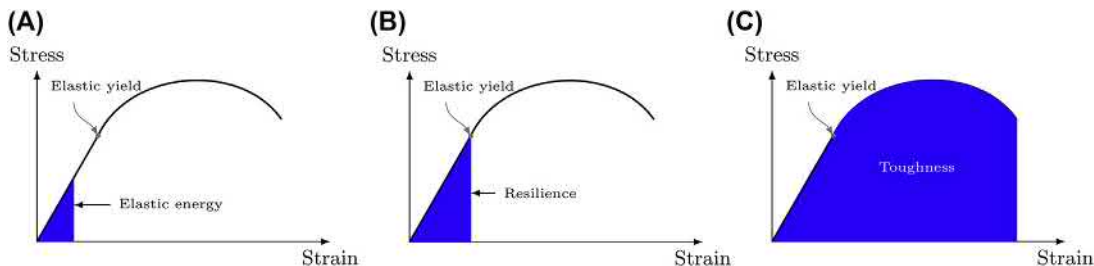
The positive value suggests that the diameter of the rod is becoming wider due to a compressive force.

2. Use a stress-strain curve to depict the determination of the followings: (A) strain energy, (B) resilience, and (C) toughness.

Solution:

Using the stress-strain curve of a typical metallic material, we can sketch the followings.

- (A) Strain energy is typically obtained by the area under the stress-strain curve at a given stress which is below the elastic yield point.
 (B) Resilience is determined by the area under the stress-strain curve up to the point where stress reaches the elastic yield point.
 (C) Toughness is determined by the area under the stress-strain curve up to the point where stress reaches the breaking point.



3. Referring to the generalized Hooke's Law relation and the $[c]$ matrix given in Fig. 1.2.3.5A for an isotropic material, derive the reduced stress-strain relation for a 2D plane-strain and plane-stress situation.

Solution:

With the $[c]$ matrix for an isotropic material given in Fig. 1.2.3.5A, we can write its stress and strain relations according to the generalized Hooke's Law as,

$$\begin{Bmatrix} \sigma_x \\ \sigma_y \\ \sigma_z \\ \tau_{yz} \\ \tau_{xz} \\ \tau_{xy} \end{Bmatrix} = \begin{bmatrix} c_{11} & c_{12} & c_{12} & 0 & 0 & 0 \\ c_{12} & c_{11} & c_{12} & 0 & 0 & 0 \\ c_{12} & c_{12} & c_{11} & 0 & 0 & 0 \\ 0 & 0 & 0 & \frac{c_{11} - c_{12}}{2} & 0 & 0 \\ 0 & 0 & 0 & 0 & \frac{c_{11} - c_{12}}{2} & 0 \\ 0 & 0 & 0 & 0 & 0 & \frac{c_{11} - c_{12}}{2} \end{bmatrix} \begin{Bmatrix} \epsilon_x \\ \epsilon_y \\ \epsilon_z \\ \gamma_{yz} \\ \gamma_{xz} \\ \gamma_{xy} \end{Bmatrix}$$

By substituting the given expressions in this chapter for c_{11} and c_{12} , we have

$$\begin{Bmatrix} \sigma_x \\ \sigma_y \\ \sigma_z \\ \tau_{yz} \\ \tau_{xz} \\ \tau_{xy} \end{Bmatrix} = \frac{E}{(1+\nu)(1-2\nu)} \begin{bmatrix} 1-\nu & \nu & \nu & 0 & 0 & 0 \\ \nu & 1-\nu & \nu & 0 & 0 & 0 \\ \nu & \nu & 1-\nu & 0 & 0 & 0 \\ 0 & 0 & 0 & 0.5-\nu & 0 & 0 \\ 0 & 0 & 0 & 0 & 0.5-\nu & 0 \\ 0 & 0 & 0 & 0 & 0 & 0.5-\nu \end{bmatrix} \begin{Bmatrix} \epsilon_x \\ \epsilon_y \\ \epsilon_z \\ \gamma_{yz} \\ \gamma_{xz} \\ \gamma_{xy} \end{Bmatrix}$$

For a plane-strain situation, by referring to Fig. 1.2.3.8B the following three strain components are zero: $\epsilon_z = \gamma_{yz} = \gamma_{xz}$. Plugging in these zero components into the above matrix equation we have

$$\begin{Bmatrix} \sigma_x \\ \sigma_y \\ \sigma_z \\ \tau_{yz} \\ \tau_{xz} \\ \tau_{xy} \end{Bmatrix} = \frac{E}{(1+\nu)(1-2\nu)} \begin{bmatrix} 1-\nu & \nu & \nu & 0 & 0 & 0 \\ \nu & 1-\nu & \nu & 0 & 0 & 0 \\ \nu & \nu & 1-\nu & 0 & 0 & 0 \\ 0 & 0 & 0 & 0.5-\nu & 0 & 0 \\ 0 & 0 & 0 & 0 & 0.5-\nu & 0 \\ 0 & 0 & 0 & 0 & 0 & 0.5-\nu \end{bmatrix} \begin{Bmatrix} \epsilon_x \\ \epsilon_y \\ \epsilon_z \\ \gamma_{yz} \\ \gamma_{xz} \\ \gamma_{xy} \end{Bmatrix}$$

With simplification, we obtain the following reduced stress-strain relation for a 2D plane-strain situation:

$$\begin{Bmatrix} \sigma_x \\ \sigma_y \\ \tau_{xy} \end{Bmatrix} = \frac{E}{(1+\nu)(1-2\nu)} \begin{bmatrix} 1-\nu & \nu & 0 \\ \nu & 1-\nu & 0 \\ 0 & 0 & 0.5-\nu \end{bmatrix} \begin{Bmatrix} \epsilon_x \\ \epsilon_y \\ \gamma_{xy} \end{Bmatrix}$$

along with

$$\sigma_z = E\nu(\epsilon_x + \epsilon_y)/[(1+\nu)(1-2\nu)], \quad \tau_{yz} = \tau_{xz} = 0$$

For a plane-stress situation, we first express the above generalized stress-strain relations in strain-stress relations by taking the inverse of the generalized Hooke's Law matrix equation as

$$\begin{Bmatrix} \epsilon_x \\ \epsilon_y \\ \epsilon_z \\ \gamma_{yz} \\ \gamma_{xz} \\ \gamma_{xy} \end{Bmatrix} = \frac{1}{E} \begin{bmatrix} 1 & -\nu & -\nu & 0 & 0 & 0 \\ -\nu & 1 & -\nu & 0 & 0 & 0 \\ -\nu & -\nu & 1 & 0 & 0 & 0 \\ 0 & 0 & 0 & 2(1+\nu) & 0 & 0 \\ 0 & 0 & 0 & 0 & 2(1+\nu) & 0 \\ 0 & 0 & 0 & 0 & 0 & 2(1+\nu) \end{bmatrix} \begin{Bmatrix} \sigma_x \\ \sigma_y \\ \sigma_z \\ \tau_{yz} \\ \tau_{xz} \\ \tau_{xy} \end{Bmatrix}$$

Referring to Fig. 1.2.3.8A, we have the three zero stress components: $\sigma_z = \tau_{yz} = \tau_{xz}$ for a plane-stress situation. Plugging in these zero components into this equation we have

$$\begin{Bmatrix} \epsilon_x \\ \epsilon_y \\ \epsilon_z \\ \gamma_{yz} \\ \gamma_{xz} \\ \gamma_{xy} \end{Bmatrix} = \frac{1}{E} \begin{bmatrix} 1 & -\nu & -\nu & 0 & 0 & 0 \\ -\nu & 1 & -\nu & 0 & 0 & 0 \\ -\nu & -\nu & 1 & 0 & 0 & 0 \\ 0 & 0 & 0 & 2(1+\nu) & 0 & 0 \\ 0 & 0 & 0 & 0 & 2(1+\nu) & 0 \\ 0 & 0 & 0 & 0 & 0 & 2(1+\nu) \end{bmatrix} \begin{Bmatrix} \sigma_x \\ \sigma_y \\ 0 \\ 0 \\ 0 \\ \tau_{xy} \end{Bmatrix}$$

With simplification, we obtain the reduced strain-stress relation for a 2D plane-stress situation:

$$\begin{Bmatrix} \epsilon_x \\ \epsilon_y \\ \gamma_{xy} \end{Bmatrix} = \frac{1}{E} \begin{bmatrix} 1 & -\nu & 0 \\ -\nu & 1 & 0 \\ 0 & 0 & 2(1+\nu) \end{bmatrix} \begin{Bmatrix} \sigma_x \\ \sigma_y \\ \tau_{xy} \end{Bmatrix}$$

or its inverse stress-strain relation

$$\begin{Bmatrix} \sigma_x \\ \sigma_y \\ \tau_{xy} \end{Bmatrix} = \frac{E}{(1-\nu^2)} \begin{bmatrix} 1 & \nu & 0 \\ \nu & 1 & 0 \\ 0 & 0 & (1-\nu)/2 \end{bmatrix} \begin{Bmatrix} \epsilon_x \\ \epsilon_y \\ \gamma_{xy} \end{Bmatrix}$$

along with

$$\epsilon_z = -\nu(\sigma_x + \sigma_y)/E, \quad \gamma_{yz} = \gamma_{xz} = 0$$

4. For an isotropic elastic material having Young's modulus of $E = 210$ GPa and Poisson's ratio of $\nu = 0.33$, find the $[c]$ matrix for 2D simplified plane-stress and plane-strain situations.

Solution:

For a plane-strain situation, by plugging the given values for E and ν into the reduced stress-strain relations found in Question 3, we have

$$[c] = 10^{11} \times \begin{bmatrix} 3.110 & 1.530 & 0 \\ 1.530 & 3.110 & 0 \\ 0 & 0 & 0.789 \end{bmatrix}$$

For a plane-stress situation, by plugging the given values for E and ν into the reduced stress-strain relations found in Question 3, we get

$$[c] = 10^{11} \times \begin{bmatrix} 2.360 & 0.778 & 0 \\ 0.778 & 2.360 & 0 \\ 0 & 0 & 0.789 \end{bmatrix}$$

Apparently, the two $[c]$ matrices are not the same. The $[c]$ matrix of the plane-strain situation is stiffened as compared with that of the plane-stress situation. The two terms in the first row are 3.110×10^{11} GPa and 1.530×10^{11} GPa for the plane-strain situation, which are approximately 1.32 and 1.97 times higher than the respective terms in the plane-stress situation (i.e., 2.360×10^{11} GPa and 0.778×10^{11} GPa). This suggests that treating a plane-stress problem by mistake as a plane-strain problem would lead to stiffening the material significantly. On the contrary, treating a plane-strain problem as a plane-stress one would lead to softening the material.

5. The constitutive relations between strains and stresses for a 2D plane-stress simplified problem can be expressed in a reduced 3×3 matrix equation as follows

$$\begin{Bmatrix} \epsilon_x \\ \epsilon_y \\ \gamma_{xy} \end{Bmatrix} = \frac{1}{E} \begin{bmatrix} 1 & -\nu & 0 \\ -\nu & 1 & 0 \\ 0 & 0 & 2(1+\nu) \end{bmatrix} \begin{Bmatrix} \sigma_x \\ \sigma_y \\ \tau_{xy} \end{Bmatrix}$$

Show that when the situation can be further simplified to a 1D problem, a simple relationship between stress and strain as

$$\sigma_x = E\epsilon_x$$

Will govern the constitutive relation.

Solution:

For a 1D situation, we can further assume $\sigma_y = \tau_{xy} = 0$. By plugging these two zero terms into the given relations, we have

$$\begin{Bmatrix} \epsilon_x \\ \epsilon_y \\ \gamma_{xy} \end{Bmatrix} = \frac{1}{E} \begin{bmatrix} 1 & -\nu & 0 \\ -\nu & 1 & 0 \\ 0 & 0 & 2(1+\nu) \end{bmatrix} \begin{Bmatrix} \sigma_x \\ 0 \\ 0 \end{Bmatrix}$$

With simplification, we obtain

$$\sigma_x = E\epsilon_x \text{ along with } \epsilon_y = -\frac{\nu\sigma_x}{E} \text{ and } \gamma_{xy} = 0$$

The first equation is the 1D Hooke's Law governed constitutive relation, and the first two equations will lead to the Poisson's ratio equation

$$-\frac{\epsilon_y}{\epsilon_x} = -\frac{-\frac{\nu\sigma_x}{E}}{\frac{\sigma_x}{E}} = \nu$$

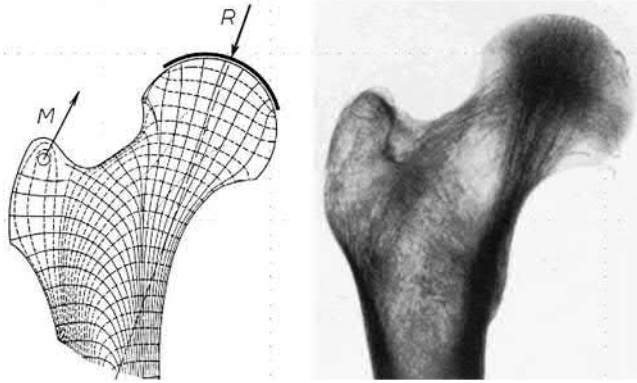
6. The image given below shows a helical fracture in a femur bone. Explain your observation.



Solution:

A helical fracture line is surely the result of torsional loading. Referring to the Mohr's circle and stress elements shown in Fig. 1.2.3.6, it is known that under a torsional load, the femur could break either in a shear failure mode or a tensile failure mode. If in a shear-failure mode, the fracture surface should be in a cross-cutting plane perpendicular to the shaft of the femur because the this plane is where the maximum shear stress lies, and if in tensile-failure mode, the fracture surface will follow a helical line due to the existence of the maximum tensile stress following a helical pattern. From the fracture shown, it is believed that the bone fractured under a torsional load. However, the load was applied very likely at a relatively high speed such that the bone behaves more like a brittle material. In this situation, the tensile strength of the bone becomes the weakest link because it will not be able to resist the highest tensile stress generated in the bone, thereby leading to a tensile-stress induced helical fracture due to the high-speed torsional load. This example highlights the fact that regardless the external loading situations, the actual fracture mode in a material is always dictated by the internal stress state and the nature of material, as well as the loading speed in the case of materials of viscoelastic nature.

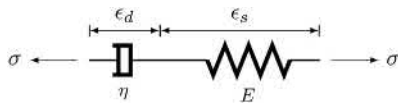
7. Of the two images given below, one showing the stress trajectories obtained from a finite element analysis of a 2D femoral-head-like structure, and the other showing the X-ray microarchitectures in a femoral head. Explain your observations.



Solution:

Inside the thin layer of strong cortical (or compact) bone of a femoral head is coarsely structured trabecular (or cancellous, spongy) bony structure. The microarchitecture of the spongy bony structure is not random, instead it appears to follow the stress trajectories inside the femoral head. According to Wolff's Law, living bones will remodel in adaptation to the external loads they experience. The microarchitecture of the spongy bone is likely the result of the bone remodeling process in meeting the strengthening needs of human/animal growth and daily activities, guided by the stress trajectories dictated by the internal stress state.

8. A viscoelastic material represented by a spring (with modulus of E) and a dashpot (with viscosity of η) connected in series is illustrated below. The spring is regarded as governed by Hooke's Law and the dashpot by Newton's Law. Derive the governing differential equation for the material and find the time-dependent stress function in response to a step function of strain.



Solution:

Since the spring and dashpot are connected in series, the stress in the material (σ) will be experienced by the spring ($\sigma_s = \sigma$) and the dashpot ($\sigma_d = \sigma$), and the strain in the material will be shared by the spring and dashpot in the following relationship:

$$\varepsilon = \varepsilon_s + \varepsilon_d$$

By applying Hooke's Law to the spring, we have:

$$\varepsilon_s = \frac{\sigma}{E}$$

and by applying the Newton's Law to the dashpot, we have:

$$\frac{d\varepsilon_d}{dt} = \frac{\sigma}{\eta}$$

Taking the time derivative of the first two equations, we obtain

$$\frac{d\varepsilon}{dt} = \frac{d\varepsilon_s}{dt} + \frac{d\varepsilon_d}{dt} \text{ and } \frac{d\varepsilon_s}{dt} = \frac{1}{E} \frac{d\sigma}{dt}$$

With the three derivative expressions, we can eliminate the ε_s and ε_d terms, and arrive at the following governing differential equation in time domain for the viscoelastic material:

$$\frac{d\varepsilon}{dt} = \frac{1}{E} \frac{d\sigma}{dt} + \frac{\sigma}{\eta}$$

To find the time-dependent stress function in response to a step function of strain, we first multiply the above differential equation by E and rearrange it to

$$\frac{d\sigma}{dt} + \frac{E}{\eta} \sigma = E \frac{d\varepsilon}{dt}$$

Then by taking the Laplace transformation of the above equation, we arrive at the following frequency-domain differential equation

$$\sigma(s) \left(s + \frac{E}{\eta} \right) = E \varepsilon(s) s$$

in which $\sigma(s)$ and $\varepsilon(s)$ are stress and strain in frequency domain, corresponding to the $\sigma(t)$ and $\varepsilon(t)$ in time domain, respectively, and s is the Laplace variable.

Let a step function of strain take the following form

$$\varepsilon(t) = \begin{cases} \varepsilon_0, & t \geq 0 \\ 0, & t < 0 \end{cases}$$

then its Laplace transformed function will be

$$\varepsilon(s) = \frac{\varepsilon_0}{s}$$

Substituting this expression into the frequency-domain differential equation with some rearrangement, we obtain the stress response function in frequency-domain as

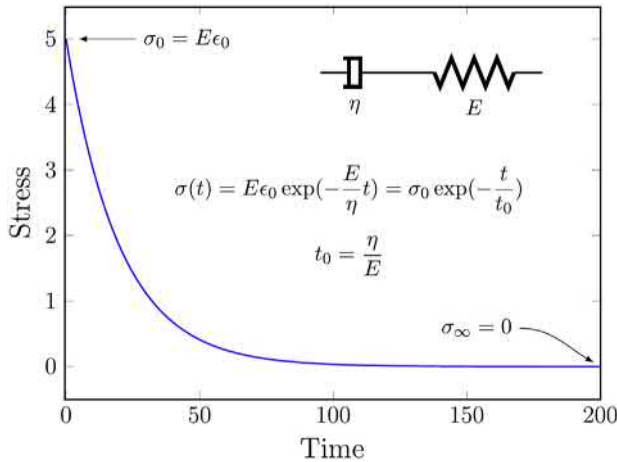
$$\sigma(s) = \frac{E \varepsilon_0}{\left(s + \frac{E}{\eta} \right)}$$

To find the time-dependent stress function, we will just take the inverse Laplace transformation. Do so leads us to the following stress response function in time domain:

$$\sigma(t) = E \varepsilon_0 \exp\left(-\frac{E}{\eta} t\right)$$

Clearly, the time-dependent stress function in response to a step function of strain is an exponential delaying function. This behavior is commonly referred to as the stress

relaxation behavior of viscoelastic materials. Obviously, the stress decays exponentially from $E\epsilon_0$ at $t = 0$ to zero as $t \rightarrow \infty$,



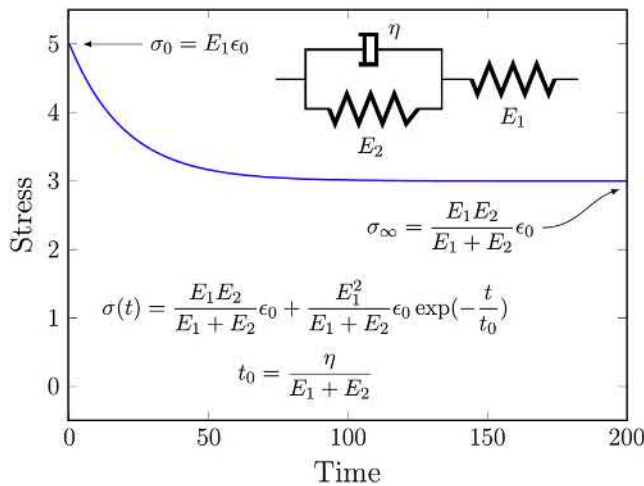
as illustrated in the plot given below.

9. For a viscoelastic material represented by two springs and a dashpot as illustrated in the given figure, show its governing differential equation as

$$\frac{d\sigma}{dt} + \frac{E_1 + E_2}{\eta} \sigma = E_1 \frac{d\epsilon}{dt} + \frac{E_1 E_2}{\eta} \epsilon$$

and its time-dependent stress function in response to a step function of strain as

$$\epsilon(t) = \epsilon_0, \quad \sigma(t) = \frac{E_1 E_2}{E_1 + E_2} \epsilon_0 + \frac{E_1^2}{E_1 + E_2} \epsilon_0 \exp(-t/t_0) \eta$$



Solution:

Since spring 2 (E_2) is connected in parallel with the dashpot (η), they will experience the same strain, $\epsilon_d = \epsilon_{2s} = \epsilon_2$. Moreover, because spring 1 (E_1) is in series with the parallel combo of spring 2 and the dashpot, the stress in the material (σ) will be experienced by spring 1 ($\sigma_{1s} = \sigma$)

and by the combined spring 2 and dashpot ($\sigma_d + \sigma_{2s} = \sigma$), and the strain in the material will be shared by spring 1 and the combo of spring 2 and dashpot in the following relationship:

$$\epsilon = \epsilon_{1s} + \epsilon_2$$

By applying Hooke's Law to the springs, we have:

$$\sigma = \sigma_{1s} = E_1 \epsilon_{1s}$$

and

$$\sigma_{2s} = E_2 \epsilon_{2s} = E_2 \epsilon_2$$

and by applying the Newton's Law to the dashpot, we have:

$$\sigma_d = \eta \frac{d\epsilon_d}{dt} = \eta \frac{d\epsilon_2}{dt}$$

Substituting the last two expressions into $\sigma_d + \sigma_{2s} = \sigma$, we have

$$\sigma = \eta \frac{d\epsilon_2}{dt} + E_2 \epsilon_2$$

With further substitution using $\epsilon = \epsilon_{1s} + \epsilon_2$, $\sigma = E_1 \epsilon_{1s}$,

and $\frac{d\sigma}{dt} = E_1 \frac{d\epsilon_{1s}}{dt}$, we obtain

$$\sigma = \eta \frac{d\epsilon_2}{dt} + E_2 \epsilon_2 = \eta \frac{d\epsilon - d\epsilon_{1s}}{dt} + E_2 (\epsilon - \epsilon_{1s}) = \eta \left(\frac{d\epsilon}{dt} - \frac{d\sigma}{E_1 dt} \right) + E_2 \left(\epsilon - \frac{\sigma}{E_1} \right)$$

After rearranging it, we obtain the following time-domain governing differential equation for the viscoelastic material as

$$\sigma \left(1 + \frac{E_2}{E_1} \right) + \frac{\eta}{E_1} \frac{d\sigma}{dt} = E_2 \epsilon + \eta \frac{d\epsilon}{dt}$$

Or in the following form after some further rearrangement,

$$\sigma + \frac{\eta}{E_1 + E_2} \frac{d\sigma}{dt} = \frac{E_1 E_2}{E_1 + E_2} \epsilon + \frac{E_1 \eta}{E_1 + E_2} \frac{d\epsilon}{dt}$$

This is the governing differential equation for the viscoelastic material represented by the given model. This equation, with some rearrangement, is exactly the same as that given in the question.

To find the time-dependent stress function in response to a step function of strain, we take the Laplace transformation of the above equation, and arrive at the following frequency domain differential equation

$$\sigma(s) \left(1 + \frac{\eta s}{E_1 + E_2} \right) = \epsilon(s) \left(\frac{E_1 E_2}{E_1 + E_2} + \frac{E_1 \eta s}{E_1 + E_2} \right)$$

in which $\sigma(s)$ and $\epsilon(s)$ are stress and strain in the frequency domain, corresponding to the $\sigma(t)$ and $\epsilon(t)$ in the time domain, respectively, and s is the Laplace variable.

Let a step function of strain take the following form

$$\varepsilon(t) = \begin{cases} \varepsilon_0, & t \geq 0 \\ 0, & t < 0 \end{cases}$$

then its Laplace transformed function is

$$\varepsilon(s) = \frac{\varepsilon_0}{s}$$

Substituting this expression into the frequency-domain differential equation along with some rearrangement, we obtain

$$\sigma(s) = \frac{\varepsilon_0 \left(\frac{E_1 E_2}{E_1 + E_2} + \frac{E_1 \eta s}{E_1 + E_2} \right)}{1 + \frac{\eta s}{E_1 + E_2}} = \frac{\varepsilon_0 \left(\frac{E_1 E_2}{\eta} + E_1 s \right)}{s \left(s + \frac{E_1 + E_2}{\eta} \right)}$$

This equation can be further expressed by the partial-fraction decomposition method as

$$\sigma(s) = \varepsilon_0 \frac{\left(\frac{E_1 E_2}{\eta} + E_1 s \right)}{s \left(s + \frac{E_1 + E_2}{\eta} \right)} = \varepsilon_0 \left(\frac{A}{s} + \frac{B}{s + \frac{E_1 + E_2}{\eta}} \right) = \varepsilon_0 \left(\frac{\frac{E_1 E_2}{E_1 + E_2}}{s} + \frac{\frac{E_1^2}{E_1 + E_2}}{s + \frac{E_1 + E_2}{\eta}} \right)$$

$$\text{with } A = \frac{E_1 E_2}{E_1 + E_2} \text{ and } B = \frac{E_1^2}{E_1 + E_2}.$$

Taking the inverse Laplace transformation of the above equation, we obtain the following stress response function in time domain:

$$\sigma(t) = \frac{E_1 E_2}{E_1 + E_2} \varepsilon_0 + \frac{E_1^2}{E_1 + E_2} \varepsilon_0 \exp \left(- \frac{E_1 + E_2}{\eta} t \right)$$

Apparently, the time-dependent stress function in response to a step function of strain for this viscoelastic material is still an exponential relaxation function. In this case, the stress decays exponentially from $E_1 \varepsilon_0$ at $t = 0$ to $\frac{E_1 E_2}{E_1 + E_2} \varepsilon_0$, not zero, as $t \rightarrow \infty$.

1.2.4

Surface Properties and Surface Characterization of Biomaterials

BUDDY D. RATNER¹, DAVID G. CASTNER²

¹Bioengineering and Chemical Engineering, Director of University of Washington Engineered Biomaterials (UWEB), Seattle, WA, United States

²University of Washington, Seattle, WA, United States

Introduction

Nothing is rich but the inexhaustible wealth of nature. She shows us only surfaces, but she is a million fathoms deep.

Ralph Waldo Emerson.

Biomaterials “show” to the world (and the biological environment) only surfaces. Atoms and molecules make up the outermost surface of a biomaterial (the interface between the material and the world). As we shall discuss in this section, these atoms and molecules that reside at the surface have a special organization and reactivity. They require special methods to characterize them, novel methods to tailor them, and they drive many of the biological reactions that occur in response to the biomaterial (protein adsorption, cell adhesion, cell growth, blood compatibility, etc.). The importance of surfaces for biomaterials science has been appreciated since the 1960s. Almost every biomaterials meeting will have sessions addressing surfaces and interfaces. In this chapter we focus on the special properties of surfaces, definitions of terms, methods to characterize surfaces, and some implications of surfaces as the drivers of bioreactions to biomaterials.

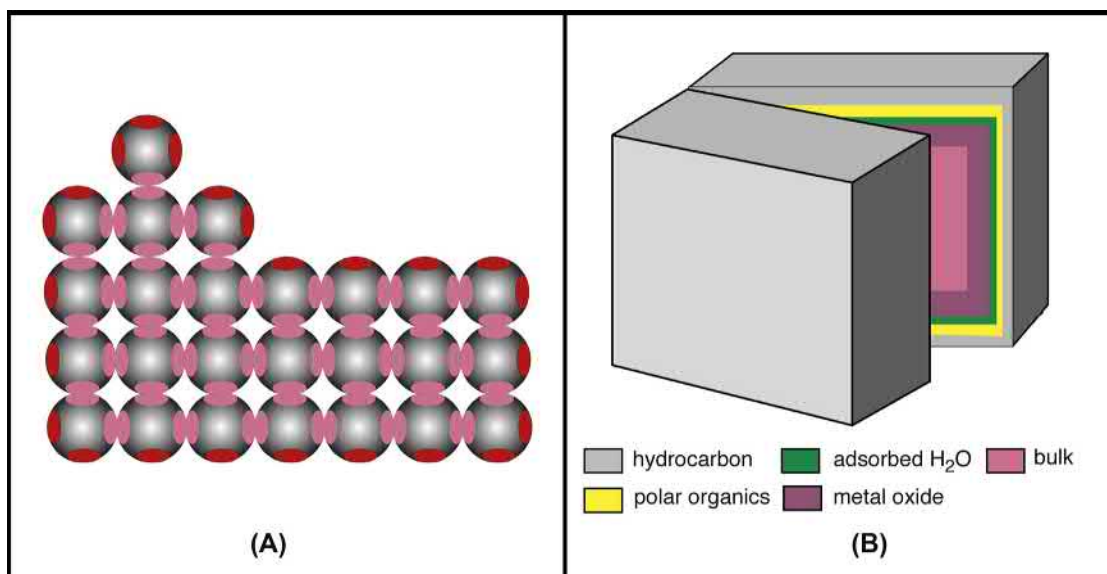
Atoms and molecules that reside at the surface of a biomaterial have special reactivity and a direct biological response.

During the development of biomedical implant devices and materials, we are concerned with physical properties, durability, and biocompatibility. The understanding of physical properties (e.g., mechanical strength, permeability, elasticity) has evolved over hundreds of years and is relatively well understood—the standard tools of engineers and materials scientists are appropriate to characterize and study physical properties (see [Chapters 1.2.2 and 1.2.3](#)). Durability, particularly in the biological environment, is less

well understood. Still, the tests we need to evaluate durability are clear (see [Chapters 1.2.2, 2.4.3, and 2.4.4](#)). Biocompatibility represents a frontier of knowledge in this field, and its study is often assigned to the biochemist, biologist, and physician (see [Chapters 2.3.2, 2.3.3, and 2.3.4](#)). However, an important question in biocompatibility is how the device or material “transduces” its structural makeup to direct or influence the response of proteins, cells, and the organism to that material. For devices and materials that do not leach undesirable substances (i.e., that have passed routine toxicological evaluation; see [Chapter 2.3.3](#)), this transduction occurs through the surface structure. The body “reads” the surface structure and responds to the particular chemistry and organization. For this reason we must understand the surface structure of biomaterials, and thus there is an important role for the physical scientist in understanding surface-driven biointeractions. [Chapter 3.1.9](#) elaborates on the biological implications of this idea.

General Surface Considerations and Definitions

This is the appropriate point to highlight general ideas about surfaces, especially solid surfaces. First, the surface region of a material is known to be of unique reactivity ([Fig. 1.2.4.1A](#)). Catalysis (for example, as used in petrochemical processing) and microelectronics both capitalize on special *surface* organization and reactivity—biology also exploits this enhanced surface reactivity to do its work. Second, the surface of a material is inevitably different from the bulk. The traditional techniques used to analyze the bulk structure of materials are not suitable for surface determination because they typically do not have the sensitivity to observe the small amount of material comprising the unique surface chemistry/structure. Third, there is not much total mass of material at a surface. An example may help us to appreciate



• **Figure 1.2.4.1** (A) A two-dimensional representation of a crystal lattice suggesting bonding orbitals (red or pink ovals). For atoms in the center (bulk) of the crystal (pink ovals), all binding sites have associations with those of other atoms (sharing electrons). At planar exterior surfaces, one of the bonding sites is unfulfilled (red oval). At corners, two bonding sites are unfulfilled. The single atom on top of the crystal (an adatom) has three unfulfilled valencies. Energy is minimized where more of these unfulfilled valencies can interact. Where interactions do not satisfy all binding orbitals, there is an asymmetric electrical field driving a surface dipole. (B) In a “real-world” material (a block of metal from an orthopedic device, for example), if we cleave the block (under ultrahigh vacuum to prevent recontamination), we should find hydrocarbon on the outermost layer (perhaps 3nm, surface energy ~ 22 ergs/cm²), polar organic molecules (>1 nm, surface energy ~ 45 ergs/cm²), adsorbed water (<1 nm, surface energy ~ 72 ergs/cm²), metal oxide (approximately 5nm, surface energy ~ 200 ergs/cm²), and finally, the uniform bulk interior (surface energy ~ 1000 ergs/cm²). The interface between air and material has the lowest interfacial energy (~ 22 ergs/cm²). The layers are not drawn to scale.

this—on a 1 cm³ cube of titanium, the 100Å oxide surrounding the cube is in the same proportion as a 5 m-wide beach on each coast of the United States is to the roughly 5,000,000 m distance from coast to coast. Fourth, surfaces readily contaminate with components from the vapor phase (some common examples are hydrocarbons, silicones, sulfur compounds, iodine). Under ultrahigh vacuum conditions (pressures $<10^{-7}$ Pa) we can retard this contamination. However, in view of the atmospheric pressure conditions under which all biomedical devices are used, we must learn to live with some contamination. The key questions here are whether we can make devices with controlled and acceptable levels of contamination and also avoid undesirable contaminants. This is critical so that a laboratory experiment on a biomaterial generates the same results when repeated after 1 day, 1 week, or 1 year, and so that the biomedical device is dependable and has a reasonable shelf-life. Finally, the surface structure of a material is often mobile. A modern view of what might be seen at the surface of a real-world material is illustrated in Fig. 1.2.4.1B.

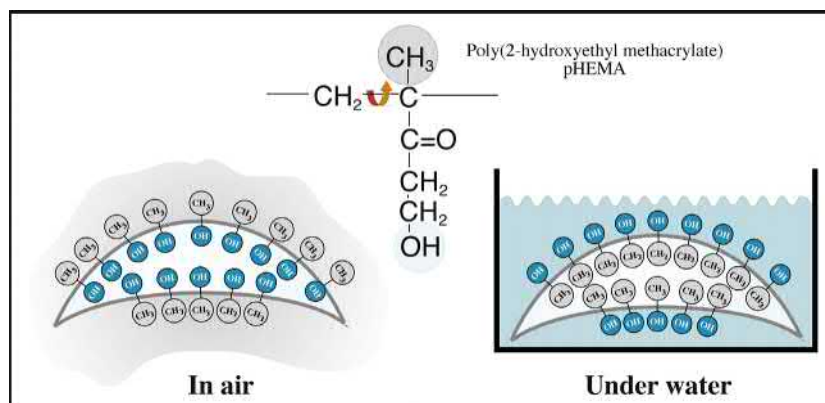
Five points about surfaces include:

1. Surfaces have unique reactivity.
2. The surface is inevitably different from the bulk.
3. The mass of material that makes up the surface zone is very small.
4. Surfaces readily contaminate.
5. Surface molecules can exhibit considerable mobility.

The movement of atoms and molecules near the surface in response to the outside environment is often highly significant. In response to a hydrophobic environment (e.g., air), more hydrophobic (lower energy) components may migrate to the surface of a material—a process that reduces interfacial energy (Fig. 1.2.4.1B). Responding to an aqueous environment, the surface may reverse its structure and point polar (hydrophilic) groups outward to interact with the polar water molecules. Again, energy minimization drives this process. An example of this is schematically illustrated in Fig. 1.2.4.2. For metal alloys, one metal tends to dominate the surface, for example, silver in a silver–gold alloy or chromium in stainless steel.

The nature of surfaces is complex and the subject of much independent investigation. The reader is referred to one of many excellent monographs on this important subject for a complete and rigorous introduction (see Somorjai, 1981; Somorjai and Li, 2010; Adamson and Gast, 1997; Andrade, 1985; Garbassi et al., 1998). Biosurfaces, with particular relevance for biomaterials, are overviewed in articles and books (Castner and Ratner, 2002; Kasemo, 2002; Tirrell et al., 2002; Ratner, 1988; Castner, 2017).

When we say “surface,” a question that immediately comes to mind is, “how deep into the material does it extend?” Although formal definitions are available, for all practical purposes, the surface is the zone where the structure and composition, influenced by the interface, differ from the average (bulk) composition and structure. This value often



• **Figure 1.2.4.2** Many materials can undergo a reversal of surface structure when transferred from air into a water environment. In this schematic illustration, a hydroxylated polymer (for example, a pHEMA contact lens) exhibits a surface rich in methyl groups (from the polymer chain backbone) in air, and a surface rich in hydroxyl groups under water. This has been observed experimentally [Ratner et al., *J. Appl. Polym. Sci.*, 1978; 22, 643; Chen et al., *J. Am. Chem. Soc.*, 1999; 121 (2); 446].

scales with the size of the molecules making up the surface. For an “atomic” material, for example gold, after penetration of about five atomic layers (0.5–1 nm), the composition becomes uniform from layer to layer (i.e., you are seeing the bulk structure). At the outermost atomic layer, the organization of the gold atoms at the surface (and their reactivity) can be substantially different from the organization in the averaged bulk (Barth et al., 1990), but it is not the atomic/molecular rearrangements we are discussing here. The gold surface, in air, will always have a contaminant overlayer, largely hydrocarbon, that may be roughly 2 nm thick. This results in a difference in composition between bulk and surface. For a polymer, the unique surface zone may extend from 10 to 100 nm (depending on the polymeric system and the chain molecular weight). Fig. 1.2.4.1B addresses some of these issues about surface definitions. Two more definitions must be considered. An interface is the transition between two phases, in principle an infinitely thin separation plane. An interphase is the unique compositional zone between two phases. For the example, for gold, we might say that the interphase between gold and air is 3 nm thick (the structurally rearranged gold atoms + the contaminant layer).

What Surface Properties Are We Interested in?

A surface is fully described by many parameters (Fig. 1.2.4.3). The more of these parameters we measure, the more we can piece together a complete description of the surface. A complete characterization requires a cadre of techniques to examine the many facets that contribute to the surface properties. Unfortunately, we cannot yet specify which parameters are most important for understanding specific biological responses to surfaces. Studies have been published on the importance of roughness, patterns, wettability, surface mobility, chemical composition, electrical charge, crystallinity, modulus, and heterogeneity to biological reaction. Since we cannot be certain which surface factors are predominant in each situation, the controlling variable or variables must be independently measured and correlated. We use surface analysis techniques to measure these surface properties.

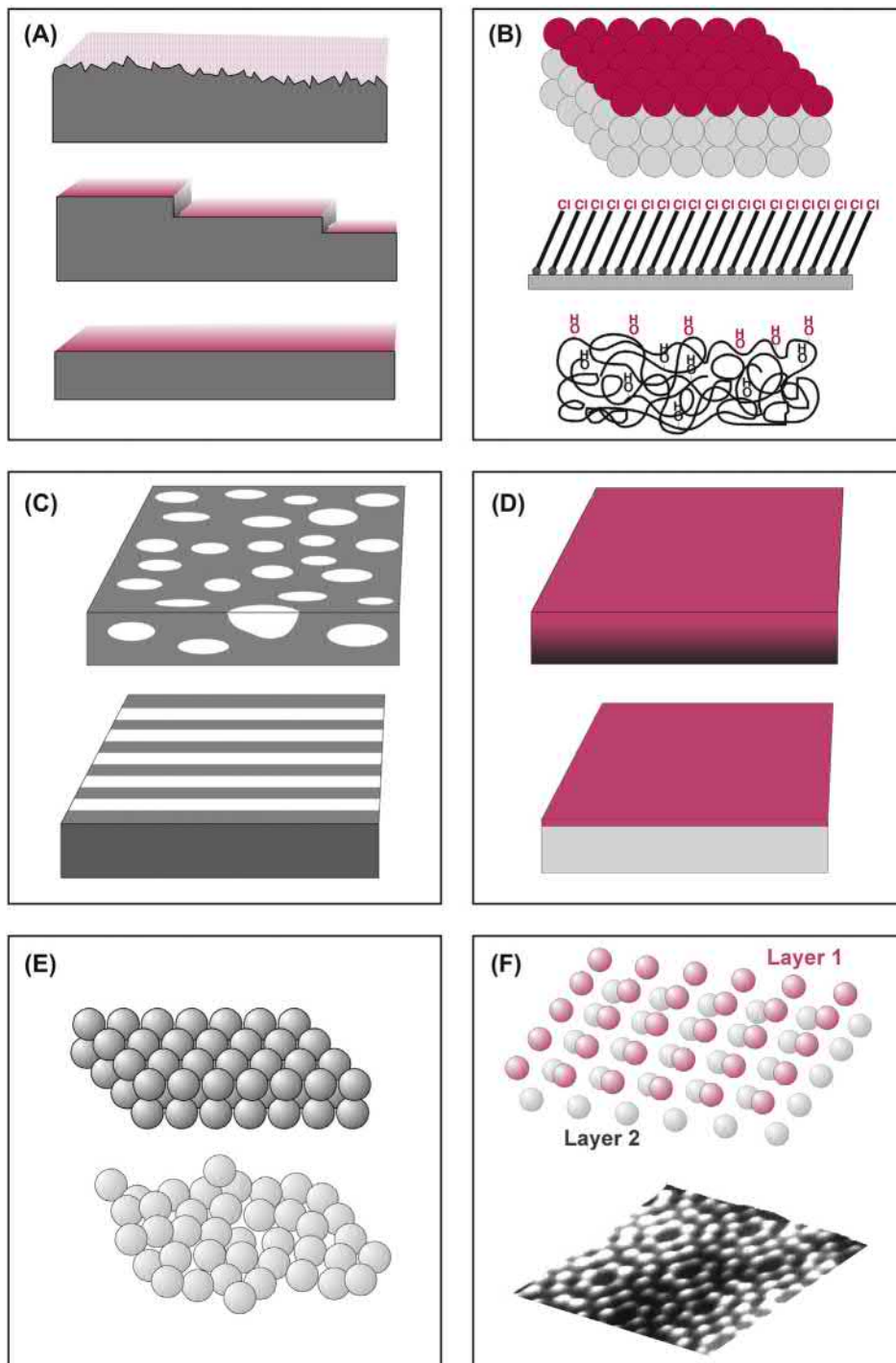
Surface Analysis Techniques: Principles and Methods

Sample Preparation

A guiding principle of surface analysis sample preparation is that the sample should resemble, as closely as possible, the material or device in the form that it is used for biological testing or implantation. Needless to say, fingerprints on the surface of the sample will obscure surface properties of interest. If the sample is placed in a package for shipping or storage prior to surface analysis, it is critical to know whether the packaging material can deliver surface contamination. Plain paper in contact with most specimens will transfer contaminants (often metal ions) to the surface of the material. Many plastics are processed with silicone oils or other additives that can migrate to the specimen. The packaging material used should be examined by surface analysis methods to ascertain its purity. Samples can be surface analyzed prior to and after storage in containers to ensure that the surface composition measured is not due to the container. As a general rule, the polyethylene press-close bags used in electron microscopy and cell culture plastic ware are clean storage containers. However, abrasive contact must be avoided, and each brand must be evaluated so that a meticulously prepared specimen is not ruined by contamination. Many brands of aluminum foil are useful for packing specimens, but some are treated with a surface layer of stearic acid that can surface-contaminate biomaterials, implants, or medical devices. Aluminum foil should be checked for surface contamination layers by surface analysis methods prior to wrapping important specimens.

Surface Analysis General Comments

Two general principles guide sample analysis. First, all methods used to analyze surfaces also have the potential to alter the surface. The analyst must be aware of the damage potential of the method used. Second, because of the potential for



• **Figure 1.2.4.3** What might be measured to define surface structure? (A) Surfaces can be rough, stepped, or smooth. (B) Surfaces can be comprised of different chemistries (atomic, supramolecular, macromolecular). (C) Surfaces may be structurally or compositionally inhomogeneous in the plane of the surface such as phase-separated domains or microcontact printed lanes. (D) Surfaces may be inhomogeneous with depth into the specimen or simply overlayered with a thin film. (E) Surfaces may be highly crystalline or disordered. (F) Crystalline surfaces are found with many organizations such as a silicon (100) unreconstructed surface or a silicon (111) (7×7) reconstructed surface.

artifacts and the need for corroborative information to construct a complete picture of the surface (Fig. 1.2.4.3), more than one method should be used whenever possible. The data derived from two or more methods should be internally consistent. When data are contradictory, be suspicious and

question why. A third or fourth method may then be necessary to draw confident conclusions about the nature of a surface. These general principles are applicable to all materials.

There are properties (only a few of which will be presented here) that are specific to specific classes of materials.

TABLE 1.2.4.1 Common Methods to Characterize Biomaterial Surfaces

Method	Principle	Depth Analyzed	Spatial Resolution	Analytical Sensitivity	Cost
Contact angles	Liquid wetting of surfaces is used to estimate the energy of surfaces	3–20Å	1 mm	Low or high depending on the chemistry	\$
ESCA (XPS)	X-rays induce the emission of electrons of characteristic energy	10–250Å	5–150µm	0.1 atom %	\$\$\$
Auger electron spectroscopy ^a	A focused electron beam stimulates the emission of auger electrons	50–100Å	80Å	0.1 atom %	\$\$\$
SIMS	Ion bombardment sputters secondary ions from the surface	10Å–1µm ^b	100Å	Very high	\$\$\$
FTIR-ATR	IR radiation is adsorbed and excites molecular vibrations	1–5µm	10µm	1 mol %	\$\$
STM	Measurement of the quantum tunneling current between a metal tip and a conductive surface	5Å	1Å	Single atoms	\$\$
SEM	Secondary electron emission induced by a focused electron beam is spatially imaged	5Å	10–40Å	High, but not quantitative	\$\$-\$\$\$

\$, up to \$5000; \$\$, \$5000–\$250,000; \$\$\$, >\$250,000.
^aAuger electron spectroscopy is damaging to organic materials, and best used for inorganics.
^bStatic SIMS=10Å, dynamic SIMS to 1µm.

Compared to metals, ceramics, and glasses, organic and polymeric materials are more easily damaged by surface analysis methods. Polymeric systems also exhibit greater surface molecular mobility than inorganic systems. The surfaces of inorganic materials are contaminated more rapidly than polymeric materials because of their higher surface energy. Electrically conductive metals and carbons will often be easier to characterize than insulators using electron, X-ray, and ion interaction methods. Insulators accumulate a surface electrical charge that requires special methods (e.g., a low-energy electron beam) to neutralize. To learn about other concerns in surface analysis that are specific to specific classes of materials, published papers become a valuable resource for understanding the pitfalls that can lead to artifact or inaccuracy.

Table 1.2.4.1 summarizes the characteristics of many common surface analysis methods, including their depth of analysis under standard conditions and their spatial resolution (spot size analyzed). A few of the more frequently applied techniques are described in the next section. However, space limitations prevent an intensive discussion of these methods. The reader is referred to many comprehensive books on the general subject of surface analysis (Andrade, 1985; Briggs and Seah, 1983; Feldman and Mayer, 1986; Vickerman and Gilmore, 2009). References describing specific surface analysis methods will be presented in sections on each of the key methods.

Contact Angle Methods

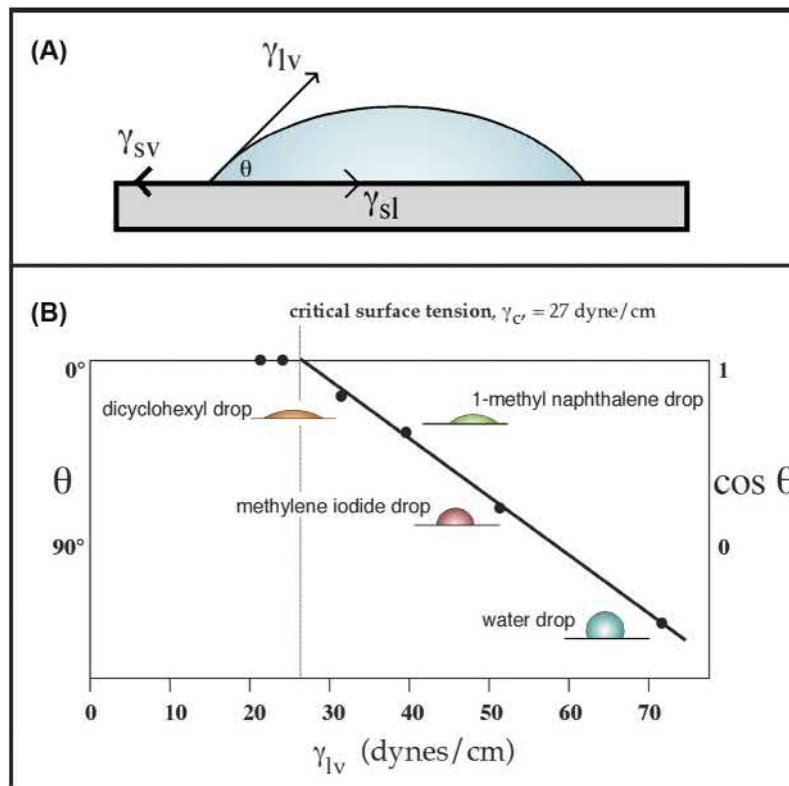
A drop of liquid sitting on a solid surface represents a simple, but potentially powerful, method to probe surface

properties. Experience tells us that a drop of water on a highly polished automobile body surface will stand up (bead up), while on an old, weathered car, the liquid will flow evenly over the surface. This observation, for those knowledgeable about contact angles, tells us that the highly polished car probably has silicones or hydrocarbons at its surface, while the unpolished car surface is oxidized material. Quantitative contact angle measurement has, in fact, been used to predict the performance of vascular grafts and the adhesion of cells to surfaces.

The phenomenon of the contact angle can be explained as a balance between the force with which the molecules of the drop liquid are being attracted to each other (a cohesive force) and the attraction of the liquid molecules for the surface (an adhesive force). An equilibrium is established between these forces. The force balance between the liquid–vapor surface tension (γ_{lv}) of a liquid drop and the interfacial tension between a solid and the drop (γ_{sl}), manifested through the contact angle (θ) of the drop with the surface, can be used to quantitatively characterize the energy of the surface (γ_{sv}) (Fig. 1.2.4.4A). The basic relationship describing this force balance is:

$$\gamma_{sv} = \gamma_{sl} + \gamma_{lv} \cos \theta$$

The surface energy, closely related to wettability, is a useful parameter that has often been correlated with biological interaction. Unfortunately, γ_{sv} cannot be directly obtained since this equation contains two unknowns, γ_{sl} and γ_{sv} . Therefore, the γ_{sv} is sometimes approximated by the Zisman method for obtaining the critical surface tension (Fig. 1.2.4.4B), or calculated by solving simultaneous equations



• **Figure 1.2.4.4** (A) An equilibrium is established between surface tension forces contracting a liquid drop to a spherical shape and forces interacting the drop with the surface. The force balance between the liquid–vapor surface tension (γ_{lv}) of a liquid drop and the interfacial tension between a solid and the drop (γ_{sl}), manifested through the contact angle (θ) of the drop and can be used to quantitatively characterize the surface–vapor interfacial tension (γ_{sv}). (B) The Zisman method permits a critical surface tension value, an approximation to the solid surface tension, to be measured. Drops of liquids of different surface tensions are placed on the solid, and the contact angles of the drops are measured. The plot of liquid surface tension versus angle is extrapolated to zero contact angle to give the critical surface tension value.

TABLE 1.2.4.2 Critical Surface Tension Values for Common Polymeric Materials Calculated From Contact Angle Measurements

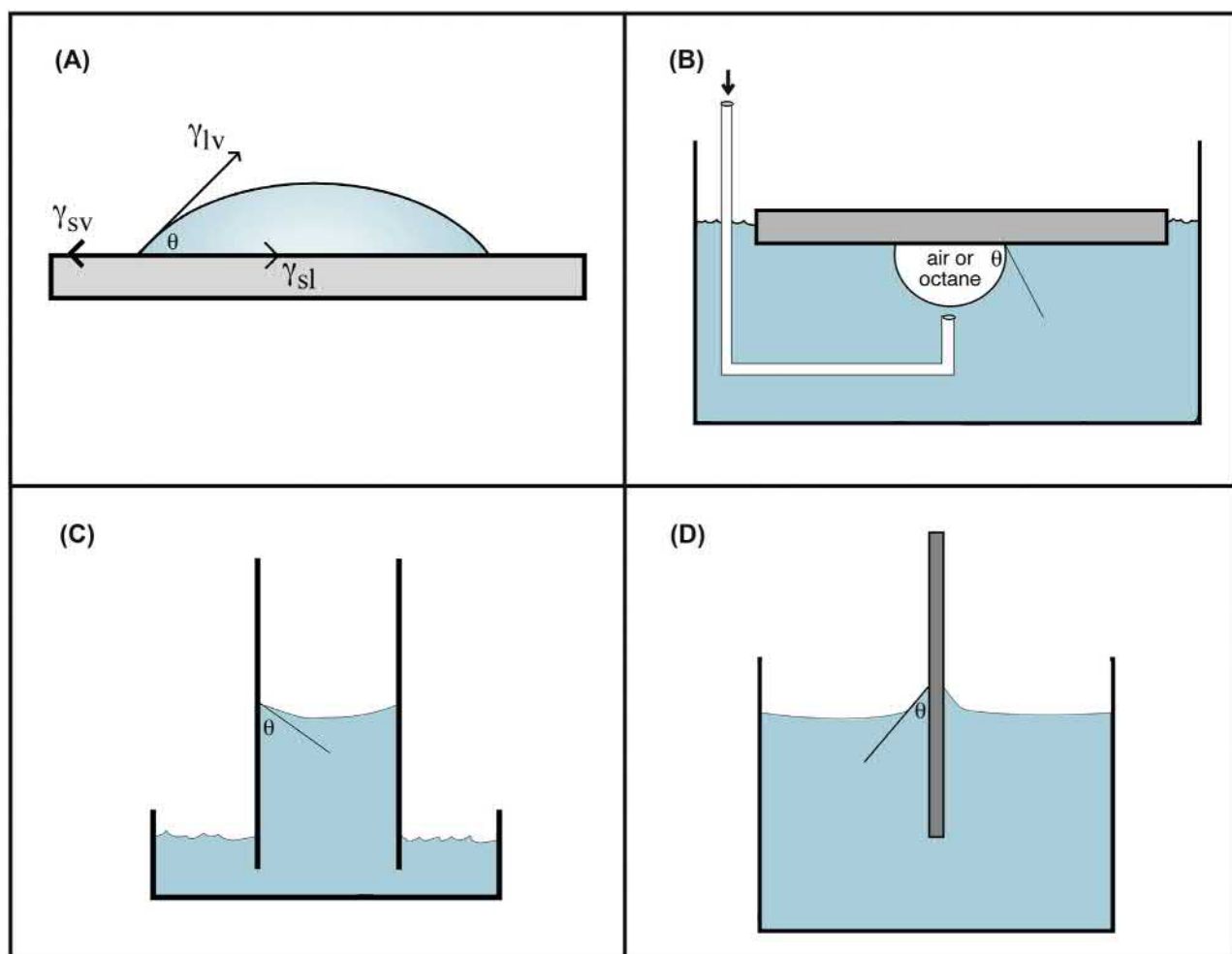
Material	Critical Surface Tension (dynes/Cm)
Polytetrafluoroethylene	19
Poly(dimethyl siloxane)	24
Poly(vinylidene fluoride)	25
Poly(vinyl fluoride)	28
Polyethylene	31
Polystyrene	33
Poly(2-hydroxyethyl methacrylate)	37
Poly(vinyl alcohol)	37
Poly(methyl methacrylate)	39
Poly(vinyl chloride)	39
Polycaproamide (nylon 6)	42
Poly(ethylene oxide)-diol	43
Poly(ethylene terephthalate)	43
Polyacrylonitrile	50

with data from liquids of different surface tensions. Some critical surface tensions for common materials are listed in [Table 1.2.4.2](#).

Experimentally, there are a number of ways to measure the contact angle. Some of these are illustrated in [Fig. 1.2.4.5](#). Contact angle methods can be inexpensive, and, with some practice, easy to perform. A contact angle goniometer (a telescope to observe the drop that is equipped with a protractor eyepiece) is the least expensive method for contact angle measurement. A number of companies now offer video systems that compute the contact angle and other surface energy parameters from digital image analysis of the liquid drop profile. Accessories to control humidity and temperature and deposit drops of liquid are available.

Contact angles directly measure surface wettability and indirectly probe surface energy, roughness, heterogeneity, contamination, and molecular mobility.

Contact angle measurements provide a “first-line” characterization of materials and can be performed in any laboratory. Contact angle measurements provide a unique insight into how the surface will interact with the external world. However, in performing such



• **Figure 1.2.4.5** Four possibilities for contact angle measurement: (A) sessile drop; (B) captive air bubble method; (C) capillary rise method; (D) Wilhelmy plate method.

TABLE 1.2.4.3 Concerns in Contact Angle Measurement

- The measurement is operator dependent (for manual, goniometer instruments)
- Surface roughness influences the results
- Surface heterogeneity influences the results
- The liquids used are easily contaminated (typically reducing their γ_{lv})
- Liquid evaporation and temperature changes can impact measurement
- The liquids used can reorient the surface structure
- The liquids used can absorb into the surface, leading to swelling
- The liquids used can dissolve the surface
- Few sample geometries are appropriate for contact angle measurement
- Information on surface structure must be inferred from the data obtained

measurements, a number of concerns must be addressed to obtain meaningful data (Table 1.2.4.3). Review articles are available on contact angle measurement for surface characterization (Andrade, 1985; Good, 1993; Zisman, 1964; Ratner, 1988).

Electron Spectroscopy for Chemical Analysis

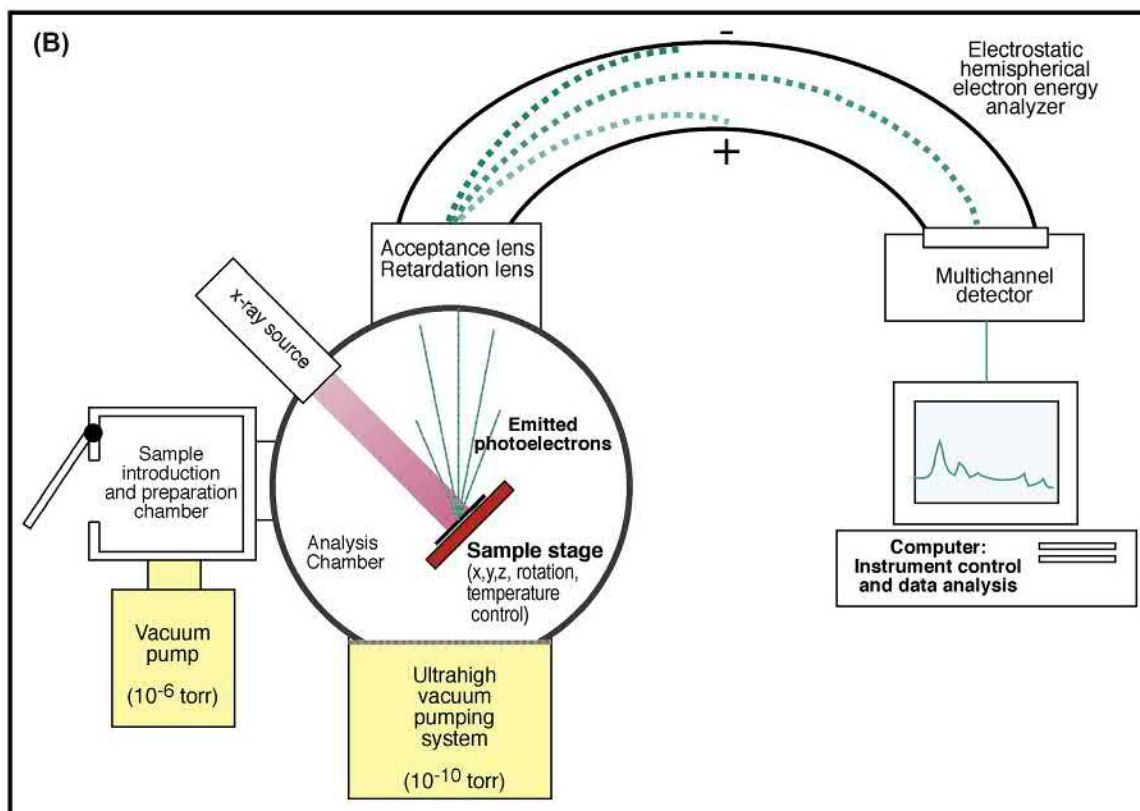
Electron spectroscopy for chemical analysis (ESCA) provides a comprehensive qualitative and quantitative overview of a surface that would be challenging to obtain by other means (Andrade, 1985; Ratner, 1988; Dilks, 1981; Ratner and McElroy, 1986; Ratner and Castner, 2009; Watts and Wolstenholme, 2003; McArthur, 2006). In contrast to the contact angle technique, ESCA requires complex, expensive apparatus (Fig. 1.2.4.6A) and demands considerable training to perform the measurements. However, since ESCA is available from commercial laboratories, university analytical facilities, national centers (for example, NESAC/BIO at the University of Washington), and specialized research laboratories, most biomaterials scientists can access instrumentation for sample analysis. ESCA has contributed significantly to the development of biomaterials and medical devices, and to understanding the fundamentals of biointeraction.

The ESCA method (also called X-ray photoelectron spectroscopy, XPS) is based on the photoelectric effect, properly described by Einstein in 1905. X-rays are focused upon a specimen. The interaction of the X-rays with the atoms in the specimen causes the emission of core level (inner shell)

(A)



(B)



• **Figure 1.2.4.6** (A) Photograph of a contemporary ESCA instrument. (B) Schematic diagram of a monochromatized ESCA instrument. (Photo by Kratos Axis Ultra DLD – contemporary ESCA instrument).

TABLE 1.2.4.4 Information Derived From an ESCA Experiment

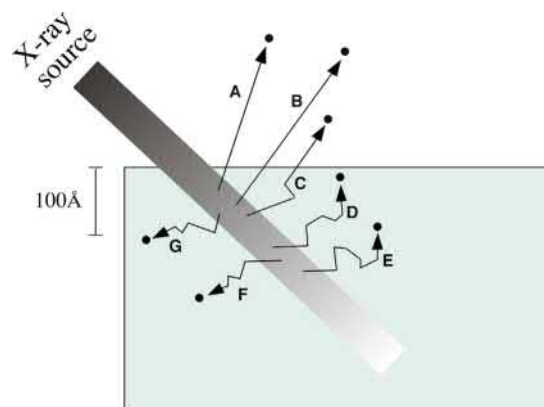
- In the outermost 100Å of a surface, ESCA can provide:
- Identification of all elements (except H and He) present at concentrations >0.1 atomic %
 - Semiquantitative determination of the approximate elemental surface composition ($\pm 10\%$)
 - Information about the molecular environment (oxidation state, bonding atoms, etc.)
 - Information about aromatic or unsaturated structures from shake-up ($\pi^* \leftarrow \pi$) transitions
 - Identification of organic groups using derivatization reactions
 - Nondestructive elemental depth profiles 100Å into the sample and surface heterogeneity assessment using angular-dependent ESCA studies and photoelectrons with differing escape depths
 - Destructive elemental depth profiles several thousand angstroms into the sample using argon ion etching (for inorganics) or cluster beam etching (for organics)
 - Lateral variations in surface composition (spatial resolution 5–150 μm , depending upon the instrument)
 - “Fingerprinting” of materials using valence band spectra and identification of bonding orbitals
 - Studies on hydrated (frozen) surfaces

electrons. The energy of these electrons is measured and their values provide information about the nature and environment of the atom or atoms from which they originated. The basic energy balance describing this process is given by the relationship:

$$BE = h\nu - KE$$

where BE is the energy binding the electron to an atom (the value desired), KE is the kinetic energy of the emitted electron (the value measured in the ESCA spectrometer), and $h\nu$ is the energy of the X-rays, a known value. A schematic diagram illustrating an ESCA instrument is shown in Fig. 1.2.4.6B. Table 1.2.4.4 lists the types of information about the nature of a surface that can be obtained using ESCA. The origin of the surface sensitivity of ESCA is described in Fig. 1.2.4.7.

ESCA has many advantages, and a few disadvantages, for studying biomaterials. The advantages include high information content, surface localization of the measurement (outermost 8–10 nm), speed of analysis, low damage potential, and the ability to analyze most samples with no special specimen preparation. The latter advantage is particularly important since biomedical devices (or parts of devices) can often be inserted, as fabricated and sterilized, directly in the analysis chamber for study. The disadvantages include the need for vacuum compatibility (i.e., no outgassing of volatile components), the vacuum environment and its impact on the specimen (particularly for hydrated specimens), the possibility of sample damage by X-rays if long analysis times are used, the need for experienced operators, and the cost associated with this complex instrumentation. The vacuum limitations can be



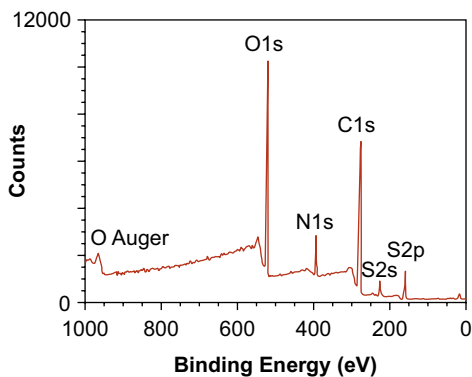
• **Figure 1.2.4.7** ESCA is a surface-sensitive method. Although the X-ray beam can penetrate deeply into a specimen, electrons emitted deep in the specimen (D, E, F, G) will lose their energy in inelastic collisions and never emerge from the surface. Only those electrons emitted near the surface that lose no energy (A, B) will contribute to the ESCA signal used analytically. Electrons that lose some energy, but still have sufficient energy to emerge from the surface (C) contribute to the background signal.

sidestepped by using an ESCA system with a cryogenic sample stage. At liquid nitrogen temperatures, samples with volatile components, or even wet, hydrated samples, can be analyzed.

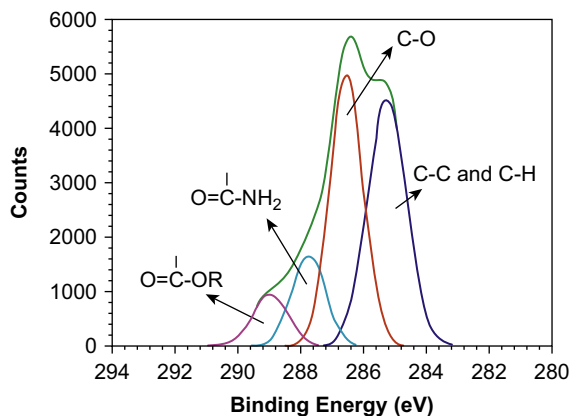
ESCA analyzes to approximately 10 nm and gives information on elements present, their concentrations, and their bonding environments.

The use of ESCA is best illustrated with a brief example. A poly(methyl methacrylate) (PMMA) ophthalmologic device is to be examined. Taking care not to touch or damage the surface of interest, the device is inserted into the ESCA instrument introduction chamber. The introduction chamber is then pumped down to 10^{-7} torr (1.33×10^{-5} Pa) or lower pressure. A gate valve between the introduction chamber and the analytical chamber is opened and the specimen is moved into the analysis chamber. In the analysis chamber, at 10^{-9} torr (1.33×10^{-7} Pa) or lower pressure, the specimen is positioned using a microscope or TV camera and the X-ray source is turned on. The ranges of electron energies to be observed are computer-controlled with the retardation lens on the spectrometer. First, a wide scan is made in which the energies of all emitted electrons over a 1000 eV range are detected (Fig. 1.2.4.8). Then, narrow scans are made in which each of the elements detected in the wide scan is examined in higher resolution (Fig. 1.2.4.9).

From the wide scan, we learn that the specimen contains carbon, oxygen, nitrogen, and sulfur. The presence of sulfur and nitrogen is unexpected for PMMA. We can calculate the atomic % composition from the wide scan spectral data. The sample surface contains 58.2% carbon, 27.7% oxygen, 9.5% nitrogen, and 4.5% sulfur. The narrow scan for the carbon region (C1s spectrum) suggests four classes of compounds: hydrocarbons, carbons singly bonded to oxygen



• **Figure 1.2.4.8** ESCA wide scan of a surface-modified poly(methyl methacrylate) ophthalmologic device.



• **Figure 1.2.4.9** The carbon 1s narrow scan ESCA spectrum of a surface-modified poly(methyl methacrylate) ophthalmologic device. Narrow scan spectra can be generated for each element seen in low energy resolution mode in Fig. 1.2.4.8.

(the predominant species), carbons in amide-like molecular environments, and carbons in carboxylic acid or ester environments. This is quite different from the spectrum expected for pure PMMA. An examination of the peak position in the narrow scan of the sulfur region (S2p spectrum) suggests sulfonate-type groups. The shape of the C1s spectrum, the position of the sulfur peak, and the presence of nitrogen all suggest that heparin was immobilized to the surface of the PMMA device. Since the stoichiometry of the lens surface does not match that for pure heparin, this suggests that we are seeing either some of the PMMA substrate through a $<100\text{\AA}$ layer of heparin, or we are seeing some of the bonding links used to immobilize the heparin to the lens surface. Further analysis with ESCA and other surface analysis techniques will permit the extraction of more detail about this surface-modified device, including an estimate of surface modification thickness, further confirmation that the coating is indeed heparin, and additional information about the nature of the immobilization chemistry.

Secondary Ion Mass Spectrometry

Secondary ion mass spectrometry (SIMS) is an information-rich tool that the surface analyst can bring to bear on

TABLE 1.2.4.5 Analytical Capabilities of SIMS

	Static SIMS	Dynamic SIMS
Identify hydrogen and deuterium	✓	✓
Identify other elements (often must be inferred from the data)	✓	✓
Suggest molecular structures (inferred from the data)	✓	
Observe extremely high-mass fragments (proteins, polymers)	✓	
Detection of extremely low concentrations	✓	✓
Depth profile to $1\ \mu\text{m}$ into the sample	^a	✓
Observe the outermost 1–2 atomic layers	✓	
High spatial resolution (features as small as approximately 400\AA)	✓	✓
Semiquantitative analysis (for limited sets of specimens)	✓	✓
Useful for polymers	✓	^a
Useful for inorganics (metals, ceramics, etc.)	✓	✓
Useful for powders, films, fibers, etc.	✓	✓

^aCluster ion sources allow depth profiling with static-SIMS-like information content.

a biomedical problem. SIMS, in the static mode, produces a mass spectrum of the outermost 1–2 nm of a surface. Like ESCA, it requires complex instrumentation and an ultra-high vacuum chamber for the analysis. However, it provides unique information that is complementary to ESCA and greatly aids in understanding surface composition. Some of the analytical capabilities of SIMS are summarized in Table 1.2.4.5. Review articles on SIMS are available (Ratner, 1988; Scheutzle et al., 1984; Briggs, 1986; Davies and Lynn, 1990; Vickerman et al., 1989; Benninghoven, 1983; Van Vaeck et al., 1999; Belu et al., 2003; Michel and Castner, 2006; Bich et al., 2015; Fletcher and Vickerman, 2013; Fletcher, 2015; Nunez et al., 2018).

In SIMS analysis, a surface is bombarded with a beam of accelerated ions. The collision of these ions with the atoms and molecules in the surface zone can transfer enough energy that they sputter from the surface into the vacuum phase. The process is analogous to racked pool balls that are ejected from the ball cluster by the impact of the cue ball; the harder the cue ball hits the rack of balls, the more balls are emitted from the rack. In SIMS, the “cue balls” are positive ions (cesium, gallium, bismuth, C60-buckyballs, and cluster ions are commonly used) that are accelerated at the surface to be analyzed with energies of 5000–20,000 eV.

The particles ejected from the surface are positive and negative ions (secondary ions), radicals, excited states, and neutrals. Only the secondary ions are measured in SIMS. In ESCA, the energy of emitted particles (electrons) is measured. SIMS measures the mass of emitted ions (more rigorously, the ratio of mass to charge, m/z) using a time-of-flight (TOF) mass analyzer, magnetic sector analyzer or, in older instruments, a quadrupole mass analyzer.

Historically SIMS analysis has been divided into two modes, dynamic and static. Dynamic SIMS uses high ion doses over a given analysis time. The primary ion beam sputters sufficient material from the surface that the surface erodes away at an appreciable rate. We can capitalize on this to depth-profile into a specimen, and this works particularly well for metallic, semiconductor, and ceramic materials. The intensity of the m/z peak of a species of interest (e.g., sodium ion, $m/z=23$) might be followed as a function of time. If the ion beam is well controlled and the sputtering rate is constant, the sodium ion signal intensity measured at any time will be directly related to its concentration at the erosion depth of the ion beam into the specimen. A concentration depth profile (sodium concentration vs. depth) can be constructed from the outermost atoms to a micron or more into the specimen. Depending on the primary ion used, for example, cesium or gallium, and its energy, the high-flux ion beam can destroy organic samples and relevant organic fragments and predominantly atomic fragments (e.g., C^- , CH^- , O^- , OH^- , Na^+ , etc.) will be detected. Also, as the beam erodes deeper into the specimen, more artifacts are introduced in the data by “knock-in” and scrambling of atoms. However, by using methods like isotope labeling, techniques such as nanoSIMS that fall into the dynamic SIMS category can provide 3D imaging of biological samples (Nunez et al., 2018; Steinhäuser et al., 2012).

Static SIMS, in contrast, induces minimal surface destruction. The ion dose is adjusted so that during the period of the analysis less than 10% of one monolayer of surface atoms is sputtered. Since there are typically 10^{13} – 10^{15} atoms in 1 cm^2 of surface, a total ion dose of less than 10^{12} ions/ cm^2 during the analysis period is appropriate. Under these conditions, extensive degradation and rearrangement of the chemistry at the surface does not take place, and large, relatively intact molecular fragments can be ejected into the vacuum for measurement. Examples of molecular fragments are shown in Fig. 1.2.4.10. This figure also introduces some of the ideas behind SIMS spectral interpretation. A more complete introduction to the concepts behind static SIMS spectral interpretation can be found in Van Vaeck et al. (1999) or in standard texts on mass spectrometry.

Static SIMS provides qualitative information on the atomic and molecular composition in the outermost 1–2 nm of surface with high analytical sensitivity and excellent x,y spatial resolution.

Magnetically or electrostatically focusing the primary ion beam permits the SIMS technique to have high spatial resolution in the x,y plane. In fact, SIMS analysis can be

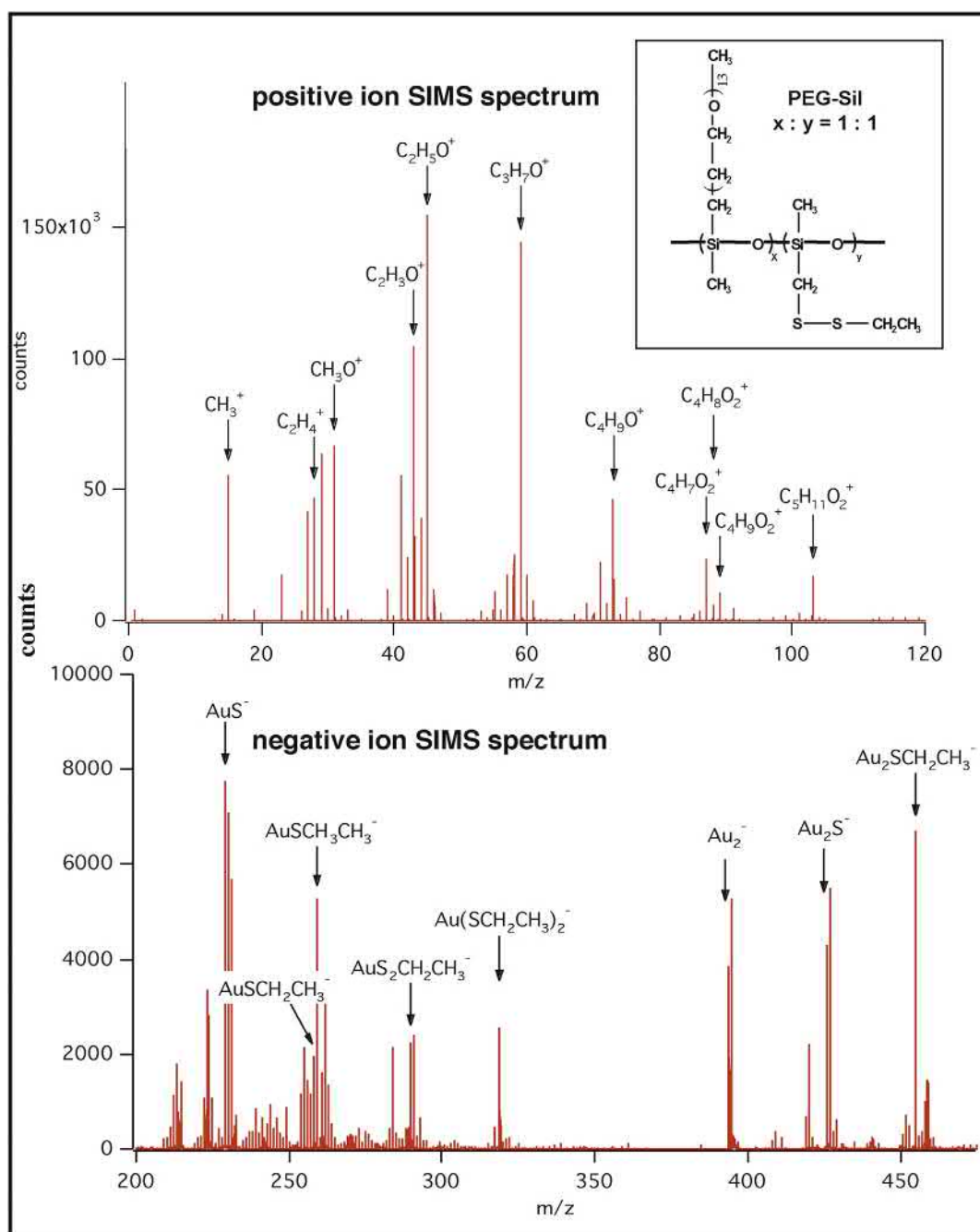
performed in surface regions of 10 nm diameter on optimal specimens. For static SIMS analysis, only 1%–10% of the atoms in any area are sampled. Thus, as the spot size gets smaller, the challenge to achieve high analytical sensitivity increases sharply. Still, static SIMS measurements have been performed in areas as small as 40 nm. Newly developed cluster ion sources (for example, using Bi_3 , C_{60} , or large gas clusters as the impacting primary particles) show high secondary ion yields and relatively low surface damage. These improve spatial resolution and also permit depth profiling of organic surfaces by sputtering down into a surface while monitoring secondary ion emission as a function of time (Ninomiya et al., 2009; Brison et al., 2010; Winograd, 2005). Thus, the advent of ion beams such as C_{60} and large Ar clusters for etching has blurred the difference between static and dynamic SIMS.

If the focused primary ion beam is rastered over the surface, and the x,y position of the beam correlated with the signal emitted from a given spot, the SIMS data can be converted into an elemental image. Patterning and spatial control of chemistry is becoming increasingly important in biomaterials surface design. For example, microcontact printing allows patterned chemistry to be transferred to surfaces at the micron level using a relatively simple rubber stamp. Imaging SIMS is well suited to studying and monitoring such spatially defined chemistry (Dubey et al., 2009; Bolles et al., 2010). An example is presented in Fig. 1.2.4.11. Imaging SIMS is also valuable for observing defects in thin films (pinholes), analyzing the chemistry of fine particulates, or assessing causes of implant failure. SIMS instrumentation continues to rapidly evolve. New cluster ion beams are being developed to further enhance the yield of secondary ions (Winograd, 2018; Sheraz et al., 2015). Recently MS/MS capabilities have been added to ToF-SIMS instruments to aid in the identification of high mass species in biological samples. Also, the importance of acquiring images at both high mass resolution and high spatial resolution has been demonstrated (Brison et al., 2013). Now modern instruments can acquire images in the high spatial and mass resolution modes with the option for MS/MS analysis (Passerelli et al., 2017; Fisher et al., 2016; Hill et al., 2011).

Scanning Electron Microscopy

Scanning electron microscopy (SEM) images of surfaces have great resolution and depth of field, with a three-dimensional quality that offers a visual perspective familiar to most users. SEM images are widely used and much has been written about the technique. The comments here are primarily oriented toward SEM as a surface analysis tool.

SEM functions by focusing and rastering a relatively high-energy electron beam (typically, 5–100 keV) on a specimen that is under vacuum. Low-energy secondary electrons (1–20 eV) are emitted from each spot where the focused electron beam impacts. The intensity of the secondary electron emission is a function of the atomic composition of the

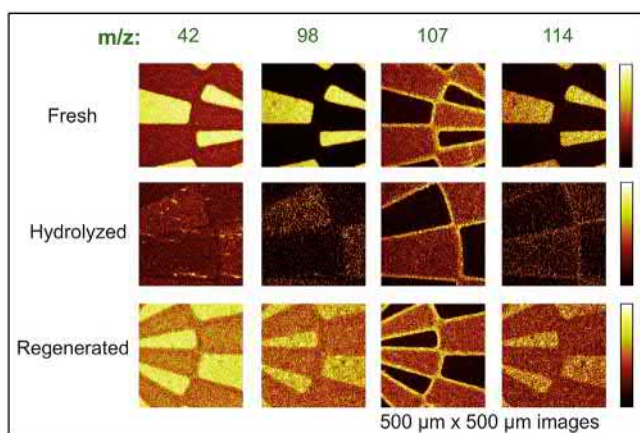


• **Figure 1.2.4.10** Static positive and negative ion SIMS spectra of a poly(ethylene glycol)–poly(dimethyl siloxane) copolymer containing disulfide side groups on a gold surface. The primary peaks are identified. The low mass region of the negative ion spectrum offers little insight into the polymer structure but the high mass region is rich in information. In this case, the low mass positive spectrum is rich in information. (Further details on this class of polymers can be found in Xia, N., Hu, Y., Grainger, D.W., Castner, D.G., 2002. Functionalized poly(ethylene glycol)-grafted polysiloxane monolayers for control of protein binding, *Langmuir*, 18, 3255–3262).

sample and the geometry of the features under observation. The image of the surface is spatially reconstructed on a phosphor screen (or CCD detector) from the intensity of the secondary electron emission at each point. Because of the shallow penetration depth of low-energy electrons produced by the primary electron beam, only the secondary electrons generated near the surface can escape and be detected (this is analogous to the surface sensitivity described in Fig. 1.2.4.7). Consequently, SEM is a surface analysis method.

SEM provides a high-resolution image of the surface. On insulating materials, a metallic coating is required and the image is actually of the coating surface, not the underlying material.

Nonconductive materials observed in the SEM are typically coated with a thin, electrically grounded layer of metal to minimize negative charge accumulation from the electron beam. However, this metal layer is always sufficiently



• **Figure 1.2.4.11** Negative ToF-SIMS ion images exploring the N-hydroxysuccinimide (NHS) reaction used to immobilize biomolecules to surfaces. Yellow colors show regions rich in NHS groups based on peaks at m/z 42, 98, 107, and 114. The image shows a spatially defined sample with freshly prepared, hydrolyzed, and regenerated photopatterned surfaces. (Further details are in Dubey, M., Emoto, K., Cheng, F., Gamble, L.J., Takahashi, H., Grainger, D.W., Castner, D.G., 2009. Surface analysis of photolithographic patterns using ToF-SIMS and PCA. *Surf. Interface Anal.* 41 (8), 645–652 (used with permission of the publisher)).

thick ($>200\text{\AA}$) that the electrons emitted from the sample beneath cannot penetrate. Therefore, in SEM analysis of nonconductors, the surface of the metal coating is, in effect, what is being monitored. If the metal coat is truly conformal, a good representation of the surface geometry will be conveyed. However, the specimen surface chemistry no longer influences secondary electron emission. Also, at very high magnifications, the texture of the metal coat and not the surface may be under observation.

SEM, in spite of these limitations, is an important corroborative method to use in conjunction with other surface analysis methods. Surface roughness and texture can have a profound influence on data from ESCA, SIMS, and contact angle determinations. Therefore, SEM provides important information in the interpretation of data from these methods.

The development of low-voltage SEM does study the surface chemistry (and geometry) of nonconductors. With the electron-accelerating voltage lowered to approximately 1 keV, charge accumulation is not as critical and metallization is not required. Low-voltage SEM has been used to study platelets and phase separation in polymers. Also, the environmental SEM (ESEM) permits wet, uncoated specimens to be studied.

The primary electron beam also stimulates the emission of X-rays. These X-rays are used to identify elements with the technique called energy-dispersive X-ray analysis (EDXA). However, the high-energy primary electron beam penetrates deeply into a specimen (a micron or more). The X-rays produced from the interaction of these electrons with atoms deep in the bulk of the specimen can penetrate through the material and be detected. Therefore, EDXA is not a surface analysis method.

The primary use of SEM is to image topography. SEM for this application is elaborated upon in the chapter on microscopy in biomaterials research (Chapter 2.3.8 in the previous edition).

Infrared Spectroscopy

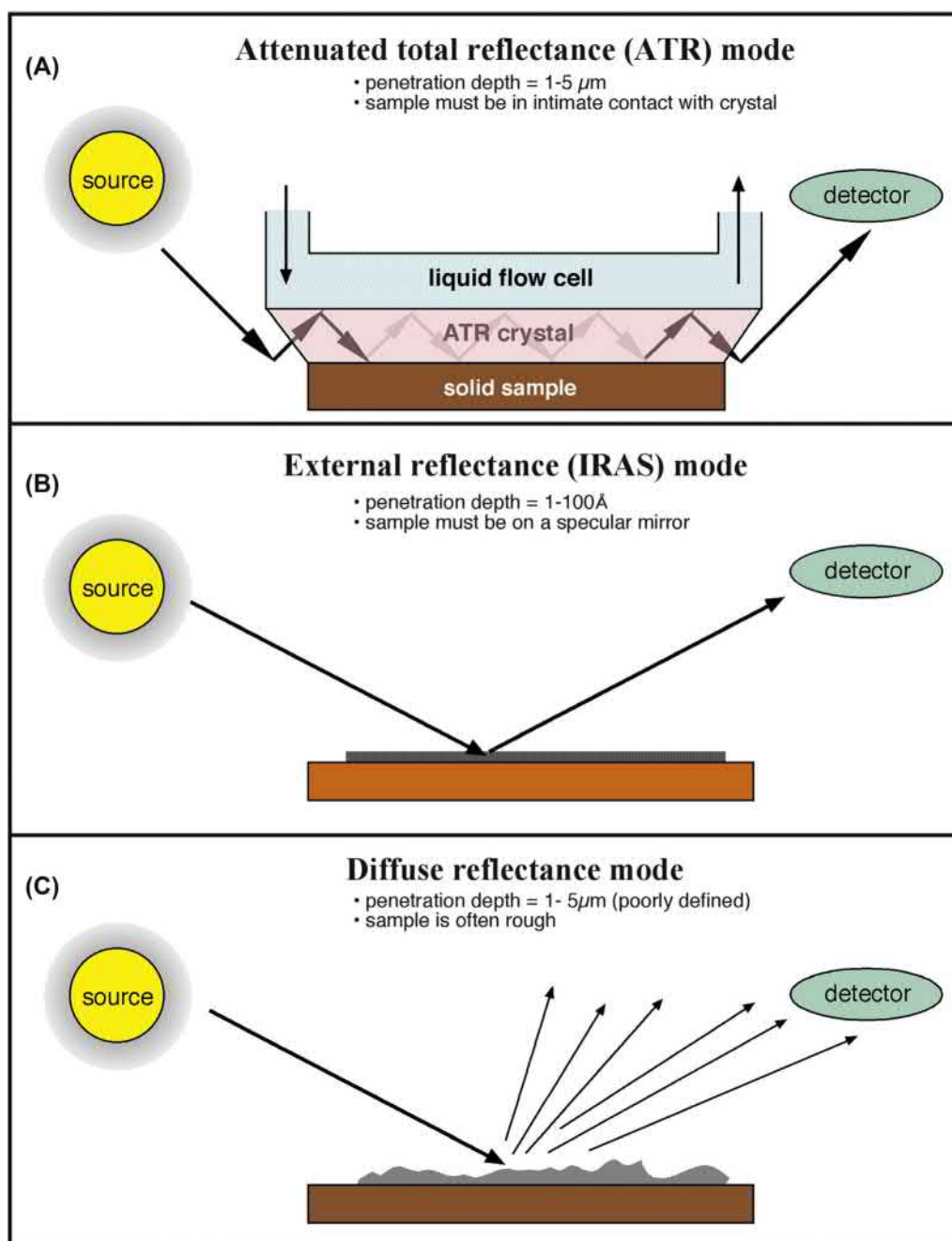
Infrared spectroscopy provides information on the bond vibrations of molecular species. It is a widely used analytical method that can reveal information on specific chemistries and the orientation of structures. Fourier transform infrared (FTIR) spectrometry offers outstanding signal-to-noise ratio (S/N) and spectral accuracy. However, even with this high S/N , the small absorption signal associated with the minute mass of material in a surface region can challenge the sensitivity of the spectrometer. Also, the problem of separating the vastly larger bulk absorption signal from the surface signal must be addressed.

Surface FTIR methods couple the infrared radiation to the sample surface to increase the intensity of the surface signal and reduce the bulk signal (Allara, 1982; Layden and Murthy, 1987; Urban, 1993; Dumas et al., 1999). Some of these sampling modes, and their characteristics, are illustrated in Fig. 1.2.4.12.

The attenuated total reflectance (ATR) mode of sampling has been used most often in biomaterials studies. The penetration depth into the sample is 1–5 μm . Therefore, ATR is not highly surface sensitive, but observes a broad region near the surface. However, it does offer the wealth of rich structural information common to infrared spectra. With extremely high S/N FTIR instruments, ATR studies of proteins and polymers adsorbed from aqueous solutions have been performed. In these experiments, the water signal (which is typically 99% or more of the total signal) is subtracted from the spectrum to leave only the surface material (e.g., adsorbed protein) under observation. Micro-ATR, coupling a microscope, IR spectrometer, and micro-ATR crystal, permits ATR analysis with high spatial resolution (approximately $1\ \mu\text{m}^2$ pixel size).

ATR-IR permits detailed molecular analysis of the outermost 1–5 microns of a sample.

Another infrared method that has proven immensely valuable for observing extremely thin films on reflective surfaces is infrared reflection absorption spectroscopy (IRAS) (Fig. 1.2.4.12). This method has been widely applied to self-assembled monolayers (SAMs), but is applicable to many surface films that are less than 10 nm thickness. The surface upon which the thin film resides must be highly reflective and metal surfaces work best though a silicon wafer can be used. IRAS gives information about composition, crystallinity, and molecular orientation. Infrared spectroscopy is one member of a family of methods called vibrational spectroscopies. Two other vibrational spectroscopies, sum frequency generation and Raman (in particular, surface enhanced), will be mentioned below in the section on newer methods.



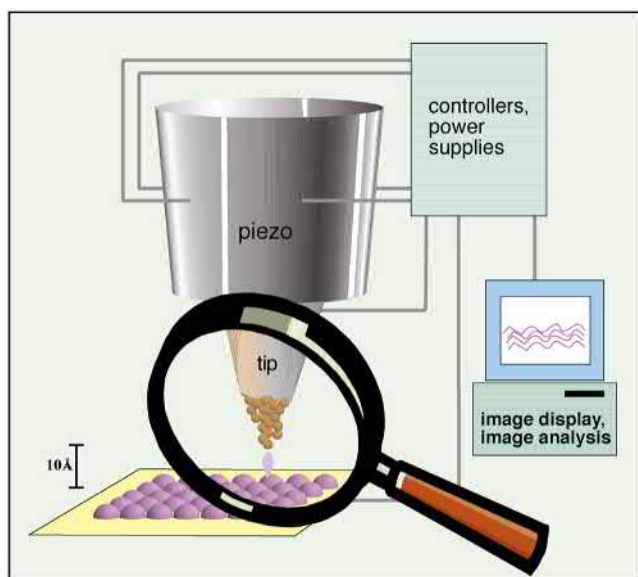
• **Figure 1.2.4.12** Three surface-sensitive infrared sampling modes: (A) attenuated total reflectance infrared (ATR-IR); (B) infrared reflection absorption spectroscopy (IRAS); (C) diffuse reflectance infrared spectroscopy.

Scanning Tunneling Microscopy (STM), Atomic Force Microscopy (AFM), and the Scanning Probe Microscopies (SPMs)

Since the first edition of this book was published in 1996, scanning tunneling microscopy (STM) and atomic force microscopy (AFM) have devolved from novel research tools to key methods for biomaterials characterization. AFM is more widely used than STM because electrically conductive surfaces are not needed with AFM and quantitative force measurements can be made. General review articles

are available (Binnig and Rohrer, 1986; Avouris, 1990; Albrecht et al., 1988) and articles oriented toward biological studies with these methods (Hansma et al., 1988; Miles et al., 1990; Rugar and Hansma, 1990; Jandt, 2001; Dufrene, 2004; Jelinek, 2017; Gross et al., 2018).

The STM was invented in 1981 and led to a Nobel Prize for G. Binnig and H. Rohrer in 1986. The STM capitalizes on quantum tunneling to generate an atom-scale, electron density image of a surface. A metal tip terminating in a single atom is brought within 5–10 \AA of an electrically conducting surface. At these distances, the electron cloud of



• **Figure 1.2.4.13** Schematic diagram illustrating the principle of the scanning tunneling microscope—a tip terminating in a single atom permits localized quantum tunneling current from surface features (or atoms) to tip. This tunneling current can be spatially reconstructed to form an image.

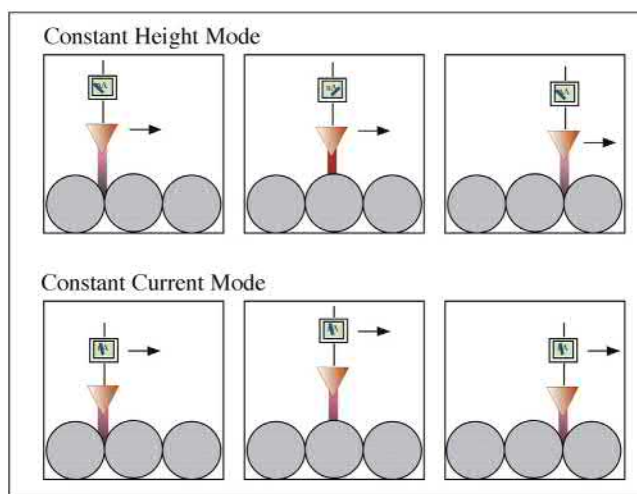
the atom at the “tip of the tip” will significantly overlap the electron cloud of an atom on the surface. If a potential is applied between the tip and the surface, an electron tunneling current will be established whose magnitude, J , follows the proportionality:

$$J \propto e^{(-AK_0S)}$$

where A is a constant, K_0 is an average inverse decay length (related to the electron affinity of the metals), and S is the separation distance in angstrom units. For most metals, a 1 Å change in the distance of the tip to the surface results in an order of magnitude change in tunneling current. Even though this current is small, it can be measured with good accuracy.

To image a surface, this quantum tunneling current is used in one of two ways. In constant current mode, a piezoelectric driver scans a tip over a surface. When the tip approaches an atom protruding above the plane of the surface, the current rapidly increases, and a feedback circuit moves the tip up to keep the current constant. Then, a plot is made of the tip height required to maintain constant current versus distance along the plane. In constant height mode, the tip is moved over the surface and the change in current with distance traveled along the plane of the surface is directly recorded. A schematic diagram of a scanning tunneling microscope is presented in Fig. 1.2.4.13. Two STM scanning modes are illustrated in Fig. 1.2.4.14.

The STM measures electrical current and therefore is well suited for conductive and semiconductor surfaces. However, biomolecules (even proteins) on conductive substrates appear amenable to imaging. STM does not “see” atoms, but rather monitors electron density. The conductive and imaging mechanism for proteins is not well understood.

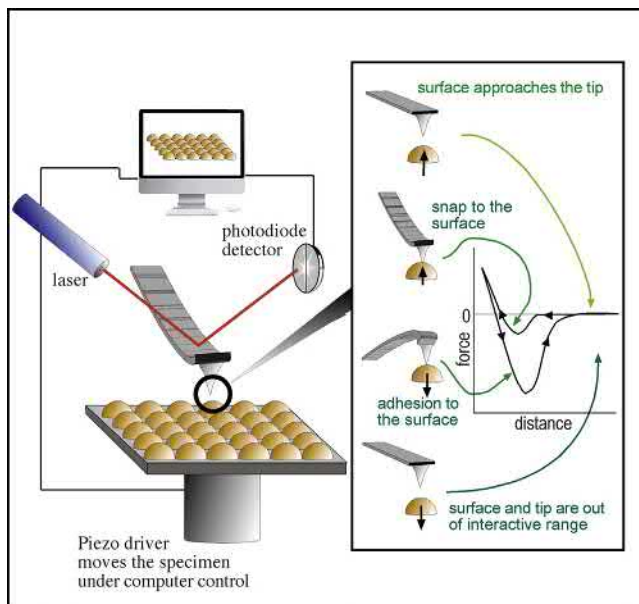


• **Figure 1.2.4.14** Scanning tunneling microscopy can be performed in two modes. In constant height mode, the tip is scanned a constant distance from the surface (typically 5–10 Å) and the change in tunneling current is recorded. In constant current mode, the tip height is adjusted so that the tunneling current is always constant, and the tip distance from the surface is recorded as a function of distance traveled in the plane of the surface.

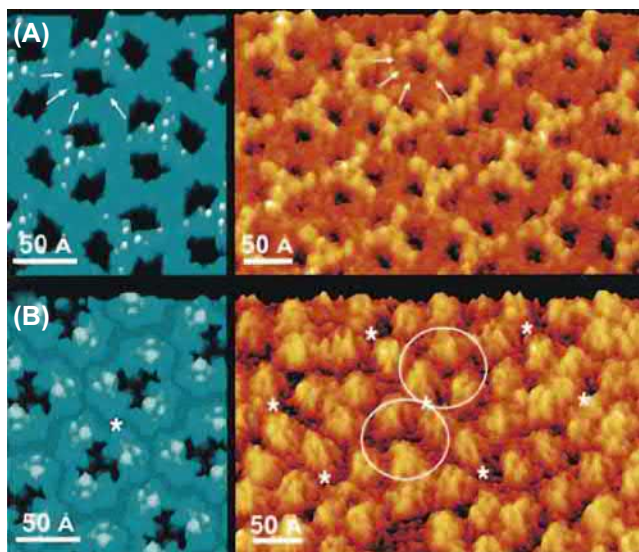
Still, publications suggest that information-rich images of biomolecules on conductive surfaces can be obtained (Campbell et al., 2007).

The AFM uses a similar piezo drive mechanism. However, instead of recording tunneling current, the deflection of a tip mounted on a flexible cantilever arm due to van der Waals forces and electrostatic repulsion/attraction between an atom at the tip and an atom on the surface is measured. Atomic-dimension measurements of cantilever arm movements can be made by reflecting a laser beam off a mirror on the cantilever arm (an optical lever). A one-atom deflection of the cantilever arm can easily be measured by monitoring the position of the laser reflection on a spatially resolved photosensitive detector. Other principles are also used to measure the deflection of the tip. These include capacitance measurements and interferometry. A diagram of a typical AFM is presented in Fig. 1.2.4.15. Images of protein molecules recorded by AFM are shown in Fig. 1.2.4.16 to demonstrate the subnanometer resolution possible on biological specimens.

Tips are important in AFM as the spatial resolution is significantly associated with tip terminal diameter and shape. Tips are made from microlithographically fabricated silicon or silicon nitride. Also carbon whiskers, nanotubes, and a variety of nanospherical particles have been mounted on AFM tips to increase their sharpness or improve the ability to precisely define tip geometry. Tips are also surface-modified to alter the strength and types of interactions with surfaces (static SIMS can be used to image these surface modifications). Finally, cantilevers are sold in a range of stiffnesses so the analysis modes can be tuned to the needs of the sample and the type of data being acquired. The forces associated with the interaction of an AFM tip with a surface as it approaches and is retracted are illustrated in Fig. 1.2.4.15.



• **Figure 1.2.4.15** Schematic diagram illustrating the principle of the atomic force microscope.



• **Figure 1.2.4.16** An AFM image of porin proteins from the outer membrane of *E. coli* imaged with nano-scale resolution. Comparison of high-resolution AFM images of OmpF crystals (in brown-yellow) and the atomic model rendered at 3 Å (in blue). (From Müller, D.J., Engel, A., 1999. *J. Mol. Biol.* 285, 1347, used with permission of the authors and publisher).

Since force is being measured and Hooke's law applies to the deformation of an elastic cantilever, AFM can be used to quantify the forces between surface and tip. Quantitative AFM is now widely used to measure the strength of interaction between biomolecules (Chilkoti et al., 1995; Muller and Dufre ne, 2008) and the mechanical properties of proteins (Li and Cao, 2010).

AFM instruments are commonly applied to surface problems using many possible tip interaction modes. Some AFM modes are contact, lateral force, noncontact, tapping, force modulation, and phase imaging. In contact mode, the tip is

in contact with the surface (or at least the electron clouds of tip and surface essentially overlap). The pressures resulting from the force of the cantilever delivered through the extremely small surface area of the tip can be damaging to soft specimens (proteins, polymers, etc.). However, for more rigid specimens, excellent topographical imaging can be achieved in contact mode. In tapping mode, the tip is oscillated at a frequency near the resonant frequency of the cantilever. The tip barely taps the surface. The force interaction of tip and surface can affect the amplitude of oscillation and the oscillating frequency of the tip. In standard tapping mode, the amplitude change is translated into topographic spatial information. Many variants of tapping mode have been developed, allowing imaging under different conditions and using the phase shift between the applied oscillation to the tip and the actual tip oscillation in the force field of the surface to provide information of the mechanical properties of the surface (in essence, the viscoelasticity of the surface can be assessed).

AFM allows imaging of surfaces at subnanometer resolutions and also probes detail on surface mechanics and molecular interactions.

The potential of the AFM to explore surface problems has been greatly expanded by ingenious variants of the technique. In fact, the term "atomic force microscopy" has been generalized to "scanning probe microscopy (SPM)." Table 1.2.4.6 lists many of these creative applications of the AFM/STM idea. Two of the more recently developed variants are photoinduced force microscopy (PiFM) and high-speed AFM imaging (Nowak et al., 2016; Dufre ne et al., 2017).

Since the AFM measures force, it can be used with both conductive and nonconductive specimens. Force must be applied to bend a cantilever, so AFM is subject to artifacts caused by damage to fragile structures on the surface. Both AFM and STM can function well for specimens under water, in air, or under vacuum. For exploring biomolecules or mobile organic surfaces, the "pushing around" of structures by the tip is a significant concern. This surface artifact can be capitalized upon to write and fabricate surface structures at the nanometer scale (Fig. 1.2.4.17) (Boland et al., 1998; Quate, 1997; Wilson et al., 2001; Rosa and Liang, 2009).

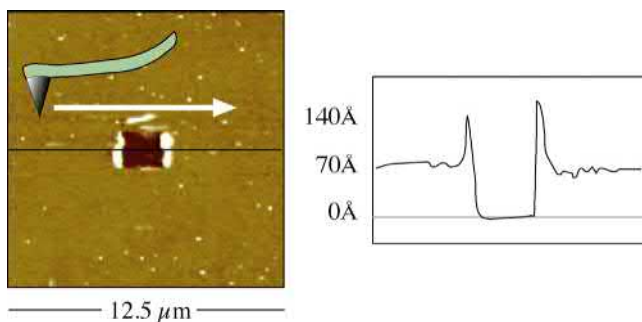
Newer Methods

There are many other surface characterization methods that have the potential to become important in future years. Some of these are listed in Table 1.2.4.7. A few of these evolving techniques that will be specifically mentioned here include nonlinear optical, Raman, and synchrotron methods.

A variety of different nonlinear optical methods have been developed to investigate biological materials (Johansson et al., 2018). Of particular interest is sum frequency generation (SFG) vibration spectroscopy, a method that looks at the outmost surface of materials in aqueous, air, or vacuum. SFG uses two high-intensity, pulsed laser beams,

TABLE 1.2.4.6 Scanning Probe Microscopy (SPM) Modes

Name	Acronym	Use
Contact mode	CM-AFM	Topographic imaging of harder specimens
Tapping (intermittent force) mode	IF-AFM	Imaging softer specimens
Noncontact mode	NCM-AFM	Imaging soft structures
Force modulation (allows slope of force–distance curve to be measured)	FM-AFM	Enhances image contrast based on surface mechanics
Scanning surface potential microscopy (Kelvin probe microscopy)	SSPM, KPM	Measures the spatial distribution of surface potential
Magnetic force microscopy	MFM	Maps the surface magnetic forces
Scanning thermal microscopy	SThM	Maps the thermal conductivity characteristics of a surface
Recognition force microscopy	RFM	Uses a biomolecule on a tip to probe for regions of specific biorecognition on a surface
Chemical force microscopy	CFM	A tip derivatized with a given chemistry is scanned on a surface to spatially measure differences of interaction strength
Lateral force microscopy	LFM	Maps frictional force on a surface
Electrochemical force microscopy	EFM	The tip is scanned under water and the electrochemical potential between tip and surface is spatially measured
Nearfield scanning optical microscopy	NSOM	A sharp optical fiber is scanned over a surface allowing optical microscopy or spectroscopy at 100nm resolution
Electrostatic force microscopy	EFM	Surface electrostatic potential is mapped
Scanning capacitance microscopy	SCM	Surface capacitance is mapped
Conductive atomic force microscopy	CAFM	Surface conductivity is mapped with an AFM instrument
Nanolithographic AFM		An AFM tip etches, oxidizes, or reacts a space permitting pattern fabrication at the 10 nm or better resolution
Dip-pen nanolithography	DPN	An AFM tip, inked with a thiol or other molecule, writes on a surface at the nanometer scale
Photoinduced force microscopy	PIFM	PIFM measures the photoinduced polarizability of a sample by imaging the force between the tip and the sample at multiple IR wavelengths



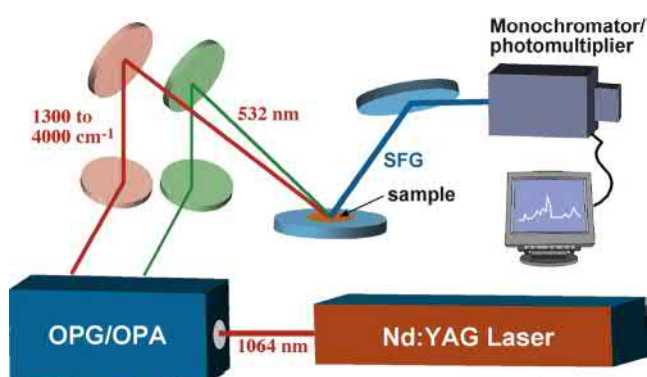
• **Figure 1.2.4.17** An AFM tip, using relatively high force, was used to scratch a rectangular feature into a thin (70 Å) plasma-deposited film. The AFM also characterized the feature created.

one in the visible range (frequency = ω_{visible}) and one in the infrared (frequency = ω_{ir}), to illuminate a specimen. The light emitted from the specimen by a nonlinear optical process, $\omega_{\text{sum}} = \omega_{\text{visible}} + \omega_{\text{ir}}$, is detected and quantified (Fig. 1.2.4.18). The intensity of the light at ω_{sum} is proportional to the square

of the sample's second-order nonlinear susceptibility ($\chi^{(2)}$). The term susceptibility refers to the effect of the light field strength in polarizing molecules (molecular polarizability). The ω_{sum} light intensity vanishes where a material has inversion symmetry, e.g., in the bulk of a crystalline material or in a disordered liquid solution. At an interface, the inversion symmetry is broken and an SFG signal is generated. Thus, SFG is exquisitely sensitive to the plane of the interface. To generate an SFG spectrum with pico-second lasers ω_{ir} is scanned over a vibrational frequency range. To generate an SFG spectrum with femto-second lasers broadband regions (each ~ 100 to 200 cm^{-1} in width) are stitched together. This leads to vibrational absorptions that occur with only interface molecules. For this case, the SFG signal is resonantly enhanced and we see a vibrational spectrum. The advantages of SFG are the superb surface sensitivity, the cancellation of bulk spectral intensity (for example, this allows measurements at a water/solid interface), the richness of information from vibrational spectra and the ability to study molecular orientation

TABLE 1.2.4.7 Additional Methods for the Surface Characterization of Biomaterials

Method	Information Obtained
Second-harmonic generation (SHG)	Detect submonolayer amounts of adsorbate at any light-accessible interface (air–liquid, solid–liquid, solid–gas)
Sum frequency generation (SFG) vibrational spectroscopy	Provides structure, orientation and ordering information about molecules at air–liquid, solid–liquid, and solid–gas interfaces
Surface-enhanced raman spectroscopy (SERS)	High-sensitivity Raman at rough metal interfaces
Ion scattering spectroscopy (ISS)	Elastically reflected ions probe only the outermost atomic layer
Laser desorption mass spectrometry (LDMS)	Mass spectra of adsorbates at surfaces
Matrix-assisted laser desorption ionization (MALDI)	Though generally a bulk mass spectrometry method, MALDI has been used to analyze large adsorbed proteins
IR photoacoustic spectroscopy (IR-PAS)	IR spectra of surfaces with no sample preparation based on wavelength-dependent thermal response
High-resolution electron energy loss spectroscopy (HREELS)	Vibrational spectroscopy of a highly surface-localized region, under ultrahigh vacuum
X-ray reflection	Structural information about order at surfaces and interfaces
Neutron reflection	Thickness and refractive index information about interfaces from scattered neutrons—where H and D are used, unique information on interface organization can be obtained
Extended X-ray absorption fine structure (EXAFS)	A synchrotron method providing atomic-level chemical and nearest-neighbor (morphological) information
Near-edge X-ray absorption fine structure (NEXAFS)	A synchrotron method providing information about bonding environments and chain orientation
Quartz Crystal microbalance with dissipation (QCM-D)	An oscillating quartz crystal provides information about the amount and viscoelastic properties of molecules interacting with a surface
Scanning auger microprobe (SAM)	Spatially defined auger analysis at the nanometer scale
Surface plasmon resonance (SPR)	Study aqueous adsorption events in real time by monitoring changes in surface refractive index
Rutherford backscattering spectroscopy (RBS)	Depth profiling of complex, multilayer interfacial systems



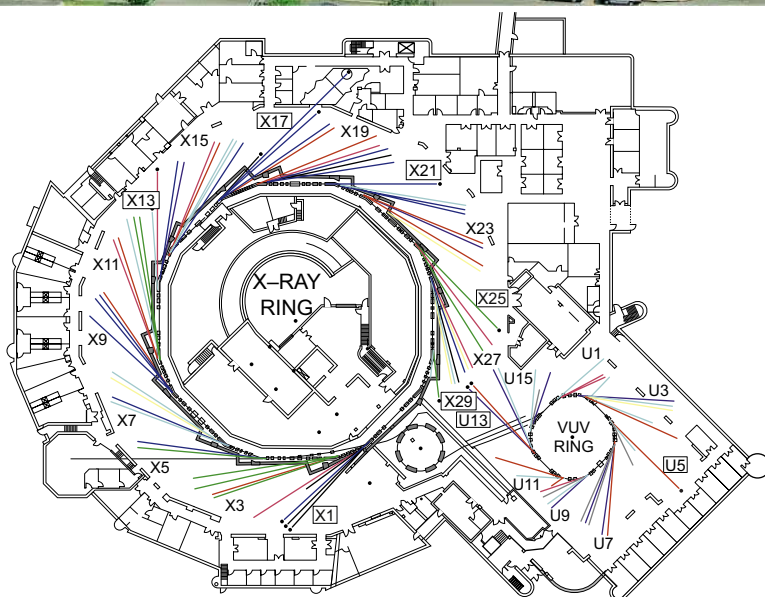
• **Figure 1.2.4.18** Schematic diagram of a sum frequency generation (SFG) apparatus. (Based upon a diagram by Polymer Technology Group, Inc).

by polarization of the laser light. SFG is not yet a routine method. The lasers and optical components are expensive and require precision alignment. However, the power of SFG for biomaterials studies has already been proven with studies on hydrated hydrogels, polyurethanes, surface-active polymer

additives, proteins, and nonfouling surfaces (Shen, 1989; Chen et al., 2002; Stein et al., 2009; Johansson et al., 2018).

SFG is among the most surface-sensitive of all surface methods. It provides vibrational spectroscopic detail on surface composition, orientation, and interactions.

In Raman spectroscopy a bright light is focused on a specimen. Most of the light scatters back at the same frequency as the incident beam. However, a tiny fraction of this light excites vibrations in the specimen and thereby loses or gains energy. The frequency shift of the light corresponds to vibrational bands indicative of the molecular structure of the specimen. The Raman spectroscopic technique has been severely limited for surface studies due to its low signal level. However, in recent years, great strides in detector sensitivity have allowed Raman to be applied for studying the minute mass of material at a surface. Also, surface-enhanced Raman spectroscopy (SERS), Raman spectra taken from molecules on a roughened metal surface, can enhance Raman signal intensity by 10^6 or more. Raman spectra will be valuable



BEAMLINE STATUS AS OF AUGUST, 2011

	VUV	X-RAY
— DIFFRACTION AND SCATTERING	0	20
— MACROMOLECULAR CRYSTALLOGRAPHY	0	9
— MICROSPECTROSCOPY	3	6
— SPECTROSCOPY	6	9
— OTHER	1	4
— DIAGNOSTIC AND INSTRUMENTATION	9	9
— CONSTRUCTION	0	4
— AVAILABLE	7	2
— UNUSED	5	3
X/U • INSERTION DEVICES		

• **Figure 1.2.4.19** The National synchrotron light Source, Brookhaven National Laboratories. (Images courtesy of Brookhaven National Laboratory).

for biomedical surface studies because water, which absorbs radiation very strongly in the infrared range, has little effect on Raman spectra that are often acquired with visible light (Storey et al., 1995; Smith, 2008; Henry et al., 2017).

Synchrotron sources generate energetic radiation that can be used to probe matter. Such sources were originally confined to the physics community and devoted to fundamental studies. However, there are now many synchrotron sources offering access to researchers in all communities, better instrumentation, and improved data interpretation. Synchrotron sources are typically national facilities costing >\$100M and often occupying hundreds of acres (Fig. 1.2.4.19). By accelerating electrons to near the speed of light in a large, circular ring, energies covering a broad swath of the electromagnetic spectrum (IR to energetic X-rays) are emitted. A synchrotron source (and ancillary equipment) permits a desired energy of the probe beam to be “dialed in” or scanned through a frequency range.

Other advantages include high source intensity (bright light) and polarized light. Some of the experimental methods that can be performed with great success at synchrotron sources include crystallography, scattering, spectroscopy, microimaging, and nanofabrication. Specific surface spectroscopic methods include scanning photoemission microscopy (SPEM, 100 nm spatial resolution) (Leung, 2010), ultraESCA (100 μm spatial resolution, high-energy resolution), and near-edge X-ray absorption fine structure (NEXAFS).

Studies With Surface Methods

Hundreds of studies have appeared in the literature in which surface methods have been used to enhance the understanding of biomaterial systems. A few studies that demonstrate the power of surface analytical methods for biomaterials science are briefly described here.

Platelet Consumption and Surface Composition

Using a baboon arteriovenous shunt model of platelet interaction with surfaces, a first-order rate constant of reaction of platelets with a series of polyurethanes was measured. This rate constant, the platelet consumption by the material, correlated in an inverse linear fashion with the fraction of hydrocarbon-type groups in the ESCA C1s spectra of the polyurethanes (Hanson et al., 1982). Thus, surface analysis revealed a chemical parameter about the surface that could be used to predict long-term biological reactivity of materials in a complex *ex vivo* environment.

Contact-Angle Correlations

The adhesion of a number of cell types, including bacteria, granulocytes, and erythrocytes, has been shown, under certain conditions, to correlate with solid–vapor surface tension as determined from contact-angle measurements. In addition, immunoglobulin G adsorption is related to γ_{sv} (Neumann et al., 1983).

Contamination of Intraocular Lenses

Commercial intraocular lenses were examined by ESCA. The presence of sulfur, sodium, and excess hydrocarbon at their surfaces suggested contamination by sodium dodecyl sulfate (SDS) during the manufacture of the lenses (Ratner, 1983). A cleaning protocol was developed using ESCA to monitor results that produced a lens surface of clean PMMA.

Titanium

The discoloration sometimes observed on titanium implants after autoclaving was examined by ESCA and SIMS (Lausmaa et al., 1985). The discoloration was found to be related to accelerated oxide growth, with oxide thicknesses to 650 Å. The oxide contained considerable fluorine, along with alkali metals and silicon. The source of the oxide was the cloth used to wrap the implant storage box during autoclaving. Since fluorine strongly affects oxide growth, and since the oxide layer has been associated with the biocompatibility of titanium implants, the authors advise avoiding fluorinated materials during sterilization of samples. Another paper by this group contains detailed surface characterization of titanium using a battery of surface methods and addresses surface preparation, contamination, and cleaning (Lausmaa, 1996).

SIMS for Adsorbed Protein Identification and Quantification

All proteins are comprised of the same 21 amino acids and thus, on the average, are compositionally similar. Surface analysis methods have shown the ability to detect and quantify surface-bound protein, but biological tools have, until recently, been needed to identify specific proteins. Modern static SIMS instrumentation, using a multivariate statistical analysis of the data, has demonstrated the ability to distinguish between

more than 13 different proteins adsorbed on surfaces (Wagner and Castner, 2001; Muramoto et al., 2011). Also, the limits of detection for adsorbed proteins on various surfaces were compared by ESCA and SIMS (Wagner et al., 2002).

Poly(Glycolic Acid) Degradation Studied by SIMS

The degradation of an important polymer for tissue engineering, poly(glycolic acid), has been studied by static SIMS. As well as providing useful information on this degradation process, the study illustrates the power of SIMS for characterizing synthetic polymers and their molecular weight distributions (Chen et al., 2000).

MultiTechnique Characterization of Adsorbed Peptides and Proteins

Though proteins at interfaces are critically important to biomaterials science, we have an incomplete picture of what proteins really look and behave like on surfaces. Multiple techniques are required to obtain detailed information about the structure of proteins at interfaces (Weidner and Castner, 2013). By combining a surface method, SFG, with a traditionally bulk analysis method, solid state NMR, an elegant picture of peptides on surfaces emerges. The study quantified, with site specificity and atomic resolution, the orientation and dynamics of side chains in labeled, synthetic model peptides adsorbed onto a polystyrene surface (Weidner et al., 2010). The combination of SFG, ToF-SIMS, and computational methods provided detailed information about the structure, orientation, and interactions of Protein G with a hydrophobic surface (Harrison et al., 2017).

Conclusions

The instrumentation of surface analysis steadily advances and newer instruments and techniques can provide invaluable information about biomaterials and medical devices. The information obtained can be used to monitor contamination, ensure surface reproducibility, and explore fundamental aspects of the interaction of biological systems with living systems. Considering that biomedical experiments, especially *in vivo* experiments, are typically expensive to perform, the costs for surface analysis are modest to ensure that the surface is as expected, stable, and identical from experiment to experiment. Surface analysis can also contribute to the understanding of medical device failure (and success). A myriad of applications for surface methods are found in device optimization, manufacture, and quality control. Predicting biological reaction based on measured surface structure is a frontier area for surface analysis.

Acknowledgments

Support was received from the UWEB21 Engineering Research Center and the NESAC/BIO National Resource, NIH grant EB-002027, during the preparation of this chapter and for some of the studies described herein.

References

- Adamson, A.W., Gast, A., 1997. *Physical Chemistry of Surfaces*, sixth ed. Wiley-Interscience, New York.
- Albrecht, T.R., Dovek, M.M., Lang, C.A., Grutter, P., Quate, C.F., Kuan, S.W.J., Frank, C.W., Pease, R.F.W., 1988. Imaging and modification of polymers by scanning tunneling and atomic force microscopy. *J. Appl. Phys.* 64, 1178–1184.
- Allara, D.L., 1982. Analysis of surfaces and thin films by IR, Raman, and optical spectroscopy. *ACS Symp. Ser.* 199, 33–47.
- Andrade, J.D., 1985. *Surface and Interfacial Aspects of Biomedical Polymers*, Vol. 1: Surface Chemistry and Physics. Plenum Publishers, New York.
- Avouris, P., 1990. Atom-resolved surface chemistry using the scanning tunneling microscope. *J. Phys. Chem.* 94, 2246–2256.
- Barth, J.V., Brune, H., Ertl, G., Behm, R.J., 1990. Scanning tunneling microscopy observations on the reconstructed Au(111) surface: atomic structure, long-range superstructure, rotational domains, and surface defects. *Phys. Rev. B* 42, 9307–9318.
- Belu, A.M., Graham, D.J., Castner, D.G., 2003. Time-of-flight secondary ion mass spectrometry: techniques and applications for the characterization of biomaterial surfaces. *Biomaterials* 24, 3635–3653.
- Benninghoven, A., 1983. Secondary ion mass spectrometry of organic compounds (review). In: Benninghoven, A. (Ed.), *Springer Series of Chemical Physics: Ion Formation from Organic Solids*, vol. 25. Springer-Verlag, Berlin, pp. 64–89.
- Bich, C., Touboul, D., Brunelle, A., 2015. Biomedical studies by ToF-SIMS imaging. *Biointerphases* 10, 018901.
- Binnig, G., Rohrer, H., 1986. Scanning tunneling microscopy. *IBM J. Res. Dev.* 30, 355–369.
- Boland, T., Johnston, E.E., Huber, A., Ratner, B.D., 1998. Ch. 21 Recognition and nanolithography with the atomic force microscope. In: Ratner, B.D., Tsukruk, V.V. (Eds.), *Scanning Probe Microscopy of Polymers*, vol. 694. American Chemical Society, Washington, DC, pp. 342–350.
- Bolles, K.M., Cheng, F., Burk-Rafel, J., Dubey, M., Ratner, D.M., 2010. Imaging analysis of carbohydrate-modified surfaces using ToF-SIMS and SPRi. *Materials* 3, 3948–3964.
- Briggs, D., 1986. SIMS for the study of polymer surfaces: a Review. *Surf. Interface Anal.* 9, 391–404.
- Briggs, D., Seah, M.P., 1983. *Practical Surface Analysis*. Wiley, Chichester, England.
- Brisson, J., Muramoto, S., Castner, D.G., 2010. ToF-SIMS depth profiling of organic films: a comparison between single beam and dual-beam analysis. *J. Phys. Chem. C* 114, 5565–5573.
- Brisson, J., Robinson, M.A., Benoit, D.S.W., Muramoto, S., Stayton, P.S., Castner, D.G., 2013. ToF-SIMS 3D imaging of native and non-native species within HeLa cells. *Anal. Chem.* 85, 10869–10877.
- Campbell, S., Smith, J., Jungblut, H., Lewerenz, H., 2007. Protein imaging on a semiconducting substrate: a scanning tunnelling microscopy investigation. *J. Electroanal. Chem.* 599, 313–322.
- Castner, D.G., 2017. Biomedical surface analysis: evolution and future directions. *Biointerphases* 12, 02C301.
- Castner, D.G., Ratner, B.D., 2002. Biomedical surface science: foundations to frontiers. *Surf. Sci.* 500, 28–60.
- Chen, J., Lee, J.-W., Hernandez, N.L., Burkhardt, C.A., Hercules, D.M., Gardella, J.A., 2000. Time-of-flight secondary ion mass spectrometry studies of hydrolytic degradation kinetics at the surface of poly(glycolic acid). *Macromolecules* 33, 4726–4732.
- Chen, Z., Ward, R., Tian, Y., Malizia, F., Gracias, D.H., Shen, Y.R., Somorjai, G.A., 2002. Interaction of fibrinogen with surfaces of end-group-modified polyurethanes: a surface-specific sum-frequency-generation vibrational spectroscopy study. *J. Biomed. Mater. Res.* 62, 254–264.
- Chilkoti, A., Boland, T., Ratner, B.D., Stayton, P.S., 1995. The relationship between ligand-binding thermodynamics and protein-ligand interaction forces measured by atomic force microscopy. *Biophys. J.* 69, 2125–2130.
- Dilks, A., 1981. X-ray photoelectron spectroscopy for the investigation of polymeric materials. In: Baker, A.D., Brundle, C.R. (Eds.), *Electron Spectroscopy: Theory, Techniques, and Applications*, vol. 4. Academic Press, London, pp. 277–359.
- Davies, M.C., Lynn, R.A.P., 1990. Static secondary ion mass spectrometry of polymeric biomaterials. *CRC Crit. Rev. Biocompat.* 5, 297–341.
- Dubey, M., Emoto, K., Cheng, F., Gamble, L.J., Takahashi, H., Grainger, D.W., Castner, D.G., 2009. Surface analysis of photolithographic patterns using ToF-SIMS and PCA. *Surf. Interface Anal.* 41 (8), 645–652.
- Dufrène, Y.F., 2004. Using nanotechniques to explore microbial surfaces. *Nat. Rev. Microbiol.* 2 (6), 451–460.
- Dufrene, Y.F., Ando, T., Garcia, R., Alsteens, D., Martinez-Martin, D., Engel, A., Gerber, C., Mueller, D.J., 2017. Imaging modes of atomic force microscopy for application in molecular and cell biology. *Nat. Nanotechnol.* 12, 295–307.
- Dumas, P., Weldon, M.K., Chabal, Y.J., Williams, G.P., 1999. Molecules at surfaces and interfaces studied using vibrational spectroscopies and related techniques. *Surf. Rev. Lett.* 6 (2), 225–255.
- Feldman, L.C., Mayer, J.W., 1986. *Fundamentals of Surface and Thin Film Analysis*. North-Holland, New York.
- Fisher, G.L., Bruinen, A.L., Potocnik, N.O., Hammond, J.S., Bryan, S.R., Larson, P.E., Heeren, R.M.A., 2016. A new method and mass spectrometer design for TOF-SIMS parallel imaging MS/MS. *Anal. Chem.* 88, 6433–6440.
- Fletcher, J.S., 2015. Latest applications of 3D ToF-SIMS bio-imaging. *Biointerphases* 10, 018902.
- Fletcher, J.S., Vickerman, J.C., 2013. Secondary ion mass spectrometry: characterizing complex samples in two and three dimensions. *Anal. Chem.* 85, 610–639.
- Garbassi, F., Morra, M., Occhiello, E., 1998. *Polymer Surfaces: From Physics to Technology*. John Wiley and Sons, Chichester, UK.
- Good, R.J., 1993. Contact angle, wetting, and adhesion: a critical review. In: Mittal, K.L. (Ed.), *Contact Angle, Wettability and Adhesion*. VSP Publishers, The Netherlands.
- Gross, L., Schuler, B., Pavlicek, N., Fatayer, S., Majzik, Z., Moll, N., Pena, D., Meyer, G., 2018. Atomic force microscopy for molecular structure elucidation. *Angew. Chem. Int. Ed.* 57, 3888–3908.
- Hansma, P.K., Elings, V.B., Marti, O., Bracker, C.E., 1988. Scanning tunneling microscopy and atomic force microscopy: application to biology and technology. *Science* 242, 209–216.
- Hanson, S.R., Harker, L.A., Ratner, B.D., Hoffman, A.S., 1982. Evaluation of artificial surfaces using baboon arteriovenous shunt model. In: Winter, G.D., Gibbons, D.F., Plenk, H. (Eds.), *Biomaterials 1980, Advances in Biomaterials*, vol. 3. Wiley, Chichester, pp. 519–530.
- Harrison, E.T., Weidner, T., Castner, D.G., Interlandi, G., 2017. Predicting the orientation of protein G B1 on hydrophobic surfaces using Monte Carlo simulations. *Biointerphases* 12, 04B304.
- Henry, A.-I., Ueltschi, T., McAnally, M.O., Van Duyne, R.P., 2017. Surface-enhanced Raman spectroscopy: from single particle/molecule spectroscopy to angstrom-scale spatial resolution and femto-second time resolution. *Faraday Discuss.* 205, 9–30.

- Hill, R., Blenkinsopp, P., Thompson, S., Vickerman, J., Fletcher, J.S., 2011. A new time-of-flight SIMS instrument for 3D imaging and analysis. *Surf. Interface Anal.* 43, 6652–6659.
- Jandt, K.D., 2001. Atomic force microscopy of biomaterials surfaces and interfaces. *Surf. Sci.* 491, 303–332.
- Jelinek, P., 2017. High resolution SPM imaging of organic molecules with functionalized tips. *J. Phys. Condens. Mat.* 29, 343002.
- Johansson, P.K., Schmöser, L., Castner, D.G., 2018. Nonlinear optical methods for characterization of molecular structure and surface chemistry. *Top. Catal.* 61, 1101–1124.
- Kasemo, B., 2002. Biological surface science. *Surf. Sci.* 500, 656–677.
- Lausmaa, J., Kasemo, B., Hansson, S., 1985. Accelerated oxide growth on titanium implants during autoclaving caused by fluoride contamination. *Biomaterials* 6, 23–27.
- Lausmaa, J., 1996. Surface spectroscopic characterization of titanium implant materials. *J. Electron. Spectrosc. Relat. Phenom.* 81, 343–361.
- Leung, B.O., Brash, J.L., Hitchcock, A.P., 2010. Characterization of biomaterials by soft X-ray spectromicroscopy. *Materials* 3 (7), 3911–3938.
- Leyden, D.E., Murthy, R.S.S., 1987. Surface-selective sampling techniques in Fourier transform infrared spectroscopy. *Spectroscopy* 2, 28–36.
- Li, H., Cao, Y., 2010. Protein mechanics: from single molecules to functional biomaterials. *Acc. Chem. Res.* 43 (10), 1331–1341.
- McArthur, S.L., 2006. Applications of XPS in bioengineering. *Surf. Interface Anal.* 38, 1380–1385.
- Michel, R., Castner, D.G., 2006. Advances in time-of-flight secondary ion mass spectrometry analysis of protein films. *Surf. Interface Anal.* 38 (11), 1386–1392.
- Miles, M.J., McMaster, T., Carr, H.J., Tatham, A.S., Shewry, P.R., Field, J.M., Belton, P.S., Jeenes, D., Hanley, B., Whittam, M., Cairns, P., Morris, V.J., Lambert, N., 1990. Scanning tunneling microscopy of biomolecules. *J. Vac. Sci. Technol. A* 8, 698–702.
- Muller, D.J., Dufrene, Y.F., 2008. Atomic force microscopy as a multifunctional molecular toolbox in nanobiotechnology. *Nat. Nanotechnol.* 3 (5), 261–269.
- Muramoto, S., Graham, D.J., Wagner, M.S., Lee, T.G., Moon, D.W., Castner, D.G., 2011. ToF-SIMS analysis of adsorbed proteins: principal component analysis of the primary ion species effect on the protein fragmentation patterns. *J. Phys. Chem. C* 115, 24247–24255.
- Neumann, A.W., Absolom, D.R., Francis, D.W., Omenyi, S.N., Spelt, J.K., Policova, Z., Thomson, C., Zingg, W., Van Oss, C.J., 1983. Measurement of surface tensions of blood cells and proteins. *Ann. New York Acad. Sci.* 416, 276–298.
- Ninomiya, S., Ichiki, K., Yamada, H., Nakata, Y., Seki, T., Aoki, T., Matsuo, J., 2009. Precise and fast secondary ion mass spectrometry depth profiling of polymer materials with large Ar cluster ion beams. *Rapid Commun. Mass Spectrom.* 23 (11), 1601–1606.
- Nowak, D., Morrison, W., Wickramasinghe, H.K., Jahng, J., Potma, E., Wan, L., Ruiz, R., Albrecht, T.R., Schmidt, K., Frommer, J., Sanders, D.P., Park, S., 2016. Nanoscale chemical imaging by photoinduced force microscopy. *Sci. Adv.* 2, e1501571.
- Nunez, J., Renslow, R., Cliff, J.B., Anderton, C.R., 2018. NanoSIMS for biological applications: current practices and analyses. *Biointerphases* 13, 03B301.
- Passarelli, M.K., Pirk, A., Moellers, R., Grinfeld, D., Kollmer, F., Havelund, R., Newman, C.F., Marshall, P.S., Arlinghaus, H., Alexander, M.R., West, A., Horning, S., Niehuis, E., Makarov, A., Dollery, C.T., Gilmore, I.S., 2017. The 3D OrbiSIMS-label-free metabolic imaging with subcellular lateral resolution and high mass-resolving power. *Nat. Methods* 14, 1175–1183.
- Quate, C.F., 1997. Scanning probes as a lithography tool for nanostructures. *Surf. Sci.* 386, 259–264.
- Ratner, B.D., 1983. Analysis of surface contaminants on intraocular lenses. *Arch. Ophthalmol.* 101, 1434–1438.
- Ratner, B.D., 1988. *Surface Characterization of Biomaterials*. Elsevier, Amsterdam.
- Ratner, B.D., McElroy, B.J., 1986. Electron spectroscopy for chemical analysis: applications in the biomedical sciences. In: Gendreau, R.M. (Ed.), *Spectroscopy in the Biomedical Sciences*. CRC Press, Boca Raton, FL, pp. 107–140.
- Ratner, B.D., Castner, D.G., 2009. Electron spectroscopy for chemical analysis. In: Vickerman, J.C., Gilmore, I.S. (Eds.), *Surface Analysis – The Principal Techniques*, second ed. John Wiley and Sons, Ltd., Chichester, UK, pp. 47–112.
- Rosa, L.G., Liang, J., 2009. Atomic force microscope nanolithography: dip-pen, nanoshaving, nanografting, tapping mode, electrochemical and thermal nanolithography. *J. Phys. Condens. Matter* 21, 483001.
- Rugar, D., Hansma, P., 1990. Atomic force microscopy. *Phys. Today* 43, 23–30.
- Shen, Y.R., 1989. Surface properties probed by second-harmonic and sum-frequency generation. *Nature* 337 (6207), 519–525.
- Scheutle, D., Riley, T.L., deVries, J.E., Prater, T.J., 1984. Applications of high-performance mass spectrometry to the surface analysis of materials. *Mass Spectrom.* 3, 527–585.
- Sheraz, S., Razo, I.B., Kohn, T., Lockyer, N., Vickerman, J.C., 2015. Enhancing ion yields in time-of-flight-secondary ion mass spectrometry: a comparative study of argon and water cluster primary beams. *Anal. Chem.* 87, 2367–2374.
- Smith, W.E., 2008. Practical understanding and use of surface enhanced Raman scattering/surface enhanced resonance Raman scattering in chemical and biological analysis. *Chem. Soc. Rev.* 37 (5), 955.
- Somorjai, G.A., 1981. *Chemistry in Two Dimensions: Surfaces*. Cornell University Press, Ithaca, NY.
- Somorjai, G.A., Li, Y., 2010. *Introduction to Surface Chemistry and Catalysis*, second ed. John Wiley and Sons, Inc., Hoboken, NJ.
- Stein, M., Weidner, T., McCrea, K., Castner, D., Ratner, B., 2009. Hydration of sulphobetaine and tetra (ethylene glycol)-terminated self-assembled monolayers studied by sum frequency generation vibrational spectroscopy. *J. Phys. Chem. B* 113 (33), 11550–11556.
- Steinhauser, M.L., Bailey, A.P., Senyo, S.E., Guillemer, C., Perlstein, T.S., Gould, A.P., Lee, R.T., Lechene, C.P., 2012. Multi-isotope imaging mass spectrometry quantifies stem cell division and metabolism. *Nature* 481, 516–519.
- Storey, J.M.E., Barber, T.E., Shelton, R.D., Wachter, E.A., Carron, K.T., Jiang, Y., 1995. Applications of surface-enhanced Raman scattering (SERS) to chemical detection. *Spectroscopy* 10 (3), 20–25.
- Tirrell, M., Kokkoli, E., Biesalski, M., 2002. The role of surface science in bioengineered materials. *Surf. Sci.* 500, 61–83.
- Urban, M.W., 1993. *Vibrational Spectroscopy of Molecules and Macromolecules on Surfaces*. Wiley-Interscience, NY.
- Van Vaec, L., Adriaens, A., Gijbels, R., 1999. Static secondary ion mass spectrometry: (S-SIMS) Part I. Methodology and structural interpretation. *Mass Spectrom. Rev.* 18, 1–47.
- Vickerman, J.C., Gilmore, I., 2009. *Surface Analysis: The Principal Techniques*, second ed. John Wiley and Sons, Chichester, UK.
- Vickerman, J.C., Brown, A., Reed, N.M., 1989. *Secondary Ion Mass Spectrometry, Principles and Applications*. Clarendon Press, Oxford.

- Wagner, M.S., Castner, D.G., 2001. Characterization of adsorbed protein films by time-of-flight secondary ion mass spectrometry with principal component analysis. *Langmuir* 17, 4649–4660.
- Wagner, M.S., McArthur, S.L., Shen, M., Horbett, T.A., Castner, D.G., 2002. Limits of detection for time of flight secondary ion mass spectrometry (ToF-SIMS) and X-ray photoelectron spectroscopy (XPS): detection of low amounts of adsorbed protein. *J. Biomater. Sci. Polym. Ed.* 13 (4), 407–428.
- Watts, J.F., Wolstenholme, J., 2003. *An Introduction to Surface Analysis by XPS and AES*. John Wiley & Sons, Chichester, UK.
- Weidner, T., Breen, N.F., Li, K., Drobny, G.P., Castner, D.G., 2010. Sum frequency generation and solid-state NMR study of the structure, orientation, and dynamics of polystyrene-adsorbed peptides. *Proc. Natl. Acad. Sci. U.S.A.* 107 (30), 13288–13293.
- Weidner, T., Castner, D.G., 2013. SFG analysis of surface bound proteins: a route towards structure determination. *Phys. Chem. Chem. Phys.* 15, 12516–12524.
- Wilson, D.L., Martin, R., Hong, S., Cronin-Golomb, M., Mirkin, C.A., Kaplan, D.L., 2001. Surface organization and nanopatterning of collagen by dip-pen nanolithography. *PNAS* 98 (24), 13660–13664. <https://doi.org/10.1073/pnas.241323198>.
- Winograd, N., 2005. The magic of cluster SIMS. *Anal. Chem.* 77, 142A–149A.
- Winograd, N., 2018. Gas cluster ion beams for secondary ion mass spectrometry. *Annu. Rev. Anal. Chem.* 11, 29–48.
- Zisman, W.A., 1964. Relation of the equilibrium contact angle to liquid and solid constitution. In: Fowkes, F.M. (Ed.), *Contact Angle, Wettability and Adhesion*, ACS Advances in Chemistry Series, vol. 43. American Chemical Society, Washington, DC, pp. 1–51.

Chapter Questions

1. Scan the table of contents and abstracts from the last three issues of *Journal of Biomedical Materials Research or Biomaterials*. List all the surface analysis methods used in the articles therein and briefly describe what was learned by using them.
2. How is critical surface tension related to wettability? For the polymers in [Table 1.2.4.2](#), draw the chemical formulas of the chain repeat units and attempt to relate the structures to the wettability. Where inconsistencies are noted, explain those inconsistencies using [Table 1.2.4.3](#).
3. A titanium dental implant was manufactured by the Biomatter Company for the past 8 years. It performed well clinically. For economic reasons, manufacturing of the titanium device was outsourced to Metalsmed, Inc. Early clinical results on this Metalsmed implant, supposedly identical to the Biomatter implant, suggested increased inflammation. How would you compare the surface chemistry and structure of these two devices to see if a difference that might account for the difference in clinical performance could be identified?

1.2.5

Role of Water in Biomaterials

BUDDY D. RATNER¹, ROBERT A. LATOUR²

¹Bioengineering and Chemical Engineering, Director of University of Washington Engineered Biomaterials (UWEB), Seattle, WA, United States

²Bioengineering Department, Clemson University, Clemson, SC, United States

This chapter first introduces the physical and chemical properties of water, and then expands upon water's significance for biomaterials and biology. This chapter encourages you to think about how the phenomena you are reading about may be driven or controlled by the water that comprises such a large fraction of all biological systems.

In the world there is nothing more submissive and weak than water. Yet for attacking that which is hard and strong nothing can surpass it.

LAO TZU.

Water! Omnipresent, chemically inert, a simple diluent—these words come to mind and prompt the question: “why is there a section of this textbook devoted to water?” The special properties of water, this substance that is critical for life as we know it, significantly impact the “materials-centric” subject of biomaterials, and the biology closely associated with biomaterials.

As will be presented in this chapter, water is not simply a passive molecule that represents the major component of the solvent for biological systems, but instead it is a very dynamic molecule that is an important mediator of essentially all biological interactions. Water is thus a unique, remarkable substance—in this instance, the word “unique” can be used without hyperbole. Although its chemical composition was elucidated in the 1770s by Lavoisier and others, its liquid structure continues to be explored today using state-of-the-art physical characterization methods. The importance of water for life as we know it was appreciated as early as 1913 in an interesting historical volume, *The Fitness of the Environment* (Henderson, 1913; available in reprint).

This chapter will first introduce the physical and chemical properties of water. Then water's significance for biomaterials and biology will be expanded upon.

Water: The Special Molecule

The simple “H₂O” structure of the water molecule does not immediately communicate the ability of one water

molecule to interact with many other water molecules, in particular to interact not too strongly, and not too weakly. This interaction, largely via the hydrogen bond, is associated with the dipole of the water molecule (slightly more negatively charged at the oxygen and positively charged at the hydrogen, i.e., partial negative and positive charges). This dipole, combined with the bent shape (bond angle of 104.6 degrees) of the molecule and its small size contributes to the special properties of liquid water. Fig. 1.2.5.1 illustrates schematically the geometry of the water molecule, and suggests some hydrogen bonding possibilities with neighboring water molecules (as well as the occasional H⁺ or OH⁻).

The physical properties of water are profoundly unique compared with all other substances.

The unique physical and chemical properties of water, attributable to the 104.6 degree bond angle and the ability to form up to four hydrogen bonds per molecule despite the fact that it is made up of only three atoms, are discussed here. Note how special water is compared with other liquid and solid substances.

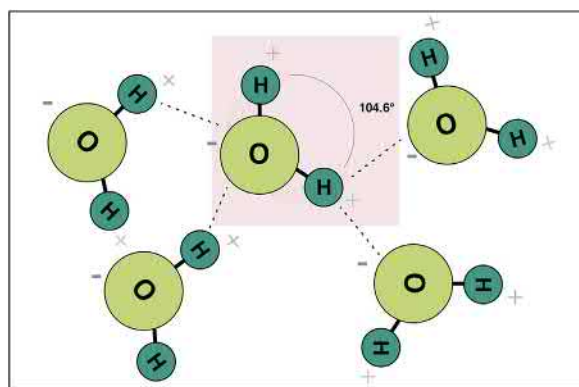
Melting Point and Boiling Point

The physical properties of H₂O that make it stand out from all other related molecules are best appreciated from the data in Table 1.2.5.1.

As the molecular weight for compounds in this series of related molecules decreases, the boiling points also decrease, until you reach water, where the boiling point is (unexpectedly) up to 160°C higher. At common temperatures and pressures on Earth, all the other compounds exist as gases, except water. A similar dramatic trend is seen in the freezing point.

Density and Surface Tension

Water has a density of 0.997 g/mL at 25°C and 1.0 atm pressure. As the temperature decreases, water, like most



• **Figure 1.2.5.1** Schematic illustration of five water molecules suggesting their geometry and dipole. A hydrogen bond is represented by a dotted line. Consider the many possibilities for these electrostatic (charge) interactions.

TABLE 1.2.5.1 Boiling Point and Freezing Point of Water Contrasted to Other H_2X Compounds

H_2X Compound		Molecular Weight	Boiling Point	Freezing Point
H_2Te	Hydrogen telluride	130	$-2^\circ C$	$-49^\circ C$
H_2Se	Hydrogen selenide	81	$-41^\circ C$	$-66^\circ C$
H_2S	Hydrogen sulfide	34	$-60^\circ C$	$-82^\circ C$
H_2O	Water	18	$100^\circ C$	$0^\circ C$

substances, increases in density, until $4^\circ C$ where its density is 1.00 g/mL . Then, as temperature is decreased further, an unusual phenomenon is observed. The density actually decreases as the temperature is lowered. At $0^\circ C$, the density is 0.92 g/mL . This phenomenon occurs because when water freezes, its hydrogen-bonded structure causes the molecules to crystallize in a manner such as to increase the volume of space that each water molecule occupies. Thus, ice floats on liquid water and metal pipes filled with water may burst when the water freezes. There is special significance to this. If bodies of water froze from the bottom to the top (i.e., if ice were heavier than water), during cold periods in Earth's geological history most aquatic life might have been destroyed.

Surface tension is a measure of the magnitude of cohesive forces holding molecules of a liquid together at an interface. For substances at ambient temperature and pressure, water has the highest surface tension with one exception—mercury. The water surface tension is 72.8 dyne/cm . Compare this to, for example, ethanol at 22.3 dyne/cm and ethylene glycol at 47.7 dyne/cm . This surface tension permits a water strider insect (family Gerridae) to transport across lakes riding on the “surface skin” of water, a metal paper clip to float (Fig. 1.2.5.2), and assists with the transport of water from soil to the tops of tall trees.



• **Figure 1.2.5.2** A metal paper clip floats on the water surface “skin,” a manifestation of water's high surface tension. (Photograph by Buddy Ratner.)

Specific Heat and Latent Heats of Fusion and Evaporation

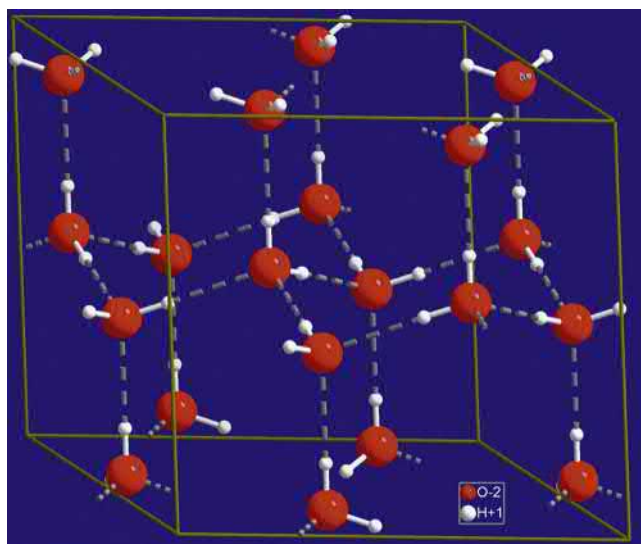
Water has a specific heat of $1.0\text{ cal/g}^\circ C$, that is, the heat per unit mass required to raise the temperature of water $1^\circ C$. For comparison, copper has a specific heat of $0.1\text{ cal/g}^\circ C$, and ethyl alcohol has a specific heat of $0.6\text{ cal/g}^\circ C$. Water has a higher specific heat than any other common substance. Related to the specific heat is the latent heat of fusion or evaporation. The latent heat is the energy in calories per gram taken up or released by matter changing phase (liquid/solid or solid/liquid) with no change in temperature. Again, water has anomalously high values compared to other common substances.

Water as a Solvent

Water is a remarkably powerful and versatile solvent. It will dissolve proteins, ions, sugars, gases, many organic liquids, and even lipids (up to the critical micelle concentration). In fact, it is the most versatile solvent known.

Water: Structure

Fig. 1.2.5.1 illustrates how water can form extended hydrogen bonding structures. These structures grow in three dimensions. The molecular crystal structure of ice is shown in Fig. 1.2.5.3. At temperatures of $0^\circ C$ and below, thermal fluctuations of molecules (referred to as kT vibrations, where k is Boltzmann's constant and T is absolute temperature) are low and a continuous, ordered three-dimensional network of water molecules can form. The hydrogen bonds in water are relatively low strength, approximately 5 kcal/mol (21 kJ/mol); in contrast, a $C-H$ bond is approximately 100 kcal/mol . However, unlike covalent bonds, hydrogen bonding is readily reversible, which enables the bonded state of water molecules to rapidly and dynamically respond

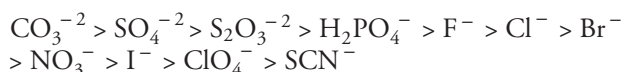


• **Figure 1.2.5.3** The hexagonal ice structure. (Wikipedia public domain image.)

to their surrounding molecular environment. At room temperature, the thermal fluctuations of water molecules can disrupt this hydrogen-bond association—if it were not so, water would coalesce into a solid at room temperature. An oft-cited model of water molecule organization suggests that disrupted groupings of water molecules rapidly form new clusters (dimers, trimers, tetramers, pentamers, hexamers, etc.) (Keutsch and Saykally, 2001). This is the “flickering cluster” model of water structure. More recently, it has been established that liquid water is closer to a hydrogen-bonded continuum with much bond-angle distortion from the tetrahedral organization seen in the ice structure, and with bonds breaking and reforming so rapidly (in the order of 200 fs), that the cluster model is not an accurate description (Smith et al., 2005). The continuum model is now the most accepted model for water structure, though there is still much controversy about water structure, and new insights are frequently reported.

The water structure discussion, above, applies to bulk, pure water. The water continuum organization can be disrupted or reorganized by dissolved ions or solutes, by absorption into hydrophilic polymers (e.g., hydrogels when the polymer is cross-linked), and by solid surfaces. Each of these cases will be very briefly addressed.

Dissolved ions and solutes may have a profound impact on water organization (Marcus, 2009). Dissolved salts are dissociated to form an anion and a cation, with each ion having a shell of water of different structure from the bulk. This hydration shell perturbs the structure of water adjacent to it (Marcus, 2009). Much of the study of dissolved ions has centered around studies of the Hofmeister series of anions:



Ions to the left of the series are referred to as kosmotropes (“order makers”)—they generally precipitate proteins

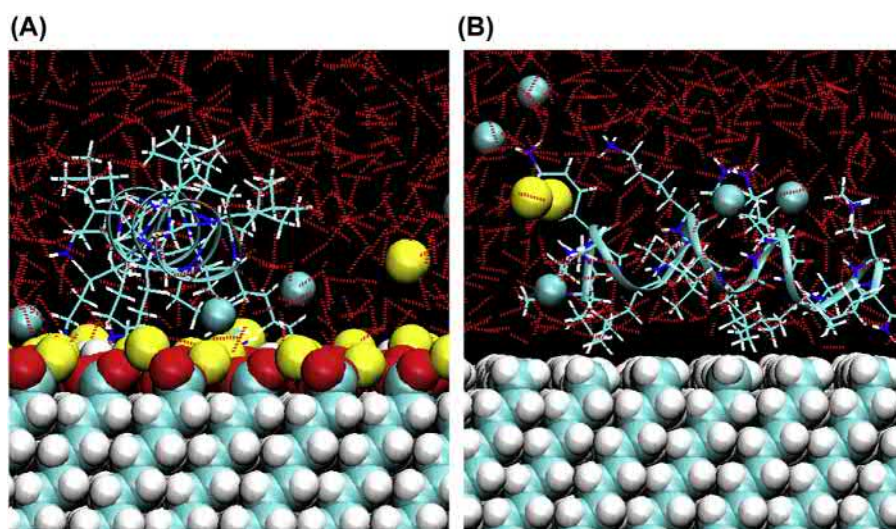
from solution and inhibit denaturation. Ions on the right side of the series are considered chaotropes (“disorder makers”), and these are more denaturing. Note that chloride is roughly at the center of the series, and thus might be expected to induce little change in proteins and water. Though earlier theories on the Hofmeister series suggested that ions to the left enhanced water structure while those to the right destructured or disordered water, this concept is not fully supported by recent experiments. The Hofmeister effect is impacted by the degree of hydration of ions in water, which cation is involved, and specific interactions of ions with solutes. Review articles that discuss the complexities of the Hofmeister effect and consider contemporary experimental and theoretical work are available (Zhang and Cremer, 2010; Paschek and Ludwig, 2011).

The “swelling” water entrained in gels (hydrogels, see Chapter 1.3.2E) is thought to be in three possible forms. Different nomenclatures are used to describe these forms, but basically three states have been proposed: (1) free water (similar to bulk water); (2) tightly bound water (more structured and with limited mobility); and (3) intermediate water (with characteristics of both free and bound water) (Jhon and Andrade, 1973; Akaike et al., 1979). Below, when the hydrophobic effect is discussed, other possibilities will be suggested. Evidence for different forms of water in gels continues to accumulate (Sekine and Ikeda-Fukazawa, 2009) and implications for biomaterials and biocompatibility have been discussed (Tsuruta, 2010). The nature of the water in the gel may also impact on the diffusion of molecules through it, blood interactions, and its performance as a cell-support in tissue engineering and regenerative medicine. The water that swells a hydrogel is impacted by the polymer chains at a nanoscale, because of its close proximity to the polymer that comprises the mesh of the hydrogel. When macroscopic pores are introduced into the hydrogel, the polymer will impact the water in a different fashion, i.e., the surface of the pores will interact with water in a manner similar to surface effects discussed in the next paragraph; in the interior of the pore (away from the pore wall), the water will have an organization more similar to bulk water.

When a solid surface or biomaterial disrupts the continuum structure of water, the water near the solid surface will adopt a new organization to achieve free-energy minimization for the total system. Since all our biomaterials will first see water before proteins or cells ever diffuse or transport to the surface, the nature of this surface-water layer may be, from a biomaterials-science standpoint, the most important event driving biointeractions at interfaces.

The nature of water in proximity to surfaces may be the primary driver for interactions between biomaterials and biological systems.

There is ample evidence from many analytical techniques, and also from computational methods, that water organization is altered close to a surface compared to the bulk. Most experimental data suggest this difference persists over a length of one to four water molecules (i.e., about 0.3–1.2 nm), before reverting to a structure



• **Figure 1.2.5.4** Snapshots from molecular simulations of a helical leucine-lysine (LK) peptide adsorbing onto (A) a negatively charged hydrophilic surface [self-assembled monolayer (SAM) with COOH/COO⁻ surface groups], and (B) a hydrophobic surface (SAM with nonpolar CH₃ surface groups) (from studies conducted by Collier et al., 2012). Color coding: greenish-blue surface atoms and “sticks” in the LK peptide=C, white surface atoms and sticks in the peptide=H, red surface atoms and sticks in the LK peptide=O, dark blue sticks in the peptide=N, yellow spheres in solution=Na⁺ ions, greenish-blue spheres in solution=Cl⁻ ions, red dotted lines=hydrogen bonds formed by water molecules. Molecular images created using VMD software (Humphrey et al., 1996).

indistinguishable from the bulk water. There is much research on the adsorption of the first layer of water on materials. Clearly, the organization of this first layer will dictate the structure of subsequent layers. On many close-packed metal crystal surfaces (for example, Pt, Ni, Pd) results suggest that a water bilayer exists with a structure analogous to ice (Hodgson and Haq, 2009). This may have led to the somewhat misleading term for interfacial water, “ice-like water.” Although the water structure is different from the bulk liquid at all surfaces, the specific ice-like organization is predominantly seen at these close-packed metal crystal surfaces. Above the water bilayer directly in contact with the metal, water structure is altered for a few molecular layers until it becomes indistinguishable from bulk water.

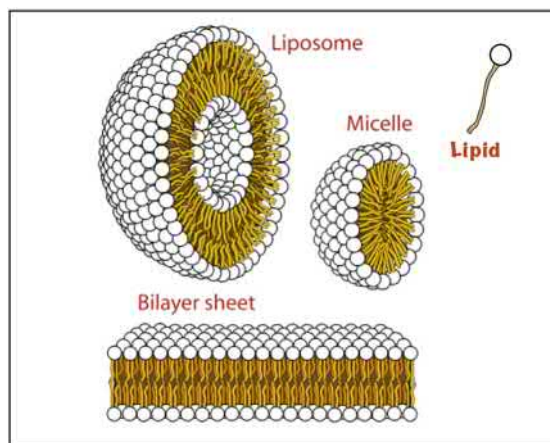
Other studies demonstrate differences between hydrophilic and hydrophobic surfaces as to their interactions with water (Howell et al., 2010). Both types of surfaces have a substantial effect on water organization, but in very different ways. Hydrophilic surfaces have functional groups that are attractive to water molecules by forming hydrogen bonds with them (e.g., surfaces with polar functional groups like O–H or N–H), or strong electrostatic interactions (e.g., charged functional groups), thus resulting in a closely bound layer of water over the surface. In contrast to this, for hydrophobic interfaces, which lack the ability to form hydrogen bonds or strong electrostatic interactions with water molecules, there appears to be a low water density zone, sometimes called a depletion zone, a few angstroms thick over the surface. Fig. 1.2.5.4 presents results from molecular dynamics simulations that illustrate these effects. In this figure, the presence of hydrogen bonds

formed by the water molecules over a negatively charged hydrophilic surface (Fig. 1.2.5.4A) and a hydrophobic surface (Fig. 1.2.5.4B) are indicated by the red dotted lines. Over the hydrophilic surface, hydrogen bonds are clearly formed with either the negatively charged surface functional groups or the tightly adsorbed counter-ions with these hydrogen bonds primarily oriented perpendicular to the surface. However, over the hydrophobic surface, which does not have the capability to form hydrogen bonds with the interfacial water molecules, there is a distinct gap a few angstroms thick directly over the surface (i.e., a depletion zone). The hydrogen bonds formed by the water molecules directly above this layer are primarily oriented parallel to the surface, indicating hydrogen bonding only between the water molecules themselves. The resulting hydrophobic effect is also clearly shown in this molecular model, with nonpolar side-chains of the adsorbing peptide being excluded by the surrounding water and tightly adsorbed to the hydrophobic surface.

There are hundreds of recent studies on the water–solid interface, mostly in physical chemistry journals. A comprehensive review of this complex and still controversial subject would be impossible in this textbook. However, the take-home message is relatively straightforward—the presence of an interface alters the water structure adjacent to it.

Water: Significance for Biomaterials

When a protein or a cell approaches a biomaterial, it interacts with the surface water first. This final section will briefly review some implications of this surface water for biomaterials.



• **Figure 1.2.5.5** Lipid molecules with polar head groups (white) and hydrophobic tails (brown), when placed in water, organize themselves to minimize surface area contact between the hydrophobic tail (typically comprised of methylene units, $-\text{CH}_2-$) and water. This minimization of contact area, depending on precise conditions, can lead to micelles, liposomes, or bilayer sheets. (Modified from a public domain image on Wikimedia Commons.)

Hydrophobic Effect, Liposomes, and Micelles

If we place a drop of oil under water it will round up to a sphere as it floats to the water surface. The common explanation for this is that because oil molecules do not hydrogen bond with water molecules the oil cannot strongly interact with the bulk water phase. Another way to say this is that the oil disrupts the bulk (continuum) structure of water, and the water molecules at the oil interface then have to restructure to a new (more ordered) organization. This decrease in water entropy is energetically unfavorable according to the second law of thermodynamics (i.e., it results in an increase in the free energy of the system). Therefore, the oil minimizes its interfacial area with the water by coalescing into a sphere (a sphere has the lowest surface area for a given volume). This is called the hydrophobic effect (Tanford, 1978; Widom et al., 2003). It is not driven by the oil–water molecular interactions, but rather by the necessity to minimize the more structured (lower entropy, higher free energy) organization of water molecules.

If we now take a surfactant molecule comprised of an “oily” segment and a polar (water-loving) segment, by shielding the oily phase from the water with the hydrophilic head groups, contact between oil and water is minimized. Fig. 1.2.5.5 illustrates some hydrophobic-effect-driven supramolecular aggregate structures that lead to this free-energy minimization. Liposomes and block copolymer micelles are widely used in drug delivery, where the hydrophobic region (micelle core or liposome bilayer) or the aqueous center (liposome) can carry a hydrophobic drug or hydrophilic drug, respectively (see Chapters 1.3.8A and 1.3.8B). Bilayer sheets are used in biosensors to orient and stabilize receptor proteins.

Hydrogels

The structured water within hydrogels has been discussed. Water structure associated with hydrogels has been implicated in their interactions with blood (Garcia et al., 1980; Tanaka and Mochizuki, 2004). Water structure in hydrogels is also thought to be important in the performance of hydrogel contact lenses, specifically the rate of lens dehydration (Maldonado-Codina and Efron, 2005).

Protein Adsorption

Protein adsorption is discussed in detail in Chapter 2.1.2, and is critically important for understanding the performance of biomaterials. A question commonly posed is: “Why do proteins bind rapidly and tenaciously to almost all surfaces?” A model that can explain this considers structured water at interfaces. All surfaces will organize water structure differently from the bulk structure; this organization almost always gives more structured (lower entropy, higher free energy) water. If a protein can displace the ordered water in binding to the surface, the entropy of the system will increase, and thus the free energy will decrease as the water molecules are released and gain freedom in bulk water. This is probably the driving force for protein adsorption at most interfaces. There are some specially engineered surfaces referred to as “nonfouling” or “protein-resistant” (see Chapter 1.4.3A). These surfaces may resist protein adsorption by binding or structuring water so strongly that the protein molecule cannot “melt” or displace the organized or tightly bound water, and thus there is no driving force for adsorption.

Life

Living systems self-assemble from smaller molecular units. For example, think about the organizational processes in going from an egg, to a fetus, to a mature creature. Much of this assembly is driven by hydrophobic interactions (i.e., entropically by water structure). Another area where water structure has a major impact on life involves DNA and its unique binding of water (Khesbak et al., 2011). Also, consider enzymes that are so essential to life. A substrate molecule enters the active site of an enzyme by displacing water molecules. The unique mechanical properties of cartilage under compression can be modeled by considering water organization. In fact, the average human is 57% by weight water, on a molar basis by far the major component in the human body. Thus we can well appreciate, as Henderson surmised in 1913, that water is essential to this phenomenon we call life.

As you work through this textbook, think about how the phenomena you are reading about may be driven or controlled by water that comprises such a large fraction of all biological systems.

References

- Akaike, T., Sakurai, Y., Kosuge, K., Kuwana, K., Katoh, A., et al., 1979. Study on the interaction between plasma proteins and synthetic polymers by circular dichroism. *ACS Polym. Prepr.* 20 (1), 581–584.

- Collier, G., Vellore, N.A., Yancey, J.A., Stuart, S.J., Latour, R.A., 2012. Comparison between empirical protein force fields for the simulation of the adsorption behavior of structured LK peptides on functionalized surfaces. *Biointerphases* 7 (1), 1–19 article 24.
- Garcia, C., Anderson, J.M., Barenberg, S.A., 1980. Hemocompatibility: effect of structured water. *Trans. Am. Soc. Artif. Intern. Organs* 26, 294–298.
- Henderson, L.J., 1913. *The Fitness of the Environment*. The Macmillan Company, New York, NY.
- Hodgson, A., Haq, S., 2009. Water adsorption and the wetting of metal surfaces. *Surf. Sci. Rep.* 64 (9), 381–451.
- Howell, C., Maul, R., Wenzel, W., Koelsch, P., 2010. Interactions of hydrophobic and hydrophilic self-assembled monolayers with water as probed by sum-frequency-generation spectroscopy. *Chem. Phys. Lett.* 494 (4–6), 193–197.
- Humphrey, W., Dalke, A., Schulten, K., 1996. Vmd – visual molecular dynamics. *J. Mol. Graph.* 14 (1), 33–38.
- Jhon, M.S., Andrade, J.D., 1973. Water and hydrogels. *J. Biomed. Mater. Res.* 7, 509–522.
- Keutsch, F.N., Saykally, R.J., 2001. Water clusters: untangling the mysteries of the liquid, one molecule at a time. *Proc. Natl. Acad. Sci.* 98 (19), 10533–10540.
- Khesbak, H., Savchuk, O., Tsushima, S., Fahmy, K., 2011. The role of water H-bond imbalances in B-DNA substrate transitions and peptide recognition revealed by time-resolved FTIR spectroscopy. *J. Am. Chem. Soc.* 133 (15), 5834–5842.
- Maldonado-Codina, C., Efron, N., 2005. An investigation of the discrete and continuum models of water behavior in hydrogel contact lenses. *Eye Contact Lens* 31 (6), 270–278.
- Marcus, Y., 2009. Effect of ions on the structure of water: structure making and breaking. *Chem. Rev.* 109, 1346–1370.
- Paschek, D., Ludwig, R., 2011. Specific ion effects on water structure and dynamics beyond the first hydration shell. *Angew. Chem.* 50 (2), 352–353.
- Sekine, Y., Ikeda-Fukazawa, T., 2009. Structural changes of water in a hydrogel during dehydration. *034501 J. Chem. Phys.* 130 (3), 034501.
- Smith, J.D., Cappa, C.D., Wilson, K.R., Cohen, R.C., Geissler, P.L., et al., 2005. Unified description of temperature-dependent hydrogen-bond rearrangements in liquid water. *Proc. Natl. Acad. Sci. U. S. A.* 102 (40), 14171–14174.
- Tanaka, M., Mochizuki, A., 2004. Effect of water structure on blood compatibility: thermal analysis of water in poly (meth) acrylate. *J. Biomed. Mater. Res.* 68A, 684–695.
- Tanford, C., 1978. The hydrophobic effect and the organization of living matter. *Science* 200 (4345), 1012–1018.
- Tsuruta, T., 2010. On the role of water molecules in the interface between biological systems and polymers. *J. Biomater. Sci. Polym. Ed.* 21 (14), 1831–1848.
- Widom, B., Bhimalapuram, P., Koga, K., 2003. The hydrophobic effect. *Phys. Chem. Chem. Phys.* 5 (15), 3085.
- Zhang, Y., Cremer, P.S., 2010. Chemistry of Hofmeister anions and osmolytes. *Annu. Rev. Phys. Chem.* 61 (1), 63–83.

Chapter Exercises

Consider having two types of homogeneous surface chemistries: one with hydrophilic hydroxyl (-OH) groups and the other with hydrophobic methyl (-CH₃) groups.

(a) Which surface would more strongly adsorb a protein in air?

(b) Which surface would more strongly adsorb a protein in water?

Answers:

(a) In air, the -OH surface would more strongly adsorb the protein due to the fact that it would be able to form the strongest type of van der Waals (vdW) interactions (i.e., hydrogen bonds) with the polar groups of the protein, as well as forming moderately strong dipole-induced dipole vdW interactions with the nonpolar groups of the protein. In comparison, the -CH₃ surface would only be able to form the moderate and very weak vdW interactions

with the protein (i.e., induced dipole-dipole and induced dipole-induced dipole interactions, respectively).

(b) In water, the -CH₃ surface would more strongly adsorb the protein due to the ability of water molecules to form hydrogen bonds with the -OH groups of the surface, which will directly compete with the protein, thus weakening the -OH surface's bonding with the protein. In contrast, the -CH₃ surface would form very strong hydrophobic interactions with the hydrophobic domains of the protein due to the thermodynamically unfavorable interactions between the -CH₃ groups of the surface and the surrounding water.

Suggested External Reading

Voet, D., Voet, J.G., Pratt, C.W., 2016. *Fundamentals of Biochemistry: Life at the Molecular Level*, fifth edition, Chapter 2: Physical and Chemical Properties of Water, John Wiley & Sons, pp. 23–41.

1.3.1

The Materials Side of the Biomaterials Relationship

WILLIAM R. WAGNER

Departments of Surgery, Bioengineering & Chemical Engineering, McGowan Institute for Regenerative Medicine, University of Pittsburgh, Pittsburgh, PA, United States

When seeking to cover the “Classes of Materials Used in Medicine,” as this section of the book states, a quick overview of the landscape, together with some caveats and definitions, is in order. What are these materials that will be brought to bear as biomaterials in devices? Materials employed as biomaterials will need to serve many needs: replacement of physiologic functions lost to trauma, disease, or congenital conditions (e.g., cardiac valves); sensing (e.g., ultrasound contrast agents); delivery of materials within the body (e.g., stent-delivery catheters); temporary mechanical support (e.g., sutures); or extracorporeal processes (e.g., dialyzers). It is not surprising that the array of applied biomaterials is very broad and growing.

However, this chapter will not consider specific classes of materials that are used daily in the clinic to meet some of the needs just outlined. Specifically, consider biomedical devices that seek to replace a given physiologic function and the analogous situation with an automobile. For an automobile, tires that no longer grip on wet roads or a battery that cannot start the vehicle elicit a trip to the mechanic’s shop and replacement of these parts with “devices” that are fully capable of restoring those functions, or perhaps even exceeding the capabilities and duration of the original equipment manufacturer. The parts are designed to be fully compatible and are readily available for a quick and unambiguous replacement procedure. The situation in the clinic from a needs perspective is similar, but unfortunately society has not advanced to the state where off-the-shelf replacement parts of compositional and functional equivalence are available. Arguably, the best source for such materials in many cases is from the patient: autograft materials. Muscle flaps moved by plastic surgeons for reconstructive procedures, saphenous veins and arteries used for arterial bypass, and skin harvested and mechanically processed to increase its

coverage area for burn treatment all represent current gold-standard materials used to meet clinical needs for replacement tissues. Which of these autograft materials are best selected for specific conditions and how they are isolated and processed is the focus of surgical textbooks, but may only be peripherally mentioned here. Yet the reader should be aware that biomaterials and medical device technology falls usually well short of addressing clinical needs as effectively as autografts may. This is true despite the downsides associated with autografting, such as donor site morbidity.

Similar to autografts, allografts (from organ and tissue donation) fill critical needs for tissue replacement where autografts and other material-based approaches are not possible or fall short. For instance, the best option for patients in end-stage cardiac, kidney, liver, and pulmonary failure is currently to receive an allograft. Despite the morbidity associated with immunosuppressant therapy, and issues associated with a limited supply, the quality of life and survival for allograft recipients exceeds similar populations that would be supported by the best current medical support devices for heart, lung, or kidney. The considerations, particularly immunology, surrounding allograft materials are beyond the scope of this text, but the target populations for important classes of medical devices are similar. For both auto- and allografts used in the manner already described, these materials are utilized in a minimally processed state. Particularly for allografts and certainly for xenograft materials, the application of processing methods, from decellularization to cryopreservation and cross-linking, bring these materials into the realm of biomaterials that are considered in this text.

With the preceding discussion the need for extensive consideration of surgical principles as well as broad coverage of allografting, immunology, and immunosuppressive therapy has been taken off the table. At the same time, two critically

important classes of materials used in medicine have been noted, but largely dismissed. Having recognized this, the focus for Section 1.3 is to cover the remaining major classes of materials used in medicine. Studying biomaterials requires the study of the interface between the material and the biological, and in this section the material side of this relationship is covered. To fulfill the design requirements of diverse medical devices, diverse materials are needed that can meet mechanical, chemical, and biological requirements. For some applications it may be that very different material types are being considered due to different design considerations. For instance, in articulating joint replacement devices, some parts have been made from polymer, metal, or ceramic in different designs. In vascular stents a variety of metals have been used, but with recent consideration of degradable stents, both degradable polymeric stents from poly(lactide) and degradable metallic stents made of a magnesium alloy have been tested clinically. Understanding what different material classes and subclasses offer in terms of properties and how structure relates to function is essential knowledge for the biomaterials expert. The chapters here are generally grouped into categories of polymers, metals, ceramics, natural materials, composites, and particulates with subchapters devoted to particularly important material types.

An major trend in the biomaterials community over the past several decades has been the harnessing of advances in molecular biology to design materials with specific biological functionalities. Some of these advances will be covered in this section (Chapter 1.3.2G) and also in select chapters later in the book. More recently there has been a dramatic increase in research focused on particulate biomaterials,

where biological knowledge is critically leveraged to impart targeting potential, responsiveness to conditions at a targeted site (e.g., pH), and to orchestrate specific interactions at a cellular level upon arrival. Traditional bulk materials such as polymers, ceramics, and metals may be used as part of these designs, but self-assembly of macromolecules is also often a feature. Chapters 1.3.8A and 1.3.8B seek to summarize this rapidly advancing area in the biomaterials community. Finally, the use of biologically derived materials has been of growing interest and clinical impact. These materials range from highly purified single components that may be from plant or animal sources, to engineered natural materials where functionality such as photocross-linking activity may be added, to materials derived from the extracellular matrix or tissues with processing for degradation resistance (fixation) or intended remodeling (decellularized tissues). The subsections of Chapter 1.3.6 seek to cover this space.

While the theme for this section is firmly on the materials side of the biomaterials relationship, as the field progresses the knowledge bases that inform either side of the material and biological interface are merging, and with some materials the design and control of the biological response has become the critical issue in engineering the intended effect. At the same time, the reality in today's clinics and hospitals is that when autografts and allografts are not available or when devices are needed for other purposes beyond tissue replacement, the vast majority of medical devices remain comprised of materials adopted from the broader materials community to meet the principal design objectives. There remains the need for understanding and working with the fundamentals of materials science.

1.3.2

Polymers: Basic Principles

GARRETT BASS¹, MATTHEW L. BECKER¹, DANIEL E. HEATH², STUART L. COOPER²

¹Departments of Chemistry, Mechanical Engineering and Materials Science, Biomedical Engineering and Orthopaedic Surgery, Duke University, Durham, NC, United States

²William G. Lowrie Department of Chemical and Biomolecular Engineering, The Ohio State University, Columbus, OH, United States

Polymers represent the largest class of materials used in medicine. They have a range of unique properties making them useful in biomaterial applications, including orthopedics, dental, hard and soft tissue replacements, drug delivery, and cardiovascular devices. This chapter explains the basic principles of polymer science, illustrates how polymer materials can be specifically designed to fill needs in the biomaterials field, and provides examples of how this class of materials is currently used in medical applications. Structure–property relationships, including molecular architecture, molecular mass, and chemical composition related to the physical and chemical properties of the macroscopic material, are included. A biomaterials scientist aware of structure–property relationships can engineer a polymer system for a specific need.

Introduction

Polymer materials possess an array of unique properties that make them useful in a variety of biomaterial applications such as orthopedics, dental, hard and soft tissue replacements, drug delivery and cardiovascular devices. In fact, polymers represent the largest class of materials used in medicine. This chapter introduces the basic principles in polymer science, illustrates how polymer materials can be specifically designed to fill needs in the biomaterials field, and provides examples of how this class of materials is currently used in medical applications.

The central idea of this chapter is structure–property relationships, which means how molecular characteristics such as molecular architecture, molecular mass, and chemical composition are directly related to the physical and chemical properties of the macroscopic material. It also includes a brief introduction to polymer synthesis, presents advantages and disadvantages of these methods, and outlines recent developments in postpolymerization functionalization. For instance, polymer scientists in other fields have been able to

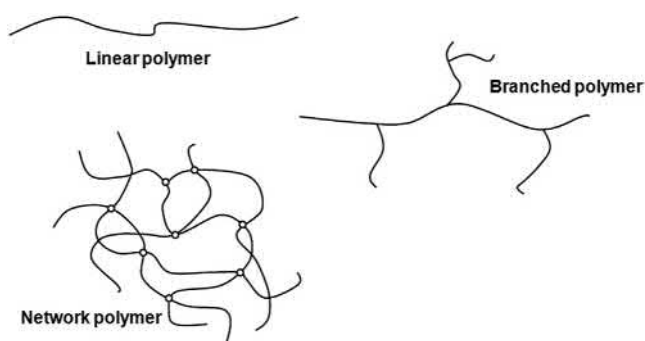
exploit structure–property relationships to create nonstick coatings, pressure-sensitive adhesives, and the penetration-resistant materials used in bulletproof vests. A biomaterials scientist aware of structure–property relationships can rationally engineer a polymer system for a specific need.

The Polymer Molecule

Molecular Structure of Single Polymer Molecules

The hallmark of polymer molecules is high molecular mass. A single polymer molecule could have a molecular mass of 2,000,000 Da compared to a water molecule, which has a molecular mass of 18 Da. Furthermore, polymer molecules are organized into very interesting architectures. Common architectures of polymer molecules are shown in Fig. 1.3.2.1. The simplest is the linear chain where there is a single molecular backbone. When linear chains of two different compositions (e.g., polymers A and B) are linked together, the resultant polymer is called an A–B block copolymer. If another chain is added to the second chain, it may be called an A–B–C triblock copolymer, or more simply an A–B–C block copolymer. Differences in monomer reactivity can also lead to random or gradient copolymers where the chain sequence of monomer addition is altered. Branched structures are also possible where a central polymer backbone has smaller side chains extending from it. Branches can occur due to undesired side reactions during synthesis, or can be purposefully incorporated into the molecular structure. The type and extent of branching introduces significant changes in properties to a polymer system.

Star-shaped polymers consist of a multifunctional core molecule from which at least three polymer chains (arms) radiate. These arms can be chemically identical (homostars) or different (heteroarm stars). Star polymers have been widely used in biomedical applications such as drug and



• **Figure 1.3.2.1** Three polymer architectures commonly seen.

gene delivery, tissue engineering, diagnostics, and antifouling biomaterials. The intensified interest in star polymers is attributed to their unique topological structures and physical/chemical properties.

Polymer brushes are a branched polymer system in which chains of polymer molecules are attached along a linear polymer backbone in such a way that the graft density of the polymers is sufficiently high to force stretching of the tethered chains away from the backbone. Some examples of naturally occurring polymer brushes include extracellular polysaccharides on bacterial surfaces and the proteoglycans of cartilage.

Dendrimers are monodisperse, precisely branched macromolecules in which all bonds emerge radially from a central focal point with a regular branching pattern and with repeat units that each contribute a branch point. These structures exhibit a high degree of molecular uniformity, precise molecular mass, tunable size, shape, and number of functional groups.

So far we have discussed polymer systems in which there are discrete polymer molecules. However, what would happen if you took a linear polymer molecule and covalently bonded it to the backbone of another linear chain? A few of these bonding events would produce a branched structure as noted previously. If you repeated this act many times over you would eventually link all of the polymer chains together into one very large *network* polymer. This is also possible by using small di- or trifunctional “cross-linker” molecules to react with pendant or terminal reactive groups on linear polymer chains, eventually yielding a network polymer.

Chemical Structure of Single Polymer Molecules

If you were able to see the individual atoms making up a polymer molecule, you would notice the same basic structure repeats over and over again. This structure is called the *repeat unit* of a polymer molecule. Etymologically, polymer comes from the Greek “poly,” meaning many, and “meros,” meaning part—many parts. In polymer molecules the “mer” is the repeat unit. [Fig. 1.3.2.2](#) shows a schematic of a linear polypropylene molecule. The polymer chain is composed of many $(-\text{CH}_2-\text{CHCH}_3)-$ repeat units covalently linked end to

end. The repeat unit itself consists of the polymer backbone, a series of carbon–carbon single bonds, while the hydrogen atoms and methyl group are *pendant groups*. The repeat unit can be controlled through choice of synthetic method and plays a large role in the macroscopic behavior of the polymer. [Fig. 1.3.2.3](#) shows the repeat units of several synthetic and natural polymers commonly used in the biomaterials field.

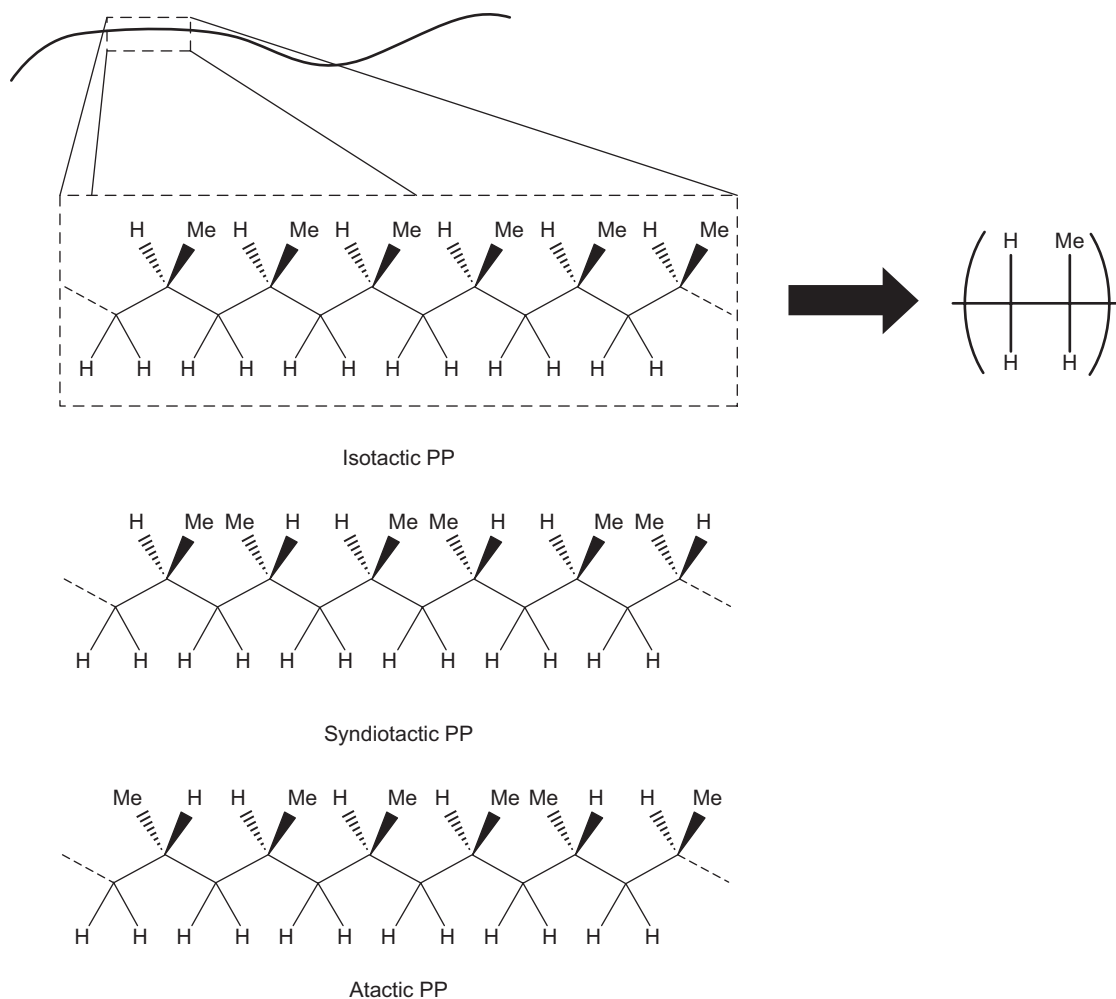
Copolymers

Sometimes it is advantageous to synthesize copolymers—polymers containing more than one chemically distinct repeat unit. For instance, a researcher may synthesize a polymer that contains repeat units “A” and “B.” As shown in [Fig. 1.3.2.4](#), there are many different ways the repeat units could be organized. Random copolymers occur when the “A” and “B” repeat units have no order in the backbone; however, alternating, block, gradient, and graft copolymers are also possible and the arrangement of repeat units affects the physical behavior of the biomaterial. The repeat units of two random copolymers commonly used in the biomaterials field are shown in [Fig. 1.3.2.5](#).

Determination of Chemical Composition

A researcher will often need to verify the chemical structure of polymers or determine the composition of copolymer systems. Two common techniques a scientist would use are nuclear magnetic resonance (NMR) spectroscopy and infrared (IR) spectroscopy. NMR is an analytical technique that exploits the magnetic moments associated with isotopes that contain an odd number of protons and/or neutrons. These atoms have an intrinsic nuclear magnetic moment and angular momentum, in other words a nonzero nuclear spin, while all nuclides with even numbers of both have a total spin of zero. The most commonly used nuclei are ^1H , ^{13}C , and ^{19}F although isotopes of many other elements can be studied by high-field NMR spectroscopy as well. In a typical experiment, these nuclei are excited to a higher energy state through a burst of radiofrequency radiation. The nuclei relax to a lower energy state, which is measured as an electric signal. Fourier transform analysis is used to convert this time domain electrical signal into the frequency domain. Due to electron shielding, protons attached to different structural units will display chemical shifts, meaning their resonances in the NMR spectrum will be at different frequencies. Through analysis of the resonance placement, splitting patterns, and intensity, the chemical structure of molecules can be determined.

IR spectroscopy is also used to determine the chemical composition of polymers. In a typical experiment, a sample of interest is irradiated with IR radiation. The sample absorbs certain wavelengths, resulting in specific molecular motion or vibrations (such as C–H stretching). The IR spectrum is created by plotting absorbance versus wavelength. Like NMR, analysis of the spectra can lead to the verification of a polymer's composition.



• **Figure 1.3.2.2** Polypropylene repeat unit and its different tactic isomers. In the schematic Me indicates a methyl group.

Often the chemical composition of the polymer surface is different from the bulk. For a medical implant the surface composition is highly important, since it will interface with the biological environment. To probe the surface composition, X-ray photoelectron spectroscopy—also known as electron spectroscopy for chemical analysis—is a common technique. A sample is bombarded with X-rays, which results in the ejection of inner shell electrons from the atoms displayed on the material surface. The kinetic energies of the ejected electrons are measured and interpreted into information about the chemical composition of the surface (for more information on surface characterization techniques, see [Chapter 1.2.4](#)).

Tacticity

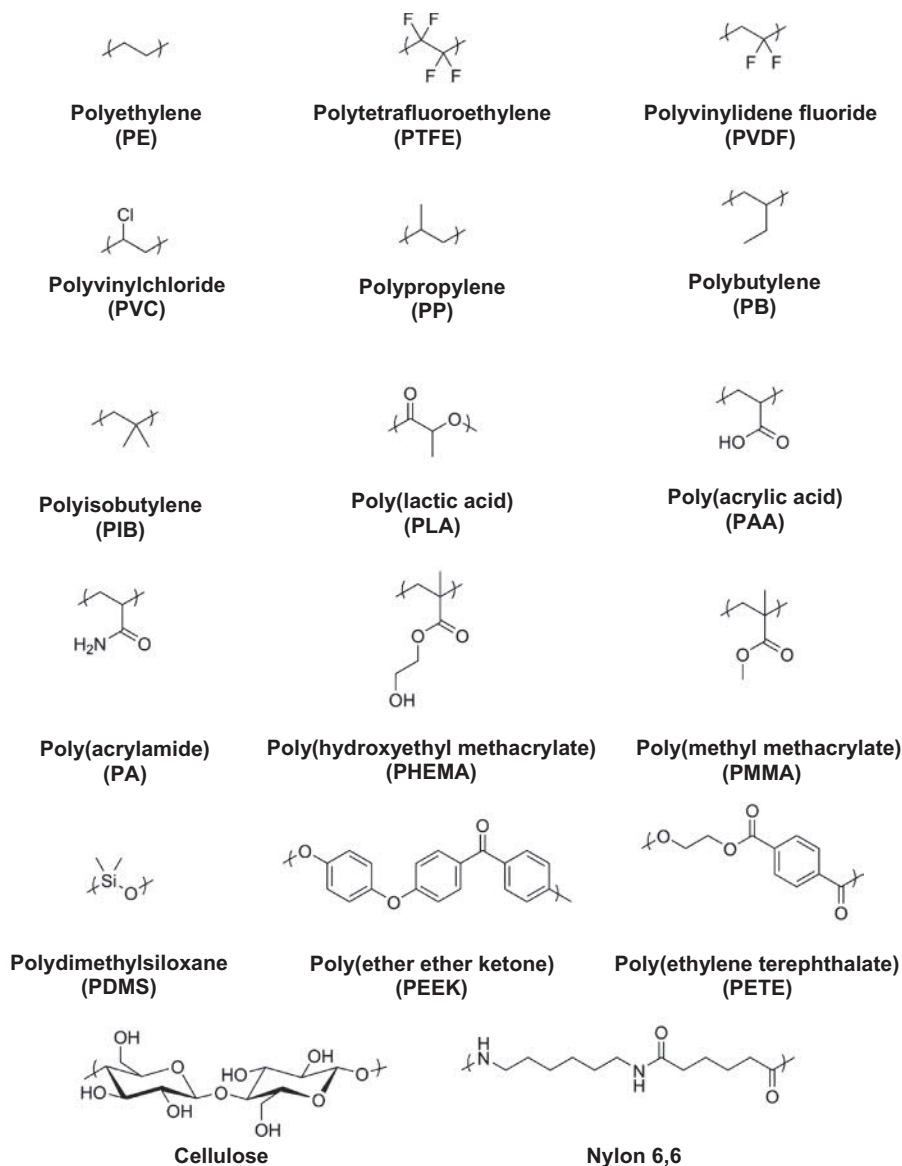
Tacticity describes the stereochemistry of the repeat units in polymer chains. To illustrate the discussion on tacticity, let us consider a molecule of polypropylene (PP). When stretched into its *planar zigzag* form, as seen in [Fig. 1.3.2.2](#), you can see that sometimes the methyl groups are all on one side of the backbone, sometimes they alternate from side to side, and sometimes they are randomly distributed. During routine

synthesis, a polymer chemist would normally produce an *atactic* version of PP, one where the methyl group is randomly located in front of and behind the polymer backbone. However, when a special catalyst is used during synthesis a chemist can produce *isotactic* PP, where all the methyl groups are located on one side of the “stretched-out” polymer backbone, or *syndiotactic* PP, where the methyl groups regularly alternate from side to side. As will be discussed later, tacticity can drastically affect the physical behavior of the polymer system, largely by affecting the ability of the polymer molecules to crystallize. Tactic isomers occur whenever an atom in the polymer backbone has the capacity to form tetrahedral bonding and is bonded to four different chemical groups. Such atoms (generally carbon) are referred to as *asymmetric*.

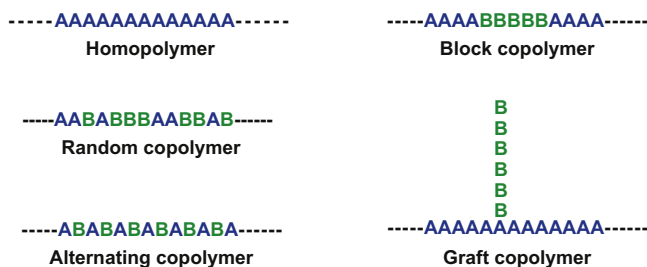
Molecular Mass

The Molecular Mass Distribution and Its Averages

During polymerization, polymer chains are built up from monomers to a desired molecular mass. Polymers with identical composition but different molecular mass (different chain length) may exhibit different physical properties. The number of monomer repeat units in each polymer chain is called the *degree of polymerization* (DP).



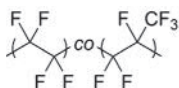
• **Figure 1.3.2.3** Repeat units of common polymer biomaterials.



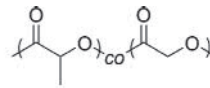
• **Figure 1.3.2.4** Various copolymers formed by varying the arrangement of two monomers.

For a homopolymer, there is only one type of monomeric unit and the number average degree of polymerization is given by $M_n = M_0 \times DP$, where M_n is the number average molecular mass and M_0 is the molecular mass (or formal weight) of the monomer unit.

However, in a traditional free radical or condensation polymerization synthesis, each polymer chain will not have the same DP. For instance, in the free radical polymerization of polyethylene (PE), one polymer chain may add 3000 monomers, a second may add 4500 monomers, and a third may only add 1500. Therefore most polymer systems have a *distribution of molecular masses*. Since polymer materials are made from molecules with a variety of molecular mass, it is incorrect to talk about *the* molecular mass of a polymer system. Instead, polymer systems are described by average values of molecular mass. The two most commonly used averages are the number average molecular mass (M_n) and the weight average molecular weight (M_w). The mathematical definitions of these averages are supplied in Eqs. (1.3.2.1) and (1.3.2.2), where N_i is the number of molecules with “ i ” repeat units and M_i is the molecular weight of a polymer chain with “ i ”



**Poly(tetrafluoroethylene-co-hexafluoropropylene)
random copolymer**



**Poly(lactic-co-glycolic acid)
random copolymer**

• **Figure 1.3.2.5** Repeat units of two common copolymer biomaterials.

repeat units. Since M_w is calculated using the square of the molecular weight it is almost always greater than or equal to M_n :

$$D_m > 1 \quad (1.3.2.1)$$

$$M_n = \frac{\sum_i N_i M_i}{\sum_i N_i} \quad (1.3.2.2)$$

$$M_w = \frac{\sum_i N_i M_i^2}{\sum_i N_i M_i}$$

The ratio of M_w to M_n is the molecular mass distribution (D_m) (Eq. 1.3.2.3), which is a measurement of the breadth of the chain length populations. If the D_m of a polymer system is unity (1), the number average and weight average molecular masses are identical, meaning the polymer sample is monodisperse (all chains have the same degree of polymerization). This level of precision is only found in dendrimers and biopolymers.

For most condensation polymers, the D_m is approximately 2:

$$D_m = \frac{M_w}{M_n} \quad (1.3.2.3)$$

The higher the average molecular mass, the stronger a polymer material will be (up to a point). However, the melt/solution viscosity increases with increasing average molecular mass, making the material more difficult to process. Often a molecular mass range exists within which most desired physical behaviors are achieved, yet the material is still easily processed. Generally, condensation polymerizations are suitable for a number average molecular mass range from 25,000 to 50,000 Da, while addition polymerizations are preferred for values from about 50,000 Da up to hundreds of thousands.

Characterizing the Molecular Mass Distribution

Through understanding the importance of molecular mass and its mass distribution, polymer scientists have developed many methods for measuring average molecular mass values. For instance, M_n can be determined through techniques such as end-group analysis by NMR, vapor pressure lowering, and freezing point depression. In the following paragraphs we will first discuss common methods historically used to measure M_n

(osmotic pressure) and M_w (light scattering). Although osmotic pressure and light scattering are powerful and useful techniques in the field of polymer science, they have been replaced in recent years by size exclusion chromatography (SEC), which gives much more detail about the molecular mass distribution, and does so much quicker. From the molecular mass distribution obtained by SEC, the first and second moments of the distribution, M_n and M_w are readily determined.

In osmotic pressure experiments, a dilute polymer solution is separated from pure solvent by a semipermeable membrane through which solvent can freely pass but which excludes polymer. The activity of the pure solvent differs from that of the solvent molecules in the solution phase resulting in a thermodynamic driving force—the osmotic pressure (π or P) causes molecules of pure solvent to diffuse across a membrane (which is permeable only to solvent) and into a compartment containing a solute (e.g., polymer) in solution. This causes the fluid level in the solution compartment to rise, resulting in a hydrostatic pressure head. Equilibrium is reached when the pressure head exactly offsets the osmotic pressure. By measuring the rise in fluid level, the osmotic pressure can be calculated and related to the number average molecular weight. A number of polymer solutions are prepared, each with a distinct concentration. The osmotic pressure is measured for each solution and plotted against concentration, the concentration is then extrapolated to zero, and the number average molecular weight can be determined from the intercept of the regression line.

Light scattering is a common technique to determine the M_w of a polymer system. In dilute solutions, the scattering of light is directly proportional to the number of molecules. The scattered intensity is observed at a distance r and angle Q from the incident beam, and is related to the size or weight average molecular weight of the molecule. The light-scattering behavior of a series of polymer solutions with varying concentrations is measured and the data are extrapolated to zero concentration to determine M_w . Once the M_n and M_w values are determined, the D_m of the polymer system can be calculated.

SEC is the most commonly used molecular mass characterization technique in modern polymer science laboratories. Unlike osmotic pressure and light scattering, which provide *average* values of molecular mass, SEC provides the entire molecular mass distribution from which all the desired average values can be calculated. Different average values can be defined using SEC, depending on the statistical method applied. In practice, two averages are commonly used, representing the weighted mean taken with the mole fraction and the weight fraction. In an SEC experiment, a dilute polymer solution flows through a column packed with solid

separation media that contains pores on the same size scale as the polymer molecules. As the polymer molecules flow through the column, smaller chains diffuse into the pores and thus must travel a further distance, while larger polymer chains move through the column faster since they are excluded from the pore structure, resulting in higher molecular mass material eluting from the column first, followed by lower molecular mass species. The concentration of the effluent stream is monitored and a plot of detector signal (which is proportional to polymer concentration) versus retention time can be generated. The use of narrow molecular mass distribution standards allows the user to correlate retention time with molecular mass, although the actual correlation is with the hydrodynamic volume of the known standards. If the relationship between molar mass and the hydrodynamic volume changes (i.e., the polymer is not the same shape in solution, i.e., branched, cyclic, as the standard, or is of a differing chemical makeup), then the calibration for mass is in error.

Connecting Physical Behavior With Chemical Characteristics

We have discussed the key characteristics of polymer molecules (molecular architecture, chemical composition, tacticity, and molecular mass). Now we will relate these molecular characteristics to macroscopic properties, and illustrate how these characteristics can be manipulated to create a polymer system with the desired behavior. We will focus on the tensile properties, hydrophilicity, and biodegradability of polymer systems.

Physical States of Linear Polymers

When designing a biomaterial, physical properties are key features. For instance, if you were creating a cement for use in loadbearing bones (tibia or femur) you would have to ensure the material is both strong enough to act as a cement, but not so brittle that it would fail due to low fracture toughness. The physical properties of a polymer stem from the intermolecular interactions occurring between individual polymer molecules; thus the molecular characteristics we have discussed up to this point are of extreme importance. As you will see in the following text, the four most fundamental molecular characteristics of polymer chains that determine the physical behavior of a polymer are chain stiffness, chain composition or polarity, chain architecture or regularity, and molecular mass. They determine two important temperatures that characterize polymer molecules: T_g , the glass transition temperature, and T_m , the crystalline melting temperature. T_m is only present when there are crystalline regions in a polymer.

In Fig. 1.3.2.2, we see polypropylene molecules extended into planar zigzags. Although this is a convenient way to draw polymer molecules, this type of extended structure is rarely seen in nature. More often, polymer molecules are found as unorganized and three-dimensional structures called a *random coil*. In an *amorphous* structure, each random coil is highly entangled with its neighbors. Polymers in the rubbery state or the glassy state have this amorphous

molecular arrangement. Under certain conditions, some polymers will arrange themselves into highly organized crystalline domains resulting in a semicrystalline material. Each of these states will now be explored in more depth.

The Rubbery State

Rubbery polymers are amorphous. However, the random coils have enough thermal energy for rotation to occur around single bonds. If you were able to look at polymer molecules in the melt state, you would see that each random coil is continuously changing shape (conformation). This molecular motion becomes more intense as the thermal energy in the system increases. Macroscopically these materials are soft, flexible, and extensible, due to the molecular motion available to the molecules.

The Glassy State

As the polymer system is cooled, rotation around bonds becomes hindered due to energy barriers created by a segment of a chain having to move (rotate) past a neighboring segment. As the temperature drops, the rate of segmental motion in a polymer chain becomes slower and slower, and the chain gets stiffer and stiffer. As the system approaches the T_g the interpenetrated random coils become frozen in space. This is called the glassy state. A material below its T_g is called a glass because it is hard, stiff, and brittle. Molecules in the glassy state can no longer rearrange themselves under applied stress, so deformation results in straining the secondary interactions between molecules. The opposite occurs when an amorphous polymer is heated: the amorphous region goes from hard and glassy, to “leathery,” to rubbery, and if the material is not cross-linked, it will eventually flow as a viscous fluid and can be processed into shapes.

RAMEN NOODLES: GLASSY VERSUS RUBBERY POLYMER CHAINS

If you are reading this you are probably a college student, which means you are very familiar with Ramen noodles. A package of noodles can be cooked in about 10 min. When you first remove the noodles from the package, you will notice that the individual noodles are rather random in shape and intertwined with their neighbors. Furthermore, before boiling, these noodles are very rigid and fixed in relation to one another. This food product is a pretty good example of a polymer in the glassy state, where each noodle represents one polymer molecule. As the noodles are boiled, they become flexible and can easily change their shape and slip around; however, they retain their intertwined character. These noodles are a good example of a polymer material in the rubbery state.

The Semicrystalline State

All polymer systems form glasses at sufficiently low temperatures. However, as a melt is cooled, certain polymers have the ability to pack into a regular lattice, leading to the formation of stable crystalline domains. In PE, these stable crystalline domains are formed by chains in the planar zigzag conformation, while the crystalline chains

TABLE 1.3.2.1 Physical Properties and Equilibrium Water Absorption of Common Polymeric Biomaterials

Material	Tensile Modulus (GPa)	Tensile Strength (MPa)	Elongation at Break (%)	Water Absorption (%)
Polyethylene	0.8–2.2	30–40	130–500	0.001–0.02
Poly(methyl methacrylate)	3–4.8	38–80	2.5–6	0.1–0.4
Polytetrafluoroethylene	1–2	15–40	250–550	0.1–0.5
Poly(lactide)	3.4	53	4.1	<0.5
Poly(hydroxyethyl methacrylate) ^a	0.29	0.15	71	40
Polypropylene	1.6–2.5	21–40	100–300	0.01–0.035
Poly(ethylene terephthalate)	3–4.9	42–80	50–500	0.06–0.3
Poly(ether ether ketone) (Liu et al., 2018)	3.6–5.0	92	9	0.1
Poly(vinylidene fluoride) (Shackelford and Alexander, 2001)	1.7–2.0	5.2 – 8.6	200–300	0.03–0.06
Poly(lactic-co-glycolic acid) (Gentile et al., 2014; Avgoustakis, 2008)	2.0–4.0	6.0–10.0	3–10	0.06–0.08

^aTensile properties were measured after the polymer was equilibrated with water.

in syndiotactic poly(vinyl chloride) (PVC) have a helical conformation. Since only a portion of the long polymer chains can crystallize (some segments will not be able to pack into the crystallites) this state is called semicrystalline. Crystallites act to stiffen and reinforce the bulk material, and extend the stiffness and strength properties of a material well above the T_g until the T_m is reached.

The Physical Behavior of Linear and Amorphous Polymers

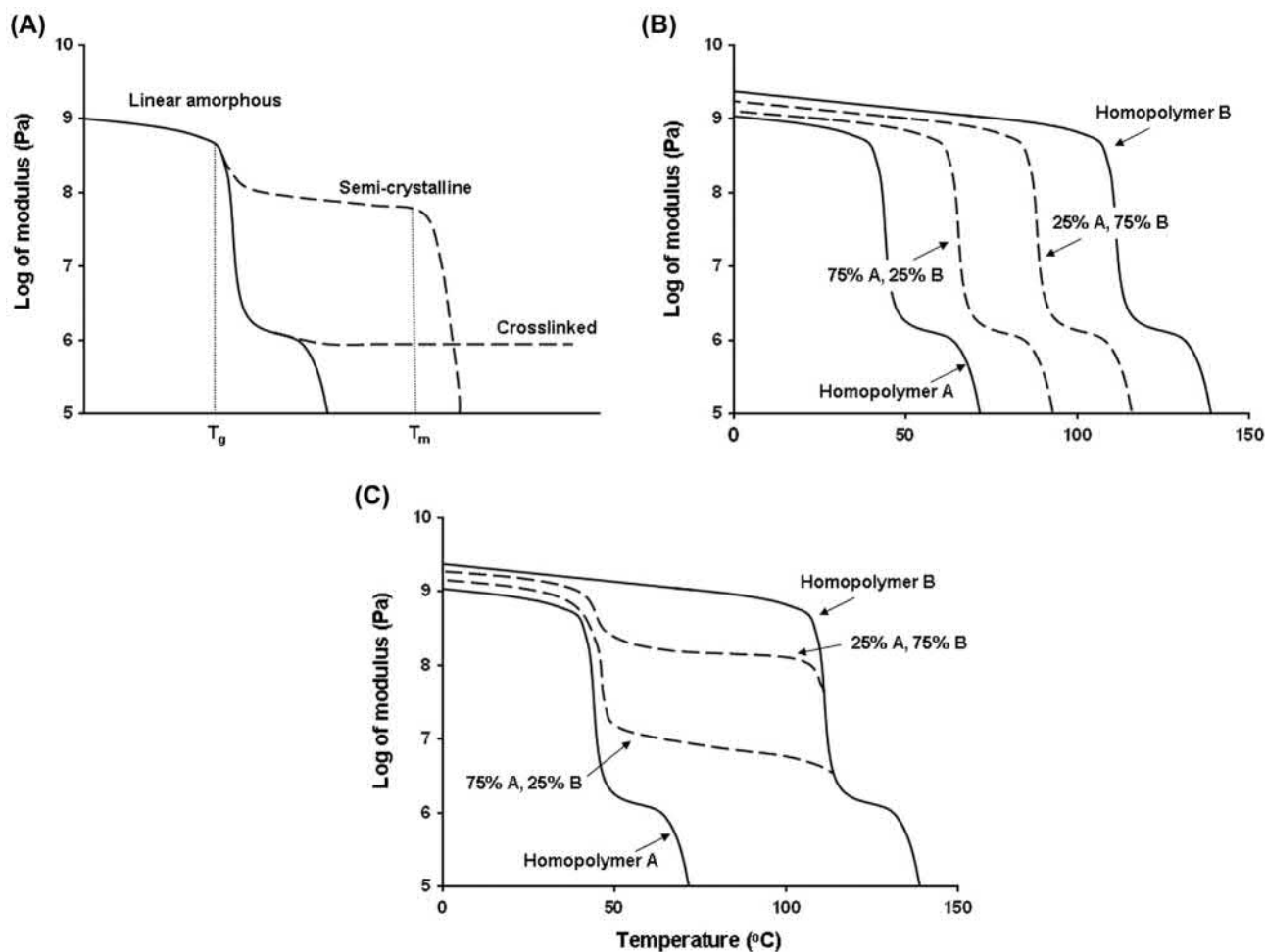
Unlike metals, which are held together by metallic bonds, and atomic crystals, which are held together by covalent bonds, polymer materials are held together by secondary interactions such as van der Waals forces, dipole–dipole interactions, and hydrogen bonding. For this reason, polymers are often mechanically weaker than other classes of materials; however, they can display physical behavior more similar to native tissue.

The simplest polymer system is an amorphous rubbery or glassy polymer composed of linear polymer chains. When rubbery materials are strained, the polymer molecules are able to deform and extend resulting in a material that is macroscopically soft and weak, yet highly extensible. However, as the T_g of the material approaches and exceeds the environmental conditions, the material becomes a glass and is much stronger and stiffer. The mechanical behavior of polymer systems is often probed through stress–strain analysis. From this analysis, several key material properties can be determined: modulus (a measurement of material stiffness); tensile strength (the

stress at failure); and percent elongation (the amount of deformation at failure). The room temperature mechanical properties of several polymeric biomaterials are presented in Table 1.3.2.1.

The Physical Behavior of Other Physical States

Cross-linking, crystallinity, and copolymerization greatly affect the physical behavior of polymer systems, and controlling these parameters gives polymer scientists ways of specifying the physical behavior of a polymer system. Fig. 1.3.2.6 illustrates how each of these parameters affects polymer modulus as a function of temperature. In Fig. 1.3.2.6A we see the standard modulus–temperature behavior of a linear and amorphous polymer system (solid line). Below the T_g the material is a glass and has a high modulus. However, at the T_g we see a dramatic drop in modulus due to the increased mobility within the polymer structure. At temperatures just higher than the T_g we see a plateau on the curve where modulus declines more slowly with temperature. This is called the rubbery plateau, and in this region the polymer is still solid-like but soft, flexible, and extensible. Eventually, as the temperature is increased more, we see the modulus curve take another drop corresponding to the material beginning to flow. Notice that amorphous materials do not have a melting temperature. Melting refers to the loss of crystallinity, and since these materials are noncrystalline, they never truly melt. As we will discover later, the architecture of the polymer chains, especially where there is a specific tacticity, determines if segments of a polymer chain can pack together and form crystallites.



• **Figure 1.3.2.6** Modulus versus temperature behavior for: (A) linear amorphous, semi-crystalline, and cross-linked polymer; (B) random copolymer; and (C) block or graft copolymer.

In Fig. 1.3.2.6A we can also see the modulus–temperature behavior of a semicrystalline material. In this curve we see a small drop in the modulus at the T_g , due to the onset of backbone rotation in the amorphous regions of the polymer. Since crystallites are unaffected by the T_g , the magnitude of this drop is greatly affected by the amount of crystallinity in the system. After the T_g we see that the modulus holds steady until the melting point, illustrating that crystallinity is a way to increase the window of temperatures in which a polymer can be employed. At T_m the crystallites melt and the polymer begins to flow. The ability of chains to crystallize is a special feature of chain architecture that is sometimes called “symmetry” or “regularity,” i.e., a streamline profile in cross-section with small side groups that allows the chain segments to pack into crystallites. In special cases, a stereospecific property of some chains with asymmetric atoms is called tacticity; it can also control the ability of a polymer to crystallize. Polymers without asymmetric atoms in the backbone (and therefore having no tactic isomers) can crystallize along with isotactic and syndiotactic polymers. However, atactic materials cannot organize themselves into a lattice due to the irregularity in their chemical structure, and are

therefore permanently amorphous. Branched polymers have difficulty crystallizing, since the branch sites interfere with the ability of the polymer to organize into a lattice. In cases where branch sites are purposefully incorporated into the material, they will lower the extent of crystallization (such as in the case of low-density PE).

Also, in Fig. 1.3.2.6A one can see the modulus–temperature behavior of a cross-linked polymer. Again, at the T_g you will see a decrease in modulus due to the onset of single bond rotation; however, above the T_g the modulus is relatively independent of temperature because the crosslinks act to tether the polymer chains in place. In fact, the crosslinked polymer will not experience a large decrease in modulus until the temperature is high enough to begin thermally degrading the bonds holding the structure together.

Copolymerization of more than one monomer unit could also be used to control the physical behavior of a material. Fig. 1.3.2.6B shows modulus–temperature curves for a random copolymer system where the shape of the curve is maintained, but shifted laterally. If block or graft copolymers are produced, one would see the distinct transition of both materials used to generate the copolymer, as seen in Fig. 1.3.2.6C.

TABLE 1.3.2.2 Structural Factors Affecting the Glass Transition Temperature and the Crystalline Melting Point of Polymers

Material	T_g (°C)	T_m (°C)
 Polyethylene	-113 to -103	125–135
 Polydimethylsiloxane	-125	-40
 Polypropylene ^a	-30 to -3	160–180
 Polyisobutylene	-73	44
 Polybutylene ^a	-38 to -33	126–139
 Poly(vinyl chloride)	87	150 ^b
 Poly(tetrafluoroethylene) (Calleja et al., 2013)	-110 ^c	330 ^b
 Poly(vinylidene fluoride) (Cao et al., 2016)	-42 to -35	162 to 167 ^b

^aIsotactic.
^bDecomposition temperature.
^cReports vary drastically.

Table 1.3.2.2 provides the repeat unit, T_g , and T_m of common polymers. Chemical characteristics that facilitate backbone rotation result in lower T_g materials, while structural characteristics that hinder backbone rotation result in higher T_g materials. For instance, the $-\text{Si}-\text{O}-$ bond in polydimethylsiloxane is unhindered, and is a freely rotating bond down to very low temperatures, resulting in a very low T_g . As pendant group bulkiness increases, the polymer chains along the backbone have more difficulty rotating due to steric hindrances, illustrated by the much higher T_g of polystyrene in comparison with PE. However, pendant groups of four or more carbon atoms tend to create “free volume” around the polymer backbone, making main chain rotation easier, and the T_g may be lowered, as seen in the alkyl methacrylate family as the alkyl group increases in length. Increased polarity, especially where hydrogen bonds may act between side groups, increases the polar interactions between chains,

slowing the rate of main chain rotations and resulting in a higher T_g . In general, the structural factors that affect the T_g (backbone flexibility, pendant group structure and polarity, main chain symmetry and polarity) similarly affect T_m , as illustrated by the data in Table 1.3.2.2.

A TRAGEDY CAUSED BY A CHANGE IN TEMPERATURE AND ITS EFFECT ON T_g AND POLYMER PROPERTIES

In 1986 the space shuttle *Challenger* broke apart during lift-off, killing the seven crew members aboard and halting all US space flights for the next two and a half years. This tragedy was caused by the failure of an O-ring—a polymer gasket—connecting the shuttle’s external fuel tank to one of its solid rocket boosters. The O-ring failed, in part, due to the abnormally cold weather on the morning of the launch, causing stiffening of the gasket as the polymer approached its T_g , and that undermined its ability to form a tight seal. The gasket failure allowed a tongue of flame to reach both the solid rocket booster and the external fuel tank, and resulted in the structural failure of both. The shuttle then broke apart due to extreme aerodynamic loads (see NASA, 1986).

Characterizing a Polymer's Physical State and Behavior

Crystallinity plays a large role in determining polymer behavior. The *degree of crystallinity*—a measurement of how much of the polymer is incorporated into crystalline regions—can be studied with techniques such as measurement of density, X-ray diffraction (XRD), and IR spectroscopy. In XRD experiments a polymer sample is bombarded with X-ray radiation and the intensity of the scattered X-rays is measured as a function of scattering angle. A fully amorphous material would produce a very broad peak, covering all scattering angles. However, crystalline materials will produce sharp peaks at specific angles. Furthermore, the placement of these peaks corresponds to a particular crystalline structure. By integrating the areas under the amorphous peak and the crystalline peaks, and then calculating the fractional area of the crystalline peaks relative to the total area, a researcher can determine the degree of crystallinity.

Stress–strain analysis provides information about the mechanical behavior of a polymeric biomaterial. In this test a polymer sample of known dimensions is deformed at a given rate, and the force needed to cause the deformation is recorded.

Measuring the Transition Temperatures Between States

Measuring transition temperatures (T_g and T_m) is important to understanding how a material will behave in a certain application. Two common methods for determining the transition temperatures in polymer systems are differential

scanning calorimetry (DSC) and dynamic mechanical analysis (DMA). In DSC experiments a polymer sample is heated at a constant temperature rate (generally 10–20°C/min) and the amount of heat supplied to the sample to obtain the temperature increase is recorded. The output from this experiment is a plot of supplied heat versus temperature. The curves exhibit a step change at T_g due to a change in heat capacity at the onset of backbone rotation. An endothermic peak occurs in the DSC spectra at the melting point of the polymer due to the increased energy needed to melt the crystalline regions.

When performing a DMA experiment, one measures the modulus (stiffness) of the material over a temperature range, yielding the types of curves shown in Fig. 1.3.2.6. The T_g of the material is physically observed as the softening point of the material. In a DMA study the modulus drops by approximately three orders of magnitude at the T_g . At the T_m , another drop is observed, associated with softening due to melting of the polymer crystalline units and the onset of flow behavior.

Interactions With Water

Biomaterials are often employed in highly hydrated environments, so their interaction with water is an important design characteristic. Relatively nonpolar and electrically neutral polymers such as PE or poly(methyl methacrylate) (PMMA) are very hydrophobic and absorb <1 wt% water. However, as polarity and, in some cases, ionic character are incorporated into the polymer, it will imbibe more water due to polar (and coulombic) interactions. For instance, poly(hydroxyethyl methacrylate) (PHEMA) (the first soft contact lens) absorbs approximately 40 wt% water due to the polar hydroxyl moieties of the pendant groups. Eventually, if enough polarity or ionic character is incorporated into the material, it becomes water soluble, e.g., poly(ethylene glycol) and poly(methacrylic acid). The equilibrium water absorption of common biomaterials is presented in Table 1.3.2.1.

One can tailor the interaction of a polymer with water in several ways, such as by controlling the ratio of hydrophobic and hydrophilic monomers in a copolymer. Also, crystalline regions in polymers usually resist infiltration of water molecules. If a polymer is processed in a way to control the degree of crystallization, the swelling character of the polymer can thereby be controlled. Cross-linked hydrophilic polymers generate hydrogels that can imbibe upward of 200 wt% water. However, increasing the cross-link density can reduce the swelling of such a material, providing another method of tailoring the interactions of a polymer with water.

In addition to swelling behavior, the surface hydrophilicity of a polymer is also an important design feature. Though it is beyond the scope of this chapter, you will learn elsewhere in this text that a biomaterial surface can be physically or chemically coated with peptides or proteins to enhance cellular attachment and growth. Surfaces may also

be treated to be “antifouling,” i.e., to resist protein adsorption and cell attachment.

Measuring the Hydrophilicity of Polymer Materials

Equilibrium swelling experiments are performed to study the interactions between bulk polymer and water. A dry sample of polymer of known mass is submerged in water, and the change in mass is recorded over time. Eventually the sample weight will become constant, and from this value the equilibrium water absorption can be calculated.

The surface hydrophilicity is probed through either static or dynamic contact angle experiments. In static experiments, a droplet of water is placed on a flat polymer surface and the angle the droplet makes with the material (as measured through the water phase) is measured. The degree to which water spreads on the surface is a measurement of the polarity of the interface. For instance, a material with a water contact angle of 20 degrees has a *more polar* surface than a material with a water contact angle of 95 degrees.

The surface composition of some materials can change depending on the external environment. For instance, a polymer may expose its hydrophobic portions to an air environment, yet it will reorganize its surface to display its hydrophilic portions when exposed to water (unless the interface has been oxidized to increase hydrophilicity). Dynamic contact angle experiments allow a researcher to probe the ability of the surface molecules to rearrange depending on the phase to which they are exposed. In such an experiment a polymer film is dipped into a bath of water and then removed. The force between the polymer sample and water is measured during immersion and retraction, and converted into contact angles. Materials with surface molecules that have the mobility to rearrange in air versus water will exhibit contact angle hysteresis, and the advancing and receding contact angles will not be the same. The advancing angle is always greater than the receding angle.

Degradation Characteristics

Depending on the application, one may desire a polymer material that is either biodegradable or biostable. For instance, a polymer that will be used for a tissue-engineered scaffold needs to be biodegradable, and to “disappear” or be resorbed as functioning tissue is regenerated by cells. However, some biomaterials, such as dental implants, vascular grafts, and intraocular lenses need to be biostable so that they retain their function for the lifetime of the patient. The main type of polymer degradation reaction occurring in the body is *hydrolysis*, i.e., the reaction of the polymer backbone bonds with water, which results in the cleavage of those bonds and loss of the polymer's mechanical properties. Eventually the polymer breaks up into small fragments that are metabolized and/or dissolve, and the residual molecules are eliminated from the body. The ultimate stability of polymers in the body

depends on two key factors: water absorption and the susceptibility of main chain bonds to hydrolysis.

The carbon–carbon single bond is very stable and those materials with main chain C–C bonds, such as PE, PP, or PMMA, do not lose their properties due to degradation of the backbone. However, the presence of other bonds in the polymer backbone (*heterochain* polymers) can lead to hydrolytic breakdown, and the rate of this hydrolysis is greatly affected by the polymer's molecular structure. For instance, the hydrolysis of amide bonds in nylon 6,6 is so slow that it is almost nonexistent at physiological conditions, making polyamide biomaterials relatively biostable. On the other hand, water can hydrolyze ester bonds (–CO–O–C–) present in some polymers. For example, poly(lactide-*co*-glycolide) copolymers (Fig. 1.3.2.5) degrade by such hydrolysis. An exception to this is poly(ethylene terephthalate) or PET, which is crystalline and hydrophobic, so that even though it has main chain ester bonds, water absorption is so low it is resistant to hydrolysis. The reader is referred to Chapter 2.4.1 on degradation of biomaterial implants and to Chapter 2.5.12 on drug delivery from degradable matrices for further discussion of this important topic.

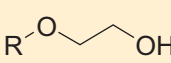
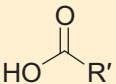
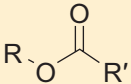
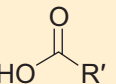
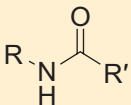
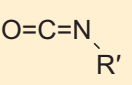
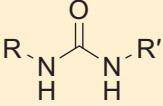
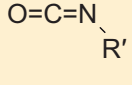
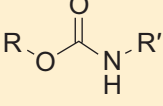
Polymer Synthesis

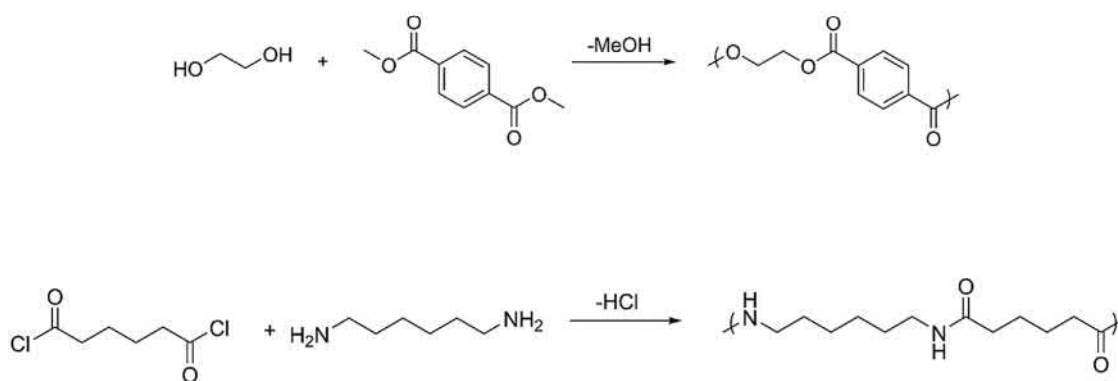
A polymer scientist who understands structure–property relationships can design polymer molecules to fit a particular application. In this section we discuss the synthesis of polymers.

Polymerization Mechanisms

Condensation and *addition polymerization* are the two most common methods for polymer synthesis. In organic chemistry, reactions are described that occur between different functional groups. For instance, a carboxylic acid group can react with an amine group to form an amide bond and liberate a water molecule. Table 1.3.2.3 illustrates some of these major organic reactions for bond formation. The same reactions as those seen in Table 1.3.2.3 are used to produce a number of condensation polymers. The only difference is that instead of using monofunctional molecules (which contain only one functional group) difunctional monomers (which contain two functional groups) are used. Fig. 1.3.2.7A illustrates the formation of a PET repeat unit through the

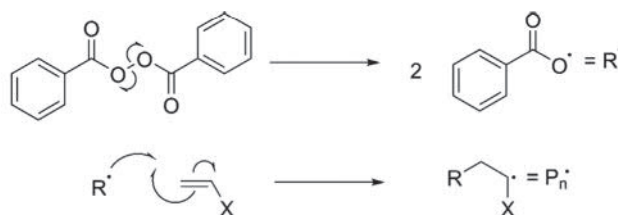
TABLE 1.3.2.3 Examples of Common Organic Reactions

Reactants		Product
R–OH	+ 	
Alcohol	Epoxide	Ether bond
R–OH	+  $\xrightarrow{-H_2O}$	
Alcohol	Carboxylic Acid	Ester bond
R–NH ₂	+  $\xrightarrow{-H_2O}$	
Amine	Carboxylic Acid	Amide bond
R–NH ₂	+ 	
Amine	Isocyanate	Urea bond
R–OH	+ 	
Alcohol	Isocyanate	Urethane bond



• **Figure 1.3.2.7** Condensation reactions between: (A) ethylene glycol and dimethyl terephthalate to produce poly(ethylene terephthalate); and (B) adipoyl chloride and hexamethylenediamine to produce Nylon 6,6.

(A) Initiation: Benzoyl peroxide initiator undergoes homolytic cleavage to produce two free radicals, which can then initiate polymerization by adding to a monomer unit.



(B) Propagation: Polymer chain ends continue to add monomer units, increasing the chain length.



(C) Termination: Termination of polymer chain ends can occur by two methods. Combination occurs with two radical chain ends coupling to result in linking of two polymers. Disproportionation occurs when a proton is transferred from one chain to another, resulting in an elimination reaction.



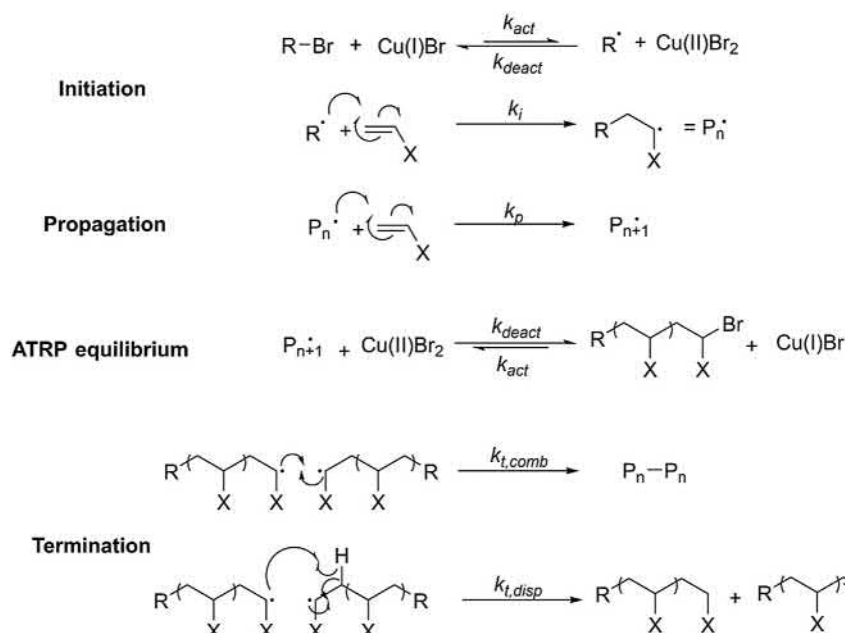
• **Figure 1.3.2.8** Free radical polymerization of a vinyl monomer to a polymer chain: (A) the initiation step where the free radical is produced and is added to a monomer unit; (B) the propagation step where the chain end free radical adds across the vinyl monomer's double bond; and (C) the termination step where two radicals react to produce dead polymer chains. In the schematic, X represents a generic side group.

reaction of ethylene glycol and dimethyl terephthalate, while Fig. 1.3.2.7B shows the production of a nylon 6,6 repeat unit through the reaction of adipoyl chloride and hexamethylenediamine. Notice that all of the monomers are difunctional molecules. Furthermore, the products from each reaction are also difunctional, allowing further, similar reactions to gradually produce higher molecular mass linear polymer chains.

The addition or chain-growth polymerization mechanisms are quite different from condensation polymerization. Chain-growth polymerization includes radical polymerization but also cationic polymerization and anionic polymerization. In chain-growth polymerization, the only chain-extension reaction step is

the addition of a monomer to a growing chain that possesses an active center such as a free radical or ion (cation or anion). Once the growth of a chain is initiated by formation of an active species, chain propagation is usually rapid by addition of a sequence of monomers. Chain-growth polymerization often involves the linking together of molecules incorporating unsaturated double (alkene) or triple (alkyne) carbon-carbon bonds. Chain-growth polymerization is used heavily by industry in the manufacture of polymers such as PE, PP, polyisobutylene, and PVC.

Fig. 1.3.2.8 is a schematic of a typical radical polymerization. Chains are initiated by radicals, formed from an initiator, which then adds to the monomer. These chains



• **Figure 1.3.2.9** Atom transfer radical polymerization (ATRP) of a vinyl monomer. Initiation begins when a radical species is formed through redox chemistry. Propagation occurs until the growing chain end is reversibly deactivated in the ATRP equilibrium. Termination can occur through chain combination or chain disproportionation by hydrogen abstraction (Wang and Matyjaszewski 1995; Ribelli et al., 2019).

propagate by sequential addition of monomer units. Chain termination occurs when the propagating radicals self-react by combination or disproportionation. Continuous initiation and termination yield a steady-state radical concentration of $\sim 10^{-7} M$ and the lifetimes of individual chains are typically $\sim 5\text{--}10 s$ within a reaction span that may be many hours. In the absence of chain transfer, the lengths (DP) of the chains formed during the early stages of polymerization are high. The breadth of the molecular mass distribution is governed by statistical factors. The molecular mass distribution (\mathcal{D}_m) is ideally 2.0 if termination is by disproportionation or chain transfer, or 1.5 if termination is by combination.

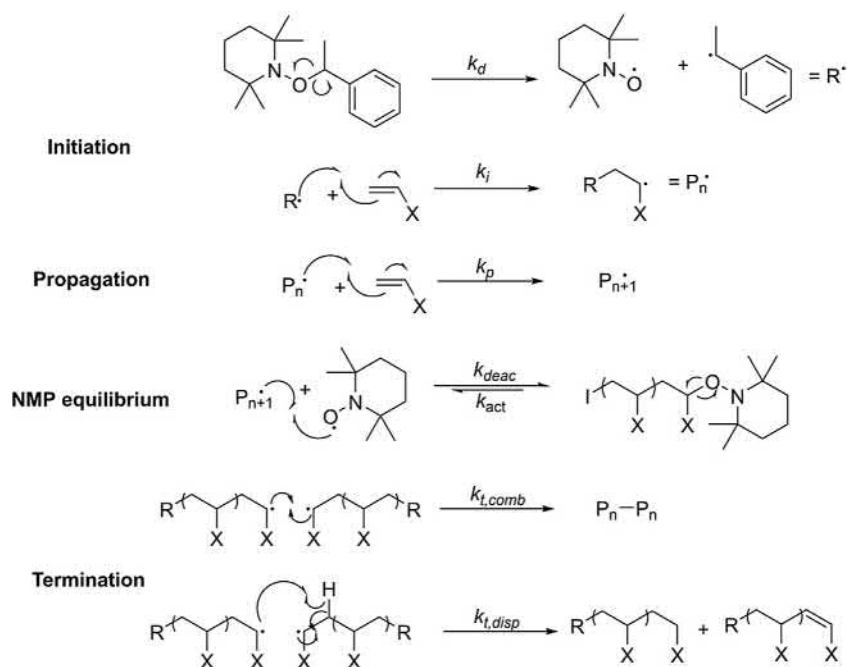
There are newer polymerization techniques that are known as “controlled living free radical polymerizations” or “reversible-deactivation radical polymerizations” (RDRPs) where the growth, chain transfer, and termination reactions are controlled to yield polymers with a desired molecular mass and narrow \mathcal{D}_m . The most popular of these techniques are known as atom transfer radical polymerization (ATRP) (Kato et al., 1995; Wang and Matyjaszewski, 1995), nitroxide-mediated radical polymerization (NMP) (Moad and Rizzardo, 1995; Nicolas et al., 2013), and reversible addition-fragmentation chain-transfer polymerization (RAFT) (Chiefari et al., 1998). A commonality between these techniques is the use of reversible activation and deactivation reactions to limit the concentration of active chains at any one time, effectively increasing the polymerization control.

ATRP is a catalytic process that can be mediated by several redox-active transition metal complexes. In ATRP, radicals are generated through a reversible redox process in which the transition metal complex undergoes a single-electron

oxidation with simultaneous abstraction of a halogen atom, X, from a dormant species, R–X. This process, which generates an active chain end, follows rate constants k_{act} and k_{deact} , corresponding to the formation of the active and dormant species, respectively. The active species propagates and terminates as in conventional free radical polymerization with a rate constant k_p and a termination constant k_t , but the low concentration of active species prevents significant termination events. The result is well-defined polymer chains with defined end groups and narrow molecular mass distribution ($\mathcal{D}_m < 1.2$) (Fig. 1.3.2.9).

Like ATRP, NMP is also based on a reversible termination mechanism, but this time between a propagating radical and a stable nitroxide radical. At high temperatures, the initiator species undergoes homolytic cleavage to produce a stable nitroxide radical and an alkyl radical that can initiate the polymerization. The chain is then able to propagate or form the dormant species by addition to the nitroxide radical. This reversible termination event establishes the activation–deactivation equilibrium between the dormant and active species. As with ATRP, termination events are possible, but not significant under appropriate conditions (Fig. 1.3.2.10).

RAFT is also an RDRP technique as with ATRP and NMP, but instead uses reversible radical transfer reactions to limit the number of active chain ends. While ATRP and NMP rely on reversible termination events to limit the concentration of radicals, RAFT relies on these reactions to reversibly transfer the radical to the chain transfer agent (CTA), thus temporarily deactivating the polymer chain. A thiocarbonylthio compound, such as dithioesters, thiocarbamates, or xanthates, serves as a CTA, and is required for



• **Figure 1.3.2.10** Nitroxide-mediated radical polymerization (NMP) of a vinyl monomer. Initiation begins through homolytic cleavage of a nitroxide-containing molecule to generate radical species. Propagation continues until the active chain-end is reversibly deactivated by the nitroxide species in the NMP equilibrium. Termination can occur through chain combination or chain disproportionation by hydrogen abstraction (Moad and Rizzardo 1995; Nicolas et al. 2013).

RAFT polymerization. RAFT offers excellent control over the polymerization, such as predefined molecular weights and narrow molecular mass distributions, and is experimentally simple compared to ATRP, often involving only the addition of a CTA to the conventional free radical polymerization (Fig. 1.3.2.11).

The reader is referred to recent polymer textbooks (see Bibliography) for further reading on polymerization and controlled radical polymerization techniques.

Using Synthesis Conditions to Build the Desired Polymer

The first step toward producing a material with the desired behavior is selection of the appropriate monomer species. For instance, a researcher developing a bone cement could select a monomer with a bulky pendant group to produce a glassy polymer, while another biomaterials scientist creating a hydrogel could select a monomer with a polar pendant group to improve hydrogen bonding interactions with water.

Physical behavior can be further tailored through crystallinity and cross-linking. Addition polymers containing asymmetric carbon atoms are generally atactic, meaning the polymer will be predominantly amorphous. However, one can use special catalysts to produce isotactic or syndiotactic addition polymers that can crystallize.

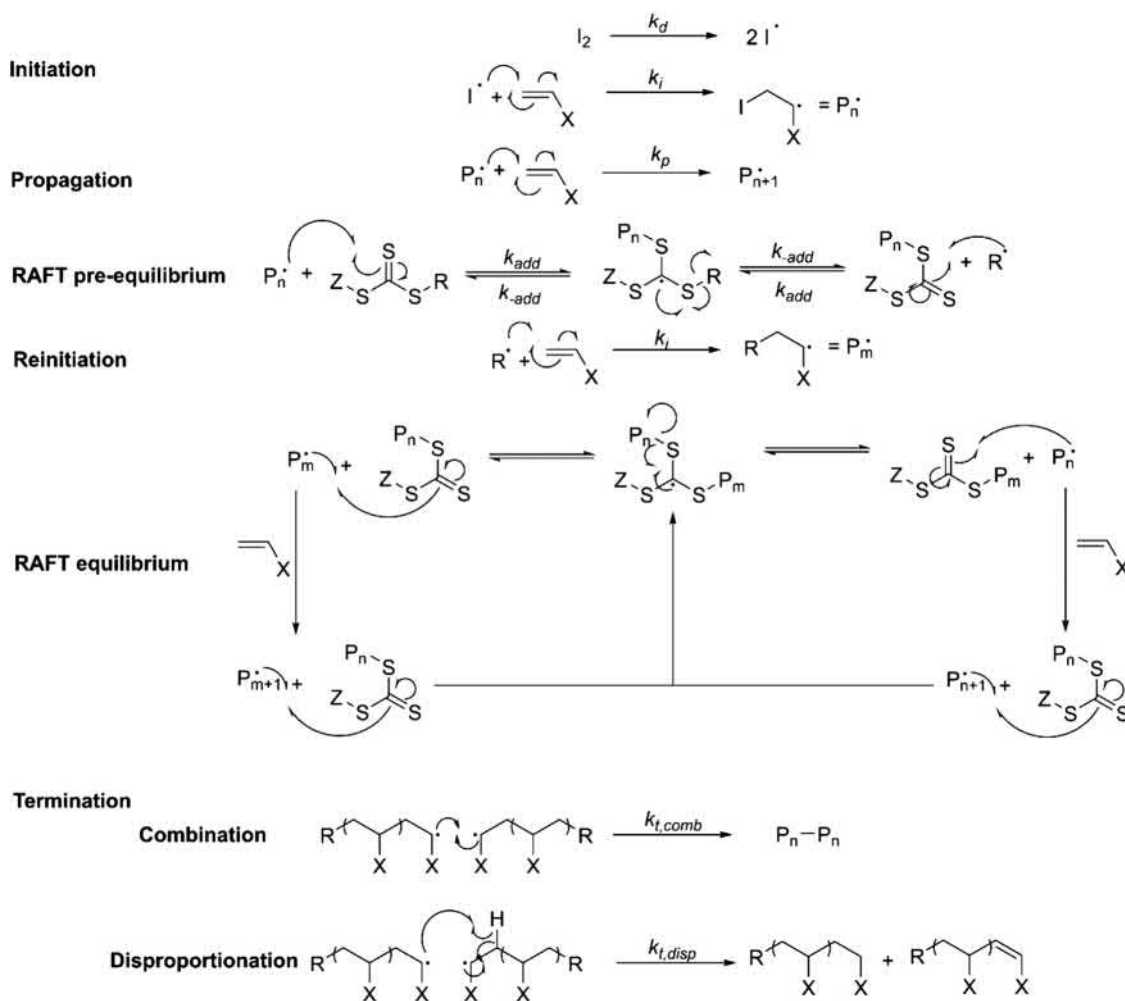
In condensation polymerization, monomers containing two functional groups produce linear polymer chains.

However, if one adds a small amount of a monomer with three or more functional groups, cross-linked materials are produced. Similarly, addition of vinyl-type monomers containing two or more vinyl groups can produce networked materials. Linear polymers can also be cross-linked after synthesis through techniques such as vulcanization, or UV or gamma ray irradiation.

SO WHAT IS A NETWORK POLYMER?

A common example of a network polymer is an automobile tire. The main polymer component of a tire tread is a polystyrene/polybutadiene copolymer (SBR). The individual SBR polymer chains are covalently cross-linked into a network polymer through reaction with sulfur (a process known as vulcanization). There are other additives in car tires (carbon black, for instance, which gives the tire its black color); however, the polymer component of the tire is actually one very large, covalently cross-linked molecule.

If degradation characteristics are desired, they can be achieved through control of the composition of the backbone groups. Addition or chain-growth polymerization produces polymers with carbon-carbon backbones that are generally biostable. Sometimes condensation polymerization mechanisms may produce a water molecule as a residual. The reverse reaction can occur between the polymer bonds being formed and the water molecule, resulting in hydrolytic degradation of the polymer. In that case, water must be removed as it is formed.



• **Figure 1.3.2.11** Reversible addition-fragmentation chain-transfer (RAFT) polymerization of a vinyl monomer. The initiation phase occurs with homolytic cleavage of an initiator to form two radicals, followed by addition to the double bond of the monomer. Propagation continues until radicals are transferred to the RAFT chain transfer agent (CTA), deactivating the polymer chain. Homolytic cleavage of the CTA “R” group reinitiates, forming a new polymer chain. The polymer chains then enter the RAFT equilibrium phase, where polymer chains alternate between active propagation and deactivated dormant phases. Termination can occur through chain combination or chain disproportionation by hydrogen abstraction (Chieffari et al., 1998; Perrier 2017).

Case Studies

We have discussed the basic molecular characteristics that govern polymer behavior, and how to exploit chemistry to build polymers with the desired characteristics. Table 1.3.2.4 compiles the chemical characteristics of several polymeric biomaterials, and reports their clinical applications. We will also look in more depth at the development of three polymer biomaterials that have achieved clinical success.

The Present and the Future

In the early days of biomaterials science, materials were not designed for biomedical applications. Preexisting materials were used and their biocompatibility was empirically assessed. As you will learn through this book, much of the current work in the biomaterials field focuses on creating materials that exhibit specific interactions with biology to achieve improved performance and better healing.

TABLE 1.3.2.4 Common Polymeric Biomaterials With Their Applications and the Properties That Make Them Useful in the Medical Field

Material	Characteristics	Uses
Poly(methyl methacrylate)	Hydrophobic polymer that is hard, rigid, and biostable. The amorphous material is clear allowing light transmittance	Bone cement Intraocular lenses Hard contact lenses
Polyacrylamide	Cross-linking produces a hydrogel with molecular-sized pores that allow the gel to be used as a separation medium	Separation gel used in electrophoresis
Poly(acrylic acid)	The liquid monomer can be cured with a photoinitiator. If inorganic salts are added, ionic cross-linking can occur. The material is glassy and rigid, and has the potential to bond to enamel.	Glass ionomer cement used in dental restoration
Polyethylene (high density) (PE)	Low-density PE cannot withstand sterilization temperatures; however, high-density PE has good toughness and wear resistance	Tubing for drains and catheters Prosthetic joints
Poly(vinyl chloride) (PVC)	PVC is plasticized to make flexible materials. This material is used for short-term applications since plasticizers can be leached resulting in embrittlement of the material.	Tubing Blood storage bags
Polypropylene (PP)	Isotactic PP is semicrystalline, has high rigidity and tensile strength, and good biostability	Nondegradable sutures Hernia repair
Polydimethylsiloxane	Due to its silicone backbone, this material has a very low T_g making it extremely flexible and providing it with good fatigue resistance at physiological conditions	Finger joints Heart valves Breast implants Ear, chin, and nose reconstruction
Poly(ethylene terephthalate)	The aromatic rings in the backbone generate a polymer with a high melting point ($T_m = 267^\circ\text{C}$). It is semicrystalline and possesses excellent tensile strength.	Vascular grafts Fixation of implants Hernia repair Ligament reconstruction
Cellulose acetate	Unique transport properties make it excellent for use in the separation of complex biological mixtures	Dialysis membranes Osmotic drug delivery devices
Polyether ether ketone (PEEK)	PEEK is a semicrystalline polyaromatic thermoplastic. It is chemically resistant and displays high thermal transitions ($T_g = 145^\circ\text{C}$, $T_m = 334^\circ\text{C}$). It is often used as a composite material for biomedical applications.	Engineering plastics Cranial defect repair Dental implants
Poly(lactic acid) (PLA)	PLA is a biodegradable polyester that can range from amorphous to crystalline depending on the stereochemical makeup, which also influences its mechanical properties	3D-printing filaments Surgical screws, pins, and meshes Drug delivery
Poly(lactic-co-glycolic acid)	This copolymer shows enhanced processability over the corresponding homopolymers and allows for tunable glass transition temperatures and degradation rates based on composition	Degradable sutures Implantable meshes

CASE STUDY I: RESORBABLE SUTURES**What Problems can Occur?**

Sutures are often needed to hold tissue together after injury, incision, or surgery. If a nonbiodegradable material is used to suture an internal wound, a secondary surgery would be necessary to remove the stitches after healing.

What Properties are Required of the Biomaterial?

For a suture material, the most fundamental property required is appropriate tensile strength, so the wound does not reopen during healing. Also, the suture materials should degrade in the body during healing, making retrieval or removal unnecessary. Further, the degradation must occur at an appropriate rate, and the degradation products must be nontoxic.

What Polymeric Biomaterial is Used?

Early resorbable sutures were made from sheep or beef gut. However, synthetics are more commonly used due to their ease of handling, low cost, consistent performance, and low chance of disease transfer. One commonly used material is a poly(lactide-co-glycolide) copolymer. This is a random copolymer so the material is permanently amorphous; however, it still possesses the high tensile strength and flexibility required for this application. Also, the material biodegrades through hydrolysis of the ester bonds in the polymer backbone into lactic and glycolic acids. Both of these chemicals occur naturally in the body's metabolic pathway, and so are nontoxic in small amounts. Furthermore, the ester bonds in the lactide and glycolide repeat units hydrolyze at different rates, allowing the degradation rate to be tailored.

CASE STUDY II: SOFT CONTACT LENSES

What Problem was Addressed?

The first contact lens, developed in 1888, was made of glass, and could not be worn for long periods of time. A generation of PMMA lenses were developed (hard contact lenses) and experienced clinical success. However, these rigid lenses caused eye irritation, and did not allow enough oxygen to be transported to the cornea of the eye (an avascular tissue that must receive oxygen from the environment for normal metabolism to occur). The Czech scientists Wichterle and Lim wanted to make a lens that was more comfortable and would allow better transport of oxygen to the cornea. (Otto Wichterle and Drahoslav Lim, "Process for producing shaped articles from three-dimensional hydrophilic high polymers", US Patent 2,976,576, March 28, 1961.)

What Properties Were Required of the Biomaterial?

Strong mechanical properties were not a major factor in the design of soft contact lenses, since the device does not need to support large stresses. However, a successful lens needed to: (1) be transparent so that clear vision could be achieved; (2) be dimensionally stable to maintain the optical correction desired; (3) be soft and flexible to minimize eye irritation; (4) allow appropriate transport of oxygen and nutrients to the cornea; and (5) have sufficient surface wettability so as not to damage the corneal cells.

What Polymeric Biomaterial is Used?

The major component of most modern soft contact lenses is loosely cross-linked PHEMA. Semicrystalline polymers are often translucent due to light refracted by crystallites. Since PHEMA is atactic the polymer is transparent. When dry, PHEMA is glassy, allowing the lens to be fabricated through milling procedures (as is done with hard contact lenses). However, the hydroxyl-containing pendant group results in a hydrophilic polymer that imbibes 40 wt% water. The absorbed water plasticizes the polymer, producing a soft and supple material that is less irritating to the eye. Pure PHEMA lenses are not capable of providing the necessary oxygen to the cornea of the eye, so PHEMA is often copolymerized with other monomers, such as fluorinated or "siliconized" methacrylates, to improve oxygen transport either by increasing the oxygen solubility in the lens or by allowing the fabrication of a thinner lens.

Recently, much research in contact lens development has focused on the design of extended wear lenses (contacts that can be worn for up to 7–14 days without removal). A leading material for extended wear contacts is a silicone hydrogel that is composed of a silicone polymer network with an entrapped water-soluble polymer such as poly(vinyl pyrrolidone). This combination creates a material with excellent oxygen and ion permeability, and good lubricity of the lens against the cornea (for example, see http://en.wikipedia.org/wiki/Contact_lens).

CASE STUDY III: ARTIFICIAL HIP JOINTS

What Problem was Addressed?

A surgeon may perform hip arthroplasty (implantation of an artificial hip) to alleviate the pain and stiffness of severe arthritis or to repair the joint after physical damage. An artificial hip implant has two pieces: the femoral ball and stem, and the acetabular cup. The femoral ball and stem implant is a metal shaft that inserts into the femoral bone core, and is capped by a ball that articulates with the acetabular cup.

What Properties Were Required of the Biomaterial?

Sir John Charnley— a British orthopedic surgeon— conceived the initial concept that led to the modern artificial hip. Focusing on the acetabular component, tribology (the study of friction, lubrication, and wear) is of utmost importance. The ideal polymer for use in an articulating joint would be low friction and resistant to wear.

What Polymeric Biomaterial was Used?

Initially, Charnley used poly(tetrafluoroethylene) (PTFE), a very nonpolar and low-friction material, for the acetabular cup. He also used stainless steel for the femoral ball and stem. Two problems arose: first, PTFE did not have the necessary wear resistance, and small pieces of PTFE debris eroded from the surface of the cup, causing severe inflammation of the surrounding tissue. Second, Charnley had to force-fit the femoral stem into the femur, and it loosened during use. Although PE has a higher-friction surface than PTFE, very high molecular weight PE is a superior biomaterial for this application, since PE did not produce excessive wear debris. Also, PE could be simultaneously gamma radiation sterilized and cross-linked, increasing its wear resistance. It could also be machined to a fine smoothness to further minimize wear. Charnley was advised by Dennis Smith, a biomaterials chemist working on dental implants, to use PMMA dental cement to hold the femoral stem in place during wear, and that solved the second problem.

References

- Avgoustakis, k., 2008. Poly(lactic-Co-Glycolic Acid (PLGA)). In: Gary, E., Wnek, Gary L. (Eds.), *Bowlin: Encyclopedia of Biomaterials and Biomedical Engineering*, Second ed. CRC Press.
- Calleja, G., Jourdan, A., Arneduri, B., Habas, J., 2013. Where is the glass transition temperature of poly(tetrafluoroethylene)? A new approach by dynamic rheometry and mechanical tests. *Eur. Polym. J.* 49 (8), 2214–2222.
- Cao, Y., Liang, M., Liu, Z., Wu, Y., Xiong, X., Li, C., Wang, X., Jiang, N., Yu, J., Lin, C., 2016. Enhanced thermal conductivity for poly(vinylidene fluoride) composites with nano-carbon fillers. *RSC Adv* 6, 68357–68362.
- Chiefari, J., Chong, Y.K., Ercole, F., Krstina, J., Jeffery, J., et al., 1998. Living free-radical polymerization by reversible addition–fragmentation chain transfer: the RAFT process. *Macromolecules* 31, 5559–5562.
- Gentile, P., Chiono, V., Carmagnola, I., Hatton, P.V., 2014. An overview of poly(lactic-co-glycolic) acid (PLGA)-based biomaterials for bone tissue engineering. *Int. J. Mol. Sci.* 15, 3640–3659.
- Kato, M., Kamigaito, M., Sawamoto, M., Higashimura, T., 1995. Polymerization of methyl methacrylate with the carbon tetrachloride/dichlorotris-(triphenylphosphine)ruthenium(II)/methylaluminum bis (2,6-di-tert-butylphenoxide) initiating system: possibility of living radical polymerization. *Macromolecules* 28, 1721–1723.

- Liu, H., Wang, J., Jiang, P., Yan, F., 2018. Accelerated degradation of polyetheretherketone and its composites in the deep sea. *R. Soc. open sci.* 5, 171775.
- Moad, G., Rizzardo, E., 1995. Alkoxyamine-initiated living radical polymerization: Factors affecting alkoxyamine homolysis rates. *Macromolecules* 28, 8722–8728.
- NASA, 1986. Challenger Accident Investigation Report. (Chapter 4): The Cause of the Accident.
- Nicolas, J., Guillaneuf, Y., Lefay, C., Bertin, D., Gignes, D., Charleux, B., 2013. Nitroxide-mediated polymerization. *Prog. Polym. Sci.* 38 (1), 63–235.
- Perrier, S., 2017. 50th anniversary perspective: RAFT polymerization – A user guide. *Macromolecules* 50 (19), 7433–7447.
- Ribelli, T.G., Lorandi, F., Fantin, M., Matyjaszewski, K., 2019. Atom transfer radical polymerization: Billion times more active catalysts and new initiation systems. *Macromol. Rapid Commun.* 40 (1), 1800616.
- Shackelford, J.F., Alexander, W., 2001. *CRC materials science and engineering handbook*. CRC Press, Boca Raton, FL.
- Wang, J., Matyjaszewski, K., 1995. Controlled/“living” radical polymerization: atom transfer radical polymerization in the presence of transition-metal complexes. *J. Am. Chem. Soc.* 117, 5614–5615.
- Brandrup, J., Immergut, E.H., Grukle, E.A., 1999. *Polymer Handbook*, fourth ed. Wiley-Interscience, New York, NY.
- Charnley, J., Halley, D.K., 1975. Rate of wear in total hip replacement. *Clin. Orthop. Relat. Res.* 112, 170–179.
- Dumitriu, S., 2002. *Polymeric Biomaterials*, second ed. Marcel Dekker Inc, New York, NY.
- Flory, P.J., 1953. *Principles of Polymer Chemistry*. Cornell University Press, Ithaca, NY.
- Gilding, D.K., Reed, A.M., 1979. Biodegradable polymers for use in surgery: poly (glycolic)/poly (lactic acid) homo- and copolymers. *Polymer* 20, 1459–1464.
- Painter, P.C., Coleman, M.M., 2009. *Essentials of Polymer Science and Engineering*. DEStech Publications, Lancaster, PA.
- Rodriguez, F., Cohen, C., Ober, C.K., Archer, L.A., 2003. *Principles of Polymer Systems*, fifth ed. Taylor & Francis, New York, NY.
- Vert, M., 2007. Polymeric biomaterials: strategies of the past vs. strategies of the future. *Prog. Polym. Sci.* 32, 755–761.
- Wang, J., Wu, W., 2005. Swelling behaviors, tensile properties and thermodynamic studies of water sorption of 2-hydroxyethyl methacrylate/opoxy methacrylate copolymeric hydrogels. *Eur. Polym. J.* 41, 1143–1151.
- Ward, I.M., Sweeney, J., 2004. *An Introduction to the Mechanical Properties of Solid Polymers*, second ed. John Wiley & Sons Ltd, West Sussex, UK.
- Wichterle, O., Lim, D., 1960. Hydrophilic gels for biological use. *Nature* 185, 117–118.

Further Reading

- Allcock, H.R., Lampe, F.W., Mark, J.E., 2004. *Contemporary Polymer Chemistry*, third ed. Prentice Hall, Inc, Englewood Cliffs, NJ.

1.3.2A

Polyurethanes

DANIEL E. HEATH¹, SCOTT A. GUELCHER², STUART L. COOPER¹

¹William G. Lowrie Department of Chemical and Biomolecular Engineering, The Ohio State University, Columbus, OH, United States

²Department of Chemical and Biomolecular Engineering, Vanderbilt University, Nashville, TN, United States

Introduction

Polyurethanes are widely used in medical devices such as pacemakers, artificial hearts, and other blood-contacting applications. Their excellent mechanical properties, stability, and good biocompatibility give them a special place in medicine (Lamba et al., 1998). Polyurethanes were developed in the 1930s. Around that time, Nylon 6,6—a condensation polymer of hexamethylenediamine and adipic acid—was developed and patented by Du Pont. This polymer achieved commercial success due to its good mechanical properties and fiber-producing ability. German scientists led by Otto Bayer began to explore new polymerization techniques in the hope of creating a material competitive with nylon. Initial work reacted difunctional isocyanates and amines to produce polyureas; however, these materials were too hydrophilic to be used as plastics or textiles. Diisocyanates were also reacted with diols to produce polyurethanes. One nylon-like polyurethane produced through the reaction of 1,4-butanediol and hexamethylene diisocyanate, as shown in Fig. 1.3.2A.1, was used commercially in Germany. Chemically the polymer is the same as nylon except for the two additional oxygens per repeat unit, and the properties are similar except that the polyurethane has a lower melting point. These early polyurethanes also had lower water absorption, and better electrical and mechanical stability upon aging compared to nylon. Subsequently block polymers including polyester or polyether polyols were developed both in Germany and the United States (Saunders and Frisch, 1965).

Today, polyurethanes (PUs) are a class of polymer which has achieved industrial relevance due to their tough and elastomeric properties, and good fatigue resistance (Randall and Lee, 2002). PUs are used as adhesives, coatings, sealants, rigid and flexible foams, and textile fibers. Furthermore, PUs have also been employed in biomaterial applications such as artificial pacemaker lead insulation, catheters,

vascular grafts, heart assist balloon pumps, artificial heart bladders, wound dressings, tissue adhesives, bone grafts, and drug-delivery vehicles.

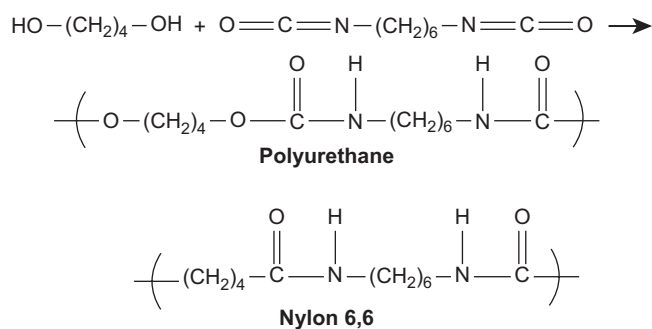
Anatomy of a Polyurethane Molecule

The polyurethane molecule presented in Fig. 1.3.2A.1 has a very simple architecture. Most commercially relevant PUs today are actually block copolymers (as seen in Chapter 1.3.2, Figure 1.3.2.4) meaning there are alternating segments in the polymer molecules composed of solely “A” or “B” repeat units. Furthermore, the materials are designed so that one of the segments—called the *hard segment*—is glassy or crystalline at the use temperature, while the other segment—referred to as the *soft segment*—is rubbery. If the monomers are appropriately selected, the hard and soft segments of the polyurethane will be incompatible, leading to phase separation so that the composition of the bulk polymer will not be homogeneous. Instead, there will be nanometer-sized regions which are rich in hard segments, and other regions rich in soft segments. The unique block copolymer structure and phase separation of PUs results in unique and useful properties. One can consider the hard phase domains as providing highly efficient reinforcing microdomains which give rise to the unusual and very attractive properties of polyurethanes, such as strength and toughness.

The Physical Properties of Polyurethanes

Thermosets

Most polymer elastomers—such as rubber bands—are produced by lightly cross-linking a low T_g polymer into a loose network (as seen in Chapters 1.2.2 and 1.3.2, Figure 1.3.2.3). When such a material is strained, the segments between cross-links can deform and elongate; however,



• **Figure 1.3.2A.1** Synthesis scheme of a polyurethane through the condensation of 1,4-butanediol and hexamethylene diisocyanate. The repeat units of the PU and of Nylon 6, 6 are presented for comparison.

when the load is removed the cross-links result in the material returning to its original form. Although these elastomers are useful, they are *thermosets*. Since the material is essentially one large molecule it cannot be dissolved, neither can it be made to flow through the introduction of heat and pressure. This means that once a thermoset elastomer is formed, it cannot be processed further. Prior to completion of the setting reaction, PU thermosets are flowable, making them useful as injectable or moldable biomedical devices (e.g., tissue adhesives, scaffolds, and bone grafts) that cure in situ after implantation.

Thermoplastic Elastomers

The unique segmented structure of PUs allows *thermoplastic elastomers* to be formed. When such materials are strained, the polymer segments in the soft phase will deform and elongate, while the hard phase will stabilize the structure, resulting in recovery of the original form once the load is removed. However, unlike the covalent cross-links in thermosets, the physical cross-links present between hard segments can be undermined through the application of heat, and then reformed upon cooling, allowing the useful properties of elastomers to be combined with the simple processing procedures of thermoplastics. In addition to elastomeric properties, PUs have several useful interfacial characteristics. Foremost, PUs are abrasion- and impact-resistant, making them useful as coatings, and the materials also have good blood-contacting properties, making them useful in biomaterial applications.

Polyurethane Synthesis

Precursors

When synthesizing most PU block copolymers a two-step synthesis strategy is typically employed which involves three precursor molecules: diisocyanates, diols, and chain extenders. In the final polymer molecule the diisocyanates and chain extenders will form the hard segments, while the diols form the soft segments. Table 1.3.2A.1 illustrates the chemical structure of molecules often used to synthesize PU block copolymers. Thermoplastic PU elastomers are synthesized

from diisocyanates and diols (functionality equal to two), while PU thermosets are synthesized from polyisocyanates and polyols with functionality greater than two.

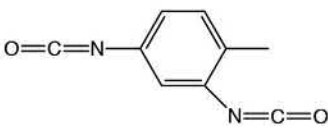
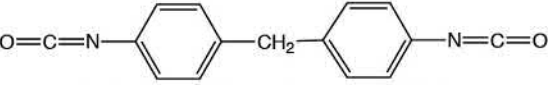
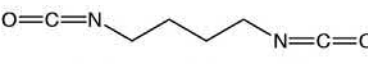
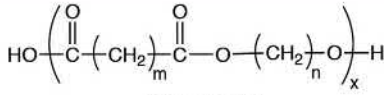
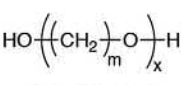
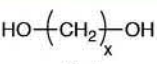
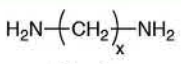
The diisocyanate molecules used in biostable polyurethane synthesis can be aliphatic (such as Fig. 1.3.2A.1), but most often aromatics are used (Table 1.3.2A.1). The two most commonly used diisocyanates employed in biostable PU synthesis are 2,4 and 2,6 mixed-toluene diisocyanates (TDI) and methylene-bis(4) phenyl isocyanate (MDI). The soft segments are formed from polyether or polyester diols (sometimes referred to as *polyols*). These molecules have a molecular weight of 1000–2000 Da, and are well above their T_g s and melting points at use conditions, which impart a rubbery character to the resulting polyurethane. Polyether diols are often preferred to form the soft segments since they are more resistant to hydrolytic degradation than polyesters. The last precursor is the chain extender. These molecules are often short aliphatic diols or diamines containing two to six carbon atoms, and are used to build the polymer up to its final high molecular weight.

Aromatic diisocyanates can result in carcinogenic degradation products; therefore, resorbable PUs for tissue engineering applications require the use of diisocyanates other than MDI and TDI (Table 1.3.2A.1). Resorbable PU segmented elastomers and thermosets have been synthesized using lysine-diisocyanate (LDI), hexamethylene diisocyanate (HDI), and 1,4 diisocyanatobutane (BDI), which degrade to nontoxic breakdown products (Takanari et al., 2017). Soft segment structure is often designed to build in the appropriate degradability. For instance, soft segments containing copolymers of lactide, glycolide, and ϵ -caprolactone have been investigated, all of which are susceptible to hydrolytic degradation, and the degradation rates vary based on chemical composition (Santerre et al., 2006). Similar to biostable polyurethanes, short-chain aliphatic diols or diamines are often used as chain extenders, although recent work has focused on synthesizing cell-degradable or biologically active chain extenders (Xu et al., 2015). In some applications, water is used as a chain extender to generate porous foam scaffolds for tissue regeneration or to facilitate in situ cure after implantation in the body (Guelcher, 2008).

Synthesis Reactions

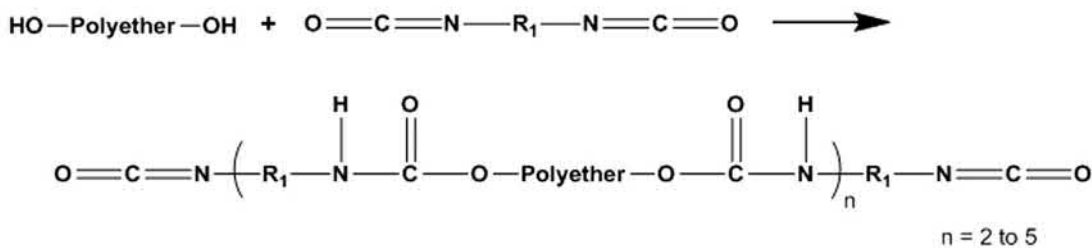
The isocyanate group contains two unsaturated bonds and is a highly reactive moiety. When reacted with a hydroxyl group, the result is a urethane bond, as illustrated in Fig. 1.3.2A.1. The first step in PU synthesis reacts the diisocyanates with the polyether or polyester diols. Excess diisocyanate is used to ensure the resulting materials are end terminated with isocyanate groups, as seen in Fig. 1.3.2A.2A. The result of this reaction is a *prepolymer* with a degree of polymerization commonly between two and five. Next, the prepolymer is further reacted with the chain extenders to produce high-molecular-weight polyurethane molecules, as shown in Fig. 1.3.2A.2B.

TABLE 1.3.2A.1 Chemical Structure of Common Precursors Used in Polyurethane Block Copolymer Synthesis: Diisocyanates, Chain Extenders, and Polyester or Polyether Diols

Diisocyanates		
<p>Biostable</p>  <p>2,4-toluene diisocyanate (TDI)</p>	<p>Resorbable</p>  <p>L-Lysine ethyl ester diisocyanate (LDI)</p>	
 <p>Methylene-bis(4)phenyl isocyanate (MDI)</p>	 <p>1,4-Diisocyanatobutane (BDI)</p>	
Diols		
 <p>Polyester diol</p>	<p>MW = 1000 to 2000 Da</p>	 <p>Polyether diol</p>
Chain extenders		
 <p>Diol</p>	<p>x = 2 to 6 carbons</p>	 <p>Diamine</p>

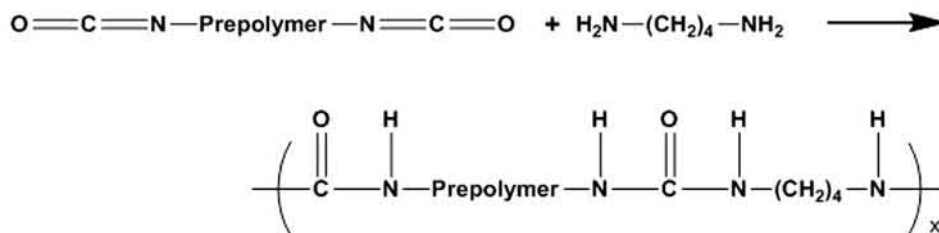
(A)

Preparation of isocyanate terminated prepolymer from polyetherdiol and excess diisocyanate.



(B)

Building prepolymer to high molecular weight through chain extension with diamine.



• **Figure 1.3.2A.2** Two-step synthesis of a polyurethane block copolymer: (A) isocyanate-terminated prepolymer synthesis from excess diisocyanate and polyether diol; (B) reaction of prepolymer with diamines to build high-molecular-weight polyurethane chains.

CASE STUDY I

What Problem Was Addressed?

An individual may require an artificial pacemaker to regulate their heartbeat. The pacemaker is an implanted device which monitors heartbeat and provides electrical stimulation to the muscles of the heart, resulting in muscle contraction when needed. The pacemaker is connected to the appropriate heart muscles through pacemaker leads, electrically conductive wires which are fed to the heart through the vasculature.

The pacemaker leads require insulation. Initially poly(dimethyl siloxane) (PDMS) or polyethylene was used as the insulator for the leads. However, both of these materials resulted in a fibrous endocardial reaction. Furthermore, PDMS has a low tensile modulus and poor tear resistance.

What Properties Were Required of the Biomaterial?

A successful insulator for pacemaker leads would not elicit a fibrous reaction from the heart, and would have high tensile strength and resistance to tearing, allowing for thinner lead insulations to be produced.

What Polymeric Biomaterial is Used?

In 1978, polyurethane was introduced as a lead insulator. Although not as flexible as PDMS, the PU had superior tensile properties and tear resistance. This allowed much thinner lead insulations to be fabricated without compromising handling properties. The thinner insulation allows multiple leads to be inserted per vein, enabling sequential pacing. Furthermore, the PU surface has lower friction in contact with blood and tissue than the PDMS surface, allowing easier insertion of the leads.

The search for the optimum lead insulation material is not over yet, however. In the 1980s it was found that metal-induced oxidation from lead metals resulted in undesired degradation of the polyurethane insulation. Lower ether content in the polyurethane was one solution to this problem, although this results in higher modulus insulation. In subsequent years there have been changes to the material used for the lead wire, and silicone rubber remains in use as well as polyurethanes for pacemaker insulation. Research is under way to find more biostable polyurethanes for this application.

CASE STUDY II: RESORBABLE POLYURETHANE ADHESIVE

What Problem Was Addressed?

An individual may require an abdominoplasty procedure, in which excess skin and fat are removed from the abdomen to tighten the muscle of the abdominal wall. Most patients who undergo large flap procedures require implantation of drains to remove fluid that accumulates under the skin at the surgical site. Drains can cause discomfort and lead to complications for the patient. Tissue adhesives, such as cyanoacrylates, can be used to hold the remaining layers of tissue in place and reduce the voids between layers, thereby eliminating the need for drains. However, cyanoacrylates are nonresorbable and are potentially toxic to patients and health professionals.

What Properties Were Required of the Biomaterial?

A successful surgical adhesive would be easily administered, cure inside the body within minutes to form a strong tissue

bond, and break down into nontoxic and resorbable components as the tissues continue to heal.

What Polymeric Biomaterial is Used?

In 2015, TissuGlu polyurethane surgical adhesive was approved by the FDA for use during abdominoplasty. TissuGlu consists of a prepolymer prepared by reacting lysine diisocyanate ethyl ester with trimethylolpropane. The prepolymer, which is delivered by a handheld applicator, reacts with moisture present at the surgical site to form a strong tissue bond that eliminates voids between tissue layers. In clinical trials, TissuGlu was found to be a safe and effective alternative to postoperative fluid collection drains. Patients treated with TissuGlu Surgical Adhesive required fewer postoperative treatments and resumed daily activities sooner than those receiving surgical drains. Research is under way to expand the use of TissuGlu Surgical Adhesive to other surgical procedures, including mastectomy, inguinal lymph node dissection, and colorectal anastomosis.

Tailoring Polyurethane Behavior

Many of the techniques described in [Chapter 1.3.2](#) to modulate polymer properties can easily be applied to polyurethanes. For instance, monomers with functionality greater than two can be used in order to produce cross-linked PU thermosets. Also, as the cross-link density in thermosets controls material stiffness, the relative amounts of hard and soft segments in the PU can vary the modulus. Similarly, the length and chemical nature of the soft segment can be adjusted to further tune physical behavior.

Resorbable PUs have been explored more recently for tissue regeneration and repair. For these applications, the degradation rate must be controlled to match that of tissue

ingrowth and the degradation products need to be nontoxic and readily cleared from the body. Examples include moisture-cure surgical adhesives as an alternative to surgical drains ([Ohlinger et al., 2018](#)), resorbable electrospun elastomers for tissue reconstruction and repair ([Takanari et al., 2017](#)), resorbable bone cements for repair of weight-bearing fractures ([Lu et al., 2018](#)), and injectable high internal phase emulsions (polyHIPEs) for production of high-porosity scaffolds ([Moglia et al., 2011](#)).

There have been many advances in the application of polyurethane chemistry to create novel biomaterials. Examples include smart materials for drug delivery that exhibit pH and/or temperature sensitivity ([Zhao et al., 2011](#)),

shape change materials (Zheng et al., 2016), and antimicrobial polyurethanes (Grapski et al., 2001). Additionally, thermoplastic polyurethanes lend themselves to electrospinning and additive manufacturing techniques (3D printing) for a variety of tissue engineering applications (Cooper and Guan, 2016).

Concluding Remarks

Polyurethanes are a unique family of polymers with interesting properties which arise from their block copolymer nature and the resulting phase separation. These materials have achieved industrial success in everyday applications, as well as in the biomaterials field.

References

- Cooper, S.L., Guan, J. (Eds.), 2016. *Advances in Polyurethane Biomaterials*. Woodhead Publishing/Elsevier, London, UK.
- Grapski, J.A., Cooper, S.L., 2001. Synthesis and characterization of non-leachable biocidal polyurethanes. *Biomaterials* 22, 2239–2346.
- Guelcher, S.A., 2008. Biodegradable polyurethanes: synthesis and applications in regenerative medicine. *Tissue Eng. Part B* 14, 3–17.
- Lamba, N.M.K., Woodhouse, K.A., Cooper, S.L., 1998. *Polyurethanes in Biomedical Applications*. CRC Press, Boca Raton, FL.
- Lu, S., McGough, M.A.P., Shiels, S.M., Zienkiewicz, K.J., Merkel, A.R., Vanderburgh, J.P., Nyman, J.S., Sterling, J.A., Tennent, D.J., Wenke, J.C., Guelcher, S.A., 2018. Settable polymer/ceramic composite bone grafts stabilize weight-bearing tibial plateau slot defects and integrate with host bone in an ovine model. *Biomaterials* 179, 29–45.
- Moglia, R.S., Holm, J.L., Sears, N.A., Wilson, C.J., Harrison, D.M., Cosgriff-Hernandez, E., 2011. Injectable polyHIPEs as high-porosity bone grafts. *Biomacromolecules* 12, 3621–3628.
- Ohlinger, R., Gieron, L., Rutkowski, R., Kohlmann, T., Zygmunt, M., Unger, J., 2018. The use of TissuGlu surgical adhesive for mastectomy with or without lymphonodectomy. *In Vivo* 32, 625–631.
- Randall, D., Lee, S., 2002. *The Polyurethanes Book*. John Wiley & Sons, Ltd, West Sussex, UK.
- Santerre, J.P., Woodhouse, K., Laroche, G., Labow, R.S., 2006. Understanding the biodegradation of polyurethanes: from classical implants to tissue engineering materials. *Biomaterials* 26, 7457–7470.
- Saunders, J.H., Frisch, K.C., 1965. *Polyurethanes: Chemistry and Technology, Part 1*. Chemistry. Interscience Publishers, New York, NY.
- Takanari, K., Hashizume, R., Hong, Y., Amoroso, N.J., Yoshizumi, T., Gharaibeh, B., Yoshida, O., Nonaka, K., Sato, H., Huard, J., Wagner, W.R., 2017. Skeletal muscle derived stem cells microintegrated into a biodegradable elastomer for reconstruction of the abdominal wall. *Biomaterials* 113, 31–41.
- Xu, C., Huang, Y., Wu, J., Tang, L., Hong, Y., 2015. Triggerable degradation of polyurethanes for tissue engineering applications. *ACS Appl. Mater. Interfaces* 7, 20377–20388.
- Zhao, L., Yu, L., Ding, M., Li, J., Tan, H., Wang, Z., Fu, Q., 2011. Synthesis and characterization of pH sensitive biodegradable polyurethane for potential drug delivery application. *Macromolecules* 44, 857–864.
- Zheng, Y., Dong, R., Shen, J., Guo, S., 2016. Tunable shape memory performances via multilayer assembly of thermoplastic polyurethane and polycaprolactone. *Adv. Appl. Mater. Interfaces* 8, 1371–1380.

Further Reading

- Dumitriu, S., 2002. *Polymeric Biomaterials*, second ed. Marcel Dekker Inc, New York, NY.
- Rodriguez, F., Cohen, C., Ober, C.K., Archer, L.A., 2003. *Principles of Polymer Systems*, fifth ed. Taylor & Francis, New York, NY.

Chapter Exercises

1. Describe the structure of the polyurethane molecule and how it gives rise to the favorable properties of polyurethanes, such as high strength and toughness.
2. Describe the differences between thermosets and thermoplastic elastomers and give examples of each of these types of materials that are useful for biomedical devices.
3. Draw schematics of monodentate and bidentate hydrogen bonding between urethane and urea groups in the hard segments of polyurethanes. Discuss how hydrogen bonding between adjacent hard segments enhances polyurethane properties.
4. Discuss the targeted design properties for resorbable polyurethanes for tissue repair and nonresorbable polyurethane permanent implants. How can the properties of the polyurethane be tailored to the application by modifying the structure?
5. Draw the schematic for synthesizing a nonresorbable thermoplastic elastomer from MDI, butanediol, and poly(tetramethylene oxide) (PTMO, 2000 g/mol). Highlight the hard and soft blocks in the polyurethane molecule.
6. Draw the schematic for synthesizing a resorbable polyurethane thermoset from LDI and a polyester triol (900 g/mol).
7. List the optimal mechanical, rheological, biological, and degradation properties of polyurethane elastomers for 3D printing scaffolds for tissue repair using fused deposition modeling.

1.3.2B

Silicones

JIM CURTIS, STEPHANIE D. STEICHEN

DuPont Health Care Solutions, Midland, MI, United States

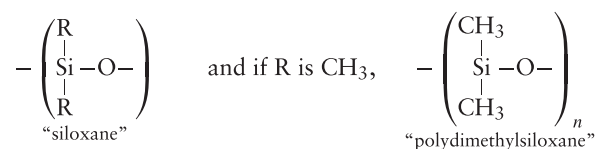
Silicone materials have been extensively used in a variety of industries for over 70 years. These materials are typically composed of an alternating inorganic silicon–oxygen backbone with pendant organic groups. The simultaneous presence of inorganic and organic moieties provides unique chemical and physical properties, while also enabling control over those characteristics through molecular architecture. Silicones are available in an assortment of material types including fluids, emulsions, compounds, resins, etc., which can be further formulated into elastomers, gels, adhesives, and more.

Silicones have remarkably low glass-transition temperatures and maintain their flexibility over a wide temperature range, permitting them to withstand conditions from cold storage to steam autoclaving. This robust temperature performance makes them ideal for use in the aerospace and automotive industries. In the electronics field, silicones are used as electrical insulation, potting compounds, and in other applications specific to semiconductor manufacture. Their long-term durability has made silicone sealants, adhesives, and waterproof coatings commonplace in the construction industry. Silicones possess high permeability to gases and many drugs, advantageous, respectively, in wound care or transdermal drug delivery. Excellent biocompatibility, facilitated by low surface tension and remarkable chemical stability, makes many silicones well suited for use in personal care, pharmaceutical, and medical device applications, including long-term implant applications. Since the 1960s, silicones have enjoyed expanded medical applications and today are one of the most widely used biomaterials.

Chemical Structure and Nomenclature

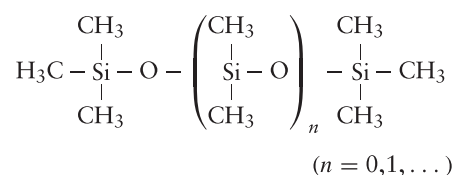
Silicones were so named due to their similarity with ketones, specifically because, in most cases, there is on average one silicon atom for one oxygen and two methyl groups (Kipping, 1904). Later, as these materials and their applications flourished, more specific nomenclature was developed. Key milestones in the development of silicone chemistry are summarized in Table 1.3.2B.1.

The basic repeating unit became known as “siloxane,” and the most common silicone is polydimethylsiloxane, abbreviated as PDMS.



Many other groups (e.g., phenyl, vinyl, and trifluoropropyl) can be substituted for the methyl groups along the chain.

The most common silicones are the trimethylsilyloxy end-blocked polydimethylsiloxanes, with the following structure:



These are linear polymers and remain liquids, even for large values of n . The main chain unit, $-(\text{Si}(\text{CH}_3)_2\text{O})-$, or alternatively $(\text{CH}_3)_2\text{SiO}_{2/2}$, is often represented by the letter D, because when the silicon atom is connected to two oxygen atoms, this unit is capable of expanding the polymer in two directions. M, T, and Q units are defined in a similar manner, being capable of expanding the chain in one, three, and four directions, respectively. These are shown in Table 1.3.2B.2.

The system is sometimes modified by the use of superscript letters to designate nonmethyl substituents, for example, $\text{D}^{\text{H}} = \text{H}(\text{CH}_3)\text{SiO}_{2/2}$ and M^{O} or $\text{M}^{\text{Ph}} = (\text{CH}_3)_2(\text{C}_6\text{H}_5)\text{SiO}_{1/2}$ (Smith, 1991). Further examples are shown in Table 1.3.2B.3.

Preparation

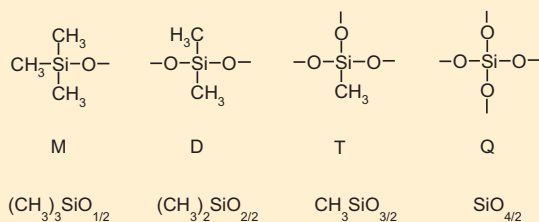
Silicone Polymers

The modern synthesis of silicone polymers is a complex, multistage process. It typically involves the four basic steps described in Table 1.3.2B.4. Only step 4 in this table will be elaborated upon here.

TABLE 1.3.2B.1 Key Milestones in the Development of Silicone Chemistry (Lane and Burns, 1996; Rochow, 1945; and Noll, 1968)

1824	Berzelius discovers silicon by the reduction of potassium fluorosilicate with potassium: $4K + K_2SiF_6 \rightarrow Si + 6KF$. Reacting silicon with chlorine gives a volatile compound later identified as tetrachlorosilane, $SiCl_4$: $Si + 2Cl_2 \rightarrow SiCl_4$
1863	Friedel and Crafts synthesize the first silicon organic compound, tetraethylsilane: $2Zn(C_2H_5)_2 + SiCl_4 \rightarrow Si(C_2H_5)_4 + 2ZnCl_2$
1871	Ladenburg observes that diethyldiethoxysilane $(C_2H_5)_2Si(OC_2H_5)_2$, in the presence of a diluted acid gives an oil that decomposes only at a "very high temperature."
1901–1930s	Kipping lays the foundation of organosilicon chemistry with the preparation of various silanes by means of Grignard reactions and the hydrolysis of chlorosilanes to yield "large molecules." The polymeric nature of the silicones is confirmed by the work of Stock.
1940s	In the 1940s, silicones become commercial materials after Hyde of Dow Corning demonstrates the thermal stability and high electrical resistance of silicone resins, and Rochow of General Electric finds a direct method to prepare silicones from silicon and methylchloride.

TABLE 1.3.2B.2 Shorthand Notation for Siloxane Polymer Units

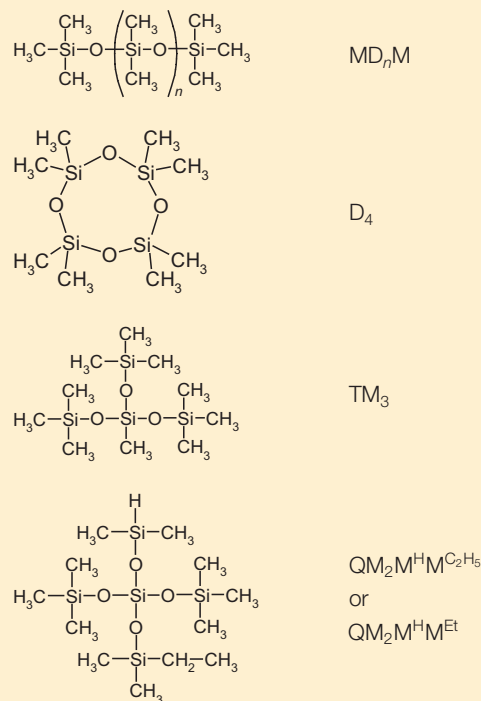


Polymerization and Polycondensation

The linear and cyclic oligomers resulting from dimethyldichlorosilane hydrolysis (step 3) have chain lengths too short for most applications. The cyclics must be polymerized, and the linears condensed, to give macromolecules of sufficient length (Noll, 1968).

Catalyzed by acids or bases, cyclosiloxanes $(R_2SiO)_m$ are ring-opened and polymerized to form long linear chains. At equilibrium, the reaction results in a mixture of cyclic oligomers plus a distribution of linear polymers. The proportion of cyclics depends on the substituents along the Si–O chain, the temperature, and the presence of a solvent. Polymer chain length depends on the presence and concentration of substances capable of giving chain ends. For example, in the KOH-catalyzed

TABLE 1.3.2B.3 Examples of Silicone Shorthand Notation



polymerization of the cyclic tetramer octamethylcyclotetrasiloxane $(\text{Me}_2\text{SiO})_4$ (or D₄ in shorthand notation), the average length of the polymer chains depends on the KOH concentration:



A stable hydroxy-terminated polymer, $\text{HO}(\text{Me}_2\text{SiO})_z\text{H}$, can be isolated after neutralization by stripping the mixture under vacuum at elevated temperature. This removes the remaining cyclics and leaves a distribution of linear chains with different lengths.

The reaction can also be made in the presence of $\text{Me}_3\text{SiOSiMe}_3$, which acts as a chain end-blocker:



where --- represents the main chain.

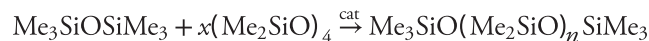
The Me_3SiOK formed attacks another chain to reduce the average molecular weight of the linear polymer formed.

Substitution of the KOH catalyst for ME_4NOH and introduction of the chain end-blocker, $\text{Me}_3\text{SiOSiMe}_3$, has significant and interesting effects on the copolymerization of $(\text{Me}_2\text{SiO})_4$ (Noll, 1968). The cyclics are initially polymerized into very long, viscous chains that are subsequently reduced in length by the addition of terminal groups provided by the end blocker, which is slower to react. The viscosity of the material correspondingly peaks at the beginning of the reaction and then decreases. This behavior is attributed to the silicon in the cyclics being more susceptible to nucleophilic attack by the base catalyst because of its

TABLE 1.3.2B.4 The Basic Steps in Silicone Polymer Synthesis

1. Silica reduction to silicon	$\text{SiO}_2 + 2\text{C} \rightarrow \text{Si} + 2\text{CO}$
2. Chlorosilanes synthesis	$\text{Si} + 2\text{CH}_3\text{Cl} \rightarrow (\text{CH}_3)_2\text{SiCl}_2 + \text{CH}_3\text{SiCl}_3 + (\text{CH}_3)_3\text{SiCl} + \text{CH}_3\text{HSiCl}_2 + \dots$
3. Chlorosilanes hydrolysis	$\text{Cl}-\underset{\text{CH}_3}{\overset{\text{CH}_3}{\text{Si}}}-\text{Cl} + 2\text{H}_2\text{O} \rightarrow \text{HO}-\underset{\text{CH}_3}{\overset{\text{CH}_3}{\text{Si}}}-\text{O}-\text{H} + \left(\underset{\text{CH}_3}{\overset{\text{CH}_3}{\text{Si}}}-\text{O}\right)_{3,4,5} + \text{HCl}$ <p style="text-align: center;">linears cyclics</p>
4. Polymerization and poly-condensation	$\left(\underset{\text{CH}_3}{\overset{\text{CH}_3}{\text{Si}}}-\text{O}\right)_{3,4,5} \rightarrow \left(\underset{\text{CH}_3}{\overset{\text{CH}_3}{\text{Si}}}-\text{O}\right)_y$ <p style="text-align: center;">cyclics polymer</p> $\text{HO}-\underset{\text{CH}_3}{\overset{\text{CH}_3}{\text{Si}}}-\text{O}-\text{H} \rightarrow \text{HO}-\underset{\text{CH}_3}{\overset{\text{CH}_3}{\text{Si}}}-\text{O}-\text{H} + z\text{H}_2\text{O}$ <p style="text-align: center;">linears polymer</p>

two flanking oxygen atoms, as opposed to the silicon in the end-blocker, which is substituted by only one oxygen atom. This reaction can be described as follows:



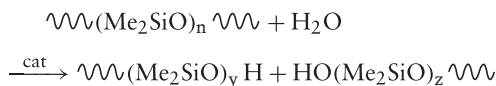
or, in shorthand notation:



where $n = 4x$ (theoretically).

The ratio between D and M units defines the average molecular weight of the polymer formed.

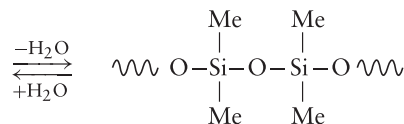
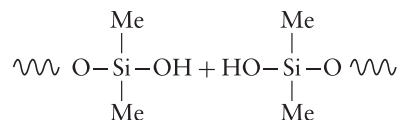
Catalyst removal (or neutralization) is always an important step in silicone preparation. Most catalysts used to prepare silicones can also catalyze the depolymerization (attack along the chain), particularly at elevated temperatures when in the presence of traces of water.



It is therefore essential to remove all remaining traces of the catalyst to provide the silicone optimal thermal stability. Labile catalysts have been developed that either decompose or volatilize above the optimum polymerization temperature and can, consequently, be eliminated. Thus, catalyst neutralization or filtration can be avoided (Noll, 1968).

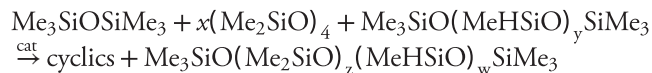
The cyclic trimer $(\text{Me}_2\text{SiO})_3$, D_3 , has internal ring tension and can be polymerized without reequilibration of the resulting polymers. With this cyclic, polymers with narrow molecular weight distribution can be prepared, as well as polymers only carrying one terminal reactive functionality (living polymerization). Starting from a mixture of cyclics with different internal ring tensions also allows preparation of block or sequential polymers (Noll, 1968).

When catalyzed, linears can combine into long chains by intermolecular condensation of the silanol terminal groups (Noll, 1968; Stark et al., 1982).

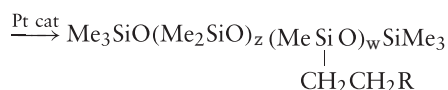


This reaction yields a distribution of chain lengths. Adjustment of reaction conditions, e.g., reduction or residual water by increasing temperature or applying vacuum, can shift the distribution.

In addition to the polymers described above, reactive polymers can also be prepared. This result can be achieved when reequilibrating oligomers or existing polymers to first produce a polydimethylmethylhydrosiloxane, $\text{MD}_2\text{D}^{\text{H}}_w\text{M}$.

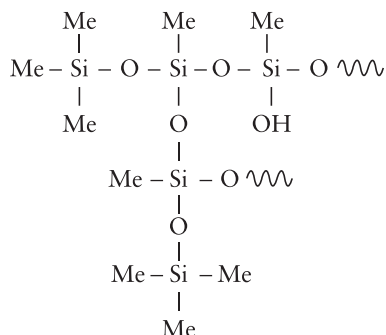
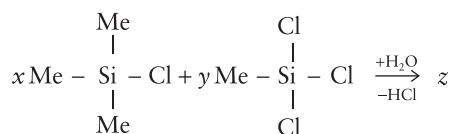


Additional functional groups can be attached to this polymer using an addition reaction.



All the polymers heretofore shown are linear or cyclic, comprising mainly of difunctional units, D. Branched polymers, or resins, can be prepared if, during hydrolysis of the chlorosilanes, a certain amount of T or Q units are included; this allows molecular expansion in three or four directions, as opposed to just two. For example, consider

the hydrolysis of methyltrichlorosilane in the presence of trimethylchlorosilane, which leads to a branched polymer:



The resulting polymer can be described as $(\text{Me}_3\text{SiO}_{1/2})_x$, $(\text{MeSiO}_{3/2})_y$, or M_xT_y using shorthand notation. The formation of three silanols on the MeSiCl_3 by hydrolysis yields a three-dimensional structure, or resin, after condensation, rather than a linear polymer. The average molecular weight depends upon the number of M units that come from the trimethylchlorosilane, which limits the growth of the resin molecule. Most of these resins are prepared in a solvent and usually contain some residual hydroxyl groups. These groups could subsequently be used to cross-link the resin and form a continuous network.

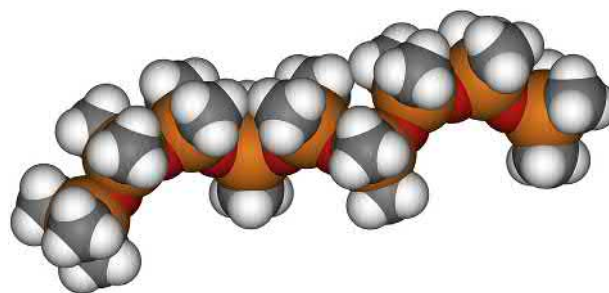
Physicochemical Properties

The position of silicon just under carbon in the periodic table led to a belief in the existence of analog compounds where silicon would replace carbon. Most of these analog compounds do not exist, or behave very differently from their carbon counterparts. There are few similarities between Si–X bonds and C–X bonds (Stark et al., 1982; Corey, 1989; Hardman, 1989; Lane and Burns, 1996).

Between any given element and Si, bond lengths are longer than for the element and C. The lower electronegativity of silicon ($\chi_{\text{Si}} \approx 1.80$, $\chi_{\text{C}} \approx 2.55$) leads to a very polar Si–O bond compared to C–O. This bond polarity also contributes to strong silicon bonding; for example, the Si–O bond is highly ionic and has a high bond energy. To some extent, these values explain the stability of silicones. The Si–O bond is highly resistant to homolytic scission. On the other hand, heterolytic scissions are easy, as demonstrated by the reequilibration reactions occurring during polymerizations catalyzed by acids or bases.

Silicones exhibit the unusual combination of an inorganic chain similar to silicates and often associated with high surface energy, but with side methyl groups that are very organic and often associated with low surface energy (Owen, 1981). The Si–O bonds are moderately polar, and without protection would lead to strong intermolecular interactions (Stark et al., 1982). Yet, the methyl groups, only weakly interacting with each other, shield the main chain (see Fig. 1.3.2B.1).

This shielding is made easier by the high flexibility of the siloxane chain. Rotation energy around a $\text{H}_2\text{C}-\text{CH}_2$ bond in



• **Figure 1.3.2B.1** Space-filling model of polydimethylsiloxane (PDMS).

polyethylene is 13.8 kJ/mol, but is only 3.3 kJ/mol around a $\text{Me}_2\text{Si}-\text{O}$ bond, corresponding to nearly free rotation. Thus, barriers to rotation are low, enabling the siloxane chain to adopt many configurations. In general, the configuration adopted by the siloxane chain will expose the maximum number of methyl groups to the outside. Conversely, the relative rigidity of the hydrocarbon polymer backbone will not allow selective exposure of the organic and hydrophobic methyl groups. In silicones, chain-to-chain interactions are low and the distance between adjacent chains is also great. Despite a very polar chain, silicones can be compared to paraffin, with a low critical surface tension of wetting (Owen, 1981).

Types, Properties, and Preparation of Silicone Materials

The versatility of silicone polymers enables their formulation into a variety of materials with vastly different cure chemistries, material properties, and processing requirements. The end-use will dictate the appropriate material selection and covers a diverse set of applications ranging from orthopedic soft-gel inserts to tubing for bio-pharma processing to prosthetic attachment. A brief overview of these silicone-based materials is described below and summarized in Table 1.3.2B.5.

Silicone Elastomers

Silicone polymers can easily be transformed into a three-dimensional network by way of a cross-linking reaction (often called “curing”), which allows formation of chemical bonds between adjacent chains. The majority of silicone elastomers are cross-linked according to one of the following three reactions, which are summarized in Table 1.3.2B.6.

1. Cross-linking with radicals
2. Cross-linking by condensation
3. Cross-linking by addition.

The preferred cure system can vary by application. For example, silicone medical bonding adhesives often use acetoxy cure (condensation cross-linking), while platinum cure (cross-linking by addition) is typically used for precise silicone parts with no byproducts.

Elastomer Filler

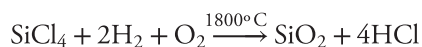
Most silicone elastomers incorporate “filler.” Besides acting as a material extender, as the name implies, filler acts to reinforce the cross-linked matrix. The strength of silicone polymers without filler is unsatisfactory for most applications (Noll, 1968).

TABLE 1.3.2B.5 Types of Silicone Materials and Processing for Medical Applications

Type of Silicone Material	Primary Processing Technique(s)	Examples of Use in Medical Applications
High consistency rubber	High-shear mixing (e.g., two-roll mill, twin conical screw mixer) followed by compression, transfer, or injection molding	Catheters, shunts, drains, tubing for bio-pharma processing
Liquid silicone rubber	Liquid injection molding	High-volume silicone parts molding
Room-temperature vulcanizing elastomer	Hand-mixing, de-airing, and casting	Dental impression molds, encapsulation
Silicone gel	Mixing and filling into envelope shell	Breast, testicular, and soft-tissue implants or external prosthetics
Silicone bonding adhesives	Application onto surfaces to be adhered	Medical device assembly, electrical component encapsulation
Silicone pressure-sensitive adhesives	Coating onto substrate, optional heating to remove solvent	Attachment of hairpieces, prosthetics, and other devices to the body; Transdermal drug delivery
Silicone gel adhesives	Two-parts mixed coated onto a substrate and then heated to cure	Soft skin adhesive for wound and scar-care applications
Silicone film-in-place, fast-cure elastomers	Spreading or spraying onto surface; cures at ambient temperature	Spray-on wound dressings Drug-loaded lotions Topical analgesics

The addition of reinforcing fillers reduces the tackiness of the silicone, increases its hardness, and enhances its mechanical strength. Fillers might also be employed to affect other properties; for example, carbon black is added for electrical conductivity, or barium sulfate to increase radiopacity. These and other materials are used to pigment the otherwise colorless elastomer; however, care must be taken to select only pigments suitable for the processing temperatures and end-use application.

The most widely used reinforcement is obtained by using fumed silica, such as Cab-O-Sil, Aerosil, or Wacker HDK. Fumed silica is produced by the vapor phase hydrolysis of silicon tetrachloride vapor in a hydrogen/oxygen flame:



Unlike many naturally occurring forms of crystalline silica, fumed silica is amorphous. The very small spheroid silica particles (in the order of 10 nm in diameter) fuse irreversibly while still semimolten, creating aggregates. When cool, these aggregates become physically entangled to form agglomerates. Silica produced in this way possesses remarkably high surface area (100–400 m²/g) (Noll, 1968; Cabot Corporation, 1990). Reinforcement occurs with polymer adsorption encouraged by the large surface area of the silica, and when hydroxyl groups on the filler surface lead to hydrogen bonds between the filler and the silicone polymer. In this way, reinforcing filler contributes to the high tensile strength and elongation capability of silicone rubber (Lynch, 1978).

The incorporation of silica filler into silicone polymers is accomplished prior to cross-linking, by mixing the silica into the silicone polymers. This addition increases the already high viscosity of the polymer, resulting in viscosities from 10,000 to well over 100,000 mPas. The mixing, therefore, typically occurs

on a two-roll mill, in a twin-screw extruder, or in a Z-blade mixer capable of processing materials with this rheology.

Chemical treatment of the silica filler with silanes enhances its incorporation in, and reinforcement of, the silicone elastomer, resulting in increased material strength and tear resistance (Fig. 1.3.2B.2).

Processing of Silicone Elastomers

After blending the silicone polymer with amorphous silica filler, an initiator and/or cross-linker, and catalyst are needed to cure the elastomer. To avoid premature cure these ingredients must be separated until use. Consequently, products for making silicone elastomers are generally supplied as two-component or two-part kits, for example, a base and a peroxide paste, or a kit made of part A containing polymer and catalyst, and part B containing polymer and cross-linker. These two components are mixed at a fixed ratio at the point of use and formed into the desired shape before cure.

Silicone elastomers are thermosetting materials. Unlike a thermoplastic, which can be remelted and formed again, a cured silicone elastomer part cannot be reprocessed. They must be formed into the appropriate shape and configuration prior to cross-linking. Suitable methods for shaping silicone elastomers include casting, extrusion, and molding. The process selected depends on the viscosity of the feedstock elastomer material and the shape of the desired cured elastomer part.

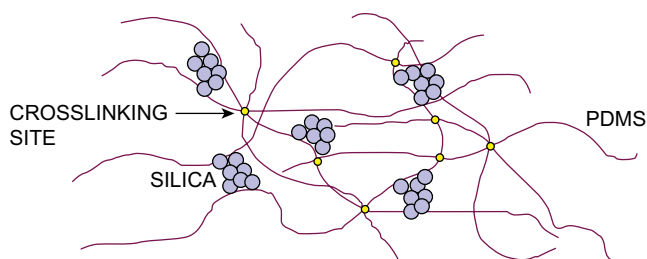
High Consistency Rubber (HCR). If very high-molecular-weight silicone polymers are used (silicone “gums” in the trade) to produce an elastomer, the resulting material is an HCR. These materials have high tear strengths and tensile elongations. Uncured HCRs are putty-like materials that require high shear equipment for processing. The most common technique for HCR processing is extrusion and is

TABLE 1.3.2B.6 Types of Cross-linking (Curing) of Silicone Materials

Crosslinking Scheme/ Mechanism	Usual Components	Main Reaction(s)	Typical Uses	Pros	Cons
<ul style="list-style-type: none"> Radical Cross-linking Free-radical polymerization 	<ul style="list-style-type: none"> Vinyl-containing polymers^a Organic peroxide initiator 	$\begin{aligned} R' + CH_2 = CH - Si \equiv &\rightarrow R - CH_2 - CH' - Si \equiv \\ RCH_2 - CH' - Si \equiv + CH_3 - Si \equiv & \\ \rightarrow RCH_2 - CH_2 - Si \equiv + \equiv Si - CH_2' & \\ \equiv Si - CH_2' + CH_2 = CH - Si \equiv & \\ \rightarrow \equiv Si - CH_2 - CH_2 - CH' - Si \equiv & \\ \equiv Si - CH_2 - CH_2 - CH' - Si \equiv + CH_3 - Si \equiv & \\ \rightarrow \equiv Si - CH_2 - CH_2 - CH_2 - Si \equiv + \equiv Si - CH_2' & \\ 2 \equiv Si - CH_2' \rightarrow \equiv Si - CH_2 - CH_2 - Si \equiv & \end{aligned}$	High consistency silicone rubbers, such as those used in extrusion, compression, or injection molding	Can be used at high temperatures	<ul style="list-style-type: none"> Depending on the peroxide initiator selected, voids can form due to volatile residues during processing Post-cure may be needed to remove volatiles, which can catalyze depolymerization at high temperatures
<ul style="list-style-type: none"> Condensation, one-part RTV (room-temperature vulcanization) Moisture-initiated condensation reaction 	<ul style="list-style-type: none"> Hydroxy end-blocked polydimethyl siloxane Methyl triacetoxysilane^b Tin-catalyst 	$\begin{aligned} &\text{Me} && \text{Me} \\ & && \\ \sim\text{O}-\text{Si}-\text{OAc} & \xrightarrow[\text{-AcOH}]{+\text{H}_2\text{O}} & \sim\text{O}-\text{Si}-\text{OH} \\ & && \\ &\text{OAc} && \text{OAc} \end{aligned}$ $\begin{aligned} &\text{Me} && \text{Me} \\ & && \\ \sim\text{O}-\text{Si}-\text{OH} & + & \text{AcO}-\text{Si}-\text{O} \sim \\ & && \\ &\text{OAc} && \text{OAc} \end{aligned} \quad [8]$ $\xrightarrow{-\text{AcOH}} \begin{aligned} &\text{Me} && \text{Me} \\ & && \\ \sim\text{O}-\text{Si}-\text{O}-\text{Si}-\text{O} \sim \\ & && \\ &\text{OAc} && \text{OAc} \end{aligned}$	Medical device bonding adhesives, encapsulants, and sealants	Cure at room temperature	<ul style="list-style-type: none"> Acetic acid byproduct can be undesirable for certain applications^b Can take significant time for complete cure, ~24 h, because reaction proceeds from outside in as moisture diffuses into the material Needs base levels of moisture to initiate and sustain cure Can have limited shelf-life
<ul style="list-style-type: none"> Condensation, two-part RTV Condensation reaction initiated by component mixing 	<ul style="list-style-type: none"> Hydroxy end-blocked polydimethyl siloxane Alkoxysilane, such as tetra-<i>n</i>-propoxysilane, Si(OnPr)₄ Organotin salt catalyst 	$\begin{aligned} &\text{Me} && n\text{Pr} \\ & && \\ 4 \sim\text{Si}-\text{OH} & + & n\text{Pr}-\text{O}-\text{Si}-\text{O}-n\text{Pr} \\ & && \\ &\text{Me} && \text{O} \\ &&& \\ &&& n\text{Pr} \end{aligned}$ $\xrightarrow[\text{-4nPr OH}]{\text{cat}} \begin{aligned} &\text{Me} && \text{Me} \\ & && \\ \sim\text{Si}-\text{O}-\text{Si}-\text{O}-\text{Si}-\text{O} \sim \\ & && \\ &\text{Me} && \text{Me} \end{aligned}$	Medical device bonding adhesives, encapsulants and sealants	<ul style="list-style-type: none"> Cure at room temperature Cure byproduct is alcohol Longer shelf-life than the corresponding one-part system 	<ul style="list-style-type: none"> Shrinkage can occur after cure at room temperature (0.5%–2% linear shrinkage). Not recommended for use in parts with precise tolerances Organotin salt catalyst limits stability of resulting elastomer at high temperatures
<ul style="list-style-type: none"> Addition-Cure Platinum-catalyzed addition reaction 	<ul style="list-style-type: none"> Vinyl end-blocked polymers Si-H groups carried by a functional oligomer Pt "Karstedt" catalyst 	$\begin{aligned} \equiv\text{Si}-\text{CH}=\text{CH}_2 + \text{H}-\text{Si} \equiv &\xrightarrow{\text{Pt}} \\ \equiv\text{Si}-\text{CH}=\text{CH}_2 & \\ & \\ \text{Pt} & \\ & \\ \text{Si} & \\ & \\ \text{H} & \end{aligned}$ $\begin{aligned} \text{---} &\equiv\text{Si}-\text{CH}_2-\text{CH}_2-\text{Pt}-\text{Si} \equiv \\ \text{---} &\equiv\text{Si}-\text{CH}_2-\text{CH}_2-\text{Si} \equiv \end{aligned}$	<ul style="list-style-type: none"> Molded silicone elastomer components Silicone gel 	<ul style="list-style-type: none"> Can eliminate shrinkage issue in condensation reactions No byproducts 	<ul style="list-style-type: none"> Two-part product, which will begin to react immediately upon mixing (unless an inhibitor is used) Pt in the complex is easily rendered inactive, or "poisoned," if inadvertently bonded to electron-donating substances such as amine or organosulfur compounds

^aEfficient cross-linking with radicals is achieved only when some vinyl groups are present on the polymer chains; using so-called vinyl-specific peroxides; however peroxide-initiated cross-linking of unsubstituted poly(dimethylsiloxane) can be practiced.

^bThe methyltriacetoxysilane can be replaced by oximosilane RSi(ON=CR)₃ or alkoxysilane RSi(OR)₃ to avoid acetic acid by-product.



• **Figure 1.3.2B.2** Silicone elastomer/silica network.

primarily used to produce tubing for bio-pharma processing (Colas et al., 2004). Less common processing techniques include compression, transfer, and injection molding.

Liquid Silicone Rubber (LSR). To obtain a liquid silicone rubber, lower molecular weight silicone polymers are blended with silica. The viscosity of the resulting LSR is correspondingly lowered as compared to an HCR. The LSRs are supplied as two-part kits, which can be pumped, metered, mixed, and directly injected into the molding cavity. Their processing is further eased by the shear-thinning effect that occurs during pumping and injection, reducing the viscosity and injection pressure of the LSR blend.

LSRs are particularly well-suited for long automated production runs as the pumping, metering, and injecting into the molding cavity can be both accomplished and precisely controlled with automation. This does incur higher up-front equipment costs and initial process development time to ensure proper mold temperature control, allowance for venting (air escape from mold cavity during injection), appropriate mold filling rate (to not over- or underfill the mold), prevention of premature curing, and complete product ejection after cure. This acquisition cost is usually justified for large production runs as they provide for more efficiency in terms of mold cycle time, overall processing time, and material usage (Sommer, 2003).

Room Temperature Vulcanizing (RTV) Elastomers. In addition to HCRs and LSRs, which are designed to cure by exposure to heat, other silicone elastomers, known as RTVs, are intended to be cured at room temperature. These materials rely on moisture in the air to cure via a condensation reaction (described in Table 1.3.2B.6), but can also be prepared using a platinum-catalyzed two-part addition reaction.

Typically, RTV elastomers are provided in two-part systems and can be viewed as a variation of LSR, but with lower viscosity and less inhibitor. They can be mixed either by hand or a simple lab mixer, de-aired, and then cast. They are commonly used in laboratory trials as a product development tool, but also have medical commercial applicability, e.g., for dental impression molding.

Silicone Gels

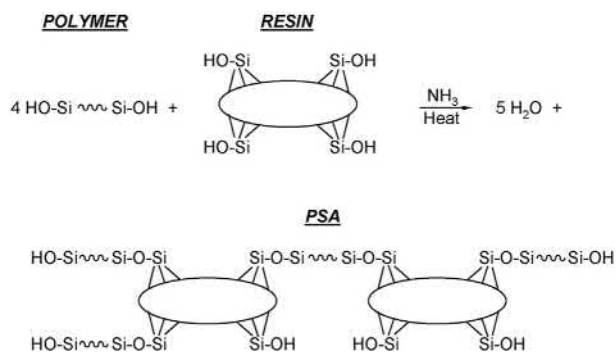
Silicone gels are typically composed of a very lightly cross-linked silicone elastomer whose polymer network has been swollen with silicone fluids or, less commonly, nonsilicone fluids, such as mineral oil. However, these gels contain no silica or other fillers. Silicone gel is often supplied in a two-part fluid system and

cures via a platinum-catalyzed addition reaction. Parts A and B are mixed at a desired ratio and cured (usually by exposure to elevated temperature) to yield a sticky, but cohesive mass. The consistency of the material can be controlled by the degree of cross-linking and the type and quantity of swelling fluid. After mixing, but before cure, the mixture is still liquid and can be cast onto substrates or pushed through a large-gauge needle, enabling the filling of voids e.g., preformed shells, molds, or pouches.

Silicone Adhesives

Three basic types of silicone adhesives are used in medical applications: bonding, pressure-sensitive, and gel.

1. **Bonding adhesives.** Silicone bonding adhesives are used to attach components together and to seal seams and junctions. Electrical components can also be encapsulated and insulated using silicone bonding adhesive. Silicone bonding adhesives are most commonly formulated as one-part RTV elastomer systems that use a condensation cross-linking reaction, as described earlier in this chapter.
2. **Pressure-sensitive adhesives.** Silicone PSAs are typically formulated in solvent. Silanol end-blocked PDMS undergoes a polycondensation reaction with silicate resin in the presence of ammonia as catalyst. The ammonia is stripped with heat and usually the solvent is exchanged. For some applications, a hot-melt PSA can be used with no solvent.



The resulting materials, in addition to being adhesive to skin and other substrates, are highly flexible and permeable to moisture vapor, CO₂, and oxygen. An additional class of silicone PSAs has been developed by incorporating a subsequent reaction step that converts the pendant ≡SiOH groups into ≡SiOSi(CH₃)₃ groups via a reaction with hexamethyldisilazane.

3. **Gel adhesives.** Silicone gel adhesives are supplied in a solventless, two-part system and are cured via a platinum-catalyzed addition reaction run at elevated temperatures. The materials can be coated as a thin film onto a backing substrate such as polyurethane. These materials, also called soft-skin adhesives, have gentler and less traumatic removal from skin than the pressure-sensitive alternatives.

Silicone Film-in-Place, Fast-Cure Elastomers

In addition to the cured silicone elastomers in skin contact applications, in situ cure materials have been developed.

These materials form films when spread or sprayed on the skin, and then undergo RTV cure. The ability of silicone to spread and form films is related to its low surface tension as described in the Physicochemical Properties section above (Maxon et al., 2004).

Biocompatibility of Silicones

There has been much discussion regarding the various definitions of the term *biocompatibility*. We now take it to mean “the ability of a material to perform with an appropriate host response in a specific situation” (Black, 1992; Remes and Williams, 1992). The material properties of silicone, such as hydrophobicity, have been related to biocompatibility properties such as reduced hemolytic potential. Additionally, the relative purity of silicone, its high-molecular-weight polymeric nature, and its chemical structure provide a theoretical basis for its lack of toxicity. Historically it has been tacitly understood that silicone materials are intrinsically biocompatible, since they have been used successfully in so many healthcare applications. However, given the modern definition of the term, no material can be assumed to be universally biocompatible, since this implies that it is suitable for every conceivable healthcare application involving contact with the host patient.

Numerous silicone materials have undergone biocompatibility testing. Many have passed every bioqualification test; however, others have not. Several factors can affect the results of such testing, including the composition of the material. As described previously, the basic polydimethylsiloxane (PDMS) polymer can be modified by replacing the methyl groups with other functional groups. In some cases, those groups may be responsible for an untoward host response. There may be byproducts from the preparation of silicone materials that might trigger tissue reaction, e.g., acetic acid, peroxide initiator, etc.

Purity is another factor that can affect biotest results. Medical silicone materials, including fluids, gels, elastomers, and adhesives, are manufactured by several companies today. Some of these firms manufacture these medical materials following good manufacturing practice (GMP) principles in dedicated, registered, and inspected facilities. Others sell materials generated on their industrial production line into the healthcare market.

Selection of appropriate preclinical material bioqualification tests for their application is the responsibility of the medical device or pharmaceutical manufacturer. Several national, international, and governmental agencies have provided guidance or regulation. Several silicone manufacturers offer special grades of materials that have met these specific requirements. The buyer should carefully investigate the supplier’s definition, since there are no universal special-grade definitions.

At DuPont, BioMedical Grade materials have been qualified to meet or exceed the requirements of ISO 10993-1, USP (United States Pharmacopeia) Class V Plastics tests (acute systemic toxicity and intracutaneous reactivity), hemolysis, cell culture, skin sensitization, mutagenicity, pyrogenicity, and 90-day implant testing. Other physicochemical qualification tests have been conducted, such as certain tests from

the *European Pharmacopoeia*. Specific information regarding material biotesting can be found in other chapters of this text. Testing of the device in finished form should follow material bioqualification tests such as those described above.

Biodurability of Silicones

Traditionally we have thought of *biocompatibility* as the situation in which the biomaterial has minimal adverse impact on the host. Conversely, *biodurability* is where the host has a minimal adverse effect on the biomaterial. The biodurability of silicone in medical applications is likely related to its exceptional thermal and chemical stability.

Silicones are used in numerous applications requiring high temperature resistance (Noll, 1968; Stark et al., 1982). During thermogravimetric analysis and in the absence of impurities, poly-dimethylsiloxane degradation only starts at around 400°C. Thus, silicones remain essentially unaffected by repeated sterilization by autoclaving and they can usually also be dry-heat sterilized. Other sterilization methods can be used, such as ethylene oxide exposure and gamma and e-beam irradiation—although care must be taken to ensure complete sterilant outgassing in the former and that the dosage does not affect performance properties in the latter.

Although silicones can be chemically degraded, particularly at elevated temperatures, by substances capable of acting as depolymerization catalysts (Stark et al., 1982), their hydrophobic nature limits the extent of contact with many aqueous solutions. Typically, the biologic milieu does not present a particularly hostile chemical environment for silicone. A notable exception, however, is the stomach, which excretes large amounts of hydrochloric acid, capable of attacking PDMS if it remains there too long. Based on silicone elastomer performance in long-term implantation applications in other sites, its biodurability is generally considered excellent (Table 1.3.2B.7).

The chemical stability associated with silicones became so well-established that it has been formulated into other biomaterials, such as polyurethane, to enhance their biodurability (Pinchuk et al., 1988; Ward, 2000; Christenson et al., 2002; Ward et al., 2006a,b).

Notwithstanding the chemical stability of silicone, certain factors have been shown to affect its durability in terms of long-term in vivo performance. The hydrophobic elastomer is somewhat lipophilic and can be swollen by lipids or other nonpolar agents. Early experience with in vivo failure of silicone-containing heart valves was traced to elastomer absorption of lipids from the blood that resulted in significant dimensional swelling (McHenry et al., 1970). In most cases the absorption was low and failures did not occur, but in a small percentage of cases the silicone was absorbing quantities sufficient to affect valve performance. Researchers speculated that variations in silicone poppet manufacture, such as cure, might have been a factor (Carmen and Mutha, 1972). Absorption of lipids was a variable reported by Swanson and LeBeau (1974) and Langley and Swanson (1976). The work of Brandon et al. (2002, 2003) has shown that the shells of silicone gel-filled breast implants also absorb silicone fluid (from the gel), causing a minor diminution in mechanical properties, one that is reversed after extraction of the elastomer.

TABLE 1.3.2B.7 Biodurability Studies of Silicone Elastomer and Medical Implants

Year	Researchers	Synopsis
1960	Ames	Explant examination of a clinical silicone ventriculocisternostomy shunt used in the treatment of hydrocephalus showed “the silicone rubber tubing was unchanged by three years implantation in the tissues of the brain and in the cervical subarachnoid space.” Similarly, after over 3 years implantation of silicone tubing in the peritoneal cavity of dogs, Ames wrote, “The physical properties of the tubing itself are apparently unchanged by prolonged contact with tissues.”
1963	Sanislow and Zuidema	Silastic T-tubes were placed in the common ducts of dogs and explanted 9 months later. They were found to be free of bile-salt precipitation and completely patent. Four were tested for tensile strength and compared with a control sample from the same lot of elastomer. “These tests suggested that little physical change occurred in the Silastic as a result of prolonged contact with animal bile.” The tensile strength after 9 months was reported as 1130 psi (7.8MPa), the same value as reported for the nonimplanted control.
1964	Leininger et al.	The Battelle Memorial Institute examined the biodurability of five plastics by implanting films in dogs for 17 months’ duration. The material’s tensile strength and elongation were measured and compared with nonimplanted controls. Although sizable changes were seen in the tensile properties of polyethylene, Teflon, and nylon, the results for Mylar and Silastic remained essentially the same.
1974	Swanson and LeBeau	“Dog-bone”-shaped specimens of medical-grade silicone rubber were implanted subcutaneously in dogs. Tensile properties and lipid content were measured at 6 months and 2 years post-implantation. A slight but statistically significant decrease in measured ultimate tensile strength and elongation were observed, as well as a small weight increase attributed to lipid absorption.
1976	Langley and Swanson	Mechanical test specimens were implanted in dogs for 2 years. Tensile strength, elongation, and tear resistance showed no statistically significant changes. Lipid absorption into the elastomer ranged from 1.4% to 2.6%.
2000	Curtis et al.	Six silicone breast implants surgically excised after 13.8–19.3 years and 10 similar nonimplanted units were tested to determine shell tensile properties and molecular weight of silicone gel extracts. The “study observed only minor changes (less than the explant or implant lot-to-lot variation range) in the tensile strength of Dow Corning silicone breast implants after nearly twenty years of human implantation.” The gel extract molecular weight was either unchanged by implantation or increased slightly.
2003	Brandon et al.	In the most comprehensive study of breast implant biodurability heretofore published, the authors reported their results of tensile, cross-link density, and percent extractable measurements made on 42 explants and 51 controls. The study included some of the oldest explants, with human implantation durations up to 32 years. The researchers also performed a literature search and plotted all published explant tensile modulus data against implantation duration, finding no temporal relationship. Neither was a relationship with implant time seen for the cross-link density results, supporting the biodurability of the silicone elastomer utilized in the implant shells. The researchers concluded, “There was little or no degradation of the base polydimethylsiloxane during in vivo aging in any of the implants we examined.”
2008	Taylor et al.	Silicone biodurability after long-term implantation was examined by a highly sensitive NMR spectroscopy technique as well as NMR relaxometry measurements of explanted gel breast implants and matched nonimplanted controls. No evidence of chemical degradation of the cross-linked silicone matrix was observed in specimens explanted after as many as 32 years in vivo underscoring the biostability of the cross-linked silicone shell and gel.

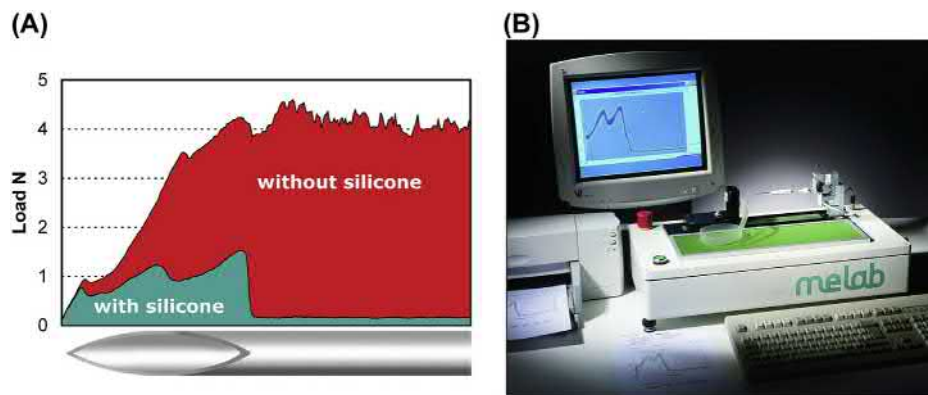
Medical Applications

Silicones, with their unique set of material properties, have found widespread use in the healthcare field. These properties include hydrophobicity, low surface tension, and thermal and chemical stability, which enable both the biocompatibility and biodurability of silicones.

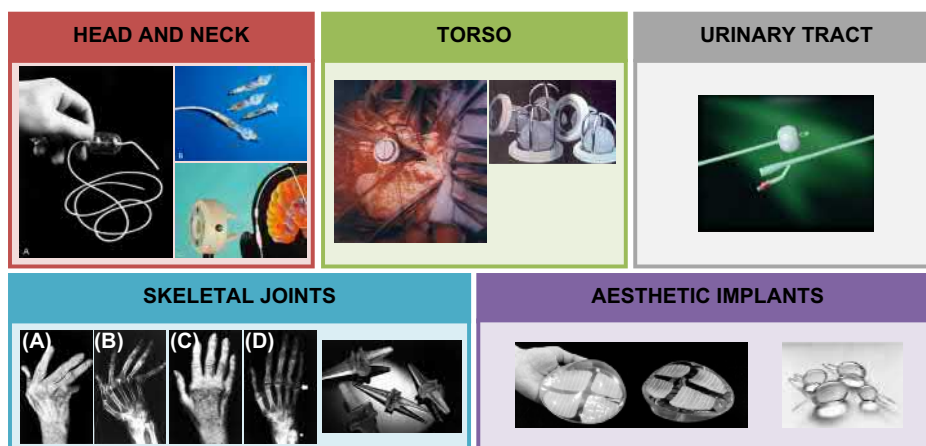
Siliconization

The hydrophobic character of silicone materials led to their consideration for blood coagulation prevention in the mid-1940s. Researchers from the Universities of Toronto and Manitoba obtained a methylchlorosilane from the Canadian General Electric Company and coated syringes,

needles, and vials with the material. When rinsed with distilled water, the silane hydrolyzed, forming a silicone coating on the substrate. The researchers found that the silicone treatment “on glassware and needles gives a surface which preserves blood from clotting for many hours” (Jaques et al., 1946). According to researchers at the Mayo Clinic, silicone: “was the most practical of any known [substance] for coating needle, syringe and tube” (Margulies and Barker, 1949). They further demonstrated that leaving blood in silicone-coated syringes had no significant persistent effect on the blood as a measure of coagulation time after being dispensed. Soon the use of silicone precoating of needles, syringes, and blood collection vials became commonplace. In addition to the blood-preserving quality of silicone, it



• **Figure 1.3.2B.3** (A) Penetration force of silicone coated and noncoated hypodermic needles as measured by (B) Melab equipment using DIN 13097. (Photo courtesy of Melab GmbH.)



• **Figure 1.3.2B.4** Examples of silicone medical devices. (Head and neck) (A) Original Silastic hydrocephalus shunt. (B, C) Modern Codman Hakim programmable valve shunt. (Courtesy of Integra LifeSciences Corporation. (Torso) Examples of early heart valves containing silicone elastomer. (Urinary tract) Silastic Foley catheter. Courtesy of C. R. Bard, Inc. (Skeletal joints) Silicone elastomer finger joint implants: (A, B) Photograph and X-ray of arthritic right hand prior to restorative implantation surgery. (C, D) Postoperative photograph and X-ray view of the same hand. (Aesthetic implants) Silastic mammary prosthesis, 1964.)

was discovered that coated needles were less painful (Fig. 1.3.2B.3). Today most hypodermic needles, syringes, and other blood-collecting apparatus are coated or lubricated with silicone.

Silicone materials have also found uses in the medical laboratory, including silicone tubing for fluid transport between vessels, e.g., bio-pharma processing, and silicone impression materials for dentistry (Starke, 1975; Colas et al., 2004).

Extracorporeal Equipment

Silicone tubing and membranes have found applications in numerous extracorporeal machines, e.g., kidney dialysis, blood oxygenators, and heart bypass machines; silicone is particularly well suited for these applications due in large part to its hemocompatibility and gas-permeability properties. Blood compatibility was also a factor in the incorporation of silicone in several mechanical heart valves (Fig. 1.3.2B.4). The use of silicone in extracorporeal applications continues today.

Medical Inserts and Implants

Silicone implants are literally found from head-to-toe, as detailed in Table 1.3.2B.8 and shown in Fig. 1.3.2B.4. Their use ranges from silicone vitreous fluid replacement in the eye to encapsulation of the electronics on a cardiac pacemaker to finger and toe joint replacements. Material selection will depend on numerous factors including intended function, required mechanical integrity, length of residence in the body, location, etc.

Catheters, Drains, and Shunts

Silicone elastomers are widely used in female and male urinary catheters for intermittent and longer term usage. These include devices composed entirely of extruded silicone elastomers and devices composed of nonsilicone substrates that are subsequently coated to reduce the host reaction. For example, the Silastic Foley is a latex catheter whose interior and exterior are coated with a silicone elastomer (Fig. 1.3.2B.4). Depending on their construction, these silicone catheters can

TABLE 1.3.2B.8 Anatomic Placement of Example Silicone Implants

Head and Neck	
Brain	Hydrocephalus shunts
Skull	Burr hole covers
Eye	Scleral bands and buckles Vitreous fluid replacement Intraocular lenses Contact lenses
Ear	Elastomer tubes for ontological ventilation Cochlear implants (encased in silicone)
Throat	Voice-box prostheses, post-laryngectomy
Torso	
Cardiac	Pacemaker encapsulated and leads insulated with silicone Mechanical heart valves
Gastric	Gastric band implant (Lap-Band, Realize) Angelchik antireflux device
Urinary System	
Urinary tract	Silicone urological catheters Urethral stents Artificial urethra
Bladder	Suprapubic drainage systems
Skeletal Joints	
Hip	Silicone elastomer cement restrictor (bone plug) for total hip replacement
Knee	Shock-absorbing silicone bumper for knee replacement
Hand	Wrist, hand, and finger joint implants
Foot	Foot and toe joint implants
Other	
Breast	Breast implants for post-mastectomy reconstruction or aesthetic augmentation
Scrotum	Testicular implants for congenital defects or post-orchietomy surgery

be used for temporary insertion or as long-term implants for urethra replacement (DeNicola, 1950).

A particularly notable early example of a silicone medical device was the hydrocephalus shunt, which is implanted in patients suffering a dangerous and often fatal buildup of cerebrospinal fluid (CSF) in the brain. This one-way valve, composed of Silastic brand silicone elastomer and tubing from Dow Corning, allowed excess cerebrospinal fluid (CSF) to drain from the brain into the heart when pressure began to build, but closed to prevent backflow once the pressure equalized (Baru et al., 2001). The silicone used in the shunt could be autoclaved without loss of performance and was stable during long-term implantation. This shunt, now known as the Holter valve, was developed by John Holter, a machinist, when his son, Casey, contracted meningitis and subsequently

developed hydrocephalus (LaFay, 1957). It is still being made, almost unchanged, today. The Holter valve and more recent valve/shunt designs have helped save the lives of over one million patients worldwide (Aschoff et al., 1999) (Fig. 1.3.2B.4).

Aesthetic Implants

Silicones have been used extensively in aesthetic and reconstructive plastic surgery for over 50 years. Silicone elastomer is used in implanted prosthetics of numerous descriptions, including breast, scrotum, chin, nose, cheek, calf, and buttocks. Some of these devices may also employ silicone gel, which is a softer feeling substance, contained within a silicone elastomer shell. These are often used for breast, testicular, and chin implants. Surgeons implant these medical devices for aesthetic reasons, to correct congenital deformity, or during reconstructive surgery after trauma or cancer treatment.

The most prominent of these aesthetic implants is the silicone breast implant. Breast enlargement by surgical means has been practiced for over a century. In 1895, Czerny reported transplanting a lipoma to a breast in order to correct a defect resulting from the removal of a fibroadenoma (Czerny, 1895). The insertion of glass balls into the breasts was described by Schwartzmann in 1930 and again by Thorek in 1942. The Ivalon sponge, introduced by Pangman in 1951, was the first augmentation prosthesis to be implanted fairly consistently. This surgical sponge, formulated of poly(vinyl alcohol) cross-linked with formaldehyde, was initially hand-trimmed to the desired shape by the implanting surgeon, and later preformed by Clay Adams, Inc. There was some early recognition of the tendency for tissue growth into the open-cell foam, and in 1958 Pangman patented the concept of encapsulating the foam with an alloplastic (manmade) envelope. His patent also contemplated the use of other fill materials, such as silicone, in place of foam. The Polystan and Ethern polyurethane sponge implants began to be used as breast implants in 1959 and 1960, respectively. These sponge implants became popular in the early 1960s, later being supplanted by the Cronin-type silicone gel-filled breast implants.

With silicone materials and prototypes supplied free of charge from Dow Corning, Doctors Cronin and Gerow developed and tested their silicone gel-filled breast implant in 1961. They implanted the first pair in 1962 (Cronin and Gerow, 1963). Word of their success and the superiority of these silicone implants to the existing foam type led to the popularity of the silicone gel breast implant (Gerow, 1976).

Fig. 1.3.2B.4 shows the appearance of these implants in 1964. The shells of Cronin-type implants were vacuum-molded with anterior and posterior elastomer pieces sealed together, creating a seam around the perimeter of the base. The posterior shell had exposed loops of Dacron mesh attached. The surgeons believed that prosthesis fixation to the chest wall was necessary to prevent implant migration.

Since this early 1964 design, Dow Corning and numerous other companies made prosthesis design improvements, including elimination of the seam and realization that fixation is frequently unnecessary.

In the early 1990s, these popular devices became the subject of a torrent of contentious allegations regarding their safety. The controversy in the 1990s initially involved breast cancer, then evolved to autoimmune connective tissue disease, and continued to evolve to the frequency of local or surgical complications such as rupture, infection, or capsular contracture. Epidemiology studies have consistently found no association between breast implants and breast cancer (McLaughlin et al., 1998, 2007; Park et al., 1998; Brinton et al., 2000; Mellemkjær et al., 2000). In fact, some studies suggest that women with implants may have decreased risk of breast cancer (Brinton et al., 1996; Deapen et al., 1997). Reports of cancer at sites other than the breast are inconsistent or attributed to lifestyle factors (Herdman and Fahey, 2001). The epidemiologic research on autoimmune or connective-tissue disease has also been remarkably uniform, and concludes there is no causal association between breast implants and connective-tissue disease (Gabriel et al., 1994; Sánchez-Guerrero et al., 1995; Hennekens et al., 1996; Edworthy et al., 1998; Nyrén et al., 1998; Kjølner et al., 2001; McLaughlin et al., 2007).

It can be argued that, as a consequence of this examination into the safety of silicone breast implants, silicones are among the most thoroughly tested biomaterials available.

Conclusion

Polydimethylsiloxanes, often referred to as silicones, are a robust class of materials used in a variety of different industries and applications. The inorganic backbone can be functionalized with methyl or other organic groups, while introduction of tri- or tetrafunctional siloxane units leads to a wide range of possible structures. The polymers are easily cross-linked at room or elevated temperatures to form elastomers and other structures. The materials typically exhibit many advantageous properties, including chemical and thermal stability, low surface tension, hydrophobicity, and high gas permeability. These properties combine to result in a biodurable and biocompatible material utilized for medical applications, such as long-term implants, skin-contact adhesives, and transdermal drug delivery.

SIDEBAR 1—LIMITATIONS OF PRESENT-DAY SILICONE MATERIALS

However, versatile as they are, present-day silicone materials still have limitations. The mechanical properties of silicone elastomers, such as tensile strength or tear resistance, are somewhat lower than for other implantable elastomers such as polyurethanes (although generally speaking, polyurethanes are less biodurable). While resistant to a wide array of chemical environments, silicone elastomers are susceptible to degradation in very strongly basic or acidic conditions, such as those found in the stomach. Like all hydrophobic implant materials, silicones are quickly coated with proteins when placed in tissue contact; and a scar tissue capsule forms to surround an implant during wound healing, walling it off from the host. Additionally, silicone elastomers are thermosetting materials, requiring different processing from conventional thermoplastics, such as Teflon or polyetheretherketone (PEEK).

SIDEBAR 2—SURFACE ACTIVITY AND LOW INTERMOLECULAR INTERACTIONS OF SILICONE

The surface activity of silicones is evident in many ways (Owen, 1981):

- Polydimethylsiloxanes have low surface tension (20.4 mN/m) and are capable of wetting most surfaces. With the methyl groups facing outward, this configuration gives very hydrophobic films and a surface with good release properties, particularly if the film is cross-linked after application. Silicone surface tension resides in the range considered most promising for biocompatible elastomers (20–30 mN/m) (Baier, 1985).
- Silicones have a critical surface tension of wetting (24 mN/m), which is higher than their own surface tension. This means silicones are capable of wetting themselves, which promotes good film formation and surface coverage.
- Silicone organic copolymers can be prepared with surfactant properties, with the silicone acting as the hydrophobic part (i.e., in silicone glycol copolymers).

The low intermolecular interactions in silicones have other consequences (Owen, 1981):

- Glass transition temperatures are very low (i.e., 146 K for a polydimethylsiloxane compared to 200 K for polyisobutylene, the analog hydrocarbon).
- The presence of a high free volume compared to hydrocarbons explains the high solubility and high diffusion coefficient of gas into silicones. Silicones have a high permeability to oxygen, nitrogen, and water vapor, even though liquid water is not capable of wetting a silicone surface. As expected, silicone compressibility is also high.
- The viscous movement activation energy is very low for silicones. Their viscosity is less dependent on temperature compared to hydrocarbon polymers. Furthermore, chain entanglements are involved at higher temperature, and contribute to limit viscosity reduction (Stark et al., 1982).

SIDEBAR 3—FILLERS FOR SILICONE ELASTOMERS

Silicone elastomers for medical applications normally use fumed silica as filler, and, occasionally, appropriate pigments or barium sulfate. Because of their low glass transition temperatures, these compounded and cured silicone materials are elastomeric at room and body temperatures without the use of plasticizers, unlike other medical materials such as PVC.

SIDEBAR 4—CURE INHIBITION OF SILICONE ELASTOMERS

Fabricators of silicone elastomer parts should be aware that these LSRs and other addition-cure products contain an inhibitor, a substance that weakly bonds to the platinum catalyst to moderate its activity, permitting sufficient pot life by avoiding premature cure. If contamination occurs with substances capable of bonding more strongly to the platinum catalyst (e.g., amino or thio compounds), the catalyst (which is present in only minute quantities, typically about 10 ppm) may lose activity, resulting in inhibition of cure.

SIDEBAR 5—SILICONE BREAST IMPLANT SAFETY

Numerous systematic reviews (UK IEAG, 1993; France ANDEM, 1996; US IOM, 2000; Australia TDEC, 1997; Germany BgVV, 1998; UK IRG, 1998; EU EQUAM, 2000; US NSP/MDL926, 2001; Spain/EU STOA, 2003) commissioned by various governments have repeatedly and consistently borne out that the evidence fails to support a cause-and-effect relationship between silicone breast implants and systemic diseases. Following FDA approval action on November 17, 2006 making silicone gel breast implants widely available in the United States again, the controversy had diminished.

Recently, however, the controversy has been stoked by the identification of a new, albeit rare, condition called breast implant associated-anaplastic large cell lymphoma (BIA-ALCL). As the nomenclature indicates, the condition is associated with breast implants. The first case was reported in 1997 (Keech and Creech, 1997), the FDA indicated their preliminary interest in the condition in 2011 (US FDA CDRH, 2011), and the World Health Organization designated BIA-ALCL as a provisional disease diagnosis in 2016 (Swerdlow et al., 2016). BIA-ALCL presents as fluid accumulation and edema in the patient's breast implant capsule. Biopsy and serology usually confirm the differential diagnosis. ALCL patients have atypical, monoclonal T-cell proliferation with positive immunohistochemical results for CD30. Like other non-Hodgkin's lymphoma patients, they test negative for anaplastic lymphoma kinase (ALK) (Fleming et al., 2018). Of the estimated 35 million women globally who have received breast implants, there are just over 500 reported cases of BIA-ALCL and 12 associated deaths (Sieber et al., 2017).

Current epidemiology strongly suggests that this disease often has an indolent course, although most patients do undergo explantation and resection of the capsule around the implant. BIA-ALCL is not typically a cancer that will inevitably progress without treatment, in some cases spontaneous regression and resolution have been observed (Fleming et al., 2018).

As this chapter was being revised in late 2018, hypotheses regarding the etiology of BIA-ALCL focused mainly on chronic inflammation and biofilm infection with *Ralstonia* species (a Gram-negative bacilli in the *Burkholderiaceae* family) (Hu et al., 2016). An extremely interesting factor in the development of this condition is that virtually all of the women diagnosed had implants with textured surfaces (Brody et al., 2010). While this disease has been observed in women with polyurethane foam-covered implants and in implants whose shells were imprinted with the negative texture of such foam, most BIA-ALCL patients had implants with very rough surfaces prepared through the use of a lost-salt process (Brody et al., 2010). In animal implantation studies of several implant surface textures, we observed intensities of inflammation that were consistent with the later clinical outcomes. It is evident that surface properties of alloplastic biomaterials can have a profound and determining effect on biocompatibility and that not all implants, nor implant textures, are created equal (Curtis and Klykken, 2015).

In addition to ALCL being associated almost exclusively with textured breast implants, it is also important to note that it has occurred with saline-filled as well as silicone gel-filled implant types. Material of composition does not appear to be related to the development of this condition as ALCLs have been observed adjacent to multiple implant types with varied materials of construction (Palraj, 2010).

Acknowledgments

A portion of this chapter (here updated) was authored by André Colas and originally published in *Chimie Nouvelle*, the journal of the Société Royale de Chimie (Belgium), Vol. 8 (30), 847 (1990) and is reproduced here with the permission of the editor.

The authors thank S. Hoshaw, Ph.D. and P. Klein, Ph.D. for their contributions regarding breast implant epidemiology.

References

- Ames, R.H., 1960. Response to silastic tubing. Bull. Dow Corning Center Aid Med. Res. 2 (4), 1.
- Aschoff, A., Kremer, P., Hashemi, B., Kunze, S., 1999. The scientific history of hydrocephalus and its treatment. Neurosurg. Rev. 22, 67.
- Australia TDEC (Therapeutic Devices Evaluation Committee, Therapeutic Goods Administration), 1997. Aust. Ther. Device Bull. 33, 3.
- Baier, R.E., 1985. Adhesion in the biologic environment. Biomater. Med. Dev. Artif. Organs 12, 133–159.
- Baru, J.S., Bloom, D.A., Muraszko, K., Koop, C.E., 2001. John Holtzer's shunt. J. Am. Coll. Surg. 192, 79.
- Black, J., 1992. Biological Performance of Materials: Fundamentals of Biocompatibility. Marcel Dekker, New York.
- Brandon, H.J., Jerina, K.L., Wolf, C.J., Young, V.L., 2002. *In vivo* aging characteristics of silicone gel breast implants compared to lot-matched controls. Plast. Reconstr. Surg. 109 (6), 1927.
- Brandon, H.J., Jerina, K.L., Wolf, C.J., Young, V.L., 2003. Biodurability of retrieved silicone gel breast implants. Plast. Reconstr. Surg. 111 (7), 2295.
- Brinton, L.A., Lubin, J.H., Burich, M.C., Colton, T., Brown, S.L., Hoover, R.N., 2000. Breast cancer following augmentation mammoplasty (United States). Cancer Causes Control 11, 819.
- Brinton, L.A., Malone, K.E., Coates, R.J., Schoenberg, J.B., Swanson, C.A., Daling, J.R., Stanford, J.L., 1996. Breast enlargement and reduction: results from a breast cancer case-control study. Plast. Reconstr. Surg. 97 (2), 269.
- Brody, G.S., Deapen, D., Gill, P., Epstein, A., Martin, S., Elatra, W., March 20–23, 2010. T Cell Non-Hodgkin's Anaplastic Lymphoma Associated with One Style of Breast Implants. American Society of Plastic Surgeons Annual Conference, San Antonio, Texas. Scientific Session IX: Breast B, Oral communication and abstract 42.
- Cabot Corporation, 1990. CAB-O-SIL Fumed Silica Properties and Functions. Cabot Corporation, Tuscola, IL.
- Carmen, R., Mutha, S.C., 1972. Lipid absorption by silicone rubber heart valve poppets—in-vivo and in-vitro results. J. Biomed. Mater. Res. 6, 327.
- Christenson, E.M., Dadestan, M., Wiggins, M.J., Ebert, M., Ward, R., Hiltner, A., Anderson, J.M., 2002. The effect of silicone on the biostability of poly(ether urethane). Soc. Biomater. 28th Ann. Meeting Trans. 111.
- Colas, A., 1990. Silicone chemistry overview. Chimie Nouvelle. J. Soc. R Chim. Belgium 8 (30), 847.
- Colas, A., Malczewski, R., Ulman, K., 2004. Silicone tubing for pharmaceutical processing. Der Pharma Chem. 30–36.

- Corey, J.Y., 1989. Historical overview and comparison of silicon with carbon. In: Patai, S., Rappoport, Z. (Eds.), *The Chemistry of Organic Silicon Compounds*. John Wiley & Sons, New York, NY, pp. 1–56. Part 1.
- Cronin, T.D., Gerow, F.J., 1963. Augmentation mammoplasty: a new “natural feel” prosthesis. *Trans. Third Int. Congress Plastic Surg.—Excerpt. Med., Int. Congr. Ser.* 66, 41.
- Curtis, J., Klykken, P., 2015. Breast implant-associated anaplastic large cell lymphoma: report of 2 cases and review of the literature. *Aesthet. Surg. J.* 35 (3), 75–77.
- Curtis, J.M., Peters, Y.A., Swarthout, D.E., Kennan, J.J., VanDyke, M.E., 2000. Mechanical and chemical analysis of retrieved breast implants demonstrate material durability. *Trans. Sixth World Biomater. Congress* 346.
- Czerny, V., 1895. Plastischer ersatz der brustdruse durch ein lipoma. *Zentralbl. Chir.* 17, 72.
- Deapen, D.M., Bernstein, L., Brody, G.S., 1997. Are breast implants anticarcinogenic? A 14-year follow-up of the Los Angeles Study. *Plast. Reconstr. Surg.* 99 (5), 1346.
- DeNicola, R.R., 1950. Permanent artificial (silicone) urethra. *J. Urol.* 63 (1), 168–172.
- Edworthy, S.M., Martin, L., Barr, S.G., Birdsell, D.C., Brant, R.F., Fritzler, M.J., 1998. A clinical study of the relationship between silicone breast implants and connective tissue disease. *J. Rheumatol.* 25 (2), 254.
- European Committee on Quality Assurance & Medical Devices in Plastic Surgery (EQUAM), 2000. Consensus Declaration of Breast Implants and Consensus Declaration of Advanced Technologies and Devices in Plastic Surgery. 4th Consensus Conference, 22nd–24th June 2000 at Herzliya, Israel.
- Fleming, D., Stone, J., Tansley, P., 2018. Spontaneous regression and resolution of breast implant-associated anaplastic large cell lymphoma: implications for research, diagnosis and clinical management. *Aesthet. Plast. Surg.* 42, 672–678 2018.
- France, 1996. Agence Nationale pour le Développement de l'Evaluation Médicale (ANDEM) Silicone gel-filled breast implants.
- Gabriel, S.E., O'Fallon, W.M., Kurland, L.T., Beard, C.M., Woods, J.E., Melton 3rd, L.J., 1994. Risk of connective-tissue diseases and other disorders after breast implantation. *N. Engl. J. Med.* 330 (24), 1697.
- Germany, 1998. Bundesinstitut für gesundheitlichen Verbraucherschutz und Veterinärmedizin (BgVV).
- Gerow, F.J., 1976. Breast implants. In: Georgiade, N.G. (Ed.), *Reconstructive Breast Surgery*. Mosby, St. Louis.
- Hardman, B., 1989. Silicones. 204. *Encyclopedia of Polymer Science and Engineering*, vol. 15. John Wiley & Sons, New York, NY, p. 204.
- Hennekens, C.H., Lee, I.M., Cook, N.R., Hebert, P.R., Karlson, E.W., LaMotte, E., Manson, J.E., Buring, J.E., 1996. Self-reported breast implants and connective-tissue diseases in female health professionals. A retrospective cohort study. *JAMA* 275 (8), 616.
- Herdman, R.C., Fahey, T.J., 2001. Silicone breast implants and cancer. *Canc. Invest.* 19 (8), 821.
- Hu, H., et al., 2016. Bacterial biofilm infection detected in breast implant-associated anaplastic large-cell lymphoma. *Plast. Reconstr. Surg.* 137 (6), 1659–1669.
- Jaques, L.B., Fidler, E., Feldsted, E.T., MacDonald, A.G., 1946. Silicones and blood coagulation. *Can. Med. Assoc. J.* 55, 26.
- Keech Jr., J.A., Creech, B.J., 1997. Anaplastic T-cell lymphoma in proximity to a saline-filled breast implant. *Plast. Reconstr. Surg.* 100 (2), 554–555.
- Kipping, F.S., 1904. Organic derivative of silicon. Preparation of alkylsilicon chlorides. *Proc. Chem. Soc.* 20, 15.
- Kjøller, K., Friis, S., Mellekjær, L., McLaughlin, J.K., Winther, J.F., Lipworth, L., Blot, W.J., Fryzek, J., Olsen, J.H., 2001. Connective tissue disease and other rheumatic conditions following cosmetic breast implantation in Denmark. *Arch. Intern. Med.* 161, 973.
- LaFay, H., January 1957. A father's last-chance invention saves his son. *Reader's Digest*, pp. 29–32.
- Lahey, F.H., 1946. Comments made following the speech “results from using Vitallium tubes in biliary surgery,” read by Pearse HE before the American Surgical Association, Hot Springs, VA. *Ann. Surg.* 124, 1027.
- Lane, T.H., Burns, S.A., 1996. Silica, silicon and silicones ... unraveling the mystery. *Curr. Top. Microbiol. Immunol.* 210, 3–12.
- Langley, N.R., Swanson, J.W., 1976. Effects of Subcutaneous Implantation, through Two Years, on the Physical Properties of Medical Grade Tough Rubber (MDF-0198). Internal Dow Corning Report Number 1976-10030-4571, Produced to FDA and in Litigation Discovery. MDL926 number P-000004408.
- Leininger, R.I., Mirkovitch, V., Peters, A., Hawks, W.A., 1964. Change in properties of plastics during implantation. *Trans. Am. Soc. Artif. Intern. Organs* X, 320.
- Lynch, W., 1978. *Handbook of Silicone Rubber Fabrication*. Van Nostrand Reinhold, New York, NY, pp. 25–34.
- Margulies, H., Barker, N.W., 1949. The coagulation time of blood in silicone tubes. *Am. J. Med. Sci.* 218 (1), 42.
- Maxon, B.D., Starch, M.S., Raul, V.A., 2004. New silicone film-forming technologies for topical delivery and beyond. In: Orlando, FL: Proceedings of the 23rd International Federation of the Society of Cosmetic Chemists (IFSCC) Congress.
- McHenry, M.M., Smeloff, E.A., Fong, W.Y., Miller, G.E., Ryan, P.M., 1970. Critical obstruction of prosthetic heart valves due to lipid absorption by Silastic. *J. Thorac. Cardiovasc. Surg.* 59 (3), 413.
- McLaughlin, J.K., Lipworth, L., Murphy, D.K., Walker, P.S., 2007. The safety of silicone gel-filled breast implants – a review of the epidemiologic evidence. *Ann. Plast. Surg.* 59 (5), 569–580.
- McLaughlin, J.K., Nyrén, O., Blot, W.J., Yin, L., Josefsson, S., Fraumeni, J.F., Adami, H.O., 1998. Cancer risk among women with cosmetic breast implants: a population-based cohort study in Sweden. *J. Natl. Cancer Inst. (Bethesda)* 90 (2), 156.
- Mellekjær, L., Kjøller, K., Friis, S., McLaughlin, J.K., Hogsted, C., Winther, J.F., Breiting, V., Krag, C., Kruger Kjær, S., Blot, W.J., Olsen, J.H., 2000. Cancer occurrence after cosmetic breast implantation in Denmark. *Int. J. Cancer* 88, 301.
- Noll, W., 1968. *Chemistry and Technology of Silicones*. Academic Press, New York, NY.
- Nyrén, O., Yin, L., Josefsson, S., McLaughlin, J.K., Blot, W.J., Engqvist, M., Hakelius, L., Boice Jr., J.D., Adami, H.O., 1998. Risk of connective tissue disease and related disorders among women with breast implants: a nation-wide retrospective cohort study in Sweden. *Br. Med. J.* 316 (7129), 417.
- Owen, M.J., 1981. Why silicones behave funny. *Chemtech* 11, 288.
- Palraj, B., et al., 2010. Soft tissue anaplastic large T-cell lymphoma associated with a metallic orthopedic implant: case report and review of the current literature. *J. Foot Ankle Surg.* 49 (6), 561–564.
- Pangman, W.J., 1958. U.S. Patent No. 2,842,775.
- Park, A.J., Chetty, U., Watson, A.C.H., 1998. Silicone breast implants and breast cancer. *Breast* 7 (1), 22.
- Pinchuk, L., Martin, J.B., Esquivel, M.C., MacGregor, D.C., 1988. The use of silicone/polyurethane graft polymers as a means of eliminating surface cracking of polyurethane prostheses. *J. Biomater. Appl.* 3 (2), 260.

- Remes, A., Williams, D.F., 1992. Immune response in biocompatibility. *Biomaterials* 13 (11), 731.
- Rochow, E.G., 1945. The direct synthesis of organosilicon compounds. *J. Am. Chem. Soc.* 67, 963–965.
- Sánchez-Guerrero, J., Colditz, G.A., Karlson, E.W., Hunter, D.J., Speizer, F.E., Liang, M.H., 1995. Silicone breast implants and the risk of connective-tissue diseases and symptoms. *N. Engl. J. Med.* 332 (25), 1666.
- Sanislow, C.A., Zuidema, G.D., 1963. The use of silicone T-tubes in reconstructive biliary surgery in dogs. *J. Sur. Res.* III (10), 497.
- Schwartzmann, E., 1930. Die technik der mammoplastik. *Der. Chirurg.* 2 (20), 932–945.
- Sieber, D.A., Adams Jr., W.P., 2017. What's your micromort? A patient-oriented analysis of breast implant-associated anaplastic large cell lymphoma (BIA-ALCL). *Aesthet. Surg. J.* 37 (8), 887–891.
- Smith, A.L., 1991. Introduction to silicones. 3–19. *The Analytical Chemistry of Silicones*. John Wiley & Sons, New York, NY, pp. 3–19.
- Sommer, J.G., 2003. *Elastomer Molding Technology: A Comprehensive and Unified Approach to Materials, Methods, and Mold Design for Elastomers*. Elastech, Hudson, OH.
- Spain/EU, 2003. European parliament Scientific and technological Options Assessment (STOA). In: Updated Report on the “Health Risks Posed by Silicone Implants in General, with a Special Attention to Breast Implants”.
- Stark, F.O., Falender, J.R., Wright, A.P., 1982. Silicones. In: Wilkinson, G., Sone, F.G.A., Ebel, E.W. (Eds.), *Comprehensive Organometallic Chemistry*, vol. 2. Pergamon Press, Oxford, UK, pp. 288–297.
- Starke Jr., E.N., 1975. A historical review of complete denture impression materials. *JADA* 91, 1037–1041.
- Swanson, J.W., LeBeau, J.E., 1974. The effect of implantation on the physical properties of silicone rubber. *J. Biomed. Mater. Res.* 8, 357.
- Swerdlow, S.H., et al., 2016. The 2016 revision of the World Health Organization classification of lymphoid neoplasms. *Blood* 127, 2375–2390.
- Taylor, R.B., Eldred, D.E., Kim, G., Curtis, J.M., Brandon, H.J., Klykken, P.C., 2008. Assessment of silicone gel breast implant biodurability by NMR and EDS techniques. *J. Biomed. Mater. Res. A.* 85, 684–691.
- Thorek, M., 1942. Amastia, hypomastia and inequality of the breasts. In: *Plastic Surgery of the Breast and Abdominal Wall*. C. C. Thomas, Springfield, IL.
- UK Independent Expert Advisory Group (IEAG), 1993. Evidence for an Association between the Implantation of Silicones and Connective Tissue Disease. UK Medical Devices Agency.
- UK Independent Review Group (IRG), 1998. *Silicone Gel Breast Implants — the Report of the Independent Review Group*. US FDA, CDRH, January 2011. Anaplastic Large Cell Lymphoma (ALCL) in Women with Breast Implants: Preliminary FDA Findings and Analyses.
- US Institute of Medicine (IOM), 2000. *Safety of Silicone Breast Implants*. Bondurant, Ernster, and Herdman. National Academy Press.
- US National Science Panel (NSP), 2001. In re: Silicone Gel Breast Implant Products Liability Litigation (MDL926). Rule 706 National Science Panel Report www.fjc.gov/BREIMLIT/SCIEN/CE/report.htm.
- Ward, R.S., 2000. Thermoplastic silicone-urethane copolymers: a new class of biomedical elastomers. *Med. Device Diagn. Ind.* 22 (4), 68–77.
- Ward, R., Anderson, J., Ebert, M., McVenes, R., Stokes, K., 2006a. *In vivo* biostability of polysiloxane polyether polyurethanes: resistance to metal ion oxidation. *J. Biomed. Mater. Res. A.* 77 (2), 380–389.
- Ward, R., Anderson, J., McVenes, R., Stokes, K., 2006b. *In vivo* biostability of polysiloxane polyether polyurethanes: resistance to biologic oxidation and stress cracking. *J. Biomed. Mater. Res. A.* 77 (3), 580–589.

Further Reading

- Braley, S.A., 1973. *Spare Parts for Your Body*. Dow Corning Center for Aid to Medical Research, Midland, MI.
- Brunauer, S., Emmett, P.H., Teller, E., 1938. Adsorption of gases in multimolecular layers. *J. Am. Chem. Soc.* 60, 309.
- Ciapetti, G., Granchi, D., Stea, S., Savarino, L., Verri, E., Gori, A., Savioli, F., Montanaro, L., 1998. Cytotoxicity testing of materials with limited *in vivo* exposure is affected by the duration of cell-material contact. *J. Biomed. Mater. Res.* 42, 485–490.
- Colas, A., 1990. Silicone chemistry overview. *Chimie Nouvelle. J. Soc. R Chim. Belgium* 8 (30), 847.
- Delank, K.W., Scheuermann, K., 2008. Praktische Aspekte der prothetischen Stimmrehabilitation nach Laryngektomie. *Laryngo-Rhino-Otol.* 87 (3), 160–166.
- Dillehay, S.M., 2007. Does the level of available oxygen impact comfort in contact lens wear?: a review of the literature. *Eye Contact Lens* 33 (3), 148–155.
- Harmand, M.F., Briquet, F., 1999. In vitro comparative evaluation under static conditions of the hemocompatibility of four types of tubing for cardiopulmonary bypass. *Biomaterials* 20 (17), 1561.
- Mazas, F.B., 1973. Guepar total knee prosthesis. *Clin. Orthop. Relat. Res.* 94, 211.
- O'Brien, L., Jones, D.J., 2013. Silicone gel sheeting for preventing and treating hypertrophic and keloid scars. *Cochrane Database Syst. Rev.* (9) CD003826.pub3.
- Swanson, A.B., 1968. Silicone rubber implants for replacement of arthritic or destroyed joints in the hand. *Surg. Clin. N. Am.* 48, 1113.
- Timoney, A.G., Kelly, J.M., Welfare, M.R., 1990. The Angelchik anti-reflux device: a 5-year experience. *Ann. R. Coll. Surg. Engl.* 72, 185–187.

Chapter Questions

- Which material property was the basis for Charles Holter's selection of silicone rubber for the hydrocephalic shunt valve?
 - Biostability
 - Hemocompatibility
 - Thermal stability
 - Viscoelasticity
 - All of the above
- Among the following applications where silicones are still in use today, which was the first reported human implantation of a silicone elastomer medical device?
 - Breast augmentation
 - Bile duct repair
 - Hydrocephalus shunt
 - Urethra repair
- What functions can fillers serve in silicone elastomers?
 - Material extender to reduce bulk cost
 - Reinforce the cross-linked polymer matrix
 - Provide color pigmentation
 - Enhance visibility on X-ray
 - All of the above
- Draw the molecular structure represented by the shorthand notation $\text{TM}_2\text{M}^{\text{H}}$. What is its chemical name?
- What properties of silicones are responsible for their (a) biodurability and (b) biocompatibility?
- For the following biomaterials design scenarios, select the preferred material and provide your assumptions and justifications for doing so.
 - Your customer is designing a syringe. They want to select a material capable of lubricating the interior surface of the syringe to reduce the force required to depress the plunger. Would you select a silicone fluid or a silicone elastomer?
 - You have two material options for designing an indwelling urinary catheter: (1) silicone elastomer or (2) thermoplastic polymer, e.g., polyvinyl chloride (PVC). Which would you select?
 - You are designing a wound dressing. It is intended to be used on geriatric patients who are suffering from chronic wounds. The adhesive must be selected such that it provides secure attachment yet gentle release from the skin. Would you select an acrylic adhesive or a silicone tacky gel adhesive?
 - An artificial tendon is being designed and is intended for implantation. You are primarily concerned about the tensile strength of the material. Would you select a silicone elastomer, a polyurethane elastomer, or PEEK (polyether ether ketone)?
- Case Study: Sterilization of a silicone elastomer (Foley catheter, neonatal catheter, tubing).

One of the most significant challenges to consider when designing a medical device is whether and how to sterilize it. Sterilization, which can help to ensure the safety of the device for implantation, can also drastically affect material properties and ultimate stability. Discuss each of the following topics as they would affect the sterilization of a silicone elastomer being used as a Foley catheter, neonatal catheter, tubing, etc.

- Would a standard manufacturing facility be sufficient for the production of the catheter or would either cGMP (good manufacturing practice) or clean room facilities be required? How would each process affect the bio-burden and subsequent sterilization required?
- What types of sterilization techniques can be used with silicone elastomers?
- What are the considerations for each sterilization technique?
- What are the consequences of selecting an inappropriate sterilization technique?
- How would the biomaterial or device be assessed post-sterilization? How do you guarantee sufficient sterilization?

Chapter Answers

Question 1

The most correct answer is c. While hemocompatibility, biostability, and viscoelastic properties are all related to silicone's successful application in shunts for the treatment of hydrocephalus, thermal stability was the basis for Holter to select silicone rubber for his valve. Steam sterilization deformed other rubbers he tried.

Question 2

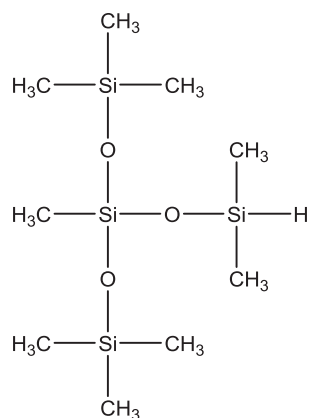
The correct answer is b. While many believe that Holter's silicone hydrocephalic shunts in 1956 were the earliest use, the first reported human implantation of a silicone elastomer medical device was actually a decade before. In April 1946, Dr. Frank Lahey used silicone elastomer materials from the experimental laboratory of General Electric Company called "bouncing clay" for bile duct repair. Silicone materials continue to be used in each of these applications today. The vast majority of today's breast implants still have shells made of silicone elastomer. Silicone stents and T-tubes remain in use for biliary repair. Valved hydrocephalus shunts of silicone—including the popular Pudenz-Schulte and Holter types—continue to save lives. Silicone tubes and catheters continue to find wide urologic use, including in the surgical repair of epi- and hypospadias.

Question 3

The correct answer is e, all of the above. Fillers such as fumed amorphous silica can be used to both extend the material and reinforce the cross-linked polymer matrix. Silicone-compatible dyes and pigments can modify the color of the elastomer. And additives such as barium sulfate increase radiopacity if necessary so implants are visible on X-ray.

Question 4

The long-hand name for $\text{TM}_2\text{M}^{\text{H}}$ is 3-dimethylsiloxy-heptamethyltrisiloxane. Its structure is below:



Question 5

- a. The biocompatibility of silicone materials is attributed to their tremendous thermal and chemical stability, afforded to them by three specific properties:
- (1) Silicon, when compared to carbon, has much lower electronegativity ($\chi^{\text{Si}} \approx 1.80$, $\chi^{\text{C}} \approx 2.55$). In the case of the Si–O bond, this electronegativity difference leads to a more polar bond with a high bond energy, which is highly resistant to homolytic scission. This provides improved stability over organic polymers with primarily C–C bonds.
 - (2) The side methyl groups on the siloxane polymers shield the polar Si–O backbone from strong intermolecular interactions that could result in degradation.
 - (3) Additionally, the Si–O bonds have a low barrier to rotation (3.3 kJ/mol around a Me₂Si–O bond, compared to 13.8 kJ/mol for an H₂C–CH₂ bond). This enables silicone polymers to adopt the most energetically favorable configuration.
- b. The biocompatibility of silicones is also due to a combination of unique properties:
- (1) Due to its hydrophobic nature, any implanted silicone material undergoes rapid protein adsorption (opsonization) to its surface. This can limit the host response to the foreign material.
 - (2) The cross-linked and/or long-chain silicone polymers used in medical materials will not leach over time in the relatively aqueous environments found within the body. This is due to their hydrolytic stability, which prevents the degradation of these larger silicone molecules into lower molecular weight silicones that would leach more readily. The one exception is in the acidic environment of the stomach, where the elevated level of hydrochloric acid is capable of attacking PDMS over long residence times.
 - (3) Silicones have high permeability to oxygen, nitrogen, and water vapor due to their high free volume compared to hydrocarbons.
 - (4) Silicones are widely considered to be hemocompatible, having very low hemolytic potential.
 - (5) Finally, silicones are able to be manufactured with high levels of purity, with tight controls over the

polydispersity of silicone polymers and over the resulting material properties.

Question 6

- The correct answer is silicone fluid. Silicone elastomers, even when filled with silica that tends to reduce bulk adhesion, remain very tacky and sticky and would not impart a lubricious surface to the interior of a syringe. Silicone fluids, on the other hand, are able to readily form a film on the interior surface (e.g., barrel) of a syringe due to their critical surface tension of wetting being lower than their own surface tension. This leaves a lubricating surface on the syringe and, additionally, can help prevent blood coagulation.
- The correct answer is the silicone elastomer. Although widely used in urinary catheters due to their low cost, PVC (and other thermoplastic) catheters are less flexible than their silicone counterparts and the plasticizers required to soften the material can have deleterious effects over long-term use. Silicone elastomer catheters have excellent biocompatibility, but can require lubrication to easily insert the catheter into the urinary tract.
- The correct answer is the silicone tacky gel adhesive. In patients with compromised skin, such as the geriatric population, a silicone soft skin adhesive dressing will provide secure attachment of a wound dressing while maintaining a gentle release profile, which is less likely to further damage the skin. Acrylic adhesives are inexpensive, can be coated at low coat weights, and provide strong attachment to the skin. This strong attachment, coupled with acrylic adhesives potentially sensitizing skin over repeated exposures, makes it a less gentle alternative for wound dressings.
- The correct answer is PEEK. The silicone elastomer, even at comparable durometers, will have significantly lower tensile strength than either polyurethane or PEEK. In an artificial tendon application, the implant must be able to match the tensile strength of a tendon to withstand the mechanical loads required in use without failure.

Question 7

- The cleaner the manufacturing facility, the cleaner the surface of the material will be prior to sterilization. A cleaner surface will require less exposure to harsh sterilization conditions, which will limit the possibility of the sterilization process negatively impacting the robustness of the material/device. This needs to be balanced with the feasibility of manufacturing in these environments, e.g., cost, access.
- Among the most common methods, ethylene oxide, dry heat, and autoclaving can be used to sterilize devices comprised of silicone elastomers. Depending on the material and other parameters, gamma sterilization and e-beam (also known as beta) sterilization can also be used with silicone materials.

- c. What are the considerations for each sterilization technique?
- (1) Ethylene oxide. Exposure to ethylene oxide will successfully sterilize silicone elastomers. However, complete outgassing of the ethylene oxide gas must be verified. Any remaining EtO and/or byproducts of its reaction with water, e.g., ethylene glycol, can have significant and deleterious effects upon implantation. The device packaging, therefore, must be permeable to not only EtO, but those other byproducts.
 - (2) Autoclave/Dry Heat. Due to the thermal and moisture resistance of silicone elastomers, autoclaving is generally considered a well-tolerated sterilization technique for these materials. Similarly, dry heat sterilization is used regularly with silicone elastomers due to their thermal resistance.
 - (3) Gamma Sterilization/e-Beam. Although these techniques will sterilize the silicone elastomer, they can potentially further cross-link the material and change its mechanical properties. The dose will directly affect the extent of the change.
- d. One needs to balance the sterilant dose that a material can withstand with the dose it receives. For polymers, in particular, you need to minimize the amount of radiation a material receives while still ensuring a sufficient sterilization effect. An inappropriate sterilization technique will not allow the user this balance, resulting in either an insufficiently sterilized material or a material whose properties have been negatively impacted and that can no longer perform as needed.
- e. According to ISO 10993-1, a battery of biological evaluation tests shall be performed either on the final product, or representative samples from the final product, or

materials processed in the same manner as the final product (including sterilization). This is important because the processing, especially sterilization, impacts these materials and their properties. The critical performance parameters should also be reevaluated with the sterilized material to ensure no significant change has occurred. The challenge is to balance sufficient sterilization with maintaining the material properties of the device. Sufficient sterilization ensures that the dosage exceeds the bioburden with adequate safety margin (overkill). Typically, sterilization assurance is performed by either dosimetric or parametric release or a combination of both. Dosimetric release is defined as the release of terminally sterilized batches or lots of sterile products based on physical data from the irradiation process instead of direct sterility testing. This includes appropriate process qualification to verify that the irradiation cycle provided the required minimum dose to the product. Parametric release is defined as the release of terminally sterilized batches or lots of sterile products based upon compliance with the defined critical parameters of sterilization without having to perform the requirements under pharmacopeial sterility tests, such as USP <71>. Parametric release is a possibility when the mode of sterilization is very well understood, the physical parameters of processing are well defined, predictable, and measurable, and the lethality of the cycle has been microbiologically validated through the use of appropriate biological indicators or, in the case of ionizing radiation, the appropriate microbiological and dosimetric tests. The use of parametric release for sterilization processes requires prior FDA approval.

1.3.2C

Fluorinated Biomaterials

DAVID W. GRAINGER^{1,2}

¹Department of Biomedical Engineering, University of Utah, Salt Lake City, UT, United States

²Department of Pharmaceutics and Pharmaceutical Chemistry, University of Utah, Salt Lake City, UT, United States

Introduction

Fluorinated biomaterials have a long history of biomedical device and biomaterials applications. These materials are generally carbon-based polymers, liquids, and gas precursors to films that all contain large amounts of chemically bonded fluorine (i.e., perfluorocarbons). Fluorinated materials can be solids, liquids, thin films, coatings, or gels, depending on their chemistry, processing, and mode of use. Fluoropolymers in general are thermoplastic polymers analogous to hydrocarbon-based polyethylene (PE), but highly fluorinated; some or all of the hydrogen atoms attached to the PE carbon polymer chain are replaced by fluorine (F) or fluorinated alkyl (perfluorocarbon) side groups. In some cases, other halogen atoms (e.g., chlorine, Cl) are also included with F to slightly modify polymer properties (Drobny, 2005). Notably, fluoropolymers show unique properties not achievable by other polymer materials, including chemical inertness, extreme hydrophobicity and solvent resistance, low coefficients of friction, high design tolerances for device fabrication, and temperature resistance (Drobny, 2005). These properties facilitate fluoropolymer use in specific technologies where most hydrocarbon-based materials do not perform well, either in device manufacturing or their applications. Nevertheless, as with all biomaterials, fluoropolymers perform best only in certain biomedical applications, and often carry a considerably greater cost than their hydrocarbon analogs into medical device designs.

Just 2 years after the first commercial launch of completely fluorinated polytetrafluoroethylene (PTFE), as DuPont's now well-known Teflon product, after World War II ended, this new polymer was implanted in animals for the first time (Leveen and Barberio, 1949). However, early PTFE materials processing difficulties limited device capabilities. In 1963, Japanese researchers reported a new process for expanding PTFE films to produce highly uniform, continuous fibrous porous structures that, after thermal processing, retained this microstructure with vastly improved mechanical strength (Oshige, 1967). In 1972, this expanded fibrous material

was first used experimentally as a venous graft substitute (Soyer et al., 1972), and a year later as an arterial bypass implant (Matsumoto et al., 1973). Several years later (1976), expanded PTFE (ePTFE) was refined to production scales by Gore, allowing increased access and clinical use of this more versatile PTFE form in commercialized biomedical products (Gore, 1976). This enabled fluorinated biomaterials to be employed in biomedical applications both inside and outside the living host, facilitating entry as an important class of polymeric biomaterials that are seen in the field today.

Biomedical interest in fluorinated biomaterials focuses on several unique properties: lubricity; high sizing tolerances for device fabrication; and select aspects of reasonable biocompatibility resulting from both unique chemical and morphological properties. Understanding certain aspects of fluorinated chemistry is important to appreciate their material properties and broad utility in biomedical products.

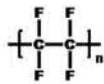
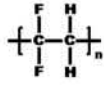
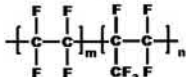
Interesting Fluoropolymer Chemical and Physical Properties Derived From Their Polymer Chemistry, Molecular Structure, and Bonding

Replacing large amounts of hydrogen in C–H and C–C bonds in organic materials with fluorine as C–F chemistry, using several different chemical means, results in dramatic changes to the fluoromaterial's physical and chemical properties. Technologically desirable characteristics of perfluorinated materials are identified from how they interact distinctly with other media (e.g., heated fabrication machines and device-extruding dyes, as well as tissue, blood, proteins, and other polymers). Single fluorine bonds with carbon are the strongest carbon bonds, some 25 kcal/mol⁻¹ stronger than C–Cl (Smart, 1994). Fluorination also strengthens adjacent aliphatic bonds: the CF₃–CF₃ bond is 10 kcal/mol⁻¹ stronger than the CH₃–CH₃ bond (Smart, 1994). This makes alkyl fluorides 10²–10⁶ times more stable than

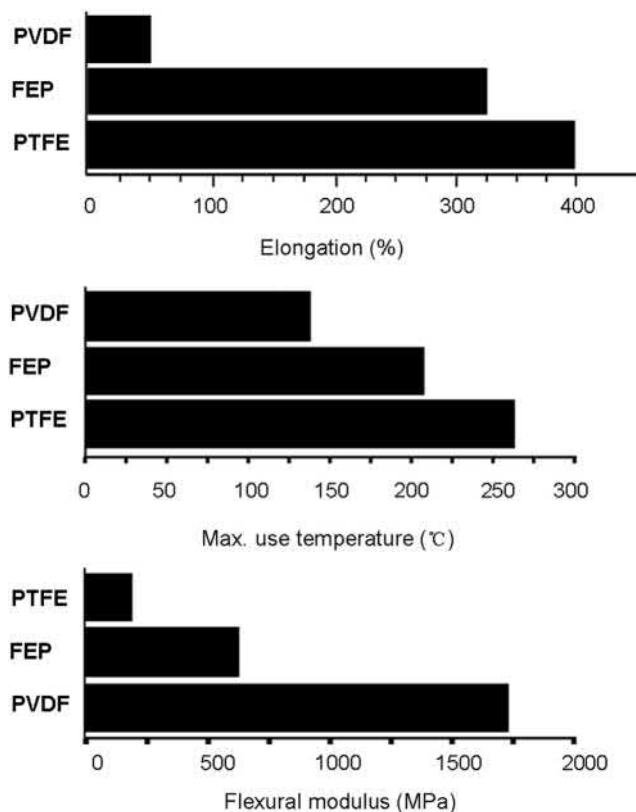
the corresponding alkyl chlorides in solvent and thermal reactions (Smart, 1994). Exceptional thermal and chemical stabilities observed for perfluorinated materials then result. Fluorine's high ionization potential energy and low polarizability provide relatively weak intermolecular forces, low interfacial energies, and low refractive indices in fluorinated materials. This is important to interfacial applications (see section on Surfaces Modified by Fluorination Treatments later). Fluorine's larger atomic radius compared to hydrogen provides a rational basis for the observed structural differences between perfluorocarbons and hydrocarbons; chain movement energies (i.e., C–C chain rotational barriers) for various fluorine-substituted bonds are significantly higher than barriers in analogous hydrocarbon systems (Smart, 1994). Partially fluorinated commercial polymers, polyvinylidene fluoride (PVDF), and ethylene-trifluoroethylene copolymer, have zigzag polymer chain conformations with different C–F dipole alignments along the chain (Smart, 1994), while perfluorocarbons with only C–F bonds (e.g., PTFE, see later) assume helical chain orientations with C–F dipoles distributed axially around the chain helix (Doeff and Lindner, 1989; Zhang et al., 1989; Sun et al., 1994a, 1994b; Kobayashi and Owen, 1995; Bar et al., 1997; Stone et al., 1998). PTFE, for example, as a model for high molecular weight perfluorocarbon chains, is known to have a rich phase diagram of several distinct helical solid phases (Scheirs, 1997). This polymer helix basically encases the inner carbon–carbon polymer backbone with a tight outer shell of fluorine groups, protecting the carbon bonds from reactants, and also contributing to unique chain–chain interactions in PTFE and helical fluorinated polymers. Although most fluoropolymers share unique properties (e.g., thermal and chemical stability, lubricity), their mechanical properties are slightly different, depending on whether they are fully fluorinated or contain a number of hydrogen atoms. Generally, partially hydrogenated fluoropolymers (e.g., PVDF, see later) exhibit higher stiffness than fully fluorinated polymers (i.e., perfluoropolymers). Perfluoropolymers exhibit greater elongation and higher maximum service temperatures that benefit device engineering and thermal processing.

Distinguishing the Different Fluoropolymers

Fluoropolymers can be classified into homopolymers and copolymers by the monomer(s) used in their polymerization. They are divided into either “partially fluorinated” or “perfluorinated” (i.e., 100% C–F bonds) based on the amounts of fluorine in the polymer chain. Fig. 1.3.2C.1 lists currently available commercial biomedical fluoropolymers. Polymer chemical composition affects the resulting materials' properties; only certain fluoropolymers exhibit properties attractive for biomedical products. As one selection criterion, Fig. 1.3.2C.2 (Scheirs, 1997) compares some selected mechanical properties for different biomedical fluoropolymers (Drobny, 2005).

Abbreviation	Generic polymer name	Structure
PTFE	Poly(tetrafluoroethylene)	
PVDF	Poly(vinylidene fluoride)	
FEP	Fluorinated ethylene-propylene	

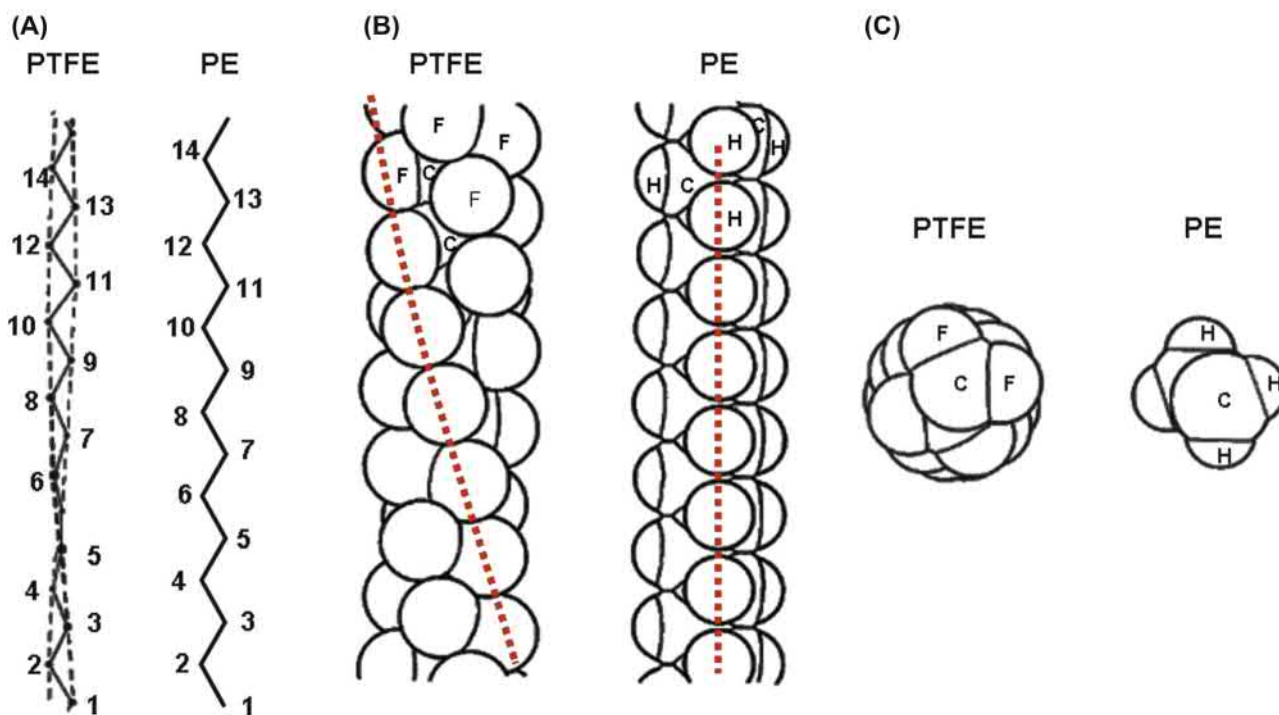
• **Figure 1.3.2C.1** Abbreviated names and molecular structures for some biomedical fluoropolymers.



• **Figure 1.3.2C.2** Comparison of mechanical properties of some select biomedical fluoropolymers, FEP, Fluorinated ethylene propylene; PTFE, polytetrafluoroethylene; PVDF, polyvinylidene fluoride. (Adapted by permission from Modern Fluoropolymers. Scheirs, J. (Ed.), John Wiley & Sons, Ltd., copyright 1997).

Polytetrafluoroethylene

PTFE (DuPont tradename Teflon) is perhaps the most commonly analyzed fluoropolymer. As described previously, fluorine's large size and mutual repulsion of adjacent fluorine atoms causes PTFE macromolecule chains to exhibit a twisting helix, comprising 13 CF₂ groups per 180-degree turn, distinct from the classic planar zigzag chain typical for PE (Bunn and Howells, 1954). Fig. 1.3.2C.3 shows this important conformational chain distinction that imparts certain unique physical properties to the fluoropolymer. Helical PTFE chains are often of very high molecular weight (>10⁶) from their polymerization by reactive tetrafluoroethylene (TFE) gas. The helical polymer chains pack into solid



• **Figure 1.3.2C.3** (A) Polytetrafluoroethylene (PTFE) twisted zigzag chain compared to polyethylene (PE) molecular zigzag chain; (B) side space-filling views and (C) top views of PTFE chain versus hydrocarbon chain (PE). (Adapted by permission from Macmillan Publishers Ltd: Bunn, C.W., Howells, E.R., 1954. Structures of molecules and crystals of fluoro-carbons. *Nature* 174, 550, <http://www.nature.com/npj/indexnpj.html>).

• BOX 1.3.2C.1 Sir John Charnley and the PTFE Replacement Hip Bearing

Convinced that hip joint repair could not use metal-on-metal bearings, Professor Sir John Charnley's early work on hip arthroplasty techniques in the early 1950s used a Teflon-on-Teflon solid bearing to resurface the arthritic femoral head and acetabulum. These Teflon-on-Teflon bearings failed within 2 years from mechanical creep and particulate issues. His further innovations created a femoral stem and metal head articulating against a Teflon cup socket inserted into the acetabulum. High Teflon wear occurred with joint articulation, producing severe osteolysis, loosening in the surrounding bone, and, as a result, requiring many revision surgeries. Teflon's poor performance in this articulating joint application prompted the adoption of high molecular weight polyethylene as a better bearing surface—an innovation that persists today.

crystallites like long, parallel, stiff molecular rods; individual PTFE polymer molecules can slip on each other as quasicylinders sliding under shear stress. Tight helical packing and chain–chain slip make PTFE the most lubricious polymer available, with a low coefficient of friction (0.1). This is a major selection criterion for manufacturing fluoropolymer tubing for catheters. Unfortunately, this also makes PTFE solids very susceptible to cold flow (creep) under stress—a major reason for their contraindication in mechanical applications (i.e., poor bearing and joint surfaces) (Box 1.3.2C.1). Mutual repulsive forces of adjacent fluorine atoms keep the PTFE chain backbone from bending. Low-energy barriers to

chain–chain slip events result from low chain–chain interaction energies. PTFE's very high bulk solid fractional crystallinity means that it scatters most visible light wavelengths, resulting in its characteristic opaque white color. PTFE's high molecular weight and rigid helical chain conformation also produce high melt viscosities (e.g., 1012 Pa/s), ~6 times higher than most thermoplastic polymers. This viscosity is excessive for conventional melt processing fabrication methods for thermoplastic medical devices (e.g., extrusion and injection molding). This requires a high continuous service temperature (~260°C) for processing PTFE into devices. Therefore, as PTFE does not dissolve in any solvents, PTFE processing technologies are similar to those of powder metallurgy. This involves form casting of prepolymerized PTFE granulated powders or latex formulations, followed by mold compression and thermal sintering. PTFE's high thermal stability is key to success under the extreme processing conditions required for molded device parts (Drobny, 2005).

Fluorinated Ethylene Propylene

Fluorinated ethylene propylene (FEP) is a copolymer of TFE and hexafluoropropylene (HFP), first produced by DuPont in 1956 (Teflon FEP) to reduce PTFE's high crystallinity and melt viscosity. This improves FEP processing characteristics while maintaining high perfluorination. Bulky FEP perfluoromethyl groups produce defects in solid fluoropolymer crystallites, reducing polymer melting point, impeding chain slip, and reducing solid cold flow (Drobny, 2001).

FEP combines the unique mechanical and chemical properties of PTFE with the melt processability of more conventional polymers. FEP has a maximum service temperature of 204°C, and a slightly higher coefficient of friction than PTFE. It is used in biomedical devices in place of PTFE.

Polyvinylidene Fluoride

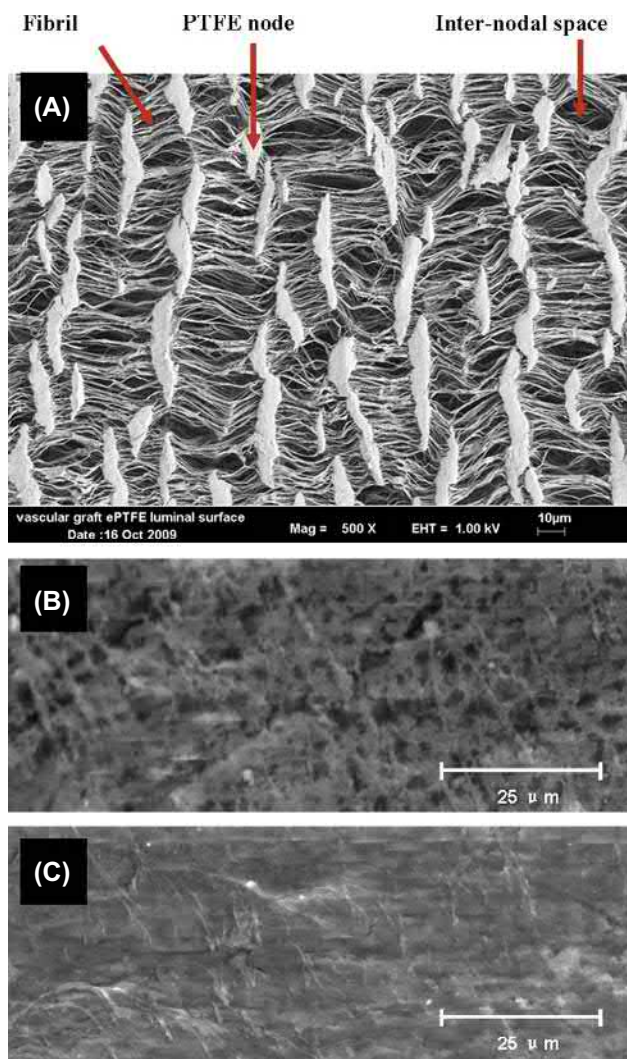
PVDF is a homopolymer of the vinylidene monomer (CH_2CF_2), and is sold as Kynar. PVDF has the highest flexural modulus of all fluoropolymers, due to the interpenetration of larger CF_2 groups crystallizing with adjacent smaller CH_2 groups on adjacent chains. Unlike other fluoropolymers, PVDF is soluble in highly polar solvents (dimethylformamide, tetrahydrofuran), acetone, and esters (Drobny, 2005). PVDF's unique high dielectric constant, high dielectric loss factor, and interesting piezoelectric behavior under certain conditions result from this chemistry and result in solid-state structures. Fluorine's shielding effects to all neighboring CH_2 groups provides PVDF with good chemical resistance and thermal stability (Scheirs, 1997; Drobny, 2001). These are all valuable properties sought in specific medical device applications.

Fluoropolymer Melt Processing

Because most perfluorinated polymers do not dissolve in many solvents, their biomedical products are often made by melt extrusion, where polymers develop flow upon melting in normal extrusion equipment. This technique, common to all polymer devices and chemistries, exposes fluoropolymers to very high temperatures to reduce their viscosity and improve flow characteristics for extended device production runs and product lengths. Fluoropolymers FEP and PVDF will readily melt flow when heated, typically above 260°C. This permits uninterrupted feed of fluoropolymer resin into the parts extruder to produce long continuous lengths of product (i.e., medical tubing). By contrast, PTFE extrusion is limited due to difficulties in its materials handling, size of the stock preforms, and tubing. However, PTFE's poor melt processing presents an important opportunity: PTFE tubing can be manufactured to very small dimensions, with wall thicknesses as small as 2.54×10^{-3} cm and tolerances of $\pm 1 \times 10^{-3}$ cm. This engineering benefit is largely due to PTFE's inability to melt flow, allowing more precise control over its use in small-dimensional, high-tolerance extrusion forms. This unique PTFE property is essential for producing medical products requiring tight size tolerances, such as small diameter and multilumen tubing with multiple precision passages for advanced catheters.

Original Gore-Tex and Generic Equivalents

PTFE film extrusion under anisotropic loading conditions produces expanded Teflon (ePTFE). Its microarchitecture exhibits pores axially aligned along the stretch direction, resulting in a unique fluoropolymer fabric material



• **Figure 1.3.2C.4** (A) Scanning electron micrograph (SEM) of expanded polytetrafluoroethylene (ePTFE) showing regular node-fiber open materials structure (scale bar, lower right corner = 10 microns) (B. Wagner, W. L. Gore & Associates, Flagstaff, USA, is acknowledged for ePTFE micrographs). (B) SEM of solid Teflon showing the cross-sectional porous structure resulting from the compressed sintering of PTFE particles (P. Högbe, SEM micrographs). (C) Dense continuous top surface (scale bar = 25 microns).

with an oriented microporous architecture. This was originally commercialized as the fabric-like Gore-Tex material (Gore, 1976). ePTFE's porous structure is characterized by regular PTFE nodes interconnected by PTFE fibrils (Fig. 1.3.2C.4A), distinct from solid PTFE shown in Fig. 1.3.2C.4B. In ePTFE, internodal spacing or distance (i.e., PTFE fibril length between solid PTFE nodes) is important to control device implant behavior (McClurken et al., 1986), and this can be controlled from 1 to 100 microns (Santiago et al., 1981) while retaining some properties similar to PTFE, e.g., biological adsorption, low tensile strength, low modulus of elasticity, water penetration control, and easy sterilizability. Porous ePTFE structures also allow important mechanical modulus-matching properties in tissue sites better than other polymers for many soft biological tissue applications (Mole, 1992). Porosity also importantly

TABLE 1.3.2C.1 Surface Energies for Perfluorocarbons Versus Analogous Hydrocarbons^a

Substance	Solid Interfacial Energy γ_c (mN/M)	
	Perfluorocarbon	Hydrocarbon
PTFE ^b	18.5	31
PVDF	25	31
HDPE ^c	18.5	31
<i>n</i> -Pentane	9.4	15.2
<i>n</i> -Hexane	11.4	17.9
<i>n</i> -Octane	13.6	21.1
Decalin	17.6	29.9
Benzene	22.6	28.5

HDPE, High-density polyethylene; *PTFE*, polytetrafluoroethylene; *PVDF*, polyvinylidene fluoride.
^aSmart, B.E., 1994. Characteristics of C–F systems. Chapter 3. In: Banks, R.E., Tatlow, J.C., Smart, B.E. (Eds.), *Organofluorine Chemistry: Principles and Commercial Applications*, Plenum Press, New York, NY, Chapter 3.
^b γ_c values.
^c γ_{IV} values.

encourages in-growth of tissue, and hence moderate levels of tissue mechanical fixation. Bulk PTFE does not exhibit this property. The micropores also present active sites for stable blood clotting, an important property for conditioning implanted vascular graft surfaces to limit their chronic blood coagulation.

Surfaces Modified by Fluorination Treatments (Grainger and Stewart, 2001)

Bulk perfluorinated materials' intrinsically higher costs and often substandard mechanical properties limit their applications. When only fluorinated polymer interfacial properties are desired, then fluorinated surface layers can be chemically deposited or coated over other mechanically superior substrates to impart fluorinated properties only at the surface. This surface application limits bulk fluorocarbon costs and their performance liabilities. As developed further later, fluorinated surfaces can be produced by plasma deposition of gaseous precursor monomers, direct solid powder or solution overcoating and casting/evaporation, and solution phase fluorinated component blooming. High surface fluorocarbonation produces unique interfacial properties, imparting specific, technologically attractive features, including low solid-state surface free energy (or low water wettability and permeability), surface lubricity, and chemical resistance and durability, to device surfaces. Table 1.3.2C.1 shows that perfluorinated polymer surfaces exhibit low interfacial energies (indicated by Zisman γ_c values), correlating directly with their utility as low-adhesion, low-water-wetting, and low-friction surfaces. Substituting either hydrogen or another halogen for fluorine along

the polymer backbone results in significant increases in γ_c values (as seen in comparisons of PTFE with high-density polyethylene [HDPE]); PVDF:poly(CH₂CHF) has a $\gamma_c \sim 25$ mN/m, approaching that for polyethylene (HDPE, see Table 1.3.2C.1). Another important outcome of this low interfacial fluoromaterial energy is that fluorinated species thermodynamically prefer to coat a material's surface exposed to air. Hence fluorinated components will migrate from deep inside fluid coating mixtures to "bloom" and enrich as a coated overlayer at the solid–air interface.

Surface-enriched films of fluorinated components reside at surfaces even if fluorinated components are doped only at trace or minority components into bulk coating materials. Therefore fluorinated surfaces can be fabricated using minority fluorinated components added to a bulk material if they are allowed to move to that material's surface (e.g., from coating solutions), offsetting the intrinsically high costs of fluorinated materials. Emphasis on surface-fluorinated coatings and films has therefore increased as technological needs drive new, improved, and less expensive methods to put this chemistry over biomaterial surfaces. Several coating strategies have sought to create, organize, and orient –CF₃ and –SF₅ terminal groups from films over any surface to provide such properties. High surface density and organization of these groups is necessary to achieve their technological properties. Alignment of perfluorinated chains terminating in this –CF₃ or –SF₅ chemistry at the surface is required. Orienting the side chains in fluoroalkyl side chain acrylate and methacrylate films enriches surfaces with side chain-terminating –CF₃ groups (Bunn and Howells, 1954; Clark and Muus, 1962; Russell et al., 1986; Naselli et al., 1989), and lowers solid interfacial energies. Perfluoroalkyl-grafted polysiloxanes also exhibit side chain orientation of their perfluorinated chemistry, sometimes with spontaneous perfluorinated group organization as a film or coating (Hare et al., 1954; Pittman, 1972; Schneider et al., 1989; Tsao et al., 1997; Clark, 1999). Gas plasma-deposited thin fluorinated coatings are also well developed for this purpose (D'Agostino, 1990), representing a mature industry and biomedically relevant materials treatment (e.g., for vascular devices and intraocular lenses; Ratner, 1995).

Biomedical Applications

Biomedical applications of fluoropolymers, fluorocarbon coatings, and perfluorinated fluids and gels all include clinical interventional and luminal access devices (catheters in many forms), and more permanent implants (cardiovascular (Stanley, 1982), dental (Ratner, 1993), ocular (Legeais et al., 1998), craniofacial (Valdevit et al., 2000), urological (Reid et al., 1995), and abdominal (Grannis and Wagman, 1995) applications) as well as substantial nonimplanted medical tubing and biotechnology components (protein blotting and filtration membranes). Annually, millions of perfluorinated polymer components are used worldwide in biological milieu both in vitro and in vivo. PTFE (Teflon) and ePTFE (Gore-Tex) are widely used in medical tubing,

TABLE 1.3.2C.2 Fluorinated Biomaterials Biomedical Applications

Decade	Biomedical Applications
1970s	Implantable vascular grafts, peripheral catheters, and catheter introducers
1980s	Guiding catheters, protein blotting membranes, tissue meshes, tubing
1990s	Endoluminal stents, blood substitutes
2000s	Drug-eluting stents

advanced catheters, vascular grafts, meshes, sutures, and other medical implants. PVDF is used for biotechnology blotting/separation membranes. Table 1.3.2C.2 provides biomedical applications of more popular fluoropolymers. Clinically, ePTFE vascular grafts, including dialysis-access grafts, and Teflon-FEP catheter components are the most widely used fluorinated material medical devices. Other biomedical applications are described next.

Fluorinated Material Biological Response

Fluoropolymers are often regarded as chemically inert under most biological conditions. As noted earlier, they have some mechanical shortcomings under cyclic or continuous shear (creep). This makes applications in loadbearing situations (i.e., joint replacement, wear surfaces) difficult. Additionally, fluoropolymer surfaces are not inert to host biological reactions, including protein adsorption and blood clotting, either in vitro or in vivo. In fact, extremely tight binding of serum albumin to fluoroplasma-deposited surfaces (Kiaei et al., 1992), high levels of fibronectin and hemoglobin on PVDF (Paynter and Ratner, 1985) and various serum proteins (Dekker et al., 1991), including significant fibrinogen (Chandy et al., 2000), and high levels of both fibronectin and albumin (Grainger et al., 2003) on PTFE are observed in vitro. Importantly, protein adsorption to fluoropolymers is also observed in vivo (van Wachem et al., 1985; Roald et al., 1994), including fibrinogen activation, fibrin deposition, and platelet activation from blood, often deliberately promoted to stabilize blood reactivity on ePTFE vascular graft materials in vivo (Hoffman et al., 1986; Callow, 1988; Roald et al., 1994). Therefore nonspecific protein adsorption is significant, often irreversible, on fluoropolymer surfaces, leading to their desired utility as efficient protein-blotting membranes. But different proteins from different media (i.e., serum vs. plasma vs. blood) produce different interfacial reactions to fluorinated surfaces. From serum in vitro, for example, substantial amounts of albumin adsorption hinder serum-mediated cell attachment to fluoropolymers. This albumin passivation against further biological reactivity helps render the surface biofouling resistant. Clinical human cell-based vascular graft endothelialization to improve their blood compatibility is also generally poor on nonporous fluoropolymer chemistries (Kempczinski et al.,

1985; Callow, 1988; Dekker et al., 1991; Schmidt et al., 1991; van Kooten et al., 1992; Roald et al., 1994; Legeais et al., 1998). This poor cell–fluoropolymer attachment has often been interpreted as “biological inertness,” but results instead from substantial plasma protein adsorption on fluoropolymers (Baier et al., 1984) that does not support cell attachment and growth. Serum albumin, the most abundant protein in blood, blocks most cell attachment and other protein binding (Kesler et al., 1986; Zilla et al., 1989). Fibronectin, collagens, and other trace extracellular matrix proteins (e.g., osteopontin, laminin, vitronectin) are cell-adhesive proteins. The observed general inability of nonporous fluoropolymers to support cell attachment has been related to excessive adsorption of albumin over cell-adhesive proteins (e.g., fibronectin) from serum—a medium lacking clot-forming fibrinogen (Grainger et al., 2003). PreadSORption of specific cell-adhesive proteins (e.g., collagen or fibronectin) to fluoropolymers is used to promote reliable cell adhesion (McClary et al., 2000; Koenig et al., 2003). Therefore little evidence suggests that fluoropolymers can be intrinsically “biologically inert.” In fact, the opposite is true; solid fluoropolymers are intrinsically reactive and adsorptive to almost every protein studied, and the nature of what types of proteins are adsorbed dictates the fluoropolymer’s biological reactivity. For example, porous fluoropolymers with 60–80 μm voids, including ePTFE, can facilitate rapid blood clotting and cell and bacterial in-growth in blood. These interactions occur by blood-based protein adsorption, clotting, and cell/bacterial adhesion, with additional physical integration and engagement into the ePTFE pores (Clark et al., 1974; Clowes et al., 1986).

PTFE (Teflon) Mesh and Fabric Vascular Implants

The innovation that enabled the spinning of PTFE paste into a fiber that could be woven or knitted into fabric or mesh produced a fabric-like fluorinated material (Berry, 1951). Attracted by solid PTFE’s reported “blood compatibility” claimed in early animal acute in vivo studies, PTFE weaves were applied early in vascular grafts (Edwards, 1959). However, these early woven vascular grafts exhibited both high early failure rates and substantial late failure rates. Graft thrombosis was the most frequent early complication, accompanied by a high mortality rate (Boyd and Midell, 1971). Gore-Tex (ePTFE) vascular grafts supplanted these earlier PTFE weaves in this application and are discussed next. Thrombosis is a general property of fluoropolymer meshes and weaves in blood, passivating surfaces rapidly for acute short-term use, but limiting long-term blood-contacting applications.

ePTFE and Teflon Soft Tissue Repair Meshes

Teflon fibrous mesh has been used to repair abdominal wall defects (Ludington and Woodward, 1959) and hernias (Gibson and Stafford, 1964; Snijders, 1969; Kalsbeek,

• BOX 1.3.2C.2 ePTFE Hernial Mesh

Nearly a million hernial repairs are performed annually in the United States. Clinically, hernial repair meshes are implanted to bulk the abdominal wall at the herniated site. Tissue in-growth and organized fibrogenesis are deliberately promoted in these meshes to stabilize them in the abdominal tissue. ePTFE meshes and their combinations with polypropylene meshes are clinically available as a hernial repair product. However, ePTFE's lack of resistance to infection and inability to effectively engage tissue, promote on-growth, and organize fibrogenesis makes these meshes inferior to more popular polypropylene and polyester synthetic polymer meshes.

1974). However, it does not reliably integrate into body tissues, is not sufficiently infection resistant, and exhibits wound complication rates too high for routine hernia or abdominal repair use. ePTFE mesh is clinically used to repair hernias of many types (DeBord, 1998), reducing risks of several complications (DeGuzman et al., 1995; Lo Monte et al., 2009) (Box 1.3.2C.2). Infection and intestinal obstructions remain an issue for ePTFE mesh. However, they are better controlled with antibiotic therapies without mesh removal. ePTFE meshes have also been used as abdominal surgery barriers against surgical adhesions (Tulandi, 1997; Morris-Stiff and Hughes, 1998). ePTFE is also Food and Drug Administration (FDA) approved for many different plastic surgical facial defect reconstructions and augmentations, but is contraindicated in cosmetic lip augmentation, temporomandibular joint reconstruction, cardiovascular defects, and dermal placement (Levine and Berman, 1995). Nonetheless, commercial sources for these plastic surgery materials are discontinued.

ePTFE Vascular Implants

Because of abundant protein adsorption, ePTFE's porous inner surface is often claimed in vascular implants (blood) to clot blood rapidly to stabilize further surface coagulation and promote formation of a host “pseudointimal lining” that maintains blood compatibility under high-flow, high-shear applications. Its porous outer surface promotes perigraft cell and tissue infiltration that mechanically stabilizes the prosthesis in place, preventing kinking (White, 1988). Unlike most animal models, humans do not reliably form stable cellular “neointimal” endothelial cell linings in these grafts, limiting their success. ePTFE is currently used most widely to fabricate medium-sized (4–10 micron internode) vascular grafts for use in specific clinical blood vessel replacement indications (Kannan et al., 2005), including major vessels affected by disease or trauma, and arteriovenous hemodialysis grafts (Jenkins, 1976; Konner, 2005). ePTFE vascular prostheses are most clinically successful in high blood flow, low -resistance conditions (i.e., large peripheral arteries >5–6 mm diameter, such as the descending aorta). They are generally not suitable for smaller arterial reconstructions (e.g., coronary circulation and peripheral

vascular placements) under high-resistance, low-flow conditions that allow continued clotting and loss of patency. Typically, ePTFE suffers from thrombosis, poor healing, lack of compliance, and excessive intimal and anastomotic hyperplasia leading to stenotic complications. Their routine placement in high-flow vascular environments allows them to remain patent despite their thrombus generation (Box 1.3.2C.3).

Arteriovenous ePTFE Grafts for Dialysis Access

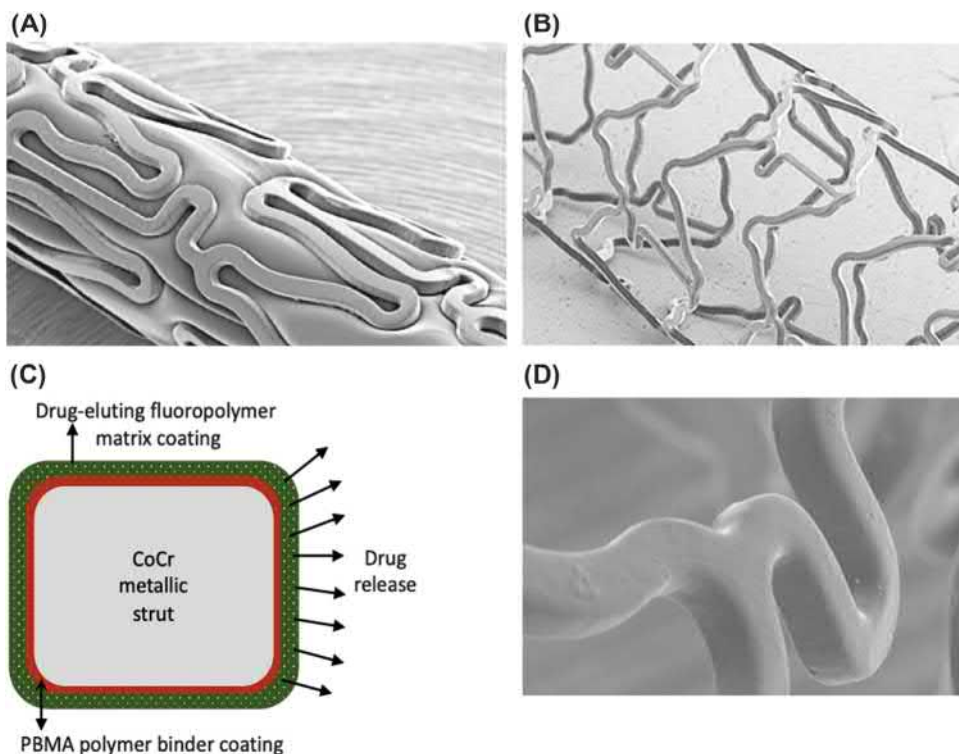
Hemodialysis—essential for patients with end-stage renal disease—often requires regular, repeated (weekly) access to large blood vessels capable of producing high flow rates through an external artificial kidney device. Hemodialysis patients typically undergo cannula puncture of skin, underlying tissue, and vasculature to provide this access to the external artificial kidney. Repeated trauma to patient skin, tissue, and blood vessels from 13- to 17-gauge access needles produces notable complications, including hyperplasia, thrombosis, hematoma, occlusion, infection, and other morbidities. Vascular access complications remain the main reason for hemodialysis patient hospitalization. Synthetic ePTFE arteriovenous (A–V) grafts are surgically placed across the basilic vein and brachial artery to permit cannula access and reduce tissue trauma complications. A–V prosthetic graft failure rates are substantial (>50%), leading to increasing use of native fistulas and catheters (Li et al., 2008). However, synthetic grafts reliably provide high blood flow rates shortly after placement, as they do not require maturation before use. In A–V ePTFE grafts, stenosis occurs most commonly at the graft–venous anastomosis. Histologically, macrophages are seen in large numbers in the adventitial and medial layers in the anastomotic tissues from A–V ePTFE grafts (Kapadia et al., 2008) (Box 1.3.2C.4).

Multilumen Catheters

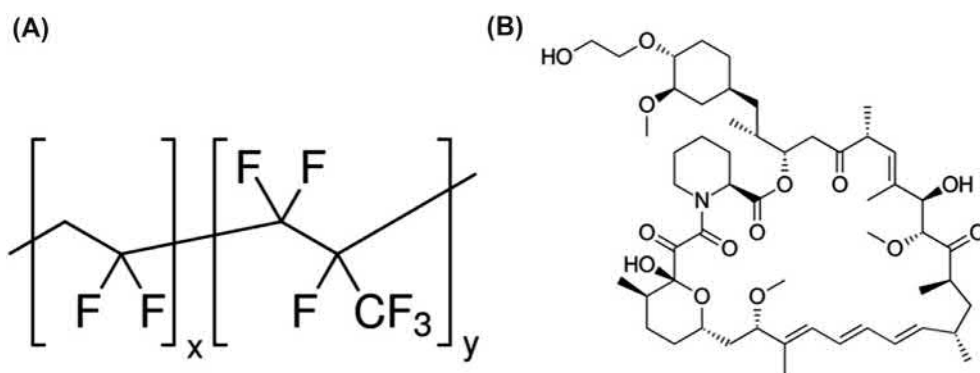
Fluoropolymers are important for biomedical tubing, and are central to advanced multilumen small-gauge medical-grade tubing required in many new minimally invasive catheters. These catheters permit surgeons to perform several invasive procedures through several lumens in a single inserted catheter device without removing one entire catheter to insert another. Catheter in vivo exposures are usually short term, typically using endoluminal access, and are increasingly minimally invasive. As described earlier, PTFE's unique properties and stable thermal processing methods allow PTFE multilumen tubing precision manufacture unlike any other material, and this is a very important fluoropolymer in this particular use.

Guiding Catheters

An important clinical device with a long track record, the guiding catheter helps the clinician deliver stents and other devices endoluminally. Central to the guiding catheter is a



• **Figure 1.3.2C.5** Drug-eluting stent (DES) implantable medical device: (A) metallic DES stent mounted on cardiovascular catheter, with fluoropolymer matrix coating around the struts incorporating a drug payload for local delivery to the vascular tissue bed adjacent to the implant, assisting stent biocompatibility; (B) expanded stent postdeployment; (C) cross-section view of the XIENCE (Abbott Vascular) stent design with CoCr metal struts, poly(butyl methacrylate) (PBMA) primer interlayer, and polyvinylidene fluoride-co-hexafluoropropylene fluoroelastomer drug-releasing matrix overlayer; (D) magnified view of expanded stent struts showing conformal integrity of polymer coating after expansion. (Courtesy: Abbott Vascular).



• **Figure 1.3.2C.6** (A) Polyvinylidene fluoride-hexafluoropropylene fluoropolymer coating molecular structure, and (B) everolimus drug.

• BOX 1.3.2C.3 Notable Clinical Success for Fluoropolymer Coatings on Cardiovascular Stents

Stent coatings comprising one or more polymers with a drug are widely used on coronary and peripheral DESs and deemed essential for producing controlled drug release kinetics to locally influence vascular site tissue healing, stent thrombogenicity, and stent patency. Among several patient factors, including health status, cardiovascular disease, and physiological factors, stent coating designs are known to influence stent blood compatibility, local tissue healing, and chronic inflammatory responses. Many durable and biodegradable polymers are used as coatings, combined with an equally diverse selection of drugs released from these polymers (Fig. 1.3.2C.5).

Two different fluoropolymer coatings are currently used in the majority of cardiovascular stents deployed clinically. Abbott Vascular's XIENCE family of endovascular coronary stents is the

world's leading DES, with twice as many implants as any other DES. First introduced in 2006, this stent model has undergone several design changes and product improvements to now represent four different XIENCE stents. Each XIENCE stent employs polymers PBMA as a primer layer and PVDF-HFP overlayers in conformal wire stent coatings (6–7 microns thick). PBMA base primer over the metallic stent metal wires (struts) adheres the stent to the overlying fluoropolymer polymer-drug coating. PVDF-HFP is employed in the drug matrix layer to hold the drug everolimus on the stent and control its release, as well as ease its release from the deploying catheter expansion balloon.

PVDF-HFP is a semicrystalline fluorinated copolymer of vinylidene fluoride and hexafluoropropylene monomers (Fig. 1.3.2C.6).

• BOX 1.3.2C.3 Notable Clinical Success for Fluoropolymer Coatings on Cardiovascular Stents—cont'd

The PVDF-HFP copolymer backbone is comprised of entirely saturated carbon-carbon single bonds, >50% of which are fluorinated, resulting in unusual $-CF_2$ main chain and $-CF_3$ side group polymer dipole properties and polymer hydrophobicity. Significantly, the PVDF-HFP copolymer exhibits high elasticity and fatigue resistance attributed to its low glass transition temperature, T_g (-29°C), and semicrystallinity. It is considered a durable coating as it is resistant to hydrolytic, oxidative, or enzymatic breakdown. Introduction of the HFP comonomer to the PVDF polymer chains restricts polymer crystal content, forming nano-sized crystalline domains that alter polymer interchain distances and dipolar mobility, and reducing the polymer T_g . This allows this fluoropolymer the requisite mechanical properties (polymer elongation 600%–750%) to expand as the metallic stent is expanded in vivo, retaining a conformal, adherent, and defect-resistant coating character important to its biocompatibility. XIENCE's drug is everolimus (Fig. 1.3.2C.2B; $100\ \mu\text{g}/\text{cm}^2$ stent surface area loading on-stent). The PVDF-HFP copolymer drug matrix controls drug release to 80% in 1 month.

Like many other blood-contacting polymers, fluoropolymer surfaces are hydrophobic. They are recognized to elicit a unique biological response in contact with plasma or blood known as "fluoropassivation," reducing fibrin deposition, platelet reactivity, thrombogenicity, and inflammatory responses, and enhancing more rapid, reliable vascular neointimal healing (Lavery et al., 2017; Xie et al., 2010; Chin-Quee et al., 2010; Garfinkle et al., 1984; Kiaei, 1988; Massa et al., 2007; Lin et al., 2000). Preferential affinity of fluorinated surfaces for albumin, with respect to fibrin, fibrinogen, or fibronectin, and the inhibitory effect of materials fluorination on platelet adhesion/activation or leukocyte recruitment while encouraging more rapid neointima formation and endothelialization, are proposed mechanisms to explain this consistently observed phenomenon (Grainger et al., 2003; Szott et al., 2016).

Commercially available (currently only in CE-mark countries) fluoropolymer-based peripheral stents (FP-PESs, Eluvia) are now sold by Boston Scientific. The Eluvia FP-PES uses the same dual-layer polymer coating as XIENCE, comprising the primer layer

PBMA to promote adhesion to the stent of an active polymer layer comprising a combination of drug, paclitaxel (concentration is $167\ \mu\text{g}/\text{cm}^2$ stent surface area), and PVDF-HFP, controlling drug release for 12 months upon deployment (Gasoir et al., 2017).

Another fluoropolymer stent coating, Polyzene-F (PzF; CeloNova BioSciences, Inc., TX, USA) is a formulation of poly[bis(trifluoroethoxy) phosphazene], an inorganic hydrophobic polymer possessing a backbone of alternating nitrogen and phosphorus atoms bearing trifluoroethoxy side groups. The COBRA-PzF (CeloNova BioScience, Inc.) coronary stent system is a cobalt chromium metallic stent design using this Polyzene-F polymer coating without drug, and was recently approved by the FDA for clinical use (Richter and Stampfl, 2005; Hiroyoshi et al., 2018).

Importantly, as stents undergo substantial mechanical manipulations, structural change, and deformation during expansion and deployment in vivo, coatings must adapt to the stent deformations with structural integrity and reliable metal-polymer adhesion. Select fluoropolymers seem to exhibit superiority in this regard, withstanding mechanical deformations required for stent assembly, deployment, expansion, and placement without any adverse effect on the mechanical and biological functionality of the coated device. The majority of struts on the XIENCE PVDF-HFP fluoropolymer coating lacked coating defects after stent in vivo explantation at 180 days. This coating also has been shown to remain intact at maximum stent postdilatation without exhibiting any mechanical constraints on stent final dimensions (Yazdani et al., 2016). The ability of the fluoropolymer coating to remain intact without defects, exhibit reliable fluoropassivation in blood, and deliver drug is a clear stent performance advantage. Recent metaanalyses have established that durable fluoropolymer (PVDF-HFP)-coated everolimus-eluting stents (FP-EESs) have lower rates of stent thrombosis and target vessel revascularization than bare metal stents (BMSs) or thick-strut biodegradable polymer drug-eluting stents (BP-DESs). Additionally, preclinical ex vivo porcine shunt data confirmed superior acute thromboresistance for FP-EES versus BMS and BP-DES (Otsuka et al., 2015; Torri et al., 2018).

PTFE inner liner with its superior lubricity and low friction coefficient that slides within an outer lumen. Lubricity is so critical to this device function that FEP, as the second-most lubricious material available, is insufficient as a catheter liner. During catheter construction, PTFE is chemically bonded onto the tube's outer diameter to enable slip. Bonding is accomplished by using an FEP heat-shrinkable fusing sleeve. After depositing PTFE over the liner the FEP mold is removed from the device, leaving a smooth outer PTFE jacket on the liner within the catheter outer liner.

PTFE Catheter Introducers

Now over three decades old, the PTFE "introducer" facilitates catheter insertion into a patient's vein, taking full advantage of PTFE's endoluminal lubricity and precision tubing processing. Once the catheter is inserted, the PTFE outer sheath can be removed from the patient, leaving the implanted catheter behind. The introducer exploits PTFE processing that molecularly orients the fluoropolymer

material in the tubing-based sleeve over the catheter. This allows PTFE tubing to be readily split and torn longitudinally from the catheter in situ, enabling the surgeon to remove a PTFE introducer from a patient while the primary catheter remains in place.

Perfluorocarbon Liquids and Emulsions as Oxygen-Carrying Blood Substitutes

Low molecular weight perfluoro-fluids can be aspirated into the lungs directly or injected as submicron-sized emulsion droplets into the blood to facilitate oxygen transport, exploiting their high oxygen-carrying capacities (Winslow, 2005). Liquid perfluorocarbons in the lung eliminate the gas-lung interface, acting to reduce tension in the lung alveolus, and reducing mechanical work required to breathe during respiratory distress and lung surfactant deficiency. Emulsions made from dispersing perfluoro-fluids into water using interfacial droplet stabilizers (emulsifiers) create submicron perfluoro-droplets, much smaller than red blood cells. This provides

• BOX 1.3.2C.4 The ePTFE Vascular Graft and a Bizarre and Costly Patent Dispute

The 1974 patent filing from W. L. Gore & Associates, Inc. for the invention of the vascular graft resulted in the eruption of one of the most expensive and notorious medical device patent disputes in history. To challenge Gore's patent validity, a competing company started from former Gore employees and consultants—International Medical Prosthetics Research Associates, Inc. (IMPRA)—filed their own competing patent based on work from a pediatric heart surgeon, Dr. Goldfarb, investigating ePTFE at Arizona State University. IMPRA also agreed to fund Goldfarb's research in exchange for exclusive rights to Goldfarb's patent. But, after an extended period without IMPRA support, Goldfarb dissolved his IMPRA ties. Eventually, IMPRA returned patent rights to the doctor, but not without a nasty struggle. Goldfarb then licensed his still-pending patent to the C. R. Bard medical device company, seeking to obtain a piece of the vascular graft market from Gore and IMPRA. In 1995, the US Patent and Trade Office Interference Board declared that the Goldfarb patent (still pending) invalidated the Gore patent on the vascular graft—a decision upheld twice in the US appeals court. Goldfarb was finally awarded his patent in 2002, still licensed to C. R. Bard, invalidating the Gore patent. But Gore continued to sell its ePTFE vascular grafts until Bard filed suit in 2003. The trial, first “settled” in 2007, found Goldfarb to be the rightful graft inventor, that his patent was valid, and that Gore had willfully infringed the patent in its vascular products. But it was not over yet: in 2009, Gore's claims of inequitable conduct against Bard were denied, and damages against Gore were increased to a total of \$410 million. Gore then appealed this verdict (Frankel, 2009). In 2012, citing “substantial evidence” that Gore infringed a patent for vascular grafts, the US Court of Appeals upheld assessed penalties on Gore for past interest, royalties, and fees. Resolution of the case was estimated to have yielded about \$1 billion for Bard from Gore, and is among one of the largest settlements in patent litigation history. Interestingly, the judgment also allowed Gore to keep selling their products on the markets as it was in the public interest to allow competition in the medical device arena.

enormous oxygen-carrying capacity in blood to supplement normal oxygenation in microcirculation. Several commercial products have been clinically available, most recently Oxygen (Alliance Pharmaceutical, USA), consisting of two different perfluorocarbon fluids stabilized as a microemulsion using egg phospholipids. The product is eliminated from the blood after injection by macrophage/monocyte clearance, and is exhaled eventually from the lung.

Fluorinated Liquids in the Eye as Experimental Vitreous Substitutes

Detached retinal repair and other ophthalmic surgeries require oxygen-permeable viscous liquid vitreous substitutes. Perfluorinated oils and polymers have intrinsic high oxygen permeabilities and solubilities with suitable viscosity control. Perfluoropolyethers, perfluorinated alkanes, and perfluorinated silicone oils have all been studied in ocular vitreous applications, but still lack convincing safety, toxicity, or efficacy to date to produce an approved product in this context.

Fluorinated (Meth)Acrylates and (Meth)Acrylated Perfluoroalkyl Silicones as Cross-Linked Polymer Cores for Soft Contact Lenses

Exploiting the intrinsic high oxygen permeability well known for perfluorinated materials, rigid gas permeable contact lenses (RGPs) have used many variations on cross-linked perfluorinated acrylates and perfluorinated polyether silicone gels as lens cores to improve extended-wear contact lens on-eye performance. Increased ocular acuity under high-throughput inexpensive but precise lens fabrication methods, with high lens oxygen transport, is sought. Many patents describe many fluorinated polymer gels in this regard, with most major lens manufacturers developing these lens core materials.

Fluorinated Materials as Antifouling Coatings for Intraocular Lenses

General cellular reactions to implanted polymer intraocular lenses (IOLs) replacing cataracts can result in cell migration onto, and adhesion to, the lens, with optical interference (clouding) requiring IOL replacement. To prevent cells from migrating onto and coating the IOL's optical lens surface (typically a thermoplastic), thin optically transparent plasma-deposited fluorocarbon films or layers of other fluorinated polymers are deposited on the IOL rear surface. Several patents describe this approach and application.

PTFE Paste Injectable Bulking Agent

Teflon particles formulated as an injectable paste have been reported for the treatment of vesicoureteric reflux (VUR) (Puri, 1995), corrected by subureteric injection of a PTFE paste (Puri and O'Donnell, 1984). Subureteric paste injection by endoscopy has successfully addressed primary and secondary VUR in children for nearly two decades (Le Guillou et al., 1984; Dodat and Paulhac, 1987; Puri, 2000). Similarly, PTFE paste was introduced nearly four decades ago to treat female stress urinary incontinence (Beckingham et al., 1992; Politano, 1992; Meschia et al., 2002). However, this device does not have regulatory approval, due to high risks for PTFE microparticle migration and granuloma induction, especially in lymph nodes, kidneys, lungs, and brain (Aronson et al., 1993). Applications of Teflon paste injection are still reported (Harrison et al., 1993; Lopez et al., 1993; Herschorn and Glazer, 2000), but its side effect concerns limit clinical use.

Ligament Replacement

The Gore-Tex ligament prosthesis comprises a single long fiber of ePTFE woven into loops. Mechanical testing shows that the resulting ultimate tensile strength is ~3 times that of the human anterior cruciate ligament (ACL). Creep and bending fatigue testing validate this ePTFE device as a strong synthetic ACL replacement material (Bolton and Bruchman, 1985). The Gore-Tex ACL prosthesis is

currently FDA approved for use in patients with failed autogenous intraarticular graft procedures (Mascarenhas and Macdonald, 2008). However, while acute performance shows promising stability in the knee, extended use and implant time produce significant ligament loosening, and other knee stability problems.

Sutures

PTFE also finds limited use as a suture fiber in various forms. Both PTFE monofilament and ePTFE fibers are surgically proven, with clinically accepted surgeon-handling and lubricity properties. Additionally, PTFE is blended into other common surgical sutures used for myocardial heart valve prostheses fixation. Poly(ethylene terephthalate) (polyester)-braided sutures are impregnated with PTFE polymer to limit wrinkling of the braid and consequent swelling. PTFE hydrophobic properties likely help protect the polyester braid from water uptake and hydrolysis (Bhat, 2002).

The Money Joint

Most biomaterials used for jaw joint reconstruction were introduced to markets prior to the 1976 Medical Devices Amendment Act that required device manufacturers to prove that their devices were safe and effective. A legal loophole that required manufacturers only to prove that their devices were “substantially equivalent” to a pre-Amendment device allowed temporal mandibular joint (TMJ) implants marketed soon after 1976 to enter the market without testing. Two designs widely used as TMJ replacement surfaces were Dow Corning’s Silastic and Vitek’s Proplast-Teflon product. Vitek developed and sold Proplast sheeting (Teflon FEP film laminated with a porous composite material of PTFE and carbon) in the 1970s. Implants modified in the 1980s comprised Teflon film laminated to PTFE and aluminum oxide. These implants, ~1 cm² in size, were cut from sheets in the operating room and sutured into the TMJ joint. In 1983, the FDA allowed Vitek to market a precut disc because, under the law, the company needed only to convince the FDA that its device was “substantially equivalent” to Dow’s Silastic disc marketed years earlier. In 1986, several reports of catastrophic biomechanical failure of the PTFE implant were linked to a giant cell reaction leading to bone resorption and pain. Further analysis documented device failure rates of 10%–25%. By 1992, implant success rates below 20% were reported. Animal studies performed only after failures in humans began showed complete erosion of the TMJ implant within a “few months.” In early 1990, with implant failures increasing, the FDA recalled Vitek’s products. Predictably, Vitek declared bankruptcy with its rising product litigation costs, but continued to market their TMJ implants. Surgeons continued to implant them until eventually the FDA seized all products from Vitek, as well as its subsidiaries.

Summary

Due to their unique chemistry, fluorinated materials, primarily fluoropolymers, have attractive properties of

biomaterials interest, including chemical stability, low adhesion/friction, nonwetting, high protein adsorption, high oxygen permeability, and precision tubing manufacturing. Low cell adhesion in serum and high intrinsic blood coagulation in plasma and blood both result from distinct media-dependent protein adsorption treatments and the physical form of the material. Expanded PTFE provides fabric-like properties with controlled pores and high surface area to alter device-related mechanics, processing, and tissue responses, while promoting rapid blood clotting. Solid fluoropolymers also have attractive precision-engineering and device-processing properties essential to producing several medical device classes where fine dimensional tolerances and biocompatibility are required. This enables fabrication of multilumen, high-tolerance, small-dimensional tubing for advanced catheters.

Glossary

- Blooming** a term used to describe the spontaneous enrichment of certain chemistries at the surface of a bulk matrix, usually associated with surface enrichment by low surface energy chemistry-like fluorinated materials. This phenomenon is used to promote a surface enriched in trace components like expensive added fluorinated chemistry by allowing them to spontaneously diffuse from the bulk material to the surface.
- Blotting membrane** a thin, porous, hydrophobic, high protein-binding capacity polymer membrane (e.g., PVDF) used to transfer proteins from a gel electrophoresis separation process for further probing with antibodies to identify the proteins as a blot or spot.
- Drug-eluting stent** small mesh tubes inserted into arteries to maintain patency after a procedure called angioplasty. The mesh is coated with a polymer/drug combination that deploys with the stent placement and elutes drug to the vascular bed adjacent to the stent for weeks to months.
- ePTFE** expanded polytetrafluoroethylene, produced from PTFE films under anisotropic stretching to yield a unique node–fibril microporous morphology in a fabric-like sheet form deemed important to biomedical utility in implanted biomaterials.
- Fluorinated biomaterial** a material intended for a biomedical application made from a base material that contains significant amounts of chemically bonded fluorine.
- Fluoropolymer** fluorinated polymer, also perfluoropolymer, usually thermoplastic, with high content of fluorine atoms replacing hydrogen atoms along the carbon-based polymer chain.
- Perfluorinated material** a material wherein all hydrogen atoms are replaced with fluorine, generally making C–F bonds.
- PTFE** polytetrafluoroethylene, a high molecular weight, highly crystalline perfluoropolymer solid also known as Teflon, discovered at DuPont in 1938, with unique solid properties and processing requirements.

References

- Aaronson, I.A., Rames, R.A., Greene, W.B., Walsh, L.G., Hasal, U.A., et al., 1993. Endoscopic treatment of reflux: migration of Teflon to the lungs and brain. *Eur. Urol.* 23, 394–399.
- Baier, R.E., Meyer, A.E., Natiella, J.R., Natiella, R.R., Carter, J.M., 1984. Surface properties determine bioadhesive outcomes: methods and results. *J. Biomed. Mater. Res.* 18, 327–355.
- Bar, G., Thomann, Y., Brandsch, R., Cantow, H.J., Whangbo, M.H., et al., 1997. Factors affecting the height and phase images in tapping mode atomic force microscopy. Study of phase-separated polymer blends of poly(ethene-co-styrene) and poly(2,6-dimethyl-1,4-phenylene oxide). *Langmuir* 13, 3807–3812.
- Beckingham, I.J., Wemyss-Holden, G., Lawrence, W.T., 1992. Long-term follow-up of women treated with perurethral Teflon injections for stress incontinence. *Br. J. Urol.* 69, 580–583.
- Berry, K.L., 1951. United States Patent 2559750.
- Bhat, S.V., 2002. *Biomaterials*. Kluwer Academic Publishers, Boston, MA.
- Bolton, C.W., Bruchman, W.C., 1985. The GORE-TEX expanded polytetrafluoroethylene prosthetic ligament. An in vitro and in vivo evaluation. *Clin. Orthop. Relat. Res.* 196, 202–213.
- Boyd, D.P., Midell, A.I., 1971. Woven teflon aortic grafts. An unsatisfactory prosthesis. *Vasc. Surg.* 5, 148–153.
- Bunn, C.W., Howells, E.R., 1954. Structures of molecules and crystals of fluorocarbons. *Nature* 174, 549–551.
- Callow, A.D., 1988. Problems in the construction of a small diameter graft. *Int. Angiol.* 7, 246–253.
- Chandy, T., Das, G.S., Wilson, R.F., Rao, G.H., 2000. Use of plasma glow for surface-engineering biomolecules to enhance blood compatibility of Dacron and PTFE vascular prosthesis. *Biomaterials* 21, 699–712.
- Chin-Quee, S.L., Hsu, S.H., Nguyen-Ehrenreich, K.L., Tai, J.T., Abraham, G.M., Pacetti, S.D., Chan, Y.F., Nakazawa, G., Kolodgie, F.D., Virmani, R., Ding, N.N., Coleman, L.A., 2010. Endothelial cell recovery, acute thrombogenicity, and monocyte adhesion and activation on fluorinated copolymer and phosphorylcholine polymer stent coatings. *Biomaterials* 31, 648–657. <https://doi.org/10.1016/j.biomaterials.2009.09.079>.
- Clark, E.S., 1999. The molecular conformations of polytetrafluoroethylene: forms II and IV. *Polymer* 40, 4659–4665.
- Clark, E.S., Muus, L.T., 1962. Partial disordering and crystal transitions in polytetrafluoroethylene. *Z. Kristallogr.* 117, 119–127.
- Clark, R.E., Boyd, J.C., Moran, J.F., 1974. New principles governing the tissue reactivity of prosthetic materials. *J. Surg. Res.* 16, 510–522.
- Clowes, A.W., Kirkman, T.R., Reidy, M.A., 1986. Mechanisms of arterial graft healing. Rapid transmural capillary ingrowth provides a source of intimal endothelium and smooth muscle in porous PTFE prostheses. *Am. J. Pathol.* 123, 220–230.
- D'Agostino, R., 1990. *Plasma Deposition, Treatment, and Etching of Polymers*. Academic Press, Boston, MA.
- DeBord, J.R., 1998. The historical development of prosthetics in hernia surgery. *Surg. Clin. North Am.* 78, 973–1006.
- DeGuzman, L.J., Nyhus, L.M., Yared, G., Schlesinger, P.K., 1995. Colocutaneous fistula formation following polypropylene mesh placement for repair of a ventral hernia: diagnosis by colonoscopy. *Endoscopy* 27, 459–461.
- Dekker, A., Reitsma, K., Beugeling, T., Bantjes, A., Feijen, J., et al., 1991. Adhesion of endothelial cells and adsorption of serum proteins on gas plasma-treated polytetrafluoroethylene. *Biomaterials* 12, 130–138.
- Dodat, H., Paulhac, J.B., 1987. Endoscopic treatment of vesico-ureteral reflux by injection of Teflon in children. Preliminary results. *Pediatric* 42, 211–214.
- Doeff, M.M., Lindner, E., 1989. Structure and surface energy characteristics of a series of pseudo-perfluoroalkyl polysiloxanes. *Macromolecules* 22, 2951–2957.
- Drobny, J.G., 2001. *Technology of Fluoropolymers*. CRC Press, Boca Raton, FL.
- Drobny, J.G., 2005. *Fluoroplastics (Rapra Review Report 184)*. Smithers Rapra Press, Boca Raton, FL.
- Edwards, W.S., 1959. Progress in synthetic graft development; an improved crimped graft of Teflon. *Surgery* 45, 298–309.
- Frankel, A., November, 2 2009. Blood Money: The American Lawyer. <https://www.lw.com/mediaCoverage/blood-money-american-lawyer-article>.
- Garfinkle, A.M., Hoffman, A.S., Ratner, B.D., Reynolds, L.O., Hanson, S.R., 1984. Effects of a tetrafluoroethylene glow discharge on patency of small diameter Dacron vascular grafts. *Trans. Am. Soc. Artif. Intern. Organs* 30, 432–439.
- Gasior, P., Cheng, Y., Valencia, A.F., McGregor, J., Conditt, G.B., Kaluza, G.L., Granada &, J.F., 2017. Impact of fluoropolymer-based paclitaxel delivery on neointimal proliferation and vascular healing: a comparative peripheral drug-eluting stent study in the familial hypercholesterolemic swine model of femoral restenosis. *Circ. Cardiovasc. Interv* 10, e004450. <https://doi.org/10.1161/CIRCINTERVENTIONS.116.004450>.
- Gibson, L.D., Stafford, C.E., 1964. Synthetic mesh repair of abdominal wall defects: follow up and reappraisal. *Am. Surg.* 30, 481–486.
- Gore, R.W., 1976. United States Patent 3953566.
- Grainger, D.W., Stewart, C.W., 2001. Fluorinated coatings and films: motivation and significance. Chapter 1. In: Castner, D.G., Grainger, D.W. (Eds.), *Fluorinated Surfaces, Coatings, and Films*. American Chemical Society, Washington, DC, pp. 1–14, (Chapter 1).
- Grainger, D.W., Pavon-Djavid, G., Migonney, V., Josefowicz, M., 2003. Assessment of fibronectin conformation adsorbed to polytetrafluoroethylene surfaces from serum protein mixtures and correlation to support of cell attachment in culture. *J. Biomater. Sci. Polym. Ed.* 14, 973–988.
- Grannis Jr., F.W., Wagman, L.D., 1995. Repair of a complex body wall defect using polytetrafluoroethylene patches. *Ann. Thorac. Surg.* 60, 197–199.
- Hare, E.F., Shafrin, E.G., Zisman, W.A., 1954. Properties of films of adsorbed fluorinated acids. *J. Chem. Phys.* 58, 236–239.
- Harrison, S.C., Brown, C., O'Boyle, P.J., 1993. Periurethral Teflon for stress urinary incontinence: medium-term results. *Br. J. Urol.* 71, 25–27.
- Herschorn, S., Glazer, A.A., 2000. Early experience with small volume periurethral polytetrafluoroethylene for female stress urinary incontinence. *J. Urol.* 163, 1838–1842.
- Hiroyoshi, M., Jinnouchi, H., Diljon, C., Torii, S., Sakamoto, A., Kolodgie, F.D., Virmani, R., Finn, A.V., 2018. A new category stent with novel polyphosphazene surface modification. *Future Cardiol.* 14 (3), 225–235.
- Hoffman, A.S., Ratner, B.D., Garfinkle, A.M., Reynolds, L.O., Horbett, T.A., Hanson, S.R., 1986. A new plasma discharge treatment for cardiovascular implants. In: Williams, J.M., Nichols, M.F., Zingg, W. (Eds.), *Biomedical Materials*, pp. 3–17 Pittsburgh, USA: Mater. Res. Soc. Proc.
- Jenkins, A., 1976. Gore-Tex: a new prosthesis for vascular access. *Br. Med. J.* 2, 280.

- Kalsbeek, H.L., 1974. Experience with the use of Teflon mesh in the repair of incisional hernias. *Arch. Chir. Neerl.* 26, 71–75.
- Kannan, R.Y., Salacinski, H.J., Butler, P.E., Hamilton, G., Seifalian, A.M., 2005. Current status of prosthetic bypass grafts: a review. *J. Biomed. Mater. Res. B Appl. Biomater.* 74, 570–581.
- Kapadia, M.R., Popowich, D.A., Kibbe, M.R., 2008. Modified prosthetic vascular conduits. *Circulation* 117, 1873–1882.
- Kempczinski, R.F., Rosenman, J.E., Pearce, W.H., Roedersheimer, L.R., Berlatzky, Y., et al., 1985. Endothelial cell seeding of a new PTFE vascular prosthesis. *J. Vasc. Surg.* 2, 424–429.
- Kesler, K.A., Herring, M.B., Arnold, M.P., Glover, J.L., Park, H.M., et al., 1986. Enhanced strength of endothelial attachment on polyester elastomer and polytetrafluoroethylene graft surfaces with fibronectin substrate. *J. Vasc. Surg.* 3, 58–64.
- Kiaei, D., Hoffman, A.S., Horbett, T.A., 1992. Tight binding of albumin to glow discharge treated polymers. *J. Biomater. Sci. Polym. Ed.* 4, 35–44.
- Kiaei, D., Hoffman, A.S., Ratner, B.D., Horbett, T.A., Reynolds, L.O., 1988. Interaction of blood with gas discharge treated vascular grafts. *J. Appl. Polym. Sci. Appl. Polym. Symp.* 42, 269–283.
- Kobayashi, H., Owen, M.J., 1995. Surface properties of fluorosilicone. *Trends Polym. Sci.* 3, 330–335.
- Koenig, A.L., Gambillara, V., Grainger, D.W., 2003. Correlating fibronectin adsorption with endothelial cell adhesion and signaling on polymer substrates. *J. Biomed. Mater. Res. A.* 64, 20–37.
- Konner, K., 2005. History of vascular access for hemodialysis. *Nephrol. Dial. Transplant.* 20, 2629–2635.
- Lavery, K.S., Rhodes, C., McGraw, A., Eppihimer, M.J., 2017. Anti-thrombotic technologies for medical devices. *Adv. Drug Deliv. Rev.* 112, 2–11.
- Le Guillou, M., Ferriere, J.M., Pourquie, J., Barthaburu, D., Amory, J.P., et al., 1984. Primary vesico-ureteral reflux in adults. 1977–1982. Department experience of 6-years. *Ann. Urol.* 18, 121–123.
- Legeais, J.M., Werner, L.P., Legeay, G., Briat, B., Renard, G., 1998. In vivo study of a fluorocarbon polymer-coated intraocular lens in a rabbit model. *J. Cataract Refract. Surg.* 24, 371–379.
- Leveen, H.H., Barberio, J.R., 1949. Tissue reaction to plastics used in surgery with special reference to Teflon. *Ann. Surg.* 129, 74–84.
- Levine, B., Berman, W.E., 1995. The current status of expanded polytetrafluoroethylene (Gore-Tex) in facial plastic surgery. *Ear Nose Throat J.* 74, 681–682.
- Li, L., Terry, C.M., Shiu, Y.-T.E., Cheung, A.K., 2008. Neointimal hyperplasia associated with synthetic hemodialysis grafts. *Kidney Int.* 74, 1247–1261.
- Lin, J.C., Tiong, S.L., Chen, C.Y., 2000. Surface characterization and platelet adhesion studies on fluorocarbons prepared by plasma-induced graft polymerization. *J. Biomater. Sci. Polym. Ed.* 11 (7), 701–714.
- Lo Monte, A.I., Damiano, G., Maione, C., Gioviale, M.C., Lombardo, C., et al., 2009. Use of intraperitoneal ePTFE Gore dual-mesh plus in a giant incisional hernia after kidney transplantation: a case report. *Transpl. Proc.* 41, 1398–1401.
- Lopez, A.E., Padron, O.F., Patsias, G., Politano, V.A., 1993. Transurethral polytetrafluoroethylene injection in female patients with urinary continence. *J. Urol.* 150, 856–858.
- Ludington, L.G., Woodward, E.R., 1959. Use of Teflon mesh in the repair of musculofascial defects. *Surgery* 46, 364–373.
- Mascarenhas, R., Macdonald, P.B., 2008. Anterior cruciate ligament reconstruction: a look at prosthetics – past, present and possible future. *J. Med.* 11, 29–37.
- Massa, T.M., McClung, W.G., Yang, M.L., Ho, J.Y., Brash, J.L., Santerre, J.P., 2007. Fibrinogen adsorption and platelet lysis characterization of fluorinated surface-modified polyetherurethanes. *J. Biomed. Mater. Res. A* 81 (1), 178–185.
- Matsumoto, H., Hasegawa, T., Fuse, K., Yamamoto, M., Saigusa, M., 1973. A new vascular prosthesis for a small caliber artery. *Surgery* 74, 519–523.
- McClary, K.B., Ugarova, T., Grainger, D.W., 2000. Modulating fibroblast adhesion, spreading, and proliferation using self-assembled monolayer films of alkythiolates on gold. *J. Biomed. Mater. Res.* 50, 428–439.
- McClurken, M.E., McHaney, J.M., Colonel, W.M., 1986. Physical properties and test methods for expanded polytetrafluoroethylene (PTFE) grafts. In: Kobic, H.E., Katrowitz, A., Sung, P. (Eds.), *Vascular Graft Update: Safety and Performance*. ASTM Publications, Philadelphia, PA, pp. 82–94.
- Meschia, M., Pifarotti, P., Gattei, U., Crosignani, P.G., 2002. Injection therapy for the treatment of stress urinary incontinence in women. *Gynecol. Obstet. Invest.* 54, 67–72.
- Mole, B., 1992. The use of Gore-Tex implants in aesthetic surgery of the face. *Plast. Reconstr. Surg.* 90, 200–206.
- Morris-Stiff, G.J., Hughes, L.E., 1998. The outcomes of nonabsorbable mesh placed within the abdominal cavity: literature review and clinical experience. *J. Am. Coll. Surg.* 186, 352–367.
- Naselli, C., Swalen, J.D., Rabolt, J.F., 1989. Order–disorder transitions in Langmuir–Blodgett films. IV. Structure of [F(CF₂)₈(CH₂)₁₀COO–]₂ Cd²⁺ multilayers at ambient and elevated temperatures. *J. Chem. Phys.* 90, 3855.
- Oshige, S., 1967. Japanese Patent No. 42–13560(67/13560).
- Otsuka, F., Cheng, Q., Yahagi, K., Acampado, E., Sheehy, A., Yazdani, S.K., Sakakura, K., Euler, K., Perkins, L.E.L., Kolodgie, F.D., Virmani, R., Joner, M., 2015. Acute thrombogenicity of a durable polymer everolimus-eluting stent relative to contemporary drug-eluting stents with biodegradable polymer coatings assessed ex vivo in a swine shunt model. *JACC Cardiovasc. Interv.* 8 (9), 1248–1260. <https://doi.org/10.1016/j.jcin.2015.03.029>.
- Paynter, R.W., Ratner, B.D., 1985. *Surface and Interfacial Aspects of Biomedical Polymers*, second ed. Springer, New York, NY.
- Pittman, A.G., 1972. Surface properties of fluorocarbon polymers”. Chapter 13. In: Wall, L.A. (Ed.), *Fluoropolymers*. Wiley, New York, NY, pp. 413–431, (Chapter 13).
- Politano, V.A., 1992. Transurethral polytef injection for post-prostatectomy urinary incontinence. *Br. J. Urol.* 69, 26–28.
- Puri, P., 1995. Ten year experience with subureteric Teflon (polytetrafluoroethylene) injection (STING) in the treatment of vesicoureteric reflux. *Br. J. Urol.* 75, 126–131.
- Puri, P., 2000. Endoscopic correction of vesicoureteral reflux. *Curr. Opin. Urol.* 10, 593–597.
- Puri, P., O'Donnell, B., 1984. Correction of experimentally produced vesicoureteric reflux in the piglet by intravesical injection of Teflon. *Br. Med. J.* 289, 5–7.
- Ratner, B.D., 1993. New ideas in biomaterials science: a path to engineered biomaterials. *J. Biomed. Mater. Res.* 27, 837–850.
- Ratner, B.D., 1995. Plasma deposition of organic thin films for surface modification. *J. Photopolym. Sci. Technol.* 8, 481–494.
- Reid, G., Busscher, H.J., Sharma, S., Mittelman, M.W., McIntyre, S., 1995. Surface properties of catheters, stents and bacteria associated with urinary tract infections. *Surf. Sci. Rep.* 21, 251–273.
- Richter, G.M., Stampfl, U., 2005. A new polymer concept for coating of vascular stents using PTFEP (poly(bis(trifluoroethoxy)phosphazene) to reduce thrombogenicity and late in-stent stenosis. *Invest. Radiol.* 40 (4), 210–218.
- Roald, H.E., Barstad, R.M., Bakken, I.J., Roald, B., Lyberg, T., 1994. Initial interactions of platelets and plasma proteins in

- flowing non-anticoagulated human blood with the artificial surfaces Dacron and PTFE. *Blood Coagul. Fibrinolysis* 5, 355–363.
- Russell, T.P., Rabolt, J.F., Twieg, R.J., Siemens, R.L., Farmer, B.L., 1986. Structural characterization of semifluorinated n-alkanes. 2. Solid–solid transition behavior. *Macromolecules* 19, 1135–1143.
- Santiago, E.J., Chatamra, K., Taylor, D.E., 1981. Haemodynamic aspects of lower limb arterial reconstruction using Dacron and GoreTex prostheses. *Ann. R. Coll. Surg. Engl.* 63, 253–256.
- Scheirs, J., 1997. *Modern Fluoropolymers*. Wiley, New York, NY.
- Schmidt, S., Decler, W., Wagner, U., Kindermann, D., Pringle, K., et al., 1991. An approach to fetal surgery: endoscopic use of excimer laser. *Eur. J. Obstet. Gynecol. Reprod. Biol.* 42 (Suppl. 1), S84–S86.
- Schneider, J., Erdelen, C., Ringsdorf, H., Rabolt, J.F., 1989. Structural studies of polymers with hydrophilic spacer groups. 2. Infrared spectroscopy of Langmuir–Blodgett multilayers of polymers with fluorocarbon side chains at ambient and elevated temperatures. *Macromolecules* 22, 3475–3480.
- Smart, B.E., 1994. Characteristics of C–F systems. Chapter 3. In: Banks, R.E., Tatlow, J.C., Smart, B.E. (Eds.), *Organofluorine Chemistry: Principles and Commercial Applications*. Plenum Press, New York, NY. ISBN 978-1-4899-1202-2.
- Snijders, H., 1969. The use of Teflon gauze in the treatment of medial and recurrent inguinal hernias. *Arch. Chir. Neerl.* 21, 199–202.
- Soyer, T., Lempien, M., Cooper, P., Norton, L., Eiseman, B., 1972. A new venous prosthesis. *Surgery* 72, 864–872.
- Stanley, J.C., 1982. *Biologic and Synthetic Vascular Prostheses*. Grune & Stratton, New York, NY.
- Stone, M., Nevell, T.G., Tsibouklis, J., 1998. Surface energy characteristics of poly(perfluoroacrylate) film structures. *Mater. Lett.* 37, 102–105.
- Sun, F., Grainger, D.W., Castner, D.G., Leach-Scampavia, D.K., 1994a. Adsorption of ultrathin films of sulfur-containing siloxane oligomers on gold surfaces and their in situ modification. *Macromolecules* 27, 3053–3062.
- Sun, F., Mao, G., Grainger, D.W., Castner, D.G., 1994b. Polymer ultrathin films by self-assembly: bound perfluorinated monolayers and their modification using in situ derivatization strategies. *Thin Solid Films* 242, 106–111.
- Szott, L.M., Irvin, C.A., Trollsas, M., Hossainy, S., Ratner, B.D., 2016. Blood compatibility assessment of polymers used in drug eluting stent coatings. *Biointerphases* 11 (2), 029806.
- Torii, S., Cheng, Q., Mori, H., Lipinski, M.J., Acampado, E., Perkins, L.E.L., Hossainy, S.F., Pacetti, S.D., Kolodgie, F.D., Virmani, R., Finn, A.V., 2018. Acute thrombogenicity of fluoropolymer-coated versus biodegradable and polymer-free stents. *EuroIntervention*. <https://doi.org/10.4244/EIJ-D-17-00728>. pii: EIJ-D-17-00728.
- Tsao, M.W., Hoffmann, C.L., Rabolt, J.F., Johnson, H.E., Castner, D.G., et al., 1997. Studies of molecular orientation and order in self-assembled semifluorinated n-alkanethiols: single and dual component mixtures. *Langmuir* 13, 4317–4322.
- Tulandi, T., 1997. How can we avoid adhesions after laparoscopic surgery? *Curr. Opin. Obstet. Gynecol.* 9, 239–243.
- Valdevit, A., Turegun, M., Kambic, H., Siemionow, M., Zins, J., 2000. Cranial defect repair using e-PTFE: Part I. Evaluation of bone stiffness. *J. Biomed. Mater. Res.* 53, 62–66.
- van Kooten, T.G., Schakeraad, J.M., Van der Mei, H.C., Busscher, H.J., 1992. Influence of substratum wettability on the strength of adhesion of human fibroblasts. *Biomaterials* 13, 897–904.
- van Wachem, P.B., Beugeling, T., Feijen, J., Bantjes, A., Detmers, J.P., et al., 1985. Interaction of cultured human endothelial cells with polymeric surfaces of different wettabilities. *Biomaterials* 6, 403–408.
- White, R.A., 1988. The effect of porosity and biomaterial on the healing and long-term mechanical properties of vascular prostheses. *ASAIO (Am. Soc. Artif. Intern. Organs) Trans.* 34, 95–100.
- Winslow, R.W., 2005. *Blood Substitutes*. Academic Press, London, UK, p. 91.
- Xie, X., Guidoin, R., Nutley, M., Zhang, Z., 2010. Fluoropassivation and gelatin sealing of polyester arterial prostheses to skip preclotting and constrain the chronic inflammatory response. *J. Biomed. Mater. Res. B Appl. Biomater.* 93, 497–509.
- Yazdani, S., Sheehy, A., Pacetti, S., Rittlemeier, B., Kolodgie, F., Virmani, R., 2016. Stent coating integrity of durable and biodegradable coated drug eluting stents. *J. Interv. Cardiol.* 29. <https://doi.org/10.1111/joic.12303>.
- Zhang, Y.X., Da, A.H., Hogen-Esch, T.E., Butler, G.B., 1989. A fluorocarbon-containing hydrophobically associating polymer. *J. Polym. Sci. C. Polym. Lett. Ed.* 28, 213–218.
- Zilla, P., Fasol, R., Preiss, P., Kadletz, M., Deutsch, M., et al., 1989. Use of fibrin glue as a substrate for in vitro endothelialization of PTFE vascular grafts. *Surgery* 105, 515–522.

Chapter Exercises

1. Fluoropolymers are commonly considered “inert.” Teflon PTFE for example does not dissolve in any known solvents. Are fluoropolymers biologically inert? Explain.
Answer: Fluoropolymers of all types and chemistries are well recognized to interact actively with all biological components: proteins, platelets, bacteria, fungus, algae, cells. Tight protein adsorption to fluoropolymer surfaces from different fluids (e.g., serum, plasma, blood, simple buffered protein solutions) is reported. Blood coagulation and complement activation are well documented. In fact, some fluorinated implants (e.g., ePTFE vascular grafts) are preclotted in patient fluids (e.g., whole blood) to passivate them prior to implantation. Cells and bacteria also adhere and proliferate under both in vitro and in vivo conditions. Fluoropolymers are not biologically inert. They do, however, appear to prefer to adsorb certain proteins from mixtures that then bias their subsequent interactions with other biological components. PVDF protein blotting membranes are passivated with various masking proteins (e.g., casein) to prevent adsorption of other proteins during protein blotting and transfers. Additionally, many fluorinated surfaces will adsorb high amounts of serum albumin from blood, plasma fractions, and mammalian sera. This “albumin passivation” renders these surfaces resistant to other protein adsorption, cell and platelet adhesion, and blood coagulation activation.
2. PTFE under mechanical loading suffers from creep: describe this problem and its impact on implant

applications where durable mechanical properties under compression or cyclic loading are essential.

Answer: Creep and cold flow are classic problems for PTFE polymers under continuous loading that result in deformation. PTFE failures in certain biomechanical applications experiencing loading (e.g., temporal mandibular knee hip joint bearing surfaces) are notable examples. Despite low coefficients of friction that make PTFE attractive in loadbearing surfaces, PTFE implant experiences to date in mechanical loading have not been promising (witness the early Charnley hip bearing and TMJ joint failures).

3. RGP contact lens materials based on glassy polymethylmethacrylates have included fluorinated copolymers with either silicone polymers or as perfluorohydrocarbons. What is the functional advantage for including fluorinated materials in these contact lenses?

Answer: Due to their polymer chemistry, RGP lenses do not contain significant amounts of water, affecting their mechanical properties, comfort, and oxygen through-lens transmissibility. RGP lenses rely instead on microscopic pores in the lens to transmit oxygen to the cornea. But RGP lenses exhibit limited oxygen permeability, compromising several contact lens properties. As highly fluorinated materials have intrinsically high oxygen permeability, fluorinated lenses provide an alternative transport mechanism to improve oxygen permeability through the lens compared to the aqueous phase in conventional soft lens materials. Additionally, fluorine content in an RGP lens influences lens flexibility, lipid/protein deposition properties, and cost considerations.

1.3.2D

The Organic Matrix of Restorative Composites and Adhesives

JACK L. FERRACANE¹, CARMEM S. PFEIFER²

¹Department of Restorative Dentistry, Oregon Health & Science University, Portland, Oregon

²Biomaterials and Biomechanics, Oregon Health & Science University, Portland, Oregon

Introduction—Historical Perspective

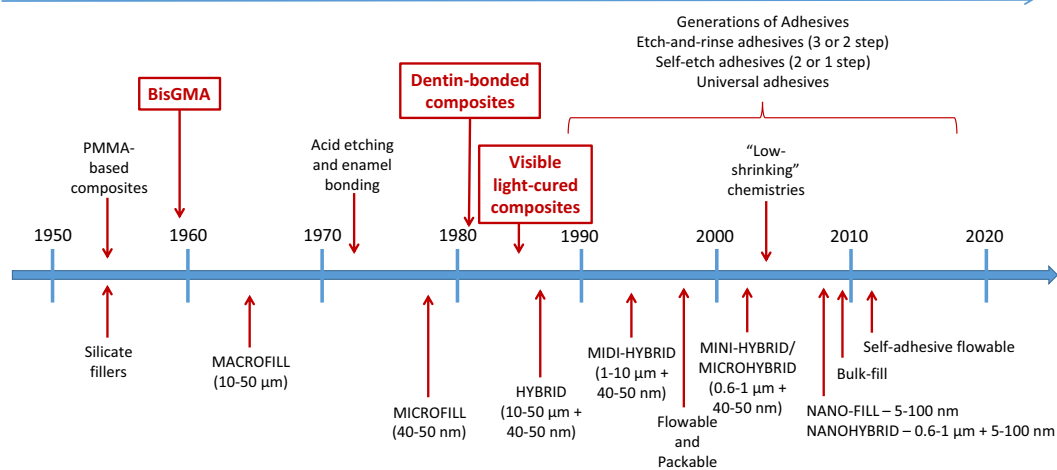
The use of polymeric materials to build directly-placed dental restorations dates to the 1950s (Fig. 1.3.2D.1) (Bayne, 2005). The first materials relied on polymethyl methacrylate as the organic matrix, which confined their use to small, nonload-bearing applications. Owing to low mechanical properties and high volumetric shrinkage, and in the absence of an adhesive system, these materials were found to be unsuitable for most dental restorations (Anusavice et al., 2013). In the early 1960s, Dr. Rafael Bowen synthesized a dimethacrylate monomer referred to as Bis-GMA (bisphenol A diglycidyl dimethacrylate) that revolutionized restorative composites (Bowen, 1956, 1939, 1962) and is still used in the majority of currently available commercial materials (Anusavice et al., 2013). The fillers used in the early “macrofill” composites were comprised of quartz, ground into particles of 10–100 μm. Though the mechanical properties were significantly increased in comparison to the polymethyl methacrylate-based materials, early formulations exhibited severe wear due to the large particle size (Lee et al., 1975, 1974). Clinical use of dental composites became well accepted for anterior teeth in the early 1970s when the mechanism of adhesion to enamel through phosphoric acid etching was popularized, based on the technique first described by Dr. Michael Buonocore in the late 1950s (Bayne, 2005; Anusavice et al., 2013; Zero, 2013; Buonocore, 1955). Early adhesives consisted of a resin of BisGMA and TEGDMA, and were very hydrophobic compared to the modern formulations (Bowen and Molineaux, 1969). The concept of “total etching,” now known as “etch-and-rinse,” in which phosphoric acid was applied to both the dentin and enamel surfaces, was only introduced 10–15 years later, and it was not until the 1980s that Nakabayashi first described the potential formation of a “hybrid layer” of resin-reinforced dentin with the use of an etch-and-rinse technique (Nakabayashi et al., 1982; Nakabayashi, 1985).

The first composite materials were self-cured, requiring the mixing of two pastes containing appropriate amine and peroxide catalysts to produce polymerization within minutes. The concept of “on command” polymerization led to the replacement of the two-paste system with a single paste polymerized via a photocatalyzed redox reaction (Lee et al., 1976). The initial materials employed UV-mediated photocuring, which was later replaced by visible light photocuring based on camphorquinone/amine initiator systems (Bassiouny and Grant, 1980).

Thus, the beginning of the development of dental composites experienced three major ground-breaking discoveries that facilitated their acceptance by the profession: the introduction of BisGMA as a base monomer for the composite, the acquisition of adhesion to dentin through the hybrid layer formation, and the advent of visible light-mediated, on-command photocuring (Fig. 1.3.2D.1). Subsequently, composites underwent dramatic development in the inorganic portion, primarily to produce heavily filled materials with small filler sizes. Some current materials employ nanotechnology that allows for the incorporation of up to 80% by weight of nanometer-sized fillers (Chen, 2010).

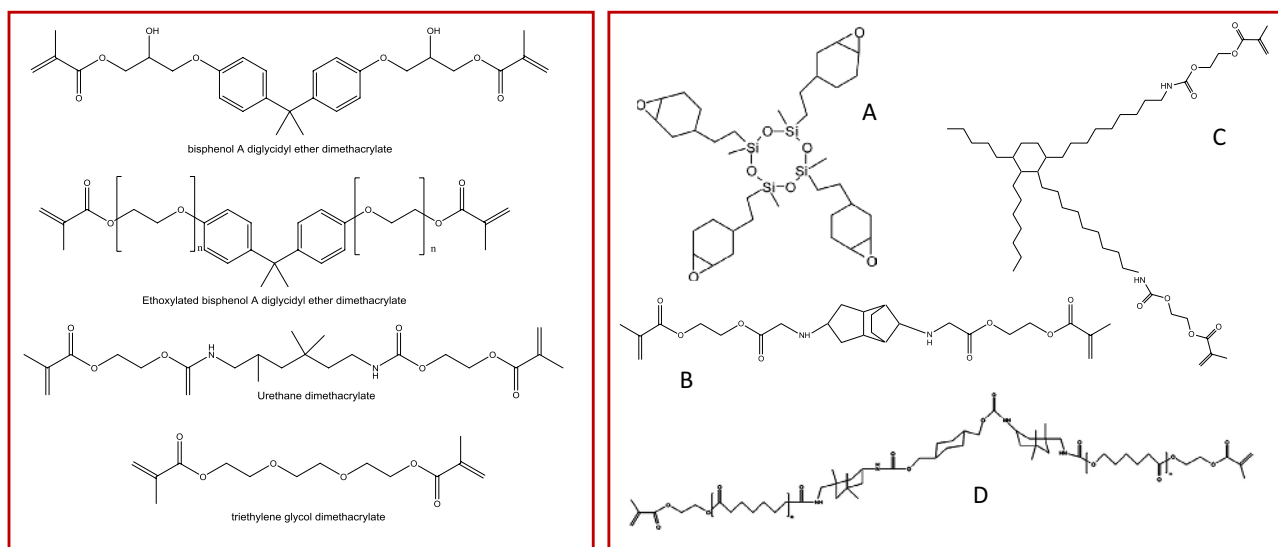
Interestingly, however, the chemistry used in the organic matrix continues to rely on methacrylates, and it is only in the past 10 years that attempts have been made to replace these monomers. Dental composite restorations may last on average less than 10 years in service, with the main causes for restoration replacement being secondary caries and fracture (Demarco et al., 2015, 2012). New alternatives being investigated aim at overcoming the drawbacks of ester bond hydrolysis, high polymerization stress, and gap formation, which combined lead to instability at the tooth–restoration interface and loss of mechanical integrity (Fugolin et al., 2019; Gonzalez-Bonet et al., 2015; Podgorski et al., 2015). Novel materials also aim at not being merely inert (not cytotoxic/allergenic), but rather capable of eliciting desirable biological responses, such as remineralization and antimicrobial activity.

Resins are still largely reliant on BisGMA (and HEMA for adhesives), with novel chemistries in the last 10 years



Fillers decreased in size; surface functionalization technology allowed for incorporation of larger amounts

• **Figure 1.3.2D.1** Timeline for improvements in dental composites and adhesives. (Adapted from Figure 5 in Bayne, S.C., 2005. Dental biomaterials: where are we and where are we going? *J. Dent. Educ.* 69, 571–585).



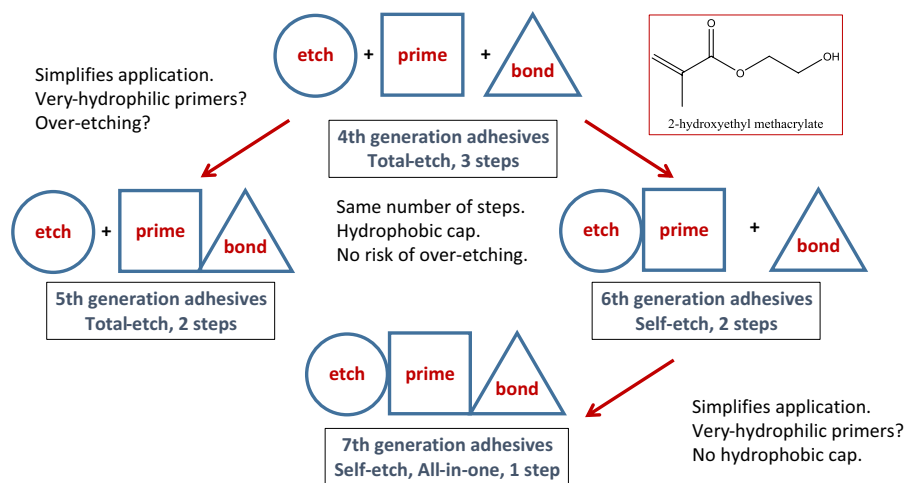
• **Figure 1.3.2D.2** Molecular structure of conventional dimethacrylates (box on the left) and alternative monomers (box on the right) used in commercial products. (A) Oxirane (Filtek LS, 3M-ESPE); (B) TCD-urethane (Venus Diamond, Heraeus Kulzer); (C) Dimeracid dimethacrylate (N'Durance, ConfiDental-Septodont); (D) DuPont DX-511 (Kalore, GC America). (Adapted from Figures 1 and 5 in "Dental Composites — Chemistry and Composition" (Pfeifer, CS. Chapter 11 in *Dental Biomaterials* (Pfeifer, 2017))).

The Monomer Matrix—Conventional Systems

Dimethacrylates (Base and Diluent Monomers) Used in Commercial Composites

BisGMA remains the most common dimethacrylate monomer used in dental composites and adhesives (Fig. 1.3.2D.2). The success of this monomer is related to a combination of properties afforded by BisGMA's structure: a rigid BPA (bisphenol A) core, strong hydrogen bonding potential imparted by the two hydroxyl groups in the backbone, and the potential to form cross-linked networks by virtue of two methacrylate functionalities per molecule (Asmusen and Peutzfeldt, 1998). The strong hydrogen bonding

in BisGMA imparts intermolecular reinforcement, but also results in high viscosity (1200 MPa/s) (Lemon et al., 2007). The high viscosity, in turn, hinders the addition of a high volume of inorganic filler particles, which are the component mainly responsible for producing high mechanical properties (El-Safty et al., 2012; Ilie and Hickel, 2009). In addition, the low mobility of BisGMA in a polymerizing medium also means that diffusion-controlled acceleration takes place early in conversion (Oadian, 2004), leading to low conversion for the homopolymer (Gajewski et al., 2012). To allow for the incorporation of larger amounts of filler and also to adjust clinical handling properties, so-called "diluent" monomers are combined with BisGMA (Froes-Salgado et al., 2015). The most commonly used diluent monomer is triethyleneglycol dimethacrylate (TEGDMA), which has



• **Figure 1.3.2D.3** Representation of the different generations of dental adhesives. The structure of 2-hydroxyethyl methacrylate (HEMA) is shown at the top right corner.

a much lower viscosity [0.1 MPas (Gajewski et al., 2012)] and lower molecular weight (286 g/mol) compared to BisGMA (512 g/mol). TEGDMA has a flexible ethylene glycol unit backbone, with the homopolymer reaching around 100 MPa in flexural strength and 1.8 GPa in flexural modulus (Gajewski et al., 2012). The lower viscosity and greater molecular flexibility leads to delayed diffusional limitations to conversion when combined with BisGMA, in a well-documented synergistic effect (Asmussen and Peutzfeldt, 1998). The molar shrinkage coefficient of TEGDMA is also much higher than that of BisGMA, due to the lower molecular weight of the former (Patel et al., 1987). Therefore, when combined with BisGMA, TEGDMA's lower viscosity allows for the incorporation of larger amounts of particles and for increased conversion; however its smaller size, flexible backbone, and lack of strong intermolecular interactions increase shrinkage and decrease mechanical properties (Froes-Salgado et al., 2015; Goncalves et al., 2010). For this reason, other dimethacrylates have been used as diluents, including urethane dimethacrylate (UDMA) and ethoxylated bisphenol A dimethacrylate (BisEMA). UDMA and BisEMA have molecular weights (470 and 512 g/mol, respectively) comparable to BisGMA, but have much lower viscosity (23 and 0.9 MPas, respectively) (Gajewski et al., 2012; Goncalves et al., 2009). Though lower than for BisGMA, UDMA has a significant hydrogen bonding potential via intermolecular interaction on the imino group, which reinforces the network (Bowen and Moliniaux, 1969). BisEMA only has hydrogen bonding acceptor capability via ethylene glycol units, but still presents a stiff BPA core. With recent concerns over the potential exposure to BPA upon degradation of these materials, alternatives have been developed (Fig. 1.3.2D.2), such as the dimethacrylate monomer known as TCD-urethane used in one specific commercial material (Venus Diamond, Kerr). This monomer also has a stiff core based on a ring moiety, and relatively high molecular weight (507 g/mol). Another example is the dimethacrylate monomer DX-511, patented by Dupont and used in Kalore from GC Corporation. Its molecular weight is 895 g/mol.

The commercial materials containing conventional and alternative monomers have been extensively characterized in vitro and in clinical studies. The rationale for their development was to produce low-viscosity diluents for high filler loading that have higher molecular weights, thus producing much lower shrinkage than TEGDMA. Indeed, the volumetric shrinkage of some of the new materials was lower than conventional materials at the same filler level (Boaro et al., 2010), but the correlation with polymerization stress and the consequent interfacial gap formation is more complex. Polymerization stress is complex, resulting from a combination of shrinkage, final conversion, and elastic modulus (Goncalves et al., 2008; Pfeifer et al., 2008). In fact, some of the “low-shrinking” materials have not shown reduced stress (Boaro et al., 2010). In addition, controlled clinical trials have failed to demonstrate improved performance and longevity of restorations made with these materials compared with their conventional counterparts (Baracco et al., 2016; Kruly et al., 2018; Magno et al., 2016; Mahmoud et al., 2014; Schmidt et al., 2015).

Adhesive Monomers

Most modern adhesives are composed of a combination of a dimethacrylate monomer (generally BisGMA) that provides cross-linking and increased polymer stability, and one or more monomethacrylate monomers with hydrophilic characteristics (Cadenaro et al., 2019). The most common example is hydroxyethyl methacrylate (HEMA), whose complete miscibility with water allowed for “wet bonding” to be performed on the dentin substrate via the formation of a hybrid layer (Nakabayashi et al., 1982). HEMA is used mostly in fourth and fifth generation, etch-and-rinse adhesives, but can also be present in sixth and seventh generation, self-etching compositions, including the most recent “universal” adhesives (Fig. 1.3.2D.3). The rationale for the different generations of adhesives is to simplify the technique-sensitive application of fourth generation, three-step, etch-and-rinse adhesives (Lane et al., 2016) by either combining the primer and bond steps (two-step, etch-and-rinse, or fifth-generation adhesives), or by using self-etching (acidic) monomers that eliminate the

need for a separate etching step. These self-etch adhesives have either a separate final resin bond step (self-etch, two-step, or sixth-generation adhesives) or without a separate bond step (all-in-one, or seventh-generation adhesives). In the early 2000s, the concept of very hydrophilic adhesives started to be investigated, with the phenomenon of adhesive layer degradation by water percolation being described and the term “water-treering” being coined (Tay and Pashley, 2003). Water treering describes the seepage of water through adhesives, especially those where the hydrophilic primer step is combined with the hydrophobic bond step (fifth and seventh generations), resulting in an adhesive layer that serves as a semipermeable membrane (Chersoni et al., 2004; Tay et al., 2004, 2003). The adhesive polymer network is intrinsically less cross-linked than that of composites, and also much more prone to water sorption (Cadenaro et al., 2019). This means that the hydrolysis-prone ester bonds in methacrylates are exposed to degradative conditions. In fact, some studies have shown that the adhesive layer can be severely compromised after only 6 months (Tay and Pashley, 2003), especially for materials where the bond step is not separate from the primer application.

Self-etching has the potential to decrease dentin permeability because the dentinal tubules do not become completely exposed during demineralization, as is the case when phosphoric acid is applied to dentin. Because there is no acid rinsing step, the demineralized dentin material becomes incorporated within the bonding layer with self-etch adhesives. Therefore, the hybrid layer is much thinner, and primer and adhesive more easily penetrate the full depth of the demineralization. In contrast, for the etch-and-rinse systems, there is potential for a band of collagen to remain exposed and not penetrated by the adhesive (Cadenaro et al., 2019), which increases the likelihood of water permeability. Self-etching monomers present a pKa of 1.7–2.5 (Salz et al., 2006), and rely either on carboxylic acid or phosphonic acid moieties (Fig. 1.3.2D.4). Several different monomer structures have been investigated, with 10-MDP (10-methacryloyloxydecyl dihydrogen phosphate) showing the best overall

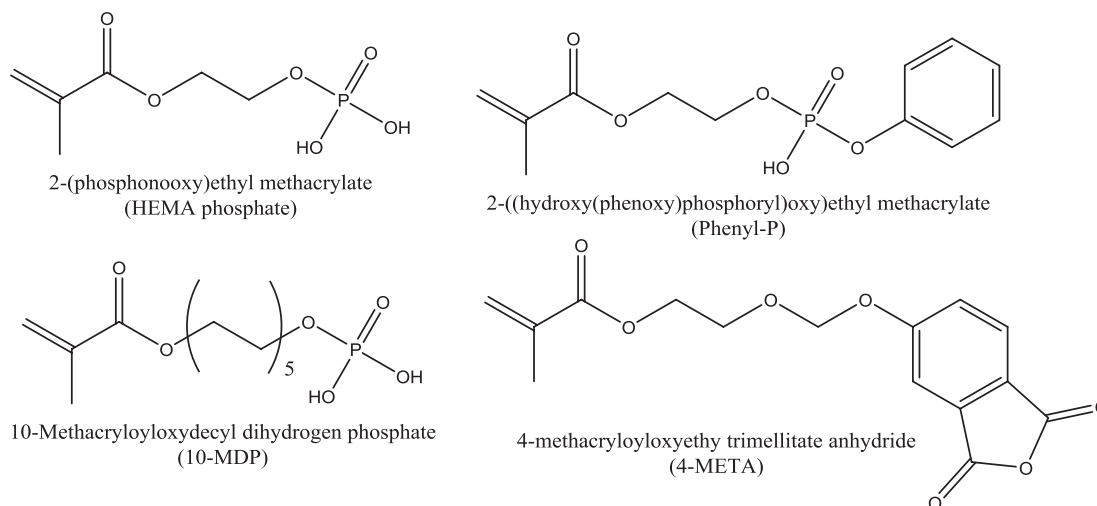
results (Feitosa et al., 2014; Yoshihara et al., 2013) and now being used in most commercial universal dental adhesives (since the expiration of the original patent by Kuraray Inc.).

The Monomer Matrix—Novel Systems

Lower Stress Resin Systems

Low-Shrinkage Materials

As composites undergo polymerization, bonding to the cavity wall causes the shrinkage inherent in the process to take place under confinement (Feilzer et al., 1987). Being unable to accommodate all of the change in volume, the polymerizing material transfers stress to the bonded interface (Feilzer et al., 1987). If the bond strengths are insufficient, a gap opens at the interface, potentially leading to staining, bacterial infiltration, and ultimately recurring decay (Peutzfeldt and Asmussen, 2004). The management of polymerization stress is complex, since many factors affect the magnitude of the forces transferred to the interface, including the size of the cavity preparation and the free surface area (Goncalves et al., 2008), as well as the interplay between conversion, shrinkage, and modulus development (Pfeifer et al., 2008). Any strategy aiming at reducing stress should not jeopardize conversion or elastic modulus, so tackling the shrinkage was the first approach used in stress management. In the 2000s, novel materials claiming to produce less polymerization shrinkage and stress were marketed using monomers with higher molecular weight or those polymerizing via a ring-opening mechanism. In either case, the rationale was to reduce the molar shrinkage coefficient of the material (Patel et al., 1987). In other words, the loss in free volume among polymerizing chains is expected to be diminished for monomers that either occupy more space initially (higher molecular weight) or that polymerize by expansion of a ring-opening system, such as in the case of epoxides (Patel and Braden, 1989). Examples of higher molecular weight monomers are shown in Fig. 1.3.2D.2, along with the only commercial dental composite example of a ring-opening monomer.



• **Figure 1.3.2D.4** Molecular structures of common acidic monomethacrylate monomers used in the formulation of self-etching adhesives.

In vitro studies indeed demonstrated reduced polymerization shrinkage and stress with these materials, albeit at times correlated to reduced conversion and/or mechanical properties (Boaro et al., 2010). Other ring-opening systems based on spiro-ortho carbonates (Stansbury, 1992) have also been proposed (Fig. 1.3.2D.5). The main advantage of ring-opening systems is their reduced shrinkage (Yoo and Kim, 2010), but they are also ester-free and generally more hydrophobic than methacrylate-based systems, which explains their reduced water sorption and solubility (Gonzalez-Bonet et al., 2015). Complications associated with these systems include the cationic polymerization mechanism which requires specialized initiator and adhesive systems that are sensitive to moisture and pH (Vitale et al., 2014).

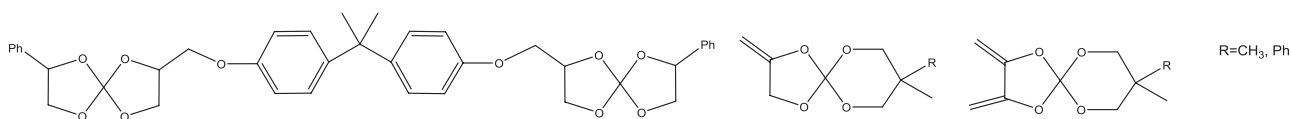
Polyhedral oligomeric silsesquioxanes (POSS) have also been proposed to improve the properties of dental composites (Chen, 2010; Schreck et al., 2011; Fong et al., 2005). These molecules are comprised of distinctive nanocage structures, with an inner inorganic framework of silicon and oxygen atoms, and an outer shell of organic functional groups (Ghanbari et al., 2011). They were at first designed to reduce polymerization shrinkage in dental composites due to their high molecular weight (Fong et al., 2005). Early reports indicated that the mechanical properties of composites are reduced with the addition of even modest concentrations of these oligomers (Fong et al., 2005). More recent reports indicate the potential use of POSS additives to reinforce other classes of polymeric materials, such as those used in maxillofacial applications (Mohammad et al., 2010).

The inclusion of prepolymerized resin particles has been proposed to reduce polymerization shrinkage and stress in dental composites, and more recent examples have included nanogels (Morales et al., 2011; D'Ovidio et al., 2018; Liu et al., 2012) and other oligomers (Carioscia et al., 2005; Bacchi et al., 2014; Bacchi et al., 2016; Bacchi and Pfeifer, 2016). In the case of nanogels, prepolymerized particles of around 230–650 kDa are synthesized in solution (Dailing et al., 2014), producing a cross-linked network bearing different functional groups, such as methacrylates. These networks are swollen by the secondary monomer matrix they are added to and as the polymerization progresses, become covalently attached to the newly forming polymer (Morales et al., 2011). Studies have demonstrated reduced polymerization shrinkage and stress without compromising conversion and mechanical properties (Morales et al., 2011). These materials have also been successfully used in adhesives having increased longevity of the bonded interface (Gotti et al., 2016; Morales et al., 2012). Stress reductions have also been shown with the addition of thiol-ene and thiourethane oligomers, through

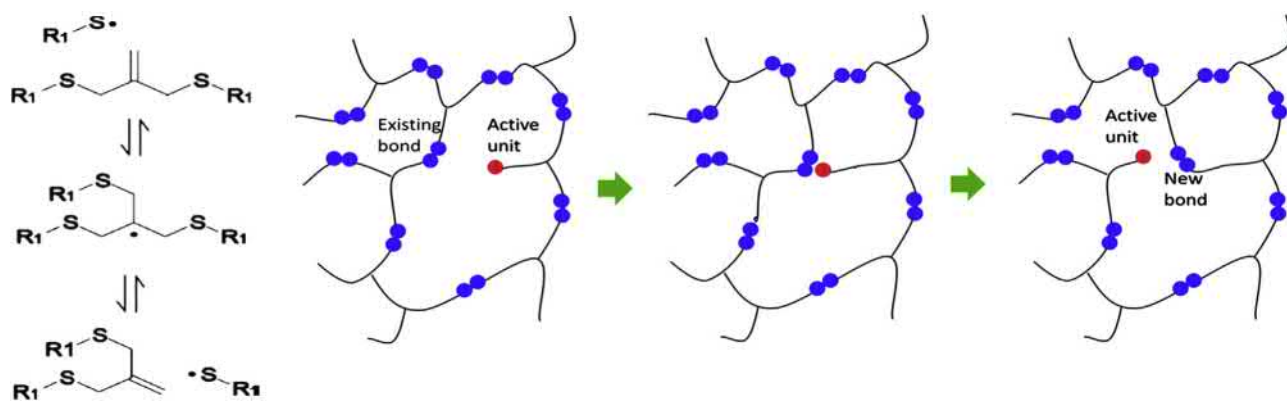
reduced shrinkage, but more closely related to network rearrangement, as explained in detail in the next section.

Network Modulation

Apart from decreasing shrinkage, polymerization stress reduction can also be achieved by controlling network formation. One specific approach is to delay the time in conversion at which modulus develops rapidly (Cramer et al., 2010). One study demonstrated that in cross-linked methacrylates, most of the stresses develop after the material achieves approximately 60% conversion (Lu et al., 2004a,b). At that point in conversion, diffusional limitations and network formation have progressed sufficiently to inhibit significant stress relaxation within the material (Oadian, 2004), leading to the buildup of stress and an overall limited conversion (Oadian, 2004; Lovell et al., 1999). Another study demonstrated that the gel point in methacrylates occurs at around 5% conversion and that the modulus presents a significant increase at around 60% conversion (Pfeifer et al., 2011), coinciding with the most significant increase in stress reported by Lu et al. (Lu et al., 2004a, b). This is typical of methacrylates, which undergo polymerization via a chain-growth mechanism. In contrast, the gelation/vitrification in polymers formed via step-growth mechanisms only takes place at very high conversions (Oadian, 2004). One example of step-growth polymers is thiol-enes, which are not generally useful for dental material applications when used alone due to their intrinsically low mechanical properties (Shin et al., 2009). However, hybrid systems based on combined chain-growth (methacrylates) and step-growth (thiol-containing) polymers have been developed, showing significantly reduced polymerization stress with similar (Cramer et al., 2010; Boulden et al., 2011; Ye et al., 2011) or improved (Bacchi et al., 2015) conversion and mechanical properties. Chain transfer reactions of the thiol functionality to the vinyl-containing monomer during polymerization are responsible for delaying the development of diffusional limitations to termination and propagation until higher levels of conversion have been reached (Berchtold et al., 2001; Lovell et al., 2001). As a consequence, final conversion is increased and the overall polymerization stress is decreased (Cramer et al., 2010). There is a chance for reduced cross-linking and, consequently, reduced mechanical properties, since chain-transfer events are chain breaking (Berchtold et al., 2001). Indeed, in some ternary thiol-ene-methacrylate systems the flexural strength and modulus may be compromised in comparison to the neat methacrylate control, in spite of increased conversion (Cramer et al., 2010a,b). However, the toughness and fracture toughness increase due



• **Figure 1.3.2D.5** Molecular structure of a few examples of monomers based on spiro-orthocarbonate chemistry (Stansbury, 1992; Yoo and Kim, 2010; Stansbury, 1990). (Adapted from Figure 6 in “Dental Composites — Chemistry and Composition” [Pfeifer, CS. Chapter 11 in *Dental Biomaterials* (Pfeifer, 2017)]).



• **Figure 1.3.2D.6** Mechanistic step of the chain-transfer reactions that take place in allyl disulfide networks (left) and cartoon illustration of the bond forming/breaking events within a cross-linked network. (Adapted from Yang, H., Yu, K., Mu, X., Shi, X., Wei, Y., Guo, Y., et al., 2015. A molecular dynamics study of bond exchange reactions in covalent adaptable networks. *Soft Matter*. 11, 6305–6317. and Park, H.Y., Kloxin, C.J., Scott, T.F., Bowman, C.N., 2010. Covalent adaptable networks as dental restorative resins: stress relaxation by addition-fragmentation chain transfer in allyl sulfide-containing resins. *Dent. Mater.* 26, 1010–1016).

to enhanced stress relaxation and crack arrest mechanisms, owing to the low T_g (glass transition temperature) afforded by thiol-carbon bonds (Cramer et al., 2010). The use of multifunctional thiols (Cramer et al., 2010) and multi-thiol oligomers (Carioscia et al., 2005) alleviates concerns over decreased cross-linking. In addition, the use of thiol-functionalized thiourethane oligomers has been shown to reduce polymerization stress via the same chain-transfer reactions, but at the same time to significantly increase fracture toughness via the presence of tough thio-carbamate bonds within the oligomer network (Bacchi et al., 2016).

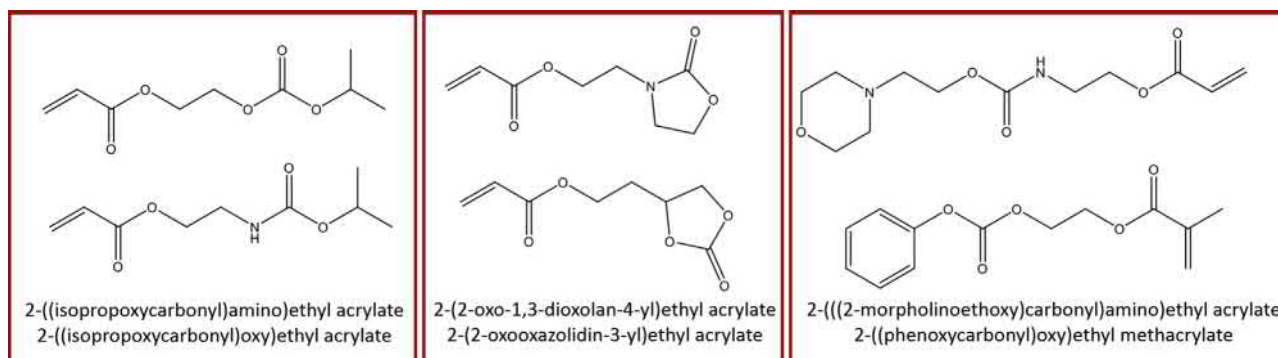
Another approach to control network formation is to use allyl disulfide-based monomers, capable of network rearrangement via covalently adaptable networks (CANs) (Yang et al., 2015). The cross-links in CANs are capable of undergoing reversible rearrangement reactions, as illustrated in Fig. 1.3.2D.6. The chain-breaking/chain-forming reactions provide a mechanism for macroscopic flow and stress relaxation that are initiated at the molecular level, and activated by an external stimulus to the cured polymer (Kloxin and Bowman, 2013). In addition, during the polymerization reaction, the cross-linking chain strand rearrangements actively work to delay or at least partially offset diffusional limitations to conversion, ultimately reducing the overall polymerization stress without reducing the cross-linking density (Bowman and Kloxin, 2012). These monomers have been proposed for use in dental materials in combination with multithiol and dimethacrylate monomers, with the advantages of reducing stress while producing supra-ambient T_g networks (“glassy networks”) (Park et al., 2010). This technology has been translated into a commercial material (Filtek Bulk-Fill Posterior, 3M-ESPE), incorporating the addition-fragmentation moiety directly into the backbone of a proprietary dimethacrylate monomer (<http://multimedia.3m.com/mws/media/976634O/filtek-bulk-fill-posterior-restorative-technical-product-profile.pdf>). In vitro studies demonstrated that this material leads to a reduction in polymerization stress and an

increase in depth of cure compared to a conventional methacrylate control (Fronza et al., 2015), while a 1-year clinical evaluation did not show a difference in performance compared to conventional materials (Bayraktar et al., 2017).

Finally, polymerization-induced phase-separation and interpenetrating network formation have also been proposed as means to control polymerization stress in dimethacrylate networks (Pfeifer et al., 2014). In such systems, two distinct but interconnected phases are formed as the material polymerizes, and the differential in stiffness among the several formed domains is leveraged to accommodate the change in volume, and alleviate part of the stresses being generated (Li and Lee, 2000; Li and Lee, 2000). This can be accomplished by using “low-profile additives” (prepolymerized particles, commonly PMMA) (Szczepanski et al., 2012), metastable mixtures of monomers (Pfeifer et al., 2014), or a combination of monomers in which each polymerizes via a different mechanism (Cook et al., 2006). One example of phase-separating monomer [dimer acid dimethacrylate, $M_w=849$ g/mol, Fig. 1.3.2D.2 (Trujillo-Lemon et al., 2006)] is used in the composition of a commercial material (N'Durance, Septodont), which in theory provides a reduction in shrinkage via polymerization-induced phase separation, and also due to the high molecular weight of the monomer (Bracho-Troconis et al., 1995; Lu et al., 2010).

Fast Polymerizing Monomers

In several applications, including in dentistry, the speed of polymerization is almost equally as important as other physicochemical properties of the polymer. Faster reacting monomers allow for high conversions to be achieved with shorter light exposure times, lower light intensities, and/or lower initiator concentrations. A few examples of monomers with ultra-fast polymerizations have been developed and showed increased degrees of conversions and improved mechanical properties (Lu et al., 2005; Berchtold et al., 2004), including when used to replace TEGDMA in a BisGMA/TEGDMA



• **Figure 1.3.2D.7** Examples of fast polymerizing methacrylate-based monomers. The top and bottom IUPAC names in each box correspond to the top and bottom molecules, respectively.

system (Lu et al., 2005). These monomers (Fig. 1.3.2D.7) are based on carbamates, carbonates, and oxazolidones (Decker and Moussa, 1991), among others. The mechanism for faster polymerization has been correlated to efficient chain-transfer reactions involving labile hydrogens from the functional groups (Decker and Moussa, 1991), and/or potentially inefficient termination reactions (Decker and Moussa, 1990). Hydrogen bonding has also been hypothesized to play a role in preorganizing monomer molecules (and thus increasing the polymerization rate), which may also explain the increased stiffness observed with these materials (Jansen et al., 2003). No commercial example exists for dental applications.

Antimicrobial Resins

Secondary decay is one of the leading causes for composite restoration replacement (van de Sande et al., 2013; Neshchadin et al., 2013). Caries formation at the interface may be promoted by gap formation due to polymerization stress and/or material degradation through hydrolysis (Cenci et al., 2009; Kuper et al., 2014; Maske et al., 2019). Bacterial recolonization in those areas may lead to the formation of acidogenic biofilms that demineralize the tooth structure and lead to marginal breakdown (Maske et al., 2018). More recently, the role of the biofilm itself on material degradation has been described, with bacteria-derived esterases potentially being responsible for the breakdown of ester-containing methacrylates into by-products which, in turn, can upregulate the function of the bacteria (Stewart and Finer, 2019). Therefore, the development of materials that can avoid the recolonization of the surface and interface with the tooth by caries-forming bacteria has gained interest in recent years (Stewart and Finer, 2019; Zhou et al., 2019).

Quaternary ammonium is the most commonly studied antimicrobial moiety attached to polymerizable methacrylates, with several studies demonstrating its efficacy in impeding biofilm formation (Zhou et al., 2019; Han et al., 2017). Quaternary ammonium methacrylates (QAMs) are positively charged monomers characterized as broad-spectrum antibiotics (Wang et al., 2018). The concentration of such monomers into composite systems is limited by their hydrophilicity, which may lead to decreased mechanical properties due to excessive water

sorption (Zhang et al., 2015). However, even at relatively low concentrations (up to 10 wt.%), they have shown efficacy in reducing biofilm formation, with the bacterial content on the surface decreasing linearly with the surface charge (Zhang et al., 2015). The length of the side chain on the quaternized nitrogen has also been correlated with the antibacterial potential against *S. mutans* (Zhang et al., 2016). The optimal chain length has been demonstrated to be between 12 and 16 carbons, and the proposed killing mechanism has been described as the positive charge attracting the bacteria to the surface while the side chain interacts with the thick bacterial wall, leading to its rupture (Zhang et al., 2016). However, no study has confirmed this proposed mechanism. Drawbacks of this system include: (1) the contact–kill mechanism limits their potency to the very first layer of bacteria, with little effect on the bulk of the biofilm; (2) since the QAMs are generally monofunctional ester-containing monomers, they are likely to either leach out as unreacted monomers or as degradation products, which poses toxicity concerns; and (3) QAMs are not selective to dysbiotic bacteria, and instead also eliminate protective (commensal) early colonizers such as *S. sanguinis* (Cheng et al., 2017). Other compounds, such as imidazolium, have also been made polymerizable by functionalization with methacrylates, with encouraging results in terms of antimicrobial activity (Hwang et al., 2017). However, they also rely on broad-spectrum antibiotics, acting via contact–kill mechanisms.

Enhanced Chemical Stability

Material degradation in the harsh conditions of the oral environment is likely one of the causes for marginal breakdown and bulk fracture of the composite. The oral environment experiences variations in temperature, pH, and mechanical loading throughout the day, and in conjunction with the individual's oral microbiome, creates significant challenges for polymeric materials. The vast majority of all adhesives and composites currently in use are based on methacrylates, which contain hydrolyzable ester bonds. To various degrees, the different methacrylate-based materials are prone to water sorption and solubility, with leachates from materials comprising unreacted monomers, oligomers, and degradation products (Finer and Santerre, 2004). Common degradation

products include methacrylic acid, BisHPP (2,2-bis[4(2,3-hydroxypropoxy)phenyl]propane), ethylene glycol, and ethylene glycol monomethacrylate, among others (Finer and Santerre, 2004). BPA has also been detected in the oral cavity after placement of certain orthodontic resins and pit and fissure sealants (Deviot et al., 2018; Eliades et al., 2011; Kloukos et al., 2013). The hydrolysis of the ester bonds has been demonstrated to be catalyzed by several esterases present in the saliva (Finer and Santerre, 2004) and produced by oral bacteria (Marashdeh et al., 2018; Huang et al., 2018).

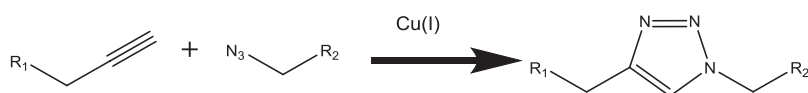
In an attempt to reduce material degradation in the oral environment, research efforts have focused on designing alternative monomers to methacrylates that have fewer or no ester linkages. Examples of ester-free monomers include acrylamides (Fugolin et al., 2019; Moszner et al., 2006), vinyl ethers (Gonzalez-Bonet et al., 2015), alkyne-azides (Zajdowicz et al., 2018), and thiol-vinyl sulfones (Podgórski et al., 2014), all of which are very distinct in their properties and polymerization schemes (Fig. 1.3.2D.8).

Acrylamides and methacrylamides are chemically very similar to methacrylates, with the exception that the oxygen in the ester bond is replaced by a nitrogen atom in the amide bond. The presence of the lone electron pair in nitrogen provides resonance stabilization to the bond, and the trigonal planar conformation about the nitrogen-carbon shortens the bonds in comparison with the conformation in methacrylates, both of which make hydrolysis of the amide bond less likely than that of the ester in methacrylates (Bruice, 2016). However, the carbon-carbon double bonds on some of these monomers are also less prone to attack by free-radicals, which explains the lower reactivity and lower overall conversion observed (Tauscher et al., 2017). These monomers are also intrinsically more hydrophilic than methacrylates, and this greatly limits their usefulness in the formulation of dental composites. However, they may be well suited for use in

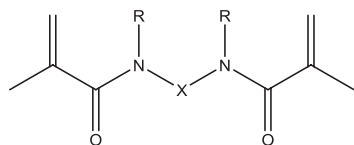
adhesives where hydrophilicity is an asset (Salz and Bock, 2010), and in fact, commercial examples exist (AdheSE One F, Ivoclar-Vivadent; Xeno V, Dentsply Sirona). More recent iterations have shown significantly improved bond strengths, and maintenance of the integrity of the bonded interface for up to 6 months (Fugolin et al., 2019; Rodrigues et al., 2018). The slower reactivity may conceivably be circumvented by the addition of more reactive initiator systems containing iodonium salts and/or others based on germanium initiators (Moszner et al., 2008; Bouzrati-Zerelli et al., 2016), but this yet to be demonstrated. One clear concern with acrylamides is the potential for cytotoxicity (Sahinturk et al., 2018), something that needs to be thoroughly investigated before new materials are brought to the marketplace.

Vinyl ethers are another ester-free alternative to methacrylates. They have been shown to reach reasonably high conversion levels and produce extremely stable materials, even after being subjected to low pH storage and biofilm challenges (Gonzalez-Bonet et al., 2015). However, their polymerization progresses via a cationic mechanism that can be sensitive to moisture and produces networks with low T_g (Kirschbaum et al., 2015). When combined with methacrylates, these monomers produce stable composites with similar elastic modulus and Knoop hardness, and up to 30% greater conversion and fracture toughness compared to a BisGMA/TEGDMA control (Wang et al., 2018).

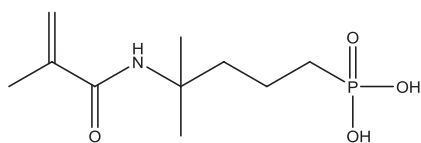
Thiol-vinyl sulfones and alkyne-azide polymerizations are both examples of materials that polymerize via click reactions (Adzima and Bowman, 2012), as well as being free of hydrolyzable ester bonds. The recent development of photo-base generators has allowed for thiol-vinyl sulfones to be photopolymerized on command, making them attractive for use in dental applications (Claudino et al., 2016). These materials present mechanical properties that are similar or better than methacrylate controls, with the advantage of increased conversion



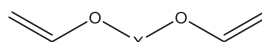
General reaction scheme for alkyne-azides, catalyzed by copper I. Copper I is reduced from copper II either by reaction with sodium ascorbate or in the presence of a photoinitiator.



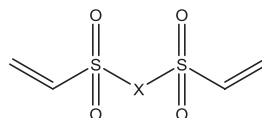
General structure of a multifunctional methacrylamide
R = H, CH₃, C₂H₅



Example of methacrylamide phosphonic acid



General structure of a multifunctional vinyl ether



General structure of a multifunctional vinyl sulfone

• **Figure 1.3.2D.8** Molecular structure of ester-free monomers. (Adapted from Figures 12 and 13 in “Dental Composites — Chemistry and Composition” [Pfeifer, C.S. Chapter 11 in *Dental Biomaterials* (Pfeifer, 2017)]).

and improved resistance to degradation, as well as significantly reduced polymerization stress (Podgorski et al., 2015; Podgórski et al., 2014). Alkyne-azides rely on copper-catalyzed click-reactions (Demko and Sharpless, 2002). Photoactivated copper reduction has been recently demonstrated (Gong et al., 2013) and proposed for use in dental materials. Its advantages include low water sorption and solubility (very stable materials), potential antibacterial properties, reduced polymerization stress, and increased energy absorption (Zajdowicz et al., 2018; Song et al., 2016; Song et al., 2017). Potential disadvantages include a lower T_g compared to methacrylates, poorer color stability, and potential biocompatibility concerns due to the presence of the reduced copper catalyst (Song et al., 2016).

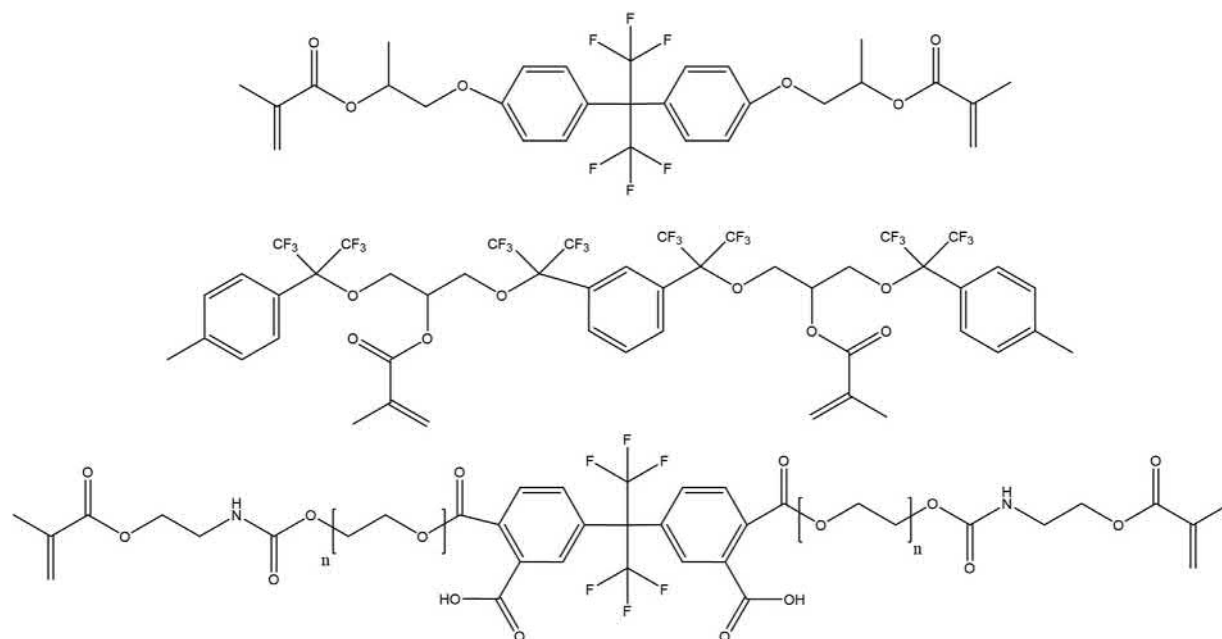
Enhanced Toughness

Historically, the most common strategy to increase the mechanical properties of composites has been to maximize filler content (Finer and Santerre, 2007; Rodriguez et al., 2019). Recently, modifications to the organic matrix have been proposed, such as the use of toughening additives (Bacchi et al., 2016; Fugolin et al., 2019). One example of such additives is thiourethane oligomers, produced through a thiol-isocyanate click reaction, and resulting in a preformed network with lower T_g that can then be added into a methacrylate matrix (Bacchi et al., 2014). The use of such networks has been described for applications where increased toughness and impact resistance are necessary (Li et al., 2009), including in dental materials (Bacchi et al., 2014; Bacchi et al., 2016; Fugolin et al., 2019). Along with a twofold increase in fracture toughness, these materials also result in lower polymerization stress (Bacchi and Pfeifer, 2016). The increase in toughness is in part explained by the

low T_g of the oligomer. In addition, the flexible thiocarbamate bonds have been demonstrated to produce more homogeneous networks compared to urethane counterparts, as evidenced by narrowing tan delta peaks observed with dynamic mechanical analysis (Li et al., 2009). These characteristics likely impart some type of crack arrest capability, but it can also be hypothesized that active strand behavior is at play, similar to what is observed in other carbamate-containing materials (Kuhl et al., 2018), in covalent adaptable networks (Bowman and Kloxin, 2012), and in other urethane-containing materials (Zheng et al., 2016).

Hydrophobic Resins

Enhancing the hydrophobicity of the cured polymer would be an advantage in the oral environment. Fluorine-containing materials are intrinsically hydrophobic, with many examples in the literature demonstrating significantly reduced water sorption and solubility, increased contact angle, and similar to reduced mechanical properties compared to conventional methacrylates (Stansbury and Antonucci, 1999; Liu et al., 2018; Luo et al., 2016). Potential miscibility issues with other monomers could explain the reduction in properties, and in fact studies evaluating the effect of the addition of moderate amounts of solvents (aldehydes and ketones) (Prakki et al., 2009; Prakki et al., 2007), as well as the use of urethane-derived formulations (Liu et al., 2018; Luo et al., 2016), have demonstrated improved mechanical performance. Hydrophobic monofunctional monomers have also been synthesized with this chemistry to produce less water-permeable dental adhesives (Buruiana et al., 2016). Examples of these molecules are shown in Fig. 1.3.2D.9, but no commercial examples exist.



• **Figure 1.3.2D.9** Molecular structure of a few examples of fluorinated monomers proposed for dental applications (Stansbury and Antonucci, 1999; Prakki et al., 2009; Buruiana et al., 2016). (Adapted from Figure 11 in “Dental Composites — Chemistry and Composition” [Pfeifer, CS. Chapter 11 in *Dental Biomaterials* (Pfeifer, 2017)]).

CASE STUDIES I AND II

Describe the chemical characteristics and properties that would be most ideal for a dental resin-based restorative to be used in the following applications.

Case 1: A patient visits the dental office and complains to the dentist that one of their teeth is very sensitive when they drink cold liquids. The tooth is in the front of the mouth (see Fig. A) in their maxilla (upper jaw), and upon inspection the dentist notices that the surface of the tooth is eroded near the gum line. Blowing of light air from the dental unit onto the tooth elicits a rapid pain response. The dentist makes the choice to restore the tooth lesion (defect) with an adhesively bonded composite restorative material. What specific things should the dentist consider when choosing a material to restore this tooth? (Hint: Consider the importance of the following characteristics/properties for this application: high mechanical properties, high wear resistance, excellent esthetics, strong adhesion to dentin and enamel, high color stability, fast polymerization reaction, and resistance to degradation by moisture, enzymes, and bacteria.)

Case 2: A patient visits the dental office and complains to the dentist that one of their teeth is sore and it is hard to chew on that side of their mouth. The tooth is a second molar (see Fig. B) in their mandible (lower jaw), and upon inspection the dentist notices that the tooth already has a composite restoration but suspects that a new lesion is present. The dentist takes an X-ray and sees obvious evidence of a large lesion, not limited to the occlusal surface, but also extending to the distal portion of the tooth. The dentist decides to restore the tooth with an adhesively bonded composite restorative material that will replace the occlusal and distal parts of the tooth, and will extend all the way down to the gum line. What specific things should the dentist consider when choosing a material to restore this tooth? (Hint: Consider the importance of the following characteristics/properties for this application: high mechanical

properties, high wear resistance, excellent esthetics, strong adhesion to dentin and enamel, high color stability, fast polymerization reaction, and resistance to degradation by moisture, enzymes, and bacteria.)



Silane Coupling Agents

The coupling between the organic matrix and the inorganic filler phase in dental composites is accomplished with the functionalization of the surface of silica-containing particles with a silane agent (Bowen, 1962). The majority of the currently available commercial materials use 3-(trimethoxysilyl) propyl methacrylate (TMPS), which provides a chemical bond with the filler via the hydrolysis of its methoxysilane groups, and provides covalent attachment to the organic matrix via copolymerization with the methacrylate (Matinlinna et al., 2011). TMPS is a small molecule, which likely forms close to a monolayer on the filler surface (Sideridou and Karabela, 2009), and this is enough to improve mechanical properties in resin composites. Without the silane coupling, the filler particles essentially behave as voids in the material, providing a facile path for crack propagation (Condon and Ferracane, 1998; Condon and Ferracane, 2002). The caveat of silanization, however, is the potential for stress concentration at the filler–matrix interface, given that the shrinkage inherent to the polymerization of the resin is constrained by the bond to the stiff inorganic particle (Condon and Ferracane, 1998; Condon and Ferracane, 2002). Other silane coupling agents have been proposed, bearing thiol functionalities that would help alleviate part of the stress via

chain-transfer reactions between the thiol and the methacrylate in the organic matrix (Matinlinna et al., 2011). More recently, the use of prepolymerized species has been proposed to harness potential stress relaxation (Fugolin et al., 2019; Faria et al., 2018) and crack arrest mechanisms (Fugolin et al., 2019; Fronza et al., 2019; Ye et al., 2012) specifically at this vulnerable interface. This is hypothesized to be accomplished by functionalizing the surface with thicker layers of more compliant compounds, such as hyperbranched oligomers (Ye et al., 2012), thiourethane oligomers (Fugolin et al., 2019), or nanogels (Fronza et al., 2019).

References

- Adzima, B.J., Bowman, C.N., 2012. The emerging role of click reactions in chemical and biological engineering. *AIChE J.* 58, 2952–2965.
- Anusavice, K.J., Phillips, R.W., Shen, C., Rawls, H.R., 2013. *Phillips' Science of Dental Materials*, twelfth ed. Elsevier, United States.
- Asmussen, E., Peutzfeldt, A., 1998. Influence of UEDMA BisGMA and TEGDMA on selected mechanical properties of experimental resin composites. *Dent. Mater.* 14, 51–56.
- Bacchi, A., Pfeifer, C.S., 2016. Rheological and mechanical properties and interfacial stress development of composite cements modified with thio-urethane oligomers. *Dent. Mater.* 32, 978–986.

- Bacchi, A., Dobson, A., Ferracane, J.L., Consani, R., Pfeifer, C.S., 2014. Thio-urethanes improve properties of dual-cured composite cements. *J. Dent. Res.* 93, 1320–1325.
- Bacchi, A., Consani, R.L., Martim, G.C., Pfeifer, C.S., 2015. Thio-urethane oligomers improve the properties of light-cured resin cements. *Dent. Mater.* 31, 565–574.
- Bacchi, A., Nelson, M., Pfeifer, C.S., 2016. Characterization of methacrylate-based composites containing thio-urethane oligomers. *Dent. Mater.* 32, 233–239.
- Baracco, B., Fuentes, M.V., Ceballos, L., 2016. Five-year clinical performance of a silorane- vs a methacrylate-based composite combined with two different adhesive approaches. *Clin. Oral Investig.* 20, 991–1001.
- Bassiouny, M.A., Grant, A.A., 1980. Physical properties of a visible-light-cured composite resin. *J. Prosthet. Dent.* 43, 536–541.
- Bayne, S.C., 2005. Dental biomaterials: where are we and where are we going? *J. Dent. Educ.* 69, 571–585.
- Bayraktar, Y., Ercan, E., Hamidi, M.M., Colak, H., 2017. One-year clinical evaluation of different types of bulk-fill composites. *J. Investig. Clin. Dent.* 8.
- Berchtold, K.A., Hacıoğlu, B., Lovell, L., Nie, J., Bowman, C.N., 2001. Using changes in initiation and chain transfer rates to probe the kinetics of cross-linking photopolymerizations: effects of chain length dependent termination. *Macromolecules* 34, 5103–5111.
- Berchtold, K.A., Nie, J., Stansbury, J.W., Hacıoğlu, B., Beckel, E.R., Bowman, C.N., 2004. Novel monovinyl methacrylic monomers containing secondary functionality for ultrarapid polymerization: steady-state evaluation. *Macromolecules* 37, 3165–3179.
- Boaro, L.C., Goncalves, F., Guimaraes, T.C., Ferracane, J.L., Versluis, A., Braga, R.R., 2010. Polymerization stress, shrinkage and elastic modulus of current low-shrinkage restorative composites. *Dent. Mater.* 26, 1144–1150.
- Boulden, J.E., Cramer, N.B., Schreck, K.M., Couch, C.L., Brachotroconis, C., Stansbury, J.W., et al., 2011. Thiol-ene-methacrylate composites as dental restorative materials. *Dent. Mater.* 27, 267–272.
- Bouzrati-Zerelli, M., Maier, M., Dietlin, C., Fabrice, M.S., Fouassier, J.P., Klee, J.E., et al., 2016. A novel photoinitiating system producing germyl radicals for the polymerization of representative methacrylate resins: camphorquinone/R₃GeH/iodonium salt. *Dent. Mater.* 32, 1226–1234.
- Bowen, R.L., 1962. In: Office, U.S.P. (Ed.), *Dental Filling Material Comprising Vinyl Silane-Treated Fused Silica and A Binder Consisting of the Reaction Product of Bis Phenol A and Glycidyl Acrylate* United States of America.
- Bowen, R.L., 1939. Properties of a silica-reinforced polymer for dental restorations. *JADA (J. Am. Dent. Assoc.)* 66, 57–64.
- Bowen, R.L., 1956. Use of epoxy resins in restorative materials. *J. Dent. Res.* 35, 360–369.
- Bowen, R.L., Molineaux, A.L., 1969. Adhesive restorative materials. *Dental abstracts; a selection of world dental literature.* 14, 80–82.
- Bowman, C.N., Kloxin, C.J., 2012. Covalent adaptable networks: reversible bond structures incorporated in polymer networks. *Angew. Chem. Int. Ed.* 51, 4272–4274.
- Bracho-Troconis, C., Trujillo-Lemon, M., Boulden, J., Wong, N., Wall, K., Esquibel, K., 2010. Characterization of N'Durance: a nanohybrid composite based on new nano-dimer technology. *Compend. Contin. Educ. Dent. (Jamesburg, NJ:1995)* 31 Spec No 2, 5–9.
- Bruice, P.Y., 2016. *Organic Chemistry*, eighth ed. Pearson Education, Santa Barbara, CA.
- Buonocore, M.G., 1955. A simple method of increasing the adhesion of acrylic filling materials to enamel surfaces. *J. Dent. Res.* 34, 849–853.
- Buruiana, T., Melinte, V., Aldea, H., Pelin, I.M., Buruiana, E.C., 2016. A new fluorinated urethane dimethacrylate with carboxylic groups for use in dental adhesive compositions. *Mat. Sci. Eng. C* 62, 96–104.
- Cadenaro, M., Maravic, T., Comba, A., Mazzoni, A., Fanfoni, L., Hilton, T., et al., 2019. The role of polymerization in adhesive dentistry. *Dent. Mater.* 35, e1–e22.
- Carioscia, J.A., Lu, H., Stanbury, J.W., Bowman, C.N., 2005. Thiol-ene oligomers as dental restorative materials. *Dent. Mater.* 21, 1137–1143.
- Cenci, M.S., Pereira-Cenci, T., Cury, J.A., Ten Cate, J.M., 2009. Relationship between gap size and dentine secondary caries formation assessed in a microcosm biofilm model. *Caries Res.* 43, 97–102.
- Chen, M.H., 2010. Update on dental nanocomposites. *J. Dent. Res.* 89, 549–560.
- Cheng, L., Zhang, K., Zhang, N., Melo, M.A.S., Weir, M.D., Zhou, X.D., et al., 2017. Developing a new generation of antimicrobial and bioactive dental resins. *J. Dent. Res.* 96, 855–863.
- Chersoni, S., Suppa, P., Grandini, S., Goracci, C., Monticelli, F., Yiu, C., et al., 2004. In vivo and in vitro permeability of one-step self-etch adhesives. *J. Dent. Res.* 83, 459–464.
- Claudino, M., Zhang, X., Alim, M.D., Podgórski, M., Bowman, C.N., 2016. Mechanistic kinetic modeling of thiol-michael addition photopolymerizations via photocaged “superbase” generators: an analytical approach. *Macromolecules* 49, 8061–8074.
- Condon, J.R., Ferracane, J.L., 1998. Reduction of composite contraction stress through non-bonded microfiller particles. *Dent. Mater.* 14, 256–260.
- Condon, J.R., Ferracane, J.L., 2002. Reduced polymerization stress through non-bonded nanofiller particles. *Biomaterials* 23, 3807–3815.
- Cook, W.D., Chen, F., Ooi, S.K., Moorhoff, C., Knott, R., 2006. Effect of curing order on the curing kinetics and morphology of bisGMA/DGEBA interpenetrating polymer networks. *Polym. Int.* 55, 1027–1039.
- Cramer, N.B., Couch, C.L., Schreck, K.M., Carioscia, J.A., Boulden, J.E., Stansbury, J.W., et al., 2010a. Investigation of thiol-ene and thiol-ene-methacrylate based resins as dental restorative materials. *Dent. Mater. : Official Publication of the Academy of Dental Materials* 26, 21–28.
- Cramer, N.B., Couch, C.L., Schreck, K.M., Boulden, J.E., Wydra, R., Stansbury, J.W., et al., 2010b. Properties of methacrylate-thiol-ene formulations as dental restorative materials. *Dent. Mater. : Official Publication of the Academy of Dental Materials* 26, 799–806.
- D'Ovidio, T.J., Roberts, R.M., Gautam, D., Marks, Z.D., Saraswathy, M., Stansbury, J.W., et al., 2018. Photopolymerization kinetics of methyl methacrylate with reactive and inert nanogels. *J. Mech. Behav. Biomed. Mater.* 85, 218–224.
- Dailing, E.A., Lewis, S.H., Barros, M.D., Stansbury, J.W., 2014. Construction of monomer-free, highly crosslinked, water-compatible polymers. *J. Dent. Res.* 93, 1326–1331.
- Decker, C., Moussa, K., 1990. Photopolymerisation de monomeres multifonctionnels-III. analyse cinetique par spectroscopie infrarouge resolue dans le temps (RTTR). *Eur. Polym. J.* 26, 393–401.
- Decker, C., Moussa, K., 1991. Photopolymerisation de monomeres multifonctionnels-IV. Acrylates a structure carbamate ou oxazolodone. *Eur. Polym. J.* 27, 403–411.
- Demarco, F.F., Correa, M.B., Cenci, M.S., Moraes, R.R., Opdam, N.J., 2012. Longevity of posterior composite restorations: not only a matter of materials. *Dent. Mater.* 28, 87–101.
- Demarco, F.F., Collares, K., Coelho-de-Souza, F.H., Correa, M.B., Cenci, M.S., Moraes, R.R., et al., 2015. Anterior composite restorations: a systematic review on long-term survival and reasons for failure. *Dent. Mater.* 31, 1214–1224.

- Demko, Z.P., Sharpless, K.B., 2002. A click chemistry approach to tetrazoles by Huisgen 1,3-dipolar cycloaddition: synthesis of 5-acyltetrazoles from azides and acyl cyanides. *Angew. Chem. Int. Ed.* 41, 2113–2116.
- Deviot, M., Lachaise, I., Hogg, C., Durner, J., Reichl, F.X., Attal, J.P., et al., 2018. Bisphenol A release from an orthodontic resin composite: a GC/MS and LC/MS study. *Dent. Mater.* 34, 341–354.
- El-Safty, S., Akhtar, R., Silikas, N., Watts, D.C., 2012. Nanomechanical properties of dental resin-composites. *Dent. Mater.* 28, 1292–1300.
- Eliades, T., Voutsas, D., Sifakakis, I., Makou, M., Katsaros, C., 2011. Release of bisphenol-A from a light-cured adhesive bonded to lingual fixed retainers. *Am. J. Orthod. Dentofacial Orthop.* 139, 192–195.
- Faria, E.S.A.L., Dos Santos, A., Tang, A., Giroto, E.M., Pfeifer, C.S., 2018. Effect of thiourethane filler surface functionalization on stress, conversion and mechanical properties of restorative dental composites. *Dent. Mater.* 34, 1351–1358.
- Feilzer, A.J., De Gee, A.J., Davidson, C.L., 1987. Setting stress in composite resin in relation to configuration of the restoration. *J. Dent. Res.* 66, 1636–1639.
- Feitosa, V.P., Sauro, S., Ogliari, F.A., Ogliari, A.O., Yoshihara, K., Zanchi, C.H., et al., 2014. Impact of hydrophilicity and length of spacer chains on the bonding of functional monomers. *Dent. Mater.* 30, e317–e323.
- Finer, Y., Santerre, J.P., 2004. The influence of resin chemistry on a dental composite's biodegradation. *J. Biomed. Mater. Res. A* 69, 233–246.
- Finer, Y., Santerre, J.P., 2004. Salivary esterase activity and its association with the biodegradation of dental composites. *J. Dent. Res.* 83, 22–26.
- Finer, Y., Santerre, J.P., 2007. Influence of silanated filler content on the biodegradation of bisGMA/TEGDMA dental composite resins. *J. Biomed. Mater. Res. A* 81, 75–84.
- Fong, H., Dickens, S.H., Flaim, G.M., 2005. Evaluation of dental restorative composites containing polyhedral oligomeric silsesquioxane methacrylate. *Dent. Mater.* 21, 520–529.
- Froes-Salgado, N.R., Gajewski, V., Ornaghi, B.P., Pfeifer, C.S., Meier, M.M., Xavier, T.A., et al., 2015. Influence of the base and diluent monomer on network characteristics and mechanical properties of neat resin and composite materials. *Odontology* 103, 160–168.
- Fronza, B.M., Rueggeberg, F.A., Braga, R.R., Mogilevych, B., Soares, L.E., Martin, A.A., et al., 2015. Monomer conversion, microhardness, internal marginal adaptation, and shrinkage stress of bulk-fill resin composites. *Dent. Mater.* 31, 1542–1551.
- Fronza, B.M., Rad, I.Y., Shah, P.K., Barros, M.D., Giannini, M., Stansbury, J.W., 2019. Nanogel-based filler-matrix interphase for polymerization stress reduction. *J. Dent. Res.* 98(7), 779–785. <https://doi.org/10.1177/0022034519845843>.
- Fugolin, A.P., Sundfeld, D., Ferracane, J.L., Pfeifer, C.S., 2019. Toughening of dental composites with thiourethane-modified filler interfaces. *Sci. Rep.* 9, 2286.
- Fugolin, A.P., Dobson, A., Mbiya, W., Navarro, O., Ferracane, J.L., Pfeifer, C.S., 2019. Use of (meth)acrylamides as alternative monomers in dental adhesive systems. *Dent. Mater.* 35, 686–696.
- Gajewski, V.E., Pfeifer, C.S., Froes-Salgado, N.R., Boaro, L.C., Braga, R.R., 2012. Monomers used in resin composites: degree of conversion, mechanical properties and water sorption/solubility. *Braz. Dent. J.* 23, 508–514.
- Ghanbari, H., Cousins, B.G., Seifalian, A.M., 2011. A nanocage for nanomedicine: polyhedral oligomeric silsesquioxane (POSS). *Macromol. Rapid Commun.* 32, 1032–1046.
- Goncalves, F., Pfeifer, C.S., Ferracane, J.L., Braga, R.R., 2008. Contraction stress determinants in dimethacrylate composites. *J. Dent. Res.* 87, 367–371.
- Goncalves, F., Pfeifer, C.S., Meira, J.B., Ballester, R.Y., Lima, R.G., Braga, R.R., 2008. Polymerization stress of resin composites as a function of system compliance. *Dent. Mater.* 24, 645–652.
- Goncalves, F., Kawano, Y., Pfeifer, C., Stansbury, J.W., Braga, R.R., 2009. Influence of BisGMA, TEGDMA, and BisEMA contents on viscosity, conversion, and flexural strength of experimental resins and composites. *Eur. J. Oral Sci.* 117, 442–446.
- Goncalves, F., Pfeifer, C.C., Stansbury, J.W., Newman, S.M., Braga, R.R., 2010. Influence of matrix composition on polymerization stress development of experimental composites. *Dent. Mater.* 26, 697–703.
- Gong, T., Adzima, B.J., Baker, N.H., Bowman, C.N., 2013. Photopolymerization reactions using the photoinitiated copper (I)-catalyzed azide-alkyne cycloaddition (CuAAC) reaction. *Adv. Mater.* 25, 2024–2028.
- Gonzalez-Bonet, A., Kaufman, G., Yang, Y., Wong, C., Jackson, A., Huyang, G., et al., 2015. Preparation of dental resins resistant to enzymatic and hydrolytic degradation in oral environments. *Biomacromolecules* 16, 3381–3388.
- Gotti, V.B., Correr, A.B., Lewis, S.H., Feitosa, V.P., Correr-Sobrinho, L., Stansbury, J.W., 2016. Influence of nanogel additive hydrophilicity on dental adhesive mechanical performance and dentin bonding. *Dent. Mater.* 32, 1406–1413.
- Han, Q., Li, B., Zhou, X., Ge, Y., Wang, S., Li, M., et al., 2017. Anti-Caries Effects of Dental Adhesives Containing Quaternary Ammonium Methacrylates with Different Chain Lengths. *Materials (Basel, Switzerland)* 10.
- Huang, B., Siqueira, W.L., Cvitkovitch, D.G., Finer, Y., 2018. Esterase from a cariogenic bacterium hydrolyzes dental resins. *Acta Biomater.* 71, 330–338.
- Hwang, G., Koltisko, B., Jin, X., Koo, H., 2017. Nonleachable imidazolium-incorporated composite for disruption of bacterial clustering, exopolysaccharide-matrix assembly, and enhanced biofilm removal. *ACS Appl. Mater. Interfaces* 9, 38270–38280.
- Ilie, N., Hickel, R., 2009. Investigations on mechanical behaviour of dental composites. *Clin. Oral Investig.* 13, 427–438.
- Jansen, J.F.G.A., Dias, A.A., Dorsch, M., Coussens, B., 2003. Fast monomers: factors affecting the inherent reactivity of acrylate monomers in photoinitiated acrylate polymerization. *Macromolecules* 36, 3861–3873.
- Kirschbaum, S., Landfester, K., Taden, A., 2015. Unique curing properties through living polymerization in crosslinking materials: polyurethane photopolymers from vinyl ether building blocks. *Angew. Chem.* 54, 5789–5792.
- Kloukos, D., Pandis, N., Eliades, T., 2013. In vivo bisphenol-a release from dental pit and fissure sealants: a systematic review. *J. Dent.* 41, 659–667.
- Kloxin, C.J., Bowman, C.N., 2013. Covalent adaptable networks: smart, reconfigurable and responsive network systems. *Chem. Soc. Rev.* 42, 7161–7173.
- Kruly, P.C., Giannini, M., Pascotto, R.C., Tokubo, L.M., Suga, U.S.G., Marques, A.C.R., et al., 2018. Meta-analysis of the clinical behavior of posterior direct resin restorations: low polymerization shrinkage resin in comparison to methacrylate composite resin. *PLoS One* 13 e0191942.
- Kuhl, N., Abend, M., Geitner, R., Vitz, J., Zechel, S., Schmitt, M., et al., 2018. Urethanes as reversible covalent moieties in self-healing polymers. *Eur. Polym. J.* 104, 45–50.
- Kuper, N.K., Opdam, N.J., Ruben, J.L., de Soet, J.J., Cenci, M.S., Bronkhorst, E.M., et al., 2014. Gap size and wall lesion development next to composite. *J. Dent. Res.* 93, 1085–1135.
- Lane, J.A., Hughey, S.J., Gregory, P.N., Versluis-Tantbirojn, D., Simon, J.F., Harrison, J., et al., 2016. Is your dental adhesive forgiving? How to address challenges. *Compend. Contin. Edu. Dent.* 37, 621–625 quiz 6.

- Lee, H.L., Orlowski, J.A., Kidd, P.D., Glace, R.W., Enabe, E., 1974. Evaluation of wear resistance of dental restorative materials. In: *Advances in Polymer Friction and Wear, Polymer Science and Technology*, 5 B, .
- Lee, H.L., Orlowski, J.A., Kidd, P.D., 1975. Surface roughness of composite filling materials. *Biomater. Med. Devices Artif. Organs* 3, 503–519.
- Lee, H.L., Orlowski, J.A., Rogers, B.J., 1976. A comparison of ultraviolet-curing and self-curing polymers in preventive, restorative and orthodontic dentistry. *Int. Dent. J.* 26, 134–151.
- Lemon, M.T., Jones, M.S., Stansbury, J.W., 2007. Hydrogen bonding interactions in methacrylate monomers and polymers. *J. Biomed. Mater. Res. A* 83, 734–746.
- Li, W., Lee, L.J., 2000. Low temperature cure of unsaturated polyester resins with thermoplastic additives: II. Structure formation and shrinkage control mechanism. *Polymer* 41, 697–710.
- Li, W., Lee, L.J., 2000. Low temperature cure of unsaturated polyester resins with thermoplastic additives I. Dilatometry and morphology study. *Polymer* 41, 685–696.
- Li, Q., Zhou, H., Wicks, D.A., Hoyle, C.E., Magers, D.H., McAlexander, H.R., 2009. Comparison of small molecule and polymeric urethanes, thiourethanes, and dithiourethanes: hydrogen bonding and thermal, physical, and mechanical properties. *Macromolecules* 42, 1824–1833.
- Liu, J., Howard, G.D., Lewis, S.H., Barros, M.D., Stansbury, J.W., 2012. A study of shrinkage stress reduction and mechanical properties of nanogel-modified resin systems. *Eur. Polym. J.* 48, 1819–1828.
- Liu, X., Wang, Z., Zhao, C., Bu, W., Zhang, Y., Na, H., 2018. Synthesis, characterization and evaluation of a fluorinated resin monomer with low water sorption. *J. Mech. Behav. Biomed. Mater.* 77, 446–454.
- Lovell, L.G., Newman, S.M., Bowman, C.N., 1999. The effects of light intensity, temperature, and comonomer composition on the polymerization behavior of dimethacrylate dental resins. *J. Dent. Res.* 78, 1469–1476.
- Lovell, L.G., Berchtold, K.A., Elliott, J.E., Lu, H., Bowman, C.N., 2001. Understanding the kinetics and network formation of dimethacrylate dental resins. *Polym. Adv. Technol.* 12, 335–345.
- Lu, H., Trujillo-Lemon, M., Ge, J., Stansbury, J.W., 2010. Dental resins based on dimer acid dimethacrylates: a route to high conversion with low polymerization shrinkage (Jamesburg, NJ : 1995) *Compend. Contin. Edu. Dent.* 31 Spec No 2, 1–4.
- Lu, H., Stansbury, J.W., Dickens, S.H., Eichmiller, F.C., Bowman, C.N., 2004a. Probing the origins and control of shrinkage stress in dental resin-composites: I. Shrinkage stress characterization technique. *J. Mater. Sci. Mater. Med.* 15, 1097–1103.
- Lu, H., Stansbury, J.W., Dickens, S.H., Eichmiller, F.C., Bowman, C.N., 2004b. Probing the origins and control of shrinkage stress in dental resin composites. II. Novel method of simultaneous measurement of polymerization shrinkage stress and conversion. *J. Biomed. Mater. Res. B Appl. Biomater.* 71, 206–213.
- Lu, H., Stansbury, J.W., Nie, J., Berchtold, K.A., Bowman, C.N., 2005. Development of highly reactive mono-(meth)acrylates as reactive diluents for dimethacrylate-based dental resin systems. *Biomaterials* 26, 1329–1336.
- Luo, S., Zhu, W., Liu, F., He, J., 2016. Preparation of a bis-GMA-free dental resin system with synthesized fluorinated dimethacrylate monomers. *Int. J. Mol. Sci.* 17.
- Magno, M.B., Nascimento, G.C., Rocha, Y.S., Ribeiro, B.D., Loretto, S.C., Maia, L.C., 2016. Silorane-based composite resin restorations are not better than conventional composites – a meta-analysis of clinical studies. *J. Adhesive Dent.* 18, 375–386.
- Mahmoud, S.H., Ali, A.K., Hegazi, H.A., 2014. A three-year prospective randomized study of silorane- and methacrylate-based composite restorative systems in class II restorations. *J. Adhesive Dent.* 16, 285–292.
- Marashdeh, M.Q., Gitalis, R., Levesque, C., Finer, Y., 2018. *Enterococcus faecalis* hydrolyzes dental resin composites and adhesives. *J. Endod.* 44, 609–613.
- Maske, T.T., Kuper, N.K., Hollanders, A.C.C., Bronkhorst, E.M., Cenci, M.S., Huysmans, M., 2018. Secondary caries development and the role of a matrix metalloproteinase inhibitor: a clinical in situ study. *J. Dent.* 71, 49–53.
- Maske, T.T., Hollanders, A.C.C., Kuper, N.K., Bronkhorst, E.M., Cenci, M.S., Huysmans, M., 2019. A threshold gap size for in situ secondary caries lesion development. *J. Dent.* 80, 36–40.
- Matinlinna, J.P., Vallittu, P.K., Lassila, L.V.A., 2011. Effects of different silane coupling agent monomers on flexural strength of an experimental filled resin composite. *J. Adhes. Sci. Technol.* 25, 179–192.
- Mohammad, S.A., Wee, A.G., Rumsey, D.J., Schricker, S.R., 2010. Maxillofacial materials reinforced with various concentrations of polyhedral silsesquioxanes. *J. Dent. Biomech.* 2010, 701845.
- Moraes, R.R., Garcia, J.W., Barros, M.D., Lewis, S.H., Pfeifer, C.S., Liu, J., et al., 2011. Control of polymerization shrinkage and stress in nanogel-modified monomer and composite materials. *Dent. Mater.* 27, 509–519.
- Moraes, R.R., Garcia, J.W., Wilson, N.D., Lewis, S.H., Barros, M.D., Yang, B., et al., 2012. Improved dental adhesive formulations based on reactive nanogel additives. *J. Dent. Res.* 91, 179–184.
- Moszner, N., Fischer, U.K., Angermann, J., Rheinberger, V., 2006. Bis-(acrylamide)s as new cross-linkers for resin-based composite restoratives. *Dent. Mater.* 22, 1157–1162.
- Moszner, N., Fischer, U.K., Ganster, B., Liska, R., Rheinberger, V., 2008. Benzoyl germanium derivatives as novel visible light photoinitiators for dental materials. *Dent. Mater.* 24, 901–907.
- Nakabayashi, N., 1985. Bonding of restorative materials to dentine: the present status in Japan. *Int. Dent. J.* 35, 145–154.
- Nakabayashi, N., Kojima, K., Masuhara, E., 1982. The promotion of adhesion by the infiltration of monomers into tooth substrates. *J. Biomed. Mater. Res.* 16, 265–273.
- Neshchadin, D., Rosspeintner, A., Griesser, M., Lang, B., Mosquera-Vazquez, S., Vauthey, E., et al., 2013. Acylgermanes: photoinitiators and sources for Ge-centered radicals. insights into their reactivity. *J. Am. Chem. Soc.* 135, 17314–17321.
- Odian, G., 2004. *Principles of Polymerization*.
- Park, H.Y., Kloxin, C.J., Scott, T.F., Bowman, C.N., 2010. Covalent adaptable networks as dental restorative resins: stress relaxation by addition-fragmentation chain transfer in allyl sulfide-containing resins. *Dent. Mater.* 26, 1010–1016.
- Patel, M.P., Braden, M., 1989. Cross-linking and ring opening during polymerization of heterocyclic methacrylates and acrylates. *Biomaterials* 10, 277–280.
- Patel, M.P., Braden, M., Davy, K.W., 1987. Polymerization shrinkage of methacrylate esters. *Biomaterials* 8, 53–56.
- Peutzfeldt, A., Asmussen, E., 2004. Determinants of in vitro gap formation of resin composites. *J. Dent.* 32, 109–115.
- Pfeifer, C.S., 2017. *Dental composites? Chemistry and composition*. World Scientific. *Dental Biomater.* 295–333.
- Pfeifer, C.S., Ferracane, J.L., Sakaguchi, R.L., Braga, R.R., 2008. Factors affecting photopolymerization stress in dental composites. *J. Dent. Res.* 87, 1043–1047.
- Pfeifer, C.S., Wilson, N.D., Shelton, Z.R., Stansbury, J.W., 2011. Delayed gelation through chain-transfer reactions: mechanism for stress reduction in methacrylate networks. *Polymer* 52, 3295–3303.
- Pfeifer, C.S., Shelton, Z.R., Szczpanski, C.R., Barros, M.D., Wilson, N.D., Stansbury, J.W., 2014. Tailoring heterogeneous polymer networks through polymerization-induced phase separation: influence of composition and processing conditions on reaction kinetics and optical properties. *J. Polym. Sci. A Polym. Chem.* 52, 1796–1806.

- Podgórski, M., Chatani, S., Bowman, C.N., 2014. Development of glassy step-growth thiol-vinyl sulfone polymer networks. *Macromol. Rapid Commun.* 35, 1497–1502.
- Podgórski, M., Becka, E., Chatani, S., Claudino, M., Bowman, C.N., 2015. Ester-free thiol-X resins: new materials with enhanced mechanical behavior and solvent resistance. *Polym. Chem.* 6, 2234–2240.
- Prakki, A., Tallury, P., Mondelli, R.F., Kalachandra, S., 2007. Influence of additives on the properties of Bis-GMA/Bis-GMA analog comonomers and corresponding copolymers. *Dent. Mater.* 23, 1199–1204.
- Prakki, A., Pereira, P.N., Kalachandra, S., 2009. Effect of propionaldehyde or 2,3-butanedione additives on the mechanical properties of Bis-GMA analog-based composites. *Dent. Mater.* 25, 26–32.
- Rodrigues, S.B., Petzhold, C.L., Gamba, D., Leitune, V.C.B., Colares, F.M., 2018. Acrylamides and methacrylamides as alternative monomers for dental adhesives. *Dent. Mater.* 34, 1634–1644.
- Rodriguez, H.A., Kriven, W.M., Casanova, H., 2019. Development of mechanical properties in dental resin composite: effect of filler size and filler aggregation state. *Mat. Sci. Eng. C* 101, 274–282.
- Sahinturk, V., Kacar, S., Vejselova, D., Kutlu, H.M., 2018. Acrylamide exerts its cytotoxicity in NIH/3T3 fibroblast cells by apoptosis. *Toxicol. Ind. Health* 34, 481–489.
- Salz, U., Bock, T., 2010. Adhesion performance of new hydrolytically stable one-component self-etching enamel/dentin adhesives. *J. Adhesive Dent.* 12, 7–10.
- Salz, U., Mucke, A., Zimmermann, J., Tay, F.R., Pashley, D.H., 2006. pKa value and buffering capacity of acidic monomers commonly used in self-etching primers. *J. Adhesive Dent.* 8, 143–150.
- Schmidt, M., Dige, I., Kirkevang, L.L., Vaeth, M., Horsted-Bindslev, P., 2015. Five-year evaluation of a low-shrinkage Silorane resin composite material: a randomized clinical trial. *Clin. Oral Investig.* 19, 245–251.
- Schreck, K.M., Leung, D., Bowman, C.N., 2011. Hybrid organic/inorganic thiol-ene-based photopolymerized networks. *Macromolecules* 44, 7520–7529.
- Shin, J., Nazarenko, S., Hoyle, C.E., 2009. Effects of chemical modification of thiol-ene networks on enthalpy relaxation. *Macromolecules* 42, 6549–6557.
- Sideridou, I.D., Karabela, M.M., 2009. Effect of the amount of 3-methacryloxypropyltrimethoxysilane coupling agent on physical properties of dental resin nanocomposites. *Dent. Mater.* 25, 1315–1324.
- Song, H.B., Sowan, N., Shah, P.K., Baranek, A., Flores, A., Stansbury, J.W., et al., 2016. Reduced shrinkage stress via photo-initiated copper(I)-catalyzed cycloaddition polymerizations of azide-alkyne resins. *Dent. Mater.* 32, 1332–1342.
- Song, H.B., Wang, X., Patton, J.R., Stansbury, J.W., Bowman, C.N., 2017. Kinetics and mechanics of photo-polymerized triazole-containing thermosetting composites via the copper(I)-catalyzed azide-alkyne cycloaddition. *Dent. Mater.* 33, 621–629.
- Stansbury, J.W., 1990. Cyclopolymerizable monomers for use in dental resin composites. *J. Dent. Res.* 69, 844–848.
- Stansbury, J.W., 1992. Synthesis and evaluation of new oxaspiro monomers for double ring-opening polymerization. *J. Dent. Res.* 71, 1408–1412.
- Stansbury, J.W., Antonucci, J.M., 1999. Dimethacrylate monomers with varied fluorine contents and distributions. *Dent. Mater.* 15, 166–173.
- Stewart, C.A., Finer, Y., 2019. Biostable, antidegradative and antimicrobial restorative systems based on host-biomaterials and microbial interactions. *Dent. Mater.* 35, 36–52.
- Szczepanski, C.R., Pfeifer, C.S., Stansbury, J.W., 2012. A new approach to network heterogeneity: polymerization induced phase separation in photo-initiated, free-radical methacrylic systems. *Polymer* 53, 4694–4701.
- Tauscher, S., Angermann, J., Catel, Y., Moszner, N., 2017. Evaluation of alternative monomers to HEMA for dental applications. *Dent. Mater.* 33, 857–865.
- Tay, F.R., Pashley, D.H., 2003. Water treeing – a potential mechanism for degradation of dentin adhesives. *Am. J. Dent.* 16, 6–12.
- Tay, F.R., Pashley, D.H., Peters, M.C., 2003. Adhesive permeability affects composite coupling to dentin treated with a self-etch adhesive. *Oper. Dent.* 28, 610–621.
- Tay, F.R., Lai, C.N., Chersoni, S., Pashley, D.H., Mak, Y.F., Suppa, P., et al., 2004. Osmotic blistering in enamel bonded with one-step self-etch adhesives. *J. Dent. Res.* 83, 290–295.
- Trujillo-Lemon, M., Ge, J., Lu, H., Tanaka, J., Stansbury, J.W., 2006. Dimethacrylate derivatives of dimer acid. *J. Polym. Sci. A Polym. Chem.* 44, 3921–3929.
- van de Sande, F.H., Opdam, N.J., Rodolpho, P.A., Correa, M.B., Demarco, F.F., Cenci, M.S., 2013. Patient risk factors' influence on survival of posterior composites. *J. Dent. Res.* 92, 785–835.
- Vitale, A., Sangermano, M., Bongiovanni, R., Burtscher, P., Moszner, N., 2014. Visible light curable restorative composites for dental applications based on epoxy monomer. *Materials* 7, 554–562.
- Wang, S., Wang, H., Ren, B., Li, X., Wang, L., Zhou, H., et al., 2018. Drug resistance of oral bacteria to new antibacterial dental monomer dimethylaminohexadecyl methacrylate. *Sci. Rep.* 8, 5509.
- Wang, X., Huyang, G., Palagummi, S.V., Liu, X., Skrtic, D., Beauchamp, C., et al., 2018. High performance dental resin composites with hydrolytically stable monomers. *Dent. Mater.* 34, 228–237.
- Yang, H., Yu, K., Mu, X., Shi, X., Wei, Y., Guo, Y., et al., 2015. A molecular dynamics study of bond exchange reactions in covalent adaptable networks. *Soft Matter* 11, 6305–6317.
- Ye, S., Cramer, N.B., Smith, I.R., Voigt, K.R., Bowman, C.N., 2011. Reaction kinetics and reduced shrinkage stress of thiol-yne-methacrylate and thiol-yne-acrylate ternary systems. *Macromolecules* 44, 9084–9090.
- Ye, S., Azarnoush, S., Smith, I.R., Cramer, N.B., Stansbury, J.W., Bowman, C.N., 2012. Using hyperbranched oligomer functionalized glass fillers to reduce shrinkage stress. *Dent. Mater.* 28, 1004–1011.
- Yoo, S.H., Kim, C.K., 2010. Synthesis of a novel spiro orthocarbonate containing bisphenol-a unit and its application to the dental composites. *Macromol. Res.* 18, 1013–1020.
- Yoshihara, K., Yoshida, Y., Nagaoka, N., Hayakawa, S., Okihara, T., De Munck, J., et al., 2013. Adhesive interfacial interaction affected by different carbon-chain monomers. *Dent. Mater.* 29, 888–897.
- Zajdowicz, S., Song, H.B., Baranek, A., Bowman, C.N., 2018. Evaluation of biofilm formation on novel copper-catalyzed azide-alkyne cycloaddition (CuAAC)-based resins for dental restoratives. *Dent. Mater.* 34, 657–666.
- Zero, D.T., 2013. How the introduction of the acid-etch technique revolutionized dental practice. *JADA (J. Am. Dent. Assoc.)* 144, 475–515.
- Zhang, N., Ma, J., Melo, M.A., Weir, M.D., Bai, Y., Xu, H.H., 2015. Protein-repellent and antibacterial dental composite to inhibit biofilms and caries. *J. Dent.* 43, 225–234.
- Zhang, K., Cheng, L., Weir, M.D., Bai, Y.X., Xu, H.H., 2016. Effects of quaternary ammonium chain length on the antibacterial and remineralizing effects of a calcium phosphate nanocomposite. *Int. J. Oral Sci.* 8, 45–53.
- Zheng, N., Fang, Z., Zou, W., Zhao, Q., Xie, T., 2016. Thermoset shape-memory polyurethane with intrinsic plasticity enabled by transcarbamoylation. *Angew. Chem. Int. Ed.* 55, 11421–11425.
- Zhou, Y., Wang, S., Zhou, X., Zou, Y., Li, M., Peng, X., et al., 2019. Short-time antibacterial effects of dimethylaminododecyl methacrylate on oral multispecies biofilm in vitro. *BioMed. Res. Int.* 2019 6393470.

Chapter Exercises

1. Identify the major milestones in the evolution of dental composite restorative materials and predict what future modifications may be forthcoming to produce more ideal formulations.
2. Describe the chemistry involved in the initiation and propagation of the polymerization of dimethacrylate monomers and explain the importance of maximizing the extent of the curing reaction.
3. Describe the origin of polymerization stress in dental composite restorations, and explain what chemical modifications to current formulations have been attempted to mitigate it.
4. Identify the chemical difference between the monomers used in self-adhesive and etch-and-rinse dental adhesive formulations, and explain the mechanism of adhesion of each to dentin and enamel tissues.
5. Explain what clinical benefit may be derived from the incorporation of an antimicrobial monomer in a dental resin, and discuss how such monomers demonstrate their activity.
6. Discuss how the monomers used in dental composite and adhesive formulations can be chemically and physically degraded within the oral cavity, and identify potential changes in formulation that can protect the polymerized resin and make it more degradation resistant.
7. Explain chemical approaches to enhance the toughness of dental resins used for composite restorations, as well as the need for improved toughness.

1.3.2E

Hydrogels

NICHOLAS A. PEPPAS¹, ALLAN S. HOFFMAN²

¹Department of Chemical Engineering and Biomedical Engineering, Pediatrics, Surgery and Molecular Pharmaceutics and Drug Delivery, The University of Texas, Austin, TX, United States

²Bioengineering and Chemical Engineering, University of Washington, Seattle, WA, United States

Introduction

Hydrogels have received significant attention because of their high-water contents and related potential for many biomedical applications. Hydrogels are polymeric structures held together as water-swollen gels by: (1) primary covalent cross-links; (2) ionic forces; (3) hydrogen bonds; (4) affinity or “bio-recognition” interactions; (5) hydrophobic interactions; (6) polymer crystallites; (7) physical entanglements of individual polymer chains; or (8) a combination of two or more of the above interactions.

Early work on hydrogels was initiated in the mid 1930s, mostly in Germany, with studies on kinetics of cross-linked polymers. In the 1940s, the research of 1094 Nobel laureate Paul Flory led to a detailed, fundamental understanding of the hydrogels’ cross-linked structure, their swelling/syneresis characteristics and the small and large deformation behavior in pure water and physiological fluids. The pioneering book by Andrade (1976) offered some of the early work that was available prior to 1975. Since then, numerous reviews and several books have addressed the preparation, structure, characterization, and applications of hydrogels (e.g., Peppas, 1987, 2001; Brannon-Peppas and Harland, 1990; Lee and Mooney, 2001; Qiu and Park, 2001; Hennink and van Nostrum, 2002; Jeong et al., 2002; Miyata et al., 2002; Drury and Mooney, 2003; Patterson et al., 2010).

Here, we focus on the preparation and characterization of the structure, and chemical and physical properties of *synthetic* hydrogels. Many natural polymers such as collagen, gelatin, fibrin, hyaluronic acid, heparin, alginates, pectins, chitosan, and others can be used to form hydrogels, and some of these gels have been used in biomedical applications. Details on these types of materials can be found throughout this textbook in other chapters.

Classification and Basic Structures of Hydrogels

Depending on their method of preparation, ionic charge, or physical structure features, hydrogels may be classified in several categories. Based on the method of preparation, they may be: (1) *homopolymer hydrogels*; (2) *copolymer hydrogels*; (3) *multipolymer hydrogels*; and (4) *interpenetrating network (IPN) hydrogels*. *Homopolymer hydrogels* are cross-linked networks of one type of hydrophilic monomer unit, whereas *copolymer hydrogels* are produced by cross-linking of chains composed of two comonomer units, at least one of which must be hydrophilic to render them water-swallowable. *Multipolymer hydrogels* are produced from three or more comonomers reacting together (e.g., Lowman and Peppas, 1997, 1999). Finally, *interpenetrating network (IPN) hydrogels* are produced by two methods, one within a preformed network and the other in solution; the most common method is to polymerize one monomer within a different cross-linked hydrogel network. The monomer polymerizes to form a polymer or a second cross-linked network that is intermeshed with the first network.

There are several other ways that hydrogels may be classified. *Ionic hydrogels*, with ionic charges on the backbone polymers, may be classified as: (1) *neutral hydrogels* (uncharged); (2) *anionic hydrogels* (having negative charges only); (3) *cationic hydrogels* (having positive charges only); or (4) *ampholytic hydrogels* (having both positive and negative charges). These last gels may end up with a net negative, positive, or neutral charge.

Based on physicochemical structural features of the network, hydrogels may also be classified as: (1) *amorphous hydrogels* (having covalent cross-links); or (2) *semicrystalline hydrogels* (may or may not have covalent cross-links). In amorphous hydrogels, the macromolecular chains are arranged randomly.

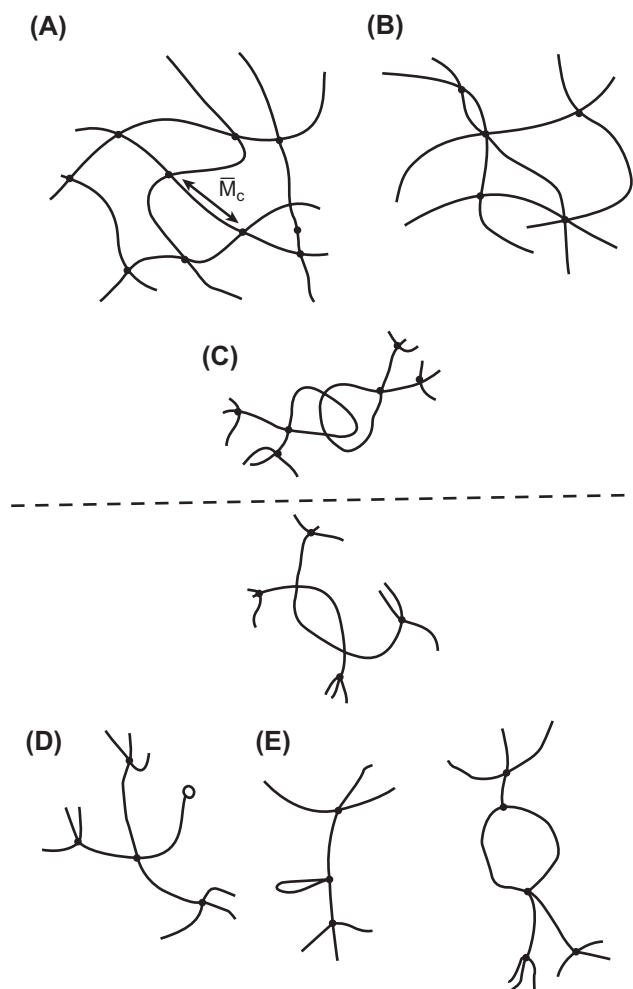
Semicrystalline hydrogels are characterized by self-assembled regions of ordered macromolecular chains (crystallites).

Another type of classification of hydrogels includes the “complexation” hydrogels, which are held together by specific types of secondary forces. These include hydrogen bonds, hydrophobic group associations, and affinity “complexes” [e.g., (1) heterodimers (peptide/peptide interactions called “coil-coil”); (2) biotin/streptavidin; (3) antibody/antigen; (4) conA/glucose; (5) poly(D-lactic acid)/poly(L-lactic acid) (PDLA/PLLA) stereocomplexes; and (6) cyclodextrin (CD) inclusion complexes]. The physical properties of the gels held together by such secondary associations are critically dependent on the network density of these interactions, as well as on the many environmental conditions that can affect them. Hydrogels may also be classified as stable or degradable, with the latter further categorized as hydrolytically or enzymatically degradable.

Structural evaluation of hydrogels reveals that ideal networks are only rarely observed. Fig. 1.3.2E.1A shows an ideal macromolecular network (hydrogel) indicating tetrafunctional cross-links (junctions) produced by covalent bonds. However, in real networks it is possible to encounter

multifunctional junctions (Fig. 1.3.2E.1B) or physical molecular entanglements (Fig. 1.3.2E.1C) playing the role of semipermanent junctions. Hydrogels with molecular defects are always possible. Fig. 1.3.2E.1D and E indicate two such effects: unreacted functionalities with partial entanglements (Fig. 1.3.2E.1D) and chain loops (Fig. 1.3.2E.1E).

The terms “cross-link,” “junction,” or “tie-point” (shown by an open circle symbol in Fig. 1.3.2E.1D) indicate the covalent or secondary connection points of several chains. In the case of covalent linkages, these junctions may be carbon atoms, but they are usually small chemical bridges [e.g., an acetal bridge in cross-linked poly(vinyl alcohol), or an ethylene glycol diester bridge in the polyHEMA contact lens gel] with molecular weights much smaller than those of the cross-linked polymer chains. In other situations, a junction may be crystallites or other secondary interactions, such as described above, of a permanent or semipermanent nature. Thus, in reality, the junctions should never be considered as points without volume, which is the usual assumption made when developing theoretical models for prediction of the properties of cross-linked hydrogels (Flory, 1953). Instead, they have a finite size and contribute to the physical properties during biomedical applications.

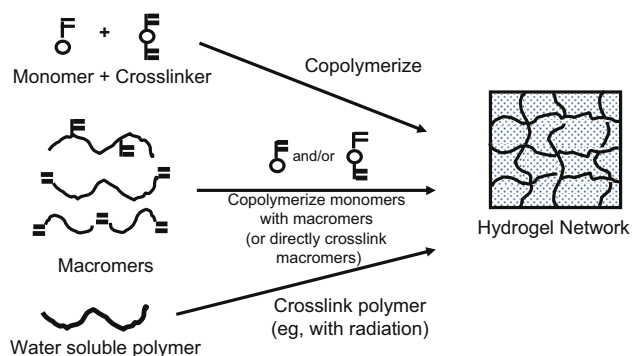


• **Figure 1.3.2E.1** (A) Ideal macromolecular network of a hydrogel; (B) network with multifunctional junctions; (C) physical entanglements in a hydrogel; (D) unreacted functionality in a hydrogel; (E) chain loops in a hydrogel.

Synthesis of Hydrogels

Covalently cross-linked hydrogels are usually prepared by bringing together small multifunctional molecules such as monomers and oligomers, and reacting to form a network structure. Sometimes large polymer molecules may be cross-linked with the same small multifunctional molecules. Such cross-linking may be achieved by reaction of two chemical groups on two different molecules, which can be initiated by catalysts, by photo-polymerization, or by radiation cross-linking (see reviews by Peppas et al., 2000; Hoffman, 2002; Ottenbrite et al., 2010; Jin and Dijkstra, 2010).

Several methods for forming cross-linked hydrogels are based on free radical reactions. The first involves a copolymerization-cross-linking reaction between one or more monomers and one multifunctional monomer that are present in relatively small quantities. In a related method, two water-soluble polymers may be cross-linked together by formation of free radicals on both polymer molecules, which combine to form the cross-link (Fig. 1.3.2E.2). These



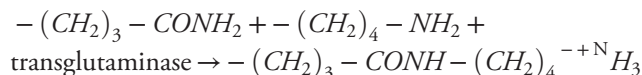
• **Figure 1.3.2E.2** Synthesis of hydrogels by free radical polymerization reactions and cross-linking reactions (Hoffman, 2002).

reactions are free radical polymerization or cross-linking reactions, and such processes for synthesis of cross-linked hydrogels can be initiated by decomposition of peroxides or azo compounds, or by using ionizing radiation or UV light. Ionizing radiation methods utilize electron beams, gamma rays, or X-rays to excite a polymer and produce a cross-linked structure via free radical reactions (e.g., [Chapiro, 1962](#)). Such free radical reactions can lead to rapid formation of a three-dimensional network, and are usually carried out in the absence of oxygen or air (note: some polymers are degraded by radiation, especially in air).

In another method, chemical cross-linking calls for direct reaction of a linear or branched polymer with a difunctional or multifunctional, low-molecular-weight, cross-linking agent. This agent usually links two higher-molecular-weight chains through its di- or multifunctional groups ([Fig. 1.3.2E.3A](#)). There are a number of well-known reactions that can be used for linking hydrophilic polymers together with each other or with cross-linkers to form hydrogels, including some recent methods with growing popularity, such as the Michael addition of dithiol compounds with divinyl compounds (e.g., see [Schoenmakers et al., 2004](#); [van de Wetering et al., 2005](#)) and the reaction of alkynes plus azides to form triazoles (click reaction; see [Kolb et al., 2001](#)). The reader is referred to the excellent, comprehensive book detailing such chemistries, *Bioconjugate Techniques* ([Hermanson, 2008](#)).

A similar method involves the reaction of a small bifunctional molecule and linear polymeric chains having pendant or terminal reactive groups such as $-\text{OH}$, $-\text{NH}_2$, NCO , or $-\text{COOH}$ that are cross-linked by the bifunctional molecule ([Fig. 1.3.2E.3B](#)). Natural polymers such as proteins can also be cross-linked in a similar way using enzymes. For example,

transglutaminase catalyzes the reaction of protein glutamine amide groups with lysine amino groups (or with pendant or terminal amine groups on a synthetic polymer backbone) ([Sperinde and Griffith, 1997, 2000](#)). This reaction is:

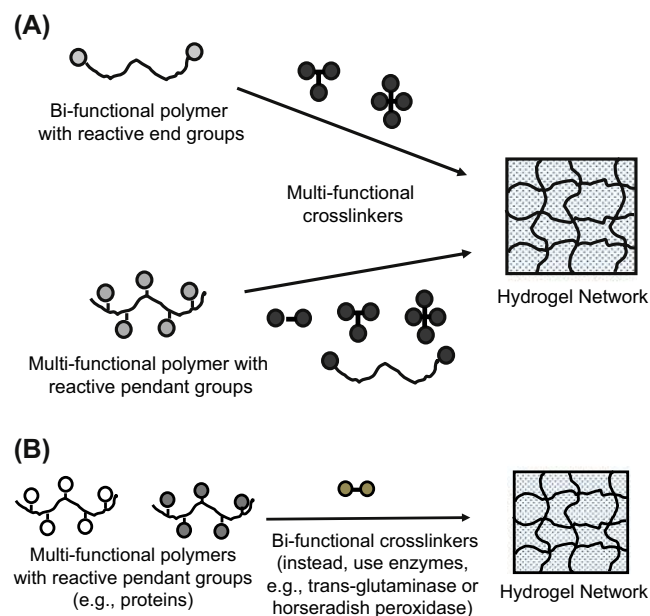


In another enzyme-catalyzed cross-linking reaction, hydroxyphenylpropionic acid (tyramine) was conjugated to gelatin and cross-linked to form a hydrogel by the horseradish peroxidase (HRP)-catalyzed oxidation reaction with hydrogen peroxide (H_2O_2) ([Wang et al., 2010](#); [Jin and Dijkstra, 2010](#)).

The formation of hydrogel networks may also result from physicochemical interactions, and some examples are highlighted below.

Poly(ethylene glycol) (PEG) molecules or block polymers containing PEG can “thread” through cyclodextrins (CDs), and sequences of CDs threaded on different PEG molecules can then self-associate, helping to hold together the hydrogel that is formed ([Harada et al., 1992](#); [Li et al., 2001, 2003a,b, 2006](#)). Heterodimer peptide sequences that are conjugated as pendant groups on different polymer chains can complex together in “coil-coil” associations, and thereby “tie” chains together to form hydrogels ([Yang et al., 2006](#); [Xu and Kopecek, 2008](#)). Stereocomplexes can form between D and L forms of poly(lactic acid) (known as PDLA/PLLA stereocomplexes); this complexation can lead to hydrogel formation if block copolymers that contain both PDLA and PLLA blocks, along with hydrophilic blocks as PEG, are mixed together ([Jin and Dijkstra, 2010](#)).

[Fig. 1.3.2E.4](#) shows the formation of interpenetrating network (IPN) hydrogels. [Fig. 1.3.2E.5](#) shows how hydrogels can be formed by ionic interactions. [Fig. 1.3.2E.6A and B](#) show how hydrogels can be formed by affinity recognition reactions (see also [Miyata, 2010](#), for more on the formation of affinity recognition hydrogels).

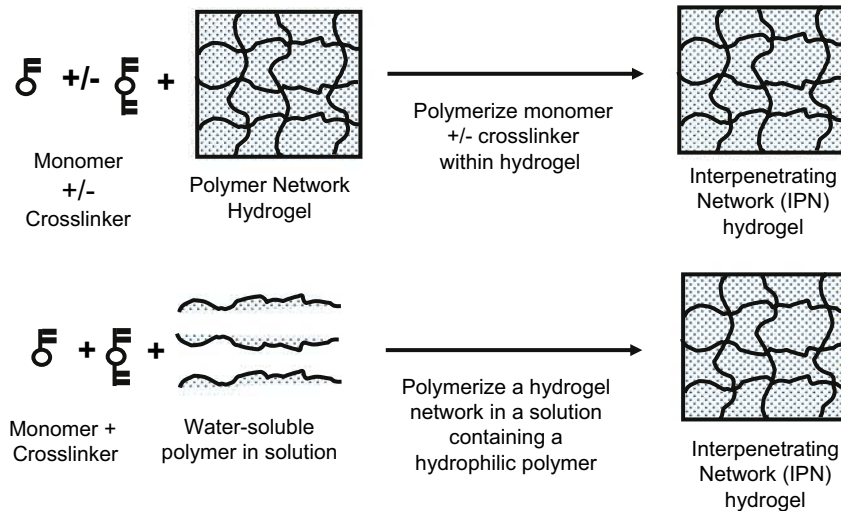


• **Figure 1.3.2E.3** (A) Synthesis of hydrogels by cross-linking reactive polymers with multifunctional cross-linkers ([Hoffman, 2002](#)). (B) Synthesis of hydrogels by cross-linking of multifunctional polymers with small bifunctional molecules ([Hoffman, 2002](#)).

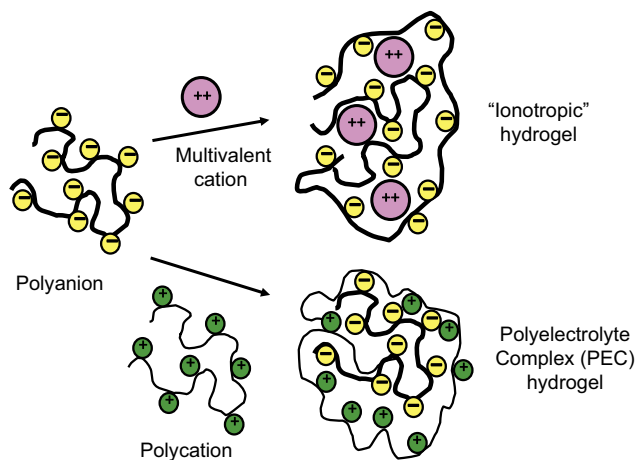
Swelling Behavior of Hydrogels

The physical behavior of biomedical hydrogels is dependent on their dynamic swelling and equilibrium in water and in aqueous solutions. Much of the water within swollen hydrogels may be bound to the polymer chains by either polar or hydrophobic interactions (e.g., [Ilavsky, 1982](#)). Many solutes can diffuse into and through hydrogels only within unbound or “free” water channels. Solutes that are chaotropic may diffuse into and through hydrogels by destructuring such bound water layers around the polymer chains.

The Flory–Huggins theory is an ideal thermodynamic description of polymer solutions, and it does not consider network imperfections or the real, finite volumes of network chains and cross-links, and in the case of aqueous solutions it does not consider the presence of “bound” (vs. “free”) water around the network chains. It can be used to calculate thermodynamic quantities related to that mixing process.



• **Figure 1.3.2E.4** Two methods for formation of an interpenetrating network (IPN) hydrogel (Hoffman, 2002).



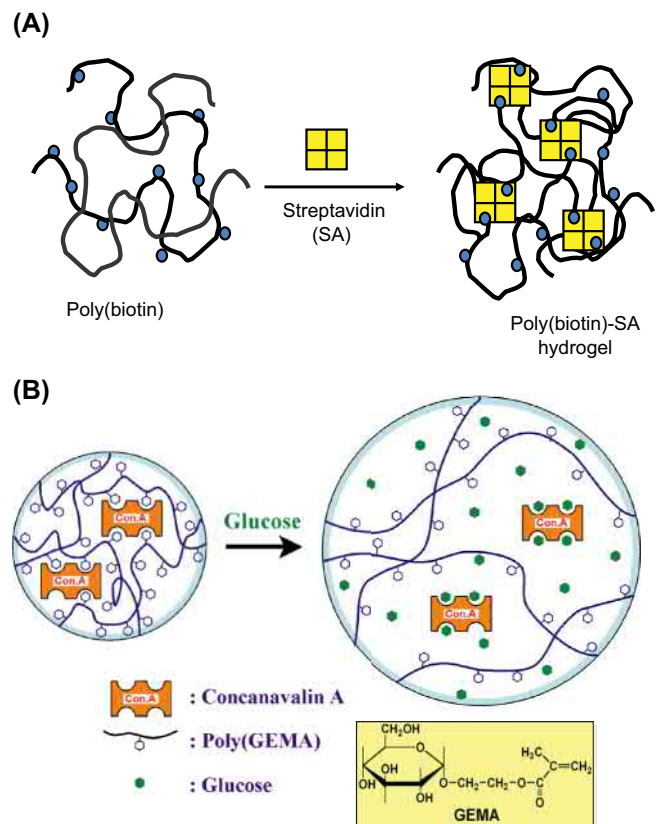
• **Figure 1.3.2E.5** Formation of ionic hydrogels (Hoffman, 2002).

Flory (1953) developed the initial theory of the swelling of cross-linked polymer gels using a Gaussian distribution of the polymer chains. His model describing the equilibrium degree of cross-linked polymers postulated that the degree to which a polymer network swelled was governed by the elastic retractive forces of the polymer chains and the thermodynamic compatibility of the polymer and the solvent molecules. In terms of the free energy of the system, the total free energy change upon swelling was written as:

$$\Delta G = \Delta G_{\text{elastic}} + \Delta G_{\text{mix}} \quad (1.3.2E.1)$$

Here, $\Delta G_{\text{elastic}}$ is the contribution due to the elastic retractive forces and ΔG_{mix} represents the thermodynamic compatibility of the polymer and the swelling agent (water).

Upon differentiation of Eq. (1.3.2E.1) with respect to the water molecules in the system, an expression can be derived for the chemical potential change of water in terms of the elastic and mixing contributions due to swelling.



• **Figure 1.3.2E.6** (A) Formation of an affinity hydrogel between polybiotin and streptavidin (Morris et al., 1993). (B) Glucose-responsive hydrogel swells when free glucose competes with polymeric glucose groups in a ConA-cross-linked GEMA hydrogel (Miyata et al., 1996).

$$\mu_1 - \mu_{1,0} = \Delta \mu_{\text{elastic}} + \Delta \mu_{\text{mix}} \quad (1.3.2E.2)$$

Here, μ_1 is the chemical potential of water within the gel and $\mu_{1,0}$ is the chemical potential of pure water.

At equilibrium, the chemical potentials of water inside and outside of the gel must be equal. Therefore, the elastic

and mixing contributions to the chemical potential will balance one another at equilibrium. The chemical potential change upon mixing can be determined from the heat of mixing and the entropy of mixing. Using the Flory–Huggins theory, the chemical potential of mixing can be expressed as:

$$\Delta \mu_{mix} = RT (\ln (1 - v_{2,s}) + v_{2,s} + \chi_1 v_{2,s}^2) \quad (1.3.2E.3)$$

where χ_1 is the polymer–water interaction parameter, $v_{2,s}$ is the polymer volume fraction of the gel, T is absolute temperature, and R is the gas constant.

This thermodynamic swelling contribution is counterbalanced by the retractive elastic contribution of the cross-linked structure. The latter is usually described by the rubber elasticity theory and its variations (Peppas, 1987). Equilibrium is attained in a particular solvent at a particular temperature when the two forces become equal. The volume degree of swelling, Q (i.e., the ratio of the actual volume of a sample in the swollen state divided by its volume in the dry state) can then be determined from Eq. (1.3.2E.4).

$$\Delta \mu_{mix} = RT (\ln (1 - v_{2,s}) + v_{2,s} + \chi_1 v_{2,s}^2) \quad (1.3.2E.4)$$

Researchers working with hydrogels for biomedical applications prefer to use other parameters in order to define the equilibrium-swelling behavior. For example, Yasuda et al. (1969) introduced the use of the so-called hydration ratio, H , which has been accepted by those researchers who use hydrogels for contact lens applications (Peppas and Yang, 1981). Another definition is that of the weight degree of swelling, q , which is the ratio of the weight of the swollen sample over that of the dry sample.

In general, highly water-swollen hydrogels include those of cellulose derivatives, poly(vinyl alcohol), poly(N-vinyl 2-pyrrolidone) (PNVP), and poly(ethylene glycol), among others. Moderately and poorly swollen hydrogels are those of poly(hydroxyethyl methacrylate) (PHEMA) and many of its copolymers. In general, a basic hydrophilic monomer can be copolymerized with other more or less hydrophilic monomers to achieve desired swelling properties. Such processes have led to a wide range of swellable hydrogels, as Gregonis et al. (1976), Peppas (1987, 1997), and others have noted. Park and co-workers have developed a family of high water content, rapid swelling hydrogels (Omidian and Park, 2010), and superabsorbent hydrogels (Mun et al., 2010). Knowledge of the swelling characteristics of a polymer is of utmost importance in biomedical and pharmaceutical applications since the equilibrium degree of swelling influences: (1) the solute diffusion coefficient through these hydrogels; (2) the surface properties and surface molecule mobility; (3) the optical properties, especially in relation to contact lens applications; and (4) the mechanical properties.

Determination of Structural Characteristics

The parameter that describes the basic structure of the hydrogel is the molecular weight between cross-links, \dot{M}_c (as shown in Fig. 1.3.2E.1A). This parameter defines the average molecular size between two consecutive junctions regardless of the nature of those junctions and can be calculated by Eq. (1.3.2E.5).

$$\frac{1}{\dot{M}_c} = \frac{2}{\dot{M}_n} - \frac{(v/V_1) [\ln (1 - v_{2,s}) + v_{2,s} + \chi_1 v_{2,s}^2]}{\left(v_{2,s}^{1/3} - \frac{v_{2,s}}{2}\right)} \quad (1.3.2E.5)$$

An additional parameter of importance in structural analysis of hydrogels is the cross-linking density, ρ_x , which is defined by Eq. (1.3.2E.6).

$$\rho_x = \frac{1}{\dot{v}\dot{M}_c} \quad (1.3.2E.6)$$

In these equations, v is the specific volume of the polymer (i.e., the reciprocal of the amorphous density of the polymer), and \dot{M}_n is the initial molecular weight of the uncross-linked polymer.

Biomedical Hydrogels

Acrylic Hydrogels

Hydrogels with desired physical or chemical properties for a specific biomedical application may be “molecularly engineered” by choosing among the many types of acrylic monomers and cross-linkers available. This has led to many publications, describing a large family of acrylic hydrogels (e.g., Peppas et al., 2000; Peppas, 2001; Ottenbrite et al., 2010).

The most widely used hydrogel is water-swollen, cross-linked PHEMA, which was introduced as a biological material by Wichterle and Lim (1960). The hydrogel is inert to normal biological processes, shows resistance to degradation, is permeable to metabolites, is not absorbed by the body, is biocompatible, withstands heat sterilization without damage, and can be prepared in a variety of shapes and forms. The swelling, mechanical, diffusional, and biomedical characteristics of PHEMA gels have been studied extensively. The properties of these hydrogels are dependent upon their method of preparation, polymer volume fraction, degree of cross-linking, temperature, and swelling agent (Michalek et al., 2010).

Other acrylic hydrogels of biomedical interest include polyacrylamides and their derivatives. Tanaka (1979) has carried out extensive studies on the abrupt swelling and deswelling of partially hydrolyzed acrylamide gels with changes in swelling agent composition, curing time, degree of cross-linking, degree of hydrolysis, and temperature.

These studies have shown that the ionic groups produced in an acrylamide gel upon hydrolysis give the gel a structure that shows a discrete transition in equilibrium-swollen volume with environmental changes.

Discontinuous swelling in partially hydrolyzed polyacrylamide gels has been studied by Gehrke et al. (1986). Copolymers of HEMA and acrylamides with methacrylic acid (MAA) and methyl methacrylate (MMA) have proven useful as hydrogels in biomedical applications (see below).

Small amounts of MAA as a comonomer have been shown to dramatically increase the swelling of PHEMA polymers. Owing to the hydrophobic nature of MMA, copolymers of MMA and HEMA have a lower degree of swelling than pure PHEMA (Brannon-Peppas and Peppas, 1991a). One particularly interesting IPN is the double network (DN) hydrogel of Gong and Murosaki (Murosaki and Gong, 2010). These DN hydrogels are composed of two interpenetrating cross-linked networks of PAAm and PAMPS, and exhibit the unusual combination of exceptionally strong mechanical properties and high water contents. All of these materials have potential uses in advanced technology applications, including biomedical separations, drug-delivery devices, and as scaffolds for tissue engineering (Neves et al., 2017).

Poly(Vinyl Alcohol) (PVA) Hydrogels

Another hydrophilic polymer that has received much attention is poly(vinyl alcohol). This material holds great promise as a biological drug-delivery matrix because it is nontoxic. Two methods exist for the preparation of PVA gels. In the first method, linear PVA chains are cross-linked using glyoxal, glutaraldehyde, or borate. In the second method, semicrystalline gels are prepared by exposing aqueous solutions of PVA to repeated freezing and thawing (Peppas and Hassan, 2000). The freezing and thawing induces crystal formation in the materials and allows for the formation of a network structure cross-linked with the quasipermanent crystallites. The latter method is the preferred method for preparation as it allows for the formation of a “pure” network without the need to add cross-linking agents. Ficek and Peppas (1993) used PVA gels for the release of bovine serum albumin using novel PVA microparticles.

Poly(Ethylene Glycol) (PEG) Hydrogels

Hydrogels of poly(ethylene oxide) (PEO) and poly(ethylene glycol) (PEG) have received increasing attention recently for biomedical applications because of the nontoxic behavior of PEG, and its wide use in PEGylation of nanoscale drug carriers (e.g., Graham, 1992; Harris, 1992; Griffith and Lopina, 1995; Kofinas et al., 1996; Lee and He, 2010; Oishi and Nagasaki, 2010).

Three major techniques exist for the preparation of PEG networks: (1) chemical cross-linking between PEG chains, such as reaction of difunctional PEGs and multifunctional cross-linking agents; (2) radiation cross-linking

of PEG chains to each other; and (3) physical interactions of hydrophobic blocks of triblock copolymers containing both hydrophobic blocks and PEG blocks (e.g., see Jeong et al., 2002, and Lee and He, 2010 for detailed discussion of pioneering work by S.W. Kim and co-workers on such block copolymer hydrogels. See also discussions of PEG hydrogels in the sections on Degradable Hydrogels and Temperature-Sensitive Hydrogels in this chapter).

The advantage of using radiation-cross-linked PEG networks is that no toxic cross-linking agents are required. However, it is difficult to control the network structure of these materials. Stringer and Peppas (1996) prepared PEG hydrogels by radiation cross-linking. In this work, they analyzed the network structure in detail. Additionally, they investigated the diffusional behavior of lower-molecular-weight drugs, such as theophylline, in these gels. Kofinas et al. (1996) have prepared PEG hydrogels by a similar technique. In this work, they studied the diffusional behavior of various macromolecules in these gels. They noted an interesting, yet previously unreported, dependence between the cross-link density and protein diffusion coefficient, and the initial molecular weight of the linear PEGs.

Lowman et al. (1997) described a method for the preparation of PEG gels with controllable structures. In this work, highly cross-linked and tethered PEG gels were prepared from PEG-dimethacrylates and PEG-monomethacrylates. The diffusional behavior of diltiazem and theophylline in these networks was studied. The technique described in this work has been used for the development of a new class of functionalized PEG-containing gels that are used for a variety of drug-release applications.

Degradable Hydrogels

Hydrogels may degrade and dissolve by either of two mechanisms: hydrolysis or enzymolysis of main chain, side chain, or cross-linker bonds (e.g., Gombotz and Pettit, 1995). Degradable hydrogels have mainly been designed and synthesized for applications in drug delivery and, more recently, as tissue engineering scaffolds (e.g., Park, 1993; Atzet et al., 2008; Garcia et al., 2010).

Hydrolytically degradable hydrogels have been synthesized from triblock copolymers of A–B–A structure that form hydrogels held together by hydrophobic forces, where A (or B) may be PLA, PLGA, or other hydrophobic polyesters that form hydrophobic blocks, and B (or A) is PEG, a hydrophilic block. These polyester hydrogels degrade into natural, endogenous metabolites such as lactic or glycolic acids, and the PEG block is then excreted through the kidneys (e.g., Lee and He, 2010; Jeong et al., 2002). A variation of this type of degradable hydrogel is formed by an A–B–A triblock copolymer composed of PEG-degradable polyester-PEG blocks mixed with cyclodextrin (CD) molecules, which thread onto the PEG blocks, after which the CDs self-assemble, forming the hydrogel [e.g., see the work of Harada et al., 1992; Li et al., 2001, 2003(a,b), 2006; Li, 2009].

Polymerizable, cross-linked, and degradable PEG gels have been prepared from acrylate- or methacrylate-terminated block copolymers that include PEG as a hydrophilic block (see the work of Hubbell and co-workers, e.g., Sawhney et al., 1993; Schoenmakers et al., 2004; van de Wetering et al., 2005; Lutolf and Hubbell, 2005; Raeber et al., 2005; Patterson et al., 2010; Patterson and Hubbell, 2010). These gels may have the simple A–B–A triblock structure of (methacrylate)–PEG–methacrylate which is photo-polymerized and later degrades by hydrolysis of the ester bonds linking PEG to the methacrylate cross-links. Another gel was formed with a more elaborate structure, (methacrylate–oligolactide–PEG–oligolactide–methacrylate), which is photo-polymerized, and later degrades and dissolves mainly by hydrolysis of the PLA in the main chains (see also Atzet et al., 2008; Kloxin et al., 2009). A third type of PEG gel may include a fibrin peptide cross-linking block, where the peptide is sequenced from fibrin that is a substrate for a naturally occurring, fibrinolytic enzyme. The peptide block reacts by thiol addition of HS–peptide–SH to the acrylate vinyl groups, cross-linking the (acrylate)–PEG–acrylate triblock, to form: {–peptide–S–acrylate–PEG–acrylate–S–peptide–}, which then degrades and dissolves by proteolysis of the peptide by a natural, endogenous fibrinolytic enzyme.

Star Polymer and Dendrimer Hydrogels

Dendrimers and star polymers (Dvornik and Tomalia, 1996; Oral and Peppas, 2004) are exciting new materials because of the large number of functional groups available in a very small molecular volume. Such systems could have great promise in drug-targeting applications. In 1993 Merrill published an exceptional review of PEO star polymers and applications of such systems in the biomedical and pharmaceutical fields. Griffith and Lopina (1995) prepared gels of controlled structure and large biological functionality by irradiation of PEO star polymers. Such structures could have particularly promising drug-delivery applications when combined with emerging new technologies such as molecular imprinting.

Self-Assembled Hydrogel Structures

Recently there have been new, creative methods of preparation of novel hydrophilic polymers and hydrogels that may have significant drug-delivery applications in the future [e.g., Li et al., 2001, 2003(a,b); Yang et al., 2006; Jin and Dijkstra, 2010; Wang et al., 2010; Miyata, 2010]. In one unusual example, Stupp et al. (1997) synthesized self-assembled triblock copolymer nanogels having well-defined molecular architectures.

Hydrogels usually exhibit swelling behavior dependent on the external environment. Over the last 30 years there has been a significant interest in the development and analysis of environmentally responsive hydrogels. These types of gels show large and significant changes in their swelling ratio due to small changes in environmental conditions, such as

pH, temperature, ionic strength, nature, and composition of the swelling agent (including affinity solutes), light (visible vs. UV), electrical, and magnetic stimuli (e.g., Peppas, 1991; 1993; Hoffman, 1997; Hoffman et al., 2000; Yoshida and Okano, 2010). In most responsive networks, a critical point exists at which this transition occurs. These gels are sometimes referred to as “smart” or “intelligent” hydrogels.

“Smart” or “Intelligent,” Stimuli-Responsive Hydrogels and Their Applications

An interesting characteristic of numerous stimuli-responsive “smart” gels is that the mechanism causing the network structural changes can be entirely reversible in nature (Koetting et al., 2015). The ability of pH- or temperature-responsive gels to exhibit rapid changes in their swelling behavior and pore structure in response to changes in environmental conditions lends these materials favorable characteristics as carriers for delivery of drugs, including peptides and proteins. This type of behavior may also allow these materials to serve as self-regulated, pulsatile, or oscillating drug-delivery systems (Yoshida and Okano, 2010).

pH-Sensitive Hydrogels

One of the most widely studied types of physiologically responsive hydrogels is pH-responsive hydrogels. These hydrogels are swollen ionic networks containing either acidic or basic pendant groups. In aqueous media of appropriate pH and ionic strength, the pendant groups can ionize and develop fixed charges on the gel, leading to rapid swelling. All ionic hydrogels exhibit both pH and ionic strength sensitivity, especially around the pK of the pH-sensitive group. These gels typically contain ionizable pendant groups such as carboxylic acids or amine groups. The most commonly studied ionic polymers include poly(acrylic acid) (PAA), poly(methacrylic acid) (PMAA), poly(diethylaminoethyl methacrylate) (PDEAEMA), and poly(dimethylaminoethyl methacrylate) (PDMAEMA). The swelling and drug-delivery characteristics of anionic copolymers of PMAA and PHEMA (PHEMA-co-MAA) have been investigated (Koetting et al., 2015). In acidic media, the gels did not swell significantly; however, in neutral or basic media, the gels swelled to a high degree due to ionization of the pendant acid group (this is similar behavior to that of polymers used as enteric coatings). Brannon-Peppas and Peppas (1991b) have also studied the oscillatory swelling behavior of these gels.

One interesting example of pH-responsive “smart” polymers with great sensitivity to pK is the behavior of two poly(alkylacrylic acids): poly(ethylacrylic acid) (PEAA) (Tirrell et al., 1985) and poly(propylacrylic acid) (PPAA) (Cheung et al., 2001). These polymers phase separate sharply as pH is lowered below their pK, and this can lead to lipid bilayer membrane disruption in acidic liposome solutions or within the acidic environments of endosomes and

lysosomes of cells, where the membranes of those vesicles contain proton pumps. This behavior makes such polymers very useful for endosomal escape and cytosolic delivery of biomolecular drugs such as protein and nucleic acid drugs (Stayton and Hoffman, 2008).

The swelling forces developed in pH-responsive gels are significantly increased over nonionic hydrogels. This increase in swelling is due to the presence of mobile counter-ions (such as Na^+) that electrostatically balance the fixed charges on the polymer backbone. The concentration of such counter-ions will be dependent on the concentration of the fixed polymer charges, which in turn will be dependent on the composition of the network polymer and the pH. As a result, the water content and mesh size of an ionic polymeric network can change significantly with small changes in pH, as the osmotic pressure of the counter-ions within the gel changes.

pH-Responsive Complexation Hydrogels

Another promising class of hydrogels that exhibits responsive behavior is complexing hydrogels. Bell and Peppas (1995) have discussed a class of graft copolymer gels of PMAAc grafted with PEG: poly(MAAc-g-EG). These gels exhibited pH-dependent swelling behavior due to the presence of acidic pendant groups and the formation of inter-polymer H-bonded complexes at low pH between the ether groups on the graft chains and protonated pendant groups. In these covalently cross-linked, complexing poly(MAAc-g-EG) hydrogels, complexation resulted in the formation of temporary physical cross-links due to hydrogen bonding between the PEG grafts and the pendant and protonated $-\text{COOH}$ groups in PMAAc. The physical cross-links were reversible in nature and dependent on the pH and ionic strength of the environment. As a result, these complexing hydrogels exhibit drastic changes in their mesh size in response to small changes of pH, which could be useful for drug delivery in varying pH environments in the body, such as in the GI tract, mouth, and vagina, and on the skin.

In another study of complexation hydrogels, Hayashi et al. (2007) formed gels from PEGylated papain and PAAc at low pH. They showed how the molecular weight of the PEG and the addition of free PEG significantly affected the release rate of the PEGylated protein from the gel. A complexation gel formed as a result of H-bonding between PAAc and PAAm chains at low pH. It was unusual in that it exhibited temperature-responsive behavior, and went from a gel to a solution state as temperature rose above 30°C (Katono et al., 1991).

Temperature-Sensitive Hydrogels

Another class of environmentally sensitive gels exhibits sharp temperature-sensitive swelling-deswelling behavior due to a change in the polymer/swelling agent compatibility over the temperature range of interest. Temperature-sensitive polymers typically exhibit a lower critical solution

temperature (LCST), below which the polymer is soluble. Above this temperature, the polymers may lose their hydrophobically bound water, and phase separate, causing the gel to collapse. Below the LCST, the cross-linked gel reswells to significantly higher degrees because of the increased hydrophobic bonding with water. Poly(N-isopropyl acrylamide) (PNIPAAm) has been the most widely studied temperature-responsive polymer and hydrogel, with an LCST of around $32\text{--}34^\circ\text{C}$ (Dong and Hoffman, 1986; Park and Hoffman, 1990; 1992; Kim, 1996; Hoffman et al., 2000; Yoshida and Okano, 2010).

Some of the earliest work with PNIPAAm hydrogels was carried out by Dong and Hoffman (1986). They immobilized an enzyme in copolymer hydrogels of NIPAAm and AAm, and observed a maximum in the specific activity of the enzyme in each hydrogel as the temperature was raised. They concluded that above the maximum the gel collapsed as the copolymer LCST was surpassed, and the collapse blocked substrate diffusion into, and product out of, the gel. As the ratio of AAm/NIPAAm increased, the maximum shifted to higher temperatures due to the increasing hydrophilicity, which caused an increase in the LCST of the copolymer hydrogel. Most interesting was the fact that the curves were reversible up to the maximum reached for the highest AAm/NIPAAm ratio; above that LCST the enzyme was denatured due to the high temperature.

In another early work, Hirotsu et al. (1987) synthesized cross-linked PNIPAAm gels and determined that the LCST of the gels was 34.3°C ; below this transition temperature significant gel swelling occurred. They noted that the deswelling-swelling above and below the LCST was reversible. Similar to Dong and Hoffman (1986), they also noted that the transition temperature was raised by copolymerizing PNIPAAm with small amounts of hydrophilic ionic monomers. Dong and Hoffman (1991) prepared heterogeneous PNIPAAm gels containing silicone polymer regions; these unusual gels collapsed at significantly faster rates than homopolymers of PNIPAAm. Park and Hoffman (1990, 1992) studied the effect of temperature cycling on the efficiency of enzyme turnover in a temperature-controlled packed bed of PNIPAAm hydrogel microparticles containing the enzyme. They noted a significant increase in the productivity of the reactor with thermal cycling of temperatures from above to below the LCST, where the increased efficiency was due to the collapse of the gel particles above the LCST, “squeezing” out the product followed by reswelling of the gel below the LCST, enhancing uptake of substrate.

Yoshida et al. (1995) and Kaneko et al. (1996) developed an ingenious method to prepare comb-type graft hydrogels of PNIPAAm chains grafted to a PNIPAAm hydrogel network. Under conditions of gel collapse (above the LCST), hydrophobic regions were developed in the pores of the gel by the collapse of the grafted chains, drawing the network chains together with the collapsing grafted chains, resulting in very rapid collapse of the gel. These materials had the ability to collapse from a fully swollen conformation in less than 20 min, while comparable gels that did not contain

graft chains required up to a month to fully collapse. Such systems show promise for rapid or oscillatory release of drugs such as peptides and proteins.

There is a whole class of thermally sensitive hydrogels based on physical interactions of hydrophobic blocks of tri-block copolymers that also contain PEG blocks. Pluronic block polymers (e.g., PPO-PEO-PPO) form such gels, but they are not degradable. The most interesting block copolymers for biomedical applications are hydrolytically degradable since they contain blocks of PLA or PLGA (e.g., PLGA-PEG-PLGA or PEG-PLA-PEG), which hydrolyze and release PEG chains that can be eliminated through the kidneys. These thermally gelling block copolymers form in situ gels when injected subcutaneously, and act as drug-delivery depots, releasing entrapped drugs as they degrade (e.g., see Jeong et al., 2002, and Lee and He, 2010 for detailed discussion of pioneering work by S. W. Kim and co-workers on such block copolymer hydrogels). One very interesting class of such degradable block copolymer hydrogels is formed by stereocomplexation of the two stereoisomers of PLA in PLLA-PEG and PDLA-PEG block copolymers (Fujiwara et al., 2010; Gaharwar et al., 2014).

Affinity Hydrogels

Some hydrogels may exhibit environmental sensitivity due to the formation of complexes between chains that hold them together as a gel. Polymer complexes are macromolecular structures formed by the noncovalent association of groups on multifunctional molecules or on polymer chains that exhibit affinity for different groups on another polymer molecule. Sometimes this complexation is due to affinity recognition interactions, such as between streptavidin, with four binding sites for biotin, and a polymer with multiple pendant biotins (see Fig. 1.3.2E.7A and Morris et al., 1993), or concanavalin A with four binding sites for glucose and a polymer with multiple pendant glucose units (see Fig. 1.3.2E.7B and Miyata et al., 1996), or an antibody with two binding sites for its antigens (Miyata, 2010). The complexes may form by association of repeating units on different chains (interpolymer complexes) or on separate regions of the same chain (intrapolymer complexes). The stability of these affinity hydrogels is dependent on such factors as the affinity constant of the association, the concentration of a competing, mobile affinity agent, temperature, pH, ionic strength, network composition, and structure, especially the length of the network polymer chains between association points. In these types of hydrogel, complex formation results in the formation of physical cross-links in the gel. As the degree of such physical cross-linking is increased, the network mesh size and degree of swelling will be significantly reduced. As a result, if such hydrogels are used as drug carriers, the rate of drug release will decrease dramatically upon the formation of interpolymer complexes.

The hydrophilic character of hydrogels makes them attractive for a variety of biomedical and pharmaceutical applications. Because of their normally high water

contents, hydrogels have been useful for delivering drugs from ingested tablets and osmotic pumps. Further, they have been successful as contact lenses applied to the eye, or as drug-releasing coatings on mucosal, skin, or open-wound surfaces. They have also been applied as nonfouling coatings on implants and devices that may contact blood, such as catheters. More recently they are being developed as scaffolds for tissue engineering implants.

Biomedical Applications of Hydrogels

Contact Lenses

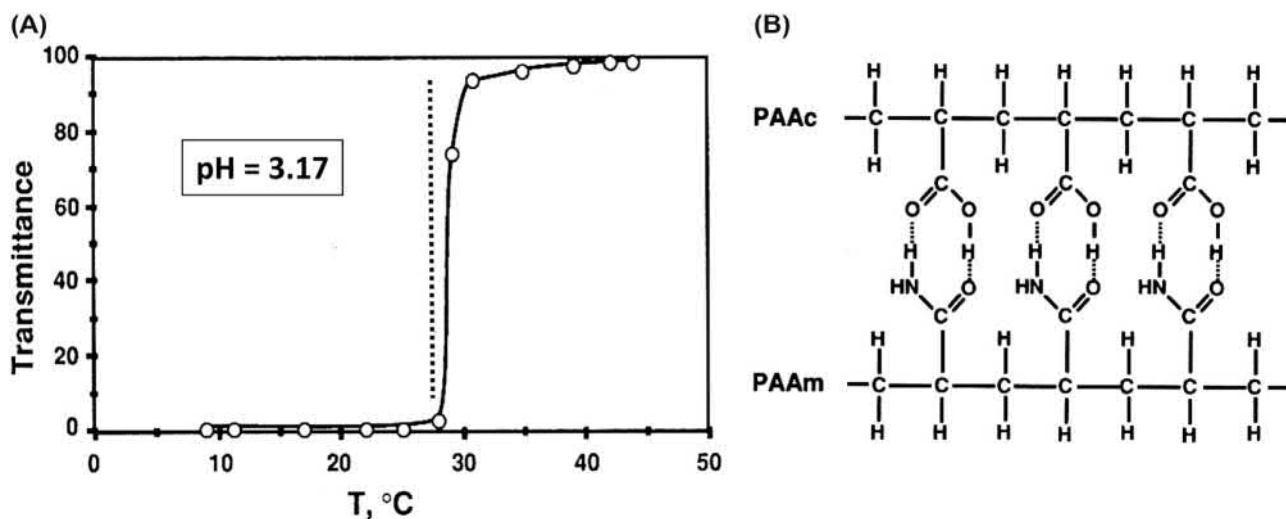
One of the earliest biomedical applications of hydrogels was the use of PHEMA hydrogels in contact lenses (Wichterle and Lim, 1960). Hydrogels are particularly useful as contact lenses because of their relatively good mechanical stability and favorable refractive index (see also Tighe, 1976; Pappas and Yang, 1981; Michalek et al., 2010). More recently, extended-wear contact lenses have been fabricated from an IPN composed of PNVP chains entrapped within a silicone hydrogel network. In this system, silicone monomers and cross-linkers are polymerized in a solution containing PNVP, and an IPN hydrogel is formed. The PNVP acts to lubricate the surface of the lens against the cornea, and the silicone hydrogel provides high oxygen transport to the cornea, as well as enhanced permeability of small nutrient molecules and ions.

Blood-Contacting Hydrogels

Hydrogels also exhibit properties that make them desirable candidates for blood-contacting biomaterials (Merrill et al., 1987). Nonionic hydrogels have been prepared from poly(vinyl alcohol), polyacrylamides, PNVP, PHEMA, and poly(ethylene oxide) (PEO, sometimes also referred to as PEG) (Peppas et al., 1999). Heparinized polymer hydrogels (Sefton, 1987) and heparin-based hydrogels (Tae et al., 2007) also show promise as materials for blood-contacting applications.

Drug Delivery From Hydrogels

Applications of hydrogels in controlled drug-delivery systems (DDS) have become very popular in recent years. They include equilibrium-swollen hydrogels, i.e., matrices that have a drug incorporated in them and are swollen to equilibrium, releasing the drug. This category of *solvent-activated*, matrix-type, controlled-release devices comprises two important types of systems: (1) *rapidly swelling, diffusion-controlled devices*; and (2) *slowly swelling, swelling-controlled devices*. In general, a drug-loaded hydrogel may be prepared by swelling the hydrogel to equilibrium in a drug solution, and carefully drying it. In the dry state it becomes a glassy polymer that can be swollen when brought in contact with water or simulated biological fluids. This swelling process may or may not be the controlling mechanism for



• **Figure 1.3.2E.7** Temperature dependence of light transmission for two H-bonded polymers, PAAc [poly(acrylic acid)] and PAAm (polyacrylamide) at pH 3.17; (A) shows the temperature dependence of light transmission and (B) shows the hypothetical H-bonded structure that would exist at low pH and at temperatures below 30°C, where the COOH groups are protonated and the polymer chains are complexed. The H-bonding is disrupted as temperature rises above 30°C. Data are for an aqueous solution at pH 3.17 (adjusted by HCl). Polymer concentration (wt.%): PAAc, 0.5%; PAAm, 0.5%. (Katono et al. (1991).

diffusional release, depending on the relative rates of the macromolecular relaxation of the polymer and drug diffusion from the gel.

In swelling-controlled release systems, the bioactive agent is dispersed into the polymer to form nonporous films, disks, or spheres. Upon contact with an aqueous dissolution medium, a distinct front (interface) is observed that corresponds to the water penetration front into the polymer and separates the glassy from the rubbery (gel-like) state of the material. Under these conditions, the macromolecular relaxation of the polymer influences the diffusion mechanism of the drug through the rubbery state. This water uptake can lead to considerable swelling of the polymer, with a thickness that depends on time. The swelling process proceeds toward equilibrium at a rate determined by the water activity in the system and the structure of the polymer. If the polymer is cross-linked, or if it is of sufficiently high molecular weight (so that chain entanglements can maintain structural integrity), the equilibrium state is a water-swollen gel. The equilibrium water content of such hydrogels can vary from ~30% to over 90%. If the dry hydrogel contains a water-soluble drug, the drug is essentially immobile in the glassy matrix, but begins to diffuse out as the polymer swells with water. Drug release thus depends on the simultaneous rate processes of water migration into the device, polymer chain hydration and relaxation, followed by drug dissolution and diffusion outward through the swollen gel. An initial burst effect is frequently observed in matrix devices, especially if the drying process brings a higher concentration of drug to the surface. The continued swelling of the matrix causes the drug to diffuse increasingly easily, mitigating the slow tailing off of the release curve. The net effect of the swelling process is to prolong and “linearize” the release curve. Details of the process of drug delivery from hydrogels have been

presented by Kormsmeier and Peppas (1981) for poly(vinyl alcohol) systems, and by Reinhart et al. (1981) for PHEMA systems and their copolymers. One of numerous examples of such swelling-controlled systems was reported by Franson and Peppas (1983) who prepared cross-linked copolymer gels of poly(HEMA-co-MAA) of varying compositions. Theophylline release was studied and it was found that near zero-order release could be achieved using copolymers containing 90% PHEMA. For sensing devices see also Snelling Van Blarcom and Peppas (2011).

Targeted Drug Delivery From Hydrogels

Promising new methods for the delivery of chemotherapeutic agents using hydrogels have been recently reported. Novel bio-recognizable sugar-containing copolymers have been investigated for use in targeted delivery of anticancer drugs. For example, Peterson et al. (1996) have used poly(N-2-hydroxypropyl methacrylamide) carriers for the treatment of ovarian cancer. Sharpe et al. (2014) used hydrogels for advanced drug-delivery release.

Tissue Engineering Scaffolds From Hydrogels

This is an application area that continues to expand. It is driven by the same attractive properties that drive the use of hydrogels for drug-delivery applications: high water content gels that may be synthesized with degradable backbone polymers, with an added advantage of being able to attach cell adhesion ligands to the network polymer chains. There are a number of natural polymer-based hydrogel scaffolds that have been studied (e.g., collagen, gelatin, alginates, hyaluronic acid, chitosan, etc.) and the reader is referred to three chapters in this text (see Chapters 1.3.6A, 1.3.6B and 2.6.3)

and some excellent review articles (Lee and Mooney, 2001; Lutolf and Hubbell, 2005; Jin and Dijkstra, 2010).

One very interesting observation with hydrogels that has recently been reported is that they may stimulate stem cell differentiation; that is, when stem cells are deposited on some hydrogel surfaces, depending on the composition and/or mechanical stiffness of the surface, differentiation of the stem cells into certain phenotypes may occur (e.g., Liu et al., 2010; Nguyen et al., 2011). An important recent review of hydrogel design for regenerative medicine applications can be found in Annabi et al. (2014).

Miscellaneous Biomedical Applications of Hydrogels

Other potential applications of hydrogels mentioned in the literature include artificial tendon materials, wound-healing bio-adhesives, artificial kidney membranes, articular cartilage, artificial skin, maxillofacial and sexual organ reconstruction materials, and vocal cord replacement materials (Byrne et al., 2002a,b).

References

- Andrade, J.D., 1976. In: *Hydrogels for Medical and Related Applications*. ACS Symposium Series, vol. 31. American Chemical Society, Washington, DC.
- Annabi, N., Tamayol, A., Uquillas, J.A., Akbari, M., Bertassoni, L., Cha, C., Camci-Unal, G., Dokmeci, M., Peppas, N.A., Khademhosseini, 2014. Emerging frontiers in rational design and application of hydrogels in regenerative medicine. *Adv. Mat.* 26, 85–124.
- Atzet, S., Curtin, S., Trinh, P., Bryant, S., Ratner, B., 2008. Degradable poly(2-hydroxyethyl methacrylate)-co-polycaprolactone hydrogels for tissue engineering scaffolds. *Biomacromolecules* 9, 3370–3377.
- Bell, C.L., Peppas, N.A., 1995. Biomedical membranes from hydrogels and interpolymer complexes. *Adv. Polym. Sci.* 122, 125–175.
- Brannon-Peppas, L., Harland, R.S., 1990. *Absorbent Polymer Technology*. Elsevier, Amsterdam.
- Brannon-Peppas, L., Peppas, N.A., 1991a. Equilibrium swelling behavior of dilute ionic hydrogels in electrolytic solutions. *J. Control. Release* 16, 319–330.
- Brannon-Peppas, L., Peppas, N.A., 1991b. Time-dependent response of ionic polymer networks to pH and ionic strength changes. *Int. J. Pharm.* 70, 53–57.
- Byrne, M.E., Henthorn, D.B., Huang, Y., Peppas, N.A., 2002a. Micropatterning biomimetic materials for bioadhesion and drug delivery. In: Dillow, A.K., Lowman, A.M. (Eds.), *Biomimetic Materials and Design: Biointerfacial Strategies, Tissue Engineering and Targeted Drug Delivery*. Dekker, New York, NY, pp. 443–470.
- Byrne, M.E., Park, K., Peppas, N.A., 2002b. Molecular imprinting within hydrogels. *Adv. Drug Deliv. Rev.* 54, 149–161.
- Chapiro, A., 1962. *Radiation Chemistry of Polymeric Systems*. Interscience, New York, NY.
- Cheung, C.Y., Murthy, N., Stayton, P.S., Hoffman, A.S., 2001. A pH-sensitive polymer that enhances cationic lipid-mediated gene transfer. *Bioconjug. Chem.* 12, 906–910.
- Dong, L.C., Hoffman, A.S., 1986. Thermally reversible hydrogels: III. Immobilization of enzymes for feedback reaction control. *J. Control. Release* 4, 223–227.
- Dong, L.C., Hoffman, A.S., 1991. A novel approach for preparation of pH-sensitive hydrogels for enteric drug delivery. *J. Control. Release* 15, 141–152.
- Drury, J.L., Mooney, D.J., 2003. Hydrogels for tissue engineering: scaffold design variables and applications. *Biomaterials* 24, 4337–4351.
- Dvornik, P.R., Tomalia, D.A., 1996. Recent advances in dendritic polymers. *Curr. Opin. Colloid Interface Sci.* 1, 221–235.
- Ficek, B.J., Peppas, N.A., 1993. Novel preparation of poly(vinyl alcohol) microparticles without cross-linking agent. *J. Control. Release* 27, 259–264.
- Flory, P.J., 1953. *Principles of Polymer Chemistry*. Cornell University Press, Ithaca, NY.
- Franson, N.M., Peppas, N.A., 1983. Influence of copolymer composition on water transport through glassy copolymers. *J. Appl. Polym. Sci.* 28, 1299–1310.
- Fujiwara, T., Yamaoka, T., Kimura, Y., 2010. Thermo-responsive biodegradable hydrogels from stereocomplexed polylactides. In: Ottenbrite, R.M., Park, K., Okano, T. (Eds.), *Biomedical Applications of Hydrogels Handbook*. Springer, New York, NY, pp. 157–178.
- Gaharwar, A.K., Peppas, N.A., Khademhosseini, A., 2014. Nanocomposite hydrogels for biomedical applications. *Biotechnol. Bioeng.* 111, 441–453.
- Garcia, L., Aguilar, M.R., San Román, J., 2010. Biodegradable hydrogels for controlled drug delivery. In: Ottenbrite, R.M., Park, K., Okano, T. (Eds.), *Biomedical Applications of Hydrogels Handbook*. Springer, New York, NY, pp. 147–155.
- Gehrke, S.H., Andrews, G.P., Cussler, E.L., 1986. Chemical aspects of gel extraction. *Chem. Eng. Sci.* 41, 2153–2160.
- Gombotz, W.R., Pettit, D.K., 1995. Biodegradable polymers for protein and peptide drug delivery. *Bioconjug. Chem.* 6, 332–351.
- Graham, N.B., 1992. Poly(ethylene glycol) gels and drug delivery. In: Harris, J.M. (Ed.), *Poly(Ethylene Glycol) Chemistry, Biotechnical and Biomedical Applications*. Plenum Press, New York, NY, pp. 263–281.
- Gregonis, D.E., Chen, C.M., Andrade, J.D., 1976. The chemistry of some selected methacrylate hydrogels. In: Andrade, J.D. (Ed.), *ACS Symposium Series: Hydrogels for Medical and Related Applications*, vol. 31. American Chemical Society, Washington, DC, pp. 88–104.
- Griffith, L., Lopina, S.T., 1995. Network structures of radiation cross-linked star polymer gels. *Macromolecules* 28, 6787–6794.
- Harada, A., Li, J., Kamachi, M., 1992. The molecular necklace: a rotaxane containing many threaded α -cyclodextrins. *Nature* 356, 325–327.
- Harris, J.M., 1992. *Poly(Ethylene Glycol) Chemistry, Biotechnical and Biomedical Applications*. Plenum Press, New York, NY.
- Hayashi, Y., Harris, J.M., Hoffman, A.S., 2007. Delivery of PEGylated drugs from mucoadhesive formulations by pH-induced disruption of H-bonded complexes of PEG-drug with poly(acrylic acid). *React. Funct. Polym.* 67, 1330–1337.
- Hennink, W.E., van Nostrum, C.F., 2002. Novel cross-linking methods to design hydrogels. *Adv. Drug Deliv. Rev.* 54, 13–36.
- Hermanson, G.T., 2008. *Bioconjugate Techniques*, second ed. Elsevier, New York, NY.
- Hirotsu, S., Hirokawa, Y., Tanaka, T., 1987. Swelling of gels. *J. Chem. Phys.* 87, 1392–1395.
- Hoffman, A.S., 1997. Intelligent polymers. In: Park, K. (Ed.), *Controlled Drug Delivery*. ACS Publications, ACS, Washington, DC.
- Hoffman, A.S., 2002. Hydrogels for biomedical applications. *Adv. Drug Deliv. Rev.* 43, 3–12.

- Hoffman, A.S., Stayton, P.S., Bulmus, V., Chen, J., Cheung, C., et al., 2000. Really smart bioconjugates of smart polymers and receptor proteins. *J. Biomed. Mater. Res.* 52, 577–586.
- Ilavsky, M., 1982. Phase transition in swollen gels. *Macromolecules* 15, 782–788.
- Jeong, B., Kim, S.W., Bae, Y.H., 2002. Thermosensitive sol-gel reversible hydrogels. *Adv. Drug Deliv. Rev.* 54, 37–51.
- Jin, R., Dijkstra, P.J., 2010. Hydrogels for tissue engineering applications. In: Ottenbrite, R.M., Park, K., Okano, T. (Eds.), *Biomedical Applications of Hydrogels Handbook*. Springer, New York, NY, pp. 203–226.
- Kaneko, Y., Saki, K., Kikuchi, A., Sakurai, Y., Okano, T., 1996. Fast swelling/deswelling kinetics of comb-type grafted poly(N-isopropyl acrylamide) hydrogels. *Macromol. Symp.* 109, 41–53.
- Katono, H., Maruyama, A., Sanui, K., Ogata, N., Okano, T., Sakurai, Y., 1991. Thermo-responsive swelling and drug release switching of interpenetrating polymer networks composed of poly(acrylamide-co-butyl methacrylate) and poly(acrylic acid). *J. Control. Release* 16, 215–227.
- Kim, S.W., 1996. Temperature sensitive polymers for delivery of macromolecular drugs. In: Ogata, N., Kim, S.W., Feijen, J., Okano, T. (Eds.), *Advanced Biomaterials in Biomedical Engineering and Drug Delivery Systems*. Springer, Tokyo, pp. 125–133.
- Kloxin, A.M., Kasko, A., Salinas, C.N., Anseth, K.S., 2009. Photodegradable hydrogels for dynamic tuning of physical and chemical properties. *Science* 324, 59–63.
- Koetting, M.C., Peters, J.T., Steichen, S.D., NA Peppas, N.A., 2015. Stimulus-responsive hydrogels: theory, modern advances and applications. *Mat. Sci. Engin. R: Report* 93, 1–49.
- Kofinas, P., Athanassiou, V., Merrill, E.W., 1996. Hydrogels prepared by electron beam irradiation of poly(ethylene oxide) in water solution: unexpected dependence of cross-link density and protein diffusion coefficients on initial PEO molecular weight. *Biomaterials* 17, 1547–1550.
- Kolb, H.C., Finn, M.G., Sharpless, K.B., 2001. Click chemistry: diverse chemical function from a few good reactions. *Angew. Chem. Int. Ed.* 40 (11), 2004–2021.
- Korsmeyer, R.W., Peppas, N.A., 1981. Effects of the morphology of hydrophilic polymeric matrices on the diffusion and release of water soluble drugs. *J. Membr. Sci.* 9, 211–227.
- Lee, D.S., He, C., 2010. *In-situ* gelling stimuli-sensitive PEG-based amphiphilic copolymer hydrogels. In: Ottenbrite, R.M., Park, K., Okano, T. (Eds.), *Biomedical Applications of Hydrogels Handbook*. Springer, New York, NY, pp. 123–146.
- Lee, K.Y., Mooney, D.J., 2001. Hydrogels for tissue engineering. *Chem. Rev.* 101, 1869–1879.
- Li, J., 2009. Cyclodextrin inclusion polymers forming hydrogels. *Adv. Polym. Sci.* 222, 79–113.
- Li, J., Li, X., Zhou, Z., Ni, H., Leong, K.W., 2001. Formation of supramolecular hydrogels induced by inclusion complexation between Pluronics and cyclodextrin. *Macromolecules* 34, 7236–7237.
- Li, J., Ni, X., Zhou, Z., Leong, K.W., 2003a. Preparation and characterization of polypseudorotaxanes based on block-selected inclusion complexation between poly(propyleneoxide)-poly(ethylene oxide)-poly(propylene oxide) triblock copolymers and α -cyclodextrin. *J. Am. Chem. Soc.* 125, 1788–1795.
- Li, J., Ni, X., Leong, K.W., 2003b. Injectable drug-delivery systems based on supramolecular hydrogels formed by poly(ethylene oxide)s and cyclodextrin. *J. Biomed. Mater. Res.* 65A, 196–202.
- Li, J., Li, X., Ni, X., Wang, X., Li, H., Leong, K.W., 2006. Self-assembled supramolecular hydrogels formed by biodegradable PEO-PHB-PEO triblock copolymers and α -cyclodextrin for controlled drug delivery. *Biomaterials* 27, 4132–4140.
- Liu, S.Q., Tay, R., Khan, M., Lai, P., Ee, R., et al., 2010. Synthetic hydrogels for controlled stem cell differentiation. *Soft Matter* 6, 67–81.
- Lowman, A.M., Peppas, N.A., 1997. Analysis of the complexation/decomplexation phenomena in graft copolymer networks. *Macromolecules* 30, 4959–4965.
- Lowman, A.M., Peppas, N.A., 1999. Hydrogels. In: Mathiowitz, E. (Ed.), *Encyclopedia of Controlled Drug Delivery*. Wiley, New York, NY, pp. 397–418.
- Lowman, A.M., Dziubla, T.D., Peppas, N.A., 1997. Novel networks and gels containing increased amounts of grafted and cross-linked poly(ethylene glycol). *Polym. Prepr.* 38, 622–623.
- Lutolf, M.P., Hubbell, J.A., 2005. Synthetic biomaterials as instructive extracellular microenvironments for morphogenesis in tissue engineering. *Nat. Biotechnol.* 23, 47–55.
- Merrill, E.W., 1993. Poly(ethylene oxide) star molecules: synthesis, characterization, and applications in medicine and biology. *J. Biomater. Sci. Polym. Ed.* 5, 1–11.
- Merrill, E.W., Pekala, P.W., Mahmud, N.A., 1987. Hydrogels for blood contact. In: Peppas, N.A. (Ed.), *Hydrogels in Medicine and Pharmacy*, vol. 3. CRC Press, Boca Raton, FL, pp. 1–16.
- Michalek, J., Hobzova, R., Pradny, M., Duskova, M., 2010. Hydrogel contact lenses. In: Ottenbrite, R.M., Park, K., Okano, T. (Eds.), *Biomedical Applications of Hydrogels Handbook*. Springer, New York, NY, pp. 303–316.
- Miyata, T., 2010. Biomolecule-responsive hydrogels. In: Ottenbrite, R.M., Park, K., Okano, T. (Eds.), *Biomedical Applications of Hydrogels Handbook*. Springer, New York, NY, pp. 65–86.
- Miyata, T., Jikihara, A., Nakamae, K., Uragami, T., Hoffman, A.S., Kinomura, K., Okumura, M., 1996. Preparation of glucose-sensitive hydrogels by entrapment or copolymerization of concanavalin A in a glucosyloxyethyl methacrylate hydrogel. In: Ogata, N., Kim, S.W., Feijen, J., Okano, T. (Eds.), *Advanced Biomaterials in Biomedical Engineering and Drug Delivery Systems*. Springer, pp. 237–238.
- Miyata, T., Uragami, T., Nakamae, K., 2002. Biomolecule-sensitive hydrogels. *Adv. Drug Deliv. Rev.* 54, 79–98.
- Morris, J.E., Fischer, R., Hoffman, A.S., 1993. Affinity precipitation of proteins with polyligands. *J. Anal. Biochem.* 41, 991–997.
- Mun, G., Suleimenov, I., Park, K., Omidian, H., 2010. Superabsorbent hydrogels. In: Ottenbrite, R.M., Park, K., Okano, T. (Eds.), *Biomedical Applications of Hydrogels Handbook*. Springer, New York, NY, pp. 375–392.
- Murosaki, T., Gong, J.P., 2010. Double network hydrogels as tough, durable tissue substitutes. In: Ottenbrite, R.M., Park, K., Okano, T. (Eds.), *Biomedical Applications of Hydrogels Handbook*. Springer, New York, NY, pp. 285–302.
- Nguyen, L.H., Kudva, A.K., Guckert, N.L., Linse, K.D., Roy, K., 2011. Unique biomaterial compositions direct bone marrow stem cells into specific chondrocyte phenotypes corresponding to the various zones of articular cartilage. *Biomaterials* 32, 1327–1338.
- Neves, M.I., Wechsler, M.E., Gomes, M.E., Reis, R., Granja, P.L., Peppas, N.A., 2017. Molecularly imprinted intelligent scaffolds for tissue engineering applications. *Tissue Eng. B* 23, 27–43.
- Oishi, M., Nagasaki, Y., 2010. Stimuli-responsive PEGylated nanogels for smart nanomedicine. In: Ottenbrite, R.M., Park, K., Okano, T. (Eds.), *Biomedical Applications of Hydrogels Handbook*. Springer, New York, NY, pp. 87–106.
- Omidian, H., Park, K., 2010. Engineered high swelling hydrogels. In: Ottenbrite, R.M., Park, K., Okano, T. (Eds.), *Biomedical*

- Applications of Hydrogels Handbook. Springer, New York, NY, pp. 351–374.
- Oral, E., Peppas, N.A., 2004. Responsive and cognitive hydrogels using star polymers. *J. Biomed. Mater. Res.* 68A, 439–447.
- Ottenbrite, R.M., Park, K., Okano, T., 2010. Biomedical Applications of Hydrogels Handbook. Springer, New York, NY.
- Park, K., 1993. Biodegradable Hydrogels for Drug Delivery. Technomic Publishing Co., Inc, Lancaster, PA.
- Park, T.G., Hoffman, A.S., 1990. Immobilized biocatalysts in reversible hydrogels. *NY Acad. Sci.* 613, 588–593.
- Park, T.G., Hoffman, A.S., 1992. Synthesis and characterization of pH and temperature-sensitive hydrogels. *J. Appl. Polym. Sci.* 46, 659–671.
- Patterson, J., Hubbell, J.A., 2010. Enhanced proteolytic degradation of molecularly-engineered PEG hydrogels in response to MMP-1 and MMP-2. *Biomaterials* 31, 7836–7845.
- Patterson, J., et al., 2010. Biomimetic materials in tissue engineering. *Mater. Today* 13, 14–22.
- Peppas, N.A., 1987. Hydrogels in Medicine and Pharmacy. CRC Press, Boca Raton, FL.
- Peppas, N.A., 1991. Physiologically-responsive hydrogels. *J. Bioact. Compat Polym.* 6, 241–246.
- Peppas, N.A., 1993. Fundamentals of pH- and temperature-sensitive delivery systems. In: Gurny, R., Junginger, H.E., Peppas, N.A. (Eds.), *Pulsatile Drug Delivery*. Wissenschaftliche Verlagsgesellschaft, Stuttgart, pp. 41–56.
- Peppas, N.A., 1997. Hydrogels and drug delivery. *Critical Opinion in Colloid and Interface Science* 2, 531–537.
- Peppas, N.A., 2001. Gels for drug delivery. In: *Encyclopedia of Materials: Science and Technology*. Elsevier, Amsterdam, pp. 3492–3495.
- Peppas, N.A., Yang, W.H.M., 1981. Properties-based optimization of the structure of polymers for contact lens applications. *Contact Intraocular Lens*. *Med. J.* 7, 300–321.
- Peppas, N.A., Keys, K.B., Torres-Lugo, M., Lowman, A.M., 1999. Poly(ethylene glycol)-containing hydrogels in drug delivery. *J. Control. Release* 62, 81–87.
- Peppas, N.A., Huang, Y., Torres-Lugo, M., Ward, J.H., Zhang, J., 2000. Physicochemical foundations and structural design of hydrogels in medicine and biology. *Annu. Rev. Biomed. Eng.* 2, 9–29.
- Peterson, C.M., Lu, J.M., Sun, Y., Peterson, C.A., Shiah, J.G., Straight, R.C., Kopecek, J., 1996. Combination chemotherapy and photodynamic therapy with N-(2-hydroxypropyl) methacrylamide copolymer-bound anticancer drugs inhibit human ovarian carcinoma hetero-transplanted in nude mice. *Cancer Res.* 56, 3980–3985.
- Qiu, Y., Park, K., 2001. Environment-sensitive hydrogels for drug delivery. *Adv. Drug Deliv. Rev.* 53, 321–339.
- Raeber, G.P., Lutolf, M., Hubbell, J.A., 2005. Molecularly engineered PEG hydrogels: a novel model system for proteolytically mediated cell migration. *Biophys. J.* 89, 1374–1388.
- Reinhart, C.T., Korsmeyer, R.W., Peppas, N.A., 1981. Macromolecular network structure and its effects on drug and protein diffusion. *Int. J. Pharm. Technol.* 2 (2), 9–16.
- Sawhney, A.S., Pathak, C.P., Hubbell, J.A., 1993. Bioerodible hydrogels based on photopolymerized poly(ethylene glycol)-co-poly(alpha-hydroxy acid) diacrylate macromers. *Macromolecules* 26, 581–587.
- Schoenmakers, R.G., van de Wetering, P., Elbert, D.L., Hubbell, J.A., 2004. The effect of the linker on the hydrolysis rate of drug-linked ester bonds. *J. Control. Release* 95, 291–300.
- Sefton, M.V., 1987. Heparinized hydrogels. In: Peppas, N.A. (Ed.), *Hydrogels in Medicine and Pharmacy*, vol. 3. CRC Press, Boca Raton, FL, pp. 17–52.
- Sharpe, L.A., Daily, A., Horava, S., Peppas, N.A., 2014. Therapeutic applications of hydrogels in oral drug Delivery. *Expert Opin. Drug Deliv.* 11, 901–915.
- Snelling Van Blarcom, D., Peppas, N.A., 2011. Microcantilever sensing arrays from biodegradable, pH-responsive hydrogels. *Biomed. Microdevices* 13, 829–836.
- Sperinde, J.J., Griffith, L.G., 1997. Synthesis and characterization of enzymatically-cross-linked poly(ethylene glycol) hydrogels. *Macromolecules* 30, 5255–5264.
- Sperinde, J.J., Griffith, L.G., 2000. Control and prediction of gelation kinetics in enzymatically cross-linked poly(ethylene glycol) hydrogels. *Macromolecules* 33, 5476–5480.
- Stayton, P.S., Hoffman, A.S., 2008. Smart pH-responsive carriers for intracellular delivery of biomolecular drugs. In: Torchilin, V. (Ed.), *Multifunctional Pharmaceutical Nanocarriers*. Springer, New York, NY.
- Stringer, J.L., Peppas, N.A., 1996. Diffusion in radiation-cross-linked poly(ethylene oxide) hydrogels. *J. Control. Release* 42, 195–202.
- Stupp, S.I., LeBonheur, V., Walker, K., Li, L.S., Huggins, K.E., et al., 1997. Supramolecular materials: self-organized nanostructures. *Science* 276, 384–389.
- Tae, G., Kim, Y.J., Choi, W.I., Kim, M., Stayton, P.S., et al., 2007. Formation of a novel heparin-based hydrogel in the presence of heparin-binding biomolecules. *Biomacromolecules* 8, 1979–1986.
- Tanaka, T., 1979. Phase transitions in gels and a single polymer. *Polymer* 20, 1404–1412.
- Tighe, B.J., 1976. The design of polymers for contact lens applications. *Br. Polym. J.* 8, 71–90.
- Tirrell, D.A., Takigawa, D.Y., Seki, K., 1985. pH sensitization of phospholipid vesicles via complexation with synthetic poly(carboxylic acid)s. *Ann. NY Acad. Sci.* 446, 237–248.
- van de Wetering, P., Metters, A.T., Schoenmakers, R.G., Hubbell, J.A., 2005. Poly(ethylene glycol) hydrogels formed by conjugate addition with controllable swelling, degradation, and release of pharmaceutically active proteins. *J. Control. Release* 102, 619–627.
- Wang, L.S., Boulaire, J., Chan, P.P.Y., Chung, J.E., Kurisawa, M., 2010. The role of stiffness of gelatin-hydroxyphenylpropionic acid hydrogels formed by enzyme-mediated cross-linking on the differentiation of human mesenchymal stem cell. *And* 8608–8616 *Biomaterials* 31, 8608–8616 1148–1157.
- Wichterle, O., Lim, D., 1960. Hydrophilic gels for biological use. *Nature* 185, 117–118.
- Xu, C., Kopecek, J., 2008. Genetically engineered block copolymers: influence of the length and structure of the coiled-coil block on hydrogel self-assembly. *Pharm. Res.* 25, 674–682.
- Yang, J., Xu, C., Wang, C., Kopecek, J., 2006. Refolding hydrogels self-assembled from HPMA graft copolymers by antiparallel coiled-coil formation. *Biomacromolecules* 7, 1187–1195.
- Yasuda, H., Peterlin, A., Colton, C.K., Smith, K.A., Merrill, E.W., 1969. Permeability of solutes through hydrated polymer membranes. III. Theoretical background for the selectivity of dialysis membranes. *Makromol. Chem.* 126, 177–186.
- Yoshida, R., Okano, T., 2010. Stimuli-responsive hydrogels and their application to functional materials. In: Ottenbrite, R.M., Park, K., Okano, T. (Eds.), *Biomedical Applications of Hydrogels Handbook*. Springer, New York, NY, pp. 19–44.
- Yoshida, R., Uchida, K., Kaneko, Y., Sakai, K., Kikuchi, A., et al., 1995. Comb-type grafted hydrogels with rapid deswelling response to temperature changes. *Nature* 374, 240–242.

Further Reading

- Hassan, C.M., Peppas, N.A., 2000. Cellular Freeze/thawed PVA hydrogels. *J. Appl. Polym. Sci.* 76, 2075–2079.
- Hickey, A.S., Peppas, N.A., 1995. Mesh size and diffusive characteristics of semicrystalline poly(vinyl alcohol) membranes. *J. Membr. Sci.* 107, 229–237.
- Okano, T., 1993. Molecular design of temperature-responsive responsive polymers as intelligent materials. In: Dusek, K. (Ed.), *Gels: Volume Transitions II*. Springer-Verlag, New York, NY.
- Peppas, N.A., Wood, K.M., Blanchette, J.O., 2004. Hydrogels for oral delivery of therapeutic proteins. *Expert Opin. Biol. Ther.* 4, 881–887.
- Peppas, N.A., Hilt, J.Z., Khademhosseini, A., Langer, R., 2006. Hydrogels in biology and medicine: from fundamentals to bionanotechnology. *Adv. Mater.* 18, 1345–1360.
- Ratner, B.D., Hoffman, A.S., 1976. Synthetic hydrogels for biomedical applications. In: Andrade, J.D. (Ed.), *Hydrogels for Medical and Related Applications*, vol. 31. ACS Symposium Series, American Chemical Society, Washington, DC, pp. 1–36.

1.3.2F

Degradable and Resorbable Polymers

LAURA MACDOUGALL^{1,2}, HEIDI CULVER¹, CHIEN-CHI LIN³, CHRISTOPHER BOWMAN¹, KRISTI ANSETH^{1,2}

¹Department of Chemical and Biological Engineering, University of Colorado, Boulder, CO, United States

²Biofrontiers Institute, University of Colorado, Boulder, CO, United States

³Department of Biomedical Engineering, Indiana University-Purdue University Indianapolis, Indianapolis, IN, United States

Introduction

Degradable polymers offer many advantages when used in biomaterial applications (e.g., temporary implants, degradable sutures, or drug delivery platforms), because of their ability to degrade in different environments, over different time scales, and without the production of toxic by-products (Piskin, 1995; Shalaby and Burg, 2003). Degradation is often desirable, as it can circumvent the need for additional surgeries to remove nondegradable medical implants/sutures, and hence reduce recovery time and risk of infection, as well as lower healthcare costs. Applications of degradable polymers are not limited to short-term applications, as tailoring polymer properties allows for controlled degradation rates to enable long-term support for tissue regeneration and sustained drug delivery over a defined period of time. Although degradable polymers offer a range of benefits, one must also consider the biocompatibility of the degradation products in addition to the polymer itself. Furthermore, uncontrolled or accelerated polymer degradation rates can lead to premature implant failure or side effects from depositing high concentrations of an encapsulated therapeutic. However, with careful consideration of polymer design, chemistry, and function, degradable biomaterials can be synthesized with precise and relevant degradation timescales, producing nontoxic, and in some cases functional, degradation products (e.g., release of a drug) (He and Benson, 2017).

While natural polymers are also able to degrade, given the correct conditions and timescale, synthetic polymers offer specific advantages with respect to controlled synthetic routes, resulting in highly defined polymers with user-designed degradability and tunable material properties. This chapter, in the context of biomaterials applications, focuses on synthetic degradable polymers, including: (1) degradable polymer properties, (2) types of different degradation processes

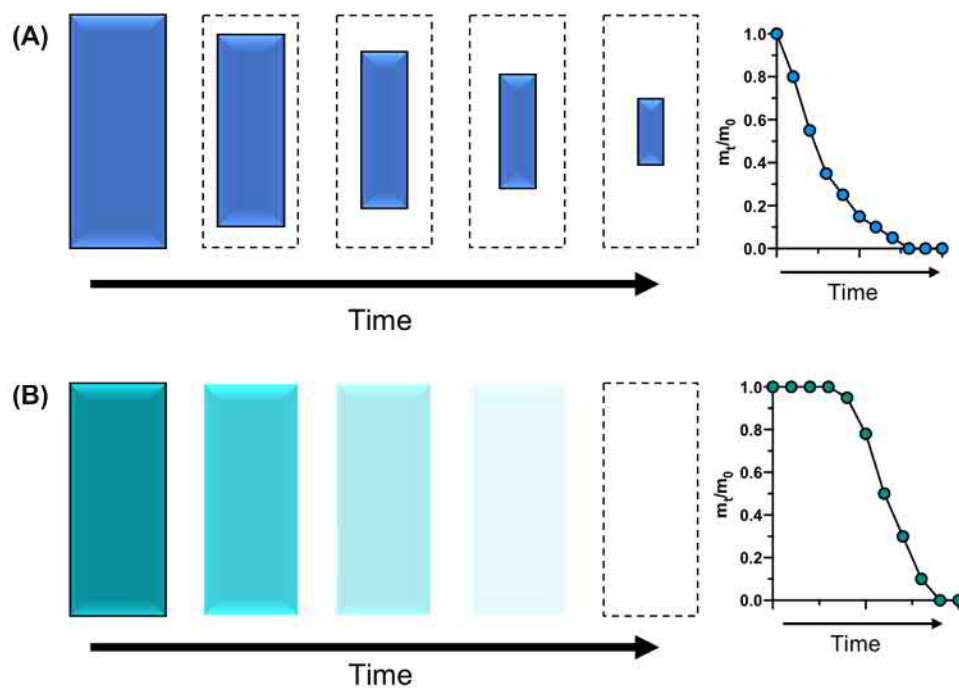
and their kinetics, (3) design and processing considerations, and (4) performance metrics unique to degradable biomaterials. The chapter concludes with case studies of commercially available degradable polymers that are used in medical devices and drug delivery systems, demonstrating the importance of degradable polymers to the field of biomaterials.

Brief History of Degradable Polymers

The application of degradable polymers in medicine can be dated back to the early 1960s when polymers (e.g., poly(glycolic acid) (PGA)), which were initially found unstable due to rapid degradation, were used as suture materials (Dardik et al., 1971; Morgan, 1969; Vert, 1989). Since then, numerous degradable biomaterials have been investigated and continue to play a critical role in clinical applications, as well as laboratory research. In recent decades, there have been major advances in the design and applications of synthetic polymeric degradable materials (Vert et al., 1992; Anderson and Shive, 1997; Langer and Tirrell, 2004). Through theoretical and experimental investigations, degradable polymers have found numerous applications, particularly in the fields of drug delivery (Siepmann and Göpferich, 2001) and tissue engineering (Langer and Tirrell, 2004; Tibbitt et al., 2015; Tibbitt and Anseth, 2009), and have resulted in high levels of commercialization (Deshayes and Kasko, 2013).

Definition of Degradation, Erosion, Bulk, and Surface Processes

Many of the important terms related to biodegradable materials are explained in this section and their definitions are summarized in Table 1.3.2F.1. Degradation is defined as a bond cleavage event leading to a change in structure of a material,



• **Figure 1.3.2F.1** Schematics (left) and representative mass loss as a function of time (right) for (A) surface erosion (B) bulk erosion. (Adapted from Figures 1 and 4 of [Burkersroda et al., 2002](#)).

characterized by a loss of properties and/or fragmentation ([Göpferich, 1996](#); [Williams and Zhang, 2019a](#)). Bond cleavage can occur through a variety of processes (i.e., hydrolysis, enzymatic activity, or exposure to light). Consequently, the molecular weight of the polymer decreases to form lower molecular weight oligomers and monomers, and ultimately results in the loss of mechanical stability of the material. While polymers can be degraded through a variety of mechanisms, such as thermal, mechanical, and photodegradation, the most common modes of degradation in a therapeutically relevant *in vivo* environment are either hydrolytic or enzymatic degradation. The term “biodegradation” is typically reserved for situations where the degradation involves biological entities and environments, such as bodily fluids, cellular activity, and/or enzymatic reactions. The conditions of the biological environment therefore determine the rate of polymer degradation to a great extent. For example, the degradation of a polymeric biomaterial may proceed faster when implanted in a highly inflammatory environment, due to excessive biological and biochemical activity. Thus context matters when selecting a degradable polymer for implantation. The pH and temperature of the local biological environment, enzyme concentrations, and cell infiltration/recruitment to the implant sites affect the rate of polymer degradation.

Erosion is defined as a process in which mass is lost that may result in a change in the physical size or shape of a device. How a material erodes is also an important consideration for polymer design ([Burkersroda et al., 2002](#)). Bulk erosion entails mass loss throughout a material, whereas surface erosion is restricted to the surface of the material and proceeds via an erosion front ([Tamada and Langer, 1993](#); [Woodard and Grunlan, 2018](#)). Surface erosion is useful in drug delivery applications, as the release rate of a drug from surface-eroding polymers is independent of diffusion and is easily altered by

changing the device geometry ([Tabata et al., 1993](#); [Wei et al., 2015](#)). It is important to note that both degradation and erosion processes can occur without the presence of water ([Fig. 1.3.2F.1](#)). Following this, bioerosion is defined as the process of erosion in a biological setting (e.g., enzymatic erosion).

Resorption is the process of eliminating the products produced through degradation. Resorption occurs in a variety of ways. For example, the degradation product of PGA is glycolic acid, which can be used in the Krebs cycle when produced *in vivo*. This example also highlights bioresorption, where the process of removal is via cellular activity and/or the dissolution of a material is in a biological environment ([Williams and Zhang, 2019b](#)).

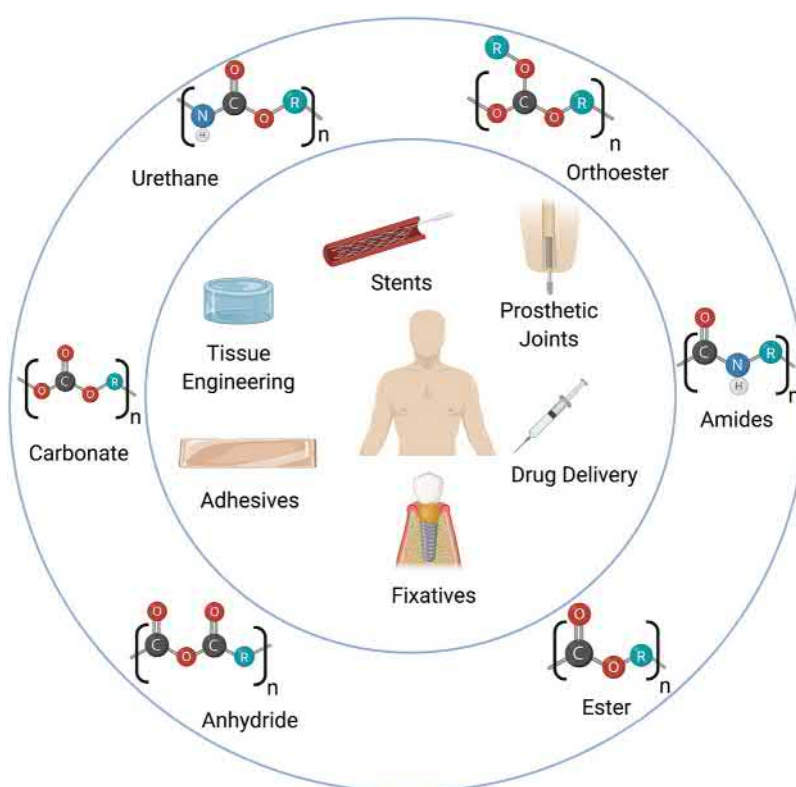
While this chapter primarily discusses degradation that is engineered into the polymer and its structure by design, one should always remember that *in vivo* implantation of any degradable polymer device can result in unintended degradation. For example, polyesters can be degraded *in vivo* by cell-secreted esterases in addition to hydrolysis.

Degradable Polymer Properties

Since the concept of polymerization emerged in the 1920s, development of polymers with defined molecular weights and chemical functionality has grown, especially as precursors to synthesize degradable biomaterials ([Fig. 1.3.2F.2](#)). To date, a wide range of degradable polymers has been developed to achieve controlled and tailorable degradation behavior ([Langer and Tirrell, 2004](#); [Nair and Laurencin, 2007](#); [Piskin, 1995](#)). In this section, important polymer properties that affect biomaterial degradation (e.g., polymer backbone functionality, polymer architecture, hydrophobicity/hydrophilicity, crystallinity) are discussed.

TABLE 1.3.2F.1 Definition and Examples of Key Processes

Term	Definition	Example
Degradation	A chemical process by which bonds are cleaved	Hydrolysis of poly(lactic acid)
Resorbable	The process of eliminating the degradation products	Bone resorption
Erosion	A process that results in the mass loss of a material that may result in a change of size, shape, or mass	Release of a drug through layer-by-layer erosion of a nanoparticle
Biodegradation	Cleavage of bonds as a consequence of a biological agent, such as an enzyme, cell, or microorganism	Enzymatic degradation of amorphous poly(L-lactide) by proteinase K
Bioerosion	Erosion in a biological setting	Microborers graze on the surface of coral slowly breaking down limestone
Surface Erosion	Erosion that is restricted to the surface of a material and proceeds via an erosion front	Surface erosion of polyanhydrides
Bulk Erosion	Erosion that occurs throughout a sample causing the whole material to degrade	Degradation of poly(glycolic acid)



• **Figure 1.3.2F.2** Overview of degradable polymer backbone functionalities and some of their applications as biomaterials. (Image created with biorender.com).

Polymer Backbone Functionality

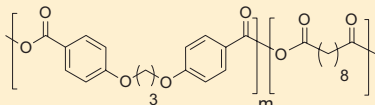
The most common backbone functionalities incorporated into polymer chains are hydrolytically susceptible groups (i.e., covalent bonds that degrade in the presence of water), which enables polymer degradation under biologically relevant conditions (Table 1.3.2F.2). In general, anhydrides and carbonates are among the fastest degrading chemical bonds, followed by ester and urethane bonds. Ortho esters and amides have the lowest rate of hydrolysis (Fig. 1.3.2F.3). The degradation rates of these chemical bonds, however, are

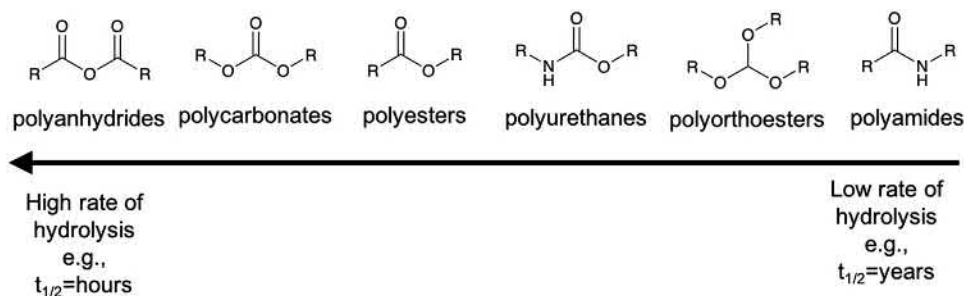
affected by several factors, such as the presence of nearby hydrophobic groups, changes in local pH due to degradation products, molecular weights of the polymer, and polymer architecture (Gombotz and Pettit, 1995).

Polyanhydrides

The anhydride linkage is among the least hydrolytically stable, so polyanhydrides are typically synthesized from hydrophobic diacids (Rosen et al., 1983). Hydrophobicity, which limits water penetration into the polymer, combined with the fast

TABLE 1.3.2F.2 Examples of Degradable Polymers and Their Commercial Uses as Biomaterials

Functional Group	Structure	Commercial Example	Commercial Use
Polyanhydrides	 Poly(PCPP-SA anhydride)	Gliadel	The treatment of glioblastoma multiforme
Polyesters	 Poly(lactic acid)	Lactosorb	Meniscal staples
	 Poly(glycolic acid)	Unify	Surgical sutures
Polycarbonates	 Poly(ε-caprolactone)	Monocryl	Drug delivery sutures
	 Poly(trimethylene carbonate)	Maxon	Monofilament resorbable sutures



• **Figure 1.3.2F.3** Relative hydrolytic rates of degradable functional groups. The rate at which the functional group degrades also depends on pH, crystallinity, equilibrium water content and architecture. (Adapted from Gombotz and Pettit (1995)).

hydrolysis rate of the anhydride linkage, leads to surface erosion, producing diacid monomers that can be metabolized by the body. Due to the fast-degrading anhydride bonds (days to weeks) and the nontoxic acid degradation products, polymers made from polyanhydrides have been used for short-term drug release for more than three decades (Leong et al., 1986; Rosen et al., 1983). The unique properties of polyanhydrides result in near zero-order drug release profiles from thin disks, but the geometry of the polymer (e.g., porous scaffolds, microspheres, disks) and composition of the diacids used to synthesize the polymers allow further tailoring of the release profile (Tabata et al., 1993; Tamada and Langer, 1992).

Poly(Ortho Esters)

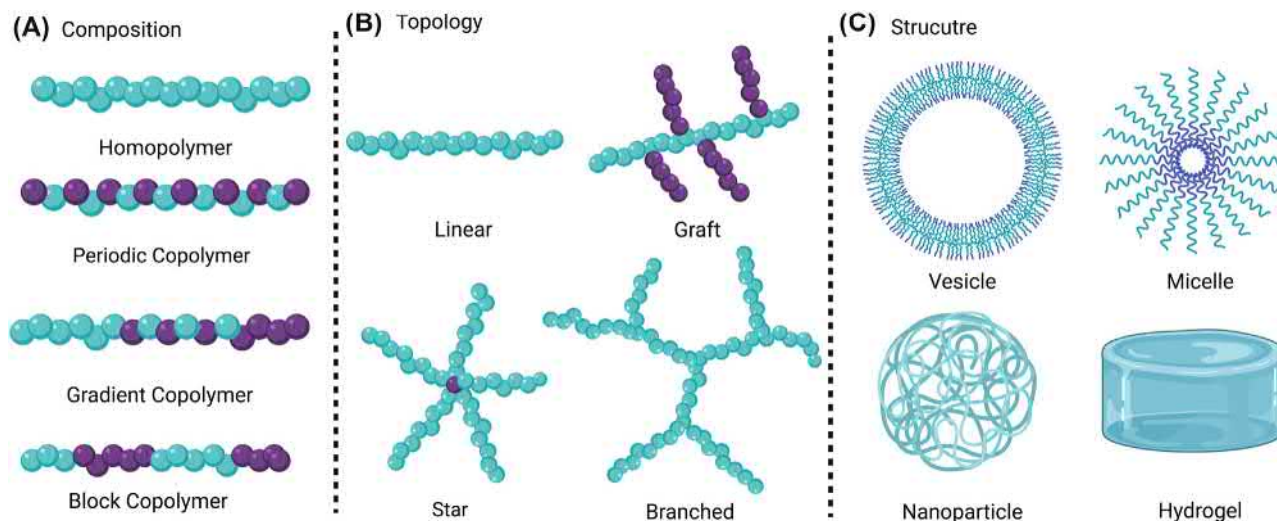
Compared to polyanhydrides, poly(ortho esters) are more hydrophobic, but still undergo surface erosion when degrading, albeit with slower degradation rates compared to polyanhydrides (Heller et al., 2002). The degradation of poly(ortho esters) produces esters as initial degradation products, followed by further degradation into acids and alcohols. The use of poly(ortho esters) as controlled release devices dates back to

the early 1970s (Heller and Barr, 2004). Since the polymers are surface eroding, drug release rates are controlled by the rate of polymer erosion, similar to the polyanhydrides, and can be tuned by the polymer composition and geometry of the device.

Polyesters and Polycarbonates

One of the most popular classes of degradable polymers, poly(α -hydroxy esters), falls into this category and includes poly(lactic acid) (PLA), PGA, and their copolymer, poly(lactic-co-glycolic acid) (PLGA). Poly(α -hydroxy esters) were among the first synthetic polymers with clinical applications (Gilding and Reed, 1979; Reed and Gilding, 1981). For example, PGA has long been used as a suture material due to its rapid erosion rate.

The hydrolysis of poly(α -hydroxy esters) occurs at the ester bonds in the polymer backbone, and is governed by the accessibility of water to those bonds. Upon cleavage, acidic degradation products (e.g., lactic acid and glycolic acid) are released that can lower the local pH and accelerate the hydrolytic degradation rate (Cha and Pitt, 1989). In addition, the monomers of PLA, lactic acid, and lactide have chiral centers (i.e., four different groups attached to a carbon atom, L and D form)



• **Figure 1.3.2F.4** Different polymer (A) compositions, (B) topology and (C) structures. (Images created with biorender.com).

enabling different stereo polymeric isomers to form (e.g., poly(L-lactic acid) and poly(D-lactic acid) (PDLA)). These PLA isomers have different degradation rates as a consequence of the accessibility of the ester groups to water molecules. The effect of crystallinity and hydrophobicity as a function of PLGA composition or stereochemistry of PLA and the influence on the degradation rate are discussed later in this chapter.

This category also includes poly(ϵ -caprolactone) (PCL), a commercially available polycarbonate, which has high solubility and a low melting temperature (59–64°C). It is a semicrystalline polymer with a low glass transition temperature, T_g . As such, in comparison to PGA, PCL has a lower mechanical strength but has been commercialized as an implantable contraceptive device, Capronor ([Brannigan and Dove, 2017](#)).

Many degradable devices are made from polymers with nondegradable backbone functionalities (e.g., poly(ethylene glycol) (PEG), polycyanoacrylates, and polyphosphazenes). Devices made from these polymers can be engineered to degrade through the addition of degradable functional end groups, side chains, or cross-linkers. Nondegradable polymers confer advantageous properties to the polymeric device. For example, PEG is a hydrophilic and nonfouling material that has been used extensively in the formation of degradable hydrogels through functionalization of pendant hydroxyl groups (see [Chapter 1.3.2E](#)). These polymer systems have found applications in adhesives, bandages, and photodegradable scaffolds ([Doppalapudi et al., 2014](#)).

Polymer Architecture

Polymerization Routes

Varying the architecture of a polymer, rather than its backbone chemistry and pendant functional groups, is equally important for controlling the final degradation pathways and kinetics. By considering polymerization conditions, polymers can be synthesized in a controlled manner with predictable degradation routes and products ([Nair and Laurencin, 2007](#); [Shalaby and Burg, 2003](#)). Many degradable polymers are synthesized through condensation and

addition polymerization routes (discussed in [Chapter 1.3.2](#) ([Odián, 2004](#))). Polycondensation of difunctional monomers preferentially yield low molecular weight polymers that can reduce the mechanical properties of the material ([Vroman and Tighzert, 2009](#)). Ring-opening polymerization reactions are commonly used to prepare polyesters from six- or seven-membered lactones that result in high molecular weight polymers ([Albertsson and Varma, 2003](#)).

To increase the predictable nature and to enhance the sophistication of the polymeric biomaterial, degradable polymers are synthesized through controlled radical polymerization routes, which allow for precise molecular weights and lower polymer dispersity to be obtained. The ratio of comonomers is included in a controlled, statistical manner. Two examples of controlled radical polymerization routes are reversible addition–fragmentation chain transfer (RAFT) and atom transfer radical polymerization (ATRP). RAFT is a living radical polymerization technique using a chain transfer agent, typically a thiocarbonylthio, that influences reaction kinetics and, consequently, properties of the resultant polymer ([Barner-Kowollik, 2008](#)). Alternatively, ATRP uses a metal complex to control the rate of monomer addition to the propagation polymer chain end, reducing termination of polymer end groups and lowering the dispersity of the polymer ([Wang and Matyjaszewski, 1995](#)). Both of these routes form polymers with predictable molecular weights, high functionality, and low dispersity, three important factors with regards to polymer degradation rate (see [Chapter 1.3.2](#) for more details).

In addition, these routes enable controlled synthesis of copolymers with different polymer compositions (e.g., statistical, gradient, and block copolymers, [Fig. 1.3.2F.4A](#)) and topologies (e.g., graft, dendritic, and star polymers, [Fig. 1.3.2F.4B](#)), each with different degradation profiles. For example, high ratios of hydrophilic monomers in a block copolymer would accelerate the degradation rate. Furthermore, star polymers synthesized with a degradable core (in which water can easily infiltrate) exhibit rapid degradation of pendant arms under the correct environmental conditions ([Rosselgong et al., 2013](#)). Copolymers are also able to self-assemble into different

structures (e.g., micelles, vesicles, and worm structures) (Fig. 1.3.2F.4C), facilitating sustained release of a drug or layer-by-layer degradation of a nanoparticle, with and without the use of external stimuli (e.g., light or pH) (Kocak et al., 2017; Rinkenauer et al., 2015; Zhang et al., 2015).

Molecular Weight

Degradation rate is also influenced by polymer molecular weight and is therefore an important consideration when designing a degradable polymeric device. The degradation rate increases as molecular weight increases as a consequence of the accessibility of functional groups for the degrading species. For example, PDLA with a molecular weight higher than 5000 Da is hard and rigid, making it difficult for the degrading species (e.g., water or enzymes) to access the backbone of the polymer. As a result, the time it takes to degrade high molecular weight PDLA is longer than for softer, lower molecular weight PLDA devices (Niaounakis, 2013).

Morphology

Depending on the structure, packing, and chemistry of the polymer chains, the resultant polymeric devices will have different rates of degradation. One of the most important polymer properties in the context of degradation is the T_g . T_g is the temperature at which a polymer transitions from a “glassy” to a “rubbery” state as the polymer chains gain sufficient thermal energy to undergo coordinated movement. Therefore a more rapid diffusion of degrading species occurs within the polymer matrix and, consequently, more rapid degradation is expected at temperatures above the T_g of the polymer. These characteristics are especially important when the T_g is near body temperature (37°C), which could lead to abrupt or unexpected changes in the bioerosion kinetics of the device.

In addition to polymers being classified as glassy or rubbery, polymers are also classified based on how the polymer chains pack together. Specifically, polymers have amorphous regions, where the polymer chains are randomly and loosely packed, and sometimes crystalline regions, where the polymer chains are densely packed in an ordered structure. Polymers that have both amorphous and crystalline regions are characterized as semicrystalline. For further explanation of these polymer characteristics, see Chapter 1.3.2. In the crystalline state, the crystalline domains resist the infiltration of the degrading specie (e.g., water, enzyme) because the polymer chains are densely packed, often leading to surface erosion in these areas (Fig. 1.3.2F.5A). Degradation is faster in the amorphous regions of semicrystalline polymers, where transport of degrading species is more facile, compared to the crystalline regions. A classic example of a strong dependence of degradation and erosion as a function crystallinity is PLGA. Both PLA and PGA have higher degrees of crystallinity, but the copolymers lead to decreased organization and lower degrees of crystallinity. Miller et al. showed that the half-life of the homopolymers to copolymers decreased from 5 months for 100% PGA to 1 week for 50:50 PGA:PLA and rapidly increased to 6.1 months for 100% PLA (Miller et al., 1977; Reed and Gilding, 1981)

(Fig. 1.3.2F.5B). This effect has been exploited in the commercialization of these polymers tailoring the degradation rate to specific applications by using different monomer ratios (Middleton and Tipton, 2000).

Stereochemistry also affects morphology and crystallinity and thereby the degradation rates of degradable polymers. One predominant example is in the synthesis of PLA from different stereoisomers (D-lactide, L-lactide, DL-lactide). Although both monomers lead to the same chemical backbone structure and degree of hydrophobicity, biomaterials made from the L isomer will degrade slower than identical polymers made from a mixture of the D and L isomers. This is a consequence of the stereoregularity of the pure L isomer making it a semicrystalline polymer, whereas the racemic polymer (made from D and L isomers) is amorphous (Farah et al., 2016) (Fig. 1.3.2F.5C).

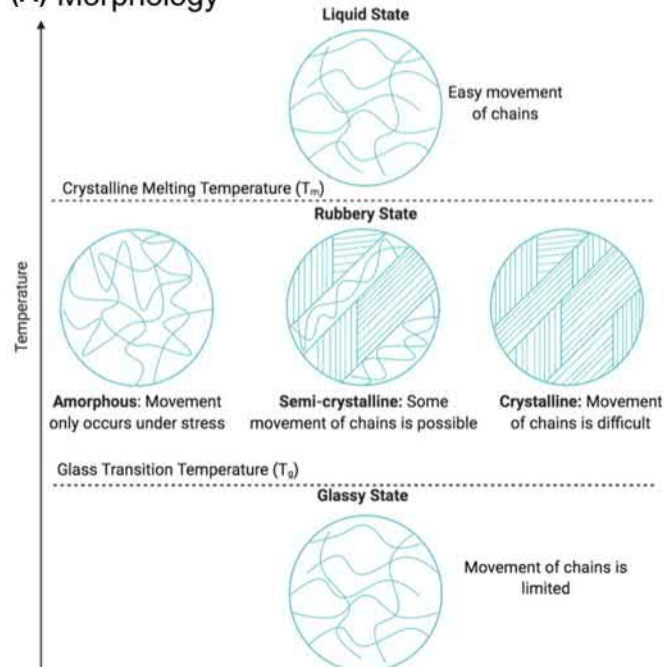
Relative Hydrophobicity versus Hydrophilicity

Although polymers can degrade through many different processes, in most biomedical cases water is present and will affect the rate of degradation. For hydrolytic degradation the amount of water surrounding the polymer and its proximity to neighboring functional groups underpins the rate of degradation. For enzymatic degradation, enzyme diffusion into polymeric matrices, and thereby accessibility to the enzyme labile linkages, is also directly influenced by water distribution. Therefore the hydrophilic/hydrophobic nature of the polymer will affect the degradation rate of both hydrolytically and enzymatically degradable biomaterials. For example, the erosion rate of polyanhydrides can be controlled through the addition of a more hydrophobic monomer, bis(carboxy phenoxy)propane (CPP), compared to sebacic acid (SA) as the monomeric starting material (Tamada and Langer, 1993). Pure P(CPP) has a lifetime of over 3 years, whereas after copolymerization with 80% SA the lifetime is reduced to a few days, allowing this material to be used for drug delivery (Leong et al., 1986) (Fig. 1.3.2F.5D). P(CPP:SA) (20:80) is approved by the US Food and Drug administration (FDA) for the treatment of malignant glioma as Gliadel wafers. It is processed into a wafer with the chemotherapy drug carmustine dispersed throughout. The hydrophobic nature of P(CPP:SA) provides the encapsulated drug with some protection from hydrolytic degradation before release from the wafer. This is important as carmustine has a half-life of only 52 min at 37°C (pH 7.4) (Fleming and Saltzman, 2002). For more information on Gliadel wafers, see Case Study III (Askeland et al., 1996).

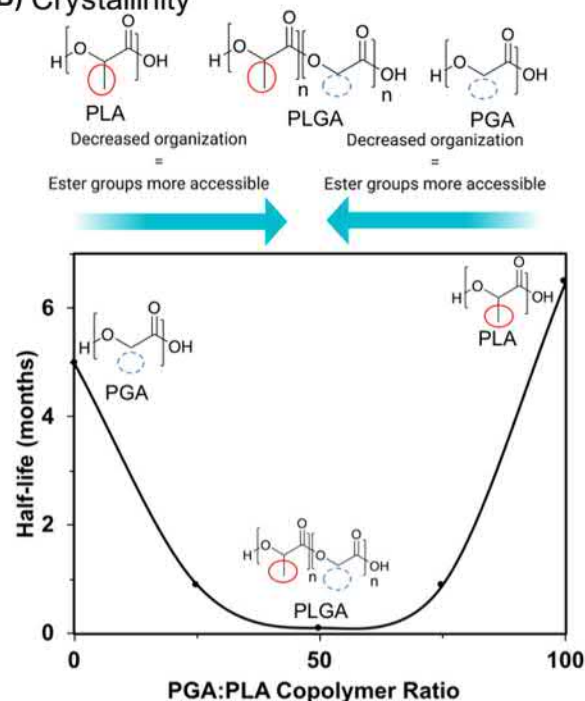
Degradation Routes and Kinetics

The route of polymer degradation depends not only on the linkers within the polymer backbone and its pendant functionalities, but also external stimuli. As noted previously, degradable polymers are designed to break down under biologically relevant conditions, primarily through hydrolysis or enzymatic activity. However, other unintended degradation routes can occur as a consequence of insertion of a biomaterial into the body, including oxidative and physical degradation. Oxidative degradation typically occurs as a result of

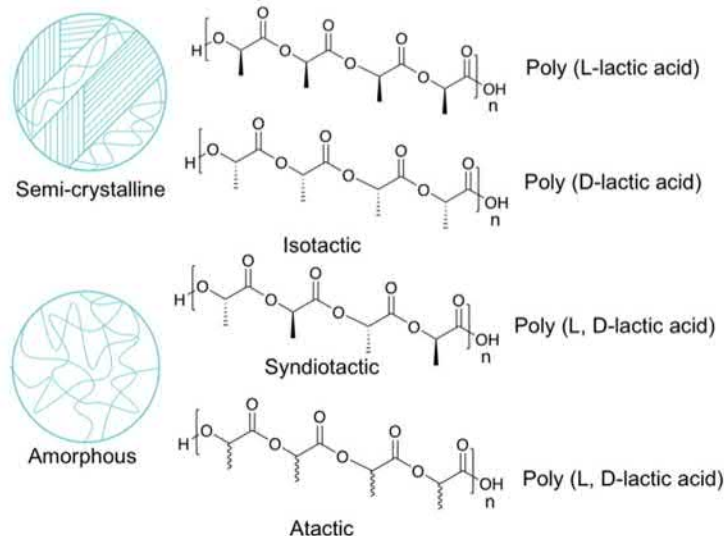
(A) Morphology



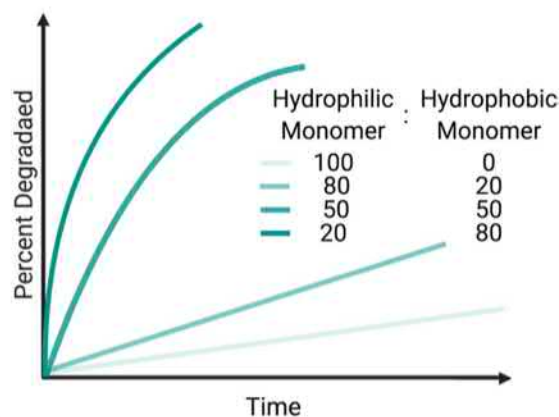
(B) Crystallinity



(C) Stereochemistry



(D) Hydrophobicity



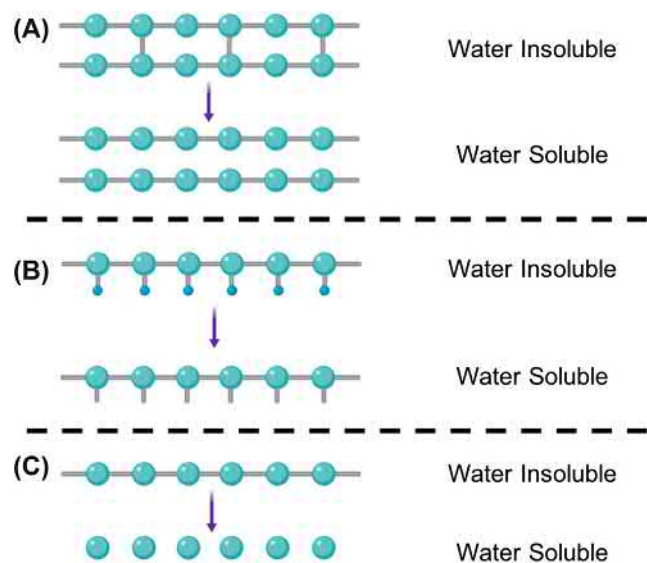
• **Figure 1.3.2F.5** Effect of: (A) Morphology; where increasing temperature allows a polymer to go from a glassy structure where polymer chains are unable to move, reducing degradation rate to above their T_g and are able to degrade depending on the stacking of the polymeric chains. Adapted from *The Science and Engineering of Materials*, Donald. R. Askeland, 2nd Edition, Chapman and Hall, (B) Crystallinity; the addition of disorder through copolymerization of PLA with PGA to form PLGA, reduces crystallinity decreasing the rate of degradation. Figure adapted from [Miller et al. \(1977\)](#) (C) Stereochemistry; Isotactic PLA leads to stereoregularity reducing degradation. Syndiotactic (alternating isomers) and atactic (no regular repeating stereochemical configuration) forms racemic polymers increasing degradation (D) effect of increasing the hydrophobic nature of a copolymer on the rate of degradation. (Adapted from [Leong et al. \(1986\)](#)). Images created with [biorender.com](#).

an inflammatory response. Macrophages from the inflamed site produce peroxide radicals that react with covalent bonds within the polymeric structure, leading to polymer degradation. Physical degradation is often attributed to mechanical forces on the implanted material, including mechanical loading of the implant, discussed in detail in [Chapter 2.4.2](#). This

section will primarily focus on intended or engineered chemical degradation pathways, including hydrolytic, photo-, and enzymatic degradation, and their kinetics.

Chemical degradation is the term used when covalent bonds are cleaved through a stimulus (e.g., hydrolysis, enzymes, pH, or light). Three mechanisms of chemical degradation by which

cleavage of bonds leads to the formation of water-soluble polymers or oligomers have been identified: (1) cleavage of crosslinks between polymer chains, (2) cleavage of side chains, or (3) cleavage of the polymer backbone (Rosen et al., 1983) (Fig. 1.3.2F.6). In reality, a combination of these routes is used for the degradation of polymeric biomaterials.



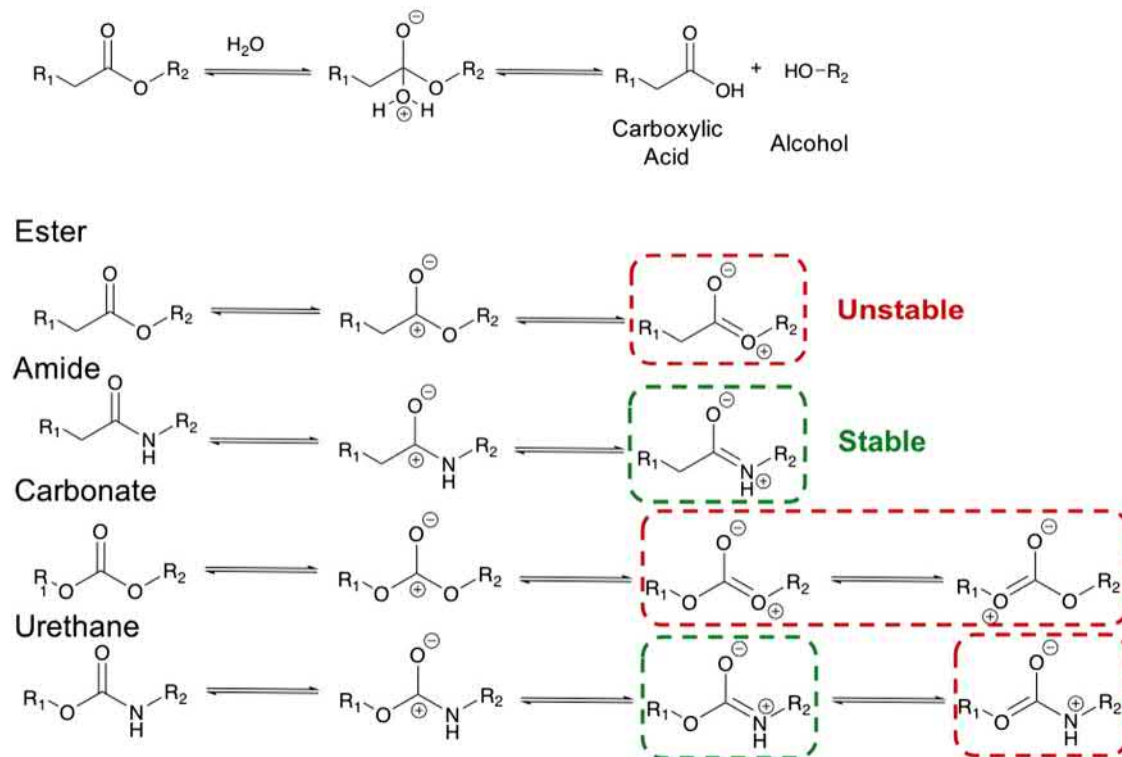
• **Figure 1.3.2F.6** Mechanism of chemical degradation, adapted from Gombotz and Pettit 1995, (A) Mechanism 1: Cleavage of crosslinks between water soluble polymer chains, (B) Mechanism 2: Cleavage of side chains leading to polar groups or charged groups, (C) Mechanism 3: Cleavage of backbone linkages between polymer repeat units. (Images created with biorender.com).

Hydrolytic Degradation

Hydrolysis is defined as the reaction of water with susceptible bonds in a compound to form two or more products (Göpferich, 1996). The susceptibility of a covalent bond to hydrolysis is dependent on the charge of the reacting carbon, steric effects, and the conjugated structures formed (Fig. 1.3.2F.7). The more stable the conjugated structure, the lower the rate of its hydrolysis (e.g., amides, carbonates, urea). For hydrolytic degradation of polymer chains, chemically identical bonds should have equal reactivity irrespective of chain position, unless steric hindrance, hydrophobicity of repeating unit, or pH of the local environment changes (Brannigan and Dove, 2017; Lyu and Untereker, 2009). Depending on the rate of the hydrolysis reaction relative to the rate of water penetration, the degradation either occurs uniformly throughout the polymer device (i.e., bulk degradation) or is confined to an interface (i.e., surface erosion). These processes are discussed in more detail below.

Surface Erosion

The kinetics of surface-eroding polymers has been well studied. The hydrolysis of surface-eroding polymers starts at any exposed interface and gradually proceeds to the interior. If a drug or other molecule is entrapped in the polymer, the release rates are often correlated directly to the mass loss. To facilitate experimental observation, surface-eroding polymers, such as polyanhydrides, are often fabricated as disks with high aspect ratios (e.g., large diameter compared to the thickness of the polymer), such that the surface area of the



• **Figure 1.3.2F.7** Stability of conjugated structures of hydrolyzable bonds. (Adapted from Brannigan and Dove (2017)).

polymer remains roughly constant throughout degradation. Thus the rate of polymer erosion can be expressed as:

$$\frac{dM}{dt} = -k \quad (1.3.2F.1)$$

where M is the polymer mass at any given time (t) and k is the kinetic rate constant of the degradation. Assuming one-dimensional erosion and constant density, Eq. (1.3.2F.1) can be rearranged into:

$$\frac{dl}{dt} = -k' \quad (1.3.2F.2)$$

where l is the dimension of the polymer in the direction of degradation front at any given time (t) and k' is the adjusted rate constant.

Eq. (1.3.2F.2) can be easily solved to obtain:

$$l = l_0 - k' t \quad (1.3.2F.3)$$

Eq. (1.3.2F.3) illustrates a linear decrease in polymer thickness as the polymer degrades. This linear relationship is very useful in controlled release applications, as drug release rates can be stringently controlled by the rate of polymer mass loss and approach zero-order release. Eqs. (1.3.2F.1)–(1.3.2F.3) dictate the kinetics of surface erosion when the device is fabricated as thin slabs. For other geometries, such as cylinders and spheres, similar equations can be derived accordingly, and once k' is known, multidimensional degradation profiles can be predicted as well.

Experimental Tools for Characterizing Surface Erosion Kinetics

Qualitatively, surface erosion is often characterized using imaging methods, including scanning electron microscopy and atomic force microscopy, which show changes in the surface of the device (e.g., nonuniform surfaces). Other tools, including ellipsometry, surface plasmon resonance (SPR), and Fourier transform infrared (FTIR) spectroscopy, are being used to experimentally quantify degradation and erosion kinetics as a function of polymer thickness (Deng et al., 2019). Ellipsometry, SPR, and FTIR are all optical techniques, where signal changes correspond to changes in the sample's thickness, refractive index, and/or composition. These are useful tools for characterizing hydrolytic degradation, because as water diffuses into a polymer matrix or erodes the surface of the polymer, the refractive index and/or thickness decreases, leading to a detectable change in signal.

Bulk Degradation

For hydrolytic bulk degradation, a majority of studies focus on the mechanism of polyester degradation, particularly PLA and its copolymers with PGA. More contemporary examples include the bulk degradation of hydrogels with degradable cross-links, in which case the water content is much higher compared to PLA and PGA. For the purpose of this discussion, we focus on polyester degradation, as it is one of the most widely used linkers in polymeric biomaterials. Hydrolysis of a polyester is usually described as

a random polymer chain scission throughout the polymer and is auto accelerated by increasing carboxylic acid end groups. The hydrolysis of ester bonds to produce carboxylic acids can be expressed as:

$$-\frac{d[\text{Ester}]}{dt} = k [\text{Ester}] [\text{H}_2\text{O}] \quad (1.3.2F.4)$$

Here, $[\text{Ester}]$ is the concentration of ester bonds in the polymer, t is the degradation time, k is the kinetic rate constant, and $[\text{H}_2\text{O}]$ is the concentration of water. As a simplifying assumption for bulk degrading polyesters, the water concentration is often considered constant. Then, Eq. (1.3.2F.4) simplifies to:

$$-\frac{d[\text{Ester}]}{dt} = k' [\text{Ester}] \quad (1.3.2F.5)$$

where k' is a pseudo-first-order rate constant. Integrating Eq. (1.3.2F.5) yields the following equation:

$$\frac{[\text{Ester}]}{[\text{Ester}]_0} = e^{-k' t} \quad (1.3.2F.6)$$

where $[\text{Ester}]_0$ is the initial ester bond concentration. Since $[\text{Ester}]$ is related to the molecular weight (M_n) of the polymer at any time during degradation, Eq. (1.3.2F.6) can be expressed as:

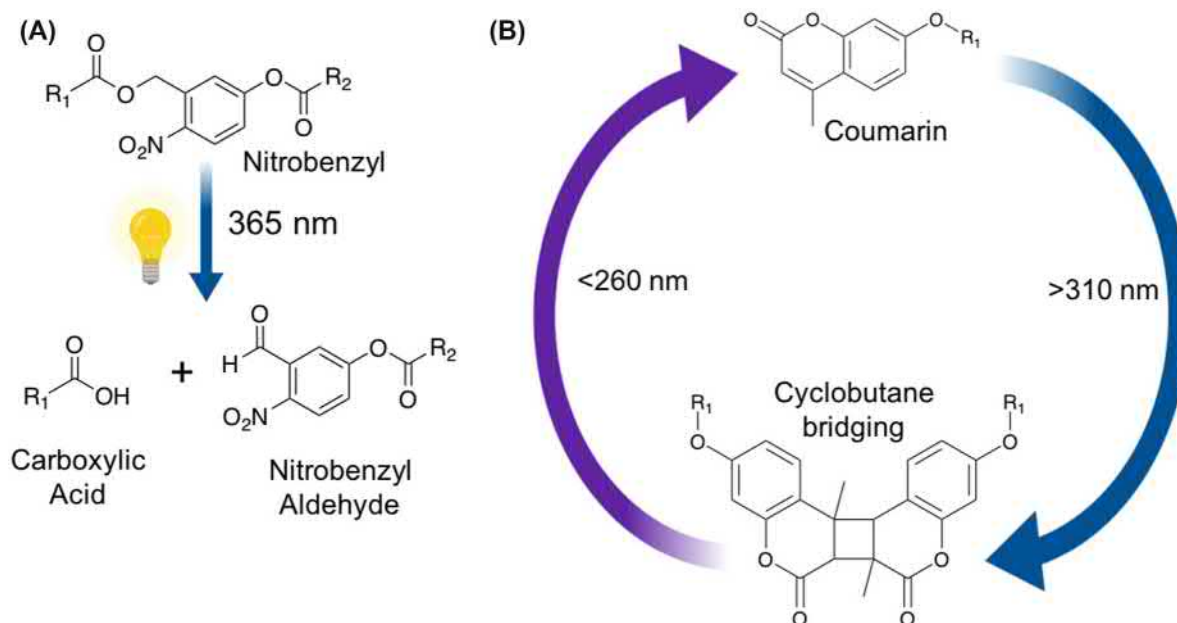
$$\frac{M_n}{M_{n0}} = e^{-k' t} \quad (1.3.2F.7)$$

In examining Eq. (1.3.2F.7), one readily notes that the molecular weight of the degrading polymer decreases exponentially. It should be noted that Eq. (1.3.2F.7) only holds until significant degradation causes the loss of oligomers and carboxylic acids. It has been observed that this relationship is approximately true until the molecular weight of the polymer decreases to below 5000 Da (Pitt et al., 1981). Substitution of the Mark–Houwink equation ($[\eta] = KM_n^\alpha$) into Eq. (1.3.2F.7) yields:

$$[\eta] = [\eta]_0 \cdot e^{-\alpha k' t} \quad (1.3.2F.8)$$

Here, η is the intrinsic viscosity of the polymer, and α is the Mark–Houwink exponent, which depends on the solvent in which the polymer degrades. Eq. (1.3.2F.8) is practical as it allows the experimenter to monitor polymer degradation by measuring the change in its intrinsic viscosity.

Eqs. (1.3.2F.4)–(1.3.2F.8) only illustrate the basic kinetics of ester bond hydrolysis in bulk-degrading polymers. The prediction of mass loss kinetics in the bulk-degrading polymers, however, often requires more sophisticated mathematical models, as simple cleavage of bonds does not accurately reflect loss of mass from the polymer device (e.g., hydrogel networks). For more information on hydrogel degradation and statistical models, see Wong and Bronzino (2007).



• **Figure 1.3.2F.8** Examples of photodegradable groups, (A) nitrobenzyl degrades with 365 nm light, (B) 2+2 cycloaddition of coumarin at 310 nm to form a cyclobutene link. The group degrades back to coumarin at wavelengths below 260 nm. (Images created with [biorender.com](https://www.biorender.com)).

Photodegradation

In recent decades, the advantage of using light as a tool to synthesize and degrade biomaterials has been recognized. Photodegradable polymers have been used in numerous applications for biopatterning, photo(un)caging of biologics, and drug delivery using different polymeric structures, including block copolymers, surfaces, and hydrogels (Bajaj et al., 2014; Li et al., 2014). Light offers specific advantages over more traditional degradation routes, as it allows for precise temporal and spatial control by controlled illumination via photomasks, using focused laser light, or varying the light intensity or shuttering the light source. There are a variety of photodegradable groups that have been incorporated into polymers depending on the application and function of the device (e.g., nitrobenzyl derivatives, coumarins, vinyl ketones, pyrene esters) (Fig. 1.3.2F.8, Pasparakis et al., 2012). Through careful choice of wavelength and intensity, cytocompatible light (e.g., >365 nm) can be used to degrade biomaterials in the presence of cells. Photodegradable biomaterials have predominantly been used in tissue engineering, allowing for precise spatio-temporal control over material properties, capturing extracellular matrix heterogeneity in a synthetic scaffold (Brown and Anseth, 2017). Furthermore, photodegradation has been applied for release of biomolecules from a network, as well as spatially controlled photopatterning (Kloxin et al., 2010; DeForest and Anseth, 2011; Arakawa et al., 2017).

In this field, a common method involves incorporation of photolabile cross-linkers into a network, especially hydrogels. When irradiated with a specific wavelength, the cross-linked molecules absorb light causing bond rearrangement and cleavage of the cross-links. The reactions depend on the intensity and wavelength of light, as well as the photophysical properties of the photodegradable linker. First-order kinetics

are often relevant to describe the rate of cleavage through a material with uniform illumination, Eq. (1.3.2F.9):

$$\frac{dC}{dt} = -kC, \quad k = \frac{\Phi \epsilon I}{N_A h \nu} \quad (1.3.2F.9)$$

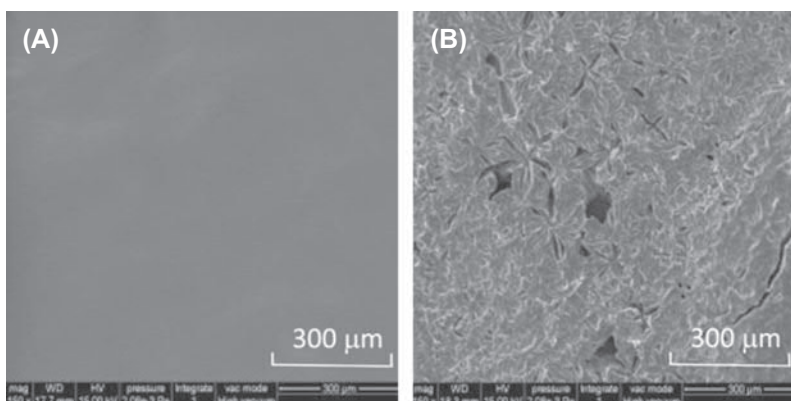
Here, C is the concentration of absorbing species and the kinetic rate constant k is a product of the quantum yield (Φ) and absorptivity (ϵ) of the photoactive species at the wavelength used along with the light intensity (I), light frequency (ν), Planck's constant (h), and Avogadro's number (N_A). For elastomers, the rate of cleavage of a photolabile cross-linker can be related to a network's storage modulus (G') and cross-link density (ρ_x), which can be used to predict changes in material properties and mass loss with time, Eq. (1.3.2F.10):

$$\frac{G'}{G'_0} = \frac{\rho_x}{\rho_{x,0}} = e^{-kt} \quad (1.3.2F.10)$$

Enzymatic Degradation

Several synthetic polymers are susceptible to enzymatic degradation. For example, amorphous PLA can be degraded by proteinase K, while both amorphous and crystalline PCL can be degraded by lipases of various origins (Liu et al., 2000, 2019) (Fig. 1.3.2F.9).

Enzymatic degradation of synthetic polymers can occur by either surface or bulk mechanisms, depending on the location and stability of the acting enzyme. However, due to the limited water accessibility of most hydrophobic polymers, surface erosion is often the dominant degradation mechanism, described in an earlier section of this chapter. The degradation for a hydrophilic polymer, permitting the diffusion of the



• **Figure 1.3.2F.9** Scanning electron micrographs of esterase degraded PCL films after 48 h; (A) control PCL film (no enzyme present), (B) Lipase degraded film, Magnification 150x. (Adapted from Liu et al. (2019)).

enzyme to the interior of the polymer, can also be mediated by a surface erosion mechanism if the rate of enzymatic polymer bond cleavage is faster than the rate of enzyme diffusion. Bulk degradation of synthetic polymers induced by enzymatic activity may occur under two conditions: (1) the enzyme is able to infiltrate and distribute uniformly throughout the bulk of the polymer, and (2) the rate of enzymatic bond cleavage is slower than the diffusion of the enzyme. Typically, hydrogels containing enzymatically cleavable units in their polymer backbone fall into this category of degradation. Under these assumptions, Michaelis–Menten enzymatic kinetics are commonly used to predict the enzymatic degradation rates of synthetic polymers via a bulk degradation mechanism:

$$v_0 = v_{max} \frac{[S]}{K_M + [S]} \quad (1.3.2F.11)$$

Here, v_0 and v_{max} are the initial and maximum reaction rate of degradation, respectively. $[S]$ is the degradable polymeric substrate concentration, and K_M is the Michaelis–Menten constant.

In Eq. (1.3.2F.11), v_{max} can also be expressed as:

$$v_{max} = k_{cat} [E] \quad (1.3.2F.12)$$

where k_{cat} is the catalytic constant describing the rate of enzymatic degradation of polymer bonds and $[E]$ is the concentration of enzyme catalytic sites.

As in other enzymatic reactions, both k_{cat} and K_M are important parameters in characterizing the enzymatic degradation of polymers. While k_{cat} represents the sensitivity of an enzyme for a specific polymeric substrate, K_M is the substrate concentration needed to achieve a half-maximum enzyme velocity. Factors affecting these parameters will also determine the rate of polymer degradation.

While simple Michaelis–Menten kinetics can be used to describe enzymatic polymer bond cleavage, they do not provide information regarding the mass loss behavior of the polymers. Sophisticated mathematical models are often required to correlate microscopic enzymatic bond cleavage to macroscopic polymer mass loss, and it depends on the structure and connectivity of the polymer. For example, to describe the mass

loss of cross-linked hydrogels containing enzymatic cleavable substrate (e.g., PCL), a statistical-kinetic model integrating the structural information of the hydrogels with the enzyme degradation kinetics is required (Rice et al., 2006).

Orthogonal Stimuli-Labile Strategies

While most degradable polymer systems rely on single degradation pathways, materials capable of undergoing multiple routes of degradation have emerged in recent years. For example, release of model therapeutics from hydrogels with orthogonal stimuli-labile linkers was demonstrated. The degradation routes were reduction of disulfide bonds, enzymatic cleavage, photodegradation, or combinations thereof, leading to logic-based, controlled release (Ruskowitz et al., 2019). Adopting such a strategy to include light, enzyme, or other stimuli-degradable linkages within a hydrolytically degradable scaffold will enable development of other tailorable scaffolds for precision medicine applications.

Polymer Design and Processing

The chemical structure (e.g., backbone functional groups, crystallinity, and architecture) of a polymer significantly influences its degradation mechanism and rate. Because of this, it is often desirable to use well-studied degradable polymers (e.g., PLA, PLGA) for the synthesis of biomaterial devices, because their breakdown is better understood *in vivo* and they are used in many FDA-approved applications, giving precedent for use in other applications. As biomaterials are required for a growing number of clinical applications, from synthetic replacements for biological tissue to materials as diagnostics (Langer and Tirrell, 2004), more sophisticated polymers are continually being developed. However, in designing a new degradable biomaterial, one must first understand the unique performance requirements and constraints for the intended application, including lifetime, location, mechanical properties, and delivery method (Table 1.3.2F.3). Then, different polymer-processing strategies can be applied to meet the design requirements, in terms of both degradation rate and overall performance. This section covers the design and processing considerations that are especially important for degradable biomaterials, providing examples of degradable systems that are commercially available or are being explored in academia.

TABLE 1.3.2F.3 Design Criteria of Different Degradable Biomaterial Application With Polymer Examples

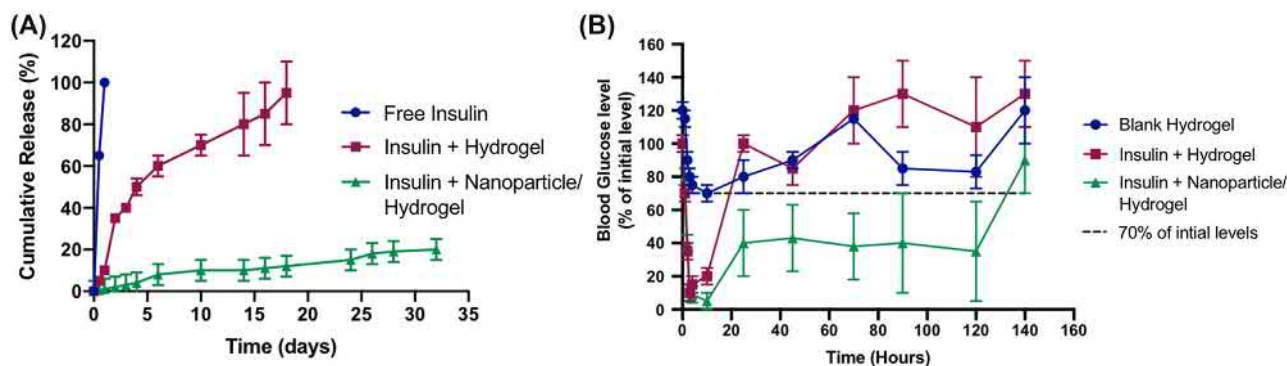
Application	Function	Lifetime/ Biodegradation Time	Location in the Body	Mechanical Properties	Mechanism of Delivery	Degradable Polymer Examples
Bone Fixatives	Provide support to the joint, alleviate pain/arthritis	More than 10 years	Bone joint, high mechanical load	High modu- lus, good fracture toughness	Surgery	Poly(lactic acid), poly(glycolic acid), poly(caprolactone)
Sutures	Allow improved healing process without secondary surgery/reduce inflammation	1 week–1 month	Organ, skin	High tensile strength	Surgery	Poly(trimethylene carbonate), polydioxanone
Drug Delivery	Releases drug to a target site	Dependent on location/deliv- ery short term/ long term	Digestive track, blood stream, tumor	Not critical	Oral/ injection	Poly(ortho-esters), polyphospha- zenes
Adhesives	Wound healing, hemorrhage control, drug car- riers, closure of pulmonary leaks	1 week–Years	Skin	High adhe- sion strength	Surgery	Poly(lactic-co- glycolic acid), degradable hydrogels

Lifetime—How Long Does the Biomaterial Need to Function?

For any given device, the time that a biomaterial is required to perform a desired function must be known. Some materials are only required for a short period of time, on the order of days to week, serving a temporary function that allows for rapid tissue healing (e.g., sutures). Other biomaterials are required to last longer and degrade slowly over months and years as regrowing tissue infiltrates the scaffold (e.g., some bone fixation devices). In drug delivery, an important aspect is to deliver a drug at a constant rate over a predictable amount of time and at a dose that can be tuned for the patient (Sershen and West, 2002). The lifetime of a biomaterial can be controlled by varying different aspects of the polymer design (e.g., backbone functionality, porosity, shape). For example, diabetic patients require daily intravenous insulin injections, which could lead to “peak-and-valley-shaped” drug-concentration profiles in the body and cause gastrointestinal side effects and patient discomfort (Bratlie et al., 2012). Through the use of biodegradable polymeric nanoparticles (e.g., poly(3-hydroxybutyrate-co-3-hydroxyhexanoate) embedded in a thermosensitive, injectable hydrogels), the release rate of insulin can be tightly controlled, a strategy with significant potential to meet the therapeutic needs of diabetic patients (Peng et al., 2013) (Fig. 1.3.2F.10).

Location—Where Will the Biomaterial Perform Its Task?

The body is made up of a range of different environments (e.g., different pH levels, high vs. low moisture environments, varied enzyme concentrations) that need to be considered collectively when designing a functional polymeric biomaterial for any given setting. For example, when designing gastric devices (e.g., weight loss balloons, ingestible diagnostic devices, oral drug delivery formulations) the biomaterial needs to reach its target area intact after traveling through areas with vastly different pH and enzyme profiles (Knipe et al., 2015). For example, Zhang et al. designed a gastric-retentive device from a supramolecular hydrogel (e.g., poly(acryloyl 6-aminocaproic acid) and poly(methacrylic acid-co-ethyl acrylate) system) that could respond to changes in pH through protonation and deprotonation of carboxylic acid side chains (Zhang et al., 2015). The elastic nature of the polymer enabled packing of the structure into a gelatin capsule to allow for oral delivery. The material was designed to change shape as it moved through the digestive tract, retaining its extended shape in the gastric environment to perform its function (e.g., release of a drug or delivery of a gastric balloon) before degrading at neutral pH once it moved into the small intestines, preventing intestinal obstructions (Fig. 1.3.2F.11). This application demonstrates how the application of degradable polymers can increase the safety and efficacy of biomaterials.



• **Figure 1.3.2F.10** (A) In vitro release of free insulin (circle), free insulin-loaded hydrogel (square) and nanoparticle-loaded hydrogel (triangle) in PBS (pH 7.4) at 37°C, (B) Blood glucose level-time curve after subcutaneous injection into mice of blank blank hydrogel (circle), free insulin loaded hydrogel (square) and nanoparticle-loaded hydrogels (triangle) to male diabetic rats. Showing the nanogels had a remarkable retaining effect enabling the therapeutic effects to last 5 days. Data presented as mean \pm SD (n = 5). (Adapted from Peng et al. (2013)).

Mechanical Properties—What Mechanical Properties Are Required for the Task?

The mechanical properties required for the application should be determined based on both the location of the device and the timescale of degradation required (Engelberg and Kohn, 1991). While nondegradable devices have stable and predictable mechanical properties throughout their duration of use, degradable devices will exhibit a decrease in most mechanical properties (e.g., strength, modulus) as the polymer degrades. In some cases, especially those that involve implantation in a load-bearing site, it is critical to match the breakdown of the polymer mechanical properties with the biological repair time. For example, sutures must maintain sufficient tensile strength to keep the wound closed until it heals. The polymer used to make sutures should also allow doctors to easily stitch and tie the sutures without breaking. For orthopedic applications, polymeric devices with initially high mechanical strength and good fracture toughness, comparable to the mechanical properties of the native tissue, are required to support load bearing. Ideally, gradual stress transfer will occur as the biomaterial degrades and the tissue heals (Brauer et al., 2008) (Fig. 1.3.2F.12).

Delivery—How Will the Biomaterial Reach the Required Site?

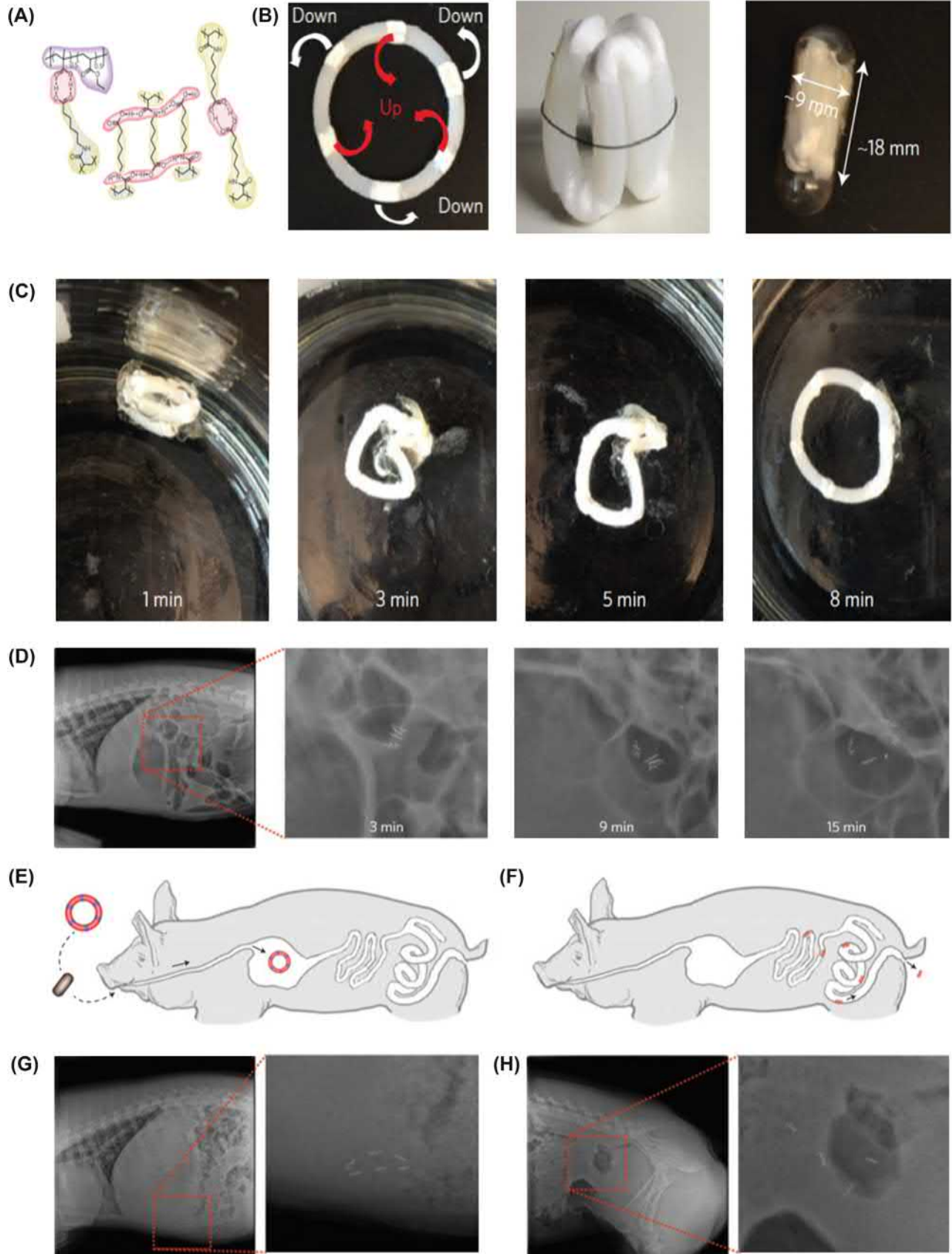
The delivery mechanism by which the biomaterial will reach its intended site without degrading should also be carefully considered when designing degradable polymeric biomaterials. Popular modes of delivery are injection, surgical implantation, or ingestion. Injections are commonly used to deliver shear thinning hydrogels that serve as drug and cell delivery vehicles (Bakaic et al., 2015). Injections minimize invasive surgery, leading to faster recovery times and reduced infection rates and costs. Furthermore, the material injected can fill voids and pack defects specific to the patient, without needing to preshape the material, which leads to improved comfort and efficacy. A range of different approaches is available to make degradable polymers injectable, including use of covalent adaptable

networks (e.g., oxime and hydrazine chemistries) or use of in situ-forming devices that rely on thermoresponsive chemistries (Kretlow et al., 2007), photopolymerization (Rydholm et al., 2005), or solvent-exchange strategies (Parent et al., 2013).

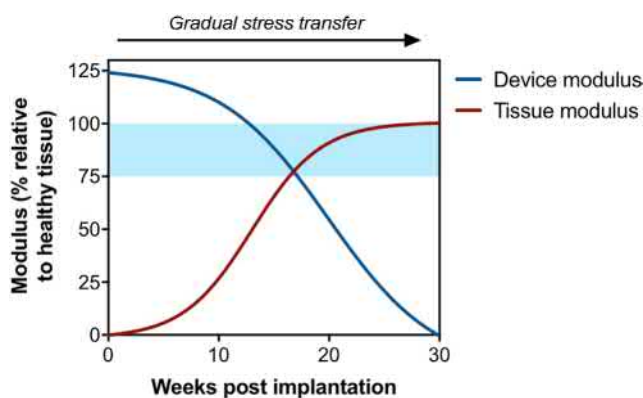
Covalent Adaptable Networks

Covalent adaptable networks are structures that incorporate exchangeable chemical bonds that undergo cleavage and reformation in response to an external stimulus (e.g., mechanical force, heat, base). An active species undergoes a reaction that results in bond exchange and the formation of new active species, which subsequently undergoes an additional exchange reaction (Bowman and Kloxin, 2012). Covalent adaptable chemistries used in polymeric biomaterials include boronate esters (Smithmyer et al., 2018), Diels–Alder (Kalaoglu-Altan et al., 2017), imines (i.e., oxime and hydrazone) (Boehnke et al., 2015), and thioester chemistries (Brown et al., 2018). The presence of these dynamic chemistries can lead to depolymerization or dynamic changes in mechanical properties. In tissue-engineering applications, covalent adaptable hydrogel networks have been synthesized to more closely mimic tissue viscoelasticity and support matrix deposition by encapsulated cells. For example, hydrazones and their network reorganization allow stress relaxation in a hydrogel with encapsulated, proliferating chondrocytes. The relaxation can be tuned to foster the deposition of a collagen and proteoglycan-rich matrix by the encapsulated cells (Richardson et al., 2019).

Injectable, in situ-forming devices or implants that rely on solvent-exchange strategies have been designed such that they set into their shape inside the body by relying on insolubility of the polymer in water. Specifically, degradable polymers (e.g., PLGA) are dissolved in a biocompatible solvent, such as *N*-methyl-2-pyrrolidone or dimethylsulfoxide, before injection. Upon injection, solvent exchange occurs, increasing the concentration of water near the polymer as the solvent diffuses away from the injection site. When the surrounding concentration of water is sufficiently high, phase inversion occurs, causing the polymer to precipitate. The shape that the polymer takes depends on the concentration of polymer in the solvent and the miscibility of the solvent with water. The rate of in situ formation and the structure formed by the polymer, which are



• **Figure 1.3.2F.11** A pH-responsive supramolecular polymer gel as an enteric elastomer for use in gastric devices. (A) Supramolecular polymer gel network. Structures in yellow, synthesized poly(acryloyl 6-aminocaproic acid) (PA6ACA); structures in purple, linear poly(methacrylic acid-co-ethyl acrylate) (EUDRAGIT L); red, inter-polymer hydrogen bonds. (B) Folding of the ring into a standard gelatin 000 capsule by using the elasticity of the polymer gel. (C) Escape from the capsule and recovery to the ring shape after dissolution of the gelatin capsule in simulated gastric fluid at 37°C. (D) Recovery of the ring shape after delivery of an encapsulated ring-shaped device through the esophagus and dissolution of the gelatin capsule in the stomach of a Yorkshire pig. (E) Schematic representation of the delivery and gastric retention of a ring-shaped device. (F) Schematic illustration of safe passage of PCL arcs through the small and large intestine on dissociation of the ring-shaped device as a result of the total or partial dissolution of enteric elastomer linkers. (G) X-ray image of a ring-shaped device residing in the gastric cavity of a Yorkshire pig. (H) X-ray image of four PCL arcs passing through the intestine after dissolution of the enteric elastomer linker. For visualization purposes, six to ten radio-opaque stainless steel beads (1 mm diameter) were incorporated in every PCL arm. The total bead mass was 200 mg and the weight of the whole device (with iron beads) was 1,000 mg. Figure adapted from Zhang et al. (2015).



• **Figure 1.3.2F.12** The mechanical properties (e.g., modulus) of degradable scaffolds decreases over time. In orthopedic applications, where the scaffold is expected to be load bearing, the mechanical properties as a function of time need to be characterized. In well-designed materials, gradual stress transfer will occur as the tissue re-grows.

dictated by polymer concentration and solvent identity, determine the burst and sustained release kinetics of drugs from the in situ-formed device (Parent et al., 2013).

While noninvasive strategies are preferred for many applications, other applications, such as joint replacements, still require open surgery to get the biomaterial to the correct site in the body. The joint replacement is often a prefabricated, synthetic joint shaped to match the native joint. Alternatively, bone cement, which cures in situ to take the shape of the cavity, can be used. Both delivery techniques are invasive processes and pose a high risk of infection, causing postoperative pain and numerous side effects for the patient (ter Boo et al., 2015). To help prevent infections, prosthetic joints and implants have been designed with degradable polymer coatings that deliver a local dose of antibiotics, thereby reducing the changes of infection and localizing the antibiotics to a specific region of the body. A clinical example is ETN PROtect, where gentamicin-loaded PDLA (Fuchs et al., 2011; Metsemakers et al., 2015) is coated on intramedullary nails to reduce infection. Clinical studies with this degradable polymer coating revealed no deep wound infections, good fracture healing, and increased weight-bearing capacity after 6 months compared to the nail alone (Fig. 1.3.2F.13). These results were found even in patients with complex fractures and multiple traumas.

Composites—When Should a Composite Be Used and How Will Additives Affect Degradation?

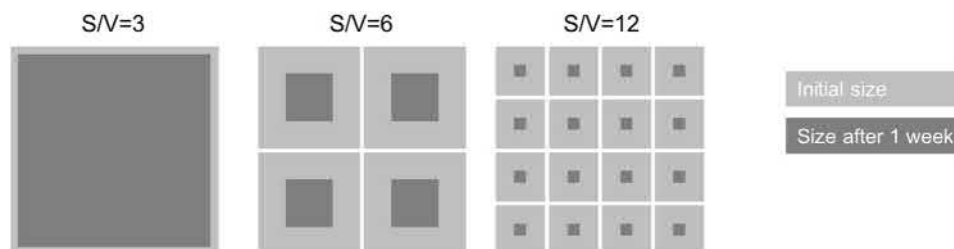
If the desired mechanical properties of a temporary support device or erosion kinetics of a controlled release system are not accessible through changing the degradable polymer composition alone, composites with nondegradable materials can be used. For example, low concentrations of natural materials (e.g., ceramic fibers or particles) are often embedded within degradable polymers used to increase the mechanical properties of degradable scaffolds for orthopedic applications (Rezwan et al., 2006). The effect of nondegradable additives on the final mechanical properties, and degradation, of the device/materials is dependent on both the loading density and hydrophobicity of the additive. For example, low loadings (<5%) of hydrophilic nanohydroxyapatite were shown to reinforce PLGA scaffolds, improving the storage modulus, while higher loadings acted as defects and weakened the scaffolds and accelerated erosion (Jose et al., 2009).

The effect of additives on degradation kinetics is especially important to understand when designing controlled release systems, which are inherently composites because of the addition of therapeutic molecules and/or excipients. For example, if there is a well-studied, commercially available PLGA formulation that has been used to deliver a specific compound, the release profile of a different drug from the same polymer may be significantly different depending on the drug loading and properties (i.e., molecular weight, hydrophobicity) of the drug (Jain et al., 2000). During the embedding or encapsulation process, hydrophobic drugs tend to lead to formation of more compact particles, which ultimately impedes water adsorption such that degradation and release are slowed (Rodrigues de Azevedo et al., 2017). Options for tuning the release/degradation include changing the polymer composition or using combinations of additives until the desired release kinetics are achieved (Shikanov et al., 2005; Song et al., 1997).

In another composite-based strategy for controlled release, degradable particles can be embedded in a nondegradable matrix, such as a hydrogel, to slow down



• **Figure 1.3.2F.13** A 36-year-old male polytrauma patient presented with an open, Gustilo grade 2, tibia fracture after a motor vehicle accident. (A) After 1 week of primary external fixation, nailing of the defect fracture using an ETN PROtect™ was performed. (B) Before definitive wound closure a polymethylmethacrylate (PMMA) spacer was left in place (Masquelet procedure). (C) In a second stage, the spacer was replaced by autologous bone graft. (D) Healing of the fracture 18 months after the injury. Figure adapted from [Metsemakers et al. \(2015\)](#).



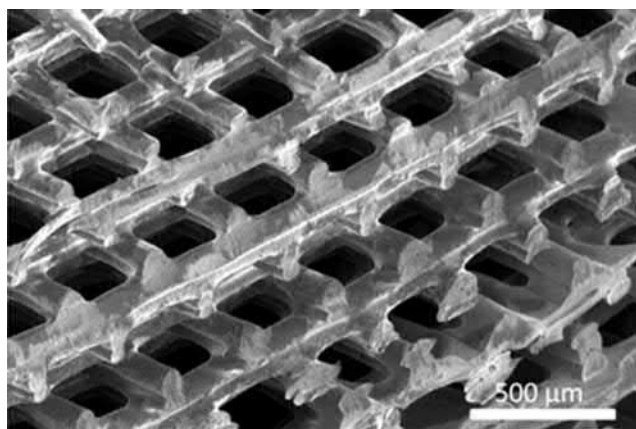
• **Figure 1.3.2F.14** Effect of surface area to volume ratio (S/V) on degradation rates. Biomaterials made from the same surface eroding polymer and that have the same initial volume but different S/V will have different degradation kinetics. The biomaterials with the highest S/V will have the fastest degradation, because there are more hydrolytically labile bonds accessible to water.

degradation and therapeutic release ([Liu et al., 2007](#)). Commercially, this strategy has been employed in Urolon, a bioresorbable urethral implant for stress-induced incontinence, which consists of degradable PCL microparticles embedded in a hydrogel matrix.

Shape—How Will the Material Be Shaped and How Does Shape Affect Degradation Kinetics?

The shape of the biomaterial is dictated by the intended application. In particular, the surface area-to-volume ratio is an important determinant of degradation kinetics for surface-eroding polymers, but can be less important for polymers that undergo bulk erosion ([Chew et al., 2016](#)). Larger surface areas mean increased exposure to water at the polymer interfaces and, consequently,

faster erosion ([Fig. 1.3.2F.14](#)). Some examples of shapes that have large surface area-to-volume ratios are fibers, micro/nanoparticles, thin flat slabs, and porous scaffolds. In all of these cases, if a surface-eroding polymer is used, the rate of degradation can be tuned by changing the dimensions of the material. For example, several small, thin, polyanhydride Gliadel wafers (up to eight), rather than one large wafer, are implanted for the treatment of glioblastoma ([Kleinberg, 2016](#)). Polyanhydride micro/nanoparticles are being extensively explored in academia for controlled release applications ([Basu and Domb, 2018](#)). As with hydrolytic degradation, surface area-to-volume ratios also dictate the rate of enzymatic degradation, where the larger the surface area, the better the accessibility for enzymes to reach and cleave polymer bonds, as explained earlier in this chapter. Thin,



• **Figure 1.3.2F.15** SEM images of 3D[HYPHEN]printed, biodegradable PLA orthogonal displaced structure. (Adapted from [Serra et al. \(2013\)](#)).

photodegradable scaffolds will also degrade more quickly than thick scaffolds, because light absorbance can lead to significant attenuation with depth ([Tibbitt et al., 2013](#)).

While a biomaterial of a certain composition and shape may be seemingly perfect for a certain application because of its expected degradation properties, it is also necessary to consider if and how the polymer can be processed into the desired shape. There are many options for making micro/nanoparticles from biodegradable polymers, including emulsion polymerizations, photolithography, and nanoprecipitation ([Jain, 2000](#)). In cases where the shape must exactly match the shape of the void or have a shape for a specific purpose (e.g., a bone screw), the shape can be achieved via a wide range of processing methods, depending on the polymer melting temperature and desired architecture. For example, porous PLGA scaffolds have been synthesized from methods including injection molding plus particulate leaching ([Wu et al., 2006](#)), extrusion plus solvent casting ([Widmer et al., 1998](#)), or additive manufacturing ([Serra et al., 2013](#)). Of all the options, additive manufacturing gives the most precise control over scaffold geometry, an important feature for controlling degradation ([Fig. 1.3.2F.15](#)).

Custom, Degradable Inks for 3D Printing

Significant progress in both additive manufacturing and polymer chemistry over the past several decades has led to the development of custom-designed 3D printable biomaterials. Through rational design, polymers with specific chemical and mechanical properties that make them 3D printable, biologically functional, and degradable can be achieved. For example, a novel polyester-based copolymer with pendant reactive alkene and alkyne functional groups was synthesized and formed into a scaffold using an extrusion-based printing method. The reactive groups on the polymer allowed functionalization of the scaffolds with bioactive molecules for diverse tissue-engineering applications ([Ji et al., 2019](#)).

Sterilization—Will Degradation Properties Be the Same After Sterilization?

The last step in processing a new device before it can be put in the body is sterilization, a physical or chemical process used to remove or inactivate microorganisms present

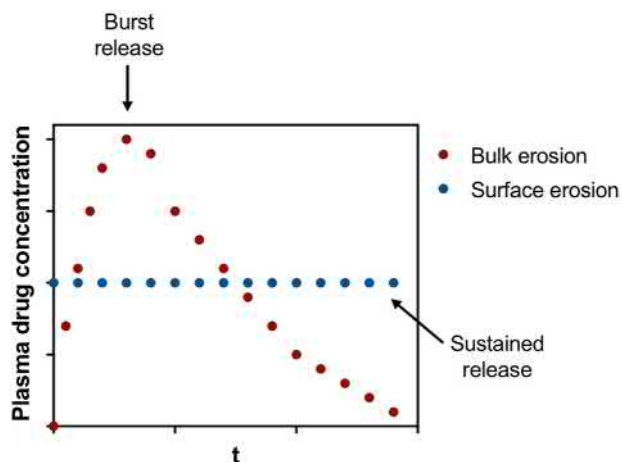
on the biomaterial. While most nondegradable biomaterials are sterilized via autoclaving (i.e., using high-temperature steam), this sterilization procedure is not a good choice for hydrolytically degradable polymers because of their inherent sensitivity to moisture and heat. However, autoclaving may be an option for sterilizing nonhydrolytically degradable materials (e.g., enzyme or photodegradable polymers). Regardless of the mechanism, materials that are designed to degrade need to be sterilized in facilities with strict control over environmental conditions (i.e., heat, humidity, light) to avoid premature degradation. For scaffolds containing living cells or biological agents, which cannot handle harsh sterilization conditions, sterility must be maintained throughout the course of the manufacturing process ([Treiser et al., 2013](#)).

Degradable biomaterials not containing biological agents are most commonly sterilized by gamma irradiation or ethylene oxide gas (EOG) treatment. It is important to test how the degradation properties of these materials change after such treatments. For example, gamma irradiation of PLGA devices lowers the average molecular weight and deteriorates the original mechanical properties of the device ([Jo et al., 2012](#)). EOG treatment is a more common choice for PLA-, PGA-, and PLGA-based biomaterials because of their poor tolerance to radiation ([Treiser et al., 2013](#)). Polymers treated with EOG, however, pose another serious concern: the toxicity of residual EOG. The International Organization for Standardization defined an EOG exposure limit of 25 ppm to minimize potential health risks associated with EOG exposure ([Shintani, 2017](#)). For this reason, devices sterilized by EOG require extensive degassing prior to use to minimize health risks for patients.

Performance Metrics

Every biodegradable material designed for in vivo use must undergo careful evaluation to ensure it performs as expected. As with any material, the polymer must be evaluated for cytotoxicity, efficacy, and storage stability. However, for polymers that degrade over time, it is particularly important to consider and carefully evaluate the cytotoxicity of their degradation products as well. While monomers are typically more cytotoxic than polymers, some degradable polymers degrade into monomers that are natural metabolites. For example, PLGA degrades into lactic acid and glycolic acid, which are natural metabolites. In any case, cytotoxicity studies should always be performed on both the intact polymers and degradation products before advancing to in vivo studies.

In addition to establishing cytocompatibility, degradation properties of new degradable biomaterials should be carefully characterized in vitro, following well-vetted experimental protocols. This is important especially for slowly degrading materials, for which accelerated degradation studies are often used rather than quantifying degradation of the material over the course of months to years. When characterizing a new biodegradable material,



• **Figure 1.3.2F.16** Typical time course profiles of plasma drug concentrations released from bulk eroding and surface eroding polymers. Bulk eroding formulations exhibit burst release, while surface eroding polymers exhibit sustained release.

experimental variables should be kept consistent with those used in previously performed studies on materials designed for similar applications (e.g., nanoparticles for insulin delivery, antibiotic-containing sutures for wound healing). Some examples of experimental variables that will affect degradation properties of controlled release devices include solution-to-specimen mass ratio, pH, temperature, mixing rates, light exposure, and ionic strength. While literature searches provide a good starting point for identifying best practices, standardized methods for evaluating degradable biomaterials still need to be established (Woodard and Grunlan, 2018).

Following *in vitro* cytocompatibility and degradation studies, degradable polymer devices should be characterized *in vivo* for a better understanding of the complex interactions that will occur between the material and the body. For example, release of lactic acid and glycolic acid can lower the pH of the environment quite dramatically, depending on the volume of the implant, and this can elicit a foreign body and inflammatory response to PLGA biomaterials, which in turn will alter the degradation kinetics (Ji et al., 2012).

Other *in vivo* studies for characterizing degradable biomaterials depend on the application. For controlled release studies, pharmacokinetic and bioavailability studies provide important information on the burst and sustained release of the therapeutic payload (Steinijans, 1990). Bulk-eroding polymers exhibit characteristic burst release profiles, while the concentration of drugs released from surface-eroding polymers is more constant (Fig. 1.3.2F.16). Even when theoretical and *in vitro* studies suggest that the drug release will occur over the desired timescale, biological responses to the materials may lead to dramatically different results. For example, opsonization of nanoparticles, leading to uptake by phagocytes, may lead to clearance on a much shorter timescale than the expected degradation timescale. Modifications to particle surfaces, such as PEGylation, can be performed to improve the distribution

and circulation time of the particles (Owens and Peppas, 2006). For temporary support devices, mechanical testing is often performed on devices both preimplantation and on the explanted device to learn about how cell–material interactions, which lead to scaffold remodeling, affect the mechanical properties of the device (Hong et al., 2011). Additionally, histology of explanted temporary support devices provides invaluable information regarding cell–material interactions.

While degradation in the body is the goal, it is critical to avoid premature degradation during storage. As such, materials made from degradable polymers require strict storage conditions because of their inherent sensitivity to moisture and heat. In cases where living cells or sensitive biological agents are included, shelf life is very limited. The properties (e.g., tensile strength, degradation rate) should be characterized over different storage time periods to ensure the device performs as expected.

Worked Examples

Question

Cells have been encapsulated in a polymeric hydrogel composed of polyamides and polyesters. When immersed in cell culture media, the material swells over time. Identify the routes of degradation and explain why the hydrogel has swollen and why the hydrogel will not completely degrade in a week.

Solution

The polymer chains reorganize when placed in water, causing swelling as water infiltrates the network. With time, hydrolytic degradation will break the ester bonds, reducing the cross-linking density and increasing the water influx to the network, leading to additional swelling. In addition, the cell will secrete enzymes accelerating the rate of degradation. As amide bonds are present, the network will not completely degrade as amides form stable conjugates when in the presence of water.

Question

Sculptra is an injectable PLA cosmetic filler that is used to reduce the signs of aging. The formulation, which can last for 2 years, consists of PLA microspheres in water that initiate a twofold mechanism of action. Identify the benefits of using PLA as a degradable polymer for this application. What are the two steps of action and why are the effects sustained for 2 years?

Solution

PLA is a biodegradable, biocompatible, and immunologically inert polymer. It is a polyester and therefore can degrade through hydrolytic and enzymatic degradation

pathways. It is beneficial to use PLA as it is already FDA approved and is one of the most researched and utilized biodegradable polyesters. The mechanism of degradation is well understood and the kinetics of degradation can be controlled. The monomers are produced from a nontoxic renewable feedback and it is also a naturally occurring acid. PLA microspheres cause a gradual tissue response and stimulate collagen production. Initially, the volume of the injected area increases before collagen synthesis. After 1 month, the microparticles have been shown to increase vascularity and the capsule thickness starts to decrease until the area is composed of collagen fibers. After 18 months, the microparticles are still present with the collagen that has formed, with no inflammation (Engelhard et al., 2005; Humble and Mest, 2004).

PLA is more hydrophobic compared to PLGA and the single L isomer makes the polymer stereoregular, increasing the degradation rate and sustaining the effects of the PLA filler for longer as water cannot infiltrate as efficiently. The metabolism of the polymer involves bioadsorption and then hydrolysis of the ester bonds into monomers and oligomers. The degraded products can then be phagocytized by macrophages and ultimately degraded as CO₂ or converted into glucose.

Question

You need to fill a void of certain dimensions with a biomaterial made from a poly(sebacic anhydride) to support tissue regrowth. You are deciding between using a device that has been finely tuned to match the exact shape of that void or using smaller particles that will assemble and pack together with some space between particles. Assuming the total mass of material and chemical composition used are

the same in both cases, should you use the large plug or small particles if you want to maximize the lifetime of the implant? Why? What if the biomaterials were made from PLGA?

Solution

Because poly(sebacic anhydride) is a hydrophilic polyanhydride, it is expected to undergo surface rather than bulk degradation. For surface-degrading polymers, the small particles would be expected to degrade much faster than the single large plug, because of larger surface area-to-volume ratio, and degradation is proportional to surface area. Thus the large plug would be the better choice for extending the lifetime of the implant. If PLGA, a bulk-degrading polymer, had been used instead, both the large plug and small particles should degrade at the same rate, because bulk degradation depends on composition and total amount of material (which was constant) but are less dependent on material shape or size.

Case Studies on Degradable Polymers Used in Medicine

The use of degradable polymers in medicine has grown significantly since their initial use as sutures more than 50 years ago. Scientists have many avenues by which they can tailor the properties of these degradable biomaterials, ranging from simply changing the chemical composition to developing sophisticated composite materials and shapes. The following case studies focus on materials design considerations as they relate to commercially available devices made from degradable polymers.

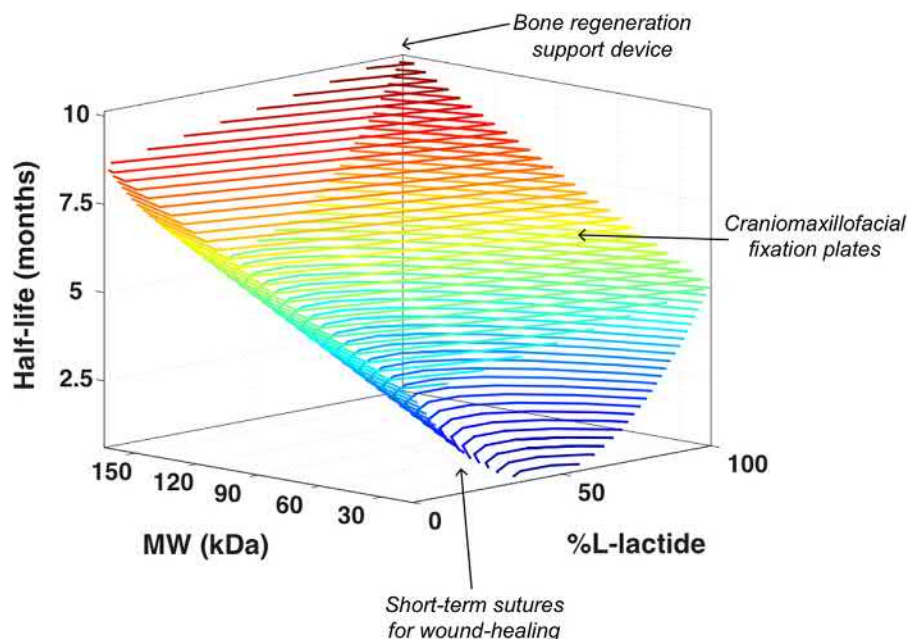
CASE STUDY I

PLGA in Temporary Support Devices

PLGA is a widely used, FDA-approved copolymer with tunable properties that depends on the ratio of glycolide:lactide (G:L) monomers, molecular weight, and processing of the material (Fig. 1.3.2F.17). PLGA copolymers with low G:L ratios are well suited for orthopedic applications because their high degree of crystallinity improves their mechanical strength and toughness. For example, OSSIOfiber is a support device for bone regeneration that is made from 100% poly(L,D,-lactic acid) that is initially stronger than bone, enabling the device to bear the load of the broken bone until the bone heals. It degrades over the course of 78 weeks, during which time the bone can heal and gradually bear more of its original load. As another example, LactoSorb temporary craniomaxillofacial fixation systems use 18:82 PLGA. With a T_g well above body temperature (58°C), doctors are able to soften plates with gentle heating to mold the plates to a patient's skull, after which the plate hardens in place as it cools.

For soft tissue applications, PLGA copolymers with high G:L ratios are preferred. For example, a suite of Pectryl sutures

is available for surgeons to choose from, depending on the application. By changing the composition from 100% PGA to 90:10 glycolide/L-lactide, the tensile strength of the sutures is reduced and the lifetime is decreased. For these reasons, 100% PGA is better suited for orthopedic applications, while 90:10 PLGA is better for soft tissue suturing. Both of these sutures retain 70%–75% of their tensile strength after 2 weeks, so for the shorter term (e.g., wound healing), doctors prefer sutures made from lower molecular weight 90:10 PLGA, which retains only 50% of its tensile strength after 5 days. PLGA copolymers of the same composition (90:10) are also used in VICRYL fiber meshes, which are used as temporary supports for wound and organ healing to foster soft tissue regrowth. Here, meshes with different degradation rates and mechanical properties are achieved by processing (i.e., either weaving or knitting the PLGA fibers into the mesh). When the fibers are knit, the mesh is more porous, causing faster degradation and lower burst strength compared to the woven meshes.



• **Figure 1.3.2F.17** Variations in PLGA molecular weight (MW), percent L-lactide, and processing allow development of a wide-range of biomaterials with distinctive degradation and mechanical properties, making them suitable for a variety of applications.

CASE STUDY II

PLGA in Controlled Release Devices—Formulation Considerations

For controlled release applications, PLGA copolymers with intermediate G:L ratios are often chosen because their shorter half-lives better match the desired pharmacokinetics, where 50:50 copolymers have the shortest half-lives. Ideally, these devices can be delivered through minimally invasive procedures (i.e., injection) to minimize discomfort for patients. FDA-approved, injectable PLGA formulations include in situ-forming systems and suspensions of microparticles. For example, Eligard is an in situ-forming system used for controlled release of leuprolide acetate for the treatment of advanced prostate cancer. Different polymer compositions and dosages are offered to control the duration of treatments, but the most common is a 75:25 PLGA capped with hexanediol in *N*-methyl 2-pyrrolidone

(NMP) as a biocompatible solvent. Upon injection, quick displacement of the NMP by water causes precipitation and formation of a subcutaneous drug depot. Having the hydroxyl rather than carboxylic acid end groups slows the degradation of the depot, allowing sustained release for 1–6 months (Parent et al., 2013). For even faster release, the composition of the PLGA used in the formulation can be decreased to 50:50 PLGA. For example, Bydureon BCise, a treatment for type 2 diabetes, uses microparticles made from 50:50 PLGA to achieve release of exenatide on the order of weeks. Rather than daily insulin injections, people with type 2 diabetes can inject themselves once per week using this controlled release system (Cai et al., 2013; DeYoung et al., 2011).

CASE STUDY III

Polyanhydrides in Controlled Release Devices

There are fewer examples of FDA-approved biomaterials made from polyanhydrides than there are of polyesters, but the surface-eroding nature of polyanhydrides is crucial for certain controlled release applications. The best example of this is Gliadel wafers, which are implanted in the brains of patients with malignant glioblastoma. The wafers are made from poly(bis(*p*-carboxyphenoxy) propane-*co*-sebacic acid) (poly(CPP-*co*-SA) at a ratio of 20:80 CPP:SA and are loaded with carmustine, a potent chemotherapeutic. Because the wafer degrades by surface erosion, the release of carmustine is steady and sustained rather than undergoing the initial burst release seen with PLGA-based devices. This is important because the Gliadel wafers are implanted directly into the brain, and carmustine is a potent drug that kills cells by cross-linking DNA and RNA. Slow release mitigates off-target toxicity (overdose) and also prolongs

the mechanism of action, which is critical because brain surgery is dangerous and leads to many complications. For this reason, Gliadel wafers are advantageous because they are implanted once, slowly release carmustine from the wafers to continue killing cancer cells as they proliferate over the course of 2–3 weeks, and then are fully resorbed by the body, eliminating the need for a second surgery to remove the wafers (Kleinberg, 2016).

Unlike with PLGA, initial studies on the poly(CPP-*co*-SA) wafers showed that initial molecular weight of the polymers used did not affect erosion rate (Dang et al., 1996). Beyond the benefit of steady release as a result of surface hydrolysis, polyanhydrides have also been extensively investigated in vaccine development because of the inherent adjuvant properties of these polymers (Kipper et al., 2006; Vela Ramirez et al., 2016).

References

- Albertsson, A.-C., Varma, I.K., 2003. Recent developments in ring opening polymerization of lactones for biomedical applications. *Biomacromolecules* 4, 1466–1486. <https://doi.org/10.1021/bm034247a>.
- Anderson, J.M., Shive, M.S., 1997. Biodegradation and biocompatibility of PLA and PLGA microspheres. *Adv. Drug Deliv. Rev.* 28, 5–24. [https://doi.org/10.1016/S0169-409X\(97\)00048-3](https://doi.org/10.1016/S0169-409X(97)00048-3).
- Arakawa, C.K., Badeau, B.A., Zheng, Y., DeForest, C.A., 2017. Multicellular vascularized engineered tissues through user-programmable biomaterial photodegradation. *Adv. Mater.* 29, 1703156. <https://doi.org/10.1002/adma.201703156>.
- Askeland, D.R., Haddleton, F., Green, P., Robertson, H., 1996. *The Science and Engineering of Materials*. Springer, US. <https://doi.org/10.1007/978-1-4899-2895-5>.
- Bajaj, P., Schweller, R.M., Khademhosseini, A., West, J.L., Bashir, R., 2014. 3D biofabrication strategies for tissue engineering and regenerative medicine. *Annu. Rev. Biomed. Eng.* 16, 247–276. <https://doi.org/10.1146/annurev-bioeng-071813-105155>.
- Bakaic, E., Smeets, B., Hoare, N.M.T., 2015. Injectable hydrogels based on poly(ethylene glycol) and derivatives as functional biomaterials. *RSC Adv.* 5, 35469–35486. <https://doi.org/10.1039/C4RA13581D>.
- Barner-Kowollik, C., 2008. *Handbook of RAFT Polymerization*. John Wiley & Sons.
- Basu, A., Domb, A.J., 2018. Recent advances in polyanhydride based biomaterials. *Adv. Mater.* 30, 1706815. <https://doi.org/10.1002/adma.201706815>.
- Boehnke, N., Cam, C., Bat, E., Segura, T., Maynard, H.D., 2015. Imine hydrogels with tunable degradability for tissue engineering. *Biomacromolecules* 16, 2101–2108. <https://doi.org/10.1021/acs.biomac.5b00519>.
- Bowman, C.N., Kloxin, C.J., 2012. Covalent adaptable networks: reversible bond structures incorporated in polymer networks. *Angew. Chem. Int. Ed.* 51, 4272–4274. <https://doi.org/10.1002/anie.201200708>.
- Brannigan, R., Dove, A., 2017. Synthesis, properties and biomedical applications of hydrolytically degradable materials based on aliphatic polyesters and polycarbonates. *Biomater. Sci.* 5, 9–21. <https://doi.org/10.1039/C6BM00584E>.
- Bratlie, K.M., York, R.L., Invernale, M.A., Langer, R., Anderson, D.G., 2012. Materials for diabetes therapeutics. *Adv. Healthc. Mater.* 1, 267–284. <https://doi.org/10.1002/adhm.201200037>.
- Brauer, D.S., Rüssel, C., Vogt, S., Weisser, J., Schnabelrauch, M., 2008. Degradable phosphate glass fiber reinforced polymer matrices: mechanical properties and cell response. *J. Mater. Sci. Mater. Med.* 19, 121–127. <https://doi.org/10.1007/s10856-007-3147-x>.
- Brown, T., Anseth, K., 2017. Spatiotemporal hydrogel biomaterials for regenerative medicine. *Chem. Soc. Rev.* 46, 6532–6552. <https://doi.org/10.1039/C7CS00445A>.
- Brown, T.E., Carberry, B.J., Worrell, B.T., Dudaryeva, O.Y., McBride, M.K., Bowman, C.N., Anseth, K.S., 2018. Photopolymerized dynamic hydrogels with tunable viscoelastic properties through thioester exchange. *Biomaterials* 178, 496–503. <https://doi.org/10.1016/j.biomaterials.2018.03.060>.
- Burkersroda, F. von, Schedl, L., Göpferich, A., 2002. Why degradable polymers undergo surface erosion or bulk erosion. *Biomaterials* 23, 4221–4231. [https://doi.org/10.1016/S0142-9612\(02\)00170-9](https://doi.org/10.1016/S0142-9612(02)00170-9).
- Cai, Y., Liangming Wei, L., Ma, L., Huang, X., Tao, A., Liu, Z., Yuan, W., 2013. Long-acting preparations of exenatide. *Drug Des. Dev. Ther.* 963. <https://doi.org/10.2147/DDDT.S46970>.
- Cha, Y., Pitt, C.G., 1989. The acceleration of degradation-controlled drug delivery from polyester microspheres. *J. Control. Release* 8, 259–265. [https://doi.org/10.1016/0168-3659\(89\)90047-3](https://doi.org/10.1016/0168-3659(89)90047-3).
- Chew, S.A., Arriaga, M.A., Hinojosa, V.A., 2016. Effects of surface area to volume ratio of PLGA scaffolds with different architectures on scaffold degradation characteristics and drug release kinetics: effects of surface area to volume ratio of PLGA scaffolds. *J. Biomed. Mater. Res. A* 104, 1202–1211. <https://doi.org/10.1002/jbm.a.35657>.
- Dang, W., Daviau, T., Ying, P., Zhao, Y., Nowotnik, D., Clow, C.S., Tyler, B., Brem, H., 1996. Effects of GLIADEL® wafer initial molecular weight on the erosion of wafer and release of BCNU. *J. Control. Release* 42, 83–92. [https://doi.org/10.1016/0168-3659\(96\)01371-5](https://doi.org/10.1016/0168-3659(96)01371-5).
- Dardik, H., Dardik, I., Laufman, H., 1971. Clinical use of polyglycolic acid polymer as a new absorbable synthetic suture. *Am. J. Surg.* 121, 656–660. [https://doi.org/10.1016/0002-9610\(71\)90039-0](https://doi.org/10.1016/0002-9610(71)90039-0).
- DeForest, C.A., Anseth, K.S., 2011. Cytocompatible click-based hydrogels with dynamically tunable properties through orthogonal photoconjugation and photocleavage reactions. *Nat. Chem.* 3, 925–931. <https://doi.org/10.1038/nchem.1174>.
- Deng, Z., Schweigerdt, A., Norow, A., Lienkamp, K., 2019. Degradation of polymer films on surfaces: a model study with poly(sebacic anhydride). *Macromol. Chem. Phys.* 220, 1900121. <https://doi.org/10.1002/macp.201900121>.
- Deshayes, S., Kasko, A.M., 2013. Polymeric biomaterials with engineered degradation. *J. Polym. Sci. Part Polym. Chem.* 51, 3531–3566. <https://doi.org/10.1002/pola.26765>.
- DeYoung, M.B., MacConell, L., Sarin, V., Trautmann, M., Herbert, P., 2011. Encapsulation of exenatide in poly-(D,L-Lactide-Co-glycolide) microspheres produced an investigational long-acting once-weekly formulation for type 2 diabetes. *Diabetes Technol. Ther.* 13, 1145–1154. <https://doi.org/10.1089/dia.2011.0050>.
- Doppalapudi, S., Jain, A., Khan, W., Domb, A.J., 2014. Biodegradable polymers—an overview. *Polym. Adv. Technol.* 25, 427–435. <https://doi.org/10.1002/pat.3305>.
- Engelberg, I., Kohn, J., 1991. Physico-mechanical properties of degradable polymers used in medical applications: a comparative study. *Biomaterials* 12, 292–304.
- Engelhard, P., Humble, G., Mest, D., 2005. Safety of Sculptra®: a review of clinical trial data. *J. Cosmet. Laser Ther.* 7, 201–205. <https://doi.org/10.1080/14764170500451404>.
- Farah, S., Anderson, D.G., Langer, R., 2016. Physical and mechanical properties of PLA, and their functions in widespread applications — a comprehensive review. *Adv. Drug Deliv. Rev.* 107, 367–392. <https://doi.org/10.1016/j.addr.2016.06.012>.
- Fleming, A.B., Saltzman, W.M., 2002. Pharmacokinetics of the carmustine implant. *Clin. Pharmacokinet.* 41, 403–419. <https://doi.org/10.2165/00003088-200241060-00002>.
- Fuchs, T., Stange, R., Schmidmaier, G., Raschke, M.J., 2011. The use of gentamicin-coated nails in the tibia: preliminary results of a prospective study. *Arch. Orthop. Trauma Surg.* 131, 1419–1425. <https://doi.org/10.1007/s00402-011-1321-6>.
- Gilding, D.K., Reed, A.M., 1979. Biodegradable polymers for use in surgery—polyglycolic/poly(lactic acid) homo- and copolymers: 1. *Polymer* 20, 1459–1464. [https://doi.org/10.1016/0032-3861\(79\)90009-0](https://doi.org/10.1016/0032-3861(79)90009-0).
- Gombotz, W.R., Pettit, D.K., 1995. Biodegradable polymers for protein and peptide drug delivery. *Bioconjug. Chem.* 6, 332–351. <https://doi.org/10.1021/bc00034a002>.
- Göpferich, A., 1996. Mechanisms of polymer degradation and erosion. *Biomaterials* 17, 103–114. [https://doi.org/10.1016/0142-9612\(96\)85755-3](https://doi.org/10.1016/0142-9612(96)85755-3).

- He, W., Benson, R., 2017. 8 - polymeric biomaterials. In: Kutz, M. (Ed.), *Applied Plastics Engineering Handbook*, Plastics Design Library, second ed. William Andrew Publishing, pp. 145–164. <https://doi.org/10.1016/B978-0-323-39040-8.00008-0>.
- Heller, J., Barr, J., 2004. Poly(ortho esters) from concept to reality. *Biomacromolecules* 5, 1625–1632. <https://doi.org/10.1021/bm040049n>.
- Heller, J., Barr, J., Ng, S.Y., Abdellouai, K.S., Gurny, R., 2002. Poly(ortho esters): synthesis, characterization, properties and uses. *Adv. Drug Deliv. Rev.* 54, 1015–1039. [https://doi.org/10.1016/S0169-409X\(02\)00055-8](https://doi.org/10.1016/S0169-409X(02)00055-8).
- Hong, Y., Huber, A., Takanari, K., Amoroso, N.J., Hashizume, R., Badylak, S.F., Wagner, W.R., 2011. Mechanical properties and in vivo behavior of a biodegradable synthetic polymer microfibrillar extracellular matrix hydrogel biohybrid scaffold. *Biomaterials* 32, 3387–3394. <https://doi.org/10.1016/j.biomaterials.2011.01.025>.
- Humble, G., Mest, D., 2004. Soft tissue augmentation using sculptra. *Facial Plast. Surg.* 20, 157–163. <https://doi.org/10.1055/s-2004-861758>.
- Jain, R.A., 2000. The manufacturing techniques of various drug loaded biodegradable poly(lactide-co-glycolide) (PLGA) devices. *Biomaterials* 21, 2475–2490. [https://doi.org/10.1016/S0142-9612\(00\)00115-0](https://doi.org/10.1016/S0142-9612(00)00115-0).
- Jain, R.A., Rhodes, C.T., Raikar, A.M., Malick, A.W., Shah, N.H., 2000. Controlled release of drugs from injectable in situ formed biodegradable PLGA microspheres: effect of various formulation variables. *Eur. J. Pharm. Biopharm. Off. J. Arbeitsgemeinschaft Pharm. Verfahrenstechnik EV* 50, 257–262.
- Ji, S., Dube, K., Chesterman, J.P., Fung, S.L., Liaw, C.-Y., Kohn, J., Guvendiren, M., 2019. Polyester-based ink platform with tunable bioactivity for 3D printing of tissue engineering scaffolds. *Biomater. Sci.* 7, 560–570. <https://doi.org/10.1039/C8BM01269E>.
- Ji, W., Yang, F., Seyednejad, H., Chen, Z., Hennink, W.E., Anderson, J.M., van den Beucken, J.J.P., Jansen, J.A., 2012. Biocompatibility and degradation characteristics of PLGA-based electrospun nanofibrous scaffolds with nanoapatite incorporation. *Biomaterials* 33, 6604–6614. <https://doi.org/10.1016/j.biomaterials.2012.06.018>.
- Jo, S.-Y., Park, J.-S., Gwon, H.-J., Shin, Y.-M., Khil, M.-S., Nho, Y.-C., Lim, Y.-M., 2012. Degradation behavior of poly (l-lactide-co-glycolide) films through gamma-ray irradiation. *Radiat. Phys. Chem.* 81, 846–850. <https://doi.org/10.1016/j.radphyschem.2012.03.013>.
- Jose, M., Thomas, V., Johnson, K., Dean, D., Nyairo, E., 2009. Aligned PLGA/HA nanofibrous nanocomposite scaffolds for bone tissue engineering. *Acta Biomater.* 5, 305–315. <https://doi.org/10.1016/j.actbio.2008.07.019>.
- Kalaoglu-Altan, O.I., Kirac-Aydin, A., Sumer Bolu, B., Sanyal, R., Sanyal, A., 2017. Diels–alder “clickable” biodegradable nanofibers: benign tailoring of scaffolds for biomolecular immobilization and cell growth. *Bioconj. Chem.* 28, 2420–2428. <https://doi.org/10.1021/acs.bioconjchem.7b00411>.
- Kipper, M.J., Wilson, J.H., Wannemuehler, M.J., Narasimhan, B., 2006. Single dose vaccine based on biodegradable polyanhydride microspheres can modulate immune response mechanism. *J. Biomed. Mater. Res. A* 76A, 798–810. <https://doi.org/10.1002/jbm.a.30545>.
- Kleinberg, L., 2016. Polifeprosan 20, 3.85% carmustine slow release wafer in malignant glioma: patient selection and perspectives on a low-burden therapy. *Patient Prefer. Adherence* Volume 10, 2397–2406. <https://doi.org/10.2147/PPA.S93020>.
- Kloxin, A.M., Tibbitt, M.W., Kasko, A.M., Fairbairn, J.A., Anseth, K.S., 2010. Tunable hydrogels for external manipulation of cellular microenvironments through controlled photodegradation. *Adv. Mater.* 22, 61–66. <https://doi.org/10.1002/adma.200900917>.
- Knipe, J.M., Chen, F., Peppas, N.A., 2015. Enzymatic biodegradation of hydrogels for protein delivery targeted to the small intestine. *Biomacromolecules* 16, 962–972. <https://doi.org/10.1021/bm501871a>.
- Kocak, G., Tuncer, C., Bütün, V., 2017. pH-Responsive polymers. *Polym. Chem.* 8, 144–176. <https://doi.org/10.1039/C6PY01872F>.
- Kretlow, J.D., Klouda, L., Mikos, A.G., 2007. Injectable matrices and scaffolds for drug delivery in tissue engineering. *Adv. Drug Deliv. Rev.* 59, 263–273. <https://doi.org/10.1016/j.addr.2007.03.013>.
- Langer, R., Tirrell, D.A., 2004. Designing materials for biology and medicine. *Nature* 428, 487–492. <https://doi.org/10.1038/nature02388>.
- Leong, K.W., Kost, J., Mathiowitz, E., Langer, R., 1986. Polyamides for controlled release of bioactive agents. *Biomaterials* 7, 364–371. [https://doi.org/10.1016/0142-9612\(86\)90007-4](https://doi.org/10.1016/0142-9612(86)90007-4).
- Li, L., Deng, X.-X., Li, Z.-L., Du, F.-S., Li, Z.-C., 2014. Multifunctional photodegradable polymers for reactive micropatterns. *Macromolecules* 47, 4660–4667. <https://doi.org/10.1021/ma501019c>.
- Liu, J., Zhang, S.M., Chen, P.P., Cheng, L., Zhou, W., Tang, W.X., Chen, Z.W., Ke, C.M., 2007. Controlled release of insulin from PLGA nanoparticles embedded within PVA hydrogels. *J. Mater. Sci. Mater. Med.* 18, 2205–2210. <https://doi.org/10.1007/s10856-007-3010-0>.
- Liu, L., Li, S., Garreau, H., Vert, M., 2000. Selective enzymatic degradations of poly(l-lactide) and poly(ε-caprolactone) blend films. *Biomacromolecules* 1, 350–359. <https://doi.org/10.1021/bm000046k>.
- Liu, M., Zhang, T., Long, L., Zhang, R., Ding, S., 2019. Efficient enzymatic degradation of poly (ε-caprolactone) by an engineered bifunctional lipase–cutinase. *Polym. Degrad. Stab.* 160, 120–125. <https://doi.org/10.1016/j.polymdegradstab.2018.12.020>.
- Lyu, S., Untereker, D., 2009. Degradability of polymers for implantable biomedical devices. *Int. J. Mol. Sci.* 10, 4033–4065. <https://doi.org/10.3390/ijms10094033>.
- Metsemakers, W.J., Reul, M., Nijs, S., 2015. The use of gentamicin-coated nails in complex open tibia fracture and revision cases: a retrospective analysis of a single centre case series and review of the literature. *Injury* 46, 2433–2437. <https://doi.org/10.1016/j.injury.2015.09.028>.
- Middleton, J.C., Tipton, A.J., 2000. Synthetic biodegradable polymers as orthopedic devices. *Biomaterials* 21, 2335–2346. [https://doi.org/10.1016/S0142-9612\(00\)00101-0](https://doi.org/10.1016/S0142-9612(00)00101-0).
- Miller, R.A., Brady, J.M., Cutright, D.E., 1977. Degradation rates of oral resorbable implants (polylactates and polyglycolates): rate modification with changes in PLA/PGA copolymer ratios. *J. Biomed. Mater. Res.* 11, 711–719. <https://doi.org/10.1002/jbm.820110507>.
- Morgan, M.N., 1969. New synthetic absorbable suture material. *Br. Med. J.* 2, 308.
- Nair, L.S., Laurencin, C.T., 2007. Biodegradable polymers as biomaterials. *Prog. Polym. Sci.* 32, 762–798. <https://doi.org/10.1016/j.progpolymsci.2007.05.017>.
- Niaounakis, M., 2013. 7 - degradability on demand. In: Niaounakis, M. (Ed.), *Biopolymers Reuse, Recycling, and Disposal*, Plastics Design Library. William Andrew Publishing, Oxford, pp. 193–241. <https://doi.org/10.1016/B978-1-4557-3145-9.00007-5>.

- Odian, G., 2004. Principles of Polymerization. John Wiley & Sons.
- Owens, D., Peppas, N., 2006. Opsonization, biodistribution, and pharmacokinetics of polymeric nanoparticles. *Int. J. Pharm.* 307, 93–102. <https://doi.org/10.1016/j.ijpharm.2005.10.010>.
- Parent, M., Nouvel, C., Koerber, M., Sapin, A., Maincent, P., Boudier, A., 2013. PLGA in situ implants formed by phase inversion: critical physicochemical parameters to modulate drug release. *J. Control. Release* 172, 292–304. <https://doi.org/10.1016/j.jconrel.2013.08.024>.
- Pasparakis, G., Manouras, T., Argitis, P., Vamvakaki, M., 2012. Photodegradable polymers for biotechnological applications. *Macromol. Rapid Commun.* 33, 183–198. <https://doi.org/10.1002/marc.201100637>.
- Peng, Q., Sun, X., Gong, T., Wu, C.-Y., Zhang, T., Tan, J., Zhang, Z.-R., 2013. Injectable and biodegradable thermosensitive hydrogels loaded with PHBHHx nanoparticles for the sustained and controlled release of insulin. *Acta Biomater.* 9, 5063–5069. <https://doi.org/10.1016/j.actbio.2012.09.034>.
- Piskin, E., 1995. Biodegradable polymers as biomaterials. *J. Biomater. Sci. Polym. Ed.* 6, 775–795. <https://doi.org/10.1163/156856295X00175>.
- Pitt, G.G., Gratzl, M.M., Kimmel, G.L., Surles, J., Sohindler, A., 1981. Aliphatic polyesters II. The degradation of poly (DL-lactide), poly (ϵ -caprolactone), and their copolymers in vivo. *Biomaterials* 2, 215–220. [https://doi.org/10.1016/0142-9612\(81\)90060-0](https://doi.org/10.1016/0142-9612(81)90060-0).
- Reed, A.M., Gilding, D.K., 1981. Biodegradable polymers for use in surgery — poly(glycolic)/poly(lactic acid) homo and copolymers: 2. In vitro degradation. *Polymer* 22, 494–498. [https://doi.org/10.1016/0032-3861\(81\)90168-3](https://doi.org/10.1016/0032-3861(81)90168-3).
- Rezwan, K., Chen, Q.Z., Blaker, J.J., Boccaccini, A.R., 2006. Biodegradable and bioactive porous polymer/inorganic composite scaffolds for bone tissue engineering. *Biomaterials* 27, 3413–3431. <https://doi.org/10.1016/j.biomaterials.2006.01.039>.
- Rice, M.A., Sanchez-Adams, J., Anseth, K.S., 2006. Exogenously triggered, enzymatic degradation of photopolymerized hydrogels with polycaprolactone Subunits: experimental observation and modeling of mass loss behavior. *Biomacromolecules* 7, 1968–1975. <https://doi.org/10.1021/bm060086+>.
- Richardson, B.M., Wilcox, D.G., Randolph, M.A., Anseth, K.S., 2019. Hydrazone covalent adaptable networks modulate extracellular matrix deposition for cartilage tissue engineering. *Acta Biomater.* 83, 71–82. <https://doi.org/10.1016/j.actbio.2018.11.014>.
- Rinkenauer, A.C., Schubert, S., Traeger, A., Schubert, U.S., 2015. The influence of polymer architecture on in vitro pDNA transfection. *J. Mater. Chem. B* 3, 7477–7493. <https://doi.org/10.1039/C5TB00782H>.
- Rodrigues de Azevedo, C., von Stosch, M., Costa, M.S., Ramos, A.M., Cardoso, M.M., Danhier, F., Pr eat, V., Oliveira, R., 2017. Modeling of the burst release from PLGA micro- and nanoparticles as function of physicochemical parameters and formulation characteristics. *Int. J. Pharm.* 532, 229–240. <https://doi.org/10.1016/j.ijpharm.2017.08.118>.
- Rosen, H.B., Chang, J., Wnek, G.E., Linhardt, R.J., Langer, R., 1983. Bioerodible polyanhydrides for controlled drug delivery. *Biomaterials* 4, 131–133. [https://doi.org/10.1016/0142-9612\(83\)90054-6](https://doi.org/10.1016/0142-9612(83)90054-6).
- Rosselgong, J., Williams, E.G.L., Le, T.P., Grusche, F., Hinton, T.M., Tizard, M., Gunatillake, P., Thang, S.H., 2013. Core degradable star RAFT polymers: synthesis, polymerization, and degradation studies. *Macromolecules* 46, 9181–9188. <https://doi.org/10.1021/ma402122z>.
- Ruskowitz, E.R., Comerford, M.P., Badeau, B.A., DeForest, C.A., 2019. Logical stimuli-triggered delivery of small molecules from hydrogel biomaterials. *Biomater. Sci.* 7, 542–546. <https://doi.org/10.1039/C8BM01304G>.
- Rydholm, A.E., Bowman, C.N., Anseth, K.S., 2005. Degradable thiol-acrylate photopolymers: polymerization and degradation behavior of an in situ forming biomaterial. *Biomaterials* 26, 4495–4506. <https://doi.org/10.1016/j.biomaterials.2004.11.046>.
- Serra, T., Mateos-Timoneda, M.A., Planell, J.A., Navarro, M., 2013. 3D printed PLA-based scaffolds: a versatile tool in regenerative medicine. *Organogenesis* 9, 239–244. <https://doi.org/10.4161/org.26048>.
- Sershen, S., West, J., 2002. Implantable, polymeric systems for modulated drug delivery. *Adv. Drug Deliv. Rev.* 54, 1225–1235. [https://doi.org/10.1016/S0169-409X\(02\)00090-X](https://doi.org/10.1016/S0169-409X(02)00090-X).
- Shalaby, S.W., Burg, K.J.L., 2003. Absorbable and Biodegradable Polymers. CRC Press.
- Shikanov, A., Ezra, A., Domb, A.J., 2005. Poly(sebacic acid-co-ricinoleic acid) biodegradable carrier for paclitaxel—effect of additives. *J. Control. Release* 105, 52–67. <https://doi.org/10.1016/j.jconrel.2005.02.018>.
- Shintani, H., 2017. Ethylene oxide gas sterilization of medical devices. *Biocontrol. Sci.* 22, 1–16. <https://doi.org/10.4265/bio.22.1>.
- Siepmann, J., G pferich, A., 2001. Mathematical modeling of bioerodible, polymeric drug delivery systems. *Adv. Drug Deliv. Rev.* 48, 229–247. [https://doi.org/10.1016/S0169-409X\(01\)00116-8](https://doi.org/10.1016/S0169-409X(01)00116-8).
- Smithmyer, M.E., Deng, C.C., Cassel, S.E., LeValley, P.J., Sumerlin, B.S., Kloxin, A.M., 2018. Self-healing boronic acid-based hydrogels for 3D Co-cultures. *ACS Macro Lett.* 7, 1105–1110. <https://doi.org/10.1021/acsmacrolett.8b00462>.
- Song, C.X., Labhasetwar, V., Levy, R.J., 1997. Controlled release of U-86983 from double-layer biodegradable matrices: effect of additives on release mechanism and kinetics. *J. Control. Release* 45, 177–192. [https://doi.org/10.1016/S0168-3659\(96\)01551-9](https://doi.org/10.1016/S0168-3659(96)01551-9).
- Steinijans, V.W., 1990. Pharmacokinetic characterization of controlled-release formulations. *Eur. J. Drug Metab. Pharmacokinet.* 15, 173–181. <https://doi.org/10.1007/BF03190201>.
- Tabata, Y., Gutta, S., Langer, R., 1993. Controlled delivery systems for proteins using polyanhydride microspheres. *Pharm. Res.* 10, 487–496. <https://doi.org/10.1023/A:1018929531410>.
- Tamada, J., Langer, R., 1992. The development of polyanhydrides for drug delivery applications. *J. Biomater. Sci. Polym. Ed.* 3, 315–353. <https://doi.org/10.1163/156856292X00402>.
- Tamada, J.A., Langer, R., 1993. Erosion kinetics of hydrolytically degradable polymers. *Proc. Natl. Acad. Sci.* 90, 552–556. <https://doi.org/10.1073/pnas.90.2.552>.
- ter Boo, G.-J.A., Grijpma, D.W., Moriarty, T.F., Richards, R.G., Eglin, D., 2015. Antimicrobial delivery systems for local infection prophylaxis in orthopedic- and trauma surgery. *Biomaterials* 52, 113–125. <https://doi.org/10.1016/j.biomaterials.2015.02.020>.
- Tibbitt, M.W., Anseth, K.S., 2009. Hydrogels as extracellular matrix mimics for 3D cell culture. *Biotechnol. Bioeng.* 103, 655–663. <https://doi.org/10.1002/bit.22361>.
- Tibbitt, M.W., Kloxin, A.M., Anseth, K.S., 2013. Modeling controlled photodegradation in optically thick hydrogels. *J. Polym. Sci. Part Polym. Chem.* 51, 1899–1911. <https://doi.org/10.1002/pola.26574>.
- Tibbitt, M.W., Rodell, C.B., Burdick, J.A., Anseth, K.S., 2015. Progress in material design for biomedical applications. *Proc. Natl. Acad. Sci.* 112, 14444–14451. <https://doi.org/10.1073/pnas.1516247112>.
- Treiser, M., Abramson, S., Langer, R., Kohn, J., 2013. Chapter I.2.6 - degradable and resorbable biomaterials. In: Ratner, B.D., Hoffman, A.S., Schoen, F.J., Lemons, J.E. (Eds.), *Biomaterials Science*, third ed. Academic Press, pp. 179–195. <https://doi.org/10.1016/B978-0-08-087780-8.00021-8>.

- Vela Ramirez, J.E., Tygrett, L.T., Hao, J., Habte, H.H., Cho, M.W., Greenspan, N.S., Waldschmidt, T.J., Narasimhan, B., 2016. Poly-anhydride nanovaccines induce germinal center B cell formation and sustained serum antibody responses. *J. Biomed. Nanotechnol.* 12, 1303–1311. <https://doi.org/10.1166/jbn.2016.2242>.
- Vert, M., 1989. Bioresorbable polymers for temporary therapeutic applications. *Angew. Makromol. Chem.* 166, 155–168. <https://doi.org/10.1002/apmc.1989.051660111>.
- Vert, M., Li, S.M., Spenlehauer, G., Guerin, P., 1992. Bioresorbability and biocompatibility of aliphatic polyesters. *J. Mater. Sci. Mater. Med.* 3, 432–446. <https://doi.org/10.1007/BF00701240>.
- Vroman, I., Tighzert, L., 2009. Biodegradable polymers. *Materials* 2, 307–344. <https://doi.org/10.3390/ma2020307>.
- Wang, J.-S., Matyjaszewski, K., 1995. Controlled/“living” radical polymerization. atom transfer radical polymerization in the presence of transition-metal complexes. *J. Am. Chem. Soc.* 117, 5614–5615. <https://doi.org/10.1021/ja00125a035>.
- Wei, B., Tao, Y., Wang, X., Tang, R., Wang, J., Wang, R., Qiu, L., 2015. Surface-eroding poly(ortho ester amides) for highly efficient oral chemotherapy. *ACS Appl. Mater. Interfaces* 7, 10436–10445. <https://doi.org/10.1021/acsami.5b01687>.
- Widmer, M.S., Gupta, P.K., Lu, L., Meszlenyi, R.K., Evans, G.R.D., Brandt, K., Savel, T., Gurlek, A., Patrick, C.W., Mikos, A.G., 1998. Manufacture of porous biodegradable polymer conduits by an extrusion process for guided tissue regeneration. *Biomaterials* 19, 1945–1955. [https://doi.org/10.1016/S0142-9612\(98\)00099-4](https://doi.org/10.1016/S0142-9612(98)00099-4).
- Williams, D., Zhang, X. (Eds.), 2019a. I - Introduction, in: *Definitions of Biomaterials for the Twenty-First Century*. Elsevier, pp. 1–14. <https://doi.org/10.1016/B978-0-12-818291-8.00001-8>.
- Annex A - provisional list of terms to be discussed and examples of possible definitions. In: Williams, D., Zhang, X. (Eds.), 2019b. *Definitions of Biomaterials for the Twenty-First Century*. Elsevier, pp. 257–267. <https://doi.org/10.1016/B978-0-12-818291-8.00017-1>.
- Wong, J.Y., Bronzino, J.D., 2007. *Biomaterials*. CRC Press.
- Woodard, L.N., Grunlan, M.A., 2018. Hydrolytic degradation and erosion of polyester biomaterials. *ACS Macro Lett.* 7, 976–982. <https://doi.org/10.1021/acsmacrolett.8b00424>.
- Wu, L., Jing, D., Ding, J., 2006. A “room-temperature” injection molding/particulate leaching approach for fabrication of biodegradable three-dimensional porous scaffolds. *Biomaterials* 27, 185–191. <https://doi.org/10.1016/j.biomaterials.2005.05.105>.
- Zhang, S., Bellinger, A.M., Glettig, D.L., Barman, R., Lee, Y.-A.L., Zhu, J., Cleveland, C., Montgomery, V.A., Gu, L., Nash, L.D., Maitland, D.J., Langer, R., Traverso, G., 2015a. A pH-responsive supramolecular polymer gel as an enteric elastomer for use in gastric devices. *Nat. Mater.* 14, 1065–1071. <https://doi.org/10.1038/nmat4355>.
- Zhang, X., Malhotra, S., Molina, M., Haag, R., 2015b. Micro- and nanogels with labile crosslinks – from synthesis to biomedical applications. *Chem. Soc. Rev.* 44, 1948–1973. <https://doi.org/10.1039/C4CS00341A>.

Chapter Exercises

1. Define the term erosion.
2. What are the major routes of degradation for an orally administered drug? How could the activity of this drug be extended?
3. What factors should be considered when designing a photodegradable polymeric device?
4. How could a nondegradable polymer be useful in a degradable biomaterial?
5. Proteinase K has been added to a PLA device. How quickly will the device degrade? What are the degradation products?
6. How would the rate of degradation change for polymers made with a macrolactone (C₈–C₁₇) over PCL? Why does the degradation rate change?
7. What polymer composition, degradation rate, and delivery route would you use for a dental fixative?
8. What are the important factors to consider when designing biodegradable nanoparticles to deliver therapeutics?
9. Research an FDA-approved commercial PLGA product of your choice that was not covered in this chapter. Identify as much information about the polymer properties as you can (G:L ratio, molecular weight, end group chemistry, processing, etc.) and then use this information to explain why this specific design was well suited for the biomaterial's application.
10. Biochronomer, a poly(ortho ester)-based technology for controlled release applications, is used in two commercially available therapeutics, CINVANTI and SUSTOL, loaded with aprepitant and granisetron, respectively. Aprepitant has a logP value of 4.5 while granisetron has a logP value of 2.6, where a higher logP corresponds to more lipophilic drugs. Assuming the polymer formulation and drug loading are the same in both therapeutics, which treatment would you expect to have faster drug release? Why?

1.3.2G

Applications of “Smart Polymers” as Biomaterials

ALLAN S. HOFFMAN¹, PATRICK S. STAYTON²

¹Bioengineering and Chemical Engineering, University of Washington, Seattle, WA, United States

²Bioengineering, University of Washington, Seattle, WA, United States

Introduction

Stimulus-responsive, “intelligent” polymers are polymers that respond to small changes in physical or chemical conditions near a critical condition with sharp and relatively large phase or property changes. They are also known as “smart,” stimuli-responsive, or “environmentally sensitive” polymers. These polymers can take many forms; for example, they may be dissolved in aqueous solutions, adsorbed or grafted on aqueous–solid interfaces, or cross-linked in the form of hydrogels. They may also be combined chemically or physically with other molecules, especially a variety of bioactive molecules. A number of reviews over the past 20–25 years have highlighted applications of smart polymers in the biomedical field (Hoffman, 1987, 1995, 1997; Hoffman et al., 2000; Okano et al., 2000; Roy and Gupta, 2003; Roy et al., 2010; Hoffman, 2013; Moad, 2017, MacEwan and Chilkoti, 2017; Reineke, 2016). In this chapter, we have prioritized earlier historical examples with some exciting and representative more recent developments. The reader is referred to classical and more recent reviews of the ever-expanding applications of smart polymers in the biomaterial field (e.g., Hoffman, et al., 2000; Heredia and Maynard, 2007; Hoffman and Stayton, 2010; Grover and Maynard, 2010; Broyer et al., 2011). The reader is also referred to the chapter by Benoit on Drug Delivery Systems (Chapter 2.5.12) for more details.

Many different stimuli-responsive polymers have been investigated, and the various stimuli that researchers have used are listed in Table 1.3.2G.1. Typically, when the polymer’s smart response is stimulated, the resultant behavior will depend on the initial state of the polymer (Fig. 1.3.2G.1). Four examples of this are described below:

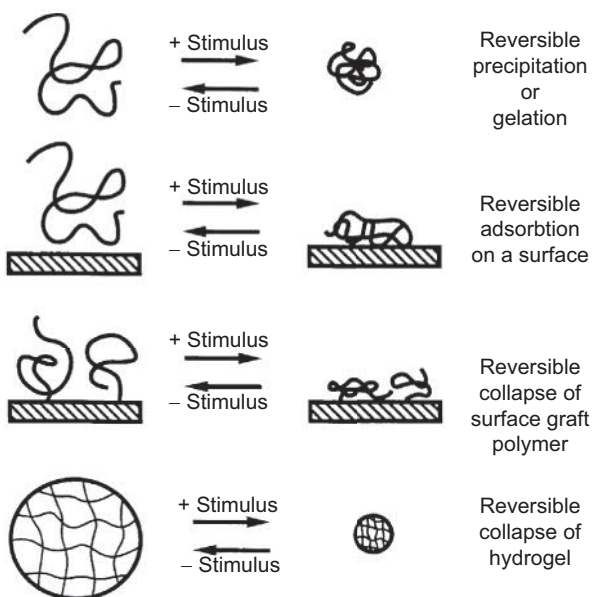
- When a smart polymer is dissolved in an aqueous solution, it will exhibit a sudden onset of turbidity as it phase separates, and if its concentration is high enough it may convert from a viscous solution to a gel.

- When a smart polymer is designed as a block copolymer it can be stimulated to phase separate as a segment that forms a hydrophobic core of a micelle, that can load drugs, and then stimulated to reversibly release the drugs as the polymer is switched back to unimeric soluble chains.
- When a smart polymer is chemically grafted to an aqueous–solid interface and is stimulated to phase separate, it will collapse, converting that interface from a hydrophilic to a hydrophobic interface. If the smart polymer is dissolved in solution and is stimulated to phase separate in the presence of a solid–aqueous interface, it may physically adsorb at the interface, especially when the surface composition has a balance of hydrophobic and polar groups similar to the phase-separating smart polymer.
- A smart polymer may be chemically cross-linked into a network. When it is swollen in an aqueous solution below its critical condition, it may be called a “smart hydrogel.” When the polymer network chains are stimulated to phase separate at their critical condition, the hydrogel will collapse and release much of its swelling solution as a burst.

These phenomena all reverse when the stimulus is reversed. The phase separation of a water-solvated smart polymer chain is driven by the release of the hydrophobically bound water molecules on the polymer backbone, which creates a large gain in entropy in the system. Often the rate of reversion back to the hydrated state is slower than the collapse, because the reverse process of water moving back into the collapsed phase and to the apolar groups of the polymer is slower than the original release of waters to bulk solution. The rehydration of the hydrophobic groups of the polymer as a process is thermodynamically opposed by the resultant decline in entropy of the system (the reswelling process is favored by the exothermic hydration and expansion of the polymer chains). The rate of collapse of smart

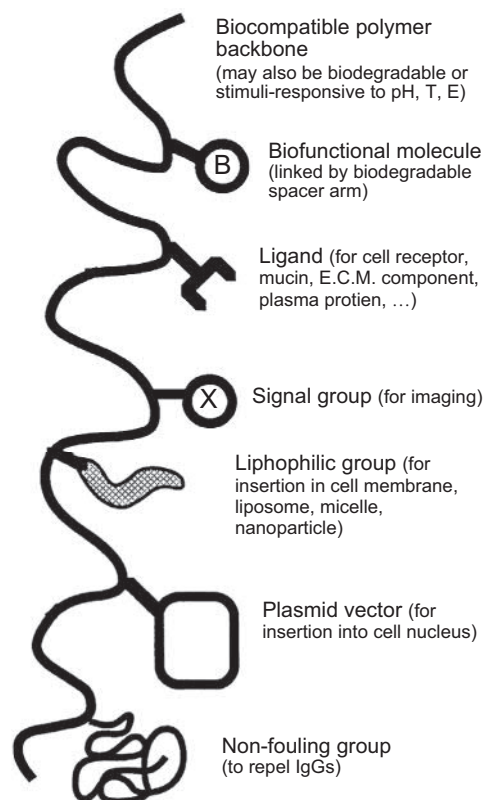
TABLE 1.3.2G.1 Environmental Stimuli

Physical
Temperature
Ionic strength
Solvents
Radiation (UV, visible)
Electric fields
Mechanical stress
High pressure
Sonic radiation
Magnetic fields
Chemical
pH
Specific ions
Chemical agents
Biochemical
Enzyme substrates
Affinity ligands
Other biological agents



• **Figure 1.3.2G.1** Schematic illustration showing the different types of responses of “intelligent” polymer systems to environmental stimuli. Note that all systems are reversible when the stimulus is reversed. (Hoffman et al., (2000) *Journal of Biomedical Materials Research* (JBMR): Reproduced with permission of JBMR, J. Wiley, Publisher.)

polymer systems and its reversal can also depend on the dimensions of the smart polymer system. Rates will be more rapid for systems with smaller dimensions, e.g., nanoscale versus microscale dimensions.



• **Figure 1.3.2G.2** Schematic illustration showing the variety of natural or synthetic biomolecules that may be conjugated to a smart polymer. In some cases, only one molecule may be conjugated, such as a recognition protein, which may be linked to the protein at a reactive terminal group of the polymer, or it may be linked at a reactive pendant group along the polymer backbone. In other cases more than one molecule may be conjugated along the polymer backbone, such as a targeting ligand along with many drug molecules. (Hoffman et al., (2000) *Journal of Biomedical Materials Research* (JBMR): Reproduced with permission of JBMR, J. Wiley, Publisher.)

The rate of collapse of smart polymer systems and its reversal can depend on the dimensions of the smart polymer system. Rates will be more rapid for systems with smaller dimensions, e.g., nanoscale versus microscale dimensions.

Smart polymers may be physically mixed with, complexed with, or chemically conjugated to biomolecules, small-molecule drugs, and/or imaging agents to yield a large and diverse family of biomaterials that can respond to biological, as well as to physical and chemical, stimuli. Biomolecules that may be combined with smart polymer systems include proteins and peptides, sugars and polysaccharides, single- and double-stranded oligonucleotides, RNA and DNA, simple lipids and phospholipids, and a wide spectrum of recognition ligands and synthetic drug and contrast agents. In addition, other polymer compositions such as polyethylene glycol (PEG) may be conjugated to the smart polymer backbone to provide it with “stealth” properties (Fig. 1.3.2G.2 schematically shows many different molecules, one or several together, which may be conjugated to a single smart polymer chain).

Smart polymer–biomolecule conjugates in solution, on surfaces, and within hydrogels represent an important and exciting extension of polymeric biomaterials beyond their well-known uses in implants, medical devices, and drug delivery.

Smart Polymers in Solution

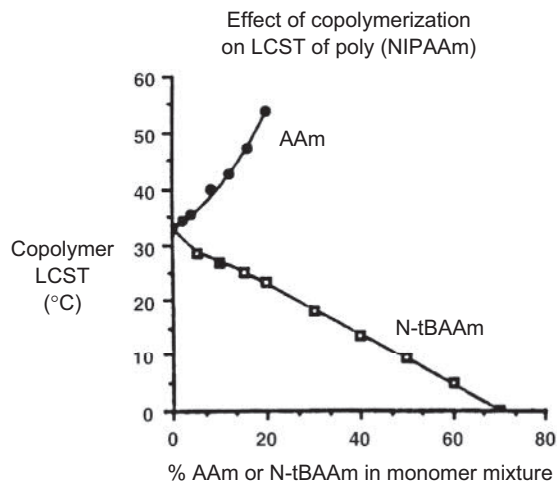
There are many polymers that exhibit thermally induced precipitation out of aqueous solutions (Table 1.3.2G.2), and the polymer that has been most extensively studied is poly(*N*-isopropyl acrylamide), or PNIPAAm. This polymer is soluble in water below 32°C, and precipitates sharply as temperature is raised above 32°C (Heskins and Guillet, 1968; Schild, 1992). The precipitation temperature is called the lower critical solution temperature, or LCST. If the solution contains buffer and salts the LCST may be reduced several degrees. If NIPAAm monomer is copolymerized with more hydrophilic monomers, such as acrylamide, the LCST will increase and may even disappear. If NIPAAm monomer is copolymerized with more hydrophobic monomers, such as *n*-butylacrylamide, the LCST decreases (Priest et al., 1987).

pH-responsive polymers have also been extensively studied due to the many biomaterial settings where physiological or device-related pH gradients can be used to couple phase transitions to useful actions such as drug delivery. The incorporation of carboxylic acid-derived monomers, such as acrylic acid (AA) or methacrylic acid (MAA), has been used to impart pH sensitivity in a variety of copolymers. By copolymerizing these monomers with more hydrophobic monomers, the pH transition can be tuned to higher pH values. Peppas and coworkers have extensively studied pH-sensitive acrylic acid-acrylate copolymer smart gels (e.g., Peppas et al., 1999, 2000; Robinson and Peppas, 2002; Peppas, 1997, 2001). This work is discussed in more detail in Chapter 1.3.2E on Hydrogels. The synthesis of longer alkyl-segment members such as propyl(acrylic acid), butyl(acrylic acid), and longer apolar segments also has provided new opportunities to tune the pH transition point. Tirrell originally characterized a newer member of the alkylacrylic acid family in ethyl(acrylic acid) and more recently, Stayton, Hoffman, and coworkers have studied the behavior of pH-sensitive alpha-alkylacrylic acid polymers in solution (Tirrell, 1987; Lackey et al., 1999; Murthy et al., 1999; Stayton et al., 2000; Murthy et al., 2003a,b; Yin et al., 2006; Stayton and Hoffman, 2008). As pH is lowered, these polymers become increasingly protonated and hydrophobic, and eventually phase separate; this transition can be sharp, resembling the phase transition at the LCST. Bae and coworkers also developed interesting temperature- and pH-sensitive polymers for endosomal release of drug formulations (e.g., Na et al., 2006; Kang and Bae, 2007).

Dual-sensitive smart polymers have also been developed to provide further tunability. NIPAAm may be copolymerized with pH-sensitive monomers, leading to random copolymers with both temperature- and pH-responsive behavior (Murthy, et al., 1999; Zareie et al., 2000; Murthy

TABLE 1.3.2G.2 Some Polymers and Surfactants That Exhibit Thermally-Induced Phase Separation in Aqueous Solutions

Polymers/Surfactants with Ether Groups
Poly(ethylene oxide) (PEO)
Poly(ethylene oxide/propylene oxide) random copolymers [poly(EO/PO)]
PEO–PPO–PEO triblock surfactants (Polyoxamers or Pluronic)
PLGA–PEO–PLGA triblock polymers
Alkyl–PEO block surfactants (Brij)
Poly(vinyl methyl ether)
Polymers with Alcohol Groups
Poly(hydropropyl acrylate)
Hydroxypropyl cellulose
Methylcellulose
Hydroxypropyl methylcellulose
Poly(vinyl alcohol) derivatives
Polymers with Substituted Amide Groups
Poly(<i>N</i> -substituted acrylamides)
Poly(<i>N</i> -acryloyl pyrrolidine)
Poly(<i>N</i> -acryloyl piperidine)
Poly(acryl- <i>l</i> -amino acid amides)
Others
Poly(methacrylic acid)



• **Figure 1.3.2G.3** Copolymerization of a thermally sensitive polymer, PNIPAAm, with a more hydrophilic comonomer, AAm, raises the LCST of the copolymer, whereas copolymerization with a more hydrophobic comonomer, N-tBAAm, lowers the LCST. (Hoffman et al., (2000) *Journal of Biomedical Materials Research* (JBMR): Reproduced with permission of JBMR, J. Wiley, Publisher.)

et al., 2003a,b; Yin, et al., 2006). NIPAAm has been copolymerized with pH-responsive macromonomers of acrylic acid (AAc), which yielded graft copolymers that independently exhibit two distinct stimuli responses, one for the backbone PNIPAAm and one for the side chain PAAc (Chen and Hoffman, 1995). Block copolymers of two such smart polymers also exhibit two distinct stimuli responses if the two individual blocks are each long enough. Such smart polymers can form physical hydrogels in response to changes in temperature and/or pH and have been broadly investigated for use as injectable drug-delivery systems (their high water content provides good biocompatibility, and the lack of chemical cross-links facilitates eventual elimination from the body (see also Chapter 2.5.12 on Drug Delivery Systems for more details). A family of thermally gelling and biodegradable triblock copolymers has been developed by Sung Wan Kim and coworkers for injectable formulations that form degradable, drug depot masses at body conditions (Vernon et al., 2000; Lee et al., 2001; Jeong et al., 2002). The formulation is a medium viscosity, injectable solution at room temperature, and a phase-separated hydrogel mass at 37°C. Doo Sung Lee, You Han Bae, and coworkers have developed similar biocompatible and degradable A–B–A triblock copolymers having both pH and temperature sensitivity; they are based on two blocks of poly(caprolactone-co-lactic acid) copolymers (PCLA), combined with a central PEG block. The pH sensitivity is derived from short blocks containing the sulfonamide group (OSM) that are attached at each end of the triblock (Shim et al., 2005, 2006).

In addition to vinyl-based polymers, there have been exciting advances in developing stimuli-responsive biopolymers for biomaterial applications. Urry and colleagues first developed elastin polypeptides that showed temperature- and pH-responsive behavior, i.e., LCST properties. Subsequently, elastin-like polypeptides (ELPs) have been developed extensively by Chilkoti and coworkers. Because the ELPs are genetically encoded and produced biologically, the sequence and size of ELPs can be exactly designed and controlled. This precision in engineering their sequences and molecular weights is thus unattainable by synthetic chemistry and as a result they have been rapidly developed into biomaterial applications. By controlling the incorporation of hydrophobic or charged amino acids, different trigger points for temperature and pH transitions can be engineered. Block architectures have also been developed with similar architectural transitions as smart synthetic block copolymers. Finally, they can be engineered as genetic fusions to therapeutic or targeting peptides and proteins and thus do not always require bioconjugation. Due to these versatile attributes, ELPs have been used extensively as scaffolds for tissue engineering, in drug-delivery systems as soluble biopolymer therapeutics, micelles, nano- and microparticles, and as thermally triggered drug depots (Urry et al., 1991; Meyer and Chilkoti, 2002; MacEwan and Chilkoti, 2017; Panitch et al., 1999).

Smart Polymer–Protein Bioconjugates

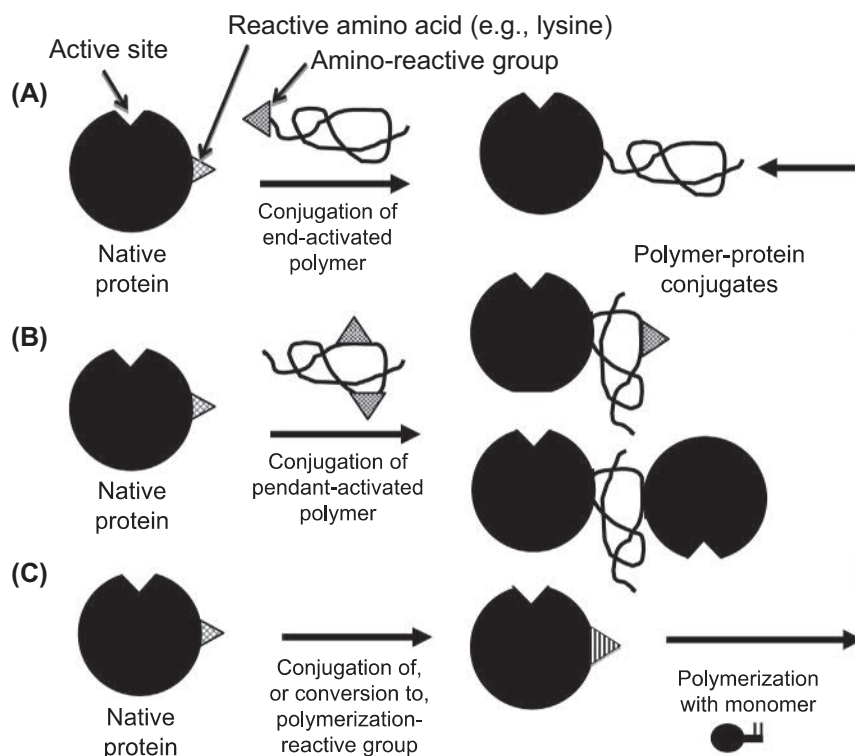
Smart polymers may be conjugated randomly to proteins by binding the reactive end of the polymer or reactive pendant groups along the polymer backbone to reactive sites on the protein. One may utilize functionalized free radical initiator or chain transfer agents to synthesize oligomers with one functional end group, which can then be derivatized to form a reactive group that can be conjugated to the protein. For example, NIPAAm has been copolymerized with reactive monomers such as *N*-hydroxysuccinimide acrylate (NHS acrylate) to yield a random copolymer with pendant NHS groups, which have then been conjugated to the protein. (These synthesis methods are described in Cole et al., 1987; Monji and Hoffman, 1987; Chen et al., 1990; Chen and Hoffman, 1990; Yang et al., 1990; Takei et al., 1993a; Chen and Hoffman, 1994; Ding et al., 1996, 1998.) Vinyl monomer groups may also be conjugated to proteins to provide “comonomer” vinyl groups for copolymerization with free monomers such as NIPAAm (Shoemaker et al., 1987).

Normally the lysine amino groups are the most reactive protein sites for random polymer conjugation to proteins, and *N*-hydroxysuccinimide (NHS) attachment chemistry is often utilized. Other possible sites include –COOH groups of aspartic or glutamic acid residues, –OH groups of serine or tyrosine residues, –SH groups of cysteine residues, and terminal amino groups. Fig. 1.3.2G.4 shows various ways that polymers may be directly conjugated to proteins or formed by growth from the protein (Hoffman and Stayton, 2010).

Random conjugation of temperature-sensitive (mainly) and pH-sensitive (occasionally) polymers to proteins has been extensively investigated, and applications of these conjugates have been focused on immunoassays, affinity separations, enzyme recovery, and drug delivery. One of the earliest applications of a smart polymer–biomolecule conjugate was an immunoassay developed by Hoffman, along with coworkers at a Seattle company called Genetic Systems Corp. They conjugated PNIPAAm to an antibody and used it to capture an antigen, then added a second, labeled antibody to the antigen, and warmed to phase separate the labeled immune complex sandwich. The assay was similar to an ELISA assay, but was much faster and was as accurate as ELISA. (Other interesting early work on soluble–insoluble polymer–biomolecule conjugates can be found in the following references: Schneider et al., 1981; Okamura et al., 1984; Nguyen and Luong, 1989; Taniguchi et al., 1989; Chen and Hoffman, 1990; Monji et al., 1990; Pecs et al., 1991; Taniguchi et al., 1992; Takei et al., 1993b, 1994a; Galaev and Mattiasson, 1993; Fong et al., 1999; Anastase-Ravion et al., 2001; Pelegri-O’Day, 2014; Broyer et al., 2011; De et al., 2008).

Site-Specific Smart Polymer Bioconjugates

Conjugation of a responsive polymer to specific and designed sites of proteins opened new opportunities for

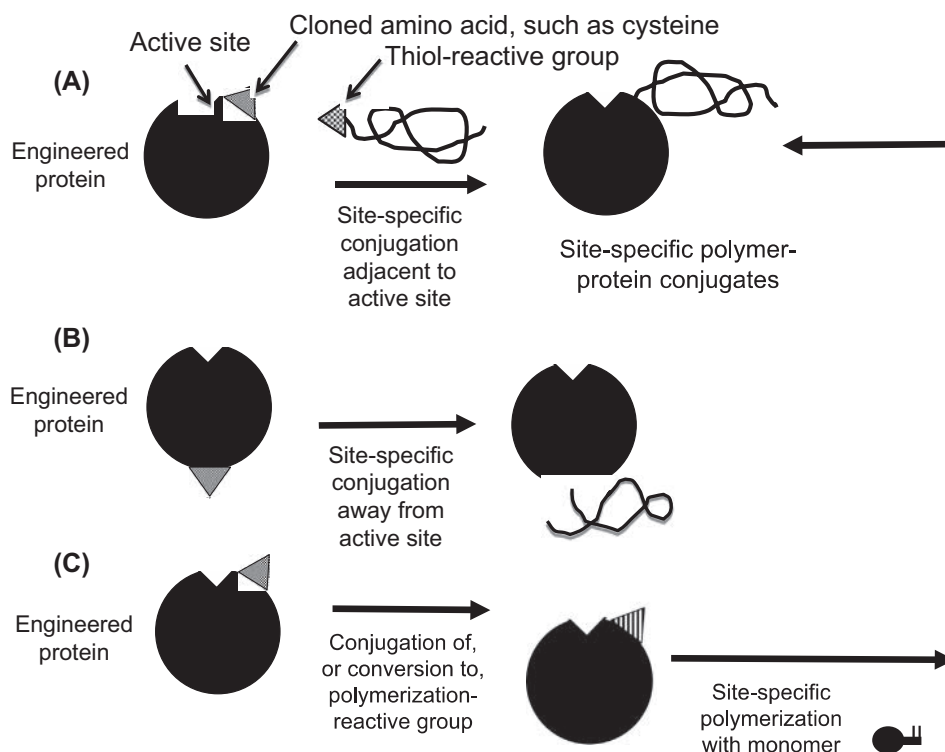


• **Figure 1.3.2G.4** Various methods for synthesizing polymer-protein bioconjugates.

the bioconjugate field (Chilkoti et al., 1994; Stayton and Hoffman et al., 1995, 2000). The possibilities of exploiting the polymer chain transitions to control the desired protein/enzyme activities were opened by this site-selective design of the conjugation site (Stayton and Hoffman et al., 1995). The first application was an “affinity switch” where protein activity was shown to be switchable by the smart polymer switches triggered by external stimuli such as temperature, pH, or light. The molecular switching capabilities were shown to depend on polymeric parameters, such as the composition, MW, attachment site, and magnitude of its conformational and physical change. The switching efficiency was also engineered based on the size of the ligands or substrates, and their affinity for the active site. Smart polymers were conjugated to a reactive –SH thiol group from a cysteine that had been inserted by site-specific mutagenesis at a site nearby the active site of the protein (Fig. 1.3.2G.5). Typical SH-reactive polymer end groups include maleimide and vinyl sulfone groups. The specific site for polymer conjugation can also be located far away from the active site (Chilkoti et al., 1994), in order to avoid interference with the biological functioning of the protein, or nearby or even within the active site, in order to control the ligand-protein recognition process, and the resulting biological activity of the protein (Fig. 1.3.2G.5) (see also Stayton et al., 1995). Temperature-, pH-, and light-sensitive smart polymers have been used to form such novel, “really smart” bioconjugates (Ding et al., 1999, 2001; Bulmus et al., 1999; Stayton et al., 2000; Shimoboji et al., 2001, 2002a,b, 2003).

Similar strategies were shown to create reversible smart polymer shields to reversibly control protein-protein associations (Stayton et al., 1995), and have enabled separation of biotinylated proteins according to the size of the protein (Ding et al., 2001). The smart polymers could serve as dual-sensitive enzyme activity switches. For the site-specific enzyme conjugates, a combined temperature- and light-sensitive polymer was conjugated to specific sites on endocellulase, which provided “on-off” control of the enzyme activity with either light or temperature (Shimoboji et al., 2001, 2002a,b, 2003). Bulmus et al. (1999) conjugated a pH- and temperature-responsive PNIPAAm copolymer to a specific site on streptavidin. Triggered release of bound drugs by the smart polymer-engineered protein bioconjugates could be used to release therapeutics, such as for topical drug delivery to the skin or mucosal surfaces of the body, and also for localized delivery of drugs within the body by stimulated release at pretargeted sites using noninvasive, focused stimuli such as ultrasound or delivery of light stimuli from catheters. Triggered release could also be used to release and recover affinity-bound ligands from chromatographic and other supports in eluate-free conditions, including capture and release of specific cell populations to be used in stem cell and bone marrow transplantation.

A method for thermally induced switching of enzyme activity has been developed, based on the site-directed conjugation of end-reactive temperature-responsive polymers to a unique cysteine (Cys) residue positioned near the enzyme active site. The reversible temperature-induced collapse of



• **Figure 1.3.2G.5** Schematic illustration of various processes for preparing a site-specific conjugate of a polymer with a genetically-engineered, mutant protein.

N,N-dimethylacrylamide (DMA)/N-4-phenylazo-phenylacrylamide (AZAAM) copolymers (DMAAm) has been used as a molecular switch to control the catalytic activity of endoglucanase 12A (EG 12A). The polymer was conjugated to the EG 12A site-directed mutant N55C, directly adjacent to the cellulose binding cleft, and to the S25C mutant, where the conjugation site is more distant. The N55C conjugate displayed a larger activity shut-off efficiency in the collapsed polymer state than the S25C conjugate. Increasing the polymer molecular weight was also shown to increase the shut-off efficiency of the switch.

Block copolymers containing stimuli-responsive segments provide important new opportunities for controlling the activity and aggregation properties of protein–polymer conjugates. Kulkarni et al. prepared an RAFT block copolymer of a biotin-terminated poly(*N*-isopropylacrylamide) (PNIPAAm)–*b*–poly(acrylic acid) (PAA). The number-average molecular weight (M_n) of the (PNIPAAm)–*b*–(PAA) copolymer was determined to be 17.4 kDa ($M_w/M_n = 1.09$). The PNIPAAm block had an M_n of 9.5 kDa and the PAA block had an M_n of 7.9 kDa. This block copolymer was conjugated to streptavidin (SA) via the terminal biotin on the PNIPAAm block. This controls the molecular orientation of the PNIPAAm block to be near the streptavidin surface with the PAA block oriented further away toward bulk solution. It was found that the PNIPAAm still went through its chain collapse via thermal stimulation, while the PAA chain in its ionized state prevented the usual PNIPAAm-induced aggregation. Thus the activity switching could be separated from protein aggregation and the molecular switch could

operate on isolated polymer–protein conjugates. If aggregation was also desired, reducing the pH to protonate the PAA could remove the charge repulsive properties of the outer segment and protein aggregation could be triggered by dual temperature and pH stimulation.

Smart Polymers on Surfaces

Smart polymers, especially PNIPAAm, have been coated on various surfaces by physical adsorption, chemical conjugation, affinity complexation, radiation-induced polymerization, direct or chain-transfer initiated polymerization from the surface, and plasma discharge deposition. These methods and various applications of them are discussed in this section.

Smart polymers, especially PNIPAAm, have been coated on various surfaces by physical adsorption, chemical conjugation, affinity complexation, radiation-induced polymerization, direct or chain-transfer initiated polymerization from the surface, and plasma discharge deposition.

One may covalently graft PNIPAAm to a surface by exposing the surface to ionizing radiation in the presence of the monomer (and in the absence of air) or by preirradiating the polymer surface in air, and later contacting the surface with the monomer solution and heating in the absence of air to expose trapped radicals. These surfaces exhibit stimulus-responsive changes in wettability (e.g., Uenoyama and Hoffman, 1988; Takei et al., 1994b; Kidoaki et al., 2001). Okano, Yamato, and coworkers have been pioneers in the

area of smart polymer cell culture surfaces. They applied the radiation grafting technique to form surfaces having a surface layer of grafted PNIPAAm (Yamato and Okano, 2001; Shimizu et al., 2003). They cultured cells to confluent sheets on these surfaces at 37°C, which is above the LCST of the polymer. When the PNIPAAm collapses, the interface becomes hydrophobic and leads to physical adsorption of cell adhesion proteins from the culture medium, enhancing the cell culture process. Then, when the temperature is lowered, the interface becomes hydrophilic as the PNIPAAm chains rehydrate, and the cell sheets are released from the surface along with the cell adhesion proteins, which remain bound to the cell surfaces. The cell sheet can be recovered and used in tissue engineering, e.g., for artificial corneas and heart patches, and in periodontal applications. These exciting new applications of smart surface cell sheets are being pursued in the clinic. Patterned PNIPAAm surfaces have also been prepared for cell culture (Yamato et al., 2001).

Ratner and coworkers used a gas plasma discharge technique to deposit temperature-responsive coatings from a NIPAAm monomer vapor phase plasma discharge. When cells are cultured on these surfaces, they also form reversible cell sheets in a manner similar to Okano and Yamato's PNIPAAm-grafted surfaces (Pan et al., 2001).

Smart polymers may also be grafted to surfaces by polymerizing the monomer directly from the surface. This may be done by first attaching to the surface either a radical initiator, such as an azo or peroxide initiator, or a chain transfer agent (CTA) for controlled radical polymerizations such as reversible addition-fragmentation chain transfer polymerization (RAFT) (e.g., Chiefari et al., 1998; McCormick and Lowe, 2004; Moad et al., 2008) or atom transfer radical polymerization (ATRP) (e.g., Wang and Matyjaszewski, 1995; Matyjaszewski and Xia, 2001; Matyjaszewski and Tsarevsky, 2009). (The ATRP of the smart polymer from a biomolecule such as a protein to form the bioconjugate directly was discussed earlier in this chapter.) Then the polymerization is initiated at the surface or in the surrounding solution, and the result is a smart polymer grafted to the surface. In the case of RAFT or ATRP controlled radical polymerizations, the molecular weights of the grafted polymer can be controlled to a narrow range. In a recent example, Golden and coworkers conjugated an RAFT CTA to the surface of a microporous, hydroxylated nylon membrane, and graft-polymerized NIPAAm directly from the surface, forming a graft polymer of around 9000 MW (Golden et al., 2010). Then this surface was heated, and the collapsed PNIPAAm-coated porous membrane was used in a microfluidic channel to sequester dilute PNIPAAm-antibody conjugates that had earlier captured a biomarker antigen in a blood test sample. In this way, the captured biomarker was concentrated on the membrane surface and later released by cooling to provide a concentrated pulse flowing downstream in the channel for this smart polymer microfluidic immunoassay.

The research team of Stayton, Hoffman, and coworkers developed a variety of nanoparticles coated with PNIPAAm for various applications in diagnostic immunoassays. They

include polystyrene latex nanoparticles, magnetic nanoparticles, and gold nanoparticles. For example, PNIPAAm- and antibody-functionalized beads were then used to capture labeled, biotinylated antigens in a diagnostic test sample, to produce a smart polymer competition immunoassay carried out in a microfluidic device (Malmstadt et al., 2003a,b, 2004). Such PNIPAAm-antibody coatings were also developed on magnetic and gold nanoparticles, which were used to capture dilute antigen biomarkers in a test sample, then later were captured on the PNIPAAm-grafted porous membrane surface described above (Golden et al., 2010). After that they were released by cooling, forming a concentrated pulse of labeled nanoparticles for a global health infectious disease assay downstream in a microfluidic device. PNIPAAm-coated magnetic and gold NPs were also applied in lateral flow, “dipstick” assay for diagnostics in global health infectious disease applications by the Stayton–Hoffman group.

In a process for coating magnetic nanoparticles with PNIPAAm, the Stayton–Hoffman group developed responsive magnetic nanoparticles in the presence of a dodecyl-terminated PNIPAAm. The dodecyl-terminated PNIPAAm polymer formed micelles that concentrated the pentacarbonyl iron precursor of magnetic iron oxides in the dodecyl core of the micelle before it was converted at high temperature to magnetic iron oxide (Lai et al., 2007, 2009). To coat the gold nanoparticles, Nash bound RAFT-polymerized PNIPAAm chains to the gold surface via sulfur's affinity to gold, utilizing the sulfur-containing groups in the dithioester or trithiocarbonate terminal groups from the original CTA of the RAFT polymer chain (Nash et al., 2010a,b,c). The coated magnetic particles were mainly used for separating and concentrating the captured antigen, and the coated gold particles were mainly used as color (red) labels to indicate the approximate concentration of the captured antigen.

Smart polymers may also be grafted in gradients to surfaces to provide surfaces of gradually varying hydrophilicity and hydrophobicity as a function of the polymer composition and conditions. This phenomenon has been applied by Okano, Kikuchi, and coworkers to prepare chromatographic column packing for use in eluate-free (“green”) chromatographic separations (Kobayashi et al., 2001; Kikuchi and Okano, 2002). Ishihara et al. (1982, 1984) developed photo-responsive coatings and membranes that reversibly change surface wettability or swelling due to the photo-induced isomerization of an azobenzene-containing polymer.

Smart Polymer Hydrogels

When a smart polymer is cross-linked to form a gel, it will collapse and reswell in water as a stimulus raises or lowers it through its critical condition. PNIPAAm hydrogels have been extensively studied, starting with the pioneering work of Toyochi Tanaka in 1981 (Tanaka, 1981). In the mid-to late-1980s, Hoffman and coworkers were among the first to recognize the potential of PNIPAAm hydrogels

as biomaterials; they showed that smart gels could be used to entrap enzymes and cells, and then by inducing cyclic collapse and swelling of the gel, the enzymes (or enzymes within the cells) could be turned “on” and “off.” Park and Hoffman also showed enhanced enzyme efficiency for an entrapped enzyme in a packed bed, hydrogel bead reactor, since the collapse delivered product faster than it could diffuse out, and the reswelling imbibed substrate faster than it could diffuse in. They also could deliver drugs or remove toxic biomolecules, by stimulus-induced collapse or swelling. Dong and Hoffman developed an interesting pH- and temperature-responsive gel that swelled linearly at 37°C and pH 7.4, at rates depending on the AAc monomer content in the gel (Dong and Hoffman, 1986, 1987, 1990, 1991; Park and Hoffman, 1988, 1990a,b,c, 1994) (Fig. 1.3.2G.6).

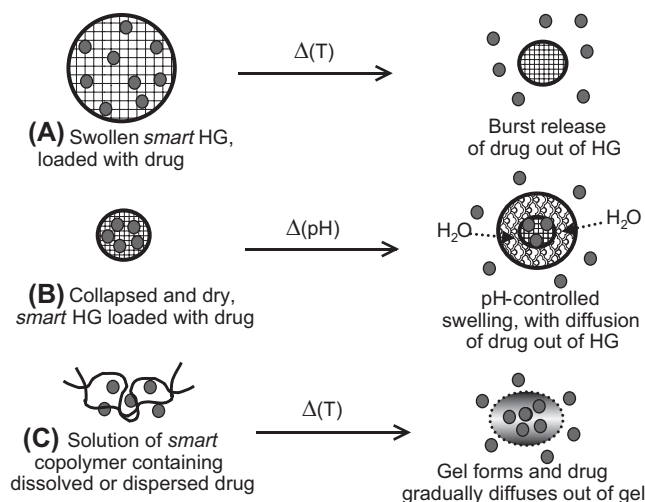
The research team of Kim, Okano, Bae, and coworkers was also actively studying smart hydrogels in the late 1980s and 1990s. For example, they investigated smart gels containing entrapped cells that could be used as artificial organs (Vernon et al., 2000). Since then, the properties of PNIPAAm hydrogels have been widely investigated in the form of beads, slabs or discs, and multilamellar laminates (Park and Hoffman, 1992a,b; Hu et al., 1995, 1998; Mitsumata et al., 2001; Gao and Hu, 2002; Kaneko et al., 2002).

Okano and coworkers designed and synthesized PNIPAAm gels that collapse much more rapidly than PNIPAAm gels that are simply cross-linked with a divinyl comonomer. Yoshida, Okano, and coworkers copolymerized NIPAAm monomer with a PNIPAAm macromer and a cross-linker, which yielded a gel with PNIPAAm chains grafted to the PNIPAAm network. The grafted chains collapsed first at the LCST, enhancing the rate of collapse of the network, along with the related rate of expulsion of water from the gel (Yoshida et al., 1995; Masahiko et al., 2003).

Peppas and coworkers (e.g., Peppas et al., 2000; Robinson and Peppas, 2002) have extensively studied pH-sensitive acrylic acid-acrylate copolymer smart gels. This work is discussed in more detail in Chapter 1.3.2E on Hydrogels (see also Peppas, 1997, 2001; Peppas et al., 1999, 2000).

Matsuda and coworkers incorporated PNIPAAm into physical mixtures with natural polymers such as hyaluronic acid and gelatin, for use as tissue-engineering scaffolds (Ohya et al., 2001a,b). Park and Hoffman developed a unique process for synthesizing mm-size spherical microgels of PNIPAAm (Park and Hoffman, 1992b). Nakamae, Hoffman, and coworkers developed novel compositions of smart gels containing phosphate groups that were used to bind cationic proteins as model drugs, and then to release them by a combination of thermal stimuli and ion exchange (Nakamae et al., 1992, 1997; Miyata et al., 1994).

A number of smart hydrogel drug-delivery systems have been designed to respond to biologic signals in a feedback manner. Many of these gels contain an immobilized enzyme. They are discussed in the Chapter 2.5.12 on Drug Delivery Systems.



• **Figure 1.3.2G.6** Schematic illustration showing three ways that smart gel formulations may be stimulated to release bioactive agents: (A) thermally-induced collapse, which is relevant to skin or mucosal drug delivery; (B) pH-induced swelling, which is relevant to oral drug delivery, where the swelling is induced by the increase in pH in going from the gastric to enteric regions; and (C) sol-to-gel formation, which is relevant to injectable or topical formulations of a triblock copolymer solution that are thermally gelled at body temperature. For in vivo uses, the block copolymer is designed to be degradable. The first two apply to cross-linked gels applied topically or orally, and the third is relevant to thermally-induced formation of gels from polymer solutions that are delivered topically or by injection. (See also Chapter 2.5.12 Drug Delivery Systems.)

Stimuli-Responsive Polymer Micelles and Carriers

One of the most rapidly developing biomaterial applications of smart polymers involves their development as drug-delivery systems. This includes pioneering work of Kataoka with pH-responsive and light-responsive photodynamic polymers for both small-molecule and nucleic acid drugs. Their group has carried such small-molecule carriers into advanced clinical trials. Bae and coworkers have done seminal work on sharply pH-responsive micelles that introduced elements of biodegradable, targeting, and triggered drug release (connected to work by Kim on polyhistidine polymers for nucleic acid delivery, see below). For example, they developed drug-delivery systems composed of PLA-*b*-PEG-*b*-P(His)-TAT and P(His) block of P(His)-*b*-PEG, where the surface of the particles was covered by hydrophilic PEG. They showed the targeting and intracellular carrier TAT peptide could be concealed during circulation but be exposed after the hydrophobic transition coupled to histidine protonation in the lower pH environment of tumors. This system showed higher anticancer activity and triggered release compared to free drug in animal models.

There have been many more developments using temperature, pH, redox and other signals to trigger better delivery and also imaging (for recent reviews see). One creative example of couple “theranostic” imaging and therapy was reported by Koo et al., 2011. They described the

development of pH-responsive MPEG poly(β -amino ester) polymeric micelles, which are designed to undergo a sharp pH-dependent transition to unimers in the lower pH environment of tumors. The tertiary amine groups are copolymerized into the hydrophobic amino ester block and these become protonated and highly destabilizing to the micelle core when they localize into the tumor when pH falls below 6.5. By coupling the imaging agent and drug release to this micelle destabilization they showed this theranostic system enabled in vivo tumor diagnosis and therapy simultaneously.

The area of nucleic acid delivery and the advent of gene medicine and other biologic drugs has driven considerable development of stimuli-responsive carriers over the past two decades. Stimuli-responsive polymers have played a continuing part of the nucleic acid carrier field as it has developed from and across plasmid, siRNA, mRNA, and most recently gene-editing technologies. Considerable effort has in particular been aimed at overcoming one of the most significant barriers for the delivery of biomolecular therapeutics that function inside the cell—endosomal release and cytosolic delivery (e.g., Stayton and Hoffman, 2008; also see Chapter 2.5.12 on Drug Delivery Systems). Many exciting developments continue today—and are still badly needed for ever-evolving biologic drugs that could benefit from DDS—to produce carriers that better target, enhance intracellular delivery, and maintain necessary ADME and manufacturing requirements.

Many cationic polymers were initially developed and some were designed as proton sponges to aid in endosomal escape. Early work with smart polymers from the group of Sung Wan Kim developed pH-responsive carriers that exploited biomimetic polyhistidine, such as in *N*-Ac-poly(L-histidine)-graft-poly(L-lysine) to trigger better endosomal release. These carriers demonstrated the potential of sharply triggered polymers to become endosome-releasing for plasmid DNA as the endosome acidified. Another approach was developed by Stayton and Hoffman with polymers that were engineered to undergo a pH-responsive transition in the endosome to directly destabilize the endosomal membrane. These polymers and the original monomer developed were inspired by the mechanism exploited by pathogens that must deliver nucleic acids and proteins to the cytosol for activity. The polymers also contain similar constituent pH-sensing chemical functionalities such as hydrophobized carboxylate groups—originally with a new member of the alkyl(acrylic acid) family in propyl(acrylic acid) (PAA). These polymers were initially built into DDS as an endosomal-releasing polymer for plasmid delivery, and were subsequently built out to be stand-alone carriers that retained the built-in segments for pH-responsive endosomal release. These new carriers incorporated a targeting component, a versatile conjugation or complexation element that allows biomolecules to be incorporated and released through pH- or redox-triggered release, the endosomal releasing segment, and a stealth component as necessary to optimize circulation stability. These carriers have been applied to siRNA and mRNA therapeutics in academia and are still being further developed in the

biotechnology industry. They have been further developed in vaccine applications, for intracellular delivery of adjuvants where access to cytosolic danger receptors is critical, and for peptide and protein therapeutics, including de novo designer proteins that act against intracellular disease target. With the advent of modern biologic and vaccine drug space, including cell therapies, the field continues to expand and the reader is referred to many recent reviews (Lu et al., 2014; Zhao et al., 2018; Reineke, 2016; Shae et al., 2019).

Conclusions

Smart polymers in solution, on surfaces and as hydrogels, have been utilized in many interesting ways, especially in combination with biomolecules such as proteins and drugs. Important applications include affinity separations, enzyme processes, immunoassays, drug delivery, and toxin removal. These smart polymer–biomolecule systems represent an important extension of polymeric biomaterials beyond their well-known uses in implants and medical devices.

References

- Anastase-Ravion, S., Ding, Z., Pelle, A., Hoffman, A.S., Letourneur, D., 2001. New antibody purification procedure using a thermally-responsive polyNIPAAm-dextran derivative conjugate. *J. Chromatogr. B* 761, 247–254.
- Broyer, R.M., Grover, G.N., Maynard, H.D., 2011. Emerging synthetic techniques for protein–polymer conjugations. *Chem. Commun.* 47, 2212–2226.
- Bulmus, V., Ding, Z., Long, C.J., Stayton, P.S., Hoffman, A.S., 1999. Design, synthesis and site-specific conjugation of a pH- and temperature-sensitive polymer to streptavidin for pH-controlled binding and triggered release of biotin. *Bioconj. Chem.* 11, 78–83.
- Chen, J.P., Hoffman, A.S., 1990. Polymer-protein conjugates. II. Affinity precipitation of human IgG by poly(N-isopropyl acrylamide)-protein A conjugates. *Biomaterials* 11, 631–634.
- Chen, G., Hoffman, A.S., 1994. Synthesis of carboxylated poly(NIPAAm) oligomers and their application to form thermoreversible polymer-enzyme conjugates. *J. Biomater. Sci. Polymer. Edn.* 5, 371–382.
- Chen, G., Hoffman, A.S., 1995. Graft copolymer compositions that exhibit temperature-induced transitions over a wide range of pH. *Nature* 373, 49–52.
- Chen, J.P., Yang, H.J., Hoffman, A.S., 1990. Polymer–protein conjugates. I. Effect of protein conjugation on the cloud point of poly(N-isopropyl acrylamide). *Biomaterials* 11, 625–630.
- Chiefari, J., Chong, Y.K., Ercole, F., Krstina, J., Jeffery, J., et al., 1998. Living free-radical polymerization by reversible addition-fragmentation chain transfer: The RAFT process. *Macromolecules* 31 (16), 5559–5562.
- Chilkoti, A., Chen, G., Stayton, P.S., Hoffman, A.S., 1994. Site-specific conjugation of a temperature-sensitive polymer to a genetically-engineered protein. *Bioconj. Chem.* 5, 504–507.
- Cole, C.A., Schreiner, S.M., Priest, J.H., Monji, N., Hoffman, A.S., 1987. N-isopropyl acrylamide and N-acryl succinimide copolymers: A thermally reversible water soluble activated polymer for protein conjugation. In: Russo, P. (Ed.), *Reversible Polymeric Gels and Related Systems*, ACS Symposium Series, 350. ACS, Washington, DC, pp. 245–254.

- Dong, L.C., Hoffman, A.S., 1986. Thermally reversible hydrogels: III. Immobilization of enzymes for feedback reaction control. *J. Contr. Rel.* 4, 223–227.
- Dong, L.C., Hoffman, A.S., 1987. Thermally reversible hydrogels: Swelling characteristics and activities of copoly(NIPAAm-AAm) gels containing immobilized asparaginase. In: Russo, P. (Ed.), *Reversible Polymeric Gels and Related Systems*, ACS Symposium Series, 350. ACS, Washington, DC, pp. 236–244.
- Dong, L.C., Hoffman, A.S., 1990. Synthesis and application of thermally-reversible heterogels for drug delivery. *J. Contr. Release* 13, 21–32.
- Dong, L.C., Hoffman, A.S., 1991. A novel approach for preparation of pH- and temperature-sensitive hydrogels for enteric drug delivery. *J. Contr. Release* 15, 141–152.
- De, P., Li, M., Gondi, S.R., Sumerlin, B.S., 2008. Temperature-Regulated Activity of Responsive Polymer-Protein Conjugates Prepared by Grafting-from via RAFT Polymerization. *J. Am. Chem. Soc.* 130, 11288–11289.
- Ding, Z.L., Chen, G., Hoffman, A.S., 1996. Synthesis and purification of thermally-sensitive oligomer-enzyme conjugates of poly(NIPAAm)-trypsin. *Bioconj. Chem.* 7, 121–125.
- Ding, Z.L., Chen, G., Hoffman, A.S., 1998. Properties of polyNIPAAm-trypsin conjugates. *J. Biomed. Mater. Res.* 39, 498–505.
- Ding, Z.L., Long, C.J., Hayashi, Y., Bulmus, E.V., Hoffman, A.S., et al., 1999. Temperature control of biotin binding and release with a streptavidin-polyNIPAAm site-specific conjugate. *J. Bioconj. Chem.* 10, 395–400.
- Ding, Z.L., Shimoboji, T., Stayton, P.S., Hoffman, A.S., 2001. A smart polymer shield that controls the binding of different size biotinylated proteins to streptavidin. *Nature* 411, 59–62.
- Fong, R.B., Ding, Z.L., Long, C.J., Hoffman, A.S., Stayton, P.S., 1999. Thermoprecipitation of streptavidin via oligonucleotide-mediated self-assembly with poly(NIPAAm). *Bioconj. Chem.* 10, 720–725.
- Galae, I.Y., Mattiasson, B., 1993. Affinity thermoprecipitation: Contribution of the efficiency and access of the ligand. *Biotechnol. Bioeng.* 41, 1101–1106.
- Gao, J., Hu, Z.B., 2002. Optical properties of N-isopropylacrylamide microgel spheres in water. *Langmuir* 18, 1360–1367.
- Golden, A.L., Battrell, C.F., Pennell, S., Hoffman, A.S., Lai, J.J., et al., 2010. Simple fluidic system for purifying and concentrating diagnostic biomarkers using stimuli-responsive antibody conjugates and membranes. *Bioconj. Chem.* 21, 1820–1826.
- Grover, G.N., Maynard, H.D., 2010. Protein-polymer conjugates: Synthetic approaches by controlled radical polymerizations and interesting applications. *Current Opin. Chem. Biol.* 14, 818–827.
- Heredia, K.L., Maynard, H.D., 2007. Synthesis of protein-polymer conjugates. *Organic & Biomol. Chem.* 5, 45–53.
- Heskins, H., Guillet, J.E., 1968. Solution properties of poly(*N*-isopropyl acrylamide). *J. Macromol. Sci. Chem.* A2 (6), 1209.
- Hoffman, A.S., 1987. Applications of thermally reversible polymers and hydrogels in therapeutics and diagnostics. *J. Contr. Rel.* 6, 297–305.
- Hoffman, A.S., 1995. Intelligent polymers in medicine and biotechnology. *Macromol. Symp.* 98, 645–664.
- Hoffman, A.S., 1997. Intelligent polymers in medicine and biotechnology. In: Park, K. (Ed.), *Controlled Drug Delivery*. ACS Publications, Washington, DC.
- Hoffman, A.S., 2013. Stimuli-responsive polymers: Biomedical applications and challenges for clinical translation. *Adv. Drug Del. Rev.* 65, 10–16.
- Hoffman, A.S., Stayton, P.S., 2010. Conjugates of stimuli-responsive polymers and proteins. *Prog. Polym. Sci.* 32, 922–932.
- Hoffman, A.S., Stayton, P.S., Bulmus, V., Chen, G., Chen, J., et al., 2000. Really smart bioconjugates of smart polymers and receptor proteins. *J. Biomed. Mater. Res.* 52, 577–586.
- Hu, Z.B., Zhang, X.M., Li, Y., 1995. Synthesis and application of modulated polymer gels. *Science* 269, 525.
- Hu, Z.B., Chen, Y.Y., Wang, C.J., Zheng, Y.Y., & Li, Y., 1998. Polymer gels with engineered environmentally responsive surface patterns. *Nature* 393, 149.
- Ishihara, K., Okazaki, A., Negishi, N., Shinohara, I., Okano, T., et al., 1982. Photo-induced change in wettability and binding ability of azaromatic polymer. *J. Appl. Polymer Sci.* 27, 239–245.
- Ishihara, K., Hamada, N., Kato, S., Shinohara, I., 1984. Photo-induced swelling control of amphiphilic azaromatic polymer membrane. *Polymer Sci. (Polymer Chem. Ed.)* 22, 21–128.
- Jeong, B., Kim, S.W., Bae, Y.H., 2002. Thermosensitive sol-gel reversible hydrogels. *Adv. Drug. Delivery. Rev.* 54, 37–51.
- Kang, H.C., Bae, Y.H., 2007. pH-Tunable endosomolytic oligomers for enhanced nucleic acid delivery. *Advanced Functional Materials* 17, 1263–1272.
- Kaneko, D., Gong, J.P., Osada, Y., 2002. Polymer gels as soft and wet chemomechanical systems: An approach to artificial muscles. *J. Mater. Chem.* 12, 2169–2177.
- Kidoaki, S., Ohya, S., Nakayama, Y., Matsuda, T., 2001. Thermoresponsive structural change of a PNIPAAm graft layer measured with AFM. *Langmuir* 17, 2402–2407.
- Kikuchi, A., Okano, T., 2002. Intelligent thermoresponsive polymeric stationary phases for aqueous chromatography of biological compounds. *Progr. Polymer Sci.* 27, 1165–1193.
- Koo, H., Huh, M.S., Sun, I.-C., Yuk, S.H., Choi, K., Kim, K., Kwon, I.C., 2011. *Acc. Chem. Res.* 44, 1018–1028.
- Kobayashi, J., Kikuchi, A., Sakai, K., Okano, T., 2001. Aqueous chromatography utilizing pH-/temperature-responsive polymers as column matrix surfaces for separation of ionic bioactive compounds. *Anal. Chem.* 73, 2027–2033.
- Lackey, C.A., Murthy, N., Press, O.W., Tirrell, D.A., Hoffman, A.S., et al., 1999. Hemolytic activity of pH-responsive polymer-streptavidin bioconjugates. *Bioconj. Chem.* 10, 401–405.
- Lai, J., Hoffman, A.S., Stayton, P.S., 2007. Dual magnetic-temperature responsive nanoparticles for microfluidic separations and assays. *Langmuir* 23, 7385–7391.
- Lai, J.J., Nelson, K.E., Nash, M.A., Hoffman, A.S., Yager, P., et al., 2009. Dynamic bioprocessing and microfluidic transport control with smart magnetic nanoparticles in laminar-flow devices. *Lab. Chip* 9, 1997–2002.
- Lee, D.S., Shim, M.S., Kim, S.W., Lee, H., Park, I., et al., 2001. Novel thermoreversible gelation of biodegradable PLGA-block-PEO-block-PLGA triblock copolymers in aqueous solution. *Macromol. Rapid. Commun.* 22, 587–592.
- Lu, Y., Sun, W., Gu, Z., 2014. Stimuli-responsive nanomaterials for therapeutic protein delivery. *J. Cont. Rel.* 194, 1–19.
- McCormick, C., Lowe, A.B., 2004. Aqueous RAFT polymerization: Recent developments in synthesis of functional water-soluble (co)polymers with controlled structures. *Accounts of Chemical Research* 37, 312–325.
- MacEwan, S., Chilkoti, A., 2017. Applications of elastin-like polypeptides in drug delivery. *J. Control. Release* 190, 314–330.
- Malmstadt, N., Yager, P., Hoffman, A.S., Stayton, P.S., 2003. A Smart Microfluidic Affinity Chromatography Matrix Composed of Poly(*N*-isopropylacrylamide)-Coated Beads. *Anal. Chem.* 75, 2943–2949.

- Malmstadt, N., Hyre, D., Ding, Z., Hoffman, A.S., Stayton, P.S., 2003. Affinity Thermoprecipitation and Recovery of Biotinylated Biomolecules via a Mutant Streptavidin-Smart Polymer Conjugate. *Bioconj. Chem.* 14, 575–580.
- Malmstadt, N., Hoffman, A.S., Stayton, P.S., 2004. Smart Mobile Affinity Matrix for Microfluidic Immunoassays. *Lab. Chip.* 4, 412–415.
- Masahiko, A., Matsuura, T., Kasai, M., Nakahira, T., Hara, Y., et al., 2003. Preparation of comb-type N-isopropylacrylamide hydrogel beads and their application for size-selective separation media. *Biomacromolecules* 4, 395–403.
- Matyjaszewski, K., Xia, J., 2001. Atom transfer radical polymerization. *Chem. Rev.* 101, 2921–2990.
- Matyjaszewski, K., Tsarevsky, N.V., 2009. Nanostructured functional materials prepared by atom transfer radical polymerization. *Nature Chemistry* 1, 276–288.
- Meyer, D.E., Chilkoti, A., 2002. Genetically Encoded Synthesis of Protein-Based Polymers with Precisely Specified Molecular Weight and Sequence by Recursive Directional Ligation: Examples from the Elastin-like Polypeptide System. *BioMacromolecules* 3, 357–367.
- Mitsumata, T., Gong, J.P., Osada, Y., 2001. Shape memory functions and motility of amphiphilic polymer gels. *Polymer. Adv. Technol.* 12, 136–150.
- Miyata, T., Nakamae, K., Hoffman, A.S., Kanzaki, Y., 1994. Stimuli-sensitivities of hydrogels containing phosphate groups. *Macromol. Chem. Phys.* 195, 1111–1120.
- Moad, G., 2017. RAFT polymerization to form stimuli-responsive polymers. *Polym. Chem.* 8, 177–219.
- Moad, G., Rizzardo, E., Thang, S.H., 2008. Radical addition-fragmentation chemistry in polymer synthesis. *Polymer* 49, 1079–1131.
- Monji, N., Hoffman, A.S., 1987. A novel immunoassay system and bioseparation process based on thermal phase separating polymers. *Appl. Biochem. Biotechnol.* 14, 107–120.
- Monji, N., Cole, C.A., Tam, M., Goldstein, L., Nowinski, R.C., et al., 1990. Application of a thermally-reversible polymer-antibody conjugate in a novel membrane-based immunoassay. *Biochem. Biophys. Res. Commun.* 172, 652–660.
- Murthy, N., Stayton, P.S., Hoffman, A.S., 1999. The design and synthesis of polymers for eukaryotic membrane disruption. *J. Controlled Release* 61, 137–143.
- Murthy, N., Campbell, J., Fausto, N., Hoffman, A.S., Stayton, P.S., 2003a. Bioinspired polymeric carriers that enhance intracellular delivery of biomolecular therapeutics. *Bioconj. Chem.* 14, 412–419.
- Murthy, N., Campbell, J., Fausto, N., Hoffman, A.S., Stayton, P.S., 2003b. Design and synthesis of pH-responsive polymeric carriers that target uptake and enhance the intracellular delivery of oligonucleotides to hepatocytes. *J. Contr. Rel.* 89 (3), 365–374.
- Na, K., Lee, D.H., Hwang, D.J., Lee, K.H., & Bae, Y.H., 2006. pH-Sensitivity and pH-dependent structural change in polymeric nanoparticles of poly(vinyl sulfadimethoxine)-deoxycholic acid conjugate. *Eur. Polym. J.* 42, 2581–2588.
- Nakamae, K., Miyata, T., Hoffman, A.S., 1992. Swelling behavior of hydrogels containing phosphate groups. *Macromol. Chem.* 193, 983–990.
- Nakamae, K., Miyata, T., Jikihara, A., Hoffman, A.S., 1994. Formation of poly(glucosyloxyethyl methacrylate)-concanavalin a complex and its glucose sensitivity. *J. Biomater. Sci. (Polymer Ed)* 6, 79–90.
- Nakamae, K., Nizuka, T., Miyata, T., Furukawa, M., Nishino, T., et al., 1997. Lysozyme loading and release from hydrogels carrying pendant phosphate groups. *J. Biomater. Sci. (Polymer Ed)* 9, 43–53.
- Nash, M.A., Yager, P., Hoffman, A.S., Stayton, P.S., 2010. Mixed stimuli-responsive magnetic and gold nanoparticle system for rapid purification, enrichment and detection of biomarkers. *Bioconj. Chem.* 21, 2197–2204.
- Nash, M.A., Lai, J.J., Hoffman, A.S., Yager, P., Stayton, P.S., 2010. "Smart" diblock copolymers as templates for magnetic-core gold-shell nanoparticle synthesis. *Nano. Lett.* 10, 85–91.
- Nash, M.A., Hoffman, J.M., Stevens, D.Y., Hoffman, A.S., Stayton, P.S., et al., 2010. Laboratory-scale protein striping system for patterning biomolecules onto paper-based immunochromatographic test strips. *Lab. Chip.* 10, 2279–2282.
- Nguyen, A.L., Luong, J.H.T., 1989. Syntheses and application of water soluble reactive polymers for purification and immobilization of biomolecules. *Biotechnol. Bioeng.* 34, 1186–1190.
- Ohya, S., Nakayama, Y., Matsuda, T., 2001. Thermoresponsive artificial extracellular matrix for tissue engineering: Hyaluronic acid bioconjugated with poly(N-isopropylacrylamide) grafts. *Biomacromolecules* 2, 856–863.
- Ohya, S., Nakayama, Y., Matsuda, T., 2001. Material design for an artificial extracellular matrix: Cell entrapment in poly(N-isopropylacrylamide) (PNIPAM)-grafted gelatin hydrogel. *J. Artif. Organs* 4, 308–314.
- Okamura, K., Ikura, K., Yoshikawa, M., Sakaki, R., Chiba, H., 1984. Soluble-insoluble interconvertible enzymes. *Agric. Biol. Chem.* 48, 2435–2440.
- Okano, T., Kikuchi, A., Yamato, M., 2000. Intelligent hydrogels and new biomedical applications. In: *Biomaterials and Drug Delivery toward the New Millennium*. Han Rim Won Publishing Co, Seoul, Korea, pp. 77–86.
- Park, T.G., Hoffman, A.S., 1988. Effect of temperature cycling on the activity and productivity of immobilized β -galactosidase in a thermally reversible hydrogel bead reactor. *Appl. Biochem. Biotechnol.* 19, 1–9.
- Park, T.G., Hoffman, A.S., 1990a. Immobilization and characterization of β -galactosidase in thermally reversible hydrogel beads. *J. Biomed. Mater. Res.* 24, 21–38.
- Park, T.G., Hoffman, A.S., 1990b. Immobilization of *A. simplex* cells in a thermally-reversible hydrogel: Effect of temperature cycling on steroid conversion. *Biotech. Bioeng.* 35, 52–159.
- Park, T.G., Hoffman, A.S., 1990c. Immobilized biocatalysts in reversible hydrogels. In: Tanaka, A. (Ed.), *Enzyme Engineering X* Ann NY Acad Sci, 613, pp. 588–593.
- Park, T.G., Hoffman, A.S., 1992a. Synthesis and characterization of pH- and/or temperature-sensitive hydrogels. *J. Appl. Polymer. Sci.* 46, 659–671.
- Park, T.G., Hoffman, A.S., 1992b. Preparation of large, uniform size temperature-sensitive hydrogel beads. *J. Poly. Sci. A., Poly. Chem.* 30, 505–507.
- Park, T.G., Hoffman, A.S., 1994. Estimation of temperature-dependent pore sizes in poly(NIPAAm) hydrogel beads. *Biotechnol. Progr.* 10, 82–86.
- Pan, Y.V., Wesley, R.A., Luginbuhl, R., Denton, D.D., Ratner, B.D., 2001. Plasma-polymerized N-isopropylacrylamide: Synthesis and characterization of a smart thermally responsive coating. *Biomacromolecules* 2, 32–36.
- Panitch, A., Yamaoka, T., Fournier, M.J., Mason, T.L., Tirrell, D., 1999. Design and biosynthesis of elastin-03-like artificial extracellular matrix proteins containing periodically spaced fibronectin CS5 domains. *Macromolecules* 32, 1701–1703.

- Pecs, M., Eggert, M., Schügerl, K., 1991. Affinity precipitation of extracellular microbial enzymes. *J. Biotechnol.* 21, 137–142.
- Pelegri-O'Day, E., Lin, E.-W., Maynard, H.D., 2014. Therapeutic Protein-Polymer Conjugates: Advancing Beyond PEGylation". *J. Am. Chem. Soc.* 136, 14323–14332.
- Peppas, N.A., 1997. Hydrogels and drug delivery. *Critical Opinion in Colloid and Interface Science* 2, 531–537.
- Peppas, N.A., 2001. Gels for drug delivery. In: *Encyclopedia of Materials: Science and Technology*. Elsevier, Amsterdam, pp. 3492–3495.
- Peppas, N.A., Keys, K.B., Torres-Lugo, M., Lowman, A.M., 1999. Poly(ethylene glycol)-containing hydrogels in drug delivery. *J. Controlled Release* 62, 81–87.
- Peppas, N.A., Huang, Y., Torres-Lugo, M., Ward, J.H., Zhang, J., 2000. Physicochemical foundations and structural design of hydrogels in medicine and biology. *Ann. Revs. Biomed. Eng.* 2, 9–29.
- Priest, J.H., Murray, S., Nelson, R.G., Hoffman, A.S., 1987. LCSTs of aqueous copolymers of N-isopropyl acrylamide and other N-substituted acrylamides. In: Russo, P. (Ed.), *Reversible Polymeric Gels and Related Systems*, ACS Symposium Series, 350. ACS, Washington, DC, pp. 255–264.
- Reineke, T.M., 2016. Stimuli-responsive polymers for biological detection and delivery. *ACS Macro Lett* 5, 14–18.
- Robinson, D.N., Peppas, N.A., 2002. Preparation and characterization of pH-responsive poly(methacrylic acid-g-ethylene glycol) nanospheres. *Macromolecules* 35, 3668–3674.
- Roy, D., Cambre, J.N., Sumerlin, B.S., 2010. Future perspectives and recent advances in stimuli-responsive materials. *Prog. in Polymer Sci.* 35, 278–301.
- Roy, I., Gupta, M.N., 2003. Smart polymeric materials: Emerging biochemical applications. *Chemistry & Biology* 10, 1161–1171.
- Shae, D., Becker, K.W., Christov, P., Yun, D.S., Lytton-Jean, A.K.R., Sevimli, S., Ascano, M., Kelley, M., Johnson, D.B., Balko, J., Wilson, J.T., 2019. Endosomolytic polymersomes increase activity of cyclic dinucleotide STING agonists to enhance cancer immunotherapy. *Nature Nanotechnology* 14, 269–278.
- Schild, H.G., 1992. Poly(N-isopropylacrylamide): Experiment, theory and application. *Prog. Polym. Sci.* 17, 163–249.
- Schneider, M., Guillot, C., Lamy, B., 1981. The affinity precipitation technique: Application to the isolation and purification of trypsin from bovine pancreas. *Ann. NY Acad. Sci.* 369, 257–263.
- Shim, W.S., Yoo, J.S., Bae, Y.H., Lee, D.S., 2005. Novel injectable pH and temperature sensitive block copolymer hydrogel. *Biomacromolecules* 6, 2930–2934.
- Shim, W.S., Kim, J.H., Park, H., Kim, K., Kwon, I.C., et al., 2006. Biodegradability and biocompatibility of a pH- and thermo-sensitive hydrogel formed from a sulfonamide-modified poly(*ε*-caprolactone-co-lactide)-poly(ethylene glycol)-poly(*ε*-caprolactone-co-lactide) block copolymer. *Biomaterials* 27, 5178–5185.
- Shimizu, T., Yamato, M., Kikuchi, A., Okano, T., 2003. Cell sheet engineering for myocardial tissue reconstruction. *Biomaterials* 24, 2309–2316.
- Shimoboji, T., Ding, Z., Stayton, P.S., Hoffman, A.S., 2001. Mechanistic investigation of smart polymer-protein conjugates. *Bioconj. Chem.* 12, 314–319.
- Shimoboji, T., Ding, Z.L., Stayton, P.S., Hoffman, A.S., 2002a. Photoswitching of ligand association with a photoresponsive polymer-protein conjugate. *Bioconj. Chem.* 13, 915–919.
- Shimoboji, T., Larenas, E., Fowler, T., Kulkarni, S., Hoffman, A.S., et al., 2002b. Photoresponsive polymer-enzyme switches. *Proc. Natl. Acad. Sci. USA* 99, 16592–16596.
- Shimoboji, T., Larenas, E., Fowler, T., Hoffman, A.S., Stayton, P.S., 2003. Temperature-induced switching of enzyme activity with smart polymer-enzyme conjugates. *Bioconj. Chem.* 14, 517–525.
- Shoemaker, S., Hoffman, A.S., Priest, J.H., 1987. Synthesis of vinyl monomer-enzyme conjugates. *Appl. Biochem. and Biotechnology* 15, 11.
- Stayton, P.S., Hoffman, A.S., 2008. Smart pH-responsive carriers for intracellular delivery of Biomolecular Drugs. In: Torchilin, V. (Ed.), *Multifunctional Pharmaceutical Nanocarriers*. New. Springer Publishers, York, NY.
- Stayton, P.S., Shimoboji, T., Long, C., Chilkoti, A., Chen, G., et al., 1995. Control of protein-ligand recognition using a stimuli-responsive polymer. *Nature* 378, 472–474.
- Stayton, P.S., Hoffman, A.S., Murthy, N., Lackey, C., Cheung, C., et al., 2000. Molecular engineering of proteins and polymers for targeting and intracellular delivery of therapeutics. *J. Contr. Rel.* 65, 203–220.
- Tanaka, T., 1981. Gels. *Scientific American* 244, 124.
- Takei, Y.G., Aoki, T., Sanui, K., Ogata, N., Okano, T., et al., 1993a. Temperature-responsive bioconjugates. 1. Synthesis of temperature-responsive oligomers with reactive end groups and their coupling to biomolecules. *Bioconj. Chem.* 4, 42–46.
- Takei, Y.G., Aoki, T., Sanui, K., Ogata, N., Okano, T., et al., 1993b. Temperature-responsive bioconjugates. 2. Molecular design for temperature-modulated bioseparations. *Bioconj. Chem.* 4, 341–346.
- Takei, Y.G., Matsukata, M., Aoki, T., Sanui, K., Ogata, N., et al., 1994a. Temperature-responsive bioconjugates. 3. Antibody-poly(N-isopropylacrylamide) conjugates for temperature-modulated precipitations and affinity bioseparations. *Bioconj. Chem.* 5, 577–582.
- Takei, Y.G., Aoki, T., Sanui, K., Ogata, N., Sakurai, Y., et al., 1994b. Dynamic contact angle measurements of temperature-responsive properties for PNIPAAm grafted surfaces. *Macromolecules* 27, 6163–6166.
- Taniguchi, M., Kobayashi, M., Fujii, M., 1989. Properties of a reversible soluble-insoluble cellulase and its application to repeated hydrolysis of crystalline cellulose. *Biotechnol. Bioeng.* 34, 1092–1097.
- Taniguchi, M., Hoshino, K., Watanabe, K., Sugai, K., Fujii, M., 1992. Production of soluble sugar from cellulosic materials by repeated use of a reversibly soluble-autoprecipitating cellulase. *Biotechnol. Bioeng.* 39, 287–292.
- Tirrell, D., 1987. Macromolecular switches for bilayer membranes. *J. Contr. Rel.* 6, 15–21.
- Uenoyama, S., Hoffman, A.S., 1988. Synthesis and characterization of AAm/NIPAAm grafts on silicone rubber substrates. *Radiat. Phys. Chem.* 32, 605–608.
- Urry, D.W., Luan, C.H., Parker, T.M., Channe Gowda, D., Prasad, K.U., Reid, M.C., Safavy, A., 1991. *J. Am. Chem. Soc.* 113, 4346–4348.
- Vernon, B., Kim, S.W., Bae, Y.H., 2000. Thermoreversible copolymer gels for extracellular matrix. *J. Biomed. Mater. Res.* 51, 69–79.
- Wang, J., Matyjaszewski, K., 1995. Controlled/"living" radical polymerization. Atom transfer radical polymerization in the presence of transition-metal complexes. *J. Am. Chem. Soc.* 117, 5614–5615.
- Yamato, M., Okano, T., 2001. Cell sheet engineering for regenerative medicine. *Macromol. Chem. Symp.* 14 (2), 21–29.
- Yamato, M., Kwon, O.H., Hirose, M., Kikuchi, A., Okano, T., 2001. Novel patterned cell co-culture utilizing thermally responsive grafted polymer surfaces. *J. Biomed. Mater. Res.* 55, 137–140.

- Yang, H.J., Cole, C.A., Monji, N., Hoffman, A.S., 1990. Preparation of a thermally phase-separating copolymer with a controlled number of active ester groups per polymer chain. *J. Polymer. Sci. A. Polymer. Chem.* 28, 219–226.
- Yin, X., Stayton, P.S., Hoffman, A.S., 2006. Temperature- and pH-responsiveness of poly(n-isopropylacrylamide-co-propylacrylic acid) copolymers prepared by RAFT polymerization. *Biomacromol* 7, 1381–1385.
- Yoshida, R., Uchida, K., Kaneko, Y., Sakai, K., Kikuchi, A., et al., 1995. Comb-type grafted hydrogels with rapid de-swelling response to temperature changes. *Nature* 374, 240–242.
- Zareie, H.M., Bulmus, V., Gunning, P.A., Hoffman, A.S., Piskin, E., et al., 2000. Investigation of a pH- and temperature-sensitive polymer by AFM. *Polymer* 41, 6723–6727.
- Zhao, Y., Guo, Y., Tang, L., 2018. Engineering cancer vaccines using stimuli-responsive biomaterials. *Nano Research* 11, 5355–5371.

1.3.3

Metals: Basic Principles

JEREMY L. GILBERT

Department of Bioengineering, Clemson University, Charleston, SC, United States

Introduction

Medical Devices and Metals in the Body

The use of metals in the body has in many ways paralleled and enabled the advancement of medicine in the 20th and 21st centuries. A majority of medical devices (joint replacements, spinal devices, cardiovascular stents, mechanical heart valves, fracture fixation devices, dental implants) require the presence of a metal alloy to provide the strength and fatigue resistance to perform over the life of the patient. Indeed, the adaptation of metals and alloys for use in skeletal repairs and dentistry has foundations that go back millennia. Bechtol, Fergusson, and Laing (Bechtol et al., 1959) in 1959 provided an excellent review of the development and use of metals in the body from the first half of the 20th century. Many of the concepts and directions of study of metallic biomaterials are outlined in this monograph and many of these are the subject of ongoing research around metals in the body. Here, as early as 1775, iron wires were explored for use in internal fracture fixation and in 1829 tests in dogs of platinum, gold, silver, and lead showed promise. As early as 1908 there was research around the cellular reaction to metal fragments. In addition, coimplantation of copper and zinc induced periodic muscular contractions.

Early studies identified scientific topics that included magnesium (Mg) alloy corrosion and its ability to induce bone formation or inhibit cancerous tumors, and that infections may be limited by copper (Cu), silver (Ag), and other elements. Significant advances in metallurgy up to the 1920s began to introduce stainless steels (AISI-302, AISI-304, AISI-316, and AISI-317 versions), and Stellite and/or Vitallium (cobalt–chromium–molybdenum [CoCrMo] alloys) for use in internal fracture fixation devices (screws, plates). In the late 1950s up to the 1970s, titanium and its alloys were also found to exhibit excellent properties in strength, corrosion resistance, and biocompatibility for use in a wide range of medical device applications and were subsequently introduced into use in medical devices. Other

alloys related to platinum (e.g., Pt-10% Ir for electrodes), gold (Au–Cu alloys for dentistry), silver–mercury (Ag–Hg amalgams), and others have been in use for decades or longer in various applications and have resulted in significant enhancements in the health and quality of life for millions of patients.

Metals, in general, are required for medical devices because they have the requisite mechanical properties necessary for many applications that no other class of biomaterials can replicate. The human body is, essentially, a fatigue machine where millions to tens of millions of loading cycles are generated in specific locations every year. For example, at 70 beats per min, the human heart contracts about 37 million times per year, and a typical human who walks 10,000 steps per day (5000 per leg) loads their joints about 1.8 million times per year. These loads can be significant and result in stresses that can reach hundreds of megapascals. Cyclic loading results in fatigue failure modes, sustained wear mechanisms, the potential for mechanically assisted corrosion mechanisms, and other effects. No other biomaterial class can perform at the stress and degradation-inducing levels that metals can. Metallic biomaterials have provided the medical device community with a large and successful toolbox of alloys with which to perform many of the required functions, and new alloys are being investigated even today. These facts are likely to continue to be the case for decades to come and metal and alloys will remain an essential part of the biomaterials armamentarium for the foreseeable future.

The Major Alloy Systems (Ti, NiTi, CoCrMo, SS, Pt, Au, Mg, Ag)

While greater detail of each group of metals currently in use or under development will be described in later sections of this text, this introduction is intended to give the reader basic insights into the metallic biomaterial alloys available today and the underlying basic metallurgical science associated with them.

In part due to the enactment of the Medical Device Amendments of 1976 (Wizemann, 2010), as well as the limited number of alloys with the right combination of mechanical, corrosion, and biocompatibility properties, there are a limited set of alloys currently used in the human body. Most of these alloys had been in widespread use prior to the enactment of the Medical Device Amendments and were therefore grandfathered in to be used in medical devices after passage. However, it is also the case that the alloys in use today represent some of the most corrosion resistant, highest strength alloys available and have shown themselves to be successful in their application to medical devices by their decades of use. Since 1976, the experience within the body of the major alloys used has elucidated the safety and effectiveness of these alloys for most applications. It has also raised new concerns related to degradation and biological–biomaterial interactions, including immune responses, hypersensitivity, and allergic responses that are often multifactorial and interacting degradation processes.

The major alloys in use today consist of metals intended for indefinite use within the body (permanently implantable) and those that are designed to be temporary, ultimately degrading or biocorroding over time (biodegradable alloys). The permanently implantable alloys are the principal ones applied to a wide range of medical devices currently in use today, while the biodegradable alloys are in development or used in a small set of approved applications.

The three major permanently implantable alloy systems used in the body across the spectrum of medical devices are: (1) stainless steels (primarily 316L stainless steel [ASTM F-138]), (2) cobalt–chromium–molybdenum (CoCrMo [ASTM F-75; ASTM F-799; ASTM F1537]) alloys, and (3) titanium (ASTM-F76) and its alloys (ASTM F136). Other permanently implantable alloys include Pt, Au (ASTM-F72), and Ag alloys. The degradable alloys under consideration include Mg, tin (Sn), iron (Fe), and zinc (Zn) alloys. One needs only look at the periodic table to realize that there are a wide range of metallic elements present that may be able to serve as potential biomedical alloys. Some of the more promising ones include zirconium (Zr) (ASTM-F2384), niobium (Nb), palladium (Pd), and tantalum (Ta). There are others as well such as rhenium (Re), molybdenum (Mo), and alloys of these two elements that are beginning to be considered for medical device use. Recent research is evaluating these alloys, and while some advantages in strength or other properties may be present, the three major alloy systems described earlier (stainless steel, CoCrMo, and Ti-alloys) remain the workhorse alloys in biomaterials.

For degradable alloys, the primary interest is to find alloys that will remain capable of carrying the applied loads and wear processes until the body has healed sufficiently that they are no longer required, and will then corrode away and be resorbed and eliminated by the body. Magnesium alloys (Witte, 2010) have been investigated the most. This alloy is known to corrode rapidly in physiological solutions and that the oxidation products are mostly Mg oxide (MgO or Mg(OH)₂), which is relatively innocuous, and hydrogen

gas, which can be problematic. Other alloy systems, including Sn, Fe, and Zn, are under consideration as degradable alloys for biomaterials applications as well.

The alloys comprised of Au, Ag, and Pt, which are noble alloys, typically utilize their electrical properties to serve as electrodes, their noble electrochemical properties to resist corrosion or degradation, and/or other properties to serve in certain dental applications. Silver is also being adopted for its antibacterial properties, typically as a coating, nanoparticles, or other approaches to place the silver on the surface of a medical device. It is also used in silver–mercury amalgams in dentistry. Other alloys are also being considered for their antibacterial effects. These include alloys that rapidly corrode, and in so doing generate significant reduction reaction products (reactive oxygen intermediates) that can induce killing effects as well.

The big three—stainless steel, CoCrMo, and Ti—have a number of alloy systems that have seen widespread adoption for applications within the body. Stainless steels (primarily 316LVM stainless steel [ASTM F-138]) are used in surgical instrumentation, but also, importantly, in many medical devices, including screws, rods, and plates for bone fixation and in spinal fusion devices. Cobalt–chromium–molybdenum alloys (ASTM F-75; F-799; F-1537) are typically used in applications where high strength, fatigue resistance, and wear resistance are needed. CoCrMo is one of the most wear resistant alloys known and has been used for decades in total joint applications. Titanium and its principal alloy (Ti-6Al-4V) are used in dental implants as well as total joint replacements among other applications (ASTM F-67; ASTM F-136). This alloy has high strength, low modulus, and is particularly good at interfacing with the biological system. Bone ingrowth into porous titanium surfaces, known as biological fixation, is a primary means by which orthopedic implants affix to bone directly.

Metal Processing

Metals can be processed in many different ways to result in the end-products used in medical devices. Typically, to start, metals must be obtained from ore, which is mostly metal oxides found in nature. The metal cations in these metal oxides need to be reduced to elemental metals and this is often done in high-temperature furnaces under low (to no) oxygen-reducing conditions. In some cases, chemical reactions are used to pull the ions from the ore and then to subsequently reduce the ions to an elemental state.

Once elemental metals are formed, they can be melted together to form alloys of specific weight or atomic concentrations. Heating to melting and then casting the mixture is typically the first step. Once this billet of metal is cast, it is usually immediately hot worked (i.e., wrought or otherwise thermomechanically processed) into rod, sheet, plate, or bar stock. Continuous casting systems with follow-on thermomechanical treatment systems are often used. In some cases, like CoCrMo orthopedic devices, the alloy is cast directly into the near net final shape.

Forging, drawing, extruding, and other deformation processes are typically applied to metals under high-temperature conditions (i.e., thermomechanically processed) to allow the metal to recover and refine its grain size and allow far larger deformations to occur without damaging the alloy. These processing steps can affect the structure and properties of the materials (see later). Typically, metals are received in rod, bar, sheet, tube, or plate form for further processing by machining or thermomechanical processes.

Thermomechanical processing is the combination of high temperature and plastic deformation so that the effects of each can work together to obtain the final form of the metal. Plastic deformation at low temperature, known as cold working or work hardening, imparts plastic deformation into the alloy. This is manifested structurally as the generation, movement, and entanglement of dislocations (see the Section “Line Defects”). These defect structures act to increase the yield stress and lower the ductility of the metal. Often, alloys can be prepared with some amount of cold working in them to raise their strength. However, the loss of ductility associated with plastic deformation can raise the risk of fracture of the alloy and care must be taken to assure that the proper conditions for the metal are obtained (e.g., annealed vs. cold worked).

Thermal treatments, known as annealing, are often performed on previously cold-worked alloys to provide thermal energy to the microstructure so that dislocations can be eliminated (recovery) or new deformation-free grains can be nucleated and grown (recrystallization) from the prior deformed (or cold-worked) grains. Annealed alloys are those metals that have been cold worked and then heated to remove the effects of deformation. Thus annealed alloys tend to have lower yield strengths than their cold-worked counterparts, and higher ductility. Thus ASTM standards (e.g., *ASTM F-138*) have specifications that link to the cold-worked state of the alloy.

In some cases, powders of these alloys are generated by high-temperature spraying of molten alloy into a fine mist that solidifies into spherical powders. These powders can then be used in subsequent processes where either hot isostatic pressing (HIPing) (Pilliar, 2009) or selective laser sintering (or selective laser melting (Hedberg et al., 2014) can be used in 3D printers. HIPing is a process where powders are placed in a near net shape of the part and then put into a high-temperature and -pressure container and the powder alloy particles are diffusion bonded (or sintered) together to make a fully condensed and consolidated part. This occurs by raising the temperature of the alloy to a high temperature while still in the solid state. With this increased temperature, surface diffusional processes allow atoms of the surface to move and result in a metallurgical bond (diffusion bond or sintering) to form between adjacent surfaces in contact. The advantage of this approach is that the grain size is governed by the starting particles and can be very small, which results in very high-strength alloys (see later on grain size strengthening). For 3D printing, powdered alloy particles can be sintered or melted together by a short laser pulse, or electron

beam methods that are used in a fixed pattern to print the part. Such selective laser (or e-beam) sintering methods are gaining in use and application in the medical device industry.

For many of the alloys in biomaterials the presence of oxygen during fabrication is detrimental and often inert gas environments are required to limit oxidation of the surface or the alloy, or uptake of oxygen into the alloy. This is particularly true for titanium and its alloys. It has a high affinity for oxygen uptake into the hexagonal close-packed (HCP) phase of the alloy. A small amount of oxygen may increase the strength of the titanium (through interstitial solid solution strengthening), but too much can make the alloy brittle and easily fractured. Indeed, surface diffusion of oxygen can result in a so-called alpha case on titanium that can reduce the fracture resistance of the alloy.

Ultimately, for many parts, manufacturing requires machining of the metal into a final shape. Such milling machines, lathes, and CNC machines are highly precise and require very hard and sharp cutting tools to make the precision cuts necessary. Tool-driven localized plastic deformation of the surface can induce effects like the formation of residual stresses that may impact the surface strength (hardness) of the alloy.

Finally, the surfaces of metals will require several different potential treatments to impart specific surface properties. These include shot peening (or glass beading) where high-velocity particles are blasted at a surface to induce compressive deformation of the surface. This has the effect of generating large compressive residual stresses on the surface and these can be beneficial in improving the fatigue strength of the part. Other processes may include grinding, polishing, electropolishing, anodizing, thermally oxidizing, nitriding, and/or plasma coating (physical vapor deposition or chemical vapor deposition coatings).

Surfaces of metals are typically treated to a passivation step where the part is immersed in an acid (typically nitric or citric acid) to remove unwanted surface contaminants and to induce the passive oxide film to become more chemically uniform and provide increased corrosion resistance. Such passivation treatments (*ASTM F-86*) typically consist of 30% nitric acid at 130°F for 30 min. In some cases, citric acid has been considered for passivation treatments. These treatments, while they are applied to the three main alloy systems, have not been shown to have the same effects on different alloy surfaces. This passivation method was initially developed for stainless-steel passive films to remove iron and other elements from the oxide and to drive the oxide to be mostly a Cr-based oxide (Cr_2O_3). Use of this treatment may not have similar effects on CoCr alloys or Ti alloys; however, it is considered standard practice for the preparation of metals for use in the body and is generally applied across all alloy systems. At the end of fabrication, sterilization steps are needed and these may include gamma irradiation, ethylene oxide treatment, or even steam sterilization (as in the case of reused surgical instruments).

Passive oxide films are not static and are affected by immersion in electrolyte and time. They can also be modified by changes to the oxidizing power of the body solution

or the electrode potential across the metal electrolyte interface. Passive oxides are known to grow with time and to change chemistry. In some cases the oxides can incorporate other ions (phosphates, calcium, etc.).

Processing–Structure–Properties–Performance Paradigm

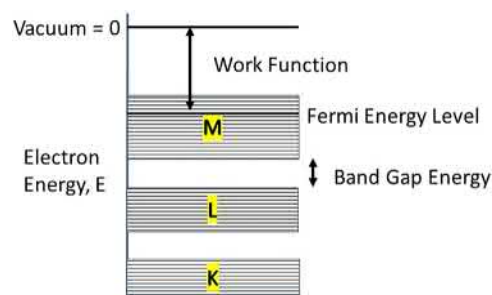
To understand these alloys, it is important to understand the processing–structure–properties–performance paradigm for alloys. That is, the processes used to make the alloy, in its final form, result in structures, from atomic scale (defects), to grain size (grain boundaries, texture), to a whole device, which determine the specific bulk and surface properties for the alloy. These properties, including strength, ductility, fracture toughness, fatigue strength, and wear resistance, in turn, determine the ultimate performance of the alloy. Since the surfaces of alloys are where the biological interactions occur and where many of the initiating events for failure begin (fatigue crack initiation mechanisms are typically surface driven), the surface processing of the alloy is an important element of the overall performance.

Thus processing affects structure, structure affects properties, and properties affect performance, and this approach to metallurgical control of medical devices has been a foundational element of the success of metal-based implants for decades. Below is a short discussion of the structure of metals.

Structure of Metals and Alloys

Electronic and Atomic Structure: Crystal Structures

To understand metal alloy performance, it is important to discuss the structural elements of metals from the atomic through the bulk size scales. Metal atoms consist of a nucleus made of protons and neutrons with electrons orbiting the nucleus in specific and quantized energy levels out to the outer valence electrons. The electrons occupy quantized energy levels starting with the inner-most bound electrons (K or 1s) and moving out from there (L, M, N, or 2s-2p, 3s-3p-3d, etc.). In a metal, no two electrons can occupy the same energy level and have the same spin, thus alloys are considered to have electron energy bands (Reed-Hill, 1973) made up of discrete (or quantized) electron energy levels that are occupied by electrons from the lowest K-level bands up to the outermost valence band for the alloy (Fig. 1.3.3.1). Since transition metals have unfilled valence bands (typically in the M or N, or “3” or “4” orbital), these bands are only partially filled with electrons up to the highest energy level called the Fermi energy level. The empty levels above the Fermi level represent energies available to electrons to jump into and conduct. This is why metals are high electron conductors (availability of energy levels immediately above the Fermi level provide easy conduction of electrons). In addition, there are energy gaps between the main quantum



• **Figure 1.3.3.1** Electron energy levels associated with the band energy theory of electrons in metals.

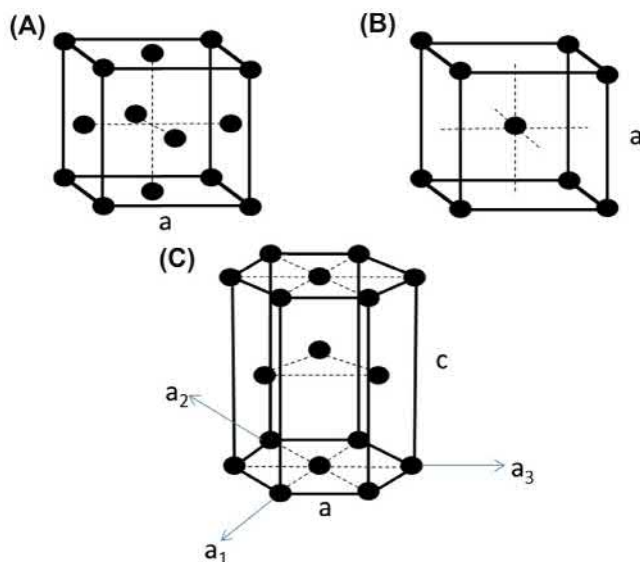
levels called band gaps, and there is a work function of the material, which is the energy required to raise an electron from the Fermi level to the vacuum (or to pull an electron out of the metal). The work function plays a significant role in photoelectric methods of materials analysis (e.g., X-ray photoelectron spectroscopy, Auger spectroscopy, etc.).

Because of the distinct and unique energy levels for inner bound electrons for each element, measurement of the energy of these electrons using various high-vacuum photoelectric methods (e.g., energy dispersive spectroscopy of characteristic X-rays, etc.) allows for the detection and quantification of these elements using an electron microprobe, scanning electron microscopy with energy dispersive spectroscopy, etc.

For the most part, atoms can be considered roughly spherical in their outer orbital and thus will act like hard spheres where each atom is attracted to every other atom. These attractive forces form the metallic bond and result in the hard sphere atoms coming together into crystalline forms or lattices. The short-range repulsive forces from atomic overlap (a result of the Pauli exclusion principle) keep the atoms as separate and distinct hard spheres.

Thus attractive electrostatic forces pull the atoms together and will drive them to form specific ordered crystalline structures (known as crystal lattices). There are 14 different lattice structures (Bravais lattices (Calister and Rethwisch, 2010)) that can form crystals (long-range repeating symmetry of atomic placement). For the most part, metallic biomaterials form either cubic or HCP structures (Fig. 1.3.3.2). In the cubic system there are face-centered cubic (FCC) and body-centered cubic (BCC) structures. For example, HPC elements (at room temperature) include Ti and Mg. Austenitic stainless steel (Fe–Cr–Ni–Mo alloy) is FCC, while iron alone at body temperature is BCC.

The crystal-forming electrostatic attractive forces (i.e., metallic bonds) are counteracted by thermal (kinetic) energy associated with increasing temperatures above 0 K. That is, thermal energy, given by kT (Boltzmann’s constant, 1.38×10^{-23} J/K, times temperature, in K), is the average kinetic (or vibrational) energy present in a system and drives increasing entropy. This thermal energy acts on metal crystals to generate phonons (quantized atomic mechanical vibrations) and plasmons (quantized plasma [or electron] vibrations). The higher the temperature, the greater are these oscillations. Ultimately, at sufficient temperatures,



• **Figure 1.3.3.2** Crystal structures of typical alloys. (A) Face-centered cubic, (B) body-centered cubic, (C) hexagonal close packed.

the thermal (vibrational) energy of the system overwhelms the attractive electrostatic forces and changes in the atomic structure can occur. This is known as a phase transition (from one solid phase to another, or from a solid to a liquid, in which case it is called melting). Some metals (e.g., Fe) may have multiple solid crystal structure phases (allotropes) that arise at different temperatures (pure iron is BCC at room temperature, FCC, and then a different BCC, with different lattice parameters, as the temperature is raised, until it ultimately melts). Thus the temperature of the system relative to the transition temperature for different allotropes determines the possibility of forming different crystal structures. Similarly, the stronger the electrostatic interatomic bonding forces, the higher will be the melt temperature of the metal.

Alloying, Microstructure, and Phase Diagrams

Alloys, typically used in metallic biomaterials, are metals that consist of more than one element combined together. The addition of carbon into iron results in steel, for example. When relatively small atoms (C, O, N, H) are mixed with larger atoms (Fe, Ti, Cr, etc.) they can fit in the open or interstitial spaces between the larger atom crystal structure and become **interstitial** atoms. When two elements of about equal size are mixed, the lower concentration atoms (the solute) will replace the higher concentration atoms (solvent) on the crystal lattice of the solvent atoms. This is called a **substitutional solid solution**. Thus adding nickel (Ni) to Fe would result in a substitutional solid solution.

When multiple elements are mixed together, several factors come into play to dictate the types of atomic structures that form. These have to do with the various attractive (or ordering) forces and the disordering forces (entropy) and their relative magnitudes. These combined effects lead to a wide variety of changes in crystal structures, distribution of different solid phases that may arise within an alloy, and the

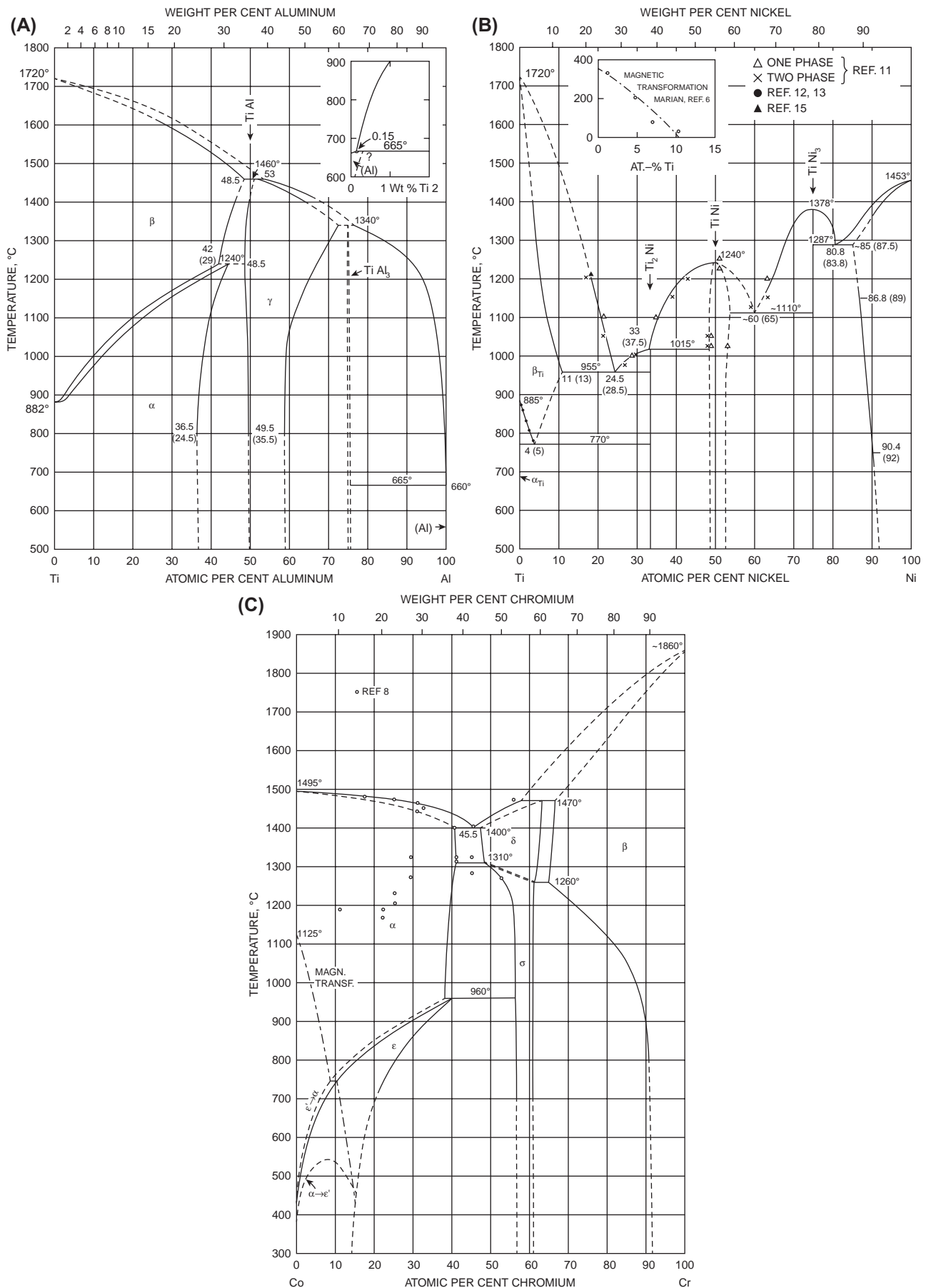
shape, size, and distribution of multiple phases. That is, the microstructure of the alloy can be affected by the processing methods used. For example, Ti-6Al-4V is a two-phase alloy. The alpha phase (HCP) is comprised primarily of titanium and has most of the aluminum in it since Al is a so-called alpha stabilizer (i.e., it stabilizes the HCP crystal structure). The beta phase (BCC) is comprised of Ti and most of the V present. Vanadium is a beta stabilizer and drives the Ti to form the BCC structure instead of the HCP structure. Thus this alloy has two phases due to the Al and V present.

In terms of steel, the Fe atoms form a BCC crystal structure (at room temperature) and the addition of carbon (C) into the Fe crystal (i.e., steel) results in an interstitial solid solution. If enough carbon is present and it is possible that second-phase metal carbides can form within the alloy, to minimize carbide formation, low levels of carbon are typically present in steels used in biomaterials. If Ni is added to Fe, the Ni atoms will begin to replace the Fe atoms on the BCC Fe lattice. However, because Ni is naturally an FCC structure, as more is added to the Fe, the BCC structure becomes less stable as Ni drives the crystal structure to want to transform into the FCC structure (i.e., Ni is an FCC stabilizer or austenitic stabilizer). With sufficient Ni, the Fe crystal structure will become an FCC structure, which is what occurs with austenitic stainless steel (where about 8% Ni is added to stabilize the FCC structure). Thus the alloy 316L stainless steel is an austenitic stainless steel with an FCC crystal structure.

Not all elements can mix together in any proportion and there are rules for mixing of elements to get high solubility of one element in a crystal structure of another. These are called the Hume–Rothery rules for substitutional alloying. The rules include the relative size of solute and solvent (within about 15% for full solubility), the native crystal structure for each (it should be the same for full solubility), and the electronegativity of the element (should be close). When these rules are not met, more complex microstructures may arise and even nonequilibrium crystal structures (i.e., those not present in phase diagrams) can arise.

Phase diagrams are a graphical means for showing what equilibrium phases (i.e., crystal structures, liquids, etc.) are present at which temperatures, concentrations of elements, and pressure. They provide insight into the microstructures that may arise with certain specific thermal processes (heating and cooling). They can show, for example, the solubility of one solute metal in another solvent metal, or if two distinct phases can exist in the alloy at the same temperature. Phase diagrams are a representation of the equilibrium conditions associated with specific compositions and do not provide for the formation of metastable or nonequilibrium phases that may arise from nonequilibrium treatment, for example, rapid cooling (quenching) of the alloy. Thus while very useful, phase diagrams are not a complete representation of the possible conditions of the alloy, only that which may form if equilibrium (long times) is achieved.

Examples of two-component phase diagrams for Ti–Al, Ni–Ti and CoCr metallic biomaterials are shown in Fig. 1.3.3.3 (Massalski et al., 1990). The plot of temperature



• Figure 1.3.3.3 Phase diagrams for: (A) Ti-Al, (B) Ni-Ti, and (C) Co-Cr binary alloys.

versus composition is shown and it is assumed that the pressure is held constant (typically atmospheric). The lines on the diagram represent solubility limits of one metal in another and define the boundaries between different regions of phase stability. On the far left (Fig. 1.3.3.3A), for example, a single solid α phase in the Ti–Al alloy system with limited solubility of the solute (Al) atom is present. At some critical composition, the single solid phase cannot take any more of the solute atoms (i.e., saturation is reached). At this point (temperature and composition), if additional solute atoms are added, they start to make a second phase that is more solute rich and based on the crystal structure of the solute–solvent combination. The topic of phase diagrams and their specific scientific underpinnings are beyond the scope of this chapter and the reader is referred to a basic physical metallurgy text.

The diagrams in Fig. 1.3.3.3 show what phases are stable at specific temperature–composition points on the graph. For example, for the Ti–Al phase diagram (Fig. 1.3.3.3A), the HCP alpha phase is stable at low temperatures up to about 6wt% Al and the Al increases the temperature where alpha is stable (i.e., where alpha-to-beta transformation may occur). Higher amounts of Al begin to generate Ti_3Al intermetallics. At higher temperatures (above about 880°C), Ti transforms from the alpha (HCP) to the beta (BCC) phase. The NiTi phase diagram (Fig. 1.3.3.3B) shows that the near-50 atomic % NiTi compositions used as metallic biomaterials are single phase. However, this alloy's shape memory and superelastic behavior are highly sensitive to the specific composition and deformation state of the alloy around this 50% compositional range. Nonequilibrium phases (e.g., martensite) may arise and the transition from deformation-induced martensitic to austenitic phases with temperature increases is the major mechanism for the shape memory behavior of this alloy.

For the CoCr phase diagram (Fig. 1.3.3.3C) the alloy is an FCC crystal structure at body temperature, but transforms to HCP at higher temperatures. However, it is possible for both FCC and HCP structures to be present due to more metastable behavior of the alloy and its low stacking fault energy (i.e., the energy associated with the area between partial dislocations). A stacking fault in a metal occurs when the normal plane stacking of the FCC phase is shifted, which results in an HCP stacking sequence. This can arise when dislocations break into two partial dislocations and the region between these two partial dislocations has an HCP stacking fault. When an alloy has a low stacking fault energy, the distance between partials can be large, resulting in a large faulted region. Thus both FCC and HCP structures can arise in heavily deformed CoCr alloys.

Defects in Crystals

Many metal crystals come together to make an alloy (i.e., polycrystalline) and these crystals can be randomly oriented to one another or partially aligned such that the axes of the multiple crystals are close to one another. This is called texture and can arise from deformation processes and affect

local mechanical properties of the alloy. The size and shape of the crystals also can be affected by the prior thermomechanical history of the metal and this can affect the properties of the material in significant ways. For example, rolling of plate or sheet alloy can flatten crystals and make them elongated. Such changes can affect the mechanical and other properties of the alloy. To understand the processing–structure–property relationships in metals, one needs to understand the nature of the defects that arise in these polycrystalline materials, and how such defects affect properties.

Briefly, there are point, line, area, and volume defects that can arise in metals. Each has a significant effect on the properties of the metal and affects the metal in different ways. A brief summary of the role of each type of defect on the properties of metals is described next.

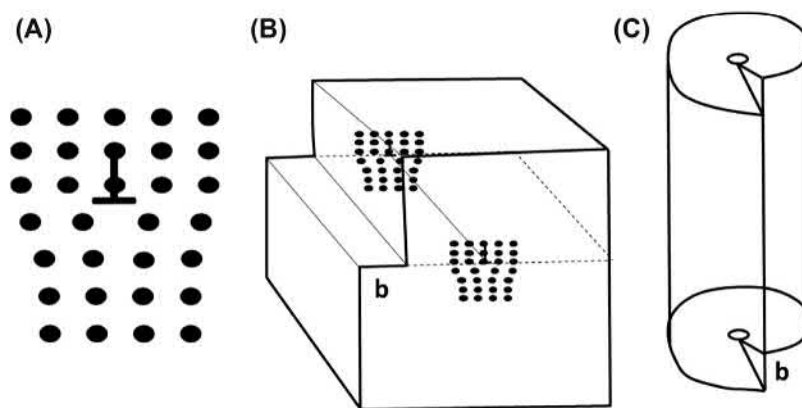
Point Defects

Point defects include vacancies and interstitial atoms. A vacancy is a position within the crystal lattice where an atom should be present but it is missing. An interstitial atom is one of the small atoms that occupies the available interstitial space of the crystal lattice (e.g., O in Ti, C in Fe). Vacancies can have an effect on the diffusion behavior of substitutional atoms in the metal and for most biomaterials applications these have a limited effect on properties. Interstitial atoms, however, can have profound effects on the strength properties of a metal. Whether it is oxygen in titanium alloys or carbon in iron alloys (i.e., steel), these small interstitial atoms increase the yield strength and ultimate strength, and affect the work hardening of metals by creating dislocation atmospheres that can pin dislocations requiring higher stresses to induce plastic deformation (i.e., raising the yield strength). Both substitutional and interstitial atoms affect the mechanical properties of the alloy.

Line Defects

Line defects in crystals include a particular type of defect called a dislocation. These crystal defects are associated with plastic deformation of crystalline materials and are the principal means by which metals deform permanently (i.e., plastically). That is, plastic deformation of metals is associated with the sliding of atom planes over one another and dislocations are a localized elastic distortion of the crystal associated with this plane sliding. There are both edge and screw dislocations that are present, and edge dislocations can be thought of as the distortion around the termination of an extra half-plane of atoms in the crystal lattice (Fig. 1.3.3.4).

Since this distortion is only present at the end of the half-plane, it appears as a line defect. When shear stresses of a sufficient magnitude (critical shear stresses) arise on specific planes (known as slip planes, typically the close-packed planes), in specific directions (slip directions, close-packed directions), dislocations can be generated and moved through the crystal affecting a sliding of the upper plane of atoms relative to the lower plane and inducing plastic



• **Figure 1.3.3.4** Schematic representation of dislocations. (A) Edge dislocation showing the region around the termination of an extra half-plane of atoms in the crystal. (B) Another representation of an edge dislocation where the edge of the crystal is pushed in one plane and the extra half-plane terminates within the crystal at the dislocation line. (C) Representation of a screw dislocation. The variable b is known as the Burgers vector. ((A) Olivera, VMCA., et al., 2017. Corrosion behavior analysis of plasma-assisted PVD coated Ti-6Al-4V alloy in 2 M NaOH solution. *Mat. Res.* 20 (2), 436–444. (B) Muñoz-Portero, M. J., García-Antón, J., Guiñón, J. L., & Pérez-Herranz, V., 2009. Pourbaix diagrams for chromium in concentrated aqueous lithium bromide solutions at 25 °C. *Corrosion Sci.* 51 (4), 807–819.)

deformation. Dislocations are well documented and critical to the understanding of the strength of metals and alloys. Most mechanisms of strengthening of metals rely on affecting and controlling the density (generation and elimination of dislocations) and movement of dislocations. For example, plastic deformation (i.e., cold working) can dramatically increase the density of dislocations in a metal, create entanglements of dislocations (known as dislocation substructure), raise the alloy's strength, and lower its ductility. A heat treatment known as annealing provides thermal energy to allow elimination of dislocations, which then lowers the strength and raises the ductility. Thus annealing treatments are often applied to a metal at the end of processing to reduce the deformation state in the alloy, lowering the yield strength and increasing the ductility.

Area Defects

Area defects can be thought of as grain boundaries (boundaries between adjacent grains or crystals of metal) or free surfaces. Both are locations of higher disorder (randomness or entropy) and both have interfacial energies associated with them that affect the behavior of the crystals. For example, dislocations cannot easily pass highly disordered grain boundaries, and therefore they are piled up at the grain boundary. Thus, increasing the grain boundary area present in a volume of metal (by making smaller grains) creates more barriers to dislocation motion and thereby raises the strength of the alloy.

Free surfaces are another place where defects are present. In the case of most metallic biomaterials, the surfaces of the alloy are covered with a chemically reacted layer of metal oxide, where oxygen from air or water reacts with the metal to form an oxide film on the surface. These are known as passive oxide films in many cases and are critically important for the corrosion resistance and biological interaction of the metal with the body. In other alloys (e.g., Mg alloys) oxides

form, but they are not passive and do not substantially slow corrosion at the surface. Thus Mg alloys corrode rapidly and are known as biocorrosible or biodegradable alloys.

Volume Defects

Finally, volume defects can be present as well. These are typically voids (from, say, casting) or cracks, both of which can significantly reduce the fracture toughness or fatigue resistance of the alloy.

Each of these forms of defects are important for the properties of alloys and ultimately their performance as a biomaterial. Of course, metallic biomaterials go to make medical devices and it is the combination of the mechanical properties of these alloys and their corrosion resistance that are critical for success.

Bulk Mechanical Properties of Metallic Biomaterials

As discussed earlier, metals are required for a wide range of medical devices because, simply, they have the strength and fatigue resistance to survive in the hostile mechanical environment of the body.

The mechanical properties of metals are highly dependent on the structure (atomic, crystalline, defect) of the alloys. The following is a short description of the basic strengthening mechanisms in metals and the structural elements that give rise to these properties. The properties of interest include: modulus, strength (yield strength and ultimate strength), fracture toughness, and fatigue resistance, among others. Of these, modulus and fatigue resistance play important roles in medical device design, where the modulus is linked to effects like stress shielding bone resorption, and fatigue strength dictates the ability of the metal to withstand cyclic stresses.

To understand mechanical properties of metallic biomaterials, a tensile test of the material is often performed. These tests provide a significant amount of insight into the mechanical properties of the alloy.

Elastic and Plastic Deformation of Metals

When subjected to tensile or compressive loading, metals will engage, first, in elastic deformation if the stresses are below the proportional limit, and then plastic deformation if the stress reaches a critical level. The yield stress of metals is defined as the engineering stress required to induce 0.2% of plastic strain in the metal and is a common term used to describe the strength of the alloy. Very different processes occur in elastic and plastic deformation. During elastic deformation, atoms of the metal remain fixed within their lattices, but they become stretched (or compressed) from their equilibrium position. In plastic deformation, the deformation results in the permanent movement of atoms within the crystal. These movements occur mostly by dislocation motion, resulting in the sliding of specific planes of atoms over one another, or twinning (a deformation mechanism that kinks the crystal lattice). The sliding of planes of atoms is caused by the creation and movement of dislocations. Interestingly, elastic deformation is not a constant volume process, but plastic deformation is a constant volume process. That is, dislocation movement slides atoms around changing the shape, but does not increase or decrease the volume of metal present. In addition, the modulus of the alloy (i.e., the slope of the elastic portion of the stress–strain curve) reflects pulling atoms slightly away from their equilibrium positions, and not other processes. Thus the modulus of alloys is dependent on the chemistry of the alloy, but not other factors like cold-worked state.

One important point about the modulus of alloys is that they can range from a low of about 50 GPa (some Mg alloys) to as high as 400 GPa (molybdenum alloys) or more depending on the alloy. The workhorse alloys (Ti, CoCr, 316L SS) have moduli of 110, 230, and 210 GPa, respectively.

Strength of Metals and Strengthening Mechanisms

The strength of metals is determined from a number of different tests that basically assess the stresses required to induce some amount of permanent (or plastic) deformation in the metal. There are a variety of strengths that can be reported for metals that include: tensile yield strength (σ_{ys}), flexural strength, compressive strength, ultimate strength, etc. Hardness is another description of the yield strength of an alloy that relates to the stress applied to a surface to induce permanent deformation of the surface. There are a number of different hardness tests that range from Rockwell hardness measurements (more macroscopic indentation tests), to microhardness tests (Brinell and Vickers hardness). Hardness values are meant to describe the stress required to induce plastic surface deformation and are an easy way to assess the strength of an alloy.

In addition to strength, the ductility of metals, defined in terms of the percent elongation, plays an important role in performance as well where higher ductility alloys tend to have high fracture toughness. Ductility measures the amount of plastic deformation a metal can undertake prior to failure and is an important property that allows for the potential of some amount of yielding without fracture.

The strength and ductility of metals can be affected by processing methods that change the structure. Typically, those processes that result in structural changes that increase strength tend also to decrease ductility, and vice versa, for an alloy of a fixed composition. In addition, the fracture toughness (the ability to resist the propagation of a crack in the material) is also a property that combines both strength and ductility.

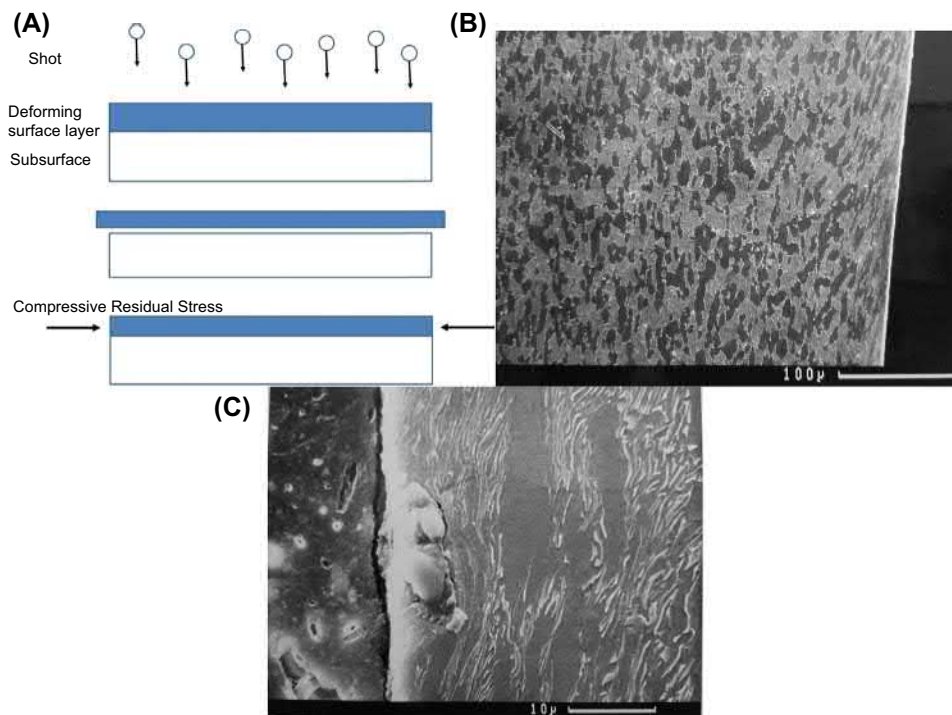
Strengthening Mechanisms: Alloying

Alloying to increase strength has already been described and relates to the increase in yield and ultimate strength that results from the addition of alloying elements to a metal. Pure, single element metals (e.g., iron) have very low strength. That is, their resistance to plastic deformation (i.e., dislocation generation and motion) is low. Such pure metals like iron in an annealed condition (i.e., with low amounts of cold working) can have yield stresses as low as 50 MPa, typical of some plastics. However, with small additions of carbon (e.g., 0.03%), the strength of iron–carbon alloys (steel) rises rapidly to 250–690 MPa depending on other factors. Thus small additions of alloying elements, particularly the interstitial atoms, can have a large effect on the strength of the metal. Carbon additions to iron to make steel is just one example of such interstitial solid solution strengthening. These small interstitial atoms are mobile and tend to accumulate around dislocations, creating dislocation atmospheres (or Cottrell atmospheres) and act to pin them in place requiring higher applied stresses to move such pinned dislocations. These dislocation atmospheres have a pronounced effect on the yield strength of the alloy.

Substitutional elements can also increase the yield strength. These do so by creating elastic strain distortions in the crystal lattice that make movement of dislocations more difficult. In addition, the local modulus is altered by the presence of the substitutional element and this too affects the local strain energy impeding dislocation motion.

Strengthening Mechanisms: Cold Working

A second factor that impacts the strength of alloys is the extent of plastic deformation that is imparted to the alloy during processing. This is called cold working or work hardening. Plastic deformation induces dislocation generation, movement, and entanglement. These changes make it more difficult to induce additional dislocation generation and motion and therefore higher amounts of applied stress are needed to generate additional plastic deformation. Alloys can be purposefully deformed during rolling, forging, extrusion, or other processes to induce high



• **Figure 1.3.3.5** (A) Schematic of shot peening and the development of surface compressive residual stresses. Shot impacts the surface layer of the metal inducing plastic deformation of the outer region (stretching it). (B and C) Scanning electron microscopy micrographs of a Ti-6Al-4V alloy microstructure after shot-peening processes. The surface layer has a heavily deformed surface region and the subsurface region is not deformed. The subsurface constrains the surface layer from stretching, thus creating compressive surface residual stresses. The substrate layer will develop tensile residual stresses to balance the compression of the surface.

amounts of dislocation density and entanglement, which will raise the yield and ultimate strength of the alloy. For example, [ASTM F138](#) describes annealed (undeformed) and cold-worked ultimate strengths for 316L stainless steel. Minimum annealed yield strength is 200 MPa, while the minimum cold-worked yield strength is upward of 690 MPa. One effect of cold working is that the residual ductility of the alloy decreases with increasing cold working. This will make the alloy more brittle and more susceptible to fracture.

One form of cold working used to increase the strength of a surface is **shot peening**. This is a deformation process where high-velocity particles (alumina, glass beads, steel shot) are impacted onto the surface of a metal inducing plastic deformation of the outer layer of the alloy ([Fig. 1.3.3.5](#)). This deformation cold works the surface and imparts compressive residual stresses into the metal. Such residual stresses have important technological effects on the alloy's surface strength and can significantly increase the fatigue strength of the alloy.

In this case ([Fig. 1.3.3.5](#)) Ti-6Al-4V has been shot peened, sectioned to reveal the microstructure, and imaged in scanning electron microscopy to show the surface deformation that can occur during shot peening. Note the heavily deformed surface layer with the grains flattened and distorted compared to the internal microstructure.

Strengthening Mechanisms: Grain Size

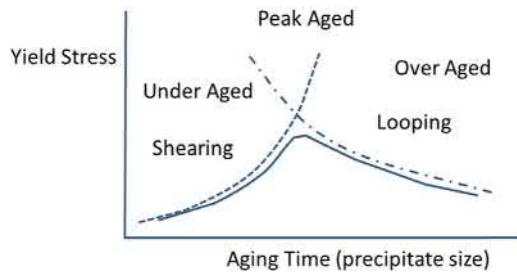
As already described, the size of crystals in a polycrystalline alloy affects the yield strength. In fact, this relationship is known as the **Hall-Petch relationship** where the yield strength increases with decreasing grain diameter to the $\frac{1}{2}$ power:

$$\sigma = \sigma_0 + kd^{-1/2}$$

where σ_0 is the stress that causes yielding in large grain alloy and k is a material-dependent factor. Thus smaller grain sizes for a particular alloy will raise the strength of the alloy. This is one reason why titanium alloys and CoCrMo alloys are currently being fabricated with grains in the 5 μm range. Thus fine-grained alloys will have significantly higher yield and ultimate strengths compared to higher grain size equivalent alloys.

Strengthening Mechanisms: Precipitation Strengthening

A final strengthening mechanism is the generation of multiple phases in a single alloy. These second-phase particles may be intermetallics, carbides, oxides, or other crystal structures (phases) and are sometimes referred to as precipitates. Such second-phase precipitates embedded within the primary alloy matrix act to limit dislocation motion in the parent matrix. Two basic mechanisms can be present



• **Figure 1.3.3.6** Effect of particle size (aging time) on the yield strength of precipitation-strengthened alloys.

depending on the size and density of the second-phase precipitates: (1) particle shearing (at small particle sizes) and (2) dislocation looping (Orowan looping, at larger particle sizes). Depending on the particle size, the way in which dislocations interact with the particles changes from shearing of the particle at small particle sizes to generating dislocation loops around particles at larger sizes. It turns out that the stress to shear small particles increases with particle size and the stress to drive dislocations to loop around particles decreases with particle size. Fig. 1.3.3.6 schematically shows the effect of particle size on the yield strength of a precipitation-strengthened alloy. This figure shows that there is an optimal particle size to achieve the highest yield stress.

The particle size of precipitates can be manipulated by a heat treatment process known as aging. As the precipitation-strengthened alloy is heated (or subjected to an aging process) the particles will grow in size and decrease in density (a process known as coarsening). Thus aging first increases the strength, up to the optimal precipitate size, and then decreases with continued aging. Precipitation-strengthened alloys can be under-aged (many small precipitates where shearing occurs), optimally (or peak) aged (where the precipitates are at the ideal size), or overaged (where the precipitates become large and dislocation looping occurs).

Fracture of Metals

The process of fracture has many distinctly different elements compared to the processes of yielding. In the case of fracture, a crack must be initiated and once this geometry is present, the tip of the crack serves as a high-stress concentrator that focuses deformation to the crack tip and once the local plasticity of the alloy is exhausted at the crack tip, propagation of the crack occurs. The concepts of stress concentrations are critically important in understanding crack propagation. The geometry of a surface, for example, can induce local increases of the applied stress. A circular hole in a plate that is subjected to a uniaxial tensile stress, for example, will induce a stress concentration of about $3\times$ immediately adjacent to the hole in the tensile direction. If such a geometry is converted into an ellipse (a = major axis, b = minor axis), then the stress concentration factor becomes

$$\sigma = \sigma_{\text{far}} \left(1 + 2 \frac{a}{b} \right) = \sigma_{\text{far}} \left(1 + 2 \frac{\sqrt{a}}{\sqrt{\rho}} \right)$$

where $\rho = b^2/a$ is the radius of curvature for the ellipse and σ_{far} is the far-field applied stress.

This shows that the stress at the tip of the crack is increased due to the sharpness of the crack, ρ , and the length of the crack, a . In addition, fracture propagation depends on the energy associated with growth of the crack, the so-called strain energy release rate, and the energy required to grow a crack of some length. When the strain energy released per crack length is larger than the energy needed to grow the crack, catastrophic crack propagation results.

This, basically, is how fracture occurs. However, these analyses presume the existence of a crack of some length being already present in the material. In most cases such cracks would need to develop or initiate and in medical devices, most applications involve cyclic loading and hence fatigue crack initiation behavior becomes important.

The fracture toughness (or mode I critical stress intensity factor, K_{Ic}) of a material is found by loading a precracked test geometry (compact tension sample or three- or four-point bending sample) and measuring the load needed to advance the crack. From this, one can calculate the stress intensity factor needed to fracture. There are ASTM standards for testing the fracture toughness of metal samples (ASTM E-399) where the sample geometry, testing methods, and analysis are described. Such tests provide a measure of a metal's ability to resist fracture once a crack is already present.

The typical fracture toughness analysis is that for mode I opening (where the two fracture surfaces are pulled perpendicularly to the fracture surface), and the fracture toughness is given by the general formula

$$K_{Ic} = \sigma \sqrt{a} Y \left(\frac{a}{w} \right)$$

where a is the crack length, w is the width, $Y(a/w)$ is a geometric factor to account for the sample shape, and σ is the far-field stress applied to the sample. Typical sample geometries include the compact tension sample and the three-point bend sample. In these tests, the crack length should be within the $0.45\text{--}0.55w$ range (ASTM E-399).

Fatigue of Metals

When metals are subjected to cyclic stresses, for example, due to walking, a beating heart, chewing, etc., there is a process of fracture that may result from the initiation and propagation of a crack in a subcritical fashion. This process of initiation and propagation to fracture of a crack in response to cyclic applied stresses is called fatigue. The stresses needed to induce a failure by fatigue are typically well below the yield stress or ultimate stress of the material and ultimate fracture of the alloy may require millions of cycles of loading before complete failure occurs. During these cyclic stresses the alloy is being subjected to small-scale, localized damage accumulation processes where local plastic deformation

in some grains, typically at or near the surface, takes place. This damage accumulation ultimately leads to the initiation of a small crack at the surface. Once this fatigue crack is initiated, the sharpness of the crack localizes additional plastic deformation to the crack tip and the crack begins to propagate cyclically. That is, the crack grows intermittently with cyclic loading, advancing little by little. This fatigue crack propagation will ultimately grow the crack to a critical size where the next single cycle of loading will result in catastrophic fracture of the metal.

Fatigue strength is assessed by subjecting a part or sample to a cyclic stress, counting the number of cycles applied until failure, and plotting the stress versus the log of the number of cycles to failure (N_f). These $S-N$ curves (or Wohler diagrams, Fig. 1.3.3.7) then demonstrate the fatigue strength of the material by finding the cyclic stress required to induce fracture in some preset number of cycles (e.g., 10^6 or 10^7 cycles) (Fig. 1.3.3.7). An alternative description is the fatigue life, which represents the number of cycles to failure at some preset applied cyclic stress.

An alternative method to assess fatigue crack propagation behavior is to start with a precracked sample of some known geometry, for example, a compact tension sample (see schematic in Fig. 1.3.3.8). Then, the crack length, a , is measured as a function of the number of cycles applied. From these plots, the crack growth rate, da/dN , is determined over a range of crack lengths. The applied cyclic stress

intensity factor, ΔK , can be determined from the instantaneous crack length and the applied cyclic stress:

$$\Delta K = \Delta \sigma \sqrt{a} Y \left(\frac{a}{w} \right)$$

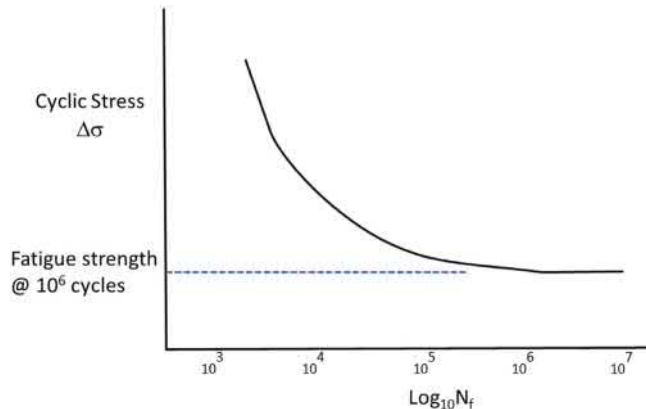
The Paris law crack growth behavior can be determined from

$$\frac{da}{dN} = C \Delta K^m$$

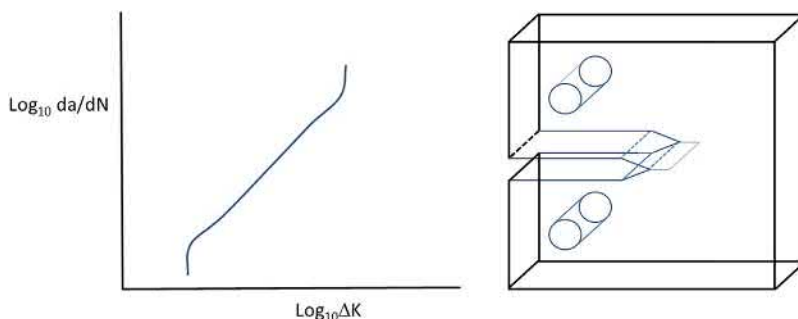
where m is the exponent (typically in the range of 4 for metals) and C is a material-dependent constant (i.e., the crack growth rate when the cyclic stress intensity factor is equal to 1).

Fatigue of metals is often delineated by high-cycle and low-cycle fatigue behavior. In biomaterials, since the intent is for medical devices subjected to cyclic loading to last for the life of the patient (or at least several years), these metals are subjected to the high-cycle fatigue regime. This distinction is important to understand in that the structures and properties that govern high-cycle fatigue response are different to those of low-cycle fatigue. High-cycle fatigue occurs when the cyclic stresses are smaller and fatigue failure occurs generally at 10^5 cycles or higher, while low-cycle fatigue is typically thought of when the cyclic stresses are larger (closer to the yield stress) and require 10^4 or lower cycles to induce failure.

In most high-cycle fatigue cases the overwhelming preponderance of cycles is spent in accumulating damage within the surface or near the surface of the material up to the point that a crack is initiated. This can require 95%–98% of the total number of cycles applied in a high-cycle fatigue test. The remaining few percent of cycles of load result in the propagation of the initiated crack to failure. Thus structural factors that impede nucleation of a crack are most important. For metals, the initiation process is directly linked to the yield and ultimate strength of the alloy at or near the surface. The higher the yield stress (or hardness) of the material, the better it can resist initiation of the fatigue crack. In addition, factors like surface topography, surface residual stresses (e.g., from shot peening), etc. can raise the fatigue crack initiation resistance of the alloy. Since almost all fatigue cracks initiate at or near the free



• **Figure 1.3.3.7** Wohler diagram (cyclic stress vs. log of number of cycles to failure) plots obtained from fatigue experiments.



• **Figure 1.3.3.8** Fatigue crack propagation test schematic. Crack growth rate versus log of the cyclic stress intensity.

surface, control of the surface topography and residual stress can be an effective method to enhance the fatigue strength of the alloy. In addition, microstructures that are designed to raise the yield strength (e.g., grain size reduction) will also increase the fatigue strength. For example, Ti-6Al-4V alloys are expected to have small (3–5 μm) grains that are equiaxed with blocky beta phases. The alloy cannot have a transformed beta (acicular alpha-beta) structure, which may arise from heating to above the alpha-beta transformation temperature (about 880°C). This is primarily to assure that the highest fatigue strength possible for this alloy is obtained by the proper control of its microstructure.

Fatigue initiation processes typically occur at or near free surfaces (as mentioned) and can sometimes be the result of metallurgical flaws in the device. As an example, Fig. 1.3.3.9 shows scanning electron micrographs of an example of a cast CoCrMo alloy femoral component that failed by fatigue. The fatigue crack initiation site (Fig. 1.3.3.9A, white circle) is very close to the lateral side of the femoral stem component where the tensile stresses are highest. The arrow in Fig. 1.3.3.9A identifies a region where the characteristic fatigue “clam shell markings” are present. These markings are a direct result of the cyclic propagation of the fatigue crack and point back to the site of initiation. At higher magnifications there are features called “fatigue striations” that are characteristic of this fracture process. This failure, however, was contributed to by the presence of significant casting porosity found within the stem as can be seen in Fig. 1.3.3.9B–D. Casting porosity may arise when solidification of the metal alloy, which is accompanied by a contraction in volume from liquid to solid, leaves behind regions of the alloy that have voids present. Such casting voids can act as stress concentration sites and will locally raise the stresses leading to fatigue failure. Fig. 1.3.3.9B–D are increasing magnification images of the initiation region showing the casting porosity structure and the fracture surface emanating from the casting voids. Fig. 1.3.3.9D shows the characteristic fatigue striations seen in CoCrMo alloy fatigue failures. These exhibit the cyclic planar crack propagation and deformation processes leading to fatigue fracture in the alloy.

Ti-6Al-4V fatigue fracture processes generate characteristic features of failure as well (Fig. 1.3.3.10). These data came from a corrosion fatigue test set up for hip stems (Gilbert, 1987; ASTM F1612). The fatigue fracture initiation, propagation, and fast fracture regions typical for such failures can be seen. Fatigue striations, characteristic of fatigue fractures, are also shown for this alloy.

Surfaces of Metals: Oxide Films and Passivity

The three major alloys used in biomaterials (Ti, CoCr, and stainless steel) each owe their corrosion resistance to the presence of a thin (nanometer scale) metal oxide film that forms by the reaction of the surface metal atoms with the surrounding oxygen in contact with the surface. For titanium, the oxide

that forms is typically TiO_2 , while for CoCrMo and stainless steel, the oxide's principal chemical form is Cr_2O_3 but other oxide-forming reactions can also be present (e.g., NiO, Fe_2O_3 , CoO, MoO_3 , etc.). When in air, the oxygen to make the oxide can come from molecular oxygen and from water vapor present, while in aqueous solution, oxygen comes from water molecules or dissolved molecular oxygen. These oxide thin film surfaces, known as passive oxide films, are the ultimate smart, self-healing nanobiomaterials. That is, passive oxide films can be manipulated electrochemically (smart), they spontaneously form and reform if any oxygen is present (self-healing), and they are only a few nanometers thick (nanomaterial).

To be a passive film, the oxide that forms on these alloy surfaces must be fully covering, compact, and highly resistive to both electronic and ionic transport of charge across the interface. That is, passive films act as kinetic barriers to the transport and reaction associated with corrosion processes and the films dramatically slow the rate of corrosion that occurs. The alloys with passive films typically have high thermodynamic driving forces (free energy of oxidation) for corrosion, but these passive films limit the rate of transport and reaction by orders of magnitude. Passive films impart compressive residual stresses to the oxide since the volume per cation of oxide is typically larger (1.5–2.0 times) than the volume of the metal atom from which it came. This is known as the Pilling–Bedworth ratio and it is given by

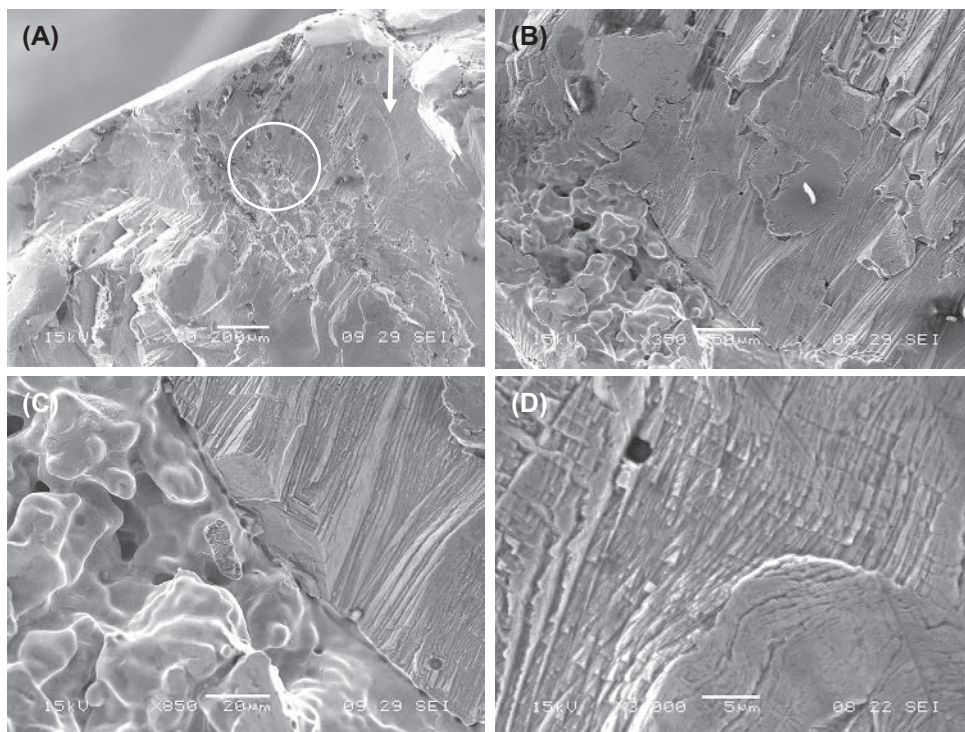
$$PBR = \frac{V_{\text{oxide}}}{V_{\text{metal}}} = \frac{M_{\text{oxide}} \rho_{\text{metal}}}{n \rho_{\text{oxide}} M_{\text{metal}}}$$

where n is the number of metal cations per oxide molecule, the M 's are the molecular or atomic mass of oxide or metal, respectively, and the ρ 's are the densities of metal and oxide. The Pilling–Bedworth ratio for TiO_2 is 1.7, for Cr_2O_3 it is 2.0, and for Mg it is 0.8. As can be seen by these values, Pilling–Bedworth ratios outside of the 1.5–2 range typically do not result in good passive films (e.g., Mg is not a passive alloy).

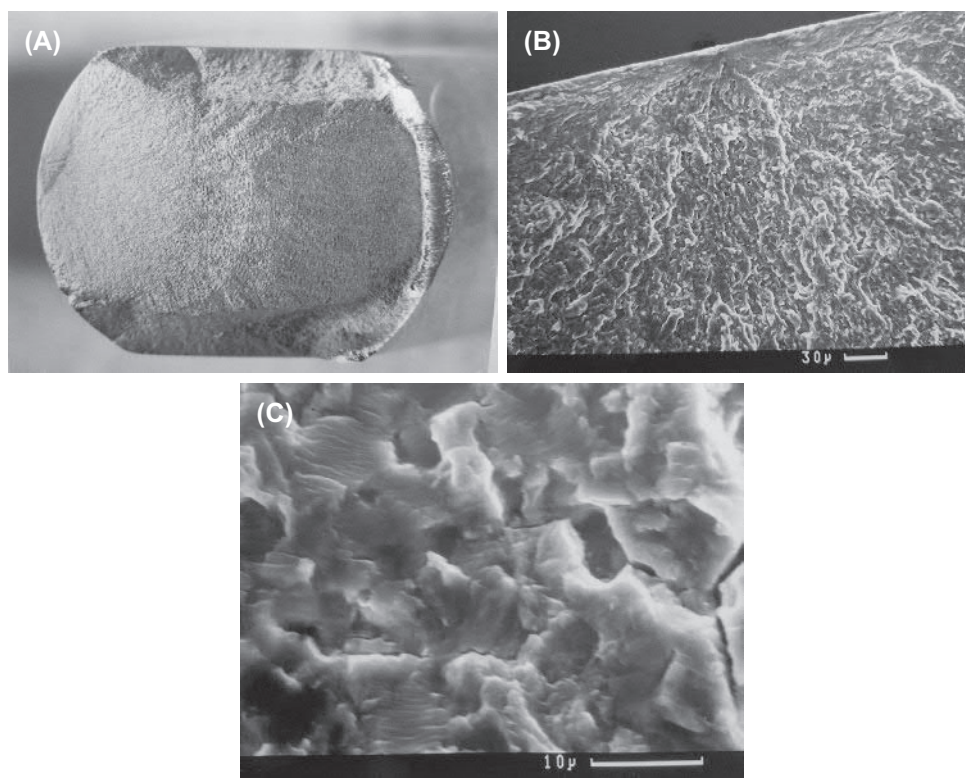
Passive oxide films also have a nanostructure that can be affected by processing, immersion in solution, and potential (Bearinger et al., 2003; Liu and Gilbert, 2018). An example of the evolution of oxide morphology of TiO_2 on Ti-6Al-4V with immersion in phosphate-buffered saline and application of potential from –1 V to +1 V is shown in Fig. 1.3.3.11.

High-Field, Low-Temperature Oxide Film Growth

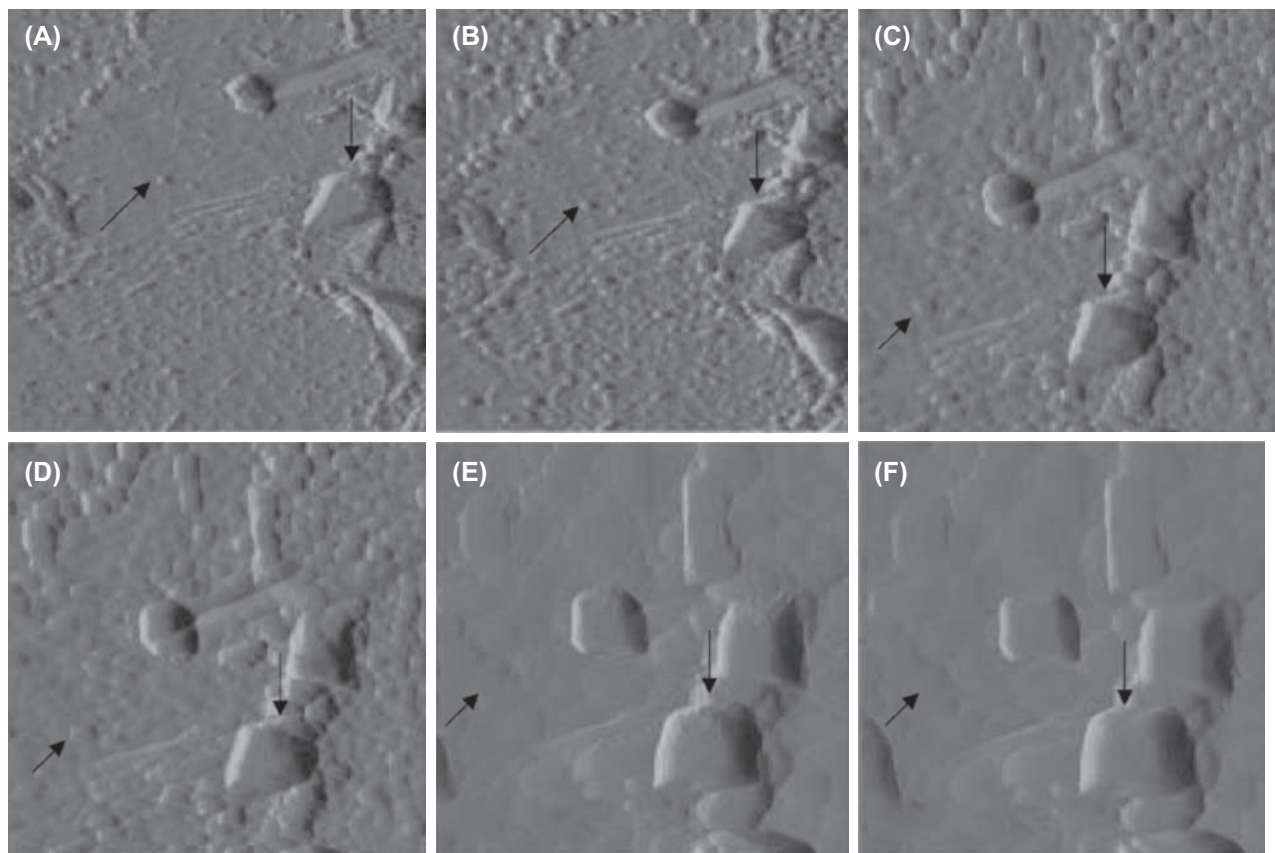
The passive film formation process involves a complex set of reactions at the surface where electrons in the metal tunnel out to the near surface region outside of the metal (see the schematic in Fig. 1.3.3.12). Oxygen atoms in this vicinity can trap these electrons and set up a charge separation (with positive ions inside the metal and negative oxygen ions just outside). This results in the development of a very high-strength electric field (voltage/distance, on the order of 10^5 V/cm) across the interface. This field then drives ion transport by electromigration with positive ions driven out of the surface and negative ions driven inward.



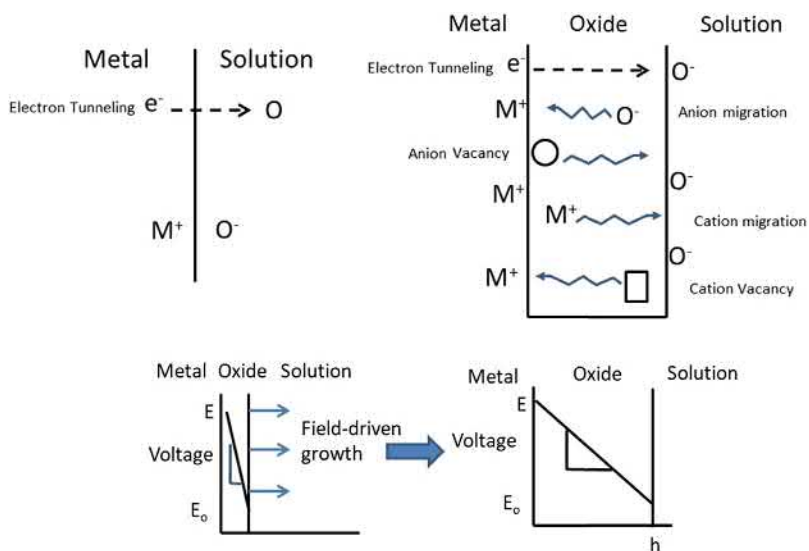
• **Figure 1.3.3.9** (A) 20× magnification of a CoCrMo alloy hip stem that suffered a fatigue failure in vivo. (B) Higher magnification (350×) image of the initiation site showing casting porosity and the fatigue fracture emanating from the porosity. (C) Higher magnification (850×) scanning electron micrograph of the casting-fracture interface. (D) High-magnification (3000×) image of the characteristic features of fatigue striations associated with fatigue crack propagation in CoCrMo alloy.



• **Figure 1.3.3.10** Fatigue fracture surface of a Ti-6Al-4V hip stem from a simulated corrosion fatigue test similar to [ASTM F-1612](#). (A) Optical micrograph of the entire cross-section of the stem. Fatigue crack initiation occurred on the left center (*rounded portion*) and propagated from left to right with fast fracture and final plastic hinge on the far right. (B) Fatigue crack initiation site (*top center*) of one such fatigue failure. (C) High-magnification scanning electron micrograph of the fatigue fracture surface showing fatigue striations and secondary cracking characteristic of fatigue of this alloy ([Gilbert, 1987](#)).



• **Figure 1.3.3.11** Atomic force microscope images of Ti oxide films on Ti-6Al-4V while in air (A) and while immersed in phosphate-buffered saline; potential was applied from -1 V (B) to $+1$ V (F). (From Bearinger, J.P., Orme, C.A., Gilbert, J.L., 2003. In-situ imaging and impedance measurements of titanium surfaces using AFM and SPIS. *Biomaterials* 24 (11), 1837–1852, with permission.)



• **Figure 1.3.3.12** High-field oxide film growth model. Electron tunneling out of the metal is captured by oxygen traps that create high electric fields across the metal oxide–solution interface. These high fields drive cation and anion migration and film growth.

There are corresponding cationic and anionic vacancies also present (i.e., holes in the oxide lattice where cations and anions should be present) that also migrate to enable cations and anions to move in response to the electric field. Reactions between cation and anion form the metal oxide and this process continues to thicken the oxide film, which, in turn, decreases the field strength. Ultimately, the passive film thickness is limited by the decreasing field strength and the oxides cease growing after just a few nanometers. This is known as the high-field, low-temperature film growth law first articulated by [Cabrera and Mott \(1949\)](#), [Gunterschultz and Betz \(1931\)](#).

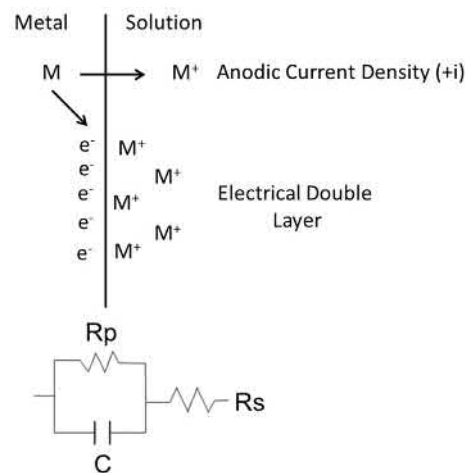
Once the film is established, transport processes through the film are dictated by the field strength and the mobility of charged species through the film. The mobility is linked to atomistic aspects of the film that include the presence of anionic and cationic vacancies, and the semiconducting nature of the film (for electron and hole transport processes). The so-called point-defect model of oxide films has been generally accepted as the atomistic description of how passive films behave ([Chao et al., 1981](#)).

Electrically, passive oxides behave like semiconductors with both capacitive and resistive character where charge transport across the film has a resistive character and charge accumulation across in the film leads to capacitive charging effects. These electronic, semiconducting characteristics of passive oxide films can be measured using electrochemical impedance spectroscopy (EIS) methods and other electrochemical techniques.

Passive films are affected by applied voltages across the metal film–solution interface. For example, with titanium, application of high positive potentials across the interface will induce growth of the oxide films by a process known as anodization. It is generally known that titanium oxide films grow about 2 nm/V with application of an external potential. This technique is used in medical devices, particularly spinal and fracture fixation devices, to create surfaces that have different films that result in different colors. That is, when anodized, titanium takes on a range of colors that are affected by the film thickness and the presence of specific anions. Titanium surfaces can become blue, green, purple, or gold, depending on the anodization thickness obtained. Implants are often color coded to assure the proper screw is used with the proper rod, for example.

Introduction to Metallic Corrosion

Corrosion is comprised of a set of electrochemical reactions in which one chemical species oxidizes (i.e., liberates electrons and increases its valence state) and another chemical species reduces (i.e., consumes electrons in the reaction and decreases its valence state). Each of these reactions is called a half-cell reaction in that it is one of the two required reactions needed for corrosion to progress. Reduction–oxidation (redox) reactions are not limited to metallic biomaterials; in fact, there are a wide number of redox reactions that may arise in the body. Often, these are called anabolic



• **Figure 1.3.3.13** Schematic representation of the metal oxidation half-cell where metal ions are generated and electrons remain in the surface.

(reduction) or catabolic (oxidation) reactions. Cells often require maintenance of redox homeostasis to remain viable and active. Oxidative stress may arise in cells that experience an excess amount of oxidizing species in the biological system. These can include reactive oxygen species, among other chemistries.

Electrochemical Reactions (Oxidation and Reduction) and the Nernst Equation

All metallic biomaterials are susceptible to corrosion processes in the body ([Fig. 1.3.3.13](#)). Metal atoms are present at the surface of the anode and they oxidize by liberating electrons. The electrons remain behind in the surface of the metal (i.e., charge in a conductor moves to its surface), while the metal cations can be released into the adjacent solution (as depicted) or can go to form other compounds, including metal oxides. This process generates a current as the metal ion moves from the electrode to the solution, and there is an inherent resistance to this movement of charge (R_p known as the polarization resistance). In addition, the separation of charge means the electrode surface establishes an electrical double layer with the electrons in the metal and the metal ions in the solution, as if the interface is a charged capacitor (C). In addition, the solution also has an intrinsic resistance to the movement of charged ions (R_s) and the electrical circuit shown is the typical one used to represent an electrode surface. This is known as the Randles circuit and is discussed later.

The oxidation half-cell reaction ([Fig. 1.3.3.13](#)) would result in the accumulation of metal ions in solution and electrons accumulated in the metal. This separation of charge results in a capacitive-based electrical energy developing that resists the chemical oxidation free energy (ΔG_{ox}) and the continuation of the half-cell reaction. Ultimately, an equilibrium is reached where the chemical free energy driving oxidation equals the electrical energy resulting from the charge separation inhibiting the reaction. At this

equilibrium condition, there are equal forward and reverse reactions (i.e., metal ions leave the metal and return to the metal in equal rates) and there is an electrode potential established as a result of this process. If the potential is altered, then the reaction will shift to reestablish the equilibrium condition. For example, a more positive potential will increase the amount of metal ion dissolution, raising the concentration in the solution until equilibrium is reestablished.

At equilibrium, the chemical and electrical energies are equal:

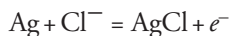
$$\Delta G_{\text{ox}} = nFE^{\text{eq}}$$

where ΔG_{ox} is the chemical free energy driving oxidation, n is the charge per cation, F is Faraday's constant (96,485 coulombs of charge/mole of electrons), and E^{eq} is the electrode potential (i.e., the voltage drops across the metal–electrolyte interface resulting from the accumulation of the charge at the interface).

This equation, known as the Nernst equation, is a measure of the driving force for oxidation and the more negative the potential, the greater is the chemical energy driving the oxidation of the metal (i.e., the more negative is ΔG_{ox}). Some metals have very negative electrode potentials (e.g., Mg, Ti) and are called active, while others have more positive potentials (e.g., Au, Pt) and are called noble. Thus the scale of electrode potential from negative potentials to positive is referred to as the electromotive series, or sometimes the galvanic series depending on the solution in which the electrode is placed.

The Nernst equation can also be related to the chemical activity of species involved in the half-cell reaction. That is, one can relate the free energy of oxidation to the chemical activity (or concentration) of the species involved.

For example, a commonly used electrode in biomedical applications is that of the silver chloride electrode. The half-cell reaction for the Ag/AgCl electrode is



where AgCl is a solid oxidation product of the oxidation of Ag in a chloride-containing solution. The Nernst equation for this reaction, using the chemical potential of species to relate to the free energy of the reaction is

$$E^{\text{eq}} = E_0 + \frac{RT}{nF} \ln \left[\frac{[\text{AgCl}]}{[\text{Ag}][\text{Cl}^-]} \right]$$

where E_0 is the electrode potential when all chemical species are at unit activity (i.e., saturated or pure), and is called the standard half-cell potential. Here, the bracketed values are concentrations, or activities, of each chemical species. Since AgCl is a pure substance (activity of 1) and Ag is a pure metal (activity of 1), the equation results in

$$E^{\text{eq}} = E_0 - \frac{RT}{F} \ln [\text{Cl}^-] = E_0 - \frac{2.303RT}{F} \log_{10} [\text{Cl}^-]$$

This equation shows that a chlorided silver wire's electrode potential will depend on the concentration of chloride in the solution. The factor $2.303RT/F$ is known as the thermal potential and has a value of 0.059 V per decade of $[\text{Cl}^-]$ concentration (i.e., factor of 10 change in concentration) at room temperature. If the chloride concentration remains below the saturation point (4 M, activity of 1), then for every factor of 10 change in the chloride concentration, the wire electrode potential will change by 59 mV at 300 K (or 61.5 mV at 37°C). This is known as an ion-specific electrode and is a means of determining Cl ion concentrations in solutions. In addition, when the solution is maintained saturated in Cl ions, then the Ag/AgCl electrode is highly stable and fixed in its potential and is often used in corrosion experiments as a reference electrode to fix all potentials relative to a stable fixed value (222 mV vs. the normal hydrogen electrode [NHE]). Another reference electrode often used in biomaterials experiments is the saturated calomel electrode (SCE, Hg/Hg₂Cl₂, 242 mV vs. NHE). In each of these cases the reference voltage is for the case where the solution bathing the electrode is saturated in the ions of the electrode (e.g., 4 M KCl).

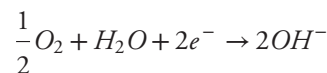
In general, the Nernst equation relates to any redox reaction, $r \rightleftharpoons O + ne^-$:

$$E^{\text{eq}} = E_0 + \frac{RT}{nF} \ln \left[\frac{[O]}{[r]} \right]$$

where R is the ideal gas constant (8.314 J/mol K) and O is the oxidized form of the half-cell, while r is the reduced form. Thus all electrode half-cell reactions have an associated Nernst equation that describes how the electrode potential is affected by the concentration of the reactants and products of the reaction.

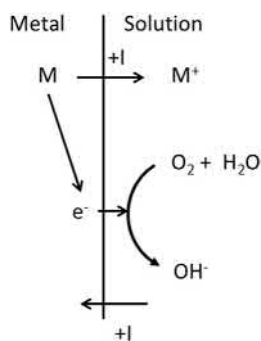
The Principal Reduction Reaction in Biomaterials (Oxygen Reduction)

In most biomaterials applications, it is thought that the primary reduction half-cell reaction is the reduction of oxygen and water according to



This reaction, however, is overly simplified and has a number of reactive oxygen intermediates, including hydrogen peroxide and hydroxide radicals, that may arise depending on the potential and solution conditions. It is important to note, however, that there are myriad other chemical species present in the body that are redox active and may participate in reactions related to corrosion.

Together, the oxidation of metal (to form ions or oxides) and the reduction of oxygen combine to form the corrosion reaction (Fig. 1.3.3.14). Importantly, when both reactions are present, electrons do not accumulate at the surface since the reduction reaction consumes them, and there is charge transport (ionic and electronic) across the interface with positive



• **Figure 1.3.3.14** Simplified two half-cell redox reactions to generate corrosion.

current going from the metal to the solution where metal ions are released (i.e., the oxidation reaction), and positive current is returned to the electrode at the site of the reduction reaction. Thus both reactions together complete an electrical circuit and may continue to generate currents at multiple sites on the metal surface as both oxidation and reduction reactions occur. Essentially, the electrical circuit is closed with currents leaving the electrode into the solution at the anode (site of oxidation), while the current returns to the electrode at the cathode (site of reduction). Because the metal electrode is a conductor, these two half-cell reactions may be in close proximity to one another, or they may be spatially separated depending on the conditions, and the local currents associated with these reactions may also be close or separate.

Polarizable and Nonpolarizable Electrodes

Another feature of electrodes used for stimulation or recording of potentials is the concept of polarizability and nonpolarizability. A nonpolarizable electrode is one where even if a current is being passed across the electrode interface, there is little to no change in its electrode potential. A polarizable electrode is one where its electrode potential can be shifted by the injection of charge into the electrode. Ag/AgCl electrodes are excellent reference electrodes because of their nonpolarizability, where even if a small amount of current is passing the interface, the potential of the electrode is not significantly affected. On the other hand, Pt as well as Hg are excellent polarizable electrodes where the potential can reach a wide range simply by injecting charge into the metal. This property results from the high charge transfer resistance (or low exchange current density) typically seen in these metal surfaces. Thus the electrode potential is a measure of the thermodynamics of corrosion reactions. What reactions are possible depends on the reactants present and the electrode potential.

The kinetics of electrode reactions requires additional considerations. As can be seen from the foregoing, the metal oxidation half-cell results in the transport of positive charge across the metal–solution interface. This gives rise to a current that is distributed over the area of the electrode. Current per unit area of the electrode is known as the current density and is in units of amps per cm^2 . Thus current density is a direct measure of the rate of an electrode reaction.

Pourbaix Diagrams (Electrode Potentials vs. pH)

Electrode potential is directly linked to the chemical free energy driving the half-cell reaction by the Nernst equation. This relationship can be used to assess when specific electrochemical reactions are thermodynamically favored (i.e., in which direction a half-cell reaction will occur). For example, the metal dissolution half-cell reaction can either be driven toward more dissolution (i.e., oxidation) by increasing the electrode potential (making it more positive) or toward reduction of the metal ions to metal atoms, by applying a potential more negative than the equilibrium potential. The equilibrium potential itself is also dependent on the concentration of the metal ions in the solution.

In many half-cell reactions, the pH of the electrolyte solution is related to the electrode potential because hydrogen ions are involved in the reaction. In these cases it is useful to make plots of the electrode potential versus the pH of the solution. These plots are known as Pourbaix diagrams and they depict the combined conditions of potential and pH where specific products of electrode reactions are thermodynamically stable. For example, when a metal reacts with water to form a metal oxide, the half-cell reaction may appear as

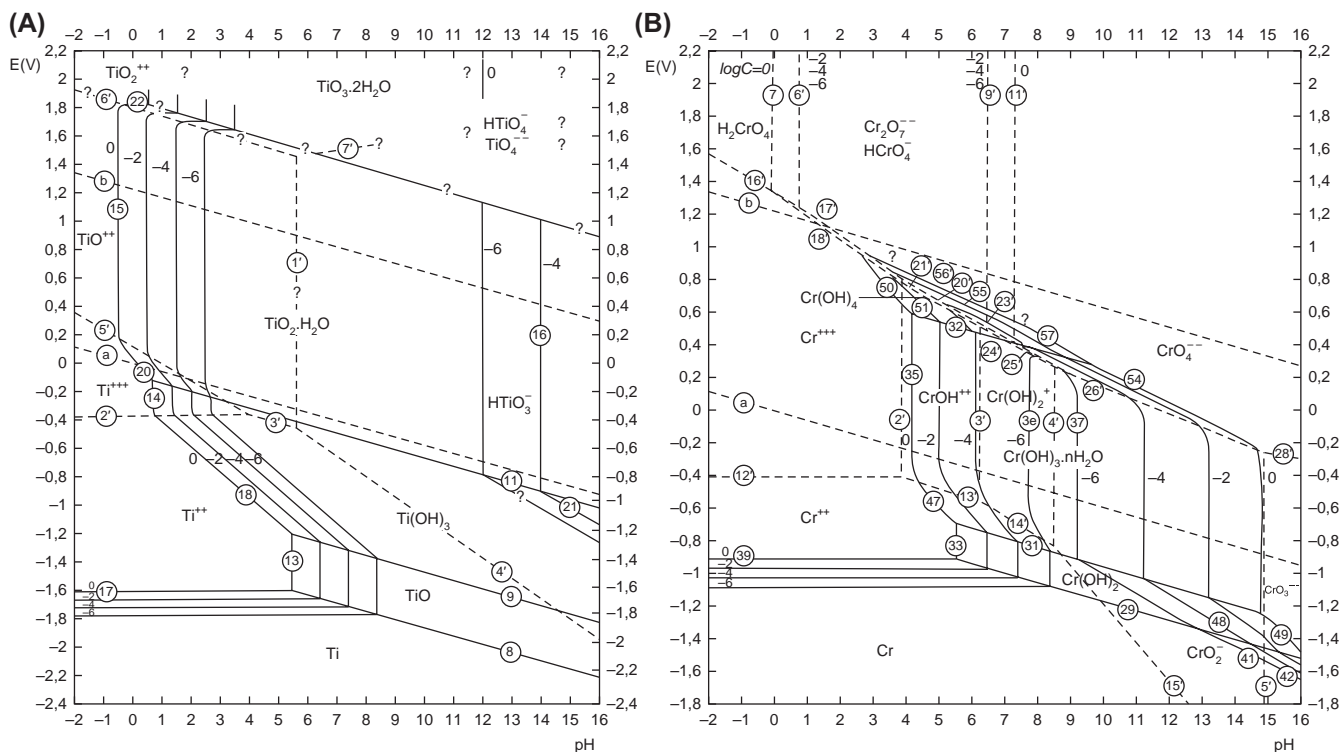


The Nernst equation depends on the hydrogen ion concentration. Using pH as the measure of hydrogen ion concentration (i.e., $\text{pH} = -\log_{10}[\text{H}^+]$), the Nernst equation can be written as

$$E^{eq} = E_0 - k\text{pH}$$

where $k = 2.303RT/F$. This equation shows that the potential of an electrode in which hydrogen ions participate shifts negatively by about 59 mV (at room temperature) for every unit of pH increase in the solution. An example in which pH plays a role in a half-cell reaction is in the reduction of water $H_2O + e^- \rightarrow 1/2H_2 + OH^-$, which can also be written as $H^+ + e^- \rightarrow 1/2H_2$ (the normal hydrogen electrode reaction). Here, the Nernst equation is $E = E_0 - k\text{pH}$ where E_0 is the potential when the electrode is in a solution with a unit activity of H^+ (i.e., $\text{pH} = 0$). In the normal hydrogen electrode ($\text{pH} = 0$, $[H_2] = 1$), $E_0 = 0.0$ and for every pH unit shift from 0, the electrode potential drops 59 mV. At pH 7.4, E for reduction of water is -436 mV versus NHE or -658 mV versus Ag/AgCl. Thus water starts to be reduced at a potential of about -658 mV versus Ag/AgCl at metal electrode surfaces. The water reduction curve is always represented on the Pourbaix diagram as a dashed line with negative slope starting at $\text{pH} = 0$ at 0V. When the electrode potential sits above this line, then water is thermodynamically stable. When the electrode potential sits below this line, then the thermodynamics of the system drive it to reduce water to hydrogen gas and hydroxide ions.

Pourbaix diagrams were developed (Pourbaix, 1964) to demonstrate the potential and pH where specific chemical species would be thermodynamically stable and where transitions in reactions would occur. These diagrams represent equilibrium conditions and do not



• Figure 1.3.3.15 Pourbaix diagrams for (A) Ti and (B) Cr in chloride-containing solutions.

speak to the kinetics of any of the reactions. Pourbaix diagrams for Cr and Ti in chloride-containing solutions (Fig. 1.3.3.15) have been determined and are reproduced here. These diagrams show, for example, the potential and pH range where oxides, ions, or metal states of the element are stable.

Electrochemical Currents (Evans Diagrams)

Several factors affect the rate at which corrosion reactions occur. In the case of an active metal undergoing corrosion, where there are no passive films or other limiting structures, the rate of oxidation (i.e., the current density or current per unit area of electrode) is controlled by the chemical reaction rate theory, known as the activated complex theory (Bard and Faulkner, 1980). This theory, under the assumption that there are no other mass transfer limiting processes, results in the Butler–Volmer equation for a single half-cell reaction. This is shown as

$$i = i_0 \left[e^{\frac{\eta}{\beta_a}} - e^{-\frac{\eta}{\beta_c}} \right]$$

where i_0 is known as the exchange current density (i.e., the current density of the electrode reaction when it is at equilibrium [equal forward and reverse reaction]), β_a and β_c are the anodic and cathodic Tafel slopes, and η is the overpotential (i.e., $\eta = E - E^{eq}$). This equation shows that the current density rises exponentially with potential when the electrode potential is either anodically or cathodically shifted from the equilibrium potential. The Tafel slopes for active electrode reactions governed by reaction rate kinetics

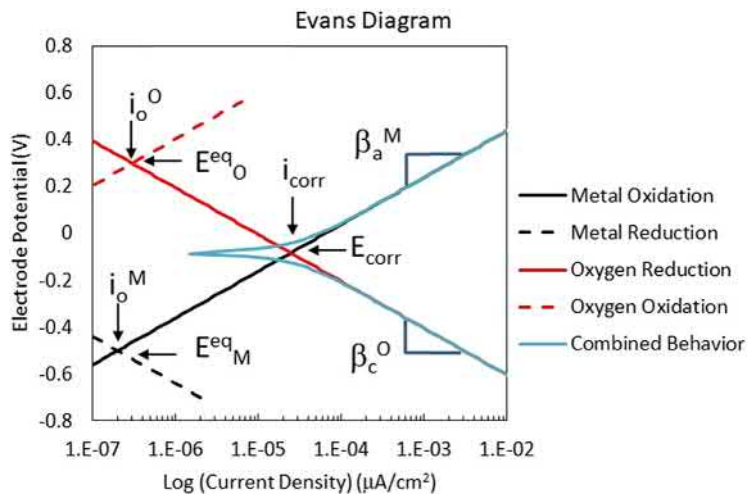
are typically given approximately by $2.303RT/0.5F$, which is roughly a 120 mV/decade change in current density. That is, the currents change by a factor of 10 with every 120 mV away from the equilibrium potential for the half-cell reaction.

Importantly, the Butler–Volmer equation is limited to those electrodes where so-called activation-limited reactions dominate. This is not the case typically when passive oxide films are present and thus the Butler–Volmer equation and analyses based on it are not accurate when dealing with passivating electrodes.

Each half-cell reaction has a Butler–Volmer equation and when oxidation from one reaction interacts with the reduction of another reaction, then two Butler–Volmer equations can be combined.

This equation, which is based on the fact that there is an activation energy barrier to electrode reactions that can be modified by the application of an electrical potential across the interface, results in an exponential dependence of the current density on the application of a potential away from the equilibrium (Nernst) potential of the electrode.

Graphical representations of the Butler–Volmer equation are often very useful in understanding electrode reactions when multiple half-cells are present and help to explain how an electrode's current varies with variation in applied potential. Such plots are known as Evans diagrams, which plot the electrode potential versus the \log_{10} of the absolute value of the current density (Fig. 1.3.3.16). The experiments performed to obtain the next response are called potentiodynamic polarization plots. Shown in Fig. 1.3.3.16 are two half-cell reactions, one for metal oxidation and the other for

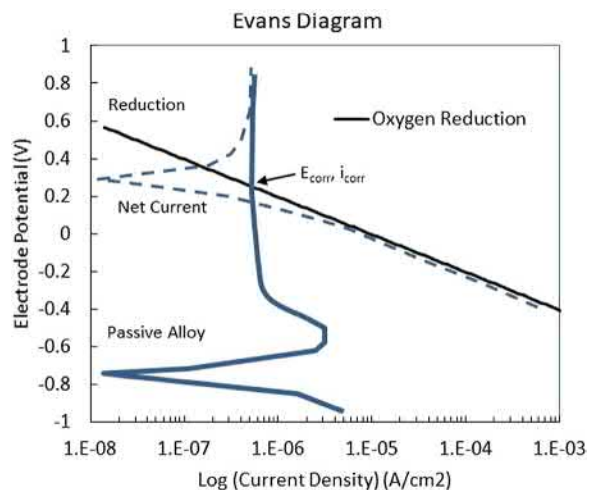


• **Figure 1.3.3.16** Evans diagram (polarization plots— E vs. $\log i$).

oxygen reduction. Each has its own equilibrium (Nernst) potential and exchange current density (identified in Fig. 1.3.3.16). For the combined reactions (Fig. 1.3.3.13), because the metal equilibrium potential is more negative (active) than the oxygen reduction potential, the metal will be driven to corrode and the oxygen will be reduced. The rate of increase in the redox reactions is given by the slope of these lines, which are the Tafel slopes in the Butler–Volmer equation for each half-cell. During corrosion processes, the sum of the oxidation currents must equal the sum of all reduction reactions on average over time when there is no external source or sink of electrons. This is known as the mixed potential theory (Jones, 1996) of electrode processes. The point on the Evans diagram where the oxidation currents equal the reduction currents (or current densities in this case, assuming the same electrode area) is given by E_{corr} and i_{corr} . The total current density (i.e., the difference between the anodic and cathodic current densities [blue line—combined behavior]) can be measured with polarization tests and the total external current versus potential will be measured. Note, polarization tests do not identify the underlying equilibrium potentials or exchange current densities for the individual half-cell reactions, but rather capture the combined behavior of the two electrode processes.

The Evans diagram helps to elucidate the interplay between half-cell reactions to predict corrosion potentials, corrosion currents in the role of different oxidizing species, and the effects of galvanic interactions. However, there are some limitations to the ability of Evans diagrams since they derive from the analysis of activation-limited electrode reactions and are not predictive of passive alloy behavior. Changes in E_{corr} and i_{corr} are easily explained based on shifts either of equilibrium potentials (up or down) or exchange current densities (left or right) and help to visualize the overall electrode behavior with such changes.

Evans diagrams become more complicated (and less well described mathematically) when passivating alloys are involved. Such a schematic polarization plot is shown in Fig. 1.3.3.17. Here, the anodic reaction (blue) is more



• **Figure 1.3.3.17** Evans diagram for the case of a passivating alloy and a reduction reaction.

complicated due to the formation of the passive oxide film. This acts to limit the current passing the interface (kinetic barrier) and the intersection of the reduction reaction with the oxidation reaction defines the corrosion potential and corrosion current (also sometimes called the passive current density). Again, the total behavior of the electrode will be based on the mixed potential theory, and the complex behavior of the anode at the negative potentials will typically not appear in the polarization plot because it is overwhelmed by the cathodic reduction reaction.

Electrochemical Impedance Spectroscopy (an Introduction)

Resistive (Faradaic) and Capacitive (Non-Faradaic) Behavior

From the foregoing discussion of a single half-cell reaction, it can be seen that there are current densities (charge transfer across the interface) and charge accumulation processes. These

are known as Faradaic (charge transfer) and non-Faradaic (charge accumulating) processes. Since charge transfer results in currents across the interface that depend on the electrode potential, one can see that there is a resistive character to the interface. There is also charge accumulation, which results in a capacitive character of the electrode. This capacitance can arise from several sources, including the electrical double layer that may arise at such metal–electrolyte surfaces, but also from charge accumulation that can arise in the oxide film (so-called space charge layer) and even across the oxide–metal interface. These different capacitive effects act in series and since capacitors in series add as the reciprocal, the smallest of these will dominate the charging-based response. These impedance-based properties are an important element of the electrode behavior.

Basic Impedance Concepts

Since electrode surfaces (even with passive films) have both resistive and capacitive character, and these properties reflect the nature of the surface of the electrode and its activity within the electrolyte, an important tool to assess the surface behavior is known as EIS (Gilbert, 2011). This approach to understanding electrochemical systems has been in place for decades and as a result the basic concepts (MacDonald, 1987) for this are described here.

In EIS, a very small cyclic voltage is applied over some fixed potential (typically the E_{corr} , but could be any potential), with the amplitude of the voltage oscillation around 10 mV and the frequency of the oscillation varying between 1 mHz (sometimes less) and 10^5 Hz (sometimes more). At each frequency the current response is captured and will consist of an amplitude, i_o , frequency, ω , and a phase angle that will depend on the extent of resistive and capacitive character present at the frequency. The phase angle can vary from 0 to -90 degrees depending on the resistive (0) to capacitive (-90) character. That is, in general, the applied potential will be

$$V = V_o \sin(\omega t)$$

and the current response will be

$$I = I_o \sin(\omega t + \theta)$$

From these measurements, one can obtain the real (Z') and imaginary (Z'') part of the impedance, $Z(\omega)$, of the interface over the range of frequencies tested:

$$Z(\omega) = Z' + iZ'' = \frac{V_o}{I_o} (\cos \theta - i \sin \theta)$$

Both I_o and θ are frequency dependent, thus the real (Z') and imaginary (Z'') impedances will vary with frequency. Note, that

$$\tan(\theta) = \frac{Z''}{Z'}$$

To analyze EIS data, equivalent electrical circuits are used. These circuits are not “models” per se of the electrode

surface but are electrical analogs that can reproduce the observed behavior. Care must be taken not to ascribe too much meaning to a particular circuit element in terms of the impedance behavior.

To obtain the equivalent circuit impedance, two simple concepts are needed. First is the frequency-based impedance of a simple resistor and capacitor. These are $Z_R = R$ and $Z_C = \frac{1}{i\omega C}$, where i is the imaginary number.

The second concept is to recall how resistors and capacitors add in series and parallel. Resistors (impedances) add in series and add as the reciprocal in parallel, while capacitors add as the reciprocal in series and simply add in parallel. Since impedance, Z , is like a resistor, impedances add like resistors. Using these two concepts, the frequency-based impedance response of R – C circuits can be readily obtained.

The simplest R – C circuit is the series sum of R and C . Here, the impedance is just

$$Z = R + \frac{1}{i\omega C} = R - i \frac{1}{\omega C}$$

where $i = \sqrt{-1}$, $Z' = R$ and $Z'' = 1/i\omega C$, and $\tan \theta = 1/\omega\tau$, where τ is the time constant (RC) for the circuit.

The most typically used electrical circuit analog for an electrode interface is the Randles circuit (Fig. 1.3.3.16), where there is an electrode-based resistor, R_p , and capacitor, C , which are in parallel, and the solution resistance (R_s) in series with this combination. The impedance for the Randle circuit is

$$Z = R_s + R_p \left[\frac{1 - i\omega\tau}{1 + (\omega\tau)^2} \right]$$

where

$$Z' = R_s + R_p \left[\frac{1}{1 + (\omega\tau)^2} \right]$$

and

$$Z'' = -R_p \left[\frac{\omega\tau}{1 + (\omega\tau)^2} \right]$$

where $\tau = R_p C$.

From these results, one can make several different plots. These are known as Bode plots and Nyquist plots. In Bode plots, the $\log_{10}|Z|$ and θ are plotted against $\log_{10}\omega$, while Nyquist plots are a plot of Z'' versus Z' . Each provides some insight into the overall behavior of the electrode circuit and can assist in determining the values of the circuit elements (R_s and C). Typically, the software used for fitting these functions to the obtained data relies on an iterative nonlinear least squares fitting algorithm contained in the software that depends on the starting values chosen and the quality of the data. The solution resistance in a Randles circuit is found

from the high-frequency response, where the capacitor acts like a short circuit and all of the voltage drop is across R_s (i.e., $R_s = |Z|$ as $\omega \rightarrow \infty$), while the R_p can be found at very low frequency (i.e., $R_p + R_s = |Z|$ as $\omega \rightarrow 0$).

Equivalent circuit impedance models can be more complicated to include defected coated models, where additional R - C elements are added into the Randles circuit. In addition, electrode surfaces often do not behave as ideal capacitors and in these cases a nonideal capacitive element, known as a constant phase element (CPE), is used to replace the capacitor in the circuit. The CPE element is of the form

$$Z_{CPE} = \frac{1}{(i\omega)^\alpha Q}$$

where Q is the capacitive-like element and α is the CPE exponent that can range between 0 and 1. When α is 0 the element acts like a resistor ($R = 1/Q$), and when α is 1, the CPE element acts like an ideal capacitor and $Q = C$. Typically, passive film-covered alloys exhibit α between 0.7 and 0.95 and have mostly capacitive behavior. There is some thought that increased heterogeneity of the surface impedance over the area of the electrode contributes to the non-ideality of this circuit element.

When a CPE element is used in a Randles circuit, the equation for Z is

$$Z = R_s + R_p \left[\frac{\left(1 + (\omega\tau)^\alpha \cos\left(\alpha\frac{\pi}{2}\right) - i(\omega\tau)^\alpha \sin\left(\alpha\frac{\pi}{2}\right)\right)}{1 + 2(\omega\tau)^\alpha \cos\left(\alpha\frac{\pi}{2}\right) + (\omega\tau)^{2\alpha}} \right]$$

where $\tau^\alpha = R_p Q$.

This comes about using the identity

$$i^\alpha = e^{i\alpha\frac{\pi}{2}} = \cos\alpha\frac{\pi}{2} + i\sin\alpha\frac{\pi}{2}$$

Semiconducting Oxide Impedance (Mott-Schottky Analysis)

With the passivating alloys typically used in biomaterials, the semiconducting properties of the oxide are at times of interest. One impedance-based technique used is the Mott-Schottky analysis. Here, the capacitance of the surface is measured across a range of potentials and a plot of $1/C^2$ versus potential is constructed. The capacitance measured is directly linked to the semiconducting space charge region, and, based on an analysis similar to the electrical double layer analysis for ionic electrolytes adjacent to charged surfaces, the Mott-Schottky equation comes from a similar approach (i.e., analysis of the Poisson equation (Gilbert, 2011)):

$$C^{-2} = \frac{2}{A^2 \epsilon \epsilon_0 e^- N_D} \left(V - V_{fb} - \frac{kT}{e^-} \right)$$

where A is the area, ϵ is the dielectric constant of the oxide, ϵ_0 is the permittivity of free space, e^- is the charge on an

electron, N_D is the number of charge carriers in the oxide, k is Boltzmann's constant, T is temperature, and V_{fb} is the flat-band potential of the semiconductor (i.e., the potential where there is no band bending taking place (Gilbert, 2011)). This equation shows that the square of the reciprocal of capacitance is a linear function of voltage rising from the flat band potential. The slope of the line depends on the dielectric constant and the number of charge carriers. More defective films will have higher numbers of charge carriers.

The impedance of passive oxide-covered alloys (Ti and CoCr alloys) tend to show very high-resistance films in the most simplified, yet physiologically representative solutions (e.g., Ringer's, Hanks balanced salt solution, phosphate-buffered saline, etc.). The resistance can reach upwards of $10^7 \Omega\text{cm}^2$ and, because these films are thin, they exhibit significant capacitive effects as well. This latter property is an important one to understand in that significant charging/discharging of the surface can arise and these capacitive charging currents may affect polarization data and other voltage-changing measurements of the electrode. That is, passive films have significant capacitive charging currents that depend on the voltage scan rate and these electrodes can store significant amounts of charge over time. EIS is an important tool for understanding electrode interfaces and new methods are being developed to make such analyses more facile and better understood in terms of the electrochemical properties of these surfaces.

References

- ASTM F-1612 (95) (withdrawn), Standard Practice for Cyclic Fatigue Testing of Metallic Stemmed Hip Arthroplasty Femoral Components with Torsion, Amer Soc for Test and Mat. ASTM International, West Conshohocken, PA.
- ASTM F-86, Standard Practice for Preparation and Marking of Metallic Surgical Implants, Amer Soc for Test and Mat. ASTM International, West Conshohocken, PA.
- ASTM F-138 (Stainless steel), Standard Specification for Wrought 18Chromium-14Nickel-2.5Molybdenum Stainless Steel Bar and Wire for Surgical Implants, Amer Soc for Test and Mat. ASTM International, West Conshohocken, PA.
- ASTM F-75, Standard Specification for Cobalt-28 Chromium-6 Molybdenum Castings and Casting Alloy for Surgical Implants, Amer Soc for Test and Mat. ASTM International, West Conshohocken, PA.
- ASTM F-799, Standard Specification for Cobalt- 28 Chromium - 6 Molybdenum Alloy Forgings for Surgical Implants, Amer Soc for Test and Mat. ASTM International, West Conshohocken, PA.
- ASTM F-1537, Standard Specification for Wrought Cobalt - 28 Chromium - 6 Molybdenum Alloys for Surgical Implants, Amer Soc for Test and Mat. ASTM International, West Conshohocken, PA.
- ASTM F-67, Standard Specification for Unalloyed Titanium, for Surgical Implant Applications, Amer Soc for Test and Mat. ASTM International, West Conshohocken, PA.
- ASTM F-136, Standard Specification for Wrought Titanium- 6 Aluminum - 4 Vanadium ELI (Extra Low Interstitial) Alloy for Surgical Implant Applications, Amer Soc for Test and Mat. ASTM International, West Conshohocken, PA.
- ASTM F-72, Standard Specification for Gold Wire for Semiconductor Lead Bonding, Amer Soc for Test and Mat. ASTM International, West Conshohocken, PA.

- ASTM F-2384, Standard Specification for Wrought Zirconium – 2.5 Niobium Alloy for Surgical Implant Applications, Amer Soc for Test and Mat. ASTM International, West Conshohocken, PA.
- Bard, A.J., Faulkner, L.R., 1980. *Electrochemical Methods: Fundamentals and Applications*. J Wiley and Sons, Hoboken, NJ.
- Bearinger, J.P., Orme, C.A., Gilbert, J.L., 2003. In-situ imaging and impedance measurements of titanium surfaces using AFM and SPIS. *Biomaterials* 24 (11), 1837–1852.
- Bechtol, Fergusson, Laing, 1959. *Metals and Engineering in Bone and Joint Surgery*. Williams and Wilkins, Baltimore.
- Cabrera, N., Mott, N.F., 1949. Theory of the Oxidation of Metals, *Reports on Progress in Physics*, pp. 163–184.
- Callister, W.D., Rethwisch, D.G., 2010. *Materials Science and Engineering: An Integrated Approach*, eighth ed. J Wiley and Sons, Hoboken, NJ.
- Chao, C.Y., Lin, L.F., Macdonald, D.D., 1981. A Point defect model for anodic passive films”. *J. Electrochem. Soc.* 128 (No 6), 1187–1194.
- Gilbert, J.L., 2011. Electrochemical behaviour of metals in the biological Milieu. In: Ducheyne, P. (Ed.), Chapter 3, *Comprehensive Biomaterials*. Elsevier Press, pp. 21–40.
- Gilbert, J.L., 1987. *Corrosion Fatigue Crack Initiation in Ti-6Al-4V Hip Prostheses*. Carnegie Mellon University, PhD thesis.
- Gunterschultze, A., Betz, H., 1931. *Z. Elektrochem* 37, 730.
- Hedberg, Y.S., Qian, B., Shen, Z., Virtanen, S., Wallinder, I.O., 2014. In vitro biocompatibility of CoCrMo dental alloys fabricated by selective laser melting. *Dent. Mat.* 30, 525–534.
- Jones, D., 1996. *Principles and Prevention of Corrosion*. Prentice Hall.
- Liu, Y., Gilbert, J.L., 2018. Effect of simulated Inflammatory conditions and potential on dissolution and surface oxide of CoCrMo alloy: in situ electrochemical atomic force microscopy study. *Electrochem. Acta* 262, 252–263. <https://doi.org/10.1016/j.elect-acta.2017.12.151>.
- Macdonald, J.R., 1987. *Impedance Spectroscopy: Emphasizing Solid Materials and Systems*. J Wiley and Sons, Hoboken, NJ.
- Massalski, T.B., Okamoto, H., Subramanian, P.R., Kacprzak, L., 1990. *Binary Alloy Phase Diagrams*, second ed. ASM International, Novelty, OH.
- Pilliar, R.M., 2009. *Metallic biomaterials*. In: Narayan, R. (Ed.), *Biomedical Materials*. Springer, Boston, MA.
- Pourbaix, M., 1964. Atlas D equilibres electrochimiques. *J. Electrochem. Soc.* 11 (1).
- Reed-Hill, 1973. *Physical Metallurgy Principles*, second ed. Van Nostrand and Co., NY, pp. 81–143.
- Witte, F., 2010. A history of biodegradable magnesium implants: a review. *Acta Biomat.* 6 (5), 1680–1692.
- Wizemann, T. (Ed.), 2010. *Institute of Medicine (US) Committee on the Public Health Effectiveness of the FDA 510(k) Clearance Process. Public Health Effectiveness of the FDA 510(k) Clearance Process: Balancing Patient Safety and Innovation: Workshop Report, vol. 2*. National Academies Press (US), Washington (DC). Legislative History of the Medical Device Amendments of 1976. Available from: <https://www.ncbi.nlm.nih.gov/books/NBK209793/>.

Further Reading

- Meyers, M.A., Chawla, K.K., 1999. *Mechanical Behavior of Materials*. Prentice Hall, NY.

Questions

1. For the titanium–TiO₂ surface, find the Pilling–Bedworth ratio for this system. Would you expect this alloy–oxide film system to result in a passive behavior based on this result? Why or why not?
2. For a metal–solution interface with properties of the solution resistance of 100 Wcm², polarization resistance of 10⁶ Ωcm², and constant phase impedance $Z_{CPE} = 1 / ((i\omega)^{0.89} 10^{-5})$, plot the Bode diagrams (for log|Z| and θ). Also, plot the Nyquist diagram and the Z'' vs. log ω , A'' vs. log ω . Finally, find the frequencies (in rad/s) associated with the reciprocal of the time constants, $\tau_1 = (R_s Q)^{1/\alpha}$, $\tau_2 = (R_p Q)^{1/\alpha}$, and identify these on the log|Z| versus log ω Bode plot. Where do these sit?
3. For an oxide film-covered surface, plot the Mott–Schottky plot for $N_D = 10^{22}$ carriers/cm³ and 10¹² carriers/cm³. How does the change in carrier density affect the plot and the ability of the charge to transit the oxide?
4. Explain how shot peening results in the development of compressive residual stresses in the surface of a metal and how these stresses enhance the fatigue crack initiation resistance of the alloy?
5. Using the Butler–Volmer equation (see equation in the section “Electrochemical Currents [Evans Diagrams]”) recreate the plot in Fig. 1.3.3.17 (use Excel or Matlab). Using this diagram show an additional plot and explain why increased cathodic reaction exchange current density will shift the corrosion current and corrosion potential for the anodic reaction.

1.3.3A

Titanium Alloys, Including Nitinol

SERTAN OZAN^{1,2}, KHURRAM MUNIR¹, ARNE BIESIEKIERSKI¹, RASIM IPEK³,
YUNCANG LI¹, CUIE WEN¹

¹School of Engineering, RMIT University, Bundoora, VIC, Australia

²Department of Mechanical Engineering, Yozgat Bozok University, Yozgat, Turkey

³Department of Mechanical Engineering, Ege University, Izmir, Turkey

Introduction

Metals, polymers, ceramics, and composites can all be used as biomaterials (Martz et al., 1997). When compared with ceramic and polymeric biomaterials, metallic biomaterials stand out for their high strength, ductility, fracture toughness, hardness, and formability in addition to their reasonable biocompatibility (Nouri et al., 2010). Metallic biomaterials have a long history of use, dating back to antiquity; considering only modern surgical implants, stainless-steel and cobalt (Co)-based alloys have found use since the 1930s (Niinomi, 2002), with titanium (Ti) and its alloys subsequently finding applications in these areas due to their excellent properties (Niinomi, 1998). Ti alloys, which have become indispensable for the biomedical industry (Abdel-Hady Gepreel and Niinomi, 2013; Niinomi, 2008; Niinomi and Nakai, 2011), are also used in the aviation (Peters et al., 2003), maritime (Candel et al., 2010), armored vehicle (Moxson et al., 2000), chemical (Cui et al., 2011), and sports materials (Moxson and Froes, 2001) industries due to their high specific strength and corrosion resistance; furthermore, their usage area is expanding daily (Ozan and Ipek, 2012). Ti and some of its alloys have become the preferred metallic biomaterials for orthopedic implant applications because of their excellent mechanical, physical, and biological performance in comparison with other metallic biomaterials (Long and Rack, 1998; Niinomi, 1998; Rack and Qazi, 2006).

The need for these materials is increasing, with expected major orthopedic surgeries in the United States showing large increases over the period of 2005–30; total hip arthroplasties are predicted to increase by 174% to 572,000, with revision hip arthroplasties increasing by 137% (Kurtz et al., 2007). Meanwhile, total knee arthroplasties are predicted to grow by an enormous 673%, up to 3.48 million, with a similar 601% increase in knee revisions (Kurtz et al., 2007). Taken together, it is thus apparent that joint replacement

biomaterials may profoundly influence the lives of millions of patients. To this end, it is vital to avoid the use of implant materials with low wear and corrosion resistance, low fracture toughness, low fatigue strength and a high elastic modulus, and/or use of poorly biocompatible alloying elements in the alloys, as any or all of these may lead to incompatibility between the bone tissue and implant materials (Geetha et al., 2009).

The primary consideration in designing new biomedical Ti alloys is to select alloying elements with a known, high degree of biocompatibility, e.g., without any biological concerns (Abdel-Hady Gepreel and Niinomi, 2013; Geetha et al., 2009). In the event that the elements chosen are inherently poorly biocompatible, it would then be possible that the implant material as a whole may be nonbiocompatible, causing severe problems in the physiological environment (Abdel-Hady Gepreel and Niinomi, 2013). Following this step, the designers should also consider the criteria of yield strength, elastic modulus, fatigue strength, fracture toughness, wear resistance, corrosion resistance, and surface bioactivity parameters based on the area of use of Ti alloys (Geetha et al., 2009). The development of new Ti alloys for biomedical applications have attracted increasing attention in recent years (Cui and Ping, 2009; Cui et al., 2010; Miyazaki et al., 2006; You and Song, 2012; Zhang et al., 2011a). Biomedical Ti-based materials with both biomechanical and biological compatibility pose an important necessity for orthopedic implant applications.

Biocompatibility

As defined earlier in the Introduction chapter of this book, an important question in biocompatibility is how the device or material “transduces” its structural make-up to direct or influence the response of proteins, cells, and the organism to it. As such, it is clear that the cytotoxic, genotoxic,

mutagenic, carcinogenic, allergenic, and neurological effects must all be taken into consideration, along with corrosion tendencies, when evaluating the biocompatibility of metallic biomaterials (Biesiekierski et al., 2012a).

Nickel (Ni), Co, chromium (Cr), and iron (Fe) ions were released to the physiological environment by stainless steels and Co-Cr alloy implants (Okazaki and Gotoh, 2005). There are serious concerns regarding the carcinogenic effects of Ni and Co (Beyersmann and Hartwig, 2008). In addition, Cr and Fe are not listed as biocompatible elements (Biesiekierski et al., 2012a).

Implant materials may also cause allergic reactions (Biant et al., 2010; Granchi et al., 2008; Rushing et al., 2007; Sesia et al., 2013; Shah et al., 2014; Zhubrak and Bar-David, 2014). Metal allergy due to ion release has become a significant modern issue (Niinomi, 2002), with 20% of young European women and 4% of young European men affected by Ni allergy (Niinomi, 2002). For orthopedic biomaterials specifically, it is estimated that allergic reactions take place in between 1% and 5% of orthopedic cases (Zhubrak and Bar-David, 2014). Figs. 1.3.3A.1 and 1.3.3A.2 show the allergic reactions of patients to the Ni content of stainless-steel screws (Fig. 1.3.3A.1) and bars (Fig. 1.3.3A.2); in both cases, the allergic reaction seems to be caused by the implant, but disappears shortly after removal/substitution for a Ti alloy implant (Zhubrak and Bar-David, 2014; Sesia et al., 2013).

These responses are not limited to stainless steel; even though the wear and corrosion resistance of Co-Cr-based alloys are better than stainless-steel alloys, some of the Co-Cr-based alloys contain high amounts of Ni (Niinomi, 2002).



• **Figure 1.3.3A.1** Nickel allergy reaction following implantation of stainless-steel screws in bunion surgery. (Reprinted from Zhubrak, M., Bar-David, T., 2014. Systemic nickel allergy after internal fixation of a bunions. *J. Foot Ankle Surg.* 53 (4), 466–467, Copyright (2014), with permission from Elsevier.)

Furthermore, Co and Cr are also potentially concerning (Biesiekierski et al., 2012a), with metal allergies observed in patients even when Co-Cr alloys with less than 1% Ni are used as biomedical materials in total knee arthroplasty, leading to revision surgery (Gao et al., 2011).

These case studies highlight the importance of designing biocompatible materials that are comprised fully of elements without major physiological concerns; coupled with biomechanical problems, this has increasingly contributed to the replacement of stainless steels and Co-Cr alloys in orthopedic implant applications (Abdel-Hady Gepreel and Niinomi, 2013). Beyond stainless steels and Co-Cr-based alloys, some Ti alloys are increasingly considered unsuitable, in part because they contain nonbiocompatible alloying elements (Abdel-Hady Gepreel and Niinomi, 2013). For instance, one of the most commonly used Ti alloys, Ti-6Al-4V, contains vanadium (V) and aluminum (Al). V and its compounds are noted to be carcinogenic (Beyersmann and Hartwig, 2008), while Al displayed neurological side effects (Flaten, 2001) and genotoxicity (Lima et al., 2011).

Related to this topic is the development of novel shape-memory alloys (SMAs). SMAs are alloys that display the



• **Figure 1.3.3A.2** The occurrence of metal allergy in a patient as a result of the use of stainless-steel bars in pectus excavatum correction surgery. (Reprinted from Sesia, S.B., Haecker, F.-M., Shah, B., Goretsky, M.J., Kelly Jr., R.E., Obermeyer, R.J., 2013. Development of metal allergy after Nuss procedure for repair of pectus excavatum despite preoperative negative skin test. *J. Pediatr. Surg. Case Rep.* 1 (6), 152–155, Copyright (2013), with permission from Elsevier.)

desirable thermomechanical shape-memory and superelasticity effects (SMEs and SEs, respectively); while SMAs are desirable for a range of biomedical applications (Otsuka and Ren, 2005), the SMA currently displaying the strongest SME and SE is nitinol (NiTi), with recoverable strains of 8% in polycrystalline forms (Buehler et al., 1963). This is increasingly a subject of concern due to the high Ni concentrations, and so there is a push to develop comparable, Ni-free SMAs (Cui et al., 2010; Kim et al., 2006; Li et al., 2012; Xiong et al., 2008; Zhang et al., 2011a).

The biocompatibilities of the transition elements were comprehensively reviewed based on the carcinogenic, mutagenic, genotoxic, cytotoxic, allergic, hemolysis, and neurological effects of alloying elements as well as their corrosion resistances (Biesiekierski et al., 2012a). It has been indicated that Ti, gold (Au), tin (Sn), tantalum (Ta), niobium (Nb), ruthenium (Ru), and zirconium (Zr) are biocompatible (Biesiekierski et al., 2012a); however, Sn has a tendency for pathogenic bacterial adhesion, thus its concentration in Ti alloys should be limited and this should be taken into consideration during the design stage (Mediaswanti et al., 2012). Hafnium (Hf) and rhenium (Re) are promising Ti-alloying elements; however, their carcinogenic, genotoxic, mutagenic, allergenic, and neurological effects are still not well known and need further in-depth study (Biesiekierski et al., 2012a); the remaining elements of the 3d, 4d, and 5d d-blocks, as well as Zn and Al, were deemed insufficiently biocompatible (Biesiekierski et al., 2012a).

Biocompatible Titanium Alloys

Ti and some of its alloys are promising metallic biomaterials due to their excellent biocompatibility and corrosion resistance as well as relatively low elastic moduli (Long and Rack, 1998). Ti alloys can be classified as α -, α - β -, and β -type alloys based on their room temperature microstructures. The strength of α -type Ti alloys does not increase with heat treatment since it is a stable phase (Boyer et al., 1994). This is also a fundamental property that distinguishes the α -type Ti alloys from α - β - and β -type Ti alloys (Boyer et al., 1994). In addition, the cold-forming capabilities of β -type Ti alloys that have attracted significant attention in recent years as orthopedic implant materials are much better than those of α - β -type Ti alloys (Boyer et al., 1994). This superior cold-forming ability of β -type Ti alloys decreases the production cost for the use of such alloys, thereby providing advantages for transforming them into commercial products (Abdel-Hady Gepreel and Niinomi, 2013).

To reduce the number of revision surgeries, it is desirable that the orthopedic implants exhibit long service life and have a rigidity (elastic modulus, E) close to that of bone tissue (Abdel-Hady Gepreel and Niinomi, 2013). However, designing orthopedic implant materials with both high mechanical strength and low elastic modulus is challenging, and it appears that the β -type Ti alloys are a promising candidate for orthopedic applications, as can be seen in Table 1.3.3A.1 (Abdel-Hady Gepreel and Niinomi, 2013).

Recent Efforts in Fabrication Processes

Ti alloys may be produced via casting and powder metallurgy (PM) methods (Nouri et al., 2010). Items made of Ti-based alloys have a much higher cost compared with other metallic biomaterials such as stainless steels due to a combination of high reactivity and poor machinability. This has resulted in an increasing preference for manufacturing methods such as PM, which enables the production of net shape or near net shape parts without needing to melt the alloy, so as to minimize the production costs (Biesiekierski et al., 2012b; Moxson and Froes, 2001; Peter et al., 2012; Qian et al., 2012).

Many powder compaction methods such as die pressing, vacuum hot pressing, cold isostatic pressing, and hot isostatic pressing (HIP) are used to produce compacts with high density (Peter et al., 2012). PM methods have especially been sought for usage in industries such as aviation, where mechanical performance is of utmost importance and where the products used are subject to cyclic loading (Peter et al., 2012). HIP can be used to produce Ti alloy parts with near theoretical density and low porosities, but is very costly (Dewidar et al., 2006). It is one of the most frequently used methods in producing high-density Ti alloys (Donachie, 2000).

The fundamental properties expected from artificial joint prostheses are as follows: restoration of patient ability/mobility, biocompatibility, sufficient mechanical performance, ease of production, ease of implantation, and economic advantage (Dewidar et al., 2006). Thus economics is typically the last factor considered, since cost cannot be a significant factor when human health is taken into consideration (Dewidar et al., 2006).

The mechanical performance indicators include the mechanical strength, elastic modulus, toughness, and fatigue strength since load-bearing implants are generally subjected to cyclic load. For example, the femoral stems of hip prostheses are subject to serious cyclic loading because people may walk several thousands of steps daily (Vadivraj and Kamaraj, 2006). Biomedical materials subjected to cyclic loading may be damaged with the occurrence of fatigue (Buttaro et al., 2007; Chen et al., 2005; Ramos and Simões, 2009).

While modern-day bioengineers use solid and nonporous materials in their designs for load-bearing structures, nature makes use of porous structures that adapt properties such as elastic modulus and strength according to the situation faced in its own cycle (Ashby, 1983). A 100-m-tall alder tree with a weight of around 2500 tons is an excellent example of a load-bearing, naturally porous structure (Ashby, 1983). Coral, fungi, and trabecular bone tissues are also examples of natural porous materials (Ashby, 1983).

To eliminate the mechanical incompatibility between the osseous tissue and the implant material (de Vasconcellos et al., 2010; Dewidar et al., 2008), porous structures may be used, yielding decreased moduli as a function of increasing porosity (Ashby, 1983). But as these pores also aid implant

TABLE 1.3.3A.1 Mechanical Properties of Titanium Alloys

Ti Alloy (wt%)	Microstructure	Young's Modulus (GPa)	Yield Strength (MPa)	Tensile Strength (MPa)	References
Ti-6Al-4V ELI (mill annealed)	$\alpha + \beta$	110	875	965	Wang (1996)
Ti-6Al-7Nb (annealed)	$\alpha + \beta$	105	800	900	Boyer et al. (1994)
Ti-15Mo (annealed)	β	78	544	874	Wang (1996)
Ti-35.3Nb-5.1Ta-7.1Zr (annealed)	β	55	547	597	Niinomi (1998)
Ti-12Mo-6Zr-2Fe	β	74–85	1000–1060	1060–1100	Wang (1996)
Ti-11.5Mo-6Zr-4.5Sn (annealed)	β	79	620	690	Boyer et al. (1994)
Tiadyne 1610 (aged)	β	81	736	851	Wang (1996)
Ti-13Nb-13Zr (aged)	$\alpha + \beta$	79–84	836–908	973–1037	Wang (1996)
Ti-32Nb-6Zr (aged)	$\beta + \alpha''/\omega$	53–97	400–820	400–840	Biesiekierski et al. (2018)
Ti-32Zr-30Nb (annealed)	β	62	710	722	Ozan et al. (2018a)
Ti-32Zr-30Nb (cold rolled)	$\beta + \alpha''$	57–69	629–899	692–961	Ozan et al. (2018a)
Ti-35.4Zr-28Nb (annealed)	β	63	611	633	Ozan et al. (2018b)
Ti-35.4Zr-28Nb (cold rolled)	$\beta + \alpha'' + \omega$	70–79	708–890	763–941	Ozan et al. (2018b)

Hence, β -type Ti alloys with lower elastic moduli than those of α - β Ti alloys are being developed for orthopedic applications by numerous researchers. Hao et al. (2007), Kuroda et al. (1998), Li et al. (2012), Matsumoto et al. (2005), Miyazaki et al. (2006), Ozaki et al. (2004), Yang and Zhang (2005), Ozan et al. (2015).

fixation via bone ingrowth into the implant (Dewidar et al., 2006), research efforts in developing porous Ti and its alloys have gained significant attention in recent years (Ahn et al., 2014; Asik and Bor, 2015; Rao et al., 2014; Rivard et al., 2014). Some negative aspects include: (1) the presence of porosity will compromise the mechanical strength of these implants with low moduli (Li et al., 2009b; Wang et al., 2009, 2010), and (2) the corrosion resistance and fatigue life of foam alloys are generally lower than nonporous materials (Ryan et al., 2006).

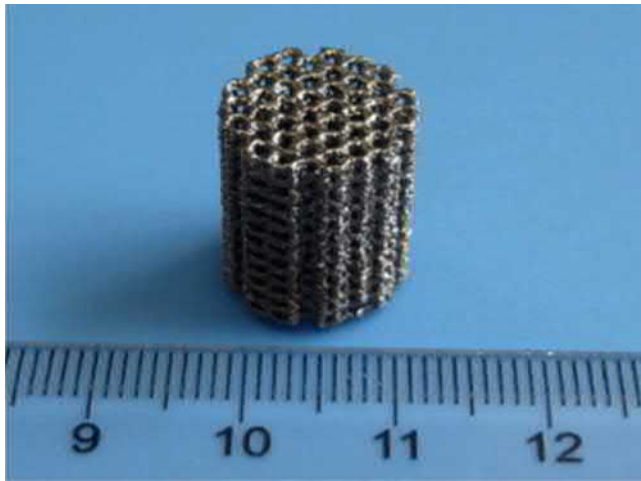
Ti foam materials can be produced by PM in a number of different ways. It is possible to create a porous structure simply by sintering loose powders, but it is difficult to produce parts with high porosity using this method. When higher porosities are desired, methods such as space-holder sintering are more effective method choices, for they provide some degree of choice over pore morphology (Biesiekierski et al., 2012b). Porosity, pore shape and size, and interconnectivity, in addition to appropriate mechanical properties, are important factors determining the bone ingrowth and the biological fixation of an implant material (Ryan et al., 2006).

Carbamide (Bhattarai et al., 2008; Bram et al., 2000), magnesium (Mg) (Asik and Bor, 2015; Esen and Bor, 2007), ammonium bicarbonate (Nouri et al., 2011; Wang et al., 2011), tapioca starch (Mansourighasri et al., 2012), sodium chloride (Ye and Dunand, 2010), and sodium fluoride

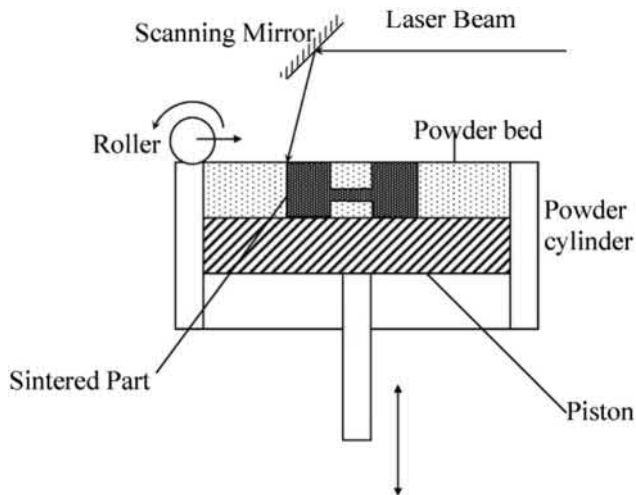
(Bansiddhi and Dunand, 2007) have all been used as space-holders in the production of porous Ti materials. It should also be taken into consideration that the space-holder materials used may contaminate the porous Ti materials, thereby resulting in degradation of mechanical properties, corrosion resistance, and biocompatibility.

Porous materials with the desired porosity and pore size may also be produced directly, without the use of any space-holders, via additive manufacturing (AM) methods, such as selective laser sintering (SLS) (Shishkovsky et al., 2008; Xie et al., 2013), selective laser melting (SLM) (Chen et al., 2017), and electron beam melting (EBM) (Heinl et al., 2007; Horn et al., 2014; Springer et al., 2014). Fig. 1.3.3A.3 shows a porous Ti-6Al-4V alloy scaffold produced via EBM (Li et al., 2009a) and Fig. 1.3.3A.4 shows the schematic of the SLS process (Yang and Evans, 2007).

The manufacturing process varies somewhat depending on the method chosen. For instance, in the SLS method, powdered material is first spread out as a layer, then sintered in a targeted manner by a computer-controlled laser beam, resulting in metallurgical bonding between metal powders in shapes that may be defined based on CAD or equivalent software files (Munir et al., 2017). When the process is completed, the platform at the base is lowered by a layer thickness and a new powder-bed layer is deposited and then sintered, with this repeating until the target part is produced

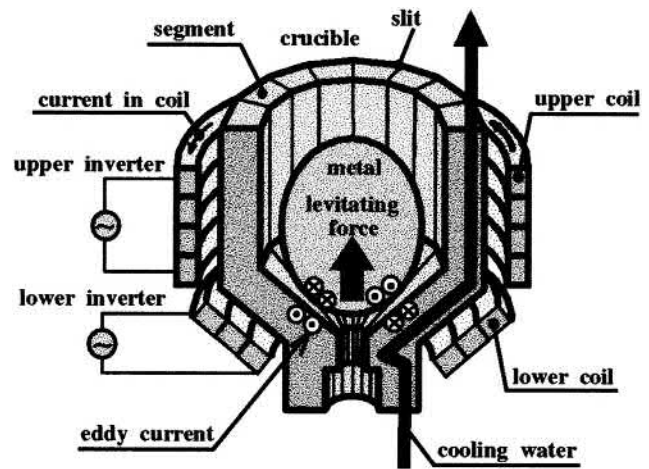


• **Figure 1.3.3A.3** Porous Ti6Al4V alloy sample produced via electron beam melting. (Reprinted from Li, X., Wang, C., Zhang, W., Li, Y., 2009a. Fabrication and characterization of porous Ti6Al4V parts for biomedical applications using electron beam melting process. *Mater. Lett.* 63 (3–4), 403–405, Copyright (2009), with permission from Elsevier.)



• **Figure 1.3.3A.4** Schematic illustration of selective laser sintering. (Reprinted from Yang, S., Evans, J.R.G., 2007. Metering and dispensing of powder; the quest for new solid freeforming techniques. *Powder Technol.* 178 (1), 56–72, Copyright (2007), with permission from Elsevier. AM has emerged as a promising method for producing biomedical implants with complex shapes. AM is so named because, unlike traditional methods such as machining or forming, production is carried out by systematically adding materials. Comprehensive studies have been carried out examining the use of AM for production of porous bone scaffolds (Ataee et al., 2018; Eldesouky et al., 2017) and dental implants (Jamshidinia et al., 2014, 2015). SLS, SLM, laser-engineered net shaping (LENS), and EBM are the most frequently used AM methods for manufacturing biomedical implants (Harun et al., 2018).)

(Liu et al., 2006). The SLM method is an evolution of the SLS method that allows the metal powder to fully melt to produce a homogeneous part, in contrast to the SLS process where the raw powder is only partially melted or heated to the sintering point (Harun et al., 2018). Similarly, the EBM method also employs complete particle melting, but unlike the SLM method, it uses an electron beam instead of a laser.



• **Figure 1.3.3A.5** Schematic illustration of cold crucible levitation melting method. (Reprinted from Morita, A., Fukui, H., Tadano, H., Hayashi, S., Hasegawa, J., Niinomi, M., 2000. Alloying titanium and tantalum by cold crucible levitation melting (CCLM) furnace. *Mater. Sci. Eng. A* 280 (1), 208–213, Copyright (2000), with permission from Elsevier.)

Notably, this limits the EBM method to be operable under high vacuum due to the inherent characteristics of the electron beam (Harun et al., 2018). Atmospheric control is also required for the SLM and SLS methods, typically an argon (Ar) atmosphere throughout the entire work area, due to the high reactivity of Ti powders. This can be avoided in the LENS method, however, as the powders are fed through Ar-pressurized nozzles using a high-power laser. The use of pressurized nozzles acts as a local shield to keep potential contaminants out of the melt pool without requiring evacuation of the entire work area (Harun et al., 2018).

Aside from the PM and AM methods, casting also finds use as a near net shape method. However, it is not an easy process to melt and cast Ti, Nb, and/or Ta metals, as these elements have both very high melting points and chemical reactivities (Morita et al., 2000). The density difference between those elements also makes it more difficult to obtain a homogeneous microstructure by traditional casting methods (Morita et al., 2000).

To overcome this challenge, the cold crucible levitation melting (CCLM) method, shown schematically in Fig. 1.3.3A.5, proves to be a very useful method in casting Ti alloys (Morita et al., 2000). In CCLM, both heating and effective mixing are carried out via electromagnetic forces, thereby yielding a uniform microstructure even for metals with high melting points and differences in density (Morita et al., 2000). As the magnetic fields used to heat the material also induce levitation, contamination resulting from crucible contact is also avoided (Morita et al., 2000).

Mechanical Properties of Titanium Alloys

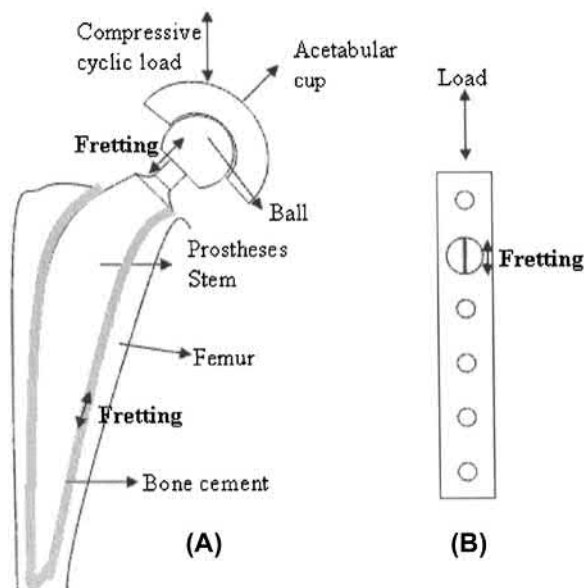
The elastic moduli of Ti alloys (55–110 GPa) are lower than those of stainless steels (~210 GPa) and Co-based alloys (~240 GPa) (Geetha et al., 2009), but their corrosion resistance is higher than that of the aforementioned materials

(Liu et al., 2004), thereby making Ti alloys promising candidate materials in orthopedic implant applications. The fatigue strength should also be high for Ti alloys as implant materials (Niinomi and Nakai, 2011). Since fatigue limit is related to tensile strength (Pang et al., 2014), orthopedic implant materials should have a low elastic modulus and high mechanical strength so that they can be used as implant materials such that the implant can have a longer service life without a need for revision surgeries (Abdel-Hady Gepreel and Niinomi, 2013). In addition, long fretting fatigue life and high wear resistance are two other important characteristics expected from orthopedic implant materials (Niinomi, 2008). Fig. 1.3.3A.6 shows a schematic illustration of the expected locations of fretting motion as a result of cyclic loading experienced by a total hip prosthesis or bone plate (Vadiraj and Kamaraj, 2006).

Inadequacy in these mechanical properties may lead to revision surgeries even when biocompatible alloying elements are used. This was seen in the recall of the Stryker modular hip replacements, made of Ti-12Mo-6Zr-2Fe, in 2011 (Yang and Hutchinson, 2016). In addition to the significant economic burden resulting from those revision surgeries, they show poorer success rates than primary surgeries (Geetha et al., 2009). Therefore the wear resistance, fatigue strength, and elastic modulus of the orthopedic implant material used should be mechanically sufficient for minimizing revision surgeries of Ti implants designed using biocompatible alloying elements (Geetha et al., 2009).

Elastic Modulus

It is inevitable that the number of revision surgeries will increase when biochemically and biomechanically



• **Figure 1.3.3A.6** Fretting fatigue of (A) total hip prosthesis and (B) bone plate. (Reprinted from Vadiraj, A., Kamaraj, M., 2006. Characterization of fretting fatigue damage of PVD TiN coated biomedical titanium alloys. *Surf. Coat. Technol.* 200 (14–15), 4538–4542, Copyright (2006), with permission from Elsevier.)

incompatible materials are used for implant applications (Abdel-Hady Gepreel and Niinomi, 2013). Stress shielding may develop in cases where an implant material exhibits an elastic modulus exceeding that of the surrounding bone (Huiskes et al., 1992). Stress shielding occurs due to the applied stresses being taken by the stiffer implant rather than the surrounding tissue, and as a result it leads to bone atrophy via the adaptive remodeling process of bone (Torres et al., 2011). Fig. 1.3.3A.7 shows the right hip radiographies for a 63-year-old female (Kawate et al., 2009). Excessive stress shielding can be observed in Fig. 1.3.3A.7C (Kawate et al., 2009), and it may result in implant loosening, increased susceptibility to bone fracture, and worsened revision surgery prognoses due to insufficient bone structure for subsequent implant fixation (Heinl et al., 2007).

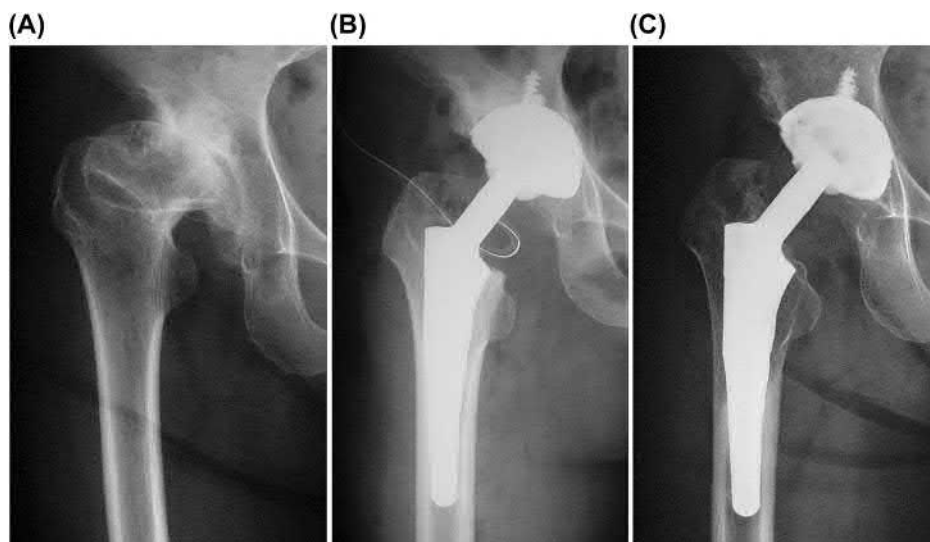
The use of Ti alloys as orthopedic implant materials is becoming increasingly popular due to their high compatibility with bone (Geetha et al., 2009). However, stress shielding remains an open issue. The elastic moduli of Ti alloys, at 40–110 GPa, are still high in comparison with the elastic moduli of osseous tissue, which range between 0.1 and 30 GPa (Wang et al., 2011). For femoral and knee prostheses in particular, it is worth noting that human femur has an elastic modulus of 16–18 GPa (Rogers and Zioupos, 1999).

As seen in Table 1.3.3A.1, while the Young's moduli of β -type Ti alloys are lower than those of $\alpha + \beta$ -type Ti alloys, they are still higher than that of bones. By contrast, the most used biomaterial, the Ti-6Al-4V alloy, has a Young's modulus value that is ~ 6 – 7 times higher than that of femur bones.

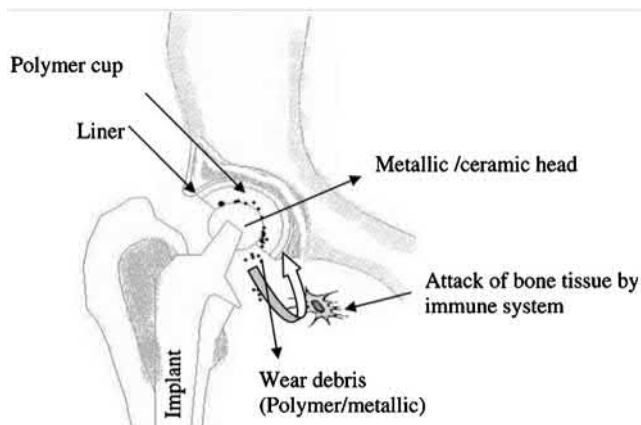
Wear Resistance

Ti alloys are known for their poor tribological characteristics (Budinski, 1991). Low thermal conductivity, low strain hardening, and inadequate covering of surface oxides are indicated as reasons for the low wear resistance of Ti alloys (Molinari et al., 1997; Straffelini et al., 2004). If the high wear resistance needed for long service lifetimes cannot be attained, wear debris forms on the material, which may lead to inflammation, osteolysis, metallosis, and bone resorption, leading to the loosening of the implant material (Geetha et al., 2009). Notably, it is not suggested at this stage to use metal-on-metal hip prostheses until they are confirmed as reliable (van Raay, 2012). Fig. 1.3.3A.8 shows schematically the formation of the wear particles (Geetha et al., 2009).

Co-based alloys have better wear resistance when compared with Ti alloys (Long and Rack, 1998). However, the higher elastic moduli and elemental toxicity of Co-based alloys make Ti alloys the preferred option (Long and Rack, 1998). Therefore it is necessary to improve the wear resistance of Ti alloys for implant applications (Niinomi, 2008). While there are many different surface-hardening procedures available for enhancing the tribological properties of biomedical Ti alloys, two methods are of particular note due to their ease of application: oxidation and gas nitriding. The wear resistances of Ti-29Nb-13Ta-4.6Zr and



• **Figure 1.3.3A.7** Radiographs belonging to a 63-year-old woman: (A) preoperative anteroposterior radiography of the right hip, (B) anteroposterior radiography of the right hip taken immediately after surgery, (C) anteroposterior radiography of the right hip taken 7.5 years after surgery. (Reprinted from Kawate, K., Ohneda, Y., Ohmura, T., Yajima, H., Sugimoto, K., Takakura, Y., 2009. Computed Tomography-based Custom-made stem for Dysplastic hips in Japanese patients. *J. Arthroplast.* 24 (1), 65–70, Copyright (2009), with permission from Elsevier.)



• **Figure 1.3.3A.8** Implant wear. (Reprinted from Geetha, M., Singh, A.K., Asokamani, R., Gogia, A.K., 2009. Ti based biomaterials, the ultimate choice for orthopaedic implants – a review. *Prog. Mater. Sci.* 54 (3), 397–425, Copyright (2009), with permission from Elsevier.)

Ti-6Al-4V were improved significantly in Ringer's solution by the nitriding process as compared to those of their as-solutionized counterparts (Niinomi, 2008).

Fatigue Behavior

The use of implant materials with high fatigue strength is as crucial as that of low modulus for achieving a long service life (Niinomi and Nakai, 2011). The strength of Ti alloys may be improved by different methods such as strain hardening, grain refinement, and aging (Niinomi and Nakai, 2011). When orthopedic implant materials are evaluated regarding the location of failures due to fatigue, fractures mostly occur near the hole of plates and bars, on screws and



• **Figure 1.3.3A.9** Anteroposterior radiograph of the left hip showing the fracture of the total hip prosthesis. (Reprinted from Buttaro, M.A., Mayor, M.B., Van Citters, D., Piccaluga, F., 2007. Fatigue fracture of a Proximally modular, distally tapered fluted implant with diaphyseal fixation. *J. Arthroplast.* 22 (5), 780–783, Copyright (2007), with permission from Elsevier.)

spinal implants, and on joints of hip prostheses (Okazaki, 2012). Orthopedic implant materials may fail as a result of fatigue (Buttaro et al., 2007; Chen et al., 2005; Ramos and Simões, 2009). Fig. 1.3.3A.9 (Buttaro et al., 2007) shows a total hip prosthesis failure due to fatigue.

One of the methods for improving the fatigue strength of the β -type Ti alloys is aging treatment after solution treatment, which allows α - and/or ω -phases to precipitate. This provides increased mechanical strength, as the secondary phases interfere with dislocation movement (Helth et al., 2017). However, the increase in mechanical strength also coincides with increased elastic moduli of the material, since the elastic moduli of the precipitating secondary phases is significantly higher compared with that of the β -phase (Helth et al., 2017).

Assuming equal yield strength, fatigue strength is generally lower for the β -type Ti alloys with lower elastic moduli than that for the α - β Ti alloys (Long and Rack, 1998; Rack and Qazi, 2006). Taking the Ti-6Al-4V ELI alloy, the most common Ti alloy for biomedical applications due to its satisfactory tensile (listed in Table 1.3.3A.1) and fatigue properties (varying between 610 and 800 MPa; Akahori et al., 2000), as a reference point, it is crucial for β -type Ti alloys to possess improved fatigue strength, but it is quite difficult to improve fatigue strength without also raising modulus (Niinomi and Nakai, 2011). For this purpose, short-term aging at low temperatures, excessive cold rolling, and trace addition of ceramic particles may keep the elastic modulus as low as possible while improving fatigue strength (Niinomi and Nakai, 2011).

Effects of Interstitial Atoms on Mechanical Properties

Precipitation hardening is commonly used to produce Ti alloys with satisfactory strengths, but at the cost of substantially increased elastic moduli (Helth et al., 2017). Thankfully, however, other mechanisms to improve the strength of metallic materials are possible, notably the use of interstitial atoms for strengthening (Cho et al., 2013).

For commercial Ti alloys, one of the major avenues of interstitial or solid-solution strengthening is via controlled oxygen content (Liu et al., 2015). The α - and/or β -phase in Ti have a high capacity for oxygen or other interstitial elements, hence encouraging the use of interstitial elements for solid-solution strengthening (Ouchi et al., 1998). Indeed, commercially pure Ti and Ti alloys generally contain oxygen levels in excess of 0.06% (wt%), while the oxygen content of pure Ti produced via the Kroll method varies between about 0.02% and 0.04% (Ouchi et al., 1998). This mechanism has been shown to contribute to strengthening Ti alloys (Liu et al., 2015; Ji et al., 2018), and it has also been reported that this strengthening can be achieved with no increase in the elastic modulus value of β -type Ti alloys when oxygen content is maintained under 0.33% (wt%) (Geng et al., 2011). That said, care must be taken, as excessive oxygen could degrade the ductility of Ti alloys (Yan, 2014). It is therefore crucial for the strengthening of the β -type Ti alloys: the amount of oxygen must be controlled to just provide a solid-solution strengthening effect to improve the tensile and fatigue properties, and at the same time keep the elastic modulus value almost constant.

Surface Modification of Titanium Alloys

Ti and its alloys have good biocompatible characteristics due to their protective surface oxide layer (Yamamuro, 1989). Implant materials with good biocompatibility have traditionally been preferred to eliminate undesirable tissue reactions such as necrosis after implantation. One issue with this class of biomaterial is that fibrous tissue formation may occur at the bone/implant interface (Liu et al., 2004), which could lead to implants loosening due to the greater compliance of the fibrous tissue (Frenkel et al., 2004). This fibrous tissue also limits bone growth by isolating the implant from the surrounding bone tissue. Fibrous tissue formation can be minimized when excessive micromotion of the implant can be avoided or prevented, e.g., using a bone-like apatite layer directly on the surface of the implant to bond the implant to the surrounding bone (Liu et al., 2004). This process is known as osseointegration, and is defined as a direct contact between bone and implant with no interfering fibrous tissue (Carlsson et al., 1986). While this leads to more rigid fixation than fibrous encapsulation, it has been acknowledged that a better degree of fixation may be achieved with the latter case (Anselme, 2011). As such, there is increasing interest in the property of osteoconductivity or bioactivity, that is, the ability of a material to promote the development of hydroxyapatite (HA) directly onto the implant surface (Skripitz and Aspenberg, 1998).

Integration between bone and implant has importance with respect to clinical requirements (Hanawa, 2012). It is expected that these artificial joints integrate easily with the bone tissue and preserve this integration (Simka et al., 2013a). Because artificial joints are often used in patients with damaged joints to restore bodily functions lost by the damaged natural joints, implants that do not promote new osseous tissue are at best a temporary measure. These patients will need artificial joints throughout their lives. Consequently, an artificial joint that can successfully bond with bone is crucial for the patient to be able to carry out daily activities comfortably throughout life (Fujibayashi and Nakamura, 2004). Alkali heat treatment (Xiong et al., 2008), acidic procedures (Wen et al., 1997), anodic oxidation (Simka et al., 2013b), hydrogen peroxide (Karthega and Rajendran, 2010), plasma spray (Roy et al., 2011a), sandblasting (Kim et al., 2011), and sol-gel (Domínguez-Trujillo et al., 2018) are among the primary methods used to improve the bonding between the implant and bone. Anodic oxidation stands out among those methods for improving surface bioactivity due to its cost effectiveness and ease of application.

Recent Efforts in the Anodization Process

Recent progress in the development of Ti implants has shown that clinical success of such implants relies on the degree of osseointegration in the host environment (Cheng et al., 2010). In this context, biocompatibility of such implants preferentially depends upon the structure,

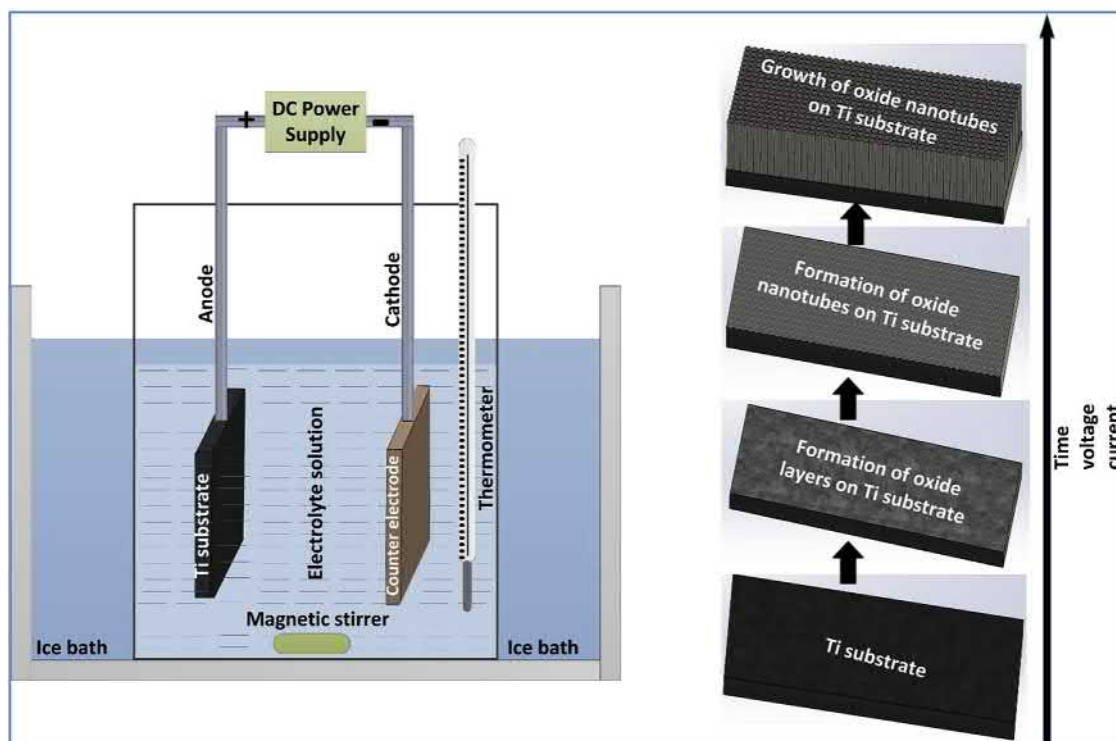
morphology, and composition of oxide layers on their surfaces. Thus additional surface treatments are essential to ensure formation of stable passive films on the surface of Ti implants with desirable surface chemistry (Liu et al., 2017; Minagar et al., 2012). Anodization has emerged as a promising electrochemical surface modification technique for Ti implants to achieve faster, more secure bonding to the host bone (Minagar et al., 2012; Yao and Webster, 2006). Anodization results in the formation of the desired surface by manipulating its ability and tendency to tailor a self-protective oxide layer. In the presence of fluoride-containing electrolyte solutions and an applied electrical potential, controlled oxidation–reduction reactions form a characteristic, patterned, nanoporous, tubular structure on the surface of the oxide layer, with a conical closed-bottom configuration (Kapusta-Kołodziej et al., 2017; Michalska-Domańska et al., 2018). Fig. 1.3.3A.10 shows schematically a typical anodization set-up and events during the anodization of Ti-based substrates.

In similar studies (Crawford and Chawla, 2009; Crawford et al., 2009), the anodization technique was used to modify the surfaces by fabricating a dual-porous, hierarchical structure on Ti substrates. The characteristic hierarchical structure consisted of a dual-porous structure of TiO₂ nanotubes and randomly distributed microscale pores. Fig. 1.3.3A.11 shows microscopic images of typical configurations of TiO₂ tubes grown on Ti substrates via anodization at different applied potentials. It has also been established that electrochemical conditions such as applied potential, current density, electrolyte type, time, and temperature govern the characteristic dimensions of these nanotubular

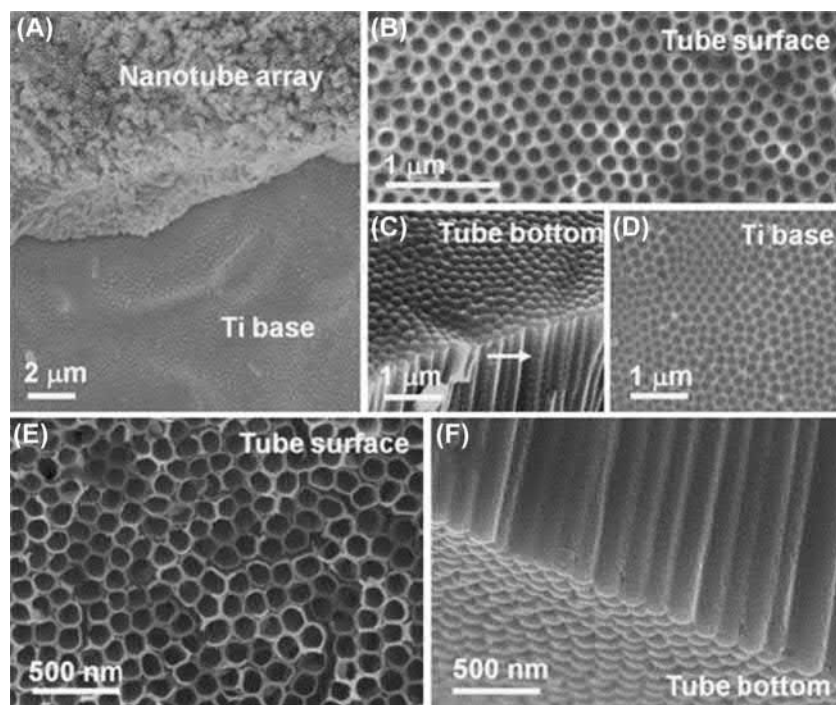
configurations, such as diameter, length, and wall thickness (Kapusta-Kołodziej et al., 2017; Ozkan et al., 2018; Roy et al., 2011b). In contrast to the study by Bauer et al. (2009), which indicated that the nanotube length does not affect the cell behavior, other studies suggest that the characteristic length and wall thickness of grown TiO₂ nanotubes on Ti substrates could affect cell adhesion, proliferation, and differentiation because the resultant wettability and surface energy of a Ti substrate are subject to change with changing characteristic dimensions of growth nanotubes on them (Bai et al., 2018; Minagar et al., 2013). Also, compared with surface modification of commercially pure (CP)-Ti, anodization of other β Ti alloys containing different weight fractions of niobium (Nb), zirconium (Zr), and tantalum (Ta) in Ti results in different reaction rates because of the differing electrochemical properties of these alloying elements in Ti (Allam et al., 2010; Jha et al., 2010). Such differences in oxidation rates lead to formation of a more selective and regular, self-organized pattern of anodic nanotube layers, which grow to different sizes in diameters and lengths. Table 1.3.3A.2 summarizes recent efforts in the anodization of Ti alloys.

Effects of Anodization on Corrosion and Surface Mechanical Properties

Corrosion resistance of implants in a human body environment is a critical factor, as the biocompatibility and mechanical integrity of implants can be adversely affected by a low corrosion resistance (Jacobs et al., 1998). Corrosion and dissolution of surface films introduce metal ions



• **Figure 1.3.3A.10** Schematic of a typical anodization set-up for surface modification of Ti implants.



• **Figure 1.3.3A.11** Microscopic images of TiO_2 nanotubes grown on Ti substrates via anodization under different applied potentials, times, and electrolyte types: (A–D) 60V for 16h in ethylene glycol/0.3% NH_4F /2% H_2O and (E–F) 120V for 1 h in ethylene glycol/0.5% NH_4F /1% H_2O . (Reprinted from Su, Z., Zhang, L., Jiang, F., Hong, M., 2013. Formation of crystalline TiO_2 by anodic oxidation of titanium. *Prog. Nat. Sci. Mater. Int.* 23, 294–301, Copyright (2013), with permission from Elsevier.)

from metallic implants into the physiological medium; extensive release of metal ions from these implants causes adverse biological reactions, which may lead to complete failure of the implanted medical devices (Brunette et al., 2012). It has been established that the corrosion resistance of metals can be improved by anodic oxidation via electrochemical techniques. This is mainly attributed to the formation of stable, adherent, and protective oxide films on the surfaces during anodization (Shabalovskaya, 2002; White et al., 1985). Despite the adherence of an oxide layer to its metal substrate and its self-healing ability when damaged, traces of Ti can nevertheless be observed in tissues adjacent to implant prostheses (Ducheyne et al., 1984). Addition of alloying elements in Ti such as Nb, Zr, and Ta improves the corrosion resistance of these alloys by stabilizing the surface oxide films in the human body environment (Okazaki et al., 1997).

This is particularly important in Ni-containing alloys such as NiTi. Though with high corrosion resistance, NiTi contains a high Ni content, which makes the use of NiTi debatable due to the allergenic and toxic nature of Ni (Morgan, 2004). For this reason, modification of the surfaces of NiTi to further improve the corrosion resistance of NiTi to reduce Ni ion releasing to surrounding tissues has been attempted. It was found that the anodization behavior of NiTi in acetic acid differs markedly from that of Ti, with a much lower value for the steady-state potential and thinner oxide film thickness at similar anodizing current densities. As such, surface modification of NiTi significantly

enhanced the corrosion resistance of NiTi with reduced Ni concentration on the surface.

It has also been established that in comparison with bare Ti, anodized Ti containing porous TiO_2 oxide layers enabled them to support more stable sputter-coated HA films (Lee et al., 2010). Subsequently, the corrosion resistance of HA-coated/anodized Ti was found to be higher than nonanodized Ti in Hank's solution. Karpagavalli et al. (2007) also reported enhanced corrosion resistance of anodized Ti-6Al-4V containing nanostructured TiO_2 films as compared with nonanodized substrates. Table 1.3.3A.3 summarizes the recent efforts by different research groups to evaluate the effects of anodization on corrosion and surface mechanical properties of Ti alloys.

Coloring Methods for Titanium Alloys

Coloring of Ti is beneficial for a variety of biomedical applications, as many biomedical-grade metal products in the medical industry require color coding to streamline surgical operations (Kobayashi et al., 1992). The characteristic TiO_2 films on Ti substrates exhibit a wide range of colors as the thickness of the oxide layer approaches the wavelength of visible light, which also makes them potential candidate materials to be used in jewelry and decorative applications to enhance the aesthetics (Suzuki, 2000). This occurs due to constructive and destructive interference between light waves reflected from the air–oxide and oxide–substrate interfaces. Several techniques have been used for coloring Ti substrates via this principle, including high-voltage discharge

TABLE 1.3.3A.2 Recently Established Relationships Between the Various Anodization Parameters and Characteristics of TiO₂ Nanotubes Formed on Ti Substrates

Anodization Parameters				Characteristics of Grown TiO ₂ Nanotubes			References
Electrolyte Type	Potential (V)	Time (h)	Temperature (°C)	Tube Inner Diameter (nm)	Wall Thickness (nm)	Length (μm)	
HF/ethylene glycol	30	1	RT	37–41	8–22	–	Yang and Pan (2010)
HF	20	2	–	100	–	–	Demetrescu et al. (2010)
HF/NH ₄ F				60			
HF/H ₃ PO ₄				400			
(NH ₄) ₂ SO ₄ /NaF				120			
NH ₄ F/H ₂ O/ ethylene glycol	60	1.5	10–35	83–105	–	–	Chen et al. (2010)
NH ₄ F/H ₂ O/ ethylene glycol	10–50	0.5	–	40–110	–	0.2–1.0	Lai and Sreekantan (2011)
NH ₄ F/H ₂ O/ ethylene glycol	60	1	10–80	56–110	21–30	6–7	Lai and Sreekantan (2012)
NH ₄ F/H ₂ O/ ethylene glycol	30–70	3	20	20–55	–	1.7–6.2	Sulka et al. (2013)
NH ₄ F/H ₂ O/ ethylene glycol	30	4	–	70–100	–	4	Wang et al. (2014)
NH ₄ F/H ₂ O/ ethylene glycol	5–28	3	RT	40–100	12–25	–	Roguska et al. (2016)
NH ₄ F/H ₂ O/ ethylene glycol	60	0.5	RT	98	52	1.4	Chernozem et al. (2016)
	60	4		155	32	6.2	
	30	0.5		53	50	0.9	
NH ₄ F/H ₂ O	30–70	3	10–40	20–47	–	0.15–2.62	Kapusta-Kołodziej et al. (2017)
NH ₄ F/H ₂ O/ ethylene glycol	28	18	RT	63	12	1	Giorgi et al. (2018)
HF/H ₂ O	20	0.25		84	11	0.2	
		0.80		63	7	0.2	
		0.80		104	16	0.2	
NH ₄ F/H ₂ O/ ethylene glycol	20–40	0.15–1.60	RT	20–67	–	1.0–1.6	Sang et al. (2018)

RT, Room temperature.

methods (Suzuki, 2000), AC polarization (Jerkiewicz et al., 1996), plasma and thermal oxidation (Teng et al., 1998), pulse laser treatment (Lavissee et al., 2007), and anodization (Lausmaa et al., 1990). Among these techniques, anodization has emerged as the most commonly used commercial technique for the coloring of Ti. During anodization, the nature and type of electrolyte, along with the characteristics of oxide films themselves, determine the surface coloration. These colors in turn can be manipulated to measure the

oxide thicknesses on the metallic substrates. It has also been reported that difference in composition in the Ti substrates can give rise to different colors within the same specimen due to the presence of various oxide phases (Langlade et al., 1997). A previous study (Kobayashi et al., 1992) on anodization of Ti in phosphoric acid (H₃PO₄)-based electrolytes has shown that the color of Ti changes to blue tones by applying a voltage of 25 V. Increasing the voltage from 25 V formed thicker oxide films and their progressive transformation into

TABLE 1.3.3A.3 The Effect of Anodization on Corrosion and Surface Mechanical Properties of Ti Alloys

Anodization Parameters			Characteristics of Oxide Films + Secondary Treatment	Corrosion Performance	Mechanical Property Evaluation	References
Electrolyte Type	Potential (V)	Time				
H ₂ SO ₄ /NaF/citric acid	20	15 min–4 h	TiO ₂ NTs anodized on Ti	–	<i>E</i> of TiO ₂ NTs = 36–43 GPa	Crawford et al. (2007)
H ₂ SO ₄	80–110	2 h	NP TiO ₂ on Ti and Ti alloy	Improved corrosion resistance	–	Song et al. (2007)
H ₃ PO ₄ /NaF	20	28 min	TiO ₂ NTs plus electrodeposited HA	–	σ = 7.41 MPa	Wang et al. (2008)
Glycerol/NH ₄ F	30	0.5–4 h	TiO ₂ NTs anodized on Ti	–	σ = 3.5–4.1 MPa	Narayanan et al. (2009)
HF/NH ₄ /H ₂ PO ₄	20	1 h	TiO ₂ NTs plus HA formed by SBF soaking	–	σ = 15 MPa	Feng et al. (2010)
NH ₄ F/H ₂ O/ethylene glycol	20	5 h	Superhydrophobic NP TiO ₂ on Ti	Effective corrosion resistance	–	Zhang et al. (2011b)
NaOH	–	12 min	Anodized Al-free NP oxide on Ti–6Al–7Nb	Enhanced corrosion resistance in SBFs	–	Huang et al. (2013)
H ₂ SO ₄	100	2 min	Anodized NP TiO ₂ on Ti–6Al–4V followed by alkalization, plus electrochemical deposition of HA	Enhanced corrosion performance	–	Benea et al. (2014)
H ₂ SO ₄	100	2 min	NP TiO ₂ plus electrodeposited HA on Ti–6Al–4V	Enhanced tribocorrosion resistance	–	Benea et al. (2015)
Glycerol/NH ₄ F/H ₂ O	10–60	1 h	Heat-treated TiO ₂ NTs plus HA formation via SBF soaking	Improved corrosion resistance	–	Hilario et al. (2017)
H ₃ PO ₄ /H ₂ SO ₄	180	15 min	Anodized NP oxide on Ti	Improved corrosion resistance	No obvious delamination due to fatigue wear at the worn surface	Fazel et al. (2018)

E, Young's modulus; *HA*, hydroxyapatite; *NT*, nanotube; *NP*, nanoporous; σ , bond strength.

a wide range of colors on Ti surfaces. Similarly, relationships between the pulse energy of the laser beams, during laser oxidation, and coloring of oxide films on NiTi substrates can also be identified (Wong et al., 2007). It was found that the surfaces of NiTi remained metallic gray when the pulse energy was kept below 400 mJ, and turned to uniform yellowish and then red–purple colors upon increasing the laser energy to 500 and 600 mJ, respectively. Table 1.3.3A.4 summarizes the recent efforts by different research groups for the coloring of Ti via anodization and laser oxidation.

Compared with coloring of Ti via thermal oxidation techniques, coloring via oxidation of Ti by electrochemical

anodization is advantageous as the oxide films can be more accurately controlled by the applied potentials. Another advantage of using anodization techniques for coloring Ti is that it changes the colors of Ti without significantly altering the metallurgical properties of the substrates. Fig. 1.3.3A.12 shows the typical morphology of Ti substrates after their coloring via anodization and laser oxidation techniques.

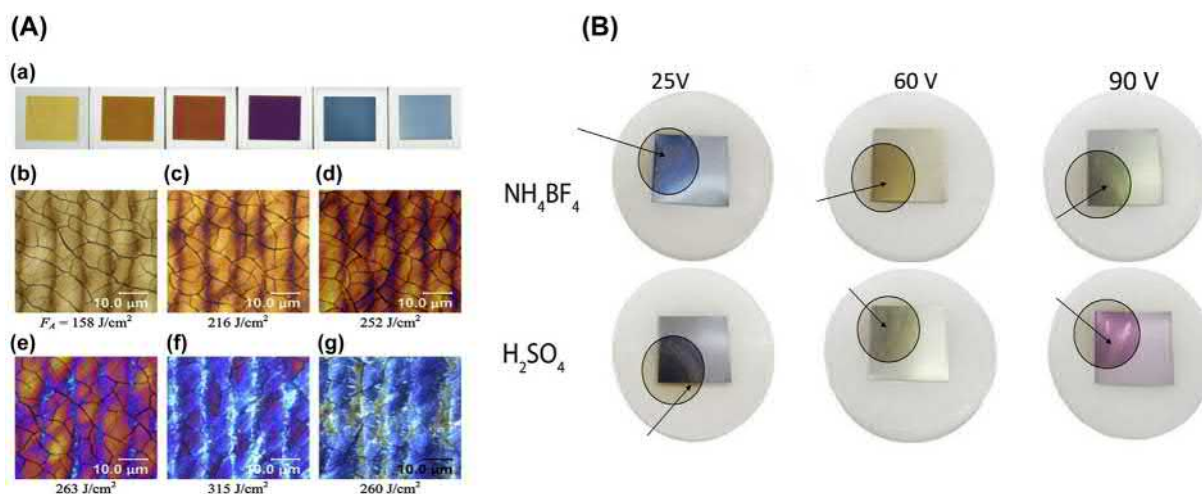
Conclusions

NiTi alloy, which is attractive with its shape memory and superelasticity, contains carcinogenic and allergic nickel

TABLE
1.3.3A.4

Recent Efforts in Coloring of Ti via Anodization and Laser Oxidation Techniques

Substrate	Surface Coloring Technique	Processing Conditions	Colors of Oxide Films on Ti Substrates	References
Ti	Anodization	Electrolyte: acetic acid Voltage: 0–100V	Golden, purple, blue, light blue, yellow, pink, green	Del Pino et al. (2004)
Ti	Laser oxidation	Nd:YAG laser with average laser intensity of 55 kW/cm ²	Golden, Purple, yellow–green, pink–golden, green–pink	
NiTi	Laser oxidation	Nd:YAG laser with average nominal pulse energy = 400–600 mJ	Yellow, red–purple	Wong et al. (2007)
Ti-6Al-4V	Anodization	Electrolyte: H ₃ PO ₄ /H ₂ SO ₄ Voltage: 10–130V	A wide range of color saturation observed, depending on jewel surface finishing	Diamanti et al. (2012)
Ti	Laser oxidation	Yb:glass fiber laser (1062 nm) with average output power 20W, laser scanning speed = 25–200 mm/s	Yellow, orange, red, purple, blue, light blue, silver, black	Antończak et al. (2014)
Ti	Laser oxidation	Yb:glass fiber laser with average output power 20W	Yellow, orange, red, purple, blue, light blue	Antończak et al. (2015)
Ti	Anodization	Electrolyte: NH ₄ NO ₃ Voltage: 80V	Black	Kaneko et al. (2018)



• **Figure 1.3.3A.12** (A) Coloring of Ti via laser oxidation showing an effect on Ti substrate upon their exposure to different values of laser fluence: (a) photos of individual samples exposed to different laser fluences, (b–g) microscope images of oxide layers on the surface of Ti for various values of accumulated fluence (in the same order as in point (a)). (B) Coloring of Ti via anodization techniques under different anodizing conditions. ((A) Reprinted from Antończak, A.J., Skowroński, Ł., Trzcinski, M., Kinzhybalo, V.V., Łazarek, Ł.K., Abramski, K.M., 2015. Laser-induced oxidation of titanium substrate: analysis of the physicochemical structure of the surface and sub-surface layers. *Appl. Surf. Sci.* 325, 217–226, Copyright (2015), with permission from Elsevier. (B) Reprinted from Diamanti, M.V., Pozzi, P., Randone, F., Del Curto, B., Pedferri, M., 2016. Robust anodic colouring of titanium: effect of electrolyte and colour durability. *Mater. Des.* 90, 1085–1091, Copyright (2016), with permission from Elsevier.)

elements, thus making it necessary to design and manufacture nickel-free Ti alloys. In this regard, it is necessary to design and manufacture Ti alloys possessing mechanical properties close to those of NiTi alloys.

This chapter aimed to inform readers about the strategies in designing new Ti alloys for orthopedic implant

applications. The first and most important step in a design process is to start designing with the biocompatible alloying elements. Following this step, designers should target not only lower elastic modulus, but also higher tensile strength, fatigue strength, wear resistance, corrosion resistance, and surface bioactivity.

SLS, SLM, EBM, and LENS methods are the most effective methods for the production of biomedical implants with complex shapes. On the other hand, the ability to achieve a higher mechanical strength in powder metallurgical methods depends on minimizing the pores originating from the nature of the PM method.

Ti alloys exhibit higher corrosion resistance and lower elastic modulus than many other metallic biomaterials (e.g., austenitic stainless steel and Co-Cr alloys). Although the use of Ti and its alloys as a biomaterial exhibits many advantages over other metallic alloys, chemical bonding to bone tissue, biochemical interaction, and incompatibility between the elastic modulus of bone and the Ti implant material are the three most challenging problems to be solved for the use of Ti alloys as orthopedic implant materials. The elastic modulus of β -type Ti alloys is closer to the elastic modulus of cortical bone tissue than the elastic moduli of other metallic alloys, thus making β -type Ti alloys a more suitable implant material in terms of minimizing the stress-shielding phenomenon. It is of great importance to use implant materials that match the mechanical properties of the target bone tissue. The high fatigue strength of the implant materials subject to cyclic loading is crucial for long-term, problem-free use. With the increase in tensile strength, fatigue strength is also improved. β -type Ti-alloys have a lower elastic modulus than $\alpha + \beta$ -type Ti alloys, but also display lower mechanical strengths.

The mechanical strength of Ti alloys can be increased via solid-solution strengthening using oxygen or other interstitial elements. It is advisable, however, to add small amounts of interstitial elements to minimize the increase in elastic modulus, while still providing high mechanical strength. Hardening mechanisms (e.g., precipitation hardening and work hardening) are also effective in increasing the mechanical strength. It is worth noting that phases formed during aging and cold-working processes may cause an increase in elastic modulus.

Alkaline heat treatment, acidic processes, anodic oxidation, hydrogen peroxide, plasma spray, sandblasting, and sol-gel are used as methods for increasing the surface bioactivity of Ti and its alloys. The anodic oxidation method for increasing surface bioactivity is widely used because of its effective role in enhancing surface bioactivity in addition to cost effectiveness and ease of application.

Acknowledgments

The authors acknowledge the financial support for this research by the National Health and Medical Research Council (NHMRC), Australia, through grant GNT1087290; and the Australian Research Council (ARC) through the discovery grant DP170102557. YL is also supported through an ARC Future Fellowship (FT160100252). Part of this chapter was originally published in the Ph.D. thesis titled “Investigation of mechanical properties of Ti-alloys developed for bone-tissue engineering applications” (in Turkish),

Ege University, Turkey (2015) by SO. SO would like to acknowledge the Council of Higher Education (CoHE) of Turkey for a Ph.D. scholarship.

The authors declare that there are no conflicts of interest.

References

- Abdel-Hady Gepreel, M., Niinomi, M., 2013. Biocompatibility of Ti-alloys for long-term implantation. *J. Mech. Behav. Biomed. Mater.* 20, 407–415.
- Ahn, M.K., Jo, I.H., Koh, Y.H., Kim, H.E., 2014. Production of highly porous titanium (Ti) scaffolds by vacuum-assisted foaming of titanium hydride (TiH₂) suspension. *Mater. Lett.* 120, 228–231.
- Akahori, T., Niinomi, M., Fukunaga, K.I., 2000. An investigation of the effect of fatigue deformation on the residual mechanical properties of Ti-6Al-4V ELI. *Metall. Mater. Trans. A-Phys. Metall. Mater. Sci.* 31 (8), 1937–1948.
- Allam, N.K., Alamgir, F., El-Sayed, M.A., 2010. Enhanced photoassisted water electrolysis using vertically oriented anodically fabricated Ti-Nb-Zr-O mixed oxide nanotube arrays. *ACS Nano* 4 (10), 5819–5826.
- Anselme, K., 2011. Biomaterials and interface with bone. *Osteoporos. Int.* 22 (6), 2037–2042.
- Antończak, A.J., Skowroński, Ł., Trzcinski, M., Kinzhybalo, V.V., Łazarek, Ł.K., Abramski, K.M., 2015. Laser-induced oxidation of titanium substrate: analysis of the physicochemical structure of the surface and sub-surface layers. *Appl. Surf. Sci.* 325, 217–226.
- Antończak, A.J., Stępak, B., Koziół, P.E., Abramski, K.M., 2014. The influence of process parameters on the laser-induced coloring of titanium. *Appl. Phys. A* 115 (3), 1003–1013.
- Asby, M.F., 1983. The mechanical-properties of cellular solids. *Metall. Trans. A-Phys. Metall. Mater. Sci.* 14 (9), 1755–1769.
- Asik, E.E., Bor, S., 2015. Fatigue behavior of Ti-6Al-4V foams processed by magnesium space holder technique. *Mater. Sci. Eng. A* 621, 157–165.
- Ataee, A., Li, Y., Fraser, D., Song, G., Wen, C., 2018. Anisotropic Ti-6Al-4V gyroid scaffolds manufactured by electron beam melting (EBM) for bone implant applications. *Mater. Des.* 137, 345–354.
- Bai, L., Yang, Y., Mendhi, J., Du, Z., Hao, R., Hang, R., Yao, X., Huang, N., Tang, B., Xiao, Y., 2018. The effects of TiO₂ nanotube arrays with different diameters on macrophage/endothelial cell response and ex vivo hemocompatibility. *J. Mater. Chem. B* 6, 6322–6333.
- Bansiddhi, A., Dunand, D.C., 2007. Shape-memory NiTi foams produced by solid-state replication with NaF. *Intermetallics* 15 (12), 1612–1622.
- Bauer, S., Park, J., Faltenbacher, J., Berger, S., von der Mark, K., Schmuki, P., 2009. Size selective behavior of mesenchymal stem cells on ZrO₂ and TiO₂ nanotube arrays. *Integr. Biol.* 1 (8–9), 525–532.
- Benea, L., Danaila, E., Ponthiaux, P., 2015. Effect of titania anodic formation and hydroxyapatite electrodeposition on electrochemical behaviour of Ti-6Al-4V alloy under fretting conditions for biomedical applications. *Corros. Sci.* 91, 262–271.
- Benea, L., Mardare-Danaila, E., Mardare, M., Celis, J.-P., 2014. Preparation of titanium oxide and hydroxyapatite on Ti-6Al-4V alloy surface and electrochemical behaviour in bio-simulated fluid solution. *Corros. Sci.* 80, 331–338.

- Beyersmann, D., Hartwig, A., 2008. Carcinogenic metal compounds: recent insight into molecular and cellular mechanisms. *Arch. Toxicol.* 82 (8), 493–512.
- Bhattarai, S.R., Khalil, K.A.R., Dewidar, M., Hwang, P.H., Yi, H.K., Kim, H.Y., 2008. Novel production method and in-vitro cell compatibility of porous Ti-6Al-4V alloy disk for hard tissue engineering. *J. Biomed. Mater. Res. A* 86A (2), 289–299.
- Biant, L.C., Bruce, W.J.M., van der Wall, H., Walsh, W.R., 2010. Infection or allergy in the painful metal-on-metal total hip arthroplasty? *J. Arthroplast.* 25 (2), 334.e311–334.e316.
- Biesiekierski, A., Lin, J., Munir, K., Ozan, S., Li, Y., Wen, C., 2018. An investigation of the mechanical and microstructural evolution of a TiNbZr alloy with varied ageing time. *Sci. Rep.* 8 (1), 5737.
- Biesiekierski, A., Wang, J., Gepreel, M.A., Wen, C., 2012a. A new look at biomedical Ti-based shape memory alloys. *Acta Biomater.* 8 (5), 1661–1669.
- Biesiekierski, A., Wang, J., Wen, C., 2012b. A brief review of biomedical shape memory alloys by powder metallurgy. *Key Eng. Mater.* 520, 195–200.
- Boyer, R., Welsch, G., Collings, E.W. (Eds.), 1994. *Materials Properties Handbook: Titanium Alloys*. ASM International, Materials Park, OH, USA.
- Bram, M., Stiller, C., Buchkremer, H.P., Stover, D., Baur, H., 2000. High-porosity titanium, stainless steel, and superalloy parts. *Adv. Eng. Mater.* 2 (4), 196–199.
- Brunette, D.M., Tengvall, P., Textor, M., Thomsen, P., 2012. *Titanium in Medicine: Material Science, Surface Science, Engineering, Biological Responses and Medical Applications*. Springer Science & Business Media.
- Budinski, K.G., 1991. Tribological properties of titanium-alloys. *Wear* 151 (2), 203–217.
- Buehler, W.J., Gilfrich, J., Wiley, R., 1963. Effect of low-temperature phase changes on the mechanical properties of alloys near composition TiNi. *J. Appl. Phys.* 34, 1475–1477.
- Buttaro, M.A., Mayor, M.B., Van Citters, D., Piccaluga, F., 2007. Fatigue fracture of a proximally modular, distally tapered fluted implant with diaphyseal fixation. *J. Arthroplast.* 22 (5), 780–783.
- Candel, J.J., Amigo, V., Ramos, J.A., Busquets, D., 2010. Sliding wear resistance of TiCp reinforced titanium composite coating produced by laser cladding. *Surf. Coat. Technol.* 204 (20), 3161–3166.
- Carlsson, L., Röstlund, T., Albrektsson, B., Albrektsson, T., Bränemark, P.-I., 1986. Osseointegration of titanium implants. *Acta Orthop.* 57 (4), 285–289.
- Chen, C.-S., Chen, W.-J., Cheng, C.-K., Jao, S.-H.E., Chueh, S.-C., Wang, C.-C., 2005. Failure analysis of broken pedicle screws on spinal instrumentation. *Med. Eng. Phys.* 27 (6), 487–496.
- Chen, J., Lin, J., Chen, X., 2010. Self-assembled TiO₂ nanotube arrays with U-shaped profile by controlling anodization temperature. *J. Nanomater.* 753253.
- Chen, S.Y., Huang, J.C., Pan, C.T., Lin, C.H., Yang, T.L., Huang, Y.S., Ou, C.H., Chen, L.Y., Lin, D.Y., Lin, H.K., Li, T.H., Jang, J.S.C., Yang, C.C., 2017. Microstructure and mechanical properties of open-cell porous Ti-6Al-4V fabricated by selective laser melting. *J. Alloy. Comp.* 713, 248–254.
- Cheng, Z., Zhang, F., He, F., Zhang, L., Guo, C., Zhao, S., Yang, G., 2010. Osseointegration of titanium implants with a roughened surface containing hydride ion in a rabbit model. *Oral Surg. Oral Med. Oral Pathol. Oral Radiol. Endod.* 110 (1), e5–e12.
- Chernozem, R.V., Surmeneva, M.A., Surmenev, R.A., 2016. Influence of anodization time and voltage on the parameters of TiO₂ nanotubes. *IOP Conf. Ser. Mater. Sci. Eng.* 116, 012025.
- Cho, K., Niinomi, M., Nakai, M., Hieda, J., Kanekiyo, R., 2013. Improvement of tensile and fatigue properties of beta-titanium alloy while maintaining low young's modulus through grain refinement and oxygen addition. *Mater. Trans.* 54 (10), 2000–2006.
- Crawford, G., Chawla, N., 2009. Porous hierarchical TiO₂ nanostructures: processing and microstructure relationships. *Acta Mater.* 57 (3), 854–867.
- Crawford, G., Chawla, N., Ringnald, J., 2009. Processing and microstructure characterization of a novel porous hierarchical TiO₂ structure. *J. Mater. Res.* 24 (5), 1683–1687.
- Crawford, G., Chawla, N., Das, K., Bose, S., Bandyopadhyay, A., 2007. Microstructure and deformation behavior of biocompatible TiO₂ nanotubes on titanium substrate. *Acta Biomater.* 3 (3), 359–367.
- Cui, C.Y., Ping, D.H., 2009. Microstructural evolution and ductility improvement of a Ti-30Nb alloy with Pd addition. *J. Alloy. Comp.* 471 (1–2), 248–252.
- Cui, C., Hu, B., Zhao, L., Liu, S., 2011. Titanium alloy production technology, market prospects and industry development. *Mater. Des.* 32 (3), 1684–1691.
- Cui, Y., Li, Y., Luo, K., Xu, H., 2010. Microstructure and shape memory effect of Ti-20Zr-10Nb alloy. *Mater. Sci. Eng. A* 527 (3), 652–656.
- de Vasconcellos, L.M.R., Leite, D.d.O., Nascimento, F.O., de Vasconcellos, L.-G.-O., Graca, M.-L.-d. A., Carvalho, Y.-R., Cairo, C.-A.-A., 2010. Porous titanium for biomedical applications: an experimental study on rabbits. *Med. Oral Patol. Oral Cirugía Bucal* 15 (2), E407–E412.
- Del Pino, A.P., Fernández-Pradas, J., Serra, P., Morenza, J., 2004. Coloring of titanium through laser oxidation: comparative study with anodizing. *Surf. Coat. Technol.* 187 (1), 106–112.
- Demetrescu, I., Ionita, D., Pirvu, C., Portan, D., 2010. Present and future trends in TiO₂ nanotubes elaboration, characterization and potential applications. *Mol. Cryst. Liq. Cryst.* 521 (1), 195–203.
- Dewidar, M.M., Yoon, H.C., Lim, J.K., 2006. Mechanical properties of metals for biomedical applications using powder metallurgy process: a review. *Met. Mater. Int.* 12 (3), 193–206.
- Dewidar, M., Mohamed, H.F., Lim, J.-K., 2008. A new approach for manufacturing a high porosity Ti-6Al-4V scaffolds for biomedical applications. *J. Mater. Sci. Technol.* 24 (6), 931–935.
- Diamanti, M.V., Del Curto, B., Masconale, V., Passaro, C., Pedferri, M., 2012. Anodic coloring of titanium and its alloy for jewels production. *Color Res. Appl.* 37 (5), 384–390.
- Diamanti, M.V., Pozzi, P., Randone, F., Del Curto, B., Pedferri, M., 2016. Robust anodic colouring of titanium: effect of electrolyte and colour durability. *Mater. Des.* 90, 1085–1091.
- Domínguez-Trujillo, C., Peón, E., Chicardi, E., Pérez, H., Rodríguez-Ortiz, J.A., Pavón, J.J., García-Couce, J., Galván, J.C., García-Moreno, F., Torres, Y., 2018. Sol-gel deposition of hydroxyapatite coatings on porous titanium for biomedical applications. *Surf. Coat. Technol.* 333, 158–162.
- Donachie Jr., M.J., 2000. Chap 7 – powder metallurgy. In: *Titanium: A Technical Guide*, second ed. ASM International, Materials Park, OH, USA.
- Ducheyne, P., Willems, G., Martens, M., Helsen, J., 1984. In vivo metal-ion release from porous titanium-fiber material. *J. Biomed. Mater. Res.* 18 (3), 293–308.
- Eldesouky, I., Harrysson, O., West, H., Elhofy, H., 2017. Electron beam melted scaffolds for orthopedic applications. *Addit. Manuf.* 17, 169–175.
- Esen, Z., Bor, Ş., 2007. Processing of titanium foams using magnesium spacer particles. *Scr. Mater.* 56 (5), 341–344.

- Fazel, M., Salimijazi, H.R., Shamanian, M., 2018. Improvement of corrosion and tribocorrosion behavior of pure titanium by sub-zero anodic spark oxidation. *ACS Appl. Mater. Interfaces* 10 (17), 15281–15287.
- Feng, B., Chu, X., Chen, J., Wang, J., Lu, X., Weng, J., 2010. Hydroxyapatite coating on titanium surface with titania nanotube layer and its bond strength to substrate. *J. Porous Mater.* 17 (4), 453–458.
- Flaten, T.P., 2001. Aluminium as a risk factor in Alzheimer's disease, with emphasis on drinking water. *Brain Res. Bull.* 55 (2), 187–196.
- Frenkel, S.R., Jaffe, W.L., Dimaano, F., Iesaka, K., Hua, T., 2004. Bone response to a novel highly porous surface in a canine implantable chamber. *J. Biomed. Mater. Res. B Appl. Biomater.* 71B (2), 387–391.
- Fujibayashi, S., Nakamura, T., 2004. Current status of bioactive coatings in Japan. In: *Fifteen Years of Clinical Experience with Hydroxyapatite Coatings in Joint Arthroplasty*. Springer, Paris, pp. 115–124.
- Gao, X., He, R.-X., Yan, S.-G., Wu, L.-D., 2011. Dermatitis associated with chromium following total knee arthroplasty. *J. Arthroplast.* 26 (4), 665.e613–665.e616.
- Geetha, M., Singh, A.K., Asokamani, R., Gogia, A.K., 2009. Ti based biomaterials, the ultimate choice for orthopaedic implants – a review. *Prog. Mater. Sci.* 54 (3), 397–425.
- Geng, F., Niinomi, M., Nakai, M., 2011. Observation of yielding and strain hardening in a titanium alloy having high oxygen content. *Mater. Sci. Eng. A* 528 (16–17), 5435–5445.
- Giorgi, L., Dikonimos, T., Giorgi, R., Buonocore, F., Faggio, G., Messina, G., Lisi, N., 2018. Electrochemical synthesis of self-organized TiO₂ crystalline nanotubes without annealing. *Nanotechnology* 29 (9), 095604.
- Granchi, D., Cenni, E., Tigani, D., Trisolino, G., Baldini, N., Giunti, A., 2008. Sensitivity to implant materials in patients with total knee arthroplasties. *Biomaterials* 29 (10), 1494–1500.
- Hanawa, T., 2012. Research and development of metals for medical devices based on clinical needs. *Sci. Technol. Adv. Mater.* 13 (6), 064102.
- Hao, Y.L., Li, S.J., Sun, S.Y., Zheng, C.Y., Yang, R., 2007. Elastic deformation behaviour of Ti-24Nb-4Zr-7.9Sn for biomedical applications. *Acta Biomater.* 3 (2), 277–286.
- Harun, W.S.W., Kamariah, M.S.I.N., Muhamad, N., Ghani, S.A.C., Ahmad, F., Mohamed, Z., 2018. A review of powder additive manufacturing processes for metallic biomaterials. *Powder Technol.* 327, 128–151.
- Heinl, P., Rottmair, A., Koerner, C., Singer, R.F., 2007. Cellular titanium by selective electron beam melting. *Adv. Eng. Mater.* 9 (5), 360–364.
- Helth, A., Pilz, S., Kirsten, T., Giebler, L., Freudenberger, J., Calin, M., Eckert, J., Gebert, A., 2017. Effect of thermomechanical processing on the mechanical biofunctionality of a low modulus Ti-40Nb alloy. *J. Mech. Behav. Biomed. Mater.* 65, 137–150.
- Hilario, F., Roche, V., Nogueira, R.P., Junior, A.M.J., 2017. Influence of morphology and crystalline structure of TiO₂ nanotubes on their electrochemical properties and apatite-forming ability. *Electrochim. Acta* 245, 337–349.
- Horn, T.J., Harrysson, O.L.A., Marcellin-Little, D.J., West, H.A., Lascelles, B.D.X., Aman, R., 2014. Flexural properties of Ti6Al4V rhombic dodecahedron open cellular structures fabricated with electron beam melting. *Addit. Manuf.* 1–4, 2–11.
- Huang, H.H., Wu, C.P., Sun, Y.S., Lee, T.H., 2013. Improvements in the corrosion resistance and biocompatibility of biomedical Ti-6Al-7Nb alloy using an electrochemical anodization treatment. *Thin Solid Films* 528, 157–162.
- Huiskes, R., Weinans, H., Vanrietbergen, B., 1992. The relationship between stress shielding and bone-resorption around total hip stems and the effects of flexible materials. *Clin. Orthop. Relat. Res.* (274), 124–134.
- Jacobs, J.J., Gilbert, J.L., Urban, R.M., 1998. Corrosion of metal orthopaedic implants. *J. Bone Jt. Surg.* 80 (2), 268–282.
- Jamshidinia, M., Wang, L., Tong, W., Kovacevic, R., 2014. The bio-compatible dental implant designed by using non-stochastic porosity produced by Electron Beam Melting® (EBM). *J. Mater. Process. Technol.* 214 (8), 1728–1739.
- Jamshidinia, M., Wang, L., Tong, W., Ajlouni, R., Kovacevic, R., 2015. Fatigue properties of a dental implant produced by electron beam melting® (EBM). *J. Mater. Process. Technol.* 226, 255–263.
- Jerkiewicz, G., Strzelecki, H., Wieckowski, A., 1996. A new procedure of formation of multicolor passive films on titanium: compositional depth profile analysis. *Langmuir* 12 (4), 1005–1010.
- Jha, H., Hahn, R., Schmuki, P., 2010. Ultrafast oxide nanotube formation on TiNb, TiZr and TiTa alloys by rapid breakdown anodization. *Electrochim. Acta* 55 (28), 8883–8887.
- Ji, X., Emura, S., Liu, T., Suzuta, K., Min, X., Tsuchiya, K., 2018. Effect of oxygen addition on microstructures and mechanical properties of Ti-7.5Mo alloy. *J. Alloy. Comp.* 737, 221–229.
- Kaneko, M., Tokuno, K., Yamagishi, K., Wada, T., Hasegawa, T., 2018. Characterization of surface oxide layers on black-colored titanium. *J. Surf. Eng. Mater. Adv. Technol.* 8 (4), 71–82.
- Kapusta-Kołodziej, J., Syrek, K., Pawlik, A., Jarosz, M., Tynkevych, O., Sulka, G.D., 2017. Effects of anodizing potential and temperature on the growth of anodic TiO₂ and its photoelectrochemical properties. *Appl. Surf. Sci.* 396, 1119–1129.
- Karpagavalli, R., Zhou, A., Chellamuthu, P., Nguyen, K., 2007. Corrosion behavior and biocompatibility of nanostructured TiO₂ film on Ti6Al4V. *J. Biomed. Mater. Res. A* 83 (4), 1087–1095.
- Karthege, M., Rajendran, N., 2010. Hydrogen peroxide treatment on Ti-6Al-4V alloy: a promising surface modification technique for orthopaedic application. *Appl. Surf. Sci.* 256 (7), 2176–2183.
- Kawate, K., Ohneda, Y., Ohmura, T., Yajima, H., Sugimoto, K., Takakura, Y., 2009. Computed tomography-based custom-made stem for dysplastic hips in Japanese patients. *J. Arthroplast.* 24 (1), 65–70.
- Kim, H.Y., Kim, J.I., Inamura, T., Hosoda, H., Miyazaki, S., 2006. Effect of thermo-mechanical treatment on mechanical properties and shape memory behavior of Ti-(26–28) at.% Nb alloys. *Mater. Sci. Eng. A* 438, 839–843.
- Kim, W.G., Ahn, K.H., Jeong, Y.H., Vang, M.S., Choe, H.C., 2011. Surface characteristics and cell proliferation of mechanical sandblasted Ti-30Ta-xNb surface. *Proc. Eng.* 10, 2399–2404.
- Kobayashi, K., Shimizu, K., Yoshioka, H., Corp, Y.K.K., 1992. Process for coloring titanium and its alloys. *U.S. Patent* 5 (160), 599.
- Kuroda, D., Niinomi, M., Morinaga, M., Kato, Y., Yashiro, T., 1998. Design and mechanical properties of new beta type titanium alloys for implant materials. *Mater. Sci. Eng. A* 243 (1–2), 244–249.
- Kurtz, S., Ong, K., Lau, E., Mowat, F., Halpern, M., 2007. Projections of primary and revision hip and knee arthroplasty in the United States from 2005 to 2030. *J. Bone Joint Surg. Am. Vol.* 89A (4), 780–785.
- Lai, C.W., Sreekantan, S., 2011. Effect of applied potential on the formation of self-organized TiO₂ nanotube arrays and its photoelectrochemical response. *J. Nanomater.* 2011, 142463.
- Lai, C.W., Sreekantan, S., 2012. Photoelectrochemical performance of smooth TiO₂ nanotube arrays: effect of anodization temperature and cleaning methods. *Int. J. Photoenergy* 2012, 356943.

- Langlade, C., Vannes, A., Piccinini, P., Baldi, G., 1997. Characterisation and applications of laser treated titanium and titanium alloys. In: Sudarshan, T.S., Jeandin, M., Kho, K.A. (Eds.), *Surface Modification Technologies XI*, pp. 634–648.
- Lausmaa, J., Kasemo, B., Mattsson, H., Odellius, H., 1990. Multi-technique surface characterization of oxide films on electropolished and anodically oxidized titanium. *Appl. Surf. Sci.* 45 (3), 189–200.
- Lavisse, L., Jouvard, J., Imhoff, L., Heintz, O., Korntheuer, J., Langlade, C., Bourgeois, S., de Lucas, M.M., 2007. Pulsed laser growth and characterization of thin films on titanium substrates. *Appl. Surf. Sci.* 253 (19), 8226–8230.
- Lee, K., Choe, H.-C., Kim, B.-H., Ko, Y.-M., 2010. The biocompatibility of HA thin films deposition on anodized titanium alloys. *Surf. Coat. Technol.* 205, S267–S270.
- Li, Q., Niinomi, M., Nakai, M., Cui, Z., Zhu, S., Yang, X., 2012. Effect of Zr on super-elasticity and mechanical properties of Ti–24at% Nb–(0, 2, 4)at% Zr alloy subjected to aging treatment. *Mater. Sci. Eng. A* 536, 197–206.
- Li, X., Wang, C., Zhang, W., Li, Y., 2009a. Fabrication and characterization of porous Ti6Al4V parts for biomedical applications using electron beam melting process. *Mater. Lett.* 63 (3–4), 403–405.
- Li, Y., Xiong, J., Wong, C.S., Hodgson, P.D., Wen, C.e., 2009b. Ti6Ta4Sn alloy and subsequent scaffolding for bone tissue engineering. *Tissue Eng. A* 15 (10), 3151–3159.
- Lima, P.D., Vasconcellos, M.C., Montenegro, R.C., Bahia, M.O., Costa, E.T., Antunes, L.M., Burbano, R.R., 2011. Genotoxic effects of aluminum, iron and manganese in human cells and experimental systems: a review of the literature. *Hum. Exp. Toxicol.* 30 (10), 1435–1444.
- Liu, H., Niinomi, M., Nakai, M., Cho, K., 2015. β -Type titanium alloys for spinal fixation surgery with high Young's modulus variability and good mechanical properties. *Acta Biomater.* 24, 361–369.
- Liu, P., Hao, Y., Zhao, Y., Yuan, Z., Ding, Y., Cai, K., 2017. Surface modification of titanium substrates for enhanced osteogenetic and antibacterial properties. *Colloids Surfaces B Biointerfaces* 160, 110–116.
- Liu, Q., Leu, M.C., Schmitt, S.M., 2006. Rapid prototyping in dentistry: technology and application. *Int. J. Adv. Manuf. Technol.* 29 (3), 317–335.
- Liu, X.Y., Chu, P.K., Ding, C.X., 2004. Surface modification of titanium, titanium alloys, and related materials for biomedical applications. *Mater. Sci. Eng. R Rep.* 47 (3–4), 49–121.
- Long, M., Rack, H.J., 1998. Titanium alloys in total joint replacement – a materials science perspective. *Biomaterials* 19 (18), 1621–1639.
- Mansourighasri, A., Muhamad, N., Sulong, A.B., 2012. Processing titanium foams using tapioca starch as a space holder. *J. Mater. Process. Technol.* 212 (1), 83–89.
- Martz, E.O., Goel, V.K., Pope, M.H., Park, J.B., 1997. Materials and design of spinal implants – a review. *J. Biomed. Mater. Res.* 38 (3), 267–288.
- Matsumoto, H., Watanabe, S., Hanada, S., 2005. Beta TiNbSn alloys with low Young's modulus and high strength. *Mater. Trans.* 46, 1070–1078.
- Mediaswanti, K., Truong, V.K., Hasan, J., Ivanova, E.P., Malherbe, F., et al., 2012. Influence of titanium alloying element substrata on bacterial adhesion. *Adv. Mater. Res.* 535–537, 992–995.
- Michalska-Domańska, M., Nyga, P., Czerwiński, M., 2018. Ethanol-based electrolyte for nanotubular anodic TiO₂ formation. *Corros. Sci.* 134, 99–102.
- Minagar, S., Berndt, C.C., Wang, J., Ivanova, E., Wen, C., 2012. A review of the application of anodization for the fabrication of nanotubes on metal implant surfaces. *Acta Biomater.* 8 (8), 2875–2888.
- Minagar, S., Wang, J., Berndt, C.C., Ivanova, E.P., Wen, C., 2013. Cell response of anodized nanotubes on titanium and titanium alloys. *J. Biomed. Mater. Res. A* 101 (9), 2726–2739.
- Miyazaki, S., Kim, H.Y., Hosoda, H., 2006. Development and characterization of Ni-free Ti-base shape memory and superelastic alloys. *Mater. Sci. Eng. A* 438–440, 18–24.
- Molinari, A., Straffellini, G., Tesi, B., Bacci, T., 1997. Dry sliding wear mechanisms of the Ti6Al4V alloy. *Wear* 208 (1–2), 105–112.
- Morgan, N., 2004. Medical shape memory alloy applications—the market and its products. *Mater. Sci. Eng. A* 378 (1–2), 16–23.
- Morita, A., Fukui, H., Tadano, H., Hayashi, S., Hasegawa, J., Niinomi, M., 2000. Alloying titanium and tantalum by cold crucible levitation melting (CCLM) furnace. *Mater. Sci. Eng. A* 280 (1), 208–213.
- Moxson, V.S., Senkov, O.N., Froes, F.H., 2000. Innovations in titanium powder processing. *JOM* 52 (5), 24–26.
- Moxson, V.S., Froes, F.H., 2001. Fabricating sports equipment components via powder metallurgy. *JOM* 53 (4), 39–41.
- Munir, K.S., Li, Y., Wen, C., 2017. 1 – metallic scaffolds manufactured by selective laser melting for biomedical applications. In: Wen, C. (Ed.), *Metallic Foam Bone*. Woodhead Publishing, pp. 1–23.
- Narayanan, R., Kwon, T.-Y., Kim, K.-H., 2009. TiO₂ nanotubes from stirred glycerol/NH₄F electrolyte: roughness, wetting behavior and adhesion for implant applications. *Mater. Chem. Phys.* 117 (2–3), 460–464.
- Niinomi, M., 1998. Mechanical properties of biomedical titanium alloys. *Mater. Sci. Eng. A* 243 (1–2), 231–236.
- Niinomi, M., 2002. Recent metallic materials for biomedical applications. *Metall. Mater. Trans. A-Phys. Metall. Mater. Sci.* 33 (3), 477–486.
- Niinomi, M., 2008. Mechanical biocompatibilities of titanium alloys for biomedical applications. *J. Mech. Behav. Biomed. Mater.* 1 (1), 30–42.
- Niinomi, M., Nakai, M., 2011. Titanium-based biomaterials for preventing stress shielding between implant devices and bone. *Int. J. Biomater.* 2011, 836587.
- Nouri, A., Hodgson, P.D., Wen, C., 2011. Effect of ball-milling time on the structural characteristics of biomedical porous Ti–Sn–Nb alloy. *Mater. Sci. Eng. C* 31 (5), 921–928.
- Nouri, A., Hodgson, P.D., Wen, C.E., 2010. Biomimetic porous titanium scaffolds for orthopedic and dental applications. In: Mukherjee, A. (Ed.), *Biomimetics Learning from Nature*. InTech, pp. 415–450.
- Okazaki, Y., 2012. Comparison of fatigue properties and fatigue crack growth rates of various implantable metals. *Materials* 5 (12), 2981–3005.
- Okazaki, Y., Gotoh, E., 2005. Comparison of metal release from various metallic biomaterials in vitro. *Biomaterials* 26 (1), 11–21.
- Okazaki, Y., Tateishi, T., Ito, Y., 1997. Corrosion resistance of implant alloys in pseudo physiological solution and role of alloying elements in passive films. *Mater. Trans., JIM* 38 (1), 78–84.
- Otsuka, K., Ren, X., 2005. Physical metallurgy of Ti–Ni-based shape memory alloys. *Prog. Mater. Sci.* 50, 511–678.
- Ouchi, C., Iizumi, H., Mitao, S., 1998. Effects of ultra-high purification and addition of interstitial elements on properties of pure titanium and titanium alloy. *Mater. Sci. Eng. A* 243 (1), 186–195.
- Ozaki, T., Matsumoto, H., Watanabe, S., Hanada, S., 2004. Beta Ti alloys with low Young's modulus. *Mater. Trans.* 45 (8), 2776–2779.

- Ozan, S., Ipek, R., 2012. Production of titanium alloy foams by space holder technique. In: P/M Method: A Review. Paper Presented at the 2nd International Scientific Conference on Engineering "Manufacturing and Advanced Technologies" MAT 2012 Antalya.
- Ozan, S., Lin, J., Li, Y., Ipek, R., Wen, C., 2015. Development of Ti-Nb-Zr alloys with high elastic admissible strain for temporary orthopedic devices. *Acta Biomater* 20, 176–187.
- Ozan, S., Li, Y., Lin, J., Zhang, Y., Jiang, H., Wen, C., 2018a. Microstructural evolution and its influence on the mechanical properties of a thermomechanically processed β Ti-32Zr-30Nb alloy. *Mater. Sci. Eng. A* 719, 112–123. <https://doi.org/10.1016/j.msea.2018.02.034>.
- Ozan, S., Lin, J., Li, Y., Zhang, Y., Munir, K., Jiang, H., Wen, C., 2018b. Deformation mechanism and mechanical properties of a thermomechanically processed β Ti-28Nb-35.4Zr alloy. *J. Mech. Behav. Biomed. Mater.* 78, 224–234. <https://doi.org/10.1016/j.jmbbm.2017.11.025>.
- Ozkan, S., Mazare, A., Schmuki, P., 2018. Critical parameters and factors in the formation of spaced TiO₂ nanotubes by self-organizing anodization. *Electrochim. Acta* 268, 435–447.
- Pang, J.C., Li, S.X., Wang, Z.G., Zhang, Z.F., 2014. Relations between fatigue strength and other mechanical properties of metallic materials. *Fatigue Fract. Eng. Mater. Struct.* 37, 958–976.
- Peter, W.H., Chen, W., Yamamoto, Y., Dehoff, R., Muth, T., et al., 2012. Current status of Ti PM: progress, opportunities and challenges. *Key Eng. Mater.* 520, 1–7.
- Peters, M., Kumpfert, J., Ward, C.H., Leyens, C., 2003. Titanium alloys for aerospace applications. *Adv. Eng. Mater.* 5 (6), 419–427.
- Qian, M., Yang, Y.F., Yan, M., Luo, S.D., 2012. Design of low cost high performance powder metallurgy titanium alloys: some basic considerations. *Key Eng. Mater.* 520, 24–29.
- Rack, H.J., Qazi, J.I., 2006. Titanium alloys for biomedical applications. *Mater. Sci. Eng. C* 26 (8), 1269–1277.
- Ramos, A., Simões, J.A., 2009. In vitro fatigue crack analysis of the Lubinus SPII cemented hip stem. *Eng. Fail. Anal.* 16 (4), 1294–1302.
- Rao, X., Chu, C.L., Zheng, Y.Y., 2014. Phase composition, microstructure, and mechanical properties of porous Ti-Nb-Zr alloys prepared by a two-step foaming powder metallurgy method. *J. Mech. Behav. Biomed. Mater.* 34, 27–36.
- Rivard, J., Brailovski, V., Dubinskiy, S., Prokoshkin, S., 2014. Fabrication, morphology and mechanical properties of Ti and metastable Ti-based alloy foams for biomedical applications. *Mater. Sci. Eng. C Mater. Biol. Appl.* 45, 421–433.
- Rogers, K.D., Zioupos, P., 1999. The bone tissue of the rostrum of a *Mesoplodon densirostris* whale: a mammalian biomineral demonstrating extreme texture. *J. Mater. Sci. Lett.* 18 (8), 651–654.
- Roguska, A., Pisarek, M., Belcarz, A., Marcon, L., Holdynski, M., Andrzejczuk, M., Janik-Czachor, M., 2016. Improvement of the bio-functional properties of TiO₂ nanotubes. *Appl. Surf. Sci.* 388, 775–785.
- Roy, M., Bandyopadhyay, A., Bose, S., 2011a. Induction plasma sprayed Sr and Mg doped nano hydroxyapatite coatings on Ti for bone implant. *J. Biomed. Mater. Res. B Appl. Biomater.* 99B (2), 258–265.
- Roy, P., Berger, S., Schmuki, P., 2011b. TiO₂ nanotubes: synthesis and applications. *Angew. Chem. Int. Ed.* 50 (13), 2904–2939.
- Rushing, G.D., Goretsky, M.J., Gustin, T., Morales, M., Kelly Jr., R.E., Nuss, D., 2007. When it is not an infection: metal allergy after the Nuss procedure for repair of pectus excavatum. *J. Pediatr. Surg.* 42 (1), 93–97.
- Ryan, G., Pandit, A., Apatsidis, D.P., 2006. Fabrication methods of porous metals for use in orthopaedic applications. *Biomaterials* 27 (13), 2651–2670.
- Sang, L., Zhao, Y., Niu, Y., Bai, G., 2018. TiO₂ with controlled nanoring/nanotube hierarchical structure: multiabsorption oscillating peaks and photoelectrochemical properties. *Appl. Surf. Sci.* 430, 496–504.
- Sesia, S.B., Haecker, F.-M., Shah, B., Goretsky, M.J., Kelly Jr., R.E., Obermeyer, R.J., 2013. Development of metal allergy after Nuss procedure for repair of pectus excavatum despite preoperative negative skin test. *J. Pediatr. Surg. Case Rep.* 1 (6), 152–155.
- Shabalovskaya, S.A., 2002. Surface, corrosion and biocompatibility aspects of Nitinol as an implant material. *Bio Med. Mater. Eng.* 12 (1), 69–109.
- Shah, B., Cohee, A., Deyerle, A., Kelly, C.S., Frantz, F., Kelly, R.E., Kuhn, M.A., Lombardo, M., Obermeyer, R., Goretsky, M.J., 2014. High rates of metal allergy amongst Nuss procedure patients dictate broader pre-operative testing. *J. Pediatr. Surg.* 49 (3), 451–454.
- Shishkovsky, I.V., Volova, L.T., Kuznetsov, M.V., Morozov, Y.G., Parkin, I.P., 2008. Porous biocompatible implants and tissue scaffolds synthesized by selective laser sintering from Ti and NiTi. *J. Mater. Chem.* 18 (12), 1309–1317.
- Simka, W., Krzakala, A., Maselbas, M., Dercz, G., Szade, J., Winiarski, A., Michalska, J., 2013a. Formation of bioactive coatings on Ti-13Nb-13Zr alloy for hard tissue implants. *RSC Adv.* 3 (28), 11195–11204.
- Simka, W., Socha, R.P., Dercz, G., Michalska, J., Maciej, A., Krzakala, A., 2013b. Anodic oxidation of Ti-13Nb-13Zr alloy in silicate solutions. *Appl. Surf. Sci.* 279, 317–323.
- Skripitz, R., Aspenberg, P., 1998. Tensile bond between bone and titanium – a reappraisal of osseointegration. *Acta Orthop. Scand.* 69 (3), 315–319.
- Song, H.-J., Kim, M.-K., Jung, G.-C., Vang, M.-S., Park, Y.-J., 2007. The effects of spark anodizing treatment of pure titanium metals and titanium alloys on corrosion characteristics. *Surf. Coat. Technol.* 201 (21), 8738–8745.
- Springer, J.C., Harrysson, O.L.A., Marcellin-Little, D.J., Bernacki, S.H., 2014. In vitro dermal and epidermal cellular response to titanium alloy implants fabricated with electron beam melting. *Med. Eng. Phys.* 36 (10), 1367–1372.
- Straffelini, G., Andriani, A., Tesi, B., Molinari, A., Galvanetto, E., 2004. Lubricated rolling-sliding behaviour of ion nitrated and untreated Ti-6Al-4V. *Wear* 256 (3–4), 346–352.
- Su, Z., Zhang, L., Jiang, F., Hong, M., 2013. Formation of crystalline TiO₂ by anodic oxidation of titanium. *Prog. Nat. Sci. Mater. Int.* 23, 294–301.
- Sulka, G.D., Kapusta-Kołodziej, J., Brzózka, A., Jaskała, M., 2013. Anodic growth of TiO₂ nanopore arrays at various temperatures. *Electrochim. Acta* 104, 526–535.
- Suzuki, A., 2000. Effect of multiply charged ions on the refractive index of titanium oxide films and an application to decorative films. *Jpn. J. Appl. Phys.* 39 (3R), 1295.
- Teng, K., Delplancke, J.-L., Zhang, J., O'keefe, T., 1998. Electrochemical characterization of copper deposited on plasma and thermally modified titanium surfaces. *Metall. Mater. Trans. B* 29 (4), 749–754.
- Torres, Y., Pavon, J.J., Nieto, I., Rodriguez, J.A., 2011. Conventional powder metallurgy process and characterization of porous titanium for biomedical applications. *Metall. Mater. Trans. B Process Metall. Mater. Process. Sci.* 42 (4), 891–900.
- Vadiraj, A., Kamaraj, M., 2006. Characterization of fretting fatigue damage of PVD TiN coated biomedical titanium alloys. *Surf. Coat. Technol.* 200 (14–15), 4538–4542.
- van Raay, J.J.A.M., 2012. Metal-on-Metal total hip arthroplasty: known and unknown side effects. *Orthopedics* 35 (6), 447–449.

- Wang, K., 1996. The use of titanium for medical applications in the USA. *Mater. Sci. Eng. A* 213 (1–2), 134–137.
- Wang, X., Li, Y., Xiong, J., Hodgson, P.D., Wen, C.e., 2009. Porous TiNbZr alloy scaffolds for biomedical applications. *Acta Biomater.* 5 (9), 3616–3624.
- Wang, X.J., Li, Y.C., Hodgson, P.D., Wen, C., 2010. Biomimetic modification of porous TiNbZr alloy scaffold for bone tissue engineering. *Tissue Eng. A* 16 (1), 309–316.
- Wang, Y., Wen, C., Hodgson, P., Li, Y., 2014. Biocompatibility of TiO₂ nanotubes with different topographies. *J. Biomed. Mater. Res. A* 102 (3), 743–751.
- Wang, Y.-Q., Jie, T., Ling, W., He, P.-T., Tao, W., 2008. HA coating on titanium with nanotubular anodized TiO₂ intermediate layer via electrochemical deposition. *Trans. Nonferrous Metals Soc. China* 18 (3), 631–635.
- Wang, Y.-Q., Tao, J., Zhang, J.-L., Wang, T., 2011. Effects of addition of NH₄HCO₃ on pore characteristics and compressive properties of porous Ti-10%Mg composites. *Trans. Nonferrous Metals Soc. China* 21 (5), 1074–1079.
- Wen, H.B., Wolke, J.G.C., de Wijn, J.R., Liu, Q., Cui, F.Z., de Groot, K., 1997. Fast precipitation of calcium phosphate layers on titanium induced by simple chemical treatments. *Biomaterials* 18 (22), 1471–1478.
- White, K., Svare, C., Taylor, T., 1985. A potentiostatic study of the corrosion behavior of anodized and nonanodized aluminum alloy. *J. Prosthet. Dent* 53 (6), 815–819.
- Wong, M., Cheng, F., Man, H., 2007. Laser oxidation of NiTi for improving corrosion resistance in Hanks' solution. *Mater. Lett.* 61 (16), 3391–3394.
- Xie, F., He, X., Lu, X., Cao, S., Qu, X., 2013. Preparation and properties of porous Ti–10Mo alloy by selective laser sintering. *Mater. Sci. Eng. C* 33 (3), 1085–1090.
- Xiong, J., Li, Y., Wang, X., Hodgson, P., Wen, C.e., 2008. Mechanical properties and bioactive surface modification via alkali-heat treatment of a porous Ti-18Nb-4Sn alloy for biomedical applications. *Acta Biomater.* 4 (6), 1963–1968.
- Yamamuro, T., 1989. Patterns of osteogenesis in relation to various biomaterials. *J. Jpn. Soc. Biomater.* 7, 19–23.
- Yan, M., Xu, W., Dargusch, M.S., Tang, H.P., Brandt, M., Qian, M., 2014. Review of effect of oxygen on room temperature ductility of titanium and titanium alloys. *Powder Metall.* 57 (4), 251–257.
- Yang, G., Zhang, T., 2005. Phase transformation and mechanical properties of the Ti50Zr30Nb10Ta10 alloy with low modulus and biocompatible. *J. Alloy. Comp.* 392 (1–2), 291–294.
- Yang, H., Pan, C., 2010. Diameter-controlled growth of TiO₂ nanotube arrays by anodization and its photoelectric property. *J. Alloy. Comp.* 492 (1–2), L33–L35.
- Yang, S., Evans, J.R.G., 2007. Metering and dispensing of powder; the quest for new solid freeforming techniques. *Powder Technol.* 178 (1), 56–72.
- Yang, X., Hutchinson, C.R., 2016. Corrosion-wear of β-Ti alloy TMZF (Ti-12Mo-6Zr-2Fe) in simulated body fluid. *Acta Biomater.* 42, 429–439.
- Yao, C., Webster, T.J., 2006. Anodization: a promising nano-modification technique of titanium implants for orthopedic applications. *J. Nanosci. Nanotechnol.* 6 (9–10), 2682–2692.
- Ye, B., Dunand, D.C., 2010. Titanium foams produced by solid-state replication of NaCl powders. *Mater. Sci. Eng. A* 528 (2), 691–697.
- You, L., Song, X., 2012. First principles; study of low Young's modulus Ti-Nb-Zr alloy system. *Mater. Lett.* 80, 165–167.
- Zhang, D.C., Lin, J.G., Jiang, W.J., Ma, M., Peng, Z.G., 2011a. Shape memory and superelastic behavior of Ti–7.5Nb–4Mo–1Sn alloy. *Mater. Des.* 32 (8–9), 4614–4617.
- Zhang, F., Chen, S., Dong, L., Lei, Y., Liu, T., Yin, Y., 2011b. Preparation of superhydrophobic films on titanium as effective corrosion barriers. *Appl. Surf. Sci.* 257 (7), 2587–2591.
- Zhubrak, M., Bar-David, T., 2014. Systemic nickel allergy after internal fixation of a bunionectomy. *J. Foot Ankle Surg.* 53 (4), 466–467.

Chapter Exercise 1

1. Explain the term “biocompatibility” in metallic biomaterials.
2. What are the two unique behaviors of NiTi alloys that make them promising for a variety of implant applications?
3. Which of the following alloys contain allergic and carcinogenic elements?
 - (a) Ti-13Nb-13Zr
 - (b) Ti-6Al-7Nb
 - (c) Co-20Cr-15W-10Ni
4. Explain “stress shielding” in metallic hip implants and its potential consequences.
5. Which of the following implant materials can possibly exhibit the stress-shielding effect when implanted as hip prostheses?
 - (a) Ti-15Mo (annealed)
 - (b) Ti-13Nb-13Zr (aged)
 - (c) Co-Cr-Mo (ASTM-F75)
6. What are the advantages of using Ti alloys over other metallic biomaterials for orthopedic implant applications?
7. Sort the elastic modulus of the following biomaterials in a descending order: (1) AZ91D magnesium alloy (AZ91D), (2) CP-Ti, (3) Co-Cr-Mo alloy (ASTM-F75) (Co-Cr-Mo), and (4) stainless steel (316L).
 - (a) AZ91D > CP-Ti > Co-Cr-Mo > 316L
 - (b) CP-Ti > AZ91D > Co-Cr-Mo > 316L
 - (c) 316L > AZ91D > CP-Ti > Co-Cr-Mo
 - (d) Co-Cr-Mo > 316L > CP-Ti > AZ91D
8. What are the advantages of using β -type Ti alloys over α -type Ti alloys for orthopedic applications?
9. Which of the following sets of properties should load-bearing implant materials have?
 - (a) High elastic modulus, high fatigue strength, high tensile strength, high wear resistance, and high corrosion resistance
 - (b) Low elastic modulus, high fatigue strength, high tensile strength, high wear resistance, high corrosion resistance
 - (c) High elastic modulus, high fatigue strength, high tensile strength, low wear resistance, high corrosion resistance

Chapter Exercise 2

1. Explain the term “osseointegration” in metallic biomaterials.
2. Which of the following biomaterials exhibit the lowest wear resistance?
 - (a) CP-Ti (Grade 1)
 - (b) Co-20Cr-15W-10Ni
 - (c) Stainless steel (316L)
3. What is the effect of interstitial oxygen atoms on the mechanical properties of Ti alloys?
4. Which of the following Ti alloys exhibit better cold-forming ability?

- (a) α -type Ti alloys
 - (b) β -type Ti alloys
5. Why is fatigue strength important for metallic biomaterials?
 6. Why do surface properties of Ti alloys differ from their bulk properties?
 7. Which of the following contains information on critical anodization parameters?
 - (a) Applied potential, type of electrolyte, time, temperature
 - (b) Laser pulse intensity, laser energy, exposure time
 8. What are the most commonly used coloring methods for Ti alloys?
 9. What are the key steps involved in the additive manufacturing of Ti structures?

Chapter Exercise 3

1. Which of the following materials exhibit shape memory property?
 - (a) CP-Ti (Grade 1)
 - (b) NiTi alloy
 - (c) Stainless steel (316 SS)
 - (d) Co-Cr-Mo (ASTM-F75)
2. Which of the following techniques can fabricate complex Ti geometrical shapes?
 - (a) Powder metallurgy
 - (b) Additive manufacturing
 - (c) Casting
3. What are the complications of using stainless steels for orthopedic applications?
4. Why cannot α -type Ti alloys be strengthened by heat treatment?
5. Porous Ti alloys with the desired porosity ratio and pore size may be produced in the required geometric shape without the use of any space-holder material via:
 - (a) Casting
 - (b) Selective laser sintering
 - (c) Powder metallurgy
6. Which of the following is an additive manufacturing process?
 - (a) Cold rolling
 - (b) Hot isostatic pressing
 - (c) Electron beam melting
7. Co-based alloys have higher wear resistances than Ti alloys?
 - (a) True
 - (b) False
8. Which of the following methods is commonly used to grow oxide nanotubes on Ti alloys?
 - (a) Forging
 - (b) Anodization
 - (c) Additive manufacturing
9. What are the key strategies to avoid stress shielding in orthopedic surgeries?

1.3.3B

Stainless Steels

PHILLIP J. ANDERSEN

Andersen Metallurgical, LLC, Madison, WI, United States

Overview

Stainless steel refers to the family of iron-based alloys having appreciable concentrations of nickel and chromium alloying elements. The term stainless derives from the corrosion resistance afforded by the protective surface oxide layer attributable to these alloying elements. Specific stainless steels are useful for biomedical applications due to their desirable shaping, joining, and mechanical properties, acceptable corrosion resistance, durability, and manufacturing economics.

History

Iron-based tools and weapons have been used since the end of the Bronze Age and the beginning of the historical record. Iron is a particularly advantageous material because material hardness and tensile strength are readily controlled by appropriate heating and quenching. A major disadvantage of iron is its propensity to react with oxygen to corrode (rust) and lose desirable mechanical properties. Humans recognized these characteristics for more than two millennia and this limited use of iron for many applications (prohibited it for biomedical use).

Discovery within the past century, showing that adding appreciable amounts of chromium and nickel to iron produced a new alloy (now known as stainless steel), was an extraordinary technological development enabling many new uses of iron-based alloys in almost every area of human endeavor, especially biomedical. While there are a large number of different types of stainless steels available commercially, only a few of these alloys have properties that enable their use as biomaterials for implantable devices. Use of stainless-steel implants began in the 1920s and 1930s and applications for stainless steels expanded as new medical procedures and material refinements were developed.

Composition and Types

Stainless steel is an iron-based alloy that contains an appreciable percentage of chromium and nickel. There

are three main classes of stainless steels: austenitic, ferritic, and martensitic. These classes are differentiated by their microstructure. Austenitic stainless steels have austenite (gamma-phase iron) as their primary phase and contain chromium and nickel (sometimes manganese and nitrogen also). The 300-series of stainless steels, i.e., Types 301 to 304, Type 316 and Type 347, are those most commonly used for biomedical purposes because of their toughness, durability, ability to be joined by welding, corrosion resistance, and manufacturing economics (ESPI Metals, 2019).

The basic composition of austenitic stainless steels is exemplified by Type 302 stainless steel. This alloy is composed of iron with 18% chromium and 8% nickel added. Austenitic steels are amenable to work hardening but cannot be hardened by heat treatment. In addition to favorable corrosion resistance and mechanical properties, austenitic stainless steel is desirable for implanted devices because it is nonmagnetic and thus has minimal or no interactions with the intense magnetic fields used in magnetic resonance imaging (MRI). The most familiar austenitic stainless steel used for surgical implants is Type 304, which contains 18%–20% chromium and 8%–10% nickel (National Specialty Alloys, 2011). Ferritic and martensitic stainless steels, as well as precipitation-hardened and cast stainless steels, lack the desirable corrosion and mechanical properties of austenitic stainless steels. For these reasons, they are not commonly used for biomedical applications and will not be discussed further.

Composition of stainless steels used for biomedical applications is closely controlled because under some processing conditions, it is possible to form different phases within the austenitic stainless-steel alloys, e.g., delta ferrite (which is magnetic). Modest amounts of heating and material displacement can occur for delta ferrite phases when exposed to the large magnetic fields accompanying MRI. Such localized heating or material motion in implants in patients exposed to high magnetic fields during MRI is deleterious, hence the need to control the composition of stainless-steel alloys used for implants.

Structure

Metals, including stainless steel alloys, are characterized by a high percentage of crystallinity. The constituent crystalline structures in metals have one of three basic types of unit cells: face-centered cubic, body-centered cubic, or hexagonal close packed. Stainless steels used for implants are face-centered cubic (Fig. 1.2.3.2, Chapter 1.2.3). Table 1.3.3B.1 shows the ranges of chemical compositions specified for several common implantable stainless steels. Chromium is present in these alloys and its primary purpose is to form a protective Cr_2O_3 surface layer (passive film) that confers corrosion resistance. Since chromium stabilizes the ferrite (body-centered cubic) phase, other alloying elements are added to stabilize the desired austenite phase. This objective is attained by addition of nickel, manganese, and nitrogen. Nitrogen added as an alloying element to stainless steel also increases mechanical strength and corrosion resistance. Molybdenum additions have a beneficial impact on the pitting corrosion resistance of stainless steels.

Carbon content in stainless-steel alloys must be limited to small percentages (the “L” in 316L designates low carbon) to prevent formation of chromium carbides. Formation of these carbides can result in a phenomenon known as sensitization. If sufficient carbon is available, chromium carbides can form when austenitic stainless steels are held at temperatures in the range of 450–815°C. The time required to form these carbides depends on temperature. Under select time and high-temperature conditions, carbides tend to form preferentially along grain boundaries, leaving the adjacent areas with depleted chromium levels. Such chromium-depleted areas then become prone to corrosion and this can lead to macroscopic material (implant) failure. Slow cooling after welding is a classic means by which sensitization can occur when time and cooling rates are unmanaged.

Examination of the chemical compositions of surgically implantable stainless steels (Table 1.3.3B.1) shows variability with time and alloy selection. While 316 and 316L stainless steels have been used successfully for implants for many decades, stronger and more corrosion-resistant alloys have subsequently been developed. The alloys, e.g., Rex 734 (also known as Ortron 90) and 22-13-5, were developed in the 1980s. They contain higher levels of chromium, manganese, and nitrogen compared to 316L, leading to improved mechanical properties and enhanced corrosion resistance. Recent concerns for adverse (allergic) patient responses to nickel (see Orthopedic Applications, Chapter 2.5.4 for additional discussion of this topic) have led to the development of stainless steels that are essentially nickel free. One example is BioDur 108 (BioDur, 2008), a stainless-steel alloy that uses manganese and nitrogen instead of nickel to stabilize the austenite phase. The nitrogen level in this alloy is much greater than the level found in the Type-300 family of stainless steels.

Structure, Composition, and Processing Effects on Mechanical Properties

The mechanical properties of metals and alloys depend on their structure, chemical composition, and processing history. To understand how these factors influence mechanical properties, consider the mechanisms involved when permanent (plastic) deformation occurs. Plastic deformation results from mechanical stress-induced movement of atoms within the crystalline structure of a metal. These movements result in irregularly distributed atoms that cause defects or disturbed regions in the crystal lattice. These disturbances are known as “dislocations.” Subsequent strain-induced movement of atoms in the presence of dislocations is typically more difficult, and in this event the mechanical properties of the material change. Typical changes accompanying increased dislocation density include increases in yield strength and decreases in ductility.

Chemical composition of an alloy influences mechanical properties by a process known as solid solution strengthening. Metallic alloying elements in stainless steels, i.e., chromium, nickel, etc., replace iron atoms at random locations within the crystal structure. Since the replacement atoms differ in size compared to iron atoms, the crystal lattice can be distorted. This distortion makes material deformation via dislocation movement more difficult and this also increases yield strength as well as generally decreases ductility. Smaller atoms, such as nitrogen, fit within the gaps between the larger metallic atoms and for this reason they are often referred to as interstitials. Additions of these chemical species leads to substantial strength increases due to interactions between solute atoms and dislocations.

Processing also affects the mechanical properties of stainless steels. While processes are commonly used to alter mechanical properties of other iron-based alloys, e.g., aging reactions during heat treatment, such processes are not applicable to austenitic stainless steels. Instead, material strengthening mechanisms such as work hardening, also known as “cold working,” are used. Work hardening involves repeated mechanical stresses applied to an unheated material. Work hardening occurs by mechanical stress-induced introduction of increasing amounts of dislocations. As the percentage of dislocations increases, motion of these dislocations becomes more difficult as more dislocations interact within the material. As the material continues deforming by the applied mechanical stress, increasing quantities of dislocations develop within the grains of the alloy. If the deformation process takes place at high temperatures typical of the large-scale processes used to produce metal products, or if the material is heated above its recrystallization temperature after deformation, then the dislocations are removed by formation of new, annealed grains (recrystallization). Deformation at lower temperatures does not eliminate dislocations. As the density of dislocations within the material increases, they interact causing increasing difficulty for further dislocation motion. This leads to increases

TABLE 1.3.3B.1 Compositions of Common Implantable Stainless Steels (Weight Percent)

Alloy	Cr	Ni	Mn	Mo	C	N	Nb	V	Si	Cu	P	S
316L ASTM F138, ISO 5832-1	17–19	13–15	<2 max	2.25–3	<0.030	<0.10	–	–	<0.75	<0.5	<0.025	<0.010
22-13-5 ASTM F1314	20.5– 23.5	11.5–13.5	4–6	2–3	<0.030	0.2–0.4	0.1–0.3	0.1–0.3	<0.75	<0.5	<0.025	<0.010
Rex 734, Ortron 90 ASTM F1586 ISO 5832-9	19.5–22	9–11	2–4.25	2–3	<0.08	0.25–0.5	0.25–0.8	–	<0.75	<0.25	<0.25	<0.010
BioDur 108 ASTM F 2229	19–23	<0.050	21–24	0.5–1.5	<0.08	0.85–1.10	–	–	<0.75	<0.25	<0.03	<0.010



• **Figure 1.3.3B.1** Microstructures of annealed 316L (*left*) and ~30% cold-worked 316L (*right*). Deformation within many of the grains of the cold-worked material is evident.

in strength and reductions in ductility. More information on solid solution strengthening and work hardening can be found in materials science textbooks (Hosford, 2005; Meyers and Chawla, 2008).

Evidence of mechanical stress-induced deformation within the grains of a moderately cold-worked 316L sample is shown in Fig. 1.3.3B.1. This compares the structure of annealed and ~30% cold-worked 316L. The amount of cold work is routinely specified by the percentage reduction of area, i.e., $(A_i - A_f/A_i) \times 100$, where A_i is the initial cross-sectional area of the product and A_f is the final cross-sectional area. As the amount of cold work increases, strength parameters (yield strength and ultimate strength) increase (along with hardness), while ductility decreases. This behavior provides designers with the ability to specify a wide range of mechanical properties by proper selection of alloy composition, processing temperature, and amount of cold work. Table 1.3.3B.2 lists approximate tensile and fatigue strength properties for some implantable stainless steels produced under different conditions. These data show the influence of chemical composition and amount of cold work on mechanical properties of stainless steels.

There are limits to the uniformity of the cold-working response of a material. This limit is a function of the material cross-sectional area. Practically speaking, this means that a large cross-section may have a cold-work gradient such that the exterior regions of the material may be more heavily worked than the interior regions. Another effect of cold working is that heavily worked stainless steels, such as Types 304 or 305, can become magnetic due to a stress-induced transformation of crystal structure from austenite (nonmagnetic) to martensite (magnetic). This can have pronounced negative results if fragments of these alloys, routinely used as guide wires, fracture and separate during an invasive clinical procedure (FDA Public Health Notification, 2008). It is also important to realize that elevated temperature processes such as welding will result in softening of a cold-worked material and reduction of mechanical properties to annealed levels.

A high level of fatigue strength is necessary for many stainless-steel medical devices (see Chapters 1.2.3 and 1.3.3 of this volume for more information on mechanical fatigue). The fatigue properties of metallic materials depend on a number of factors, including composition, grain size, processing history, surface finish, and test method. The fatigue data shown (Table 1.3.3B.2) provide approximate relative values; these data should not be used for implant design purposes since the properties of specific devices are strongly influenced by manufacturing processes, product design features, heterogeneities in raw materials, and variability in device manufacturing processes.

Corrosion

Corrosion (oxidation) is a persistent materials-engineering consideration because this ubiquitous process causes loss of desirable electrical, chemical, mechanical, or thermal properties. Corrosion is even more important for biomedical applications because in addition to loss of desired material properties, adverse cellular responses may occur when metal ion corrosion products interact with biological tissues. Corrosion-related loss of properties or adverse cellular responses to corrosion-released metal ions may cause failure of the implant.

Except for noble metals such as gold or platinum, commonly used implantable metals and alloys rely upon protective oxide films to limit corrosion to acceptable levels. These oxides are commonly referred to as passive films. They are thin (typically less than 100 microns), dense, adhere strongly to the metal alloy substrate, and limit transport of corroding metallic ions to the implant surface and into the body. Alloys containing substantial amounts of chromium (austenitic stainless steels and implantable cobalt base alloys) form a Cr_2O_3 passive film, while alloys rich in titanium (titanium alloys and Nitinol) form a TiO_2 passive film.

The internal milieu of the human body presents a hostile environment to artificial biomaterials. Given the highly corrosive nature of most body fluids, additional corrosion resistance beyond that afforded by Type 304 stainless steel is frequently needed. For such applications, Type 316 or Type

TABLE 1.3.3B.2 Approximate Mechanical Properties of Stainless Steels

Alloy	Material Condition	Ultimate Tensile Strength (MPa)	Yield Strength (MPa)	% Elongation	10 ⁷ Cycle Endurance Limit (MPa)	References
316L	Annealed	550	240	55	180	Shetty and Ottersberg (1995)
316L	30% cold worked	896	827	20	380	Shetty and Ottersberg (1995)
316L	60% cold worked	1240	1000	12	450	Shetty and Ottersberg (1995)
Rex 734	Hot forged	1140–1230	1050–1179	15–19	585	Windler and Steger (2003)
22-13-5	Annealed	965	760	35	380	Shetty and Ottersberg (1995)
22-13-5	30% cold worked	1240	1170	15	530	Shetty and Ottersberg (1995)
22-13-5	60% cold worked	1585	1480	9	670	Shetty and Ottersberg (1995)
BioDur 108	Annealed	827–930	517–605	30–50	380	ASTM F 2229 and Technical Data Sheet BioDur 108
BioDur 108	35% cold worked	1580	1350	15		Technical Data Sheet BioDur 108
BioDur 108	65% cold worked	2000	1790	5		Technical Data Sheet BioDur 108

316L stainless steel is appropriate. Alloy Type 316 or 316L is an austenitic stainless steel typically composed of iron and 12% nickel, 17% chromium, 2.4% molybdenum, 2% magnesium, and less than 0.08% carbon. The higher nickel and molybdenum content in Type 316 stainless steel provides superior overall corrosion resistance compared to Type 304, especially with regard to pitting and crevice corrosion in chloride environments. In addition, Type 316 or 316L provides excellent mechanical properties as well as outstanding formability and weldability. High-temperature benefits of Type 316 stainless alloys are also useful for manufacturing bone drill bits and bone saw blades.

In general, austenitic stainless steels are not as corrosion resistant as either cobalt–chromium alloys or titanium alloys. The more recent stainless-steel alloys, e.g., 22-13-5, Rex 734, and BioDur 108, exhibit improved corrosion resistance compared to 316L, due to their greater concentrations of Cr and N. A metric for relative corrosion resistance is the pitting potential; this is measured by an anodic polarization test. Pitting potentials vary depending on testing conditions, but one study observed 346 mV for 316L, 1030 mV for 22-13-5, and 1120 mV for BioDur 108 (Zardiackas et al., 2003). Another factor influencing corrosion of stainless steels is the presence of foreign particles (inclusions). Inclusions are typically oxide particles, such as alumina or silicates formed during the initial melting of the alloy, which become trapped within the material during subsequent processing. Since these inclusions have different corrosion behavior compared to the host alloy, they can act as corrosion initiation sites if they occur on the implant surface. Careful control of alloy melting and subsequent processing, as noted in standardized specifications (e.g., American Society for Testing and Materials, ASTM) for stainless steels, is required to minimize inclusions within these alloys.

Corrosion occurs by several specific mechanisms, i.e., uniform corrosion, pitting corrosion, crevice corrosion, intergranular corrosion, stress corrosion cracking, and galvanic corrosion. The most familiar everyday experience is a relatively even layer of rust on the surface of an iron bar exposed to the elements—this is a form of uniform corrosion. Pitting corrosion, a separate mechanism, deserves special attention due to the difficulty of predicting, detecting, and characterizing this form of corrosion. Pitting corrosion occurs when the protective oxide layer fails in a localized region on the surface of a metal. The oxidation that preferentially occurs in this region can lead to the formation of a focal deficit (hole) in the material. Even small amounts of pitting corrosion-induced material defects can ultimately lead to gross failure of the implant, particularly those subjected to repetitive mechanical loads.

To quantify the potential for pitting corrosion, an empirical relationship estimates the contribution of alloying elements to pitting corrosion resistance of austenitic stainless steels. This relationship, i.e., the pitting resistance equivalent number or PRE, depends on the percentage of chromium, molybdenum, and nitrogen in the alloy. For low nitrogen levels an appropriate approximation of the PRE is $PRE = \% Cr + 3.3 \times \% Mo + 16 \times \% N$; at nitrogen levels nearing 1% an appropriate approximation is $PRE = \% Cr + 3.2 \times \%$

$Mo + 8 \times \% N$ (Gebeau and Brown, 2001). Higher PRE numbers indicate improved resistance to pitting corrosion.

Crevice corrosion is another localized form of corrosion, but occurs chiefly due to a stagnant microenvironment that in turn causes a difference in ion concentration between two areas of a given metal. Here, corrosive agents may enter a given local microenvironment, but oxygen is prevented from entering this microenvironment thereby preventing repassivation (reformation of the protective oxide layer). The potential for crevice corrosion can be minimized by careful attention to implant design and consideration of all local microenvironments.

Galvanic corrosion occurs when two dissimilar metals are in electrical contact in an electrolytic (fluid-conducting) environment. Galvanic corrosion may occur even when two ostensibly similar corrosion-resistant alloys are in electrical contact in the body if such alloys have different alloying elements, different concentrations of the same alloying elements, or different processing methods. Galvanic corrosion can be avoided by careful management of stainless-steel alloy composition and processing.

Summary

Iron-based alloys were unsuitable for human implantation because rapid oxidation in vivo deteriorated their mechanical properties and released excessive quantities of corrosion products. The introduction of engineered quantities of chromium and nickel to iron for the creation of corrosion-inhibiting oxide layers revolutionized biomaterials by the creation of new “stainless-steel” alloys for human implants. A select group of austenitic stainless steels is especially suitable for human implantation in biomedical devices because these alloys offer favorable corrosion resistance, MRI compatibility, and desirable mechanical properties that collectively support long-term implant use in the human body. The favorable biological performance (Black, 2005) of these stainless-steel alloys is not only conferred by the types and concentrations of particular alloying elements, but also by the processing of these alloys, which collectively produces a desirable material structure conferring these favorable material properties. Although 316L is one of the oldest and most common alloys used for human implants, recent developments have led to newer stainless steels with improved mechanical strength and enhanced corrosion resistance. Alloy element type and concentration, as well as postprocessing, permits the resulting material to have a wide range of properties engineered for a specific biomaterial application. A soft, ductile, annealed condition is useful for implants requiring intraoperative contouring by the surgeon, while a higher strength, less ductile, work-hardened material can be specified for implants exposed to high amplitude fatigue loading. While ASTM and ISO standards provide valuable guidance for alloy composition, processing, machining, sterilization, and use, information obtained from retrieval studies attending long-term human usage is also important for advancing the design and biomedical applications of stainless-steel alloys for human use.

References

- BioDur, 2008. Technical Data Sheet BioDur®108. <http://www.cartech.com/techcenter.aspx?id=1692>. [Accessed 22 January 2008].
- Black, J., 2005. In: *Biological Performance of Materials: Fundamentals of Biocompatibility*, fourth ed. CRC Press, Boca Raton.
- FDA, 2008. FDA Public Health Notification: Unretrieved Device Fragments. <http://www.fda.gov/cdrh/safety/011508-udf.html>. [Accessed 22 January 2008].
- Gebeau, R.C., Brown, R.S., 2001. Biomedical Implant Alloy. *Sept Advanced Materials & Processes*, pp. 46–48 Sept.
- Hosford, W.F., 2005. *Mechanical Behavior of Materials*. Cambridge University Press.
- Metals, E.S.P.I., 2019. Stainless steel 316 – alloy composition. [Accessed 3 April 2019].
- Meyers, M.A., Chawla, K.K., 2008. *Mechanical Behavior of Materials*. Cambridge University Press.
- National Specialty Alloys, 2011. 3 Types of Stainless Steel. [Accessed 3 April 2019].
- Shetty, R.H., Ottensberg, W.H., 1995. Metals in orthopedic surgery. In: *Encyclopedic Handbook of Biomaterials and Bioengineering – Part B Applications*. Marcel Decker, New York, NY, pp. 509–540.
- Windler, M., Steger, R., 2003. Mechanical and corrosion properties of forged hip stems made of high nitrogen stainless steel. *ASTM International*. In: Winters, G.L., Nutt, M.J. (Eds.), *Stainless Steels for Medical and Surgical Applications ASTM STP 1438*. ASTM International, pp. 39–49.
- Zardiackas, L.D., et al., 2003. Comparison of anodic polarization and galvanic corrosion of a low-nickel stainless steel to 316LS and 22Cr-13Ni-5Mn stainless steels. *ASTM International*. In: Winters, G.L., Nutt, M.J. (Eds.), *Stainless Steels for Medical and Surgical Applications ASTM STP 1438*. ASTM International, pp. 107–118.

1.3.3C

CoCr Alloys

AMIT BANDYOPADHYAY, KELLEN D. TRAXEL, JOSE D. AVILA, INDRANATH MITRA, SUSMITA BOSE

W. M. Keck Biomedical Materials Research Laboratory, Washington State University, Pullman, WA, United States

Introduction

Degenerative joint disease and rheumatoid arthritis are the most common clinical conditions in which cobalt–chromium (CoCr) implants are used. In recent years, arthroplasty has seen a significant jump in numbers and is projected to grow in the future, increasing the number of implants and technological improvements needed for future patients. From 2005 to 2030, the demand for total hip arthroplasty (THA) and total knee arthroplasty (TKA) is projected to increase by 174% to 572,000 total, and 673% to 3.48 million total, respectively (Kurtz et al., 2007). In 2014, in the most recent study released by the Mayo Clinic, it was estimated that 7.2 million Americans were living with knee and hip implants; that is, 4.7 million TKAs and 2.5 million THAs performed on Americans (Maradit-Kremers et al., 2014). In response, orthopedic device manufacturers have made headway in addressing some of the issues that arise from introducing artificial materials into the body for articulating surface applications (relative motion between two surfaces). Namely, there has been significant regulatory development calling for additional bio-tribological, mechanical, and electrochemical testing due to ionic leaching from wear-induced damage. Because of this, extensive studies have been performed to understand the cellular response to ionic release of Co^{2+} and Cr^{3+} depending on particulate size range, concentration, pH, and galvanic potential at the implant site. In addition, new electrochemical testing methods have been developed to better understand the complex reactions that occur at the implant site during wear degradation, the methods of which are presented later in this Introduction. The most common CoCr-based alloys are of the cobalt–chromium–tungsten (Co–Cr–W) and cobalt–chromium–molybdenum (Co–Cr–Mo) types, where chromium provides a passive Cr_2O_3 surface oxide that is the same corrosion-resistant film that forms for “stainless” steels, and W and/or Mo both act as strengthening elements within the CoCr alloy system. The best known Co–Cr–Mo ternary system is the Co27Cr6.1Mo (ASTM-designated “F75”) alloy owing to the excellent combination

of properties that it exhibits for biomedical applications. Because of its widespread success, it has seen little change in the composition except for strict regulation on the carbon content, which affects the amount and nature of the intergranular carbide formation. Tables 1.3.3C.1 and 1.3.3C.2 outline some of the common grades and compositions, as well as their general properties.

Among the various characterization techniques for biomedical devices in articulating surface applications, electroanalytical methods (EMs) have provided a simple and standardized way to analyze and quantify the electrochemical performance of many biocompatible materials. These techniques fall within the field of analytical chemistry or the branch of chemistry that identifies and quantifies matter. EMs examine an analyte—the species of interest in an analytical test—by quantification of current and/or potential within an electrochemical cell. Specifically, in tribocorrosion testing, the analyte is generally the metal or metal–composite sample. In performing a tribocorrosion test the typical setup is of a three-electrode convention as seen in Fig. 1.3.3C.1A. The different electrodes are the reference electrode (RE), the working electrode (WE, or the analyte), and a counterelectrode (CE)—most commonly made of platinum due to its high electrochemical stability. The working electrode provides the surface for the electrochemical reactions to take place and thus allow quantification of the reacting matter—the material that corrodes. A potentiostat instrument controls the potential between the WE and RE, and subsequent data acquisition. The combination of the electrolyte, three electrodes, and the potentiostat gives rise to a specific type of EC termed a “corrosion cell” and measures the corrosion properties of an analyte surface. A corrosion cell is often configured to work in biologically relevant media and can be combined with tribological (wear) testing to study tribocorrosion (Fig. 1.3.3C.1B); this is done by implementing a counter wear material, applying a load, and allowing relative motion between the WE and counter material. An example potentiodynamic polarization curves for CoCrMo alloys are shown in Fig. 1.3.3C.2.

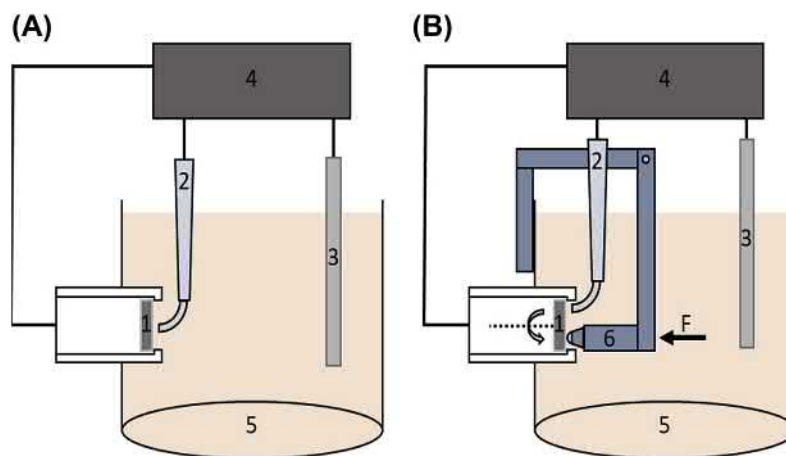
TABLE 1.3.3C.1 Common Biomedical CoCr Alloy Grades and Their Alloy Composition

ASTM Designation	Main Alloying Elements								
	Co	Cr	Mo	W	Si	Mn	C	Ni	Other
F75 (CoCrMo)	Bal.	27.0–30.0	5.0–7.0	–	0.0–1.0	0.0–1.0	0.0–0.35	1.0	Fe
F799 (CoCrMo)	Bal.	26.0–30.0	5.0–7.0	–	0.0–1.0	0.0–1.0	0.0–0.35	0.0–1.0	Fe, Al, N, La
F90 (CoCrW)	Bal.	19.0–21.0	–	14.0–16.0	0.4	1.0–2.0	0.05–0.15	9.0–11.0	Fe (3.0 max)
F562 (CoNiCrMo)	Bal.	19.0–21.0	9.0–10.5	–	0.0–0.15	0.0–0.15	0.0–0.025	33.0–37.0	Ti, B, Fe, S, P
F90 (CoCrWNi)	Bal.	19.0–21.0	–	14.0–16.0	–	–	–	9.0–11.0	–

All properties originate from each respective ASTM standard related to the designation.

TABLE 1.3.3C.2 Common Biomedical Grade Metals and Their Properties (Davis, 2000) and (Hermawan et al., 2011)

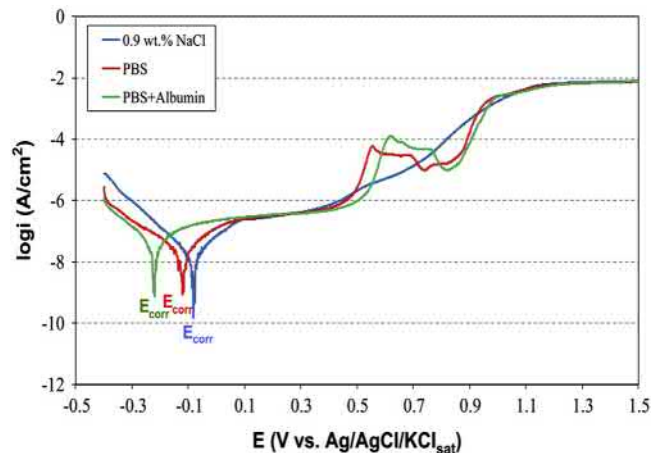
Composition	Processing	Yield Strength (MPa)	Tensile Strength (MPa)	% Elongation	Elastic Modulus (GPa)
F75 (CoCrMo)	Cast	450	655	8	248
F799 (CoCrMo)	Thermomechanically processed	827	1172	12	–
F90 (CoCrW)	Wrought	379	896	–	242
F562 (CoNiCrMo)	Annealed	241–448	793–1000	50	228
	Cold-worked and aged	1586	1793	8	–
F90 (CoCrWNi)	Annealed	310	860	20	210
F136 (Ti6Al4V)		795	860	10	116
F67 (pure Ti grade 4)		485	550	15	110
316L (stainless steel)		190	490	40	193



• **Figure 1.3.3C.1** (A) Corrosion cell setup: (1) working electrode (analyte), (2) reference electrode, (3) counter-electrode, (4) data acquisition unit (potentiostat), (5) electrolyte media, and (6) counter wear ball/pin holder with loading arm. (B) Tribocorrosion cell setup, translation or rotation is now incorporated into the analyte holder.

Microstructure, Mechanical Properties, and Manufacturing of CoCr Alloys

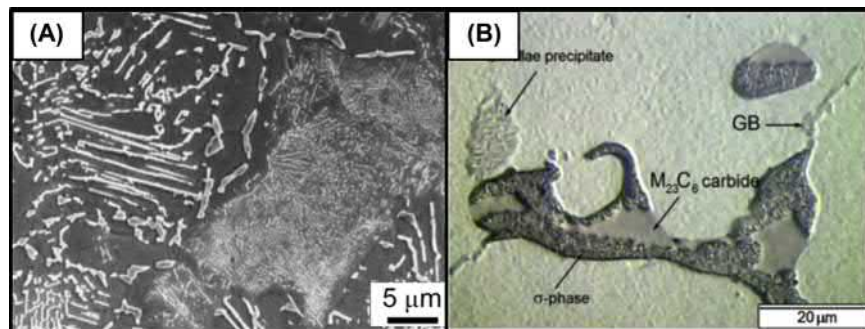
In CoCr alloys, cobalt serves as the base FCC (face-centered-cubic, α -Co) crystal structure of these alloys. On its own, it is known to have low stacking fault energy that results in relatively high strength and work-hardening rates, low damage under cyclic loading, and the ability to absorb stresses through an FCC-HCP (hexagonal closed-packed) phase transformation. These characteristics lead to its excellent wear and corrosion resistance as well as strength. Chromium provides oxidation and corrosion resistance in the form of an oxide surface layer, Cr_2O_3 , as well as a major metal-carbide source, typically forming carbides in the form of Cr_7C_3 and Cr_{23}C_6 . Chromium also provides strength to the larger solid solution when dissolved in the Co matrix, stabilizing the HCP (ϵ -Co) phase when present in amounts up to 30 wt.%. Tungsten and molybdenum provide general substitutional and interstitial solid-solution strength to the cobalt matrix due to their large atomic size, which significantly impedes dislocation motion. These elements also contribute to the metal carbide formation along the



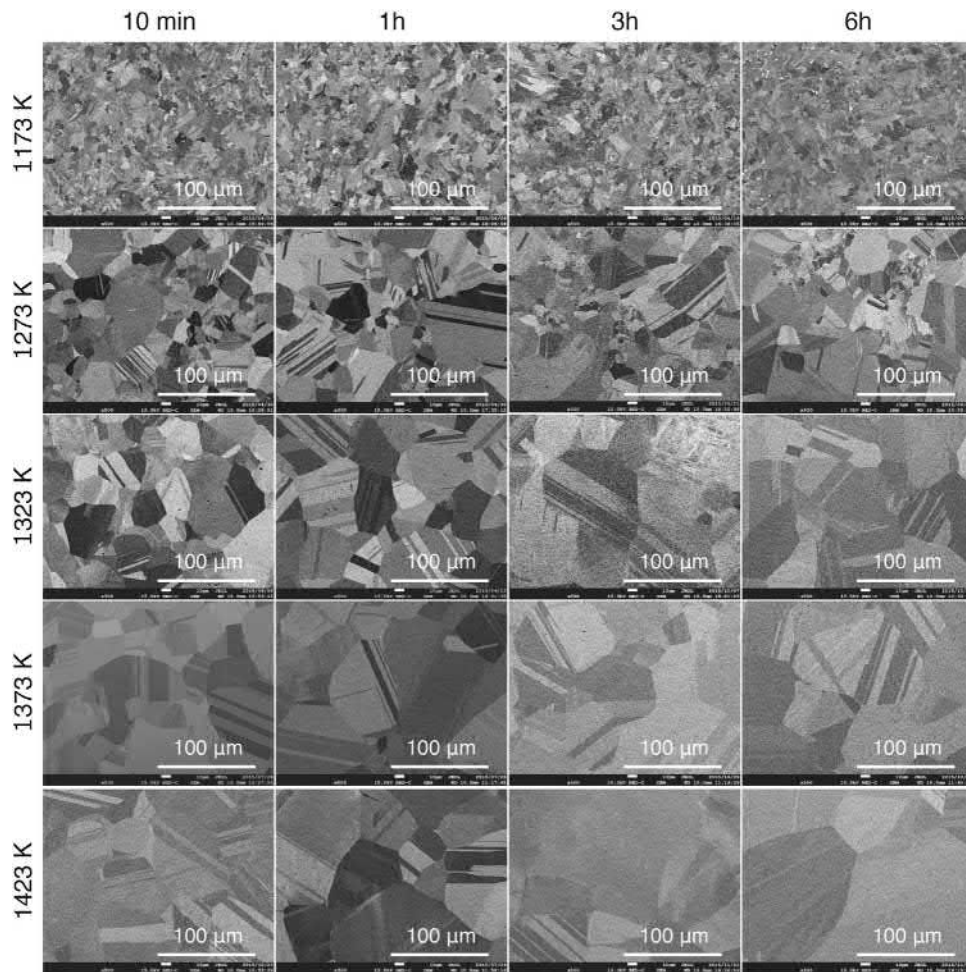
• **Figure 1.3.3C.2** Example of potentiodynamic polarization curves of CoCrMo alloy in varying media. Testing was conducted at 37°C in 9 g/L NaCl, PBS and PBS + albumin solutions (Espallargas et al., 2016).

grain boundaries of the Co-base matrix, when present in large enough amounts. Typically, these carbides are reported as being of the M_7C_3 and M_{23}C_6 types, where M denotes metal and is usually considered to be taken as Cr, Mo, or W, depending on the specific alloy composition and processing route, and any secondary solution treatments. Examples of different phases that form within these microstructures are shown in Fig. 1.3.3C.3.

The mechanical properties of CoCr alloys generally depend upon the alloying elements, processing route, as well as the thermomechanical post-processing that is used to achieve specific microstructures. As shown in Fig. 1.3.3C.4, the microstructure of cold-swaged (cold-rolled) F75 depends heavily on the heat treatment (annealing) time as well as the temperature. High-temperature annealing results in the formation of large, equiaxed grains, whereas lower temperature annealing resulted in highly refined grains. The finer grained material results in higher hardness and tensile strength, whereas the larger grained material maintains high ductility under loading. Also of note are the intergranular twins caused by the stress-induced phase transformation from γ -(FCC) to ϵ -(HCP). These annealing and/or solution treatments can result in microstructural homogeneity within both the Co-rich dendritic phases as well as the carbides that form along the grain boundaries of the main Co phase. It was shown that solution-annealing treatment to a hot-pressed F75 microstructure results in carbide-free grains which are prone to higher abrasive wear when compared with simply hot-pressed microstructures that contain large amounts of intergranular carbides (Chen et al., 2014). The microstructure of the hot-pressed condition can be seen in Fig. 1.3.3C.3A, where the darker phase represents the γ -(FCC) structure, and the lighter phases correspond to the carbides. It was also shown that the initial formation of an intermetallic σ phase, as shown in Fig. 1.3.3C.3B, and lamella precipitates can be removed from the microstructure after appropriate solution annealing treatments to force diffusion back into the Co-based grain structure (Giacchi, 2012). The σ phase is known to negatively affect the mechanical properties of these alloys, therefore removing it during solution treatment is of great importance within



• **Figure 1.3.3C.3** High-magnification microstructural characteristics of F75 material. (A) Hot-pressed condition showing γ -(FCC) phase (dark) and network of carbide structures (Chen et al., 2014). (B) As-cast features of a low-carbon CoCrMo alloy showing the precipitation of an M_{23}C_6 phase, an intermetallic σ phase, and lamella precipitates (Giacchi et al., 2012).



• **Figure 1.3.3C.4** Effect of heat treatment time (horizontal scale) and temperature (vertical scale) on the microstructural characteristics of Co₂₇Cr_{6.1}Mo (F75) alloy (Mori et al., 2016).

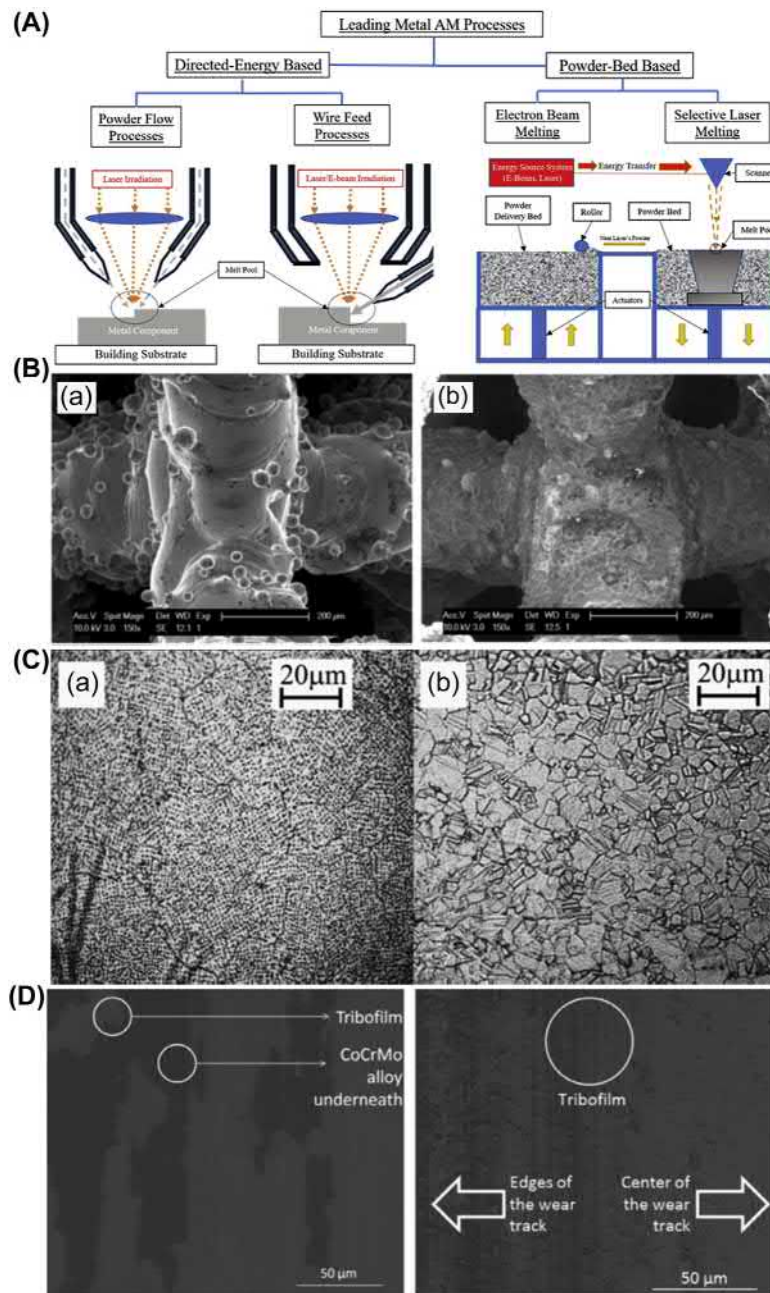
low-carbon CoCrMo alloys. Often, a compromise must be made in regard to the desired final properties in comparison with ASTM standard values.

Most CoCr implants are traditionally manufactured using investment casting or wrought processing, although alternative methods have been investigated for reducing production cost, increasing patient specificity, and enabling advanced design capabilities to increase implant longevity and performance. Castings are formed from wax molds that represent the final geometry of the implant component when the mold is covered with ceramic and hot fired with access ports, the wax burns out and a void is created where liquid metal can be cast into shape. Wrought materials are formed from ingots and shaped through various techniques. Casting alloys, while ideal for high-production volumes, are typically known for their variation in microstructure, difficulty in final machining and variations in mechanical properties in comparison to wrought materials. As shown in Table 1.3.3C.2, the mechanical properties of wrought versus cold-worked and aged F562 are significantly different when comparing the wrought versus annealed processing route. The annealing heat treatment results in larger, equiaxed grains that provide better ductility (50% elongation) at the expense of both tensile yield strength

(241–248 vs. 1586 MPa) and tensile (ultimate) strength (793–1000 MPa). Note that the range is highly dependent on the annealing temperature and time (as systematically demonstrated in Fig. 1.3.3C.4). Powder-based metal injection molding has also been investigated for manufacturing F75 and demonstrated comparable fatigue properties with increased tensile strength (1000 MPa) and ductility (40%) due to the more homogeneous microstructure in comparison to casting after post-processing and hot isostatic pressing (HIP). While these methods have shown success in producing materials that are biocompatible with adequate mechanical properties, the increase in implant failure after 10–15 years has stimulated the development of new manufacturing techniques that can simultaneously increase implant life and reduce costs for patient-matched implants.

3D Printing of CoCr Alloys

The advent of additive manufacturing or 3D printing technology has provided a layer-by-layer processing route that can introduce patient specificity as well as surface modification that are not possible using traditional methods (Bose et al., 2018). Metal-additive manufacturing processes applicable to



• **Figure 1.3.3C.5** Additive manufacturing for biomedical CoCr alloys and aspects associated with process evaluation. (A) Different AM-based processing techniques (Bandyopadhyay and Traxel, 2018). (B) Comparison of nonetched (left) to etched (right) microstructures of interconnected pores in SLM-F75 material (Van Hooreweder et al., 2017). (C) Grain size comparison of EBM F75 to wrought-processed F75 (Bordin et al., 2014). (D) Materials innovation using DED-processing (Sahasrabudhe, 2018).

biomedical applications (as shown in Fig. 1.3.3C.5A) can be combined into two distinct categories, the first being powder-bed based and the second being directed-energy-deposition (DED) methods. The DED methods utilize a powder or wire feedstock material that is melted, cooled, and rapidly solidified in a defined manner to create a layer of a component, with the deposition head moved upward to deposit subsequent layers. The DED process was utilized to make CrCo alloys for load-bearing implants and showed that a compositional gradient can be established from Ti alloys to CoCr alloys during the direct digital manufacturing (España et al., 2010). Powder-bed methods utilize a powder

delivery bed and roller system to provide a thin layer of powder which is melted by a laser or electron beam and creates a single layer. After the layer is traced out by the heat source, the powder-bed side drops a layer thickness, and the next layer of powder is rolled over from the powder delivery-bed side (Bandyopadhyay, 2018). In general, powder-bed processes utilize lower layer thickness and can create finer features than the DED processes, lending themselves well to designed porosity and internal features within patient-specific implants. Directed-energy processes are known for their ability to quickly change feedstock material as well as process metal–matrix composites, which lends them well

toward material development and testing for implants (Stenberg et al., 2018). While additive manufacturing techniques are envisioned to be the future of low-volume, patient-specific implant fabrication, challenges such as defects, residual stress, and surface roughness play a vital role in the successful implementation of this process. When parts are produced, excess powder around the parts must be removed as well as partially melted particles on the surface of the component, to ensure that no particles are loosened from the surface and put the patient's health at risk from infection or other complications. The effects of chemical etching were studied on powder removal of selective-laser-melted (SLM-processed) F75 scaffolds with interconnected pores (see Fig. 1.3.3C.5Ba and 1.3.3C.5Bb) (Van Hooreweder et al., 2017). As shown in the pre-etching images (Fig. 1.3.3C.5Ba), free particles have a tendency to sintering onto the surface of the melted and resolidified component. Etching using a combination of HCl and H₂O₂ (Fig. 1.3.3C.5Bb) resulted in a smoother surface finish without a significant compromise in fatigue performance, a property that is known to be highly dependent upon surface condition. For the same F75 material, it was demonstrated that using the SLM-processing route, changing the layer thickness from 30 to 60 μm resulted in no effect on the fatigue properties despite lower resolution and higher surface roughness, indicating that streamlining this process is possible for manufacturers of CoCr alloys in multiple different patient-specific geometries and applications (Cutolo et al., 2018). Furthermore, because of the high cooling rates that are inherent during laser-based additive manufacturing, the grain structure can vary significantly from wrought or other traditionally processed alloys and can have an effect on the machinability of the material in the as-processed condition. It has been reported that these differences (see Fig. 1.3.3C.5C) can make machining more difficult for additively processed parts than a wrought specimen of larger grain size (Bordin et al., 2014). The EBM-processed material exhibited extensive adhesive wear on the tool and resulted in cracking within the printed material. This study helps to demonstrate the importance of controlling processing parameters as well as post-processing conditions in order to achieve appropriate microstructures for machining of additively manufactured implant materials.

Materials innovation is also capable of using additive manufacturing, particularly in the case of DED systems. The ability to deposit both premixed powder compositions as well as dynamically change the composition during printing can result in unique microstructures and properties that are advantageous for improving the biomedical relevance of these materials. It was demonstrated that premixing 1–3 wt.% calcium phosphate powder into CoCrMo alloy during laser-additive manufacturing results in an in situ tribofilm on the surface of the printed component during wear testing (Sahasrabudhe, 2018). This film contributed to a lower coefficient of friction and wear debris during testing, providing a surface that is less prone to ion release during the lifetime of the implant material, and therefore decreasing the likelihood of a required secondary procedure to alleviate complications between the patient's tissue and the implant material. This

concept demonstrates a combination of materials development, design innovation, and cost reduction, to provide the best possible implant for the patient, which is truly the future of biomedical materials manufacturing.

Bio-Tribocorrosion of CoCr Alloys

One of the more relevant tests using the corrosion cell setup is measurement of the equilibrium potential or open-circuit potential (OCP). Once material is placed in the corrosion cell with its respective media, a spontaneous potential difference between WE and RE exists and may be measured. A typical setup is demonstrated in Fig. 1.3.3C.1A. For this test, an idle time is implemented to allow the potential to reach an equilibrium (Fazel et al., 2015), which is dependent on the coupled half-cell/redox reactions and can fluctuate depending on environmental factors such as oxygen, salt concentration, temperature, and the pH of the testing media. The spontaneous potential can be correlated to the chemical reactions taking place by the Nernst equation, thus allowing the proportional chemical activity to that of potential change or monitoring of the OCP. In OCP testing, the circuit is considered open with no current flow, allowing for the equilibrium potential to exist under nonpolarized conditions. Shifting from the equilibrium potential is considered “polarizing the sample,” and is achieved by introduction of a counterelectrode and control of the potential difference between the WE and the CE, as shown in Fig. 1.3.3C.1B. As the potential is varied, it gives rise to the concept of potentiodynamic polarization (PDP) Fig. 1.3.3C.3. The applied potential can allow for further reaction of the surface and is used to measure the corrosion potential (E_{corr}) and the corrosion current (I_{corr}), identifying passive and active states at varying potentials. Potentials below E_{corr} are classified as the cathodic domain, where reduction of water and dissolved oxygen determine the current, as shown in Fig. 1.3.3C.2. The second domain is characterized when a shift from cathodic current takes place to anodic current at E_{corr} , varying the applied potential in a more positive direction relative to the WE. The third domain is the passivation region; steadier current values are observed and succeed the E_{corr} peak. Certain shifts can be interpreted as the material exhibiting a lower resistance to corrosion if in the presence of the physiological environment, which has strong implications for biomedical applications. As observed in Fig. 1.3.3C.2, for example, a negative shift in E_{corr} is observed. The CoCr alloy displays a lower resistance to corrosion in a physiological environment. This displays the importance of EM for better understanding the behavior of such materials in biomedical applications—simple salt-based media testing will not suffice.

A typical tribocorrosion OCP curve for a CoCrMo alloy tested in phosphate buffered solution (PBS) and bovine serum albumin (BSA) was shown by Gil and Muñoz (2011). A sudden drop in potential by 200 mV and stability at a more negative potential occurs due to mechanical wear. The reduction in potential occurred due to the destruction of the passive layer of the WE, exposing the CoCrMo surface to the PBS and thereby activating dissolution of CoCrMo alloy. Similar results have also been reported for other biocompatible alloys (Fazel et al., 2015).

TABLE 1.3.3C.3 Bio-Tribocorrosion Results for CoCr Alloy and Ti64

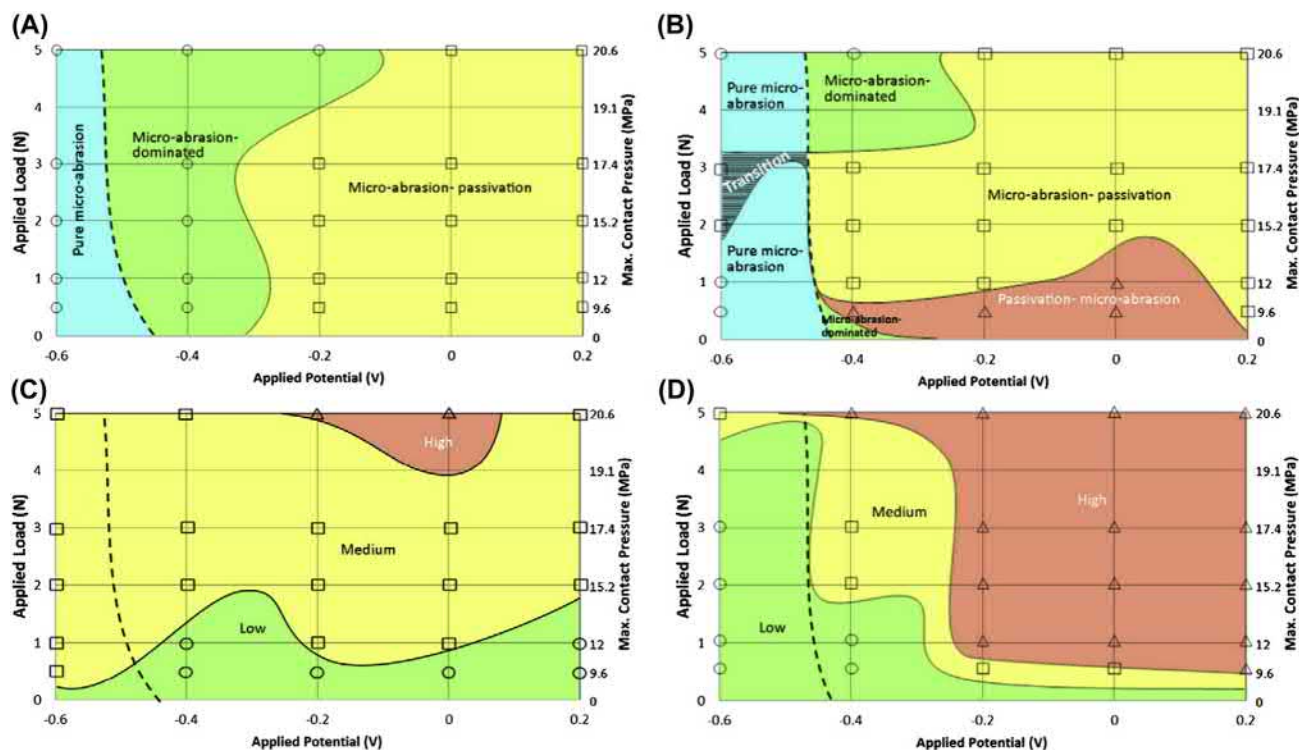
Source	Material	Processing	Medium	Counter Material	Total Slide Distance (m)	Wear Rate (mm ³ /Nm)	Idle OCP (V)	Wear OCP (V)
Sahasrabudhe et al. (2018)	CoCr alloy		DI water	SiC	1000	$3.02 \pm 0.28 \times 10^{-5}$	–	–
Dittrick et al. (2011)		LENS	Simulated body fluid	UHMWPE		4.0×10^{-6}	–	–
Balagna et al. (2012)		Cast and wrought	Bovine serum solution	Alumina	1100	2.0×10^{-5} – 3.0×10^{-6}	–	–
Cawley et al. (2003)		Varying heat treatments	DI water	SiC	225	0.95×10^{-3} – 1.26×10^{-3}	–	–
Doni et al. (2015)		Hot pressed	NaCl		5.4	–	–0.17	–0.5
Buciumeanu et al. (2016)		Hot pressed @ 10, 30, and 60 min	Artificial saliva	Alumina		–	–0.17 –0.09 –0.07	–0.46 –0.45 –0.42
Buciumeanu et al. (2017)	Ti64	Hot pressed	Artificial saliva	Alumina	5.4	–	–0.26	–0.75
Buciumeanu et al. (2018)		LENS deposited	Phosphate buffered saline			–	–0.02	–0.65
		Hot pressed					–0.25	–0.75
		Cast					–0.36	–0.9
Xiong et al. (2007)		Bar stock	DI water	UHMWPE	10,368	23×10^{-6}	–	–
Balla et al. (2014)		Rolled	Simulated body fluid	Hardened chrome steel	1000	6.82×10^{-4}	–	–

Reported results under PBS + BSA display an initial drop in OCP (depassivation) and a subsequent increase in OCP, meaning that the surface's electrochemical response is dictated by mechanical factors applied to the surface. The upward shift in OCP is due to the mixed potential of the active and unstable passive surface area attempting to reach an equilibrium. In comparison, for Ti6Al4V (Ti64), an overall negative shift in the OCP curve occurs. This shift in the OCP may be seen in Table 1.3.3C.3 for reported OCP values of Ti64. The exception is LENS processed Ti64, which at idle state exhibits a higher potential when compared with CoCr alloys but falls below during mechanical wear. The negative shift is interpreted as an increase in dissolution kinetics and results in reduced corrosion resistance at idle state and under mechanical wear conditions.

Another typical EM is performed under nondynamic polarization when a constant potential is applied and current values are measured, which are typically normalized by the exposed surface area. Unlike the potentiodynamic polarization curves, which only display the electrochemical properties of the material at idle, i.e., no mechanical wear, holding the potential constant and performing mechanical

wear can display the evolution of the anodic current over time. In one example, CoCrMo alloy was tested initially at rest and then under mechanical wear with a constant applied passive potential of 0.05 V in a base solution of 0.14 M NaCl, 0.5 g/L BSA, and bovine serum (BS) (Casabá N Juliá and Muñ Oz, 2011). Upon the initiation of mechanical wear, a rise in current is observed which is due to removal of the passivation layer. Corrosion of the exposed material occurs as the passive film is regenerated but is subsequently removed. This cycle is known as depassivation/repassivation, and results in wear-accelerated corrosion, or synergistic wear. It was observed that the protein-containing solutions allowed for a third body layer to adhere to the surface, protecting the underlying metal and therefore reducing wear and corrosion by lower current values.

The application of different normal loads can allow for microabrasion corrosion (MAC) and wastage mapping. These maps are similar to a typical metal phase diagram, or Pourbaix diagram, as the stable ionic phase is identified via a potential versus pH diagram. Wastage maps are the result of weight loss as a function of applied load and potential and are derived by



• **Figure 1.3.3C.6** (A, B) MAC wear maps of CoCrMo alloy against UHMWPE ball in FCS solution at 25°C; (C, D) wastage maps (Sadiq, 2015).

taking the ratio of weight loss due to corrosion or microabrasion corrosion. Depending on the magnitude of the ratio, regimens such as “micro-abrasion,” “micro-abrasion passivation,” or “passivation microabrasion” may be established (Sadiq et al., 2015) and can be seen in Fig. 1.3.3C.6. Wear regimens and transition zones are defined by the MAC maps within the testing parameters. The severity of material loss is defined by the wastage maps. Being able to develop these maps can prove useful when considering the fabrication of a medical device for load-bearing articulating applications. A major contributor to the development of these maps is volume loss. CoCr alloys have been reported to exhibit less wear volume than Ti64, and a summary of the reported wear rate values is displayed in Table 1.3.3C.3.

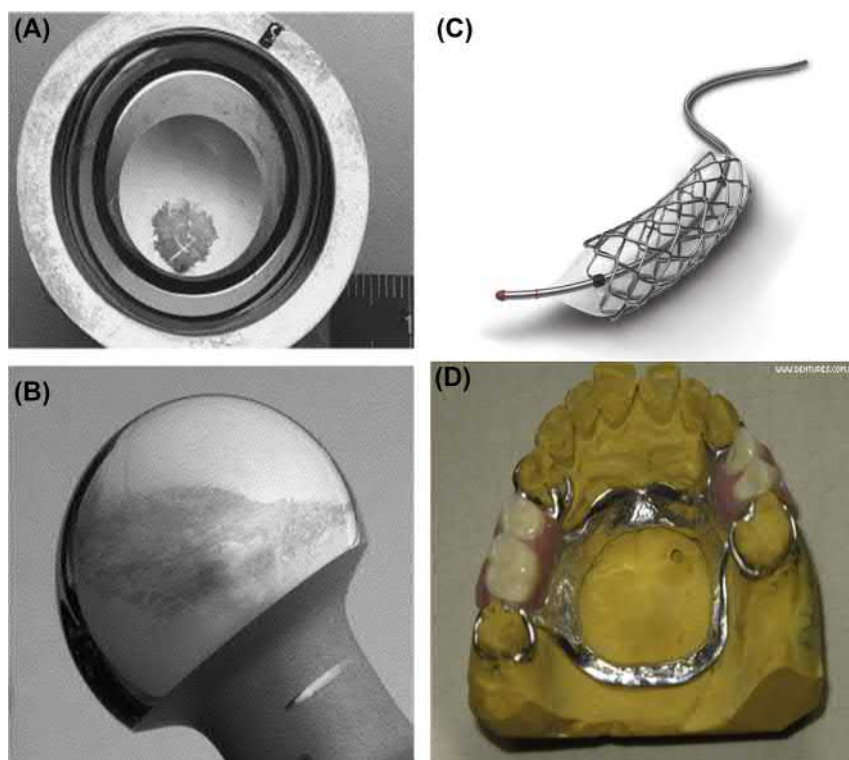
A final bio-tribological metric, electrochemical impedance spectroscopy (EIS), relates the effect of adsorbed species on the surface of the material as well as characterization of the passive film formed. The manner in which EIS is performed is by application of an alternating current (AC) potential signal through the material, current signal measurement, and calculation of the impedance of the system. Larger impedance values signify greater resistance to corrosion across a frequency range. In one example of a high-carbon CoCrMo alloy, higher impedance is reported in NaCl-based solutions and not so much in protein-based bovine serum (Igal Muñoz and Casabán Julián, 2010). The reason for this is the higher dissolution occurring in the NaCl solution, enhanced at a higher passive potential.

The general and most important take-away from CoCr alloys is the significant reduction in volume loss and positive shift in equilibrium potential. In comparing reported wear rates from

Table 1.3.3C.3 with comparable wear tests, the results display lower wear rate values associated with CoCr alloys across the board. The reported wear rates when using UHMWPE as the counter material are approximately six times lower for a CoCr alloy than they are for Ti64. This is directly proportional to the working life of an implant and reduction of wear debris. Moreover, the positive shift in the OCP is ideal for CoCr alloys. It was previously discussed that a negative shift is indicative of reduced corrosion resistance, therefore a positive shift means increased corrosion resistance. The reason for this is the phenomenon of cathodic protection—a common electrochemical method for the protection of metals. The method typically involves what is referred to as a “sacrificial metal,” which must exhibit a lower equilibrium potential than the metal needing protection. The greater the potential difference, the faster the corrosion kinetics. CrCo alloys having more positive equilibrium potential, as seen in Table 1.3.3C.3, can allow for a reduction of the drive for the corrosion mechanism to occur.

Application of CoCr Alloys in Biomedical Devices

CoCr as biomaterials were originally introduced by Austenal Laboratories (Stryker, MI) in the early 1930s for dental applications. Since then, this particular class of alloys has seen significant market demand over the past 90 years for their durability and versatility. Under the brand name of Vitallium, this class of alloys was soon adopted by the orthopedic industry because of its excellent corrosion resistance and biocompatibility. Vitallium also found its application in



• **Figure 1.3.3C.7** CoCr alloy based (A,B) McKee-Farrar prosthesis (Wimmer et al., 2003), (C) cardiac stent (Confluent Medical Technologies, 2017), (D) orthodontic wire (Cheng et al., 2010).

articulating joint arthroplasty and fracture fixation devices. In the 1970s, the alloy underwent modification in response to reports of fatigue failure in forged Vitallium.

First-generation CoCr THA implants were called Charnley prostheses, and these implants introduced an acetabular cup and small femoral head with low friction design. Later, the Harris Design 2 THA Prosthesis was brought to the market due to several recalls and failure of the Charnley prosthesis. The Harris Design 2 THA implants gained popularity by changing the original Charnley design into a collared prosthesis. These implants were also made both cemented and cementless. Following this, the introduction of tapered stem designs for THA led to better stabilization of the implant within the bony matrix. These implants were called “anatomic stems” because they incorporated an anteroposterior curve to match the bent shape of a patient’s femur. The anatomic stems came to market also due to recall of the first-generation Charnley implants and showed >92% stem survivorship along with increased bony growth, reduced stress shielding, and reduced thigh pain.

To date, CoCr alloys have been extensively used in dental, spinal, and orthopedic applications. Properties such as excellent wear and corrosion resistance, good castability, strength, and toughness make these materials viable for such applications. The first CoCr prosthetic heart valve was implanted in 1960, and lasted over 30 years due to its high wear resistance. Long-term stability, surface hardness that resists abrasive wear, and good coating properties are other key attractive characteristics for CoCr alloys to be used in biomedical devices. Several rare and noble metals in combination with CoCr possess the desired properties needed for

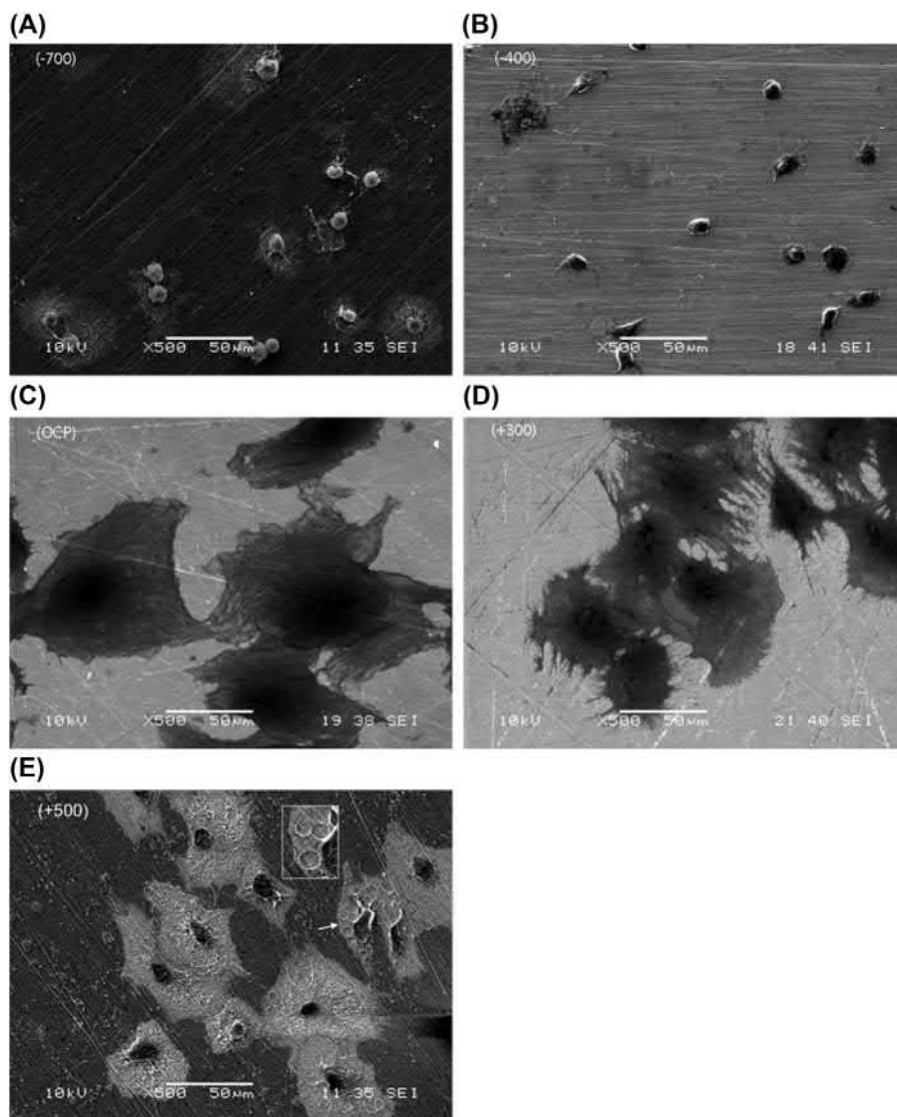
specific applications. For example, CoCrMo (CoCr–molybdenum) alloys are used in cardiac stents (Kereiakes et al., 2003), bone plates/screws/pins (Ogawa et al., 2012) (Fig. 1.3.3C.7), orthodontic wire (Cheng et al., 2010), and some craniofacial applications due to their high wear resistance. Their application as load-bearing ankle implants, however, have been fashioned out of CoNiCrMo alloys.

CoCr alloys have comparable mechanical properties to stainless steel (another material used for biomedical orthopedic applications). Heat treatment can increase tensile and fatigue strength. However, CoCr alloys have low ductility, which can result in component failure, posing a serious concern in load-bearing applications. CoCr alloys in combination with other metals can help overcome this drawback, usually by stabilizing the γ phase. The hardness and tensile strength of CoCr range from 550 to 800 MPa and 145 to 250 MPa, respectively. Table 1.3.3C.2 lists the mechanical properties of CoCr alloys in comparison with other metals used for similar applications. A complete understanding of biocompatibility, which is the most relevant property with respect to safe biological application of these implants, can provide a clear picture of the advantages and disadvantages of CoCr alloys.

Properties Leading to Biocompatibility of CoCr Alloys and Their Applications

Corrosion Resistance

Among the various material properties, corrosion resistance of CoCr alloys has gained the most significant interest in terms of



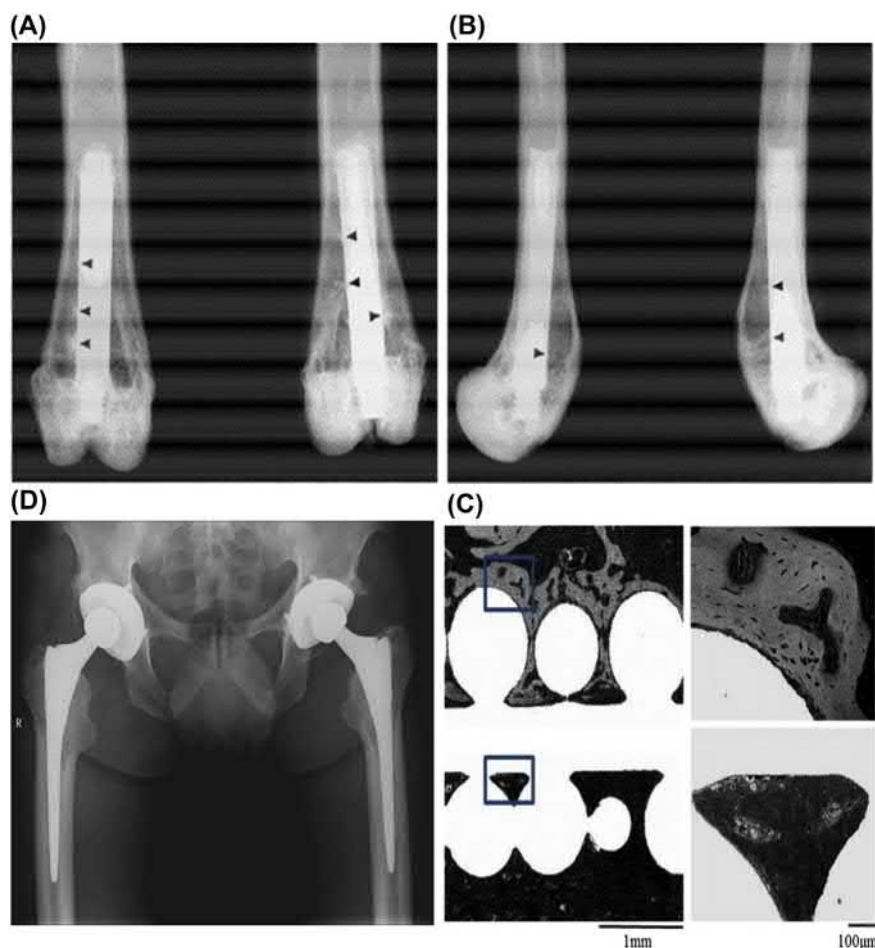
• **Figure 1.3.C.8** Topography of MC3T3 preosteoblast cells from SEM micrographs exposed to different polarization voltages for 24h. (A, B) Negative polarization voltages show rounded MC3T3 cellular morphology indicating unfavorable conditions for cellular proliferation. (C) The open-circuit potential varies from -400mV to -200mV and shows adequate cellular flattening and attachment. (D, E) Positive/increased circuit potential shows enhanced cellular proliferation and flattened morphology.

host responses. The presence of chromium helps in self-passivation of the alloy surface as mentioned above, thereby providing corrosion resistance in devices such as dental prosthetics. Under low pH conditions, Cr ions remain associated with the alloy and are responsible for the development of the corrosion-resistant surface oxide layer (Haynes et al., 2000). Dental crown and other prosthetics run the risk of getting damaged due to chemical reactions from food and enzymes. The self-passivating chromium oxide layer on the surface of CoCr prosthetics provides resistance to such damage, thereby increasing the service life. Corrosion resistance of CoCr alloys also plays an important part in medical implants by reducing complications with irritation and immune response in the surrounding tissue.

CoCr Alloys in Biological Environments

CoCr alloys under different pH conditions result in Co^{2+} particulate leaching for at least the initial 24 h compared

with Cr^{3+} ions. These alloys show markedly lower cellular toxicity at pH 4.5 due to corrosion resistance from the self-passivating oxide layer (Haynes et al., 2000). Electroactive metals, in close apposition to cellular structures, influence electrochemical processes related to cellular adhesion, proliferation, membrane transport, and other cellular redox reactions. Electrical stimulation on these materials results in cell–electrode interactive effects. Materials such as CoCr alloys, owing to their proneness to mechanically assisted corrosion, undergo large shifts in positive and negative voltage during redox reactions in a corrosive environment such as body fluid/cell culture media. The effect of these voltage changes has been shown to have positive effects on cell–material interactions between CoCr alloys and MC3T3-E1 preosteoblast cells (Haeri et al., 2012). Fig. 1.3.C.8 shows enhanced MC3T3-E1 cell attachment and proliferation with increased circuit potential.



• **Figure 1.3.3C.9** (A,B) MicroCT images of Ti6AL4V (left) and CoCr (right) showing multiple localized bone apposition regions after 12 weeks post-implantation (Jinno et al., 1998), (B) first-generation DePuy CoCr hip implant at 10-year follow up (Learnmonth, 2007), (C) electron microscope image of bone growth around CoCr implants after 3 weeks post-surgery (Ogawa et al., 2012), (D) first-generation Co-Cr implant called “anatomic stems.”

CoCr implants bypass the disadvantages often encountered with the use of NiCr implants in dental prosthetic applications, which is primarily due to cytotoxic Ni ion release. CoCr femoral prostheses have also been shown to be effective for load-bearing applications in terms of stability. In *in vivo* conditions, CoCr alloys have good biocompatibility characterized by new bone formation as early as 3 weeks post-implantation. Lamellar contact and bony-bridge formation are characteristic responses of CoCr alloys *in vivo* (Fig. 1.3.3C.9A,B) (Jinno et al., 1998). Tissue engineering has also been explored with CoCr alloys using mesenchymal stem cells and differentiated osteoblasts on the surface of the implants prior to implantation, which has been shown to improve bone interlocking as early as 3 weeks (Fig. 1.3.3C.9C) (Ogawa et al., 2012).

Clinical Concerns Related to Metal Ion Release From CoCr Alloys

Although load-bearing implants are popular, revision surgeries are also common. Some of the main reasons

for revision surgeries include wear-induced osteolysis, aseptic loosening, metal ion release, and mismatch of modulus between the implant and the bone. Moreover, it is worth noting that wear- and corrosion-induced metal ion release from CoCrMo alloys from devices used in articulating joints can potentially cause cancers and metallosis (Sansone, 2013). A recent study, with 8343 patients over 9 years, showed that the risk of cancer in tissues including bone, prostate, kidney, and skin, is higher for patients with THA that have either metal-on-metal (MOM) or metal-on-polymer (MOP) devices (Levašič, 2018). In almost all cases, these cancers were linked to release of Co^{2+} and Cr^{3+} ions due to wear and biocorrosion of metal implants. Moreover, toxicity from Co^{2+} may cause symptoms related to neurological (deafness and blindness), endocrine (hypothyroidism), hematological, and cardiological (Posada et al., 2015) damage. Due to some of these concerns, use of CoCr alloys has declined significantly in recent years for many load-bearing implant applications. However, it is still one of the best alloys available today that can provide excellent strength as well as both wear and fatigue resistance for *in vivo* applications.

Conclusions

CoCr–base alloys are widely used in dental, hip, knee, and spine arthroplasty applications because of their unique combination of strength, and wear and corrosion resistance, along with excellent fatigue properties. Although CoCr alloys are well-known in the biomedical field, recent developments in manufacturing capabilities and biologically relevant testing methods have provided new insights into how these base materials can be implemented in different applications. In this chapter, details are given on fundamental relationships between the main alloying elements, microstructure, mechanical and electrochemical properties, and in vitro as well as in vivo cellular responses of CoCr alloys. These aspects are crucial to building a foundational understanding of the material system, how it has been used previously, and the challenges that lie ahead for future engineers and physicians.

References

- Balagna, C., Spriano, S., Faga, M.G., 2012. Characterization of Co–Cr–Mo alloys after a thermal treatment for high wear resistance. *Mater. Sci. Eng. C* 32, 1868–1877. <https://doi.org/10.1016/j.msec.2012.05.003>.
- Balla, V.K., et al., 2014. Microstructure, mechanical and wear properties of laser surface melted Ti6Al4V alloy. *J. Mech. Behav. Biomed. Mater.* 32, 335–344. <https://doi.org/10.1016/j.jmbbm.2013.12.001>. Elsevier.
- Bandyopadhyay, A., Traxel, K.D., 2018. ‘Invited review article: metal-additive manufacturing—modeling strategies for application-optimized designs’. *Addit. Manuf.* 22, 758–774. <https://doi.org/10.1016/j.addma.2018.06.024>.
- Bordin, A., et al., 2014. Machinability characteristics of wrought and EBM CoCrMo alloys. *Procedia CIRP* 14, 89–94. <https://doi.org/10.1016/j.procir.2014.03.082>.
- Bose, S., et al., 2018. Additive manufacturing of biomaterials. *Prog. Mater. Sci.* 93, 45–111.
- Buciumeanu, M., et al., 2016. Tribocorrosion behavior of hot pressed CoCrMo alloys in artificial saliva. *Tribol. Int.* 97, 423–430. <https://doi.org/10.1016/j.triboint.2016.02.007>.
- Buciumeanu, M., et al., 2017. Study of the tribocorrosion behaviour of Ti6Al4V – HA biocomposites. *Tribol. Int.* 107, 77–84. <https://doi.org/10.1016/j.triboint.2016.11.029>. Elsevier.
- Buciumeanu, M., et al., 2018. Tribocorrosion behavior of additive manufactured Ti-6Al-4V biomedical alloy. *Tribol. Int.* 119, 381–388. <https://doi.org/10.1016/j.triboint.2017.11.032>.
- Casabá N Juliá, L., Muñ Oz, A.I., 2011. Influence of microstructure of HC CoCrMo biomedical alloys on the corrosion and wear behaviour in simulated body fluids. *Tribol. Int.* 44, 318–329. <https://doi.org/10.1016/j.triboint.2010.10.033>.
- Cawley, J., et al., 2003. A tribological study of cobalt chromium molybdenum alloys used in metal-on-metal resurfacing hip arthroplasty. *Wear* 255, 999–1006. [https://doi.org/10.1016/S0043-1648\(03\)00046-2](https://doi.org/10.1016/S0043-1648(03)00046-2).
- Chen, Y., et al., 2014. Effects of microstructures on the sliding behavior of hot-pressed CoCrMo alloys. *Wear* 319 (1–2), 200–210. <https://doi.org/10.1016/j.wear.2014.07.022>.
- Cheng, H., et al., 2010. Cyclic fatigue properties of cobalt-chromium alloy clasps for partial removable dental prostheses. *J. Prosthet. Dent* 104 (6), 389–396.
- Confluent Medical Technologies, 2017. Tech Note: Confluent Medical Technologies Adds Cobalt Chromium Manufacturing Capabilities Enabling Production of Balloon Expandable Stent Assemblies – Confluent Medical.
- Cutolo, A., et al., 2018. Influence of layer thickness and post-process treatments on the fatigue properties of CoCr scaffolds produced by laser powder bed fusion. *Addit. Manuf.* 23, 498–504. <https://doi.org/10.1016/j.addma.2018.07.008>.
- Davis, J.R., 2000. Nickel, Cobalt, and Their Alloys. ASM International, Materials Park, OH. <https://doi.org/10.1361/ncta2000p013>.
- Dittrick, S., et al., 2011. In vitro wear rate and Co ion release of compositionally and structurally graded CoCrMo–Ti6Al4V structures. *Mater. Sci. Eng. C* 31 (4), 809–814. <https://doi.org/10.1016/j.msec.2010.07.009>. Elsevier B.V.
- Doni, Z., et al., 2015. ‘Tribocorrosion behaviour of hot pressed CoCrMo–HAP biocomposites’. *Tribol. Int.* 91, 221–227. <https://doi.org/10.1016/j.triboint.2015.04.009>.
- Espallargas, N., Torres, C., Muñoz, A.I., 2016. A metal ion release study of CoCrMo exposed to corrosion and tribocorrosion conditions in simulated body fluids. *Wear* 669–678. <https://doi.org/10.1016/j.wear.2014.12.030>. 332–333.
- España, F.A., et al., 2010. Design and fabrication of CoCrMo alloy based novel structures for load bearing implants using laser engineered net shaping. *Mater. Sci. Eng.* 30 (1), 50–57.
- Fazel, M., et al., 2015. A comparison of corrosion, tribocorrosion and electrochemical impedance properties of pure Ti and Ti6Al4V alloy treated by micro-arc oxidation process. *Appl. Surf. Sci.* 324, 751–756. <https://doi.org/10.1016/j.apsusc.2014.11.030>. Elsevier B.V.
- Giacchi, J.V., Fornaro, O., Palacio, H., 2012. ‘Microstructural evolution during solution treatment of Co–Cr–Mo–C biocompatible alloys’. *Mater. Char.* 68, 49–57. <https://doi.org/10.1016/j.matchar.2012.03.006>.
- Gil, R.A., Muñoz, A.I., 2011. Influence of the sliding velocity and the applied potential on the corrosion and wear behavior of HC CoCrMo biomedical alloy in simulated body fluids. *J. Mech. Behav. Biomed.* 4, 2090–2102.
- Haeri, M., et al., 2012. Electrochemical control of cell death by reduction-induced intrinsic apoptosis and oxidation-induced necrosis on CoCrMo alloy in vitro. *Biomaterials* 33 (27), 6295–6304. <https://doi.org/10.1016/j.biomaterials.2012.05.054>.
- Haynes, D.R., Crotti, T.N., Haywood, M.R., 2000. Corrosion of and changes in biological effects of cobalt chrome alloy and 316L stainless steel prosthetic particles with age. *J. Biomed. Mater. Res.* 49 (2), 167–175. [https://doi.org/10.1002/\(SICI\)1097-4636.200002<49:2<167::AID-JBM3>3.0.CO;2-9](https://doi.org/10.1002/(SICI)1097-4636.200002<49:2<167::AID-JBM3>3.0.CO;2-9).
- Hermawan, H., Ramdan, D., Djuansjah, J.R.P., 2011. Metals for biomedical applications. In: *Biomedical Engineering - from Theory to Applications*. InTech, p. 64. <https://doi.org/10.5772/19033>.
- Van Hooreweder, B., et al., 2017. CoCr F75 scaffolds produced by additive manufacturing: influence of chemical etching on powder removal and mechanical performance. *J. Mech. Behav. Biomed. Mater.* 68, 216–223. <https://doi.org/10.1016/j.jmbbm.2017.02.005>.
- Igual Muñoz, A., Casabán Julián, L., 2010. Influence of electrochemical potential on the tribocorrosion behaviour of high carbon CoCrMo biomedical alloy in simulated body fluids by electrochemical impedance spectroscopy. *Electrochim. Acta* 55, 5428–5439. <https://doi.org/10.1016/j.electacta.2010.04.093>.
- Jinno, T., et al., 1998. Osseointegration of surface-blasted implants made of titanium alloy and

- cobalt-chromium alloy in a rabbit intramedullary model. *J. Biomed. Mater. Res.* 42 (1), 20–29. [https://doi.org/10.1002/\(SICI\)1097-4636.199810\)42:1<20::AID-JBM4>3.0.CO;2-Q](https://doi.org/10.1002/(SICI)1097-4636.199810)42:1<20::AID-JBM4>3.0.CO;2-Q).
- Kereiakes, D.J., et al., 2003. Usefulness of a cobalt chromium coronary stent alloy. *Am. J. Cardiol.* 92 (4), 463–466. [https://doi.org/10.1016/S0002-9149\(03\)00669-6](https://doi.org/10.1016/S0002-9149(03)00669-6).
- Kurtz, S., et al., 2007. Projections of primary and revision hip and knee arthroplasty in the United States from 2005 to 2030. *J. Bone Joint Surg. Series A* 89 (4), 780–785. <https://doi.org/10.2106/JBJS.F.00222>.
- Learmonth, I.D., Young, C., Rorabeck, C., 2007. The Operation of the Century: Total Hip Replacement, p. 370. <https://doi.org/10.1016/S0140.%3c%3e%3ca href=www.thelancet.com>.
- Levašič, V., Milošev, I., Zadnik, V., 2018. Risk of cancer after primary total hip replacement: the influence of bearings, cementation and the material of the stem. *Acta Orthop.* 89 (2), 234–239. <https://doi.org/10.1080/17453674.2018.1431854>. Taylor & Francis.
- Maradit-Kremers, H., et al., 2014. 2014 AAOS Annual Meeting. In: Prevalence of Total Hip (THA) and Total Knee (TKA) Arthroplasty in the United States. New Orleans, La, pp. 8–9.
- Mori, M., et al., 2016. ‘Development of microstructure and mechanical properties during annealing of a cold-swaged Co–Cr–Mo alloy rod’. *J. Mech. Behav. Biomed. Mater.* <https://doi.org/10.1016/j.jmbbm.2016.07.009>.
- Ogawa, M., et al., 2012. Early fixation of cobalt-chromium based alloy surgical implants to bone using a tissue-engineering approach. *Int. J. Mol. Sci* 13, 13. <https://doi.org/10.3390/ijms13055528>.
- Posada, O., et al., 2015. ‘In vitro analyses of the toxicity, immunological, and gene expression effects of cobalt-chromium alloy wear debris and Co ions derived from metal-on-metal hip implants’. *Lubricants* 3 (3), 539–568. <https://doi.org/10.3390/lubricants3030539>. Multidisciplinary Digital Publishing Institute.
- Sadiq, K., Stack, M.M., Black, R.A., 2015. Wear mapping of CoCrMo alloy in simulated bio-tribocorrosion conditions of a hip prosthesis bearing in calf serum solution. *Mater. Sci. Eng. C* 49, 452–462. <https://doi.org/10.1016/j.msec.2015.01.004>.
- Sahasrabudhe, H., Bose, S., Bandyopadhyay, A., 2018. Laser processed calcium phosphate reinforced CoCrMo for load-bearing applications: processing and wear induced damage evaluation. *Acta Biomater.* 66, 118–128. <https://doi.org/10.1016/j.actbio.2017.11.022>.
- Sansone, V., Pagani, D., Melato, M., 2013. The effects on bone cells of metal ions released from orthopaedic implants. A review. *Clinical Cases Miner. Bone Metab.* Available at: <https://www.ncbi.nlm.nih.gov/pmc/articles/PMC3710008/pdf/34-40.pdf>.
- Stenberg, K., et al., 2018. Influence of simultaneous addition of carbon nanotubes and calcium phosphate on wear resistance of 3D-printed Ti6Al4V. *JMR* 33 (14), 2077–2086.
- Wimmer, M.A., et al., 2003. Tribochemical reaction on metal-on-metal hip joint bearings A comparison between in-vitro and in-vivo results. *Wear* 255, 1007–1014. [https://doi.org/10.1016/S0043-1648\(03\)00127-3](https://doi.org/10.1016/S0043-1648(03)00127-3).
- Xiong, D., Gao, Z., Jin, Z., 2007. Friction and wear properties of UHMWPE against ion implanted titanium alloy. *Surf. Coat. Tech.* 201, 6847–6850. <https://doi.org/10.1016/j.surfcoat.2006.09.043>.

Further Reading

- Sadiq, K., Black, R.A., Stack, M.M., 2014. Bio-tribocorrosion mechanisms in orthopaedic devices: mapping the micro-abrasion-corrosion behaviour of a simulated CoCrMo hip replacement in calf serum solution. *Wear* (316), 58–69. <https://doi.org/10.1016/j.wear.2014.04.016>.

Questions

1. Describe the advantages and disadvantages of CrCr alloys for biomedical applications.
2. What are the typical processing routes for CrCo alloys?
3. Why is additive manufacturing becoming popular for making CoCr alloy-based implants?
4. Describe typical biocorrosion testing methods for CoCr alloys. What parameters can influence biocorrosion of CoCr alloys?
5. What kind of microstructures are preferred for CoCr alloys and why? What is the purpose of adding Mo or W in CoCr alloys? What is the role of Cr in CoCr alloys?

1.3.3D

Biodegradable Metals

FRANK WITTE

Professor for Bioactive Implants, Department of Prosthodontics, Geriatric Dentistry and Craniomandibular Disorders, Berlin, Germany

Introduction

The current definitions of biodegradable metals are:

A pure metal, alloy, or metal matrix composite that is intended to degrade in vivo. (Ai et al., 2019).

or

Metals are expected to corrode gradually in vivo, with an appropriate host response elicited by released corrosion products, which can pass through or be metabolized or assimilated by cells and/or tissue, and then dissolve completely upon fulfilling the mission to assist with tissue healing with no implant residues. (Liu et al., 2019).

The majority of metal implants are designed on the assumption that the device will remain in the human body for the patient's lifetime or until the device's service life has ended and requires surgical removal. However, there are some situations where permanent implants are not needed and in fact it would be beneficial if an alternative biodegradable device could be utilized. This is especially the case when load-bearing tissues are accidentally or surgically injured and complete healing is intended by the use of auxiliary implantable devices, which provide mechanical support of the healing tissue until sufficient repair or regeneration is achieved.

In these cases, biodegradable metals are advantageous due to their specific strength (strength/density), which allows the design of thin and low-volume biodegradable metal implants with higher strength than alternative biodegradable polymers. Such mechanical properties are attractive to minimize the necessary strut thickness for cardiovascular stents or for low-volume fixation screws in small bones. An advantage of the low implant volume achievable with biodegradable metals is that less material needs to be cleared or diffused from the healing site. Moreover, more space is available for the increasingly strong healing tissue, and there is a lower release of ions and secondary formed material that could potentially interact locally or systemically with the body.

A principal question when considering the use of a biodegradable metal in a medical device is which element should be chosen as a base metal? From a toxicological perspective, all obviously nontoxic elements that can form a technical metal could be selected from the mass elements (>50 mg/kg body weight), e.g., Mg or Ca, or from trace elements (<50 mg/kg body weight) in our body, e.g., Mn, Fe, or Zn. All other elements could be candidates as alloying elements. To understand which base metal might be suitable for large- or small-volume implants, the concentration of an administered element at which no adverse response is recognized (NOAEL = no observable adverse effect level) might provide some guidance (EFSA Journal, 2009; ATSDR, 2012).

According to these guidelines, the daily dosage of Mg is 6.7 mg/kg/day making Mg suitable for larger-volume implants compared to Fe (0.28 mg/kg/day) or Zn (0.07–0.23 mg/kg/day), where the NOAEL is an order of magnitude lower than for Mg-based implants and thus might be suitable for small-volume implants such as coronary stents. From the regulatory perspective, good advice is the use of minor amounts and low diversity of alloying elements (so-called lean alloys), to achieve the intended corrosion rate and mechanical strength as well as processing properties of newly designed biodegradable metals. Further selection criteria for the choice of metal or alloy may be based on the local anatomical situation, which may limit the dimensions of the implant, but also overall toxicity levels of the released ions, or the requirement for the service lifetime of the intended implant, may lead to the choice of the base metal and alloying elements.

A general agreement is that temporary implants should provide sufficient mechanical support until healing of the tissue is completed. Both loading pattern over the healing period and the time until the tissue is healed are meaningful parameters, but sound data for many clinical applications in humans are rare. Moreover, most data refer to physiological situations while implants are placed in pathological situations—or data from similar pathological situations in animals are available. Thus, one is still left alone with the scalpel

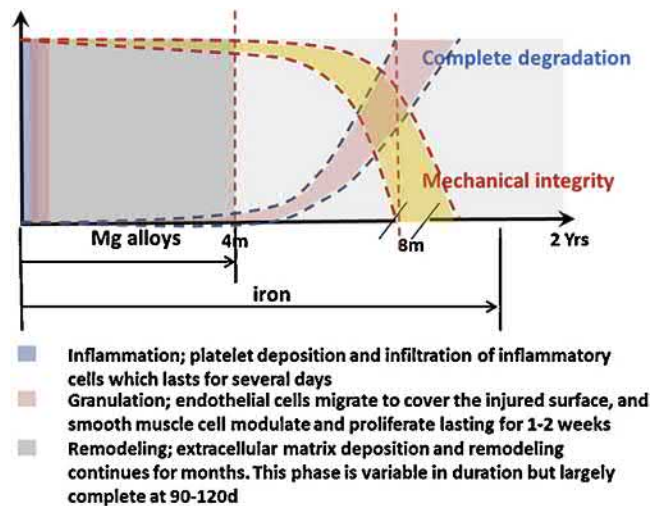
problem from animals to humans. Moreover, changes in loads at the tissue level, structural level, or whole-body level may also be considered within the various loading phases after implantation and the recovery phase for the patient. Good estimations can be drawn from biomechanical textbooks and further references (Verheul et al., 2019; Van den Bogert, 1994).

A basic truth in biomaterials is the appearance of an inflammatory phase after any implantation. This phase might be longer and more intense if degradation products need to be locally cleared, but if this reaction is only temporary and local, and the mechanical support function of the implant for the healing tissue is not compromised, the injured tissue might be completely repaired or regenerated without a persisting device made of a permanent implant material. This concept should receive more attention especially when the biological response to biodegradable metals is histologically or clinically evaluated.

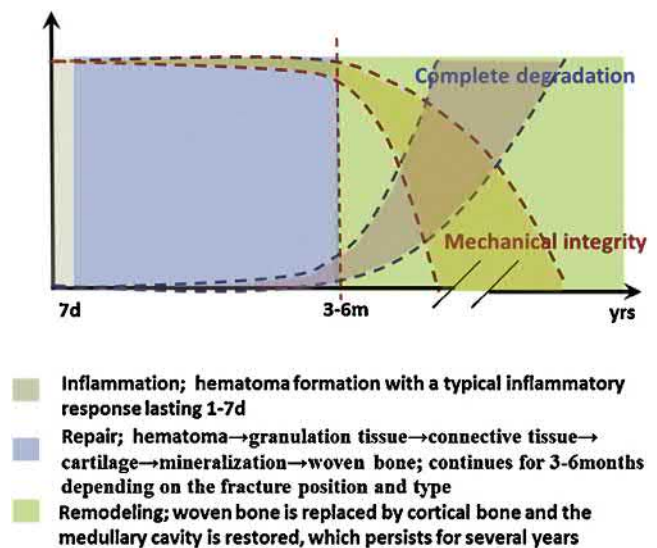
General Considerations of Corrosion Design of Biodegradable Metals

Some very general considerations on the design of the corrosion rate of temporary metal implants will be discussed. Based on standard electrode potential, reactivity, and galvanic series (corrosion potential), all the metallic elements with standard electrode potential lower than zero exhibit the potential to initiate corrosion in a neutral aqueous environment. Furthermore, metals with an electrode potential slightly higher than zero may be degraded under certain microenvironments inside the human body. In general, electrode potential and galvanic series show the tendency for corrosion, but the corrosion kinetics or extent of the degradation process is dependent on certain specific aspects such as the surface film condition and environmental parameters such as pH and flow of the media or tissue fluid around the implant (Li et al., 2014). To prevent local accumulation of corrosion products and to estimate the initial corrosion attack, the local tissue perfusion needs to be considered. In particular, changes in local perfusion after trauma or operation can dramatically reduce tissue perfusion (more than 80%) for several days after implantation (Melnik et al., 2008). Moreover, the general pathological situations of patients (e.g., cardiovascular or metabolic diseases) may also influence local perfusion.

A “holy grail” remains the prediction of cyclic fatigue of biodegradable metals in vivo, since there are still many unknown values for parameters such as local loads, changes of these loads over time, changes in perfusion and tissue coverage (corrosive environment) over the healing period, mechanical capacity of the healing tissue, time point when tissue is considered to be healed/repared, number of cycles until tissue healing/repair is accomplished, and frequency and amplitude changes over time. A general idea of the service lifetime for corroding implants in a healing tissue situation (either cardiovascular or musculoskeletal) is given in Figs. 1.3.3D.1 and 1.3.3D.2.



• **Figure 1.3.3D.1** Vascular injury after following balloon angioplasty is often observed in three overlapping phases: inflammation, granulation, and remodeling. The vessel remodeling phase, which is usually completed at 90–120 days, and the minimal luminal diameter tend to stabilize after the 90th day. Even though experts still debate whether full mechanical support in stented lesions is mandatory during the first 4 months after implantation, it would certainly be wise to use this clinical opinion as a safety design parameter and a benchmark for market approval evaluations based on the fact that there are insufficient human in vivo data available especially for mechanical vessel wall properties during the healing/remodeling phase (Zheng et al., 2014). (Reprint with permission from Elsevier.)



• **Figure 1.3.3D.2** Bone fracture healing occurs in three stages: inflammation, repair, and remodeling phases. A similar illustration is valid for absorbable bone implants, but the mechanical integrity should remain high for the first 3–6 months to allow bone repair processes to take place (Zheng et al., 2014). (Reprint with permission from Elsevier.)

It might be wise to consider a very low corrosion rate in some situations. Therefore, either a very corrosion-resistant metal/alloy can be used, but the implant may not completely dissolve, or a surface treatment or coating could be employed to protect the base material from initially high corrosion attack; however, the coating needs to dissolve/degrade as well, leaving no remnants of the implant or coating behind.

General Ideas on the Influence of Alloying Elements, Corrosion Behavior, and the Biocompatibility of Zn and Mg

It is well known that the mechanical properties, corrosion behaviors, and biocompatibility of metallic alloys are strongly influenced by alloying elements as well as by microstructure. Another effective way to improve the mechanical and corrosion properties of biodegradable metals is the use of mechanical deformation techniques such as rolling (hot/cold), extrusion, equal-channel angular pressing, high-pressure torsion, or drawing. While these techniques are known for Mg, they can also be adopted for Zn-based biodegradable metals (Zheng et al., 2014).

Materials with amorphous, nano-, or quasicrystalline structure can exhibit very promising physical, mechanical, and chemical properties, e.g., high corrosion resistance, about one to two orders of magnitude higher than polycrystalline alloys with the same alloy composition (Zberg et al., 2009; Zberg et al., 2009). In general, nanocrystallinity is assumed to improve the mechanical behavior as well as the corrosion resistance of an alloy as compared to its conventional counterpart. A reason for such a behavior might be a higher diffusivity due to the high ratio of surface to volume due to the presence of a high number of grain boundaries, thus improving the formation of a protective layer. Furthermore, the higher homogeneity allows better distribution of contaminants because of the increased area of grain boundaries, thus reducing local segregation (Liu et al., 2019; Zheng et al., 2014).

Iron-Based Biodegradable Metals

Introduction to Fe-Based Implants

Iron-based biodegradable metal implants can provide high strength (up to 1450 MPa) and high ductility (up to 80% elongation), and thus make them favored candidates for biodegradable stents (Li et al., 2014). Iron stents are characterized by high radial strength, which enables the fabrication of thin struts, while the high ductility of the Fe stents allows good plastic deformation during vascular deployment (Davim, 2019). Other attempts to use Fe-based biodegradable metals in clinical applications such as bone substitutes or osteosynthesis material have not yet been very successful (Wegener et al., 2011; Ray et al., 2018; Kraus et al., 2014). For further reading regarding the biological role of Fe in the human body, please see the following references (Yiannikourides and Latunde-Dada, 2019; Coates and Cazzola, 2019).

Modifications to Accelerate the Corrosion Rate of Fe-Based Biodegradable Metals

The advantage of a biodegradable iron implant is limited when incomplete corrosion leads to residual implant material, as has been reported with pure Fe stents. A solution to

accelerate corrosion of Fe implants but maintain mechanical strength is alloying. Among such attempts, alloying with elements such as manganese and palladium has been successful. Alloying with manganese turns the ferromagnetic iron into nonmagnetic, as a single austenitic phase is formed (Feng et al., 2016; Hufenbach et al., 2017), which is beneficial for magnetic resonance (MR) compatibility of the Fe-based device.

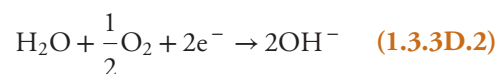
The alloying elements, including Mn, Co, W, B, C, and S, were found to improve the yield tensile stress and ultimate tensile stress (UTS) of iron, whereas the alloying element Sn led to a severe reduction in mechanical properties (Liu and Zheng, 2011; Liu et al., 2011). However, techniques such as silver ion implantation using a vapor vacuum arc technique, or by making composites with its oxides or bioceramics, have also been investigated (Li et al., 2014; Moravej and Mantovani, 2011). A more promising approach seems to be enhancing the surface of the implant and utilizing iron in its porous structure for potential scaffold applications, which has been achieved by creating a nanoporous surface via a dealloying zinc-diffused process on Fe–Mn alloys or electroforming (Li et al., 2014; Moravej et al., 2010a,b). The smaller grains of electroformed iron provide a higher grain boundary area and are more susceptible to corrosive attack. The high density of microstructural defects in electroformed iron is another reason for the higher corrosion rate with a more uniform morphology (Moravej et al., 2010a,b). The mechanical properties can be adjusted by thermomechanical treatment (Moravej et al., 2010a,b, 2011). For more details on properties of Fe-based biodegradable materials, please refer to the following references (Li et al., 2014; Moravej and Mantovani, 2011).

The Proposed Degradation Process of Fe-Based Biodegradable Metals

Iron-based biodegradable devices undergo local corrosion in the presence of dissolved oxygen with a lower tendency to dissolve relative to other biodegradable metals. This is based on the formation of a protective oxide layer that acts as a barrier to the rapid degradation. An explanation for the corrosion processes in vivo follows from the electrochemical processes found in the literature (Schinhammer et al., 2013). The anodic partial reaction (oxidation) usually proceeds rapidly in physiological media:



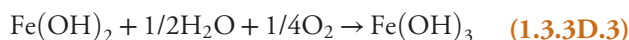
The cathodic partial reaction (reduction) in oxygen-containing aqueous solutions with a pH range between 4 and 10 is:



This pH range is representative for most of the potential implantation sites in a living body, except, e.g., for implantation in the gastrointestinal tract. The reaction kinetics of

the coupled reduction (2) and oxidation reaction (1) are dependent on the locally dissolved oxygen reaching the Fe metal surface. The critical factor for the local degradation of Fe-based implants is the local availability of oxygen in the surrounding tissue. This consideration explains the different corrosion rates of Fe stents in blood vessels and Fe pins in bone (Kraus et al., 2014; Schinhammer et al., 2013).

The degradation mechanism of Fe-based alloys and the formation of degradation products is schematically illustrated in Fig. 1.3.3D.3. This degradation process could be applied for all iron-containing alloys. In detail, the Fe ions, which are usually formed in the corrosion process, react with hydroxyl ions (OH^- ions) to form hydrous ferrous oxide ($\text{FeO} \cdot n\text{H}_2\text{O}$). Dissolved oxygen causes the ferrous (Fe^{2+}) oxides to be further oxidized to ferric (Fe^{3+}) oxides according to the following reaction:

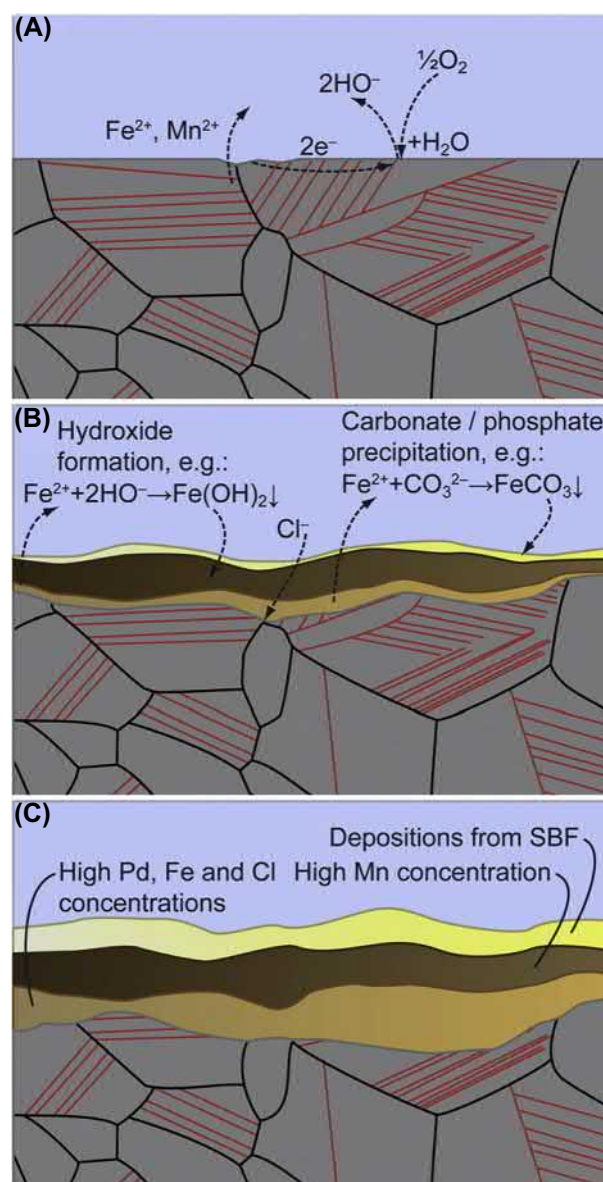


Based on the oxygen gradient in the corrosion layer, oxidation to the ferric form usually commences in the outer layers and subsequently progresses toward the *metal* surface. The formation of such Fe-oxide degradation products has been observed in vitro (Li et al., 2014), but also in vivo by Peuster et al. (Peuster et al., 2006; Peuster et al., 2001).

Another important factor influencing the degradation rate in vivo is the formation of degradation products on the implant surface, especially the formation of a complex iron phosphate layer (Schinhammer et al., 2013). The precipitation of carbonates and phosphates comprises the formation of hydroxides/oxides in the oxide layer, which allows Cl^- ions to diffuse to the metal surface, causing localized corrosive attacks (Schinhammer et al., 2013).

Biocompatibility Evaluations

Several animal tests have been reported, but one of the first in vivo experiments with Fe-based materials was performed by Peuster et al. who implanted a pure Fe stent into the descending aorta of New Zealand white rabbits that showed a moderate local macrophage infiltration and complete neointima coverage after 18 months (Peuster et al., 2001). In further studies, a biodegradable stent in a minipig model could maintain mechanical properties during the implantation without failure. However, these results also clearly demonstrated the need for faster-degrading Fe-based implants (Peuster et al., 2006; Peuster et al., 2001). Today the appropriate corrosion rate for Fe implants remains unclear since the formation of by-products of iron oxide degradation as well as the controlled release of Fe ions into the surrounding tissues is concomitant. In this regard, the biological role of Fe, especially its role in oxygen transport, needs to be considered (Silva and Faustino, 2015). Its ability to mediate electron transfer, changing between the +2 and +3 oxidation states, may elicit the production of reactive oxygen species responsible for cellular and tissue damage. To avoid those negative effects, iron is usually found coupled with



• **Figure 1.3.3D.3** The degradation process and formation of degradation products for TWIP-1Pd alloys. Schematic illustration of the degradation process and the formation of degradation products for TWIP-1Pd alloys. (A) Initiation of the corrosion reaction: the anodic partial reactions are metal oxidation, whereas the cathodic partial reaction is oxygen reduction. (B) Formation of hydroxides/oxides, and precipitation of carbonates and phosphates that comprise the degradation products. Cl^- ions diffuse to the surface, causing localized attacks. (C) Further build up of degradation products. The Pd remains in the layer close to the sample surface and acts as a macrogalvanic element to increase degradation. SBF, Simulated body fluid; TWIP = twinning-induced plasticity. (Reproduced with permission of Elsevier from Schinhammer et al., 2013.)

proteins. In serum, it is mainly associated with transferrin, while within the cells it is driven by chaperones or stored within ferritin (Silva and Faustino, 2015). The role of Fe ions for inflammation and healing tissues has to be carefully considered. For further reading on Fe metabolism and its disorders, please refer to the following references (Andrews, 1999; Ponka et al., 2015).

TABLE 1.3.3D.1 Mechanical Properties for Common Mg Alloys and Other Polymers/Metals (Han et al., 2019; Zheng et al., 2014; Katarivas Levy et al., 2017; Helsen et al., 2010)

Metal/Alloy/Polymer	E (GPa)	YS (MPa)	YS/ ρ	UTS (MPa)	UTS/ ρ	Elongation%	ρ (kg/m ³)
Mg cp	45	90	52	198	114		1738
AZ91	46	160	88	276	152	6.5	1820
WE21	46						
PA	2.1			83	73	300	1130
PLA	3.0			48		2	
Zn		160	22	200	28	0.32	7140
Zn-1.2Mg		220		362		21	
Fe (electroformed)		360	46	423	54		7874
FeMn35		230					
CoCr (ASTM1537)		928	106	1403	160		8768
Ti6Al4V	113.8	880	199	950	214	14	4430

PA, Polyamide; PLA, resorbable poly-L-lactic acid.

Current Perspective on Fe-Based Degradable Implants

Fe-based biodegradable metals are a challenging choice for temporary implants. Research efforts address very interesting potential clinical applications such as triggering drug release by using external magnetic fields, using the heat generated locally for thermal therapy of cancer, or treating implant-associated infections. Given the biocompatibility considerations, small volume implants seem to be most feasible for Fe-based alloys, such as biodegradable stents. Their main design characteristics can be given as: (1) high strength approaching 316L SS alloy with sufficient remaining ductility; (2) biocompatibility, including MR compatibility; and (3) controlled degradation within a reasonable period (1–2 years) (Moravej and Mantovani, 2011; Francis et al., 2015).

Zinc-Based Biodegradable Metals

Introduction to Zn-Based Implants

Zn-based biodegradable metals have been applied in tissues with high tolerances to Zn ions, such as vessels and muscles, but mainly in cardiovascular stent applications. The predominant processes responsible for the corrosion of zinc are the cathodic reduction of the oxygen dissolved, anodic dissolution, and pH level of the surrounding environment. The corrosion rate of Zn is comparatively lower than that of pure Mg, but higher compared to Fe-based alloys. Enhanced corrosion resistance as well as improved mechanical properties are obtained by combining Zn with Mg (Heiden, 2015). Zn-based biodegradable stents do not lead to extended inflammatory responses, which was evident when Zn stents were implanted into rat arteries. Zn and its alloys have also been explored for fixation of

fractures, besides their applications for stents (Bowen et al., 2016). The locally released concentration of zinc ions needs to be critically discussed since this essential element serves as a cofactor of many enzymes and regulatory proteins. For further reading regarding the biological role of zinc in the human body, please see the following references (Sandstead, 2015; Coleman, 1998; Vallee, 1988).

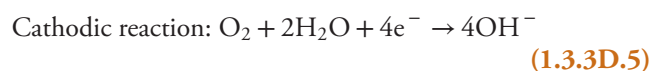
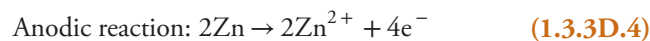
Zn-Based Materials Under Investigation

Zinc has been widely used as an alloying element in Mg-based biodegradable metals. However, the limitation of pure zinc as an implant material is based on its low strength (UTS 30 MPa) and plasticity ($\epsilon < 0.25\%$), which are inappropriate for most clinical devices. Therefore, a higher strength and hardness are the main focus of current zinc research. This can be achieved by metallurgical engineering of the zinc alloy's chemical composition and microstructure by solid-solution and second-phase strengthening as well as thermomechanical deformation techniques to improve the mechanical and corrosion properties. Currently investigated zinc alloys exhibit a wide range of ultimate tensile strengths and elongations, from 87 to 399 MPa and from 0.9% to about 170% (Katarivas Levy et al., 2017). Even minor alloying can significantly improve the mechanical properties, for example, adding 1.2% Mg to pure zinc improves its ultimate tensile strength from 18 to 362 MPa, and the elongation fraction from 0.32% to 21% (Table 1.3.3D.1). Moreover, hot rolling and hot extrusion contribute to the strength and ductility of zinc alloys, particularly in Zn-based ternary alloys. Thus conventional metallurgical approaches can be used to adjust the required mechanical properties of Zn-based biodegradable metals. Furthermore, Zn-based bulk metallic glasses have been intensively studied for their magnetic

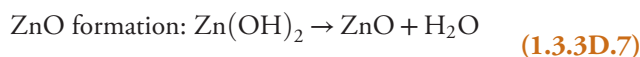
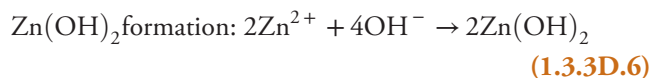
susceptibility, mechanical properties, corrosion behavior, and cytocompatibility, aiming to develop Zn-based alloys for bone repair and fracture fixation. Zn-based metallic glasses ($\text{Zn}_{38}\text{Ca}_{32}\text{Mg}_{12}\text{Yb}_{18}$) exhibited higher strength (above 600 MPa) than conventional Mg (about 200 MPa) crystalline materials, much lower magnetic susceptibility than that of commonly used biomedical alloys, and a slower degradation rate than pure Mg. During corrosion immersion testing in Hank's solution for 30 days, minimal hydrogen was generated and its compression fracture strength was retained. Based in part on its slow corrosion, Zn-based metallic glass exhibited good cytocompatibility with MG63 osteoblast cells (Zheng et al., 2014).

The Proposed Degradation Process of Zn-Based Biodegradable Metals

In general, the standard electrode potential (vs. standard hydrogen electrode) for Mg is -2.37V , for Zn -0.763V , and for Fe -0.440V , which means that Zn has a corrosion rate faster than Fe, but slower than Mg. The degradation model for Zn-based biodegradable metals in a neutral physiological environment has been proposed by Zheng et al. (2014) and generally occurs via a cathodic and anodic reaction:

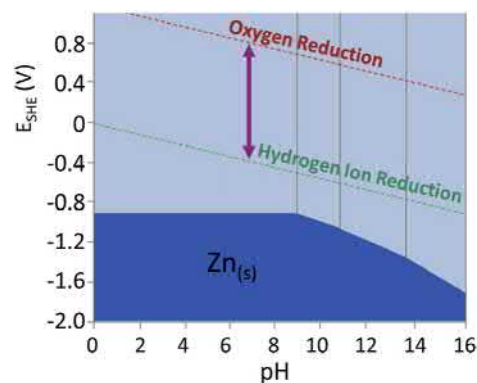
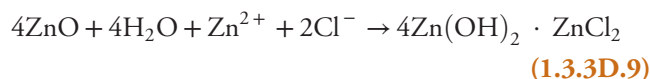
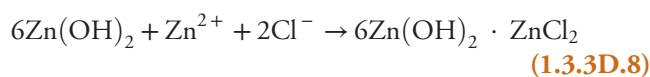


When exposed to body fluid, zinc is oxidized into metal cations following the anodic reaction in Eq. (1.3.3D.4). The generated electrons are consumed by a cathodic reaction, corresponding to the dissolved oxygen reduction in Eq. (1.3.3D.5). The corrosion reaction produces zinc hydroxides and oxides via a number of intermediate species, according to the following:



The corrosion products Zn(OH)_2 and ZnO are likely to form on the metal surface according to Eqs. (1.3.3D.6) and (1.3.3D.7).

The high concentration of chloride ions in the physiological environment destabilizes the equilibrium between dissolution and formation of the corrosion product layer, which enables chloride ions to convert the corrosion layer into soluble chloride salts as follows:



• **Figure 1.3.3D.4** Pourbaix diagram of zinc. The purple arrow shows the range of biological standard reduction potentials at pH 7.4: from ~ -820 to $\sim -670\text{mV}$ (Katarivas Levy et al., 2017). (Reprinted with permission from MDPI.)

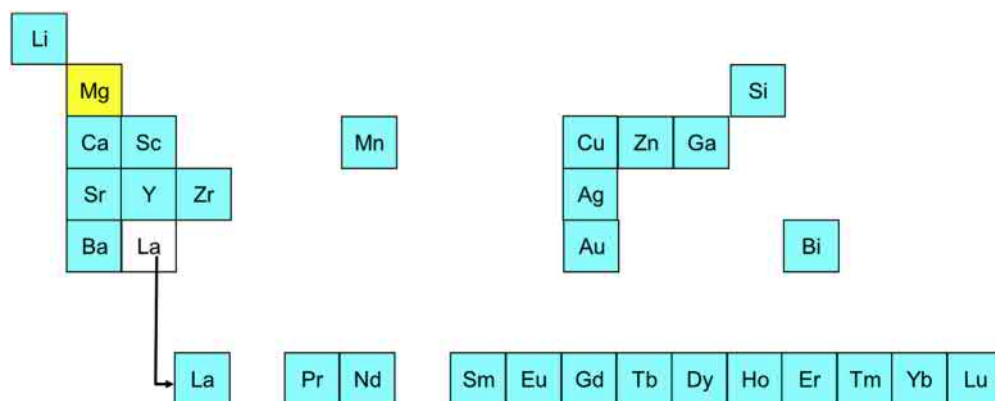
The dissolution of the Zn(OH)_2 and ZnO surface film components promotes further dissolution of the exposed metal. With progressing corrosion, irregular particles may be separated from the zinc-based metal and released into the surrounding tissue (Katarivas Levy et al., 2017).

Another important factor that needs to be considered in the corrosion of zinc is the pH value of the physiological solution or surrounding tissue (Katarivas Levy et al., 2017). According to a Pourbaix diagram, shown in Fig. 1.3.3D.4, zinc is present as hydrated $\text{Zn}^{2+}(\text{aq})$, over the entire physiological range of pH values and biological standard reduction potentials (~ -820 to $\sim -670\text{mV}$) (Fig. 1.3.3D.4).

In vivo experiments by Bowen et al. (Bowen et al., 2013, 2014) demonstrated thin layers of zinc oxide during early stages of implantation (1.5 and 3 months) on the surface of zinc wires (99.99% purity) in the rat aorta. As corrosion progressed (4.5 and 6 months), the corrosion layer thickened and contained three different phases/layers: calcium phosphate, zinc oxide, and zinc carbonate (Fig. 1.3.3D.5). The calcium phosphate layer appeared on the exterior surface without forming a true bulk product. Hence, the calcium phosphate layer was not thought to play a significant role in zinc biocorrosion. The compact corrosion layer included the two other phases, zinc oxide and zinc carbonate, with ZnO appearing in formations isolated from one another by the zinc carbonate phase. This complex corrosion layer is reminiscent of the composition reported for Mg-based biodegradable metals. These ceramic degradation products can accumulate as a function of the local tissue's physiological mass transfer rate and therefore may impact tissue healing and remodeling.

Biocompatibility of Dissolved Zn Corrosion Products

A number of zinc alloys have been developed considering nontoxicity for the choice and amount of the used alloying elements (lean alloys). As an example, for lean Zn alloys, Zn–Mg and Zn–Al with alloying element concentrations of less than 1%, enhanced mechanical properties and



• **Figure 1.3.3D.7** Alloying elements for Mg-based implants. (With courtesy from Norbert Hort.)

fixation screws (Magnezix, Syntellix AG) in patients (Fig. 1.3.3D.6). Most interestingly, both implants are made of Mg–Y–RE (WE) alloys, but both have different processing routes and serve in two different clinical applications. The benefit of biodegradable implant materials is enormous when applied in pediatrics, where the patient’s tissue often continues to grow after implantation.

Even though successful clinical applications have been proven in humans, the basic understanding of the complex processes at the implant surface and in the surrounding tissue is still not clear, primarily due to the lack of nondestructive and noninvasive methods with suitable spatial and temporal resolution for local perfusion, pH, and osmolality. For the biological role of Mg ions in the human body the reader may refer to established literature for further reading (Ala, 1958). The following text will summarize the general approach to Mg-based implants and specific biological and clinical findings.

Impact of Alloying Elements on Mg Processing and Microstructure

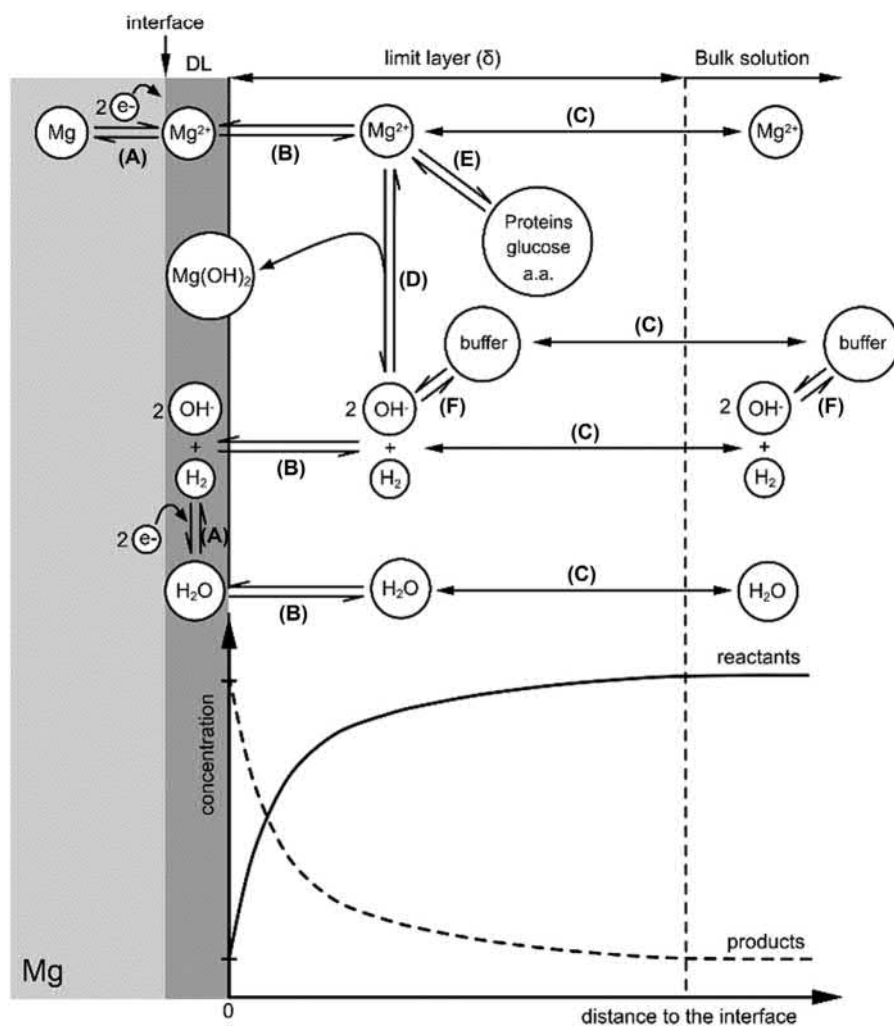
Critical properties (e.g., corrosive or mechanical) stem from the metal microstructure, which is a result of the combined alloying elements and specific processing routes, including surface conditioning. Therefore, appropriate elements for alloying have to be selected and checked for their suitability in all intended following processing steps. The first processing steps, melting and casting, are already influenced by the selected alloying elements. In a next step, wrought processes such as extrusion, rolling, and forging are often combined with heat treatments that are highly impacted by the alloying elements. However, the processing also influences the microstructure and element distribution. With respect to the biological performance, only a few elements remain as possible alloying elements as depicted in Fig. 1.3.3D.7. Due to improved casting and processing properties, Al is often chosen as an alloying element regardless of the possibility that it may be involved in Alzheimer’s disease. Other elements are also under evaluation. Still it is unpredictable which element and at what amount an alloying element can be used to achieve intended corrosive and mechanical properties in the implant material, as well as offering appropriate biocompatibility. Therefore, Mg-based alloy development is based on multiple experiments, even though first principle

calculations may be applied to guide the selection of alloying elements and their concentration.

Remarkable progress to achieve improved mechanical and corrosion characteristics has been made by using rare earth elements (REE) as alloying elements (Han et al., 2019). REEs can be categorized depending on their solubility in Mg in a high solid-solubility group (Y, Gd, Tb, Dy, Ho, Er, Tm, Yb, Lu) and a limited solid-solubility group (Nd, La, Ce, Pr, Sm, Eu). To improve the mechanical properties of Mg for cardiovascular stents, REEs may promote grain refinement upon thermomechanical treatment. REEs (e.g., Nd, Gd) may also improve the corrosion resistance of Mg alloys by suppressing microgalvanic coupling between Mg and impurities by precipitating secondary phases with similar electrochemical potentials with respect to the matrix (Chen et al., 2014; Hort et al., 2010). REEs may arouse toxicological concerns due to insufficient in vivo data, but most published preclinical literature report on biocompatible REE systems. As an alternative, Zr can be used as a grain refiner (Chen et al., 2014).

If the solid-solubility limit of Ca in Mg (1.34wt%) is exceeded, Ca saturation results in the secondary Mg_2Ca phase, which can cause accelerated corrosion (Li et al., 2008). However, the corrosion rate can be controlled by selectively doping Zn into Mg_2Ca to synchronize the corrosion potentials of the two constituent phases (i.e., Mg and Mg_2Ca). Additionally, extrusion processes have been used to break down the connectivity of the Mg_2Ca phases to prevent continuous corrosion and the formation of galvanic circuits. Adjustments to this microstructure have led to an Mg–Ca–Zn alloy (Resomet), which was approved by the Korean government in 2015 for clinical applications (Han et al., 2019).

Bulk metallic glass (BMG) materials have been created from Zn-containing Mg systems. In contrast to conventional metallic materials with crystalline structures, non-crystalline amorphous BMGs are obtained by processes such as extremely rapid cooling, ion irradiation, or physical vapor deposition. Based on their unique irregular atomic arrangement, BMGs provide low elasticity, high strength, and improved corrosion resistance due to the absence of grain boundaries (Zberg et al., 2009). However, BMGs are very brittle and may shatter during implantation or under severe loading (Han et al., 2019). For further reading on

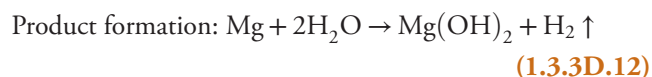
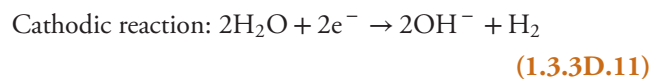
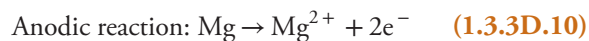


• **Figure 1.3.3D.8** Schematic description of the degradation process involving (A) electrochemical reactions, (B) absorption–desorption processes, (C) mass transfer processes, (D) precipitation reactions, (E) complexation reaction, (F) acid–base reactions (Gonzalez et al., 2018). (Reprinted with permission of Bioactive Materials.)

fundamentals in Mg alloy metallurgy the following reference is recommended (Pekguleryuz et al., 2013).

Current Models of the Corrosion Process In Vitro

When an Mg alloy is immersed in a physiological medium, the contact between the fresh metal surface and an electrolyte-containing aqueous medium initiates high corrosion rates. This process involves the release of hydrogen and the alkalization of the environment as described by the following reactions:



The formed $\text{Mg}(\text{OH})_2$ is the first product in the degradation process and precipitates on the metal surface due to its low solubility in water (12 mg/L). The consolidation or dissolution of this layer depends on the other elements present in the electrolyte and the immersion time. However, it has been shown that MgO , $\text{Mg}(\text{OH})_2$, and MgCO_3 are the main degradation products formed with the application of Hank's balanced salt solution, simulated body fluid, and Dulbecco's modified Eagle's medium (Gonzalez et al., 2018). Moreover, the solubility of the various corrosion products is dependent on environmental factors such as temperature, pH, and flow of the electrolyte.

The flow of the electrolyte or media in the in vitro setup—and probably in vivo too—can modulate the kinetics of electrochemical processes. Fig. 1.3.3D.8 displays the surface electrochemical and chemical processes involved in magnesium degradation, including the necessary mass transfer processes between the region of the metal surface and the bulk solution. As a consequence of this mass transfer process and the natural tendency of a fluid to stick to a solid surface,

a gradient of reactants (e.g., H_2O) and products (e.g., Mg^{2+} and OH^-) is stabilized (Gonzalez et al., 2018). Depending on the hydrodynamic conditions, the contribution of the mass transfer can be the major rate-determining parameter of the overall degradation process (Fig. 1.3.3D.8) (Gonzalez et al., 2018).

The best explanation for different corrosion rates of Mg-based biodegradable metals in *in vitro* and *in vivo* setups is based on different environmental conditions as depicted in Fig. 1.3.3D.9. A study investigating the reported corrosion rates across various publications on Mg-based biodegradable metals has been published by Martinez-Sanchez et al., which showed that the corrosion rate *in vitro* is about 1–5 times higher than *in vivo* (Martinez Sanchez et al., 2015).

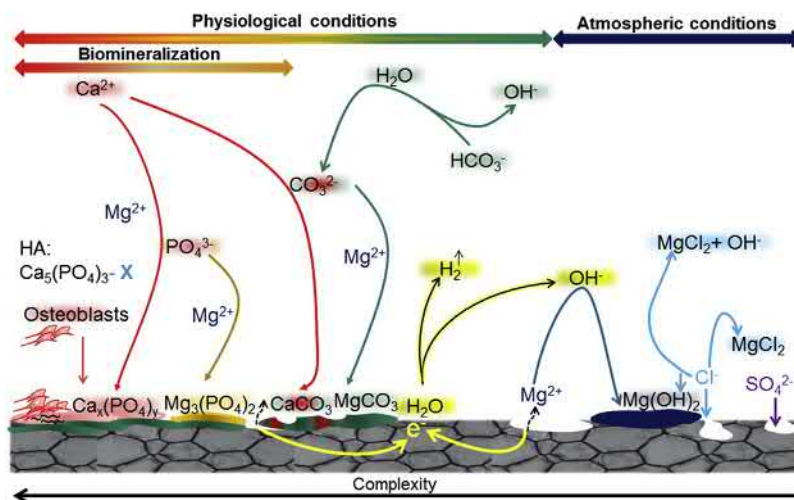
While under atmospheric conditions, $\text{Mg}(\text{OH})_2$ and MgCl_2 are the main degradation products, and carbonates (CO_3^{2-}) and phosphates (PO_4^{3-}) stabilize the corrosion layer under physiological conditions and may interact with further protein and cell adhesion. The cells themselves can influence the condition of the corrosion layer *in vitro* and *in vivo*. Especially *in vivo* the reactive zone influencing the corrosion layer on the implant is increasing and becoming more complex in terms of active parameters (cells, proteins, reactants, loads) and their constituent variations over time compared to the *in vitro* situation.

Situation In Vivo: Tissue Perfusion, pH, and the Issue of Gas Formation

It is evident that after implantation the perfusion at the implantation site is changing, disturbed by the associated mechanical damage. Ischemic tissues (low oxygen, low perfusion) influence the initial degradation behavior of the material. Generally, the blood flow in bone is rather low (Kane, 1968; Kiær et al., 1989) and after fracture or implantation there are significant changes. First, the direction of blood flow is changing from centrifugal to centripetal, thereby inducing a healing cascade, which includes cells

from the periosteum and the surrounding soft tissue (Einhorn, 1995; Rhinelander, 1974). Second, the perfusion at the fracture or implantation site shows a transient diminishing for 3–10 days, depending on the site of implantation. This reduction in perfusion can reach up to nearly 20% of the baseline value (Melnyk et al., 2008). Afterward the blood flow is successively restored and even increases compared to the flow in the healthy counterpart (Retzepi et al., 2007; Vendégh et al., 2012). This implies a highly complex interaction: not only the magnesium degradation shows a variable and time-dependent behavior, but also the tissue environment is far from stable. Consequently, a reduction of blood flow initiates a change in mass transport and oxygen saturation and raises the possibility of pH changes and degradation product accumulation. As an example, *in vitro* studies revealed that magnesium degradation, oxygen saturation, and pH are interlinked (Feyerabend et al., 2012; Willumeit et al., 2013). From the tissue side, hypoxia is essential for bone regeneration via hypoxia-inducible transcription factors (HIF-1 α and HIF-2 α) (Araldi and Schipani, 2010; Street et al., 2005) and the vascular endothelial growth factor pathway (Genetos et al., 2010), but can also be a sign of transitional pathological conditions, then upregulating osteoclast activity (Knowles, 2015).

It also seems true that the spontaneous mineralization of the corrosion layer stabilizes the corrosion *in vivo*. This phenomenon can be reduced if matrix GLA protein is locally present (Hong et al., 2019). Recent research also shows that the calcium ions in the corrosion layer seem to determine also if cells migrate on the implant surface (Amberg et al., 2019). This might lead to a thickening of the corrosion layer, which in turn reduces the velocity of mass exchange at the implantation site leading to an additional phenomenon: the formation of gas pockets around the implant. It is widely believed that these gas pockets indicate high hydrogen formation and an accumulation of hydrogen in the vicinity of the implant. However, it has been demonstrated in *in vivo*



• **Figure 1.3.3D.9** Degradation products formed under physiological conditions and the corresponding chemical reactions. As an overview, current knowledge on degradation products under physiological conditions is shown.

experiments (Kuhlmann et al., 2013) that these gas pockets do not contain high levels of hydrogen, but a substitution by other gases with a much higher tissue retention than hydrogen (Witte et al., 2008). Although these pockets may be formed by a too high initial hydrogen release, the replacement of hydrogen by other gases (nitrogen, oxygen, carbon dioxide) leads to temporary gas cavities, which can separate tissue layers. However, all in vivo observations demonstrated that these gas cavities are transient. Gas cavity may push the bone marrow locally; however, in long-term observations the final bone healing result is sufficient (Han et al., 2019).

In several clinical reports of Mg-based implants with different Mg alloys, processing and coating background, an early appearance of locally hypomineralized zones around the Mg-based implant could be observed in bone applications (Fig. 1.3.3D.10) 6–12 weeks after surgery. However, these hypomineralized zones disappear on radiographic images at the time of complete bone healing. The scientific understanding of this phenomenon is still pending. It is not clear if the stiffness changes in the hypomineralized zones are critical for the overall mechanical stability of the

fracture/osteotomy or if the temporary reduced stiffness in the implant interface could even have beneficial effects on bone healing as reported elsewhere (Weinkamer et al., 2019).

The ability of Mg implants to promote bone growth has been fully validated in various preclinical animal models using computed tomography, fluorescent imaging, and histological analysis (Han et al., 2019) and is evident from various clinical trials (Witte, 2015; Windhagen et al., 2013). The periosteal bone growth is based on the enhanced release of calcitonin gene-related peptide (CGRP) from sensory nerve endings in the periosteum, which promotes osteogenic differentiation of periosteal-derived stem cells. The peripheral release of CGRP in the sensory nerve endings upregulates the CGRP production in the dorsal root ganglion and continues until the Mg^{2+} ion-triggered release of CGRP ends (Zhang et al., 2016). However, in the bone marrow space, Mg^{2+} ions seem to stimulate an osteogenic effect by activating the canonical Wnt signaling pathway, which in turn causes bone marrow-derived stem/stromal cells to differentiate toward the osteoblast lineage (Hung et al., 2019).



• **Figure 1.3.3D.10** Clinical translation of biodegradable metallic implant materials in orthopedics. X-ray images showing fixation of the distal radius fracture with conventional stainless-steel pin implant and the scaphoid nonunion with Resomet screws at preoperative, postoperative, 6-month follow-up, and 12-month follow-up. Complete degradation of screw and bone healing was observed at 12-month follow-up. (Reprinted from Han, H.-S., et al., 2019. Current status and outlook on the clinical translation of biodegradable metals. *Mater. Today* 23, 57–71.)

Methods to Measure Mg-Based Implant Corrosion In Vitro and In Vivo

The observed corrosion of Mg-based biodegradable metals (in vitro and in vivo) is highly dependent on the environment. Therefore, samples under atmospheric conditions exhibit a black surface, typically consisting of $\text{Mg}(\text{OH})_2$, while samples immersed under cell culture conditions show various precipitates, where the main constituent has been identified as MgCO_3 . Additionally, the introduction of cell culture conditions accelerates the degradation rate of all Mg-based materials, as monitored by the increase of osmolality. Therefore, the most relevant corrosion setup for prediction of in vivo behavior includes immersion of the Mg-based sample in complex physiological solutions (e.g., HBSS) with the addition of physiological serum levels of Ca^{2+} ions, tested at cell culture conditions (37°C, 95% RH, 5% CO_2 , 21% O_2) in at least slow flowing media (Reynolds number <1000) (Gonzalez et al., 2018). The ratio of the media volume to the sample surface should be kept the same for all tested samples and needs to be reported. The level of NaHCO_3 in the media should be kept at physiological concentrations, since NaHCO_3 and CaCl_2 in the media promote the formation of MgCO_3 , which influences the measured corrosion rate. For cocultures of the material with cells, the required media and additives as well as the cells themselves can interfere with the corrosion process, which needs to be carefully checked and reported (Gonzalez et al., 2018).

Mass loss measurements are the simplest approach to analyze the degradation of Mg-based materials using ASTM standards. Chromic acid treatment (180 g/L in distilled water) facilitates the removal of the degradation layer providing an opportunity to visualize the degraded metal surface morphology (Gonzalez et al., 2018). To prevent surface-entrapped Cl^- aggregates from reacting with chromic acid and continue corrosion locally, compounds such as silver nitrate (AgNO_3 ; 2 g/L in distilled water) are added to the chromic acid. Most of the alloying elements are inert in contact with chromic acid; however, certain elements such as silicon, zirconium, and others may interact with chromates. Therefore, it is of importance to check possible interaction of magnesium alloys with chromic acid treatment. However, if Ag-containing Mg alloys are analyzed, the addition of AgNO_3 should be avoided. Another method to determine the degradation rate is with eudiometric measurements of generated hydrogen (Gonzalez et al., 2018; Tie et al., 2013). As under physiological conditions, eudiometric experiments are performed either in a gaseous atmosphere in the incubator or by gassing of the medium (Gonzalez et al., 2018). However, not many studies have been conducted with eudiometric setups. A general concern about the validity of this determination of mass loss/degradation rate should be stated, as (1) magnesium degradation influences directly the amount of O_2 and CO_2 in solution and (2) many ingredients of physiological solutions have hydrogen-binding capacities, including the medium buffering systems as stated before. Therefore, if eudiometric methods are used, the escaped gas should be analyzed (Gonzalez et al., 2018; Agha et al., 2016).

Several analytical methods have been successfully applied to investigate the corrosion of Mg-based biodegradable metals in vivo. Especially, microtomography (lab devices or synchrotron radiation based) seem to be useful to determine nondestructively the remaining metal volume and therefore can be used to estimate the corrosion rate and describe the corrosion morphology (Witte et al., 2006; Witte et al., 2010). Retrieved tissue-implant samples need special sample treatments to minimize artifacts, e.g., histological techniques requiring plastic embedding and thin microtome sections for immunohistology (Willbold and Witte, 2010). These techniques can also be used to prepare samples to analyze the locally dispersed alloying elements or impurities at ultratrace level, e.g., by laser ablation-inductively coupled plasma-mass spectrometry or synchrotron radiation-induced micro-X-ray fluorescence (Gruhl et al., 2009). High-field magnetic resonance imaging technology seems to be promising for functional imaging (Witte, 2013) as well as hydrogen measurements in vivo via hydrogen selective electrodes (Kuhlmann et al., 2013).

Preclinical and Clinical Observations for Mg-Based Biodegradable Metals

Various preclinical studies using different Mg-based materials with various processing histories and different coatings have been published for soft and hard tissue applications. A good summary can be found in the following references (Han et al., 2019; Zheng et al., 2014). In general, a low initial corrosion rate after implantation can reduce or prevent side effects such as gas cavity formation or the observation of locally hypomineralized zones. However, most of the studies provide short- to mid-term postoperative follow-ups and it is hard to predict when the implant is completely degraded. Some of the remarkable results are the effect of Mg on bone healing, but Mg-based implants might also be beneficial for soft tissue repair such as anterior cruciate ligament reconstruction in rabbits (Wang et al., 2018). An accumulation of bone morphogenetic protein-2 and vascular endothelial growth factor and reduction in the expression of matrix metalloproteinase-13 have been found around corroding pure Mg implants, which facilitated early phase healing of the tendon in bone without bone tunnel widening, implying its potential application in clinical settings (Wang et al., 2018). The result seems not to be material specific, since similar results can be obtained with interference screws made of Mg-REE alloys (Diekmann et al., 2016). Another interesting study showed the application of an Mg-6Zn alloy system as a pin stapler to treat intestinal anastomosis leading to stimulation and accumulation of the extracellular matrix and promoting healing of the anastomotic site (Cao et al., 2013).

Clinical data for Mg-based biodegradable metals are abundant for a coronary stent made by the company Biotronik AG, while only a few reports from three companies are available for orthopedic applications. The interested reader may want to study further literature for the fascinating development from preclinical studies to the final Mg stent called Magmaris, which received CE mark approval in

TABLE 1.3.3D.2 Summary of Recent Clinical Trials of Orthopedic Devices Made of Mg-Based Biodegradable Metals (Han et al., 2019)

Device Material/ Trade Name	Study Type and Identifier [#]	No. of Patients	Application	Total Duration	Outcomes
Magnezix	Prospective and randomized controlled (according to EN ISO 14155–1:2009 and EN ISO 14155–2:2009)	26	Mild hallux valgus	6 mo	Outstanding results for ROM, MTPJ, AOFAS. Equivalent performance to titanium screws for treatment of mild hallux valgus deformities.
Resomet (K-MET)	Prospective, single center, single group, open (KFDA clinical trial approval for medical device no. 362), NCT02456415	53	Hand fractures	12 mo	Normal range of grip power. No change in ROM, DASH. At 12 months, screws were completely replaced by new bones.
Pure magnesium	Prospective and randomized pilot (registered in the Chinese Clinical Trial registry), ChiCTR-TRC-13003238	48	Osteonecrosis of the femoral head	2 mo	Increased bone flap stability. Serum levels were normal. Two patients suffered collapse of the femoral head. At 12 months, higher Harris hip score than control.

AOFAS, American Orthopaedic Foot and Ankle Society; *DASH*, disabilities of the arm, shoulder, and hand; *MTPJ*, metatarsophalangeal joint; *ROM*, range of motion.

[#]Clinical trial identifiers were Retrieved From www.clinicaltrials.gov.

2016 (Han et al., 2019; Erbel et al., 2007; G et al., 2019; Haude et al., 2013; Haude et al., 2019; Hideo-Kajita et al., 2019; Joner et al., 2018; Verheye et al., 2020). The clinical studies for orthopedic applications are summarized in Table 1.3.3D.2 and briefly introduced as follows:

Orthopedic Devices Based on MgYREZr Alloy (Magnezix)

The first orthopedic application of an MgYREZr alloy screw was to treat patients with a mild hallux valgus (bunion) (Windhagen et al., 2013). In a prospective and randomized controlled study, a chevron osteotomy was performed in 26 patients who were randomly assigned to two groups and treated using either the titanium or MgYREZr alloy screws. No complications during the 6-month follow-up period were reported, but one patient from each group dropped out of the study after surgery for personal reasons. Equivalent performance of MgYREZr alloy screws compared to the conventional titanium screws was demonstrated by the range of motion of the first metatarsophalangeal joint, the visual analog scale for pain assessment, and the postoperative American Orthopaedic Foot and Ankle Society score for hallux. After receiving a CE mark in 2013, a modified chevron osteotomy study with a larger group of patients (44 total) was performed showing similar results (Plaass et al., 2016; Plaass et al., 2018; Han et al., 2019). Moreover, recent case studies have reported the application of

MgYREZr alloy systems in the fixation of distal fibular and intraarticular fractures (Biber et al., 2016).

Orthopedic Devices Based on MgCaZn Alloy (Resomet)

In a postmarket approval study (KFDA Clinical Trial Approval for Medical Device No. 362), the Mg–Ca–Zn alloy system was tested in a prospective single group clinical trial in 53 patients to evaluate its performance in the treatment of hand fractures (Lee et al., 2016). All patients revealed normal healing after 12 months with continuity of the cortical bone and a reduced diameter of the Mg–Ca–Zn alloy screws after implantation without any adverse events (Fig. 1.3.3D.10). None of the patients had any indication of pain and reported recovery of their range of motion and grip power. Even though hypomineralized zones could be seen as early as 6–12 weeks postoperatively (Fig. 1.3.3D.10, after surgery), the fracture appeared to be healed at that time point. Furthermore, the Mg–Ca–Zn screws were completely replaced by new bone after 1 year of implantation. Mg–Ca–Zn screws were approved by the KFDA for clinical use in 2015, and various prototypes are currently being developed to utilize this newly approved alloy system (Han et al., 2019).

Orthopedic Devices Based on Pure Mg

Patients with osteonecrosis of the femoral head (ONFH) received a vascularized bone flap that was fixed with screws made of high-purity (99.99%) magnesium (Zhao et al.,

TABLE 1.3.3D.3 Specific Standards Under Development for Absorbable Metals (Han et al., 2019)

Topic of Standard	Title of Standard	Status
Umbrella document	ISO/DTS 20721: Implants for surgery—guidance for the assessment of absorbable metal implants (as revised)	Under development in ISO/TC 150
Material Characterization	ASTM F3160-16: Standard guide for metallurgical characterization of absorbable metallic materials for medical implants	Published 2016
Degradation guidance	ASTM WK52640: Standard guide to in vitro degradation testing of absorbable metals	Ballot approved; expected publication 2018
Fatigue Testing	ASTM WK61103: Standard guide for corrosion fatigue evaluation of absorbable metals	Updated draft review May 2018
Biological evaluation	ISO/NP TS 37137-1: Biological evaluation of medical devices—Part 1: Guidance for absorbable implants	Under development in ISO/TC 194
	ISO/DTR 37137-2: Biological evaluation of medical devices—Part 2: Guidance for absorbable metal implants	Under development in ISO/TC 194

2016). In a prospective, randomized clinical trial (ChiCTR-TRC-13003238) with 48 patients (18–55 years) suffering from femoral head osteonecrosis of the ARCO stage II/III (Association Research Circulation Osseous), 23 patients received the Mg screw fixation of the bone flaps during ONFH and the remaining 25 patients received the vascularized bone grafting without fixation. Computed tomography analysis showed higher mineral density around the Mg screws, and continuous degradation of the Mg screw after implantation from $3.7 \pm 0.4\%$ at 1 month postoperative to $25.2 \pm 1.8\%$ at 12 months postoperative. A collapse of the femoral head was observed twice in the Mg screw group and six times in the control group. After 12 months, the Mg screw group had a significantly higher Harris hip score than the control group. The Chinese FDA (CFDA now National Medical Products Administration) recently approved high-purity Mg screws as medical devices for various applications, e.g., in fractures of the femoral neck, femoral head, and metatarsals (Han et al., 2019).

Current Perspective on Mg-Based Degradable Implants

Mg-based biodegradable metals have been intensively investigated during the past decades and have finally been introduced as medical devices in the clinic. Further clinical applications, e.g., as clips in general surgery or in oral surgery as barrier membranes or membrane fixation screws, may be available soon.

Summary

Biodegradable metals have been established as a new class of biomaterials. About one decade after rediscovery of this biomaterial class in 2000, Mg-based biodegradable metals were introduced as medical devices in cardiovascular and orthopedic applications. Medical devices based on Fe-based or Zn-based biodegradable metals seem to be promising, but

the technology needs to meet the right market and investment situation before it can be seen as medical devices on the market.

In general, it might be advisable for biodegradable metals to look for small volume implant applications that require high-specific strength materials. These applications may be safe and the clinical performance design of these implants seem to be achievable by biodegradable metals.

In this regard, iron-based biodegradable metals may have a challenging future as large-volume, solid, and bulky implants. However, there might be some advantageous applications for very low-volume Fe-based implants in well-perfused tissues. Zinc-based implants seemed to be promising for temporary implants, but they are still mainly used in academic research.

The term “absorbable” has been introduced to “biodegradable metals” in the regulatory language to harmonize the language with already existing guidelines for “absorbable polymers.” Even though it seems to be confusing, the terms “absorbable” and “biodegradable” can both be used equally for biodegradable metal implants. The standards and guidelines that are under development by ISO and ASTM (Table 1.3.3D.3) will serve as a platform that allows the comparison of results from different labs. These new standards will certainly promote a faster translation of biodegradable metals toward their clinical use.

Acknowledgment

The author appreciates the intensive discussions and help of Frank Feyerabend and Norbert Hort.

References

- Ai, H., et al., 2019. Attendees at chengdu definitions in biomaterials conference 2019. In: *Definitions of Biomaterials for the Twenty-First Century*, pp. vii–viii.

- Agency for Toxic Substances and Disease Registry (ATSDR), 2012. Toxicological profile for Manganese. Department of Health and Human Services. Public Health Service, Atlanta, GA: U.S.
- Agha, N.A., et al., 2016. Magnesium degradation influenced by buffering salts in concentrations typical of in vitro and in vivo models. *Mater. Sci. Eng. C Mater. Biol. Appl.* 58, 817–825.
- Ala, P., 1958. Biological role of magnesium. *Clin. Chem.* 4 (6), 429–451.
- Amberg, R., et al., 2019. Effect of physical cues of altered extract media from biodegradable magnesium implants on human gingival fibroblasts. *Acta Biomater.* 98, 186–195.
- Andrews, N.C., 1999. Disorders of iron metabolism. *N. Engl. J. Med.* 341 (26), 1986–1995.
- Araldi, E., Schipani, E., 2010. Hypoxia, HIFs and bone development. *Bone* 47 (2), 190–196.
- Biber, R., et al., 2016. Magnesium-based absorbable metal screws for intra-articular fracture fixation. *Case Rep. Orthop.* 2016, 9673174.
- Bowen, P.K., et al., 2016. Biodegradable metals for cardiovascular stents: from clinical concerns to recent Zn-alloys. *Adv. Healthc. Mater.* 5 (10), 1121–1140.
- Bowen, P.K., Drelich, J., Goldman, J., 2013. Zinc exhibits ideal physiological corrosion behavior for bioabsorbable stents. *Adv. Mater.* 25 (18), 2577–2582.
- Bowen, P.K., Drelich, J., Goldman, J., 2014. Magnesium in the murine artery: probing the products of corrosion. *Acta Biomater.* 10 (3), 1475–1483.
- Cao, J., et al., 2013. Animal experimental study of biodegradable magnesium alloy stapler for gastrointestinal anastomosis. *Zhonghua Wei Chang Wai Ke Za Zhi* 16 (8), 772–776.
- Chen, Y., et al., 2014. Recent advances on the development of magnesium alloys for biodegradable implants. *Acta Biomater.* 10 (11), 4561–4573.
- Coates, T.D., Cazzola, M., 2019. Introduction to a review series on iron metabolism and its disorders. *Blood* 133 (1), 1–2.
- Coleman, J.E., 1998. Zinc enzymes. *Curr. Opin. Chem. Biol.* 2 (2), 222–234.
- Davim, J.P., 2019. *Mechanical Behavior of Biomaterials*. Woodhead Publishing, p. 146.
- Diekmann, J., et al., 2016. Examination of a biodegradable magnesium screw for the reconstruction of the anterior cruciate ligament: a pilot in vivo study in rabbits. *Mater. Sci. Eng. C Mater. Biol. Appl.* 59, 1100–1109.
- Einhorn, T.A., 1995. Enhancement of fracture-healing. *JBJS* 77 (6), 940–956.
- Erbel, R., et al., 2007. Temporary scaffolding of coronary arteries with bioabsorbable magnesium stents: a prospective, non-randomised multicentre trial. *Lancet* 369 (9576), 1869–1875.
- Feng, Y.P., et al., 2016. Novel Fe–Mn–Si–Pd alloys: insights into mechanical, magnetic, corrosion resistance and biocompatibility performances. *J. Mater. Chem. B* 4 (39), 6402–6412.
- Feyerabend, F., et al., 2012. Ion release from magnesium materials in physiological solutions under different oxygen tensions. *J. Mater. Sci. Mater. Med.* 23 (1), 9–24.
- Francis, A., et al., 2015. Iron and iron-based alloys for temporary cardiovascular applications. *J. Mater. Sci. Mater. Med.* 26 (3), 138.
- Front matter, 2013. In: Pekguleryuz, M.O., Kainer, K.U., Arslan Kaya, A. (Eds.), *Fundamentals of Magnesium Alloy Metallurgy*. Woodhead Publishing, pp. i–iii.
- G, G.T., et al., 2019. Resorbable magnesium scaffold in coronary bifurcations - report of in vitro experiments. *Cardiovasc. Revasc. Med.* 20 (10), 858–864.
- Genetos, D.C., et al., 2010. Hypoxia decreases sclerostin expression and increases Wnt signaling in osteoblasts. *J. Cell. Biochem.* 110 (2), 457–467.
- Gonzalez, J., et al., 2018. Magnesium degradation under physiological conditions - best practice. *Bioact. Mater.* 3 (2), 174–185.
- Gruhl, S., et al., 2009. Determination of concentration gradients in bone tissue generated by a biologically degradable magnesium implant. *J. Anal. At. Spectrom.* 24 (2), 181–188.
- Han, H.-S., et al., 2019. Current status and outlook on the clinical translation of biodegradable metals. *Mater. Today* 23, 57–71.
- Haude, M., et al., 2013. Safety and performance of the drug-eluting absorbable metal scaffold (DREAMS) in patients with de-novo coronary lesions: 12 month results of the prospective, multicentre, first-in-man BIOSOLVE-I trial. *Lancet* 381 (9869), 836–844.
- Haude, M., et al., 2020. Sustained safety and performance of the second-generation drug-eluting absorbable metal scaffold (DREAMS 2G) in patients with de novo coronary lesions: 3-year clinical results and angiographic findings of the BIOSOLVE-II first-in-man trial. *EuroIntervention* 15 (15), e1375–e1382. <https://doi.org/10.4244/EIJ-D-18-01000>.
- Heiden, M., 2015. Magnesium, iron and zinc alloys, the trifecta of bioresorbable orthopaedic and vascular implantation - a review. *J. Biotechnol. Biomater.* 05.
- Helsen, J.A., Missirlis, Y., 2010. *Biomaterials*. In: *Biological and Medical Physics, Biomedical Engineering*. Springer-Verlag Berlin Heidelberg.
- Hideo-Kajita, A., et al., 2019. First report of edge vascular response at 12Months of Magmaris, A second-generation drug-eluting resorbable magnesium scaffold, assessed by grayscale intravascular ultrasound, virtual histology, and optical coherence tomography. A biosolve-II trial sub-study. *Cardiovasc. Revasc. Med.* 20 (5), 392–398.
- Hong, D., et al., 2019. Controlling magnesium corrosion and degradation-regulating mineralization using matrix GLA protein. *Acta Biomater.* 98, 142–151.
- Hort, N., et al., 2010. Magnesium alloys as implant materials-principles of property design for Mg-RE alloys. *Acta Biomater.* 6 (5), 1714–1725.
- Hufenbach, J., et al., 2017. Novel biodegradable Fe-Mn-C-S alloy with superior mechanical and corrosion properties. *Mater. Lett.* 186, 330–333.
- Hung, C.C., et al., 2019. The role of magnesium ions in bone regeneration involves the canonical Wnt signaling pathway. *Acta Biomater.* 98, 246–255.
- Joner, M., et al., 2018. Preclinical evaluation of degradation kinetics and elemental mapping of first- and second-generation bioresorbable magnesium scaffolds. *EuroIntervention* 14 (9), e1040–e1048.
- Kane, W.J., 1968. Fundamental concepts in bone-blood flow studies. *J. Bone Jt. Surg.* 50 (4), 801–811.
- Katarivas Levy, G., Goldman, J., Aghion, E., 2017. The prospects of zinc as a structural material for biodegradable implants—a review paper. *Metals* 7 (10).
- Kiær, T., Grønlund, J., Sørensen, K.H., 1989. Intraosseous pressure and partial pressures of oxygen and carbon dioxide in osteoarthritis. *Semin. Arthritis Rheum.* 18 (4), 57–60.
- Knowles, H.J., 2015. Hypoxic regulation of osteoclast differentiation and bone resorption activity. *Hypoxia* 3, 73–82.
- Kraus, T., et al., 2014. Biodegradable Fe-based alloys for use in osteosynthesis: outcome of an in vivo study after 52 weeks. *Acta Biomater.* 10 (7), 3346–3353.
- Kuhlmann, J., et al., 2013. Fast escape of hydrogen from gas cavities around corroding magnesium implants. *Acta Biomater.* 9 (10), 8714–8721.

- Lee, J.W., et al., 2016. Long-term clinical study and multiscale analysis of in vivo biodegradation mechanism of Mg alloy. *Proc. Natl. Acad. Sci. U. S. A.* 113 (3), 716–721.
- Li, Z., et al., 2008. The development of binary Mg–Ca alloys for use as biodegradable materials within bone. *Biomaterials* 29 (10), 1329–1344.
- Li, H., Zheng, Y., Qin, L., 2014. Progress of biodegradable metals. *Prog. Nat. Sci.: Materials International* 24 (5), 414–422.
- Liu, Y., et al., 2019. Fundamental theory of biodegradable metals—definition, criteria, and design. *Adv. Funct. Mater.* 29 (18).
- Liu, B., Zheng, Y.F., 2011. Effects of alloying elements (Mn, Co, Al, W, Sn, B, C and S) on biodegradability and in vitro biocompatibility of pure iron. *Acta Biomaterialia* 7 (3), 1407–1420.
- Liu, B., Zheng, Y.F., Ruan, L., 2011. In vitro investigation of Fe30Mn6Si shape memory alloy as potential biodegradable metallic material. *Mater. Lett.* 65 (3), 540–543.
- Martinez Sanchez, A.H., et al., 2015. Mg and Mg alloys: how comparable are in vitro and in vivo corrosion rates? A review. *Acta Biomater.* 13, 16–31.
- Melnyk, M., et al., 2008. Revascularisation during fracture healing with soft tissue injury. *Arch. Orthop. Trauma Surg.* 128 (10), 1159–1165.
- Moravej, M., et al., 2010a. Electroformed iron as new biomaterial for degradable stents: development process and structure-properties relationship. *Acta Biomater.* 6 (5), 1726–1735.
- Moravej, M., et al., 2010b. Electroformed pure iron as a new biomaterial for degradable stents: in vitro degradation and preliminary cell viability studies. *Acta Biomater.* 6 (5), 1843–1851.
- Moravej, M., et al., 2011. Effect of electrodeposition current density on the microstructure and the degradation of electroformed iron for degradable stents. *Mater. Sci. Eng. B* 176, 1812–1822.
- Moravej, M., Mantovani, D., 2011. Biodegradable metals for cardiovascular stent application: interests and new opportunities. *Int. J. Mol. Sci.* 12 (7), 4250–4270.
- Peuster, M., et al., 2001. A novel approach to temporary stenting: degradable cardiovascular stents produced from corrodible metal—results 6–18 months after implantation into New Zealand white rabbits. *Heart* 86 (5), 563–569.
- Peuster, M., et al., 2006. Long-term biocompatibility of a corrodible peripheral iron stent in the porcine descending aorta. *Biomaterials* 27 (28), 4955–4962.
- Plaass, C., et al., 2016. Early results using a biodegradable magnesium screw for modified chevron osteotomies. *J. Orthop. Res.* 34 (12), 2207–2214.
- Plaass, C., et al., 2018. Bioabsorbable magnesium versus standard titanium compression screws for fixation of distal metatarsal osteotomies - 3 year results of a randomized clinical trial. *J. Orthop. Sci.* 23 (2), 321–327.
- Ponka, P., Tenenbein, M., Eaton, J.W., 2015. Chapter 41 - iron. In: Nordberg, G.F., Fowler, B.A., Nordberg, M. (Eds.), *Handbook on the Toxicology of Metals*, fourth ed. Academic Press, San Diego, pp. 879–902.
- Ray, S., et al., 2018. Strontium and bisphosphonate coated iron foam scaffolds for osteoporotic fracture defect healing. *Biomaterials* 157, 1–16.
- Retzepi, M., Tonetti, M., Donos, N., 2007. Comparison of gingival blood flow during healing of simplified papilla preservation and modified Widman flap surgery: a clinical trial using laser Doppler flowmetry. *J. Clin. Periodontol.* 34 (10), 903–911.
- Rhineland, F.W., 1974. Tibial blood supply in relation to fracture healing. *Clin. Orthop. Relat. Res.* 105, 34–81.
- Sandstead, H.H., 2015. Chapter 61 - zinc. In: Nordberg, G.F., Fowler, B.A., Nordberg, M. (Eds.), *Handbook on the Toxicology of Metals*, fourth ed. Academic Press, San Diego, pp. 1369–1385.
- Schinhammer, M., et al., 2013. Degradation performance of biodegradable Fe–Mn–C–(Pd) alloys. *Mater. Sci. Eng. C Mater. Biol. Appl.* 33 (4), 1882–1893.
- Scientific Opinion of the Panel on Food Additives and Nutrient Sources added to Food on iron (II) taurate, magnesium taurate and magnesium acetyl taurate as sources for iron or magnesium to be added as a nutritional substance in food supplements following a request from the European Commission, 2009. *The EFSA Journal* 947, 1–30.
- Silva, B., Faustino, P., 2015. An overview of molecular basis of iron metabolism regulation and the associated pathologies. *Biochim. Biophys. Acta* 1852 (7), 1347–1359.
- Street, J.T., et al., 2005. Hypoxia regulates the paracrine coupling of angiogenesis and bone formation. *Eur. J. Orthop. Surg. Traumatol.* 15 (3), 214–225.
- Tie, D., et al., 2013. Antibacterial biodegradable Mg–Ag alloys. *Eur. Cells Mater.* 25, 284–298 discussion 298.
- Vallee, B.L., 1988. Zinc: biochemistry, physiology, toxicology and clinical pathology. *Biofactors* 1 (1), 31–36.
- Van Den Bogert, A.J., 1994. Analysis and simulation of mechanical loads on the human musculoskeletal system: a methodological overview. *Exerc. Sport Sci. Rev.* 22 (1), 23–52.
- Vendéghe, Z., et al., 2012. Effects of vasoactive substances on the neurovascular structures and microcirculation in the developing callus 10 and 15 days after bone injury. *Clin. Hemorheol. Microcirc.* 50, 279–291.
- Verheul, J., Nedergaard, N., Vanrenterghem, J., Robinson, M., 2019. Measuring biomechanical loads in team sports – from lab to field. *SportRxiv*. 1–9. <https://doi.org/10.31236/osf.io/5pt3y>.
- Verheyne, S., et al., 2020. Safety and performance of a resorbable magnesium scaffold under real-world conditions: 12-month outcomes of the first 400 patients enrolled in the BIOSOLVE-IV registry. *EuroIntervention* 15 (15), e1383–e1386. <https://doi.org/10.4244/EIJ-D-18-01058>.
- Wang, J., et al., 2018. Magnesium alloy based interference screw developed for ACL reconstruction attenuates peri-tunnel bone loss in rabbits. *Biomaterials* 157, 86–97.
- Wegener, B., et al., 2011. Microstructure, cytotoxicity and corrosion of powder-metallurgical iron alloys for biodegradable bone replacement materials. *Mater. Sci. Eng. B* 176 (20), 1789–1796.
- Weinkamer, R., Eberl, C., Fratzl, P., 2019. Mechanoregulation of bone remodeling and healing as inspiration for self-repair in materials. *Biomimetics* 4 (3).
- Willbold, E., Witte, F., 2010. Histology and research at the hard tissue-implant interface using Technovit 9100 New embedding technique. *Acta Biomater.* 6 (11), 4447–4455.
- Willumeit, R., Feyerabend, F., Huber, N., 2013. Magnesium degradation as determined by artificial neural networks. *Acta Biomater.* 9 (10), 8722–8729.
- Windhagen, H., et al., 2013. Biodegradable magnesium-based screw clinically equivalent to titanium screw in hallux valgus surgery: short term results of the first prospective, randomized, controlled clinical pilot study. *Biomed. Eng. Online* 12, 62.
- Witte, F., Bobe, K., 2013. MRI based perfusion measurements in bone after implantation of biodegradable magnesium rods. *eCM Meeting Abstracts*, 5th Symposium on Biodegradable Metals.
- Witte, F., 2015. Reprint of: the history of biodegradable magnesium implants: a review. *Acta Biomater.* 23 (Suppl. 1), S28–S40.
- Witte, F., et al., 2006. In vitro and in vivo corrosion measurements of magnesium alloys. *Biomaterials* 27 (7), 1013–1018.
- Witte, F., et al., 2008. Degradable biomaterials based on magnesium corrosion. *Curr. Opin. Solid State Mater. Sci.* 12, 63–72.

- Witte, F., et al., 2010. In vivo corrosion and corrosion protection of magnesium alloy LAE442. *Acta Biomater.* 6 (5), 1792–1799.
- Yiannikourides, A., Latunde-Dada, G.O., 2019. A short review of iron metabolism and pathophysiology of iron disorders. *Medicine* 6 (3).
- Zberg, B., et al., 2009. Tensile properties of glassy MgZnCa wires and reliability analysis using Weibull statistics. *Acta Mater.* 57 (11), 3223–3231.
- Zberg, B., Uggowitzer, P.J., Löffler, J.F., 2009. MgZnCa glasses without clinically observable hydrogen evolution for biodegradable implants. *Nat. Mater.* 8 (11), 887–891.
- Zhang, Y., et al., 2016. Implant-derived magnesium induces local neuronal production of CGRP to improve bone-fracture healing in rats. *Nat. Med.* 22 (10), 1160–1169.
- Zhao, D., et al., 2016. Vascularized bone grafting fixed by biodegradable magnesium screw for treating osteonecrosis of the femoral head. *Biomaterials* 81, 84–92.
- Zheng, Y.F., Gu, X.N., Witte, F., 2014. Biodegradable metals. *Mater. Sci. Eng. R Rep.* 77, 1–34.

1.3.4

Ceramics, Glasses, and Glass-Ceramics: Basic Principles

JULIAN R. JONES¹, IAIN R. GIBSON²

¹Department of Materials, Imperial College London, South Kensington Campus, London, United Kingdom

²Institute of Medical Sciences, School of Medicine, Medical Sciences and Nutrition, University of Aberdeen, Aberdeen, United Kingdom

Introduction

Ceramic, glass, and glass-ceramic implant materials can be broadly grouped as bioceramics. These materials often contain a broad range of hard inorganic components that are generally used to repair, replace, or regenerate bone or teeth, and their applications are becoming broader with time.

This chapter will consider bioceramic implant materials that are designed to be nearly bioinert and those that are bioactive (and biodegradable). No material implanted in living tissue is completely inert because all materials elicit a response from living tissues. Nearly-inert bioceramics tend to be used where a robust hard surface is needed, e.g. a joint replacement with articulating bearing surface or dental restoration. Nearly-inert implants are commonly surrounded by fibrous capsules in the body due to the body's inflammatory response to foreign objects. Bioactivity is regarded as the provocation of a beneficial biological response from the body's host environment to the implanted devices. In the case of bioactive ceramics, glasses, and glass-ceramics, this has traditionally been regarded as the ability to form a direct bond with bone tissue without fibrous encapsulation. This chapter will discuss these two types of bioceramics (nearly inert bioceramics and bioactive bioceramics) with a focus on materials that have been utilized in clinical applications.

Nearly-Bioinert Ceramics

Common nearly-bioinert bioceramics are alumina (aluminum oxide) and/or zirconia (zirconium oxide)-based biomaterials. A medical device, or part of it, made of these nearly-inert bioceramics is often formed from fine-grained particulate solids, e.g. by mixing the particulates with water and an organic binder, then pressing them in a

mold. Subsequently, the temperature is raised to evaporate the water (i.e., drying) and the binder is burned out. At a very much higher temperature, the part is densified during firing. After cooling to ambient temperature, one or more finishing steps, such as polishing, may be applied.

Without the densification stage, pores will remain in between the particles, which can act as defects under mechanical loads. The process of densification closes those pores in a process commonly known as sintering and for bioceramics this is typically by solid-state sintering. In some systems when the temperature is raised to a certain point at which some liquid phases form at grain boundaries, while the majority of the material remains solid, densification can occur by "liquid-phase sintering." Here, as the liquid penetrates between the grains and fills the pores, it will draw the grains together by capillary attraction, thereby decreasing the volume of the powdered compact (densification). The microstructure resulting from this "liquid-phase sintering" will consist of small grains from the original powder compact surrounded by a liquid phase. As the compact is cooled, the liquid phase will crystallize into a fine-grained matrix surrounding the original grains. A powder compact can also be densified without the presence of a liquid phase by a process called solid-state sintering. In this case, atoms move to fill up the pores and channels between the grains of the powder compact, causing the grains of crystals to bond together more tightly, thereby leading to greatly improved density, strength, and fatigue resistance for the sintered ceramic object. The rate of densification for solid-state sintering is typically slower than that for liquid-phase sintering, because material transport is slower in a solid state than in a liquid state. However, a higher degree of purity and uniformity in fine-grained microstructures can be obtained via the solid-state sintering process, making it a common process for forming many bioceramics.

Alumina and Zirconia Ceramics

Alumina (Al_2O_3) has been used in orthopedic surgery for over 50 years. High-density, high-purity (>99.5%), fine-grained polycrystalline $\alpha\text{-Al}_2\text{O}_3$ is used in the articulating surfaces of total joint prostheses because of its excellent corrosion resistance, high wear resistance, and high strength (Chevalier and Gremillard, 2009; De Aza et al., 2002). To form these ceramics, ceramic powder is pressed and sintered at 1600–1700°C. A very small amount of MgO (<0.5%) is used to aid sintering and limit grain growth during sintering. Too much sintering aid would be detrimental (Rahman et al., 2007).

The strength, fatigue resistance, and fracture toughness of polycrystalline $\alpha\text{-Al}_2\text{O}_3$ ceramics are functions of grain size and percentage of sintering aid (i.e., purity) (Chevalier and Gremillard, 2009; De Aza et al., 2002). Al_2O_3 ceramics with an average grain size of $\sim 4\ \mu\text{m}$ and >99.7% purity can exhibit good flexural strength (e.g. 55 MPa) and excellent compressive strength (e.g. 4.5 GPa), which are needed to reach the International Standards Organization (ISO) requirements for alumina implants (ISO 6474).

The use of polished alumina as part of the articulating joint was motivated mainly by its exceptionally low coefficient of friction and low wear rates. The superb tribology properties (friction and wear) of alumina occur only when the grains are very small (<4 μm) and have a very narrow size distribution. These conditions lead to very low surface roughness values ($R_a < 0.02\ \mu\text{m}$). If large grains are present, they can be pulled out, leading to very rapid wear of bearing surfaces because of local dry friction.

Yttria-stabilized zirconia was later introduced for articulating applications in hip and knee implants (Chevalier and Gremillard, 2009; De Aza et al., 2002). Specifically, zirconia stabilized with 3 mol% yttria, termed Y-TZP, results in a ceramic with excellent fracture toughness. However, a series of implant failures around the year 2000 resulted in the withdrawal of zirconia for these applications. This is because of unforeseen aging of the ceramic postimplantation, where the crystal structure of the ceramic changed from tetragonal to monoclinic, making the ceramic more brittle. Today, development of zirconia-toughened alumina (ZTA) is used as it has enhanced strength and toughness properties over $\alpha\text{-Al}_2\text{O}_3$. Small zirconia grains within the alumina matrix will not only slow down the aging process but also prevent crack propagation. ZTA is now in widespread use for the articulating surfaces of knee implants and trials are currently under way for hip arthroplasty, which could benefit younger patients as it will help preserve much of the underlying bone in the femoral head. Alumina and zirconia ceramics are described in more detail in Chapter 1.3.4B.

Bioactive Ceramics and Glasses

Bioactive ceramics and glasses are designed to elicit a biological response that supports tissue repair, specifically

bone formation and integration. The types of biological responses to such bioactive materials, alongside bioinert ceramics, are discussed in detail in Chapter 2.2.2 and the classic descriptions of these are summarized in Table 1.3.4.1.

The responses described in Table 1.3.4.1 are not simply dictated by material type; the physical form that a given material takes will also influence the local tissue response, such as dense or porous, low or high surface area, among others. In the context of bone repair, a bioactive material would be associated with bone formation at the implant surface, but it may also undergo osteoclast resorption (Hasegawa et al., 2003), activation of a proinflammatory response (Zhao et al., 2018), or new blood vessel formation (Arkudas et al., 2013), in addition to being chemically resorbed. Clinical applications of bioactive ceramics and bioactive glasses are quite broad and Table 1.3.4.2 lists some of the example cases.

These different applications require the use of bone grafts. Synthetic bone graft substitutes derived from bioactive ceramics and bioactive glasses offer advantages over other grafts such as autografts, allografts, and demineralized bone matrix (DBM) (Oryan et al., 2014). The properties of these synthetic materials will depend on their chemical compositions, their physical micro- and macrostructures, and the forms in which they are used within an implant. These different attributes of bioactive ceramics and bioactive glasses will now be described separately. It should be noted that bioactive ceramics and glasses also have a role as scaffolds in orthopedic tissue engineering and this is described elsewhere in this book (see Chapters 2.6.3 and 2.6.5).

TABLE 1.3.4.1 Types of Implant-Tissue Response Observed With Bioceramics

Type of Tissue Response to Biomaterial	Description of Tissue Response
Biologically active (bioactive)	An interfacial bond with tissue forms. For bone repair, implants may allow/support the formation of bone (osteoconductive) or may induce the formation of bone.
Biologically inactive (nearly inert, or bioinert)	The material is tolerated by the formation of a fibrous tissue layer for variable thickness
Resorbable	Implant material is resorbed/ degraded by chemical and/or biological processes, typically designed to allow new tissue to replace it. Degradation products should be biocompatible.
Toxic	Toxic response, surrounding tissue death (local), with potential systemic toxicity

Bioactive Ceramics

A number of ceramic materials have been shown to be bioactive but the most widely studied group is calcium phosphate-based bioceramics. These materials share a similarity in chemical composition to the mineral component of bone and teeth. A wide range of distinct calcium phosphate phases exist that can be found in mineralized tissue in nature. This family of calcium phosphate phases is typically classed in terms of the molar ratio of calcium-to-phosphorus (Ca/P), their polymorphs (same chemical composition but different crystal structure), the presence/absence of structural water, and whether any crystalline phases can only form at high temperatures (e.g., tetracalcium phosphate). Some of the main phases that are relevant to bioactive calcium phosphate ceramics and bone graft substitutes are listed in Table 1.3.4.3.

TABLE 1.3.4.2 Types of Clinical Indications That Utilize Bioactive Ceramics and/or Glasses as Synthetic Bone Graft Substitutes

Orthopedics	
General	Filling of bone defects, including after removal of bone cysts
Trauma	Long-bone nonunion fractures Tibial plateau fractures Repair of long bone fractures Hand surgery
Spine	Posterolateral spinal fusion Interbody spinal fusion
Craniomaxillofacial/Dental	
Trauma	Cranioplasty Repair of orbital floor fracture
Disease	Sinus obliteration Repair after cyst removal
General oral/ dental defects	Ridge augmentation Repair of tooth extraction sites Periodontal regeneration

One of the major differences in the properties of these different calcium phosphate phases is their relative solubility. At physiological pH and at 37°C, the solubility of the CaPs listed in Table 1.3.4.3 has the following order: dicalcium phosphate anhydrous (DCPA) = dicyclopentadiene (DCPD) > α -tricalcium phosphate (α -TCP) > β -TCP > TCP > Ca-deficient apatite (CDA) > octacalcium phosphate (OCP) > hydroxyapatite (HA) (LeGeros, 2002). The application of a number of these phases (DCPA, DCPD, α -TCP, and TCP) is predominantly as reactant phases in calcium phosphate bone cements, due to their inherent high solubility at physiological pH; these cements will be discussed later.

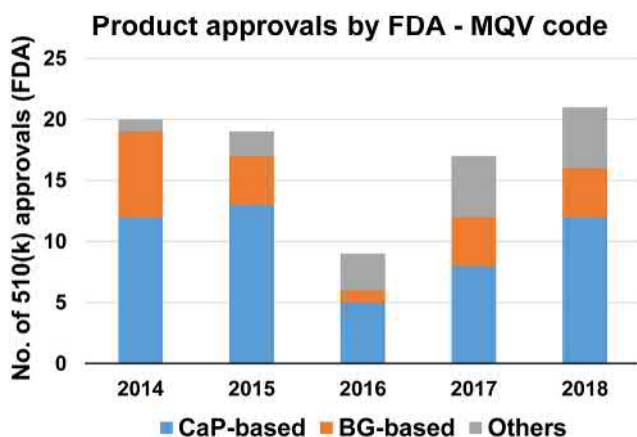
DCPD, DCPA, and OCP, although not traditionally classed as ceramics as they form by aqueous precipitation at or close to room temperature and would transform to different calcium phosphate phases through traditional high-temperature ceramic processing, have been studied as potential bone graft substitutes (Tamimi et al., 2010; Komlev et al., 2014; Sheikh et al., 2017; Kawai et al., 2017).

Calcium phosphates can be used to coat metallic and polymeric implants to provide a bioactive surface on a bulk material that is biologically inert. The most studied coating is HA on metallic implants and it is usually applied to the implant surface using a high-temperature plasma-spraying method. This, along with other coating methods, is described in more detail in Chapter 1.3.4A.

Of the calcium phosphate phases listed in Table 1.3.4.3, HA and TCP are the two compositions that are widely studied as bioactive ceramics. They are mainly used as bone graft substitutes, which sometimes are referred to as bone void fillers (BVs). They are typically used in the form of porous ceramics, often within a natural (e.g., collagen) or synthetic (e.g., polyethylene glycol [PEG]) polymeric carrier, or as cements. These different forms offer distinct advantages, depending on the nature of the bone defect to be repaired. In the United States, calcium salt BVFs approved for orthopedic use by the Food and Drug Administration (FDA) are classed with a product code MQV, whereas for dental application they have the code LYC. To give some context of the number of synthetic bone graft substitutes available

TABLE 1.3.4.3 Different Calcium Phosphate Phases Relevant to Bioceramics

Chemical Name	Chemical Formula	Ca/P Molar Ratio	Mineral Name
Dicalcium phosphate anhydrous	CaHPO ₄	1.0	Monetite
Dicalcium phosphate anhydrous	CaHPO ₄ ·2H ₂ O	1.0	Brushite
Octacalcium phosphate	Ca ₈ (HPO ₄) ₂ (PO ₄) ₄ ·5H ₂ O	1.33	
Tricalcium phosphate (α -, β -) (TCP)	Ca ₃ (PO ₄) ₂	1.50	Whitlockite (β -TCP)
Ca-deficient apatite	Ca _{10-x} (HPO ₄) _x (PO ₄) _{6-x} ·(OH) _{2-x}	0 < x ≤ 1, (1.50 ≤ Ca/P < 1.67)	
Hydroxyapatite	Ca ₁₀ (PO ₄) ₆ (OH) ₂	1.67	Apatite, hydroxyapatite
Tricalcium phosphate	Ca ₄ O(PO ₄) ₂	2.0	Hilgenstockite



• **Figure 1.3.4.1** The number of synthetic bone graft substitutes approved annually by the Food and Drug Administration (FDA) under the MQV product code (calcium salt bone void fillers) between 2014 and 2018; the approvals may be for trauma indications and/or posterolateral spinal fusion indications (CaP based include hydroxyapatite, tricalcium phosphate, and biphasic calcium phosphate-based bone grafts and CaP cements; bioactive glass [BG]-based includes Bioglass containing bone grafts; others include demineralized bone matrices, calcium carbonate-based bone grafts, and polymer-based bone grafts).

commercially, a summary of the number of MQV products approved by the FDA between 2014 and 2018 is depicted in Fig. 1.3.4.1.

Porous Calcium Phosphate Ceramics

Bone graft substitutes produced from porous calcium phosphates usually consist of either HA or β -TCP, or a mixture of these two phases to produce biphasic calcium phosphates (BCPs). The relative solubility of β -TCP is much higher than that of HA. Both of these materials are osteoconductive, providing a surface that encourages new bone formation, with their major difference being the rate of degradation in vivo (Klein et al., 1983). In cases where rapid resorption of the bone graft is required, the use of β -TCP could be preferred to HA, but the challenge could be that the β -TCP resorbs faster than the rate of bone formation. The limited solubility of HA ceramics can result in a material with an osteoconductive surface that, once host bone forms on the surface, shows limited further integration and is not remodeled.

The rationale for BCP compositions with a biphasic mixture of HA and β -TCP is that it provides a material offering a mixture of these biological responses (Bouler et al., 2017). The relative amounts of these two phases has been shown to have an effect on bone formation (Jensen et al., 2009), soft tissue response (Ghanaati et al., 2012), material degradation/resorption (Yamada et al., 1997; Daculsi et al., 1989), and even osteoinduction (Arinze et al., 2005; Tang et al., 2017).

Calcium phosphate phases utilized as bioceramics can be synthesized using a number of methods; these are described in detail for the case of HA in Chapter 1.3.4A, and all these

methods may also be used to synthesize TCP and BCP bioceramics. Briefly, aqueous precipitation reactions involving calcium and phosphate reactants are preferred methods (Osaka et al., 1991; Jarcho et al., 1976). The Ca/P molar ratio of the product formed can be controlled by the synthesis conditions, principally the pH but also the concentration of reactants and the temperature, and this method can be easily scaled to large volumes for translation to commercial manufacture. In these methods the product formed is described by the composition in Table 1.3.4.2 of a CDA, and the value of x can vary from 0 to 1 depending on the synthesis design. When the formed composition is heated/sintered to temperatures above 750°C and water is lost, the final composition will form with either HA ($x=0$), TCP ($x=1$), or BCP ($1 > x > 0$, with the amount of TCP relative to HA increasing as x increases). If excess calcium is present, or reaction conditions have allowed large drops in pH to below 7, it is possible that other CaP phases may be present in the product phase (DCPD, DCPA, or OCP) and this would affect the final bioceramic composition on heating/sintering. Aqueous precipitation reactions can also be used to synthesize DCPD, DCPA, or OCP, but these would not involve a heating/sintering step to form the final composition.

There is an increased interest in producing nanoparticles of calcium phosphates, primarily apatites, and these can be produced by aqueous precipitation reactions but can also be synthesized by other methods such as biomimetic synthesis, sol-gel synthesis, and hydrothermal methods (see Chapter 1.3.4A).

Synthesized CaP bioceramics can be characterized by a number of methods and ISO 13175-3 (2012) and ASTM F1185-03 (2014), F1088-18 (2018) standards describe the requirements of characterization methods and the expected parameters for use of these compositions as bone replacement materials. Primary measures of chemical characteristics of these materials include phase composition/phase purity (X-ray diffraction), chemical composition (Ca/P molar ratio, impurity content, using, e.g., X-ray fluorescence and/or inductively coupled plasma-optical emission spectrometry), presence of specific functional groups (Fourier transform infrared and/or Raman spectroscopy), surface area, and density. The identification of different calcium phosphate phases can be achieved by reference to standard powder diffraction files from the International Centre for Diffraction Data. Some of these main CaP phases and the most common impurity phases are listed in Table 1.3.4.4.

Infrared and Raman spectroscopy have been used to characterize naturally occurring calcium phosphates and also synthetic calcium phosphates (Koutsopoulos, 2002), providing a complementary method for distinguishing different CaP phases and small changes that may occur in these materials during synthesis and/or processing, such as the inclusion of carbonate ions or the loss of structural water.

In addition to the chemistry of bone graft substitute ceramics affecting their behavior, the physical form in which they are manufactured is as, if not more, influential. HA, TCP, and BCP ceramics can be produced by typical ceramic approaches such as optimizing the powder properties in

TABLE 1.3.4.4 Powder Diffraction Files (PDFs) for the Main Calcium Phosphate Phases and Most Common Impurity Phases

Chemical Name	Chemical Formula	PDF No.
Hydroxyapatite (hexagonal)	$\text{Ca}_{10}(\text{PO}_4)_6(\text{OH})_2$	00-009-0432
Tricalcium phosphate	$\beta\text{-Ca}_3(\text{PO}_4)_2$	00-009-0169
Tricalcium phosphate	$\alpha\text{-Ca}_3(\text{PO}_4)_2$	00-009-0348
Dicalcium phosphate anhydrous	CaHPO_4	00-009-0080
Dicalcium phosphate anhydrous	$\text{CaHPO}_4 \cdot 2\text{H}_2\text{O}$	00-009-0077
Octacalcium phosphate	$\text{Ca}_8(\text{HPO}_4)_2(\text{PO}_4)_4 \cdot 5\text{H}_2\text{O}$	00-026-1056
Calcium oxide (lime)	CaO	00-037-1497
Ca-deficient apatite	$\text{Ca}_{10-x}(\text{HPO}_4)_x(\text{PO}_4)_{6-x} \cdot (\text{OH})_{2-x}$	00-046-0905
Calcium carbonate (calcite)	CaCO_3	00-041-1425
Calcium carbonate (aragonite)	CaCO_3	00-041-1475

terms of particle size, surface area, and composition of HA, and the sintering conditions, including compaction pressure, sintering temperature, and sintering atmosphere (Patel et al., 2001; Gibson et al., 2001; Champion 2013). As calcium phosphate ceramics exhibit relatively poor mechanical properties compared with other bioceramics, dense monolithic calcium phosphate ceramics have limited applications. Production of macroporous ceramics as bone graft substitutes from natural sources such as converted coral and bovine bone still relies on the sintering/densification of the calcium phosphate in a structure that contains large macropores, typically 100–1000 μm in size (Seebach et al., 2010). Other methods for producing macroporous ceramics of calcium phosphates are: space holder, e.g., polymer sphere, burnout (Bouler et al., 1996); use of polymer foam templates (Ramay and Zhang, 2003); gas-inducing reactions such as decomposition of hydrogen peroxide (Almirall et al., 2004); mechanically induced foaming procedures (Binner and Reichert, 1996); and more recently using 3D printing methods (reviewed by Yu et al., 2017). The latter provides a significant amount of design control that is not available with other methods, and this opens up the feasibility of making individualized patient-specific scaffolds. Currently, scalable additive manufacturing of large volumes may be limited to more simple architectures.

The characteristics of the porosity produced by these different methods, such as pore size, pore size distribution, total porosity, and pore interconnectivity, can be controlled and they have significant effects on bone ingrowth and integration (Gauthier et al., 1998). Typical macroporous calcium phosphate bone graft substitutes have cancellous bone-like foam architectures with 50%–90% total porosity and macropore sizes of 100–1000 μm , with a high level of interconnectivity between the pores (Seebach et al., 2010). Calcium phosphate particles form the struts or the “skeleton” of the material and to improve the scaffolds’ resistance to crushing or damage they need to undergo densification/sintering, and the powder properties and sintering parameters can be optimized to achieve this.

Macroporous calcium phosphate bone graft substitutes and scaffolds are designed to have an interconnecting network of pores to encourage host bone ingrowth and formation. Characterization of this pore structure requires specific techniques (Jones et al., 2007). Scanning electron microscopy (SEM) is often used to study pore shape/structure, either on the material surface or from 2D sections cut through the material. Mercury intrusion porosimetry allows quantification of pore size distribution and an indication of interconnectivity/presence of trapped, isolated pores, and pore windows. An effective nondestructive alternative to these methods is using microcomputed tomography, which is effective at quantifying macroporosity but requires smaller pixel sizes to effectively quantify microporosity in the porous structures (Cengiz et al., 2017).

For bone regeneration, large pores are needed that allow for blood (carrying cells) flow into the scaffold and space for 3D growth of immature bone and, perhaps most importantly, population by blood vessels. The morphology and degree of interconnectivity of pores may be more critical than the pore size. Comparing 3D printed scaffolds with orthogonal pore channels with cancellous bone-like porous foams both in the form of synthetic HA, which has similar sizes of interconnections between the pores (Barba et al., 2017), it was found that bone ingrowth was more rapid in the foam scaffold than in the printed scaffold. This was attributed to bone progenitor cells preferring the concave niche of the pores in the foams.

As shown in Fig. 1.3.4.1, a large number of synthetic bone graft substitutes have been approved for clinical use and examples of some commercially available calcium phosphate-based bone graft substitutes are listed in Table 1.3.4.5, including the calcium phosphate phase(s) present in these materials and the form that the CaP takes in the product. This selection is chosen to represent the broad range of CaP compositions chosen for use in bone graft substitutes and does not represent a selection based on any clinical performance. Clinical data showing the efficacy of different synthetic bone graft substitutes are very limited, in terms of the number of studies, the size and design of published studies that do exist, and the broad range of fusion techniques/approaches studied. Some recent clinical studies compared clinical outcomes in spinal fusion of a synthetic

TABLE 1.3.4.5 A Selection of Commercially Available Calcium Phosphate-Based Bone Graft Substitutes, Selected to Show the Range of CaP Material Compositions Used

Product Name	Calcium Phosphate Phase	Product Form	References
NanoBone Granulate (Artoss)	Nanocrystalline HA and a silica gel matrix	Granules	Abshagen et al. (2009)
Chronos Granules (Synthes)	β -TCP	Macroporous granules	Seebach et al. (2010)
Actifuse ABX (Baxter)	(Silicated) HA	Macroporous granules in a poloxamer hydrogel carrier	Miramond et al. (2013)
In'Oss (Biomatlante)	BCP (60% HA:40% β -TCP)	Macroporous granules in a carboxymethyl cellulose hydrogel carrier	Miramond et al. (2013)
Attrax Putty (NuVasive)	BCP (4% HA:96% β -TCP)	Macroporous BCP granules in an AOC polymer carrier	Barbieri et al. (2017)
Mastergraft Strip (Medtronic)	BCP (85% HA:15% β -TCP)	Macroporous BCP granules in a bovine collagen scaffold	Qiu et al. (2015)
Vitoss BA (Stryker)	β -TCP and bioactive glass particles	Macroporous β -TCP granules in a bovine collagen scaffold, with BG particles	Barbieri et al. (2017)

BCP, Biphasic calcium phosphate; BG, bioactive glass; HA, hydroxyapatite; TCP, tricalcium phosphate.

bone graft substitute against autograft, which is the clinical gold standard ([Parker and Malham, 2017](#); [Lechner et al., 2017](#)). This fact may suggest that there is a shift toward obtaining more clinical data on new bone graft substitutes that will enable comparisons to be made. The efficacy of synthetic bone graft substitutes in general was reviewed in comparison with allograft or autograft in spinal fusion surgery, and a lack of clinical data limiting strong conclusions to be made was highlighted ([Buser et al., 2016](#)).

Calcium phosphate bone graft substitutes typically consist of macro- and/or microporous ceramics of HA, TCP, or BCP in a granular form, with typical sizes in the range of 0.4–2 mm. Some examples of synthetic calcium phosphate bone graft substitutes and of bone graft substitutes derived from human or bovine bones are presented in [Fig. 1.3.4.2](#), highlighting the differences in sintered grain structures and microporosity ([Seebach et al., 2010](#)).

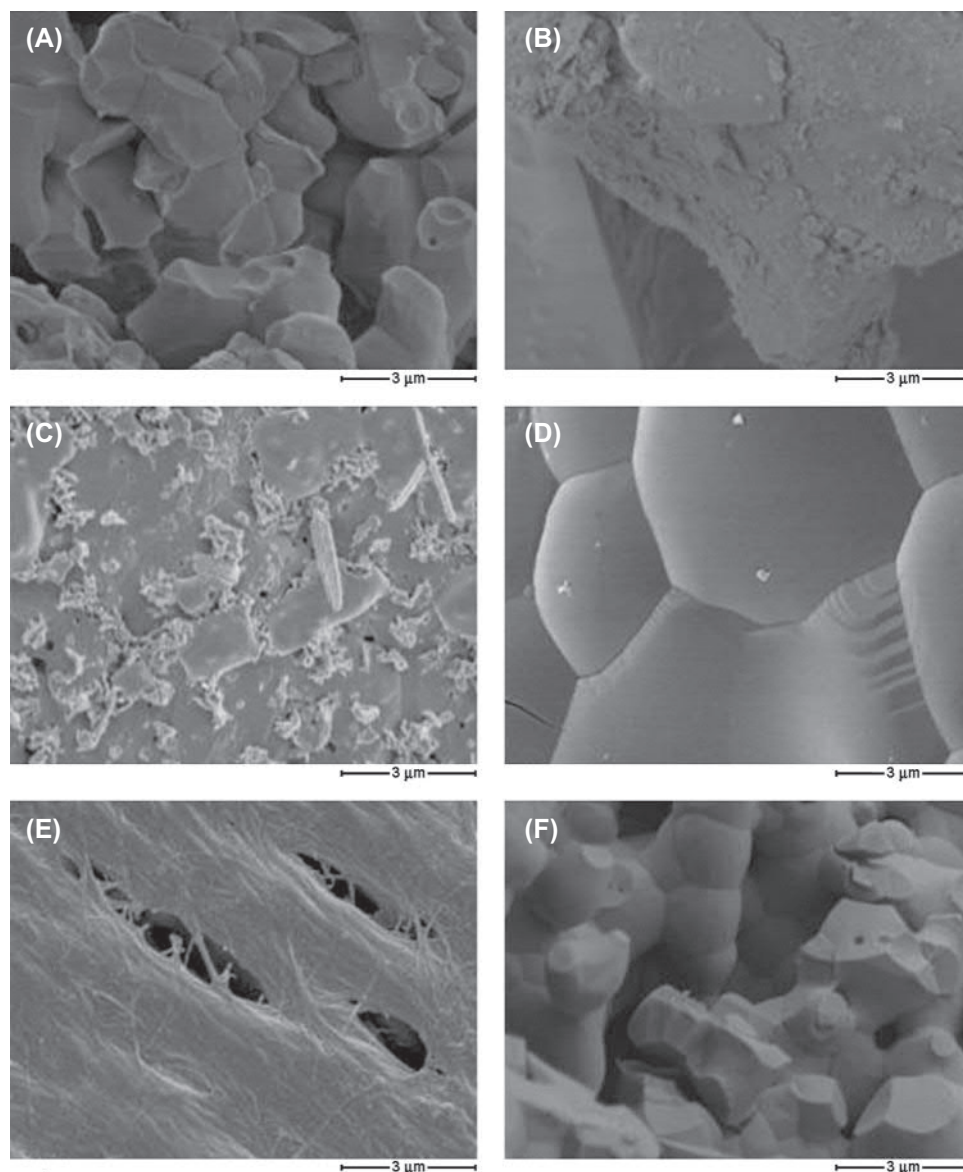
Granules are often mixed with saline, blood, or bone marrow aspirate (BMA) to improve their handling and to potentially introduce biological factors (from blood or BMA). Actifuse ABX (Baxter, UK) is a silicon-substituted synthetic HA available in the form of foamed granules (~3 mm dimensions). Microcomputed tomography imaging ([Fig. 1.3.4.3](#)) and subsequent image analysis showed how the pore network can be imaged and quantified and how its open pore architecture and modal interconnect size of 120 μ m are important for its efficacy ([Midha et al., 2013](#)).

Most bone graft substitutes are designed to consist of granules in either a hydrogel carrier, anhydrous polymeric carrier, or collagen (or gelatin) scaffold (usually bovine or porcine collagen), with examples of these listed in [Table 1.3.4.5](#). These formulations are designed to improve the

intraoperative handling and placement of the synthetic bone graft substitute. They also allow surgeons to shape the graft material (if in the form of a putty) and/or combine with the patient's BMA, providing a cell population that might contribute toward bone repair. Some surgical procedures require delivery of a synthetic bone graft into a confined defect, possibly via a minimally invasive procedure, and/or a graft material that will set and harden in situ, which are cases where a cement has significant advantages.

Calcium Phosphate Cements

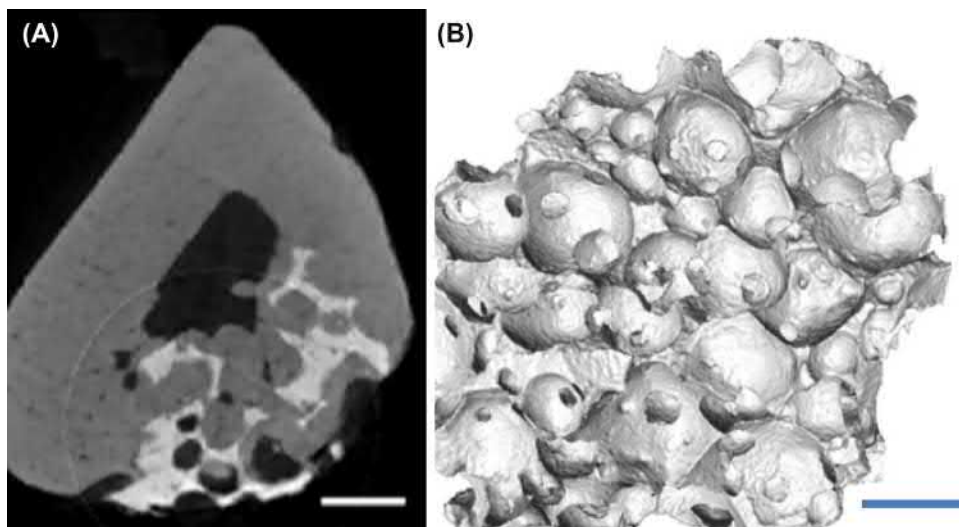
A calcium phosphate bone cement involves mixing certain calcium phosphate phases with an aqueous solution to form a paste, which then undergoes a chemical dissolution and reprecipitation reaction analogous to calcium silicate construction cements, leading to interlocking/entanglement of new crystals of the product calcium phosphate phase and producing a set and hardened mass. This provides some unique advantages over typical ceramics for filling bone defects such as (1) being able to inject the paste into the defect, (2) creating a hardened mass that has a compressive strength similar to cancellous bone, and (3) incorporation of drugs or biomolecules into the aqueous phase, such as antibiotics. The final product of a calcium phosphate bone cement reaction is either brushite or an apatite phase (typically CDA), and which product phase is obtained will depend on the reactant phases chosen. The first calcium phosphate bone cement that led to a clinically used formulation was described in the early 1980s and consisted of mixtures of tetracalcium phosphate and dicalcium phosphate anhydrous or dihydrate (DCPA or



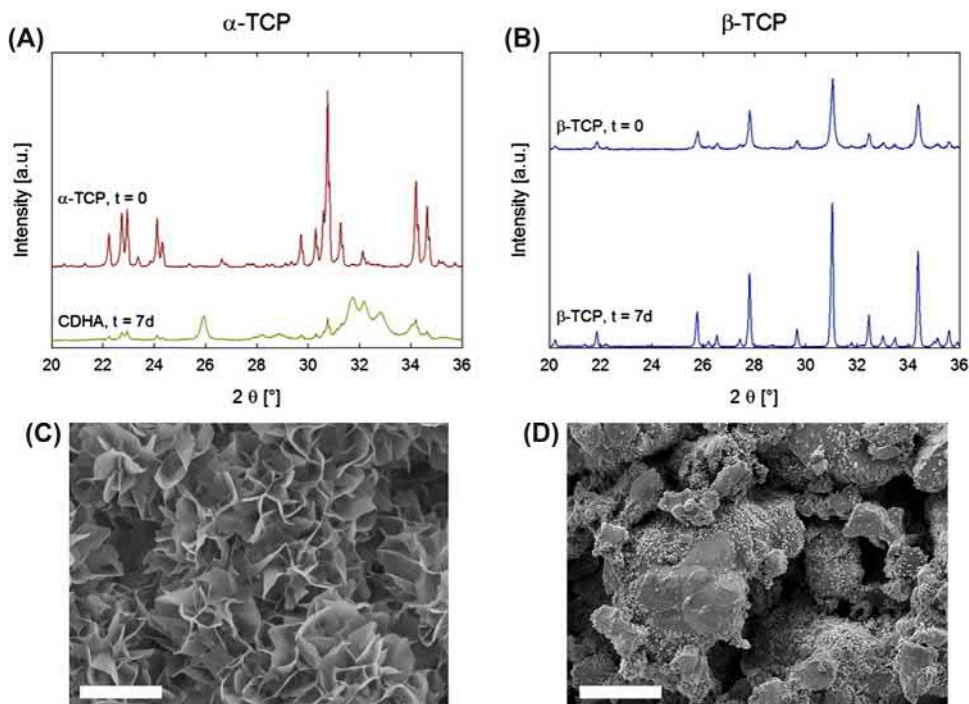
• **Figure 1.3.4.2** Scanning electron microscope images of a range of commercial synthetic and natural (derived from human or bovine bone) calcium phosphate bone graft substitutes: (A) synthetic silicate-substituted porous hydroxyapatite (Actifuse ABX); (B) synthetic α -TCP (Biobase); (C) processed bovine hydroxyapatite ceramic (Cerabone); (D) synthetic β -TCP (Chronos); (E) processed human cancellous allograft (Tutoplast); (F) synthetic β -TCP (Vitoss). TCP, Tricalcium phosphate. (Adapted from Seebach, C., Schultheiss, J., Wilhelm, K., Frank, J., Henrich, D., 2010. Comparison of six bone-graft substitutes regarding to cell seeding efficiency, metabolism and growth behaviour of human mesenchymal stem cells (MSC) in vitro. *Injury* 41, 731–738.)

DCPD), which formed an apatite as the product phase (Brown and Chow, 1983). An alternative cement formulation that produces an apatite product phase is a mixture of α -TCP and DCPA, with small amounts of precipitated HA (Fernández et al., 1996) or calcium carbonate (Fernández et al., 1998) added, and these formulations have led to clinically used cements. Many other mixtures of phases that result in an apatite product have been studied, but the TTCP/DCPA-DCPD and the α -TCP and DCPA systems provide optimum setting and handling characteristics. The effect of parameters such as particle size, surface area, liquid/powder ratio, and composition of aqueous

solution used to form the cement on the properties of the paste/hardened cement has been studied extensively and reviewed elsewhere (Zhang et al., 2014). An example of the effect of the calcium phosphate used as a reactant in a cement is shown in Fig. 1.3.4.4, where the cement setting reaction of a cement composed of α -TCP is compared to a cement composed of β -TCP after immersion in water for 7 days (Montufar et al. 2013). The X-ray diffraction patterns show almost complete conversion of the α -TCP to a CDA product phase, with associated entanglement of apatite crystals observed by SEM, compared with minimal reaction in the β -TCP cement.



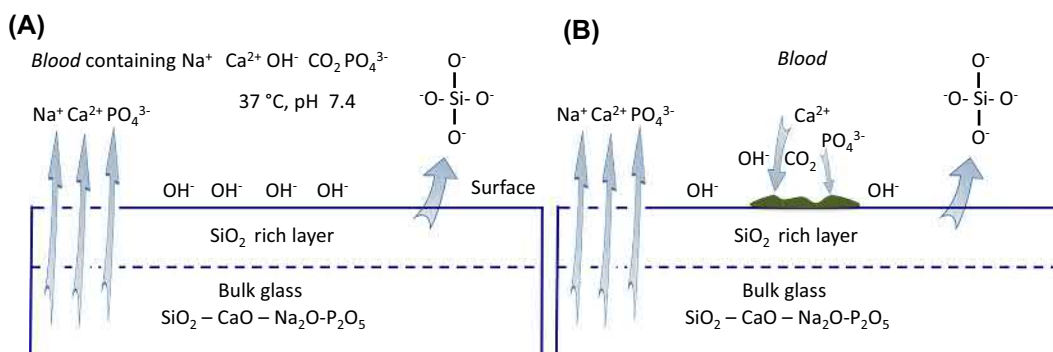
• **Figure 1.3.4.3** Microcomputed tomography images of Actifuse (porous silicon containing synthetic hydroxyapatite) bone graft: (A) 2D slice view (cross-section) of a rat tibia bone defect regenerating through the Actifuse granules 11 weeks after implantation, scale bar is 1 mm; (B) 3D image of an Actifuse granule, scale bar = 400 μm . (Images adapted from Midha, S., Kim, T.B., van den Bergh, W., Lee, P.D., Jones, J.R., Mitchell, C.A., 2013. Preconditioned 70S30C bioactive glass foams promote osteogenesis in vivo. *Acta Biomater.* 9, 9169–9182.)



• **Figure 1.3.4.4** X-ray diffraction patterns of (A) α -TCP and (B) β -TCP cements and the microstructures observed by scanning electron microscopy of (C) α -TCP and (D) β -TCP cements after immersion in water for 7 days at 37°C (scale bar is 5 μm). The α -TCP cement reacts to form Ca-deficient apatite after 7 days, whereas the β -TCP cements exhibits minimal reactivity. *TCP*, Tricalcium phosphate. (Figure taken from Montufar, E.B., Maazouz, Y., Ginebra, M.P., 2013. Relevance of the setting reaction to the injectability of tricalcium phosphate pastes. *Acta Biomater.* 9, 6188–6198.)

In the case of a cement with brushite as the product phase, a combination of β -TCP and monocalcium phosphate monohydrate with an aqueous phase led to the dissolution of the reactant phases and the precipitation of brushite crystals (Mirtchi et al., 1989). Although these cements are less common than the apatite-forming cement formulations,

an interesting aspect of a brushite cement is that the product phase that forms is inherently unstable at physiological pH, and will undergo gradual dissolution during which it may be replaced by new bone. Brushite cements and their potential clinical applications have been reviewed in detail (Tamini et al., 2012).



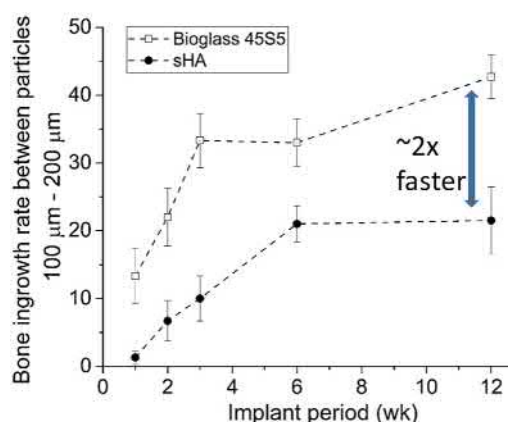
• **Figure 1.3.4.5** Schematic of the bone mineral-like hydroxycarbonate apatite (HCA) layer forming on the surface of a bioactive glass during solution-mediated dissolution: (A) cation exchange between the glass and protons in blood/solution; (B) deposition of amorphous calcium phosphate deposition, which crystallizes into HCA as glass dissolution continues.

Bioglass and Bioactive Glass

Bioglass was the first material to bond with bone, rather than be encapsulated by fibrous tissue, launching the field of bioactive ceramics (Hench, 2015). Bioglass degrades by dissolution in solution. Bioglass has two modes of bioactivity in terms of bone repair: (1) bone bonding is due to a hydroxycarbonate apatite (HCA) layer on the glass that forms following dissolution of the glass and precipitation of HCA on the glass surface (Hench et al., 1971), which is thought to integrate with collagen fibrils of the host bone, and (2) the osteogenic property of the bioactive glass due to the dissolution products of the glass, i.e., soluble silica and calcium ions, that stimulate bone cells to produce more bone (Hench and Polak, 2002; Silver et al., 2001). The first bioactive glass was discovered by Larry Hench (Hench, 2015) and was termed 45S5 Bioglass, having a composition of 46.1 mol% SiO_2 , 24.4 mol% Na_2O , 26.9 mol% CaO , and 2.6 mol% P_2O_5 (Hench et al., 1971).

The mechanism for HCA layer formation on the surface of the glass is solution mediated. Cations in the glass, e.g., Na^+ and Ca^{2+} , exchange with protons (H^+) from the water in the blood/solution, leaving a silica-rich layer and $\text{Si}-\text{OH}$ bonds on the glass surface. The low connectivity of the silica-rich layer means that some of the silica will also be lost and also enables continual ion transport out from the bulk of the glass. The blood already has high concentrations of calcium and phosphate and a further increase, plus a pH rise at the glass surface (due to the loss of H^+ from the solution), promotes calcium phosphate deposition on the glass surface, with $\text{Si}-\text{OH}$ groups being suitable sites. The amorphous calcium phosphate then crystallizes as it incorporates OH^- and carbonate from the solution/blood, forming HCA (Fig. 1.3.4.5).

In vivo comparative studies between 45S5 and similar sized particles of synthetic HA showed that Bioglass produces more rapid and higher quality bone regeneration than HA (Oonishi et al., 1999) with 17 times more bone in defects filled with Bioglass after a week, and twice as much bone 24 weeks after implantation, compared to defects filled with sHA (Fig. 1.3.4.6) (Oonishi et al., 1997, 1999, 2000; Wheeler et al., 2000).



• **Figure 1.3.4.6** Percentage bone ingrowth into defects in rabbit femoral chondyle filled with particles of synthetic bone grafts of 45S5 Bioglass and synthetic hydroxyapatite (sHA). (Data replotted from Oonishi, H., Hench, L.L., Wilson, J., Sugihara, F., et al., 2000. Quantitative comparison of bone growth behavior in granules of Bioglass (R), A-W glass-ceramic, and hydroxyapatite. *J. Biomed. Mater. Res.* 51, 37–46.)

In vitro studies indicated that the reason for the improved bone growth was due to the dissolution products stimulating bone cells at the genetic level. The experiments involving human osteoblast cell media collected from the dissolution products of Bioglass, without the glass itself, showed that seven families of genes that support osteogenesis are upregulated within 48 h of exposure to the ion “soup” (Xynos et al., 2001). The dissolution media were prepared simply by soaking the glass in culture media, extracting the dissolution of the glass, before removing the glass. The dissolution products were then given to the cells that were cultured in conventional tissue culture well plates. Transcription of at least five extracellular matrix components was also induced. Extracellular matrix secretion increased, which mineralized without addition of osteogenic supplements or growth factors (Xynos et al., 2000a, b). The gene expression was dose dependent, with the highest observed at $\sim 20 \mu\text{g mL}^{-1}$ of soluble silica, accompanied by $60\text{--}90 \mu\text{g mL}^{-1}$ of calcium ions (Hench, 2009).

The results enabled NovaBone Products LLC (Jacksonville, FL), the company that was producing the Bioglass



• **Figure 1.3.4.7** PerioGlas and NovaBone packaging with a scanning electron microscopy image of the Bioglass particulate grafts (scale bar is 200 μm) and BonAlive packaging with BonAlive granules in a delivery device.

particulate product at the time, to claim the term “Osteostimulation.” Many research groups have since investigated incorporation of other cations with potential therapeutic benefits into bioactive glasses, but they are yet to reach clinical use (Hoppe et al., 2011).

Bioglass Granules

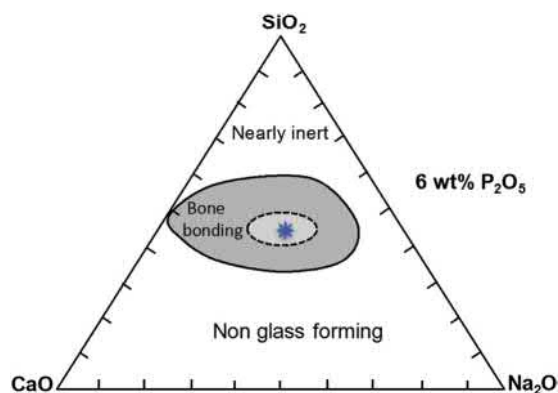
The original Bioglass 45S5 has been used in more than 1.5 million patients (Pomrink, 2016) in the form of a particulate synthetic bone graft, marketed under the trade name NovaBone, to repair bone defects in orthopedics and maxillofacial reconstruction (Hench, 2011). However, NovaBone particulate did not reach the market until 2005. The first particulate Bioglass was PerioGlas, which was launched in 1993 as a synthetic bone graft for the repair of pockets in the jaw bone that resulted from periodontal disease. It is usually applied by mixing first with saline solution. Fig. 1.3.4.7 shows PerioGlas and NovaBone packaging and an SEM image of the particulate (90–710 μm). Clinical studies (Low et al., 1997; Lovelace et al., 1998; Rosenberg et al., 2004; Anderegge et al., 1999; Yukna et al., 2001; Park et al., 2001; Norton and Wilson, 2002; Sculean et al., 2002; Mengel et al., 2003; Froum et al., 1998; Shapoff et al., 1997; Zamet et al., 1997a, b) showed that bone pockets treated with PerioGlas were ~70% filled with new bone compared to ~35% for controls, which were often bovine

bone mineral, which is slower to biodegrade/remodel. The product has also been used with polymeric membranes, which periodontists term guided tissue regeneration (Yadav et al., 2011).

For orthopedic applications, NovaBone is usually mixed with blood from the bone defect by the surgeon before being pressed into place. It was compared with autograft in posterior spinal fusion operations in clinical trials for the treatment of adolescent idiopathic scoliosis (curvature of the spine), wherein the grafts were compressed in place by the neighboring vertebrae via metal screws (Ilharreborde et al., 2008). NovaBone performed as well as autograft over the 4-year follow-up period, with the benefit that a donor site was not needed with NovaBone.

Biogran (Biomet 3i, Palm Beach Gardens, FL) is a 45S5 glass particulate graft with a narrow (300–350 μm) particle size range, and it is used in periodontal regeneration. In vivo studies showed that the HCA layer forms and then the particles hollow out within 4 weeks of implantation because of phagocytes entering the particles through cracks in the HCA shell to break down the glass core (Schepers and Ducheyne, 1997). Clinical trials showed that Biogran outperformed synthetic HA in bone pockets in the jaw (Schepers et al., 1993).

The 45S5 Bioglass composition is not the only glass composition that is considered bioactive. Fig. 1.3.4.8 shows a composition map, with the composition region marked that is predicted to be bioactive.



• **Figure 1.3.4.8** Composition map with a predicted area in which a glass composition will bond with bone; 4555 Bioglass composition is denoted with a star (phosphate content fixed at 6wt%). The dashed region indicates a composition region that is likely to also bond with soft tissue (note: this is not a phase diagram).

The S53P4 composition (53.8 mol% SiO₂, 21.8 mol% CaO, 22.7 mol% Na₂O, 1.7 mol% P₂O₅) is another synthetic bone graft called BonAlive (BonAlive Biomaterials, Turku, Finland), which also has a larger particle size range (1–4 mm) (Andersson et al., 1990). In vitro studies indicated that the glass may have antimicrobial properties (Stoor et al., 1998) and clinical reports suggest that BonAlive can help treat chronic osteomyelitis (bone infection, usually caused by bacteria), even when antibiotics alone have been ineffective. In a clinical study, 11 patients with chronic osteomyelitis (*Staphylococcus aureus*) in the spine (Lindfors et al., 2010a) were treated with S53P4 with a 10–38-month follow-up. Nine patients healed without complications, while the other two had unrelated complications.

There are many more journal articles on clinical trials of S53P4 compared with those featuring the original 45S5 Bioglass. It is important in such trials to be able to compare with the clinical gold standard (autograft). BonAlive granules (1–4 mm, 14 patients) were compared with autograft (11 patients) for regeneration of defects created by the removal of benign bone tumors, with a 14-year follow-up (Lindfors et al., 2010b). Following treatment with BonAlive, the cortical bone thickness was twice as thick as it was after treatment with autograft. However, some of the glass remained in the bone, even after 14 years. NovaBone is thought to biodegrade in 1–2 years (Hupa et al., 2010). An 11-year follow-up on BonAlive in subchondral bone defects also showed some glass particles were still present, even at 11 years postoperation (Heikkila et al., 2011). The glass began to degrade between 12 and 36 months and stimulated remodeling of the bone (Lindfors et al., 2009) but remodeling was slower than in the case of autograft (at 12 months) (Lindfors et al., 2008). Slower resorption of S53P4 compared with 45S5 is due to glass composition, which has higher silica content and network connectivity than 45S5.

Network connectivity (Eq. 1.3.4.1) is a method of predicting the bioactivity of bioactive glasses based on their nominal composition (Hill and Brauer, 2011). It uses the glass composition (in mol%), where M_f is the molar fraction

of the network oxide (e.g., SiO₂) and M_2^I O and M^{II} O are molar fractions of the mono- and divalent modifier oxides, e.g., Na₂O and CaO. This calculation (NC') assumes that phosphate forms its own orthophosphate network, charged balanced by divalent cations.

$$NC' = \frac{4(M_f) - 2(M_2^I O + M^{II} O) + 6(M_{P_2O_5})}{M_f} \quad (1.3.4.1)$$

The relationship of network connectivity and bioactivity is limited by certain assumptions: that the glass is homogeneous; that once a bridging oxygen bond is broken, it will be replaced with a nonbridging oxygen; and that the user has to define what role a particular atom will play within the network. The last assumption may not be obvious, for example, magnesium in a silicate glass can act as a former (MgO₄) and/or a modifier (Mg²⁺), with ~14% of the total magnesium acting as a network former (Watts et al., 2010).

The slow resorption rate of S53P4 becomes useful for dentists and maxillofacial surgeons who need to replace bone lost in the maxilla (upper jaw), for example, in patients with periodontitis. The treatment is termed a sinus floor lift, where bone grows partially into the sinus cavity. A mixture of S53P4 granules mixed with autograft showed more rapid bone repair compared to autograft alone (Turunen et al., 2004).

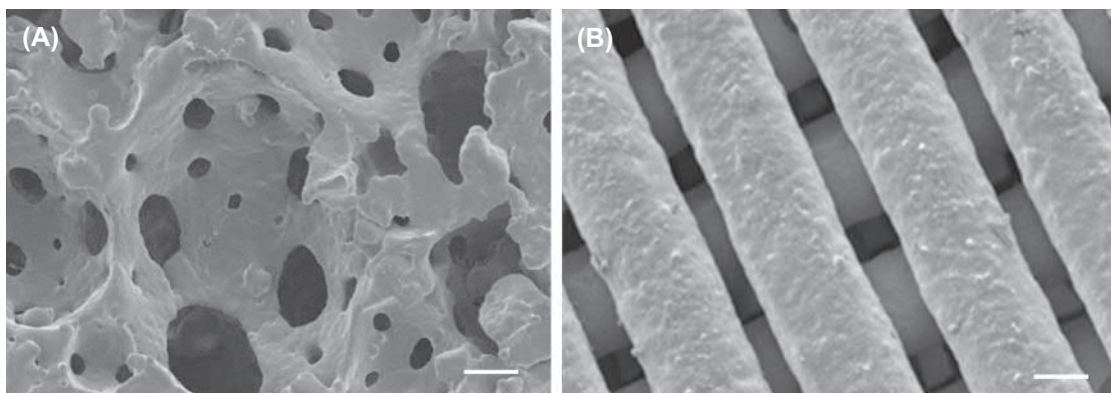
Bioactive Glass Composites and Putties for Bone Repair

NovaBone (45S5), GlassBone (45S5, Noraker, Lyon, France), and BonAlive (S53P4) are available in bioresorbable putty form (Schallenberger et al., 2014), which consists of a carrier matrix of PEG and glycerin containing the glass particles, with the aim of providing clinicians with easier delivery methods. Common bone graft devices combine bioactive glass with a natural polymeric matrix to partially mimic natural bone, e.g., Vitoss Bioactive Bone Graft (Stryker, NJ) and NanoFuse (Amend Surgical, Alachua, FL), which have been shown to improve bone over DBM alone (Kirk et al., 2013). The DBM-based devices are a mixture of components, with little mechanical integrity, rather than true composites.

Structural composites containing bioactive glasses can be made for sustaining cyclic loads. Noraker have developed a screw for anterior cruciate ligament reconstruction called LockActiv (CE marked in 2015), which is a poly(L-lactide)-*co*-poly(D,L)lactide polymer matrix containing 45S5 Bioglass particles. The screw must fix a detached ligament into a hole that the surgeon has drilled into the host bone. A problem with such a composite is that much of the bioactive glass particles will be embedded within the polymer, reducing its bioactivity.

Porous Bioactive Glasses

Porous synthetic hydroxyapatite (porous sHA) has been used successfully in the clinic but the 45S5 and S53P4 compositions cannot be made into porous constructs while



• **Figure 1.3.4.9** Scanning electron microscopy images of bioactive glass scaffolds: (A) gel-cast foam; (B) Robocast 3-D printed. Scale bars are 200 μm . (Courtesy of Dr. Amy Nommeets-Nomm.)

maintaining their amorphous glass structure. This is due to the small difference between their glass transition temperatures (T_g) and crystallization onset temperatures (T_{Conset}) (Wu et al., 2011). To enable sintering, glass particles must be heated above T_g to enable the viscous flow of the glass and fusion of the particles, but if the temperature reaches T_{Conset} the glass will crystallize, which reduces bioactivity and can cause instability, unless the glass is fully crystallized intentionally (a glass-ceramic) (Filho et al., 1996). New compositions have been designed with an increased sintering thermal processing window, allowing thermal processing postmelt quenching (Elgayar et al., 2005; O'Donnell and Hill, 2010).

Three processes are most commonly used for making porous glasses: the foam replica (reticulation) method, direct foaming (gel-cast foaming process), and additive manufacturing. Foam reticulation uses polyurethane foam as a sacrificial template. A glass particle slurry coats the foam and the foam is burned out during sintering, creating porous scaffolds (Chen and Boccaccini, 2006). However, the struts can remain hollow, reducing the compressive strength of the scaffold (Hoppe et al., 2014; Baino et al., 2013).

The additive manufacturing technique is termed robocasting, direct ink writing, or extrusion 3D printing (different names for the same technique). Robocasting prints glass particles dispersed within a polymer binder. The binder must exhibit shear thinning properties and burn out below the T_g of the glass. Typically, 3D grid-like structures with straight channels are printed (Fu et al., 2011a).

The glass composition 13-93 (54.6 mol% SiO_2 , 22.4 mol% CaO , 6 mol% Na_2O , 1.7 mol% P_2O_5 , 7.9 mol% K_2O , 7.7 mol% MgO) has an excellent processing window. 13-93 scaffolds have been produced by foam reticulation, with porosities of 85%, pore interconnect (windows between pores) diameters in the range 100–500 μm , and compressive strengths of 11 ± 2 MPa (Fu et al., 2008). Robocast scaffolds with interconnects of 500 μm in the xy direction and 100 μm in z direction, with a porosity of 60%, had a mean compressive strength of 136 ± 22 MPa (Fu et al., 2011b). While 13-93 sinters nicely without crystallizing, it has a much higher network connectivity (2.58)

compared to 45S5 Bioglass (2.11). The ICIE16 composition (49.46 mol% SiO_2 , 36.6 mol% CaO , 6.6 mol% Na_2O , 1.07 mol% P_2O_5 , 6.6 mol% K_2O) was designed to enable glass scaffold production with a network connectivity as close to 2.11 as possible (2.13).

Gel-cast foaming involves direct foaming of a glass particle slurry with the aid of a surfactant (Wu et al., 2011). The surfactant stabilizes air bubbles and rapid gelation then solidifies the slurry so that bubbles remain and form the pores. Foam scaffolds produced from ICIE16 glass had porosities of 79%, with modal pore diameters of 379 μm and compressive strength of 1.9 MPa (Fig. 1.3.4.9) (Wu et al., 2011; Nommeets-Nomm et al., 2017).

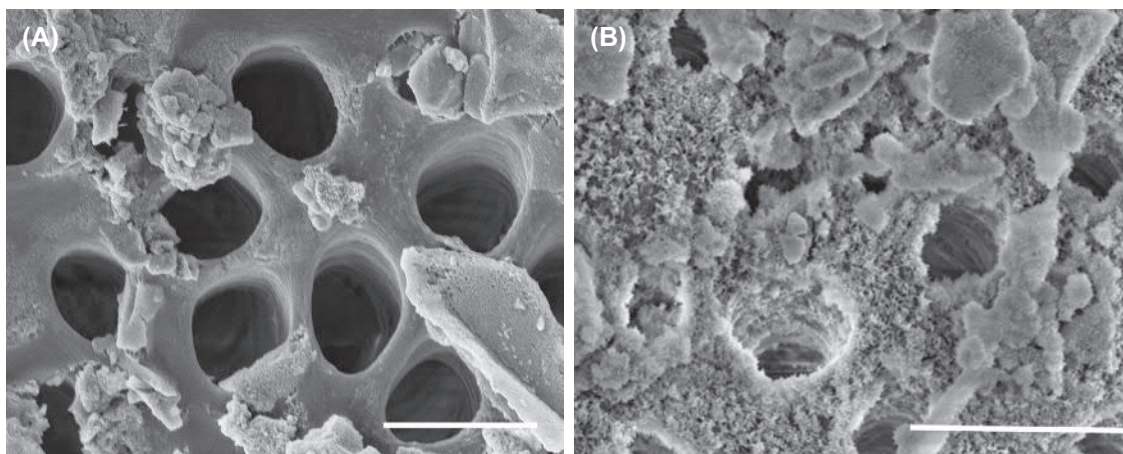
Wound Healing

Bioactive glass is thought to be useful in many applications aside from bone repair. One reason is that the amorphous glass can release many different ions with potentially therapeutic benefits as it biodegrades (Hoppe et al., 2011). The delivery of the ions is sustained and controlled by the degradation rate of the glass, which can be tailored more easily than drug release from conventional biodegradable polymers.

Another reason is the FDA approval of borate-based bioactive glasses for healing chronic wounds, e.g., diabetic venous ulcers (Rahaman et al., 2011). The cotton candy-like glass, named MIRRAGEN (ETS Woundcare, Rolla, MO), biodegrades rapidly in the wound bed (under a dressing) and encourages the wound-healing process in wounds that did not heal under conventional treatment (Jung et al., 2011).

Bioactive Glass in Toothpaste

Bioactive glass is not only used as a medical device or implant, it has also has an impact in consumer healthcare, with the largest commercial use of a bioactive material being in toothpaste. Enamel and dentine of the tooth are very similar to bone, in that they contain HCA mineral and collagen. The pain felt by 35% of the adult population



• **Figure 1.3.4.10** Scanning electron microscopy images of human dentin treated with Sensodyne Repair and Protect (UK formulation) toothpaste that contains NovaMin (45S5) particles: (A) immediately after application of NovaMin in artificial saliva; (B) 24 h after application. Scale = 5 μm . (Modified from Earl, J.S., Leary, R.K., Muller, K.H., Langford, R.M., Greenspan, D.C., 2011. Physical and chemical characterization of dentin surface, following treatment with NovaMin® technology. *J. Clin. Dent.* 22, 62–67.)

that suffer from hypersensitivity is due to exposure of the microtubules of the dentine (Fig. 1.3.4.10) that lead to the pulp cavity and nerves (Rees and Addy, 2002). A fine Bioglass 45S5 particulate ($\sim 18 \mu\text{m}$), termed NovaMin, which has been owned by GlaxoSmithKline, UK, since 2010, has been used in toothpaste. NovaMin releases calcium and phosphate species during glass dissolution, which then form HCA on the dentine (Gillam et al., 2002). Fig. 1.3.4.10A shows exposed dentine tubules following a brief acid etch with the NovaMin immediately after it was brushed onto the dentine in artificial saliva. The particles attached and, within 24 h, the surface was almost completely covered by an HCA (Fig. 1.3.4.10B) mineralization.

The success of NovaMin has led to the development of more complex glass compositions, such as those designed to stimulate the formation of fluorapatite on the dentine, which is more resistant to acid attack than HCA, leading to a fluoride-releasing bioactive glass, BioMinF (BioMin Technologies Ltd., London, UK) for use in toothpaste (Hill et al., 2011).

Glasses for Cancer Therapy

Insoluble (nonbioactive) glass microspheres (TheraSphere, BTG, London, UK) are used as a microinjectable delivery system for in situ treatment of tumors. The glass microspheres contain ^{90}Y isotopes in the glass composition and are therefore radioactive and deliver a local dose of radiotherapy from inside the tissue. They travel to the site of a tumor through the blood and become lodged in the tissue, where they emit the radiation energy to kill the cancer cells with very little damage to surrounding tissues. This mode of action is currently considered the most effective in treating liver cancer, as the tumor blood supply comes almost entirely from the hepatic artery, making delivery of the spheres to the tumor possible.

Glass-Ceramics

The formation of a glass-ceramic material often starts as a glass and ends up as a polycrystalline ceramic. This is accomplished by first quenching a melt to form the glass object. A reason for doing this is that more complex compositions of a crystalline material can be made by first making a glass. The molten glass can also be poured into a mold to provide shape. The glass is transformed into a glass-ceramic in two steps. First, the glass is heated at a temperature range of $500\text{--}700^\circ\text{C}$ to produce a large concentration of nuclei from which crystals can grow. When enough nuclei are present to ensure that a fine-grained structure will be obtained, the temperature of the object is raised to a range of $600\text{--}900^\circ\text{C}$ to promote crystal growth. Crystals grow from the nuclei until they impinge with up to 100% crystallization achieved. The resulting microstructure contains fine-grained, randomly oriented crystals. When phase separation occurs, a microstructure can be produced that consists of glass phases suspended in a glass matrix. Crystallization of phase-separated glasses results in very complex glass-ceramic microstructures, as reviewed in Höland and Beall (2001). Glass-ceramics can also be made by pressing powders and a grain boundary glassy phase (Kokubo, 1991). Due to their high strength and the ability to closely mimic the color and aesthetics of natural teeth, glass-ceramics are used for dental restorations, including inlays, onlays, crowns, and multiunit bridges.

Summary

Bioceramics consist of ceramics, glasses, and glass-ceramics for biomedical applications. They can be nearly inert or bioactive/biodegradable. Nearly-inert bioceramics are used for their hardness and resistance to wear and degradation. Bioactive ceramics are good bone graft substitute materials. Bioactive glass was the first material found to bond to

bone. Bioactive glass can outperform sHA in terms of rate and quality of bone ingrowth. It is, however, challenging to produce it in a porous scaffold form. Porous sHA is widely used in orthopedic applications.

References

- Abshagen, K., Schrodi, I., Gerber, T., Vollmar, B., 2009. In vivo analysis of biocompatibility and vascularization of the synthetic bone grafting substitute NanoBone®. *J. Biomed. Mater. Res.* 91A, 557–566.
- Almirall, A., Larrecq, G., Delgado, J.A., Martínez, S., Pannel, J.A., Ginebra, M.P., 2004. Fabrication of low temperature macroporous hydroxyapatite scaffolds by foaming and hydrolysis of an α -TCP paste. *Biomaterials* 25, 3671–3680.
- Anderegg, C.R., Alexander, D.C., Freidman, M., 1999. A bioactive glass particulate in the treatment of molar furcation invasions. *J. Periodontol.* 70, 384–387.
- Andersson, O.H., Liu, G.Z., Karlsson, K.H., Niemi, L., Miettinen, J., Juhanoja, J., 1990. In vivo behavior of glasses in the SiO_2 - Na_2O - CaO - P_2O_5 - Al_2O_3 - B_2O_3 system. *J. Mater. Sci. Mater. Med.* 1, 219–227.
- Arinze, T.L., Tran, T., Mcalary, J., Daculsi, G., 2005. A comparative study of biphasic calcium phosphate ceramics for human mesenchymal stem-cell-induced bone formation. *Biomaterials* 26, 3631–3638.
- Arkudas, A., Balzer, A., Buehrer, G., Arnold, I., Hoppe, A., Detsch, R., Newby, P., Fey, T., Greil, P., Horch, R.E., Boccaccini, A.R., Kneser, U., 2013. Evaluation of angiogenesis of bioactive glass in the arteriovenous loop model. *Tissue Eng. C.* 19, 479–486.
- ASTM F1185-03, 2014. Standard Specification for Composition of Hydroxylapatite for Surgical Implants. ASTM International, West Conshohocken, PA. www.astm.org.
- ASTM F1088-18, 2018. Standard Specification for Beta-Tricalcium Phosphate for Surgical Implantation. ASTM International, West Conshohocken, PA. 2014 www.astm.org.
- Baino, F., Ferraris, M., Bretcanu, O., Verne, E., Vitale-Brovarone, C., 2013. Optimization of composition, structure and mechanical strength of bioactive 3-D glass-ceramic scaffolds for bone substitution. *J. Biomater. Appl.* 27, 872–890.
- Barba, A., Diez-Escudero, A., Maazouz, Y., Rappe, K., Espanol, M., Montufar, E.B., et al., 2017. Osteoinduction by foamed and 3D-printed calcium phosphate scaffolds: effect of nanostructure and pore architecture. *ACS Appl. Mater. Interfaces* 9, 41722–41736.
- Barbieri, D., Yuan, H., Ismailoğlu, A.S., de Bruijn, J.D., 2017. Comparison of two moldable calcium phosphate-based bone graft materials in a noninstrumented canine interspinous implantation model. *Tissue Eng. A.* 23, 1310–1320.
- Binner, J.G.P., Reichert, J., 1996. Processing of hydroxyapatite ceramic foams. *J. Mater. Sci.* 31, 5717–5723.
- Bouler, J.M., Trecant, M., Delecrin, J., Royer, J., Passuti, N., Daculsi, G., 1996. Macroporous biphasic calcium phosphate ceramics: influence of five synthesis parameters on compressive strength. *J. Biomed. Mater. Res.* 32, 603–609.
- Bouler, J.M., Pilet, P., Gauthier, O., Verron, E., 2017. Biphasic calcium phosphate ceramics for bone reconstruction: a review of biological response. *Acta Biomater.* 53, 1–12.
- Brown, W.E., Chow, L.C., 1983. A new calcium phosphate setting cement. *J. Dent. Res.* 62, 672–679.
- Buser, Z., Brodke, D.S., Youssef, J.A., Meisel, H.J., Myhre, S.L., Hashimoto, R., Park, J.B., Tim Yoon, S., Wang, J.C., 2016. Synthetic bone graft versus autograft or allograft for spinal fusion: a systematic review. *J. Neurosurg. Spine* 25, 509–516.
- Cengiz, I.F., Oliveira, J.M., Reis, R.L., 2017. Micro-computed tomography characterization of tissue engineering scaffolds: effects of pixel size and rotation step. *J. Mater. Sci. Mater. Med.* 28, 129–133.
- Champion, E., 2013. Sintering of calcium phosphate bioceramics. *Acta Biomater.* 9, 5855–5875.
- Chen, Q.Z., Boccaccini, A.R., 2006. Poly(D,L-lactic acid) coated 45S5 Bioglass (R)-based scaffolds: processing and characterization. *J. Biomed. Mater. Res. A* 77A, 445–457.
- Chevalier, J., Gremillard, L., 2009. Ceramics for medical applications: a picture for the next 20 years. *J. Eur. Ceram. Soc.* 29, 1245–1255.
- Daculsi, G., Legeros, R.Z., Nery, E., Lynch, K., Kerebel, B., 1989. Transformation of biphasic calcium phosphate ceramics in vivo: ultrastructural and physicochemical characterization. *J. Biomed. Mater. Res.* 23, 883–894.
- De Aza, A.H., Chevalier, J., Fantozzi, G., Schehl, M., Torrecillas, R., 2002. Crack growth resistance of alumina, zirconia and zirconia toughened alumina ceramics for joint prostheses. *Biomaterials* 23, 937–945.
- Earl, J.S., Leary, R.K., Muller, K.H., Langford, R.M., Greenspan, D.C., 2011. Physical and chemical characterization of dentin surface, following treatment with NovaMin® technology. *J. Clin. Dent.* 22, 62–67.
- Elgayar, I., Aliev, A.E., Boccaccini, A.R., Hill, R.G., 2005. Structural analysis of bioactive glasses. *J. Non-Cryst. Solids* 351, 173–183.
- Fernández, E., Ginebra, M.P., Boltong, M.G., Driessens, F.C., Ginebra, J., De Maeyer, E.A., Verbeeck, R.M., Planell, J.A., 1996. Kinetic study of the setting reaction of a calcium phosphate bone cement. *J. Biomed. Mater. Res.* 32, 367–374.
- Fernández, E., Gil, F.J., Best, S.M., Ginebra, M.P., Driessens, F.C., Planell, J.A., 1998. Improvement of the mechanical properties of new calcium phosphate bone cements in the CaHPO_4 - α - $\text{Ca}_3(\text{PO}_4)_2$ system: compressive strength and microstructural development. *J. Biomed. Mater. Res.* 4, 560–567.
- Filho, O.P., La Torre, G.P., Hench, L.L., 1996. Effect of crystallization on apatite-layer formation of bioactive glass 45S5. *J. Biomed. Mater. Res.* 30, 509–514.
- Froum, S.J., Weinberg, M.A., Tarnow, D., 1998. Comparison of bioactive glass synthetic bone graft particles and open debridement in the treatment of human periodontal defects. A clinical study. *J. Periodontol.* 69, 698–709.
- Fu, Q., Rahaman, M.N., Bal, B.S., Brown, R.F., Day, D.E., 2008. Mechanical and in vitro performance of 13-93 bioactive glass scaffolds prepared by a polymer foam replication technique. *Acta Biomater.* 4, 1854–1864.
- Fu, Q., Saiz, E., Tomsia, A.P., 2011a. Bioinspired strong and highly porous glass scaffolds. *Adv. Funct. Mater.* 21, 1058–1063.
- Fu, Q., Saiz, E., Tomsia, A.P., 2011b. Direct ink writing of highly porous and strong glass scaffolds for load-bearing bone defects repair and regeneration. *Acta Biomater.* 7, 3547–3554.
- Gauthier, O., Bouler, J.M., Aguado, E., Pilet, P., Daculsi, G., 1998. Macroporous biphasic calcium phosphate ceramics: influence of macropore diameter and macroporosity percentage on bone ingrowth. *Biomaterials* 19, 133–139.
- Ghanaati, S., Barbeck, M., Detsch, R., Deisinger, U., Hilbig, U., Rausch, V., Sader, R., Unger, R.E., Ziegler, G., Kirkpatrick, C.J., 2012. The chemical composition of synthetic bone substitutes influences tissue reactions in vivo: histological and histomorphometrical analysis of the cellular inflammatory response to hydroxyapatite, beta-tricalcium phosphate and biphasic calcium phosphate ceramics. *Biomed. Mater.* 7, 015005.

- Gibson, I.R., Ke, S., Best, S.M., Bonfield, W., 2001. Effect of powder characteristics on the sinterability of hydroxyapatite powders. *J. Mater. Sci. Mater. Med.* 12, 163–171.
- Gillam, D.G., Tang, J.Y., Mordan, N.J., Newman, H.N., 2002. The effects of a novel Bioglass (R) dentifrice on dentine sensitivity: a scanning electron microscopy investigation. *J. Oral Rehabil.* 29, 305–313.
- Hasegawa, M., Doi, Y., Uchida, A., 2003. Cell-mediated bioresorption of sintered carbonate apatite in rabbits. *J. Bone Joint Surg. Br.* 85B, 142–147.
- Heikkilä, J.T., Kukkonen, J., Aho, A.J., Moisander, S., Kyyronen, T., Mattila, K., 2011. Bioactive glass granules: a suitable bone substitute material in the operative treatment of depressed lateral tibial plateau fractures: a prospective, randomized 1 year follow-up study. *J. Mater. Sci. Mater. Med.* 22, 1073–1080.
- Hench, L.L., Splinter, R.J., Allen, W.C., Greenlee, T.K., 1971. Bonding mechanisms at the interface of ceramic prosthetic materials. *J. Biomed. Mater. Res. Symp.* 2, 117–141.
- Hench, L.L., Polak, J.M., 2002. Third-generation biomedical materials. *Science* 295, 1014–1017.
- Hench, L.L., 2009. Genetic design of bioactive glass. *J. Eur. Ceram. Soc.* 29, 1257–1265.
- Hench, L.L., 2011. Bioactive materials for gene control. In: Hench, L.L., Jones, J.R., Fenn, M.B. (Eds.), *New Materials and Technologies for Healthcare*. World Scientific, Singapore, pp. 25–48.
- Hench, L.L., 2015. Opening paper 2015- some comments on bioglass: four eras of discovery and development. *Biomed. Glasses* 1, 1–11.
- Hill, R.G., Brauer, D.S., 2011. Predicting the bioactivity of glasses using the network connectivity or split network models. *J. Non-Cryst. Solids* 357, 3884–3887.
- Hill, R., Brauer, D., Gillam, D.G., Karpukhina, N., Bushby, A., Mneimne, M., inventors, 2011. Bioactive Glass Composition. Queen Mary and Westfield College, UK, assignee. WO patent WO 2011/161422 A1. 2011 29 December 2011.
- Höland, W., Beall, G.H., 2001. In: *Glass Ceramic Technology*, second ed. John Wiley & Sons, Hoboken, NJ.
- Hoppe, A., Güldal, N.S., Boccaccini, A.R., 2011. A review of the biological response to ionic dissolution products from bioactive glasses and glass-ceramics. *Biomaterials* 32, 2757–2774.
- Hoppe, A., Jokic, B., Janackovic, D., Fey, T., et al., 2014. Cobalt-releasing 1393 bioactive glass-derived scaffolds for bone tissue engineering applications. *ACS Appl. Mater. Interfaces* 6, 2865–2877.
- Hupa, L., Karlsson, K.H., Hupa, M., Aro, H.T., 2010. Comparison of bioactive glasses in vitro and in vivo. *Glass Technol. Eur. J. Glass Sci. Technol. A* 51, 89–92.
- Ilharreborde, B., Morel, E., Fitoussi, F., Presedo, A., et al., 2008. Bioactive glass as a bone substitute for spinal fusion in adolescent idiopathic scoliosis a comparative study with iliac crest autograft. *J. Pediatr. Orthop.* 28, 347–351.
- ISO 13175-3, 2012. *Implants for Surgery – Calcium Phosphates – Part 3: Hydroxyapatite and Beta-Tricalcium Phosphate Bone Substitutes*.
- Jarcho, M., Bolen, C.H., Thomas, M.B., Babock, J., Kay, J.F., Doremus, R.H., 1976. Hydroxyapatite synthesis and characterization in dense polycrystalline form. *J. Mater. Sci.* 11, 2027–2035.
- Jensen, S.S., Bornstein, M.M., Dard, M., Bosshardt, D.D., Buser, D., 2009. Comparative study of biphasic calcium phosphates with different HA/TCP ratios in mandibular bone defects. A long-term histomorphometric study in minipigs. *J. Biomed. Mater. Res. B Appl. Biomater.* 90, 171–181.
- Jones, J.R., Poologasundarampillai, G., Atwood, R.C., Bernard, D., Lee, P.D., 2007. Non-destructive quantitative 3D analysis for the optimisation of tissue scaffolds. *Biomaterials* 28, 1404–1413.
- Jung, S.B., Day, D.E., Day, T., Stoecker, W., Taylor, P., 2011. Treatment of non-healing diabetic venous stasis ulcers with bioactive glass nanofibers. *Wound Repair Regen.* 19, A30.
- Kawai, T., Suzuki, O., Matsui, K., Tanuma, Y., Takahashi, T., Kamakura, S., 2017. Octacalcium phosphate collagen composite facilitates bone regeneration of large mandibular bone defect in humans. *J. Tissue Eng. Regen. Med.* 11, 1641–1647.
- Klein, C.P.A.T., Driessen, A.A., de Groot, K., van den Hooff, A., 1983. Biodegradation behavior of various calcium phosphate materials in bone tissue. *J. Biomed. Mater. Res.* 17, 769–784.
- Kirk, J.F., Ritter, G., Waters, C., Narisawa, S., Millan, J.L., Talton, J.D., 2013. Osteoconductivity and osteoinductivity of Nano-FUSE (R) DBM. *Cell Tissue Bank.* 14, 33–44.
- Komlev, V.S., Barinov, S.M., Bozo, I.I., Deev, R.V., Eremin, I.I., Fedotov, A.Y., Gurin, A.N., Khromova, N.V., Kopnin, P.B., Kuvshinova, E.A., Mamonov, V.E., Rybko, V.A., Sergeeva, N.S., Teterina, A.Y., Zorin, V.L., 2014. Bioceramics composed of octacalcium phosphate demonstrate enhanced biological behavior. *ACS Appl. Mater. Interfaces* 6, 16610–16620.
- Kokubo, T., 1991. Bioactive glass-ceramics – properties and applications. *Biomaterials* 12, 155–163.
- Koutsopoulos, S., 2002. Synthesis and characterization of hydroxyapatite crystals: a review study on the analytical methods. *J. Biomed. Mater. Res.* 62, 600–612.
- Lechner, R., Putzer, D., Liebensteiner, M., Bach, C., Thaler, M., 2017. Fusion rate and clinical outcome in anterior lumbar interbody fusion with beta-tricalcium phosphate and bone marrow aspirate as a bone graft substitute. A prospective clinical study in fifty patients. *Int. Orthop.* 41, 333–339.
- LeGeros, R.Z., 2002. Properties of osteoconductive biomaterials: calcium phosphates. *Clin. Orthop. Relat. Res.* 395, 81–98.
- Lindfors, N.C., Heikkilä, J.T., Aho, A.J., 2008. Long-term evaluation of blood silicon and osteocalcin in operatively treated patients with benign bone tumors using bioactive glass and autogenous bone. *J. Biomed. Mater. Res. B* 87B, 73–76.
- Lindfors, N.C., Heikkilä, J.T., Koski, I., Mattila, K., Aho, A.J., 2009. Bioactive glass and autogenous bone as bone graft substitutes in benign bone tumors. *J. Biomed. Mater. Res. B* 90B, 131–136.
- Lindfors, N.C., Hyvonen, P., Nyyssönen, M., Kirjavainen, M., et al., 2010a. Bioactive glass S53P4 as bone graft substitute in treatment of osteomyelitis. *Bone* 47, 212–218.
- Lindfors, N.C., Koski, I., Heikkilä, J.T., Mattila, K., Aho, A.J., 2010b. A prospective randomized 14-year follow-up study of bioactive glass and autogenous bone as bone graft substitutes in benign bone tumors. *J. Biomed. Mater. Res. B* 94B, 157–164.
- Lovelace, T.B., Mellonig, J.T., Meffert, R.M., Jones, A.A., Nummikoski, P.V., Cochran, D.L., 1998. Clinical evaluation of bioactive glass in the treatment of periodontal osseous defects in humans. *J. Periodontol.* 69, 1027–1035.
- Low, S.B., King, C.J., Krieger, J., 1997. An evaluation of bioactive ceramic in the treatment of periodontal osseous defects. *Int. J. Periodontics Restor. Dent.* 17, 359–367.
- Mengel, R., Soffner, M., Flores-De-Jacoby, L., 2003. Bioabsorbable membrane and bioactive glass in the treatment of intrabony defects in patients with generalized aggressive periodontitis: results of a 12-month clinical and radiological study. *J. Periodontol.* 74, 899–908.
- Midha, S., Kim, T.B., van den Bergh, W., Lee, P.D., Jones, J.R., Mitchell, C.A., 2013. Preconditioned 70S30C bioactive glass foams promote osteogenesis in vivo. *Acta Biomater.* 9, 9169–9182.
- Miramond, T., Aguado, E., Goyenvall, E., Borget, P., Baroth, S., Daculis, G., 2013. In vivo comparative study of two injectable/

- moldable calcium phosphate bioceramics. *Key Eng. Mater.* 529–530, 291–295.
- Mirtchi, A.A., Lemaitre, J., Terao, N., 1989. Calcium-phosphate cements—study of the beta-tricalcium-phosphate–monocalcium phosphate system. *Biomaterials* 10, 475–480.
- Montufar, E.B., Maazouz, Y., Ginebra, M.P., 2013. Relevance of the setting reaction to the injectability of tricalcium phosphate pastes. *Acta Biomater.* 9, 6188–6198.
- Nommeots-Nomm, A., Labbaf, S., Devlin, A., Todd, N., et al., 2017. Highly degradable porous melt-derived bioactive glass foam scaffolds for bone regeneration. *Acta Biomater.* 57, 449–461.
- Norton, M.R., Wilson, J., 2002. Dental implants placed in extraction sites implanted with bioactive glass: human histology and clinical outcome. *Int. J. Oral Maxillofac. Implant.* 17, 249–257.
- O'Donnell, M.D., Hill, R.G., 2010. Influence of strontium and the importance of glass chemistry and structure when designing bioactive glasses for bone regeneration. *Acta Biomater.* 6, 2382–2385.
- Oonishi, H., Kushitani, S., Yasukawa, E., Iwaki, H., et al., 1997. Particulate bioglass compared with hydroxyapatite as a bone graft substitute. *Clin. Orthop. Relat. Res.* 334, 316–325.
- Oonishi, H., Hench, L.L., Wilson, J., Sugihara, F., et al., 1999. Comparative bone growth behavior in granules of bioceramic materials of various sizes. *J. Biomed. Mater. Res.* 44, 31–43.
- Oonishi, H., Hench, L.L., Wilson, J., Sugihara, F., et al., 2000. Quantitative comparison of bone growth behavior in granules of Bioglass (R), A-W glass-ceramic, and hydroxyapatite. *J. Biomed. Mater. Res.* 51, 37–46.
- Oryan, A., Alidadi, S., Moshiri, A., Maffulli, N., 2014. Bone regenerative medicine: classic options, novel strategies, and future directions. *J. Orthop. Surg. Res.* 9, 18.
- Osaka, A., Miuro, Y., Takeuchi, K., Asada, M., Takahashi, K., 1991. Calcium apatite prepared from calcium hydroxide and orthophosphoric acid. *J. Mater. Sci. Mater. Med.* 2, 51–55.
- Park, J.S., Suh, J.J., Choi, S.H., Moon, I.S., et al., 2001. Effects of pretreatment clinical parameters on bioactive glass implantation in intrabony periodontal defects. *J. Periodontol.* 72, 730–740.
- Parker, R.M., Malham, G.M., 2017. Comparison of a calcium phosphate bone substitute with recombinant human bone morphogenetic protein-2: a prospective study of fusion rates, clinical outcomes and complications with 24-month follow-up. *Eur. Spine J.* 26, 754–7763.
- Patel, N., Gibson, I.R., Ke, S., Best, S.M., Bonfield, W., 2001. Calcining influence on the powder properties of hydroxyapatite. *J. Mater. Sci. Mater. Med.* 12, 181–188.
- Pomrinc, G., 2016. Personal Communication. NovaBone Products LLC.
- Qiu, Z.Y., Cui, Y., Tao, C.S., Zhang, Z.Q., Tang, P.F., Mao, K.Y., Wang, X.M., Cui, F.Z., 2015. Mineralized collagen: rationale, current status, and clinical applications. *Materials* 8, 4733–4750.
- Rahaman, M.N., Yao, A.H., Bal, B.S., Garino, J.P., Ries, M.D., 2007. Ceramics for prosthetic hip and knee joint replacement. *J. Am. Ceram. Soc.* 90, 1965–1988.
- Rahaman, M.N., Day, D.E., Bal, B.S., Fu, Q., et al., 2011. Bioactive glass in tissue engineering. *Acta Biomater.* 7, 2355–2373.
- Ramay, H.R., Zhang, M.Q., 2003. Preparation of porous hydroxyapatite scaffolds by combination of the gel-casting and polymer sponge methods. *Biomaterials* 24, 3293–3302.
- Rees, J.S., Addy, M., 2002. A cross-sectional study of dentine hypersensitivity. *J. Clin. Periodontol.* 29, 997–1003.
- Rosenberg, E.S., Cho, S.C., Elian, N., Jalbout, Z.N., Froum, S., Evian, C.I., 2004. A comparison of characteristics of implant failure and survival in periodontally compromised and periodontally healthy patients: a clinical report. *Int. J. Oral Maxillofac. Implant.* 19, 873–879.
- Schallenger, M.A., Rossmeier, K., Lovick, H.M., Meyer, T.R., Aberman, H.M., Juda, G.A., 2014. Comparison of the osteogenic potential of OsteoSelect demineralized bone matrix putty to NovaBone calcium-phosphosilicate synthetic putty in a cranial defect model. *J. Craniofac. Surg.* 25, 657–661.
- Schepers, E.J.G., Ducheyne, P., 1997. Bioactive glass particles of narrow size range for the treatment of oral bone defects: a 1–24 month experiment with several materials and particle sizes and size ranges. *J. Oral Rehabil.* 24, 171–181.
- Schepers, E., Ducheyne, P., Barbier, L., Schepers, S., 1993. Bioactive glass particles of narrow size range: a new material for the repair of bone defects. *Implant Dent.* 2, 151–156.
- Sculean, A., Barbe, G., Chiantella, G.C., Arweiler, N.B., Berakdar, M., Brex, M., 2002. Clinical evaluation of an enamel matrix protein derivative combined with a bioactive glass for the treatment of intrabony periodontal defects in humans. *J. Periodontol.* 73, 401–408.
- Seebach, C., Schultheiss, J., Wilhelm, K., Frank, J., Henrich, D., 2010. Comparison of six bone-graft substitutes regarding to cell seeding efficiency, metabolism and growth behaviour of human mesenchymal stem cells (MSC) in vitro. *Injury* 41, 731–738.
- Shapoff, C.A., Alexander, D.C., Clark, A.E., 1997. Clinical use of a bioactive glass particulate in the treatment of human osseous defects. *Compend. Contin. Educ. Dent.* 18, 352–358.
- Sheikh, Z., Zhang, Y.L., Tamimi, F., Barralet, J., 2017. Effect of processing conditions of dicalcium phosphate cements on graft resorption and bone formation. *Acta Biomater.* 53, 526–535.
- Silver, I.A., Deas, J., Erecinska, M., 2001. Interactions of bioactive glasses with osteoblasts in vitro: effects of 45S5 Bioglass (R), and 58S and 77S bioactive glasses on metabolism, intracellular ion concentrations and cell viability. *Biomaterials* 22, 175–185.
- Stoor, P., Soderling, E., Salonen, J.I., 1998. Antibacterial effects of a bioactive glass paste on oral microorganisms. *Acta Odontol. Scand.* 56, 161–165.
- Tamimi, F., Torres, J., Bassett, D., Barralet, J., Cabarcos, E.L., 2010. Resorption of monetite granules in alveolar bone defects in human patients. *Biomaterials* 31, 2762–2769.
- Tamini, F., Sheikh, Z., Barralet, J., 2012. Dicalcium phosphate cements: brushite and monetite. *Acta Biomater.* 8, 474–487.
- Tang, Z., Tan, Y., Ni, Y., Wang, J., Zhu, X., Fan, Y., Chen, X., Yang, X., Zhang, X., 2017. Comparison of ectopic bone formation process induced by four calcium phosphate ceramics in mice. *Mater. Sci. Eng. C* 70, 1000–1010.
- Turunen, T., Peltola, J., Yli-Urpo, A., Happonen, R.P., 2004. Bioactive glass granules as a bone adjunctive material in maxillary sinus floor augmentation. *Clin. Oral Implant. Res.* 15, 135–141.
- Watts, S.J., Hill, R.G., O'Donnell, M.D., Law, R.V., 2010. Influence of magnesia on the structure and properties of bioactive glasses. *J. Non-Cryst. Solids* 356, 517–524.
- Wheeler, D.L., Eschbach, E.J., Hoellrich, R.G., Montfort, M.J., Chamberland, D.L., 2000. Assessment of resorbable bioactive material for grafting of critical-size cancellous defects. *J. Orthop. Res.* 18, 140–148.
- Wu, Z.Y., Hill, R.G., Yue, S., Nightingale, D., Lee, P.D., Jones, J.R., 2011. Melt-derived bioactive glass scaffolds produced by a gel-cast foaming technique. *Acta Biomater.* 7, 1807–1816.
- Xynos, I.D., Edgar, A.J., Buttery, L.D.K., Hench, L.L., Polak, J.M., 2000a. Ionic products of bioactive glass dissolution increase

- proliferation of human osteoblasts and induce insulin-like growth factor II mRNA expression and protein synthesis. *Biochem. Biophys. Res. Commun.* 276, 461–465.
- Xynos, I.D., Hukkanen, M.V.J., Batten, J.J., Buttery, L.D., Hench, L.L., Polak, J.M., 2000b. Bioglass 45S5 stimulates osteoblast turnover and enhances bone formation in vitro: implications and applications for bone tissue engineering. *Calcif. Tissue Int.* 67, 321–329.
- Xynos, I.D., Edgar, A.J., Buttery, L.D.K., Hench, L.L., Polak, J.M., 2001. Gene-expression profiling of human osteoblasts following treatment with the ionic products of Bioglass (R) 45S5 dissolution. *J. Biomed. Mater. Res.* 55, 151–157.
- Yadav, V.S., Narula, S.C., Sharma, R.K., Tewari, S., Yadav, R., 2011. Clinical evaluation of guided tissue regeneration combined with autogenous bone or autogenous bone mixed with bioactive glass in intrabony defects. *J. Oral Sci.* 53, 481–488.
- Yamada, S., Heymann, D., Bouler, J.M., Daculsi, G., 1997. Osteoclastic resorption of calcium phosphate ceramics with different hydroxyapatite/beta-tricalcium phosphate ratios. *Biomaterials* 18, 1037–1041.
- Yu, W., Sun, X., Meng, H., Sun, B., Chen, P., Liu, X., Zhang, K., Yang, X., Peng, J., Lu, S., 2017. 3D printed porous ceramic scaffolds for bone tissue engineering: a review. *Biomater. Sci.* 5, 1690–1698.
- Yukna, R.A., Evans, G.H., Aichelmann-Reidy, M.B., Mayer, E.T., 2001. Clinical comparison of bioactive glass bone replacement graft material and expanded polytetrafluoroethylene barrier membrane in treating human mandibular molar Class II furcations. *J. Periodontol.* 72, 125–133.
- Zamet, J.S., Darbar, U.R., Griffiths, G.S., Bulman, J.S., et al., 1997a. Particulate bioglass(R) as a grafting material in the treatment of periodontal intrabony defects. *J. Clin. Periodontol.* 24, 410–418.
- Zamet, J.S., Darbar, U.R., Griffiths, G.S., Burgin, W., Newman, H.N., 1997b. Particulate bioglass (Perioglas(R)) in the treatment of periodontal intrabony defects. *J Dent Res.* SI 76 2219–2219.
- Zhang, J., Liu, W., Schnitzler, V., Tancrét, F., Bouler, J.M., 2014. Calcium phosphate cements for bone substitution: chemistry, handling and mechanical properties. *Acta Biomater.* 10, 1035–1049.
- Zhao, F.J., Lei, B., Li, X., Mo, Y.F., Wang, R.X., Chen, D.F., et al., 2018. Promoting in vivo early angiogenesis with sub-micrometer strontium-contained bioactive microspheres through modulating macrophage phenotypes. *Biomaterials* 178, 36–47.

Chapter Questions

- (a) Explain why “nearly bionert” bioceramics are not completely bionert. [3 marks]
- (b) Define the term “bioactive ceramic”. [2 marks]
- (c) Explain how the general immune response to implants leads to the mechanism of bone bonding for a synthetic hydroxyapatite (sHA) bone graft. [5 marks]
- (d) Explain how biological apatite and stoichiometric sHA differ. [3 marks]
- (e) Discuss how the bioactivity mechanism of Bioglass differs from that of sHA. [4 marks]
- (f) Describe the synthesis chemistry and processing required to produce an sHA powder. [4 marks]
- (g) Describe the design criteria for bioactive ceramic scaffold for bone regeneration. [6 marks]
- (h) Explain why Actifuse contains some Si [2 marks]
- (i) Explain why it is challenging to produce porous 45S5 Bioglass. [2 marks]

Questions with answers

Here are the answers

- (a) Explain why “nearly bionert” bioceramics are not completely bionert. [3 marks]
- Answer: They do illicit a response from the body in that the body recognises them as foreign, triggering an inflammatory response
- (b) Define the term “bioactive ceramic”. [2 marks]
- Answer: Historically a hard crystalline material (ceramic) that can form bond with bone. Now modified to one that stimulates a positive biological response from the body.
- (c) Explain how the general immune response to implants leads to the mechanism of bone bonding for a synthetic hydroxyapatite (sHA) bone graft. [5 marks]
- Answer: macrophages recruited: macrophages become osteoclasts; digestion of HA as it is similar to bone mineral; Ca and phosphate ion release; precipitation of Ca and phosphate as HCA; osteoblasts produce new bone

- (d) Explain how biological apatite and stoichiometric sHA differ. [3 marks]

Answer: biological apatite is calcium deficient and carbonate substituted (for phosphate) sHA has Ca/P ratio of 1.67

- (e) Discuss how the bioactivity mechanism of Bioglass differs from that of sHA. [4 marks]

Answer: Bioglass dissolution is Solution mediated via ion exchange, silica rich layer formation. Ions cause Osteostimulation– ions stimulate osteogenic cells to produce more bone

- (f) Describe the synthesis chemistry and processing required to produce an sHA powder. [4 marks]

Answer: solution precipitation by the equation



Once aged, the precipitate is thoroughly washed, filtered and dried.

- (g) Describe the design criteria for bioactive ceramic scaffold for bone regeneration. Answers [expected to be able to list at least 6 of]:

- Biocompatible
- Inflammation?
- No immuno-rejection
- No formation of fibrous capsules;
- Be easily and cheaply produced to ISO/FDA/CE standards (must be easily sterilised)
- Have mechanical properties similar to the host tissue
- Act as template for tissue growth in 3D;
- Have an interconnected macroporous network for vascularisation, tissue ingrowth and nutrient delivery;
- Bond to the host tissue without the formation of scar tissue;
- Resorb at the same rate as the tissue is repaired
- Provide signals to the cells

[6 marks]

- (h) Explain why Actifuse contains some Si [2 marks]

Answer: to increase dissolution rate by introducing some disorder in the crystal structure (particularly at grain boundaries); soluble silica dissolution (Si release) can stimulate osteogenesis

- (i) Explain why it is challenging to produce porous 45S5 Bioglass. [2 marks]

Answer: the original Bioglass composition will crystallise on sintering, losing its amorphous structure.

1.3.4A

Natural and Synthetic Hydroxyapatites

IAIN R. GIBSON

Institute of Medical Sciences, School of Medicine, Medical Sciences and Nutrition, University of Aberdeen, Aberdeen, United Kingdom

Introduction

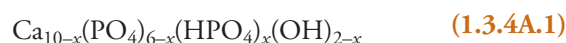
Hydroxyapatite (HA, also described as hydroxyapatite, HAp) is a stoichiometric calcium phosphate phase with a composition $\text{Ca}_{10}(\text{PO}_4)_6(\text{OH})_2$. This is a very specific composition that defines an absolute material but its chemistry allows a range of nonstoichiometric compositions to be described as apatite phases. The interest in HA in the biomedical field is due to its similarity to the calcium phosphate apatite phase in bone and tooth mineral. Bone mineral consists of nanoscale crystals of calcium phosphate but the chemical composition of this is not fixed and can vary with age, anatomical location, diet, disease, etc. Considering stoichiometric HA first, this is defined as having a calcium-to-phosphorus molar ratio of 10:6, or typically written 1.67. The structure has been commonly reported as having hexagonal crystal structure, with space group $\text{P6}_3/\text{m}$ (Kay et al., 1964) and typical unit cell parameters of $a=9.422$ and $c=6.883$ Å (Young and Elliott, 1966). It has also been reported as having a monoclinic crystal structure $\text{P2}_{1/b}$ (Elliott et al., 1973), with typical unit cell parameters $a=9.426$, $b=18.856$, and $c=6.887$ Å, with $\gamma=119.97$ degrees (Ikoma et al., 1999). This difference is ascribed to the hydroxyl groups existing in an ordered (monoclinic) or disordered (hexagonal) crystal lattice and is thought to be related to preparation conditions (Ikoma et al., 1999). Representations of the crystal structure of hydroxyapatite are provided in Fig. 1.3.4A.1 (Uskoković and Uskoković, 2011).

When HA is termed crystalline HA it can be considered analogous to naturally occurring mineral forms and it usually relates to an HA that has been heated to greater than $\sim 800^\circ\text{C}$ to form a ceramic. It should be noted that HA can be prepared using hydrothermal synthesis methods to produce large (up to 3 mm in dimension) crystals, which are clearly crystalline (Arends et al., 1979). Crystalline HA produces an X-ray diffraction pattern as shown in Fig. 1.3.4A.2A, with narrow diffraction peaks and a very high signal-to-noise ratio. X-ray (Kay et al., 1964) and neutron (Arcos et al., 2004) diffraction data have been used to describe the crystal structure of HA and several ICDD

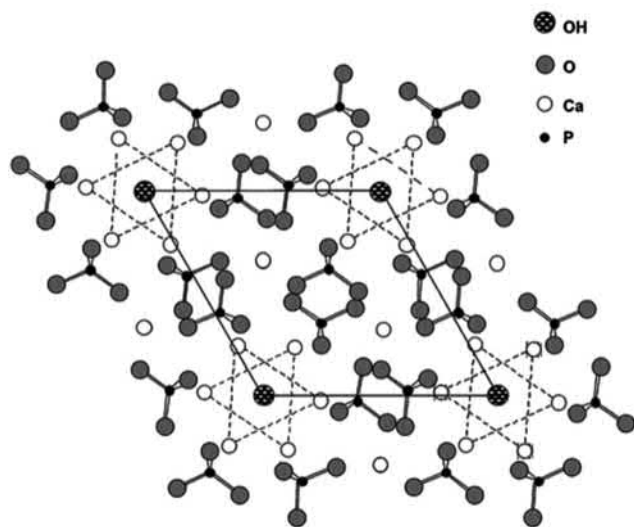
Powder Diffraction Files (PDFs) exist as “fingerprints” of HA with hexagonal symmetry, e.g., PDF no. 00-009-0432, and monoclinic symmetry, e.g., PDF no. 01-089-4405 (ICDD, 2013).

The X-ray diffraction pattern of crystalline HA differs from that of the calcium phosphate phase of bone mineral (Fig. 1.3.4A.2B) in that the diffraction peaks of the latter are very broad. This is due mostly to the very small crystallite size of the bone mineral apatite phase, but also due to crystal imperfections or lattice strain (Venkateswarlu et al., 2014). Indeed, the crystallites of bone mineral apatite can be described as nanoparticles, or nanocrystals, with a mean dimension in the c -axis of approximately 32 nm and a thickness of approximately 5 nm, as determined by dark-field transmission electron microscopy (Jackson et al., 1978). It should be noted that this phase is not amorphous because, although the diffraction peaks are broad, within a nanocrystal there is structural order. If bone mineral is heated to temperatures above $\sim 800^\circ\text{C}$, analogous to sintering synthetic HA, then a diffraction pattern similar to that of crystalline HA is observed, although secondary phases may develop depending upon the absolute composition of the bone mineral apatite.

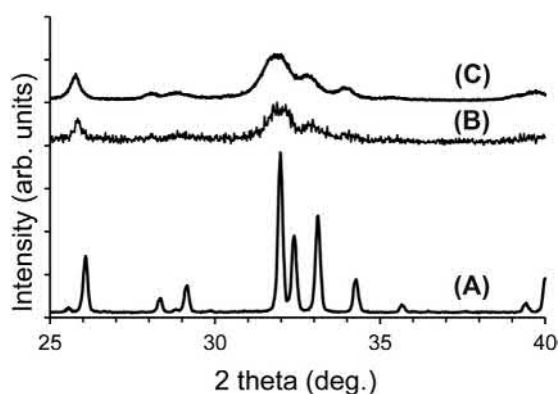
This brings us full circle to the synthesis of bone-like apatite phases. Using various aqueous-based synthesis methods we can prepare nanocrystals of apatite compositions, including stoichiometric HA, that have a similar size scale to bone mineral apatite and have a similar X-ray diffraction pattern (Fig. 1.3.4A.2C). As for bone mineral apatite, heating these synthetic nanocrystals to temperatures above $\sim 800^\circ\text{C}$ results in crystal growth and a diffraction pattern of “crystalline HA.” A better description of the composition of HA and apatites produced by such methods is given in Eq. (1.3.4A.1), with $0 \leq x \leq 1$.



For $x=0$, this gives the composition of stoichiometric HA and when $0 < x \leq 1$ a calcium-deficient apatite phase is



• **Figure 1.3.4A.1** The crystal structure of hydroxyapatite. The unit cell is projected on the *ab* (001) plane showing the location of Ca, P, O, and H within the unit cell. (Reproduced and adapted from Uskoković, V., Uskoković, D.V., 2011. Nanosized hydroxyapatite and other calcium phosphates: chemistry of formation and application as drug and gene delivery agents. *J. Biomed. Mater. Res. B. (Appl. Biomater.)* 96, 152–191.)



• **Figure 1.3.4A.2** Representative X-ray diffraction patterns of (A) a crystalline synthetic hydroxyapatite prepared by an aqueous precipitation reaction then heated at 900°C in air, (B) bone mineral apatite, and (C) “poorly crystalline” synthetic hydroxyapatite prepared by an aqueous precipitation reaction and dried at 90°C.

obtained, which produces an X-ray diffraction pattern that is largely indistinguishable from that obtained when $x=0$ (Fig. 1.3.4A.2C). Heating Ca-deficient apatite compositions to temperatures above ~800°C will result in the formation of HA and tricalcium phosphate (TCP, $\text{Ca}_3(\text{PO}_4)_2$) and the relative proportion of these phases will depend on the value of x ; it should be noted that the value of $x=1$ results in a Ca-deficient apatite that would produce only TCP upon heating to above ~740°C (Gibson et al., 2000).

Another major difference between bone mineral apatite and the crystalline or nanocrystal HA (or apatites) described so far is that bone mineral contains various other ions and also vacancies, partially substituting at the various Ca, PO_4 , and OH sites in the structure. The types of ion substituted in bone mineral and tooth dentine and enamel have been

TABLE 1.3.4A.1 The Comparative Chemical Composition of Human Enamel, Dentine, and Bone Mineral

	Enamel (wt%)	Dentine (wt%)	Bone (wt%)
Calcium, Ca^{2+}	37.1	38.6	37.7
Phosphorus, PO_4^{3-} as P	18.2	18.6	16.1
Sodium, Na^+	0.5	0.5	1.1
Potassium, K^+	0.08	0.07	0.05
Magnesium, Mg^{2+}	0.45	1.6	0.85
Carbonate, CO_3^{2-}	2.4	6.4	8.9
Fluoride, F^-	0.01	0.07	0.03
Chloride, Cl^-	0.3	0.01	0.1
Calculated Ca/P molar ratio	1.57	1.60	1.80

Data taken from Legeros R.Z., 1981. Apatites in biological systems. *Prog. Cryst. Growth Charact.* 4, 1–45, and normalized to the reported total inorganic component.

reviewed extensively and are summarized in Table 1.3.4A.1 (Legeros, 1981). The composition of bone mineral apatite is not fixed, and the amount of different substitutions varies with age and most notably the carbonate content (LeGeros et al., 1987).

This observation led researchers to consider synthesis of HA compositions with various ion substitutions, partly to understand better various biological apatites, but more recently to test the hypothesis that including one or more of these ion substitutions in HA would result in improved biological responses (Shepherd et al., 2013). In terms of mimicking bone mineral, the main substitutions studied include sodium (Driessens et al., 1983), magnesium (Bigi et al., 1996), or strontium (O'Donnell et al., 2008) for calcium; carbonate (Nelson and Featherstone, 1982; Vignoles et al., 1988) for phosphate; carbonate (Ito et al., 1997), fluoride (Jha et al., 1997), or chloride (LeGeros, 1975) for hydroxyl ions; or carbonate for both phosphate and hydroxyl ions (Gibson and Bonfield, 2002).

This chapter will now discuss in more depth the various methods used to synthesize HA, the processing of HA to form medical devices, characterization of these materials as well as clinical use of HA. Reference will be made to the application of HA as a coating on biologically inert implant materials, but the focus will be on HA ceramics, principally as macroporous bone graft substitutes.

Synthesis of Hydroxyapatite Ceramics

Many synthesis methods have been used to prepare HA compositions and the suitability of each of these will depend on the final application but also the scale of product required. Some of the first HA ceramics were produced from natural

apatites or reactants. Coral-derived HA ceramics have been prepared by Roy and Linnehan (1974) and Sivakumar et al. (1996), where calcium carbonate coral acts not only as a template for the macroporous structure but also as a reactant in the hydrothermal reaction with a phosphate source to produce a macroporous HA product. HA ceramics have also been prepared by thermal and/or chemical conversion of bovine cancellous bone to form a macroporous HA ceramic that is then deproteinated. It is often described as inorganic bone (Spector, 1994). Such composition of inorganic bone should comply with ASTM F1581-08 (2016) that describes the standard specification for use as surgical implants. Many other natural sources of reactants and/or templates to synthesize HA include fish bones and shells, algae and egg shells and they have been reviewed elsewhere (Akram et al., 2014). The use of naturally occurring materials as templates/reactants may provide economically viable routes to manufacture HA, particularly when the process utilizes waste material (Inyang and Ibitoye, 2018).

Solid-state synthesis is a traditional method that is used to synthesize inorganic oxide materials as it allows excellent control of chemical stoichiometry. Challenges exist, however, when formation of the phase composition of the desired product is not compatible with the high temperatures and long thermal treatment times required to obtain complete solid-state reaction. This method is also not suitable when product with a high surface area is required, as the high thermal energy used in solid-state synthesis usually results in low surface area powders. HA can be synthesized by solid-state reaction of a mixture of reactant oxides, for example, between a mixture of calcium pyrophosphate and calcium carbonate at 1100°C in a vacuum, followed by further heating in 1.5 atm H₂O between 900 and 1100°C; after prolonged reaction times, including remixing of the product, a single-phase polycrystalline HA sample was obtained (Fowler, 1974).

The most widely used method to synthesize HA samples is an aqueous precipitation reaction, typically involving a calcium salt and a phosphate salt/acid mixed at alkaline pH. An example of an aqueous precipitation method to make dense HA ceramics used Ca(NO₃)₂·4H₂O and (NH₄)HPO₄ as the reactants, and gradual mixing of these at an alkaline pH maintained with addition of NH₄OH produced a precipitate consisting of nanoscale crystals of HA (Jarcho et al., 1976). An alternative aqueous precipitation reaction uses a mixture of Ca(OH)₂ suspension and phosphoric acid solution, again mixed slowly at alkaline pH (Osaka et al., 1991). Calcium hydroxide has low solubility in water, but gradual dissolution is associated with a very high pH value; slow addition of phosphoric acid to a Ca(OH)₂ suspension results in a precipitation reaction to form nanocrystals of HA, and the pH can be maintained at high alkaline pH during the whole reaction by the addition of ammonia. These methodologies of producing a precipitate of nanoscale crystals of HA, which is then dewatered by, e.g., filtering and drying the filter cake, have been used extensively in the synthesis of HA powders and ceramics. A distinct advantage of

aqueous precipitation methods as a route to synthesize HA is the ability to scale up the process to the large-scale manufacture of a product that has a high surface.

A number of other synthesis methods have been reported, including: sol-gel synthesis (Deptula et al., 1992); biomimetic synthesis using supersaturated solutions (Tas, 2000a); hydrolysis of a calcium phosphate precursor, for example, brushite (Monma and Kamiya, 1987); microwave solid-state sintering (Cao et al., 2005); mechanochemical synthesis (Yeong et al., 2001); sonochemical synthesis (Fang et al., 1992); emulsion techniques (Lim et al., 1997); hydrothermal synthesis (Yoshimura et al., 1994); combustion synthesis (Tas, 2000b); and pyrolysis methods (Itatani et al., 1994). These methods have been optimized and/or adapted to control chemical and phase composition, morphology, and other specific properties of the synthesized HA, with recent reviews describing in detail the current status of HA synthesis (Zakaria et al., 2013; Haider et al., 2017). An HA or Ca-deficient HA composition can also be produced as the product phase of calcium phosphate cement-setting reactions, whereby reactant phases (typically one or more calcium phosphate phases) is mixed with water and the paste undergoes a dissolution/reprecipitation reaction forming interlocking apatite crystals producing a hardened mass (Fukase et al., 1990; TenHuisen and Brown, 1998).

A feature of a number of these synthesis methods is that the primary (smallest) crystallite size has nanoscale dimensions and these nanoparticles can have a wide variety of morphologies, depending on the method but also specific parameters within the chosen synthesis method. The range of morphologies has been reviewed by Lin et al. (2014), ranging from very small spherical (Nathanael et al., 2011) nanoparticles to nanoneedles (Kobayashi et al., 2012), nanorods (Manafi and Rahimpour, 2011), nanowires (Lin et al., 2011), nanowhiskers (Teshima et al., 2012), nanosheets (Xiao et al., 2010), hollow nanospheres (Cai et al., 2007), nanotubes (Lester et al., 2013), nanobelts (Ma et al., 2018), and whiskers (Zhang and Darvell, 2011). Although synthetic HA has conventionally been utilized as a ceramic or as a coating, these nanoscale morphologies open up new possibilities for potential applications of HA in medicine, including drug delivery (Li et al., 2016), gene delivery (Curtin et al., 2015), delivery of cells in tissue engineering/regenerative medicine (Zannettino et al., 2010), hyperthermia therapy of cancer (Hou et al., 2009), and in vivo imaging (Altinoglu et al., 2008; Ashokan et al., 2010).

In addition to the various synthesis methods just described, which can alter the morphology of the formed HA crystals, many studies have focused on modifying the chemical composition of HA to incorporate ions that exist in bone mineral or may have a biological function. As mentioned previously, studies have reported the substitution of sodium, magnesium, strontium, carbonate, fluoride, and chloride ions, but other ions, including potassium (Nordström and Karlsson, 1992), lithium (Wang et al., 2016), barium (Bigi et al., 1984), silicate

(Gibson et al., 1999), copper (Gomes et al., 2018), cobalt (Ignjatović et al., 2013), silver (Shi et al., 2016), and zinc (Thian et al., 2013), have been described. Some of these ions have been shown to have osteogenic (e.g., Li et al., 2018), angiogenic (e.g., Birgani et al., 2016), or antibacterial (Shi et al., 2016) properties in vitro and their potential mechanisms by which ions may enhance osteogenesis and angiogenesis have been reviewed comprehensively (Bose et al., 2013).

Another approach to alter the properties of HA ceramics is the synthesis of compositions that are a mixture of HA and β -TCP, termed biphasic calcium phosphate (BCP) ceramics (reviewed in Bouler et al., 2017). BCPs are described in detail in Chapter 1.3.4.

HA has been utilized as a bioactive coating on the surfaces of implant materials that are considered biologically nearly inert, such as some metals (Sun et al., 2001) and polymers (Barkarmo et al., 2013). This changes the mode of fixation of these implants to the host bone and may improve integration of joint replacements (Goosen et al., 2009), dental tooth root implants (Zhou et al., 2011), and spinal cages (Daentzer et al., 2005). The most widely applied HA coating method in the area of medical devices is plasma spraying, where HA powder is fed into a high-temperature plasma torch that then sprays semimolten HA powder particles onto the substrate to be coated (de Groot et al., 1987). A number of spraying parameters and powder properties can be modified to control the properties of the final coating. ASTM 1609-2014 (Standard Specification for Calcium Phosphate Coatings for Implantable Materials) describes the requirements of HA coatings on surgical implants; a number of other coating methods in addition to plasma spraying are described within this ASTM. An ISO standard also exists that describes the requirements of an HA coating that is specifically applied by thermal spraying: ISO 13779-2:2018 (Implants for surgery—Hydroxyapatite—Part 2: Thermally sprayed coatings of hydroxyapatite).

Examples of other coating methods used to coat HA include sol-gel (Weng and Baptista, 1998), electrophoretic deposition (Shirkhanzadeh, 1995), biomimetic coating (Habibovic et al., 2002), and various sputter-coating methods (Yang et al., 2005). Although most of the published literature focuses on HA-coated metallic implants there has been a recent growth in studies that aim to apply HA coatings to polymeric implants such as polyether ether ketone spinal cages (Hahn et al., 2013), with the purpose of improving implant fixation and integration.

A major application of HA, along with other BCPs and β -TCP, is as synthetic bone graft substitutes. These require both the densification of the calcium phosphate and the introduction of micro- and macroporosity during sintering. These somewhat conflicting processes require optimization of the powder properties and also of the method of introducing the macroporosity. These processes are described in detail in Chapter 1.3.4.

TABLE 1.3.4A.2 The Key Chemical and Physical Variables Used to Describe a Synthetic Hydroxyapatite Bone Graft Substitute (BGS)

Possible Variable	Description/Examples
Chemical composition	Ca/P molar ratio, presence of substituted ions, e.g., carbonate, sodium, strontium, magnesium, silicate ions
Phase composition	100% hydroxyapatite, or the presence of additional phases, e.g., β -tricalcium phosphate, CaO, CaCO ₃
Density/porosity	Density (often expressed as a percentage of theoretical density), porosity (often expressed as a percentage of theoretical density)
Pore size and size range	Diameter and range, including distinguishing between macropores (e.g., 100–200 μ m) and micropores (e.g., 2–5 μ m)
Pore interconnectivity	Trapped pores or fully interconnected pore structures
Grain size	Submicron or micron size range of grains, e.g., 1 μ m
Physical form of BGS	Granule, block, putty, foam, paste, etc.
Granule size and size range	Diameter and range, e.g., 200–300 μ m or 1–2 mm
Additive (putty, foam, paste)	Description of organic additives, e.g., collagen, gelatin, carboxy-methyl cellulose, hyaluronic acid, saline, etc.

Characterization of Hydroxyapatite Ceramics

Physicochemical Characterization

HA ceramics can be characterized using a number of different methods that establish key parameters, including phase composition and chemical composition, including Ca/P molar ratio and trace metal content. HA materials intended for use in medical devices can be characterized as guided by ASTM F1185-03 (2014)—Standard Specification for Composition of Hydroxyapatite for Surgical Implants. A standard reference material of HA is also available from the National Institute of Standards and Technology (Markovic et al., 2004). Some of the key chemical and physical characteristics of HA and products composed of HA are summarized in Table 1.3.4A.2. These characteristics are all parameters that can be varied to modify or optimize the properties of the product.

X-ray diffraction analysis of HA was described earlier in terms of comparing the diffraction patterns of biological apatite and synthetic HA (nanoscale and sintered HA). Extensive

information can be derived from diffraction data, including determination of crystallite size (Venkateswarlu et al., 2014), unit cell parameters, and the effect of composition on these structural parameters (Legeros, 1981), as well as phase composition, namely the presence and quantification of any additional crystalline phases (Keller, 1995). Estimations of the relative amount of amorphous phase to crystalline phase have also been reported, which are particularly relevant to HA coatings produced by high-temperature methods (Wang et al., 1995).

Infrared spectroscopy, most typically Fourier transform infrared spectroscopy (FTIR) and Raman spectroscopy, also provide significant information on synthetic and biological apatites (Koutsopoulos, 2002). The phosphate and hydroxyl groups in stoichiometric HA produce various vibrations in the FTIR spectra of HA samples and the presence of other ions can also be identified, notably carbonate ions, in substituted HA and biological apatites. The specific infrared (IR) vibration peaks for PO_4^{3-} , OH^- , and CO_3^{2-} groups in synthetic and biological apatites are summarized in Table 1.3.4A.3 (Koutsopoulos, 2002). These vibration peaks can provide significant information on the effect of synthesis or processing conditions on synthetic HA, and they can also help distinguish other calcium phosphate phases. IR data can also be used to identify and characterize the substitution site of carbonate in HA, on the phosphate site (B-type) and/or hydroxyl site (A-type) (Fleet, 2009), and the crystallinity of apatites can be assessed from analysis of the phosphate vibrations at $550\text{--}600\text{ cm}^{-1}$ (Termine and Posner, 1966). Example FTIR spectra of synthetic HA (nanocrystals and sintered) are presented in Fig. 1.3.4A.3. Raman spectroscopy provides complementary data to IR data (Khan et al., 2013), with some advantages of minimal sample preparation and high spatial resolution using a Raman microscope.

The chemical composition of HA can be determined by a number of analytical techniques, but the most common method for determining the Ca/P molar ratio and the elemental content of a number of different trace elements such as sodium, magnesium, potassium, strontium, and silicon that may be present in the reactants used is X-ray fluorescence spectroscopy. Trace elements that may be present at ppm levels (such as As, Hg, Pb, and Cd) are more effectively measured using, e.g., ion-coupled plasma optical emission spectroscopy. Solid-state nuclear magnetic resonance (NMR) spectroscopy also provides additional information about local structure in HA compositions, with ^{43}Ca , ^{31}P , ^1H solid-state NMR all providing insights into the structure of synthetic HA and natural apatites (Ben-Nissan et al., 2001; Laurencin et al., 2008; Kafak and Kolodziejski, 2007). Additionally, ion substitutions in HA can also be probed by solid-state NMR, such as carbonate using ^{13}C and silicate using ^{29}Si solid-state NMR (Beshah et al., 1990; Gillespie et al., 2010). X-ray photoelectron spectroscopy and time-of-flight secondary ion mass spectrometry provide the ability to study phase composition on very small samples and the very surface layers of a material, which has aided the understanding of correlations of the bulk composition with surface composition of HA (Chusuei and Goodman, 1999; Lu et al., 2000). These techniques have

TABLE 1.3.4A.3 The Specific Infrared Vibrations for PO_4^{3-} , OH^- , and CO_3^{2-} Groups in Synthetic Hydroxyapatites

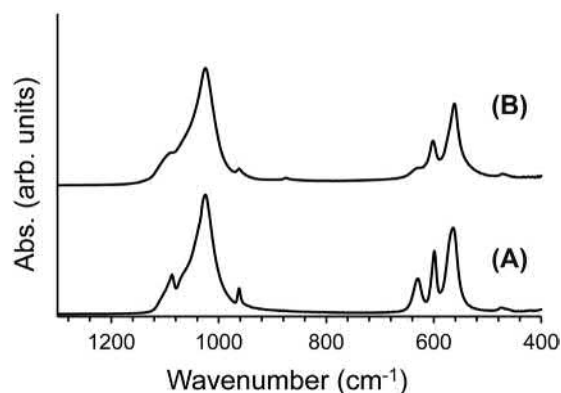
	Peak (cm^{-1})
Hydroxyl group, stretching mode, ν_s	3572
Hydroxyl group, librational mode, ν_L	631
Phosphate group, triply degenerated asymmetric stretching mode, ν_{3a}	1087
Phosphate group, triply degenerated asymmetric stretching mode, ν_{3b}	1046
Phosphate group, triply degenerated asymmetric stretching mode, ν_{3c}	1032
Phosphate group, nondegenerated symmetric stretching mode, ν_1	962
Phosphate group, triply degenerated bending mode, ν_{4a}	602
Phosphate group, triply degenerated bending mode, ν_{4b}	574
Phosphate group, triply degenerated bending mode, ν_{4c}	561
Phosphate group, doubly degenerated bending mode, ν_{2a}	472
Phosphate group, doubly degenerated bending mode, ν_{2b}	462
Carbonate group, bending mode in A-type CHA, ν_4	1550
Carbonate group, stretching mode in CHA, ν_3	1500
Carbonate group, stretching mode in A-type CHA, ν_1	1465
Carbonate group, bending mode in A- and B-type CHA, ν_4 or ν_3	1452–1455
Carbonate group, stretching mode in B-type CHA, ν_1	1430
Carbonate group, bending mode in A-type CHA, ν_2	883
Carbonate group, bending mode in B-type CHA, ν_2	875

CHA, Carbonate hydroxyapatite.
Taken from review by Koutsopoulos, S., 2002. Synthesis and characterization of hydroxyapatite crystals: a review study on the analytical methods. *J. Biomed. Mater. Res.* 62, 600–612.

also been used extensively to characterize the chemical and physical properties of bone mineral and tooth enamel apatite crystals dating back to the 1950s, and these have been reviewed in detail elsewhere (Rey et al., 2009).

In Vitro and In Vivo Characterization

HA ceramics are long established as being biocompatible, osteoconductive, and bioactive, typically evaluated by cell



• **Figure 1.3.4A.3** Fourier transform infrared spectroscopy spectra of (A) a crystalline synthetic hydroxyapatite prepared by an aqueous precipitation reaction then heated at 900°C in air and (B) “poorly crystalline” synthetic hydroxyapatite prepared by an aqueous precipitation reaction and dried at 90°C.

culture studies (Seebach et al., 2010), in vivo bone healing response (Peric et al., 2015), and surface apatite layer formation when immersed in a physiological salt solution, such as simulated body fluid (Kim et al., 2004). These responses can be evaluated following established ISO protocols, including ISO 10993-5, ISO 10993-6, and ISO 23317, and ASTM standards, including ASTM F2721-09 (2014) and ASTM F3207-17 (2017). In addition to the osteogenic response of mesenchymal stem cells, preosteoblasts or osteoblasts to HA surfaces (Samavedi et al., 2013), the response of osteoclasts (Yamada et al., 1997; Nakamura et al., 2016), endothelial cells (Pezzatini et al., 2007), and macrophages (Linares et al., 2016) have also been studied. Moreover, aside from being very dependent on culture model and cell source, the surface physical properties of the HA, such as the surface roughness (Yang et al., 2016), will also have a significant effect on any cell response and this should be considered in addition to the HA chemistry.

The shift in application of HA from coatings and monolithic dense ceramics toward use as macroporous bone graft substitutes or scaffolds for bone tissue engineering/repair has led to an increase in the in vivo evaluation of these materials in models for repair of critical size bone defects (Kon et al., 2000), spinal fusion (Walsh et al., 2009), and osteoinductivity (Ripamonti, 1996; Duan et al., 2018). The development of specific macroporous structures, HA chemistry, and microstructures has led to HA-based bone graft substitutes that exhibit osteoinductive properties, whereby bone is formed within the porous structure when the material is implanted into an intramuscular or subcutaneous defect (LeGeros, 2008; Barradas et al., 2011; García-Gareta et al., 2015; Bohner and Miron, 2019). The mechanisms for this response are not yet clear and a single pathway may not describe osteoinductive response in all these different materials. Proposed mechanisms have included an influence on the inflammatory/wound-healing response, localized changes in Ca and PO₄ concentrations, or localized adhesion/capture of exogenous osteoinductive growth factors such as BMP-2 (Bohner and Miron, 2019).

TABLE 1.3.4A.4 Different Forms That Hydroxyapatite has Been Utilized in as, or as Part of, a Medical Device

Granules (porous or dense)—typically between 200 μm and 5 mm
Granules within a putty (polymeric carrier)
Granules within a collagen matrix
Coating on metallic or polymeric device
Injectable paste or slurry (small particles dispersed in a carrier)
Cement
Porous blocks or wedges
Filler phase of a composite
Nanoparticles

With the increased development of HA nanomaterials there has been a renewed interest in the specific in vitro and in vivo response that these materials may produce. As with most materials that consist of nanoparticles, these nanoparticles typically agglomerate to form a larger secondary particle or a cluster. In applications where the use of HA nanoparticles is reliant on the size of the primary particle, such as cell transfection (Tenkumo et al., 2016), which requires the nanoparticles to cross the cell membrane, methods to functionalize the HA nanoparticles to improve dispersion can be utilized (Xu et al., 2015).

The in vitro and in vivo inflammatory responses to nanoparticles of HA in different morphologies, including dots, sheets, long rods, and fibers, were shown to have the highest acute inflammation in vivo (Pujari-Palmer et al., 2016). Studying a broader range of particle sizes and particle shapes, a similar result was observed, with small needle-shaped particles producing a strong inflammatory response compared with spherical nanoparticles (Lebre et al., 2017). A recent review noted “the risk associated with an exposition to nanoparticulate calcium phosphate in doses that are usually applied in biomedicine, health care products, and cosmetics is very low and most likely not present at all” (Epple, 2018).

Clinical Use of Hydroxyapatite Ceramics

The use of HA for medical applications has been largely as a ceramic, where a solid mass can be obtained by sintering a compacted powder at temperatures greater than 1100°C, or as a coating on biologically inert materials, traditionally on metals (Sun et al., 2001) but more recently on polymers (Barkarmo et al., 2013). As noted, however, the ability to synthesize HA as a nanocrystal has created applications in drug delivery (Li et al., 2016) and gene delivery (Curtin et al., 2015). HA can be used in a variety of forms and these are listed in Table 1.3.4A.4.

The use of HA as a coating on medical devices has been most closely associated with orthopedic hip and knee implants and with dental tooth root implants, hence a significant body of data on their clinical use is available now. The coating of metallic hip or knee implants provides an alternative method of fixation to the use of polymeric bone cements. A challenge for understanding the clinical outcome of using HA-coated implants is that there are a considerable number of variables in the plasma-spraying process and also in the HA powder used.

A systematic review of randomized clinical trials attempted to identify if there was a difference in clinical outcome when an HA coating was applied to uncemented porous titanium-coated femoral hip prostheses (Goosen *et al.*, 2009). Exclusion criteria meant that only a small percentage of the initial publications were identified in their search, but data pooled from the five studies that met the strict criteria showed that there was no significant difference in Harris hip score and that there was no clear benefit of an HA coating in radiographic or clinical success. In a metaanalysis from a systematic review of randomized clinical trials of HA-coated uncemented knee implants versus cemented implants (Nakama *et al.*, 2012), the authors showed that the HA-coated implants had a much lower risk of future failure by aseptic loosening compared with the cemented implants, but again only five studies met the strict exclusion criteria for this study. Clinical studies using HA-coated dental implants have shown good early fixation of the implants, but the survivorship of the implants is inferior after longer periods. For instance, the 8-year survivorship of titanium plasma-sprayed dental implants was at 92.7% compared with that at 77.8% for HA-coated implants (Wheeler, 1996).

The main use of hydroxyapatite and other calcium phosphate ceramics (TCP or BCP) is as synthetic bone graft substitutes, where they can be used as an alternative to autograft bone to fill bone defects (Campana *et al.*, 2014; de Grado *et al.*, 2018). They are typically in the form of porous granules or blocks, sometimes within a polymeric carrier or dispersed within a collagen foam strip. The porous structure encourages bone ingrowth and integration and the granules or blocks can act as a carrier for growth factors, antibiotics, bone marrow aspirate, or platelet-rich plasma. More than 2 million bone-grafting procedures have been performed globally (Campana *et al.*, 2014). A large number of synthetic bone graft substitutes that contain HA have been approved for clinical use but clinical trial data are still very limited to support specific products. These products (some are listed in Chapter 1.3.4) have different permutations of the features described in Table 1.3.4A.2, so understanding which of these parameters affects clinical outcomes is challenging. The use of various ceramic bone graft substitutes in spinal surgery was described in a systematic review (Fischer *et al.*, 2013). The authors noted that a lack of good clinical data limited the grading of these materials in comparison with bone graft alternatives, restricting their recommendation on the

efficacy of calcium phosphate bone graft substitutes. They further noted that the situation would likely improve as more studies showing stronger evidence became available. This lack of high-level clinical efficacy data is also observed in other clinical studies reporting the use of bone graft substitutes (Buser *et al.*, 2016). Although many clinical studies reporting the efficacy of specific synthetic bone graft substitute products have been reported in the last 5 years, these are typically observational studies or open label interventional trials, thereby lacking high-quality clinical evidence. This is one area in general that needs to be addressed to help translate the development of the science of biomaterials into improved clinical treatments, and it is not exclusive to synthetic bone graft substitutes.

References

- Akram, M., Ahmed, R., Shakir, I., Ibrahim, W., Hussain, R., 2014. Extracting hydroxyapatite and its precursors from natural resources. *J. Mat Sci.* 49, 1461–1475.
- Altinoglu, E.I., Russin, T.J., Kaiser, J.M., Barth, B.M., Eklund, P.C., Kester, M., Adair, J.H., 2008. Near-infrared emitting fluorophore-doped calcium phosphate nanoparticles for in vivo imaging of human breast cancer. *ACS Nano* 2, 2075–2084.
- Arcos, D., Rodríguez-Carvajal, J., Vallet-Regí, M., 2004. The effect of the silicon incorporation on the hydroxylapatite structure. A neutron diffraction study. *Solid State Sci.* 6, 987–994.
- Arends, J., Schuthof, J., van der Lindwen, W.H., Bennema, P., van der Berg, P.J., 1979. Preparation of pure hydroxyapatite single crystals by hydrothermal recrystallization. *J. Cryst. Growth* 46, 213–220.
- Ashokan, A., Menon, D., Nair, S., Koyakutty, M., 2010. A molecular receptor targeted, hydroxyapatite nanocrystal based multi-modal contrast agent. *Biomaterials* 31, 2606–2616.
- ASTM F1185-03, 2014. Standard Specification for Composition of Hydroxylapatite for Surgical Implants. ASTM International, West Conshohocken, PA. www.astm.org.
- ASTM F1581-08, 2016. Standard Specification for Composition of Anorganic Bone for Surgical Implants. ASTM International, West Conshohocken, PA. www.astm.org.
- ASTM F2721-09, 2014. Standard Guide for Pre-clinical In Vivo Evaluation in Critical Size Segmental Bone Defects. ASTM International, West Conshohocken, PA. www.astm.org.
- ASTM F3207-17, 2017. Standard Guide for In Vivo Evaluation of Rabbit Lumbar Intertransverse Process Spinal Fusion Model. ASTM International, West Conshohocken, PA. www.astm.org.
- Barkarmo, S., Wennerberg, A., Hoffman, M., Kjellin, P., Breiding, K., Handa, P., Stenport, V., 2013. Nanohydroxyapatite-coated PEEK implants: a pilot study in rabbit bone. *J. Biomed. Mater. Res.* 101A, 465–471.
- Barradas, A.M., Yuan, H., van Blitterswijk, C.A., Habibovic, P., 2011. Osteoinductive biomaterials: current knowledge of properties, experimental models and biological mechanisms. *Eur. Cells Mater.* 21, 407–429.
- Ben-Nissan, B., Green, D.D., Kannangara, G.S.K., Chai, C.S., Milev, A., 2001. ³¹P NMR studies of diethyl phosphite derived nanocrystalline hydroxyapatite. *J. Sol. Gel Sci. Technol.* 21, 27–37.
- Beshah, K., Rey, C., Glimcher, M.J., Schimizu, M., Griffin, R.G., 1990. Solid state carbon-13 and proton NMR studies of carbonate-containing calcium phosphates and enamel. *J. Solid State Chem.* 84, 71–81.

- Bigi, A., Foresti, E., Marchetti, F., Ripamonti, A., Roveri, N., 1984. Barium calcium hydroxyapatite solid solutions. *J. Chem. Soc. Dalton Trans.* 6, 1091–1093.
- Bigi, A., Falini, G., Foresti, E., Gazzano, M., Ripamonti, A., Roveri, N., 1996. Rietveld structure refinements of calcium hydroxylapatite containing magnesium. *Acta Crystallogr. B* 52, 87–92.
- Birgani, Z.T., Fennema, E., Gijbels, M.J., de Boer, J., van Blitterswijk, C.A., Habibovic, P., 2016. Stimulatory effect of cobalt ions incorporated into calcium phosphate coatings on neovascularization in an in vivo intramuscular model in goats. *Acta Biomater.* 36, 267–276.
- Bohner, M., Miron, R.J., 2019. A proposed mechanism for material induced heterotopic ossification. *Mater. Today* 22, 132–141.
- Bose, S., Fielding, G., Tarafder, S., Bandyopadhyay, A., 2013. Understanding of dopant-induced osteogenesis and angiogenesis in calcium phosphate ceramics. *Trends Biotechnol.* 31, 594–605.
- Bouler, J.M., Pilet, P., Gauthier, O., Verron, E., 2017. Biphasic calcium phosphate ceramics for bone reconstruction: a review of biological response. *Acta Biomater.* 53, 1–12.
- Buser, Z., Brodke, D.S., Youssef, J.A., Meisel, H.J., Myhre, S.L., Hashimoto, R., Park, J.B., Tim Yoon, S., Wang, J.C., 2016. Synthetic bone graft versus autograft or allograft for spinal fusion: a systematic review. *J. Neurosurg. Spine* 25, 509–516.
- Cai, Y., Pan, H., Xu, X., Hu, Q., Li, L., Tang, R., 2007. Ultrasonic controlled morphology transformation of hollow calcium phosphate nanospheres – a smart and biocompatible drug release system. *Chem. Mater.* 19, 3081–3083.
- Campana, V., Milano, G., Pagano, E., Barba, M., Cicione, C., Salonna, G., Lattanzi, W., Logroscino, G., 2014. Bone substitutes in orthopaedic surgery: from basic science to clinical practice. *J. Mater. Sci. Mater. Med.* 25, 2445–2461.
- Cao, J.M., Feng, J., Deng, S.G., Chang, X., Wang, J., Liu, J.S., Lu, P., Lu, H.X., Zheng, M.B., Zhang, F., Tao, J., 2005. Microwave-assisted solid-state synthesis of hydroxyapatite nanorods at room temperature. *J. Mater. Sci.* 40, 6311–6313.
- Chusuei, C.C., Goodman, D.W., 1999. Calcium phosphate phase identification using XPS and time-of-flight cluster SIMS. *Anal. Chem.* 71, 149–153.
- Curtin, C.M., Tierney, E.G., McSorley, K., Cryan, S.A., Duffy, G.P., O'Brien, F.J., 2015. Combinatorial gene therapy accelerates bone regeneration: non-viral dual delivery of VEGF and BMP2 in a collagen-nanohydroxyapatite scaffold. *Adv. Healthc. Mater.* 4, 223–227.
- Daentzer, D., Asamoto, S., Böker, D.K., 2005. HAC-titanium as an implant for interbody fusion in spinal canal stenosis of the cervical spine. Six-year clinical trial. *Der Orthopäde* 34, 234–240.
- de Grado, G.F., Keller, L., Idoux-Gillet, Y., Wagner, Q., Musset, A., Benkirane-Jessel, N., Bornert, F., Offner, D., 2018. Bone substitutes: a review of their characteristics, clinical use, and perspectives for large bone defects management. *J. Tissue Eng.* 9, 1–18.
- de Groot, K., Greesink, R.G.T., Klein, C.P.A.T., Serekian, P., 1987. Plasma-sprayed hydroxyapatite coatings of hydroxyapatite. *J. Biomed. Mater. Res.* 21, 1375–1381.
- Deptula, A., Lada, W., Olczak, T., Borello, A., Alvani, C., di Bartolomeo, A., 1992. Preparation of spherical powders of hydroxyapatite by sol-gel process. *J. Non-Cryst. Solids* 147/148, 537–541.
- Driessens, F.C.M., Verbeeck, R.M.H., Heijligers, H.J.M., 1983. Some physical properties of Na- and CO₃-containing apatites synthesized at high temperatures. *Inorg. Chim. Acta* 80, 19–23.
- Duan, R., Barbieri, D., Luo, X., Weng, J., Bao, C., de Bruijn, J.D., Yuan, H., 2018. Variation of the bone forming ability with the physicochemical properties of calcium phosphate bone substitutes. *Biomater. Sci.* 6, 136–145.
- Elliott, J.C., Mackie, P.E., Young, R.A., 1973. Monoclinic hydroxyapatite. *Science* 180, 1055–1057.
- Epple, M., 2018. Review of potential health risks associated with nanoscopic calcium phosphate. *Acta Biomater.* 77, 1–14.
- Fang, Y., Agrawal, D.K., Roy, D.M., Roy, R., Brown, P.W., 1992. Ultrasonically accelerated synthesis of hydroxyapatite. *J. Mater. Res.* 7, 2294–2298.
- Fischer, C.R., Cassilly, R., Cantor, W., Edusei, E., Hammouri, Q., Errico, T., 2013. A systematic review of comparative studies on bone graft alternatives for common spine fusion procedures. *Eur. Spine J.* 22, 1423–1435.
- Fleet, M.E., 2009. Infrared spectra of carbonate apatites: v₂-Region bands. *Biomaterials* 30, 1473–1481.
- Fowler, B.O., 1974. Infrared studies of apatites II, 1974. Preparation of normal and isotopically substituted calcium, strontium, and barium hydroxyapatites and spectra-structure-composition correlations. *Inorg. Chem.* 13, 207–214.
- Fukase, Y., Eanes, E.D., Takagp, S., Chow, L.C., Brown, W.E., 1990. Setting reactions and compressive strengths of calcium phosphate cements. *J. Dent. Res.* 69, 1852–1856.
- García-Gareta, E., Coathup, M.J., Blunn, G., 2015. Osteoinduction of bone grafting materials for bone repair and regeneration. *Bone* 81, 112–121.
- Gibson, I.R., Best, S.M., Bonfield, W., 1999. Chemical characterization of silicon-substituted hydroxyapatite. *J. Biomed. Mater. Res.* 44, 422–428.
- Gibson, I.R., Rehman, I., Best, S.M., Bonfield, W., 2000. Characterization of the transformation from calcium-deficient apatite to β-tricalcium phosphate. *J. Mater. Sci. Mater. Med.* 11, 533–539.
- Gibson, I.R., Bonfield, W., 2002. Novel synthesis and characterization of an AB-type carbonate-substituted hydroxyapatite. *J. Biomed. Mater. Res.* 59, 697–708.
- Gillespie, P., Wu, G., Sayer, M., Stott, M.J., 2010. Si complexes in calcium phosphate biomaterials. *J. Mater. Sci. Mater. Med.* 21, 99–108.
- Gomes, S., Vichery, C., Descamps, S., Martinez, H., Kaur, A., Jacobs, A., Nedelec, J.M., Renaudin, G., 2018. Cu-doping of calcium phosphate bioceramics: from mechanism to the control of cytotoxicity. *Acta Biomater.* 65, 462–474.
- Goosen, J.H.M., Kums, A.J., Kollen, B.J., Verheven, C.C.P.M., 2009. Porous-coated femoral components with or without hydroxyapatite in primary uncemented total hip arthroplasty: a systematic review of randomized controlled trials. *Arch. Orthop. Trauma Surg.* 129, 1165–1169.
- Habibovic, P., Barrère, F., van Blitterswijk, C.A., de Groot, K., Layrolle, P., 2002. Biomimetic hydroxyapatite coating on metal implants. *J. Am. Ceram. Soc.* 85, 517–522.
- Hahn, B.D., Park, D.S., Choi, J.J., Ryu, J., Yoon, W.H., Choi, J.H., Kim, J.W., Ahn, C.W., Kim, H.E., Yoon, B.H., Jung, I.K., 2013. Osteoconductive hydroxyapatite coated PEEK for spinal fusion surgery. *Appl. Surf. Sci.* 283, 6–11.
- Haider, A., Haider, S., Han, S.S., Kang, I.K., 2017. Recent advances in the synthesis, functionalization and biomedical applications of hydroxyapatite: a review. *RSC Adv.* 7, 7442–7458.
- Hou, C.H., Hou, S.M., Hsueh, Y.S., Lin, J., Wu, H.C., Lin, F.H., 2009. The in vivo performance of biomagnetic hydroxyapatite nanoparticles in cancer hyperthermia therapy. *Biomaterials* 30, 3956–3960.
- ICDD, 2013. PDF-2 2013. International Centre for Diffraction Data. Newtown Square, PA, USA.

- Ignjatović, N., Ajduković, Z., Savić, V., Najman, S., Mihailović, D., Vasiljević, P., Stojanović, Z., Uskoković, V., Uskoković, D., 2013. Nanoparticles of cobalt-substituted hydroxyapatite in regeneration of mandibular osteoporotic bones. *J. Mater. Sci. Mater. Med.* 24, 343–354.
- Ikoma, T., Yamazaki, A., Nakamura, S., Akao, M., 1999. Preparation and structure refinement of monoclinic hydroxyapatite. *J. Solid State Chem.* 144, 272–276.
- Inyang, A.O., Ibitoye, S.A., 2018. Quality assessment of hydroxyapatite derived from bovine bone wastes. *Int. J. Appl. Ceram. Technol.* 15, 1439–1445.
- Itatani, K., Nishioka, T., Seike, S., Howell, F.S., Kishioka, A., Kinoshita, M., 1994. Sinterability of β -calcium orthophosphate powder prepared by spray pyrolysis. *J. Am. Ceram. Soc.* 77, 801–805.
- Ito, A., Maekawa, K., Tsutsumi, S., Ikazaki, F., Tateishi, T., 1997. Solubility product of OH-carbonated hydroxyapatite. *J. Biomed. Mater. Res.* 36, 522–528.
- Jackson, S.A., Cartwright, A.G., Lewis, D., 1978. The morphology of bone mineral crystals. *Calcif. Tissue Res.* 25, 217–222.
- Jarcho, M., Bolen, C.H., Thomas, M.B., Babock, J., Kay, J.F., Doremus, R.H., 1976. Hydroxyapatite synthesis and characterization in dense polycrystalline form. *J. Mater. Sci.* 11, 2027–2035.
- Jha, L.J., Best, S.M., Knowles, J.C., Rehman, I., Santos, J.D., Bonfield, W., 1997. Preparation and characterization of fluoride-substituted apatites. *J. Mater. Sci. Mater. Med.* 8, 185–191.
- Kaflak, A., Kolodziejski, W., 2007. Phosphorus-31 spin-lattice NMR relaxation in bone apatite and its mineral standards. *Solid State Nucl. Magn. Reson.* 31, 174–183.
- Kay, M.I., Young, R.A., Posner, A.S., 1964. Crystal structure of hydroxyapatite. *Nature* 204, 1050–1052.
- Keller, L., 1995. X-ray powder diffraction patterns of calcium phosphates analyzed by the Rietveld method. *J. Biomed. Mater. Res.* 29, 1403–1413.
- Khan, A.F., Awais, M., Khan, A.S., Tabassum, S., Chaudhry, A.A., Rehman, I.U., 2013. Raman spectroscopy of natural bone and synthetic apatites. *Appl. Spectrosc. Rev.* 48, 329–355.
- Kim, H.M., Himeno, T., Kawashita, M., Kokubo, T., Nakamura, T., 2004. The mechanism of biomineralization of bone-like apatite on synthetic hydroxyapatite: an in vitro assessment. *J. R. Soc. Interface* 1, 17–22.
- Kobayashi, T., Ono, S., Hirakura, S., Oaki, Y., Imai, H., 2012. Morphological variation of hydroxyapatite grown in aqueous solution based on simulated body fluid. *CrystEngComm* 14, 1143–1149.
- Kon, E., Muraglia, A., Corsi, A., Bianco, P., Marzetti, M., Martin, I., Boyde, A., Ruspanini, I., Chistolini, P., Rocca, M., Giardino, R., Cancedda, R., Quarto, R., 2000. Autologous bone marrow stromal cells loaded onto porous hydroxyapatite ceramic accelerate bone repair in critical-size defects of sheep long bones. *J. Biomed. Mater. Res.* 49, 328–337.
- Koutsopoulos, S., 2002. Synthesis and characterization of hydroxyapatite crystals: a review study on the analytical methods. *J. Biomed. Mater. Res.* 62, 600–612.
- Laurencin, D., Wong, A., Dupree, R., Smith, M.E., 2008. Natural abundance ^{43}Ca solid-state NMR characterisation of hydroxyapatite: identification of the two calcium sites. *Magn. Reson. Chem.* 46, 347–350.
- Lebre, F., Sridharan, R., Sawkins, M.J., Kelly, D.J., O'Brien, F.J., Lavelle, E.C., 2017. The shape and size of hydroxyapatite particles dictate inflammatory responses following implantation. *Sci. Rep.* 7, 2922.
- LeGeros, R.Z., 1975. The unit-cell dimensions of human enamel apatite: effect of chloride incorporation. *Arch. Oral Biol.* 20, 63–71.
- Legeros, R.Z., 1981. Apatites in biological systems. *Prog. Cryst. Growth Charact.* 4, 1–45.
- LeGeros, R.Z., Balmain, N., Bonel, G., 1987. Age-related changes in mineral of rat and bovine cortical bone. *Calcif. Tissue Int.* 41, 137–144.
- LeGeros, R.Z., 2008. Calcium phosphate-based osteoinductive materials. *Chem. Rev.* 108, 4742–4753.
- Lester, E., Tang, S.V.Y., Khlobystov, A., Rose, V.L., Buttery, L., Roberts, C.J., 2013. Producing nanotubes of biocompatible hydroxyapatite by continuous hydrothermal synthesis. *CrystEngComm* 15, 3256–3260.
- Li, D., Huang, X., Wu, Y., Li, J., Cheng, W., He, J., Tian, H., Huang, Y., 2016. Preparation of pH-responsive mesoporous hydroxyapatite nanoparticles for intracellular controlled release of an anticancer drug. *Biomater. Sci.* 4, 272–280.
- Li, D., Xie, X., Yang, Z., Wang, C., Wei, Z., Jang, P., 2018. Enhanced bone defect repairing effects in glucocorticoid-induced osteonecrosis of the femoral head using a porous nano-lithium hydroxyapatite/gelatin microsphere/erythropoietin composite scaffold. *Biomater. Sci.* 6, 519–537.
- Lim, G.K., Wang, J., Ng, S.C., Chew, C.H., Gan, L.M., 1997. Processing of hydroxyapatite via microemulsion and emulsion routes. *Biomaterials* 18, 1433–1439.
- Lin, K., Liu, X., Chang, J., Zhu, Y., 2011. Facile synthesis of hydroxyapatite nanoparticles, nanowires and hollow nano-structured microspheres using similar structured hard-precursors. *Nanoscale* 3, 3052–3055.
- Lin, K., Wu, C., Chang, J., 2014. Advances in synthesis of calcium phosphate crystals with controlled size and shape. *Acta Biomater.* 10, 4071–4102.
- Linares, J., Fernández, A.B., Feito, M.J., Matesanz, M.C., Sánchez-Salcedo, S., Arcos, D., Vallet-Regí, M., Rojo, J.M., Portolés, M.T., 2016. Effects of nanocrystalline hydroxyapatites on macrophage polarization. *J. Mater. Chem. B* 4, 1951–1959.
- Lu, H.B., Campbell, C.T., Graham, D.J., Ratner, B.D., 2000. Surface characterization of hydroxyapatite and related calcium phosphates by XPS and TOF-SIMS. *Anal. Chem.* 72, 2886–2894.
- Ma, X., Pend, W., Su, W., Yi, Z., Chen, G., Chen, X., Guo, B., Li, X., 2018. Delicate assembly of ultrathin hydroxyapatite nanobelts with nanoneedles directed by dissolved cellulose. *Inorg. Chem.* 57, 4516–4523.
- Manafi, S., Rahimpour, M.R., 2011. Synthesis of nanocrystalline hydroxyapatite nanorods via hydrothermal conditions. *Chem. Eng. Technol.* 34, 972–976.
- Markovic, M., Fowler, B.O., Tung, M.S., 2004. Preparation and comprehensive characterization of a calcium hydroxyapatite reference material. *J. Res. Natl. Inst. Stand. Technol.* 109, 553–568.
- Monma, H., Kamiya, T., 1987. Preparation of hydroxyapatite by the hydrolysis of brushite. *J. Mater. Sci.* 22, 4247–4250.
- Nakama, G.Y., Peccin, M.S., Almeida, G.J., Lira Neto, A., Queiroz, A.A., Navarro, R.D., 2012. Cemented, cementless or hybrid fixation options in total knee arthroplasty for osteoarthritis and other non-traumatic diseases. *Cochrane Database Syst. Rev.* 10, CD006193.
- Nakamura, M., Hiratai, R., Hentunen, T., Salonen, J., Yamashita, K., 2016. Hydroxyapatite with high carbonate substitutions promotes osteoclast resorption through osteocyte-like cells. *ACS Biomater. Sci. Eng.* 2, 259–267.
- Nathanael, A.J., Hong, S.I., Mangalaraj, D., Chen, P.C., 2011. Large scale synthesis of hydroxyapatite nanospheres by high gravity method. *Chem. Eng. J.* 173, 846–854.
- Nelson, D.G.A., Featherstone, J.D.B., 1982. Preparation, analysis and characterization of carbonated apatites. *Calcif. Tissue Int.* 34, S69–S81.

- Nordström, E.G., Karlsson, K.H., 1992. Chemical characterization of a potassium hydroxyapatite prepared by soaking in potassium chloride and carbonate solutions. *Bio Med. Mater. Eng.* 2, 185–189.
- O'Donnell, M.D., Fredholm, Y., de Rouffignac, A., Hill, R.G., 2008. Structural analysis of a series of strontium-substituted apatites. *Acta Biomater.* 4, 1455–1464.
- Osaka, A., Miuro, Y., Takeuchi, K., Asada, M., Takahashi, K., 1991. Calcium apatite prepared from calcium hydroxide and orthophosphoric acid. *J. Mater. Sci. Mater. Med.* 2, 51–55.
- Peric, M., Domic-Cule, I., Grcevic, D., Matijasic, M., Verbanac, D., Paul, R., Grgurevic, L., Trkulja, V., Bagi, C.M., Vukicevic, S., 2015. The rational use of animal models in the evaluation of novel bone regenerative therapies. *Bone* 70, 73–86.
- Pezzatini, S.I., Morbidelli, L., Solito, R., Paccagnini, E., Boanini, E., Bigi, A., Ziche, M., 2007. Nanostructured HA crystals up-regulate FGF-2 expression and activity in microvascular endothelium promoting angiogenesis. *Bone* 41, 523–534.
- Pujari-Palmer, S., Chen, S., Rubino, S., Weng, H., Xia, W., Engqvist, H., Tang, L., Ott, M.K., 2016. In vivo and in vitro evaluation of hydroxyapatite nanoparticle morphology on the acute inflammatory response. *Biomaterials* 90, 1–11.
- Rey, C., Combes, C., Drouet, C., Glimcher, M.J., 2009. Bone mineral: update on chemical composition and structure. *Osteoporos. Int.* 20, 1013–1021.
- Ripamonti, U., 1996. Osteoinduction in porous hydroxyapatite implanted in heterotopic sites of different animal models. *Biomaterials* 17, 31–35.
- Roy, D.M., Linnehan, L.K., 1974. Hydroxyapatite formed from coral skeletal carbonate by hydrothermal exchange. *Nature* 247 (5438), 220–222.
- Samavedi, S., Whittington, A.R., Goldstein, A.S., 2013. Calcium phosphate ceramics in bone tissue engineering: a review of properties and their influence on cell behaviour. *Acta Biomater.* 9, 8037–8045.
- Seebach, C., Schultheiss, J., Wilhelm, K., Frank, J., Henrich, D., 2010. Comparison of six bone-graft substitutes regarding to cell seeding efficiency, metabolism and growth behaviour of human mesenchymal stem cells (MSC) in vitro. *Injury* 41, 731–738.
- Shepherd, J.H., Shepherd, D.V., Best, S.M., 2013. Substituted hydroxyapatites for bone repair. *J. Mater. Sci. Mater. Med.* 23, 2335–2347.
- Shi, C., Gao, J., Wang, M., Shao, Y., Wang, L., Wang, D., Zhu, Y., 2016. Functional hydroxyapatite bioceramics with excellent osteoconductivity and stern-interface induced antibacterial ability. *Biomater. Sci.* 4, 699–710.
- Shirkhanzadeh, M., 1995. Calcium phosphate coatings prepared by electrocrystallization from aqueous electrolytes. *J. Mater. Sci. Mater. Med.* 60, 90–93.
- Sivakumar, M., Kumar, T.S., Shantha, K.L., Rao, K.P., 1996. Development of hydroxyapatite derived from Indian coral. *Biomaterials* 17, 1709–1714.
- Spector, M., 1994. Anorganic bovine bone and ceramic analogs of bone mineral as implants to facilitate bone regeneration. *Clin. Plast. Surg.* 21, 437–444.
- Sun, L., Berndt, C.C., Gross, K.A., Kucuk, A., 2001. Material fundamentals and clinical performance of plasma-sprayed hydroxyapatite coatings: a review. *J. Biomed. Mater. Res. (Appl. Biomater.)* 58, 570–592.
- Tas, A.C., 2000a. Synthesis of biomimetic Ca-hydroxyapatite powders at 37 degrees C in synthetic body fluids. *Biomaterials* 21, 1429–1438.
- Tas, A.C., 2000b. Combustion synthesis of calcium phosphate bioceramic powders. *J. Eur. Ceram. Soc.* 20, 2389–2394.
- TenHuisen, K.S., Brown, P.W., 1998. Formation of calcium-deficient hydroxyapatite from alpha-tricalcium phosphate. *Biomaterials* 19, 2209–2217.
- Tenkumo, T., Vanegas Sáenz, J.R., Takada, Y., Takahashi, M., Rotan, O., Sokolova, V., Epple, M., Sasaki, K., 2016. Gene transfection of human mesenchymal stem cells with a nano-hydroxyapatite-collagen scaffold containing DNA-functionalized calcium phosphate nanoparticles. *Genes Cells* 21, 682–695.
- Termine, J.D., Posner, A.S., 1966. Infrared analysis of rat bone: age dependency of amorphous and crystalline mineral fractions. *Nature* 153 (3743), 1523–1525.
- Teshima, K., Wagata, H., Sakurai, K., Enomoto, H., Mori, S., Yubuta, K., Shishido, T., Oishi, S., 2012. High quality ultralong hydroxyapatite nanowhiskers grown directly on titanium surfaces by novel low-temperature flux coating method. *Cryst. Growth Des.* 12, 4890–4896.
- Thian, E.S., Konishi, T., Kawanobe, Y., Lim, P.N., Choong, C., Ho, B., Aizawa, M., 2013. Zinc-substituted hydroxyapatite: a biomaterial with enhanced bioactivity and antibacterial properties. *J. Mater. Sci. Mater. Med.* 24, 437–445.
- Uskoković, V., Uskoković, D.V., 2011. Nanosized hydroxyapatite and other calcium phosphates: chemistry of formation and application as drug and gene delivery agents. *J. Biomed. Mater. Res. B. (Appl. Biomater.)* 96, 152–191.
- Venkateswarlu, K., Sandhyarani, M., Nellaippan, T.A., Rameshbabu, N., 2014. Estimation of crystallite size, lattice strain and dislocation density of nanocrystalline carbonate substituted hydroxyapatite by X-ray peak variance analysis. *Proc. Mater. Sci.* 5, 212–221.
- Vignoles, M., Bonel, G., Holcomb, D.W., Young, R.A., 1988. Influence of preparation conditions on the composition of type-B carbonated hydroxyapatite and on the localization of the carbonate ions. *Calcif. Tissue Int.* 43, 33–34.
- Walsh, W.R., Vizesi, F., Cornwall, G.B., Bell, D., Oliver, R., Yu, Y., 2009. Posterolateral spinal fusion in a rabbit model using a collagen–mineral composite bone graft substitute. *Eur. Spine J.* 18, 1610–1620.
- Wang, B.C., Chang, E., Lee, T.M., Yang, C.Y., 1995. Changes in phases and crystallinity of plasma-sprayed hydroxyapatite coatings under heat treatment: a quantitative study. *J. Biomed. Mater. Res.* 29, 1483–1492.
- Wang, Y., Yang, X., Gu, Z., Qin, H., Li, L., Liu, J., Yu, X., 2016. In vitro study on the degradation of lithium-doped hydroxyapatite for bone tissue engineering scaffold. *Mater. Sci. Eng. C* 66, 185–192.
- Weng, W., Baptista, J.L., 1998. Sol-gel derived porous hydroxyapatite coatings. *J. Mater. Sci. Mater. Med.* 9, 159–163.
- Wheeler, S.L., 1996. Eight-year clinical retrospective study of titanium plasma-sprayed and hydroxyapatite-coated cylinder implants. *Int. J. Oral Maxillofac. Implant.* 11, 340–350.
- Xiao, J., Zhu, Y., Ruan, Q., Liu, Y., Zeng, Y., Xu, F., Zhang, L., 2010. Biomacromolecule and surfactant complex matrix for oriented stack of 2-dimensional carbonated hydroxyapatite nanosheets as alignment in calcified tissues. *Cryst. Growth Des.* 10, 1492–1499.
- Xu, X.L., Yang, H.Y., Ou, B., Lin, S.D., Wu, H., He, W., Jiang, Q.C., Luo, B.M., Li, G.P., 2015. Hydroxyapatite nanoparticles modified by branched polyethylenimine are effective non-viral vectors for siRNA transfection of hepatoma cells in vitro. *Int. J. Oncol.* 46, 2138–2142.
- Yamada, S., Heymann, D., Bouler, J.M., Daculsi, G., 1997. Osteoclastic resorption of calcium phosphate ceramics with different

- hydroxyapatite/beta-tricalcium phosphate ratios. *Biomaterials* 18, 1037–1041.
- Yang, Y., Kim, K.H., Ong, J.L., 2005. A review on calcium phosphate coatings produced using a sputtering process—an alternative to plasma spraying. *Biomaterials* 26, 327–337.
- Yang, W., Han, W., He, W., Li, J., Wang, J., Feng, H., Qian, Y., 2016. Surface topography of hydroxyapatite promotes osteogenic differentiation of human bone marrow mesenchymal stem cells. *Mater. Sci. Eng. C* 60, 45–53.
- Yeong, K.C.B., Wang, J., Ng, S.C., 2001. Mechanochemical synthesis of nanocrystalline hydroxyapatite from CaO and CaHPO₄. *Biomaterials* 22, 2705–2712.
- Yoshimura, M., Suda, H., Okamoto, K., Ioku, K., 1994. Hydrothermal synthesis of biocompatible whiskers. *J. Mater. Sci.* 29, 3399–3402.
- Young, R.A., Elliott, J.C., 1966. Atomic scale bases for several properties of apatites. *Arch. Oral Biol.* 11, 699–707.
- Zakaria, S.M., Zein, S.H.S., Othman, M.R., Yang, F., Jansen, J.A., 2013. Nanophase hydroxyapatite as a biomaterial in advanced hard tissue engineering: a review. *Tissue Eng. B* 19, 431–441.
- Zannettino, A.C.W., Paton, S., Itescu, S., Gronthos, S., 2010. Comparative assessment of the osteoconductive properties of different biomaterials in vivo seeded with human or ovine mesenchymal stem/stromal cells. *Tissue Eng. A* 16, 3579–3587.
- Zhang, H., Darvell, B.W., 2011. Morphology and structural characteristics of hydroxyapatite whiskers: effect of the initial Ca concentration, Ca/P ratio and pH. *Acta Biomater.* 7, 2960–2968.
- Zhou, W., Liu, Z., Xu, S., Hao, P., Xu, F., Sun, A., 2011. Long-term survivability of hydroxyapatite-coated implants: a meta-analysis. *Oral Surg* 4, 2–7.

1.3.4B

Structural Ceramic Oxides

GARY FISCHMAN, PhD.

Future Strategy Solutions, LLC, Gambrills, MD, United States

Introduction

Structural ceramics are materials of significant importance in medical applications. They are strong and hard, desirable for load-bearing and structural support applications in many biomedical devices. Within medical devices, known examples of structural ceramics include articulating surfaces for hip and knee joints, including femoral heads, acetabular cups, and femoral condyles, as well as dental implants. They have also been used as electrical feedthroughs, internal support structures, and enclosures for devices such as cochlear implants. The advantages of these materials include high strength and hardness, good electrical insulation, low solubility, good biocompatibility, and radiofrequency (RF) transparency, and they can be machined to achieve extremely high degrees of surface smoothness, which is ideal for many articulating applications. One tradeoff aspect of these advantages is that their very high Young's modulus as compared with bones makes these materials prone to problems such as stress shielding, which is detrimental to bone healing and repair.

In orthopedics, structural ceramics are used most often in wear surface applications such as femoral hip (ball) and acetabular (cup) structures; they are also used the same way for other joints. In spinal applications, they are used for wear purposes in cervical implants as well as spacers for intervertebral systems. In dentistry, structural ceramics have been used for dental implants as well as articulation restoratives such as crowns. Other products that are less obvious include protective housings for implanted electronics such as pacemakers and cochlear implants; structural internal parts for the electronics for implants; as well as electronic feedthroughs for products like pacemakers and electro-surgical units. Structural ceramics have also been used as bone spacers, for ear, nose, and throat applications, and in maxillo-facial surgeries. Implants from these materials have been used in neurosurgical operations such as cranioplasties. Alumina, which can be made transparent, has been used in keratoprostheses (corneal replacement). Porous alumina has been used for controlled delivery of hormones, vaccines, and drugs for dose rates needed over long periods of time. Interestingly, zirconia has been used as an oxygen filter and generator due to the high diffusion rate of oxygen within the material.

This chapter provides an overview of structural oxide ceramics with a focus on biomedical applications with load-bearing and/or load-transferring requirements. Of the ceramics being used for biomedical applications, the oxide materials are more common, though to a lesser extent nonoxide ceramic materials such as carbides (silicon carbide) and nitrides (e.g., silicon nitride) are also used for these purposes. An example of oxide ceramics for such applications is the BIOLOX delta, a zirconia-toughened alumina (ZTA) composite used as an arthroplasty material. Overall, devices made of nonoxide structural ceramics represent only a small share of the market, and they therefore will not be discussed further here. For a broader perspective on structural ceramics, readers are encouraged to consult specific texts on the subjects, including [Carter and Norton \(2007\)](#), [Callister \(2009\)](#), or [Morrell \(2011\)](#).

Structural Ceramic Oxides

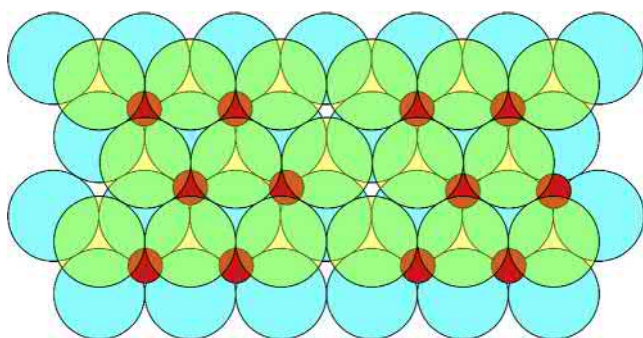
Ceramics are materials that are physically nonmetallic and chemically inorganic. They are generally derived from commonly mined materials such as silica sand (silicon dioxide or silica), bauxite (aluminum hydroxide mineral), zircon sands (zirconium sulfate minerals), and others. Like metals, they are mined from sands and ores, but their commonality ends there: ceramics tend to have ionocovalent bond structures. Moreover, ceramics tend to form three-dimensional amorphous (glassy) as well as lattice (crystalline) structures. Structural ceramic oxides like alumina and zirconia are formed based on an oxygen anion lattice structure with metal cations (such as aluminum, zirconium, and silicon) in interstitial locations within the oxygen anion structure. The properties of structural ceramics can vary depending upon the full chemical makeup of the materials and the thermal processing (the heating profile) that is used to coalesce them in a process known as sintering.

The three most commonly used materials in structural ceramics for medical devices are alumina, zirconia, and a composite of alumina in which zirconia is added to make a material called ZTA. We will discuss all three of these materials here.

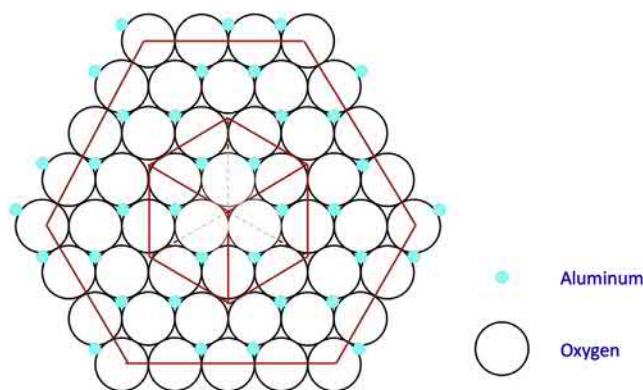
Aluminum Oxide (Alumina)

Aluminum oxide, Al_2O_3 , corundum sapphire, and alumina are all the same material. Gemological specimens of aluminum oxide, sapphire, abound from clear to red to blue depending on the impurities that are found in the material. Chrome-doped alumina, which is also used in medical-grade ceramics (see the Section “Zirconia-Toughened Alumina”) is known gemologically as ruby and has a red color. Both sapphire and ruby are types of alumina and are extremely hard, brittle materials.

Alumina was the first ceramic used in a major way for medical applications. Crystallographically, alumina is classified as rhombohedral. It is based upon a hexagonal close-packed



• **Figure 1.3.4B.1** Alumina structure with two layers of oxygen atoms (blue below, yellow above) and aluminum in two-thirds of the octahedral interstitial sites.



• **Figure 1.3.4B.2** Adaptation of the alpha alumina crystal structure (see Krönberg, 1958).

structure of oxygen anions. This structure has aluminum cations sitting in two-thirds of the octahedral interstitial sites (Fig. 1.3.4B.1). The aluminum sits between the first (A) layer and the second (B) layer creating an AaB structure. For electroneutrality, the alumina in each layer moves over by one interstitial site, meaning that it takes three layers to come back to the original layer positions. This means that it takes six oxygen layers ([AaBbAcBaAbBc]Aa) to create the repeat unit for the alumina structure and it is within this thickness of layers that the rhombohedral unit cell for alumina exists (Fig. 1.3.4B.2).

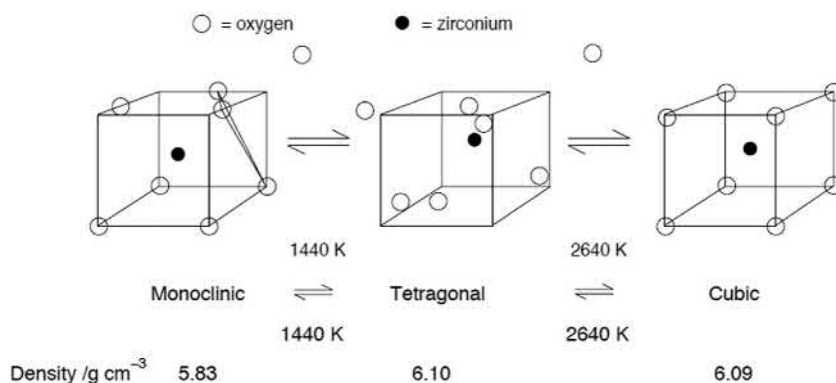
Zirconia

Zirconia is a material that also has been around for decades. It is made up of oxygen anions that are not set in a hexagonally structured close-packed arrangement but, more or less, in a square pattern. Zirconia was known for decades for its use in highly reactive glass furnaces. It had limited use until the last quarter of the 20th century because of the destructive nature of the reversible phase transformation to and from tetragonal to monoclinic. Zirconia has also become a synthetic gem quality replacement for diamond in its cubic form.

There are three polymorphs of zirconia as shown in Fig. 1.3.4B.3. Starting by cooling a zirconia liquid, the cooling liquid solidifies to the cubic phase of zirconia at approximately 2750°C. Upon further cooling, the cubic phase then transforms at 2370°C to the tetragonal phase. At 1170°C the tetragonal phase transforms to the monoclinic phase. If we look at the changes in volume of the phases as they transform we see that the phase transformation from cubic to tetragonal is accompanied by a 0.18% decrease (based on the higher temperature material in the denominator) in volume, whereas the transformation of tetragonal to monoclinic is accompanied by a relatively large (4.4%) increase in volume. Because of the very large change in volume, the microcrystalline structure of a material cannot maintain its integrity during the tetragonal-to-monoclinic transformation.

Yttria and Magnesia-Stabilized Zirconias

Yttria tetragonal zirconia polycrystalline (YTZP) ceramic and magnesia partially stabilized zirconia (MgPSZ) are both types of zirconia. As discussed earlier, zirconia goes through



• **Figure 1.3.4B.3** Unit cells for the three polymorphs of pure zirconia and their transition temperatures.

a set of phase transformations when it is heated and cooled (Fig. 1.3.4B.3). Though they do so differently, yttria and magnesia promote toughness in zirconia through control of the transformation from tetragonal to monoclinic zirconia within the material.

Like other chemically forced phase change manipulations (like the freezing point depression of water), zirconias can be chemically or morphologically stabilized so that a particular polymorph of zirconia such as cubic, tetragonal, or monoclinic is stable beyond the temperature ranges defined by the pure form. For instance, cubic zirconia (which looks similar to diamond) can be designed to be stable with the appropriate dopants (elements) at room temperature. Appropriate dopants and thermal processing can create a metastable tetragonal phase in the material. This tetragonal phase can be transformed to the monoclinic phase through a diffusionless martensitic transformation. Because of the martensitic nature of the change, stress can cause the material within a stress region to transform to monoclinic. Because of the major volume increase that the transformation from tetragonal to monoclinic zirconia causes, a designed transformation can create a high compressive stress when the transformation occurs. This is the basic idea behind the zirconias that are used in medical devices.

Depending on the dopant used to create the metastable tetragonal phase (in medical ceramics this is usually yttrium or magnesium) the phases and microstructures that form (and therefore the risks) are different.

In YTZP, the whole zirconia microstructure is designed to be made up of small tetragonal zirconia crystals. If a crack forms, there is a stress region emanating from the crack front that leads the crack as it moves through a solid. When the crack front moves through a region of YTZP, it causes the tetragonal zirconia within the crack front zone to martensitically transform to the monoclinic phase. This change is accompanied by an increase in volume and so causes a compression in front of the crack tip. This compressive stress is similar to pushing the crack together so that the stress is used to slow down or stop the crack.

One of the problems that had to be overcome in YTZP was its sensitivity to transformation when in water (US FDA, 1997). Water can replace some of the bonds in the structure and cause the material to spontaneously transform from tetragonal to monoclinic. This issue was mitigated through the optimization of YTZP both by further chemical additives and by grain size adjustments.

Different to YTZP, the MgPSZ microstructure is made up mostly of large cubic zirconia crystals. In this particular type of zirconia, the large, stabilized cubic grains of zirconia have transformable tetragonal seeds embedded within the larger crystal. When a crack front approaches, the seeds inside the grain transform creating a compressive stress to the material.

Zirconia-Toughened Alumina

Another currently commonly used structural ceramic is a ceramic matrix composite called ZTA. ZTA is a composite

of alumina in which zirconia is added. The zirconia modifies the alumina by utilizing zirconia's ability to create a compressive stress region (through transformation) if a crack moves through the region. This material maintains much of the hardness of alumina and adds much of the toughness of zirconia into an optimized material.

Current ZTAs are toughened with YTZP. The ZTAs used in orthopedics are currently further toughened by the addition of strontium, which causes the alumina to grow disproportionately in a platelet configuration. Many ZTAs are also pink because of the addition of chromium, which was originally added to improve the hardness that was lowered due to the addition of the softer zirconia to the alumina matrix.

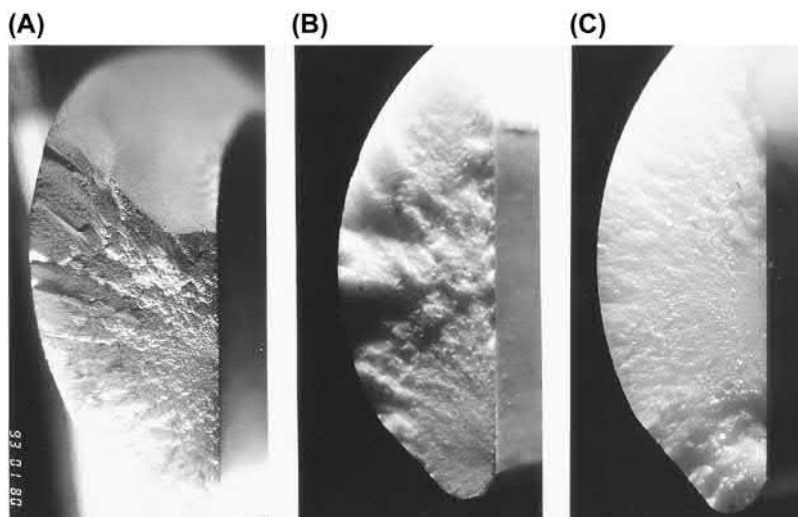
A History of These Structural Materials in Medical Devices

These three materials, namely alumina, zirconia, and ZTA, are the basic materials that are used in biomedical applications. Dentistry and orthopedic surgery have led the introduction of these materials into the medical device industry. Alumina was an obvious place to start, zirconia matured appropriately at an ideal time in history, and ZTAs were in exactly in the right place at the right time.

Alumina was the first biomedically important structural ceramic. It is one of the earliest and most heavily researched ceramics available. It has been used commercially at least since the 1930s as an insulator for spark plugs. It has been studied heavily to model and better understand the science of sintering and structure–property relationships in ceramics. When Boutin considered ceramics for hip implants in the early 1970s, alumina became a material for the manufacture of components for prostheses and surgical devices. Before this, metal was the femoral end (ball) that was used. Unfortunately, the metal system usually failed because of wear based on CoCr grinding away at the polyethylene cup. Much of this was because the metal could only be polished to a certain level of smoothness. The failure was accompanied by a large amount of wear debris in the joint space. The result of this wear debris was characterized as particle disease.

To mitigate the wear–failure–particle problem, implant manufacturers turned to a very highly polished alumina. Alumina is extremely hard. On a Mohs hardness scale (the geological scratch test) alumina tests at 9, just under diamond, which tests at 10. From this perspective, alumina can scratch metal, glass, and most natural minerals. If manufactured properly, alumina can be polished to be very smooth. It also is resistant to corrosion in an *in vivo* environment, elicits minimal response from biological tissues, and remains stable for many years of service.

In testing, a polished alumina femoral end (head) replacing the metal femoral end basically doubled the life of the total hip replacement (THR) implant based on wear rates. The abrasion rate on ultrahigh molecular weight polyethylene (UHMWPE) in switching from metal to alumina improved from 0.2 mm/year (loss of thickness of UHMWPE) to less than 0.1 mm/year (Willmann, 2000).



• **Figure 1.3.4B.4** Fracture surfaces of alumina hips: (A) fractured in testing as per ISO 7206-5; (B) head fractured in vivo; (C) head fractured via proof test. (From Richter, H., 1998. Application of Proof-Testing to Ceramic Hip Joint Heads, 3rd Ceramtec Symposium, Stuttgart.)

The major problem with alumina has always been its brittleness. When a crack forms, there is very little that can be done to stop the crack from worsening and so a device (such as a femoral head) fractures catastrophically (Fig. 1.3.4B.4). Failure of ceramic heads for hip replacements due to brittleness then became a problem. In the 1990s the failure rate of alumina heads varied greatly and in some cases it could be as high as 0.5% (1 out of every 200 heads could fail) (Richter, 1998). This failure rate was a barrier to the acceptance of alumina as a material for high-load THR and was mitigated through the use of a proof-testing tool. Improvements in manufacturing along with the proof-testing tool brought the failure rate in alumina down to a very acceptable 0.01%. In the 1980s, alumina was the up and coming material for hip joint replacement.

Attempting to further reduce wear caused primarily by the loss of UHMWPE from the cup, alumina was considered for the acetabular cup as well using a “hard-on-hard” alumina system. The hard-on-hard Mittelmeier system failed by wearing at a phenomenally high rate. This was due to a combination of placement and the unforgivingly high rigidity of the alumina. Today, designs have dealt well with this issue, further reducing wear without creating a high failure risk.

The proneness to fracture of alumina created an opportunity for another ceramic described as “ceramic steel”¹ (Garvie, 1975). Zirconium oxide, or zirconia, which is derived from zircon (mostly in sands), is a much more complicated material. For many years it was not an easy material to use because of a high-volume phase change occurring in the material. The “pure” material has three basic crystal phases and it can undergo transformation from one phase to another. At 2400°C, it is in the cubic crystal form. As it cools, it transforms at 2370°C to the tetragonal crystal form and then at 1173°C it transforms yet again to the

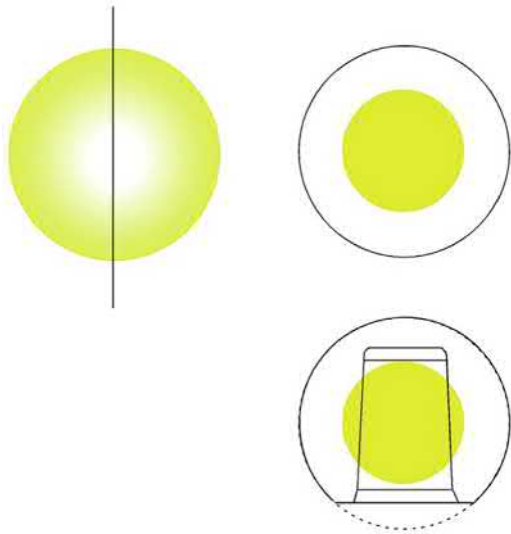
monoclinic crystal form, which is its natural stable state at room temperature. This in itself does not pose a serious problem, but the phase transformation from a tetragonal to a monoclinic crystal results in a martensitic phase transformation which causes a diffusionless volume change of about 5 vol%, which can totally destroy the structure. If pure zirconia powder is pressed, machined, formed, and then sintered by placing it in an oven, heating it up to its sintering temperature and then cooling it down, the result would likely result in a broken or defective part.

It was known that additives like magnesium oxide (MgO) could stabilize the cubic phase, creating a hard, brittle ceramic. However, in the 1960s, people started realizing they could delay the monoclinic-to-tetragonal transformation and thereby create a metastable phase. The partially stabilized material is much more flaw tolerant than alumina or its stabilized counterpart because when a crack starts propagating, the metastable material transforms martensitically and the volume change from the transformation creates a compressive layer that slows the crack down. This is the basic idea behind zirconia toughening in ceramics. There are basically two ways that the metastable tetragonal zirconia structure is formed, namely partially stabilized zirconia and tetragonal zirconia polycrystalline materials, which we will go into more depth later.

In medical devices, there are basically two different zirconia-based materials that have been cleared for use by the Food and Drug Administration (FDA) as of 2018: (1) YTZP ceramic, and (2) MgPSZ. The highest market share in the 1990s was by far YTZP, which became the “go-to” material for arthroplasty instead of alumina. Although not as hard as alumina, its toughness (see the high Weibull modulus in Table 1.3.4B.2) suggested that it was not expected to have the same problems with catastrophic failure. In the late 1990s, the desire for YTZP heads outpaced the manufacturers’ capabilities.

It is more nuanced to properly manufacture partially stabilized zirconias than it is to manufacture an alumina.

¹R.C. Garvie, R.H. Hannink, R.T. Pascoe, “Ceramic steel?”, *Nature* 258, 703–704 (1975).

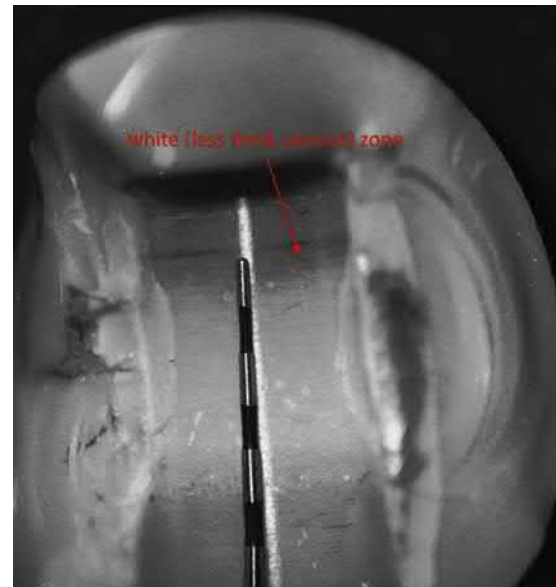


• **Figure 1.3.4B.5** St. Gobain Prozyr fast transformation region based on discussions with St. Gobain following the 2001 recall.

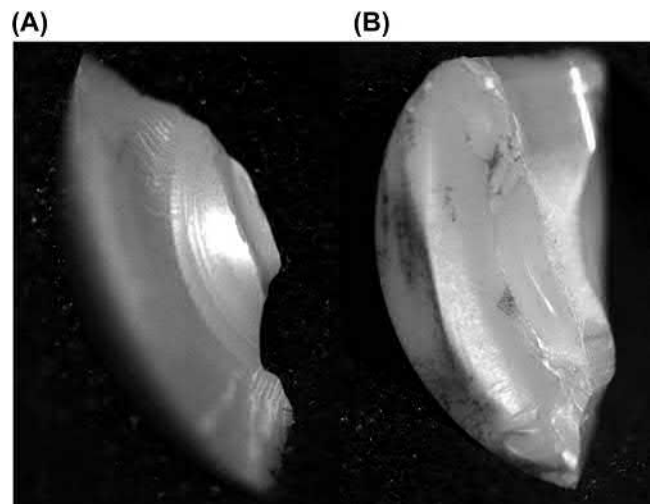
Depending on whether it is a YTZP or MgPSZ, there are different issues to resolve and different things that must be done to make sure the material is and remains appropriately stable. As an example, YTZP has a problem with water-initiated degradation. Water replaces the oxygen in the material and destabilizes it. This prompted the FDA to issue a “do not steam resterilize” warning to medical facilities ([US FDA Dear Dr Letter, 1997](#)). Beyond requirements against steam sterilization, the issue was controlled by adjustments in chemistry as well as the grain size of the structure. Thus the YTZPs that were used for medical implants were highly optimized materials. This created a very good material, but the optimization also made this material more challenging to manufacture.

In the late 1990s, due to a high demand for the material, the major manufacturer of YTZP upgraded its manufacturing process. One of the changes was switching from a batch furnace (kitchen oven) to a belt furnace (pizza oven), which changed the temperature profile of the process, which was followed by another change in temperature variable (i.e., weather). These changes led to serious quality issues. Of a series of seven lots from this new process there were known failure rates well above the 0.001% anticipated. For example, of the seven lots in question, the failure rates were 36%, 13%, 0.42%, 0.17%, 0.56%, 0.14%, and 0.68%, respectively. These failures were devastating to the zirconia medical implant industry.

Because the forming process of zirconia was so highly optimized, it was extremely sensitive to manufacturing changes. The change in thermal processing profile left very little room for error. When ambient conditions changed, the center of the material was not properly fired. The company made the heads by forming a sphere, firing the sphere, and then machining the bore in the finished sphere. Machining the bore in the sphere cut into the improperly fired region and opened material that could easily transform to an environment that included a water-intense body fluid environment. These materials failed dramatically, often revealing an internal, spherical transformation core ([Fig. 1.3.4B.5](#)).



• **Figure 1.3.4B.6** Failed head from the recalled material with the fast transformation region showing up as a white band. (From author's private collection.)



• **Figure 1.3.4B.7** Other views of a failed head. (A) shows a crack emanating from the spherical fast transformation region and (B) shows the crushed bore surface where the metal stem articulated against the bore in the head. (From the author's private collections.)

The resulting failures were usually a crushed region that presented itself as a band ([Fig. 1.3.4B.6](#)) in the fast transformation region where cracks emanated and moved outward toward the surface, creating orange slice-like pieces of ceramics ([Fig. 1.3.4B.7](#)). The failed materials were recalled globally by the company and zirconia became an uncomfortable term in the industry. Because there was no other material besides alumina and zirconia on the market, the ceramic hip replacement industry was in peril. As the industry was considering returning to alumina, another ceramic was already in the later stages of development.

The dwindling in market share for alumina caused by the success of zirconia pushed CeramTec, the major alumina head manufacturer, to become innovative. A material that

TABLE 1.3.4B.1 Properties of Various Grades of Alumina Offered by Kyocera and CoorsTek

Property and Unit	Kyocera	CoorsTek	Kyocera	Kyocera	Kyocera	CoorsTek	CoorsTek	Kyocera
Alumina content (wt%)	99	99.5	99.5	99.5	99.7	99.8	99.9	99.9
Density (g/mL)	3.8	3.9	3.9	3.9	3.9	3.92	3.92	3.9
Flexural strength (MPa)	310	379	360	370	380	390	400	400
Elastic modulus (GPa)	360	370	370	370	70	380	386	380
Thermal conductivity (w/(m*K))	29	30	32	32	32	31	33	34

was used for other purposes (such as machine tools) was already available. It was an alumina that was toughened with a little bit of zirconia, hardened with the addition of chromium, and further toughened by adding strontium, which enabled the alumina to grow in hexagonal platelets. This material became the new Biolox delta material in the early 2000s. Its introduction at about the time of the zirconia failure was fortuitous because it was not alumina, which zirconia replaced due to better toughness, and not zirconia, which just had a major failure, but rather a mixture of both, which made it both harder and tougher. These materials are by and large the materials still used today.

Properties in General

Structural ceramics are used in medical devices because they are very hard, very strong, not soluble, and can be made with an extremely smooth surface. Because of this, they gained a great deal of popularity in orthopedic implants, mostly hips, and they have been a major factor in the reduction of failure of these devices due to wear of the articulating surfaces.

Another property that has made them important structurally is their use as electrical insulators, which have made them ideal materials for electrical feedthroughs in electrical packages for devices. Moreover, because they are relatively transparent to RF frequencies, they can be used for containers for electronics and batteries allowing communication and battery charging of an implanted device.

It is simple reality that materials, including ceramics, are not absolutely pure. Elements that are different from the material but found naturally in it are generally called impurities. If an element is desired or added to the material to modify its properties, that element is called a dopant. One should be aware that material properties will be affected by the impurities and dopants that are found in that material. Determining the level of impurities that exist and what those impurities are is important in both the manufacturing and final properties of the material itself. As an example of the comparable² final property difference, Table 1.3.4B.1 lists a number of different aluminas from Kyocera³

and CoorsTek⁴ (both companies make ceramics for medical devices) between 99 and 100 wt% alumina.

The properties of these materials will vary depending on their manufacturing processes, phase content, and impurities. For other applications beyond medical devices, readers are encouraged to refer to specific ceramic topic books (e.g., Carter and Norton, 2007). Commercially, medical-grade aluminas, zirconias, and ZTAs adhere to international specifications that have been developed for these materials by the industry and regulatory bodies through the standards development agencies of ASTM and ISO. A comparison of these materials with respect to specified properties considered significant for medical device manufacture in general is given in Table 1.3.4B.2. These properties are based on standard specifications from both ISO and ASTM, which means that these properties are minimum allowable values. The Biolox data are actual data for the product used here as an example and therefore should be higher than the values for ZTA Type X, which is the specification for that material.

One significant aspect of Table 1.3.4B.2 is that both alumina and ZTA have two different types of materials. There is a high strength (Type A alumina, Type X ZTA) and a low strength (Type B alumina, Type S ZTA) material found in the specifications. When the specifications were first developed, it was important to make clear that an alumina (or later a ZTA) used for a feedthrough does not need to have the same property as an alumina (or later a ZTA) used for a hip replacement.

While any of the three materials (alumina, zirconia, and ZTA) would make a good, strong, inert electrically insulative material that would be transparent, there are nuances as to why one would choose alumina over zirconia or ZTA. For instance, alumina is quite hard and very strong, but it is very flaw sensitive. Once a crack propagates in alumina, it is very difficult to stop. This makes alumina highly sensitive to flaws such as scratches externally and voids internally in the structure. One might choose not to use zirconia over alumina because the former is quite dense (~6 vs. ~3 g/mL), hence in terms of minimizing the weight of the material, alumina would be the preferred material. When X-ray translucency is important, alumina would be preferable over zirconia or ZTA. When toughness is important zirconia or ZTA would be preferable over alumina.

²Tests are done the same way.

³<https://global.kyocera.com/prdct/fc/list/material/alumina/alumina.html>.

⁴<https://www.coorstek.com/media/1715/advanced-alumina-brochure.pdf>.

TABLE 1.3.4B.2 Property Sets of Various Structural Ceramics for Medical Implants Based on Their Standard Specifications by ASTM and ISO

Property	Units	Alumina Type A ^a	Alumina Type B ^a	YTZP ^b	MgPSZ ^c	ZTA Type X ^d	ZTA Type S ^d	BioloX delta ^e
Density	g/cm ³	≥3.94	3.90	≥6.00	Not specified (but ~6.04)	Given in % theoretical density and varies by composition	Given in % theoretical density and varies by composition	4.36
Strength (4 point bend)	MPa	≥500	≥250	≥800	≥600	≥1.000	≥750	≥1000
Weibull modulus		≥8	≥8	≥8	≥10	≥8	≥8	13
Young's modulus	GPa	≥380	≥370	≥200	≥180	≥320	≥320	350
Hardness	GPa	≥18	≥17	≥11.8	≥10.0	≥16.0	≥15.5	19.75

MgPSZ, Magnesia partially stabilized zirconia; YTZP, yttria tetragonal zirconia polycrystalline; ZTA, zirconia-toughened alumina.

^aISO 6474-1 (2018) Implants for surgery—Ceramic materials: Part 1: Ceramic materials based on high purity alumina.

^bISO 13356 (2014) Implants for surgery—Ceramic materials based on yttria-stabilized tetragonal zirconia (YTZP).

^cASTM F2393-12 (reapproved 2016) Standard Specification for High-Purity Dense Magnesia Partially Stabilized Zirconia (Mg-PSZ) for Surgical Implant Applications.

^dISO 6474-2 (2008) Implants for surgery—Ceramic materials: Part 2: Composite materials based on a high purity alumina matrix with zirconia reinforcement.

^eBioloX delta (since 2004) in CeramTec BioloX delta—compiled from various publicly available product literatures.

References

- Callister W.D. and Retthwisch D.G., 2009. *Materials Science and Engineering, An Introduction: Eighth Edition*. Wiley, ISBN 978-0-470-41997-7.
- Carter, C.B., Norton, M.G., 2007. *Ceramic Materials: Science and Engineering*. Springer. 0-387-46271-6.
- Garvie, R.C., Hannink, R.H., Pascoe, R.T., 1975. Ceramic steel? *Nature* 258, 703–704.
- International Organization for Standardization – ISO 13356, 2014. *Implants for Surgery – Ceramic Materials Based on Yttria-Stabilized Tetragonal Zirconia (YTZP)*.
- International Organization for Standardization – ISO 6474-1, 2018. *Implants for Surgery – Ceramic Materials: Part 1 Ceramic Materials Based on High Purity Alumina*.
- International Organization for Standardization – ISO 6474-2, 2008. *Implants for Surgery – Ceramic Materials: Part 2: Composite Materials Based on High Purity Alumina Matrix with Zirconia Reinforcement*.
- Kronberg, M.L., 1958. Plastic deformation of single crystal sapphire, basal slip and twinning. *Acta Metall.* 5.
- Morrell, R., 2011. Structural ceramics. In: *Kirk Othmer Encyclopedia of Chemical Technology*. <https://doi.org/10.1002/0471238964.1920182116011903.a01.pub2>.
- Richter, H., 1998. Application of Proof-Testing to Ceramic Hip Joint Heads. In: *3rd Ceramtec Symposium Stuttgart*.
- US Food and Drug Administration, Dear Colleague Letter, May 21, 1997. Center for Devices and Radiological Health.
- Willmann, G., 2000. Ceramic femoral heads for total hip arthroplasty. *Adv. Eng. Mater.* 2 (3), 114–122.
- ASTM International ASTM F2393-12, 2016. *Standard Specification for High-Purity Dense Magnesia Partially Stabilized Zirconia (Mg-PSZ) for Surgical Implant Applications*. reapproved.
- BioloX® Delta (Since 2004) in Ceramtec BioloX® Delta – Compiled from Various Available Public Literature Products.
- Cavalcanti, A.N., Foxton, R.M., Watson, T.F., Oliveira, M.T., Giannini, M., Marchi, G.M., 2009. Y-TZP ceramics: key concepts for clinical application. *Oper. Dent.* 34, 344–351.
- Chevalier, J., et al., 2009. The tetragonal-monoclinic transformation in zirconia: lessons learned and future trends. *J. Am. Ceram. Soc.* 92 (9), 1901–1920.
- Christel, P.S., 1992. Biocompatibility of surgical-grade dense polycrystalline alumina. *Clin. Orthop. Relat. Res.* 10–18.
- Della Bona, A., Kelly, J.R., 2008. The clinical success of all-ceramic restorations. *J. Am. Dent. Assoc.* 139 (Suppl.), 8S–13S.
- Dörre, E., Hübner, H., 1984. *Alumina, Processing, Properties and Applications*. Springer Verlag. 3-540-13576-6 [added].
- Evans, A.G., 1990. Perspective on the development of high-toughness ceramics. *J. Am. Ceram. Soc.* 73 (2), 187–206.
- Evans, A.G., Heuer, A.H., 1980. Review – transformation toughening in ceramics: martensitic transformations in crack-tip stress fields. *J. Am. Ceram. Soc.* 63 (5–6), 241–248.
- Hannink, R.H.J., Kelly, P.M., Muddle, B.C., 2000. Transformation toughening in zirconia containing ceramics. *J. Am. Ceram. Soc.* 83 (3), 461–487.
- Hench, L.L., Wilson, J., 1991. Bioceramics. In: *MRS Bulletin XVI* [9], pp. 62–74.
- International Organization for Standardization – ISO 7206-5, 1992. *Implants for Surgery – Partial and Total Hip Joint Prostheses – Part 5: Determination of Resistance to Static Load of Head and Neck Region of Stemmed Femoral Components*. Withdrawn.
- Kelly, J.R., Denry, I., 2008. Stabilized zirconia as a structural ceramic: an overview. *Dent. Mater.* 24, 289–298.
- Kobayashi, S., Hara, H., Okudera, H., Takemae, T., Sugita, K., 1987. Usefulness of ceramic implants in neurosurgery. *Neurosurgery* 21, 751–755.

Further Reading

- Andriotelli, M., Wenz, H.J., Kohal, R.J., 2009. Are ceramic implants a viable alternative to titanium implants? A systematic literature review. *Clin. Oral Implant. Res.* 20 (Suppl. 4), 32–47.

- Lang, J.E., Whiddon, D.R., Smith, E.L., Salyapongse, A.K., 2008. Use of ceramics in total hip replacement. *J. Surg. Orthop. Adv.* 17, 51–57.
- Oonishi, H., et al., 2009. Ceramic versus cobalt-chrome femoral components; wear of polyethylene insert in total knee prosthesis. *J. Arthroplast.* 24 (3).
- Piconi, C., et al., 1998. Y-TZP ceramics for artificial joint replacements. *Biomaterial* 19, 1489–1494.
- Polack, F.M., Heimke, G., 1980. Ceramic keratoprotheses. *Ophthalmology* 87, 693–698.
- Popat, K.C., Leary Swan, E.E., Mukhatyar, V., Chatvanichkul, K.I., Mor, G.K., Grimes, C.A., Desai, T.A., 2005. Influence of nanoporous alumina membranes on long-term osteoblast response. *Biomaterials* 26, 4516–4522.
- Schneider, S. (Ed.), 1991. *ASM Engineered Materials Handbook, Volume 4: Ceramics and Glasses*. 0-87170-282-7.
- Tateiwa, T., Clarke, I.C., Williams, P.A., Garino, J., Manaka, M., Shishido, T., Yamamoto, K., Imakiire, A., 2008. Ceramic total hip arthroplasty in the United States: safety and risk issues revisited. *Am. J. Orthop. (Belle Mead NJ)* 37, E26–E31.
- Willmann, G., 2001. Improving bearing surfaces of artificial joints. *Adv. Eng. Mater.* 3 (3), 135–141.

Questions

1. What are the differences in properties between alumina, zirconia, and ZTA and why are these differences important?
2. Materials are often sensitive to thermal history. Why would a batch furnace and a belt furnace yield different thermal histories?
3. What was the original reason for the addition of chrome to the ZTAs used for hip replacements in the early 2000s?
4. What different toughening mechanisms are available in medical-grade zirconia?
5. What are the different hardening and toughening mechanisms found in the ZTAs used in medical devices?
6. In zirconia, what is the transformation that causes toughness and how does it work?

1.3.5

Carbon Biomaterials

ARTUR M. PINTO¹, ANDREIA T. PEREIRA^{2,3,4}, INÊS C. GONÇALVES^{2,3}

¹LEPABE - Laboratory of Process Engineering, Environment, Biotechnology and Energy, Faculty of Engineering, University of Porto, Portugal

²3S - Instituto de Inovação e Investigação em Saúde, Universidade do Porto, Rua Alfredo Allen 208, Porto, Portugal

³INEB - Instituto de Engenharia Biomédica, Universidade do Porto, Rua Alfredo Allen 208, Porto, Portugal

⁴Graduate Program in Areas of Basic and Applied Biology, Instituto de Ciências Biomédicas Abel Salazar, Universidade do Porto, Rua Jorge de Viterbo Ferreira 228, Porto, Portugal

Introduction

The recognition of the biocompatibility of carbon dates back to ancient times, where manmade permanent tattoos using pulverized charcoal could be placed under the skin without apparent adverse effects. However, it was only in the late 1960s that a pyrolytic form of carbon was found to have remarkable blood compatibility and the structural properties needed for application in long-term artificial heart valves (Haubold et al., 2016). Since then, several forms of carbon have sparked investigation for application as medical devices. This chapter outlines the existing forms of carbon biomaterials and their main biomedical applications to date. The main properties and production techniques of all existing carbon biomaterials are firstly presented. Following, the biomedical applications of carbon biomaterials are described taking into consideration their use as colloids, free-standing materials, coatings or composites. Focus was given to commercially available and under research uses in drug delivery, phototherapy and imaging, biosensors, antimicrobial therapy, cardiovascular, orthopedic, dental, neurological and ophthalmological applications, catheters and guidewires among others. Short considerations are presented at the end of the chapter to raise awareness about safety of carbon biomaterials.

Carbon Biomaterials

Carbon atoms consist of six electrons, which are arranged in the $1s^2 2s^2 2p^2$ electronic configuration. Their unique properties and high plasticity allow them to form covalent bonds with other carbon atoms or elements,

which empower their presence from small organic molecules to complex structures such as carbon materials (Fig. 1.3.5.1) with distinct and remarkable properties.

SIDEBAR #1

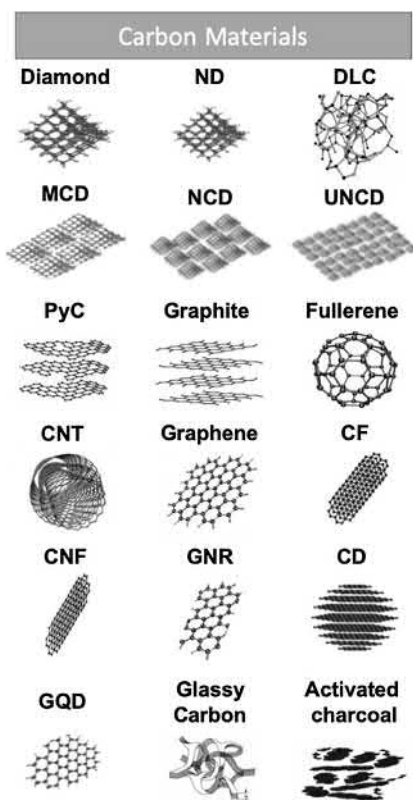
Carbon biomaterials can be characterized regarding: (1) dimension, ranging from 0D materials, which have all the dimensions in nanometric size, such as nanodiamonds, fullerenes, graphene quantum dots, and carbon dots, to 3D materials, which have 3 dimensions out of the nanometric size range, such as diamond, pyrolytic carbon, diamond-like carbon, carbon fibers, and graphite; (2) crystallinity, ranging from entirely crystalline allotropic materials, such as diamond and graphite, to entirely amorphous, like pyrolytic carbon, diamond-like carbon, and carbon dots; and (3) carbon atoms hybridization state, ranging from materials that display only sp^2 hybridized carbons, such as graphite, to materials which mainly contain sp^3 hybridized carbons, as diamond.

Fig. 1.3.5.2 displays the organization of the most common carbon biomaterials regarding their dimension, crystallinity, and carbon atoms hybridization state.

Diamond and Diamond-Like Carbon

Diamond

Diamond is a 3D material with a fully crystalline form of carbon, containing sp^3 hybridized atoms. It presents a cubic structure in which each carbon atom is linked to four other carbon atoms arranged tetrahedrally around it. Its crystalline structure and the strength of its chemical bonds score diamond as the hardest known material. Diamond-based materials comprise microcrystalline, nanocrystalline, and ultrananocrystalline diamond films or coatings, mostly



• **Figure 1.3.5.1** Carbon biomaterials structure. *CD*, Carbon dots; *CF*, Carbon fibers; *CNF*, Carbon nanofibers; *CNT*, Carbon nanotubes; *DLC*, Diamond-like carbon; *GNR*, Graphene nanoribbons; *GQD*, Graphene quantum dots; *MCD*, Microcrystalline diamond; *NCD*, Nanocrystalline diamond; *ND*, Nanodiamonds; *PyC*, Pyrolytic carbon; *UNCD*, Ultrananocrystalline diamond.

produced by chemical vapor deposition (CVD), or nanodiamond (ND) particles produced by top-down methods such as detonation or grinding (Fig. 1.3.5.3). Diamond and diamond-like carbon (DLC) materials exhibit excellent features for applications that require high wear resistance such as hip, knee, and other joint prostheses.

Microcrystalline Diamond. Microcrystalline diamond (MCD) is a material with a crystalline form of carbon containing a high fraction of sp^3 hybridized atoms. MCD grows as a film, having grain sizes larger than $0.1\ \mu\text{m}$, therefore being considered 3D. sp^2 hybridized atoms as well as amorphous carbon are commonly observed at the grain boundaries.

Nanocrystalline Diamond. Nanocrystalline diamond (NCD) is a material with a crystalline form of carbon containing sp^3 hybridized atoms. NCD grows as a film, having grain sizes below $100\ \text{nm}$, therefore being considered 0D. As grain size decreases, more sp^2 hybridized atoms and amorphous carbon are present at diamond grain boundaries, consequently, the degree of sp^3 bonding also decreases with the grain size.

Ultrananocrystalline Diamond. Ultrananocrystalline diamond (UNCD) is a material with a crystalline form of carbon containing sp^3 hybridized atoms. UNCD grows as a film, having grain sizes below $10\ \text{nm}$, therefore being considered 0D. Among MCD, NCD and UNCD, UNCD has the lowest fraction of sp^3 hybridized atoms.

Nanodiamonds. Nanodiamonds (ND) are 0D materials with a crystalline form of carbon containing sp^3 hybridized atoms. These nanoparticles have a diameter range from 1 to $20\ \text{nm}$. Nanostructures with higher sizes ($> 20\ \text{nm}$) are similar to bulk diamonds and the ones with lower sizes ($< 1\ \text{nm}$), called diamondoids, appear naturally in petroleum deposits. ND production techniques have high influence on their size, shape, and quality.

Detonation nanodiamonds (DND) are produced by the detonation of an explosive mixture of certain carbon-containing compounds (such as trinitrotoluene). Particles of $5\ \text{nm}$ are usually produced with narrow size distribution and in large scale. The main disadvantage of this procedure is the formation of aggregates coated with a graphitic layer, which are not dispersible in organic or aqueous solvents. However, DND's large surface area and small size, which allow the attachment of large amounts of drugs, and the reproducibility of their particle size are major assets as drug delivery systems. DND are not suitable for labeling or sensing applications due to their small size and high amount of impurities. However, nitrogen vacancy (NV) centers can be introduced in deep locations, conferring fluorescence even after surface modification, unlike in other carbon materials such as quantum dots (QD).

ND from grinding are particles with different features obtained by grinding larger diamonds (typically high-pressure high-temperature diamonds). These ND have a flake-like shape and different sizes that can be selected by centrifugation. They are purer and contain fewer defects than DND.

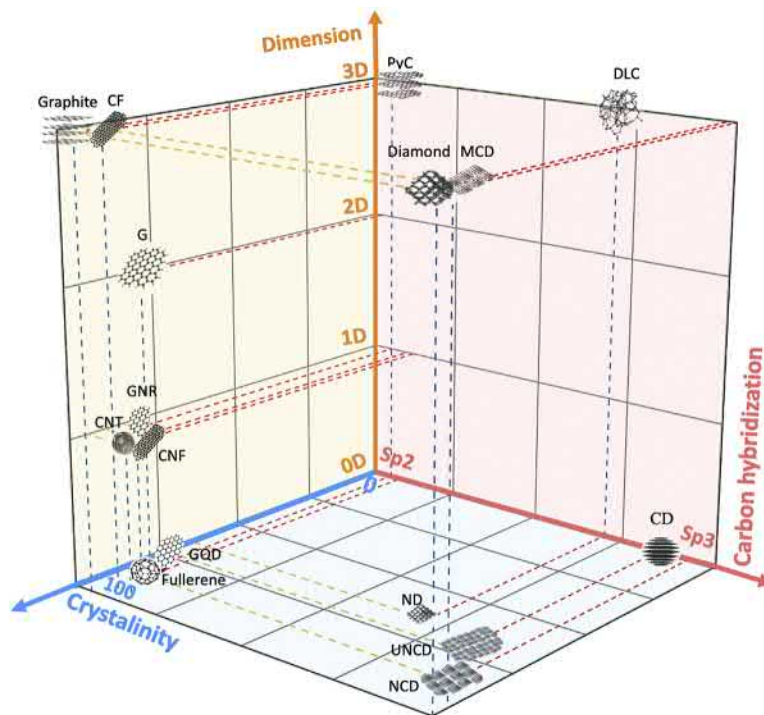
Besides these, other techniques have been developed to produce ND. One possibility is to use a predefined adamantane (small molecule with a diamond-like position of molecules), which already has the atoms required for defects, and then grow a diamond around it. ND can also be produced by microfabricating bulk diamond, resulting in very pure materials with controlled shape. Despite the promising features for sensing or labeling, the low yields of these methods are a disadvantage.

Diamond-Like Carbon

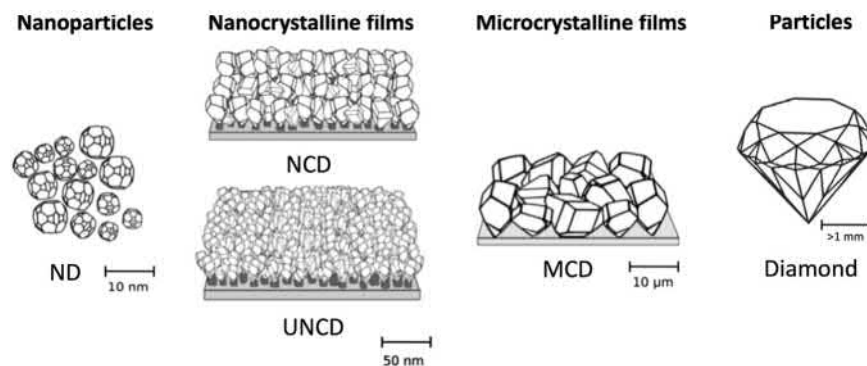
Diamond-like carbon (DLC), a 3D material, is a variety of amorphous carbon material film containing significant amounts of sp^3 hybridized atoms and varying amounts of hydrogen.

DLC is characterized into four categories by their predominant bonding type (either trigonal sp^2 bonding or tetrahedral sp^3 bonding) and hydrogen content. The forms that contain low levels of hydrogen (around 1%) may have low amounts of sp^3 bonds, being referred to as amorphous carbon (a-C), or high amounts of sp^3 bonds (up to 85%), being referred to as tetrahedral amorphous carbon (ta-C). The forms that contain high levels of hydrogen (up to 50%) may have low amounts of sp^3 bonds, being referred to as hydrogenated amorphous carbon (a-C:H), or high amounts of sp^3 bonds (up to 85%), being referred to as hydrogenated tetrahedral amorphous carbon (ta-C:H).

The mechanical, electronic, and optical properties of DLC are closely related to the sp^3/sp^2 ratio, which in turn



• **Figure 1.3.5.2** Organization of carbon biomaterials regarding dimension, crystallinity, and carbon hybridization. Dimension was classified taking into account their size/grain size (0D: all dimensions < 100 nm; 1D: 1 dimension > 100 nm; 2D: 2 dimensions > 100 nm; 3D: all dimensions > 100 nm). Crystallinity was classified taking into account their 3D structure, therefore considering graphite and diamond as fully crystalline, since besides having a crystalline form of C, they have well-organized 3D structures. CD, Carbon dot; CF, Carbon fiber; CNF, Carbon nanofiber; CNT, Carbon nanotube; DLC, Diamond-like carbon; G, Graphene; GNR, Graphene nanoribbon; GQD, Graphene quantum dot; MCD, Microcrystalline diamond; NCD, Nanocrystalline diamond; ND, Nanodiamond; PyC, Pyrolytic carbon; UNCD, Ultrananocrystalline diamond.



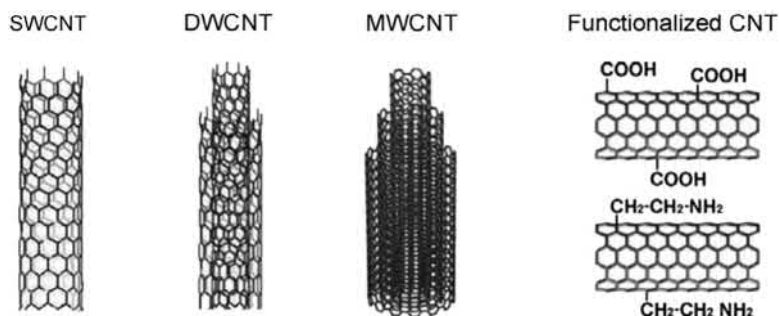
• **Figure 1.3.5.3** Diamond-based materials. MCD, Microcrystalline diamond; NCD, Nanocrystalline diamond; ND, nanodiamond; UNCD, Ultrananocrystalline diamond. Adapted from (Pennisi et al., 2014).

is dependent on the substrate material, growth method, and growth parameters (*e.g.*, growth temperature and ion energy) (Ducheyne, 2011). DLC films' high hardness, wear resistance, chemical inertness, and biological properties make them attractive coatings for biomedical devices.

Pyrolytic Carbon

Pyrolytic carbon (PyC) is a 3D turbostratic form of carbon with an amorphous structure containing sp^2 hybridized

atoms. This material is produced by pyrolysis (thermal decomposition) of hydrocarbon precursors and consists of randomly layered, kinked or curved “graphene-like sheets” (turbostratic), generating large gaps between layers. PyC is one of the best thermal conductors available and exhibits high wear resistance and low thrombogenicity, being mostly applied as coatings in commercially available mechanical heart valves, vascular stents, and orthopedic implants.



• **Figure 1.3.5.4** Carbon nanotubes (CNT): single-walled carbon nanotubes (SWCNT), double-walled carbon nanotubes (DWCNT), and multiwalled carbon nanotubes (MWCNT), and possible surface modification by adding functional groups to the CNT surface (functionalization) (Jackson et al., 2013).

Hexagonally Bonded Carbon

Graphite

Graphite (Gt) is a 3D material with a crystalline form of carbon containing sp^2 hybridized atoms. This material consists of hexagonally bonded carbon atom-stacked sheets connected to each other through van der Waals interaction that allows slipping of graphene (G) sheets past one another; it is consequently a soft material but an excellent lubricant.

Fullerenes

Fullerenes are 0D materials with a crystalline form of carbon containing sp^2 hybridized atoms. These materials are closed hollow cages made of 12 pentagons and a number of hexagons dependent on the total number of carbon atoms ($20 + 2n$, where n is the number of hexagons). C_{60} is the most abundant and studied fullerene and the smallest carbon nanostructure, with a size of 0.71 nm. Fullerenes show a high reactivity, which is associated with the pyramidalization of the carbon atoms in a spherical shape and small size, allowing their use in several biomedical applications, mainly as imaging contrast agents and drug delivery systems.

Carbon Nanotubes

Carbon nanotubes (CNT) are 1D materials with a hexagonal lattice crystalline form of carbon mostly constituted by sp^2 hybridized atoms. CNT can be single-walled (SWCNT), having a single G layer in the wall and a diameter ranging from 0.2 to 2 nm, double-walled (DWCNT), or multiwalled (MWCNT), with two layers or more, respectively, and several micrometers long (Fig. 1.3.5.4).

CNT can be produced by laser ablation, electric arc discharge, catalytic CVD, catalytic plasma-enhanced CVD, or template-based CVD. They present high aspect ratio (more than 10,000 length/diameter ratio), are mechanically robust, electrical and thermal conductors, and have unique optical properties. These features are highly dependent on aspect ratio, chirality of carbon tubes, and also on the number of walls. Despite being chemically inert, they can be modified to obtain chemically reactive groups (Fig. 1.3.5.4). CNT can be potentially applied in the design of tissue-engineered scaffolds, providing electrical conductivity and mechanical

reinforcement, as biosensors, in drug delivery systems, and in phototherapy.

Graphene-Based Materials

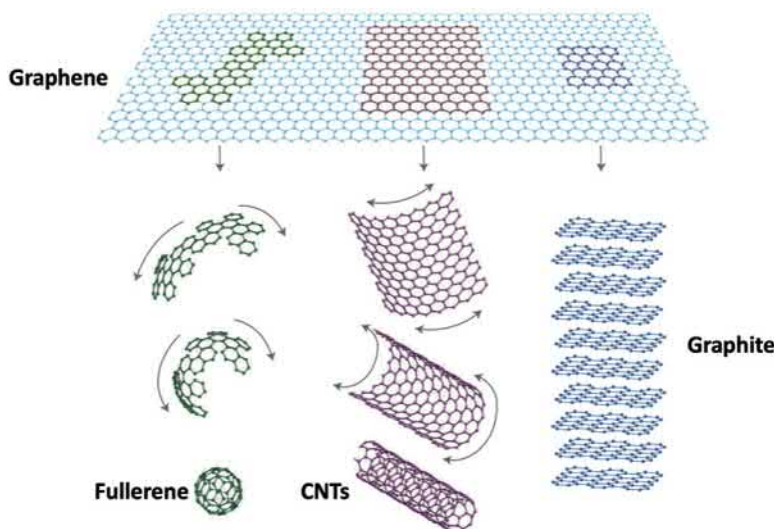
Graphene (G) is a 2D material with a crystalline form of carbon containing sp^2 hybridized atoms. It is the basic building block of hexagonally bonded carbon materials and consists of a 6-ring honeycomb lattice structure where each carbon atom is bonded to three neighboring carbon atoms (Fig. 1.3.5.5).

SIDEBAR #2

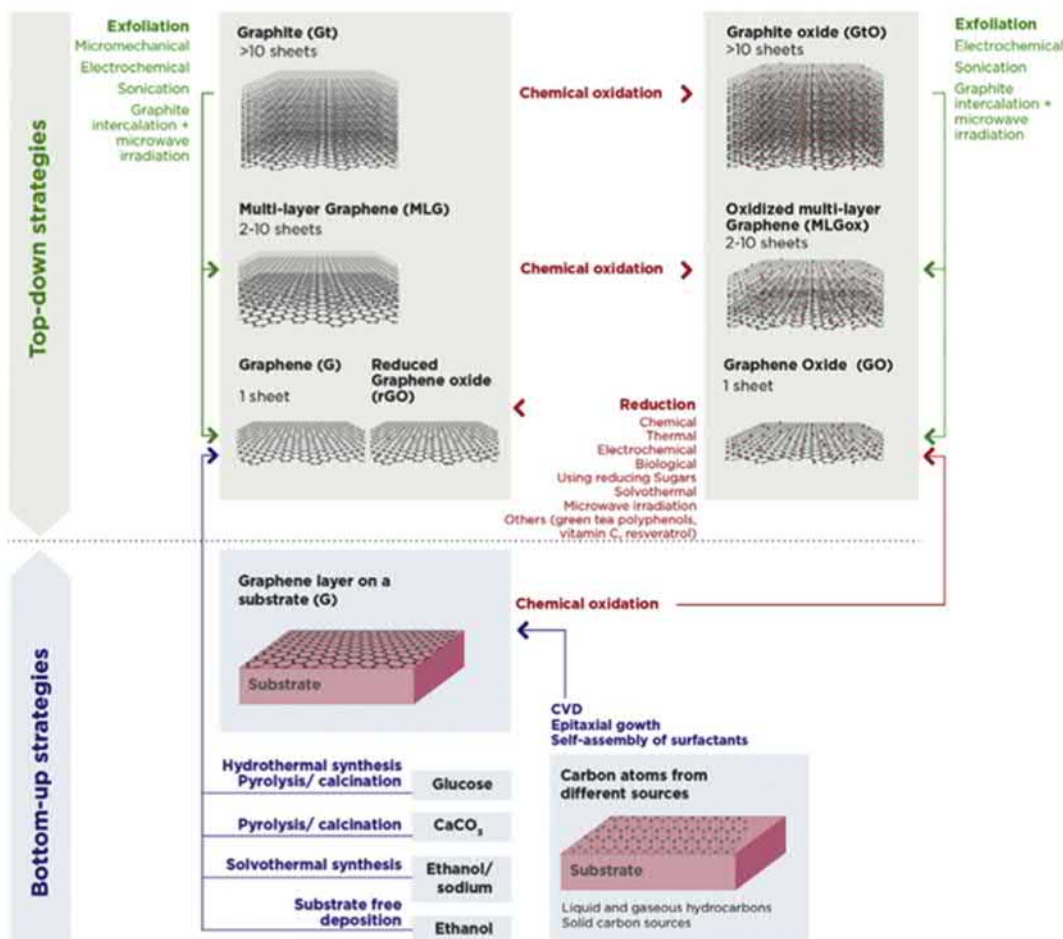
Despite many of us not always being aware of it, carbon materials are part of our daily routines, being present in things like coal, jewelry, pencils, biomaterials, graphite lubricants, etc., but two of these materials have even reached higher stages ... the Nobel Prize ceremony! In 1996, Professor Robert Curl Jr. and Richard Smalley from Rice University, Houston (USA), and Professor Sir Harold Kroto from the University of Sussex, Brighton (UK), won the Nobel Prize in Chemistry due to the discovery of fullerene. These three scientists wanted to evaluate the formation of carbon chains in interstellar space and circumstellar shells, and when they laser irradiated graphite, it was vaporized, producing C_{60} , which was believed impossible to build. This discovery opened the door for a wide range of applications such as the creation of tiny carbon-based and superfast computers. Later on, in 2010, Professors Andre Geim and Konstantin Novoselov from the University of Manchester (UK) won the Nobel Prize in Physics due to groundbreaking experiments in graphene. By peeling off graphite using regular tape, these two scientists isolated graphene for the first time, obtaining a single layer of the carbon atom, which was believed impossible to obtain due to its instability. Graphene is considered a breakthrough material with potential to revolutionize the world of materials science.

G was first isolated in 2004, and since then, along with its derived graphene-based materials (GBM), has been remarkably studied. G can be produced by top-down approaches, using Gt as raw material, and/or bottom-up approaches, using alternative carbon sources as raw material (Henriques et al., 2018).

GBM are a broad class of materials that involve single-layer G, few-layer G (FLG, 2–5 G layers packed together), and multilayer G (MLG) also called G nanoplatelets (GNP)



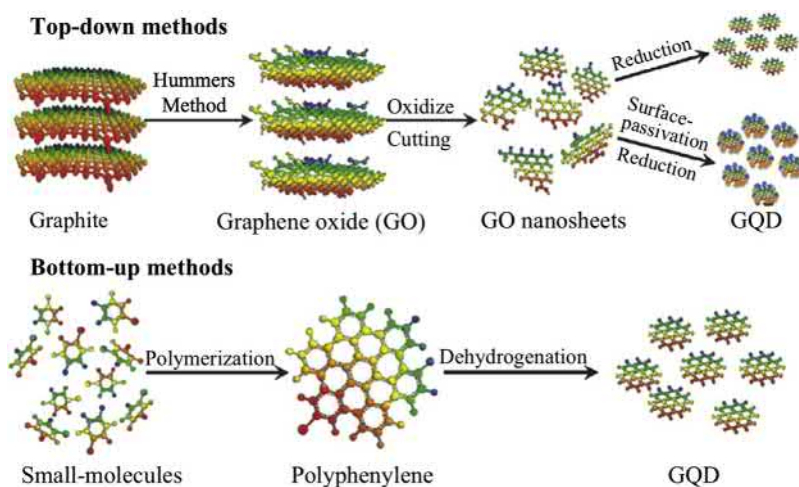
• **Figure 1.3.5.5** Graphene is the 2D building block of hexagonally bonded carbon materials, being wrapped up to form fullerene, rolled to generate carbon nanotubes (CNT), or stacked to create 3D graphite. Adapted from (Geim et al., 2007).



• **Figure 1.3.5.6** Graphene-based materials family and their production methods (Henriques et al., 2018).

(2–10 layers), while materials with more than 10 layers are considered Gt. Each of this class of materials can be oxidized (usually by the modified Hummers method), being referred as G oxide (GO), oxidized FLG, oxidized MLG, and Gt oxide (Fig. 1.3.5.6).

In addition to its unique thermal and electrical conductivity, G is the strongest, thinnest, and one of the lightest materials in the world. However, with the increase in G layers a decrease in electric conductivity is observed. GBM oxidation disrupts the aromatic system, introducing oxygen



• **Figure 1.3.5.7** Schematic diagram of the top-down and bottom-up methods for synthesizing graphene quantum dots (GQD). Adapted from (Shen et al., 2012).

in the form of hydroxyl and ether groups at the bulk surface and carboxyl and carbonyl at the edges of the sheets. This also leads to a decrease in conductivity, which can be partially reestablished by reduction, resulting in reduced GO (rGO) when GO is used.

Other Hexagonally Bonded Carbons

Graphene Quantum Dots. Graphene quantum dots (GQD) are 0D materials (2–20 nm) with a crystalline form of carbon containing sp^2 hybridized atoms. These materials can be produced by top-down techniques, applying a cutting process to Gt, carbon black, GO, and CNT, or by bottom-up techniques, which are associated with the assembling of large aromatic molecules (reviewed by Chen et al., 2018) (Fig. 1.3.5.7). Their optoelectronic and electronic properties are highly dependent on their lateral size, with smaller particles having nonzero band gaps, which exhibit outstanding properties. GQD can be potentially applied in bioimaging and phototherapy as discussed later in this chapter.

Carbon Fibers. Carbon fibers (CF) are a 3D material (diameter: 5–10 μm) with a crystalline form of carbon containing sp^2 hybridized atoms. These materials are produced by drawing a precursor polymer, commonly polyacrylonitrile, into long strands or fibers followed by heating in vacuum to a very high temperature, causing a violent vibration in the molecules and expelling most of the noncarbon atoms (carbonization). CF exhibit high mechanical resistance and thermal conductivity and have been explored as biomaterials for the past 30 years, mainly incorporated as composites in commercially available orthopedic implants (Saito et al., 2011). More recently, a nanosized CF was developed, named carbon nanofiber (CNF).

Carbon Nanofibers. Carbon nanofibers (CNF) are noncontinuous 1D materials with a crystalline form of carbon containing sp^2 hybridized atoms. CNF consist of stacked and curved G with a cylindrical or conical shape. The main differences between CNF and CNT is the absence or presence of a hollow cavity, respectively. CNF are produced in a similar way to CF, through the

carbonization of electrospun nanofibers using polymeric precursors (Georgakilas et al., 2015).

Graphene Nanoribbons. Graphene nanoribbons (GNR) are 1D materials with a crystalline form of carbon containing sp^2 hybridized atoms. GNR are commonly produced by the chemical unzipping of MWCNT under strong oxidizing conditions, which causes the graphitic layers of the tube to unfold one by one, releasing them as GNR rich in oxygen-containing groups. Similarly to the oxidized forms of GBM, the electrical conductivity of these GNR is poor, despite it being substantially increased by reduction using hydrazine or annealing under H_2 .

Other Carbon Biomaterials

Carbon Dots

Carbon dots (CD) are quasispherical 0D materials (2–10 nm in diameter) with an amorphous form of carbon, mostly containing sp^3 hybridized atoms. These materials consist of combinations of turbostratic and graphitic carbon with a high oxygen content. CD can be produced by laser ablation followed by oxidation and surface passivation, which results in the production of nanoparticles with a mean diameter of about 5 nm, by thermal decomposition or carbonization of organic compounds in high-boiling solvents, by pyrolysis of polymer–silica nanocomposites, by ultrasonic carbonization, or by microwave hydrothermal or solvothermal treatment of organic compounds, organosilanes, polymers, or natural products such as carbohydrates. CD present a very high photoluminescence (PL) capacity, which depends on the excitation wavelength, size, and surface functionalization.

Glassy Carbon

Glassy carbon (GC) is a 3D material with an amorphous form of carbon containing sp^2 hybridized atoms. This bulk solid has a turbostratic structure with strongly curved and poorly

organized bonded G sheets being arranged in ribbons, as in polymers. GC can be produced by pyrolysis of organic polymers. It combines glassy and ceramic properties with those of Gt. GC is unsuitable for applications that are mechanically demanding, but its biological properties are similar to that of PyC, being suitable for blood contact applications.

Activated Charcoal

Activated charcoal is a 3D material with an amorphous form of carbon. These solid particles have very high porosity and a very large internal surface area. It can be produced from organic natural carbon-based materials by heating at high temperatures in the presence of oxidizing gases or impregnation with chemicals and heating. Activated charcoal can be processed into powder, granular, and pellet forms. It can adsorb molecules from both the liquid and gas phases and is therefore used in purification and cleaning processes, including the biomedical field (Hasirci and Hasirci, 2018).

Biomedical Applications of Carbon Biomaterials

The existing wide variety of carbon biomaterials and their inherent unique properties have instilled their investigation and/or commercialization in a wide range of biomedical applications. Depending on the application, carbon biomaterials are currently used as colloids, free-standing materials, coatings, or composites (Table 1.3.5.1).

Colloids in the form of carbon micro- and nanoparticles, mostly ND, fullerenes, CNT, GBM, and CD, have been mainly explored for drug and gene delivery, phototherapy, imaging (diagnostics), and as antimicrobial agents (Table 1.3.5.1). Despite no products being commercially available, their efficacy has been shown both *in vitro* and *in vivo*.

Free-standing materials comprise free-standing films that can be quickly and cheaply produced through vacuum filtration or direct evaporation methods (Kong, 2013; Gong et al., 2018), and carbon aerogels, generally produced by critical point drying, 3D printing, or freeze-drying methods (Duong et al., 2016). CNT, GBM, and CF free-standing materials have been mainly explored for the development of biosensors, cardiac, orthopedic, and neurological tissue engineering applications, skin wound healing, and antibacterial surfaces (Table 1.3.5.1).

Carbon-based coatings have been used for decades to enhance biomaterial performance. Coatings can be performed by diverse methods, being the most common, CVD, electrophoretic deposition, and dip, drop, spin or spray coating. Table 1.3.5.1 shows examples of commercially available carbon-coated implants and the most relevant potential applications under investigation of carbon-based material coatings. DLC and PyC coatings are commercialized in ventricular-assisted devices, vascular stents, urethral stents, mechanical heart valves (MHV), or orthopedic implants. NCD, UNCD, DLC, fullerenes, CNT, GBM, and CD are being investigated for cardiovascular, orthopedic, dental, neurological, and ophthalmological

applications and as biosensors, antimicrobial materials, catheters, and guidewires.

As for carbon composites, these presuppose that carbon materials are combined with polymers, ceramics, or metals. Carbon composites can be produced using different techniques, such as *in situ* polymerization, melt blending, and solvent mixing (followed by casting, doctor blading, electrospinning, 3D printing, etc.) (Henriques et al., 2018). The final features of the produced materials are highly dependent on the used carbon material, production technique, and base polymer. Thus, playing with all these features allows the production of a wide range of biomaterials. CF and ND containing composites are commercialized for orthopedic and dental applications, respectively. ND, Gt, CNT, GBM, or CQD composites are widely explored for the development of drug and gene delivery systems, biosensors, antibacterial materials, and medical implants, including both permanent prosthesis and regenerative medicine approaches, as summarized in Table 1.3.5.1.

The following subsections highlight the most common biomedical applications in which the different carbon materials are being applied or investigated.

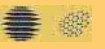
Drug Delivery

Most of the drug delivery systems containing carbon materials can load the drug directly at their surface. Nevertheless, carbon materials can also be functionalized to improve biocompatibility or drug interaction, as reviewed in Kumar et al. (2017), Mohajeri et al. (2018), and Swetha et al. (2018).

DND with a primary particle size of 4–5 nm are of particular interest for biomedical applications due to their small dimensions, inertness, generally good biocompatibility, and higher purity compared to other carbon nanomaterials such as CNT. Drugs, biological molecules, or imaging agents can be loaded at ND surface through chemical functionalization or by physical interaction. Because ND possess the ability to penetrate through tissues and cell membranes, they have been explored for the delivery of drugs (cisplatin, purvalanol A, 4-hydroxytamoxifen), proteins (insulin, bone morphogenetic proteins), and genetic material (DNA) (Fig. 1.3.5.8) (van der Laan et al., 2018; Passeri et al., 2015; Kaur and Badea, 2013; Zhang et al., 2016).

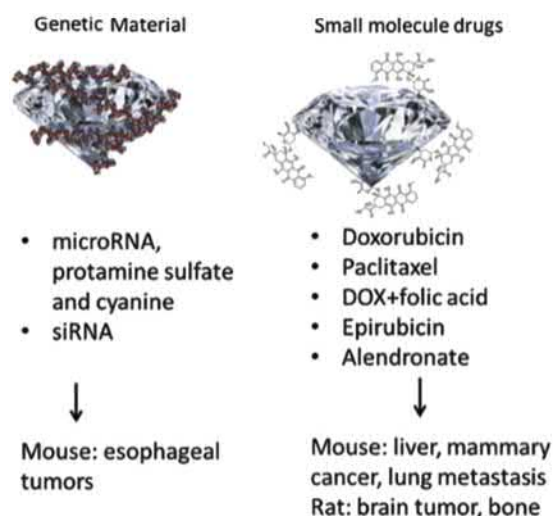
Pristine fullerenes are highly hydrophobic and form colloidal aggregates in aqueous biological solutions, which have hindered their study for biomedical applications for several years. However, strategies have been developed to increase their water solubility, such as solvent exchange stabilization, external chemical functionalization of their cage (e.g., hydroxylation, carboxylation, amination, quaternary ammonium salts), and stabilization/encapsulation with macromolecules (e.g., surfactants, saccharides, proteins, lipids, polymers). Modifications are often performed with bioactive compounds that have affinity to target nucleic acids, cell receptors, or proteins (Bakry et al., 2007; Rasovic, 2017; Torres and Srdjenovic, 2011;

TABLE 1.3.5.1 Examples of the Main Commercially Available Devices and Potential Applications Under Investigation for Different Carbon Biomaterials in the Form of Colloids, Free-Standing Films, Coatings, and Composites. In the Case of Commercially Available Products, the Major Manufacturers are Identified

										
	NCD/UNCD	ND	DLC	PyC	Graphite	Fullerene	CNT	GBM	CF	CD/GQD
Colloids	Not applicable	Under research - Drug delivery - Imaging - Antimicrobial	Not applicable	Not applicable		Under research - Drug delivery - Phototherapy - Imaging - Antimicrobial - Sunscreen	Under research - Drug delivery - Phototherapy - Imaging - Antimicrobial	Under research - Drug delivery - Phototherapy - Antimicrobial		Under research - Drug delivery - Phototherapy - Imaging - Antimicrobial
Free standing								Under research - Biosensors - Antimicrobial - T.E. (cardiac; bone; Neuronal; muscle) - Skin wound healing	Under research - Orthopedic implants - T.E. (Bone)	
Coatings	Under research - Mechanical heart valves - Orthopedic implants - Antimicrobial - TE (bone; neuronal)		Commercially available - Ventricular assist devices Sun Medical technology (JP) Ventricor (AU) - Vascular stents Phytis (DE) Plasma chem (DE) Bekaert (BE) - Urethral stents Optimed (DE) Under research - Antimicrobial - Mechanical heart valves - Orthopedic implants - Catheters - Contact lenses - Oral implants - Guidewires	Commercially available - Mechanical heart valves St. Jude Medical (USA) On-X life tech (USA) Medtronic (USA) Sorin Biomedica (IT) Edward (USA) - Vascular stents Sorin (IT) - Orthopedic implants Tornier/Wright-Medical (FR) Integra life Sciences (USA)		Under research - TE (bone; neuronal) - Biosensors - Dental implants	Under research - Biosensors - Antimicrobial - T.E. (neuronal; cardiac; bone)	Under research - Biosensors - Antimicrobial - Orthopedic Implants - Catheter - Contact lenses - Dental implants - T.E. (cardiac; bone)		Under research - Biosensors
Composites		Commercially available - Dental fillers - Kulzer - Polishing paste - Kavo kerr (USA) Under research - Contact lenses - TE (bone)			Under research - TE (neuronal; bone)		Under research - Biosensors - Antimicrobial - Mechanical heart valves - Orthopedic implants - T.E. (cardiac; bone; cartilage; neuronal)	Under research - Drug delivery - Antimicrobial - Mechanical heart valves - T.E. (cardiac; bone; cartilage; neuronal; muscle) - Skin wound healing		Commercially available - Orthopedic Implants DePuy synthes™ (US) Invibio™ (US) Össur® (IS) Under research - T.E. (cardiac; Bone)

CD, Carbon dots; CF, Carbon fibers; CNF, Carbon nanofibers; CNT, Carbon nanotubes; DLC, Diamond-like carbon; GBM, Graphene-Based Materials; GNR, Graphene nanoribbons; GQD, Graphene quantum dots; Gt, Graphite; MCD, Microcrystalline diamond; NCD, Nanocrystalline diamond; ND, Nanodiamond; PyC, Pyrolytic carbon; TE, Tissue engineering; UNCD, Ultrananocrystalline diamond.

Dellinger et al., 2013; Castro et al., 2017). Due to their small size (≈ 0.7 nm), fullerenes can easily penetrate mammalian cell membranes and are therefore used for gene and drug delivery, presenting comparable or better efficiency than some commercial lipid vectors. Moreover, they can protect DNA during delivery, increasing its lifetime in liposomes, leading to more effective chromosomal incorporation. Taking advantage of its amphiphilicity, functionalized fullerenes have also been used for delivery of hydrophobic drugs, such as anticancer chemotherapeutics (Bakry et al., 2007; Dellinger et al., 2013). Fullerenes have also improved the bioavailability of erythropoietin upon small intestinal administration in rats (Venkatesan et al., 2005). Finally, the ability of fullerenes to penetrate through skin makes them an ideal carrier for transdermal delivery of pharmaceutical formulations (Bakry et al., 2007; Dellinger et al., 2013).

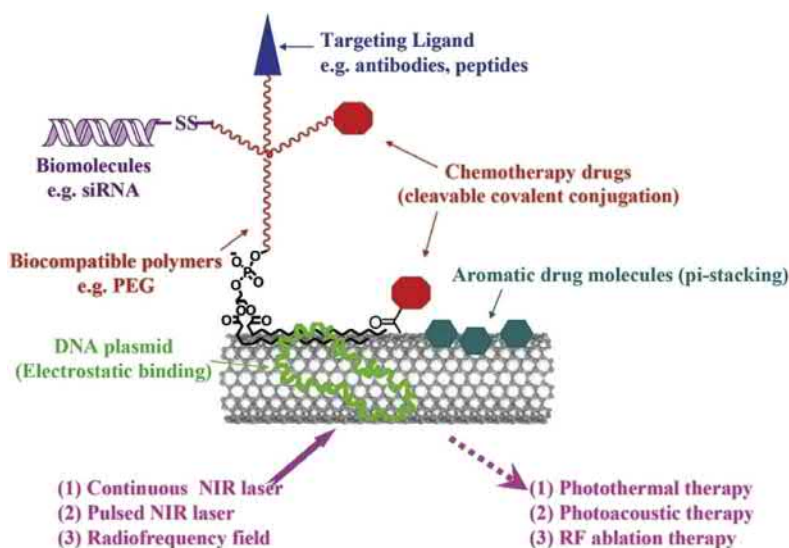


• **Figure 1.3.5.8** Examples of nanodiamond (ND)-based drug and gene delivery approaches tested in *in vivo* models. Adapted from (van der Laan et al., 2018).

CNT in their different unfunctionalized forms, from single to multiwalled, are water insoluble. Several covalent and noncovalent functionalization strategies have been employed to improve their solubility and stability in physiological medium, which can also be used for biological properties enhancement. Due to their high surface area and aspect ratio, CNT can be attached with suitable delivery vectors (e.g., antibodies, peptides), permeate cell membranes, and accumulate intracellularly, with enhanced permeability and retention effect being reported. Also, their hollow interior facilitates the loading of molecules through noncovalent interactions (π - π stacking, hydrophobic) as aromatic drugs, proteins, DNA, siRNA, and antisense oligodeoxynucleotides. Covalent bonding can be performed with some small drugs and biomacromolecules. Some of these modifications are represented in the following section (Fig. 1.3.5.9). Several anticancer drugs (e.g., paclitaxel, cisplatin, epirubicin, doxorubicin, methotrexate) have been conjugated with CNT and successfully delivered *in vitro* and *in vivo* (Liu et al., 2011b; Saito et al., 2014; Sharma et al., 2016; Grumezescu, 2018; Alshehri et al., 2016; Sajid et al., 2016).

GBM edges and large surface, allow chemical modification by oxidation or functionalization with groups of interest, to improve dispersibility in water or interaction with molecules to be loaded. The large delocalized π -conjugated network allows effective loading of aromatic drugs. GO can be used for delivery and targeting of small drug molecules, and when functionalized with cationic polymers, it has been used for delivery of biomacromolecules, such as plasmid DNA and siRNA (Zhang et al., 2016; Grumezescu, 2018; Liu et al., 2011b; Pinto et al., 2013).

CD and GQD have sizes below 10 nm, possessing oxygen-containing surface groups that confer them good water solubility and biocompatibility. Chemical surface modifications with several polymeric, inorganic, organic, or biological entities have been tried to tune their drug/gene delivery and targeting ability, as well as their performance for



• **Figure 1.3.5.9** Illustration of carbon nanotube possible modifications for theranostic uses. *NIR*, Near-infrared; *PEG*, Poly(ethylene glycol); *RF*, Radiofrequency (Liu et al., 2011b).

phototherapeutic and bioimaging applications. Cell uptake of CD can occur passively due to their small size and surface charge, by active delivery (e.g., reversible membrane permeabilization, nanochannel electroporation, microfluidic cell squeezing), or through facilitated delivery, using peptides, polymers, or small molecules (Grumezescu, 2018; Namdari et al., 2017; Venkatesan et al., 2005; Nurunnabi et al., 2014).

Some GBM-containing composites with good biocompatibility have also been described, such as CaCO_3 /tetraethylenepentamine-rGO, which shows pH-sensitive delivery of doxorubicin (Li et al., 2016) and G-oleate-poly(amidoamine) dendrimer hybrids used as gene delivery vectors with gene transfection capacity (Liu et al., 2014). Moreover, drug delivery systems based on GO/polyethylenimine allow an effective loading of DNA and RNA, preventing their degradation, which is promising for nonviral gene delivery and stem cell differentiation (Choi et al., 2016).

Phototherapy and Imaging

Phototherapy is a minimally invasive treatment that can be used for several complications, from skin diseases to cancer. Photosensitizers (PS) or photothermal agents are often used to improve its effectiveness. Carbon materials have been generally reported to have strong light absorption while maintaining their stability, therefore being a promising new class of agents for phototherapy. Moreover, they can also be used as platforms for imaging and/or diagnostics. Table 1.3.5.2 summarizes the main properties of the carbon biomaterials that are currently under investigation for use in phototherapy and imaging.

While ND with ideal crystalline structure are not fluorescent or optically absorptive in near-infrared (NIR) radiation, they can be implanted with color centers, mainly nitrogen-vacancies, or covalently conjugated with specific

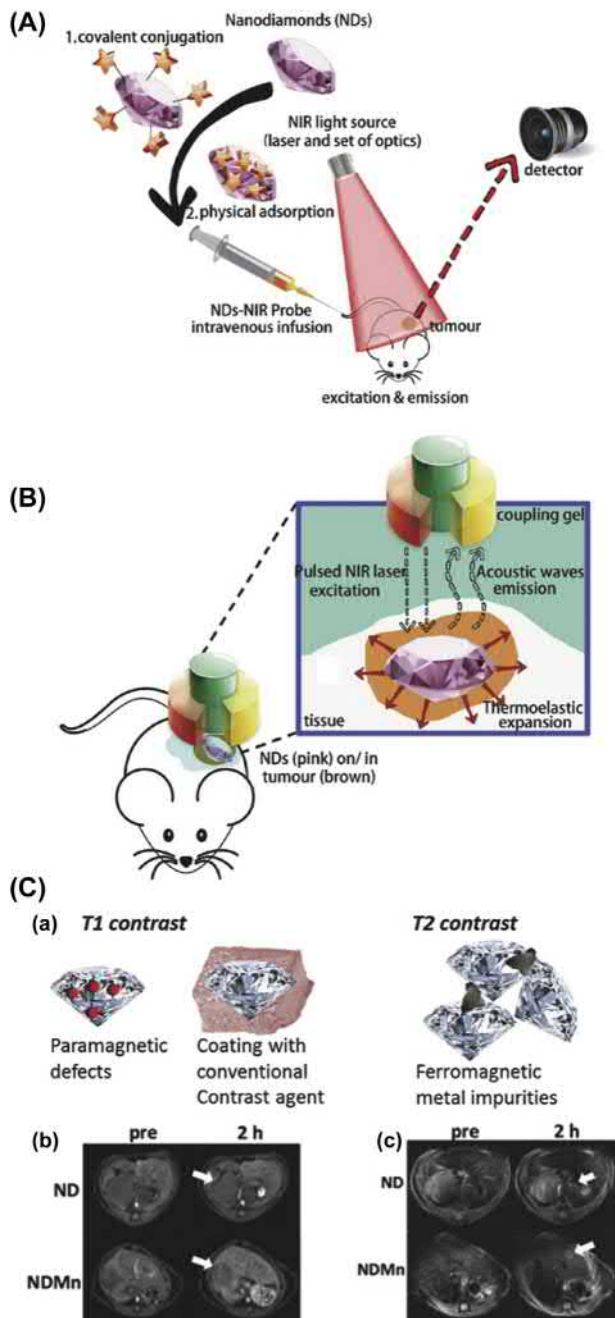
molecules, such as octadecylamine, to provide them with photoproperties. Fluorescent ND are highly photostable and do not photobleach or blink on relatively long time scales. For those reasons, they have been used as contrast agents to visualize internalization pathways and cellular uptake of several molecules. ND exhibit a sharp Raman peak ($\approx 1330\text{ cm}^{-1}$), which facilitates distinction from tissue signals, allowing mapping up to small space resolutions ($\approx 100\text{ nm}$). ND have also been used for bioimaging with several other techniques, such as tip-enhanced Raman spectroscopy, electron spin resonance, photoacoustic imaging, or magnetic resonance imaging (MRI). Examples of ND *in vivo* applications can be found in Fig. 1.3.5.10 (van der Laan et al., 2018; Passeri et al., 2015; Kaur and Badea, 2013; Zhang et al., 2016).

Functionalized fullerenes have been widely studied as PS for the photodynamic therapy (PDT) of tumors. Fullerenes present weak absorbance at wavelengths above the ultraviolet (UV) region, which limits radiation penetration depth in tissues. However, functionalization with donor chromophore antennae are performed to improve absorbance, resulting in compounds that produce a substantial amount of reactive oxygen species (ROS) in aqueous biomedical solutions, especially superoxide anion, which leads to cell apoptosis. Photothermal therapy (PTT) of tumors has also been successfully performed in mice using fullerenes irradiated in the NIR region (Chen et al., 2012; Krishna et al., 2010; Torres and Srdjenovic, 2011; Huang et al., 2014). A poly(ethylene glycol)-conjugated fullerene containing Gd^{3+} ions was shown to be effective for both PDT and MRI in tumor-bearing mice (Liu et al., 2007). Also, other works have reported metallofullerenes being used as contrast agents or in the development of novel platforms for theranostics (Zhang et al., 2016; Castro et al., 2017; Rasovic, 2017).

TABLE 1.3.5.2 Absorption Wavelengths for Phototherapy and Current Imaging Techniques of the Most Commonly Used Pristine Carbon Biomaterials for Theranostics

						
	Carbon Colloids	ND	Fullerene	CNT	GBM	CD
Photodynamic therapy	–	UV	UV	UV (strong absorption)	UV (strong absorption)	UV Visible light laser
Photothermal therapy	–	NIR (weak absorption—requires modification to increase it)	NIR (strong absorption)	NIR (strong absorption)	NIR (strong absorption)	Visible light laser NIR (only deeply colored)
Type of imaging	Raman Tip-Raman Photoacoustic MRI ESR	MRI	Fluorescence Raman Photoacoustic MRI Radiation Multiplexed	–	Fluorescence	Fluorescence

CD, Carbon dots; *CNT*, Carbon nanotubes; *ESR*, Electron spin resonance; *GBM*, Graphene-based materials; *MRI*, Magnetic resonance imaging; *ND*, Nanodiamonds; *NIR*, Near-infrared radiation; *Tip-Raman*, tip-enhanced Raman spectroscopy; *UV*, Ultraviolet radiation.



• **Figure 1.3.5.10** The mechanics of nanodiamond (ND)-based near-infrared (NIR) fluorescence imaging. (A) NIR emitting dyes (indicated by an orange star) are linked to the diamond covalently (1) or adsorbed nonspecifically (2). The conjugate is intravenously injected into mice. Excitation is performed with a laser or LED in the NIR range and is read out optically. The mechanics of ND-based photoacoustic imaging (B). ND absorb energy of nonionizing laser pulses and convert it into heat, resulting in thermoelastic expansion and ultrasonic waves. Meanwhile, the ultrasound signal is monitored via ultrasonic transducers. Blue color indicates medical ultrasound gel, which distributes between the skin and the detector for ultrasonic signal conduction (van der Laan et al., 2018). (C) ND for conventional MRI imaging: (a) different ways how ND can create a contrast in MRI. T1 signal contrast can be achieved by using the paramagnetic defects in the diamond itself or by coating with conventional contrast agents. T2 signal contrast has been achieved via metallic impurities in the diamond material. (b) A T1 signal-weighted image, which was taken from mice liver; arrow indicates a tumor. The images were taken using ND or ND conjugated with a manganese contrast agent (NDMn). (c) The same in T2 contrast mode. Adapted from (Hou et al., 2017).

CNT present strong absorption and fluorescence in the NIR region, and strong Raman signals. This makes them ideal platforms for cancer phototherapy (through ablation or increasing tumor permeability) and bioimaging, more specifically by lowering autofluorescence during imaging, as Raman probes for specific detection and multiplexed imaging, and for photoacoustic imaging with high sensitivity and resolution (Fig. 1.3.5.9). Also, CNT have been proven to be effective for other techniques, such as MRI and radioimaging (Liu et al., 2011b; Saito et al., 2014; Sharma et al., 2016; Grumezescu, 2018; Alshehri et al., 2016; Sajid et al., 2016).

GBM have been shown to improve the stability, bioavailability, tumor accumulation, and photodynamic efficiency of PS. They have also been reported to behave as electron sinks for UV-based PDT. GBM also absorb in the NIR region, allowing a combination of both PDT and/or PTT. A study using tumor-bearing mice has demonstrated that the intravenous injection of reduced nanographene oxide-polyethylene glycol (average diameter of 27 nm) together with NIR irradiation induced complete tumor ablation. The laser (808 nm) power density (0.15 W/cm^2) was lower than usually applied when using other nanomaterials, with irradiation time being 5 min (Yang et al., 2010). Moreover, combined platforms with other carbon biomaterials can be developed to obtain synergistical phototherapeutic effects (Li et al., 2015a; Yang et al., 2010; Hu et al., 2015).

GBM have lower quantum yields than other carbon materials, which limits their use for *in vivo* imaging. For that reason, they have been conjugated with fluorescent dyes and PS. However, because of the strong π - π stacking interaction between dye/sensitizer porphyrin rings with the GBM plane, fluorescence quenching was observed. Thus other luminescent inorganic materials (e.g., QD, metal clusters, upconversion nanoparticles) have been used to achieve efficient fluorescent imaging and even MRI (Grumezescu, 2018; Chen and Wang, 2016).

CD present nonblinking photoluminescence and excellent photostability, in contrast to organic fluorophores. The nonblinking PL ability enables single-molecule tracking, while the photostability allows long-term real-time imaging. PL can be tuned by size, edge configuration, shape, attached chemical functionalities, heteroatom doping, and defects. Usually, CD present strong fluorescence in the visible region upon excitation with UV light; however, particles with excitation and emission in visible to NIR regions can be obtained (Chen and Wang, 2016; Namdari et al., 2017; Nurunnabi et al., 2014). As an example, GQD (average diameter $\approx 5 \text{ nm}$) were able to destroy both cancer cells *in vitro* and tumor cells in mice, while allowing real-time imaging. GQD acted as a PS generating singlet oxygen, and also led to temperature increase resulting in tumor ablation (Fig. 1.3.5.11) (Nurunnabi et al., 2014).

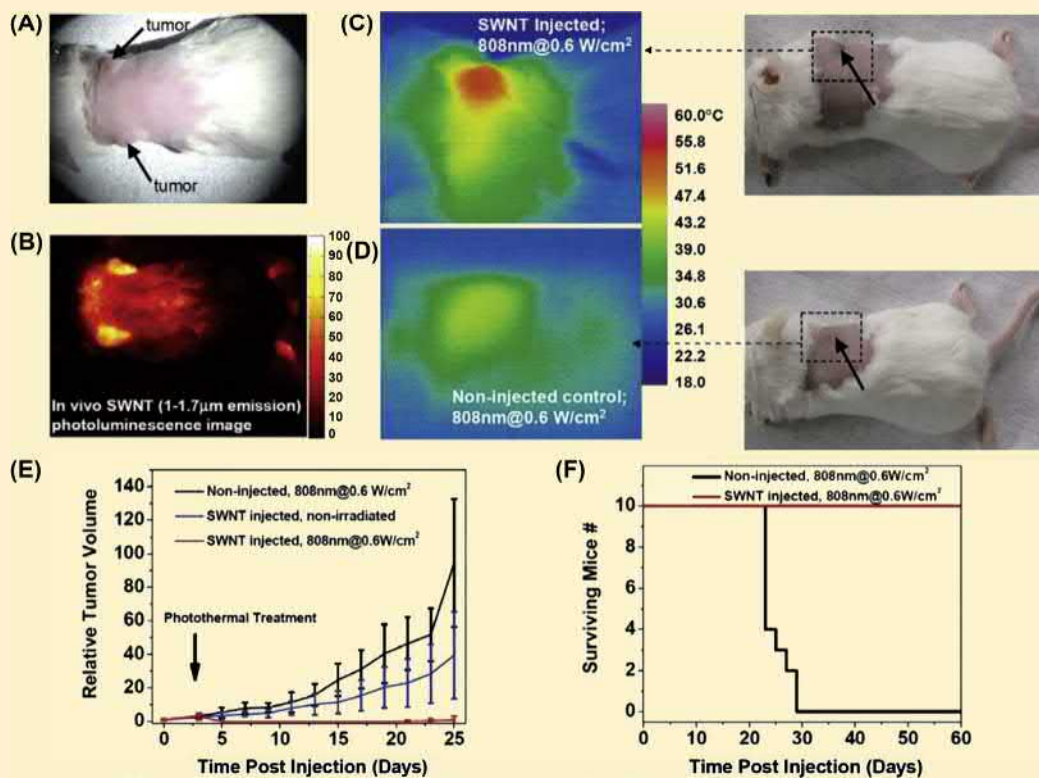
Biosensors

Disease diagnostics play an important role in the clinical treatment and outcomes of several diseases. During disease,

SIDEBAR #3

Short single-walled carbon nanotubes functionalized with PEGylated phospholipids (SWNT) are biologically nontoxic nanomaterials with intrinsic near infrared (NIR) photoluminescence and strong optical absorbance in the NIR. It has been shown that after intravenous injection in tumor bearing mice (A), SWNT migrate to the tumor and serve as photoluminescent agents for *in vivo* tumor imaging in the 1.0–1.4 μm emission region (B) and as NIR absorbers and heaters at 808 nm for photothermal

tumor elimination, reaching temperatures around 52 °C (C, D), decreasing the tumor volume (E) and increasing mice survival (F) (Robinson et al., 2010). The performance of these materials was also compared to gold nanorods (AuNR), being verified that higher tumor elimination was achieved with SWNT at 10x lower injected doses and lower irradiation powers than for AuNR. These results highlight the potential of the intrinsic properties of SWNT for combined cancer imaging and therapy.

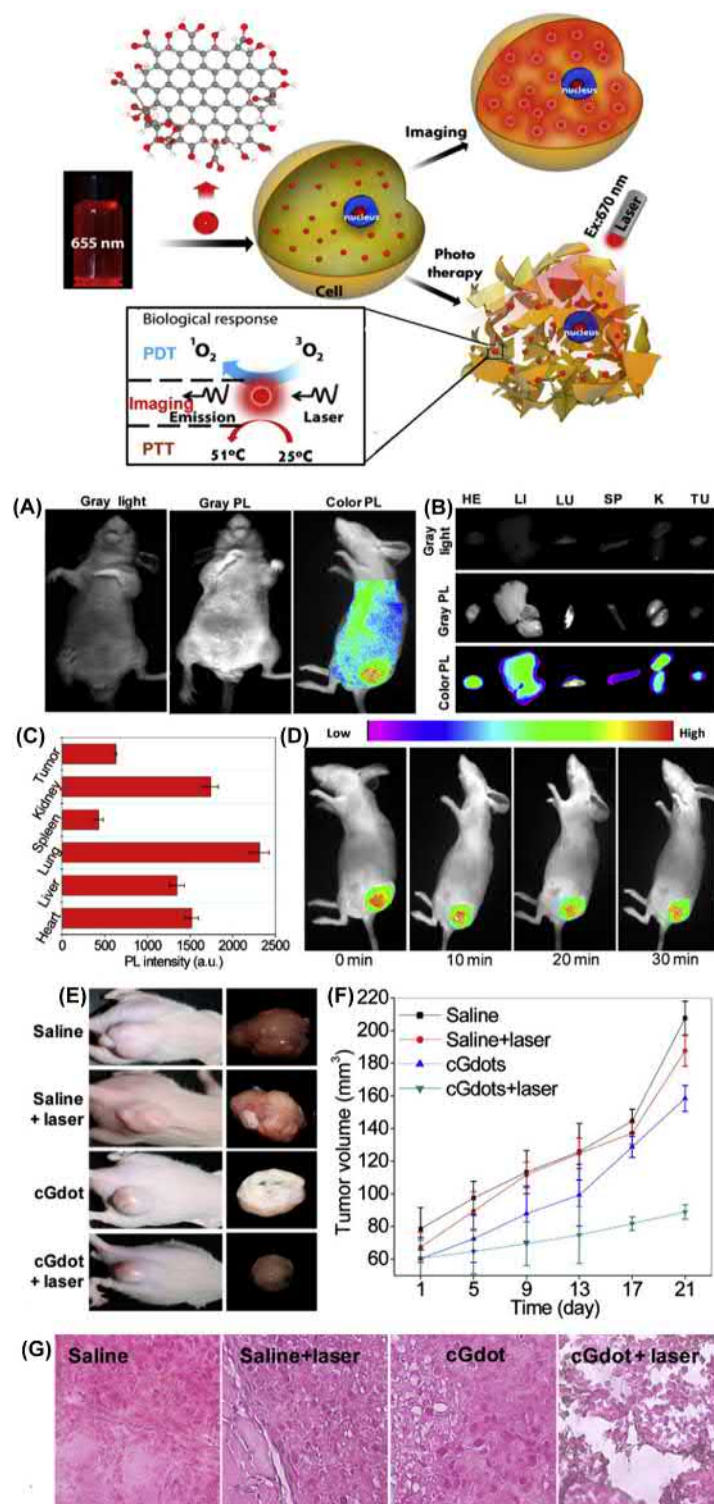


the profile of some biomolecules is altered in body fluids allowing their use as biomarkers of such illnesses. These molecules could be identified using an analytical tool such as a biosensor. Conventionally, a biosensor consists of three parts: a receptor that detects the molecule, a signaling transducer that converts the physical/chemical signal, and a signal processor. Biosensors can be electrochemical (physical/chemical signal is transduced to an electrical signal), piezoelectric (mass bound to the piezoelectric crystal surface sensor promotes a change in oscillation), optical (recognition of a target changes light emission), and electrochemiluminescent (electrochemical reactions produce a luminescence signal). Carbon nanomaterials have shown excellent performance in biosensor development due to their unique mechanical, electronic, and optical properties, high specific surface area, and biocompatibility, as reviewed by Pasinszki et al. (2017), Liu et al. (2017), and Teradal and Jelinek (2017). Among all carbon materials, CNT, GBM, and CD are the most applied materials in the development of biosensors, despite fullerenes also being used. These materials

can be used for the recognition of target molecules, for target molecule labeling, and in the transducer component, by either adsorbing molecules at their surface or being functionalized, despite the latter potentially compromising their conductivity properties.

Fullerene-C60 has been used to improve the sensitivity of electrochemical biosensors, due to its high conductivity. It provides a suitable immobilization platform for DNA and antibodies and has the ability to induce the proper orientation of redox-active proteins, which results in better electron transfer properties (Pilehvar and Wael 2015).

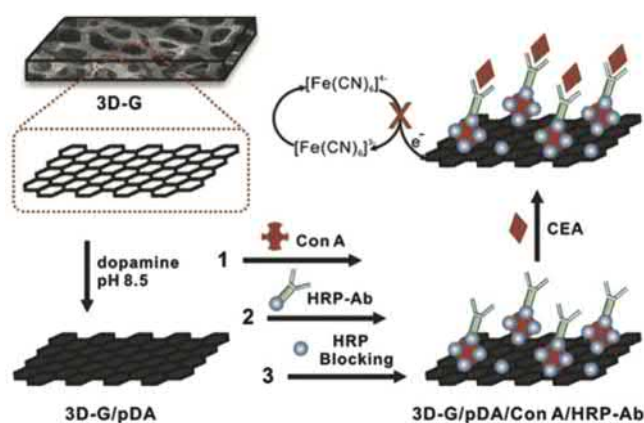
CNT-based biosensors have been assembled for the detection of several molecules such as dopamine, uric acid, glucose, prostate-specific antigen (PSA), osteopontin, miRNA, DNA, K-ras, carcinoma antigen-125, alpha-fetoprotein, and amyloid- β (Pasinszki et al., 2017). In most of these cases, biosensors have a low limit of detection and high linear range, showing suitable sensor performance (Pasinszki et al., 2017). A piezoelectric biosensor that recognizes carbohydrate antigen 19–9, which is a marker for colorectal,



• **Figure 1.3.5.11** Near-infrared graphene quantum dot (GQD) ($\lambda_{\text{ex}}=655\text{ nm}$) for optical imaging and phototherapy. Schematic representation of GQD chemical structure with carboxyl and hydroxyl functional groups located at the edges. Singlet oxygen generation occurs under laser exposure upon internalization. However, the photothermal effect occurs even without internalization. Cellular uptake was monitored in real time by confocal laser scanning microscopy, with the enhanced permeability and retention effect being identified. (A) Noninvasive images of GQD-treated MDA-MB231 breast cancer cell-bearing mice after injection. (B) *Ex-vivo* images of harvested organs. (C) Fluorescence intensity for harvested organs. (D) *In vivo* photoquenching profile for intratumoral-injected GQD upon laser irradiation up to 30 min. (E) Tumor morphology 21 days after treatment. (F) Progress of tumor volume along treatment. (G) Histological analysis of tumor tissue at day 21. Approximately 70% of the cells treated with GQD plus laser irradiation were necrotic. Magnification=400 \times . Adapted from (Nurunnabi et al., 2014). HE, Heart; K, kidney; LI, liver; LU, lung; SP, spleen; TU, tumor.

pancreatic, and hepatic cancer, was developed using a quartz crystal microbalance probe modified with poly-L-lysine/hydroxyapatite/CNT nanocomposite functionalized with antibody. This biosensor exhibits a high marker-binding activity (Ding et al., 2008). In a uric acid electrochemical biosensor, SWCNT are used as a matrix for enzyme immobilization (uricase) and as a mediator (Chen et al., 2010). Signal transduction is based on electrocatalytic reduction of H_2O_2 produced upon uricase activity. This biosensor has a low detection limit, high sensitivity, a wide linear range, and good stability (Chen et al., 2010).

Similarly to CNT, GBM have been incorporated in several biosensors for the detection of glucose, dopamine, uric acid, PSA, and carcinoembryonic antibody (CEA). A 3D-G foam was modified with concanavalin using polydopamine as adhesive, and the antibody (anti-CEA) labeled with horseradish peroxidase added to concanavalin (Fig. 1.3.5.12) (Liu et al., 2015). This biosensor shows a



• **Figure 1.3.5.12** Schematic illustration of the fabrication and carcinoembryonic antibody (CEA) detection process of the immunosensor (Liu et al., 2015). Concanavalin A (Con A) was immobilized in 3D graphene foam using polydopamine (pDA) as adhesive. Anti-CEA contains a sugar protein conjugated (HRP) that links to Con A allowing its immobilization. Upon recognition of CEA by anti-CEA, there is a change in solution-phase redox probes ($[Fe(CN)_6]^{4-/3-}$), which is measured by differential pulse voltammetry.

low detection limit, a linear range, and decreased incubation time (Liu et al., 2015).

A glassy carbon electrode coated with gold nanoparticles hybridized with hydrazine-modified GQD showed strong electrochemiluminescence activity in the presence of H_2O_2 after CEA binding to the surface. This biosensor could be used for the rapid, sensitive detection of CEA (Dong et al., 2015).

Antimicrobial Therapy

The antimicrobial properties of carbon materials have been mostly explored using ND, fullerenes, CNT, GBM, and CD as colloids (Table 1.3.5.3). However, much interest has arisen regarding their incorporation in surfaces, with research using CNT and GBM films, DLC coatings, and CNT-, GBM-, and CD-containing composites also being described.

ND antibacterial effect depends on size, surface chemistry, and composition of biological medium. ND with a size of 5 nm have more effective antibacterial activity against *Escherichia coli*, while ND with sizes between 18 and 50 nm are more effective against *Bacillus subtilis*. Both ND types were found interacting with bacterial surfaces, which might have affected bacterial cell wall and/or membrane permeability (Beranova et al., 2014). It has also been observed that fully carboxylated ND do not show antibacterial activity, while partially oxidized ND show similar potency to silver nanoparticles toward both Gram-positive (*B. subtilis*) and Gram-negative (*E. coli*) bacteria at concentrations of 50 mg/L. This might be explained based on reactive oxygen-containing surface groups fostering interactions with cellular components, while the anisotropic distribution of charges on ND surfaces facilitates alterations in bacterial surfaces. However, the bactericidal potential is gradually inhibited as protein concentration in culture media increases (Wehling et al., 2014). Several antiadhesive nanoparticles displaying activity against *Staphylococcus aureus* and *E. coli* biofilms have been developed using glycan-modified ND, revealing themselves to be of great promise for combating microbial infections

TABLE 1.3.5.3 Mechanisms of Action and Photoactivation Wavelengths of Antibacterial Carbon Colloids

Carbon Colloids	ND	Fullerene	CNT	GBM	CD
Membrane action	Destabilization	Oxidation (functionalized forms)	Piercing Oxidation Destabilization Wrapping	Piercing Oxidation Destabilization Wrapping	Destabilization
Oxidative stress	–	Yes (hydrophobic forms)	Yes (reduced impact)	Yes	Yes
Photo activation	–	UV (ROS production)	NIR (thermal effect)	UV NIR	Visible light (ROS production)

CD, Carbon dots; CNT, Carbon nanotubes; GBM, Graphene-based materials; ND, Nanodiamonds; NIR, Near-infrared radiation; ROS, Reactive oxygen species; UV, Ultraviolet radiation.

(Szunerits et al., 2016). Also, menthol-modified ND were shown to decrease surface adhesion of these two bacteria (Maas, 2016).

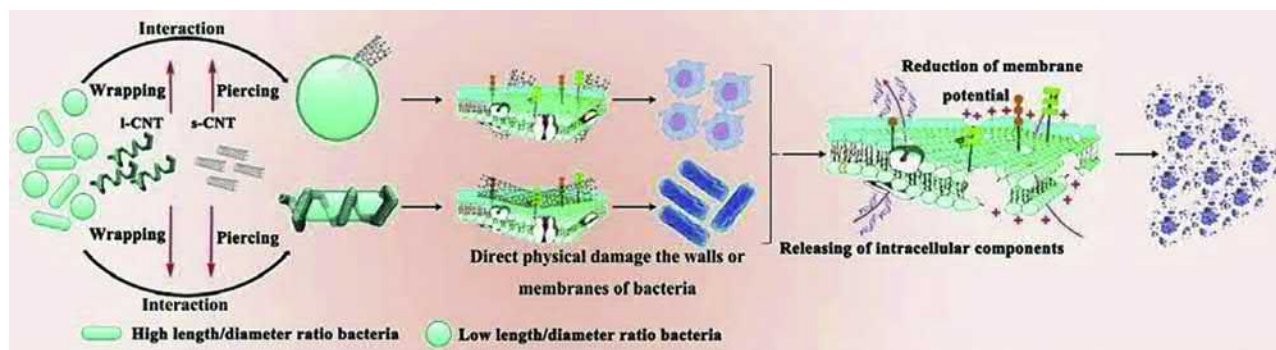
Hydrophobic fullerenes do not cause membrane damage to bacteria, instead they adsorb onto it and cause ROS-independent oxidative stress. In contrast, functionalized fullerenes were reported to insert and damage bacterial cell walls, much like GBM or CNT as described later. Fullerene derivatives have been reported to be effective against different bacterial types (e.g., *S. aureus*, *B. subtilis*, *E. coli*), and even fungus (*Candida albicans*). Upon photoirradiation, functionalized fullerenes are able to produce superoxide anion, which is generally more toxic toward bacterial than mammalian cells. (Al-Jumaili et al., 2017; Dizaj et al., 2015; Maas, 2016). Functionalized fullerene-mediated UV phototherapy was shown to be effective to treat skin wounds in mice infected with different Gram-positive and Gram-negative bacteria. This perspective is applied in infection treatment where antibiotics are ineffective, such as in many infected burn wounds (Huang et al., 2014). Fullerenes have been extensively studied for HIV treatment, because they specifically bind to the HIV-1 protease active site, inhibiting virus replication (Chen and Wang, 2016; Castro et al., 2017). Fullerenes also present activity against several other viruses, such as influenza and hepatitis (Bakry et al., 2007; Torres and Srdjenovic, 2011).

CNT have been found to selectively lyse the walls and membranes of pathogenic and nonpathogenic, Gram-positive and Gram-negative, spherical and rod-shaped bacterial strains, depending not only on the length and surface functional groups of CNT, but also on the bacteria features. Thin and rigid SWCNT show more effective wall/membrane piercing on spherical bacteria than MWCNT. Long MWCNT may wrap around bacteria, increasing the area contacting the bacterial wall (Fig. 1.3.5.13). Generally, short MWCNT and functionalized MWCNT are more toxic to bacteria than long MWCNT (Chen et al., 2013b). Membrane disruption can be caused by powerful electrostatic forces between the microbial outer surface and CNT, leading to membrane

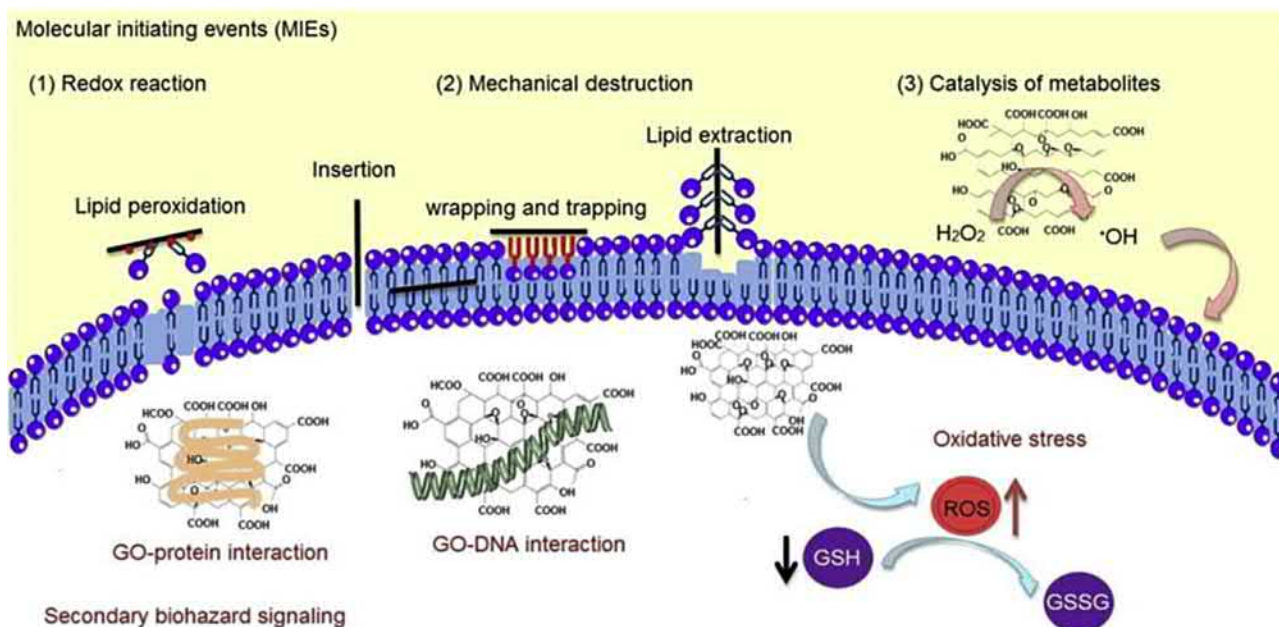
oxidation. Oxidative stress contributes to the CNT antibacterial effect; however, it has been described as less relevant than direct membrane damage. Since impurities remaining from CNT production (metallic nanoparticles, catalysts) can present an antibacterial effect, suitable cleaning of the materials is essential prior to biological testing (Al-Jumaili et al., 2017; Maas, 2016). Photothermal ablation of *E. coli* has been demonstrated using SWCNT and MWCNT upon NIR irradiation. Additionally, anti-*Streptococcus* group A antibody-functionalized MWCNT were employed to demonstrate effective targeted photothermal ablation (NIR) of planktonic bacteria and bacteria living within a biofilm using an *ex vivo* full-thickness porcine skin model (Mocan et al., 2017).

The antibacterial activity of GBM is described to be higher for GO than for rGO (Liu et al., 2011a; Gurunathan et al., 2012). Differences are explained by the different states of dispersion and amounts of oxygen-containing functional groups, which impact on both membrane and oxidative stress. Large GO nanosheets, which can cover bacteria preventing proliferation, have been pointed out as having a stronger antibacterial effect. By contrast, some results indicate that small GO sheets have higher oxidative and antibacterial capacity (Shi et al., 2016; Zheng et al., 2018). There are three different molecular initiating events caused by GBM that lead to the antibacterial effect: redox reaction with biomolecules, mechanical destruction of membranes, and catalysis of extracellular metabolites (Fig. 1.3.5.14). UV radiation has been described as possibly activating GO basal and edge radicals, leading to a superior antibacterial effect than that of nonirradiated GO, and even the standard antibiotic kanamycin (Veerapandian et al., 2013). Potential for *in vivo* antibacterial and antifungal PTT leading to wound healing has already been demonstrated, as GO absorbs NIR radiation increasing local temperature, which acts synergistically with its intrinsic antimicrobial mechanisms (Khan et al., 2015).

CD show a strong broad-spectrum antibacterial and antifungal activity. Due to their small size, they can enter microorganisms by diffusion, destroy the cell wall, bind



• **Figure 1.3.5.13** Carbon nanotubes (CNT) antibacterial mechanisms of action. Short CNT (s-CNT) are more prone to pierce spherical bacteria walls/membranes than long CNT (l-CNT), which wrap around and interact with the cell surface. Induced release of intracellular components (DNA, RNA) and loss of membrane potential lead to bacterial cell integrity loss (Chen et al., 2013b).



• **Figure 1.3.5.14** Graphene-based material (GBM) antibacterial mechanisms of action. Three different molecular initiating events (MIEs) have been described for GBM: (1) redox reaction with biomolecules; (2) mechanical destruction of membranes; and (3) catalysis of extracellular metabolites. The downstream signaling pathways may include reactive oxygen species (ROS) generation and glutathione (GSH) depletion, protein and DNA damage. GO, Graphene oxide; GSSG, Glutathione disulfide (Zheng et al., 2018).

to DNA and RNA, inhibit gene expression, and lead to apoptosis even at low concentrations. Moreover, they are easily biodegradable and eliminated from the body (Li et al., 2018; Jhonsi et al., 2018; Bing et al., 2016). CD bactericidal activity depends on their surface chemistry. Nitrogen-doped CD have higher antibacterial effect than sulfur-doped ones. This is explained by electrostatic interactions between CD-protonated forms and bacterial cell membrane lipids (Travlou et al., 2018). CD can be photoactivated under visible light for antibacterial effect enhancement through ROS production (Al Awak et al., 2017; Bing et al., 2016; Meziiani et al., 2016; Ristic et al., 2014). They are also fluorescent allowing real-time bacterial imaging and selective staining (Gram-positive over Gram-negative) (Yang et al., 2016). GQD-based band-aids for wound disinfection have been successfully tested in mice (Sun et al., 2014).

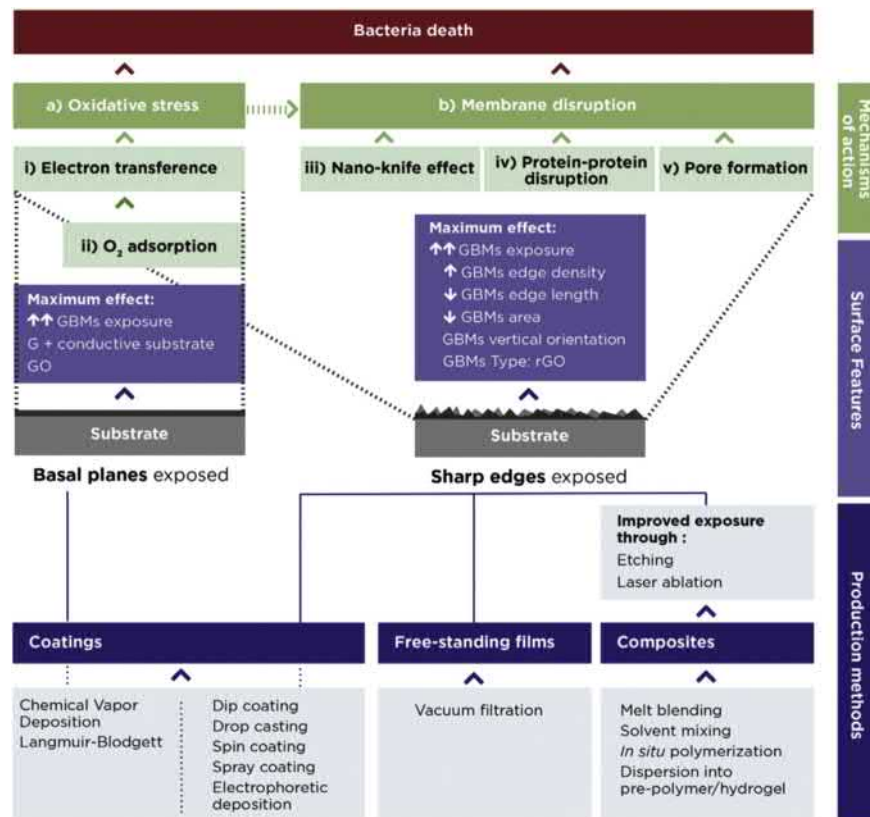
The carbon biomaterials previously mentioned in the form of micro/nanoparticles also have potential to be used as antibacterial films, coatings, or composites, retaining most of their properties when incorporated in a biomaterial. New factors must be taken into account, for example the exposure angle of sharp particles should be maximized to obtain effective mechanical damage at the bacterial membrane, and stability of the coatings assured.

The antimicrobial activity of GBM free-standing 2D films has been assessed in a review (Henriques et al., 2018). Despite the controversy, since some authors defend

that GBM free-standing 2D films could indeed support bacterial growth (Park et al., 2010; Ruiz et al., 2011; Aryal et al., 2017), the particles' lateral size and oxidation degree seem to have a crucial impact on antimicrobial activity (Fig. 1.3.5.15). Films containing smaller GO particles have a stronger antimicrobial effect than films containing large particles and/or rGO (Henriques et al., 2018; Perreault et al., 2015; Singh et al., 2017), and these smaller GO particles seem to induce higher oxidative stress in bacteria. Besides surface chemistry, the roughness of GBM free-standing 2D films also influences their antimicrobial properties. When using G, rough surfaces that expose the sharp edges promote bacteria killing while smooth surfaces promote bacterial adhesion (Henriques et al., 2018; Pham et al., 2015). Possible piercing of the bacterial cell wall and membrane by exposure of sharp edges has been pointed out as the main mechanism for this phenomenon, although some authors defend a low probability of it occurring (Pham et al., 2015; Romero-Vargas Castrillón, 2015).

The application of UNCD, DLC, CNT, and GBM coatings in the development of antimicrobial surfaces has also been suggested.

UNCD and DLC coatings have been used to improve the surface properties of biomedical implants (Al-Jumaili et al., 2017). DLC films are highly hydrophobic, which leads to variations in bacterial cell membrane, and prevents bacterial adhesion. However, differences in antibacterial



• **Figure 1.3.5.15** Relation between graphene-based materials (GBM)-containing surface production methods, surface features, and antibacterial mechanisms of action. G, Graphene; GO, graphene oxide; rGO, reduced graphene oxide (Henriques et al, 2018).

effects have been found according to fabrication conditions, which lack reproducibility. A widely observed factor is that decreasing the sp^3/sp^2 ratio has a positive effect on surface antibacterial properties.

Paper coated with functionalized SWCNT that contain amine, phosphate, and carboxylic groups at their surface exhibits an antimicrobial action against *S. aureus* and *E. coli*. This effect is higher in Gram-positive *S. aureus*, being correlated with CNT direct contact that promotes the piercing of bacterial membrane leading to the loss of cell shape integrity (Deokar et al., 2013). CNT films on silicon substrate also inhibit the growth of *S. aureus* (Narayan et al., 2005).

Depending on the coating production technique, it is possible to obtain surfaces with different features that can promote a wide range of effects in bacteria. GBM-containing surfaces produced by CVD and Langmuir-Blodgett techniques have a high exposition of G and GO basal planes at the surface, promoting oxidative stress, which culminates in bacterial death. In the case of G, the presence of conductive substrate seems to be a necessary condition to exhibit an antimicrobial effect (Li et al., 2014; Henriques et al., 2018). Surfaces produced by dip, spray, or spin coating, drop casting, and electrophoretic deposition expose GBM in a random orientation. As such,

besides basal planes, they also expose sharp edges, which promote bacterial cell membrane disruption by piercing (nanoknife effect), protein–protein interaction, or pore formation (Fig. 1.3.5.15).

Regarding the incorporation of carbon biomaterials as composites, the antimicrobial effect of composites containing CNT is highly dependent on CNT type, length, and amount in the polymeric matrix. As observed for CNT powders, when incorporated in polymeric matrices, SWCNT with shorter lengths are the most effective in killing bacteria, forming a poly(lactic-co-glycolic acid) (PLGA) composite with antimicrobial activity of 98% (Mocan et al., 2017; Aslan et al., 2010). Incorporation of CNT in ZnO (Akhavan et al., 2011), poly(vinyl acetate) (Youssef et al., 2019), Ag–TiO₂ (Hossain et al., 2018), and gelatin-fluoroquinolones (Spizzirri et al., 2015) leads to a general increase of their antimicrobial activity. Electrospun polysulfone-SWCNT mats reveal an antibacterial effect of 76%, even in the presence of very low amounts of SWCNT and after a short contact time of 15 min or less (Schiffman and Elimelech, 2011).

The antimicrobial performance of GBM-containing composites depends not only on the incorporated GBM and its amount but also on the adopted composite production technique. Production techniques that promote GBM

exposure at composite surfaces generate materials with higher antimicrobial properties (Henriques et al., 2018). Due to the poor characterization of incorporated GBM and resulting composites, comparisons between different studies are difficult. However, incorporation of GO to create polymeric composites such as chitosan (CS)/GO (Mazaheri et al., 2014), CS/polyvinylpyrrolidone/GO (Mahmoudi et al., 2016), polylactic acid/polyurethane (PU)/GO (An et al., 2013), PCL/GO fibrous scaffolds (Melo et al. 2020) and agar/GO (Papi et al., 2016) hydrogel promoted an antimicrobial effect between 50% and 100% in different bacteria species.

Upon excitation with visible light, a CD-decorated $\text{Na}_2\text{W}_4\text{O}_{13}$ composite with WO_3 photocatalyst (CD/ $\text{Na}_2\text{W}_4\text{O}_{13}/\text{WO}_3$) exhibited excellent antimicrobial activity against *E. coli* without promoting cytotoxicity. Similarly to what happens in CD colloids, ROS production during light activation plays a critical role in composites' bactericidal effect (Zhang et al., 2018a). Also, an epoxide-functionalized CD/

organomontmorillonite composite exhibits great antimicrobial properties inhibiting biofilm formation (De et al., 2015).

Cardiovascular Applications

According to the World Health Organization, cardiovascular diseases are the number one cause of death globally. Biomaterials have long been used in cardiovascular applications, with carbon-based materials playing an important role mostly as coatings of long-term implants, where devices are already commercially available, despite also being investigated for tissue-engineering approaches.

Long-Term Implants

Mechanical Heart Valves

Mechanical heart valves (MHV) are composed of man-made materials (e.g., stainless steel, ceramic, carbon materials) and have been developed into different shapes (e.g., caged ball, monoleaflet, bileaflet).

CASE STUDY: MECHANICAL HEART VALVES

In the past, MHV design and materials were optimized to reduce wear and thromboembolism, which were much more severe, until a drastic improvement was found when carbon materials were tested (Musumeci et al., 2018; Nachlas et al., 2017). The Gott–Daggett bileaflet valve was first produced in 1963 with a Gt-benzalkonium-heparin coating, upon Dr. Vincent Gott's findings of its high potential to reduce blood clotting on rings implanted in canine vena cava. Later, in 1965, Dr. Jack Bokros proposed a collaboration to try to bind heparin to a highly polished PyC, which he had developed at General Atomic, and which proved not to be suitable to bind heparin, but to have outstanding thromboresistance performance on canine *in vivo* assays. Following these finds, Bokros developed the ball puppet for the DeBakey-Surgitool valve, also discs and leaflets for most of the MHV produced thereafter. Since then, PyC has been used in more than 25 different MHV designs, and nowadays 95% of all MHV have at least one structural component made of this carbon biomaterial. The balance between blood compatibility, physical and mechanical properties, and durability made PyC the best material option available in MHV. This allowed MHV anticoagulation therapy dose reduction, despite it not being suppressed. It is still uncertain if hemocompatibility issues arise from the biointeractions with the PyC itself or from hemodynamic interaction of the devices in which it is

integrated. However, it has been observed that PyC first adsorbs and denatures albumin over other proteins, forming a surface passivating layer. Also, adsorbed fibrinogen is rapidly converted to a nonelutable form, which is less reactive to platelets (Robert et al., 2013; Gott et al., 2003).

Nowadays, MHV are composed of two hemidisks in a housing, both made of pyrolytic carbon, being commercialized by several companies (Fig. 1.3.5.16). A 17-year follow-up study in 500 patients implanted with Sorin mechanical valves revealed that only five reoperations were necessary, and that there was a total of 15 valve-related deaths (Kheradvar et al., 2015). A study comparing contemporary bileaflet valves revealed that On-X MHV presented the lowest incidence of thrombosis, stenosis, and hemolysis in the aortic position (Chaudhary et al., 2017). However, strategies to further decrease thrombogenicity are still being pursued, in the search for an MHV that does not require lifelong anticoagulation therapy.

In 2018 the Food and Drug Administration (FDA) approved the world's smallest MHV, which was produced with PyC, and commercialized by Abbott. This new valve can be used to treat babies and toddlers in need of a mitral or aortic valve replacement, who until now could not be submitted for treatment due to the small size of their hearts. More than 50 years after started being used in MHV, PyC is still integrated on those devices, even for the most demanding procedures.



• **Figure 1.3.5.16** Images of mechanical heart valves from the major manufacturers (Kheradvar et al., 2015).

As described in this chapter's case study, MHV made of PyC present a satisfactory performance. Despite being commercialized, further improvement is desired and therefore research on this topic is still ongoing. The potential use of UNCD (Zeng et al., 2016) and DLC (Tran et al., 1999) coatings on MHVs have been proposed. These types of coatings have desirable chemical inertness, mechanical durability, and biocompatibility (Dearnaley and Arps, 2005; Roy and Lee, 2007; Ma et al., 2009).

Materials used in the production of heart valves, such as poly(tetrafluoroethylene), polyvinyl chloride, segmented PU, silicon rubber, and poly(ether urethane urea), have a low cycle fatigue strength, which impacts their durability. As previously mentioned, incorporation of carbon materials in polymeric matrices improves their mechanical performance significantly (Vellayappan et al., 2015). Thus, some carbon biomaterial-containing composites have been developed for application as cardiac prostheses.

The incorporation of low amounts of CNT in PU induces higher mechanical performance, but high amounts of CNT decrease material fatigue strength (Vellayappan et al., 2015; Rozeik et al., 2017). Besides the mechanical improvement, incorporation of MWCNTs with oxygen-containing functional groups in a PU matrix promotes anticoagulant activity at the polymer surface.

Incorporation of 2-(methacryloyloxy) ethyl phosphor-ylcholine functionalized GO in PU improves its hemocompatibility, even when a small amount of GBM is used (Vellayappan et al., 2015; Rozeik et al., 2017). Incorporation of 2-(methacryloyloxy) ethyl phosphorylcholine functionalized GO in PU improves its hemocompatibility, even when a small amount of GBM is used (Vellayappan et al., 2015).

Vascular Stents

Stent development has focused on the mitigation of in-stent thrombosis, flexibility, and ease of implantation. Carbon material coatings can be used to encapsulate metallic stents, preventing toxic ion release and providing a low friction, bioinert surface for biointeraction. This leads to better cell adhesion and proliferation, suppression of immune response, increased albumin adsorption, and low platelet activation, decreasing thrombogenicity and preventing restenosis.

Vascular stents coated with DLC or PyC are currently available on the market (Table 1.3.5.1).

Carbostent (Sorin, Italy) has a coating of a turbostratic structure equivalent to that of PyC, produced by physical vapor deposition, which has been used both in stents and MHV.

a-C:H DLC coatings are used in Diamond Flex (Phytis, Germany), BioDiamond (Plasma Chem, Germany) (Fig. 1.3.5.17), and DLN or Dylyn (Bekaert, Belgium). ta-C coatings have been reported to adhere less to platelets than PyC, and to be less inflammatory toward macrophages than uncoated stainless steel. Thus this might be a coating material for future consideration for biocompatibility improvement

of medical devices (Dearnaley and Arps, 2005; Roy and Lee, 2007; Ma et al., 2009).

A study on nitinol coated with CVD-transferred G has revealed no significant *in vitro* toxicity to endothelial and smooth muscle cell lines. Coatings were chemically inert, durable, and impermeable, revealing low fibrinogen/albumin ratio, which might result in good hemocompatibility (Podila et al., 2013). This promotes G as a new candidate coating material for stents, with patents already registered for this use.

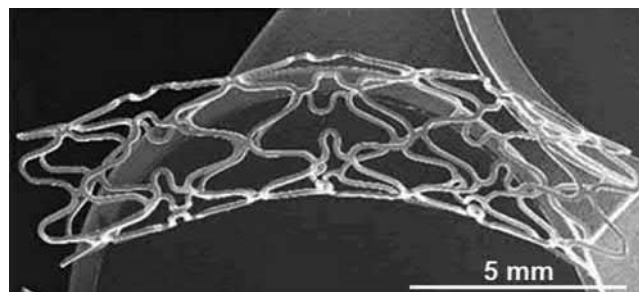
Ventricular Assist Devices

Ventricular assist device (VAD) is an alternative to patients with severe heart failure with secondary pulmonary hypertension, for whom transplant may be contraindicated. Its rotary blood pumps are commonly made of titanium alloy (Ti 6Al4V), but strategies to reduce its thrombogenicity are needed.

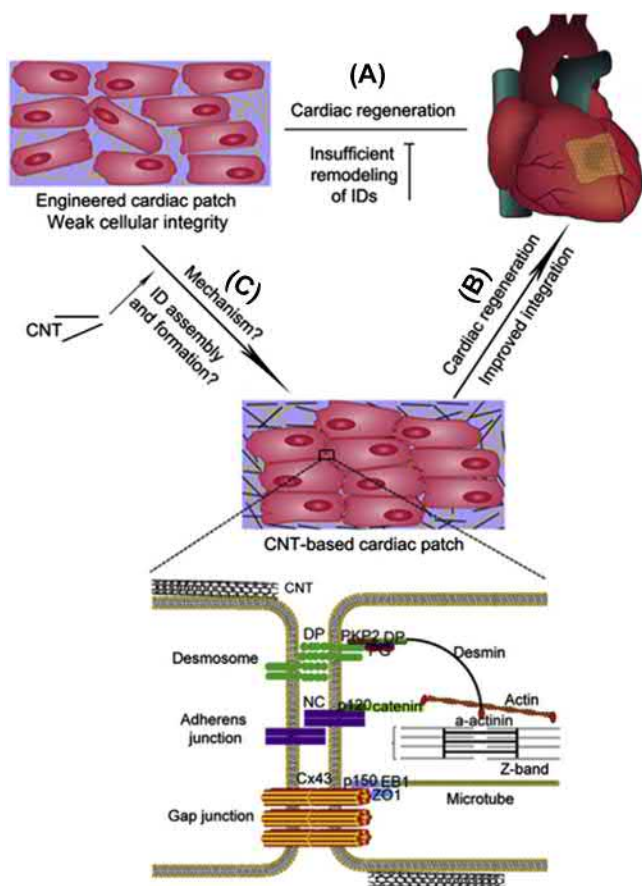
A DLC coating was tested in a centrifugal VAD (Sun-Medical Technology, Japan), maintaining a stable performance without any adverse effect over 6 months in calves under postoperative anticoagulation protocol. Blood-contacting surfaces of the DLC coating were entirely free from thrombus formation and there were no major organ infarcts except a few small-sized ones at the kidneys. The wear rate of the seal face was 10 μm after 200 days of continuous operation and there was no measurable wear at the hydrodynamic journal bearing (Yamazaki et al., 1998). An FDA-approved DLC-coated centrifugal VAD, VentrAssist (Ventracor, Australia), is already on the market.

Tissue-Engineering Approaches

Cardiovascular diseases comprise problems in blood vessels and/or the heart, and usually culminate in the occurrence of heart attacks and strokes. In the heart, myocardial infarction leads to large-scale loss of cardiomyocytes that exceeds the limited regenerative capacity of the myocardium leading to a collagen-based scar and loss of function (Prabhu and Frangogiannis, 2016). Tissue engineering is one promising strategy to allow cardiac repair but has revealed to be challenging, since cardiac scaffolds must merge exactly the mechanical and electrical features of the natural tissue. Most of the biocompatible polymers such as alginate, collagen, polycaprolactone (PCL), CS, gelatin methacrylate



• **Figure 1.3.5.17** Images of BioDiamond (Plasma Chem, Germany), a diamond-like carbon-coated stent. Adapted from (Roy and Lee, 2007).



• **Figure 1.3.5.18** Proposed hypothesis that carbon nanotubes (CNT) promote cardiomyocyte organization and functional integration with host tissue. (A) Currently used cardiac patches with insufficient remodeling of intercalated discs (ID). (B) CNTs offer a new paradigm for constructing CNT-based functional cardiac patches to repair myocardial infarction. (C) Questions that remain unraveled (Sun et al., 2015). *Cx43*, Connexin43; *NC*, N-cadherin. ((B) Images courtesy of Eclipse, cited from the article of Garcia-Elias, M., 2007. Eclipse: partial ulnar head replacement for the isolated distal radio-ulnar joint arthrosis. *Tech. Hand Upper Extremity Surg.* 11, 121–128 with original copyright holder's permission.)

(GelMA), polyglycerol sebacate, and PLGA have weak mechanical properties and are insulators, which impair the electrical signal propagation compromising the contractile behavior of cardiac cells (Pok et al., 2014). The mechanical properties and electricconductive capacity of some carbon materials such as CNT and GBM prompted their investigation as materials for cardiac regeneration, mostly as free-standing materials or as composites.

The potential application of CNT in cardiac tissue engineering has been validated by several studies as reviewed by Gorain et al. (Gorain et al., 2018). CNT films stimulate the expression of genes involved in growth and in the differentiation process of neonatal cardiomyocytes (Martinelli et al., 2013). Additionally, these cardiomyocytes have an upregulation of the genes involved in the formation of intercalated discs (Fig. 1.3.5.18), which establish a network between cardiomyocytes, enabling the rapid transmission of electrical impulses and coordinated contraction of the myocardium (Sun et al., 2015). Superaligned CNT sheets present improved conductivity along the alignment and promote

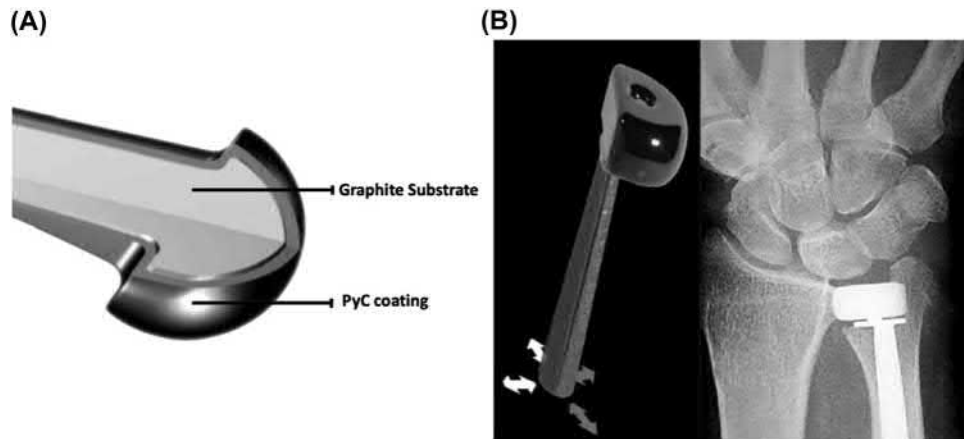
growth of cardiomyocytes with regular and synchronized contractions, exhibiting an elongated morphology with alignment similar to the natural myocardium (Ren et al., 2017). The incorporation of CNT as composites improves electrical conductivity and/or mechanical performance of the base polymers (Gorain et al., 2018; Vellayappan et al., 2015), promoting the adhesion of cardiomyocytes and supporting their function, growth, and maturation (Gorain et al., 2018) without inducing toxicity and/or apoptosis (Kroustalli et al., 2013). Early differentiation of human mesenchymal stem cells into cardiomyocytes has also been described using CNT-containing 3D poly(ϵ -caprolactone) scaffolds, due to the high similarity to the native tissue regarding conductivity and mechanical strength (Crowder et al., 2013a). Likewise, increased cardiac differentiation of embryoid bodies was reported for gelatin methacryloyl hydrogels containing aligned CNT (Ahadian et al., 2016).

GBM have also been applied in the design of scaffolds for cardiac regeneration. Overall, all GBM exhibit the capacity to improve cardiomyocyte adhesion and proliferation. The chemical features and conductive capacity of GBM play a critical role in the beating capacity of cardiomyocytes. G films produced by CVD showed stable cardiac cell attachment and excellent biocompatibility (Kim et al., 2013b). Despite the conductive capacity of GO being lower than G, GO incorporation in polymeric matrices such as CS (Jing et al., 2017), tropoelastin (Annabi et al., 2016), and collagen (Norahan et al., 2019) still promotes cell adhesion, proliferation, electrical signal propagation, and expression of specific cardiac markers. rGO reestablishes its conductivity, and its incorporation in GelMA hydrogel induces a faster spontaneous beating rate and stronger contractility of cardiomyocytes compared to GO-GelMA (Shin et al., 2016). Multilayer cardiac constructs have been attempted using layer-by-layer assembly of poly-L-lysine-functionalized GO and cardiac and endothelial cells, revealing that these engineering 3D tissue structures present improved cell organization, electrophysiological function, and mechanical integrity (Shin et al., 2014). GO incorporation in thermoplastic PU, besides improving the mechanical properties of electrospun fibers, increases human umbilical vein endothelial cell adhesion and proliferation, revealing to be promising for the development of tissue-engineered vascular grafts (Jing et al., 2015).

Orthopedic Applications

Aging of the world population leads to an increase in musculoskeletal and cartilage-associated diseases. The traditional materials conventionally used in orthopedic applications, namely polymers, ceramics, and metals, commonly induce wear, debris, inflammation, mechanical loosening, implant fracture, and bone resorption caused by foreign body reaction.

The mechanical properties of available polymers are not suitable for load-bearing orthopedic applications. Thus they need a mechanical reinforcement to be applied in such a field. The remarkable mechanical properties, biocompatibility, and large surface-specific area of most carbon materials make



• **Figure 1.3.5.19** Pyrolytic carbon (PyC) coatings used in orthopedic applications. (A) PyC coating (0.5–1.0mm PyroCarbon) on a graphite substrate used in joint arthroplasty (Integra Life Sciences, USA). (B) The Eclipse partial ulnar head replacement (Tornier Surgical Implants, France) consists of an expandable titanium stem with a mobile PyC spacer (*left*). When implanted, the prosthesis preserves the ulnar styloid and attachment of the triangular fibrocartilage complex (*right*). Adapted from (Garcia-elias et al., 2007).

them perfect candidates to explore in the orthopedics field, either as composites or coatings, decreasing wear-related failures and adverse tissue reactions (bone resorption), while sustaining compatibility with cartilage and bone tissues.

Long-Term Implants

PyC implants are commonly used in hand and wrist arthroplasty, with some having more than 10 years of clinical follow-up. As an alternative to silicone, Dr. Beckenbaugh developed the first PyC metacarpophalangeal (MCP) implant, which was tested in patients between 1979 and 1987 resulting in improved function and esthetics. MCP implants were first commercialized by Ascension Orthopedics (USA). Several PyC-coated implants are currently marketed by Integra Life Science (USA) and Tornier/Wright Medical (France) (Fig. 1.3.5.19). These PyC hand and wrist implants for replacement of MCP, proximal interphalangeal and carpometacarpal (CMC) joints, radial head, lunate, and interpositional articulating surface spacers for use in CMC joints have overcome the previously mentioned implant-associated complications verified when using materials such as silicone, metal, and polyethylene. Moreover, follow-up studies usually report good pain relief, improved grip and pinch strength, and better appearance (Bellemere, 2018; Ross, 2008). PyC has also been investigated for use in scaphoid trapezium implants, in the femoral head-articulating surfaces of hip joint prostheses, and in femoral implants to enhance bone ingrowth (Bohem et al., 2011).

Due to its excellent tribological properties, DLC has been extensively investigated in the last few decades as a coating to decrease wear and corrosion of orthopedic materials. Several studies have shown considerable wear rate improvement, markedly reduced corrosion and leaching of metal into body fluids, good osteointegration, low immunoreactivity, and harmless debris release when DLC coatings are applied. In 2001, Diamond Rota Gliding (Implant Design,

Switzerland), a DLC-coated ultrahigh molecular weight polyethylene (UHMWPE) knee joint, was commercialized. However, some of the implants showed increased wear and partial delamination, with the residual coating on the upper side of the implant leading to inadequate bone ingrowth. As such, the use of this implant was forbidden. In 2003, results were published from an 8-year clinical follow-up of 100 patients implanted with DLC-coated Adamante (Biomécanique, France) femoral heads, articulating against polyethylene. After 1.5 years, aseptic loosening was found, with implant revision being needed, and after 8 years almost half of the implants had to be replaced. DLC coatings presented numerous small pits, and delamination of the carbon layer led to excessive release of polyethylene debris, and in some cases even of the metallic substrate of the heads. Despite DLC coatings having high potential to be used to enhance orthopedic implant performance, instability caused by their high level of residual stress and poor adhesion in aqueous environments must be addressed (Ma et al., 2009; Roy and Lee, 2007; Dearnaley and Arps, 2005; Taeger et al., 2003).

UNCD coatings usually reveal appropriate interfacial structure and chemistry, presenting good adherence on a variety of steels. Also, they enhance the growth of osteogenic cells, including mesenchymal stem cells (MSC). Control of cell adhesion, proliferation, and subsequent bone formation can be achieved by altering UNCD surface properties, influencing protein adsorption toward a beneficial biointeraction. Despite UNCD coatings being able to reduce friction and wear of metallic implants, increasing their longevity, the *in vivo* response of macrophages to the possible wear debris and the fate of phagocytosed nanoparticles are not well understood. For that reason, further toxicological studies are needed (Catledge et al., 2013).

The use of CNT as coatings has also been attempted using a hydroxyapatite/CNT composite coating on Ti alloys produced

by laser-surface alloying, revealing that it hardens the surface and makes it more resistant to wear (Chen et al., 2007).

Being impermeable, GBM meet the most relevant requirements for orthopedic implant coating materials, such as good biocompatibility, excellent mechanical strength, and tribological properties. GBM-based coatings have been shown to prevent bacterial adhesion and proliferation, potentially preventing implant-related infections (Henriques et al., 2018; Shadjou and Hasanzadeh, 2016).

Regarding the use of composites containing carbon biomaterials, commercially available prosthetic foot designs for patients with regular activities and elite running and jumping events are constituted by CF in their keel and/or heel part. These prostheses need to resist impact and at the same time should be lighter than an intact limb so that amputee athletes may have a similar energy cost to non-disabled athletes (Nelham, 1981; Saito et al., 2011). For this, fiber alignment in angles concerning applied stress is essential to fit the required properties (Nelham, 1981). Besides their usage in this type of prosthesis, CF were also incorporated in polyether ether ketone (PEEK) and calcium phosphate composites, reinforcing their mechanical properties to improve their performance for bone replacement (Park and Vasilos, 1997; Scotchford et al., 2003). CF/PEEK composites are currently commercialized as spinal fixation cages, hip joint sockets, and knee, limb, and foot prostheses (Table 1.3.5.1). Compared with titanium or stainless-steel prosthesis, CF/PEEK composites exhibit similar mechanical properties but prevent interface disruption and bone loss (Scotchford et al., 2003). However, when CF were incorporated in UHMWPE, the resulting scaffolds did not show good performance for the development of artificial hip and knee joints. This has been associated with the loss of interaction between CF and polyethylene over time (Saito et al., 2011; Kurtz et al., 1999; Korkala and Syrjanen, 1998).

Given the promising results of CF/PEEK composites, the use of CNT was also attempted for PEEK reinforcement. These composites exhibit high strength and low wear, enabling their application as orthopedic implants, essentially in joint replacement (Diez-Pascual et al., 2009). Incorporation of MWCNT into polymethyl-methacrylate led to the reinforcement of neat polymer exhibiting a lower crack propagation (Marrs et al., 2006). GO incorporation in pHEMA suppressed its mechanical limitations, allowing uses in load-bearing applications, such as orthopedic implants (Pereira et al., 2019).

Tissue-Engineering Approaches

Besides the remarkable ability of bone to regenerate and heal itself, large bone defects are still a difficult issue in the biomedical field (Roseti et al., 2017; Agarwal and Garcia, 2015). Bone remodeling is a dynamic process that involves formation of bone matrix by osteoblasts and resorption of bone tissue by osteoclasts. In bone tissue engineering, most of the strategies aim to promote the natural process of bone remodeling and regeneration, meaning that an ideal scaffold must have

the required mechanical properties, promote cell adhesion, proliferation and differentiation, and enhance intravascularization and host integration (Roseti et al., 2017; Agarwal and Garcia, 2015). The regenerative capacity of cartilage is limited due to its lack of vascularization. Cartilage development shares several growth factors with bone development, namely the bone morphogenic proteins. Thus development of scaffolds for cartilage regeneration have the additional challenge of privileging the development of cartilaginous tissue instead of ossification (Kessler and Grande, 2008).

NCD films proved to be excellent substrates for the adhesion, growth, and functioning of bone cells, which has been attributed mainly to the surface nanostructure of these films (Grausova et al., 2008, 2009). When functionalized NCD is used, cells tend to adhere preferentially to *O*-terminated domains (Rezek et al., 2010). The roughness of UNCD surfaces promotes high adsorption of apatite at the surface (Fox et al., 2013).

Unlike freshly produced fullerene films that do not show much potential to adhere to osteoblasts (Bacakova et al., 2014), aged fullerene films or Ti/fullerene films lead to improvement in osteoblast adhesion compared with glass substrate (Vandrovcova, 2008).

GBM have been used as films, revealing that the high surface/area ratio of GBM allows effective adsorption of osteogenic inducers at their surface, such as dexamethasone, β -glycerophosphate, and ascorbic acid, which promote osteogenic differentiation (Lee et al., 2011; Akhavan et al., 2013). Moreover, by playing with the surface chemistry of GBM it is possible to modulate the adsorption of different osteogenic markers at their surface: while rGO adsorbs higher amounts of dexamethasone and β -glycerophosphate, GO adsorbs more vitamin C (Lee et al., 2011). Also, negatively charged GO promotes higher calcium absorption, while amine-functionalized GO promotes higher phosphate adsorption (Kumar et al., 2015). Osteogenic differentiation of human MSCs has also been induced by 3D-G aerogels (Crowder et al., 2013b).

Regarding cartilage repair, aligned sheets of CNT induce growth of primary chondrocytes, particularly under electrical stimulation (King et al., 2017).

Application of CF for cartilage regeneration was first attempted by incorporation of these fibers in an osteochondral defect, revealing excellent repair capacity (Kaar et al., 1998; Minns and Muckle, 1989). Since then, many papers have reported *in vivo* the potential of CF as scaffolds for bone regeneration and cartilage repair as reviewed by Saito et al. (Saito et al., 2011). The dimension of CF has a high impact on osteoblast activity, being higher for fibers with diameters <100 nm (Saito et al., 2011).

Regarding the use of composites, incorporation of ND in PLGA and poly(L-lactic acid) leads to improved mechanical properties of both polymers, despite having an adverse effect on cell viability and the production of osteodifferentiation factors, which could be explained by the release of ND for cell culture medium (Parizek et al., 2012; Bacakova et al., 2014). However, when ND are coated with phospholipids and then incorporated in PLGA, the high mechanical properties, good

in vitro and *in vivo* biocompatibility, acceptable immune response, and increased mineralization capability suggest that these biodegradable composites may potentially be useful for bone tissue engineering (Zhang et al., 2016).

EMO-GO/poly(lactic acid) fibrous scaffolds promote MSC attachment and proliferation through provision of a 3D porous environment, showing no acute toxicity when implanted *in vivo* (Ding et al., 2014).

The improvement of the mechanical properties and/or conductivity of CNT-containing scaffolds induces higher cell adhesion, growth, differentiation, and elongation (Newman et al., 2013; Wang et al., 2014; Lin et al., 2011; Mikael et al., 2014). Moreover, incorporation of MWCNT in a scaffold has decreased the number of osteoclasts, inhibiting the resorption of bone (Abarrategi et al., 2008; Tonelli et al., 2012). Surface chemistry of CNT seems to affect the *in vivo* inflammatory response, since when incorporated in PLGA scaffolds, OH-modified MWCNT are less reactive, followed by unmodified MWCNT, with COOH-modified MWCNT exhibiting the highest response (Mikael et al., 2014). CNT were also used to substantially enhance the mechanical properties of decellularized articular cartilage (Ghassemi et al., 2017) and poly(3-hydroxybutyrate)/CS electrospun scaffolds (Karbasi and Alizadeh, 2017) while maintaining their biocompatibility.

GO incorporation in polymer matrices such as CS (Depan et al., 2011), CS/gelatin (Saravanan et al., 2017), and PCL (Kumar et al., 2015) leads to an increase in mechanical properties, protein absorption, and apatite deposition compared with neat polymers. Likewise, GBM incorporation in bioceramic matrices, such as hydroxyapatite and calcium phosphate (Wu et al., 2015), has resulted in mechanical improvements. In hydroxyapatite/rGO composites, rGO leads to an increase in fracture toughness, enabling its application for bone repair (Lee et al., 2015b) and improvement of proliferation and alkaline phosphatase activity of MSC (Nie et al., 2017). *In vivo* studies showed that these scaffolds have accelerated the healing process of circular calvarial defects in rabbits (Nie et al., 2017).

Dental Applications

DLC-coated nitinol orthodontic archwires show excellent mechanical and adhesion properties under the mechanical brushing test. Coatings significantly decrease corrosion and Ni release in degradation tests in physiological saline (Kobayashi et al., 2005).

A carbon coating produced by ion-beam deposition using C₆₀ fullerene molecules presents a unique nanocomposite structure, reduced internal stress, high adhesion to substrate, and few defects. It results in a 100–400-fold higher wear resistance compared to Co/Cr and Ti alloys, and improved biocompatibility regarding tissue regeneration, absence of necrosis, and demineralization (Penkov et al., 2016).

Some studies show GBM potential to be used as coatings to prevent bacterial adhesion and biofilm formation in dental implant material (Guazzo et al., 2018).

Composites containing diamond have been commercialized as a nanohybrid filler system (Charisma Diamond) and also as a polishing paste (DiaSheen, Couture Polishing Paste). Charisma Diamond has high strength, conferred by diamond incorporation, which allows perfect handling of this bonding material. Polishing paste containing diamonds has been shown to promote a smooth dental surface, limiting bacteria adherence and therefore preventing the development of gingivitis and periodontal disease. Gutta percha is a filler used to load root canal space that reveals poor mechanical properties, leakage, and occurrence of infection when tested in mice. However, the incorporation of amoxicillin-functionalized ND improved its mechanical performance and inhibited bacterial growth (Lee et al., 2015a).

Incorporation of FLG in poly(acrylic acid) revealed mechanical performance suitable to develop dental prostheses (Malik et al., 2018). However, it is important to point out that incorporation of GBM in polymeric matrices leads to color change, turning them gray, which could be an issue in the development of dental implants.

Neurological Applications

Due to central nervous system complexity, repairing and recovering the full function of injured nerves are authentic riddles in the tissue engineering field (Bosi et al., 2013). Neuronal scaffolds should mimic the natural structure of the nerve pathway within the brain and spinal cord, namely their physical–chemical (conductivity, porosity, and permeability), mechanical (flexibility and resistance), and biological (biocompatibility and nonimmunogenicity) properties.

Carbon materials have been revealed as promising materials, namely CNT, due to their tubular structures, which resemble natural structures such as microtubules, ion channels, and axons. Moreover, several studies have reported that electrical stimulation could improve neuronal stem cell proliferation and differentiation and boost neuronal outgrowth, which are promoted in scaffolds containing CNT and GBM.

ND- and UNCD-coated substrates have shown remarkable capacity to sustain cell attachment and neurite outgrowth, as well as to promote neuronal excitability and function (Chen et al., 2008; Erriquez et al., 2005). The topography of the ND film is an important feature to promote cell adhesion since it is much lower on flat surfaces. Moreover, UNCD presents the capacity to guide neural stem cell differentiation (Chen et al., 2009; Pradhan et al., 2006), an effect that has been associated with the capacity of NCD and UNCD films to adhere proteins at their surface, influencing the cell phenotypes (Ariano et al., 2009; Chen et al., 2013a).

Fullerene films can differentiate and develop neurons, indicating their possible application as scaffolds for neural tissue engineering (Hsieh et al., 2017; Krishnan et al., 2015).

CNT films support neuronal cell growth, increase the area of the cell body, and promote the neurite outgrowth

(Malarkey et al., 2009; Galvan-Garcia et al., 2007; Bosi et al., 2013). By controlling CNT orientation, it is possible to guide the growth of neuronal cells, as they tend to orient in the direction of the electrical signal. Moreover, neuronal cells seem to adhere preferentially to the edges of long CNT, which has been associated with their extreme flexibility (Zhang et al., 2005).

Similarly to CNT, 2D films of GBM promote cell attachment and differentiation (Bramini et al., 2018). The surface chemistry of GBM influences cell differentiation, with GO promoting a better neuronal differentiation of MSC despite its lower conductivity compared to rGO (Feng et al., 2018; Halim et al., 2018). These features are maintained in 3D free-standing GBM scaffolds (Zhang et al., 2018b). *In vivo* implantation of these scaffolds in spinal cord injury promotes partial axonal regeneration and angiogenesis without causing toxicity (Lopez-Dolado et al., 2016).

CF films containing fibers with larger diameter (>100 nm) and low surface energy are associated with poor adhesion of astrocytes. A lower adhesion and function of astrocytes leads to a decrease in glial scar tissue formation, which could facilitate neuronal regeneration (Mckenzie et al., 2004). An analogous behavior has been observed in CF/polycarbonate urethane composites (Khang et al., 2004).

Similarly to what is observed with other carbon material composites, incorporation of graphite in PCL increases electrical conductivity and roughness of base polymer showing the highest attachment and proliferation of PC12 cells (Gopinathan et al., 2016).

Composites incorporating CNT or GBM in different polymeric matrices have been developed for neuronal repair using polymers such as agarose (Lewitus et al., 2011), CS (Gupta et al., 2015; Wu et al., 2017; Kim et al., 2013a), collagen (Cho and Borgens, 2010; Ryan et al., 2018), gelatin (Wan et al., 2011), PCL (Gattazzo et al., 2015; Fan et al., 2010), collagen/PCL (Yu et al., 2014), poly(ethylene glycol) (Shah et al., 2015), poly(lactic acid) (Scapin et al., 2015), PLGA (Lee et al., 2009), poly(L-lactic acid-co-caprolactone) (Lee et al., 2009), and poly(3,4-ethylenedioxythiophene) (Tian et al., 2014), showing an increase in cell attachment, differentiation, and neurite outgrowth.

Ophthalmologic Applications

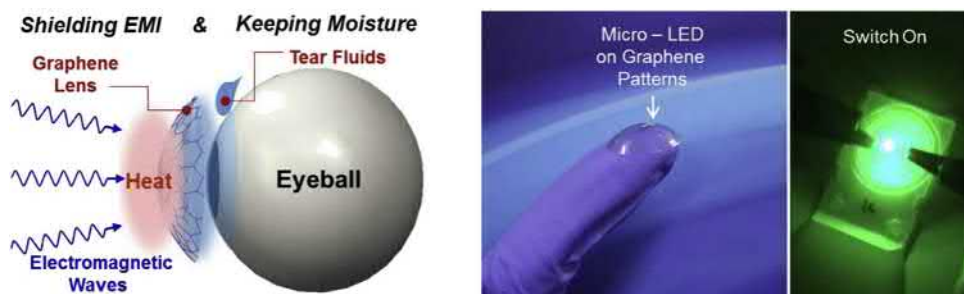
Contact Lenses

Contact lenses and contact lens cases are prone to bacterial contamination and biofilm formation. DLC thin coatings (20–200 nm) were shown to be free of any bacterial contamination after 1 year in contrast to original materials. Besides presenting antibacterial properties, DLC coatings improve biocompatibility, chemical inertness, and resistance to sterilization, as well as mechanical properties, extending poly(methyl methacrylate) lens usage time. The main disadvantage might be some light transmission reduction, whose extension depends on coating thickness (Roy and Lee, 2007; Elinson et al., 1999). Smart contact lenses based on a CVD-transferred G coating were shown to be effective at shielding electromagnetic waves, which may cause eye disease such as cataracts, as well as protecting eyes from dehydration. Also, the assembly of a functional LED on G-coated lenses was achieved (Fig. 1.3.5.20) (Lee et al., 2017).

Drug-loaded contact lenses have been developed for the treatment of ocular diseases, aiming to replace traditional eye drops and drug-soaked lenses without continuous therapeutic delivery. Timolol maleate-containing ND embedded in CS were incorporated in poly(2-hydroxyethyl methacrylate), the conventional polymer used in contact lenses, allowing a controlled release of timolol maleate (used in glaucoma treatment) in the presence of lysozyme. It was shown that ND incorporation in drug delivery systems helps to elute therapeutic compounds (Kim et al., 2014).

Catheters

DLC coatings on PU and nylon, polymers used in catheters, resulted in improved coefficient of friction, abrasion, and puncture resistance and also reduced fibrinogen adsorption, which might lead to reduced thrombogenicity (Nakagawa et al., 2009). Another study also showed that DLC coatings on a PU surface present good adhesion without delamination and prevent *C. albicans* biofilm formation (Santos et al., 2017). Double-J urethral stents were coated with DLC and tested in 10 patients with previous heavy encrustation with crystalline bacterial microfilm. The mean stent indwelling



• **Figure 1.3.5.20** Graphene-coated poly(methyl methacrylate) contact lens advantages, and working demonstrator integrating an LED. EMI, Electromagnetic interference. Adapted from (Lee et al., 2017).

time was 97 days, with no primarily stent-related complications or biofilm formation. Facile handling and less painful replacement were reported due to lower friction (Laube et al., 2007). Ureteral stents (CarboSoft) are currently commercialized by Optimed (Germany).

Silicone rubber (SR)/oxidized graphene-nanoplatelets coatings on SR revealed good surface adherence, preserving bacterial adhesion levels of silicone while increasing bacterial death to around 80%. GBM degree of oxidation and SR coating methods influenced the antibacterial properties (Gomes et al., 2018). In general, increased GBM edge exposure and oxidized state contribute to a more effective antibacterial effect (Henriques et al., 2018). GO incorporation in polyethylene, a material also used in catheter fabrication, generates a hemocompatible and bacteriostatic material (Jin et al., 2013).

Guidewires

Medical guidewires are used to introduce stents, catheters, and other medical devices through blood vessels. They are often made of stainless-steel coated with polytetrafluoroethylene or silicone rubber. These coatings can be released due to poor adhesion and are sometimes not uniform. Due to their optimal tribological properties, DLC coatings have been proposed to enhance the performance of guidewires. Studies show that DLC coatings present better adhesion to the substrate, uniformity, and lower coefficient of friction than polymer coatings and are less inflammatory and less thrombogenic than stainless steel (Dearnaley and Arps, 2005; Roy and Lee, 2007).

Other Biomedical Applications

Fullerenes present high electron accommodating capacity and strong electron-withdrawing ability. For that reason, fullerene derivatives act as free radical sponges, having the potential to be used for the treatment of diseases like diabetes, neurodegenerative disorders, atherosclerosis, and autoimmune diseases, among others where free radicals play a role in pathology (Bakry et al., 2007; Rasovic, 2017; Torres and Srdjenovic, 2011; Castro et al., 2017). Carboxyfullerenes and polyhydroxyfullerenes are the most advanced classes in current clinical and pharmaceutical research (Torres and Srdjenovic, 2011). Dendrofullerene has been shown to be as effective as FDA-approved radioprotector amifostine, preventing radiation-induced ROS in zebrafish, without causing detectable adverse effects (Daroczi et al., 2006). Several studies report that fullerenes possess immunomodulatory properties, with different functionalization eliciting either proinflammatory or immunosuppressive responses, enabling the development of therapeutic biomaterials for different goals (Torres and Srdjenovic, 2011; Castro et al., 2017).

ND increase the bioactivity of pharmaceutical formulations acting as nanocarriers and provide protection from UV light in a similar way to titanium and zinc oxide, which are used in sunscreen formulations. Even after intensive UVB irradiation, ND do not penetrate the deeper layers of the

skin, and further study of their long-term fate is still needed (van der Laan et al., 2018). After injection into mice, ND can carry and maintain the conformational stability of the antigen mussel adhesive protein, leading to antibody production (Passeri et al., 2015). Finally, ND have been found to be highly effective binding to aflatoxins, therefore they have the potential to be explored as enterosorbents for toxic substances when ingested by the oral route or for accidental spills (Schrand et al., 2009). Activated charcoal has been used for a long time in this role as a sorbent for detoxification.

GBM 2D films revealed the capacity to adhere and promote differentiation of skeletal muscle cells (Zhang et al., 2018b). Surface chemistry of these films plays a critical role in the differentiation of stem cells into skeletal muscle cells, with rGO being more efficient than G (Ahadian et al., 2014; Zhang et al., 2018b). GBM composites have improved myoblast growth and myogenic differentiation, forming multinucleated myotubes (Patel et al., 2018; Du et al., 2018; Zhang et al., 2018b).

Regarding skin tissue, 3DG foams containing MSC implanted *in vivo* in a wound promoted upregulation of neovascularization and reduced the scarring effect, revealing promise as a material for skin wound healing (Li et al., 2015b). It has also been shown that rGO/polydimethylsiloxane composite induces reepithelialization and granulation tissue formation *in vivo*, accelerating wound healing (Qian et al., 2018). Composites of PLGA/GO, CS/GO (Azarniya et al., 2016), and extracellular matrices/GO (Nyambat et al., 2018) are also being extensively studied for skin wound healing. Similarly, the incorporation of GO into CS-/polyvinylpyrrolidone-based electrospun porous membranes not only improved the mechanical properties of the resulting membranes, but also enhanced interactions with human fibroblasts, accelerating the wound healing rate on rat skins by more than 90% (Zhang et al., 2017).

Safety of Carbon Biomaterials: Short Considerations

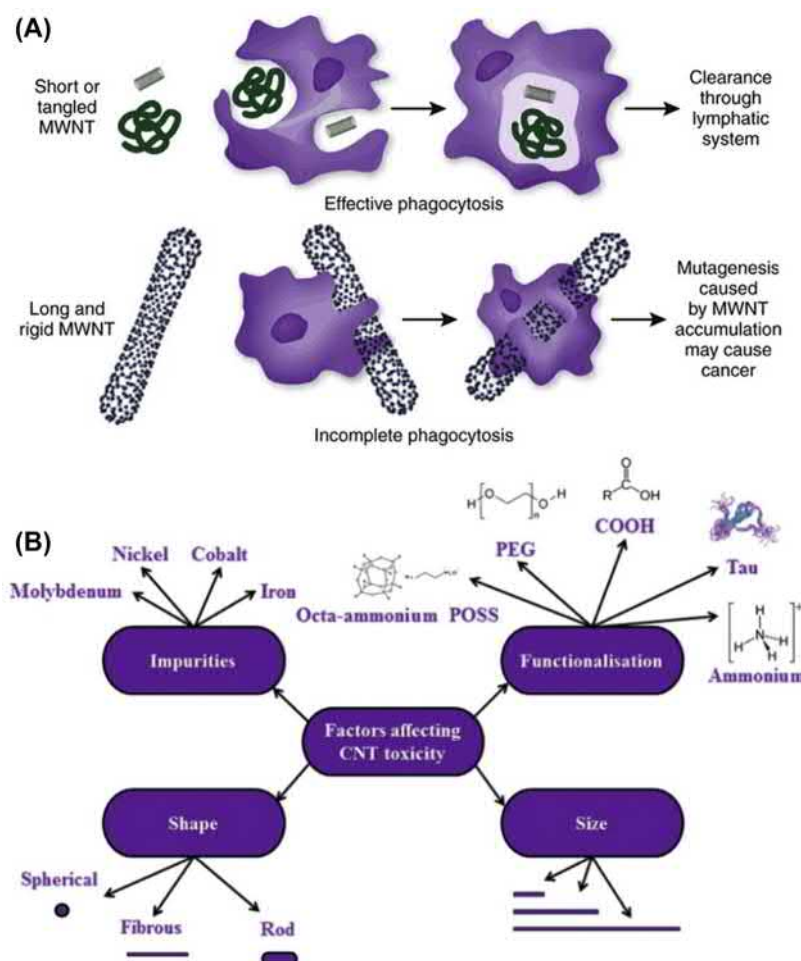
Carbon biomaterials have been used in clinics for more than 50 years. PyC containing mechanical heart valves and orthopedic implants, stents coated with PyC or DLC, and DLC-coated ventricular-assisted devices are available on the market without toxicity being reported so far. This opens the door for the development of implant material composed of or coated with other carbon material types. However, care should be taken as DLC commercial orthopedic implant failure has happened in the past. Thus long-term stability of carbon implants and coatings is paramount to prevent delamination, wear, and eventual release of toxic particles. To minimize toxicity risks, it is also important to assure proper removal of contaminants (e.g., metals, graphitic materials, solvent residues) resulting from carbon biomaterial manufacturing processes (Zhang et al., 2016). Possible mechanisms for carbon nanomaterials toxicity have been proposed, including damage to membrane integrity, lipid and protein destabilization and oxidation, cell damage via

ROS, and release of metal ions (Chen and Wang, 2016). However, different carbon materials and their derivatives vary substantially (e.g., carbon structure, carbon number, size, thickness, charge, aggregation, degree of functionality) and can be altered *in vivo*. Therefore individual characterization is advisable over results extrapolation (Dellinger et al., 2013; Zhang et al., 2016).

FDA guidance documents on the application of nanotechnology products state that the specific characteristics and effects of nanomaterials in the particular biological context of each product and its intended use should be assessed. The International Agency for Research on Cancer released a report mentioning that only certain types of rigid MWCNT can be classified as being possibly carcinogenic to humans (Bengt Fadeel et al., 2018). Despite CNT being the carbon biomaterial generally raising more toxicity issues, they can be designed to improve biocompatibility and be biodegradable and body clearable (Fig. 1.3.5.21). Besides their dimensions, other concerns should be taken into consideration when it comes to the safety of CNT, such as preventing

aggregation and increasing their solubility, which makes excretion easier, preventing accumulation. Similar strategies can be applied to other carbon biomaterials.

GO and graphene showed potential to be degraded by active molecules present in blood plasma (e.g., $\bullet\text{OH}$ and $\bullet\text{O}_2$) being the degradation rate higher for GO since these molecules attack oxygen-containing groups (Li et al., 2019). GO has also been reported to be intra- and extracellularly degradable by immune system cells. Degradation of graphene with lateral size < 200 nm was also reported *in vivo* (Girish et al., 2018). GO generally elicits less lung toxicity than certain CNT. However, reports on toxicity towards neural cells have been made. Therefore further study is needed on GBM toxicity (Bengt Fadeel et al., 2018). Most fullerenes are usually not toxic unless photoexcited or used at very high concentrations, which is hard to achieve in the environment or during therapy. However, some reports on inflammation and genotoxicity have been found, raising some concerns about their use (Singh and Nalwa, 2007; Rasovic, 2017). Well-purified and dispersed ND are better tolerated by cells than



• **Figure 1.3.5.21** Factors affecting carbon nanotube (CNT) toxicity and elimination. (A) Illustration showing how the structure of CNT can affect phagocytosis by macrophages and tissue clearance. Low aspect ratio multiwalled carbon nanotubes (MWCNT) can be engulfed by macrophages, while it is not the case with high aspect ratio MWCNT. (B) Schematic illustration of the factors affecting CNT toxicity (Alshehri et al., 2016). PEG, poly(ethylene glycol); POSS, polyhedral oligomeric silsesquioxane.

fullerenes or CNT. They have proven to be generally biocompatible in several *in vivo* studies. However, inflammation, embryotoxicity, and teratogenicity reports have been made, therefore detailed study is needed on those subjects for each newly designed ND-based biomaterial (Zhang et al., 2016). When administered through different routes, CD are readily cleared out of mice through the renal route, with no detectable toxicity, due to being small and biodegradable. However, a more comprehensive toxicological evaluation is still needed on this carbon biomaterial class (Chen and Wang, 2016).

Carbon nanomaterials have become the most common nanoproducts according to “The Nanotechnology Consumer Products Inventory.” Their production, use, and disposal inevitably lead to environmental release (Chen and Wang, 2016). Therefore biocompatibility evaluation is pertinent not only in the context of their incorporation in biomaterials, but also regarding environmental exposition.

Summary

The different forms of carbon biomaterials differ in crystallinity, dimension, and carbon hybridization. This variation, along with their different physical–chemical properties, allows a wide range of biomedical applications.

PyC and DLC are both amorphous forms of carbon, being applied as coatings for biomedical devices. PyC has been used for more than 50 years in commercially available MHV and orthopedic implants, due to its outstanding mechanical, tribological, and hemocompatibility properties. PyC- and DLC-coated vascular stents and DLC-coated urethral stents and VAD are also currently marketed. Coatings with other carbon biomaterials such as DLC, NCD, UNCD, fullerenes, CNT, and GBM are under investigation for MHV, orthopedic implants, catheters, contact lenses, oral implant guidewires, biosensors, neuronal tissue engineering, and antimicrobial materials.

The hexagonally bonded carbons - fullerenes, CNT, GBM, and CF - are also being investigated for use as free-standing films or scaffolds in bone implants, antimicrobial materials, skin wound healing, and cardiac, bone, neuronal, and muscle tissue-engineering approaches.

Carbon materials can also be combined with polymers, ceramics, or metals to produce composites with improved biocompatibility and/or mechanical, conductive, and antimicrobial properties. ND-containing dental fillers and polishing pastes are already commercialized, as well as a wide variety of PEEK/CF composite orthopedic implants for joint replacement. Along with ND and CF; G, fullerenes, CNT, GBM, or CD/GQD are under research for use as MHV, biosensors, orthopedic implants, drug delivery systems, antimicrobial materials, contact lenses, skin wound healing, and different tissue-engineering applications (cardiac, bone, cartilage, neuronal, and muscle).

Due to their small size, radiation absorption properties, large surface area, and tunable surface properties, carbon biomaterials can also be used for bioapplications in the form of micro/nanocolloids. Fullerenes, CNT, and

CD/GQD are applied to drug delivery, imaging, PTT and PDT, and antimicrobial applications. These uses are also under investigation using ND and GBM, except for ND-based phototherapy (poor radiation absorption) and GBM-based imaging (low quantum yield). Additionally, fullerenes have also been applied in sunscreen formulations.

Besides the successful use of some carbon biomaterials in commercially available products, new materials and many applications have arisen in the past years and therefore toxicological studies are still lacking to guaranty their safety and to reach the market.

References

- Abarrategi, A., Gutierrez, M.C., Moreno-Vicente, C., Hortiguera, M.J., Ramos, V., Lopez-Lacomba, J.L., Ferrer, M.L., Del Monte, F., 2008. Multiwall carbon nanotube scaffolds for tissue engineering purposes. *Biomaterials* 29, 94–102.
- Agarwal, R., Garcia, A.J., 2015. Biomaterial strategies for engineering implants for enhanced osseointegration and bone repair. *Adv. Drug Deliv. Rev.* 94, 53–62.
- Ahadian, S., Ramón-Azcón, J., Chang, H., Liang, X., Kaji, H., Shiku, H., Nakajima, K., Ramalingam, M., Wu, H., Matsue, T., Khademhosseini, A., 2014. Electrically regulated differentiation of skeletal muscle cells on ultrathin graphene-based films. *RSC Adv.* 4, 9534–9541.
- Ahadian, S., Yamada, S., Ramon-Azcon, J., Estili, M., Liang, X., Nakajima, K., Shiku, H., Khademhosseini, A., Matsue, T., 2016. Hybrid hydrogel-aligned carbon nanotube scaffolds to enhance cardiac differentiation of embryoid bodies. *Acta Biomater.* 31, 134–143.
- Akhavan, O., Azimirad, R., Safa, S., 2011. Functionalized carbon nanotubes in ZnO thin films for photoinactivation of bacteria. *Mater. Chem. Phys.* 130, 598–602.
- Akhavan, O., Ghaderi, E., Shahsavari, M., 2013. Graphene nanogrids for selective and fast osteogenic differentiation of human mesenchymal stem cells. *Carbon* 59, 200–211.
- Al Awak, M.M., Wang, P., Wang, S.Y., Tang, Y.A., Sun, Y.P., Yang, L.J., 2017. Correlation of carbon dots' light-activated antimicrobial activities and fluorescence quantum yield. *RSC Adv.* 7, 30177–30184.
- Al-Jumaili, A., Alancherry, S., Bazaka, K., Jacob, M.V., 2017. Review on the antimicrobial properties of carbon nanostructures. *Materials* 10 (9), 1052–1066.
- Alshehri, R., Ilyas, A.M., Hasan, A., Arnaout, A., Ahmed, F., Memci, A., 2016. Carbon nanotubes in biomedical applications: factors, mechanisms, and remedies of toxicity. *J. Med. Chem.* 59, 8149–8167.
- An, X.L., Ma, H.B., Liu, B., Wang, J.Z., 2013. Graphene oxide reinforced polylactic acid/polyurethane antibacterial composites. *J. Nanomater.* 2013, 7.
- Annabi, N., Shin, S.R., Tamayol, A., Miscuglio, M., Bakooshli, M.A., Assmann, A., Mostafalu, P., Sun, J.Y., Mithieux, S., Cheung, L., Tang, X.S., Weiss, A.S., Khademhosseini, A., 2016. Highly elastic and conductive human-based protein hybrid hydrogels. *Adv. Mater.* 28, 40–49.
- Ariano, P., Budnyk, O., Dalmazzo, S., Lovisolò, D., Manfredotti, C., Rivolo, P., Vittone, E., 2009. On diamond surface properties and interactions with neurons. *Eur. Phys. J. E Soft Matter* 30, 149–156.
- Aryal, N., Halder, A., Zhang, M., Whelan, P.R., Tremblay, P.L., Chi, Q., Zhang, T., 2017. Freestanding and flexible graphene papers as

- bioelectrochemical cathode for selective and efficient CO₂ conversion. *Sci. Rep.* 7, 9107.
- Aslan, S., Loebick, C.Z., Kang, S., Elimelech, M., Pfeifferle, L.D., Van Tassel, P.R., 2010. Antimicrobial biomaterials based on carbon nanotubes dispersed in poly(lactic-co-glycolic acid). *Nanoscale* 2, 1789–1794.
- Azarniya, A., Eslahi, N., Mahmoudi, N., Simchi, A., 2016. Effect of graphene oxide nanosheets on the physico-mechanical properties of chitosan/bacterial cellulose nanofibrous composites. *Compos. Appl. Sci. Manuf.* 85, 113–122.
- Bacakova, L., Kopova, I., Stankova, L., Liskova, J., Vacik, J., Lavrentiev, V., Kromka, A., Potocky, S., Stranska, D., 2014. Bone cells in cultures on nanocarbon-based materials for potential bone tissue engineering: a review. *Phys. Status Solidi A* 211, 2688–2702.
- Bakry, R., Vallant, R.M., Najam-Ul-Haq, M., Rainer, M., Szabo, Z., Huck, C.W., Bonn, G.K., 2007. Medicinal applications of fullerenes. *Int. J. Nanomed.* 2, 639–649.
- Bellemere, P., 2018. Pyrocarbon implants for the hand and wrist. *Hand Surg. Rehabil.* 37, 129–154.
- Bengt Fadeel, C.B., Merino, S., Vázquez, E., Flahaut, E., Mouchet, F., Evariste, L., Gauthier, L., Koivisto, A.J., Vogel, U., Martín, C., Delogu, L.G., Buerki-Thurnherr, T., Wick, P., Beloin-Saint-Pierre, D., Hischier, R., Pelin, M., Carniel, F.C., Tretiach, M., Cesca, E., Benfenati, F., Scaini, D., Ballerini, L., Kostarelos, K., Prato, M., Bianco, A., 2018. Safety assessment of graphene-based materials: focus on human health and the environment. *ACS Nano* 12, 10582–10620.
- Beranova, J., Seydlova, G., Kozak, H., Benada, O., Fiser, R., Artemenko, A., Konopasek, I., Kromka, A., 2014. Sensitivity of bacteria to diamond nanoparticles of various size differs in gram-positive and gram-negative cells. *FEMS Microbiol. Lett.* 351, 179–186.
- Bing, W., Sun, H.J., Yan, Z.Q., Ren, J.S., Qu, X.G., 2016. Programmed bacteria death induced by carbon dots with different surface charge. *Small* 12, 4713–4718.
- Bohem, R.D., Jin, C., Narayan, R.J., 2011. Carbon and diamond. In: Ducheyne, P. (Ed.), *Comprehensive Biomaterials*. Elsevier.
- Bosi, S., Ballerini, L., Prato, M., 2013. Carbon nanotubes in tissue engineering. In: Marcaccio, M., Paolucci, F. (Eds.), *Making and Exploiting fullerenes, graphene, and carbon nanotubes*. Springer.
- Bramini, M., Alberini, G., Colombo, E., Chiacchiarretta, M., Difrancesco, M.L., Maya-Vetencourt, J.F., Maragliano, L., Benfenati, F., Cesca, F., 2018. Interfacing graphene-based materials with neural cells. *Front. Syst. Neurosci.* 12, 12.
- Castro, E., Garcia, A.H., Zavala, G., Echegoyen, L., 2017. Fullerenes in biology and medicine. *J. Mater. Chem. B* 5, 6523–6535.
- Catledge, S.A., Thomas, V., VOHRA, Y.K., 2013. Nanostructured diamond coatings for orthopaedic applications. In: Narayan, R. (Ed.), *Diamond-based Materials for Biomedical Applications*. Woodhead Publishing, Cambridge, UK.
- Chaudhary, R., Garg, J., Krishnamoorthy, P., Shah, N., Feldman, B.A., Martinez, M.W., Freudenberg, R., 2017. On-x valve the next generation aortic valve. *Cardiol. Rev.* 25, 77–83.
- Chen, Y.C., Lee, D.C., Tai, N.H., Chiu, I.M., 2013a. Ultrananocrystalline diamond (UNCD) for neural applications. In: Narayan, R. (Ed.), *Diamond-based materials for biomedical applications*. Woodhead Publishing.
- Chen, Y., Zhang, T.H., Gan, C.H., Yu, G., 2007. Wear studies of hydroxyapatite composite coating reinforced by carbon nanotubes. *Carbon* 45, 998–1004.
- Chen, Y.C., Zhong, X.Y., Konicek, A.R., Grierson, D.S., Tai, N.H., Lin, I.N., Kabius, B., Hiller, J.M., Sumant, A.V., Carpick, R.W., Auciello, O., 2008. Synthesis and characterization of smooth ultrananocrystalline diamond films via low pressure bias-enhanced nucleation and growth. *Appl. Phys. Lett.* 92, 133113.
- Chen, Y.C., Lee, D.C., Hsiao, C.Y., Chung, Y.F., Chen, H.C., Thomas, J.P., Pong, W.F., Tai, N.H., Lin, I.N., Chiu, I.M., 2009. The effect of ultra-nanocrystalline diamond films on the proliferation and differentiation of neural stem cells. *Biomaterials* 30, 3428–3435.
- Chen, D., Wang, Q., Jin, J., Wu, P., Wang, H., Yu, S., Zhang, H., Cai, C., 2010. Low-potential detection of endogenous and physiological uric acid at uricase-thionine-single-walled carbon nanotube modified electrodes. *Anal. Chem.* 82, 2448–2455.
- Chen, Z.Y., Ma, L.J., Liu, Y., Chen, C.Y., 2012. Applications of functionalized fullerenes in tumor theranostics. *Theranostics* 2, 238–250.
- Chen, H.Q., Wang, B., Gao, D., Guan, M., Zheng, L.N., Ouyang, H., Chai, Z.F., Zhao, Y.L., Feng, W.Y., 2013b. Broad-spectrum antibacterial activity of carbon nanotubes to human gut bacteria. *Small* 9, 2735–2746.
- Chen, C., Wang, H., 2016. *Biomedical applications and toxicology of carbon nanomaterials*. Wiley, Germany.
- Chen, W.F., Lv, G., Hu, W.M., Li, D.J., Chen, S.N., Dai, Z.X., 2018. Synthesis and applications of graphene quantum dots: a review. *Nanotechnol. Rev.* 7, 157–185.
- Cho, Y., Borgens, R.B., 2010. The effect of an electrically conductive carbon nanotube/collagen composite on neurite outgrowth of PC12 cells. *J. Biomed. Mater. Res. A* 95, 510–517.
- Choi, H.Y., Lee, T.J., Yang, G.M., Oh, J., Won, J., Han, J., Jeong, G.J., Kim, J., Kim, J.H., Kim, B.S., Cho, S.G., 2016. Efficient mRNA delivery with graphene oxide-polyethylenimine for generation of footprint-free human induced pluripotent stem cells. *J. Control. Release* 235, 222–235.
- Crowder, S.W., Liang, Y., Rath, R., Park, A.M., Maltais, S., Pintauro, P.N., Hofmeister, W., Lim, C.C., Wang, X., Sung, H.-J., 2013a. Poly(*ε*-caprolactone)-carbon nanotube composite scaffolds for enhanced cardiac differentiation of human mesenchymal stem cells. *Nanomedicine* 8, 1763–1776.
- Crowder, S.W., Prasai, D., Rath, R., Balikov, D.A., Bae, H., Bolotin, K.I., Sung, H.J., 2013b. Three-dimensional graphene foams promote osteogenic differentiation of human mesenchymal stem cells. *Nanoscale* 5, 4171–4176.
- Daroczi, B., Kari, G., Mcaleer, M.F., Wolf, J.C., Rodeck, U., Dicker, A.P., 2006. In vivo radioprotection by the fullerene nanoparticle DF-1 as assessed in a zebrafish model. *Clin. Cancer Res.* 12, 7086–7091.
- De, B., Gupta, K., Mandal, M., Karak, N., 2015. Biocide immobilized OMMT-carbon dot reduced Cu₂O nano-hybrid/hyperbranched epoxy nanocomposites: mechanical, thermal, antimicrobial and optical properties. *Mater. Sci. Eng. C Mater. Biol. Appl.* 56, 74–83.
- Dearnaley, G., Arps, J.H., 2005. Biomedical applications of diamond-like carbon (DLC) coatings: a review. *Surf. Coat. Technol.* 200, 2518–2524.
- Dellinger, A., Zhou, Z.G., Connor, J., Madhankumar, A.B., Pamujula, S., Sayes, C.M., Kepley, C.L., 2013. Application of fullerenes in nanomedicine: an update. *Nanomedicine* 8, 1191–1208.
- Deokar, A.R., Lin, L.Y., Chang, C.C., Ling, Y.C., 2013. Single-walled carbon nanotube coated antibacterial paper: preparation and mechanistic study. *J. Mater. Chem. B* 1, 2639–2646.
- Depan, D., Girase, B., Shah, J.S., Misra, R.D., 2011. Structure-property relationship of the polar graphene oxide-mediated cellular response and stimulated growth of osteoblasts on hybrid chitosan network structure nanocomposite scaffolds. *Acta Biomater.* 7, 3432–3445.

- DIEZ-Pascual, A.M., Naffakh, M., Gomez, M.A., Marco, C., Ellis, G., Martinez, M.T., Anson, A., Gonzalez-Dominguez, J.M., Martinez-Rubi, Y., Simard, B., 2009. Development and characterization of PEEK/carbon nanotube composites. *Carbon* 47, 3079–3090.
- Ding, Y., Liu, J., Jin, X., Lu, H., Shen, G., Yu, R., 2008. Poly-L-lysine/hydroxyapatite/carbon nanotube hybrid nanocomposite applied for piezoelectric immunoassay of carbohydrate antigen 19-9. *Analyst* 133, 184–190.
- Ding, Q.X., Liao, J.F., Yang, Y., Qu, Y., Peng, J.R., Fan, M., Luo, F., Qian, Z.Y., 2014. Preparation and characterization of epoxidized methyl oleate-graphite oxide/poly(L-lactide) electrospun hybrid fibrous scaffolds for tissue engineering applications. *Sci. Adv. Mater.* 6, 1769–1777.
- Dizaj, S.M., Mennati, A., Jafari, S., Khezri, K., Adibkia, K., 2015. Antimicrobial activity of carbon-based nanoparticles. *Adv. Pharmaceut. Bull.* 5, 19–23.
- Dong, Y.Q., Wu, H., Shang, P.X., Zeng, X.T., Chi, Y.W., 2015. Immobilizing water-soluble graphene quantum dots with gold nanoparticles for a low potential electrochemiluminescence immunosensor. *Nanoscale* 7, 16366–16371.
- Du, Y., Ge, J., Li, Y., Ma, P.X., Lei, B., 2018. Biomimetic elastomeric, conductive and biodegradable polycitrate-based nanocomposites for guiding myogenic differentiation and skeletal muscle regeneration. *Biomaterials* 157, 40–50.
- Ducheyne, P., 2011, *Comprehensive Biomaterials*. Elsevier.
- Duong, H.M., Fan, Z., Nguyen, S.T., 2016. Graphene/carbon nanotube Aerogels. In: Sattler, K.D. (Ed.), *Carbon Nanomaterials Source Book*.
- Elinson, V.M., Sleptsov, V.V., Laymin, A.N., Potraysay, V.V., Kostuychenko, L.N., Moussina, A.D., 1999. Barrier properties of carbon films deposited on polymer-based devices in aggressive environments. *Diam. Relat. Mater.* 8, 2103–2109.
- Erriquez, J., Gilardino, A., Ariano, P., Munaron, L., Lovisolò, D., Distasi, C., 2005. Calcium signals activated by arachidonic acid in embryonic chick ciliary ganglion neurons. *Neurosignals* 14, 244–254.
- Fan, H., Wang, L., Zhao, K., Li, N., Shi, Z., Ge, Z., Jin, Z., 2010. Fabrication, mechanical properties, and biocompatibility of graphene-reinforced chitosan composites. *Biomacromolecules* 11, 2345–2351.
- Feng, Z.Q., Yan, K., Shi, C., Xu, X., Wang, T., Li, R., Dong, W., Zheng, J., 2018. Neurogenic differentiation of adipose derived stem cells on graphene-based mat. *Mater. Sci. Eng. C Mater. Biol. Appl.* 90, 685–692.
- Fox, K., Palamara, J., Judge, R., Greentree, A.D., 2013. Diamond as a scaffold for bone growth. *J. Mater. Sci. Mater. Med.* 24, 849–861.
- Galvan-Garcia, P., Keefer, E.W., Yang, F., Zhang, M., Fang, S., Zakhidov, A.A., Baughman, R.H., Romero, M.I., 2007. Robust cell migration and neuronal growth on pristine carbon nanotube sheets and yarns. *J. Biomater. Sci. Polym. Ed.* 18, 1245–1261.
- Garcia-Elias, M., 2007. Eclipse: Partial Ulnar Head Replacement for the Isolated Distal Radio-ulnar Joint Arthritis. *Techniques in Hand and Upper Extremity Surgery* 11, 121–128.
- Gattazzo, F., De Maria, C., Whulanza, Y., Taverni, G., Ahluwalia, A., Vozzi, G., 2015. Realisation and characterization of conductive hollow fibers for neuronal tissue engineering. *J. Biomed. Mater. Res. B Appl. Biomater.* 103, 1107–1119.
- Geim, A.K., Novoselov, K.S., 2007. The rise of graphene. *Nat. Mater.* 6, 183–191.
- Georgakilas, V., Perman, J.A., Tucek, J., Zboril, R., 2015. Broad family of carbon nanoallotropes: classification, chemistry, and applications of fullerenes, carbon dots, nanotubes, graphene, nanodiamonds, and combined superstructures. *Chem. Rev.* 115, 4744–4822.
- Ghassemi, T., Saghatolslami, N., Matin, M.M., Gheshlaghi, R., Moradi, A., 2017. CNT-decellularized cartilage hybrids for tissue engineering applications. *Biomed. Mater.* 12, 065008.
- Girish, C.M., Sasidharan, A., Gowd, G.S., Nair, S., Koyakutty, M., 2018. Confocal Raman imaging study showing macrophage mediated biodegradation of graphene in vivo. *Adv. Healthc. Mater.* 11, 1489–1500.
- Gomes, R.N., Borges, I., Pereira, A.T., Maia, A.E., Pestana, M., Magalhaes, F.D., Pinto, A.M., Goncalves, I.C., 2018. Antimicrobial graphene nanoplatelets coatings for silicone catheters. *Carbon* 139, 635–647.
- Gong, F., Li, H., Wang, W.B., Xia, D.W., Liu, Q.M., Papavassiliou, D.V., Xu, Z.Q., 2018. Recent advances in graphene-based free-standing films for thermal management: synthesis, properties, and applications. *Coatings* 8 (2), 63.
- Gopinathan, J., Quigley, A.F., Bhattacharyya, A., Padhye, R., Kapsa, R.M., Nayak, R., Shanks, R.A., Houshyar, S., 2016. Preparation, characterisation, and in vitro evaluation of electrically conducting poly(varepsilon-caprolactone)-based nanocomposite scaffolds using PC12 cells. *J. Biomed. Mater. Res. A* 104, 853–865.
- Gorain, B., Choudhury, H., Pandey, M., Kesharwani, P., Abeer, M.M., Tekade, R.K., Hussain, Z., 2018. Carbon nanotube scaffolds as emerging nanoplatform for myocardial tissue regeneration: a review of recent developments and therapeutic implications. *Biomed. Pharmacother.* 104, 496–508.
- Gott, V.L., Alejo, D.E., Cameron, D.E., 2003. Mechanical heart valves: 50 years of evolution. *Ann. Thorac. Surg.* 76, S2230–S2239.
- Grausova, L., Kromka, A., Bacakova, L., Potocky, S., Vanecek, M., Lisa, V., 2008. Bone and vascular endothelial cells in cultures on nanocrystalline diamond films. *Diam. Relat. Mater.* 17, 1405–1409.
- Grausova, L., Bacakova, L., Kromka, A., Potocky, S., Vanecek, M., Nesladek, M., Lisa, V., 2009. Nanodiamond as promising material for bone tissue engineering. *J. Nanosci. Nanotechnol.* 9, 3524–3534.
- Grumezescu, A., (Ed.), 2018. *Fullerenes, Graphenes and Nanotubes: A Pharmaceutical Approach*. Elsevier, UK, p.724, 489.
- Guazzo, R., Gardin, C., Bellin, G., Sbricoli, L., Ferroni, L., Ludovichi, F.S., Piattelli, A., Antoniac, I., Bressan, E., Zavan, B., 2018. Graphene-based nanomaterials for tissue engineering in the dental field. *Nanomaterials* 8.
- Gupta, P., Sharan, S., Roy, P., Lahiri, D., 2015. Aligned carbon nanotube reinforced polymeric scaffolds with electrical cues for neural tissue regeneration. *Carbon* 95, 715–724.
- Gurunathan, S., Han, J.W., Dayem, A.A., Eppakayala, V., Kim, J.H., 2012. Oxidative stress-mediated antibacterial activity of graphene oxide and reduced graphene oxide in *Pseudomonas aeruginosa*. *Int. J. Nanomed.* 7, 5901–5914.
- Halim, A., Luo, Q., Ju, Y., Song, G., 2018. A mini review focused on the recent applications of graphene oxide in stem cell growth and differentiation. *Nanomaterials* 8.
- Hasirci, V., Hasirci, N., 2018. Carbon as a biomaterial. In: Hasirci, V., Hasirci, N. (Eds.), *Fundamentals of Biomaterials*. Springer.
- Haubold, A.D., More, R.B., Bokros, J.C., 2016. *Carbons*. In: Murphy, W., Black, J., Hastings, G. (Eds.), *Handbook of Biomaterial Properties*.
- Henriques, P.C., Borges, I., Pinto, A.M., Magalhaes, F.D., Goncalves, I.C., 2018. Fabrication and antimicrobial performance of surfaces integrating graphene-based materials. *Carbon* 132, 709–732.

- Hossain, M.A., Elias, M., Sarker, D.R., Diba, Z.R., Mithun, J.M., Azad, M.A.K., Siddiquey, I.A., Rahman, M.M., Uddin, J., Uddin, M.N., 2018. Synthesis of Fe- or Ag-doped TiO₂-MWCNT nanocomposite thin films and their visible-light-induced catalysis of dye degradation and antibacterial activity. *Res. Chem. Intermed.* 44, 2667–2683.
- Hou, W.X., Toh, T.B., Abdullah, L.N., Yvonne, T.W.Z., Lee, K.J., Guenther, I., Chow, E.K.H., 2017. Nanodiamond-Manganese dual mode MRI contrast agents for enhanced liver tumor detection. *Nanomed. Nanotechnol. Biol. Med.* 13, 783–793.
- Hsieh, F.Y., Shrestha, L.K., Ariga, K., Hsu, S.H., 2017. Neural differentiation on aligned fullerene C60 nanowhiskers. *Chem. Commun. (Camb)* 53, 11024–11027.
- Hu, Z., Li, J., Huang, Y.D., Chen, L., Li, Z.H., 2015. Functionalized graphene/C-60 nanohybrid for targeting photothermally enhanced photodynamic therapy. *RSC Adv.* 5, 654–664.
- Huang, L.Y., Wang, M., Dai, T.H., Sperandio, F.F., Huang, Y.Y., Xuan, Y., Chiang, L.Y., Hamblin, M.R., 2014. Antimicrobial photodynamic therapy with decacationic monoadducts and bisadducts of [70] fullerene: in vitro and in vivo studies. *Nanomedicine* 9, 253–266.
- Jackson, P., Jacobsen, N.R., Baun, A., Birkedal, R., Kuhnel, D., Jensen, K.A., Vogel, U., Wallin, H., 2013. Bioaccumulation and ecotoxicity of carbon nanotubes. *Chem. Cent. J.* 7.
- Jhonsi, M.A., Ananth, D.A., Nambirajan, G., Sivasudha, T., Yamini, R., Bera, S., Kathiravan, A., 2018. Antimicrobial activity, cytotoxicity and DNA binding studies of carbon dots. *Spectrochim. Acta A Mol. Biomol. Spectrosc.* 196, 295–302.
- Jin, S., Xu, D., Zhou, N., Yuan, J., Shen, J., 2013. Antibacterial and anticoagulation properties of polyethylene/geneO-MPC nanocomposites. *J. Appl. Polym. Sci.* 129, 884–891.
- Jing, X., Mi, H.Y., Napiwocki, B.N., Peng, X.F., Turng, L.S., 2017. Mussel-inspired electroactive chitosan/graphene oxide composite hydrogel with rapid self-healing and recovery behavior for tissue engineering. *Carbon* 125, 557–570.
- Jing, X., Mi, H.Y., Salick, M.R., Cordie, T.M., Peng, X.F., Turng, L.S., 2015. Electrospinning thermoplastic polyurethane/graphene oxide scaffolds for small diameter vascular graft applications. *Mater. Sci. Eng. C Mater. Biol. Appl.* 49, 40–50.
- Kaar, T.K., Fraher, J.P., Brady, M.P., 1998. A quantitative study of articular repair in the Guinea pig. *Clin. Orthop. Relat. Res.* 228–243.
- Karbasi, S., Alizadeh, Z.M., 2017. Effects of multi-wall carbon nanotubes on structural and mechanical properties of poly(3-hydroxybutyrate)/chitosan electrospun scaffolds for cartilage tissue engineering. *Bull. Mater. Sci.* 40, 1247–1253.
- Kaur, R., Badea, I., 2013. Nanodiamonds as novel nanomaterials for biomedical applications: drug delivery and imaging systems. *Int. J. Nanomed.* 8, 203–220.
- Kessler, M.W., Grande, D.A., 2008. Tissue engineering and cartilage. *Organogenesis* 28–32.
- Khan, M.S., Abdelhamid, H.N., Wu, H.F., 2015. Near infrared (NIR) laser mediated surface activation of graphene oxide nanoflakes for efficient antibacterial, antifungal and wound healing treatment. *Colloid Surf. B Biointer.* 127, 281–291.
- Khang, D., McKenzie, J.L., Webster, T.J., 2004. Carbon nanofibers: polycarbonate urethane composites' as a neural biomaterial. In: *Proceedings of the IEEE 30th Annual Northeast Bioengineering Conference*, pp. 241–242.
- Kheradvar, A., Groves, E.M., Goergen, C.J., Alavi, S.H., Tranquillo, R., Simmons, C.A., Dasi, L.P., Grande-Allen, K.J., Mofrad, M.R.K., Falahatpisheh, A., Griffith, B., Baaijens, F., Little, S.H., Canic, S., 2015. Emerging trends in heart valve engineering: Part II. Novel and standard technologies for aortic valve replacement. *Ann. Biomed. Eng.* 43, 844–857.
- Kim, J., Kim, Y.R., Kim, Y., Lim, K.T., Seonwoo, H., Park, S., Cho, S.P., Hong, B.H., Choung, P.H., Chung, T.D., Choung, Y.H., Chung, J.H., 2013a. Graphene-incorporated chitosan substrata for adhesion and differentiation of human mesenchymal stem cells. *J. Mater. Chem. B* 1, 933–938.
- Kim, T., Kahng, Y.H., Lee, T., Lee, K., Kim, D.H., 2013b. Graphene films show stable cell attachment and biocompatibility with electrogenic primary cardiac cells. *Mol. Cells* 36, 577–582.
- Kim, H.J., Zhang, K.Y., Moore, L., Ho, D., 2014. Diamond nanogel-embedded contact lenses mediate lysozyme-dependent therapeutic release. *ACS Nano* 8, 2998–3005.
- King, A.A.K., Matta-Domjan, B., Large, M.J., Matta, C., Ogilvie, S.P., Bardi, N., Byrne, H.J., Zakhidov, A., Jurewicz, I., Velliou, E., Lewis, R., La Ragione, R., Dalton, A.B., 2017. Pristine carbon nanotube scaffolds for the growth of chondrocytes. *J. Mater. Chem. B* 5, 8178–8182.
- Kobayashi, S., Ohgoe, Y., Ozeki, K., Gei, L., Hirakuri, K.K., Aoki, H., 2005. Biocompatibility of diamond-like carbon coated NiTi orthodontic wire and acrylic resin teeth. *Bioceramics* 17 (284–286), 783–786.
- Kong, H.X., 2013. Hybrids of carbon nanotubes and graphene/graphene oxide. *Curr. Opin. Solid State Mater. Sci.* 17, 31–37.
- Korkala, O., Syrjanen, K.J., 1998. Intrapelvic cyst formation after hip arthroplasty with a carbon fibre-reinforced polyethylene socket. *Arch. Orthop. Trauma. Surg.* 118, 113–115.
- Krishna, V., Singh, A., Sharma, P., Iwakuma, N., Wang, Q., Zhang, Q., Knapik, J., Jiang, H., Grobmyer, S.R., Koopman, B., Moudgil, B., 2010. Polyhydroxy fullerenes for non-invasive cancer imaging and therapy. *Small* 6, 2236–2241.
- Krishnan, V., Kasuya, Y., Ji, Q., Sathish, M., Shrestha, L.K., Ishihara, S., Minami, K., Morita, H., Yamazaki, T., Hanagata, N., Miyazawa, K., Acharya, S., Nakanishi, W., Hill, J.P., Ariga, K., 2015. Vortex-aligned fullerene nanowhiskers as a scaffold for orienting cell growth. *ACS Appl. Mater. Interfaces* 7, 15667–15673.
- Kroustalli, A., Zisimopoulou, A.E., Koch, S., Rongen, L., Deligianni, D., Diamantouros, S., Athanassiou, G., Kokozidou, M., Mavrilas, D., Jockenhoevel, S., 2013. Carbon nanotubes reinforced chitosan films: mechanical properties and cell response of a novel biomaterial for cardiovascular tissue engineering. *J. Mater. Sci. Mater. Med.* 24, 2889–2896.
- Kumar, S., Raj, S., Kolanthai, E., Sood, A.K., Sampath, S., Chatterjee, K., 2015. Chemical functionalization of graphene to augment stem cell osteogenesis and inhibit biofilm formation on polymer composites for orthopedic applications. *ACS Appl. Mater. Interfaces* 7, 3237–3252.
- Kumar, S., Rani, R., Dilbaghi, N., Tankeshwar, K., Kim, K.H., 2017. Carbon nanotubes: a novel material for multifaceted applications in human healthcare. *Chem. Soc. Rev.* 46, 158–196.
- Kurtz, S.M., Muratoglu, O.K., Evans, M., Edidin, A.A., 1999. Advances in the processing, sterilization, and crosslinking of ultra-high molecular weight polyethylene for total joint arthroplasty. *Biomaterials* 20, 1659–1688.
- Laube, N., Kleinen, L., Bradenahl, J., Meissner, A., 2007. Diamond-like carbon coatings on ureteral stents - a new strategy for decreasing the formation of crystalline bacterial biofilms? *J. Urol.* 177, 1923–1927.
- Lee, H.J., Yoon, O.J., Kim, D.H., Jang, Y.M., Kim, H.W., Lee, W.B., Lee, N.E., Kim, S.S., 2009. Neurite outgrowth on nanocomposite scaffolds synthesized from PLGA and carboxylated carbon nanotubes. *Adv. Eng. Mater.* 11, B261–B266.

- Lee, W.C., Lim, C.H., Shi, H., Tang, L.A., Wang, Y., Lim, C.T., Loh, K.P., 2011. Origin of enhanced stem cell growth and differentiation on graphene and graphene oxide. *ACS Nano* 5, 7334–7341.
- Lee, D.K., Kim, S.V., Limansubroto, A.N., Yen, A., Soundia, A., Wang, C.Y., Shi, W., Hong, C., Tetradis, S., Kim, Y., Park, N.H., Kang, M.K., Ho, D., 2015a. Nanodiamond-gutta percha composite biomaterials for root canal therapy. *ACS Nano* 9, 11490–11501.
- Lee, J.H., Shin, Y.C., Lee, S.M., Jin, O.S., Kang, S.H., Hong, S.W., Jeong, C.M., Huh, J.B., Han, D.W., 2015b. Enhanced osteogenesis by reduced graphene oxide/hydroxyapatite nanocomposites. *Sci. Rep.* 5, 18833.
- Lee, S., Jo, I., Kang, S., Jang, B., Moon, J., Park, J.B., Lee, S., Rho, S., Kim, Y., Hong, B.H., 2017. Smart contact lenses with graphene coating for electromagnetic interference shielding and dehydration protection. *ACS Nano* 11, 5318–5324.
- Lewitus, D.Y., Landers, J., Branch, J., Smith, K.L., Callegari, G., Kohn, J., Neimark, A.V., 2011. Biohybrid carbon nanotube/agarose fibers for neural tissue engineering. *Adv. Funct. Mater.* 21, 2624–2632.
- Li, D., Hu, X., Zhang, S., 2019. Biodegradation of graphene-based nanomaterials in blood plasma affects their biocompatibility, drug delivery, targeted organs and antitumor ability. *Biomaterials* 202, 12–25.
- Li, J.H., Wang, G., Zhu, H.Q., Zhang, M., Zheng, X.H., Di, Z.F., Liu, X.Y., Wang, X., 2014. Antibacterial activity of large-area monolayer graphene film manipulated by charge transfer. *Sci. Rep.* 4.
- Li, Y., Dong, H.Q., Li, Y.Y., Shi, D.L., 2015a. Graphene-based nanovehicles for photodynamic medical therapy. *Int. J. Nanomed.* 10, 2451–2459.
- Li, Z., Wang, H., Yang, B., Sun, Y., Huo, R., 2015b. Three-dimensional graphene foams loaded with bone marrow derived mesenchymal stem cells promote skin wound healing with reduced scarring. *Mater. Sci. Eng. C Mater. Biol. Appl.* 57, 181–188.
- Li, J., Jiang, H., Ouyang, X., Han, S., Wang, J., Xie, R., Zhu, W., Ma, N., Wei, H., Jiang, Z., 2016. CaCO₃/Tetraethylenepentamine-Graphene hollow microspheres as biocompatible bone drug carriers for controlled release. *ACS Appl. Mater. Interfaces* 8, 30027–30036.
- Li, H., Huang, J., Song, Y.X., Zhang, M.L., Wang, H.B., Lu, F., Huang, H., Liu, Y., Dai, X., Gu, Z.L., Yang, Z.X., Zhou, R.H., Kang, Z.H., 2018. Degradable carbon dots with broad-spectrum antibacterial activity. *ACS Appl. Mater. Interfaces* 10, 26936–26946.
- Lin, C., Wang, Y., Lai, Y., Yang, W., Jiao, F., Zhang, H., Ye, S., Zhang, Q., 2011. Incorporation of carboxylation multiwalled carbon nanotubes into biodegradable poly(lactic-co-glycolic acid) for bone tissue engineering. *Colloids Surf. B Biointer.* 83, 367–375.
- Liu, J., Ohta, S., Sonoda, A., Yamada, M., Yamamoto, M., Nitta, N., Murata, K., Tabata, Y., 2007. Preparation of PEG-conjugated fullerene containing Gd³⁺ ions for photodynamic therapy. *J. Control. Release* 117, 104–110.
- Liu, S.B., Zeng, T.H., Hofmann, M., Burcombe, E., Wei, J., Jiang, R.R., Kong, J., Chen, Y., 2011a. Antibacterial activity of graphite, graphite oxide, graphene oxide, and reduced graphene oxide: membrane and oxidative stress. *ACS Nano* 5, 6971–6980.
- Liu, Z., Robinson, J.T., Tabakman, S.M., Yang, K., Dai, H.J., 2011b. Carbon materials for drug delivery and cancer therapy. *Mater. Today* 14, 316–323.
- Liu, X., Ma, D., Tang, H., Tan, L., Xie, Q., Zhang, Y., Ma, M., Yao, S., 2014. Polyamidoamine dendrimer and oleic acid-functionalized graphene as biocompatible and efficient gene delivery vectors. *ACS Appl. Mater. Interfaces* 6, 8173–8183.
- Liu, J., Wang, J., Wang, T., Li, D., Xi, F., Wang, J., Wang, E., 2015. Three-dimensional electrochemical immunosensor for sensitive detection of carcinoembryonic antigen based on monolithic and macroporous graphene foam. *Biosens. Bioelectron.* 65, 281–286.
- Liu, H.Y., Zhang, L.N., Yan, M., Yu, J.H., 2017. Carbon nanostructures in biology and medicine. *J. Mater. Chem. B* 5, 6437–6450.
- Lopez-Dolado, E., Gonzalez-Mayorga, A., Gutierrez, M.C., Serrano, M.C., 2016. Immunomodulatory and angiogenic responses induced by graphene oxide scaffolds in chronic spinal hemisectioned rats. *Biomaterials* 99, 72–81.
- Ma, W., Ruys, A.J., Zreiqat, H., 2009. Diamond-like carbon (DLC) as a biocompatible coating in orthopaedic and cardiac medicine. In: Silvio, L.D. (Ed.), *Cellular Response to Biomaterials*. CRC Press, Boca Raton, USA.
- Maas, M., 2016. Carbon nanomaterials as antibacterial colloids. *Materials* 9, 617.
- Mahmoudi, N., Ostadhossein, F., Simchi, A., 2016. Physicochemical and antibacterial properties of chitosan-polyvinylpyrrolidone films containing self-organized graphene oxide nanolayers. *J. Appl. Polym. Sci.* 133.
- Malarkey, E.B., Fisher, K.A., Bekyarova, E., Liu, W., Haddon, R.C., Parpura, V., 2009. Conductive single-walled carbon nanotube substrates modulate neuronal growth. *Nano Lett.* 9, 264–268.
- Malik, S., Ruddock, F.M., Dowling, A.H., Byrne, K., Schmitt, W., Khalakhan, I., Nemoto, Y., Guo, H.X., Shrestha, L.K., Ariga, K., Hill, J.P., 2018. Graphene composites with dental and biomedical applicability. *Beilstein J. Nanotechnol.* 9, 801–808.
- Marrs, B., Andrews, R., Rantell, T., Pienkowski, D., 2006. Augmentation of acrylic bone cement with multiwall carbon nanotubes. *J. Biomed. Mater. Res. A* 77, 269–276.
- Martinelli, V., Cellot, G., Toma, F.M., Long, C.S., Caldwell, J.H., Zentilin, L., Giacca, M., Turco, A., Prato, M., Ballerini, L., Mestroni, L., 2013. Carbon nanotubes instruct physiological growth and functionally mature syncytia: nongenetic engineering of cardiac myocytes. *ACS Nano* 7, 5746–5756.
- Mazaheri, M., Akhavan, O., Simchi, A., 2014. Flexible bactericidal graphene oxide–chitosan layers for stem cell proliferation. *Appl. Surf. Sci.* 301, 456–462.
- Mckenzie, J.L., Waid, M.C., Shi, R., Webster, T.J., 2004. Decreased functions of astrocytes on carbon nanofiber materials. *Biomaterials* 25, 1309–1317.
- Melo, S.F., Neves, S.C., Pereira, A.T., Borges, I., Granja, P., Magalhães, F., Gonçalves, I.C., 2020. Incorporation of graphene oxide into poly(ϵ -caprolactone) 3D printed fibrous scaffolds improves their antimicrobial properties. *Mat. Sci. Eng C* 109, 110537.
- Meziani, M.J., Dong, X.L., Zhu, L., Jones, L.P., Lecroy, G.E., Yang, F., Wang, S.Y., Wang, P., Zhao, Y.P., Yang, L.J., Tripp, R.A., Sun, Y.P., 2016. Visible-light-Activated bactericidal functions of carbon "quantum" dots. *ACS Appl. Mater. Interfaces* 8, 10761–10766.
- Mikael, P.E., Amini, A.R., Basu, J., Josefina Arellano-Jimenez, M., Laurencin, C.T., Sanders, M.M., Barry Carter, C., Nukavarapu, S.P., 2014. Functionalized carbon nanotube reinforced scaffolds for bone regenerative engineering: fabrication, in vitro and in vivo evaluation. *Biomed. Mater.* 9, 035001.
- Minns, R.J., Muckle, D.S., 1989. Mechanical and histological response of carbon fibre pads implanted in the rabbit patella. *Biomaterials* 10, 273–276.
- Mocan, T., Matea, C.T., Pop, T., Mosteanu, O., Buzoianu, A.D., Suci, S., Puia, C., Zdrehus, C., Iancu, C., Mocan, L., 2017.

- Carbon nanotubes as anti-bacterial agents. *Cell. Mol. Life Sci.* 74, 3467–3479.
- Mohajeri, M., Behnam, B., Sahebkar, A., 2018. Biomedical applications of carbon nanomaterials: drug and gene delivery potentials. *J. Cell. Physiol.* 234, 298–319.
- Musumeci, L., Jacques, N., Hego, A., Nchimi, A., Lancellotti, P., Oury, C., 2018. Prosthetic aortic valves: challenges and solutions. *Front. Cardiovasc. Med.* 5, 46.
- Nachlas, A.L.Y., Li, S., Davis, M.E., 2017. Developing a clinically relevant tissue engineered heart valve—A review of current approaches. *Adv. Healthc. Mater.* 6.
- Nakagawa, T., Ohishi, R., Ohtake, N., Takai, O., Tsutsui, N., Tsutsui, Y., Muraki, Y., Ogura, J., 2009. Segment-Structured Diamond-Like Carbon Coatings on Polymer Catheter.
- Namdari, P., Negahdari, B., Eatemadi, A., 2017. Synthesis, properties and biomedical applications of carbon-based quantum dots: an updated review. *Biomed. Pharmacother.* 87, 209–222.
- Narayan, R.J., Berry, C.J., Brigmon, R.L., 2005. Structural and biological properties of carbon nanotube composite films. *Mat. Sci. Eng. B Solid State Mat. Adv. Technol.* 123, 123–129.
- Nelham, R.L., 1981. Carbon fibre reinforced plastic applied to prosthetics and orthotics. *J. Biomed. Eng.* 3, 305–314.
- Newman, P., Minnett, A., ELLIS-Behnke, R., Zreiqat, H., 2013. Carbon nanotubes: their potential and pitfalls for bone tissue regeneration and engineering. *Nanomedicine* 9, 1139–1158.
- Nie, W., Peng, C., Zhou, X.J., Chen, L., Wang, W.Z., Zhang, Y.Z., Ma, P.X., He, C.L., 2017. Three-dimensional porous scaffold by self-assembly of reduced graphene oxide and nano-hydroxyapatite composites for bone tissue engineering. *Carbon* 116, 325–337.
- Norahan, M.H., Amroon, M., Ghahremanzadeh, R., Mahmoodi, M., Baheiraei, N., 2019. Electroactive graphene oxide-incorporated collagen assisting vascularization for cardiac tissue engineering. *J. Biomed. Mater. Res. A* 107, 204–219.
- Nurunnabi, M., Khatun, Z., Reeck, G.R., Lee, D.Y., Lee, Y.K., 2014. Photoluminescent graphene nanoparticles for cancer phototherapy and imaging. *ACS Appl. Mater. Interfaces* 6, 12413–12421.
- Nyambar, B., Chen, C.H., Wong, P.C., Chiang, C.W., Satapathy, M.K., Chuang, E.Y., 2018. Genipin-crosslinked adipose stem cell derived extracellular matrix-nano graphene oxide composite sponge for skin tissue engineering. *J. Mater. Chem. B* 6, 979–990.
- Papi, M., Palmieri, V., Bugli, F., DE Spirito, M., Sanguinetti, M., Ciancico, C., Braidotti, M.C., Gentilini, S., Angelani, L., Conti, C., 2016. Biomimetic antimicrobial cloak by graphene-oxide agar hydrogel. *Sci. Rep.* 6, 12.
- Parizek, M., Douglas, T.E., Novotna, K., Kromka, A., Brady, M.A., Renzing, A., Voss, E., Jarosova, M., Palatinus, L., Tesarek, P., Ryparova, P., Lisa, V., DOS Santos, A.M., Warnke, P.H., Bacakova, L., 2012. Nanofibrous poly(lactide-co-glycolide) membranes loaded with diamond nanoparticles as promising substrates for bone tissue engineering. *Int. J. Nanomed.* 7, 1931–1951.
- Park, K., Vasilos, T., 1997. Characteristics of carbon fibre-reinforced calcium phosphate composites fabricated by hot pressing. *J. Mater. Sci. Lett.* 16, 985–987.
- Park, S., Mohanty, N., Suk, J.W., Nagaraja, A., An, J., Piner, R.D., Cai, W., Dreyer, D.R., Berry, V., Ruoff, R.S., 2010. Biocompatible, robust free-standing paper composed of a TWEEN/graphene composite. *Adv. Mater.* 22, 1736–1740.
- Pasinszki, T., Krebsz, M., Tung, T.T., Losic, D., 2017. Carbon nanomaterial based biosensors for non-invasive detection of cancer and disease biomarkers for clinical diagnosis. *Sensors* 17.
- Passeri, D., Rinaldi, F., Ingallina, C., Carafa, M., Rossi, M., Terranova, M.L., Marianecchi, C., 2015. Biomedical applications of nanodiamonds: an overview. *J. Nanosci. Nanotechnol.* 15, 972–988.
- Patel, A., Xue, Y., Hartley, R., Sant, V., Eles, J.R., Cui, X.T., Stolz, D.B., Sant, S., 2018. Hierarchically aligned fibrous hydrogel films through microfluidic self-assembly of graphene and polysaccharides. *Biotechnol. Bioeng.* 115, 2654–2667.
- Penkov, O.V., Pukha, V.E., Starikova, S.L., Khadem, M., Starikov, V.V., Maleev, M.V., Kim, D.E., 2016. Highly wear-resistant and biocompatible carbon nanocomposite coatings for dental implants. *Biomaterials* 102, 130–136.
- Pennisi, C.P., Alcaide, M., 2014. Nanocrystalline diamond films for biomedical applications. In: *Frontiers in Biomaterials*.
- Pereira, A.T., Henriques, P.C., Costa, P.C., Martins, M.C.L., Magalhães, F.D., Gonçalves, I.C., 2019. Graphene oxide-reinforced poly(2-hydroxyethyl methacrylate) hydrogels with extreme stiffness and high-strength. *Compos. Sci. Technol* 184, 107819.
- Perreault, F., DE Faria, A.F., Nejati, S., Elimelech, M., 2015. Antimicrobial properties of graphene oxide nanosheets: why size matters. *ACS Nano* 9, 7226–7236.
- Pham, V.T., Truong, V.K., Quinn, M.D., Notley, S.M., Guo, Y., Baulin, V.A., AL Kobaisi, M., Crawford, R.J., Ivanova, E.P., 2015. Graphene induces formation of pores that kill spherical and rod-shaped bacteria. *ACS Nano* 9, 8458–8467.
- Pilehvar, S., Wael, K., 2015. Recent advances in electrochemical biosensors based on Fullerene-C60 Nano-Structured platforms. *Biosensors* 5, 712–735.
- Pinto, A.M., Goncalves, I.C., Magalhaes, F.D., 2013. Graphene-based materials biocompatibility: a review. *Colloids Surf. B Biointerfaces* 111, 188–202.
- Podila, R., Moore, T., Alexis, F., Rao, A.M., 2013. Graphene coatings for enhanced hemo-compatibility of nitinol stents. *RSC Adv.* 3, 1660–1665.
- Pok, S., Vitale, F., Eichmann, S.L., Benavides, O.M., Pasquali, M., Jacot, J.G., 2014. Biocompatible carbon nanotube-chitosan scaffold matching the electrical conductivity of the heart. *ACS Nano* 8, 9822–9832.
- Prabhu, S.D., Frangogiannis, N.G., 2016. The biological basis for cardiac repair after myocardial infarction: from inflammation to fibrosis. *Circ. Res.* 119, 91–112.
- Pradhan, D., Lee, Y.C., Pao, C.W., Pong, W.F., Lin, I.N., 2006. Low temperature growth of ultrananocrystalline diamond film and its field emission properties. *Diam. Relat. Mater.* 15, 2001–2005.
- Qian, W., Hu, X., He, W., Zhan, R., Liu, M., Zhou, D., Huang, Y., Hu, X., Wang, Z., Fei, G., Wu, J., Xing, M., Xia, H., Luo, G., 2018. Polydimethylsiloxane incorporated with reduced graphene oxide (rGO) sheets for wound dressing application: preparation and characterization. *Colloids Surf B Biointerfaces* 166, 61–71.
- Rasovic, I., 2017. Water-soluble fullerenes for medical applications. *Mater. Sci. Technol.* 33, 777–794.
- Ren, J., Xu, Q., Chen, X., Li, W., Guo, K., Zhao, Y., Wang, Q., Zhang, Z., Peng, H., Li, Y.G., 2017. Superaligned carbon nanotubes guide oriented cell growth and promote electrophysiological homogeneity for synthetic cardiac tissues. *Adv. Mater.* 29.
- Rezek, B., Ukrainsev, E., Kromka, A., Ledinsky, M., Broz, A., Noskova, L., Hartmannova, H., Kalbacova, M., 2010. Assembly of osteoblastic cell micro-arrays on diamond guided by protein pre-adsorption. *Diam. Relat. Mater.* 19, 153–157.
- Ristic, B.Z., Milenkovic, M.M., Dakic, I.R., Todorovic-Markovic, B.M., Milosavljevic, M.S., Budimir, M.D., Paunovic, V.G., Dramicanin, M.D., Markovic, Z.M., Trajkovic, V.S., 2014. Photodynamic antibacterial effect of graphene quantum dots. *Biomaterials* 35, 4428–4435.

- Robert, B., More, A.D.H., Bokros, J.C., Buddy, D., 2013. Pyrolytic carbon for long-term medical implants. In: Ratner, A.S.H., Schoen, F.J., Lemons, Jack E. (Eds.), *Biomaterials Science: An Introduction to Materials in Medicine*, third ed. Elsevier, Oxford, UK.
- Robinson, J.T., Welsher, K., Tabakman, S.M., Sherlock, S.P., Wang, H.L., Luong, R., Dai, H.J., 2010. High performance in vivo near-IR ($> 1 \mu\text{m}$) imaging and photothermal cancer therapy with carbon nanotubes. *Nano Res.* 3, 779–793.
- Romero-Vargas Castrillón, S.P.F.F., Fonseca, A., Menachem, E., 2015. Interaction of graphene oxide with bacterial cell membranes: insights from force spectroscopy. *Environ. Sci. Technol. Lett.* 2, 112–117.
- Roseti, L., Parisi, V., Petretta, M., Cavallo, C., Desando, G., Bartolotti, I., Grigolo, B., 2017. Scaffolds for bone tissue engineering: state of the art and new perspectives. *Mater. Sci. Eng. C Mater. Biol. Appl.* 78, 1246–1262.
- Ross, M., James, C., Couzens, G., 2008. Pyrocarbon small joint arthroplasty of the extremities. In: Revell, P.A. (Ed.), *Joint Replacement Technology*. Woodhead Publishing, Cambridge, UK.
- Roy, R.K., Lee, K.R., 2007. Biomedical applications of diamond-like carbon coatings: a review. *J. Biomed. Mater. Res. B Appl. Biomater.* 83, 72–84.
- Rozeik, M.M., Wheatley, D.J., Gourlay, T., 2017. Investigating the suitability of carbon nanotube reinforced polymer in transcatheter valve applications. *Cardiovasc. Eng. Technol.* 8, 357–367.
- Ruiz, O.N., Fernando, K.A., Wang, B., Brown, N.A., Luo, P.G., Mcnamara, N.D., Vangsness, M., Sun, Y.P., Bunker, C.E., 2011. Graphene oxide: a nonspecific enhancer of cellular growth. *ACS Nano* 5, 8100–8107.
- Ryan, A.J., Kearney, C.J., Shen, N., Khan, U., Kelly, A.G., Probst, C., Brauchle, E., Bicca, S., Garcarena, C.D., Vega-Mayoral, V., Loskill, P., Kerrigan, S.W., Kelly, D.J., Schenke-Layland, K., Coleman, J.N., O'Brien, F.J., 2018. Electroconductive biohybrid collagen/pristine graphene composite biomaterials with enhanced biological activity. *Adv. Mater.* 30, e1706442.
- Saito, N., Aoki, K., Usui, Y., Shimizu, M., Hara, K., Narita, N., Oghihara, N., Nakamura, K., Ishigaki, N., Kato, H., Haniu, H., Taruta, S., Kim, Y.A., Endo, M., 2011. Application of carbon fibers to biomaterials: a new era of nano-level control of carbon fibers after 30-years of development. *Chem. Soc. Rev.* 40, 3824–3834.
- Saito, N., Haniu, H., Usui, Y., Aoki, K., Hara, K., Takanashi, S., Shimizu, M., Narita, N., Okamoto, M., Kobayashi, S., Nomura, H., Kato, H., Nishimura, N., Taruta, S., Endo, M., 2014. Safe clinical use of carbon nanotubes as innovative biomaterials. *Chem. Rev.* 114, 6040–6079.
- Sajid, M.I., Jamshaid, U., Jamshaid, T., Zafar, N., Fessi, H., Elaissari, A., 2016. Carbon nanotubes from synthesis to in vivo biomedical applications. *Int. J. Pharm.* 501, 278–299.
- Santos, T.B., Vieira, A.A., Paula, L.O., Santos, E.D., Radi, P.A., Khouri, S., Maciel, H.S., Pessoa, R.S., Vieira, L., 2017. Flexible camphor diamond-like carbon coating on polyurethane to prevent *Candida albicans* biofilm growth. *J. Mech. Behav. Biomed. Mater.* 68, 239–246.
- Saravanan, S., Chawla, A., Vairamani, M., Sastry, T.P., Subramanian, K.S., Selvamurugan, N., 2017. Scaffolds containing chitosan, gelatin and graphene oxide for bone tissue regeneration in vitro and in vivo. *Int. J. Biol. Macromol.* 104, 1975–1985.
- Scapin, G., Salice, P., Tescari, S., Menna, E., DE Filippis, V., Filippini, F., 2015. Enhanced neuronal cell differentiation combining biomimetic peptides and a carbon nanotube-polymer scaffold. *Nanomedicine* 11, 621–632.
- Schiffman, J.D., Elimelech, M., 2011. Antibacterial activity of electrospun polymer mats with incorporated narrow diameter single-walled carbon nanotubes. *ACS Appl. Mater. Interfaces* 3, 462–468.
- Schrand, A.M., Hens, S.A.C., Shenderova, O.A., 2009. Nanodiamond particles: properties and perspectives for bioapplications. *Crit. Rev. Solid State Mater. Sci.* 34, 18–74.
- Scotchford, C.A., Garle, M.J., Batchelor, J., Bradley, J., Grant, D.M., 2003. Use of a novel carbon fibre composite material for the femoral stem component of a THR system: in vitro biological assessment. *Biomaterials* 24, 4871–4879.
- Shadjou, N., Hasanazadeh, M., 2016. Graphene and its nanostructure derivatives for use in bone tissue engineering: recent advances. *J. Biomed. Mater. Res. A* 104, 1250–1275.
- Shah, K., Vasileva, D., Karadaghy, A., Zustiak, S.P., 2015. Development and characterization of polyethylene glycol-carbon nanotube hydrogel composite. *J. Mater. Chem. B* 3, 7950–7962.
- Sharma, P., Mehra, N.K., Jain, K., Jain, N.K., 2016. Biomedical applications of carbon nanotubes: a critical review. *Curr. Drug Deliv.* 13, 796–817.
- Shen, J.H., Zhu, Y.H., Yang, X.L., Li, C.Z., 2012. Graphene quantum dots: emergent nanolights for bioimaging, sensors, catalysis and photovoltaic devices. *Chem. Commun.* 48, 3686–3699.
- Shi, L., Chen, J.R., Teng, L.J., Wang, L., Zhu, G.L., Liu, S., Luo, Z.T., Shi, X.T., Wang, Y.J., Ren, L., 2016. The antibacterial applications of graphene and its derivatives. *Small* 12, 4165–4184.
- Shin, S.R., Aghaei-Ghareh-Bolagh, B., Gao, X., Nikkha, M., Jung, S.M., Dolatshahi-Pirouz, A., Kim, S.B., Kim, S.M., Dokmeci, M.R., Tang, X.S., Khademhosseini, A., 2014. Layer-by-layer assembly of 3D tissue constructs with functionalized graphene. *Adv. Funct. Mater.* 24, 6136–6144.
- Shin, S.R., Zihlmann, C., Akbari, M., Assawes, P., Cheung, L., Zhang, K., Manoharan, V., Zhang, Y.S., Yuksekaya, M., Wan, K.T., Nikkha, M., Dokmeci, M.R., Tang, X.S., Khademhosseini, A., 2016. Reduced graphene oxide-gelma hybrid hydrogels as scaffolds for cardiac tissue engineering. *Small* 12, 3677–3689.
- Singh, S., Nalwa, H.S., 2007. Nanotechnology and health safety - toxicity and risk assessments of nanostructured materials on human health. *J. Nanosci. Nanotechnol.* 7, 3048–3070.
- Singh, S.P., Li, Y., Be'er, A., Oren, Y., Tour, J.M., Arnusch, C.J., 2017. Laser-induced graphene layers and electrodes prevents microbial fouling and exerts antimicrobial action. *ACS Appl. Mater. Interfaces* 9, 18238–18247.
- Spizzirri, U.G., Hampel, S., Cirillo, G., Mauro, M.V., Vittorio, O., Cavalcanti, P., Giraldo, C., Curcio, M., Picci, N., Iemma, F., 2015. Functional gelatin-carbon nanotubes nanohybrids with enhanced antibacterial activity. *Int. J. Polym. Mater. Polym. Biomater.* 64, 439–447.
- Sun, H.J., Gao, N., Dong, K., Ren, J.S., Qu, X.G., 2014. Graphene quantum dots-band-aids used for wound disinfection. *ACS Nano* 8, 6202–6210.
- Sun, H., Lu, S., Jiang, X.X., Li, X., Li, H., Lin, Q., Mou, Y., Zhao, Y., Han, Y., Zhou, J., Wang, C., 2015. Carbon nanotubes enhance intercalated disc assembly in cardiac myocytes via the beta1-integrin-mediated signaling pathway. *Biomaterials* 55, 84–95.
- Swetha, P.D.P., Manisha, H., Sudhakaraprasad, K., 2018. Graphene and graphene-based materials in biomedical science. *Part. Part. Syst. Charact.* 35.
- Szunerits, S., Barras, A., Boukherroub, R., 2016. Antibacterial applications of nanodiamonds. *Int. J. Environ. Res. Public Health* 13, 413.
- Taeger, G., Schmidt, L.E.P.B., Ziegler, M., Nast-Kolb, D., 2003. Comparison of diamond-like-carbon and alumina-oxide articulating with polyethylene in total hip arthroplasty. *Mater. Sci. Eng. Technol.* 34, 1094–1100.

- Teradal, N.L., Jelinek, R., 2017. Carbon nanomaterials in biological studies and biomedicine. *Adv. Healthc. Mater.* 6.
- Tian, H.C., Liu, J.Q., Wei, D.X., Kang, X.Y., Zhang, C., Du, J.C., Yang, B., Chen, X., Zhu, H.Y., Nuli, Y.N., Yang, C.S., 2014. Graphene oxide doped conducting polymer nanocomposite film for electrode-tissue interface. *Biomaterials* 35, 2120–2129.
- Tonelli, F.M., Santos, A.K., Gomes, K.N., Lorencon, E., Guatimosim, S., Ladeira, L.O., Resende, R.R., 2012. Carbon nanotube interaction with extracellular matrix proteins producing scaffolds for tissue engineering. *Int. J. Nanomed.* 7, 4511–4529.
- Torres, V., Srdjenovic, B., 2011. Biomedical applications of fullerenes. In: Verner, R.F.B., C. (Ed.), *Handbook on Fullerene: Synthesis, Properties and Applications*. Nova Science.
- Tran, H.S., Puc, M.M., Hewitt, C.W., Soll, D.B., Marra, S.W., Simonetti, V.A., Cilley, J.H., Delrossi, A.J., 1999. Diamond-like carbon coating and plasma or glow discharge treatment of mechanical heart valves. *J. Investig. Surg.* 12, 133–140.
- Travlou, N.A., Giannakoudakis, D.A., Algarra, M., Labella, A.M., Rodriguez-Castellon, E., Bandosz, T.J., 2018. S- and N-doped carbon quantum dots: surface chemistry dependent antibacterial activity. *Carbon* 135, 104–111.
- van der Laan, K., Hasani, M., Zheng, T., Schirhagl, R., 2018. Nanodiamonds for in vivo applications. *Small* 14, e1703838.
- Vandrovcova, M.V.J., Svorcik, V., Slepicka, P., Kasalkova, N., Vorlicek, V., Lavrentiev, V., Vosecek, V., Grausova, L., Lisa, V., Bacakova, L., 2008. Fullerene C60 and hybrid C60/Ti films as substrates for adhesion and growth of bone cells. *Physica Status Solidi (A)* 205, 2252–2261.
- Veerapandian, M., Zhang, L.H., Krishnamoorthy, K., Yun, K., 2013. Surface activation of graphene oxide nanosheets by ultraviolet irradiation for highly efficient anti-bacterials. *Nanotechnology* 24.
- Vellayappan, M.V., Balaji, A., Subramanian, A.P., John, A.A., Jagannathan, S.K., Murugesan, S., Mohandas, H., Supriyanto, E., Yusuf, M., 2015. Tangible nanocomposites with diverse properties for heart valve application. *Sci. Technol. Adv. Mater.* 16, 033504.
- Venkatesan, N., Yoshimitsu, J., Ito, Y., Shibata, N., Takada, K., 2005. Liquid filled nanoparticles as a drug delivery tool for protein therapeutics. *Biomaterials* 26, 7154–7163.
- Wan, C., Frydrych, M., Chen, B., 2011. Strong and bioactive gelatin–graphene oxide nanocomposites. *Soft Matter* 7, 6159–6166.
- Wang, W., Zhu, Y., Liao, S., Li, J., 2014. Carbon nanotubes reinforced composites for biomedical applications. *BioMed Res. Int.* 2014, 518609.
- Wehling, J., Dringen, R., Zare, R.N., Maas, M., Rezwani, K., 2014. Bactericidal activity of partially oxidized nanodiamonds. *ACS Nano* 8, 6475–6483.
- Wu, C.X.L., Han, P., Xu, M., Fang, B., Wang, J., Chang, J., Xiao, Y., 2015. Graphene-oxide-modified β -tricalcium phosphate bioceramics stimulate in vitro and in vivo osteogenesis. *Carbon* 93, 116–129.
- Wu, S., Duan, B., Lu, A., Wang, Y., Ye, Q., Zhang, L., 2017. Biocompatible chitin/carbon nanotubes composite hydrogels as neuronal growth substrates. *Carbohydr. Polym.* 174, 830–840.
- Yamazaki, K., Litwak, P., Tagusari, O., Mori, T., Kono, K., Kameleva, M., Watach, M., Gordon, L., Miyagishima, M., Tomioka, J., Umezu, M., Outa, E., Antaki, J.F., Kormos, R.L., Koyanagi, H., Griffith, B.P., 1998. An implantable centrifugal blood pump with a recirculating purge system (Cool-Seal system). *Artif. Organs* 22, 466–474.
- Yang, K., Zhang, S.A., Zhang, G.X., Sun, X.M., Lee, S.T., Liu, Z.A., 2010. Graphene in mice: ultrahigh in vivo tumor uptake and efficient photothermal therapy. *Nano Lett.* 10, 3318–3323.
- Yang, J.J., Zhang, X.D., Ma, Y.H., Gao, G., Chen, X.K., Jia, H.R., Li, Y.H., Chen, Z., Wu, F.G., 2016. Carbon dot-based platform for simultaneous bacterial distinguishment and antibacterial applications. *ACS Appl. Mater. Interfaces* 8, 32170–32181.
- Youssef, A.M., EL-Naggar, M.E., Malhat, F.M., El Sharkawi, H.M., 2019. Efficient removal of pesticides and heavy metals from wastewater and the antimicrobial activity of f-MWCNTs/PVA nanocomposite film. *J. Clean. Prod.* 206, 315–325.
- Yu, W., Jiang, X., Cai, M., Zhao, W., Ye, D., Zhou, Y., Zhu, C., Zhang, X., Lu, X., Zhang, Z., 2014. A novel electrospun nerve conduit enhanced by carbon nanotubes for peripheral nerve regeneration. *Nanotechnology* 25, 165102.
- Zeng, H., Yin, W., Catausan, G., Moldovan, N., Carlisle, J., 2016. Ultrananocrystalline diamond integration with pyrolytic carbon components of mechanical heart valves. *Diam. Relat. Mater.* 61, 97–101.
- Zhang, X., Prasad, S., Niyogi, S., Morgan, A., Ozkan, M., Ozkan, C., 2005. Guided neurite growth on patterned carbon nanotubes. *Sens. Actuators B Chem.* 106, 843–850.
- Zhang, M., Nalk, R.R., Limin, D., (Eds.), 2016. *Carbon Nanomaterials for Biomedical Applications*. Springer, p.576, 486.
- Zhang, F., Song, Q.X., Huang, X., Li, F.N., Wang, K., Tang, Y.X., Hou, C.L., Shen, H.X., 2016. A novel high mechanical property PLGA composite matrix loaded with nanodiamond-phospholipid compound for bone tissue engineering. *ACS Appl. Mater. Interfaces* 8, 1087–1097.
- Zhang, Q., Du, Q.Y., Zhao, Y.A., Chen, F.X., Wang, Z.J., Zhang, Y.X., Ni, H., Deng, H.B., Li, Y.P., Chen, Y., 2017. Graphene oxide-modified electrospun polyvinyl alcohol nanofibrous scaffolds with potential as skin wound dressings. *RSC Adv.* 7, 28826–28836.
- Zhang, J., Liu, X., Wang, X., Mu, L., Yuan, M., Liu, B., Shi, H., 2018. Carbon dots-decorated Na2W4O13 composite with WO3 for highly efficient photocatalytic antibacterial activity. *J. Hazard Mater.* 359, 1–8.
- Zhang, Z., Klausen, L.H., Chen, M., Dong, M., 2018. Electroactive scaffolds for neurogenesis and myogenesis: graphene-based nanomaterials. *Small* 14, e1801983.
- Zheng, H.Z., Ma, R.L., Gao, M., Tian, X., Li, Y.Q., Zeng, L.W., Li, R.B., 2018. Antibacterial applications of graphene oxides: structure-activity relationships, molecular initiating events and biosafety. *Sci. Bull.* 63, 133–142.

Chapter Questions and Answers

1. Classify the following carbon materials regarding their dimension (size/grain size) and carbon hybridization

	DIMENSION (size/grain size)				HYBRIDIZATION RATIO	
	0D	1D	2D	3D	$\frac{Sp^2}{Sp^3} > 1$	$\frac{Sp^2}{Sp^3} < 1$
Diamond				X		X
MCD				X		X
NCD	X					X
UNCD	X					X
ND	X					X
DLC				X		X
PyC				X	X	
Graphite				X	X	
Fullerene	X				X	
CNT		X			X	
Graphene			X		X	
CF				X	X	
CNF		X			X	
GNR		X			X	
CD	X					X
GQD	X				X	

2. One of the major constraints associated to the application of carbon materials colloids in biological systems is their aggregation in aqueous media. Describe a currently used strategy to improve it, explaining the changes in interfacial properties.

Answer: Due to the high content of carbon atoms, carbon materials exhibit a high hydrophobicity which compromises their solubility and/or dispersion in aqueous media, such as the biological systems. The most common strategies to prevent aggregation are carbon materials oxidation or their functionalization with hydrophilic molecules such as polyethylene glycol, since these will increase their oxygen containing groups and therefore make them more hydrophilic.

3. Classify the following sentences as true (T) or false (F)

- 3.1. Discovery of PyC, fullerene and G is associated to attribution of three Nobel prizes. **F**
- 3.2. For biomedical applications, carbon materials can be used as colloids, free-standing materials, coatings, or composites. **T**
- 3.3. PyC, and MCD, NCD and UNCD are synthesized as a film being frequently used as a surface coating of biomaterials. **T**
- 3.4. DLC, PyC and ND are carbon materials already applied in commercially available biomaterials. **T**
- 3.5. Despite their small size, fullerenes can't penetrate the mammalian cell membrane. **F**
- 3.6. Drugs can only interact with carbon materials by covalent interaction. **F**
- 3.7. Due to their high surface area and aspect ratio, CNT can be loaded with high amounts of molecules (e.g., drugs, antibodies, peptides) and used

to deliver them intracellularly, by permeating cell membranes. **T**

- 3.8. The good dispersion in water and biocompatibility of CD and GQD are attributed to their small size (<10 nm) and oxygen content. **T**
 - 3.9. ND present strong absorption and fluorescence in the UV region, and strong Raman signals. **T**
 - 3.10. GBM outstanding optical properties perspective their application in bioimaging. **F**
 - 3.11. CNT and GBM have strong absorption of NIR radiation, enabling their use in photothermal therapy. **T**
 - 3.12. Most colloidal carbon based materials have anti-bacterial effect by acting on bacterial membrane. **T**
4. Select the correct answer:
- 4.1. Carbon-based coatings:
 - a) have been used for decades to enhance biomaterials performance.
 - b) of DLC are used in commercially available orthopedic implants.
 - c) of DLC are used in commercially available stents and ventricular assisted devices.
 - d) Two of the above.**
 - e) All of the above.
 - 4.2. Carbon materials composites:
 - a) of CNT and GBM are used to improve the polymer conductivity.
 - b) of CNT and GBM are used to improve the polymer mechanical properties.
 - c) of ND are commercially available for dental applications.

- d) of CF are commercially available for dental applications.
e) all of the above.
- 4.3. Mechanical heart valves that contain carbon materials:
 a) can be made of PyC.
 b) are commercially available.
 c) have good hemocompatibility and therefore do not require systemic anticoagulation therapy.
d) Two of the above.
 e) All of the above.
- 4.4. Considering carbon materials application in phototherapy:
 a) ND with ideal crystalline structure are fluorescent.
 b) Fullerenes present strong absorbance at wavelengths above UV region.
 c) Graphene decreases fluorescence quenching of dyes and sensitizers.
 d) CD have poor photostability.
e) None of the above.
- 4.5. Considering application in biosensors, carbon materials:
 a) can be used as the receptor that detects the molecule.
 b) can be used as the signaling transducer which converts the physical/chemical signal.
 c) can be used as a signal processor.
 d) Two of the above.
e) All of the above.
- 4.6. Considering carbon materials application in antimicrobial therapy:
 a) Fullerenes have an inherent antiviral action.
 b) GBM antimicrobial mechanisms of action are different for GBM colloidal dispersions and GBM containing-surfaces.
 c) The coating production technique influences the antibacterial outcome of the surface
 d) Two of the above.
e) All of the above.
5. Identify the main applications under study or commercially available for the carbon biomaterials presented in the table below:

	Drug delivery	Phototherapy	Imaging	Biosensors	Antimicrobial	Cardiovascular	Orthopaedics	Neuronal	Dental
NCD/UNCD					X	X	X	X	
ND	X		X		X			X	X
DLC					X	X	X		
PyC						X	X		
Graphite								X	
Fullerene	X	X	X	X	X	X	X	X	X
CNT	X	X	X	X	X	X	X	X	
GBM	X	X		X	X	X	X	X	X
CF				X			X	X	
CD/GQD	X	X	X	X	X				

6. Using a carbon nanomaterial of your choice, describe its main properties and give an example of a biomedical application, explaining how/why it can be used.

Answer: This question can have numerous possible answers. However, it should be taken into account that carbon nanomaterials have at least one dimension smaller than 100 nm, so only 0D, 1D or 2D carbon materials should be selected. Students are intended to highlight the main properties of one of these nanomaterials and correlate them with a selected biomedical application, explaining the rationale for the design of the medical device.

7. Provide example of one success and one failure on carbon-based materials applications in clinics.

Answer: For more than 50 years, pyrolytic carbon has been used in more than 25 different mechanical heart valves (MHV) designs, and nowadays 95% of all MHV have at least one structural component made of this carbon biomaterial. The balance between blood compatibility, physical

and mechanical properties, and durability made PyC the best material option available in MHV. A 17-year follow-up study in 500 patients implanted with Sorin MHV revealed that only five reoperations were necessary, and that there was a total of 15 valve-related deaths.

Failures were observed in diamond-like carbon (DLC) coated implants for orthopaedics. In 2001, Diamond Rota Gliding (Implant Design, Switzerland), a DLC-coated ultra-high molecular weight polyethylene (UHMWPE) knee joint, was commercialized. However, some of the implants showed increased wear and partial delamination, with the residual coating on the upper side of the implant leading to inadequate bone ingrowth. As such, the use of this implant was forbidden. In 2003, results were published from an 8-year clinical follow-up of 100 patients implanted with DLC-coated Adamante (Biomécanique, France) femoral heads, articulating against polyethylene. After 1.5 years, aseptic loosening was found, with implant revision being needed, and after 8 years almost half of the implants had to be replaced.

1.3.6

Natural Materials

MANUEL GÓMEZ-FLORIT^{1,2,3}, RUI M.A. DOMINGUES^{1,2,3}, SYEDA MAHWISH BAKHT^{1,2,3}, BÁRBARA B. MENDES^{1,2,3}, RUI L. REIS^{1,2,3}, MANUELA E. GOMES^{1,2,3}

¹3B's Research Group, I3Bs-Research Institute on Biomaterials, Biodegradables and Biomimetics, University of Minho, Headquarters of the European Institute of Excellence on Tissue Engineering and Regenerative Medicine, Guimarães, Portugal

²ICVS/3B's-PT Government Associate Laboratory, Braga/Guimarães, Portugal

³The Discoveries Centre for Regenerative and Precision Medicine, Headquarters at University of Minho, Guimarães, Portugal

Introduction to Natural Materials

The use of naturally occurring materials as matrices or scaffolds to support cell growth and proliferation significantly impacted the origin and progress of tissue engineering and regenerative medicine (TERM). However, the majority of these materials failed to provide adequate cues to guide cell differentiation toward the formation of new tissues. Over the past decade, a new generation of multifunctional and smart natural-based materials has been developed to provide biophysical and biochemical cues intended to specifically guide cell behavior.

Natural-based polymers originate from millions of years of nature's evolution in different environments, which resulted in an outstanding range of well adapted macromolecular designs to perform multiple structural and biological functions (Mano et al., 2007). In general, these can be categorized into three types of biopolymers: (1) proteins—chains of amino acids (e.g., collagen, elastin); (2) polysaccharides—chains of sugar (e.g., chitin, cellulose, glycosaminoglycans); and (3) nucleic acids—chains of nucleotides (DNA, RNA) (Table 1.3.6.1). From the point of view of origin, they might be derived from plants, animals (xenogenic), or humans (allogenic and autologous). Natural polymers offer several advantages with respect to synthetic polymers (Fig. 1.3.6.1): (1) they frequently avoid the immunogenic response and toxicity typical of synthetic polymers, thus presenting higher biocompatibility; (2) they contain bioactive motifs enabling local remodeling and cell spreading and a fibrillar architecture that can be deformed by cells, thus better mimicking the extracellular matrix (ECM); and (3) they can be recognized and metabolically processed by the body. However, natural polymers have historically been

associated with some disadvantages, including batch-to-batch variability, lower modularity, and inadequate biomechanical properties. Recent developments in the field have led to a reduction in these drawbacks, and allowed exploration of the full potential of naturally occurring polymers to develop a number of biomaterials that mimic key aspects of the native ECM (Mano et al., 2007).

In this chapter, we first review the use of ECM proteins and blood-derivatives intrinsic capacity to mimic the biophysical and biological characteristics of native tissues. Furthermore, the design of a variety of nanostructures using the well-explored characteristics of nucleic acids is summarized. In the second section, the exploitation of supramolecular chemistry to create new dynamic functional hydrogels that mimic the ECM structure and/or composition is surveyed. Finally, we focus on the incorporation of nanoelements in polymeric networks for the design of smart nanocomposite materials with tailored functionalities to guide cell behavior.

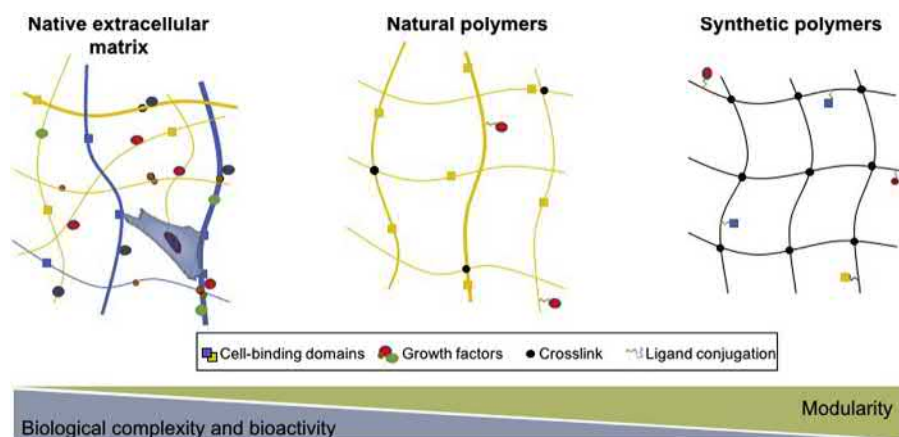
Natural Based-Biomaterials Exploring Structural Molecules

Extracellular Matrix-Based Biomaterials

The ECM comprises a complex milieu of proteins and glycosaminoglycans (GAGs) that provides a physical scaffold for maintaining the structural integrity of tissues, serves as an adhesive substrate for cell attachment and organization, and as a reservoir for biochemical cues to support cell survival and differentiation (Hussey et al., 2018; Mecham, 2001). These results in the establishment of specialized environments that contribute to the specific cell phenotypes and functions, making the ECM composition

TABLE 1.3.6.1 Origin and Relevant Properties of Selected Natural Polymers

Natural Material	Source	Relevant Properties
Proteins		
Collagen or denatured collagen (gelatin)	Animal tissues/cell culture	ECM protein. Provides cell-binding sites. Thermal gelation. Easy chemical modification
Decellularized ECM	Animal tissues/cell culture	ECM composition and structure mimetic. Tissue-specific. Provides cell-binding sites
Blood derivatives	Blood	ECM mimetic. Provides biochemical cues related to tissue healing/regeneration. Natural enzymatic gelation with thrombin (clot formation). Provides cell-binding sites
Polysaccharides		
Chondroitin sulfate	Animal tissues	Sulfated GAG present in connective tissues. Different sulfation patterns/growth factors affinity depending on source
Hyaluronic acid	Animal tissues/bacterial fermentation	ECM component. Nonsulfated GAG. Easy chemical modification
Cellulose nanocrystals	Plants, bacteria and tunicates (marine invertebrate animal)	High strength and aspect ratio. Used as nanofiller and reinforcement element
Nucleic acids		
DNA	Cells	Predictable biophysical and biochemical behavior. Different applications



• **Figure 1.3.6.1** Native extracellular matrix is a heterogeneous fibrillar network that provides biochemical and biophysical cues to cells. The use of natural polymers aims to mimic the native ECM complexity, which is very difficult to achieve using synthetic polymers. On the other hand, the modularity and chemical modification possibilities are wider on synthetic polymers.

tissue/organ-specific. Most ECMs are formed by a hydrogel-like porous network of fibrous proteins and linear GAGs. This fibrillar structure of the ECM influences its physical properties, signaling of growth factors (GFs), cell fate, and transport of nutrients and waste (Prince and Kumacheva, 2019). In order to recreate the biophysical and biochemical characteristics of the native tissues, the use of ECM-based biomaterials has gained interest in the last few years.

Proteins

Naturally occurring materials processed from purified or recombinant ECM proteins, such as collagen, laminin, fibrin,

fibronectin, or elastin, have been widely used to create a myriad of biomimetic hydrogels and scaffolds for diverse TERM applications. The most abundant and well-studied protein of mammalian ECM is collagen, which accounts for nearly 90% of the dry weight of most tissues and organs. Other abundant ECM proteins include fibronectin and elastin. Collagen and its partially hydrolyzed form, gelatin, are among the most preferred ECM proteins used in TERM due to their wide availability in nature (bovine, porcine, and marine), and ease of processing and modification using various techniques and chemistries. For example, the modification of gelatin with methacryloyl residues (also known as GelMA) has been

widely used to generate constructs with controlled architectures using micromolding, photomasking, bioprinting, self-assembly, and microfluidic techniques. The derived structures have been explored in a wide range of applications including bone, cartilage, cardiac, vascular tissues engineering, and drug and gene delivery (Yue et al., 2015).

Elastin is an extremely durable ECM protein responsible for the repetitive and reversible elastic recoil of tissues. The insoluble nature of elastin makes its processing challenging and incompatible with some techniques, which restricts its use in TERM approaches. Tropoelastin, on the other hand, is the soluble precursor of elastin and combines the similarities to elastin with easy handling, making this monomer a versatile building block to engineer biomaterials (Mithieux et al., 2013; Wise et al., 2009). It has been incorporated as a bulk material to build highly elastic hydrogels (Annabi et al., 2017, 2010), films produced through casting (Hu et al., 2011), or electrospun fibrous scaffolds (Machula et al., 2014; Nivison-Smith et al., 2010) to enhance cell adhesion, proliferation and migration, neovascularization, and even direct stem cell commitment (Yeo and Weiss, 2019). It has also been used as surface coatings to enhance cell interaction with the interface and to potentiate integration within the body (Yeo et al., 2017, 2012). In a different approach, recombinant and synthetic elastin-like polypeptides [repetition of the pentapeptide valine-proline-glycine-valine-glycine (VPGVG) from elastin], which mimic the extensibility and thermal properties of natural elastin, have been used to produce a range of biomaterials, including nanoparticles, electrospun fibers, and hydrogels cross-linked using different chemical strategies (Rodríguez-Cabello et al., 2018). These polypeptides also have been modified to incorporate “clickable” sequences (azides and alkynes) that react orthogonally to form an irreversible covalent bond, which resulted in hydrogels with fully tunable viscoelastic properties (González de Torre et al., 2014; Testera et al., 2015).

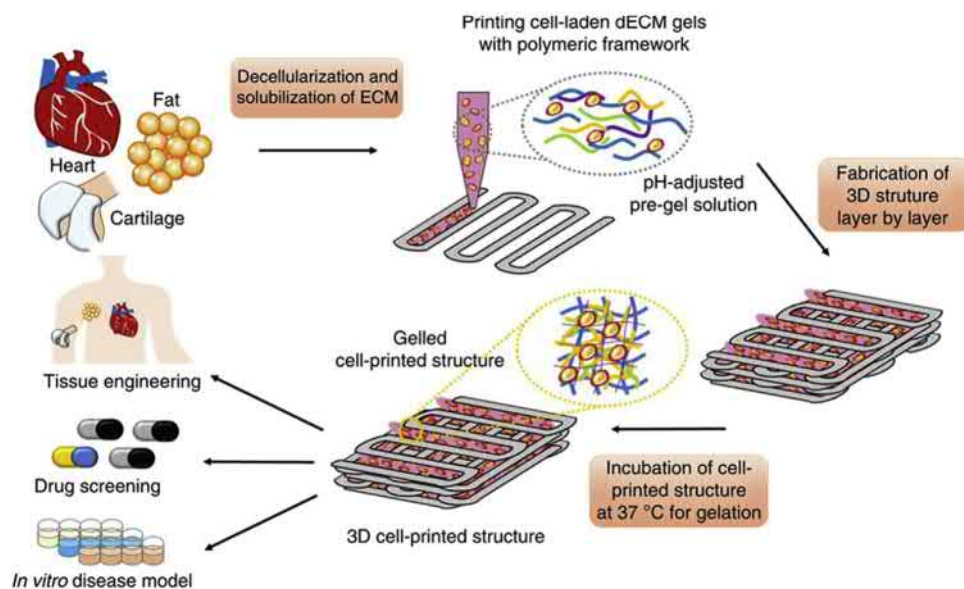
In order to recapitulate the cell-binding properties of ECM proteins, different biomaterials/formats have been conjugated with the bioactive domains of these proteins. The majority of the published studies (89%, from 1979 to early 2018) used the tripeptide arginine-glycine-asparagine (RGD), which is the minimal binding domain of some ECM proteins such as fibronectin, vitronectin, and laminin to integrin receptors (Huettner et al., 2018). Beyond this, many binding domains derived from ECM proteins have been recently described, which has opened new avenues for designing complex strategies to target diverse cell receptors (Huettner et al., 2018). For example, PCL scaffolds coated with RGD and tyrosine-isoleucine-glycine-serine-arginine (YIGSR) promoted axonal regeneration, functional recovery, and vascularization within regenerating nerve tissues in vivo through the activation of independent signaling pathways (Zhu et al., 2017a). Nevertheless, although the short binding domains can support cell attachment, migration, and activation of specific pathways, they have severely reduced binding affinity and specificity compared with the same peptide presented within its associated full-length 3D

protein structure (Li et al., 2017; Martino et al., 2009). Interestingly, the presentation of RGD in fibronectin sequences containing the major integrin-binding domain has been shown to improve binding affinity and modulate GF signaling (Martino et al., 2011). Therefore, the presentation of multiple cell-adhesion domains in their correct three-dimensional (3D) structural context can open new avenues for precisely controlling cell function and identifying synergistic effects that promote tissue regrowth and regeneration.

In addition, decellularized ECM (dECM)-based hydrogels have emerged as promising “game-changer” materials to develop biomimetic bioinks for 3D bioprinting (Choudhury et al., 2018). These bioinks are prepared from decellularized tissues and organs that are typically mixed and/or cross-linked using different natural and synthetic polymers or cross-linking agents to make them printable alone or in combination with biocompatible thermoplastics (e.g., PCL) to obtain mechanically reinforced scaffolds (Fig. 1.3.6.2). So far, different dECM bioinks have been derived from various organs such as heart, liver, fat, cartilage, skeletal muscle, skin, and vascular tissue (Choudhury et al., 2018). In a pioneering work, heart dECM bioink was developed, which allowed myoblasts to produce the cardiac-specific proteins actinin and fast myosin heavy chain-6, when compared with a collagen bioink (Pati et al., 2015, 2014). Thus, dECM bioinks have great potential to direct and mediate the differentiation of stem cells to create biomimetic and functional tissues, which would have applications in drug screening, disease modeling, and regenerative medicine. Nevertheless, since dECM is prepared either from human donors or animals, immunological issues need to be considered as well as the batch-to-batch high variability and limited availability of tissues. In order to overcome these issues, the use of cell-culture-derived matrix to produce dECM could offer a reliable alternative (Hussey et al., 2018). Using this approach, autologous cells can be cultured to obtain specific ECMs, avoiding concerns about the immune response. Furthermore, it could be obtained on a larger scale with higher reproducibility using cell expansion factories, although it remains very far from clinical translation.

Glycosaminoglycans

GAGs are negatively charged linear polysaccharides frequently found in the ECM conjugated with proteins, forming proteoglycans. They play important structural and regulatory roles in the ECM and are involved in many important cellular signaling processes governing tissue growth and development. Important types of GAGs that differ in chemical composition, structure, and function include the nonsulfated hyaluronan, the sulfated heparan sulfate and the closely related heparin, the sulfated chondroitin sulfate and the related dermatan sulfate, and keratan sulfate. Considering the diverse cell-instructive roles of GAGs in native tissues, GAG-based biomaterials have attracted huge attention in the field of TERM (Dinoro et al., 2019; Freudenberg et al., 2016).



• **Figure 1.3.6.2** Three-dimensional printing using specific cell-laden dECM bioinks. (Reproduced with permission from Pati, F., Jang, J., Ha, D.-H., Won Kim, S., Rhie, J.-W., Shim, J.-H., Kim, D.-H., Cho, D.-W., 2014. Printing three-dimensional tissue analogues with decellularized extracellular matrix bioink. *Nat. Commun.* 5, 3935. <https://doi.org/10.1038/ncomms4935>.)

Chondroitin sulfate (CS) is composed of repeating glucuronic acid and N-acetylgalactosamine units and has a high negative charge density. The main sources of CS for biomedical applications are cartilaginous tissues from bovine trachea and, in recent years, also from marine sources such as shark cartilage (Valcarcel et al., 2017). CS is a very heterogeneous family of polysaccharides with high variability in terms of sulfation pattern and chain length, which depend mainly on their sources. CS has traditionally been used for polyelectrolyte complexation strategies to build, e.g., membranes, fibers, and nanoparticles (Costa-Almeida et al., 2016; Santo et al., 2015; Silva et al., 2016).

Hyaluronic acid (HA) is the only nonsulfated GAG, and consists of repeating disaccharide units of N-acetylglucosamine and glucuronic acid. For biomedical and biotechnological use, it has been traditionally isolated from animal sources, mainly rooster combs, but in recent years microbial fermentation has emerged as the preferred alternative in industrial production of HA (Liu et al., 2011). Although HA is among the preferred polymers for hydrogel matrices in the biomedical field, it does not have any natural and effective physical mechanisms of gelling (e.g., thermal, ionic) and therefore, chemical modification is required for this type of application (Highley et al., 2016). Readers are addressed to the section “Dynamic Hydrogels Exploring Supramolecular Chemistry” of this chapter and to the excellent reviews from Burdick’s group to gain a better overview of HA-based biomaterials for biomedical applications (Burdick and Prestwich, 2011; Highley et al., 2016). Among several strategies, recent works have developed an injectable hydrogel using a combination of dynamic covalent cross-linking with thermoresponsive engineered proteins provided by hydrazine-modified elastin-like protein and aldehyde-modified HA. This biomaterial allowed the

encapsulated cells maintain their ability to differentiate into multiple lineages after injection (Wang et al., 2017) and the increase in cartilage-marker gene expression and GAG deposition while minimizing undesirable fibrocartilage phenotype (Zhu et al., 2017b).

Blood Derivatives as a Source of Bioinstructive Materials

Upon tissue injury, blood components, together with the provisional fibrillar matrix, are crucial to achieve hemostasis, to support cell infiltration, and to establish a spatial-temporal chemotactic gradient of proteins (e.g., GFs, cytokines, morphogens) that can tightly regulate the complex wound healing microenvironment (Anitua et al., 2019; Mendes et al., 2018a). During normal wound repair, the mimetic fibrillar network embedded with biologically active proteins is remodeled, being gradually degraded and replaced by mature ECM, until tissue repair is achieved. In a biomimetic approach, blood derivative formulations have been extensively studied to guide the wound healing process into regenerative pathways by tailoring the biophysical and biochemical cues present on the biomimetic ECM (Mendes et al., 2018a). In particular, platelet-rich blood derivative strategies led to the development of a panoply of novel human-based biomaterials that are making their way to clinical application.

Under physiological conditions, activated platelets release an enriched milieu of proteins, while circulating fibrinogen is polymerized, producing an insoluble fibrin matrix (clot) through multiple molecular mechanisms (Piechocka et al., 2010; Ryan et al., 1999). Briefly, fibrin polymerization is initiated by thrombin cleavage, which exposes the central domain of fibrinogen-binding sites to interact with

complementary sites at the terminal domains of other fibrin molecules. These noncovalent interactions induce the self-assembly of fibrin monomers and the formation of half-staggered two-stranded protofibrils. When protofibrils achieve a threshold length, they start to associate laterally to form fibers that branch into a stable three-dimensional network due to plasma transglutaminase (factor XIIIa) covalent cross-linking and calcium ions presence. It is clear that the self-assembled fibrin matrix not only provides a provisional hierarchical ECM to facilitate cellular infiltration, but also contains numerous binding domains for the cells, ECM proteins, and secreted GFs (Brown and Barker, 2014; Laurens et al., 2006). Interestingly, fibrin contains binding sequences for integrins, which facilitate the adhesion of platelets, endothelial cells, smooth muscle cells, fibroblasts, and leukocytes (Lishko et al., 2004). Moreover, fibrin through its heparin-binding domain shows a promiscuous high affinity to bind platelet-derived GF (PDGF), vascular endothelial GF (VEGF), and fibroblast GF (FGF), which can be released from the activated/disrupted platelets (Martino et al., 2013). The complex and hierarchical fibrin structure, in combination with the unique molecules binding interactions, highlight the important and ubiquitous role of fibrin as a bioinstructive platform that provides the biophysical and biochemical cues to modulate a number of complex cellular responses.

In a biomimetic regenerative medicine approach, blood derivatives composed by a high content of structural proteins have been easily produced from autologous or heterologous whole blood samples (Mendes et al., 2018a). Thus, blood derivative formulations can be used directly as a liquid or a liquid-to-gel fibrin-based scaffold through the activation of collagen, calcium, or/and thrombin. The modulation of fibrinogen, thrombin, and calcium/salt concentrations has a marked impact over fibrin polymerization dynamics and the resulting fibrin scaffold properties, namely on fiber diameter, mechanical properties, and bioactive molecule sequestration (Brown and Barker, 2014; Dohan Ehrenfest et al., 2012; Piechocka et al., 2010). Throughout the last few decades, fibrin-based blood derivative formulations have been already successfully translated to the clinics (e.g., fibrin glue) due to their positive effects in the localized and sustained delivery of therapeutic GFs in the treatment, for instance, of periodontal and soft tissue wound healing (Anitua et al., 2019; Heher et al., 2018; Miron et al., 2017; Weisel and Litvinov, 2013). However, the lack of standardization in the formulations' preparation, poor characterization of formulations, and conflicting co-delivery of multifunctional biomolecules led to conflicting results in the therapeutic outcomes, opening a debate on their real potential within the field (Marx, 2004; Wang and Avila, 2007). Moreover, the use of fibrillar gels produced from blood derivative precursors has attracted significant interest in the promotion of vascularization in regenerative strategies due to their natural reservoir in angiogenic GFs (e.g., VEGF) (Fortunato et al., 2016). Nevertheless, these strategies also exhibit limited ability to protect biomolecules

from fast clearance and proteolytic degradation, have low mechanical properties, and show a high contractile effect upon cell encapsulation, which severely limits their potential as wound-healing modulators (Robinson et al., 2016; Sadeghi-Ataabadi et al., 2017).

In order to overcome the above-mentioned drawbacks, a wide range of natural and synthetic polymers, inorganic materials, or their blends have been recently combined with blood derivatives to tightly modulate spatiotemporal biomolecules delivery and to reinforce its inherent mechanical and structural properties (Mendes et al., 2018a). Recently, Faramarzi et al. embedded the inert alginate polymer matrix with the enriched bioactive milieu of platelet-rich plasma (platelets suspended in platelet-poor plasma at 1×10^6 platelet μL^{-1} concentration) to obtain a biofunctional alginate bioink for 3D bioprinting (Faramarzi et al., 2018). The engineered patient-specific bioink exhibited a gradual release of bioactive proteins and positively affected the function of mesenchymal stem cells and human umbilical vein endothelial cells, which could be explored to induce a healing response in cardiovascular and musculoskeletal bioprinted tissue constructs. Our research group has been focused on the modulation of biomolecule release kinetics from platelet lysate (platelet disruption by freeze–thaw cycles) hydrogels in a timely and a controlled space by solely using magnetic stimulation (Silva et al., 2018). The incorporation of magnetic nanoparticles in a methacrylated chondroitin sulfate hydrogel loaded with platelet lysate enabled the modulation of hydrogel physical properties (swelling, matrix stability, and degradation) and control over the GF profile release. This magnetic stimulation control led to a synergistic impact on cell morphology and synthesis of tendon- and bone-like matrix in an in vitro interfacial coculture model. In a different work, using polyelectrolyte complexation between two oppositely charged polysaccharides—chitosan and CS—resulted in the formation of nanoparticles that were loaded with PL and human adipose-derived stem cells. These particles showed an initial burst release of growth factors that correlated with higher cell proliferation, compared to cultures on unloaded particles and in the form of cell pellets (Santo et al., 2015). Along the modulation of bioactive molecules profile release, nanomaterials have also been explored to fine-tune hydrogel mechanical properties to trigger specific cellular responses (Memic et al., 2015). This concept was explored on the development of an injectable fibrillar nanocomposite hydrogel based on platelet lysate combined with cellulose nanocrystals (CNC) (Mendes et al., 2018b). Here, by increasing CNC loading it was possible to increase stiffness, improve biomolecule sequestering, and hinder the typical extensive retraction upon 3D cell culture, enabling therefore the modulation of encapsulated human adipose-derived stem cell behavior.

The development of blood derivatives-based biomaterials with biochemically, mechanically, and structurally tunable properties will clearly improve control over the proteins' milieu composition and kinetics release profile. These findings can be explored to fine-tune stem cell behavior toward specific

lineages and, in combination with recent developments in the regenerative mechanisms, to engineer the wound-healing microenvironment toward tissue regeneration.

Multifunctional Biomaterials Based on DNA

Deoxyribonucleic acid (DNA) is a very old and well-known molecule due to its role as genetic information carrier. However, recently, it has also become a key player in materials science. Exploiting the biophysical and biochemical features of single- and double-stranded DNA, a variety of DNA-based materials showing programmable and multifunctional characteristics are used for biomedical applications (Ke et al., 2018; Shahbazi et al., 2018; Zhang et al., 2018). In this section, we focus on hydrogels, aptamers, and nanostructures based on DNA for tissue engineering applications.

The hydrated nature of DNA hydrogels, which can mimic the properties of natural tissues, has awakened the interest in the design of DNA-based tissue engineering scaffolds. DNA hydrogels are normally created using ligase cross-linking or self-assembly reactions, enabling the gelling to occur under physiological conditions and, thus, the encapsulation of cells. These gels have shown excellent biocompatibility and biodegradation (Stoll et al., 2017). In addition, they have been designed to respond to a variety of stimuli, such as temperature, pH, enzymes, light, or magnetic forces to alter their conformation (Shahbazi et al., 2018; Zhang et al., 2018). For example, Liu's group reported a DNA hydrogel that undergoes a pH-driven conformational transition (called the DNA motor), which influences the spatial distance between cross-linking points and subsequently the stiffness of the hydrogel. By changing the pH between 5.0 and 8.0, the storage modulus of the hydrogel could be tuned reversibly from 1000 to 250 Pa (Zhou et al., 2016).

The aptamers, also known as “nucleic acid antibodies,” are designed to specifically bind with high affinity to a target molecule, have been classically used for disease diagnosis and therapy (Keefe et al., 2010; Zhang et al., 2018). DNA aptamers are generated using SELEX, an *in vitro* selection and evolution process, it being theoretically possible to create aptamers that target any molecule of interest (Gelinas et al., 2016). Unlike antibodies, the generation of aptamers is much cheaper and easier and reduces ethical and immunogenic constraints, offering new perspectives in biomedical applications. In a pioneering work using DNA aptamers to design GF mimetics for regenerative medicine, an aptamer for the hepatocyte GF (HGF) receptor (also known as c-Met), which plays a key role in cancer metastasis, inhibited HGF-induced c-Met activation, which suppressed cancer cell mobility *in vitro* (Ueki and Sando, 2014). More recently, aptamers were engineered to bind the PDGF-BB and VEGF. One end of the aptamer was linked to an RGD peptide and the other end to a functional group able to covalently link the aptamer to different material systems such as glass, polymers, or collagen scaffolds. In this new strategy the specific GFs are delivered using cell traction forces on the ECM, avoiding the need for exogenous triggers (Stejskalová et al., 2019).

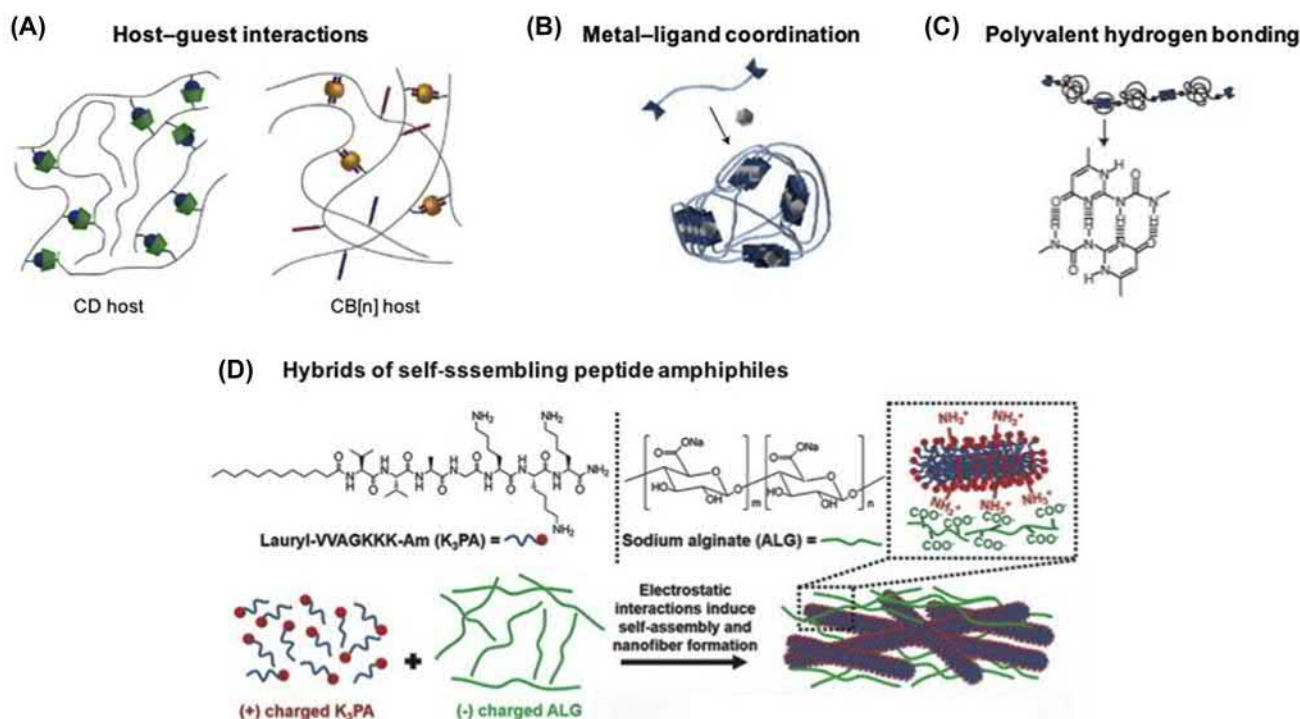
Exploiting nitrogenous bases complementarity and DNA predictable folding, the DNA origami technique provides a versatile platform to engineer nanoscale structures and devices that can sense, compute, and actuate (Hong et al., 2017; Zhang et al., 2018). This has opened a wide range of applications in chemistry, biology, physics, material science, and computer science (Hong et al., 2017). In the field of biomedicine, the most frequent application of these nanostructures is for targeted drug delivery of anticancer drugs, while its use in classical tissue engineering approaches is still limited to a conceptual stage, which is addressed in the last section of this chapter.

Dynamic Hydrogels Exploring Supramolecular Chemistry

A plethora of biocompatible hydrogel cross-linking mechanisms have been developed along the years to recreate hydrated mesh-like architectures of native tissue ECM. Nonetheless, conventional hydrogel systems typically rely on stable, permanent covalent cross-linking bonds that do not capture its highly dynamic character. The inability to relax and dissipate stress, a phenomenon that happens in native ECM by reorganization of physical cross-links or entanglements, or the restrictions that they pose to the spreading, migration, and proliferation of encapsulated cells, are limitations of most static hydrogels (Rosales and Anseth, 2016). In some cases, hydrogel degradation may proceed through hydrolytic or cell-mediated enzymatic degradation (Kharkar et al., 2013). However, the degradation of permanently cross-linked hydrogels presents several drawbacks in TERM applications, such as fast disappearance or deterioration and spatial inhomogeneity of mechanical properties over time. These features pose significant challenges in studying and controlling how cells respond to local biophysical cues, which is increasingly recognized as a key parameter in determining the fate of cells (McKinnon et al., 2014; Rodin et al., 2010).

Reversible Hydrogels Based on Supramolecular Cross-Linking of Polymeric Precursors

Hydrogels based on reversible (or adaptable) linkages that can be broken and reformed in a reversible manner (self-healing) under physiological conditions without external triggers (such as changes in pH or temperature) are becoming increasingly popular in the design of biomaterials (Fig. 1.3.6.3). Several comprehensive reviews covering this topic can be found in the literature (Mann et al., 2018; Saunders and Ma, 2019; Wang and Heilshorn, 2015). The dynamic nature of the linkages (built through physical associations or dynamic covalent bonds) applied to obtain reversible hydrogel systems has significant advantages over static hydrogels. Inherently, it enables the spatiotemporally controlled addition and removal of biochemical signals, repeated changes in matrix mechanics and, having shear-thinning (viscous flow under shear stress) and self-healing (time-dependent



• **Figure 1.3.6.3** Supramolecular biomaterials formed by cross-linking of polymeric precursors through (A) host-guest complexation using macrocyclic hosts, (B) coordination of metals with ligands (end-terminated or grafted on polymer chains), and (C) multiple hydrogen-bonding motifs. (D) Hybrid supramolecular combining high-molecular-weight biopolymers and oppositely charged low-molecular-weight peptide amphiphiles. (Figure adapted with permissions from: (A) Mann, J.L., Yu, A.C., Agmon, G., Appel, E.A., 2018. Supramolecular polymeric biomaterials. *Biomater. Sci.* 6, 10–37. <https://doi.org/10.1039/C7BM00780A>; (B) Burnworth, M., Tang, L., Kumpfer, J.R., Duncan, A.J., Beyer, F.L., Fiore, G.L., Rowan, S.J., Weder, C., 2011. Optically healable supramolecular polymers. *Nature* 472, 334–337. <https://doi.org/10.1038/nature09963>; (C) Dankers, P. Y. W., Harmsen, M. C., Brouwer, L. A., Van Luyn, M. J. A., Meijer, E. W., 2005. A modular and supramolecular approach to bioactive scaffolds for tissue engineering. *Nat. Mater.* 4, 568–574. <https://doi.org/10.1038/nmat1418>; and (D) Borges, J., Sousa, M.P., Cinar, G., Caridade, S.G., Guler, M.O., Mano, J.F., 2017. Nanoengineering hybrid supramolecular multilayered biomaterials using polysaccharides and self-assembling peptide amphiphiles. *Adv. Funct. Mater.* 27, 1605122. <https://doi.org/10.1002/adfm.201605122>.)

recovery upon relaxation) characteristics, they allow the encapsulation and delivery of cells through minimal invasive strategies (Guvendiren et al., 2012; Rosales and Anseth, 2016). This set of characteristics further makes them interesting materials to be applied as bioink for 3D bioprinting (Wang and Heilshorn, 2015). This biofabrication strategy is an emerging and rapidly expanding field of research in which additive manufacturing techniques in combination with cell printing are exploited to generate hierarchical tissue-like structures. In fact, the bioinks, materials that combine printability with cytocompatibility, are currently one of the biggest bottlenecks of 3D bioprinting technology. Thus, new polymeric biomaterials that can overcome these limitations are particularly needed, making reversible hydrogel systems appealing alternatives in this field. Moreover, self-healing hydrogel with rapid self-integrating properties may provide a novel injectable solution for the regeneration of tissue interfaces needing different spatiotemporal biochemical and biophysical cues but that seamlessly integrate at their interfaces (e.g., bone-cartilage tissue complex).

Among the possible approaches to produce reversible hydrogels, systems based on transient polymeric networks

formed through supramolecular cross-linking of polymer chains such as host-guest inclusion complexes (Fig. 1.3.6.3A), multiple hydrogen bonding, or metal-ligand coordination (Fig. 1.3.6.3B–C) are currently among the most promising strategies (Appel et al., 2012; Webber et al., 2016). Here, we highlight some representative studies exploring these reversible hydrogel design strategies with potential application in TERM.

Functionalization of polymers and macromers with pendant host-guest motifs has been among the preferred strategies to produce building blocks of reversibly cross-linked hydrogels. Examples of these systems are the host-guest inclusion complexes using macrocyclic host molecules such as cyclodextrin (CD) and cucurbit[*n*]uril (CB[*n*], *n* = 5–8), showing high affinity for small hydrophobic guest molecules (Mann et al., 2018; Wang and Heilshorn, 2015; Webber et al., 2016). Although other macrocyclic hosts have been explored (e.g., crown ethers, catenanes, and cyclophanes), CD and CB[*n*] are the most commonly applied in TERM. This is mainly because of their compatibility with aqueous use since the interaction between host and guest occurs in a hydrophobic cavity that minimizes

polar solvent interactions (Assaf and Nau, 2015; Mann et al., 2018). Both CD and CB[n] bind guest molecules through hydrophobic and van der Waals interactions in the hydrophobic cavity. However, CB[n] has a higher bind versatility. Whereas CB[6] tends to bind neutral and positively charged organic guests, CB[7] binds larger amphiphilic guests, and CB[8] binds positively charged and large organic guests (Assaf and Nau, 2015; Mann et al., 2018). These different affinities contribute to widening the number of possible hydrogel designs. Moreover, different binding affinities exist not only between CB[n], but also between the host and different guest molecules, a particular behavior that has been recently explored to develop hydrogels with a broad range of bulk dynamic properties without changing network topology (Zou et al., 2019). Both natural (e.g., HA) and synthetic polymeric (e.g., polyacrylamide or PEG) precursors have been cross-linked using these recognition motifs to produce reversible supramolecular hydrogels. The precursor polymers can be grafted with either a host or its complementary guest molecule to form hydrogels when the pairs are mixed. This cross-linking strategy has as an additional advantage the possibility of using the same grafted supramolecular motifs for the modular noncovalent functionalization of polymer hydrogel through biorthogonal synthesis pathways.

Numerous hydrogel systems based on these supramolecular cross-linking strategies have been developed and optimized in the past for 3D cell encapsulation and as injectable cell carriers (Wang and Heilshorn, 2015). The β -CD–adamantane host–guest pair is perhaps one of most well-known cross-linking systems explored in the TERM field. For example, HA has been modified with these pendant moieties to produce a hydrogel that enables shear-thinning injection and high target site retention (>98%) (Rodell et al., 2015). Stabilization of the network through secondary Michael addition reaction (between thiol- and Michael-acceptor modified HA macromers) further improved the positive outcomes on the treatment of myocardial infarct in an in vivo mouse model. In a similar approach, the low stability and mechanical properties of β -CD–adamantane cross-linked HA has been improved by first promoting the host–guest complexation between monoacrylated β -CD host monomers and adamantane-functionalized HA guest polymers, to fabricate the supramolecular hydrogels by UV-induced polymerization of preassembled host–guest complexes (Wei et al., 2016). These hydrogels demonstrated self-healing behavior and showed promising results as injectable cell carriers, supporting chondrogenesis of human mesenchymal stem cells (hMSCs) and promoting cartilage regeneration in a rat model. Injectable and cytocompatible hydrogels have also been produced based on CB[6]-modified HA mixed with the respective complementary guest, diaminohexane conjugated HA (DAH-HA), that was applied for the controlled chondrogenesis of hMSCs (Jung et al., 2014). Interestingly, this host–guest pair was not only used to produce the hydrogel as a cell carrier, but was also leveraged to functionalize the polymer backbone

with a prochondrogenic drug conjugated to CB[6], demonstrating the modular nature of these type of systems. The versatility of this strategy was later explored to support the long-term survival and prolonged transgene expression of bioengineered MSCs, a potential platform biomaterial that can be applied in the treatment of cancer and other intractable diseases (Yeom et al., 2015).

Functionalization of polymers or macromers with multiple hydrogen bonding motifs, such as the quadruple hydrogen bonding motif ureidopyrimidinone (UPy), is another widely reported strategy for the production of supramolecular hydrogels with viscoelasticity, shear-thinning, and self-healing behavior (Saunders and Ma, 2019; Webber et al., 2016). Several hydrogels based on UPy cross-linking have been used as biologic, and recently, also as cell delivery systems. A notable example of this strategy is a dextran-based hydrogel where the polymer backbone was functionalized with multiple pendant UPy units per chain (Hou et al., 2015). This supramolecular hydrogel was used as a cell carrier and drug-delivery system (chondrocytes, bone marrow stem cells, and bone morphogenetic protein 2). Moreover, due to its self-healing and shear-thinning nature, the system has the potential to be applied in the regeneration of complex tissue interfaces.

Metal–ligand interactions are an alternative cross-linking strategy that are gaining relevance in the biomaterials field. This class of supramolecular cross-linking, in which two or more ligands donate a nonbinding electron pair to empty orbitals in a transition metal cation, include the well-known Fe-catechol coordination complexes that have stability and strength approaching covalent bonds (Mann et al., 2018; Webber et al., 2016). Several mussel-inspired metal–ligand hydrogels based on Fe-catechol cross-linking have been developed in the past few years. For example, HA functionalized with pendent catechol can be cross-linked with Fe^{3+} ions, resulting in reversible, self-healable, and tissue-adhesive hydrogels (Lee et al., 2016; Park et al., 2016; Shin et al., 2015). These biocompatible injectable hydrogels were demonstrated to be effective for cell transplantation (Shin et al., 2015) and could potentiate the in vivo stem cell-mediated angiogenesis and osteogenesis potential in tissue defect models (Park et al., 2016), making them promising materials for TERM applications.

The unique rheology and gelation properties of the above-mentioned supramolecular hydrogels make them obvious candidates as bioinks materials for 3D bioprinting. Burdick's research group has published a representative example of such applications. Their approach explores an interesting printing strategy based on HA bioink that cross-links through supramolecular assembly of β -CD–adamantane host–guest complexes (Highley et al., 2015; Ouyang et al., 2016). Since the host–guest supramolecular bonds can be disrupted by the shearing stress applied during the extrusion process and rapidly reform after printing without any further trigger, this system allows reaching new levels of 3D printing complexity, such as the direct writing of shear-thinning bioinks at any position of a 3D space into

supporting self-healing hydrogels made of similar materials. The printed structures can be further stabilized by secondary cross-linking by, e.g., introducing methacrylates into the HA and post-printing photopolymerization. The versatility of this platform has shown that supramolecular cross-linked hydrogels are biomaterials with new and existing properties to be explored in the field of 3D bioprinting.

Hydrogels Based on Natural Supramolecular Self-Assembly

Based on DNA self-assembly capacity, hybrid DNA hydrogels can be developed using short DNA sequences mixed or coupled onto the polymer backbones physically or chemically. Contrary to DNA-based hydrogels addressed in the section “Multifunctional Biomaterials Based on DNA,” hybrid hydrogels only require a small quantity of DNA, and self-assembled DNA acts as both the cross-linker and switchable element (Shahbazi et al., 2018; Shao et al., 2017). For example, Li and colleagues combined single-stranded (ss) DNA attached to a polymer backbone with a double-stranded DNA with ending sequences complementary to the ssDNA to develop a biodegradable bioink with encapsulated cells (Li et al., 2015). The hydrogel was biocompatible and could be used for rapid formation of 3D constructs for tissue engineering.

In another very interesting approach, a stimuli-responsive liposome–DNA hydrogel was created by the functionalization of polyacrylamide with cholesterol-modified DNA motifs (Lyu et al., 2018). The cholesterol interacts with the lipid bilayers of the liposomes and cross-links the polymer in a reversible manner (sol–gel–sol transitions) due to the thermosensitive nature of DNA motifs. Moreover, the system can serve as a release system upon the presence of a restriction endonuclease enzyme.

Peptides are versatile building blocks for supramolecular assembly of tissue engineering constructs. The use of peptides to create biomaterials provides a number of advantages such as natural biodegradation, and the possibility to mimic the structural and functional aspects of native ECM. Peptides can be used alone, or designed for conjugation or coassembly with polymers in order to improve bioactivity and structural complexity. In particular, the supramolecular assembly capacity of peptide amphiphiles (PAs), consisting of a charged hydrophilic head, a β -sheet forming domain, and a hydrophobic alkyl tail (Fig. 1.3.6.3D), has been used to create one-dimensional self-assembled fibrillar structures with many applications in biomedicine (Borges et al., 2017; Brito et al., 2019; Radvar and Azevedo, 2019; Webber et al., 2016). Although not covered in this chapter, for more information readers are directed to a recent review on the topic by the Stupp’s group, pioneers in the field (Hendricks et al., 2017).

PA also can be coassembled with hydrophobic polymer tails or polypeptides to construct self-assembling bioactive and biomimetic hydrogels (Borges et al., 2017; Radvar and Azevedo, 2019). In a recent work, a biodegradable

self-healing polymer–peptide hydrogel consisting of a poly(γ -glutamic acid) polymer network was physically cross-linked via conjugated β -sheet peptide sequences (Clarke et al., 2017). The authors could tailor the mechanical properties of the hydrogels over an order of magnitude range of 10–200 kPa, which is in the region of many soft tissues, by altering the β -sheet peptide graft density and concentration. In a different approach, using hybrid PA–protein systems, Mata and colleagues produced complex hierarchical fibrillar membranes and 3D printed constructs for tissue engineering applications. On one hand, hybrid PA–elastin-like polypeptides were used as building blocks to fabricate foldable bioactive membranes that guide the growth of endothelial and adipose-derived stem cells into tubular structures (Inostroza-Brito et al., 2015). In a later work, using a range of ECM biomolecules as the protein component of the hybrid system, adipose-derived stem cells were bioprinted with high viability into complex hierarchical structures, demonstrating that the combination of self-assembly with 3D bioprinting has a huge potential in the field (Hedegaard et al., 2018).

Soft Nanocomposite Smart Materials

The nanoscale interactions between the cells and the tissue microenvironment control the function and fate of the cells. Hence, the rational design of biomimetic and functional biomaterials is subjective to these cues (Memic et al., 2015). The design of “smart materials,” stimuli-responsive materials that respond to external stimuli such as pH, temperature, magnetic, electric, or any other stimulus, is gaining increased relevance in the biomedical field (Merino et al., 2015). Among the numerous strategies to incorporate new and tunable functionalities in biomaterials, the incorporation of nanoparticles in hydrogels has become a popular option, not only as mere reinforcement nanofillers, but also as functional nanoelements to meet the specific needs of the different tissues (Alarçin et al., 2016). These nanoelements can be manipulated to interfere with cell processes like growth, differentiation, proliferation, and alignment in a controlled manner (Carrow and Gaharwar, 2015). In this section, we highlight some of the latest developments on soft nanocomposites developed using natural materials.

Stimuli-Responsive Soft Nanocomposites

The intrinsic properties of iron-based magnetic nanoparticles (MNPs) are highly attractive to produce responsive biomaterials providing the liberty to control the spatial distribution and orientation of MNPs through remote magnetic fields (Tibbitt et al., 2015). For example, a hybrid hydrogel composed of type II collagen, hyaluronic acid, and polyethylene glycol, incorporating MNPs was guided to defect tissue sites using a remote magnetic field (Zhang et al., 2015). This work paves a path for further investigation of tunable magneto-responsive nanocomposites for minimally invasive tissue engineering strategies.

Furthermore, the use of rod-shaped CNC, the nature's "carbon nanotubes," has been explored by our group and others to cross-link and reinforce soft HA hydrogel networks (Domingues et al., 2015) and to produce anisotropic domains within natural and synthetic 3D hydrogels (Araújo-Custódio et al., 2019; De France et al., 2017). These CNC could also be decorated with MNPs to create injectable gelatin hydrogels presenting an aligned microstructure, which was achieved by the alignment of the nanoparticles under the influence of low magnetic fields (106 mT) (Araújo-Custódio et al., 2019). At the same time, hydrogel 3D anisotropy induced the alignment of encapsulated and seeded adipose tissue-derived stem cells, when compared with isotropic hydrogels.

In a different approach, the incorporation of electroconductive nanoelements can play a key role in the improvement of regenerative strategies for electro-responsive organs/tissue, such as the heart, muscles, and neural tissue (Palza et al., 2019). For example, an electro-responsive nanogel was achieved via incorporation of gold nanoparticles in a chitosan hydrogel. The amount of nanoparticle in the hydrogel was directly proportional to electrical conductivity. Mesenchymal stem cells seeded on these hydrogels showed high viability and were able to migrate and proliferate, while showing evidence of accelerated cardiomyogenic differentiation in comparison with control hydrogels (Baei et al., 2016).

Future Perspectives

Tissue engineering was born with the promise of revolutionizing health care by providing artificially engineered functional tissue and organ substitutes (Langer and Vacanti, 1993). During the last few decades, extraordinary accomplishments have been achieved and significant scientific knowledge spanning from cell biology up to advanced biomaterials synthesis and processing technologies has been produced. However, the vast majority of strategies has been developed as "one-size-fits-all." Addressing the increasing demand for precision and personalized medicine treatments, in which health care is tailored on the basis of individual complexities (Hodson, 2016), the extension of this concept to the field of TERM will allow to produce biomaterials with precise and specific functions that will be integrated with technological advances such as microfabrication, 3D bioprinting, and stem cells, to select the most suitable approach to treat diseases or injuries in a specific patient or subset of patients (Aguado et al., 2018). Furthermore, using the same principles, personalized tissue constructs have the incomparable potential to be used as disease models that will change the future of drug-discovery pipelines in a manner that substantially deviates from traditional platforms, namely, 2D cell monolayer cultures and animal disease models (Skardal et al., 2016).

The combination of blood derivatives with biomaterials has emerged as a synergistic strategy to modulate the release of signaling molecules that orchestrate the swing

between tissue regeneration, tissue repair, and scar formation (Mendes et al., 2018a). In this sense, the use of biomimetic biomaterials described in this chapter incorporating standardized blood derivatives might enable engineering the wound-healing environment toward tissue regeneration. In a translational perspective, we think that this strategy holds great potential to produce biomimetic and bioactive materials for different TERM applications due to the increasing trend on the production and use of standardized clinical-grade human PL as a xeno-free alternative to animal-derived serum in cell culture, which represents an advantage over similar materials such as dECM. This further strengthens the use of blood derivative formulations not only for research purposes, but also in terms of compliance with good manufacturing practices and clinical relevance.

DNA-based materials represent a forefront frontier for the biomaterials field due to their versatility. In particular, an underexplored area is the use of DNA origami for TERM applications. These nanostructures could be used to provide direct cell behavior on surfaces (2D) and hydrogel (3D) environments. For example, the creation of anisotropic DNA origami patterns, as shown in a chemically modified graphene surface (Yun et al., 2012), could be used to provide enough biophysical cues to guide the appropriate stem cells toward the regeneration of anisotropic tissues. Furthermore, the potential of DNA origami nanostructures to bind serum proteins could be explored for the selective/preferential binding of GFs and to control its delivery to target tissues.

In addition, so far mostly the methods to achieve anisotropy within hydrogel matrices depend on external stimuli such as magnetic or electrical, which is not universally practical for large-scale production (Chen et al., 2018). Hence, we believe that continued development in this area of soft nanocomposites is essential to acquire scalable orderly structures, with excellent mechanical properties, and novel responses to stimuli for use in innovative applications in the fields of biomedicine, sensors, actuators, and biomimetic materials.

Using an out-of-the-box concept, a new generation of living biomaterials that contain genetically modified bacteria have been proposed to modulate the microenvironment in a dynamic way. For this, bacteria are engineered to produce proteins and GFs triggered by external stimuli such as molecules and drugs, in a dose-dependent manner (Hay et al., 2018; Sankaran et al., 2018). Furthermore, the combination of additive manufacturing or other advanced technologies and bacteria (Liu et al., 2018; Schaffner et al., 2017) might bring a new generation of living responsive materials on demand, if serious bacterial safety concerns are addressed.

Despite the added functionalities that provide many new materials, the clinical translation of tissue-engineered products has been significantly slower than would be expected. The complexity of some strategies represents the main barrier for clinical translation, as practical, economic, and

regulatory barriers favor simplicity (Abou-El-Enein et al., 2017; Darnell and Mooney, 2017). However, tissues and organs have multiscaled architectures, multiple cell types and ECM components, and possess a complex vascular, neural, and lymphatic network to support cell activity in a finely orchestrated dynamic microenvironment. Balancing the need for simplicity with this natural complexity creates the necessity for biomaterials researchers to identify the strategies, within the large design space now available, with the minimum necessary complexity to recreate native tissues.

Acknowledgments

The authors acknowledge the financial support of the European Union Framework Programme for Research and Innovation Horizon 2020, under the TEAMING grant agreement No 739572 – The Discoveries CTR, Marie Skłodowska-Curie grant agreement No 706996 and European Research Council grant agreement No 726178; FCT (Fundação para a Ciência e a Tecnologia) and the Fundo Social Europeu através do Programa Operacional do Capital Humano (FSE/POCH) in the framework of Ph.D. grants PD/BD/113807/2015 (BBM) and PD/BD/129403/2017 (SMB), Post-Doc grant SFRH/BPD/112459/2015 (RMD) and project SmarTendon (PTDC/NAN-MAT/30595/2017); Project NORTE-01-0145-FEDER-000021 supported by Norte Portugal Regional Operational Programme (NORTE 2020), under the PORTUGAL 2020 Partnership Agreement, through the European Regional Development Fund (ERDF).

References

- Abou-El-Enein, M., Duda, G.N., Gruskin, E.A., Grainger, D.W., 2017. Strategies for derisking translational processes for biomedical technologies. *Trends Biotechnol.* 35, 100–108. <https://doi.org/10.1016/j.tibtech.2016.07.007>.
- Aguado, B.A., Grim, J.C., Rosales, A.M., Watson-Capps, J.J., Anseth, K.S., 2018. Engineering precision biomaterials for personalized medicine. *Sci. Transl. Med.* 10. <https://doi.org/10.1126/scitranslmed.aam8645>.
- Alarçin, E., Guan, X., Kashaf, S.S., Elbaradie, K., Yang, H., Jang, H.L., Khademhosseini, A., 2016. Recreating composition, structure, functionalities of tissues at nanoscale for regenerative medicine. *Regen. Med.* 11, 849–858. <https://doi.org/10.2217/rme-2016-0120>.
- Anitua, E., Nurden, P., Prado, R., Nurden, A.T., Padilla, S., 2019. Autologous fibrin scaffolds: when platelet- and plasma-derived biomolecules meet fibrin. *Biomaterials* 192, 440–460. <https://doi.org/10.1016/j.biomaterials.2018.11.029>.
- Annabi, N., Mithieux, S.M., Weiss, A.S., Dehghani, F., 2010. Cross-linked open-pore elastic hydrogels based on tropoelastin, elastin and high pressure CO₂. *Biomaterials* 31, 1655–1665. <https://doi.org/10.1016/j.biomaterials.2009.11.051>.
- Annabi, N., Rana, D., Shirzaei Sani, E., Portillo-Lara, R., Gifford, J.L., Fares, M.M., Mithieux, S.M., Weiss, A.S., 2017. Engineering a sprayable and elastic hydrogel adhesive with antimicrobial properties for wound healing. *Biomaterials* 139, 229–243. <https://doi.org/10.1016/j.biomaterials.2017.05.011>.
- Appel, E.A., del Barrio, J., Loh, X.J., Scherman, O.A., 2012. Supramolecular polymeric hydrogels. *Chem. Soc. Rev.* 41, 6195. <https://doi.org/10.1039/c2cs35264h>.
- Araújo-Custódio, S., Gomez-Florit, M., Tomás, A.R., Mendes, B.B., Babo, P.S., Mithieux, S.M., Weiss, A.S., Domingues, R., Reis, R.L., Gomes, M.E., 2019. Injectable and magnetic responsive hydrogels with bioinspired ordered structures. *ACS Biomater. Sci. Eng. acsbiomaterials*. <https://doi.org/10.1021/acsbiomaterials.8b01179>.
- Assaf, K.I., Nau, W.M., 2015. Cucurbiturils: from synthesis to high-affinity binding and catalysis. *Chem. Soc. Rev.* 44, 394–418. <https://doi.org/10.1039/C4CS00273C>.
- Baei, P., Jalili-Firoozinezhad, S., Rajabi-Zeleti, S., Tafazzoli-Shadpour, M., Baharvand, H., Aghdami, N., 2016. Electrically conductive gold nanoparticle-chitosan thermosensitive hydrogels for cardiac tissue engineering. *Mater. Sci. Eng.* C 63, 131–141. <https://doi.org/10.1016/j.msec.2016.02.056>.
- Borges, J., Sousa, M.P., Cinar, G., Caridade, S.G., Guler, M.O., Mano, J.F., 2017. Nanoengineering hybrid supramolecular multilayered biomaterials using polysaccharides and self-assembling peptide amphiphiles. *Adv. Funct. Mater.* 27, 1605122. <https://doi.org/10.1002/adfm.201605122>.
- Brito, A., Abul-Haija, Y.M., da Costa, D.S., Novoa-Carballal, R., Reis, R.L., Ulijn, R.V., Pires, R.A., Pashkuleva, I., 2019. Minimalistic supramolecular proteoglycan mimics by co-assembly of aromatic peptide and carbohydrate amphiphiles. *Chem. Sci.* <https://doi.org/10.1039/C8SC04361B>.
- Brown, A.C., Barker, T.H., 2014. Fibrin-based biomaterials: modulation of macroscopic properties through rational design at the molecular level. *Acta Biomater.* 10, 1502–1514. <https://doi.org/10.1016/j.actbio.2013.09.008>.
- Burdick, J.A., Prestwich, G.D., 2011. Hyaluronic acid hydrogels for biomedical applications. *Adv. Mater.* 23, H41–H56. <https://doi.org/10.1002/adma.201003963>.
- Carrow, J.K., Gaharwar, A.K., 2015. Bioinspired polymeric nanocomposites for regenerative medicine. *Macromol. Chem. Phys.* 216, 248–264. <https://doi.org/10.1002/macp.201400427>.
- Chen, T., Hou, K., Ren, Q., Chen, G., Wei, P., Zhu, M., 2018. Nanoparticle-polymer synergies in nanocomposite hydrogels: from design to application. *Macromol. Rapid Commun.* 39, 1800337. <https://doi.org/10.1002/marc.201800337>.
- Choudhury, D., Tun, H.W., Wang, T., Naing, M.W., 2018. Organ-derived decellularized extracellular matrix: a game changer for bioink manufacturing? *Trends Biotechnol.* <https://doi.org/10.1016/j.tibtech.2018.03.003>.
- Clarke, D.E., Pashuck, E.T., Bertazzo, S., Weaver, J.V.M., Stevens, M.M., 2017. Self-healing, self-assembled β -sheet peptide-poly(γ -glutamic acid) hybrid hydrogels. *J. Am. Chem. Soc.* 139, 7250–7255. <https://doi.org/10.1021/jacs.7b00528>.
- Costa-Almeida, R., Gasperini, L., Borges, J., Babo, P.S., Rodrigues, M.T., Mano, J.F., Reis, R.L., Gomes, M.E., 2016. Microengineered multi-component hydrogel fibers: combining polyelectrolyte complexation and microfluidics. *ACS Biomater. Sci. Eng. acsbiomaterials*.6b00331. <https://doi.org/10.1021/acsbiomaterials.6b00331>.
- Darnell, M., Mooney, D.J., 2017. Leveraging advances in biology to design biomaterials. *Nat. Mater.* 16, 1178–1185. <https://doi.org/10.1038/nmat4991>.
- De France, K.J., Yager, K.G., Chan, K.J.W., Corbett, B., Cranston, E.D., Hoare, T., 2017. Injectable Anisotropic nanocomposite hydrogels direct in situ growth and alignment of myotubes. *Nano Lett.* 17, 6487–6495. <https://doi.org/10.1021/acs.nanolett.7b03600>.

- Dinoro, J., Maher, M., Talebian, S., Jarfarkhani, M., Mehrali, M., Orive, G., Foroughi, J., Lord, M.S., Dolatshahi-Pirouz, A., 2019. Sulfated polysaccharide-based scaffolds for orthopaedic tissue engineering. *Biomaterials*. <https://doi.org/10.1016/j.biomaterials.2019.05.025>.
- Dohan Ehrenfest, D.M., Bielecki, T., Jimbo, R., Barbé, G., Del Corso, M., Inchingolo, F., Sammartino, G., 2012. Do the fibrin architecture and leukocyte content influence the growth factor release of platelet concentrates? An evidence-based answer comparing a pure platelet-rich plasma (P-PRP) gel and a leukocyte- and platelet-rich fibrin (L-PRF). *Curr. Pharmaceut. Biotechnol.* 13, 1145–1152.
- Domingues, R.M.A., Silva, M., Gershovich, P., Betta, S., Babo, P., Caridade, S.G., Mano, J.F., Motta, A., Reis, R.L., Gomes, M.E., 2015. Development of injectable hyaluronic acid/cellulose nanocrystals bionanocomposite hydrogels for tissue engineering applications. *Bioconjug. Chem.* 26, 1571–1581. <https://doi.org/10.1021/acs.bioconjchem.5b00209>.
- Faramarzi, N., Yazdi, I.K., Nabavinia, M., Gemma, A., Fanelli, A., Caizzone, A., Ptaszek, L.M., Sinha, I., Khademhosseini, A., Ruskin, J.N., Tamayol, A., 2018. Patient-specific bioinks for 3D bioprinting of tissue engineering scaffolds. *Adv. Healthc. Mater.* 7, 1701347. <https://doi.org/10.1002/adhm.201701347>.
- Fortunato, T.M., Beltrami, C., Emanuelli, C., De Bank, P.A., Pula, G., 2016. Platelet lysate gel and endothelial progenitors stimulate microvascular network formation in vitro: tissue engineering implications. *Sci. Rep.* 6, 25326. <https://doi.org/10.1038/srep25326>.
- Freundenberg, U., Liang, Y., Kiick, K.L., Werner, C., 2016. Glycosaminoglycan-based biohybrid hydrogels: a sweet and smart choice for multifunctional biomaterials. *Adv. Mater.* 28, 8861–8891. <https://doi.org/10.1002/adma.201601908>.
- Gelinas, A.D., Davies, D.R., Janjic, N., 2016. Embracing proteins: structural themes in aptamer–protein complexes. *Curr. Opin. Struct. Biol.* 36, 122–132. <https://doi.org/10.1016/j.sbi.2016.01.009>.
- González de Torre, I., Santos, M., Quintanilla, L., Testera, A., Alonso, M., Rodríguez Cabello, J.C., 2014. Elastin-like recombinamer catalyst-free click gels: characterization of poroelastic and intrinsic viscoelastic properties. *Acta Biomater.* 10, 2495–2505. <https://doi.org/10.1016/j.actbio.2014.02.006>.
- Guvendiren, M., Lu, H.D., Burdick, J.A., 2012. Shear-thinning hydrogels for biomedical applications. *Soft Matter* 8, 260–272. <https://doi.org/10.1039/C1SM06513K>.
- Hay, J.J., Rodrigo-Navarro, A., Petaroudi, M., Bryksin, A.V., García, A.J., Barker, T.H., Dalby, M.J., Salmeron-Sanchez, M., 2018. Bacteria-based materials for stem cell engineering. *Adv. Mater.* 30, 1804310. <https://doi.org/10.1002/adma.201804310>.
- Hedegaard, C.L., Collin, E.C., Redondo-Gómez, C., Nguyen, L.T.H., Ng, K.W., Castrejón-Pita, A.A., Castrejón-Pita, J.R., Mata, A., 2018. Hydrodynamically guided hierarchical self-assembly of peptide-protein bioinks. *Adv. Funct. Mater.* 28, 1703716. <https://doi.org/10.1002/adfm.201703716>.
- Heher, P., Mühleder, S., Mittermayr, R., Redl, H., Slezak, P., 2018. Fibrin-based delivery strategies for acute and chronic wound healing. *Adv. Drug Deliv. Rev.* 129, 134–147. <https://doi.org/10.1016/j.addr.2017.12.007>.
- Hendricks, M.P., Sato, K., Palmer, L.C., Stupp, S.I., 2017. Supramolecular assembly of peptide amphiphiles. *Acc. Chem. Res.* 50, 2440–2448. <https://doi.org/10.1021/acs.accounts.7b00297>.
- Highley, C.B., Prestwich, G.D., Burdick, J.A., 2016. Recent advances in hyaluronic acid hydrogels for biomedical applications. *Curr. Opin. Biotechnol.* 40, 35–40. <https://doi.org/10.1016/j.copbio.2016.02.008>.
- Highley, C.B., Rodell, C.B., Burdick, J.A., 2015. Direct 3D printing of shear-thinning hydrogels into self-healing hydrogels. *Adv. Mater.* 27, 5075–5079. <https://doi.org/10.1002/adma.201501234>.
- Hodson, R., 2016. Precision medicine. *Nature* 537. <https://doi.org/10.1038/537S49a>. S49–S49.
- Hong, F., Zhang, F., Liu, Y., Yan, H., 2017. DNA origami: scaffolds for creating higher order structures. *Chem. Rev.* 117, 12584–12640. <https://doi.org/10.1021/acs.chemrev.6b00825>.
- Hou, S., Wang, X., Park, S., Jin, X., Ma, P.X., 2015. Rapid self-integrating, injectable hydrogel for tissue complex regeneration. *Adv. Healthc. Mater.* 4, 1491–1495. <https://doi.org/10.1002/adhm.201500093>.
- Hu, X., Park, S.H., Gil, E.S., Xia, X.X., Weiss, A.S., Kaplan, D.L., 2011. The influence of elasticity and surface roughness on myogenic and osteogenic-differentiation of cells on silk-elastin biomaterials. *Biomaterials* 32, 8979–8989. <https://doi.org/10.1016/j.biomaterials.2011.08.037>.
- Huettner, N., Dargaville, T.R., Forget, A., 2018. Discovering cell-adhesion peptides in tissue engineering: beyond RGD. *Trends Biotechnol.* 36, 372–383. <https://doi.org/10.1016/j.tibtech.2018.01.008>.
- Hussey, G.S., Dziki, J.L., Badylak, S.F., 2018. Extracellular matrix-based materials for regenerative medicine. *Nat. Rev. Mater.* 1–15. <https://doi.org/10.1038/s41578-018-0023-x>.
- Inostroza-Brito, K.E., Collin, E., Siton-Mendelson, O., Smith, K.H., Monge-Marcet, A., Ferreira, D.S., Rodríguez, R.P., Alonso, M., Rodríguez-Cabello, J.C., Reis, R.L., Sagués, F., Botto, L., Bitton, R., Azevedo, H.S., Mata, A., 2015. Co-assembly, spatiotemporal control and morphogenesis of a hybrid protein–peptide system. *Nat. Chem.* 7, 897–904. <https://doi.org/10.1038/nchem.2349>.
- Jung, H., Park, J.S., Yeom, J., Selvapalam, N., Park, K.M., Oh, K., Yang, J.-A., Park, K.H., Hahn, S.K., Kim, K., 2014. 3D tissue engineered supramolecular hydrogels for controlled chondrogenesis of human mesenchymal stem cells. *Biomacromolecules* 15, 707–714. <https://doi.org/10.1021/bm401123m>.
- Ke, Y., Castro, C., Choi, J.H., 2018. Structural DNA nanotechnology: artificial nanostructures for biomedical research. *Annu. Rev. Biomed. Eng.* 20, 375–401. <https://doi.org/10.1146/annurev-bioeng-062117-120904>.
- Keefe, A.D., Pai, S., Ellington, A., 2010. Aptamers as therapeutics. *Nat. Rev. Drug Discov.* 9, 537–550. <https://doi.org/10.1038/nrd3141>.
- Kharkar, P.M., Kiick, K.L., Kloxin, A.M., 2013. Designing degradable hydrogels for orthogonal control of cell microenvironments. *Chem. Soc. Rev.* 42, 7335–7372. <https://doi.org/10.1039/C3CS60040H>.
- Langer, R., Vacanti, J., 1993. Tissue engineering. *Science* 260, 920–926. <https://doi.org/10.1126/science.8493529>.
- Laurens, N., Koolwijk, P., de Maat, M.P.M., 2006. Fibrin structure and wound healing. *J. Thromb. Haemost.* 4, 932–939. <https://doi.org/10.1111/j.1538-7836.2006.01861.x>.
- Lee, J., Chang, K., Kim, S., Gite, V., Chung, H., Sohn, D., 2016. Phase controllable hyaluronic acid hydrogel with iron(III) ion-catechol induced dual cross-linking by utilizing the gap of gelation kinetics. *Macromolecules* 49, 7450–7459. <https://doi.org/10.1021/acs.macromol.6b01198>.
- Li, C., Faulkner-Jones, A., Dun, A.R., Jin, J., Chen, P., Xing, Y., Yang, Z., Li, Z., Shu, W., Liu, D., Duncan, R.R., 2015. Rapid formation of a supramolecular polypeptide-DNA hydrogel for in situ three-dimensional multilayer bioprinting. *Angew. Chem. Int. Ed.* 54, 3957–3961. <https://doi.org/10.1002/anie.201411383>.
- Li, S., Nih, L.R., Bachman, H., Fei, P., Li, Y., Nam, E., Dimatteo, R., Carmichael, S.T., Barker, T.H., Segura, T., 2017. Hydrogels with precisely controlled integrin activation dictate vascular

- patterning and permeability. *Nat. Mater.* 16, 953–961. <https://doi.org/10.1038/nmat4954>.
- Lishko, V.K., Podolnikova, N.P., Yakubenko, V.P., Yakovlev, S., Medved, L., Yadav, S.P., Ugarova, T.P., 2004. Multiple binding sites in fibrinogen for integrin alphaMbeta2 (Mac-1). *J. Biol. Chem.* 279, 44897–44906. <https://doi.org/10.1074/jbc.M408012200>.
- Liu, L., Liu, Y., Li, J., Du, G., Chen, J., 2011. Microbial production of hyaluronic acid: current state, challenges, and perspectives. *Microb. Cell Fact.* 10, 99. <https://doi.org/10.1186/1475-2859-10-99>.
- Liu, X., Yuk, H., Lin, S., Parada, G.A., Tang, T.-C., Tham, E., de la Fuente-Nunez, C., Lu, T.K., Zhao, X., 2018. 3D printing of living responsive materials and devices. *Adv. Mater.* 30, 1704821. <https://doi.org/10.1002/adma.201704821>.
- Lyu, D., Chen, S., Guo, W., 2018. Liposome crosslinked polyacrylamide/DNA hydrogel: a smart controlled-release system for small molecular payloads. *Small* 14, e1704039. <https://doi.org/10.1002/sml.201704039>.
- Machula, H., Ensley, B., Kellar, R., 2014. Electrospun tropoelastin for delivery of therapeutic adipose-derived stem cells to full-thickness dermal wounds. 3, 367–375. <https://doi.org/10.1089/wound.2013.0513>.
- Mann, J.L., Yu, A.C., Agmon, G., Appel, E.A., 2018. Supramolecular polymeric biomaterials. *Biomater. Sci.* 6, 10–37. <https://doi.org/10.1039/C7BM00780A>.
- Mano, J., Silva, G., Azevedo, H., Malafaya, P., Sousa, R., Silva, S., Boesel, L., Oliveira, J., Santos, T., Marques, A., Neves, N., Reis, R., 2007. Natural origin biodegradable systems in tissue engineering and regenerative medicine: present status and some moving trends. *J. R. Soc. Interface* 4, 999–1030. <https://doi.org/10.1098/rsif.2007.0220>.
- Martino, M.M., Briquez, P.S., Ranga, A., Lutolf, M.P., Hubbell, J.A., 2013. Heparin-binding domain of fibrin(ogen) binds growth factors and promotes tissue repair when incorporated within a synthetic matrix. *Proc. Natl. Acad. Sci.* 110, 4563–4568. <https://doi.org/10.1073/pnas.1221602110>.
- Martino, M.M., Mochizuki, M., Rothenfluh, D.A., Rempel, S.A., Hubbell, J.A., Barker, T.H., 2009. Controlling integrin specificity and stem cell differentiation in 2D and 3D environments through regulation of fibronectin domain stability. *Biomaterials* 30, 1089–1097. <https://doi.org/10.1016/j.biomaterials.2008.10.047>.
- Martino, M.M., Tortelli, F., Mochizuki, M., Traub, S., Ben-David, D., Kuhn, G.A., Muller, R., Livne, E., Eming, S.A., Hubbell, J.A., 2011. Engineering the growth factor microenvironment with fibronectin domains to promote wound and bone tissue healing. *Sci. Transl. Med.* 3. <https://doi.org/10.1126/scitranslmed.3002614>. 100ra89-100ra89.
- Marx, R.E., 2004. Platelet-rich plasma: evidence to support its use. *J. Oral Maxillofac. Surg.* 62, 489–496.
- McKinnon, D.D., Domaille, D.W., Brown, T.E., Kyburz, K.A., Kiyotake, E., Cha, J.N., Anseth, K.S., 2014. Measuring cellular forces using bis-aliphatic hydrazone crosslinked stress-relaxing hydrogels. *Soft Matter* 10, 9230–9236. <https://doi.org/10.1039/c4sm01365d>.
- Mecham, R.P., 2001. Overview of extracellular matrix. *Curr. Protoc. Cell Biol.* <https://doi.org/10.1002/0471143030.cb1001s00>. (Chapter 10), Unit 10.1.
- Memic, A., Alhadrami, H.A., Hussain, M.A., Aldhahri, M., Al Nowaiser, F., Al-Hazmi, F., Oklu, R., Khademhosseini, A., 2015. Hydrogels 2.0: improved properties with nanomaterial composites for biomedical applications. *Biomed. Mater.* 11. <https://doi.org/10.1088/1748-6041/11/1/014104>. 014104.
- Mendes, B.B., Gómez-Florit, M., Babo, P.S., Domingues, R.M., Reis, R.L., Gomes, M.E., 2018a. Blood derivatives awaken in regenerative medicine strategies to modulate wound healing. *Adv. Drug Deliv. Rev.* 129, 376–393. <https://doi.org/10.1016/j.addr.2017.12.018>.
- Mendes, B.B., Gómez-Florit, M., Pires, R.A., Domingues, R.M.A., Reis, R.L., Gomes, M.E., 2018b. Human-based fibrillar nanocomposite hydrogels as bioinstructive matrices to tune stem cell behavior. *Nanoscale* 10, 17388–17401. <https://doi.org/10.1039/C8NR04273J>.
- Merino, S., Martín, C., Kostarelos, K., Prato, M., Vázquez, E., 2015. Nanocomposite hydrogels: 3D polymer-nanoparticle synergies for on-demand drug delivery. *ACS Nano* 9, 4686–4697. <https://doi.org/10.1021/acs.nano.5b01433>.
- Miron, R.J., Fujioka-Kobayashi, M., Bishara, M., Zhang, Y., Hernandez, M., Choukroun, J., 2017. Platelet-rich fibrin and soft tissue wound healing: a systematic review. *Tissue Eng. B Rev.* 23, 83–99. <https://doi.org/10.1089/ten.TEB.2016.0233>.
- Mithieux, S.M., Wise, S.G., Weiss, A.S., 2013. Tropoelastin — a multifaceted naturally smart material. *Adv. Drug Deliv. Rev.* 65, 421–428. <https://doi.org/10.1016/j.addr.2012.06.009>.
- Nivison-Smith, L., Rnjak, J., Weiss, A.S., 2010. Synthetic human elastin microfibers: stable cross-linked tropoelastin and cell interactive constructs for tissue engineering applications. *Acta Biomater.* 6, 354–359. <https://doi.org/10.1016/j.act-bio.2009.08.011>.
- Ouyang, L., Highley, C.B., Rodell, C.B., Sun, W., Burdick, J.A., 2016. 3D printing of shear-thinning hyaluronic acid hydrogels with secondary cross-linking. *ACS Biomater. Sci. Eng.* 2, 1743–1751. <https://doi.org/10.1021/acsbomaterials.6b00158>.
- Palza, H., Zapata, P., Angulo-Pineda, C., Palza, H., Zapata, P.A., Angulo-Pineda, C., 2019. Electroactive smart polymers for biomedical applications. *Materials* 12, 277. <https://doi.org/10.3390/ma12020277>.
- Park, H.-J., Jin, Y., Shin, J., Yang, K., Lee, C., Yang, H.S., Cho, S.-W., 2016. Catechol-functionalized hyaluronic acid hydrogels enhance angiogenesis and osteogenesis of human adipose-derived stem cells in critical tissue defects. *Biomacromolecules* 17, 1939. <https://doi.org/10.1021/acs.biomac.5b01670>.
- Pati, F., Ha, D.-H., Jang, J., Han, H.H., Rhie, J.-W., Cho, D.-W., 2015. Biomimetic 3D tissue printing for soft tissue regeneration. *Biomaterials* 62, 164–175. <https://doi.org/10.1016/j.biomaterials.2015.05.043>.
- Pati, F., Jang, J., Ha, D.-H., Won Kim, S., Rhie, J.-W., Shim, J.-H., Kim, D.-H., Cho, D.-W., 2014. Printing three-dimensional tissue analogues with decellularized extracellular matrix bioink. *Nat. Commun.* 5, 3935. <https://doi.org/10.1038/ncomms4935>.
- Piechocka, I.K., Bacabac, R.G., Potters, M., Mackintosh, F.C., Koenderink, G.H., 2010. Structural hierarchy governs fibrin gel mechanics. *Biophys. J.* 98, 2281–2289. <https://doi.org/10.1016/j.bpj.2010.01.040>.
- Prince, E., Kumacheva, E., 2019. Design and applications of man-made biomimetic fibrillar hydrogels. *Nat. Rev. Mater.* <https://doi.org/10.1038/s41578-018-0077-9>.
- Radvar, E., Azevedo, H.S., 2019. Supramolecular peptide/polymer hybrid hydrogels for biomedical applications. *Macromol. Biosci.* 19, 1800221. <https://doi.org/10.1002/mabi.201800221>.
- Robinson, S.T., Douglas, A.M., Chadid, T., Kuo, K., Rajabalan, A., Li, H., Copland, I.B., Barker, T.H., Galipeau, J., Brewster, L.P., 2016. A novel platelet lysate hydrogel for endothelial cell and mesenchymal stem cell-directed neovascularization. *Acta Biomater.* 36, 86–98. <https://doi.org/10.1016/j.act-bio.2016.03.002>.
- Rodell, C.B., MacArthur, J.W., Dorsey, S.M., Wade, R.J., Wang, L.L., Woo, Y.J., Burdick, J.A., 2015. Shear-thinning supramolecular hydrogels with secondary autonomous covalent crosslinking to

- modulate viscoelastic properties in vivo. *Adv. Funct. Mater.* 25, 636–644. <https://doi.org/10.1002/adfm.201403550>.
- Rodin, S., Domogatskaya, A., Ström, S., Hansson, E.M., Chien, K.R., Inzunza, J., Hovatta, O., Tryggvason, K., 2010. Long-term self-renewal of human pluripotent stem cells on human recombinant laminin-511. *Nat. Biotechnol.* 28, 611–615. <https://doi.org/10.1038/nbt.1620>.
- Rodríguez-Cabello, J.C., González de Torre, I., Ibañez-Fonseca, A., Alonso, M., 2018. Bioactive scaffolds based on elastin-like materials for wound healing. *Adv. Drug Deliv. Rev.* 129, 118–133. <https://doi.org/10.1016/j.addr.2018.03.003>.
- Rosales, A.M., Anseth, K.S., 2016. The design of reversible hydrogels to capture extracellular matrix dynamics. *Nat. Rev. Mater.* 1, 15012. <https://doi.org/10.1038/natrevmats.2015.12>.
- Ryan, E.A., Mockros, L.F., Weisel, J.W., Lorand, L., 1999. Structural origins of fibrin clot rheology. *Biophys. J.* 77, 2813–2826. [https://doi.org/10.1016/S0006-3495\(99\)77113-4](https://doi.org/10.1016/S0006-3495(99)77113-4).
- Sadeghi-Ataabadi, M., Mostafavi-pour, Z., Vojdani, Z., Sani, M., Latifi, M., Talaei-Khozani, T., 2017. Fabrication and characterization of platelet-rich plasma scaffolds for tissue engineering applications. *Mater. Sci. Eng. C* 71, 372–380. <https://doi.org/10.1016/j.msec.2016.10.001>.
- Sankaran, S., Zhao, S., Muth, C., Paez, J., del Campo, A., 2018. Toward light-regulated living biomaterials. *Adv. Sci.* 5, 1800383. <https://doi.org/10.1002/advs.201800383>.
- Santo, V.E., Popa, E.G., Mano, J.F., Gomes, M.E., Reis, R.L., 2015. Natural assembly of platelet lysate-loaded nanocarriers into enriched 3D hydrogels for cartilage regeneration. *Acta Biomater.* 19, 56–65. <https://doi.org/10.1016/j.actbio.2015.03.015>.
- Saunders, L., Ma, P.X., 2019. Self-healing supramolecular hydrogels for tissue engineering applications. *Macromol. Biosci.* 19, 1800313. <https://doi.org/10.1002/mabi.201800313>.
- Schaffner, M., Rühls, P.A., Coulter, F., Kilcher, S., Studart, A.R., 2017. 3D printing of bacteria into functional complex materials. *Sci. Adv.* 3. <https://doi.org/10.1126/sciadv.aao6804>. eao6804.
- Shahbazi, M.-A., Bauleth-Ramos, T., Santos, H.A., 2018. DNA hydrogel assemblies: bridging synthesis principles to biomedical applications. *Adv. Ther.* 1, 1800042. <https://doi.org/10.1002/adtp.201800042>.
- Shao, Y., Jia, H., Cao, T., Liu, D., 2017. Supramolecular hydrogels based on DNA self-assembly. *Acc. Chem. Res.* 50, 659–668. <https://doi.org/10.1021/acs.accounts.6b00524>.
- Shin, J., Lee, J.S., Lee, C., Park, H.-J., Yang, K., Jin, Y., Ryu, J.H., Hong, K.S., Moon, S.-H., Chung, H.-M., Yang, H.S., Um, S.H., Oh, J.-W., Kim, D.-I., Lee, H., Cho, S.-W., 2015. Tissue adhesive catechol-modified hyaluronic acid hydrogel for effective, minimally invasive cell therapy. *Adv. Funct. Mater.* 25, 3814–3824. <https://doi.org/10.1002/adfm.201500006>.
- Silva, E.D., Babo, P.S., Costa-Almeida, R., Domingues, R.M.A., Mendes, B.B., Paz, E., Freitas, P., Rodrigues, M.T., Granja, P.L., Gomes, M.E., 2018. Multifunctional magnetic-responsive hydrogels to engineer tendon-to-bone interface. *Nanomed. Nanotechnol. Biol. Med.* 14, 2375–2385. <https://doi.org/10.1016/j.nano.2017.06.002>.
- Silva, J.M., Reis, R.L., Mano, J.F., 2016. Biomimetic extracellular environment based on natural origin polyelectrolyte multilayers. *Small* 4308–4342. <https://doi.org/10.1002/smll.201601355>.
- Skardal, A., Shupe, T., Atala, A., 2016. Organoid-on-a-chip and body-on-a-chip systems for drug screening and disease modeling. *Drug Discov. Today* 21, 1399–1411. <https://doi.org/10.1016/j.drudis.2016.07.003>.
- Stejskalová, A., Oliva, N., England, F.J., Almquist, B.D., 2019. Biologically inspired, cell-selective release of aptamer-trapped growth factors by traction forces. *Adv. Mater.* 1806380. <https://doi.org/10.1002/adma.201806380>.
- Stoll, H., Steinle, H., Stang, K., Kunnakattu, S., Scheideler, L., Neumann, B., Kurz, J., Degenkolbe, I., Perle, N., Schlensak, C., Wendel, H.P., Avci-Adali, M., 2017. Generation of large-scale DNA hydrogels with excellent blood and cell compatibility. *Macromol. Biosci.* 17, 1600252. <https://doi.org/10.1002/mabi.201600252>.
- Testera, A.M., Girotti, A., de Torre, I.G., Quintanilla, L., Santos, M., Alonso, M., Rodríguez-Cabello, J.C., 2015. Biocompatible elastin-like click gels: design, synthesis and characterization. *J. Mater. Sci. Mater. Med.* 26, 105. <https://doi.org/10.1007/s10856-015-5435-1>.
- Tibbitt, M.W., Rodell, C.B., Burdick, J.A., Anseth, K.S., 2015. Progress in material design for biomedical applications. *Proc. Natl. Acad. Sci.* 112, 14444–14451. <https://doi.org/10.1073/pnas.1516247112>.
- Ueki, R., Sando, S., 2014. A DNA aptamer to c-Met inhibits cancer cell migration. *Chem. Commun.* 50, 13131–13134. <https://doi.org/10.1039/C4CC06016D>.
- Valcarcel, J., Novoa-Carballal, R., Pérez-Martín, R.I., Reis, R.L., Vázquez, J.A., 2017. Glycosaminoglycans from marine sources as therapeutic agents. *Biotechnol. Adv.* 35, 711–725. <https://doi.org/10.1016/j.biotechadv.2017.07.008>.
- Wang, H.-L., Avila, G., 2007. Platelet rich plasma: myth or reality? *Eur. J. Dermatol.* 1, 192–194.
- Wang, H., Heilshorn, S.C., 2015. Adaptable hydrogel networks with reversible linkages for tissue engineering. *Adv. Mater.* 27, 3717–3736. <https://doi.org/10.1002/adma.201501558>.
- Wang, H., Zhu, D., Paul, A., Cai, L., Enejder, A., Yang, F., Heilshorn, S.C., 2017. Covalently adaptable elastin-like protein-hyaluronic acid (ELP-HA) hybrid hydrogels with secondary thermoresponsive crosslinking for injectable stem cell delivery. *Adv. Funct. Mater.* 27, 1605609. <https://doi.org/10.1002/adfm.201605609>.
- Webber, M.J., Appel, E.A., Meijer, E.W., Langer, R., 2016. Supramolecular biomaterials. *Nat. Mater.* 15, 13–26. <https://doi.org/10.1038/nmat4474>.
- Wei, K., Zhu, M., Sun, Y., Xu, J., Feng, Q., Lin, S., Wu, T., Xu, J., Tian, F., Xia, J., Li, G., Bian, L., 2016. Robust biopolymeric supramolecular “host-guest macromer” hydrogels reinforced by in situ formed multivalent nanoclusters for cartilage regeneration. *Macromolecules* 49, 866–875. <https://doi.org/10.1021/acs.macromol.5b02527>.
- Weisel, J.W., Litvinov, R.I., 2013. Mechanisms of fibrin polymerization and clinical implications. *Blood* 121, 1712–1719. <https://doi.org/10.1182/blood-2012-09-306639>.
- Wise, S.G., Mithieux, S.M., Weiss, A.S., 2009. Engineered tropoelastin and elastin-based biomaterials. *Adv. Protein Chem. Struct. Biol.* 78, 1–24. [https://doi.org/10.1016/S1876-1623\(08\)78001-5](https://doi.org/10.1016/S1876-1623(08)78001-5).
- Yeo, G.C., Baldock, C., Tuukkanen, A., Roessle, M., Dyksterhuis, L.B., Wise, S.G., Matthews, J., Mithieux, S.M., Weiss, A.S., 2012. Tropoelastin bridge region positions the cell-interactive C terminus and contributes to elastic fiber assembly. *Proc. Natl. Acad. Sci.* 109, 2878–2883. <https://doi.org/10.1073/pnas.1111615108>.
- Yeo, G.C., Kondyurin, A., Kosobrodova, E., Weiss, A.S., Bilek, M.M.M., 2017. A sterilizable, biocompatible, tropoelastin surface coating immobilized by energetic ion activation. *J. R. Soc. Interface* 14, 20160837. <https://doi.org/10.1098/rsif.2016.0837>.
- Yeo, G.C., Weiss, A.S., 2019. Soluble matrix protein is a potent modulator of mesenchymal stem cell performance. *Proc.*

- Natl. Acad. Sci. 116, 2042–2051. <https://doi.org/10.1073/pnas.1812951116>.
- Yeom, J., Kim, S.J., Jung, H., Namkoong, H., Yang, J., Hwang, B.W., Oh, K., Kim, K., Sung, Y.C., Hahn, S.K., 2015. Supramolecular hydrogels for long-term bioengineered stem cell therapy. *Adv. Healthc. Mater.* 4, 237–244. <https://doi.org/10.1002/adhm.201400304>.
- Yue, K., Trujillo-de Santiago, G., Alvarez, M.M., Tamayol, A., Annabi, N., Khademhosseini, A., 2015. Synthesis, properties, and biomedical applications of gelatin methacryloyl (GelMA) hydrogels. *Biomaterials* 73, 254–271. <https://doi.org/10.1016/j.biomaterials.2015.08.045>.
- Yun, J.M., Kim, K.N., Kim, J.Y., Shin, D.O., Lee, W.J., Lee, S.H., Lieberman, M., Kim, S.O., 2012. DNA origami nanopatterning on chemically modified graphene. *Angew. Chem.* 124, 936–939. <https://doi.org/10.1002/ange.201106198>.
- Zhang, N., Lock, J., Sallee, A., Liu, H., 2015. Magnetic nanocomposite hydrogel for potential cartilage tissue engineering: synthesis, characterization, and cytocompatibility with bone marrow derived mesenchymal stem cells. *ACS Appl. Mater. Interfaces* 7, 20987–20998. <https://doi.org/10.1021/acsami.5b06939>.
- Zhang, Y., Tu, J., Wang, D., Zhu, H., Maity, S.K., Qu, X., Bogaert, B., Pei, H., Zhang, H., 2018. Programmable and multifunctional DNA-based materials for biomedical applications. *Adv. Mater.* 1–44. <https://doi.org/10.1002/adma.201703658>. 1703658.
- Zhou, X., Li, C., Shao, Y., Chen, C., Yang, Z., Liu, D., 2016. Reversibly tuning the mechanical properties of a DNA hydrogel by a DNA nanomotor. *Chem. Commun.* 52, 10668–10671. <https://doi.org/10.1039/C6CC04724F>.
- Zhu, D., Wang, H., Trinh, P., Heilshorn, S.C., Yang, F., 2017a. Elastin-like protein-hyaluronic acid (ELP-HA) hydrogels with decoupled mechanical and biochemical cues for cartilage regeneration. *Biomaterials* 127, 132–140. <https://doi.org/10.1016/j.biomaterials.2017.02.010>.
- Zhu, L., Wang, K., Ma, T., Huang, L., Xia, B., Zhu, S., Yang, Y., Liu, Z., Quan, X., Luo, K., Kong, D., Huang, J., Luo, Z., 2017b. Noncovalent bonding of RGD and YIGSR to an electrospun poly(ϵ -caprolactone) conduit through peptide self-assembly to synergistically promote sciatic nerve regeneration in rats. *Adv. Healthc. Mater.* 6, 1600860. <https://doi.org/10.1002/adhm.201600860>.
- Zou, L., Braegelman, A.S., Webber, M.J., 2019. Dynamic supramolecular hydrogels spanning an unprecedented range of host-guest affinity. *ACS Appl. Mater. Interfaces* *acsami*. <https://doi.org/10.1021/acsami.8b22151>. 8b22151.

Questions

1. What strategies can be used to control the temporal, spatial, and type of released bioactive molecules from blood derivatives?
2. Which advantages and disadvantages do natural polymers offer?
3. What characteristics should an ideal ECM-mimetic hydrogel have?
4. What characteristics of DNA are critical to enable its use as a biomaterial?
5. Identify two different types of supramolecular cross-linking strategies that can be applied to produce reversible hydrogels using polymeric precursors.

1.3.6A

Processed Tissues

RAYMOND M. WANG^a, PAMELA DURAN^a, KAREN L. CHRISTMAN^{*}

Department of Bioengineering, Sanford Consortium of Regenerative Medicine,
University of California San Diego, La Jolla, CA, United States

Introduction

The prevalence of chronic tissue injuries and diseases has spurred extensive research into developing methods to preserve, process, and modify tissues for treating and understanding these sources of morbidity and mortality. Healthy donor tissue is consistently under heavy demand, with over 10,000 patients added annually to the organ transplant waitlist, which was over 110,000 in the United States in 2016 (OPTN/SRTR, 2018). Unfortunately, a large amount of viable tissue is not successfully transplanted before expiring. Standard practice preserving tissue before transplantation is on ice with a reported storage life of several hours. With logistical challenges, difficulty of surgical transplantation, and limited medical resources, utilizing all organs for transplant becomes impossible given the available time. Furthermore, the ever-growing patient population with chronic tissue diseases increases both demand and shortage of available healthy donor tissue, thus prompting investigation into methods for enhanced tissue preservation and alternative treatments. In particular, tissue decellularization methods isolating the extracellular matrix (ECM) scaffold have shown promise for developing novel proregenerative materials. These naturally derived materials provide biocompatible and bioactive scaffolds that can be improved by modification of native properties or utilization as a delivery vehicle. Processing methods also allow use of nonhuman tissue sources by masking or removing epitopes that initiate immune rejection responses from xenogeneic derived materials. We will discuss methods and developments in the preservation of tissue, methods of decellularization to isolate the tissue ECM scaffold, and finally, how decellularized tissues have been utilized to create new clinical treatments and improve understanding of tissue diseases.

Cryopreservation and Vitrification

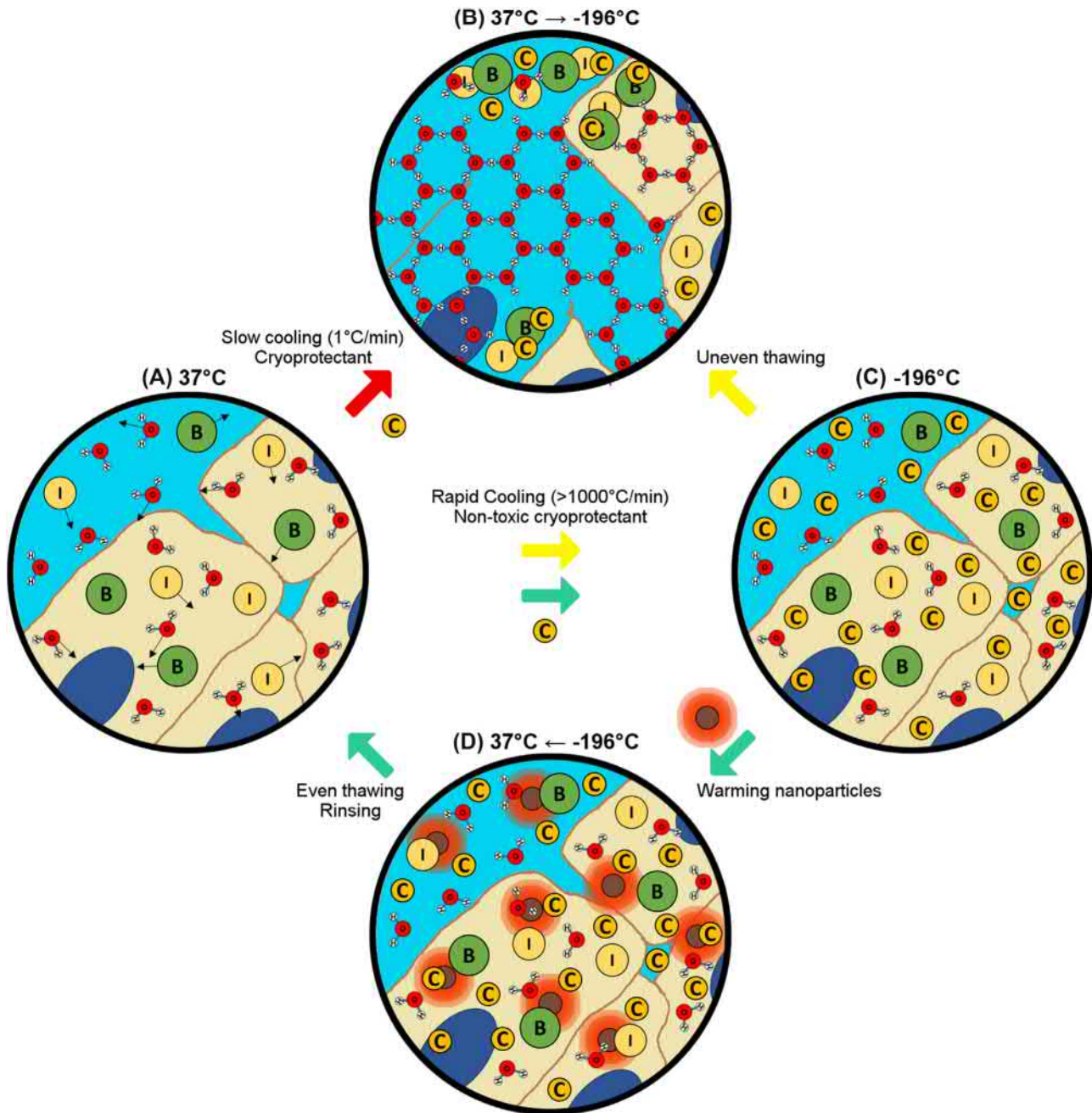
In its ideal form, tissue preservation is the principle of maintaining quality of a biological sample outside its host for

extended time periods and allowing relatively stable restoration to a healthy functional state upon reintroduction into a metabolically active system. As sustaining tissue by mimicking host system conditions *ex vivo* is impractical long term, technology has focused on cooling methods to halt unregulated processes within tissue samples. From a thermodynamic point of view, activity within an isolated system is a consequence of the motion of matter and transfer of energy among its constituents. As the temperature of a system is a measure of motion of molecular constituents, minimizing temperature to a low enough point provides a mechanism for diminishing the molecular motion in a system (Wovk, 2010). Based on a biochemical viewpoint, this logical approach similarly applies as temperature influences the rate of chemical reactions and enzymatic activity, with these processes effectively halting at sufficiently low temperatures.

For tissue preservation, two phases of the process are particularly sensitive: (1) the cooling of tissue and (2) restoration to normal conditions. Two cryogenic or cooling to low temperature methods for extended tissue preservation are cryopreservation and vitrification. Cryopreservation is the conventional idea of freezing biological samples for long-term storage. However, simple freezing of tissue alone is lethal as it mainly consists of water. Water organizes into ice crystals below 0°C that push away other tissue components, causing intracellular rupture, extracellular tearing, and osmotic shock as solute components are locally concentrated from displacement by crystal formation (Fig. 1.3.6A.1A and B). To minimize these effects, cryoprotectants (e.g., cell-permeable dimethyl sulfoxide) hindering organized ice crystal formation along with optimal cooling rates for equilibrating osmotic pressures are required (Gao and Critser, 2000). As optimal cooling rates are cell specific (Leibo and Pool, 2011), cryopreservation has seen limited preclinical and clinical success for densely packed multicellular organs (Bakhach, 2009). The large volumetric size of human tissue is also an issue as temperature changes do not permeate evenly throughout. Otherwise, cryopreservation is more conventionally utilized with cellular suspensions, most notably for preservation of red blood cell (Al-Otaibi et al., 2019), gamete (Cil and Seli, 2013), and stem

*Corresponding author.

^aContributed equally to this chapter.



• **Figure 1.3.6A.1** Issues with ice crystal formation for tissue preservation by cryopreservation (red arrow) or vitrification and restoration through uneven thawing (yellow arrows) versus even thawing methods throughout the tissue (green arrow). (A) Tissue at 37°C homeostatic conditions with Brownian motion of components such as water molecules (H₂O), ions (I) and biomolecules (B). (B) Tissue classically cryopreserved using cryoprotectants (C) at low concentrations and slow cooling rates (1°C/min) allows water molecules to assemble into ice crystals causing cell lysis, disruption of cell-cell contacts, and toxic localized segregation of components. (C) Vitrification by rapid cooling rates (>1000°C/min) and high cryoprotectant concentrations creates a high-viscosity, glassy state preventing ice crystal organization and halting molecular motion and activity. However, restoration by uneven thawing with slow heating methods can allow ice crystal organization to arise. (D) Even thawing methods with magnetic nanoparticles provide distributed inductive warming for restoring molecular activity throughout and allow for return to the original tissue state.

cell storage (Jang et al., 2017b) with standardized guidelines for certain cell types readily available.

Clinical success utilizing cryopreserved arterial allografts has been demonstrated for vascular conditions such as peripheral artery bypasses for treating critical limb ischemia.

Cryopreservation of arterial allografts minimizes tissue degradation, preventing calcification and dilation over time. Treatment of patients by cryopreserved arterial allografts for limb salvage and abdominal aorta reconstruction showed favorable results compared with outcomes from conventional

synthetic grafts (Castier et al., 1999; Gournier et al., 1995). Interestingly, lack of temperature control freezing and rapidly thawing grafts utilized in these studies is known to elicit extensive cellular damage and death (Pascual et al., 2001). However, these studies have speculated the rapid freeze–thaw procedure and extensive rinsing to remove dimethyl sulfoxide cryoprotectant partially acted as a decellularization method (Castier et al., 1999). Thus, these results could instead imply efficacy of decellularized ECM scaffold grafts for vascular reconstruction in humans versus actual cryopreservation of viable tissue. For other densely packed tissues that require viability throughout for functionality, cryopreservation has shown limited feasibility for translation.

Vitrification addresses biophysical issues from cryopreservation by solidifying tissue with high concentrations of nontoxic cryoprotectants such as sucrose or antifreeze proteins (Kim et al., 2017) forming a high-viscosity, glassy state with immediate cooling from physiological to -196°C liquid nitrogen storage temperatures in under a second, leading to minimal ice crystal formation. This method reduces mechanical disruption from freezing and does not require cell- or tissue-optimized cooling rates (Fig. 1.3.6A.1C). Following vitrification, long-term preservation theoretically only requires maintaining storage temperatures with relevant equipment (Fahy and Wowk, 2015). However, tissue damage is still a potential issue with larger volumes during the thawing process as uneven heating can create nonhomogeneous molecular arrangements and ice crystal formation with standard convection heating or slow thawing methods (Gao and Critser, 2000). Breakthroughs in heating nanotechnology, such as utilizing nanoscale mesoporous silica-coated iron oxide particles that excite with radiofrequency, have demonstrated scalable capabilities of evenly warming vitrified tissue throughout (Fig. 1.3.6A.1D). Porcine aortic heart valve leaflet and carotid artery tissue sample up to 50 mL volumes maintained similar cell viability and mechanical properties to fresh tissue, while standard convective methods caused extensive cell death (Manuchehrabadi et al., 2017).

Since early attempts to preserve tissue, vitrification has made great strides in long-term preservation, and incorporation of nanotechnology has suggested the potential of tissue restoration with minimal damage. Continued testing and optimization for whole human tissue volumes and different architectural structures will need to be confirmed. Tissue functionality and suitability for transplantation still need assessment as high cryoprotectant concentrations and cold temperatures can elicit undesirable cellular shock responses (Corwin et al., 2009). Addressing clinical setting feasibility and logistical challenges will also be important for future translation of this technology (Giwa et al., 2017).

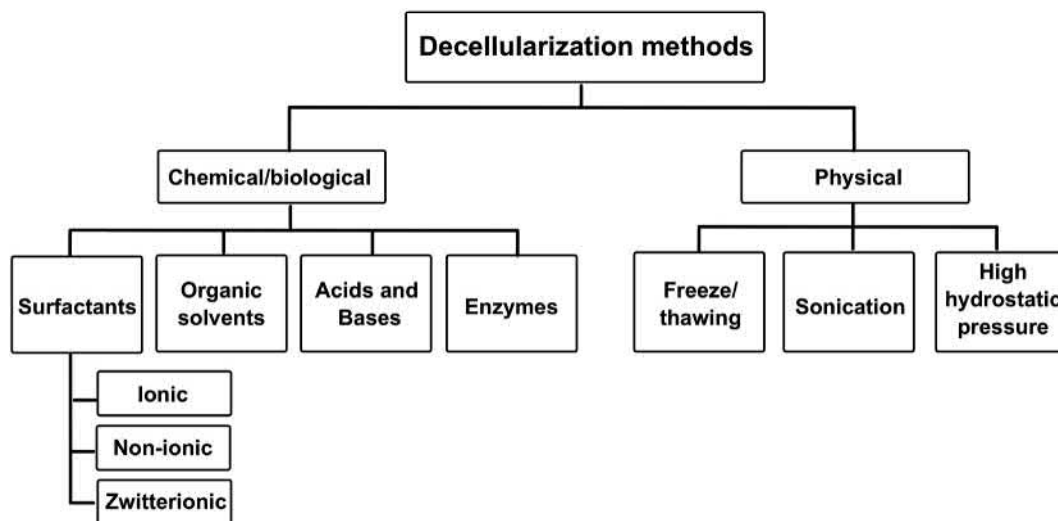
Tissue Cross-Linking

Different cross-linking methods have been utilized with tissue to augment the durability and decrease the rate of *in vivo* enzymatic degradation. Bioprosthetic heart valves have been extensively fabricated with various cross-linking methods.

Glutaraldehyde-treated heart valves were introduced in the late 1960s (Jayakrishnan, 1996). Glutaraldehyde reacts with amino acids, such as histidine and tyrosine, forming covalent bonds between adjacent collagen chains. Aside from reducing biodegradation, glutaraldehyde preserves tissue viscoelastic properties (i.e., strength and flexibility). Allografts and xenografts, fabricated from porcine aortic valves or bovine pericardium, have been used for total valve replacement, with the former representing the largest proportion (Simionescu, 2004). However, glutaraldehyde-treated valves commonly cause long-term calcification after implantation. One reason for this calcification is the presence of cytotoxic aldehyde group residuals from incomplete binding of glutaraldehyde to the collagen network (Siddiqui et al., 2009). To prevent or reduce calcification, reagents to neutralize free aldehyde groups or different nonaldehyde cross-linker agents have been used. Amino acids with reactive primary amines can neutralize aldehyde residues, such as glutamine and lysine, amino-bisphosphonates, toluidine blue, and alpha-amino-oleic acid. Even though these reagents elicit decreased calcification, associated host cellular reactions can occur. Glutaraldehyde-treated valves pretreated with alpha-amino-oleic acid induced chronic inflammatory responses characterized by macrophage, plasma cell, and lymphocyte infiltration at the host and porcine tissue interface (Butany et al., 2007). Inadequate fixation, leading to retention of antigenicity, might also induce a humoral immune response (Human, 2001).

Nonaldehyde fixation methods have also been investigated. The agent 1-ethyl-3-(3-dimethyl aminopropyl) carbodiimide hydrochloride (EDC) coupled with N-hydroxysulfosuccinimide (sulfo-NHS) cross-links nonspecifically all proteins by linking amine and carboxyl groups by amide bonds. The byproducts of the fixation process are water soluble, easily rinsed away, and nontoxic (Girardot and Girardot, 1996; Simionescu, 2004). EDC/NHS cross-linking with porcine aortic roots and porcine pericardium in a short-term study demonstrated decreased calcification after implantation *in vivo* in a rat model. However, long-term preclinical and clinical studies are still necessary to evaluate this technique (Girardot and Girardot, 1996; Timek et al., 2002). Other processes based on photochemical reaction provide an efficient and rapid method. Dye-mediated photooxidation consists of dye treatment (i.e., methylene blue) and delivering oxygen while exposing tissue to ultraviolet light. This results in modification of tyrosine, methionine, and histidine residues. Studies demonstrated successful calcification reduction after implantation of a bovine pericardium-derived prosthetic heart valve in a sheep model. While pericardial tissue tears occurred in clinical trials, issues stemmed from biomaterial design as higher compliance of cross-linked tissue lead to abrasion-induced tearing (Svendsen CA., 2000; Vesely, 2003).

Aldehyde-fixed bioprosthetic heart valves have been used for 50 years, demonstrating hemocompatibility and tissue compliance, however, there are still issues regarding clinical durability and biocompatibility. Other methods have been investigated, but long-term results are still an open question. To increase xenogeneic material biocompatibility,



• **Figure 1.3.6A.2** Schematic of decellularization methods.

decellularized scaffolds have become widely adopted not only for prosthetic valves, but also for reconstruction and treatment of different tissue types as discussed in following sections.

Decellularization

Over the past two decades, tissue decellularization has shown promise for tissue engineering and regenerative medicine approaches. Decellularized scaffolds retain non-cellular components (i.e., ECM) representative of native tissue. These characteristics promote cell growth, survival, and development (Hussein et al., 2018; Sasaki, 2009). An effective decellularization process depends on the type, age of tissue and method used. A summary of decellularization methods (Fig. 1.3.6A.2) is presented below, while in-depth reviews on methods and effects on composition and structure of decellularized scaffolds have been previously published (Crapo et al., 2011; Keane et al., 2015).

Decellularization Methods

Chemical/biological methods: Different chemical agents are commonly used as the main agent of the decellularization process; these include surfactants, organic solvents, acids, and bases. Enzymes are used in combination with these chemical agents to enhance removal of DNA (e.g., DNase, RNase, trypsin). Surfactants are classified as ionic, nonionic, or zwitterionic. They disorganize the phospholipid cellular membrane leading to cell lysing. Examples include sodium dodecyl sulfate (SDS), Triton X-100, and sodium deoxycholate. SDS, an ionic detergent, has been widely used in the decellularization process for diverse tissue types, from tissues to whole-organ decellularization. In the early 2000s, small intestinal submucosa (SIS) and urinary bladder were decellularized by mechanical delamination followed by treatments with acids and bases (Abraham et al., 2000; Hodde et al., 2002). SDS has been associated with efficient cellular removal, though loss of ECM components and structure to varying degrees are

expected due to the strength of this agent. For additional preservation of the organ structure, perfusion of the surfactant through the native vasculature allows for whole-organ decellularization first demonstrated with a rat heart (Ott et al., 2008). Isolation of a whole decellularized organ initiated an entirely new field of study for recellularization of whole decellularized tissue as a potential alternative source of transplant tissue (see “Applications of Decellularized Tissues”). Similar methods for SDS perfusion have since been applied for numerous tissues including rabbit bladder (Miyazaki and Maruyama, 2014), liver (Shupe et al., 2010; Baptista et al., 2011), rat lung (Petersen et al., 2010), rat uterus (Miyazaki and Maruyama, 2014), porcine urethra (Simoes et al., 2017), porcine kidneys (Hussein et al., 2018), and rat spleen (Zheng et al., 2015). Alternatively, thin or minced tissue under agitation allows for diffusion of SDS throughout. Agitation of human tendon, with SDS, resulted in preservation of collagen content and ultimate tensile stress and elastic modulus similar to native tissue (Pridgen et al., 2011). Decellularized minced porcine skeletal muscle resulted in cellular removal and preservation of ECM components (e.g., sulfated glycosaminoglycans) (Ungerleider et al., 2015). In contrast, SDS (0.1%–1%) decellularization of minced porcine pancreas removed over 30% of ECM proteins compared to native tissue, as analyzed by mass spectrometry, leaving mainly fibrillar collagen (Gaetani et al., 2018). Loss of collagen fiber organization was also observed with 24 h SDS treatment of porcine heart valve leaflets (Zhou et al., 2010). Thus, selection of SDS based on efficient decellularization alone is not always an ideal choice due to tissue- and processing-specific effects on native ECM properties.

Triton X-100 is another surfactant that is used for the fabrication of acellular scaffolds. This nonionic agent has been mainly used in combination with other surfactants or enzymes. For whole-organ decellularization, such as rat kidneys, triton X-100 alone led to incomplete cellular removal, and disruption of basement membrane. However, triton combined with SDS resulted in efficient absence of nuclei, preservation of growth factors and underlying vasculature,

with a small loss of collagen IV (Caralt et al., 2015). Human urethra decellularization by triton and SDS preserved biomechanical properties compared to native tissue, defined by similar Young's modulus (Kajbafzadeh et al., 2017). Triton X-100 has also been used with another ionic surfactant, sodium deoxycholate, which dissociates cellular membrane protein interactions. Rat spinal cord decellularization with triton and sodium deoxycholate preserved collagen bundles and porous structure (Zhu et al., 2018).

Tri(n-butyl) phosphate (TnBP) is an organic solvent that disrupts protein–protein interactions (Keane et al., 2016). TnBP has been used in soft tissues, especially in tendon decellularization, due to high protein content. TnBP alone maintained ECM composition, and mechanical properties of porcine diaphragm tendon (Deeken et al., 2011). However, TnBP treatment alone can cause a decreased degree of collagen cross-linking, which may affect the long-term biomechanical properties of the tissue. Thus, surfactants can be used in combination with this organic solvent to stabilize it. TnBP with SDS resulted in preservation of collagen structure and elastic modulus (Xing et al., 2014).

Enzymes have been used in combination with chemical agents to break down DNA (DNase) or RNA (RNase) fragments, and to break cell–matrix interactions (trypsin). Decellularization of human cornea only by SDS led to cytoplasmic debris removal, but was inefficient for nuclear debris; addition of DNase eliminated nuclear debris, resulting in increased tissue transparency (He, 2016). Enzyme agents have been used for blood vessel decellularization in rabbit, porcine, and human tissue sources. Combination of triton X-100, TnBP, and DNase led to efficient cellular removal of human saphenous vein (Kumar Kuna et al., 2018). Rat sciatic nerve decellularization with DNase and RNase resulted in cellular removal, and preserved collagen and laminin content (Philips et al., 2018).

Physical methods: Mechanical processes decellularize ECM by eliminating cell–matrix interactions and lysis of cells. These methods include freeze and thawing, sonication by ultrasound, and high hydrostatic pressure. Alternating between freezing (at -80°C or immersion in liquid nitrogen) and thawing (37°C) cycles has been demonstrated to preserve ECM composition and biomechanical properties. Decellularization of bovine tendon after five cycles of this physical method, together with DNase led to removal of cell nuclei, and preservation of collagen III and growth factors (Ning et al., 2017). However, the freezing and thawing method is often not efficient for other tissue types. Addition of this physical method to porcine uterus decellularization led to increased protein content, but also maintained nuclei content as compared to a chemical agent process without freezing/thawing (Campo et al., 2017).

Exposure of tissue to ultrasound at high frequencies can increase the effectiveness of the decellularization process. Sonication alone has been inefficient for cellular removal as demonstrated in human cornea processing (He, 2016). However, in skeletal muscle, combination of this method with enzymes efficiently removed cellular nuclei, retained sulfate glycosaminoglycans, and preserved biomechanical properties similar to native tissue (Lin et al., 2014).

Pressures around 1000 MPa, with an onset temperature set at 10 or 30°C , have also been applied to tissues as a decellularization method. After the applied pressure, porcine corneas were efficiently decellularized, with preservation of glycosaminoglycan content (Sasaki, 2009). In another study of porcine aortic blood vessels, the mechanical properties were also similar to native tissue (Funamoto et al., 2010). A further in vitro study with endothelial and smooth muscle cells demonstrated that a pressure of 200 MPa for only 10 min was enough to cause cellular disruption (Mahara et al., 2014).

Quality of Decellularization

Besides solely evaluating removal of cellular content, ideally decellularized material also retains the vast majority of extracellular components to most faithfully represent the native extracellular environment. Realistically, removal of cellular content with decellularization methods also strips ECM of its native components and structure to some extent. Therefore, complete removal of cellular content is impossible without excessive destruction of the ECM. Instead, decellularization methods require balancing preserving original ECM qualities and sufficient removal of cellular debris and other content that could stimulate undesirable responses. This can be accomplished by optimizing selection of the decellularization agents along with amount and time of exposure.

Commonly, ECM proteins are investigated for retention post-decellularization. Although largely consisting of structural proteins such as different isoforms of collagen, the ECM consists of a spectrum of proteins providing a multitude of functions including mechanical stiffness, elasticity, adhesion sites, and mechanotransduction signaling (Chapter 2.1.5). General composition can be assessed by histological or more specific immunolabeling staining, or breaking down the scaffold for gel electrophoresis. For broad coverage analysis, high-throughput proteomic methods such as mass spectrometry allow for determining the protein profile. Furthermore, targeted proteomics methods have demonstrated the potential for quantitative comparison of decellularized ECM protein composition to native tissue, which can measure the quality of ECM retention versus effective decellularization (Calle et al., 2016; Gaetani et al., 2018).

Carbohydrate structures maintained in decellularized ECM such as proteoglycans and glycoproteins provide additional functional properties including mechanical strength and compressive resistance, maintaining the charge and hydration of the ECM, regulating cellular activity through environmental cues, and growth factor retention by covalent binding or electrostatic interaction. These properties provide functional benefits such as enhanced local retention of heparin-binding growth factors from endogenous sources or exogenous growth factor delivery (Pieper et al., 2002; Seif-Naraghi et al., 2012; Sonnenberg et al., 2015). For quantification of the sulfated glycosaminoglycan content, Blyscan or dimethylmethylene blue assays can be used, while more specific assessment requires immunolabeling or mass spectroscopy methods (Klein et al., 2018; Noborn et al., 2016). In-depth evaluation of carbohydrate composition in

decellularized tissues and influence on downstream applications is an understudied area despite their known importance in the native tissue, and standardized evaluations could be important for future decellularized material development.

Remaining nucleic acid content such as microRNA encapsulated into matrix-bound nanovesicles has been implicated as a contributor to the bioactive responses of decellularized ECM scaffolds. Based on RNA-sequencing analysis, these responses have included proremodeling macrophage polarization, cell survival, cellular growth and development, and cell cycle progression (van der Merwe et al., 2017, 2019; Huleihel et al., 2016, 2017). Given these characteristics and observations of matrix-derived nanovesicles, their content might be another property that should be more commonly evaluated.

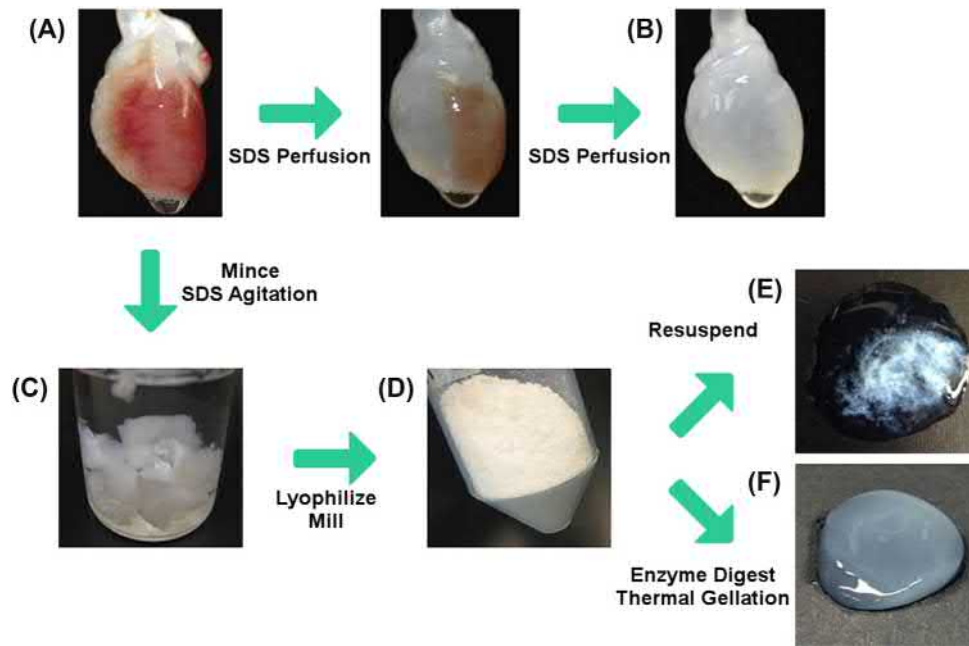
Besides compositional retention, structural and mechanical preservation is also important. Structural organization can be generally studied by histological staining (Aamodt and Grainger, 2016) or electron microscopy for high-resolution imaging of nanoscale architecture (Stephenson et al., 2016). Mechanical properties at the macroscale can be evaluated by biomechanics testing methods such as uniaxial, biaxial, or indentation loading for measuring the stress versus strain relationship of the processed tissue (Black et al., 2008; Griffin et al., 2016). Assessments of mechanical features relevant to the cellular microenvironment can be achieved by atomic force microscopy methods (Klaas et al., 2016; Jorba et al., 2017; Giménez et al., 2017). Since these are commonly used for studying properties of native tissue, comparisons between the pre- and post-decellularization state can be readily adapted.

Decellularization, by definition, seeks to isolate ECM by removal of cellular content and debris that can elicit adverse immune responses. Ensuring sufficient decellularization is critically important before clinical translation as inadequate decellularization, such as with early decellularized heart valves, can elicit severe immune rejection and harm to patients (Simon et al., 2003). Double-stranded DNA content from lyzed nuclei is a common surrogate marker for measuring the extent of decellularization as it is known to stimulate inflammatory responses, such as type I interferon pathways in macrophages (King et al., 2017; Brown et al., 2009). In general, cutoffs of <50 ng/mg dry ECM weight, <200 base pair DNA fragment length, and lack of visible nuclear material with nuclear counterstains, are commonly cited based on empirical observations of minimal adverse host responses from commercial and custom decellularized materials fitting these parameters (Gilbert et al., 2009; Brown et al., 2009; Crapo et al., 2011). However, these thresholds may not correlate with biological significance and specific understanding of the underlying mechanism is needed before the field sets such specifications (see Section 2.2). Furthermore, other cellular debris such as remnant mitochondria and cell membranes can elicit persistent proinflammatory macrophage responses (Londono et al., 2017).

As opposed to evaluating acellularity that has sometimes demonstrated poor prediction of graft acceptance

(Kasimir et al., 2006), other optimized methods have focused on specifically targeting sourcing of antigenicity for removal. Several xenogeneic epitopes such as the α -Gal, a carbohydrate structure absent in humans and Old World monkeys, elicit immune rejection responses from anti- α -Gal antibodies. These adverse host responses act as a major immunological barrier for xenografts. For therapeutic applications, decellularization and further processing (i.e., partial enzymatic digestion) have been shown to reduce α -Gal content to minimal quantities along with demonstration of a lack of anti- α -Gal antibody-driven host responses in Old World primate models (Wang et al., 2017b; McPherson et al., 2000; Daly et al., 2009). However, given the repercussions detergents have on ECM preservation, milder stepwise methods have been developed utilizing optimized solvents for solubilization of hydrophilic and lipophilic sources of antigenicity (Wong and Griffiths, 2014). These methods have demonstrated improved preservation of ECM properties such as collagen alignment, elastin content, and mechanical properties, while eliciting similar or improved immunological outcomes such as milder cellular infiltration and lesser fibrous capsule thickness (Wong et al., 2013, 2016). Interestingly, residual antigenicity based on IgG binding from antiovine conditioned rabbit serum on treated bovine-derived scaffolds determined no correlation between the degree of antigen removal and residual nuclei content. This result indicates limitations of DNA content quantification for predicting graft acceptance (Wong et al., 2011). For evaluation, specific antigens within decellularized materials can be immunolabeled for staining or ELISA analysis. Unknown graft-specific antigens can be evaluated by collection and analysis of serum-isolated antibodies in an animal model post-implantation (Sandor et al., 2008). High-throughput methods utilizing serum IgG immunoprecipitation and liquid chromatography tandem mass spectrometry have demonstrated broad coverage and identification of sources of antigenicity from native bovine tissue that could provide rapid antigen identification of tissue-derived materials (Gates et al., 2017).

Lipids are overall undesirable in decellularized tissue as they can interfere with proper decellularization and further scaffold processing (e.g., digestion), and elicit cellular responses uncharacteristic of the tissue of interest. Although decellularization methods remove some content, additional rinsing steps in organic solvent such as isopropyl alcohol are usually needed for complete removal (Ungerleider et al., 2015). These steps are especially important with older human tissue due to higher fat content compared to young adult porcine tissue commonly used in protocols (Sackett et al., 2018; Johnson et al., 2014). Confirmation by histology such as Oil Red or with a quantitative assay such as colorimetric sulfo-phospho-vanillin interaction with lipid content (Cheng, 2011) can assure adequate lipid content removal. Ultimately, understanding of isolated ECM characteristics and higher scrutiny of antigenicity are critical for continued advancement and successful clinical implementation of decellularized materials.



• **Figure 1.3.6A.3** Representative examples of processing heart tissue for various decellularized material applications. (A) Isolated rat heart decellularized by perfusion of sodium dodecyl sulfate (SDS) through native vasculature leading to (B) isolated extracellular matrix (ECM) scaffold maintaining whole-organ structure. (C) Alternatively, minced porcine left ventricular tissue decellularized by diffusion of SDS under agitation. (D) Lyophilized or freeze-during and milling of the tissue into a fine ECM particulate. (E) ECM particulate directly mixed with a liquid carrier for injection or (F) partially enzymatically digested into an ECM suspension that can undergo thermal gelation by 37°C incubation or injection in vivo. (Modified with permission from Ott, H.C., Matthiesen, T.S., Goh, S.K., Black, L.D., Kren, S.M., Netoff, T.I., Taylor, D.A., 2008. Perfusion-decellularized matrix: using nature's platform to engineer a bioartificial heart. *Nat. Med.* 14, 213–221; Singelyn, J.M., Sundaramurthy, P., Johnson, T.D., Schup-Magoffin, P.J., Hu, D.P., Faulk, D.M., Wang, J., Mayle, K.M., Bartels, K., Salvatore, M., Kinsey, A.M., Demaria, A.N., Dib, N., Christman, K.L., 2012. Catheter-deliverable hydrogel derived from decellularized ventricular extracellular matrix increases endogenous cardiomyocytes and preserves cardiac function post-myocardial infarction. *J. Am. Coll. Cardiol.* 59, 751–763; Spang, M.T., Christman, K.L., 2017. Extracellular matrix hydrogel therapies: in vivo applications and development. *Acta Biomater.*)

Post-decellularization Processing and Modifications

Milling for ECM Powder and Partial Enzymatic Digestion for Hydrogel Formation

Additional processing can be performed on isolated ECM material based on intended application (see “Applications of Decellularized Tissues”). Following decellularization, isolated ECM can be frozen and lyophilized for characterization and long-term storage. Although useable as its native scaffold, mechanical breakdown of the native architecture into a homogeneous ECM powder provides flexibility for applying material in *in vitro* and *in vivo* platforms. ECM powders can be formed with a mortar and pestle following freezing with liquid nitrogen or more uniformly ground by milling lyophilized material (Fig. 1.3.6A.3D). This powder can be directly mixed with a liquid carrier (Fig. 1.3.6A.3E) or alternatively processed into a hydrogel by partial enzymatic digestion (Fig. 1.3.6A.3F). This can be accomplished with pepsin in acidic solution, followed by neutralization and reconstitution to physiological salt and pH conditions (Freytes et al., 2008; Voytik-Harbin et al., 1998). Similar to collagen alone, injection of the digested ECM suspension or incubation at 37°C can cause self-assembly into a

nanofibrous hydrogel. Generally, reported times between 24 and 96 h have been sufficient for digesting particles into a homogeneous solution (Saldin et al., 2017). Notably, adjusting parameters such as salt concentration and digestion time has been shown to affect material properties (Johnson et al., 2011) and solubilized protein fragments influencing *in vitro* cellular responses (Agrawal et al., 2011; Williams et al., 2015b), respectively.

Cross-Linking

Like other biomaterials, cross-linking methods can be utilized to modulate degradation rate and mechanical strength of decellularized ECM. These methods include chemical, natural, and physical agents. Chemical cross-linker glutaraldehyde has been widely used for vascular tissue engineering applications (Chapter 1.2.5; Zhao et al., 2011). As previously mentioned, glutaraldehyde treatment can potentially lead to calcification (see “Tissue Cross-linking” section) resulting in failure of the implanted decellularized tissue (Perrotta et al., 2011; Hussein et al., 2017). Treatment with organic solvents and amino acids can decrease calcification (Park et al., 2017). Another well-known chemical cross-linker genipin forms covalent bonds between free primary amine groups of lysine and

TABLE 1.3.6A.1 Partial List of Commercial Decellularized Tissue Products and Clinical Use

Tissue	Source	Form	Demonstrated Uses	Product	References	
Skin	Human	Scaffold	Wound and abdominal hernia repair; breast reconstruction	AlloDerm	(Breuing and Warren, 2005; Slavin and Lin, 2012; Skovsted Yde et al., 2016; Krishnan et al., 2014)	
				AlloMax	Hinchcliff et al., (2017)	
	Porcine	Scaffold	Wound, abdominal and chest wall repair; breast reconstruction	Rotator cuff repair	GraftJacket	(Brigido, 2006; Derwin et al., 2006)
				Wound repair; soft tissue facial augmentation; vocal cord paralysis	Micronized AlloDerm	(Sclafani et al., 2000, 2001)
				Strattice	(Begum et al., 2016; Salzberg et al., 2013)	
Bovine	Scaffold		Surgimend	Ball et al. (2017)		
Urinary Bladder	Porcine	Scaffold	Wound, hernia and ulcer repair; treating volumetric muscle loss	MatriStem	(Kim et al., 2016b; Howell et al., 2018; Sicari et al., 2014)	
		Powder	Wound and ulcer repair	MicroMatrix	(Dorman and Bass, 2016; Rommer et al., 2013; Lecheminant and Field, 2012; Frykberg et al., 2016; Ahmed et al., 2012; Kruper et al., 2013)	
Small Intestinal Submucosa	Porcine	Scaffold	Wound, hernia, and ulcer repair	Surgisis	(Oelschlager et al., 2003; Holcomb et al., 2005; Franklin et al., 2004; Edelman and Hodde, 2006)	
				Oasis	(Mostow et al., 2005; Romanelli et al., 2010)	
			Vascular, pericardial, valve, atrial, septal, and ventricular wall repair	CorMatrix	(Eckhauser et al., 2013; Stelly and Stelly, 2013; Poulin et al., 2013; Cua et al., 2014; Yanagawa et al., 2014; Holubec et al., 2015; Szczeklik et al., 2015; Gerdisch et al., 2014; Mosala Nezhad et al., 2016)	
Pulmonary Valve	Human	Scaffold	Valve replacement	CryoValve SG	(Hawkins et al., 2003b; Brown et al., 2010)	
	Porcine	Scaffold		Synergraft	(Simon et al., 2003; Goldstein et al., 2000)	
	Porcine	Scaffold		Matrix P	(Konertz et al., 2011; Voges et al., 2013)	
Cartilage/ bone	Human	Scaffold	Focal cartilage defects	Chondrofix	Gomoll (2013)	

hydroxylysine residues in collagen. A previous study with genipin-cross-linked liver ECM scaffold demonstrated increased tensile strength and elastic modulus compared to glutaraldehyde-treated scaffolds (Gao et al., 2018). Other examples of cross-linking agents include EDC/NHS and transglutaminases. EDC/NHS cross-linking significantly improved compression modulus and reduced degradation of porcine acellular dermal matrix (Li et al., 2013). Transglutaminase is a natural cross-linking enzyme that produces a reaction between glutamine and lysine residues on proteins, resulting in covalent amide bond formation (Williams et al., 2015a). Liver scaffolds cross-linked by transglutaminase showed increased elastic modulus and tensile stress response, decreased porosity, and maintained cell attachment (Takeda and Xu, 2014).

Other cross-linking methods, such as photooxidation, increased acellular blood vessel thermal stability and mechanical strength (Moore, 1998; Lu et al., 2009). Also, gamma and ultraviolet irradiation (UV) have been used, which produce free radicals leading to polymer chain scission and cross-linking (Park et al., 2013). These methods can be combined with chemical agents. Decellularized porcine cornea cross-linked by carbodiimide and gamma irradiation showed increased thermal stability and mechanical strength compared to native tissue (Lin et al., 2017).

Applications of Decellularized ECM

Decellularized tissues in various forms have become commercial products for clinical use (Table 1.3.6A.1) with more

TABLE 1.3.6A.2 Partial List of Decellularized Tissue Therapies Along the Translational Pipeline (Large Animal, Clinical Trial)

Tissue	Source	Form	Product	Treatment	Clinical	Preclinical Models	References
Small Intestinal Submucosa	Porcine	Scaffold	CorMatrix®	Small bowel defect		Dog	Chen and Badylak, (2001)
				Ureteral replacement		Pig	Liatsikos et al. (2001)
		Powder	CorMatrix ECM Particulate	Postinfarct and heart failure	Phase I: RESTORE: NCT02139189	Rat, Bovine	(Zhao et al., 2010; Slaughter et al., 2014; Soucy et al., 2015)
Adipose	Human	Powder	Renuva (Musculoskeletal Transplant Foundation)	Soft-tissue defect and reconstruction	Phase I: NCT02445118	Mouse	Kokai et al., (2019)
			A3T01 (Aegeria Soft Tissue)		Phase I: NCT02817984	Rat	Wu et al., (2012)
					Phase I: NCT01992315		
Myocardium	Porcine	Hydrogel	Ventrigel (Ventrix)	Postinfarct and heart failure	Phase I: NCT02305602	Rat, Pig	(Singelyn et al., 2012; Seif-Naraghi et al., 2013; Traverse et al., 2019)
Aortic valve	Porcine	Scaffold		Valve replacement		Pig	Gallo et al., (2012)

products on the translational pipeline based on promising preclinical results in large animal models and evaluations under way at the clinical trial stage (Table 1.3.6A.2). A summary of decellularized tissue applications is provided below to demonstrate the progression and trends in the field for research and clinical use.

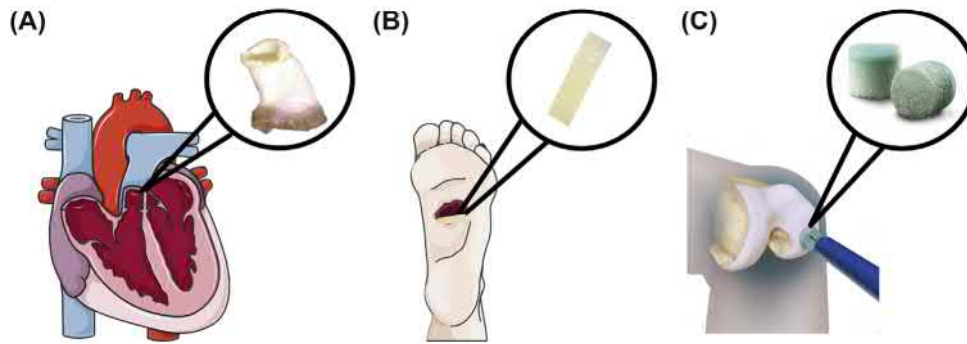
Scaffold-Based Therapies

In vivo implantation of decellularized ECM scaffolds into different tissue sources provides a three-dimensional structure for cellular infiltration and restoration of function to a particular tissue. These biomaterials can be implanted into the same tissue source (orthotopic) or alternative environments (heterotopic). Allogeneic or xenogeneic acellular scaffolds from heart valves, skin, SIS, and bladder among others, are commercially available, while others are in preclinical to clinical development.

Heart valves: Clinical studies with decellularized human valve allografts were developed in the late 1990s, with three options currently available. The widely known option, CryoValve SG, is an acellular pulmonary valve which demonstrated in a clinical trial maintenance of structural integrity

and hemodynamic function after 4 years of implantation (Brown et al., 2010; Hawkins et al., 2003a). Two other products have demonstrated positive results in early and midterm studies, but long-term outcomes are still necessary (Cebotari et al., 2011; Sarikouch et al., 2016; da Costa et al., 2010).

Apart from allogeneic valves, xenografts (Fig. 1.3.6A.4A) have been tested in preclinical and clinical stages. SynerGraft, the first developed decellularized porcine valve, was implanted in a sheep model of right ventricular outflow tract reconstruction. Infiltration of fibroblasts toward the leaflet supportive tissue with no evidence of calcification was observed 6 months after implantation (O'Brien MF, 1999). In clinical trials, both positive and negative results have been observed. Negative outcomes included an inflammatory response, possibly due to incomplete decellularization (Simon et al., 2003; Goldstein et al., 2000). A xenogeneic pulmonary valve (Matrix P), was also developed with sodium deoxycholate treatment. In a clinical study, implantation of the scaffold maintained normal structural integrity (Konertz et al., 2011). However, another study resulted in a foreign-body reaction against the xenograft with severe inflammation



• **Figure 1.3.6A.4** Scaffold-based therapies for different tissue-engineering and regenerative medicine applications. (A) Replacement of pulmonary heart valves, (B) dermis for diabetic foot ulcers, (C) hyaline cartilage and subchondral bone for focal cartilage defects (Chondrofix). (Modified with permission from Wolkers, W., Oldenhof, H., 2015. Cryopreservation and Freeze-Drying Protocols. Springer, New York; Lee, J.H., Park, K.R., Kim, T.G., Ha, J.H., Chung, K.J., Kim, Y.H., Lee, S.J., Kang, S.H., 2013. A comparative study of CG CryoDerm and AlloDerm in direct-to-implant immediate breast reconstruction. Arch Plast Surg. 40, 374–379, Zimmer Biomet and Creative Commons License 3.0.)

and fibrotic tissue (Voges et al., 2013). Controversial results with both xenogeneic valves indicate the need to carefully evaluate biocompatibility in preclinical stages, improve preimplant conditioning, or removal of xenantigens after the decellularization process.

Skin: Several decellularized skin tissues are already FDA cleared for different applications, such as superficial and deep burns, and ulcers. In 1995, the first acellular human dermal matrix by sodium deoxycholate and freeze-drying decellularization methods, AlloDerm (Fig. 1.3.6A.4B), was developed for full-thickness skin injury (Wainwright, 1995). Over the years, this scaffold has been used for other approaches, such as breast reconstruction and abdominal hernia repair (Breuing and Warren, 2005; Slavin and Lin, 2012; Skovsted Yde et al., 2016; Krishnan et al., 2014). Other acellular human dermis matrices have been developed using different decellularization methods, such as AlloMax, which is treated with hyper/hypotonic solutions and sodium hydroxide (Chauviere et al., 2014; Orenstein et al., 2010; Hinchcliff et al., 2017). GraftJacket, another FDA-cleared commercial product, is used in orthotopic (e.g., chronic wound healing) and heterotopic (e.g., rotator cuff tendon repair) locations (Brigido, 2006) (Derwin KA, 2006). Xenografts include Strattice and Surgimend, derived from porcine and bovine sources, respectively. These scaffolds are used for breast reconstruction, hernia repair, and abdominal and chest wall repair (Begum et al., 2016; Salzberg et al., 2013; Ball et al., 2017).

Other tissues: Different tissues, besides heart valves and skin, have been decellularized for scaffold-based therapies. Acellular porcine SIS is widely used in diverse fields such as gastroenterology, dermatology, orthopedic, and cardiovascular fields. SIS (Surgis) has been used since 1999 for hernia repair, and different clinical studies have indicated success with this product (Oelschlager et al., 2003; Holcomb et al., 2005; Franklin et al., 2004; Edelman and Hodde, 2006). Another application of SIS includes wound healing of chronic leg ulcers (Oasis) or arterial and venous ulcers (Mostow et al., 2005; Romanelli et al., 2010).



• **Figure 1.3.6A.5** Porcine urinary bladder matrix for wound healing applications. (Modified with permission from Acell.)

Moreover, SIS has been tested in preclinical studies of cardiovascular surgery, such as valve replacement and myocardial repair (Rosen et al., 2005; Fallon et al., 2014; Mosala Nezhad et al., 2016). The variety of preclinical results has supported SIS (CorMatrix) use in numerous clinical studies (Mosala Nezhad et al., 2016; Quarti et al., 2011; Gerdisch MW, 2014). Even though results of SIS application in the cardiovascular field are promising, large-scale and long-term clinical studies are needed to better assess integration in a heterotopic environment. The need for additional evaluations has been especially evident in pediatric applications, as mentioned in the case study.

Chondrofix (Fig. 1.3.6A.4C), a decellularized cadaveric human hyaline cartilage and subchondral bone, was implanted in patients with focal cartilage defects. After 28 months of implantation, allografts led to decreased knee pain with maintenance of subchondral bone (Gomoll, 2013). However, another study indicated the need for reoperation due to structural damage of the graft after 2 years (Farr et al., 2016). As a relatively new option for osteochondral defects, long-term clinical studies are needed to efficiently evaluate applications in the orthotopic scenario.

Acellular porcine urinary bladder (MatriStem) (Fig. 1.3.6A.5) has been tested in clinical studies of deep burns demonstrating reepithelialization and also effective treatment of acute diabetic or venous ulcerations (Kim et al., 2016b; Balland et al., 2016). Hernia repair application has also been assessed in clinical studies involving a large cohort of patients, without postoperative complications (Howell et al., 2018). The porcine urinary bladder was also tested in a pilot clinical study for volumetric muscle loss, where three of the five patients involved had an improved functional capacity of the damaged limb 6 months after the scaffold implantation (Sicari et al., 2014).

Whole Organ Recellularization

To address the critical shortage of donor organs, tissue-engineering approaches developing functional organs from decellularized xenogenic or allogeneic sources seeded with different cell populations have been investigated. Whole-organ recellularization is a complicated task that takes into consideration three main factors: cell source, cell seeding approach, and a bioreactor. Successful organ regeneration is dependent on complete recellularization of the parenchyma (functional tissue of an organ), vasculature, and supportive structures (Badylak et al., 2011; Scarritt et al., 2015). Furthermore, the method of cellular delivery is important, since fluid shear stress and pressure can affect cell adhesion to the scaffold and proliferation. Finally, a bioreactor is essential for adequate delivery of nutrients to the center of the organ. Besides perfusion, mechanical and electrical cues may be necessary depending on the organ to recellularize.

Over the past years, different organs from various animal sources have been recellularized. In 2008, the field of whole-organ recellularization started when adult rat heart was decellularized and perfused with neonatal rat cardiac or endothelial cells. After 8 days in culture under electrical stimulation and load, the construct started to pump at a rate equivalent to 2% of adult heart function (Ott et al., 2008). After this breakthrough, researchers started to recellularize different organs including kidney, liver, and lungs. In one study, recellularization of kidney scaffold with epithelial and endothelial cells led to urine production in vitro. The construct when orthotopically implanted and connected to native vasculature in the recipient rat, was well perfused, and urine, creatinine, urea, and albumin were produced (Song et al., 2013). Furthermore, decellularized liver matrix seeded with primary rat hepatocytes maintained hepatocyte viability after 2 days in culture. After 8 h of transplantation in rats, hepatocytes maintained their morphology and parenchymal positions (Uygun et al., 2010). Lung scaffolds have been seeded with epithelial and endothelial cells, leading to gas exchange after 5 days in culture. This was also observed 6 h after the construct was implanted and ventilated by the airways and respiratory muscles of recipient rats (Ott et al., 2010). In another study, lung constructs seeded with neonatal rat lung epithelial and endothelial cells replaced lungs of rats and gas exchange was documented



• **Figure 1.3.6A.6** ECM powder from porcine urinary bladder (MicroMatrix). (Modified with permission from Acell.)

during the 45–120 min of implantation (Petersen et al., 2010). Another example includes recellularization of acellular rhesus macaque lung scaffold, done by airway seeding with macaque bone marrow mesenchymal stem cells, and further vascular seeding perfusion with endothelial cells (Bonvillain et al., 2013). From the reproductive system, decellularized porcine uterus repopulated with human endometrial stem cells resulted in a contracted scaffold and organized seeded cells (Campo et al., 2017). Although successful studies have been done in small animal models, several issues with organ transplantation need to be considered (see “Current Challenges and Future Directions of Decellularized Tissues” section).

Powder and Injectable Decellularized ECM Therapies

For tissue conditions not requiring volumetric replacement of tissue structures, ECM scaffolds further processed into powder or hydrogel forms can be utilized (see “Milling for ECM Powder and Partial Enzymatic Digestion for Hydrogel Formation”). As volumetric organization in these platforms is broken down, these therapies can be evenly applied onto tissue surfaces or act as space-filling material.

Several ECM powder products that can be applied as a dry powder, hydrated paste, or injectable are commercially available, such as MicroMatrix (Acell) (Fig. 1.3.6A.6) from porcine urinary bladder, micronized AlloDerm (Allergan) from human dermal tissue, Powder Extracellular Matrix (Cook Biotech), and ECM Particulate (CorMatrix) from decellularized SIS. Clinical use has been mainly for enhanced recovery and comfort of slow or nonhealing percutaneous wounds, ulcers, and surgical operations compared to traditional treatment methods (Dorman and Bass, 2016; Rommer et al., 2013; Lecheminant and Field, 2012; Frykberg et al., 2016; Ahmed et al., 2012; Kruper et al., 2013). At the preclinical stage, surgical implantation of ECM powders with carriers has been demonstrated for several tissues including bone (Brown et al., 2012; Peterson et al., 2004) and cardiac (Tabuchi et al., 2015). However, required

invasive surgery for directly applying ECM powders has limited translation compared to less invasive injection delivery.

Application and efficacy of injectable ECM powders have been applied to a wider range of tissue including liver (Nakamura and Ijima, 2013), lung (Manni et al., 2011), bone (Teng et al., 2017; Peterson et al., 2004), and adipose (Wu et al., 2012; Beachley et al., 2015; Gibson et al., 2014; Kokai et al., 2019). In the clinical setting, micronized Alloderm has been applied for facial soft tissue augmentation (Sclafani et al., 2000, 2001) and treating unilateral vocal fold paralysis (Pearl et al., 2002; Milstein et al., 2005; Morgan et al., 2007; Vinson et al., 2010) with beneficial long-term functional outcomes at least up to 1 year postinjection. Based on evaluation for treatment, postmyocardial infarction in small (Zhao et al., 2010) and large animal models (Slaughter et al., 2014; Soucy et al., 2015), ECM Particulate (CorMatrix) has undergone a phase I clinical trial (RESTORE: NCT02139189) delivered in tandem with coronary artery bypass operation for patients with an ejection fraction between 25% and 40%. Several injectable decellularized adipose ECM powders have been evaluated in phase I clinical trials for the treatment of soft tissue defects: Acellularized Adipose Tissue 01 or A3T01 (Aegeria Soft Tissue) (NCT01992315, NCT02817984) and Renuva (NCT02445118), with the latter showing safe implantation and greater than 40% volumetric retention at 16 weeks (Kokai et al., 2019).

Due to the shear thinning properties of enzymatically digested ECM suspension that forms a hydrogel postinjection (Ungerleider et al., 2015), these materials are highly compatible with less invasive delivery methods. The digestion process also renders a hemocompatible material (Seif-Naraghi et al., 2013). For tissues that normally require invasive surgery for treatment, such as the heart, this advantage helps reduce risk and hastens patient recovery from deployment. Many promising results have been produced for ECM hydrogels in preclinical animal models from a variety of different source tissues for orthotopic and heterotopic applications including cerebral, skeletal muscle, tendon, and cardiac applications (Saldin et al., 2017; Spang and Christman, 2018). Potentially due to delivery advantages, the development and preclinical testing of ECM hydrogels across a wide variety of tissues has been gaining interest and could prompt an upcoming wave of clinically applied hydrogel products in the near future.

Generally, ECM hydrogels are still at an early phase of the translation process and are not yet available as a clinical therapy (Spang and Christman, 2018). Currently, VentriGel (Ventrix, Inc.) is the only product to reach the clinical stage. VentriGel made from myocardial matrix of decellularized porcine left ventricular tissue has demonstrated feasibility, safety, and efficacy in both small and large animal models (Singelyn et al., 2009, 2012; Seif-Naraghi et al., 2013). Accompanying mechanistic evaluation by transcriptomic and immunohistochemistry analysis has demonstrated increased arteriogenesis, immune cell infiltration, cardiomyocyte preservation, cardiac tissue development, and oxidative metabolism along with reduced apoptosis, hypertrophy, and fibrosis

among a plethora of modulated pathways in matrix versus saline-injected controls (Wassenaar et al., 2016). Evaluation in a phase I trial (NCT02305602) in patients with ejection fraction between 25% and 45% was recently completed, demonstrating safety of an ECM hydrogel in patients for the first time (Traverse et al., 2019).

Aside from advancements testing and translating ECM hydrogels alone, these methods have also been demonstrated as a useful codelivery vehicle with other therapeutic agents for synergistic benefits. Cellular codelivery in hydrogels (Lee et al., 2014; Rao et al., 2017; Yuan et al., 2017) has commonly demonstrated enhanced viability of cellular payload with some improved outcomes for ECM compared to single-component systems. Additional noncovalent interactions with native ECM components such as heparin-binding glycosaminoglycans have been demonstrated to further elevate sustained delivery of exogenously loaded proteins, nucleic acid therapeutics, and exosomes in ECM hydrogels (Hernandez Melissa et al., 2018; Seif-Naraghi et al., 2012; Kwon et al., 2013; Smith et al., 2014) that would typically require additional components or modification for these properties in nondecellularized ECM hydrogel systems (Brouwer et al., 2013; Purcell et al., 2014). Thus, a plethora of options are available to apply these ECM materials and improve efficacy in the clinical setting.

Tissue-Specific In Vitro Models of the Native Microenvironment

Decellularized tissue can be utilized as an in vitro model representative of biophysical, biomechanical, and biochemical cues in a 3D architecture of a native ECM microenvironment. The influence of these environmental signals can help functionally and phenotypically maintain cells difficult to grow on tissue culture plastic or single ECM coating systems such as preventing dedifferentiation postisolation of culture primary esophageal epithelial cells (Ozeki et al., 2006; Bhrany et al., 2006; Hussey et al., 2017). Alterations and influence of the healthy ECM microenvironment can be studied by decellularizing tissue from disease animal models or patient biopsies for assessing disease progression or as a therapeutic screening model such as studying the influence of ECM on human breast cancer progression and efficacy of therapeutics against those cues (Liu et al., 2019).

ECM processed into a powder or an enzymatically digested suspension can be readily utilized for 2D coatings of cell adhesion surfaces (DeQuach et al., 2010; Shakouri-Motlagh et al., 2017; Lee et al., 2014; Zhang and Dong, 2015), resuspended as a soluble form in cell culture solution or formed into a 3D ECM hydrogel scaffold (Gaetani et al., 2018; Kim et al., 2016a; Wolf et al., 2014). Although processed forms lose 3D architecture, organization, and mechanical properties representative of the native tissue, batching from different tissue samples improves compositional consistency, and implementation in these different forms provides a flexible platform more readily incorporated into existing in vitro model systems. Similar to the scaffold form, cues from processed ECM can aid in maintenance of

cell behavior, viability, and function of primary isolated cell cultures such as enhancing insulin release from cultured pancreatic islets that are normally difficult to maintain *in vitro* (Chaimov et al., 2017). Culture on these ECM materials has also been shown to promote enhanced differentiation of stem and progenitor cells toward tissue-specific lineages such as heart, nerve, and immune cell populations (Lee et al., 2014; Rao et al., 2017; DeQuach et al., 2011; Wolf et al., 2012). Mechanistic study of therapeutics can also be improved by utilizing diseased tissue-derived ECM. Mesenchymal stem cell in *in vitro* culture on infarcted cardiac tissue-derived ECM demonstrated regressed expression of cardiac lineage markers while expression of pro-survival cytokine was elevated compared to healthy cardiac ECM, supporting cellular therapy efficacy by a paracrine mechanism (Sullivan et al., 2014). For the hydrogel form, cellular responses are elicited by eluted soluble fragments and hydrogel fractions. Variations of secreted cytokines from macrophages incubated with different hydrogel fractions made from urinary bladder have been observed (Slivka et al., 2014).

Aside from utilizing decellularized ECM alone, incorporation with other materials and in *in vitro* systems recapitulating additional properties of the native tissue environment can enhance representation of the healthy and diseased microenvironment. These allow study of how multiple environmental variables influence tissue development, disease progression, and screening of therapeutic efficacy. Incorporation of fetal versus adult brain ECM into an *in vitro* 3D model of cortical brain tissue with a silk and collagen I base scaffold enhanced neural network formation and neural firing function of seeded cortical neurons with fetal ECM compared to adult or collagen alone. These results support that the fetal ECM aids in early growth and development, differentiation, and organization of the cortical network (Sood et al., 2016). More specific organization of decellularized ECM for 3D cell culture can be achieved by combining with bio-ink printing platforms either alone (Jang et al., 2017a) or onto mechanically supportive synthetic (Pati et al., 2014) or naturally derived filler material (Bejleri et al., 2018) allowing for multilayered cell-laden tissue analogues. Utilizing photo-initiated cross-linking of the ECM allows further control of the local mechanical properties with these bioprinting platforms (Jang et al., 2016; Grover et al., 2014). Mechanical properties can be bulk or regionally controlled for mimicking different tissue conditions such as emulating heterogeneous stiffness profiles in healthy versus cirrhotic liver with photo-cross-linked decellularized liver ECM (Ma et al., 2018). Ultimately, isolation of the native decellularized ECM and flexibility implementing these materials redefined our general capabilities to represent tissue-specific properties *in vitro*.

Current Challenges and Future Directions for Decellularized Tissues

Despite several decellularized tissues being commercially available, there are still challenges involving optimization

and variability of the decellularization process. The need for a standard technique is required, especially for scaling-up production for clinical translation. Another crucial factor to consider is minimizing sources of immunogenicity, especially for treating demographics with abnormal immune responses such as pediatric patients. Decellularization protocols are being developed to specifically address these issues (Iop et al., 2014; Gallo et al., 2012). Pursuing improvements and more standardized use of animal models that better represent the human immune response and aspects of the targeted patient population can also prevent limited efficacy and unexpected safety issues at the clinical stage (Wang et al., 2017a; Mortell et al., 2006).

Along with optimizing methods, elevating mechanistic understanding of material properties supporting proregenerative cellular responses will aid future improvements in decellularized tissue-based therapies. Although commonly used adult porcine tissue provides abundant quantity and convenience utilizing commercial waste, whether this is an ideal source material is unknown. Mass spectrometry and transcriptomic analysis have suggested ECM components and properties from younger tissue may support greater tissue repair. For example, the neonatal mouse heart has a short regenerative window postgestation that is lost with aging. Transiently abundant agrin protein (Bassat et al., 2017) and lesser cross-linking (Notari et al., 2018) found in neonatal mouse heart ECM were determined to elicit repair in adult cardiac tissue postinjury and prolong the regenerative capability during the neonatal stages, respectively. Alternatively, decellularized myocardial matrix hydrogels from zebrafish hearts, which can fully regenerate 20% amputated cardiac tissue volume, elicited greater cardiac function, lesser negative remodeling, and increased number of cycling cardiomyocytes in infarcted mouse hearts compared with murine-derived hydrogels (Chen et al., 2016). Although translation feasibility from these sources is limited by tissue yield, isolating underlying contributors to tissue regeneration could allow adoption into other platforms.

Whole-organ recellularization in the clinical stage is still likely a long pathway. Further studies should include long-term graft function in healthy and diseased animal models. Before implantation, there are some challenges that still need to be optimized. Recellularization protocols would need to be refined to organ size, species, and donor characteristics (Song and Ott, 2011). Moreover, a durable vascular network is one of the major hurdles (Soto-Gutierrez et al., 2012) as incomplete reendothelialized vasculature is at risk for acute thrombosis because of exposed ECM. Furthermore, the immune response following implantation can lead to scar tissue formation, further inhibiting vascularization (Badylak et al., 2011). In summary, whole-organ recellularization is a promising field to decrease the number of patients with end-stage failure, however, the mentioned issues need to be addressed before clinical translation can be considered with recellularized constructs.

CASE STUDY: CONSIDERATIONS APPLYING DECELLULARIZED SCAFFOLDS AT INFANCY VERSUS ADULTS

Appropriate scaffolds for valve or myocardial wall repair should be bio- and hemocompatible, provide mechanical support while being resorbed with surrounding tissue, and not calcify. One option is CorMatrix ECM, a decellularized porcine small intestinal submucosa (SIS) extracellular matrix (ECM) sheet scaffold. Products with CorMatrix ECM initially received a European CE mark in 2010 and were later FDA cleared as devices for vascular repair, pericardial closure, and tissue reconstruction. While there have not been large randomized controlled clinical trials, CorMatrix ECM has demonstrated some favorable outcomes in adult cardiovascular surgical procedures based on case reports and reviews of vascular (Szczeplik et al., 2015), valvular (Gerdisch et al., 2014), pericardial (Stelly and Stelly, 2013), and myocardial wall repair (Holubec et al., 2015; Yanagawa et al., 2014). For example, CorMatrix ECM was implanted in 19 adults for mitral valve replacement. During the 10.9-months mean follow-up, no evidence of calcifications or development of stenosis was observed with partial vascularization of the graft and without valve-related complications in 17 recipients. Two patients experienced complications with limited scaffold resorption, though these patients had distinct complicating medical histories for treatment of other conditions such as cancer (Gerdisch et al., 2014).

More mixed results have been observed in pediatric applications when utilized for congenital cardiac defect surgical reconstruction. While positive outcomes in explanted scaffolds from pediatric patients have been reported showing reabsorption and replacement with collagen, reendothelialization, and no evidence of calcification (Scholl et al., 2010), histological evaluation of some explanted CorMatrix material collected due to complications or reoperations has shown cases of chronic inflammation and limited material resorption (Witt et al., 2013; Zaidi et al., 2014; Rosario-Quinones et al., 2015; Wong et al., 2016; Padalino et al., 2015). In one study, negative outcomes occurred in 9 of 47 recipients (0.1–14.5 years old), where the longest follow-up was approximately 9 months (Zaidi et al., 2014). In all explanted samples, a mild to severe inflammatory response was observed from macrophage, lymphocyte, and eosinophil infiltration. Mild calcification with neointima formation at the scaffold surface was also visualized, without scaffold reabsorption. Another evaluation

in 25 recipients (5 days to 57 years old), six infant recipients required reoperation with evidence of prolonged inflammatory response, hypersensitivity reaction, and fibrosis in explants (Rosario-Quinones et al., 2015). In a study of infantile intracardiac repair (4–8 months), 10 of 12 CorMatrix patches explanted at a median of 21 months postimplantation had calcification, fibrosis, and chronic inflammation in the scaffold (Nelson et al., 2016). While extensive preclinical research supports the biocompatibility of these scaffolds, the contrasting outcomes and number of pediatric cases experiencing complications compared to adult recipients suggests that further considerations are required for pediatric applications.

One reason for differences in the outcomes between the adult and pediatric populations could be related to the immune modulation in infants and young children (Nelson et al., 2016). For immune tolerance of maternal alloantigens, an antiinflammatory, immune-suppressed state is maintained in infants for several months postgestation (Simon et al., 2015). This state is caused by the high percentage of T-cell-independent B1 cells secreting IL-10 and TGF- β promoting differentiation of T cells toward the regulatory T-cell phenotype (Hannet et al., 1992; Mold et al., 2010). Although an immune suppressed state could be considered ideal for safe uptake of a biomaterial implant, studies have demonstrated the importance of activation and transitioning between proinflammatory and proremodeling states of macrophages and T cells for biomaterial-induced tissue repair and associated tissue remodeling responses (Nassiri et al., 2015). Furthermore, the transient immune-tolerant state at infancy has been shown to not reliably prevent rejection of xenogeneic grafts (Mattis et al., 2014). As decellularization quality batch variability has been observed in some CorMatrix scaffolds (Wong et al., 2016), xenogeneic antigens could elicit a progressive humoral response in the developing immune system, leading to later graft rejection. These issues could also limit efficacy in senior patients or patients with medical histories that hinder normal activity of their immune system (Gerdisch et al., 2014). These issues, coupled with potential genetic deviations with congenital tissue diseases, support heightened caution and scrutiny when applying these materials in infant patients.

Conclusion

Progress in tissue processing has immense promise to address the increasing need for available donor tissue and to create new standards of therapy for tissue diseases with decellularized ECM materials. With the extensive research being performed, improvements in preservation of tissue and whole-organ recellularization have potential to minimize human donor tissue waste and overcome shortages by expanding resources with xenogeneic tissue sources, respectively. Application and advancement of decellularized ECM treatments can further reduce the patient population

awaiting transplant by mitigating negative outcomes and promoting tissue repair. With further understanding of complex diseases and tissue repair processes, an increased impact of these processed tissues is expected on the scientific community and medical practice.

Acknowledgments

This work was supported by the NIH NHLBI (R01HL113468, R01HL146147), the NIH NICHD (R21HD094566), NIH NIAMS (R21AR072523), and the California Institute for Regenerative Medicine

(TRAN1-09814). RMW was supported through the NHLBI as a T32 training grant recipient (2T32HL105373-06A1) and a NIH F31 Predoctoral fellowship (F31HL137347). PD was supported through the NIAMS T32 Predoctoral Training Grant (T32AR060712) and a NIH F31 Predoctoral fellowship (F31HD098007). KLC is co-founder, consultant, board member, holds equity interest, and receives income from Ventrix, Inc.

References

- Aamodt, J.M., Grainger, D.W., 2016. Extracellular matrix-based biomaterial scaffolds and the host response. *Biomaterials* 86, 68–82.
- Abraham, G.A., Murray, J., Billiar, K., Sullivan, S.J., 2000. Evaluation of the porcine intestinal collagen layer as a biomaterial. *J. Biomed. Mater. Res.* 51, 442–452.
- Agrawal, V., Tottey, S., Johnson, S.A., Freund, J.M., Siu, B.F., Badylak, S.F., 2011. Recruitment of progenitor cells by an extracellular matrix cryptic peptide in a mouse model of digit amputation. *Tissue Eng. A* 17, 2435–2443.
- Ahmed, T., Marcal, H., Johnson, S., Brown, B.N., Foster, L.J., 2012. Coalescence of extracellular matrix (ECM) from porcine urinary bladder (UBM) with a laser-activated chitosan-based surgical adhesive. *J. Biomater. Sci. Polym. Ed.* 23, 1521–1538.
- Al-Otaibi, N.A.S., Slater, N.K.H., Rahmoune, H., 2019. Cryopreservation of red blood cells. *Methods Mol. Biol.* 1916, 233–238.
- Badylak, S.F., Taylor, D., Uygun, K., 2011. Whole-organ tissue engineering: decellularization and recellularization of three-dimensional matrix scaffolds. *Annu. Rev. Biomed. Eng.* 13, 27–53.
- Bakhach, J., 2009. The cryopreservation of composite tissues: principles and recent advancement on cryopreservation of different type of tissues. *Organogenesis* 5, 119–126.
- Ball, J.F., Sheena, Y., Tarek Saleh, D.M., Forouhi, P., Benyon, S.L., Irwin, M.S., Malata, C.M., 2017. A direct comparison of porcine (Strattice™) and bovine (Surgimend™) acellular dermal matrices in implant-based immediate breast reconstruction. *J. Plast. Reconstr. Aesthet. Surg.* 70, 1076–1082.
- Balland, O., Poinard, A.S., Famose, F., Gouille, F., Isard, P.F., Mathieson, I., Dulaurent, T., 2016. Use of a porcine urinary bladder acellular matrix for corneal reconstruction in dogs and cats. *Vet. Ophthalmol.* 19, 454–463.
- Baptista, P.M., Siddiqui, M.M., Lozier, G., Rodriguez, S.R., Atala, A., Soker, S., 2011. The use of whole organ decellularization for the generation of a vascularized liver organoid. *Hepatology* 53, 604–617.
- Bassat, E., Mutlak, Y.E., Genzelinakh, A., Shadrin, I.Y., Baruch Umansky, K., Yifa, O., Kain, D., Rajchman, D., Leach, J., Riabov Bassat, D., Udi, Y., Sarig, R., Sagi, I., Martin, J.F., Bursac, N., Cohen, S., Tzahor, E., 2017. The extracellular matrix protein agrin promotes heart regeneration in mice. *Nature* 547, 179–184.
- Beachley, V.Z., Wolf, M.T., Sadtler, K., Manda, S.S., Jacobs, H., Blatchley, M.R., Bader, J.S., Pandey, A., Pardoll, D., Elisseeff, J.H., 2015. Tissue matrix arrays for high-throughput screening and systems analysis of cell function. *Nat. Methods* 12, 1197–1204.
- Begum, T., Farrelly, P.J., Craigie, R.J., 2016. Non-cross-linked porcine acellular dermal matrix (Strattice Tissue Matrix) in pediatric reconstructive surgery. *J. Pediatr. Surg.* 51, 461–464.
- Bejleri, D., Streeter, B.W., Nachlas, A.L.Y., Brown, M.E., Gaetani, R., Christman, K.L., Davis, M.E., 2018. A bioprinted cardiac patch composed of cardiac-specific extracellular matrix and progenitor cells for heart repair. *Adv. Healthc. Mater.* 7, e1800672.
- Bhrany, A.D., Beckstead, B.L., Lang, T.C., Farwell, D.G., Giachelli, C.M., Ratner, B.D., 2006. Development of an esophagus acellular matrix tissue scaffold. *Tissue Eng.* 12, 319–330.
- Black, L.D., Allen, P.G., Morris, S.M., Stone, P.J., Suki, B., 2008. Mechanical and failure properties of extracellular matrix sheets as a function of structural protein composition. *Biophys. J.* 94, 1916–1929.
- Bonvillain, R.W., Scarritt, M.E., Pashos, N.C., Mayeux, J.P., Meshberger, C.L., Betancourt, A.M., Sullivan, D.E., Bunnell, B.A., 2013. Nonhuman primate lung decellularization and recellularization using a specialized large-organ bioreactor. *J. Vis. Exp.* e50825.
- Breuing, K.H., Warren, S.M., 2005. Immediate bilateral breast reconstruction with implants and inferolateral AlloDerm slings. *Ann. Plast. Surg.* 55, 232–239.
- Brigido, S.A., 2006. The use of an acellular dermal regenerative tissue matrix in the treatment of lower extremity wounds: a prospective 16-week pilot study. *Int. Wound J.* 3, 181–187.
- Brouwer, K.M., Wijnen, R.M., Reijnen, D., Hafmans, T.G., Daamen, W.F., Van Kuppevelt, T.H., 2013. Heparinized collagen scaffolds with and without growth factors for the repair of diaphragmatic hernia: construction and in vivo evaluation. *Organogenesis* 9, 161–167.
- Brown, B.N., Chung, W.L., Almarza, A.J., Pavlick, M.D., Reppas, S.N., Ochs, M.W., Russell, A.J., Badylak, S.F., 2012. Inductive, scaffold-based, regenerative medicine approach to reconstruction of the temporomandibular joint disk. *J. Oral Maxillofac. Surg.* 70, 2656–2668.
- Brown, B.N., Valentin, J.E., Stewart-Akers, A.M., McCabe, G.P., Badylak, S.F., 2009. Macrophage phenotype and remodeling outcomes in response to biologic scaffolds with and without a cellular component. *Biomaterials* 30, 1482–1491.
- Brown, J.W., Elkins, R.C., Clarke, D.R., Tweddell, J.S., Huddleston, C.B., Doty, J.R., Fehrenbacher, J.W., Takkenberg, J.J., 2010. Performance of the CryoValve SG human decellularized pulmonary valve in 342 patients relative to the conventional CryoValve at a mean follow-up of four years. *J. Thorac. Cardiovasc. Surg.* 139, 339–348.
- Butany, J., Zhou, T., Leong, S.W., Cunningham, K.S., Thangaroopan, M., Jegatheeswaran, A., Feindel, C., David, T.E., 2007. Inflammation and infection in nine surgically explanted Medtronic Freestyle stentless aortic valves. *Cardiovasc. Pathol.* 16, 258–267.
- Calle, E.A., Hill, R.C., Leiby, K.L., Le, A.V., Gard, A.L., Madri, J.A., Hansen, K.C., Niklason, L.E., 2016. Targeted proteomics effectively quantifies differences between native lung and detergent-decellularized lung extracellular matrices. *Acta Biomater.* 46, 91–100.
- Campo, H., Baptista, P.M., Lopez-Perez, N., Faus, A., Cervello, I., Simon, C., 2017. De- and recellularization of the pig uterus: a bioengineering pilot study. *Biol. Reprod.* 96, 34–45.
- Caralt, M., Uzarski, J.S., Iacob, S., Obergfell, K.P., Berg, N., Bijonowski, B.M., Kiefer, K.M., Ward, H.H., Wandinger-Ness, A., Miller, W.M., Zhang, Z.J., Abecassis, M.M., Wertheim, J.A., 2015. Optimization and critical evaluation of decellularization strategies to develop renal extracellular matrix scaffolds as biological templates for organ engineering and transplantation. *Am. J. Transplant.* 15, 64–75.

- Castier, Y., Leseche, G., Palombi, T., Petit, M.D., Cerceau, O., 1999. Early experience with cryopreserved arterial allografts in below-knee revascularization for limb salvage. *Am. J. Surg.* 177, 197–202.
- Cebotari, S., Tudorache, I., Ciubotaru, A., Boethig, D., Sarikouch, S., Goerler, A., Lichtenberg, A., Cheptanaru, E., Barnaciuc, S., Cazacu, A., Maliga, O., Repin, O., Maniuc, L., Breyman, T., Haverich, A., 2011. Use of fresh decellularized allografts for pulmonary valve replacement may reduce the reoperation rate in children and young adults: early report. *Circulation* 124, S115–S123.
- Chaimov, D., Baruch, L., Krishtul, S., Meivar-Levy, I., Ferber, S., Machluf, M., 2017. Innovative encapsulation platform based on pancreatic extracellular matrix achieve substantial insulin delivery. *J. Control. Release* 257, 91–101.
- Chauviere, M.V., Schutter, R.J., Steigelman, M.B., Clark, B.Z., Grayson, J.K., Sahar, D.E., 2014. Comparison of AlloDerm and AlloMax tissue incorporation in rats. *Ann. Plast. Surg.* 73, 282–285.
- Chen, M.K., Badylak, S.F., 2001. Small bowel tissue engineering using small intestinal submucosa as a scaffold. *J. Surg. Res.* 99, 352–358.
- Chen, W.C., Wang, Z., Missinato, M.A., Park, D.W., Long, D.W., Liu, H.J., Zeng, X., Yates, N.A., Kim, K., Wang, Y., 2016. Decellularized zebrafish cardiac extracellular matrix induces mammalian heart regeneration. *Sci Adv* 2, e1600844.
- Cheng, Y., Zheng, Y., Vanderghenst, J., 2011. Rapid quantitative analysis of lipids using a colorimetric method in a microplate format. *Lipids* 46, 95–103.
- Cil, A.P., Seli, E., 2013. Current trends and progress in clinical applications of oocyte cryopreservation. *Curr. Opin. Obstet. Gynecol.* 25, 247–254.
- Corwin, W.L., Baust, J.M., Vanbuskirk, R.G., Baust, J.G., 2009. In vitro assessment of apoptosis and necrosis following cold storage in a human airway cell model. *Biopreserv. Biobanking* 7, 19–27.
- Crapo, P.M., Gilbert, T.W., Badylak, S.F., 2011. An overview of tissue and whole organ decellularization processes. *Biomaterials* 32, 3233–3243.
- Cua, C.L., Kollins, K., McConnell, P.I., 2014. Echocardiographic analysis of an extracellular matrix tricuspid valve. *Echocardiography* 31, E264–E266.
- Da Costa, F.D., Costa, A.C., Prestes, R., Domanski, A.C., Balbi, E.M., Ferreira, A.D., Lopes, S.V., 2010. The early and midterm function of decellularized aortic valve allografts. *Ann. Thorac. Surg.* 90, 1854–1860.
- Daly, K.A., Stewart-Akers, A.M., Hara, H., Ezzelarab, M., Long, C., Cordero, K., Johnson, S.A., Ayares, D., Cooper, D.K., Badylak, S.F., 2009. Effect of the alphaGal epitope on the response to small intestinal submucosa extracellular matrix in a nonhuman primate model. *Tissue Eng. A* 15, 3877–3888.
- Deeken, C.R., White, A.K., Bachman, S.L., Ramshaw, B.J., Cleveland, D.S., Loy, T.S., Grant, S.A., 2011. Method of preparing a decellularized porcine tendon using tributyl phosphate. *J. Biomed. Mater. Res. B Appl. Biomater.* 96, 199–206.
- Dequach, J.A., Mezzano, V., Miglani, A., Lange, S., Keller, G.M., Sheikh, F., Christman, K.L., 2010. Simple and high yielding method for preparing tissue specific extracellular matrix coatings for cell culture. *PLoS One* 5, e13039.
- Dequach, J.A., Yuan, S.H., Goldstein, L.S., Christman, K.L., 2011. Decellularized porcine brain matrix for cell culture and tissue engineering scaffolds. *Tissue Eng. A* 17, 2583–2592.
- Derwin Ka, B.A., Spragg, R.K., Leigh, D.R., Iannotti, J.P., 2006. Commercial extracellular matrix scaffolds for rotator cuff tendon repair. Biomechanical, biochemical, and cellular properties. *J. Bone Joint Surg. Am.* 88, 2665–2672.
- Derwin, K.A., Baker, A.R., Spragg, R.K., Leigh, D.R., Iannotti, J.P., 2006. Commercial extracellular matrix scaffolds for rotator cuff tendon repair. Biomechanical, biochemical, and cellular properties. *J. Bone Joint Surg. Am.* 88, 2665–2672.
- Dorman, R.M., Bass, K.D., 2016. Novel use of porcine urinary bladder matrix for pediatric pilonidal wound care: preliminary experience. *Pediatr. Surg. Int.* 32, 997–1002.
- Eckhauser, A.W., Hannon, D., Molitor, M., Scaife, E., Gruber, P.J., 2013. Repair of traumatic aorto innominate disruption using CorMatrix. *Ann. Thorac. Surg.* 95, e99–e101.
- Edelman, D., Hodde, J.P., 2006. Bioactive prosthetic material for treatment of hernias. *Surg. Technol. Int.* 15, 104–108.
- Fahy, G.M., Wovk, B., 2015. Principles of cryopreservation by vitrification. *Methods Mol. Biol.* 1257, 21–82.
- Fallon, A.M., Goodchild, T.T., Cox, J.L., Matheny, R.G., 2014. In vivo remodeling potential of a novel bioprosthetic tricuspid valve in an ovine model. *J. Thorac. Cardiovasc. Surg.* 148, 333–340 e1.
- Farr, J., Gracitelli, G.C., Shah, N., Chang, E.Y., Gomoll, A.H., 2016. High failure rate of a decellularized osteochondral allograft for the treatment of cartilage lesions. *Am. J. Sports Med.* 44, 2015–2022.
- Franklin Jr., M.E., Gonzalez, J.J., Glass, J.L., 2004. Use of porcine small intestinal submucosa as a prosthetic device for laparoscopic repair of hernias in contaminated fields: 2-year follow-up. *Hernia* 8, 186–189.
- Freytes, D.O., Martin, J., Velankar, S.S., Lee, A.S., Badylak, S.F., 2008. Preparation and rheological characterization of a gel form of the porcine urinary bladder matrix. *Biomaterials* 29, 1630–1637.
- Frykberg, R.G., Cazzell, S.M., Arroyo-Rivera, J., Tallis, A., Reyzelman, A.M., Saba, F., Warren, L., Stouch, B.C., Gilbert, T.W., 2016. Evaluation of tissue engineering products for the management of neuropathic diabetic foot ulcers: an interim analysis. *J. Wound Care* 25 (Suppl. 7), S18–S25.
- Funamoto, S., Nam, K., Kimura, T., Murakoshi, A., Hashimoto, Y., Niwaya, K., Kitamura, S., Fujisato, T., Kishida, A., 2010. The use of high-hydrostatic pressure treatment to decellularize blood vessels. *Biomaterials* 31, 3590–3595.
- Gaetani, R., Aouad, S., Demaddalena, L.L., Straessle, H., Dzieciatkowska, M., Wortham, M., Bender, H.R., Nguyen-Ngoc, K.V., Schmid-Schoenbein, G.W., George, S.C., Hughes, C.C.W., Sander, M., Hansen, K.C., Christman, K.L., 2018. Evaluation of different decellularization protocols on the generation of pancreas-derived hydrogels. *Tissue Eng. C Methods*.
- Gallo, M., Naso, F., Poser, H., Rossi, A., Franci, P., Bianco, R., Micciolo, M., Zanella, F., Cucchini, U., Aresu, L., Buratto, E., Busetto, R., Spina, M., Gandaglia, A., Gerosa, G., 2012. Physiological performance of a detergent decellularized heart valve implanted for 15 months in Vietnamese pigs: surgical procedure, follow-up, and explant inspection. *Artif. Organs* 36, E138–E150.
- Gao, D., Critser, J.K., 2000. Mechanisms of cryoinjury in living cells. *ILAR J.* 41, 187–196.
- Gao, M., Wang, Y., He, Y., Li, Y., Wu, Q., Yang, G., Zhou, Y., Wu, D., Bao, J., Bu, H., 2018. Comparative Evaluation of Decellularized

- Porcine Liver Matrices Crosslinked with Different Chemical and Natural Crosslinking Agents. *Xenotransplantation*, p. e12470.
- Gates, K.V., Dalglish, A.J., Griffiths, L.G., 2017. Antigenicity of bovine pericardium determined by a novel immunoproteomic approach. *Sci. Rep.* 7, 2446.
- Gerdisch, M.W., Shea, R.J., Barron, M.D., 2014. Clinical experience with CorMatrix extracellular matrix in the surgical treatment of mitral valve disease. *J. Thorac. Cardiovasc. Surg.* 148, 1370–1378.
- Gibson, M., Beachley, V., Coburn, J., Bandinelli, P.A., Mao, H.Q., Elisseff, J., 2014. Tissue extracellular matrix nanoparticle presentation in electrospun nanofibers. *Biomed Res. Int.* 2014, 469120.
- Gilbert, T.W., Freund, J.M., Badylak, S.F., 2009. Quantification of DNA in biologic scaffold materials. *J. Surg. Res.* 152, 135–139.
- Giménez, A., Uriarte, J.J., Vieyra, J., Navajas, D., Alcaraz, J., 2017. Elastic properties of hydrogels and decellularized tissue sections used in mechanobiology studies probed by atomic force microscopy. *Microsc. Res. Tech.* 80, 85–96.
- Girardot, J.M., Girardot, M.N., 1996. Amide cross-linking: an alternative to glutaraldehyde fixation. *J. Heart Valve Dis.* 5, 518–525.
- Giwa, S., Lewis, J.K., Alvarez, L., Langer, R., Roth, A.E., Church, G.M., Markmann, J.F., Sachs, D.H., Chandraker, A., Wertheim, J.A., Rothblatt, M., Boyden, E.S., Eidbo, E., Lee, W.P.A., Pomahac, B., Brandacher, G., Weinstock, D.M., Elliott, G., Nelson, D., Acker, J.P., Uygun, K., Schmalz, B., Weegman, B.P., Tocchio, A., Fahy, G.M., Storey, K.B., Rubinsky, B., Bischof, J., Elliott, J.A.W., Woodruff, T.K., Morris, G.J., Demirci, U., Brockbank, K.G.M., Woods, E.J., Ben, R.N., Baust, J.G., Gao, D., Fuller, B., Rabin, Y., Kravitz, D.C., Taylor, M.J., Toner, M., 2017. The promise of organ and tissue preservation to transform medicine. *Nat. Biotechnol.* 35, 530–542.
- Goldstein, S., Clarke, D., Walsh, S., Black, K., Brien, M., 2000. Transpecies heart valve transplant: advanced studies of a bioengineered xeno-autograft. *Ann. Thorac. Surg.* 70, 1962–1969.
- Gomoll, A.H., 2013. Osteochondral allograft transplantation using the chondrofix implant. *Oper. Tech. Sport. Med.* 21, 90–94.
- Gournier, J.P., Favre, J.P., Gay, J.L., Barral, X., 1995. Cryopreserved arterial allografts for limb salvage in the absence of suitable saphenous vein: two-year results in 20 cases. *Ann. Vasc. Surg.* 9 (Suppl) S7-14.
- Griffin, M., Premakumar, Y., Seifalian, A., Butler, P.E., Szarko, M., 2016. Biomechanical characterization of human soft tissues using indentation and tensile testing. *J. Vis. Exp. : J. Vis. Exp.* 54872.
- Grover, G.N., Rao, N., Christman, K.L., 2014. Myocardial matrix-polyethylene glycol hybrid hydrogels for tissue engineering. *Nanotechnology* 25, 014011.
- Hawkins, J.A., Hillman, N.D., Lambert, L.M., Jones, J., Di Russo, G.B., Profaizer, T., Fuller, T.C., Minich, L.L., Williams, R.V., Shaddy, R.E., 2003a. Immunogenicity of decellularized cryopreserved allografts in pediatric cardiac surgery: comparison with standard cryopreserved allografts. *J. Thorac. Cardiovasc. Surg.* 126, 247–252.
- Hawkins, J.A., Hillman, N.D., Lambert, L.M., Jones, J., Di Russo, G.B., Profaizer, T., Fuller, T.C., Minich, L.L., Williams, R.V., Shaddy, R.E., 2003b. Immunogenicity of decellularized cryopreserved allografts in pediatric cardiac surgery: comparison with standard cryopreserved allografts. *J. Thorac. Cardiovasc. Surg.* 126, 247–252 Discussion 252-3.
- He, Z., Forest, F., Bernard, A., Gauthier, A., Montard, R., Peoc'h, M., Jumelle, C., Courrier, E., Perrache, C., Gain, P., Thuret, G., 2016. Cutting and decellularization of multiple corneal stromal lamellae for the bioengineering of endothelial grafts. *Invest. Ophthalmol. Vis. Sci.* 57.
- Hernandez Melissa, J., Gaetani, R., Pieters Vera, M., Ng Nathan, W., Chang Audrey, E., Martin Taylor, R., Ingen, E., Mol Emma, A., Dzieciatkowska, M., Hansen Kirk, C., Sluijter Joost, P.G., Christman Karen, L., 2018. Decellularized extracellular matrix hydrogels as a delivery platform for MicroRNA and extracellular vesicle therapeutics. *Adv. Ther.* 1, 1800032.
- Hinchcliff, K.M., Orbay, H., Busse, B.K., Charvet, H., Kaur, M., Sahar, D.E., 2017. Comparison of two cadaveric acellular dermal matrices for immediate breast reconstruction: a prospective randomized trial. *J. Plast. Reconstr. Aesthet. Surg.* 70, 568–576.
- Hodde, J.P., Record, R.D., Tullius, R.S., Badylak, S.F., 2002. Retention of endothelial cell adherence to porcine-derived extracellular matrix after disinfection and sterilization. *Tissue Eng.* 8, 225–234.
- Holcomb 3rd, G.W., Ostlie, D.J., Miller, K.A., 2005. Laparoscopic patch repair of diaphragmatic hernias with Surgisis. *J. Pediatr. Surg.* 40, 1–5.
- Holubec, T., Caliskan, E., Bettex, D., Maisano, F., 2015. Repair of post-infarction left ventricular free wall rupture using an extracellular matrix patch. *Eur. J. Cardiothorac. Surg.* 48, 800–803.
- Howell, R.S., Fazzari, M., Petrone, P., Barkan, A., Hall, K., Servide, M.J., Anduaga, M.F., Brathwaite, C.E.M., 2018. Paraesophageal hiatal hernia repair with urinary bladder matrix graft. *JSLs* 22.
- Huleihel, L., Bartolacci, J.G., Dziki, J.L., Vorobyov, T., Arnold, B., Scarritt, M.E., Pineda Molina, C., Lopresti, S.T., Brown, B.N., Naranjo, J.D., Badylak, S.F., 2017. Matrix-bound nanovesicles recapitulate extracellular matrix effects on macrophage phenotype. *Tissue Eng. A* 23, 1283–1294.
- Huleihel, L., Hussey, G.S., Naranjo, J.D., Zhang, L., Dziki, J.L., Turner, N.J., Stolz, D.B., Badylak, S.F., 2016. Matrix-bound nanovesicles within ECM bioscaffolds. *Sci. Adv.* 2 e1600502-e1600502.
- Human, P., Zilla, P., 2001. Characterization of the immune response to valve bioprostheses and its role in primary tissue failure. *Ann. Thorac. Surg.* 71, 385–388.
- Hussein, K.H., Park, K.M., Lee, Y.S., Woo, J.S., Kang, B.J., Choi, K.Y., Kang, K.S., Woo, H.M., 2017. New insights into the pros and cons of cross-linking decellularized bioartificial organs. *Int. J. Artif. Organs* 40, 136–141.
- Hussein, K.H., Saleh, T., Ahmed, E., Kwak, H.H., Park, K.M., Yang, S.R., Kang, B.J., Choi, K.Y., Kang, K.S., Woo, H.M., 2018. Biocompatibility and hemocompatibility of efficiently decellularized whole porcine kidney for tissue engineering. *J. Biomed. Mater. Res. A* 106, 2034–2047.
- Hussey, G.S., Cramer, M.C., Badylak, S.F., 2017. Extracellular matrix bioscaffolds for building gastrointestinal tissue. *Cell. Mol. Gastroenterol. Hepatol.* 5, 1–13.
- Iop, L., Bonetti, A., Naso, F., Rizzo, S., Cagnin, S., Bianco, R., Dal Lin, C., Martini, P., Poser, H., Franci, P., Lanfranchi, G., Busetto, R., Spina, M., Basso, C., Marchini, M., Gandaglia, A., Ortolani, F., Gerosa, G., 2014. Decellularized allogeneic heart valves demonstrate self-regeneration potential after a long-term preclinical evaluation. *PLoS One* 9, e99593.
- Jang, J., Kim, T.G., Kim, B.S., Kim, S.W., Kwon, S.M., Cho, D.W., 2016. Tailoring mechanical properties of decellularized extracellular matrix bioink by vitamin B2-induced photo-crosslinking. *Acta Biomater.* 33, 88–95.

- Jang, J., Park, H.J., Kim, S.W., Kim, H., Park, J.Y., Na, S.J., Kim, H.J., Park, M.N., Choi, S.H., Park, S.H., Kim, S.W., Kwon, S.M., Kim, P.J., Cho, D.W., 2017a. 3D printed complex tissue construct using stem cell-laden decellularized extracellular matrix bioinks for cardiac repair. *Biomaterials* 112, 264–274.
- Jang, T.H., Park, S.C., Yang, J.H., Kim, J.Y., Seok, J.H., Park, U.S., Choi, C.W., Lee, S.R., Han, J., 2017b. Cryopreservation and its clinical applications. *Integr. Med. Res.* 6, 12–18.
- Jayakrishnan, A., Jameela, S.R., 1996. Glutaraldehyde as a fixative in bioprostheses and drug delivery matrices. *Biomaterials* 17, 471–484.
- Johnson, T.D., Dequach, J.A., Gaetani, R., Ungerleider, J., Elhag, D., Nigam, V., Behfar, A., Christman, K.L., 2014. Human versus porcine tissue sourcing for an injectable myocardial matrix hydrogel. *Biomater. Sci.* 2014, 60283D.
- Johnson, T.D., Lin, S.Y., Christman, K.L., 2011. Tailoring material properties of a nanofibrous extracellular matrix derived hydrogel. *Nanotechnology* 22, 494015.
- Jorba, I., Uriarte, J.J., Campillo, N., Farré, R., Navajas, D., 2017. Probing micromechanical properties of the extracellular matrix of soft tissues by atomic force microscopy. *J. Cell. Physiol.* 232, 19–26.
- Kajbafzadeh, A.M., Abbasioun, R., Sabetkish, S., Sabetkish, N., Rahmani, P., Tavakkolatabassi, K., Arshadi, H., 2017. Future prospects for human tissue engineered urethra transplantation: decellularization and recellularization-based urethra regeneration. *Ann. Biomed. Eng.* 45, 1795–1806.
- Kasimir, M.T., Rieder, E., Seebacher, G., Nigisch, A., Dekan, B., Wolner, E., Weigel, G., Simon, P., 2006. Decellularization does not eliminate thrombogenicity and inflammatory stimulation in tissue-engineered porcine heart valves. *J. Heart Valve Dis.* 15, 278–286 Discussion 286.
- Keane, T.J., Saldin, L.T., Badylak, S.F., 2016. Decellularization of mammalian tissues. In: *Characterisation and Design of Tissue Scaffolds*.
- Keane, T.J., Swinehart, I.T., Badylak, S.F., 2015. Methods of tissue decellularization used for preparation of biologic scaffolds and in vivo relevance. *Methods* 84, 25–34.
- Kim, E.J., Choi, J.S., Kim, J.S., Choi, Y.C., Cho, Y.W., 2016a. Injectable and thermosensitive soluble extracellular matrix and methylcellulose hydrogels for stem cell delivery in skin wounds. *Biomacromolecules* 17, 4–11.
- Kim, H.J., Koo, B.W., Kim, D., Seo, Y.S., Nam, Y.K., 2017. Effect of marine-derived ice-binding proteins on the cryopreservation of marine microalgae. *Mar. Drugs* 15.
- Kim, J.S., Kaminsky, A.J., Summitt, J.B., Thayer, W.P., 2016b. New innovations for deep partial-thickness burn treatment with ACell MatriStem matrix. *Adv. Wound Care* 5, 546–552.
- King, K.R., Aguirre, A.D., Ye, Y.-X., Sun, Y., Roh, J.D., Ng Jr., R.P., Kohler, R.H., Arlauckas, S.P., Iwamoto, Y., Savol, A., Sadreyev, R.I., Kelly, M., Fitzgibbons, T.P., Fitzgerald, K.A., Mitchison, T., Libby, P., Nahrendorf, M., Weissleder, R., 2017. IRF3 and type I interferons fuel a fatal response to myocardial infarction. *Nat. Med.* 23, 1481.
- Klaas, M., Kangur, T., Viil, J., Mäemets-Allas, K., Minajeva, A., Vadi, K., Antsov, M., Lapidus, N., Järvekülg, M., Jaks, V., 2016. The alterations in the extracellular matrix composition guide the repair of damaged liver tissue. *Sci. Rep.* 6, 27398.
- Klein, J.A., Meng, L., Zaia, J., 2018. Deep sequencing of complex proteoglycans: a novel strategy for high coverage and site-specific identification of glycosaminoglycan-linked peptides. *Mol. Cell. Proteom.* 17, 1578–1590.
- Kokai, L.E., Schilling, B.K., Chnari, E., Huang, Y.-C., Imming, E.A., Karunamurthy, A., Khouri, R.K., D'amico, R.A., Coleman, S.R., Marra, K.G., Rubin, J.P., 2019. Injectable allograft adipose matrix supports adipogenic tissue remodeling in the nude mouse and human. *Plast. Reconstr. Surg.* 143, 299e–309e.
- Konertz, W., Angeli, E., Tarusinov, G., Christ, T., Kroll, J., Dohmen, P., Krogmann, O., Franzbach, B., Napoleone, C., Gargiulo, G., 2011. Right ventricular outflow tract reconstruction with decellularized porcine xenografts in patients with congenital heart disease. *J. Heart Valve Dis.* 20.
- Krishnan, N.M., Chatterjee, A., Rosenkranz, K.M., Powell, S.G., Nigriny, J.F., Vidal, D.C., 2014. The cost effectiveness of acellular dermal matrix in expander-implant immediate breast reconstruction. *J. Plast. Reconstr. Aesthet. Surg.* 67, 468–476.
- Kruper, G.J., Vandegriend, Z.P., Lin, H.-S., Zuliani, G.F., 2013. Salvage of failed local and regional flaps with porcine urinary bladder extracellular matrix aided tissue regeneration. *Case Rep. Otolaryngol.* 2013, 5.
- Kumar Kuna, V., Xu, B., Sumitran-Holgersson, S., 2018. Decellularization and recellularization methodology for human saphenous veins. *J. Vis. Exp.*
- Kwon, J.S., Yoon, S.M., Shim, S.W., Park, J.H., Min, K.J., Oh, H.J., Kim, J.H., Kim, Y.J., Yoon, J.J., Choi, B.H., Kim, M.S., 2013. Injectable extracellular matrix hydrogel developed using porcine articular cartilage. *Int. J. Pharm.* 454, 183–191.
- Lecheminant, J., Field, C., 2012. Porcine urinary bladder matrix: a retrospective study and establishment of protocol. *J. Wound Care* 21 (476), 478–480 482.
- Lee, J.H., Park, K.R., Kim, T.G., Ha, J.H., Chung, K.J., Kim, Y.H., Lee, S.J., Kang, S.H., 2013. A comparative study of CG CryoDerm and AlloDerm in direct-to-implant immediate breast reconstruction. *Arch. Plast. Surg.* 40, 374–379.
- Lee, J.S., Shin, J., Park, H.M., Kim, Y.G., Kim, B.G., Oh, J.W., Cho, S.W., 2014. Liver extracellular matrix providing dual functions of two-dimensional substrate coating and three-dimensional injectable hydrogel platform for liver tissue engineering. *Biomacromolecules* 15, 206–218.
- Leibo, S.P., Pool, T.B., 2011. The principal variables of cryopreservation: solutions, temperatures, and rate changes. *Fertil. Steril.* 96, 269–276.
- Li, J., Ren, N., Qiu, J., Jiang, H., Zhao, H., Wang, G., Boughton, R.I., Wang, Y., Liu, H., 2013. Carbodiimide crosslinked collagen from porcine dermal matrix for high-strength tissue engineering scaffold. *Int. J. Biol. Macromol.* 61, 69–74.
- Liatsikos, E.N., Dinlenc, C., Kapoor, R., Alexianu, M., Yohannes, P., Anderson, A.E., Smith, A.D., 2001. Laparoscopic ureteral reconstruction with small intestinal submucosa. *J. Endourol.* 15, 217–220.
- Lin, C.H., Yang, J.R., Chiang, N.J., Ma, H., Tsay, R.Y., 2014. Evaluation of decellularized extracellular matrix of skeletal muscle for tissue engineering. *Int. J. Artif. Organs* 37, 546–555.
- Lin, Y., Zheng, Q., Hua, S., Meng, Y., Chen, W., Wang, Y., 2017. Cross-linked decellularized porcine corneal graft for treating fungal keratitis. *Sci. Rep.* 7, 9955.
- Liu, G., Wang, B., Li, S., Jin, Q., Dai, Y., 2019. Human breast cancer decellularized scaffolds promote epithelial-to-mesenchymal transitions and stemness of breast cancer cells in vitro. *J. Cell. Physiol.* 234, 9447–9456.

- Londono, R., Dziki, J.L., Haljasmaa, E., Turner, N.J., Leifer, C.A., Badylak, S.F., 2017. The effect of cell debris within biologic scaffolds upon the macrophage response. *J. Biomed. Mater. Res. A* 105, 2109–2118.
- Lu, W.D., Zhang, M., Wu, Z.S., Hu, T.H., 2009. Decellularized and photooxidatively crosslinked bovine jugular veins as potential tissue engineering scaffolds. *Interact. Cardiovasc. Thorac. Surg.* 8, 301–305.
- Ma, X., Yu, C., Wang, P., Xu, W., Wan, X., Lai, C.S.E., Liu, J., Korolova-Maharajh, A., Chen, S., 2018. Rapid 3D bioprinting of decellularized extracellular matrix with regionally varied mechanical properties and biomimetic microarchitecture. *Biomaterials* 185, 310–321.
- Mahara, A., Morimoto, N., Sakuma, T., Fujisato, T., Yamaoka, T., 2014. Complete cell killing by applying high hydrostatic pressure for acellular vascular graft preparation. *Biomed. Res. Int.* 2014, 379607.
- Manni, M.L., Czajka, C.A., Oury, T.D., Gilbert, T.W., 2011. Extracellular matrix powder protects against bleomycin-induced pulmonary fibrosis. *Tissue Eng. A* 17, 2795–2804.
- Manuchehrabadi, N., Gao, Z., Zhang, J., Ring, H.L., Shao, Q., Liu, F., Mcdermott, M., Fok, A., Rabin, Y., Brockbank, K.G., Garwood, M., Haynes, C.L., Bischof, J.C., 2017. Improved tissue cryopreservation using inductive heating of magnetic nanoparticles. *Sci. Transl. Med.* 9.
- Mcpherson, T.B., Liang, H., Record, R.D., Badylak, S.F., 2000. Galalpha(1,3)Gal epitope in porcine small intestinal submucosa. *Tissue Eng.* 6, 233–239.
- Milstein, C.F., Akst, L.M., Hicks, M.D., Abelson, T.I., Strome, M., 2005. Long-term effects of micronized Alloderm injection for unilateral vocal fold paralysis. *Laryngoscope* 115, 1691–1696.
- Miyazaki, K., Maruyama, T., 2014. Partial regeneration and reconstruction of the rat uterus through recellularization of a decellularized uterine matrix. *Biomaterials* 35, 8791–8800.
- Moore, M., Phillips, R., Mcllory, B., Walley, V., Hendry, P., 1998. Evaluation of porcine valves prepared by dye-mediated photooxidation. *Ann. Thorac. Surg.* 66, S245–S248.
- Morgan, J.E., Zraick, R.I., Griffin, A.W., Bowen, T.L., Johnson, F.L., 2007. Injection versus medialization laryngoplasty for the treatment of unilateral vocal fold paralysis. *Laryngoscope* 117, 2068–2074.
- Mortell, A., Montedonico, S., Puri, P., 2006. Animal models in pediatric surgery. *Pediatr. Surg. Int.* 22, 111–128.
- Mosala Nezhad, Z., Poncelet, A., De Kerchove, L., Gianello, P., Feraille, C., El Khoury, G., 2016. Small intestinal submucosa extracellular matrix (CorMatrix(R)) in cardiovascular surgery: a systematic review. *Interact. Cardiovasc. Thorac. Surg.* 22, 839–850.
- Mostow, E.N., Haraway, G.D., Dalsing, M., Hodde, J.P., King, D., Group, O.V.U.S., 2005. Effectiveness of an extracellular matrix graft (OASIS Wound Matrix) in the treatment of chronic leg ulcers: a randomized clinical trial. *J. Vasc. Surg.* 41, 837–843.
- Nakamura, S., Ijima, H., 2013. Solubilized matrix derived from decellularized liver as a growth factor-immobilizable scaffold for hepatocyte culture. *J. Biosci. Bioeng.* 116, 746–753.
- Ning, L.J., Jiang, Y.L., Zhang, C.H., Zhang, Y., Yang, J.L., Cui, J., Zhang, Y.J., Yao, X., Luo, J.C., Qin, T.W., 2017. Fabrication and characterization of a decellularized bovine tendon sheet for tendon reconstruction. *J. Biomed. Mater. Res. A* 105, 2299–2311.
- Noborn, F., Gomez Toledo, A., Green, A., Nasir, W., Sihlbom, C., Nilsson, J., Larson, G., 2016. Site-specific identification of heparan and chondroitin sulfate glycosaminoglycans in hybrid proteoglycans. *Sci. Rep.* 6, 34537.
- Notari, M., Ventura-Rubio, A., Bedford-Guaus, S.J., Jorba, I., Mulero, L., Navajas, D., Marti, M., Raya, A., 2018. The local microenvironment limits the regenerative potential of the mouse neonatal heart. *Sci. Adv.* 4 eaao5553.
- O'Brien, M.F., Goldstein, S., Walsh, S., Black, K.S., Elkins, R., Clarke, D., 1999. The SynerGraft valve: a new acellular (nonglutardaldehyde-fixed) tissue heart valve for autologous recellularization first experimental studies before clinical implantation. *Semin. Thorac. Cardiovasc. Surg.* 11, 194–200.
- Oelschlager, B.K., Barreca, M., Chang, L., Pellegrini, C.A., 2003. The use of small small intestine submucosa in the repair of paraesophageal hernias: initial observations of a new technique. *Am. J. Surg.* 186, 4–8.
- Optn/Srtr, 2018. OPTN/SRTR 2016 annual data report: introduction. *Am. J. Transplant.* 18 (Suppl. 1), 10–17.
- Orenstein, S., Qiao, Y., Kaur, M., Klueh, U., Kreutzer, D., Novitsky, Y., 2010. In vitro activation of human peripheral blood mononuclear cells induced by human biologic meshes. *J. Surg. Res.* 158, 10–14.
- Ott, H.C., Clippinger, B., Conrad, C., Schuetz, C., Pomerantseva, I., Ikononou, L., Kotton, D., Vacanti, J.P., 2010. Regeneration and orthotopic transplantation of a bioartificial lung. *Nat. Med.* 16, 927–933.
- Ott, H.C., Matthiesen, T.S., Goh, S.K., Black, L.D., Kren, S.M., Netoff, T.I., Taylor, D.A., 2008. Perfusion-decellularized matrix: using nature's platform to engineer a bioartificial heart. *Nat. Med.* 14, 213–221.
- Ozeki, M., Narita, Y., Kagami, H., Ohmiya, N., Itoh, A., Hirooka, Y., Niwa, Y., Ueda, M., Goto, H., 2006. Evaluation of decellularized esophagus as a scaffold for cultured esophageal epithelial cells. *J. Biomed. Mater. Res. A* 79, 771–778.
- Park, C.S., Kim, Y.J., Lee, J.R., Lim, H.G., Chang, J.E., Jeong, S., Kwon, N., 2017. Anticalcification effect of a combination of decellularization, organic solvents and amino acid detoxification on glutaraldehyde-fixed xenopericardial heart valves in a large-animal long-term circulatory model. *Interact. Cardiovasc. Thorac. Surg.* 25, 391–399.
- Park, S., Kim, S.H., Lim, H.G., Lim, C., Kim, Y.J., 2013. The anticalcification effect of dithiobispropionimidate, carbodiimide and ultraviolet irradiation cross-linking compared to glutaraldehyde in rabbit implantation models. *Korean J. Thorac. Cardiovasc. Surg.* 46, 1–13.
- Pascual, G., Garcia-Honduvilla, N., Rodriguez, M., Turegano, F., Bujan, J., Bellon, J.M., 2001. Effect of the thawing process on cryopreserved arteries. *Ann. Vasc. Surg.* 15, 619–627.
- Pati, F., Jang, J., Ha, D.H., Won Kim, S., Rhie, J.W., Shim, J.H., Kim, D.H., Cho, D.W., 2014. Printing three-dimensional tissue analogues with decellularized extracellular matrix bioink. *Nat. Commun.* 5, 3935.
- Pearl, A.W., Woo, P., Ostrowski, R., Mojica, J., Mandell, D.L., Costantino, P., 2002. A preliminary report on micronized AlloDerm injection laryngoplasty. *Laryngoscope* 112, 990–996.
- Perrotta, I., Russo, E., Camastra, C., Filice, G., Di Mizio, G., Colosimo, F., Ricci, P., Tripepi, S., Amorosi, A., Triumbari, F., Donato, G., 2011. New evidence for a critical role of elastin in

- calcification of native heart valves: immunohistochemical and ultrastructural study with literature review. *Histopathology* 59, 504–513.
- Petersen, T.H., Calle, E.A., Zhao, L., Lee, E.J., Gui, L., Raredon, M.B., Gavrilov, K., Yi, T., Zhuang, Z.W., Breuer, C., Herzog, E., Niklason, L.E., 2010. Tissue-engineered lungs for in vivo implantation. *Science* 329, 538–541.
- Peterson, B., Whang, P.G., Iglesias, R., Wang, J.C., Lieberman, J.R., 2004. Osteoinductivity of commercially available demineralized bone matrix. Preparations in a spine fusion model. *J. Bone Joint Surg. Am.* 86-A, 2243–2250.
- Philips, C., Campos, F., Roosens, A., Sanchez-Quevedo, M.D.C., Declercq, H., Carriel, V., 2018. Qualitative and quantitative evaluation of a novel detergent-based method for decellularization of peripheral nerves. *Ann. Biomed. Eng.* 46, 1921–1937.
- Pieper, J.S., Hafmans, T., Van Wachem, P.B., Van Luyn, M.J., Brouwer, L.A., Veerkamp, J.H., Van Kuppevelt, T.H., 2002. Loading of collagen-heparan sulfate matrices with bFGF promotes angiogenesis and tissue generation in rats. *J. Biomed. Mater. Res.* 62, 185–194.
- Poulin, F., Horlick, E.M., David, T., Woo, A., Thavendirathan, P., 2013. 3-Dimensional transesophageal echocardiography-guided closure of a Gerbode shunt due to CorMatrix patch dehiscence. *J. Am. Coll. Cardiol.* 62, e5.
- Pridgen, B.C., Woon, C.Y., Kim, M., Thorfinn, J., Lindsey, D., Pham, H., Chang, J., 2011. Flexor tendon tissue engineering: acellularization of human flexor tendons with preservation of biomechanical properties and biocompatibility. *Tissue Eng. C Methods* 17, 819–828.
- Purcell, B.P., Lobb, D., Charati, M.B., Dorsey, S.M., Wade, R.J., Zellars, K.N., Doviak, H., Pettaway, S., Logdon, C.B., Shuman, J.A., Freels, P.D., Gorman 3rd, J.H., Gorman, R.C., Spinale, F.G., Burdick, J.A., 2014. Injectable and bioresponsive hydrogels for on-demand matrix metalloproteinase inhibition. *Nat. Mater.* 13, 653–661.
- Quarti, A., Nardone, S., Colaneri, M., Santoro, G., Pozzi, M., 2011. Preliminary experience in the use of an extracellular matrix to repair congenital heart diseases. *Interact. Cardiovasc. Thorac. Surg.* 13, 569–572.
- Rao, N., Agmon, G., Tierney, M.T., Ungerleider, J.L., Braden, R.L., Sacco, A., Christman, K.L., 2017. Engineering an injectable muscle-specific microenvironment for improved cell delivery using a nanofibrous extracellular matrix hydrogel. *ACS Nano* 11, 3851–3859.
- Romanelli, M., Dini, V., Bertone, M., 2010. Randomized comparison of OASIS wound matrix versus moist wound dressing in the treatment of difficult-to-heal wounds of mixed arterial/venous etiology. *Adv. Skin Wound Care* 23.
- Rommer, E.A., Peric, M., Wong, A., 2013. Urinary bladder matrix for the treatment of recalcitrant nonhealing radiation wounds. *Adv. Skin Wound Care* 26, 450–455.
- Rosen, M., Roselli, E., Faber, C., Ratliff, N., Ponsky, J., Smedira, N., 2005. Small intestinal submucosa intracardiac patch: an experimental study. *Surg. Innov.* 12, 227–231.
- Sackett, S.D., Tremmel, D.M., Ma, F., Feeney, A.K., Maguire, R.M., Brown, M.E., Zhou, Y., Li, X., O'Brien, C., Li, L., Burlingham, W.J., Odorico, J.S., 2018. Extracellular matrix scaffold and hydrogel derived from decellularized and delipidized human pancreas. *Sci. Rep.* 8, 10452.
- Saldin, L.T., Cramer, M.C., Velankar, S.S., White, L.J., Badylak, S.F., 2017. Extracellular matrix hydrogels from decellularized tissues: structure and function. *Acta Biomater.* 49, 1–15.
- Salzberg, C.A., Dunavant, C., Nocera, N., 2013. Immediate breast reconstruction using porcine acellular dermal matrix (Strattice): long-term outcomes and complications. *J. Plast. Reconstr. Aesthet. Surg.* 66, 323–328.
- Sandor, M., Xu, H., Connor, J., Lombardi, J., Harper, J.R., Silverman, R.P., Mcquillan, D.J., 2008. Host response to implanted porcine-derived biologic materials in a primate model of abdominal wall repair. *Tissue Eng. A* 14, 2021–2031.
- Sarikouch, S., Horke, A., Tudorache, I., Beerbaum, P., Westhoff-Bleck, M., Boethig, D., Repin, O., Maniuc, L., Ciubotaru, A., Haverich, A., Cebotari, S., 2016. Decellularized fresh homografts for pulmonary valve replacement: a decade of clinical experience. *Eur. J. Cardiothorac. Surg.* 50, 281–290.
- Sasaki, S., Funamoto, S., Hashimoto, Y., Kimura, T., Honda, T., Hattori, S., Kobayashi, H., Kishida, A., Mochizuki, 2009. In vivo evaluation of a novel scaffold for artificial corneas prepared by using ultrahigh hydrostatic pressure to decellularize porcine corneas. *Mol. Vis.* 15, 2022–2028.
- Scarritt, M.E., Pashos, N.C., Bunnell, B.A., 2015. A review of cellularization strategies for tissue engineering of whole organs. *Front Bioeng. Biotechnol.* 3, 43.
- Sclafani, A.P., Romo 3rd, T., Jacono, A.A., McCormick, S., Cocker, R., Parker, A., 2000. Evaluation of acellular dermal graft in sheet (AlloDerm) and injectable (micronized AlloDerm) forms for soft tissue augmentation. Clinical observations and histological analysis. *Arch. Facial Plast. Surg.* 2, 130–136.
- Sclafani, A.P., Romo 3rd, T., Jacono, A.A., McCormick, S.A., Cocker, R., Parker, A., 2001. Evaluation of acellular dermal graft (AlloDerm) sheet for soft tissue augmentation: a 1-year follow-up of clinical observations and histological findings. *Arch. Facial Plast. Surg.* 3, 101–103.
- Seif-Naraghi, S.B., Horn, D., Schup-Magoffin, P.J., Christman, K.L., 2012. Injectable extracellular matrix derived hydrogel provides a platform for enhanced retention and delivery of a heparin-binding growth factor. *Acta Biomater.* 8, 3695–3703.
- Seif-Naraghi, S.B., Singelyn, J.M., Salvatore, M.A., Osborn, K.G., Wang, J.J., Sampat, U., Kwan, O.L., Strachan, G.M., Wong, J., Schup-Magoffin, P.J., Braden, R.L., Bartels, K., Dequach, J.A., Preul, M., Kinsey, A.M., Demaria, A.N., Dib, N., Christman, K.L., 2013. Safety and efficacy of an injectable extracellular matrix hydrogel for treating myocardial infarction. *Sci. Transl. Med.* 5, 173ra25.
- Shakouri-Motlagh, A., O'Connor, A.J., Brennecke, S.P., Kalionis, B., Heath, D.E., 2017. Native and solubilized decellularized extracellular matrix: a critical assessment of their potential for improving the expansion of mesenchymal stem cells. *Acta Biomater.* 55, 1–12.
- Shupe, T., Williams, M., Brown, A., Willenberg, B., Petersen, B.E., 2010. Method for the decellularization of intact rat liver. *Organogenesis* 6, 134–136.
- Sicari, B.M., Rubin, J.P., Dearth, C.L., Wolf, M.T., Ambrosio, F., Boninger, M., Turner, N.J., Weber, D.J., Simpson, T.W., Wyse, A., Brown, E.H., Dziki, J.L., Fisher, L.E., Brown, S., Badylak, S.F., 2014. An acellular biologic scaffold promotes skeletal muscle formation in mice and humans with volumetric muscle loss. *Sci. Transl. Med.* 6, 234ra58.

- Siddiqui, R.F., Abraham, J.R., Butany, J., 2009. Bioprosthetic heart valves: modes of failure. *Histopathology* 55, 135–144.
- Simionescu, D.T., 2004. Prevention of calcification in bioprosthetic heart valves: challenges and perspectives. *Expert Opin. Biol. Ther.* 4, 1971–1985.
- Simoes, I.N., Vale, P., Soker, S., Atala, A., Keller, D., Noiva, R., Carvalho, S., Peleteiro, C., Cabral, J.M., Eberli, D., Da Silva, C.L., Baptista, P.M., 2017. Acellular urethra bioscaffold: decellularization of whole urethras for tissue engineering applications. *Sci. Rep.* 7, 41934.
- Simon, P., Kasimir, M.T., Seebacher, G., Weigel, G., Ullrich, R., Salzer-Muhar, U., Rieder, E., Wolner, E., 2003a. Early failure of the tissue engineered porcine heart valve SYNERGRAFT in pediatric patients. *Eur. J. Cardiothorac. Surg.* 23, 1002–1006 Discussion 1006.
- Singelyn, J.M., Dequach, J.A., Christman, K.L., 2009. Injectable myocardial matrix as a scaffold for myocardial tissue engineering. *Conf. Proc. IEEE Eng. Med. Biol. Soc.* 2009, 2406–2408.
- Singelyn, J.M., Sundaramurthy, P., Johnson, T.D., Schup-Magoffin, P.J., Hu, D.P., Faulk, D.M., Wang, J., Mayle, K.M., Bartels, K., Salvatore, M., Kinsey, A.M., Demaria, A.N., Dib, N., Christman, K.L., 2012. Catheter-deliverable hydrogel derived from decellularized ventricular extracellular matrix increases endogenous cardiomyocytes and preserves cardiac function post-myocardial infarction. *J. Am. Coll. Cardiol.* 59, 751–763.
- Skovsted Yde, S., Brunbjerg, M.E., Damsgaard, T.E., 2016. Acellular dermal matrices in breast reconstructions – a literature review. *J. Plast. Surg. Hand Surg.* 50, 187–196.
- Slaughter, M.S., Soucy, K.G., Matheny, R.G., Lewis, B.C., Hennick, M.F., Choi, Y., Monreal, G., Sobieski, M.A., Giridharan, G.A., Koenig, S.C., 2014. Development of an extracellular matrix delivery system for effective intramyocardial injection in ischemic tissue. *ASAIO J.* 60, 730–736.
- Slavin, S.A., Lin, S.J., 2012. The use of acellular dermal matrices in revisional breast reconstruction. *Plast. Reconstr. Surg.* 130, 70S–85S.
- Slivka, P.F., Dearth, C.L., Keane, T.J., Meng, F.W., Medberry, C.J., Riggio, R.T., Reing, J.E., Badylak, S.F., 2014. Fractionation of an ECM hydrogel into structural and soluble components reveals distinctive roles in regulating macrophage behavior. *Biomater. Sci.* 2, 1521–1534.
- Smith, E.L., Kanczler, J.M., Gothard, D., Roberts, C.A., Wells, J.A., White, L.J., Qutachi, O., Sawkins, M.J., Peto, H., Rashidi, H., Rojo, L., Stevens, M.M., El Haj, A.J., Rose, F.R., Shakesheff, K.M., Oreffo, R.O., 2014. Evaluation of skeletal tissue repair, part 1: assessment of novel growth-factor-releasing hydrogels in an ex vivo chick femur defect model. *Acta Biomater.* 10, 4186–4196.
- Song, J.J., Guyette, J.P., Gilpin, S.E., Gonzalez, G., Vacanti, J.P., Ott, H.C., 2013. Regeneration and experimental orthotopic transplantation of a bioengineered kidney. *Nat. Med.* 19, 646–651.
- Song, J.J., Ott, H.C., 2011. Organ engineering based on decellularized matrix scaffolds. *Trends Mol. Med.* 17, 424–432.
- Sonnenberg, S.B., Rane, A.A., Liu, C.J., Rao, N., Agmon, G., Suarez, S., Wang, R., Munoz, A., Bajaj, V., Zhang, S., Braden, R., Schup-Magoffin, P.J., Kwan, O.L., Demaria, A.N., Cochran, J.R., Christman, K.L., 2015. Delivery of an engineered HGF fragment in an extracellular matrix-derived hydrogel prevents negative LV remodeling post-myocardial infarction. *Biomaterials* 45, 56–63.
- Sood, D., Chwalek, K., Stuntz, E., Pouli, D., Du, C., Tang-Schomer, M., Georgakoudi, I., Black 3rd, L.D., Kaplan, D.L., 2016. Fetal brain extracellular matrix boosts neuronal network formation in 3D bioengineered model of cortical brain tissue. *ACS Biomater. Sci. Eng.* 2, 131–140.
- Soto-Gutierrez, A., Wertheim, J.A., Ott, H.C., Gilbert, T.W., 2012. Perspectives on whole-organ assembly: moving toward transplantation on demand. *J. Clin. Investig.* 122, 3817–3823.
- Soucy, K.G., Smith, E.F., Monreal, G., Rokosh, G., Keller, B.B., Yuan, F., Matheny, R.G., Fallon, A.M., Lewis, B.C., Sherwood, L.C., Sobieski, M.A., Giridharan, G.A., Koenig, S.C., Slaughter, M.S., 2015. Feasibility study of particulate extracellular matrix (P-ECM) and left ventricular assist device (HVAD) therapy in chronic ischemic heart failure bovine model. *ASAIO J.* 61, 161–169.
- Spang, M.T., Christman, K.L., 2017. Extracellular matrix hydrogel therapies: in vivo applications and development. *Acta Biomater.*
- Spang, M.T., Christman, K.L., 2018. Extracellular matrix hydrogel therapies: in vivo applications and development. *Acta Biomater.* 68, 1–14.
- Stelly, M., Stelly, T.C., 2013. Histology of CorMatrix bioscaffold 5 years after pericardial closure. *Ann. Thorac. Surg.* 96, e127–e129.
- Stephenson, M.K., Lenihan, S., Covarrubias, R., Huttinger, R.M., Gumina, R.J., Sawyer, D.B., Galindo, C.L., 2016. Scanning electron microscopy of macerated tissue to visualize the extracellular matrix. *J. Vis. Exp.*
- Sullivan, K.E., Quinn, K.P., Tang, K.M., Georgakoudi, I., Black 3rd, L.D., 2014. Extracellular matrix remodeling following myocardial infarction influences the therapeutic potential of mesenchymal stem cells. *Stem Cell Res. Ther.* 5, 14.
- Svensen, C.A., Kreykes, N., Butany, J., Bianco, R., 2000. In-vivo assessment of a photofixed bovine pericardial valve. *J. Heart Valve Dis.* 9, 813–820.
- Szczeklik, M., Gupta, P., Amersey, R., Lall, K.S., 2015. Reconstruction of the right atrium and superior vena cava with extracellular matrix. *J. Card. Surg.* 30, 351–354.
- Tabuchi, M., Negishi, J., Yamashita, A., Higami, T., Kishida, A., Funamoto, S., 2015. Effect of decellularized tissue powders on a rat model of acute myocardial infarction. *Mater. Sci. Eng. C Mater. Biol. Appl.* 56, 494–500.
- Takeda, Y.S., Xu, Q., 2014. Fabrication of 2D and 3D constructs from reconstituted decellularized tissue extracellular matrices. *J. Biomed. Nanotechnol.* 10, 3631–3637.
- Teng, Y., Li, X., Chen, Y., Cai, H., Cao, W., Chen, X., Sun, Y., Liang, J., Fan, Y., Zhang, X., 2017. Extracellular matrix powder from cultured cartilage-like tissue as cell carrier for cartilage repair. *J. Mater. Chem. B* 5, 3283–3292.
- Timek, T.A., Lai, D.T., Tibayan, F.A., Dagum, P., Daughters, G.T., Liang, D., Ingels, N.B., Miller, D.C., 2002. Hemodynamic performance of an unstented xenograft mitral valve substitute. *J. Thorac. Cardiovasc. Surg.* 124, 541–552.
- Traverse, J.H., Henry, T.D., Dib, N., Patel, A.N., Pepine, C., Schaefer, G.L., Dequach, J.A., Kinsey, A.M., Chamberlin, P., Christman, K.L., 2019. First-in-Man Study of a Cardiac Extracellular Matrix

- Hydrogel in Early and Late Myocardial Infarction Patients. *JACC Basic Transl Sci* 4, 659–669.
- Ungerleider, J.L., Johnson, T.D., Rao, N., Christman, K.L., 2015. Fabrication and characterization of injectable hydrogels derived from decellularized skeletal and cardiac muscle. *Methods* 84, 53–59.
- Uygun, B.E., Soto-Gutierrez, A., Yagi, H., Izamis, M.L., Guzzardi, M.A., Shulman, C., Milwid, J., Kobayashi, N., Tilles, A., Berthiaume, F., Hertl, M., Nahmias, Y., Yarmush, M.L., Uygun, K., 2010. Organ reengineering through development of a transplantable recellularized liver graft using decellularized liver matrix. *Nat. Med.* 16, 814–820.
- Van Der Merwe, Y., Faust, A.E., Sakalli, E.T., Westrick, C.C., Hussey, G., Conner, I.P., Fu, V.L.N., Badylak, S.F., Steketee, M.B., 2019. Matrix-bound nanovesicles prevent ischemia-induced retinal ganglion cell axon degeneration and death and preserve visual function. *Sci. Rep.* 9, 3482.
- Van Der Merwe, Y., Faust, A.E., Steketee, M.B., 2017. Matrix bound vesicles and miRNA cargoes are bioactive factors within extracellular matrix bioscaffolds. *Neural Regen. Res.* 12, 1597–1599.
- Vesely, I., 2003. The evolution of bioprosthetic heart valve design and its impact on durability. *Cardiovasc. Pathol.* 12, 277–286.
- Vinson, K.N., Zraick, R.I., Ragland, F.J., 2010. Injection versus medialization laryngoplasty for the treatment of unilateral vocal fold paralysis: follow-up at six months. *Laryngoscope* 120, 1802–1807.
- Voges, I., Bräsen, J., Entenmann, A., Scheid, M., Scheewe, J., Fischer, G., Hart, C., Andrade, A., Pham, H., Kramer, H., Rickers, C., 2013. Adverse results of a decellularized tissue-engineered pulmonary valve in humans assessed with magnetic resonance imaging. *Eur. J. Cardiothorac. Surg.* 44.
- Voytik-Harbin, S.L., Brightman, A.O., Waisner, B.Z., Robinson, J.P., Lamar, C.H., 1998. Small intestinal submucosa: a tissue-derived extracellular matrix that promotes tissue-specific growth and differentiation of cells in vitro. *Tissue Eng.* 4, 157–174.
- Wainwright, D.J., 1995. Use of an acellular allograft dermal matrix (AlloDerm) in the management of full-thickness burns. *Burns* 21, 243–248.
- Wang, R.M., He, J., Xu, Y., Christman, K.L., 2017a. Humanized mouse model for evaluating biocompatibility and human immune cell interactions to biomaterials. *Drug Discov. Today Dis. Model.* 24, 23–29.
- Wang, R.M., Johnson, T.D., He, J., Rong, Z., Wong, M., Nigam, V., Behfar, A., Xu, Y., Christman, K.L., 2017b. Humanized mouse model for assessing the human immune response to xenogeneic and allogeneic decellularized biomaterials. *Biomaterials* 129, 98–110.
- Wassenaar, J.W., Gaetani, R., Garcia, J.J., Braden, R.L., Luo, C.G., Huang, D., Demaria, A.N., Omens, J.H., Christman, K.L., 2016. Evidence for mechanisms underlying the functional benefits of a myocardial matrix hydrogel for post-MI treatment. *J. Am. Coll. Cardiol.* 67, 1074–1086.
- Williams, C., Budina, E., Stoppel, W.L., Sullivan, K.E., Emani, S., Emani, S.M., Black 3rd, L.D., 2015a. Cardiac extracellular matrix-fibrin hybrid scaffolds with tunable properties for cardiovascular tissue engineering. *Acta Biomater.* 14, 84–95.
- Williams, C., Sullivan, K., Black 3rd, L.D., 2015b. Partially digested adult cardiac extracellular matrix promotes cardiomyocyte proliferation in vitro. *Adv. Healthc. Mater.* 4, 1545–1554.
- Wolf, M.T., Daly, K.A., Brennan-Pierce, E.P., Johnson, S.A., Caruthers, C.A., D'Amore, A., Nagarkar, S.P., Velankar, S.S., Badylak, S.F., 2012. A hydrogel derived from decellularized dermal extracellular matrix. *Biomaterials* 33, 7028–7038.
- Wolf, M.T., Dearth, C.L., Ranallo, C.A., Lopresti, S.T., Carey, L.E., Daly, K.A., Brown, B.N., Badylak, S.F., 2014. Macrophage polarization in response to ECM coated polypropylene mesh. *Biomaterials* 35, 6838–6849.
- Wolkers, W., Oldenhof, H., 2015. Cryopreservation and Freeze-Drying Protocols. Springer, New York.
- Wong, M.L., Griffiths, L.G., 2014. Immunogenicity in xenogeneic scaffold generation: antigen removal vs. decellularization. *Acta Biomater.* 10, 1806–1816.
- Wong, M.L., Leach, J.K., Athanasiou, K.A., Griffiths, L.G., 2011. The role of protein solubilization in antigen removal from xenogeneic tissue for heart valve tissue engineering. *Biomaterials* 32, 8129–8138.
- Wong, M.L., Wong, J.L., Athanasiou, K.A., Griffiths, L.G., 2013. Stepwise solubilization-based antigen removal for xenogeneic scaffold generation in tissue engineering. *Acta Biomater.* 9, 6492–6501.
- Wong, M.L., Wong, J.L., Vapniarsky, N., Griffiths, L.G., 2016. In vivo xenogeneic scaffold fate is determined by residual antigenicity and extracellular matrix preservation. *Biomaterials* 92, 1–12.
- Wovk, B., 2010. Thermodynamic aspects of vitrification. *Cryobiology* 60, 11–22.
- Wu, I., Nahas, Z., Kimmerling, K.A., Rosson, G.D., Elisseeff, J.H., 2012. An injectable adipose matrix for soft-tissue reconstruction. *Plast. Reconstr. Surg.* 129, 1247–1257.
- Xing, S., Liu, C., Xu, B., Chen, J., Yin, D., Zhang, C., 2014. Effects of various decellularization methods on histological and biomechanical properties of rabbit tendons. *Exp. Ther. Med.* 8, 628–634.
- Yanagawa, B., Rao, V., Yau, T.M., Cusimano, R.J., 2014. Potential myocardial regeneration with CorMatrix ECM: a case report. *J. Thorac. Cardiovasc. Surg.* 147, e41–e43.
- Yuan, X., Wei, Y., Villasante, A., Ng, J.J.D., Arkonac, D.E., Chao, P.G., Vunjak-Novakovic, G., 2017. Stem cell delivery in tissue-specific hydrogel enabled meniscal repair in an orthotopic rat model. *Biomaterials* 132, 59–71.
- Zhang, X., Dong, J., 2015. Direct comparison of different coating matrix on the hepatic differentiation from adipose-derived stem cells. *Biochem. Biophys. Res. Commun.* 456, 938–944.
- Zhao, Y., Zhang, Z., Wang, J., Yin, P., Wang, Y., Yin, Z., Zhou, J., Xu, G., Liu, Y., Deng, Z., Zhen, M., Cui, W., Liu, Z., 2011. Preparation of decellularized and crosslinked artery patch for vascular tissue-engineering application. *J. Mater. Sci. Mater. Med.* 22, 1407–1417.
- Zhao, Z.Q., Puskas, J.D., Xu, D., Wang, N.P., Mosunjac, M., Guyton, R.A., Vinten-Johansen, J., Matheny, R., 2010. Improvement in cardiac function with small intestine extracellular matrix is associated with recruitment of C-kit cells, myofibroblasts, and macrophages after myocardial infarction. *J. Am. Coll. Cardiol.* 55, 1250–1261.

- Zheng, X.L., Xiang, J.X., Wu, W.Q., Wang, B., Liu, W.Y., Gao, R., Dong, D.H., Lv, Y., 2015. Using a decellularized splenic matrix as a 3D scaffold for hepatocyte cultivation in vitro: a preliminary trial. *Biomed. Mater.* 10, 045023.
- Zhou, J., Fritze, O., Schleicher, M., Wendel, H.P., Schenke-Layland, K., Harasztosi, C., Hu, S., Stock, U.A., 2010. Impact of heart valve decellularization on 3-D ultrastructure, immunogenicity and thrombogenicity. *Biomaterials* 31, 2549–2554.
- Zhu, J., Lu, Y., Yu, F., Zhou, L., Shi, J., Chen, Q., Ding, W., Wen, X., Ding, Y.Q., Mei, J., Wang, J., 2018. Effect of decellularized spinal scaffolds on spinal axon regeneration in rats. *J. Biomed. Mater. Res. A* 106, 698–705.

Questions

1. What are the issues with classical cryopreservation (freezing) on tissue preservation? How are these issues addressed with vitrification? What limitations still exist with tissue preservation despite minimizing structural damage to tissue at low temperatures?
 - a. Classical cryopreservation causes immobilization of solute components by freezing of water and formation of ice crystals causing extracellular tearing, cell membrane lysis, and segregation of solute molecules, leading to a toxically high concentration of solute molecules due to displacement from organized crystal structure.
 - b. Vitrification creates a high-viscosity, glass state due to the relatively high concentration of cryoprotectant and rapid freezing leading to immobilization of solute components faster than ice crystal formation can take place.
 - c. Despite improvements in reaching the “frozen” state, standard methods cause uneven thawing throughout large volumes of tissue, causing similar issues with classical cryopreservation as different regions regain mobility of solute components. The cellular response during these freezing and thawing processes also can cause pathological responses that limit the actual restoration of the tissue, however, this requires further evaluation.
2. What is the purpose of tissue cross-linking and cross-linking for decellularized materials? Why does glutaraldehyde still have issues regarding durability and biocompatibility? Give an example of a chemical cross-linking method together with the mechanism of action.
 - a. Tissue cross-linking decreases the rate of enzymatic digestion by the host cells and delays the hyper-acute and acute immune response by masking antigens. For decellularized ECM, besides modulating the degradation rate, cross-linking also tailors the mechanical properties of the material.
 - b. Incomplete binding of glutaraldehyde to the collagen network leads to the presence of cytotoxic aldehyde groups that might be involved in long-term calcification as observed in bioprosthetic heart valves.
 - c. An example of a chemical cross-linker is carbodiimide coupled with N-hydroxysulfosuccinimide. These agents cross-link nonspecifically all proteins by linking the amine and the carboxyl groups by amide bonds.
3. Why is DNA commonly utilized as a surrogate marker of decellularization quality? What are the limitations of this approach? How do methods of antigen removal address some of these limitations?
 - a. DNA is commonly measured as a remnant of cellular content because it has been linked to the activation of inflammatory mechanisms.
 - b. A limitation of this method is that DNA is not the only source of antigenicity that could elicit an inflammatory response for in vivo applications as other remnant cellular components and especially xenogeneic epitopes can elicit immune rejection responses.
 - c. Antigen removal focuses specifically on assessing content during the decellularization that interacts with antibodies that could elicit immune responses of engrafted tissue-derived materials, thus being a more direct measure of content that could stimulate an immune rejection response.
4. Give an example of three commercially available ECM-based products. Mention the tissue source, together with the application.
 - a. AlloDerm is an acellular human dermal matrix used for full-thickness skin injury, breast reconstruction, and abdominal hernia repair. Oasis is a porcine small intestinal submucosa matrix applied in chronic leg ulcers, myocardial repair, and arterial and venous grafting. MatriStem is an acellular porcine urinary bladder matrix used for deep burns, and acute diabetic or venous ulcerations.
5. What is an advantage of injectable ECM particulate and ECM hydrogels as therapies?
 - a. Injectable therapies can be delivered through less invasive or minimally invasive methods, which can improve the recovery times and safety of the procedure. For hydrogels, in particular, their shear thinning properties allow them to be delivered by catheter methods, allowing delivery to organs that require highly invasive and risky surgeries such as the heart.
6. What current medical issues do tissue-processing methods seek to address? How do these methods address limitations of the standard practices in the medical field?
 - a. Tissue-processing methods seek to improve the resources and treatments for patients with chronic tissue injuries and diseases, especially ones that can only be addressed by eventual organ transplant.
 - b. Tissue-processing methods address the limitations of current medical technology in a variety of ways. These methods hope to improve the preservation of donated organ tissue, expand the available sources of organs used for transplant with xenogeneic-derived substitutes, and develop alternative treatments that can be utilized to promote repair for damaged and diseased tissue in patients.

Burlingham, W.J., Grailer, A.P., Heisey, D.M., Claas, F.H., Norman, D., Mohanakumar, T., Brennan, D.C., De Fijter, H., Van Gelder, T., Pirsch, J.D., Sollinger, H.W., Bean, M.A., 1998. The effect of tolerance to noninherited maternal HLA antigens on the survival of renal transplants from sibling donors. *N. Engl. J. Med.* 339, 1657–1664.

Hannet, I., Erkeller-Yuksel, F., Lydyard, P., Deneys, V., Debruyere, M., 1992. Developmental and maturational changes in human blood lymphocyte subpopulations. *Immunol. Today* 13, 215–218.

Luk, A., Rao, V., Cusimano, R.J., David, T.E., Butany, J., 2015. CorMatrix extracellular matrix used for valve repair in the adult: is there de novo valvular tissue seen? *Ann. Thorac. Surg.* 99, 2205–2207.

- Mattis, V.B., Wakeman, D.R., Tom, C., Dodiya, H.B., Yeung, S.Y., Tran, A.H., Bernau, K., Ornelas, L., Sahabian, A., Reidling, J., Sareen, D., Thompson, L.M., Kordower, J.H., Svendsen, C.N., 2014. Neonatal immune-tolerance in mice does not prevent xenograft rejection. *Exp. Neurol.* 254, 90–98.
- Mold, J.E., Venkatasubrahmanyam, S., Burt, T.D., Michaelsson, J., Rivera, J.M., Galkina, S.A., Weinberg, K., Stoddart, C.A., McCune, J.M., 2010. Fetal and adult hematopoietic stem cells give rise to distinct T cell lineages in humans. *Science* 330, 1695–1699.
- Nelson, J.S., Heider, A., Si, M.S., Ohye, R.G., 2016. Evaluation of explanted CorMatrix intracardiac patches in children with congenital heart disease. *Ann. Thorac. Surg.* 102, 1329–1335.
- Padalino, M.A., Quarti, A., Angeli, E., Frigo, A.C., Vida, V.L., Pozzi, M., Gargiulo, G., Stellin, G., 2015. Early and mid-term clinical experience with extracellular matrix scaffold for congenital cardiac and vascular reconstructive surgery: a multicentric Italian study. *Interact. Cardiovasc. Thorac. Surg.* 21, 40–49; Discussion 49.
- Rosario-Quinones, F., Magid, M.S., Yau, J., Pawale, A., Nguyen, K., 2015. Tissue reaction to porcine intestinal submucosa (CorMatrix) implants in pediatric cardiac patients: a single-center experience. *Ann. Thorac. Surg.* 99, 1373–1377.
- Scholl, F.G., Boucek, M.M., Chan, K.C., Valdes-Cruz, L., Perryman, R., 2010. Preliminary experience with cardiac reconstruction using decellularized porcine extracellular matrix scaffold: human applications in congenital heart disease. *World J. Pediatr. Congenit. Heart Surg.* 1, 132–136.
- Witt, R.G., Raff, G., Van Gundy, J., Rodgers-Ohlau, M., Si, M.S., 2013. Short-term experience of porcine small intestinal submucosa patches in paediatric cardiovascular surgery. *Eur. J. Cardiothorac. Surg.* 44, 72–76.
- Woo, J.S., Fishbein, M.C., Reemtsen, B., 2016. Histologic examination of decellularized porcine intestinal submucosa extracellular matrix (CorMatrix) in pediatric congenital heart surgery. *Cardiovasc. Pathol.* 25, 12–17.
- Zaidi, A.H., Nathan, M., Emani, S., Baird, C., Del Nido, P.J., Gauvreau, K., Harris, M., Sanders, S.P., Padera, R.F., 2014. Preliminary experience with porcine intestinal submucosa (CorMatrix) for valve reconstruction in congenital heart disease: histologic evaluation of explanted valves. *J. Thorac. Cardiovasc. Surg.* 148, 2216–4, 2225 e1.

1.3.6B

Use of Extracellular Matrix Proteins and Natural Materials in Bioengineering

KATJA SCHENKE-LAYLAND^{1,2,3,4}, SIMONE LIEBSCHER¹, SHANNON LEE LAYLAND¹

¹Department of Women's Health, Research Institute for Women's Health, Eberhard Karls University Tübingen, Tübingen, Germany

²Natural and Medical Sciences Institute (NMI) at the University of Tübingen, Reutlingen, Germany

³Cluster of Excellence iFIT (EXC 2180) "Image-Guided and Functionally Instructed Tumor Therapies", Eberhard Karls University Tübingen, Tübingen, Germany

⁴Department of Medicine/Cardiology, Cardiovascular Research Laboratories (CVRL), University of California (UCLA), Los Angeles, CA, United States

Introduction

The fields of bioengineering and regenerative medicine aim to develop new strategies to treat or replace failing organs. While ongoing pathological changes of the extracellular matrix (ECM) may contribute to the failing of a tissue or organ, specific ECM proteins could be the key to a successful treatment, potentially supporting a higher regenerative capacity or overcoming limitations of cell therapy approaches.

ECM proteins or naturally occurring materials, such as alginates or chitosan, can offer several advantages for bioengineering and regenerative medicine applications in terms of biocompatibility, since the surrounding biological environment can recognize and metabolically process implanted substances through established pathways (Shin et al., 2003). A unique advantage of naturally-derived materials is that through either enzymatic or hydrolytic degradation the host can successfully clear and metabolize the implanted substance (Prestwich and Atzet, 2012). While this may not be desirable in permanent and long-term implants such as hip replacements, it is extremely advantageous when timed biological resorption is desired, i.e., in delivery vehicles for drugs or therapeutic cells. ECM proteins and natural materials can be chemically modified and cross-linked to match the degradation rate to a particular biological application (Augst et al., 2006; Badylak and Gilbert, 2008; Prestwich and Atzet, 2012).

One frequent concern about ECM proteins derived from animals and natural materials is the immunogenic response that can occur following implantation (Prestwich and Atzet, 2012). This response results from the fact that the implanted materials, although similar to the endogenous host ECM component, may not be identical, and thus contain antigenic determinants (Prestwich and Atzet, 2012). This issue is mainly common among animal-based ECM proteins. The immunogenic effect can be reduced by either chemical modification or through sourcing of the ECM material (Badylak and Gilbert, 2008).

Chemical modification and cross-linking are common methods for altering mechanical properties such as elasticity and tensile strength of natural materials that are often not appropriate for dynamic physiologic environments (Prestwich and Atzet, 2012). However, the complex structures of natural materials can complicate technical modifications that are simple to perform in synthetic polymers (Prestwich and Atzet, 2012). Nonetheless, numerous research studies have demonstrated the successful modification and purification of natural-based materials (Prestwich and Atzet, 2012).

Another common issue arising with ECM proteins is the lot-to-lot variability in molecular structure that can occur due to, for example, animal sourcing (Prestwich and Atzet, 2012). But variability arises not only due to species-to-species variation, but also from tissue-to-tissue variation, which can complicate processing and quantification of the materials. As a complex mixture of various molecules arranged

in a three-dimensional (3D) manner, the ECM features the fundament for cell anchorage and migration as well as regulatory functions for all types of cells (Votteler et al., 2010). The ECM's constitutions can be divided into three kinds of classes: (1) proteins with primarily structural functions such as collagens and elastic fibers, (2) proteoglycans (PGs) or glycosaminoglycans (GAGs), which are first of all responsible for regulatory processes, and (3) matricellular proteins. The structure and function of a tissue depends on the relative proportion of these constituent molecules. Those tissues that have to withstand large tensional forces tend to be particularly rich in fibrillar collagens and elastic fibers, while tissues that are exposed to compressive forces usually contain high levels of PGs and GAGs (Votteler et al., 2010). Although most of the ECM components are well known, the precise composition of this mixture of molecules varies from tissue to tissue and remains underinvestigated. However, in recent years it has been acknowledged that the 3D architecture of the ECM is an important driver of cell modulation, as it regulates signal transduction mechanisms, which in turn can impact ECM remodeling (Votteler et al., 2010). Understanding the spatial distribution of ECM components within tissues and organs often provides insight into their function and basic mechanisms of action. A detailed analysis of the miscellaneous elements of the ECM is of great value in gaining structural and diagnostic information, particularly with regard to bioengineering efforts.

The following sections will discuss common types of ECM proteins as well as natural-based biomaterials. We will conclude this chapter highlighting different strategies to produce recombinant human ECM proteins and manufacturing approaches that utilize ECM proteins and natural materials.

Collagens

Collagens are the most abundant and ubiquitous ECM proteins in mammals, which are not only critically important for the biomechanical stability of tissues, but are also intimately involved in cell adhesion and migration during growth, differentiation, morphogenesis, and wound healing (Schenke-Layland, 2008; Votteler et al., 2010). To date, various types of collagens (more than 28) have been identified, each with a unique biological function (Hulmes, 2008) (Table 1.3.6B.1).

Although both fibrillar and nonfibrillar collagens are found in mammalian tissues, the fibril-forming collagens (types I, II, III, V, XI, XXIV, and XXVII) account for the majority of the body's collagen mass (Leitinger and Hohenester, 2007; Hulmes, 2008; Schenke-Layland, 2008). Each fibrillar collagen molecule consists of three polypeptide chains, called α -chains. Molecules can be homotrimeric, consisting of three identical α -chains, or heterotypic, consisting of up to three genetically distinct α -chains (Hulmes, 2008). Individual α -chains are identified by the following nomenclature: $\alpha_n(N)$, where N is the Roman numeral

TABLE 1.3.6B.1 Collagen Types

Subfamily	Types
Fibrillar collagens	I, II, III, V, XI, XXIV, and XXVII
Fibril-associated collagens	IX, XII, XIV, XVI, XIX, XX, XXI, and XXII
Beaded filament-forming collagens	VI
Basement-membrane (BM) and BM-associated collagens	IV, VII, XV, and XVIII
Short-chain collagens	VIII and X; inner ear-specific or saccular collagen
Transmembrane collagens	XXVI and XXVIII

indicating collagen type and n is the number of the α -chain (Hulmes, 2008). Thus the chain composition of collagen II is $[\alpha_1(\text{II})]_3$, while that of collagen type I (ColI), a heterotrimer with two identical α_1 -chains and a third distinct α_2 -chain, is $[\alpha_1(\text{I})]_2\alpha_2(\text{I})$ (Hulmes, 2008). The common characteristic of the classical fibrillar collagens is a long central triple-helical region in each α -chain, consisting of a continuous $(\text{Gly-X-Y})_n$ repeat, where n is 337–343 (depending on the collagen type). All fibrillar collagens are synthesized in the form of soluble precursor molecules, called procollagens, with large N- and C-terminal propeptide domains (Hulmes, 2008). The C-propeptides are removed during the later stages of biosynthesis, usually by specific metalloproteinases, leaving short C-telopeptides (Hulmes, 2008). The extent of N-terminal processing depends on the collagen type (Hulmes, 2008).

Collagen biosynthesis is a highly complex process, involving numerous intra- and extracellular steps, all of which then contribute to the structure and biomechanical properties of the collagen fibrils. While there are several types of collagen, the fibrils all share the characteristic triple-helical structure, but have variations in the length of the nonhelical and helical sections, variations in the number of carbohydrates attached to the helical fraction, and the formation of covalent cross-links (Stenzel et al., 1974; Hulmes, 2008).

There are four types of collagen that are mainly focused on in bioengineering applications: fibrillar ColI is commonly found in skin, bone, and tendons, while type II (ColII) is mainly synthesized in cartilage (Votteler et al., 2010). Type III collagen (ColIII) is prevalent in vascular structures (i.e., blood vessel walls), and can also be found in skin and the peritoneum. The nonfibrillar collagen type IV (ColIV) is a crucial element within the basement membrane underlying epithelial cells (Votteler et al., 2010). The small ColIV molecules link also to GAGs with much larger structural proteins such as ColI and thus contribute to the gel properties of the ECM (Votteler et al., 2010). ColIV is unique in that it is largely nonhelical and does not form fibrils.

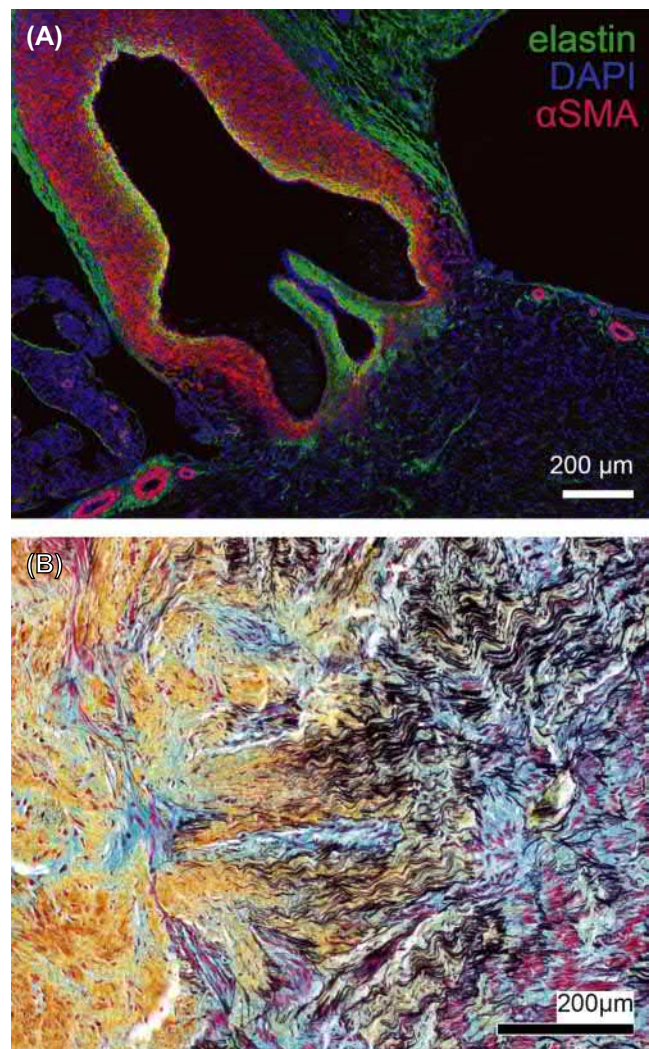
Gelatin is an irreversibly denatured and hydrolyzed form of collagen that is commonly used in pharmaceuticals, cosmetics, and foods. Most medical-grade collagens and gelatin are obtained from closely regulated bovine and porcine tissue. However, human collagens can be obtained by recombinant methodology (see section “Manufacturing Approaches Utilizing Natural Materials” in this chapter), isolation from tissues such as lung and placenta, or from human cell culture (Lee et al., 2001).

Collagens, in most cases Coll, are used as a biomaterial because of their widespread abundance in nature and ease of modification (Stenzel et al., 1974; Stone et al., 1997; Friess, 1998). Collagens are composed of ~20 amino acids, each providing pendant side groups available for chemical modifications (White et al., 1973; Hulmes, 2008). The prevalence of hydroxyl, amine, and carboxylic acid groups allows simple cross-linking between and within collagen units (Prestwich and Atzet, 2012). Cross-linking collagen can also decelerate the degradation of implanted materials, and is thought to reduce to some extent the immunogenicity in xenografted collagen materials (Nimni et al., 1987; Prestwich and Atzet, 2012). Exposure to glutaraldehyde produces collagens with firm covalent cross-links and elastic behavior (Prestwich and Atzet, 2012). Numerous commercial products have been developed from collagen-based technologies. CosmoDerm (Allergan) is, for example, a human collagen-based implant generated and purified from human fibroblast cell culture. Coll is the major component of this material with some presence of CollIII, as determined by Western blot analysis (Prestwich and Atzet, 2012). Zyderm (Allergan) is based on bovine-derived Coll. Both products, CosmoDerm and Zyderm, are chemically cross-linked by treatment with glutaraldehyde (Prestwich and Atzet, 2012). Gelfoam (Pfizer) is an absorbable, water-soluble, nonelastic, and porous sterile compressed sponge produced from denatured Coll from porcine skin. It is used for compression of wounds and in combination with human thrombin as a hemostat (Prestwich and Atzet, 2012).

Elastin, Elastic Fibers, and Elastin-Like Peptides

Elastic fibers provide the essential recoil for all tissues that are exposed to constantly repeated strain, such as blood vessels or heart valve leaflets (Fig. 1.3.6B.1) (Votteler et al., 2013). They are also abundantly expressed in lung tissue, the eye, ligaments, and skin; all organs that commonly stretch and relax (Geutjes et al., 2006; Daamen et al., 2007; Vindin et al., 2019).

The processes underlying elastic fiber formation are highly complex and require the interplay of various molecules. To date, the mechanisms that drive elastic fiber formation, termed “elastogenesis,” are, although well explored, not very well understood. They are currently the subject of intense research by many groups. It is well known that elastic fibers consist of various ECM proteins such as microfibrillar proteins (fibrillins), linking proteins (fibulins, elastin



• **Figure 1.3.6B.1** (A) Fluorescence image of a human 9-week outflow tract heart valve. Tropoelastin/elastin protein expression (green) is seen in the valve leaflets and the entire outflow tract vasculature. (B) Bright-field image of an adult porcine aortic vessel section stained with Movat's pentachrome to visualize collagens (yellow) and elastic fibers (black), as well as muscle tissue (red), proteoglycans, and glycosaminoglycans (green-blue). DAPI, 4',6-Diamidino-2-phenylindole; SMA, smooth muscle actin.

microfibril interfacers), microfibril-associated glycoproteins, soluble factors (transforming growth factor beta), and the core protein elastin (Sherratt, 2009; Wagenseil and Mecham, 2007, 2009; Wise and Weiss, 2009; Hubmacher et al., 2014). Due to its extremely long half-life (e.g., elastin turnover in human lung is approximately 74 years (Shapiro et al., 1991)), elastin is believed to remain functional, under normal physiological conditions, during a human lifetime. For the assembly of elastic fibers, specifically for the assembly of fibrillins and consequently of microfibrils, a fibronectin network is also needed (Sabatier et al., 2009). It is known that microfibrils provide a microenvironment that controls tropoelastin/elastin arrangement and cross-linking processes (Kielty et al., 2002).

Although there have been many attempts to engineer elastic fibers in human tissues, the in vitro generation of elastic

fibers represents a major bottleneck in bioengineering. Neonatal or adult rat vascular smooth muscle cells and neonatal human dermal fibroblasts are routinely used to synthesize tropoelastin *in vitro*, showing elastin deposition in two-dimensional cell cultures (Hinderer et al., 2015). Hinderer et al. used a customized bioreactor, combined with a 3D hybrid electrospun fibrillar polymer scaffold, to induce an elastic fiber-containing network, including elastogenesis-associated proteins (Hinderer et al., 2015). However, there have been no reports of the generation of fully functional human-based elastic fibers in 3D tissue-engineered constructs.

A different approach is the utilization of tropoelastin as biomaterial to engineer elastic tissues *in vitro*. The ability of tropoelastin to self-assemble has driven investigations into utilizing coacervation to facilitate the fabrication of tropoelastin-based materials such as hydrogels and electrospun scaffolds for tissue repair (Yeo et al., 2015; Vindin et al., 2019). The introduction of the recombinant technology to produce synthetic tropoelastin (see also section “Manufacturing Approaches Utilizing Natural Materials” in this chapter) helped to provide scalable host overexpression systems to meet the demands of industrial applications. In the development of these systems, gene optimization is, however, critically important. This was exemplified by poor yields in early implementations of an *Escherichia coli* overexpression system, due to rare bacterial codons populating up to 35% of the native human tropoelastin gene (Indik et al., 1990). By engineering a synthetic gene highly optimized for bacterial expression, significantly enhanced protein yields of multigram quantities were obtainable for biomaterial fabrication (Martin et al., 1995).

Elastin-like peptides (ELPs) have been synthetically produced (Urry et al., 2002; McHale et al., 2005). These polypeptides are composed of the highly repetitive amino acid sequences found in elastin. Physical properties of the ELPs can be manipulated based on amino acid sequence and resulting hydrophobicity. The polypeptides can coacervate and then be cross-linked by gamma irradiation. Researchers have produced nonwoven fabrics and fibers by electrospinning ELPs (Huang et al., 2000).

Proteoglycans and Glycosaminoglycans

In humans, PGs are the first ECM elements, emerging in the early developing embryo (Fig. 1.3.6B.2). Therefore they are supposed to be the most critical factors of regulatory mechanism for normal cell function and tissue development (Voteler et al., 2010). PGs persist in core protein and covalently attached sulfated GAGs, including chondroitin sulfate (CS), heparan sulfate (HS), and hyaluronic acid (HA). Within the ECM, they offer a huge water-holding and growth factor-binding capacity and have a significant impact on cell adhesion, migration, and differentiation through the regulation of their various protein partners (Badylak et al., 2008).

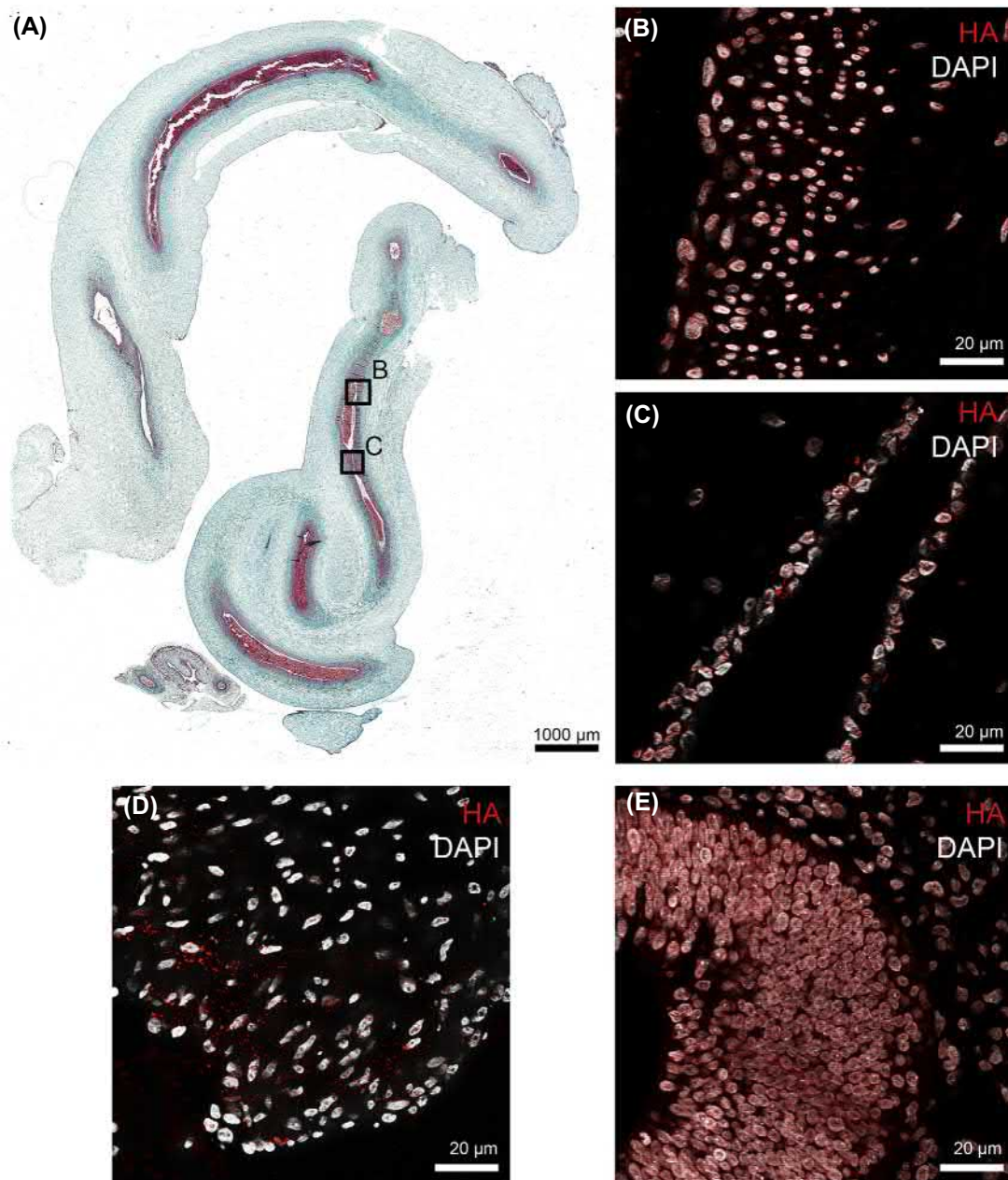
GAGs are a family of polysaccharides that can generally be described as an alternating copolymer, which are found in all animal tissues. The repeat units of GAGs consist of a



• **Figure 1.3.6B.2** Bright-field image of a 4-week embryo stained with Movat's pentachrome. Proteoglycans and glycosaminoglycans are depicted in green-blue.

hexamine unit (glucosamine or galactosamine) and a sugar (galactose, glucuronic acid, or iduronic acid) (Prestwich and Atzet, 2012). GAGs are found on all cell surfaces and in the ECM, and they are well preserved among species (Hildebrandt, 2002; Prestwich and Kuo, 2008; Prestwich and Atzet, 2012). The molecular weights of GAGs generally range from 5 to 5000 kDa (Prestwich and Atzet, 2012). There are several specific GAGs used as biomaterials, including heparin, HS, keratan sulfate, dermatan sulfate, CS, and HA.

Heparin is a highly sulfated GAG and is widely used as an anticoagulant (Breckwoldt et al., 1991; van der Giessen et al., 1998; Hildebrandt, 2002). Due to the sulfation levels it is very strongly negatively charged. Pharmaceutical-grade heparin is routinely derived from bovine or porcine mucosal tissues. Heparin is chemically related to HS and is composed of variably sulfated disaccharides. The predominant saccharide units are D-glucosamine and uronic acid (either D-glucuronic acid or L-iduronic acid) with sulfation of some hydroxyl groups (Prestwich and Atzet, 2012). Due to the strong negative charge, heparin has been found to bind to growth factors, such as vascular endothelial growth factor and basic fibroblast growth factor, and stabilize them *in vivo*, thus regulating their release (Peattie et al., 2008). Growth factor release is dependent on the strength of association with heparin, and can vary depending on the growth factor and environment from days to weeks (Peattie et al., 2008). Heparin was one of the first biological molecules to be covalently immobilized to biomaterials (Hoffman et al., 1972; Schmer, 1972; Basmadjian and Sefton, 1983), and



• **Figure 1.3.6B.3** (A) Human embryonic (10-week) umbilical cord section stained with Movat's pentachrome. Proteoglycans and glycosaminoglycans are depicted in green-blue. Blood vessels and embryonic blood cells are shown in dark red. (B, C) Fluorescence images of hyaluronic acid (HA)-stained human umbilical cord tissue. HA can also be found in (D) 15-week embryonic heart muscle and (E) 5-week embryonic eye tissue. (B–E) Cells are shown in white (4',6-diamidino-2-phenylindole [DAPI]).

has since been used extensively for coating in catheters, stents, and other medical devices (Breckwoldt et al., 1991; van der Giessen et al., 1998; Cauda et al., 2008; Jiang et al., 2009; FDA TyCo, 2010).

CS is a negatively charged GAG that is composed of repeating glucuronic acid and *N*-acetylgalactosamine units. Most disaccharide units contain a single sulfate at C-4 or C-6 hydroxyl groups, as well as a carboxyl group that can be chemically modified (Yuan et al., 2008; Baldwin and Kiick, 2010). CS is a major component of cartilage tissue with a huge capacity to absorb water, which is crucial for the compressive strength of that tissue. CS is commonly attached

to proteoglycans as a structural protein or it can be found on cell surfaces or basement membranes where it functions as a receptor. Commercial CS is often sourced and purified from shark or whale cartilage, or it is harvested from bovine or porcine tissues (Baldwin and Kiick, 2010).

HA is found in the ECM of all tissues of the body, and is particularly abundant in umbilical cords, as well as embryonic hearts, the eye, and cartilage (Laurent, 1989) (Fig. 1.3.6B.3). HA is the only nonsulfated glycosaminoglycan, and consists of repeating disaccharide units of *N*-acetylglucosamine and glucuronic acid. In addition to being unsulfated, HA is unique among GAGs in that it exists in

much higher molecular weights (50–6000 kDa), is secreted by cells, and (with a few exceptions) does not occur as a proteoglycan, that is, bound to a protein core (Prestwich and Kuo, 2008; Prestwich and Atzet, 2012). HA has been extensively studied as a biomaterial, in part due to these and other unique properties (Shu et al., 2002, 2004, 2006). HA occurs primarily as the sodium salt under physiological conditions; collectively, HA, sodium HA, and other HA salts are often referred to as hyaluronan (Prestwich and Atzet, 2012). There exist three major commercial sources of HA: a product that was isolated (1) from rooster combs (>2000 kDa HA), (2) from bacterial fermentation (50–100 kDa HA), and (3) HA oligosaccharides that are produced enzymatically (ranging from only a few disaccharide units up to 20 kDa) (DeAngelis et al., 2003; Prestwich and Atzet, 2012). HA forms lubricious and viscoelastic solutions that can protect, for example, eye tissues during ophthalmic surgeries, provide viscosupplementation in joints, reduce post-surgical adhesions, and can also help to deliver drugs in vivo (Kuo, 2006; Prestwich and Atzet, 2012). However, a rather short residence time in vivo and its poor mechanical properties led to many chemical modifications of HA (Shu and Prestwich, 2004; Allison and Grande-Allen, 2006). In the past two decades, HA-based medical devices and coatings have addressed many clinical needs with different levels of success. A detailed overview of monolithic and living HA as well as the applications of HA in bioengineering and regenerative medicine applications are provided in Prestwich and Atzet (2012). Moreover, the chemistry and biology of HA is exhaustively reviewed on the Glycoforum website (<http://glycoforum.gr.jp/science/hyaluronan/>).

Alginates

Alginates constitute a family of linear anionic polysaccharides isolated from coastal brown algae species (commonly known as kelp) such as *Laminaria hyperborean* (Augst et al., 2006; Prestwich and Atzet, 2012). Alginates are composed of (1,4)-linked β -D-mannuronic acid (M) and α -L-guluronic acid (G) residues in homopolymer blocks of either similar or strictly alternating sections (i.e., MMMMM, GGGGG, MGMGMG) (Rowley et al., 1999). The relative amounts of the blocks are dependent on the origin of the alginate (Prestwich and Atzet, 2012). Due to axial links, G blocks are stiffer than M blocks and alternating sequences in turn increase the solubility of the alginate (Prestwich and Atzet, 2012). The molecular weight of alginates can vary between 50 kDa and 100,000 kDa (Prestwich and Atzet, 2012). Alginate hydrogels can be formed by various cross-linking methods. One common technique is to use a divalent cation (Ca^{2+} or Ba^{2+}) to form ionic bonds between the carboxylic groups of neighboring strands, thereby inducing chain–chain associations (Prestwich and Atzet, 2012). Alginate can also be cross-linked by partial oxidation of the poly(guluronate), followed by reaction with adipic dihydrazide to form covalent cross-links (Prestwich and Atzet, 2012). A third cross-linking strategy uses polyethylene glycol diamines to

covalently link alginate chains (Prestwich and Atzet, 2012). Gel stiffness and elasticity vary with composition and cross-linking method. The stiffness of divalent cation cross-linked alginate increases with the following trends in composition: $\text{MG} < \text{MM} < \text{GG}$, whereas elasticity increases following $\text{GG} < \text{MM} < \text{MG}$ (Prestwich and Atzet, 2012). Thus the M:G ratio, cross-linking method, and molecular weight can all be used to tune mechanical properties of alginate gels (Prestwich and Atzet, 2012).

Because alginate is foreign to mammalian cells, alginate materials are not naturally broken down enzymatically after implantation in vivo. As a result they have a poorly controlled in vivo degradation. When the divalent cations are exchanged with Na^+ ions, ionically cross-linked alginate typically undergoes slow uncontrolled dissolution at neutral pH (i.e., greater than 3 months) (Mi et al., 2002a; FDA PhytaCare 510(k), 2010; FDA HemCon 510(k), 2010; Prestwich and Atzet, 2012). Degradation kinetics of covalently cross-linked alginate generally depends on the type and density of cross-linker (Mi et al., 2002b). However, there are strategies to adjust degradation kinetics by modifying polymer molecular weight, composition (M:G), and partial oxidation.

Another unique property of alginate is that it is relatively biologically inert. Cells do not naturally adhere to alginate, which has fostered investigations into the attachment of ECM proteins and peptide sequences to hydrogels (Prestwich and Atzet, 2012). Adhesion proteins such as laminins, fibronectin, and collagens have all been coupled to alginate, as well as the integrin-binding, fibronectin-derived, cell adhesive peptide arginine–glycine–aspartic acid and its derivatives (FDA PhytaCare 510(k), 2010; FDA Collamend 510(k), 2010; Prestwich and Atzet, 2012). These modifications have led to significant improvements in cellular attachment to alginate materials.

Specifically tailored alginate hydrogels have numerous proposed uses, including bulking agents, drug delivery vehicles, and scaffolds for regenerative medicine (Prestwich and Atzet, 2012). Alginate hydrogels have also been clinically investigated as a carrier for transplanted chondrocytes to treat intrinsic sphincter disease, and as a delivery vehicle for mineralization-promoting proteins (Prestwich and Atzet, 2012). Alginate-based biomaterials have been approved by the Food and Drug Administration (FDA) for topical use in wound healing. The PhytaCare Alginate Hydrogel and the Silverlon Calcium Alginate Dressing products both have 510(k) clearance as barrier wound dressings that provide a microbial barrier for partial to full thickness wounds, including ulcers, graft sites, surgical wounds, and burns (Prestwich and Atzet, 2012).

Chitosan

Chitosan is a polycationic copolymer of *N*-acetyl-glucosamine and *N*-glucosamine, and is generally obtained by alkaline deacetylation of chitin, a linear homopolymer of *N*-acetyl-glucosamine (Prestwich and Atzet, 2012). Chitin

is structurally related to glycosaminoglycans, but lacks the uronic acid groups. It is the primary component in fungi cell walls, and the exoskeleton of crustaceans such as shrimp, crab, and lobster (Khor and Lim, 2003; Prestwich and Atzet, 2012). When the degree of deacetylation (conversion to *N*-glucosamine) is greater than 50%, the biopolymer is termed chitosan (Prestwich and Atzet, 2012). The biopolymer is soluble in dilute acidic solutions, such as acetic acid or hydrochloric acid, and as a result the amino groups become protonated (Jiang et al., 2008). Chitosan hydrogels can be formed by entangled networks, ionic cross-links/polyelectrolyte complexes, or by covalent cross-linking (Mi et al., 2002b; Berger et al., 2004). Once dissolved, entangled networks of chitosan can gel by increasing the pH or extruding the solution into a nonsolvent. Entangled networks have limited use due to a lack of mechanical strength and a tendency to dissolve (Prestwich and Atzet, 2012). Due to the cationic nature of chitosan, combination with a negatively charged polymer, such as chondroitin sulfate or hyaluronan, will result in an ionic-bound network (Prestwich and Atzet, 2012). Covalently cross-linked hydrogels can be prepared by reaction with various difunctional molecules such as glutaraldehyde, poly (ethylene glycol), dialdehyde diethyl acetal, or genipin (Dal Pozzo et al., 2000). Chitosan is metabolized by human enzymes such as lysozyme, and thus can be considered biodegradable. Degradation rates depend, however, on the type of hydrogel network, and specifically for covalent networks, the type and density of cross-linker (Freier et al., 2005a). As with alginate, much research has explored the conjugation of biomolecules to chitosan, by either ionic, adsorption, or covalent modification of ECM proteins and peptide sequences to modify cellular response (Suh and Matthew, 2000; Ho et al., 2005). Chitosan provides multiple hydroxyl and amino functional sites for chemical modification opportunities (Berger et al., 2005). Chitosan-based hydrogels have been researched and developed for applications in drug and growth factor delivery, scaffold-based tissue regeneration, and wound dressings (Rao and Sharma, 1997; VandeVord et al., 2002; Mi et al., 2003; Freier et al., 2005b). Chitosan-based biomaterials have also been approved by the FDA for topical use in wound healing and as hemostats. Scion Cardio-Vascular, Inc. developed and markets a soft absorbent pad called the Clo-Sur P.A.D as a noninvasive topical approach to hemostasis based on chitosan and its absorbent properties (Prestwich and Atzet, 2012). This product has been cleared as a Class III medical device by the FDA. Other devices with FDA 510(k) clearance are Aquanova's superabsorbent dressing for wounds such as ulcers, and Celox's granulated chitosan for hemostasis (Prestwich and Atzet, 2012).

Fibrin

Fibrin is a naturally occurring biodegradable matrix that can be produced via polymerization of fibrinogen and thrombin to form a mesh network (Ahmed et al., 2008). Fibrinogen is a glycoprotein synthesized by the liver and is soluble in the

bloodstream (Linnes et al., 2007). Thrombin, also produced in the liver and found in the bloodstream, initiates end-to-end polymerization of the soluble fibrinogen to form long strands that precipitate to form a fibrin mesh (Prestwich and Atzet, 2012). This polymerization occurs naturally at a wound site and contributes, in conjunction with platelets, to form a clot. In vivo, fibrin gels are degraded by the proteolytic enzyme plasmin.

Fibrin gels often do not possess the required mechanical strength for some physically dynamic environments. To overcome this, researchers have combined various natural or synthetic polymers, such as collagen or polyglactin, to provide stronger gels (Eyrich et al., 2007; Dare et al., 2009). Using fibrin-based gels, 3D mitral valve constructs were produced as an experimental platform to serve as a test system to study mitral valve cellular phenotype behavior (Liu et al., 2018). Commercially available fibrin sealants are used to control bleeding and speed wound healing. Fibrinogen can be isolated from animal plasma, including human plasma; thus autologous scaffolds for tissue engineering applications can be generated from a patient's own blood (Prestwich and Atzet, 2012).

Manufacturing Approaches Utilizing Natural Materials

Human Recombinant ECM Protein Production

For the safety and efficacy of a high-quality human-based protein product like an injectable hydrogel with defined composition and protein concentrations, several points must be taken into account. For safe clinical application, the identity of the ECM proteins should be ideally human. Protein sequences among different species may show high homology to the human sequence, but even slight differences might be detected and trigger a response from the immune system of a patient (Courtman et al., 2001; Scherthaner, 1993; Meyer et al., 1988). With regard to a possible protein extraction from human tissue, it should be noted that these tissues are rare, of varying origin and quality, and with uncertain infection background. Also, the purification of a specific protein from a tissue with complex protein composition can require harsh methods (Nandi et al., 1987). These can damage the protein and impair or abolish its natural activity. Therefore the recombinant production of a protein of interest is much preferred compared to its extraction from human tissue. Progress in genetics allowed a better understanding of protein production and the possibilities of genetic manipulation (Urlaub et al., 1983; Seth et al., 2006; Korke et al., 2002). One of the most important accomplishments of this development is recombinant protein production in high-yield host cell lines (Seth et al., 2006; Korke et al., 2002). The recombinant production of protein products and therapeutics is an important branch of the pharmaceutical industry, which achieves turnovers measured in the billions worldwide. Compared to protein extractions from tissues, recombinant protein production has the advantage

of granting the secured availability of the human protein of interest in a reproducible high quality (Wurm, 2004). To generate high-quality protein products, the recombinant production of the human ECM proteins of interest by a safe host cell line under defined conditions and in defined media is preferable to other options. The careful selection of the host cell line, transfection, clone selection, production, and purification method needs to be based on the requirements for recombinant human ECM protein production under good manufacturing practice-translatable conditions.

For proteins to be synthesized in biologically active forms, they need to be properly folded and posttranslationally modified. There are more than 200 different posttranslational protein modifications possible in mammalian cells. Glycosylation is one of the most common and important posttranslational modifications (Palomares et al., 2004; Bhatia and Mukhopadhyay, 1999). When glycans are attached to asparagine residues on the core protein this is defined as *N*-linked glycosylation and when glycans are attached to serine or threonine residues as *O*-linked glycosylation (Bhatia and Mukhopadhyay, 1999). This posttranslational modification cannot be done in microbial hosts like *E. coli* because these organisms lack the required machinery to synthesize the appropriate mammalian glycoforms (Korke et al., 2002; Palomares et al., 2004; Zhu et al., 2007). Many ECM proteins carry complex glycosylations that are important for activities such as growth factor sequestering and can enable interactions with cells or other ECM components. Therefore an adequate host with the required enzymes for posttranslational modification of human proteins needs to be chosen.

Chinese hamster ovary (CHO) cells are the most commonly used cell line for the production of recombinant protein therapeutics in the pharmaceutical industry (Wurm, 2004; Omasa et al., 2010). CHO cells are robust protein expression hosts that are easy to maintain, which have the ability to adapt to suspension cultures (Sinacore et al., 2000). Suspension culture results in enhanced cell density and cell productivity levels compared to cultures employing adherent cells and therefore is the most common cell culture format for recombinant protein production with CHO cells (Wurm, 2004). Using a mutant CHO cell line deficient in the dihydrofolate reductase (DHFR) enzyme, an improved selection of stable clones and coamplification of the gene of interest can be achieved with rising methotrexate (MTX) levels (Urlaub and Chasin, 1980; Kellems, 1991).

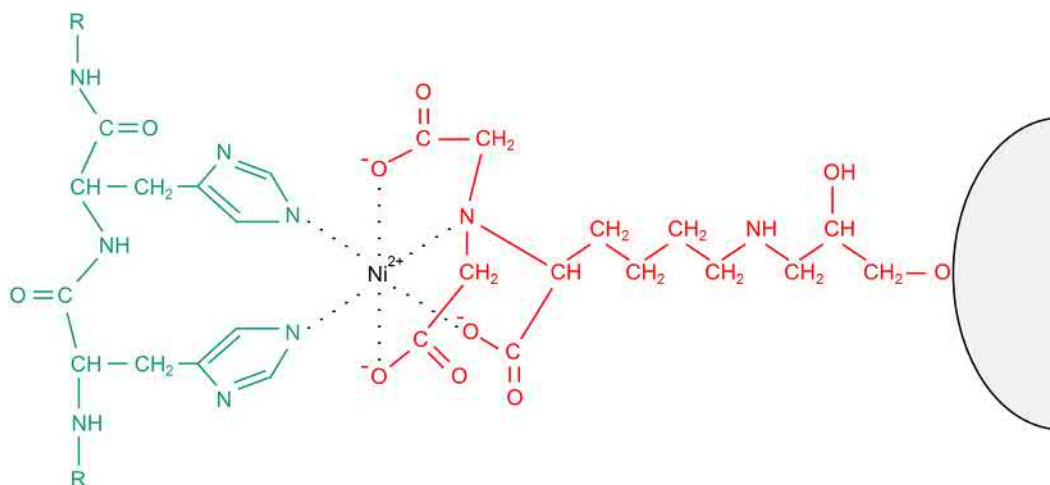
The increased number of copies of the gene of interest in the host genome due to coamplification with the DHFR gene results in a higher productivity of the production clone. The DHFR enzyme catalyzes the reaction of dihydrofolate to tetrahydrofolate, thereby playing a central role in the synthesis of this nucleic acid precursor in all organisms and eventually for DNA replication and cell growth. MTX is a potent competitive inhibitor of the DHFR enzyme, with a 1000-fold higher affinity to DHFR than folate. Making use of this coamplification system, specific productivity levels are expected to be highly increased (Wurm et al., 1986,

2004). For a further increase of product expression, codon adaptation can be applied to the gene sequence of ECM proteins (Zhou et al., 2004). The genetic code is degenerated, which means that many amino acids are encoded by more than one triplet codon. The concept of codon adaptation is based on the usage of the most frequently used triplet code for an amino acid, resulting in an optimized gene sequence, matching the codon usage of the rodent host while still encoding the same human protein (Ikemura, 1981). This is how codon adaptation can bypass predictable bottlenecks in transfer (tRNA) availability for a certain codon in the host cell line. Additional to permanent recombinant protein production, an inducible production of ECM proteins can be beneficial. This is the case if the permanent amplified recombinant protein production causes a metabolic burden to the host cell, leading, for example, to a reduced cell proliferation (Gu et al., 1992). Undesired inhibition of host cell proliferation during the clone selection phase could also be caused by the biological effects of the protein of interest (Yamaguchi and Ruoslahti, 1988). Therefore instead of conventionally designed plasmids for permanent protein production, the inducible production system uses plasmids with the protein of interest under the transcriptional control of an inducible promoter (Gossen et al., 1995). For this system, it is necessary to stably transfect the host cells with a plasmid for the permanent production of an activator protein (Gossen et al., 1995; Urlinger et al., 2000). Subsequently, this stable activator clone is transfected with the plasmid for inducible production of the ECM protein of interest. In this plasmid an inducible promoter controls the transcription of the gene of interest, and can only be activated by the permanently produced activator ECM protein in the presence of doxycycline (Gossen et al., 1995; Urlinger et al., 2000).

Purification of Recombinant ECM Proteins

For easier protein purification without the need for a lysis step as well as intact protein activity, recombinant ECM proteins should be secreted to the culture media by the host cells, just like these ECM proteins are secreted into the interstitial space in the human body (Sheehan and O'Sullivan, 2004). For secretion purposes, the ECM protein's natural secretion peptide needs to be included in the ECM gene sequence in the production plasmid. Incomplete protein secretion of the recombinant ECM proteins could cause protein aggregate formation in the host cell, impairing its metabolism as well as the protein purification and protein activity (Sheehan and O'Sullivan, 2004). Protein purification of secreted proteins from the culture media leads to higher yields with maintained protein activity as no cell lysis or chemical extraction of the protein-containing cell compartment and refolding of the protein to bioactive conformation needs to be performed (Mukhopadhyay, 1997; Sheehan and O'Sullivan, 2004).

Affinity chromatography is one of the most efficient and selective chromatographic protein purification methods



• **Figure 1.3.6B.4** A protein with a polyhistidine tag (in green) is bound to a nickel ion (Ni^{2+}). The nickel ion is immobilized to a solid support (sepharose bead) by the chelating agent nitrilotriacetic acid (in red) and a linker (in red).

(Zhu et al., 2007). Several small affinity tags are widely used as an efficient tool for recombinant protein purification, histidine tags being one of the most known and also favored (Yip and Hutchens, 1994; Hochuli et al., 1987). The main step in the purification of a secreted, histidine-tagged protein is based on a specific type of affinity chromatography, the so-called immobilized metal affinity chromatography (IMAC) (Porath et al., 1975). In this case the natural affinity of the amino acid histidine to immobilized nickel ions on an affinity chromatography column is used for the protein purification (Hochuli et al., 1987; Yip et al., 1989). A nickel ion-charged sepharose bead matrix ensures a high binding capacity for histidine-tagged proteins (Hochuli et al., 1987). The molecular interaction, which is the basis of this affinity chromatography, is depicted in Fig. 1.3.6B.4.

Reproducible IMAC purification with defined equilibration, wash and elution buffers, constant flow rates through the affinity chromatography column, and monitoring of important measurement data can be accomplished with a fast protein liquid chromatography system (Sheehan and O'Sullivan, 2004). Monitoring and recording of flow rate, conductivity, pressure, and absorption at 280 and 256 nm provide an informative basis for the different sections of the purification process. Automated elution fraction collection and subsequent desalting and buffer exchange, concentration, wash, and sterile filtration of the protein solution result in a high-quality pure protein product that can be stored until its use for biomedical applications such as 3D bioprinting or electrospinning at -80°C .

3D Bioprinting

3D scaffolds can either be produced by laser-based, printer-based, or nozzle-based printing, whereas the printer-based method is suitable for printing cells (Hinderer et al., 2016). Compared to printing, bioprinting includes the addition of cells, growth factors, and other functional elements (Murphy and Atala, 2014). It has been demonstrated that ECM

proteins are suitable for generating 3D bioprinted scaffolds. Collagens (Chang et al., 2012), fibrin (Cui and Boland, 2009), and methacrylated gelatin (Hoch et al., 2013) have been used in bioprinting applications. Hoch et al. introduced living chondrocytes to an in-house manufactured gelatin solution to create an ink for bioprinting. In their study, the authors showed that the printed chondrocytes exhibited excellent viability, concluding that this method is suitable for generating ECM-based cell carriers for application in cartilage tissue engineering (Hoch et al., 2013; Hinderer et al., 2016). Due to the layer-by-layer deposition of the material, complex and well-defined 3D structures, such as whole organs, can be realized. Sun et al. developed a printing and coating method termed “Patterning on Topography” (PoT) that enables the layering of proteins such as fibronectin, laminin, collagen type IV, and other ECM proteins onto printed geometric surfaces ranging from smooth to very topographically complex surfaces with high fidelity (Hinderer et al., 2016). In this method, thermally sensitive poly(*N*-isopropylacrylamide) are spin coated onto glass coverslips and then sandwiched with ECM proteins that have been microcontact printed with a polydimethylsiloxane stamp. The sandwiched layers are dipped in distilled water and allowed to cool to room temperature (Hinderer et al., 2016). This allows the transfer of the printed ECM protein layer onto the printed topography layer, where the ECM adheres via hydrophobic interactions, resulting in a highly defined ECM-layered surface that can be used for cell culture or potentially on implant surfaces. In this work, the printed ECM was used to elucidate how competing physical and chemical microenvironment cues influence cardiomyocyte behavior (Hinderer et al., 2016). Joo et al. performed similar work where their group used PoT to investigate the effects of ECM patterns on the migration and differentiation of adult neural stem cells (Joo et al., 2015; Hinderer et al., 2016). Using humidified microcontact printing, Ricoult et al. printed ECM proteins onto smooth surfaces without the need of harsh chemicals that are typically involved in

this process, thus protecting the proteins from denaturalization (Ricoult et al., 2014; Hinderer et al., 2016). They created vascularized printed topographies with nanometer resolution as a proof of principle for the possibility of the solvent-assisted printing of proteins and nanoparticles. Further options and current applications of 3D bioprinting in regenerative medicine as well as current challenges in the field, including improvement of resolution, generation of more adequate printable biomaterials, and upscaling to clinical relevant sizes, have been intensively reviewed by Murphy and Atala (Murphy and Atala, 2014).

Electrospinning of ECM Proteins and Natural Materials

Electrospinning is an attractive method to generate fibrous and porous matrices with a high surface area for regenerative medicine applications. Varying matrix properties, such as fiber and pore sizes, enable the control of cellular responses, including migration, proliferation, and progenitor cell differentiation (Hinderer et al., 2016). The basic experimental set-up for electrospinning includes a syringe that is connected to a pump, as well as a conductive flat or rotating electrode (=collector), and a high-voltage power supply. A polymer solution is pumped through the syringe and forms a droplet on the needle tip. By applying high voltage, the droplet adopts a conical shape, and as soon as the electrical field strength exceeds the surface tension, a thin fiber develops. Due to equal charges, instabilities occur and the fiber travels in spinning motions to the collector, the solvent evaporates, and a solid fibrous network is generated. Depending on the collector shape, different scaffold types can be obtained. Therefore it is possible to spin flat sheets, tubes, or even the shape of a heart valve (Hinderer et al., 2016). Today, there are various methods described to electrospin synthetic polymers from different solvents (Hinderer et al., 2014, 2016). One of the first examples of electrospinning ECM proteins was performed by the Chaikof group where they spun a 1 wt% solution of type I collagen with polyethylene oxide to create a collagen mesh (Huang et al., 2001). Fourteen years after the first ECM scaffolds were spun, groups have electrospun natural decellularized ECM (Wen et al., 2014), or ECM components such as collagen blends, HA, or proteoglycans (Hinderer et al., 2016). Rao et al. used coaxial electrospinning to create a brain white matter in vitro model to study the migration of malignant brain tumors. They tested HA, collagens, and Matrigel, an extract of the Engelbreth-Holm-Swarm mouse tumor, in the outer shell of the nanofibers to analyze the effects of different proteins on cell migration (Rao et al., 2013). Electrospun scaffolds can be layered using multiple methods. For example, a positively charged chitosan and negatively charged ColI were used to create a layered scaffold to promote wound healing (Huang et al., 2015). Although electrospinning is a simple and cost-effective method to generate 3D fiber-containing materials, due to the need of high electrical fields and harsh

solvents, it is quite challenging to maintain a physiological protein function. Although there are a few publications focusing on functional electrospinning of ECM molecules (Hinderer et al., 2012), a clinical translation has not yet been demonstrated.

Summary

Regenerative strategies such as stem cell-based therapies and tissue engineering applications are being developed with the aim of replacing, remodeling, regenerating, or supporting damaged tissues and organs. When aiming for ultimately clinical applications, in addition to, or instead of, a careful cell type selection, the design of appropriate 3D scaffolds is essential for the generation of bioinspired replacement tissues. Such scaffolds are composed of degradable or nondegradable biomaterials. The development of effective and efficient drug carrier systems is also highly relevant for novel therapeutic treatment strategies. ECM and natural materials have a great potential to be utilized as scaffolds for bioengineering and regenerative medicine. The native ECM is a heterogeneous network of soluble and fibrous proteins, PGs, and GAGs, which is maintained by both covalent and noncovalent interactions. Recapitulating the composition and structure, and moreover the native function of the ECM, is a highly challenging task to bioengineers and biochemists. This said, researchers have worked successfully over the past decades on many novel approaches either to produce and further manufacture ECM proteins and natural materials, or to harness the knowledge obtained from studies focusing on the ECM. This has enabled them to mimic the native function of the ECM using ECM-like materials supporting cell attachment, growth, and proliferation as well as differentiation. The fundamental role of such natural materials is to enhance the natural biological repair processes mediated by endogenous cells. However, no technology will reach patients and physicians unless it is commercialized. Upscaling of the laboratory-grade processes is often a hurdle. Advanced process development, such as the introduction of technologies that allows recombinant protein production, has and will further push great ideas to the market.

As already stipulated by Prestwich and Atzet, while we must embrace the complexity of biology, we cannot let this complexity dominate the design of a clinical biomaterial (Prestwich and Atzet, 2012). There will be not one formulation that can fulfill every need. As seen lately in therapeutic approaches, personalized medicine, in this case personalized materials design, will likely dominate the future. Technologies such as 3D (bio) printing and electrospinning will further allow us to design and shape the ideal biomaterial for a defined clinical application. However, the penetration of a new technology into any market is not only determined by improvement in patient outcome, but also by the true limiting factors of cost, familiarity, and ease of use (Prestwich and Atzet, 2012).

References

- Ahmed, T.A., Dare, E.V., Hincke, M., 2008. Fibrin: a versatile scaffold for tissue engineering applications. *Tissue Eng. B Rev.* 14 (2), 199–215.
- Allison, D., Grande-Allen, K., 2006. Hyaluronan: a powerful tissue engineering tool. *Tissue Eng.* 12 (8), 2131–2140.
- Augst, A.D., Kong, H.J., Mooney, D.J., 2006. Alginate hydrogels as biomaterials. *Macromol. Biosci.* 6 (8), 623–633.
- Badylak, S.F., Gilbert, T.W., 2008. Immune response to biologic scaffold materials. *Semin. Immunol.* 20 (2), 109–116.
- Badylak, S., Gilbert, T., Myers-Irvin, J., 2008. The extracellular matrix as a biologic scaffold for tissue engineering. In: van Blitterswijk, C. (Ed.), *Tissue Engineering*. Elsevier, pp. 121–143.
- Bhatia, P.K., Mukhopadhyay, A., 1999. Protein glycosylation: implications for in vivo functions and therapeutic applications. *Adv. Biochem. Eng. Biotechnol.* 64, 155–201.
- Baldwin, A.D., Kiick, K.L., 2010. Polysaccharide-modified synthetic polymeric biomaterials. *Biopolymers* 94 (1), 128–140.
- Basmadjian, D., Sefton, M.V., 1983. Relationship between release rate and surface concentration for heparinized materials. *J. Biomed. Mater. Res.* 17 (3), 509–518.
- Berger, J., Reist, M., Mayer, J.M., Felt, O., Peppas, N.A., et al., 2004. Structure and interactions in covalently and ionically cross-linked chitosan hydrogels for biomedical applications. *Eur. J. Pharm. Biopharm.* 57 (1), 19–34.
- Berger, J., Reist, M., Chenite, A., Felt-Baeyens, O., Mayer, J.M., et al., 2005. Pseudo-thermosetting chitosan hydrogels for biomedical application. *Int. J. Pharm.* 288 (1), 17–25.
- Breckwoldt, W.L., Belkin, M., Gould, K., Allen, M., Connolly, R.J., et al., 1991. Modification of the thrombogenicity of a self-expanding vascular stent. *J. Investig. Surg.* 4 (3), 269–278.
- Cauda, F., Cauda, V., Fiori, C., Onida, B., Garrone, E., 2008. Heparin coating on ureteral Double J stents prevents encrustations: an in vivo case study. *J. Endourol.* 22 (3), 465–472.
- Chang, C.C., Krishnan, L., Nunes, S.S., Church, K.H., Edgar, L.T., Boland, E.D., Weiss, J.A., Williams, S.K., Hoying, J.B., 2012. Determinants of microvascular network topologies in implanted neovasculatures. *Arterioscler. Thromb. Vasc. Biol.* 32, 5–14.
- Courtman, D.W., Errett, B.F., Wilson, G.J., 2001. The role of cross-linking in modification of the immune response elicited against xenogenic vascular acellular matrices. *J. Biomed. Mater. Res.* 55 (4), 576–586.
- Cui, X., Boland, T., 2009. Human microvasculature fabrication using thermal inkjet printing technology. *Biomaterials* 30, 6221–6227.
- Daamen, W.F., Veerkamp, J.H., van Hest, J.C., van Kuppevelt, T.H., 2007. Elastin as a biomaterial for tissue engineering. *Biomaterials* 28 (30), 4378–4398.
- Dal Pozzo, A., Vanini, L., Fagnoni, M., Guerrini, M., De Benedittis, A., et al., 2000. Preparation and characterization of poly (ethylene glycol)-cross-linked reacylated chitosans. *Carbohydr. Polym.* 42, 201–206.
- Dare, E.V., Griffith, M., Poitras, P., Kaupp, J.A., Waldman, S.D., et al., 2009. Genipin cross-linked fibrin hydrogels for in vitro human articular cartilage tissue-engineered regeneration. *Cells Tissues Organs* 190 (6), 313–325.
- DeAngelis, P.L., Oatman, L.C., Gay, D.F., 2003. Rapid chemoenzymatic synthesis of monodisperse hyaluronan oligosaccharides with immobilized enzyme reactors. *J. Biol. Chem.* 278 (37), 35199–35203.
- Eyrich, D., Brandl, F., Appel, B., Wiese, H., Maier, G., et al., 2007. Long-term stable fibrin gels for cartilage engineering. *Biomaterials* 28 (1), 55–65.
- FDA Collamend 510(k), 2010. http://www.accessdata.fda.gov/cdrh_docs/pdf8/K082687.pdf.
- FDA HemCon 510(k), 2010. http://www.accessdata.fda.gov/cdrh_docs/pdf8/K080818.pdf.
- FDA PhytaCare 510(k), 2010. http://www.accessdata.fda.gov/cdrh_docs/pdf5/K053538.pdf.
- FDA TyCo Healthcare Heparin Coated Catheter (3/24/10), 2010. http://www.accessdata.fda.gov/cdrh_docs/pdf6/K062671.pdf.
- Freier, T., Koh, H.S., Kazazian, K., Shoichet, M.S., 2005a. Controlling cell adhesion and degradation of chitosan films by N-acetylation. *Biomaterials* 26 (29), 5872–5878.
- Freier, T., Montenegro, R., Shan Koh, H., Shoichet, M.S., 2005b. Chitin-based tubes for tissue engineering in the nervous system. *Biomaterials* 26 (22), 4624–4632.
- Friess, W., 1998. Collagen: biomaterial for drug delivery. *Eur. J. Pharm. Biopharm.* 45 (2), 113–136.
- Geutjes, P.J., Daamen, W.F., Buma, P., Feitz, W.F., Faraj, K.A., et al., 2006. From molecules to matrix: construction and evaluation of molecularly defined bioscaffolds. *Adv. Exp. Med. Biol.* 585, 279–295.
- Gossen, M., et al., 1995. Transcriptional activation by tetracyclines in mammalian cells. *Science* 268 (5218), 1766–1769.
- Gu, M.B., et al., 1992. Effect of amplification of dhfr and lac Z genes on growth and beta-galactosidase expression in suspension cultures of recombinant CHO cells. *Cytotechnology* 9 (1–3), 237–245.
- Hildebrandt, P., 2002. Glycosaminoglycans: all round talents in coating technology. *Biomed. Tech. (Berl.)* 47 (Suppl. 1 Pt. 1), 476–478.
- Hinderer, S., Schesny, M., Bayrak, A., Ibold, B., Hampel, M., Walles, T., Stock, U.A., Seifert, M., Schenke-Layland, K., 2012. Engineering of fibrillar decorin matrices for a tissue-engineered trachea. *Biomaterials* 33, 5259–5266.
- Hinderer, S., H., Seifert, J., Votteler, M., Shen, N., Rheinlaender, J., Schäffer, T.E., Schenke-Layland, K., 2014. Engineering of a bio-functionalized hybrid off-the-shelf heart valve. *Biomaterials* 35, 2130–2139.
- Hinderer, S., Shen, N., Ringuette, L.J., Hansmann, J., Reinhardt, D.P., Brucker, S.Y., Davis, E.C., Schenke-Layland, K., 2015. *Biomed. Mater.* 10 (3), 034102.
- Hinderer, S., Layland, S.L., Schenke-Layland, K., 2016. ECM and ECM-like materials – biomaterials for applications in regenerative medicine and cancer therapy. *Adv. Drug Deliv. Rev.* 97, 260–269.
- Ho, M.H., Wang, D.M., Hsieh, H.J., Liu, H.C., Hsien, T.Y., et al., 2005. Preparation and characterization of RGD-immobilized chitosan scaffolds. *Biomaterials* 26 (16), 3197–3206.
- Hoch, E., Hirth, T., Tovar, G.E.M., Borchers, K., 2013. Chemical tailoring of gelatin to adjust its chemical and physical properties for functional bioprinting. *J. Mater. Chem. B* 1, 5675–5685.
- Hochuli, E., Dobeli, H., Schacher, A., 1987. New metal chelate adsorbent selective for proteins and peptides containing neighbouring histidine residues. *J. Chromatogr.* 411, 177–184.
- Hoffman, A.S., Schmer, G., Harris, C., Kraft, W.G., 1972. Covalent binding of biomolecules to radiation-grafted hydrogels on inert polymer surfaces. *Trans. Am. Soc. Artif. Intern. Organs* 18 (1), 10–18.
- Hubmacher, D., Reinhardt, D.P., Plesec, T., Schenke-Layland, K., Apte, S.S., 2014. Human eye development is characterized by coordinated expression of fibrillin isoforms. *Investig. Ophthalmol. Vis. Sci.* 55, 7934–7944.
- Hulmes, D.J.S., 2008. Collagen diversity, synthesis and assembly. In: Fratzl, P. (Ed.), *Collagen: Structure and Mechanics*. Springer Science+Business Media, LLC, pp. 15–47.

- Huang, L., McMillan, R.A., Apkarian, R.P., Pourdeyehimi, B., 2000. Generation of synthetic elastin-mimic small diameter fibers and fiber networks. *Macromolecules* 33, 2989–2997.
- Huang, L., Apkarian, R.P., Chaikof, E.L., 2001. High-resolution analysis of engineered type I collagen nanofibers by electron microscopy. *Scanning* 23, 372–375.
- Huang, L.W., Li, W., Lv, X., Lei, Z., Bian, Y., Deng, H., Wang, H., Li, J., Li, X., 2015. Biomimetic LBL structured nanofibrous matrices assembled by chitosan/collagen for promoting wound healing. *Biomaterials* 53, 58–78.
- Ikemura, T., 1981. Correlation between the abundance of *Escherichia coli* transfer RNAs and the occurrence of the respective codons in its protein genes. *J. Mol. Biol.* 146 (1), 1–21.
- Indik, Z., Abrams, W.R., Kucich, U., Gibson, C.W., Mecham, R.P., Rosenbloom, J., 1990. *Arch. Biochem. Biophys.* 280, 80.
- Jiang, T., Kumbar, S.G., Nair, L.S., Laurencin, C.T., 2008. Biologically active chitosan systems for tissue engineering and regenerative medicine. *Curr. Top. Med. Chem.* 8 (4), 354–364.
- Jiang, T., Wang, G., Qiu, J., Luo, L., Zhang, G., 2009. Heparinized poly(vinyl alcohol): small intestinal submucosa composite membrane for coronary covered stents. *Biomed. Mater.* 4 (2), 025012.
- Joo, K.J., Lee, E., Hong, N., Sun, W., Nam, Y., 2015. Effects of ECM protein micropatterns on the migration and differentiation of adult neural stem cells. *Sci. Rep.* 5, 13043.
- Kielty, C.M., Wess, T.J., Haston, L., Ashworth, J.L., Sherratt, M.J., Shuttleworth, C.A., 2002. Fibrillin-rich microfibrils: elastic biopolymers of the extracellular matrix. *J. Muscle Res. Cell Motil.* 23, 581–596.
- Kellems, R.E., 1991. Gene amplification in mammalian cells: strategies for protein production. *Curr. Opin. Biotechnol.* 2 (5), 723–729.
- Khor, E., Lim, L.Y., 2003. Implantable applications of chitin and chitosan. *Biomaterials* 24 (13), 2339–2349.
- Korke, R., et al., 2002. Genomic and proteomic perspectives in cell culture engineering. *J. Biotechnol.* 94 (1), 73–92.
- Kuo, J.W., 2006. *Practical Aspects of Hyaluronan Based Medical Products*. CRC/Taylor & Francis, Boca Raton.
- Laurent, T., 1989. The biology of hyaluronan. *Introduction*. *Ciba Found. Symp.* 143, 1–20.
- Lee, C.H., Singla, A., Lee, Y., 2001. Biomedical applications of collagen. *Int. J. Pharm.* 221 (1–2), 1–22.
- Leitinger, B., Hohenester, E., 2007. Mammalian collagen receptors. *Matrix Biol.* 3, 146–155.
- Linnes, M.P., Ratner, B.D., Giachelli, C.M., 2007. A fibrinogen-based precision microporous scaffold for tissue engineering. *Biomaterials* 28 (35), 5298–5306.
- Liu, M.M., Flanagan, T.C., Jockenhoefel, S., Black, A., Lu, C.C., French, A.T., Argyle, D.J., Corcoran, B.M., 2018. Development and evaluation of a tissue-engineered fibrin-based canine mitral valve three-dimensional cell culture system. *J. Comp. Pathol.* 160, 23–33.
- Martin, S.L., Vrhovski, B., Weiss, A.S., 1995. *Gene* 154, 159.
- McHale, M.K., Setton, L.A., Chilkoti, A., 2005. Synthesis and in vitro evaluation of enzymatically cross-linked elastin-like polypeptide gels for cartilaginous tissue repair. *Tissue Eng.* 11 (11–12), 1768–1779.
- Meyer, A.A., et al., 1988. Antibody response to xenogeneic proteins in burned patients receiving cultured keratinocyte grafts. *J. Trauma Acute Care Surg.* 28 (7), 1054–1059.
- Mi, F.L., Sung, H.W., Shyu, S.S., 2002a. Drug release from chitosan-alginate complex beads reinforced by a naturally occurring cross-linking agent. *Carbohydr. Polym.* 48, 61–72.
- Mi, F.L., Tan, Y.C., Liang, H.F., Sung, H.W., 2002b. In vivo biocompatibility and degradability of a novel injectable-chitosan-based implant. *Biomaterials* 23 (1), 181–191.
- Mi, F.L., Shyu, S.S., Lin, Y.M., Wu, Y.B., et al., 2003. Chitin/PLGA blend microspheres as a biodegradable drug delivery system: a new delivery system for protein. *Biomaterials* 24 (27), 5023–5036.
- Mukhopadhyay, A., 1997. Inclusion bodies and purification of proteins in biologically active forms. *Adv. Biochem. Eng. Biotechnol.* 56, 61–109.
- Murphy, S.V., Atala, A., 2014. 3D bioprinting of tissues and organs. *Nat. Biotechnol.* 32, 773–785.
- Nandi, J., Zhou, M.A., Ray, T.K., 1987. Purification and partial characterization of the (H⁺,K⁺)-transporting adenosinetriphosphatase from fundic mucosa. *Biochemistry* 26 (14), 4264–4272.
- Nimni, M.E., Cheung, D., Strates, B., Kodama, M., Sheikh, K., 1987. Chemically modified collagen: a natural biomaterial for tissue replacement. *J. Biomed. Mater. Res.* 21 (6), 741–771.
- Omasa, T., Onitsuka, M., Kim, W.D., 2010. Cell engineering and cultivation of Chinese hamster ovary (CHO) cells. *Curr. Pharmaceut. Biotechnol.* 11 (3), 233–240.
- Palomares, L.A., Estrada-Mondaca, S., Ramirez, O.T., 2004. Production of recombinant proteins: challenges and solutions. *Methods Mol. Biol.* 267, 15–52.
- Peattie, R.A., Pike, D.B., Yu, B., Cai, S., Shu, X.Z., et al., 2008. Effect of gelatin on heparin regulation of cytokine release from hyaluronan-based hydrogels. *Drug Deliv.* 15 (6), 389–397.
- Porath, J., et al., 1975. Metal chelate affinity chromatography, a new approach to protein fractionation. *Nature* 258 (5536), 598–599.
- Prestwich, G.D., Kuo, J.W., 2008. Chemically-modified HA for therapy and regenerative medicine. *Curr. Pharmaceut. Biotechnol.* 9 (4), 242–245.
- Prestwich, G.D., Atzet, S., 2012. Biomaterials science: an introduction to materials in medicine. In: Ratner, B.D., Hoffman, A.S., Schoen, F.J., Lemons, J.E. (Eds.). Elsevier Academic Press.
- Rao, S.B., Sharma, C.P., 1997. Use of chitosan as a biomaterial: studies on its safety and hemostatic potential. *J. Biomed. Mater. Res.* 34 (1), 21–28.
- Rao, S.S., Nelson, M.T., Xue, R., DeJesus, J.K., Viapiano, M.S., Lannutti, J.J., Sarkar, A., Winter, J.O., 2013. Mimicking white matter tract topography using core-shell electrospun nanofibers to examine migration of malignant brain tumors. *Biomaterials* 34, 5181–5190.
- Ricoult, S.G., Nezhad, A.S., Knapp-Mohammady, M., Kennedy, T.E., Juncker, D., 2014. Humidified microcontact printing of proteins: universal patterning of proteins on both low and high energy surfaces. *Langmuir* 30, 12002–12010.
- Rowley, J.A., Madlambayan, G., Mooney, D.J., 1999. Alginate hydrogels as synthetic extracellular matrix materials. *Biomaterials* 20 (1), 45–53.
- Sabatier, L., Chen, D., Fagotto-Kaufmann, C., Hubmacher, D., McKee, M.D., Annis, D.S., et al., 2009. Fibrillin assembly requires fibronectin. *Mol. Biol. Cell* 20, 846–858.
- Schenke-Layland, K., 2008. Non-invasive multiphoton imaging of extracellular matrix structures. *J. Biophot.* 6, 451–462.
- Scherthaner, G., 1993. Immunogenicity and allergenic potential of animal and human insulins. *Diabetes Care* 16 (Suppl. 3), 155–165.
- Schmer, G., 1972. The biological activity of covalently immobilized heparin. *333Trans. Am. Soc. Artif. Intern. Organs* 18 (1), 321–324 333.
- Seth, G., et al., 2006. Engineering cells for cell culture bioprocessing-physiological fundamentals. *Adv. Biochem. Eng. Biotechnol.* 101, 119–164.
- Shapiro, S.D., Endicott, S.K., Province, M.A., Pierce, J.A., Campbell, E.J., 1991. Marked longevity of human lung parenchymal elastic fibers deduced from prevalence of D- aspartate and nuclear weapons-related radiocarbon. *J. Clin. Investig.* 87, 1828–1834.

- Sheehan, D., O'Sullivan, S., 2004. Fast protein liquid chromatography. In: Cutler, P. (Ed.), *Protein Purification Protocols*. Humana Press, pp. 253–258.
- Sherratt, M.J., 2009. Tissue elasticity and the ageing elastic fibre. *Age (Dordr)*. 31, 305–325.
- Shin, H., Jo, S., Mikos, A.G., 2003. Biomimetic materials for tissue engineering. *Biomaterials* 24 (24), 4353–4364.
- Shu, X.Z., Liu, Y., Luo, Y., Roberts, M.C., Prestwich, G.D., 2002. Disulfide cross-linked hyaluronan hydrogels. *Biomacromolecules* 3 (6), 1304–1311.
- Shu, X.Z., Prestwich, G.D., 2004. Therapeutic biomaterials from chemically modified hyaluronan. In: Garg, H.G., Hales, C.A. (Eds.), *Chemistry and Biology of Hyaluronan*. Elsevier, Amsterdam, pp. 475–504.
- Shu, X.Z., Ahmad, S., Liu, Y., Prestwich, G.D., 2006. Synthesis and evaluation of injectable, in situ cross-linkable synthetic extracellular matrices for tissue engineering. *J. Biomed. Mater. Res. A* 79 (4), 902–912.
- Sinacore, M.S., Drapeau, D., Adamson, S.R., 2000. Adaptation of mammalian cells to growth in serum-free media. *Mol. Biotechnol.* 15 (3), 249–257.
- Stenzel, K.H., Miyata, T., Rubin, A.L., 1974. Collagen as a biomaterial. *Annu. Rev. Biophys. Bioeng.* 3 (0), 231–253.
- Stone, K.R., Steadman, J.R., Rodkey, W.G., Li, S.T., 1997. Regeneration of meniscal cartilage with use of a collagen scaffold. Analysis of preliminary data. *J. Bone. Joint Surg. Am.* 79 (12), 1770–1777.
- Suh, J.K., Matthew, H.W., 2000. Application of chitosan-based polysaccharide biomaterials in cartilage tissue engineering: a review. *Biomaterials* 21 (24), 2589–2598.
- Urlaub, G., Chasin, L.A., 1980. Isolation of Chinese hamster cell mutants deficient in dihydrofolate reductase activity. *Proc. Natl. Acad. Sci. U. S. A.* 77 (7), 4216–4220.
- Urlaub, G., et al., 1983. Deletion of the diploid dihydrofolate reductase locus from cultured mammalian cells. *Cell* 33 (2), 405–412.
- Urlinger, S., et al., 2000. Exploring the sequence space for tetracycline-dependent transcriptional activators: novel mutations yield expanded range and sensitivity. *Proc. Natl. Acad. Sci. U. S. A.* 97 (14), 7963–7968.
- Urry, D.W., Hugel, T., Seitz, M., Gaub, H.E., Sheiba, L., et al., 2002. Elastin: a representative ideal protein elastomer. *Philos. Trans. R. Soc. Lond. B Biol. Sci.* 357 (1418), 169–184.
- van der Giessen, W.J., van Beusekom, H.M., Eijgelshoven, M.H., Morel, M.A., Serruys, P.W., 1998. Heparin-coating of coronary stents. *Semin. Interv. Cardiol.* 3 (3–4), 173–176.
- VandeVord, P.J., Matthew, H.W., DeSilva, S.P., Mayton, L., Wu, B., et al., 2002. Evaluation of the biocompatibility of a chitosan scaffold in mice. *J. Biomed. Mater. Res.* 59 (3), 585–590.
- Vindin, H., Mithieux, S.M., Weiss, A.S., 2019. Elastin architecture. *Matrix Biol.* <https://doi.org/10.1016/j.matbio.2019.07.005> (in press).
- Votteler, M., Kluger, P.J., Waller, H., Schenke-Layland, K., 2010. *Macromol. Biosci.* 10, 1302–1315.
- Votteler, M., Carvajal Berrio, D.A., Horke, A., Sabatier, L., Reinhardt, D.P., Nsair, A., Aikawa, E., Schenke-Layland, K., 2013. *Development* 140, 2345–2353.
- Wagenseil, J.E., Mecham, R.P., 2007. New insights into elastic fiber assembly. *Birth Defects Res. C Embryo Today* 81, 229–240.
- Wagenseil, J.E., Mecham, R.P., 2009. Vascular extracellular matrix and arterial mechanics. *Physiol. Rev.* 89, 957–989.
- Wen, X., Wang, Y., Guo, Z., Meng, H., Huang, J., Zhang, L., Zhao, B., Zhao, Q., Zheng, Y., Peng, J., 2014. Cauda equina-derived extracellular matrix for fabrication of nanostructured hybrid scaffolds applied to neural tissue engineering. *Tissue Eng. A* 21, 1095–1105.
- Wise, S.G., Weiss, A.S., 2009. Tropoelastin. *Int. J. Biochem. Cell Biol.* 41, 494–497.
- White, M.J., Kohno, I., Rubin, A.L., Stenzel, K.H., Miyata, T., 1973. Collagen films: effect of cross-linking on physical and biological properties. *Biomater. Med. Devices Artif. Organs* 1 (4), 703–715.
- Wurm, F.M., Gwinn, K.A., Kingston, R.E., 1986. Inducible overproduction of the mouse *c-myc* protein in mammalian cells. *Proc. Natl. Acad. Sci. U. S. A.* 83 (15), 5414–5418.
- Wurm, F.M., 2004. Production of recombinant protein therapeutics in cultivated mammalian cells. *Nat. Biotechnol.* 22 (11), 1393–1398.
- Yamaguchi, Y., Ruoslahti, E., 1988. Expression of human proteoglycan in Chinese hamster ovary cells inhibits cell proliferation. *Nature* 336 (6196), 244–246.
- Yeo, G.C., Aghaei-Ghareh-Bolagh, B., Brackenreg, E.P., Hiob, M.A., Lee, P., Weiss, A.S., 2015. Fabricated elastin. *Adv. Healthc. Mater.* 4 (16), 2530–2556.
- Yip, T.T., Nakagawa, Y., Porath, J., 1989. Evaluation of the interaction of peptides with Cu(II), Ni(II), and Zn(II) by high-performance immobilized metal ion affinity chromatography. *Anal. Biochem.* 183 (1), 159–171.
- Yip, T.T., Hutchens, T.W., 1994. Immobilized metal ion affinity chromatography. *Mol. Biotechnol.* 1 (2), 151–164.
- Yuan, N., Tsai, R., Ho, M., Wang, D., Lai, J., et al., 2008. Fabrication and characterization of chondroitin sulfate-modified chitosan membranes for biomedical applications. *Desalination* 23 (1–3), 166–174.
- Zhou, Z., et al., 2004. Enhanced expression of a recombinant malaria candidate vaccine in *Escherichia coli* by codon optimization. *Protein Expr. Purif.* 34 (1), 87–94.
- Zhu, M., Mollet, M., Hubert, R., 2007. Industrial production of therapeutic proteins: cell lines, cell culture, and purification. In: Kent, J. (Ed.), *Kent and Riegel's Handbook of Industrial Chemistry and Biotechnology*. Springer US, pp. 1421–1448.

Further Reading

- Chunduru, S.K., et al., 1994. Methotrexate-resistant variants of human dihydrofolate reductase. Effects of Phe31 substitutions. *J. Biol. Chem.* 269 (13), 9547–9555.

1.3.7

Composites

GUIGEN ZHANG¹, HELEN LU², SACHIN MAMIDWAR³, MIN WANG⁴

¹F Joseph Halcomb III, M.D. Department of Biomedical Engineering, University of Kentucky, Lexington, KY, United States

²Department of Biomedical Engineering, Columbia University, New York, NY, United States

³Orthogen, LLC, Springfield, NJ, United States

⁴Department of Mechanical Engineering, The University of Hong Kong, Pok Fu Lam, Hong Kong, China

Introduction

Biomedical composites are materials that are formed by combining multiple components of materials such as metals, polymers, and ceramics. For certain targeted biomedical applications, they provide improved properties that a typical metal, polymer, or ceramic material alone cannot provide. A main advantage of composites is that their properties can be tailored by changing the composition ratio of constituting materials, their placement, and the interfaces. In the history of biomaterial developments, the class of biomedical composites is relatively young. But its unmatched advantage in certain implants and medical devices makes this class of biomaterials desirable for applications ranging from orthopedics, dentistry, and drug delivery to frontiers such as cancer theragnostics.

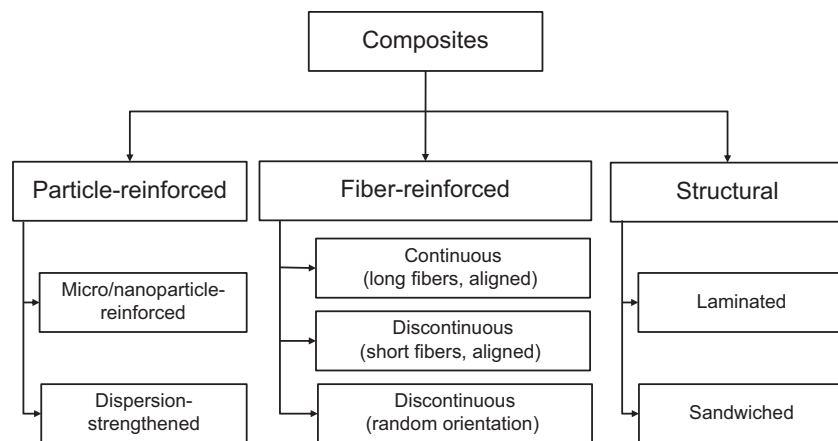
In a composite material, the component forming the major and continuous phase (>50% by volume, usually having relatively low stiffness and strength) is termed “matrix” and the component existing as a minor, discontinuous, and dispersed phase (<50% by volume, usually exhibiting relatively high stiffness and strength) is termed “reinforcement.” The boundary between matrix and reinforcement is the “interface.” Depending on the types of matrix materials, composites may be classified as polymer, metal, or ceramic matrix composites. Alternatively, composites are often categorized by the geometry of the reinforcement, for example, particle-reinforced composites, fiber-reinforced composites, and structural composites (Fig. 1.3.7.1). Generally, particle-reinforced composites use micro- or nanosized particles as reinforcements. In fiber-reinforced composites, fibrous reinforcements can be in a form of long continuous fibers either aligned or woven, or of short fibers either aligned or randomly oriented.

Fiber-reinforced composites generally exhibit significant improvements in stiffness and strength, which are required for load-bearing implants. For example, continuous carbon fiber (CF)-reinforced polymers have been explored as the stem of hip prosthesis. Mechanical properties of fibrous composites are highly related to the type, volume fraction, length, and orientation of fibers. Structural composites are laminates and sandwich panels. They are not often designed and studied for implants or medical devices. Like other biomaterials, biomedical composites can also be made as bioactive and biodegradable. Bioactivity here means the ability of the material to form a chemical (or physiological) bond with a tissue in a human body (typically, the bone). A bioactive composite must have at least one component (either matrix or reinforcement) that can bond to a tissue. A biodegradable composite can be totally degradable or partially degradable.

Matrix and Reinforcement in Composites

Matrix Materials

Because of the availability of many biomedical polymers, their good biocompatibility, excellent ductility and flexibility, low cost, and ease of fabrication into final products (as compared with metals and ceramics), polymer matrix composites are the most investigated biomedical composites. The polymer matrices have been mainly synthetic polymers, though natural polymers are making good inroads into composite development due to their own distinctive advantages. For synthetic polymers, polyethylene (PE), polypropylene, polyurethane (PU), poly(ethylene terephthalate) (PET), polytetrafluoroethylene (PTFE), poly(methyl methacrylate) (PMMA),



• **Figure 1.3.7.1** Classification of composites according to the geometry of reinforcements.

polycarbonate, polyetheretherketone (PEEK), polysulfone (PSU), and ultra-high molecular weight polyethylene (UHMWPE) have been used for biomedical composites for different applications. PTFE/PU artificial vascular grafts and UHMWPE tendon/ligament/joint substitutes are good examples. Moreover, biodegradable polymers such as poly(L-lactic acid) (PLLA), poly(lactic-co-glycolic acid) (PLGA), poly(ϵ -caprolactone) (PCL), and poly(3-hydroxybutyrate-co-3-hydroxyvalerate) (PHBV) are used as matrices for composites. An example is a PLLA-matrix bone fracture fixation plate. Natural polymers such as collagen, gelatin, hyaluronic acid, silk fibroin, chitosan, alginate, and PHBV are now frequently used for different biomedical devices because of their excellent biocompatibility. Hydrogels also find their way into composites. For example, poly(hydroxyethyl methacrylate) (PHEMA), poly(vinyl alcohol), poly(ethylene glycol), poly(acrylic acid), PMMA, and thermoresponsive poly(*N*-isopropylacrylamide), and natural polymers, such as collagen, gelatin, hyaluronic acid, and alginate, are now used to make nanocomposite hydrogels with improved mechanical properties and tailored functions such as desired physical, chemical, electrical, and biological properties. Even though there are many advantages for using polymers for biomedical composites, the low stiffness and strength and other properties (e.g., creep) of polymers have limited their scope for biomedical applications. There have also been investigations using metals or ceramics as matrices for biomedical composites. For example, a Ti-6Al-4V matrix with dispersed hydroxyapatite (HA) particles was made for potential load-bearing orthopedic applications. Ceramic matrix composites are investigated, in fact more often than metal matrix, for biomedical applications. One major effort in the field is the toughening of weak bioceramics (e.g., HA, $\text{Ca}_{10}(\text{PO}_4)_6(\text{OH})_2$) using biocompatible glasses. There is also the development of biphasic calcium phosphate, which is a physical mixture of HA and tricalcium phosphate (TCP, $\text{Ca}_3(\text{PO}_4)_2$) in different proportions. The biodegradation rate of this material can be controlled by varying the HA-to-TCP ratio, giving it an advantage for some clinical applications.

Reinforcements

To overcome some shortcomings of polymers, ceramics and metals in medical applications, hard bioceramic particles are often used for achieving different effects or properties such as strengthening, bioactivity, or wear resistance. They are usually dispersed in ductile matrices (commonly, polymers but sometimes metals). Mechanical and biological properties of particle-reinforced composites are significantly affected by the characteristics (e.g., type, composition, size, shape, etc.) of reinforcing particles. Decades ago, microparticles were the main particulate materials used for composites. With advances in nanotechnology, recent years have seen the surge of applying nanoparticles in composites, which can offer both mechanical and biological benefits. Bioactive bioceramic particles, such as HA, TCP, Bioglass, and apatite-wollastonite (A-W) glass-ceramic particles are used for making bone-mimicking bioactive composites for orthopedic and/or dental applications. Many micro- or nanoparticles are spherical in shape. But commercially available particulate calcium phosphates (e.g., HA and TCP) and Bioglass particles are usually irregularly shaped. Particulate reinforcements with irregular shapes are preferred for their surface to form a stable mechanical interlock with the matrix, whereas smooth-surfaced and spheroid-shaped particulate reinforcements are easily detached from the matrix when stressed in the absence of chemical bonding between the reinforcement and matrix. Apart from these particulate bioceramics, it has been shown that alumina particles can be mixed with dental resins for filling cavities in the teeth, with these alumina particles providing enhanced wear resistance for the dental filling. For “brittle” polymers such as PMMA, which is commonly used as bone cement in total hip replacement, toughening of the polymer is needed and hence in some investigations rubber particles are mixed with PMMA, resulting in a toughened bone cement.

Biomedical composites with fibrous reinforcements can provide much improved mechanical properties (modulus, strength, etc.), which are heavily influenced by the mechanical properties of the fibers used, fiber diameter, fiber volume fraction, aspect ratio (i.e., the fiber length-to-fiber diameter ratio) in the case of short fibers, etc. For continuous fiber-reinforced composites, long fibers are generally polymer

fibers or ceramic fibers. Polymer fibers often include Kevlar fibers, nylon fibers, PE fibers, PLLA fibers, PLGA fibers, PCL fibers, and more recently cellulose fibers. PLLA, PLGA, PCL, and cellulose fibers are very useful for developing biodegradable composites. Commonly used ceramic fibers for biomedical composites are the very fine carbon fibers (CFs) whose diameters are about 10 μm . These CFs possess high modulus (200–500 GPa) and high strength (over 2 GPa) and are also flexible. They can be braided with polymer fibers to form artificial ligaments/tendons. A common example is CF-reinforced PEEK or PSU for the stem of hip prostheses. Absorbable calcium phosphate or glass fibers have also been used to reinforce biodegradable polymers to make internal fracture fixation devices.

In manufacturing biomedical composites in a large quantity, producing particle-reinforced composites is the most economical, whereas fabricating long fiber-reinforced composites is the most time-consuming and expensive. When significant improvements in stiffness and strength are required for the materials and particle-reinforced composites cannot meet the requirements, short-fiber reinforced composites can fill this need. Depending on the manufacturing technology and processing parameters, the short fibers in composites can be either aligned or randomly oriented. Mechanical properties of composites reinforced by aligned short fibers are anisotropic, while randomly oriented fiber-reinforced composites appear to be nearly isotropic. The aspect ratio of short fibers significantly affects properties of the composite. Also, short fibers must be longer than a critical length to provide the desired reinforcing effect. Short fibers can be whiskers or chopped fibers cut from long fiber strands. Whiskers can be viewed as much elongated particulate materials and are produced by carefully controlling the synthesis parameters. They are generally thin single crystals of materials such as calcium phosphates, alumina, and silicon carbide and have nearly perfect crystalline structures. Therefore they possess extremely high stiffness, enabling significant mechanical property improvements for metal or ceramic matrices. Chopped CFs or polymer fibers can be used as reinforcements in polymer matrix composites. A few investigations have found chopped stainless-steel wires (which can be viewed as chopped fibers) useful in reinforcing and toughening bioactive HA or glass matrices.

Nonporous and Porous Composites

From a structure standpoint, biomedical composites can be either nonporous or porous (with pore sizes ranging from a few micrometers to hundreds of micrometers). Bulk, nonporous composites exhibit good structural integrity and normally possess required mechanical properties. They can be used for biomedical applications under high mechanical loading such as bone substitution and dental filling. For manufacturing these composites, various conventional technologies are available (Wang et al., 2019). For example, particle-reinforced polymer matrix composites can be conveniently and efficiently made using extrusion and injection molding. Ceramic matrix

composites can be produced using pressureless sintering, hot pressing, or hot-isostatic pressing. In comparison, a porous composite usually has a much lower strength than the nonporous composite of the same composition but has advantages such as light weight and high surface area-to-volume ratio. Porous biodegradable composites are now extensively investigated as novel tissue engineering scaffolds, which can provide microenvironments with suitable physical, chemical, and biological cues for living cells, leading to new tissue formation. The fabrication of porous polymer matrix composites can use solvent casting, freeze drying, electrospinning, 3D printing, etc. All these techniques can form porous composites with interconnected pores, which are essential for cell migration, cell–cell connection, and tissue formation and growth. The size of the interconnected pores in porous composites must be controlled and also tailored for different tissue engineering applications. Porosity is another important parameter that must be controlled for porous composites as tissue engineering requires high porosity in scaffolds. A balance then needs to be struck to achieve high porosity while maintaining sufficient mechanical strength for the porous structures.

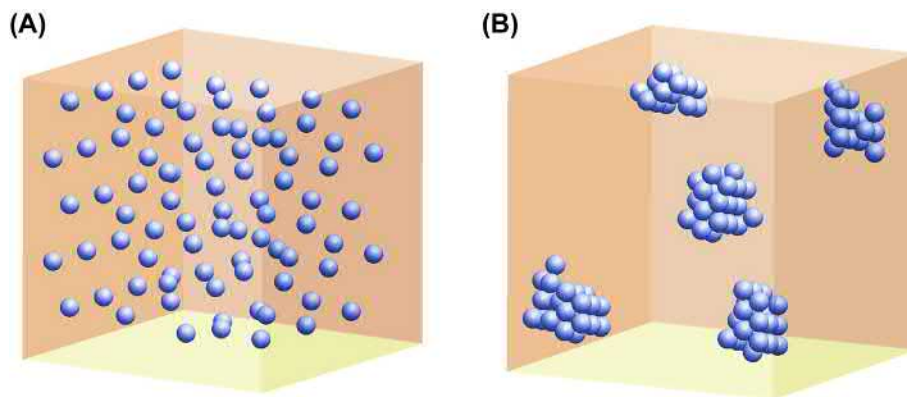
Properties of Composites

Major Influencing Factors

Properties (physical, structural, mechanical, electrical, biological, etc.) of composites can be affected by many factors. The major influencing factors for biomedical composites include:

1. matrix property (the average molecular weight of a polymer, average grain size of a metal or ceramic, strength, stiffness and ductility of the material, etc.);
2. stability or biodegradability of the matrix or reinforcement;
3. bioactivity of the reinforcement or matrix;
4. reinforcement shape, size, and size distribution;
5. reinforcement property (strength, stiffness, ductility, etc.) and volume percentage in the composite;
6. distribution (and orientation) of the reinforcement in the composite;
7. reinforcement–matrix interfacial state.

Biomedical composites have gone through different stages of development from nonporous biostable composites to nonporous biodegradable composites to porous tissue engineering scaffolds. Biodegradable materials, including biodegradable polymers such as PLLA, PLGA, PCL, collagen, chitosan, and alginate, and biodegradable ceramics such as TCP and a few bioactive glasses are increasingly used for biomedical composites. The bioactivity of composites is usually achieved by the incorporation of bioactive bioceramics (HA, TCP, Bioglass, etc.) in composites. To achieve enhanced tissue repair or regeneration, bioactive molecules such as growth factors can be encapsulated in biodegradable composites, which are released later *in vivo* in a controlled manner. To combat bacterial infection, antibiotics can be incorporated in biodegradable composites for their later release. The manufacture of biodegradable composites and composites containing biomolecules or drugs



• **Figure 1.3.7.2** Schematic 3D views of dispersion and distribution of particulate reinforcements in composites: (A) ideal dispersion and distribution of the particles; (B) particles existing as aggregates in composites.

can be a challenge and hence different fabrication techniques are needed for achieving the optimal outcome.

Geometry and Size of the Dispersed Phase and Its Distribution in Composite

For a particle-reinforced composite, the geometry and size of particles are important in determining composite properties such as mechanical properties. Particle dispersion and distribution in a composite play a critical role in determining composite properties. To form high-quality and high-performance particulate bioceramic–polymer composites, the particle agglomerates or aggregates must be broken down during composite processing into primary particles (i.e., the smallest particulate pieces of the minor component existing in as-fabricated or as-received ceramic powder), which show sufficient dispersion and reasonable distribution in the polymer matrix (Fig. 1.3.7.2A). Dispersing particles from the condensed state only to the aggregate state (Fig. 1.3.7.2B) is not adequate as the particle contacting points in aggregates will provide crack initiation sites or act to enhance crack propagation, thus causing premature failure of the composite when the composite is under mechanical stresses. Ideally, particles present in the composite should be in a dispersed state. Therefore specially designed processing equipment and/or good fabrication procedures are often required, which produces shear forces large enough to overcome various particle adhesion forces during composite processing so that particle agglomerates or aggregates can be reduced to primary particles and primary particles can be evenly distributed in the composite. Generally, there is a critical amount of particulate reinforcement for the composite, only above which desired properties can be obtained for the composite. In such a situation of highly filled polymers, processing of the composites becomes a challenge, sometimes insurmountable. Surface treatment of bioceramic particles may ease processing difficulties but may not necessarily lead to enhanced particle dispersion.

Fiber Arrangement

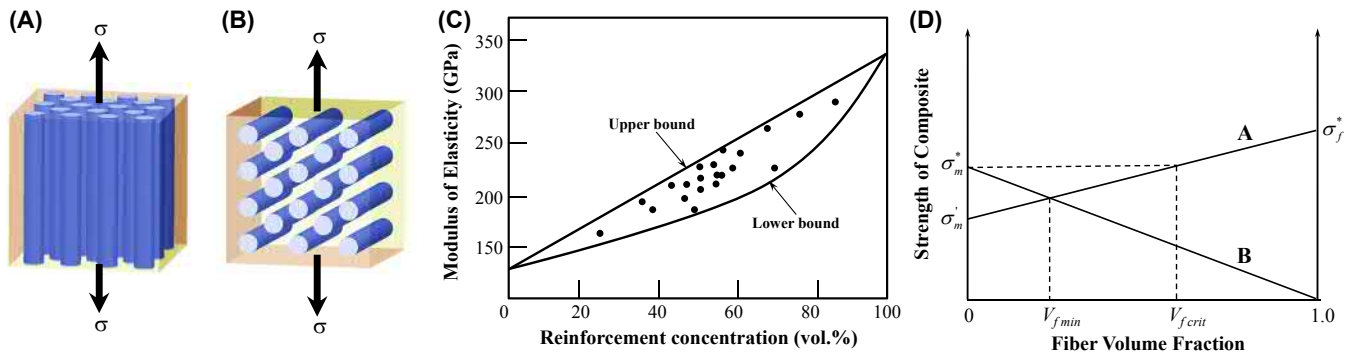
For long-fiber composites, fiber arrangement such as fiber orientation, fiber stacking pattern, and the angle and

packing sequence of fiber-reinforced sheets is a critical factor affecting the performance of long-fiber reinforced composites. For short-fiber composites, the fiber length, aspect ratio, and fiber orientation are key influencing factors. While the fiber length affects the load transfer between short fibers and the matrix locally, fiber orientation affects the macroscopic properties of the composite. The random orientation or alignment in one direction of short fibers in composites results in isotropic or anisotropic materials. However, isotropic short-fiber composites (i.e., those with randomly oriented short fibers) can become “anisotropic” upon unidirectional tension when the fibers are “forced” aligned to some extent due to the effect of the elongational flow.

For uniaxial long-fiber composites, the fiber-stacking pattern is an important factor that influences their mechanical properties as the interfiber spacing is varied by different fiber stacking arrangements. For example, in a cross-sectional view, fibers can be arranged in a hexagonal pattern or square array. For other fibrous composites, woven, braided, and knitted fiber arrays are used, which affect macroscopic properties of the composites because different texture patterns result in distinct fiber arrangements. In structural composites, laminates are formed by the sequential stacking of continuous and aligned long-fiber composite ply sheets. Therefore the angle and the sequence for stacking sheets must be carefully considered. Each of the unidirectional sheets is stacked according to a certain sequence and with a certain angle by design to produce the composite to meet the requirements for specific anisotropic mechanical properties in the targeted composite applications. Because this laminate class of composites is rarely used in the biomedical field, we intentionally leave it out, since it would take a whole chapter to discuss it at a level to benefit readers. We therefore encourage readers to consult other books on this specific subject should such a need occur.

Interfaces in Composites

The interface between the reinforcement and matrix in a composite is governed by the bonding mechanism(s) involved, which in turn strongly affects the properties of



• **Figure 1.3.7.3** Two simple models for long-fiber reinforced composites: (A) Voigt model; (B) Reuss model. Upper and lower bounds of composite modulus of elasticity as a function of fiber volume fraction (C). Longitudinal tensile strength of long-fiber composites as a function of fiber volume fraction (D), where σ_m^* = strength of the matrix, σ_f^* = strength of the fiber, and σ_m^* = strength of the matrix at the fiber fracture strain.

the composite. Normally, a strong interface results in a high strength but a low toughness of the composite. Conversely, a weak interface leads to a composite with a low strength but a relatively high toughness. There are different bonding mechanisms at the interface, from physical or mechanical bonds to chemical bonds. The interface formed by chemical bonding is several orders of magnitude stronger than that by physical bonding. However, chemical bonding, in which the reinforcement chemically reacts with the matrix at the interface, is generally avoided for biomedical composites due to biocompatibility concerns of these composites. Therefore most composite interfaces rely on physical bonding, including mechanical interlocking, electrostatic attraction, cation–anionic interaction, and molecular entanglement following interdiffusion at the interface. Consequently, surface features and properties (surface topography, surface electric charge, surface energy, etc.) of reinforcements and matrices are highly important for interfacial bonding.

Mechanical Properties of Composites

Tensile Properties of Fibrous Composites

The mechanics of composites have been well established. The micromechanics of long-fiber reinforced composites can be dealt with by using relatively simple models with simplified assumptions. In determining the elastic properties (e.g., Young's modulus) of unidirectional fibrous composites, it is often assumed that (1) the fiber and matrix have different elastic moduli but identical Poisson's ratio, (2) fibers are perfectly aligned, (3) fibers and matrix are perfectly bonded, and (4) initially, there are neither voids nor internal stresses in the composite.

There are two distinct limiting cases on the elastic properties of long-fiber composites. The first case possesses the upper limit for the modulus of the composites. It is when the composite is stretched along the fibers' axis as illustrated in Fig. 1.3.7.3A for a two-component composite (a matrix with only one type of fibers as the reinforcement), and the

following equation can be deduced for the modulus using the concept of a Voigt model:

$$E_c = E_f \cdot V_f + E_m \cdot V_m \quad (1.3.7.1)$$

where E_c , E_f and E_m are elastic moduli of the composite, reinforcing fiber, and matrix, respectively, and V_f and V_m are volume fractions of the fiber and matrix, respectively. The second case is when a tensile force is applied perpendicular to the fibers' axis in the two-component composite, as shown in Fig. 1.3.7.3B, and for this situation the following equation is deduced based on the concept of a Reuss model, giving the lower bound:

$$1/E_c = E_f/V_f + E_m/V_m \quad (1.3.7.2)$$

While neither of these models is rigorously correct, the two models do provide the upper and lower bounds, respectively, for the Young's modulus of a long-fiber reinforced composite (Fig. 1.3.7.3C). When the moduli of the reinforcement and matrix differ by no more than a factor of two or three, the simple linear superimposition of Voigt and Reuss values provides a good approximation. When the Poisson's ratios of the reinforcement and matrix are not equal, a correction term needs to be introduced into the equations.

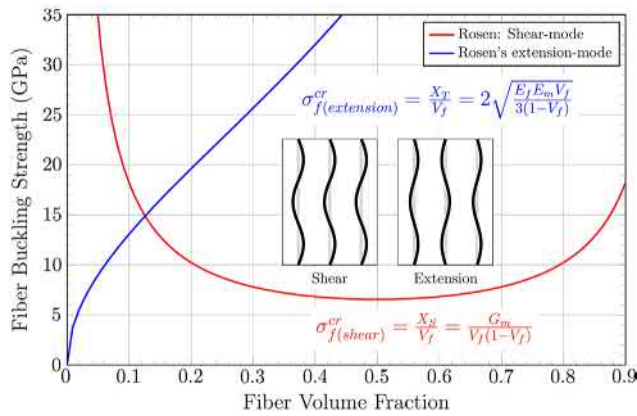
Using the Voigt model, the longitudinal strength of the composite can be deduced:

$$\sigma_c = \sigma_f \cdot V_f + \sigma_m \cdot V_m \quad (1.3.7.3)$$

where σ_c , σ_f and σ_m are the strength of the composite, reinforcing fiber, and matrix, respectively assuming that (1) all fibers have equal strength, (2) both matrix and fibers exhibit linear elastic behavior up to failure, and (3) there is equal longitudinal strain in the composite, fibers, and matrix.

When the fiber failure strain is smaller than that of the matrix, for fibrous composites to achieve the reinforcing effect of fibers, the fiber volume fraction must exceed a critical value $V_{f,crit}$ as illustrated in Fig. 1.3.7.3D. For short-fiber composites, the critical fiber length l_c is

$$l_c = \sigma_f^* \tau / \tau \quad (1.3.7.4)$$



• **Figure 1.3.7.4** Variation of fiber compressive strength with volume fraction when undergoing microbuckling in a uniaxial composite as predicted by Rosen's model.

where σ_f^* , r , and τ are fiber fracture strength, fiber radius, and interfacial shear strength, respectively.

Compressive Properties of Fibrous (CF/PEEK) Composites: A New Perspective

Rosen's Microbuckling Model and the Contradictions

The compressive behavior of uniaxial long-fiber composites has been the subject of many investigations since the development of these materials. Many factors, including manufacturing processes, material constituent properties, specimen geometry, method of load introduction, fiber orientation and waviness, voids, and stress concentration, have all been shown to play a role in affecting the predominant mode of compressive failure. The failure mode includes global Euler buckling, microbuckling, transverse tension, fiber kinking, and fiber or matrix delamination, among others. One of the first analytical models predicting the compressive strength of such composites through addressing fiber microbuckling was presented by Rosen (1965). Using a 2D model, Rosen suggested that compressive failure for a uniaxial composite material occurs when the fibers buckle into either an extension mode or a shear mode. In the extension mode, the deformation of the matrix material between fibers was solely by extension or compression in a direction perpendicular to the fibers. In the shear mode, pure shear deformation was considered to occur in the matrix material between fibers. Fig. 1.3.7.4 shows the variation of fiber buckling strength based on Rosen's equations as a function of fiber volume fraction (V_f) for a CF/PEEK uniaxial composite, where X_T and X_S are composite compressive strength in the extension and shear mode, respectively, and σ_f^{cr} represents the corresponding buckling strength of a fiber.

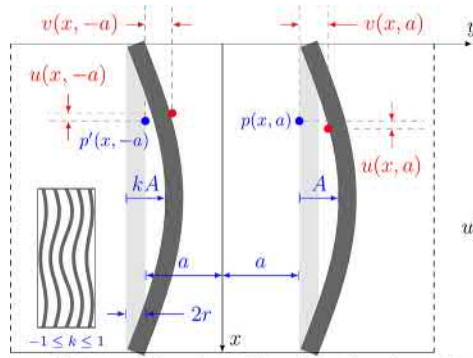
The curves exhibit two different trends for the shear and extension modes. Rosen argued that the likely failure

mode for such a composite is the one that exhibits a lower strength value, hence the conclusion that the shear mode will prevail when V_f is high and the extension mode when V_f is low. This was the prevailing knowledge for predicting the microbuckling behavior for uniaxial composites for many decades. However, a close inspection reveals a contradiction when V_f becomes very small: the diverged fiber-buckling strength values in the shear and extension modes when V_f becomes very small. It does not make any sense because as $V_f \rightarrow 0$, fibers in both the extension and shear mode cases will be located far away from each other, such that they could be regarded as individual ones. So, a converged, not a diverged, result should be expected. Another issue is that the theoretical predicted strength values are much higher than the experimentally observed values. Moreover, in a uniaxial composite with fiber volume fraction in the range of 55%–60%, shear mode long wavelength microbuckling is predicted, but experimentally, short wavelength fiber kinking is typically observed as the compressive failure mode.

A First-Principles-Based Compressive Microbuckling Model

Zhang and Latour (1994) used the first-principles approach to reexamine the microbuckling problem of uniaxial fibrous composites and developed an analytical model based on the theory of elasticity. Unlike in Rosen's model, where only extension deformation of the matrix was considered in the extension mode, and shear deformation was considered in the shear mode, this elasticity-based analytical model accounts for both the shear and normal interfacial stresses because of fiber and matrix deformation and establishes relationships between microbuckling strength, microbuckling wavelength, fiber volume fraction, and interfacial stresses, among others. Here we briefly discuss the important aspects of this new model.

Deformations in fibers and matrix: A 2D unidirectional composite model with a unit thickness under uniform compression is considered as depicted on the left in Fig. 1.3.7.5. Fibers are assumed to have a width of $2r$ and placed at a distance $2a$ apart from each other. When this uniaxial composite is subject to compressive loading, fibers are assumed to undergo in-plane microbuckling in the Cartesian xy -coordinate system. When microbuckling of fibers occurs, each fiber is assumed to deform in a sinusoidal pattern: $Y = A \sin \alpha x$. For considering a general case, it is assumed that neighboring fibers can undergo microbuckling with different amplitudes. For example, for the two fibers shown in Fig. 1.3.7.5, one is assumed to deform in a sinusoidal pattern with amplitude A , and the other kA , where k is an interaction coefficient varying from -1 to 1 ($-1 \leq k \leq 1$). When $k = 1$, the situation reduces to Rosen's shear mode, and when $k = -1$, it becomes Rosen's extension mode. This general consideration can be termed the k -mode of microbuckling.



• **Figure 1.3.7.5** A 2D uniaxial composite undergoing microbuckling, along with a list of equations describing the deformations of fibers and matrix, the constitutive relations, the induced stresses and strains, and an Airy stress function.

In the sinusoidal expression ($Y = kA \sin \alpha x$), α is a microbuckling parameter expressed as $m\pi/L = \pi/l_0$, where L is the length of fibers, m is the buckling wave number, and l_0 is the microbuckling wavelength. To consider the deformations in the fibers, matrix, and at the interfaces, the displacements of two arbitrary points, $p(x, a)$ and $p'(x, -a)$, are considered. With the sinusoidal expression for fiber microbuckling, the displacement components in the x and y directions of the points p and p' , namely, $u(x, a)$, $v(x, a)$, $u(x, -a)$, and $v(x, -a)$, are expressed as given in the equation list on the right in Fig. 1.3.7.5.

The matrix is considered as an isotropic linear elastic medium. The deformation of the matrix is caused by the microbuckling deformation of the fibers, assuming the fibers and matrix to be perfectly bonded. Due to the 2D consideration, the matrix deformation problems can be treated as a plane-stress problem, for which an Airy stress function Φ (given at the bottom of Fig. 1.3.7.5) satisfying the biharmonic equation (given at the top of the equation list in Fig. 1.3.7.5) is used. With the selected Airy stress function, in which c_1 through c_4 are constants to be determined, the stresses in the matrix (σ_x , σ_y , τ_{xy}) are derived as:

$$\begin{aligned} \sigma_x &= \sin \alpha x \begin{bmatrix} c_1 \alpha^2 \cosh \alpha y + c_2 \alpha^2 \sinh \alpha y + c_3 \alpha \\ (2 \sinh \alpha y + \alpha y \cosh \alpha y) + c_4 \alpha \\ (2 \cosh \alpha y + \alpha y \sinh \alpha y) \end{bmatrix} \\ \sigma_y &= -\sin \alpha x \begin{bmatrix} c_1 \alpha^2 \cosh \alpha y + c_2 \alpha^2 \sinh \alpha y + \\ c_3 \alpha^2 y \cosh \alpha y + c_4 \alpha^2 y \sinh \alpha y \end{bmatrix} \\ \tau_{xy} &= -\alpha \cos \alpha x \begin{bmatrix} c_1 \alpha \sinh \alpha y + c_2 \alpha \cosh \alpha y + c_3 \\ (\cosh \alpha y + \alpha y \sinh \alpha y) + c_4 \\ (\sinh \alpha y + \alpha y \cosh \alpha y) \end{bmatrix} \end{aligned} \quad (1.3.7.5)$$

Through the stress-strain relationships and the strain-displacement expressions listed in Fig. 1.3.7.5, the displacement fields of the matrix, $u(x, y)$ and $v(x, y)$, are solved as follows, where E_m is the matrix Young's modulus and ν_m is the matrix Poisson's ratio:

$$\frac{\partial^4 \Phi}{\partial x^4} + 2 \frac{\partial^4 \Phi}{\partial x^2 \partial y^2} + \frac{\partial^4 \Phi}{\partial y^4} = 0$$

$$\sigma_x = \frac{\partial^2 \Phi}{\partial y^2}, \quad \sigma_y = \frac{\partial^2 \Phi}{\partial x^2}, \quad \tau_{xy} = -\frac{\partial^2 \Phi}{\partial x \partial y}$$

$$Y = A \sin \alpha x, \quad \alpha = \frac{m\pi}{L} = \frac{\pi}{l_0}$$

$$u(x, a) = A \alpha r \cos \alpha x, \quad v(x, a) = A \sin \alpha x$$

$$u(x, -a) = -kA \alpha r \cos \alpha x, \quad v(x, -a) = kA \sin \alpha x$$

$$\epsilon_x = \frac{1}{E_m} (\sigma_x - \nu_m \sigma_y), \quad \epsilon_y = \frac{1}{E_m} (\sigma_y - \nu_m \sigma_x)$$

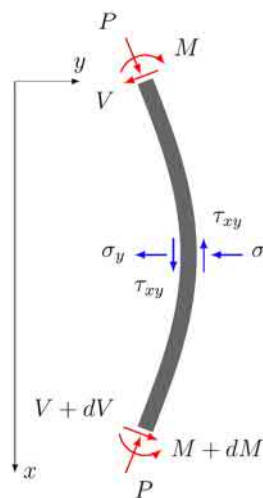
$$\epsilon_x = \frac{\partial u}{\partial x}, \quad \epsilon_y = \frac{\partial v}{\partial y}, \quad \gamma_{xy} = \frac{\partial u}{\partial y} + \frac{\partial v}{\partial x}$$

$$\begin{aligned} u(x, y) &= -\frac{(1 + \nu_m) \cos \alpha x}{E_m} \\ &\left\{ c_1 \alpha \cosh \alpha y + c_2 \alpha \sinh \alpha y \right. \\ &\left. + c_3 \left[\frac{2}{1 + \nu_m} \sinh \alpha y + \alpha y \cosh \alpha y \right] \right. \\ &\left. + c_4 \left[\frac{2}{1 + \nu_m} \cosh \alpha y + \alpha y \sinh \alpha y \right] \right\} \end{aligned} \quad (1.3.7.6)$$

$$\begin{aligned} v(x, y) &= -\frac{(1 + \nu_m) \sin \alpha x}{E_m} \\ &\left\{ c_1 \alpha \sinh \alpha y + c_2 \alpha \cosh \alpha y \right. \\ &\left. + c_3 \left[\alpha y \sinh \alpha y - \frac{1 - \nu_m}{1 + \nu_m} \cosh \alpha y \right] \right. \\ &\left. + c_4 \left[\alpha y \cosh \alpha y - \frac{1 - \nu_m}{1 + \nu_m} \sinh \alpha y \right] \right\} \end{aligned}$$

Applying Eq. (1.3.7.6) to the four displacement expressions given in Fig. 1.3.7.5 for $u(x, a)$, $v(x, a)$, $u(x, -a)$, and $v(x, -a)$, we find the four unknown constants as

$$\begin{aligned} c_1 &= (1 - k) \frac{E_m A \{ [2 - \alpha \alpha^2 r (1 + \nu_m)] \cosh \alpha a + [\alpha \alpha (1 + \nu_m) + (1 - \nu_m) \alpha r] \sinh \alpha a \}}{\alpha (1 + \nu_m) [2 \alpha \alpha (1 + \nu_m) - (3 - \nu_m) \sinh 2 \alpha a]} \\ c_2 &= -(1 + k) \frac{E_m A \{ [2 - \alpha \alpha^2 r (1 + \nu_m)] \sinh \alpha a + [\alpha \alpha (1 + \nu_m) + (1 - \nu_m) \alpha r] \cosh \alpha a \}}{\alpha (1 + \nu_m) [2 \alpha \alpha (1 + \nu_m) + (3 - \nu_m) \sinh 2 \alpha a]} \\ c_3 &= (1 + k) \frac{E_m A (\sinh \alpha a - \alpha r \cosh \alpha a)}{2 \alpha \alpha (1 + \nu_m) + (3 - \nu_m) \sinh 2 \alpha a} \\ c_4 &= -(1 - k) \frac{E_m A (\cosh \alpha a - \alpha r \sinh \alpha a)}{2 \alpha \alpha (1 + \nu_m) - (3 - \nu_m) \sinh 2 \alpha a} \end{aligned} \quad (1.3.7.7)$$



$$E_f I \frac{d^4 Y}{dx^4} - 2r \frac{d\tau_{xy}}{dx} + 2\sigma_y + P \frac{d^2 Y}{dx^2} = 0$$

$$\sum F_y = 0 : \frac{dV}{dx} - 2\sigma_y - P \frac{d^2 Y}{dx^2} = 0; \quad \sum M = 0 : \frac{dM}{dx} + 2r\tau_{xy} - V = 0$$

$$M = -E_f I \frac{d^2 Y}{dx^2}, \quad I = \frac{2r^3}{3}, \quad \sigma_f = \frac{P}{2r}, \quad \beta = \frac{a}{r} = \frac{1}{V_f} - 1, \quad t = \alpha r, \quad a\alpha = \beta t$$

$$\sigma_y = E_m A \alpha f_1 \sin \alpha x, \quad \tau_{xy} = E_m A \alpha f_2 \cos \alpha x$$

$$f_1 = (1+k) \frac{(1+\nu_m)\beta t^2 + (1-\nu_m)t \sinh \beta t \cosh \beta t + 2 \sinh^2 \beta t}{(1+\nu_m)[2\beta t(1+\nu_m) + (3-\nu_m) \sinh 2\beta t]} + (1-k) \frac{(1+\nu_m)\beta t^2 - (1-\nu_m)t \sinh \beta t \cosh \beta t - 2 \cosh^2 \beta t}{(1+\nu_m)[2\beta t(1+\nu_m) - (3-\nu_m) \sinh 2\beta t]}$$

$$f_2 = (1+k) \frac{(1+\nu_m)\beta t + (1-\nu_m) \sinh \beta t \cosh \beta t + 2t \cosh^2 \beta t}{(1+\nu_m)[2\beta t(1+\nu_m) + (3-\nu_m) \sinh 2\beta t]} + (1-k) \frac{(1+\nu_m)\beta t - (1-\nu_m) \sinh \beta t \cosh \beta t - 2t \sinh^2 \beta t}{(1+\nu_m)[2\beta t(1+\nu_m) - (3-\nu_m) \sinh 2\beta t]}$$

• **Figure 1.3.7.6** A free-body diagram of a fiber segment undergoing microbuckling, along with a list of equations describing the governing equilibrium equations and interfacial stresses.

Plugging Eq. (1.3.7.7) into Eq. (1.3.7.5) along with letting $y = a$, or $y = -a$, we arrive at the expressions for the normal and shear interfacial stresses as listed in Fig. 1.3.7.6.

Fiber equilibrium equation: Fibers are considered as elastic beams supported by a surrounding elastic matrix. A free-body diagram of a fiber segment is shown on the left in Fig. 1.3.7.6, where P is the applied longitudinal compressive force, M is the bending moment in the fiber, V is the transverse shear force, and σ_y and τ_{xy} are the interfacial normal and shear stresses, respectively, acting on the fiber surface.

From the force and moment equilibrium equations, namely $\sum F_y = 0$ and $\sum M = 0$, the governing equivalent equation for the fiber is derived as given at the top of the equation list on the right in Fig. 1.3.7.6, in which E_f is the fiber axial Young’s modulus and I is the fiber’s area moment of inertia.

By substituting the interfacial stresses into the microbuckling governing equation along with the following expressions: $I = 2r^3/3$, $P = 2r\sigma_f$, $\beta = ar = (1/V_f - 1)$, $t = \alpha r$, and $a\alpha = \beta t$, the compressive stress in a fiber is derived as a function of E_f , E_m , ν_m , k , β , and t , as follows:

$$\sigma_f = \frac{E_f t^2}{3} + (1+k) E_m \frac{2\beta t(1+\nu_m) + (1-\nu_m) \sinh 2\beta t + \frac{2 \sinh^2 \beta t}{t} + 2t \cosh^2 \beta t}{(1+\nu_m)[2\beta t(1+\nu_m) + (3-\nu_m) \sinh 2\beta t]} + (1-k) E_m \frac{2\beta t(1+\nu_m) - (1-\nu_m) \sinh 2\beta t - \frac{2 \cosh^2 \beta t}{t} - 2t \sinh^2 \beta t}{(1+\nu_m)[2\beta t(1+\nu_m) - (3-\nu_m) \sinh 2\beta t]} \quad (1.3.7.8)$$

TABLE 1.3.7.1 Material Properties of CF/PEEK and CF/PSF Composite Systems

Young’s modulus for AS4 fibers (E_f , GPa)	248.0
Young’s modulus for PEEK matrix (E_m , GPa)	4.646
Radius of AS4 fibers (r , μm)	3.5
Poisson’s ratio for PEEK matrix (ν_m)	0.42

CF/PEEK, Carbon fiber/polyetheretherketone; CF/PSF, carbon fiber/poly(sulfone)

For the two particular cases, the shear mode of the microbuckling case can be obtained by letting $k = 1$, and the extension mode with $k = -1$. The critical compressive strength for a fiber (σ_f^{cr}) is obtained by finding the minimum value of σ_f with respect to t for a given set of E_f , E_m , ν_m , k , and β values, as

$$\sigma_f^{cr} = \sigma_f(t = t_{cr}); \quad \text{when } \left. \frac{\partial \sigma_f}{\partial t} \right|_{t=t_{cr}} = 0 \quad \text{and} \quad \left. \frac{\partial^2 \sigma_f}{\partial t^2} \right|_{t=t_{cr}} > 0 \quad (1.3.7.9)$$

The associated microbuckling wavelength, normalized by the fiber diameter, is then determined as

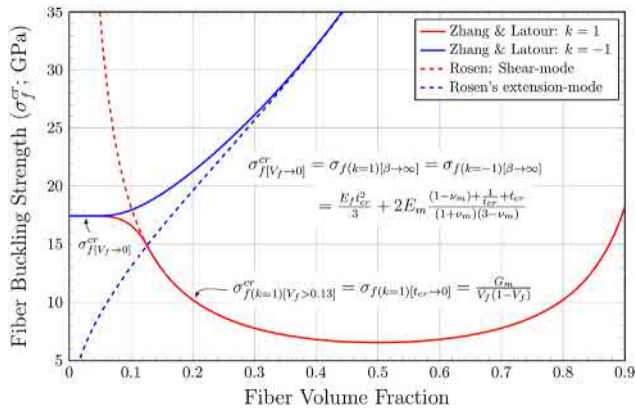
$$l_r = \frac{l_0}{2r} = \frac{\pi r}{2rt_{cr}} = \frac{\pi}{2t_{cr}} \quad (1.3.7.10)$$

Selected Results

To illustrate the results as predicted by this first-principle-based analytical model, we consider an example case using the material properties of an AS4 (CF/PEEK composite (Table 1.3.7.1).

Fiber critical compressive strength: Fig. 1.3.7.7 plots the variation of fiber critical compressive strength (or fiber buckling strength), σ_f^c , with V_f for the CF/PEEK composite. The results of the $k=1$ and $k=-1$ cases are compared with those of Rosen's shear and extension modes. An excellent agreement exists between the two corresponding curves at high V_f but agreement is not found at low V_f . In Zhang and Latour's model, however, when $V_f \rightarrow 0$, both the $k=1$ and $k=-1$ cases converge to a single value for the fiber buckling strength. The equation given in the inset, $\sigma_f^c|_{V_f \rightarrow 0}$, provides the analytical expression for this converged buckling strength. The convergence predicted here makes perfect sense because as $V_f \rightarrow 0$, fibers in both cases will be located far away from one another such that they will deform individually as in a single fiber composite.

Fiber-matrix interfacial stresses: This result sheds some important light on the contradiction in Rosen's model, whereas diverged strength values are predicted for the shear and extension modes when V_f becomes very small. It is known that in Rosen's model, only the matrix transverse deformation is considered in the extension mode (which



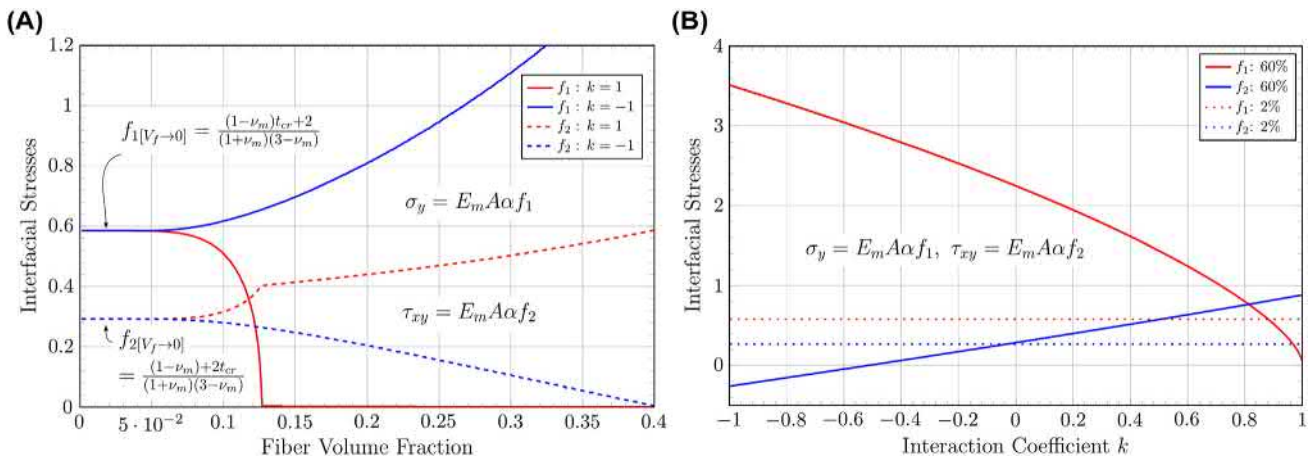
• **Figure 1.3.7.7** Variation of fiber compressive strength with volume fraction in a uniaxial carbon fiber/polyetheretherketone composite due to fiber microbuckling.

accounts only for the interfacial normal stresses) and the shear deformation is considered in the shear mode (which accounts only for the interfacial shear stresses). In this first-principle-based model, all interfacial stresses resulting from fiber microbuckling deformation are inherently considered because of the use of Airy stress function. To show these stresses, their magnitude (note that σ_{y-max} occurs at $\sin \alpha x = 1$, and τ_{xy-max} at $\cos \alpha x = 1$) normalized by $E_m A \alpha$ are determined and presented in Fig. 1.3.7.8A as a function of V_f .

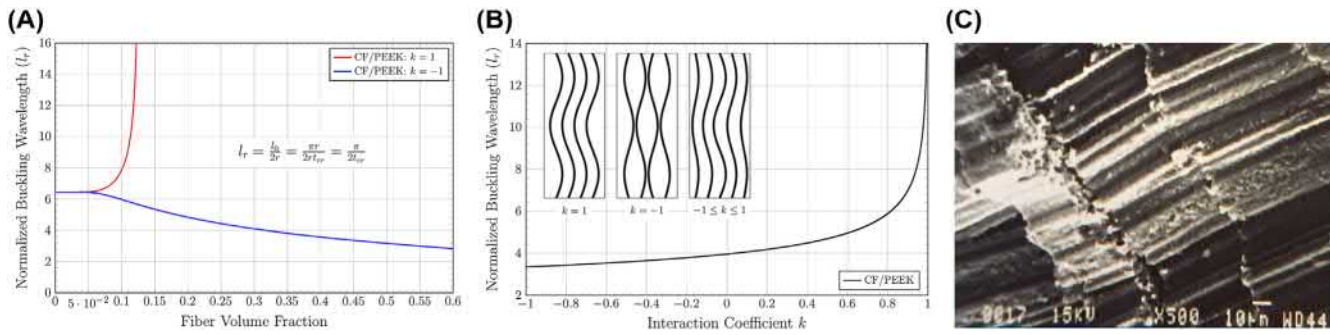
In the $k=1$ case, the normal stress (red solid line) drops quickly to zero as V_f increases from 0 to approximately 0.13, and in the $k=-1$ case, the shear stress (blue dashed line) decreases gradually with increasing V_f . These facts suggest that the contributions of normal stress in the shear mode ($k=1$) and the shear stress in the extension mode ($k=-1$) are only negligible when V_f is high, but they cannot be neglected when V_f is low. That these stresses are not accounted for in Rosen's model provides a reasonable explanation why good agreement is seen between the corresponding results when V_f is high and no agreement was seen at low V_f .

In Fig. 1.3.7.8A it is seen that for the case of $k=1$, both σ_y and τ_{xy} (red solid and dashed lines) curves exhibit a sharp transition at around $V_f = 0.13$, marking a change in fiber microbuckling deformation from short to long wavelength buckling. Moreover, when $V_f \rightarrow 0$, both the $k=1$ and $k=-1$ cases see the same normal and shear stresses, confirming that in both situations fibers deform individually with the same support from the matrix, thereby yielding the same buckling deformation.

Fig. 1.3.7.8B looks at the variation of the normal and shear stresses with k when $V_f = 2\%$ and 60% . When $V_f = 2\%$, both stresses remain constant and they do not change with k . This result provides yet another confirmation that when V_f is very low, all fibers in the composite will deform individually, independent of what the value of k is. When $V_f = 60\%$, the normal stress (red solid line) decreases from a high value at $k=-1$ to zero at $k=1$, while the shear stress



• **Figure 1.3.7.8** Variation of normal and shear interfacial stresses with fiber volume fraction (A), and variation of normal and shear interfacial stresses with interaction coefficient at $V_f = 2\%$ and 60% (B).



• **Figure 1.3.7.9** Variation of normalized microbuckling wavelength with fiber volume fraction (A), and variation of normalized microbuckling wavelength with interaction coefficient (B). A scanning electron microscopy image of a fractured surface of a uniaxial carbon fiber/polyetheretherketone (CF/PEEK) composite ($V_f=60\%$) tested under compression (C).

(blue solid line) increases from a slightly negative value at $k=-1$ to a positive value at $k=1$. With this insight in mind, we can be certain that the $k=1$ case always produces a lower σ_c^{cr} value, except for the condition of $V_f < 0.05$, in which case both the $k=1$ and $k=-1$ cases converge to the case of individual fibers surrounded by an infinitely wide matrix.

Microbuckling wavelength: Fig. 1.3.7.9A shows the variation of l_r with V_f . When $V_f < 0.05$, l_r is approximately 6.4 for the CF/PEEK composite for both the $k=1$ and $k=-1$ cases. When $V_f > 0.05$, l_r for the $k=1$ case increases rapidly toward infinity, and l_r for the $k=-1$ case decreases gradually from ~ 6.4 to ~ 3 . Fig. 1.3.7.9B shows the variation of l_r with k (at $V_f=0.6$). Clearly, l_r increases gradually as k increases, but it goes rapidly to infinity as k approaches 1. With a decrease in k value of only 0.1%, i.e., $k=0.999$, the predicted l_r will take a value of ~ 13 , which falls within the range for experimentally observed microbuckling wavelength, as confirmed by the scanning electron microscopy image of a compressively fractured surface of a uniaxial CF/PEEK composite (Zhang et al., 1996) shown in Fig. 1.3.7.9C. This fracture surface shows that fibers do appear to break due to short wavelength ($3 < l_r < 13$) buckling or kinking, supporting the argument for a k mode microbuckling with k being close to, but not equal to, 1.

Contrary to Rosen's predictions, it is shown that shear mode is always the preferred microbuckling mode, except for the case where fibers perform individually in a single fiber composite. Based on the k -mode concept, a short microbuckling wavelength is predicted to occur in uniaxial fibrous composites because fibers in these composites will always have some degree of imperfection in their alignment (with k being close to but equal to 1). Regarding the resulting interfacial stresses, a k value less than 1.0 would lead to an increase in the normal stress and a decrease in shear stress. This result likely suggests that the combined effect of fiber misalignment, interfacial debonding, and matrix yielding would be responsible for the failure of uniaxial composites, thereby resulting in a lower than predicted experimental compressive strength. Hahn and Williams (1986) demonstrated that fiber misalignment did have a significant effect on the compressive

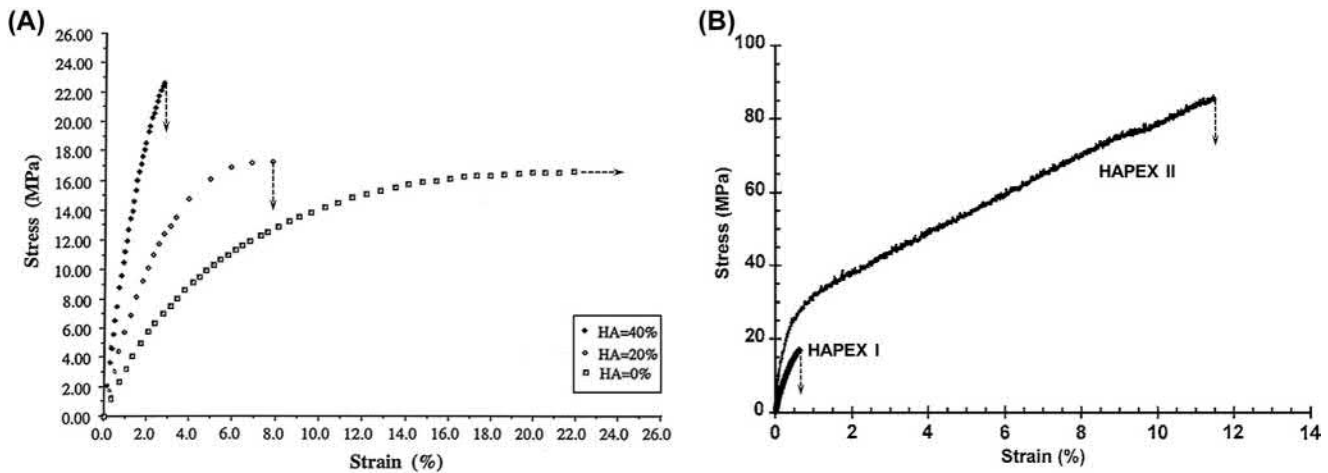
strength of uniaxial composites. In addition, interfacial bond strength, void content, and matrix nonlinearity have also been recognized as factors influencing compressive strength (Zhang and Latour, 1994).

Medical Applications of Composites

Biomedical Composites in Orthopedic Applications

Biomedical composites have been investigated for different orthopedic applications, including bone fracture fixation devices (internal or external fixation), biodegradable bone screws, bone filling and grafting, total hip replacement, and repair of ruptured tendon or ligament. One of the earliest investigations was the use of CF to reinforce an epoxy resin in an attempt to solve the stress-shielding problem under metal fracture fixation plates. The Young's modulus of these composite plates could be tailored to approach that of cortical bone but there were other problems in the clinical application of these fixation plates.

Subsequent work in this area by other researchers looked into other nonbiodegradable composites such as CF/PEEK. This composite has been extensively used in various orthopedic applications. Brantigan et al. (1993) demonstrated successful radiographic results after 2 years when CF/PEEK implant cages were used for posterior lumbar interbody fusion. Clinically, 20 out of 26 patients were categorized as either excellent or good. Only two patients were considered to have poor results, but the reasons were not related to the material. CF/PEEK interbody cages were also used for the treatment of degenerative lumbar spine disorders and successful clinical as well as radiographic results were observed after an average follow-up period of 5.7 years. Definite fusion was observed in 56 out of 57 patients. Pace et al. (2008) reported a study where CF/PEEK was used for acetabular cup. Patients were followed up after 3 years. Harris hip score improved from 52 to 90. Radiographic examination revealed that every patient was stable. One revision surgery was performed due to septic



• **Figure 1.3.7.10** Typical tensile curves of HAPEX developed as bone substitutes: HAPEX I (A) and HAPEX II (B).

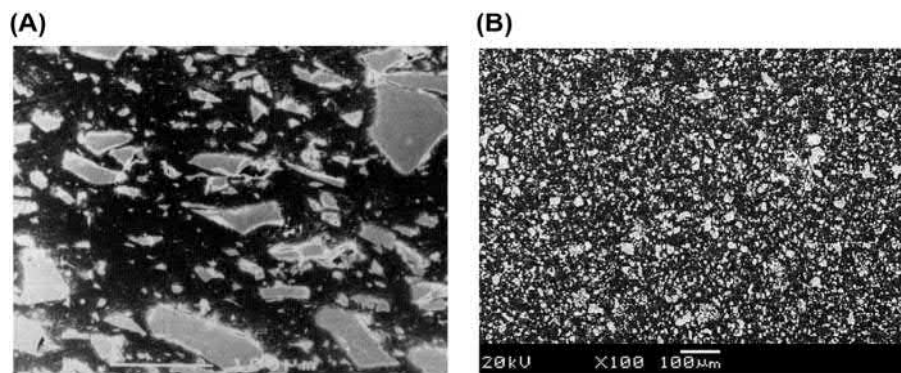
loosening. Heary et al. (2011) demonstrated excellent clinical and radiographic results in 39 out of 40 patients when CF cages were used for the treatment of thoracolumbar fusion. Misuse or wrong use of CFs to develop composites for orthopedic devices often occurs. For example, a CF-reinforced UHMWPE composite was investigated for the acetabulum cup of hip prosthesis. However, there are major concerns regarding the generation of CF debris during wear of the cup.

Biodegradable composites such as PLLA fiber-reinforced poly(glycolic acid) (PGA) or PCL and self-reinforced poly(D,L-lactic acid)(PDLA)/PLLA composites are also investigated because they could be processed into the forms of rods, screws, tacks, plates, etc., which can be used in traumatology and orthopedic surgery. Using high-strength and high-modulus CFs to reinforce high-strength polymers can attain the strength of metallic biomaterials with a tailored modulus approaching that of bone. Fibrous composites have also been investigated for the substitution of tendon and ligament. In replacing a ruptured tendon or ligament in the body, some successes were achieved by using tendon/ligament prostheses made of either nonbiodegradable fibrous composites (CF/PTFE, aramid fiber/PE, PET/PHEMA, etc.) or partially degradable composites (CF/PLLA, CF/PU, etc.), which have comparable mechanical properties (elastic properties) to those of native tendon and ligament and also excellent fatigue performance. Problems with abrasion and abrasion products such as brittle ceramic fiber fragments have hindered their development and clinical use.

HA particles have been used as a bioactive and reinforcing phase for high-density polyethylene (HDPE) to produce HAPEX, a bone analog (Bonfield et al., 1998). Numerous bioactive composites consisting of bioactive bioceramic particles and biomedical polymers have been investigated for bone substitution. HAPEX is the first bioactive ceramic-polymer composite that is designed to mimic the structure and match the properties of bone. It is the first successful, commercialized composite for bone tissue substitution in the clinic. It can contain up to 40 vol% of HA

with acceptable ductility and machinability when intricate small medical devices are made from it. HDPE was chosen as the matrix material because (1) it is a proven biocompatible polymer widely used in orthopedics, (2) it is a ductile polymer that allows the incorporation of a large amount of bioceramic particles in the system, (3) the polymer having high content of bioceramic particles can still be melt processed using conventional plastics technology, and (4) it is a linear polymer whose molecular chains can be aligned for property enhancement when advanced polymer processing technology is used. HA in the composite provides bone-bonding ability for HAPEX. Like other particle-reinforced composites, with an increasing amount of HA in the composite, the stiffness and strength of HAPEX increase but its ductility drastically decreases (Fig. 1.3.7.10). When the HA content is above 45 vol%, the composite is a very brittle material that is not suitable for bone implants. It has also been shown that to achieve good bioactivity for the composite, HAPEX must have at least 20 vol% of HA. The higher the HA content in the composite, the better the bioactivity of HAPEX.

Implants made of HAPEX can form good bonding with bone within 6 months after implantation. HAPEX has been used for bone substitution such as orbital floor implants and middle ear implants. Hydrostatic extrusion aligns HDPE molecule chains along the extrusion direction, resulting in much improved mechanical properties for HAPEX II. HA particles in HAPEX I and HAPEX II show excellent dispersion and even distribution, which are necessary for their high mechanical and biological performance. Many other bioceramic particle-reinforced composites were investigated for bone substitution, including Bioglass/HDPE, A-W glass-ceramic/HDPE, HA/PSU, and HA/PEEK. Seeking new biodegradable materials for bone tissue repair, many researchers have also investigated biodegradable particulate composites such as HA/PLLA, TCP/PLLA, HA/PHBV, and TCP/PHBV. Natural biodegradable polymers such as collagen and chitosan have also been used to incorporate HA or TCP as bioactive and biodegradable composites.



• **Figure 1.3.7.11** Scanning electron microscopy views of the microstructure of bioceramic particle-reinforced polymer composites: nonbiodegradable Bioglass/high-density polyethylene (A) and totally biodegradable tricalcium phosphate/poly(3-hydroxybutyrate-co-3-hydroxyvalerate) (B).

For attaining the desired performance for the composite, no matter what the combination is for the particle reinforcement and matrix and no matter what the fabrication technique is for composite manufacture, the bioceramic particles must be sufficiently dispersed and well distributed in the composite (Fig. 1.3.7.11). For obtaining high load-bearing capabilities, composites of metal matrices instead of polymer matrices are investigated. A typical example is the HA/Ti–6Al–4V composite. This composite can withstand much higher loads than polymer matrix composites because of the load-carrying ability of the metal alloy. However, the interfacial reaction between HA particles and Ti–6Al–4V matrix during composite manufacture involving high temperature is a serious problem. Ceramic matrix composites such as the HA particle–zirconia composite have appeared. But its development lacks sound justification and manufacture of this type of composite possesses particular technical challenges.

A composite of calcium sulfate, poly(D,L-lactide-co-glycolide), PGA, and surfactant has been developed and is in clinical use for bone grafting applications. In this case, addition of surfactant has made the composite easier to handle and moldable. In another case, a nanocomposite of calcium sulfate and PLLA was developed; however, it is not extensively used in practice (Mamidwar et al., 2008). An important lesson was that the manufacturing process of the composite had a huge impact on the properties of the composite that was developed. Composites formed by combining calcium sulfate and carboxymethyl cellulose or hydroxymethyl cellulose were also developed and extensively used clinically. Cellulose component mainly helped in the handling properties of the bone graft. A composite of calcium sulfate and PGA has been developed and commercialized by Osteobiologics under the trade name PolyGraft (Dahabreh et al., 2014; Kline et al., 2008). It is available in various forms such as wedges and granules. It has much better mechanical properties compared to calcium sulfate or HA alone. Although composites of bone graft such as calcium sulfate or HA and antibiotics were never approved in the United States, it is fairly common for surgeons to mix the two in the operating room and use them clinically.

Biomedical Composites in Dental Applications

One area where composites are extensively used clinically is dental restorative materials. Such dental composites are usually composites of polymeric acrylic or methacrylic matrix reinforced with ceramic particles. Clinically available formulations are made up of bisphenol-A-glycidylmethacrylate (bis-GMA) and triethylene glycoldimethacrylate. The manufacturing process is again important as monomer-polymer conversion significantly effects the mechanical and biological properties of the composites. Bridges are made up of composites of carbon and UHMWPE or glass-reinforced polycarbonate (Schedle et al., 1999). Removable prostheses are made up of glass fiber-reinforced polycarbonate. Bone cements are used in orthopedics and dentistry. Usually, bone cement is PMMA powder mixed with a methacrylate-type monomer, which is polymerized during fixation. To increase fatigue life and reduce creep formation, small amounts of Kelvar, carbon, graphite, or ultrahigh molecular weight fibers are added to PMMA-based bone cement (Pillar et al., 1976; Pourdeyhimi et al., 1989).

Alumina micro- or nanoparticle-reinforced bis-GMA-based resins were investigated as new dental filling materials. It was shown that the particulate alumina filler can increase the wear resistance of the new filling material. However, issues relating to bonding of resin to the tooth need to be solved to avoid leakage of hot or cold liquid along the filling material-tooth interface, which can cause severe toothache. For the same purpose, others followed this idea and have produced other hard ceramic particle-resin composites as dental filling materials. Another area of high interest is the polymer fiber-reinforced or toughened denture for elderly dental patients. High-performance PE fibers, either woven or chopped (over 30 vol%), have been used to strengthen and toughen acrylic denture-based resin. The composite dentures have much higher stiffness and strength and do not break into fragments upon high impact. For artificial teeth, dental posts are traditionally made of metals, e.g., Co-Cr and Ti alloys. Along the same rationale for using long-fiber composites for the stem of hip prosthesis, dental posts comprising an epoxy resin matrix and carbon or glass fibers have

been investigated. In addition, finite element analysis indicates that ideal dental posts should possess varied stiffness along their length (with relatively low stiffness at the apical end and high stiffness at the coronal end), which are impossible to achieve using homogeneous materials. Composite dental posts with a specific design can meet this requirement. Overall, dental applications of biomedical composites are not as numerous as in the orthopedic field and hence there is still a large scope for exploration.

Biomedical Composites for Tissue Engineering

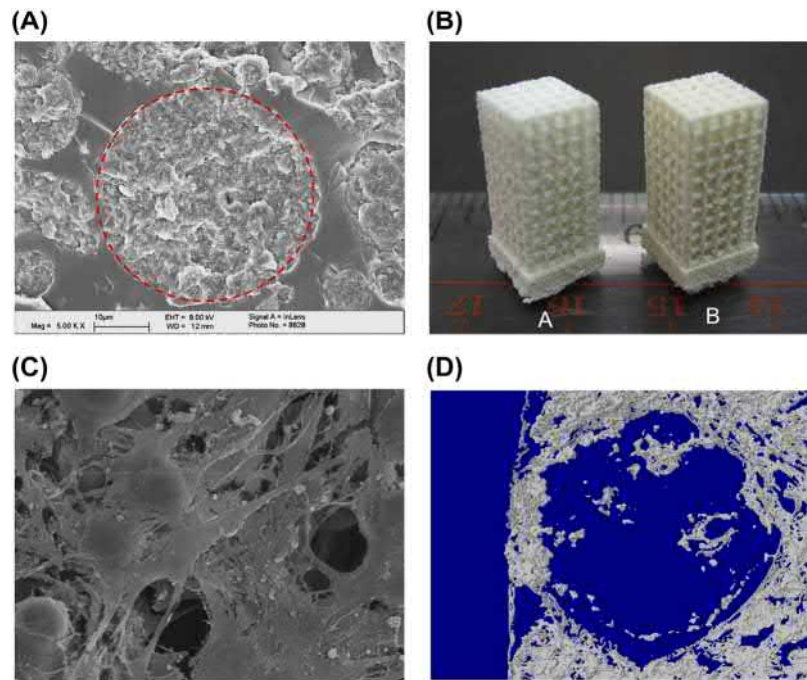
Biomedical composites can play a great role in forming the essential tissue engineering scaffolds. Tissue engineering scaffolds are biodegradable, porous, synthetic extracellular matrices that provide a conducive environment for cells to migrate, adhere, proliferate, and differentiate, leading to new tissue formation and growth in the body. The basic requirements for biodegradable scaffolds include (1) a highly porous body having a 3D, interconnecting pore network structure, (2) a controlled degradation rate, and (3) scaffold degradation and degradation products being unharmed to the tissue and body. Basic scaffolds are simple porous structures made of mostly biodegradable polymers such as PLLA, PLGA, and PCL, with porous metals and ceramics also being investigated. They are useful for regenerating “simple tissues” in the body (human body tissues are never simple). However, for achieving enhanced tissue regeneration or for regenerating complex tissues, advanced, multifunctional tissue engineering scaffolds are needed (Zhao and Wang, 2017).

Biomimetic composites have been investigated for bone tissue engineering. Selection of a proper material in the design of the bone regeneration process has some important implications to maintaining mechanical strength, structural support, and providing the optimal culturing environment for bone formation. The ideal composite for bone regeneration is biocompatible, supports bone formation (osteoconductive), induces bone formation (osteoinductive), is chemically bonded to bone (osteointegrative), is able to support angiogenesis, and is structurally and mechanically compatible to bone (Robinson et al., 2017). The development of bioactive ceramic-polymer composites has been largely inspired by the make-up of the native bone matrix, which is comprised predominantly of a biopolymer or collagen-rich matrix with a controlled dispersion of bone apatite nanoparticles. The native anisotropic microstructure formed by the biopolymer and mineral organization is responsible for the complex mechanical properties of bone and promotes bioactive signaling to stimulate remodeling. Particulate strengthening achieved via the addition of ceramic particles effectively reinforces and stiffens the polymeric matrix, resulting in a superior material for bone scaffolding.

The two most common types of ceramic-polymer composites are calcium phosphate-polymer composites and bioactive glass-polymer composites. Both biodegradable and nondegradable polymers have been explored as the matrix.

Given its inherent biomimicry, calcium phosphate-polymer composites have been studied widely for bone regeneration. A range of bioactivity and degradation rates exist for calcium phosphates depending on the Ca/P ratio, crystallinity, and phase purity. Calcium and phosphate ions released from the ceramic serve as building blocks and nucleation sites for mineralization, with both particle size and ceramic degradation rate regulating cell response over time and resultant bone formation. With the increasing understanding of mechanisms underlying bone formation, bioactive materials have been developed to better guide the response of bone-forming cells and promote functional host integration. To this end, incorporation of bioactive glasses (Hench, 1991) into polymer-composite design has also been investigated. Bioactive glasses promote osteointegration by forming a surface calcium phosphate layer, from which bone cells can be remodeled and used to chemically integrate the material with the host bone, with superior bone bonding strength and osteoinductivity when compared to traditional HA. An additional advantage of these materials is the potential to neutralize the acidic degradation products with the alkaline ion released as bioactive glass transforms into calcium phosphate (Lu et al., 2003).

The majority of the earlier designs of ceramic-polymer composites were in the form of cement-like pastes and films, later progressing to 3D porous scaffolds as well as the introduction of ceramic and glass nanoparticles. More recent efforts have focused on recapitulating the native micro- and nanoscale topography and organization of the native bone matrix in ceramic-polymer composite design, with the aid of 3D printing and additive manufacturing. Advanced manufacturing technologies are now increasingly used to fabricate multifunctional composite scaffolds. For achieving enhanced regeneration of bone, nanocomposites, 3D printing, and controlled release of growth factor have been combined to produce advanced bone tissue-engineering scaffolds (Duan and Wang, 2010). First, nanocomposite microspheres comprising bioactive and biodegradable calcium phosphate (Ca-P) nanoparticles and biodegradable PHBV matrix are made. The Ca-P nanoparticles are evenly distributed inside the microspheres (Fig. 1.3.7.12A). Using selective laser sintering (a 3D printing technology), Ca-P/PHBV nanocomposite scaffolds are fabricated from the nanocomposite microspheres (Fig. 1.3.7.12B). Subsequently, the Ca-P/PHBV scaffolds are chemically modified and molecules of bone morphogenetic protein-2 (BMP-2), an osteoinductive factor, are attached to the struts of scaffolds. These 3D printed scaffolds are therefore both osteoconductive (due to the incorporated Ca-P particles) and osteoinductive (due to the attached BMP-2). After scaffold implantation in animal bodies, Ca^{2+} , PO_4^{3-} , and BMP-2 molecules can be gradually released from scaffolds, promoting bone tissue formation. The Ca-P/PHBV nanocomposite scaffolds have significant advantages for bone tissue engineering because of their designed architecture, biodegradability, osteoconductivity, osteoinductivity, and mechanical properties. *In vitro* experiments show that because of the



• **Figure 1.3.7.12** 3D printed Ca-P/poly(3-hydroxybutyrate-co-3-hydroxyvalerate) (PHBV) composite tissue-engineering scaffolds: microstructure of a nanocomposite microspherule (A), a photo showing 3D printed PHBV (left) and Ca-P/PHBV (right) scaffolds (B), mesenchymal stem cells seeded on a Ca-P/PHBV scaffold (C), and a microcomputed tomography image showing bone formation inside and outside a Ca-P/PHBV scaffold (D).

In vitro gradual release of BMP-2, Ca^{2+} , and PO_4^{3-} from nanocomposite scaffolds, human umbilical cord-derived mesenchymal stem cells seeded on scaffolds have proliferated and are induced for osteogenic differentiation (Fig. 1.3.7.12C). After 6 weeks of intraosseous implantation of the advanced nanocomposite scaffolds in animals, new bone forms inside as well as outside the original scaffolds (Fig. 1.3.7.12D).

The composite approach has achieved remarkable success in tissue engineering, particularly for bone tissue regeneration. However, successful tissue engineering strategies do not depend solely on scaffolds and scaffold materials. Cells and various cues (biochemical, topographical, mechanical, etc.) are also important. New manufacturing technologies need to be developed, which can produce directly composite scaffolds incorporated with living cells and delicate biomolecules.

References

- Bonfield, W., Wang, M., Tanner, K.E., 1998. Interfaces in analogue biomaterials. *Acta Materialia* 46 (7), 2509–2518.
- Brantigan, J.W., Steffee, A.D., 1993. A carbon fiber implant to aid interbody lumbar fusion. Two-year clinical results in the first 26 patients. *Spine* 18 (14), 2106–2107.
- Dahabreh, Z., Panteli, M., Pountos, I., Howard, M., Campbell, P., Giannoudis, P., 2014. Ability of bone graft substitutes to support the osteoprogenitor cells: an in-vitro study. *World J. Stem Cells* 6 (4), 497–504.
- Duan, B., Wang, M., 2010. Customized Ca-P/PHBV nanocomposite scaffolds for bone tissue engineering: design, fabrication, surface modification and sustained release of growth factor. *J. R. Soc. Interface* 7, S615–S629.
- Hahn, H.T., Williams, J.G., 1986. Compression failure mechanisms in unidirectional composites. In: *Composite Materials*, pp. 115–139 Philadelphia, PA.
- Heary, R.F., Kheterpal, A., Mammis, A., Kumar, S., 2011. Stackable carbon fiber cages for thoracolumbar interbody fusion after corpectomy: long-term outcome analysis. *Neurosurgery* 68 (3), 810–818 discussion 818–9.
- Hench, L.L., 1991. Bioceramics: from concept to clinic. *J. Am. Ceram. Soc.* 74 (7), 1487–1510.
- Kline, A.D.P.M., 2008. Freiberg's infraction of the second metatarsal head with bioorthologic repair using the NEXA Osteocure™ bone graft: a case report. *Foot Ankle J.* 1 (11), 4.
- Lu, H.H., Scott, K., El-Amin, S.F., Laurencin, C.T., 2003. Three-dimensional, bioactive, biodegradable polymer-bioactive glass composite scaffolds with improved mechanical properties support collagen synthesis and mineralization by human osteoblast-like cells *in vitro*. *J. Biomed. Mater. Res.* 64A, 465–474.
- Mamidwar, S., Weiner, M., Alexander, H., Ricci, J., 2008. In vivo bone response to calcium sulfate/PLLA composite. *Implant Dent.* 17 (2), 208–216.
- Pace, N., Marinelli, M., Spurio, S., 2008. Technical and histological analysis of a retrieved carbon fiber-reinforced poly-ether-ether-ketone composite alumina bearing linear 28 months after implantation. *J. Arthroplast.* 23 (1), 151–155.
- Pillar, R.M., Blackwell, R., Macnab, I., Cameron, H.U., 1976. Carbon fiber-reinforced bone cement in orthopedic industry. *J. Biomed. Mater. Res.* 10, 893–906.
- Pourdeyhimi, B., Wagner, H.D., 1989. Elastic and ultimate properties of acrylic bone cement reinforced with ultra-high-molecular-weight polyethylene fibers. *J. Biomed. Mater. Res.* 23, 63–80.
- Robinson, J., Brudnicki, Lu, H.H., 2017. Polymer-bioactive ceramic composites. In: Ducheyne, P., et al. (Ed.), *Comprehensive Biomaterials*, second ed. Elsevier.

- Rosen, B.W., 1965. Mechanics of composite strengthening. In: *Fiber Composite Materials*. American Society for Metals, pp. 37–75.
- Schedle, A., Franz, A., Rausch-Fan, X., et al., 1999. Cytotoxic effects of dental composites, adhesive substance, compomers and cements. *Dent. Mater.* 15, 262–267.
- Wang, M., Guo, L., Sun, H., 2019. Manufacturing technologies for biomaterials. In: Narayan, R.J. (Ed.). *Encyclopedia of Biomedical Engineering*, vol. 1. Elsevier, the Netherlands, pp. 116–134.
- Zhao, Q., Wang, M., 2017. Chapter 20 Smart multifunctional tissue engineering scaffolds. In: Wang, Q. (Ed.), *Smart Materials for Tissue Engineering: Applications*. Royal Society of Chemistry, UK, pp. 558–595.
- Zhang, G., Latour, R.A., 1994. An analytical and numerical study of fiber microbuckling. *Compos. Sci. Technol.* 51, 95–109.
- Zhang, G., Latour, R.L., Kennedy, J.M., Schutte, H.D., Friedman, R.J., 1996. Long-term compressive property durability of carbon fiber-reinforced polyetheretherketone composite in physiological saline. *Biomaterials* 17, 781–789. ceramic-polymer composites.

Chapter Questions

1. A unidirectionally reinforced carbon fiber-polyetheretherketone (CF/PEEK) composite is investigated for the stem of hip prostheses. The composite contains 30% by volume of the carbon fiber. Properties of carbon fiber and PEEK are summarized in the table below.

Table 1 Properties of Carbon Fiber and PEEK

Constituent of the Composite	Property		
	Young's Modulus (GPa)	Tensile Strength (MPa)	Density (g/cm ³)
Carbon fiber	360	1800	2.10
PEEK	5.0	100	1.40

(A) Calculate the Young's modulus and tensile strength of this composite according to the composite theory.

(B) If an elderly man having a body weight of 800N has been implanted with a total hip prosthesis made of this composite and he is walking slowly, what is the maximum load borne by carbon fibers and what is the maximum load applied to the polymer matrix in the stem of the hip prosthesis? (You can assume that the direction of the load applied to the stem is parallel to carbon fibers in the stem.)

Solution:

(A) At $V_f = 30\%$, we have $V_m = 1 - V_f = 70\%$
Young's modulus of the composite:

$$E_c = E_f V_f + E_m V_m = 360 \times 0.3 + 5.0 \times 0.7 = 111.5 \text{ GPa}$$

Tensile strength of the composite:

$$\sigma_c = \sigma_f V_f + \sigma_m V_m = 1800 \times 0.3 + 100 \times 0.7 = 610 \text{ MPa}$$

(B) Knowing $P = \sigma A$, $L_c = L_f$, $\sigma = E \varepsilon$ and $\varepsilon_c = \varepsilon_f$, the loads shared by carbon fibers and PEEK can be found as

$$P_f/P_c = \sigma_f A_f / \sigma_c A_c = \sigma_f A_f L_f / \sigma_c A_c L_c = \sigma_f V_f / \sigma_c = E_f \varepsilon_f V_f / E_c \varepsilon_c = E_f V_f / E_c$$

During walking, the maximum force in the vertical direction of the hip is typically 5 times the body weight. The load borne by carbon fibers is

$$P_f = P_c E_f V_f / E_c = 5 \times 800 \times 360 \times 0.3 / 111.5 = 3874 \text{ N}$$

and the load borne by PEEK is

$$P_m = 5 \times 800 - 3874 = 126 \text{ N}$$

2. As discussed in this chapter, in the k -mode microbuckling the compressive strength of a uniaxial fiber embedded in a matrix as predicted by Equation (1.3.7.8) will reduce to that of a single-fiber composite case when the fiber volume fraction (V_f) becomes very small. Referring

to Equation (1.3.7.8) and Figure 1.3.7.7, show the following relations

$$\sigma_f(V_f \rightarrow 0) = \frac{E_f t^2}{3} + 2E_m \frac{(1 - \nu_m) + \frac{1}{t} + t}{(1 + \nu_m)(3 - \nu_m)}$$

when $V_f \rightarrow 0$, or $\beta \rightarrow \infty$.

Solution:

With $V_f \rightarrow 0$ or $\beta \rightarrow \infty$, by applying the L'Hôpital's Rule with respect to β to the following expressions along with the relationships between the hyperbolic sine/cosine functions and the exponential function, one establishes the following relations

$$\begin{aligned} \lim_{\beta \rightarrow \infty} \frac{2\beta t}{\sinh 2\beta t} &= \lim_{\beta \rightarrow \infty} \frac{2t}{2t \cosh 2\beta t} \\ &= \lim_{\beta \rightarrow \infty} \frac{1}{\cosh 2\beta t} = \lim_{\beta \rightarrow \infty} \frac{2}{e^{2\beta t} + e^{-2\beta t}} = 0 \end{aligned}$$

$$\begin{aligned} \lim_{\beta \rightarrow \infty} \frac{2 \sinh^2 \beta t}{\sinh 2\beta t} &= \lim_{\beta \rightarrow \infty} \frac{2 \sinh^2 \beta t}{2 \sinh \beta t \cosh \beta t} \\ &= \lim_{\beta \rightarrow \infty} \frac{\sinh \beta t}{\cosh \beta t} = \lim_{\beta \rightarrow \infty} \frac{e^{\beta t} - e^{-\beta t}}{e^{\beta t} + e^{-\beta t}} = 1 \end{aligned}$$

$$\begin{aligned} \lim_{\beta \rightarrow \infty} \frac{2 \cosh^2 \beta t}{\sinh 2\beta t} &= \lim_{\beta \rightarrow \infty} \frac{2 \cosh^2 \beta t}{2 \sinh \beta t \cosh \beta t} \\ &= \lim_{\beta \rightarrow \infty} \frac{\cosh \beta t}{\sinh \beta t} = \lim_{\beta \rightarrow \infty} \frac{e^{\beta t} + e^{-\beta t}}{e^{\beta t} - e^{-\beta t}} = 1 \end{aligned}$$

To take advantage of these relations, it is necessary to rearrange Equation (1.3.7.8) slightly, hence one has

$$\sigma_f = \frac{E_f t^2}{3} + (1+k) E_m \frac{\frac{2\beta t(1+\nu_m)}{\sinh 2\beta t} + \frac{(1-\nu_m) \sinh 2\beta t}{\sinh 2\beta t} + \frac{2 \sinh^2 \beta t}{t \sinh 2\beta t} + \frac{2t \cosh^2 \beta t}{\sinh 2\beta t}}{(1+\nu_m) \left[\frac{2\beta t(1+\nu_m)}{\sinh 2\beta t} + (3-\nu_m) \right]}$$

$$\begin{aligned} &+ (1-k) E_m \frac{\frac{2\beta t(1+\nu_m)}{\sinh 2\beta t} - \frac{(1-\nu_m) \sinh 2\beta t}{\sinh 2\beta t} - \frac{2 \cosh^2 \beta t}{t \sinh 2\beta t} - \frac{2t \sinh^2 \beta t}{\sinh 2\beta t}}{(1+\nu_m) \left[\frac{2\beta t(1+\nu_m)}{\sinh 2\beta t} - (3-\nu_m) \right]} \end{aligned}$$

Plugging in the above derived relationships, one obtains

$$\begin{aligned} \sigma_f &= \frac{E_f t^2}{3} + (1+k) E_m \frac{(1-\nu_m) + \frac{1}{t} + t}{(1+\nu_m)(3-\nu_m)} \\ &+ (1-k) E_m \frac{(1-\nu_m) + \frac{1}{t} + t}{(1+\nu_m)(3-\nu_m)} \end{aligned}$$

Apparently, regardless what the k value is, one has

$$\sigma_f(V_f \rightarrow 0) = \frac{E_f t^2}{3} + 2E_m \frac{(1 - \nu_m) + \frac{1}{t} + t}{(1 + \nu_m)(3 - \nu_m)}$$

By taking the critical value of the above expression with respect to t_{cr} one arrives at the following expression

$$\sigma_f^{cr}(V_f \rightarrow 0) = \frac{E_f t_{cr}^2}{3} + 2E_m \frac{(1 - \nu_m) + \frac{1}{t_{cr}} + t_{cr}}{(1 + \nu_m)(3 - \nu_m)}$$

This relation supports the converged result for the $k=1$ and $k=-1$ cases of microbuckling when $V_f \rightarrow 0$, as shown in Figure 1.3.7.7.

3. Use the values provided in Table 1.3.7.1 for a CF/PEEK composite, determine the critical value for the compressive strength of a fiber undergoing microbuckling as predicted by the following expression

$$\sigma_f^{cr}(V_f \rightarrow 0) = \frac{E_f t_{cr}^2}{3} + 2E_m \frac{(1 - \nu_m) + \frac{1}{t_{cr}} + t_{cr}}{(1 + \nu_m)(3 - \nu_m)}$$

Solution:

For the given expression, its critical value can be determined by finding its minimum with respect to t . So, by taking the first-order derivative of the above expression and setting it to zero, one can find the t_{cr} value for the given E_f , E_m and ν_m : $t_{cr} = 0.243$. By plugging this t_{cr} value and the known E_f , E_m and ν_m values into the above expression, one arrives at:

$$\sigma_f^{cr} = 17.417 \text{ GPa}$$

4. As shown in Figure 1.3.7.7, for $V_f > 0.13$, the compressive strength of a uniaxial fiber reinforced composite predicted by the $k=1$ case of the k -mode microbuckling will be the same as that predicted by Rosen's theory. Show that

$$\sigma_{f_{cr}} = \frac{G_m}{V_f(1 - V_f)}$$

when V_f is sufficiently large (e.g., $V_f > 0.13$ for CF/PEEK composite).

Solution:

When V_f is sufficiently large, β will be a finite value. In this situation, the critical value of the compressive strength of a uniaxial fiber reinforced composite as predicted by Equation (1.3.7.8) will be reached when $t \rightarrow 0$. By applying the L'Hôpital's Rule with respect to t to the following expressions, one establishes the following relations

$$\begin{aligned} \lim_{t \rightarrow 0} \frac{\sinh 2\beta t}{2\beta t} &= \lim_{t \rightarrow 0} \frac{2t \cosh 2\beta t}{2\beta t} \\ &= \lim_{t \rightarrow 0} \cosh 2\beta t = \lim_{t \rightarrow 0} \frac{e^{2\beta t} + e^{-2\beta t}}{2} = 1 \end{aligned}$$

$$\begin{aligned} \lim_{t \rightarrow 0} \frac{2 \sinh^2 \beta t}{2\beta t^2} &= \lim_{t \rightarrow 0} \frac{4 \sinh \beta t \cosh \beta t}{4\beta t} \\ &= \lim_{t \rightarrow 0} \frac{\sinh 2\beta t}{2t} = \lim_{t \rightarrow 0} \beta \cosh 2\beta t = \beta \end{aligned}$$

$$\begin{aligned} \lim_{t \rightarrow 0} \frac{2t \cosh^2 \beta t}{2\beta t} &= \lim_{t \rightarrow 0} \frac{\cosh^2 \beta t}{\beta} \\ &= \lim_{t \rightarrow 0} \left(\frac{e^{\beta t} + e^{-\beta t}}{2} \right) = \frac{1}{\beta} = \frac{1}{\beta} \end{aligned}$$

Letting $k=1$ and rearranging Equation (1.3.7.8), one has

$$\sigma_f^{cr} = \lim_{t \rightarrow 0} \sigma_f = \lim_{t \rightarrow 0} \left[\frac{E_f t^2}{3} + \frac{2E_m \left[(1 + \nu_m) + (1 - \nu_m) \frac{\sinh 2\beta t}{2\beta t} + \frac{\sinh^2 \beta t}{2\beta t^2} + \frac{2t \cosh^2 \beta t}{2\beta t} \right]}{(1 + \nu_m) \left[(1 - \nu_m) + (3 - \nu_m) \frac{\sinh 2\beta t}{2\beta t} \right]} \right]$$

Plugging in the above derived relationships along with the relationships of $\beta = \frac{1}{V_f} - 1$ and $G_m = \frac{E_m}{2(1 + m)}$, one obtains

$$\begin{aligned} \sigma_f^{cr} &= 2E_m \frac{(1 + \nu_m) + (1 - \nu_m) + \beta + \frac{1}{\beta}}{(1 + \nu_m) [(1 + \nu_m) + (3 - \nu_m)]} \\ &= \frac{E_m}{2(1 + \nu_m) V_f (1 - V_f)} = \frac{G_m}{V_f (1 - V_f)} \end{aligned}$$

5. Referring to Figures 1.3.7.6 and 1.3.7.8, find the expression for f_1 when $V_f \rightarrow 0$ (or $\beta \rightarrow \infty$) for an arbitrary k value ($-1 \leq k \leq 1$).

Solution:

From Figure 1.3.7.6 one copies the expression for f_1 as follows:

$$\begin{aligned} f_1 &= (1 + k) \frac{(1 + \nu_m) \beta t^2 + (1 - \nu_m) t \sinh \beta t \cosh \beta t + 2 \sinh^2 \beta t}{(1 + \nu_m) [2\beta t (1 + \nu_m) + (3 - \nu_m) \sinh 2\beta t]} \\ &+ (1 - k) \frac{(1 + \nu_m) \beta t^2 - (1 - \nu_m) t \sinh \beta t \cosh \beta t - 2 \sinh^2 \beta t}{(1 + \nu_m) [2\beta t (1 + \nu_m) - (3 - \nu_m) \sinh 2\beta t]} \end{aligned}$$

With some rearrangement one further writes

$$f_1 = (1+k) \frac{(1+\nu_m) \frac{\beta t^2}{\sinh 2\beta t} + (1-\nu_m) \frac{t \sin \beta t \cosh \beta t}{\sinh 2\beta t} + \frac{2 \sinh^2 \beta t}{\sinh 2\beta t}}{(1+\nu_m) \left[(1+\nu_m) \frac{2\beta t}{\sinh 2\beta t} + (3-\nu_m) \right]} + (1-k) \frac{(1+\nu_m) \frac{\beta t^2}{\sinh 2\beta t} - (1-\nu_m) \frac{t \sin \beta t \cosh \beta t}{\sinh 2\beta t} - \frac{2 \sinh^2 \beta t}{\sinh 2\beta t}}{(1+\nu_m) \left[(1+\nu_m) \frac{2\beta t}{\sinh 2\beta t} - (3-\nu_m) \right]}$$

By substituting the limits relations obtained in Question 2 into the above f_1 expression along with some elimination and simplification, one obtains

$$\lim_{\beta \rightarrow \infty} f_1 = (1+k) \frac{(1-\nu_m) \frac{t}{2} + 1}{(1+\nu_m)(3-\nu_m)} + (1-k) \frac{(1-\nu_m) \frac{t}{2} + 1}{(1+\nu_m)(3-\nu_m)} = \frac{(1-\nu_m)t + 2}{(1+\nu_m)(3-\nu_m)}$$

Apparently, the above expression is not a function of k , indicating that when $V_f \rightarrow 0$ (or $\beta \rightarrow \infty$), the function of f_1 is independent of the k parameter.

6. Referring to Figures 1.3.7.6 and 1.3.7.8, find the expression for f_2 when $V_f \rightarrow 0$ (or $\beta \rightarrow \infty$) for an arbitrary k value ($-1 \leq k \leq 1$).

Solution:

From Figure 1.3.7.6 one copies the expression for f_2 as follows:

$$f_2 = (1+k) \frac{(1+\nu_m)\beta t + (1-\nu_m) \sinh \beta t \cosh \beta t + 2t \cosh^2 \beta t}{(1+\nu_m) [2\beta t(1+\nu_m) + (3-\nu_m) \sinh 2\beta t]} + (1-k) \frac{(1+\nu_m)\beta t - (1-\nu_m) \sinh \beta t \cosh \beta t - 2t \cosh^2 \beta t}{(1+\nu_m) [2\beta t(1+\nu_m) - (3-\nu_m) \sinh 2\beta t]}$$

With some rearrangement one writes

$$f_2 = (1+k) \frac{(1+\nu_m) \frac{\beta t}{\sinh 2\beta t} + (1-\nu_m) \frac{\sinh \beta t \cosh \beta t}{\sinh 2\beta t} + \frac{2t \cosh^2 \beta t}{\sinh 2\beta t}}{(1+\nu_m) \left[(1+\nu_m) \frac{\beta t}{\sinh 2\beta t} + (3-\nu_m) \right]} + (1-k) \frac{(1+\nu_m) \frac{\beta t}{\sinh 2\beta t} - (1-\nu_m) \frac{\sinh \beta t \cosh \beta t}{\sinh 2\beta t} - \frac{2t \cosh^2 \beta t}{\sinh 2\beta t}}{(1+\nu_m) \left[(1+\nu_m) \frac{\beta t}{\sinh 2\beta t} - (3-\nu_m) \right]}$$

By substituting the limits relations in Question 2 into the above f_2 expression along with some elimination and simplification, one obtains

$$\lim_{\beta \rightarrow \infty} f_2 = (1+k) \frac{\frac{1}{2}(1-\nu_m) + t}{(1+\nu_m)(3-\nu_m)} + (1-k) \frac{\frac{1}{2}(1-\nu_m) + t}{(1+\nu_m)(3-\nu_m)} = \frac{(1-\nu_m) + 2t}{(1+\nu_m)(3-\nu_m)}$$

Apparently, the above expression is not a function of k , indicating that when $V_f \rightarrow 0$ (or $\beta \rightarrow \infty$), the function of f_2 is independent of the k parameter.

7. The biphasic calcium phosphate (BCP) bioceramic is actually a composite material. Its composition can be 60% of hydroxyapatite (HA) and 40% of tricalcium phosphate (TCP). It is developed for biodegradable implants for human hard tissue repair.

(A) Non-porous BCP rods are now used in *in vitro* degradation tests. It is found that the strength of this BCP decreases to 70% of the original strength after 10 weeks' immersion in phosphate buffered saline solution (PBS). It further decreases to 50% of the original strength after another 10 weeks' immersion. How many more weeks will it take for the strength of this BCP to be reduced to 5% of the original strength? You can assume that the strength (σ) of this BCP follows the relationship shown below:

$$\sigma = \sigma_0 + C \ln t$$

where t is the immersion time (week) in PBS, and σ_0 and C are constants.

(B) The degradation rate of BCP can be controlled by changing proportions of HA and TCP in the BCP. In order to increase the degradation rate of BCP, do you need to increase or decrease the percentage of TCP in BCP? Provide the reason for your decision.

Solution:

(A) Knowing

$$\sigma = \sigma_0 + C \ln t$$

by assuming the original strength of BCP before degradation tests as σ_i

we have

$$0.70\sigma_i = \sigma_0 + C \ln 10 = \sigma_0 + 2.303C$$

and

$$0.50\sigma_i = \sigma_0 + C \ln 20 = \sigma_0 + 2.996C$$

By taking the difference of the two above equations, we have

$$0.20\sigma_i = -0.693C$$

This leads to

$$C = -0.289\sigma_i$$

and

$$\sigma_0 = 0.70\sigma_i - 2.303C = 1.366\sigma_i$$

We can calculate the time required ($t_{0.05}$) for the strength of BCP to be reduced to 5% of the original strength by solving the following equation:

$$0.05\sigma_i = 1.366\sigma_i - 0.289\sigma_i \ln t_{0.05}$$

By elimination, we then have

$$\ln t_{0.05} = 1.316 / 0.289 = 4.554$$

therefore

$$t_{0.05} = 95.01 \text{ weeks}$$

$$t = 95.01 - 24 = 75.01 \text{ weeks}$$

that is to say, it would take another 75 weeks for the BCP rods to degrade to 5% of the original strength.

(B) Increase the amount of TCP in BCP will do.

HA is perceived to be stable in the human body environment and TCP is a proven biodegradable bioceramic. Increasing TCP in BCP enhances biodegradation of BCP.

1.3.8A

Microparticles

YANG LI, DANIEL S. KOHANE

Laboratory for Biomaterials and Drug Delivery, Department of Anesthesiology, Division of Critical Care Medicine, Boston Children's Hospital, Harvard Medical School, Boston, MA, United States

Introduction

Particulate drug-delivery systems (DDSs) can be advantageous for delivering therapeutic compounds, for local and systemic effects, providing extended duration of action, reduced systemic (although perhaps not local) toxicity, and improved patient compliance (Tiwari et al., 2012; Uhrich et al., 1999). Over the past several decades, particulate drug-delivery systems have gone from being scientific curiosities to areas of very active research interest, to clinical applications. Microparticles fabricated from natural or synthetic polymers have been used in a wide range of biomedical applications including drug delivery, molecular imaging, and immune adjuvants.

In general, the term “microparticle” refers to particles whose dimensions range from 1 to 1000 μm . There are no clear universally recognized cut-offs to differentiate microparticles from nanoparticles. The larger the particles are, the more likely they behave as microparticles (as will be discussed below), and require similar fabrication processes (Kohane, 2007).

This chapter outlines key concepts in the design of polymeric microparticles for biomedical applications. An overview of commonly used materials for the synthesis of microparticles is provided. Classic formulation and characterization techniques in the preparation of microparticles are covered. The mechanism of drug release from microparticles is summarized. This chapter also discusses several microparticle-based drug-delivery systems and analyzes the features that lead to success. This chapter emphasizes microparticles as drug-delivery systems for biomedical applications. Their use as embolic materials (Matsumaru et al., 1997), structural materials (Mikkelsen et al., 2017), radiotherapeutic agents (Hamoudeh et al., 2008), etc. is covered elsewhere, as are their applications in pet care (Singh and T O'Hagan, 2003), food science (Gharsallaoui et al., 2007), agriculture (Asrar et al., 2010), cosmetics (Li et al., 2011), and environmental remediation (Wang et al., 2008).

Why Size Matters

Particle size has a direct impact on the potential routes by which particles can be delivered. Perhaps the most notable

limitation is that larger vehicles cannot be delivered directly into the circulation (e.g., intravenously), because of concerns over embolic phenomena (obstruction of blood vessels). Therefore, most intravenously delivered particles tend to be nanoscale. Microparticles tend to be depot formulations, taken orally, deposited on mucosae (e.g., inhaled), or injected into tissue (subcutaneous, intramuscular, etc.). From those sites, the microparticles release drugs to achieve effects locally (e.g., local anesthesia, bronchodilation) or systemically (e.g., growth hormone, antipsychotics). Particle size also has practical implications. For example, larger particles are more likely to clog needles, or settle in a solution intended for injection.

Size has a major impact on particles' abilities to cross biological barriers (Yang et al., 2017). Barriers can be large and obvious like skin, or finer structures like epithelia, that limit access to organs e.g., the blood–brain barrier (Chen and Liu, 2012). Mucus or loose connective tissue can be barriers. In general, microscale devices will not cross these barriers spontaneously; they have to be injected across them. As a corollary to that, microparticles injected into a tissue have a much greater tendency to remain where injected than do nanoscale devices (Kohane et al., 2006). Larger particles are less likely than smaller ones to be cleared from the bloodstream by the kidney, or to leave the bloodstream and enter tissues with highly permeable endothelia (e.g., tumors).

Microparticles are less likely to be able to penetrate into cells than nanoparticles. One exception to that is with phagocytic cells such as neutrophils and dendritic cells, which can ingest particles up to 10 μm in diameter (Tabata and Ikada, 1988). The fact that microparticles can only be taken up by such cells—which often have immunological roles—has been exploited to provide passive targeting to phagocytic cells, e.g., for vaccines. The nature of the cellular inflammatory response is also determined by particle size. While smaller particles can be ingested by the inflammatory cells that arrive at the site of injection, larger ones cannot and tend to become walled off by a syncytium of monocytes—the giant foreign body cells (Anderson, 1994).

Size affects many particle properties that are important for their function as drug-delivery systems, including drug loading, pharmacokinetics, and degradation rate. The surface area to volume ratio of particulate systems is inversely proportional to the diameter. Consequently, smaller particles tend to release encapsulated drugs more rapidly, both during some types of production processes (e.g., emulsion-based production) and after administration. Water will penetrate into smaller particles more rapidly, which accelerates drug release and—in particles that can be degraded hydrolytically—degradation.

Materials for the Synthesis of Microparticles

The composition of materials used for the fabrication of microparticles determines the mechanism and duration of drug release (Uhrich et al., 1999). Microparticles can be readily prepared with polymers or nonpolymeric materials by a variety of well-established formulation methods. Although there are examples of nondegradable polymeric microparticles (Kawashima et al., 1992; Ting et al., 1992; De Ascentiis et al., 1995; Köse et al., 2003; Kunioka and Doi, 1990; Chen and Tong, 2012), most microparticles for drug delivery are fabricated with biodegradable materials, especially degradable polymers. Commonly used polymers for the fabrication of microparticles fall into two categories: natural polymers and synthetic polymers (Fig. 1.3.8A.1).

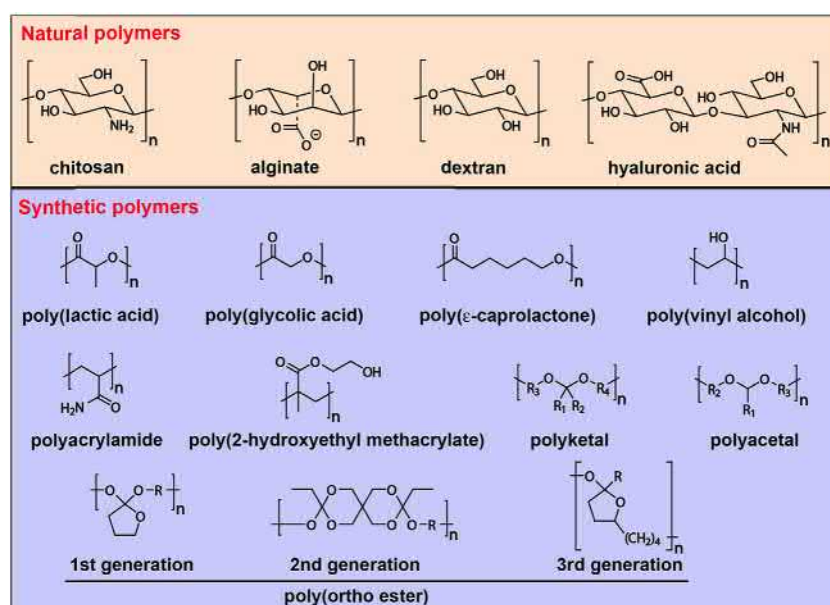
Natural Polymers

Natural polymers have been widely applied in biomedical applications due to their intrinsic biocompatibility. Natural polymers like polysaccharides are abundant in nature, and

are often inexpensive, nontoxic, and biodegradable, making them useful building blocks for the design of biomaterials including microparticles (Yang et al., 2015). Their production often does not require synthetic chemistry. Many natural polymer-derived self-assemblies have porous structures, which can be beneficial for drug encapsulation and release. Natural polymers can also be easily processed (Dang and Leong, 2006) and chemically modified (John and Anandjiwala, 2008). Polysaccharides usually contain multiple free carboxyl, hydroxyl, and amino groups which provide reactive sites for chemical modification and functionalization such as oxidation, esterification, amidation, and sulfation (Mizrahy and Peer, 2012). The hydrophobicity, surface chemistry, and adhesiveness of polymers can be tailored for the delivery of various drugs (Lehr et al., 1992; Surini et al., 2009).

Chitosan. Chitosan is a linear polysaccharide composed of β -(1–4)-linked D-glucosamine and N-acetyl-D-glucosamine randomly distributed within the backbone (Bhattarai et al., 2010). Chitosan is obtained by deacetylation of chitin, a main component of the exoskeleton of crustaceans. It has been approved by the Food and Drug Administration (FDA) for use in wound dressings (Wedmore et al., 2006). Chitosan is generally believed to have good biocompatibility (Croisier and Jérôme, 2013), although adverse tissue reactions have also been reported (Yeo et al., 2006). Chitosan is positively charged at physiological pH due to the protonation of primary amines, which facilitates its adherence to negatively charged tissues such as mucosal surfaces (He et al., 1998). Positively charged chitosan has been used to deliver payloads with negative charges, such as nucleic acids and some proteins (Bhattarai et al., 2010).

The degradation of chitosan microparticles can be accelerated by increasing the hydrophilicity of the chitosan backbone (Prashanth and Tharanathan, 2007), decreasing deacetylation (Tomihata and Ikada, 1997), decreasing molecular weight



• **Figure 1.3.8A.1** Structures of commonly used natural and synthetic polymers for the fabrication of microparticles.

(Zhang and Neau, 2001) and by chemical modification [e.g., PEGylation (Cui et al., 2012)]. The degradation rate of chitosan microparticles (1–10 μm) can also be fine-tuned by incorporation of electrostatic cross-linkers (Mi et al., 2002). Chitosan microspheres have been extensively used in drug delivery. For example, chitosan microparticles smaller than 20 μm have been used to encapsulate the antiviral drug acyclovir (Genta et al., 1997). Compared to free acyclovir, microencapsulation significantly prolonged the release of acyclovir following a single instillation into the conjunctival sac.

Alginate. Alginate is a linear anionic polysaccharide copolymer composed of 1,4-linked β -D-mannuronic acid (M) and α -L-guluronic acid (G) residues. It is obtained primarily from brown seaweed and bacteria (Lee and Mooney, 2012). Ionic bridges between divalent cations like Ca^{2+} and the G monomers of alginate can effectively cross-link alginate chains to generate hydrogels and scaffolds. The mechanical rigidity, pore size, and degradation rate of ionically cross-linked alginate microspheres can be easily tuned by altering the cation to monomer ratio or M to G ratio (Lee and Mooney, 2012). Alginate is often combined with other polymers such as chitosan to generate a more rigid matrix for prolonged release of entrapped payloads (Ribeiro et al., 2005). Alginate has been used in drug delivery due to its biocompatibility, relatively strong mucosal adhesion, and abundance in nature (Lee and Mooney, 2012). For instance, alginate microspheres with diameters ranging from 20 to 300 μm have been designed to protect insulin from degradation by the harmful pH and enzymes in the gut (Silva et al., 2006).

Dextran. Dextran is a polysaccharide composed of glucan with side chains attached to the 3-positions of the backbone glucose units (Hovgaard and Brøndsted, 1995). Dextran can be produced by several bacterial strains, such as *Leuconostoc mesenteroides* (Suarez et al., 2013; Cheung et al., 2005). Dextran is available in various molecular weights, with differing degradation rates (Stenekes et al., 1998). Dextran microparticles have been used for encapsulation and sustained release of various payloads, such as chemotherapeutics (Cheung et al., 2005), proteins (Franssen et al., 1999), and nucleic acids (Cohen et al., 2010). Dextran can be easily modified via its reactive hydroxyl groups, e.g. by acetylation. For example, acetylated dextran microparticles 1–3 μm in diameter enabled prolonged release of protein antigens over 42 days (Chen et al., 2018).

Other natural materials. Many other natural materials have also been investigated for the preparation of microparticles. For example, collagen microparticles have been used for the delivery of glucocorticosteroids (Berthold et al., 1998) and lipophilic drugs (Swatschek et al., 2002). Hyaluronic acid microparticles have been studied to deliver biomolecules (e.g. recombinant human growth hormone) (Kim et al., 2005) and antibiotics (Park et al., 2004).

Synthetic Polymers

Progress in the methodology of polymer synthesis (Hawker et al., 2001), especially metal-free polymerization

(Treat et al., 2014), has markedly facilitated the preparation of synthetic polymers (Ueda et al., 2005). Synthetic polymers can be prepared in a controlled manner, resulting in materials with well-defined compositions, low polydispersities, and predetermined molecular weights (Campos et al., 2013). By choosing appropriate monomers with specified physicochemical properties such as hydrophobicity or charge, polymers can be specifically designed for the delivery of various payloads ranging from hydrophobic or hydrophilic small molecules, proteins, and DNA (Duncan et al., 2006). Synthetic smart polymers have enabled triggerable drug release from microparticles (Schmaljohann, 2006; Haining et al., 2004). Although microparticles are predominantly prepared from degradable polymers, nondegradable polymers with high mechanical strength have also been used for the fabrication of microparticles for long-term use, such as orthopedic (Yaszemski, 2003) and dental applications (Fu and Kao, 2010; Chergn et al., 2013).

Poly(α -hydroxy acid). The best-known members of this family of molecules are composed of varying proportions of lactic and glycolic acids. Poly(lactic-co-glycolic acid) (PLGA) refers to a copolymer of lactic acid and glycolic acid (Makadia and Siegel, 2011). Hydrolysis of ester linkages leads to degradation into lactic and/or glycolic acids, which are natural products of human metabolism. PLGA has been approved by the United States Food and Drug Administration (FDA) and the European Medicines Agency (EMA) for use in a wide range of applications (Han et al., 2016). It has been extensively investigated for the delivery of nucleic acids, proteins, and peptides, and hydrophilic and hydrophobic small-molecule drugs (Makadia and Siegel, 2011).

Drug release from PLGA microparticles occurs via diffusion and homogeneous bulk erosion of the matrix (Klose et al., 2006). Drug release from PLGA microparticles can be extended by increasing the molecular weight of PLGA polymers (Klose et al., 2006). Lactic acid is more hydrophobic than glycolic acid because it has a methyl substituent at the α -carbon of glycolic acid rather than a hydrogen. As a result, increasing the molar ratio of lactic acid in PLGA polymers reduces their capability to absorb water molecules and decreases their degradation rate (Visscher et al., 1985; Visscher et al., 1986; Visscher et al., 1988).

Poly(ϵ -caprolactone) (PCL). Poly- ϵ -caprolactone (PCL) is an aliphatic polyester which is usually synthesized by ring-opening polymerization of ϵ -caprolactone using a wide range of catalysts (Chasin, 1990). The degradation rate of PCL is slow due to its hydrophobicity and high crystallinity (Sinha et al., 2004; Kweon et al., 2003). The hydrolytic degradation of PCL microspheres can proceed via both surface and bulk erosion pathways (Woodruff and Huttmacher, 2010). Increasing the molecular weight of PCL polymers decreases the drug release rate from PCL-based devices (Woodruff and Huttmacher, 2010). Modulation of porosity has also been used to alter the degradation of PCL microparticles. Strong hydrogen bonding between the encapsulated drug and the PCL matrix can further extend the duration

of drug release (Rai et al., 2016). PCL microparticles have been widely used for drug-delivery applications (Woodruff and Hutmacher, 2010). For example, 100 μm PCL microspheres showed sustained release of the antibiotic vancomycin over 50 days (Rai et al., 2016). Albumin-loaded PCL microparticles 30 μm in diameter exhibited burst release within the first 24 h followed by continuous release over 28 days (Youan et al., 1999).

Poly(ortho ester) (POE). Poly(ortho esters) (POEs) are another class of synthetic polymers designed specifically to inhibit drug release by diffusion and to only allow drug release after the hydrolysis of polymer chains on the surface of particles (Heller et al., 2002). POEs can be readily synthesized by addition of diols or polyols to diketene acetals (Heller, 1993). Poly(ortho esters) are surface-eroding polymers (Heller, 1985). The drug release duration from POE microparticles can be altered by changing the molecular weight and hydrophilicity of the diol monomers (Heller and Barr, 2004). Modification of the POE backbone with lactic acid or glycolic acid increases the degradation rate (Heller et al., 2002). POE microparticles have been used to deliver various payloads including hydrophobic (Deng et al., 2003) and hydrophilic (Schwach-Abdellaoui et al., 2002) drugs, proteins (van de Weert et al., 2002), and nucleic acids (Wang et al., 2004). For example, POE microparticles have shown continuous release of entrapped albumin for over 40 days. Poly(ortho ester) microspheres have been designed to protect loaded DNA from degradation and improve uptake by phagocytic antigen-presenting cells (Wang et al., 2004).

Polyanhydrides. Polyanhydrides are hydrophobic polymers with water-sensitive linkages, which can readily react with water molecules to form carboxylic acids (Rosen et al., 1983). They can be synthesized from aromatic or aliphatic diacids by many methods, including melt condensation, ring opening polymerization, and dehydration (Leong et al., 1987). The degradation of polyanhydride particles is believed to occur through surface erosion, and release kinetics can be close to zero-order (Rosen et al., 1983). The degradation rate can be controlled by changing the polymer composition. Polyanhydrides synthesized with more hydrophobic monomers have slower erosion by reducing water penetration. Aromatic polyanhydrides have much slower degradation compared to aliphatic ones (Leong et al., 1985). Polyanhydrides are FDA approved for use in humans (Katti et al., 2002; Kumar et al., 2002) and have been extensively studied for drug delivery (Mathiowitz et al., 1997).

Polyacetals. Polyacetals and polyketals are acid-labile polymers in which two ether bonds are connected to the same carbon atom. Their pH-triggered degradation is of interest since acidosis is associated with many diseases such as cancer and inflammatory diseases (Heffernan and Murthy, 2005). Degradation of ketal bonds produces neutral products (ketones and diols) instead of acidic ones (Lee et al., 2007). Polyketal microparticles have been used to deliver siRNA (Lee et al., 2009), DNA (Goh et al., 2004), and proteins (Kumar et al., 2002; Lee et al., 2007; Heffernan et al., 2009) for the treatment of acute inflammatory

disease, ischemic heart disease, and cancer, respectively. Conventional polyketal particulate formulations have relatively short durations of drug release. Microparticles prepared from an estradiol-polyketal conjugate—in which the drug was incorporated into the polymer backbone—showed increased loading efficiency and significantly prolonged drug release (Guo et al., 2016).

PEGylation. Poly(ethylene glycol) (PEG) has been one of the most widely used polymers for biomedical applications including microparticle-based drug-delivery systems, due to its biocompatibility and low immunogenicity (Wattendorf and Merkle, 2008). Due to its neutral charge and hydrophilicity, PEG has been extensively used in tuning the loading efficiency and hydrolytic degradation rate of microparticles. For example, in the preparation of microparticles with diameters ranging from 2 to 10 μm for the delivery of ovalbumin, blending PLGA with poly(ethylene glycol) increased the protein entrapment fourfold (Yeh et al., 1995).

Smart polymers. Smart polymers are designed to undergo changes in conformation, phase, integrity, and volume due to physical, chemical, or biological changes (stimuli) in the surrounding environment (Aguilar and San Román, 2014). There has been considerable interest in the development of drug delivery systems made of such “smart” polymers (Liu et al., 2016), where the release of payload can be accelerated or slowed as a result of stimuli. There are numerous smart polymers for biomedical applications (Mura et al., 2013; Bajpai et al., 2008); here we will focus on pH- (Haining et al., 2004) and thermo-responsive polymers due to their prevalence in the field (Oh et al., 2008; Lyon et al., 2009).

Local pH can vary in different organs, tissues, and cellular compartments (Lu et al., 2017). pH-responsive polymers can allow the fabrication of devices that are intact (and don't release drug) at one pH, but swell or degrade or dissolve at another pH (and release drug). For example, pH-responsive poly(acrylic acid) microspheres 200–300 μm in diameter have been developed to deliver the antiinflammatory drug diclofenac sodium (DS) to the intestines following oral administration (Kurkuri and Aminabhavi, 2004). In the acidic environment of the stomach, the acrylic acid remains in a neutral, protonated state, and the microparticles therefore remain intact, preventing drug release. In the relatively alkaline intestine, the acrylic acid is deprotonated and the particles swell due to increased hydrophilicity and electrostatic repulsion, which induces the accelerated release of payload (Kurkuri and Aminabhavi, 2004). In another example, particles with an acid-labile polymer were used to produce 4–6 μm microparticles carrying a peptide antigen for a vaccine (Haining et al., 2004). Phagocytosis of the particles by antigen-presenting cells into the acidic environment of the phagosome led to rapid intracellular release of the antigen, enhancing antigen presentation and cytotoxic T lymphocyte responses (Haining et al., 2004).

Thermo-responsive polymers can undergo a dynamic phase transition as a result of a temperature-dependent

change in the hydrogen bonding network (Ward and Georgiou, 2011), usually called a “solution–gel transition” (Jeong et al., 2012). Temperature-induced transition from the solution state to the gel state may significantly decrease the release of encapsulated payloads. In one relatively common application, polymers have been made which are liquid at a lower temperature (e.g., room temperature) but become gel-like at a higher temperature (e.g., body temperature); this is referred to as reversed thermal gelation. Thus, when injected into the body, the polymers are heated above a given temperature (the lower critical solution temperature, LCST) and become gel-like, and, being more viscous, slow the release of drugs. For example, 1–3 μm N-isopropyl acrylamide (NIPAAm) microgels with an LCST of 32° enabled sustained release of fibroblast growth factor over 14 days (Joshi et al., 2013). Thermo-responsive microgels that undergo volume expansion at higher temperatures (above an upper critical solution temperature, UCST) have also been described (Serrano-Ruiz et al., 2013). These $\sim 5 \mu\text{m}$ spherical microgels, composed of random copolymers of acrylic acid (AAc) and acrylamide (AAm), swelled by 60% when heated from 37 to 45°C.

Other degradable synthetic polymers. Many other biodegradable polymers have been synthesized for the fabrication of microparticles; we provide a few examples here. Poly(vinyl alcohol) (PVA) is a swellable hydrophilic polymer widely used for medical applications such as contact lenses, implants, and artificial organs (Baker et al., 2012). PVA microparticles 150–1400 μm in diameter have been studied for the prolonged release of proteins (Ficek and Pappas, 1993). Poly(2-hydroxyethyl methacrylate) (PHEMA) has been widely used in biomedical applications, such as contact lenses (Nicolson and Vogt, 2001) and implants (Chirila et al., 1993). Mucoadhesive PHEMA microspheres 300–400 μm in diameter have been studied for prolonged release of protein drugs to the intestine (Lehr et al., 1992). Poly(3-hydroxybutyrate-co-3-hydroxyvalerate) (PHBV) microspheres have also been studied for the delivery of chemotherapeutics (Khang et al., 2001) and antibiotics (Sendil et al., 1999).

Nonpolymeric Materials

Microparticles can also be prepared from nonpolymeric materials. We will focus on liposomes and lipid microparticles here since they are most extensively investigated for biomedical applications.

Liposomes are spherical particles composed of phospholipid bilayers. They can be smaller than 100 nm in diameter (Kirby et al., 1980), or tens of μm across (Akashi et al., 1996). Liposomes have been successfully translated into clinical use due to their biocompatibility (Bulbake et al., 2017), and can be used to encapsulate hydrophilic drugs within the inner water phase and hydrophobic drugs within the lipid membranes (Sharma and Sharma, 1997). Liposomes have been used for the encapsulation and release of various payloads, including chemotherapeutics (Barenholz,

2012), protein drugs (Tan et al., 2010), and nucleic acids (Balazs and Godbey, 2011). Drug release from liposomal carriers can be tuned by changing the composition of phospholipids (Gabizon et al., 1990) and incorporation of cholesterol (Coderch et al., 2000). Coencapsulation of drugs and sensitizers enabled drug release from liposomes that can be triggered by external stimuli such as light and ultrasound (Rwei et al., 2015; Zhan et al., 2015; Rwei et al., 2017).

Lipid vesicles consist of a hydrophobic core surrounded by a layer of surfactant (Jaspart et al., 2005). Various lipids can be used for the fabrication of solid lipid microparticles, including triglycerides, fatty acids, steroids, or a combination of these (Scalia et al., 2015). A hydrophobic payload is dispersed in the solid lipid matrix (Jaspart et al., 2007). Solid lipid microparticles can be well tolerated in the body since they are composed of biocompatible and degradable lipids. Naturally occurring surfactants such as phosphatidylcholine and bile acids are usually used to minimize potential safety concerns. Inflammation may occur in the surrounding tissues following subcutaneous administration of lipid particles (Reithmeier et al., 2001).

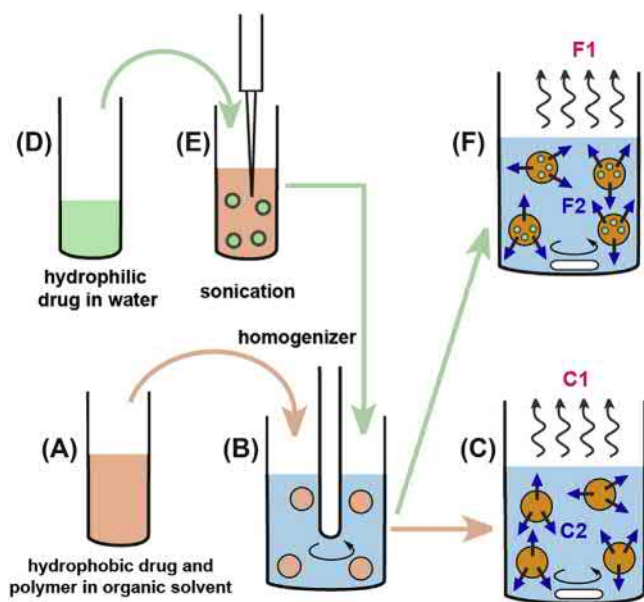
Microparticle Preparation

Many methods have been described for the fabrication of microscale particulate systems include single and double emulsion, coacervation, and spraying drying. Here we described some of the more commonly employed ones.

Single and double emulsion. Emulsification followed by solvent evaporation (or extraction into a second solvent) is one of the most commonly used techniques in microparticle preparation, particularly for drug encapsulation (Fig. 1.3.8A.2) (Lee et al., 2016). The polymer, along with a drug, is dissolved in solvent. The solution of drug and polymer is then dispersed (by homogenization or another form of mechanical agitation) in an immiscible liquid: e.g., an organic solvent, or “oil,” in water (O/W emulsion). In this section, we will focus on the O/W emulsion, but an analogous approach disperses water in the oil [W/O emulsion (Xu et al., 2012)]. The O/W method is generally used for the microencapsulation of hydrophobic drugs, and sometimes for hydrophilic ones. (To encapsulate hydrophilic drugs using the O/W method, either a double emulsion [W/O/W] method is used, or solid forms of the hydrophilic drug are dispersed in the oil phase (Thomas et al., 2004).

The dispersion described above forms emulsion droplets. PLGA microparticles can be prepared by O/W emulsion. To prevent droplet coalescence, surfactants such as polyvinyl alcohol are used, and the emulsions are continuously stirred.

In an O/W system (e.g., PLGA and hydrophobic drug both dissolved in an organic solvent dispersed in water), microparticles harden as the volatile organic solvent diffuses out of the droplets. Solvent evaporation is often performed at atmospheric pressure, or can be accelerated by use of negative pressure and/or heating. The solvent can also be extracted



• **Figure 1.3.8A.2** Example of microspheres production by the emulsion system. (A–C) The single emulsion system, for encapsulating hydrophobic drugs. (A) A hydrophobic drug and polymer are dissolved in an organic solvent. (B) They are then poured into an aqueous solution of a surfactant [poly(vinyl alcohol)] under agitation, forming droplets (i.e., an emulsion) of organic solvent (with drug and polymer) dispersed in water (O/W). (C) The droplets in the emulsion are allowed to harden, by solvent evaporation (C1) or extraction (C2) under gentle agitation. (D–F) The double emulsion system, for coencapsulating hydrophilic drugs. (D) A hydrophilic drug is dissolved in an aqueous solution. (E) It is then mixed under agitation with the solution in (A), forming a primary emulsion (W/O) of aqueous droplets dispersed in organic solvent. This emulsion is then treated as in step (B), forming the secondary emulsion of droplets of organic solvent (with solutes) containing aqueous droplets (with solutes) as shown in (F); W/O/W. The droplets in the emulsion are allowed to harden by solvent evaporation (F1) or extraction (F2) under gentle agitation. O = oil, i.e., organic solvents immiscible with water; W = water, i.e., aqueous solvents.

by introducing a second liquid into the external phase, into which the first solvent is miscible, but the polymer and drug are not soluble. This process is termed solvent extraction. An example of this approach is placing isopropyl alcohol in the external aqueous phase surrounding an O/W emulsion; the methylene chloride in the internal organic phase is miscible in it and will be extracted, but PLGA is not and will remain in the nascent particle. With some drugs (e.g., relatively hydrophilic ones), acceleration of hardening can greatly improve drug loading by entrapping drugs before they can partition into the external aqueous phase. However, rapid solvent evaporation often results in more porous microspheres.

The outcome of particle production by emulsification is affected by a wide range of parameters, including the geometry of the system, the concentration of each ingredient, polymer molecular weight, solution viscosity, method and speed of solvent extraction, emulsifier type and concentration, osmolarity and pH of the external phase, and others. The effects of the method of mechanical agitation are particularly obvious. For example, the speed of homogenization is inversely related to the size of the resulting particles, and to

the polydispersity of size (i.e., faster homogenization yields smaller but more uniform particles).

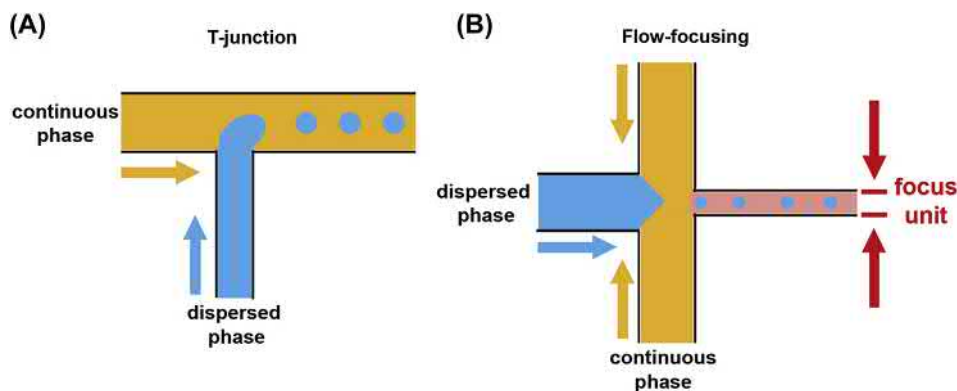
The double emulsion process or water-in-oil-in-water (W/O/W) method is often used for the encapsulation of hydrophilic drugs of all sizes. The therapeutic payload is dissolved in water, which is then dispersed in an organic solvent (oil) containing a polymer (and optionally hydrophobic drugs), forming a primary emulsion (Dorati et al., 2008). That emulsion is then dispersed in an aqueous phase, forming a secondary emulsion (W/O/W). The double emulsion system is otherwise analogous to the single emulsion system.

Microfluidic emulsion. Microparticles prepared by emulsification may be relatively polydisperse in size (Sandsdrap and Moës, 1993). Microfluidic technologies offer precise control over the flow rate of fluid, which facilitates the continuous, reproducible, scalable production of microparticles with precise tunable compositions, structures, and polydispersities (Wang et al., 2013; Duncanson et al., 2012; Wang et al., 2017).

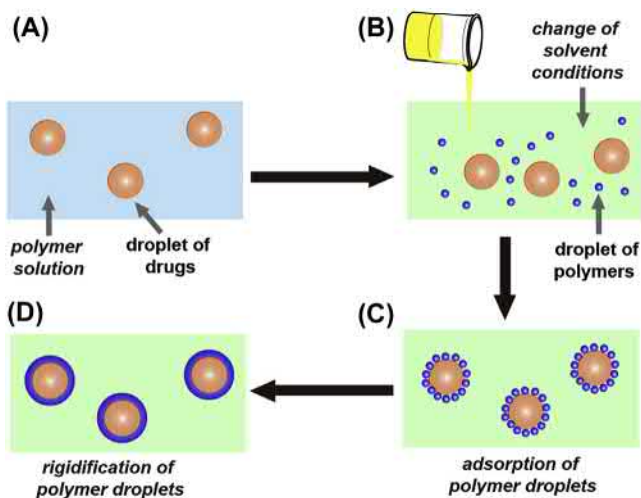
The generation of microparticles involves the formation of a dispersed phase (containing drug and polymer) in an immiscible continuous phase by a device with either a T-junction or a flow-focusing nozzle (Fig. 1.3.8A.3). The viscous shear force in the T-junction breaks up the immiscible two-phase mixture into droplets (Li et al., 2018). With flow-focusing, the dispersed phase is surrounded by the continuous phase before going through a focus unit with a diameter smaller than that of the channel providing the dispersed, which enhances the viscous shear forces and enables the formation of droplets (Li et al., 2018).

Coacervation phase separation. Coacervation relies on the changes in solubility of polymers, leading to phase separation and microparticle formation (Alvim and Grosso, 2010; Reverchon et al., 2008) (Fig. 1.3.8A.4). Polymers are dissolved in an organic solvent, in which drugs are dispersed in aqueous droplets (Fig. 1.3.8A.4A). A change of solution conditions [e.g., mixing with another component (Yeo et al., 2005) or changing the solvent system (Kaibara et al., 2000) so that the polymer(s) are no longer soluble] leads to the formation of polymer droplets (Fig. 1.3.8A.4B). These polymer droplets are adsorbed onto the surface of the aqueous (drug) droplets and coalesce into a coating (Fig. 1.3.8A.4C). Microparticles are obtained after rigidification of polymer droplets by washing, centrifugation, and lyophilization (Fig. 1.3.8A.4D). In a typical coacervation process for the encapsulation of proteins into PLGA microparticles (Nihant et al., 1995), the PLGA was first dissolved in methylene chloride. An aqueous solution of albumin was dispersed in the PLGA solution leading to the formation of albumin droplets. A polymer (silicone oil) immiscible with the PLGA solution was added to the dispersion, which caused the formation of PLGA droplets and its adsorption onto the surface of the albumin droplets. Albumin-loaded PLGA microparticles were obtained by washing with heptane, centrifugation, and lyophilization.

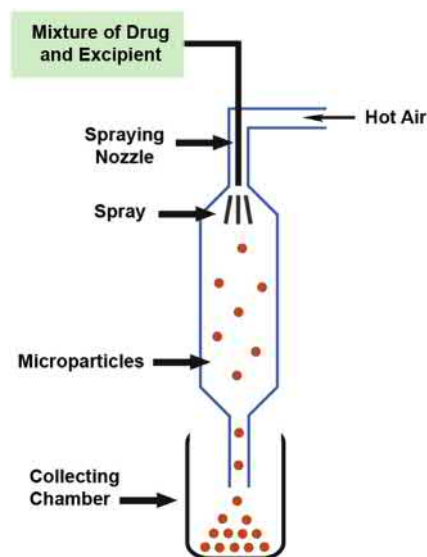
Coacervation has a relatively high loading efficiency. It can be operated at low temperature, which is particularly suitable for the encapsulation of sensitive payloads like



• **Figure 1.3.8A.3** Schematic illustration of chip designs for microfluidic devices. (A) A T-junction microfluidic device with planar rectangular channels where the dispersed phase (blue) is injected into a perpendicular stream of the continuous phase (yellow). (B) A flow-focusing device where the dispersed phase (blue) encounters continuous phase (yellow) coming from two perpendicular side channels before entering a narrow focusing unit (red).



• **Figure 1.3.8A.4** Schematic illustration of coacervation. (A) Dispersion of drug droplets (orange) in the polymer solution (blue). (B) Formation of polymer droplets (blue) by changing solution conditions (green). (C) Adsorption of polymer droplets onto the surface of drug droplets. (D) Rigidification of polymer droplets by washing, centrifugation, and lyophilization.



• **Figure 1.3.8A.5** Schematic illustration of microparticle production by spray drying. A mixture of drugs and excipients is sprayed through a nozzle into a chamber where hot air evaporates the solvent and leads to the formation of microspheres.

insulin (Black et al., 2014). Microencapsulation via coacervation phase separation has been used for the delivery of various payloads, including hydrophilic drugs (Thote et al., 2005), hydrophobic drugs (Dong and Bodmeier, 2006), and proteins (Jay and Saltzman, 2009).

Spray drying. This technique involves dispersion of drugs and/or excipients in a solvent system, which is then sprayed through a fine nozzle into a chamber (Fig. 1.3.8A.5) (Bakry et al., 2016). The hot air within the chamber causes the evaporation of the solvent, forming microparticles. Since the droplets are traveling through air during hardening, there is no external phase for drugs to escape to. Consequently, drug loading can be essentially whatever was put into the sprayed solution, and can be very high. Microparticles prepared by this method are usually 1–100 μm in diameter (Jain, 2000; Wagenaar and Müller, 1994).

Drug–polymer interactions, solution viscosity, and nozzle characteristics are important determinants of particle properties. Spray drying has been used with synthetic polymers such as PLGA, PLA, and PCL, natural polymers including gelatin and chitosan (Vehring, 2008), and other excipients (Edwards et al., 1997). Many parameters influence particle size, including nozzle radius, chamber temperature, air and solvent flow rate, and pressure. Mass loss due to particle aggregation and adhesion to the chamber walls can markedly curtail yield.

Characterization of Microparticles

There are a number of characterizations that are routinely done after manufacture of microparticles. The purpose is to verify that they are intact and of the expected size, shape,

and charge; to assess their drug loading, release, and degradation, etc. These studies are crucial to guide optimization and for quality control.

Morphology. Light microscopy can provide a quick qualitative assessment of the size and shape of particles, particularly if one of the eyepieces is equipped with a reticle. More detailed images of surface features (e.g., pores and defects) can be obtained by electron microscopy (EM) [i.e., scanning electron microscope (SEM) and transmission electron microscopy (TEM)]. Fig. 1.3.8A.6A shows a representative SEM image of PLGA microspheres, showing a spherical shape with a smooth surface (Zhao and Rodgers, 2006). EM also provides a qualitative appreciation of size distribution. Fluorescence microscopy, such as confocal laser scanning microscopy (CLSM) can also be used to visualize fluorescent dyes or drugs encapsulated in microparticles (Fig. 1.3.8A.6B) (Guo et al., 2016).

Size and polydispersity. Light scattering is the most commonly used method for measuring the size and polydispersity of particles (Lawrie et al., 2009). It measures particle size based on the intensity of the scattered light passing through a medium, which changes with many parameters including the size of particles in the medium (Goldburg, 1999). Light scattering is often confirmed by other techniques such as microscopy.

The Coulter counter is another tool for the measurement of size and concentration of particles (Henriquez et al., 2004). It has been used with nanoparticles, microparticles, cells, and viruses (Zhe et al., 2007). Particle size measurement is performed by allowing a suspension of microparticles to flow through a microchannel which separates two chambers containing electrolyte solutions. When particles pass through the channel, there is a transient change in the electrical resistance of the channel (DeBlois and Bean, 1970), which is correlated with the size, shape, surface charge, and concentration of the particles (Qin et al., 2011).

Surface charge. Surface properties of colloidal particles play a critical role in their physical stability as well as their interactions with cells (Zhang et al., 2008) and biomacromolecules (Singh et al., 2000). Zeta potential is a commonly used

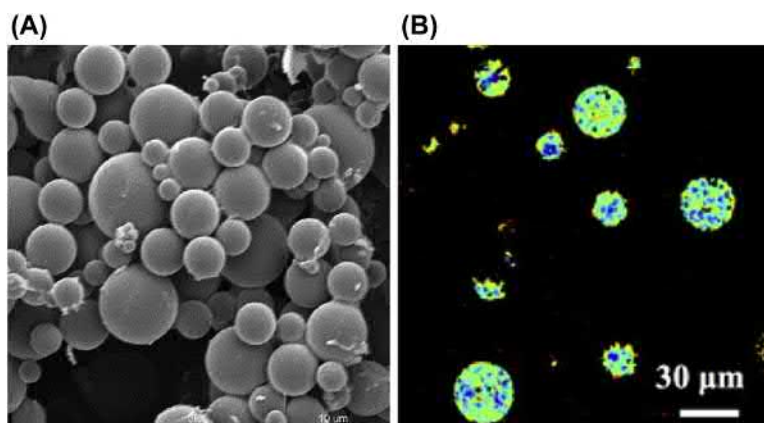
measure of the electrokinetic potential at the interface of a colloid particle and its surrounding medium (Bhattacharjee, 2016). Microparticles with a large absolute value of zeta potential are more stable in suspension and less likely to aggregate, due to the particles' mutual repulsion. Cationic particles are often suitable for delivery of nucleic acids (which are anionic) (Singh et al., 2000). For example, PLGA microparticles with positively charged surfaces can adsorb negatively charged plasmid DNA for gene delivery (Denis-Mize et al., 2000).

Other physicochemical properties. Infrared spectra (IR or FTIR) can be used to analyze interactions between the payload and microparticle matrix, such as hydrogen bonding (Huang et al., 2008). Atomic force microscopy (AFM) can provide information on particle shape, size, and morphology. AFM is often used to quantify a particle's elastic modulus (Moner-Girona et al., 2003), its adhesion to surfaces, and deformation (Vakarelski et al., 2001). AFM can measure the surface tension of colloidal particles, which is the surface energy per unit area (Cuenot et al., 2004). Colloidal particles with large surface tensions tend to aggregate in aqueous suspension. X-ray photoelectron spectroscopy (XPS) can provide information on the chemical composition of the particle surface, including the presence of biomolecules, dopants, and drugs.

Drug loading. Two parameters are commonly used in the evaluation of microencapsulation: drug encapsulation and encapsulation efficiency. The drug encapsulation is the ratio of the measured mass of encapsulated drug to the measured mass of drug and excipients. Encapsulation efficiency is a metric of how well the encapsulation process works, and is the ratio of the measured drug content of a given mass of particles to the theoretical content (i.e., the mass of drug used in creating the particles). Various methods have been used for the quantification of drugs, including UV absorption, liquid chromatography, and enzyme-linked immunosorbent assays.

$$\text{Drug Encapsulation (\%)} = \frac{\text{Mass of encapsulated drug}}{\text{Mass of microparticle}} \times 100$$

$$\text{Encapsulation efficiency (\%)} = \frac{\text{Mass of drug encapsulated}}{\text{Mass of drug used}}$$



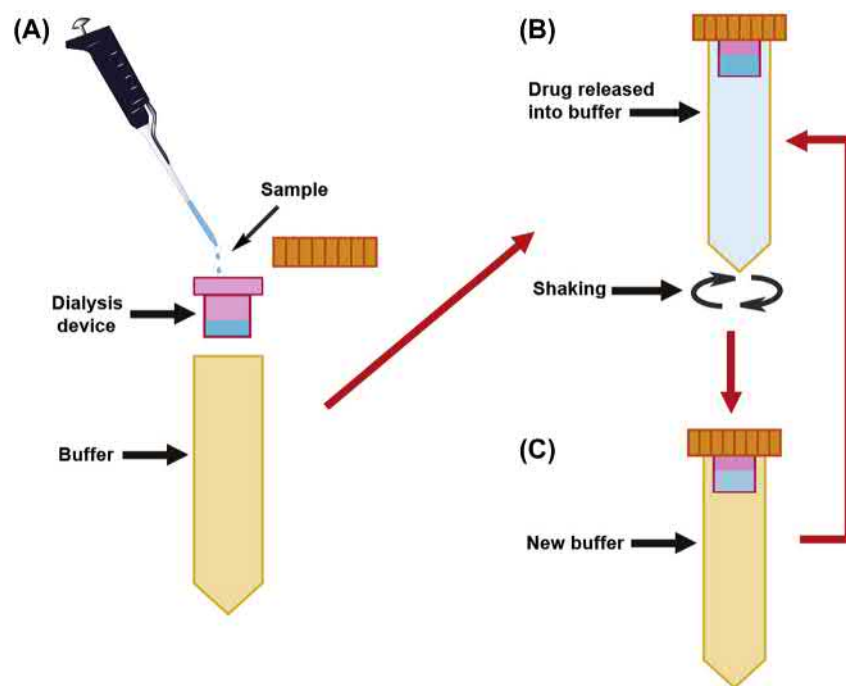
• **Figure 1.3.8A.6** Morphology of microparticles. (A) SEM image of PLGA microspheres (Zhao and Rodgers, 2006). (B) Confocal laser scanning microscopy image of rhodamine-loaded polyketal microparticles (Guo et al., 2016).

Release Kinetics. In polymeric drug-delivery systems, an initial rapid release is often observed, termed “burst release” (Huang and Brazel, 2001). In most cases, burst release results from drug located near the surface of microparticles (Mao et al., 2007) or drug diffusion to the surface during fabrication or storage, especially in porous systems (Yeo and Park, 2004). While a rapid initial release of encapsulated drugs may be desirable in certain circumstances, burst release may lead to excessive drug levels, causing toxicity which can be either systemic (Verrijck et al., 1992) or local (Padera et al., 2008). It is also potentially wasteful of drug, which might be better used—if released more slowly—to extend the duration of effect. Burst release of payload from microparticles can be reduced by using more hydrophobic polymers or materials (Huang and Brazel, 2001), polymers with higher molecular weight (Cohen et al., 1991), decreasing pore size (Wang et al., 2002), or increasing particle diameter (Berkland et al., 2002). The subsequent release kinetics can similarly be fine-tuned by altering key design parameters of microparticles such as material composition (Makadia and Siegel, 2011), size (Mitrugotri and Lahann, 2009), morphology (Champion et al., 2007), and surface properties (Yoo et al., 2011). Drug release from microparticles can also be made inducible by stimuli in cellular compartments such as phagosome pH (Haining et al., 2004), or external stimuli such as heating (Lopes et al., 2013).

Release kinetics should be tested in a system that reflects the properties of the intended site of use in vivo, including temperature, pH, fluid turnover, shear forces, and other factors that may potentially impact the drug release

behavior (D’souza and DeLuca, 2006). However, the correlation between in vitro release kinetics and in vivo findings is generally (although not always) poor. Another common method of assessing release kinetics is using “infinite sink” conditions, using a system where drug release is not impeded by accumulating drug levels in the external aqueous phase. (The latter is particularly important with hydrophobic drugs.) There are many ways to study release kinetics in this way. Particles may be suspended in a buffer solution, then spun down at predetermined intervals (Padera et al., 2008; McAlvin et al., 2013); the supernatant (“release medium”) is removed for analysis then replaced. Alternatively, the particles may be placed in a dialysis bag then immersed in buffer (Zhou et al., 2016); the buffer outside the bag is removed for analysis at predetermined intervals (Fig. 1.3.8A.7). Preventing drug accumulation in the release media may involve relatively large volumes of buffer, or frequent replacement. Frequent sampling is particularly important early on in the release experiment, due to possible burst release. In studies in infinite sink conditions, the goal is not to mimic the rate of drug release in vivo, but to study the inherent ability of the particle to control drug release. Such studies can be useful for optimizing particles in vitro.

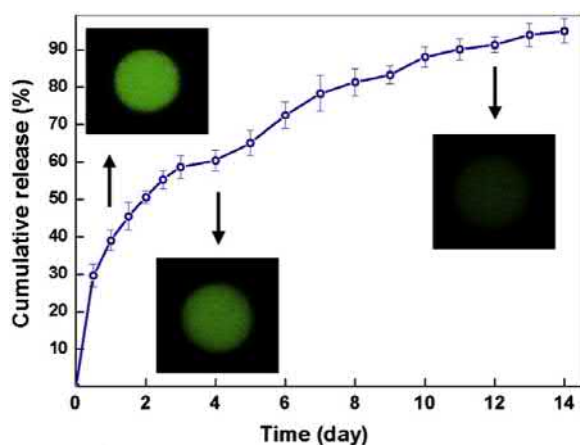
The technique used for quantification of drug concentrations in release media depends on the nature of the encapsulated payload. Commonly used methods include enzyme-linked immunosorbent assays (ELISAs), high-performance liquid chromatography (HPLC), UV spectrophotometry, and liquid chromatography-mass spectrometry (LC-MS).



• **Figure 1.3.8A.7** Schematic illustration of a release experiment. (A) A sample is placed into a dialysis device which is placed into buffer. (B) The system is agitated at an appropriate temperature. (C) At predetermined intervals, the dialysis buffer is removed for analysis and replaced, after which the process returns to (B).

Drug release kinetics are often represented graphically with time on the x-axis and drug release on the y-axis. The y-axis often represents cumulative release, i.e., each time point shows the total release of drug up to that point. The y-axis is also often the drug release at the particular time points studied. In a representative release of insulin from microparticles (Fig. 1.3.8A.8), burst release was observed in the first 2 days, followed by slower release over 14 days (Zhang et al., 2011).

Mathematical modeling can help predict drug release from a polymeric drug-delivery system (Siepmann and Göpferich, 2001). It may offer insights regarding potential approaches to release therapeutic levels of drugs for a prolonged duration as well as reduce systemic toxicities. Mathematical modeling of drug release from microparticles has been reviewed elsewhere (Brazel and Peppas, 2000; Narasimhan, 2001; Weiser and Saltzman, 2014).



• **Figure 1.3.8A.8** Cumulative release over time of Alexa Fluor 488 labeled insulin release from chitosan-modified alginate microspheres (Zhang et al., 2011). Insets are laser scanning confocal microscopy images of Alexa Fluor-488-insulin in microspheres at selected time points.

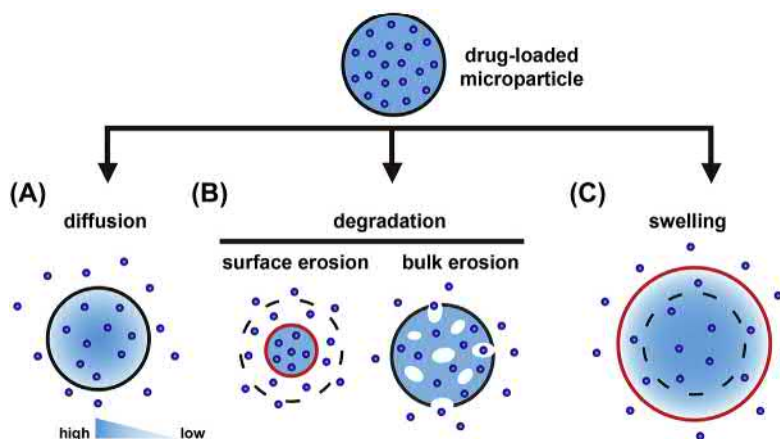
Drug Release Mechanisms

Drug release is a transport process in which a drug migrates from within the matrix or from the surface of drug carriers to the surrounding environment (Langer, 1990). Classic drug release mechanisms include diffusion, degradation, and swelling (Fig. 1.3.8A.9); release from microparticles can (and usually does) happen by more than one mechanism. Particle design parameters including composition, size, and geometry all play important roles in determining the drug release mechanism and kinetics.

Diffusion. Diffusional release is driven by the chemical potential gradient across the matrix of the drug-delivery system to the outside, and affected by the physicochemical properties of the microparticles, such as permeability/porosity, thickness, and electrochemical interactions if any between drug and particle. This is a prominent drug release mechanism in many drug-delivery depot systems (Fu and Kao, 2010).

Degradation. Polymers containing ester, amide, and anhydride bonds are most commonly used in the fabrication of biodegradable microparticles. “Degradation” refers to the cleavage of these chemical bonds by hydrolysis or enzymatic degradation in the body (Uhrich et al., 1999). Some excipients’ degradation can be accelerated by environmental factors such as pH and enzymatic activity (see “Smart Polymers” section). Degradation leads to particle erosion, i.e., the depletion of materials (Batycky et al., 1997). There are two principal types of erosion of polymeric materials, surface and bulk erosion.

Surface erosion occurs when the degradation of polymeric materials is confined to the exterior surface of particles as a result of slow water penetration (Uhrich et al., 1999). Surface-eroding microparticles are usually composed of hydrophobic monomers prohibiting penetration of water molecules. Examples of surface-erodible systems include poly(anhydrides) and poly(ortho esters). Surface erosion



• **Figure 1.3.8A.9** Classic mechanisms of drug release from microparticles. (A) Diffusion driven by chemical potential gradient. (B) Degradation at the surface or throughout the matrix of microparticles. In surface erosion, the size of a microparticle decreases due to mass loss. (C) Swelling-driven drug release due to increased mesh size of the polymer network. In (B) and (C), dashed lines indicate the original boundary of microparticles and red lines indicate the boundary of microparticles after erosion or swelling.

leads to zero-order drug release, where the release rate is proportional to the surface area (Möckel and Lippold, 1993). Slow water penetration in surface-eroding materials may be desirable for the delivery of water-labile drugs.

Bulk erosion occurs when water molecules are able to easily penetrate into the bulk of the polymer, which results in homogeneous depletion of the entire matrix. Many biodegradable polymers used in the fabrication of microparticles are bulk-eroding systems, such as those based on poly(ester) polymers. For many biodegradable systems, the erosion of the polymer matrix occurs by a combination of bulk and surface erosion, the relative proportion depending on the chemical structure of the polymers (von Burkersroda et al., 2002).

Swelling. Swelling of particles can accelerate the release of entrapped payloads. Simple hydration of polymer chains may lead to the swelling of microparticles and accelerate release of payload (Keegan et al., 2012). Swelling is the basis of some stimulus-sensitive drug-delivery systems. Physical or chemical changes in the environment trigger the swelling, which allows release of entrapped drugs due to the increased mesh size of the polymer network. Most microparticles that release drugs primarily through swelling are hydrogels containing noncovalent cross-links such as alginate microgels (Lee et al., 2000). Hydrogels are three-dimensional networks of hydrophilic polymers that can be fabricated into various forms including microparticles (Hoare and Kohane, 2008). An example of triggered swelling is seen with poly(vinylpyridine) microparticles: the amine groups were protonated when the ambient pH decreased from 7.4 (physiological pH) to 4.5, causing electrostatic repulsion, which in turn caused swelling and release of the encapsulated antiseptic compound cetylpyridinium chloride (Bradley and Vincent, 2008). Temperature has also been used as the trigger for swelling: microgels made of the thermo-responsive polymer poly(acrylic acid)-*b*-poly(acrylamide) swelled by 60% when the ambient temperature increased from 37 to 45°C (Serrano-Ruiz et al., 2013).

Biomedical Applications of Microparticles

Drug Delivery

Microparticles have been predominantly investigated for drug-delivery applications. Microparticles have been used for the delivery of a wide range of drugs by different routes of administration, singly or in combination. The literature on the encapsulation of small-molecule (and other) drugs is very large, and has also been reviewed extensively (Edlund and Albertsson, 2002; Lam and Gambari, 2014; Ramazani et al., 2016). Here we focus on a few relatively specialized topics.

Encapsulation and Sustained Release of Biopharmaceuticals. Microencapsulation has been widely used for sustained release of nucleic acids (Guliyeva et al., 2006) and proteins (Putney and Burke, 1998). However, the encapsulation of biological pharmaceuticals like proteins and

nucleic acids poses substantial challenges due to their large size (Radomsky et al., 1990), high viscosity (Yadav et al., 2010), and lability (Mitragotri et al., 2014) compared to small molecules. The preservation of their intrinsic structural complexity, crucial for their therapeutic potency and specificity, may also be difficult. Factors during formulation and storage such as organic solvents and high temperature may lead to denaturation and loss of activity (Sah, 1999). In addition, they are susceptible to enzymatic or hydrolytic degradation (Estey et al., 2006) following administration.

Improving the loading efficiency can be important for achieving long-term release of protein drugs. The loading capacity of proteins can be improved by changing the composition (Han et al., 2016), molecular weight (Blanco and Alonso, 1998), the mass ratio of polymers and proteins (Rafati et al., 1997), formulation method (Bilati et al., 2005), incorporation of surfactants (De Rosa et al., 2000) and formation of amorphous glasses using sugars or polyols (Weers et al., 2007). The release of peptide and protein drugs from microspheres can be tuned by changing key structural parameters such as particle size (Park et al., 2006), surface pore diameter (Kim et al., 2006), and others. Surface modification of microparticles such as PEGylation, which significantly decreases the uptake of drug-loaded microparticles by macrophages, has also been used to improve the sustained release of protein drugs (Simón-Yarza et al., 2013). The sustained release of microencapsulated proteins can vary from days to months (Ye et al., 2010), depending on the formulation. Further detail on the encapsulation of proteins and nucleic acids can be reviewed elsewhere (Mitragotri et al., 2014; Ye et al., 2010; Bhavsar and Amiji, 2007; Luo et al., 1999).

Local Injection. Most commonly, microparticles are delivered by injection at a specific site in the body, where they act as a depot, for local or systemic effect. They are very well-suited to situations where a therapeutic drug level is desired at a specific location, with minimal systemic drug distribution. This is well illustrated by microparticles used to prolong local anesthesia (Santamaria et al., 2017; McAlvin and Kohane, 2014). A variety of local anesthetics, with or without other compounds that enhance their performance, have been encapsulated in many different types of microscale vehicles composed of a range of materials. They are injected along the course of a peripheral nerve, where the resulting high drug concentration and sustained release provide local anesthesia that can last hours to days, much longer than could be safely achieved by free drug. Systemic drug distribution—and therefore toxicity—is minimal. Conceptually similar devices have been used to treat conditions in many other organs, such as the heart (Sy et al., 2008), brain (Kohane et al., 2002; Tamargo et al., 2002), eyes (Lavik et al., 2011), and others.

Microparticles can also be used to provide prolonged systemic drug delivery from a single injection, often with relatively zero-order release kinetics. Such formulations are useful for convenience and patient compliance (Kohane and Langer, 2005). Microparticles loaded with growth hormone

deposited in soft tissue can slowly release the drug for effect throughout the body (Johnson et al., 1996). Similarly, microparticles containing psychoactive medications can provide a prolonged effect (Lu et al., 2014; Ramstack et al., 1997).

Microparticles can also be delivered through the major portals of delivery into the body. They can be ingested or delivered by enema, for treatment of local conditions within the gut (Lamprecht et al., 2000) (e.g., inflammatory bowel disease), or for systemic disease (Cheng et al., 2006) (e.g., diabetes). They can be inhaled to treat local pulmonary disease [e.g., asthma (Edwards et al., 1997) and pulmonary hypertension (Evgenov et al., 2007)].

Oral Delivery. Oral administration remains the preferred route for the application of pharmaceuticals due to its convenience (Sastry et al., 2000). Microencapsulation of labile biopharmaceuticals including proteins and nucleic acids has improved their bioavailability by decreasing chemical or enzymatic degradation inside the gastrointestinal tract (Mahato et al., 2003). Polysaccharide (e.g., chitosan)-based microparticles have been studied for the oral delivery of insulin (Zhang et al., 2011; Jose et al., 2012). Less than 3% of encapsulated insulin was released in 1.5 h after exposure to simulated gastric fluid containing pepsin at pH \sim 1.2, suggesting that microencapsulation preserves the chemical stability of encapsulated insulin. The blood glucose level of diabetic rats could be effectively reduced for over 60 h after oral administration of the insulin-loaded microspheres. Orally administered dextran microspheres have been used to improve the bioavailability of drugs delivered to the colon (Hovgaard and Brøndsted, 1995). The dextran matrix remains intact in the stomach and small intestine and degrades in the colon due to dextranase secreted by bacteria (Sinha and Kumria, 2001).

Pulmonary Delivery. Pulmonary administration is a noninvasive method of drug administration with fast absorption and direct targeting of the lungs (Abdelaziz et al., 2017). Microparticles have been used to deliver particles to the lung. This can be either to achieve systemic effect [e.g., insulin (Amidi et al., 2008)], or local delivery [e.g., bronchodilators (Ben-Jebria et al., 1999)]. Direct pulmonary delivery can achieve local effect while minimizing systemic effect (Edwards et al., 1997; Evgenov et al., 2007). Porous PLGA microspheres have been used for pulmonary delivery of protein drugs like insulin (Amidi et al., 2008), and small molecules like testosterone (Edwards et al., 1997) and doxorubicin (Fig. 1.3.8A.10) (Kim et al., 2012). The size of microparticles plays a key role in their retention in the lungs, and the level in the lungs (e.g., small airways) at which they are deposited (Adjei and Garren, 1990; Kutscher et al., 2010).

Ophthalmic Delivery. Microencapsulation has emerged as a promising approach to provide sustained release of drugs at a number of locations on or in the eye (Ludwig, 2005). Mucoadhesive \sim 10 μ m PLGA microparticles can remain on the ocular surface for over 30 min, compared to \sim 5 min for a conventional eye drop formulation (Choy et al., 2008). Subconjunctival administration of 4 μ m PLGA

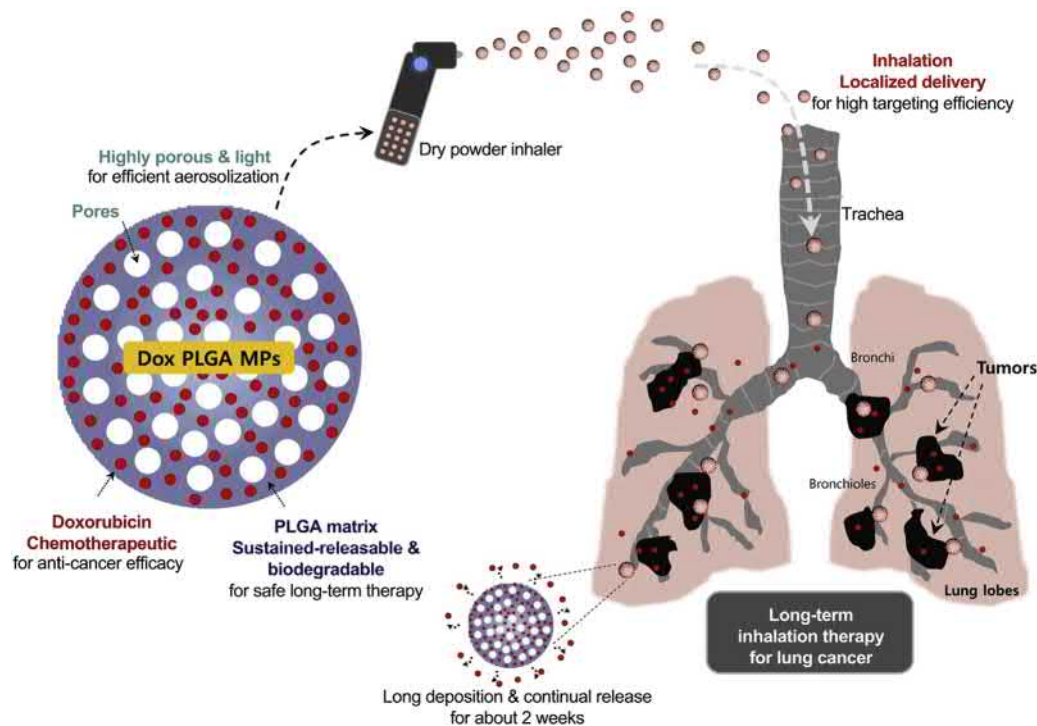
microparticles enabled release of celecoxib, which effectively inhibited diabetes-induced retinal oxidative damage for 14 days in rats (Ayalasomayajula and Kompella, 2005). Intravitreally injected \sim 10 μ m PLGA microspheres released proteins for 7 weeks for the treatment of acute retinal ischemia in a pig model (Kyhn et al., 2009).

Vaccines and Immune Adjuvants. There has been considerable interest in particulate approaches to enhancing vaccines. Microparticles have been used in part because their relatively large size makes it only possible for them to be taken up by phagocytic cells such as antigen-presenting cells (APCs) (Haining et al., 2004). For example, 0.1–10 μ m ovalbumin-loaded microparticles induced an antigen-specific immune response after being phagocytosed by dendritic cells (Dierendonck et al., 2014).

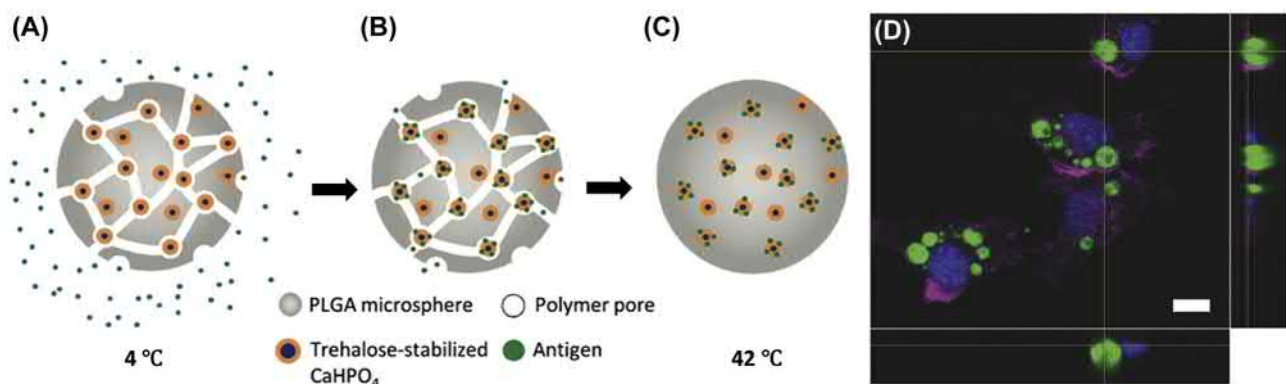
Another major challenge in the design of biomaterial-derived vaccines is the instability of encapsulated antigen and loss of immunogenicity. PLGA microspheres have been used for the encapsulation of vaccine antigens such as ovalbumin (OVA) with encapsulation efficiencies ranging from 4% to 13% (Uchida et al., 1994). A modified microencapsulation technique has been developed to increase protein antigen encapsulation efficiency and decrease exposure of antigens to organic solvents during formulation (Reinhold et al., 2012). PLGA microspheres loaded with trehalose and calcium phosphate (CaHPO₄) nanogels were formulated via a standard double emulsion and solvent evaporation technique (Fig. 1.3.8A.11A) (Bailey et al., 2017). Trehalose created a porous network inside the microsphere matrix and prevented CaHPO₄ gels from aggregating during lyophilization. The dried microspheres were incubated at 4°C in an aqueous solution of protein antigens, allowing the antigens to diffuse into the porous network created by the trehalose and bind to the calcium phosphate gel (Fig. 1.3.8A.11B). Pores were closed, keeping antigens inside by heating the aqueous solution above the glass-transition temperature of PLGA (Fig. 1.3.8A.11C). The encapsulation efficiency was 56%, compared to 10% with a conventional double emulsion method (Uchida et al., 1994). The obtained 7 μ m PLGA microspheres enabled single-dose vaccination with sustained antigen release over 40 days (Bailey et al., 2017). Confocal microscopy confirmed that rhodamine-labeled microspheres were readily taken up by dendritic cells (Fig. 1.3.8A.11D), enabling the targeted delivery of antigens.

Radiotherapy

Radiotherapy uses high doses of radiation to kill cancer cells and shrink tumors (Delaney et al., 2005). However, external irradiation can have trouble reaching deep-seated cancers without damaging healthy tissues. Radioactive microparticles to be placed in situ have been developed to address these concerns. For example, 35 μ m glass microspheres containing yttrium-90 have been applied by intratumoral injection in rabbits for tumor suppression (Yan et al., 1993). In situ radiotherapy provided localized β -irradiation with a



• **Figure 1.3.8A.10** Inhalable highly porous large PLGA microparticles for delivering doxorubicin for the treatment of lung cancer. After pulmonary administration, doxorubicin-containing PLGA microparticles remained in the lungs and delivered drug for ~2 weeks (Kim et al., 2012).



• **Figure 1.3.8A.11** PLGA microspheres for single-dose vaccination (Bailey et al., 2017). (A) Preparation of antigen-free PLGA microspheres loaded with trehalose and calcium phosphate (CaHPO₄) nanogels. (B) Diffusion and entrapment of protein antigens. (C) Closure of the pores and encapsulation of antigens. (D) Confocal microscopy of dendritic cells that internalized PLGA microspheres schematized in panel (C) labeled with rhodamine (green). Actin filaments were stained with Alexa Fluor 647-phalloidin (violet) and nuclei were stained with DAPI (blue). Scale bar represents 10 μm.

penetration depth of less than 3 mm, with minimal toxicity to surrounding normal tissues (Kawashita et al., 2003).

Other Applications

The use of particulate-delivery systems and microencapsulation technology has gone beyond pharmaceuticals. Over the past several decades, the food and beverage industries have been using microencapsulation for controlled release of food ingredients. A simple example of encapsulation-enabled controlled release is the flavoring of chewing gums

(Witzel and Patents, 1976). Flavor compounds were encapsulated into polysaccharide-based microspheres with sizes ranging from 1 to 100 μm, which were then deposited on the surface of a gum stick. Microencapsulation achieved release of sufficient flavoring ingredients to maintain an acceptable taste over 60 min (Witzel and Patents, 1976). Microencapsulation protects sensitive, reactive, or volatile food ingredients against heat, moisture, and pH during storage (Yeo et al., 2005). Microencapsulation may also turn liquid or gas ingredients into powders, enabling easier handling (Ho et al., 2014). For example, expansible thermoplastic

CASE STUDY: TRIAMCINOLONE ACETONIDE-ENCAPSULATED PLGA MICROSPHERES FOR MANAGEMENT OF OSTEOARTHRITIC PAIN OF THE KNEE

Osteoarthritis (OA) is a common chronic condition of the joints, characterized by intraarticular inflammation, deterioration of articular cartilage, and degenerative changes to periarticular and subchondral bone. OA occurs most often in large weight-bearing joints such as the knees and hips, but also occurs in the shoulders, lower back, neck, small joints of the fingers, and the bases of the thumb and big toe. About 13% of women and 10% of men aged 60 years and older have symptomatic OA of the knee, with rates likely to increase due to the aging of the population and the rate of obesity or overweight individuals in the general population.

During the early stages of knee OA, conservative management including weight loss, the use of ambulatory aids, simple analgesics, and nonsteroidal antiinflammatory drugs is the first line of treatment; however, as the disease progresses and the joints become increasingly painful, the effectiveness of these treatment options becomes limited. Intraarticular administration of immediate-release corticosteroid or hyaluronic acid has been clinically used to relieve symptoms of knee OA. However, the duration of pain reduction from intraarticular corticosteroid

injections is less than 1 week, which is insufficient for chronic knee osteoarthritis.

Triamcinolone acetonide (TCA) is an FDA-approved short-acting corticosteroid for the treatment of various disease conditions including osteoarthritis. A PLGA microsphere-based formulation (Zilretta) has been developed to provide extended release of TCA. It is prepared as TCA-loaded microspheres with a drug loading of 25% (w/w) to provide more persistent pain relief than currently available immediate-release formulations of TCA. The excipient is biodegradable PLGA polymer. In a nearly 500-patient phase three study, Zilretta significantly lowered pain intensity scores compared to placebo 3 months following a single dose intraarticular administration. Compared to conventional immediate-release formulations, microencapsulation provides the following benefits: (1) extended drug release; (2) potent therapeutic response through targeted local delivery; (3) minimal systemic exposure; (4) long-lasting local pain relief from a single injection; and (5) safety profile with treatment-related side effects comparable to placebo. In 2017, Zilretta was approved by FDA for the treatment for patients with OA-related knee pain.

polymers synthesized with alkenyl aromatic monomers have been used for the preparation of microparticles 3–50 μm in diameter for the encapsulation of volatile fluid foaming agents for applications such as coffee foam (Morehouse Jr et al., 1971). Changes in physiological conditions such as pH have been used for triggered release of food ingredients from microparticles (Zhang et al., 2015). Microparticles have been applied in cosmetics (Takezaki et al., 2015) as in the preparation of perfume by encapsulation of volatile fragrances (Tekin et al., 2013). Microencapsulation has also been used in the development of agricultural products (Gimeno, 1996). Microparticle-based pesticide-delivery systems have been designed for sustained release of encapsulated pesticides, resulting in improved handling safety and increased time intervals between applications of pesticides (Tsuji, 2001; Delin, 2000).

Concluding Remarks

Microparticles have many desirable properties for biomedical applications. They are excellent depot systems for sustained release of a wide range of therapeutic compounds. The formulation methods are readily tunable to allow variation in a range of particle parameters, resulting in the potential for release over a range of time frames, or stimulus-responsive release. Microparticles can be administered by a variety of routes and are generally small enough to be injectable.

References

- Adjei, A., Garren, J., 1990. Pulmonary delivery of peptide drugs: effect of particle size on bioavailability of leuprolide acetate in healthy male volunteers. *Pharm. Res.* 7 (6), 565–569.
- Abdelaziz, H.M., Gaber, M., Abd-Elwakil, M.M., Mabrouk, M.T., Elgohary, M.M., Kamel, N.M., Kabary, D.M., Freag, M.S., Samaha, M.W., Mortada, S.M., 2017. Inhalable particulate drug delivery systems for lung cancer therapy: nanoparticles, microparticles, nanocomposites and nanoaggregates. *J. Control. Release* 269 (10), 374–392.
- Aguilar, M.R., San Román, J., 2014. *Smart Polymers and Their Applications*. Elsevier.
- Akashi, K.-i., Miyata, H., Itoh, H., Kinoshita Jr., K., 1996. Preparation of giant liposomes in physiological conditions and their characterization under an optical microscope. *Biophys. J.* 71 (6), 3242–3250.
- Alvim, I.D., Grosso, C.R.F., 2010. Microparticles obtained by complex coacervation: influence of the type of reticulation and the drying process on the release of the core material. *Food Sci. Technol.* 30 (4), 1069–1076.
- Amidi, M., Pellikaan, H.C., de Boer, A.H., Crommelin, D.J., Hennink, W.E., Jiskoot, W., 2008. Preparation and physicochemical characterization of supercritically dried insulin-loaded microparticles for pulmonary delivery. *Eur. J. Pharm. Biopharm.* 68 (2), 191–200.
- Anderson, J.M., 1994. In vivo biocompatibility of implantable delivery systems and biomaterials. *Eur. J. Pharm. Biopharm.* 40 (1), 1–8.
- Asrar, J., Ding, Y., 2010. Google Patents.
- Ayalasomayajula, S.P., Kompella, U.B., 2005. Subconjunctivally administered celecoxib-PLGA microparticles sustain retinal drug levels and alleviate diabetes-induced oxidative stress in a rat model. *Eur. J. Pharmacol.* 511 (2–3), 191–198.
- Bailey, B.A., Ochyl, L.J., Schwendeman, S.P., Moon, J.J., 2017. Toward a single-dose vaccination strategy with self-encapsulating PLGA microspheres. *Adv. Healthc. Mater.* 6 (12), 1601418.
- Bajpai, A.K., Shukla, S.K., Bhanu, S., Kankane, S., 2008. Responsive polymers in controlled drug delivery. *Prog. Polym. Sci.* 33 (11), 1088–1118.
- Baker, M.I., Walsh, S.P., Schwartz, Z., Boyan, B.D., 2012. A review of polyvinyl alcohol and its uses in cartilage and orthopedic applications. *J. Biomed. Mater. Res. B Appl. Biomater.* 100 (5), 1451–1457.

- Bakry, A.M., Abbas, S., Ali, B., Majeed, H., Abouelwafa, M.Y., Mousa, A., Liang, L., 2016. Microencapsulation of oils: a comprehensive review of benefits, techniques, and applications. *Compr. Rev. Food Sci. Food Saf.* 15 (1), 143–182.
- Balazs, D.A., Godbey, W., 2011. Liposomes for use in gene delivery. *J. Drug Deliv.* 2011.
- Barenholz, Y.C., 2012. Doxil®—the first FDA-approved nano-drug: lessons learned. *J. Control. Release* 160 (2), 117–134.
- Batycky, R.P., Hanes, J., Langer, R., Edwards, D.A., 1997. A theoretical model of erosion and macromolecular drug release from biodegrading microspheres. *J. Pharm. Sci.* 86 (12), 1464–1477.
- Ben-Jebria, A., Chen, D., Eskew, M.L., Vanbever, R., Langer, R., Edwards, D.A., 1999. Large porous particles for sustained protection from carbachol-induced bronchoconstriction in guinea pigs. *Pharm. Res.* 16 (4), 555–561.
- Berkland, C., King, M., Cox, A., Kim, K.K., Pack, D.W., 2002. Precise control of PLG microsphere size provides enhanced control of drug release rate. *J. Control. Release* 82 (1), 137–147.
- Berthold, A., Cremer, K., Kreuter, J., 1998. Collagen microparticles: carriers for glucocorticosteroids. *Eur. J. Pharm. Biopharm.* 45 (1), 23–29.
- Bhattacharjee, S., 2016. DLS and zeta potential—What they are and what they are not? *J. Control. Release* 235, 337–351.
- Bhattarai, N., Gunn, J., Zhang, M., 2010. Chitosan-based hydrogels for controlled, localized drug delivery. *Adv. Drug Deliv. Rev.* 62 (1), 83–99.
- Bhavsar, M.D., Amiji, M.M., 2007. Polymeric nano- and microparticle technologies for oral gene delivery. *Expert Opin. Drug Deliv.* 4 (3), 197–213.
- Bilati, U., Allémann, E., Doelker, E., 2005. Poly (D, L-lactide-co-glycolide) protein-loaded nanoparticles prepared by the double emulsion method—processing and formulation issues for enhanced entrapment efficiency. *J. Microencapsul.* 22 (2), 205–214.
- Black, K.A., Priftis, D., Perry, S.L., Yip, J., Byun, W.Y., Tirrell, M., 2014. Protein encapsulation via polypeptide complex coacervation. *ACS Macro Lett.* 3 (10), 1088–1091.
- Blanco, D., Alonso, M.a.J., 1998. Protein encapsulation and release from poly (lactide-co-glycolide) microspheres: effect of the protein and polymer properties and of the co-encapsulation of surfactants. *Eur. J. Pharm. Biopharm.* 45 (3), 285–294.
- Bradley, M., Vincent, B., 2008. Poly (vinylpyridine) core/poly (N-isopropylacrylamide) shell microgel particles: their characterization and the uptake and release of an anionic surfactant. *Langmuir* 24 (6), 2421–2425.
- Brazel, C.S., Peppas, N.A., 2000. Modeling of drug release from swellable polymers. *Eur. J. Pharm. Biopharm.* 49 (1), 47–58.
- Bulbake, U., Doppalapudi, S., Kommineni, N., Khan, W., 2017. Liposomal formulations in clinical use: an updated review. *Pharmaceutics* 9 (2), 12.
- Campos, E., Branquinho, J., Carreira, A.S., Carvalho, A., Coimbra, P., Ferreira, P., Gil, M., 2013. Designing polymeric microparticles for biomedical and industrial applications. *Eur. Polym. J.* 49 (8), 2005–2021.
- Champion, J.A., Katare, Y.K., Mitragotri, S., 2007. Particle shape: a new design parameter for micro- and nanoscale drug delivery carriers. *J. Control. Release* 121 (1–2), 3–9.
- Chasin, M., 1990. Biodegradable Polymers as Drug Delivery Systems. Informa Health Care.
- Chen, Y., Liu, L., 2012. Modern methods for delivery of drugs across the blood–brain barrier. *Adv. Drug Deliv. Rev.* 64 (7), 640–665.
- Chen, W., Tong, Y.W., 2012. PHBV microspheres as neural tissue engineering scaffold support neuronal cell growth and axon–dendrite polarization. *Acta Biomater.* 8 (2), 540–548.
- Chen, N., Johnson, M.M., Collier, M.A., Gallovic, M.D., Bachelder, E.M., Ainslie, K.M., 2018. Tunable degradation of acetylated dextran microparticles enables controlled vaccine adjuvant and antigen delivery to modulate adaptive immune responses. *J. Control. Release* 273, 147–159.
- Cheng, J., Teply, B.A., Jeong, S.Y., Yim, C.H., Ho, D., Sherifi, I., Jon, S., Farokhzad, O.C., Khademhosseini, A., Langer, R.S., 2006. Magnetically responsive polymeric microparticles for oral delivery of protein drugs. *Pharm. Res.* 23 (3), 557–564.
- Cherng, J.Y., Hou, T.Y., Shih, M.F., Talsma, H., Hennink, W.E., 2013. Polyurethane-based drug delivery systems. *Int. J. Pharm.* 450 (1–2), 145–162.
- Cheung, R.Y., Ying, Y., Rauth, A.M., Marcon, N., Wu, X.Y., 2005. Biodegradable dextran-based microspheres for delivery of anticancer drug mitomycin C. *Biomaterials* 26 (26), 5375–5385.
- Chirila, T.V., Constable, I.J., Crawford, G.J., Vijayasekaran, S., Thompson, D.E., Chen, Y.-C., Fletcher, W.A., Griffin, B.J., 1993. Poly (2-hydroxyethyl methacrylate) sponges as implant materials: in vivo and in vitro evaluation of cellular invasion. *Biomaterials* 14 (1), 26–38.
- Choy, Y.B., Park, J.-H., Prausnitz, M.R., 2008. Mucoadhesive microparticles engineered for ophthalmic drug delivery. *J. Phys. Chem. Solids* 69 (5–6), 1533–1536.
- Coderch, L., Fonollosa, J., De Pera, M., Estelrich, J., De La Maza, A., Parra, J., 2000. Influence of cholesterol on liposome fluidity by EPR: relationship with percutaneous absorption. *J. Control. Release* 68 (1), 85–95.
- Cohen, S., Yoshioka, T., Lucarelli, M., Hwang, L.H., Langer, R., 1991. Controlled delivery systems for proteins based on poly (lactic/glycolic acid) microspheres. *Pharm. Res.* 8 (6), 713–720.
- Cohen, J.A., Beaudette, T.T., Cohen, J.L., Broaders, K.E., Bachelder, E.M., Fréchet, J.M., 2010. Acetal–modified dextran microparticles with controlled degradation kinetics and surface functionality for gene delivery in phagocytic and non–phagocytic cells. *Adv. Mater.* 22 (32), 3593–3597.
- Croisier, F., Jérôme, C., 2013. Chitosan-based biomaterials for tissue engineering. *Eur. Polym. J.* 49 (4), 780–792.
- Cuenot, S., Frétygny, C., Demoustier-Champagne, S., Nysten, B., 2004. Surface tension effect on the mechanical properties of nanomaterials measured by atomic force microscopy. *Phys. Rev. B* 69 (16), 165410.
- Cui, L., Tang, C., Yin, C., 2012. Effects of quaternization and PEGylation on the biocompatibility, enzymatic degradability and antioxidant activity of chitosan derivatives. *Carbohydr. Polym.* 87 (4), 2505–2511.
- D'souza, S.S., DeLuca, P.P., 2006. Methods to assess in vitro drug release from injectable polymeric particulate systems. *Pharm. Res.* 23 (3), 460–474.
- Dang, J.M., Leong, K.W., 2006. Natural polymers for gene delivery and tissue engineering. *Adv. Drug Deliv. Rev.* 58 (4), 487–499.
- De Ascentiis, A., Bowman, C.N., Colombo, P., Peppas, N.A., 1995. Mucoadhesion of poly (2-hydroxyethyl methacrylate) is improved when linear poly (ethylene oxide) chains are added to the polymer network. *J. Control. Release* 33 (1), 197–201.
- De Rosa, G., Iommelli, R., La Rotonda, M.I., Miro, A., Quaglia, F., 2000. Influence of the co-encapsulation of different non-ionic surfactants on the properties of PLGA insulin-loaded microspheres. *J. Control. Release* 69 (2), 283–295.

- DeBlois, R., Bean, C., 1970. Counting and sizing of submicron particles by the resistive pulse technique. *Rev. Sci. Instrum.* 41 (7), 909–916.
- Delaney, G., Jacob, S., Featherstone, C., Barton, M., 2005. The role of radiotherapy in cancer treatment: estimating optimal utilization from a review of evidence-based clinical guidelines. *Cancer* 104 (6), 1129–1137.
- Delin, G., 2000. Applications of microencapsulation technologies in pesticide formulations [J]. *Mod. Chem. Ind.* 2.
- Deng, J.-S., Li, L., Tian, Y., Ginsburg, E., Widman, M., Myers, A., 2003. In vitro characterization of polyorthoester microparticles containing bupivacaine. *Pharm. Dev. Technol.* 8 (1), 31–38.
- Denis-Mize, K., Dupuis, M., MacKichan, M., Singh, M., Doe, B., O'hagan, D., Ulmer, J., Donnelly, J., McDonald, D., Ott, G., 2000. Plasmid DNA adsorbed onto cationic microparticles mediates target gene expression and antigen presentation by dendritic cells. *Gene Therapy* 7 (24), 2105.
- Dierendonck, M., Fierens, K., De Rycke, R., Lybaert, L., Maji, S., Zhang, Z., Zhang, Q., Hoogenboom, R., Lambrecht, B.N., Grooten, J., 2014. Nanoporous hydrogen bonded polymeric microparticles: facile and economic production of cross presentation promoting vaccine carriers. *Adv. Funct. Mater.* 24 (29), 4634–4644.
- Dong, W., Bodmeier, R., 2006. Encapsulation of lipophilic drugs within enteric microparticles by a novel coacervation method. *Int. J. Pharm.* 326 (1–2), 128–138.
- Dorati, R., Genta, I., Tomasi, C., Modena, T., Colonna, C., Pavanetto, F., Perugini, P., Conti, B., 2008. Polyethylenglycol-co-poly-D, L-lactide copolymer based microspheres: preparation, characterization and delivery of a model protein. *J. Microencapsul.* 25 (5), 330–338.
- Duncan, R., Ringsdorf, H., Satchi-Fainaro, R., 2006. Polymer therapeutics—polymers as drugs, drug and protein conjugates and gene delivery systems: past, present and future opportunities. *J. Drug Target.* 14 (6), 337–341.
- Duncanson, W.J., Lin, T., Abate, A.R., Seiffert, S., Shah, R.K., Weitz, D.A., 2012. Microfluidic synthesis of advanced microparticles for encapsulation and controlled release. *Lab Chip* 12 (12), 2135–2145.
- Edlund, U., Albertsson, A.-C., 2002. In: *Degradable Aliphatic Polyesters*. Springer.
- Edwards, D.A., Hanes, J., Caponetti, G., Hrkach, J., Ben-Jebria, A., Eskew, M.L., Mintzes, J., Deaver, D., Lotan, N., Langer, R., 1997. Large porous particles for pulmonary drug delivery. *Science* 276 (5320), 1868–1872.
- Estey, T., Kang, J., Schwendeman, S.P., Carpenter, J.F., 2006. BSA degradation under acidic conditions: a model for protein instability during release from PLGA delivery systems. *J. Pharm. Sci.* 95 (7), 1626–1639.
- Eygenov, O.V., Kohane, D.S., Bloch, K.D., Stasch, J.-P., Volpato, G.P., Bellas, E., Eygenov, N.V., Buys, E.S., Gnoth, M.J., Graveline, A.R., 2007. Inhaled agonists of soluble guanylate cyclase induce selective pulmonary vasodilation. *Am. J. Respir. Crit. Care Med.* 176 (11), 1138–1145.
- Ficek, B.J., Peppas, N.A., 1993. Novel preparation of poly (vinyl alcohol) microparticles without crosslinking agent for controlled drug delivery of proteins. *J. Control. Release* 27 (3), 259–264.
- Franssen, O., Stenekes, R., Hennink, W., 1999. Controlled release of a model protein from enzymatically degrading dextran microspheres. *J. Control. Release* 59 (2), 219–228.
- Fu, Y., Kao, W.J., 2010. Drug release kinetics and transport mechanisms of non-degradable and degradable polymeric delivery systems. *Expert Opin. Drug Deliv.* 7 (4), 429–444.
- Gabizon, A., Price, D.C., Huberty, J., Bresalier, R.S., Papahadjopoulos, D., 1990. Effect of liposome composition and other factors on the targeting of liposomes to experimental tumors: biodistribution and imaging studies. *Cancer Research* 50 (19), 6371–6378.
- Genta, I., Conti, B., Perugini, P., Pavanetto, F., Spadaro, A., Puglisi, G., 1997. Bioadhesive microspheres for ophthalmic administration of acyclovir. *J. Pharm. Pharmacol.* 49 (8), 737–742.
- Gharsallaoui, A., Roudaut, G., Chambin, O., Voilley, A., Saurel, R., 2007. Applications of spray-drying in microencapsulation of food ingredients: an overview. *Food Research International* 40 (9), 1107–1121.
- Gimeno, M., 1996. An overview of the latest development of microencapsulation for agricultural products. *J. Environ. Sci. Heal B* 31 (3), 407–420.
- Goh, S.L., Murthy, N., Xu, M., Fréchet, J.M., 2004. Cross-linked microparticles as carriers for the delivery of plasmid DNA for vaccine development. *Bioconjug. Chem.* 15 (3), 467–474.
- Goldburg, W., 1999. Dynamic light scattering. *Am. J. Phys.* 67 (12), 1152–1160.
- Guliyeva, Ü., Öner, F., Özsoy, Ş., Haziroğlu, R., 2006. Chitosan microparticles containing plasmid DNA as potential oral gene delivery system. *Eur. J. Pharm. Biopharm.* 62 (1), 17–25.
- Guo, S., Nakagawa, Y., Barhoumi, A., Wang, W., Zhan, C., Tong, R., Santamaria, C., Kohane, D.S., 2016. Extended release of native drug conjugated in polyketal microparticles. *J. Am. Chem. Soc.* 138 (19), 6127–6130.
- Haining, W.N., Anderson, D.G., Little, S.R., von Berwelt-Baildon, M.S., Cardoso, A.A., Alves, P., Kosmatopoulos, K., Nadler, L.M., Langer, R., Kohane, D.S., 2004. pH-triggered microparticles for peptide vaccination. *J. Immunol.* 173 (4), 2578–2585.
- Hamoudeh, M., Kamleh, M.A., Diab, R., Fessi, H., 2008. Radionuclides delivery systems for nuclear imaging and radiotherapy of cancer. *Adv. Drug Deliv. Rev.* 60 (12), 1329–1346.
- Han, F.Y., Thurecht, K.J., Whittaker, A.K., Smith, M.T., 2016. Biodegradable PLGA-based microparticles for producing sustained-release drug formulations and strategies for improving drug loading. *Front. Pharmacol.* 7, 185.
- Hawker, C.J., Bosman, A.W., Harth, E., 2001. New polymer synthesis by nitroxide mediated living radical polymerizations. *Chem. Rev.* 101 (12), 3661–3688.
- He, P., Davis, S.S., Illum, L., 1998. In vitro evaluation of the mucoadhesive properties of chitosan microspheres. *Int. J. Pharm.* 166 (1), 75–88.
- Heffernan, M.J., Murthy, N., 2005. Polyketal nanoparticles: a new pH-sensitive biodegradable drug delivery vehicle. *Bioconjug. Chem.* 16 (6), 1340–1342.
- Heffernan, M.J., Kasturi, S.P., Yang, S.C., Pulendran, B., Murthy, N., 2009. The stimulation of CD8+ T cells by dendritic cells pulsed with polyketal microparticles containing ion-paired protein antigen and poly (inosinic acid)–poly (cytidylic acid). *Biomaterials* 30 (5), 910–918.
- Heller, J., 1985. Controlled drug release from poly (ortho esters)—a surface eroding polymer. *J. Control. Release* 2, 167–177.
- Heller, J., 1993. *Biopolymers I*. Springer.
- Heller, J., Barr, J., 2004. Poly (ortho esters) from concept to reality. *Biomacromolecules* 5 (5), 1625–1632.
- Heller, J., Barr, J., Ng, S.Y., Abdellauoi, K.S., Gurny, R., 2002. Poly (ortho esters): synthesis, characterization, properties and uses. *Adv. Drug Deliv. Rev.* 54 (7), 1015–1039.
- Henriquez, R.R., Ito, T., Sun, L., Crooks, R.M., 2004. The resurgence of Coulter counting for analyzing nanoscale objects. *Analyst* 129 (6), 478–482.

- Ho, T.M., Howes, T., Bhandari, B.R., 2014. Encapsulation of gases in powder solid matrices and their applications: a review. *Powder Technol.* 259, 87–108.
- Hoare, T.R., Kohane, D.S., 2008. Hydrogels in drug delivery: progress and challenges. *Polymer* 49 (8), 1993–2007.
- Hovgaard, L., Brøndsted, H., 1995. Dextran hydrogels for colon-specific drug delivery. *J. Control. Release* 36 (1–2), 159–166.
- Huang, X., Brazel, C.S., 2001. On the importance and mechanisms of burst release in matrix-controlled drug delivery systems. *J. Control. Release* 73 (2–3), 121–136.
- Huang, J., Wigent, R.J., Schwartz, J.B., 2008. Drug–polymer interaction and its significance on the physical stability of nifedipine amorphous dispersion in microparticles of an ammonio methacrylate copolymer and ethylcellulose binary blend. *J. Pharm. Sci.* 97 (1), 251–262.
- Jain, R.A., 2000. The manufacturing techniques of various drug loaded biodegradable poly (lactide-co-glycolide)(PLGA) devices. *Biomaterials* 21 (23), 2475–2490.
- Jaspart, S., Piel, G., Delattre, L., Evrard, B., 2005. Solid lipid microparticles: formulation, preparation, characterisation, drug release and applications. *Expert Opin. Drug Deliv.* 2 (1), 75–87.
- Jaspart, S., Bertholet, P., Piel, G., Dogné, J.-M., Delattre, L., Evrard, B., 2007. Solid lipid microparticles as a sustained release system for pulmonary drug delivery. *Eur. J. Pharm. Biopharm.* 65 (1), 47–56.
- Jay, S.M., Saltzman, W.M., 2009. Controlled delivery of VEGF via modulation of alginate microparticle ionic crosslinking. *J. Control. Release* 134 (1), 26–34.
- Jeong, B., Kim, S.W., Bae, Y.H., 2012. Thermosensitive sol–gel reversible hydrogels. *Adv. Drug Deliv. Rev.* 64, 154–162.
- John, M.J., Anandjiwala, R.D., 2008. Recent developments in chemical modification and characterization of natural fiber–reinforced composites. *Polym. Compos.* 29 (2), 187–207.
- Johnson, O.L., Cleland, J.L., Lee, H.J., Charnis, M., Duenas, E., Jaworowicz, W., Shepard, D., Shahzamani, A., Jones, A.J., Putney, S.D., 1996. A month-long effect from a single injection of microencapsulated human growth hormone. *Nat. Med.* 2 (7), 795–799.
- Jose, S., Fangueiro, J., Smitha, J., Cinu, T., Chacko, A., Premaletha, K., Souto, E., 2012. Cross-linked chitosan microspheres for oral delivery of insulin: Taguchi design and in vivo testing. *Colloids Surf. B Biointerfaces* 92, 175–179.
- Joshi, R.V., Nelson, C.E., Poole, K.M., Skala, M.C., Duvall, C.L., 2013. Dual pH-and temperature-responsive microparticles for protein delivery to ischemic tissues. *Acta Biomater.* 9 (5), 6526–6534.
- Kaibara, K., Okazaki, T., Bohidar, H., Dubin, P., 2000. pH-induced coacervation in complexes of bovine serum albumin and cationic polyelectrolytes. *Biomacromolecules* 1 (1), 100–107.
- Katti, D., Lakshmi, S., Langer, R., Laurencin, C., 2002. Toxicity, biodegradation and elimination of polyanhydrides. *Adv. Drug Deliv. Rev.* 54 (7), 933–961.
- Kawashima, Y., Niwa, T., Takeuchi, H., Hino, T., Itoh, Y., 1992. Hollow microspheres for use as a floating controlled drug delivery system in the stomach. *J. Pharm. Sci.* 81 (2), 135–140.
- Kawashita, M., Shineha, R., Kim, H.-M., Kokubo, T., Inoue, Y., Araki, N., Nagata, Y., Hiraoka, M., Sawada, Y., 2003. Preparation of ceramic microspheres for in situ radiotherapy of deep-seated cancer. *Biomaterials* 24 (17), 2955–2963.
- Keegan, G.M., Smart, J.D., Ingram, M.J., Barnes, L.-M., Burnett, G.R., Rees, G.D., 2012. Chitosan microparticles for the controlled delivery of fluoride. *J. Dent.* 40 (3), 229–240.
- Khang, G., Kim, S.W., Cho, J.C., Rhee, J.M., Yoon, S.C., Lee, H.B., 2001. Preparation and characterization of poly (3–hydroxybutyrate–co–3–hydroxyvalerate) microspheres for the sustained release of 5–fluorouracil. *Bio Med. Mater. Eng.* 11 (2), 89–103.
- Kim, S.J., Hahn, S.K., Kim, M.J., Kim, D.H., Lee, Y.P., 2005. Development of a novel sustained release formulation of recombinant human growth hormone using sodium hyaluronate microparticles. *J. Control. Release* 104 (2), 323–335.
- Kim, H.K., Chung, H.J., Park, T.G., 2006. Biodegradable polymeric microspheres with “open/closed” pores for sustained release of human growth hormone. *J. Control. Release* 112 (2), 167–174.
- Kim, I., Byeon, H.J., Kim, T.H., Lee, E.S., Oh, K.T., Shin, B.S., Lee, K.C., Youn, Y.S., 2012. Doxorubicin-loaded highly porous large PLGA microparticles as a sustained-release inhalation system for the treatment of metastatic lung cancer. *Biomaterials* 33 (22), 5574–5583.
- Kirby, C., Clarke, J., Gregoriadis, G., 1980. Effect of the cholesterol content of small unilamellar liposomes on their stability in vivo and in vitro. *Biochem. J.* 186 (2), 591–598.
- Klose, D., Siepmann, F., Elkharraz, K., Krenzlin, S., Siepmann, J., 2006. How porosity and size affect the drug release mechanisms from PLGA-based microparticles. *Int. J. Pharm.* 314 (2), 198–206.
- Kohane, D.S., 2007. Microparticles and nanoparticles for drug delivery. *Biotechnol. Bioeng.* 96 (2), 203–209.
- Kohane, D., Langer, R., 2005. Biotechnology to improve patients’ medication compliance. *Behav. Health Manag.* 25, 26–28.
- Kohane, D.S., Lipp, M., Kinney, R.C., Anthony, D.C., Louis, D.N., Lotan, N., Langer, R., 2002a. Biocompatibility of lipid–protein–sugar particles containing bupivacaine in the epineurium. *J. Biomed. Mater. Res.* 59 (3), 450–459.
- Kohane, D.S., Plesnila, N., Thomas, S.S., Le, D., Langer, R., Moskowitz, M.A., 2002b. Lipid–sugar particles for intracranial drug delivery: safety and biocompatibility. *Brain Res.* 946 (2), 206–213.
- Kohane, D.S., Tse, J.Y., Yeo, Y., Padera, R., Shubina, M., Langer, R., 2006. Biodegradable polymeric microspheres and nanospheres for drug delivery in the peritoneum. *J. Biomed. Mater. Res. Part A* 77 (2), 351–361.
- Köse, G.T., Kenar, H., Hasırcı, N., Hasırcı, V., 2003. Macroporous poly (3-hydroxybutyrate-co-3-hydroxyvalerate) matrices for bone tissue engineering. *Biomaterials* 24 (11), 1949–1958.
- Kumar, N., Langer, R.S., Domb, A.J., 2002. Polyanhydrides: an overview. *Adv. Drug Deliv. Rev.* 54 (7), 889–910.
- Kunioka, M., Doi, Y., 1990. Thermal degradation of microbial copolyesters: poly (3-hydroxybutyrate-co-3-hydroxyvalerate) and poly (3-hydroxybutyrate-co-4-hydroxybutyrate). *Macromolecules* 23 (7), 1933–1936.
- Kurkuri, M.D., Aminabhavi, T.M., 2004. Poly (vinyl alcohol) and poly (acrylic acid) sequential interpenetrating network pH-sensitive microspheres for the delivery of diclofenac sodium to the intestine. *J. Control. Release* 96 (1), 9–20.
- Kutscher, H.L., Chao, P., Deshmukh, M., Singh, Y., Hu, P., Joseph, L.B., Reimer, D.C., Stein, S., Laskin, D.L., Sinko, P.J., 2010. Threshold size for optimal passive pulmonary targeting and retention of rigid microparticles in rats. *J. Control. Release* 143 (1), 31–37.
- Kweon, H., Yoo, M.K., Park, I.K., Kim, T.H., Lee, H.C., Lee, H.-S., Oh, J.-S., Akaike, T., Cho, C.-S., 2003. A novel degradable polycaprolactone networks for tissue engineering. *Biomaterials* 24 (5), 801–808.
- Kyhn, M.V., Klassen, H., Johansson, U.E., Warfvinge, K., Lavik, E., Kiilgaard, J.F., Prause, J.U., Scherfig, E., Young, M., la Cour, M., 2009. Delayed administration of glial cell line-derived neurotrophic factor (GDNF) protects retinal ganglion cells in a pig model of acute retinal ischemia. *Exp. Eye Res.* 89 (6), 1012–1020.
- Lam, P., Gambari, R., 2014. Advanced progress of microencapsulation technologies: in vivo and in vitro models for studying oral and transdermal drug deliveries. *J. Control. Release* 178, 25–45.

- Lamprecht, A., Torres, H.R., Schäfer, U., Lehr, C.-M., 2000. Biodegradable microparticles as a two-drug controlled release formulation: a potential treatment of inflammatory bowel disease. *J. Control. Release* 69 (3), 445–454.
- Langer, R., 1990. New methods of drug delivery. *Science* 249 (4976), 1527–1533.
- Lavik, E., Kuehn, M., Kwon, Y., 2011. Novel drug delivery systems for glaucoma. *Eye* 25 (5), 578.
- Lawrie, A., Albany, A., Cardigan, R., Mackie, I., Harrison, P., 2009. Microparticle sizing by dynamic light scattering in fresh-frozen plasma. *Vox Sang* 96 (3), 206–212.
- Lee, K.Y., Mooney, D.J., 2012. Alginate: properties and biomedical applications. *Prog. Polym. Sci.* 37 (1), 106–126.
- Lee, K.Y., Rowley, J.A., Eiselt, P., Moy, E.M., Bouhadir, K.H., Mooney, D.J., 2000. Controlling mechanical and swelling properties of alginate hydrogels independently by cross-linker type and cross-linking density. *Macromolecules* 33 (11), 4291–4294.
- Lee, S., Yang, S.C., Heffernan, M.J., Taylor, W.R., Murthy, N., 2007. Polyketal microparticles: a new delivery vehicle for superoxide dismutase. *Bioconjug. Chem.* 18 (1), 4–7.
- Lee, S., Yang, S.C., Kao, C.-Y., Pierce, R.H., Murthy, N., 2009. Solid polymeric microparticles enhance the delivery of siRNA to macrophages in vivo. *Nucleic Acids Res.* 37 (22) e145–e145.
- Lee, B.K., Yun, Y., Park, K., 2016. PLA micro- and nano-particles. *Adv. Drug Deliv. Rev.* 107, 176–191.
- Lehr, C.M., Bouwstra, J.A., Kok, W., De Boer, A.G., Tukker, J.J., Verhoef, J.C., Breimer, D.D., Junginger, H.E., 1992. Effects of the mucoadhesive polymer polycarbophil on the intestinal absorption of a peptide drug in the rat. *J. Pharm. Pharmacol.* 44 (5), 402–407.
- Leong, K., Brott, B., Langer, R., 1985. Bioerodible polyanhydrides as drug-carrier matrices. I: characterization, degradation, and release characteristics. *J. Biomed. Mater. Res.* 19 (8), 941–955.
- Leong, K., Simonte, V., Langer, R., 1987. Synthesis of polyanhydrides: melt-polycondensation, dehydrochlorination, and dehydrative coupling. *Macromolecules* 20 (4), 705–712.
- Li, D., Wu, Z., Martini, N., Wen, J., 2011. Advanced carrier systems in cosmetics and cosmeceuticals: a review. *J. Cosmet. Sci.* 62 (6), 549–563.
- Li, W., Zhang, L., Ge, X., Xu, B., Zhang, W., Qu, L., Choi, C.-H., Xu, J., Zhang, A., Lee, H., 2018. Microfluidic fabrication of microparticles for biomedical applications. *Chem. Soc. Rev.* 47 (15), 5646–5683.
- Liu, D., Yang, F., Xiong, F., Gu, N., 2016. The smart drug delivery system and its clinical potential. *Theranostics* 6 (9), 1306.
- Lopes, J.R., Santos, G., Barata, P., Oliveira, R., Lopes, C.M., 2013. Physical and chemical stimuli-responsive drug delivery systems: targeted delivery and main routes of administration. *Curr. Pharmaceut. Des.* 19 (41), 7169–7184.
- Lu, Y., Sturek, M., Park, K., 2014. Microparticles produced by the hydrogel template method for sustained drug delivery. *Int. J. Pharm.* 461 (1–2), 258–269.
- Lu, Y., Aimetti, A.A., Langer, R., Gu, Z., 2017. Bioresponsive materials. *Nat. Rev. Mater.* 2 (1), 16075.
- Ludwig, A., 2005. The use of mucoadhesive polymers in ocular drug delivery. *Adv. Drug Deliv. Rev.* 57 (11), 1595–1639.
- Luo, D., Woodrow-Mumford, K., Belcheva, N., Saltzman, W.M., 1999. Controlled DNA delivery systems. *Pharm. Res.* 16 (8), 1300–1308.
- Lyon, L.A., Meng, Z., Singh, N., Sorrell, C.D., John, A.S., 2009. Thermoresponsive microgel-based materials. *Chem. Soc. Rev.* 38 (4), 865–874.
- Mahato, R.I., Narang, A.S., Thoma, L., Miller, D.D., 2003. Emerging trends in oral delivery of peptide and protein drugs. *Crit. Rev. Ther. Drug Carrier Syst.* 20 (2&3).
- Makadia, H.K., Siegel, S.J., 2011. Poly lactic-co-glycolic acid (PLGA) as biodegradable controlled drug delivery carrier. *Polymers* 3 (3), 1377–1397.
- Mao, S., Xu, J., Cai, C., Germershaus, O., Schaper, A., Kissel, T., 2007. Effect of WOW process parameters on morphology and burst release of FITC-dextran loaded PLGA microspheres. *Int. J. Pharm.* 334 (1–2), 137–148.
- Mathiowitz, E., Jacob, J.S., Jong, Y.S., Carino, G.P., Chickering, D.E., Chaturvedi, P., Santos, C.A., Vijayaraghavan, K., Montgomery, S., Bassett, M., 1997. Biologically erodable microspheres as potential oral drug delivery systems. *Nature* 386 (6623), 410.
- Matsumaru, Y., Hyodo, A., Nose, T., Hirano, T., Ohashi, S., 1997. Embolic materials for endovascular treatment of cerebral lesions. *J. Biomater. Sci. Polym. Ed.* 8 (7), 555–569.
- McAlvin, J.B., Kohane, D.S., 2014. *Focal Controlled Drug Delivery*. Springer.
- McAlvin, J.B., Reznor, G., Shankarappa, S.A., Stefanescu, C.F., Kohane, D.S., 2013. Local toxicity from local anesthetic polymeric microparticles. *Anesth. Analg.* 116 (4), 794.
- Mi, F.-L., Tan, Y.-C., Liang, H.-F., Sung, H.-W., 2002. In vivo biocompatibility and degradability of a novel injectable-chitosan-based implant. *Biomaterials* 23 (1), 181–191.
- Mikkelsen, A., Kertmen, A., Khobaib, K., Rajňák, M., Kurimský, J., Rozynek, Z., 2017. Assembly of 1D granular structures from sulfonated polystyrene microparticles. *Materials* 10 (10), 1212.
- Mitragotri, S., Lahann, J., 2009. Physical approaches to biomaterial design. *Nat. Mater.* 8 (1), 15.
- Mitragotri, S., Burke, P.A., Langer, R., 2014. Overcoming the challenges in administering biopharmaceuticals: formulation and delivery strategies. *Nat. Rev. Drug Discov.* 13 (9), 655.
- Mizrahy, S., Peer, D., 2012. Polysaccharides as building blocks for nanotherapeutics. *Chem. Soc. Rev.* 41 (7), 2623–2640.
- Möckel, J.E., Lippold, B.C., 1993. Zero-order drug release from hydrocolloid matrices. *Pharm. Res.* 10 (7), 1066–1070.
- Moner-Girona, M., Roig, A., Molins, E., Llibre, J., 2003. Sol-gel route to direct formation of silica aerogel microparticles using supercritical solvents. *J. Sol. Gel Sci. Technol.* 26 (1–3), 645–649.
- Morehouse Jr., D.S., Tetreault, R.J., 1971. Google Patents.
- Mura, S., Nicolas, J., Couvreur, P., 2013. Stimuli-responsive nanocarriers for drug delivery. *Nat. Mater.* 12 (11), 991.
- Narasimhan, B., 2001. Mathematical models describing polymer dissolution: consequences for drug delivery. *Adv. Drug Deliv. Rev.* 48 (2–3), 195–210.
- Nicolson, P.C., Vogt, J., 2001. Soft contact lens polymers: an evolution. *Biomaterials* 22 (24), 3273–3283.
- Nihant, N., Grandfils, C., Jérôme, R., Teyssié, P., 1995. Microencapsulation by coacervation of poly (lactide-co-glycolide) IV. Effect of the processing parameters on coacervation and encapsulation. *J. Control. Release* 35 (2–3), 117–125.
- Oh, J.K., Drumright, R., Siegwart, D.J., Matyjaszewski, K., 2008. The development of microgels/nanogels for drug delivery applications. *Prog. Polym. Sci.* 33 (4), 448–477.
- Padera, R., Bellas, E., Julie, Y.T., Hao, D., Kohane, D.S., 2008. Local myotoxicity from sustained release of bupivacaine from microparticles. *Anesthesiology* 108 (5), 921–928.
- Park, S.-N., Kim, J.K., Suh, H., 2004. Evaluation of antibiotic-loaded collagen-hyaluronic acid matrix as a skin substitute. *Biomaterials* 25 (17), 3689–3698.

- Park, J.H., Ye, M., Yeo, Y., Lee, W.-K., Paul, C., Park, K., 2006. Reservoir-type microcapsules prepared by the solvent exchange method: effect of formulation parameters on microencapsulation of lysozyme. *Mol. Pharm.* 3 (2), 135–143.
- Prashanth, K.H., Tharanathan, R., 2007. Chitin/chitosan: modifications and their unlimited application potential—an overview. *Trends Food Sci. Technol.* 18 (3), 117–131.
- Putney, S.D., Burke, P.A., 1998. Improving protein therapeutics with sustained-release formulations. *Nat. Biotechnol.* 16 (2), 153.
- Qin, Z., Zhe, J., Wang, G.-X., 2011. Effects of particle's off-axis position, shape, orientation and entry position on resistance changes of micro Coulter counting devices. *Meas. Sci. Technol.* 22 (4): 045804.
- Radomsky, M.L., Whaley, K.J., Cone, R.A., Saltzman, W.M., 1990. Macromolecules released from polymers: diffusion into unstirred fluids. *Biomaterials* 11 (9), 619–624.
- Rafati, H., Coombes, A., Adler, J., Holland, J., Davis, S., 1997. Protein-loaded poly (DL-lactide-co-glycolide) microparticles for oral administration: formulation, structural and release characteristics. *J. Control. Release* 43 (1), 89–102.
- Rai, A., Senapati, S., Saraf, S.K., Maiti, P., 2016. Biodegradable poly (ϵ -caprolactone) as a controlled drug delivery vehicle of vancomycin for the treatment of MRSA infection. *J. Mater. Chem. B* 4 (30), 5151–5160.
- Ramazani, F., Chen, W., van Nostrum, C.F., Storm, G., Kiessling, F., Lammers, T., Hennink, W.E., Kok, R.J., 2016. Strategies for encapsulation of small hydrophilic and amphiphilic drugs in PLGA microspheres: state-of-the-art and challenges. *Int. J. Pharm* 499 (1–2), 358–367.
- Ramstack, J.M., Herbert, P.F., Strobel, J., Atkins, T.J., 1997. Google Patents.
- Reinhold, S.E., Desai, K.G.H., Zhang, L., Olsen, K.F., Schwendeman, S.P., 2012. Self-healing microencapsulation of biomacromolecules without organic solvents. *Angew. Chem. Int. Ed.* 51 (43), 10800–10803.
- Reithmeier, H., Herrmann, J., Göpferich, A., 2001. Lipid microparticles as a parenteral controlled release device for peptides. *J. Control. Release* 73 (2–3), 339–350.
- Reverchon, E., Adami, R., Caputo, G., De Marco, I., 2008. Spherical microparticles production by supercritical antisolvent precipitation: interpretation of results. *J. Supercrit. Fluids* 47 (1), 70–84.
- Ribeiro, A.J., Silva, C., Ferreira, D., Veiga, F., 2005. Chitosan-reinforced alginate microspheres obtained through the emulsification/internal gelation technique. *Eur. J. Pharm. Sci.* 25 (1), 31–40.
- Rosen, H.B., Chang, J., Wnek, G., Linhardt, R., Langer, R., 1983. Bioerodible polyanhydrides for controlled drug delivery. *Biomaterials* 4 (2), 131–133.
- Rwei, A.Y., Lee, J.-J., Zhan, C., Liu, Q., Ok, M.T., Shankarappa, S.A., Langer, R., Kohane, D.S., 2015. Repeatable and adjustable on-demand sciatic nerve block with photo triggerable liposomes. *Proc. Natl. Acad. Sci.* 112 (51), 15719–15724.
- Rwei, A.Y., Paris, J.L., Wang, B., Wang, W., Axon, C.D., Vallet-Regí, M., Langer, R., Kohane, D.S., 2017. Ultrasound-triggered local anaesthesia. *Nat. Biomed. Eng.* 1 (8), 644.
- Sah, H., 1999. Stabilization of proteins against methylene chloride/water interface-induced denaturation and aggregation. *J. Control. Release* 58 (2), 143–151.
- Sansdrap, P., Moës, A.-J., 1993. Influence of manufacturing parameters on the size characteristics and the release profiles of nifedipine from poly (DL-lactide-co-glycolide) microspheres. *Int. J. Pharm* 98 (1–3), 157–164.
- Santamaria, C.M., Woodruff, A., Yang, R., Kohane, D.S., 2017. Drug delivery systems for prolonged duration local anesthesia. *Mater. Today* 20 (1), 22–31.
- Sastry, S.V., Nyshadham, J.R., Fix, J.A., 2000. Recent technological advances in oral drug delivery—a review. *Pharm. Sci. Technol. Today* 3 (4), 138–145.
- Scalia, S., Young, P.M., Traini, D., 2015. Solid lipid microparticles as an approach to drug delivery. *Expert Opin. Drug Deliv.* 12 (4), 583–599.
- Schmaljohann, D., 2006. Thermo- and pH-responsive polymers in drug delivery. *Adv. Drug Deliv. Rev.* 58 (15), 1655–1670.
- Schwach-Abdellaoui, K., Moreau, M., Schneider, M., Boisramé, B., Gurny, R., 2002. Controlled delivery of metoclopramide using an injectable semi-solid poly (ortho ester) for veterinary application. *Int. J. Pharm.* 248 (1–2), 31–37.
- Sendil, D., Gürsel, I., Wise, D.L., Hasırcı, V., 1999. Antibiotic release from biodegradable PHBV microparticles. *J. Control. Release* 59 (2), 207–217.
- Serrano-Ruiz, D., Alonso-Cristobal, P., Laurenti, M., Frick, B., López-Cabarcos, E., Rubio-Retama, J., 2013. Influence of the inter-chain hydrogen bonds on the thermoresponsive swelling behavior of UCST-like microgels. *Polymer* 54 (18), 4963–4971.
- Sharma, A., Sharma, U.S., 1997. Liposomes in drug delivery: progress and limitations. *Int. J. Pharm.* 154 (2), 123–140.
- Siepmann, J., Göpferich, A., 2001. Mathematical modeling of bioerodible, polymeric drug delivery systems. *Adv. Drug Deliv. Rev.* 48 (2–3), 229–247.
- Silva, C.M., Ribeiro, A.J., Figueiredo, I.V., Gonçalves, A.R., Veiga, F., 2006. Alginate microspheres prepared by internal gelation: development and effect on insulin stability. *Int. J. Pharm.* 311 (1–2), 1–10.
- Simón-Yarza, T., Formiga, F.R., Tamayo, E., Pelacho, B., Prosper, F., Blanco-Prieto, M.J., 2013. PEGylated-PLGA microparticles containing VEGF for long term drug delivery. *Int. J. Pharm.* 440 (1), 13–18.
- Singh, M., T O'Hagan, D., 2003. Recent advances in veterinary vaccine adjuvants. *Int. J. Parasitol.* 33 (5–6), 469–478.
- Singh, M., Briones, M., Ott, G., O'Hagan, D., 2000. Cationic microparticles: a potent delivery system for DNA vaccines. *Proc. Natl. Acad. Sci.* 97 (2), 811–816.
- Sinha, V.R., Kumria, R., 2001. Polysaccharides in colon-specific drug delivery. *Int. J. Pharm.* 224 (1–2), 19–38.
- Sinha, V., Bansal, K., Kaushik, R., Kumria, R., Trehan, A., 2004. Poly- ϵ -caprolactone microspheres and nanospheres: an overview. *Int. J. Pharm.* 278 (1), 1–23.
- Stenekes, R.J., Franssen, O., van Bommel, E.M., Crommelin, D.J., Hennink, W.E., 1998. The preparation of dextran microspheres in an all-aqueous system: effect of the formulation parameters on particle characteristics. *Pharm. Res.* 15 (4), 557–561.
- Suarez, S., Grover, G.N., Braden, R.L., Christman, K.L., Almutairi, A., 2013. Tunable protein release from acetylated dextran microparticles: a platform for delivery of protein therapeutics to the heart post-MI. *Biomacromolecules* 14 (11), 3927–3935.
- Surini, S., Anggriani, V., Anwar, E., 2009. Study of mucoadhesive microspheres based on Pregelatinized. *J. Med. Sci.* 9 (6), 249–256.
- Swatschek, D., Schatton, W., Kellermann, J., Müller, W.E., Kreuter, J., 2002. Marine sponge collagen: isolation, characterization and effects on the skin parameters surface-pH, moisture and sebum. *Eur. J. Pharm. Biopharm.* 53 (1), 107–113.
- Sy, J.C., Seshadri, G., Yang, S.C., Brown, M., Oh, T., Dikalov, S., Murthy, N., Davis, M.E., 2008. Sustained release of a p38 inhibitor from non-inflammatory microspheres inhibits cardiac dysfunction. *Nat. Mater.* 7 (11), 863.

- Tabata, Y., Ikada, Y., 1988. Macrophage phagocytosis of biodegradable microspheres composed of L-lactic acid/glycolic acid homo- and copolymers. *J. Biomed. Mater. Res.* 22 (10), 837–858.
- Takezaki, H., Kobayashi, H., Saito, M., Asano, I., 2015. G. Patents.
- Tamargo, R.J., Rossell, L.A., Kossoff, E.H., Tyler, B.M., Ewend, M.G., Aryanpur, J.J., 2002. The intracerebral administration of phenytoin using controlled-release polymers reduces experimental seizures in rats. *Epilepsy Research* 48 (3), 145–155.
- Tan, M.L., Choong, P.F., Dass, C.R., 2010. Recent developments in liposomes, microparticles and nanoparticles for protein and peptide drug delivery. *Peptides* 31 (1), 184–193.
- Tekin, R., Bac, N., Erdogmus, H., 2013. *Macromolecular Symposia*, pp. 35–40.
- Thomas, T.T., Kohane, D.S., Wang, A., Langer, R., 2004. Microparticulate formulations for the controlled release of interleukin-2. *J. Pharm. Sci.* 93 (5), 1100–1109.
- Thote, A.J., Chappell Jr., J.T., Kumar, R., Gupta, R.B., 2005. Reduction in the initial-burst release by surface crosslinking of PLGA microparticles containing hydrophilic or hydrophobic drugs. *Drug Dev. Ind. Pharm.* 31 (1), 43–57.
- Ting, T.-Y., Gonda, I., Gipps, E.M., 1992. Microparticles of polyvinyl alcohol for nasal delivery. I. Generation by spray-drying and spray-desolvation. *Pharm. Res.* 9 (10), 1330–1335.
- Tiwari, G., Tiwari, R., Sriwastawa, B., Bhati, L., Pandey, S., Pandey, P., Bannerjee, S.K., 2012. Drug delivery systems: an updated review. *Int. J. Pharm. Investig.* 2 (1), 2.
- Tomihata, K., Ikada, Y., 1997. In vitro and in vivo degradation of films of chitin and its deacetylated derivatives. *Biomaterials* 18 (7), 567–575.
- Treat, N.J., Sprafke, H., Kramer, J.W., Clark, P.G., Barton, B.E., Read de Alaniz, J., Fors, B.P., Hawker, C.J., 2014. Metal-free atom transfer radical polymerization. *J. Am. Chem. Soc.* 136 (45), 16096–16101.
- Tsuji, K., 2001. Microencapsulation of pesticides and their improved handling safety. *J. Microencapsul.* 18 (2), 137–147.
- Uchida, T., Martin, S., Foster, T.P., Wardley, R.C., Grimm, S., 1994. Dose and load studies for subcutaneous and oral delivery of poly (lactide-co-glycolide) microspheres containing ovalbumin. *Pharm. Res.* 11 (7), 1009–1015.
- Ueda, J., Sato, S., Tsunokawa, A., Yamauchi, T., Tsubokawa, N., 2005. Scale-up synthesis of vinyl polymer-grafted nano-sized silica by radical polymerization of vinyl monomers initiated by surface initiating groups in the solvent-free dry-system. *Eur. Polym. J.* 41 (2), 193–200.
- Uhrich, K.E., Cannizzaro, S.M., Langer, R.S., Shakesheff, K.M., 1999. Polymeric systems for controlled drug release. *Chem. Rev.* 99 (11), 3181–3198.
- Vakarelski, I.U., Toritani, A., Nakayama, M., Higashitani, K., 2001. Deformation and adhesion of elastomer microparticles evaluated by AFM. *Langmuir* 17 (16), 4739–4745.
- van de Weert, M., Van Steenberghe, M.J., Cleland, J.L., Heller, J., Hennink, W.E., Crommelin, D.J., 2002. Semisolid, self-catalyzed poly (ortho ester) s as controlled-release systems: protein release and protein stability issues. *J. Pharm. Sci.* 91 (4), 1065–1074.
- Vehring, R., 2008. Pharmaceutical particle engineering via spray drying. *Pharm. Res.* 25 (5), 999–1022.
- Verrijck, R., Smolders, I.J., Bosnie, N., Begg, A.C., 1992. Reduction of systemic exposure and toxicity of cisplatin by encapsulation in poly-lactide-co-glycolide. *Cancer Res.* 52 (23), 6653–6656.
- Visscher, G., Robison, R., Maulding, H., Fong, J., Pearson, J., Argentieri, G., 1985. Biodegradation of and tissue reaction to 50: 50 poly (DL-lactide-co-glycolide) microcapsules. *J. Biomed. Mater. Res.* 19 (3), 349–365.
- Visscher, G., Robison, R., Maulding, H., Fong, J., Pearson, J., Argentieri, G., 1986. Biodegradation of and tissue reaction to poly (DL-lactide) microcapsules. *J. Biomed. Mater. Res.* 20 (5), 667–676.
- Visscher, G., Pearson, J., Fong, J., Argentieri, G., Robison, R., Maulding, H., 1988. Effect of particle size on the in vitro and in vivo degradation rates of poly (DL-lactide-co-glycolide) microcapsules. *J. Biomed. Mater. Res.* 22 (8), 733–746.
- von Burkersroda, F., Schedl, L., Göpferich, A., 2002. Why degradable polymers undergo surface erosion or bulk erosion. *Biomaterials* 23 (21), 4221–4231.
- Wagenaar, B., Müller, B., 1994. Piroxicam release from spray-dried biodegradable microspheres. *Biomaterials* 15 (1), 49–54.
- Wang, J., Wang, B.M., Schwendeman, S.P., 2002. Characterization of the initial burst release of a model peptide from poly (D, L-lactide-co-glycolide) microspheres. *J. Control. Release* 82 (2–3), 289–307.
- Wang, C., Ge, Q., Ting, D., Nguyen, D., Shen, H.-R., Chen, J., Eisen, H.N., Heller, J., Langer, R., Putnam, D., 2004. Molecularly engineered poly (ortho ester) microspheres for enhanced delivery of DNA vaccines. *Nat. Mater.* 3 (3), 190.
- Wang, J.J., Jiang, J., Hu, B., Yu, S.H., 2008. Uniformly shaped poly (p-phenylenediamine) microparticles: shape-controlled synthesis and their potential application for the removal of lead ions from water. *Adv. Funct. Mater.* 18 (7), 1105–1111.
- Wang, W., Zhang, M.-J., Chu, L.-Y., 2013. Functional polymeric microparticles engineered from controllable microfluidic emulsions. *Acc. Chem. Res.* 47 (2), 373–384.
- Wang, J., Li, Y., Wang, X., Wang, J., Tian, H., Zhao, P., Tian, Y., Gu, Y., Wang, L., Wang, C., 2017. Droplet microfluidics for the production of microparticles and nanoparticles. *Micromachines* 8 (1), 22.
- Ward, M.A., Georgiou, T.K., 2011. Thermoresponsive polymers for biomedical applications. *Polymers* 3 (3), 1215–1242.
- Wattendorf, U., Merkle, H.P., 2008. PEGylation as a tool for the biomedical engineering of surface modified microparticles. *J. Pharm. Sci.* 97 (11), 4655–4669.
- Wedmore, I., McManus, J.G., Pusateri, A.E., Holcomb, J.B., 2006. A special report on the chitosan-based hemostatic dressing: experience in current combat operations. *J. Trauma Acute Care Surg.* 60 (3), 655–658.
- Weers, J.G., Tarara, T.E., Clark, A.R., 2007. Design of fine particles for pulmonary drug delivery. *Expert Opin. Drug Deliv.* 4 (3), 297–313.
- Weiser, J.R., Saltzman, W.M., 2014. Controlled release for local delivery of drugs: barriers and models. *J. Control. Release* 190, 664–673.
- Witzel, F., 1976. Google Patents.
- Woodruff, M.A., Hutmacher, D.W., 2010. The return of a forgotten polymer—polycaprolactone in the 21st century. *Prog. Polym. Sci.* 35 (10), 1217–1256.
- Xu, J.H., Zhao, H., Lan, W.J., Luo, G.S., 2012. A novel microfluidic approach for monodispersed chitosan microspheres with controllable structures. *Adv. Healthc. Mater.* 1 (1), 106–111.
- Yadav, S., Shire, S.J., Kalonia, D.S., 2010. Factors affecting the viscosity in high concentration solutions of different monoclonal antibodies. *J. Pharm. Sci.* 99 (12), 4812–4829.
- Yan, Z.P., Lin, G., Zhao, H.Y., Dong, Y.H., 1993. An experimental study and clinical pilot trials on Yttrium-90 glass microspheres through the hepatic artery for treatment of primary liver cancer. *Cancer* 72 (11), 3210–3215.
- Yang, J., Han, S., Zheng, H., Dong, H., Liu, J., 2015. Preparation and application of micro/nanoparticles based on natural polysaccharides. *Carbohydr. Polym.* 123, 53–66.

- Yang, R., Wei, T., Goldberg, H., Wang, W., Cullion, K., Kohane, D.S., 2017. Getting drugs across biological barriers. *Adv. Mater.* 29 (37), 1606596.
- Yaszemski, M.J., 2003. *Biomaterials in Orthopedics*. CRC Press.
- Ye, M., Kim, S., Park, K., 2010. Issues in long-term protein delivery using biodegradable microparticles. *J. Control. Release* 146 (2), 241–260.
- Yeh, M.-K., Jenkins, P., Davis, S., Coombes, A., 1995. Improving the delivery capacity of microparticle systems using blends of poly (DL-lactide co-glycolide) and poly (ethylene glycol). *J. Control. Release* 37 (1–2), 1–9.
- Yeo, Y., Park, K., 2004. Control of encapsulation efficiency and initial burst in polymeric microparticle systems. *Arch Pharm. Res.* 27 (1), 1.
- Yeo, Y., Bellas, E., Firestone, W., Langer, R., Kohane, D.S., 2005. Complex coacervates for thermally sensitive controlled release of flavor compounds. *J. Agric. Food Chem.* 53 (19), 7518–7525.
- Yeo, Y., Burdick, J.A., Highley, C.B., Marini, R., Langer, R., Kohane, D.S., 2006. Peritoneal application of chitosan and UV-cross-linkable chitosan. *J. Biomed. Mater. Res. Part A* 78 (4), 668–675.
- Yoo, J.-W., Doshi, N., Mitragotri, S., 2011. Adaptive micro and nanoparticles: temporal control over carrier properties to facilitate drug delivery. *Adv. Drug Deliv. Rev.* 63 (14–15), 1247–1256.
- Youan, B., Benoit, M.-A., Baras, B., Gillard, J., 1999. Protein-loaded poly (epsilon-caprolactone) microparticles. I. Optimization of the preparation by (water-in-oil)-in water emulsion solvent evaporation. *J. Microencapsul.* 16 (5), 587–599.
- Zhan, C., Wang, W., McAlvin, J.B., Guo, S., Timko, B.P., Santamaria, C., Kohane, D.S., 2015. Phototriggered local anesthesia. *Nano Letters* 16 (1), 177–181.
- Zhang, H., Neau, S.H., 2001. In vitro degradation of chitosan by a commercial enzyme preparation: effect of molecular weight and degree of deacetylation. *Biomaterials* 22 (12), 1653–1658.
- Zhang, Y., Yang, M., Portney, N.G., Cui, D., Budak, G., Ozbay, E., Ozkan, M., Ozkan, C.S., 2008. Zeta potential: a surface electrical characteristic to probe the interaction of nanoparticles with normal and cancer human breast epithelial cells. *Biomed. Micro-devices* 10 (2), 321–328.
- Zhang, Y., Wei, W., Lv, P., Wang, L., Ma, G., 2011. Preparation and evaluation of alginate–chitosan microspheres for oral delivery of insulin. *Eur. J. Pharm. Biopharm.* 77 (1), 11–19.
- Zhang, Z., Zhang, R., Decker, E.A., McClements, D.J., 2015. Development of food-grade filled hydrogels for oral delivery of lipophilic active ingredients: pH-triggered release. *Food Hydrocolloids* 44, 345–352.
- Zhao, A., Rodgers, V., 2006. Using TEM to couple transient protein distribution and release for PLGA microparticles for potential use as vaccine delivery vehicles. *J. Control. Release* 113 (1), 15–22.
- Zhe, J., Jagtiani, A., Dutta, P., Hu, J., Carletta, J., 2007. A micromachined high throughput Coulter counter for bioparticle detection and counting. *J. Micromech. Microeng.* 17 (2), 304.
- Zhou, Y., He, C., Chen, K., Ni, J., Cai, Y., Guo, X., Wu, X.Y., 2016. A new method for evaluating actual drug release kinetics of nanoparticles inside dialysis devices via numerical deconvolution. *J. Control. Release* 243, 11–20.

Chapter Exercises

- Which of the following cell types is least likely to take up microparticles?
 - Dendritic cells
 - Macrophages
 - Endothelial cells
- Which of the following routes of administration is not commonly used for drug-loaded microparticles?
 - Oral delivery
 - Intravenous injection
 - Pulmonary delivery
 - Local injection
- Which is the principal mechanism underlying drug release from poly(ortho ester) microparticles?
 - Surface erosion
 - Bulk erosion
 - Diffusion
 - Swelling
- Why do microparticles usually exhibit more prolonged release of drugs compared to nanoparticles?
- What is burst release? What are the potential consequences of burst release? What parameters of polymers and microparticles may affect burst release?
- Discuss strategies to improve microencapsulation efficiency of proteins. What factors in the microencapsulation process may lead to the loss of biological activity of proteins?
- A new hydrophobic drug which absorbs light at 580 nm has been developed. PLGA microspheres are used for the encapsulation of this drug by a conventional o/w emulsion and solvent evaporation method. Twenty mg of drug and 200 mg of PLGA polymer were dissolved in methylene chloride and the final volume was made to 2 mL. The absorption of polymer and drug solution at 580 nm was 0.8. The solution was then emulsified in 10 mL PBS buffer with a surfactant, using a homogenizer. Microspheres underwent solvent evaporation, washing and freeze-drying. To quantify drug encapsulation, 50 mg of the 210 mg of drug-loaded PLGA microspheres obtained were redissolved in methylene chloride and the final volume was made to 5 mL. The absorption of the redissolved solution at 580 nm was 0.065. What were the drug encapsulation and encapsulation efficiency in this example?

1.3.8B

Nanoparticles

LICHEN YIN¹, ZHIYUAN ZHONG²

¹Jiangsu Key Laboratory for Carbon-Based Functional Materials and Devices, Institute of Functional Nano and Soft Materials (FUNSOM), the Collaborative Innovation Center of Suzhou Nano Science and Technology, Soochow University, Suzhou, Jiangsu, China

²Biomedical Polymers Laboratory and Jiangsu Key Laboratory of Advanced Functional Polymer Design and Application, College of Chemistry, Chemical Engineering and Materials Science, Soochow University, Suzhou, Jiangsu, China

Chapter Objectives

- To provide an overview of nanoparticles (NPs)
- To outline various types of NPs and their preparation as well as characterization methods
- To highlight the intelligent design of NPs in overcoming multiple biological barriers
- To elucidate the numerous applications of NPs toward diagnosis and disease treatment

Introduction

NPs are colloidal solid particles with the size range of 1–1000 nm. In the field of nanomedicine and nanodiagnosis, NPs are more preferentially referred to as particles of 5–100 nm that are favorable for overcoming various systemic barriers. NPs have demonstrated extensive utilities for biomedical applications because of their unique physicochemical properties including changes in biochemical, magnetic, optical, and electronic properties at cellular, atomic, and molecular levels due to their high surface-to-volume ratio. Biomaterials-based NPs have received particular attention because they hold the promise to revolutionize medical treatment with more potent, less toxic, and smart therapeutics. For the purpose of drug delivery, NPs can encapsulate or covalently conjugate hydrophobic drugs to greatly enhance their aqueous solubility. They can also encapsulate hydrophilic drugs or biomacromolecules (such as proteins, peptides, or nucleic acids) to enhance their stability in vivo, prolong blood circulation time, and facilitate transmembrane delivery. The nanoscale diameter of NPs allows targeting to tumors via the enhanced permeability and retention (EPR) effect, and can dramatically reduce the nonspecific toxicity of chemodrugs. In addition, NPs with large surface area, improved circulation time, and high stability offer a

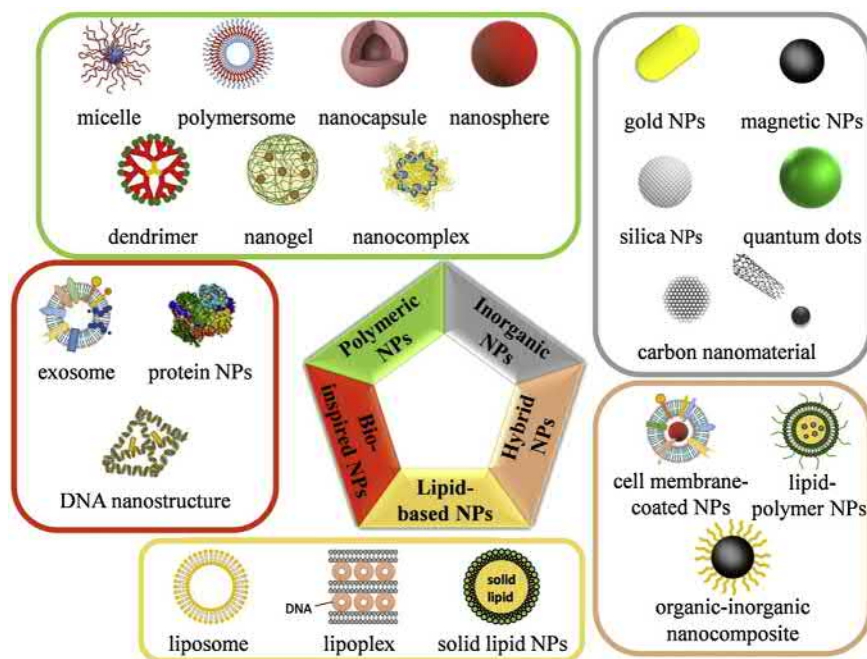
platform for highly specific and sensitive molecular imaging, by delivering the imaging probe or contrast agent to the target tissues or cells. Various ligands or antibodies can be grafted onto NP surfaces to increase the targeting efficiency and specificity. Alternatively, certain NPs, especially inorganic NPs with desired optical properties, have intrinsic imaging or therapeutic properties. These NPs, such as gold NPs or superparamagnetic iron-oxide NPs, often allow multimodal imaging due to production of the imaging contrast by themselves, and can mediate photothermal therapy due to photon-to-heat conversion.

Categories of NPs

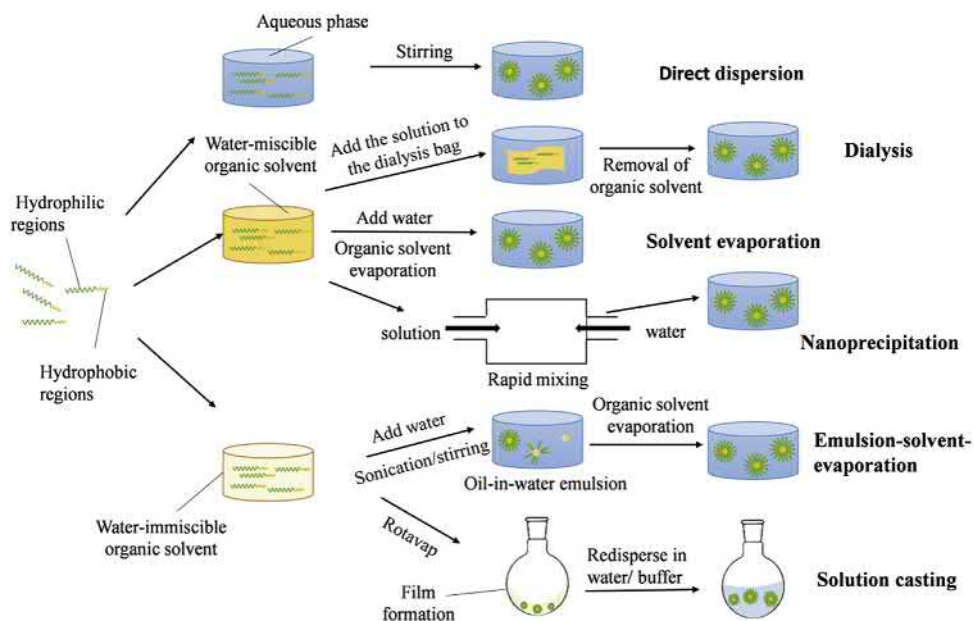
Depending on the type of fabricated materials, NPs can be classified into five major categories, including polymeric NPs, lipid-based NPs, inorganic NPs, bio-inspired NPs, and hybrid NPs (Fig. 1.3.8B.1).

Polymeric NPs

Polymeric micelles. Polymeric micelles (PMs) typically possess a core/shell structure with sizes of 20–200 nm. PMs are formed via the self-assembly of amphiphilic copolymers, driven by the hydrophobic interactions of the hydrophobic blocks of amphiphilic copolymers, generating a hydrophobic core surrounded by a hydrophilic shell (Kataoka et al., 2001). This thermodynamically driven process occurs when the copolymer concentration is higher than the critical micellar concentration (CMC), an important indicator of micelle stability that is affected by the hydrophilic-lipophilic balance (HLB). In general, with the same hydrophilic portion, a longer hydrophobic chain correlates to a lower CMC, and thus better micelle stability. The CMC can be determined by fluorescence spectroscopy, surface tension measurement,



• **Figure 1.3.8B.1** Categories of NPs.



• **Figure 1.3.8B.2** Methods for the preparation of polymeric micelles (Cagel et al., 2017).

UV-vis spectroscopy, and dynamic light scattering (DLS). A preferred technique to determine the CMC involves the use of fluorogenic dyes, such as pyrene, due to its high sensitivity. When PMs are formed, pyrene is preferentially partitioned into the hydrophobic core and thus a CMC value can be determined. Commonly used amphiphilic copolymers to prepare micelles include poly(ethylene oxide)-poly(propylene oxide)-poly(ethylene oxide) (PEO-PPO-PEO), poly(ethylene glycol)-poly(lactic acid) (PEG-PLA), PEG-poly(lactic-co-glycolic acid) (PEG-PLGA), and PEG-poly(ϵ -caprolactone) (PEG-PCL), approved by the FDA for biomedical applications. In addition, other biodegradable copolymers with

hydrophobic segments covalently bonded to PEG have also been used to build PMs. These hydrophobic segments include polyanhydrides, such as poly(sebacic anhydride) (PSA), and hydrophobic poly(L-amino acid) and derivatives. Hydrophobic drugs can be encapsulated into the hydrophobic core of PMs via hydrophobic interactions.

There are various methods for micelle preparation such as direct dispersion, nanoprecipitation, emulsion-solvent evaporation, solvent evaporation, dialysis, and film formation. The dispersion method involves direct dispersion of the polymer in an aqueous solution, which is usually employed for intermediate hydrophobic polymers (Fig. 1.3.8B.2).

The advantages of this method are simplicity, short processing time, and avoidance of organic solvent. However, only a few drugs could be encapsulated using this method. The nanoprecipitation method involves copolymer dissolution in a water-miscible organic solvent, and the organic solution is afterward added dropwise to an aqueous solution under vigorous stirring. Subsequently, the organic solvent is removed by evaporation. In the method of emulsion-solvent evaporation, copolymers are dissolved in a water-immiscible organic solvent. After the solvent is emulsified in an aqueous solution, the solvent is removed by evaporation. The solvent evaporation method is similar to the emulsion-solvent evaporation method, except that the organic solvent is miscible with water. The organic solvent is removed through evaporation, and the change in solvent quality from organic to aqueous is gradual, which allows the polymer and drug to aggregate into micelles rather than precipitate from the solution in bulk. The solvent of choice is usually acetone, due to its high water miscibility and low vapor pressure, which simplifies the solvent removal. The dialysis method involves the use of water-miscible organic solvent to dissolve copolymers with low water solubility. The micelles are assembled when the organic phase is removed by dialysis against water, and the hydrophobic core could encapsulate poorly water-soluble drugs. Another method is based on the formation of a thin film. The organic phase containing copolymers and hydrophobic drugs are evaporated using a rotary evaporator to form a thin film. The micelles are formed when the thin film is rehydrated with an aqueous phase (Cagel et al., 2017).

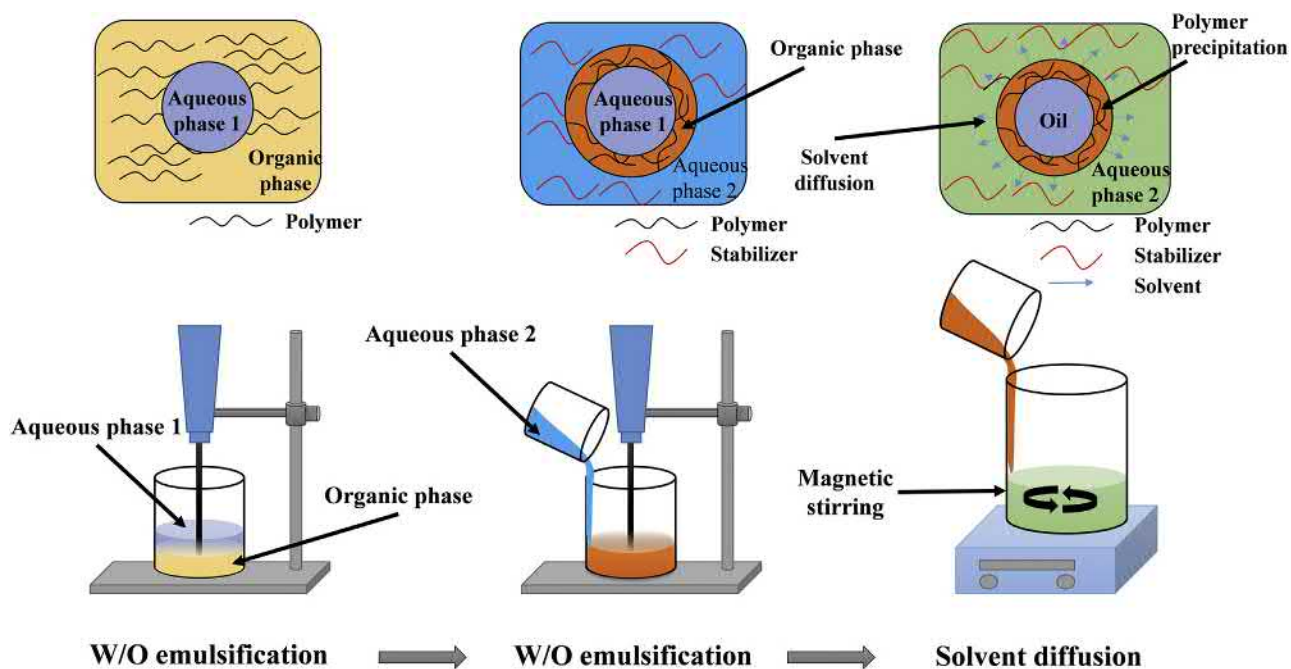
Nevertheless, micelle-based nanomedicines will suffer from premature disintegration upon dilution in the bloodstream. Core-cross-linked or shell-cross-linked PMs have thus evolved to overcome this critical issue. Either the core or the shell of micelles can be cross-linked via covalent bonding, hydrogen bonding, or π - π stacking, and the obtained PMs have no CMC values to completely resist dilution-induced disassembly. By incorporating stimuli-responsive domains in the cross-linker, the cross-linked PMs allow stable drug retention yet tailored release kinetics.

In addition to noncharged polymeric micelles, polyion complex (PIC) micelles with sizes lower than 100 nm are developed from a pair of oppositely charged block copolymers through electrostatic interactions. For example, upon mixing aqueous solutions of PEG-poly(L-lysine) (PEG-PLys) and PEG-poly(aspartic acid) (PEG-PAsp), PIC micelles with an extremely narrow size distribution are formed without exchanging solvent. This behavior could be explained by the segregation of the PIC structure from the aqueous polyion exterior to form the core of the micelles.

Nanospheres. Polymeric nanospheres are defined as matrix-type, solid colloidal particles based on hydrophobic polymers stabilized via surfactants assembled on the nanosphere surfaces. Generally, these particles are larger than micelles with diameters between 100 and 200 nm. The hydrophobic surfaces of nanospheres are highly

susceptible to opsonization and clearance by the reticulo-endothelial system (RES). There are two methods to prepare nanospheres. One method involves either emulsion polymerization in the case of poly(methylmethacrylate) and poly(ethylcyanoacrylate) or interfacial polymerization for poly(alkylcyanoacrylate). The monomers are usually dissolved in the aqueous phase containing stabilizers (such as PVA) or surfactants (such as Span 80), and polymerization is initiated upon contact of the monomers present in continuous phase with an initiator molecule that can be an ion, a free radical, or by high-energy radiation. Polymerization leads to the formation and precipitation of solid nanospheres. Another method is based on emulsification/solvent evaporation and nanoprecipitation. Polymers are dissolved in water-miscible organic solvent, and then added to the aqueous phase. Upon contact with the aqueous phase, the organic solvent immediately diffuses out, resulting in the formation of nanospheres. Alternatively, the organic phase is emulsified in an aqueous phase containing surfactant or stabilizer using high-energy homogenization or sonication. Subsequently, the organic phase is evaporated under vacuum, leading to the formation of nanospheres.

Nanocapsules. Nanocapsules are defined as nano-vesicular systems consisting of an inner liquid core surrounded by a polymeric membrane. Frequently, the core is an oily liquid, and the surrounding polymer is a single layer of polymer. Polyesters such as PLA, PLGA, and PCL, have been widely used to construct nanocapsules. Generally, there are six classical methods to prepare nanocapsules, including nanoprecipitation, emulsion-diffusion, double emulsification, emulsion-coacervation, polymer-coating, and layer-by-layer assembly (Mora-Huertas et al., 2010). The nanoprecipitation method, also known as solvent displacement or interfacial deposition, produces nanocapsules as a colloidal suspension when the organic phase containing polymers is added slowly to the aqueous phase under stirring. For the emulsion-diffusion method, the procedure requires three phases, organic, aqueous, and dilution. The organic solvent should be partially water-miscible and the aqueous phase should be solvent-saturated, while the dilution phase is usually water. The organic phase is emulsified under vigorous agitation in the aqueous phase. Addition of dilution solvent into the system leads to the diffusion of solvent into the external phase, resulting in nanocapsule formation. The double emulsification method, also called “emulsion of emulsion,” often involves water-oil-water emulsion, that requires two surfactants, a hydrophobic one to stabilize the interface of the w/o internal emulsion and a hydrophilic one to stabilize the external interface of the oil globules (Fig. 1.3.8B.3). The emulsion-coacervation method is based on the formation of a coacervate phase that causes polymer precipitation from the continuous emulsion phase to form a film on the template. This method is suitable for naturally occurring polymers, such as sodium alginate and gelatin. Polymer is dissolved in an aqueous phase and o/w emulsion is formed by mechanical stirring or ultrasound. Subsequently, a coacervation process is performed by using either



• **Figure 1.3.8B.3** Preparation of nanocapsules by the double emulsification method (Mora-Huertas et al., 2010).

electrolytes with a sodium alginate–calcium chloride system, or by addition of a water-miscible nonsolvent or a dehydration agent with a gelatin–isopropanol–sodium sulfate system. The polymer-coating method is based on depositing a thin layer of polymer on the nanoparticle surface during the final stage of conventional methods such as nanoprecipitation and double emulsification to allow simultaneous layer formation. Nanocapsules obtained by the layer-by-layer assembly process are called polyelectrolyte capsules with well-defined chemical and structural properties. This technique requires a colloidal template on which a polymer layer is adsorbed via electrostatic attraction. This procedure is repeated using a second polymer with opposite charge.

With regard to drug encapsulation efficiency, nanoprecipitation, emulsion-diffusion, and layer-by-layer methods exhibit excellent encapsulation efficiencies (80% or more). In the case of the layer-by-layer method, the solid drug serves as the template to ensure high encapsulation efficiency. However, for the nanoprecipitation and emulsion-diffusion methods, various factors including the chemical nature and polarity of the drug may influence the encapsulation efficiency. Hydrophilic drugs can reach maximum values of 10%, while lipophilic compounds can reach higher than 70%. Regarding the double emulsification method, encapsulation efficiency ranges from 65% to 75%, depending on both the polymers and the surfactants used. For the emulsion-coacervation method, its encapsulation efficiency is obviously low in comparison to other nanoencapsulation methods. Although nanocapsules are considered as stable systems due to Brownian motion, they can be subject to instability due to polymer degradation, migration of the active substance from the inner liquid, and microbiological contamination of aqueous systems.

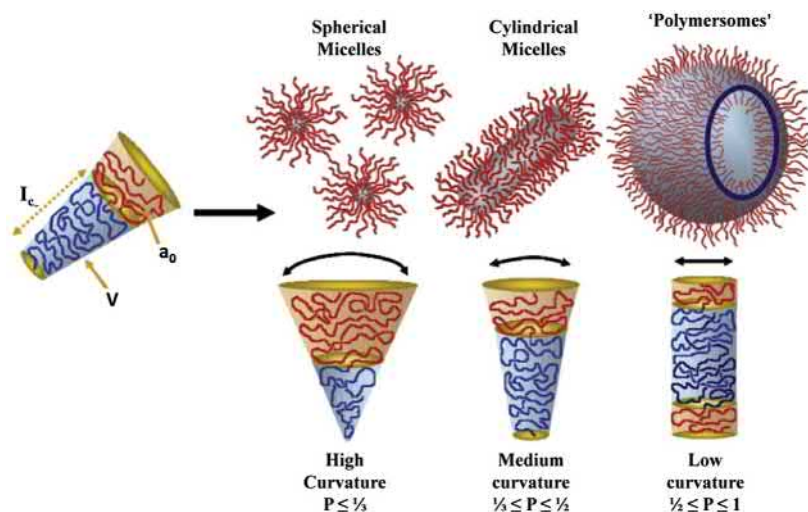
Polymersomes. Polymersomes self-assembled from block or graft amphiphilic copolymers afford similar properties to liposomes yet higher stability. Regarding the specific self-assembled nanostructure of amphiphilic block copolymers, a dimensionless “packing parameter,” p , defined in the following equation, is developed to indicate the most likely morphology.

$$p = v/a_o l_c$$

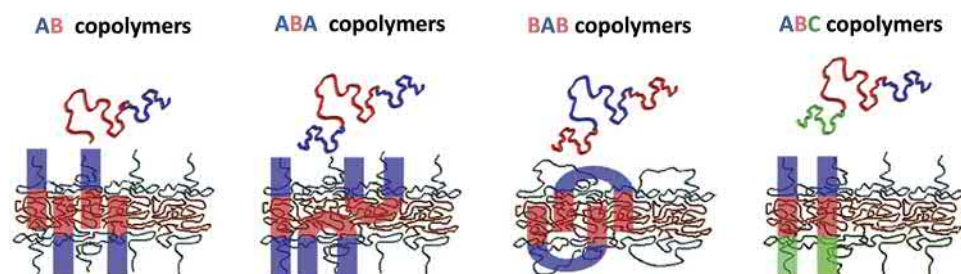
where v is the volume of the hydrophobic chain, a_o is the optimal area of the head group, and l_c is the length of the hydrophobic tail.

Generally, spherical micelles are favored at $p \leq 1/3$; cylindrical micelles are obtained at $1/3 \leq p \leq 1/2$; and polymersomes are formed at $1/2 \leq p \leq 1$ (Fig. 1.3.8B.4) (Blanzaz et al., 2009).

Typical polymersomes are hollow spheres that contain an aqueous solution in the core surrounded by a bilayer membrane. The bilayer membrane is composed of hydrated hydrophilic coronas both at the inside and outside of the hydrophobic middle part of the membrane separating and protecting the fluidic core from the outside medium. Water-soluble drugs could be encapsulated in the core of polymersomes, and hydrophobic drugs are integrated within the hydrophobic membrane. In general, the composition and molecular weight of synthetic amphiphilic polymers can be varied, offering polymersomes with different membrane thicknesses and permeability. Usually, polymersomes from amphiphilic copolymers with high molecular weight have relatively thick (3–4 nm) and robust membranes (Lee and Feijen, 2012). The possible bilayer assemblies in the aqueous environment are schematically illustrated in Fig. 1.3.8B.5 for AB diblock, and ABA, BAB, and ABC triblock



• **Figure 1.3.8B.4** The self-assembled nanostructures of block copolymers. (Reproduced from Blanazs, A., Armes, S. P., Ryan, A. J., 2009. Self-assembled block copolymer aggregates: from micelles to vesicles and their biological applications. *Macromol. Rapid Commun.* 30, 267–277.)

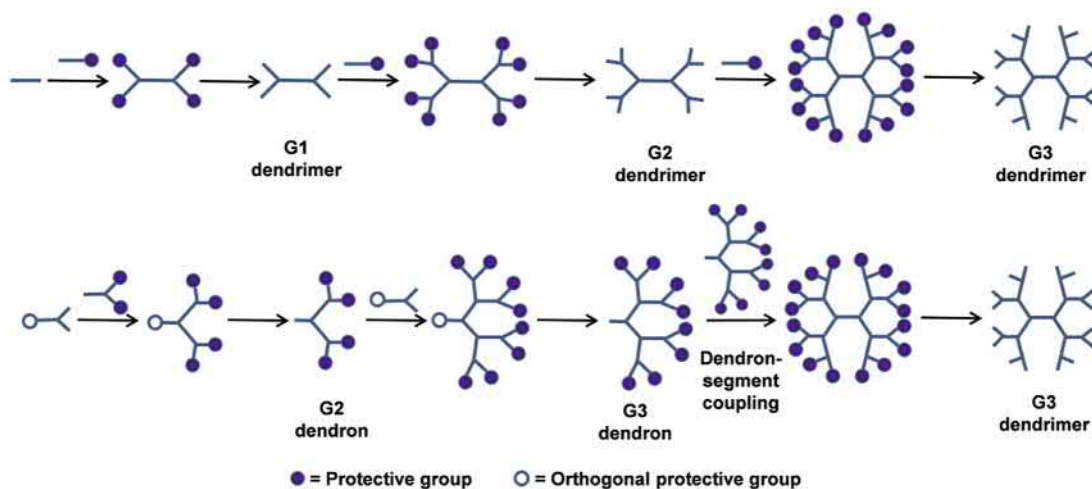


• **Figure 1.3.8B.5** Membrane conformation of polymersomes formed by diblock and triblock copolymers. (Reproduced from Lee, J. S., Feijen, J., 2012, Polymersomes for drug delivery: design, formation and characterization. *J. Control. Release* 161, 473–483.)

copolymers, where A and C are different hydrophilic blocks and B is the hydrophobic block. The geometric shapes of the amphiphiles in the aqueous environment are driven by complementary hydrophobic–hydrophobic interactions between the polymer chains. For AB and BAB copolymers, there is only one molecular conformation that can result in bilayer membrane formation (cylindrical shape for AB and curved shape for BAB). The hydrophobic chains are entangled in the middle of the membrane to minimize the interfacial area with water and the hydrophilic block is positioned to the outside of the membranes. In the case of ABA copolymer, there are two possible conformations. The hydrophobic block can either form a curved loop so that both hydrophilic chains are faced toward the outside of the membrane or they can stretch to form a cylindrical shape with the two hydrophilic blocks at the opposite sides of the membrane. Additionally, ABC copolymers can self-assemble into polymersomes with asymmetric membranes. Due to the difference in MW, charge, and solubility of the hydrophilic blocks, polymer chains with relatively larger fraction are preferentially positioned to the outer surface of the polymersomes (Blanazs et al., 2009).

Solvent-switching and polymer rehydration are two major techniques to prepare polymersomes. For the

solvent-switching method, also called the phase inversion method, polymersomes are formed by first dissolving amphiphilic copolymers in an organic solvent, followed by hydration of the solution either through slow addition of water into the organic phase or injection of the organic solution into water. This procedure causes the hydrophobic blocks to become insoluble, thus triggering copolymer self-assembly into polymersomes due to increasing interfacial tension between the hydrophobic blocks and water. In this method, the size and size distribution of the polymersomes can be varied by selecting different organic solvents. The polymer rehydration method involves the hydration of amphiphilic block copolymer films to induce self-assembly. Polymers are first dissolved in an organic solvent followed by evaporation of the organic solvent to form a thin film. Then, water is added to hydrate the film, and the successive processes of water permeation through defects in the polymer layers driven by hydration forces, inflation of polymer layers, and formation of bulges finally yield polymersomes upon separation from the surface. Polymersomes produced by this method have a broad size distribution, and desired polymersomes are obtained by sequential extrusion through filters with different pore sizes under high pressure. In general, polymersomes are more stable in the blood circulation



• **Figure 1.3.8B.6** Synthesis of dendrimer. (Top) Divergent strategy; (bottom) convergent strategy (Boas and Heegaard, 2004).

than liposomes. Hydrophilic, hydrophobic, or amphiphilic compounds can be loaded in either the aqueous core or the bilayer membrane of polymersomes, which makes them highly attractive for drug delivery, bio-imaging, and diagnosis.

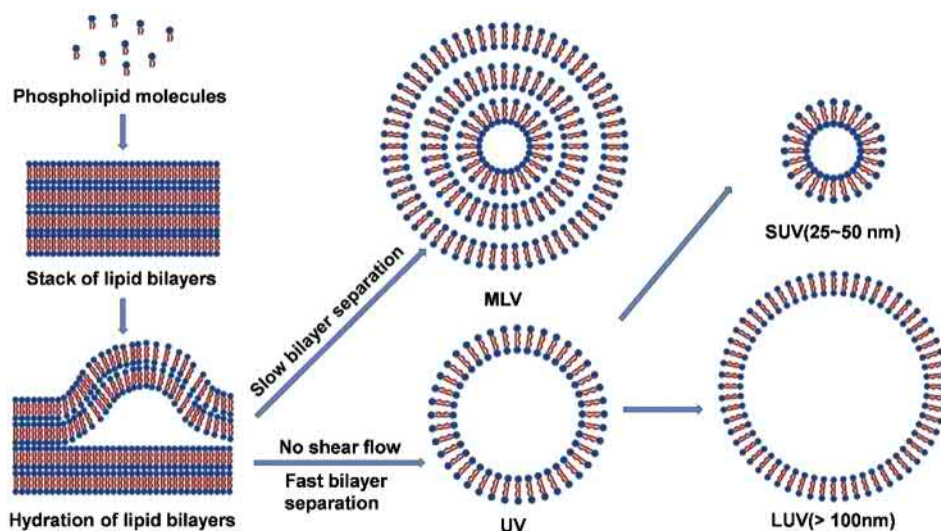
Nanogels. Nanogels are nanoscale three-dimensional polymer networks with a high capacity to hold water, without dissolving into the aqueous medium. Nanogels with high loading capacity for drug cargoes and unique physical properties offer distinct advantages over other nanomaterials for biomedical applications. Their size, charge, porosity, amphiphilicity, softness, and degradability can be fine-tuned by flexible design. Nanogels can be prepared by physical or chemical cross-linking. Amphiphilic polysaccharides were first used to create physically cross-linked nanogels via hydrophobic interactions in water. However, physically cross-linked nanogels tend to be more fragile because they are stabilized by relatively weak interactions such as hydrophobic or ionic interactions. Meanwhile, the control over the particle size is another critical challenge, which is affected by the polymer concentrations, temperature, pH, and ionic strength. Chemically cross-linked nanogels are therefore developed via covalent bond formation during the polymerization of monomers or cross-linking of polymer precursors via thiol-disulfide exchange, amide cross-linking, click chemistry, Schiff-base reactions, photo-induced cross-linking, and enzyme-mediated cross-linking.

Dendrimers. Dendrimers are unimolecular NPs with a well-defined, homogeneous, and monodisperse architecture consisting of three distinct domains: (1) a core at the center of the dendrimer consisting of an atom or a molecule having at least two identical chemical functions; (2) branches, emanating from the core, constituted of repeating units having at least one branch junction, whose repetition is organized in a geometrical progression that results in a series of radially concentric layers called “generations”; and (3) multiple terminal functional groups, located on

the surface of the dendritic architecture. The nomenclature dendrimer is derived from a Greek term *dendron* that means “tree.” Divergent and convergent methods are most frequently used for dendrimer synthesis (Fig. 1.3.8B.6). The divergent approach comprises two steps, the activation of functional surface groups and the addition of branching monomer units. In this approach, the core is reacted with two or more equivalents of reagent containing at least two protecting/branching sites, followed by removal of the protecting groups, leading to the formation of a first-generation dendrimer. This process is repeated several times until dendrimers with specific generations and sizes are formed. One advantage of this approach is the ability to modify the surface of dendrimer molecules by changing the end groups at the outermost layer, while the main constraint is that only one type of functional group is placed on the outermost generation.

The convergent growth method would overcome this issue, and involves two stages, reiterative coupling of protected/deprotected branch to produce a focal point functionalized dendron, followed by a divergent core anchoring step to produce various multidendron dendrimers. Precise control over molecular weight and production of dendrimers with functionalities in precise positions and numbers are unique advantages of this method. However, difficulty in synthesizing dendrimers in large quantities is a significant limitation. Dendrimers with uniform and well-defined molecular structure, size, and shape are of prominent interest in biomedical applications because of their ability to cross cell membranes as well as reduce premature clearance from the body. Amine-terminated polyamidoamine (PAMAM) and polypropyleneimine (PPI) dendrimers display concentration-dependent toxicity and hemolysis, which, nevertheless, can be overcome by partial or complete modification of their periphery with negatively charged or neutral groups.

Nanocomplexes. Nanocomplexes are functional supramolecular nanocomposites formed from the self-assembly



• **Figure 1.3.8B.7** Preparation of different liposomes. (Reproduced from Yingchoncharoen, P., Kalinowski, D. S., Richardson, D. R., 2016. Lipid-based drug delivery systems in cancer therapy: what is available and what is yet to come. *Pharmacol. Rev.* 68, 701–787.)

of polymers and biomacromolecular drug cargoes, such as protein and nucleic acids, via specific intra- and intermolecular interactions. Cationic polymers can condense negatively charged nucleic acids to form nanocomplexes, called polyplexes. Polyplex formation is usually kinetically controlled; it is performed at ionic strengths where the polycation/polyanion association is rapid and almost irreversible. The sequence of addition of components during the complexation procedure (involving either the addition of a polymer solution to the DNA solution, or vice versa) influences the resulting polyplex size, as well as the transfection efficiency. Besides nucleic acid-based nanocomplexes, proteins can serve to form nanocomposites with various materials by self-assembly via electrostatic interactions, hydrogen bonding, hydrophobic interactions, or salt bridging. In addition, proteins can be fabricated into fluoroamphiphilic nanocomplexes via the fluorination effect.

Lipid-Based NPs

Liposomes. Liposomes are a class of nano- or micrometer-sized phospholipid vesicles composed of one or multiple lipid bilayers that envelope the inner aqueous cores. The polar head groups of phospholipids are oriented in the pathway of the interior and exterior aqueous phases. The liposome size can vary from very small (25 nm) to large (2.5 μm). On the basis of their size and number of bilayers, liposomes can be classified into two categories, multilamellar vesicles (MLVs) with sizes of 0.05–10 μm and unilamellar vesicles (ULVs) with sizes ranging from 25 nm to several hundred nm. ULVs can also be classified into large unilamellar vesicles (LUVs) and small unilamellar vesicles (SUVs) (Fig. 1.3.8B.7). Hydrophilic drugs can be encapsulated in the aqueous core and hydrophobic drugs are entrapped in the lipid bilayer, making them ideal candidates for drug delivery. Major methods to prepare liposomes include thin-film

hydration, solvent injection, reverse-phase evaporation, detergent depletion, and microfluidics.

As a common technique for liposome preparation, thin-film hydration (also called the Bangham method) involves dissolution of the lipid in an organic solvent, evaporation of the solvent, and dispersion of the lipid film in aqueous media. However, the encapsulation efficiency of water-soluble drugs is often low (5%–15%). Moreover, this method produces large and heterogeneous MLVs that require additional sonication or extrusion to produce homogeneous small ULVs. Another technique is solvent injection. A lipid solution (diethyl ether or ethanol) is injected to an aqueous solution or a huge excess of buffer, and liposomes are obtained after removal of organic solvent. The major disadvantage of this technique is the heterogeneous population and difficulty to remove organic solvent. The reverse-phase evaporation method is based on the creation of inverted micelles. The inverted micelles are shaped upon sonication of a mixture of a buffered aqueous phase, which contains the water-soluble drug cargoes and an organic phase containing amphiphilic molecules. The slow elimination of the organic solvent leads to conversion of inverted micelles into viscous state and finally gel forms. At a critical point in this process, the gel state collapses, and some of the inverted micelles were disturbed. The excess of phospholipids in the environment donates to the formation of a complete bilayer around the residual micelles, which results in the liposomes. The detergent-depletion method involves the hydration of a lipid film with a detergent solution and leads to the formation of large MLVs. However, this method usually suffers from a long preparation time and poor trapping efficiency. The microfluidic-based method for liposome preparation allows strict control over lipid hydration, thus enabling precise control over liposome size and size distribution by controlling the flow rate and mixing conditions.

Solid lipid NPs (SLNs). SLNs, also known as lipospheres or solid lipid nanospheres, consist of lipid matrix that remain

in the solid state at room and body temperature coated with a monolayer of phospholipid and exhibit a size range of 50–1000 nm. Compared with liposomes, SLNs feature easy preparation, low cost, and amenability to scale up. Various techniques have been developed to prepare SLNs, including high-pressure homogenization, microemulsion, and precipitation via solvent evaporation. High-pressure homogenization further involves hot and cold homogenization. For hot homogenization, the drug is firstly dissolved in the lipid at the temperature 5–10°C above its melting point. The mixture is dispersed in an aqueous surfactant solution at the same temperature to form a pre-emulsion. After homogenization, the hot oil-in-water (o/w) nanoemulsion is allowed to cool down to recrystallize the lipid and form SLNs. For temperature-sensitive drugs, cold homogenization is required. The mixture of melted lipid and drug is cooled down to form the solid lipid which is ground to form microparticles (50–100 μm). The microparticles are further dispersed in a cold surfactant solution, homogenized at room temperature or lower, and cut into SLNs by the cavitation forces produced by the high-pressure homogenizer.

With regard to the microemulsion method, water, cosurfactants, and surfactants at the same temperature are mixed under mild stirring. Subsequently, the microemulsion is dispersed in cold water (2–3°C) under mild stirring and small particles are formed upon precipitation. This method allows preparation of SLNs on a large scale. The precipitation method by solvent evaporation is similar to PMs. Lipid is dissolved in organic solvent, emulsified in an aqueous phase, and then organic solvent is evaporated, leading to precipitation of the lipid to form SLNs. The main challenge of this method is the difficulty in removing organic solvent.

Lipoplexes. Cationic lipids can condense negatively charged nucleic acids at particular weight ratios to form nanocomplexes, termed lipoplexes. The lipid can fuse with cell membranes and endolysosomal membranes to potentiate intracellular gene delivery. The concentration, temperature, environment, and kinetics of mixing could affect the characteristics and transfection potential of lipoplexes. X-ray diffraction (XRD) studies have demonstrated the existence of different lipoplex structures. One is a multilamellar structure, with DNA monolayers sandwiched between cationic membranes, and the other is an inverted hexagonal structure, also called the inverted “honeycomb” phase, with DNA encapsulated within cationic lipid monolayer tubes. Similar to the gene complexes, cationic lipids can also assemble with negatively charged proteins/peptides to form lipopolyplexes.

Inorganic NPs

Gold NPs. Gold nanoparticles (GNPs) have unique chemical and physical properties for diagnosis and drug delivery. First, the gold core is essentially inert with low toxicity. Second, monodispersed GNPs are easy to synthesize, with sizes ranging from 1 to 150 nm. Via thiol linkages, GNPs can be facilely functionalized. Moreover, their photophysical

properties can be used to trigger drug release at a remote place. GNPs can be prepared via various methods based on the reduction of gold salts in the presence of appropriate stabilizers, such as ligands, surfactants, and polymers. However, the most robust GNPs are stabilized by thiolates using a strong Au–S bond. A variety of monolayer-protected clusters (MPCs) can be formed rapidly and in scalable manner using the one-pot protocol developed by Schiffrin et al. in 1994 (Brust et al., 1994). In particular AuCl₄⁻ salts are reduced with NaBH₄ in the presence of the thiol capping ligand. The core size of the particles can be varied from 1.5 nm to ~6 nm by varying the thiol-gold stoichiometry. Tunable size and functionality make GNPs a useful scaffold for efficient recognition and delivery of biomolecules. GNPs also have several advantages in diagnosis over quantum dots and organic dyes due to their better contrast for imaging, and surface-enhanced and distance- and refractive index-dependent spectroscopic properties. Moreover, GNPs can cause local heating to eradicate tumors when they are irradiated with light in the “water window” (800–1200 nm), which enables so-called photothermal therapy.

Magnetic NPs. Magnetic nanoparticles (MNPs) are being actively investigated as magnetic resonance imaging (MRI) contrast agents and nanocarriers for targeted drug delivery. Colloidal iron oxide nanoparticles, such as superparamagnetic iron oxides (SPIO) and ultrasmall superparamagnetic iron oxides (USPIO), are the most extensively investigated MNPs for biomedical applications. Typically composed of nanocrystalline magnetite (Fe₃O₄) or maghemite (γ-Fe₂O₃) protected with a polymeric coating, these ferrite NPs possess a spinel crystal structure with oxygen ions forming a close-packed cubic lattice and iron ions located at interstices. Efficient synthesis approaches including co-precipitation, thermal decomposition, hydrothermal synthesis, microemulsion, and sonochemical synthesis have been developed to produce the shape-controlled, stable, biocompatible, and monodispersed iron oxide NPs. In addition, electrochemical synthesis, laser pyrolysis techniques, microorganism or bacterial synthesis are also used to fabricate MNPs. The most conventional method for obtaining Fe₃O₄ or γ-Fe₂O₃ is by co-precipitation. This method consists of mixing ferric and ferrous ions in highly basic solutions at room temperature or at an elevated temperature. The size and shape of the iron oxide NPs depend on the type of salt used, the ferric and ferrous ions ratio, the reaction temperature, pH value, ionic strength, and other reaction parameters (e.g., stirring rate, dropping speed of basic solution). However, this method generates particles with a wide particle size distribution, which sometimes requires secondary size selection.

Silica NPs. Silica NPs are widely utilized for bioimaging and drug delivery due to their easy synthesis, uniform morphology, high surface area-to-volume ratio, controlled size, easy surface functionalization, and biocompatibility. In addition, silica NPs with size <5 nm show significant optical properties due to the quantum confinement effect. Generally, there are two types of silica NPs, the solid core/shell silica NPs and mesoporous silica NPs (MSNs).

The solid NPs can be used to deliver imaging probes doped into the core. MSNs contain mesopores with high surface area (600–1000 m²/g) and pore volume (0.6–1.0 mL/g), and thus allow high drug loading and controllable release. The most well-known MSNs include MCM-41, MCM-48, and SBA-15, with different pore sizes (2–10 nm) and structures (2D hexagonal and 3D cubic).

There are two general routes for the synthesis of silica NPs, reverse microemulsion, and the Stöber method. The reverse microemulsion is an isotropic and thermodynamically stable single-phase system. Water nanodroplets formed in the bulk oil phase act as nanoreactors for the formation of discrete NPs. The Stöber method involves the hydrolysis of tetraalkyl silicates in a mixture of alcohol and water using ammonia as a catalyst. The synthesis of MSNs typically relies on the cooperative self-assembly of oligomeric silica species and supramolecular surfactant assemblies that act as structure-directing agents. MSNs are obtained after removal of the structure-directing agent, which leads to opening of the pores. By tuning the synthesis conditions and/or by variation of the reactants, elongated MSNs with tunable aspect ratios can be synthesized.

Quantum dots. Quantum dots (QDs) are semiconductor NPs with sizes ranging from 2 to 10 nm, often made from hundreds to thousands of atoms of group II and VI elements (e.g., CdSe and CdTe) or group III and V elements (e.g., InP and InAs). Physical size smaller than the exciton Bohr radius results in a three-dimensional quantum confinement of charge carriers within the QD and limits the number of possible energy states that an electron can occupy, thus giving NPs novel properties including unique photophysical properties and versatile surface chemistry that are not achievable in bulk materials. However, QDs are water-insoluble, limiting their biological applications. To address this issue, one approach involves replacing the hydrophobic trioctyl phosphine oxide (TOPO) coating with bifunctional ligands, which presents both a surface-anchoring group (e.g., thiol) and a hydrophilic end group (e.g., carboxyl or hydroxyl). An alternative approach is to retain the native TOPO coating and encapsulate the hydrophobic QDs with amphiphilic molecules such as polymers, or phospholipids. By decorating QDs with biomolecules that mediate specific interactions with living systems, QDs are effectively used for bioimaging, detection, and drug delivery. To this end, QDs can be conjugated with biomolecules via covalent bonding or coordination with metal atoms of the QD core/shell.

Nanocarbons. Nanocarbons, including carbon nanodots (CNDs), carbon nanotubes (CNTs), and graphene oxide, have been widely developed. Carbon dots (C-dots) contain many carboxylic acid moieties at their surface, thus imparting them with excellent water solubility and the suitability for subsequent functionalization. Approaches for synthesizing CNDs include top-down and bottom-up methods. Top-down methods consist of arc discharge, laser ablation, and electrochemical oxidation, where the CNDs are formed or “broken off” from a larger carbon structure. Bottom-up approaches consist of combustion/thermal, supported synthetic, or microwave methods during which the CNDs are

formed from molecular precursors. Typically, their surfaces are oxidized by nitric acid (HNO₃) and further purified by using centrifugation, dialysis, etc.

Graphene is a 2D single layer of carbon atoms with a hexagonal packed structure. The highly reactive surface of graphene makes it difficult to be suspended in solution, which can be overcome by oxidizing graphene into graphene oxide (GO). The oxidized portion of the surface offers functional groups for further conjugation and the unmodified part of the surface is capable of loading drugs through hydrophobic interactions and π - π stacking.

CNTs are rolled-up seamless cylinders of graphene sheets, exhibiting unparalleled physical, mechanical, and chemical properties. Depending on the number of graphene layers, CNTs are classified into single-walled carbon nanotubes (SWCNTs) or multiwalled carbon nanotubes (MWCNTs). SWCNTs are one-dimensional (1D) nanomaterials with diameters of 1–2 nm and lengths ranging from 50 nm to 1 cm, and they may behave distinctly from spherical NPs in biological environments. MWCNTs are formed by multiple layers of graphene and have much larger diameters (10–100 nm). Surface functionalization of CNTs can be covalent or noncovalent. Covalent modification includes oxidation reaction using nitric acid to introduce carboxyl at the end of CNTs or at the defects on the sidewalls. Cycloaddition reaction via photochemical reaction of CNTs with azides is also commonly utilized. However, intrinsic physical properties of CNTs such as photoluminescence and Raman scattering are often destroyed after chemical reactions. In contrast, noncovalent functionalization of CNTs can be carried out by coating CNTs with amphiphilic surfactant molecules or polymers. The polyaromatic graphitic surface of CNTs is accessible to the binding of aromatic molecules via π - π stacking. Moreover, various amphiphiles have been used to suspend CNTs in aqueous solutions, with hydrophobic domains attached to the nanotube surface via van der Waals forces and hydrophobic effects, and polar heads for water solubility.

Bio-Inspired NPs

Exosomes. Exosomes are inherent carriers of genetic and proteomic information, and are believed to be a central form of cell–cell communication. This makes them attractive as delivery vehicles. Exosomes are formed intracellularly via endocytic invagination within the endosomal network. Early endosomes then undergo a series of alterations to become late endosomes or multivesicular bodies (MVBs), and the fusion of MVBs with plasma membrane results in the release of exosomes into extracellular space. Exosomes have a characteristic lipid bilayer with an average thickness of ~5 nm.

To date, five major exosome isolation techniques including differential ultracentrifugation-based techniques, size-based techniques, immunoaffinity capture-based techniques, exosome precipitation, and microfluidics-based techniques have been developed (Li et al., 2017). Ultracentrifugation-based exosome isolation is a gold standard method, wherein particulate constituents in a heterogeneous mixture can be

sedimented under the condition of centrifugation according to their density, size, and shape. More dense and/or larger particles settle out first. A variation of ultracentrifugation is density gradient ultracentrifugation including isopycnic ultracentrifugation and moving-zone ultracentrifugation. Ultrafiltration is a popular size-based exosome isolation technique, wherein the separation of suspended particles is primarily dependent on their size or molecular weight. Therefore, exosomes can be isolated using membrane filters with defined molecular weight or size exclusion limit. Ultrafiltration is faster than ultracentrifugation and does not require special equipment. However, the mechanical force may result in the deformation and breakage of large vesicles. Immunoaffinity capture involves immunoaffinitive interactions between antigens on exosomes and their antibodies. With respect to the precipitation method, exosomes can be settled out from biological fluids by altering their solubility or dispersibility. Generally, samples are incubated with a precipitation solution containing PEG (8000 Da), which tie up water molecules and force less soluble components out of the solution. The precipitate containing exosomes is isolated by means of either low-speed centrifugation or filtration. With the aid of microfluidics devices, exosomes can also be isolated with significantly reduced sample volume, reagent consumption, and isolation time (Li et al., 2017).

Protein NPs. Proteins have been used to construct NPs due to their biodegradability, nonantigenicity, abundant renewable sources, emulsification, gelation, foaming and water-binding capacity, and extraordinary binding capacity of various drugs. Additionally, protein NPs undergo less opsonization by the reticuloendothelial system (RES) through an aqueous steric barrier. Moreover, protein NPs can be easily prepared and scaled up, and they are amenable to surface modification due to abundant functional groups (i.e., carboxylic and amino groups) on the NP surface. Generally, animal proteins including gelatin, collagen, albumin, silk proteins, elastin, and milk proteins, and plant proteins including zein, gliadin, soy proteins, and lectins are widely used to construct protein NPs.

The techniques to prepare protein NPs include desolvation, coacervation-phase separation, emulsification-solvent evaporation, reverse-phase evaporation, nanoprecipitation, nano spray drying, and liquid-liquid dispersion (Elzoghby et al., 2012). For example, paclitaxel-loaded gelatin NPs are prepared by a coacervation-phase separation method. An aqueous solution of sodium sulfate is added slowly to gelatin solution containing Tween 20 followed by addition of isopropanol containing paclitaxel. The liquid-liquid dispersion method is used to fabricate zein NPs. Zein and drugs are dissolved in 70% ethanol, followed by shearing the solution into deionized water. Zein becomes insoluble when the ethanol concentration in the emulsified droplets decreases below a certain level, and precipitates to form NPs. However, proteins as natural polymers are heterogeneous mixtures of different sizes with a wide range of molecular weights, which will cause heterogeneous size distribution with batch-to-batch variation. Recombinant protein technology can

be used to overcome this drawback, such as recombinant human serum albumin (HSA) and recombinant gelatin.

DNA nanostructure. The unique programmability of DNA enables the design of uniform nanostructures with well-defined geometries and topologies. DNA nanostructures are designed by precise self-recognition of A–T and C–G pairings. The superior biocompatibility is attributed to the degradability of DNA by DNase in tissues. Meanwhile, though free DNA is cell membrane-impermeable, a DNA nanostructure could readily enter cells via endocytosis. Single-stranded DNA could self-assemble into small building block materials called tiles. DNA tiles with “sticky ends” are able to further self-assemble into larger arrays with distinct geometries based on Watson-Crick base pairing (Pei et al., 2014). Various DNA nanostructures can be obtained, such as cubes, networks, arrays, or arbitrary shapes on a DNA canvas.

Generally, the process of DNA self-assembly can be divided into four categories. (1) The quick mix approach, wherein a set of DNA strands designed with unique sticky ends associate at definite positions to form the entire architecture. (2) Hierarchical self-assembly, wherein DNA strands are mixed in a particular order to minimize the unique set of strands required to generate individually formed multitile DNA structure. (3) Algorithmic self-assembly, wherein the DNA tiles are programmed with built-in instructions following algorithmic rules. (4) Nucleated self-assembly, wherein a longer strand is used as a nucleation site to attach the associated strands to generate a complex pattern. More recently, DNA origami has been developed, which is based on folding a long single-stranded DNA (ss-DNA, also called a scaffold strand) into a customized shape with a set of short synthetic ss-DNA strands (also called staple strands). DNA origami nanostructures could be further used as modular elements to form supernanostructures, making it possible to design complex nanostructures with one, two, and three dimensions. Moreover, rolling circle amplification (RCA), a polymerase chain reaction-based method, has also attracted considerable attention in assembling DNA nanostructure, which amplifies repeated single-stranded DNA from a circular single-strand template.

Hybrid NPs

Cell membrane-coated NPs. Cell membrane-coated NPs are characterized by a synthetic nanoparticulate core cloaked with a layer of natural cell membrane, which inherently mimics the properties of the source cells such as long circulation and disease-specific targeting. For example, red blood cells' (RBC) membrane coating prolongs the blood circulation of NPs. Platelet membrane coating renders an entire array of platelet surface markers, such as collagen-binding proteins and immunomodulatory proteins CD47, therefore allowing binding to human type IV collagen and reducing macrophage uptake. White blood cells' (WBC) membrane coating enables site-specific targeting to the vasculature of tumors or inflammatory tissues. Cancer cell membrane-coated NPs feature self-targeting and antigenic displays which could be used for immune modulation. Stem cell

membrane-coated NPs also feature tumor-targeting due to the tumor tropism of stem cells.

The cell membrane coating technology was first reported in 2011 (Hu et al., 2011). By transferring the outermost layer of a cell directly onto the surface of NPs, the complexity of the membrane, with all of its lipids, proteins, and carbohydrates, can be faithfully preserved. Cell membrane-coated NPs can be fabricated using several different methods. The extrusion method was firstly adopted, wherein the nanoparticulate cores and purified membrane were coextruded through a porous membrane. This method is adapted from the synthesis of liposomes, and the mechanical force provided by the extrusion is believed to disrupt the membrane structure and enable it to reform around the nanoparticulate cores. Another method is based on sonication. The cell membrane and NPs are subjected to disruptive forces provided by ultrasonic energy, resulting in the spontaneous formation of a core-shell nanostructure with less material loss. Recently, a microfluidic system that combines rapid mixing with electroporation has been employed for membrane coating. By fine-tuning the pulse voltage, pulse duration, and flow velocity, high-quality particles with complete coatings and exceptional stability are fabricated. Besides coating of NPs with purified membranes, an alternative approach is based on the in situ packaging of NPs using live cells. Cells are first incubated with NPs to allow internalization, and after incubation in serum-free media, the cells secrete vesicles containing the exogenous NPs.

Organic-inorganic nanocomposites. Organic-inorganic nanocomposites, also known as polymeric nanocomposites, are often obtained by grafting polymers onto inorganic NPs or by adding modified NPs into polymer matrices. The produced composite materials are intended to combine the unique optical, magnetic, and electronic properties of inorganic NPs and in the meantime enable desired colloidal stability as well as biological activity. Inorganic NPs have a strong tendency to aggregate in the polymer matrix and thus cause insufficient dispersion, and therefore it is essential that the NP surface is modified by polymer surfactant molecules or other modifiers. Commonly used methods for surface modification of inorganic NPs include chemical treatment, grafting of synthetic polymer, and ligand exchange. Various types of inorganic NPs, such as metals (e.g., Al, Fe, Au, and Ag), metal oxides (e.g., ZnO, Al₂O₃, CaCO₃, and TiO₂), nonmetal oxides (e.g., SiO₂), and others (e.g., SiC), have been incorporated into polymeric nanocomposites.

The conventional and simple method for the preparation of polymeric nanocomposites is direct mixing of NPs with the polymer matrix, which can be done by solution blending, emulsion blending, or melt blending. Solution blending is a liquid-state powder processing method, which is widely used when the polymer and inorganic NPs are dissolved in solution. Emulsion blending, also known as suspension blending, is similar to solution blending, but requires the use of an emulsion or suspension solution instead of a simple solution, which is an effective method for polymers difficult to dissolve. Regarding melt

blending, NPs are dispersed in the polymer melt and the polymeric nanocomposites are obtained by extrusion. Sol-gel processing is another method for the synthesis of polymeric nanocomposites. The sol-gel processing of NPs inside a polymer dissolved in aqueous solutions leads to the formation of interpenetrating networks between inorganic and organic moieties at mild temperature. The network improves the compatibility between components and builds a strong interfacial interaction between the two phases. In situ fabrication of polymeric nanocomposites is another simple and efficient method, wherein the NPs are generated from their respective precursors in the presence of the polymer matrix. After the nanocomposites are formed, the undesired or unbound chemical products are removed. Another in situ fabrication approach consists of the simultaneous formation of both the polymer matrix and the inorganic NPs. In this method, precursors of the NPs are dispersed in the polymerizable monomers, and the inorganic NPs and the polymer matrix are generated simultaneously. The in situ formed metal surface can catalyze or initiate the polymerization via electron transfer from the metal surface atoms to the monomers. Thus, the degree of dispersion of the inorganic component is an important parameter, which may affect the formation of inorganic NPs and in turn the degree of polymerization.

Lipid-polymer NPs (LPNs). LPNs are a class of core-shell NPs consisting of three components, a polymer core, an inner lipid layer enveloping the polymer core, and an outer lipid-PEG layer. The LPNs combine the characteristics of both polymeric NPs and liposomes, and feature high structural stability, membrane fusion capability, biocompatibility, and bioavailability. Generally, the preparation of LPNs can be realized via a two-step or one-step method. In the two-step method, polymeric NPs and lipid vesicles are mixed together, and the lipid vesicles are adsorbed on the NPs via electrostatic interactions. Alternatively, polymeric NPs can be added to a dried thin lipid film. For both of these approaches, LPNs are produced by either vortexing or ultrasonication of the mixture. Afterward, the LPNs are separated from the nonadsorbed lipid by centrifugation. By passing through a porous membrane, monodisperse LPNs are obtained in the determined size range. Other methods such as spray drying and soft lithography particle molding have also been developed to prepare LPNs via mixing of polymeric NPs and lipids. The soft lithography particle molding technique, also called particle replication in non-wetting templates (PRINT), is a promising technique for scalable fabrication of particles with definite shape and size. In this technique, the polymer is dissolved in an organic solvent and cast onto a polyethylene terephthalate (PET) sheet which is heated to allow flow of the polymer into the mold and then solidifying at room temperature. The NPs are thus formed, and harvested using a poly(vinyl alcohol) (PVA)-coated PET sheet. The NPs are released from the sheet by dissolving PVA in an aqueous solution of lipids, thus forming the LPNs. Based on this technique, a variety of shapes can be prepared. The main disadvantage of the

two-step method is that polymeric NPs and lipid vesicles have to be separately prepared in advance.

In comparison, the one-step method that only involves the mixing of polymer and lipid solutions followed by nanoprecipitation or emulsion is more effective. In the nanoprecipitation approach, polymer is dissolved in a water-miscible organic solvent, while the lipid and/or the lipid-PEG are dissolved in water and heated. The organic solution is added dropwise into the aqueous solution under continuous stirring, leading to formation of NPs and self-assembly of the lipids on the surface via hydrophobic interactions. The emulsion approach is divided into single and double emulsification. For single emulsification, polymer dissolved in a water-immiscible solvent is added to an aqueous solution containing lipids with continuous stirring or ultrasonication to form an oil-in-water (o/w) emulsion. After removal of the oil phase by evaporation, LPNs are formed via self-assembly. The single emulsification approach is suitable for encapsulating cargoes soluble in the water-immiscible solvent. In contrast, double emulsification is employed when the encapsulated substance is insoluble in any organic solvent. In this case, the substance is dissolved in aqueous phase, and emulsified in an oil phase containing the polymer and lipid. The w/o emulsion is further emulsified for the second time in aqueous phase containing lipid-PEG to form w/o/w emulsion. The LPNs are obtained after evaporation of the oil phase.

Characterization of NPs

Physicochemical properties of NPs, such as size, surface properties, and morphology, are major determinants of their behavior in biological systems. By modulating these physicochemical properties, researchers can obtain NPs with tailored structures to meet their purposes of application. In addition, the biocompatibility of NPs is another crucial property consideration for biomedical applications. In this section, the common methods to characterize the size, surface charge, morphology, and biocompatibility of NPs are introduced.

Size

Various characterization methods of NP size have been developed. First, size can be determined by direct visualization via microscopy techniques such as scanning electron microscopy (SEM), transmission electron microscopy (TEM), and atomic force microscopy (AFM). Among them, SEM and TEM can directly observe the size and shape of NPs. The thickness of the particles can be estimated, and the size distribution can be analyzed in combination with statistics. In addition, the microstructure inside NPs can be analyzed after slicing the samples. The SEM resolution is lower than TEM, but the preparation of the sample is simpler, and nonconductive samples need to be sprayed with Pt or Au. The size measured by both SEM and TEM is aggregate size, and due to the small number of samples it may

not be representative and the results may not be statistical. Therefore, it is necessary to fully disperse the NPs during sample preparation. For AFM, the reaction of the probe to the forces that the sample imposes on it can be used to form an image of the three-dimensional shape of NPs at high resolution. AFM can not only measure the size and shape of the sample at a near-atomic resolution, but can also measure the force between surface atoms, the surface elasticity, plasticity, hardness, friction, and other properties. However, AFM can only observe a small number of samples and takes a long time, which is the main obstacle.

Dynamic light scattering (DLS) is the most widely used characterization method for determining NP size. This method obtains particle size information by utilizing time variation of scattered light from suspended particles under Brownian motion to obtain their hydrodynamic size distribution. DLS can accurately measure NP size below 5 μm . However, DLS results are susceptible to interference. Sample preparation is crucial, and should be clear, homogeneous, and without haze. A higher concentration of NPs results in multiscattering, where the scattered light from one particle interacts with other particles before reaching the detector and loses intensity, which will result in a size estimate that is too low. Overdiluted samples cannot generate enough scattered light for analysis. As a result, it is necessary to run DLS experiments on serial dilutions. NP shape and size distribution have a great influence on the DLS measurement results. Irregular particle shape and wide particle size distribution may cause more errors.

X-ray diffraction (XRD) and light Raman scattering (LRS) can be used to calculate crystal size. When NP size is smaller than 100 nm, it can be calculated from the diffraction peak width of XRD. LRS can measure the average diameter of nanocrystalline grains. In addition, NP size can be calculated by the specific surface area and density.

In practical applications, the size characterization method is selected according to the particle size range and morphology. It is recommended to use two or more characterization methods to verify each other.

Surface Charge

Until now, there is no satisfactory technique to directly determine the surface charge of NPs in liquid. Common practice is to determine the electric potential of NPs at a location away from the particle surface, somewhere in the diffuse layer, which is called the slipping or shear plane. The potential measured is called the zeta potential (ζ -potential), which is related to the movement of NPs in liquid. Zeta potential is usually used to represent the surface charge of NPs, and is closely related to NP suspension stability. In the solution state, the absolute value of the zeta potential is larger and the repulsive force between particles is larger, and thus the system is more stable. On the contrary, if the absolute value of zeta potential is small, NPs tend to aggregate. Zeta potential can be affected by pH, the electrolyte type, as well as concentration.

There are three existing methods to measure zeta potential, electrophoretic light scattering (ELS), acoustic, and electroacoustic. The acoustic method yields only average values with low sensitivity provided that the solid concentration is known. ELS, characterized with desired sensitivity, accuracy, and versatility, is the most widely used method. Its principle is that under the action of an electric field, the charged particles will move along a set direction. By irradiation with the laser, the velocity of the particles can be calculated and, from that, the zeta potential can be calculated. Recently, commercial instruments have been widely used for measuring zeta potential. Zetasizer Nano series (Malvern, UK) can effectively eliminate electroosmosis and analyze samples in nonaqueous dispersions.

Morphology

Morphology of NPs can be observed by microscopy, such as SEM, TEM, and AFM. Several factors can be used to describe the morphology, including circularity, aspect ratio, elongation, convexity, and fractal dimension. Diffraction technology such as powder XRD, small angle X-ray scattering (SAXS), small angle neutron scattering (SANS), and electron diffraction (ED) can also be used to characterize NP morphology. XRD determines the atomic and molecular structure of a crystal. The principle of XRD is that the crystalline structure causes incident X-rays to diffract into many specific directions. By measuring the angles and intensities of these diffracted beams, a three-dimensional picture of the density of electrons within the crystal can be produced. From that, the mean positions of the atoms in the crystal can be determined, as well as their chemical bonds, crystallographic disorder, and other information. SAXS is suitable for characterizing the structure of NPs at lower resolutions and the crystalline sample is not required. In addition, techniques such as nuclear magnetic resonance (NMR) can be used for morphology characterization.

Biocompatibility

Biocompatibility of NPs refers to the ability of NPs to perform their desired function without eliciting any undesirable local or systemic effects. When NPs enter the body, there may be a series of interactions between NPs and cells or the extracellular environment, which could eventually cause the NPs to be contained, removed, degraded, metabolized, or undergo toxicological reactions leading to tissue damage. To ensure the safe use of NPs for biomedical applications, the biocompatibility must be studied and clearly characterized. In fact, a thorough evaluation of the biocompatibility of NPs is central and possibly a first key step for the safe delivery of drugs.

In Vitro Toxicity

Cell viability test. The cell viability test is an *in vitro* method to detect the cytotoxicity of NPs, and is usually based on the measurement of metabolic activity. The most common

method to measure metabolic activity of cells involves the utilization of tetrazolium reagent chemistries (e.g., MTT, MTS, XTT, WST). For example, MTT can be reduced by viable cells into an intensely colored formazan precipitate that is subsequently solubilized followed by absorbance measurement. Detection of ATP is another viability assay that has become the gold standard for high-throughput screening. The process of cell death results in a loss of ability to synthesize new ATP along with a rapid depletion of cytoplasmic ATP by endogenous ATPases, which makes ATP a valid marker of viable cells. Protease activities (such as caspase-3) can also be used as a marker of cell viability.

Oxidative stress test. Oxidative stress (OS) caused by the presence of reactive oxygen species (ROS) is an important cause of NP toxicity. ROS can cause damage to biomolecules including DNA, RNA, proteins, and lipids, and the OS levels can be evaluated using the following assays. Direct ROS measurement is the most common method, which involves the use of fluorescent probes and electron paramagnetic resonance. However, ROS are extremely unstable and difficult to measure directly. Therefore, indirect approaches such as measurement of proteins, DNA, RNA, lipids, or other biomolecules levels are utilized. An alternative approach is to measure the levels of antioxidant enzymes and other redox molecules which serve to counterbalance ROS generated in the cells.

Cellular stress response test. NPs can cause nonfatal damage or changes in cell behavior that are mainly due to changes in protein and gene expression, regulation of phagocytic capacity, and inflammatory response. Changes in protein and gene expression relevant to inflammatory responses can be determined by PCR, immunoblotting, and total protein analysis (e.g., BCA method, Bradford method).

Hemocompatibility

Hemocompatibility refers to the properties that allow NPs to maintain contact with flowing blood without causing adverse reactions, releasing leachable components, or triggering adverse reactions. Regardless of the administration method used, NPs may be translocated to the blood circulation, which makes hemocompatibility of critical importance. Generally, erythrocyte composition (hemolysis and hemagglutination), thrombogenicity, cytokine assays, and complement activation (protein adsorption) are the major parameters during hemocompatibility assessment.

In Vivo Toxicity

Acute toxicity. Acute toxicity testing of NPs is designed to determine the serious toxicological effects produced within a certain period of time after single or multiple administrations. It serves to determine the doses that should be used in subsequent studies, and it renders another opportunity to find out what effects the NPs have in clinical chemistry, and also gives an early indication of possible target organs. Acute toxicology testing may have multistage exposures, with escalating doses to find the maximum tolerance dose (MDT). In general, these studies include 3–4 animals per sex per

group for nonrodent species, and 5–10 rodents per sex per group. Most studies include clinical observations and pathology determinations. LD₅₀, also known as the median lethal dose, is an important parameter for acute toxicity testing, which represents the dose required to kill half of the tested animals within a specified test duration.

Subacute/subchronic/chronic toxicity. The objective of these tests is to define the toxic effect of NPs over a period of repeated administrations. It is performed by giving NPs at multiple doses with certain intervals that will produce animal intolerance. Additionally, these studies may identify the minimal doses harmful to animals. Importantly, such long-term toxicity testing is designed to serve clinical trials and clinical medications. Therefore, attention should be paid to predicting the possible clinical adverse reactions of NPs, judging the target organs or target tissues when they are repeatedly administered, and estimating the range of clinical doses. In addition, the choice of experimental animal species and strains should enhance the predictability of the studies for human subjects. When choosing the species and strain of animals, the therapeutic target and the similarity of its distribution in the experimental animals to that in humans are important. The similarity of the pathophysiological mechanisms in the target organ should also be taken into consideration.

Genotoxicity and carcinogenicity. The genotoxicity and carcinogenicity of NPs are mainly attributed to factors such as direct interaction of NPs with the genetic material, indirect damage due to ROS generation, release of toxic ions, interaction with cytoplasmic/nuclear proteins, binding with the mitotic spindle or its components, increased oxidative stress, disturbance of cell cycle checkpoint functions, and inhibition of antioxidant defense. The genotoxicity of the NPs can be assessed using the prokaryotic system, either in *in vitro* cell cultures or in *in vivo* models. The bacterial reverse mutation assay (Ames test) is used for initial screening for genotoxicity. Subsequently, the ability of NPs to induce DNA damage is assessed in multiple cell lines using different assays such as the comet assay, gene mutation assay, micronucleus assay, and chromosomal aberration assay. The genotoxic potential of NPs is finally confirmed using animal models. Carcinogenicity tests are intended to identify the carcinogenicity risk in experimental animals and predict carcinogenic potential in clinical medication. Long-term exposure of animals, such as 2-year chronic administration in mice and rats, is required to express any carcinogenic potential.

Drug Delivery Applications of NPs

Drug Loading

Drug delivery using nanocarriers has various advantages, such as increasing drug solubility, prolonging blood circulation, enhancing tumor distribution, and decreasing systemic toxicity. Drugs can be loaded into NPs via covalent bonding and noncovalent encapsulation.

Covalent Bonding (Prodrug)

Drugs can be conjugated to NPs via covalent bonding, which affords advantages such as high drug-loading efficiency, stability of covalent bonds during circulation, and minimal side toxicity in nondiseased tissues. The covalent bonds need to be cleaved in tumor tissues/cells, thus realizing drug release and recovery of drug activity. Polymer–drug conjugates which can self-assemble into NPs have been widely developed. Polymers including block copolymers, dendritic polymers, and comb-like copolymers have a large number of active functional groups, and anticancer drugs can be coupled onto side chains to achieve high drug loading.

The most widely used polymers include poly(ethylene glycol) (PEG)-based block copolymers, poly(amino acid)s, polypeptides, and polysaccharides. For example, NPs self-assembled from PEG-b-PCPTM have been developed for camptothecin (CPT) delivery, in which PCPTM is a polymerized block of a CPT prodrug monomer with a reduction-responsive drug release manner. Drugs can also serve to control the polymerization for preparing polymer–drug conjugates. For example, paclitaxel (PTX) with multiple hydroxyl groups can be used to initiate the controlled polymerization of lactide for the formulation of polymeric NPs (Tong and Cheng, 2008).

Besides polymer–drug conjugates, drugs can also be connected to each other to form drug–drug conjugates. For example, PTX can be connected via a thioketal linker to form ROS-responsive PTX dimer. Camptothecin (CPT) can also be connected to form the dimeric CPT derivative, which can prevent the π – π interaction among drug monomers, thus prohibiting the drug aggregation in the aqueous solution to achieve ultra-high drug loading in NPs.

Different from polymer–drug conjugates and drug–drug conjugates, one drug molecule can be coupled to another nondrug small molecule, and the prodrugs themselves can self-assemble into NPs. These drug conjugates mainly include four categories: (1) lipid–drug conjugates (e.g., squalenoylations, cholesteryl, and palmityl prodrugs of anticancer agents); (2) low-molecular-weight oligo(ethylene glycol) (OEG)–drug conjugates; (3) amphiphilic peptidic prodrugs; and (4) tocopherol succinate–drug conjugates. An advantage of a low-molecular-weight prodrug delivery system lies in their smaller particle size and higher drug-loading capacity. However, they also have limitations, such as short circulation time in the blood due to lack of a dense shield layer (e.g., long-chain PEG) and poor structural stability owing to the relatively higher CMC. Therefore, NPs self-assembled from low-molecular-weight conjugates are usually stabilized by using an amphiphilic block copolymer containing a long PEG chain to achieve both long blood circulation time and high structural stability.

Noncovalent Encapsulation

Prodrug design features precise control over chemical composition, which unfortunately can be associated with tedious synthesis that would result in high cost and difficulty in quality control as well as scale up. As an alternative, drugs can be

noncovalently encapsulated into various NPs, which allows easy manipulation and scale up. Common noncovalent interactions include hydrophobic interaction, π - π interaction, hydrogen bonding, electrostatic force, van der Waals force, coordination bonding, and physical combination.

Hydrophobic interaction. Hydrophobic interaction (10–60 kJ/mol) is most widely utilized for drug encapsulation, in particular in micelles. Hydrophobic chemodrugs are efficiently encapsulated in the hydrophobic core of micelles via hydrophobic interactions. Various factors, such as the chemical characteristics of the drug, the hydrophobic nature of the copolymers, and the miscibility of both, affect the strength of the hydrophobic interaction and accordingly the entrapment efficiency, drug-loading capacity, and stability of the drug-loaded micelles.

π - π interaction. π - π interaction, although featuring relatively low bonding energy (8–9 kJ/mol), plays an important role in improving the loading capacity of aromatic drugs in NPs bearing aromatic rings. For example, nanographene with polyaromatic surfaces features efficient loading of aromatic drug molecules (i.e., DOX, hypocrellin B, chlorin e6, and epirubicin hydrochloride) via π - π stacking.

Hydrogen bonding. Hydrogen bonds with relatively high bonding strength (10–40 kJ/mol) can be introduced between NPs and drug molecules to enhance the drug-loading capacity. For example, NPs can be modified with thymine and cyanuric acid to enhance the loading of methotrexate (MTX) by forming three-point hydrogen bonds.

Electrostatic force. Electrostatic interaction (~500 kJ/mol) is totally nondirectional and by far the strongest physical interaction. It can be attractive or repulsive, and can function over distances much longer than those of covalent bonds. Electrostatic interaction plays an important role for drug loading, since many active substances carry charged groups. For instance, the charged drug can be efficiently encapsulated inside the liposomes by forming an insoluble ion complex through a strong electrostatic interaction between drug and particular ions such as ammonium sulfate, manganese, citrate, and phosphate. Drug can also be efficiently encapsulated in liposomes based on the direct electrostatic interactions between the drug and lipid.

van der Waals force. van der Waals force (~1 kJ/mol) includes three distinct types of forces, induction, orientation, and dispersion forces. The dispersion force is solely involved in the interactions between nonpolar molecules (i.e., hydrocarbons), and plays a dominant role in the drug-NP interactions when hydrocarbons are used as hydrophobic regions. Usually, the nonpolar groups (i.e., cholesterol and aliphatic hydrocarbons) are grafted to the hydrophilic polymer (i.e., polyvinyl alcohol, PEG, polysaccharide, and peptides) to allow them to form micelles.

Coordination bonding. Coordination bonding, also known as donor-acceptor interaction, is a common molecular force between electron donors and acceptors. The donor-acceptor bond energy is usually weaker than covalent bonds, whereas it is stronger than hydrophobic interactions. Ultra-high drug loading (50%) and

quantitative loading efficiency (>99%) can be achieved for DOX using micelles, by incorporating the coordination effect between the pendant phenylboronic acid (electron-acceptor unit) on micelles and DOX (donor acceptor) (Lv et al., 2018).

Physical combination. Drug can be physically loaded into NPs via embedding. Mesoporous materials, especially mesoporous silica NPs, are commonly used to physically encapsulate drugs that can diffuse into channels or empty cores of these materials. To prevent the preleakage of drug cargoes, the mesoporous NPs are often surface-decorated with gating materials, and the gates can be opened under specific conditions to allow selective cargo release.

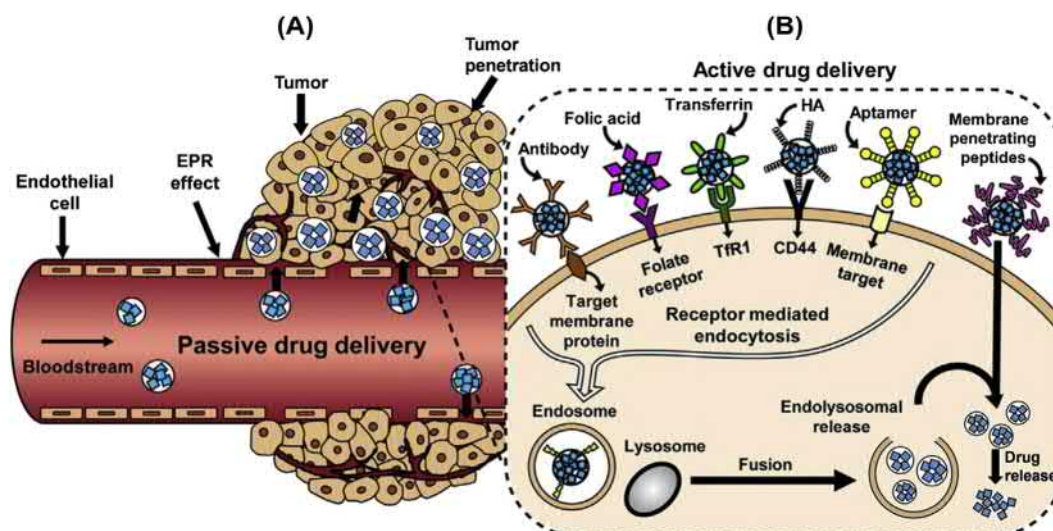
Systemic Barriers Against Drug Delivery

NP delivery to tumors is impeded by multiple systemic barriers, including clearance by renal filtration and the reticuloendothelial system (RES), extravasation through the enlarged endothelial gaps in tumors, the dense stroma in the tumor microenvironment that impedes penetration of NPs, cellular membranes blocking internalization of NPs, and release of the drug cargoes to induce a pharmacological effect (Fig. 1.3.8B.8).

Circulation. Short circulation time can greatly limit the performance of chemodrugs. The RES interaction can scavenge NPs from the blood circulation, especially positively charged NPs, because phagocytic cells such as macrophages will engulf particles bearing recognized opsonins (negatively charged serum proteins) that have adsorbed to NPs via electrostatic interaction. Factors affecting opsonization and the RES interaction include size, surface composition, zeta potential, and the shape of NPs. Interaction of NPs with the RES will shorten the blood circulation time, and accordingly reduce tumor accumulation.

Tumor accumulation. The tumor blood vessels are dense, immature, chaotically branched, and dilated. Limited perfusion becomes a barrier against extravasation of NPs from the bloodstream into the tumor tissues. Typical tumor vascular characteristics, such as irregular leakage, poor perfusion, and compressed blood vessels, limit the accumulation and distribution of NPs.

Tumor penetration. NPs that have successfully extravasated into tumor tissues face another barrier consisting of high interstitial fluid pressure (IFP), dense stromal tissue, and complex interactions with macrophages, fibroblasts, and tumor cells, which collectively impedes the penetration of NPs into deep tumor tissues. The lack of lymphatic vessels and the vascular hyperpermeability inside tumors results in interstitial hypertension. High IFP in tumors disrupts normal convective flow, and NPs that rely on convective flow cannot efficiently transport into the deep tumor compartment. In addition, tumors are often rich in stromal tissues. Fibroblasts in tumors are unregulated, continuously proliferate, and do not senesce. The dense extracellular matrix (ECM) produced by the activated fibroblast impedes the convective and diffusive transport of NPs.



• **Figure 1.3.8B.8** Critical steps in nanomedicine-mediated delivery of chemodrugs into cancer cells, including circulation in blood compartments, accumulation and penetration in tumors, cellular internalization, and intracellular drug release. (Reproduced from Bar-Zeev, M., Livney, Y. D., Assaraf, Y. G., 2017, Targeted nanomedicine for cancer therapeutics: towards precision medicine overcoming drug resistance. *Drug Resist. Updates* 31, 15–30.)

Cellular internalization and efflux. Phagocytosis and endocytosis are two major internalization mechanisms by which cells take up NPs. Endocytosis can be further divided into caveolae- or clathrin-mediated endocytosis, as well as clathrin-independent or caveolae-independent endocytosis. Different mechanisms of endocytosis put forward different requirements for NP design. For example, in clathrin-mediated endocytosis, endosomal escape must occur before fusion with the lysosome to prevent cargo degradation. For NPs entering the lysosomal compartments, the released drug must be resistant to the lysosomal environment and be able to escape into the cytosol. Besides internalization, the efflux system also plays a pivotal role in eliminating chemodrugs. The ATP-binding cassette transports (such as P-glycoprotein) work in concert with drug-metabolizing enzymes to pump out drugs and their metabolites, thus provoking multidrug resistance (MDR).

On-demand drug release. The drug cargoes need to be released effectively and selectively in tumor tissues/cells to realize their anticancer efficacy and reduce undesired toxicity to normal tissues/cells. Excessive stability of NPs will impair the drug release efficiency. For example, Doxil (a liposomal formulation of DOX) delivers 10–15 times more DOX to the tumor compared to standard therapy, but slow release results in low bioavailability (40%–50%). Additionally, the excessively slow drug release may cause drug resistance, due to the insufficient drug concentration to potently kill cancer cells. On the other hand, excessive instability can also be a persistent challenge. In the application of Genexol and NK105, the taxanes rapidly partition out of the polymeric micelles and bind with serum proteins during blood circulation. Excessive instability can also cause additional toxicity, because the prematurely released drugs would distribute in normal organs.

Approaches to Overcome Systemic Barriers

Long-Circulating NPs

In order to prolong the circulation time, hydrophilic stealth polymers such as PEG, poly(acrylic acid), and polysaccharides have been used as surface coating materials. PEGylation is the most commonly used strategy, because PEGylated NPs experience reduced opsonization by blood proteins and clearance by RES. Due to its hydrophilic nature, PEG chains grafted on the NP surface generate a hydrated cloud with a large excluded volume that sterically precludes NPs from interacting with neighboring NPs and blood components. The surface charge shielding effect of PEG on positively charged NPs is also an important factor to prolong circulation, because positively charged NPs will not only increase the adsorption of opsonins, leading to their recognition by macrophages, followed by phagocytosis and elimination, but also increase electrostatic interactions with the vascular wall to increase the clearance rate. In addition, the large conformational freedom provided by the flexibility of PEG renders interpenetration of foreign matters into the PEG corona thermodynamically unfavorable. Thus, PEG coatings on NPs prevent aggregation, opsonization, and phagocytosis, thereby prolonging the blood circulation time. The first PEGylated polymeric NPs based on poly(lactic-co-glycolic acid) (PLGA) were developed in 1994 by Ruxandra Gref et al. (Gref et al., 1994).

However, PEGylation also has some shortcomings. First, PEG impedes the interaction with target cells because of its superhydrophilicity that is rejected by the phospholipid bilayer of the cell membrane. Second, PEG possesses accelerated blood clearance effect, because repeated administration of PEG may result in anti-PEG IgG in the human body. After being connected with neutralizing antibodies

secreted by B cells, the PEG-modified NPs that are repeatedly administered will be recognized and cleared by phagocytes, resulting in a significantly shortened half-life.

Various strategies have been developed to overcome these shortcomings. Sheddable PEGylation is a commonly used approach, which removes the PEG coating from NPs at the target site. For example, PEG could be conjugated to the liposomal surface via a matrix metalloproteinase-2 (MMP-2) cleavable peptide. MMP-2 overexpressed in the ECM of tumor tissues can cleave the peptide and remove PEG to promote cancer cell internalization. Besides PEG, other materials have also been investigated for NP surface decoration. Polyvinyl pyrrolidone (PVP) is a common example used for the modification of metal NPs or upconversion NPs to enhance their solubility. Recently, zwitterion as an alternative to PEG has demonstrated good performance. Besides endowing the NPs with good solubility, decreased immunogenicity, and excellent mucus-penetrating ability, the zwitterion provides monolayer-type coverage with minimal thickness, while the PEG appears to yield a more three-dimensional coating.

In addition to covalent modification, the noncovalent surface coating strategy is also used. For example, negatively charged hyaluronic acid can be coated onto positively charged NPs via electrostatic interaction, thus neutralizing the positive surface charge of NPs to prolong blood circulation. Recently, cell membrane-coated NPs have attracted tremendous attention due to their desired capabilities to prolong the systemic circulation. Among them, erythrocyte membrane displays the strongest long-circulation property, and thus erythrocyte membrane-coated NPs can bypass macrophage uptake and systemic clearance.

Suitable NP morphology design contributes to extension of the circulation time. The importance of NP shape was first demonstrated by Dennis Discher in 2007, with the persistent circulation of soft filamentous or worm-like micelles for ~1 week in mice or rats (Geng et al., 2007). NPs in cylindrical shape display a longer circulation time than those with a spherical shape, and this prolonged circulation effect stems from the interplay between surface properties, nanoparticle core rigidity, length or aspect ratio, and shape. Phagocytosis by macrophages exhibits a strong dependence on NP morphology, as NPs with higher aspect ratios are less likely to undergo phagocytosis than spherical ones of the same volume. The reason is that the interactions between long cylindrical micelles and cell surfaces are easily disrupted under strong hydrodynamic shear forces that minimize the opportunity for cell uptake. In contrast, spherical NPs are less influenced by shear and are able to interact more strongly with cell surfaces to enhance cellular uptake. In addition, nonspherical NPs show a deviating hydrodynamic behavior in comparison to spherical ones, which allows them to align with the blood flow and contributes to the extension of circulation time. Apart from this, nonspherical NPs exhibit more complex motions with tumbling and rolling, which can be exploited to the action of drifting laterally toward the vessel walls under flow without

the need for lateral external forces. Thus, they can exit the main vasculature more easily than quasihemispherical and spherical NPs in the bloodstream. Other NP shapes such as disks and lamellae can also prolong the circulation time.

Targeted Drug Delivery

Targeted delivery of chemodrugs has always been an important direction of modern pharmacy. Most chemodrugs have great toxic and side effects because they kill not only cancer cells but also normal cells. Targeted drug delivery can reduce cytotoxicity, promote entry into tumor tissues and cells, and overcome MDR.

Passive targeting (EPR effect). Unlike the compact and well-structured microvascular endothelial spaces in normal tissues, the vasculature in solid tumor is characterized by poor structural integrity, wide vessel wall spaces, and abundant blood vessels. Such leaky vasculature thus promotes the transport of NPs from the blood circulation into tumor tissues. Additionally, solid tumors lack lymphatic reflux, thus impeding the clearance of NPs from the interstitial space of tumor tissues. Such a phenomenon is called the EPR effect, and EPR effect-enhanced tumoral accumulation of NPs is defined as passive targeting.

The EPR effect is mainly based on leaky blood vessels within tumors, with transvascular endothelium gaps ranging between 100 and 780 nm in diameter. The size and shape of NPs can significantly affect their passive targeting to the tumor tissue. The sizes should be larger than 4–5 nm to avoid quick kidney filtration while being less than 200 nm to extravasate the leaky vasculature. NPs in the size range of 20–200 nm tend to penetrate inside the interstitial space due to the poorly aligned defective endothelial cells. The biodistribution pattern of NPs is also highly dependent on their shape. Nonspherical NPs exhibit different in vivo behaviors. For example, filomicelles have limited accumulation in healthy organs or tissues because of the hydrodynamic flow effect, but they are able to move around obstacles and reptate into tumors through small leaky vasculatures, while spherical NPs of the same volume must deform to pass through small tubular pores into tumors. Surface charge is another important factor. Positively charged NPs can bind to the luminal surface of vascular walls and be cleared rapidly from the blood circulation, as the blood vessels have a negatively charged surface. In contrast, negatively charged NPs show higher accumulation in the liver due to charge-selective filtration.

Several strategies have been applied to improve EPR-mediated passive targeting, which includes the use of inflammatory cytokines and vasomodulators to permeabilize blood vessels and increase blood flow. Several vasomodulators such as histamine, serotonin, bradykinin, and tumor necrosis factor- α (TNF- α) have been coupled with nano-delivery systems to enhance vascular permeability in tumors. Nitric oxide (NO), as a potent endothelium-derived vasomodulator, is also utilized to enhance vascular permeability, thus inducing vasodilation and increasing blood flow. Nitroglycerin (NG) is a pharmacological agent, which

dilates blood vessels and increases blood flow by releasing NO, by modulating denitrase and nitrite reductases. NG has been employed to enhance drug delivery, and works particularly well in tumors characterized by clogging problems. The use of angiotensin-II (AT-II) is an alternative approach to enhance blood flow and promote vascular permeability in tumors, because it induces blood vessel constriction in healthy tissues and raises the systemic blood pressure. Using anticoagulants can also achieve the goal of enhancing blood flow. Vascular disruption is another strategy to enhance the EPR effect. Several vascular disrupting agents (VDAs) have been evaluated over the years, including combretastatin A4 phosphate (CA4P), a tubulin-binding agent which induces vessel disruption by inhibiting tubulin polymerization. Another well-known VDA is the flavonoid acetic acid-based agent 5,6-dimethylxanthenone-4-acetic acid (DMXAA), which increases NO and serotonin production, leading to endothelial damage.

Active targeting. Active targeting of tumors is an approach utilizing a high-affinity targeting ligand for selective recognition of a specific receptor or antigen overexpressed on the surface of cancer cells to achieve targeted drug delivery. To accomplish this goal, the surface of the NPs is typically functionalized with a targeting ligand/antibody, followed by receptor-mediated endocytosis. Active targeting enhances drug specificity and accumulation to the tumor tissues/cells. Therefore, it enhances the cytotoxic activity of anticancer drugs against tumor cells while avoiding adverse effects on healthy tissues.

Commonly used cancer-targeting moieties include antibodies and ligands that can respectively bind to overexpressed antigens and receptors on cancer cell membranes. For instance, folic acid receptors, CD44, transferrin receptors, HER2, PSMA, and EGFR are overexpressed on cancer cells, and thus folic acid, hyaluronic acid, transferrin, and antibodies against HER2, PSMA, and EGFR are widely used as active targeting domains toward cancer cells. Peptides can also serve as cancer cell targeting ligands, among which the “cilengitide-like” cyclopentapeptides (i.e., cRGDfK, cRGDyK, and cRGDfC) that target overexpressed integrins on cancer cells are widely utilized. Additionally, aptamers, short single-stranded oligonucleotides (DNA or RNA) or peptides with specific tertiary structures, have emerged as effective targeting ligands to tumors. Compared with DNA aptamers, RNA aptamers have smaller physical size and more flexible 3D structures, making it easier to be conjugated with NPs and to penetrate target cells. Multiple antibody/ligand-based targeted drug-delivery NPs are under clinical trial, including MM-302 (HER2-targeting liposome), BIND-014 (PSMA-targeting polymeric NPs), and MBP-426 (TfR-targeting liposome).

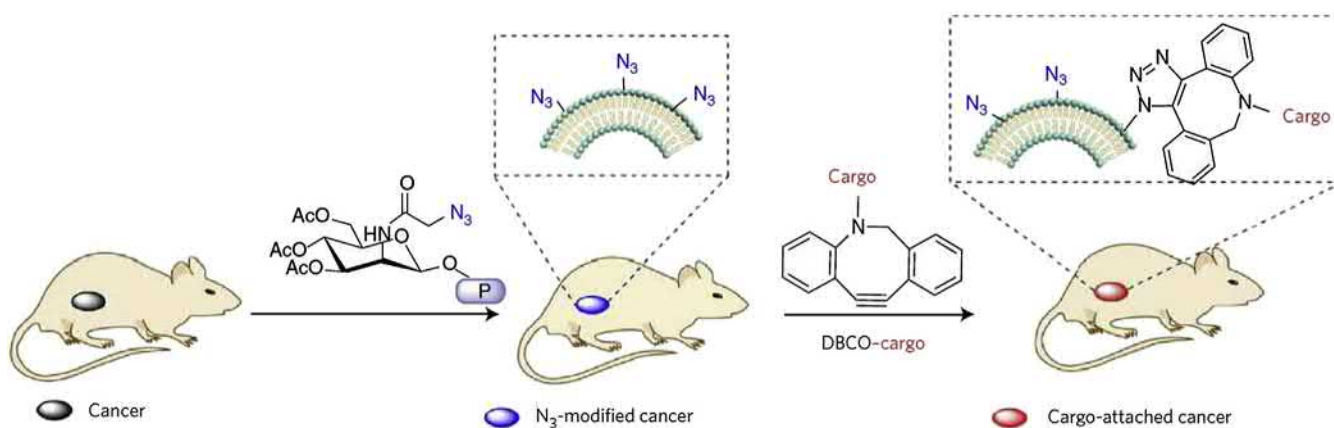
The active targeting mechanism heavily relies on the overexpression of specific biomarkers on cancer cells. However, the number of cancer-specific antigens/receptors on different cancer cells is heterogeneous and often not high enough. Some cancer types, such as the triple negative breast cancer (TNBC), lack any specific receptors, thus preventing

traditional antibody/ligand-based active targeting. To overcome such issues, two major strategies have been exploited to manually manipulate cell-surface receptors. The first strategy is to directly amplify the expression of existing cell-surface protein receptors using a gene transfection method. However, this strategy is of limited translational applicability given the stringent technical requirements, nonselectivity over cell types, and potential detrimental effects on the treated cells.

A different strategy, instead of directly increasing the amount of cell-surface protein receptors, is to introduce unique chemical functional groups onto the cell surface as an alternative to protein receptors. These externally introduced chemical functional groups can mimic the receptor function of cell-surface proteins, which can be utilized for cell binding via efficient chemical reactions. Among them, an unprecedented targeting technology called active tissue targeting via anchored click chemistry (ATTACK), is based on unnatural sugar-mediated cancer-selective labeling followed by reagent-free click chemistry. In this technique, Ac_4ManAz as a mannose derivative bearing an azide group was reversibly caged, and its metabolic activity could be recovered selectively in cancer cells after decaging, thus labeling the cancer cells with abundant azide groups to enable further targeting of DBCO-modified NPs via the DBCO-azide bioorthogonal chemistry (Fig. 1.3.8B.9) (Wang et al., 2017). Besides ATTACK, there are other methods to introduce artificial targets onto cancer cell membranes, such as inserting targets into cell membranes via lipids.

Tumor Penetration

There are two major approaches to promote the tumor penetration of NPs, manipulation of the tumor microenvironment and transformation of the NP structures. The former approach is often realized via IFP reduction and stromal depletion. Reducing IFP to restore a normalized flow pattern can enhance convective transport and intratumoral penetration of NPs. Using antiangiogenic drugs which target VEGF (i.e., bevacizumab and cediranib) can normalize tumor vasculature and thus decrease IFP. Tumor-associated fibroblasts have also been identified as good targets to alleviate high IFP, reduce tumorigenic stimuli, debulk the tumor, and restore perfusion and drug delivery. For example, prostaglandin inhibitors such as Imatinib can reduce IFP and improve tumor penetration of NPs, because prostaglandins can interact with fibroblasts to increase contractile forces and therefore decrease IFP. In addition, debulking the ECM or stromal cells can also reduce IFP. Treatment of ECM with ECM-degrading enzymes (i.e., hyaluronidase and collagenase), or debulking tumor cells with drugs (i.e., PTX) can reduce IFP and greatly enhance tumor penetration of NPs. Several stromal depletion approaches are being tested in clinical trials, including Abraxane (PTX-albumin NPs) and Hedgehog inhibitors. In the clinical evaluation of a combination with gemcitabine, Abraxane reduced pancreatic ECM, possibly due to increased interactions with stromal cells via an SPARC (secreted protein acidic and



• **Figure 1.3.8B.9** Schematic illustration of ATTACK technology, in vivo selective labeling of cancer cells with azido groups and subsequent cancer targeting via efficient click chemistry. (Reproduced from Wang, H., Wang, R. B., Cai, K. M., He, H., Liu, Y., Yen, J., et al., 2017. Selective in vivo metabolic cell-labeling-mediated cancer targeting. *Nat. Chem. Biol.* 13, 415.)

rich in cysteine)-mediated mechanism. The latter approach could be achieved via size shrinkage of NPs. In general, NPs with sizes of 50–100 nm are suitable for prolonged blood circulation and efficient tumor accumulation via the EPR effect. However, the tumor-associated fibroblasts and dense ECM are major barriers to the deep interstitial penetration of large NPs. On the other hand, NPs with sizes below 10 nm are characterized by better intratumoral penetrating efficiency but possibly a reduced EPR effect. Thus, ideal NPs should be relatively large (50–100 nm) during blood circulation to achieve effective EPR-dependent tumor accumulation, but once inside the tumors, they ought to be small enough for enhanced penetration. These systems are usually composed of a mothership nanocarrier with larger size (approximately 50 nm) and 10 nm-sized babyship nanocarriers encapsulated in the NPs or conjugated on the surface. The mothership NPs are stable during systemic delivery and concentrate in tumor tissues via the EPR effect. Subsequently, the babyship NPs are released by the acidic pH or overexpressed enzymes in the tumors, thus triggering deep tumor penetration.

Stimuli-Responsive Drug Delivery

One of the most important requirements for NP-mediated drug delivery is that the cargos need to be released effectively and selectively in the target disease site. Stimuli-responsive delivery systems serve as a promising modality to meet the demand of precision delivery, because they can release the payloads upon exposure to endogenous or exogenous triggers such as chemical, physical, or biological stimuli. These drug delivery systems enable target-activated release of the drug to potentiate the pharmacological activity while minimizing systemic toxicity. Significant inherent differences between the tumor microenvironment and normal tissues can be exploited for designing internal stimuli-responsive NPs, while exogenous stimuli such as light or heat can also be utilized to trigger transformation of the NPs (Meng et al., 2009).

Internal stimuli in tumors mainly include acidic pH, high intracellular GSH concentration, high levels of reactive oxygen species (ROS), high APT levels, overexpressed enzymes, and hypoxia. In particular, the pH condition in the extracellular compartment of tumors is more acidic (pH 6.5–7.2) than in the normal neighboring tissues (pH ~7.4), whereas endolysosomes typically exhibit even more acidic pH values (pH 4.5–6.5). The GSH and ATP concentrations are notably different between extracellular (~10 mM and <0.4 mM) and intracellular (~2 μM and 1–10 mM) compartments. The endogenous ROS are maintained at a low level in normal cells by the intracellular reduction–oxidation balance, while ROS levels are much higher in tumor cells. Tumor tissues or cells also express a higher amount of specific enzymes, which include extracellular [i.e., matrix metalloproteinase (MMP), hyaluronidase, phospholipase, and alkaline phosphatase] and intracellular (i.e., cysteine caspase, cathepsin, furin, telomerase, and azoreductase) enzymes. Solid tumors often undergo hypoxia because of the uncontrollable tumor cell proliferation and irregular vascular system.

By responding to these stimuli, NPs can change their morphology, solubility, or assembly state to allow drug release. For example, NPs with pH-labile or ROS-responsive linkages can change their hydrophilicity/hydrophobicity to enable dissociation of NPs. Alternatively, reversibly cross-linked polymeric particles containing GSH-cleavable disulfides can undergo decross-linking by GSH, thus triggering on-demand drug release in tumor cells (Chen et al., 2010; Zou et al., 2016a,b). Nanoparticulate prodrugs can also mediate drug release via cleavage of the stimuli-cleavable linkers (such as redox-responsive disulfide, pH-responsive ketal, ROS-responsive thioketal, and hypoxia-responsive azobenzene). NPs that can respond to extracellular stimuli (such as slightly acidic condition or extracellular enzymes) are often constructed to undergo PEG removal or charge reversal in the extracellular compartment, thus exposing the membrane-penetrating domains to enhance tumor cell uptake. In the case that internal stimuli

are of an insufficient level to trigger effective transformation of NPs, their concentration could be artificially elevated. For instance, photodynamic therapy is often coupled with ROS-responsive NPs to artificially generate ROS in tumor cells, which not only triggers drug release but also kills cancer cells via ROS-mediated cell apoptosis/necrosis.

Compared with internal triggers, external triggers such as light, heat, and magnetic field show unique advantages such as spatiotemporal precision, relative safety, and minimal cross-reaction with cellular signaling networks. Ultraviolet (UV) light (<400 nm)-responsive NPs are widely developed for drug delivery, while the low penetration depth of UV light greatly restricts their *in vivo* utility. As such, NPs responsive to near-infrared (NIR) light (700–1000 nm) with better penetration and safety have been developed. Alternatively, upconversion materials are incorporated into UV-responsive NPs, which can change NIR light into UV light to realize NIR light responsiveness. The disadvantage of this approach is the heat damage caused by high-power-density light irradiation. To overcome this dilemma, indirect photo-responsive NPs utilizing an internal trigger as “mediator” have been proposed and explored. Particularly, thermal-responsive NPs can be coupled with photothermal materials to enable light-to-heat transfer and thereafter heat-responsive drug release. Similarly, light-triggered NPs can also be fabricated via the combination of ROS (or hypoxia)-responsive NPs with photodynamic therapy that generates a tremendous amount of ROS or local hypoxia in tumor tissues/cells (Zhou et al., 2018).

Besides light-responsive NPs, thermo-responsive NPs can also change their macroscopic properties and thus enable drug release by changing the interaction force between polymer molecules and solvent molecules upon temperature alteration. For instance, the principle of the thermo-responsive NPs (e.g., nanogels) is based on their solubility behavior that changes in response to temperature alterations. Most often, the thermo-responsive behavior is obtained by utilizing the LCST (low critical solution temperature) of polymers. The solubility of thermo-responsive NPs is increased by decreasing the temperature below the LCST. Subsequently, a volume phase transition and swelling of the nanogels occur by means of the formation of hydrogen bonds. Such polymeric NPs are called “negative thermo-sensitive” polymers. The problem with these NPs is that heating may damage normal cells around the tumor. Furthermore, magnetic NPs have been widely developed and combined with flexible polymeric materials to achieve magneto-responsive drug delivery. By integration with thermo-responsive materials, the localized heating caused by magnetic particles under an alternating current magnetic field can be used to realize controlled drug release. Alternatively, the magnetic material integrated with flexible polymers is able to deform by stretching, compressing, or bending to release the drug upon exposure to the magnetic field.

Clinical Development

The application of nanotechnology in drug delivery has developed rapidly in the past few decades, and many

nanodrugs have been approved or are in clinical trials (Table 1.3.8B.1). The first anticancer nanodrug, Abraxane, was approved by the FDA in 2005. By 2018, 38 nanodrugs had been approved by FDA, and more than 60 nanodrugs were in clinical trials. Liposomes, as the first class of therapeutic NPs to receive clinical approval for cancer treatment, have tremendously developed in the past decades. Nowadays, various stimuli-responsive or active-targeting liposomes have been developed. Other nanodrug delivery systems such as polymeric micelles or even inorganic NPs are also being gradually applied in clinical practice.

Nucleic Acid Delivery Applications of NPs

Since the discovery of DNA in the 1950s, nucleic acids have not only revolutionized our capability to understand the fundamental basis of life, but also have encouraged us to develop novel nucleic acid-based therapeutics. Gene therapy has drawn tremendous attention as a promising modality for the treatment of numerous gene-associated diseases, which is implemented via the introduction of nucleic acids into the pathological cells to correct, replace, or silence defective genes. Therapeutic nucleic acids mainly include plasmid DNA, messenger RNA (mRNA), oligodeoxynucleotides (ODNs), small interference RNA (siRNA), micro-RNA (miRNA), and ribozymes. The majority of nucleic acids function within cells at either transcriptional or posttranscriptional states, and thus transmembrane delivery of nucleic acids is essential for their biological function. Viral vectors, although highly efficient in terms of gene transfection, often suffer from safety concerns such as carcinogenicity, immunogenicity, and insertional mutagenesis. In contrast, nanoscale non-viral vectors possess desired biocompatibility and minimal mutagenesis, and thus serve as an alternatives to viral vectors for gene delivery.

Intracellular Barriers Against Nucleic Acid Delivery

After injection of a nucleic acid delivery system into the body, it will face multiple systemic barriers before reaching the target site to initiate gene transfection. Extracellular barriers, such as circulation in the blood, tissue distribution, and disease targeting, have been summarized in the section on drug delivery. Intracellular barriers against gene delivery mainly include cell membranes, endolysosomal entrapment, intracellular gene release, and nuclear transport (Fig. 1.3.8B.10).

Cell membrane and endocytosis. Nucleic acids are hydrophilic and negatively charged macromolecules, and are thus expelled by cell membranes that adopt lipophilic and negatively charged structures. Therefore, cationic materials are normally used to condense nucleic acids into nanocomplexes to facilitate cellular internalization. To date, the majority of nanocomplexes are internalized via endocytosis.

TABLE 1.3.8B.1 Representative Examples of Clinical-Stage NPs for Anticancer Drug Delivery

	Nano-Platform	Generic Name	Active Ingredients	Status	
Polymeric NPs	Nontargeted polymeric NPs	Genexol PM	Paclitaxel	Approved in Korea	
		NK 105	Paclitaxel	Phase III	
		SMANCS	Neocarzinostatin	Approved in Japan	
Inorganic NPs	PSMA-targeting polymeric NPs	BIND-014	Docetaxel	Phase II	
		Iron oxide NPs	NanoTherm	NA	Approved in Europe
		Hafnium oxide NPs	NBTR3	NA	Phase II/III
Lipid-based NPs	Liposome	CYT-6091	TNF	Phase I	
		DaunoXome	DNR	Approved by FDA	
		Marqibo	Vincristine sulfate		
Lipid-based NPs	Thermo-responsive liposome	Myocet	DOX	Approved in Europe	
		Mepact	MTP-PE		
		Tecemotide	MUC1 antigen	Phase III	
		CPX-351/Vyxeos	AraC and DNR		
		Doxil	DOX	Approved by FDA	
		Onivyde/MM-398	Irinotecan		
		MM-302	DOX	Phase II/III	
Bio-inspired NPs	Albumin NPs	ThermoDox	DOX		
		Abraxane	Paclitaxel	Approved by FDA	

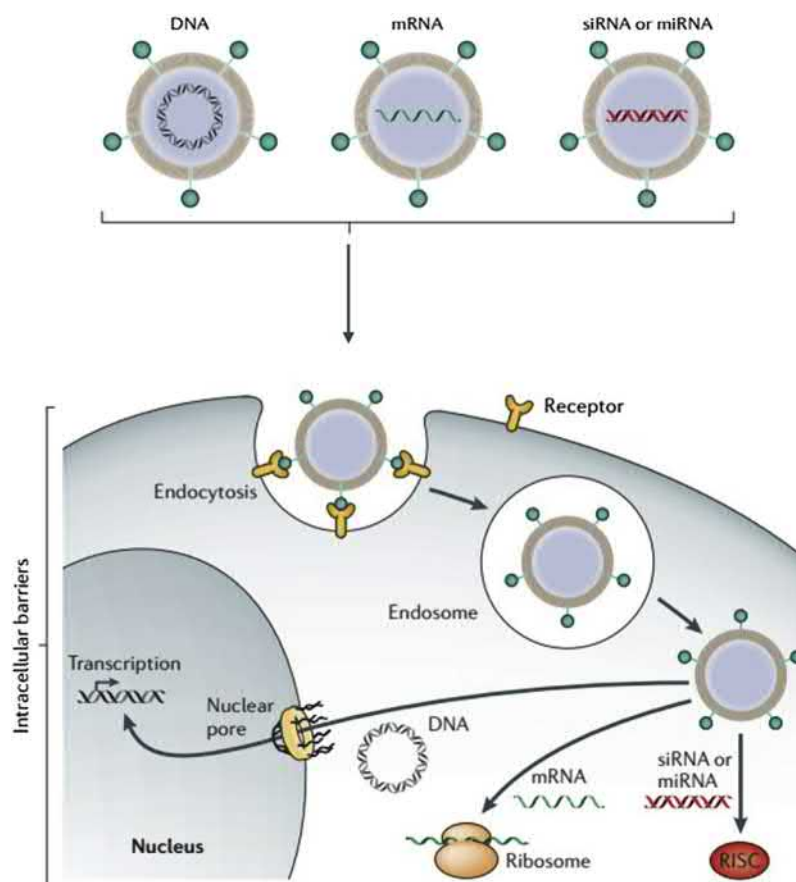
Reproduced from Ref Shi, J. J., Kantoff, P. W., Wooster, R., Farokhzad, O. C., 2017. Cancer nanomedicine: progress, challenges and opportunities. Nat. Rev. Cancer 17, 20–37.

Endocytosis is an energy-dependent process that mainly includes clathrin-mediated endocytosis (CME), caveolae, and macropinocytosis. Many factors determine the endocytosis pathway, including both cell lines and complex properties, such as chemical structure, presence of ligands, size, and surface charge. Nanocomplexes internalized via CME will be trapped in acidic and digestive endosomes and lysosomes, unless the nanocomplexes can enable particular mechanisms to escape the endosomes. Therefore, the CME pathway is ineffective toward gene transfection. In contrast, caveolae take part in a non-acidic and nondigestive process, wherein the nanocomplexes experience association with the cell membrane, encapsulation within caveolae, uptake by caveosomes, and direct transport to the Golgi or endoplasmic reticulum to facilitate nuclear transport. Thus, caveolae are an effective pathway for gene transfection. Macropinocytosis, which involves a large volume of extracellular fluid and vesicles (~200 nm–5 μm) via the cell membrane, is a prevalent pathway for dendritic cells and antigen-presenting cells. The innate leaky property of macropinosomes allows the nanocomplexes to easily transport into the cytosol to enhance gene transfection.

Endolysosomal entrapment. After CME, nanocomplexes are usually transported to the late endosomes, which are

rapidly acidified to pH 5–6 by the activation of ATPase proton-pump enzyme in the endosomal membrane. Afterward, complexes are trafficked to lysosomes, which further acidify to pH 4.5 and with abundant digestive enzymes. The acidic environment of lysosomes accelerates substrate denaturation and aids lysosomal hydrolases, leading to the degradation of nucleic acids that fail to escape from these acidic vesicles. Therefore, endosomal/lysosomal entrapment is a main bottleneck step for successful nucleic acid delivery.

Intracellular gene release. Another important barrier that should be overcome is the kinetics of nucleic acid release from the NPs. Nanocarriers with higher cationic charge density afford stronger nucleic acid condensation capacities and will facilitate cellular internalization via electrostatic interactions with cell membranes. However, the excessively strong binding affinity toward nucleic acids will impede intracellular release. While the negatively charged components in the cytoplasm such as polysaccharides or proteins can competitively replace the nucleic acid from the nanocomplexes, its efficiency is low. Therefore, a proper balance between gene condensation and gene release needs to be achieved for NPs to synchronize the multiple transfection processes such as cellular internalization and intracellular release, thus synergistically contributing to effective gene transfection.



• **Figure 1.3.8B.10** Intracellular barriers to successful delivery of nucleic acids. (Reproduced from Yin, H., Kanasty, R. L., Eltoukhy, A. A., Vegas, A. J., Dorkin, J. R., Anderson, D. G., 2014, Non-viral vectors for gene-based therapy. *Nat. Rev. Genet.* 15, 541–555.)

Nuclear transport. For DNA delivery, nuclei transport is another critical barrier because DNA needs to be transcribed in the cell nuclei. The nucleus is coated with a double-bilayer membrane with tightly regulated pores that allow the passage of small particles (≤ 10 nm) freely into or out of the nuclei, while large macromolecules or NPs enter the nuclei with difficulty via the nuclear pore complex (NPC). Evidence has proven that it is easier to achieve nuclear transport in proliferating cells. During cell division, the nuclear membrane disintegrates for a short time, allowing transport of exogenous nucleic acids into the nuclei. To this end, for nondividing cells or slowly dividing cells, nuclear transport of DNA is difficult, thus conferring low transfection efficiency.

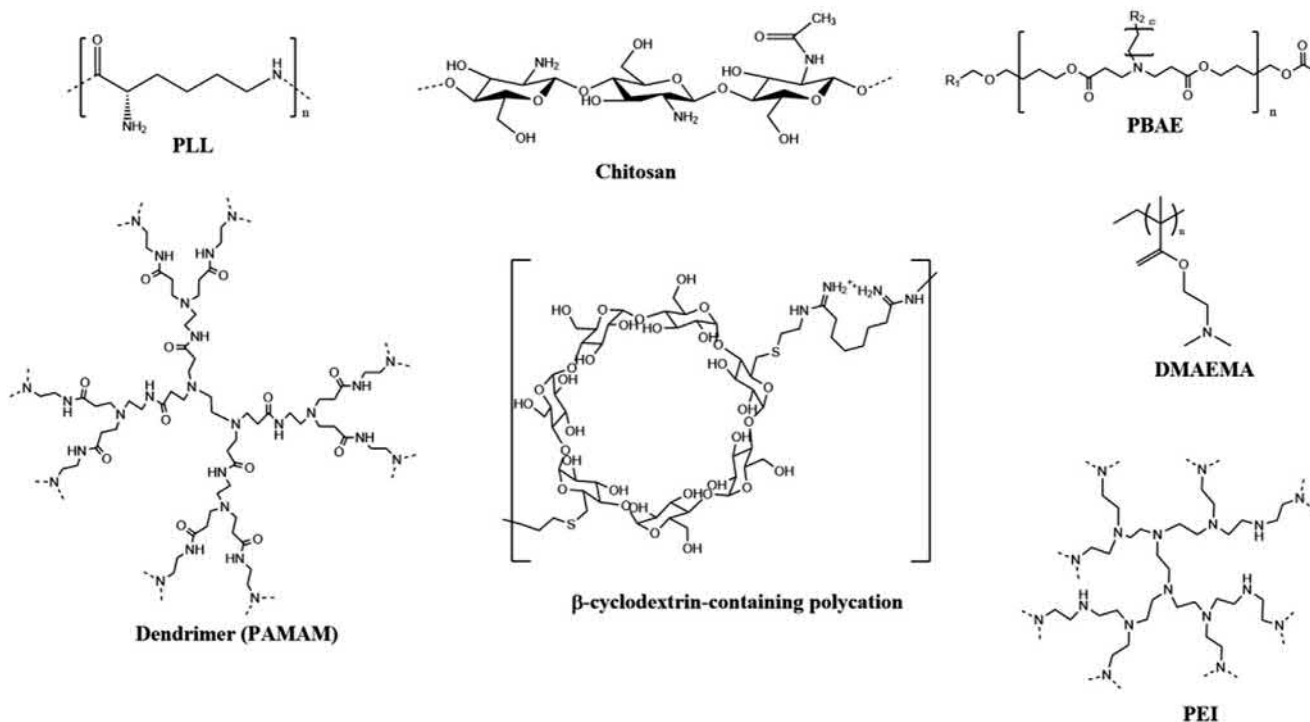
Strategies to Overcome Intracellular Barriers

Nucleic Acid Condensation and Cellular Internalization

Nucleic acids are often condensed by cationic materials, exemplified by cationic polymers (polycations) and lipids, to form positively charged and nano-scale complexes, thus favoring the cellular internalization.

Polycations. Commonly utilized polycations include poly(L-lysine) (PLL), polyethylenimine (PEI), poly(β -amino ester)

(PBAE), cationic dendrimer, 2-dimethyl(aminoethyl) methacrylate (pDMAEM), cyclodextrin, or carbohydrate-based polymers such as chitosan (Fig. 1.3.8B.11). Cationic groups, including primary, secondary, tertiary, and quaternary amines, as well as other positively charged groups such as amidines, are incorporated into the polymer backbone or side chain to facilitate binding with nucleic acids. Protonation of amines can increase the net positive charge of cationic polymers, and thus cationic polymers often exhibit a pH-dependent interaction with nucleic acids in which higher charge-density polyamines show stronger binding affinity. Based on the flexible chemistries of polycations, they can provide various functions used for efficient gene delivery and feature biocompatibility, easy manufacturing, and controllable formulation. The molecular weight and chain length of a polymer also have a significant impact on its nucleic acid condensation capability and cellular uptake level. Polycations with higher molecular weight (MW) usually afford higher nucleic acid condensation capability, cellular uptake level, and transfection efficiency, while polycations with lower MW have less cytotoxicity and better DNA unpackaging. The excessively strong binding affinity endowed by high-MW polycations will impede the intracellular release of gene cargos and induce stronger posttransfection cytotoxicity, which impairs the transfection efficiency.



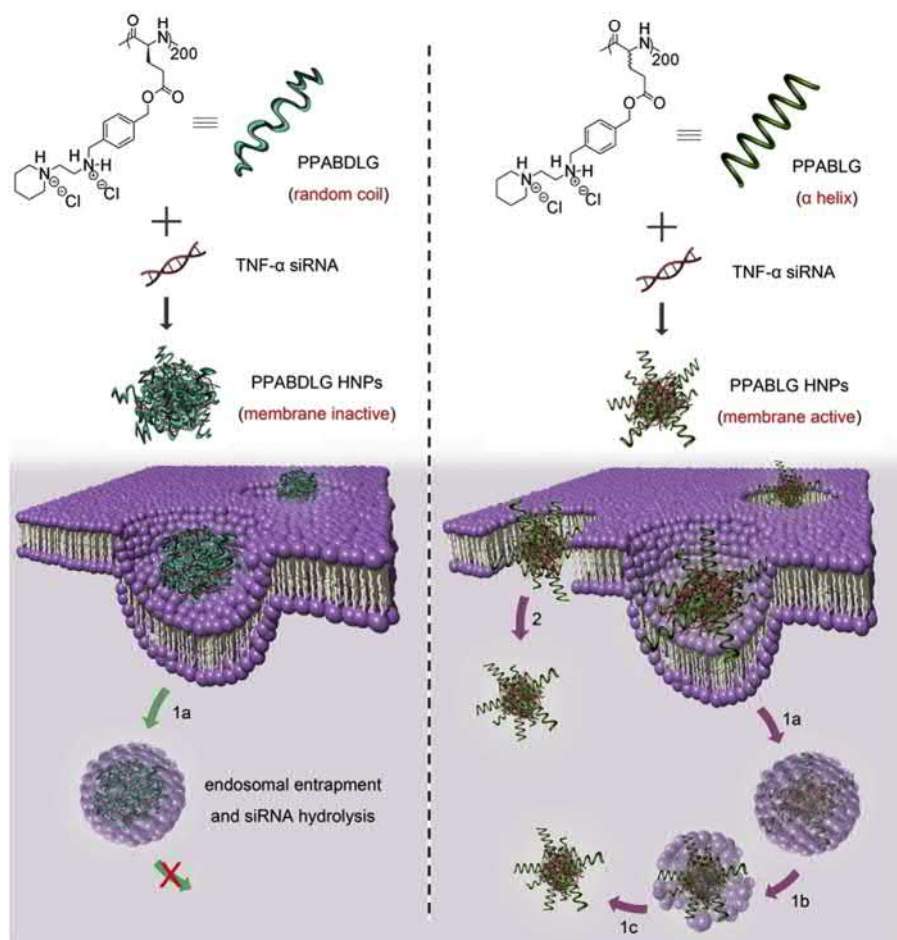
• **Figure 1.3.8B.11** Chemical structures of commonly used polycations for the construction of gene delivery NPs.

Tremendous efforts have been devoted to enhancing transfection efficiency while reducing the toxicity of polycations. The salt bridge is an effective method to improve gene condensation, which is formed between positively charged groups of polycations (such as guanidines or Zn-DPA) and the phosphate groups of nucleic acids. Hydrophobic modification of polycations has also received much attention. Mounting evidence shows that the incorporation of hydrophobic domains, especially aromatic motifs, can enhance gene delivery efficiency, due to the hydrophobic interactions with lipophilic cell membranes that enhance cellular uptake. To achieve a proper balance between cationic charge and hydrophobicity, large library screening is often performed. For instance, a library of PBAEs with different backbone structures, side chain functionality, and terminal groups has been prepared via the Michael addition reaction between different diacrylates and amine-containing molecules (Lynn and Langer, 2000). Alternatively, fluorinated polycations are both hydrophobic and lipophilic, and have a high phase-separation tendency in polar and nonpolar conditions, which can enhance the affinity between polycations and cell membrane as well as endo/lysosomal membrane, accelerating the entry of complexes into cells and escape from endo/lysosomes. Moreover, the fluorinated polycations have low surface energy and tend to connect with others at low concentrations, which allows the formulation of complexes at low nitrogen to phosphorus (N/P) ratios to minimize the toxicity (Wang et al., 2014).

The topological structure of complexes alters how the cells interact with material surfaces, affects cell migration, and modulates endocytosis, and thus manipulation of the topological structure of polycations can potentially

enhance the membrane affinity and transfection efficiency. Polycations with branched, dendritic, or brush topologies often exhibit higher affinity with nucleic acids and cell membranes due to their multivalent structure, and accordingly lead to higher transfection efficiency. One important example is branched PEI and branched PBAE, which demonstrate notably higher transfection efficiencies than their linear counterparts. Similar to the NPs used for anticancer drug delivery, incorporation of targeting ligands/antibodies onto the surface of nanocomplexes can enhance the affinity with specific cell membranes, thus enhancing the intracellular delivery efficiency of gene cargoes.

Cationic lipids. The use of cationic lipids for nucleic acid delivery was first introduced by Felgner in 1987. The lipid structure has significant influence on the interaction with DNA or RNA, and thus has a strong relationship with gene delivery efficiency. Based on their high transfection efficiency, cationic lipids have been widely used for nonviral gene delivery. A typical liposomal formulation needs a mixture of cationic lipid and neutral lipid, wherein cationic lipids, such as DOTMA, DOSPA, DOTAP, DMRIE, and DC-cholesterol, play a key role in gene binding and transfection. The structure of cationic lipids consists of a cationic head group, a hydrophobic tail, and a linker region. Alternatively, neutral lipids, such as phospholipids DSPC, DOPE, and cholesterol serve as “helper lipids” to enhance complex stability and transfection efficiency. Particularly, Lipofectamine 2000, as a commercial product, has been widely used for gene transfection. However, lipid-based gene delivery demonstrates crucial drawbacks, including cytotoxicity, poor in vivo stability, and low condensation efficiency.



1a. Endocytosis; 1b. Pore formation on endosomal membrane; 1c. endosomal escape;
2. Direct transduction via pore formation on cell membranes;

• **Figure 1.3.8B.12** Schematic illustration of the formation of stable helix in polypeptides and their trans-membrane gene-delivery mechanisms. (Reproduced from He, H., Zheng, N., Song, Z. Y., Kim, K. H., Yao, C., Zhang, R. J., et al., 2016. Suppression of hepatic inflammation via systemic siRNA delivery by membrane-disruptive and endosomolytic helical polypeptide hybrid nanoparticles. *ACS Nano* 10, 1859–1870.)

Currently, a combinatorial series of lipid-like materials called “lipidoids” has been developed, and they have been widely used as carriers for delivering nucleic acids. These lipidoids are synthesized by reacting amines with lipophilic acrylates, acrylamides, and epoxide, which generate a large library of materials followed by screening to identify the top-performing candidate (Akinc et al., 2008). These lipidoids have various advantages for nucleic acid delivery, such as low cost, facile synthesis, and structural diversity of the starting materials.

Cell-penetrating peptides (CPPs). Cell-penetrating peptides, such as HIV-Tat, oligoarginine, Pep-1, MPG, TP10, and melittin, are sequence-specific oligopeptides with distinguished membrane-penetrating properties. As such, they have been utilized for the transmembrane delivery of nucleic acids. CPPs often adopt an inherent helical structure or form a helix during membrane penetration, which strengthens the interactions with cell membranes to facilitate cellular internalization. However, because of their short length and lack of sufficient cationic charges, CPPs have difficulty effectively delivering genes by themselves. To address this dilemma, cationic polypeptides with long backbones

and stable helical structures have been developed by elongating the separation distance between backbone and charged side groups, which reduced the side-chain charge repulsion to stabilize the helix (Fig. 1.3.8B.12). Such helical polypeptides possess strong membrane penetration capability via the “pore formation” mechanism, outperforming classical CPPs such as Arg9 and HIV-Tat by 1–2 orders of magnitude (Tang et al., 2013). Because of their sufficient backbone length, these polypeptides demonstrate potent transfection efficiencies for both DNA and siRNA, notably outperforming commercial reagents such as PEI and Lipofectamine 2000 (Tang et al., 2013; He et al., 2016).

Endosomal Escape

“Proton sponge” effect. Polymers with high buffering ability, such as PEI and polyamidoamine (PAMAM) dendrimers, possess secondary and tertiary amines in their structures with pKa values between physiological and lysosomal pH. These polymers absorb protons in the endolysosomes, and in order to maintain the endolysosomal pH, the ATPase enzymes pump protons from the cytosol into endosomes

along with passive entry of chloride ions. The increased ion concentration in the endolysosomes induces water diffusion into the endolysosomes to maintain the balance of ion concentration, which finally induces osmotic swelling and rupture of the endosomal membrane. This mechanism is called the “proton sponge” effect.

Fusion with endosomal membranes. Lipoplexes coated with a lipid membrane can fuse with the endosomal membrane, resulting in the release of nucleic acid into the cytosol. The charge of cationic liposomes ensures close interaction with and destabilization of the endosomal membrane, leading to fusion and release of the nucleic acid. The cationic liposomes incorporated with fusogenic “helper” lipids, such as DOPE, further facilitate endosomal fusion and escape via conformational change upon acidification and enhancing a nonlamellar lipid phase change. Incorporation of cholesterol in cationic liposomes can also enhance fusogenicity in a pH-dependent way at the plasma membrane.

CPPs. Most CPPs have a similar mechanism of membrane activity, which is mediated by endosomal pH. Acidic environment in the endosome causes conformational transition of CPPs from a random coil to α -helix, which interacts with endosomal membrane phospholipids and induces pore formation. HIV-Tat is a commonly used CPP and derives from the transcriptional activator protein of human immunodeficiency virus type 1 (HIV-1), which significantly enhances complex-mediated gene delivery. Enlightened by the CPPs, various new peptides with endosomal membrane-destabilizing activity have been developed. Although these peptides have a random coil conformation in the neutral environment, the structure is converted to an amphiphilic α -helical conformation in endosomes, resulting in the endosomal membrane disruption.

Photochemical disruption. Photosensitizers can produce reactive oxygen species (ROS) upon light irradiation, which disrupts the endolysosomal membranes to facilitate endosomal escape, the so-called photochemical internalization (PCI) effect. Many studies have demonstrated that the incorporation of photosensitizers with nucleic acid carriers can notably improve gene transfection efficiency as a result of PCI-facilitated endosomal escape. However, ROS will also destabilize the nucleic acid cargoes via oxidation, and thus photosensitizers need to be encapsulated in the gene carrier in a separate compartment from the gene cargo, avoiding direct contact between generated ROS and genes. Alternatively, the photosensitizer can be localized on the NP shells, which is removed from the NPs before light irradiation and thus avoids ROS-induced gene damage.

Stimuli-Responsive NPs for Intracellular Gene Release

One major approach to trigger on-demand gene release is to use intracellularly degradable carriers. These carriers have potent DNA/RNA binding affinity to facilitate cellular internalization, but can degrade into small segments inside the cells to release cargoes instantaneously. Various cationic polyesters have been developed as degradable gene carriers due to hydrolysis of the ester bonds by the

esterases rich in the cytoplasm. Among them poly [α -(4-aminobutyl)-L-glycolic acid] (PAGA), a biodegradable analogue of polylysine, demonstrates lower cytotoxicity and higher transfection efficiency than polylysine. Another important cationic polyester is PBAE, which possesses ester bonds in its backbone. However, hydrolysis of the ester bonds occurs on the time scale of several hours to a few days, and is largely affected by the polymer structure as well as the cellular condition. As such, it is difficult to precisely control when and where gene release will occur. As a structural-mimicking analogue of PBAE, a poly(amido amine) has been developed which contains stable amide bonds instead of hydrolysable ester bond in the backbone. To enable controlled and fast degradation of these materials inside cells, trigger-cleavable domains are introduced into the backbone, such as disulfide, thioketal, ketal, or nitrobenzyl linkers that can be cleaved by intracellular redox, ROS, acidic pH, or external UV light, respectively. Similarly, cross-linking of low-MW oligocations with cleavable linkers to synthesize high-MW polymers is also a commonly utilized approach. For example, low-MW PEI can be cross-linked by disulfide-, ketal-, thioketal-, or nitrobenzyl-containing linkers to achieve high-MW PEI. Using these approaches, the inconsistency between nucleic acid condensation and intracellular gene release are harmonized. Additionally, the posttransfection material toxicity can also be reduced as a result of polymer degradation.

Charge reversal is another efficient method to facilitate intracellular nucleic acid release. Upon internal or external triggers, the responsive polycations transform to neutral or negatively charged materials, thus repelling the gene cargoes to potentiate transfection (Yin et al., 2013).

Nuclear Transport

Many proteins are naturally targeted to the nucleus by nuclear localization signals (NLSs), which are short amino acid sequences recognized by importins. NLSs are often rich in arginine or lysine, and widely used NLSs include SV40 large T-antigen (PKKKRKV) and the bipartite NLSs. NPs conjugated with NLSs can improve nuclear entry in both dividing and nondividing cells. Therefore, the incorporation of NLSs in nucleic acid delivery NPs through electrostatic complexation or covalent conjugation holds great promise for the nuclear transport of DNA cargoes that have to be transcribed in the nuclei.

Clinical Development

Gene therapy is a promising strategy for the treatment of many gene-associated human diseases by altering gene expression, such as cancer, hemophilia, hypercholesterolemia, neurodegenerative diseases, and autoimmune diseases (Table 1.3.8B.2). Despite some clinical trials of NPs for gene delivery showing promising results, the wide use of gene therapy for disease treatment still faces great challenges. The primary factor is the delivery, including fast degradation and clearance in circulation, nonspecific uptake, inability for endosomal escape, and cytotoxicity.

TABLE 1.3.8B.2 NP-Based Gene Therapy Under Clinical Evaluation

Delivery System	Product	Sponsor	Disease	Administration	Phase	Status	Gov Identifier
PEI-based NPs	BC-819/PEI	BioCancell	BC	Local	2	Active	NCT00595088
	BC-819	BioCancell	OC	IP	1/2	Completed	NCT00826150
	DTA-H19	BioCancell	PN	Local	1/2	Completed	NCT00711997
	EGEN-001	Gynecologic Oncology Group	Cancer	IP	2	Active	NCT01118052
Lipid-based NPs	TKM-080301	National Cancer Institute	HM	IA	1	Completed	NCT01437007
	TKM-080301	Tekmira Pharmaceuticals Corporation	HC	IV	1/2	Recruiting	NCT02191878
	TKM-080301	Tekmira Pharmaceuticals Corporation	NET; ACC	IV	1/2	Completed	NCT01262235
	Atu027	Silence Therapeutics GmbH	ASC	IV	1	Completed	NCT00938574
	ALN-TTR02	Amylam Pharmaceuticals	TTR-A	IV	2	Completed	NCT01617967
	DOTAP-Chol-fus1	MD Anderson Cancer Center	LC	IV	1	Completed	NCT00059605
	DCR-MYC	Dicerna Pharmaceuticals	ST; MM; NHL	IV	1	Recruiting	NCT02110563
	DCR-MYC	Dicerna Pharmaceuticals	HC	IV	1/2	Recruiting	NCT02314052
	ND-L02-s0201 Injection	Nitto Denko Corporation	EHF	IV	1	Recruiting	NCT02227459
	PLGA-based NPs	siG12D LODER	Silenseed	PC	Local	2	Active

ACC, adrenocortical carcinoma; ASC, advanced solid cancer; BC, bladder cancer; EHF, extensive hepatic fibrosis; HC, hepatocellular carcinoma; HM, hepatic metastases; IA, intraarterial; LC, lung cancer; MM, multiple myeloma; NET, neuroendocrine tumors; NHL, non-Hodgkins lymphoma; OC, ovarian cancer; PC, pancreatic cancer; PEI, polyethylenimine; PLGA, poly(lactic-co-glycolic acid); PN, pancreatic neoplasms; ST, solid tumors; TTR-A, transthyretin amyloidosis.

Reproduced from Ref Chen, J., Guo, Z., Tian, H., Chen, X., 2016. Production and clinical development of nanoparticles for gene delivery. *Mol. Ther. Methods Clin. Dev.* 3.

NPs have been used as gene delivery systems to overcome the delivery barriers based on their desirable properties such as safety, nonimmunogenicity, controllability, and low cost. The first NP-based siRNA delivery system called CALAA-01, has been studied in a phase 1 clinical trial against cancer, and shows potent antiproliferative activity to many cancer cells (Davis et al., 2010). Many other NP-based gene delivery systems have also been widely studied for clinical trials, such as PEI-, lipid-, and PLGA-based NPs. Most of these contain polycations or cationic lipids for condensing nucleic acids, PEG for stabilization, and targeting ligands for binding to the receptors on the target cells.

Diagnostic/Theranostic Applications of NPs

In Vitro Diagnosis

In vitro diagnosis is an essential component of clinical care that performs a diagnostic test on biological samples (blood, urine, tissue, etc.). In vitro diagnosis tests have received great attention due to their unique features in the medical area. For example, these tests do not directly interact with the human body, making them accessible without invasive surgeries and possible biological safety problems for patients. Moreover, an in vitro diagnosis test can quickly provide valuable information on the health status of patients and

can even enable early diagnosis, thus leading to the easier treatment of severe diseases.

Although much progress has been made in the biotechnology field, only limited in vitro diagnostic systems have been successfully translated into clinical use. Therefore, the pursuit of simple but efficient tools is highly desirable. In addition, the increasing requirement for in vitro diagnosis with enhanced properties is pushing the exploitation of highly sensitive and easily processed sensors. In recent years, with the rapid development of nanoscience and nanotechnology, advances have been made in the design of in vitro diagnostic tools using NPs. NPs large surface areas can carry various kinds of functional molecules (such as organic dye, DNA, and enzyme), allowing the detection of analytes with very low concentrations. Moreover, the surface groups of NPs can be easily functionalized using physical or chemical linkages, thus enabling analysis for real-time and direct detection of multiple targets. Up to now, a variety of NPs, such as polymeric NPs, gold NPs, carbon nanotubes, silica nanostructures, QDs, and magnetic NPs, have been utilized for constructing high-sensitivity in vitro diagnostic systems. These highly sensitive analytical systems can detect biomarkers at pico-, femto-, atto-, and even zepto-molar levels, which would open a new era of early diagnosis and certainly provide more valuable information for better treatment of diseases.

Detection of glucose. Diabetes is a major cause of death and disability around the world. Frequent measurement of blood glucose levels is a requisite for the confirmation of effective treatment. As a result, the development of highly sensitive, low-cost, and reliable glucose biosensors is in great demand. While glucose oxidase (GOx)-based glucose biosensors have been popularly utilized over the past several decades, they have disadvantages such as complicated enzyme immobilization, critical operating conditions, and chemical instability. Another important glucose detection method is amperometric nonenzymatic sensing based on the direct electrochemical oxidation of glucose, which addresses the problem of insufficient long-term stability usually encountered with enzymatic glucose sensors. In recent years, the regulation of glucose biosensors at a molecular level has become possible using various functional NPs. The conducting NPs can greatly enhance the electron communication between enzymes and electrodes. Amperometric glucose biosensors based on various NPs (carbon NPs, nanostructured metal oxides, etc.) have been extensively studied.

Detection of prostate-specific antigen (PSA). Early detection of cancer enables more timely treatment and would significantly improve therapeutic outcomes. One promising method for the early detection of cancer is to detect a specific biomarker in the blood or other body fluids that are closely related with the occurrence of cancer. These cancer biomarkers may be carbohydrates, nucleic acids, or proteins (e.g., surface glycoproteins, secreted proteins). Analyzing the levels of particular cancer biomarkers from a patient could achieve the detection of cancer at

early stages, identification of tumor recurrence, prediction of a patient's risk for cancer, as well as monitoring of therapeutic efficacy. As one of the most widely measured biomarkers for prostate cancer, PSA is a serine protease generated by the prostate epithelium to maintain liquefaction of seminal fluid. Generally, PSA tests are performed at specialized laboratories using large automated instruments, which require sample transportation that leads to increased waiting time and medical cost. Nanotechnology has been frequently utilized to address these concerns, since the unique characteristics of certain classes of NP probes endow the potential to produce rapid, inexpensive, and high-throughput assays with high sensitivity and selectivity. The resultant nanoparticulate sensor usually comprises two distinct components: (1) a recognition segment, usually high-affinity intact antibodies, to recognize and bind PSA; and (2) a transducing element that converts the interactions of biomolecules (e.g., antibody and antigen) into a quantifiable signal, such as fluorescence, surface plasmon resonance, electrochemical signal, etc.

Detection of circulating tumor cells (CTCs). With the progression of cancer, metastasis happens and drastically diminishes the prognosis of patients. Metastatic cancer formation occurs through the spread of cancer cells from the primary tumor site to the bloodstream and lymphatic system, and to new sites at distal organs and tissues to form secondary tumors. CTCs are a key component in this prognosis process, and thus the early detection of CTCs in the blood offers an efficient way to predict metastatic risk. To realize this, the correlation of CTC presence with cancer patient prognosis needs to be established.

Current technology to detect CTCs depends on the immunomagnetic separation of cells based upon their expression of cell surface antigens, such as epithelial cell adhesion molecule (EpCAM). Although this methodology has been successfully commercialized, it is often restricted by the need to recognize the antigens on the cell surface and can result in the failure to distinguish CTCs whose protein expression level is too low for isolation. It has been reported that several kinds of NPs are especially suitable for the design of nanoparticulate probes that could detect small populations of CTCs through the production of a fluorescent output (Shen et al., 2017). For instance, QDs modified with moieties that bind and recognize CTC surface markers demonstrate competitive advantages over organic dyes, such as high quantum yields, size-dependent emission tunability, improved photostability, and longer fluorescence lifetimes. The continuing progresses in the use of NP probes for CTC detection significantly strengthens the existing methods to detect CTCs, and may produce potential impacts for cancer patient prognosis in the clinic.

In Vivo Imaging

In contrast to in vitro diagnosis mentioned above, "in vivo" tests are generally conducted. Noninvasive in vivo imaging, including magnetic resonance imaging (MRI),

ultrasonography (US), X-ray computed tomography (CT), positron emission tomography (PET), optical imaging (OI), single-photon emission computed tomography (SPECT), and photoacoustic imaging (PAI), is an essential tool for the diagnosis of many diseases, such as cancer, cardiovascular diseases, and infectious diseases. A fundamental goal of in vivo imaging is to determine and localize specific molecular targets, pathways, as well as physiology in the disease state. In the imaging techniques based on contrast agents, diseases are generally identified by the accumulation of an agent at the site of pathological changes. Hence, these agents should be able to produce a signal recognized by an imaging modality. Customarily, the agents are mostly small molecules and sometimes may be linked to peptides, proteins, oligonucleotides, or antibodies. These small-molecule imaging agents are usually injected systemically and designed to accumulate at disease sites based on the difference in the fundamental biology between the diseased and normal tissues.

Although small-molecule imaging agents can make a trip easily within the body and often are able to enter cells, their small size will inevitably result in high nonspecific uptake, which is one of their greatest weakness. Other drawbacks include the increased time and expense of synthesizing the agents, the difficulty of incorporating a signaling segment without significantly changing the property of the original molecule, the low payload, and the minimal circulation half-life. The size of NPs is advantageous for in vivo imaging because it is sufficiently large to carry much more contrast than small molecules, while keeping the ability to systemically travel through the body. In other words, NPs fill in a critical gap between small molecular and larger imaging agents. Moreover, NPs provide the ability to selectively enter cancer sites other than small-molecule agents or larger agents due to the EPR effect. NPs designed for in vivo imaging require a suitable reporter moiety for the imaging application and a biocompatible coating that serves not only to control the toxicological and pharmacological properties of NPs but also serves as the functional linkage between the reporter and other molecules (e.g., targeting ligands, other imaging agents, and even therapeutic agents). On the other hand, multimodal imaging techniques using NPs are also being exploited to overcome the respective limitations of an individual imaging modality and to provide more precise physiological and anatomical data for diagnosis and treatment.

Magnetic resonance imaging (MRI). MRI is a noninvasive and nonionizing imaging technique based on the principle of NMR. In a strong magnetic field, the hydrogen nuclei absorb resonant radiofrequency pulses, and then the excited nuclei return to the initial state by emitting the absorbed energy. MR contrast is thus generated by the different relaxation characteristics of the hydrogen atoms in tissues that are influenced by the nearby magnetic materials. MRI offers information that can hardly be accessed by other imaging methods since its sufficient penetration depths enable imaging throughout the entire human body, and the spatial resolution is usually down to 10 μm . Over the last 2 decades,

various NPs or composites have been investigated as MRI contrast agents, and several formulations have been approved for clinical use. These contrast agents are mostly formed by transition and lanthanide metals, iron oxide NPs, and more recently ferrite NPs. A new generation of T1 contrast agents is developed by Gd complexes embedded in various NPs, such as porous silica NPs, dendrimers, perfluorocarbon NPs, and nanotubes. Iron oxide NPs with varying diameters can be used for MRI of different organs. For example, superparamagnetic iron oxide NPs with overall diameters greater than 50 nm can be used for imaging of liver, spleen, and bone marrow; ultra-small superparamagnetic iron oxide NPs with diameters smaller than 50 nm have been used for lymph node imaging. In addition, iron oxide NPs modified with bioactive moieties have been used for targeted imaging. The most notable restrictions associated with such MR contrast agents are the current detection limits and the lack of tissue specificity. The successful overcoming of these issues would inevitably accelerate the clinical translation of NP-based MRI to in vivo applications.

Optical imaging (OI). OI is a noninvasive and highly sensitive imaging method that can detect a concentration of up to 10^{-9} – 10^{-12} M. OI applies nonionizing radiation ranging from ultraviolet to infrared light that offers desired safety. A key advantage of OI is the accessibility to interactions between tissue and light plus the corresponding photo-physicochemical processes at the molecular level. The lower risk for patients and faster analysis procedure of OI enables long-term or repetitive observations of disease progression. In terms of cancer study, OI is mainly applied for the localization and metastases of tumors, as well as the monitoring of progression or regression of pathological sites. A critical issue for the OI technique is to maximize the penetration depth, which comes at the price of decreasing spatial resolution, and minimizing background signal, while retaining resolution and signal intensity. Multifunctional NPs have been widely utilized to manipulate and greatly amplify these optical signals. Many of these NPs provide an improvement in sensitivity and can even achieve the same imaging results using tiny amounts of material. Currently, several kinds of NPs have been used for OI application, such as quantum dots (CdSe, Ag₂S, etc.), carbon nanomaterials (carbon dots, single-walled carbon nanotubes, graphene, and nanodiamonds), as well as upconversion nanomaterials. Moreover, some other NPs (e.g., polymer-, silicon-, and lipid-based nanomaterials) have also been applied in OI, yet the vast majority are made fluorescent through incorporating organic fluorescent dyes either covalently linked to the surface or incorporated inside the NPs.

X-ray computed tomography (CT). CT is a radiography imaging technology that constructs 3D images of a body structure, which can easily distinguish between electron-dense structures (e.g., bone) and relatively electron-poor moieties (e.g., soft tissues). However, its soft-tissue contrast is quite poor and extrinsic contrast agents are thus needed to generate high contrast. The current small molecule-based CT contrast agents, especially the most commonly used iodinated compounds, usually require a relatively higher

dosage (molar concentration range) than other imaging modalities, such as MRI (millimolar concentration range) and OI (nanomolar concentration range). NPs can make intriguing CT contrast agents since they can carry a high-contrast payload, circulate for a long period of time, and can easily be prepared with electron-dense contrast materials. Such denser materials (e.g., gold over iodine) with higher absorption coefficients can achieve better contrast structures. Some other typical inorganic NPs with high atomic number apart from gold include lanthanides (e.g., Gd, Eu, and Yb) and heavy metal-based agents such as tantalum oxides and bismuth sulfides. Because of the long circulation time of NPs, delineation of soft tissues such as the vasculature has become a major application of the CT technique. Nevertheless, the critical issue in NP-based CT is its low sensitivity. The minimum detectable concentration difference between target and background is on the order of mM. Therefore, the main bottleneck of nanoparticulate CT is the total accumulation of NPs in the target sites, thus making the delivery of contrast agent the most important factor that limits the clinical application of nanoparticulate CT.

Photoacoustic imaging (PAI). PAI has emerged as a promising noninvasive imaging modality that harvests the advantages of both optical and acoustic imaging by directing (laser) light pulses into a sample and receiving acoustic information in the form of ultrasound to generate images. The key advantage of PAI is that the light in/sound out paradigm allows a detection depth into tissues of up to 5 cm at a relatively high spatial resolution. As the contrast mechanism in PAI is highly dependent on the optical absorption of the sample, NP-based contrast agents have great potential in PAI applications because they can be facilely engineered for optimum absorption in the visible or near-infrared (NIR) region with very high cross sections. Generally, NPs designed for PAI can be classified into two major types on the basis of the physical mechanism of light absorption, NPs based on surface plasmon resonance (SPR) and dye-containing NPs.

For SPR-based NPs, nanoscale metallic films, usually gold, are deposited onto the surface of NPs. The peak absorption can be facilely controlled, ranging from visible to NIR regions by simply tuning the physical dimensions of the metallic layer. For dye-encapsulated NPs, they are usually composed of NIR organic dyes (such as indocyanine green) embedded inside the NPs to enhance optical absorption. A recent advance in PAI material lies in the development of semiconducting polymer-based NPs, which offer a number of advantages (e.g., highly photostable, optically active, versatile in chemistry) over many traditional nondegradable inorganic contrast agents. The use of NP-based contrast agents greatly extends the applications of PAI. For example, it allows PAI to image deeper tissues with enhanced contrast, and targeting molecules can be conjugated onto the surface of NPs for cell-specific imaging. Moreover, PAI can be potentially integrated with photothermal therapy to achieve combined imaging and therapy because both techniques share similar mechanisms.

The past few years have witnessed enormous progress in *in vivo* imaging with NPs, which usually shows considerable advantages over small-molecule imaging agents. Novel NPs have displayed unprecedented properties that were seldom imagined over a decade ago, including imaging sensitivity, penetration depth, and multimodality capability. Because of this, they have also raised expectations from researchers and the public. A key to fulfilling these expectations is a sophisticated balance between safety concerns, synthetic simplicity or efficient scale-up production, and a suitable match to clinical needs. If these goals are realized satisfactorily, the above expectations of nanoparticulate imaging will be achieved.

Theranostics

A theranostic represents an agent that combines diagnostic capability (typically imaging) with a therapeutic property. Theranostics are being developed for both imaging and therapy using either a special probe or a drug that has diagnostic and therapeutic capabilities or linking therapeutic agents with imaging probes. The utilization of a theranostic approach can bring about the following benefits, such as providing simultaneous imaging and therapy, reducing the frequency of administration, enhancing patient compliance, decreasing the burden on patients and caregivers, and offering useful information on the biodistribution and clearance of drug. Accordingly, theranostics has recently become one of the core keywords in cancer research because of the assumption that if cancer growth can be hampered during the diagnostic stage, the subsequent cancer treatment would be much easier as cancer growth is retarded.

We have described above how multifunctional NPs realize imaging with many modalities or treatments with diverse therapeutic functionalities. NPs reflect the ideal design form for theranostics due to their highly modular characteristics. Advanced multifunctional NPs usually possess many of the properties that can meet the theranostics field requirements, such as targetable delivery, sustained and stimuli-responsive controlled release, enhanced delivery efficiency, synergistic therapeutics (e.g., multidrug combination therapy or drug plus heating/radiation/other therapeutic), as well as multimodality imaging capability. In general, theranostic NPs can be composed of at least three components including biomedical payload, carrier, and surface modifier. Biomedical payloads comprise imaging agents (e.g., organic dyes, quantum dots, MRI or CT contrast agents, etc.) and therapeutic agents (anticancer drugs, therapeutic DNA and small interfering RNA, proteins, ROS-generating agents, etc.). Carriers should provide sufficient physical protection for the payloads under physiological conditions during delivery to the desired target sites. Also, it is better to make the carriers become cancer-specifically disintegrated for better imaging or therapeutic efficacies. Finally, surface modifiers are often attached to the carriers to endow theranostic NPs with additional functions, such as long circulation time, barrier-crossing capability, as well as targeting ability. These three components have been extensively investigated for the

development of tailored multifunctional theranostics. While the clinical translation of nanoparticulate theranostics is virtually nonexistent at present and the future prospects seem challenging, it is undeniable that NPs have highly relevant properties and provide opportunities for exploitation of new diagnostic and therapeutic agents.

Imaging-Guided Surgery

As previously described, improvements in preoperative imaging tools have offered much help in the diagnosis of cancer by facilitating early detection, increasing diagnostic accuracy, and improving preoperative planning. Nevertheless, the eyes and hands of surgeons remain the dominant “imaging modalities” during surgery that are used to decide which tissues need to be removed or preserved. Palpation and visual inspection are not always accurate for discriminating between abnormal and normal tissues, which can lead to incomplete resections of malignant tissues or unnecessary removal of healthy tissue. For instance, many breast tumors are nonpalpable and hence the positive surgical margin rates are in the range of 5%–49%, which will inevitably increase patient pain. In order to successfully treat and cure patients with solid cancers, it is of great importance to precisely localize the tumor followed by complete removal of the tumor, while preserving healthy tissues as far as possible. To this end, molecular imaging techniques have tremendous potential in imaging-guided cancer surgery.

Ultrasonography and X-ray fluoroscopic imaging are sometimes utilized during cancer surgery to find occult tumors and define tumor vasculature. Furthermore, intraoperative MRI and CT have also been frequently used in preoperative staging and intraoperative planning of resection, especially in the field of neurosurgical image guidance. Nevertheless, these intraoperative techniques are expensive, require a complex infrastructure, and are mainly used for neurosurgery only at some specialized hospitals. In the past several years, intraoperative imaging using invisible NIR fluorescent light has entered the surgical consideration to fill the niche between preoperative imaging and intraoperative reality. In contrast to the case that visible light penetrates tissue on the micrometer scale, NIR light can travel millimeters—even up to centimeters—through blood and tissue. This greatly enhanced photon transport improves the recognition of targets below the background. Since the tissue shows almost no autofluorescence in the NIR spectrum range, the signal-to-background contrast can be maximized using fluorescent contrast agents responsive to NIR light. In addition, NIR light is invisible to the human eye and NIR imaging does not use ionizing radiation, making it an inherently safe technique. Therefore, to date, some specialized intraoperative imaging systems for open surgery, laparoscopy, and robot-assisted surgery have become available. Using these instruments, NIR fluorescent contrast agents can be visualized with acquisition time in the millisecond range, realizing real-time guidance during surgery.

In recent years, researchers have found that compared with NIR imaging at wavelengths in the 700–900 nm range (NIR-I region), increasingly more favorable optical properties of tissues can be exploited well when imaging at progressively longer wavelengths in the 1000–1700 nm range (NIR-II region). NIR-II fluorescence imaging can offer an even higher signal-to-noise ratio because of lower tissue autofluorescence and deeper tissue penetration because of lower signal attenuation. Although NIR-II imaging is a newly emerging field, numerous NIR-II fluorophores from small organic molecules to organic and inorganic NPs have been successfully developed, and their wide biomedical applications have been demonstrated. It is anticipated that the forthcoming crucial breakthrough in research into NIR-II fluorophores and imaging systems will make a substantial impact on precise imaging-guided cancer surgery.

Conclusion

NPs have gained tremendous popularity in the field of drug delivery, gene delivery, and diagnosis with great success. The major advantages of NPs lie in enhancing drug solubility, improving drug stability, facilitating biodistribution, controlling cargo release, realizing disease targeting, and interacting with biological barriers. Thus, nanoparticulate systems have demonstrated great promise for applications such as antitumor therapy, antiinflammation therapy, gene therapy, antiviral therapy, phototherapy, molecular imaging, and macromolecular delivery across multiple physiological barriers. Additionally, at the intersection between treatment and diagnosis, interest has grown in combining both paradigms into clinically effective formulations. With a proper combination thereof, precision nanomedicine that can simultaneously detect, image, and treat disease may one day become the norm rather than the exception. However, there is still major scope for improvement in the development of efficient NPs for biomedical utility. These improvements involve precise manipulation of NP properties (such as small size with low dispersity), controlled synthesis of materials with scale-up amenability, reduced material complexity with lower cost, synchronized nano-properties toward overcoming multiple biological barriers, long-term safety, and in vivo biodegradability. Various NPs are currently being developed for diagnosis and therapy, and with the elegant solution of the above-mentioned issues, it is envisioned that novel therapeutic/diagnostic NPs will realize ideal personalized medicines in the near future and contribute greatly to optimized therapy for individual patients in clinical fields.

References

- Akinc, A., Zumbuehl, A., Goldberg, M., Leshchiner, E.S., Busini, V., Hossain, N., et al., 2008. A combinatorial library of lipid-like materials for delivery of RNAi therapeutics. *Nat. Biotechnol.* 26, 561–569.
- Bar-Zeev, M., Livney, Y.D., Assaraf, Y.G., 2017. Targeted nanomedicine for cancer therapeutics: towards precision medicine overcoming drug resistance. *Drug Resist. Updates* 31, 15–30.

- Blanazs, A., Armes, S.P., Ryan, A.J., 2009. Self-assembled block copolymer aggregates: from micelles to vesicles and their biological applications. *Macromol. Rapid Commun.* 30, 267–277.
- Boas, U., Heegaard, P.M.H., 2004. Dendrimers in drug research. *Chem. Soc. Rev.* 33, 43–63.
- Brust, M., Walker, M., Bethell, D., Schiffrin, D.J., Whyman, R., 1994. Synthesis of thiol-derivatized gold nanoparticles in a 2-phase liquid-liquid system. *J. Chem. Soc., Chem. Commun.* 801–802.
- Cagel, M., Tesan, F.C., Bernabeu, E., Salgueiro, M.J., Zubillaga, M.B., Moretton, M.A., et al., 2017. Polymeric mixed micelles as nanomedicines: achievements and perspectives. *Eur. J. Pharm. Biopharm.* 113, 211–228.
- Chen, W., Meng, F.H., Cheng, R., Zhong, Z.Y., 2010. pH-Sensitive degradable polymersomes for triggered release of anticancer drugs: a comparative study with micelles. *J. Control. Release* 142, 40–46.
- Chen, J., Guo, Z., Tian, H., Chen, X., 2016. Production and clinical development of nanoparticles for gene delivery. *Mol. Ther. Methods Clin. Dev.* 3.
- Davis, M.E., Zuckerman, J.E., Choi, C.H.J., Seligson, D., Tolcher, A., Alabi, C.A., et al., 2010. Evidence of RNAi in humans from systemically administered siRNA via targeted nanoparticles. *Nature* 464 1067–U140.
- Elzoghby, A.O., Samy, W.M., Elgindy, N.A., 2012. Protein-based nanocarriers as promising drug and gene delivery systems. *J. Control. Release* 161, 38–49.
- Geng, Y., Dalhaimer, P., Cai, S.S., Tsai, R., Tewari, M., Minko, T., et al., 2007. Shape effects of filaments versus spherical particles in flow and drug delivery. *Nat. Nanotechnol.* 2, 249–255.
- Gref, R., Minamitake, Y., Peracchia, M.T., Trubetskoy, V., Torchilin, V., Langer, R., 1994. Biodegradable long-circulating polymeric nanospheres. *Science* 263, 1600–1603.
- He, H., Zheng, N., Song, Z.Y., Kim, K.H., Yao, C., Zhang, R.J., et al., 2016. Suppression of hepatic inflammation via systemic siRNA delivery by membrane-disruptive and endosomolytic helical polypeptide hybrid nanoparticles. *ACS Nano* 10, 1859–1870.
- Kataoka, K., Harada, A., Nagasaki, Y., 2001. Block copolymer micelles for drug delivery: design, characterization and biological significance. *Adv. Drug Deliv. Rev.* 47, 113–131.
- Lee, J.S., Feijen, J., 2012. Polymersomes for drug delivery: design, formation and characterization. *J. Control. Release* 161, 473–483.
- Li, P., Kaslan, M., Lee, S.H., Yao, J., Gao, Z., 2017. Progress in exosome isolation techniques. *Theranostics* 7, 789–804.
- Lv, S.X., Wu, Y.C., Cai, K.M., He, H., Li, Y.J., Lan, M., et al., 2018. High drug loading and sub-quantitative loading efficiency of polymeric micelles driven by donor-receptor coordination interactions. *J. Am. Chem. Soc.* 140, 1235–1238.
- Lynn, D.M., Langer, R., 2000. Degradable poly (β -amino esters): synthesis, characterization, and self-assembly with plasmid DNA. *J. Am. Chem. Soc.* 122, 10761–10768.
- Meng, F.H., Zhong, Z.Y., Feijen, J., 2009. Stimuli-responsive polymersomes for programmed drug delivery. *Biomacromolecules* 10, 197–209.
- Mora-Huertas, C.E., Fessi, H., Elaissari, A., 2010. Polymer-based nanocapsules for drug delivery. *Int. J. Pharm.* 385, 113–142.
- Pei, H., Zuo, X., Zhu, D., Huang, Q., Fan, C., 2014. Functional DNA nanostructures for theranostic applications. *Acc. Chem. Res.* 47, 550–559.
- Shen, Z.Y., Wu, A.G., Chen, X.Y., 2017. Current detection technologies for circulating tumor cells. *Chem. Soc. Rev.* 46, 2038–2056.
- Shi, J.J., Kantoff, P.W., Wooster, R., Farokhzad, O.C., 2017. Cancer nanomedicine: progress, challenges and opportunities. *Nat. Rev. Cancer* 17, 20–37.
- Tang, H.Y., Yin, L.C., Kim, K.H., Cheng, J.J., 2013. Helical poly (arginine) mimics with superior cell-penetrating and molecular transporting properties. *Chem. Sci.* 4, 3839–3844.
- Tong, R., Cheng, J.J., 2008. Paclitaxel-initiated, controlled polymerization of lactide for the formulation of polymeric nanoparticulate delivery vehicles. *Angew. Chem. Int. Ed.* 47, 4830–4834.
- Wang, M., Liu, H., Li, L., Cheng, Y., 2014. A fluorinated dendrimer achieves excellent gene transfection efficacy at extremely low nitrogen to phosphorus ratios. *Nat. Commun.* 5.
- Wang, H., Wang, R.B., Cai, K.M., He, H., Liu, Y., Yen, J., et al., 2017. Selective in vivo metabolic cell-labeling-mediated cancer targeting. *Nat. Chem. Biol.* 13, 415.
- Yin, L.C., Tang, H.Y., Kim, K.H., Zheng, N., Song, Z.Y., Gabrielson, N.P., et al., 2013. Light-responsive helical polypeptides capable of reducing toxicity and unpacking DNA: toward nonviral gene delivery. *Angew. Chem. Int. Ed.* 52, 9182–9186.
- Yin, H., Kanasty, R.L., Eltoukhy, A.A., Vegas, A.J., Dorkin, J.R., Anderson, D.G., 2014. Non-viral vectors for gene-based therapy. *Nat. Rev. Genet.* 15, 541–555.
- Yingchoncharoen, P., Kalinowski, D.S., Richardson, D.R., 2016. Lipid-based drug delivery systems in cancer therapy: what is available and what is yet to come. *Pharmacol. Rev.* 68, 701–787.
- Zhou, Y., Ye, H., Chen, Y.B., Zhu, R.Y., Yin, L.C., 2018. Photo-responsive drug/gene delivery systems. *Biomacromolecules* 19, 1840–1857.
- Zou, Y., Meng, F.H., Deng, C., Zhong, Z.Y., 2016a. Robust, tumor-homing and redox-sensitive polymersomal doxorubicin: a superior alternative to Doxil and Caelyx? *J. Control. Release* 239, 149–158.
- Zou, Y., Fang, Y., Meng, H., Meng, F.H., Deng, C., Zhang, J., et al., 2016b. Self-crosslinkable and intracellularly decrosslinkable biodegradable micellar nanoparticles: a robust, simple and multifunctional nanoplatform for high-efficiency targeted cancer chemotherapy. *J. Control. Release* 244, 326–335.

Chapter Assessment Questions

1. Define NPs, and mention three major types of NPs.
2. Please list the major advantages and disadvantages of polymeric micelles, polymersomes, liposomes, and nanocapsules.
3. Define the term “critical micellar concentration.” List three strategies to reduce the critical micellar concentration.
4. List at least five examples concerning the correlation between NP properties (size, surface charge, morphology, etc.) and functions.
5. Explain different mechanisms to noncovalently and covalently load drugs into NPs and compare their advantages/disadvantages.
6. Summarize the major systemic barriers to anticancer drug delivery and existing approaches to overcome these barriers.
7. List different endolysosomal escape mechanisms mediated by gene-delivery vectors.
8. List different intracellular gene release mechanisms mediated by polycationic vectors.
9. What are passive targeting and active targeting? List three approaches to realize passive targeting or active targeting, respectively.
10. List five different types of internal or external stimuli-responsive mechanisms in drug delivery.

1.4.1

Introduction to Materials Processing for Biomaterials

SHELLY E. SAKIYAMA-ELBERT

Department of Biomedical Engineering, The University of Texas at Austin, Austin, TX, United States

The processing of materials can be critical for altering their physical properties to modulate the biological response to the material. It can also greatly expand the number of applications that the material can be used for. In this section a number of different types of modifications will be covered, including surface modification to decrease fouling and increase specific interactions with cells, as well as fabrication of textiles and more three-dimensional structures through additive manufacturing.

The first chapter in this section focuses on physiochemical modifications of material surfaces to alter biological responses. Methods for the modification of surface chemistry through chemical reaction, grafting, and changing texture will all be discussed, as well as the characterization of modifications. The second chapter focuses specifically on nonfouling surfaces that have reduced protein adsorption and methods to generate such surfaces. In particular there is an emphasis on polymer grafting and thin films that can be applied to a broad variety of materials to lower protein adsorption.

For materials that come into contact with blood, and particularly for materials used in vascular applications, the risk of promoting undesired clot formation is one of the biggest challenges faced in medical device design, as the risk of myocardial infarctions or strokes can result. The third chapter focuses on key steps in thrombus formation and processing methods to reduce the thrombogenicity of materials either through preventing the activation of the coagulation cascade or preventing platelet activation. Specific surface modification strategies and polymer grafting are the primary methods, as well as use of antiplatelet agents and immobilization of fibrinolytic agents.

Beyond just pacifying materials surfaces or reducing protein adsorption, surface modification can also be used to promote specific interactions between biomaterials and biological

systems. This can be accomplished through the grafting of peptides or proteins that can interact specifically with cell surface receptors or catalyze biological reactions (enzymes). The fourth chapter focuses on methods that can be used to functionalize surfaces, largely through covalent reactions and the use of “capture tags.” Beyond uniform modification of surfaces, for some applications nonuniform surface modification can enhance the functionality of materials and further modulate the biological response. For example, cell migration to certain regions of the material or cell adhesion in specific shapes or patterns can improve tissue integration of materials. This chapter focuses on a variety of patterning techniques that can be used with different materials.

In addition to patterning, another key processing method for material is the texture and three-dimensional structure of the material. By processing biomaterials into fibers that can further be woven into textiles, the properties of the materials can be further altered. The fiber structure allows a much greater surface area-to-volume ratio and textiles can further increase the porosity and flexibility of materials. Woven biomaterials have been used for a variety of applications, which are highlighted in the fourth chapter along with methods for processing fiber and textile formation. More broadly textured surfaces can play a critical role in the enhancement of integration of materials with host tissue in both hard and soft tissues. This chapter specifically focuses on using texture materials to enhance cellular ingrowth and methods for fabricating texture materials on both the nano- and microscales. These approaches provide great versatility for materials processing.

The explosion of low-cost 3D printers has made additive manufacturing much more accessible for both researchers and the lay public. It has also led to the broad development of printers that can be used with biologics that cannot be processed under traditional printing conditions, and open source

hardware that can be adapted to specific user needs. The result is that complex three-dimensional materials can be printed to provide structures that are not accessible through other processing methods to provide porosity or complex architecture

that better supports tissue integration or even recapitulates the structure of complex organs. The fifth chapter focuses on the different techniques that are currently available for additive manufacturing of materials with complex structures.

1.4.2

Physicochemical Surface Modification of Materials Used in Medicine

BUDDY D. RATNER¹, ALLAN S. HOFFMAN², SALLY L. MCARTHUR^{3,4}

¹Bioengineering and Chemical Engineering, Director of University of Washington Engineered Biomaterials (UWEB), Seattle, WA, United States

²Bioengineering and Chemical Engineering, University of Washington, Seattle, WA, United States

³Bioengineering Research Group, Swinburne University of Technology, Melbourne, VIC, Australia

⁴Biomedical Manufacturing, CSIRO Manufacturing, Melbourne, VIC, Australia

Introduction

Much effort goes into the design, synthesis, and fabrication of biomaterials and devices to ensure that they have the appropriate mechanical properties, durability, and functionality. To cite a few examples, a hip joint should withstand the high stresses associated with walking and running, a hemodialyzer should have the requisite permeability characteristics, and the pumping bladder in an artificial heart should flex for millions of cycles without failure. The bulk composition and organization of materials govern these properties.

The biological response to biomaterials and devices, on the other hand, is influenced by their surface chemistry and structure (see [Chapters 1.2.4, 2.1.3 and 2.1.4](#)). The rationale for the surface modification of biomaterials is therefore straightforward: to retain the key physical properties of a biomaterial while modifying only the outermost surface to influence the biointeraction. If such surface modification is properly effected, the mechanical properties and functionality of the device will be unaffected, but the bioresponse related to the tissue–device interface will be improved or modulated.

Materials can be surface modified by using biological, mechanical or physicochemical methods. Many biological surface modification schemes are covered in [Chapter 1.4.4](#). Surface modification for creating nonfouling surfaces is reviewed in [Chapter 1.4.2](#). Generalized examples of physicochemical surface modifications, the focus of this chapter, are illustrated schematically in [Fig. 1.4.2.1](#). Surface modification with Langmuir–Blodgett (LB) films has elements of both biological modification and physicochemical

modification. LB films will be discussed later in this chapter. Some applications for surface modified biomaterials are listed in [Table 1.4.2.1](#). Physical and chemical surface modification methods, and the types of materials to which they can be applied, are listed in [Table 1.4.2.2](#). Methods to modify or create surface texture or roughness will not be explicitly covered here (see [Chapter 1.4.7](#)).

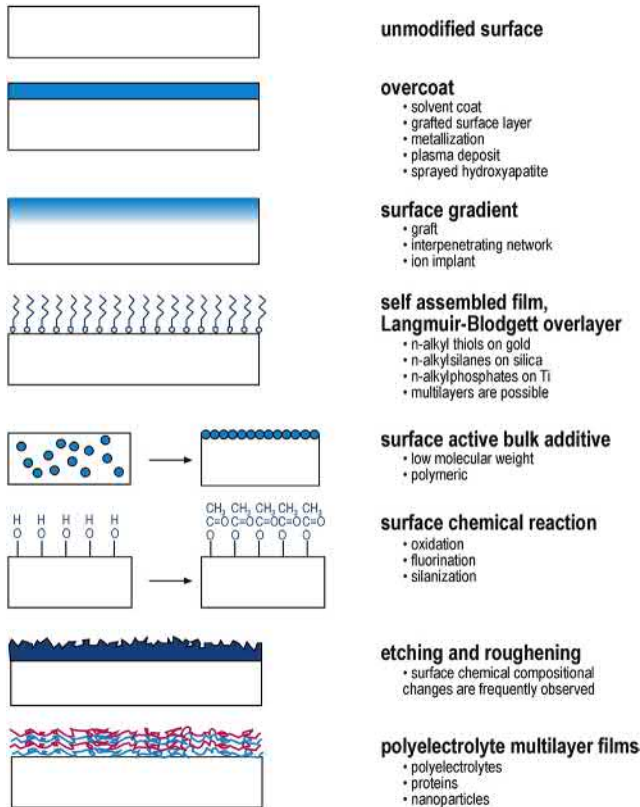
General Principles

Surface modifications fall into three categories: (1) chemically or physically altering the atoms, compounds, or molecules in the existing surface (chemical modification, etching, mechanical roughening); (2) overcoating the existing surface with a material having a different composition (coating, grafting, thin film deposition); and (3) creating surface textures or patterns ([Fig. 1.4.2.1](#)). A few general principles provide guidance when undertaking surface modifications.

Thin Surface Modifications

Thin surface modifications are desirable. Modified surface layers that are too thick can change the mechanical and functional properties of the material. Thick coatings are also more subject to delamination and cracking. How thin should a surface modification be? Ideally, alteration of only the outermost few molecular layers (3–10 nm) should be sufficient. In practice, thicker films than this will be necessary, since it is difficult to ensure that the original surface is uniformly covered when coatings and treatments are molecularly thin. This is because of intrinsic nonuniformities in

Surface Modification Possibilities



• **Figure 1.4.2.1** Schematic representations of methods to modify surfaces.

many coating processes, and also because of surface roughness that exists on almost all surfaces at the nanometer scale. Also, extremely thin layers may be more subject to surface reversal (see below) and mechanical erosion. Some coatings intrinsically have a specific thickness. For example, the thickness of LB films is related to the length of the amphiphilic molecules that comprise them (2–5 nm). Other coatings, such as poly(ethylene glycol) (PEG) protein-resistant layers, may require a minimum thickness (a dimension related to the molecular weight of chains) to function (see [Chapter 1.4.3A](#)). In general, surface modifications should be the minimum thickness needed for uniformity, durability, and functionality, but no thicker. This is often experimentally defined for each system.

Delamination Resistance

The surface modified layer should be resistant to delamination and cracking. Resistance to delamination is achieved by covalently bonding the modified region to the substrate, intermixing the components of the substrate and the surface film at an interfacial zone (for example, an interpenetrating network or IPN), applying a compatibilizing (“primer”) layer at the interface or incorporating appropriate functional groups for strong intermolecular adhesion between a substrate and an overlayer (Wu, 1982). Where the mechanical properties of the substrate and overlayer are significantly mismatched, delamination becomes increasingly of concern.

TABLE 1.4.2.1 Examples of Surface-Modified Biomaterials by Physicochemical Methods

To Modify Blood Compatibility

Octadecyl group attachment to surfaces (albumin affinity)

Silicone-containing block copolymer additive

Plasma fluoropolymer deposition

Plasma siloxane polymer deposition

Grafted poly(ethylene glycol) (PEG) or PEG-containing polymers

Chemically modified polystyrene for heparin-like activity

To Modulate Cell Adhesion and Growth

Oxidized polystyrene surface

Ammonia plasma-treated surface

Plasma-deposited acetone or methanol film

Plasma fluoropolymer deposition (reduce corneal endothelial adhesion and modify blood interactions)

Varying surface modulus

Antibacterial treatments?

To Control Protein Adsorption

Surface with immobilized poly(ethylene glycol) (reduce adsorption)

Treated ELISA dish surface (increase adsorption)

Affinity chromatography column

Surface cross-linked contact lens (reduce adsorption)

To Improve Lubricity

Plasma treatment?

Radiation grafting (hydrogels)

Interpenetrating polymeric networks

To Improve Wear Resistance and Corrosion Resistance

Ion implantation

Diamond deposition

Anodization

To Alter Transport Properties

Polyelectrolyte grafting

Surface self-assembled film barrier

Plasma-deposited barrier layer

To Modify Electrical Characteristics

Polyelectrolyte grafting

Magnetron sputtering of titanium

Surface fluoropolymer insulation

Surface Rearrangement

Surface rearrangement can readily occur. It is driven by a thermodynamic minimization of interfacial energy and enhanced by molecular mobility. Surface chemistries and structures can

TABLE 1.4.2.2 Physical and Chemical Surface Modification Methods

	Polymer	Metal	Ceramic	Glass
Noncovalent Coatings				
Solvent coating	✓	✓	✓	✓
Langmuir–Blodgett film deposition	✓	✓	✓	✓
Surface active additives	✓	✓	✓	✓
Vapor deposition of carbons and metals ^a	✓	✓	✓	✓
Vapor deposition of parylene (p-xylylene)	✓	✓	✓	✓
Covalently Attached Coatings				
Radiation grafting (electron accelerator and gamma)	✓	–	–	–
Photografting (UV and visible sources)	✓	–	–	✓
Plasma (gas discharge) (RF, microwave, acoustic)	✓	✓	✓	✓
Gas Phase Deposition:				
• Ion beam sputtering	✓	✓	✓	✓
• Chemical vapor deposition (CVD)	–	✓	✓	✓
• Flame spray deposition	–	✓	✓	✓
Chemical grafting (e.g., ozonation + grafting)	✓	✓	✓	✓
Silanization	✓	✓	✓	✓
Biological modification (biomolecule immobilization)	✓	✓	✓	✓
Modifications of the Original Surface				
Ion beam etching (e.g., argon, xenon)	✓	✓	✓	✓
Ion beam implantation (e.g., nitrogen)	–	✓	✓	✓
Plasma etching (e.g., nitrogen, argon, oxygen, water vapor)	✓	✓	✓	✓
Corona discharge (in air)	✓	✓	✓	✓
Ion exchange	✓ ^b	✓	✓	✓
UV irradiation	✓	✓	✓	✓
Chemical Reaction				
• Nonspecific oxidation (e.g., ozone)	✓	✓	✓	✓
• Functional group modifications (oxidation, reduction)	✓	–	–	–
• Addition reactions (e.g., acetylation, chlorination)	✓	–	–	–
Conversion coatings (phosphating, anodization)	–	✓	–	–
Mechanical roughening and polishing	✓	✓	✓	✓

^aSome covalent reaction may occur.
^bFor polymers with ionic groups.

“switch” due to diffusion or translation of surface atoms or molecules in response to the external environment (see [Chapter 1.2.4](#) and [Fig. 1.2.4.2](#) in that chapter). A newly formed surface chemistry can migrate from the surface into the bulk or molecules from the bulk can diffuse to cover the surface. Such reversals occur in metallic and other inorganic systems, as well as in polymeric systems. Terms such as “reconstruction,” “relaxation,” and “surface segregation” are often used to describe mobility-related alterations in surface structure and chemistry ([Ratner and Yoon, 1988](#); [Garbassi et al., 1989](#); [Somorjai, 1990, 1991](#); [Cometa et al., 2010](#)). The driving

force for these surface changes is a minimization of the interfacial energy. However, sufficient atomic or molecular mobility must exist for the surface changes to occur in reasonable periods of time. For a modified surface to remain as intended, surface reversal must be prevented or inhibited. This can be done by cross-linking, by sterically blocking the ability of surface structures to move, by incorporating a rigid, impermeable layer between the substrate material and the surface modification, or by reducing the hydrophilic character of the modified surface, which will reduce water uptake and the mobility of surface atoms.

Surface Analysis

Surface modification and surface analysis are complementary and sequential technologies. The surface-modified region is usually thin, and consists of only minute amounts of material. Undesirable contamination can readily be introduced during modification reactions. The potential for surface reversal to occur during surface modification is also high. The surface reaction should be monitored to ensure that the intended surface is indeed being formed. Since conventional analytical methods are often insufficiently sensitive to detect surface modifications, special surface analytical tools are called for to probe the physical, chemical, and biological behaviors of the coating (Chapter 1.2.4).

Manufacturability and Commercializability

The end products of biomaterials research are devices and materials that are manufactured to exacting specifications for use in humans. A surface modification that is too complex will be challenging and expensive to reproducibly manufacture and commercialize. In many instances, surface modification will require significant investment in infrastructure, may change the regulatory approach to the product (i.e., introducing nanoparticles), or simply add too much cost to the final product. It is also best to minimize the number of steps in a surface modification process, and to design each step to be relatively insensitive to small changes in the preparation processes.

Methods for Modifying the Surfaces of Materials

General methods to modify the surfaces of materials are illustrated in Fig. 1.4.2.1, with many examples listed in Table 1.4.2.2. A few of the more widely used of these methods will be briefly described. Some of the conceptually simpler methods, such as solution coating of a polymer onto a substrate or metallization by sputtering or thermal evaporation, will not be elaborated upon here.

Chemical Reaction

There are hundreds of chemical reactions that can be used to modify the chemistry of a surface. Chemical reactions, in the context of this chapter, are those performed with reagents that react with atoms or molecules at the surface, but do not overcoat those atoms or molecules with a new layer. Chemical reactions can be classified as nonspecific and specific.

Nonspecific reactions leave a distribution of different functional groups at the surface. An example of a nonspecific surface chemical modification is the chromic acid oxidation of polyethylene surfaces leading to numerous surface oxygen species including carboxylic acid, carbonyl, hydroxyl, etc. Other examples include the corona discharge modification

of materials in air; radio frequency glow discharge (RFGD) (plasma) treatment of materials in oxygen, argon, nitrogen, carbon dioxide, fluorinated gases, or water vapor; and the oxidation of metal surfaces to a mixture of metallic suboxides.

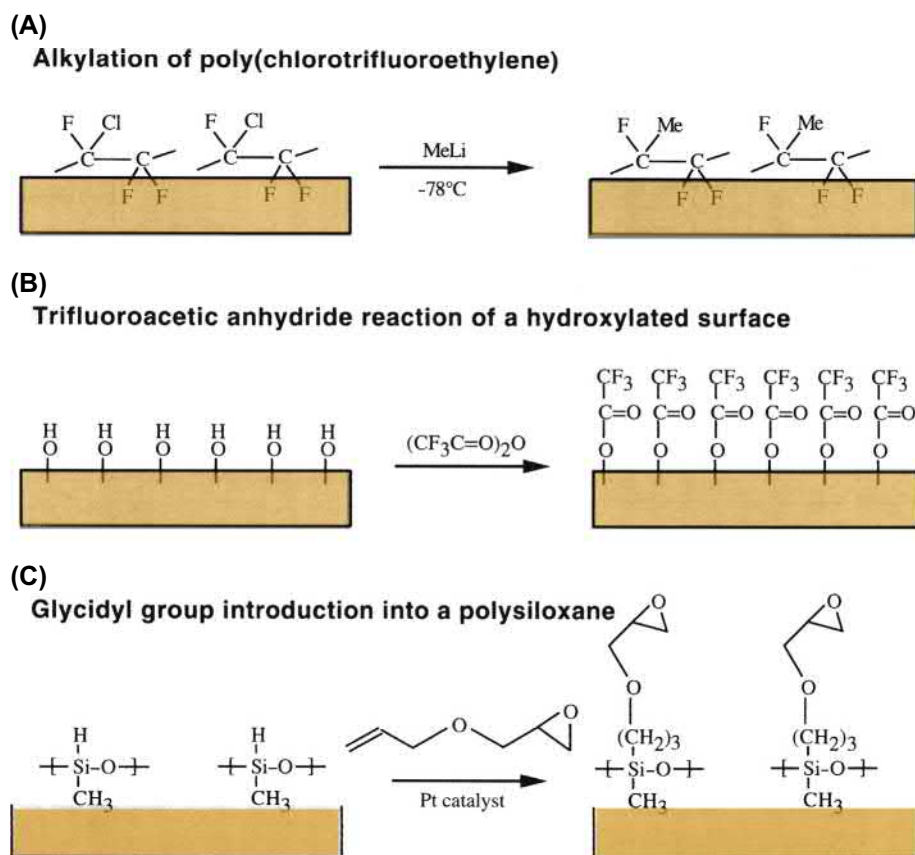
Specific chemical surface reactions change only one functional group into another with a high yield and few side reactions. A few examples of specific chemical surface modifications for polymers are presented in Fig. 1.4.2.2. Certain specific reactions can be used for inorganic (silicon) surfaces as well as polymeric surfaces (Filler and Bent, 2003). Still another example (expanded upon in the section, below, titled “Specific Chemical Reactions for Forming Surface Grafts”) uses atomic transfer radical polymerization (ATRP) chain growth on surfaces (Hucknall et al., 2009). Others have also used radical addition chain transfer polymerization (RAFT) to graft polymer chains to a surface with high precision. This may be done by conjugating the chain transfer agent (CTA) to the surface and then initiating graft polymerization of a monomer to the CTA using a typical free radical initiator (Boyer et al., 2009; Golden et al., 2010).

Protein immobilization is typically (although not always) a surface modification reaction performed with high chemical specificity. Detailed chemistries for biomolecule immobilization are described in Chapter 1.4.4.

Surface Grafting: Radiation Grafting, Photografting, and Newer Methods

Surface grafting methods have been widely applied for the surface modification of biomaterials since the early days of the field (Hoffman et al., 1972). Comprehensive review articles are available (Ratner, 1980; Hoffman, 1981; Hoffman et al., 1983; Stannett, 1990; Safrany, 1997; Ma et al., 2007). Surface grafting methods can be divided into two general categories: (1) using energetic or highly reactive species to activate a chemically inert surface, permitting the attachment of desired surface species; and (2) taking advantage of well-defined, reactive surface chemical groups to covalently attach the surface-modifying species (a polymer, a low-molecular-weight compound, a drug, a protein, etc.). These category (2)-specific reactions for forming surface grafts will be addressed in a separate section below.

The earliest biomedical surface modification studies focused on attaching chemically reactable groups ($-\text{OH}$, $-\text{COOH}$, $-\text{NH}_2$, etc.) to the surfaces of relatively inert hydrophobic polymers using methods from category (1), above. Four types of reactions can be distinguished in category (1): grafting using ionizing radiation sources (most commonly, a cobalt 60 or cesium 137 gamma radiation source) (Dargaville et al., 2003; Luk et al., 2017); grafting using UV radiation (photografting) (Matsuda and Inoue, 1990; Dunkirk et al., 1991; Swanson, 1996; Sebra et al., 2007); grafting using high-energy electron beams (Singh and Silverman, 1992); and grafting using a reactive, surface-activating species such as ozone (Chiang et al., 2009). In all cases, similar processes occur. The radiation or reactive chemical breaks chemical bonds in the material to be grafted, forming free radicals, peroxides, or



• **Figure 1.4.2.2** Some specific chemical reactions to modify surfaces.

other reactive species. These reactive surface groups are then exposed to a monomer. The monomer reacts with the free radicals at the surface and propagates as a free radical chain reaction incorporating other monomers into a surface-grafted polymer. Electron beams and gamma radiation sources are also used for biomedical device sterilization (see [Chapter 3.1.2](#) Total Product Lifecycle for Biomaterial-based Medical Devices). Note that glow discharge plasma reactions to surfaces also have similarities to these nonspecific surface modification approaches. Plasma reaction will be discussed in its own section, below.

High-energy surface modification technologies are strongly dependent on the source energy, the radiation dose rate, and the amount of the dose absorbed. The energy of the radiation produced by gamma sources is roughly 1 MeV (1 eV = 23.06 kcal/mol; for comparison, a carbon-carbon bond has a strength of approximately 85 kcal/mol). Typical energies for electron beam processing are in the range 5–10 MeV. UV radiation sources are of much lower energy (<6 eV). Radiation dose rates are low for UV and gamma, and very high for electron beams. The amount of energy absorbed is measured in units of Grays (Gy), where 1 kGy (Kgy) = 1000 J/kg. Units of megarads (MR) are often used for gamma sources, 1 MR = 1×10^6 erg/g.

Three distinct reaction modes can be described: (1) in the mutual irradiation method, the substrate material is immersed in an oxygen-free solution (monomer ± solvent) that is then exposed to the radiation source; (2) the substrate materials can also be exposed to the radiation under

an inert atmosphere or at low temperatures (to stabilize free radicals) (in this case, the materials are later contacted with a monomer solution to initiate the graft process); (3) finally, the exposure to the radiation can take place in air or oxygen, leading to the formation of peroxide groups on the surface. Heating the material to be grafted in the presence of monomer or addition of a redox reactant (e.g., Fe^{2+}) which will decompose the peroxide groups to form free radicals can initiate the graft polymerization (in O_2 -free conditions).

Graft layers formed by energetic irradiation of the substrate are often relatively thick (>1 μm) and are comprised of high-molecular-weight polymer chains. However, they are typically well-bonded to the substrate material, and thus resist delamination. Since many polymerizable monomers are available, a wide range of surface chemistries can be created. Mixtures of monomers can form unique graft copolymers ([Ratner and Hoffman, 1980](#)). For example, the hydrophilic/hydrophobic ratio of surfaces can be controlled by varying the ratio of a hydrophilic and a hydrophobic monomer in the grafting mixture ([Ratner et al., 1979](#); [Ratner and Hoffman, 1980](#)).

Photoinitiated grafting (usually with visible or UV light) represents a unique subcategory of surface modifications for which there is growing interest ([Deng et al., 2009](#); [Park et al., 2009](#)). There are many approaches to effect this photoinitiated covalent coupling. For example, a phenyl azide group can be converted to a highly reactive nitrene upon UV exposure. This nitrene will quickly react with many organic groups. If a synthetic polymer is prepared with phenyl azide side groups,

and this polymer is exposed simultaneously to UV light and a substrate polymer or polymeric medical device, the polymer containing the phenyl azide side groups will be immobilized to the substrate (Matsuda and Inoue, 1990). Another method involves the coupling of a benzophenone molecule to a hydrophilic polymer (Dunkirk et al., 1991). In the presence of UV irradiation, the benzophenone is excited to a reactive triplet state that can covalently couple with many polymers. As still another example, a dithiocarbamate-functionalized polyurethane was used to photo-pattern an extracellular-matrix-like coating (Sebra et al., 2007).

Radiation, electron beam, and photografting have frequently been used to bond hydrogels to the surfaces of hydrophobic polymers (Matsuda and Inoue, 1990; Dunkirk et al., 1991; Sebra et al., 2007; Luk et al., 2015). Electron beam grafting of N-isopropyl acrylamide to polystyrene has been used to create a new class of temperature-dependent surfaces for cell growth (Kwon et al., 2000) (also see Chapter 1.4.4). The protein interactions (Horbett and Hoffman, 1975), cell interactions (Ratner et al., 1975; Matsuda and Inoue, 1990), blood compatibility (Chapiro, 1983; Hoffman et al., 1983), and tissue reactions (Greer et al., 1979) of hydrogel graft surfaces have been investigated.

RFGD Plasma Deposition and Other Plasma Gas Processes

RFGD plasmas, as used for surface modification, are low-pressure ionized gas environments typically at ambient (or slightly above ambient) temperature. They are also referred to as glow discharge or gas discharge depositions or treatments. Plasmas can be used to modify existing surfaces by ablation or etching reactions or, in a deposition mode, to overcoat surfaces (Fig. 1.4.2.1). Good review articles on plasma deposition and its application to biomaterials are available (Yasuda and Gazicki, 1982; Hoffman, 1988; Ratner et al., 1990; Chu et al., 2002; Kitching et al., 2003; Desmet et al., 2009). Some biomedical applications of plasma-modified biomaterials are listed in Table 1.4.2.3.

RFGD plasma surface modifications are widely used in biomaterials research and development. Because such coatings and treatments are now used in commercialized biomaterials products and have special promise for improved biomaterials, they will be emphasized in this chapter. The specific advantages of plasma-deposited films (and to some extent, plasma-treated surfaces) for biomedical applications are:

1. They are conformal. Because of the penetrating nature of a low-pressure gaseous environment in which mass transport is governed by both molecular (line-of-sight) diffusion and convective diffusion, complex geometric shapes can be treated.
2. They are generally free of voids and pinholes. This continuous barrier structure is suggested by transport studies and electrical property studies (Charlson et al., 1984). However, at short deposition times (very thin films), substrate-dependence and less than uniform coatings may be noted (Vasilev et al., 2010).

TABLE 1.4.2.3 Biomedical Applications of Glow Discharge Plasma-Induced Surface Modification Processes

- A. Plasma treatment (etching)
 1. Clean
 2. Sterilize
 3. Cross-link surface molecules
- B. Plasma treatment (etching) and plasma deposition
 1. Form barrier films
 - a. Protective coating
 - b. Electrically insulating coating
 - c. Reduce absorption of material from the environment
 - d. Inhibit release of leachables
 - e. Control drug delivery rate
 2. Modify cell and protein reactions
 - a. Modulate biointeractions
 - b. Promote selective protein adsorption
 - c. Enhance cell adhesion
 - d. Improve cell growth
 - e. Form nonfouling surfaces
 - f. Increase lubricity

Antibacterial Properties?

3. Provide reactive sites
 - a. For grafting or polymerizing polymers
 - b. For immobilizing biomolecules

3. Plasma-deposited films can coat almost any clean solid, including polymers, metals, ceramics, and semiconductors. Other surface grafting or surface modification technologies are highly dependent upon the chemical nature of the substrate.
4. They can be tuned to give good adhesion to the substrate. The energetic nature of the gas phase species in the plasma reaction environment can induce mixing, implantation, penetration, and reaction between the overlayer film and the substrate.
5. Unique film chemistries can be produced. The chemical structure of the polymeric overlayer films generated from the plasma environment usually cannot be synthesized by conventional chemical methods.
6. They can serve as excellent aqueous barrier films, or can be tuned to be hydrogel-like and permeable to water (Förch et al., 2005; Lopez et al., 1993).
7. Plasma-deposited layers generally show low levels of leachables. Due to their highly cross-linked nature, plasma-deposited films contain negligible amounts of low-molecular-weight components that might lead to an adverse biological reaction. They can also inhibit leaching of low-molecular-weight material from the substrate and, in the case of drug-delivery implants or inserts, they can reduce the rate of drug diffusion out of the device (Hendricks et al., 2000).
8. These films are easily prepared. Once the apparatus is set up and optimized for a specific deposition, treatment of additional substrates is rapid and simple.

9. Plasma deposition is a mature technology. The microelectronics industry has made extensive use of inorganic plasma-deposited films for many years (Sawin and Reif, 1983; Nguyen, 1986).
10. Plasma surface modifications, although chemically complex, can be characterized by:
 - (a) infrared (IR) spectroscopy (Inagaki et al., 1983; Haque and Ratner, 1988; Krishnamurthy et al., 1989)
 - (b) nuclear magnetic resonance (NMR) (Kaplan and Dilks, 1981),
 - (c) electron spectroscopy for chemical analysis (ESCA) (Chilkoti et al., 1991a; Nisol and Reniers, 2015; McArthur, 2006)
 - (d) chemical derivatization methods (Everhart and Reilley, 1981; Gombotz and Hoffman, 1988; Griesser and Chatelier, 1990; Chilkoti et al., 1991a; Pippig et al., 2009)
 - (e) static secondary ion mass spectrometry (SIMS) (Chilkoti et al., 1991b, 1992; Johnston and Ratner, 1996; Delcorte et al., 2015; Bernard et al., 2018; Mishra et al., 2010).

Also, their behaviors and structure in aqueous environments can be characterized using:

- (a) quartz crystal microbalance (QCM) (Askew, 2018)
 - (b) surface plasmon resonance (SPR) (Förch et al., 2005)
 - (c) atomic force microscopy (Hartley et al., 2000).
11. Plasma-treated surfaces are sterile when removed from the reactor, offering an additional advantage for cost-efficient production of medical devices.
 12. New developments in the generation of atmospheric pressure plasmas may permit plasma processing without the need for a vacuum environment (Pappas, 2011).

Although plasma treatments have many advantages, there are concerns with plasma surface modification that should be discussed. First, the chemistry produced on a surface is often ill-defined. For example, if tetrafluoroethylene gas is introduced into the reactor, polytetrafluoroethylene (PTFE) will not be deposited on the surface. Rather, a complex, branched fluorocarbon polymer will be produced with a stoichiometry different from PTFE. This scrambling of monomer structure has been addressed in studies dealing with retention of monomer structure in the final film (Lopez and Ratner, 1991; Lopez et al., 1993; Panchalingam et al., 1993; Shard et al., 2004; Mishra and McArthur, 2010). Second, the apparatus used to produce plasma depositions can be expensive. A good laboratory-scale reactor will cost \$10,000–\$30,000, and a production reactor can cost \$100,000 or more. Third, uniform reaction within tubes and narrow pores can be difficult to achieve. Finally, contamination can be a problem, and care must be exercised to prevent extraneous gases and pump oils from entering the reaction zone. However, the advantages of plasma reactions outweigh these potential disadvantages for many types of modifications that cannot be accomplished by other methods.

The Nature of the Plasma Environment

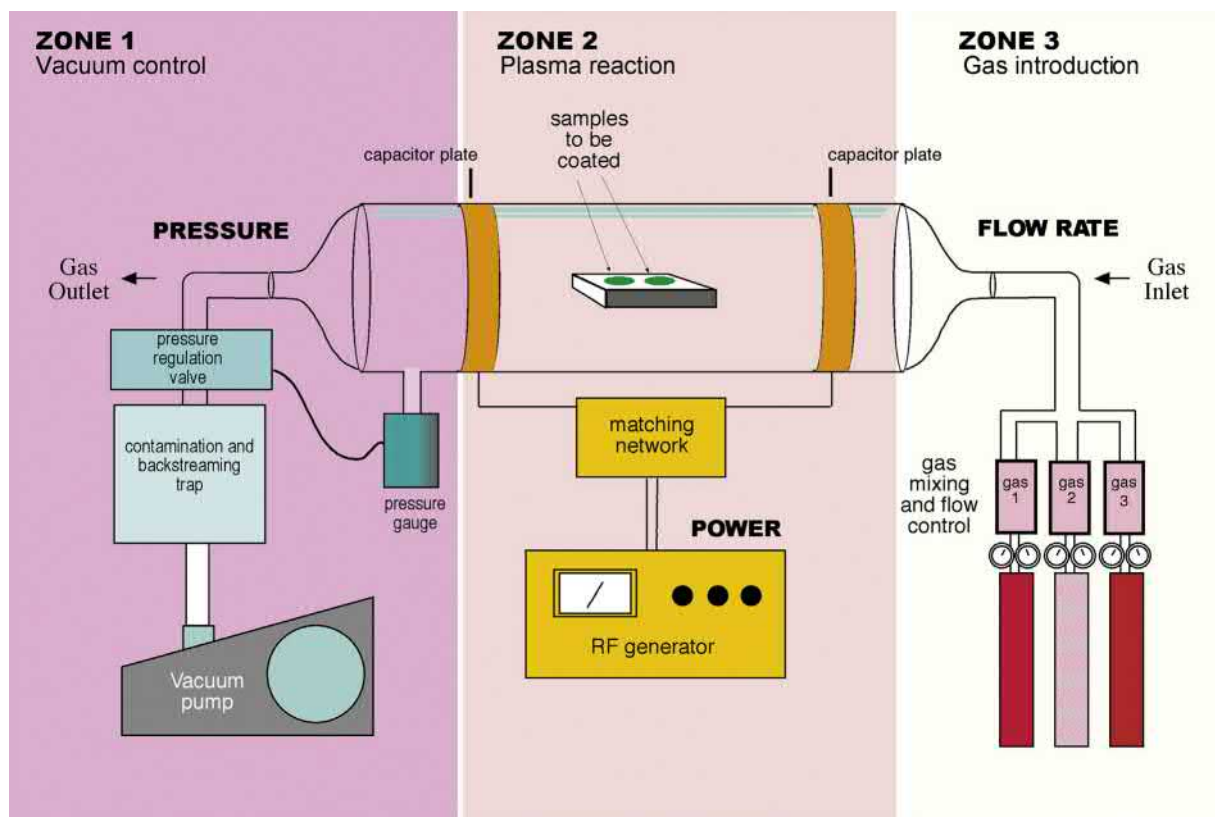
Plasmas are atomically and molecularly dissociated gaseous environments. A plasma environment contains positive ions, negative ions, free radicals, electrons, atoms, molecules, and photons (visible and near UV). Typical conditions within the plasma include an electron energy of 1–10 eV, a gas temperature of 25–60°C, an electron density of 10^{-9} to 10^{-12} /cm³, and an operating pressure of 0.025–1.0 torr.

Many processes can occur on the substrate surface that lead to the observed surface modification or deposition. First, a competition takes place between deposition and etching by the high-energy gaseous species (ablation) (Yasuda, 1979). When ablation is more rapid than deposition, no deposition will be observed. Because of its energetic nature, the ablation or etching process can result in substantial chemical and morphological changes to the substrate.

A number of mechanisms have been postulated for the deposition process. The reactive gaseous environment may create free radical and other reactive species on the substrate surface that react with and polymerize molecules from the gas phase. Alternatively, reactive small molecules in the gas phase could combine to form higher molecular weight units or particulates that may settle or precipitate onto the surface. Most likely, the depositions observed are formed by some combination of these two processes.

The Apparatus to Generate Plasmas for Surface Modification

Many experimental variables relating both to reaction conditions and to the substrate onto which the deposition is placed affect the final outcome of the plasma deposition process. A diagram of a typical capacitively coupled radio frequency plasma reactor is presented in Fig. 1.4.2.3. The major subsystems that comprise this apparatus are a gas introduction system (control of gas mixing, flow rate, and mass of gas entering the reactor), a vacuum system (measurement and control of reactor pressure and inhibition of backstreaming of molecules from the pumps), an energizing system to efficiently couple energy into the gas phase within the reactor, and a reactor zone in which the samples are treated. Radio frequency, acoustic, or microwave energy can be coupled to the gas phase. Devices for monitoring the molecular weight of the gas phase species (mass spectrometers), the optical emission from the glowing plasma (spectrophotometers), and the deposited film thickness (ellipsometers, vibrating quartz crystal microbalances) are also commonly found on plasma reactors. Technology has been developed permitting atmospheric pressure plasma deposition (Klages et al., 2000; Massines et al., 2000; Pappas, 2011). Another important development is “reel-to-reel” (continuous) plasma processing opening the way to low-cost, high-throughput treatment of films, fibers, and tubes. Finally, methods have been developed to assist in the retention of polymer chemical structure during plasma deposition. These methods include using pulsed plasmas



• **Figure 1.4.2.3** A capacitively coupled RF plasma reactor. Reddish colors indicate gas storage and mixing. Yellow colors are components that power the reactor. Zone 1: vacuum system (pressure measurement and control); zone 2: plasma generation and sample placement; zone 3: gas introduction and flow control.

(Panchalingam et al., 1993; Mishra and McArthur, 2010), condensing vapors on a cold stage during the plasma process (Lopez and Ratner, 1991), and using very low plasma powers (Pan et al., 2001; Förch et al., 2005). Such controlled chemistry plasma deposition might be thought of as at some intermediate location on a continuum between the scrambled surface chemistries achieved with conventional plasma deposition of polymers, and the precise graft structures described in the section below titled “Specific Chemical Reactions for Forming Surface Grafts.”

RFGD Plasmas for the Immobilization of Molecules

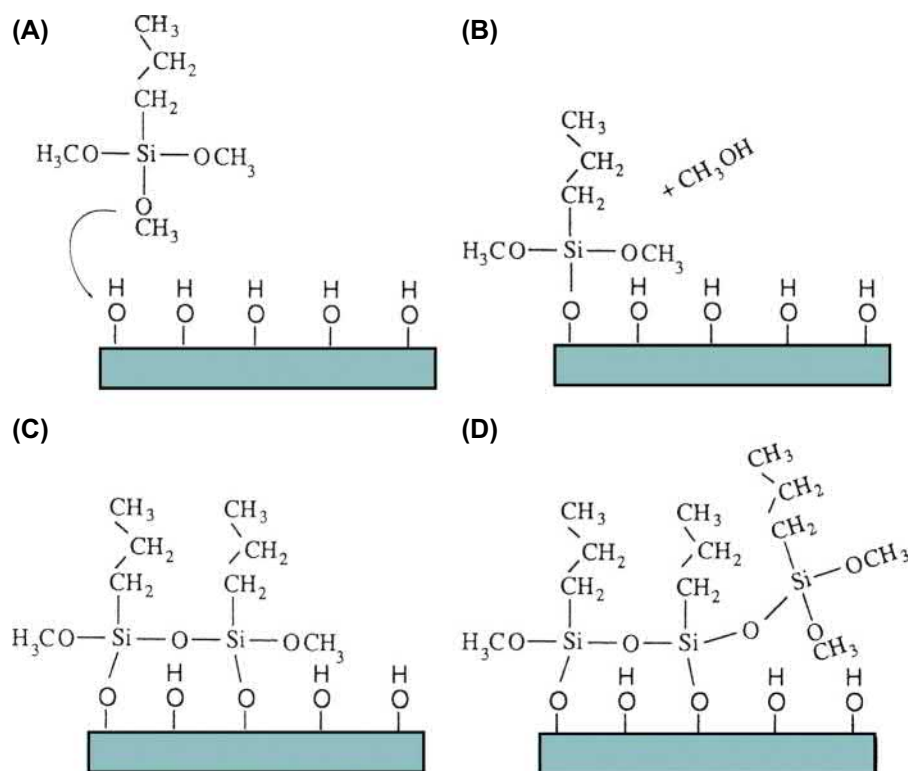
Plasmas have often been used to introduce reactive organic functional groups (e.g., amine, hydroxyl) on a surface that can be activated to attach biomolecules (see Chapter 1.4.4). Certain reactive gas environments can also be used for directly immobilizing organic molecules such as surfactants. For example, a poly(ethylene glycol)-*n*-alkyl surfactant will adsorb to polyethylene (PE) via the hydrophobic alkyl block. If the polyethylene surface with the adsorbed surfactant is briefly exposed to an argon plasma, the *n*-alkyl chains will cross-link to surface atoms of PE, thereby leading to the covalent attachment of pendant poly(ethylene glycol) chains (Sheu et al., 1992).

High-Temperature and High-Energy Plasma Treatments

The plasma environments described above are of relatively low energy and low temperature. Consequently, they can be used to deposit organic layers on polymeric or inorganic substrates. Under higher energy conditions, plasmas can effect unique and important inorganic surface modifications on inorganic substrates. For example, flame-spray deposition involves injecting a high-purity, relatively finely divided (~100 mesh) metal powder into a high-velocity plasma or flame. The melted or partially melted particles impact the surface and rapidly solidify (see Chapter 1.3.3). Examples of plasma thermal spray coating on titanium are seen in Gruner (2001), and Vidigal et al. (2009).

Specific Chemical Reactions for Forming Surface Grafts

Techniques such as radiation grafting and plasma deposition create polymer surface grafts, although the polymeric species are generally highly cross-linked, chemically rearranged, and difficult to characterize. A new generation of polymer reactions permits surface grafts with precision in chain length, control of chain architectures (for example, diblock and triblock units), and minimization of unwanted branching and other side reactions (Zhou et al., 2016; Matyjaszewski et al., 2007; Lego et al., 2009). These polymer reactions applied



• **Figure 1.4.2.4** The chemistry of a typical silane surface modification reaction: (A) a hydroxylated surface is immersed in a solution containing n-propyl trimethoxysilane (nPTMS); (B) one of the methoxy groups of the nPTMS couples with a hydroxyl group releasing methanol; (C) two of the methoxy groups on another molecule of the nPTMS have reacted, one with a hydroxyl group and the other with a methoxy group from the first nPTMS molecule; (D) a third nPTMS molecule has reacted only with a methoxy group. This molecule is tied into the silane film network, but is not directly bound to the surface.

to surface grafting include ATRP (Hucknall et al., 2009; Siegwart et al., 2012), reversible addition-fragmentation chain transfer (RAFT) polymerization (Boyer et al., 2009; Golden et al., 2010), and CLICK chemistry (Fleischmann et al., 2008; Arslan and Tasdelen, 2018; Escorihuela et al., 2015).

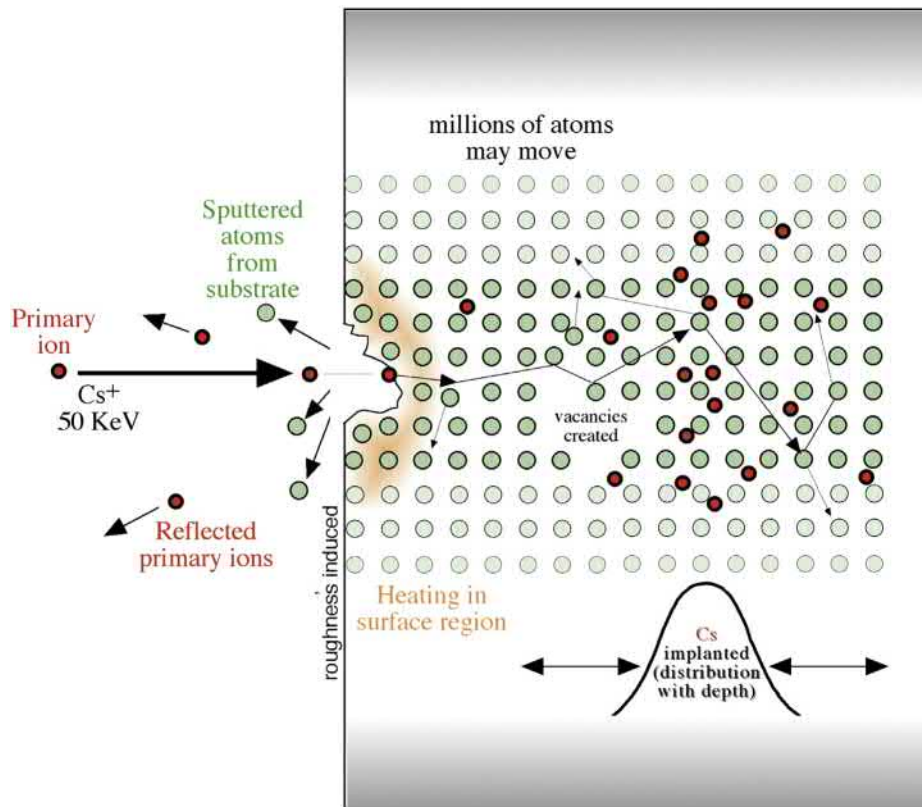
Silanization

Silane treatments of surfaces involve a liquid phase or vapor phase chemical reaction, and are straightforward to perform and of low cost. A typical silane surface modification reaction is illustrated in Fig. 1.4.2.4 (although some details of this reaction have been questioned, see Schlecht and Maurer, 2011). Silane reactions are most often used to modify hydroxylated surfaces. Since glass, silicon, alumina, titania, and quartz surfaces, as well as other metal oxide surfaces, are rich in hydroxyl groups, silanes are particularly useful for modifying these materials. Numerous silane compounds are commercially available, permitting a broad range of chemical functionalities to be incorporated on surfaces (Table 1.4.2.4). The advantages of silane reactions are their simplicity and stability, attributed to their covalent, cross-linked structure. However, the linkage between a silane and a hydroxyl group is also subject to hydrolysis, and film breakdown under some conditions must be considered (Wasserman et al., 1989).

TABLE 1.4.2.4 Silanes for Surface Modification of Biomaterials

X=Leaving Group	X	R=Functional Group
	$\begin{array}{c} \text{X} \\ \\ \text{X} - \text{Si} - \text{R} \\ \\ \text{X} \end{array}$	
-Cl		-(CH ₂) _n CH ₃
-OCH ₃		-(CH ₂) ₃ NH ₂
-OCH ₂ CH ₃		-(CH ₂) ₂ (CF ₂) ₅ CF ₃
		-(CH ₂) ₃ O-C(CH ₃)=CH ₂
		-CH ₂ CH ₂ -C(=O)-C ₆ H ₅

Silanes can form two types of surface film structures. If only surface reaction occurs (perhaps catalyzed by traces of adsorbed surface water), a structure similar to that shown in Fig. 1.4.2.4 can be formed. However, if more water is present, a thicker silane layer can be formed consisting of both Si-O groups bonded to the surface, and silane units participating in a “bulk,” three-dimensional, polymerized



• **Figure 1.4.2.5** Ion impact and implantation considerations with a 50 KeV cesium ion accelerated into a surface.

network. The initial stages in the formation of a thicker silane film are suggested by the further reaction of the group at the right side of Fig. 1.4.2.4D with solution phase silane molecules. Without careful control of silane liquid purity, water, and reaction conditions, thicker silane films can form and be rough and inhomogeneous.

A new class of silane-modified surfaces based upon monolayer silane films and yielding self-assembled, highly ordered structures is of particular interest in the precision engineering of surfaces (Pomerantz et al., 1985; Maoz et al., 1988; Heid et al., 1996; Haensch et al., 2010). These self-assembled monolayers are described in more detail later in this chapter.

Many general reviews and basic science studies on surface silanization are available (Arkles, 1977; Plueddemann, 1980; Rye et al., 1997). Applications for silanized surface-modified biomaterials are on the increase, and include cell attachment (Hickman and Stenger, 1994; Matsuzawa et al., 1997), biomolecule and polymer immobilization (Mao et al., 1997; Xiao et al., 1997), nonfouling surfaces (Lee and Laibinis, 1998), surfaces for DNA studies (Hu et al., 1996), biomineralization (Archibald et al., 1996), and model surfaces for biointeraction studies (Jenny and Anderson, 1999).

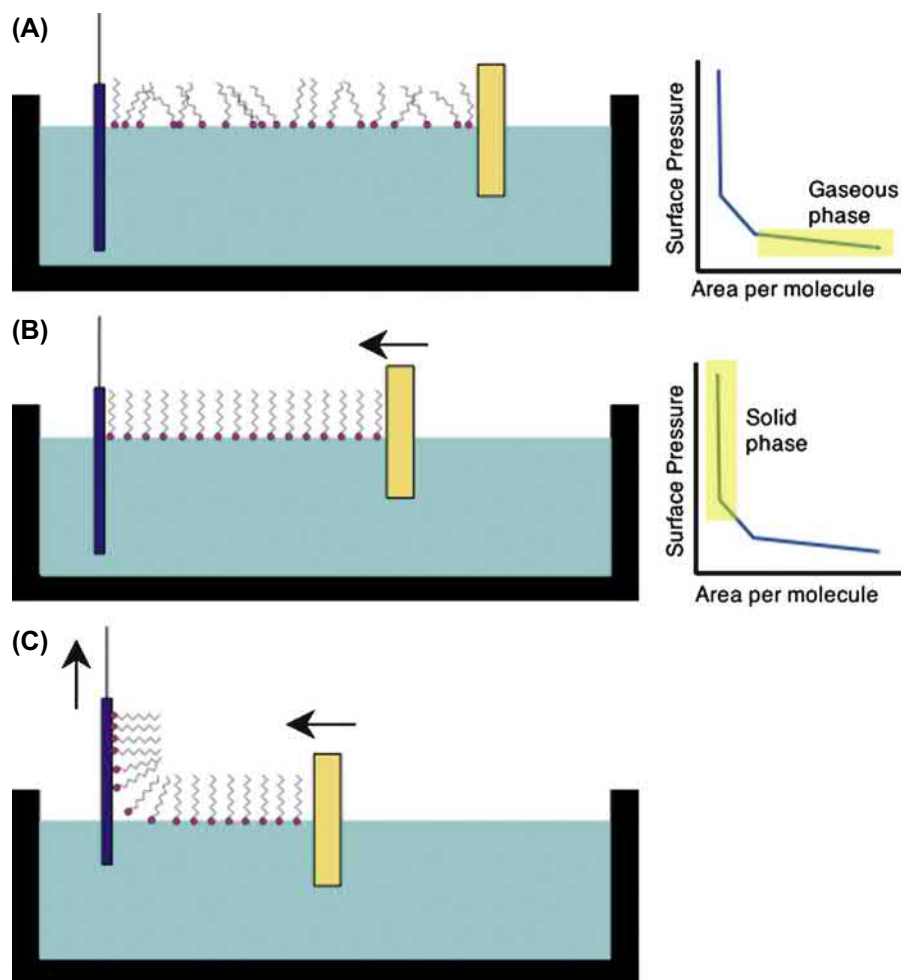
Ion Beam Implantation

The ion beam method injects accelerated ions with energies ranging from 10^1 to 10^6 eV ($1 \text{ eV} = 1.6 \times 10^{-19} \text{ J}$) into the surface zone of a material to alter its properties. It is

largely, but not exclusively, used with metals and other inorganics such as ceramics, glasses, and semiconductors. Ions formed from most of the atoms in the periodic table can be implanted, but not all provide useful modifications to the surface properties. Important potential applications for biomaterial surfaces include modification of hardness (wear), lubricity, toughness, corrosion, conductivity, and bioreactivity.

If an ion with kinetic energy greater than a few electron volts impacts a surface, the probability that it will enter the surface is high. The impact transfers much energy to a localized surface zone in a very short time interval. Some considerations for the ion implantation process are illustrated in Fig. 1.4.2.5. These surface changes must be understood quantitatively for engineering of modified surface characteristics. Many review articles and books are available on ion implantation processes and their application for tailoring surface properties (Picraux and Pope, 1984; Colligon, 1986; Sioshansi, 1987; Nastasi et al., 1996; Rautray et al., 2010).

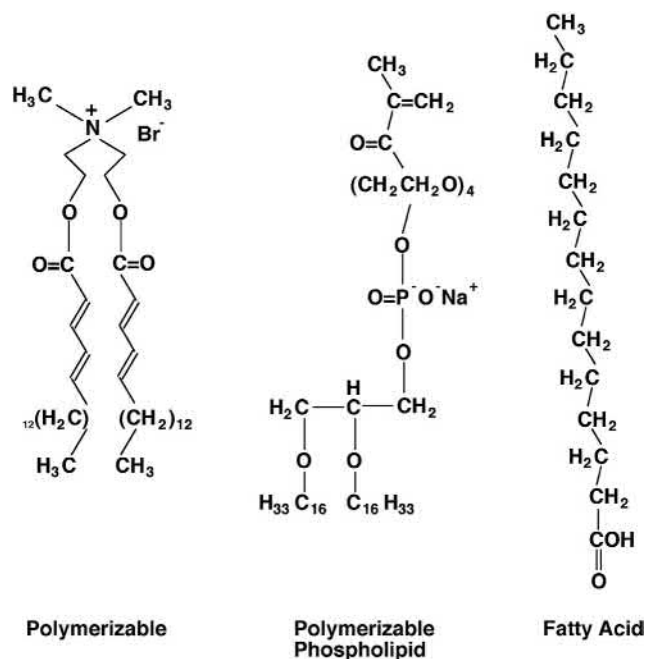
Specific examples of biomaterials that have been surface altered by ion implantation processes are plentiful. Iridium was ion implanted in a Ti-6Al-4V alloy to improve corrosion resistance (Buchanan et al., 1990). Nitrogen implanted into titanium greatly reduces wear (Sioshansi, 1987). The ion implantation of boron and carbon into type 316L stainless steel improves the high cycle fatigue life of these alloys (Sioshansi, 1987). Silver ions implanted into polystyrene permit cell attachment (Tsuji et al., 1998).



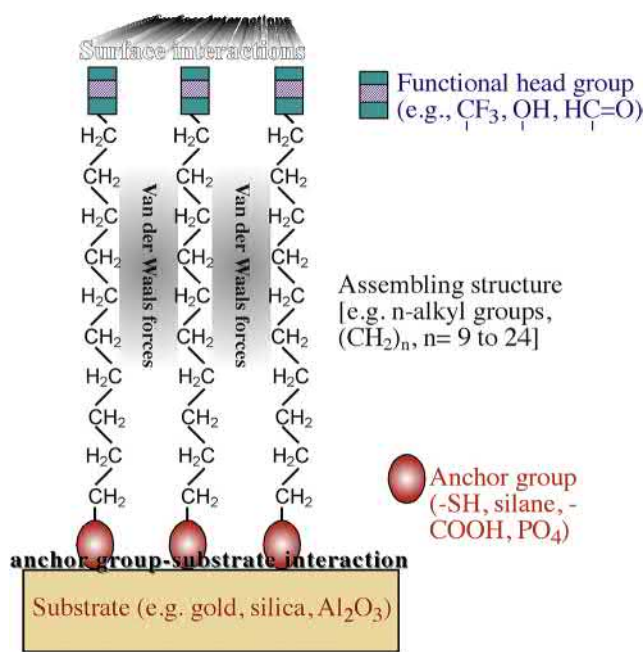
• **Figure 1.4.2.6** Deposition of a lipid film onto a glass slide by the Langmuir–Blodgett method: (A) the lipid film is floated on the aqueous layer; (B) the lipid film is compressed by a moveable barrier; (C) the vertical glass slide is withdrawn while pressure is maintained on the floating lipid film with the moveable barrier.

Langmuir–Blodgett Deposition

The Langmuir–Blodgett (LB) deposition method overcoats a surface with one or more highly ordered layers of surfactant molecules. Each of the molecules that assemble into this layer contains a polar “head” group and a nonpolar “tail” group. The deposition of an LB film using an LB trough is illustrated schematically in Fig. 1.4.2.6. By withdrawing the vertical plate out of the aqueous phase and through the air–water interface (keeping the surface film at the air–water interface compressed at all times, as illustrated in Fig. 1.4.2.6), an assembled structure coats the glass with the hydrophilic tail group contacting the hydrophilic glass surface. By next pushing the plate back down through the air–water interface, another layer can be deposited, this time with the hydrophobic tails of the two layers in contact; dipping in and out with the film at the water surface always compressed permits multilayer structures to be created. Some compounds that form organized LB layers are shown in Fig. 1.4.2.7. Other techniques to create such ordered lipid structures at surfaces include Langmuir–Schaefer transfer and vesicle fusion (Li et al., 2008). The advantages of films deposited on surfaces by this method are their high degree of order and uniformity, and also their resemblance to the lipid



• **Figure 1.4.2.7** Three examples of molecules that form organized Langmuir–Blodgett Films.



• **Figure 1.4.2.8** General characteristics of molecules that form self-assembled monolayers.

bilayer membranes surrounding living cells. Also, since a wide range of chemical structures can form LB films, there are many options for incorporating new chemistries at surfaces. The stability of LB films can be improved by cross-linking or internally polymerizing the molecules after film formation, often through double bonds in the alkyl portion of the chains (Meller et al., 1989). A number of research groups have investigated LB films for biomedical applications (Hayward and Chapman, 1984; Bird et al., 1989; Cho et al., 1990; Heens et al., 1991; Knoll et al., 2008). A cross between silane thin films and LB layers has been developed for biomedical surface modification (Takahara et al., 2000). Many general reviews on these surface structures are available (Knobler, 1990; Ulman, 1991; Park and Advincula, 2011).

Self-Assembled Monolayers

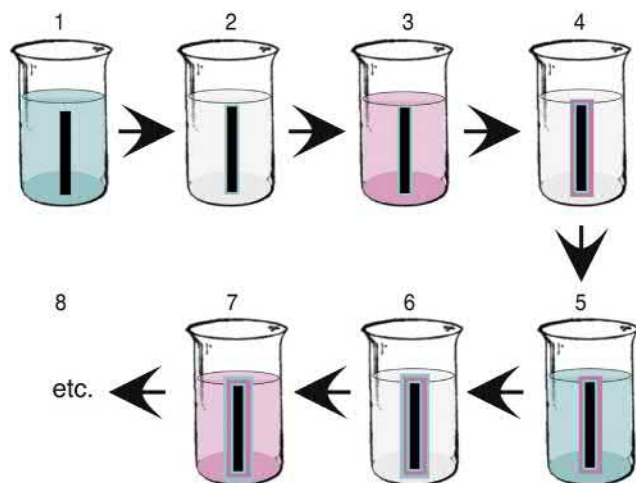
Self-assembled monolayers (SAMs) are surface films that spontaneously form as highly ordered structures (two-dimensional crystals) on specific substrates (Maaz et al., 1988; Ulman, 1990, 1991; Whitesides et al., 1991; Knoll, 1996; Raynor et al., 2009). In some ways SAMs resemble LB films, but there are important differences, in particular their ease of formation. Examples of SAM films include n-alkyl silanes on hydroxylated surfaces (silica, glass, alumina), alkane thiols [e.g., $\text{CH}_3(\text{CH}_2)_n\text{SH}$] and disulfides on coinage metals (gold, silver, copper), amines and alcohols on platinum, carboxylic acids on aluminum oxide, and silver and phosphates (phosphoric acid or phosphonate groups) on titanium or tantalum surfaces. Silane SAMs and thiols on gold are the most commonly used types. Most molecules that form SAMs have the general characteristics illustrated in Fig. 1.4.2.8. Two processes are particularly important for the formation

of SAMs (Ulman, 1991): a moderate-to-strong adsorption of an anchoring chemical group to the surface (typically 30–100 kcal/mol), and van der Waals interaction of the alkyl chains. The bonding to the substrate (chemisorption) provides a driving force to fill every site on the surface, and to displace contaminants from the surface. This process is analogous to the compression to the LB film by the movable barrier in the trough. Once adsorption sites are filled on the surface, the chains will be in sufficiently close proximity so that the weaker van der Waals interactive forces between chains can exert their influence and lead to a crystallization of the alkyl groups. Too few CH_2 groups do not provide sufficient interactive force to stabilize the two-dimensional quasi-crystal and are difficult to assemble. More than 24 CH_2 groups have too many options for defects in the crystal, and are also difficult to assemble. Molecules with lengths between 9 and 24 methylene groups will assemble well. Molecular mobility is an important consideration in this surface crystal formation process, so that: (1) the molecules have sufficient time to maneuver into position for tight packing of the binding end groups at the surface; and (2) the chains can enter the quasi-crystal.

The advantages of SAMs are their ease of formation, their chemical stability (often considerably higher than chemically related LB films), and the many options for changing the outermost group that interfaces with the external environment. Many biomaterials applications have already been suggested for SAMs (Lewandowska et al., 1989; Mrksich and Whitesides, 1996; Ferretti et al., 2000; Raynor et al., 2009). Useful SAMs for creating molecularly engineered functional surfaces include headgroups of ethylene glycol oligomers, biotin, free-radical initiators, N-hydroxysuccinimide esters, ATRP or RAFT chain transfer agents, anhydrides, perfluoro groups, and amines, to list only a small sample of the many possibilities. Although most SAMs are based on n-alkyl chain assembly, SAMs can form from other classes of molecules including peptides, proteins (Sara and Sleytr, 1996), porphyrins, nucleotide bases, and aromatic ring hydrocarbons.

Layer-By-Layer Deposition and Multilayer Polyelectrolyte Deposition

Layer-by-layer (L-b-L) deposition of thin films, and the most common variant of this method, multilayer polyelectrolyte adsorption, has become an important strategy for the surface modification of biomaterials (Decher, 1996; Ariga et al., 2007). For L-b-L surface treatment, a molecule (or polymer or protein) is chosen that adsorbs strong to the substrate (adsorbate 1). Then the substrate is rinsed (retaining adsorbate 1), and dipped in a solution of a molecule that interacts strongly with adsorbate 1 (adsorbate 2). After rinsing, the surface layer is again dipped in a solution of adsorbate 1. Adsorbate 1, adsorbate 2, and the rinsing step are alternated until the coating has the desired multilayer thickness (Fig. 1.4.2.9). Commonly, the substrate has a fixed positive or negative charge, permitting multilayers of polyanions and polycations. The rinse step is important for the removal of any unadsorbed polyions, as well as for removal of

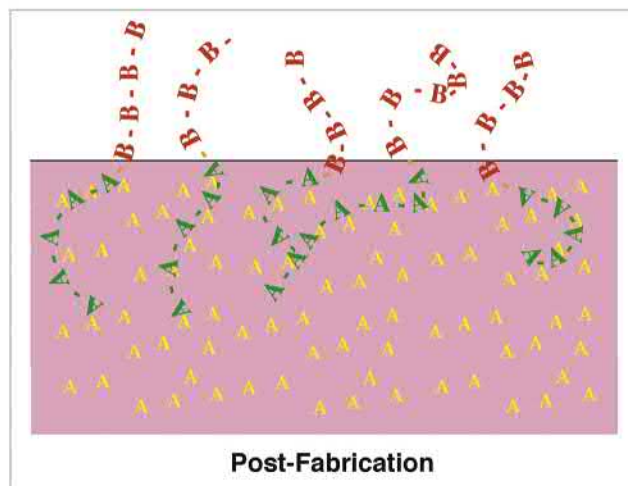
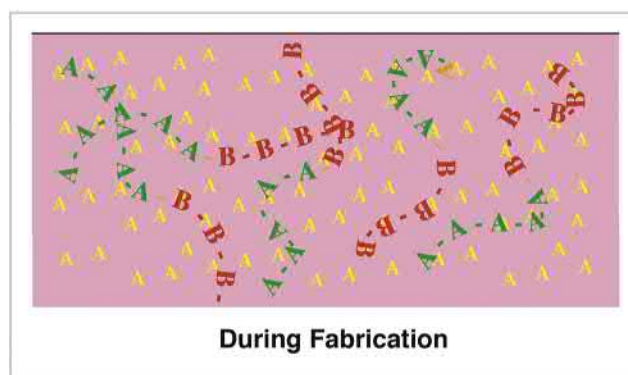


• **Figure 1.4.2.9** Layer-by-layer deposition of a multilayer surface coating. A series of adsorption-rinse steps lead to a multilayer surface deposition: (1) the “blue” compound is adsorbed to the substrate; (2) the adsorbed layer is rinsed in solvent (frequently water) to remove weakly adherent material; (3) the “pink” compound is adsorbed to the blue layer on the substrate; (4) the adsorbed layer is rinsed in solvent to remove weakly adherent material; (5) the “blue” compound is adsorbed to the “pink” adsorbed layer; (6) the adsorbed layer is rinsed in solvent to remove weakly adherent material; (7) the “pink” compound is adsorbed to the blue layer; (8) this process continues to build as many layers as desired.

the counter-ions released upon formation of each layer of the polyion complex. Some surfaces are intrinsically charged (for example, mica), others can be modified with methods already described in this chapter. Once a thin layer of a charged component adsorbs, it will repel additional adsorption of the component of the same charge, thus tightly controlling the layer thickness and uniformity. The outermost layer can be the positively or negatively charged component. This strategy works well with charged biomolecules, for example hyaluronic acid (–) and chitosan (+). Layers formed are durable, and assembly of these multilayer structures is simple. The pH and ionic strength of polyelectrolyte solutions are important process variables. The L-b-L process has been used with interacting layers of proteins, nucleotides, saccharides, nanoparticles, acid–base pairs, and H-bonding pairs. L-b-L has been used to coat surfaces (Hsu et al., 2016), microspheres, nanoparticles (Correa et al., 2016), electrospun scaffolds (Easton et al., 2014) and even living cells (Fukuda et al., 2018; Zeng and Matsusaki, 2019). L-b-L layers can be used as reservoirs to contain drug for release or as rate-limiting diffusion barriers. L-b-L films have been used to treat contact lenses, to improve comfort and retard biofilm build-up.

Surface-Modifying Additives

Specifically designed and synthesized surface-active compositions can be added in low concentrations to a material during fabrication, and will spontaneously rise to and dominate the surface (Ward, 1989; Wen et al., 1997). These surface-modifying additives (SMAs) are well-known for both organic and inorganic systems. A driving force to minimize the interfacial energy leads to the concentration of the SMA at the surface after blending homogeneously with a material. For efficient



• **Figure 1.4.2.10** A block copolymer surface-modifying additive comprised of an “A” block and a “B” block is blended into a support polymer (the bulk) with a composition similar to “A” block. During fabrication, the block copolymer is randomly distributed throughout the support polymer. After curing or annealing, the “A” block anchors the surface-modifying additive into the support, while the low-energy “B” block migrates to the air–polymer interface.

surface concentration, two factors must be considered. First, the magnitude of interfacial energy difference between the system without the additive and the same system with the SMA at the surface will determine the driving force leading to an SMA-dominated surface. Second, the molecular mobility of the bulk material and the SMA additive molecules within the bulk will determine the rate at which the SMA reaches the surface or if it will get there at all. An additional concern is the durability and stability of the SMA at the surface.

A typical SMA designed to alter the surface properties of a polymeric material will be a relatively low-molecular-weight diblock or triblock copolymer (see Chapter 1.3.2). The “A” block will be soluble in, or compatible with, the bulk material into which the SMA is being added. The “B” block will be incompatible with the bulk material and will have lower surface energy. Thus, the A block will anchor the B block into the material to be modified at the interface. This is suggested schematically in Fig. 1.4.2.10. During initial fabrication, the SMA might be distributed uniformly throughout the bulk. After a period for curing or an annealing step, the SMA will migrate to the surface. Low-molecular-weight

endgroups on polymer chains can also provide the driving force to bring the endgroup to the surface.

As an example, an SMA for a polyurethane might have a low-molecular-weight polyurethane “A” block and a poly(dimethyl siloxane) (PDMS) “B” block. The PDMS component on the surface may confer improved blood compatibility to the polyurethane. The “A” block will anchor the SMA in the polyurethane bulk (the polyurethane “A” block should be reasonably compatible with the bulk polyurethane), while the low surface energy, highly flexible, silicone “B” block will be exposed at the air surface to lower the interfacial energy (note that air is “hydrophobic”). The “A” block anchor should confer stability to this system. However, consider that if the system is placed in an aqueous environment, a low surface energy polymer (the “B” block) is now in contact with water—a high interfacial energy situation. If the system, after fabrication, still exhibits sufficient chain mobility, it might phase-invert to bring the bulk polyurethane or the “A” block to the surface. Unless the system is specifically engineered to do such a surface phase reversal, this inversion is undesirable. Proper choice of the bulk polymer and the “A” block can impede surface phase inversion.

An example of a polymer additive that was developed by 3M specifically to take advantage of this surface chemical inversion phenomenon is a stain inhibitor for fabric. Although not intended as a biomaterial, it illustrates design principles for this type of system. The compound has three “arms.” A fluoropolymer arm, the lowest energy component, resides at the fabric surface in air. Fluoropolymers and hydrocarbons (typical stains) do not mix, so hydrocarbons are repelled. A second arm of hydrophilic poly(ethylene oxide) will come to the surface in water, and assist with the washing out of any material on the surface. Finally, a third arm of hydrocarbon anchors this additive into the fabric.

Many SMAs for inorganic systems are known. For example, very small quantities of nickel will completely alter the structure of a silicon (111) surface (Wilson and Chiang, 1987). Copper or silver will accumulate at the surface of gold alloys (Tanaka et al., 1988). Also, in stainless steels, chromium will concentrate (as the oxide) at the surface, imparting corrosion resistance.

There are a number of additives that spontaneously surface-concentrate, but are not necessarily designed as SMAs. A few examples for polymers include PDMS, some extrusion lubricants (Ratner, 1983), and some UV stabilizers (Tyler et al., 1992). The presence of such additives at the surface of a polymer may be unplanned, and they will not necessarily form stable, durable surface layers. However, they can significantly contribute (either positively or negatively) to the bioresponse to the surface.

Conversion Coatings

Conversion coatings modify the surface of a metal into a dense oxide-rich layer that imparts corrosion protection (Sørensen et al., 2009), enhanced adhesivity, altered appearance (e.g., color), and sometimes lubricity to the metal. For

example, steel is frequently phosphated (treated with phosphoric acid) or chromated (treated with chromic acid). Aluminum is electrochemically anodized in chromic, oxalic, or sulfuric acid electrolytes. Electrochemical anodization may also be useful for surface modifying titanium and Ti–Al alloys (Kasemo and Lausmaa, 1985; Bardos, 1990).

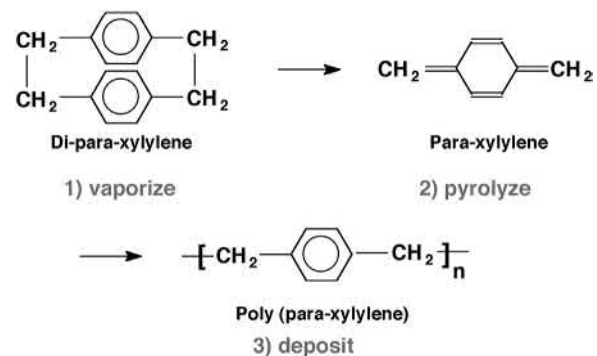
The conversion of metallic surfaces to “oxide-like,” electrochemically passive states is a common practice for base metal alloy systems used as biomaterials. Standard and recommended techniques have been published (e.g., ASTM F4-86), and are relevant for most musculoskeletal load-bearing surgical implant devices. The background literature supporting these surface passivation technologies has been summarized (von Recum, 1986).

Base metal alloy systems, in general, are subject to electrochemical corrosion ($M \rightarrow M^+ + e^-$) within saline environments. The rate of this corrosion process is reduced 10^3 – 10^6 times by the presence of a dense, uniform, minimally conductive, relatively inert oxide surface. For many metallic devices, exposure to a mineral acid (e.g., nitric acid in water) for times up to 30 min will provide a passivated surface. Plasma-enhanced surface passivation of metals, laser surface treatments, and mechanical treatments (e.g., “shot peening”) can also impart many of these characteristics to metallic systems.

The reason that many of these surface modifications are called “oxide-like” is that the structure is complex, including OH, H, and subgroups that may or may not be crystalline. Since most passive surfaces are thin films (5–500 nm), and are transparent or metallic in color, the surface appears similar before and after passivation. Further details on surfaces of this type can be found in Chapters 1.2.4, 1.3.2E and 2.4.4.

Parylene Coating

Parylene (para-xylylene) coatings occupy a unique niche in the surface modification literature, because of their wide application to biomedical devices and the good quality of the thin-film coatings formed (Loeb et al., 1977a; Nichols et al., 1984; Kim and Meng, 2016). The deposition method is also unique and involves the simultaneous evaporation, pyrolysis, deposition, and polymerization of the monomer, di-para-xylylene (DPX), according to the following reaction:



The DPX monomer is vaporized at 175°C and 1 torr, pyrolyzed at 700°C and 0.5 torr, and finally deposited on a substrate at 25°C and 0.1 torr. The coating has excellent

electrical insulation and moisture barrier properties, and has been used for protection of implant electrodes (Loeb et al., 1977b; Nichols et al., 1984) and implanted electronic circuitry (Spivack and Ferrante, 1969). A parylene coating has been used on stainless steel cardiovascular stents between the metal and a drug-eluting polymer layer (see Chapter 2.5.2B).

Laser Methods

Lasers can rapidly and specifically induce surface changes (roughness, crystallinity, chemistry) in organic and inorganic materials (Picraux and Pope, 1984; Dekumbis, 1987; Chrisey et al., 2003). The advantages of using lasers for such modifications are precise control of the frequency of the light, the wide range of frequencies available, the high energy density, the ability to focus and raster the light, the possibilities for using both heat and specific excitation to effect change, and the ability to pulse the source and control reaction time. Lasers commonly used for surface modification include ruby, neodymium:yttrium aluminum garnet (Nd:YAG), argon, argon-fluoride excimer, and CO₂. Treatments are pulsed (nanosecond to picoseconds pulse times) and continuous wave (CW), with interaction times often less than 1 ms. Laser-induced surface alterations include annealing, etching, deposition, and polymerization. Polymers, metals, ceramics, and even tooth dentin have been effectively surface modified using laser energy. The major considerations in designing a laser surface treatment include the absorption (coupling) between the laser energy and the material, the penetration depth of the laser energy into the material, the interfacial reflection and scattering, and heating induced by the laser.

Hundreds of papers have been published on laser surface modification. Examples include: (1) an Nd:YAG laser was used to treat titanium implants permitting improved hydroxyapatite nucleation and more rapid integration into bone (Faeda et al., 2009); (2) laser irradiation at 810 nm of silicone rubber induced a “lotus leaf-like” texture that imparted superhydrophobic properties to the silicone polymer (Yoon et al., 2008); (3) excimer laser irradiation at 193 nm permitted fine spatial patterning of polystyrene for improved protein adsorption and cell interactions (Pfleger et al., 2009).

Patterning

Essentially all of the surface modification methods described in this chapter can be applied to biomaterial surfaces, either as a uniform surface treatment or as patterns on the surface with length scales of millimeters, microns, or even nanometers. There are many options to pattern biomaterial surfaces. These include ion beam etching, electron beam lithography, laser methods, inkjet printers, and stochastic patterns made by phase separation of two components (Takahara et al., 2000). Chapter 1.4.5 elaborates on methods to pattern biomaterials.

Conclusions

Surface modifications are widely applied to modulate or enhance the biointeractions of biomedical devices and improve other aspects of performance. Surface modification is used in the laboratory setting, and also for the treatment of medical devices used in the clinic. Since a medical device may already have appropriate physical properties and be well-understood in the clinic, surface modification provides a means to alter only the biointeractions of the device without the need for redesign, retooling for manufacture, and retraining of medical personnel.

References

- Archibald, D.D., Qadri, S.B., Gaber, B.P., 1996. Modified calcite deposition due to ultrathin organic films on silicon substrates. *Langmuir* 12, 538–546.
- Ariga, K., Hill, J.P., Ji, Q., 2007. Layer-by-layer assembly as a versatile bottom-up nanofabrication technique for exploratory research and realistic application. *Phys. Chem. Chem. Phys.* 9 (19), 2319–2340.
- Arkles, B., 1977. Tailoring surfaces with silanes. *Chemtech* 7, 766–778.
- Arslan, M., Tasdelen, M.A., 2018. Click chemistry in macromolecular design: complex architectures from functional polymers. *Chem. Afr.* <https://doi.org/10.1007/s42250-018-0030-8>.
- Askwew, H.J., Jarvis, K.L., McArthur, S.L., 2018. Multitechnique investigation into the aqueous behavior of plasma polymers. *Bio-interphases* 13 (6), 06E410.
- Bardos, D.L., 1990. Titanium and titanium alloys. In: Williams, E., Cahn, R.W., Bever, M.B. (Eds.), *Concise Encyclopedia of Medical and Dental Materials*, first ed. Pergamon Press, Oxford, UK, pp. 360–365.
- Bernard, L., Rupper, P., Faccio, G., Hegemann, D., Scholder, O., Heuberger, M., Maniura-Weber, K., Vandenbossche, M., 2018. Plasma polymer film designs through the eyes of ToF-SIMS. *Bio-interphases* 13 (3), 03B417.
- Bird, R.R., Hall, B., Hobbs, K.E.F., Chapman, D., 1989. New haemocompatible polymers assessed by thrombelastography. *J. Biomed. Eng.* 11, 231–234.
- Boyer, C., Bulmus, V., Davis, T., Ladmiral, V., Liu, J., et al., 2009. Bioapplications of RAFT polymerization. *Chem. Rev.* 109, 5402–5436.
- Buchanan, R.A., Lee, I.S., Williams, J.M., 1990. Surface modification of biomaterials through noble metal ion implantation. *J. Biomed. Mater. Res.* 24, 309–318.
- Chapiro, A., 1983. Radiation grafting of hydrogels to improve the thrombo-resistance of polymers. *Eur. Polym. J.* 19, 859–861.
- Charlson, E.J., Charlson, E.M., Sharma, A.K., Yasuda, H.K., 1984. Electrical properties of glow-discharge polymers, parylenes, and composite films. *J. Appl. Polym. Sci. Appl. Polym. Symp.* 38, 137–148.
- Chiang, Y.C., Chang, Y., Higuchi, A., Chen, W.Y., Ruaan, R.C., 2009. Sulfobetaine-grafted poly (vinylidene fluoride) ultrafiltration membranes exhibit excellent antifouling property. *J. Membr. Sci.* 339 (1), 151–159.
- Chilkoti, A., Ratner, B.D., Briggs, D., 1991a. Plasma-deposited polymeric films prepared from carbonyl-containing volatile precursors: XPS chemical derivatization and static SIMS surface characterization. *Chem. Mater.* 3, 51–61.

- Chilkoti, A., Ratner, B.D., Briggs, D., 1991b. A static secondary ion mass spectrometric investigation of the surface structure of organic plasma-deposited films prepared from stable isotope-labeled precursors. Part I. Carbonyl precursors. *Anal. Chem.* 63, 1612–1620.
- Chilkoti, A., Ratner, B.D., Briggs, D., Reich, F., 1992. Static secondary ion mass spectrometry of organic plasma deposited films created from stable isotope-labeled precursors. Part II. Mixtures of acetone and oxygen. *J. Polym. Sci. Polym. Chem. Ed.* 30, 1261–1278.
- Cho, C.S., Takayama, T., Kunou, M., Akaike, T., 1990. Platelet adhesion onto the Langmuir–Blodgett film of poly(γ -benzyl L-glutamate)-poly(ethylene oxide)-poly(γ -benzyl L-glutamate) block copolymer. *J. Biomed. Mater. Res.* 24, 1369–1375.
- Chrisey, D.B., Piqué, A., McGill, R.A., Horowitz, J.S., Ringeisen, B.R., et al., 2003. Laser deposition of polymer and biomaterial films. *Chem. Rev.* 103, 553–576.
- Chu, P.K., Chen, J.Y., Wang, L.P., Huang, N., 2002. Plasma surface modification of biomaterials. *Mater. Sci. Eng. Rep.* 36, 143–206.
- Colligon, J.S., 1986. Surface modification by ion beams. *Vacuum* 36, 413–418.
- Cometa, S., Chiellini, F., Bartolozzi, I., Chiellini, E., De Giglio, E., et al., 2010. Surface segregation assessment in poly(ϵ -caprolactone)-poly(ethylene glycol) multiblock copolymer films. *Macromol. Biosci.* 10 (3), 317–327.
- Correa S., Choi K.Y., Dreaden E.C., Renggli K., Shi A., Gu L., Shopowitz K.E., Quadir M.A., Ben-Akiva E., Hammond P.T., 2016. Highly Scalable, Closed-Loop Synthesis of Drug-Loaded, Layer-by-Layer Nanoparticles. *Advanced Functional Materials.* 26(7), 991–1003. <https://doi.org/10.1002/adfm.201504385>.
- Dargaville, T.R., George, G.A., Hill, D.J.T., Whittaker, A.K., 2003. High energy radiation grafting of fluoropolymers. *Prog. Polym. Sci.* 28, 1355–1376.
- Decher, G., 1996. Layered nanoarchitectures via directed assembly of anionic and cationic molecules. In: Sauvage, J.-P., Hosseini, M.W. (Eds.), *Comprehensive Supramolecular Chemistry Templating, Self-Assembly and Self-Organization*, vol. 9. Pergamon Press, Oxford, UK, pp. 507–528.
- Dekumbis, R., 1987. Surface treatment of materials by lasers. *Chem. Eng. Prog.* 83, 23–29.
- Delcorte, A., Cristaudo, V., Zarshenas, M., Merche, D., Reniers, F., Bertrand, P., 2015. Chemical analysis of plasma-treated organic surfaces and plasma polymers by secondary ion mass spectrometry. *Plasma Process. Polym.* 12 (9), 905–918.
- Deng, J., Wang, L., Liu, L., Yang, W., 2009. Developments and new applications of UV-induced surface graft polymerizations. *Prog. Polym. Sci.* 34 (2), 156–193.
- Desmet, T., Morent, R., Geyter, N.D., Leys, C., Schacht, E., et al., 2009. Nonthermal plasma technology as a versatile strategy for polymeric biomaterials surface modification: a review. *Biomacromolecules* 10 (9), 2351–2378.
- Dunkirk, S.G., Gregg, S.L., Duran, L.W., Monfils, J.D., Haapala, J.E., et al., 1991. Photochemical coatings for the prevention of bacterial colonization. *J. Biomater. Appl.* 6 (2), 131–156.
- Easton, C.D., Bullock, A.J., Gigliobianco, G., McArthur, S.L., MacNeil, S., 2014. Application of layer-by-layer coatings to tissue scaffolds – development of an angiogenic biomaterial. *J. Mater. Chem. B* 2 (34), 5558–5568.
- Escorihuela, J., Marcelis, A.T.M., Zuilhof, H., 2015. Metal-free click chemistry reactions on surfaces. *Adv. Mater. Interfaces* 2, 1500135.
- Everhart, D.S., Reilley, C.N., 1981. Chemical derivatization in electron spectroscopy for chemical analysis of surface functional groups introduced on low-density polyethylene film. *Anal. Chem.* 53, 665–676.
- Faeda, R.S., Tavares, H.S., Sartori, R., Guastaldi, A.C., Marcantonio, E., 2009. Biological performance of chemical hydroxyapatite coating associated with implant surface modification by laser beam: biomechanical study in rabbit tibias. *J. Oral Maxillofac. Surg.* 67 (8), 1706–1715.
- Ferretti, S., Paynter, S., Russell, D.A., Sapsford, K.E., 2000. Self-assembled monolayers: a versatile tool for the formulation of bio-surfaces. *Trends Anal. Chem.* 19 (9), 530–540.
- Filler, M.A., Bent, S.F., 2003. The surface as molecular reagent: organic chemistry at the semiconductor interface. *Prog. Surf. Sci.* 73, 1–56.
- Fleischmann, S., Hinrichs, K., Oertel, U., Reichelt, S., Eichhorn, K.J., et al., 2008. Modification of polymer surfaces by click chemistry. *Macromol. Rapid Commun.* 29 (12–13), 1177–1185.
- Förch, R., Zhang, Z., Knoll, W., 2005. Soft plasma treated surfaces: tailoring of structure and properties for biomaterial applications. *Plasma Process. Polym.* 2 (5), 351–372.
- Fukuda, Y., Akagi, T., Asaoka, T., Eguchi, H., Sasaki, K., Iwagami, Y., Yamada, D., Noda, T., Kawamoto, K., Gotoh, K., Kobayashi, S., Mori, M., Doki, Y., Akashi, M., 2018. Layer-by-layer cell coating technique using extracellular matrix facilitates rapid fabrication and function of pancreatic beta-cell spheroids. *Biomaterials* 160, 82–91.
- Garbassi, F., Morra, M., Occhiello, E., Barino, L., Scordamaglia, R., 1989. Dynamics of macromolecules: a challenge for surface analysis. *Surf. Interface Anal.* 14, 585–589.
- Golden, A.L., Battrell, C.F., Pennell, S., Hoffman, A.S., Lai, J.J., et al., 2010. Simple fluidic system for purifying and concentrating diagnostic biomarkers using stimuli-responsive antibody conjugates and membranes. *Bioconjug. Chem.* 21, 1820–1826.
- Gombotz, W.R., Hoffman, A.S., 1988. Functionalization of polymeric films by plasma polymerization of allyl alcohol and allylamine. *J. Appl. Polym. Sci. Appl. Polym. Symp.* 42, 285–303.
- Greer, R.T., Knoll, R.L., Vale, B.H., 1979. Evaluation of tissue-response to hydrogel composite materials. *SEM* 2, 871–878.
- Griesser, H.J., Chatelier, R.C., 1990. Surface characterization of plasma polymers from amine, amide and alcohol monomers. *J. Appl. Polym. Sci. Appl. Polym. Symp.* 46, 361–384.
- Gruner, H., 2001. Thermal spray coating on titanium. In: Brunette, D.M., Tengvall, P., Textor, M., Thomsen, P. (Eds.), *Titanium in Medicine*. Springer-Verlag, Berlin.
- Haensch, C., Hoepfner, S., Schubert, U.S., 2010. Chemical modification of self-assembled silane based monolayers by surface reactions. *Chem. Soc. Rev.* 39 (6), 2323–2334.
- Haque, Y., Ratner, B.D., 1988. Role of negative ions in the RF plasma deposition of fluoropolymer films from perfluoropropane. *J. Polym. Sci. Polym. Phys. Ed.* 26, 1237–1249.
- Hartley, P.G., Thissen, H., Vaithianathan, T., Greisser, H.J., 2000. A surface masking technique for the determination of plasma polymer film thickness by AFM. *Plasma Polym.* 5, 47–60.
- Hayward, J.A., Chapman, D., 1984. Biomembrane surfaces as models for polymer design: the potential for haemocompatibility. *Biomaterials* 5, 135–142.
- Heens, B., Gregoire, C., Pireaux, J.J., Cornelio, P.A., Gardella Jr., J.A., 1991. On the stability and homogeneity of Langmuir–Blodgett films as models of polymers and biological materials for surface studies: an XPS study. *Appl. Surf. Sci.* 47, 163–172.
- Heid, S., Effenberger, F., Bierbaum, K., Grunze, M., 1996. Self-assembled mono- and multilayers of terminally functionalized organosilyl compounds on silicon substrates. *Langmuir* 12 (8), 2118–2120.

- Hendricks, S.K., Kwok, C., Shen, M., Horbett, T.A., Ratner, B.D., et al., 2000. Plasma-deposited membranes for controlled release of antibiotic to prevent bacterial adhesion and biofilm formation. *J. Biomed. Mater. Res.* 50 (2), 160–170.
- Hickman, J.J., Stenger, D.A., 1994. Interactions of cultured neurons with defined surfaces. In: Stenger, D.A., Mckenna, T.N. (Eds.), *Enabling Technologies for Cultured Neural Networks*. Academic Press, San Diego, CA, pp. 51–76.
- Hoffman, A.S., 1981. A review of the use of radiation plus chemical and biochemical processing treatments to prepare novel biomaterials. *Radiat. Phys. Chem.* 18, 323–342.
- Hoffman, A.S., 1988. Biomedical applications of plasma gas discharge processes. *J. Appl. Polym. Sci. Appl. Polym. Symp.* 42, 251–267.
- Hoffman, A.S., Schmer, G., Harris, C., Kraft, W.G., 1972. Covalent binding of biomolecules to radiation-grafted hydrogels on inert polymer surfaces. *Trans. Am. Soc. Artif. Intern. Organs* 18, 10–17.
- Hoffman, A.S., Cohn, D.C., Hanson, S.R., Harker, L.A., Horbett, T.A., et al., 1983. Application of radiation-grafted hydrogels as blood-contacting biomaterials. *Radiat. Phys. Chem.* 22, 267–283.
- Horbett, T.A., Hoffman, A.S., 1975. Bovine plasma protein adsorption on radiation-grafted hydrogels based on hydroxyethyl methacrylate and N-vinyl-pyrrolidone. In: Baier, R.E. (Ed.), *Applied Chemistry at Protein Interfaces, Advances in Chemistry Series*. American Chemical Society, Washington, DC, pp. 230–254.
- Hsu, B.B., Hagerman, S.R., Hammond, P.T., 2016. Rapid and efficient sprayed multilayer films for controlled drug delivery. *J. Appl. Polym. Sci.* 133 (25).
- Hu, J., Wang, M., Weier, U.G., Frantz, P., Kolbe, W., et al., 1996. Imaging of single extended DNA molecules on flat (aminopropyl)triethoxysilane-mica by atomic force microscopy. *Langmuir* 12 (7), 1697–1700.
- Hucknall, A., Simick, A.J., Hill, R.T., Chilkoti, A., Garcia, A., et al., 2009. Versatile synthesis and micropatterning of nonfouling polymer brushes on the wafer scale. *Biointerphases* 4 (2), FA50–FA57.
- Inagaki, N., Nakanishi, T., Katsuura, K., 1983. Glow discharge polymerizations of tetrafluoroethylene, perfluoromethylcyclohexane and perfluorotoluene investigated by infrared spectroscopy and ESCA. *Polym. Bull.* 9, 502–506.
- Jenney, C.R., Anderson, J.M., 1999. Alkylsilane-modified surfaces: inhibition of human macrophage adhesion and foreign body giant cell formation. *J. Biomed. Mater. Res.* 46, 11–21.
- Johnston, E.E., Ratner, B.D., 1996. XPS and SSIMS characterization of surfaces modified by plasma deposited oligo(glyme) films. In: Ratner, B.D., Castner, D.G. (Eds.), *Surface Modification of Polymeric Biomaterials*. Plenum Press, New York, NY, pp. 35–44.
- Kaplan, S., Dilks, A., 1981. A solid state nuclear magnetic resonance investigation of plasma-polymerized hydrocarbons. *Thin Solid Films* 84, 419–424.
- Kasemo, B., Lausmaa, J., 1985. Metal selection and surface characteristics. In: Branemark, P.I., Zarb, G.A., Albrektsson, T. (Eds.), *Tissue-Integrated Prostheses*. Quintessence Publishing, Chicago, IL, pp. 99–116.
- Kim, B.J., Meng, E., 2016. Micromachining of parylene C for bioMEMS. *Polym. Adv. Technol.* 27 (5), 564–576.
- Kitching, K.J., Pan, V., Ratner, B.D., 2003. Biomedical applications of plasma-deposited thin films. In: Biederman, H. (Ed.), *Plasma Polymer Films*. Imperial College Press, London, UK.
- Klages, C.-P., Höpfner, K., Kläke, N., 2000. Surface functionalization at atmospheric pressure by dbd-based pulsed plasma polymerization. *Plasma Polym.* 5, 79–89.
- Knobler, C.M., 1990. Recent developments in the study of monolayers at the air–water interface. *Adv. Chem. Phys.* 77, 397–449.
- Knoll, W., 1996. Self-assembled microstructures at interfaces. *Curr. Opin. Colloid Interface Sci.* 1, 137–143.
- Knoll, W., Naumann, R., Friedrich, M., Robertson, J., Lösche, M., et al., 2008. Solid supported lipid membranes: new concepts for the biomimetic functionalization of solid surfaces. *Biointerphases* 3 (2), FA125–FA135.
- Krishnamurthy, V., Kamel, I.L., Wei, Y., 1989. Analysis of plasma polymerization of allylamine by FTIR. *J. Polym. Sci. Polym. Chem. Ed.* 27, 1211–1224.
- Kwon, O.H., Kikuchi, A., Yamato, M., Sakuri, Y., Okano, T., 2000. Rapid cell sheet detachment from poly(n-isopropylacrylamide)-grafted porous cell culture membranes. *J. Biomed. Mater. Res.* 50, 82–89.
- Lee, S.-W., Laibinis, P.E., 1998. Protein-resistant coatings for glass and metal oxide surfaces derived from oligo(ethylene glycol)-terminated alkytrichlorosilane. *Biomaterials* 19, 1669–1675.
- Lego, B., Francois, M., Skene, W.G., Giasson, S., 2009. Polymer brush covalently attached to OH-functionalized mica surface via surface-initiated ATRP: control of grafting density and polymer chain length. *Langmuir* 25 (9), 5313–5321.
- Lewandowska, K., Balachander, N., Sukenik, C.N., Culp, L.A., 1989. Modulation of fibronectin adhesive functions for fibroblasts and neural cells by chemically derivatized substrata. *J. Cell. Physiol.* 141, 334–345.
- Li, M., Chen, M., Sheepwash, E., Brosseau, C.L., Li, H., et al., 2008. AFM studies of solid-supported lipid bilayers formed at an Au (111) electrode surface using vesicle fusion and a combination of Langmuir–Blodgett and Langmuir–Schaefer techniques. *Langmuir* 24 (18), 10313–10323.
- Loeb, G.E., Bak, M.J., Salzman, M., Schmidt, E.M., 1977a. Parylene as a chronically stable, reproducible microelectrode insulator. *IEEE Trans. Biomed. Eng.* 24, 121–128.
- Loeb, G.E., Walker, A.E., Uematsu, S., Konigsmark, B.W., 1977b. Histological reaction to various conductive and dielectric films chronically implanted in the subdural space. *J. Biomed. Mater. Res.* 11, 195–210.
- Lopez, G.P., Ratner, B.D., 1991. Substrate temperature effects of film chemistry in plasma deposition of organics. I. Nonpolymerizable precursors. *Langmuir* 7, 766–773.
- Lopez, G.P., Ratner, B.D., Rapoza, R.J., Horbett, T.A., 1993. Plasma deposition of ultrathin films of poly(2-hydroxyethyl methacrylate): surface analysis and protein adsorption measurements. *Macromolecules* 26, 3247–3253.
- Luk, J.Z., Cooper-White J., Rintoul L., Taran E., & Grondahl L. 2013. Functionalised polycaprolactone films and 3D scaffolds via gamma irradiation-induced grafting. *Journal of Materials Chemistry B* 1(33), 4171–4181. <https://doi.org/10.1039/c3tb20267d>.
- Luk, J.Z., Cork, J., Cooper-White, J., Grondahl, L., 2015. Use of two-step grafting to fabricate dual-functional films and site-specific functionalized scaffolds. *Langmuir* 31 (5), 1746–1754.
- Ma, Z., Mao, Z., Gao, C., 2007. Surface modification and property analysis of biomedical polymers used for tissue engineering. *Colloids Surfaces B Biointerphases* 60 (2), 137–157.
- Mao, G., Castner, D.G., Grainger, D.W., 1997. Polymer immobilization to alkylchlorosilane organic monolayer films using sequential derivatization reactions. *Chem. Mater.* 9 (8), 1741–1750.
- Maoz, R., Netzer, L., Gun, J., Sagiv, J., 1988. Self-assembling monolayers in the construction of planned supramolecular structures and as modifiers of surface properties. *J. Chim. Phys.* 85, 1059–1064.
- Massines, F., Gherardi, N., Sommer, F., 2000. Silane-based coatings of polypropylene, deposited by atmospheric pressure glow discharge plasmas. *Plasma Polym.* 5, 151–172.
- Matsuda, T., Inoue, K., 1990. Novel photoreactive surface modification technology for fabricated devices. *Trans. Am. Soc. Artif. Intern. Organs* 36, M161–M164.

- Matsuzawa, M., Umemura, K., Beyer, D., Sugioka, K., Knoll, W., 1997. Micropatterning of neurons using organic substrates in culture. *Thin Solid Films* 305, 74–79.
- Matyjaszewski, K., Dong, H., Jakubowski, W., Pietrasik, J., Kusumo, A., 2007. Grafting from surfaces for “everyone”: ARGET ATRP in the presence of air. *Langmuir* 23 (8), 4528–4531.
- McArthur, S.L., 2006. Applications of XPS in bioengineering. *Surf. Interface Anal.* 38 (11), 1380–1385.
- Meller, P., Peters, R., Ringsdorf, H., 1989. Microstructure and lateral diffusion in monolayers of polymerizable amphiphiles. *Colloid Polym. Sci.* 267, 97–107.
- Mishra, G., Easton, C.D., McArthur, S.L., 2010. Physical vs photolithographic patterning of plasma polymers: an investigation by ToF-SSIMS and multivariate analysis. *Langmuir* 26 (5), 3720–3730.
- Mishra, G., McArthur, S.L., 2010. Plasma polymerization of maleic anhydride: just what are the right deposition conditions? *Langmuir* 26 (12), 9645–9658.
- Mrksich, M., Whitesides, G.M., 1996. Using self-assembled monolayers to understand the interactions of manmade surfaces with proteins and cells. *Annu. Rev. Biophys. Biomol. Struct.* 25, 55–78.
- Nastasi, M., Mayer, J., Hirvonen, J.K., 1996. *Ion–Solid Interactions: Fundamentals and Applications*. Cambridge University Press, Cambridge, UK.
- Nguyen, S.V., 1986. Plasma assisted chemical vapor deposited thin films for microelectronic applications. *J. Vac. Sci. Technol. B.* 4, 1159–1167.
- Nichols, M.F., Hahn, A.W., James, W.J., Sharma, A.K., Yasuda, H.K., 1984. Evaluating the adhesion characteristics of glow-discharge plasma-polymerized films by a novel voltage cycling technique. *J. Appl. Polym. Sci. Appl. Polym. Symp.* 38, 21–33.
- Nisol, B., Reniers, F., 2015. Challenges in the characterization of plasma polymers using XPS. *J. Electron. Spectrosc. Relat. Phenom.* 200, 311–331.
- Pan, Y.V., Wesley, R.A., Luginbuhl, R., Denton, D.D., Ratner, B.D., 2001. Plasma polymerized *n*-isopropylacrylamide: synthesis and characterization of a smart thermally responsive coating. *Biomacromolecules* 2 (1), 32–36.
- Panchalingam, V., Poon, B., Huo, H.H., Savage, C.R., Timmons, R.B., et al., 1993. Molecular surface tailoring of biomaterials via pulsed RF plasma discharges. *J. Biomater. Sci. Polym. Ed.* 5 (1/2), 131–145.
- Pappas, D., 2011. Status and potential of atmospheric plasma processing of materials. *J. Vac. Sci. Technol. A* 29 020801–1–17.
- Park, J.Y., Advincula, R.C., 2011. Nanostructuring polymers, colloids, and nanomaterials at the air–water interface through Langmuir and Langmuir–Blodgett techniques. *Soft Matter* 7 (21), 9829–9843.
- Park, E.J., Carroll, G.T., Turro, N.J., Koberstein, J.T., 2009. Shedding light on surfaces: using photons to transform and pattern material surfaces. *Soft Matter* 5 (1), 36.
- Pfleging, W., Torge, M., Bruns, M., Trouillet, V., Welle, A., et al., 2009. Laser- and UV-assisted modification of polystyrene surfaces for control of protein adsorption and cell adhesion. *Appl. Surf. Sci.* 255 (10), 5453–5457.
- Picraux, S.T., Pope, L.E., 1984. Tailored surface modification by ion implantation and laser treatment. *Science* 226, 615–622.
- Pippig, F., Sarghini, S., Holländer, A., Paulussen, S., Terryn, H., 2009. TFAA chemical derivatization and XPS. Analysis of OH and NH_x polymers. *Surf. Interface Anal.* 41 (5), 421–429.
- Plueddemann, E.P., 1980. Chemistry of silane coupling agents. In: Leyden, D.E. (Ed.), *Silylated Surfaces*. Gordon and Breach Science Publishers, New York, NY, pp. 31–53.
- Pomerantz, M., Segmuller, A., Netzer, L., Sagiv, J., 1985. Coverage of Si substrates by self-assembling monolayers and multilayers as measured by IR, wettability and x-ray diffraction. *Thin Solid Films* 132, 153–162.
- Ratner, B.D., 1980. Characterization of graft polymers for biomedical applications. *J. Biomed. Mater. Res.* 14, 665–687.
- Ratner, B.D., 1983. ESCA studies of extracted polyurethanes and polyurethane extracts: biomedical implications. In: Mittal, K.L. (Ed.), *Physicochemical Aspects of Polymer Surfaces*. Plenum Publishing, New York, NY, pp. 969–983.
- Ratner, B.D., Hoffman, A.S., 1980. Surface grafted polymers for biomedical applications. In: Szycher, M., Robinson, W.J. (Eds.), *Synthetic Biomedical Polymers. Concepts and Applications*. Technomic Publishing, Westport, CT, pp. 133–151.
- Ratner, B.D., Yoon, S.C., 1988. Polyurethane surfaces: solvent and temperature induced structural rearrangements. In: Andrade, J.D. (Ed.), *Polymer Surface Dynamics*. Plenum Press, New York, NY, pp. 137–152.
- Ratner, B.D., Horbett, T.A., Hoffman, A.S., Hauschka, S.D., 1975. Cell adhesion to polymeric materials: implications with respect to biocompatibility. *J. Biomed. Mater. Res.* 9, 407–422.
- Ratner, B.D., Hoffman, A.S., Hanson, S.R., Harker, L.A., Whiffen, J.D., 1979. Blood compatibility–water content relationships for radiation grafted hydrogels. *J. Polym. Sci., Polym. Symp.* 66, 363–375.
- Ratner, B.D., Chilkoti, A., Lopez, G.P., 1990. Plasma deposition and treatment for biomaterial applications. In: D’Agostino, R. (Ed.), *Plasma Deposition, Treatment and Etching of Polymers*. Academic Press, San Diego, CA, pp. 463–516.
- Rautray, T.R., Narayanan, R., Kwon, T.-Y., Kim, K.-H., 2010. Surface modification of titanium and titanium alloys by ion implantation: a review. *J. Biomed. Mater. Res.* 93B, 581–591.
- Raynor, J.E., Capadona, J.R., Collard, D.M., Petrie, T.A., García, A.J., 2009. Polymer brushes and self-assembled monolayers: versatile platforms to control cell adhesion to biomaterials (Review). *Biointerphases* 4 (2), FA3–FA16.
- Rye, R.R., Nelson, G.C., Dugger, M.T., 1997. Mechanistic aspects of alkylchlorosilane coupling reactions. *Langmuir* 13 (11), 2965–2972.
- Safrany, A., 1997. Radiation processing: synthesis and modification of biomaterials for medical use. *Nucl. Instrum. Methods Phys. Res. Sect. B* 131, 376–381.
- Sara, M., Sleytr, U.B., 1996. Crystalline bacterial cell surface layers (S-layers): from cell structure to biomimetics. *Prog. Biophys. Mol. Biol.* 65 (1/2), 83–111.
- Sawin, H.H., Reif, R., 1983. A course on plasma processing in integrated circuit fabrication. *Chem. Eng. Educ.* 17, 148–152.
- Schlecht, C.A., Maurer, J.A., 2011. Functionalization of glass substrates: mechanistic insights into the surface reaction of trialkoxysilanes. *RSC Adv.* 1 (8), 1446–1448.
- Sebra, R.P., Reddy, S.K., Masters, K.S., Bowman, C.N., Anseth, K.S., 2007. Controlled polymerization chemistry to graft architectures that influence cell–material interactions. *Acta Biomater.* 3 (2), 151–161.
- Shard, A.G., Whittle, J.D., Beck, A.J., Brookes, P.N., Bullett, N.A., Talib, R.A., Mistry, A., Barton, D., McArthur, S.L., 2004. A NEX-AFS examination of unsaturation in plasma polymers of allylamine and propylamine. *J. Phys. Chem. B* 108 (33), 12472–12480.
- Sheu, M.-S., Hoffman, A.S., Feijen, J., 1992. A glow discharge process to immobilize PEO/PPO surfactants for wettable and non-fouling biomaterials. *J. Adhes. Sci. Technol.* 6, 995–1101.
- Siegiwart, D.J., Oh, J.K., Matyjaszewski, K., 2012. ATRP in the design of functional materials for biomedical applications. *Prog. Polym. Sci.* 37 (1), 18–37.

- Singh, A., Silverman, J. (Eds.), 1992. *Radiation Processing of Polymers*. Oxford University Press, New York, NY.
- Sioshansi, P., 1987. Surface modification of industrial components by ion implantation. *Mater. Sci. Eng.* 90, 373–383.
- Somorjai, G.A., 1990. Modern concepts in surface science and heterogeneous catalysis. *J. Phys. Chem.* 94, 1013–1023.
- Somorjai, G.A., 1991. The flexible surface. Correlation between reactivity and restructuring ability. *Langmuir* 7, 3176–3182.
- Sørensen, P.A., Kiil, S., Dam-Johansen, K., Weinell, C.E., 2009. Anticorrosive coatings: a review. *J. Coat. Technol. Res.* 6 (2), 135–176.
- Spivack, M.A., Ferrante, G., 1969. Determination of the water vapor permeability and continuity of ultrathin parylene membranes. *J. Electrochem. Soc.* 116, 1592–1594.
- Stannett, V.T., 1990. Radiation grafting: state-of-the-art. *Radiat. Phys. Chem.* 35, 82–87.
- Swanson, M.J., 1996. A unique photochemical approach for polymer surface modification. In: Mittal, K.L., Lee, K.W. (Eds.), *Polymer Surfaces and Interfaces: Characterization, Modification and Application*. The Netherlands: VSP.
- Takahara, A., Ge, S., Kojio, K., Kajiyama, T., 2000. In situ atomic force microscopic observation of albumin adsorption onto phase-separated organosilane monolayer surface. *J. Biomater. Sci. Polym. Ed.* 11 (1), 111–120.
- Tanaka, T., Atsuta, M., Nakabayashi, N., Masuhara, E., 1988. Surface treatment of gold alloys for adhesion. *J. Prosthet. Dent.* 60, 271–279.
- Tsuiji, H., Satoh, H., Ikeda, S., Ikemoto, N., Gotoh, Y., et al., 1998. Surface modification by silver-negative-ion implantation for controlling cell-adhesion properties of polystyrene. *Surf. Coat. Technol.* 103–104, 124–128.
- Tyler, B.J., Ratner, B.D., Castner, D.G., Briggs, D., 1992. Variations between Biomer™ lots. 1. Significant differences in the surface chemistry of two lots of a commercial polyetherurethane. *J. Biomed. Mater. Res.* 26, 273–289.
- Ulman, A., 1990. Self-assembled monolayers of alkyltrichlorosilanes: building blocks for future organic materials. *Adv. Mater.* 2, 573–582.
- Ulman, A., 1991. *An Introduction to Ultrathin Organic Films*. Academic Press, Boston, MA.
- Vasilev, K., Michelmore, A., Martinek, P., Chan, J., Sah, V., Griesser, H.J., Short, R.D., 2010. Early stages of growth of plasma polymer coatings deposited from nitrogen- and oxygen-containing monomers. *Plasma Process. Polym.* 7 (9–10), 824–835.
- Vidigal, G.M., Groisman, M., De Sena, L.Á., De Almeida Soares, G., 2009. Surface characterization of dental implants coated with hydroxyapatite by plasma spray and biomimetic process. *Implant Dent.* 18 (4), 353–361.
- von Recum, A.F., 1986. *Handbook of Biomaterials Evaluation*, first ed. Macmillan Publishing Company, New York, NY.
- Ward, R.S., June 1989. Surface modifying additives for biomedical polymers. *IEEE Eng. Med. Biol.* 22–25.
- Wasserman, S.R., Tao, Y.-T., Whitesides, G.M., 1989. Structure and reactivity of alkylsiloxane monolayers formed by reaction of alkyltrichlorosilanes on silicon substrates. *Langmuir* 5, 1074–1087.
- Wen, J.M., Gabor, S., Lim, F., Ward, R., 1997. XPS study of surface composition of a segmented polyurethane block copolymer modified by PDMS end groups and its blends with phenoxy. *Macromolecules* 30, 7206–7213.
- Whitesides, G.M., Mathias, J.P., Seto, C.T., 1991. Molecular self-assembly and nanochemistry: a chemical strategy for the synthesis of nanostructures. *Science* 254, 1312–1319.
- Wilson, R.J., Chiang, S., 1987. Surface modifications induced by adsorbates at low coverage: a scanning-tunneling-microscopy study of the Ni/Si(111) $\sqrt{19}$ surface. *Phys. Rev. Lett.* 58, 2575–2578.
- Wu, S., 1982. *Polymer Interface and Adhesion*. Marcel Dekker, New York, NY.
- Xiao, S.J., Textor, M., Spencer, N.D., Wieland, M., Keller, B., et al., 1997. Immobilization of the cell-adhesive peptide arg-gly-asp-cys (RGDC) on titanium surfaces by covalent chemical attachment. *J. Mater. Sci. Mater. Med.* 8, 867–872.
- Yasuda, H.K., 1979. Competitive ablation and polymerization (CAP) mechanisms of glow discharge polymerization. In: Shen, M., Bell, A.T. (Eds.), *ACS Symposium Series 108: Plasma Polymerization*. American Chemical Society, Washington DC, pp. 37–52.
- Yasuda, H.K., Gazicki, M., 1982. Biomedical applications of plasma polymerization and plasma treatment of polymer surfaces. *Biomaterials* 3, 68–77.
- Yoon, T.O., Shin, H.J., Jeoung, S.C., Park, Y.I., 2008. Formation of superhydrophobic poly(dimethylsiloxane) by ultrafast laser-induced surface modification. *Opt. Express* 16 (17), 12715–12725.
- Zeng, J., Matsusaki, M., 2019. Layer-by-layer assembly of nanofilms to control cell functions. *Polym. Chem.* 10 (23), 2960–2974.
- Zhou, T., Zhu, Y., Xia, L., Liu, X., Yeung, K.W.K., Wu, S., Wang, X., Cui, Z., Yang, X., Chu, P.K., 2016. Surface functionalization of biomaterials by radical polymerization. *Prog. Mater. Sci.* 83, 191–235.

Further Reading

- Folch, A., Toner, M., 2000. Microengineering of cellular interactions. *Ann. Rev. Bioeng.* 2, 227–256.
- Goessl, A., Garrison, M.D., Lhoest, J., Hoffman, A.S., 2001. Plasma lithography: thin-film patterning of polymeric biomaterials by RF plasma polymerization I: surface preparation and analysis. *J. Biomater. Sci. Polym.* 12 (7), 721–738.

1.4.3A

Nonfouling Surfaces

PENG ZHANG¹, BUDDY D. RATNER^{2,*}, ALLAN S. HOFFMAN^{3,*}, SHAOYI JIANG^{4,*}

¹Department of Chemical Engineering, University of Washington, Seattle, WA, United States

²Bioengineering and Chemical Engineering, Director of University of Washington Engineered Biomaterials (UWEB), Seattle, WA, United States

³Bioengineering and Chemical Engineering, University of Washington, Seattle, WA, United States

⁴Departments of Chemical Engineering and Bioengineering, Seattle, WA, United States

Introduction

“Nonfouling” surfaces (NFSs) refer to surfaces that resist the adsorption of proteins and/or adhesion of cells. They are also loosely referred to as protein-resistant surfaces and “stealth” surfaces. It is generally acknowledged that surfaces that strongly adsorb proteins will generally bind cells, and that surfaces that resist protein adsorption will also resist cell adhesion. It is also generally recognized that hydrophilic surfaces are more likely to resist protein adsorption, and that hydrophobic surfaces will usually adsorb a monolayer of tightly adsorbed protein. Exceptions to these generalizations exist but, overall, they are accurate statements. Further details on protein adsorption can be found in [Chapter 2.1.2](#).

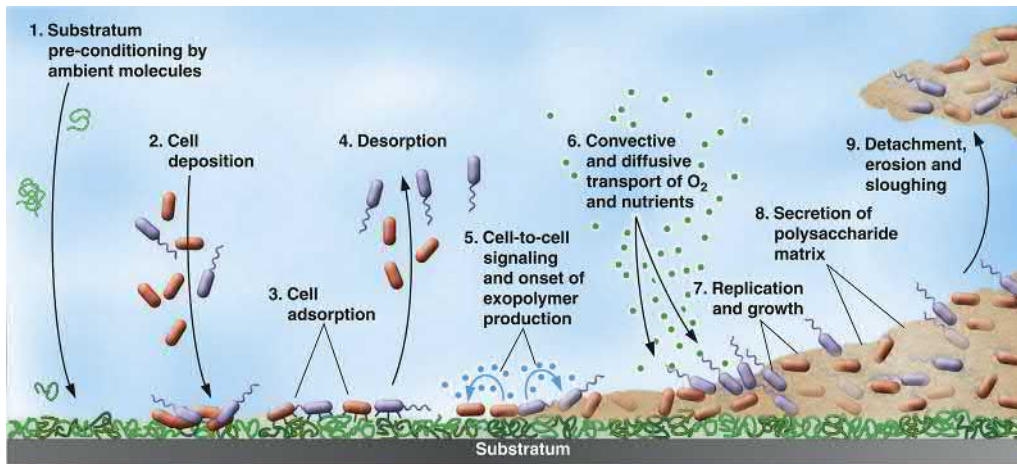
Given that proteins have a strong tendency to adsorb to almost all surfaces, how might NFSs work to inhibit such adsorption? Although there are many potential mechanisms for action, most NFSs seem to have strong interactions with water. This water–polymer interaction highly hydrates and expands surface hydrophilic polymer chains. Also, the NFSs bind water tightly, and this water shield separates the proteins from the material of the surface. These mechanisms will be elaborated on later.

An important area for NFSs focuses on bacterial biofilms (see [Chapter 2.2.8](#)). Bacteria are believed to adhere to surfaces via a “conditioning film” of organic molecules that adsorbs first to the surface. The bacteria stick to this conditioning film and begin to exude a gelatinous slime

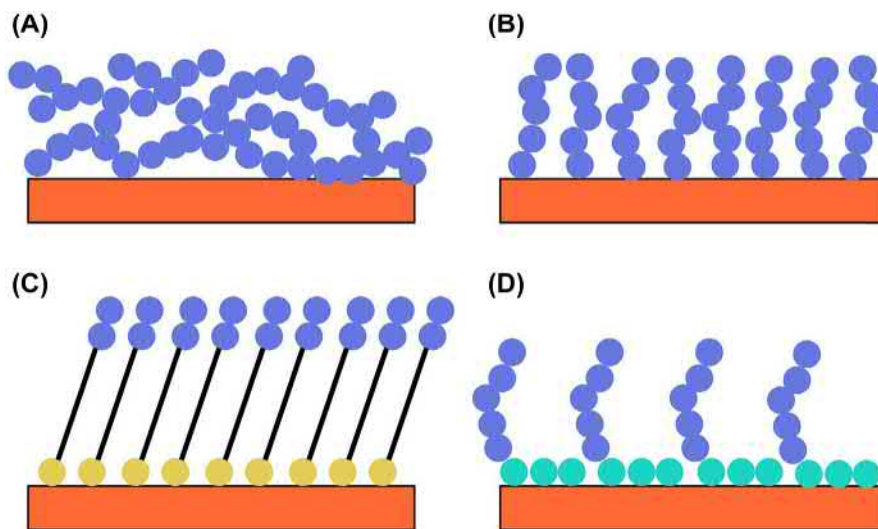
layer (the biofilm) that aids in their protection from external agents (for example, antibiotics) ([Fig. 1.4.3A.1](#)). Such layers are particularly troublesome in devices such as urinary catheters and endotracheal tubes. However, they also form on vascular grafts, hip joint prostheses, heart valves, and other long-term implants, where they can stimulate significant inflammatory reaction to the infected device. If the conditioning film can be inhibited, bacterial adhesion and biofilm formation can also be reduced. NFSs offer this possibility.

NFSs have medical and biotechnology uses as blood-compatible materials (where they may resist fibrinogen adsorption and platelet attachment), implanted devices (where they may reduce the foreign-body reaction and simplify device removal), biosensors (where they may minimize nonspecific protein adsorption and maximize specific binding), urinary catheters, affinity separation processes, microchannel flow devices, intravenous syringes and tubing, and nonmedical uses such as biofouling-resistant heat exchangers and ship hulls. It is important to note that many of these applications involve in vivo implants or extracorporeal devices, while others involve in vitro diagnostic assays, sensors, and affinity separation processes. As well as having considerable medical and economic importance, all these applications are closely related to an important phenomenon in biomaterials science: protein adsorption. Hence NFSs have been the subject of many investigations. Aspects of NFSs are addressed in many other chapters of this textbook, including the chapters on water at interfaces ([Chapter 1.2.5](#)), surface modification ([Chapter 1.4.2](#)), and protein adsorption ([Chapter 2.1.2](#)).

* Corresponding author.



• **Figure 1.4.3A.1** Several distinct processes govern biofilm formation (Bryers and Ratner, 2004).



• **Figure 1.4.3A.2** Four surfaces that can show nonfouling behavior. The *blue dot* represents a nonfouling chemical moiety such as $(\text{CH}_2\text{CH}_2\text{O})_n$. (A) Cross-linked network of long, polymeric chains; (B) polymer brushes grown from the surface; (C) oligo-nonfouling headgroups on a self-assembled monolayer (the *yellow dot* is the anchor group such as a thiol); (D) surfactant or copolymer adsorbed to the surface. The hydrophobic tails are represented by *turquoise dots*.

The significant portion of the literature on NFSs focuses on surfaces containing the relatively simple polymer poly(ethylene glycol) (PEG):



When n is in the range 15–3500 (molecular weights of approximately 400–100,000), the PEG designation is used. When molecular weights are greater than 100,000, the molecule is commonly referred to as poly(ethylene oxide). When n is in the range 2–15, the term oligo(ethylene glycol) (OEG) is often used. Other natural and synthetic polymers besides PEG show nonfouling behavior, and they will also be discussed in this chapter. Fig. 1.4.3A.2 schematically illustrates types of surfaces that show nonfouling properties.

NFSs are important in medical devices where they may inhibit bacterial colonization and blood cell adhesion. They are also valuable for ship hulls where they prevent marine organism build-up, and heat exchangers where they reduce biofilm formation. For further reading, see Jiang and Cao (2010).

Background and Mechanism

The published literature on protein and cell interactions with biomaterial surfaces has grown significantly in the past 40 years, and the following concepts have emerged:

- It is well established that hydrophobic surfaces have a strong tendency to adsorb proteins, often irreversibly (Hoffman, 1986; Horbett and Brash, 1987, 1995). The driving force for this action is most likely the unfolding of the protein on the surface, accompanied by release of many bound water molecules from the solid surface at the interface (see Chapter 1.2.5), leading to a large entropy gain for the system (Hoffman, 1999). Note that adsorbed proteins can be displaced (or “exchanged”) from the surface by solution-phase proteins (Brash et al., 1974).
- It is also well known that, at low ionic strengths, cationic proteins bind to anionic surfaces and anionic proteins bind to cationic surfaces (Horbett and Hoffman, 1975; Bohnert et al., 1988; Hoffman, 1999). The major

thermodynamic driving force for these actions is a combination of ion–ion coulombic interactions, accompanied by an entropy gain due to the release of counter-ions along with their bound water molecules. However, these interactions are diminished under physiologic conditions by shielding of the protein ionic groups at an ionic strength of 0.15 N (Horbett and Hoffman, 1975). Still, lysozyme, a highly charged cationic protein at physiologic pH, strongly binds to hydrogel contact lenses containing anionic monomers (see Bohnert et al., 1988, and Chapter 2.5.6).

- It has been a common observation that proteins tend to adsorb in monolayers, i.e., proteins do not adsorb non-specifically onto their own monolayers (Horbett, 1993). This is probably due to retention of hydration water by the adsorbed protein molecules, preventing close interactions of the protein molecules in solution with the adsorbed protein molecules. In fact, adsorbed protein films are, in themselves, reasonable NFSs with regard to other proteins (but not necessarily to cells). For example, albumin or casein is often used as a blocking agent to reduce nonspecific protein adsorption.
- The mechanism of protein resistance by the polymeric PEG surfaces may be due to a combination of factors, including the resistance of the PEG molecule to release both bound and free water from within the hydrated coil (called “osmotic repulsion”) (Gombotz et al., 1991; Antonsen and Hoffman, 1992; Heuberger et al., 2005) plus the resistance of the polymer coil to compression due to its desire to retain the more expanded volume of a random coil (called “entropic repulsion” or “elastic network” resistance) (Jeon et al., 1991). Surface hydration often plays a key role, as conformational flexibility will strengthen, but is not required to achieve NFSs (Chen et al., 2006).
- The surface-packing density of the nonfouling groups/polymers on a surface is recognized as another crucial factor that affects protein adsorption. Both molecular simulation (Zheng et al., 2004) and experimental (Li et al., 2007) studies of OEG self-assembled monolayers (SAMs) showed that there is a correlation between OEG surface density and its resistance to protein adsorption.
- It has been realized that protein solution concentration and complexity also determine protein adsorption on NFSs. Although some NFSs (e.g., OEG SAMs) resist nonspecific protein adsorption in a single protein solution or 10% blood serum, these surfaces may fail when contacting biologically complex media (e.g., whole blood or undiluted blood plasma or serum). Surfaces consisting of long nonfouling polymers improve nonfouling behavior due to the high surface-packing density of nonfouling groups (Ladd et al., 2008).

The thermodynamic principles governing the adsorption of proteins onto surfaces involve a number of enthalpic and entropic terms favoring or resisting adsorption. These terms are summarized in Table 1.4.3A.1. The major factors favoring adsorption will be the entropic gain of released water and the enthalpy loss due to cation–anion attractive interactions

TABLE 1.4.3A.1 Thermodynamics of Protein Adsorption

Favoring Adsorption

ΔH_{ads}	– Van der Waals interactions (short range)
	– Ion–ion interactions (long range)
ΔS_{ads}	+ Desorption of many H_2O 's
	+ Unfolding of protein

Opposing Adsorption

ΔH_{ads}	+ Dehydration (interface between surface and protein)
	+ Unfolding of protein
	+ Chain compression (PEG)
ΔS_{ads}	– Adsorption of protein
	– Protein hydrophobic exposure
	– Chain compression (PEG)
	– Osmotic repulsion (PEG)

PEG, Poly(ethylene glycol).

between ionic protein groups and surface groups. The major factors favoring resistance to protein adsorption will be the retention of bound water in the case of an immobilized hydrophilic polymer along with the entropic and osmotic repulsion of the polymer coils.

Observations on SAMs (described in Chapter 1.4.2) with different head groups have been particularly important in the understanding of NFSs. OEG SAMs prepared to explore NFSs were formed on gold surfaces with a set of molecules based on this alkyl thiol structure: $\text{HS}(\text{CH}_2)_{11}(\text{OCH}_2\text{CH}_2)_n\text{OH}$. The OEG chain length, n , was 0, 1, 2, 4, 6, or 17. OEGs with larger n (more ethylene glycol units) were more protein resistant, but the minimum of $n = 3$ is needed. The surface packing density of these OEG-thiol units needed to achieve nonfouling behavior decreased with increasing n (Prime and Whitesides, 1993). Thus the improved nonfouling behavior of this surface can be attributed to both chain flexibility and the ability of ethylene glycol units to interact with water. Thus protein resistance by OEG-coated surfaces may be related to a “cooperativity” between the hydrated, short OEG chains in the “plane of the surface,” wherein the OEG chains interact together to bind water to the surface in a manner analogous to the hydrated coil and its osmotic repulsion, as previously described. While hydration is the primary factor to achieve NFSs, chain flexibility, although helpful, is not necessary when hydration is strong enough. The excellent nonfouling ability of mixed SAMs containing charged pairs was achieved due to their strong electrostatically induced hydration (Chen et al., 2006) although the lattice structure of the mixed SAMs (or the absence of chain flexibility) was observed from atomic force microscopy experiments.

Four common properties shared by many nonfouling groups were summarized after a survey of structure–property

relationships of surfaces that resist protein adsorption (Ostuni et al., 2001): hydrophilic, electrically neutral, and containing groups that are hydrogen-bond acceptors, but not hydrogen-bond donors. While the first three factors are well recognized, hydrogen-bond donors are more complicated. Hydroxyl-terminated PEG surfaces (Li et al., 2007) and mannitol (Luk et al., 2000) with abundant hydrogen-bond donors or hydroxyl groups exhibit excellent nonfouling behavior. However, cellulose surfaces with abundant hydroxyl groups generated high complement activation (Poppelaars et al., 2018).

The packing density of nonfouling groups on surfaces is clearly an important factor in preparing NFSs. Nevertheless, one may conclude that the one common factor connecting all NFSs is their resistance to the release of bound water molecules from the surface. This argument is supported by neutron reflectivity measurements by Skoda et al. (2009), where they found a depletion of protein concentration around 4–5 nm above an OEG surface that might be attributable to a tightly bound water layer interfering with the protein approach to the actual surface. Also, direct measurements by D₂O exchange and sum frequency generation (see Chapter 1.2.4) of water organization at the interface of nonfouling and fouling SAMs demonstrate that NFSs lead to a more bound, organized water (Stein et al., 2009). Interfacial water may be reorganized both by hydrophobic groups and by hydrophilic interactions. In the latter case, the water may be H-bonded to neutral polar groups, such as hydroxyl (–OH) or ether (–C–O–C–) groups, or it may be polarized by ionic groups, such as COO[–] or –NH₃⁺. The more profound molecular reorganizations of water seen in NFSs are associated with certain hydrophilic surfaces. The overall conclusion from all of these observations is that resistance to protein adsorption at biomaterial interfaces is directly related to retention by interfacial groups of their bound water molecules of hydration.

The significance of protein solution concentration for surface protein resistance requires further discussion. In relatively dilute protein solutions, such as are used in diagnostic assays and sometimes in cell culture, all of the surfaces described so far will demonstrate nonfouling behavior. However, at protein concentrations similar to that in the bloodstream or in body fluids, many of these surfaces no longer appear nonfouling. The surfaces that exhibit nonfouling behavior at higher protein concentrations are comprised of longer hydrophilic chains with high conformational freedom (Zhang et al., 2008; Ma et al., 2004). Surfaces comprised of short oligo units of nonfouling chemistries probably function by tightly binding water. It may be that at high solution protein content, the protein molecules compete for the bound surface water, and the nonfouling effect vanishes. On the other hand, when longer, flexible chains are present, more bound water molecules along with the entropic repulsion effect described earlier permit these surfaces to remain free of adsorbed protein, as long as the hydrophilic polymer surface density is high enough.

TABLE 1.4.3A.2 “Nonfouling” Materials

Nonionic Synthetic Materials

- PEG polymers and surfactants
- Poly[poly(ethylene glycol) methyl ether methacrylate]
- Poly(2-methoxyethyl acrylate)
- Poly(2-hydroxyethyl methacrylate)
- Poly[N-(2-hydroxypropyl) methacrylamide]
- Polyacrylamide and poly(N-methyl acrylamide)
- Poly(N-vinyl 2-pyrrolidone)
- Poly(2-methyl-2-oxazoline)
- Gas discharge-deposited coatings (especially from PEG-like monomers)

Zwitterionic Synthetic Materials

- Poly(2-methacryloyloxyethyl phosphorylcholine)
- Poly(sulfobetaine)
- Poly(carboxybetaine)
- Mixed-charge synthetic polymers or polyampholytes
- Amino acid-derived zwitterionic polymers

Natural Hydrophilic Materials

- Passivating proteins (e.g., albumin and casein)
- Polysaccharides (e.g., hyaluronic acid)
- Liposaccharides
- Phospholipid bilayers
- Glycoproteins (e.g., mucin)

PEG, Poly(ethylene glycol).

Resistance to protein adsorption at biomaterial interfaces is directly related to resistance of interfacial groups to the release of their bound waters of hydration. For further reading, see Antonsen and Hoffman (1992), Heuberger et al. (2005), and Shao and Jiang (2015).

Nonfouling Materials and Methods

Based on these conclusions, it is obvious why the most common materials used to reduce protein adsorption and cell adhesion on surfaces have been those that strongly interact with water. Some commonly used nonfouling materials are listed in Table 1.4.3A.2.

As discussed earlier, the nonfouling property of the materials is tightly correlated with a hydration layer near the surface, which forms a physical and energetic barrier to prevent protein adsorption onto the surface. Water molecules residing on and/or penetrating into nonfouling materials can be classified into two types of “surface-bound” waters: formed by hydrogen bonding or ionic solvation. Thus nonfouling materials may also be classified into two types correspondingly. The first type of material is neutral and hydrophilic, interacting with water via hydrogen bonding. These materials consist of hydroxyl (–OH), ether (–C–O–C–), or amide (–CONH–) groups. Nonionic synthetic materials listed in Table 1.4.3A.2 belong to this type. Some natural hydrophilic materials, such as polysaccharides and liposaccharides, also belong to this type. Another class of nonfouling materials is characterized by their ionic nature, interacting with water via electrostatically induced hydration. Materials with ionic solvation can

hold water even stronger than those with hydrogen bonding. However, since negatively charged materials adsorb positively charged proteins and vice versa via electrostatic interactions, only those zwitterionic materials with overall neutral charge demonstrate strong resistance to nonspecific protein adsorption (Chen et al., 2005; Kane et al., 2003; Chen et al., 2009; Shao et al., 2015). While zwitterionic materials containing both positively and negatively charged groups in the same unit exhibit excellent nonfouling properties, these oppositely charged groups do not need to be in the same molecule. Surfaces prepared with mixed-charge SAMs or copolymers demonstrate strong resistance to nonspecific protein adsorption when positively and negatively charged components are uniformly mixed with a ratio of 1:1 (Kane et al., 2003; Chen et al., 2009). Interestingly, abundant glutamic acid (E) and lysine (K) residues were found to be randomly distributed on the surfaces of proteins and molecular chaperones, which form mixed-charge surfaces and contribute to the reduction of nonspecific interactions (White et al., 2012).

To achieve NFSs of biomaterials or medical devices, one can coat nonfouling materials discussed previously via various chemical or physical approaches. These approaches can be generally classified into two categories as “graft-to-surface” and “graft-from-surface.” In the so-called “graft-to-surface” approach, nonfouling materials adsorb or bind onto a surface out of a solution. In the “graft-from-surface” approach, nonfouling polymer brushes are initiated and propagated from a surface. The “graft-to-surface” approach is easier to perform, but requires extensive optimization to achieve high surface-packing densities. On the other hand, the “graft-from-surface” approach is easier to achieve high surface-packing densities, but they often require specific surface pretreatments and sophisticated chemistries in controlled environments. Examples of some of these strategies are:

- Physical adsorption of surfactants or other surface-active molecules that are coupled to nonfouling moieties. Examples include: adsorption of poly(ethylene glycol-propylene glycol) block copolymers (Lee et al., 1989); surface attachment of biomimetic analogs of muscle adhesive peptides coupled to PEG chains (Dalsin et al., 2003); and surface coating by zwitterionic block copolymers consisting of poly(propylene oxide) and poly(sulfobetaine methacrylate) (Chang et al., 2006).
- Immobilization of nonfouling polymers onto surfaces via covalent bonds. Examples include: nonfouling surfactants such as Pluronic polyols used to covalently bind polymer surfaces in gas discharge (Sheu et al., 1993); photoreactive polymers bearing zwitterionic phosphorylcholine and benzophenone groups on the side chain immobilized on polyolefin surfaces via ultraviolet irradiation to form antifouling coatings (Lin et al., 2015); and poly(carboxybetaine) hydrogel coated onto multiple surfaces via superglue to fabricate durable NFSs (Wang et al., 2017).
- Grafting nonfouling polymers from surfaces via different chemistries. Examples include: fouling resistant brushes of poly[poly(ethylene glycol) methyl ether methacrylate] or poly(carboxybetaine) chains grown from surfaces via atom

transfer radical polymerization (Ma et al., 2004; Ladd et al., 2008); NFSs prepared on polydimethylsiloxane with poly(2-methacryloyloxyethyl phosphorylcholine) grafted via surface-initiated photoinduced radical polymerization (Goda et al., 2006); and substrate-independent surface modification for controlled protein adsorption achieved by chemical vapor deposition (Rong Yang et al., 2012).

A variety of methods have been reported to fabricate NFSs on biomaterial surfaces. However, it is hard to coat all surfaces via one universal approach due to huge differences among material surfaces in terms of physical and chemical properties. The coating approach critically affects the grafting density, defects, and durability of the resulting NFSs. An appropriate approach needs to be chosen for a specific material surface to achieve the optimum antiprotein adsorption performance.

While PEG and other hydrophilic materials achieve hydration via hydrogen bonding, zwitterionic materials, such as poly(2-methacryloyloxyethyl phosphorylcholine), poly(sulfobetaine), and poly(carboxybetaine), can bind water molecules even more strongly via electrostatically induced hydration. As a result of strong hydration, polyzwitterions demonstrate superhydrophilicity and strong repulsion to nonspecific protein adsorption. Some examples of the applications of polyzwitterions include: poly(2-methacryloyloxyethyl phosphorylcholine) used for medical devices, such as contact lenses and artificial hip joint implants (Lewis, 2000; Ishihara, 2015); poly(sulfobetaine) applied to coat membranes to improve blood compatibility (Chang et al., 2011); and poly(carboxybetaine) used as an implant material to prevent foreign body reaction (Zhang et al., 2013).

Conclusions and Perspectives

It is remarkable how many different surface compositions appear to be nonfouling although the majority of surfaces used in medicine and biology adsorb protein. Although the unifying mechanisms require further studies, it appears that the major factor favoring resistance to protein adsorption is the retention of bound water by the surface molecules. Entropic and osmotic repulsion of the polymer coils also play an important role. In addition to the nonfouling material itself, surface coating density also plays a key role when the nonfouling material is attached to a surface.

Here are a few considerations for future perspectives. First, little is known about how long a NFS will remain nonfouling in vivo. Longevity and stability for nonfouling biomaterials remain an uncharted frontier. Also, it has been pointed out that susceptibility of PEGs to oxidative damage may reduce their utility and longevity as nonfouling surfaces in real-world situations (Kane et al., 2003; Li et al., 2007). Second, resistance to bacterial adhesion and biofilm formation remains an unsolved problem. It should be noted that bacteria tend to adhere to and colonize almost any surface, including many protein-resistant NFSs. The best NFSs can often provide acute resistance to or delay biofilm build-up better than others (Johnston et al., 1997). Defects (e.g., pits and uncoated areas) in NFSs may provide “footholds” for bacteria and cells to begin colonization. A deeper understanding of how to

optimize the surface density and composition of NFSs will lead to improvements in coating quality with fewer micro-defects. Strategies that incorporate antimicrobial activities into NFSs may potentially help solve these problems (Cheng et al., 2008; Mi et al., 2014). Third, in addition to bulk materials and surfaces, NFSs are also very important in nanotechnology for nanoparticles (NPs) used in drug delivery and diagnostics. Similar to many bulk surfaces, proteins tend to adsorb on the surfaces of NPs and form protein corona. The protein corona may destabilize NPs, affect surface ligands, increase cellular uptake and trigger immune responses in vivo. Protecting NPs with NFSs could efficiently prolong their blood circulation half-life and increase delivery efficiency. Exploration of NFSs for drug delivery NPs remains an active research topic. Selection of NFSs for drug delivery NPs is challenging due to the complexity of in vivo environments and the immune systems. Although PEG has been the most widely used NFSs for NPs, the development of anti-PEG immunity has brought complications in these applications (Zhang et al., 2016). Alternative nonfouling materials are needed to overcome these challenges.

References

- Antonsen, K.P., Hoffman, A.S., 1992. Water structure of PEG solutions by DSC measurements. In: Harris, J.M. (Ed.), *Polyethylene Glycol Chemistry: Biotechnical and Biomedical Applications*. Plenum Press, New York, NY, pp. 15–28.
- Bohnert, J.L., Horbett, T.A., Ratner, B.D., Royce, F.H., 1988. Adsorption of proteins from artificial tear solutions to contact lens materials. *Investig. Ophthalmol. Vis. Sci.* 29 (3), 362–373.
- Brash, J.L., Uniyal, S., Samak, Q., 1974. Exchange of albumin adsorbed on polymer surfaces. *Trans. Am. Soc. Artif. Intern. Organs* 20, 69–76.
- Bryers, J.D., Ratner, B.D., 2004. Bioinspired implant materials befuddle bacteria. *ASM News* 70 (5), 232–237.
- Chang, Y., Chen, S., Zhang, Z., Jiang, S., 2006. Highly protein-resistant coatings from well-defined diblock copolymers containing sulfobetaines. *Langmuir* 22, 2222–2226.
- Chang, Y., Chang, W.-J., Shih, Y.-J., Wei, T.-C., Hsiue, G.-H., 2011. Zwitterionic sulfobetaine-grafted poly(vinylidene fluoride) membrane with highly effective blood compatibility via atmospheric plasma-induced surface copolymerization. *ACS Appl. Mater. Interfaces* 3, 1228–1237.
- Chen, S., Yu, F., Yu, Q., He, Y., Jiang, S., 2006. Strong resistance of a thin crystalline layer of balanced charged groups to protein adsorption. *Langmuir* 22 (19), 8186–8191.
- Chen, S., Li, L., Jiang, S., 2005. Strong resistance of phosphorylcholine self-assembled monolayers to protein adsorption: insights into nonfouling properties of zwitterionic materials. *J. Am. Chem. Soc.* 127, 14473–14478.
- Chen, S., Cao, Z., Jiang, S., 2009. Ultra-low fouling peptide surfaces derived from natural amino acids. *Biomaterials* 30, 5892–5896.
- Cheng, G., Xue, H., Zhang, Z., Chen, S., Jiang, S., 2008. A switchable biocompatible polymer surface with self-sterilizing and non-fouling capabilities. *Angew. Chem. Int. Ed. Engl.* 47, 8831–8834.
- Dalsin, J.L., Hu, B.-H., Lee, B.P., Messersmith, P.B., 2003. Mussel adhesive protein mimetic polymers for the preparation of nonfouling surfaces. *J. Am. Chem. Soc.* 125 (14), 4253–4258.
- Goda, T., Konno, T., Takai, M., Moro, T., Ishihara, K., 2006. Biomimetic phosphorylcholine polymer grafting from polydimethylsiloxane surface using photo-induced polymerization. *Biomaterials* 27, 5151–5160.
- Gombotz, W.R., Wang, G.H., Horbett, T.A., Hoffman, A.S., 1991. Protein adsorption to PEO surfaces. *J. Biomed. Mater. Res.* 25, 1547–1562.
- Heuberger, M., Drobek, T., Spencer, N.D., 2005. Interaction forces and morphology of a protein-resistant poly(ethylene glycol) layer. *Biophys. J.* 88 (1), 495–504.
- Hoffman, A.S., 1986. A general classification scheme for hydrophilic and hydrophobic biomaterial surfaces. *J. Biomed. Mater. Res.* 20 (9), ix–xi.
- Hoffman, A.S., 1999. Non-fouling surface technologies. *J. Biomater. Sci. Polym. Ed.* 10, 1011–1014.
- Horbett, T.A., 1993. Principles underlying the role of adsorbed plasma proteins in blood interactions with foreign materials. *Cardiovasc. Pathol.* 2, 137S–148S.
- Horbett, T.A., Brash, J.L., 1987. Proteins at interfaces: current issues and future prospects. In: Horbett, T.A., Brash, J.L. (Eds.), *Proteins at Interfaces, Physicochemical and Biochemical Studies ACS Symposium Series*, vol. 343. American Chemical Society, Washington, DC, pp. 1–33.
- Horbett, T.A., Brash, J.L., 1995. Proteins at interfaces: an overview. In: Horbett, T.A., Brash, J.L. (Eds.), *Proteins at Interfaces II: Fundamentals and Applications ACS Symposium Series*, vol. 602. American Chemical Society, Washington, DC, pp. 1–25.
- Horbett, T.A., Hoffman, A.S., 1975. Bovine plasma protein adsorption to radiation grafted hydrogels based hydroxyethylmethacrylate and N-Vinyl-Pyrrolidone. In: Baier, R. (Ed.), *Advances in Chemistry Series*, 145, Applied Chemistry at Protein Interfaces. American Chemical Society, Washington DC, pp. 230–254.
- Ishihara, K., 2015. Highly lubricated polymer interfaces for advanced artificial hip joints through biomimetic design. *Polym. J.* 47, 585–597.
- Jeon, S.I., Lee, J.H., Andrade, J.D., De Gennes, P.G., 1991. Protein-surface interactions in the presence of polyethylene oxide. *J. Colloid Interface Sci.* 142, 149–158.
- Jiang, S., Cao, Z., 2010. Ultralow-fouling, functionalizable, and hydrolyzable zwitterionic materials and their derivatives for biological applications. *Adv. Mater.* 22 (9), 920–932.
- Johnston, E.E., Ratner, B.D., Bryers, J.D., 1997. RF plasma deposited PEO-like films: surface characterization and inhibition of *Pseudomonas aeruginosa* accumulation. In: d'Agostino, R., Favia, P., Fracassi, F. (Eds.), *Plasma Processing of Polymers*. Kluwer Academic Publishers, Dordrecht, Netherlands, pp. 465–476.
- Kane, R.S., Deschatelets, P., Whitesides, G.M., 2003. Kosmotropes form the basis of protein-resistant surfaces. *Langmuir* 19, 2388–2391.
- Ladd, J., Zhang, Z., Chen, S., Hower, J.C., Jiang, S., 2008. Zwitterionic polymers exhibiting high resistance to nonspecific protein adsorption from human serum and plasma. *Biomacromolecules* 9, 1357–1361.
- Lee, J.H., Kopecek, J., Andrade, J.D., 1989. Protein-resistant surfaces prepared by PEO-containing block copolymer surfactants. *J. Biomed. Mater. Res.* 23, 351–368.
- Lewis, A.L., 2000. Phosphorylcholine-based polymers and their use in the prevention of biofouling. *Colloids Surfaces B Biointerfaces* 18, 261–275.
- Li, L., Chen, S., Jiang, S., 2007. Protein interactions with oligo(ethylene glycol) (oeg) self-assembled monolayers: oeg stability, surface packing density and protein adsorption. *J. Biomater. Sci. Polym. Ed.* 18, 1415–1427.

- Lin, X., Fukazawa, K., Ishihara, K., 2015. Photoreactive polymers bearing a zwitterionic phosphorylcholine group for surface modification of biomaterials. *ACS Appl. Mater. Interfaces* 7, 17489–17498.
- Luk, Y.Y., Kato, M., Mrksich, M., 2000. Self-assembled monolayers of alkanethiolates presenting mannitol groups are inert to protein adsorption and cell attachment. *Langmuir* 16, 9604–9608.
- Ma, H., Hyun, J., Stiller, P., Chilkoti, A., 2004. “Nonfouling” oligo(ethylene glycol)-functionalized polymer brushes synthesized by surface-initiated atom transfer radical polymerization. *Adv. Mater.* 16 (4), 338–341.
- Mi, L., Jiang, S., 2014. Integrated antimicrobial and nonfouling zwitterionic polymers. *Angew. Chem. Int. Ed. Engl.* 53 (7), 1746–1754.
- Ostuni, E., Chapman, R.G., Holmlin, R.E., Takayama, S., Whitesides, G.M., 2001. A survey of structure-property relationships of surfaces that resist the adsorption of protein. *Langmuir* 17, 5605–5620.
- Poppelaars, F., Faria, B., Gaya da Costa, M., Franssen, C.F.M., van Son, W.J., Berger, S.P., Daha, M.R., Seelen, M.A., 2018. The complement system in dialysis: a forgotten story? *Front. Immunol.* 9, 71.
- Prime, K.L., Whitesides, G.M., 1993. Adsorption of proteins onto surfaces containing end-attached oligo(ethylene oxide): a model system using self-assembled monolayers. *J. Am. Chem. Soc.* 115, 10714–10721.
- Shao, Q., Jiang, S., 2015. Molecular understanding and design of zwitterionic materials. *Adv. Mater.* 27, 15–26.
- Sheu, M.-S., Hoffman, A.S., Terlingen, J.G.A., Feijen, J., 1993. A new gas discharge process for preparation of non-fouling surfaces on biomaterials. *Clin. Mater.* 13, 41–45.
- Skoda, M., Schreiber, F., Jacobs, R., Webster, J., Wolff, M., et al., 2009. Protein density profile at the interface of water with oligo (ethylene glycol) self-assembled monolayers. *Langmuir* 25 (7), 4056–4064.
- Stein, M., Weidner, T., McCrea, K., Castner, D., Ratner, B.D., 2009. Hydration of sulphobetaine and tetra(ethylene glycol)-terminated self-assembled monolayers studied by sum frequency generation vibrational spectroscopy. *J. Phys. Chem. B* 113 (33), 11550–11556.
- Wang, W., Lu, Y., Zhu, H., Cao, Z., 2017. Superdurable coating fabricated from a double-sided tape with long term “zero” bacterial adhesion. *Adv. Mater.* 29, 1606506.
- White, A.D., Nowinski, A.K., Huang, W.J., Keefe, A.J., Sun, F., Jiang, S.Y., 2012. Decoding nonspecific interactions from nature. *Chem. Sci.* 3, 3488–3494.
- Yang, R., Asatekin, A., Gleason, K.K., 2012. Design of conformal, substrate-independent surface modification for controlled protein adsorption by chemical vapor deposition (CVD). *Soft Matter* 8, 31–43.
- Zhang, Z., Zhang, M., Chen, S., Horbett, T.A., Ratner, B.D., Jiang, S., 2008. Blood compatibility of surfaces with superlow protein adsorption. *Biomaterials* 29, 4285–4291.
- Zhang, L., Cao, Z., Bai, T., Carr, L., Ella-Menye, J.-R., Irvin, C., Ratner, B.D., Jiang, S., 2013. Zwitterionic hydrogels implanted in mice resist the foreign-body reaction. *Nat. Biotechnol.* 31, 553–556.
- Zhang, P., Sun, F., Liu, S., Jiang, S., 2016. Anti-peg antibodies in the clinic: current issues and beyond pegylation. *J. Control. Release* 244, 184–193.
- Zheng, J., Li, L., Chen, S., Jiang, S., 2004. Molecular simulation study of water interactions with oligo (ethylene glycol)-terminated alkanethiol self-assembled monolayers. *Langmuir* 20, 8931–8938.

1.4.3B

Nonthrombogenic Treatments and Strategies

MICHAEL V. SEFTON¹, MAUD B. GORBET²

¹Department of Chemical Engineering and Applied Chemistry, Institute of Biomaterials and Biomedical Engineering, University of Toronto, ON, Canada

²Department of Systems Design Engineering, University of Waterloo, ON, Canada

Introduction

This chapter addresses the methods to improve the blood compatibility of biomaterials, the subject of a large body of literature in the biomaterials field and a topic of great importance clinically. To appreciate the contents of this chapter, a familiarity with materials in [Chapters 1.4.2, 1.4.4, 2.2.6 and 2.3.5](#) is expected. A recent set of reviews “The Blood Compatibility Challenge,” emphasizes the features of broad agreement and provides commentary on those aspects of the problem that remain in dispute ([Sefton et al., 2019](#); [Jaffer and Weitz, 2019](#); [Brash et al., 2019](#); [Gorbet et al., 2019](#); [Maitz et al., 2019](#)). The intent of that set of reviews was to encourage fresh approaches to address this long-standing but as yet unsolved challenge.

Historical

In 1963, Dr. Vincent Gott at the Johns Hopkins University changed the field of biomaterials by failing to reproduce an earlier experiment. He was trying to show that an applied electric field could minimize thrombus formation on a metal surface. He obtained this result, but was somewhat mystified when he discovered that the wire leading to his negative graphite electrode was broken. He soon realized the importance of rinsing his electrode with a common disinfectant (benzalkonium chloride) and heparin prior to implantation. Thus, the first heparinized material was born. [Lehninger et al. \(1966\)](#) at Battelle Memorial Institute in Columbus, Ohio, followed up with better quaternary ammonium compounds, and soon afterward a host of chemical derivatization methods were devised to adapt the original GBH (graphite benzalkonium heparin) method to plastics and other materials. The principles underlying these

strategies and others for lowering the thrombogenicity of materials are detailed here with examples.

Criteria for Nonthrombogenicity

Thrombogenicity is defined ([Williams, 1987](#)) as the ability of a material to induce or promote the formation of thromboemboli ([Box 1.4.3.B.1](#)). Here we are concerned with strategies to lower thrombogenicity, if not actually reduce it to zero, “nonthrombogenicity.” Thrombogenicity should be thought of as a rate parameter, since low rates of thrombus or emboli formation are probably tolerable because the fibrinolytic or other clearance systems exist to remove “background” levels of thromboemboli. We are principally concerned with rates of thrombi formation that are sufficient to occlude flowpaths in medical devices (e.g., block the lumen of catheters) or rates of emboli formation that cause downstream problems such as myocardial infarction or transient ischemic attacks. The mechanisms of thrombogenicity are described in [Chapter 2.2.6](#), the methods to measure thrombogenicity are described in [Chapter 2.3.5](#), while the effects of fluid flow on thrombus development and embolization are described in [Chapters 2.3.5 and 2.1.6](#).

Thrombi are produced through aggregation of activated platelets and/or the thrombin-dependent polymerization of fibrinogen into fibrin. Thrombin is directly responsible for fibrin formation but it is also an important agonist of platelet activation. Computational models have been developed to provide a better understanding of the interactions between surface thrombogenicity, variation in flow, and platelet activation ([Wu et al., 2017](#); [Tomaiuolo et al., 2014](#)). These novel simulation tools may help in the design of low thrombogenic surfaces as recently highlighted by [Wu et al. \(2016\)](#).

• BOX 1.4.3B.1 Associated Facts: Characterizing Thrombogenicity

Many investigators exploring methods of improving thrombogenicity rely on protein adsorption (especially fibrinogen) and platelet adhesion as surrogate markers of thrombogenicity to demonstrate the success of their modification. Surrogate markers are typically easier, indirect measurements of the potential for thrombus formation. However, these represent a limited assessment of the thrombogenicity of a surface, and imply a causative mechanism of action that is often not warranted. For example, the lack of platelet adhesion does not always correlate with the absence of platelet activation. In vitro and in vivo studies by Hanson et al. (1980), as well as Gemmell et al. (1995, 1997), have demonstrated significant platelet activation in the fluid phase in the absence of platelet adhesion. Many factors contribute to material-induced thrombogenicity (Gorbet and Sefton, 2004), and a limited understanding of the mechanism means that assessing thrombogenicity requires more than looking at surface adsorption and adhesion.

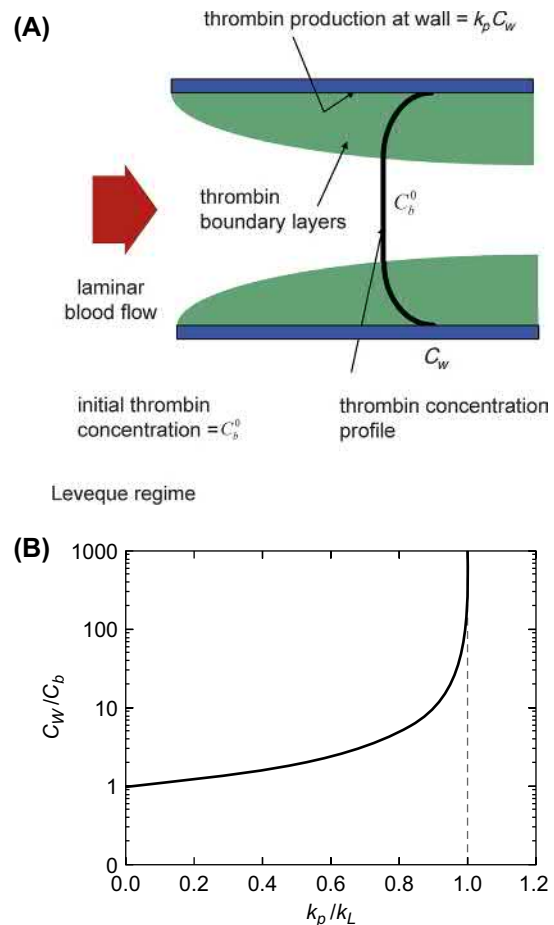
A simple, analytical, model of thrombin generation is illustrated in Fig. 1.4.3B.1A. The variety of mechanisms that lead to thrombin generation are lumped into a single parameter, k_p (cm/s), a rate constant that relates the rate of production of thrombin (per unit area), R_p (g/cm²s), to the thrombin concentration at the surface of a material C_w (g/mL):

$$R_p = k_p C_w \quad (1.4.3B.1)$$

k_p includes both the procoagulant effect of the material (via clotting factors and platelets) less any coagulation inhibition processes. A material balance (Basmadjian, 1990; Rollason and Sefton, 1992) equating the rate of production at the surface to the rate of transport away from the surface $k_L(C_w - C_b)$ for tubes greater than about 0.1 mm in diameter (Leveque region) gives:

$$\frac{C_w}{C_b^0} = \frac{1}{1 - k_p / k_L(x)} \quad (1.4.3B.2)$$

where C_b^0 is the concentration of thrombin at the inlet to a tube. $k_L(x)$ is the local mass transfer coefficient which is infinite at the tube inlet and decreases as one proceeds down the tube. Hence, C_w/C_b^0 increases progressively down the tube (Fig. 1.4.3B.1B). When $k_L = k_p$, C_w becomes infinite and a thrombus is expected. For a simple tube in laminar flow, k_L is in the order of 10^{-3} cm/s, and so k_p must be less than this to avoid a thrombus. Experimental results suggest that k_p is in the order of 10^{-3} for simple materials like polyethylene, but $<10^{-4}$ for heparinized materials (Rollason and Sefton, 1992). According to this model, only such low k_p materials can be expected to minimize thrombin production. This is one of the reasons heparinization and other active methods of inhibiting thrombin formation are so popular as strategies for imparting low thrombogenicity. There are, however, other criteria that must also be met.



• **Figure 1.4.3B.1** (A) Model illustrating thrombin production at the surface of a tube as a balance between auto-accelerative production at the surface and mass transfer away from the wall. (B) Schematic illustration of Eq. (1.4.3B.2) showing the dramatic increase in wall to bulk concentration ratio as the mass transfer coefficient k_L becomes equal to the first-order autocatalytic production constant (k_p). Since k_L decreases with increasing axial position down a tube, increasing k_p/k_L corresponds to increasing x . (Adapted from Rollason, G., Sefton, M.V., 1992. Measurement of the rate of thrombin production in human plasma in contact with different materials. J. Biomed. Mat. Res. 26, 675–693.)

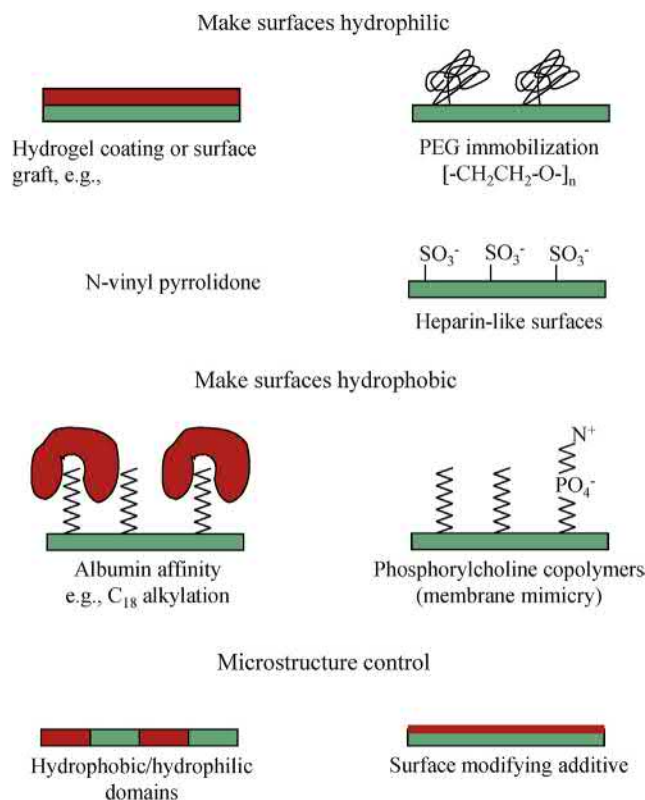
It is also a requirement that platelet interactions with the surface do not lead to thrombosis. To some extent, platelet adhesion is inevitable. Once adherent, platelets change shape and release their granule contents which can activate bulk platelets. While it is intuitive to suggest that a nonthrombogenic surface should not support platelet adhesion it has not, unfortunately, been that simple. While most studies focus on evaluating the platelet compatibility of surfaces by measuring in vitro platelet adhesion, some ex vivo studies (Hanson et al., 1980; Cholakis et al., 1989) have demonstrated that even in the absence of adhesion, platelets can be “consumed.” That is, the platelets are activated by the material leading to their premature removal from the circulation (Chapter 2.3.5). This becomes apparent as a significant shortening of platelet lifespan, if not also a decrease in systemic platelet count. Whether this process is initiated by nonadhesive direct contact with the

material or is the result of adherent platelet release, or even the effect of complement activation is currently unknown. Nevertheless, such an observation suggests that low platelet adhesion is not a sufficient criterion of *in vivo* platelet compatibility. Rather, low thrombogenicity is characterized by both low platelet adhesion and low platelet activation (see Chapter 2.2.6 for a definition of activation); the latter may even be more important than the former. Leukocyte activation (expression of procoagulant activities such as tissue factor or CD11b upregulation; Gorbet and Sefton, 2004) and complement activation may also be key components in thrombogenicity (see Chapters 2.2.4 and 2.2.6), and in the future these too may become critical parameters defining the thrombogenicity of the surface (Gorbet et al., 2019). In an attempt to evaluate more than just platelet adhesion on biomaterials, flow cytometric techniques have been developed to measure bulk (or circulating) activated platelets, platelet microparticles, platelet–leukocyte aggregates, and activated leukocytes (such as C11b upregulation) (Gemmell et al., 1995; Baker et al., 1998; Snyder et al., 2007). It is expected that such assays will result in better correlation between *in vitro* and *ex vivo/in vivo* performances.

While blood cells play an important role in material-induced thrombosis, concerns over *in-stent* thrombosis have renewed the interest in developing biomaterials to support and promote endothelialization. The potential thrombogenicity of these cells on a biomaterial adds another dimension to this topic (McGuigan and Sefton, 2007).

Inert Materials

Much of the effort in biomaterials research over the past 35 years has been directed toward the development of inert materials that do not react with platelets and coagulation factors. As outlined in Fig. 1.4.3B.2, a number of approaches, often conflicting, have been developed. For example, there is still no consensus as to whether a surface should be hydrophilic or hydrophobic. The lack of agreement is largely due to our incomplete understanding of the biological pathways to materials failure and our inability to fully evaluate blood–material responses. In developing materials with lower thrombogenicity, researchers have primarily focused their efforts on modifying the surfaces of existing polymeric materials, like polyurethanes, silicone rubber, and polyethylene. This approach is reasonable, since it is only the surface chemistry of a material that should dictate its biological responses. As illustrated by the following discussion, the full range of surface modification strategies outlined in Chapter 1.4.2 has been used, albeit with limited success. On the other hand, in comparing many plasma-modified surfaces, Sefton et al. (2001) did not identify a modification chemistry that was superior to the base material in terms of platelet or leukocyte activation. Despite the successes in reducing protein and cellular deposits on some materials, a truly nonthrombogenic surface does not yet exist.

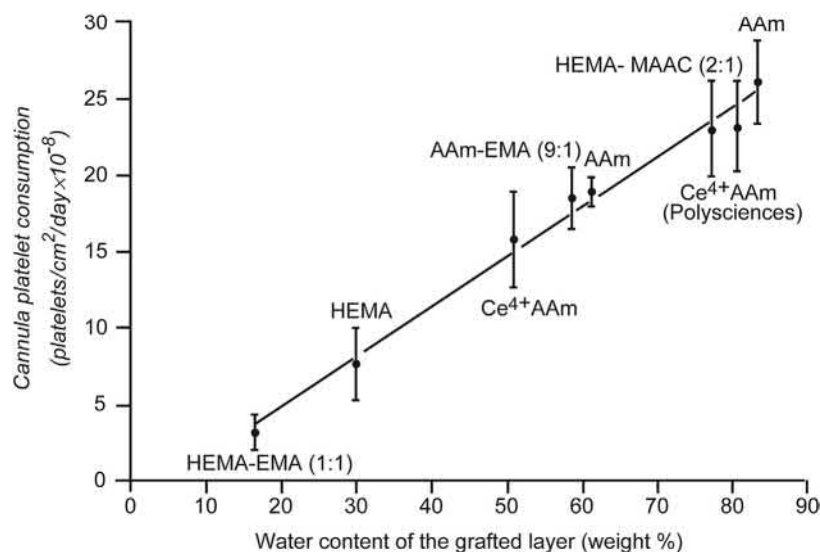


• **Figure 1.4.3B.2** Potential strategies for preparing inert surfaces with low thrombogenicity.

Hydrogels

A popular method to improve the blood compatibility of biomaterials is to increase surface hydrophilicity by incorporating a hydrogel at the surface. All commonly used hydrogels (see Chapter 1.3.2E) that can be cast, chemically cross-linked, or surface-grafted have been used. By definition, hydrogels permit the retention of large amounts of water without dissolution of the polymer itself. This makes them similar to biological tissues, in that they are permeable to small molecules and possess low interfacial tension. It was Andrade who first postulated that since the interfacial free energy between blood and vascular endothelium was near zero, material surfaces which tend to have an interfacial energy of zero should have minimal thrombogenicity (Andrade et al., 1973). Today, considerable experimental evidence supports the claim that materials with minimal interfacial energy, like hydrogels, do not strongly support cell and/or thrombus adhesion. Unfortunately, such generalizations are always flawed by exceptions. A hydrogel (cellulose) used as a dialysis membrane material (Cellophane) is well recognized as being thrombogenic, possibly because it is also a strong activator of the complement system (Chapter 2.2.4). Furthermore, low adhesion (or low protein adsorption) is not the same as low thrombogenicity.

In the early 1980s, a number of polymers were grafted with hydrogel surfaces in an effort to decrease their thrombogenicity. For example, in a large *ex vivo* study (Hanson et al., 1980), a variety of surface-grafted copolymers were



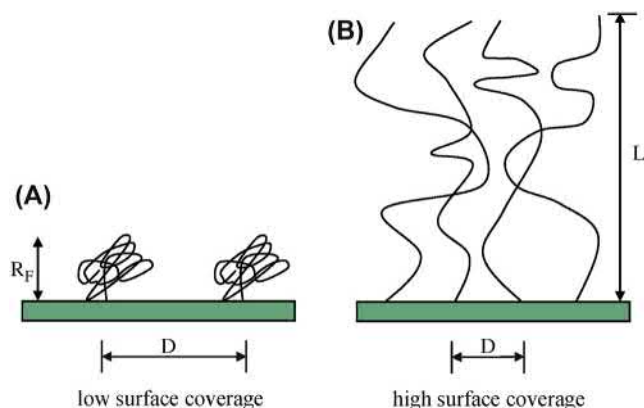
• **Figure 1.4.3B.3** Rate of cannula platelet consumption per unit area (in baboons) is directly related to the graft water content of shunts grafted with eight acrylic and methacrylic polymers and copolymers. *AAm*, acrylamide; *EMA*, ethyl methacrylate; *HEMA*, hydroxyethyl methacrylate; *MAAC*, methacrylic acid. Mean values ± 1 S.E. (From Hanson, S.R., Harker, L.A., Ratner, B.D., Hoffman, A.S., 1980. In vivo evaluation of artificial surfaces with a nonhuman primate model of arterial thrombosis. *J. Lab. Clin. Med.* 95, 289–304, with permission.)

prepared and evaluated for platelet consumption in a baboon shunt model of arterial thrombogenesis. Although few platelets were found adherent to the graft surface, the higher the water content, the greater the rate at which the graft tubing caused the destruction of the circulating platelets (Fig. 1.4.3B.3). Even though this study concluded that hydrogels did not possess low thrombogenicity, utilization of hydrogels remains a popular approach to lower thrombogenicity. It is likely that platelet consumption will be of concern only in applications with large surface areas. On the other hand, platelet consumption is evidence of platelet activation, and the local (as opposed to systemic) consequences of such activation have yet to be defined.

Rather than radiation grafting of hydrogels onto materials, surfaces can also be simply coated with hydrophilic polymers, such as poly(vinyl pyrrolidone) (PVP). While coating with PVP is intended to increase lubricity and ease catheter insertion, benefits on thrombogenicity (and bacterial adhesion) have also been noted (Francois et al., 1996).

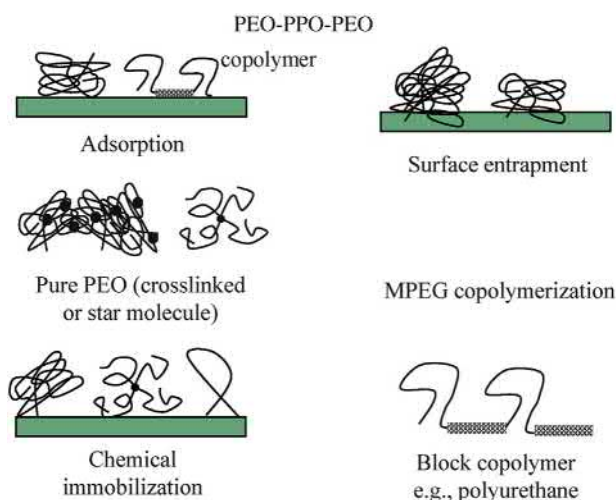
Polyethylene Glycol (PEG) Immobilization

Immobilization of the water-soluble synthetic polymer, polyethylene glycol (PEG, $-\text{CH}_2\text{CH}_2\text{O}-$), is a widely used approach to making a biomaterial surface more protein and cell resistant. It also makes the surface hydrogel-like. This approach was promoted by Edward Merrill, who recognized the lack of hydrogen bond donor sites on the PEG molecule and postulated that such sites might be involved with protein binding (Merrill and Salzman, 1983). A widely recognized theory that helps to explain the nonthrombogenicity of PEG-containing surfaces was presented by Nagaoka et al. (1984). They reasoned that the presence of diffuse



• **Figure 1.4.3B.4** Structure of polyethylene glycol (PEG)-modified surfaces. (A) At low surface coverage ($D \gg R_F$), molecules assume conformation and size similar to random coil. (B) At high surface coverage ($D \ll R_F$), molecules are more extended, chain-like, and form a dense brush. (Adapted from de Gennes, P.G., 1980. Conformation of polymers attached to an interface. *Macromolecules* 13, 1069–1075.)

hydrophilic polymers, covering a significant portion of a biomaterial surface, would exert a steric repulsion effect toward blood proteins and cells (Fig. 1.4.3B.4). The dominance of steric repulsion over the van der Waals attractive forces was hypothesized to be dependent on the extension and flexibility of the polymer chain in the bulk solution. The resulting excluded volume effect results from a loss in configurational entropy of the PEG that in turn results from the rise in the local osmotic pressure occurring when PEG chains are compressed when blood elements approach the surface. This effect is dependent on both the chain length (N , monomers/chain), and the surface density of chains (σ , number of chains per unit area). A simple scaling relationship relates these parameters (and a , the monomer size) to



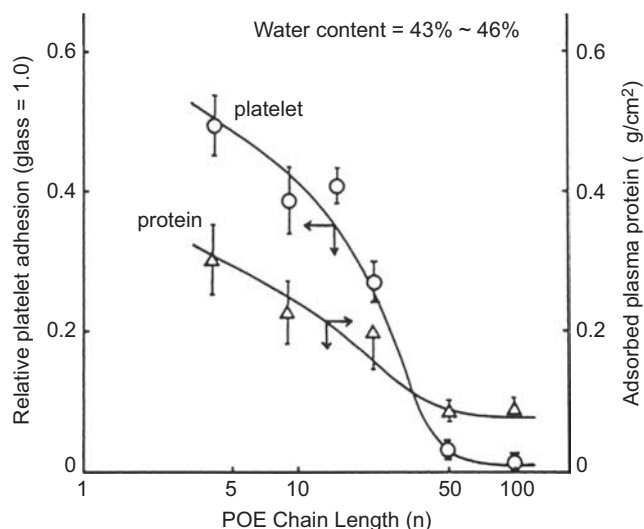
• **Figure 1.4.3B.5** Methods for incorporating poly(ethylene glycol) (PEG) onto the surfaces of materials. *MPEG*, methoxypoly(ethylene glycol) methacrylate; *PEO*, poly(ethylene oxide); *PPO*, poly(propylene oxide).

the thickness, L , of the polymer layer at the surface, for the case of a good solvent (specifically an athermal solvent), and when the chain density is high (the distance between chains (D) is less than the Flory radius (RF)) (de Gennes, 1980):

$$L \approx Na\sigma^{1/3} \quad (1.4.3B.3)$$

Jeon et al. (1991) and Jeon and Andrade (1991), among others, have theoretically modeled protein–surface interactions in the presence of PEG and concluded that steric repulsion by surface-bound PEG chains was largely responsible for the prevention of protein adsorption on PEG-rich surfaces.

As shown in Fig. 1.4.3B.5, a number of approaches have been used to enrich surfaces with PEG. For example, it has been grafted to surfaces via a backbone hydrogel polymer, such as in the preparation of methoxypoly(ethylene glycol) monomethacrylate copolymers (Nagaoka et al., 1984). It has also been covalently bonded directly to substrates via derivatization of its hydroxyl end groups with an active coupling agent or, alternatively, the hydroxyl end groups have been reacted with active coupling agents introduced onto the surface (Desai and Hubbell, 1991a; Chaikof et al., 1992; Tseng and Park, 1992). The commercial availability of a large number of reactive PEG molecules (e.g., amino-PEG, tresyl-PEG, N-hydroxysuccinimidyl-PEG) has greatly facilitated the use of covalent immobilization strategies. Unfortunately, it is difficult to achieve the required high surface coverages by immobilization, since the first molecules immobilized sterically repel later molecules that are attached, unless thermodynamically poor solvents are used. The surface fraction may then be too low to completely “mask” the other functional groups that may be present. Pure monolayers of star PEG have been grafted to surfaces in an attempt to increase surface coverage (Sofia and Merrill, 1998), and radio frequency plasma polymerization of tetraglyme has been used to the same end (Shen et al., 2001). Other investigators have used block copolymers (e.g., Pluronic)



• **Figure 1.4.3B.6** Effect of PEG (or “POE”) chain length (n) on the adhesion of platelets (from activated platelet-rich plasma) and adsorption of plasma proteins (from plasma) onto poly(methyl methacrylate-co-methoxypoly(ethylene glycol) methacrylate) gels. Mean values and standard deviation are shown. Both protein adsorption and platelet adhesion were measured by total protein analysis. A relative platelet adhesion value of 0.3 corresponded to a scanning electron microscopy (SEM) platelet adhesion density of ~ 80 platelets/ $1000\mu\text{m}^2$. (From Nagaoka, S., Mori, Y., Takiuchi, H., Yokota, K., Tanzawa, H., Nishiumi, S., 1984. Interaction between blood components and hydrogels with poly(oxyethylene) chains. In: Shalaby S., Hoffman A.S., Ratner, B.D., Horbett, T.A. (Eds.), *Polymers as Biomaterials*, Plenum Press, pp. 361–371, with permission.)

of PEG and PPO [poly(propylene oxide)] by adsorption, gamma irradiation, or as an additive (McPherson et al., 1997); some have combined PEG with other strategies such as phosphorylcholine (Kim et al., 2000), cyclodextrin (Zhao and Courtney, 2007), and negatively charged side groups (from vinyl sulfonic acid sodium salt) (Lee et al., 2004).

PEG has also been incorporated, by both ends, into polyetherpolyurethanes (Merrill et al., 1982; Okkema et al., 1989). Unfortunately, the results in this case depend on a combined effect of surface microphase separation and the hydrogel (hydrated chain steric exclusion) effect of the PEG side chains. While some have noted lower thrombogenicity, others have not. For example, Okkema et al. (1989) synthesized a series of poly(ether-urethanes) based on PEG and poly(tetramethylene oxide) (PTMO) soft segments, and noted that the higher PEG-containing polymers were more thrombogenic in a canine ex vivo shunt model. Since PEG-containing polyurethanes have a considerable non-PEG phase, Chaikof et al. (1989) prepared a cross-linked network of PEG chains using only small polysiloxane units.

A number of investigators have noted that the beneficial effect of PEG is molecular weight dependent. Nagaoka et al. (1984) were among the first to demonstrate that increasing the PEG chain length of hydrogels containing methoxy poly(ethylene glycol) monomethacrylates led to reductions in protein and platelet adhesion (Fig. 1.4.3B.6). To some extent, however, the benefit of high-molecular-weight

PEO¹ is compromised by the crystallizability of long-chain PEO. In some cases, the benefit of longer chains may reflect particular process advantages (such as surface entrapment). Chaikof et al. (1992), with end-linked PEO, and Desai and Hubbell (1991b), with physically entrapped PEO, found lowest protein and platelet or cell deposition with high-molecular-weight PEO (>18,000 Da). However, when studying PEG-modified polyurethanes, Tan and Brash (2008) noted the importance of PEG surface density over length: the shortest PEG chain (MW: 550) allowed for a higher surface density and provided the greatest reduction in protein reduction compared to modification with longer chains of PEG (MW 2000 and 5000).

It is clear that incorporation of PEG results in reduced levels of cell (including platelet) adhesion and protein adsorption when compared to unmodified and typically hydrophobic substrates. It is far less clear whether the reduced adhesion or adsorption translates to lower material thrombogenicity (Llanos and Sefton, 1993a,b). Further, it is not clear whether reduced adhesion/adsorption is due specifically to the thermodynamic effects of PEG or PEO, or to the increase in surface hydrophilicity after its immobilization [refer to Brash et al., 2019, for a critical discussion on how protein adsorption is thought to govern (or not) blood reactivity]. While the in vitro results have looked promising, the lack of correlation between the few in vitro and ex vivo studies is of concern. Efforts with plasma deposited tetraglyme (Shen et al., 2001) have led to surfaces with ultra-low adsorbed fibrinogen, suggesting that previous attempts at using PEG modification have not been successful because of the inability to achieve the desired ultra-low (<5 ng/cm²) levels of adsorbed protein. On the other hand, other studies from the same group (Zhang et al., 2008; Zhang and Horbett, 2009) show that such surfaces are not as resistant to protein adsorption as expected when exposed to physiological conditions (undiluted plasma). Low amounts of adsorbed von Willebrand factor (vWF) (and not fibrinogen only) also played a significant role in platelet adhesion under high shear rates. There is also evidence that properties of PEO and PEG surfaces may also be affected by the sterilization process (see Box 1.4.3B.2). This highlights the importance of testing modified surfaces under physiological conditions before drawing conclusions from in vitro studies using (surrogate) markers such as platelet adhesion or fibrinogen adsorption.

Albumin Coating and Alkylation

The early observation that surfaces coated with albumin did not support protein adsorption and platelet adhesion (reviewed by Andrade and Hlady, 1986) led many investigators to lower material thrombogenicity by either albumin coating or enhancing the affinity of albumin for surfaces via alkylation. Albumin adsorbs relatively tightly onto hydrophobic surfaces, while having a poor affinity for hydrophilic surfaces. Consequently, utilization of this strategy

¹ PEG >10 kD is called PEO [poly(ethylene oxide)], reflecting the different monomer and polymerization process used.

• BOX 1.4.3B.2 Associated Facts: Effect of Sterilization Procedure on Hydrogel Properties

Most in vitro blood experiments are completed in 2 hours or less and little consideration is given to sterilization. However, sterilization may affect the materials' surface properties and thrombogenicity. For example, sterilizing PEG hydrogels using current methods (ethylene oxide, gamma, or plasma) may result in changes in surface roughness, protein adsorption, or the presence of radical species (Leixa et al., 2008; Kanjickal et al., 2008). These changes lead to significant differences in the biocompatibility response between unsterilized and sterilized samples. Thus, it is important to test a surface-modified material in a "final product state," since processing may significantly alter its ability to reduce thrombogenicity in vivo. Removing endotoxin is another important consideration, at least in understanding the role of leukocytes and endothelial cells (Gorbet and Sefton, 2005a).

entails increasing the hydrophobicity of the surface, which is the opposite of the above-discussed strategies whereby the hydrophilicity of the surface was increased. Albumin coating is consistent with another hypothesis, developed early in the 1970s, which suggested that hydrophobic surfaces with critical surface tensions (conceptually related to surface free energy) around 20–30 dyn/cm would have a lower thrombogenicity (Baier et al., 1970).

A limitation of relying on albumin coating is that other proteins will adsorb to the surface displacing the albumin, limiting the long-term effectiveness of this strategy (see Chapter 2.1.2). To prevent displacement, glutaraldehyde cross-linking (Kottke-Marchant et al., 1989) or covalent immobilization has been used (Hoffman et al., 1972; Matsuda and Inoue, 1990). Reduced platelet adhesion was observed in vitro with a multilayer of albumin on polyether-sulfone deposited using a layer-by-layer technique (Sperling et al., 2006). Since albumin has binding pockets for long alkyl chains, Munro et al. (1981) demonstrated that surfaces with long carbon chains (C-16 or C-18) have a high affinity for albumin, and provided for a dynamically renewable natural albumin layer. Albumin adsorption (from diluted plasma) was enhanced on alkylated cellulose membranes (Frautschi et al., 1995). Butylation (but not longer alkyl chains) of polyvinyl alcohol hydrogel also dramatically reduced platelet reactivity in a dog shunt (Strzinar and Sefton, 1992), suggesting that some of the observed benefit was due to the creation of a hydrophobic surface (Duncan et al., 1997).

Zwitterionic Group/Phospholipid-Mimicking Surfaces

A number of investigators have hypothesized that a surface similar to the external zwitterionic outer phospholipid membrane of cells should be nonthrombogenic.² Since

² Upon cell activation, the negatively-charged phospholipids that are preferentially located on the cytoplasmic face of the cell membrane flip to the outer membrane, which accelerates blood clotting by enabling assembly of the prothrombinase and tenase complexes.

phosphorylcholine (PC) is the major lipid head group on the external surface of blood cells and red blood cells are inert in coagulation assays, PC has been the choice of many investigators for incorporation into surfaces.

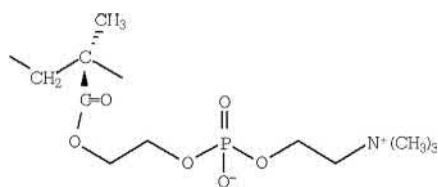
Durrani et al. (1986) prepared a series of reactive derivatives of phosphorylcholine that were designed to react with surface hydroxyl groups and surface acid chlorides on various materials. Another approach involved coating materials (Campbell et al., 1994; Lewis et al., 2000; Iwasaki et al., 2002), or blending a polyurethane (Ishihara et al., 1995, 1999) with a methacryloylphosphorylcholine (MPC; Fig. 1.4.3B.7)/polyacrylate copolymer. Platelet adhesion was significantly reduced on phosphorylcholine-coated expanded polytetrafluoroethylene (ePTFE) grafts at 90 min in dogs, and anastomotic neointimal hyperplasia and neointimal cell proliferation were also reduced (Chen et al., 1998). Ishihara et al. (1998) have attributed the low protein adsorption of their phospholipid polymers to the high free water fraction, a mechanism that has been confirmed by other investigations (Chen et al., 2005). A further modification has involved grafting only the polar part of phosphorylcholine onto ammonia plasma-treated ePTFE to promote more of the red blood cell-like properties while preventing lipid uptake (Chevallier et al., 2005). This led to a significant reduction in both platelet and leukocyte adhesion.

A recent approach has also been to modify materials (for example polyurethane) using zwitterionic polymers/monomers such as carboxybetaine or sulfobetaine (Fig. 1.4.3B.8A,B) to mimic the cell membrane (Yuan et al., 2003; Jiang et al., 2004; Kitano et al., 2005). Zhang et al.

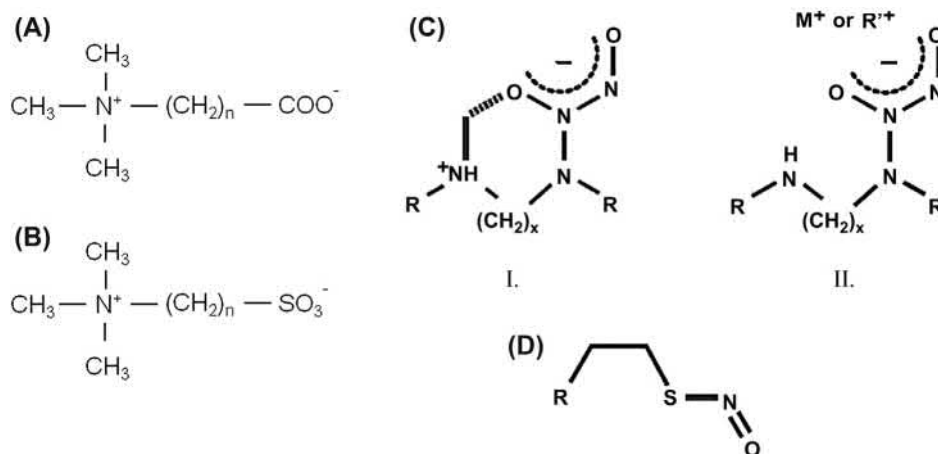
(2008) prepared polymeric brushes containing zwitterionic groups by surface-initiated atom transfer radical polymerization using sulfobetaine methacrylate (polySBMA) and carboxybetaine methacrylate (polyCBMA) on gold surfaces. Not only did such zwitterionic polymeric brushes exhibit super-low protein adsorption, with the polyCBMA brushes adsorbing less than 0.4 ng total protein/cm² (experiments performed in 100% plasma), but significantly reduced platelet adhesion was also observed. The polyCBMA also demonstrated unique anticoagulant properties, suggesting that such a material may offer excellent blood compatibility, although the mechanism by which polyCBMA is superior to polySBMA is currently unclear. Most recent studies have however focused on surface coating with polySBMA; some promising results were obtained in a porcine model with minimal platelet activation and adhesion after a 26-day implantation period (Iqbal et al., 2019).

Surface-Modifying Additives (SMAs)

The blending of a copolymer, composed of polar and non-polar blocks, to a base polymer appears to be a successful means to lower material thrombogenicity. The strategy, originally developed by Thoratec Laboratories Inc., is a means to alter the surface properties of materials without affecting bulk properties (Ward et al., 1984). The copolymers, added in low concentration, migrate to the base polymer surface during and after fabrication, and dramatically change the outermost surface molecular layers that comprise the region that determines biocompatibility (Tsai et al., 1994). The copolymers have a structure which is amphipathic, that is, certain groups or segments will have an attraction for the continuous phase (major polymer component of the blend), while other portions of the molecule will have little attraction for the base polymer and will be of lower polarity (Ward et al., 1984) (see Chapter 1.4.2). They have been used to lower the thrombogenicity of cardiopulmonary bypass and hemodialysis components by using SMA-blended polymers or SMA-coated surfaces. A clinical evaluation of the effects



• **Figure 1.4.3B.7** Chemical structure of poly(2-methacryloyloxyethyl phosphorylcholine).



• **Figure 1.4.3B.8** Generic structures of zwitterionic molecules ((A) carboxybetaine and (B) sulfobetaine) and two common NO donors: (C) zwitterionic (I) and cation-stabilized (II) diazeniumdiolates, and (D) an S-nitrosothiol. (From Frost, M.C., Reynolds, M.M., Meyerhoff, M.E., 2005. Polymers incorporating nitric oxide releasing/generating substances for improved biocompatibility of blood-contacting medical devices. *Biomaterials* 26, 1685–1693.)

of SMA on cardiopulmonary bypass circuits demonstrated a reduction in platelet interactions with no effect on complement activation (Gu et al., 1998).

Fluorination

The incorporation of fluorine into materials is also a strategy to lower thrombogenicity. Polymers with fluorinated chains are highly hydrophobic, and it is believed that the fluorine group's low surface energy modulates protein adsorption and platelet adhesion/activation. Preparing fluorine-rich surfaces is often facilitated by the tendency of fluorine-containing functional groups to concentrate on the surface of the polymer during preparation. Kiaei et al. (1988) found a strong effect of a fluoropolymer plasma on thrombus formation and plasma-induced graft polymerization of a fluorocarbon on polyethylene also reduced platelet adhesion (Lin et al., 2000). Fluoroalkyl groups as chain extenders have also been used to prepare nonthrombogenic polyurethanes (Kashiwagi et al., 1993). Using a similar approach, Wang and Wei (2005) showed that increasing fluorine content in polyurethanes by decreasing soft segment length resulted in a decrease in platelet adhesion and activation (of adherent platelets). Fluorinated surface-modifying macromolecules (SMMs) used to increase polyetherurethane biostability also improved blood compatibility (Jahangir et al., 2002), although the effect does not appear to be directly correlated with a decrease in fibrinogen adsorption (Massa et al., 2005).

Heparin-Like Materials

A number of polymers have been synthesized or modified in order to prepare polymers with chemical similarity to heparin, and thus possess heparin-like activities. For example, Fougnot et al. (1983) synthesized sulfonate/amino acid sulfamide polystyrene derivatives in order to create insoluble heparin-like materials. Some investigators (e.g., Grasel and Cooper, 1989) only incorporated sulfonate groups in an effort to lower thrombogenicity by surface thrombin inhibition. Enhanced binding and inactivation of thrombin was found, suggesting that these weak heparin-like molecules are sufficiently dense to lower thrombogenicity. A later approach combined sulfonation and PEG-like materials in the use of sulfonated cyclodextrin polymers (Park et al., 2002); and improved blood compatibility was seen in a canine shunt model (Han et al., 2006).

Self-Assembled Surface Layers

Self-assembled surface layers (Whitesides et al., 1991) have been envisioned as useful templates to nucleate or organize ordered, designed biomaterials (Ratner, 1995; see Chapter 1.4.2). Self-assembled monolayers (SAMs) of alkylsilanes supported on oxidized polydimethyl siloxane (PDMS) rubber have been used as a model system (Silver et al., 1999). The authors reported that surfaces grafted with hydrophobic head groups (CH_3 and CF_3) had significantly lower platelet

and fibrinogen deposition than the surfaces composed of hydrophilic head groups in a canine ex vivo arteriovenous series shunt model. In a later in vitro study (Sperling et al., 2005), contradictory results were obtained whereby SAMs with $-\text{CH}_3$ exhibited the most platelet adhesion compared to $-\text{COOH}$ and $-\text{OH}$. Reduced thrombin formation was observed for $-\text{CH}_3$ and $-\text{COOH}$. These studies highlight the difficulty of generalizing the effect of surface modification on blood compatibility. In addition to producing zwitterionic polymeric brushes (see the section "Zwitterionic Group/Phospholipid Mimicking Surfaces"), Zhang et al. (2008) produced a series of SAM surfaces using oligoethyleneglycol, phosphorylcholine, oligophosphorylcholine, mixed $\text{SO}_3^-/\text{N}^+(\text{CH}_3)_3$, and mixed $\text{COO}^-/\text{N}^+(\text{CH}_3)_3$; there was no significant difference in platelet adhesion or fibrinogen adsorption among these SAMs.

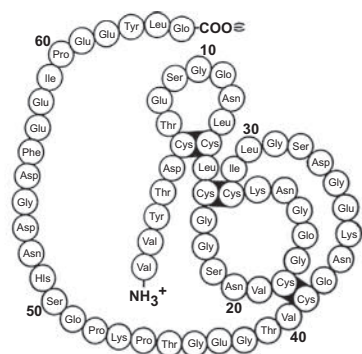
Active Materials

The limited success of the various surface treatments for lowering thrombogenicity has encouraged researchers to pursue other strategies. The most popular strategy, and the one that started the field, is the heparinization of surfaces, although the incorporation of other antithrombotic and antiplatelet agents into materials also gained popularity (Fig. 1.4.3B.9). Currently, the antithrombotic agents utilized have mainly been against thrombin (hirudin, curcumin, thrombomodulin).

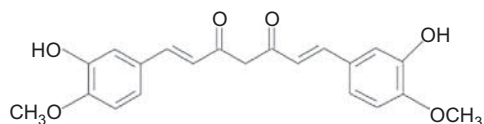
The incorporation of antiplatelet agents into materials has been limited by the instability and complex mechanism of action of these agents. Platelet GPIIb/IIIa antagonists (e.g., ReoPro, Centocor) and agents against factor Xa (low-molecular-weight heparins, LMWH) or inhibitors of tissue factor expression (extrinsic pathway) are currently being used systemically during cardiovascular surgery. There is potential for such drugs to be included in novel strategies to modify materials.

Heparinization

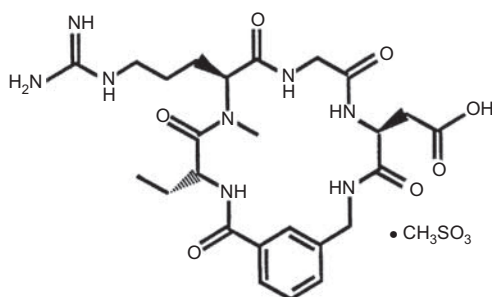
Heparinization of surfaces continues to be the most popular technique for lowering the thrombogenicity of materials. As illustrated in Fig. 1.4.3B.10, heparin is a linear, acidic carbohydrate composed of repeating disaccharide units that are O- and N-sulfated. The molecular weights of heparin chains range from 1200 to 40,000 Da, with a mean molecular weight of approximately 10,000. Depending on its molecular weight and structure, it can inhibit, in association with its cofactor (antithrombin III), the serine proteases: thrombin and factor X. Since thrombin is also a potent platelet activator, binding it into an inactive complex should help minimize platelet activation. Investigators have been able to covalently, ionically, and physically attach heparin to various substrates utilizing a number of chemistries. The main concern has been that once immobilized, the heparin should be able to assume its native conformation, and be able to interact with antithrombin III.



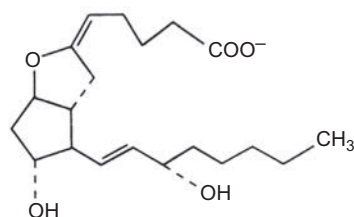
Hirudin



Curcumin



DMP 728



Prostacyclin



Thrombomodulin

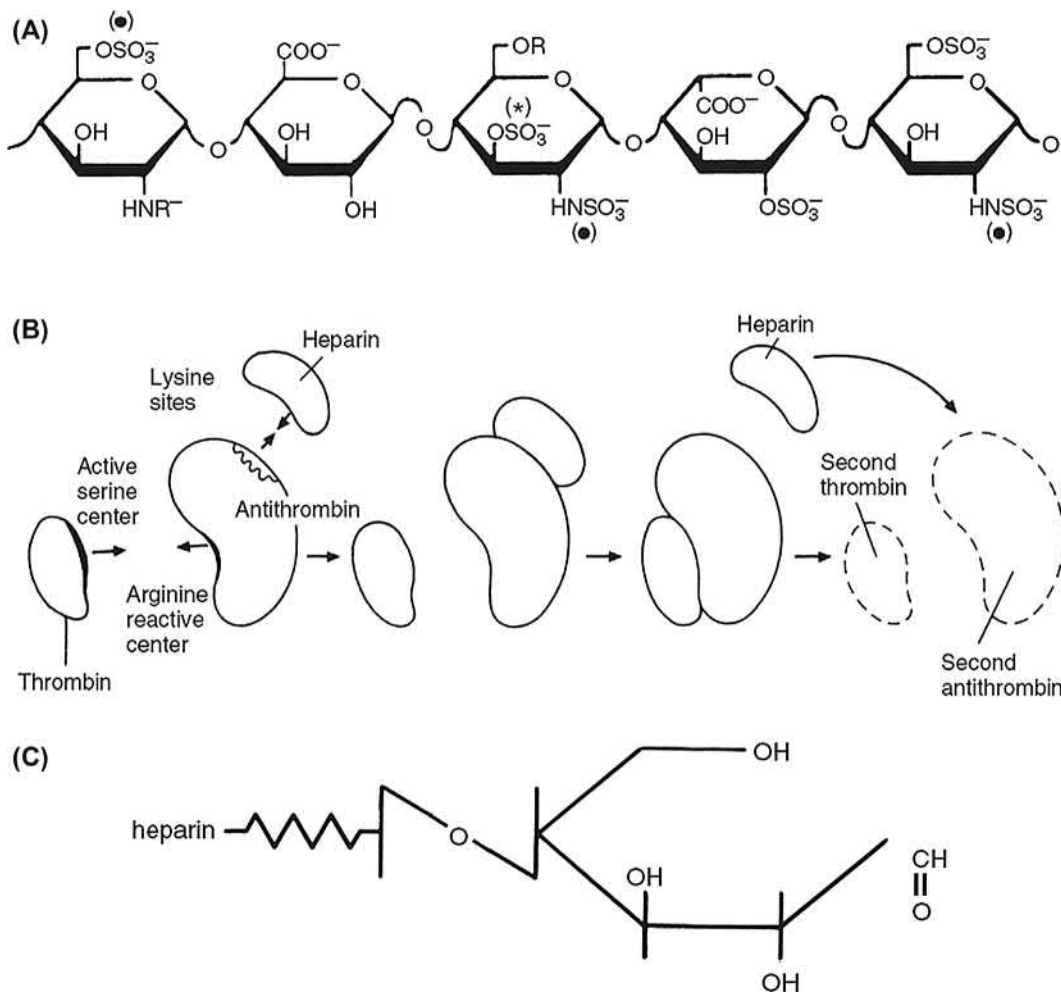
• **Figure 1.4.3B.9** Agents, other than heparin that have been incorporated into biomaterials to actively control thrombogenicity. Hirudin and curcumin are thrombin inhibitors. Prostacyclin (PGI₂) is a natural inhibitor of platelet function, while DMP728 is a small-molecule GPIIb/IIIa antagonist. Thrombomodulin inhibits thrombin by activating protein C.

The effectiveness of heparin as an agent capable of increasing synthetic venous graft patency and reducing downstream anastomotic neointimal hyperplasia and cell proliferation was demonstrated using a novel polytetrafluoroethylene-based local drug-delivery device. Heparin was infused adjacent to the graft wall and at downstream anastomotic sites for 14 days and demonstrated effectiveness (Chen et al., 1995).

Ionically Bound Heparin and Controlled-Release Systems

If negatively charged heparin is bound ionically to the surface, then heparin will be slowly released over time due to exchange with the blood. A similar effect is obtained if heparin is dispersed within a hydrophobic polymer. Selected

techniques to produce materials which release heparin at biologically significant rates have been discussed in depth by a number of investigators (Sefton et al., 1987; Amiji and Park, 1993). Ionic approaches involve binding the highly negatively charged heparin onto a cationic surface through ionic binding. The limitation is that the leaching of heparin will eventually leave the surface unprotected. Certain non-ionic approaches are also characterized by high release rates (due to relatively unstable bonds), so that determining the heparin release rate (in addition to amount bound) is a primary means of characterizing these surfaces. Limitations to the use of dispersed systems include the loading capacity of heparin, which prevents long-term usage and the heterogeneity of heparin, leading to the early release of lower molecular weight chains.



• **Figure 1.4.3B.10** (A) Antithrombin III-binding pentasaccharide of heparin. The pentasaccharide sequence is composed of three glucosamine (units 1, 3, and 5), one glucuronic acid (unit 2), and one iduronic acid (unit 4) units. Structural variants are indicated by $-R'$ ($-H$ or $-\text{SO}_3^-$) or $-R''$ ($-\text{COCH}_3$ or $-\text{SO}_3^-$). The 2-O-sulfate groups (asterisk), a marker component for the antithrombin-binding region, and sulfate groups indicated by (\bullet) are essential for high-affinity binding to antithrombin. (B) The mechanism of action of heparin and antithrombin III. (C) The reducing end of heparin formed by treatment with nitrous acid. ((A) From Fiore, L., Deykin, D., 1995. Anticoagulant therapy. In: Beutler E., Lichtman M.A., Collen B.S., Kipps, T.J. (Eds.), *Williams Hematology*, fifth ed. McGraw-Hill, pp. 1563; and (B) From Bauer, K.A., Rosenberg, R.D., 1995. Control of coagulation reactions. In: Beutler E., Lichtman M.A., Collen B.S., Kipps, T.J. (Eds.), *Williams Hematology*, fifth ed. McGraw-Hill, pp. 1241, with permission.)

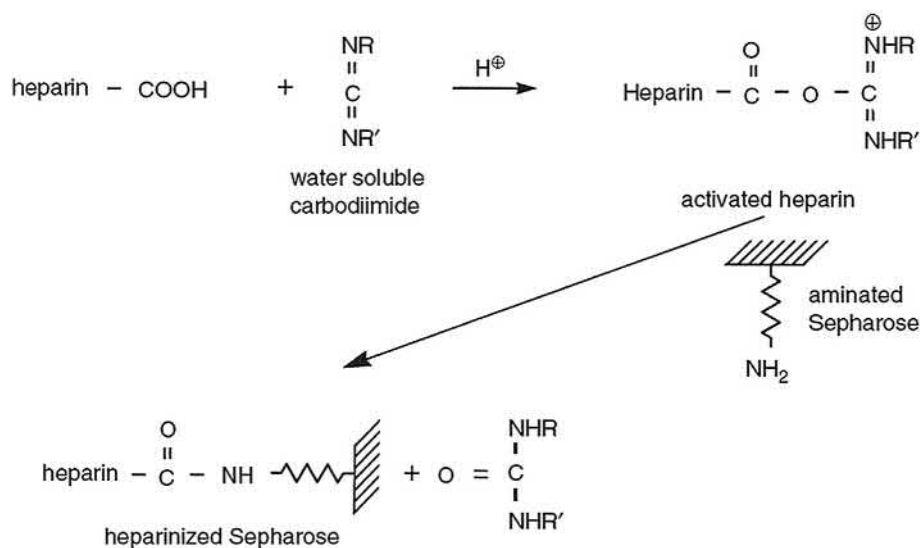
The thromboresistance of heparinized materials based on controlled release appears to be due to a microenvironment of heparin in solution at the blood–material interface. The relationship between release rate (N , g/cm²s) and surface concentration (C_s , g/cm³) for heparin or any other agent released from the inside wall of a tube of radius r_0 is given by (Basmadjian and Sefton, 1983):

$$\frac{C_s}{Nr_0/D} = 1.22 \left[\frac{x/r_0}{\text{Re}Sc} \right]^{1/3} \quad (1.4.3B.4)$$

where D = diffusivity (cm²/s); r_0 = tube radius; x = axial position; Re = Reynold's number = $2r_0v\rho/\mu$; Sc = Schmidt number = $\mu/\rho D$; v = average velocity; ρ = density; μ = viscosity. The diffusivity of heparin is $\sim 7.5 \times 10^{-7}$ cm²/s and the critical C_s (minimum therapeutic level) for heparin is ~ 0.5 $\mu\text{g}/\text{mL}$.

Use of tridodecyl methylammonium chloride (TDMAC; Lehninger, 1966), a lipophilic, cationic surfactant, eliminated the need for the graphite coating that was part of the original graphite–benzalkonium–heparin (GBH) method (Gott et al., 1963). TDMAC and the many other quaternary ammonium compounds enabled heparin to be ionically bound to a wide range of biomaterials. Unfortunately, such compounds are surfactants with potentially toxic consequences, and are known to be eluted from the surfaces within a week.

Quaternizable amino groups have also been incorporated directly into polymers to improve the stability of the ionically bound heparin. Tanzawa et al. (1973) synthesized a graft copolymer with a dimethylaminoethyl group by UV-initiated copolymerization of *N,N*-dimethylaminoethyl methacrylate (DMAEM) and methoxypolyethylene glycol



• **Figure 1.4.3B.11** One-step carbodiimide activation of carboxyl groups of heparin for binding to aminated Sepharose. For EDC, R = (CH₂)₃N(CH₃)₂. For a carboxylated substrate (e.g., hydrolyzed polymethyl acrylate) its carboxyl groups may be activated by carbodiimide in a separate step for subsequent reaction with the free amine groups of heparin.

methacrylate (MPEG). Use of this technique (Angiocath, Toray Industries) to coat poly(urethane) catheters indicated that a minimal heparin elution rate of 0.04 μg/cm²/min was needed to render the catheter thrombus free *in vivo* (Idezuki et al., 1975). This value is consistent with Eq. (1.4.3B.4).

A commercial procedure (Baxter Bentley Healthcare Systems, Irvine, CA) to ionically bind heparin (Duraflon II) has been used to coat cardiopulmonary bypass circuits and other devices. While heparin coating of extracorporeal circuits is designed to reduce surface thrombus formation, its effect on complement, contact activation, and inflammation is unclear and often contradictory (see below).

Covalently Bound Heparin

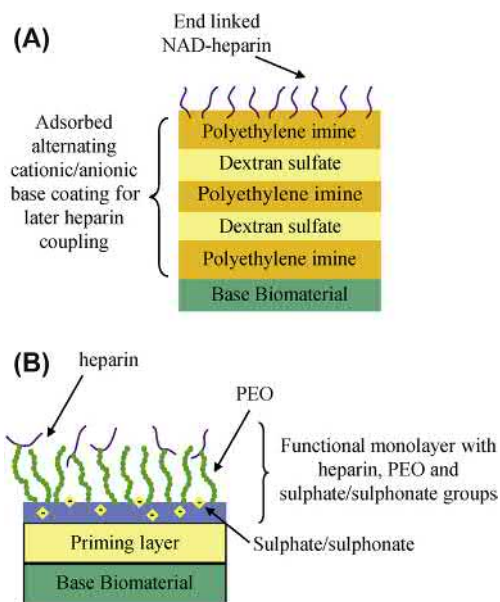
To impart a degree of activity longer than that possible with ionic linkages, heparin has been covalently immobilized to material surfaces. It is now recognized that the conformation of the attached heparin and the point of attachment (end point vs. multipoint) are critical factors determining the catalytic efficiency of the immobilized heparin. Lindhout et al. (1995) studied the antithrombin activity of surface-bound heparin under flow conditions. They demonstrated that the rate of thrombin inactivation of the antithrombin–heparin surface equals the maximal rate of transport of thrombin toward the surface when the surface coverage of antithrombin exceeds 10 pmol/cm²; thus indicating that a higher intrinsic catalytic efficiency of a surface does not necessarily result in a higher antithrombin activity.

Many of the coupling methods listed in Chapter 1.4.4 have been used for heparin. For example, Heyman et al. (1985) attached 1-ethyl-3-(3-dimethylaminopropyl) carbodiimide (EDC)-activated heparin covalently onto chemically modified polyetherurethane catheters through a diamino alkane spacer. The immobilized heparin retained its ability to bind and inactivate thrombin and factor Xa.

Unfortunately, carbodiimides (Fig. 1.4.3B.11) are recognized as less than ideal activating agents for immobilizing heparin, since the acidic conditions used can result in a loss of anticoagulant activity.

Larm et al. (1983) developed a technique by which heparin can be covalently end point-attached (commercialized as the Carmeda BioActive Surface, CBAS and marketed, for example, as Cortiva BioActive Surface by Medtronic for extracorporeal circulation devices) to the surface of plastics, as well as glass and steel. Heparin is first partially depolymerized by deaminative cleavage using nitrous acid to produce heparin fragments terminating in an aldehyde group (Fig. 1.4.3B.10C). The heparin is then covalently linked to the primary amino groups of polyethylene imine (PEI) (Fig. 1.4.3B.12A). This technique results in a highly stable, low-thrombogenicity coating that retained its efficacy *in vivo* for 4 months in dogs (Arnander et al., 1987), and during patient treatment with an artificial lung (Bindslev et al., 1987). There was also a beneficial effect on *in vivo* bacterial colonization of treated polyurethane central venous catheters (Appelgren et al., 1996).

The commercial Trillium coating (developed by Bio-Interactions Ltd. and marketed by Medtronic) combines covalently binding heparin with polyethelene oxide and sulfonate groups (Fig. 1.4.3B.12B). Clinical studies with Duraflon, Carmeda, and Trillium have shown that while they enable the use of reduced systemic anticoagulation (Ovrum et al., 2001), they do not reduce the postoperative acute phase response (van den Goor et al., 2004; Hoel et al., 2004). Complement and leukocyte activation play an important role in the biocompatibility of extracorporeal circulation devices, and while several *in vitro* studies suggest that heparin coating may have other effects (see review of Biron and Pond, 2017), it appears that the *in vivo* benefit of heparin coatings is limited to anticoagulation.



• **Figure 1.4.3B.12** Commercial surface treatments used for cardiopulmonary bypass (CPB) and potentially also for vascular grafts. (A) Carmeda method for immobilizing nitrous acid-treated heparin (end-linked heparin) to dextran sulfate and polyethylene imine-treated surface. (B) Trillium coating: The priming layer is hydrophilic and strongly binds to the base material, PEO chains and sulfate and sulfonate groups are covalently attached to the priming layer, while heparin is covalently bound to PEO. (Adapted from Shivpal, S., Luthra, A., 2002. *New biointeracting materials*. *Med. Dev. Technol.* 10, 26.)

Heparin has also been covalently immobilized via its terminal serine at the end of the protein–carbohydrate linkage region to polyvinyl alcohol hydrogel. The heparin is bound during the Lewis acid-catalyzed cross-linking of polyvinyl alcohol chains with glutaraldehyde. The heparinized polyvinyl alcohol hydrogel possessed significant anticoagulant activity, although the platelet incompatibility of the hydrogel substrate led to significant platelet consumption in an *ex vivo* canine shunt model (Cholakis et al., 1989).

Park et al. (1988) covalently bound heparin to a polyurethane using PEG spacer groups. The increasingly mobile nature of the longer hydrophilic spacer chains was considered to have increased the observed bioactivity of immobilized heparin by providing a more bulk-like environment for the heparin. An intravascular oxygenator and carbon dioxide removal device (IVOX; CardioPulmonics, Salt Lake City, UT) also uses covalent heparin bound to a PEG spacer. The PEG is grafted onto a plasma-polymerized polysiloxane on a base material after plasma amination of the surface. Heparin has also been immobilized on silicone via an N-succinimidyl carbonate PEG and the grafted heterobifunctional PEG allowed for high heparin density resulting in both low fibrinogen adsorption and high specificity for ATIII (Chen et al., 2005).

Du et al. (2007) covalently grafted an antithrombin/heparin complex onto a PEO-modified polyurethane in the presence of a free radical initiator. This increased anti-FXa activity compared to grafted heparin alone, and was

shown to significantly reduce material thrombogenicity in a chronic rabbit model (Klement et al., 2006).

There are now several commercially available heparin-coated cardiovascular devices on the market both for short-term (e.g., shunts, arteriovenous access, and extracorporeal circuits) and long-term (e.g., below-the-knee vascular grafts) use. While these coated devices cost significantly more than their uncoated counterparts, there is evidence that, in some applications, patency is significantly higher with heparin coating and thus there is a cost benefit associated with their use (Vergnaud et al., 2018; Villemoes et al., 2018). With the increased use of heparin-coated cardiovascular devices in the past 10 years, the value of heparin coating is currently an area of great debate in the cardiovascular community (Lazarides et al., 2016; Zea et al., 2016; Ashfaq et al., 2018; Samson et al., 2016). Most conclusions are based on retrospective studies and prospective studies will be needed to better assess the overall benefits of heparin coating, especially since other surface modifications to reduce thrombogenicity may be as effective at a lower cost (Giorni et al., 2019).

Thrombin Inhibition Without Heparin

Recognizing the importance of inhibiting material-induced thrombin generation, agents other than heparin have been used to inhibit thrombin and thereby lower the thrombogenicity of the material. For example, hirudin, a potent thrombin inhibitor, has been covalently bound to biomaterials. Compared with heparin, hirudin is advantageous because it has no influence on platelet function, no immune-mediated platelet-activating activity and, most importantly, it does not require the presence of endogenous cofactors like antithrombin III. Thus, the polypeptide hirudin is thought to be able to block clot-bound thrombin that is inaccessible to inhibition by a heparin/antithrombin III complex. On the other hand, heparin functions as a catalyst. That is immobilized heparin, if not blocked by adsorbed protein, can continually accelerate the inactivation of thrombin by antithrombin III. It is unclear how long a covalently immobilized hirudin surface would remain effective, and even whether an immobilized hirudin could gain access to the clot-bound thrombin. Nevertheless, Ito et al. (1991) used heterobifunctional cross-linking reagents to derivatize hirudin to form covalent cross-links between hirudin and albumin, producing active conjugates for immobilization to surfaces. Others have immobilized hirudin to a poly(lactide-glycolide) copolymer (Seifert et al., 1997). Another group has exploited controlled release of hirudin for this purpose (Kim et al., 1998). Small-molecule thrombin inhibitors, like D-Phe-Pro-Arg chloromethyl ketone (PPACK) and others may prove useful as alternatives.

Because of the affinity of benzamidine toward thrombin and its potential to reduce complement activation (which may participate in platelet activation), amidine derivatives were considered to enhance blood compatibility. Gouzy et al. (2004) immobilized a benzamidine derivative (with a hydrocarbon side chain) onto a maleic anhydride copolymer

via a PEG spacer; platelet adhesion and activation was reduced on the modified surface, as well as thrombin–anti-thrombin complex formation. They subsequently correlated thrombin binding to the amount of immobilized benzamide derivative, with the amount immobilized being dependent on spacer length and immobilization chemistry (Salchert et al., 2005). Yim and Sefton (2008) converted the surface nitrile groups of polyacrylonitrile-co-vinyl chloride films into amidine groups by first reacting nitrile with diethyl ether and hydrogen chloride followed by reaction with ammonia in ethanol. While the amidine surface modification was limited, reduced platelet adhesion and activation was observed.

Another approach involves immobilizing thrombomodulin, an endothelial cell-associated protein that inhibits thrombin by activating protein C. Using a small-scale dialyzer it was demonstrated that immobilized human thrombomodulin (on cellulose) still had co-enzyme activity for activation of protein C and anticoagulant activity (Kishida et al., 1995). An amino-terminated silane was used to couple thrombomodulin to glass, and the authors reported both anticoagulant activity and reduced platelet adhesion (Han et al., 2001). Thrombomodulin has also been immobilized (using an azido group via PEG) onto pancreatic islets, with a view to minimizing the thrombogenicity of the islet and enhancing islet engraftment after portal vein infusion (Stabler et al., 2007). Further work is needed to appreciate the potential of such surfaces.

Immobilization of Antiplatelet Agents

There has been considerable interest in incorporating antiplatelet agents into materials to lower material thrombogenicity. Endothelial cells lining the natural vessel wall help prevent thrombus formation by secreting antiplatelet agents such as nitric oxide (NO) and prostacyclin (PGI₂). Thus, a biomaterial containing antiplatelet agents is consistent with our understanding of endothelial cell function. Prostacyclin is potent yet unstable, and efforts to maintain its biological activity during immobilization, coupled with concern for the ability of platelets in the bloodstream to be affected by the immobilized prostacyclin, have limited the enthusiasm for such a strategy. On the other hand, a simpler approach, which also more closely mimics the biological environment, is to incorporate PGI₂ or NO into materials for release. Unfortunately, the inability to load sufficient drug into materials for release limits the materials' lifespan, and this approach may be limited to use in short-term cardiovascular devices such as oxygenators, sensors, and catheters. A novel approach to overcome such limitations is to use endogenous NO donors to generate NO at the blood–material interface. NO is an antiplatelet agent and a potent inhibitor of smooth muscle proliferation. This approach is described in more detail below.

Despite these challenges, many investigators have incorporated antiplatelet agents into surfaces. For example, Ebert et al. (1982) immobilized prostaglandin F₂ α using a diaminododecane spacer arm. The F₂ α was subsequently

converted to the unstable prostacyclin. The benefits of spacer arms are described elsewhere (Chapter 1.4.4). A related approach is to add an antiplatelet agent, such as prostaglandin E₁ (PGE₁), in addition to heparin into a polymer. A PGE₁-heparin compound was synthesized and incorporated into a polyurethane (Jacobs et al., 1985). Also, prostacyclin has been incorporated into polymer matrices for controlled release (McRea and Kim, 1978). Aspirin, capable of inhibiting the generation of the platelet activator thromboxane A₂, has also been incorporated into polyvinyl alcohol membranes used in hemodialysis (Paul and Sharma, 1997), while a dipyrimadole derivative was photo-immobilized on a polyurethane (Aldenhoff et al., 1997).

Two basic approaches exist to create NO-releasing polymers: N-diazeniumdiolates or S-nitrosothiols (Fig. 1.4.3B.8C,D). These can either be blended into polymers or covalently bonded to a side chain or to the polymer backbone (Frost et al., 2005). While S-nitrosothiol-based NO-releasing materials have been synthesized [e.g., with polyvinyl alcohol (PVA) and PVP (Seabra and de Oliveira, 2004)], there is currently only limited biocompatibility data on such an approach (Bohl and West, 2000). On the other hand, NO-releasing materials using diazeniumdiolates have demonstrated great efficiency in reducing thrombus formation in various animal models (Frost et al., 2005; Skrzypchak et al., 2007). Another approach is to use endogenous NO donors to produce NO locally. Duan and Lewis (2002) used endogenous S-nitrosoproteins in plasma to produce NO from immobilized cysteine to minimize platelet adhesion on a polyurethane and a poly(ethylene terephthalate). A lipophilic copper complex has also been incorporated into polyvinyl chloride (PVC) and polyurethane (PU) films that was able to generate NO from nitrite under physiological conditions (Oh and Meyerhoff, 2004) as well as in vivo in a rabbit model of extracorporeal circulation (Major et al., 2011). Significantly reduced thrombus formation as well as decreased monocyte activation were also observed in vivo with the NO-generating biomaterial (Major et al., 2011).

A new generation of antiplatelet agents based on inhibiting fibrinogen binding to activated platelet GPIIb/IIIa receptors offers a fresh approach to lowering the thrombogenicity of surfaces via drug release. These agents, from blocking monoclonal antibodies to small peptides and compounds (e.g., DMP728, Fig. 1.4.3B.9), not only block platelet aggregation, but will also likely block platelet adhesion to artificial surfaces. Some have already been incorporated into stents for release (see the section “Strategies to Lower the Thrombogenicity of Metals,” below, and Chapter 2.5.2B).

Immobilization of Fibrinolytic Agents

Some investigators have sought to promote fibrinolysis on artificial surfaces by the surface generation of plasmin. Clot lysis is achieved by the action of plasmin (formed from plasminogen) on fibrin. However, the action of such surfaces may be “too little too late.” Sugitachi and Takagi (1978) immobilized urokinase, a fibrinolytic enzyme that

acts on plasminogen, on various materials. A slightly different approach is to immobilize plasminogen and then convert it to plasmin, so as to impart fibrinolytic activity to a surface (Marconi et al., 1996). A disadvantage of utilizing streptokinase and urokinase to cleave plasminogen to plasmin is that these agents activate both circulating and fibrin-bound plasminogen. This contrasts with the action of tissue plasminogen activator (tPA), an endogenous serine protease that converts only fibrin-bound plasminogen to plasmin. A nonpharmacological approach to developing fibrinolytic surfaces for blood-contacting applications was the preparation of lysine-derivatized polyurethane surfaces (Woodhouse and Brash, 1992). The expectation was that these surfaces exhibit fibrinolytic activity because the lysine residues promote the selective adsorption of plasminogen from plasma through the lysine-binding sites in the plasminogen molecule.

Use of Endothelial Cells and RGD Peptides

It is intuitive to believe that the ideal nonthrombogenic surface for vascular grafts and other devices will consist of an intact luminal endothelial cell layer. Herring et al. (1984) seeded Dacron and ePTFE grafts with endothelial cells in a preliminary clotting step with blood and endothelial cells. Autologous endothelial cells were seeded onto ePTFE grafts (6–7 mm inner diameter) for 153 patients, and a significant improvement in the patency rate in the infrainguinal position at 7 years was reported (Meinhart et al., 2001).

To promote endothelialization of vascular grafts either in situ or in vitro, the roles of surface chemistry, pore size, and protein coatings have been investigated (McGuigan and Sefton, 2007). Using a rat model, Wang et al. (2004) found increased endothelialization in porous polyurethane grafts. To increase endothelial cell attachment and proliferation, surface modification using an anhydrous ammonia gaseous plasma technique (Sipehia, 1990; Pu et al., 2002) or UV irradiation (Olbrich et al., 2007) has proven successful in vitro. Some approaches are focused on modifying the surface with proteins or peptides that will promote adhesion and proliferation of endothelial cells. Coating or covalent binding of materials with extracellular matrix (ECM) proteins such as fibronectin (Van Wachem and Hubbell, 1987), collagen, laminin, and elastin or glycosaminoglycans such as chondroitin sulfate (Thalla et al., 2014) have shown some success in vitro. A more elegant approach (Massia and Hubbell, 1990) has been to immobilize RGD ECM peptide sequences (see Chapter 1.4.4) to encourage endothelial cell attachment. This approach has been adopted by many others, but most results remained at the proof-of-concept stage with in vitro studies (for a thorough review of the potential use of peptides to enhance vascular graft endothelialization, refer to de Mel et al., 2008).

Immobilizing growth factors, such as VEGF, or a metalloproteinase inhibitor have also been shown to promote endothelial cell proliferation on graft materials in vitro. It is important to note that while graft endothelialization might

• BOX 1.4.3B.3 Associated Facts: Endothelial Cell Activation on Vascular Grafts

When endothelial cells (ECs) are expected to adhere onto vascular grafts (or any cardiovascular material) to provide a nonthrombogenic surface, it is required that the cells express a nonactivated, nonthrombogenic phenotype, such that leukocytes and platelets do not bind to them and the endothelial cells are able to inhibit coagulation and platelet activation. While many investigators measure endothelial cell adhesion to a substrate, few characterize the actual phenotype of the adherent cells (McGuigan and Sefton, 2007). It is not a simple matter to determine adherent EC thrombogenicity in vitro, since cell seeding density, the cell origin (e.g., adipose tissue vs. umbilical vein), shear rate, and culture conditions (serum vs. no serum, human vs. bovine serum) seem to affect the expression of ICAM-1, VCAM-1 (leukocyte adhesion receptors), PECAM-1, and E-selectin (platelet adhesion receptors), and the effects are material dependent. Differences in the in vivo endothelialization process between humans and animals (e.g., canines) further complicate matters (Zilla et al., 2007).

occur from cell migration from the anastomosis or from infiltration, it is thought that endothelial progenitor cells (EPC)³ may also play a role in graft endothelialization, and thus increasing the capture of EPC through surface modification (e.g., anti-CD34 antibody immobilization; Aoki et al., 2005) is another approach.

Several coating strategies for endothelialization are also now being combined with micro- or nano-patterning as it has been shown to significantly improve EC adhesion and proliferation (Cutting et al., 2016; Ren et al., 2015).

Since considerable differences exist in the potential for endothelialization between humans (low) and animals (higher, e.g., canines), translation of results from animal studies can be problematic. A detailed discussion of this issue is presented by Zilla et al. (2007). With immobilizing adhesion peptide sequences, there is a concern that regions not covered by endothelial cells would lead to enhanced platelet and thrombus deposition, or that the attached endothelial cells might indeed be activated (see Box 1.4.3B.3).

Strategies to Lower the Thrombogenicity of Metals

While polymers represent the principal class of materials used in the cardiovascular setting, metallic surfaces are also used in mechanical heart valves and stents. Most metals are highly thrombogenic and life-long anticoagulant and anti-platelet therapies are required with the use of mechanical heart valves, while the optimum therapy for stented patients is a much discussed topic, especially with drug-eluting stents (see Box 1.4.3B.4).

To reduce the thrombogenicity of the materials used in prosthetic heart valves, three approaches for surface

³EPC are circulating bone-derived progenitor cells. They circulate in blood at low concentration and share some similarities with monocytes.

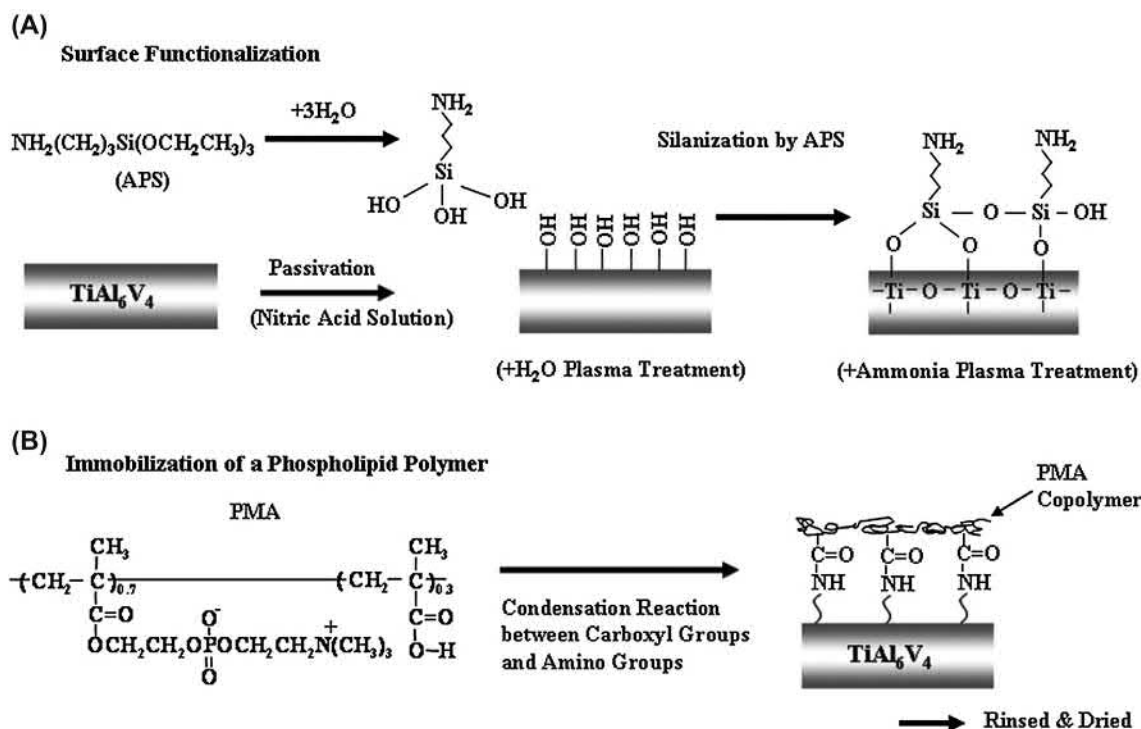
modification have been explored: coating whereby a layer of metal oxide is deposited on the metal (plasma deposition); oxidation of the metal; and ceramic or polymer coating. Deposition of tantalum-doped titanium oxide films significantly reduced platelet activation and fibrin deposition in an in vivo dog model (Huang et al., 2003). Coating with oxynitrites on stainless steel also improved overall in vitro and in vivo biocompatibility (Chen et al., 2003). A layer of oxide on titanium has also been prepared by oxidation in a solution of H_2O_2 , and this reduced platelet adhesion in vitro (Takemoto et al., 2004). Diamond-like carbon (DLC) (Mikhalovska et al., 2004) and

• BOX 1.4.3B.4 Area of Further Interest: A Benefit of “Poor” Material Blood Compatibility

While metallic stents are being modified to reduce their potential thrombogenicity, thrombogenicity may be beneficial to the promotion of osteogenesis with orthopedic implants. Upon implantation, osteogenic cells interact first with the blood clot that occupies the wound site, and platelet activation releases growth factors, such as PDGF, and cytokines, such as TGF β (both contained in platelet's α granules), that are recognized to stimulate bone growth. As such, platelet concentrates are currently being used during surgery to improve bone regeneration. More generally, thrombogenicity is a special case of inflammation (Gorbet and Sefton, 2005b), and enhancing thrombogenicity may be a strategy for creating materials with improved healing characteristics in situations such as in orthopedics.

apatite composite (Muramatsu et al., 2003) have also been coated on various metals, and both a reduction in fibrinogen adsorption and platelet adhesion have been observed in vitro. More recent approaches focus on coatings with multilayers of collagen and sulfated chitosan (Li et al., 2008), or covalently attaching a phosphorylcholine-containing polymer (see Fig. 1.4.3B.13; Ye et al., 2009). Despite these efforts, low-temperature isotropic pyrolytic carbon remains the choice for heart valves (see Chapter 2.5.2A).

Coatings for the metals currently used (stainless steel, cobalt chromium, tantalum, and Nitinol) in bare metal stents were sought as a means of reducing the thrombogenicity of such stents (Van Belle et al., 2007), and to at least indirectly influence restenosis. Due to its inertness, gold was deposited on stents, but increased restenosis rates were observed (Hara et al., 2006). Randomized clinical trials of heparin-coated tantalum stents (Blezer et al., 1998) showed that there was no significant improvement in restenosis or clinical outcomes compared to uncoated stents (Wohrle et al., 2001). Other efforts to reduce thrombogenicity included coating tantalum stents with polymers such as polyetherurethane and parylene to reduce platelet adhesion density (Fontaine et al., 1996) and radiation grafting N-vinyl-pyrrolidone (NVP) onto plasma-treated stainless steel stents (Seeger et al., 1995). Hyaluronic acid coating also reduced platelet thrombus formation on stainless steel stents and tubes in a primate



• BOX 1.4.3B.5 Clinical Correlations: Drug-Eluting Stent-Induced Thrombosis

Drug-eluting stents (DEs) have significantly reduced the rates of restenosis. However, clinical data, albeit not without dispute, suggest that DES increase the risk of late thrombosis (>30 days after implantation). While changes to the antithrombotic and anticoagulant regimen have resolved some of the concerns, ongoing animal and in vitro research (Lüscher et al., 2007) has suggested that in addition to preventing neointima formation (the intended use of the therapeutic agent being delivered), paclitaxel and sirolimus inhibit reendothelialization and induce tissue factor, thus creating a prothrombotic environment at the local site of stent implantation. The proprietary nondegradable polymers used in these stents have also been reported to be linked to inflammatory reactions at the site of implantation, although it is not clear whether these are different from what is seen with metals. A chronic inflammatory reaction would further contribute to a prothrombotic state around the stent. The clinical concerns have driven a resurgence in stent endothelialization strategies as well as a different strategy where balloons are now being considered to deliver some of the therapeutic components.

thrombosis model (Verheye et al., 2000). In another study, metal/polymer composite stents loaded (40% by weight) with a potent antiplatelet agent (GPIIb/IIIa antagonist; >90% elution in 89 h) reduced, by almost a factor of 2, platelet adhesion in dogs 2 h after stent deployment (Santos et al., 1998). r-Hirudin has also been immobilized on Nitinol stents coated with functionalized paracyclophanes (Lahann et al., 2001). As with vascular grafts, a phosphorylcholine coating has also been explored to improve stent endothelialization, however, it did not show significant improvement compared to bare metal stents in clinical trials (Abizaid et al., 2007). The relationship between thrombogenicity and clinical outcomes such as restenosis remains a hypothesis.

The early work on reducing stent thrombosis has been supplanted by drug-eluting stents (DES) to reduce restenosis rates. Rapamycin- or sirolimus-eluting stents in which the therapeutic agent is blended in a nonerodible polymer and coated onto the surface of the stent have the dramatic effect of eliminating in-stent restenosis for at least 6 months after deployment (Morice et al., 2002). Paclitaxel is an antineoplastic agent used in chemotherapies. However, the concern that DES appear to have higher risk of late thrombosis (Box 1.4.3B.5) renewed interest in developing surface strategies to lower stent thrombogenicity. Also, because of late thrombosis, there has been an interest in biodegradable stent materials with both polymeric and metallic stent systems entering clinical trials in recent years.

Summary

It is an axiom that the interactions between materials and blood are complex. Hence, it is no surprise that developing low thrombogenicity materials (let alone ones with

zero thrombogenicity) is challenging. Medical device manufacturers relying on elegant device designs and systemic pharmacological agents have significantly improved existing materials. Adverse effects are minimized and existing devices, if not risk-free, provide sufficient benefit to outweigh the risks. The focus of research in biomaterials is to make better materials that have fewer risks and greater benefits. Stents that “actively” prevent restenosis are a great example of how modifying a material can have a dramatic clinical effect. Inert materials, such as those with immobilized PEG, can resist protein and platelet deposition, but these may only be at best surrogate markers for thromboembolic phenomena. On the other hand, incorporating anticoagulants such as heparin can be an effective means of reducing thrombin production rates below critical values, but this may not be sufficient to prevent platelet activation and consumption. Many strategies for lowering thrombogenicity have been identified, and they all show a beneficial effect in at least one assay of thrombogenicity. Moreover, some have made the transition from a one-parameter benefit to multiple benefits, or from in vitro to clinical use. These issues are discussed more fully in Chapters 2.2.6 and 2.3.5.

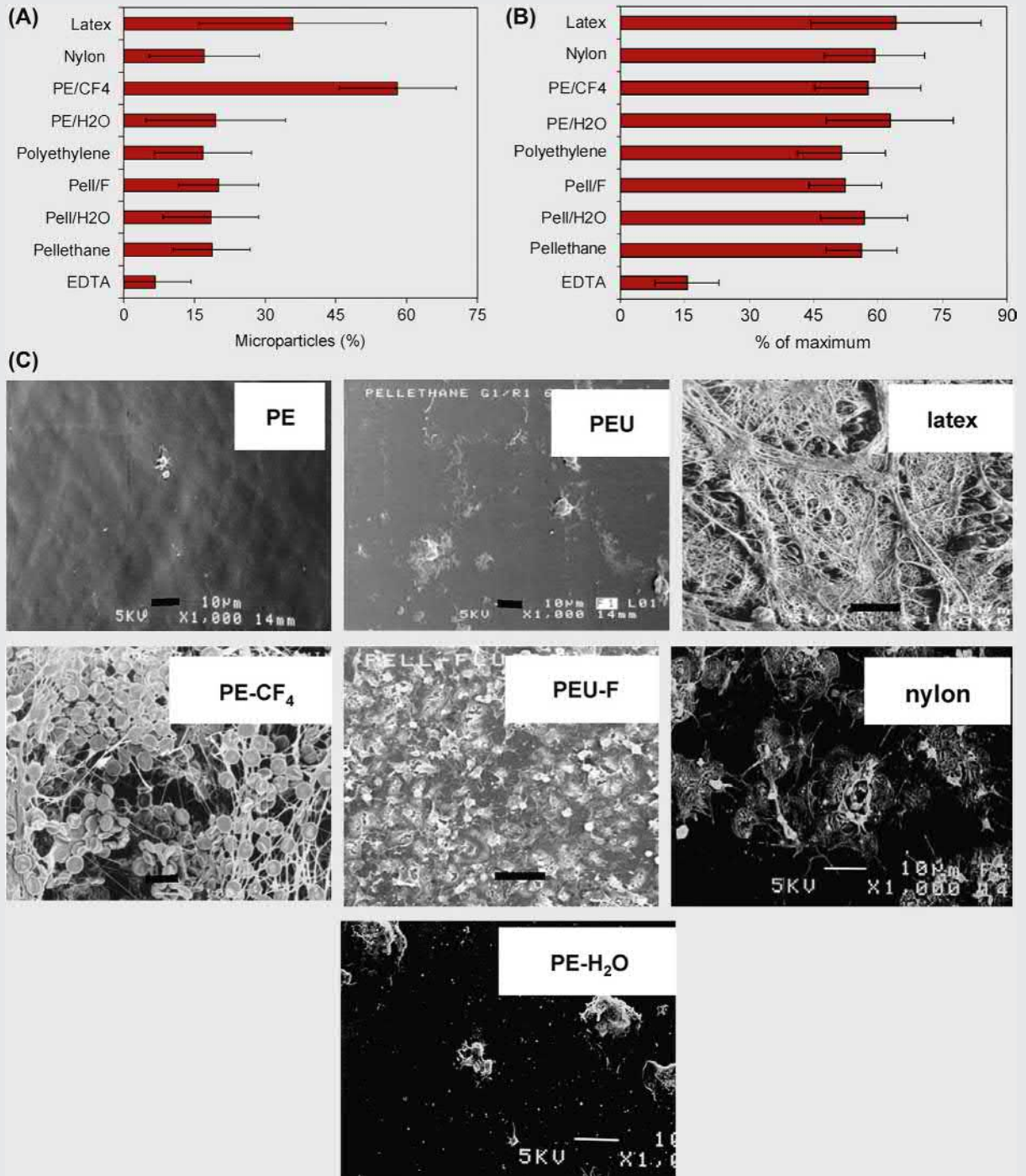
Which approaches will ultimately be successful is impossible to predict. Certainly there is much activity in biomembrane mimicry and PEG immobilization. There are many new anticoagulants and antithrombotics under development, but few have yet to be incorporated into material surfaces. In recent years, combining strategies such as reducing both protein adsorption and thrombin production while also promoting endothelialization have become prevalent and have shown promising results in small animal in vivo short-term studies (Bastijan et al., 2016; Choi et al., 2016). The commercial Trillium coating is an example of the benefit of combining various approaches. Finally, as new hypotheses are developed to understand cardiovascular material failure, new approaches will be identified for inhibiting undesired pathways. The failure to produce the ideal nonthrombogenic material, despite over 40 years of research, merely reflects our limited understanding of blood–material interactions (Jaffer and Weitz, 2019; Brash et al., 2019; Gorbet et al., 2019; Maitz et al., 2019; Ratner, 2007). A recent approach has been to consider the anticoagulant regimen that a patient is subjected to: two studies have shown that surface modification combined with single anticoagulant therapy (rather than the double anticoagulant and antiplatelet therapies) resulted in a significant improvement in blood compatibility (Yau et al., 2012; Deidre et al., 2019). Perhaps the right strategy for producing a nonthrombogenic material will have little to do with controlling platelets or thrombin, but will be directed toward leukocytes, endothelial cells, or complement (Gemmell, 1998; Wetterö et al., 2003). Ongoing research is expected to improve the blood interactions of materials used in medicine to address important clinical needs.

Nonthrombogenic Materials and Strategies

ISO10993-4, Biological Evaluation of Medical Devices Part 4: The Effects on Blood (AAMI, 1995), which manufacturers of medical devices need to use as guidance to register their products, includes thrombosis and coagulation among the tests that need to be done. However, specific test methods are not detailed. With a view to clarifying this question, a series of plasma-modified tubes (along with an unmodified control and other commercially available tubing) were prepared, surface characterized, and exposed to heparinized whole blood (1 U/mL heparin) for 1 hour

at 37°C (Sefton et al., 2001). The surface modifications included several different plasma vapors (H₂O, CF₄, and fluorine). The 1.5-mm ID tubing was incubated with whole blood on a rocking platform to gently agitate the blood and keep the cells from overtly settling. This system does not probe the effect of shear on cell activation; rather the agitation and long incubation time are thought sufficient to create “well-mixed” conditions.

Some of the results from this study are shown in Fig. 1.4.3B.14 and Table 1.4.3B.1. One of the conclusions from this



• **Figure 1.4.3B.14** Cell activation and SEM (scanning electron microscope) results after 60 min contact with whole blood (1 U/mL heparin) at 37°C in rocking platform. Flow cytometry results are mean±SD. (A) Microparticle levels (percentage of platelet events); (B) Leukocyte CD11b upregulation (expressed relative to the maximum upregulation obtained with a phorbol ester). (C) SEM. Scale bar is 10µm in all. Modified materials are designated with the name of base materials and gas introduced into plasma (H₂O, NH₄, CF₄, or F). Presented data are a subset of those studied and figures are adapted from those published (Sefton et al., 2001). PE, polyethylene; PEU, Pellethane.

CASE STUDY—CONT'D

Nonthrombogenic Materials and Strategies

TABLE 1.4.3B.1 Most Biomaterials Are the Same

Parameter	EDTA Control (or Equivalent)	Value For Most Materials
Platelet count loss (%)	0 (by definition)	25–35
P-selectin (% positive)	6.4	~8–9
Platelet–leukocyte aggregates (Fluorescent intensity)	46	~200–250
CD11b upregulation (% of maximum)	15	~50–60
L-selectin shedding	11	~70–90

study is that the materials with the lowest levels of platelet and leukocyte activation (microparticle formation, CD11b upregulation) were the unmodified materials (polyethylene, Pellethane, a polyurethane), and that the surface modifications tested here had either no effect or only made things worse from the perspective of platelet and leukocyte activation. The scanning electron micrographs showing little cellular deposit on the polyethylene or Pellethane were consistent with the flow cytometry findings. Except for those materials that were worse, the other materials expressed similar levels of activation for platelets,

leukocytes, and the other markers tested; i.e., the majority of the “inert” materials (in the absence of bioactive components like heparin) appear to have a similar nonspecific effect on blood.

The results from this study contrast sharply with other studies (many of them cited in this chapter) showing large differences in blood interactions between different biomaterials. This highlights the lack of consensus about blood–materials interactions. Reasons for this lack of consensus are discussed in [Chapter 2.3.5](#).

References

- AAMI (American Association for Medical Instrumentation), 1995. AAMI standards and recommended practice, volume 4, biological evaluation of medical devices. In: ISO Standard 10993-4: Biological Evaluation of Medical Devices Part 4: The Effects on Blood. AAMI, Washington, DC, pp. 45–68.
- Abizaid, A., Chaves, A.J., Leon, M.B., Hauptmann, K., Mehran, R., Lansky, A.J., 2007. Randomized, double-blind, multicenter study of the polymer-based 17-beta estradiol-eluting stent for treatment of native coronary artery lesions: six-month results of the ETHOS I trial. *Cathet. Cardiovasc. Interv.* 70, 654–660.
- Aldenhoff, Y.B., Blezer, R., Lindhout, T., Koole, L.H., 1997. Photo-immobilization of dipyridamole (Persantin) at the surface of polyurethane biomaterials: reduction of in vitro thrombogenicity. *Biomaterials* 18 (2), 167–172.
- Amiji, M., Park, K., 1993. Surface modification of polymeric biomaterials with poly(ethylene oxide), albumin, and heparin for reduced thrombogenicity. *J. Biomater. Sci. Polym. Ed.* 4, 217–234.
- Andrade, J.D., Hlady, V., 1986. Protein adsorption and materials biocompatibility: a tutorial review and suggested hypotheses. *Adv. Polym. Sci.* 79, 1–63.
- Andrade, J.D., Lee, H.B., John, M.S., Kim, S.W., Hibbs Jr., J.B., 1973. Water as a biomaterial. *Trans. Am. Soc. Artif. Intern. Organs* 19, 1–7.
- Aoki, J., Serruys, P.W., van, B.H., Ong, A.T., McFadden, E.P., Sianos, G., 2005. Endothelial progenitor cell capture by stents coated with antibody against CD34: the HEALING-FIM (healthy endothelial accelerated lining inhibits neointimal growth—first in man) registry. *J. Am. Coll. Cardiol.* 45, 1574–1579.
- Appelgren, P., Ransjo, U., Bindslev, L., Espersen, F., Larm, O., 1996. Surface heparinization of central venous catheters reduces microbial colonization in vitro and in vivo: results from a prospective, randomized trial. *Crit. Care Med.* 24, 1482–1489.
- Arnander, C., Bagger-Sjoberg, D., Frebelius, S., Larsson, R., Swenberg, J., 1987. Long-term stability in vivo of a thromboresistant heparinized surface. *Biomaterials* 8, 496–499.
- Ashfaq, A., Soroya, M.S., Iyengar, A., Federman, M., Reemtsen, B.L., 2018. Heparin-coated grafts reduce mortality in pediatric patients receiving systemic-to-pulmonary shunts. *Pediatr. Cardiol.* 39, 473–477.
- Baier, R.E., Gott, V.L., Furuse, A., 1970. Surface chemical evaluation of thromboresistant materials before and after venous implantation. *Trans. Amer. Soc. Artif. Org.* 16, 50–57.
- Baker, L.C., Davis, W.C., Autieri, J., Watach, M.J., Yamazaki, K., Litwak, P., Wagner, W.R., 1998. Flow cytometric assays to detect platelet activation and aggregation in device-implanted calves. *J. Biomed. Mater. Res.* 41, 312–321.
- Basmadjian, D., 1990. The effect of flow and mass transport in thrombogenesis. *Ann. Biomed. Eng.* 18 (6), 685–709.
- Basmadjian, D., Sefton, M.V., 1983. Relationship between release rate and surface concentration for heparinized materials. *J. Biomed. Mater. Res.* 17, 509–518.
- Bastjanic, J.M., Marchant, R.E., Kligman, F., Allemang, M.T., Lakin, R.O., Kendrick, D., Kashyap, V.S., Kottke-Marchant, K., 2016. *In vivo* evaluation of biomimetic fluorosurfactant polymer-coated expanded polytetrafluoroethylene vascular grafts in a porcine carotid artery bypass model. *J. Vasc. Surg.* 63, 1620–1630.
- Bauer, K.A., Rosenberg, R.D., 1995. Control of coagulation reactions. In: Beutler, E., Lichtman, M.A., Collen, B.S., Kipps, T.J. (Eds.), *Williams Hematology*, fifth ed. McGraw-Hill, p. 1241.

- Bindslev, L., Eklund, J., Norlander, O., Swedenborg, J., Olsson, P., Nilsson, E., Larm, O., Gouda, I., Malmberg, A., Scholander, E., 1987. Treatment of acute respiratory failure by extracorporeal carbon dioxide elimination performed with a surface heparinized artificial lung. *Anesthesiology* 67, 117–120.
- Biran, R., Pond, D., 2017. Heparin coatings for improving blood compatibility of medical devices. *Adv. Drug Deliv. Rev.* 112, 12–23.
- Blezer, R., Cahalan, L., Cahalan, P.T., Lindhout, T., 1998. Heparin coating of tantalum coronary stents reduces surface thrombin generation but not factor IXa generation. *Blood Coagul. Fibrinolysis* 9, 435–440.
- Bohl, K.S., West, J.L., 2000. Nitric oxide-generating polymers reduce platelet adhesion and smooth muscle cell proliferation. *Biomaterials* 21, 2273–2278.
- Brash, J.L., Horbett, T.A., Latour, R.A., Tengvall, P., 2019. The blood coagulation challenge – Part 2: protein adsorption phenomena governing blood reactivity. *Acta Biomater.* 94, 11–24.
- Campbell, E.J., O’Byrne, V., Stratford, P.W., Quirk, I., Vick, T.A., Wiles, M.C., Yianni, Y.P., 1994. Biocompatible surfaces using methacryloylphosphorylcholine laurylmethacrylate copolymer. *Am. Soc. Artif. Intern. Organs J.* 40, M853–M857.
- Chaikof, E.L., Coleman, J.E., Ramberg, K., Connolly, R.J., Merrill, E.W., Callow, A.D., 1989. Development and evaluation of a new polymeric material for small calibre vascular prostheses. *J. Surg. Res.* 47, 193–199.
- Chaikof, E.L., Merrill, E.W., Callow, A.D., Connolly, R.J., Verdon, S.L., Ramberg, K., 1992. PEO enhancement of platelet deposition, fibrinogen deposition and complement activation. *J. Biomed. Mater. Res.* 26, 1163–1168.
- Chen, C., Hanson, S.R., Lumsden, A.B., 1995. Boundary layer infusion of heparin prevents thrombosis and reduces neointimal hyperplasia in venous polytetrafluoroethylene grafts without systemic anticoagulation. *J. Vasc. Surg.* 22, 237–245.
- Chen, C., Ofenloch, J.C., Yianni, Y.P., Hanson, S.R., Lumsden, A.B., 1998. Phosphorylcholine coating of ePTFE reduces platelet deposition and neointimal hyperplasia in arteriovenous grafts. *J. Surg. Res.* 77, 119–125.
- Chen, M., Zamora, P.O., Pena, L., Som, P., Osaki, S., 2003. NH_3/O_2 mixed gas plasmas alter the interaction of blood components with stainless steel. *J. Biomed. Mater. Res. A* 67, 994–1000.
- Chen, S., Zheng, J., Li, L., Jiang, S., 2005. Strong resistance of phosphorylcholine self-assembled monolayers to protein adsorption: insights into nonfouling properties of zwitterionic materials. *J. Am. Chem. Soc.* 127, 14473–14478.
- Chevallier, P., Janvier, R., Mantovani, D., Laroche, G., 2005. In vitro biological performances of phosphorylcholine-grafted ePTFE prostheses through RFGD plasma techniques. *Macromol. Biosci.* 5, 829–839.
- Choi, W.S., Joung, Y.K., Lee, Y., Bae, J.W., Park, H.K., Park, Y.H., Park, J.C., Park, K.D., 2016. Enhanced patency and endothelialization of small-caliber vascular grafts fabricated by coimmobilization of heparin and cell-adhesive peptides. *ACS Appl. Mater. Interfaces* 8, 4336–4346.
- Cholakias, C.H., Zingg, W., Sefton, M.V., 1989. Effect of heparin-PVA hydrogel on platelets in a chronic arterial venous shunt. *J. Biomed. Mater. Res.* 23, 417–441.
- Cutiongco, M.F.A., Goh, S.H., Aid-Launais, R., Le Visage, C., Low, H.Y., Yim, E.K.F., 2016. Planar and tubular patterning of micro and nano-topographies on poly(vinyl-alcohol) hydrogel for improved endothelial cell responses. *Biomaterials* 84, 184–195.
- de Gennes, P.G., 1980. Conformation of polymers attached to an interface. *Macromolecules* 13, 1069–1075.
- de Mel, A., Jell, G., Stevens, M.M., Seifalian, A.M., 2008. Biofunctionalization of biomaterials for accelerated in situ endothelialization: a review. *Biomacromolecules* 9, 2969–2979.
- Deirdre, E.J., Anderson, K.P., Truong, M., Hagen, W., Yim, E.V.K., Hinds, M.T., 2019. Biomimetic modification of poly(vinyl alcohol): encouraging endothelialization and preventing thrombosis with antiplatelet monotherapy. *Acta Biomater.* 86, 291–299.
- Desai, N.P., Hubbell, J.A., 1991a. Biological responses to polyethylene oxide modified polyethylene terephthalate surfaces. *J. Biomed. Mater. Res.* 25, 829–843.
- Desai, N.P., Hubbell, J.A., 1991b. Solution technique to incorporate polyethylene oxide and other water-soluble polymers into surfaces of polymeric biomaterials. *Biomaterials* 12, 144–153.
- Du, Y.J., Brash, J.L., McClung, G., Berry, L.R., Klement, P., Chan, A.K., 2007. Protein adsorption on polyurethane catheters modified with a novel antithrombin-heparin covalent complex. *J. Biomed. Mater. Res. A* 80, 216–225.
- Duan, X., Lewis, R.S., 2002. Improved haemocompatibility of cysteine-modified polymers via endogenous nitric oxide. *Biomaterials* 23 (4), 1197–1203.
- Duncan, A.C., Sefton, M.V., Brash, J.L., 1997. Effect of C4-, C8- and C18-alkylation of poly(vinyl alcohol) hydrogels on the adsorption of albumin and fibrinogen from buffer and plasma: limited correlation with platelet interactions. *Biomaterials* 18, 1585–1592.
- Durrani, A.A., Hayward, J.A., Chapman, D., 1986. Biomembranes as models for polymer surfaces. II. The synthesis of reactive species for covalent coupling of phosphorylcholine to polymer surfaces. *Biomaterials* 7, 121–125.
- Ebert, C.D., Lee, E.S., Kim, S.W., 1982. The antiplatelet activity of immobilized prostacyclin. *J. Biomed. Mater. Res.* 16, 629–638.
- Fiore, L., Deykin, D., 1995. Anticoagulant therapy. In: Beutler, E., Lichtman, M.A., Collen, B.S., Kipps, T.J. (Eds.), *Williams Hematology*, fifth ed. McGraw-Hill, p. 1563.
- Fontaine, A.B., Koelling, K., Passos, S.A., Cearlock, J., Hoffman, R., Spigos, D.G., 1996. Polymeric surface modification of tantalum stents. *J. Endovasc. Surg.* 3, 276–283.
- Fougnot, C., Dupiller, M.P., Jozefowicz, M., 1983. Anticoagulant activity of amino acid modified polystyrene resins: influence of the carboxylic acid function. *Biomaterials* 4, 101–104.
- Francois, P., Vaudaux, P., Nurdin, N., Mathieu, H.J., Descouts, P., Lew, D.P., 1996. Physical and biological effects of a surface coating procedure on polyurethane catheters. *Biomaterials* 17, 667–678.
- Frautschi, J.R., Eberhart, R.C., Hubbell, J.A., 1995. Alkylated celulosic membranes with enhanced albumin affinity: influence of competing proteins. *J. Biomater. Sci. Polym. Ed.* 7, 563–575.
- Frost, M.C., Reynolds, M.M., Meyerhoff, M.E., 2005. Polymers incorporating nitric oxide releasing/generating substances for improved biocompatibility of blood-contacting medical devices. *Biomaterials* 26, 1685–1693.
- Gemmell, C.H., 1998. Platelet adhesion onto artificial surfaces: inhibition by benzamidine, pentamidine and pyridoxal-5-phosphate as demonstrated by flow cytometric quantification of platelet adhesion to microspheres. *J. Lab. Clin. Med.* 131, 84–92.
- Gemmell, C.H., Ramirez, S.M., Yeo, E.L., Sefton, M.V., 1995. Platelet activation in whole blood by artificial surfaces: identification of platelet-derived microparticles and activated platelet binding to leukocytes as material-induced activation events. *J. Lab. Clin. Med.* 125, 276–287.
- Gemmell, C.H., Yeo, E.L., Sefton, M.V., 1997. Flow cytometric analysis of material-induced platelet activation in a canine model: elevated microparticle levels and reduced platelet life span. *J. Biomed. Mater. Res.* 37, 176–181.

- Giorni, C., Pezzella, C., Bojan, M., Ricci, Z., Pouard, P., Raisky, O., Tourneur, L., La Salvia, O., Favia, I., Borgel, D., Cogo, P., Carotti, A., Lasne, D., 2019. Impact of heparin- or nonheparin-coated circuits on platelet function in pediatric cardiac surgery. *Ann. Thorac. Surg.* 107, 1241–1247.
- Gorbet, M.B., Sefton, M.V., 2004. Biomaterial-associated thrombosis: roles of coagulation factors, complement, platelets and leukocytes. *Biomaterials* 25, 5681–5703.
- Gorbet, M.B., Sefton, M.V., 2005a. Endotoxin: the uninvited guest. *Biomaterials* 26, 6811–6817.
- Gorbet, M.B., Sefton, M.V., 2005b. Complement inhibition reduces material-induced leukocyte activation with PEG modified polystyrene beads (Tentagel) but not polystyrene beads. *J. Biomed. Mater. Res. A* 74, 511–522.
- Gorbet, M., Sperling, C., Maitz, M.F., Siedlecki, C.A., Werner, C., Sefton, M.V., 2019. The blood coagulation challenge – Part 3: material associated activation of blood cascades and cells. *Acta Biomater.* 94, 25–32.
- Gott, V.L., Whiffen, J.D., Dutton, R.C., 1963. Heparin bonding on colloidal graphite surfaces. *Science* 142, 1297–1298.
- Gouzy, M.F., Sperling, C., Salchert, K., Pompe, T., Streller, U., Uhlmann, P., 2004. In vitro blood compatibility of polymeric biomaterials through covalent immobilization of an amidine derivative. *Biomaterials* 25, 3493–3501.
- Grasel, T.G., Cooper, S.L., 1989. Properties and biological interactions of polyurethane anionomers: effect of sulfonate incorporation. *J. Biomed. Mater. Res.* 23, 311–338.
- Gu, Y.J., Boonstra, P.W., Rijnsburger, A.A., Haan, J., van Oeveren, W., 1998. Cardiopulmonary bypass circuit treated with surface-modifying additives: a clinical evaluation of blood compatibility. *Ann. Thorac. Surg.* 65, 1342–1347.
- Han, H.S., Yang, S.L., Yeh, H.Y., Lin, J.C., Wu, H.L., Shi, G.Y., 2001. Studies of a novel human thrombomodulin immobilized substrate: surface characterization and anticoagulation activity evaluation. *J. Biomater. Sci. Polym. Ed.* 12 (10), 1075–1089.
- Han, D.K., Park, K., Park, K.D., Ahn, K.D., Kim, Y.H., 2006. In vivo biocompatibility of sulfonated PEO-grafted polyurethanes for polymer heart valve and vascular graft. *Artif. Organs* 30, 955–959.
- Hanson, S.R., Harker, L.A., Ratner, B.D., Hoffman, A.S., 1980. In vivo evaluation of artificial surfaces with a nonhuman primate model of arterial thrombosis. *J. Lab. Clin. Med.* 95, 289–304.
- Hara, H., Nakamura, M., Palmaz, J.C., Schwartz, R.S., 2006. Role of stent design and coatings on restenosis and thrombosis. *Adv. Drug Deliv. Rev.* 58, 377–386.
- Herring, M.B., Baughman, S., Glover, J., Kesler, K., Jesseph, J., Campbell, J., 1984. Endothelial seeding of Dacron and Polytetrafluoroethylene grafts: the cellular events of healing. *Surgery* 96, 745–754.
- Heyman, P.W., Cho, C.S., McRea, J.C., Olsen, D.B., Kim, S.W., 1985. Heparinized polyurethanes: in vitro and in vivo studies. *J. Biomed. Mater. Res.* 19, 419–436.
- Hoel, T.N., Videm, V., Baksaas, S.T., Mollnes, T.E., Brosstad, E., Svennevig, J.L., 2004. Comparison of a Duraflo II-coated cardiopulmonary bypass circuit and a trillium-coated oxygenator during open-heart surgery. *Perfusion* 19, 177–184.
- Hoffman, A.S., Schmer, G., Harris, C., Kraft, W.G., 1972. Covalent binding of biomolecules to radiation-grafted hydrogels on inert polymer surfaces. *Trans. Am. Soc. Artif. Intern. Organs* 18, 10–17.
- Huang, N., Yang, P., Leng, Y.X., Chen, J.Y., Sun, H., Wang, J., 2003. Hemocompatibility of titanium oxide films. *Biomaterials* 24, 2177–2187.
- Idezuki, Y., Watanabe, H., Hagiwara, M., Kanasugi, K., Mori, Y., 1975. Mechanism of antithrombogenicity of a new heparinized hydrophilic polymer: chronic in vivo and clinical application. *Trans. Am. Soc. Artif. Intern. Organs* 21, 436–448.
- Iqbal, Z., Kim, S., Moyer, J., Moses, W., Abada, E., Wright, N., Kim, E.J., Park, J., Fissell, W.H., Roy, S., 2019. *In vitro* and *in vivo* hemocompatibility assessment of ultrathin sulfobetaine polymer coatings for silicon-based implants. *J. Biomater. Appl.* 34, 297–312.
- Ishihara, K., Hanyuda, H., Nakabayashi, N., 1995. Synthesis of phospholipid polymers having a urethane bond in the side chain as coating material on segmented polyurethane and their platelet adhesion-resistant properties. *Biomaterials* 16, 873–879.
- Ishihara, K., Nomura, H., Mihara, T., Kurita, K., Iwasaki, Y., Nakabayashi, N., 1998. Why do phospholipid polymers reduce protein adsorption? *J. Biomed. Mater. Res.* 39, 323–330.
- Ishihara, K., Fukumoto, K., Iwasaki, Y., Nakabayashi, N., 1999. Modification of polysulfone with phospholipid polymer for improvement of the blood compatibility. Part 1. Surface characterization. *Biomaterials* 20 (17), 1545–1551.
- Ito, R.K., Phaneuf, M.D., LoGerfo, F.W., 1991. Thrombin inhibition by covalently bound hirudin. *Blood Coagul. Fibrinolysis* 2, 77–81.
- Iwasaki, Y., Uchiyama, S., Kurita, K., Morimoto, N., Nakabayashi, N., 2002. A nonthrombogenic gas-permeable membrane composed of a phospholipid polymer skin film adhered to a polyethylene porous membrane. *Biomaterials* 23, 3421–3427.
- Jacobs, H., Okano, T., Lin, J.Y., Kim, S.W., 1985. PGE1–heparin conjugate releasing polymers. *J. Control. Release* 2, 313–319.
- Jaffer, I.H., Weitz, J.I., 2019. The blood coagulation challenge – Part 1: blood contacting medical devices: the scope of the problem. *Acta Biomater.* 94, 2–10.
- Jahangir, A.R., McClung, W.G., Cornelius, R.M., McCloskey, C.B., Brash, J.L., Santerre, J.P., 2002. Fluorinated surface-modifying macromolecules: modulating adhesive protein and platelet interactions on a polyether-urethane. *J. Biomed. Mater. Res.* 60, 135–147.
- Jeon, S.I., Andrade, J.D., 1991. Protein–surface interactions in the presence of polyethylene oxide. II. Effect of protein size. *J. Colloid Interface Sci.* 142, 159–166.
- Jeon, S.I., Lee, J.H., Andrade, J.D., de Gennes, P.G., 1991. Protein–surface interactions in the presence of polyethylene oxide. I. Simplified theory. *J. Colloid Interface Sci.* 142, 149–158.
- Jiang, Y., Rongbing, B., Ling, T., Jian, S., Sicong, L., 2004. Blood compatibility of polyurethane surface grafted copolymerization with sulfobetaine monomer. *Colloids Surfaces B Biointerfaces* 36, 27–33.
- Kanjickal, D., Lopina, S., Evancho-Chapman, M.M., Schmidt, S., Donovan, D., 2008. Effects of sterilization on poly(ethylene glycol) hydrogels. *J. Biomed. Mater. Res. A* 87, 608–617.
- Kashiwagi, T., Ito, Y., Imanishi, Y., 1993. Synthesis of non-thrombogenicity of fluoralkyl polyetherurethanes. *J. Biomater. Sci. Polym. Ed.* 5, 157–166.
- Kiaei, D., Hoffman, A.S., Ratner, B.D., Horbett, T.A., 1988. Interaction of blood with gas discharge treated vascular grafts. *J. Appl. Polym. Sci. Appl. Polym. Symp.* 42, 269–283.
- Kim, D.D., Takeno, M.M., Ratner, B.D., Horbett, T.A., 1998. Glow discharge plasma deposition (GDPD) technique for the local controlled delivery of hirudin from biomaterials. *Pharm. Res.* 15 (5), 783–786.
- Kim, K., Kim, C., Byun, Y., 2000. Preparation of a PEG-grafted phospholipid Langmuir–Blodgett monolayer for blood-compatible material. *J. Biomed. Mater. Res.* 52 (4), 836–840.
- Kishida, A., Akatsuka, Y., Yanagi, M., Aikou, T., Maruyama, I., Akashi, M., 1995. In vivo and ex vivo evaluation of the antithrombogenicity of human thrombomodulin immobilized biomaterials. *Am. Soc. Artif. Intern. Organs J.* 41, M369–M374.

- Kitano, H., Tada, S., Mori, T., Takaha, K., Gemmei-Ide, M., Tanaka, M., Fukuda, M., Yokoyama, Y., 2005. Correlation between the structure of water in the vicinity of carboxybetaine polymers and their blood-compatibility. *Langmuir* 21, 11932–11940.
- Klement, P., Du, Y.J., Berry, L.R., Tressel, P., Chan, A.K., 2006. Chronic performance of polyurethane catheters covalently coated with ATH complex: a rabbit jugular vein model. *Biomaterials* 27, 5107–5117.
- Kottke-Marchant, K., Anderson, J.M., Umemura, Y., Marchant, R.E., 1989. Effect of albumin coating on the in vitro blood compatibility of Dacron arterial prostheses. *Biomaterials* 10, 147–155.
- Lahann, J., Klee, D., Pluester, W., Hoecker, H., 2001. Bioactive immobilization of r-hirudin on CVD-coated metallic implant devices. *Biomaterials* 22, 817–826.
- Larm, O., Larsson, R., Olsson, P., 1983. A new non-thrombogenic surface prepared by selective covalent binding of heparin via a modified reducing terminal residue. *Biomater. Med. Dev. Artif. Organs* 11, 161–173.
- Lazarides, M.K., Argyriou, C., Antoniou, G.A., Georgakarakos, E., Georgiadis, G.S., 2016. Lack of evidence for use of heparin-bonded grafts in access surgery: a meta-analysis. *Semin. Vasc. Surg.* 29, 192–197.
- Lee, J.H., Oh, S.H., Kim, W.G., 2004. MMA/MPEOMA/VSA copolymer as a novel blood-compatible material: ex vivo platelet adhesion study. *J. Mater. Sci. Mater. Med.* 15, 155–159.
- Lehninger, R.I., Cooper, C.W., Falb, R.D., Grode, G.A., 1966. Non-thrombogenic plastic surfaces. *Science* 152, 1625–1626.
- Lewis, A.L., Hughes, P.D., Kirkwood, L.C., Leppard, S.W., Redman, R.P., Tolhurst, L.A., Stratford, P.W., 2000. Synthesis and characterisation of phosphorylcholine-based polymers useful for coating blood filtration devices. *Biomaterials* 21 (18), 1847–1859.
- Li, Q.L., Huang, N., Chen, J., Wan, G., Zhao, A., Chen, J., Wang, J., Yang, P., Leng, Y., 2008. Anticoagulant surface modification of titanium via layer-by-layer assembly of collagen and sulfated chitosan multilayers. *J. Biomed. Mater. Res. A* 89 (3), 575–584.
- Lin, J.C., Tiong, S.L., Chen, C.Y., 2000. Surface characterization and platelet adhesion studies on fluorocarbons prepared by plasma-induced graft polymerization. *J. Biomater. Sci. Polym. Ed.* 11, 701–714.
- Lindhout, T., Blezer, R., Schoen, P., Willems, G.M., Fouache, B., Verhoeven, M., Hendriks, M., Cahalan, L., Cahalan, P.T., 1995. Antithrombin activity of surface-bound heparin studied under flow conditions. *J. Biomed. Mater. Res.* 29, 1255–1266.
- Llanos, G.R., Sefton, M.V., 1993a. Does polyethylene oxide possess a low thrombogenicity? *J. Biomater. Sci. Polym. Ed.* 4, 381–400.
- Llanos, G.R., Sefton, M.V., 1993b. Immobilization of poly(ethylene glycol) onto a poly(vinyl alcohol) hydrogel: 2. Evaluation of thrombogenicity. *J. Biomed. Mater. Res.* 27, 1383–1391.
- Lleixa, C.J., Grafahrend, D., Klee, D., Moller, M., 2008. Sterilization effects on starPEG coated polymer surfaces: characterization and cell viability. *J. Mater. Sci. Mater. Med.* 19, 1631–1636.
- Lüscher, T.F., Steffel, J., Eberli, F.R., Joner, M., Nakazawa, G., Tanner, F.C., Virmani, R., 2007. Drug-eluting stent and coronary thrombosis: biological mechanisms and clinical implications. *Circulation* 115, 1051–1058.
- Maitz, M.F., Martins, M.C.L., Grabow, N., Matschegewski, C., Huang, N., Chaikof, E.L., Barbosa, M.A., Werner, C., Sperling, C., 2019. The blood compatibility challenge. Part 4: surface modification for hemocompatible materials: passive and active approaches to guide blood-material interactions. *Acta Biomater.* 94, 33–43.
- Major, T.C., Brant, D.O., Burney, C.P., Amoako, K.A., Annich, G.A., Meyerhoff, M.E., Handa, H., Bartlett, R.H., 2011. The hemocompatibility of a nitric oxide generating polymer that catalyzes S-nitrosothiol decomposition in an extracorporeal circulation model. *Biomaterials* 32, 5957–5969.
- Marconi, W., Piozzi, A., Romoli, D., 1996. Preparation and evaluation of polyurethane surfaces containing plasminogen. *J. Biomater. Sci. Polym. Ed.* 8, 237–249.
- Massa, T.M., Yang, M.L., Ho, J.Y., Brash, J.L., Santerre, J.P., 2005. Fibrinogen surface distribution correlates to platelet adhesion pattern on fluorinated surface-modified polyetherurethane. *Biomaterials* 26, 7367–7376.
- Massia, S.P., Hubbell, J.A., 1990. Covalently attached GRGD on polymer surfaces promotes biospecific adhesion of mammalian cells. *Ann. NY Acad. Sci.* 589, 261–270.
- Matsuda, T., Inoue, K., 1990. New photoreactive surface modification technology for fabricated devices. *Trans. Am. Soc. Artif. Intern. Organs* 36, M161–M164.
- McGuigan, A.P., Sefton, M.V., 2007. The influence of biomaterials on endothelial cell thrombogenicity. *Biomaterials* 28, 2547–2571.
- McPherson, T.B., Shim, H.S., Park, K., 1997. Grafting of PEO to glass, nitinol, and pyrolytic carbon surfaces by gamma irradiation. *J. Biomed. Mater. Res.* 38, 289–302.
- McRea, J.C., Kim, S.W., 1978. Characterization of controlled release of prostaglandin from polymer matrices for thrombus prevention. *Trans. Am. Soc. Artif. Intern. Organs* 24, 746–750.
- Meinhart, J.G., Deutsch, M., Fischlein, T., Howanietz, N., Froschl, A., Zilla, P., 2001. Clinical autologous in vitro endothelialization of 153 infrainguinal ePTFE grafts. *Ann. Thorac. Surg.* 71, S327–S331.
- Merrill, E.W., Salzman, E.W., 1983. Polyethylene oxide as a biomaterial. *Am. Soc. Artif. Intern. Organs J.* 6, 60–64.
- Merrill, E.W., Salzman, E.W., Wan, S., Mahmud, N., Kushner, L., Lindon, J.N., Curme, L., 1982. Platelet-compatible hydrophilic segmented polyurethanes from polyethylene glycols and cyclohexane diisocyanate. *Trans. Am. Soc. Artif. Intern. Organs* 28, 482–487.
- Mikhailovska, L.I., Santin, M., Denyer, S.P., Lloyd, A.W., Teer, D.G., Field, S., Mikhailovsky, S.V., 2004. Fibrinogen adsorption and platelet adhesion to metal and carbon coatings. *Thromb. Haemost.* 92, 1032–1039.
- Morice, M.C., Serruys, P.W., Sousa, J.E., Fajadet, J., Ban Hayashi, E., Perin, M., Colombo, A., Schuler, G., Barragan, P., Guagliumi, G., Molnar, F., Falotico, R., RAVEL Study Group, 2002. Randomized study with the Sirolimus-coated BX velocity balloon-expandable stent in the treatment of patients with de novo native coronary artery lesions. A randomized comparison of a Sirolimus-eluting stent with a standard stent for coronary revascularization. *N. Engl. J. Med.* 346 (23), 1773–1780.
- Munro, M.S., Quattrone, A.J., Ellsworth, S.R., Kulkari, P., Eberhart, R.C., 1981. Alkyl substituted polymers with enhanced albumin affinity. *Trans. Am. Soc. Artif. Intern. Organs* 27, 499–503.
- Muramatsu, K., Uchida, M., Kim, H.M., Fujisawa, A., Kokubo, T., 2003. Thromboresistance of alkali- and heat-treated titanium metal formed with apatite. *J. Biomed. Mater. Res. A* 65, 409–416.
- Nagaoka, S., Mori, Y., Takiuchi, H., Yokota, K., Tanzawa, H., Nishiumi, S., 1984. Interaction between blood components and hydrogels with poly(oxyethylene) chains. In: Shalaby, S., Hoffman, A.S., Ratner, B.D., Horbett, T.A. (Eds.), *Polymers as Biomaterials*. Plenum Press, pp. 361–371.
- Oh, B.K., Meyerhoff, M.E., 2004. Catalytic generation of nitric oxide from nitrite at the interface of polymeric films doped with lipophilic CuII-complex: a potential route to the preparation of thromboresistant coatings. *Biomaterials* 25, 283–293.

- Okkema, A.Z., Grasel, T.G., Zdrahala, R.J., Solomon, D.D., Cooper, S.L., 1989. Bulk, surface, and blood-contacting properties of polyetherurethanes modified with polyethylene oxide. *J. Biomater. Sci. Polym. Ed.* 1, 43–62.
- Olbrich, M., Punshon, G., Frischauf, I., Salacinski, H.J., Rebollar, E., Romanin, C., Seifalian, A.M., Heitz, J., 2007. UV surface modification of a new nanocomposite polymer to improve cytocompatibility. *J. Biomater. Sci. Polym. Ed.* 18, 453–468.
- Ovrum, E., Tangen, G., Oystese, R., Ringdal, M.A., Istad, R., 2001. Comparison of two heparin-coated extracorporeal circuits with reduced systemic anticoagulation in routine coronary artery bypass operations. *J. Thorac. Cardiovasc. Surg.* 121, 324–330.
- Park, K.D., Okano, T., Nojiri, C., Kim, S.W., 1988. Heparin immobilized onto segmented polyurethane–urea surfaces: effects of hydrophilic spacers. *J. Biomed. Mater. Res.* 22, 977–992.
- Park, H.D., Lee, W.K., Ooya, T., Park, K.D., Kim, Y.H., Yui, N., 2002. Anticoagulant activity of sulfonated polyrotaxanes as blood-compatible materials. *J. Biomed. Mater. Res.* 60 (1), 186–190.
- Paul, W., Sharma, C.P., 1997. Acetylsalicylic acid loaded poly(vinyl alcohol) hemodialysis membranes: effect of drug release on blood compatibility and permeability. *J. Sci., Polym. Ed.* 8, 755–764.
- Pu, F.R., Williams, R.L., Markkula, T.K., Hunt, J.A., 2002. Effects of plasma treated PET and PTFE on expression of adhesion molecules by human endothelial cells in vitro. *Biomaterials* 23, 2411–2428.
- Ratner, B.D., 1995. Surface modification of polymers: chemical, biological and surface analytical challenges. *Biosens. Bioelectron.* 10, 797–804.
- Ratner, B.D., 2007. The catastrophe revisited: blood compatibility in the 21st century. *Biomaterials* 28, 5144–5147.
- Ren, X., Feng, Y., Guo, J., Wang, H., Li, Q., Yang, J., Hao, X., Lv, J., Ma, N., Li, W., 2015. Surface modification and endothelialization of biomaterials as potential scaffolds for vascular tissue engineering applications. *Chem. Soc. Rev.* 7, 5680–5742.
- Rollason, G., Sefton, M.V., 1992. Measurement of the rate of thrombin production in human plasma in contact with different materials. *J. Biomed. Mater. Res.* 26, 675–693.
- Salchert, K., Gouzy, M.F., Glorius, M., Kuhn, A., Nitschke, M., Werner, C., 2005. Immobilization of an anticoagulant benzamidine derivative: effect of spacer arms and carrier hydrophobicity on thrombin binding. *Acta Biomater.* 1, 441–449.
- Samson, R.H., Morales, R., Showalter, D.P., Lepore, M.R., Nair, D.G., 2016. Heparin-bonded expanded polytetrafluoroethylene femoropopliteal bypass grafts outperform expanded polytetrafluoroethylene grafts without heparin in a long-term comparison. *J. Vasc. Surg.* 64, 638–647.
- Santos, R.M., Tanguay, J.-F., Crowley, J.J., Kruse, K.R., Sanders-Millare, D., Zidar, J.P., Phillips, H.R., Merhi, Y., Garcia-Cantu, E., Bonan, R., Cote, G., Stack, R.S., 1998. Local administration of L-703,081 using a composite polymeric stent reduces platelet deposition in canine coronary arteries. *Am. J. Cardiol.* 82, 673–675.
- Seabra, A.B., de Oliveira, M.G., 2004. Poly(vinyl alcohol) and poly(vinyl pyrrolidone) blended films for local nitric oxide release. *Biomaterials* 25, 3773–3782.
- Seeger, J.M., Ingegnio, M.D., Bigatan, E., Klingman, N., Amery, D., Widenhouse, C., Goldberg, E.P., 1995. Hydrophilic surface modification of metallic endoluminal stents. *J. Vasc. Surg.* 22, 327–335.
- Sefton, M.V., Cholakis, C.H., Llanos, G., 1987. Preparation of non-thrombogenic materials by chemical modification. In: Williams, D.F. (Ed.). *Blood Compatibility*, vol. 1. CRC Press, Inc, Boca Raton, FL, pp. 151–198.
- Sefton, M.V., Sawyer, A., Gorbet, M., Black, J.P., Cheng, E., Gemmell, C., Pottinger-Cooper, E., 2001. Does surface chemistry affect thrombogenicity of surface modified polymers? *J. Biomed. Mater. Res.* 55, 447–459.
- Sefton, M.V., Sperling, C., Maitz, M.F., Werner, C., 2019. The blood compatibility challenge: editorial introduction. *Acta Biomater.* 94, 1.
- Seifert, B., Romaniuk, P., Groth, T., 1997. Covalent immobilization of hirudin improves the haemocompatibility of polylactide-polyglycolide in vitro. *Biomaterials* 8 (22), 1495–1502.
- Shen, M., Pan, Y.V., Wagner, M.S., Hauch, K.D., Castner, D.G., Ratner, B.D., Horbett, T.A., 2001. Inhibition of monocyte adhesion and fibrinogen adsorption on glow discharge plasma deposited tetraethylene glycol dimethyl ether. *J. Biomater. Sci. Polym. Ed.* 12 (9), 961–978.
- Shivpal, S., Luthra, A., 2002. New biointeracting materials. *Med. Device Technol.* 10, 26.
- Silver, J.H., Lin, J.C., Lim, F., Tegoulia, V.A., Chaudhury, M.K., Cooper, S.L., 1999. Surface properties and hemocompatibility of alkyl-siloxane monolayers supported on silicone rubber: effect of alkyl chain length and ionic functionality. *Biomaterials* 20 (17), 1533–1543.
- Sipehia, R., 1990. The enhanced attachment and growth of endothelial cells on anhydrous ammonia gaseous plasma modified surfaces of polystyrene and poly(tetrafluoroethylene). *Biomater. Artif. Cells Artif. Organs* 18, 437–446.
- Skrzypchak, A.M., Lafayette, N.G., Bartlett, R.H., Zhou, Z., Frost, M.C., Meyerhoff, M.E., Reynolds, M.M., Annich, G.M., 2007. Effect of varying nitric oxide release to prevent platelet consumption and preserve platelet function in an in vivo model of extracorporeal circulation. *Perfusion* 22, 193–200.
- Snyder, T.A., Tsukui, H., Kihara, S., Akimoto, T., Litwak, K.N., Kameneva, M.V., Yamazaki, K., Wagner, W.R., 2007. Preclinical biocompatibility assessment of the EVAHEART ventricular assist device: coating comparison and platelet activation. *J. Biomed. Mater. Res. A* 81, 85–92.
- Sofia, S.J., Merrill, E.W., 1998. Grafting of PEO to polymer surfaces using electron beam irradiation. *J. Biomed. Mater. Res.* 40, 153–163.
- Sperling, C., Schweiss, R.B., Streller, U., Werner, C., 2005. In vitro hemocompatibility of self-assembled monolayers displaying various functional groups. *Biomaterials* 26, 6547–6557.
- Sperling, C., Houska, M., Brynda, E., Streller, U., Werner, C., 2006. In vitro hemocompatibility of albumin-heparin multilayer coatings on polyethersulfone prepared by the layer-by-layer technique. *J. Biomed. Mater. Res. A* 76, 681–689.
- Stabler, C.L., Sun, X.L., Cui, W., Wilson, J.T., Haller, C.A., Chaikof, E.L., 2007. Surface re-engineering of pancreatic islets with recombinant azido-thrombomodulin. *Bioconjug. Chem.* 18, 1713–1715.
- Strzinar, I., Sefton, M.V., 1992. Preparation and thrombogenicity of alkylated polyvinyl alcohol coated tubing. *J. Biomed. Mater. Res.* 26, 577–592.
- Sugitachi, A., Takagi, K., 1978. Antithrombogenicity of immobilized urokinase-clinical application. *Int. J. Artif. Organs* 1, 88–92.
- Takemoto, S., Yamamoto, T., Tsuru, K., Hayakawa, S., Osaka, A., Takashima, S., 2004. Platelet adhesion on titanium oxide gels: effect of surface oxidation. *Biomaterials* 25, 3485–3492.
- Tan, J., Brash, J.L., 2008. Nonfouling biomaterials based on polyethylene oxide-containing amphiphilic triblock copolymers as surface modifying additives: adsorption of proteins from human plasma to copolymer/polyurethane blends. *J. Biomed. Mater. Res. A* 90 (1), 196–204.

- Tanzawa, H., Mori, Y., Harumiya, N., Miyama, H., Hori, M., Ohshima, N., Idezuki, Y., 1973. Preparation and evaluation of a new antithrombogenic heparinized hydrophilic polymer for use in cardiovascular systems. *Trans. ASAIO* 19, 188–194.
- Thalla, P.K., Fadlallah, H., Liberelle, B., Lequoy, P., De Crescenzo, G., Merhi, Y., Lerouge, S., 2014. Chondroitin sulfate coatings display low platelet but high endothelial cell adhesive properties favorable for vascular implants. *Biomacromolecules* 15, 2512–2520.
- Tomaiuolo, M., Stalker, T.J., Welsh, J.D., Diamond, S.L., Sinno, T., Brass, L.F., 2014. A systems approach to hemostasis: 2. Computational analysis of molecular transport in the thrombus microenvironment. *Blood* 124 1816–23.
- Tsai, C.-C., Deppisch, R.M., Forrestal, L.J., Ritzau, G.H., Oram, A.D., Gohn, H.J., Voorhees, M.E., 1994. Surface modifying additives for improved device-blood compatibility. *Am. Soc. Artif. Intern. Organs J.* 40, M619–M624.
- Tseng, Y.C., Park, K., 1992. Synthesis of photoreactive poly(ethylene glycol) and its application to the prevention of surface-induced platelet activation. *J. Biomed. Mater. Res.* 26, 373–391.
- Van Belle, E., Susen, S., Jude, B., Bertrand, M.E., 2007. Drug-eluting stents: trading restenosis for thrombosis? *J. Thromb. Haemost.* 5 (Suppl. 1), 238–245.
- van den Goor, J., Nieuwland, R., van den Brink, A., van Oeveren, W., Rutten, P., Tijssen, J., Eijlsman, L., 2004. Reduced complement activation during cardiopulmonary bypass does not affect the postoperative acute phase response. *Eur. J. Cardiothorac. Surg.* 26, 926–931.
- Van Wachem, P.B., Vreriks, C.N., Beugeling, T., Feijen, J., Bantjes, A., Detmers, J.P., van Aken, W.G., 1987. The influence of protein adsorption on interactions of cultured human endothelial cells with polymers. *J. Biomed. Mater. Res.* 21, 701–718.
- Vergnaud, S., Riche, V.P., Tessier, P., Mauduit, N., Kaladji, A., Gouëffic, Y., 2018. Budget impact analysis of heparin-bonded polytetrafluoroethylene grafts (Propaten) against standard polytetrafluoroethylene grafts for below-the-knee bypass in patients with critical limb ischaemia in France. *BMJ Open* 8, e017320.
- Verheye, S., Markou, C.P., Salame, M.Y., Wan, B., King III, S.B., Robinson, K.A., Chronos, N.A., Hanson, S.R., 2000. Reduced thrombus formation by hyaluronic acid coating of endovascular devices. *Arterioscler. Thromb. Vasc. Biol.* 20, 1168–1172.
- Villemoes, M.K., Lindholt, J.S., Houliind, K.C., Gottschalksen, B., Petersen, C.N., Rasmussen, M., Wedel, C., Bramsen, M.B., Sogaard, R., 2018. Cost-effectiveness evaluation of heparin coated versus standard graft for bypass surgery in peripheral artery disease alongside a randomised controlled trial. *Eur. J. Vasc. Endovasc. Surg.* 56, 87–93.
- Wang, L.F., Wei, Y.H., 2005. Effect of soft segment length on properties of fluorinated polyurethanes. *Colloids Surfaces B Biointerfaces* 41, 249–255.
- Wang, Z., Liu, S., Guidoin, R., Kodama, M., 2004. Polyurethane vascular grafts with thorough porosity: does an internal or an external membrane wrapping improve their in vivo blood compatibility and biofunctionality? *Artif. Cells Blood Substit. Immobil. Biotechnol.* 32, 463–484.
- Ward, R., White, K., Hu, C., 1984. Use of surface modifying additives in the development of a new biomedical polyurethane-urea. In: Plank, H.I., Egbers, G., Syre, I. (Eds.), *Polyurethanes in Biomedical Engineering*. Elsevier, Amsterdam, pp. 181–200.
- Wetterö, J., Askendal, A., Tengval, P., Bengtsson, T., 2003. Interactions between surface-bound actin and complement, platelets, and neutrophils. *J. Biomed. Mater. Res.* 66, 162–175.
- Whitesides, G.M., Mathias, J.P., Seto, C.T., 1991. Molecular self-assembly and nano-chemistry: a chemical strategy for the synthesis of nanostructures. *Science* 254, 1312–1319.
- Williams, D.F., 1987. In: *Definitions in Biomaterials: Proceedings of a Consensus Conference of the European Society for Biomaterials*, Chester, England, March 3–5, 1986. Elsevier, Amsterdam; NY.
- Wohrle, J., Al-Khayer, E., Grotzinger, U., Schindler, C., Kochs, M., Hombach, V., Hoher, M., 2001. Comparison of the heparin coated vs the uncoated Jostent: No influence on restenosis or clinical outcome. *Eur. Heart J.* 22, 1808–1816.
- Woodhouse, K.A., Brash, J.L., 1992. Adsorption of plasminogen from plasma to lysine-derivatized polyurethane surfaces. *Biomaterials* 13, 1103–1108.
- Wu, W.T., Yang, F., Wu, J., Aubry, N., Massoudi, M., Antaki, J.F., 2016. High fidelity computational simulation of thrombus formation in Thoratec HeartMate II continuous flow ventricular assist device. *Sci. Rep.* 6, 38025.
- Wu, W.T., Jamiolkowski, M.A., Wagner, W.R., Aubry, N., Massoudi, M., Antaki, J.F., 2017. Multi-constituent simulation of thrombus deposition. *Sci. Rep.* 7, 42720.
- Yau, J.W., Stafford, A.R., Liao, P., Fredenburgh, J.C., Roberts, R., Brash, J.L., Weitz, J.I., 2012. Corn trypsin inhibitor coating attenuates the prothrombotic properties of catheters in vitro and in vivo. *Acta Biomater.* 8, 4092–4100.
- Ye, S.H., Johnson Jr., C.A., Woolley, J.R., Snyder, T.A., Gamble, L.J., Wagner, W.R., 2009. Covalent surface modification of a titanium alloy with a phosphorylcholine-containing copolymer for reduced thrombogenicity in cardiovascular devices. *J. Biomed. Mater. Res. A.* 91 (1), 18–28.
- Yim, E.K., Sefton, M.V., 2008. Amidine surface modification of poly(acrylonitrile-co-vinyl chloride) reduces platelet adhesion. *J. Biomed. Mater. Res. A.* 89 (3), 780–790.
- Yuan, J., Zhang, J., Zhou, J., Yuan, Y.L., Shen, J., Lin, S.C., 2003. Platelet adhesion onto segmented polyurethane surfaces modified by carboxybetaine. *J. Biomater. Sci. Polym. Ed.* 14, 1339–1349.
- Zea, N., Menard, G., Le, L., Luo, Q., Bazan, H.A., Sternbergh 3rd, W.C., Smith, T.A., 2016. Heparin-bonded polytetrafluoroethylene does not improve hemodialysis arteriovenous graft function. *Ann. Vasc. Surg.* 30, 28–33.
- Zhang, M., Horbett, T.A., 2009. Tetraglyme coatings reduce fibrinogen and von Willebrand factor adsorption and platelet adhesion under both static and flow conditions. *J. Biomed. Mater. Res. A.* 89A (3), 791–803.
- Zhang, Z., Zhang, M., Chen, S., Horbett, T.A., Ratner, B.D., Jiang, S., 2008. Blood compatibility of surfaces with superlow protein adsorption. *Biomaterials* 29, 4285–4291.
- Zhao, X., Courtney, J.M., 2007. Surface modification of polymeric biomaterials: utilization of cyclodextrins for blood compatibility improvement. *J. Biomed. Mater. Res. A.* 80, 539–553.
- Zilla, P., Bezuidenhout, D., Human, P., 2007. Prosthetic vascular grafts: wrong models, wrong questions and no healing. *Biomaterials* 28, 5009–5027.

1.4.4

Surface-Immobilized Biomolecules

STEVEN J. FREY¹, ALLAN S. HOFFMAN², JEFFREY A. HUBBELL³, RAVI S. KANE¹

¹School of Chemical and Biomolecular Engineering, Georgia Institute of Technology, Atlanta, GA, United States

²Bioengineering and Chemical Engineering, University of Washington, Seattle, WA, United States

³The University of Chicago, Chicago, IL, United States

Introduction

Biomolecules such as enzymes, antibodies, affinity proteins, cell receptor ligands, and drugs of all kinds have been immobilized on and within biomaterial surfaces for a wide range of therapeutic, diagnostic, tissue regeneration, separation, and bioprocess applications. Immobilization of heparin on polymer surfaces is one of the earliest examples of a surface-modified, biologically functional biomaterial (Gott et al., 1963). Living cells may also be combined with biomaterials, especially when their surfaces contain cell adhesion peptides or proteins, and the fields of cell culture, artificial organs, and tissue engineering include important examples of cell-surface interactions. These “hybrid” combinations of natural and synthetic materials confer “biological functionality” to the synthetic biomaterial. Many sections and chapters in this textbook cover various aspects of this topic, including adsorption of proteins and adhesion of cells and bacteria on biomaterial surfaces, nonfouling surfaces, cell culture, tissue engineering, artificial organs, drug delivery, and others. This chapter will focus on the methodology involving physical adsorption and chemical immobilization of biomolecules on biomaterial surfaces, especially for applications requiring bioactivity of the immobilized biomolecule.

Among the different classes of biomaterials that could be biologically modified, synthetic polymers are especially interesting because their surfaces may contain reactive groups such as $-OH$, $-COOH$, or NH_2 groups, or they may be readily modified with other reactive groups such as azide, alkyne, and SH groups. All of these groups can be used to covalently link biomolecules.

Another advantage of polymers as supports for biomolecules is that the polymers may be fabricated in many forms, including films, membranes, tubes, fibers, fabrics, particles, capsules, and porous structures. Furthermore,

macromolecular structures can also vary substantially. The latter can include homopolymers, random, alternating, block, and graft copolymers, and hyperbranched (comb-like) and star-shaped structures (see Chapter 1.3.2 on polymers).

Living anionic polymerization techniques, along with newer methods of living free-radical polymerizations, now provide fine control of molecular weights with narrow distributions. The molecular forms of solid polymers include noncross-linked chains that are insoluble at physiologic conditions, cross-linked networks, physical blends, and interpenetrating networks (e.g., Piskin and Hoffman, 1986; see also Chapter 1.3.2). “Smart” polymers are sharply responsive in solubility behavior to stimuli, such as temperature, pH, and salt concentration (see Chapter 1.3.2G on “smart” polymers).

For surfaces of metals, metal oxides, inorganic glasses, or ceramics, biological functionality can sometimes be added via a chemically immobilized or physically adsorbed polymeric or surfactant adlayer, or by use of techniques such as plasma gas discharge, corona discharge in air, or ozone to modify polymer surface compositions with functional groups (see also Chapter 1.4.2). Several researchers have applied mussel adhesive chemistry based on self-condensation of dopamine to form tight bonding layers of polydopamine on a variety of surfaces, including metals, metal oxides, and glasses (Lee et al., 2007; Ku et al., 2010). The amine groups in these polymers may be further functionalized with biomolecules.

Patterned Surface Compositions

(See also Chapter 1.4.5).

Biomaterial surfaces may also be functionalized in geometric patterns (Bernard et al., 1998; Blawie and Reichert, 1998; James et al., 1998; Ito, 1999; Kane et al., 1999; Folch and Toner, 2000). Sometimes the patterned surfaces will

TABLE 1.4.4.1 Examples of Biologically Active Molecules That May be Immobilized on or Within Polymeric Biomaterials

Proteins/Peptides

Enzymes
Antibodies
Antigens
Cell adhesion molecules
“Blocking” proteins

Saccharides

Sugars
Oligosaccharides
Polysaccharides

Lipids

Fatty acids
Phospholipids
Glycolipids

Other

Conjugates or mixtures of the above

Drugs

Antithrombogenic agents
Anticancer agents
Antibiotics
Contraceptives
Drug antagonists
Peptide, protein drugs

Ligands

Hormone receptors
Cell surface receptor ligands (peptides, saccharides)
Avidin, biotin

Nucleic Acids, Nucleotides

Single or double stranded
DNA, RNA (e.g., antisense oligonucleotides)

have regions that are nonbinding to proteins (so-called “non-fouling” compositions), while others may contain covalently linked cell receptor ligands (Neff et al., 1999; Alsberg et al., 2002; Csucs et al., 2003; VandeVondele et al., 2003), or may have physically adsorbed cell adhesion proteins (McDevitt et al., 2002; Ostuni et al., 2003). A huge industry has also evolved based on “biochips” that contain microarrays of immobilized, single-stranded DNA (for genomic assays) or peptides or proteins (for proteomic assays) (Houseman and Mrksich, 2002; Lee and Mrksich, 2002). The majority of these microarrays utilize inorganic silica chips rather than polymer substrates directly, but it is possible to incorporate functionality through chemical modification with silane

TABLE 1.4.4.2 Application of Immobilized Biomolecules and Cells

Enzymes	Bioreactors (industrial, biomedical) Bioseparations Biosensors Diagnostic assays Biocompatible Surfaces
Antibodies, peptides, and other affinity molecules	Biosensors Diagnostic assays Affinity separations Targeted drug delivery Cell culture
Drugs	Thrombo-resistant surfaces Drug delivery systems
Lipids	Thrombo-resistant surfaces Albuminated surfaces
Nucleic acid derivatives and nucleotides	DNA probes Gene therapy
Cells	Bioreactors (industrial) Bioartificial organs Biosensors

chemistries (Puleo, 1997) or adsorption of a polymeric adlayer (Scotchford et al., 2003; Winkelmann et al., 2003).

A variety of methods have been used for the production of these patterned biochips, including photoinitiated synthesis through patterned masks (Ellman and Gallop, 1998; Folch and Toner, 2000), microfluidic fluid exposure (Ismailov et al., 2001), and protection with adhesive organic protecting layers that are lifted off after exposure to the biomolecular treatment (Jackman et al., 1999).

Immobilized Biomolecules and Their Uses

Many different biologically functional molecules can be chemically or physically immobilized on polymeric supports (Table 1.4.4.1) (Laskin, 1985; Tomlinson and Davis, 1986). Examples of applications of these immobilized biological species are listed in Table 1.4.4.2. When hydrophilic, molecularly cross-linked, or entangled solids are water swollen above about 15%–25% water content, they become hydrogels and biomolecules may be immobilized on the outer gel surface, as well as within the water-containing regions (“meshes”) of the swollen polymer gel network. It can be seen that there are many diverse uses of such biofunctional systems in both the medical and biotechnology fields. For example, a number of immobilized enzyme supports and reactor systems (Table 1.4.4.3) have been developed for therapeutic uses in the clinic (Table 1.4.4.4) (De Myttenaere et al., 1967; Kolff, 1979; Sparks et al., 1969; Chang, 1972; Nose et al., 1983, 1984; Schmer et al., 1981; Callegaro and Denri, 1983; Lavin et al., 1985; Sung et al., 1986). Advantages and disadvantages of immobilized enzymes are listed in Table 1.4.4.5.

TABLE 1.4.4.3 Bioreactors, Supports, and Designs**“Artificial Cell” Suspensions**

(microcapsules, red blood cell ghosts, liposomes, reverse micelles [w/o] microspheres)

Biologic Supports

(membranes and tubes of collagen, fibrin ± glycosaminoglycans)

Synthetic Supports

(porous or asymmetric hollow fibers, particulates, parallel plate devices)

TABLE 1.4.4.4 Examples of Immobilized Enzymes in Therapeutic Bioreactors

Medical Application	Substrate	Substrate Action
Cancer Treatment		
L-Asparaginase	Asparagine	Cancer cell nutrient
L-Glutaminase	Glutamine	Cancer cell nutrient
L-Arginase	Arginine	Cancer cell nutrient
L-Phenylalanine	Phenylalanine	Toxin lyase
Indole-3-alkane α -hydroxylase	Tryptophan	Cancer cell nutrient
Cytosine deaminase	5-Fluorocytosine	Toxin
Liver Failure (Detoxification)		
Bilirubin oxidase	Bilirubin	Toxin
UDP-Glucuronyl transferase	Phenolics	Toxin
Other		
Heparinase	Heparin	Anticoagulant
Urease	Urea	Toxin

TABLE 1.4.4.5 Some Advantages and Disadvantages of Immobilized Enzymes**Advantages**

- Enhanced stability
- Can modify enzyme microenvironment
- Can separate and reuse enzyme
- Enzyme-free product
- Lower cost, higher purity product
- No immunogenic response (therapeutics)

Disadvantages

- Difficult to sterilize
- Fouling by other biomolecules
- Mass transfer resistances (substrate in and product out)
- Adverse biological responses of enzyme support surfaces (in vivo or ex vivo)
- Greater potential for product inhibition

TABLE 1.4.4.6 Selected^a Peptide Adhesion Domains in Cell Adhesion Proteins

Fibronectin	RGDS LDV REDV
Vitronectin	RGDS
Laminin A chain	LRGDN IKVAV
Laminin B1 chain	YIGSR
Laminin B2 chain	RNIAEIKDA
Collagen I	RGDT DGEA
Thrombospondin	RGD

^aA large number of receptor-binding peptide domains have been identified in numerous adhesion proteins that are able to recapitulate some of the binding character of the entire protein. Only a small selection of widely studied peptides is listed here.

Immobilized Cell Ligands and Cells

Cell interactions with foreign materials are usually mediated by a biological intermediate, such as adsorbed proteins, as described in Chapter 2.1.2. An approach using biologically functionalized materials can be much more direct, by adsorbing or covalently grafting ligands for cell–surface adhesion receptors, such as integrins, to the material surface (Lutolf and Hubbell, 2005; Patterson et al., 2010) (Table 1.4.4.6).

This has been accomplished with peptides grafted randomly over a material surface (Massia and Hubbell, 1991), as well as with peptides presented in a preclustered manner (Irvine et al., 2001). The latter has important advantages.

Cells normally cluster their adhesion receptors into nanoscopic assemblies referred to as “focal contacts” (Geiger et al., 2009), in which both adhesion ligands and receptors are coclustered. This clustering plays an important role in both cell adhesion mechanics (Ward and Hammer, 1993) and cell signaling (Maheshwari et al., 2000; Geiger et al., 2009). In fact, Miyamoto et al. (1995) found that integrin receptors must be clustered by adhesive ligands to function as they would in a natural environment. This discovery is supported by the fact that many components of the extracellular matrix (ECM) exist as multivalent ligands. Other studies have further elucidated the impact of the multivalent presentation of adhesive ligands on cellular activity.

For instance, [Boonthekul et al. \(2008\)](#) found that the number of bonds between the integrin receptors of a cell and synthetic adhesion peptide ligands correlated with cell proliferation. Studies like these have influenced the use of multivalent adhesive ligands that cause integrin clustering in the design of synthetic biomaterial scaffolds. In addition to peptides, saccharides have also been grafted to polymer surfaces to confer biological functionality ([Griffith and Lopina, 1998](#); [Chang and Hammer, 2000](#)). Other investigations of the migration- and differentiation-inducing influences of different cell adhesion molecules have used self-assembling monolayers for the defined presentation of adhesion ligands ([Mrksich, 2009](#)).

Nanotechnology methods of ligand immobilization have been used extensively to achieve very precise control of ligand immobilization density, ligand clustering, and arrangement, and even ligand exposure from a previously hidden state or hiding after an exposed state. For example, nanopatterning methods have been used to show that cells are capable of sensing and responding to clustering on the length scale of 70 nm of the arginylglycylaspartic acid (RGD) peptide, which binds to integrins such as $\alpha_v\beta_3$ ([Huang et al., 2009](#)). At longer length scales, the cell is unable to sense clustering. In another study that examined how nanoscale ligand clustering can affect cell activity, [Petrie et al. \(2010\)](#) developed a flexible assembly of multimeric recombinant fibronectin fragments that were covalently immobilized onto a polymer brush system that had been coated onto titanium. The researchers were able to show that this multivalent display of fibronectin clustered integrin receptors for enhanced cellular adhesion, signaling, and differentiation when compared to the presentation of monomeric fibronectin fragments. Furthermore, the functionalization of titanium with the multimeric fibronectin fragments allowed for the improved integration of a titanium implant into bone.

Specific biomolecules can be immobilized to control cellular interactions. One important class of such functionalizations is the polypeptide growth factor. Such molecules can be immobilized and retain their ability to provide biological cues that signal specific cellular behavior, such as support of liver-specific function of hepatocytes ([Kuhl and Griffith-Cima, 1996](#)), induction of neurite extension in neurons ([Sakiyama-Elbert et al., 2001](#)), induction of angiogenesis ([Zisch et al., 2001](#)), or the differentiation of mesenchymal stem cells into bone-forming osteoblasts ([Lutolf et al., 2003a,b](#); [Martino et al., 2009](#)). It is important to understand that these effects are not merely induced by the mechanics of adhesion, i.e., what matters are the details of which adhesion ligand is displayed, and thus which adhesion receptor is ligated and what downstream signaling is activated. For example, stimulation of mesenchymal stem cells with a ligand for integrin $\alpha_5\beta_1$ stimulated osteogenesis, whereas stimulation with a ligand for integrin $\alpha_v\beta_3$ did not. Another example of a specific biomolecule that can be conjugated to a biomaterial scaffold to control cell behavior is Sonic Hedgehog (Shh), which naturally assembles into multimers after secretion by cells and plays a role in embryonic development. [Vazin et al. \(2014\)](#)

immobilized Shh onto linear hyaluronic acid polymers and examined the effect of its valency on the specification of human embryonic stem cells. They found that when compared to monovalent Shh, the multivalent Shh constructs could be used to more effectively drive specification of human embryonic stem cells into cell types that could be used in cell replacement therapies for Parkinson's disease or epileptic disorders. [Kaur et al. \(2010\)](#) also demonstrated the ability to control cell differentiation using a multivalent display of a specific immobilized ligand. These researchers created a two-dimensional biomaterial scaffold using tobacco mosaic virus with phosphate ligands conjugated to each capsid coat protein of the virus. The phosphate ligands induced mineralization of the scaffold through calcium incorporation, which served to upregulate osteospecific genes in bone marrow stem cells. Other molecules may be immobilized that can take part in enzymatic reactions at the surface. [McClung et al. \(2001, 2003\)](#) immobilized lysines, whose ϵ -amino groups may interact with preadsorbed tissue plasminogen activator during coagulation, to enhance fibrin clot dissolution at that surface.

The foregoing paragraphs generally deal with biomaterial surfaces as though they are two dimensional. In some devices, this is indeed the case; however, biomaterials have been developed to display their surfaces in three-dimensional situations, even with triggering by cellular remodeling. For example, biomaterial gels have been developed, consisting of cross-linked poly(ethylene glycol) (PEG) chains, where the cross-linker is sensitive to proteases, such as plasmin or matrix metalloproteinases, that are activated by cells as they migrate ([Lutolf et al., 2003a,b](#)). In this way, as cells migrate in a material and remodel it, they can expose new surfaces and be stimulated by those new surfaces. Using such materials as tools, a number of regenerative medical applications have been targeted, where the biomaterial surface displays both adhesion ligands and polypeptide growth factors ([Lutolf and Hubbell, 2005](#)). Such materials, through careful selection of adhesion ligand composition, can control very specific biological processes, such as embryonic stem cell self-renewal ([Lee et al., 2010](#)). Materials have been developed that allow for very precise control of the adhesion ligand display and cross-linked nature of the three-dimensional material, e.g., through locally controlled photochemical manipulation ([Kloxin et al., 2009, 2010](#)).

Immobilization Methods

There are three major methods for immobilizing biomolecules: physical adsorption, physical "entrapment," and covalent attachment ([Stark, 1971](#); [Zaborsky, 1973](#); [Dunlap, 1974](#)). Physical adsorption includes: (1) van der Waals interactions; (2) electrostatic interactions; and (3) affinity recognition. Once adsorbed, the molecules may be further cross-linked to each other. Physical "entrapment" systems include: (1) microcapsules; (2) hydrogels; and (3) physical mixtures such as matrix drug delivery systems. Covalent attachment includes: (1) soluble polymer conjugates; (2) conjugates on solid surfaces; or (3) conjugates within hydrogels.

It is clear that the first two are physically based, while the third is based on covalent or “chemical” attachment to the support molecules. However, sometimes the physical attachment process may involve pairs of molecules with very strong affinity interactions, verging on covalent force levels, such as biotin with streptavidin. Thus it is important to note that the term “immobilization” can refer to a short-term, long-term, or “permanent” localization of the biomolecule on or within a support. In the case of a drug delivery system, the immobilized drug is supposed to be released from the support, either over a short period or over a longer term, while an immobilized enzyme or cell adhesion peptide or protein in an artificial organ is designed to remain attached to or entrapped within the support over the duration of use. Either physical or chemical immobilization can lead to relatively long-term or “permanent” retention on or within a solid support, especially if the immobilized biomolecule is large.

If the polymer support is biodegradable, then the chemically immobilized biomolecule will be released as the matrix erodes or degrades away. Many researchers have chemically immobilized cell adhesion peptides such as RGD onto biodegradable matrices such as poly(lactic-co-glycolic acid) for use as tissue-engineering scaffolds. The cells will have the time to bind and regenerate tissue if the support is slowly degrading. If the support degrades more rapidly than the cells’ ability to reach and bind to the adhesion peptides, then the matrix will not function in the intended way. The immobilized biomolecule may also be susceptible to enzymatic degradation *in vivo*, and this remains an interesting aspect that has received relatively little attention.

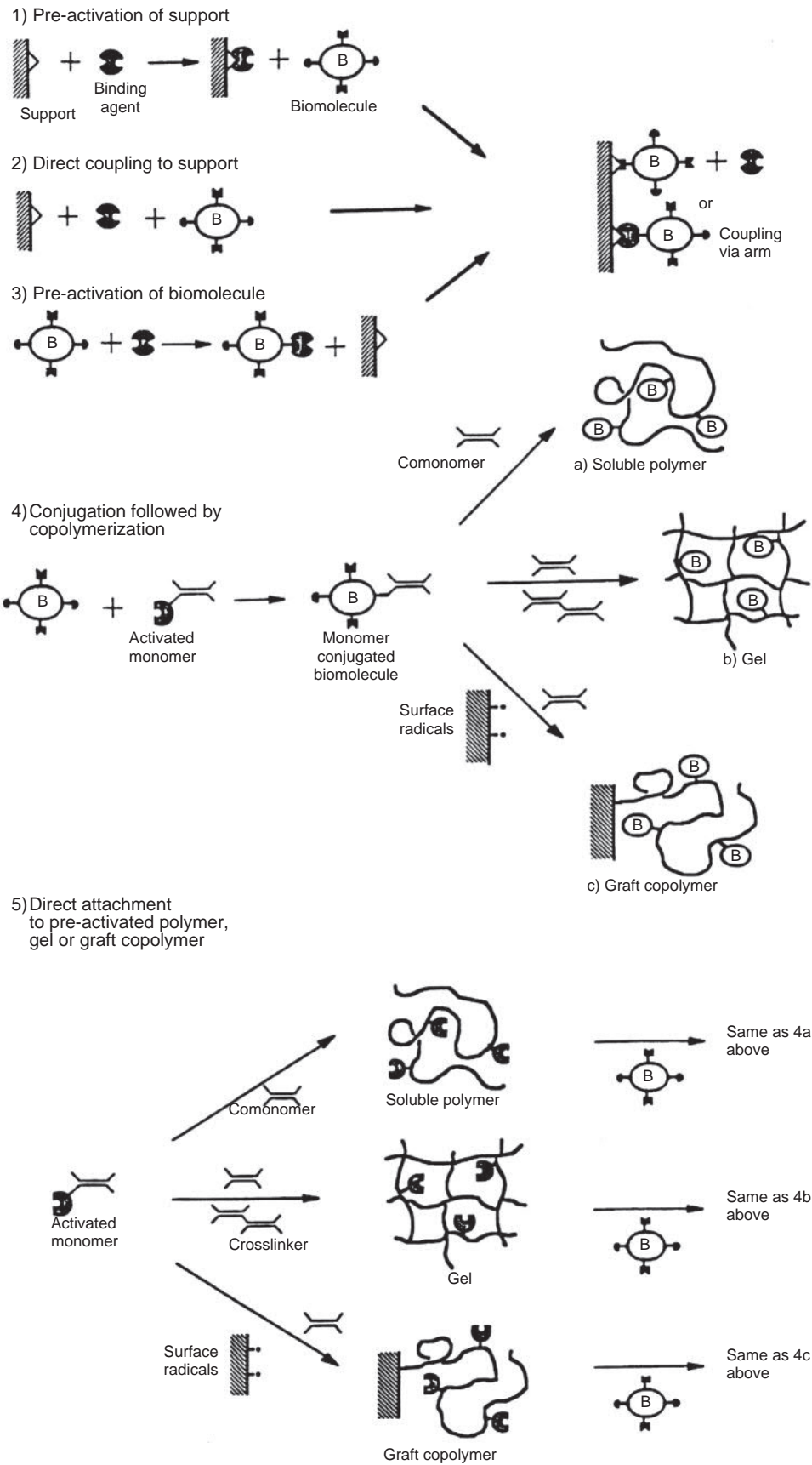
A large and diverse group of methods has been developed for covalent binding of biomolecules to soluble or solid polymeric supports (Weetall, 1975; Carr and Bowers, 1980; Dean et al., 1985; Gombotz and Hoffman, 1986; Shoemaker et al., 1987; Park and Hoffman, 1990; Yang et al., 1990; Schense and Hubbell, 1999; Lutolf et al., 2003b). Many of these methods are schematically illustrated in Fig. 1.4.4.1. The same biomolecule may be immobilized by many different methods; specific examples of the most common chemical reactions utilized are shown in Fig. 1.4.4.2. The reader is referred to Hermanson (2008) for many useful details on numerous conjugation chemistries.

Click chemistry refers to a particular set of covalent reactions often used for biomolecule immobilization. Click reactions are modular, quick, selective, and deliver a high yield under mild reaction conditions (Kolb et al., 2001). In recent years, there has been an interest in bioorthogonal click chemistries, which occur under conditions that are tolerable to cells and do not interfere with the functional groups found in cells or their media. Common bioorthogonal click chemistries include Michael addition, thiol-ene coupling, and azide-alkyne cycloaddition, among others. Examples of these reactions are shown schematically in Fig. 1.4.4.3. Many diverse applications

of bioorthogonal click chemistries exist, and a particularly relevant application for the immobilization and display of biomolecules is the formation of synthetic hydrogels. Hydrogels are hydrated networks of polymers that are often used as cell culture scaffolds due to their ability to mimic the ECM of natural tissues. Biomolecules such as adhesion ligands and growth factors can be immobilized within a hydrogel’s polymeric network to further emulate the natural ECM. Both the synthesis of the hydrogel’s polymeric network and the addition of immobilized biomolecules can be accomplished using bioorthogonal click chemistry. For example, Lutolf et al. (2003c) used base-catalyzed Michael additions to add monocysteine adhesion peptides (RGDS) in stoichiometric deficit to 4-arm-PEG tetravinyl sulfones, then cross-linked the resulting product with bis-cysteine matrix metalloproteinase-degradable peptides to form the hydrogel’s polymeric network. More complex patterning of biomolecules on hydrogels is also possible using photoresponsive click chemistry, such as the thiol-ene reaction. Grim et al. (2018) created hydrogels in which visible light could be used to initiate the reversible and repeatable conjugation of thiol-containing biomolecules to pendant allyl sulfide moieties present in the hydrogel’s polymeric matrix. This ability to spatiotemporally alter the immobilization of biomolecules within the hydrogel using photoresponsive click chemistry is important given the dynamic nature of the ECM and allows researchers to better study how a cell’s environment affects its function and behavior. While the immobilization and display of biomolecules in hydrogels is one common application of click chemistry, many other applications exist. For example, click reactions have been used to immobilize redox proteins on electrode surfaces for use in bioelectrochemical reactions (Zhang et al., 2016), anchor nucleic acids to substrates for use as biosensors (Jiménez-Meneses et al., 2018), and tether peptides to drug-encapsulating nanoparticles for targeted drug delivery (Han et al., 2015).

For covalent binding to an inert solid polymer surface such as polyethylene or silicone rubber, the surface must first be chemically modified to provide reactive groups for the subsequent immobilization step. If the “inert” polymer support does not contain such groups, then it is necessary to modify it to permit covalent immobilization of biomolecules to the surface. A wide number of solid surface modification techniques have been used, including ionizing radiation-initiated graft copolymerization, plasma gas discharge, photochemical grafting, chemical modification (e.g., ozone grafting), and chemical derivatization (Hoffman et al., 1972, 1986; Gombotz and Hoffman, 1986, 1987; Hoffman, 1987, 1988) (see also Chapter 1.4.2 on surface modification techniques).

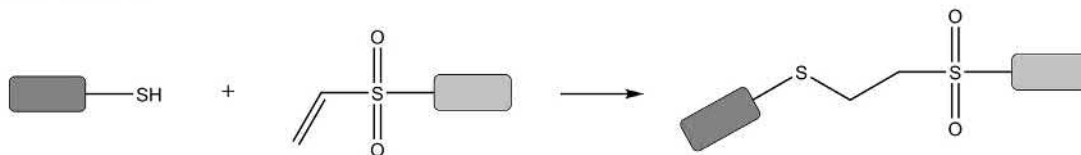
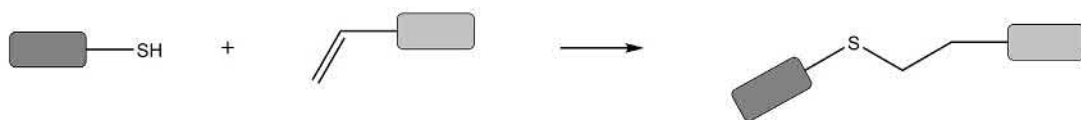
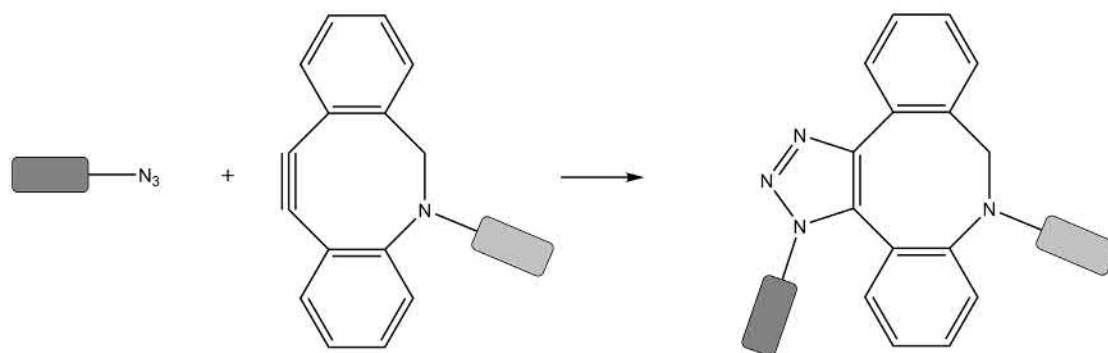
A covalently immobilized biomolecule may also be attached via a spacer group, sometimes called an “arm” or a “tether” (Cuatrecasas and Anfinsen, 1971; Hoffman et al., 1972; Hoffman, 1987). One of the most popular tethers is a PEG molecule that has been derivatized with different



• **Figure 1.4.4.1** Schematic cartoons showing various methods for covalent biomolecule immobilization.

Support function	Coupling agent	Active intermediate	Activation conditions	Coupling conditions	Major reacting groups on proteins
	CNBr		pH 11–12.5 2M carbonate	pH 9–10. 24 hr at 4°C	—NH ₂
 or 	 R = Cl, NH ₂ , OCH ₂ COOH, or NHCH ₂ COOH		Benzene 2 hr at 50°C	pH 8. 12 hr at 4°C 0.1M phosphate	—NH ₂
			10% thiophosgene CHCl ₃ , reflux reaction	pH 9–10. 0.05M HCO ₃ 2 hr at 25°C	
			Same as isothiocyanate	Same as isothiocyanate	
			2.5% Glutaraldehyde in pH 7.0, 0.1M PO ₄	pH 5–7, 0.05 M phosphate, 3 hr at R.T.	
			1% Succinic anhydride, pH 6	See carboxyl derivatives	
	HNO ₂		2N HCl: 0.2g NaNO ₂ at 4°C for 30 min (reaction conditions for aryl amine function)	pH 8, 0.05M bicarbonate. 1–2 hr at 0°C	—NH ₂ —SH
	 HNO ₂			pH 8, 0.05M bicarbonate. 1–2 hr at 0°C	—NH ₂ —SH
 or 	 C + H ⁺ R		50mg 1-cyclohexyl-3- (2-morpholinoethyl)- carbodiimide metho-p- toluene sulfate/10ml, pH 4–5 2–3 hr at R.T.	pH 4, 2–3 hr at R.T.	
		(Intermediate formed from carboxyl group are either protein or matrix) 	10% Thionyl chloride/CHCl ₃ , reflux for 4 hr	pH 8–9, 1 hr at R.T.	—NH ₂
			0.2% N-hydroxysuccinimide, 0.4% N,N-dicyclohexyl- carbodiimide/dioxane	pH 5–9, 0.1M phosphate, 2–4 hr at 0°C	—NH ₂

• **Figure 1.4.4.2** Examples of various chemical methods used to bond biomolecules directly to reactive supports (Carr and Bowers, 1980). R.T., Room temperature.

Michael addition**Thiol-ene coupling****Azide-alkyne cycloaddition**

• **Figure 1.4.4.3** Examples of common bioorthogonal click reactions.

reactive end groups (e.g., [Kim and Feijen, 1985](#)), and several companies currently offer a variety of homo- or heterobifunctional PEGs with end group chemistries such as *N*-hydroxysuccinimide, maleimide, pyridyl disulfide, thiol, vinyl sulfone, alkyne, and azide. Such spacers can provide greater steric freedom, and thus greater specific activity for the immobilized biomolecule. The spacer arm may also be either hydrolytically or enzymatically degradable, and therefore will release the immobilized biomolecule as it degrades ([Kopecek, 1977](#); [Hern and Hubbell, 1998](#)).

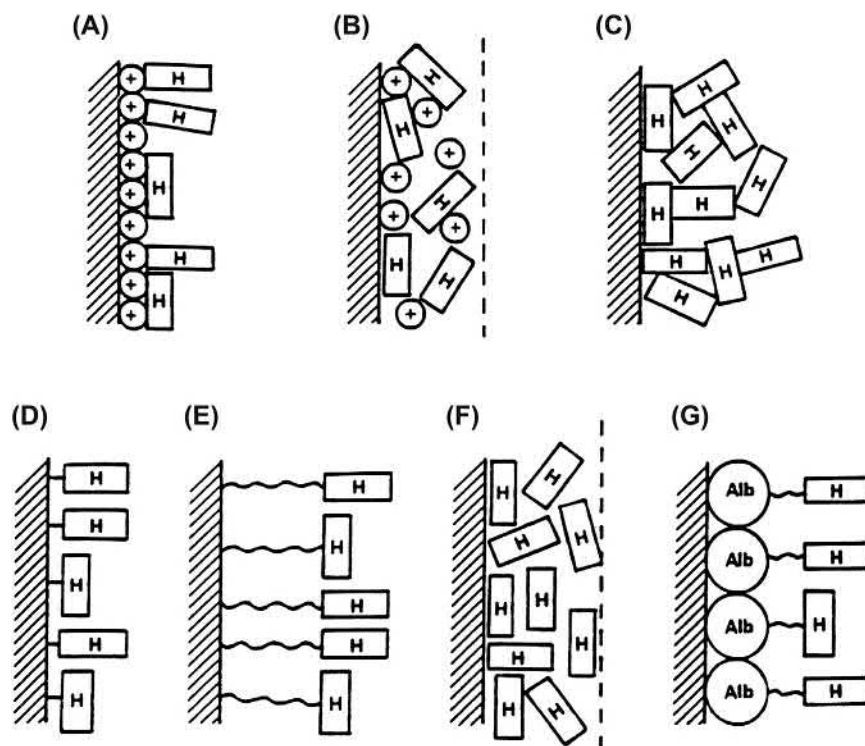
Inert surfaces, whether polymeric, metal, or ceramic, can also be functionalized through modification of a polymeric adlayer. Such physically adsorbed or chemisorbed polymers can be bound to the surface via electrostatic interactions ([VandeVondele et al., 2003](#)), hydrophobic interactions ([Neff et al., 1999](#)), or specific chemical interactions, such as that between gold and sulfur atoms ([Harder et al., 1998](#); [Bearinger et al., 2003](#)). Metal or ceramic surfaces may also be derivatized with functional groups using silane chemistry, such as with functionalized triethoxysilanes ([Massia and Hubbell, 1991](#); [Puleo, 1997](#)) or dopamine polymer chemistry, as described earlier. Plasma gas discharge has been used to deposit polymeric amino groups for conjugation of hyaluronic acid to a metal surface ([Verheye et al., 2000](#)).

As noted earlier, hydrophobic interactions have been used to functionalize hydrophobic surfaces, utilizing biomolecules such as ligands attached to hydrophobic sequences

(e.g., [Ista et al., 1999](#); [Nath and Chilkoti, 2003](#)). Surfaces with hydrophobic gradients have also been prepared for this purpose ([Detrait et al., 1999](#)). An interesting surface-active product was developed several years ago that was designed to convert a hydrophobic surface to a cell adhesion surface by hydrophobic adsorption; it had an RGD cell adhesion peptide coupled at one end to a hydrophobic peptide sequence.

Sometimes more than one biomolecule may be immobilized to the same support. For example, a soluble polymer designed to “target” a drug molecule may have separately conjugated to it a targeting moiety such as an antibody, along with the drug molecule, which may be attached to the polymer backbone via a biodegradable spacer group ([Ringsdorf, 1975](#); [Kopecek, 1977](#); [Goldberg, 1983](#)). For some nucleic acid drugs, sometimes a “nuclear localization signal” is added to enhance intracellular delivery to the nucleus (e.g., [Nair et al., 2003](#)). In another example, the wells in an immunodiagnostic microtiter plate will usually be coated first with an antibody, and then with albumin or casein (to block nonspecific adsorption during the assay); each is physically adsorbed to the well surface. In the case of affinity chromatography supports, the affinity ligand may be covalently coupled to the solid packing, and a “blocking” protein such as albumin or casein may be similarly added to block nonspecific adsorption to the support.

In certain instances, it may be important to consider the manner of presentation, or orientation, of an immobilized biomolecule. Several methods of site-specific biomolecule



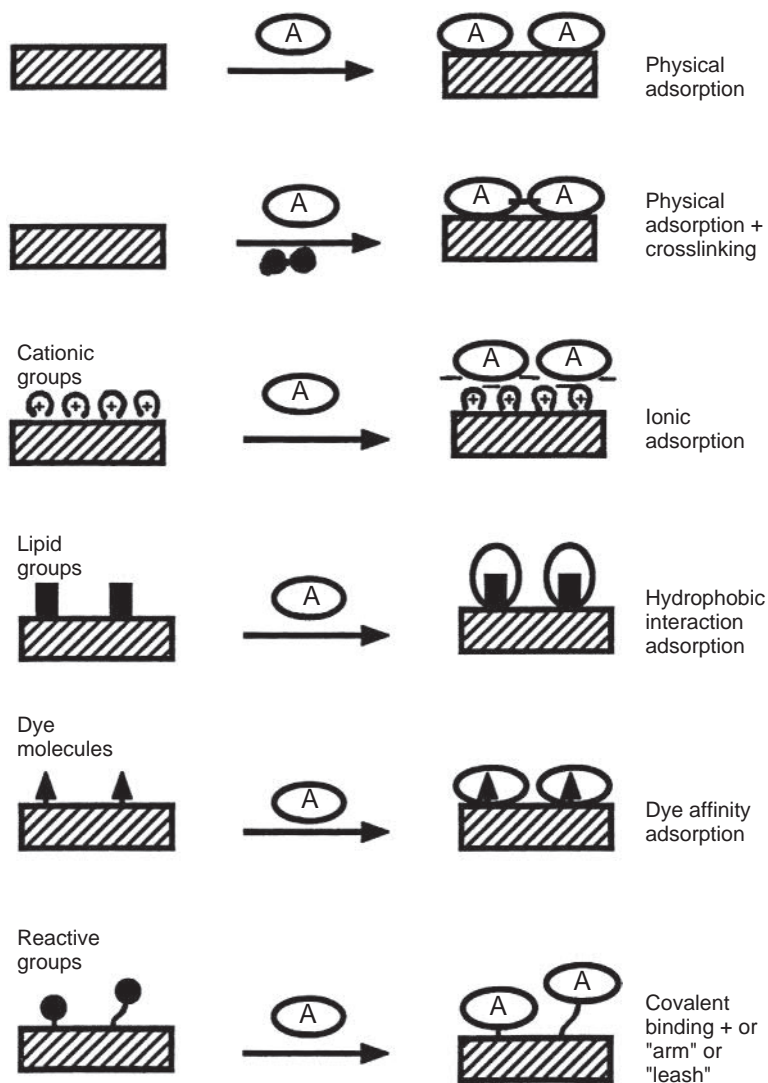
• **Figure 1.4.4.4** Various methods for heparinization of surfaces: (A) heparin bound ionically on a positively charged surface; (B) heparin ionically complexed to a cationic polymer, physically coated on a surface; (C) heparin physically coated and self-cross-linked on a surface; (D) heparin covalently linked to a surface; (E) heparin covalently immobilized via spacer arms; (F) heparin dispersed into a hydrophobic polymer; (G) heparin–albumin conjugate immobilized on a surface (Kim and Feijen, 1985).

immobilization have been developed for this purpose, some of which involve the incorporation of a single amino acid into the biomolecule to be immobilized. For example, [Torrance et al. \(2006\)](#) expressed single chain variable fragment (scFv) molecules with an added cysteine residue at the C-terminus such that the scFv could be oriented uniformly by covalent attachment to a gold surface presenting maleimide groups. This mode of attachment allowed the scFvs to be oriented such that they could sense antigen. In another example, [Lee et al. \(2009\)](#) developed a polydopamine-coated surface and synthesized a model peptide that contained histidine at the N-terminus and lysine at the C-terminus. These researchers demonstrated the ability to control the orientation of their model peptide on the polydopamine surface, as the peptide could be immobilized by either the lysine residue at low pH or the histidine residue at high pH. The addition of an unnatural amino acid can also achieve site-specific biomolecule immobilization. [Wu et al. \(2015\)](#) introduced an unnatural amino acid (*p*-propargylphenylalanine) into the enzyme T4 lysozyme such that the enzyme could be covalently immobilized onto beads presenting an azide group via the Huisgen 1,3-dipolar cycloaddition reaction. The ability to control the enzyme's orientation allowed for enhanced activity and stability when compared to random immobilization. The orientation of an immobilized protein can also be controlled through the incorporation of a peptide tag at a specific site in the protein. For instance, SpyTag forms an isopeptide bond with the protein SpyCatcher ([Zakeri et al.,](#)

[2012](#)). The SpyTag-SpyCatcher system has been used for the presentation of antigens from the surfaces of virus-like particles for use in a malaria vaccine ([Brune et al., 2016](#)). Another application of peptide tags used for biomolecule immobilization are the tags used in Sortase A-mediated ligation, where proteins with an “LPXTG” tag are covalently linked to pentaglycine in the presence of Sortase A. [Ito et al. \(2010\)](#) used Sortase A-mediated ligation to covalently attach the C-terminus of glycosyltransferases, which aid in the process of glycosylation, onto a support to enhance the stability and activity of the glycosyltransferases. In addition to controlling the orientation of immobilized proteins, it can also be desirable to control their density. To accomplish this, [Hodneland et al. \(2002\)](#) controlled the density of phosphonate-terminated “capture ligands” that were incorporated into self-assembled monolayers. Since these capture ligands were capable of forming a covalent adduct bond with cutinase, this system enabled the controlled immobilization of any protein fused with cutinase.

It is evident that there are many different ways in which the same biomolecule can be immobilized to a polymeric support. Heparin and albumin are two common biomolecules that have been immobilized by a number of widely differing methods. These are illustrated schematically in [Figs. 1.4.4.4 and 1.4.4.5](#).

Some of the major features of the different immobilization techniques are compared and contrasted in [Table 1.4.4.7](#). The important molecular criteria for



• **Figure 1.4.4.5** Schematic of various ways that albumin may be immobilized on a surface. Albumin is often used as a “passivating” protein to minimize adsorption of other proteins to a surface.

TABLE 1.4.4.7 Biomolecule Immobilization Methods

Method	Physical and Electrostatic Adsorption	Cross-Linking (After Physical Adsorption)	Entrapment	Covalent Binding
Ease	High	Moderate	Moderate to low	Low
Loading level possible	Low (unless high S/V)	Low (unless high S/V)	High	(Depends on S/V and site density)
Leakage (loss)	Relatively high (sensitive to Δ pH salts)	Relatively low	Low to none ^a	Low to none
Cost	Low	Low to moderate	Moderate	High

S/V, Surface area/Volume.
^aExcept for drug delivery systems.

successful immobilization of a biomolecule are that a large fraction of the available biomolecules should be immobilized, and a large fraction of those immobilized biomolecules should retain an acceptable level of bioactivity over an economically and/or clinically appropriate time period.

Conclusions

It can be seen that there is a wide and diverse range of materials and methods available for immobilization of biomolecules and cells on or within biomaterial supports. Combined with the great variety of possible biomedical and biotechnological applications, this represents a very exciting and fertile field for applied research in biomaterials.

References

- Alsberg, E., Anderson, K.W., Albeiruti, A., Rowley, J.A., Mooney, D.J., 2002. Engineering growing tissues. *Proc. Natl. Acad. Sci.* 99, 12025.
- Bearinger, J.P., Terrettaz, S., Michel, R., Tirelli, N., Vogel, H., et al., 2003. Chemisorbed poly (propylene sulphide)-based copolymers resist biomolecular interactions. *Nat. Mater.* 2, 259–264.
- Bernard, A., Delamarche, E., Schmid, H., Michel, B., Bosshard, H.R., et al., 1998. Printing patterns of proteins. *Langmuir* 14, 2225–2229.
- Blawas, A.S., Reichert, W.M., 1998. Protein patterning. *Biomaterials* 19, 595–609.
- Boonthekul, T., Kong, H.J., Hsiong, S.X., Huang, Y.C., Mahadevan, L., Vandenburgh, H., Mooney, D.J., 2008. Quantifying the relation between bond number and myoblast proliferation. *Faraday Discuss* 139, 53–70.
- Brune, K.D., Leneghan, D.B., Brian, I.J., Ishizuka, A.S., Bachmann, M.F., et al., 2016. Plug-and-Display: decoration of virus-like particles via isopeptide bonds for modular immunization. *Sci. Rep.* 6, 19234.
- Callegaro, L., Denri, E., 1983. Applications of bioreactors in medicine. *Int. J. Artif. Organs* 6 (Suppl. 1), 107.
- Carr, P.W., Bowers, L.D., 1980. *Immobilized Enzymes in Analytical and Clinical Chemistry: Fundamentals and Applications*. Wiley, New York, NY.
- Chang, K.C., Hammer, D.A., 2000. Adhesive dynamics simulations of sialyl-Lewis (x)/E-selectin-mediated rolling in a cell-free system. *Biophys. J.* 79, 1891–1902.
- Chang, T.M.S., 1972. *Artificial Cells*. C. C. Thomas, Springfield, IL.
- Csucs, G., Michel, R., Lussi, J.W., Textor, M., Danuser, G., 2003. Micro-contact printing of novel co-polymers in combination with proteins for cell-biological applications. *Biomaterials* 24, 1713–1720.
- Cuatrecasas, P., Anfinsen, C.B., 1971. Affinity chromatography. *Annu. Rev. Biochem.* 40, 259.
- Dean, P.D.G., Johnson, W.S., Middle, F.A. (Eds.), 1985. *Affinity Chromatography*. IRL Press, Oxford, UK.
- De Myttenaere, M.H., Maher, J., Schreiner, G., 1967. Hemo-perfusion through a charcoal column for glutethimide poisoning. *Trans. ASAIO* 13, 190.
- Detrait, E., Lhoest, J.B., Bertrand, P., de Aguilar, V.B., 1999. Fibronectin-pluronic coadsorption on a polystyrene surface with increasing hydrophobicity: relationship to cell adhesion. *J. Biomed. Mater. Res.* 45, 404–413.
- Dunlap, B.R. (Ed.), 1974. *Immobilized Biochemicals and Affinity Chromatography*. Plenum, New York, NY.
- Ellman, J.A., Gallop, M.A., 1998. Combinatorial chemistry. *Curr. Opin. Chem. Biol.* 2, 17–319.
- Folch, A., Toner, M., 2000. Microengineering of cellular interactions. *Annu. Rev. Biomed. Eng.* 2, 227–256.
- Geiger, B., Spatz, J.P., Bershadsky, A.D., 2009. Environmental sensing through focal adhesions. *Nat. Rev. Mol. Cell Biol.* 10, 21–33.
- Goldberg, E. (Ed.), 1983. *Targeted Drugs*. Wiley-Interscience, New York, NY.
- Gombotz, W.R., Hoffman, A.S., 1986. Immobilization of biomolecules and cells on and within synthetic polymeric hydrogels. In: Peppas, N.A. (Ed.), *Hydrogels in Medicine and Pharmacy*, vol. 1. CRC Press, Boca Raton, FL, pp. 95–126.
- Gombotz, W.R., Hoffman, A.S., 1987. Gas discharge techniques for modification of biomaterials. In: Williams, D. (Ed.), *Critical Reviews in Biocompatibility*, vol. 4. CRC Press, Boca Raton, FL, pp. 1–42.
- Gott, V.L., Whiffen, J.D., Dutton, R.C., 1963. Heparin bonding on colloidal graphite surfaces. *Science* 142, 1297–1298.
- Griffith, L.G., Lopina, S., 1998. Microdistribution of substratum-bound ligands affects cell function: hepatocyte spreading on PEO-tethered galactose. *Biomaterials* 19, 979–986.
- Grim, J.C., Brown, T.E., Aguado, B.A., Chapnick, D.A., Viert, A.L., et al., 2018. A reversible and repeatable thiol-ene bioconjugation for dynamic patterning of signaling proteins in hydrogels. *ACS Cent. Sci.* 4, 909–916.
- Han, S.-S., Li, Z.-Y., Zhu, J.-Y., Han, K., Zheng, Z.-Y., et al., 2015. Dual-pH sensitive charge-reversal polypeptide micelles for tumor triggered targeting uptake and nuclear drug delivery. *Small* 11, 2543–2554.
- Harder, P., Grunze, M., Dahint, R., Whitesides, G.M., Laibinis, P.E., 1998. Molecular conformation and defect density in oligo (ethylene glycol)-terminated self-assembled monolayers on gold and silver surfaces determine their ability to resist protein adsorption. *J. Phys. Chem. B* 102, 426–436.
- Hodneland, C.D., Lee, Y.S., Min, D.H., Mrksich, M., 2002. Selective immobilization of proteins to self-assembled monolayers presenting active site-directed capture ligands. *Proc. Natl. Acad. Sci.* 99, 5048–5052.
- Hermansson, G., 2008. *Bioconjugate Techniques*, second ed. Academic Press, New York, NY.
- Hern, D.L., Hubbell, J.A., 1998. Incorporation of adhesion peptides into nonadhesive hydrogels useful for tissue resurfacing. *J. Biomed. Mater. Res.* 39, 266–276.
- Hoffman, A.S., 1987. Modification of material surfaces to affect how they interact with blood. *Ann. NY Acad. Sci.* 516, 96–101.
- Hoffman, A.S., 1988. Applications of plasma gas discharge treatments for modification of biomaterial surfaces. *J. Appl. Polymer Sci. Symp.* 42, 251.
- Hoffman, A.S., Schmer, G., Harris, C., Kraft, W.G., 1972. Covalent binding of biomolecules to radiation-grafted hydrogels on inert polymer surfaces. *Trans. Am. Soc. Artif. Intern. Organs* 18, 10.
- Hoffman, A.S., Gombotz, W.R., Uenoyama, S., Dong, L.C., Schmer, G., 1986. Immobilization of enzymes and antibodies to radiation grafted polymers for therapeutic and diagnostic applications. *Radiat. Phys. Chem.* 27, 265–273.
- Houseman, B.T., Mrksich, M., 2002. Towards quantitative assays with peptide chips: a surface engineering approach. *Trends Biotechnol.* 20, 279–281.
- Huang, J., Grater, S.V., Corbellini, F., Rinck, S., Bock, E., et al., 2009. Impact of order and disorder in RGD nanopatterns on cell adhesion. *Nano Lett.* 9, 1111–1116.

- Irvine, D.J., Mayes, A.M., Griffith, L.G., 2001. Nanoscale clustering of RGD peptides at surfaces using comb polymers. 1. Synthesis and characterization of comb thin films. *Biomacromolecules* 2, 85–94.
- Ismagilov, R.F., Ng, J.M.K., Kenis, P.J.A., Whitesides, G.M., 2001. Microfluidic arrays of fluid–fluid diffusional contacts as detection elements and combinatorial tools. *Anal. Chem.* 73, 5207–5213.
- Ista, L.K., Pérez-Luna, V.H., López, G.P., 1999. Surface-grafted, environmentally sensitive polymers for biofilm release. *Appl. Environ. Microbiol.* 65, 1603–1609.
- Ito, Y., 1999. Surface micropatterning to regulate cell functions. *Biomaterials* 20, 2333–2342.
- Ito, T., Sadamoto, R., Naruchi, K., Togame, H., Takemoto, H., et al., 2010. Highly oriented recombinant glycosyltransferases: site-specific immobilization of unstable membrane proteins by using *Staphylococcus aureus* sortase A. *Biochemistry* 49, 2604–2614.
- Jackman, R.J., Duffy, D.C., Cherniavskaya, O., Whitesides, G.M., 1999. Using elastomeric membranes as dry resists and for dry lift-off. *Langmuir* 15, 2973–2984.
- James, C.D., Davis, R.C., Kam, L., Craighead, H.G., Isaacson, M., et al., 1998. Patterned protein layers on solid substrates by thin stamp microcontact printing. *Langmuir* 14, 741–744.
- Jiménez-Meneses, P., Bañuls, M.J., Puchades, R., Maquieira, A., 2018. Fluor-thiol photocoupling reaction for developing high performance nucleic acid (NA) microarrays. *Anal. Chem.* 90, 11224–11231.
- Kane, R.S., Takayama, S., Ostuni, E., Ingber, D.E., Whitesides, G.M., 1999. Patterning proteins and cells using soft lithography. *Biomaterials* 20, 2363–2376.
- Kaur, G., Wang, C., Sun, J., Wang, Q., 2010. The synergistic effects of multivalent ligand display and nanotopography on osteogenic differentiation of rat bone marrow stem cells. *Biomaterials* 31, 5813–5824.
- Kim, S.W., Feijen, J., 1985. Methods for immobilization of heparin. In: Williams, D. (Ed.), *Critical Reviews in Biocompatibility*. CRC Press, Boca Raton, FL, pp. 229–260.
- Kloxin, A.M., Kasko, A.M., Silans, C.N., Anseth, K.S., 2009. Photodegradable hydrogels for dynamic tuning of physical and chemical properties. *Science* 324, 59–63.
- Kloxin, A.M., Tibbitt, M.W., Kasko, A.M., Fairbairn, J.A., Anseth, K.S., 2010. Tunable hydrogels for external manipulation of cellular microenvironments through controlled photodegradation. *Adv. Mater.* 22, 61–66.
- Kolff, W.J., 1979. Artificial organs in the seventies. *Trans. ASAIO* 16, 534.
- Kolb, H.C., Finn, M.G., Sharpless, K.B., 2001. Click chemistry: diverse chemical function from a few good reactions. *Angew. Chem. Int. Ed.* 40, 2004–2021.
- Kopecek, J., 1977. Soluble biomedical polymers. *Polymer. Med.* 7, 191.
- Ku, S.H., Ryu, K., Hong, S.K., Lee, H., Park, C.B., 2010. General functionalization route for cell adhesion on non-wetting surfaces. *Biomaterials* 31, 2535–2541.
- Kuhl, P.R., Griffith-Cima, L.G., 1996. Tethered epidermal growth factor as a paradigm for growth factor-induced stimulation from the solid phase. *Nat. Med.* 2, 1022–1027.
- Laskin, A.I. (Ed.), 1985. *Enzymes and Immobilized Cells in Biotechnology*. Menlo Benjamin/Cummings, Park, CA.
- Lavin, A., Sung, C., Klibanov, A.M., Langer, R., 1985. Enzymatic removal of bilirubin from blood: a potential treatment for neonatal jaundice. *Science* 230, 543.
- Lee, H., Dellatore, S.M., Miller, W.M., Messersmith, P.S., 2007. Mussel inspired surface chemistry for multifunctional coatings. *Science* 318, 426–430.
- Lee, H., Rho, J., Messersmith, P.B., 2009. Facile conjugation of biomolecules onto surfaces via mussel adhesive protein inspired coatings. *Adv. Mater.* 21, 431–434.
- Lee, S.T., Yun, J.I., Jo, Y.S., Mochizuki, M., van der Vlies, A.J., et al., 2010. Engineering integrin signaling for promoting embryonic stem cell self-renewal in a precisely defined niche. *Biomaterials* 31, 1219–1226.
- Lee, Y.S., Mrksich, M., 2002. Protein chips: from concept to practice. *Trends Biotechnol.* 20, S14–S18.
- Lutolf, M.P., Hubbell, J.A., 2005. Synthetic biomaterials as instructive extracellular microenvironments for morphogenesis in tissue engineering. *Nat. Biotechnol.* 23, 47–55.
- Lutolf, M.R., Weber, F.E., Schmoekel, H.G., Schense, J.C., Kohler, T., et al., 2003a. Repair of bone defects using synthetic mimetics of collagenous extracellular matrices. *Nat. Biotechnol.* 21, 513–518.
- Lutolf, M.P., Raeber, G.P., Zisch, A.H., Tirelli, N., Hubbell, J.A., 2003b. Cell-responsive synthetic hydrogels. *Adv. Mater.* 15, 888–892.
- Lutolf, M.P., Lauer-Fields, J.L., Schmoekel, H.G., Metters, A.T., Weber, F.E., et al., 2003c. Synthetic matrix metalloproteinase-sensitive hydrogels for the conduction of tissue regeneration: engineering cell-invasion characteristics. *Proc. Natl. Acad. Sci.* 100, 5413–5418.
- McClung, W.G., Clapper, D.L., Hu, S.P., Brash, J.L., 2001. Lysine-derivatized polyurethane as a clot lysing surface: conversion of plasminogen to plasmin and clot lysis in vitro. *Biomaterials* 22, 1919–1924.
- McClung, W.G., Clapper, D.L., Anderson, A.B., Babcock, D.E., Brash, J.L., 2003. Interactions of fibrinolytic system proteins with lysine-containing surfaces. *J. Biomed. Mater. Res.* 66A, 795–801.
- McDevitt, T.C., Angelo, J.C., Whitney, M.L., Reinecke, H., Hauschka, S.D., et al., 2002. In vitro generation of differentiated cardiac myofibers on micropatterned laminin surfaces. *J. Biomed. Mater. Res.* 60, 472–479.
- Maheshwari, G., Brown, G., Lauffenburger, D.A., Wells, A., Griffith, L.G., 2000. Cell adhesion and motility depend on nanoscale RGD clustering. *J. Cell Sci.* 113, 1677–1686.
- Martino, M.M., Mochizuki, M., Rothenfluh, D.A., Rempel, S.A., Hubbell, J.A., et al., 2009. Controlling integrin specificity and stem cell differentiation in 2D and 3D environments through regulation of fibronectin domain stability. *Biomaterials* 30, 1089–1097.
- Massia, S.P., Hubbell, J.A., 1991. An RGD spacing of 440 nm is sufficient for integrin $\alpha\beta3$ -mediated fibroblast spreading and 140 nm for focal contact and stress fiber formation. *J. Cell Biol.* 114, 1089–1100.
- Miyamoto, S., Akiyama, S.K., Yamada, K.M., 1995. Synergistic roles for receptor occupancy and aggregation in integrin transmembrane function. *Science* 267, 883–885.
- Mrksich, M., 2009. Using self-assembled monolayers to model the extracellular matrix. *Acta Biomater.* 5, 823–841.
- Nair, R., Carter, P., Burkhard, R., 2003. NLSdb: database of nuclear localization signals. *Nucleic Acids Res.* 31, 397–399.
- Nath, N., Chilkoti, A., 2003. Fabrication of reversible functional arrays of proteins directly from cells using a stimuli responsive polypeptide. *Anal. Chem.* 75, 709–715.
- Neff, J.A., Tresco, P.A., Caldwell, K.D., 1999. Surface modification for controlled studies of cell–ligand interactions. *Biomaterials* 20, 2377–2393.
- Nose, Y., Malchesky, P.S., Smith, J.W. (Eds.), 1983. *Plasmapheresis: New Trends in Therapeutic Applications*. ISAO Press, Cleveland, OH.

- Nose, Y., Malchesky, P.S., Smith, J.W. (Eds.), 1984. Therapeutic Apheresis: A Critical Look. ISAO Press, Cleveland, OH.
- Ostuni, E., Grzybowski, B.A., Mrksich, M., Roberts, C.S., Whitesides, G.M., 2003. Adsorption of proteins to hydrophobic sites on mixed self-assembled monolayers. *Langmuir* 19, 1861–1872.
- Park, T.G., Hoffman, A.S., 1990. Immobilization of Arthrobacter simplex in a thermally reversible hydrogel: effect of temperature cycling on steroid conversion. *Biotechnol. Bioeng.* 35, 152–159.
- Patterson, J., Martino, M.M., Hubbell, J.A., 2010. Biomimetic materials in tissue engineering. *Mater. Today* 13, 14–22.
- Petrie, T.A., Raynor, J.E., Dumbauld, D.W., Lee, T.T., Jagtap, S., et al., 2010. Multivalent integrin-specific ligands enhance tissue healing and biomaterial integration. *Sci. Transl. Med.* 2 45ra60.
- Piskin, E., Hoffman, A.S. (Eds.), 1986. *Polymeric Biomaterials*. M. Nijhoff, Dordrecht, The Netherlands.
- Puleo, D.A., 1997. Retention of enzymatic activity immobilized on silanized Co–Cr–Mo and Ti–6Al–4V. *J. Biomed. Mater. Res.* 37, 222–228.
- Ringsdorf, H., 1975. Structure and properties of pharmacologically active polymers. *J. Polym. Sci.* 51, 135.
- Sakiyama-Elbert, S.E., Panitch, A., Hubbell, J.A., 2001. Development of growth factor fusion proteins for cell-triggered drug delivery. *FASEB J.* 15, 1300–1302.
- Schense, J.C., Hubbell, J.A., 1999. Cross-linking exogenous bifunctional peptides into fibrin gels with factor XIIIa. *Bioconjug. Chem.* 10, 75–81.
- Schmer, G., Rastelli, L., Newman, M.O., Dennis, M.B., Holcenberg, J.S., 1981. The bioartificial organ: review and progress report. *Int. J. Artif. Organs* 4, 96.
- Scotchford, C.A., Ball, M., Winkelmann, M., Voros, J., Csucs, C., et al., 2003. Chemically patterned, metal-oxide-based surfaces produced by photolithographic techniques for studying protein- and cell-interactions. II: protein adsorption and early cell interactions. *Biomaterials* 24, 1147–1158.
- Shoemaker, S., Hoffman, A.S., Priest, J.H., 1987. Synthesis and properties of vinyl monomer/enzyme conjugates: conjugation of l-asparaginase with N-succinimidyl acrylate. *Appl. Biochem. Biotechnol.* 15, 11.
- Sparks, R.E., Solemme, R.M., Meier, P.M., Litt, M.H., Lindan, O., 1969. Removal of waste metabolites in uremia by microencapsulated reactants. *Trans. ASAIO* 15, 353.
- Stark, G.R. (Ed.), 1971. *Biochemical Aspects of Reactions on Solid Supports*. Academic Press, New York, NY.
- Sung, C., Lavin, A., Klibanov, A., Langer, R., 1986. An immobilized enzyme reactor for the detoxification of bilirubin. *Biotechnol. Bioeng.* 28, 1531.
- Tomlinson, E., Davis, S.S., 1986. *Site-Specific Drug Delivery: Cell Biology, Medical and Pharmaceutical Aspects*. Wiley, New York, NY.
- Torrance, L., Ziegler, A., Pittman, H., Paterson, M., Toth, R., et al., 2006. Oriented immobilisation of engineered single-chain antibodies to develop biosensors for virus detection. *J. Virol. Methods* 134, 164–170.
- VandeVondele, S., Voros, J., Hubbell, J.A., 2003. RGD- grafted poly-L-lysine-graft-(polyethylene glycol) copolymers block non-specific protein adsorption while promoting cell adhesion. *Biotechnol. Bioeng.* 82, 784–790.
- Vazin, T., Ashton, R.S., Conway, A., Rode, N.A., Lee, S.M., et al., 2014. The effect of multivalent Sonic hedgehog on differentiation of human embryonic stem cells into dopaminergic and GABAergic neurons. *Biomaterials* 35, 941–948.
- Verheye, S., Markou, C.P., Salame, M.Y., Wan, B., King III, S.B., et al., 2000. Reduced thrombus formation by hyaluronic acid coating of endovascular devices. *Arterioscler. Thromb. Vasc. Biol.* 20, 1168–1172.
- Ward, M.D., Hammer, D.A., 1993. A theoretical analysis for the effect of focal contact formation on cell–substrate attachment strength. *Biophys. J.* 64, 936–959.
- Weetall, H.H. (Ed.), 1975. *Immobilized Enzymes, Antigens, Antibodies and Peptides: Preparation and Characterization*. Dekker, New York, NY.
- Winkelmann, M., Gold, J., Hauert, R., Kasemo, B., Spencer, N.D., et al., 2003. Chemically patterned, metal oxide based surfaces produced by photolithographic techniques for studying protein- and cell–surface interactions I: microfabrication and surface characterization. *Biomaterials* 24, 1133–1145.
- Wu, J.C.Y., Hutchings, C.H., Lindsay, M.J., Werner, C.J., Bundy, B.C., 2015. Enhanced enzyme stability through site-directed covalent immobilization. *J. Biotechnol.* 193, 83–90.
- Yang, H.J., Cole, C.A., Monji, N., Hoffman, A.S., 1990. Preparation of a thermally phase-separating copolymer, poly (N- isopropylacrylamide-co-N-acryloxysuccinimide) with a controlled number of active esters per polymer chain. *J. Polym. Sci., Polym. Chem. Ed.* 28, 219–220.
- Zaborsky, O., 1973. *Immobilized Enzymes*. CRC Press, Cleveland, OH.
- Zakeri, B., Fierer, J.O., Celik, E., Chittock, E.C., Schwarz-Linek, U., Moy, et al., 2012. Peptide tag forming a rapid covalent bond to a protein, through engineering a bacterial adhesin. *Proc. Natl. Acad. Sci.* 109, E690–E697.
- Zhang, L., Vilà, N., Klein, T., Kohring, G.-W., Mazurenko, I., et al., 2016. Immobilization of cysteine-tagged proteins on electrode surfaces by thiol-ene click chemistry. *ACS Appl. Mater. Interfaces* 8, 17591–17598.
- Zisch, A.H., Schenk, U., Schense, J.C., Sakiyama-Elbert, S.E., Hubbell, J.A., 2001. Covalently conjugated VEGF-fibrin matrices for endothelialization. *J. Control. Release* 72, 101–113.

1.4.5

Surface Patterning

JAE SUNG LEE¹, RYAN T. HILL², ASHUTOSH CHILKOTI³, WILLIAM L. MURPHY^{1,4}

¹Department of Orthopedics and Rehabilitation, University of Wisconsin–Madison, Madison, WI, United States

²Center for Biologically Inspired Materials and Material Systems, Duke University, Durham, NC, United States

³Department of Biomedical Engineering, Duke University, Durham, NC, United States

⁴Department of Biomedical Engineering, University of Wisconsin–Madison, Madison, WI, United States

Introduction

Surface patterning is the use of surface modification methods to create chemically or physically demarcated regions on a surface. The art of patterning surfaces has a long history; the recent antecedent methods to pattern biomolecules are derived, in part, from the microelectronics industry (Geissler and Xia, 2004; Whitesides et al., 2001). As hand-wiring small, complex electronic devices became increasingly difficult, new methods were developed to pattern substrates such that many electrical components and interconnects between the different components of these devices could be created on the surface of a relatively large substrate in a batch process. These processes that have been instrumental to the development of all modern electronic devices have been driven by a set of technologies to create micro- and nanoscale features on the surface of semiconductors that are collectively and somewhat loosely termed “photolithography.” Seen from this broader perspective, it might be argued that the conceptual origins of many of the techniques used to pattern biomolecules and cells on surfaces extend back to the preindustrial era, to techniques that were developed to print on paper and textiles, such as block printing, screen printing, lithography, and batik.

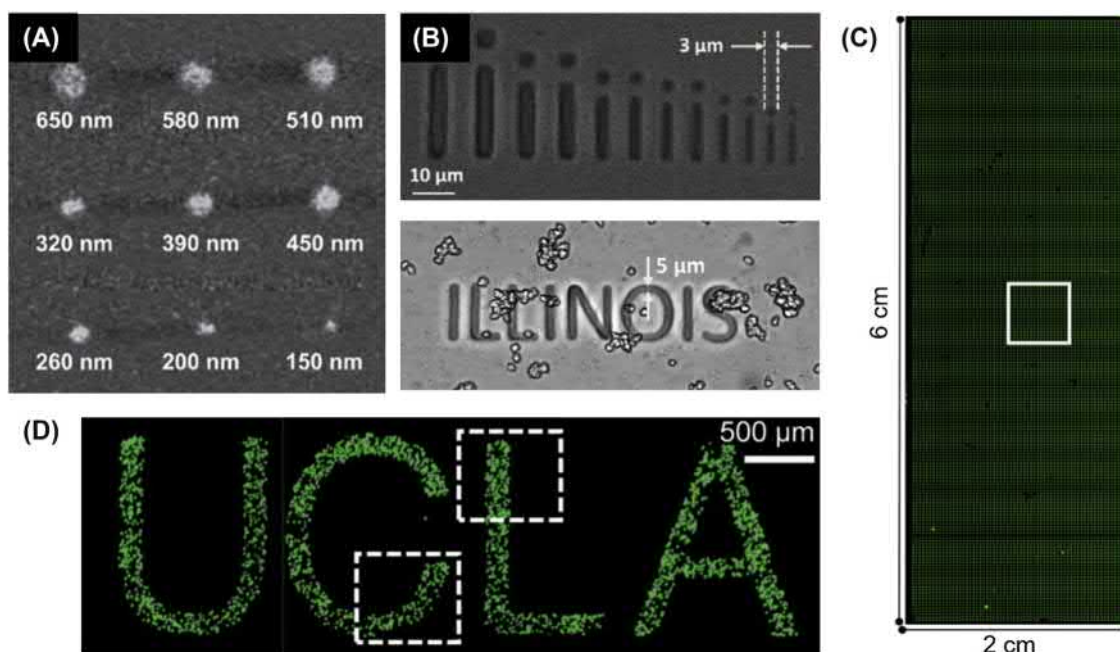
This chapter focuses on surface patterning in the realm of biomedical research. Many surface patterning techniques, especially photolithography, have become important tools for biomedical research. The unique demands of biomedical research—for example, soft hydrated materials such as proteins and hydrogels in an aqueous environment—impose a special set of requirements and constraints on patterning methods. The goal of this chapter is to familiarize the reader

with various surface patterning techniques, and how these techniques can be applied for biomedical research. First, we discuss important figure-of-merit of patterning methods that allow various methods to be compared with each other, and allow a user to identify which patterning method is most appropriate for a specific application. We then discuss various types of patterning techniques, and follow up with a brief conclusion.

Some chapters in this textbook that provide background information for this chapter include Surface Properties and Surface Characterization (Chapter 1.2.4), Non-fouling Surfaces (Chapter 1.4.3A), and Physico-chemical Surface Modification of Materials Used in Medicine (Chapter 1.4.2). However, as will quickly become apparent, this chapter has implications for many other chapters in the book.

Common Concerns In Biomolecular Surface Patterning

Surface patterning is carried out for a wide variety of reasons and, in turn, the ultimate goal of the patterned substrate defines a set of constraints or concerns that dictate how the fabrication process should be carried out. Surface patterning within the scope of biomaterials research is largely focused on the patterning of biomolecules or cells. Listed below are important figures-of-merit (FOMs) and concerns that typically need to be considered in patterning biomolecules or cells. We also briefly discuss how the selection of an appropriate patterning methodology for a particular application is not usually influenced by a single FOM, but is dictated by the technique that offers the best combination of several FOMs.



• **Figure 1.4.5.1** Examples of resolution and contrast in surface patterning. (A, B) Features of different sizes created with (A) a submicron high-resolution patterning technique (Lee et al., 2006) and (B) a relatively lower-resolution technique (Raman et al., 2016). (C) An example of a high-throughput process, enabling the patterned protein deposition on the whole glass slide (Foncy et al., 2018). (D) High-contrast cell patterning with nearly zero background defects (Wu et al., 2018).

Resolution

Resolution refers to the smallest feature size that can be reliably created by a patterning technique. Although the resolution of new techniques is constantly pushed toward smaller feature sizes and finer control, it is also beneficial to know what range of feature sizes a particular technique is capable of producing. Fig. 1.4.5.1A and B show examples of different size patterns created with a high-resolution technique, as well as patterns created with a lower-resolution technique that is capable of generating a wider range of feature sizes. The highest resolution is not necessarily better, as the desired resolution depends upon the application. Thus, in order to pattern cells whose dimension is at least several micrometers, a technique with a relatively low resolution in the micrometers range is likely adequate, as long as it can pattern a large enough area, i.e., has a high enough throughput, which is discussed next.

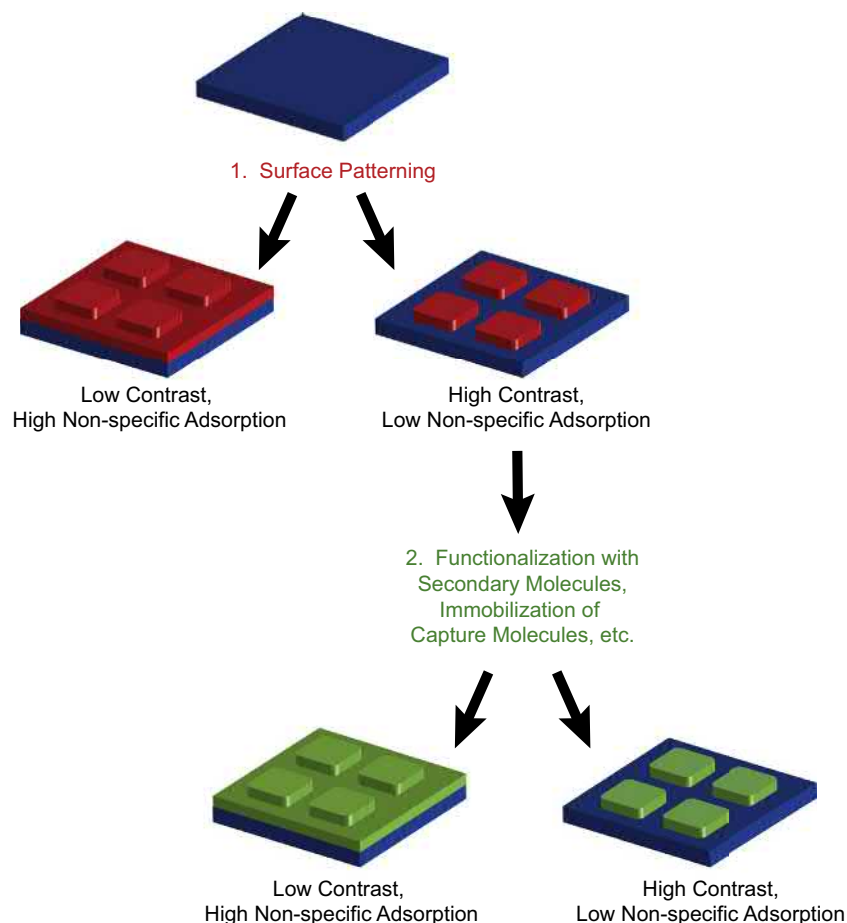
Throughput

While resolution refers to the smallest possible feature size that can be created by a patterning technique, throughput is a measure of the surface area that can be patterned in a given time. Therefore, the throughput of a patterning technique is especially important for its use in device manufacturing because scalable production is largely dependent on the length and time scale on which the patterned substrates can be manufactured (Fig. 1.4.5.1C). Although the different types of patterning techniques are discussed later in this chapter, here we briefly discuss a few patterning methods

to illustrate throughput considerations. Direct-write or “on-the-fly” types of patterning methods are those that use a stylus and ink to pattern a surface. These techniques usually provide precise control over the patterning process and finer feature sizes—often sub-100 nm—than some other printing methods, such as microcontact printing, and can often create arbitrary feature shapes. Rapid patterning over large areas (i.e., greater than hundreds of square micrometers), however, is challenging for most variants of this type of patterning. On the other hand, techniques based on printing using a mask or master can readily pattern large areas of a surface quickly (in the order of seconds to minutes), but may only be able to access certain shapes of features (e.g., circles, lines, or squares), and may have limited resolution (i.e., on the micrometer scale or greater).

Contrast

Contrast is the degree to which the patterned subjects are distinguishable from the background substrate (Fig. 1.4.5.1D). In patterning biomolecules, contrast is generally defined as the surface density of the patterned biomolecule of interest relative to biomolecules that might adventitiously be bound outside of the pattern as a consequence of the patterning process and use. Contrast in patterns of biologically active molecules, such as enzymes, cytokines, or antibodies, can be assessed by measuring the activity of the patterned molecules. For example, the pattern of biomolecules can be visualized by another molecule having a high affinity to patterned biomolecules and a fluorescent, radioactive, or plasmonic tag. Biomolecular patterning often involves



• **Figure 1.4.5.2** Contrast and nonspecific adsorption. Maintaining contrast during patterning of biomolecules often requires that: (1) the patterned materials have low nonspecific adsorption to the background substrate; and (2) any molecules used in subsequent steps (functionalization of pattern with secondary, reporter molecules, immobilization of antigens or capture molecules from solutions, etc.) also have low nonspecific adsorption to the background.

molecules with a functional activity or activity that is difficult to assess in biochemical methods. In these cases, pattern contrast is often visualized by employing a secondary processing step for pattern visualization. For example, contrast in patterned peptides that act as cues for cell adhesion can be visualized by exposing the pattern to cells in culture, and the degree of cell confinement in patterned region is an indirect measure of the fidelity and contrast of the pattern.

Contrast in biomolecular patterning is heavily dependent on surface properties of not only the pattern itself, but also of the background. Biomolecular patterns are often exposed to solutions that can contain complex mixtures of proteins and other molecules in the course of their use, and most surfaces are particularly prone to nonspecific and irreversible adsorption of poorly defined proteins. Thus, maintaining contrast in biomolecular patterning usually involves some sort of passivation step to prevent two sets of undesirable events: (1) adsorption of the molecule to be patterned on the unpatterned background regions; (2) adsorption of biomolecules—that are to be subsequently exposed to the patterned surface—onto the patterned features or the background regions of the surface (Fig. 1.4.5.2).

Nonspecific adsorption should be minimized to ensure high specificity and can be reduced by methods of varying degrees of complexity. Perhaps the most common and simplest way to reduce nonspecific adsorption is to block the background surface by absorbing known proteins, such as bovine serum albumin (BSA), under the assumption that deposition of a known protein will prevent further nonspecific adsorption of unknown, undefined biomolecules to the substrate. However, it has been shown that proteins can adsorb onto a BSA layer (Hyun et al., 2001), so that this strategy, despite its widespread use, is of limited utility. A more effective way of reducing nonspecific adsorption is to create a “nonfouling” surface. Nonfouling surfaces are typically defined as surfaces that are resistant to the protein adsorption and cell adhesion. A widely used method to create a nonfouling surface is to generate a dense layer of polyethylene glycol (PEG) on the surface. The layer of PEG molecules effectively creates a hydrated steric barrier on the surface and interferes with protein adsorption to the surface. Since the degree of protein resistance is correlated to the density, length, and molecular architecture of PEG molecules on the surface (Kingshott et al., 2002; Li et al., 2005;

Michel et al., 2005), various synthetic strategies for creating PEG nonfouling surface have been developed (Elbert and Hubbell, 1998; Herrwerth et al., 2003; Huang et al., 2001; Hucknall et al., 2009b; López et al., 1992; Ma et al., 2004), which is discussed in detail in Chapter 1.4.3A Non-fouling Surfaces.

Bioactivity

Preserving the biological activity of a biomolecule during the patterning process is a significant and nontrivial concern. Many patterning processes, especially those that are adapted from the semiconductor processing industry, can involve exposure of the surface to extreme environments, such as high vacuum, extreme temperatures, and nonaqueous conditions, which can denature or degrade biomolecules. Methods that are compatible with aqueous conditions and ambient temperature are hence preferable when deciding upon a method to pattern a biomolecule—especially proteins—on surfaces, as they are especially prone to denaturation compared to other biomolecules, such as peptides and oligonucleotides.

Shelf-Life and Durability

The shelf-life and durability of the pattern over time is another consideration when choosing a patterning methodology. This is particularly important in the case where patterns are intended for use in diagnostic or point-of-care devices. The ultimate convenience in such a situation would be one where a fully functional pattern can be stored in ambient conditions for an unspecified period of time until used. When “soft-wet” materials—including hydrated polymers, proteins, and cells—are patterned, the exposure of these materials to vacuum, high temperature, or extremes of pH becomes a critical and often limiting issue, because many of them are easily degraded, destroyed, or irreversibly denatured under such conditions. For this reason, special care is needed to ensure that all biological components involved in the patterning process are maintained in a functional state. Ensuring this may involve strategies, such as sealing the devices in a hydrated environment or an inert atmosphere during storage, taking preconditioning steps to prepare the surface prior to analysis, or integrating rinsing steps into the analysis scheme. In some instances, it may be necessary to create the patterned substrates that act as a template for patterning biomolecules, and then functionalize the pattern with the biomolecule of interest, on demand, immediately prior to its use.

In addition, it is also useful to know how long a pattern will stay intact under the end-use conditions. This is especially important for substrates patterned for cell growth or for implantation into the body that need to retain functionality for extended periods of time. For this reason, researchers often report an FOM that alludes to the life of the pattern by stating, for example, how long the cells remain confined to the pattern in cell culture.

Patterning Techniques

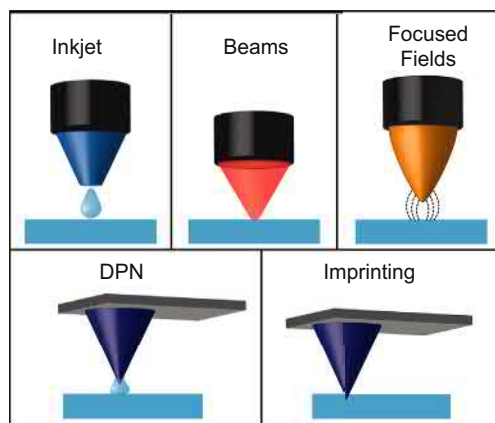
The number of surface patterning techniques is growing steadily, with new publications that present novel patterning schemes or variants of existing methodologies. This chapter seeks to provide a short discussion of the different categories of patterning techniques, and within each category points out some interesting examples; this chapter is not an exhaustive compendium of all patterning techniques. Although much of the overall organization or structure of this section owes an intellectual debt to the excellent and comprehensive review by Geissler and Xia (2004), the content of this section places greater emphasis on patterning for biomedical applications.

Direct-Write Patterning

In direct-write patterning techniques, patterns are fabricated by serially scanning a patterning element across a substrate. Direct-write patterning is a useful method because patterns of arbitrary feature shape and size—within the resolution limit of the technique—can be fabricated on-the-fly, in a process analogous to writing with a pen. In addition, direct-write patterning can generate extremely high-resolution features with great spatial accuracy. The drawbacks of direct-write patterning techniques are that they are typically slow, low-throughput, and not particularly suitable for large area patterning, because of the need to serially write the pattern. This limitation can be addressed, at the cost of greatly increased complexity of the instrumentation, by using independently actuated pens. Several direct-write techniques are described next and are grouped by the type of “pen” that is used to write the pattern (Fig. 1.4.5.3).

Writing With A Stylus

This section describes direct-write patterning techniques that use a rigid stylus as a writing tool. Inkjet printing, dip-pen nanolithography (DPN), and nanoshaving (also called nanoengraving) are typical examples of direct-write methods. DPN and nanoshaving can all produce very



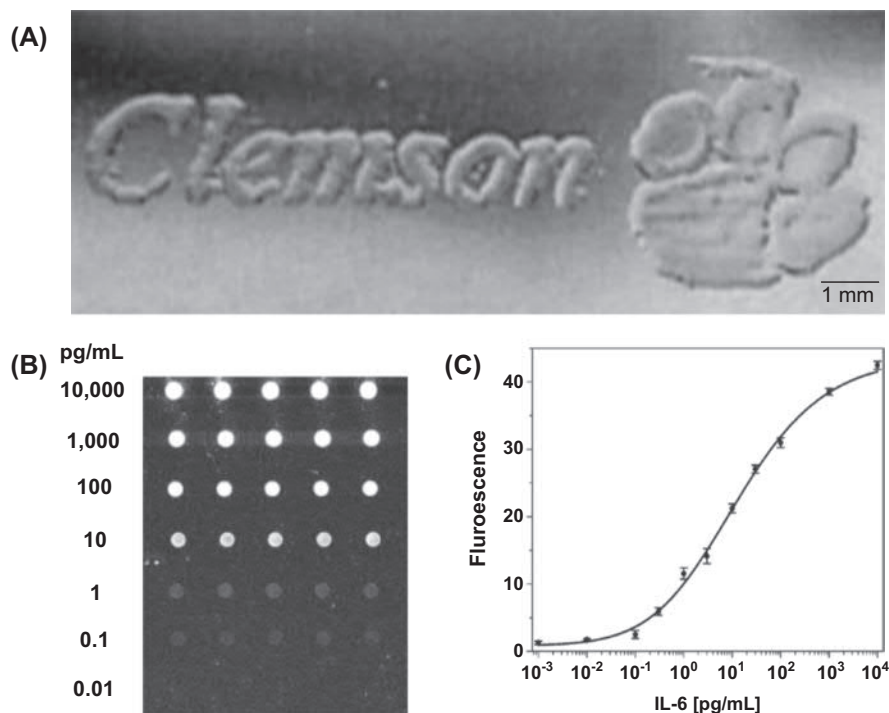
• **Figure 1.4.5.3** Types of direct-write patterning. Inkjet, beams, focused fields, dip-pen nanolithography (DPN), and imprinting.

high-resolution, sub-100 nm features, because they write patterns using very fine tips of an atomic force microscope (AFM) with nanometer-scale positional control. In contrast, inkjet printing produces coarser features, with the best lateral resolution of $\sim 10\ \mu\text{m}$, and more often in the order of $100\ \mu\text{m}$. Inkjet systems, however, can be easily multiplexed, making them very attractive for patterning biomolecules in diagnostic devices, such as protein and DNA microarrays.

Printing With Inkjets, Quills, and Pins

Inkjet printing refers to any method where liquid is pumped through a nozzle and dispensed onto a substrate in a defined pattern. Inkjet printers deliver liquid solutions as small droplets (typically $10\text{--}20\ \text{pL}$) that are either electrostatically charged and guided via electric fields or generated on demand by thermally or piezoelectrically triggered pressure pulses (Derby, 2008). Inkjet nozzles are usually very small ($20\text{--}30\ \mu\text{m}$ in diameter), which enables them to be mounted on nozzle heads that can be interfaced with computers to control the fabrication of patterns. The resolution limit of inkjet printing is in the range of tens of micrometers, and is limited by the droplet volume, droplet spreading on the substrate (which varies depending on the ink and the surface), and other mechanical factors. Some useful features of inkjet printing are: (1) patterning is contact-free and can be performed under ambient conditions on a range of solid substrates; (2) the method has high positional accuracy; (3) multiplexed printing is easily accomplished by use of multiple nozzles and/or nozzle heads; and (4) high-throughput patterning over large surface areas can be accomplished by robotic automation.

Inkjet printing of biomolecules has gained popularity, in part due to the simplicity of the technique and the availability of inexpensive printers. Thomas Boland's research group demonstrated that low-cost consumer inkjet printers could be adapted to print "biological inks" with their demonstration of the inkjet printing of proteins (Pardo et al., 2002), cells (Cui et al., 2010), and bacterial colonies (Xu et al., 2004). Fig. 1.4.5.4A shows a "living advertisement"—a colony of bacteria printed in the shape of a university logo—created by Boland and co-workers. Automated robotic inkjet printing systems designed to print "biological inks" such as DNA (Bumgarner, 2013; Hughes et al., 2001), peptide (Lin et al., 2016), or proteins (Delaney et al., 2009; Weissenstein et al., 2006) are typically called microarray printers, which are much more sophisticated and expensive than consumer-grade inkjet printers. These systems are often self-contained in an environmentally controlled chamber, and can accommodate complex protocols involving delivery of multiple biological inks as well as rinsing steps. Since the advent of the human genome project and the rise of genomics, microarrays have migrated into other fields because they provide a convenient, high-throughput, and multiplexed methodology to characterize biomolecules in proteomics (Caiazzo et al., 2009; Nagaraj et al., 2008) and diagnostics (Delehanty and Ligler, 2002; Orckowski et al., 2005). However, much of this work used arrays fabricated not by inkjet printers, but by pin-based arrayers in which pin arrays are dipped into solutions and then contact printed onto a surface, or else arrays that were fabricated by on-chip, photolithographic synthesis of spatially addressable arrays of



• **Figure 1.4.5.4** Inkjet printing. (A) Bacterial colonies printed in the shape of a university logo by a modified consumer-grade inkjet printer (Xu et al., 2004). (B, C) An inkjet-printed antibody microarray (Hucknall et al., 2009a). (B) An image of interleukin-6 (IL-6) antibody microarray on a nonfouling surface. (C) Dose-response curve for an IL-6 antibody microarray interrogated from whole blood.

oligonucleotide probes, such as the Affymetrix oligonucleotide array technology. For example, Ashutosh Chilkoti's group has used inkjet-printed microarrays of antibodies on a nonfouling polymer brush for the detection of multiple protein analytes from serum and blood with a femtomolar limit-of-detection (Figs. 1.4.5.4B and C) (Hucknall et al., 2009a).

Dip-Pen Nanolithography

Dip-pen nanolithography (DPN) is the nanoscale equivalent of writing with a quill. In DPN, AFM probes are coated with a liquid-based ink and then scanned along a substrate to write a pattern of the ink. The ink solution on the tip forms a small meniscus at the interface between the tip of the probe and the substrate, and this meniscus provides a conduit for transport of biomolecules from the tip to the surface. In this approach, patterning can be achieved either by writing a substance of interest directly from the AFM tip or by patterning functional moieties on the substrate first using the AFM tip and then exposing to a substance of interest for selective attachment to the patterned regions. DPN has been used to pattern alkanethiols (Hong et al., 1999; Piner et al., 1999), as well as a range of biomolecules including DNA (Demers et al., 2002), proteins (Hyun et al., 2004; Lee et al., 2002; Wilson et al., 2001), viruses (Smith et al., 2003; Vega et al., 2005), lipids (Hirtz et al., 2013; Lenhert et al., 2010), and nanoparticles (Santra et al., 2015; Wang et al., 2008) on many different materials including gold, metal oxides, polymers, and graphene. The resolution limit of DPN is on the order of tens of nanometers, and this method can create patterns that extend over several hundred micrometers, which is the limit of most AFM scanners. Single-probe DPN patterning is also relatively low throughput, as it is a somewhat slow and serial patterning technique. For example, in an early report on DPN, 10 min were required to create a $1 \times 1 \mu\text{m}$ feature (Piner et al., 1999). To improve throughput of conventional DPN, multiplexed DPN has been used, where parallel DPN tip arrays are scanned on the substrate simultaneously (Bullen et al., 2004; Lee et al., 2006; Ma et al., 2018). Perhaps the most impressive work

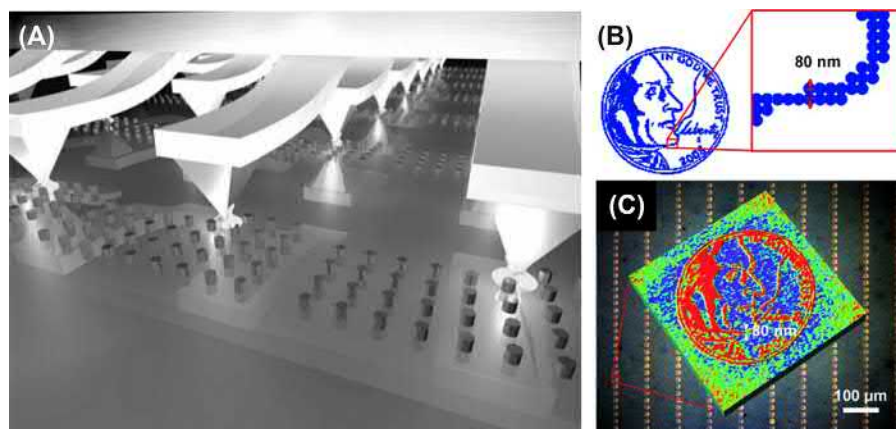
to date in this regard is that of Chad Mirkin's group, where 55,000 DPN probes were inked with a thiol solution, and used simultaneously to generate massively high-throughput, high-resolution patterns on gold (Fig. 1.4.5.5A) (Salaita et al., 2006). In this demonstration, the face of Thomas Jefferson from a US five-cent coin was generated in 55,000 duplicates, with each face containing 470 million nanoscale features, in less than 30 min (Fig. 1.4.5.5B and C). See the reviews by Salaita et al. (2007) and Wu et al. (2011) for further information on DPN.

Nanoshaving and Nanografting

Nanoshaving or nanoengraving is a term used to describe the process of scratching patterns in thin molecular layers, such as SAMs, on a bulk substrate with a hard stylus (e.g., an AFM probe) (Liu et al., 2008). These techniques have similar advantages and limitations as DPN, as the patterning mechanism is very similar. Arbitrary patterns in the molecular layer are engraved by dragging the probe on the surface. A subsequent process can be used to functionalize the exposed, underlying substrate with a secondary molecule. For example, nanoshaving has been used to selectively scrape a protein-resistant SAM on the substrate, which is then exposed to a protein solution. Nanopatterns of proteins including antibodies and ECM proteins are formed on the surface as the proteins are adsorbed only to the scraped regions of the substrate that are no longer protein-resistant (El Zubir et al., 2013; Staii et al., 2009). Nanografting—a variant of nanoshaving—involves scratching the surface in the presence of a secondary molecule with high affinity to the underlying substrate, so that the secondary molecule fills in the regions that are already cleared away by the scanning probe. Nanografting has also been used to create nanopatterns of enzymes (Jang et al., 2002), antibodies (Bano et al., 2009; Hu et al., 2005; Wadu-Mesthrige et al., 2001), and DNA (Josephs and Ye, 2010; Liu et al., 2002).

Writing With Beams

This section describes patterning methods that scan an energetic beam over a surface to create a pattern. The spatial



• **Figure 1.4.5.5** High-throughput, high-resolution dip-pen nanolithography (Salaita et al., 2006). For details of figures, please see the text.

resolution of this class of patterning techniques is generally limited by the spot size of the beam. Beams of photons are used for patterning in direct-write photolithography, and thus the spot size (and hence, resolution limit) is set by the optical diffraction limit, which is ~ 200 nm. The diffraction limit can be overcome by using near-field methods, such as scanning nearfield lithography, to create features with the dimension down to several tens of nanometers. Direct-write photolithography is particularly conducive to patterning biomolecules, as it is compatible with aqueous conditions. Electron beam lithography and focused ion beam lithography represent two other methods in this class of patterning techniques that have higher spatial resolution than conventional far-field photolithography. Electron beam lithography and focused ion beam lithography, however, usually require high vacuum and dry samples, which can be a serious impediment to patterning biomolecules.

Direct-Write Photolithography

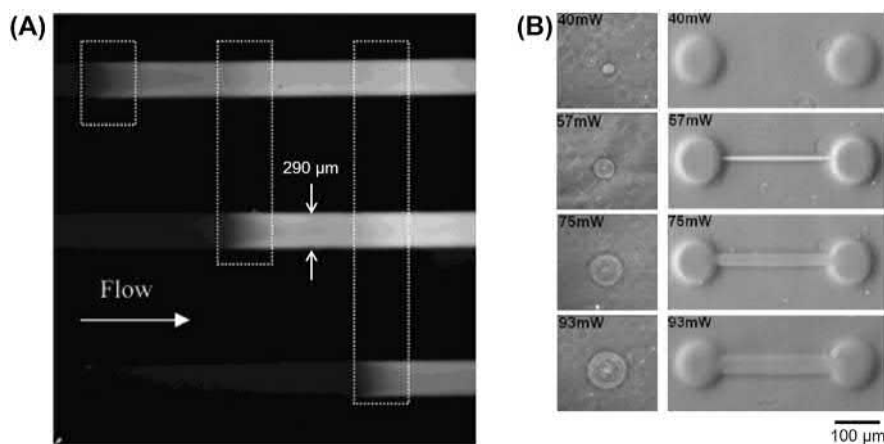
In direct-write photolithography, a beam of focused light is used to pattern a substrate directly. Light is focused into small spots using conventional light optics, and patterns are formed by photochemical or physical modification of the surface. The resolution of features that are patterned with conventionally focused light is governed by the optical diffraction limit, which is roughly half of the wavelength of the light used for excitation (Dunn, 1999). Thus, patterns formed by focused light typically have a minimum feature size of several hundred nanometers. Although broadband light sources can be used for direct-write photopatterning, lasers are more commonly used for this application, because they provide high-intensity beams of a single wavelength which allow precise control of specific photochemical reactions.

Patterning with light is generally performed using a photochemical mechanism—where the chemical reactivity of the substrate is altered by light—or a mechanism that locally induces a physical topological change on the underlying

substrate. In direct-write patterning via photochemistry, light is used to locally activate photoactive molecules on the substrate either in the presence of a substance of interest to form a pattern simultaneously or followed by an additional step where a substance to be patterned is exposed to the substrate. Photochemical patterning with light has been widely used to create patterns of proteins on a substrate. For example, Holden and Cremer used a laser to pattern enzymes directly within flow channels (Fig. 1.4.5.6A), a methodology that can be applicable to lab-on-a-chip devices (Holden et al., 2004). In another patterning methodology using light, a laser is used to pattern substrates by physically altering a localized region of a substrate. This type of patterning is conceptually similar to engraving with AFM tips, with the only difference being that the substrate materials—polymers or resins—are ablated, melted, or deformed due to the high energy of the focused laser spot, instead of being physically excavated (Joglekar et al., 2003). For example, Nielson and Shear used a high-energy pulsed laser to ablate pores in a membrane where cells are cultured and which separates adjacent flow channels (Nielson and Shear, 2006). They showed that the pores created well-defined reagent streams and dosed cells with precisely located chemical gradients. In another example, Yasuda's group used a focused infrared laser beam to photothermally etch agarose microchambers stepwise for the controlled network formation of cardiomyocytes and neurites and for use in toxicity testing (Fig. 1.4.5.6B) (Kaneko et al., 2015, 2007; Suzuki et al., 2005; Suzuki and Yasuda, 2007).

Electron Beam Lithography

Direct-write electron beam lithography (EBL) uses similar patterning principles as that of patterning with focused light. However, in EBL, a focused electron beam (e-beam) is used as a stylus to write patterns on an e-beam-sensitive material. Since the e-beam radiation is of a much shorter wavelength than that used in direct-write photolithography, the spatial resolution of EBL is superior compared to direct-write



• **Figure 1.4.5.6** Direct-write photolithography. (A) Patches of enzymes (locations indicated by dashed boxes in the figure) patterned within flow channels produce fluorescent products when exposed to fluorogenic reagents (Holden et al., 2004). (B) Microstructures are created on the agar layer by photothermal etching using infrared focused laser beam (Kojima et al., 2003).

photolithography. For this reason, EBL is a very powerful technique for creating patterns at the nanoscale, with feature sizes of 10–100 nm (Ducker et al., 2008; Schmelmer et al., 2007; Steenackers et al., 2007). Although EBL has several limitations of low throughput, high cost, and limited applicability to biological molecules, EBL is considered useful largely as a method for high-resolution fabrication of nanoscale patterns over a small area. As biological molecules generally do not remain functional in high vacuum and are vulnerable to e-beam radiation, substrates are typically first patterned by EBL and then exposed to a biological molecule of interest for selective attachment to the patterned features (Rundqvist et al., 2006; Schlapak et al., 2012; Schmelmer et al., 2007; Steenackers et al., 2007). An elegant example of EBL patterning is the work done by Heather Maynard's group, where multicomponent protein patterns were fabricated by e-beam-induced cross-linking of functionalized PEG molecules. These functional PEG patterns were then used to immobilize proteins via specific binding interactions between the soluble proteins and the ligands presented by the PEG patterns (Fig. 1.4.5.7A) (Christman et al., 2009). In a more recent approach, they demonstrated a one-step protein patterning using a trehalose glycopolymer resist, which is cross-linked by the e-beam and protects the embedded proteins from denaturation during a high-vacuum, high-energy EBL process (Fig. 1.4.5.7B).

Focused Ion Beam Lithography

A focused ion beam (FIB) can also be used for direct-write patterning. FIB patterning is similar to EBL in its advantages and limitations; however, FIB patterning makes use of high-mass ions, such as gallium ions, as the energy carriers instead of electrons in EBL. FIB patterning is an inherently destructive process, as the bombardment of a surface with ions causes atomic sputtering from the surface. For this reason, FIB is typically used as a milling technique to engrave a surface with submicrometer size features. For example, Hill et al. used an FIB to selectively sever a metallized protein-based wire to eliminate current flow in microelectronics (Hill et al., 2005). FIB can also be used to sputter metals

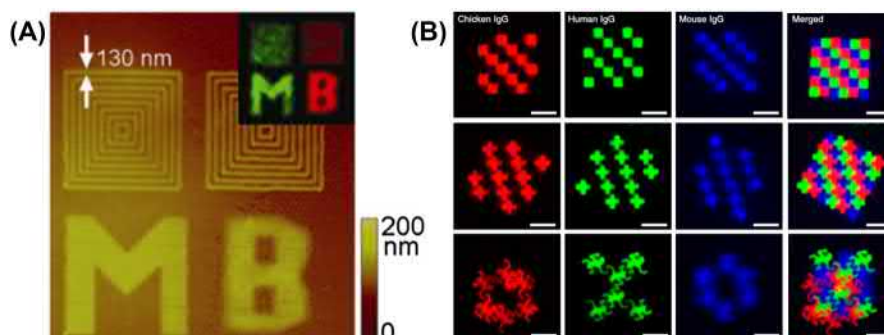
onto a surface, which makes FIB useful in repairing integrated circuits (Reetz et al., 1997).

Writing With Fields

Direct-write patterning with fields includes scanning electric and magnetic fields across a substrate to form a pattern. Features generated by direct-write electric field scanning typically have a lower spatial resolution than that attainable with other direct-write techniques. Similar to other scanning techniques, writing with fields is slow and unsuitable for large-area patterning. However, scanning electrodes allow one to perform extremely localized electrochemical reactions. Direct-write magnetic patterning is mostly geared toward data storage and, as it has not been used for sputtering biomolecules, only the underlying principle will be briefly described in this section.

Electric Field

Direct-write patterning with electric fields is accomplished by scanning an electrode near a surface to locally modify the surface using charge or current. Patterning is mediated through a variety of electrochemical processes, which include localized charging, ohmic heating, and redox reactions. Scanning electrochemical microscopy (SECM), which was developed by Allan Bard and co-workers, can be used in a patterning mode to perform localized redox reactions on a surface, resulting in the formation of microstructures (Bard et al., 1990). SECM patterning is performed with ultramicroelectrodes in electrolyte solutions, and has been used to pattern enzymes and SAMs on a surface (Shiku et al., 1997; Wittstock and Schuhmann, 1997). The feature sizes of patterns generated by SECM are typically larger than those created with other types of scanning probe techniques. Scanning tunneling microscopy (STM) and AFM can be used to generate higher resolution features. STM has the highest resolution of all proximal-probe lithography methods, as it can manipulate single atoms (Eigler and Schweizer, 1990; Manoharan et al., 2000), but as it must be operated under high vacuum to achieve atomic resolution, it is of limited utility for biomolecular patterning.



• **Figure 1.4.5.7** Electron beam lithography patterning of multicomponent patterning. Patterning is carried out by (A) two sequential reactions: local e-beam induces cross-linking of reactive PEG molecules and subsequent reaction with proteins (red: streptavidin, green: BSA) (Christman et al., 2009), and (B) one step process where an e-beam cross-linkable resist made of trehalose glycopolymer is used to protect proteins during direct-write patterning (Bat et al., 2015). Scale bars = 25 μm .

Magnetic Field

Direct-write patterning with magnetic fields has mostly been geared toward data storage applications to date, and thus this topic will not be covered in detail in this section other than to provide the reader a basic idea of its underlying physical principle. In direct-write magnetic patterning, an inductive element is scanned above a magnetizable material, such that localized regions of the surface become magnetized. These locally magnetized areas allow data to be recorded as bits, and can read the stored data using the same type of inductive element that is used to generate the patterns. For more information on magnetic direct-write patterning, see the review papers by [Chou \(1997\)](#).

Patterning With Masks

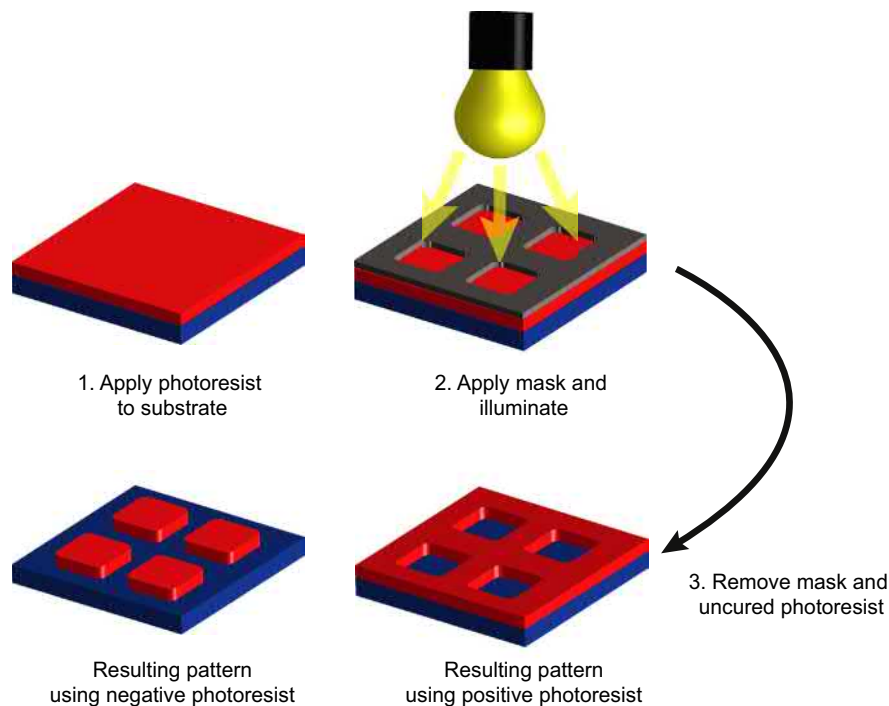
Patterning with masks is a highly developed form of patterning, as it has been the core technology of the microelectronics industry. Because of its sophistication and maturity, it has also been extensively adapted for the patterning of biomolecules and cells. A mask is broadly defined as a template that can spatially modulate a field or beam radiation that passes through it, or a template that physically protects spatially defined regions of the underlying substrate from exposure to inks or etchants. Patterning with light, generally called photolithography, is the most common form of patterning using masks, even though photolithography can be performed in a maskless, direct-write manner, as described previously. Mask-based patterning can also be performed with radiation (other than light), liquid inks, or with chemical or biological etchants. Mask-based patterning is powerful and versatile for the following reasons: (1) large areas—typically

4–6-inch wafers—can be rapidly patterned in batch mode, which makes it a high-throughput patterning technique; (2) spatially intricate patterns can be fabricated, the limitation of which is the design of the mask; and (3) layered features can be fabricated by performing multiple patterning steps in succession, each with a different etching or deposition step. With advances in light sources and optics, the spatial resolution of mask-based approaches is in the sub-100 nm regime ([Goodberlet, 2000](#); [Totzeck et al., 2007](#)).

Photolithography With Masks

In photolithography, a mask can be any material that has optically transparent and opaque regions. Masks can be rigid, such as those fabricated out of metal or printed on quartz glass, or they can be fabricated on flexible substrates such as transparencies. The critical requirement of a mask-based photolithographic patterning process is that light must pass through spatially defined regions of the mask and lead to the formation of a pattern that conforms to or is dictated by the pattern of the mask, on a substrate that is located below the mask. However, historically, the term photolithography encompasses a set of processes that were derived from the semiconductor industry, which involves more than simply using light and masks to fabricate patterns.

Patterning in photolithography is facilitated by a polymer photoresist that is spin-coated onto a silicon wafer or other substrate. The photoresist is regioselectively activated by light irradiated through a mask and then exposed to a developing solution ([Fig. 1.4.5.8](#)) to create a pattern of the photoresist, which is then subsequently processed to create a pattern in the underlying substrate. There are two types of photoresists. (1) For a positive photoresist, the areas that are



• **Figure 1.4.5.8** Mask-based photolithography.

exposed to light become soluble in the developing solution, while the unexposed regions of the photoresist are insoluble in the developing solution. (2) A negative photoresist works on the opposite principle; areas of the photoresist that are exposed to the light will become insoluble to the developing solution, so that incubation in the developing solution dissolves the unexposed regions of the photoresist. The photolithography process is completed by removing portions of photoresist that are soluble to the developing solution and exposing the underlying substrate in a pattern. Removal is usually followed by either an etching step in which the exposed thin metal/oxide films coated on a bulk substrate are dissolved or a deposition step in which metal or other materials are selectively deposited onto exposed regions.

Photolithography can be performed in three modes, depending on the location of a mask relative to the light source and substrate: contact mode, proximity mode, or projection mode. In contact mode, the mask is placed directly on the substrate. Contact mode photolithography produces patterned features at a size ratio of 1:1 relative to the features in the photomask, and thus resolution is limited by the feature size of the photomask. In contact mode, it is essential that the substrate and mask are free of particulate contaminants, as any trapped debris between the mask and substrate will contaminate the pattern and/or damage the mask or substrate. Proximity mode patterning is a variant of contact mode, in that the mask is slightly separated from the substrate along the propagating light axis. Proximity mode photolithography also produces features on the substrate with the almost same size as are patterned on the mask, but the presence of foreign contaminants is not as devastating as in contact mode. In projection mode photolithography, the mask is placed at an image plane that is well-separated from the surface of the substrate along the optical axis that is conjugate to the image plane at the surface to be patterned. Projection mode photolithography can produce a smaller feature size than the original feature in the mask, as optics can be used to project the mask pattern at a reduced dimension on the substrate. Projection mode photolithography also enables higher-throughput processing, as mask alignment can be done quickly and efficiently due to reduced risk of damaging the mask or the substrate.

Mask-based patterning has been used to create hydrogel patterns having spatially controlled physicochemical properties, such as mechanical stiffness (Guvendiren et al., 2016; Kirschner et al., 2014; Tse and Engler, 2011), pattern geometry (Jamal et al., 2013; Thérien-Aubin et al., 2013), and type and density of chemical ligands (Azagarsamy et al., 2016; Gramlich et al., 2013). In these applications, light that is applied through the photomask can regioselectively modulate the material property by varying the degree of photochemical reaction, including cross-linking and covalent conjugation. For example, Rape et al. fabricated hyaluronic acid hydrogels using orthogonal light-induced chemistry to present mutually independent and spatially continuous gradients of substrate stiffness and density of biologically

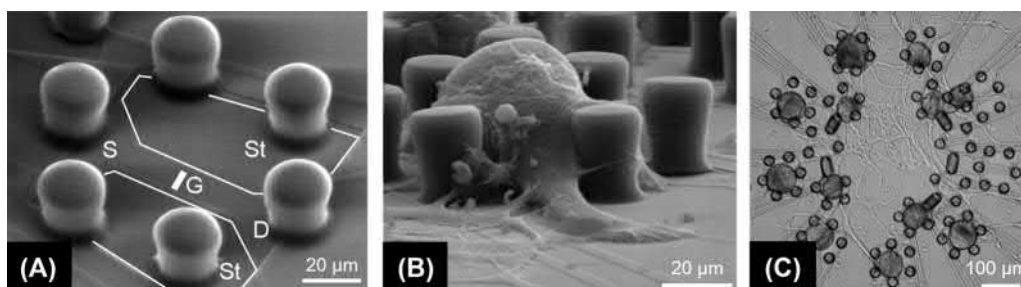
active ligand, which enabled the high-throughput study of the synergistic effects of multiple matrix parameters on cell phenotype (Rape et al., 2015).

Deposition/Etching With Masks

As mentioned above, mask-based deposition and etching is often a finishing step in a typical photolithography process. In fact, the actual photolithographic component of the process, as derived from the semiconductor/microelectronics industry, is the creation of a polymer-based mask on a substrate that is meant to protect specific parts of the underlying substrate from a subsequent deposition or etching process. However, it is beneficial to think of masked deposition and etching as standalone patterning techniques, because these techniques extend beyond the context of photolithography. Simply put, mask-based deposition is just like using a stencil to paint letters or graphics on paper, clothing, or any other material. However, other masks can be made of elastomeric polymers, such as poly(dimethyl siloxane) (PDMS), which provide the benefits of watertight seals with the substrate, compatibility with curved surfaces, and flexible peel-off (see Chapter 1.3.2B Silicones). In a deposition process, the mask is applied onto a substrate, the combination of which is then exposed to the material to be deposited. Once the mask is removed, areas protected by the mask remain free of the deposited material. In an etching process, the masked substrate is exposed to a form of radiation or an etching chemical, and the areas exposed through the mask are selectively etched.

Mask-based photolithographic patterning of biomolecules most likely started in the early 1990s with works such as Stephen Fodor's, where arrays of photoactive chemicals were patterned to create microarrays for peptide synthesis (Fodor et al., 1991). Around the same time, photolithographic processes were being used to create patterned surface chemistries to direct cell attachment and growth on substrates (Healy et al., 1994; Lom et al., 1993). This work was initiated by collaborative efforts from Kevin Healy's and Philip Hockberger's groups at Northwestern University. They combined photolithography and organosilane chemistry to produce materials with precise spatial control over presentation of surface chemistry. They went on to use these surfaces to study the mechanisms by which mammalian cells were distributed spatially when exposed to these micropatterned surfaces. These seminal studies established the utility of masked photolithography for biomolecular patterning as an important research tool in biomaterials.

An exciting biological application of mask-based photolithography combined with deposition and etching is the development of microelectronic interfaces for cells. Much work has been done creating electrode arrays and transistor arrays that can stimulate and record from cultures of neuronal cells in an attempt to elucidate brain activity on a single-cell level, as well as from controlled populations of networks of neurons (Fig. 1.4.5.9) (Patolsky et al., 2006; Zeck and Fromherz, 2001).



• **Figure 1.4.5.9** Mask-based photolithography and deposition/etching used to create microelectronics for interfacing with neurons (Zeck and Fromherz, 2001). Polymeric posts are used to confine neurons atop underlying transistors. The device is diagrammed in (A) indicating “stimulator wings” (St) and the transistor components (S, source; D, drain; G, gate). The device is shown with a single cell in (B). An array of devices is used to interface with a neuronal network (C).

Patterning With Masters

A master is a template that is used to replicate patterns, usually in a batch-type process. Rigid masters can be used directly to imprint or emboss patterns on substrates. However, the most widespread use of masters for patterning is to create a mold, typically made of an elastomeric polymer, which is subsequently used to replicate the patterns. Molds are generally fabricated by curing polymeric materials in the presence of the master, which embeds the features of the master into the mold. Once separated from the master, molds can be used for printing features on substrates using molecular inks that are first applied to ink the mold and then are transferred by contact of the protruding features of the mold with a substrate. Alternatively, they can be brought into contact with a substrate surface to create channels of the void features of the mold on a substrate, which can be used for patterning by a liquid ink flowing through the channel. Patterning with masters is a relatively cheap methodology to mass-produce features over large surface areas. In addition, the use of conformal molds allows patterning on curved surfaces (Jackman et al., 1995; Kang et al., 2013; Sun et al., 2015). Typically, patterning with masters does not offer as high spatial resolution as some direct-write patterning techniques.

Imprinting With a Master

Imprinting or embossing with a master is essentially the same concept as imprinting with a stylus, as described above, except that a master is used to imprint multiple features at once, instead of serially imprinting or writing one feature at a time using a stylus. The master is fabricated from a relatively hard material such that it resists deformation when it is pressed against the substrate. The master contains a rigid relief pattern that molds the substrate into the shape which it is pressed into. Imprinting with a master is used often to pattern polymer films; however, other substrates can be used with the main requirement being that substrate must be soft enough to be deformed by the master (Amin et al., 2016; Yang et al., 2012). The resolution of features obtained from imprinting with a master is dictated by the durability of the master, the physical properties of the substrate, and

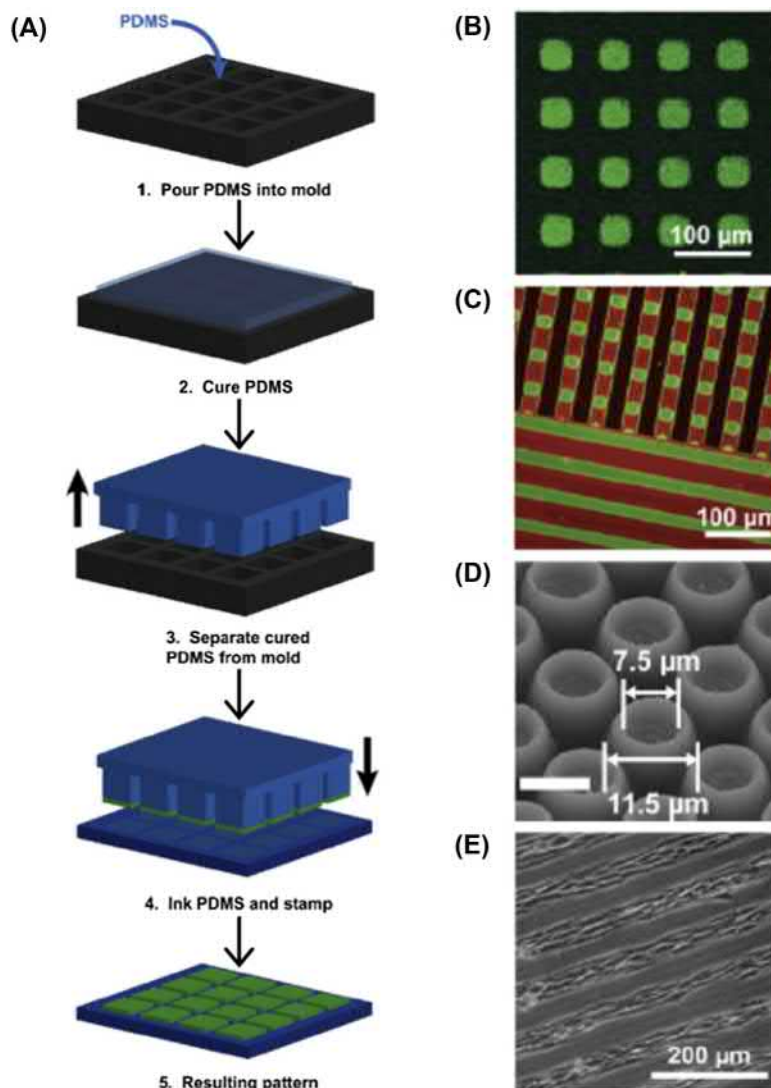
the mechanical pressure applied during embossing. Feature sizes as small as 10 nm are attainable by imprinting with masters (Guo, 2007; Pandey et al., 2019).

Printing With a Stamp

Printing of patterns using molds is most widely done by soft lithography, a suite of related techniques that generally refers to the use of soft, elastomeric polymer molds to create patterns on substrates. Polymer molds are made by pouring liquid monomer onto a rigid master and then curing it. When separated from the master, the resulting polymer mold retains the topography of the original master. These topographical features are then transferred to the substrate for patterning. Masters can be created using photolithographic techniques, direct-write patterning, or even relatively low-tech methods such as gluing rigid objects together so that they create the desired topological features on the polymer constructs (Allen et al., 2005; Hill and Shear, 2006). The most widely used polymer as a mold in soft lithography is PDMS. PDMS has numerous advantageous qualities (Ruiz and Chen, 2007), some of which include low cost, flexibility, optical transparency, resistance to harsh chemicals (e.g., hydrofluoric acid, which is a popular glass etchant), permeability to biological gases, and tight liquid-sealing to various substrates. The elasticity and adherent nature of PDMS make it an extremely versatile mold, as PDMS molds can remain in close conformation with curved or otherwise non-uniform surfaces, which allows to pattern large surface areas (up to hundreds of square centimeters) with a single mold (Xia and Whitesides, 1998a). See the review from Whiteside and co-workers for the detailed process and applications of soft lithography including microcontact printing and microfluidic systems (Whitesides et al., 2001; Xia and Whitesides, 1998b).

Microcontact Printing: Use of Protruding Features of a Stamp

Printing in the context of soft lithography is commonly referred to as microcontact printing (Fig. 1.4.5.10), where an elastomeric stamp is used to transfer molecular inks from stamp to substrate only on the regions of contact. The feature sizes of patterns range from micrometers to nanometers,



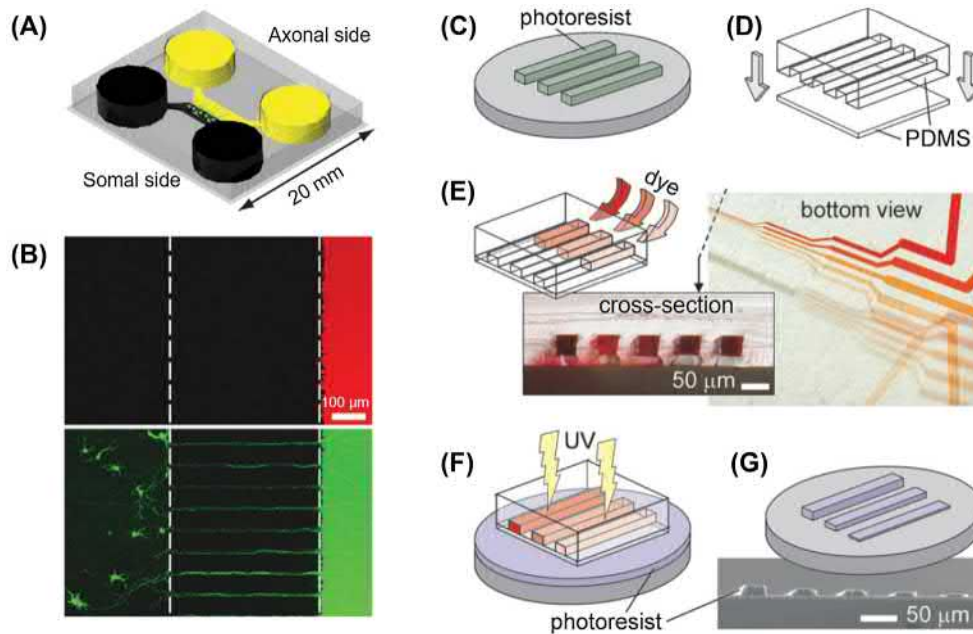
• **Figure 1.4.5.10** Microcontact printing. (A) The typical steps involved in microcontact printing. (B–E) Examples of patterns created using microcontact printing: (B) checkered pattern of fluorescent protein (Ma et al., 2006); (C) multicomponent polymer brush pattern (Zhou et al., 2006); (D) anemone-shaped patterns of stimulus-responsive polymer (Chen et al., 2009); (E) cell attachment on the fibronectin pattern (Hyun et al., 2003).

which are determined by the mechanical properties of the stamp, the deposition conditions (i.e., pressure and duration of application), and the leakiness or spreading properties of the molecular ink during the stamping process (Li et al., 2003; Whitesides et al., 2001; Xia et al., 1997).

Microcontact printing was first demonstrated in the early 1990s by George Whitesides' group at Harvard University (Kumar and Whitesides, 1993). It is benefitted from the fact that alkanethiols have a high affinity to gold and spontaneously form a dense monolayer when in contact with a gold surface. Thus, when a PDMS stamp that is inked with alkanethiol molecules comes into contact with a gold surface, alkanethiols dissociate from the PDMS stamp and self-assemble on the gold. Whitesides' group further demonstrated in the 1990s that the geometrical patterns created by microcontact printing could spatially control the adhesion and spreading of mammalian cells in culture and further

direct their function and/or behavior (Lopez et al., 1993; Singhvi et al., 1994). This approach has been expanded to systematically investigate the effect of the size and shape of patterns on the lineage commitment of stem cells (Kilian et al., 2010; McBeath et al., 2004), which revealed the power of micropatterning on the length scale of the cell.

Microcontact printing has been used to include patterning of polymers (Chen et al., 2009; Zhou et al., 2006), proteins (including functional antibodies and enzymes) (Bernard et al., 2001, 2000; Buhl et al., 2015; Ma et al., 2006), DNA (Bernard et al., 2001, 2000; Buhl et al., 2015; Lange et al., 2004; Ma et al., 2006; Thibault et al., 2005), and cells (Foncy et al., 2018; Hyun et al., 2003; Kim et al., 2015) on various surfaces, including glass, silicon, graphene, and metals. In more recent efforts to extend the utility of microcontact printing, various approaches have been developed, including surface modification of PDMS stamps, new polymeric stamp



• **Figure 1.4.5.11** Microfluidic patterning. (A, B) A microfluidic cell culture platform (Taylor et al., 2005). (A) A culture chamber consisting of a PDMS mold containing a relief pattern of somal and axonal compartments, which can fluidically isolate axons of neurons without exogenous neurotrophic factors. (B, top) Fluidic isolation of a dye (shown in red) on the axonal side of the chamber. (B, bottom) Directional growth of axons (shown in green) from somal side to axonal side. (C–G) Use of microfluidic photomasks for photolithography (Chen et al., 2003). Flow channels are created using an elastomeric PDMS mold (D) developed from a photoresist micropattern (C). The channels are filled with fluids of varying concentration of UV-absorbing dye (E), which modulates the light exposure to the underlying photoresist (F) and hence creates patterns that vary in height (G).

materials, and a wide range of inks (Kaufmann and Ravoo, 2010; Perl et al., 2009). For example, polydopamine, which can self-polymerize and is highly adhesive in wet condition, has been used as an ink of stamps, and through secondary reaction created patterns of small molecules, proteins, cells, and nanoparticles on various substrates including silicon, glass, gold, polymers, and hydrogels (Beckwith and Sikorski, 2013; Chien et al., 2012; Lee et al., 2017).

Microfluidic Patterning: Use of Void Features of a Stamp

While microcontact printing makes use of the protruding features of a mold, a complementary set of patterning techniques utilizes the void features of the mold (Xia et al., 1997, 1996). When a mold with an engraved pattern is affixed to a substrate, the voids generated between the mold and substrate form empty features or channels that can be filled with liquid to create patterns. In microfluidic patterning, a network of channels is used to deliver liquids to specific locations on a substrate. The channels in a mold can be used to deliver reagents locally to microdevices on microfluidic chips (Fig. 1.4.5.11A and B) (Juncker et al., 2002; Taylor et al., 2005), to deposit biomolecules onto the surface through adsorption and in gradients (Bernard et al., 2001; Dertinger et al., 2002; Fosser and Nuzzo, 2003), to locally dissolve parts of the underlying substrate (Rodriguez et al., 2003), or to serve as a mask for photolithography (Figs. 1.4.5.11C–G) (Chen et al., 2003). Channels can also deliver a polymer solution to a surface in a spatially delimited manner, which is then hardened

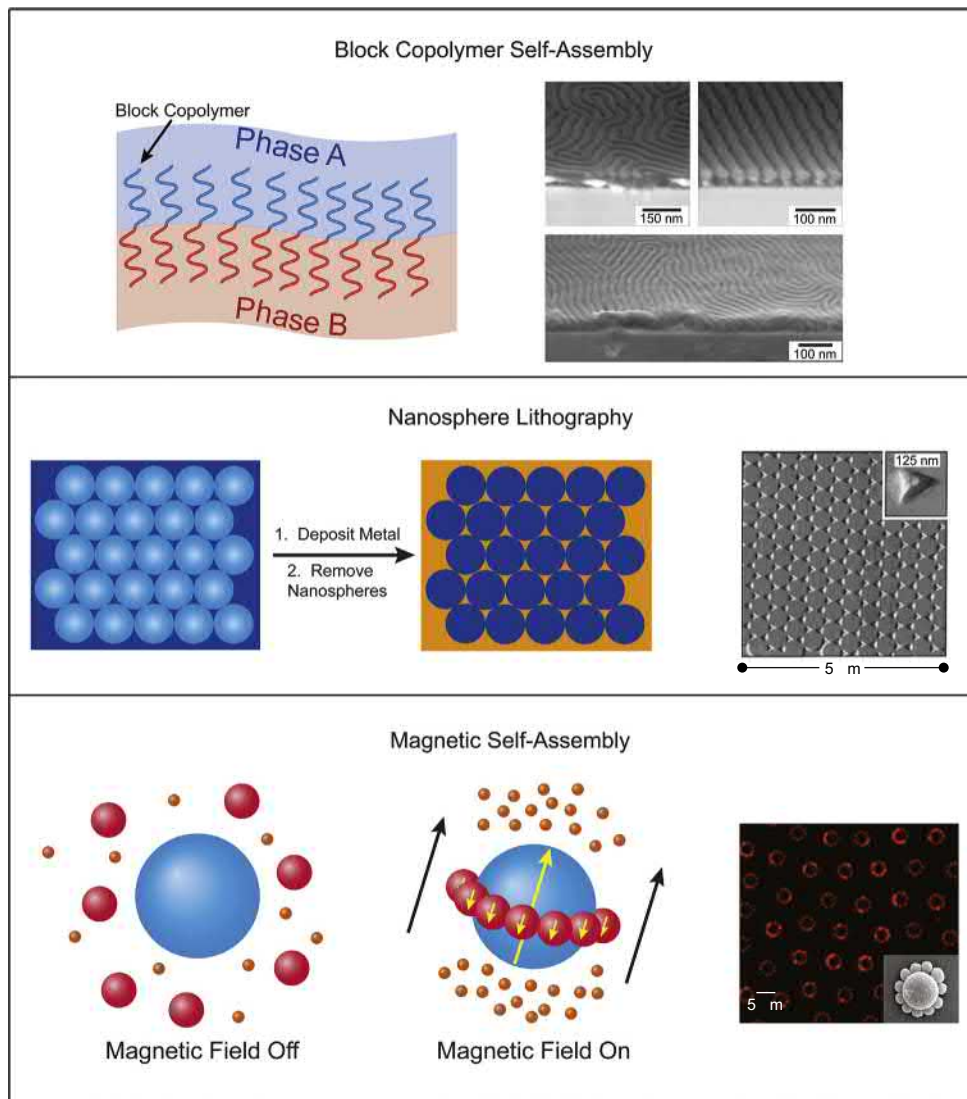
or cured. Subsequent removal of the elastomeric mold leaves microchannels behind. See the reviews by McDonald et al. (2000) and Sackmann et al. (2014) for a comprehensive review of microfluidic systems.

Patterning by Self-Assembly of Polymers and Colloids

Patterning by self-assembly of polymers and colloids is a powerful technique because, when properly executed, it requires minimal effort to produce the patterns. Self-assembled patterns are created by modulating experimental conditions where intermolecular or interparticle forces cause polymers or colloidal particles to phase separate or aggregate in a spatially defined pattern, driven by minimization of the free energy of the system. Self-assembled patterning can be used to pattern large surface areas with the feature resolution ranging from the nanoscale to the microscale. Three examples of patterning by self-assembly are highlighted in this section: block copolymer self-assembly; nanosphere lithography; and magnetic self-assembly (Fig. 1.4.5.12).

Block Copolymer Self-Assembly

Block copolymer self-assembly is an example of self-assembled patterning at the molecular level at 5–200 nm. A solution of the block copolymer having two or more blocks that are immiscible is deposited onto a surface where it undergoes phase separation as the solvent evaporates. This separation process is



• **Figure 1.4.5.12** Patterning by self-assembly. (Top) Block copolymer self-assembly where nanometer-scale patterns are created due to phase separation between the immiscible blocks of the polymer (Kim et al., 2003). (Middle) Nanosphere lithography where self-assembled, close-packed nanospheres are used as a mask for creating metallic patterns on surfaces (Haynes and Van Duyne, 2001). (Bottom) Magnetic self-assembly where magnetic fields can be used to pattern magnetically susceptible objects (Erb et al., 2009).

thermodynamically driven and then leads to the formation of highly ordered surface patterns with periods in the nanometer length scale that can readily cover large surface areas, although defects are a common problem on larger coverage areas. The nanometer-scale lateral resolution over a macroscopic surface area afforded by block copolymer self-assembly makes it a high-resolution, high-throughput patterning technique (Li and Ober, 2006). Patterns can be controlled by altering a number of variables: the sequence and length of the blocks, the degree of immiscibility of the blocks, the physicochemical properties of the solvent, the ambient conditions during thin film deposition, film thickness, and surface chemistry (Nie and Kumacheva, 2008). Patterned block copolymer films have been developed for the manufacture of integrated circuits and magnetic storage media (Ross and Cheng, 2008; Yang et al., 2013), and have also been used as photonic crystals, optical

waveguides, and templates for the growth of inorganic materials (Kim et al., 2005; Shin et al., 2002; Valkama et al., 2004). In directed block copolymer self-assembly, biomolecules are patterned either by self-assembly of block copolymers having chemical ligands (Killops et al., 2012), or by physicochemical incorporation of biomolecules on the self-assembled block copolymer films (Frith et al., 2012; Lau et al., 2008; Shen et al., 2012). For examples of block copolymer patterning, as well as reviews, see references from Ji et al. and Li and Müller (Ji et al., 2016; Li and Müller, 2016).

Nanosphere Lithography

Nanosphere lithography exploits the self-assembly of nanoscale objects to create a periodic pattern or mask. In nanosphere lithography, a solution of relatively monodisperse nanospheres—usually composed of a polymer—is delivered

to a flat substrate. Under specific conditions, the nanospheres self-assemble into a hexagonal, close-packed monolayer as the solvent evaporates, which generates voids between the nanospheres where the underlying substrate is exposed. The nanosphere monolayer is then used as a mask to pattern the underlying substrate. Typically, nanosphere masks are used for selective deposition of substances of interest onto a substrate. After deposition, the nanospheres are removed from the surface, which leaves behind metal surfaces or pyramids in the regions corresponding to the void spaces between the nanospheres. Such selective deposition allows for spatial control over biomolecule incorporation (Li et al., 2013; Malmström et al., 2010; Valsesia et al., 2008). For a detailed review on nanosphere lithography, see the reviews by Ai et al. (2017) and Haynes and Van Duyne (2001).

Magnetic Self-Assembly

In magnetic self-assembly, nano- to microscale particles with a magnetic susceptibility align or orient themselves in a magnetic field. In one implementation of this approach, magnetic nanoparticles can be located in a pattern on the surfaces under magnetic field, which can then serve as a mask for deposition of proteins or other biological materials (Bardea and Naaman, 2009). Magnetic particles have been attached to cells to enable magnetism-directed cell patterning (Alsberg et al., 2006; Ino et al., 2007). Magnetic ferrofluid can also be used to template the self-assembly of nonmagnetic materials, such as microspheres and cells (Erb et al., 2009; He et al., 2013). In this case, nonmagnetic objects are spatially manipulated by the self-assembly of the magnetic medium surrounding them in response to the external magnetic field.

Dynamic Patterning

The discussion of patterning thus far has mostly related to the formation of static patterns, which offer little control after formation, and often are subject to deformation over time. An emerging field of surface patterning is focused on the creation of dynamic or “smart” patterns. These patterns are designed to respond to external cues in the local environment. Dynamic patterning more relevant to the focus of this chapter is to enable spatiotemporal control over interfaces used to study the cellular microenvironment in microfluidic devices, as well as those used in chip-based diagnostic and sensing devices. Dynamic patterning is particularly important, because most biological processes are triggered by temporal cues in the local environment. For example, intracellular signal cascades that are driven by ligand binding to receptors, clustering of receptors on cell membranes, and remodeling of the extracellular matrix due to mechanochemical stimuli, are all dynamic processes in biology. Engineered dynamic interfaces present a biologically inspired—although abiological—methodology to provide temporal control of biological interactions at artificial surfaces. For example, Milan Mrksich’s group has created SAMs on gold that present ligands at the SAM–water interface that can be switched between an active or inactive state

via electrochemical signals from underlying gold (Mrksich, 2009, 2002). They have used these surfaces to study the interactions between cell-adhesive ligands and cells during cell attachment to micropatterned surfaces (Yeo et al., 2003) and to pattern the attachment of two different cell populations, which allows for fundamental studies of heterotypic cell–cell interactions (Yousaf et al., 2001).

Three-Dimensional Printing

Three-dimensional printing is a set of rapid prototyping, additive manufacturing techniques, where three-dimensional objects are built by adding successive layers of materials ranging from polymers, metals, ceramics, to proteins and cells (Heinrich et al., 2019; Kyle et al., 2017). A major motivation for the development of three-dimensional patterning is the fact that cells exist in a three-dimensional environment in nature. However, cell-based experimentation in laboratories typically involves cell cultures growing on planar substrates, which is often irrelevant because they do not properly recapitulate the three-dimensional environment where the cells reside in the body. The benefits of three-dimensional patterning are also relevant for the design of biosensor and diagnostics, as control of an extra dimension in device fabrication will enable the design of new sensing architectures and transduction modalities with a potentially improved figure-of-merit. Three-dimensional control of patterning will yield better control over the design of microfluidic lab-on-a-chip devices. In addition, it facilitates rapid and on-demand generation of personalized tissues and organs for applications in tissue engineering and regenerative medicine. Many of the techniques described in the preceding sections can be used for three-dimensional patterning. Three-dimensional printing is a rapidly emerging area of growing interest, and is discussed in detail in [Chapter 1.4.8](#).

Conclusions

Surface patterning has become an extremely important tool in biomedical research. The ability to precisely define the spatial location of biomolecules and/or cells on a surface or in three dimensions provides researchers with a powerful tool to examine the interplay between biomolecules, cells, and artificial materials in a highly controlled spatial environment. This chapter has reviewed a diverse set of patterning techniques, common concerns that need to be addressed in patterning biomolecules and cells, and important figures-of-merit of different patterning methods that should provide the reader with an intelligent stepping stone to sources in the primary literature for a deeper, in-depth investigation of this area of research. This chapter should also help the reader in making a rational decision about the choice of the patterning methodology that is suitable for a particular application. In conclusion, we hope that this chapter will serve as a beginner’s guide for those who wish to delve deeper into the field of biomolecular and cellular patterning in two and three dimensions.

References

- McDonald, J.C., Duffy, D.C., Anderson, J.R., Chiu, D.T., Wu, H., Schueller, O.J.A., Whitesides, G.M., 2000. Fabrication of microfluidic systems in poly(dimethylsiloxane). *Electrophoresis* 21, 27–40. [https://doi.org/10.1002/\(SICI\)1522-2683\(20000101\)21:1<27::AID-ELPS27>3.0.CO;2-C](https://doi.org/10.1002/(SICI)1522-2683(20000101)21:1<27::AID-ELPS27>3.0.CO;2-C).
- Ai, B., Möhwald, H., Wang, D., Zhang, G., 2017. Advanced colloidal lithography beyond surface patterning. *Adv. Mater. Interfaces* 4, 1600271. <https://doi.org/10.1002/admi.201600271>.
- Allen, R., Nielson, R., Wise, D.D., Shear, J.B., 2005. Catalytic three-dimensional protein architectures. *Anal. Chem.* 77, 5089–5095. <https://doi.org/10.1021/ac0507892>.
- Alsberg, E., Feinstein, E., Joy, M.P., Prentiss, M., Ingber, D.E., 2006. Magnetically-guided self-assembly of fibrin matrices with ordered nano-scale structure for tissue engineering. *Tissue Eng.* 12, 3247–3256. <https://doi.org/10.1089/ten.2006.12.3247>.
- Amin, Y.Y.I., Runager, K., Simoes, E., Celiz, A., Taresco, V., Rossi, R., Enghild, J.J., Abildtrup, L.A., Kraft, D.C.E., Sutherland, D.S., Alexander, M.R., Foss, M., Ogaki, R., 2016. Combinatorial biomolecular nanopatterning for high-throughput screening of stem-cell behavior. *Adv. Mater.* 28, 1472–1476. <https://doi.org/10.1002/adma.201504995>.
- Azagarsamy, M.A., Marozas, I.A., Spaans, S., Anseth, K.S., 2016. Photoregulated hydrazone-based hydrogel formation for biochemically patterning 3D cellular microenvironments. *ACS Macro Lett.* 5, 19–23. <https://doi.org/10.1021/acsmacrolett.5b00682>.
- Bano, F., Fruk, L., Sanavio, B., Glettenberg, M., Casalis, L., Niemeyer, C.M., Scoles, G., 2009. Toward multiprotein nanoarrays using nanografting and DNA directed immobilization of proteins. *Nano Lett.* 9, 2614–2618. <https://doi.org/10.1021/nl9008869>.
- Bard, A.J., Denuault, G., Lee, C., Mandler, D., Wipf, D.O., 1990. Scanning electrochemical microscopy - a new technique for the characterization and modification of surfaces. *Acc. Chem. Res.* 23, 357–363. <https://doi.org/10.1021/ar00179a002>.
- Bardea, A., Naaman, R., 2009. Magnetolithography: from bottom-up route to high throughput. *Small* 5, 316–319. <https://doi.org/10.1002/smll.200801058>.
- Bat, E., Lee, J., Lau, U.Y., Maynard, H.D., 2015. Trehalose glycopolymer resists allow direct writing of protein patterns by electron-beam lithography. *Nat. Commun.* 6, 6654. <https://doi.org/10.1038/ncomms7654>.
- Beckwith, K.M., Sikorski, P., 2013. Patterned cell arrays and patterned co-cultures on polydopamine-modified poly(vinyl alcohol) hydrogels. *Biofabrication* 5, 045009. <https://doi.org/10.1088/1758-5082/5/4/045009>.
- Bernard, A., Renault, J.P., Michel, B., Bosshard, H.R., Delamarche, E., 2000. Microcontact printing of proteins. *Adv. Mater.* 12, 1067–1070. [https://doi.org/10.1002/1521-4095\(200007\)12:14<1067::AID-ADMA1067>3.0.CO;2-M](https://doi.org/10.1002/1521-4095(200007)12:14<1067::AID-ADMA1067>3.0.CO;2-M).
- Bernard, A., Michel, B., Delamarche, E., 2001. Micromosaic immunoassays. *Anal. Chem.* 73, 8–12. <https://doi.org/10.1021/AC0008845>.
- Buhl, M., Vonhören, B., Ravoo, B.J., 2015. Immobilization of enzymes via microcontact printing and thiol–ene click chemistry. *Bioconjug. Chem.* 26, 1017–1020. <https://doi.org/10.1021/acs.bioconjugchem.5b00282>.
- Bullen, D., Chung, S.-W., Wang, X., Zou, J., Mirkin, C.A., Liu, C., 2004. Parallel dip-pen nanolithography with arrays of individually addressable cantilevers. *Appl. Phys. Lett.* 84, 789–791. <https://doi.org/10.1063/1.1644317>.
- Bumgarner, R., 2013. Overview of DNA microarrays: types, applications, and their future. In: *Current Protocols in Molecular Biology*. John Wiley & Sons, Inc., Hoboken, NJ, USA. <https://doi.org/10.1002/0471142727.mb2201s101>. 22.1.1–22.1.11.
- Caiazza, R.J., Maher, A.J., Drummond, M.P., Lander, C.I., Tassinari, O.W., Nelson, B.P., Liu, B.C.-S., 2009. Protein microarrays as an application for disease biomarkers. *Proteomics – Clin. Appl.* 3, 138–147. <https://doi.org/10.1002/prca.200800149>.
- Chen, C., Hirdes, D., Folch, A., 2003. Gray-scale photolithography using microfluidic photomasks. *Proc. Natl. Acad. Sci. U.S.A.* 100, 1499–1504. <https://doi.org/10.1073/pnas.0435755100>.
- Chen, T., Zhang, J., Chang, D.P., Garcia, A., Zauscher, S., 2009. Fabrication of micropatterned stimulus-responsive polymer-brush ‘anemone’. *Adv. Mater.* 21, 1825–1829. <https://doi.org/10.1002/adma.200802484>.
- Chien, H.-W., Kuo, W.-H., Wang, M.-J., Tsai, S.-W., Tsai, W.-B., 2012. Tunable micropatterned substrates based on poly(dopamine) deposition via microcontact printing. *Langmuir* 28, 5775–5782. <https://doi.org/10.1021/la300147p>.
- Chou, S.Y., 1997. Patterned magnetic nanostructures and quantized magnetic disks. *Proc. IEEE* 85, 652–671. <https://doi.org/10.1109/5.573754>.
- Christman, K.L., Schopf, E., Broyer, R.M., Li, R.C., Chen, Y., Maynard, H.D., 2009. Positioning multiple proteins at the nanoscale with electron beam cross-linked functional polymers. *J. Am. Chem. Soc.* 131, 521–527. <https://doi.org/10.1021/ja804767j>.
- Cui, X., Dean, D., Ruggeri, Z.M., Boland, T., 2010. Cell damage evaluation of thermal inkjet printed Chinese hamster ovary cells. *Biotechnol. Bioeng.* 106, 963–969. <https://doi.org/10.1002/bit.22762>.
- Delaney, J.T., Smith, P.J., Schubert, U.S., 2009. Inkjet printing of proteins. *Soft Matter* 5, 4866–4877. <https://doi.org/10.1039/b909878j>.
- Delehanty, J.B., Ligler, F.S., 2002. A microarray immunoassay for simultaneous detection of proteins and bacteria. *Anal. Chem.* 74, 5681–5687. <https://doi.org/10.1021/ac025631l>.
- Demers, L.M., Ginger, D.S., Park, S.J., Li, Z., Chung, S.-W., Mirkin, C.A., 2002. Direct patterning of modified oligonucleotides on metals and insulators by dip-pen nanolithography. *Science* 80 (296), 1836–1838. <https://doi.org/10.1126/science.1071480>.
- Derby, B., 2008. Bioprinting: inkjet printing proteins and hybrid cell-containing materials and structures. *J. Mater. Chem.* 18, 5717–5721. <https://doi.org/10.1039/b807560c>.
- Dertinger, S.K.W., Jiang, X., Li, Z., Murthy, V.N., Whitesides, G.M., 2002. Gradients of substrate-bound laminin orient axonal specification of neurons. *Proc. Natl. Acad. Sci. U.S.A.* 99, 12542–12547. <https://doi.org/10.1073/pnas.192457199>.
- Ducker, R., Garcia, A., Zhang, J., Chen, T., Zauscher, S., 2008. Polymeric and biomacromolecular brush nanostructures: progress in synthesis, patterning and characterization. *Soft Matter* 4, 1774–1786. <https://doi.org/10.1039/b804861b>.
- Dunn, R.C., 1999. Near-field scanning optical microscopy. *Chem. Rev.* 99, 2891–2928. <https://doi.org/10.1021/CR980130E>.
- Eigler, D.M., Schweizer, E.K., 1990. Positioning single atoms with a scanning tunnelling microscope. *Nature* 344, 524–526. <https://doi.org/10.1038/344524a0>.
- El Zubir, O., Barlow, I., Leggett, G.J., Williams, N.H., 2013. Fabrication of molecular nanopatterns at aluminium oxide surfaces by nanoshaving of self-assembled monolayers of alkylphosphonates. *Nanoscale* 5, 11125–11131. <https://doi.org/10.1039/c3nr04701f>.
- Elbert, D.L., Hubbell, J.A., 1998. Reduction of fibrous adhesion formation by a copolymer possessing an affinity for anionic surfaces. *J. Biomed. Mater. Res.* 42, 55–65. [https://doi.org/10.1002/\(SICI\)1097-4636\(199810\)42:1<55::AID-JBM8>3.0.CO;2-N](https://doi.org/10.1002/(SICI)1097-4636(199810)42:1<55::AID-JBM8>3.0.CO;2-N).

- Erb, R.M., Son, H.S., Samanta, B., Rotello, V.M., Yellen, B.B., 2009. Magnetic assembly of colloidal superstructures with multipole symmetry. *Nature* 457, 999–1002. <https://doi.org/10.1038/nature07766>.
- Fodor, S.P., Read, J.L., Pirrung, M.C., Stryer, L., Lu, A.T., Solas, D., 1991. Light-directed, spatially addressable parallel chemical synthesis. *Science* 251, 767–773 (80).
- Foncy, J., Estève, A., Degache, A., Colin, C., Dollat, X., Cau, J.-C., Vieu, C., Trévisiol, E., Malaquin, L., 2018. Dynamic inking of large-scale stamps for multiplexed microcontact printing and fabrication of cell microarrays. *PLoS One* 13, e0202531. <https://doi.org/10.1371/journal.pone.0202531>.
- Fosser, K.A., Nuzzo, R.G., 2003. Fabrication of patterned multicomponent protein gradients and gradient arrays using microfluidic depletion. *Anal. Chem.* 75, 5775–5782. <https://doi.org/10.1021/ac034634a>.
- Frith, J.E., Mills, R.J., Cooper-White, J.J., Wells, A., Griffith, L.G., 2012. Lateral spacing of adhesion peptides influences human mesenchymal stem cell behaviour. *J. Cell Sci.* 125, 317–327. <https://doi.org/10.1242/jcs.087916>.
- Geissler, M., Xia, Y., 2004. Patterning: principles and some new developments. *Adv. Mater.* 16, 1249–1269. <https://doi.org/10.1002/adma.200400835>.
- Goodberlet, J.G., 2000. Patterning 100 nm features using deep-ultraviolet contact photolithography. *Appl. Phys. Lett.* 76, 667–669. <https://doi.org/10.1063/1.125856>.
- Gramlich, W.M., Kim, I.L., Burdick, J.A., 2013. Synthesis and orthogonal photopatterning of hyaluronic acid hydrogels with thiol-norbornene chemistry. *Biomaterials* 34, 9803–9811. <https://doi.org/10.1016/j.biomaterials.2013.08.089>.
- Guo, L.J., 2007. Nanoimprint lithography: methods and material requirements. *Adv. Mater.* 19, 495–513. <https://doi.org/10.1002/adma.200600882>.
- Guvendiren, M., Molde, J., Soares, R.M.D., Kohn, J., 2016. Designing biomaterials for 3D printing. *ACS Biomater. Sci. Eng.* 2, 1679–1693. <https://doi.org/10.1021/acsbiomaterials.6b00121>.
- Haynes, C.L., Van Duyn, R.P., 2001. Nanosphere Lithography: a versatile nanofabrication tool for studies of size-dependent nanoparticle optics. *J. Phys. Chem. B* 105, 5599–5611. <https://doi.org/10.1021/JP010657M>.
- He, L., Wang, M., Zhang, Q., Lu, Y., Yin, Y., 2013. Magnetic assembly and patterning of general nanoscale materials through nonmagnetic templates. *Nano Lett.* 13, 264–271. <https://doi.org/10.1021/nl3040256>.
- Healy, K.E., Lom, B., Hockberger, P.E., 1994. Spatial distribution of mammalian cells dictated by material surface chemistry. *Biotechnol. Bioeng.* 43, 792–800. <https://doi.org/10.1002/bit.260430814>.
- Heinrich, M.A., Liu, W., Jimenez, A., Yang, J., Akpek, A., Liu, X., Pi, Q., Mu, X., Hu, N., Schiffelers, R.M., Prakash, J., Xie, J., Zhang, Y.S., 2019. 3D bioprinting: from benches to translational applications. *Small* 15, 1805510. <https://doi.org/10.1002/sml.201805510>.
- Herrwerth, S., Eck, W., Reinhardt, S., Grunze, M., 2003. Factors that determine the protein resistance of oligoether self-assembled monolayers: internal hydrophilicity, terminal hydrophilicity, and lateral packing density. *J. Am. Chem. Soc.* 125, 9359–9366. <https://doi.org/10.1021/ja034820y>.
- Hill, R.T., Shear, J.B., 2006. Enzyme-nanoparticle functionalization of three-dimensional protein scaffolds. *Anal. Chem.* 78, 7022–7026. <https://doi.org/10.1021/ac061102w>.
- Hill, R.T., Lyon, J.L., Allen, R., Stevenson, K.J., Shear, J.B., 2005. Microfabrication of three-dimensional bioelectronic architectures. *J. Am. Chem. Soc.* 127, 10707–10711. <https://doi.org/10.1021/ja052211f>.
- Hirtz, M., Oikonomou, A., Georgiou, T., Fuchs, H., Vijayaraghavan, A., 2013. Multiplexed biomimetic lipid membranes on graphene by dip-pen nanolithography. *Nat. Commun.* 4, 2591. <https://doi.org/10.1038/ncomms3591>.
- Holden, M.A., Jung, S.-Y., Cremer, P.S., 2004. Patterning enzymes inside microfluidic channels via photoattachment chemistry. *Anal. Chem.* 76, 1838–1843. <https://doi.org/10.1021/ac035234q>.
- Hong, S., Zhu, J., Mirkin, C.A., 1999. Multiple ink nanolithography: toward a multiple-Pen nano-plotter. *Science* 286, 523–525. <https://doi.org/10.1126/science.286.5439.523>. (80).
- Hu, Y., Das, A., Hecht, M.H., Scoles, G., 2005. Nanografting De Novo proteins onto gold surfaces. *Langmuir* 21, 9103–9109. <https://doi.org/10.1021/LA046857H>.
- Huang, N.-P., Michel, R., Voros, J., Textor, M., Hofer, R., Rossi, A., Elbert, D.L., Hubbell, J.A., Spencer, N.D., 2001. Poly(l-lysine)-g-poly(ethylene glycol) layers on metal oxide Surfaces: surface-analytical characterization and resistance to serum and fibrinogen adsorption. *Langmuir* 17, 489–498. <https://doi.org/10.1021/LA000736+>.
- Hucknall, A., Kim, D.-H., Rangarajan, S., Hill, R.T., Reichert, W.M., Chilkoti, A., 2009a. Simple fabrication of antibody microarrays on nonfouling polymer brushes with femtomolar sensitivity for protein analytes in serum and blood. *Adv. Mater.* 21, 1968–1971. <https://doi.org/10.1002/adma.200803125>.
- Hucknall, A., Simnick, A.J., Hill, R.T., Chilkoti, A., Garcia, A., Johannes, M.S., Clark, R.L., Zauscher, S., Ratner, B.D., 2009b. Versatile synthesis and micropatterning of nonfouling polymer brushes on the wafer scale. *Biointerphases* 4, FA50–FA57. <https://doi.org/10.1116/1.3151968>.
- Hughes, T.R., Mao, M., Jones, A.R., Burchard, J., Marton, M.J., Shannon, K.W., Lefkowitz, S.M., Ziman, M., Schelter, J.M., Meyer, M.R., Kobayashi, S., Davis, C., Dai, H., He, Y.D., Stephanians, S.B., Cavet, G., Walker, W.L., West, A., Coffey, E., Shoemaker, D.D., Stoughton, R., Blanchard, A.P., Friend, S.H., Linsley, P.S., 2001. Expression profiling using microarrays fabricated by an ink-jet oligonucleotide synthesizer. *Nat. Biotechnol.* 19, 342–347. <https://doi.org/10.1038/86730>.
- Hyun, J., Zhu, Y., Liebmann-Vinson, A., Beebe Jr., T.P., Chilkoti, A., 2001. Microstamping on an activated polymer Surface: patterning biotin and streptavidin onto common polymeric biomaterials. *Langmuir* 17, 6358–6367. <https://doi.org/10.1021/LA010695X>.
- Hyun, J., Ma, H., Zhang, Z., Beebe Jr., T.P., Chilkoti, A., 2003. Universal route to cell micropatterning using an amphiphilic comb polymer. *Adv. Mater.* 15, 576–579. <https://doi.org/10.1002/adma.200304496>.
- Hyun, J., Kim, J., Craig, S.L., Chilkoti, A., 2004. Enzymatic nanolithography of a self-assembled oligonucleotide monolayer on gold. *J. Am. Chem. Soc.* 126, 4770–4771. <https://doi.org/10.1021/ja049956q>.
- Ino, K., Ito, A., Honda, H., 2007. Cell patterning using magnetite nanoparticles and magnetic force. *Biotechnol. Bioeng.* 97, 1309–1317. <https://doi.org/10.1002/bit.21322>.
- Jackman, R., Wilbur, J., Whitesides, G., 1995. Fabrication of submicrometer features on curved substrates by microcontact printing. *Science* 269, 664–666. <https://doi.org/10.1126/science.7624795>. (80).

- Jamal, M., Kadam, S.S., Xiao, R., Jivan, F., Onn, T.-M., Fernandes, R., Nguyen, T.D., Gracias, D.H., 2013. Bio-origami hydrogel scaffolds composed of photocrosslinked PEG bilayers. *Adv. Healthc. Mater.* 2, 1142–1150. <https://doi.org/10.1002/adhm.201200458>.
- Jang, C.-H., Stevens, B.D., Carlier, P.R., Calter, M.A., Ducker, W.A., 2002. Immobilized enzymes as catalytically-active tools for nanofabrication. *J. Am. Chem. Soc.* 124, 12114–12115. <https://doi.org/10.1021/JA017686V>.
- Ji, S., Wan, L., Liu, C.-C., Nealey, P.F., 2016. Directed self-assembly of block copolymers on chemical patterns: a platform for nanofabrication. *Prog. Polym. Sci.* 54 (55), 76–127. <https://doi.org/10.1016/J.PROGPOLYMSCI.2015.10.006>.
- Joglekar, A.P., Liu, H., Spooner, G.J., Meyhöfer, E., Mourou, G., Hunt, A.J., 2003. A study of the deterministic character of optical damage by femtosecond laser pulses and applications to nanomachining. *Appl. Phys. B* 77, 25–30. <https://doi.org/10.1007/s00340-003-1246-z>.
- Josephs, E.A., Ye, T., 2010. Nanoscale positioning of individual DNA molecules by an atomic force microscope. *J. Am. Chem. Soc.* 132, 10236–10238. <https://doi.org/10.1021/ja1039677>.
- Juncker, D., Schmid, H., Drechsler, U., Wolf, H., Wolf, M., Michel, B., de Rooij, N., Delamarche, E., 2002. Autonomous microfluidic capillary system. *Anal. Chem.* 74, 6139–6144. <https://doi.org/10.1021/ac0261449>.
- Kaneko, T., Kojima, K., Yasuda, K., 2007. An on-chip cardiomyocyte cell network assay for stable drug screening regarding community effect of cell network size. *Analyst* 132, 892–898. <https://doi.org/10.1039/b704961g>.
- Kaneko, T., Nomura, F., Hamada, T., Abe, Y., Takamori, H., Sakakura, T., Takasuna, K., Sanbuissho, A., Hyllner, J., Sartipy, P., Yasuda, K., 2015. On-chip in vitro cell-network pre-clinical cardiac toxicity using spatiotemporal human cardiomyocyte measurement on a chip. *Sci. Rep.* 4, 4670. <https://doi.org/10.1038/srep04670>.
- Kang, H.W., Leem, J., Ko, S.H., Yoon, S.Y., Sung, H.J., 2013. Vacuum-assisted microcontact printing (μ CP) for aligned patterning of nano and biochemical materials. *J. Mater. Chem. C* 1, 268–274. <https://doi.org/10.1039/C2TC00288D>.
- Kaufmann, T., Ravoo, B.J., 2010. Stamps, inks and substrates: polymers in microcontact printing. *Polym. Chem.* 1, 371–387. <https://doi.org/10.1039/b9py00281b>.
- Kilian, K.A., Bugarija, B., Lahn, B.T., Mrksich, M., 2010. Geometric cues for directing the differentiation of mesenchymal stem cells. *Proc. Natl. Acad. Sci.* 107, 4872–4877. <https://doi.org/10.1073/PNAS.0903269107>.
- Killops, K.L., Gupta, N., Dimitriou, M.D., Lynd, N.A., Jung, H., Tran, H., Bang, J., Campos, L.M., 2012. Nanopatterning biomolecules by block copolymer self-assembly. *ACS Macro Lett.* 1, 758–763. <https://doi.org/10.1021/mz300153k>.
- Kim, S.O., Solak, H.H., Stoykovich, M.P., Ferrier, N.J., de Pablo, J.J., Nealey, P.F., 2003. Epitaxial self-assembly of block copolymers on lithographically defined nanopatterned substrates. *Nature* 424, 411–414. <https://doi.org/10.1038/nature01775>.
- Kim, D.H., Lau, K.H.A., Robertson, J.W.F., Lee, O.-J., Jeong, U., Lee, J.I., Hawker, C.J., Russell, T.P., Kim, J.K., Knoll, W., 2005. Thin films of block copolymers as planar optical waveguides. *Adv. Mater.* 17, 2442–2446. <https://doi.org/10.1002/adma.200500170>.
- Kim, T.-H., Shah, S., Yang, L., Yin, P.T., Hossain, M.K., Conley, B., Choi, J.-W., Lee, K.-B., 2015. Controlling differentiation of adipose-derived stem cells using combinatorial graphene hybrid-pattern arrays. *ACS Nano* 9, 3780–3790. <https://doi.org/10.1021/nn5066028>.
- Kingshott, P., Thissen, H., Griesser, H.J., 2002. Effects of cloud-point grafting, chain length, and density of PEG layers on competitive adsorption of ocular proteins. *Biomaterials* 23, 2043–2056. [https://doi.org/10.1016/S0142-9612\(01\)00334-9](https://doi.org/10.1016/S0142-9612(01)00334-9).
- Kirschner, C.M., Alge, D.L., Gould, S.T., Anseth, K.S., 2014. Clickable, photodegradable hydrogels to dynamically modulate valvular interstitial cell phenotype. *Adv. Healthc. Mater.* 3, 649–657. <https://doi.org/10.1002/adhm.201300288>.
- Kojima, K., Moriguchi, H., Hattori, A., Kaneko, T., Yasuda, K., 2003. Two-dimensional network formation of cardiac myocytes in agar microculture chip with 1480 nm infrared laser photo-thermal etching. *Lab Chip* 3, 292–296. <https://doi.org/10.1039/b304652d>.
- Kumar, A., Whitesides, G.M., 1993. Features of gold having micrometer to centimeter dimensions can be formed through a combination of stamping with an elastomeric stamp and an alkanethiol “ink” followed by chemical etching. *Appl. Phys. Lett.* 63. <https://doi.org/10.1063/1.110628>. 2002–2004.
- Kyle, S., Jessop, Z.M., Al-Sabah, A., Whitaker, I.S., 2017. ‘Printability’ of candidate biomaterials for extrusion based 3D printing: state-of-the-art. *Adv. Healthc. Mater.* 6, 1700264. <https://doi.org/10.1002/adhm.201700264>.
- Lange, S.A., Benes, V., Kern, D.P., Hörber, J.K.H., Bernard, A., 2004. Microcontact printing of DNA molecules. *Anal. Chem.* 76, 1641–1647. <https://doi.org/10.1021/AC035127W>.
- Lau, K.H.A., Bang, J., Kim, D.H., Knoll, W., 2008. Self-assembly of protein nanoarrays on block copolymer templates. *Adv. Funct. Mater.* 18, 3148–3157. <https://doi.org/10.1002/adfm.200800487>.
- Lee, K.-B., Park, S.-J., Mirkin, C.A., Smith, J.C., Mrksich, M., 2002. Protein nanoarrays generated by dip-pen nanolithography. *Science* 295, 1702–1705. <https://doi.org/10.1126/science.1067172>. (80).
- Lee, S.W., Oh, B.-K., Sanedrin, R.G., Salaita, K., Fujigaya, T., Mirkin, C.A., 2006. Biologically active protein nanoarrays generated using parallel dip-pen nanolithography. *Adv. Mater.* 18, 1133–1136. <https://doi.org/10.1002/adma.200600070>.
- Lee, Y.B., Kim, S., Kim, E.M., Byun, H., Chang, H., Park, J., Choi, Y.S., Shin, H., 2017. Microcontact printing of polydopamine on thermally expandable hydrogels for controlled cell adhesion and delivery of geometrically defined microtissues. *Acta Biomater.* 61, 75–87. <https://doi.org/10.1016/J.ACTBIO.2017.07.040>.
- Lenhart, S., Brinkmann, F., Laue, T., Walheim, S., Vannahme, C., Klinkhammer, S., Xu, M., Sekula, S., Mappes, T., Schimmel, T., Fuchs, H., 2010. Lipid multilayer gratings. *Nat. Nanotechnol.* 5, 275–279. <https://doi.org/10.1038/nnano.2010.17>.
- Li, W., Müller, M., 2016. Directed self-assembly of block copolymers by chemical or topographical guiding patterns: optimizing molecular architecture, thin-film properties, and kinetics. *Prog. Polym. Sci.* 54–55. <https://doi.org/10.1016/J.PROGPOLYMSCI.2015.10.008>. 47–75.
- Li, M., Ober, C.K., 2006. Block copolymer patterns and templates. *Mater. Today* 9, 30–39. [https://doi.org/10.1016/S1369-7021\(06\)71620-0](https://doi.org/10.1016/S1369-7021(06)71620-0).
- Li, H.-W., Muir, B.V.O., Fichet, G., Huck, W.T.S., 2003. Nanocontact Printing: a route to sub-50-nm-scale chemical and biological patterning. *Langmuir* 19, 1963–1965. <https://doi.org/10.1021/LA0269098>.
- Li, L., Chen, S., Zheng, J., Ratner, B.D., Jiang, S., 2005. Protein adsorption on oligo(ethylene glycol)-terminated alkanethiolate self-assembled Monolayers: the molecular basis for nonfouling behavior. *J. Phys. Chem. B* 109, 2934–2941. <https://doi.org/10.1021/JP0473321>.

- Li, Y., Zhang, J., Liu, W., Li, D., Fang, L., Sun, H., Yang, B., 2013. Hierarchical polymer brush nanoarrays: a versatile way to prepare multiscale patterns of proteins. *ACS Appl. Mater. Interfaces* 5, 2126–2132. <https://doi.org/10.1021/am3031757>.
- Lin, E., Sikand, A., Wickware, J., Hao, Y., Derda, R., 2016. Peptide microarray patterning for controlling and monitoring cell growth. *Acta Biomater.* 34, 53–59. <https://doi.org/10.1016/j.ACTBIO.2016.01.028>.
- Liu, M., Amro, N.A., Chow, C.S., Liu, G., 2002. Production of nanostructures of DNA on surfaces. *Nano Lett.* 2, 863–867. <https://doi.org/10.1021/NL025626X>.
- Liu, M., Amro, N.A., Liu, G., 2008. Nanografting for surface physical chemistry. *Annu. Rev. Phys. Chem.* 59, 367–386. <https://doi.org/10.1146/annurev.physchem.58.032806.104542>.
- Lom, B., Healy, K.E., Hockberger, P.E., 1993. A versatile technique for patterning biomolecules onto glass coverslips. *J. Neurosci. Methods* 50, 385–397. [https://doi.org/10.1016/0165-0270\(93\)90044-R](https://doi.org/10.1016/0165-0270(93)90044-R).
- López, G.P., Ratner, B.D., Tidwell, C.D., Haycox, C.L., Rapoza, R.J., Horbett, T.A., 1992. Glow discharge plasma deposition of tetraethylene glycol dimethyl ether for fouling-resistant biomaterial surfaces. *J. Biomed. Mater. Res.* 26, 415–439. <https://doi.org/10.1002/jbm.820260402>.
- Lopez, G.P., Albers, M.W., Schreiber, S.L., Carroll, R., Peralta, E., Whitesides, G.M., 1993. Convenient methods for patterning the adhesion of mammalian cells to surfaces using self-assembled monolayers of alkanethiolates on gold. *J. Am. Chem. Soc.* 115, 5877–5878. <https://doi.org/10.1021/ja00066a087>.
- Ma, H., Hyun, J., Stiller, P., Chilkoti, A., 2004. “Non-Fouling” oligo(ethylene glycol)-functionalized polymer brushes synthesized by surface-initiated atom transfer radical polymerization. *Adv. Mater.* 16, 338–341. <https://doi.org/10.1002/adma.200305830>.
- Ma, H., Wells, M., Beebe, T.P., Chilkoti, A., 2006. Surface-initiated atom transfer radical polymerization of oligo(ethylene glycol) methyl methacrylate from a mixed self-assembled monolayer on gold. *Adv. Funct. Mater.* 16, 640–648. <https://doi.org/10.1002/adfm.200500426>.
- Ma, H., Jiang, Z., Xie, X., Huang, L., Huang, W., 2018. Multiplexed biomolecular arrays generated via parallel dip-pen nanolithography. *ACS Appl. Mater. Interfaces* 10, 25121–25126. <https://doi.org/10.1021/acsami.8b07369>.
- Malmström, J., Christensen, B., Jakobsen, H.P., Lovmand, J., Foldbjerg, R., Sørensen, E.S., Sutherland, D.S., 2010. Large area protein patterning reveals nanoscale control of focal adhesion development. *Nano Lett.* 10, 686–694. <https://doi.org/10.1021/nl903875r>.
- Manoharan, H.C., Lutz, C.P., Eigler, D.M., 2000. Quantum mirages formed by coherent projection of electronic structure. *Nature* 403, 512–515. <https://doi.org/10.1038/35000508>.
- McBeath, R., Pirone, D.M., Nelson, C.M., Bhadriraju, K., Chen, C.S., 2004. Cell shape, cytoskeletal tension, and RhoA regulate stem cell lineage commitment. *Dev. Cell* 6, 483–495. [https://doi.org/10.1016/S1534-5807\(04\)00075-9](https://doi.org/10.1016/S1534-5807(04)00075-9).
- Michel, R., Pasche, S., Textor, M., Castner, D.G., 2005. Influence of PEG architecture on protein adsorption and conformation. *Langmuir* 21, 12327–12332. <https://doi.org/10.1021/LA051726H>.
- Mrksich, M., 2002. What can surface chemistry do for cell biology? *Curr. Opin. Chem. Biol.* 6, 794–797. [https://doi.org/10.1016/S1367-5931\(02\)00362-9](https://doi.org/10.1016/S1367-5931(02)00362-9).
- Mrksich, M., 2009. Using self-assembled monolayers to model the extracellular matrix. *Acta Biomater.* 5, 832–841. <https://doi.org/10.1016/j.ACTBIO.2009.01.016>.
- Nagaraj, V.J., Eaton, S., Thirstrup, D., Wiktor, P., 2008. Piezoelectric printing and probing of Lectin NanoProbeArrays for glycosylation analysis. *Biochem. Biophys. Res. Commun.* 375, 526–530. <https://doi.org/10.1016/j.bbrc.2008.08.033>.
- Nie, Z., Kumacheva, E., 2008. Patterning surfaces with functional polymers. *Nat. Mater.* 7, 277–290. <https://doi.org/10.1038/nmat2109>.
- Nielson, R., Shear, J.B., 2006. Parallel chemical dosing of subcellular targets. *Anal. Chem.* 78, 5987–5993. <https://doi.org/10.1021/AC061084I>.
- Orchekowski, R., Hamelinck, D., Li, L., Gliwa, E., VanBrocklin, M., Marrero, J.A., Vande Woude, G.F., Feng, Z., Brand, R., Haab, B.B., 2005. Antibody microarray profiling reveals individual and combined serum proteins associated with pancreatic cancer. *Cancer Res.* 65, 11193–11202. <https://doi.org/10.1158/0008-5472.CAN-05-1436>.
- Pandey, A., Tzadka, S., Yehuda, D., Schwartzman, M., 2019. Soft thermal nanoimprint with a 10 nm feature size. *Soft Matter* 15, 2897–2904. <https://doi.org/10.1039/C8SM02590H>.
- Pardo, L., Wilson, W.C., Boland, T., 2002. Characterization of patterned self-assembled monolayers and protein arrays generated by the ink-jet method. *Langmuir* 19, 1462–1466. <https://doi.org/10.1021/LA026171U>.
- Patolsky, F., Timko, B.P., Yu, G., Fang, Y., Greytak, A.B., Zheng, G., Lieber, C.M., 2006. Detection, stimulation, and inhibition of neuronal signals with high-density nanowire transistor arrays. *Science* 80 (313), 1100–1104. <https://doi.org/10.1126/science.1128640>.
- Perl, A., Reinhoudt, D.N., Huskens, J., 2009. Microcontact printing: limitations and achievements. *Adv. Mater.* 21, 2257–2268. <https://doi.org/10.1002/adma.200801864>.
- Piner, R.D., Zhu, J., Xu, F., Hong, S., Mirkin, C.A., 1999. “Dip-Pen”; nanolithography. *Science* 283, 661–663. <https://doi.org/10.1126/science.283.5402.661>. (80).
- Raman, R., Bhaduri, B., Mir, M., Shkumatov, A., Lee, M.K., Popescu, G., Kong, H., Bashir, R., 2016. High-resolution projection micro-stereolithography for patterning of neovasculature. *Adv. Healthc. Mater.* 5, 610–619. <https://doi.org/10.1002/adhm.201500721>.
- Rape, A.D., Zibinsky, M., Murthy, N., Kumar, S., 2015. A synthetic hydrogel for the high-throughput study of cell–ECM interactions. *Nat. Commun.* 6, 8129. <https://doi.org/10.1038/ncomms9129>.
- Reetz, M.T., Winter, M., Dumpich, G., Lohau, J., Friedrichowski, S., 1997. Fabrication of metallic and bimetallic nanostructures by electron beam induced metallization of surfactant stabilized Pd and Pd/Pt clusters. *J. Am. Chem. Soc.* 119, 4539–4540. <https://doi.org/10.1021/JA970054H>.
- Rodriguez, I., Spicar-Mihalic, P., Kuyper, C.L., Fiorini, G.S., Chiu, D.T., 2003. Rapid prototyping of glass microchannels. *Anal. Chim. Acta* 496, 205–215. [https://doi.org/10.1016/S0003-2670\(03\)01000-6](https://doi.org/10.1016/S0003-2670(03)01000-6).
- Ross, C.A., Cheng, J.Y., 2008. Patterned magnetic media made by self-assembled block-copolymer lithography. *MRS Bull.* 33, 838–845. <https://doi.org/10.1557/mrs2008.179>.
- Ruiz, S.A., Chen, C.S., 2007. Microcontact printing: a tool to pattern. *Soft Matter* 3, 168–177. <https://doi.org/10.1039/B613349E>.
- Rundqvist, J., Hoh, J.H., Haviland, D.B., 2006. Directed immobilization of protein-coated nanospheres to nanometer-scale patterns fabricated by electron beam lithography of poly(ethylene glycol) self-assembled monolayers. *Langmuir* 22, 5100–5107. <https://doi.org/10.1021/la052306v>.

- Sackmann, E.K., Fulton, A.L., Beebe, D.J., 2014. The present and future role of microfluidics in biomedical research. *Nature* 507, 181–189. <https://doi.org/10.1038/nature13118>.
- Salaita, K., Wang, Y., Fragala, J., Vega, R.A., Liu, C., Mirkin, C.A., 2006. Massively parallel dip-pen nanolithography with 55000-pen two-dimensional arrays. *Angew. Chem. Int. Ed.* 45, 7220–7223. <https://doi.org/10.1002/anie.200603142>.
- Salaita, K., Wang, Y., Mirkin, C.A., 2007. Applications of dip-pen nanolithography. *Nat. Nanotechnol.* 2, 145–155. <https://doi.org/10.1038/nnano.2007.39>.
- Santra, S., De Luca, A., Bhaumik, S., Ali, S.Z., Udrea, F., Gardner, J.W., Ray, S.K., Guha, P.K., 2015. Dip pen nanolithography-deposited zinc oxide nanorods on a CMOS MEMS platform for ethanol sensing. *RSC Adv.* 5, 47609–47616. <https://doi.org/10.1039/C5RA04584C>.
- Schlapak, R., Danzberger, J., Haselgrübler, T., Hinterdorfer, P., Schäffler, F., Howorka, S., 2012. Painting with biomolecules at the nanoscale: biofunctionalization with tunable surface densities. *Nano Lett.* 12. <https://doi.org/10.1021/nl2045414>. 1983–1989.
- Schmelmer, U., Paul, A., Küller, A., Steenackers, M., Ulman, A., Grunze, M., Götzhäuser, A., Jordan, R., 2007. Nanostructured polymer brushes. *Small* 3, 459–465. <https://doi.org/10.1002/sml.200600528>.
- Shen, L., Garland, A., Wang, Y., Li, Z., Bielawski, C.W., Guo, A., Zhu, X.-Y., 2012. Two dimensional nanoarrays of individual protein molecules. *Small* 8, 3169–3174. <https://doi.org/10.1002/sml.201200673>.
- Shiku, H., Uchida, I., Matsue, T., 1997. Microfabrication of alkylsilanized glass substrate by electrogenerated hydroxyl radical using scanning electrochemical microscopy. *Langmuir* 13, 7239–7244. <https://doi.org/10.1021/LA970554O>.
- Shin, K., Leach, K.A., Goldbach, J.T., Kim, D.H., Jho, J.Y., Tuominen, M., Hawker, C.J., Russell, T.P., 2002. A simple route to metal nanodots and nanoporous metal films. *Nano Lett.* 2, 933–936. <https://doi.org/10.1021/NL025656O>.
- Singhvi, R., Kumar, A., Lopez, G.P., Stephanopoulos, G.N., Wang, D.I., Whitesides, G.M., Ingber, D.E., 1994. Engineering cell shape and function. *Science* (80 264), 696–698. <https://doi.org/10.1126/SCIENCE.8171320>.
- Smith, J.C., Lee, K.-B., Wang, Q., Finn, M.G., Johnson, J.E., Mrksich, M., Mirkin, C.A., 2003. Nanopatterning the chemospecific immobilization of cowpea mosaic virus capsid. *Nano Lett.* 3, 883–886. <https://doi.org/10.1021/NL025956H>.
- Staii, C., Viesselmann, C., Ballweg, J., Shi, L., Liu, G., Williams, J.C., Dent, E.W., Coppersmith, S.N., Eriksson, M.A., 2009. Positioning and guidance of neurons on gold surfaces by directed assembly of proteins using atomic force microscopy. *Biomaterials* 30, 3397–3404. <https://doi.org/10.1016/J.BIOMATERIALS.2009.03.027>.
- Steenackers, M., Küller, A., Ballav, N., Zharnikov, M., Grunze, M., Jordan, R., 2007. Morphology control of structured polymer brushes. *Small* 3, 1764–1773. <https://doi.org/10.1002/sml.200700187>.
- Sun, Y., Jallerat, Q., Szymanski, J.M., Feinberg, A.W., 2015. Conformal nanopatterning of extracellular matrix proteins onto topographically complex surfaces. *Nat. Methods* 12, 134–136. <https://doi.org/10.1038/nmeth.3210>.
- Suzuki, I., Yasuda, K., 2007. Constructive formation and connection of aligned micropatterned neural networks by stepwise photo-thermal etching during cultivation. *Jpn. J. Appl. Phys.* 46, 6398–6403. <https://doi.org/10.1143/JJAP.46.6398>.
- Suzuki, I., Sugio, Y., Jimbo, Y., Yasuda, K., 2005. Stepwise pattern modification of neuronal network in photo-thermally-etched agarose architecture on multi-electrode array chip for individual-cell-based electrophysiological measurement. *Lab Chip* 5, 241–247. <https://doi.org/10.1039/b406885h>.
- Taylor, A.M., Blurton-Jones, M., Rhee, S.W., Cribbs, D.H., Cotman, C.W., Jeon, N.L., 2005. A microfluidic culture platform for CNS axonal injury, regeneration and transport. *Nat. Methods* 2, 599–605. <https://doi.org/10.1038/nmeth777>.
- Thérien-Aubin, H., Wu, Z.L., Nie, Z., Kumacheva, E., 2013. Multiple shape transformations of composite hydrogel sheets. *J. Am. Chem. Soc.* 135, 4834–4839. <https://doi.org/10.1021/ja400518c>.
- Thibault, C., Le Berre, V., Casimirius, S., Trévisiol, E., François, J., Vieu, C., 2005. Direct microcontact printing of oligonucleotides for biochip applications. *J. Nanobiotechnol.* 3, 7. <https://doi.org/10.1186/1477-3155-3-7>.
- Totzeck, M., Ulrich, W., Göhnermeier, A., Kaiser, W., 2007. Pushing deep ultraviolet lithography to its limits. *Nat. Photonics* 1, 629–631. <https://doi.org/10.1038/nphoton.2007.218>.
- Tse, J.R., Engler, A.J., 2011. Stiffness gradients mimicking in vivo tissue variation regulate mesenchymal stem cell fate. *PLoS One* 6:e15978. <https://doi.org/10.1371/journal.pone.0015978>.
- Valkama, S., Kosonen, H., Ruokolainen, J., Haatainen, T., Torkkeli, M., Serimaa, R., ten Brinke, G., Ikkala, O., 2004. Self-assembled polymeric solid films with temperature-induced large and reversible photonic-bandgap switching. *Nat. Mater.* 3, 872–876. <https://doi.org/10.1038/nmat1254>.
- Valsesia, A., Mannelli, I., Colpo, P., Bretagnol, F., Rossi, F., 2008. Protein nanopatterns for improved immunodetection sensitivity. *Anal. Chem.* 80, 7336–7340. <https://doi.org/10.1021/ac801021z>.
- Vega, R.A., MasPOCH, D., Salaita, K., Mirkin, C.A., 2005. Nanoarrays of single virus particles. *Angew. Chem. Int. Ed.* 44, 6013–6015. <https://doi.org/10.1002/anie.200501978>.
- Wadu-Mesthrige, K., Amro, N.A., Garino, J.C., Xu, S., Liu, G., 2001. Fabrication of nanometer-sized protein patterns using atomic force microscopy and selective immobilization. *Biophys. J.* 80, 1891–1899. [https://doi.org/10.1016/S0006-3495\(01\)76158-9](https://doi.org/10.1016/S0006-3495(01)76158-9).
- Wang, W.M., Stoltenberg, R.M., Liu, S., Bao, Z., 2008. Direct patterning of gold nanoparticles using dip-pen nanolithography. *ACS Nano* 2, 2135–2142. <https://doi.org/10.1021/nn8005416>.
- Weissenstein, U., Schneider, M.J., Pawlak, M., Cicenias, J., Eppenberger-Castori, S., Oroszlan, P., Ehret, S., Geurts-Moespot, A., Sweep, F.C.G.J., Eppenberger, U., 2006. Protein chip based miniaturized assay for the simultaneous quantitative monitoring of cancer biomarkers in tissue extracts. *Proteomics* 6, 1427–1436. <https://doi.org/10.1002/pmic.200500078>.
- Whitesides, G.M., Ostuni, E., Takayama, S., Jiang, X., Ingber, D.E., 2001. Soft lithography in biology and biochemistry. *Annu. Rev. Biomed. Eng.* 3, 335–373. <https://doi.org/10.1146/annurev.bioeng.3.1.335>.
- Wilson, D.L., Martin, R., Hong, S., Cronin-Golomb, M., Mirkin, C.A., Kaplan, D.L., 2001. Surface organization and nanopatterning of collagen by dip-pen nanolithography. *Proc. Natl. Acad. Sci. U.S.A.* 98, 13660–13664. <https://doi.org/10.1073/pnas.241323198>.
- Wittstock, G., Schuhmann, W., 1997. Formation and imaging of microscopic enzymatically active spots on the alkanethiolate-covered gold electrode by scanning electrochemical microscopy. *Anal. Chem.* 69, 5059–5066. <https://doi.org/10.1021/AC970504O>.
- Wu, C.-C., Reinhoudt, D.N., Otto, C., Subramaniam, V., Velders, A.H., 2011. Strategies for patterning biomolecules with dip-pen nanolithography. *Small* 7, 989–1002. <https://doi.org/10.1002/sml.201001749>.

- Wu, C., Zhu, X., Man, T., Chung, P.-S., Teitell, M.A., Chiou, P.-Y., 2018. Lift-off cell lithography for cell patterning with clean background. *Lab Chip* 18, 3074–3078. <https://doi.org/10.1039/C8LC00726H>.
- Xia, Y., Whitesides, G.M., 1998a. Soft lithography. *Angew. Chem. Int. Ed.* 37, 550–575. [https://doi.org/10.1002/\(SICI\)1521-3773\(19980316\)37:5<550::AID-ANIE550>3.0.CO;2-G](https://doi.org/10.1002/(SICI)1521-3773(19980316)37:5<550::AID-ANIE550>3.0.CO;2-G).
- Xia, Y., Whitesides, G.M., 1998b. Soft lithography. *Annu. Rev. Mater. Sci.* 28, 153–184. <https://doi.org/10.1146/annurev.matsci.28.1.153>.
- Xia, Y., Kim, E., Zhao, X.-M., Rogers, J.A., Prentiss, M., Whitesides, G.M., 1996. Complex optical surfaces formed by replica molding against elastomeric masters. *Science* 273, 347–349. <https://doi.org/10.1126/science.273.5273.347>. (80).
- Xia, Y., McClelland, J.J., Gupta, R., Qin, D., Zhao, X.-M., Sohn, L.L., Celotta, R.J., Whitesides, G.M., 1997. Replica molding using polymeric materials: a practical step toward nanomanufacturing. *Adv. Mater.* 9, 147–149. <https://doi.org/10.1002/adma.19970090211>.
- Xu, T., Petridou, S., Lee, E.H., Roth, E.A., Vyavahare, N.R., Hickman, J.J., Boland, T., 2004. Construction of high-density bacterial colony arrays and patterns by the ink-jet method. *Biotechnol. Bioeng.* 85, 29–33. <https://doi.org/10.1002/bit.10768>.
- Yang, Y., Mielczarek, K., Aryal, M., Zakhidov, A., Hu, W., 2012. Nanoimprinted polymer solar cell. *ACS Nano* 6, 2877–2892. <https://doi.org/10.1021/nn3001388>.
- Yang, X., Xiao, S., Hsu, Y., Feldbaum, M., Lee, K., Kuo, D., 2013. Directed self-assembly of block copolymer for bit patterned media with areal density of 1.5 teradot/inch² and beyond. *J. Nanomater.* 2013, 615896. <https://doi.org/10.1155/2013/615896>.
- Yeo, W.-S., Yousaf, M.N., Mrksich, M., 2003. Dynamic interfaces between cells and Surfaces: electroactive substrates that sequentially release and attach cells. *J. Am. Chem. Soc.* 125, 14994–14995. <https://doi.org/10.1021/JA038265B>.
- Yousaf, M.N., Houseman, B.T., Mrksich, M., 2001. Using electroactive substrates to pattern the attachment of two different cell populations. *Proc. Natl. Acad. Sci. U.S.A.* 98, 5992–5996. <https://doi.org/10.1073/pnas.101112898>.
- Zeck, G., Fromherz, P., 2001. Noninvasive neuroelectronic interfacing with synaptically connected snail neurons immobilized on a semiconductor chip. *Proc. Natl. Acad. Sci. U.S.A.* 98, 10457–10462. <https://doi.org/10.1073/pnas.181348698>.
- Zhou, F., Zheng, Z., Yu, B., Liu, W., Huck, W.T.S., 2006. Multicomponent polymer brushes. *J. Am. Chem. Soc.* 128, 16253–16258. <https://doi.org/10.1021/JA0654377>.

1.4.6

Medical Fibers and Biotextiles

CALVIN CHANG^{1,2,4}, BRIAN GINN⁶, NATALIE K. LIVINGSTON^{1,2,4}, ZHICHENG YAO^{2,4,5}, BENJAMIN SLAVIN^{2,3}, MARTIN W. KING⁷, SANGWON CHUNG^{7,8}, HAI-QUAN MAO^{1,2,4,5}

¹Department of Biomedical Engineering, Johns Hopkins University, Baltimore, MD, United States

²Translational Tissue Engineering Center, Johns Hopkins School of Medicine, Baltimore, MD, United States

³Department of Plastic and Reconstructive Surgery, Johns Hopkins School of Medicine, Baltimore, MD, United States

⁴Institute for NanoBioTechnology, Johns Hopkins University, Baltimore, MD, United States

⁵Department of Materials Science and Engineering, Johns Hopkins University, Baltimore, MD, United States

⁶Secant Group, Telford, PA, United States

⁷Department of Textile Engineering, Chemistry & Science, North Carolina State University, Raleigh, NC, United States

⁸Biomedical Engineering, Joint Department of Biomedical Engineering, North Carolina State University and University of North Carolina at Chapel Hill, Chapel Hill, NC, United States

Introduction

Biotextiles, or medical textiles, are fibrous fabrics with defined structures generated from synthetic or natural materials that are used for the prevention, treatment, or diagnosis of injury or disease. They are used as biodurable or biodegradable components of implantable medical devices, as part of systems for ex vivo manipulation of media and cells, and for in vitro cell culture and testing. Civilizations dating as early as the ancient Egyptians used natural materials such as flax, silk, linen, and cotton to create sutures and bandages for wound healing. Some natural fibers are still in use today because of their intricate and versatile structures, favorable biocompatibility, and abundance. With advancements in fields such as chemistry, biomaterials, engineering, and manufacturing, it is now common to make synthetic fibers with tailored physical and biochemical properties. Specifically, improvements in spinning and fiber assembly methods and surface modification treatments have led to a rapid growth in new products and applications.

An important application is for surgical use, for example. Implantable and topical biotextiles have become readily

available and offer a wide range of structural complexities and utilities. They can be designed to perform multiple functions, including maintenance of comfort and hygiene, prevention of injury and infection, treatment of injury and disease, and even replacement of injured tissues. Examples include vascular grafts, heart valves, ligaments, hernia meshes, and hemostatic wound dressings. Several commercially available biotextiles for surgical applications are listed in [Table 1.4.6.1](#). These applications require careful considerations of biocompatibility and biostability.

The desired properties of biotextiles vary by application. Nonetheless, favorable attributes generally include high surface area, high porosity, lightness of weight, ability to fold, good flexibility, and tunable strength. A high surface area allows for more effective tissue interface, drug delivery, and cell attachment. Lightweight and foldable materials allow for minimally invasive implantation; strong and flexible materials can tolerate damage induced during implantation. On the other hand, thin and porous materials allow for better integration, as cells and surrounding tissue can readily interact with and grow into the material. Biodegradable or

TABLE 1.4.6.1 Examples of Commercial Biotextile Products and Their Clinical Applications

Clinical Application	Devices With Biotextile Component	Polymer	Fiber Structure	Fabric Structure	Resorption Time	Examples of Commercial Products	
General surgery	Esophageal stent	PET	Monofilament	Braided	Permanent	Polyflex	
		PDO	Monofilament	Braided	11–12 weeks	SX-ELLA	
	Hernia repair mesh	PP	Microfiber	Nonwoven	Permanent	Surgimesh	
		PP	Monofilament	Warp knit	Permanent	Sepramesh	
		PTFE	Expanded film	ePTFE membrane	Permanent	Dualmesh, Dulex	
		PGCL and PP	Monofilament	Warp, knit	Partially resorbable	Ultrapro	
		PLA	Monofilament	Self-fixation, pile component	Partially resorbable	Parietex ProGrip	
	Permanent suture	P(GA-co-LA-co-TMC), P(LA-co-TMC)	Multifilament	Knit	3 years	TIGR Matrix	
			Nylon 6	Monofilament	–	Permanent	Ethilon
				Multifilament	Braided	Permanent	Nurolon
			PET	Monofilament	–	Permanent	Surgidac
				Multifilament	Braided	Permanent	Mersilene, Ethibond, Ticon
		PP	Monofilament	–	Permanent	Prolene, Surgipro	
		PBT-TMEG	Monofilament	–	Permanent	Vascufil, Novafil	
		PVDF-HFP	Monofilament	–	Permanent	Pronova	
		Silk	Multifilament	Braided	Permanent	Perma-hand, Sofsilk	
		Resorbable suture	Collagen (catgut)	Monofilament	–	70–90 days	Chromic/plain
PDO	Monofilament			–	180–250 days	PDS	
PGCL	Monofilament		–	90–120 days	Monocryl		
PLGA	Monofilament		–	40–70 days	Vicryl		
	Multifilament		Braided	Polysorb			
PGA-PCL-TMC-PLA	Monofilament		–	20–60 days	Caprosyn		
PGA-PDO-TMC	Monofilament		–	90–110 days	Biosyn		
P(GA-co-TMC)	Monofilament	–	60–180 days	Maxon			
Barbed suture	PDO	Monofilament	–	120–180 days	Quill		
	P(GA-co-TMC)	Monofilament	–	180 days	V-Loc		

TABLE 1.4.6.1 Examples of Commercial Biotextile Products and Their Clinical Applications—cont'd

Clinical Application	Devices With Biotextile Component	Polymer	Fiber Structure	Fabric Structure	Resorption Time	Examples of Commercial Products
Cardiovascular	Annuloplasty ring	PET	Multifilament	Weft knit	Permanent	Carpentier-Edwards, Duran AnCore
		PTFE	Multifilament	Weft knit	Permanent	Koehler MRS
	Arteriovenous shunt	PTFE	Expanded film	ePTFE membrane	Permanent	Vectra, Flixene
	Blood filter (ex vivo)	PET	Multifilament	Nonwoven	Permanent	MacoPharma
	Cardiac support device	PET	Multifilament	Knit	Permanent	Acorn CorCap
	Embolic vena cava filter	PTFE-FEP	Monofilament	Knotted	Permanent	Crux biomedical
	Endovascular stent graft	PET	Multifilament	Woven	Permanent	Zenith, Endurant
		PTFE	Expanded film	ePTFE membrane	Permanent	Excluder, PowerLink, Covera ^T
	Heart valve sewing ring	PET	Multifilament	Weft knit	Permanent	St. Jude Medical, sorin
		PTFE	Multifilament	Weft knit	Permanent	Edwards Lifesciences
	Septal defect repair device	PET	Multifilament	Knit	Permanent	CardioSEAL
		PTFE	Expanded film	ePTFE membrane	Permanent	Helix
Vascular prosthesis	PET	Multifilament	Warp knit, woven	Permanent	DeBakey, Gelweave, Barone	
	PTFE	Expanded film	ePTFE membrane	Permanent	Gore-Tex, Flixene	
Dental	Dental reinforcing ribbon	UHMWPE	Multifilament	Leno weave	Permanent	Ribbon
Neural	Nerve guide prosthesis	PGA	Multifilament	Woven	60–90 days	NeuraGen
Orthopedic	Bone graft/cement	Carbon fiber	Staple fiber/multifilament	Reinforced PMMA composite	Permanent	DePuy
	Ligament and tendon prosthesis	PET	Multifilament	Braided/wove/knitted	Permanent	Stryker-Meadox, Leeds-Keio
		PTFE	Expanded film	ePTFE membrane	Permanent	Gore-Tex
	Spinal disc nucleus prosthesis	UHMWPE	Multifilament	Braided	Permanent	Richards Polytex
		UHMWPE	Multifilament	Woven	Permanent	Raymedica PDN
Spinal support	Carbon fiber	Stable fiber/multifilament	Reinforced PEEK composite	Permanent	Ocelot	

(Continued)

TABLE 1.4.6.1 Examples of Commercial Biotextile Products and Their Clinical Applications—cont'd

Clinical Application	Devices With Biotextile Component	Polymer	Fiber Structure	Fabric Structure	Resorption Time	Examples of Commercial Products
Skin and wound dressing	Skin graft Wound dressing	PLGA	Multifilament	Knitted	40–70 days	Dermagraft
		Nylon	Multifilament	Knitted	Temporary	Biobrane
		Nylon/collagen	Multifilament	Knitted velour	Temporary	TransCyte
		Cotton	Staple yarn	Woven	Temporary	Kendall Curity
		UHMWPE/viscose rayon and PET	Multifilament/staple fiber	Knitted/nonwoven composite	Temporary	Acticoat
		Carboxymethyl cellulose	Staple fiber	Nonwoven	Temporary	Aquacel
		Cotton/viscose rayon	Staple yarn	Leno weave	Temporary	Jelonet
		Viscose rayon/nylon	Multifilament	Knitted	Temporary	Kband
		PET Viscose rayon	Staple fiber	Nonwoven composite	Temporary	Mepore
		PP/cellulose	Staple fiber/pulp fiber	Nonwoven composite	Temporary	Mesorb
Nylon	Multifilament	Leno weave	Temporary	Tegapore		
Calcium alginate	Staple fiber	Nonwoven	Temporary	Kaltostat		

ePTFE, Expanded polytetrafluoroethylene; *FEP*, fluorinated ethylene propylene polymer; *PBT-TMEG*, poly(butylene terephthalate-co-tetramethylene ether glycol); *PCL*, polycaprolactone; *PDO*, poly(*p*-dioxanone); *PEEK*, polyetheretherketone; *PE*, polyethylene; *PET*, poly(ethylene terephthalate); *PGA*, polyglycolide; *P(GA-co-CL)*, poly(glycolide-co- ϵ -caprolactone); *P(GA-co-LA-co-TMC)*, poly(glycolide-co-lactide-co-trimethylene carbonate); *P(GA-co-TMC)*, poly(glycolide-co-trimethylene carbonate); *PLA*, polylactide; *P(LA-co-TMC)*, poly(lactide-co-trimethylene carbonate); *PLGA*, poly(lactide-co-glycolide); *PMMA*, polymethylmethacrylate; *PP*, polypropylene; *PTFE*, poly(tetrafluoroethylene); *PVDF-HFP*, poly(vinylidene fluoride-co-hexafluoropropylene); *PTMC*, poly(trimethylene carbonate); *UHMWPE*, ultrahigh molecular weight polyethylene.

bioresorbable textiles are important for devices that serve temporary functions such as injury repair. These properties are influenced by the biotextile manufacturing process, including the choice of material or polymer, as well as the structural design of the engineered textile. In this chapter, the techniques used for fiber and textile productions, which include steps involving polymer selection and fiber formation, fiber arrangement into various textile structures, finishing, and surface modification of the biotextile products, will be described. The effects of various design parameters on the final structures, properties, and performance of biotextiles will also be discussed. Lastly, several major biotextile applications in medicine and their future R&D directions will be examined.

Fiber-Forming Polymers

Characteristics of Fiber-Forming Polymers

The primary building blocks for biotextiles are the individual fibers produced in continuous yarns or fiber fragments. The biochemical nature of these fibers largely dictates their

biocompatibility and biodegradation profiles. The basic requirement for polymer selection is the ability to form fibers, meaning the polymer chains need to share several common structural features, which include: (1) intermediate to high molecular weight (approximately 20–250 kDa) so the polymer melt or solution will have sufficient viscosity, (2) linear and ordered structure with absence of bulky side chains or cross-links to facilitate chain alignment and close packing, or crystalline phase formation when solidified from the melt or when precipitated from solution; and (3) interchain interactions that can stabilize closely packed chain segments and crystalline domains, allowing polymer chains to align and slide along the fiber axis during stretching or drawing. Fiber formation parameter requirements may also depend on the chemical structure of the polymers used. For example, a molecular weight ranging from 20 to 30 kDa is sufficient to generate fibers from polymers with strong interchain interactions such as nylon and PET, which can form hydrogen bonds and strong dipole–dipole interactions, whereas higher molecular weight is required for polymers with fewer interchain interactions, e.g., vinyl polymers and aliphatic polyesters. Polymers with a high

degree of crystallinity (e.g., silk, poly(tetrafluoroethylene) (PTFE), poly(vinylidene fluoride) (PVDF), polyethylene, and polydioxanone) typically have greater mechanical properties, and can form fibers more easily too.

The degradation of resorbable polymers in the body is driven by hydrolysis or enzymatic degradation. Biocompatible materials and implants should have nontoxic degradation by-products to minimize inflammatory response in the host. The mechanism of bioerosion and degradation for biotextiles occurs through surface or bulk degradation mechanism until the fiber has been totally resorbed. Examples of natural and synthetic fibers, including those that resorb into the biological environment postimplantation, and their relative resorption times, are provided in [Table 1.4.6.2](#). Permanent synthetic polymers were originally developed for nonmedical applications, such as poly(ethylene-terephthalate) (PET), which was first used in apparel textile fibers. Any additives, stabilizers, and antioxidants that may be cytotoxic for biomedical applications require an extensive cleaning and removal process before being adopted for implantation ([Fages et al., 1998](#); [King, 1991](#)).

Common nanofibrous polymers generated via electrospinning are poly(ϵ -caprolactone) (PCL), polyglycolide (PGA), poly(lactide-*co*-glycolide) (PLGA), and poly(*p*-dioxanone) (PDO), and are shown in [Table 1.4.6.3](#). A wide range of polymers, both natural and synthetic polymers, can be processed into fibers by electrospinning, though most of the spinning conditions are optimized through empirical trial-and-error testing. Typical electrospinning parameters that influence fiber formation include molecular weight, architecture (branched vs. linear), viscosity, and conductivity, as well as other process parameters (temperature, humidity, electrical potential, and flow rate) ([Frenot and Chronakis, 2003](#); [Kai et al., 2014](#)). More detailed discussion of the spinning process can be found in the section [Electrospinning](#).

Natural and Synthetic Polymers for Biotextile Production

Natural polymers consist of protein materials such as collagen, elastin, and silk, and polysaccharides such as cellulose, chitosan, chitin, and alginate. These natural polymers, which are isolated from plants and animal tissues ([Sionkowska, 2011](#)), feature structural complexity with functional groups that allow for postspinning modifications. Many natural polymers contain functional moieties and bioactivities such as cell receptor binding, growth factor binding and enrichment, and thrombogenic activity, as well as enhanced biocompatibility and biodegradability.

Biopolymers have evolved naturally and are particularly well suited for medical applications. Polysaccharide-based fibers, such as cellulose fibers, have been used as wound dressings and hemostats due to their thrombogenicity. Alginates from algae, chitosan from crustacean shells, and dextran from bacterial fermentation have been used for

fabricating surgical sutures and meshes. Proteins, such as collagen, elastin, fibrinogen, and silk have been spun to form fiber structures for tissue regeneration applications, notably for nerve repair and vascular repair.

Compared with natural polymers, synthetic polymers have good mechanical properties and thermal stability, and can be more easily processed into different forms with controlled batch-to-batch consistency during production. Depending on the application, synthetic polymers have high tunability of properties, such as strength, flexibility, degradation rate, resistivity, and chemical inertness. They tend to be cheaper to make into fibers and yarns. The degree of control over synthetic polymers offers great versatility for many different applications. On the other hand, biopolymers typically have better biofunctions and biodegradation property. In some applications, natural–synthetic blends are of interest, as they can combine the advantages of each polymer type while avoiding their disadvantages.

Medical Fibers and Production Methods

Introduction to Textile Fibers

The first step in creating a biotextile medical device is to generate textile fibers. Textile fiber is “a generic term for various types of matter that form the basic elements of fabrics and other textile structures. More specifically, a textile fiber is a unit of matter that is characterized by having an aspect ratio (length divided by width) of at least 100, and which can be spun into yarn or made into a fabric” ([American Society for Testing and Mater, 1985](#)).

Fibers can be spun in different ways to create either monofilaments or multifilament yarns, which can vary in length. Yarn size is usually measured in linear density, i.e., the mass in grams of a defined amount of material under standard conditions. In much of the world, the decitex (dtex) is used, which is the mass in grams of 10,000 m of fiber. In North America, linear density is measured in denier, which is the mass in grams of 9000 m of fiber. Linear density is a result of both the cross-sectional area of the fiber and its mass density. As such, it can be related to other properties such as strength and rigidity. For example, Unsealed Gelsoft, a polyester yarn for vascular prosthesis, has a reported linear density of 100 dtex. However, this yarn is a multifilament yarn made of 54 round filaments. Therefore each filament is only 1.9 dtex. Since each individual filament has a lower linear density and smaller diameter, the multifilament fiber is much more flexible than a single 100 dtex monofilament. Flexibility is critical in many medical textile applications, such as tissue scaffolds. [Fig. 1.4.6.1](#) shows scanning electron microscopy (SEM) micrographs of mono- and multifilament woven sutures ([Reinbold et al., 2017](#)).

The spinning technique chosen to form fibers and yarns affects properties such as texture, cross-section shape, and size. For example, natural fibers typically have a cross-section

TABLE 1.4.6.2 Examples of Permanent and Resorbable Fiber-Forming Polymers

Polymer ^a	Chemical and Physical Parameters	Construction/Fiber Forms	Applications	Resorption Time
Nylon 6	Thermoplastic Hydrophobic $T_m = 220^\circ\text{C}$ $T_g = 45^\circ\text{C}$ Crystallinity 50% as spun	Melt spun into monofilaments and multifilament yarns	Sutures (Nurolon; Ethilon)	Permanent
Nylon 66	Thermoplastic Hydrophobic $T_m = 265^\circ\text{C}$ $T_g = 50^\circ\text{C}$ Crystallinity 50% as spun	Melt spun into monofilaments and multifilament yarns	Sutures (Monosof [†] ; Dermalon [†] ; surglion [†])	Permanent
PE	High-density PE (HDPE) Hydrophobic $T_m = 125^\circ\text{C}$ Crystallinity up to 85%	Melt spun into fibers for polymer composite reinforcement	Orthopedic and craniofacial implants	Permanent
	Ultra-high molecular weight PE Hydrophobic $T_m = 140\text{--}150^\circ\text{C}$ High crystallinity High tensile strength and modulus	Converted to very high tenacity yarn by gel spinning	Ligament prostheses and loadbearing orthopedic composites	
PET	Thermoplastic Hydrophobic $T_m = 265^\circ\text{C}$ $T_g = 65\text{--}105^\circ\text{C}$ 100% amorphous as spun, needs to be drawn and annealed to have crystallinity	Melt spun into monofilaments and multifilament yarns for weaving, knitting, and braiding	Sutures (Mersilene [†] ; surgidac [†] ; Ticon [†]); hernia repair meshes; anterior cruciate ligament prostheses; heart valve sewing rings; vascular and endovascular grafts	Permanent
PP	Predominantly isotactic Thermoplastic Hydrophobic $T_m = 165\text{--}175^\circ\text{C}$ Crystallinity 40%–46% Higher fracture toughness than HDPE susceptible to degradation from heat and radiation	Melt spun into monofilaments, hollow fibers or spunbonded and melt blown to nonwoven fabrics	Sutures (Prolene; surgipro); hernia repair meshes; blood filters (e.g., renal dialysis machines)	Permanent
PTFE	Thermoplastic Hydrophobic $T_m = 325^\circ\text{C}$ Crystallinity 50%–75% for processed fibers	Melt spun into monofilaments and multifilaments	Sutures; vascular and endovascular grafts; heart valve sewing rings; embolic vena cava filter; anterior cruciate ligaments	Permanent
PVDF	Thermoplastic Hydrophobic $T_m = 165\text{--}175^\circ\text{C}$ Crystallinity 52%–66%	Melt spun into monofilaments and multifilaments	Sutures (Pronova)	Permanent
Silk	Biocomponent fiber prepared from fibroin protein with sericin sheath Hydrophilic Crystallinity 70% Low elastic recovery	Spun by <i>Bombyx mori</i> silkworm with sericin coating; sericin is removed before processing	Sutures (Perm-Hand; sofsilk)	Classified as permanent but known to degrade in 1–2 years
Viscose rayon	First manufactured fiber in 1892 Hydrophobic Crystallinity 33% Decomposition begins at 250°C	Wet spun from alkali sodium cellulose xanthate solution into continuous multifilaments	Wound dressing	Permanent

TABLE 1.4.6.2 Examples of Permanent and Resorbable Fiber-Forming Polymers—cont'd

Polymer ^a	Chemical and Physical Parameters	Construction/Fiber Forms	Applications	Resorption Time
PCL	Thermoplastic Rubbery at room temperature $T_m = 58\text{--}63^\circ\text{C}$ $T_g = -65^\circ\text{C}$	Melt spun into monofilaments and multifilament yarns; can be electrospun into nanofibers; can be copolymerized with other resorbable polymers	Used as scaffolds in tissue engineering	>24 months
PDO	Thermoplastic $T_m = 110\text{--}115^\circ\text{C}$ $T_g = -10\text{--}0^\circ\text{C}$ Crystallinity 55%		Sutures (PDS); intramedullar pins; ligating clips	6–9 months
PGA	Thermoplastic $T_m = 225^\circ\text{C}$ $T_g = 40\text{--}45^\circ\text{C}$ Crystallinity 45%–55% Simplest linear aliphatic polyester rigid		Sutures (Dexon); meshes (for defect repairs and periodontal inserts); used as scaffolds in tissue engineering	6–12 months
PLA	Thermoplastic $T_m = 173\text{--}178^\circ\text{C}$ $T_g = 60\text{--}65^\circ\text{C}$		Stents; drug delivery devices; used as scaffolds in tissue engineering	>24 months
Polyglactin 910 10/90	Thermoplastic $T_m = 205^\circ\text{C}$ $T_g = 43^\circ\text{C}$ Crystallinity 40%	Multifilament yarns; for weaving, knitting, and braiding	Sutures (Vicryl; Polysorb); meshes	3 months
P(GA-co-CL)	Thermoplastic $T_g = -43\text{--}18^\circ\text{C}$ depending on the copolymer ratio and molecular weight	Monofilament	Sutures (Monocryl)	3–4 months
P(GA-co-TMC)	$T_m = 206^\circ\text{C}$ $T_g = 20^\circ\text{C}$	Monofilament	Sutures (Maxon)	2–6 months

^aFor abbreviations see Table 1.4.6.1.

diameter of 10–50 μm . However, advancements in spinning methods have allowed for polymers to be spun to sizes below 1 μm , as shown in Fig. 1.4.6.2, thus allowing them to be better suited for more applications due to their high surface-to-volume ratio. In the following sections, various fiber-spinning techniques are described in greater detail.

Melt Extrusion

In melt spinning, or melt extrusion, the polymer is heated above its melting point then extruded through a spinneret. As the polymer resin is extruded, cold air is used to solidify the filaments. A yarn is immediately drawn, lubricated, twisted, and entangled before it is wound onto a bobbin. Yarns can also be texturized by blowing air through the filaments as they are drawn and twisted. A typical setup for the melt extrusion process is depicted in Fig. 1.4.6.3. A spin finish, which is scoured from the textile prior to use, is added as a lubricant to reduce friction and prepare the yarn for the next processes of texturing, weaving, and knitting.

Spinneret design, which includes the number, size, shape, and length of the spinneret's holes, affects fiber properties such

as size, number of filaments, and cross-section shape. For example, a multifilament yarn made of 50 filaments can be produced by designing a spinneret with 50 holes. Alternatively, two (same or different) yarns made of 25 filaments each could be plied together to form the 50-filament final yarn. The shape of these spinneret holes determines the fiber's cross-section. A circular cross-section is the most common fiber shape but using other cross-sectional shapes has become more popular as they can change overall fiber properties without having to change the polymer used. Unique shapes such as stars, squares, and trilobes are frequently used to increase the filaments' ratio of surface area to volume. Cross-sectional shape also influences other properties such as strain, yield stress, bending rigidity, and shrinkage.

With melt spinning, the fabrication process is quick and does not require added solvents. However, melt spinning can only be used with thermoplastic polymers, or polymers that are not significantly affected by the melting process.

Wet/Gel Spinning

Wet spinning can be used to form fibers from soluble non-thermoplastic polymers or thermoplastic polymers that have

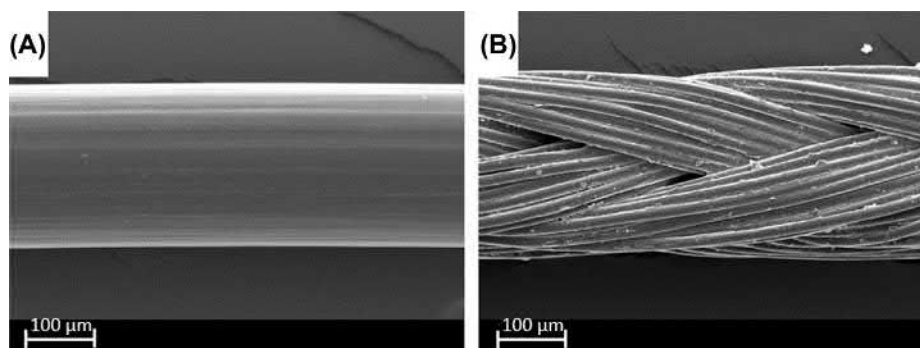
TABLE 1.4.6.3 Representative Polymers used for Electrospinning and Example Spinning Conditions

	Polymer	Solvent	Fiber Diameter	Highlight
Synthetic Polymers	PCL	THF/DMF (1:1, w/w); DMF/DCM (1:1)	100–1200 nm	As a semicrystalline polyester, PCL has slow biodegradation rate, high biocompatibility, and good drug permeability
	PLA	Acetone; DCM; chloroform; dioxane; THF; DMF; DMAc	210–1181 nm	
	PLGA	DCM; HFIP; THF; THF/DCM	500–1500 nm	Increasing the ratio of glycolide to lactide in the copolymer increased the rate of degradation
	PLA- <i>b</i> -PEG	Acetone	610–1010 nm	PLA- <i>b</i> -PEG displays good biocompatibility and increases hydrophilicity compared to pure PLA
	PEG- <i>b</i> -PCL	DMF/DCM (1:3, v/v)	350–400 nm	The hydrophilic PEG block increases the water wettability and degradation rate of PCL
	PS	DMF; THF; DMF/THF (1:1, w/w)	600–2760 nm	
	Polyanhydride	Chloroform	80–3200 nm	Polyanhydride undergoes surface erosion and gives steady degradation rate
	PU	HFIP	400–1400 nm	PU has high elasticity and low degradation rates
	PVA	Water; water/DMF (7:3, w/w)	50–1500 nm	PVA undergoes erosion in aqueous media. It has good physical and mechanical properties in dry and crystalline form.
	PVP	Water	190–1500 nm	
Natural polymers	PEO	Water		
	Collagen	HFIP	100–1200 nm	
	Gelatin	Transformation-enhancing activity; hot water	100–340 nm	
	Silk fibroin	Formic acid	30–120 nm	
	Spider silk protein	Formic acid		
	Chitosan	Formic acid		
	Alginate/PEO or PVA (coelectrospinning)	Water		Fiber swelling degree and mechanical property depend on the concentration and type of cross-linking agent used
	Fibrin	Water		Fibrin fiber is formed by cross-linking fibrinogen with thrombin in the presence of Ca ions
	Hyaluronic acid	Water		Hyaluronic acid fibers can be formed by different cross-linking methods

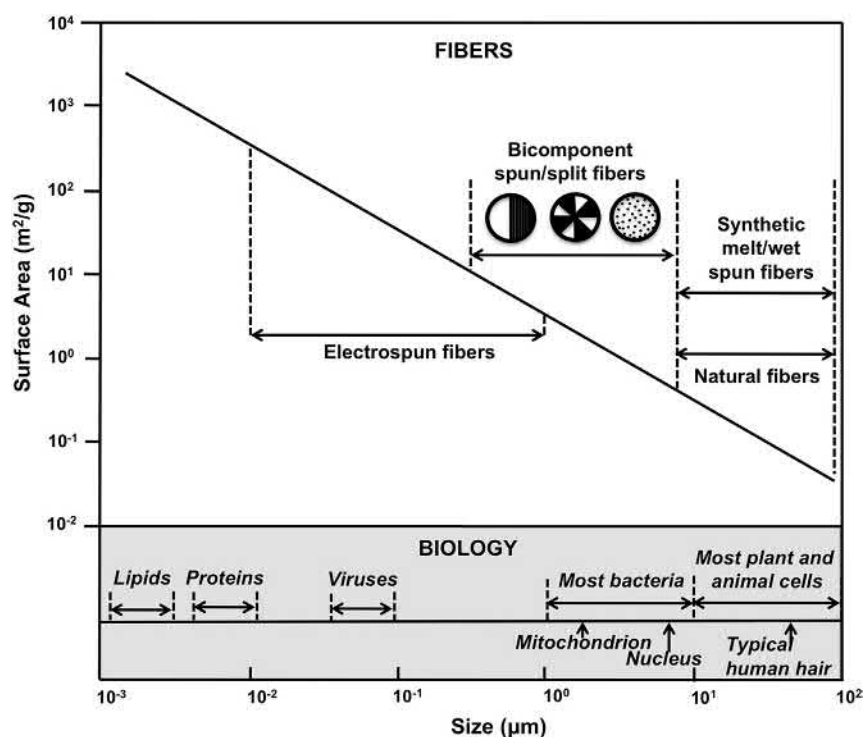
DCM, Dichloromethane; DMAc, dimethylacetamide; DMF/THF, dimethylformamide/tetrahydrofuran; HFIP, hexafluoroisopropanol; PCL, polycaprolactone; PLA, polylactide; PLGA, poly(lactide-co-glycolide); PLA-*b*-PEG, poly(lactide-*b*-ethylene glycol); PEG, polyethylene glycol; PS, polystyrene; PU, polyurethane; PVA, polyvinyl alcohol; PVP, polyvinylpyrrolidone; PEO, polyethylene oxide.

excessively high melt viscosity or melting temperature, which prevent use of melt extrusion equipment. The polymer is solubilized in either an organic or aqueous phase, extruded through a spinneret, like melt spinning, and then into a solution of opposite phase or into a cross-linking solution

to precipitate fiber as shown in Fig. 1.4.6.4A (Mather and Wardman, 2011). Alternatively, the polymer solution can be introduced directly into the coagulation bath as shown in Fig. 1.4.6.4B. The wet/gel fiber spinning method is applicable for many synthetic and biological polymers, including PCL,



• **Figure 1.4.6.1** Scanning electron microscopy micrographs of (A) a monofilament suture (Resonlon, 75 cm USP 3/0, Resorba (Nürnberg, Germany)) and (B) a multifilament suture (Ethibond Excel, 75 cm, USP 3-0 from Ethicon (Johnson and Johnson Medical GmbH, Norderstedt, Germany)). (Modified from Reinbold, J., Uhde, A.K., Müller, I., Weindl, T., Geis-Gerstorfer, J., Schlensak, C., Krajewski, S., 2017. Preventing surgical site infections using a natural, biodegradable, antibacterial coating on surgical sutures. *Molecules* 22 (9), 1570.)

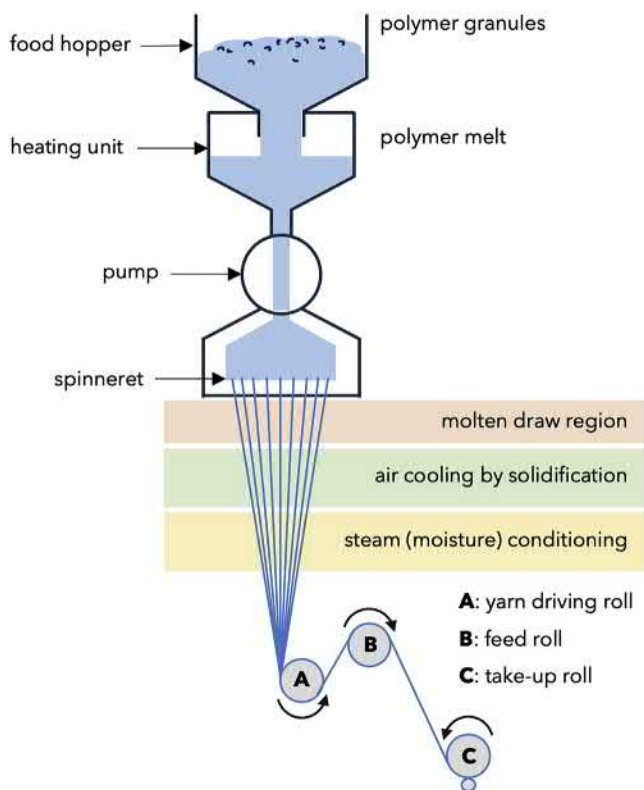


• **Figure 1.4.6.2** Relationship between fiber dimensions and surface area compared to a biological scale.

PLGA, cellulose, chitosan, alginate, cyclodextrin, fibrin, and collagen. For example, polylactide (PLA):PLGA may be solubilized in a chloroform solution and then extruded into an isopropanol solution, which it is not soluble in, to precipitate out a PLA:PLGA fiber (Razal et al., 2009). The resultant PLA:PLGA yarn can then be vacuum dried to remove residual solvent prior to use. In a similar manner, chitosan may be solubilized in acetic acid and wet spun into an ethyl alcohol or phosphate phthalate salt solution as a coagulation bath (Knaul et al., 1999). Fiber precipitation may also be induced through changes in other factors such as temperature or solution pH. Alginate fibers may be wet spun after the polysaccharide is solubilized in a sodium carbonate and caustic soda solution, via extrusion into a hydrochloric acid bath to precipitate fiber.

Electrospinning

Electrospinning is one of the most readily accessible and versatile techniques for producing ultrathin fibers with diameters on the order of hundreds of nanometers to several microns. The term “electrospinning” was coined in 1993 by Darrell H. Reneker for generating fibers from an electrically charged solution (Doshi and Reneker, 1995). Medical use of electrospun fiber mat was first developed as a wound dressing (Tucker et al., 2012). This technology has since been widely adopted for producing nanofiber structures due to its versatility, low cost, and ease of use. Although there are other approaches, such as mechanical drawing and melt blowing, which may be employed for the fabrication of nanofibers, electrospinning remains the most industrially



• **Figure 1.4.6.3** A schematic showing a typical process of melt extrusion for fiber production.

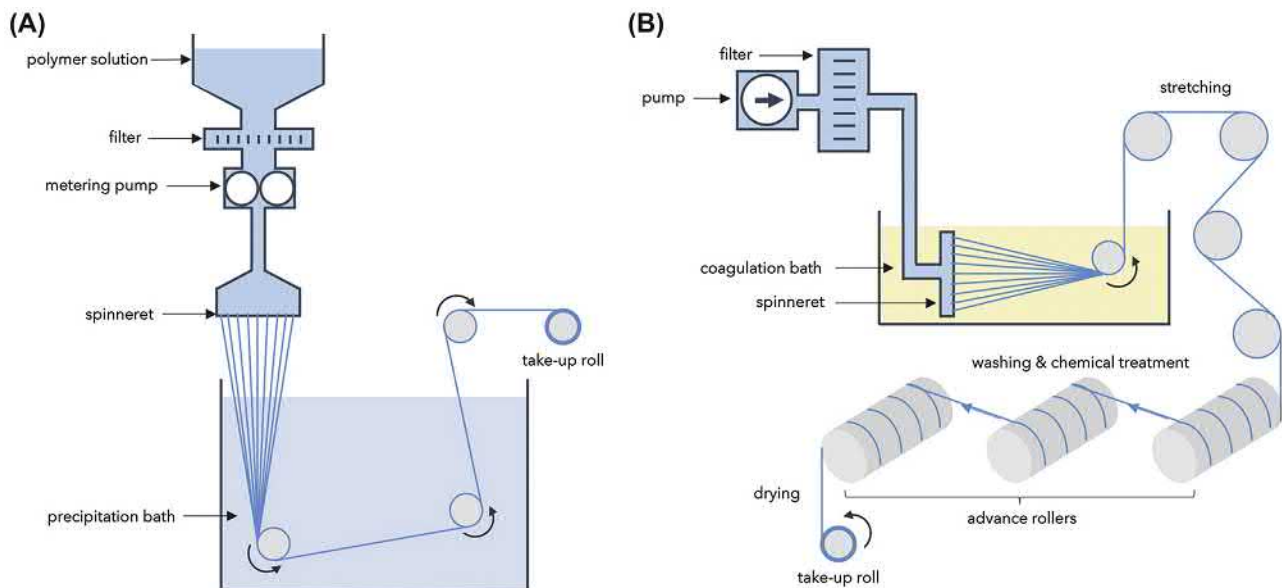
advanced as it is more suitable for producing ultrathin fibers with narrowly distributed diameters (Li and Xia, 2004).

Electrospinning Process and Spinning Parameter Optimization

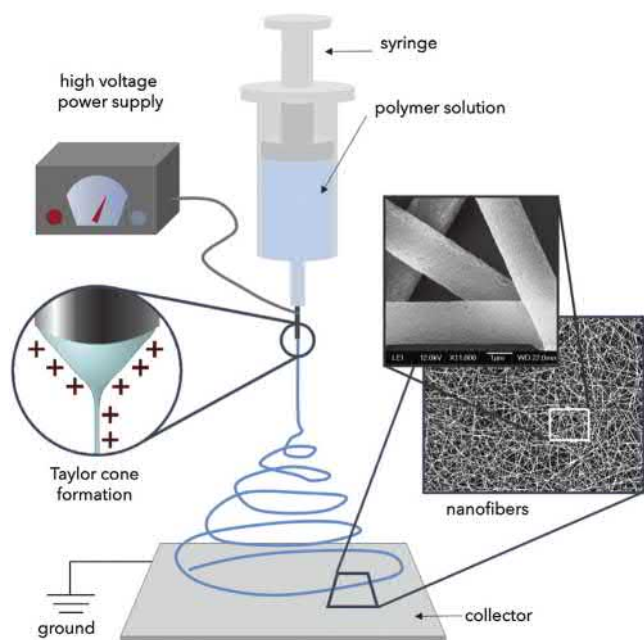
The setup for electrospinning consists of four main components: a high-voltage power supply, a syringe pump, a spinneret, and a grounded collector. When a high-voltage electrostatic field is applied to a dissolved polymer solution or melted polymer fluid with constant flow, a continuous splitting jet is ejected from the Taylor cone to form fibers, which are collected on a grounded, stationary target or rotating drum. The final fiber qualities, such as diameter, surface morphology, and alignment, can be precisely controlled by the properties of the spinning fluids and the parameters of the electrospinning process.

Exploring the formation of a Taylor cone, the most important mechanism of the electrospinning process, can help us understand how these parameters influence fiber quality. The Taylor cone is the critical condition where the shape of such a cone approaches the theoretical shape just before jet formation (Fig. 1.4.6.5) (Li and Xia, 2004; Ghorani and Tucker, 2015). To form a stable Taylor cone, the charged droplets should achieve a balance of surface tension against the electrostatic force. Therefore surface tension-related solution properties and electrostatic force-related parameters are important to consider when controlling fiber quality.

The electrospinning process is regulated by many parameters, broadly classified into solution parameters, process parameters, and ambient parameters. One example of a solution parameter is the viscosity of the spinning solution, which increases with increasing molecular weight of the



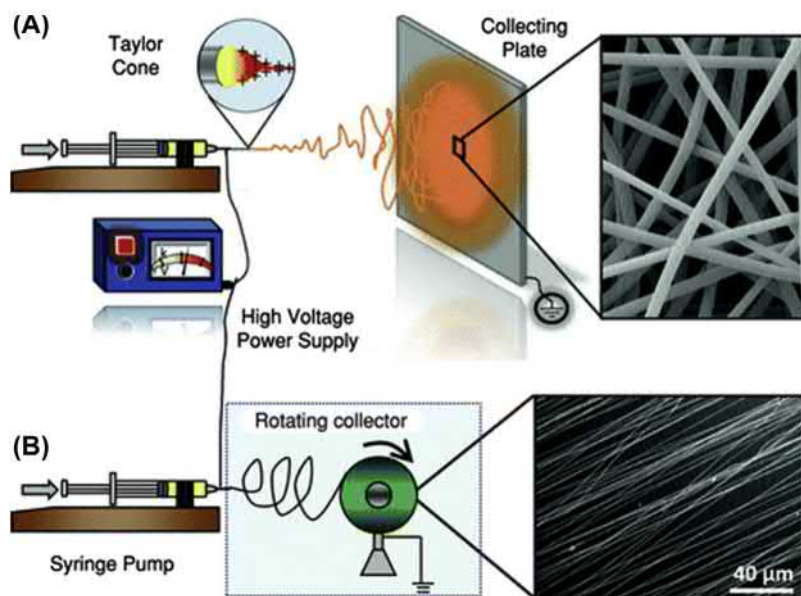
• **Figure 1.4.6.4** Examples of wet/gel spinning processes for fiber production. (A) A schematic showing a dry-jet-wet spinning process where a polymer solution is extruded out through an air gap into a precipitation bath. (B) A schematic showing a coagulation wet/gel spinning process where a polymer solution is extruded directly into a coagulation bath with a miscible but poor solvent for the polymer or with a cross-linking agent. ((A) Modified from Mather, R.R., Wardman, R.H., 2011. *The Chemistry of Textile Fibers*. R. Soc. Chem.)



• **Figure 1.4.6.5** Schematic illustration of a basic setup for electrospinning. The insets show a drawing of an electrified Taylor cone and a typical scanning electron microscopy image of the nonwoven mat of poly(ether sulfone) nanofibers deposited on a grounded collector. (Modified from Li, D., Xia, Y., 2004. Electrospinning of nanofibers: reinventing the wheel? *Adv. Mater.* 16 (14), 1151–1170.)

selected polymer or solution concentration and can increase the surface tension, thus leading to larger diameter nanofibers, while the electrostatic force will remain unchanged (Sill and von Recum, 2008). If the selected solvent possesses a higher conductivity, the electrostatic field force of the charged droplets will be greater, thus resulting in a finer jet and a thinner final fiber.

In terms of process parameters, several scaling and operational laws govern the electrospinning process, such as applied voltage, flow rate of solutions, collector distance, and shapes of spinneret and collector. Fiber diameters ranging from submicron to hundreds of nanometers have been reported (Bhardwaj and Kundu, 2010). Generally, a higher voltage results in greater stretching of the solution due to the larger coulombic forces in the jet as well as a stronger electric field. This leads to rapid evaporation of solvent from the fibers and thus reduction in the fiber diameter. Another important process parameter is flow rate. A lower flow rate is desired to get enough time to evaporate the solvent and reduce the fiber diameter. The collector distance also influences the time for solvent evaporation and fiber size distribution. The type of collector employed directly influences the fiber orientation on the collector (Fig. 1.4.6.6) (Lim and Mao, 2009; Mao et al., 2010). For example, if the collector is a roller that is rotating at high speed, the depositing fibers will be stretched, thus resulting in a highly oriented parallel fiber arrangement. Likewise, randomly oriented nanofibers can be acquired if the rotating speed is relatively slow or stationary. Additionally, collectors may be customized to obtain any needed fiber arrangement (Yee et al., 2008).



• **Figure 1.4.6.6** Two different modes of fiber collection in electrospinning, resulting in different nanofiber arrangements. (A) Randomly arranged fiber mat is produced from a polymer solution or melt when the electrospun jets are collected on a stationary grounded plate. (B) Highly aligned fibers are produced when polymer jets are collected on a wheel or frame rotating at a sufficiently high angular velocity. (Modified from (A) Mao, H.Q., Lim, S.H., Zhang, S., Christopherson, G., Kam, K., Fischer, S., 2010. The nanofiber matrix as an artificial stem cell niche. *Biomater. Stem Cell Niche*, Springer, Berlin, Heidelberg, pp. 89–118. (B) Lim, S.H., Mao, H.Q., 2009. Electrospun scaffolds for stem cell engineering. *Adv. Drug Delivery Rev.* 61 (12), 1084–1096.)

The dominant ambient parameters that can affect fiber quality during electrospinning are temperature and relative humidity (RH). After a stable polymer solution jet has been initiated from a Taylor cone, solvent evaporation and fiber deposition on the collector surface occur in ambient conditions. An increase in temperature and decrease in RH helps solvent evaporation, therefore decreasing fiber diameter. If the RH prevents solvent evaporation, the final fiber networks will be partially dissolved, thus compromising fiber quality and uniformity (Fashandi and Karimi, 2012; De Vrieze et al., 2009).

Materials Selection for Electrospinning

To date, numerous polymer materials have been fabricated into nanofibers through electrospinning. As the electrospinning technique advances, the range of materials that can be electrospun expands too. These materials include both synthetic and natural polymers, multicomponent composite polymers, and inorganic/organic composite materials. Table 1.4.6.3 summarizes the most commonly reported biomaterials used in electrospinning (Yang et al., 2018). Among them, electrospun fibers made from biodegradable polymers, including synthetic polyesters (PGA, PLA, PLGA, and PCL) and natural polymers (collagen, gelatin, silk fibroin, chitosan, and alginate), have garnered strong interests for their potential applications in regenerative medicine (Chong et al., 2007; Zhang et al., 2005). Their tunable degradation properties also allow for potential utilities in delivery of bioactive agents to control tissue regeneration or therapeutics. For example, a local anesthetic-eluting suture system, which combines the function and ubiquity of the suture with locally controlled release properties of a biodegradable polymeric matrix, was prepared by using PLGA

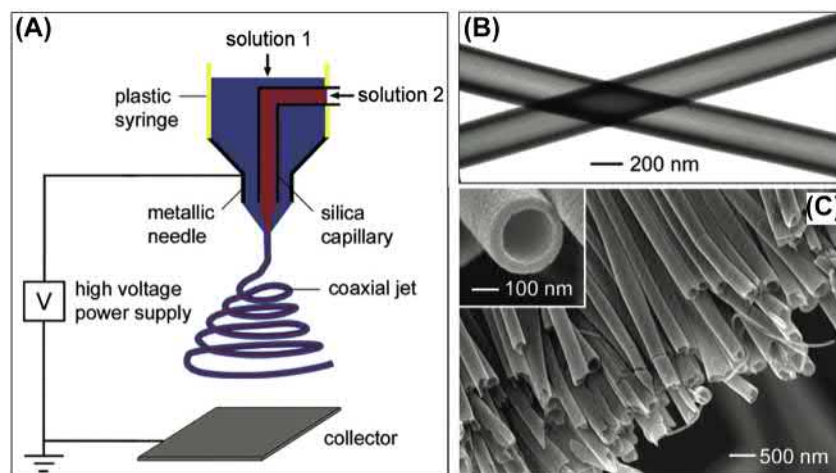
fibers (Weldon et al., 2012). Fibrous electrospun scaffolds with distinct alignment topography may guide cell migration, topography, differentiation, and growth of seeded or recruited cells (Qian et al., 2018).

Coelectrospinning

Bicomponent or multicomponent electrospun fibers can be generated for special applications. Coaxial electrospinning has been developed for preparing fibers with a core-shell or hollow structure, and emulsion electrospinning can be utilized to fabricate fibers with an embedded second component with mismatch solvent compatibility. For core-shell spinning, a spinneret fabricated from two coaxial capillaries is required, where two spinning solutions are fed into the outer and inner capillary separately. If the viscosity of the outer solution is high enough to form a stable Taylor cone, then a core-shell nanofibrous structure will eventually form, regardless of the viscosity of the inner solution, as shown in Fig. 1.4.6.7 (Hudecki et al., 2017; Sun et al., 2003). If the core component contains a bioactive agent, this core-shell nanofiber structure is capable of delaying and extending its release duration (Jiang et al., 2005). It is also possible to generate bicomponent nanofibers by electrospinning an emulsion using a typical single-nozzle spinning setup. Due to the phase separation between the oil and water phases of the emulsion, nanofibers with discontinuous phases can be generated as a result of agglomeration of droplets in the emulsion jet (Yarin, 2011).

Centrifugal Electrospinning

Centrifugal electrospinning (CES) has been developed to overcome several limitations of the electrospinning method,



• **Figure 1.4.6.7** (A) Schematic illustration of a coaxial electrospinning setup for generating nanofibers having a core-shell. The spinneret was fabricated from two coaxial capillaries, through which two feed solutions were simultaneously spun to form a continuous, coaxial jet. (B) Transmission electron microscopy image of two as-spun hollow fibers when a heavy mineral oil was used as a core solution and then extracted with octane after spinning. The walls of these tubes were made of a composite containing amorphous TiO_2 and polyvinylpyrrolidone. (C) Scanning electron microscopy image of a uniaxially aligned array of TiO_2 (anatase) hollow fibers. (Modified from Li, D., Xia, Y., 2004. Direct fabrication of composite and ceramic hollow nanofibers by electrospinning. *Nano Lett.* 4 (5), 933–938.)

such as low production yield and limited scalability in producing aligned fibers. Major equipment for CES includes a power rotation unit, high-voltage generator, spinning unit, and collection unit. The CES technique combines the centrifugal, electrostatic, gravitational, and auxiliary forces acting on the initial jet. When the combination breaks through the jet surface tension and viscous resistance, the jet is fully stretched out, forming ultrathin fibers. During the spinning, multiple formulations could be infused into the system and expelled via a rotating spinneret at a speed from the order of several hundred rpm to thousands of rpm (Mehta et al., 2019). Highly aligned PVDF, polyethylene, and chitosan fibers have been prepared by using a centrifugal electrospinning system (Edmondson et al., 2012).

Hydrogel Fiber Spinning

Hydrogels are particularly important biomaterials for cell delivery and growth, with highly porous and hydrated structures. A hydrogel can be chemically modified to incorporate cell-binding motifs and differentiation factors, while physical properties can be tuned through cross-linking type and density to provide a biomimetic microenvironment to support cell proliferation and differentiation (Hsieh et al., 2010).

Hydrogel nanofibers can be generated via electrospinning through spinning of a highly hydrophilic polymer that is cross-linked into a swellable network. For example, gelatin methacrylate nanofibers can be electrospun and then cross-linked into a hydrogel network when exposed to ultraviolet light in the presence of a photoinitiator (Sun et al., 2017). Hydrogel nanofibers produce highly extracellular matrix (ECM)-like structures capable of supporting endothelial cell and dermal fibroblast adhesion, proliferation, and migration throughout scaffolds to facilitate improved vascularization (Benton et al., 2009).

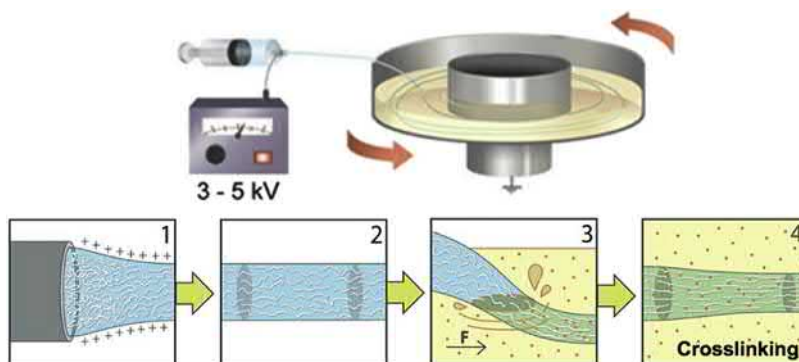
Alternatively, wet-spun fiber can also be formed through a modified electrospinning technique to produce

molecularly aligned hydrogel fibers (Fig. 1.4.6.8). The use of aqueous-based solutions enables incorporation of cells in situ during the fiber-forming process and induces alignment of cells on the fiber surface (Zhang et al., 2014). Biologically derived polymers, such as fibrin, alginate, or collagen, are used to generate fibers with this technique. Several methods of cross-linking are possible with this hydrogel fiber-forming method, including use of thrombin in the collection solution when forming fibrin fibers to mimic physiological blood coagulation or the use of calcium ions to rapidly induce ionic gelation of alginate to form fibers. Fibers produced with this method have been used to improve muscle regeneration in preclinical volumetric loss defect models (Gilbert-Honick et al., 2018a,b), while hydrated fibrin yarns have been used to study the effects of curvature on microvasculature formation and microvascular cell organization in vitro (Barreto-Ortiz et al., 2013, 2015).

Surface Functionalization

The surface chemistry of biomedical fibers plays a major role in affecting how well cells or proteins may bind to a fiber surface. Surface functionalization can be used to achieve a desired biological response or avoid an adverse response, such as increasing cell adhesion or decreasing complement deposition. Generally, surface functionalization methods can be divided into physical and chemical methods.

Physical vapor deposition (PVD) and plasma surface treatment are common physical methods used for modifying surface chemical compositions of polymer fibers. The most common PVD processes are sputtering and evaporation, which utilize a physical vapor to deposit a specific functional film onto the surface of the target substrate under a vacuum (Zussman et al., 2006). Plasma treatment is another commonly used physical surface functionalization method that employs a charged plasma to activate the target surface. For example, electrospun PCL nanofibers treated with O_2 and N_2 plasma at very low pressures will



• **Figure 1.4.6.8** Electrospinning of hydrogel fibers where biological polymer is solubilized in aqueous solution and dispensed from a syringe tip into an electric field (1). The electric field induces alignment of the polymer chains within the polymer jet (2), which is rapidly cross-linked as mechanical strain is applied upon landing in a rotating cross-linking bath (3), capturing the aligned polymer chains into a hydrogel fiber (4). (Modified from Zhang, S., Liu, X., Barreto-Ortiz, S.F., Yu, Y., Ginn, B.P., DeSantis, N.A., Gerecht, S., 2014. Creating polymer hydrogel microfibers with internal alignment via electrical and mechanical stretching. *Biomaterials* 35 (10), 3243–3251.)

have abundant hydrophilic functional groups that form on the surface, such as $-\text{OH}$, $-\text{COOH}$, and $-\text{NH}_2$ depending on the plasma selection (Formica et al., 2016).

There are many chemical methods for the surface functionalization fibers. For example, various types of cross-linkers and cross-linking techniques can be used based on the functional groups on the polymer and the extent of properties to be improved (Reddy et al., 2015). Glutaraldehyde is a widely used chemical cross linker, because of its high chemical reactivity of the aldehyde groups towards amino and hydroxyl groups found in natural polymers (Lai, 2014). Apart from glutaraldehyde, chemicals including carbodiimide, epichlorohydrin, and sodium metaphosphate, have also been used for surface functionalization (Hennink and van Nostrum, 2012). For polymers without reactive functional groups, surface-grafting methods can be adopted to modify the surface property of the fibers. For example, electrospun poly(ether sulfone) fibers can be surface grafted with poly(acrylic acid), which can then be converted to amino or hydroxyl groups through surface reactions. These surface functionalities have been shown to markedly influence hematopoietic stem cell phenotype maintenance during the expansion culture (Chua et al., 2006, 2007; Das et al., 2009).

Textile Structures

Once fibers or yarns are produced via spinning, they are fabricated into textiles using various techniques to give the final product its desired mechanical and biological properties. Structures typically used for medical textiles include weaves, knits, braids, and nonwovens. Material properties dictated by textile structure include strength, flexibility, porosity,

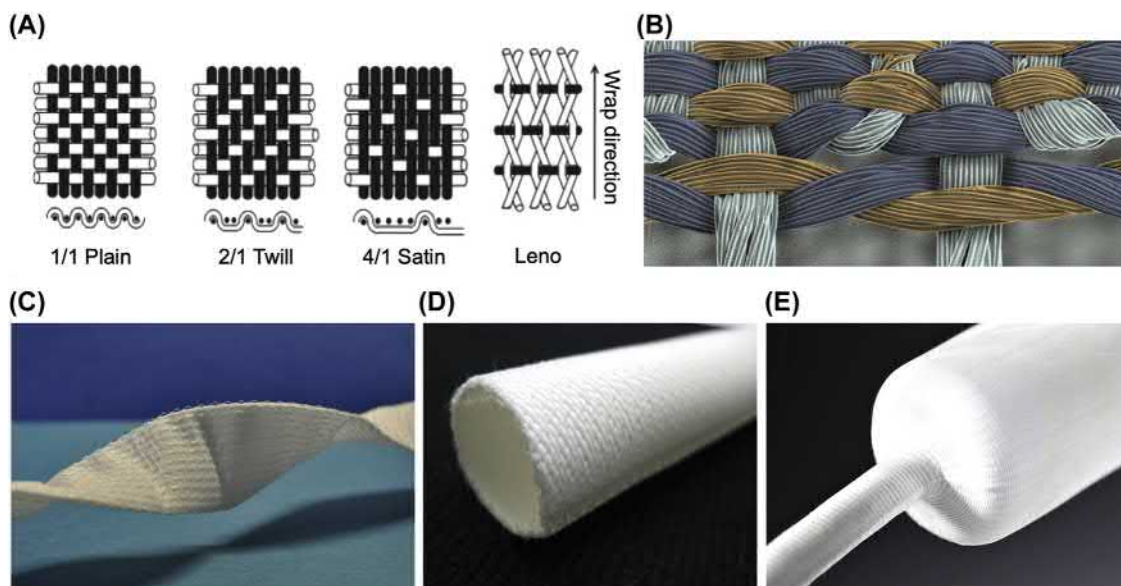
permeability, handleability, and stability. Generally, woven fabrics are strong and dimensionally stable, and have low porosity and permeability. Knit fabrics are more permeable and have higher specific surface area for tissue integration. Braided fabrics hold together well under longitudinal loads but are unstable under torsional loads while also being moderately porous. Choosing a final structure requires balancing the advantages and disadvantages of each structure. The rest of this section describes each structure in greater detail and introduces their typical use in medical applications.

Woven Textiles

Woven structures are made by interlacing primary structural yarns at right angles in directions called warp and weft. Warp yarns are held in place by a loom, while the weft yarns are drawn through warp yarns by a shuttle as warp yarns are lifted up in particular patterns to form weave structures such as plain, twill, satin, and leno weaves (Fig. 1.4.6.9A, B). Woven structures have high breaking strength in both the warp and weft directions and display low elongation. Weaves are particularly adept for vascular grafts and dental ribbon fabrications. Examples of woven textiles include planar weaves used for dressings or tubes for a variety of grafts and tissue scaffolds (Fig. 1.4.6.9C, D). Advanced textile production methods allow for the development of even more complex structures, such as tapered tubular grafts for vascular prostheses (Fig. 1.4.6.9E).

Knitted Textiles

Knitted fabrics are made of continuous interconnected chains of yarn loops. Rows of loops are called wales and vertical columns are called courses. Two major variations of



• **Figure 1.4.6.9** Woven textile structures. (A) Schematic diagram of woven textile structures. (B) False-color scanning electron microscopy images of a multifilament woven poly(ethylene-terephthalate) (PET) textile microstructure. (C) Macro view of a woven PET textile sheet. (D) Macro view of a woven PET textile tubular graft. (E) Macro view of a tapered woven PET textile tubular vascular graft. ((B–E) Courtesy of Secant Group, LLC.)

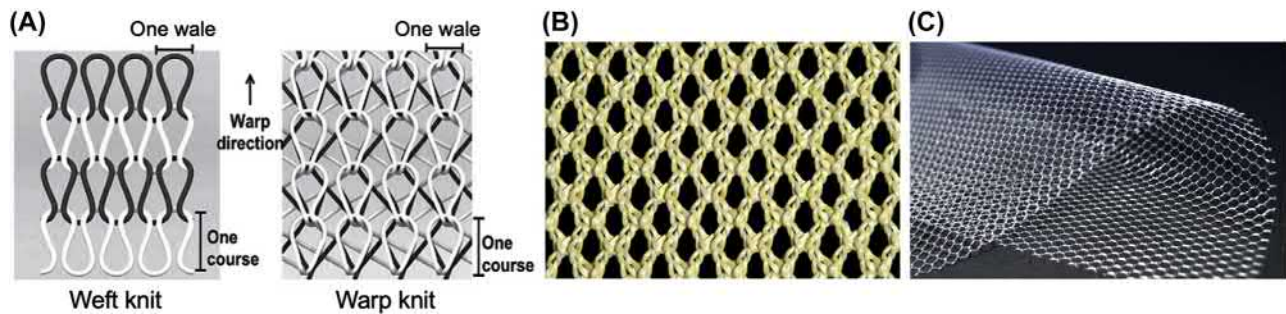
knit fabrics are the weft knit and warp knit constructions. Weft knitting is simpler; one yarn forms courses in the fabric. In warp knitting, a series of yarns forms wales in the fabric. These structures are depicted in Fig. 1.4.6.10. Warp knits are more dimensionally stable, have less stretch, and unravel less when cut compared to weft knits. Warp knits, such as velour or pile knits, are generally more versatile as they can be additionally modified by adding extra yarn to the structure to add thickness, bulk, and surface texture.

Knitted structures are generally more flexible and compliant than woven structures. Knit fabrics have a much higher porosity than woven fabrics, with typical total porosity exceeding 65%. This porosity is beneficial for tissue ingrowth but results in unacceptable water permeability. To decrease permeability, for example when a knit structure is used as a vascular graft, knits must first be coated or impregnated with collagen or gelatin to avoid the need of preclotting. Knit fabrics are often subjected to heat setting, which shrinks the yarn and tightens the loop structures to improve the fabric strength, stretchiness, softness, and

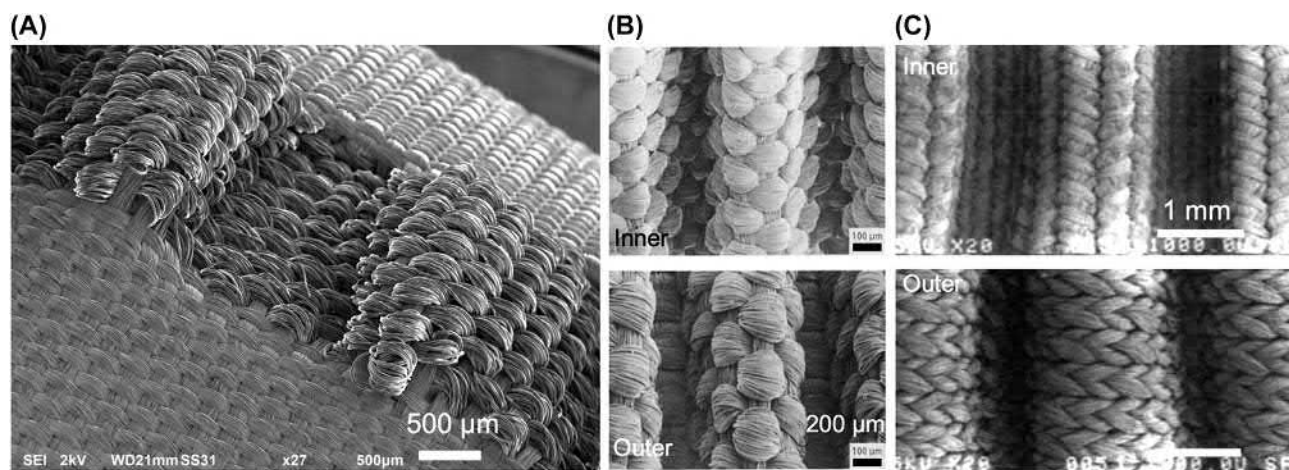
stability. The addition of pile yarn to warp knits makes the fabric softer and improves the thrombotic deposit from the initial blood contact to improve tissue ingrowth and healing (Fig. 1.4.6.11).

Braided Textiles

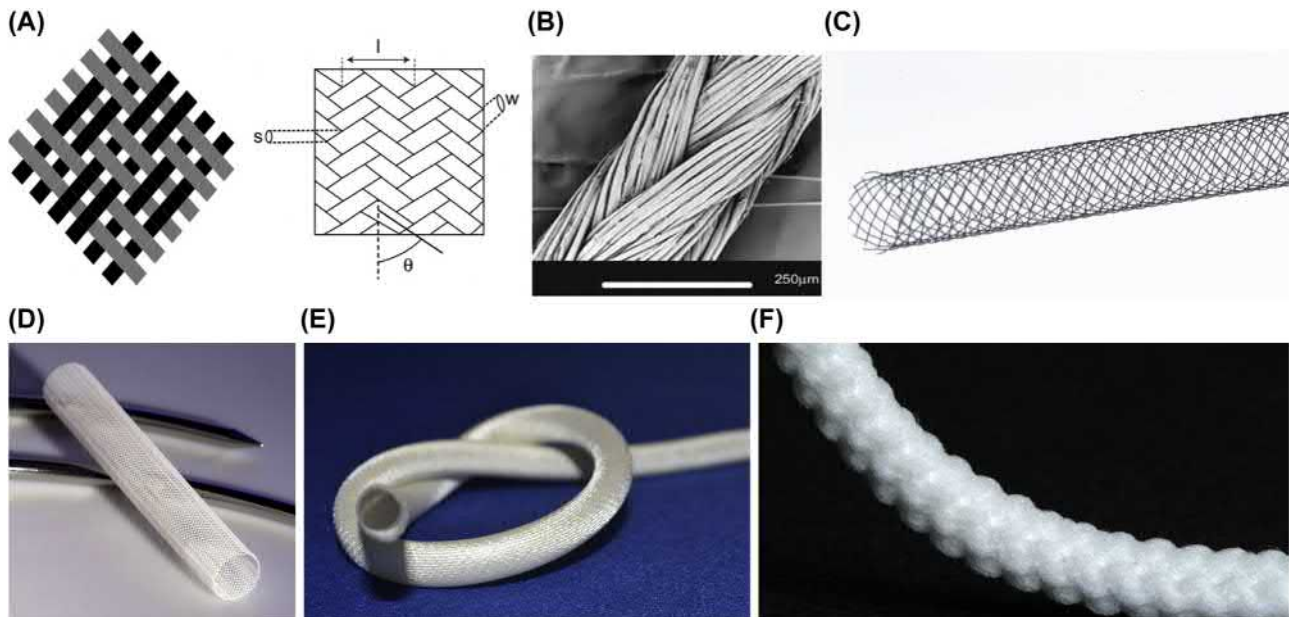
Braiding is the interweaving of three or more yarns in an angled overlapping pattern (Fig. 1.4.6.12). The structure is described by the horizontal repeat distance, called a line (l), the vertical repeat distance, called a stitch (s), the width (w) of the yarn, and the braid angle (θ) between the yarn and machine directions as seen in Fig. 1.4.6.8. Because of their inherent strength and flexibility, braided structures are the most used in surgical sutures. Advances in three-dimensional (3D) braiding have allowed for the formation of more complex structures, including “I” beams, hollow channels, and solid tubes (Chen, 2015). One application of a braided hollow tube is the vascular stent; due to the braid’s low bending rigidity and ability to radially expand, the



• **Figure 1.4.6.10** (A) Schematic diagram of knitted fabrics. (B) Closeup view of hooked loops that make up the knit structure. (C) Macro view of knit poly(ethylene-terephthalate) textile mesh. ((B and C) Courtesy of Secant Group, LLC.)



• **Figure 1.4.6.11** Scanning electron microscopy micrographs of (A) woven poly(ethylene-terephthalate) textile composed of both texturized (*center region*) and untextured (*flanking regions*) yarn, (B) woven vascular prosthesis (Cooley Verisoft) inner (*top*) and outer (*bottom*) views, and (C) warp-knitted vascular prosthesis (Dialine) inner (*left*) and outer (*right*) views. ((A) Courtesy of Secant Group, LLC. (B) Modified from Tian-Jian, R., Chin, P., Guidoin, R., Marceau, D., Roy, P.E., King, M., Xiaoping, Q., 1991. Soft filamentous woven polyester arterial prosthesis from China. *Biomaterials* 12 (3), 335–344. (C) Modified from King, M.W., Marois, Y., Guidoin, R., Ukpabi, P., Deng, X., Martin, L., Douville, Y., 1995. Evaluating the dialine® vascular prosthesis knitted from an alternative source of polyester yarns. *J. Biomed. Mater. Res.* 29 (5), 595–610.)



• **Figure 1.4.6.12** (A) Schematic diagrams of braided structures depicting the defining dimensions of the textile: stitch (s), yarn width (w), line (l), and braid angle (θ); (B) Scanning electron microscopy micrograph of a braided silk suture; (C) a braided nitinol tube with a braid structure showing that some metal fibers can be used to generate biomedical textile; (D) a braided poly(glycolic acid) fiber tube; (E) a braided poly(ethylene terephthalate) (PET) textile graft; (F) a braided PET knit fiber tube, showing a combination of textile manufacture methods that can be used to generate a biomedical device. ((C–E) Courtesy of Secant Group, LLC.)

structure is ideal for keeping arteries open and preventing clots. Another common application of braided fabrics is in anterior cruciate ligament (ACL) prostheses. ACL prostheses must exhibit sufficient mechanical strength, as the ACL is subject to myriad forces, stresses, and strains. Braided structures for this application can be designed to have pore sizes that promote tissue infiltration while still maintaining mechanical integrity. One challenge associated with braided fabrics is securing the yarn at each end of the structure. This can be addressed with finishing techniques that fuse braid ends together, or more novel approaches such as constructing the braided structure from a single wire, as has been used for an esophageal stent (Polyflex) and for thoracic aortic aneurysm repair (Murgo et al., 1998).

Textile structures may also be a combination of the three structures we have discussed thus far, allowing for more complex mechanical properties. For example, to make the PET textile shown in Fig. 1.4.6.12F, yarns were knitted together, then the knit structures were braided.

Nonwoven Textiles

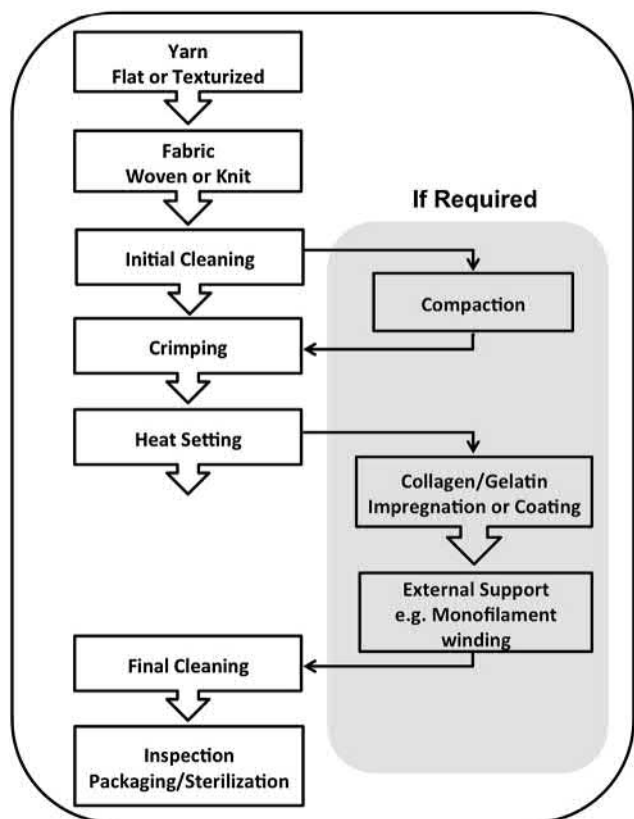
Nonwoven fabrics are produced directly from fibers or fiber fragments without the intermediate step of yarn production. Nonwovens are produced by creating a porous uniform web, often by spun-laid, wet-laid, or melt-blown processes, that is then bonded or interlocked via mechanical, thermal, chemical, or solvent means. The fibers may be randomly oriented or preferentially oriented in one or more directions, depending

on the production method. Total porosity, average pore size, and pore size distribution may be controlled by changing the density and orientation of the fibers, fiber diameter and length, and bonding method. Multiple nonwoven layers can be combined to further control the physical and mechanical properties of the textile such as permeability and strength. Nonwovens typically exhibit dimensional stability, strength, durability, and high porosity.

The properties of nonwovens are easily modified, making them highly versatile with wide-ranging applications. Nonwoven textiles are often used as bandages and wound dressings, as listed in Table 1.4.6.1, since they can be highly absorbent and gas permeable. Nonwoven wound dressings can also have release agents such as antimicrobial drugs incorporated in them for localized drug release (Giram et al., 2018). Since nonwovens can form multilayer meshes, they also work well as filters, for example, within regenerative tissue devices (Iwamoto et al., 2015) and for blood filtration (Sato et al., 2015). Nonwovens can also be implanted as tissue scaffolds for applications including nerve repair (Sarbhan et al., 2019b), intestinal prosthesis (Liu et al., 2019), tendon grafts (Sensini and Cristofolini, 2018), and osseous tissue regeneration (Krucińska et al., 2017).

Finishing and Surface Coating

After polymers have been spun into fibers and yarns, and yarns have been fashioned into textile structures, there are



• **Figure 1.4.6.13** Typical vascular graft manufacturing operations.

several processing steps that must be done before the textile is ready to be used in a medical device. Finishing operations are based on the polymer choice, the fabrication process, and the medical application. However, all finishing operations are concerned with the same properties: cytotoxicity, sterility, surface modifications, and packaging. An example of the general workflow for textile finishing for a vascular graft is diagrammed in Fig. 1.4.6.13. Each of these processes, including cleaning, heat setting, bleaching, shrinking, inspection, packaging, and sterilization, affects the textile's final properties.

Additives and solvents are often employed during various phases of the textile production process. These additions can result in cytotoxicity and other adverse events when placed in a biological environment. Many surface finishes, such as yarn lubricants, can be easily removed with cleaning and scouring techniques. Other additives such as mineral oil or silicone based require special aqueous-based or organic-based washing procedures. After wash steps, the product must be thoroughly tested to ensure there are no more harmful additives or other chemicals from the product. Finally, the product is cleaned, packaged, and sterilized. Careful packaging is necessary to protect the textile from light degradation, bacterial contamination, moisture, and oxidative stress in certain cases. Sterilization can be achieved through heat, chemical treatment, irradiation, or pressure.

There has been increasing interest in more specialized finishing that enhances the biocompatibility or functionality of the textile. For example, with any wound dressing or

implantation there is a chance of infection. Many researchers are developing antimicrobial coating agents that can be applied to textiles during production (El-Ola, 2008). Microencapsulation techniques can also be applied to medical textiles to deliver other drugs of interest through textile scaffolds or wound dressing. Other biological coatings such as collagen can be used to improve biocompatibility and promote tissue growth (Singh et al., 2015).

Applications of Medical Fibers and Biotextiles

Biotextiles of General Surgery

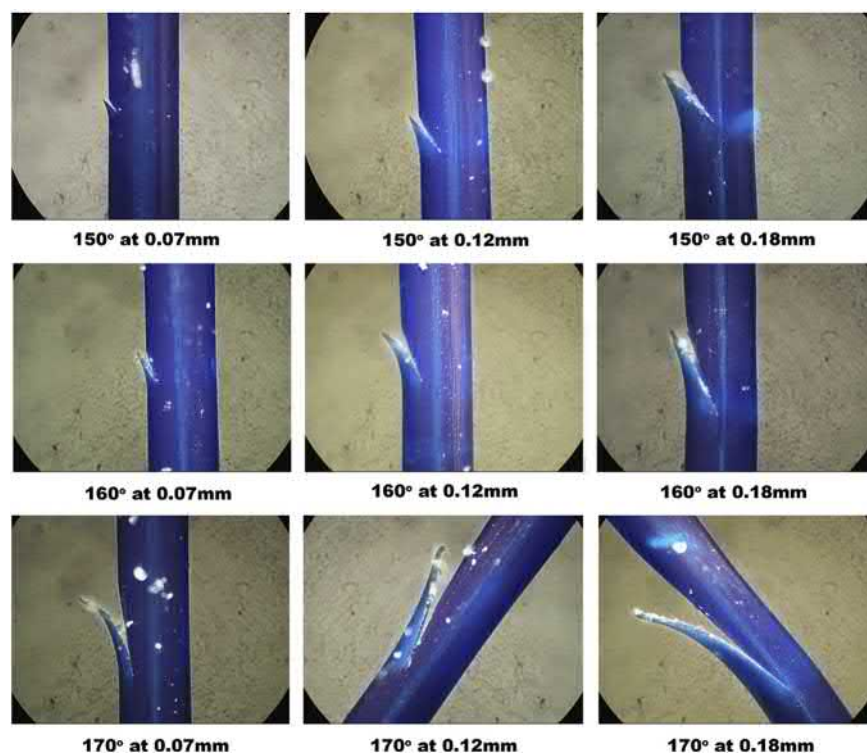
Surgical sutures and tissue repair meshes represent two of the most prominent applications of biotextiles in the general surgery field. A variety of porous mesh fabrics have been employed as a supportive material in hernia and prolapse repair, as well as in tissue patches, as listed in Table 1.4.6.1. Traditional constructions are warp knitted from polypropylene or polyester monofilaments or expanded polytetrafluoroethylene (ePTFE) membranes whose increased resistance to infection makes them preferable to multifilament yarns. More recently, 3D warp knits using polyester multifilament yarns have been found to possess increased flexibility and can be implanted endoscopically. Although the majority of these meshes are nondegradable, recent developments have included a resorbable component that allows for the promotion of a more acute inflammatory response and, ideally, faster healing.

Meshes and Sutures: Design and Materials

Sutures and meshes can be modified by a protein coating (collagen and/or gelatin) or a microporous PTFE layer applied to a single side, which reduces the risk of unwanted adhesion in vivo. As with other textile structures, specific characteristics may be engineered into the mesh to meet design goals such as added flexibility, increased strength, reduced thickness, improved handling, and a better suture-holding strength. Commercial sutures possess either a monofilament or braided multifilament structure and can be synthesized from natural materials such as silk or collagen (often referred to as “catgut,” though it is actually derived from the submucosal layer of either bovine or sheep intestine), or synthetic materials, including nylon, polyester, polypropylene, and stainless steel, as listed in Table 1.4.6.1.

Barbed and Drug-Eluting Sutures

Among the more recent innovations in surgical sutures is the development of the barbed suture (Fig. 1.4.6.14), the structure of which allows for tissue anastomosis without the need for the surgeon to tie a knot. The design concept of the barbed suture mimics the quill of a porcupine, such that angled barbs protrude from the monofilament's surface and mechanically interlock with the surrounding tissue. Advantages of these self-anchoring barbed sutures include shorter suturing time given the elimination of the



• **Figure 1.4.6.14** Single barbed suture samples with various cut angles and lengths. (Modified from Ingle, N.P., King, M.W., 2010. Optimizing the tissue anchoring performance of barbed sutures in skin and tendon tissues. *J. Biomech.* 43 (2), 302–309.)

need to tie knots, as well as a more uniform distribution of holding forces, which reduces suture slippage, tissue distortion, and necrosis, allowing for improved cosmetic outcomes. Given the previously mentioned favorable characteristics, resorbable barbed sutures are a viable clinical option for patients seeking a less invasive face-lift procedure, known as a “threadlift.” However, recent studies have shown this to be a more temporary solution with results lasting between 1 and 9 years (Wu, 2019). Additionally, Wu noted that there was an increased complication rate associated with threadlifts performed using barbed sutures versus traditional and more invasive surgical facelifts performed using nonbarbed sutures. Meanwhile, a 5-year retrospective analysis found barbed sutures to be as safe as conventional sutures for the purpose of closing the gastric pouch–jejunal anastomosis in laparoscopic gastric bypass (Pennestri et al., 2018). These findings suggest that additional work is needed to identify optimal barb dimensions, frequency, and geometry for use with different types of tissues (Ingle et al., 2010). Examples of barbed sutures currently approved by the United States Food and Drug Administration (FDA) for commercial use are included in Table 1.4.6.1.

Drug-eluting sutures represent an exciting development in the field of surgery as they simultaneously serve both a mechanical and a pharmaceutical function. The active pharmaceutical ingredient can be incorporated into the suture either during manufacturing of the suture, or after the suture has been fabricated. Current applications of this

technology include a wet-electrospun suture comprised of poly(L-lactide), polyethylene glycol, and levofloxacin as a means of providing local, postoperative delivery of antibiotics following ophthalmic procedures (Kashiwabuchi et al., 2017). Further optimization will continue to improve drug-eluting sutures, thus providing the field of surgery with encouraging prospects for decreased rates of postoperative infection.

Cardiovascular Applications of Biotextiles

Examples of biotextiles developed for cardiovascular use include heart valve sewing rings, annuloplasty rings that provide dimensional stability to incompetent cardiac heart valves, as well as vascular and endovascular stent grafts, as listed in Table 1.4.6.1. One of the most significant contributions of biotextiles to the field of cardiovascular surgery has been large (10–40 mm) diameter vascular grafts. As mentioned previously, polyester (e.g. PET) is the principal polymer used to construct vascular grafts.

Design Criteria for Vascular Prostheses

There are multiple design combinations that are possible for vascular grafts, including either a knitted or woven structure that can then be produced in a straight or bifurcated configuration. Ideally, the properties of a vascular prosthesis will meet all of the following criteria: available in different shapes and sizes, sterilizable, easy to handle and suture, cut edges that will not fray, ravel, or run,

hemostatic yet nonthrombogenic, biocompatible, low associated infection rate, capable of promoting rapid healing, dimensionally stable, and compliant (Edwards and Tapp, 1957). Although no single biomaterial has been found to meet all these requirements, textile structures designed to be flexible, porous, lightweight, and compliant are able to satisfy most of these criteria.

Woven Versus Knitted Structure

Design decisions and the goals that guide them carry significant consequences in the field of biomaterials. Woven structures can provide hemostasis and dimensional stability, whereas knitted devices are more compliant, easier to handle and suture, and promote more rapid healing. Conversely, warp knits are more dimensionally stable and do not ravel in comparison with weft knits, which are more compliant. Thus considering the key characteristics in relation to the implantation site or disease state is necessary prior to selecting the material and structure.

Examples of Cardiovascular Biotextiles

The field has a rich history of innovations that have addressed several physiological challenges, as was seen in the 1950s with Dr. Sterling Edwards' use of imparting radial folds prior to finishing, known as crimping, as a means to avoid kinking and to facilitate handling (Edwards and Tapp, 1957). Today, a substantial amount of effort is being devoted toward the development of a small vessel (<6 mm diameter) prosthesis for coronary artery bypass and tibial/popliteal artery replacement. However, high thrombogenicity, compliance mismatch of existing materials, and complications due to intimal hyperplasia have prevented the development of a successful commercial product to meet this market need. A recent study employing a cell layer-electrospun mesh composite demonstrated a construct capable of a similar J-shaped circumferential stress-strain response to that of native coronary artery, as well as an acceptable level of tensile strength. However, an extended pre-culture period and prolonged use of media additives present a significant barrier to its clinical translation (Erndt-Marino et al., 2016). In addition to the previously discussed challenges of meeting required compliance and mechanical properties, a translatable small diameter vascular graft would need its surface to be modified with an endothelial cell layer, or a specialized surface coating, growth factors, and other bioactive agents to prevent thrombosis and thromboembolic events. Thus another area of interest has been the development of biological grafts, surface-modified materials, and tissue-engineering constructs (Chung et al., 2010).

The first clinical application of an artificial vessel based on a synthetic scaffold was to reconstruct a low-pressure pulmonary outflow tract in pediatric patients with a cyanotic congenital defect (Shin'oka et al., 2005). In this approach, autologous bone marrow cells were seeded into tubes made from a copolymer of lactide and caprolactone and subsequently reinforced with a woven PGA sleeve. While the grafts were not suitable for high-pressure arterial



• **Figure 1.4.6.15** Three-dimensional computed tomography scan at 1 year after tissue-engineered vascular graft implantation (indicated by red arrows). The graft is patent and there is no aneurysmal dilation. (Modified from Hibino, N., McGillicuddy, E., Matsumura, G., Ichihara, Y., Naito, Y., Breuer, C., Shinoka, T., 2010. Late-term results of tissue-engineered vascular grafts in humans. *J. Thor. Cardiovas. Surg.* 139 (2), 431–436.)

implantation, this study demonstrated the feasibility of a tissue-engineered approach. At the most recent follow-up of a 25-patient cohort (range: 4.3–7.3 years, mean: 5.8 years), all grafts remained intact and patent (Fig. 1.4.6.15); however, there were four stenotic events and one thrombotic event that had occurred. Even though graft stenosis appeared to be the primary mode of graft failure and the mechanism of stenosis remains unclear, none of the grafts actually failed over the course of this study (Hibino et al., 2010).

Endovascular Stent Grafts

Over the past 20 years, a sizable investment of resources has been dedicated to the development of endovascular stent grafts, which have utility in minimally invasive aortic aneurysm repair, occlusive disease, and vascular trauma (Powell and Kashyap, 2016; Hinchliffe and Hopkinson, 2007). The benefits of these grafts over open surgery include decreased patient trauma, blood loss, postoperative complications, infection risk, and exposure time to anesthesia. Additionally, the costs associated with hospitalization, patient care, and the time for recovery and rehabilitation are significantly lower than for open surgery. Endovascular prostheses, or stent grafts, are tubular biotextiles with either an internal or external stent comprised of nitinol or stainless-steel wire. Given that the stent graft must be collapsed and folded onto a balloon catheter and subsequently inserted through a distal artery, the structure needs to be thin, flexible, and hemostatic. To meet these specifications, either an ePTFE

membrane or a polyester tube tightly woven from fine (45 dtex or less) untextured multifilament yarns, which allows for minimization of overall wall thickness, may be employed (Guidoin et al., 2004). However, the long-term durability and fatigue resistance of such structures require further evaluation via in vitro testing and predictive modeling.

Knitted Textile Structures as Sewing Rings

Given their high suture retention strength and ability to tolerate damage during surgery, knitted textile structures have been used as sewing rings for aortic and mitral valves. More recently, heart valve leaflets have also been fashioned from textile-based structures due to their superior flexural fatigue properties using either permanent polyester or resorbable PCL multifilament yarns (Heim et al., 2008).

Orthopedic Applications of Biotextiles

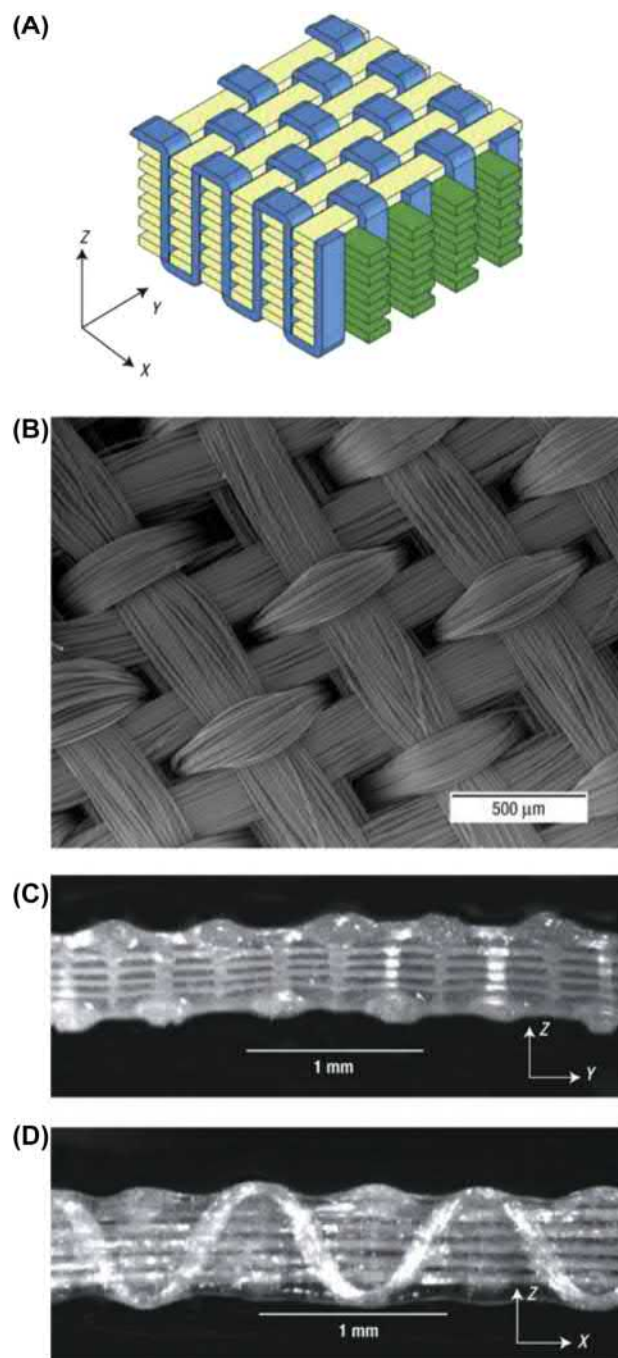
Ligament and Tendon Replacement With Woven and Braided Biotextiles

In the field of orthopedics, woven and braided textile devices have been used to construct replacement ligaments and tendons. However, issues such as abrasion and wear, inadequate strength, and poor bone attachment have been cited for premature clinical failures in ligament and tendon applications (Guidoin et al., 2000). For example, early failures in using a braided PTFE structure for ACL repair was attributed to creeping of the PTFE polymer, causing patients to experience increased knee instability over time (Roolker et al., 2000). More recently, 3D braided and woven scaffolds employing resorbable fibers spun from PGA, PLA, and their copolymers have been reported for ligament and cartilage replacement (Fig. 1.4.6.16) (Moutos et al., 2007). Although several artificial biomaterials have been brought to market to serve as ligament grafts for purposes such as repair of separated shoulder joints and ACLs, an ideal prosthesis capable of mimicking natural human tissue has yet to be found.

Another challenge for polyester implants in orthopedic surgery has been the host inflammatory response to the implanted biotextile. Coating the textile implants with antlerogenic stem cells or platelet-rich plasma (PRP) has been shown to significantly reduce inflammation and accelerate healing in a cranial cruciate ligament repair model in rabbits, leading to faster covering of the implant by host connective tissue and increased intertwinning between recipient connective tissue and polyester fiber implant, highlighting the potential benefit of combining biological components with synthetic biotextiles (Przadka et al., 2017).

Fiber Reinforcement in Bone Graft Cement

Previously, loadbearing prostheses for orthopedic applications were fabricated primarily from metals and ceramics due to their high strength and modulus. However, advances in fiber spinning technologies have allowed for



• **Figure 1.4.6.16** Fiber architecture of a three-dimensional (3D) orthogonally woven structure. (A) Schematic showing a 3D structure that is woven by interlocking multiple layers of two perpendicularly oriented sets of in-plane fibers (X- or warp direction, and Y- or weft direction) with a third set of fibers in the Z-direction; (B) Surface view of the X-Y plane (scanning electron microscope); (C) Cross-sectional view of the Y-Z plane; (D) Cross-sectional view of the X-Z plane. (Modified from Moutos, F.T., Freed, L.E., Guilak, F., 2007. A biomimetic three-dimensional woven composite scaffold for functional tissue engineering of cartilage. *Nat. Mater.* 6 (2), 162.)

the production of fibers with superior mechanical performance, including fibers comprised of ultrahigh molecular weight polyethylene, carbon, and poly(arylamide) (Kevlar). Today, these fibers are predominantly employed as a reinforced composite structure for bone graft cement as well as for spinal support devices.

Biotextiles as Wound Dressings and Skin Grafts

Wound Dressings and Hemostats

Another common application of biotextiles and fiber technology is in the synthesis of wound dressings and hemostats. Wound dressings serve primarily as a physical barrier to prevent infection and promote moisture absorption and blood coagulation, while hemostats are used clinically to stop bleeding.

Traditionally, woven cotton gauze has been used as a wound dressing due to its superior moisture absorption and blood-clotting ability. However, since it is composed of short staple fibers of cellulose, woven cotton gauze tends to adhere to the wound, consequently leading to infection and trauma upon removal. Other materials such as polyester, polypropylene, nylon, and viscose rayon, as well as the addition of antibiotics, growth factors, and a barrier layer, have been combined with absorbent cellulose as a means of fabricating a more effective wound dressing. A typical example of a layered laminate structure includes a protective outer barrier of polyester or polypropylene accompanied by an inner layer comprised of absorbent cellulose. Collagen, chitosan, and cellulose derivatives can all serve this purpose in layered fibril, foam, and powdered forms, which have hemostatic properties. Other biomaterial applications for hemostasis that have been investigated in recent years include a hydrophilic absorbent layer of poly(acrylic acid) surrounded by a flexible outer layer of electrospun ethylene-vinyl acetate (EVAc) copolymer, as well as various polysaccharide polymers, including alginate, chitosan, and dextrin (Hickman et al., 2018). Additional examples of commercial products can be found in Table 1.4.6.1.

Skin Grafting for Burn Injuries

Patients suffering from severe burn injuries or chronic diabetic ulcers require a temporary skin graft to provide protection against infection as well as maintenance of hydration prior to receiving an autologous dermal transplant. To meet this need, the first commercial skin graft product that was introduced to the market was Epicel, which is an aseptically grown wound dressing prepared from autologous keratinocytes grown *ex vivo* on a petrolatum gauze dressing in the presence of proliferation-arrested, murine fibroblasts (Wright et al., 1998). Although biocompatible, this graft consisted exclusively of biological components and consequently lacked mechanical integrity, in addition to being difficult to handle and transport. As a means of overcoming these limitations, subsequent skin graft products have been developed to incorporate both biological components, such as porcine collagen and allogenic fibroblasts, with a synthetic textile layer to provide improved mechanical stability as listed in Table 1.4.6.1.

Applications of Electrospun Fibers

Wound Dressing

Electrospun nanofiber membranes have attracted a great deal of attention as wound dressings due to their high specific

surface area, high porosity, and small-sized pores, among other characteristics. The high specific surface area enhances fluid absorption and high porosity facilitates the exchange of oxygen, water, and nutrients, as well as the removal of metabolic wastes. Additionally, the small-sized pores reduce penetration by microorganisms (Gautam et al., 2013).

Musculoskeletal Tissue Engineering

Cellular orientation and biomechanical stress on musculoskeletal tissue plays an important role in ECM deposition, neo-tissue formation, and cell phenotype maintenance. The electrospun fiber matrix can be constructed to mimic the orientation and architecture of native ECM collagen fibrils and its porous nature, and therefore suitable for muscle cell adhesion and proliferation (Abbah et al., 2015). Aligned electrospun fibers can withstand cell adhesion stress, direct cellular orientation, and maintain elasticity of the overall cell-scaffold structure. For bone reconstruction, electrospun nanofibers can be constructed to encapsulate or surface-immobilize osteo-inductive agents such as bone morphogenetic protein-2 (BMP-2) (Li et al., 2015; Perikamana et al., 2015). These functionalized nanofiber scaffolds have been shown to accelerate cranial bone regeneration by facilitating cell adhesion and growth and locally releasing osteo-inductive cues. Nanofibers also promote osteogenic differentiation and mineralization (Li et al., 2015) and guiding collagen deposition (Perikamana et al., 2015).

Neural Tissue Engineering

Electrospun fibrous scaffolds in wrap and conduit forms have been developed for neural tissue engineering due to its high porosity, small pore size, and flexibility. Alignment topography can also be incorporated inside the conduits or wraps serving as the guidance cue for Schwann cell migration and axonal re-growth. The ability to guide cell migration and maturation by aligned fibers is illustrated in a study by comparing human fetal tissue-derived Schwann cells cultured on aligned and random electrospun poly(ϵ -caprolactone) (PCL) fibers. Cell cytoskeleton and nuclei elongated along the fiber axes, emulating the structure of the bands of Büngner, which is formed during nerve repair by activated Schwann cells to guide growing axons. The aligned fibers can also condition Schwann cells into a myelinating phenotype with lowered expression of neurotrophic factors and up-regulation of an early myelination marker, myelin-associated glycoprotein. These functions may facilitate peripheral nerve regeneration. Additional functions such as local release of neurotrophic factors and immune conditioning can also be incorporated into the scaffold to promote tissue regeneration or modulating the tissue repair microenvironment. For example, nerve conduits prepared from the biodegradable poly(ϵ -caprolactone-co-ethyl ethylene phosphate) (PCLEEP) fibers with encapsulated glial cell-derived neurotrophic factor (GDNF) offer a combination of biochemical and topographical cues to facilitate peripheral nerve regeneration (Chew et al., 2008). By controlling the pore size of the electrospun fiber conduit, thus entrapping

the infiltrating macrophages, a microporous PCL nanofiber wrap creates an environment conducive to nerve repair and improves functional recovery (Sarhane et al., 2019a).

Nanofibers for Cardiovascular Repair

Electrospinning can be used to generate nanofibrous structures with various shapes and sizes to recapitulate specific architectures and functions in repairing different cardiovascular tissues, such as vascular grafts to replace blood vessels, heart valves, myocardial patches, etc. Similar to other tissue engineering applications, the multiscale topography and anisotropy, high porosity, and mechanical property make electrospun fibrous scaffolds a suitable choice (Capulli et al., 2016). Aligned fiber arrangement not only can improve the strength and elasticity of the grafts, but also can guide the organization of the endothelial cells and cardiomyocytes and the deposition of ECM molecules. Fibers with tunable degradation rates, together with the use of porogenic techniques and cell seeding methods, can be employed to facilitate cell infiltration and organization (Woods and Flanagan, 2014). Functionalization of scaffolds can be tailored for different design features of a specific product. For example, anti-thrombogenic agents can be conjugated to the surface of nanofibers to extend the patency of a small diameter vascular graft. Adhesion ligands can be conjugated to the luminal surface of the fibrous conduit to recruit endothelial cell progenitors or pre-seed autologous endothelial cells. An electrospun small-diameter vascular graft prepared with fibrin fiber tube encased in a thin sheath composed of PCL nanofiber membrane provided sufficient suture retention strength, overall mechanical property, vascular remodeling and enabled long-term graft survival (Elliott et al., 2019). The fibrin fiber tube allows successful endothelialization, remodeling of the tunica intima and media layers, abundant ECM deposition particularly collagen layers and elastin lamellae, and reduced calcification; whereas the PCL fiber sheath improves the mechanical properties that withstands the reperfusion burst pressure and maintains the integrity of the graft following implantation. Such an approach has high translational potential for generating small diameter arterial grafts for bypass surgery (Elliott et al., 2019).

Electrospun fibers prepared from elastomeric polymers such as polyurethanes (PUs) and cross-linkable polyesters have excellent elasticity, which is ideal to serve as a scaffold to generate cell populated patches to repair the myocardial tissue damaged by a heart attack. A tri-component elastomeric patch was generated from electrospun poly(carbonate-co-urethane) (PCU, Bionate®) and PLGA nanofibers using a knitted polyester fabric as a template. This approach imparted anisotropic structure to guide local cell alignment and organization, improved the overall mechanical properties of the cell-grown patch construct, and sustained the spontaneous synchronous contractility at a physiologically relevant frequency (Şenel Ayaz et al., 2014). In a different study, an elastomeric polyester poly(glycerol sebacate) (PGS) prepolymer was mixed with PCL and the mixture solution was electrospun into a nanofiber mesh with improved

mechanical properties. The PGS component allowed for direct conjugation of vascular endothelial growth factor (VEGF) to fiber surface. The functionalized nanofiber mesh permits the adhesion and proliferation of myogenic and angiogenic progenitor cells, and thus potentially improve the integration of the patch with host tissue after implantation (Rai et al., 2015). This polymer blend approach can be applied to generating fibers from a mixture solution containing synthetic and natural polymers (PGS, silk fibroin, and collagen; PFC fibers). The collagen-embedded PFC fiber mesh showed superior mechanical properties and promoted the adhesion of endothelial cells (Wang et al., 2015).

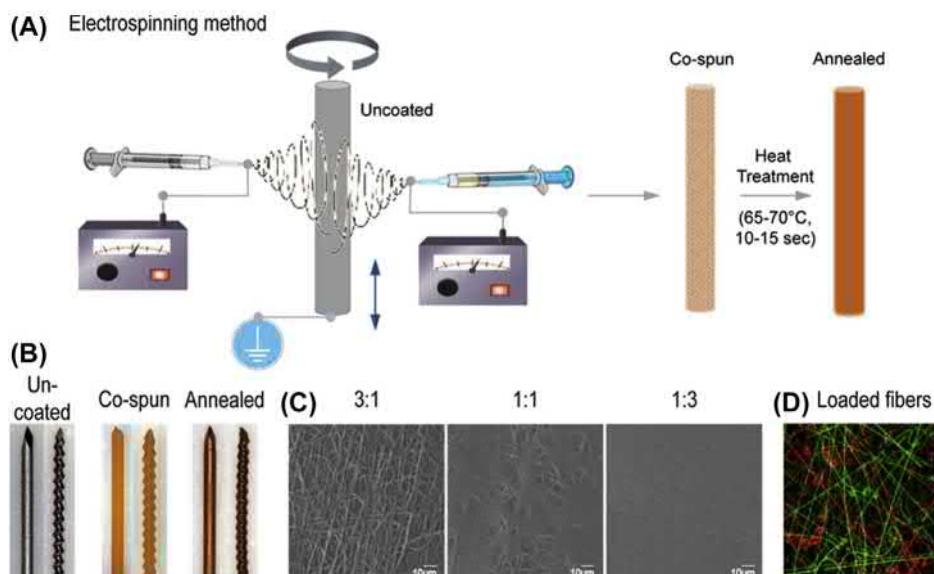
Nanofibers for Local Drug Delivery

The electrospun nanofiber structure can be used as a drug loading system to achieve controlled release of drugs locally at the site of implantation. Bioactive agents such as growth factors and cytokines can be locally delivered to influence tissue regeneration, angiogenesis, and inflammation. A wide range of bioactive agents and drugs can be loaded into the nanofibers during the electrospinning process if the agents can be dissolved or suspended in the polymer solution, or conjugated to the surface of the nanofibers through either chemical linkage or physical entrapment. Since multiple sets of fibers can be used to generate a single fibrous mesh or membrane, codelivery of multiple agents can be achieved by incorporating different drugs in different set of fibers. The release rate of each agent in one set of fibers can be independently tuned by varying the polymer-drug combination, independent of other fibers in the same fibrous mesh. This delivery feature can also be achieved by incorporating different drug-loaded nanoparticles into one set of electrospun fibers or loading different drugs into the inner or outer layer of a composite fibers with a core-shell structure through the co-axial spinning technique.

Such an approach has been applied to generate an electrospun fiber-based coating on an orthopedic prosthetic device to prevent biofilm-associated chronic infections particularly in cases involving antibiotic-resistant bacteria. A composite fiber membrane prepared from PLGA and PCL nanofibers, each loaded with a different antibiotic during electrospinning, was shown to effectively co-deliver a combination of antibiotics locally from the implant surface. The relative antibiotic release rate and duration can be adjusted by tuning drug loading and weight ratio of PLGA and PCL fibers. As tested in a mouse model for prosthetic joint infection, this conformal nanofiber coating effectively cleared bacterial infection from the implant surface and surrounding tissue without affecting osseointegration (Fig. 1.4.6.17) (Ashbaugh et al., 2016). This tunable nanofiber composite membrane or coating can be extended to other types of devices for a range of therapeutic applications.

Future Directions

The future of biotextiles development is driven by the clinical need for less-invasive and resorbable materials that do



• **Figure 1.4.6.17** Poly(lactide-co-glycolide) (PLGA)/poly(ϵ -caprolactone) (PCL) composite implant coating loaded with combinatorial antibiotics. (A) Antibiotic-loaded PLGA and PCL fibers are coelectrospun onto titanium implants to form a conformal PCL film with embedded PLGA fibers. (B) Micrographs of implants before (left) and after electrospinning (middle) and annealing of Van/Rif composite coating (right). (C) SEM images of coating surfaces with varying PLGA:PCL ratios. (D) Fluorescent micrograph of two PLGA fiber coatings (red and green fibers) embedded in PCL films. (Modified from Ashbaugh, A.G., Jiang, X., Zheng, J., Tsai, A.S., Kim, W.S., Thompson, J.M., Ordonez, A.A., 2016. Polymeric nanofiber coating with tunable combinatorial antibiotic delivery prevents biofilm-associated infection in vivo. *Proc. Nat. Acad. Sci. USA* 113 (45), E6919–E6928.)

not require explantation, as well as the emphasis on regenerative features of implanted materials to promote natural growth of viable tissue. As biotextiles are developed to become thinner, lighter, stronger, and more tunable in terms of flexibility, porosity, and functionalization, they are showing their versatility over traditional materials such as metals and ceramics. Current work is moving from permanent materials to not only resorbable materials, but also functional bioresorbable materials (Gajjar and King, 2014). The development of smart devices that rely on shape-memory, electroactivity, and self-healing properties that can respond to environmental changes in temperature, pH, and strain can serve as more than just scaffolding for biomedical applications (Lendlein and Langer, 2002). These smart devices such as biosensors, actuators, and drug delivery systems offer new ways for responsive biomaterials to improve therapeutic potential. Bioactive fiber coatings with slow release of antibacterial agents are being used to address infections resulting from implantation surgeries (Ashbaugh et al., 2016). Bioactive sutures have been developed for drug delivery, growth factor delivery, and cell delivery through surface modification and coating techniques (Alshomer et al., 2017). The growth of these new biotextiles also introduces new challenges in extrusion and sterilization practices while maintaining key functionality and structural integrity.

Prevalence in 3D printing technologies has enabled the generation of unique architectures using computer-aided designs. While these are primarily limited to microextrusion

of polymer materials, progress in this area has expanded the range of temperatures and fiber diameters to better mimic the microstructure of biological tissue (Pedde et al., 2017).

New spinning techniques and improvements in electrospinning, bicomponent spinning, and materials improvements have also expanded the range of fiber diameters ranging from sub-50 nm to 10 μ m, while also introducing new cross-sectional geometries. These enhancements facilitate the development of new therapeutic strategies as the effects of microenvironment architecture and cellular biomechanics are better understood. Moreover, new techniques to manipulate biotextiles, such as flocking, tufting, and embroidery, can create complex 3D structures (Pereira et al., 2007; Rentsch et al., 2009; Walther et al., 2007; Wollenweber et al., 2006). Additionally, techniques to improve foaming in electrospun fibers can further introduce new mechanical properties and increase porosity in these biotextile materials. These technologies contribute to the development of thicker tissue-engineered scaffolds to improve cell migration and tissue regeneration throughout the construct. As such, biotextiles and fiber-based tissue-engineering scaffolds will soon be considered as standardized “off-the-shelf” products that can be scaled up to be fabricated in large quantities for commercialization to meet growing clinical demand. The use of medical fibers and biotextiles in medicine will continue to grow as new synthetic polymers and genetically engineered biopolymers, fiber spinning technologies, 3D constructions, coatings, and surface modification processes are developed.

References

- Abbah, S.A., Delgado, L.M., Azeem, A., Fuller, K., Shologu, N., Keeney, M., Biggs, M.J., Pandit, A., Zeugolis, D.I., 2015. Harnessing hierarchical nano- and micro-fabrication technologies for musculoskeletal tissue engineering. *Adv. Healthc. Mater.* 4 (16), 2488–2499. <https://doi.org/10.1002/adhm.201500004>.
- Alshomer, F., Madhavan, A., Omar, P., Song, W., 2017. Bioactive sutures: a review of advances in surgical suture functionalisation. *Curr. Med. Chem.* 24 (2), 215–223.
- ASTM International, ASTM D123-19: Standard terminology relating to textiles. West Conshohocken, PA: American Society for Testing and Materials, 2019. www.astm.org. <https://doi.org/10.1520/D0123-19>.
- Ashbaugh, A.G., et al., 2016. Polymeric nanofiber coating with tunable combinatorial antibiotic delivery prevents biofilm-associated infection in vivo. *Proc. Natl. Acad. Sci. USA* 113 (45) E6919–E6928.
- Barreto-Ortiz, Sebastian, F., et al., 2013. A novel in vitro model for microvasculature reveals regulation of circumferential ECM organization by curvature. *PLoS One* 8 (11), e81061. <https://doi.org/10.1371/journal.pone.0081061>.
- Barreto-Ortiz, Sebastian, F., et al., 2015. Fabrication of 3-dimensional multicellular microvascular structures. *FASEB J.* 29 (8), 3302–3314. <https://doi.org/10.1096/fj.14-263343>.
- Benton, J.A., DeForest, C.A., Vivekanandan, V., Anseth, K.S., 2009. Photocrosslinking of gelatin macromers to synthesize porous hydrogels that promote valvular interstitial cell function. *Tissue Eng. A* 15, 3221–3230.
- Bhardwaj, N., Kundu, S.C., 2010. Electrospinning: a fascinating fiber fabrication technique. *Biotechnol. Adv.* 28, 325–347.
- Capulli, A.K., MacQueen, L.A., Sheehy, S.P., Parker, K.K., 2016. Fibrous scaffolds for building hearts and heart parts. *Adv. Drug. Deliv. Rev.* 96, 83–102. <https://doi.org/10.1016/j.addr.2015.11.020>.
- Chen, X., 2015. *Advances in 3D Textiles*. Woodhead Publishing Limited, in association with the Textile Institute.
- Chew, S.Y., Mi, R., Hoke, A., Leong, K.W., 2008. The effect of the alignment of electrospun fibrous scaffolds on Schwann cell maturation. *Biomaterials* 29 (6), 653–661.
- Chong, E.J., et al., 2007. Evaluation of electrospun PCL/gelatin nanofibrous scaffold for wound healing and layered dermal reconstruction. *Acta Biomater.* 3, 321–330.
- Chua, K.-N., et al., 2006. Surface-aminated electrospun nanofibers enhance adhesion and expansion of human umbilical cord blood hematopoietic stem/progenitor cells. *Biomaterials* 27 (36), 6043–6051.
- Chua, K.-N., et al., 2007. Functional nanofiber scaffolds with different spacers modulate adhesion and expansion of cryopreserved umbilical cord blood hematopoietic stem/progenitor cells. *Exp. Hematol.* 35 (5), 771–781.
- Chung, S., et al., 2010. Bioresorbable elastomeric vascular tissue engineering scaffolds via melt spinning and electrospinning. *Acta Biomater.* 6 (6), 1958–1967.
- Das, H., et al., 2009. Ex vivo nanofiber expansion and genetic modification of human cord blood-derived progenitor/stem cells enhances vasculogenesis. *Cell Transplant.* 18 (3), 305–318.
- Doshi, J., Reneker, D.H., 1995. Electrospinning process and applications of electrospun fibers. *J. Electrostat.* 35 (2–3), 151–160.
- Edmondson, D., et al., 2012. Centrifugal electrospinning of highly aligned polymer nanofibers over a large area. *J. Mater. Chem.* 22, 18646–18652.
- Edwards, W.S., Tapp, J.S., 1957. Two and a half years experience with crimped nylon grafts. *Am. Soc. Artif. Intern. Organs J.* 3 (1), 70–72.
- Elliott, M.B., Ginn, B., Fukunishi, T., Bedja, D., Suresh, A., Chen, T., Inoue, T., Dietz, H.C., Santhanam, L., Mao, H.Q., Hibino, N., Gerecht, S., 2019. Regenerative and durable small-diameter graft as an arterial conduit. *Proc. Natl. Acad. Sci. U S A.* 116 (26), 12710–12719. <https://doi.org/10.1073/pnas.1905966116>.
- El-Ola, S.M.A., 2008. Recent developments in finishing of synthetic fibers for medical applications. *Des. Monomers Polym.* 11 (6), 483–533. <https://doi.org/10.1163/156855508X363816>.
- Erndt-Marino, J.D., et al., 2016. Cell layer-electrospun mesh composites for coronary artery bypass grafts. *J. Biomed. Mater. Res. A* 104 (9), 2200–2209.
- Fages, J., et al., 1998. Use of supercritical fluid extraction as a method of cleaning anterior cruciate ligament prostheses: in vitro and in vivo validation. *Am. Soc. Artif. Intern. Organs J.* 44 (4), 278–288.
- Fashandi, H., Karimi, M., 2012. Pore formation in polystyrene fiber by superimposing temperature and relative humidity of electrospinning atmosphere. *Polymer* 53, 5832–5849.
- Formica, F.A., et al., 2016. “A bioinspired ultraporous nanofiber-hydrogel mimic of the cartilage extracellular matrix. *Adv. Healthc. Mater.* 5, 3129–3138.
- Frenot, A., Chronakis, I.S., 2003. Polymer nanofibers assembled by electrospinning. *Curr. Opin. Colloid Interface Sci.* 8 (1), 64–75. <https://www.sciencedirect.com/science/article/pii/S1359029403000049>.
- Gajjar, C.R., King, M.W., 2014. *Resorbable Fiber-Forming Polymers for Biotextile Applications*. Springer.
- Gautam, S., Dinda, A.K., Mishra, N.C., 2013. Fabrication and characterization of PCL/gelatin composite nanofibrous scaffold for tissue engineering applications by electrospinning method. *Mater. Sci. Eng. C* 33 (3), 1228–1235.
- Ghorani, B., Tucker, N., 2015. Fundamentals of electrospinning as a novel delivery vehicle for bioactive compounds in food nanotechnology. *Food Hydrocolloids* 51, 227–240.
- Gilbert-Honick, J., Ginn, B., et al., 2018a. Adipose-derived stem/stromal cells on electrospun fibrin microfiber bundles enable moderate muscle reconstruction in a volumetric muscle loss model. *Cell Transplant.* 27 (11). <https://doi.org/10.1177/0963689718805370> <https://www.ncbi.nlm.nih.gov/pubmed/30298751>.
- Gilbert-Honick, J., Iyer, S.R., et al., 2018b. Engineering functional and histological regeneration of vascularized skeletal muscle. *Biomaterials*. 164, 70–79. <http://www.sciencedirect.com/science/article/pii/S0142961218300826>.
- Giram, P.S., et al., 2018. Fast dissolving moxifloxacin hydrochloride antibiotic drug from electrospun eudragit L-100 nonwoven nanofibrous mats. *Mater. Sci. Eng. C* 92, 526–539. <https://doi.org/10.1016/j.msec.2018.06.031>.
- Guidoin, M.F., et al., 2000. Analysis of retrieved polymer fiber based replacements for the ACL. *Biomaterials* 21 (23), 2461–2474.
- Guidoin, R., et al., 2004. Biocompatibility studies of the anaconda stent-graft and observations of nitinol corrosion resistance. *J. Endovasc. Ther. Off. J. Internat. Soc. Endovas. Sp.* 11 (4), 385–403.
- Heim, F., Bernard, D., Chakfe, N., 2008. Textile heartvalve prosthesis: manufacturing process and prototype performances. *Text. Res. J.* 78 (12), 1124–1131. <https://doi.org/10.1177/0040517508092007>.
- Hennink, W.E., van Nostrum, C.F., 2012. Novel crosslinking methods to design hydrogels. *Adv. Drug Deliv. Rev.* 64, 223–236.

- Hibino, N., et al., 2010. Late-term results of tissue-engineered vascular grafts in humans. *J. Thorac. Cardiovasc. Surg.* 139 (2) 6, 436.e1-2.
- Hickman, D.A., et al., 2018. Biomaterials and advanced technologies for hemostatic management of bleeding. *Adv. Mater.* 30 (4). <https://doi.org/10.1002/adhm.201500004>.
- Hinchliffe, R.J., Hopkinson, B.R., 2007. Development of endovascular stent-grafts. *Proc. Inst. Mech. Eng. H* 221 (6), 547–560.
- Hsieh, A., et al., 2010. Hydrogel/electrospun fiber composites influence neural stem/progenitor cell fate. *Soft Matter* 6, 2227–2237.
- Hudecki, A., et al., 2017. Structure and properties of slow-resorbing nanofibers obtained by (Co-axial) electrospinning as tissue scaffolds in regenerative medicine. *PeerJ* 5, e4125.
- Ingle, N.P., King, M.W., Zikry, M.A., 2010. Finite element analysis of barbed sutures in skin and tendon tissues. *J. Biomech.* 43 (5), 879–886.
- Iwamoto, U., et al., 2015. A novel cell-containing device for regenerative medicine: biodegradable nonwoven filters with peripheral blood cells promote wound healing. *J. Artif. Organs.* 18 (4), 315–321. <https://doi.org/10.1007/s10047-015-0845-x>.
- Jiang, H., et al., 2005. A facile technique to prepare biodegradable coaxial electrospun nanofibers for controlled release of bioactive agents. *J. Control. Release* 108, 237–243.
- Kai, D., Liow, S.S., Loh, X.J., 2014. Biodegradable polymers for electrospinning: towards biomedical applications. *Mater. Sci. Eng. C.* 45, 659–670. <https://www.sciencedirect.com/science/article/pii/S0928493114002434>.
- Kashiwabuchi, F., et al., 2017. Development of absorbable, antibiotic-eluting sutures for ophthalmic surgery. *Transl. Vis. Sci. Technol.* 6 (1), 1.
- King, M.W., 1991. Designing fabrics for blood vessel replacement. *Can. Text. J.* 108 (4), 24–30.
- Knaul, J.Z., Hudson, S.M., Creber, K.A.M., 1999. Improved mechanical properties of chitosan fibers. *J. Appl. Polym. Sci.* 72 (13), 1721–1732. [https://doi.org/10.1002/\(SICI\)1097-4628\(19990624\)72:13%3C1721::AID-APP8%3E3.0.CO](https://doi.org/10.1002/(SICI)1097-4628(19990624)72:13%3C1721::AID-APP8%3E3.0.CO).
- Krucińska, I., et al., 2017. Biological properties of low-toxicity PLGA and PLGA/PHB fibrous nanocomposite implants for osseous tissue regeneration. Part I: evaluation of potential biotoxicity. *Molecules.* 22 (12), 2092. <http://www.ncbi.nlm.nih.gov/pubmed/29186078>.
- Lai, J.-Y., 2014. Interrelationship between cross-linking structure, molecular stability, and cytocompatibility of amniotic membranes cross-linked with glutaraldehyde of varying concentrations. *RSC Adv.* 4, 18871–18880.
- Lendlein, A., Langer, R., 2002. Biodegradable, elastic shape-memory polymers for potential biomedical applications. *Science* 296 (5573), 1673–1676.
- Li, D., Xia, Y., 2004. Electrospinning of nanofibers: reinventing the wheel? *Adv. Mater.* 16, 1151–1170.
- Li, L., Zhou, G., Wang, Y., Yang, G., Ding, S., Zhou, S., 2015. Controlled dual delivery of BMP-2 and dexamethasone by nanoparticle-embedded electrospun nanofibers for the efficient repair of critical-sized rat calvarial defect. *Biomaterials.* 37, 218–229. <https://doi.org/10.1016/j.biomaterials.2014.10.015>.
- Lim, S.H., Mao, H.-Q., 2009. Electrospun scaffolds for stem cell engineering. *Adv. Drug Deliv. Rev.* 61 (12), 1084–1096.
- Liu, Y., et al., 2019. Comparison of polyglycolic acid, Polycaprolactone, and collagen as scaffolds for the production of tissue engineered intestine. *J. Biomed. Mater. Res. B Appl. Biomater.* 107 (3), 750–760.
- Luo, Y., et al., 2015. Enhanced proliferation and osteogenic differentiation of mesenchymal stem cells on graphene oxide-incorporated electrospun poly (lactic-Co-glycolic acid) nanofibrous mats. *ACS Appl. Mater. Interfaces* 7 (11), 6331–6339.
- Mao, H.-Q., et al., 2010. The nanofiber matrix as an artificial stem cell niche. In: *Biomaterials as Stem Cell Niche*. Springer, pp. 89–118.
- Mather, R.R., Wardman, R.H., 2011. *The Chemistry of Textile Fibres*. The Royal Society of Chemistry.
- Mehta, P., et al., 2019. Broad scale and structure fabrication of healthcare materials for drug and emerging therapies via electrohydrodynamic techniques. *Adv. Ther.* 2 (4), 1800024.
- Moutos, F.T., Freed, L.E., Guilak, F., 2007. A biomimetic three-dimensional woven composite scaffold for functional tissue engineering of cartilage. *Nat. Mater.* 6 (2), 162–167.
- Murgo, S., et al., 1998. 21 Cardiovasc Intervent Radiol Penetrating Atherosclerotic Ulcer of the Descending Thoracic Aorta: Treatment by Endovascular Stent-Graft.
- Pedde, R.D., et al., 2017. Emerging biofabrication strategies for engineering complex tissue constructs. *Adv. Mater.* 29 (19), 1606061. <https://doi.org/10.1002/adma.201606061>.
- Pennestri, F., et al., 2019. Barbed vs conventional sutures in bariatric surgery: a propensity score analysis from a high-volume center. *Updates Surg.* 71 (1), 113–120.
- Pereira, S., Anand, S.C., Rajendran, S., Wood, C., 2007. A study of the structure and properties of novel fabrics for knee braces. *J. Ind. Text.* 36 (4), 279–300. <https://doi.org/10.1177/1528083707072357>.
- Perikamana, S.K., Lee, J., Ahmad, T., Jeong, Y., Kim, D.G., Kim, K., Shin, H., 2015. Effects of Immobilized BMP-2 and nanofiber morphology on in vitro osteogenic differentiation of hMSCs and in vivo collagen assembly of regenerated bone. *ACS Appl. Mater. Interfaces.* 7 (16), 8798–8808. <https://doi.org/10.1021/acsami.5b01340>.
- Przadka, P., et al., 2017. Reconstruction of cranial cruciate ligament in rabbits using polyester implants saturated with PRP, anterogonic stem cells MIC-1 and their homogenate. *Connect. Tissue Res.* 58 (5), 464–478.
- Qian, Y., et al., 2018. Biomimetic domain-active electrospun scaffolds facilitating bone regeneration synergistically with antibacterial efficacy for bone defects. *ACS Appl. Mater. Interfaces* 10, 3248–3259.
- Rai, R., Tallawi, M., Frati, C., Falco, A., Gervasi, A., Quaini, F., Roether, J.A., Hochburger, T., Schubert, D.W., Seik, L., Barbani, N., Lazzeri, L., Rosellini, E., Boccaccini, A.R., 2015. Bioactive electrospun fibers of poly(glycerol sebacate) and poly(ϵ -caprolactone) for cardiac patch application. *Adv. Healthc. Mater.* 4 (13), 2012–2025. <https://doi.org/10.1002/adhm.201500154>.
- Razal, J.M., et al., 2009. Wet-spun biodegradable fibers on conducting platforms: novel architectures for muscle regeneration. *Adv. Funct. Mater.* 19 (21), 3381–3388. <https://doi.org/10.1002/adfm.200900464>.
- Reddy, N., Reddy, R., Jiang, Q., 2015. Crosslinking biopolymers for biomedical applications. *Trends Biotechnol.* 33, 362–369.
- Reinbold, J., et al., 2017. Preventing surgical site infections using a natural, biodegradable, antibacterial coating on surgical sutures. *Molecules.* 22 (9), 1570. <http://www.mdpi.com/1420-3049/22/9/1570>.
- Rentsch, B., et al., 2009. Embroidered and surface modified Polycaprolactone-Co-lactide scaffolds as bone substitute: in vitro characterization. *Ann. Biomed. Eng.* 37 (10), 2118–2128. <https://doi.org/10.1007/s10439-009-9731-0>.
- Roolker, W., et al., 2000. The Gore-tex prosthetic ligament as a salvage procedure in deficient knees. *Knee Surg. Sports Traumatol. Arthrosc.* 8 (1), 20–25.

- Şenel Ayaz, H.G., Perets, A., Ayaz, H., Gilroy, K.D., Govindaraj, M., Brookstein, D., Lelkes, P.I., 2014. Textile-templated electrospun anisotropic scaffolds for regenerative cardiac tissue engineering. *Biomaterials*. 35 (30), 8540–8552. <https://doi.org/10.1016/j.biomaterials.2014.06.029>.
- Sarhane, K.A., Tuffaha, S.H., et al., 2019a. Glial cell line-derived neurotrophic factor and chondroitinase promote axonal regeneration in a chronic denervation animal model. *Neurotherapeutics* 1–13. <https://doi.org/10.1007/s13311-019-00745-0>.
- Sarhane, K.A., Ibrahim, Z., et al., 2019b. Macroporous nanofiber wraps promote axonal regeneration and functional recovery in nerve repair by limiting fibrosis. *Acta Biomater.* 88, 332–345. <https://doi.org/10.1016/j.actbio.2019.02.034>.
- Sato, N., et al., 2015. Cord blood processing by a novel filtration system. *Cell Prolif.* 48 (6), 671–681.
- Sensini, A., Cristofolini, L., 2018. Biofabrication of electrospun scaffolds for the regeneration of tendons and ligaments. *Materials* 11 (10), 1963.
- Shin'oka, T., et al., 2005. Midterm clinical result of tissue-engineered vascular autografts seeded with autologous bone marrow cells. *J. Thorac. Cardiovasc. Surg.* 129 (6), 1330–1338.
- Sill, T.J., von Recum, H.A., 2008. Electrospinning: applications in drug delivery and tissue engineering. *Biomaterials* 29, 1989–2006.
- Singh, C., Wong, C.S., Wang, X., Russell, S.J., 2015. Functional biomaterials medical textiles as vascular implants and their success to mimic natural arteries. *J. Funct. Biomater.* 6, 500–525.
- Sionkowska, A., 2011. Current research on the blends of natural and synthetic polymers as new biomaterials: review. *Prog. Polym. Sci.* 36 (9), 1254–1276.
- Sun, X., et al., 2017. Electrospun photocrosslinkable hydrogel fibrous scaffolds for rapid in vivo vascularized skin flap regeneration. *Adv. Funct. Mater.* 27 (2), 1604617.
- Sun, Z., et al., 2003. Compound core-shell polymer nanofibers by Co-electrospinning. *Adv. Mater.* 15, 1929–1932.
- Tucker, N., et al., 2012. The history of the science and technology of electrospinning from 1600 to 1995. *J. Eng. Fiber. Fabr.* 7 155892501200702S10.
- De Vrieze, S., et al., 2009. The effect of temperature and humidity on electrospinning. *J. Mater. Sci.* 44, 1357.
- Walther, A., et al., 2007. Development of novel scaffolds for tissue engineering by flock technology. *Text. Res. J.* 77 (11), 892–899. <https://doi.org/10.1177/0040517507081283>.
- Wang, R., et al., 2015. Novel nanofiber-based material for endovascular scaffolds. *J. Biomed. Mater. Res. A* 103 (3), 1150–1158.
- Weldon, C.B., et al., 2012. Electrospun drug-eluting sutures for local anesthesia. *J. Control. Release* 161, 903–909.
- Woods, I., Flanagan, T.C., 2014. Electrospinning of biomimetic scaffolds for tissue-engineered vascular grafts: threading the path. *Expert. Rev. Cardiovasc. Ther.* 12 (7), 815–832. <https://doi.org/10.1586/14779072.2014.925397>.
- Wollenweber, M., et al., 2006. Mimicked bioartificial matrix containing chondroitin sulphate on a textile scaffold of poly(3-hydroxybutyrate) alters the differentiation of adult human mesenchymal stem cells. *Tissue Eng.* 12 (2), 345–359. <https://doi.org/10.1089/ten.2006.12.345>.
- Wright, K.A., et al., 1998. Alternative delivery of keratinocytes using a polyurethane membrane and the implications for its use in the treatment of full-thickness burn injury. *Burns* 24 (1), 7–17.
- Wu, W.T.L., 2019. Commentary on: effectiveness, longevity, and complications of facelift by barbed suture insertion. *Aesthet. Surg. J.* 39 (3), 248–253.
- Yang, G., et al., 2018. From nano to micro to macro: electrospun hierarchically structured polymeric fibers for biomedical applications. *Prog. Polym. Sci.* 81, 80–113.
- Yarin, A.L., 2011. Coaxial electrospinning and emulsion electrospinning of core-shell fibers. *Polym. Adv. Technol.* 22, 310–317.
- Yee, W.A., et al., 2008. Stress-induced structural changes in electrospun polyvinylidene difluoride nanofibers collected using a modified rotating disk. *Polymer* 49, 4196–4203.
- Zhang, S., et al., 2014. Creating polymer hydrogel microfibrils with internal alignment via electrical and mechanical stretching. *Biomaterials* 35 (10), 3243–3251.
- Zhang, Y., et al., 2005. Electrospinning of gelatin fibers and gelatin/PCL composite fibrous scaffolds. *J. Biomed. Mater. Res. B Appl. Biomater.* 72, 156–165.
- Zussman, E., et al., 2006. Electrospun polyaniline/poly (methyl methacrylate)-derived turbostratic carbon micro-/nanotubes. *Adv. Mater.* 18, 348–353.

Chapter Study Questions

1. What are the general selection criteria for polymeric materials for medical fiber production?
2. Describe the main advantages and disadvantages of synthetic and natural materials as a source for producing medical fibers.
3. Give three examples each of synthetic and natural polymers and list examples of biotextile products generated from each polymer.
4. Name one clinical challenge that biotextiles have provided a solution for, and explain what specific structural features and properties are critical to accomplishing the particular tasks or serving the unique functions.
5. Consider a fiber that is 2 m long and weighs 3 g.
 - a. If the fiber is a monofilament fiber, what is the linear density of the fiber in denier and dtex?
 - b. If the fiber is a multifilament yarn made with 60 filaments, what is the linear density of each fiber in denier and dtex?
 - c. Contrast the advantages and disadvantages of monofilaments and multifilament fibers.
6. Assume that you are given a 260-denier monofilament PET yarn to prepare a vascular graft.
 - a. What is the diameter of the yarn used for this graft?
 - b. What are the advantages and disadvantages for each of the following structures for this vascular graft: woven, knit, and braided textiles?
 - c. Pick one of the three structures and describe how you could improve upon the disadvantages, which you have described, by altering the textile or yarn properties.
7. Pick a natural polymer, for example, from this list: chitosan, collagen, gelatin, alginate, and hyaluronic acid. Research and briefly describe its endogenous bioactivities and its functions in a current or potential biotextile. What properties of the biopolymer made it ideal for this application? What are the potential disadvantages of the biopolymer in this application?
8. The concept of combining naturally occurring biologic elements with artificially manufactured biotextiles has been observed with multiple products discussed in this chapter, including hybrid textiles intended for use as small vessel stent grafts and stem cell-coated polyester implants for orthopedic surgery. What are some of the advantages of products that combine textiles with biologic elements? What are some potential shortcomings of a hybrid textile compared with either the textile or biologic element alone?
9. Consider the process of producing electrospun polymer nanofibers.
 - a. Describe the basic principle of electrospinning for preparing polymeric nanofiber mesh; use a sketch or schematic to aid your description.
 - b. Explain how polymer solution properties and electrical potential applied may influence the fiber diameter.
 - c. Discuss approaches to control fiber alignment. Give two examples each for electrospun fiber products with either ordered or random alignment.
 - d. Propose one method each for encapsulating a hydrophobic drug (e.g., vancomycin) and a water-soluble drug (e.g., bone morphogenetic protein-2) into electrospun fibers.

1.4.7

Textured and Porous Biomaterials

W. BENTON SWANSON, PETER X. MA

Department of Biologic and Materials Science, School of Dentistry, University of Michigan, Ann Arbor, MI, United States

Introduction

Porous and textured biomaterial features have played an important role in the success of a myriad biomedical applications. Both the short- and long-term utility of biomaterials in medicine relies on their ability to interface with the body and deliver functionality without causing harmful complications. Biomaterial properties, including texture and porosity, are not only advantageous but necessary to facilitate successful biologic integration and influence cell adhesion, infiltration, proliferation, and nutrient and waste mass transfer. The culmination of favorable cellular responses at the tissue–material interface leads to organogenesis and accelerated healing. Biomaterial architectures at various size scales are key engineering and design considerations which require innovative fabrication strategies to impart favorable biologic compatibility to material constructs without compromising mechanical and other properties in application-specific uses.

In the past three decades there have been explosive advances and interest in porous and textured biomaterials due to new fabrication methods, particularly due to advances in the field of tissue engineering (Ma, 2008; Langer and Vacanti, 1993). As early as the 1940s, textured and porous features of successful medical devices serve as early examples of tissue engineering-like approaches to biomaterials fabrication. Biomaterial surfaces serve as critical interfaces between host and implant to coordinate many biologic processes. As demonstrated in recent literature and commercial medical products (Fig. 1.4.7.1), there is a strong appreciation for biomaterial architectural features, including surface texture and porosity, as advantageous design criteria. Hence, reliable and tunable fabrication methods are critical to the advancement of biomaterials science. Not intended to exhaustively review all textured and porous biomaterials, this chapter will focus on synthetic biomaterials and their tunable nano-, micro-, and macroscale architectures covering the following areas: (1) porous and textured synthetic matrices currently used in medical devices, (2) a comparison of the breadth of fabrication methods for biomimetic features to achieve

desirable properties, and (3) a discussion of novel processing technologies and recent advances in combining multiple fabrication technologies, with more examples from recent advances such as in tissue engineering applications.

Importance of Texture and Porosity in Facilitating Biomaterial Integration

Historically, materials with textured and porous morphologies have higher success rates than smooth constructs. The extent of a construct's success is heavily related to its ability to facilitate tissue ingrowth, prevent fibrosis, and promote angiogenesis of surrounding tissue. Of these three, tissue ingrowth—physical integration of the material into the host—is the most important. A host's natural response is to encapsulate an implant with a fibrous capsule to compartmentalize it from the rest of the body, which is minimized by textured implants and open pore architectures, leading to the formation of a thinner foreign-body capsule (Salzmann et al., 1997). Numerous materials can be textured or rendered porous, including metals, ceramics, and natural and synthetic polymers. We will discuss specific examples of successful biomedical devices and their material features.

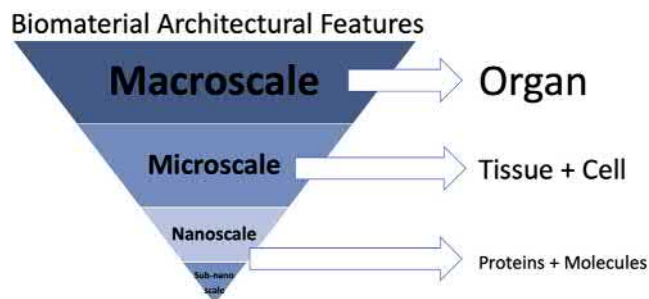
Textured Devices Promote Healing and Restore Organ Function

Dental implants, made of titanium and metal alloys as well as soft material constructs, benefit from textured surfaces. Their success in restoring normal mastication is directly related to their ability to integrate with craniofacial bone through the process of osseointegration. Branemark et al. defined osseointegration as the direct structural and functional connection between ordered living bone and the surface of a load-bearing implanted construct (Branemark, 1983). Mechanical interlocking between a synthetic prosthesis (titanium dental implant) and the living bone is critically important and can be facilitated by intentional surface texture (Esposito et al., 2005). This idea launched the

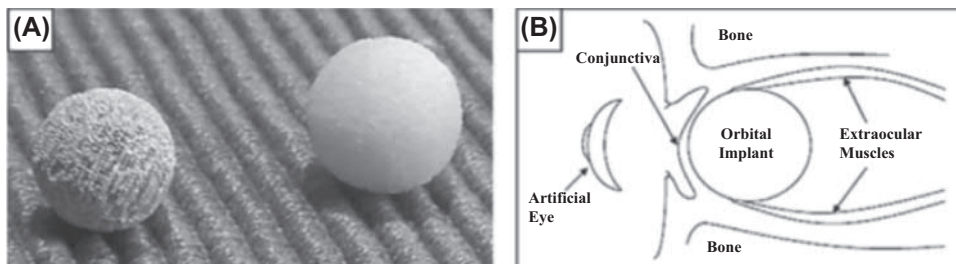
development of surface-modified implants to increase the osteoinductive potential of their surfaces (Dohan Ehrenfest et al., 2010). Macrotopography of implants can be designed in a variety of ways, strategically interfacing with local neotissue to facilitate implant integration. Additional visible geometries such as ledges, flutes, indentations, and grooves influence integration and are shown to increase implant stability and long-term success. These morphologies are primarily created by milling processes (Buser et al., 2012).

Microscale structures may also enhance the process of bone healing. Increased surface roughness has been shown to increase success by influencing cell and tissue integration. It also enhances interfacial and shear strength, important for dental implants to withstand the forces of the oral cavity over time (Strietzel et al., 2004; Wennerberg and Albrektsson, 2000). Increasing the surface area of the implant, through texture and roughness, allows greater space for cells to attach and facilitate tissue neogenesis around the implant. Microscale structures are influenced by techniques including acid etching, anodization, sandblasting, and grit blasting to mechanically impart features (Dohan Ehrenfest et al., 2010). More recently, laser micromachining has been used to modify dental implant surfaces (Nevins et al., 2010). Buser et al. evaluated the outcomes of 511 sandblasted, large grit, acid-etched dental implants (Straumann) in 303 patients over 10 years, and reported a success rate of 97%, with 98.8% of implants surviving 10 years without complication. For patients, advances in dental implant design allow for more rapid loading and return to normal lifestyle.

Breast augmentation surgeries are one of the most common cosmetic surgical procedures in the United States (Benediktsson and Perbeck, 2006; Gampper et al., 2007);



• **Figure 1.4.7.1** Biomaterial architectural scales at multiple levels are important considerations for developing fabrication methods.



• **Figure 1.4.7.2** Examples of porous hydroxyapatite (A, left) and polyethylene (A, right) orbital implants; sagittal view of human orbit showing placement of orbital implants in the eye socket (B).

15%–25% of breast implant procedures are complicated by fibrous capsular contraction and result in long-term contracture, due to the body's natural response to *any* foreign object (Taraballi et al., 2018). Fibrous capsule contracts in the months following implantation leading to patient discomfort and disfigurement, and ultimately implant failure. Implant surface texture (smooth vs. textured) is known to be a key factor influencing success (Howard, 1999; Burkhardt, 1984; Burkhardt et al., 1986).

Orbital implants (Fig. 1.4.7.2) compensate for lost tissue when the eye is enucleated due to severe trauma, intraocular cancer, or removal of a blind and painful eye (Chalasan et al., 2007; Sami et al., 2007). Key engineering considerations include fit, motility, and minimized long-term complications such as extrusion, migration, and infection (Goldberg et al., 1994). A variety of materials, including glasses, silicones, and acrylics, have been used in orbital implants; recently, porous materials such as hydroxyapatite (HAP) and polyethylene (PE) have shown increasing popularity. Their textured structure roughly resembles native surrounding trabecular bone, and thus encourages fibrovascularization of the implant within a few weeks compared to implants with smooth surfaces (Chalasan et al., 2007; Sami et al., 2007). These advantages influence patient outcomes by increasing healing rate and decreasing infection, leading to therapeutic success in compensating for lost tissue.

The cellular mechanisms of texture are not completely understood. Evidence suggests that texturing influences collagen arrangement of the surrounding extracellular matrix. Irregularly arranged collagen fibers at the textured surface may be less likely to create cooperative contractile forces and are more susceptible to collagenase degradation (Pennisi, 1990). Textured implants also show increased local macrophage number, which may degrade the capsule as it forms (Taylor and Gibbons, 1983). Additionally, texture minimizes micromotion and reduces chronic inflammation. In the case of breast implants, factors including the type of texturing, pore size, or implant material do not appear to be as important as simply disrupting surface smoothness (Caffee, 1994; Danino et al., 2001).

Porosity to Promote Tissue Ingrowth

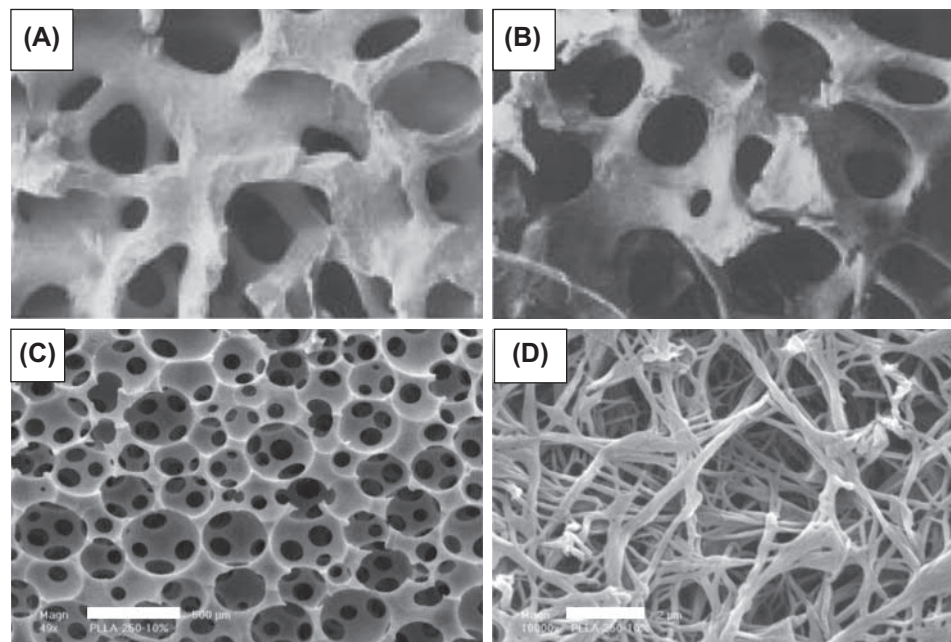
Synthetic vascular grafts used to repair damaged or occluded blood vessels are a good example of necessary

pores in biomaterial constructs. Pores are critical to support mass transport for cells and tissues and facilitate integration, both of which contribute to accelerated healing. In general, porous architectures must be sufficiently large to facilitate cell and tissue infiltration, while small enough to prevent fibrotic tissue formation and minimize interfacial cell necrosis from mechanical shear forces (Sharkawy et al., 1998; Rosengren et al., 1999). For vascular grafts, porosity helps to facilitate the formation of a stable, endothelium-lined lumen to provide an antithrombotic surface similar to native vessels (Wesolowski et al., 1961; White et al., 1983; Clowes et al., 1986; Zhu et al., 2009; Ma et al., 2010). Numerous studies demonstrate that highly porous small-diameter grafts have superior healing and long-term success compared to low-porosity grafts (Hess et al., 1984; Golden et al., 1990). Porosity allows for the ingrowth of fibrovascular tissue and infiltrating capillaries, which facilitate endothelialization and smooth muscle cell growth along the graft surface.

Macro- and microscale pores imparted to biomaterial constructs are similar to the porous organization of many physiologic tissues, such as bone (Fig. 1.4.7.3). Trabecular and cortical bone are both porous, up to 50%–90% and 3%–12%, respectively. In cortical bone, Haversian canals allow for fluid flow, which supports metabolism; pores in trabecular bone support the bone marrow that contains stem cells (Cooper et al., 2004; Lanyon and Baggott, 1976). Materials used to restore orthopedic function must be osteoconductive and capable of vascularization (Stevens,

2008; Gupte et al., 2018). Porous metals are one example of orthopedic implants, which allow bone healing and high osseointegration, similar to the dental implants mentioned earlier (Matassi et al., 2013). Highly porous metals can be fabricated from many elements, including tantalum, titanium, titanium alloy, and other alloys. Baril et al. quantified tissue response to porous metal orthopedic implants by microcomputed tomography and hard tissue histology techniques, and demonstrated that interconnected pores at the implant surface significantly improve osseointegration (Baril et al., 2011).

Critical to the success of these implants and a common theme in many implants, tissue ingrowth around and within the construct increases the likelihood of integration and long-term success and minimizes the risks of rejection. Advances in titanium porous foam manufacturing show mechanical properties similar to cancellous bone (Matassi et al., 2013). A variety of manufacturing technologies exist that allow for controlled porosity, including solid free-form machining, molding, stereolithography, laser machining, and sintering (Lewallen et al., 2015). These material modifications have a dramatic effect on clinical outcome by facilitating cell and tissue ingrowth (osseointegration) and bone formation (osteinduction), particularly in hip and knee arthroplasty (replacement) procedures (Hanzlik et al., 2013). A challenge with porous metallic foams, such as those used in orthopedic applications, is their mechanical properties, since increasing the amount of void space within the construct decreases its stiffness and fatigue strength.



• **Figure 1.4.7.3** Porous structure and composition of coralline hydroxyapatite (A), human cancellous bone (B), and macroporous, nanofibrous PLLA scaffolds fabricated by pore leaching and TIPS demonstrate well-interconnected, spherical pores (C, scale=500 μm) with a nanofibrous surface texture (D, scale=2 μm). PLLA, Poly(L-lactic acid); TIPS, thermally induced phase separation. (Modified from Wei, G.B., Ma, P. X., 2006. Macroporous and nanofibrous polymer scaffolds and polymer/bone-like apatite composite scaffolds generated by sugar spheres. *J. Biomed. Mater. Res. A* 78A (2), 306–315.)

Biomaterials for Tissue Engineering

Considering these examples of textured and porous synthetic materials in biomedical applications, it is important for engineers to develop a toolkit of fabrication strategies to achieve desirable nano-, micro-, and macrolevel material features. In the context of tissue engineering, there is no single ideal construct; scaffolds are typically designed for specific applications. Important factors in tissue-engineering scaffold design include the selection of a biodegradable and biocompatible polymer that degrades at a rate that matches tissue neogenesis, architectural features and mechanical properties specific to the target tissue that it aims to replace, with a surface that facilitates adhesion, proliferation, and differentiation of cells, and a network for nutrient exchange and diffusion (Zhang et al., 2016b). Texture and porosity address the latter needs. Advances in materials processing strategies, which allow for controlled design at the nanometer and micrometer scales, are reviewed in the following sections.

Fabrication Methods for Biomimetic Nanoscale Texture

The purpose of a tissue-engineering scaffold is to serve as an artificial extracellular matrix (ECM), which spatially supports cells, facilitates cell adhesion, provides topological cues and mechanical support (Boyan et al., 1999; Ito, 1999). Thus it is reasonable to fabricate a tissue-engineering scaffold that mimics the fibrous proteins in the ECM found in nearly all tissue types. Collagen is the most abundant extracellular protein in the human body, with a triple helix macrostructure and sub-micrometer fiber diameter (50–500 nm) (Hay, 1991; Elsdale and Bard, 1972). Collagen is a natural polymer and can be used as a scaffolding material, but significantly lacks processing control particularly in regards to mechanical properties, degradation rate, batch-to-batch consistencies, and pathogenicity (Ma and Zhang, 1999). Synthetic polymers lend themselves to the highest degree of processability and tunability (Ma and Elisseff, 2005). Poly(L-lactic acid) (PLLA) and poly(lactic-co-glycolic acid) (PLGA) are poly(aliphatic esters) and are the most commonly used biodegradable polymers because they degrade on a biologically relevant timescale, and are approved for biomedical use by the US Food and Drug Administration (Bergsma et al., 1995; Ma and Choi, 2001; Peter et al., 1998). A list of the most common biodegradable synthetic polymers is shown in Table 1.4.7.1. Electrospinning, self-assembly, and thermally induced phase separation are well-exploited processing technologies for achieving an ECM-like nanoarchitecture and surface texture in synthetic biomaterials, each with unique properties and applications, as summarized in Table 1.4.7.2.

Electrospinning

Electrospinning originates from the textile industry as a method of generating fibers using an electric field (Morton,

1900; Anton, 1934). Electrospinning imposes a difference in electrical charge between a needle and substrate to draw fine fibers from a polymer solution droplet. Electrodes between the polymer-charged needle and substrate create an electric potential, and the resulting electric field ejects a jet of polymer. The volatile organic solvent that dissolved the polymer evaporates to leave behind a polymeric nanofibrous or microfibrinous mesh (Fig. 1.4.7.4). Current advances in electrospinning technology are working toward thinner fiber diameters, most similar to the native ECM (Liu et al., 2017).

Electrospinning has proven effective for making fibers with a variety of natural and synthetic biodegradable polymers, including collagen (Matthews et al., 2002), chitosan (Bhattacharai et al., 2005), silk (Min et al., 2004), poly(glycolic acid) (Boland et al., 2001), PLLA (Yang et al., 2005), PLGA (Li et al., 2002; Kim et al., 2003), and poly(caprolactone) (Yoshimoto et al., 2003), as well as nonbiodegradable polymers (Kenawy et al., 2003; Smith and Ma, 2004). Cells are able to survive, proliferate, and differentiate to a variety of functional phenotypes on electrospun nanofibrous or microfibrinous materials (Li et al., 2003; Pham et al., 2006a,b). Electrospun nanofibrous matrices are easy to fabricate into two-dimensional (2D) sheets and meshes; however, three-dimensional (3D) constructs are difficult. It is hard to fabricate complex scaffold shapes, a critical criterion for fabricating biologically relevant tissue-engineering scaffolds. Additionally, it is difficult to incorporate an internal porous network. Construct porosity is intimately connected to nanofiber properties; in certain size ranges, it is hard to independently control fiber size and pore size/shape (Table 1.4.7.3).

Self-Assembly of Nanoscale Features

Broadly, self-assembly is defined as the autonomous organization of components into patterns or structures without intervention (Whitesides and Grzybowski, 2002). Specific to nanofiber engineering it is the rational design and chemical modification of synthetic polymers to organize into ECM-like structures. Noncovalent macromolecular bonding dictates multidimensional structures, including: hydrogen bonding, van der Waals forces, hydrophobic interactions, and electrostatic interactions (Lehn, 2002a,b). Self-assembly is advantageous for engineering very small diameter fibers (<100 nm) by exploiting ratios of copolymer section lengths with different properties. The result is self-aggregation of a 3D structure, which mimics the ECM-protein triple helix on a smaller scale (Ramachandran, 1988). Biology offers countless examples of self-assembly; this technology draws from the self-assembling nature of proteins into secondary and tertiary structures, and phospholipid macrostructures (Whitesides et al., 1991).

Synthetic peptide amphiphiles have been synthesized to mimic the ECM-protein triple helix, with a short peptide head sequence connected to a long lipid chain tail. Their

TABLE
1.4.71

Classes of Biomaterials and Methods to Render Texture in Medical Devices and Tissue-Engineering Applications

Class	Material Specific Examples	Methods to Render Texture	Advantages	Disadvantages
Synthetic polymers (Karageorgiou and Kaplan, 2005; Simske et al., 1997; Ryan et al., 2006)	<p>In order of decreasing degradation rate:</p> <ul style="list-style-type: none"> • Poly(glycolide) (Reed/Gilding, Polymer, 1981; Ma/Langer, Mat. Res. Soc., 1995) • Poly(lactide-s-glycolide) (Pitt/Langer, Biodegradable Polymers as Drug Delivery System, 1990) • Poly(lactide) (Eling, Polymer, 1982; Zhang/Ma, J. Biomed. Mater. Res., 1999) • Poly(dioxanone) (Barrow, Clin. Mater., 1986; Barber, Orthopaedic Special Edition, 1998) • Poly(trimethylene carbonate) (Barrow, Clin. Mater., 1986; Barber, Orthopaedic Special Edition, 1998) • Poly(caprolactone) (Pitt, Biomaterials, 1981) <p>Additional examples:</p> <ul style="list-style-type: none"> • Poly(ethylene glycol) • Poly(vinyl alcohol) • Poly(ethylene terephthalate) • Poly(urethane) (Lin, J. Biomed. Mater. Res., 1994) • Poly(phosphoesters) (Wang, JACS, 2001) • Poly(phosphazenes) (Caliceti, Int. J. Pharm., 2000; Aldini, J. Orthopaedic Res 2001) • Poly(anhydride) (Leong, Biomaterials, 1986) • Poly(orthoesters)/poly(orthocarbonates) (Choi, Patent 4,093,709 1978) • Poly(glycerol sebacate) (Loh, J. Mat. Chem. B, 2015). 	Discussed in detail, Tables 1.4.7.2 and 1.4.7.3	<ul style="list-style-type: none"> • Can be made to mimic natural extracellular matrix • Tunable degradation kinetics • Tunable processing lends itself to rational design • Recent facile processing technologies • Feasible to produce on large scale • Nonimmunogenic • Support cellular proliferation, migration, differentiation 	<ul style="list-style-type: none"> • No biologic specificity • Lack direct functionality
Natural polymers (Karageorgiou and Kaplan, 2005; Haarer, 2008; Ott et al., 2008)	<ul style="list-style-type: none"> • Collagen • Hyaluronic acid • Silk fibroin • Gelatin (Choi, J. Biomed. Mater. Res., 1999) • Alginate (Shapiro, Biomaterials, 1997) • Chitosan (Madhally, Biomaterials, 1999) • Decellularized extracellular matrix (Steve Badylak, Probst, BJU Int., 2000; Ott/Matthiesen, Nat. Med., 2008; Guyette, Circulation Res., 2015; Gershlak, Biomaterials, 2017) 		<ul style="list-style-type: none"> • Can be made to mimic natural extracellular matrix • Biodegradable • Amicable for biofunctionalization • Support cellular proliferation, migration, differentiation 	<ul style="list-style-type: none"> • Lack mechanical strength • Rapid degradation rates • Immunogenic and rejection potential • Degradation not tunable • Difficult processing • High cost
Composite materials	<ul style="list-style-type: none"> • Hydroxyapatite-coated poly(L-lactic acid) (Liu/Ma, Ann. Biomed. Eng., 2004; Wei/Ma, Biomaterials, 2004; Du, J. Biomed. Mater. Res., 1999) 	<ul style="list-style-type: none"> • Porosity from synthetic component 	<ul style="list-style-type: none"> • Combine biomimetic/osteoconductive ceramic properties and processability of synthetic polymers 	<ul style="list-style-type: none"> • Complex fabrication protocols

(Continued)

TABLE
1.4.71

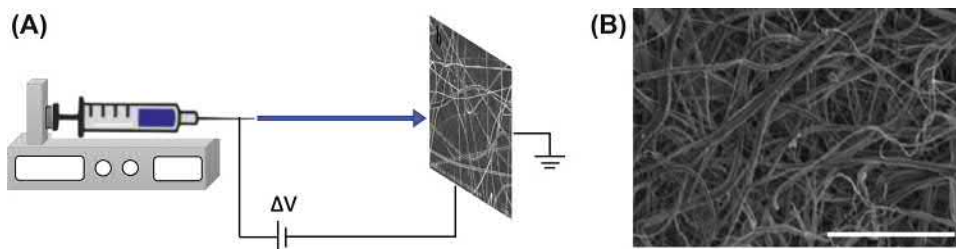
Classes of Biomaterials and Methods to Render Texture in Medical Devices and Tissue-Engineering Applications—cont'd

Material		Methods to Render Texture	Advantages	Disadvantages
Class	Specific Examples			
Ceramics (Sun et al., 2001; Karageorgiou and Kaplan, 2005; Simske et al., 1997)	<ul style="list-style-type: none"> • Hydroxyapatite • Natural coral • Calcium phosphate • Amorphous glasses 	<ul style="list-style-type: none"> • Plasma spray • Sintering 	<ul style="list-style-type: none"> • Similar compositions and structure to natural bone • Enhanced osseointegration and osteoconductivity using apatite-like materials • Biocompatible • Low corrosion • Bind some growth factors (i.e., BMP, LeGeros, Clin. Orthop. Rel. Res., 2002) 	<ul style="list-style-type: none"> • Low resorption rate • Brittle mechanical properties • Difficult to control porosity • Not amenable to large-scale production • Lack biodegradability (Maquet/Jerome, Mater. Sci. Forum, 1997)
Metals (Sun et al., 2001; Karageorgiou and Kaplan, 2005; Simske et al., 1997; Ryan et al., 2006; Bobyn et al., 1999)	<ul style="list-style-type: none"> • Titanium and Ti alloys • Cobalt-chromium and Co-Cr alloys • Tantalum 	<ul style="list-style-type: none"> • Plasma spray • Sintering • Grit blast • Wire mesh • Combustion synthesis • Vapor deposition 	<ul style="list-style-type: none"> • Bioinert • Strong mechanical properties, less susceptible to fatigue • Ideal for implants 	<ul style="list-style-type: none"> • Corrode over time • Stress shielding in vivo from high Young's modulus • Lack biodegradability (Maquet/Jerome, Mater. Sci. Forum, 1997)

TABLE
1.4.7.2

Fabrication Methods for Nanofibrous and Textured Synthetic Polymer Matrices

Method	Description	Advantages	Disadvantages
Electrospinning	Electrostatic force is used to draw a polymer solution into fibers through a capillary	<ul style="list-style-type: none"> • Reproducible • Applicable to wide range of polymers • Easily fabricates 2D constructs 	<ul style="list-style-type: none"> • Equipment investment required • Fiber diameter is larger than Type I collagen • Difficult to create 3D construct
Self-assembly	Polymer is designed to autonomously organize into cylindrical fibers based on noncovalent interactions	<ul style="list-style-type: none"> • Biomimetic fiber structure • Tunable fiber structure based on polymer composition 	<ul style="list-style-type: none"> • Polymer synthesis is labor intensive • Fiber diameter is smaller than Type I collagen • Not scalable
Thermally induced phase Separation	Decreasing system temperature of a polymer solution causes a polymer to phase separate from its solvent resulting in a nanofibrous polymer matrix	<ul style="list-style-type: none"> • Fiber diameters are most similar to Type I collagen (native extracellular matrix) • Scalable • Minimal equipment investment • Applicable to both 2D and 3D fabrication 	<ul style="list-style-type: none"> • Requires careful solvent choice (gelation temperature is critical parameter) • Requires certain degree of polymer crystallinity



• **Figure 1.4.7.4** Schematic of electrospinning equipment used to create large-diameter nanofibers. A polymer solution is drawn into fibers when an electric potential is applied between the syringe needle and a substrate (A); the resulting nanofibers have average diameters on the micron scale (B, scale=20 μm). (Adapted from 2014. RSC Adv. 4, 13652–13661.)

morphologies are governed by changes in pH and solution activity, which modulate electrostatic forces. While these supramolecular fibers are shown to support cellular activity, they do not have the same bulk structure as ECM proteins (Fields et al., 1998; Yu et al., 1999). Hartgerink et al. used this strategy to fabricate peptide amphiphile nanofibrous cylindrical micelles. These nanofibers are, on average, 5–8 nm in diameter and about 1 μm in length (Hartgerink et al., 2002). Others have formed biomimetic beta-sheet structures with two distinct surfaces—polar and nonpolar—by self-assembly of ionic self-complementary oligopeptides. Upon exposure to alkaline cations, these sheets self-assemble to a nanofibrous hydrogel, which facilitates neuronal cell attachment and differentiation (Holmes et al., 2000). Similarly, multidomain synthetic peptides have been shown to self-assemble into nanofibrous hydrogels and elicit favorable cell responses toward angiogenesis and neurogenesis (Moore et al., 2018). Scientifically, self-assembled nanofibers are interesting. Complicated chemical syntheses and potentially high cost can achieve lowest end diameters of synthetic polymer nanofibers. These self-assembly techniques are largely used to make hydrogel matrices.

Thermally Induced Phase Separation

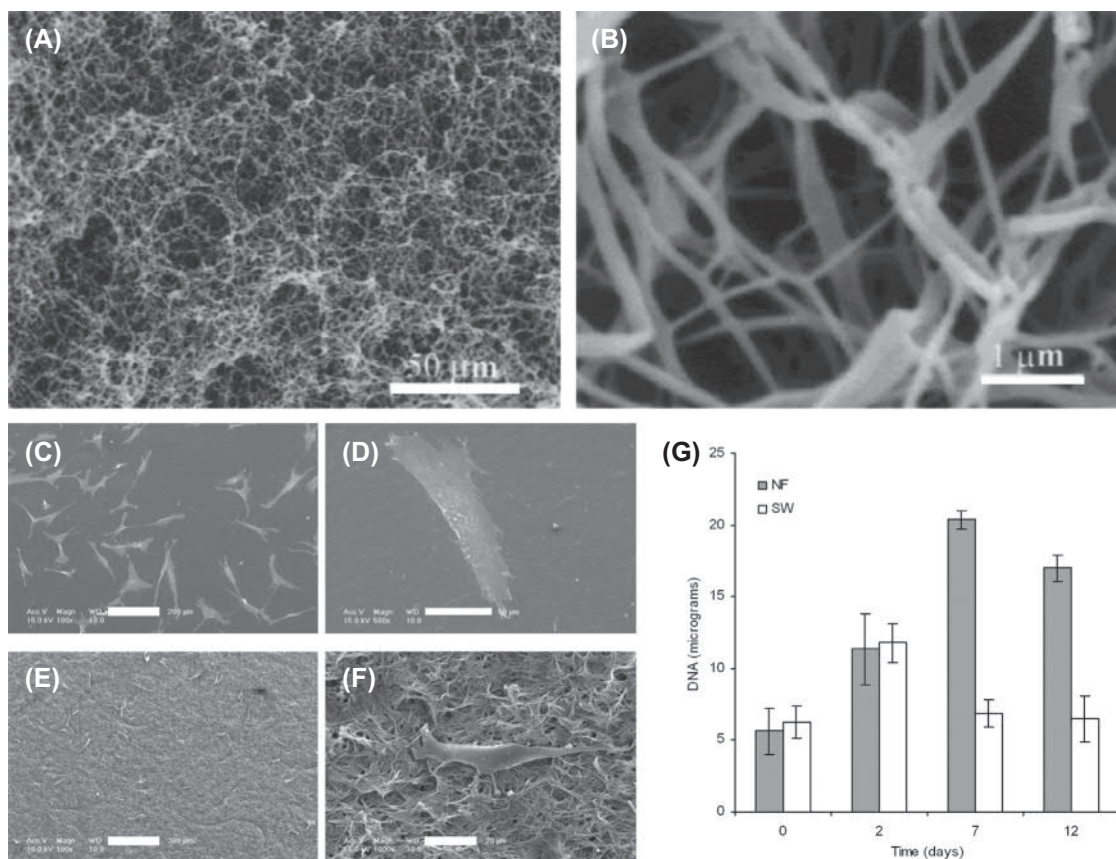
Thermally induced phase separation (TIPS) requires minimal equipment and achieves fiber diameters most similar to the native ECM. Phase separation occurs when a multicomponent system becomes thermodynamically unstable under certain conditions and separates into a multiphase system to lower its free energy (Ma et al., 2016). Originally used in the preparation of porous polymer membranes, it has since been used to fabricate porous tissue-engineering scaffolds (Zhang and Ma, 1999b) with ECM-mimicking architecture (Zhang and Ma, 2000; Peter and Ma, 1998; Wei and Ma, 2004).

In this scaffold fabrication technique, thermally induced phase separation is utilized to fabricate the nanofibrous scaffolds through the following five steps: (1) polymer dissolution in an organic solvent, typically tetrahydrofuran (THF) but other solvents are reported (Zhang and Ma, 2000), (2) phase separation and gelation induced by low temperature, (3) solvent extraction, (4) freezing, and (5) freeze drying under vacuum (Wang et al., 2007). The critical gelation step separates the solution into polymer-rich and polymer-lean phases, which control the morphology of the resulting

TABLE 1.4.7.3 Methods for Fabricating Porous Synthetic Polymer Scaffolds for Tissue-Engineering Applications

Method	Description	Advantages	Disadvantages
Porogen leaching ^a (Mikos et al., 1994)	Polymer solution is cast in preformed porogen template; porogen leaching results in 3D macropores	<ul style="list-style-type: none"> • Depends on porogen choice • Possible to have large amount of control over pore size, shape, and interconnectivity • Open pore architecture 	<ul style="list-style-type: none"> • Porogen and polymer solvent compatibilities are a key parameter
	Salt leaching	<ul style="list-style-type: none"> • Easily leached by water 	<ul style="list-style-type: none"> • Nonspherical • Low degree of connectivity
	Paraffin leaching	<ul style="list-style-type: none"> • Spherical pores of well-controlled size • High interconnectivity and tunable degree of interconnectivity 	<ul style="list-style-type: none"> • Requires organic solvents to leach paraffin • Residual paraffin is cytotoxic
	Sugar leaching	<ul style="list-style-type: none"> • Spherical pores of well-controlled size • High interconnectivity and tunable degree of interconnectivity • Easily leached with water 	
Phase Separation (Ma and Zhang, 1998)	Gelation of crystalline material induced by low temperature, below a critical gelation temperature. After solvent evaporation, nanofibrous matrices remain.	<ul style="list-style-type: none"> • Good mechanical properties • Oriented structures are possible (Ko and Ma, 2012; Zhang and Ma, 1999a,b) 	<ul style="list-style-type: none"> • Lacks control over pore shape or interconnectivity
3D printing ^a (Sachs et al., 1992; Wu et al., 1996; Yang et al., 2001; Chen et al., 2006b)	Computer-aided design and manufacturing used to fabricate a porous scaffold by direct printing of polymer or to print a scaffold mold by reverse solid freeform fabrication	<ul style="list-style-type: none"> • Reproducible • Macroarchitecture and 3D shape are tunable to fit anatomy, can be patient specific 	<ul style="list-style-type: none"> • Limited resolution for nanoscale features • Choice of material is limited
Fiber Bonding (Mikos et al., 1993)	Physical bonding of nonwoven polymer fibers to create an interconnecting mesh	<ul style="list-style-type: none"> • Large surface area 	<ul style="list-style-type: none"> • Lacks mechanical strength • Difficult to control porosity, no control over shape
Emulsion freeze drying (Whang et al., 1995)	Polymer solution is homogenized with water, quenched, and freeze dried	<ul style="list-style-type: none"> • Open pore architecture • Aqueous phase can be used to incorporate bioactive molecules 	<ul style="list-style-type: none"> • Difficult to control internal morphology—pore size, shape, and interconnectivity
Self-assembly (Nie et al., 2017)	Self-assembly of graphene oxide produces macrostructure based on electronic aggregation	<ul style="list-style-type: none"> • Allows for integration of functional moieties for improved biointegration (i.e., osteoconductive) 	<ul style="list-style-type: none"> • Synthetically involved compared to other methods
Sintering (Borden/Laurencin J. Biomed. Mater. Res., 2002)	Thermal annealing of microspheres creates an internal 3D interconnected porous network	<ul style="list-style-type: none"> • Pore interconnectivity is controlled 	<ul style="list-style-type: none"> • Difficult to control pore shape
Gas foaming ^a (Mooney 1996)	High-pressure gas dissolved to supersaturation in polymer solution to create pores	<ul style="list-style-type: none"> • Fast processing • No organic solvents required 	<ul style="list-style-type: none"> • Lacks control over pore shape • Pores are not interconnected (closed pore architecture)

^aDiscussed in this chapter.



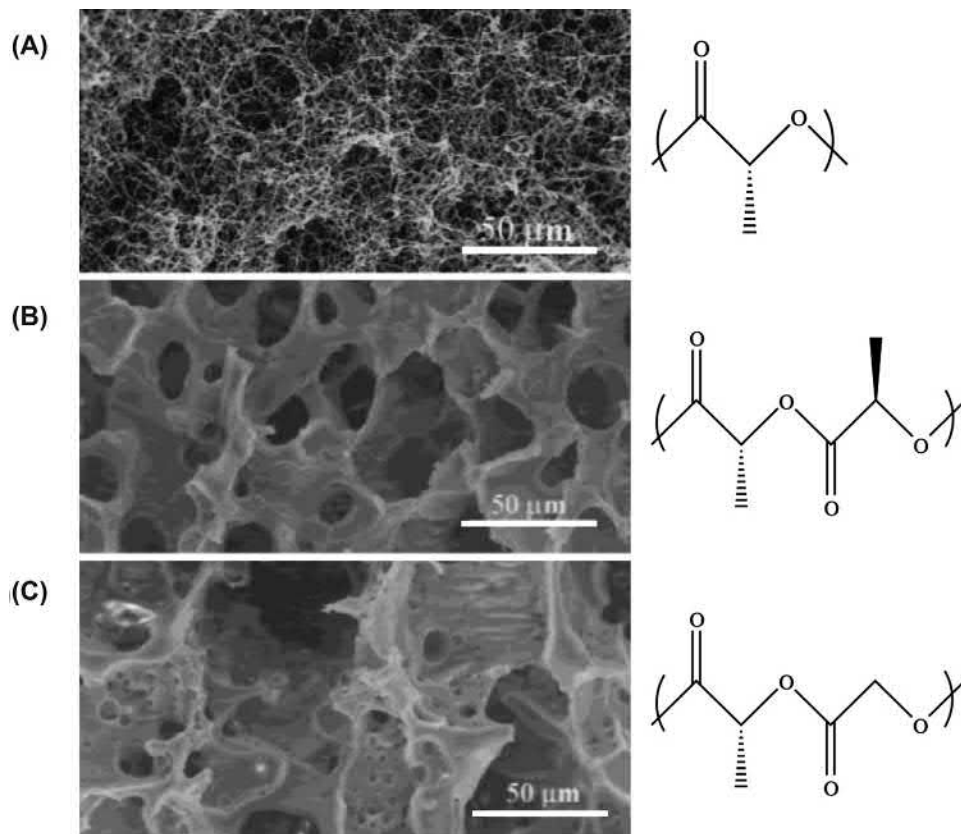
• **Figure 1.4.7.5** Scanning electron microscopy micrographs of a PLLA fibrous matrix prepared from 2.5% (wt/v) PLLA/THF solution at a gelation temperature of 8°C at 500 \times (A, scale=50 μ m) and 20K \times (B, scale=1 μ m) magnification, demonstrating nanofibers resulting from TIPS fabrication. Cells cultured on smooth (C, scale=200 μ m; D, scale=50 μ m) and nanofibrous (E, scale=200 μ m; F, scale=20 μ m) matrices for 24h. Osteoblast cell proliferation is increased on nanofibrous PLLA scaffolds compared to smooth scaffolds over the course of 12 days, when both scaffolds are initially seeded at the same cell density (G). *NF*, nanofibrous; *PLLA*, poly(L-lactic acid); *SW*, smooth walled; *THF*, tetrahydrofuran; *TIPS*, thermally induced phase separation. (Modified from (A,B) Ma, P.X., Zhang, R., 1999. Synthetic nano-scale fibrous extracellular matrix. *J. Biomed. Mater. Res.* 46, 60–72; (C–F) Hu, J., Feng, K., Liu, X., Ma, P., 2009. Chondrogenic and osteogenic differentiations of human bone marrow-derived mesenchymal stem cells on a nanofibrous scaffold with designed pore network. *Biomaterials*, 30 (28), 5061–5067; (G) Chen, V. J., Smith, L. A., Ma, P. X., 2006b. Bone regeneration on computer-designed nano-fibrous scaffolds. *Biomaterials*, 27 (21), 3973–3979.)

nanofibrous scaffold. This step is also dependent on the solvent and polymer properties (Atala and Lanza, 2001; Smith and Ma, 2004).

PLLA solution undergoes TIPS, and the solvent is exchanged to leave behind a nanofibrous matrix with fibers on the same diameter scale as natural ECM proteins, 50–500 nm (Fig. 1.4.7.5) (Ma and Zhang, 1999; Peter and Ma, 1998). Interestingly, fiber diameter does not significantly change with respect to polymer concentration, thermal annealing, solvent exchange, and freezing temperature. A lower gelation temperature (i.e., -20°C vs. liquid nitrogen) results in more well-defined fibers. At a high gelation temperature, platelet-like structures result (Ma and Zhang, 1999). These matrices have a porosity up to 98.5%, which allows cells to efficiently infiltrate the construct and facilitates nutrient exchange; they have a surface area-to-volume ratio two to three orders of magnitude higher than fibrous nonwoven fabrics made using

textile technology or foams made with particulate leaching (Ma and Zhang, 1999). Because of these features, TIPS is an excellent method for achieving biologically relevant nanofibers in polymer constructs.

The TIPS phenomenon is thought to occur through spinodal liquid–liquid phase separation, and consequential crystallization of the polymer-rich phase (Smith and Ma, 2004). The ability to form a nanofibrous matrix depends on the crystallinity of the polymer, determined by its enthalpy of melting by thermogravimetric analysis. The nanofibrous textures of PLGA and poly(D,L-lactic acid) (PDLLA) matrices are evidently different from PLLA (Fig. 1.4.7.6) (Ma and Zhang, 1999). The same is noted with many PLLA-based and other functional copolymers, which must maintain a certain degree of crystallinity to be able to form stable nanofibrous structures (Liu and Ma, 2009, 2010; Liu et al., 2009).



• **Figure 1.4.7.6** Crystallinity is a critical parameter in TIPS fabrication of nanofibrous matrices. PLLA (A) forms nanofibrous matrices while PDLLA (B) and PLGA (C) do not (scale=50 μm). *PDLLA*, Poly(D,L-lactic acid); *PLGA*, poly(lactic-co-glycolic acid); *PLLA*, poly(L-lactic acid); *TIPS*, thermally induced phase separation. (Reproduced from Ma, P.X, Zhang, R., 1999. Synthetic nano-scale fibrous extracellular matrix. *J. Biomed. Mater. Res.* 46, 60–72.)

Grooves and Micropatterns

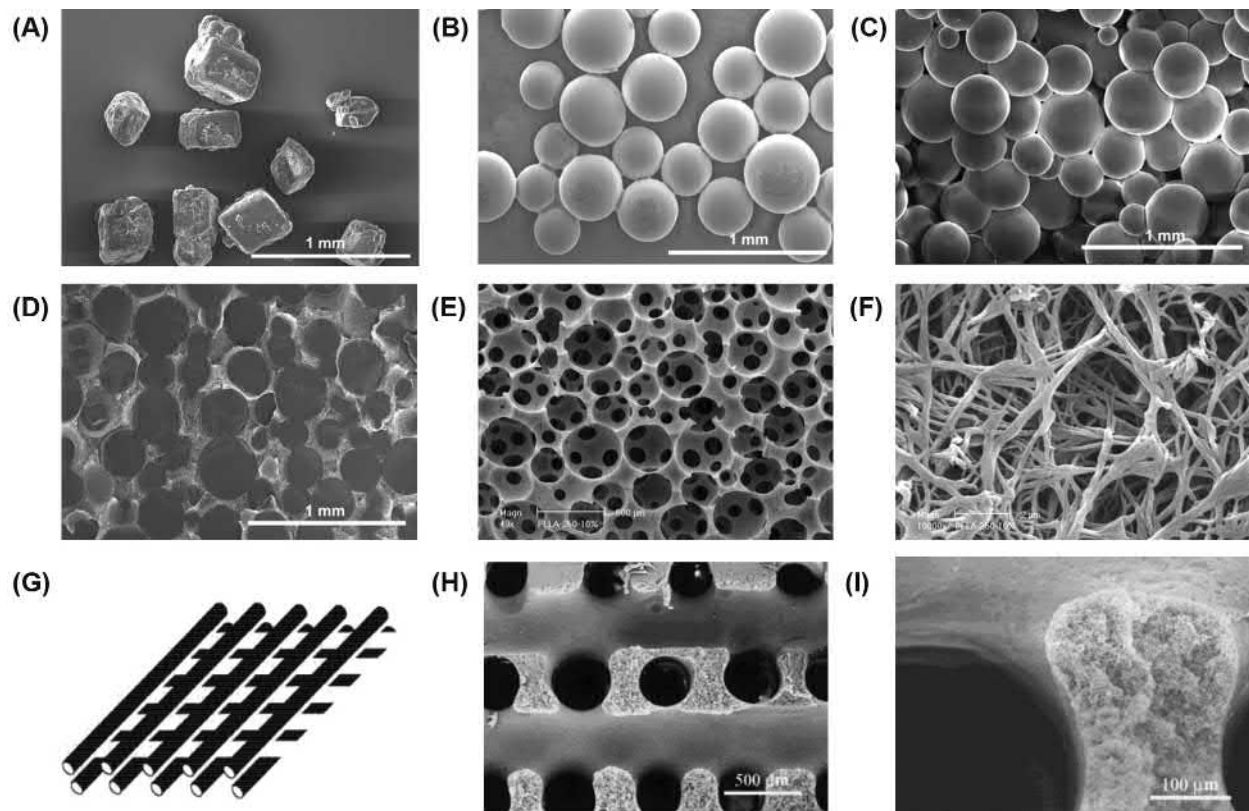
In addition to nanofibrous surface architectures, other grooved and micropatterned textured surfaces have biologic consequences on cell behavior. The ECM is critically important for organizing cell adhesion; controlling sites of cell adhesion is one method for modulating cell fate by geometric means. Capillary endothelial cells were switched from growth to apoptosis by modulating surface features of micropatterned substrates, namely so-called “adhesive islands.” Other factors, including cell spreading and cell shape, are also controlled by these geometric surface features. Decreasing island size restricted cell extension and induced apoptosis. Chen and others have pioneered this so-called geometric control of cell fate, which is an enabling technology to better understand fundamental mechanisms for 2D tissue microenvironment regulation (Chen et al., 1997, 1998; Guilak et al., 2009). For example, understanding mechanisms of angiogenesis—critical to tumor growth—is important to advancing our understanding of cancer metastasis.

Micropatterned substrates are fabricated by microcontact printing, which allows for substrate patterning with regions that are selectively modified. Silicon wafers are coated with photoresist and exposed to UV light through

a patterned mask. After developing the photoresist, the pattern is left on the mask, resulting in a substrate that is appropriate for making a polymer stamp (Singhvi et al., 1994). The substrate is stamped with sufficient pressure to cause contact, and proteins or other biologic molecules can be adsorbed to the surface to study cell–matrix interactions. Surface micropatterning has been demonstrated as a means of cell-based assays, as reviewed by Falconnet. This is a potentially important tool for organizing cells on sensors, as well as for drug discovery and screening applications (Falconnet et al., 2006).

Fabrication Methods for Micro- and Macroscale Architectural Features

Native tissues are organized hierarchically, with incorporated channels for mass transport of nutrients, waste, and signaling molecules, and a spatial organization of both cell–cell and cell–matrix interactions. In designing synthetic prostheses or tissue-engineering scaffolds, a biomimetic approach to recapitulating the native porous architecture is advantageous. Various studies have demonstrated the importance of interconnecting pores in a number of bone tissue-engineering and other biomedical



• **Figure 1.4.7.7** Fabrication process of sugar-porogen template leaching and TIPS, as shown by scanning electron microscopy micrographs. Sugar particles as received (250–425 μm , A) are fabricated into spherical particles via an emulsion method (250–425 μm , B). A sugar sphere template is heat treated to form a template for interconnected macropores (C) and polymer solution (PLLA/THF) is cast (D), phase separated, and solvent exchanged, resulting in a 3D macroporous (E, 50 \times magnification) and nanofibrous (F, 10K \times magnification) scaffold. The same method can be modified to use sugar rods stacked in an orthogonal pattern (G), used to fabricate nanofibrous scaffolds (H) with tubular macropores (I). PLLA, Poly(L-lactic acid); THF, tetrahydrofuran; TIPS, thermally induced phase separation. (Modified from (A–F) Wei, G.B., Ma, P.X., 2006. Macroporous and nanofibrous polymer scaffolds and polymer/bone-like apatite composite scaffolds generated by sugar spheres. *J. Biomed. Mater. Res. A* 78A (2), 306–315; (G–I) 2000. *J. Biomed Mater Res.* 52 (2), 430–6.)

constructs (Wei and Ma, 2006; Zhang and Ma, 1999b; Klawitter et al., 1976; Bobyn et al., 1980; Ryan et al., 2006). While optimal pore size depends on the scaffold and tissue types, there is consensus that a minimum pore size exists to allow for vascularization, tissue ingrowth, cell infiltration, and uniform cell distribution (Chalasan et al., 2007; Gupte et al., 2018). Porous materials are fabricated from synthetic and natural polymers, ceramics, and metals—each with unique processing methods and resulting mechanical properties (Ryan et al., 2006). A porous 3D construct has a high internal surface area and void space, providing a substrate for critical cell–matrix interactions to occur (Fig. 1.4.7.3) (Ma, 2005; Alberts, 2002; Sarkisov, 2012). Porosity considerations include porosity, pore size (Gupte et al., 2018), pore shape (Kawano et al., 2014; Kasten et al., 2008), inter pore connections (Chen and Ma, 2004), pore orientation (Ma and Zhang, 2001), and pore wall surface morphology (Wei and Ma, 2007). Each of these considerations and their various combinations require fabrication methods with high levels of control.

Interconnected Spherical Macropores by Porogen Methods

Porogen methods are a practical means to easily fabricate porous biomaterials with consistent macroarchitectural control, and at a low cost. Porogens are commonly used to form a template having complex pore architectures within a polymer solution by reserving free space in the matrix; once the polymer solvent evaporates and subsequently the porogen is dissolved, a porous 3D construct remains (Fig. 1.4.7.7) (Ma and Langer, 1999). Depending on the desired properties of the final construct, porogens can be solid, liquid, or gas, albeit liquid porogens are most difficult but possible in theory. For solid porogens, solvent choice and porogen/polymer solubility differences require careful consideration.

In 1991 DePonti demonstrated the first example of a porogen method using gas foaming—taking advantage of a gas-phase porogen (CO_2), which does not involve harsh solvents or high temperature to impart pores (DePonti et al., 1991). Porous PDLLA disks having up to 97% porosity

were fabricated by saturating a polymer solution with carbon dioxide for 3 days (Mooney et al., 1996). The resulting pores have a closed pore structure and solid exterior skin, both of which are not conducive to mass transport phenomena. The pores are generally nonuniform and irregularly shaped in these foams. Recent developments aim at determining appropriate parameters to achieve a more desirable pore network using supercritical fluid technology (Bhamidipati et al., 2013).

Salt was the first solid porogen and is the most frequently used method for pore fabrication (Mikos et al., 1994). First, salt is ground into small particles; particles of desired size are collected by sieving and packed into a mold. Polymer/solvent solution is cast over a packed water-soluble salt template. Salt leaching technique is discussed thoroughly in the literature (Ma and Langer, 1999). After the solvent evaporates, the solid polymer is laden with salt particles; soaking the polymer foam in water leaches away salt crystals, leaving behind pores throughout the scaffold. Salt particulate leaching can be combined with high-pressure carbon dioxide gas foaming to increase the size of pores achieved by gas foaming only, which has demonstrated utility in smooth muscle engineering (Harris et al., 1998). Despite the ease of fabrication, it is difficult to control pore shape (limited to cubic crystal structure of salt), interconnectivity (limited by nonspherical pore shape), and interpore opening size.

To improve on interconnectivity, critical to facilitate mass transport, a spherical porogen with the ability to be controllably fused is necessary. Paraffin spheres are the first example of a uniformly spherical porogen used in tissue-engineering scaffold fabrication (Ma and Choi, 2001). Spheres are fabricated by a dispersion method and annealed slightly with heat treatment in a mold. After polymer casting and solvent evaporation, a paraffin-laden polymer matrix results. Paraffin is removed in a nonpolar solvent that selectively dissolves paraffin but not the polymer, leaving behind a porous scaffold with interconnected pores.

Paraffin spheres are easily fabricated; however, it is an incompatible porogen (soluble) to many organic solvents. Additionally, its leaching can leave behind trace amounts of residual hydrophobic porogen that may have unfavorable consequences to cell activity. Sugar is an excellent alternative because it is easily processible and can be dissolved by water (Zhang and Ma, 2000). D-Fructose is emulsified in mineral oil with a nonionic surfactant, washed and sieved to desired size ranges (Fig. 1.4.7.7). Sugar is heat treated and polymer solution is cast. After leaching, scaffolds are highly porous with well-interconnected macropores and superior control over interconnectivity. Varied amounts of heat in the annealing step controls pore interconnectivity; longer heat treatment results in larger openings between pores (Ma and Choi, 2001). The compressive modulus of resulting scaffolds decreases with increasing porosity (Ma and Choi, 2001). Progress has been made in more-interconnected microchanneled and porous scaffolds by salt leaching (Tran et al., 2011) and processing salt into round particles to fabricate interconnected pores (Mukhopadhyay et al., 2010).

Nonspherical Architectural Patterning

Many tissues in the human body are naturally organized in oriented, tubular, or fibrous bundle architectures. The anisotropic properties of tissues, including nerve, muscle, dentin, tendon, and ligament, can be mimicked with carefully designed scaffolds (Ma, 2004; Ma and Zhang, 2001). Pores are incorporated by growing rod-shaped crystals in polymer solution by inducing phase separation along a uniaxial temperature gradient. Following TIPS, a network of aligned nanotubules results. When seeded with MC3T3 preosteoblasts, cells organize along tubular channels to form an oriented tissue, mimicking the organization of dentin and long bone (Ma and Zhang, 2001).

Larger oriented pores can be achieved using a tubular porogen, similar to spherical macropores discussed in detail in the section [Interconnected Spherical Macropores by Porogen Methods](#). Melted D-fructose can be drawn into thin fibers and solidified at room temperature. Their diameter, on average 100–500 μm , can be controlled by the drawing rate from melted bulk. Fibers are organized in a mold to create a porogen frame within a PLLA solution; after TIPS, sugar fibers are leached by water leaving behind a network of uniaxially oriented tubular macropores with a nanofibrous surface texture (Zhang and Ma, 2000). It is possible to fabricate scaffolds with layered orthogonal or helicoidally oriented macropores through a layer-by-layer assembly of fibers of similar diameter in varied orientations. Pores are interconnected at contacting points of the sugar fibers. Nonporogen methods for achieving these types of macroporous architectures are also achieved by 3D printing (Chen et al., 2006b) and by injection molding around objects such as needles (Sun et al., 2012).

Combining Multiple Fabrication Methods

A review of the literature supports the importance of nanofibrous surfaces that mimic the cellular ECM, and porous constructs that support diffusion and infiltration. Nanofibers provide a continuous biomimetic fiber network that, at the cellular level, selectively increases protein adsorption compared to smooth wall constructs (Woo et al., 2003), and promotes cellular adhesion and proliferation in a variety of cell types (Smith et al., 2010; Wang et al., 2011; Liu et al., 2009). Integrin expression also mediates cell–matrix interactions and may activate pathways like focal adhesion kinase, which plays a role in cell differentiation (Smith et al., 2009); nanofibers have been shown to facilitate stem cell differentiation toward multiple differentiation fates depending on culture conditions and exogenous factors (Hu et al., 2009; Gupte and Ma, 2012; Subramanian et al., 2009; Hu et al., 2010a,b; Ahmadi et al., 2011; Liu et al., 2015; Feng et al., 2012). Scaffolds should also have an internal interconnected porous network that facilitates cellular integration, uniform cell distribution, vascularization, and nutrient/waste exchange (Ma, 2008). Uniformly spherical particles are advantageous for controlling pore interconnectivity by

heat treatment. Macropores are particularly important in cell-free constructs where endogenous cells migrate and differentiate to fill a defect (Woo et al., 2009). These 3D tissue-engineering scaffolds with interconnected macropores have demonstrated regenerative potentials in a variety of tissues and physiological systems in as little as 4 weeks. It is critical for materials scientists and biomedical engineers to consider fabrication methods that can be combined to have tailorable biomaterial processing at nano-, micro-, and macroscales.

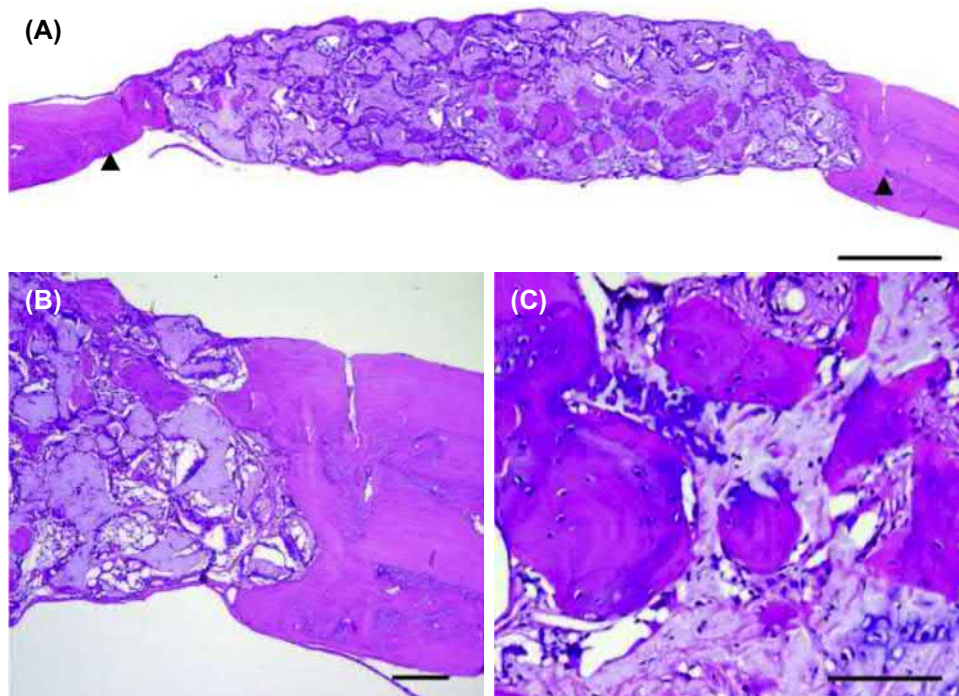
Macroporous, Nanofibrous Tissue-Engineering Scaffolds

Methods such as porogen leaching and TIPS are examples of two separate fabrication methods that are combined to yield a favorable combination of surface texture and an interconnected macroporous network. This has been demonstrated with a variety of porogens, including salt (Zhang and Ma, 2000), sugar fibers (Zhang and Ma, 2000), paraffin spheres (Chen and Ma, 2004), and sugar spheres (Wei and Ma, 2006). Porogens are chosen to be cold temperature insensitive such that polymer solutions can be cast over them and quickly chilled to gelation temperature, inducing TIPS to result in a nanofibrous matrix after solvent removal. Resulting matrices have high porosity (98%) and a high surface area (90–110 m²/g) with biomimetic nanoarchitecture features suitable for cell attachment, proliferation, and differentiation (Wei and Ma, 2006). Sugar is an ideal porogen because it is completely leached by water.

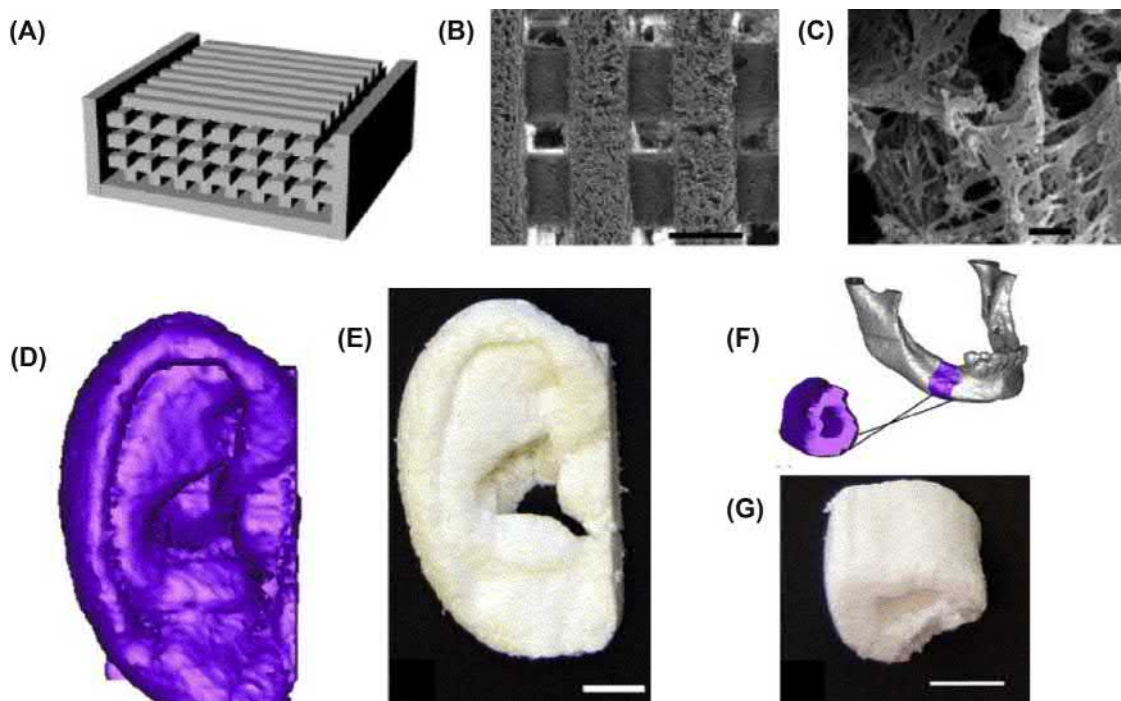
One example of the success of these constructs is seen in mineralized tissue neogenesis: odontogenesis of dental pulp stem cells in vitro and in vivo (Wang et al., 2011; Chatzistavrou et al., 2012; Soares et al., 2018), and osteogenic differentiation of multiple cell types, including embryonic stem cells (Smith et al., 2009, 2010, Hu et al., 2010) and bone marrow stromal cells in vitro (Woo et al., 2009; Hu et al., 2008). In vivo critical sized calvarial defect models have demonstrated the importance of well-interconnected macropores for vascularization as well as in supporting endogenous and exogenous osteoblasts and osteoprogenitor cells (Fig. 1.4.7.8) (Woo et al., 2009; Hu et al., 2008; Gupte et al., 2018).

Multiphasic Scaffolds

Within a single construct it is possible to incorporate multiple architectural motifs and multiple variants of the same motif. For example, in engineering a construct for the repair of an osteochondral defect it is necessary to consider the physiologic needs of cartilage and bone tissues, and their interface. It is unlikely that one scaffold design meets the needs of two distinct tissue types. However, it is equally unlikely that two unique cell-scaffold constructs, cultured separately, then combined, will result in continuous integration and distribution of cells to form a functional tissue interface (Gao et al., 2001; Alhadlaq and Mao, 2005). Patterning of architectural features can be used in directed 3D tissue differentiation within a single material construct (Hu et al., 2009). One can imagine taking advantage of



• **Figure 1.4.7.8** Histological images of H&E-stained nanofibrous scaffold implanted in a mouse calvarial defect for 8 weeks (A, arrow marks site of original defect, scale=1 mm). Peripheral (B, scale=100 μm) and central (C, scale=100 μm) images show bone tissue neogenesis throughout the scaffold construct. (Reproduced from Woo, K., Chen, V., Jung, H., Kim, T., Shin, H., Baek, J., Kim, G., 2009. Comparative evaluation of nanofibrous scaffolding for bone regeneration in critical-size calvarial defects. *Tissue Eng. A* 15 (8), 2155–2162.)



• **Figure 1.4.7.9** Computer-aided design/computer-aided manufacturing-designed three-dimensional (3D) printed tissue engineering scaffolds are advantageous because of their ability to be fabricated in complex 3D macroscale shapes with well-defined features. 3D PLLA scaffolds can be fabricated from reverse solid freeform fabrication; a negative mold (A) is used for polymer casting, where the solid struts eventually become open pores in the nanofibrous scaffold (B, scale = 500 μm ; C, scale = 2 μm). Computed tomography scans can be used to capture topographic features of a human ear (D, E, scale = 10 mm) and mandible (F, G, scale = 10 mm) in tissue-engineering scaffold. PLLA, Poly(L-lactic acid). (Reproduced from 2006. *Biomaterials* 27 (21), 3973–3979.)

the multipotency of bone marrow-derived mesenchymal stromal cells (BMSCs) to differentiate into osteoblasts or chondrocytes depending on the environment, and design a bioinstructive biphasic tissue-engineering scaffold to accommodate both tissue types in distinct zones (Caplan, 1991).

3D Printed Scaffolds

The macroscale shape of 3D tissue-engineering constructs is often a challenge for repairing clinically relevant large defects; new technologies in 3D printing can allow for controlled and customizable 3D scaffold shape. The earliest examples of 3D printed tissue-engineering constructs date to the mid-1990s (Giordano et al., 1996; Park et al., 1998). Computer-aided design (CAD) is employed to design scaffolds for solid freeform, reverse solid freeform, and rapid prototyping manufacturing (Giordano et al., 1996; Yang et al., 2002; Lin et al., 2004; Smith and Ma, 2012). One facile method for scaffold fabrication is to print a negative mold from a material that can later be dissolved (i.e., wax) by solid freeform methods. The mold can be filled with porogen, polymer cast, and frozen to induce TIPS. After dissolving the mold and porogen, a customized 3D scaffold shape with macroporous and nanofibrous features remains (Ma, 2004). To make scaffolds customized to a patient or injury site, a computed tomography scan of the void to be filled is taken and using CAD software the scaffold

or mold can be printed to an exact fit, for example, mandibular bone regeneration following trauma (Fig. 1.4.7.9) (Chen et al., 2006b). Powder inkjet printing has also been demonstrated to be feasible, but requires improvements in efficiency before it is commercially adopted (Butscher et al., 2011). 3D printing is advantageous because it is highly reproducible; however, it is currently limited by selection of materials, which are both biocompatible/biodegradable and printable, and by pixel resolution of the printers. This area has potential for significant growth in personalized medicine applications.

Injectable Tissue-Engineering Scaffolds

To accurately fit an irregular 3D defect site with minimal intervention, a biodegradable injectable scaffold is ideal, maintaining nanofibrous and macroporous architectural motifs. In the last 15 years there has been explosive interest in using micro-/nanospheres in tissue engineering (Wang et al., 2012). The first example of a microcell carrier was by Van Wezel in 1967—using dextran microcarriers to support cell attachment, growth, and proliferation in cell culture (Van Wezel, 1967). Multiple types of anchorage-dependent mammalian cells have been shown to thrive in microcarrier culture (Posillico, 1986; Tang et al., 1994; Freed et al., 1993).

Microspheres provide a unique opportunity for tunability with control over both their interior and exterior surfaces,

nanofibrous texture, macroporous architecture, and size. Depending on polymer composition and fabrication protocol, a variety of structures can be formed, including nanofibrous solid microspheres (Liu and Ma, 2010), nanofibrous hollow microspheres (Liu et al., 2011), and nanofibrous spongy microspheres (Kuang et al., 2015; Zhang et al., 2015b). Nanofibrous surface architecture is driven by the same TIPS process described earlier, and microlevel architectures are determined by emulsion conditions. Nanofibrous hollow microspheres (NF-MSs) are fabricated from star-shaped PLLA dendrimers dissolved in THF; glycerol is slowly added to the emulsion before quenching in liquid nitrogen to induce TIPS. NF-MSs are used as an injectable platform for cartilage regeneration to successfully repair a critical size osteochondral defect in rabbits, performing better than commercially available poly(ethylene glycol) hydrogels (Liu et al., 2011). Nanofibrous spongy microspheres (NF-SMSs) are made similarly, beginning from star-shaped PLLA, critical for a hollow microsphere architecture by acting as a surfactant. A reverse emulsification process is implemented where the THF/polymer solution is added into glycerol, then quenched by liquid nitrogen to induce nanofiber formation (Kuang et al., 2015; Zhang et al., 2015b) (Fig. 1.4.7.10). The combination of nanofibers and interconnected micropores is the result of a self-assembly process, controlled by the number of arms in the core dendrimer and arm length (Zhang et al., 2015b). The microporous structure maximizes cell–matrix interactions, in turn maximizing regenerative outcomes; NF-SMSs are shown to support odontogenic differentiation of human dental pulp stem cells and are a suitable injectable cell carrier for dentin regeneration (Kuang et al., 2016). Injectable cell carriers have demonstrated a great capacity for regeneration and interest in the field. Future clinically motivated research in this area will focus on how these carriers can be further tailored and modified to direct cell differentiation and be produced in mass.

Surface Modification of Biomaterial Constructs

Nanofibrous and porous materials have been explored for their very high surface area to impart additional biologic functionality. Cell–matrix interactions and cell fate can be further modulated by providing additional cues that influence growth, adhesion, proliferation, and differentiation (Ma, 2004). Early examples of scaffold modification are direct modifications of scaffold surfaces to enhance the cell–material interaction. Noncovalent deposition of biomacromolecules, including albumin, heparin, and RGD peptides, to improve or resist surface adhesion (Ratner, 1993; Amiji and Park, 1993). Plasma treatment has similarly been used to promote protein immobilization (Nitschke, 2008). Specific to bone tissue engineering, hydroxyapatite surface coatings have been used to promote bone formation and mineral deposition by providing a site for mineral nucleation (Chen et al., 2006a; Zhang and Ma, 1999a, 2004; Ma et al., 2001). Mineral can also be deposited by mineral growth

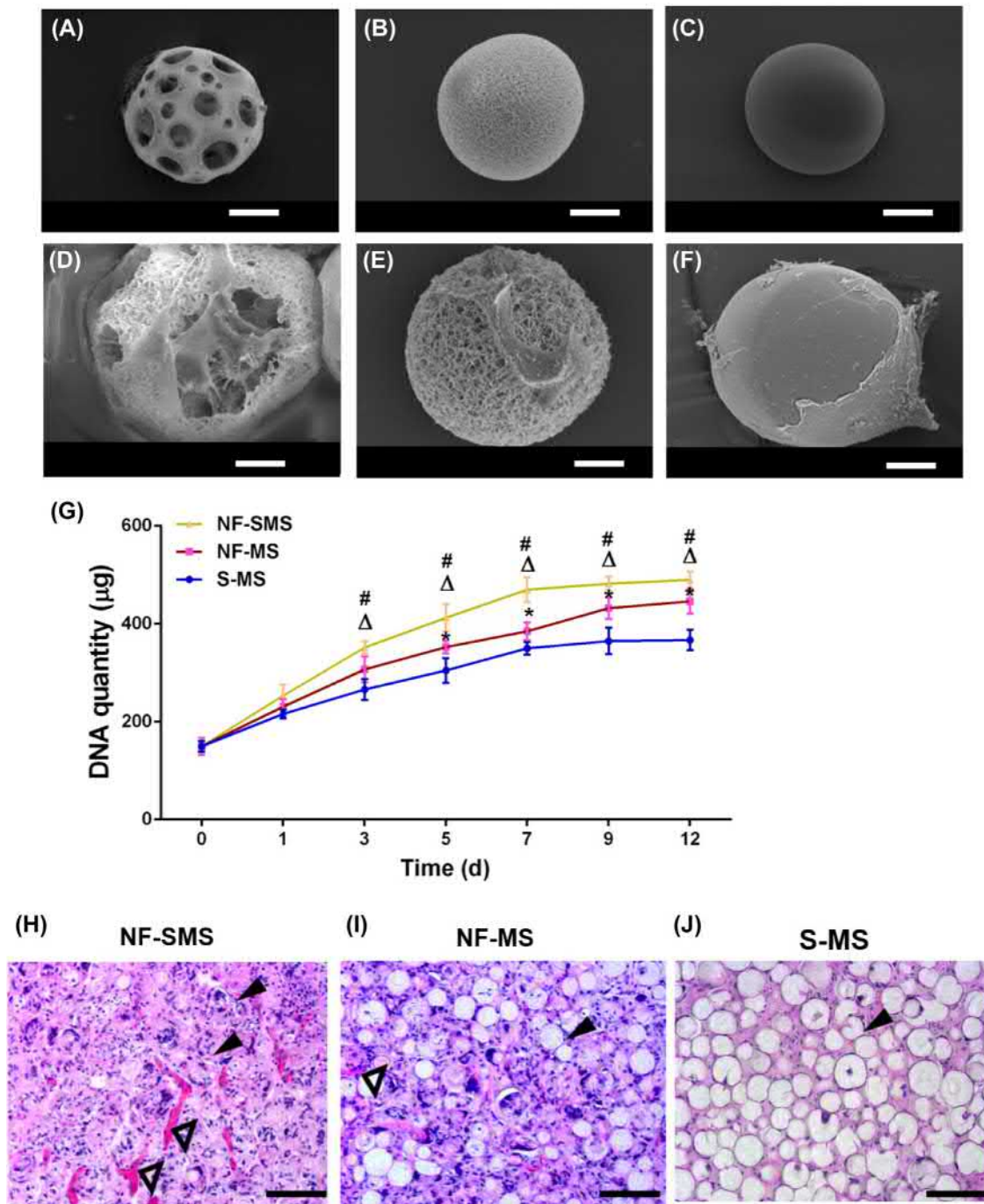
under an electric field, which helps to maintain small-scale architectures of scaffolds (He et al., 2010). Electrodeposition methods have also been developed to deposit charged biomacromolecules to the surface of scaffolds in a layer-by-layer method (Liu et al., 2005; Zhu et al., 2003). Other growth factors and small proteins are commonly coated to the surface of biomaterials to improve biologic outcomes; recent advances in phage selection and genetic engineering technologies are useful in determining application-specific surface proteins to mediate biologic outcomes (Ramaraju et al., 2017).

Chemically reactive functional groups can be incorporated into otherwise unreactive poly(aliphatic ester) chains through copolymerization, allowing for more flexible material design, which is amenable to modification (Shin et al., 2003; Quirk et al., 2001). Barrera et al. demonstrated the utility of poly(L-lactide)-*co*-poly(lysine) to attach RGD peptides to terminal lysine residues and enhance cell adhesion (Barrera et al., 1993). In the tin(II) 2-ethylhexanoate (Sn(Oct)₂)-catalyzed ring opening polymerization of L-lactide, initiators can be chosen to impart end-group functionality, for example, hydroxy(alkyl)methacrylate (Zhang et al., 2015a; Liu and Ma, 2010). Similarly, graft copolymers such as poly(hydroxyalkyl(meth)acrylate)-*g*-poly(L-lactic acid) contain repeating functional hydroxyl groups that can be functionalized with bioactive molecules to control cell–matrix interactions (Liu and Ma, 2010).

Finally, the high surface area of porous structures can be used to incorporate biomolecule delivery systems. PLGA nano- and microspheres are excellent candidates for encapsulation (Langer, 1998; Wei et al., 2004), which can be physically attached to the tissue-engineering construct by solvent wetting throughout a 3D construct (Wei et al., 2007; Hu et al., 2009; Zhang et al., 2015a). More complex delivery systems, for example, micro-RNA (Zhang et al., 2016a) and plasmid-DNA (Feng et al., 2017) delivery vectors, are incorporated through two-stage delivery systems. Growing interest in biologically derived therapeutics will require new innovation to incorporate these deliverables into adequate delivery and tissue-engineering systems. Multifunctional tissue-engineering scaffolds will be a large area of exploration in the coming years.

Summary and Future Perspectives

Textured and porous biomaterials show enhanced performance in terms of both short- and long-term successes of many biomedical devices by promoting cell adhesion, tissue infiltration, host integration, and improved biocompatibility. A high degree of fabrication controls over design architectures at both micro- and nanoscales is paramount to the diverse applications of biomaterials in clinically adopted medical products. For example, texture is important at the nanoscale to recapitulate the surface morphology of the native ECM-mimicking proteins (collagen, elastin), which supports cells and tissue organization, and porosity is important at the microscale where highly interconnected pores support



• **Figure 1.4.7.10** Scanning electron microscopy images of nanofibrous spongy microspheres (A, D), nanofibrous microspheres (B, E), and smooth microsphere (C, F) with diameters ranging from 30 to 60 μm , for use as injectable cell carriers (scale = 20 μm). hDPSCs attach to all three types of microspheres (D–F) after 24 h. Nanofibrous spongy microspheres are advantageous because of their increased porosity, which allows for cell attachment on both the inside and outside of the cell (D, G). After just 12 h this is evident by DNA quantification (G, #: $P < .05$, NF-SMS vs. S-MS, Δ : $P < .05$, NF-MS vs. S-MS). Subcutaneous injection of hDPSC–microsphere complexes generated tissue after 4 weeks in vivo; *solid triangles* indicate microspheres and *hollow triangles* indicate blood vessel formation. The most neotissue was formed with the highly porous NF-SMS (H–J, scale = 50 μm). hDPSCs, Human dental pulp stem cells; NF-MS, nanofibrous microspheres; NF-SMS, nanofibrous spongy microspheres; S-MS, solid microspheres. (Modified from Kuang, R., Zhang, Z., Jin, X., Hu, J., Shi, S., Ni, L., Ma, P.X., 2016. Nanofibrous spongy microspheres for the delivery of hypoxia-primed human dental pulp stem cells to regenerate vascularized dental pulp. *Acta Biomater.* 33, 225–234.)

nutrient transfer, and promote cell migration and proliferation, leading to host integration. Both nanofibrous texture and porosity increase construct surface area, creating space for cells to attach and proliferate, and a space to embed other signals at the surface of polymeric constructs. Such biomaterial architectural features can be achieved by using different fabrication methods discussed in this chapter. Moreover, multiple fabrication methods can be combined to fabricate constructs with multiple levels of architectural features.

In the coming years significant expansion in the fields of biomaterials science is expected, particularly in the areas of regenerative medicine and tissue engineering. Some future foreseeable challenges for porous and textured biomaterials are:

- **Scalable processing:** Many of the methods mentioned in this chapter have been developed in academic settings and are laborious in nature, making their scalability potentially challenging for future industry partners. Additionally, some steps in these processes, including solvent evaporation, are not rapid and may require days to weeks. In developing new biomaterial technologies, scalability must be considered early in development to facilitate future clinical and industry adoption.
- **Advances in 3D printing:** Macro-scale architectural control of construct shape is conveniently accomplished through 3D printing, and recently resolution has improved dramatically (Chia and Wu, 2014). Means of combining existing and new nano- and microscale feature fabrication strategies with 3D printing remains a challenge.
- **Range of biomaterial choices:** A long-standing issue with all biomaterial constructs is the limited selection of materials approved by the US Food and Drug Administration for use in humans. Materials scientists and engineers must find practical ways to maximize the functionality and bioeffectiveness of approved materials.
- **Compromised mechanical properties:** Porous materials inherently have a much higher surface area, directly responsible for cell–material interfacial interactions, at the expense of low density (Rouquerol et al., 1994; Sarkisov, 2012). Altered mechanical properties of materials as a result of processing make it difficult to match those of the surrounding tissues. Mismatch leads to insufficient integration capacity, and ultimately compromises longevity and utility of biomaterial constructs. This mismatch can lead to stress shielding, reduced interfacial stability, and ultimately rejection by the host.
- **Host reaction and long-term biosafety:** Biomaterial constructs must be strategically designed to synergize with local tissues, rather than cause local inflammation, which leads to rejection. Rather than fibrous tissue encapsulation, engineers must design biomaterial constructs that interface with native tissue. Over the last 30 years, the field of biomaterials has seen explosive growth, in particular in novel processing technologies discussed in this chapter, which increase biocompatibility and facilitate quicker, better outcomes for patients. Long-term validation of the effects of these biomaterial implants and products is still being assessed, and will inform future

directions of the field. Biocompatibility studies, complete with organ pathology studies, are necessary to demonstrate the absence of systemic toxicity. Poly(L-lactide), one of the most common synthetic biomaterials, has been demonstrated safe beyond 110 weeks of in vivo implantation (Pistner et al., 1993). The effects of processing techniques must be minimal to maintain the safety and biocompatibility of such materials.

Despite these challenges, the biomaterial market worldwide continues to expand at a rapid pace, valued at US\$134.3 billion in 2017, and will be a fruitful space for innovation in processing, fabrication, and manufacturing technologies (Rohan, 2017).

Increasing collaboration between clinicians, engineers, and biologists will continue to move the field toward clinical solutions. Recent trends in tissue engineering indicate a movement toward cell-free therapies to avoid issues with cell transplantation (Ikehara, 2013; Wei et al., 2007; Zhang et al., 2016a); tissue engineering constructs and biomedical devices require increasingly more inherent bio-instructive features to fill complex roles within physiologic systems. Therefore continued development of fabrication methods that allow for separate feature control at multiple architectural levels will increase the tunability of scaffolds. In developing new fabrication strategies, engineers and scientists in the space of biomedical innovation must keep in mind certain factors, including cost, fabrication simplicity, batch-to-batch consistency, relevant mechanical properties, biodegradability, and immune inertness. Additional work to elucidate cellular mechanisms influencing cell–artificial matrix interactions and long-term tissue-engineered construct success is necessary, with appropriate controls. In the coming years, biomaterials technology will continue to expand and be refined to suit an even wider variety of clinical needs.

References

- Ahmadi, R., Mordan, N., Forbes, A., Day, R.M., 2011. Enhanced attachment, growth and migration of smooth muscle cells on microcarriers produced using thermally induced phase separation. *Acta Biomater.* 7, 1542–1549.
- Alberts, B., 2002. *Molecular Biology of the Cell*. Garland Science, New York.
- Alhadlaq, A., Mao, J.J., 2005. Tissue-engineered osteochondral constructs in the shape of an articular condyle. *J. Bone Joint Surg. Am.* 87, 936–944.
- Amiji, M., Park, K., 1993. Surface modification of polymeric biomaterials with poly(ethylene oxide), albumin, and heparin for reduced thrombogenicity. *J. Biomater. Sci. Polym. Ed.* 4, 217–234.
- Anton, F., 1934. *Process and Apparatus for Preparing Artificial Threads*. US patent application US1975504A.
- Atala, A., Lanza, R.P., 2001. *Methods of Tissue Engineering*. Academic Press, San Diego, CA.
- Baril, E., Lefebvre, L.P., Hacking, S.A., 2011. Direct visualization and quantification of bone growth into porous titanium implants using micro computed tomography. *J. Mater. Sci. Mater. Med.* 22, 1321–1332.

- Barrera, D.A., Zylstra, E., Lansbury, P.T., Langer, R., 1993. Synthesis and RGD peptide modification of a new biodegradable copolymer: poly(lactic acid-co-lysine). *J. Am. Chem. Soc.* 115, 11010–11011.
- Benediktsson, K., Perbeck, L., 2006. Capsular contracture around saline-filled and textured subcutaneously-placed implants in irradiated and non-irradiated breast cancer patients: five years of monitoring of a prospective trial. *J. Plast. Reconstr. Aesthet. Surg.* 59, 27–34.
- Bergsma, J.E., De Bruijn, W.C., Rozema, F.R., Bos, R.R., Boering, G., 1995. Late degradation tissue response to poly(L-lactide) bone plates and screws. *Biomaterials* 16, 25–31.
- Bhamidipati, M., Scurto, A.M., Detamore, M.S., 2013. The future of carbon dioxide for polymer processing in tissue engineering. *Tissue Eng. B Rev.* 19, 221–232.
- Bhattarai, N., Edmondson, D., Veisoh, O., Matsen, F.A., Zhang, M., 2005. Electrospun chitosan-based nanofibers and their cellular compatibility. *Biomaterials* 26, 6176–6184.
- Bobyn, J.D., Pilliar, R.M., Cameron, H.U., Weatherly, G.C., 1980. The optimum pore-size for the fixation of porous-surfaced metal implants by the ingrowth of bone. *Clin. Orthop. Relat. Res.* 263–270.
- Bobyn, J.D., Stackpool, G.J., Hacking, S.A., Tanzer, M., Krygier, J.J., 1999. Characteristics of bone ingrowth and interface mechanics of a new porous tantalum biomaterial. *Journal of Bone and Joint Surgery – British Volume.* 81B, 907–914.
- Boland, E.D., Wnek, G.E., Simpson, D.G., Pawlowski, K.J., Bowlin, G.L., 2001. Tailoring tissue engineering scaffolds using electrostatic processing techniques: a study of poly(glycolic acid) electrospinning. *J. Macromol. Sci. A* 38, 1231–1243.
- Borden, M., Attawia, M., Laurencin, C.T., 2002. The sintered microsphere matrix for bone tissue engineering: in vitro osteoconductivity studies. *J. Biomed. Mater. Res.* 61, 421–429.
- Boyan, B.D., Sylvia, V.L., Liu, Y., Sagun, R., Cochran, D.L., Lohmann, C.H., Dean, D.D., Schwartz, Z., 1999. Surface roughness mediates its effects on osteoblasts via protein kinase A and phospholipase A2. *Biomaterials* 20, 2305–2310.
- Branemark, P.I., 1983. Osseointegration and its experimental background. *J. Prosthet. Dent* 50, 399–410.
- Burkhardt, B.R., 1984. Comparing contracture rates: probability theory and the unilateral contracture. *Plast. Reconstr. Surg.* 74, 527–529.
- Burkhardt, B.R., Dempsey, P.D., Schnur, P.L., Tofield, J.J., 1986. Capsular contracture: a prospective study of the effect of local antibacterial agents. *Plast. Reconstr. Surg.* 77, 919–932.
- Buser, D., Janner, S.F., Wittneben, J.G., Bragger, U., Ramseier, C.A., Salvi, G.E., 2012. 10-year survival and success rates of 511 titanium implants with a sandblasted and acid-etched surface: a retrospective study in 303 partially edentulous patients. *Clin. Implant Dent. Relat. Res.* 14, 839–851.
- Butscher, A., Bohner, M., Hofmann, S., Gauckler, L., Müller, R., 2011. Structural and material approaches to bone tissue engineering in powder-based three-dimensional printing. *Acta Biomater.* 7, 907–920.
- Caffee, H.H., 1994. Intracapsular injection of triamcinolone for intractable capsule contracture. *Plast. Reconstr. Surg.* 94, 824–828.
- Caplan, A.I., 1991. Mesenchymal stem cells. *J. Orthop. Res.* 9, 641–650.
- Chalasanani, R., Poole-Warren, L., Conway, R.M., Ben-Nissan, B., 2007. Porous orbital implants in enucleation: a systematic review. *Surv. Ophthalmol.* 52, 145–155.
- Chatzistavrou, X., Papagerakis, S., Ma, P.X., Papagerakis, P., 2012. Innovative approaches to regenerate enamel and dentin. *Int. J. Dent.* 2012, 856470.
- Chen, V.J., Ma, P.X., 2004. Nano-fibrous poly(L-lactic acid) scaffolds with interconnected spherical macropores. *Biomaterials* 25, 2065–2073.
- Chen, C.S., Mrksich, M., Huang, S., Whitesides, G.M., Ingber, D.E., 1997. Geometric control of cell life and death. *Science* 276, 1425–1428.
- Chen, C.S., Mrksich, M., Huang, S., Whitesides, G.M., Ingber, D.E., 1998. Micropatterned surfaces for control of cell shape, position, and function. *Biotechnol. Prog.* 14, 356–363.
- Chen, J., Chu, B., Hsiao, B.S., 2006a. Mineralization of hydroxyapatite in electrospun nanofibrous poly(L-lactic acid) scaffolds. *J. Biomed. Mater. Res.* 79A, 307–317.
- Chen, V.J., Smith, L.A., Ma, P.X., 2006b. Bone regeneration on computer-designed nano-fibrous scaffolds. *Biomaterials* 27, 3973–3979.
- Chia, H.N., Wu, B.M., 2014. High-resolution direct 3D printed PLGA scaffolds: print and shrink. *Biofabrication* 7, 015002.
- Clowes, A.W., Kirkman, T.R., Clowes, M.M., 1986. Mechanisms of arterial graft failure. II. Chronic endothelial and smooth muscle cell proliferation in healing polytetrafluoroethylene prostheses. *J. Vasc. Surg.* 3, 877–884.
- Cooper, D.M.L., Matyas, J.R., Katzenberg, M.A., Hallgrímsson, B., 2004. Comparison of microcomputed tomographic and microradiographic measurements of cortical bone porosity. *Calcif. Tissue Int.* 74, 437–447.
- Danino, A.M., Basmacioglu, P., Saito, S., Rocher, F., Blanchet-Bardon, C., Revol, M., Servant, J.M., 2001. Comparison of the capsular response to the Biocell RTV and Mentor 1600 Siltex breast implant surface texturing: a scanning electron microscopic study. *Plast. Reconstr. Surg.* 108, 2047–2052.
- Dohan Ehrenfest, D.M., Coelho, P.G., Kang, B.S., Sul, Y.T., Albrektsson, T., 2010. Classification of osseointegrated implant surfaces: materials, chemistry and topography. *Trends Biotechnol.* 28, 198–206.
- DePonti, R.C., Torricelli, C., Martini, A., Lardini, E., 1991. Use of Supercritical Fluids to Obtain Porous Sponges of Biodegradable Polymers. WO Patent, 91/09079.
- Elsdale, T., Bard, J., 1972. Collagen substrata for studies on cell behavior. *J. Cell Biol.* 54, 626–637.
- Espósito, M., Coulthard, P., Thomsen, P., Worthington, H.V., 2005. The role of implant surface modifications, shape and material on the success of osseointegrated dental implants. A Cochrane systematic review. *Eur. J. Prosthodont. Restor. Dent.* 13, 15–31.
- Falconnet, D., Csucs, G., Grandin, H.M., Textor, M., 2006. Surface engineering approaches to micropattern surfaces for cell-based assays. *Biomaterials* 27, 3044–3063.
- Feng, G., Zhang, Z., Jin, X., Hu, J., Gupte, M.J., Holzwarth, J.M., Ma, P.X., 2012. Regenerating nucleus pulposus of the intervertebral disc using biodegradable nanofibrous polymer scaffolds. *Tissue Eng. A* 18, 2231–2238.
- Feng, G., Zhang, Z., Dang, M., Zhang, X., Doleyres, Y., Song, Y., Chen, D., Ma, P.X., 2017. Injectable nanofibrous spongy microspheres for NR4A1 plasmid DNA transfection to reverse fibrotic degeneration and support disc regeneration. *Biomaterials* 131, 86–97.
- Fields, G.B., Lauer, J.L., Dori, Y., Forns, P., Yu, Y.C., Tirrell, M., 1998. Protein-like molecular architecture: biomaterial applications for inducing cellular receptor binding and signal transduction. *Biopolymers* 47, 143–151.
- Freed, L.E., Vunjak-Novakovic, G., Langer, R., 1993. Cultivation of cell-polymer cartilage implants in bioreactors. *J. Cell. Biochem.* 51, 257–264.
- Gampper, T.J., Khoury, H., Gottlieb, W., Morgan, R.F., 2007. Silicone gel implants in breast augmentation and reconstruction. *Ann. Plast. Surg.* 59, 581–590.

- Gao, J., Dennis, J.E., Solchaga, L.A., Awadallah, A.S., Goldberg, V.M., Caplan, A.I., 2001. Tissue-engineered fabrication of an osteochondral composite graft using rat bone marrow-derived mesenchymal stem cells. *Tissue Eng.* 7, 363–371.
- Giordano, R.A., Wu, B.M., Borland, S.W., Cima, L.G., Sachs, E.M., Cima, M.J., 1996. Mechanical properties of dense polylactic acid structures fabricated by three dimensional printing. *J. Biomater. Sci. Polym. Ed.* 8, 63–75.
- Goldberg, R.A., Dresner, S.C., Braslow, R.A., Kossovsky, N., Legmann, A., 1994. Animal model of porous polyethylene orbital implants. *Ophthalmic Plast. Reconstr. Surg.* 10, 104–109.
- Golden, M.A., Hanson, S.R., Kirkman, T.R., Schneider, P.A., Clowes, A.W., 1990. Healing of polytetrafluoroethylene arterial grafts is influenced by graft porosity. *J. Vasc. Surg.* 11, 838–844 Discussion 845.
- Guilak, F., Cohen, D.M., Estes, B.T., Gimble, J.M., Liedtke, W., Chen, C.S., 2009. Control of stem cell fate by physical interactions with the extracellular matrix. *Cell Stem Cell* 5, 17–26.
- Gupte, M.J., Ma, P.X., 2012. Nanofibrous scaffolds for dental and craniofacial applications. *J. Dent. Res.* 91, 227–234.
- Gupte, M.J., Swanson, W.B., Hu, J., Jin, X., Ma, H., Zhang, Z., Liu, Z., Feng, K., Feng, G., Xiao, G., Hatch, N., Mishina, Y., Ma, P.X., 2018. Pore size directs bone marrow stromal cell fate and tissue regeneration in nanofibrous macroporous scaffolds by mediating vascularization. *Acta Biomater.* 82, 1–11.
- Haarer, J., 2008. Proteins and amino acid-derived polymers. In: Hollinger, J.O. (Ed.), *An Introduction to Biomaterials*.
- Hanzlik, J.A., Day, J.S., Acknowledged Contributors: Ingrowth Retrieval Study, G., 2013. Bone ingrowth in well-fixed retrieved porous tantalum implants. *J. Arthroplast.* 28, 922–927.
- Harris, L.D., Kim, B.S., Mooney, D.J., 1998. Open pore biodegradable matrices formed with gas foaming. *J. Biomed. Mater. Res.* 42, 396–402.
- Hartgerink, J.D., Beniash, E., Stupp, S.I., 2002. Peptide-amphiphile nanofibers: a versatile scaffold for the preparation of self-assembling materials. *Proc. Natl. Acad. Sci. U.S.A.* 99, 5133–5138.
- Hay, E.D., 1991. *Cell Biology of Extracellular Matrix*. Plenum Press, New York.
- He, C., Xiao, G., Jin, X., Sun, C., Ma, P.X., 2010. Electrodeposition on nanofibrous polymer scaffolds: rapid mineralization, tunable calcium phosphate composition and topography. *Adv. Funct. Mater.* 20, 3568–3576.
- Hess, F., Jerusalem, C., Grande, P., Braun, B., 1984. Significance of the inner-surface structure of small-caliber prosthetic blood vessels in relation to the development, presence, and fate of a neo-intima. A morphological evaluation. *J. Biomed. Mater. Res.* 18, 745–755.
- Holmes, T.C., De Lacalle, S., Su, X., Liu, G., Rich, A., Zhang, S., 2000. Extensive neurite outgrowth and active synapse formation on self-assembling peptide scaffolds. *Proc. Natl. Acad. Sci. U.S.A.* 97, 6728–6733.
- Howard, P.S., 1999. The role of endoscopy and implant texture in transaxillary submuscular breast augmentation. *Ann. Plast. Surg.* 42, 245–248.
- Hu, J., Liu, X., Ma, P., 2008. Induction of osteoblast differentiation phenotype on poly(L-lactic acid) nanofibrous matrix. *Biomaterials* 29, 3815–3821.
- Hu, J., Feng, K., Liu, X., Ma, P., 2009. Chondrogenic and osteogenic differentiations of human bone marrow-derived mesenchymal stem cells on a nanofibrous scaffold with designed pore network. *Biomaterials* 30, 5061–5067.
- Hu, J., Smith, La, Feng, K., Liu, X., Sun, H., Ma, P.X., 2010a. Response of human embryonic stem cell-derived mesenchymal stem cells to osteogenic factors and architectures of materials during in vitro osteogenesis. *Tissue Eng. A* 16, 3507–3514.
- Hu, J.A., Sun, X.A., Ma, H.Y., Xie, C.Q., Chen, Y.E., Ma, P.X., 2010b. Porous nanofibrous PLLA scaffolds for vascular tissue engineering. *Biomaterials* 31, 7971–7977.
- Ikehara, S., 2013. Grand challenges in stem cell treatments. *Front. Cell Dev. Biol.* 1, 2.
- Ito, Y., 1999. Surface micropatterning to regulate cell functions. *Biomaterials* 20, 2333–2342.
- Karageorgiou, V., Kaplan, D., 2005. Porosity of 3D biomaterial scaffolds and osteogenesis. *Biomaterials* 26, 5474–5491.
- Kasten, P., Beyen, I., Niemeyer, P., Luginbuhl, R., Bohner, M., Richter, W., 2008. Porosity and pore size of beta-tricalcium phosphate scaffold can influence protein production and osteogenic differentiation of human mesenchymal stem cells: an in vitro and in vivo study. *Acta Biomater.* 4, 1904–1915.
- Kawano, T., Sato, M., Yabu, H., Shimomura, M., 2014. Honeycomb-shaped surface topography induces differentiation of human mesenchymal stem cells (hMSCs): uniform porous polymer scaffolds prepared by the breath figure technique. *Biomater. Sci.* 2, 52–56.
- Kenawy El, R., Layman, J.M., Watkins, J.R., Bowlin, G.L., Matthews, J.A., Simpson, D.G., Wnek, G.E., 2003. Electrospinning of poly(ethylene-co-vinyl alcohol) fibers. *Biomaterials* 24, 907–913.
- Kim, K., Yu, M., Zong, X., Chiu, J., Fang, D., Seo, Y.S., Hsiao, B.S., Chu, B., Hadjiargyrou, M., 2003. Control of degradation rate and hydrophilicity in electrospun non-woven poly(D,L-lactide) nanofiber scaffolds for biomedical applications. *Biomaterials* 24, 4977–4985.
- Klawitter, J.J., Bagwell, J.G., Weinstein, A.M., Sauer, B.W., 1976. An evaluation of bone growth into porous high density polyethylene. *J. Biomed. Mater. Res.* 10, 311–323.
- Ko, Y.G., Ma, P.X., 2012. Growth of oriented p-aminobenzoic acid crystals by directional freezing. *Cryst. Eng. Comm.* 14, 7891–7894.
- Kuang, R., Zhang, Z., Jin, X., Hu, J., Gupte, M.J., Ni, L., Ma, P.X., 2015. Nanofibrous spongy microspheres enhance odontogenic differentiation of human dental pulp stem cells. *Adv. Healthc. Mater.* 4, 1993–2000.
- Kuang, R., Zhang, Z., Jin, X., Hu, J., Shi, S., Ni, L., Ma, P.X., 2016. Nanofibrous spongy microspheres for the delivery of hypoxia-primed human dental pulp stem cells to regenerate vascularized dental pulp. *Acta Biomater.* 33, 225–234.
- Langer, R., 1998. Drug delivery and targeting. *Nature* 392, 5–10.
- Langer, R., Vacanti, J.P., 1993. Tissue engineering. *Science* 260, 920–926.
- Lanyon, L.E., Baggott, D.G., 1976. Mechanical function as an influence on the structure and form of bone. *J. Bone Joint Surg. Br.* 58-B, 436–443.
- Lehn, J.M., 2002a. Toward complex matter: supramolecular chemistry and self-organization. *Proc. Natl. Acad. Sci. U.S.A.* 99, 4763–4768.
- Lehn, J.M., 2002b. Toward self-organization and complex matter. *Science* 295, 2400–2403.
- Lewallen, E.A., Riester, S.M., Bonin, C.A., Kremers, H.M., Dudakovic, A., Kakar, S., Cohen, R.C., Westendorf, J.J., Lewallen, D.G., Van Wijnen, A.J., 2015. Biological strategies for improved osseointegration and osteoinduction of porous metal orthopedic implants. *Tissue Eng. B Rev.* 21, 218–230.
- Li, W.J., Laurencin, C.T., Caterson, E.J., Tuan, R.S., Ko, F.K., 2002. Electrospun nanofibrous structure: a novel scaffold for tissue engineering. *J. Biomed. Mater. Res.* 60, 613–621.

- Li, W.J., Danielson, K.G., Alexander, P.G., Tuan, R.S., 2003. Biological response of chondrocytes cultured in three-dimensional nanofibrous poly(epsilon-caprolactone) scaffolds. *J. Biomed. Mater. Res. A* 67, 1105–1114.
- Lin, C.Y., Kikuchi, N., Hollister, S.J., 2004. A novel method for biomaterial scaffold internal architecture design to match bone elastic properties with desired porosity. *J. Biomech.* 37, 623–636.
- Liu, X., Ma, P., 2009. Phase separation, pore structure, and properties of nanofibrous gelatin scaffolds. *Biomaterials* 30, 4094–4103.
- Liu, X., Ma, P.X., 2010. The nanofibrous architecture of poly(L-lactic acid)-based functional copolymers. *Biomaterials* 31, 259–269.
- Liu, X., Smith, L., Wei, G., Won, Y., Ma, P.X., 2005. Surface engineering of nano-fibrous poly(L-lactic acid) scaffolds via self-assembly technique for bone tissue engineering. *J. Biomed. Nanotechnol.* 1, 54–60.
- Liu, X., Smith, L., Hu, J., Ma, P., 2009. Biomimetic nanofibrous gelatin/apatite composite scaffolds for bone tissue engineering. *Biomaterials* 30, 2252–2258.
- Liu, X., Jin, X., Ma, P.X., 2011. Nanofibrous hollow microspheres self-assembled from star-shaped polymers as injectable cell carriers for knee repair. *Nat. Mater.* 10, 398–406.
- Liu, Q., Tian, S., Zhao, C., Chen, X., Lei, I., Wang, Z., Ma, P.X., 2015. Porous nanofibrous poly(L-lactic acid) scaffolds supporting cardiovascular progenitor cells for cardiac tissue engineering. *Acta Biomater.* 26, 105–114.
- Liu, J., Lin, D.Y., Wei, B., Martin, D.C., 2017. Single electrospun PLLA and PCL polymer nanofibers: increased molecular orientation with decreased fiber diameter. *Polymer* 118, 143–149.
- Ma, P.X., 2004. Scaffolds for tissue fabrication. *Mater. Today* 7, 30–40.
- Ma, P.X., 2005. Tissue engineering. In: Kroschwitz, J.I. (Ed.), *Encyclopedia of Polymer Science and Technology*, 3 ed. John Wiley & Sons, Inc, Hoboken NJ.
- Ma, P.X., 2008. Biomimetic materials for tissue engineering. *Adv. Drug Deliv. Rev.* 60, 184–198.
- Ma, P.X., Choi, J.W., 2001. Biodegradable polymer scaffolds with well-defined interconnected spherical pore network. *Tissue Eng.* 7, 23–33.
- Ma, P.X., Elisseff, J.H., 2005. *Scaffolding in Tissue Engineering*. Taylor & Francis, Boca Raton.
- Ma, P.X., Langer, R., 1999. Fabrication of biodegradable polymer foams for cell transplantation and tissue engineering. *Methods Mol. Med.* 18, 47–56.
- Ma, P.X., Zhang, R., 1998. Fibrillar Matricies. US patent application 6146892.
- Ma, P.X., Zhang, R., 1999. Synthetic nano-scale fibrous extracellular matrix. *J. Biomed. Mater. Res.* 46, 60–72.
- Ma, P.X., Zhang, R., 2001. Microtubular architecture of biodegradable polymer scaffolds. *J. Biomed. Mater. Res.* 56, 469–477.
- Ma, P.X., Zhang, R., Matricies., Fibrillar, 1998. US patent application 6146892.
- Ma, P.X., Zhang, R., Xiao, G., Franceschi, R., 2001. Engineering new bone tissue in vitro on highly porous poly(alpha-hydroxyl acids)/hydroxyapatite composite scaffolds. *J. Biomed. Mater. Res.* 54, 284–293.
- Ma, H., Hu, J., Ma, P.X., 2010. Polymer scaffolds for small-diameter vascular tissue engineering. *Adv. Funct. Mater.* 20, 2833–2841.
- Ma, P.X., Eyster, T.W., Doleys, Y., 2016. Tissue engineering biomaterials. *Encycl. Polym. Sci. Technol.* 1–47.
- Matassi, F., Botti, A., Sirleo, L., Carulli, C., Innocenti, M., 2013. Porous metal for orthopedics implants. *Clin. Cases Miner. Bone Metab.* 10, 111–115.
- Matthews, J.A., Wnek, G.E., Simpson, D.G., Bowlin, G.L., 2002. Electrospinning of collagen nanofibers. *Biomacromolecules* 3, 232–238.
- Mikos, A.G., Bao, Y., Cima, L.G., Ingber, D.E., Vacanti, J.P., 1993. Preparation of poly(glycolic acid) bonded fiber structures for cell attachment and transplantation. *J. Biomed. Mater. Res.* 27, 183–189.
- Mikos, A.G., Thorsen, A.J., Czerwonka, L.A., Bao, Y., Langer, R., Winslow, D.N., Vacanti, J.P., 1994. Preparation and characterization of poly(L-lactic acid) foams. *Polymer* 35, 1068–1077.
- Min, B.M., Lee, G., Kim, S.H., Nam, Y.S., Lee, T.S., Park, W.H., 2004. Electrospinning of silk fibroin nanofibers and its effect on the adhesion and spreading of normal human keratinocytes and fibroblasts in vitro. *Biomaterials* 25, 1289–1297.
- Mooney, D.J., Baldwin, D.F., Suh, N.P., Vacanti, J.P., Langer, R., 1996. Novel approach to fabricate porous sponges of poly(D,L-lactic-co-glycolic acid) without the use of organic solvents. *Biomaterials* 17, 1417–1422.
- Moore, A.N., Lopez Silva, T.L., Carrejo, N.C., Origel Marmolejo, C.A., Li, I.C., Hartgerink, J.D., 2018. Nanofibrous peptide hydrogel elicits angiogenesis and neurogenesis without drugs, proteins, or cells. *Biomaterials* 161, 154–163.
- Morton, W.J., 1900. Method of Dispersing Fluids. US705691A.
- Mukhopadhyay, I., Mohandas, V.P., Desale, G.R., Chaudhary, A., Ghosh, P.K., 2010. Crystallization of spherical common salt in the submillimeter size range without habit modifier. *Ind. Eng. Chem. Res.* 49, 12197–12203.
- Nevins, M., Kim, D.M., Jun, S.H., Guze, K., Schupbach, P., Nevins, M.L., 2010. Histologic evidence of a connective tissue attachment to laser microgrooved abutments: a canine study. *Int. J. Periodontics Restor. Dent.* 30, 245–255.
- Nie, W., Peng, C., Zhou, X., Chen, L., Wang, W., Zhang, Y., Ma, P.X., He, C., 2017. Three-dimensional porous scaffold by self-assembly of reduced graphene oxide and nano-hydroxyapatite composites for bone tissue engineering. *Carbon* 116, 325–337.
- Nitschke, M., 2008. Plasma modification of polymer surfaces and plasma polymerization. *Polym. Surf. Interfaces* 203–214.
- Ott, H.C., Matthiesen, T.S., Goh, S.K., Black, L.D., Kren, S.M., Netoff, T.I., Taylor, D.A., 2008. Perfusion-decellularized matrix: using nature's platform to engineer a bioartificial heart. *Nat. Med.* 14 (2), 213–221. <https://doi.org/10.1038/nm1684>.
- Park, A., Wu, B., Griffith, L.G., 1998. Integration of surface modification and 3D fabrication techniques to prepare patterned poly(L-lactide) substrates allowing regionally selective cell adhesion. *J. Biomater. Sci. Polym. Ed.* 9, 89–110.
- Pennisi, V.R., 1990. Long-term use of polyurethane breast prostheses: a 14-year experience. *Plast. Reconstr. Surg.* 86, 368–371.
- Peter, S.J., Miller, M.J., Yasko, A.W., Yaszemski, M.J., Mikos, A.G., 1998. Polymer concepts in tissue engineering. *J. Biomed. Mater. Res.* 43, 422–427.
- Pham, Q.P., Sharma, U., Mikos, A.G., 2006a. Electrospinning of polymeric nanofibers for tissue engineering applications: a review. *Tissue Eng.* 12, 1197–1211.
- Pham, Q.P., Sharma, U., Mikos, A.G., 2006b. Electrospun poly(epsilon-caprolactone) microfiber and multilayer nanofiber/microfiber scaffolds: characterization of scaffolds and measurement of cellular infiltration. *Biomacromolecules* 7, 2796–2805.
- Pistner, H., Bendi, D., Muhling, J., Reuther, J., 1993. Poly(L-lactide): a long-term degradation study in vivo Part III. Analytical characterization. *Biomaterials* 14, 291–298.
- Posillico, E.G., 1986. Microencapsulation technology for large-scale Antibody production. *Nat. Biotechnol.* 4, 114–117.

- Quirk, R.A., Chan, W.C., Davies, M.C., Tendler, S.J., Shakesheff, K.M., 2001. Poly(L-lysine)-GRGDS as a biomimetic surface modifier for poly(lactic acid). *Biomaterials* 22, 865–872.
- Ramachandran, G.N., 1988. Stereochemistry of collagen. *Int. J. Pept. Protein Res.* 31, 1–16.
- Ramaraju, H., Miller, S.J., Kohn, D.H., 2017. Dual-functioning peptides discovered by phage display increase the magnitude and specificity of BMSC attachment to mineralized biomaterials. *Biomaterials* 134, 1–12.
- Ratner, B.D., 1993. Chapter 8 characterization of biomaterial surfaces. *Cardiovasc. Pathol.* 2, 87–100.
- Rohan, 2017. Global Bio-Implants Market Worth \$134.3 Billion by 2017. [Online]. Available: <https://www.marketsandmarkets.com/PressReleases/bio-implants.asp>.
- Rosengren, A., Danielsen, N., Bjursten, L.M., 1999. Reactive capsule formation around soft-tissue implants is related to cell necrosis. *J. Biomed. Mater. Res.* 46, 458–464.
- Rouquerol, J., Avnir, D., Fairbridge, C.W., Everett, D.H., Haynes, J.M., Pernicone, N., Ramsay, J.D.F., Sing, K.S.W., Unger, K.K., 1994. Recommendations for the characterization of porous solids (Technical Report). *Pure Appl. Chem.* 66, 1739–1758.
- Ryan, G., Pandit, A., Apatsidis, D.P., 2006. Fabrication methods of porous metals for use in orthopaedic applications. *Biomaterials* 27, 2651–2670.
- Sachs, E., Cima, M., Williams, P., Brancazio, D., Cornie, J., 1992. Three Dimensional Printing: Rapid Tooling and Prototypes Directly from a CAD Model. *ASME J. Eng. Ind.* 114 (4), 481–488. <https://doi.org/10.1115/1.2900701>.
- Salzmann, D.L., Kleinert, L.B., Berman, S.S., Williams, S.K., 1997. The effects of porosity on endothelialization of ePTFE implanted in subcutaneous and adipose tissue. *J. Biomed. Mater. Res.* 34, 463–476.
- Sami, D., Young, S., Petersen, R., 2007. Perspective on orbital enucleation implants. *Surv. Ophthalmol.* 52, 244–265.
- Sarkisov, L., 2012. Accessible surface area of porous materials: understanding theoretical limits. *Adv. Mater.* 24, 3130–3133.
- Sharkawy, A.A., Klitzman, B., Truskey, G.A., Reichert, W.M., 1998. Engineering the tissue which encapsulates subcutaneous implants. II. Plasma-tissue exchange properties. *J. Biomed. Mater. Res.* 40, 586–597.
- Shin, H., Jo, S., Mikos, A.G., 2003. Biomimetic materials for tissue engineering. *Biomaterials* 24, 4353–4364.
- Simske, S.J., Ayers, R.A., Bateman, T.A., 1997. Porous materials for bone engineering. *Mater. Sci. Forum* 250, 151.
- Singhvi, R., Kumar, A., Lopez, G.P., Stephanopoulos, G.N., Wang, D.I., Whitesides, G.M., Ingber, D.E., 1994. Engineering cell shape and function. *Science* 264, 696–698.
- Smith, L.A., Ma, P.X., 2004. Nano-fibrous scaffolds for tissue engineering. *Colloids Surf. B Biointerfaces* 39, 125–131.
- Smith, L.A., Ma, P.X., 2012. Computer-designed nano-fibrous scaffolds. *Methods Mol. Biol.* 868, 125–134.
- Smith, L., Liu, X., Hu, J., Wang, P., Ma, P.X., 2009. Enhancing osteogenic differentiation of mouse embryonic stem cells by nanofibers. *Tissue Eng. A* 15, 1855–1864.
- Smith, L.A., Liu, X.H., Hu, J.A., Ma, P.X., 2010. The Enhancement of human embryonic stem cell osteogenic differentiation with nano-fibrous scaffolding. *Biomaterials* 31, 5526–5535.
- Soares, D.G., Zhang, Z., Mohamed, F., Eyster, T.W., De Souza Costa, C.A., Ma, P.X., 2018. Simvastatin and nanofibrous poly(l-lactic acid) scaffolds to promote the odontogenic potential of dental pulp cells in an inflammatory environment. *Acta Biomater.* 68, 190–203.
- Stevens, M.M., 2008. Biomaterials for bone tissue engineering. *Mater. Today* 11, 18–25.
- Strietzel, F.P., Lange, K.P., Svegar, M., Hartmann, H.J., Kuchler, I., 2004. Retrospective evaluation of the success of oral rehabilitation using the Frialit-2 implant system. Part 1: influence of topographic and surgical parameters. *Int. J. Prosthodont.* 17, 187–194.
- Subramanian, A., Krishnan, U.M., Sethuraman, S., 2009. Development of biomaterial scaffold for nerve tissue engineering: biomaterial mediated neural regeneration. *J. Biomed. Sci.* 16, 108.
- Sun, C., Jin, X., Holzwarth, J.M., Liu, X., Hu, J., Gupte, M.J., Zhao, Y., Ma, P.X., 2012. Development of channeled nanofibrous scaffolds for oriented tissue engineering. *Macromol. Biosci.* 12, 761–769.
- Sun, L.M., Berndt, C.C., Gross, K.A., Kuck, A., 2001. Material fundamentals and clinical performance of plasma-sprayed hydroxyapatite coatings: A review. *J. Biomed. Mater. Res.* 58, 570–592.
- Tang, J.S., Chao, C.F., Au, M.K., 1994. Growth and metabolism of cultured bone cells using microcarrier and monolayer techniques. *Clin. Orthop. Relat. Res.* 254–258.
- Taraballi, F., Sushnitha, M., Tsao, C., Bauza, G., Liverani, C., Shi, A., Tasciotti, E., 2018. Biomimetic tissue engineering: tuning the immune and inflammatory response to implantable biomaterials. *Adv. Healthc. Mater.* e1800490.
- Taylor, S.R., Gibbons, D.F., 1983. Effect of surface texture on the soft tissue response to polymer implants. *J. Biomed. Mater. Res.* 17, 205–227.
- Tran, R.T., Naseri, E., Kolasnikov, A., Bai, X., Yang, J., 2011. A new generation of sodium chloride porogen for tissue engineering. *Bio-technol. Appl. Biochem.* 58, 335–344.
- Van Wezel, A.L., 1967. Growth of cell-strains and primary cells on micro-carriers in homogeneous culture. *Nature* 216, 64–65.
- Whang, K., Thomas, C.H., Healy, K.E., Nuber, G., 1995. A novel method to fabricate bioabsorbable scaffolds. *Polymer* 36, 837–842.
- Wang, P., Wei, G., Liu, X., Ma, P.X., 2007. Bioinspired nanomaterials. In: Zhou, W., Wang, Z. (Eds.), *Advanced Scanning Microscopy for Nanotech.* HEP Frontiers Online.
- Wang, J., Ma, H., Jin, X., Hu, J., Liu, X., Ni, L., Ma, P.X., 2001. The effect of scaffold architecture on odontogenic differentiation of human dental pulp stem cells. *Biomaterials* 32 (31), 7822–7830. <https://doi.org/10.1016/j.biomaterials.2011.04.034>.
- Wang, H., Leeuwenburgh, S.C., Li, Y., Jansen, J.A., 2012. The use of micro- and nanospheres as functional components for bone tissue regeneration. *Tissue Eng. B Rev.* 18, 24–39.
- Wei, G., Ma, P.X., 2004. Structure and properties of nano-hydroxyapatite/polymer composite scaffolds for bone tissue engineering. *Biomaterials* 25, 4749–4757.
- Wei, G.B., Ma, P.X., 2006. Macroporous and nanofibrous polymer scaffolds and polymer/bone-like apatite composite scaffolds generated by sugar spheres. *J. Biomed. Mater. Res. A* 78A (2), 306–315.
- Wei, G., Ma, P.X., 2007. Polymeric biomaterials. In: Aldo, R., Boccaccini, J.E.G. (Eds.), *Biomaterials, Tissue Engineering Using Ceramics and Polymers.* Woodhead Publishing.
- Wei, G., Pettway, G.J., Mccauley, L.K., Ma, P.X., 2004. The release profiles and bioactivity of parathyroid hormone from poly(lactico-glycolic acid) microspheres. *Biomaterials* 25, 345–352.
- Wei, G., Jin, Q., Giannobile, W., Ma, P., 2007. The enhancement of osteogenesis by nano-fibrous scaffolds incorporating rhBMP-7 nanospheres. *Biomaterials* 28, 2087–2096.
- Wennerberg, A., Albrektsson, T., 2000. Suggested guidelines for the topographic evaluation of implant surfaces. *Int. J. Oral Maxillofac. Implant.* 15, 331–344.
- Wesolowski, S.A., Fries, C.C., Karlson, K.E., De Bakey, M., Sawyer, P.N., 1961. Porosity: primary determinant of ultimate fate of synthetic vascular grafts. *Surgery* 50, 91–96.

- White, R., Goldberg, L., Hirose, F., Klein, S., Bosco, P., Miranda, R., Long, J., Nelson, R., Shors, E., 1983. Effect of healing on small internal diameter arterial graft compliance. *Biomater. Med. Devices Artif. Organs* 11, 21–29.
- Whitesides, G.M., Grzybowski, B., 2002. Self-assembly at all scales. *Science* 295, 2418–2421.
- Whitesides, G.M., Mathias, J.P., Seto, C.T., 1991. Molecular self-assembly and nanochemistry – a chemical strategy for the synthesis of nanostructures. *Science* 254, 1312–1319.
- Woo, K.M., Chen, V.J., Ma, P.X., 2003. Nano-fibrous scaffolding architecture selectively enhances protein adsorption contributing to cell attachment. *J. Biomed. Mater. Res. A* 67A, 531–537.
- Woo, K., Chen, V., Jung, H., Kim, T., Shin, H., Baek, J., Kim, G., 2009. Comparative evaluation of nanofibrous scaffolding for bone regeneration in critical-size calvarial defects. *Tissue Eng. A* 15 (8), 2155–2162.
- Wu, B.M., Borland, S.W., Giordano, R.A., Cima, L.G., Sachs, E.M., 1996. Solid free-form fabrication of drug delivery devices. *J. Control. Release* 40, 77–87.
- Yang, S.F., Leong, K.F., Du, Z.H., Chua, C.K., 2001. The design of scaffolds for use in tissue engineering. Part 1. Traditional factors. *Tissue Eng.* 7, 679–689.
- Yang, S., Leong, K.-F., Du, Z., Chua, C.-K., 2002. The design of scaffolds for use in tissue engineering. Part II. Rapid prototyping techniques. *Tissue Eng.* 8, 1–11.
- Yang, F., Murugan, R., Wang, S., Ramakrishna, S., 2005. Electrospinning of nano/micro scale poly(L-lactic acid) aligned fibers and their potential in neural tissue engineering. *Biomaterials* 26, 2603–2610.
- Yoshimoto, H., Shin, Y., Terai, H., Vacanti, J., 2003. A biodegradable nanofiber scaffold by electrospinning and its potential for bone tissue engineering. *Biomaterials* 24, 2077–2082.
- Yu, Y.C., Roontga, V., Daragan, V.A., Mayo, K.H., Tirrell, M., Fields, G.B., 1999. Structure and dynamics of peptide-amphiphiles incorporating triple-helical proteinlike molecular architecture. *Biochemistry* 38, 1659–1668.
- Zhang, R., Ma, P., 1999a. Poly(alpha-hydroxyl acids) hydroxyapatite porous composites for bone-tissue engineering. I. Preparation and morphology. *J. Biomed. Mater. Res.* 44, 446–455.
- Zhang, R.Y., Ma, P.X., 1999b. Porous poly(L-lactic acid)/apatite composites created by biomimetic process. *J. Biomed. Mater. Res.* 45, 285–293.
- Zhang, R.Y., Ma, P.X., 2000. Synthetic nano-fibrillar extracellular matrices with predesigned macroporous architectures. *J. Biomed. Mater. Res.* 52, 430–438.
- Zhang, R.Y., Ma, P.X., 2004. Biomimetic polymer/apatite composite scaffolds for mineralized tissue engineering. *Macromol. Biosci.* 4, 100–111.
- Zhang, Z., Gupte, M.J., Jin, X., Ma, P.X., 2015a. Injectable peptide decorated functional nanofibrous hollow microspheres to direct stem cell differentiation and tissue regeneration. *Adv. Funct. Mater.* 25, 350–360.
- Zhang, Z., Marson, R.L., Ge, Z., Glotzer, S.C., Ma, P.X., 2015b. Simultaneous nano- and microscale control of nanofibrous microspheres self-assembled from star-shaped polymers. *Adv. Mater.* 27, 3947–3952.
- Zhang, X., Li, Y., Chen, Y.E., Chen, J., Ma, P.X., 2016a. Cell-free 3D scaffold with two-stage delivery of miRNA-26a to regenerate critical-sized bone defects. *Nat. Commun.* 7, 10376.
- Zhang, Z., Eyster, T.W., Ma, P.X., 2016b. Nanostructured injectable cell microcarriers for tissue regeneration. *Nanomedicine* 11, 1611–1628.
- Zhu, Y., Gao, C., He, T., Liu, X., Shen, J., 2003. Layer-by-Layer assembly to modify poly(l-lactic acid) surface toward improving its cytocompatibility to human endothelial cells. *Biomacromolecules* 4, 446–452.
- Zhu, C., Fan, D., Ma, X., Xue, W., Hui, J., Chen, L., Duan, Z., Ma, P., 2009. [Preparation and properties of novel human-like collagen-silk fibroin scaffold for blood vessel]. *Sheng Wu Gong Cheng Xue Bao* 25, 1225–1233.

Chapter Exercises

1. What are the major challenges for successful structural and functional integration of biomedical implants with native tissues?

There is a clear need for seamless and functional integration of synthetic implants with host tissue. Properties of biomedical implants must be balanced with their specific application. Important considerations include vascularization and innervation, and minimizing fibrous tissue encapsulation. Architectural and biochemical properties of the cell microenvironment, particularly at the cell–material interface, are critically important and tailorable. For example, nanofibers promote cell adhesion, proliferation, and differentiation on the material surface; porous implants facilitate tissue ingrowth and host integration.

2. Many strategies to engineer a functional tissue equivalent propose the use of an appropriate biomaterial that mimics the native ECM. What are the critical considerations of a biomaterial to be considered appropriate?

Key considerations include recapitulating native mechanical properties, physiological response, degradation rate and degradation products, cell infiltration and integration, cost, ease of manufacturing, and minimizing immune response. These factors can be modulated by selecting materials with appropriate mechanical properties, chemical composition and degradation rates, surface modification, and choosing appropriate fabrication methods for nano-, micro-, and macrolevel architectures.

3. Collagen, in the native ECM, imparts tensile strength to tissues. What aspects of collagen are structurally favorable? How can this favorable 3D structure–function relationship be recapitulated by synthetic biomaterials? What are the limitations of naturally isolated collagen as a biomaterial?

Type I collagen, which composes a majority of the native ECM, is a protein with a triple-helical fiber structure. Fiber diameters are roughly 50–500 μm . Therefore synthetic polymers must be fabricated with similar fiber diameters. This is best accomplished by TIPS. Collagen lacks processing control in regards to mechanical properties, degradation rate, batch-to-batch inconsistencies, and pathogenicity.

4. You have synthesized a new biodegradable polymer for potential use in tissue-engineering scaffold applications. What design criteria would be implicated in:

- Increasing cell adhesion to the scaffold construct? Nanofibrous surface texture.
- Directing cell alignment in the scaffold construct? Aligned macropores using a tubular porogen.

c. Promote osteogenic differentiation and calcium secretion? Use the increased surface area of a nanofibrous macroporous scaffold to adhere osteogenic factors such as bone morphogenetic proteins or hydroxyapatite.

5. Angiogenesis is critical to influence tissue neogenesis and integration of synthetic biomaterial constructs. What strategies would you employ to enhance vascularization in a synthetic prosthetic implant? Outline an appropriate experiment, with controls, to test this strategy.

To enhance vascularization, blood vessels must be able to form at the surface of and into the implanted construct. Therefore a macroporous texture is advantageous to allow cell and blood vessel infiltration. To test this hypothesis, smooth and macroporous implants could be implanted into an animal; after adequate time, histology for blood vessel formation can be quantified.

6. A patient presents with a critical size osteochondral defect (bone and cartilage) in their knee as the result of repeated athletic injury. Describe a method for fabricating a tissue-engineering scaffold that is suitable for regeneration of both tissue types in this defect.

Bone and cartilage must be combined in the same tissue-engineering construct in two distinct regions. Considerations may include pore size, pore interconnectivity, and surface decoration.

7. You are a senior staff scientist at a pharmaceutical company, working in the biomedical devices and implants division. The director of research and development has tasked you with leading a phase 1 project of an implantable biosensor for optical blood pressure sensing. What specific features would you propose to increase biocompatibility of the synthetic construct?

To increase long-term device success, you want it to integrate with the surrounding tissue without being encapsulated by fibrous tissue. Therefore ECM-like nanofibers and/or a porous surface texture are important to allow tissue ingrowth.

8. Implantation of biomaterials leads to a host of reactions that can be characterized by a series of cellular responses. You are tasked with designing a composite temporal mandibular joint implant. In general, how would you circumvent complications associated with host rejection and expedite wound healing?

ECM-like nanofibers and/or a porous surface texture are important to allow tissue ingrowth. Pores, in particular, are advantageous and must be large enough to facilitate cell and tissue infiltration, but small enough to prevent fibrous tissue formation. Nanofibers are important to disrupt capsule formation by disrupting collagen fiber orientation.

1.4.8

Biomedical Applications of Additive Manufacturing

PRACHI DHAVALIKAR¹, ZIYANG LAN¹, RONIT KAR¹, KARIM SALHADAR¹,
AKHILESH K. GAHARWAR², ELIZABETH COSGRIFF-HERNANDEZ¹

¹The University of Texas at Austin, Austin, TX, United States

²Texas A&M University, College Station, TX, United States

Introduction

Additive manufacturing, broadly known as 3D printing, is a class of manufacturing processes in which a 3D construct is built through sequential layer fabrication. This rapid prototyping methodology is transforming how medical devices are designed, developed, and manufactured by enabling low-volume and on-demand production without dedicated equipment or tooling. In brief, computer-aided design software is used to generate a 3D model that is then exported into a file format that describes the volume or surface mesh in 3D space. Another program, generally known as a “slicer,” is then used to translate the 3D data into individual layers to be printed using a multi-axis positioning system through a variety of processes, including extrusion deposition, solidification, polymerization, sintering, or binding. A subset of additive manufacturing includes living cells during the printing process and has been termed bioprinting (Jose et al., 2016). Specifically, bioprinting enables robotic deposition of cells and materials into custom shapes and patterns to replicate anatomical complexity associated with tissues and organs (Chimene et al., 2016). Bioprinting has been adopted for tissue engineering with the goal of developing highly customized cell-laden scaffolds to enable healthy human tissue to be regrown from a patient’s own stem cells (Murphy and Atala, 2014; Kang et al., 2016; Norotte et al., 2009). This chapter provides an overview of common 3D printing modalities and design considerations for bioprinting. Current applications of 3D printing technologies in different facets of the medical field are highlighted to demonstrate the current and future impact of additive manufacturing in healthcare.

3D Printing Modalities

There are numerous additive manufacturing modalities with new commercial variants under continuous development.

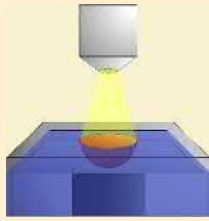
In an effort to structure this rapidly expanding portfolio of technologies, process categories were utilized to group these techniques based on the material type and method used to combine each layer. Table 1.4.8.1 provides common families of 3D printing processes as published originally in the 2012 ASTM F2792—12a Standard Terminology for Additive Manufacturing Technologies. For each of these modalities, a general description of the process and material requirements is provided with representative application cases within the medical field.

Vat Photolithography

Stereolithography (SLA) is a vat photopolymerization technique that uses a laser to cure a photopolymer reservoir layer by layer. A platform is initially positioned so that there is one layer height of the photopolymer between the platform and the light source. The laser is projected onto the surface of the photopolymer reservoir, curing a path determined by the print design (Melchels et al., 2010). Once a layer is cured, the platform is moved so that successive layers of photopolymer can be cured to form the object (Wong and Hernandez, 2012). The most common photopolymer resins used are low-molecular weight, multifunctional monomers that usually cure to form brittle constructs (Melchels et al., 2010). New polymers have been fabricated that are biocompatible (e.g., urethane dimethacrylate, diisopropyl acrylamide) and biodegradable (e.g., polypropylene fumarate, linear poly(D,L-lactide)-methacrylate) for use in biomedical applications. The print resolution is limited by the layer height, which can be as low as 20 μm (Kamran and Saxena, 2016). This is a very high accuracy and versatile technique that does not require any support material to print hollow or porous structures (Sachlos and Czernuszka, 2003). The main drawback is the limited number of commercially

TABLE 1.4.8.1 Schematics of Different 3D Printing Methodologies

Vat polymerization

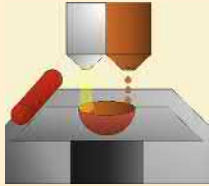


The build platform is lowered into a vat of liquid photopolymer resin. A UV light cures the resin in layers on top of the platform.

Alternative Names: SLA – Stereolithography Apparatus, DLP – Digital Light Processing

Resolution: 10 μm

Material jetting

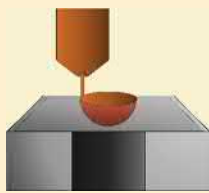


Droplets of material are deposited onto the surface using a thermal or piezoelectric method. Each layer is cooled or cured by UV light.

Alternative Names: Inkjet printing, MJM – Multi-jet modeling

Resolution: 25–100 μm

Material extrusion

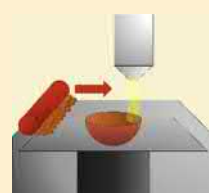


A material spool is fed and melted through a heated nozzle and deposited onto the surface, layer by layer.

Alternative Names: FDM – Fused deposition modeling

Resolution: 50–200 μm

Powder bed fusion

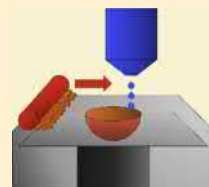


The material in powder form is spread over the surface and fused to other layers using a laser or electron beam.

Alternative Names: SMS – Selective metal sintering, SHS – Selective heat sintering, DMLS – Direct metal laser sintering

Resolution: 80–250 μm

Binder jetting

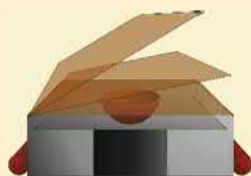


Building material in powder form is rolled/spread into a flat sheet. A liquid binding agent is selectively applied between layers as an adhesive.

Alternative Names: PB – Powder bed printing

Resolution: 80–250 μm

Sheet lamination

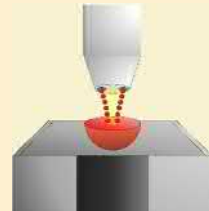


Material in sheet form is placed on a cutting bed and bonded over the surface using an adhesive. Each layer is cut to shape by laser, knife, or drill after bonding.

Alternative Names: UC – Ultrasonic consolidation, LOM – Laminated object manufacturing

Resolution: Depends of thickness of laminates

Direct energy deposition



Material, typically in the form of a powder or wire, is deposited onto the surface and melted using a laser or electron beam upon deposition.

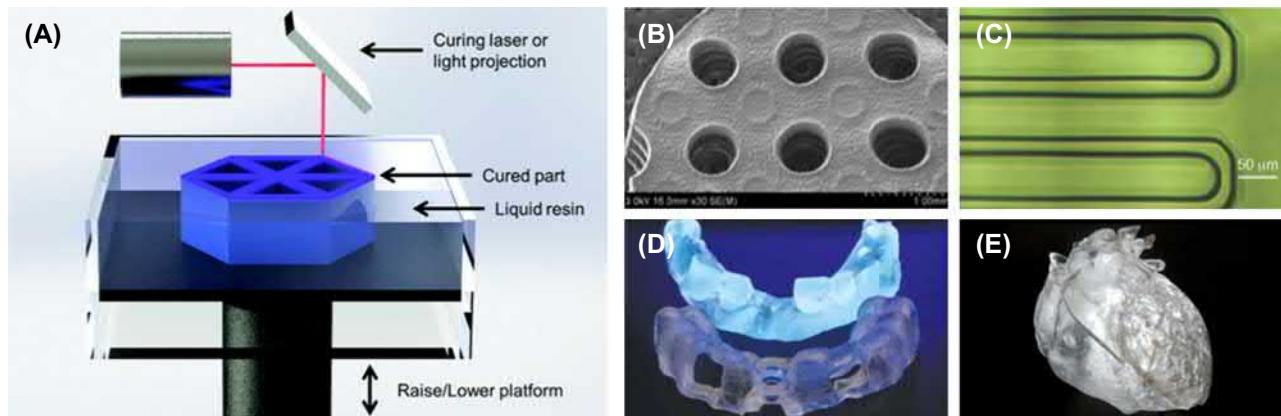
Alternative Names: LMD – Laser metal deposition, LENS – Laser engineered net shaping

Resolution: 250 μm

available photopolymers. This technique has been used to print patient-specific models and implant devices, such as noncytotoxic polyacrylate and hydroxyapatite composite bone parts (Melchels et al., 2010). The development of biodegradable resins has allowed printing of resorbable

tissue-engineered scaffolds with highly tailored pore architectures to promote cell attachment and tissue regeneration.

Like SLA, **digital light processing (DLP)** is a low-cost, high-throughput vat photopolymerization technique. It is a localized photopolymerization process, triggered by a



• **Figure 1.4.8.1** (A) A schematic of vat photopolymerization (Sears et al., 2016), (B) electron microscopy of a stereolithographic bone scaffold (Kim et al., 2010), (C) DLP-SLA-printed microfluidic channels (Gong et al., 2017), (D) SLA-printed model and surgical guide for dental reconstruction surgery (Patel et al., 2017), and (E) a transparent SLA-printed heart model for congenital heart disease intervention (Meier et al., 2017).

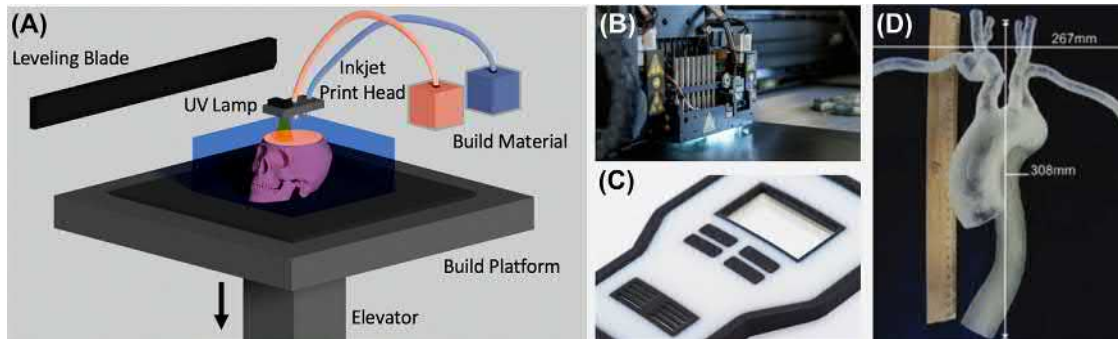
digital mirror device (DMD), a matrix of mirrors that beam light in a pixel pattern onto a bath of uncured macromer (Hornbeck, 1997). There are a limited number of liquid resin photopolymers available for DLP, and they often result in brittle prints. The photopolymer resins most often used are low-molecular weight, multifunctional monomers. This technique is capable of generating a variety of complex micro- to mesoscale structures with microscale architecture and micrometer precision, which are beneficial when printing biomaterial constructs (Kamran and Saxena, 2016). This technique also reduces printing time by curing an entire layer of resin at once. However, the resolution of the print is limited by the pixel size of the DMD, which can be as small as $16\ \mu\text{m}$ (Patel et al., 2017). This printing technique is further limited by the number of commercially available photopolymer resins. DLP has been used to print lattice metamaterials, pneumatically actuated soft robots, and structures connected with trusses or cavities. It can construct 3D-printed gel scaffolds with long-term control over cell proliferation, morphology, and geometric guidance. It can also print hearing aids, physical dental models for dental restoration, and 3D convoluted vessel-like microfluidic channels (Patel et al., 2017) (Fig. 1.4.8.1).

Material Jetting

Inkjet printing and multijet modeling are two examples of material jetting printing processes. In a simple **inkjet printing** process, droplets of material, typically in liquid form, are deposited based on a predetermined path and allowed to solidify or cool before deposition of the next layer. Droplet extrusion is dependent on a pressurized system or thermal system (Cui et al., 2012). Different materials can be printed with inkjet printing, including polymers (conductive, structural, and biological), metals, nanoparticles, ceramics, and biological materials (proteins, small molecules, and nucleic acids) (Derby, 2010). Printing resolution is controlled by changing parameters like extrusion temperature, pulse frequency, and ink viscosity. Nozzle sizes for the printers range from 10 to $30\ \mu\text{m}$, with matching resolution for the droplet

size. The advantages of using this method include the ability to precisely control the position of jetting, volume of material deposited, versatility in the material printed, and relatively high-speed printing (Nakamura et al., 2005; Bose et al., 2013). Inkjet printing is used in different fields, including optics, fabrication of transistors, and more recently in biomedical applications such as tissue engineering (Alamán et al., 2016; Siringhaus et al., 2000). Research groups have demonstrated the printing of hydrogels, stiff scaffolds, and complex matrices such as native tissue vasculature (Chia and Wu, 2015). Additional developments to the printer technology now allow for the printing of live cells, typically suspended in a material solution (Chia and Wu, 2015; Boland et al., 2006).

In **multijet modeling (MJM)**, the printer has multiple nozzles (with as many as 96 nozzles) that can be simultaneously used to deposit material. The nozzles are engaged to deposit the liquid material and support material with each layer allowed to cool, or ultraviolet (UV) cured prior to deposition of the next layer (Bikas et al., 2016). This type of printing needs support material that is typically printed in pillars along the side of the actual print and then removed using a water jet or peeled off (Vaezi et al., 2013). Photopolymers are most commonly used for building materials and gel or wax materials used for the supporting structure. These printers can process complex objects with high accuracy and resolution without the use of complex lasers or beams. The print objects have a smooth surface finish and a resolution ranging from 25 to $50\ \mu\text{m}$ in thickness (Bikas et al., 2016). It is a user-friendly instrument that can be used in any environment at high speed. However, the support pillars must be broken off and the bottom surface finish can be very poor, resulting in pitting and decreased strength of the material. For maintenance of exact layer thickness and compensation for small variations of droplet size, some of the more recent machines use a mechanical planarization, which can remove the excess material on each pass (Bikas et al., 2016; Vaezi et al., 2013). Several labs have demonstrated the use of this technique to print biomaterials as well. Biological materials, such as protein solutions, were printed onto cellular



• **Figure 1.4.8.2** (A) A schematic of material jetting, (B) image of a material jetting 3D printer demonstrating its UV curing lamp (3D Printing Hubs, 2018), (C) material jetting prototype with both rigid (white) and flexible (black) material (3D Printing Hubs, 2018), and (D) a material jetted model of an aorta used for surgical planning (Mitsouras et al., 2015). ((D) Adapted and reprinted, with permission from Markl, M., Schumacher, R., Küffer, J., Bley, T.A., Hennig, J., 2005. Rapid vessel prototyping: vascular modeling using 3T magnetic resonance angiography and rapid prototyping technology. *MAGMA* 18 (6), 288–292.)

locations on solid substrates, which allows control of bioactive surfaces of cellular scaffolds (drop-on-demand method) (Zhu et al., 2015). MJM can also be used to develop cellular colony arrays for rapid drug screening or cytotoxicity testing (Amin et al., 2016) (Fig. 1.4.8.2).

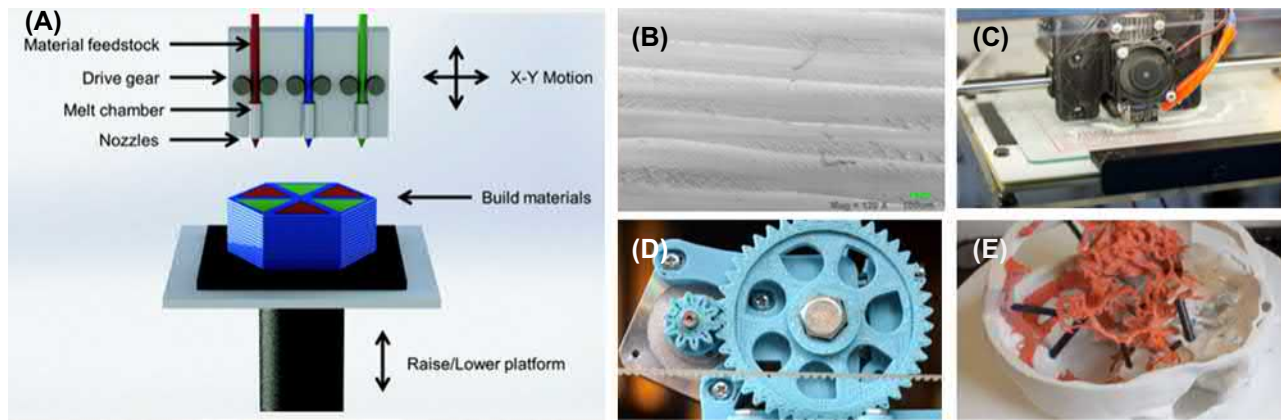
Material Extrusion

Fused Deposition Modeling (FDM) is an extrusion-based printing technique that requires the use of a nozzle to deposit material onto a platform. Extrusion of the material is dependent on pneumatic pressure or can be driven by a motor-actuated plunger system (Mohamed et al., 2015; Turner et al., 2014). Selective deposition layer by layer allows for buildup of the object from bottom to top, creating a three-dimensional (3D) object in space (Novakova-Marcincinova and Kuric, 2012). The most widely used materials for FDM printing are thermoplastic filaments, including acrylonitrile butadiene styrene, poly(lactic acid), high-impact polystyrene, thermoplastic polyurethane, and aliphatic polyamides (Nikzad et al., 2011). FDM systems can be calibrated to print materials at different temperatures and extrusion rates, and use of additional nozzles can facilitate printing of multimaterial constructs. Print resolution can depend on several different factors, including nozzle size, precision of the extruder movements in X/Y space, layer height, print speed, and shape retention of the extruded material (Ozbolat and Yu, 2013). Typical resolution is in the range of 10–300 microns (Bin et al., 2016). FDM offers several advantages, including low cost, limited use of material, accessibility, and relatively rapid turnaround, but there are several limitations to be considered (Lee et al., 2014). It is difficult to print constructs that require the printing of overhanging parts because the technique lacks an innate support system (Crump et al., 1996). This can hinder printing of certain shapes, but it has been demonstrated that secondary structures using sacrificial materials, such as sucrose or starch, can be printed to aid in the printing of overhangs. In certain cases, potential delamination of layers can introduce anisotropy and result

in mechanically unstable constructs (Ahn et al., 2002). More recent developments in technology and application of materials science now allows for a broader range of materials to be printed with this technique, broadening properties of the printed constructs. Multiple research groups have demonstrated the use of FDM to print viscous liquids such as hydrogel solutions, emulsion inks, and other paste-like compositions (Zein et al., 2002; Kalita et al., 2003). This has opened up new potential applications for the printed constructs because they maintain new properties like elasticity, the ability to respond to environmental changes like pH or heat, or can act as carriers for cells, proteins, and other biological molecules (Fig. 1.4.8.3).

Powder Bed Fusion

Electron Beam Melting (EBM) is a type of powder fusion additive manufacturing technique. The instrument setup involves a vacuum chamber that contains a moving bed with powder material and an electrical optical column from which the electron beam is generated. Briefly, a heated tungsten filament in the upper column generates an electron beam that is focused and deflected off magnetic coils in the lower column (Gong et al., 2012). For each layer, the stage rakes a new, thin layer of powder and the electron beam traces a path depending upon the designed computer-aided design model. As the electron beam traces the path, the powder material is heated (average temperature between 600 and 800°C), melted, and then rapidly solidified in an inert environment such as purified argon (Murr et al., 2012b). For each layer, this process is repeated to build an object in 3D space. The most widely used powder materials for EBM include aluminum, steel, copper, titanium, and nickel, as well as different alloys of these metals (Körner, 2016). Printed construct resolution depends on parameters like beam current and diameter, thickness of each layer (0.05–0.2 mm), and the powder size (ranging from 10 to 100 μm). EBM is an efficient printing technique, with an overall approach that has reduced cost and rapid speed. Additionally, printed



• **Figure 1.4.8.3** (A) A schematic of material extrusion (Sears et al., 2016), (B) electron microscopy of the layers of a material extrusion 3D-printed object (Cuiffo et al., 2017), (C) image of common-use material extrusion prints (Halford, 2018), (D) material extrusion 3D-printed gear mechanism prototype (Schubert et al., 2014), and (E) a material extrusion 3D-printed model used in surgical planning for neurosurgery (Ventola, 2014). ((E) 3D Print Exchange. National Institutes of Health. Available at: <http://3dprint.nih.gov>. Accessed July 9, 2014.)

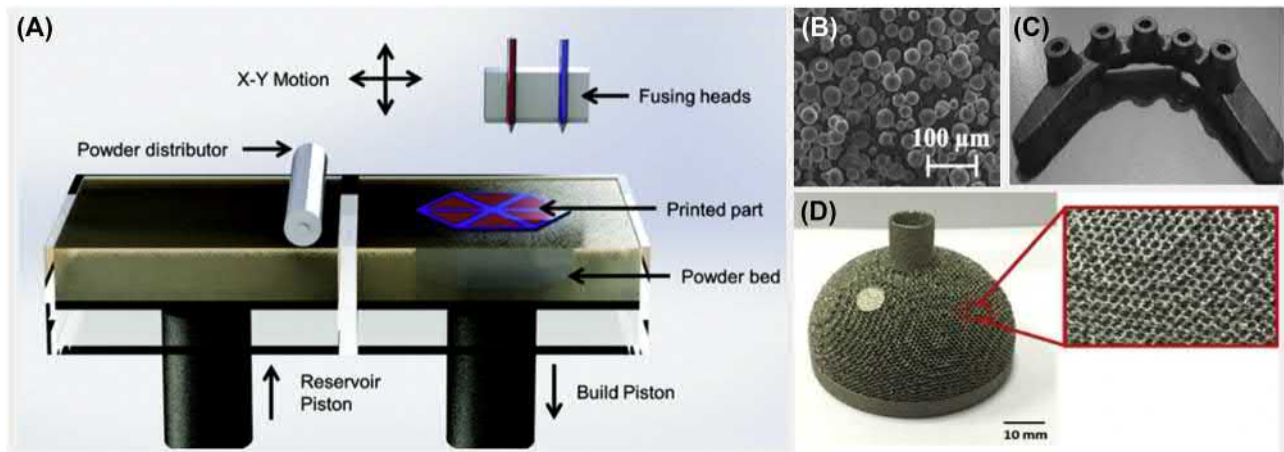
constructs maintain strong material properties because printing conditions prevent residual stresses or any distortion/warping of the prints (Seagle et al., 1962; Rafi et al., 2013). Complex prints with novel characteristics like material gradients make EBM popular for a variety of different applications. In the field of biomaterials specifically, it has been used to impart open cellular structures into solid implants to promote stiffness compatibility (Murr et al., 2010). It has been demonstrated that incorporation of these porous structures enhanced cell growth and improved implant stability by eliminating the need for using adhesive cementing, a common but invasive practice for implant strategies (Murr et al., 2012a). With the current technology, use of EBM for other biomaterial applications is relatively limited because it can print primarily metals. Additional developments to the technology have to be made to broaden its use for fabrication of other types of biomaterials.

Selective laser sintering (SLS) and **selective heat sintering (SHS)** are additive manufacturing techniques based on powder fusion binding. SLS creates 3D parts through the application of laser energy on a powder bed, based on computer-aided design descriptions. Each layer of the print is created as the laser scans a specific path over the powder, causing the particles to sinter together in thin layers. For the SHS technique, each layer of the print is created in a similar way, but the laser will melt the particles and bond them together (Merzelis and Kruth, 2006; Chia and Wu, 2015). Subsequent layers are then created as a new layer of powder is spread on top of the previously printed layer and the laser traces the path again, thus building the object in space layer by layer. Commonly used powder materials for this technique include thermoplastics, ceramics, plasters, and composites, as well as various types of metal powders (Shirazi et al., 2015; Agarwala et al., 1995). The resolution of SLS/SHS prints depends on the size of the laser or heat source, and the size of granules. To maintain higher

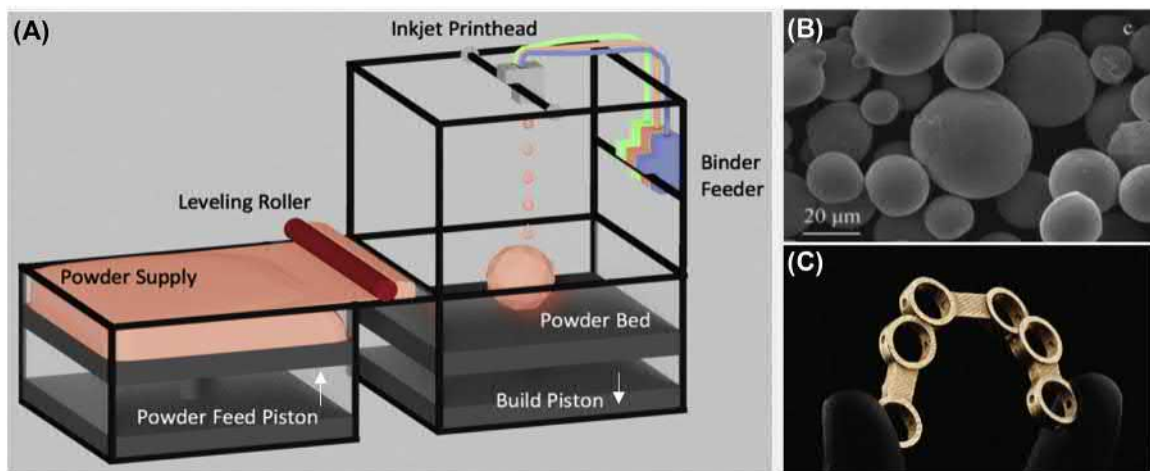
resolution in the prints, it has been observed that the preferred particle size is 10–150 μm (Exner et al., 2008). Furthermore, material properties, such as structure or mechanical stability, can also depend on process factors such as laser energy density, bed temperature, layer thickness, and hatch distance (Bhatnagar et al., 1999). Advantages of using this technique over other additive manufacturing techniques include fabrication of strong functional prints, design freedom, and minimal need for support structures for complex shapes. Although these are important benefits, products printed using this technique tend to have a rough, grainy surface (Mazoli, 2013). Additionally, large shrink rates increase the probability of the parts to shrink or warp, and SLS/SHS printed products can only be printed using the materials mentioned previously. In the field of biomaterials, various research groups have demonstrated the use of SLS to fabricate mechanically strong scaffolds that have designed geometry, compositional gradients, and surface modifications with bioactive molecules (proteins) (Tan et al., 2005; Williams et al., 2005). Their results have demonstrated that incorporating these features into the scaffolds helped improve biocompatibility, increased cell proliferation, and promoted bone regeneration, proving SLS as a competent technique for fabrication of bone replacement devices (Fig. 1.4.8.4).

Binder Jetting

Powder binding is the most typical of the binder jetting processes. In contrast to other powder bed printing processes, the **powder binding** process involves two different materials: a powder material and a liquid binding material. The manufacturing process involves spreading a thin layer of the powder material and the selective deposition of a liquid binding material using a computer-aided design model. The jetted binding droplets on the powder surface cause the powder to agglomerate (Gokuldoss et al., 2017). The next



• **Figure 1.4.8.4** (A) A schematic of powder bed fusion (Sears et al., 2016), (B) SEM micrograph of titanium powder for selective metal sintering use (Vandenbroucke and Kruth, 2007), (C) an SLM-printed titanium alloy dental prosthesis (Additive Manufacturing Group, 2018), and (D) a 3D-printed hip prosthesis (acetabular cap) with porous architecture (Sing et al., 2016).



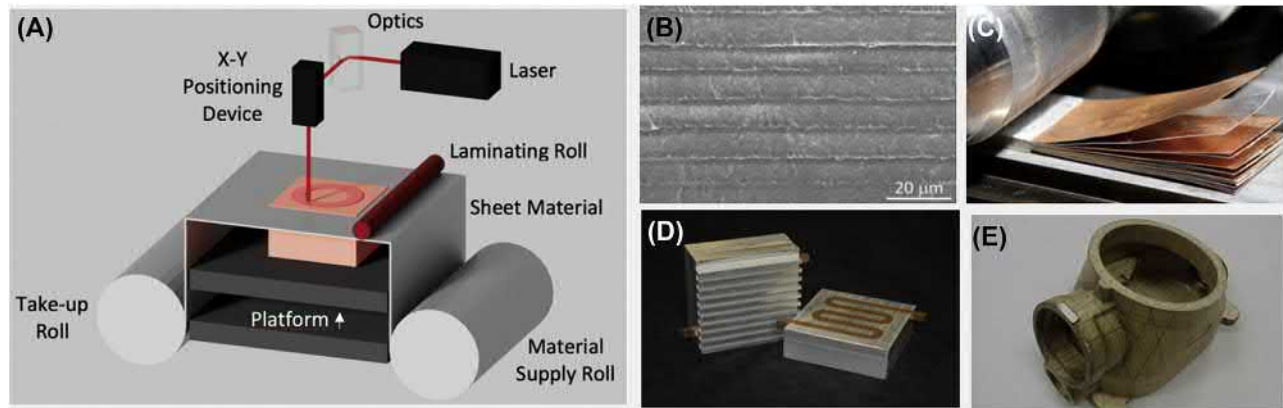
• **Figure 1.4.8.5** (A) A schematic of binder jetting (Jackson et al., 2017), (B) SEM of water-atomized powders used in powder binding printing (Mostafaei et al., 2017), and (C) metal binder jetting printed splinted framework for dental reconstruction (Cascón and Revilla-León, 2018).

layer of powder is added, spread, and the process of binder jetting is repeated. The final construct is built after all iterations of this process are completed (number of iterations varies per individual construct) (Gao et al., 2015). Common materials that can be used for this printing technique include metals/alloys (aluminum, copper, iron, nickel, and cobalt), ceramics (glass, sand, and graphite), and any other material that is available in powder form (Gonzalez et al., 2016). Product resolution depends strongly on the velocity, initial size, and path of the droplets, as well as nozzle diameter and liquid binder properties (Gibson et al., 2015a). The powder binding process is a relatively popular method as parts can be produced without support structures and it is a relatively rapid and cost-effective technique. Although the process does not involve heating during the build process, thermal treatments such as curing, sintering, and annealing after the initial printing with the binder are often required for consolidation (Gokuldoss et al., 2017).

These postprint processes are required to generate sufficient mechanical properties for use and can add significant time and cost to the prints. Additionally, the resulting coarse microstructure of the printed constructs can reduce material mechanical properties due to the presence of microscale porosity in between the sintered particles. Research groups have fabricated ceramic implants with various geometrical designs such as porous structures and cylindrical holes for bone regeneration in vivo demonstrating the potential benefit of using this technique for designing medical implants (Gokuldoss et al., 2017) (Fig. 1.4.8.5).

Sheet Lamination

Laminated Object Manufacturing (LOM) is an additive manufacturing technique based on laser cutting of cross-sections from solid materials. These materials are typically provided in a sheet form (Park et al., 2000). For every layer,



• **Figure 1.4.8.6** (A) A schematic of sheet lamination (Suresh et al., 2017), (B) SEM showing structure of laminated sheets (Yamamoto et al., 2014), (C) an image of a material-binding layer in sheet lamination (Additive Manufacturing Group, 2014), (D) a multimaterial print using ultrasonic consolidation (3D Diligent, 2019), and (E) a laminated object manufacturing (LOM) model of a valve flange (Manufacturing Technology Centre, 2018).

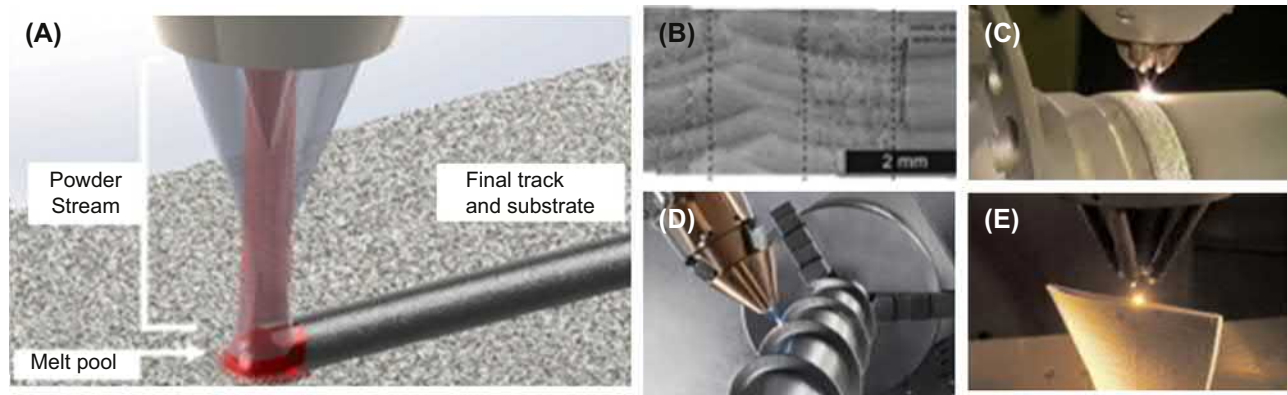
after the laser cuts along the contour of the specific part's geometry, a new sheet of material is spread over a movable substrate in preparation for cutting the next layer (Mekonnen et al., 2016). Laser cutting patterns are determined by computer-aided design models and relayed to the cutter. In postcutting, the layers are bound together with a hot roller that compresses the sheets and activates adhesives on the sheets (Zocca et al., 2015). Sheet material that can be used for this technique includes layers of paper, plastic, metal, foil, or ceramics (Wong and Hernandez, 2012; Bikas et al., 2016). Print resolution depends on parameters such as laser power/speed, temperature, and cross-hatch size. The main advantage of using this method is the high fabrication speed, largely because the laser only has to cut through one sheet at a time, not the entire cross-section of material. Additional benefits include low cost, no postprocessing or supporting material needed for printing structures, high durability parts, and use of nontoxic or reactive materials (Mueller and Kochan, 1999; Klosterman et al., 1998). Although there are numerous benefits, it has been commonly observed that the surface of LOM-generated objects typically has a poor finish due to limited control over how thick the sheets used can be and smaller pieces commonly have lower detail reproduction due to limited accuracy in the Z-dimension of the laser. Additionally, large amounts of waste can be generated depending on the design and shape of the part being printed (Gibson et al., 2015b). The LOM technique is used commonly for rapid prototyping of plastic parts, molding, and foundry, but use in the biomedical field has been limited to reproducing models of organs (Mueller and Kochan, 1999) (Fig. 1.4.8.6).

Ultrasonic Consolidation (UC) is a printing technique that combines additive manufacturing and computer numerical control to generate specific constructs from computer-aided design models. Briefly, this technique involves sequential, layer-by-layer binding of metal foils together using ultrasonic welding (White, 2003). Ultrasonic vibrations are applied to the tape (metal foils) through a sonotrode that vibrates at a specific frequency and amplitude. The

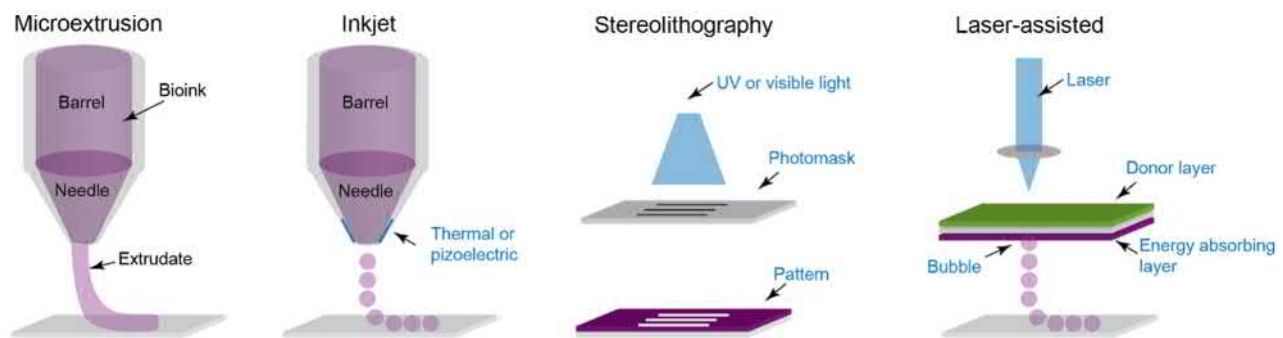
sonotrode is rolled along the length of the tape, thus bonding the tape to the ones below producing a weld between the two (Kelly et al., 2014). This technique is most commonly used to fabricate metal composite structures or metal–matrix composites, with the main foils fabricated using materials such as aluminum, copper, iron, and nickel. Several different parameters dictate resolution in UC, including: higher oscillation amplitudes for the sonotrode, high magnitude of normal force, higher substrate temperature, and lower welding speeds (Chua and Leong, 2014). Furthermore, it is important to note that these parameters often need to be modified depending on the material and vary from machine to machine. Advantages to using this technique include fabrication of parts with high dimensional accuracy, good surface finish, and fabrication of complex structures such as internal passageways, honeycomb structures, or objects made from many different types of metals. Furthermore, the fabrication process does not involve any sort of melting, limiting shrinkage, residual stresses, or distortion in finished parts. Finished part quality highly depends on the frictional conditions at the sonotrode/foil interface and can propagate defects within the part, ultimately affecting mechanical properties, surface finish, and overall quality (Kelly et al., 2014). Thus far, UC has mostly been used for the fabrication of metal parts, limiting its use in the field of biomaterials to fabrication of implants. Limited research has been done to demonstrate the utility of this technique for medical applications.

Directed Deposition

Laser Metal Deposition (LMD) is a direct energy deposition technique that is often used to 3D print metallic parts or add features to an existing metallic structure (Herzog et al., 2016). It uses a high power laser beam to melt the metal surface while simultaneously depositing a metal powder or wire (Kaiser et al., 2012). The metallic powder is extruded through one or more deposition nozzles to form a part layer by layer. Varying laser power, extrusion width, speed of



• **Figure 1.4.8.7** (A) A schematic of direct energy deposition (Pinkerton, 2015), (B) optical micrographs of the overlap of lines of a titanium alloy using DED (Saboori et al., 2017), (C) image of a laser metal deposition (DED) machine (Jackson et al., 2018), (D) using LMD to create threads on a metal shaft, and (E) a processor blade being created using Laser Engineered Net Shaping (LENS) technology (Gill).



• **Figure 1.4.8.8** Schematic overview of bioprinting processes.

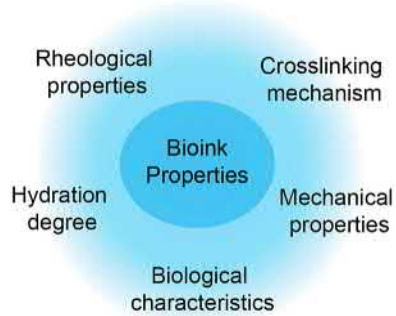
motion, and powder feed rates allow control of speed and resolution of the print (Santos et al., 2006). LMD can be used to print objects from millimeters to meters in size with a resolution as low as 1 mm (Pinkerton, 2015). Different metal materials can be used, such as nickel, cobalt, iron, copper-based metals, and carbide materials. It can also print titanium alloys, which are widely used in medical devices (Gu et al., 2012). The high level of control over the heat and positioning of the laser beam allow for very reliable results with low heat distortion and improved microstructure. However, relatively high cost and low reproducibility make it a less used method for printing parts (Kaierle et al., 2012). LMD has been used to create implants that have improved, controlled properties to promote osseointegration and cell ingrowth. It can print implants with a highly controlled and interconnected porous microarchitecture, a key property for cell ingrowth. The implants can also be printed with load-bearing capabilities and antibacterial coatings to limit infection. LMD process parameters allow for printing multiple different metals at a time, so one metal can be used to print an inner porous structure to promote bone in-growth, while another metal can be used to coat certain areas to give mechanical strength or antimicrobial properties to the implant. Fabrication of implants with even pore structure and size is a critical and distinct advantage of using LMD over other metal printing methods (Trevisan et al., 2018; Ahsan et al., 2011) (Fig. 1.4.8.7).

Bioprinting

Bioprinting involves robotic deposition of cell-laden bioinks into custom shapes to facilitate regeneration of tissue. A range of bioprinting approaches are currently used, including microextrusion, inkjet, stereolithography, and laser-assisted bioprinting. Bioinks, which are a crucial component in bioprinting, need to be designed within the “biofabrication window” by optimizing a range of material characteristics, including rheological properties, hydration characteristics, mechanical properties, cross-linking mechanism, and biological characteristics. A range of polymers are combined with bioactive agents to improve the functionality of cell-laden printed scaffolds. In this section, we will discuss some of the key components in bioprinting, including the types of bioprinting approaches and bioink design, including selection of biomaterials for bioinks.

Bioprinting Approaches

A range of additive manufacturing approaches have been developed for 3D bioprinting, including microextrusion, inkjet, stereolithography, and laser-assisted bioprinting (Fig. 1.4.8.8) (Derby 2010; Duan et al. 2014). In all these approaches cell-laden bioinks are printed to mimic native tissue structure and facilitate tissue regeneration. In



• **Figure 1.4.8.9** Bioink design parameters that need to be optimized to obtain high fidelity cell-laden constructs.

microextrusion bioprinting, cell-laden bioink is extruded through micron-sized nozzles (Exner et al., 2008). Multiple nozzles can be employed for extrusion-based bioprinting to obtain multimaterial complex structures, while in inkjet bioprinting, bioink droplets are deposited via thermal, piezoelectric, or electromagnetic means. In stereolithography, a focused UV light beam is used to cross-link liquid photopolymer via a layer-by-layer approach to fabricate scaffolds (Gong et al., 2012). In a similar approach, laser-assisted bioprinting involves use of laser energy to volatilize a sacrificial layer, propelling a payload to a receiving substrate (Ferris et al., 2015). Approaches that combine multiple modality are also investigated to obtain hybrid structures. For example, by combining extrusion bioprinting and stereolithography, cell-laden hydrogels and hard thermoplastic can be combined (Gonzalez et al., 2016). More recently, microfluidic bioprinting was developed by combining microfluidic printheads with extrusion printing for high-velocity printing of multiple materials (Gu et al., 2012). This new modality makes it possible to program sequential or simultaneous extrusion of different bioinks with complex spatiotemporal control such as printing of gradients into structures (Gunatillake and Adhikari, 2003; Haramati et al., 2002; Herzog et al., 2016).

Bioink Design Parameters

A vital aspect and bottleneck to the design and implementation of a bioprinting system is consideration of a bioink. Bioinks are mainly comprised of a polymer matrix loaded with cells and bioactive signals (Boland et al., 2006). By controlling the physical and chemical properties of the extracellular matrix (ECM), cell behavior can be regulated to accelerate tissue integration and functional recovery. Thus it is important to carefully select bioprinting process, bioink characteristics, type of cells, and bioactive signals for bioprinting to support and enhance tissue regeneration in a spatiotemporal manner (Chung et al., 2013). A range of parameters dictates the 3D bioprinting process, including rheological properties, cross-linking mechanism, hydration characteristics, mechanical properties, and biological functionality (Fig. 1.4.8.9). In this section, we will discuss how

these different aspects can affect the performance of printed scaffolds for regenerative medicine:

- **Rheological Properties:** Hydrogels are poorly suited to 3D printing, and adapting them to 3D bioprinting has proven to be a consistent challenge to the field (Chimene et al., 2016; Huebsch et al., 2010). Rheological properties of bioink, including viscoelasticity and shear-thinning characteristics, are important for obtaining high print fidelity and structural stability of 3D bioprinted structures (Das et al., 2013; Wüst et al., 2014). In addition, uniform distribution of cells within the bioink formation is also controlled by bioink viscosity. For example, low viscosity of bioink will result in sedimentation of cells during the printing process, which results in uneven distribution of cells in the printed scaffolds.
- **Cross-Linking Mechanism:** Prior to cross-linking, hydrogels are typically liquid polymer solutions that collapse into puddles, making it impossible to support subsequent layers. The type of cross-linking techniques and gelation kinetics used to obtain a 3D network depend on polymer type and printing modality. A range of cross-linking mechanisms involving use of light, ionic strength, electrostatic interactions, pH, and temperature can be employed to obtain structurally stable polymeric networks. The primary criteria for selection of cross-linking method will be to maintain high viability of encapsulated cells.
- **Hydration Degree:** The water content of bioinks dictates its viscosity, printability, and mechanical properties. In addition, porosity of hydrogel networks also controls transport of oxygen and nutrient through the cell-laden hydrogel, which is a prerequisite for successful tissue regeneration.
- **Mechanical Properties:** The mechanical properties of bioink are heavily reliant on chemical composition, polymer concentration, and cross-linking density. However, increasing polymer concentration or cross-linking density significantly interferes with the viability and function of encapsulated cells by reducing permeability and porosity. Therefore an understanding of the factors that influence mechanical behavior is required to effectively design bioink formulation.
- **Biological Characteristics:** Physical properties of bioinks influence cellular behavior and are important parameters in determining applicability of polymers for generating specific tissues. For example, polymers with cell adhesive sites are required to enhance survival and proliferation of adhesive types of cells such as osteoblasts. However, chondrocytes would prefer to be encapsulated in hydrogels with minimum cell adhesion sites.

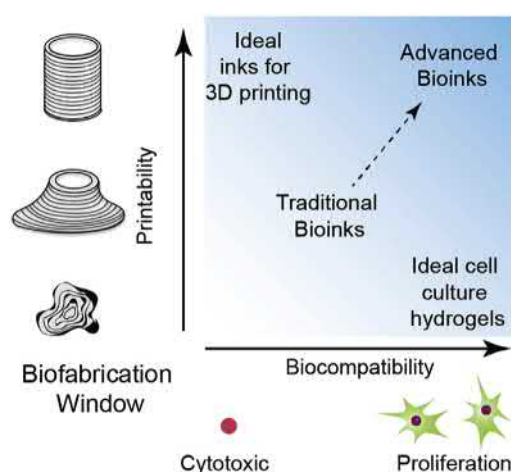
Biofabrication Window

Bioprinting living cells requires a very specific set of conditions such as aqueous environment, sufficient oxygen, and nutrient diffusion, as well as appropriate pH and osmolality along with key vitamins and minerals for cellular functions, which are best met with a special class of

biomaterial hydrogel bioinks (Michalski and Ross, 2014; Sachlos and Czernuszka, 2003). Bioinks are rationally designed materials intended to improve the functionality of cell-laden printed scaffolds within the “biofabrication window” (Chimene et al., 2016; Malda et al., 2013). The biofabrication window is a concept that describes required compromises between the printability of a bioink formulation and cell viability (Fig. 1.4.8.10). Generally, hydrogels are used as bioink in most 3D bioprinting due to high water content (70%–99%), which makes hydrogels highly porous and permeable, allowing rapid diffusion of oxygen and nutrient throughout the scaffold (Zorlutuna et al., 2012; Sachlos and Czernuszka, 2003; Ferris et al., 2013). Hydrogel networks are highly porous and provide support to cell adhesion, proliferation, and migration, which are key components to facilitate tissue regeneration. Hydrogels can also be created from synthetic as well as natural polymers. Synthetic polymers, such as poly(ethylene glycol) (PEG), provide customized physical and chemical properties, while natural polymers like collagen and hyaluronic acid provide a native-like microenvironment to help direct cellular functions. Combination of natural and synthetic polymers can provide composite hydrogels with tailored characteristics. After printing, these cell-laden hydrogels can be cross-linked using cell-friendly scaffolds. Thus hydrogels are the universal choice for 3D bioprinting as they closely mimic the native microenvironment of cells (Chimene et al., 2016; Ferris et al., 2013; Huebsch et al., 2010).

Biomaterials for Bioprinting

A range of polymers can be used to design hydrogel-based bioinks to control and direct cell functions, leading to enhanced cell motility, proliferation, and subsequent differentiation. Both natural and synthetic polymers have been investigated as hydrogel bioinks (Mano et al., 2007). Natural polymer bioinks provide a number of advantages due to their chemical and structural similarities to native ECM. Some of the natural polymers that are currently being explored for bioprinting include collagen, gelatin, alginate, fibrin, hyaluronan, and dextran. Synthetic polymers, however, can be more easily tailored for a given application by optimizing mechanical properties, degradation rates, or bioactivity (Gunatillake and Adhikari, 2003). Some of the synthetic polymers that are currently used in bioprinting include PEG, poly(lactide-co-glycolide), poly(ϵ -caprolactone), and poly(L-lactic acid). Blends of both natural and synthetic polymers can result in a combination of benefits in an attempt to enhance and tailor cellular responses within the 3D fabricated scaffolds. For example, synthetic polymers can be copolymerized with enzymatic degradation sites found in natural polymers to enhance cell migration and aggregation within the scaffold (West and Hubbell, 1999). These polymer combinations used in conjunction with the spatial resolution of many bioprinting technologies enable a more efficacious tissue and organ regeneration process.



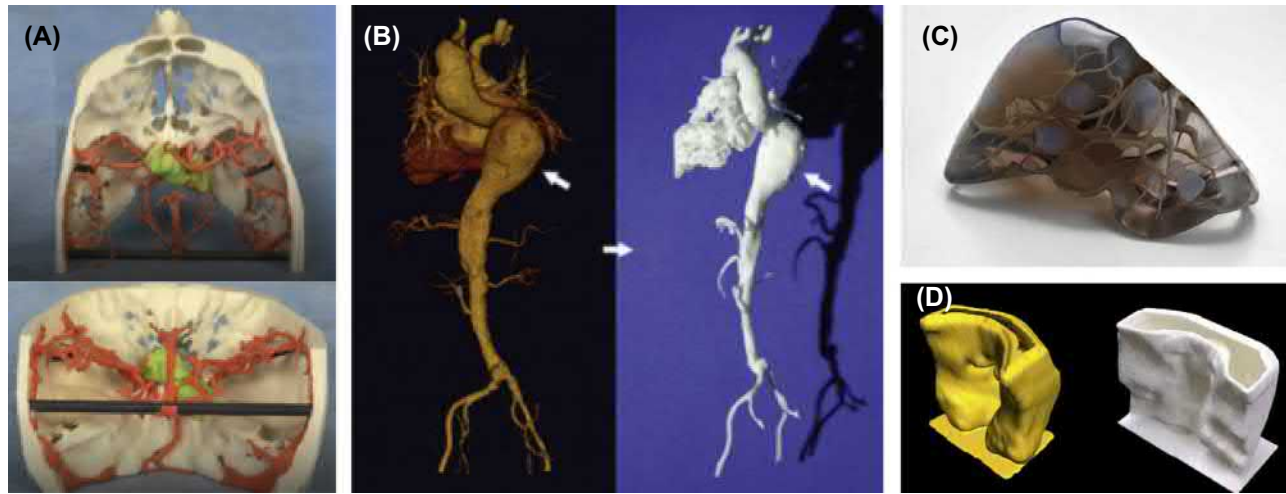
• **Figure 1.4.8.10** Biofabrication window highlighting the required compromises between the printability of a bioink formulation and cell viability.

Medical Applications of 3D Printing

This section focuses on applications of 3D printing technologies in different facets of the medical field, including surgical planning, medical training, design and fabrication of implants, and development of personalized drug delivery systems. For each category, representative application cases from both advanced studies and newly developed medical protocols will be explained, along with a discussion on different materials being used and the features or advantages of each 3D printing technology.

Surgical Planning and Medical Training

Medical imaging, such as computerized topography, magnetic resonance imaging, and ultrasound, are commonly employed for disease diagnosis and surgical planning and generate a stack of two-dimensional images to visualize the tissue or organ of interest (Vannier and Marsh, 1996; Haramati et al., 2002). With these imaging modalities, assisted by contrast agents and postimage processing, technicians can differentiate the boundary of benign and malignant tissue and identify abnormal dilation or contraction to support preliminary diagnosis and sequential surgical planning. Although the images can be converted into 3D visual models, they cannot provide direct 3D demonstration and a precise reflection of the spatial relations of the tissues. Using 3D printing technology in combination with these imaging results, researchers and surgeons can generate patient-specific anatomical structures with intricate and accurate presentation of the tissues and organs. 3D printed models can also mimic the physical properties of the targeted tissue, including compressive or tensile modulus, elasticity, and stiffness (Tymrak et al., 2014; Bose et al., 2013; Schumacher et al., 2015). Utilizing these models reduces the operation time, avoids disproportionate planning, and achieves a more cost-effective use of research and medical resources (Ventola et al., 2014). Fig. 1.4.8.11 shows several cases where 3D



• **Figure 1.4.8.11** Applications of 3D printing in surgical planning and training: (A) blood vessel reconstruction for neurosurgery guidance (Walter Reed National Military Medical Center), (B) 3D printed aorta model for thoracic complex aneurysm patient (Rengier et al., 2010), (C) a replica of liver for transplant surgical planning (Klein GT et al., 2013), (D) Personalized bolus that serves as radiological shield in skin cancer radiotherapy (Canters et al., 2016).

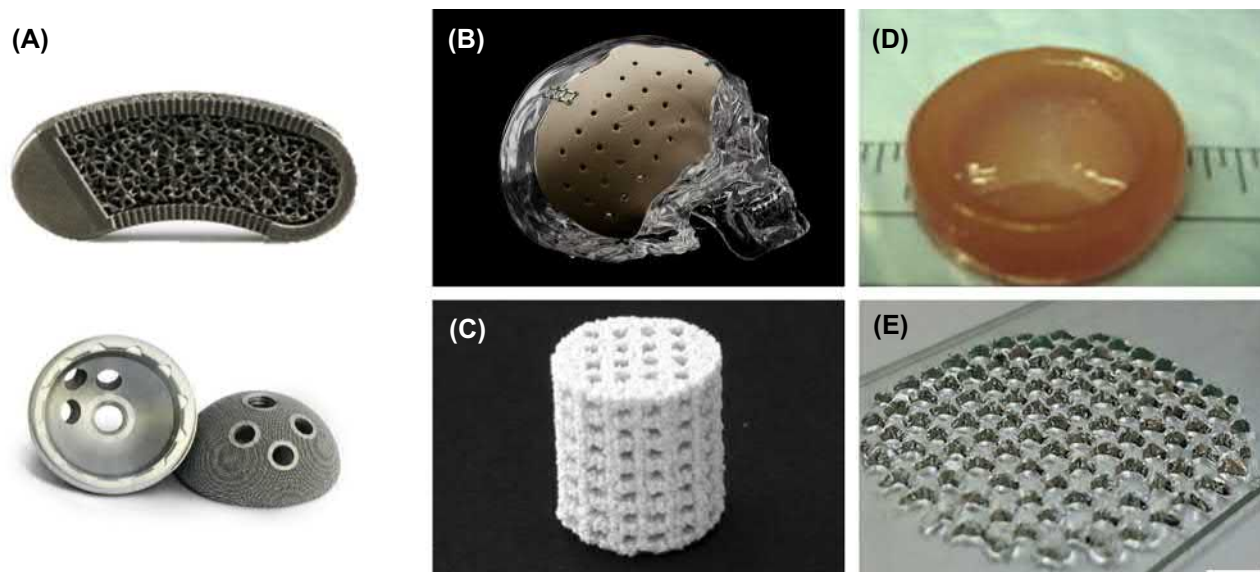
printing techniques can generate 3D replicas of patient-specific anatomies, including brain vessels, disordered aorta, and liver. Researchers from [Walter Reed National Military Medical Center](#) have been employing multimaterial 3D printing to construct skull, neural vasculature, and nerve models with various photocross-linking polymers (Fig. 1.4.8.11A). Specifically, the models with blood vessels and nerves depict the complicated spatial relationships that can be studied to avoid potential damage in surgical procedures. Surgeons can also determine reliable and effective incision and operational paths based on these models. Similarly, 3D printing techniques are being applied to cardiovascular surgical plans. In Fig. 1.4.8.11B, an aorta model was fabricated with rapid prototyping for a patient with a thoracic aortic aneurysm, displaying a well-defined vessel dilation region (Rengier et al., 2010). The model allowed the surgeons to evaluate the pathological progress and develop personalized treatment plans. It also improved communication with the patient in regard to the pathology and discussion of surgical options. In parallel to surgical applications, 3D printing is also employed in medical training for procedures such as colonoscopy. Prevalent training is performed on cadaver dissection; however, cadavers are subject to low availability, high cost, and no relevant pathology (Ventola, 2014). On the contrary, using 3D printed models can reduce the cost and replace cadaver usages.

3D printing is also playing a significant role in improving organ transplantation procedures. One of the major challenges in organ transplantation surgery is that the donor organ cannot always meet the recipient size requirements (e.g., pediatric recipient of adult organ); however, in situ organ trimming can delay and complicate the transplantation. To avoid such complications, Dr. Maki Sugimoto from Japan's Kobe University Hospital (Klein GT et al., 2013) replicated the donor's organ prior to surgery with 3D rapid

prototyping. The liver replica (Fig. 1.4.8.11C) showed the structures of different compartments and distribution of blood vessels. In addition, additive manufacturing techniques can contribute to personalizing treatments such as radiotherapy. To reduce unnecessary radiation to the normal tissue, 3D printing is applied to create patient-specific radiological shields for susceptible regions. As shown in Fig. 1.4.8.11D, a plastic bolus was made to block the radiation around the patient's nose, which has skin susceptible to radiation (Canters et al., 2016).

Fabrication of Complex Implants

Implants and prostheses are often employed to replace diseased or damaged tissue, including bone grafts (Sears et al., 2017), regenerative cartilage scaffolds (Markstedt et al., 2015), vascular grafts (Kolesky et al., 2014), or filling content, and to make adjustments in plastic and reconstructive surgeries (Kamali et al., 2016). Generally, implants can be fabricated or assembled with single materials, including metal, ceramics, and polymers, or combinations of multimaterials. With these materials, there are two categories of implant fabrication methods: negative manufacturing, based on shaving and drilling away material to generate construct, and additive/positive manufacturing with layer-by-layer addition of material to generate construct. Despite its advantage of high integrity, negative manufacturing of implants is undermined by its mismatch of detailed structures to the target tissue or organ and the possible defects that can lead to implant failure. As a novel method of additive manufacturing, 3D printing techniques are applied in implant fabrication with these advantages: (1) lower expense for implant fabrication, (2) patient-specific rapid prototyping, (3) detailed reconstruction of targeted structure, and (4) integration of multimaterial composition. Moreover,



• **Figure 1.4.8.12** Implants or scaffolds based on 3D printing techniques: (A) commercial metallic implants of Ti-4Al-6V alloy, spinal cage (top) and artificial acetabular cup (bottom) (3D Systems), (B) the OsteoFab Patient Specific Cranial Device in replacement of skull bony voids (Oxford Performance Materials), (C) synthetic bone replacement of hydroxyapatite scaffold (Leukers et al., 2005), (D) heart valve conduit with encapsulated human aortic valve interstitial cells (HAVIC) (Duan et al., 2014), (E) 3D printed polyelectrolyte gelatin-chitosan hydrogel for skin tissue engineering (Ng et al., 2016).

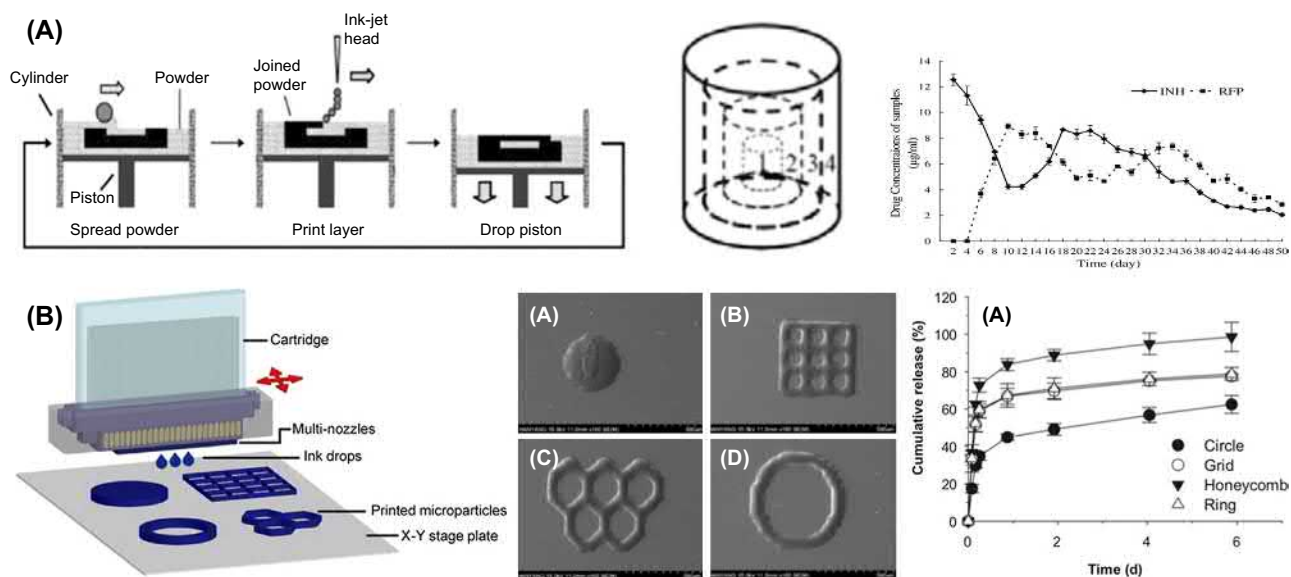
additive manufacturing techniques can be used to fabricate tissue regenerative scaffolds designed to serve as a supplementary ECM during the tissue regeneration process. Previous research probed into how these scaffolds allow for cell delivery, endogenous cell recruitment, attachment, proliferation, and differentiation to restore the functionalities of targeted tissues or organs (Do et al., 2015). The material choices for tissue regenerative scaffold range from synthetic polymers, such as poly(ϵ -caprolactone), to naturally derived materials like alginate, chitosan, cellulose, collagen, fibrinogen, and hyaluronic acid (Do, 2015). Researchers have demonstrated the use of solid free-form fabrication to create high-resolution scaffolds with or without cells. In Fig. 1.4.8.12, examples of implants or scaffolds made from different materials for various applications display the versatility of 3D printing in this field.

In Fig. 1.4.8.12A, commercially available, customized Ti-4Al-6V alloy implants are represented by a spinal cage for spinal fusion surgery and acetabular cup used in total hip replacement (3D Systems). These metal implants are designed and manufactured by 3D Systems, Inc., a company specialized in providing advanced on-demand solutions with direct digital manufacturing on the basis of metal 3D printing in a variety of fields, including dental, spinal, and orthopedic healthcare. Besides metal implants, 3D printed cranial devices made from polymer are also accessible with customization. Oxford Performance Materials, Inc. has pioneered the promotion of polymer implant development and has used an originally invented high-performance polymer, polyether-ketone-ketone. The polymer has been utilized in areas of aerospace and biomedical and industrial manufacturing. One of the exemplar products is OsteoFab,

a patient-specific cranial device that serves as a complementary structure for cranial defect caused by skull maldevelopment or major trauma (Materials) (Fig. 1.4.8.12B). Many research groups that develop all types of implants have provided promising results and potentials for eventual medical applications. Hermann Seitz and his collaborators (Leukers et al., 2005) developed a 3D printed hydroxyapatite scaffold for bone regeneration. The hydroxyapatite scaffold maintained a complex internal structure and was printed with high-resolution and important detailing (Fig. 1.4.8.12C). In this case, cell studies and histological analysis results showed invasive cell proliferation into the scaffold with a dynamic cultivation method and pointed to further inquiry of the osteogenic differentiation with high interconnection. Other groups have fabricated heart valve conduits with cell encapsulation (Duan et al., 2014) (Fig. 1.4.8.12D) and developed polyelectrolyte gelatin-chitosan hydrogel as skin constructs (Ng et al., 2016) (Fig. 1.4.8.12E). In conclusion, 3D printing techniques allow for the fabrication of implants for various tissues and tissue-engineering scaffolds with high-resolution and complicated structures, providing a low-cost, rapid solution for a diversity of surgical and therapeutic scenarios.

Personalized Drug Delivery Systems

Another medical field being redefined by 3D printing techniques is pharmaceutical research and drug delivery systems. Physicians and patients are increasingly interested in novel drug delivery systems, of which 3D printed tablets or drug delivery devices top the list (2016). The traditional manufacturing steps of tablets for drug delivery are



• **Figure 1.4.8.13** Applications of 3D printing techniques in drug delivery system design, including technique schematic (left), system model (middle), and release profile (right). (A) Temporal control on multi-drug release based on the drug spatial distribution (Wu et al., 2009) and (B) geometry-dependent kinetic control with a piezoelectric inkjet printing system (Lee et al., 2012).

mixing, milling, drying, wet granulation, and compression or molding (Prasad et al., 2016). However, these methods are limited by low drug stability caused by degradation in production and are not suitable for personalized dosage due to large-scale manufacturing. 3D printing offers the following advantages in drug delivery: (1) product consistency by standardization and mechanization, (2) customization of the drug delivery system specific to the patient's condition (e.g., multiple chronic diseases), and (3) facilitated combinations of various drugs and substrates (Prasad et al., 2016). By adjusting the drug dosing, dosage forms, and drug release profiles with the assistance of automated 3D printing systems, personalized pharmaceutical treatment can result in better patient compliance with improved therapy outcomes. To this end, researchers have invested resources and manpower in the development of reliable and tunable 3D printing-manufactured drug delivery systems. Wu et al. designed a multireservoir system to release two first-line antituberculosis drugs, isoniazid and rifampicin (Fig. 1.4.8.13A) in 2009 (Wu et al., 2009). Fabrication of the drug implant was based on a layer-by-layer sintering process to generate the multichamber structure. As shown in the middle schematic of the structure, chambers 1 and 3 contained rifampicin, while chambers 2 and 4 contained isoniazid. Therefore there was an alternating release profile of the two drugs over a timeframe of 50 days. This example provides insight into how 3D printing can be utilized to create systems that have the temporal control of drug delivery by the spatial distribution of therapeutic agents. Additionally, the shape of the delivery unit can influence the drug release kinetics. In 2012, Lee et al. investigated how the structure of drug-encapsulated microparticles can induce differences in drug release rate (Lee et al., 2012).

They fabricated microparticles of different shapes, such as a circle, grid, honeycomb, and ring, using a piezoelectric inkjet printing system. The release profiles of microparticles with different geometries showed different levels of burst release percentages and overall release rates. Thus both studies demonstrate control over the drug release profiles, maintaining difference in the mechanism and target, demonstrating the versatility of 3D printing. More importantly, given that the delivery of multiple agents has been achieved and individual agent release rates can be modified, more complicated and compositional deliveries of multiple agents will be foreseen with more advanced high-resolution 3D printing techniques and proper substrates.

Summary

Since its first introduction to researchers and industries by Charles Hull (Schubert et al., 2014), 3D printing has revolutionized traditional medical device development processes and treatment strategies (Ventola et al., 2014). The adaptation of current 3D printing techniques for biomedical applications has enabled a broad range of medical advances from patient-specific surgical guides to personalized drug delivery systems to complex cell-laden scaffolds that more closely mimic native organs and tissues. Despite the strong potential and diversity of 3D printing in the medical field, there remain many challenges that relate to both the printing process and the materials available for printing. There is a continued need for improved resolution, increased speed, and more versatile materials. In addition, there is a corollary needed for new standards and quality control systems for additive manufacturing in each of these applications.

References

- 3D Systems, I. <https://www.3dsystems.com/medical-device-manufacturing>. Date accessed November, 2018.
- Additive Manufacturing Research Group, 2018. Loughborough University. www.lboro.ac.uk/research/amrg/about/the7categoriesofadditivemanufacturing/powderbedfusion/.
- Agarwala, M., Bourell, D., Beaman, J., Marcus, H., Barlow, J., 1995. Direct selective laser sintering of metals. *Rapid Prototyp. J.* 1, 26–36.
- Ahn, S.H., Montero, M., Odell, D., Roundy, S., Wright, P.K., 2002. Anisotropic material properties of fused deposition modeling ABS. *Rapid Prototyp. J.* 8, 248–257.
- Ahsan, M.N., Paul, C.P., Kukreja, L.M., Pinkerton, A.J., 2011. Porous structures fabrication by continuous and pulsed laser metal deposition for biomedical applications; modelling and experimental investigation. *J. Mater. Process. Technol.* 211, 602–609.
- Alamán, J., Alicante, R., Peña, J., Sánchez-Somolinos, C., 2016. Inkjet printing of functional materials for optical and photonic applications. *Materials* 9, 910.
- Amin, R., Knowlton, S., Hart, A., Yenilmez, B., Ghaderinezhad, F., Katebifar, S., Messina, M., Khademhosseini, A., Tasoglu, S., 2016. 3D-printed microfluidic devices. *Biofabrication* 8, 022001.
- Bhatnagar, R.S., Qian, J.J., Wedrychowska, A., Sadeghi, M., Wu, Y.M., Smith, N., 1999. Design of biomimetic habitats for tissue engineering with P-15, a synthetic peptide analogue of collagen. *Tissue Eng.* 5, 53–65.
- Bikas, H., Stavropoulos, P., Chryssolouris, G., 2016. Additive manufacturing methods and modelling approaches: a critical review. *Int. J. Adv. Manuf. Technol.* 83, 389–405.
- Bin, Z., Baekhoon, S., Vudat, N., Doyoung, B., 2016. 3D printing of high-resolution PLA-based structures by hybrid electrohydrodynamic and fused deposition modeling techniques. *J. Micromech. Microeng.* 26, 025015.
- Boland, T., Xu, T., Damon, B., Cui, X., 2006. Application of inkjet printing to tissue engineering. *Biotechnol. J.* 1, 910–917.
- Bose, S., Vahabzadeh, S., Bandyopadhyay, A., 2013. Bone tissue engineering using 3D printing. *Mater. Today* 16, 496–504.
- Canters, R.A., Lips, I.M., Wendling, M., Kusters, M., VAN Zeeland, M., Gerritsen, R.M., Poortmans, P., Verhoef, C.G., 2016. Clinical implementation of 3D printing in the construction of patient specific bolus for electron beam radiotherapy for non-melanoma skin cancer. *Radiother. Oncol.* 121, 148–153.
- Cascón, W.P., Revilla-León, M., 2018. Digital workflow for the design and additively manufacture of a splinted framework and custom tray for the impression of multiple implants: a dental technique. *J. Prosthet. Dent.* 120 (6), 805–811.
- Chia, H.N., Wu, B.M., 2015. Recent advances in 3D printing of biomaterials. *J. Biol. Eng.* 9, 4.
- Chimene, D., Lennox, K.K., Kaunas, R.R., Gaharwar, A.K., 2016. Advanced bioinks for 3D printing: a materials science perspective. *Ann. Biomed. Eng.* 44, 2090–2102.
- Chua, C.K., Leong, K.F., 2014. *3D Printing and Additive Manufacturing: Principles and Applications (With Companion Media Pack) of Rapid Prototyping*, fourth ed. World Scientific Publishing Company.
- Chung, J.H.Y., Naficy, S., Yue, Z.L., Kapsa, R., Quigley, A., Moulton, S.E., Wallace, G.G., 2013. Bio-ink properties and printability for extrusion printing living cells. *Biomater. Sci.* 1, 763–773.
- Crump, S.S., Comb, J.W., Priedeman JR., W.R., Zinniel, R.L., 1996. Process of support removal for fused deposition modeling. Google Patents U.S. Patent 5,503,785.
- Cui, X., Boland, T., DD'lima, D., K Lotz, M., 2012. Thermal inkjet printing in tissue engineering and regenerative medicine. *Recent Pat. Drug Deliv. Formul.* 6, 149–155.
- Cuiffo, M.A., Snyder, J., Elliott, A.M., Romero, N., Kannan, S., Halada, G.P., 2017. Impact of the fused deposition (FDM) printing process on polylactic acid (PLA) chemistry and structure. *Appl. Sci.* 7 (6), 579.
- Das, S., Pati, F., Chameettachal, S., Pahwa, S., Ray, A.R., Dhara, S., Ghosh, S., 2013. Enhanced redifferentiation of chondrocytes on microperiodic silk/gelatin scaffolds: toward tailor-made tissue engineering. *Biomacromolecules* 14, 311–321.
- Derby, B., 2010. Inkjet printing of functional and structural materials: fluid property requirements, feature stability, and resolution. *Annu. Rev. Mater. Res.* 40, 395–414.
- Do, A.V., Khorsand, B., Geary, S.M., Salem, A.K., 2015. 3D printing of scaffolds for tissue regeneration applications. *Adv. Healthc. Mater.* 4, 1742–1762.
- Doyle, Melanie, 2018. “Product Development/Prototyping.” Manufacturing Technology Centre. Memorial University of Newfoundland. mtc.engr.mun.ca/prod.html.
- Doyle M., Product development/prototyping, Manufacturing Technology Centre, Memorial University of Newfoundland, <https://mtc.engr.mun.ca/prod.html>.
- Duan, B., Kapetanovic, E., Hockaday, L.A., Butcher, J.T., 2014. Three-dimensional printed trileaflet valve conduits using biological hydrogels and human valve interstitial cells. *Acta Biomaterialia* 10, 1836–1846.
- Exner, H., Horn, M., Streek, A., Ullmann, F., Hartwig, L., Regenfus, P., Ebert, R., 2008. Laser micro sintering: a new method to generate metal and ceramic parts of high resolution with sub-micrometer powder. *Virtual Phys. Prototyp.* 3, 3–11.
- Ferris, C.J., Gilmore, K.J., Beirne, S., Mccallum, D., Wallace, G.G., 2013. Bio-ink for on-demand printing of living cells. *Biomaterials Science* 1, 224–230.
- Gao, W., Zhang, Y., Ramanujan, D., Ramani, K., Chen, Y., Williams, C.B., Wang, C.C.L., Shin, Y.C., Zhang, S., Zavattieri, P.D., 2015. The status, challenges, and future of additive manufacturing in engineering. *Comput. Aided Des.* 69, 65–89.
- Gibson, I., Rosen, D., Stucker, B., 2015a. *Binder Jetting. Additive Manufacturing Technologies.* Springer.
- Gibson, I., Rosen, D., Stucker, B., 2015b. *Development of Additive Manufacturing Technology. Additive manufacturing Technologies.* Springer.
- Gokuldoss, P.K., Kolla, S., Eckert, J., 2017. Additive manufacturing processes: selective laser melting, electron beam melting and binder jetting—selection guidelines. *Materials* 10, 672.
- Gong, H., Bickham, B.P., Woolley, A.T., Nordin, G.P., 2017. Custom 3D printer and resin for 18 μm × 20 μm microfluidic flow channels. *Lab on a Chip* 17 (17), 2899–2909.
- Gong, X., Anderson, T., Chou, K., 2012. Review on Powder-Based Electron Beam Additive Manufacturing Technology, pp. 507–515.
- Gonzalez, J., Mireles, J., Lin, Y., Wicker, R.B., 2016. Characterization of ceramic components fabricated using binder jetting additive manufacturing technology. *Ceram. Int.* 42, 10559–10564.
- Gu, D., Meiners, W., Wissenbach, K., Poprawe, R., 2012. Laser additive manufacturing of metallic components: materials, processes and mechanisms. *Int. Mater. Rev.* 57, 133–164.
- Gunatillake, P.A., Adhikari, R., 2003. Biodegradable synthetic polymers for tissue engineering. *Eur Cell Mater* 5, 1–16 discussion 16.
- Halford, N., 2018. 4 Best 3D printer cameras to monitor your 3D prints. All3DP. <https://all3dp.com/2/the-4-best-3d-printer-cameras-to-monitor-your-prints/>.

- Haramati, L.B., Glickstein, J.S., Issenberg, H.J., Haramati, N., Crooke, G.A., 2002. MR imaging and CT of vascular anomalies and connections in patients with congenital heart disease: significance in surgical planning. *RadioGraphics* 22, 337–347 discussion 348–9.
- Herzog, D., Seyda, V., Wycisk, E., Emmelmann, C., 2016. Additive manufacturing of metals. *Acta Mater.* 117, 371–392.
- Hornbeck, L.J., 1997. Digital light processing for high-brightness high-resolution applications. *Projection Displays III. Intl. Soci. Optics and Photonics* 27–41.
- “How to Design Parts for Material Jetting 3D Printing.” 3D Hubs, 3D Hubs Blog, 2018. www.3dhubs.com/knowledge-base/how-design-parts-material-jetting-3d-printing.
- Huebsch, N., Arany, P.R., Mao, A.S., Shvartsman, D., Ali, O.A., Bencharif, S.A., RIVERA-Feliciano, J., Mooney, D.J., 2010. Harnessing traction-mediated manipulation of the cell/matrix interface to control stem-cell fate. *Nat. Mater.* 9, 518–526.
- “Introduction to Material Jetting 3D Printing.” 3D Hubs, 3D Hubs Blog, 2018. www.3dhubs.com/knowledge-base/introduction-material-jetting-3d-printing.
- Jackson, B., et al., 13 Dec. 2017. GE teases details of prototype H1 binder jet 3D printer. *Research News, 3D Printing Industry*. <https://3dprintingindustry.com/news/ge-teases-details-prototype-h1-binder-jet-3d-printer-126072/>.
- Jackson, B., et al., 31 May 2018. U.S. DoE applies LENS additive manufacturing to discover better magnets. *Research News, 3D Printing Industry*. <https://3dprintingindustry.com/news/us-doe-applies-lens-additive-manufacturing-discover-better-magnets-133999>.
- Jose, R.R., Rodriguez, M.J., Dixon, T.A., Omenetto, F., Kaplan, D.L., 2016. Evolution of bioinks and additive manufacturing technologies for 3D bioprinting. *ACS Biomater. Sci. Eng.* 10, 1662–1678.
- Kaierle, S., Barroi, A., Noelke, C., Hermsdorf, J., Overmeyer, L., Haferkamp, H., 2012. Review on laser deposition welding: from micro to macro. *Physics Procedia* 39, 336–345.
- Kalita, S.J., Bose, S., Hosick, H.L., Bandyopadhyay, A., 2003. Development of controlled porosity polymer-ceramic composite scaffolds via fused deposition modeling. *Mater. Sci. Eng. C* 23, 611–620.
- Kamali, P., Dean, D., Skoracki, R., Koolen, P.G., Paul, M.A., Ibrahim, A., Lin, S.J., 2016. The current role of three-dimensional printing in plastic surgery. *Plastic and reconstructive surgery*. *Plast. Reconstr. Surg.* 137, 1045–1055.
- Kamran, M., Saxena, A., 2016. A comprehensive study on 3D printing technology. *MIT Int. J. Mech. Eng.* 6, 63.
- Kang, H.-W., Lee, S.J., Ko, I.K., Kengla, C., Yoo, J.J., Atala, A., 2016. A 3D bioprinting system to produce human-scale tissue constructs with structural integrity. *Nat. Biotechnol.* 34, 312.
- Kelly, G.S., Just, M.S., Advani, S.G., Gillespie, J.W., 2014. Energy and bond strength development during ultrasonic consolidation. *J. Mater. Process. Technol.* 214, 1665–1672.
- Kim, K., Yeatts, A., Dean, D., Fisher, J.P., 2010. Stereolithographic bone scaffold design parameters: osteogenic differentiation and signal expression. *Tissue Eng. Part B Rev.* 16 (5), 523–539.
- Klein Gt, L.Y., Wang, M., 2013. 3D printing and neurosurgery—ready for prime time? *World Neurosurg* 80, 233–235.
- Klosterman, D., Chartoff, R., Graves, G., Osborne, N., Priore, B., 1998. Interfacial characteristics of composites fabricated by laminated object manufacturing. *Compos. Appl. Sci. Manuf.* 29, 1165–1174.
- Kolesky, D.B., Truby, R.L., Gladman, A.S., Busbee, T.A., Homan, K.A., Lewis, J.A., 2014. 3D bioprinting of vascularized, heterogeneous cell-laden tissue constructs. *Adv. Mater.* 26, 3124–3130.
- Körner, C., 2016. Additive manufacturing of metallic components by selective electron beam melting — a review. *Int. Mater. Rev.* 61, 361–377.
- Lee, B.K., Yun, Y.H., Choi, J.S., Choi, Y.C., Kim, J.D., Cho, Y.W., 2012. Fabrication of drug-loaded polymer microparticles with arbitrary geometries using a piezoelectric inkjet printing system. *Intl. J. Pharmaceut.* 427, 305–310.
- Lee, W.-C., Wei, C.-C., Chung, S.-C., 2014. Development of a hybrid rapid prototyping system using low-cost fused deposition modeling and five-axis machining. *J. Mater. Process. Technol.* 214, 2366–2374.
- Leukers, B., Gülkan, H., Irsen, S.H., Milz, S., Tille, C., Schieker, M., Seitz, H., 2005. Hydroxyapatite scaffolds for bone tissue engineering made by 3D printing. *J. Mater. Sci. Mater. Med.* 16, 1121–1124.
- Malda, J., Visser, J., Melchels, F.P., Jüngst, T., Hennink, W.E., Dhert, W.J., Groll, J., Huttmacher, D.W., 2013. 25th anniversary article: engineering hydrogels for biofabrication. *Adv. Mater.* 25, 5011–5028.
- Mano, J.F., Silva, G.A., Azevedo, H.S., Malafaya, P.B., Sousa, R.A., Silva, S.S., Boesel, L.F., Oliveira, J.M., Santos, T.C., Marques, A.P., Neves, N.M., Reis, R.L., 2007. Natural origin biodegradable systems in tissue engineering and regenerative medicine: present status and some moving trends. *J. R. Soc. Interface* 4, 999–1030.
- Markstedt, K., Mantas, A., Tournier, I., Martinez Avila, H., Hagg, D., Gatenholm, P., 2015. 3D bioprinting human chondrocytes with nanocellulose-alginate bioink for cartilage tissue engineering applications. *Biomacromolecules* 16, 1489–1496.
- Materials, O.P. <http://oxfordpm.com/cm/orthopedics/osteofab-implants>.
- Mazzoli, A., 2013. Selective laser sintering in biomedical engineering. *Med. Biol. Eng. Comput.* 51, 245–256.
- Meier, L.M., Meineri, M., Hiansen, J.Q., Horlick, E.M., 2017. Structural and congenital heart disease interventions: the role of three-dimensional printing. *Netherlands Heart J.* 25 (2), 65–75.
- Mekonnen, B.G., Bright, G., Walker, A., 2016. A Study on State of the Art Technology of Laminated Object Manufacturing (LOM). Springer India, New Delhi, pp. 207–216.
- Melchels, F.P., Barradas, A., Blitterswijk, C.A., Boer, J., Feijen, J., Grijpma, D.W., 2010. Effects of the architecture of tissue engineering scaffolds on cell seeding and culturing. *Acta Biomater.* 6.
- Mercelis, P., Kruth, J.P., 2006. Residual stresses in selective laser sintering and selective laser melting. *Rapid Prototyp. J.* 12, 254–265.
- Michalski, M.H., Ross, J.S., 2014. The shape of things to come: 3D printing in medicine. *JAMA* 312, 2213–2214.
- Mitsouras, D., Liacouras, P., Imanzadeh, A., Giannopoulos, A.A., Cai, T., Kumamaru, K.K., George, E., Wake, N., Caterson, E.J., Pomahac, B., Ho, V.B., 2015. Medical 3D printing for the radiologist. *Radiographics* 35 (7), 1965–1988.
- Mohamed, O.A., Masood, S.H., Bhowmik, J.L., 2015. Optimization of fused deposition modeling process parameters: a review of current research and future prospects. *Adv. Manuf.* 3, 42–53.
- Mostafaei, A., Hughes, E.T., Hilla, C., Stevens, E.L., Chmielus, M., 2017. Data on the densification during sintering of binder jet printed samples made from water-and gas-atomized alloy 625 powders. *Data Brief* 10, 116–121.
- Mueller, B., Kochan, D., 1999. Laminated object manufacturing for rapid tooling and patternmaking in foundry industry. *Comput. Ind.* 39, 47–53.
- Murphy, S.V., Atala, A., 2014. 3D bioprinting of tissues and organs. *Nat. Biotechnol.* 32, 773.

- Murr, L., Gaytan, S., Medina, F., Martinez, E., Martinez, J., Hernandez, D., Machado, B., Ramirez, D., Wicker, R., 2010. Characterization of Ti-6Al-4V open cellular foams fabricated by additive manufacturing using electron beam melting. *Mat. Sci. Engg.* 527, 1861–1868.
- Murr, L.E., Gaytan, S.M., Martinez, E., Medina, F., Wicker, R.B., 2012a. Next generation orthopaedic implants by additive manufacturing using electron beam melting. *Intl. J. Biomat.* 14 2012.
- Murr, L.E., Gaytan, S.M., Ramirez, D.A., Martinez, E., Hernandez, J., Amato, K.N., Shindo, P.W., Medina, F.R., Wicker, R.B., 2012b. Metal fabrication by additive manufacturing using laser and electron beam melting technologies. *J. Mater. Sci. Technol.* 28, 1–14.
- Turner, B.N., Strong, R., A. Gold, S., 2014. A review of melt extrusion additive manufacturing processes: I. Process design and modeling. *Rapid Prototyp. J.* 20, 192–204.
- Nakamura, M., Kobayashi, A., Takagi, F., Watanabe, A., Hiruma, Y., Ohuchi, K., 2005. Biocompatible inkjet printing technique for designed seeding of individual living cells. *Tissue Eng.* 11.
- Ng, W.L., Yeong, W.Y., Naing, M.W., 2016. Polyelectrolyte gelatin-chitosan hydrogel optimized for 3D bioprinting in skin tissue engineering. *Int. J. Bioprint.* 2, 53–62.
- Nikzad, M., Masood, S., Sbarski, I., 2011. Thermo-mechanical properties of a highly filled polymeric composites for fused deposition modeling. *Mater. Des.* 32, 3448–3456.
- Norotte, C., Marga, F.S., Niklason, L.E., Forgacs, G., 2009. Scaffold-free vascular tissue engineering using bioprinting. *Biomaterials* 30, 5910–5917.
- Novakova-Marcincinova, L., Kuric, I., 2012. Basic and advanced materials for fused deposition modeling rapid prototyping technology. *Manuf. Ind. Eng* 11, 24–27.
- Ozbolat, I.T., Yu, Y., 2013. Bioprinting toward organ fabrication: challenges and future trends. *IEEE (Inst. Electr. Electron. Eng.) Trans. Biomed. Eng.* 60, 691–699.
- Park, J., Tari, M.J., Hahn, H.T., 2000. Characterization of the laminated object manufacturing (LOM) process. *Rapid Prototyp. J.* 6, 36–50.
- Patel, D.K., Sakhaei, A.H., Layani, M., Zhang, B., Ge, Q., Magdassi, S., 2017. Highly stretchable and UV curable elastomers for digital light processing based 3D printing. *Adv. Mater.* 29, 1606000.
- Pinkerton, A.J., 2015. Advances in the modeling of laser direct metal deposition. *J. Laser Appl.* 27, S15001.
- Prasad, L.K., Smyth, H., 2016. 3D Printing technologies for drug delivery: a review. *Drug Dev. Ind. Pharm.* 42 (7), 1019–1031.
- Rafi, H.K., Karthik, N.V., Gong, H., Starr, T.L., Stucker, B.E., 2013. Microstructures and mechanical properties of Ti6Al4V parts fabricated by selective laser melting and electron beam melting. *J. Mater. Eng. Perform.* 22, 3872–3883.
- Rengier, F., Mehndiratta, A., Von Tengg-Kobligk, H., Zechmann, C.M., Unterhinninghofen, R., Kauczor, H.U., Giesel, F.L., 2010. 3D printing based on imaging data: review of medical applications. *Int. J. Comput. Assist. Radiol. Surg.* 5, 335–341.
- Saboori, A., Gallo, D., Biamino, S., Fino, P., Lombardi, M., 2017. An overview of additive manufacturing of titanium components by directed energy deposition: microstructure and mechanical properties. *Appl. Sci.* 7 (9), 883.
- Sachlos, E., Czernuszka, J., 2003. Making tissue engineering scaffolds work. Review: the application of solid freeform fabrication technology to the production of tissue engineering scaffolds. *Eur. Cell Mater.* 5, 39–40.
- Santos, E.C., Shiomi, M., Osakada, K., Laoui, T., 2006. Rapid manufacturing of metal components by laser forming. *Int. J. Mach. Tool Manuf.* 46, 1459–1468.
- Schubert, C., VAN Langeveld, M.C., Donoso, L.A., 2014. Innovations in 3D printing: a 3D overview from optics to organs. *Br. J. Ophthalmol.* 98, 159–161.
- Schumacher, C., Bickel, B., Rys, J., Marschner, S., Daraio, C., Gross, M., 2015. Microstructures to control elasticity in 3D printing. *ACM Trans. Graph.* 34, 136.
- Seagle, S.R., Martin, R.L., Berteau, O., 1962. Electron-beam melting. *JOM* 14, 812–820.
- Sears, N.A., Seshadri, D.R., Dhavalikar, P.S., Cosgriff-Hernandez, E., 2016. A review of three-dimensional printing in tissue engineering. *Tissue Eng. Part B Rev.* 22 (4), 298–310.
- Sears, N., Dhavalikar, P., Whitely, M., Cosgriff-Hernandez, E., 2017. Fabrication of biomimetic bone grafts with multi-material 3D printing. *Biofabrication* 9 (2), 025020 biofabrication, 9, 025020.
- “Sheet Lamination 3D Printing Service - Laminated Object Manufacturing.” Additive Manufacturing Research Group, 2014. Loughborough University. www.lboro.ac.uk/research/amrg/about/the7categoriesofadditivemanufacturing/sheetlamination/.
- “Sheet Lamination 3D Printing Service - Laminated Object Manufacturing.” (LOM, SDL, Electrosonic Welding), 3Diligent, 2019. www.3diligent.com/3d-printing-service/sheet-lamination/.
- Shirazi, S.F.S., Gharekhani, S., Mehrali, M., Yarmand, H., Metseelaar, H.S.C., Kadri, N.A., Osman, N.A.A., 2015. A review on powder-based additive manufacturing for tissue engineering: selective laser sintering and inkjet 3D printing. *Sci. Technol. Adv. Mater.* 16, 033502.
- Sing, S.L., An, J., Yeong, W.Y., Wiria, F.E., 2016. Laser and electron-beam powder-bed additive manufacturing of metallic implants: A review on processes, materials and designs. *J. Orthop. Res.* 34 (3), 369–385.
- Sirringhaus, H., Kawase, T., Friend, R., Shimoda, T., Inbasekaran, M., Wu, W., Woo, E., 2000. High-resolution inkjet printing of all-polymer transistor circuits. *Science* 290, 2123–2126.
- Suresh, G., Narayana, K.L., Mallik, M.K., 2017. A review on development of medical implants by rapid prototyping technology. *Int. J. Pure Appl. Math.* 117 (21), 257–276.
- Tan, K., Chua, C., Leong, K., Cheah, C., Gui, W., Tan, W., Wiria, F., 2005. Selective laser sintering of biocompatible polymers for applications in tissue engineering. *Bio Med. Mater. Eng.* 15, 113–124.
- Trevisan, F., Calignano, F., Aversa, A., Marchese, G., Lombardi, M., Biamino, S., Ugues, D., Manfredi, D., 2018. Additive manufacturing of titanium alloys in the biomedical field: processes, properties and applications. *J. Appl. Biomater. Funct. Mater.* 16, 57–67.
- Tymrak, B.M., Kreiger, M., Pearce, J.M., 2014. Mechanical properties of components fabricated with open-source 3-D printers under realistic environmental conditions. *Mater. Des.* 58, 58.
- Vaezi, M., Seitz, H., Yang, S., 2013. A review on 3D micro-additive manufacturing technologies. *Int. J. Adv. Manuf. Technol.* 67, 1721–1754.
- Vannier, M.W., Marsh, J.L., 1996. Three-dimensional imaging, surgical planning, and image-guided therapy. *Radiol Clin N. Am.* 34, 545–563.
- Vandenbroucke, B., Kruth, J.P., 2007. Selective laser melting of biocompatible metals for rapid manufacturing of medical parts. *Rapid Prototyp. J.* 13 (4), 196–203.
- Ventola, C.L., 2014. Medical applications for 3D printing: current and projected uses. *PT* 39, 704–711.
- Walter Reed National Military Medical Center. <http://www.wrnmcc.shiftpentercapmed.mil/ResearchEducation/3DMAC/SitePages/3DPrinting.aspx>. Date accessed November, 2018.

- West, J.L., Hubbell, J.A., 1999. Polymeric biomaterials with degradation sites for proteases involved in cell migration. *Macromolecules* 32, 241–244.
- White, D., 2003. Ultrasonic Object Consolidation. Google Patents.
- Williams, J.M., Adewunmi, A., Schek, R.M., Flanagan, C.L., Krebsbach, P.H., Feinberg, S.E., 2005. Bone tissue engineering using polycaprolactone scaffolds fabricated via selective laser sintering. *Biomaterials* 26.
- Wong, K.V., Hernandez, A., 2012. A Review of Additive Manufacturing. ISRN Mechanical Engineering. 2012.
- Wu, W., Zheng, Q., Guo, X., Sun, J., Liu, Y., 2009. A programmed release multi-drug implant fabricated by three-dimensional printing technology for bone tuberculosis therapy. *Biomed. Mater.* 4, 065005.
- Wüst, S., Godla, M.E., Müller, R., Hofmann, S., 2014. Tunable hydrogel composite with two-step processing in combination with innovative hardware upgrade for cell-based three-dimensional bio-printing. *Acta Biomater.* 10, 630–640.
- Yamamoto, G., Shirasu, K., Nozaka, Y., Shimamura, Y., Inoue, Y., Hashida, T., 2014. Fabrication and mechanical evaluation of aligned multi-walled carbon nanotube sheet/alumina laminated ceramic composites.
- Zein, I., Hutmacher, D.W., Tan, K.C., Teoh, S.H., 2002. Fused deposition modeling of novel scaffold architectures for tissue engineering applications. *Biomaterials* 23, 1169–1185.
- Zhu, F., Macdonald, N.P., Skommer, J., Wlodkovic, D., 2015. Biological implications of lab-on-a-chip devices fabricated using multi-jet modelling and stereolithography processes. In: *Bio-Mems and Medical Microdevices II*. International Society for Optics and Photonics, p. 951808.
- Zocca, A., Colombo, P., Gomes, C.M., Günster, J., 2015. Additive manufacturing of ceramics: issues, potentialities, and opportunities. *J. Am. Ceram. Soc.* 98, 1983–2001.
- Zorlutuna, P., Annabi, N., Camci-Unal, G., Nikkhah, M., Cha, J.M., Nichol, J.W., Manbachi, A., Bae, H., Chen, S., Khademhosseini, A., 2012. Microfabricated biomaterials for engineering 3D tissues. *Adv. Mat.* 24, 1782–1804.

Chapter Review Questions

1. Why does SLA print objects with a smoother surface finish than FDM does?

Higher resolution is possible due to the laser being smaller than the nozzle diameter, and less force being applied to the object during the printing process.

2. Why is DLP a faster printing process than SLA?
DLP prints an entire layer of resin at once using a pixel pattern, while SLA prints along a path with a laser.
3. Why is it beneficial that SLA and DLP do not use support materials?
Supporting structures require postprocessing, which makes the printing process longer and may result in damage or breaking of the surface connected to the support.
4. Why is wax often used as the support structure in MJM printing?
Wax has a lower melting temperature than most of the photopolymers used in MJM printing, so it can be melted away while the cured polymer stays intact. Melting the wax allows for hands-off postprocessing to minimize damage to the object.
5. What is the benefit of using multiple nozzles?
This allows for simultaneous printing of multiple materials in a single print to impart variable characteristics and properties.
6. Compare and contrast the following techniques: EBM, SLS, and LMD.
Similarities: Materials that are used to print these techniques include different types of metals, and all techniques can be used to generate implants.
Differences: EBM prints based on an electron beam melting down powder materials, SLS uses a laser beam to melt down powder materials, and LMD uses a laser to melt a metal surface.
7. What are the benefits of using FDM to fabricate bio-material constructs compared to SLA? What are the limitations?
FDM is an extrusion-based printing technique that can translate to limited use of material and there is rapid turnaround. Furthermore, it was previously used to print thermoplastics but now can be used to print pastes, gels, and other viscous materials. SLA has higher resolution compared to FDM, which might be better for printing biomaterials such as implants or scaffolds, but often requires the use of large volumes of material.
8. What is the advantage of using LMD for metal implants compared to other metal printing techniques such as EMD or SLS? How does this advantage make it a potentially useful technique for biomaterials?
LDM process parameters allow for printing multiple materials (metals) at a time, as compared to single material printing with EMD or SLS. Previous attempts have demonstrated fabrication of implants with coat-

ings of different types that promote antibacterial resistance and mechanical strength in one single fabrication step.

9. What is bioprinting? Please list four bioprinting methods currently used for printing cell-laden bioinks.
Bioprinting is a 3D printing strategy that involves robotic deposition of cell-laden bioinks into custom shapes for facilitating regeneration of tissue. Four bioprinting methods that are currently being used for printing bioinks include microextrusion, inkjet, stereolithography, and laser-assisted bioprinting.
10. Describe major bioink properties that affect the performance of printed scaffolds.
Specific bioink properties that affect the performance of printed scaffolds include ink rheological properties, cross-linking mechanism, degree of hydration, ink mechanical properties, and biological characteristics.
 - Rheological properties: The material for printing needs to be viscoelastic and shear thinning to allow for high print fidelity and structural stability. In addition, the viscosity of the ink must be controlled enough to allow for uniform distribution of cells within the ink.
 - Cross-linking mechanism: Enables solidification of the ink upon deposition and can be achieved via light, ionic strength, electrostatic interactions, pH, and temperature. The primary criteria to select a cross-linking method should consider how viability of encapsulated cells is affected.
 - Degree of hydration: Amount of water that is present in the ink. This can affect viscosity, print fidelity, and scaffold mechanical properties. In addition, modulation of this property can enable control over porosity, which facilitates transport of oxygen and nutrients through the scaffolds.
 - Mechanical properties: These properties are dependent on chemical composition, polymer concentration, and cross-linking density. Optimization of these parameters must be investigated thoroughly because they can significantly affect viability/functionality of encapsulated cells.
 - Biological characteristics: Presence of biological components can affect how cells encapsulated inside the bioink behave. Depending on what type of cells are encapsulated and printed, the biological properties of the ink (for example, presence or lack of adhesion sites) should be considered and designed.
11. What is the biofabrication window?
The biofabrication window is an important concept that describes the required compromises between the printability of a bioink formulation and cell viability. This allows for rational design of materials to improve the functionality of the cell-laden printed scaffolds.
12. What are the advantages and opportunities afforded by 3D printing techniques utilized in surgical planning and medical training models?

A 3D printed tissue model has the following advantages:

1. Compared with imaging examination techniques, a 3D printed model demonstrates a more straightforward and intuitive spatial relationship of targeted tissues and organs;
 2. High-resolution 3D printing can exhibit more details;
 3. A 3D printed model helps to reduce the operation time and to achieve more cost-effective management of medical resources.
 4. In medical training, 3D printing provides an alternative option with a lower cost and higher availability.
13. In 3D printing of medical implants, what parameters should be taken into consideration? Support your statement with specific examples.

Based on target tissue, one or multiple materials can be used for the fabrication of implants. The mechanical properties and bioactivity of the material should be in compliance with the application as well as its biostability or biodegradability. For example, alloys can be fabricated into bone grafts due to a similar mechanical property and a polymer with high elasticity and flexibility used to mimic the heart valve tissue.

A proper 3D printing method must be chosen to integrate multiple materials and even incorporate bioprinting with cells. The fabrication resolution requirement also differs with different implant applications. The example of the 3D printed heart valve conduit with encapsulated human cells requires a combination of hydrogel printing and bioprinting.

2.1.1

Introduction to Biology and Medicine—Key Concepts in the Use of Biomaterials in Surgery and Medical Devices

MICHAEL J. YASZEMSKI¹, BUDDY D. RATNER²

¹Orthopaedic Surgery and Biomedical Engineering, Mayo Clinic College of Medicine, Rochester, MN, United States

²Bioengineering and Chemical Engineering, Director of University of Washington Engineered Biomaterials (UWEB), Seattle, WA, United States

Biomaterials Science: An Introduction to Materials in Medicine directly addresses the multidisciplinary nature of the biomaterials field by providing concise tutorials in the key concepts essential for practitioners of biomaterials science. The word “biomaterials” implies an intersection of biology and materials. This Section 2.1 addresses the fundamental “bio” science relevant to biomaterials (Section 1.2 serves a similar function for the fundamental materials science relevant to biomaterials). The background biology is important, because this scientific foundation will help us to understand, predict, and engineer the in vivo responses observed by the biomaterials scientist/engineer, the physician, and the patient.

When a synthetic material is placed in a biological milieu (implantation in a living organism, for example), a series of reactions is initiated almost instantaneously. Water molecules (and H⁺ and OH⁻), being the lowest molecular weight species, should reach the biomaterial surface first (in milliseconds). Their considerable impact on subsequent reactions is elaborated upon in [Chapters 1.2.5 and 1.4.3A](#). Although water is not considered a biomolecule, it sets the stage for the biological reactions to follow.

Proteins, dissolved in serum at a concentration of approximately 7 g/dL, arrive next at the surface by either diffusion or convection. There are 700 or more proteins in blood. Some are relatively nonbioreactive, such as albumin, and others have numerous biological activities, such as fibrinogen or fibronectin. When proteins diffuse to a biomaterial

interface, they will arrive in order of molecular weight (small proteins like thrombin, 35 kDa, arrive before heavier proteins like IgG, at 160 kDa). Once at the surface, proteins can adsorb, desorb, exchange with other proteins, denature, and either increase or decrease their biological activity. This complex landscape, comprised of many proteins in many states of organization and elaborated upon in [Chapter 2.1.2](#), “Adsorbed Proteins on Biomaterials,” by Robert A. Latour, becomes the environment to which cells will respond (and cells do indeed respond to proteins). The fundamentals of in vitro cell interaction with surfaces (or more accurately, interactions with the protein layer on biomaterial interfaces in water) are described in [Chapter 2.1.3](#), “Cells and Surfaces in Vitro,” by Ali Khademhosseini and Nureddin Ashammakhi. This chapter is particularly relevant for surface diagnostic devices (enzyme-linked immunosorbent assays, DNA microarrays, and protein microarrays), cell culture, and biosensors, but it also addresses many reactions observed in vivo.

[Chapter 2.1.4](#), “Functional Tissue Architecture, Homeostasis, and Responses to Injury” by Frederick Schoen and Richard Neal Mitchell, discusses the biology of cells, with an emphasis on what the cells do under various conditions and what happens when they are injured (a surgical site always contains injured cells). In addition, rubbing and mechanical forces associated with medical implants can induce cell injury. Single cell types rarely exist alone. They aggregate or interact to form tissues, as discussed in [Chapter 2.1.5](#), “The Extracellular

Matrix and Cell–Biomaterial Interactions,” by Andres J. Garcia, Woojin M. Han, and Young Charles Jang. Some principles that govern tissue formation from individual cell types are relatively simple and have been elaborated upon by researchers such as Malcolm S. Steinberg, who demonstrated that cell membrane surface tension associated with cell surface cadherin molecules can drive cell aggregation into organized multicellular structures. Other aspects of tissue formation are governed by the complex mechanisms observed in studying the developmental biology of organisms. Biomaterials and medical devices interface with tissues; thus understanding tissues, their organization, and their properties is important. Furthermore, the cells in tissues make a “grout” that holds them together; this material is called the extracellular matrix (ECM). The ECM serves a mechanical function in stabilizing the tissues but is, in its own right, highly biologically active. For example, it has been shown that triple-helical collagen I, the primary component of ECM, can bind in a specific manner to more than 50 other biomolecules, including some with high biological activity such as fibronectin. Thus the ECM presents to the cells bioactive biomolecules in optimal conformation and orientation, whereby it directs their actions. This concept is particularly important to tissue engineering (Section 2.6). Also, the degradation products of ECM can be highly bioactive. For example, the work of Judah Folkman, Robert Langer, and colleagues demonstrated that degradation fragments of some collagens are inhibitory to angiogenesis. Since ECM is synthesized by tissue cells and is broken down by cells such as the macrophage, the bioactive fragments from the breakdown can impact tissue formation and biological reaction.

[Chapter 2.1.6](#), “Effects of Mechanical Forces on Cells and Tissues,” by Aaron Baker, Austin Veith, and Lei Mei, addresses mechanical forces, their effects on cells and tissues, and their importance for biomaterials. Living organisms move, and blood flows. Thus all implants in living organisms are subjected to mechanical forces. Although [Chapter 2.1.6](#) focuses on the liquid–biomaterial interface (i.e., blood interactions), the concepts of force communication from the environment external to the cell, to the cell membrane, particularly from an engineering standpoint, are elaborated upon. The work of Donald Ingber (e.g., Ingber, D.E. From mechanobiology to developmentally inspired engineering. *Phil. Trans. R. Soc. B* 373, 20170323) and others helps us to understand how this mechanical trigger at the cell membrane can signal to the cell nucleus, leading to downregulation or upregulation of specific genes, which then leads to expression of new cytokines and/or other signaling molecules. Mechanical forces can impact cells macroscopically, but also impact them at a microscopic level. Carter, S.B., January 21, 1967. Effects of cytochalasins on mammalian cells. *Nature* 213 (5073), 261–264. UI: 6067685 in which he showed that cells follow micron-dimension scratches in a plastic film, a phenomenon he named contact guidance. We use that term to this day to describe this mechanically induced response of cells to micron-scale features. [Chapters 1.4.5 and 1.4.7](#) give us patterning, texture, and porosity tools to manipulate cell–mechanical interactions at both the micro- and nano-levels.

2.1.2

Adsorbed Proteins on Biomaterials

THOMAS A. HORBETT¹, ROBERT A. LATOUR²

¹Bioengineering and Chemical Engineering, University of Washington, Seattle, WA, United States

²Bioengineering Department, Clemson University, Clemson, SC, United States

Introduction

The replacement of injured or diseased tissues with devices made from materials that are not of biologic origin has been a longstanding approach in biomaterials science and clinical practice. The prevalence of this approach is due largely to the fact that these materials are not attacked by the immune system, unlike donor tissues or organs. This fundamental difference arises from the presence of immunologically recognizable biologic motifs on donor tissue, and their absence on synthetic materials.

Nonetheless, there are other types of biological responses to implanted synthetic biomaterials that often impair their usefulness, including the clotting of blood and the foreign-body reaction. Clearly, the body does recognize and respond to these types of biomaterials. The basis for these reactions is the adsorption of adhesion proteins to the surface of the biomaterials that are recognized by the integrin receptors present on most cells. The adsorption of adhesion proteins to the biomaterial converts it into a biologically recognizable material, as illustrated in Fig. 2.1.2.1. The protein adsorption event is rapid (seconds) and generally happens on all materials implanted into biological systems with few exceptions. Note: familiarity with protein structure is essential to appreciate the content of this chapter. All introductory biochemistry textbooks can provide this critical background material.

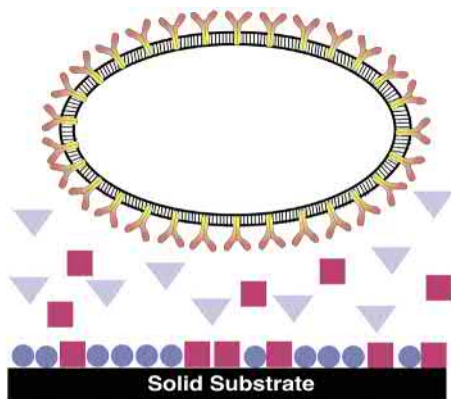
The interaction of adhesion receptors with adhesion proteins thus constitutes a major cellular recognition system for biomaterials. Therefore, the role of adsorbed adhesion proteins in mediating cellular interactions with biomaterials will be the primary focus of this chapter. Examples illustrating the ability of adsorbed adhesion proteins to influence cellular interactions with foreign materials are presented first. Then, some of the major physicochemical characteristics of protein adsorption are illustrated and discussed, including rapid kinetics, monolayer adsorption, and competitive adsorption. Molecular spreading events related to the conformational stability of the protein are presented at

some length, as background for a section on how the biological activity of adsorbed adhesion proteins is affected by the substrate. This is then followed by a section summarizing the principles underlying the role of adsorbed proteins in mediating the platelet response to biomaterials, as an illustrative case study representative of many other types of cellular responses. The next-to-last section of this chapter summarizes the development of surface chemistries that are highly resistant to protein adsorption (i.e., nonfouling surfaces), in an attempt to eliminate biological recognition of the biomaterial altogether, which is followed by concluding remarks. Each of these topical areas is discussed in greater detail in several previous journal publications and review articles (Horbett, 1993, 1994, 1996, 1999, 2003; Horbett and Brash, 1995; Latour, 2008; Latour et al., 2012; Norde et al., 2012; Thyparambil et al., 2015; Thompson et al., 2017a).

Most studies of protein interactions with biomaterials and their effects on cells have been done *in vitro* after relatively short contact periods, leading to the focus here on effects in the shorter term that involve undegraded adhesion proteins that mediate cell interactions. However, the adsorbed protein layer on biomaterials implanted in humans or animals for longer times includes smaller size fragments [observed on breast implants (Backovic et al., 2007), glucose sensors (Gifford et al., 2006), and kidney dialyzers (Cornelius and Brash, 1993)] that are presumably due to proteolytic attack. The functional role of any of these changes to the adsorbed proteins on the interaction of biomaterials with the body remains to be elucidated.

Examples of the Effects of Adhesion Proteins on Cellular Interactions With Materials

Protein adsorption to materials can be performed with a single protein, typically in a buffer solution, or from complex, multiprotein solutions, such as blood plasma, which can

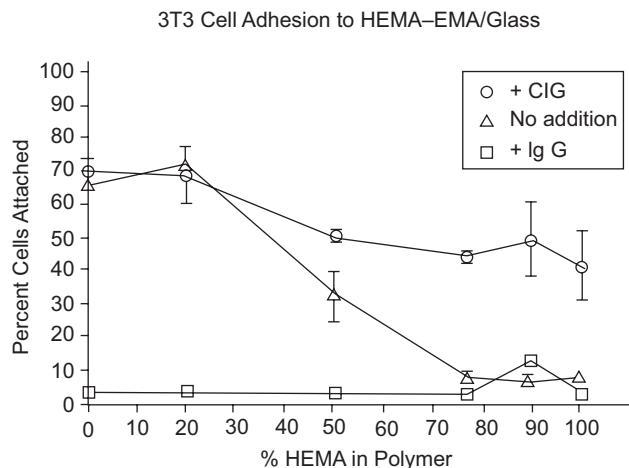


• **Figure 2.1.2.1** Cell interactions with foreign surfaces are mediated by integrin receptors with adsorbed adhesion proteins that sometimes change their biological activity when they adsorb. The cell is shown as a circular space with a bilayer membrane in which the adhesion receptor protein molecules (the slingshot-shaped objects) are partly embedded. The proteins in the extracellular fluid are represented by circles, squares, and triangles. The receptor proteins recognize and cause the cell to adhere to only the surface-bound form of one protein, the one represented by a solid blue circle. The bulk phase of this same adhesion protein is represented by a blue triangle, indicating that the solution and solid-phase forms of this same protein have a different biological activity. The figure is schematic and not to scale.

contain hundreds of proteins. Experiments done with single proteins in buffer can be used to study fundamental aspects of protein adsorption, such as adsorption rates or conformational changes, and to study biological responses, such as cell adhesion to each protein. Adsorption from complex media approximates the adsorption conditions encountered by implanted biomaterials, and thus provides a more realistic insight into the functional role of adsorbed proteins. Examples of the effects on cellular responses of protein adsorption done under both conditions are presented below.

The Effects of PreadSORption With Purified Adhesion Proteins

PreadSORption of certain proteins onto a solid substrate, such as tissue culture polystyrene, greatly increases its adhesiveness to many kinds of cells, and such proteins are called adhesion proteins. The increased adhesiveness is due to the fact that many cells have receptors in their cell membrane that bind specifically to these specialized proteins. The adhesion receptors involved in cell adhesion to biomaterials and extracellular matrices such as collagen are called integrins. For example, fibronectin preadsorption greatly increases the adhesion of fibroblasts, while albumin preadsorption prevents it (Horbett, 1994). Experiments of this type have been done with a wide variety of cells and adhesion proteins, with basically similar results. Adhesion proteins also promote the flattening out or spreading of the cell onto the surface. A specific example is provided by measuring the percentage of attached cells that spread on polystyrene surfaces pretreated with increasing concentrations of fibronectin. Spreading is only about 5% on albumin-coated surfaces, but increases to nearly 100% as the fibronectin concentrations in the



• **Figure 2.1.2.2** 3T3 cell adhesion to HEMA-EMA copolymers varying from hydrophilic (HEMA-rich) to hydrophobic (EMA-rich): effect of no adsorbed protein, preadsorption with fibronectin (designated CIG in the figure), or preadsorption with immunoglobulin G (IgG). (The data are from the Horbett laboratory.)

preadSORption solution are increased from 0.03 to 3 $\mu\text{g}/\text{mL}$ (Horbett, 1994).

In studies of protein-mediated cell adhesion, it is necessary to eliminate or reduce the role of nonspecific cell adhesion directly to the uncoated surfaces, as this is often high, so that the special ability of adhesion proteins compared to other proteins would not be masked. This nonspecific cell-adhesion process can be understood to actually be mediated by a nonspecific protein-adhesion process—but in this case, the proteins involved are the membrane-bound proteins that are presented from a cell's surface. Thus, when testing for the ability of a preadsorbed protein to specifically cause cell adhesion, any residual uncoated sites left after preadsorption with the putative adhesion protein should be filled by a second adsorption step with a known nonadhesive protein, such as albumin, which is commonly used to block exposed surface sites. Because proteins themselves are highly resistant to the nonspecific adhesion of other proteins, the complete coverage of a material surface with a layer of preadsorbed protein will thus inhibit nonspecific cell adhesion. The results for this surface with the preadsorbed adhesive protein and albumin are then compared to a control surface that is completely coated with adsorbed albumin. Under these conditions, any elevation in cell adhesion compared to the albumin control can be ascribed to the test protein, rather than nonspecific cell adhesion due to the cell's direct contact with the surface.

An example of the effect of fibronectin adsorption is shown in Fig. 2.1.2.2, which also contrasts it with the effects of the nonadhesive protein immunoglobulin G (IgG). As shown in the figure, the adhesion of the fibroblast-like 3T3 cells to a series of polymers and copolymers of 2-hydroxyethyl methacrylate (HEMA) and ethyl methacrylate (EMA) not previously adsorbed with protein (and without proteins in the cell suspension) varies, being much less on the hydrophilic polyHEMA-rich surfaces than on the hydrophobic

polyEMA-rich surfaces. These data are an example of direct or nonspecific cell adhesion in which the cells adhere directly to the surfaces, rather than to adsorbed proteins. The pre-adsorption of the surfaces with immunoglobulin G (IgG) greatly reduces the adhesion of the cells to all the surfaces, because this protein effectively blocks the nonspecific adhesion of the cells to the surfaces. In the presence of IgG, the high nonspecific cell adhesion to EMA-rich surfaces cannot occur, as the cells do not have direct contact with the surfaces. In contrast, surfaces preadsorbed with fibronectin (designated CIG in the figure) are much more adhesive than the same surface adsorbed with IgG. After fibronectin coating, even surfaces rich in HEMA that are not adhesive to the cells themselves become adhesive, as the cells now interact not with HEMA, but with the adsorbed adhesive protein.

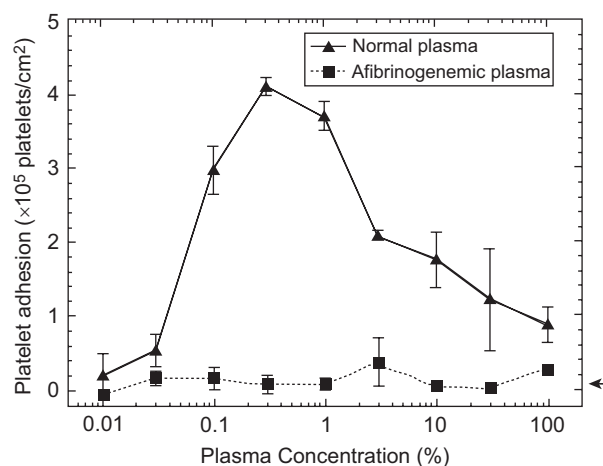
Preadsorption of adhesion proteins also affects cell interactions with surfaces studied under *in vivo* conditions. For example, blood platelet deposition onto polymeric arteriovenous shunts in dogs is greatly increased when fibrinogen or fibronectin are preadsorbed to the surfaces in comparison to albumin-coated surfaces (see Chapters 2.2.6 and 2.3.5).

Depletion Studies

Although the preadsorption of purified adhesion proteins to a surface is one way to see their effect on cell adhesion, as presented in the previous section, it does not mimic very well what occurs with implanted biomaterials. This is because biomaterials are exposed to blood and/or interstitial fluid during the surgical procedure to implant them, with these body fluids containing complex mixtures of different proteins, so the adhesion protein must compete with many others for adsorption to the biomaterial surfaces. Under those conditions, a given adhesion protein present in the biological fluid that the biomaterial is initially exposed to may really play little or no role. It is possible that very little of the adhesion protein may adsorb to the surface, as it is “out-competed” by other proteins for the limited surface sites. Thus, a more biologically relevant way to understand the role of an adhesion protein in reactions to implants is to study the effect of their selective depletion from the complex mixture. The observations presented in this section, and the articles they are based on, are presented in greater detail in a review article by Horbett (Horbett, 1999).

Selective depletion means that only one of the proteins is removed from the mixture at a time, either by immunoadsorption chromatography, by use of plasma from mutant individuals lacking the adhesion protein of interest, or by selective enzymatic degradation. Thus, the more important role of adsorbed vitronectin, as opposed to fibronectin, in mediating attachment and spreading of cells on many surfaces has emerged from immunoadsorption studies. Several studies illustrate the important role that adsorbed fibrinogen plays in the adhesion of platelets, neutrophils, and macrophages.

The effects of removal of fibronectin or vitronectin or both proteins from serum on the adhesion of endothelial



• **Figure 2.1.2.3** Platelet adhesion to Immulon I preadsorbed with normal plasma (triangles) or afibrinogenemic plasma (squares). The solid line represents the platelet adhesion to Immulon I preadsorbed with a series of dilutions of normal plasma, whereas the dotted line represents the platelet adhesion to Immulon I preadsorbed with a series of dilutions of afibrinogenemic plasma. The arrow at the lower right corner indicates platelet adhesion to Immulon I preadsorbed with 2% BSA only. BSA, bovine serum albumin. (Reproduced from Figure 4 in Tsai, W.-B., Horbett, T.A., 1999. Human plasma fibrinogen adsorption and platelet adhesion to polystyrene. *J. Biomed. Mater. Res.* 44, 130–139. Copyright permission received.)

cells depend on the surface chemistry. On tissue-culture polystyrene (TCPS) fibronectin removal has little effect, while vitronectin removal greatly reduces adhesion. These results clearly show the primary role of adsorbed vitronectin in supporting endothelial cell adhesion to TCPS. In contrast, adhesion to a surface modified by ammonia in a glow discharge (see Chapter 1.4.2) requires fibronectin, since removal of that protein greatly reduces adhesion to this surface, while vitronectin removal has little effect. However, the results for TCPS are more typical; i.e., on most surfaces studied by this method it appears that vitronectin, not fibronectin, is the primary agent responsible for cell adhesion.

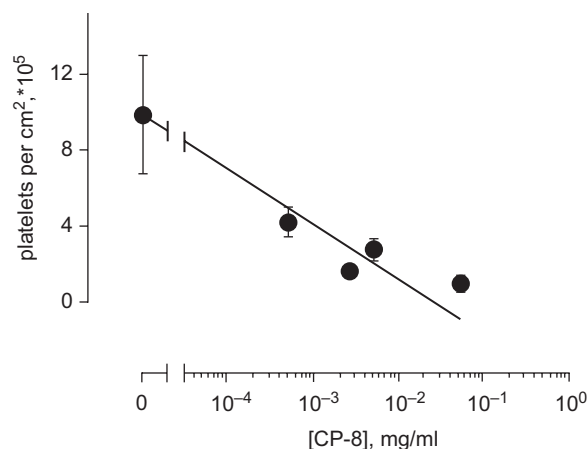
Platelet adhesion to surfaces preadsorbed with blood plasma that is deficient in fibrinogen is much less than to the same surface preadsorbed with normal plasma, as illustrated in Fig. 2.1.2.3. Most of the adhesion-supporting activity can be restored to fibrinogen-deficient plasma by the addition of exogenous fibrinogen at concentrations well below that in normal plasma. Platelets are very sensitive to fibrinogen as they adhere to some surfaces at fibrinogen adsorption levels of only 5 ng/cm², in comparison with adsorption values in the range of 100–200 ng/cm² in the presence of normal fibrinogen concentrations. In contrast, removal of fibronectin, vitronectin, or von Willebrand’s factor from plasma has little effect on platelet adhesion (data not shown), even though these other plasma proteins act as adhesion proteins when adsorbed from single-protein solutions to surfaces. It appears that too little of these other proteins adsorb from plasma to make much difference; i.e., competition from fibrinogen and other proteins keeps their surface concentration too low, and so their removal has no effect.

The apparently negligible role of von Willebrand's factor in platelet adhesion discussed above only applies when platelet adhesion from static suspensions or low wall shear strain rates is measured. At higher wall shear strain rates (e.g., $>500\text{ s}^{-1}$), platelet adhesion to biomaterials is highly dependent on the presence of adsorbed von Willebrand's factor. This dependence is most clearly illustrated by the effects of increasing the shear rate on platelet adhesion. On surfaces preadsorbed with normal plasma (i.e., containing von Willebrand's factor, fibrinogen, and the other proteins), platelet adhesion is much higher at higher shear rates than low shear rates, because of the enhanced transport of the platelets to the surface; i.e., the greater number of platelet-surface encounters at high shear rate allows for an increase in the number of adhesive outcomes. On surfaces preadsorbed with plasma deficient in von Willebrand's factor only, raising the shear rate not only does not result in an increase in adhesion, but the adhesion at high shear is actually lower than at low shear, exactly the opposite of what happens in the presence of von Willebrand's factor. Thus, von Willebrand's factor adsorption plays a major role in platelet adhesion at higher shear rates. The special role of von Willebrand's factor in high-shear adhesion is thought to be due to the ability of the platelet receptor GPIb-IX to form and break bonds very rapidly with immobilized von Willebrand's factor, causing the platelets to first adhere and then roll along the surface until they are activated and can form a permanent bond that stops the rolling. The role of von Willebrand's factor in shear-mediated adhesion was documented in several recent studies (summarized in Zhang et al., 2008). Interestingly, the adsorbed von Willebrand's factor molecule is itself subject to distortion by both mechanical and fluid shear (Siedlecki et al., 1996). That may play a role in the surface activation of von Willebrand's factor by exposing platelet-binding sites on the molecule.

When mice are depleted of fibrinogen by treatment with an enzyme that degrades it, the adhesion of neutrophils and macrophages to a polymer implanted in their peritoneal cavity is greatly reduced. The fibrinogen-depleted animals exhibited near normal neutrophil and macrophage adhesion to the implants if the implants were preadsorbed with fibrinogen. These studies clearly illustrate the power of the depletion method. Previously, it had been thought that either complement or IgG would be the main adhesion proteins for neutrophils and monocytes, due to the presence of receptors on these cells that bind these proteins. Instead, it appears that an integrin receptor for fibrinogen (CD11b/CD18, also known as Mac-1) plays a major role, at least during the initial or acute phase of the foreign-body response in the mouse peritoneal cavity.

Inhibition of Receptor Activity With Antibodies

Another way to show the role of adhesion proteins in cell interactions with biomaterials is to add specific inhibitors of their function. Adhesion proteins cause cell adhesion by binding to integrin receptors that specifically recognize the

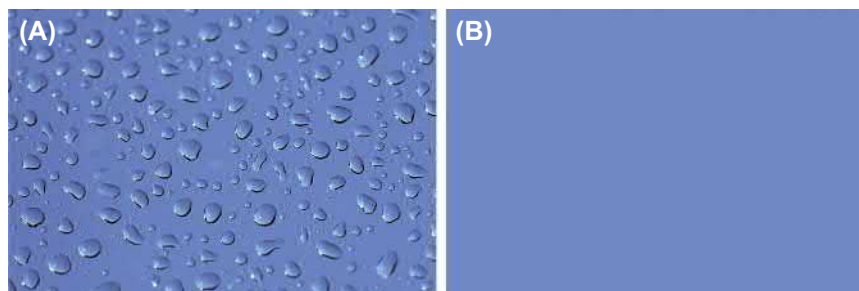


• **Figure 2.1.2.4** Effect of anti-IIb/IIIa antibody on platelet adhesion to Biomer preadsorbed with plasma. Adhesion of platelets incubated in monoclonal antibody CP-8 [monovalent Fab' fragment directed against the glycoprotein (GP) IIb/IIIa complex] to Biomer. Substrates were contacted with 1.0% plasma for 2 h, then washed with antibody-treated platelets for 2 h. (From Chinn J.A., Horbett T.A., Ratner B.D., 1991. Baboon Fibrinogen Adsorption and Platelet Adhesion to Polymeric Materials. *Thromb. Haemost.* 65, 608–17.)

adhesion protein. One way to inhibit this reaction is to add an antibody that binds to the adhesion receptor or adhesion protein. Examples of these approaches are presented next.

Platelet receptor-mediated interactions appear to be the primary mechanism of platelet interaction in vivo with certain vascular grafts, because platelet deposition is largely inhibited by antibodies to the glycoprotein IIb/IIIa receptor, the major integrin on the surface of platelets. In vitro platelet adhesion to surfaces preadsorbed with blood plasma is also inhibited by antiglycoprotein IIb/IIIa in a dose-dependent manner, as illustrated in Fig. 2.1.2.4 (Chinn et al., 1991). In this study, samples of the polyurethane Biomer were preadsorbed with plasma and then exposed to platelets in an albumin-containing buffered saline suspension that had increasing amounts of the antibody. As shown in the figure, adhesion declined to very low values when high concentrations of the antiintegrin antibody were present.

There is currently much interest in the ability of biomaterials to regulate stem-cell differentiation, including the role of proteins adsorbed to the biomaterials. Thus, antibodies to vitronectin and fibronectin were used to study the role of these two proteins in osteogenic differentiation of mesenchymal stem cells on polycaprolactone. The vitronectin antibody selectively blocked adhesion and differentiation, but the fibronectin antibody did not, showing the importance of vitronectin-mediated adhesion in the behavior of this type of stem cell (Chastain et al., 2006). Combinatorial screening methods to find biomaterials that promote neural stem-cell differentiation found a role for adsorbed fibronectin and other adhesion factors in combination with immobilized growth factors (Nakajima et al., 2007). A much broader combinatorial screen (3456 assays) for biomaterials conducive to human mesenchymal stem-cell adhesion has also been done (Anderson et al., 2005). Modification of biomaterials with various adhesion-promoting peptides



• **Figure 2.1.2.5** The conversion of nonwetable polystyrene surface (A) into one completely wettable by water (B) is due to the adsorption of proteins (simulated images based on actual observations).

to promote stem-cell adhesion and differentiation has also come under active study, because it is thought to be a good way to “provide a microenvironment where adhesive moieties are expressed in a spatial and temporal manner to control cellular behaviors” (Hwang et al., 2008).

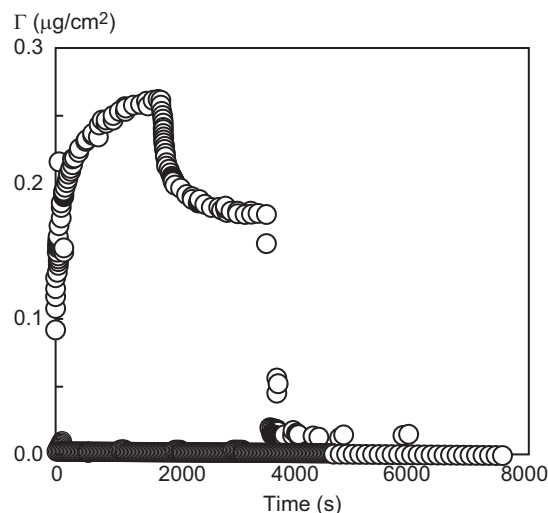
The Adsorption Behavior of Proteins at Solid–Liquid Interfaces

Adsorption Transforms the Interface

Fig. 2.1.2.5 illustrates an experiment that was performed by Horbett to demonstrate the adsorption of proteins to surfaces. As illustrated in part (A), water droplets sprayed on the surface of an unused polystyrene cell-culture dish are easily visible because they bead up, i.e., the contact angle between the droplet and the polystyrene surface is very high due to the water repellent, hydrophobic nature of polystyrene (see Chapter 1.2.4). If a cell were placed on a polystyrene dish instead of the water droplet, it would also encounter a very nonwetable surface. Part (B) of the figure illustrates the results of spraying water droplets on the surface of a polystyrene dish that had first been exposed to a protein solution for a short time, and then rinsed extensively with water. As illustrated, no water droplets can be seen on this surface, reflecting the fact that in this case the added drop of water completely spread out over the surface of the preadsorbed dish. This happens because the water in part (b) was not able to interact with the polystyrene surface, because the surface had become coated with a layer of the hydrophilic protein adsorbate. Similarly, cells that come into contact with surfaces adsorbed with proteins do not directly “see” the substrate, but instead they interact with the intervening protein adsorbate.

Rapid Adsorption Kinetics and Irreversibility

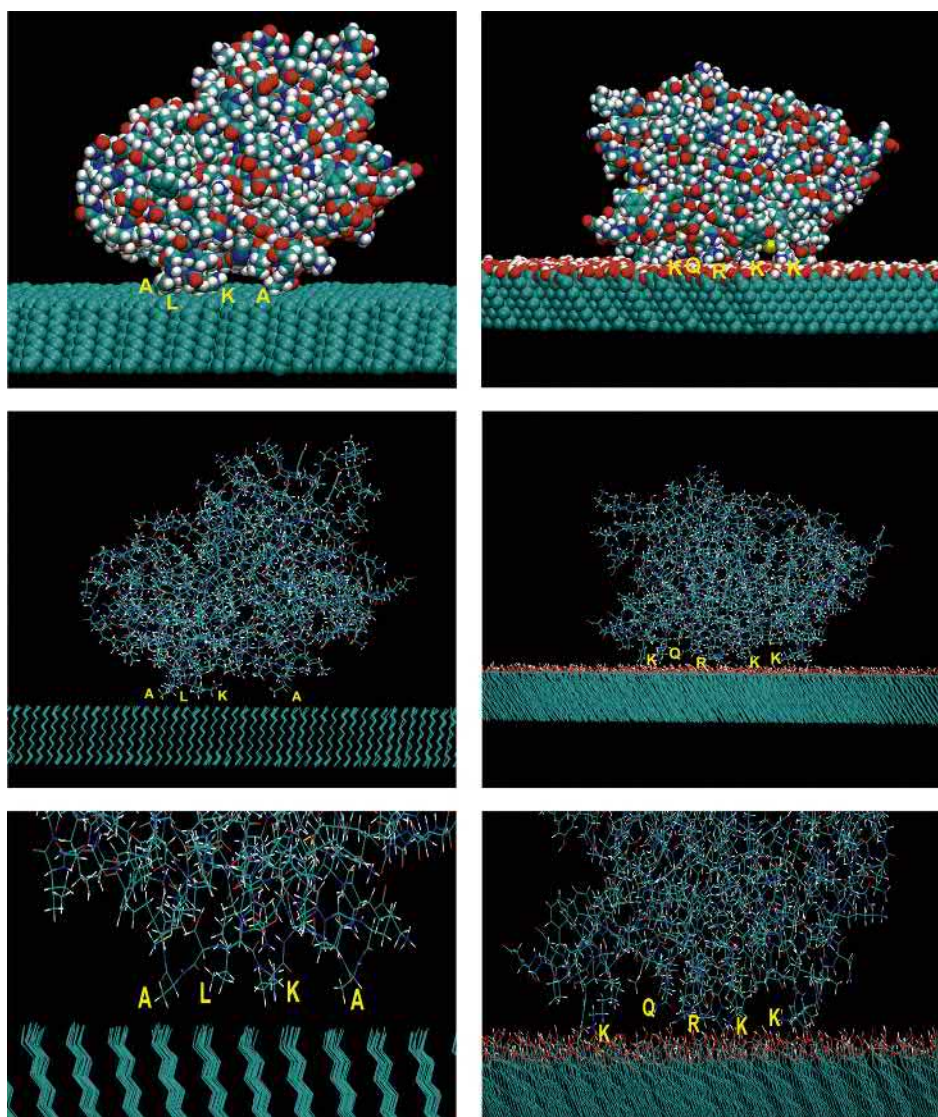
The kinetics of adsorption of proteins to solid surfaces typically consists of a very rapid initial phase, followed by a slower phase upon approach to the steady-state value. Initially, proteins adsorb as quickly as they arrive at the largely empty surface. In this phase, adsorption is linear when plotted against the square-root of time, characteristic of a diffusion-controlled process. In the later, slower phase, it is



• **Figure 2.1.2.6** The adsorption kinetics of lysozyme to a silica surface as studied with ellipsometry. The adsorbed amount versus time for adsorption of lysozyme to silica followed by buffer rinsing after 1800s, addition of surfactant (sodium dodecyl sulfate) after 3600s, and a final rinse with buffer after 5400s (open circles). Adsorption from a mixture of the protein and surfactant for 1800s followed by rinsing is also included (closed circles). The experiments were carried out at 25°C in 0.01 M phosphate buffer, 0.15 M NaCl, pH 7. (Reprinted with permission from Arnebrandt, T., Wahlgen, M., 1995. Protein–surfactant interactions at solid surfaces. In: T.A. Horbett., J. Brash. (Eds.), Proteins at Interfaces II: Fundamentals and Applications, ACS Symposium Series (pp. 239–254). Washington, DC: American Chemical Society. Copyright © 1995 American Chemical Society.)

more difficult for the arriving proteins to find and fit into an empty spot on the surface.

Fig. 2.1.2.6 shows the time course of adsorption of lysozyme on silica measured with a high-speed, automated ellipsometer capable of very rapid measurements (Arnebrandt and Wahlgen, 1995). At the earliest measurement time, less than a second into the study, the adsorption has reached almost half of the steady-state value. At 2000s, the protein solution was replaced with a buffer, resulting in some removal of loosely bound protein, but the adsorption stabilizes and would have remained at this value for much longer than shown, due to the tight, irreversible binding. At 4000s, a solution of the detergent sodium dodecyl sulfate (SDS) was infused, leading to complete removal of the protein. Thus, this experiment illustrates the rapid adsorption



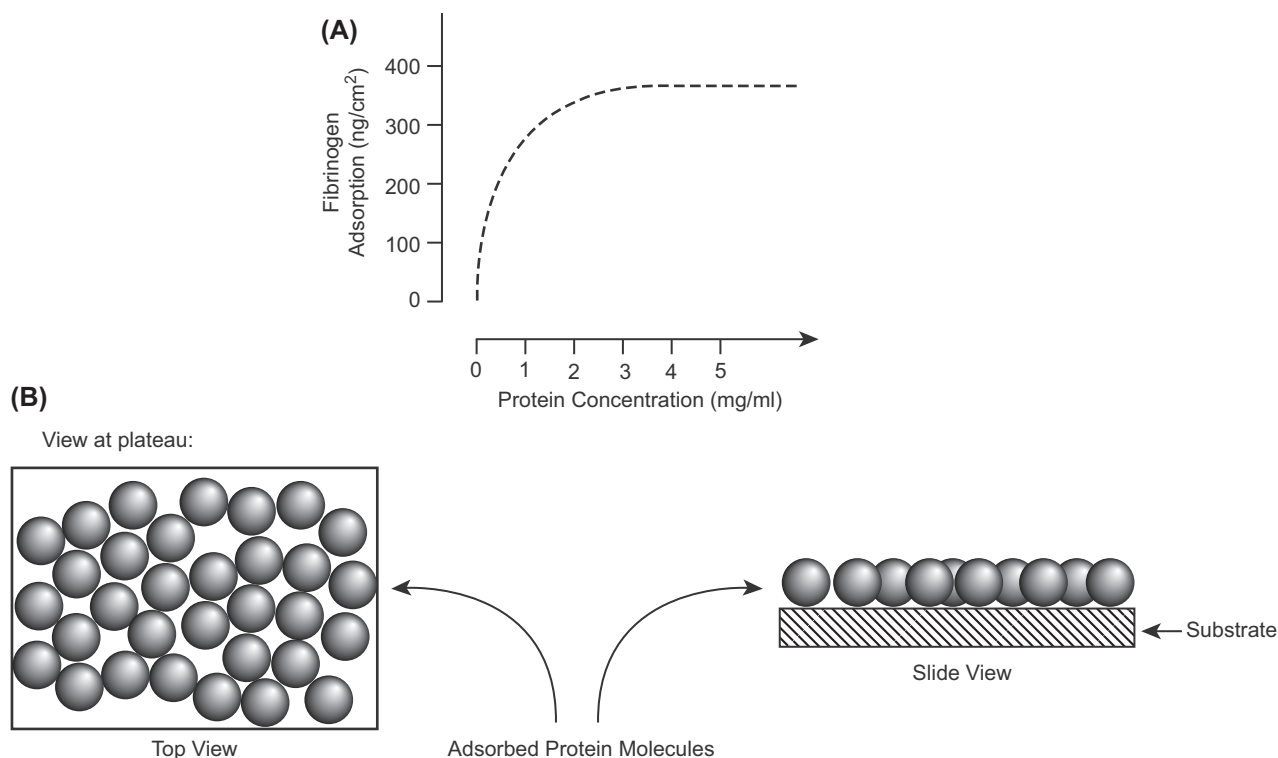
• **Figure 2.1.2.7** Molecular interactions of the 30-kDa C-terminus γ -chain fragment of fibrinogen with self-assembled monolayers with terminal CH_3 (left) and COOH (right) groups. Spacefill and wireframe models were newly created by R. Latour from the trajectory data for simulations described by [Agashe et al. \(2005\)](#). The models for the CH_3 surface show the interactions of the side chains of two alanine residues (A), one leucine (L), and the CH_2 groups of a lysine residue (K). The models for the COOH surface show the interactions of the side chains of three lysines (K), a glutamine (Q), and an arginine (R). Color code: green=C; red=O; blue=N; white=H; yellow=S. For clarity, interactions not easily seen in the full molecule views are not labeled.

of proteins. It also illustrates that most of the adsorbed protein is irreversibly bound, as indicated by the fact that washing the surface with buffer does not remove the protein. The adsorbed protein is only removed when a strong surfactant (SDS in this example) is used. All these features are characteristic of protein adsorption to solid surfaces.

[Fig. 2.1.2.7](#) provides an example from molecular modeling studies illustrating the complex array of interactions possible for a protein interacting with a surface ([Agashe et al., 2005](#)). The illustrations are for the gamma chain of fibrinogen interacting with either a CH_3 - or a COOH -terminated self-assembled monolayer (SAM) (see [Chapter 1.4.2](#)), and show that many atoms in the protein's amino acid side chains come near the surface, and could thus contribute to bonding.

These modeling studies start with high-resolution protein structures, and apply molecular dynamics calculations that allow the protein molecule and its atoms to move in space, in order to find favorable interactions with surfaces. It is found that the protein rolling over the surface eventually oriented itself with several residues near the surface, as shown.

For the CH_3 -terminated SAM, the position of the protein illustrated is a stable orientation that has hydrophobic groups, namely the side chains of alanine and leucine, and the CH_2 of a lysine side chain, lying close to the surface forming hydrophobic interactions with the methyl surface. In this orientation, the hydrophilic functional groups of the protein residues remained hydrated and well separated from the surface.



• **Figure 2.1.2.8** Adsorption isotherms (A) and the monolayer concept (B).

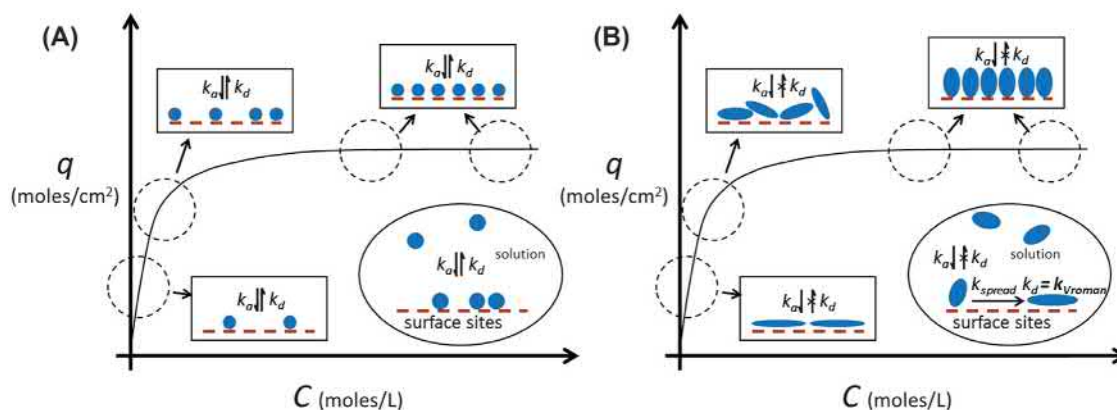
For the COOH surface, the position of the molecule that is a preferred orientation is quite different than for the CH₃ surface, as comparison of the overall shapes of the molecule against the two surfaces indicates. A clearer indication of these differences is the types of amino acid side chains found near the COOH interface. As shown, the near neighbors are three lysines (positively charged side chain), a glutamine (polar side chain), and an arginine (positively charged side chain), providing favorable interactions with the negatively charged deprotonated COOH groups presented from the surface.

The Monolayer Model

The existence of a close-packed monolayer of adsorbed protein is suggested by studies with single protein solutions, in which a saturation effect can often be observed in the adsorption isotherm (Fig. 2.1.2.8). Adsorption to surfaces exposed to different solution concentrations of protein until steady-state adsorption is achieved (2 h or more) increases steeply with increasing solution concentration at low concentrations, and then typically reaches a plateau or saturation value at some higher solution concentration. Despite the fact that protein adsorption to biomaterials is generally an irreversible process, this observed concentration dependence of adsorption for pure protein solutions thus often exhibits the shape of the Langmuir isotherm, which is only applicable for reversible adsorption processes such as gas adsorption.

One explanation for this behavior is that the space occupied per protein molecule in a close-packed layer (i.e., its

“footprint”) varies depending on the adsorption conditions. The difference between this type of adsorption behavior and true Langmuir adsorption is illustrated in Fig. 2.1.2.9. Fig. 2.1.2.9A represents true Langmuir adsorption behavior, which occurs under conditions where the adsorption process is reversible, each adsorption site is equivalent in size and in its interaction with the adsorbing solute, and the adsorbed solutes do not interact with one another. Fig. 2.1.2.9B, on the other hand, illustrates typical protein adsorption behavior. In this case, the appearance of a Langmuir-like adsorption process is caused by the fact that when adsorbed from low solution concentrations, the irreversibly bound proteins have time to molecularly spread onto the surface and form a larger footprint; i.e., a packed layer of more spread protein molecules is formed, thus resulting in a complete monolayer with a relatively low surface concentration. In contrast, when adsorption is done from higher solution concentrations, the adjacent sites are rapidly filled with other proteins, and so the spreading of each protein molecule into these sites on the surface is inhibited. In this case, a packed layer of irreversibly adsorbed protein is also formed, but the molecules are less spread, so that there can be more of them per unit area than when adsorption occurs at lower concentration (Wert and Santore, 2001; Latour, 2015). Support for the existence of variations in molecular spreading and protein footprints is provided by the fact that proteins adsorbed at lower concentrations tend to be more tightly bound, as judged by lower desorption upon exposure to buffer or other proteins or detergents. Support is also provided by circular dichroism spectropolarimetry (CD) studies that show increasingly greater degrees of protein unfolding on

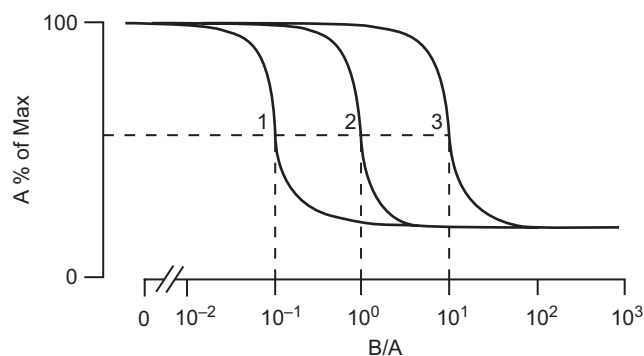


• **Figure 2.1.2.9** Adsorption isotherms; k_a , k_d , k_{spread} , k_{vroman} are the kinetic rates of adsorption, desorption, spreading, and displacement by Vroman effects, respectively. The y-axes (q) represent the moles of solute adsorbed per cm^2 of surface area. The x-axes (C) represent the concentration of the solute in solution. (A) Illustration of a reversible solute adsorption process that exhibits true Langmuir adsorption isotherm behavior. (B) Illustration of irreversible protein adsorption behavior, which exhibits a Langmuir-shaped isotherm, but does not actually represent a Langmuir adsorption process. (Reprinted with permission from The Langmuir isotherm: a commonly applied but misleading approach for the analysis of protein adsorption behavior. *J. Biomed. Mater. Res. A.* 103A, 949–958. Copyright © 2014 John Wiley and Sons.)

surfaces as the protein is adsorbed from increasingly lower solution concentrations (Sivaraman et al., 2009; Sivaraman and Latour, 2010a,b).

Because protein adsorption isotherms can take the shape of the Langmuir isotherm, there is a temptation to apply the Langmuir model to a protein adsorption isotherm and use it to calculate an equilibrium constant for the adsorption process. However, given the fact that protein adsorption tends to be an irreversible process apart from Vroman effects, and deviates from each one of the underlying requirements for Langmuir adsorption, the calculation of an equilibrium constant for protein adsorption in this manner is completely erroneous and simply should never be applied (Latour, 2015).

Usually, the plateau adsorption value observed in measured adsorption isotherms falls within the range expected for a close-packed monolayer of protein (about $0.1\text{--}0.5\ \mu\text{g}/\text{cm}^2$, depending on the diameter and orientation assumed for the protein). The adsorption values from complex protein mixtures are also typically in the monolayer range. For example, the sum total of the amount of adsorption of the three major proteins in plasma (albumin, IgG, and fibrinogen) on the HEMA-EMA series of surfaces is also in the range $0.1\text{--}0.5\ \mu\text{g}/\text{cm}^2$. In addition, the fact that competition exists between proteins for adsorption to a surface (see section “Competitive Adsorption of Proteins to Surfaces from Protein Mixtures,” below) also indicates the existence of limited sites. Thus, when a monolayer is the limit, there must be some selection for which proteins are present in the adsorbed film. It should be noted that well-defined plateaus are not always observed, but instead adsorption continues to rise as solution concentration is increased, although much more slowly than at the low solution concentrations; i.e., Freundlich isotherms do occur.



• **Figure 2.1.2.10** Competitive adsorption of two proteins from a mixture. (From Horbett, T.A., 1993. Principles underlying the role of adsorbed plasma proteins in blood interactions with foreign materials. *Cardiovasc. Pathol.* 2, 137S–148S.)

Competitive Adsorption of Proteins to Surfaces From Protein Mixtures

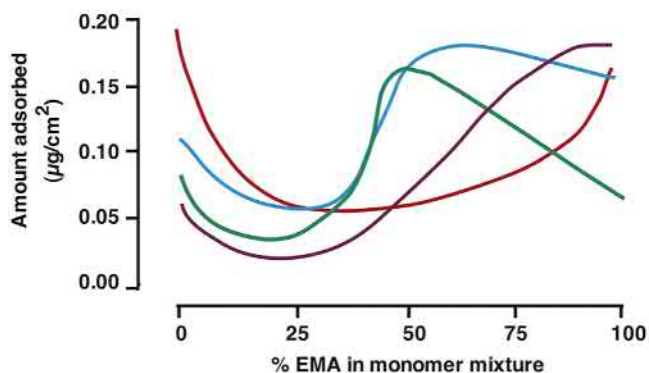
Adsorption from mixtures of proteins is selective, leading to enrichment of the surface phase in certain proteins. In this context, enrichment means that the fraction of the total mass of the adsorbed protein layer corresponding to a given protein is higher than the fraction of this protein in the bulk solution-phase mixture from which it adsorbed. Since the solid can accommodate only a small fraction of the total protein present in solution, and proteins vary greatly in their affinity for surfaces, some adsorbed proteins are present in greater amounts than others. Studies of surfaces exposed to blood plasma have shown that many different proteins are present in the adsorbed film with stoichiometries that differ greatly from plasma.

The competitive phenomena underlying differential enrichment from multiprotein mixtures are most clearly illustrated in binary mixtures of proteins. Fig. 2.1.2.10 has three separate curves in it, which overlap at the high and

low ends (Horbett, 1993). These curves represent the typical outcome of binary mixture studies, but for three different conditions. For example, when a radiolabeled protein such as fibrinogen (“A” in the figure) is mixed with various amounts of an unlabeled protein such as albumin (“B” in the figure), the adsorption of fibrinogen (“A”) always declines when sufficiently high amounts of albumin (“B”) are present. However, the amount of competing protein needed to inhibit the adsorption of the labeled protein is different in each curve. This is meant to illustrate that, for a given pair of competing proteins, the competition curves will be different if the surfaces they are competing for are different. In addition, if the surfaces are kept the same, but the competitions of different pairs of proteins are studied, the curves will differ because the ability of proteins to compete for surface sites is quite different for different proteins. A convenient way to characterize these binary competition curves is the ratio of competing protein it takes to cause 50% inhibition of the adsorption of the labeled protein. If this ratio is 1.0, it reflects the fact that the proteins are equal in affinity for the surface; if the ratio is much less (or much greater) than 1.0, it signifies that much less (or much more) of the competing protein is needed to reduce the adsorption, and so the competitor has a much higher (or much lower) affinity for the surface.

For example, inhibition of fibrinogen adsorption to polyethylene requires roughly 10-fold excess by weight of lower-affinity competing proteins such as albumin, but is effectively inhibited by the higher-affinity protein hemoglobin, even when hemoglobin is present at only 10% of the mass of fibrinogen. However, the amounts needed for this inhibition will depend on the surface chemistry, because the affinity of proteins changes with surface chemistry. Affinity variation is thus a major principle determining the outcome of the competitive adsorption processes.

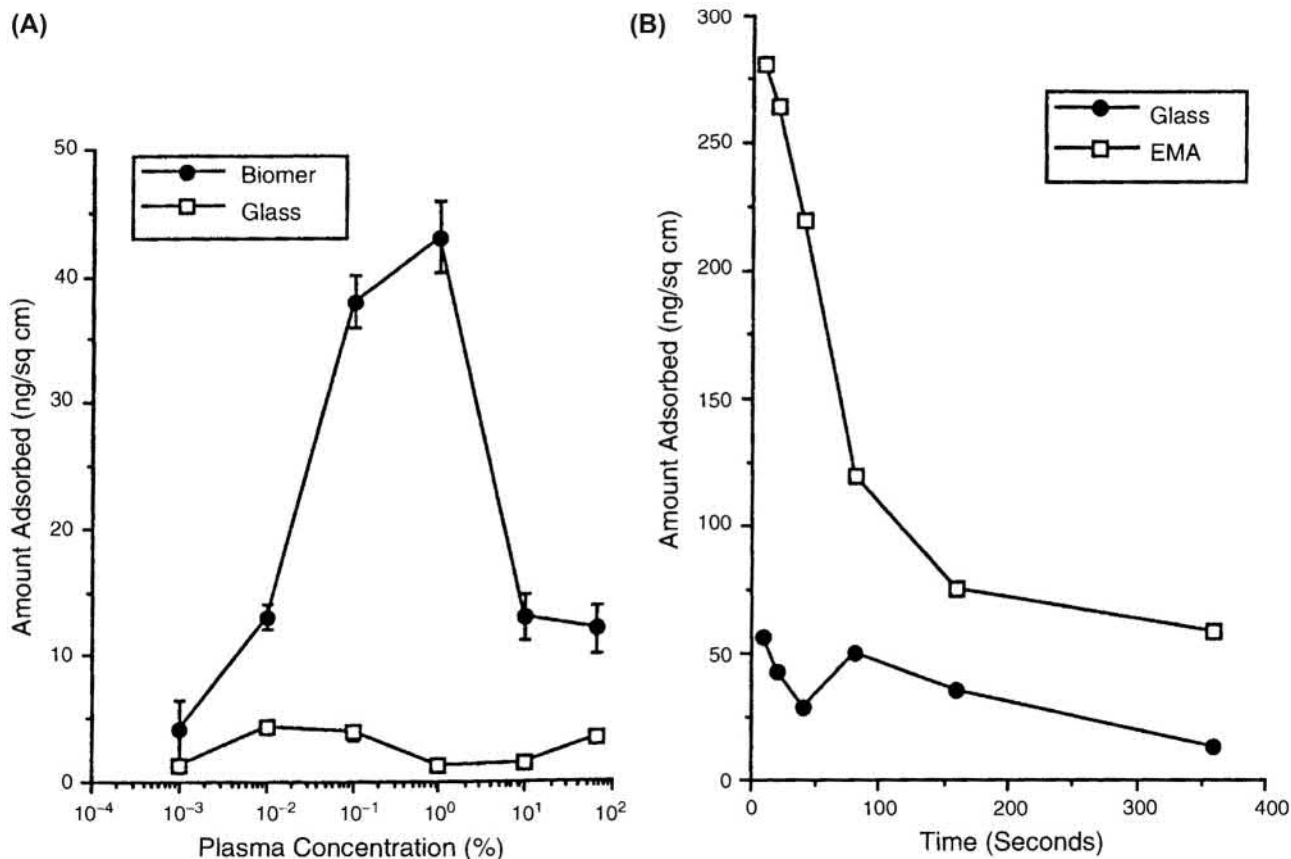
An experimental example of surface chemistry-dependent selective adsorption of proteins from a complex protein mixture is shown in Fig. 2.1.2.11 (Horbett, 1981). In these studies, a radiolabeled protein (e.g., ^{125}I -fibrinogen) added to blood plasma enabled measurement of the protein's adsorption to a series of polymers and copolymers of 2-hydroxyethyl methacrylate (HEMA) and ethyl methacrylate (EMA). This series varies greatly in its surface properties, from water-swollen hydrophilic HEMA to water-repelling hydrophobic EMA. The studies were repeated four times, once each with ^{125}I -labeled fibrinogen, albumin, IgG, or hemoglobin. The dependence of the adsorption of each protein on the changes in surface chemistry in this series is different for each protein, as reflected in the very different shape of lines for each protein. For example, albumin displayed preferential adsorption to both HEMA and EMA, in that adsorption to these polymers was much greater than to any of the HEMA–EMA copolymers. Conversely, fibrinogen adsorption was maximal at intermediate HEMA–EMA compositions. Another behavior is shown by the adsorption of hemoglobin and IgG, both of which display maximal adsorption to EMA, with minimal adsorption on surfaces made with about 20% EMA. Another



• **Figure 2.1.2.11** Differential affinity of proteins to a series of polymers: adsorption of Fg (green line); IgG (purple line); Alb (red line); and Hb (blue line) from plasma to hydroxyethyl methacrylate–ethyl methacrylate copolymers. (Redrawn version of a figure from Horbett, T.A., 1981. Adsorption of proteins from plasma to a series of hydrophilic–hydrophobic copolymers. II. Compositional analysis with the prelabelled protein technique. *J. Biomed. Mater. Res.* 15, 673–695.)

way to look at these data is to consider that the very different trends in adsorption across the series for each protein mean that the relative amount of each protein is unique to each surface, and varies quite a bit among the surfaces. On HEMA, the adsorption is seen to be in the order albumin > hemoglobin > fibrinogen > IgG, while on EMA the order is quite different: IgG, hemoglobin, and albumin are all about the same, but much greater than fibrinogen adsorption. On the 50–50 HEMA–EMA copolymer, the order is also different: fibrinogen and hemoglobin adsorption are about the same, but much greater than albumin or IgG. Examination of the amounts of adsorption for each protein on each surface shows that the overall composition of the adsorbed layer is different on each and every polymer in the series. The differences seen in these studies are typical for many other polymers that have been studied. Namely, the relative enrichment of a given protein when adsorbed from a complex mixture such as plasma is unique to each polymer studied. The effect of surface chemistry in causing differences in the relative enrichment of proteins adsorbed from the complex mixture of proteins in plasma is due to the differences in the relative competitive affinity of the proteins for each of the surfaces that were discussed above in regard to binary competitive adsorption studies.

Other examples of surface enrichment from complex protein mixtures are readily available. The examples presented in this paragraph emphasize protein-affinity differences, in contrast to the surface-affinity examples presented in the previous paragraph. Although fibrinogen is only the third most concentrated protein in blood plasma, after IgG and albumin, biomaterials exposed to plasma are typically enriched in fibrinogen in the adsorbed phase. Hemoglobin is present in very low concentrations in plasma (0.01 mg/mL or less), but it is still adsorbed in amounts similar to the more predominant proteins because of its high surface affinity. Albumin, a lower affinity protein, presents a counterexample. Albumin concentration in plasma is much higher than fibrinogen, yet the surface concentration of albumin adsorbed from plasma is typically about the same as fibrinogen. The high



• **Figure 2.1.2.12** The Vroman effect: (A) fibrinogen adsorption to Biomer and glass from various concentrations of blood plasma; (B) time course of fibrinogen adsorption to glass and poly(ethyl methacrylate) (PEMA) from undiluted plasma. (Reprinted with permission from Slack, S.M., Horbett, T.A., 1995. The Vroman effect: a critical review. In: T.A. Horbett, J. Brash (Eds.), *Proteins at Interfaces II: Fundamentals and Applications*. ACS Symposium Series (vol. 602, pp. 112–128). Washington, DC: American Chemical Society. Copyright © 1995 American Chemical Society.)

concentration of albumin in the plasma drives it onto the surface according to the law of mass action. Similarly, fibrinogen adsorption is higher from plasmas that contain higher concentrations of fibrinogen. Thus, mass concentration in the bulk solution phase is the second major factor determining competitive adsorption behavior.

The adsorption of fibrinogen from plasma exhibits some unusual behavior. On some surfaces, fibrinogen adsorption is maximal at intermediate dilutions of plasma (see example in Fig. 2.1.2.12A). In addition, fibrinogen adsorption from full-strength or moderately diluted plasma is higher at very early adsorption times than at later times (example shown in Fig. 2.1.2.12B). These are examples of the Vroman effect for fibrinogen. This phenomenon is a clear example of the unique effects of competitive adsorption on both the steady-state and the transient composition of the adsorbed layer that forms from plasma. The Vroman effect appears to involve displacement of initially adsorbed fibrinogen by later arriving, more surface-active plasma proteins, especially high-molecular-weight kininogen, and transitions in the adsorbed fibrinogen that make it less displaceable with adsorption time (reviewed in Slack and Horbett, 1995). Vroman effects, i.e., peaks in adsorption at intermediate dilution, are also observed for

fibrinectin adsorption from serum, and even for binary protein mixtures under certain conditions.

Molecular Spreading Events: Conformational and Biological Changes in Adsorbed Proteins

Proteins that adsorb to solid surfaces can undergo conformational changes, because of the relatively low structural stability of proteins and their tendency to unfold to allow further bond formation with the surface, which is driven by thermodynamics (i.e., lowering the overall free-energy state of the system) (Latour, 2008). Conformational changes can be detected with many types of physicochemical methods, and also by measuring changes in the biological activity of the adsorbed proteins.

Physicochemical Studies of Conformational Changes

“Soft” proteins are found to adsorb more readily and more tenaciously than “hard” proteins. In this context, a “soft” protein is one with a low thermodynamic stability, while

a “hard” protein is more stable to unfolding in solution in response to denaturing conditions, such as elevated temperature. This concept and the articles supporting the following discussion are presented in detail elsewhere (Horbett and Brash, 1995; Latour, 2008).

Comparison of the adsorptive behavior of different proteins to their molecular properties indicates that less stable proteins are more adsorptive. The important role of structural stability in adsorption is also supported by recent studies with engineered mutant proteins with single amino acid substitutions that vary in stability. Lysozyme adsorption at the solid–liquid interface, and tryptophan synthase occupation of the air–water interface are greater for less stable mutants, and more stable lysozyme variants tend to be displaced by less stable mutants (Lee et al., 2004).

Several studies with differential scanning calorimetry (DSC) methods seemed to indicate that adsorbed proteins may lose much of their structure, depending on how “soft” they are. Heat is taken up at a certain elevated temperature for proteins in solution, due to the unfolding of the native protein at the transition temperature. This phenomenon is analogous to the melting of a crystalline material. An absence or reduction of this effect for a preadsorbed protein suggests that the adsorbed protein has already undergone the transition; i.e., that it has already unfolded upon adsorption. The transition enthalpy of lysozyme preadsorbed to negatively charged polystyrene was much less than for the protein in solution (0–170 kJ/mol for the adsorbed protein vs. about 600 kJ/mol for the native protein in solution depending on the pH). However, for lysozyme preadsorbed on hematite, the unfolding enthalpy is only about 20% less than for the native protein in solution, indicating that changes in the enthalpy of unfolding depend on the adsorbing surface. Furthermore, for lactalbumin the heat released is nearly zero when it is preadsorbed on either the polystyrene or the hematite surface, suggesting complete unfolding of lactalbumin on both surfaces. These observations are consistent with the lower stability of lactalbumin in comparison to lysozyme. Several proteins preadsorbed to pyrolytic carbon do not show any release of heat at the expected transition temperature, suggesting that pyrolytic carbon induces complete unfolding; a result that is consistent with the tenacious binding of proteins to this surface. It has also been shown that albumin and lysozyme preadsorbed to polystyrene exhibit no transitional unfolding enthalpy, while lysozyme preadsorbed to a hydrophilic contact lens still exhibits about 50% of the heat released by the native protein in solution during its thermally induced transition. Streptavidin preadsorbed to polystyrene displays an unfolding enthalpy that is very similar to that for the native protein in solution, probably because of the greater stability of streptavidin in comparison to lysozyme or albumin.

However, more recent studies of adsorbed proteins by the DSC method in conjunction with other, more direct conformational measurements such as circular dichroism (CD), show that at least some adsorbed proteins that appear to be completely denatured, as judged by DSC, still have

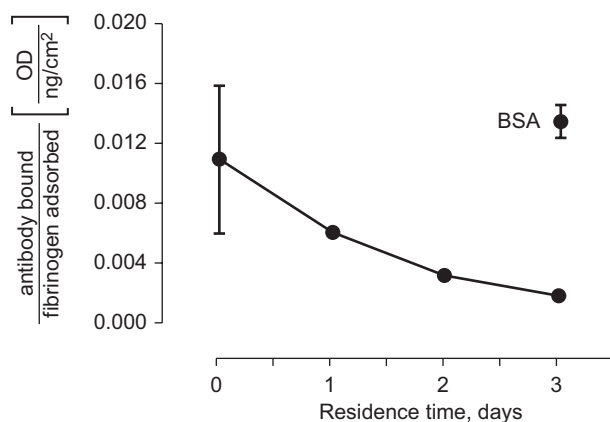
considerable amounts of their native structure, as measured by CD (Thyparambil et al., 2015). It thus appears that some proteins become somewhat more stable after adsorption, and thus do not show heat release at the normal melting temperature.

The concept of molecular spreading of the adsorbed protein suggested by these observations has been used to explain differences in the amount of IgG adsorbed during stepwise adsorption. When the final concentration of bulk protein in solution is achieved in a series of smaller concentration steps, as opposed to bringing the bulk solution concentration to its final value in one step, adsorption is smaller. This result is thought to be due to spreading and an enlarged footprint of a protein molecule that can occur at lower solution concentrations, which is the same phenomenon that leads to the appearance of Langmuir-like isotherms, as discussed above. Conformational changes upon adsorption of fibronectin to polystyrene beads and Cytodex microcarrier beads have also been detected using electron spin resonance spectroscopy. Many other physicochemical studies are consistent with partial unfolding of the adsorbed proteins (Andrade, 1985; Lundstrom, 1985; Horbett and Brash, 1995; Sivaraman et al., 2009; Sivaraman and Latour, 2010a,b; Thyparambil et al., 2015).

Changes in Biological Properties of Adsorbed Proteins

While physicochemical studies sometimes suggest complete denaturation of adsorbed proteins, most probes for biological activity suggest the changes are more limited (reviewed with citations in Horbett, 1993). Thus, enzymes retain at least some of their activity in the adsorbed state, especially when the enzyme is adsorbed from high solution concentration to minimize adsorption-induced unfolding. Measurements of enzyme activity or retention times during passage over hydrophobic chromatography matrices have shown that the degree of denaturation is highly dependent on the protein, the length of time the protein has spent on the matrix, the solvent, and other conditions, and is not necessarily complete.

Changes in the binding of a monoclonal antibody to fragment D of fibrinogen upon fibrinogen adsorption to polystyrene have been attributed to changes in the conformation of fibrinogen after adsorption. Thus, solution-phase fibrinogen does not bind the antibody raised to fragment D, but the surface-adsorbed fibrinogen does. Furthermore, fibrinogen in solution does not compete for the binding of the antibody to the surface-adsorbed fibrinogen. The RIBS (receptor-induced binding site) antibodies are similar: they bind to fibrinogen only after the fibrinogen has bound to either a solid surface or to the platelet IIb/IIIa receptor. The binding of the RIBS antibodies and others that bind to the platelet-binding regions of fibrinogen varies with the length of time after adsorption of the fibrinogen. Platelet adhesion to polymethacrylates has been correlated with the amount of antifibrinogen binding, suggesting that the adsorbed fibrinogen is in different conformations on the various polymethacrylates.



• **Figure 2.1.2.13** Transitions in adsorbed fibrinogen. The effect of 3-day residence in buffer or buffered albumin solution upon antifibrinogen binding to fibrinogen adsorbed from dilute plasma to Biomer polyurethane is shown. BSA, bovine serum albumin. (From: Fig. 3A in Chinn, J.A., Posso, S.E., Horbett, T.A., Ratner, B.D., 1992. Post-adsorptive transitions in fibrinogen adsorbed to polyurethanes: changes in antibody binding and sodium dodecylsulfate elutability. *J. Biomed. Mater. Res.* 26, 757–778.)

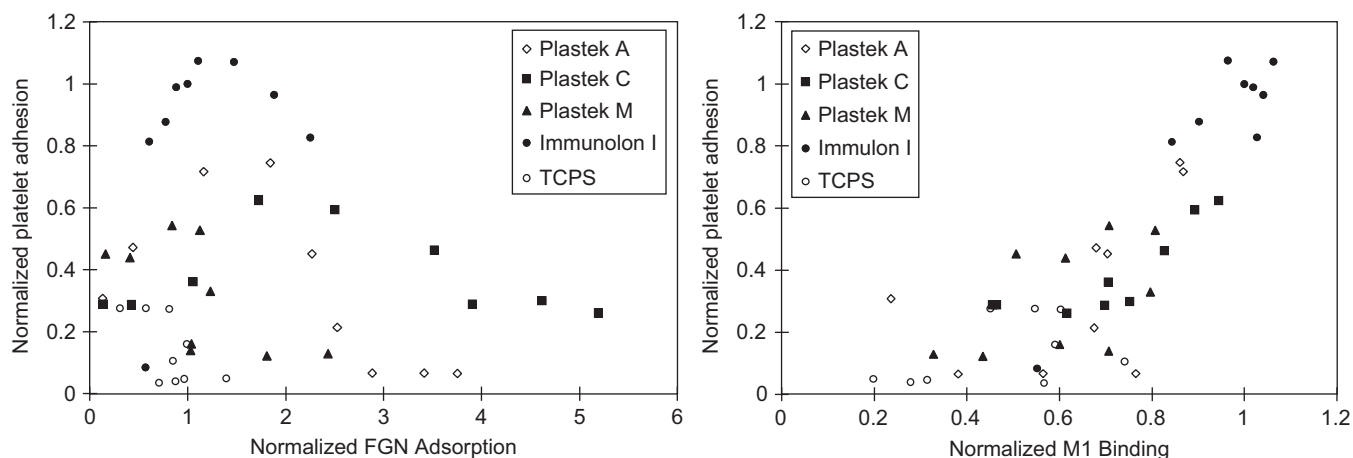
Fibrinogen undergoes a time-dependent transition after its adsorption to a surface that results in reduced platelet and antibody binding to the adsorbed fibrinogen, as well as reduction in the SDS and plasma displaceability, and changes in amide II frequency of the adsorbed fibrinogen. The losses in platelet binding, antibody binding, and SDS elutability are prevented if albumin is included in the storage buffer. An example showing time-dependent losses in antibody binding to fibrinogen and its prevention by albumin is shown in Fig. 2.1.2.13 (Chinn et al., 1992). Vitronectin also appears to undergo conformational changes upon adsorption that affect its ability to bind heparin and its infrared spectra.

Modulation of the biologic activity of fibronectin has been shown in several studies in which the ability of fibronectin adsorbed to various surfaces to support cell attachment or spreading was found to differ. For example, fibronectin adsorbed to tissue-culture-grade polystyrene was able to support cell attachment and spreading, whereas fibronectin adsorbed to ordinary polystyrene does not support spreading very well, unless some albumin is added to the fibronectin solution. Fibronectin adsorbed to self-assembled monolayer (SAM) films with various functional end groups also varies in its ability to interact with cells. On hydrophobic SAMs there is poor cell spreading unless albumin is coadsorbed (albumin “rescuing”). The albumin “rescuing” phenomenon observed for SAMs is similar to the albumin effect on fibronectin’s ability to promote cell spreading on polystyrene, and to the effect of albumin addition in preventing losses in platelet adhesion to fibrinogen-adsorbed surfaces discussed above. The ability of fibronectin adsorbed to a series of polymers to support the outgrowth of corneal epithelial cells has also been found to vary a great deal, despite the presence of similar amounts of fibronectin on the surfaces.

The effect of albumin addition in enhancing the adhesivity of fibronectin-coated surfaces is opposite to what one might expect, because the added albumin should reduce the amount of adsorbed fibronectin as albumin competes for sites on the surfaces. The explanation for the albumin effect is thought to be that by adsorbing along with the fibronectin to the surface, the albumin molecules occupy surface sites near the fibronectin molecules. The adsorbed albumin molecules thus keep the adsorbed fibronectin molecules from undergoing structural changes that they would otherwise do in trying to spread into formerly empty surface sites, but they cannot do so if albumin molecules first fill those sites.

Highly uniform SAM surfaces with different terminal functional groups have proved useful in showing how surface chemistry modulates the biologic properties of adsorbed fibronectin. When increasing amounts of fibronectin were adsorbed to SAMs with terminal OH, COOH, NH₂, or CH₃ functional groups, it was found that the amount of adsorbed fibronectin required to cause cell adhesion varied widely. Thus, on the CH₃ surface it took far higher amounts of fibronectin to obtain equivalent maximal adhesion than on the OH surfaces (Keselowsky et al., 2003). Similarly, the binding affinity of antibodies that bind to the cell-binding domain and of the integrin $\alpha_5\beta_1$ was much higher for fibronectin on the OH surface than on the CH₃ surface. Thus, there are significant differences in the functional presentation of the central cell-binding domain of fibronectin upon adsorption to different surface chemistries. The theoretical predictions of differences in preferred orientation of adsorbed molecules on surfaces with different chemistry (see Fig. 2.1.2.7) suggest that these biological effects are also due to orientational effects. With an osteogenic cell line, genes that mark osteoblastic differentiation and actual mineralization were both elevated in the cells on the fibronectin-coated OH and NH₂ surfaces compared with the COOH and CH₃ SAMs (Keselowsky et al., 2005). Myoblast differentiation on fibronectin adsorbed to this same series of SAMs also varied greatly, in the order OH > CH₃ > NH₂ = COOH (Lan et al., 2005). The ability of myoblasts to rearrange adsorbed fibronectin and deposit new fibronectin was also much greater on the CH₃ surface than on the OH surface.

Fig. 2.1.2.14 shows an experimental example of the modulation of the biologic activity of adsorbed fibrinogen, namely its ability to mediate platelet adhesion. In these studies, both fibrinogen adsorption and binding of a fibrinogen-specific antibody were measured from plasma diluted to various degrees on a series of chemically modified polystyrene surfaces. Platelet adhesion to the plasma preadsorbed surfaces was also measured. The left part of Fig. 2.1.2.14 shows that there was no obvious correlation between platelet adhesion and fibrinogen adsorption, despite the fact that we know that fibrinogen adsorption is required for adhesion, as shown in Fig. 2.1.2.3. However, when the availability of the platelet-binding region in fibrinogen adsorbed to these surfaces was measured using a monoclonal antibody (M1)



• **Figure 2.1.2.14** Cross plots of platelet adhesion against the amount of fibrinogen (FGN) adsorption or M1 antibody binding on five different surfaces. (From: Tsai, W.B., Grunkemeier, J.M., Horbett, T.A. 2003. Variations in the ability of adsorbed fibrinogen to mediate platelet adhesion to polystyrene-based materials: a multivariate statistical analysis of antibody binding to the platelet binding sites of fibrinogen. *J. Biomed. Mater. Res.* 67A, 1255–1268.)

that binds to the C-terminal region of the gamma chain of fibrinogen, it was found to vary greatly. Platelet adhesion was well correlated with the antibody binding, as shown in the right panel in Fig. 2.1.2.14. The poor correlation with total fibrinogen adsorption, and the greatly improved correlation with platelet-binding site availability, is strong support for the idea that the functional activity of adsorbed fibrinogen in supporting platelet adhesion depends on the surface to which it is adsorbed. Thus, fibrinogen's bioadhesive activity is modulated by the surface chemistry.

In another interesting set of studies, Sivaraman and Latour provided evidence that indicates that adsorption-induced unfolding of proteins can actually create platelet-binding sites. Fibrinogen was adsorbed to different surface chemistries from different solution concentrations to obtain a wide range in the degree of unfolding of the protein as determined by circular dichroism (CD) spectropolarimetry. Platelet adhesion to the adsorbed fibrinogen was then found to strongly correlate to the degree of adsorption-induced unfolding (Sivaraman and Latour, 2010a). Surprisingly, platelet adhesion was even found to then occur on surfaces with adsorbed human serum albumin, but only after the albumin unfolded beyond a critical limit, which was measured as a loss in α -helices of more than 33% (Sivaraman and Latour, 2010b). It is hypothesized that this phenomenon occurs by adsorption-induced salt-bridge separation of positively and negatively charged amino acids, causing them to effectively transition from RGE-like to RGD-like motifs, which may be a universal mechanism by which platelets are able to detect denatured proteins on a vascular or biomaterial surface. Further studies are needed to support this hypothesis.

These studies with platelets, fibroblasts, epithelial cells, osteocytic cells, and myoblasts show that substrate properties somehow modulate the ability of adsorbed proteins to interact with cells. These differences may arise, at least in part, from differences in the availability of epitopes on adhesive proteins for the cell surface receptor, which are

influenced by factors such as the orientation and conformation of the adsorbed proteins. That is, both the amount of the adsorbed adhesive protein, as well as its “bioreactivity,” are actively influenced by the properties of the surface to which it is adsorbed.

The Importance of Adsorbed Proteins in Biomaterials

Table 2.1.2.1 summarizes the principles underlying the influence of adsorbed proteins in biomaterials used in contact with the blood. All of the principles listed also apply in other environments, such as the extravascular spaces, albeit with other proteins and other cell types (e.g., macrophages in the peritoneum adhere via other receptors and other adhesion proteins). The blood platelets therefore provide a “case study,” and we close this chapter by considering this case.

The high sensitivity of platelet–surface interactions to adsorbed proteins is fundamentally due to the presence of adhesion receptors in the platelet membrane that bind to certain plasma proteins. There are generally only a few types of proteins in plasma that have native-state motifs that are bound by the adhesion receptors. The selective adsorption of these proteins to synthetic surfaces, in competition with the many nonadhesive proteins that also tend to adsorb, is thought to mediate platelet adhesion to these surfaces, which in turn leads to platelet activation events such as their ability to catalyze the formation of thrombin. However, since the dissolved plasma-phase adhesion proteins do not bind to adhesion receptors unless the platelets are appropriately stimulated, while unstimulated platelets can adhere to adsorbed adhesion proteins, it appears that adsorption of proteins to surfaces accentuates and modulates the adhesion receptor–adhesion protein interaction. The type of surface to which the adhesion protein is adsorbed affects the ability of the protein to support platelet adhesion, due to variations in the amount

TABLE 2.1.2.1 Principles Underlying the Influence of Adsorbed Plasma Proteins on Blood Platelet Interactions With Biomaterials

1. Synthetic foreign materials acquire bioreactivity only after first interacting with dissolved proteins. The principal means by which the transformation from an inert, nonthrombogenic polymer to a biologically active surface takes place is the interaction of the proteins with the surface that then mediates cell adhesion.
2. Platelets are an important example of why and how adsorbed proteins are influential in cell–biomaterials interactions.
3. Sensitivity of platelets to adsorbed proteins is due to:
 - a. Some proteins in plasma are strongly adhesive for platelets: fibrinogen, fibronectin, vitronectin, and von Willebrand factor.
 - b. Concentrating, localizing, immobilizing effects of adsorbing the proteins at the interface accentuates the receptor–adhesion protein interaction.
 - c. Platelets have receptors (IIb/IIIa and Ib/IX) that bind specifically to a few of the plasma proteins, mediating adhesion.
4. Principles of protein adsorption to biomaterials:
 - a. Monolayer adsorption and consequent competition for available adsorption sites means that not all proteins in the plasma phase can be equally represented on the surface.
 - b. Driving forces for adsorption are the intrinsic surface activity and bulk phase concentration of the proteins.
 - c. Surfaces vary in selectivity of adsorption.
 - d. Biological activity of the adsorbed protein varies on different surfaces.

of adsorbed fibrinogen (Horbett, 1993), and in the availability of the platelet-binding regions in the fibrinogen molecule (Tsai et al., 2003). The principles that determine protein adsorption to biomaterials include monolayer adsorption, the intrinsic surface activity and bulk solution concentration of the protein, and the effect of different surfaces on the selectivity of adsorption, the conformational stability, and the biologic activity of the adsorbed protein.

More generally, all proteins are known to have an inherent tendency to deposit very rapidly on surfaces as a tightly bound adsorbate that strongly influences subsequent interactions of many different types of cells with the surfaces. It is therefore thought that the particular properties of surfaces, as well as the specific properties of individual proteins, together determine the organization of the adsorbed protein layer, and that the nature of this layer in turn determines the cellular response to the adsorbed surfaces.

Surface Chemistries Highly Resistant to Protein Adsorption

The importance of adsorbed proteins in biomaterials science is also well-illustrated by the amount of effort that has been

expended to develop protein “nonfouling” or protein-repellent materials in recent years (see Chapter 1.4.3A; Horbett, 2003; Binazadeh et al., 2012; Thompson et al., 2017b).

Since adsorbed proteins are required for platelet adhesion, an obvious approach to improve blood compatibility is to produce biomaterials that prevent or at least greatly reduce protein adsorption, and thus much recent research has focused on finding protein-repellent materials. For example, many studies show that protein adsorption can be greatly reduced with poly(ethylene oxide) (PEO) or, similarly, poly(ethylene glycol) (PEG) coatings of various types [e.g., PEO/polylactide copolymers, PEO-grafted polyurethanes (PUs), PEO-grafted PU/polystyrene, ethylene glycol-terminated SAMs, or glow discharge deposited polymers of the low-molecular-weight polyether tetraglyme to make PEO-like coatings], and that platelet adhesion is reduced, both in vitro and in vivo (Gombotz et al., 1991; Shen et al., 2002; Binazadeh et al., 2012; Thompson et al., 2017b). However, since even low amounts of adsorbed fibrinogen (c. 5 ng/cm²; Tsai and Horbett, 1999) are sufficient to support nearly full-scale platelet adhesion, and many of the surfaces tested fail to reduce fibrinogen adsorption to that degree when exposed to undiluted blood plasma, it has proved difficult to make biomaterials that fully achieve this design criterion. In addition, studies have shown that PEO/PEG undergoes hydrolysis over time, thus eventually losing its protein-repellency (Shen et al., 2002; Li et al., 2007), suggesting its suitability for only relatively short-term applications.

Recent studies by Gunkel and Huck (Gunkel and Huck, 2013) and by Riedel et al. (Riedel et al., 2013) investigated the composition of the proteins that nonspecifically bind to PEG-coated surfaces following exposure to undiluted blood plasma and discovered an unusually high percentage of apolipoproteins in the adsorbed protein layer. These proteins were subsequently determined to be deposited on the surfaces via the adsorption of low-density lipoprotein (LDL) particles. These findings were further supported in a recent study by the Brash group (Cornelius and Brash, 2015). In this study, Cornelius and Brash presented the surprising results that while PEO-coated polyurethane surfaces were highly resistant to the adsorption of proteins in solution, they actually adsorbed lipoprotein particles [low-density lipoprotein (LDL), high-density lipoprotein (HDL), and very-low-density lipoproteins (VLDL)] as readily as polyurethane surfaces without a PEO coating. The significance of these findings is that lipoproteins, which are composed of phospholipid membranes encapsulating lipid molecules such as cholesterol, carry apolipoproteins on their surfaces. Thus while being highly resistant to individual proteins in solution, proteins (i.e., apolipoproteins) will still be deposited onto PEO-coated surfaces via HDL, LDL, and VLDL adsorption. The clinical significance of these findings remains to be determined, with the possibility that irreversibly adsorbed apolipoproteins may possibly initiate platelet adhesion and subsequent thrombosis (Chandy and Sharma, 1991), especially as they can be expected to eventually undergo aging-induced unfolding over time (Sivaraman and Latour, 2012).

Another category of highly protein-resistant surface chemistries that shows great potential for biomaterials applications has been provided by zwitterionic betaines [poly(carboxybetaine) (PCB) and poly(sulfobetaine) (PSB)] (Zhang et al., 2006; Jiang and Cao, 2010; Binazadeh et al., 2012; Thompson et al. 2017b). These materials show ultralow protein adsorption properties as well as being much more chemically stable than PEO/PEG functionality. In fact, zwitterionic carboxybetaine hydrogels have been shown to be stable for at least 90 days when subcutaneously implanted in mice without inducing an observable foreign-body response (Zhang et al., 2013). As with PEO/PEG coatings, these surfaces provide resistance to protein adsorption due to their ability to tightly bind water molecules, thus forming hydration layers that proteins in solution are not able to displace. It remains to be determined by further studies how long PCB- and PSB-coated surfaces will be able to maintain their resistance to protein adsorption and whether or not they are also resistant to the adsorption of lipoprotein particles when used for blood-contacting applications.

Concluding Remarks

As presented in this chapter, the adsorption of proteins to biomaterial surfaces is of fundamental importance to the understanding of cellular responses and the subsequent biocompatibility of synthetic materials that are used in implanted medical devices. Because cells do not possess receptors for synthetic materials, their response to different chemically stable materials presenting different surface chemistries is mediated not by the material itself, but by the types of proteins that adsorb to the material surface and the bioactivity of these proteins, which is influenced by their orientation, structure, and packing arrangement on the surface. While much has been learned over the past decades of research to understand and unravel the complexities involved in these processes, the understanding of protein adsorption behavior and its influence on the subsequent biological response to implanted biomaterials is far from complete and remains an important area of ongoing research in the field of biomaterials science and engineering.

References

- Agashe, M., Raut, V., Stuart, S.J., Latour, R.A., 2005. Molecular simulation to characterize the adsorption behavior of a fibrinogen γ -chain fragment. *Langmuir* 21, 1103–1117.
- Anderson, D.G., Putnam, D., Lavik, E.B., Mahmood, T.A., Langer, R., 2005. Biomaterial microarrays: rapid, microscale screening of polymer–cell interaction. *Biomaterials* 26, 4892–4897.
- Andrade, J.D., 1985. Principles of protein adsorption. In: Andrade, J.D. (Ed.), *Surface and Interfacial Aspects of Biomedical Polymers*. Plenum Press, New York, NY, pp. 1–80.
- Arnebrandt, T., Wahlgen, M., 1995. Protein–surfactant interactions at solid surfaces. In: Horbett, T.A., Brash, J. (Eds.), *Proteins at Interfaces II: Fundamentals and Applications*, ACS Symposium Series. American Chemical Society, Washington, DC, pp. 239–254.
- Backovic, A., Huang, H.L., Del Frari, B., Piza, H., Huber, L.A., et al., 2007. Identification and dynamics of proteins adhering to the surface of medical silicones *in vivo* and *in vitro*. *J. Proteome Res.* 6, 376–381.
- Binazadeh, M., Kabiri, M., Unsworth, L.D., 2012. Poly(ethylene glycol) and poly(carboxy betaine) based nonfouling architectures: review and current efforts. In: Horbett, T.A., Brash, J.L., Norde, W. (Eds.), *Proteins at Interfaces II: Fundamentals and Applications*, ACS Symposium Series, vol. 1120. American Chemical Society, Washington, DC, pp. 621–643.
- Chandy, T., Sharma, C.P., 1991. Effects of lipoproteins on protein/platelet interaction on polymers. *J. Biomed. Mater. Res.* 25, 1085–1094.
- Chastain, S.R., Kundu, A.K., Dhar, S., Calvert, J.W., Putnam, A.J., 2006. Adhesion of mesenchymal stem cells to polymer scaffolds occurs via distinct ECM ligands and controls their osteogenic differentiation. *J. Biomed. Mater. Res. A* 78, 73–85.
- Chinn, J.A., Horbett, T.A., Ratner, B.D., 1991. Baboon fibrinogen adsorption and platelet adhesion to polymeric materials. *Thromb. Haemost.* 65, 608–617.
- Chinn, J.A., Posso, S.E., Horbett, T.A., Ratner, B.D., 1992. Post-adsorptive transitions in fibrinogen adsorbed to polyurethanes: changes in antibody binding and sodium dodecylsulfate elutability. *J. Biomed. Mater. Res.* 26, 757–778.
- Cornelius, R.M., Brash, J.L., 1993. Identification of proteins absorbed to hemodialyser membranes from heparinized plasma. *J. Biomater. Sci. Polym. Ed.* 4, 291–304.
- Cornelius, R.M., Brash, J.L., 2015. Interactions of apolipoproteins AI, AII, B and HDL, LDL, VLDL with polyurethane and polyurethane-PEO surfaces. *Langmuir* 31, 12087–12095.
- Gifford, R., Kehoe, J.J., Barnes, S.L., Kornilayev, B.A., Alterman, M.A., et al., 2006. Protein interactions with subcutaneously implanted biosensors. *Biomaterials* 27, 2587–2598.
- Gombotz, W.R., Guanghui, W., Horbett, T.A., Hoffman, A.S., 1991. Protein adsorption to poly(ethylene oxide) surfaces. *J. Biomed. Mater. Res.* 25, 1547–1562.
- Gunkel, G., Huck, T.S., 2013. Cooperative adsorption of lipoprotein phospholipids, triglycerides, and cholesteryl esters are a key factor in nonspecific adsorption from blood plasma to antifouling polymer surfaces. *J. Am. Chem. Soc.* 135, 7047–7052.
- Horbett, T.A., 1981. Adsorption of proteins from plasma to a series of hydrophilic-hydrophobic copolymers. II. Compositional analysis with the prelabelled protein technique. *J. Biomed. Mater. Res.* 15, 673–695.
- Horbett, T.A., 1993. Principles underlying the role of adsorbed plasma proteins in blood interactions with foreign materials. *Cardiovasc. Pathol.* 2, 137S–148S.
- Horbett, T.A., 1994. The role of adsorbed proteins in animal cell adhesion. *Colloids Surfaces B Biointerfaces* 2, 225–240.
- Horbett, T.A., 1996. Proteins: structure, properties, and adsorption to surfaces. In: Ratner, B.D., Hoffman, A.S., Schoen, F., Lemons, J.E. (Eds.), *Biomaterials Science*. Academic Press, San Diego, CA, pp. 133–141.
- Horbett, T.A., 1999. The role of adsorbed adhesion proteins in cellular recognition of biomaterials. *BMES Bulletin* 23, 5–9.
- Horbett, T.A., 2003. Biological activity of adsorbed proteins. Chapter 15. In: Malmsten, M. (Ed.), *Biopolymers at Interfaces*, second ed. Marcel Dekker, Inc, New York, NY, pp. 393–413 (Chapter 15).
- Horbett, T.A., Brash, J.L., 1995. Proteins at interfaces: an overview. In: Horbett, T.A., Brash, J. (Eds.), *Proteins at Interfaces II: Fundamentals and Applications*, ACS Symposium Series. American Chemical Society, Washington, DC, pp. 1–25.
- Hwang, N.S., Varghese, S., Elisseeff, J., 2008. Controlled differentiation of stem cells. *Adv. Drug Deliv. Rev.* 60, 199–214.

- Jiang, S.Y., Cao, Z.Q., 2010. Ultralow-fouling, functionalizable, and hydrolyzable zwitterionic materials and their derivatives for biological applications. *Adv. Mater.* 22 (9), 920–932.
- Keselowsky, B.G., Collard, D.M., García, A.J., 2003. Surface chemistry modulates fibronectin conformation and directs integrin binding and specificity to control cell adhesion. *J. Biomed. Mater. Res.* 66A, 247–259.
- Keselowsky, B.G., Collard, D.M., García, A.J., 2005. Integrin binding specificity regulates biomaterial surface chemistry effects on cell differentiation. *Proc. Natl. Acad. Sci. U.S.A.* 102, 5953–5957.
- Lan, M.A., Gersbach, C.A., Michael, K.E., Keselowsky, B.G., García, A.J., 2005. Myoblast proliferation and differentiation on fibronectin-coated self assembled monolayers presenting different surface chemistries. *Biomaterials* 26, 4523–4531.
- Latour, R.A., 2008. Biomaterials: protein–surface interactions. In: Wnek, G.E., Bowlin, G.L. (Eds.), *Encyclopedia of Biomaterials and Biomedical Engineering*, vol. 1. second ed. Informa Healthcare, New York, NY, pp. 270–284.
- Latour, R.A., Abramyan, T., Collier, G., Kucukkal, T.G., Li, X., Snyder, J.A., Thyparambil, A.A., Vellore, N.A., Wei, Y., Yancey, J.A., Stuart, S.J., 2012. Understanding protein–surface interactions at the atomistic level through the synergistic development of experimental and molecular simulation methods. In: Horbett, T.A., Brash, J.L., Norde, W. (Eds.), *Proteins at Interfaces II: Fundamentals and Applications*, ACS Symposium Series 1120. American Chemical Society, Washington, DC, pp. 197–228.
- Latour, R.A., 2015. The Langmuir isotherm: a commonly applied but misleading approach for the analysis of protein adsorption behavior. *J. Biomed. Mater. Res. A* 103A, 949–958.
- Lee, W.-K., McGuire, J., Bothwell, M.K., 2004. Competitive adsorption of bacteriophage T4 lysozyme stability variants at hydrophilic glass surfaces. *J. Colloid Interface Sci.* 269, 251–254.
- Li, L.Y., Chen, S.F., Jiang, S.Y., 2007. Protein interactions with oligo(ethylene glycol) (OEG) self-assembled monolayers: OEG stability, surface packing density and protein adsorption. *J. Biomater. Sci. Polym. Ed.* 18, 1415–1427.
- Lundstrom, I., 1985. Models of protein adsorption on solid surfaces. *Prog. Colloid Polym. Sci.* 70, 76–82.
- Nakajima, M., Ishimuro, T., Kato, V., Ko, I.-K., Hirata, I., et al., 2007. Combinatorial protein display for the cell-based screening of biomaterials that direct neural stem cell differentiation. *Biomaterials* 28, 1048–1060.
- Norde, W., Horbett, T.A., Brash, J.L., 2012. Proteins at interfaces III: introductory overview. In: Horbett, T.A., Brash, J.L., Norde, W. (Eds.), *Proteins at Interfaces II: Fundamentals and Applications*, ACS Symposium Series, vol. 1120. American Chemical Society, Washington, DC, pp. 1–34.
- Riedel, T., Riedelová-Reicheltová, Z., Májek, P., Rodriguez-Emmenegger, C., Houska, M., Dyr, J.E., Brynda, E., 2013. Complete identification of proteins responsible for human blood plasma fouling on poly(ethylene glycol)-based surfaces. *Langmuir* 29, 3388–3397.
- Shen, M.C., Martinson, L., Wagner, M.S., Castner, D.G., Ratner, B.D., Horbett, T.A., 2002. PEO-like plasma polymerized tetra-lyme surface interactions with leukocytes and proteins: in vitro and in vivo studies. *J. Biomater. Sci. Polym. Ed.* 13, 367–390.
- Siedlecki, C.A., Lestini, B.J., Kottke-Marchant, K.K., Eppell, S.J., Wilson, D.L., et al., 1996. Shear-dependent changes in the three-dimensional structure of human von Willebrand factor. *Blood* 88, 2939–2950.
- Sivaraman, B., Fears, K.P., Latour, R.A., 2009. Investigation of the effects of surface chemistry and solution concentration on the conformation of adsorbed proteins using an improved circular dichroism method. *Langmuir* 25, 3050–3056.
- Sivaraman, B., Latour, R.A., 2010a. The relationship between platelet adhesion on surfaces and the structure versus the amount of adsorbed fibrinogen. *Biomaterials* 31, 832–839.
- Sivaraman, B., Latour, R.A., 2010b. The adherence of platelets to adsorbed albumin by receptor-mediated recognition of binding sites exposed by adsorption-induced unfolding. *Biomaterials* 31, 1036–1044.
- Sivaraman, B., Latour, R.A., 2012. Time-dependent conformational changes in adsorbed albumin and its effect on platelet adhesion. *Langmuir* 28, 2745–2752.
- Slack, S.M., Horbett, T.A., 1995. The Vroman effect: a critical review. In: Horbett, T.A., Brash, J. (Eds.), *Proteins at Interfaces II: Fundamentals and Applications*. ACS Symposium Series, vol. 602. American Chemical Society, Washington, DC, pp. 112–128.
- Thompson, M., Blaszykowski, S.S., Rodriguez-Emmenegger, C., de los Santos Pereira, A., 2017a. Protein adsorption on surfaces: understanding the complex nature of a common phenomenon. In: Thompson, M. (Ed.), *Biological Fluid-Surface Interactions in Detection and Medical Devices*. The Royal Society of Chemistry, Cambridge, UK.
- Thompson, M., Blaszykowski, S.S., Rodriguez-Emmenegger, C., de los Santos Pereira, A., 2017b. Antifouling surface chemistries to minimize signal interference from biological matrices in biosensor technology. In: Thompson, M. (Ed.), *Biological Fluid-Surface Interactions in Detection and Medical Devices*. The Royal Society of Chemistry, Cambridge, UK.
- Thyparambil, A.A., Wei, Y., Latour, R.A., 2015. Experimental characterization of adsorbed protein orientation, conformation, and bioactivity. *Biointerphases* 10, 1–14 article 19002.
- Tsai, W.-B., Horbett, T.A., 1999. Human plasma fibrinogen adsorption and platelet adhesion to polystyrene. *J. Biomed. Mater. Res.* 44, 130–139.
- Tsai, W.-B., Grunkemeier, J.M., Horbett, T.A., 2003. Variations in the ability of adsorbed fibrinogen to mediate platelet adhesion to polystyrene-based materials: a multivariate statistical analysis of antibody binding to the platelet binding sites of fibrinogen. *J. Biomed. Mater. Res.* 67A, 1255–1268.
- Wertz, C.F., Santore, M.M., 2001. Effect of surface hydrophobicity on adsorption and relaxation kinetics of albumin and fibrinogen: single-species and competitive behavior. *Langmuir* 17, 3006–3016.
- Zhang, L., Cao, Z., Bai, T., Carr, L., Ella-Menye, J.-R., Irvin, C., Ratner, B.D., Jiang, S.Y., 2013. Zwitterionic hydrogels implanted in mice resist the foreign-body reaction. *Nat. Biotechnol.* 31 (6), 553–556.
- Zhang, M., Wu, Y., Hauch, K., Horbett, T.A., 2008. Fibrinogen and von Willebrand's factor mediated platelet adhesion to polystyrene under flow conditions. *J. Biomater. Sci. Polym. Ed.* 19 (10), 1383–1410.
- Zhang, Z., Chao, T., Chen, S.F., Jiang, S.Y., 2006. Superlow fouling sulfobetaine and carboxybetaine polymers on glass slides. *Langmuir* 22 (24), 10072–10077.

Further Reading

- Dong, D.E., Andrade, J.D., Coleman, D.L., 1987. Adsorption of low density lipoproteins onto selected biomedical polymers. *J. Biomed. Mater. Res.* 21, 683–700.

Chapter Solutions to Problems

1. What are the three main driving forces that affect the competitive adsorption of proteins to biomaterials from complex mixtures such as blood plasma?
2. Calculate the amount of adsorbed protein in a close-packed monolayer for an average protein of molecular weight 100,000. Assume the protein is spherical and has a partial specific volume of proteins of 0.73 mL/g.
3. When various biomaterials are implanted in the body, the responses often depend on the chemistry of the implanted material. Yet we know that the surface is covered with adsorbed protein and thus the biological response is not due to direct interaction with the surface. How then are the differences in responses explained?
4. What are three methods that show the specific effect of adsorbed proteins on cellular interactions with biomaterials?
5. As illustrated in Fig. 2.1.2.5, polystyrene and other hydrophobic surfaces become more wettable after exposure to protein-containing media. However, for certain materials such as cleaned germanium prisms that initially have low contact angles with water (e.g., 11°) and are thus fairly wettable to begin with, exposure to protein-containing solutions has been reported to cause the contact angle to increase (to around 60°). How can this be explained?
6. Proteins are tightly bound to many biomaterials and adsorption is considered irreversible in that the protein is not washed off in the buffer used for adsorption, even after long soaking periods. Give a molecular explanation of why proteins are so tightly bound.
7. What are the two primary factors that control the kinetics of initial protein adsorption onto a biomaterial surface?
8. Which type of biomaterial surface tends to induce a greater degree of protein unfolding when the protein adsorbs onto the surface: a biomaterial functionalized with nonpolar hydrophobic surface groups (e.g., -CH₃ groups) or a biomaterial functionalized with neutral polar hydrophilic groups (e.g., -OH groups)? Explain.
9. Are Vroman effects primarily driven by kinetic or thermodynamic forces?

Chapter Solutions to Problems

1. The three main factors that are believed to control the outcome of competitive adsorption processes are: (1) the intrinsic affinity of each protein for surfaces, meaning that some proteins are more surface active and more adsorptive than others; (2) the chemical nature of the adsorbing surface, due to the fact that the variations in surface affinity among proteins one sees for a given surface are only fixed for that surface, and will differ if another surface is used; (3) the relative bulk

concentration of each protein, meaning that even a protein with high affinity for a surface will not be present in high amounts on the surface if it is present in low bulk concentration compared to the other proteins since the excess concentration of the competing proteins will overcome the affinity differences.

2. Close packing means that the molecules touch each other at their boundaries, so the problem can be solved by calculating the cross-sectional area of one molecule of the protein and dividing that into square centimeters of area, which then gives the number of molecules in that area. Using the molecular weight of the protein allows conversion of the number of molecules into the mass of molecules, and thus you end up getting mass per unit area of a close-packed monolayer.

Protein Monolayer Calculation

The specific volume (volume per gram) of a protein can be used to calculate the volume of an individual protein molecule by using the molecular weight and Avogadro's number.

$$\begin{aligned} V_{\text{molecule}} &= V_{\text{specific}} * M / N_{\text{Avogadro}} \\ &= (0.73 \text{ mL/g}) * (10^5 \text{ g/mole}) / 6.02 \times 10^{23} \\ &= 1.22 \times 10^{-19} \text{ mL/molecule} \end{aligned}$$

The volume of an individual protein molecule can be used to calculate the radius of the molecule r , assuming it is spherical.

$$\begin{aligned} r &= \left(\frac{3}{4\pi} V_{\text{molecule}} \right)^{1/3} \\ &= 3.08 \times 10^{-7} \text{ cm} \end{aligned}$$

(This radius estimate can be compared to dimensions of proteins measured by X-ray crystallography. For proteins in the range of 100,000 molecular weight, average length dimensions are around 70 Å, giving a radius of around 35 Å, fairly close to what we just calculated using the specific volume of proteins.)

The radius of the protein molecule can then be used to calculate the projected areas of an individual protein molecule A_{molecule} , which is the "footprint" or area occupied on the surface by the protein molecules.

$$\begin{aligned} A_{\text{molecule}} &= \pi r^2 \\ &= 2.97 \times 10^{-13} \text{ cm}^2 \end{aligned}$$

With the footprint area, you then can calculate the number of protein molecules that can be fit into a square centimeter n_{protein} , assuming close packing of circles representing the footprint area occupied by each spherical protein molecule. (This is a small overestimate of the occupiable area, because the tightest packing of circles on a planar surface leaves about 9% area unoccupied, according to a theory by Gauss.)

$$\begin{aligned} n_{\text{protein}} &= 1 \text{ cm}^2 / A_{\text{molecule}} \\ &= 3.36 \times 10^{12} \text{ molecules} \end{aligned}$$

Then convert the number of molecules per unit area n_{protein} into mass of protein per unit area m_{protein} using Avogadro's number and the molecular weight of the protein.

$$\begin{aligned} m_{\text{protein}} &= n_{\text{protein}} * M / N_{\text{Avo}} \\ &= 5.6 \times 10^{-7} \text{ g} \\ &= 0.56 \text{ } \mu\text{g} \end{aligned}$$

Thus, according to this calculation, there should be around 0.56 μg per square centimeter in a close-packed monolayer of a spherical protein of molecular weight 100,000.

3. Due to differences in relative competitive affinity of proteins for various surfaces, the amount of adsorption of each protein varies with surface chemistry. For example, some surfaces have more adsorbed fibrinogen, and others more adsorbed albumin, and since platelets bind only to fibrinogen, surfaces enriched in fibrinogen are more platelet reactive. Thus, the effect of surface chemistry is to vary the composition of the adsorbed protein and thus this is why the reactivity with cells varies with surface chemistry.
4. Three methods to show the role of adsorbed proteins are as follows.
 - a. If surfaces are preadsorbed with various purified proteins, it is found that most inhibit cell adhesion to the surface but a few such as fibronectin, fibrinogen, and vitronectin cause the cell adhesion to be much higher than for other proteins. Proteins that block adhesion are called passivating or blocking proteins, while those that mediate it are called adhesion proteins.
 - b. Preadsorption with complex protein mixtures such as blood plasma selectively deficient in only one protein is a more physiologically relevant way to show if a protein is contributing an important role in platelet adhesion in the presence of many other potential adhesion proteins in plasma. If cell adhesion is greatly reduced when the surface is adsorbed with the protein mixture that is missing one protein such as fibronectin, it means this protein is playing an important role in that it is not replaced by the action of other proteins still in the mixture and on the surface.
 - c. Addition of antibodies specific to a given adhesion protein or to its receptor to a cell suspension incubating with a biomaterial will result in a decrease in adhesion that is proportional to the concentration of added antibody. Because such antibody-blocking studies can be done with surfaces adsorbed with mixtures of proteins such as plasma, yet they selectively interfere in adhesion mediated by only one adhesion protein, they provide information relevant to the functional role of the adhesion protein under conditions closer to the physiological situation where biomaterials are exposed to complex mixtures of proteins.
5. An increase in contact angle after exposure to protein-containing media can be explained by adsorption of protein if the adsorbed protein layer is less wettable than the starting surface. For certain solid materials such as cleaned gallium prisms, the interaction is very strong with water and so the contact angle is low. After protein adsorption occurs, the higher contact angle must mean that adsorbed proteins interact with water less strongly than the starting germanium surface. Thus, while proteins are much more wettable than polystyrene, they evidently are not as wettable as some solid surfaces.
6. The irreversible, tight binding of proteins to surfaces is due to the large size of protein molecules so that many noncovalent bonds are formed between the surface and each molecule, i.e., "multipoint attachment" occurs. Although each bond is relatively weak and reversible, the chance that all the bonds would be broken simultaneously is low, so multivalent bonding results in strong bonding.

R. Latour adds another way to look at this issue. He notes that because of the large number of contacts between functional groups of a protein and a surface, even weak interactions will hold the protein. For example, if the interactions with the surface are equal in energy to their interactions with water in the bulk phase, and we assign the probability of a surface functional group being bonded to a protein versus a water molecule to be 0.5, the probability for all of the functional groups of an adsorbed protein to dissociate from the protein at the same time would be $P = (0.5)^n$, with n being the number of functional group contacts between the protein and surface. So even if n is as small as 20, the probability that they would all dissociate at the same time is very small. Thus, even a hydrophilic surface with OH groups (e.g., OH-SAM) will tend to irreversibly adsorb a large protein, while for hydrophobic surfaces that has favorable thermodynamics of adsorption for a nonpolar amino acid residue versus water the likelihood of desorption is even smaller.
7. Since the rate of adhesion of a protein to a biomaterial surface once it contacts the surface is generally much faster than the rate of diffusion of the protein from solution to the biomaterial surface, the kinetics of the initial process of protein adsorption is typically diffusion limited. The rate of diffusion of a protein in solution is directly proportional to the concentration of the protein in solution and inversely proportional to the square root of the protein's molecular weight. Thus, the concentration of the protein in solution and the size of the protein (i.e., its molecular weight) are the primary factors that determine the initial rate of adsorption of a given protein on a biomaterial surface.
8. Biomaterials functionalized with nonpolar hydrophobic groups will tend to induce a greater degree of protein unfolding than neutral hydrophilic groups. This occurs because proteins tend to be structured with their nonpolar hydrophobic amino acids buried within the protein with the outer surface of the protein largely containing hydrophilic groups, which enable the protein to be soluble in physiological solution. When proteins adsorb to hydrophobic surfaces, strong hydrophobic interactions tend to cause the proteins to unfold with their hydrophobic amino acid

residues tightly adsorbed to the surface. This process is driven by the thermodynamic decrease of system free energy that is caused by reducing the solvent-accessible surface area of the hydrophobic surface. However, when proteins adsorb to a hydrophilic surface, the nonpolar amino acid residues within the protein's core tend to remain buried within the protein with the

protein's outer hydrophilic residues forming hydrogen bonds with the surface, thus tending to induce a lower degree of unfolding.

9. Vroman effects represent the displacement of one adsorbed protein by a more strongly adsorbing protein, thus being thermodynamically driven to lower the overall free-energy state of the system.

2.1.3

Cells and Surfaces in Vitro

S. ADAM HACKING¹, NUREDDIN ASHAMMAKHI², ALI KHADEMHOSEINI²

¹Laboratory for Musculoskeletal Research and Innovation, Department of Orthopaedic Surgery, Massachusetts General Hospital and Harvard Medical School, Boston, MA, United States

²Center for Minimally Invasive Therapeutics (C-MIT), California NanoSystems Institute (CNSI), University of California-Los Angeles, Los Angeles, CA, United States

Introduction

There is no doubt that in vitro methods have been and will continue to be of great value to the progression of medical science. The culture of mammalian cells and the study of their behavior in vitro has led to new understandings of cell physiology, molecular biology, and many disease processes. In many experimental settings, the ability to extract and grow cells from host tissues is a powerful tool since experimental question(s) can be evaluated under standardized conditions without unwanted influences from the host physiology.

As science has progressed, new in vitro techniques have developed beyond the culture of cells in glass or plastic dishes. Cell–substrate interactions are of particular interest since cells interact physically with the extracellular matrix (ECM) and often modify it in response to various stimuli. As a result, efforts to examine and recapitulate the in vivo environment in vitro often require modification of the cell culture substrates. Cell–substrate interactions at the micro- and nano-scales have been facilitated by new techniques, applications, and approaches that have emerged from the combination of engineering and biology. In practice, the chemistry, topography, and elasticity of the culture surface may be altered, or mechanical forces can be applied to cells by physical deformation of the culture substrate.

With respect to tissue engineering and organ regeneration, advances in our understanding of cell–substrate interactions are essential to controlling cell behavior. For example, the ability to pattern cells with micron-scale precision on a variety of substrates presents new opportunities to study and recreate cell–cell interactions required to generate functional tissues in vitro for subsequent implantation in vivo. This is of primary importance since organs contain multiple cell types that are precisely arranged in close proximity to form complex tissue structures.

This chapter provides a basic understanding of in vitro principles beginning with a fundamental overview of the culture of cells and their interaction with surfaces. We then describe a number of techniques employed to manipulate the in vitro environment at the micro- and nano-scales and then discuss how these fundamental techniques can be applied to investigate and influence cell behavior.

A Basic Overview of Cell Culture

Tissue culture is a general term for the harvest of cells, tissues, or organs and their subsequent growth or maintenance in an artificial environment. Mammalian cells cultured in vitro have the same basic requirements as cells growing within an organism. Specialized approaches have been developed to replace a number of mammalian systems essential for life. In vitro, blood is replaced by the culture media, which bathes the cells and provides an energy source (glucose), essential nutrients (salts and amino acids), proteins and hormones (from added serum), and a buffer (to maintain pH balance). During culture, the byproducts of cellular metabolism are released into the media as its constituents are depleted. Since the culture media is not continually circulated and purified, it must be changed regularly to maintain optimal conditions for cell survival and function. Not surprisingly, these culture conditions are also favorable for the growth of unwanted organisms such as fungi and bacteria. Since there is no immune system to control infection in vitro, antifungal agents and antibacterial agents can be added to the culture media on a prophylactic basis. To further reduce the likelihood of contamination by microorganisms, cells are manipulated under a laminar flow hood using strict aseptic technique. Laminar hoods control and direct filtered air to facilitate a sterile working environment by reducing the contact of airborne bacteria and particulates with the culture dish and hood surfaces.

TABLE 2.1.3.1 Examples of Some Commonly Used Cell Lines

Cell Line	Organism	Tissue of Origin	Note
3T3	Mouse	Embryonic fibroblast	Fibroblast
AML-12	Mouse	Liver	Liver
HeLa	Human	Cervical cancer	Epithelium (1st cell line reported)
HUVEC	Human	Umbilical cord vein	Endothelium (stem cells)
MC3T3-E1	Mouse	Calvarial fibroblast	Differentiate to osteoblast

Cells in media are contained in culture dishes or flasks and incubated in a warm (37°C) and humidified chamber (95%). While the lids of the culture dishes cover and protect the media, they are not sealed and enable gas exchange within the incubator. The exchange of gas at the media surface acts like the lungs to maintain gas balance necessary for metabolism. CO₂ is usually added to the incubator at a low concentration (5%). The CO₂ interacts with the bicarbonate buffer in the culture media to help maintain a pH of 7.0–7.4. Buffering counteracts pH changes in the media as it accumulates waste from cellular activity. Phenol red is commonly added as an indicator to monitor pH, and a change in the color of the media is often a sign of poor culture conditions. Since the culture dishes are not sealed, they are prone to evaporation. To reduce evaporation, and prevent a subsequent change in media concentration, a water dish (with an antifungal/antibacterial agent) is usually placed in the bottom of the incubator to maintain a high level of ambient humidity.

Primary Culture

Cells for in vitro studies may be obtained from tissues (primary culture) or from cell lines. Cells for primary culture are obtained from living tissues. Cells can be obtained by passing media through the marrow cavities of the long bones, by collecting cells that grow out from a piece of tissue (*explant culture*) or by enzymatic digestion of tissue that contain cells. Enzymatic digestion of small pieces of tissue immersed in collagenase at 37°C breaks down the surrounding ECM and releases entrapped cells (*enzymatic dissociation*). After harvest, cells may be cultured in suspension or on culture substrates. Anchorage-dependent cells are plated for a few days to remove dead or unwanted (nonadherent) cell types. Cells anchored to the surface of the culture plate are “released” by adding a mixture of trypsin, a protease found in the digestive system and ethylenediaminetetraacetic acid (EDTA). Trypsin degrades proteins, including important cell adhesion proteins (CAPs) that anchor cells to

the culture surface. In short applications, trypsin is generally not harmful to cells. EDTA is a chelating agent that binds calcium and magnesium ions. EDTA increases the effectiveness of trypsin and prevents cell aggregation after release from the culture dish.

Harvested cells are often filtered to produce a suspension of single cells. The single cell suspension is counted, and portions of the initial cell population are transferred to new culture dishes for their expansion. Expansion is also referred to as *subculturing* or *passaging* the cells. Passaging cells ensures that cells are plated at a low density, so they have room to proliferate. Under appropriate conditions, most cells proliferate and form a mono-layer on the culture surface. The point at which cells completely cover the culture surface is referred to as *confluence*. At confluence, proliferation will generally cease because cell density or cell–cell contact results in *contact inhibition*. Unlike cell lines, primary cells are often cultured with little to no passaging since serial passaging can result in loss of cell characteristics (phenotype).

Cell Lines

Generating primary cultures by continually harvesting and isolating cells is a time-consuming task. Hence, it is often preferable to utilize cells that are obtained from stock maintained in the lab. Cell lines refer to cells that can be passaged many times without loss of their phenotype. Physiologically, these cells can divide repeatedly, without shortening of their telomeres (Hayflick, 1965). Cell lines differ from other cells in that they have escaped the Hayflick limit and are *immortalized* (Hayflick, 1985). Examples of a handful of commonly used cell lines, from a large number of existing cell lines, are presented in Table 2.1.3.1.

Cell lines also offer an experimental advantage. Primary cells may contain unwanted cell types and heterogeneous populations that are unintentionally collected during harvest. These variations have the potential to significantly impact experimental uniformity and reproducibility. Primary cultures may also contain slight genetic variations due to genetic differences arising from the harvest of cells from different individuals. Since cell lines are derived from a singular cell, all subsequent cells are genetic clones of the parent cell¹. As a result, experiments using cell lines can be reproduced by different labs using the same cells, which has obvious advantages for collaboration, verification, and reproducibility.

A large number of cell lines are derived from tumors or cells that have undergone spontaneous mutation or some form of manipulation. The HeLa cell line is an example that has been in use since the early 1950s and was derived from cervical cancer cells taken from Henrietta Lacks (Scherer et al., 1953). It is helpful to recognize

¹ If the cell line has not been contaminated or has not undergone spontaneous genetic change.

that while cell lines may behave similarly to normal cells, they have been obtained by repeated culture and selection (Browne and Al-Rubeai, 2007), treating or transforming normal cells (viral, oncogene, radiation, drugs, or chemicals) (Eiges et al., 2001; Groger et al., 2008; Prasad et al., 1994), from transgenic mice (Connelly et al., 1989; Wu et al., 1994) or isolated from tumors (Riches et al., 2001; Yasuda et al., 2009). For example, transformed cells may present different morphologies and altered metabolisms (Priori et al., 1975; Wittelsberger et al., 1981) and often do not exhibit robust contact inhibition (Bell, 1977; Erickson, 1978). These behaviors strongly suggested that cell lines have the inherent potential to demonstrate responses that may not be typical of primary cells (Heckman, 2009; Steele et al., 1991). Therefore, when establishing new experimental protocols using cell lines it is recommended that the results of the protocol be validated with primary cells.

Cell lines can be obtained from nonprofit organizations such as the American Type Culture Collection (ATCC), the European Collection of Cell Cultures (ECACC), and the Coriell Institute for Medical Research (CIMR). The ATCC (www.atcc.org), ECACC (www.hpacultures.org.uk), and CIMR (www.coriell.org) provide high-quality cell lines because of their careful testing and validation. The testing process ensures that cells provided are free of unwanted organisms such as mycoplasma and other unwanted cell types. Cell lines obtained from tissue banks are usually meticulously characterized and preserved to maintain these materials in a manner that permits reproducibility of results across time and among laboratories around the world. In some cases, cell lines can be obtained from other research laboratories; however, caution should be exercised since the possibility exists that the cell lines may be contaminated with microorganisms or unwanted cell types.

Characteristics of Cultured Cells

Cultured cells often display characteristic behaviors and growth patterns. A well-known characteristic is *contact inhibition*. In 1954, Abercrombie and Heaysman proposed that cells form monolayers because they do not move over or under their neighbors (Abercrombie and Heaysman, 1954). Cells exhibiting contact inhibition will preferably migrate to unoccupied areas of the culture substrate and will not use the upper surface of a confluent cell monolayer as substrate. Contact inhibition is closely related to the cessation of cell proliferation (Timpe et al., 1978) and is one reason why most cells cultured in vitro produce monolayers of cells (Garrod and Steinberg, 1973). When cultured cells are in complete contact with each other, plasma membrane ruffling and cell motility are inhibited, resulting in an overall cessation of cell growth (Heckman, 2009). For this reason, cells maintained in culture are frequently replated at lower densities so that growth and proliferation may continually occur.

SIDE BAR: DETECTING CANCEROUS CELLS IN VITRO

The phenomenon of contact inhibition has diagnostic implications for assessing malignancy. A predominant behavior of malignant cells is the loss of contact inhibition and uncontrolled cell growth. The natural phenomenon of contact inhibition has been used as a test to distinguish cancerous from noncancerous cells (Dehner, 1998). Interestingly, unlike normal cells, malignant cells will also proliferate in agar (a three-dimensional [3D] matrix), where no suitable binding sites for cell attachment exist.

Cultured cells also often display characteristic shapes that can be used as visual cues to assess the health and differentiation of a cell culture population. For example, pre-osteoblastic cells are fibroblastic in shape, possessing a long “drawn-out” morphology. Upon subsequent differentiation into mature osteoblasts, cells display a cuboidal appearance. Dead or nonadherent cells often appear spherical in shape and float in the culture media.

Understanding Cell–Substrate Interactions

In vivo, cell–surface interactions are often explored as a means to enhance or control periimplant tissue formation. Surface chemistry, topography, and elastic modulus (stiffness) of the substrate are all means that can be used to control and guide cell activity and ultimately modulate tissue formation. This triad of substrate properties is important for tissue engineering and organ regeneration, where multiple cell types must be directed to form complex tissue-like structures all in close proximity and often with micron-scale precision. In terms of 3D scaffolds, tuning of scaffold chemistry, topography, and stiffness are all means to selectively guide cell development and differentiation within the bulk material.

Since most cells interact with a substrate (or can be found within the ECM) it is often desirable to control the interaction of cells with substrates in vitro. Modulation of the culture surface by the fabrication of “engineered surfaces” comprised of micro- and nano-sized chemical and topographical patterns or coatings has been used to investigate cell behavior such as adhesion, morphology, migration, proliferation, cell–cell communication, gene expression, differentiation, production of ECM, and responsiveness to extracellular signaling.

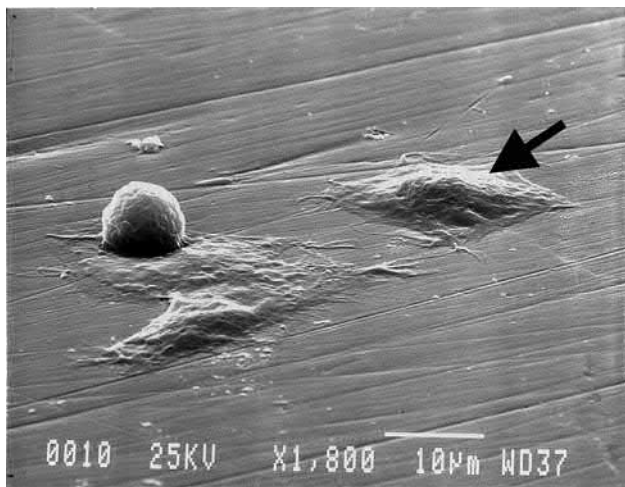
Surfaces for Cell Culture

It has long been established that most mammalian cells respond favorably to culture conditions that promote cell attachment. Cell attachment is often characterized by a change in cell morphology. Adherent cells possess a “flattened” appearance, often with an irregular cell shape and the extension of cellular processes (Fig. 2.1.3.1). Regular observation of cells in vitro is essential for successful culture as cell density, state, and contamination can all be readily assessed visually. In this regard, the use of optically clear

materials is practical as it permits simple assessment of cell growth and morphology during culture and it is well suited to many histological techniques that involve staining for quantification of cell activity. Glass, once a common form of cultureware, has been replaced by tissue culture polystyrene (TCP). While TCP is most widely used as a culture substrate, other polymers, such as polyvinylchloride, polycarbonate, and polytetrafluoroethylene, have also been used. The advantages of TCP are that it is inexpensive, clear, easily formed and treated to modify surface groups, and, unlike glass, it can be embedded and sectioned.

Process of Cell Attachment in Vitro

Cell attachment is the initial step in a cascade of cell–biomaterial interactions and it is important to cellular



• **Figure 2.1.3.1** Scanning electron microscopy image of MC3T3-E1 cells at various stages of adherence on polished titanium substrate demonstrating changes in cell morphology during attachment. Attached cells have a flattened morphology and form intimate contact with the substrate. Detached cells are round. SEM $\times 1800$.

processes such as cell guidance, proliferation, and differentiation. For many adherent cells, cell proliferation can only occur on a substrate. As a result, cell–surface interactions are fundamental to understanding cell behavior and provide an important means to control and quantify cell activity.

The process of cell attachment is largely understood (Garcia, 2005). In vitro, when hydrophilic surfaces, such as TCP, are exposed to culture media containing serum, they are rapidly coated by a thin (~ 20 nm) layer comprised mainly of proteins (Andrade and Hlady, 1987; Kasemo and Lausmaa, 1994; Nakamura et al., 2007) that adsorb to the culture surface as a monolayer. The process of cell attachment to TCP (and many other materials) is indirect since cells do not bind directly to TCP, but instead bind to the adsorbed proteins (Fredriksson et al., 1998). Cells make contact with and anchor to the adsorbed proteins at discrete regions referred to as focal contacts (Gallant and Garcia, 2007). Cells possess heterodimeric transmembrane proteins composed of α and β subunits called *integrins*. Integrins are receptors that recognize and bind to specific anchoring proteins present on the conditioned TCP surface (Peter and Ma, 2006). The adsorbed proteins present short but specific sequences (Table 2.1.3.2) that are recognized by integrins as binding sites. Integrins recognize and bind to specific ligands such as fibronectin, vitronectin, collagen, and laminin. Over 18 α and 8 β receptor subunit types have been identified and these subunits combine to produce a wide variety of receptor types (Hynes, 2002). Of these combinations, the $\alpha_v\beta_3$ integrin is one of the most abundant. It binds to vitronectin, fibronectin, von Willebrand factor, osteopontin, tenascin, bone sialoprotein, and thrombospondin (Hynes, 2002). For the majority of cells cultured in vitro, fibronectin and vitronectin are important for cell attachment to TCP (Massia and Hubbell, 1991b; Steele et al., 1993).

TABLE 2.1.3.2 Specific Peptide Sequences on Cell Anchoring Proteins

Peptide Sequence	Derived From ECM Protein	Conjugate Receptor	References
RGD	Fibronectin, laminin α -chain, collagen, vitronectin	Multiple integrins	(Massia and Hubbell, 1990a, 1991b; Erkki Ruoslahti, 1996; Ruoslahti and Pierschbacher, 1987)
YIGSR	Laminin β 1-chain	β_1 integrins	(Boateng et al., 2005; Weber and Anseth, 2008; Weber et al., 2007)
IKVAV	Laminin α -chain	LBP110	(Tashiro et al., 1989; Weber and Anseth, 2008; Weber et al., 2007)
REDV	Fibronectin	$\alpha_4\beta_1$ integrin	(Hubbell et al., 1991)
DGEA	Collagen type I	$\alpha_2\beta_1$ integrin	(Staatz et al., 1991; Weber and Anseth, 2008; Weber et al., 2007)
KQAGDV	Fibronectin γ -chain	β_3 integrins	(Gobin and West, 2003; Mann and West, 2002)
VAPG	Elastin	Elastase receptor, $\alpha_5\beta_3$ integrin	(Gobin and West, 2003; Mann and West, 2002)

While integrins mediate the physical interactions of binding, they also act as receptors that regulate cellular functions. Integrins play an important role in controlling various steps in the signaling pathways that regulate processes such as cytoskeletal organization, cell proliferation, differentiation, apoptosis, and migration. In most cell types certain biochemical signals necessary for cell survival, function, and growth are triggered by integrins upon attachment. Without attachment, the cell eventually undergoes *apoptosis*, i.e., programmed cell death (Ruoslahti and Reed, 1994).

Commercial and Experimental Modifications of Culture Surfaces

Polystyrene is a hydrophobic material that is not well suited to the attachment of most mammalian cells (Curtis et al., 1983). For the culture of nonadherent cells, untreated TCP is routinely used. As previously described, most cells require modified surfaces that are suitable for protein adsorption before cell attachment can occur.

A variety of treatment methods have been employed to improve cell attachment and growth on TCP surfaces (Table 2.1.3.3). TCP treatment methods used to enhance cell adhesion are often proprietary and vendor specific, but some of them, such as chemical treatment in sulfuric acid (Curtis et al., 1983), chemisorption (Bain and Hoffman, 2003a; Shen and Horbett, 2001), ionizing radiation (Callen et al., 1993), or exposure to plasma-based ionizing processes (such as glow discharge) (Amstein and Hartman, 1975; Koller et al., 1998), have been described in the literature. It is generally understood that these treatments impart a charge to the TCP surface that enhances its ability to interact with and bind specific CAPs present in the serum added to the culture media (Jacobson and Ryan, 1982; Lee et al., 1997).

It is important to recognize that the preparation of culture surfaces can have profound effects on the behavior of cultured cells (Bain and Hoffman, 2003b; Shen and Horbett, 2001). For some cell types, commercially available

surfaces may be far from optimal and identification of optimized substrates can be a laborious task, especially for cells that are difficult to culture in vitro. One approach has been the generation of culture surfaces comprised of mixtures of protein-adhesive and “protein-repellant” molecules or groups. Bain et al. used a combination of protein-adhesive diamine groups (N2) and repellent trifluoropropyl groups (F3) to generate a large number of culture surfaces by varying the ratio of monomers in a silanization bath (Bain and Hoffman, 2003a). The different surfaces produced possessed varying affinities for proteins and, as a result, cells. A surprising finding of the work was that the growth and activity of insulin-secreting cells was best supported by the most hydrophobic (F3) surfaces in the study (Bain and Hoffman, 2003b).

More direct approaches to tune substrate chemistry can be achieved by anchoring specific adhesion molecules to the culture substrate. In such investigations, it is often advantageous to retain only the molecule(s) of interest while reducing or excluding nonspecific protein adhesion that might occur with cells grown in normal serum-enriched media (Koepsel and Murphy, 2009). Self-assembled monolayers (SAMs) are versatile and valuable tools that have been used to study protein adhesion (Li et al., 2007; Prime and Whitesides, 1991). SAMs are comprised of long alkanethiols anchored at one end to a gold-coated substrate and at the other to small functional groups such as cell adhesion peptides or “repellant” oligo (ethylene oxide) sequences. These terminal functional groups can also be used to tether specific proteins, such as monoclonal antibodies, or can interact with proteins in the media. SAMs can be tailored to achieve a certain degree of adsorption by controlling the composition of the monolayer (mixture of functional groups).

The control of ligand density and type provides another means of modifying substrate chemistry and cell behavior. Gradients of immobilized ECM components and growth factors have also been shown to direct cell migration and shape (Byambaa et al., 2017; Inoue et al., 2009). Such experimental

TABLE 2.1.3.3 Surface Treatments to Enhance Cell Anchorage on Polymers

Approach	Technique	References
Surface modification	Corona discharge, glow discharge	(Amstein and Hartman, 1975; Chinn et al., 1994; Ertel et al., 1990; Lee et al., 1994; Lee et al., 2003)
	Oxidation	(Chang and Sretavan, 2008; Curtis et al., 1983; Frimat et al., 2009)
	Plasma etching	(Claase et al., 2003; Rhee et al., 2005)
	Surface chemical reaction	(Curtis et al., 1983; Kowalczyńska and Kaminski, 1991; Maroudas, 1977)
	Ultraviolet irradiation	(Matsuda and Chung, 1994; Nakayama et al., 1993; Welle et al., 2002)
Covalent bonding of peptide ligands	Radiation grafting	(Kallrot et al., 2006; Shen et al., 2009; Yoshii and Kaetsu, 1983; Zhu et al., 2004)
	Plasma-assisted techniques	(Larson et al., 2005; Roth et al., 2008; Sipehia et al., 1988)
	Silanization	(Muller et al., 2008; Wipff et al., 2009)

aspects can also be explored efficiently with microfluidic systems where the facile and reproducible generation of gradients utilizing small reagent volumes has been applied to the study of cell behavior *in vitro* (Du *et al.*, 2009).

Dynamic Control of Cell Culture Surfaces

Controllable surfaces for cell culture have been generated to enable a predictable change in the adhesive or morphological characteristics of the surface. Changes in surface characteristics may be achieved by mechanical or physicochemical methods, and the latter are the focus of this section. A wide variety of dynamic surfaces have been fabricated from SAMs with specific functional groups that are responsive to thermal, chemical, electrical, or electromagnetic (UV or visible light) stimuli. Dynamic culture surfaces can be used as a means to control cell adhesion. More sophisticated applications have been used to selectively pattern surfaces to generate a culture environment with multiple cell types specifically arranged in groups in close proximity to each other.

Dynamic culture surfaces have also been used to detach cells from substrates. Cell sheets have been spontaneously detached by cooling a thermally sensitive, radiation- or plasma-polymerized poly(N-isopropylacrylamide) (poly[NIPAAm]) polymer (Cheng *et al.*, 2004). Okano's group in Japan has pioneered in this method, using electron beam radiation grafting of NIPAAm monomer on the surfaces of cell culture dishes. At temperatures suitable for cell culture (above 32°C) poly[NIPAAm] surfaces are hydrophobic and readily adsorb CAPs, leading to the growth of a cell monolayer to confluence. However, when the temperature is reduced below a critical temperature (32°C) poly[NIPAAm] surfaces become hydrophilic, and the cell sheet detaches as a contiguous, confluent monolayer, carrying with it the CAP monolayer. Such dynamic thermal control of cell adhesion can be particularly useful for the safe removal of intact cell sheets by avoiding the use of proteolytic enzymes (trypsin) that can disrupt natural cell–cell networks and compromise cellular integrity. Cell sheets have a variety of applications in tissue engineering (Eloumi-Hannachi *et al.*, 2010) but are perhaps most recognized clinically by the Okano group work to provide layers of corneal cells for repairing damaged or diseased cornea of the eye.

Methods that convert surfaces from cell-adhesive to nonadhesive have also been reported using photo-responsive SAMs. These approaches generally modify the presentation of CAPs making them less accessible to the cell. Upon exposure to UV light, surfaces based on a combination of azobenzene groups and RGD ligands will “hide” the RGD groups by UV-induced conversion of the azobenzene functional group from polar to nonpolar character (Auernheimer *et al.*, 2005). Exposure to UV light reduces the exposed length of the azobenzene-RGD segments, and thus, reduces cell adhesiveness. Nitrospiropyran and methyl methacrylate polymer coatings have also been employed as photo-responsive surfaces (Higuchi

et al., 2004). Nitrospiropyran is a photo-responsive polymer that switches from a cell adhesive to a nonadhesive (hydrophilic) state upon exposure to UV light.

Investigating Cell–Substrate Interactions

The cellular microenvironment consists of a myriad of signals arising from surrounding cells, ECM, and soluble molecules. The ability to control and modulate cell behavior, through the cell microenvironment, is important for understanding cell behavior as well as controlling a wide range of cell–biomaterial interactions. In general, cell behavior can be modified by controlling substrate chemistry, topography, and elasticity, and investigations have traditionally focused on broad changes to the culture surface such as those obtained by the application of a coating. However, cell–cell and cell–ECM interactions occur over very small (micro- and nano-) length scales.

New insights into cell behavior and physiology have been gained by utilizing and extending a variety of techniques and materials that can be used to influence the cell environment at the microscale. The following sections examine some of the fundamental concepts learned from examining cell behavior in response to different substrate chemistry, topography, elasticity, and strain conditions, alone or in combination at macro-, micro-, and nano-scales.

SIDE BAR: LIMITATIONS OF BIOMATERIAL EVALUATION IN VITRO

It is important to recognize that the *in vitro* evaluation of biomaterials is subject to specific constraints, namely arising from the reduced natural complexity of the *in vitro* environment. First and foremost, there is no immune or inflammatory response *in vitro*. Nor is there the same cascade of events that normally occur with implantation, namely the interaction with components of the blood, clot formation, angiogenesis, and recruitment of a variety of cells that participate in wound healing.

Cell Response to Substrate Chemistry

Surface chemistry is perhaps the most obvious, and, in some cases, the most accessible parameter to control when modifying *in vitro* conditions to assess their effects on cell behavior. At the macroscale, a variety of strategies can be employed to modify cell culture surface chemistry. Most coating strategies aim to increase cell adhesion or to preferentially select for the adhesion of certain cell types. Uniform coatings may be achieved by simple application of the material of interest by either spin coating the substrate or by immersion in a solution of interest. Substrates have been coated with a variety of organic and inorganic compounds, such as collagen (Kataropoulou *et al.*, 2005), fibronectin (Klein-Soyer *et al.*, 1989), gelatin (Aframian *et al.*, 2000), and poly-L-lysine (Jensen and Koren, 1979). Culture surfaces have also been broadly coated with specific adhesion-related peptides. The peptide sequence arginine-glycine-aspartate (RGD) has been immobilized on a number of materials as a means to enhance cell attachment in 2D (Cutler and Garcia, 2003; Massia and

Hubbell, 1990a, b, 1991a; Petrie et al., 2008). Studies suggest that the minimal effective density of RGD is 1 pmol/mm² (Chollet et al., 2009) and that increasing RGD density (up to a limit) is generally beneficial to cell attachment (Masias and Hubbell, 1991b). Similarly, the spatial organization of various cell ligands has been achieved by controlling their density. This approach has been used to enhance the initial number of attached cells, to increase their proliferation or to preferentially select for specific cell types (Zemljic Jokhadar et al., 2007).

There are, however, instances where substrate coatings are of limited benefit and examples of such situations include cultures where the applied coating may rapidly degrade or detach from the culture substrate. A common strategy to enhance cell adhesion is to modify the substrate chemistry to encourage the adsorption and presentation of certain cell-adhesive proteins or ligands (Keselowsky et al., 2003). Ligands are present in the serum added to culture media. As previously discussed with TCP, a number of processes have been developed to enable modification of large culture surface areas to enhance protein adsorption.

Micrometer-Scale Chemical Patterns

Patterning at the microscale is associated with the control of cell shape, position, and density, and presents a powerful tool to examine and control the cell microenvironment. A common approach is to generate a pattern of CAPs on a two-dimensional (2D) surface and then deliver cells that adhere preferentially to the patterned, adhesive regions on the substrate. Usually, the nonadhesive regions are treated with polyethylene glycol (PEG), i.e., PEGylated. A multitude of patterns in various configurations have been attained using printing methods as well as methods including dynamic surfaces as previously discussed.

Cells and proteins have been previously patterned on various substrates using SAMs (Mrksich and Whitesides, 1996), metal templates (O'Neill et al., 1990), stamped proteins, peptides (Hyun et al., 2001) and biopolymers (Bhatia et al., 1997), microfluidic channels (Takayama et al., 1999), membranes (Ostuni et al., 2000), polysaccharides (Khademhosseini et al., 2004), and cross-linked PEG (Khademhosseini et al., 2003). Noncontact methods can also be used to generate protein patterns and include films that are cross-linked by photolithography that can selectively promote or exclude cell adhesion (Chien et al., 2009). In this manner, nonspecific biological molecules can be used to create patterns of adhesive and/or nonadhesive regions. Short chains of PEG have been assembled on surfaces to form a brush-like layer that resists protein adsorption and as a consequence, cell attachment.

Protein patterning has also been used to produce regions of preferential adhesion for specific cell types, to alter cell shape, to cluster cells together, to restrict their proliferation, or to position different cell types in close proximity. Components of the ECM, that participate in cell adhesion in vivo, are general candidates for studies involving chemical

patterning in vitro. Fibronectin, laminin, vitronectin, and collagen are examples of ECM molecules commonly used for patterning cell-adhesive regions.

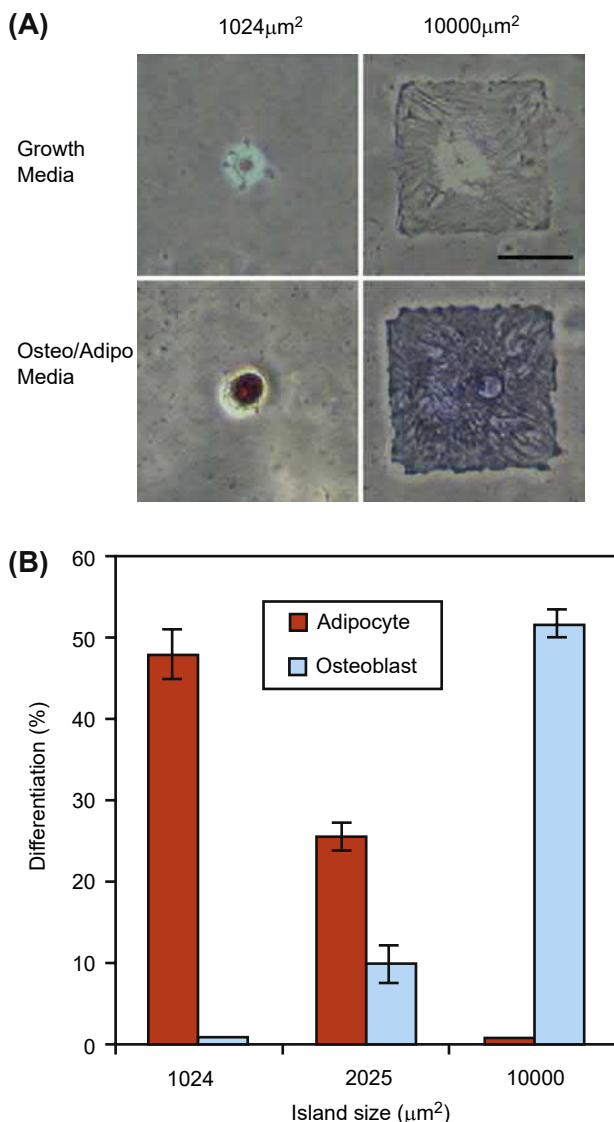
Direct transfer of proteins or cells from a stamp to the substrate can also be used to generate micro- and nanoscale patterns. Microstamping or microcontact printing (μ CP) is a technique in which polydimethylsiloxane (PDMS) molds are used to pattern substrates by the selective transfer of materials of interest (Mrksich and Whitesides, 1996). In one approach, the relief patterns on a PDMS stamp can be used to form patterns of SAMs on the surface of a substrate through conformal contact. Alkanethiols are used to pattern gold-coated surfaces by forming densely packed SAMs. The sulfur end-groups strongly interact with the metal surfaces, and the rest of the molecule can then be used to control surface chemistry, wetting, and protein and cell adhesion. For example, alkanethiols can be PEGylated at the opposite end from the thiol ($-SH$) group to render gold-coated surfaces “nonfouling,” or protein and cell resistant. To micropattern surfaces using alkanethiols, a variety of methods have been employed such as μ CP. In this approach, PDMS molds are “inked” with the alkanethiol solution and transferred to the gold surface by conformal contact between the relief pattern and the substrate. Using μ CP, micropatterns of SAMs terminated with PEG chains have been generated. These micropatterns have been used to immobilize proteins and cells on specific regions of a surface by selectively modifying surfaces with the nonfouling PEG patterns.

Using micropatterned fibronectin islands, Chen et al. reported that cell shape and the area available for cell adhesion governed whether individual cells grow or die, regardless of the type of matrix protein or antibody to integrin used to mediate adhesion (Chen et al., 1997; Dike et al., 1999) (Fig. 2.1.3.2). For bovine capillary cells, apoptosis significantly increased as fibronectin island size was reduced below 400 μm^2 . Using micropatterned fibronectin, McBeath et al. demonstrated that cell shape regulated the differentiation of human mesenchymal stem cells (hMSCs) (McBeath et al., 2004). hMSCs that were permitted to adhere, spread, and flatten differentiated into osteoblasts, while those that were not permitted to attach formed spherical cells and resulted in adipocytes.

Nonfouling Surfaces in Cell Culture

As previously described, nonfouling surfaces may be created with PEGylated alkane thiols in SAMs. Other approaches include the generation and application of nonfouling coatings or films such as plasma-deposited triglyme and tetraglyme films of the Ratner group (Johnston et al., 2005), plasma-deposited tetraglyme, and fluorocarbon-based films (Cao et al., 2007; Goessl et al., 2001).

PEG has been used in many chemical variations to generate nonfouling surfaces. Polymerization of PEG monomers to form brush-like nonfouling coatings has been investigated. Beginning with surface-initiated atom transfer radical polymerization, Lavanant et al., grew robust brush-like polymers of



• **Figure 2.1.3.2** Cell shape modulates hMSC differentiation. (A) Brightfield images of hMSCs plated onto small (1024 μm^2) or large (10,000 μm^2) fibronectin spots after 1 week. Fibronectin spots were patterned on a mixed SAM substrate by microcontact printing. Large fibronectin spots supported osteogenesis (blue), while small fibronectin spots supported adipogenesis (red). Scale bar 50 μm . (B) Differentiation of hMSCs on 1024, 2025, or 10,000 μm^2 islands after 1 week of culture. Small fibronectin spots resulted in adipogenesis, medium fibronectin spots supported both adipogenesis and osteogenesis, and large fibronectin spots resulted in osteogenesis. (Reprinted from McBeath, R., Pirone, D. M., Nelson, C. M., Bhadriraju, K., & Chen, C. S. (2004). Cell shape, cytoskeletal tension, and RhoA regulate stem cell lineage commitment. *Dev. Cell*, 6(4), 483-495., with permission from Elsevier.)

PEG methacrylate (PEGMA) on low-density poly ethylene by photobromination followed by polymerization (Lavanant et al., 2010). Functionalization of the peptide brushes with the RGD-containing peptide ligand, GGGRGDS, increased cell adhesion compared to the polymerized PEGMA surface.

Changes in the structure of the component molecules of SAMs can also reduce cell adhesion. For example, SAMs comprised of oligo(ethylene glycol) (OEG) with variable ethylene glycol side chain lengths of 4, 9 and 23 were grafted

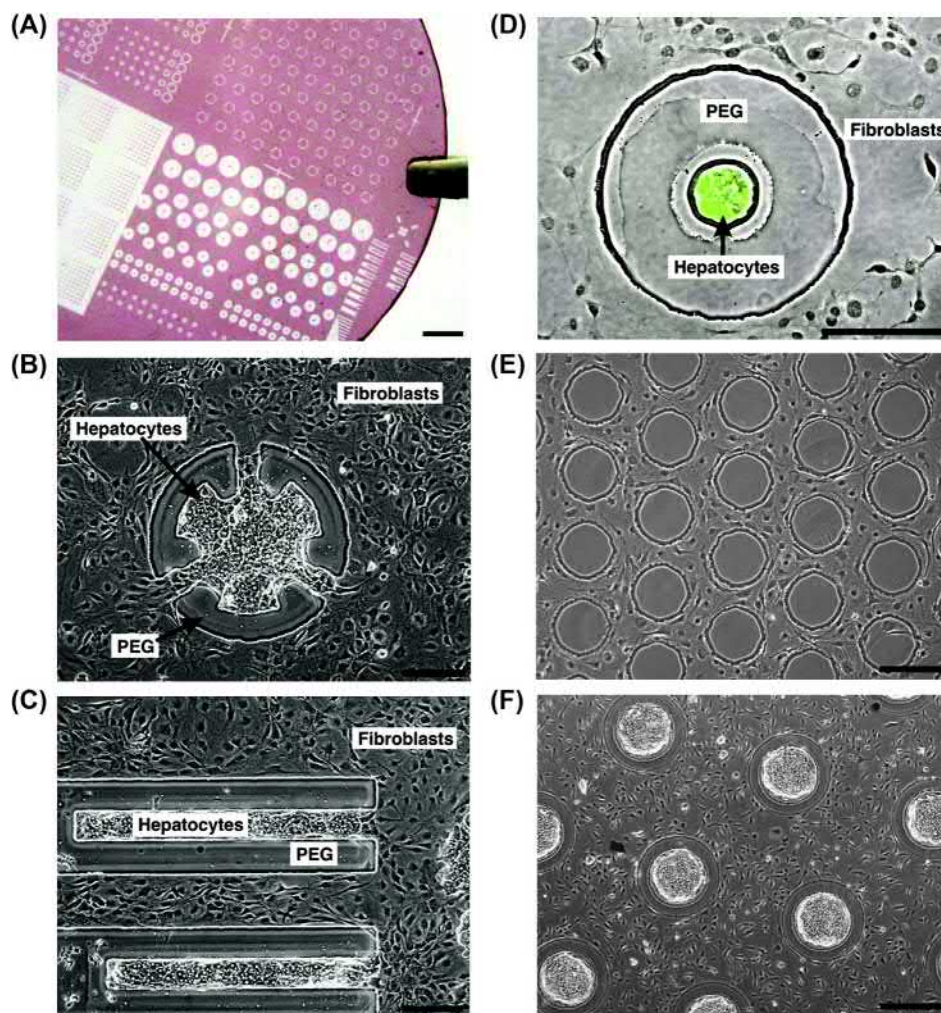
onto titanium to create a nonfouling surface. After 4h of exposure to 3T3 fibroblasts, there was no cell adhesion to any of the SAMs. At 35 days after seeding, it was observed that longer side chains resulted in reduced adhesion. This was further supported as complete cell coverage of the Ti surface was observed at 7, 10 and 11 weeks for samples with side chain lengths of 4, 9 and 23, respectively (Fan et al., 2006).

For many patterning applications, the ability to isolate or sequester cell-adhesive regions by surrounding them with surfaces that resist cell attachment is of great interest. The practical applications include the fabrication of arrays of cells for high-throughput testing as well as patterned cocultures for investigating complex interactions between different groups of homogeneous cell populations. Microarrays of captured molecules surrounded by nonfouling backgrounds are one approach that has been used to identify and screen combinations of CAPs to develop bioactive surfaces. Monchoux et al. grafted RGD and RGE (a nonadhesive control), as well as other known endothelial ligands (REDV and SVVYGLR), on a low-fouling carboxy-methyl-dextran background (Monchoux and Vermette, 2007). They concluded that RGD was necessary for cell adhesion and that endothelial cells could discriminate against and would not adhere to arg-gly-glu (RGE) sequence. Coimmobilization of the RGD peptide with vascular endothelial growth factor (VEGF) or an osteopontin-derived peptide SVVYGLR significantly enhanced endothelial cell adhesion while coimmobilization of RGD with either REDV or SVVYGLR induced a reduction in endothelial cell spreading.

The development of nonfouling surfaces from biodegradable or biologically relevant compounds is of great interest. Biodegradable ultra-low fouling peptide surfaces have been generated from natural amino acids that offer new and innovative means to control cell adhesion (Chen et al., 2009). Amino acids ($\text{H}_2\text{N}-\text{CH}-\text{R}-\text{COOH}$) are molecules that possess an amine group (H_2N), a carboxylic acid group (COOH), and an organic side chain (R) of varying length and composition. Amino acids are the building blocks of proteins and are the ubiquitous components of many organisms. Amino acids are *zwitterionic* at physiologic pH, meaning that they have both positive and negative charges on different atoms but possess no overall net charge. Ultra-low fouling surfaces based on zwitterionic molecules have been developed that can “catch and release” molecules of interest (Mi et al., 2010), potentially enabling a new generation of in vitro surfaces for diagnostic and assay-based testing.

Chemical Patterning for the Coculture of Cells

Cell-cell interactions are important for tissue development and function. During embryogenesis, the temporal and spatial signaling between cells of different origins is part of the cascade of events that support natural tissue growth and development (Yu et al., 2008). However, the process of harvesting tissues and isolating cells as well as the purification of specific cell types disrupts many of the cell-cell interactions found in in vivo cell-cell contact, signaling, structure, and general heterogeneity.



• **Figure 2.1.3.3** Examples of patterned cocultures. (A) Glass coverslip with patterned photoresist. Scale bar is 2 mm. (B,C) Spatially restricted contact between hepatocytes and fibroblasts (day 6). (D) Phase contrast and fluorescence overlay showing expression of intracellular albumin in green after 8 days of culture, indicating retained hepatocyte function. (B–D) Scale bars are 200 μm . Control of cell organization via patterned surface chemistry. (E) 3T3-J2 fibroblasts excluded from islands of PEG-disilane (day 5). (F) Hepatocytes and 3T3-J2 fibroblasts patterned on a combination of collagen and PEG-disilane, (day 2). (E,F) Scale bars 500 μm . (Reprinted in part with permission from Hui, E. E., & Bhatia, S. N. (2007). Microscale control of cell contact and spacing via three-component surface patterning. *Langmuir*, 23(8), 4103–4107. <https://doi.org/10.1021/la0630559>. Copyright 2007 American Chemical Society.)

The coculture of different cell types is one approach to enhance the in vitro environment and maintain cell phenotype in vitro (Nandkumar et al., 2002). Cocultures can be established by simply mixing two or more cell populations prior to plating, however this provides little control over cell–cell contact, spacing, or interaction. Greater control can be obtained through the use of patterned cocultures, which primarily allow to control homotypic and heterotypic cell–cell contact. Using patterning techniques, cocultures can be established where cell–cell contact, spacing, and interaction can be controlled with high resolution. Both cells and cell-adhesive proteins may be patterned using selective adhesion to micropatterned substrates (Folch and Toner, 2000; Hui and Bhatia, 2007), by flow through a microfluidic channels (Chiu et al., 2000; Takayama et al., 2001), by stamping with a stencil-based approach (Chen et al., 1998; Folch

and Toner, 2000) or by seeding on surfaces that dynamically switch from cell-adhesive to cell-repulsive (Edahiro et al., 2005; Kikuchi et al., 2009). A common requirement of most coculture (and patterning) applications is the ability to selectively control and limit cell adhesion to specific areas of the substrate. As a result, nonfouling surfaces can be of considerable benefit.

A practical application of coculturing is the study of liver cells (hepatocytes). Hepatocytes rapidly lose their ability to generate a characteristic protein (albumin) when they are cultured in vitro. Using mask-to-mask registration and photolithography, Hui and Bhatia (Hui and Bhatia, 2007) generated surfaces with three distinct chemistries for the cocultures of hepatocytes and 3T3-J2 fibroblasts. Hepatocytes preferentially adhered to collagen-coated regions and fibroblasts to serum-coated glass regions (Fig. 2.1.3.3).

A nonfouling PEG region was included that separated the two cell types and controlled the amount of contact or interaction between cocultured populations for up to 7 days (Fig. 2.1.3.3). At 8 days, hepatocytes retained the ability to produce albumin.

High-Throughput Screening

Microarrays represent a specific type of chemical patterning. The arrays consist of a large number of small spots, each with defined location and unique chemical composition. This approach is suitable for testing biomaterials and microenvironments to enable the screening of a large number of chemical combinations in a high-throughput manner. A high-throughput microarray that probes the cell–cell, cell–ECM, and cell–biomaterial interactions can be useful for studying cell adhesion, proliferation, and differentiation (Khademhosseini, 2005; Khademhosseini et al., 2006).

Typically, cell–ECM interactions are studied using purified matrix proteins adsorbed to cell culture substrates. This approach requires large amounts of protein per 96- or 384-well plate and can be prohibitively expensive. To address these challenges, new methods have been developed using pin tools (Cleveland and Koutz, 2005), piezo tips (Niles and Coassin, 2005), ultrasound (Strobl et al., 2004), and microarray (Flaim et al., 2005) technology for nanoliter liquid handling. Recently, robotic spotters capable of dispensing and immobilizing nanoliters of materials have been used to fabricate microarrays, where cell–matrix interactions can be tested and optimized in a high-throughput manner. For example, synthetic biomaterial arrays have been fabricated to test the interaction of stem cells with various extracellular signals (Anderson et al., 2004). Using this approach, thousands of polymeric materials were synthesized and their effect on differentiation of human embryonic stem cells (ESCs) (Anderson et al., 2004) and hMSCs (Anderson et al., 2005) were evaluated. These interactions have led to unexpected and novel cell–material interactions. Although the molecular mechanisms associated with the biological responses have yet to be clarified, such technology may be widely applicable in cell–microenvironment studies and in the identification of cues that may induce desired cell responses. Also, the materials which yield desired responses could be used as templates for tissue engineering scaffolds. Such an approach is a radical change from traditional methods of developing new biomaterials, where polymers have been individually developed and tested for their effect on cells. In addition to the screening of libraries of synthetic materials, the effect of natural ECM molecules on cell fate can similarly be evaluated using a high-throughput method. In one example, combinatorial matrices of various natural ECM proteins were tested for their ability to maintain the function of differentiated hepatocytes and to induce hepatic differentiation from murine ESCs (Flaim et al., 2005). A peptide and small-molecule microarray made by a DNA microarray spotter were also used to study high-throughput

cell adhesion (Falsey et al., 2001). A microarray of immobilized ligands was analyzed with three different biological assays such as protein-binding assay, functional phosphorylation assay, and cell adhesion assay. This array can be used to rapidly screen and analyze the functional properties of various ligands.

Nanometer-Scale Chemical Patterning

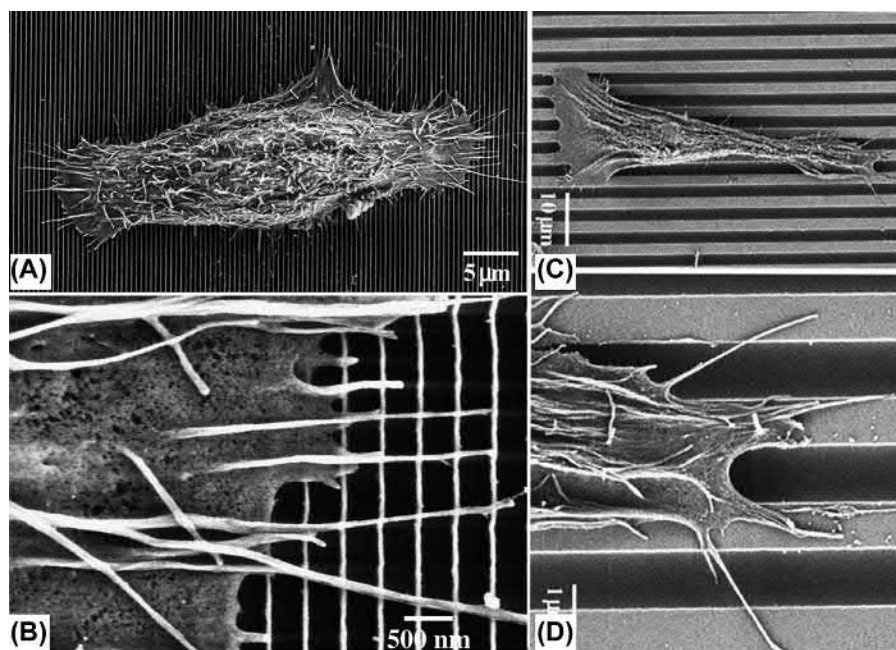
Nano-sized chemical patterns generally do not direct cell shape or orientation as a result of their extremely small size relative to the cell. Surfaces with chemical features on the nano-scale modulate cell functions such as adhesion, proliferation, migration, differentiation, and gene expression.

Cell Response to Substrate Topography

All cells are exposed to some type of physical environment in vivo. Cell–cell interactions, the ECM, and biomaterials all present a surface to the cell that is quantifiable in terms of its surface features (Liliensiek et al., 2009). As a field of study, surface topography defines the specific morphological characteristics of a surface. Surface topography may be generally described as isotropic (uniformity in all directions) or anisotropic (uniformity in one direction). Surface topography may be quantified by a number of techniques such as atomic force microscopy (AFM) or white light interferometry (WLI).

Unlike periodic surfaces typically fabricated for in vitro investigation (Clark et al., 1987), most biological surfaces present nonordered features at the macro- and micro-scales, which generally become more ordered at the nano-scale (Fratzl, 2008). Fibers in the ECM and pores in basement membranes are just a few examples of prevalent and quantifiable topographical features (Abrams et al., 2003; Liliensiek et al., 2009). Thus, it is not surprising that cells respond to topographical cues and that surface topography of the culture surface presents another means to control and study cell behavior in vitro. Micro- and nano-sized features are known to influence cell behavior, and both generally coexist in many biological surfaces. Accurate quantification of these surfaces is challenging since most tools are optimized for quantifying micro or nano features individually, but not both at the same time (Sosale et al., 2008).

In terms of cell activity, surface topography has been reported to affect proliferation, gene expression (Carinci et al., 2003), cell adhesion (Hamilton et al., 2006), motility (Clark et al., 1987), alignment (Clark et al., 1991), differentiation (Martinez et al., 2009), and matrix production (Hacking et al., 2008). In sensing and interacting with the topographical environment, evidence suggests that cells extend fine processes termed *filopodia*. While the specific mechanisms are poorly understood, changes in cell activity resulting from interaction with surface features have been linked to changes in cytoskeletal arrangement (Wojciak-Stothard et al., 1995) including actin filaments (Gerecht et al.,



• **Figure 2.1.3.4** Effect of micro- and nano-patterns on corneal epithelial cell alignment. (A) Cells were aligned perpendicularly to ridges that were 70 nm wide and 330 nm apart. (B) Expanded view of (A) showing filopodia also aligned perpendicularly to the patterns. (C) With increasing width and spacing (1900 nm ridge width, 2100 nm spacing), cells were aligned with the ridges and (D) filopodia were guided by the topographic pattern. (Reprinted from Teixeira, A.I., McKie, G.A., Foley, J.D., Bertics, P.J., Nealey, P.F., Murphy, C.J., 2006. The effect of environmental factors on the response of human corneal epithelial cells to nanoscale substrate topography. *Biomaterials* 27 (21), 3945–3954, Copyright (2006), with permission from Elsevier.)

2007), nuclear shape (Dalby et al., 2003), and ion channels (Tobasnick and Curtis, 2001). It is likely that these effects represent a small portion of the cellular events relating to interactions with surface topography and different mechanisms or combinations of mechanisms may be activated by different feature sizes and shapes (Ball et al., 2007).

Micrometer-Scale Topography

Investigations concerning the response of cells to precisely patterned, microfabricated surfaces began decades ago. Fibroblasts (Brunette, 1986a), osteoblasts (Hamilton and Brunette, 2007), macrophages (Wojciak-Stothard et al., 1996), neutrophils (Tan and Saltzman, 2002), epithelial cells (Brunette, 1986b), endothelial cells (Bettinger et al., 2006), cardiomyocytes (D. Kim et al., 2005), and neuronal cells (Clark et al., 1991) have all demonstrated a reproducible response to surface texture. Polarization or cell alignment along the direction of ridged surfaces is a phenomenon that is commonly observed when cells are cultured on linearly patterned substrates. Cell alignment to topographical features is referred to as contact guidance (Wood, 1988). With microscale-sized features, cell alignment generally increases with increasing groove depth and decreasing groove spacing (Bettinger et al., 2006), however cell response to topography is highly dependent upon cell type (Fig. 2.1.3.4). For example, epithelial cells and fibroblasts are differentially

affected by surfaces with micron-sized grooves (Clark et al., 1987, 1990). Neutrophils (Clark et al., 1987) are largely unaffected by step topographies but large differences in responses exist between fibroblastic, epithelial, and neuronal cells (Clark et al., 1990, 1991).

Nanometer-Scale Topography

It has been demonstrated that cells can sense and respond to features as small as 10–30 nm (Dalby et al., 2002; Wojciak-Stothard et al., 1996). Compared to the micron-scale, where cells may be profoundly affected by a single feature, at the nano-scale a repetition of similar features has the greatest effect and provides the most predictable results regarding cell behavior (Ball et al., 2007; Curtis et al., 2004). Once again, cell response to topography is highly dependent upon cell type. Using surfaces of aligned ridges possessing a constant ridge spacing of 260 nm and depths varying from 100 to 400 nm, Clark demonstrated that neuronal cells were highly oriented in the ridge direction for all depths, epithelial-like cells were highly oriented for all depths, whereas the orientation of fibroblast-like cells increased with increasing depth from 50% orientation at 100 nm to nearly 95% orientation at 400 nm (Clark et al., 1991).

At the microscale, increasing the depth and decreasing the width of grooved or stepped surface features increases the probability of cell alignment with the topographical

feature(s). At the nanoscale, it appears that a finite limit in feature sizes exists with respect to cell alignment to surface topography. By culturing fibroblasts on linearly patterned surfaces fabricated by e-beam lithography, it was determined that groove depths below 35 nm or ridge widths smaller than 100 nm did not result in cell alignment and that 35 nm may be the threshold for whole-cell fibroblast alignment (Loesberg et al., 2007). Similarly, Teixeira et al. demonstrated a finite limit in the response of human corneal epithelial cells to surfaces with linearly patterned surfaces with groove spacing ranging from 400 to 4000 nm (groove width 330–2100 nm) (Teixeira et al., 2006). At groove spacings greater than 400 nm, cells were oriented in an increasingly parallel manner to the linear pattern (Fig. 2.1.3.4), however at groove spacings less than 400 nm, cells were perpendicularly arranged. These findings further demonstrate a cell-specific sensitivity with regard to cell alignment to surface topography as well as imply that a limit exists in feature sizes that cells are able to recognize.

The effects of nano-topography on cell differentiation have also been reported. Proteomic-based studies have shown that cells respond to nano-sized pits and pores in irregular patterns, leading to increased differentiation and matrix production by human osteoprogenitor cells (Kantawong et al., 2009). Likewise, studies with surfaces fabricated by the arrangement of titanium nanotubes have demonstrated that nano tube diameter affects both hMSC differentiation and adhesion (Oh et al., 2009). Smaller diameter nanotubes (30 nm) increased cell adhesion, while larger diameters (100 nm) increased cell differentiation. Other authors using different cell lines and culture conditions have reported optimal nanotube diameters and spacing as low as 15 nm (Park et al., 2007). Topography at the nano-scale can also be used to effectively reduce cell adhesion. Kunzler et al. generated a constant gradient of nano-features (65 nm diameter and height) with the spacing as the only changing parameter along the gradient (Kunzler et al., 2007). This study demonstrated that the spacing or density of nonadhesive nano-scale features can disrupt cell adhesion, likely by restricting receptor–ligand interaction.

High-Throughput Screening of Surface Topography

Analogous to microarrays used to test many chemical compounds at one time in a high-throughput manner, topographical arrays have been developed to assess the effects of systematic variances in surface topography. Lovmand et al. developed a topographical array consisting of 504 topographically distinct surface structures fabricated on silicon wafers that were coated with tantalum prior to cell seeding (Lovmand et al., 2009). Each structure consisted of a topographical pattern comprised of a series of circles, squares, or rectangles that varied systematically in height from 0.6 to 2.4 μm , and feature size and spacing from 1.1 to 6.6 μm . Murine osteoblast cells (MC3T3-E1) were cultured on the array for up to 28 days to assess proliferation, cell area, and mineralization. It

was determined that the height of the features had the greatest effect on mineralization, followed by feature size, then the gap size. The combined effects of feature size and gap size became important as feature height decreased.

SIDE BAR: CLINICAL APPLICATIONS OF SURFACE MORPHOLOGY

Osteoblasts are substrate-dependent cells that have been widely used for investigating responses to surface topography. A considerable amount of work has been produced concerning the response of osteoblast cells to surface topography, and the end result of this work is widely applied clinically to enhance the long-term osseointegration of dental and orthopedic implants (Hacking et al., 1999, 2003). Mechanical fixation of an implant by the direct apposition of bone is referred to as osseointegration (Albrektsson et al., 1981; Branemark et al., 1977). Irregularly textured surfaces on titanium implants have been created by blasting the surface with small hard particles (Al_2O_3) that deform the relatively ductile titanium surface and produce a distinctly unordered micron-sized surface texture. It is common with dental implants that their surfaces are further processed by immersion in acid that superimposes a finer secondary nano-sized structure upon the textured surface and increases their osseointegration.

SIDE BAR: A NOTE ABOUT CELL LINES IN THE STUDY OF SURFACE TOPOGRAPHY

To enhance optical clarity, the TCP surface is very smooth ($R_a \sim 1.2 \text{ nm}$) (T. Y. Chang et al., 2007) and this has certain ramifications for the growth and development of cells in vitro. Adherent cell lines are selected preferentially for their ability to proliferate and differentiate on glass or tissue culture plastic. As a result, many cell lines have been selected based on their behavior on smooth, flat surfaces that are rarely found in vivo. Studies comparing the response of primary cells to cell lines derived from similar tissue sources have reported significant differences in cell activity (Fisher and Tickle, 1981; McCartney and Buck, 1981). This point becomes especially salient when working with surfaces where the effects of surface topography are the subject of primary interest (Clark et al., 1991; Hacking et al., 2008).

Cell Response to Substrate Elasticity

While surface chemistry and topography modulate cell function, it is increasingly evident that cells also respond to the physical or mechanical properties (stiffness) of the substrate. Stiffness can be described as the resistance of a solid material to deformation and is commonly defined by elastic modulus (E) and reported in “Pascals” (Pa). Excluding bone ($10\text{--}20 \times 10^9 \text{ Pa}$), most tissues have elastic moduli in the range of $10^1\text{--}10^6 \text{ Pa}$, substantially lower than the elastic moduli of most culture surfaces such as TCP ($3\text{--}3.5 \times 10^9 \text{ Pa}$).

Hydrogels are well suited to the study of cell substrate interactions since their stiffness can be varied by modifying the polymer concentration or the relative extent of cross-linking. Hydrogels can also be made from a variety of natural and synthetic materials such as hyaluronic acid (HA), fibrin, alginate, agarose, chitosan, polyacrylamide, and PEG. In

addition, natural materials can be modified to obtain hydrogels with new properties, e.g., gelatin methacryloyl (Yue et al., 2015). In terms of collagen hydrogels, gel stiffness may be increased by increasing the collagen concentration (Brigham et al., 2009) or reducing the thickness of the gel and immobilizing it on a glass substrate (Arora et al., 1999).

The stiffness of the substrate affects cell adhesion, spreading, and migration. In 2D cultures, cells preferentially migrate toward surfaces of greater stiffness, a phenomenon referred to as mechanotaxis (Lo et al., 2000). In 2D systems endothelial and fibroblast cells cultured on collagen-coated substrates that were classified as compliant ($\sim 5 \times 10^3$ Pa) or stiff ($\sim 70 \times 10^3$ Pa) demonstrated remarkably different behaviors (Opas, 1994). Cells cultured on compliant substrates had reduced spreading, increased lamellipodia activity, and greater migration. Cells cultured on stiffer substrates generally increased proliferation, however the specific preference is cell-type dependent (Pelham and Wang, 1997). There is substantial evidence that substrate stiffness also affects cell proliferation in 2D as well as 3D culture systems (Wong et al., 2003).

Substrate elasticity can also be used to direct the differentiation of certain cell types. MSCs cultured on collagen-coated substrates of varying stiffness can be directed toward neuronal, myogenic, and osteogenic lineages (Engler et al., 2006). For example, adult neural stem cells will selectively differentiate to neurons on softer substrates (1×10^2 – 5×10^2 Pa) or glial cell types on stiffer substrates (1×10^3 – 1×10^4 Pa) (Saha et al., 2008). These findings suggest that stem cells are able to recognize and differentiate according to physiologically relevant substrate stiffness. In general, stiff substrates favor myogenic differentiation, while rigid matrices favor osseous differentiation and soft ones favor neural cell differentiation (Engler et al., 2006).

Cell Response to Mechanical Deformation (Strain)

There has been considerable work assessing the response of cells to mechanical strain or deformation (Buckwalter and Cooper, 1987). Forces can be applied directly to adherent cells in vitro by either elongation or compression of their substrate (2D) or matrix (3D). With respect to cyclic tensile loads, in both 2D and 3D cultures, cells predominantly align in the direction of the applied load and assume an elongated morphology (Haghighipour et al., 2007; Henshaw et al., 2006; Toyoda et al., 1998).

Because of its load-bearing function and well-known adaptation to load, cells of the musculoskeletal system have been evaluated under conditions of tensile and compressive strain. For example, the extent of mineralization of bone and its mineral density is load dependent (Rodionova and Oganov, 2003). In vitro, cyclic strain in both tensile (Hanson et al., 2009) and compressive (Goldstein, 2002) loading enhances osteoblast mineralization. Thus, strain appears to be an important stimulus for the generation of mineralized and tendon-like tissues in vitro.

Toyoda et al. cultured cells harvested from the anterior cruciate ligament (ACL) and synovium (Toyoda et al., 1998). Cells were subjected to cyclic tensile load for 24 h via culture plates with flexible rubber bases. For both cell types, tensile load increased cell alignment and elongation, however tensile load only increased the production of collagen type I in cells derived from the ACL (Toyoda et al., 1998). These results have been supported by similar studies where fibroblasts subjected to cyclic tensile strain increased the formation of organized ECM, increased collagen production, and increased metabolic activity compared to unloaded controls (Hannafin et al., 2006; Joshi and Webb, 2008).

These findings have led to the fabrication of bioreactors that can apply physiologic loads to developing tissue to enhance the production and alignment of extracellular matrix in a number of tissues including cardiac (Kortsmit et al., 2009), bone (van Griensven et al., 2009), cartilage (Preiss-Bloom et al., 2009), and tendon (Riboh et al., 2008).

Comparison and Evaluation of Substrate Cues

As previously discussed, cells respond to a number of surface cues such as chemistry, topography, elasticity, and strain. Evaluating cell response to multiple cues is inherently difficult since substrate properties are often interrelated. In many in vitro investigations of biomaterials it may be difficult to effectively separate the effects of surface chemistry from those of morphology and elasticity. This is particularly problematic in cases where the unique properties of a material may arise from the manufacturing process (Bobyn et al., 1999; Hacking et al., 2002). In such investigations, it is important to recognize that subtle changes in biomaterial properties can have profound effects on cellular response and ultimately in vivo function. This is especially true, for example, of implant coatings where responses to surface morphology need to be dissociated from other factors such as surface chemistry. Experimental controls must not just approximate surface morphology, but match it precisely, since subtle changes in surface morphology have the potential to confound experimental findings. In many cases however, it may not be practical or even possible to produce an exact morphological control from a different biomaterial. A morphological control may be generated by coating the surface of interest with a thin film that is dense, durable, homogeneous, and does not alter the surface morphology. There are a variety of thin-film deposition techniques collectively referred to as physical vapor deposition (PVD) that have been employed by several research groups (Hacking et al., 2002, 2007; Meredith et al., 2007). While other coating methods exist, PVD is advantageous since samples can be processed at lower temperatures in a relatively inert environment.

Control of substrate elasticity can be achieved by varying the precursor components and curing conditions. PDMS, for example, can be prepared with a range of elasticity

(2.8–1882 kPa) by varying the ratio of base to curing agent (Cheng et al., 2009). Since PDMS can be cast into many shapes, patterned surfaces with varying elasticity can be created. These surfaces can be subsequently coated to achieve uniform and comparable surface chemistry. Similarly, by progressively reducing the thickness of a gel to a thin film, chemical composition can be maintained while substrate elasticity changes.

While the contributions of topography, chemistry, elasticity, and strain to cell behavior have been evaluated and documented for a wide variety of cell types, much of the literature has evaluated the effects of only one stimulus in each experimental setting. In vivo however, it is reasonable to expect that cells experience a wide range of stimuli simultaneously. Since physical cues such as chemistry, topography, elasticity, and strain can produce both synergistic and opposing effects on cell behavior, it is of interest to evaluate their simultaneous effect on cell behavior and, if possible, describe a hierarchy of cellular cues. However, since the cellular response to physical stimuli is often dependent upon cell phenotype and further subject to effects by soluble factors, broad exploration of these phenomena presents a challenging combinatorial experimental environment. Organ-on-a-chip platforms have the potential to model more complex experiments for studying cell–substrate interactions (Ashammakhi et al., 2019).

Chemistry and Topography

Using a combination of patterning techniques including photolithography, Curtis established that fibroblasts respond to both chemical and topographic patterns (Curtis and Wilkinson, 1999). However, when both chemical and topographical stimuli were combined and orthogonally opposed on the same surface, cells aligned with nanometer-sized topographical patterns. Curtis coined the term “topographic reaction” to describe these events (Curtis and Wilkinson, 1999). Similarly, a preference of cellular alignment to topographic cues in the presence of both topographic and chemical patterns has been demonstrated in a number of studies (Charest et al., 2006; Gomez et al., 2007).

Chemistry and Strain

Hyun et al. developed a system to evaluate the combined effects of chemical patterning and strain on cell alignment (Hyun et al., 2006). Thin paraffin films were patterned with adhesive regions of fibronectin to which NIH 3T3 fibroblasts adhered and aligned. After cells aligned in the direction of the chemical patterning, the paraffin films with the adherent cells were subjected to cyclical stretch. Mechanical force was applied perpendicular to the cell alignment resulting from chemical patterning and the actin cytoskeleton realigned along the axis of applied mechanical stress. Stretched cells showed altered gene expression of cytoskeletal and matrix proteins in response to mechanical deformation.

Topography and Strain

Cheng et al. (Cheng et al., 2009) fabricated patterned PDMS substrates consisting of parallel microchannels (2 μm wide, 2 μm separation, and 10 μm deep) that were subjected to cyclic compressive strain applied perpendicular to the direction of the channels. After 6 h of compression, fibroblasts cultured on the patterned PDMS substrate aligned in the direction of the microchannels (topographical cue) and perpendicular to the direction of compression. Elastic microgrooved surfaces have also been utilized to maintain the cellular orientation of mesenchymal stem cells (MSC's) while subjected to cyclic tensile strain (Kurpinski et al., 2006).

Organ-on-a-Chip 3D culture

Because 2D culture cannot mimic 3D in vivo environment and lack many aspects of native tissue such as microfluidic flow, organ-on-a-chip models were developed (Zheng et al., 2016). An organ-on-a-chip system comprises a 3D culture system that has dynamic flow through microchannels, thanks to advances made in microfluidics, microfabrication, and knowledge gained from research into bioreactors. Microfluidic work by Whitesides (Whitesides, 2006) makes the early basis for lab-on-a-chip and organ-on-a-chip systems. The platform offers several advantages over the conventional 2D culture in studying various physiological and pathological conditions. An entirely different approach is embodied in organ-on-a-chip systems where cells can be subjected to flow stress, topographical cues, and possible stimulation by embedded biomolecules and microelectrodes, and the effect can be monitored using microsensors.

In some organ-on-a-chip models, not only cells are cultured and exposed to flow, but other physiological effects are included in the system for creating movement that mimics in vivo effects. For example, by moving the membrane between alveolar and vascular space in the lung-on-a-chip (Huh et al., 2010), the mechanical cues can be recreated. Similar models were developed for the gut (Kim et al., 2012). These 3D models were used to study various diseased and pathological conditions including cancer and its metastasis (Bersini et al., 2014). In organ-on-a-chip systems, sensors can also be integrated (Shin et al., 2017) and various changes can be detected and monitored on a continuous basis making real-time follow-up and analysis possible (Ashammakhi et al., 2018, 2019). More recently, multiorgan-on-a-chip systems were developed by linking different tissue units together (Zhang et al., 2017) and the interaction between substance and cells was evaluated. The use of 3D models of organ-on-a-chip was found to be more representative to in vivo events than 2D. Cells cultured in these systems were observed to polarize in a biomimetic way (Jang and Suh, 2010) and the curvature of channels was found to influence cell function (Ferrell et al., 2012). Cell functionality was correlated to diameter, with smaller diameter resulting in increasingly functional cells.

(Normal renal tubules have a small diameter at about 50 μm [Jameson and Loscalzo, 2010]). These findings suggested that the cells could sense structural and spatial cues and that surface curvature might have a positive effect on distal tubular cell function (Ferrell et al., 2012). Thus, the system allows the manipulation and study of various material properties on cells, such as the effect of stretch (Kilinc et al., 2011), peristaltic movement (Kim and Ingber, 2013; Kim et al., 2012), as well as shear stress (Jang et al., 2013). Also, sensors and electrodes for the measurement of transepithelial electrical resistance (TEER) can be integrated to monitor renal epithelial cell growth, and the integrity of tight junctions (Ferrell et al., 2010). Jang et al. cultured primary human proximal tubular epithelial cells on microchannels comprised of collagen type IV-coated polyester membranes (Jang et al., 2013). Compared to control systems not exposed to fluid shear stress, tubular cells in microfluidic systems regained normal columnar shape, polarity, and primary cilia. They also displayed an increase in cellular uptake of albumin and an increased recovery from cisplatin-induced damage (Jang et al., 2013). Jang et al. also cultured primary rat renal collecting duct cells on a multilayer microfluidic device created from thin fibronectin-coated porous polyester membranes situated in a PDMS microchamber (Jang and Suh, 2010). Shear stress was maintained at 1 dyn/cm^2 by accounting for fluid flow rates, viscosity, and channel size in this system. At this stress level, cytoskeletal rearrangement, number of cell junctions, and cell polarity increased.

Classically, PDMS is used for the fabrication of organ-on-a-chip systems because it is transparent, has low toxicity, and high permeability to O_2 and CO_2 and (Whitesides, 2006). However, PDMS can absorb hydrophobic compounds which limits its application in for drug testing (Halldorsson et al., 2015). Other materials such as polycarbonate, polystyrene, and poly(methyl methacrylate) (PMMA) (Chan et al., 2015), can be used because they have low absorption of hydrophobic compounds (Nge et al., 2013). In addition, natural and synthetic hydrogels may be added to microfluidic devices, to better mimic the natural physiologic environment (Hasan et al., 2015). Microchannel surfaces can be coated with various biomaterials that enhance cell attachment and function. For example, Sciancalepore et al. cultured hPC progenitor cells on porous polycarbonate membranes coated with either fibronectin, laminin, or Matrigel that separated PDMS microchannels (Sciancalepore et al., 2014). In this study, fibronectin was associated with the highest number of metabolically active cells.

Summary

In vivo, cells are responsive to a myriad of substrate-related signals within the environment. At the micro- and nano-scales, interactions with the ECM expose the cell to a variety of chemical moieties and topographical features. Micro- and nano-scale technologies have provided many new tools to manipulate the in vitro environment. Cell behavior may be

modified by patterns of cell-adhesive ligands and topographical features. Further modification of cell behavior can be achieved by altering the mechanical properties of the substrate, such as elasticity or by deformation of cell shape. With respect to generating complex tissue structures, substrate cues like topography, chemistry, and matrix elasticity are promising candidates for controlling cell differentiation. Unlike soluble factors, substrate cues can provide specific information for directing and controlling cell behavior. The combination of multiple physical cues presents new and potentially useful methods to direct and control cell development and behavior. With respect to physical stimuli, evidence suggests that a hierarchy exists among cell responses to substrate characteristics.

References

- Abercrombie, M., Heaysman, J.E., 1954. Observations on the social behaviour of cells in tissue culture. II. Monolayering of fibroblasts. *Exp. Cell Res.* 6 (2), 293–306.
- Aframian, D.J., Cukierman, E., Nikolovski, J., Mooney, D.J., Yamada, K.M., Baum, B.J., 2000. The growth and morphological behavior of salivary epithelial cells on matrix protein-coated biodegradable substrata. *Tissue Eng.* 6 (3), 209–216.
- Albrektsson, T., Branemark, P.I., Hansson, H.A., Lindstrom, J., 1981. Osseointegrated titanium implants. Requirements for ensuring a long-lasting, direct bone-to-implant anchorage in man. *Acta Orthop. Scand.* 52 (2), 155–170.
- Amstein, C.F., Hartman, P.A., 1975. Adaptation of plastic surfaces for tissue culture by glow discharge. *J. Clin. Microbiol.* 2 (1), 46–54.
- Anderson, D.G., Levenberg, S., Langer, R., 2004. Nanoliter-scale synthesis of arrayed biomaterials and application to human embryonic stem cells. *Nat. Biotechnol.* 22 (7), 863–866.
- Anderson, D.G., Putnam, D., Lavik, E.B., Mahmood, T.A., Langer, R., 2005. Biomaterial microarrays: rapid, microscale screening of polymer-cell interaction. *Biomaterials* 26 (23), 4892–4897.
- Andrade, J.D., Hlady, V., 1987. Plasma protein adsorption: the big twelve. *Ann. N. Y. Acad. Sci.* 516, 158–172.
- Arora, P.D., Narani, N., McCulloch, C.A., 1999. The compliance of collagen gels regulates transforming growth factor-beta induction of alpha-smooth muscle actin in fibroblasts. *Am. J. Pathol.* 154 (3), 871–882.
- Ashammakhi, N., Hasan, A., Elkhammas, E., 2019. Translating advances in organ-on-chip platforms for supporting organs. *J. Biomed. Mater. Res.* 107 (6), 2006–2018.
- Ashammakhi, N., Wesseling-Perry, K., Hasan, A., Elkhammas, E., Zhang, Y.S., 2018. Kidney-on-a-chip: untapped opportunities. *Kidney Int.* 94 (6), 1073–1086.
- Auernheimer, J., Dahmen, C., Hersel, U., Bausch, A., Kessler, H., 2005. Photoswitched cell adhesion on surfaces with RGD peptides. *J. Am. Chem. Soc.* 127 (46), 16107–16110.
- Bain, J.R., Hoffman, A.S., 2003a. Tissue-culture surfaces with mixtures of aminated and fluorinated functional groups. Part 1. Synthesis and characterization. *J. Biomater. Sci. Polym. Ed.* 14 (4), 325–339.
- Bain, J.R., Hoffman, A.S., 2003b. Tissue-culture surfaces with mixtures of aminated and fluorinated functional groups. Part 2. Growth and function of transgenic rat insulinoma cells (betaG I/17). *J. Biomater. Sci. Polym. Ed.* 14 (4), 341–367.
- Ball, M.D., Prendergast, U., O'Connell, C., Sherlock, R., 2007. Comparison of cell interactions with laser machined micron- and nanoscale features in polymer. *Exp. Mol. Pathol.* 82 (2), 130–134.

- Bell Jr., P.B., 1977. Locomotory behavior, contact inhibition and pattern formation of 3T3 and polyoma virus-transformed 3T3 cells in culture. *J. Cell Biol.* 74 (3), 963–982.
- Bersini, S., Jeon, J.S., Dubini, G., Arrigoni, C., Chung, S., Charest, J.L., Moretti, M., Kamm, R.D., 2014. A microfluidic 3D in vitro model for specificity of breast cancer metastasis to bone. *Biomaterials* 35, 2454.
- Bettinger, C.J., Orrick, B., Misra, A., Langer, R., Borenstein, J.T., 2006. Microfabrication of poly (glycerol-sebacate) for contact guidance applications. *Biomaterials* 27 (12), 2558–2565.
- Bhatia, S.N., Yarmush, M.L., Toner, M., 1997. Controlling cell interactions by micropatterning in co-cultures: hepatocytes and 3T3 fibroblasts. *J. Biomed. Mater. Res.* 34 (2), 189–199.
- Boateng, S.Y., Lateef, S.S., Mosley, W., Hartman, T.J., Hanley, L., Russell, B., 2005. RGD and YIGSR synthetic peptides facilitate cellular adhesion identical to that of laminin and fibronectin but alter the physiology of neonatal cardiac myocytes. *Am. J. Physiol. Cell Physiol.* 288 (1), C30–C38.
- Bobyn, J.D., Stackpool, G.J., Hacking, S.A., Tanzer, M., Krygier, J.J., 1999. Characteristics of bone ingrowth and interface mechanics of a new porous tantalum biomaterial. *J. Bone Joint Surg. Br.* 81 (5), 907–914.
- Branemark, P.I., Hansson, B.O., Adell, R., Breine, U., Lindstrom, J., Hallen, O., Ohman, A., 1977. Osseointegrated implants in the treatment of the edentulous jaw. Experience from a 10-year period. *Scand. J. Plast. Reconstr. Surg. Suppl.* 16, 1–132.
- Brigham, M.D., Bick, A., Lo, E., Bendali, A., Burdick, J.A., Khademhosseini, A., 2009. Mechanically robust and bioadhesive collagen and photocrosslinkable hyaluronic acid semi-interpenetrating networks. *Tissue Eng. Part A* 15 (7), 1645–1653.
- Browne, S.M., Al-Rubeai, M., 2007. Selection methods for high-producing mammalian cell lines. *Trends Biotechnol.* 25 (9), 425–432 doi:S0167-7799(07)00182-5.
- Brunette, D.M., 1986a. Fibroblasts on micromachined substrata orient hierarchically to grooves of different dimensions. *Exp. Cell Res.* 164 (1), 11–26.
- Brunette, D.M., 1986b. Spreading and orientation of epithelial cells on grooved substrata. *Exp. Cell Res.* 167 (1), 203–217.
- Buckwalter, J.A., Cooper, R.R., 1987. Bone structure and function. *Instr. Course Lect.* 36, 27–48.
- Byambaa, B., Annabi, N., Yue, K., Trujillo-de Santiago, G., Alvarez, M.M., Jia, W., et al., 2017. Bioprinted osteogenic and vasculogenic patterns for engineering 3D. *Bone Tissue* 6 (16), 1700015.
- Callen, B.W., Sodhi, R.N., Shelton, R.M., Davies, J.E., 1993. Behavior of primary bone cells on characterized polystyrene surfaces. *J. Biomed. Mater. Res.* 27 (7), 851–859.
- Cao, L., Chang, M., Lee, C.Y., Castner, D.G., Sukavaneshvar, S., Ratner, B.D., Horbett, T.A., 2007. Plasma-deposited tetraglyme surfaces greatly reduce total blood protein adsorption, contact activation, platelet adhesion, platelet procoagulant activity, and in vitro thrombus deposition. *J. Biomed. Mater. Res. A* 81 (4), 827–837.
- Carinci, F., Pezzetti, F., Volinia, S., Francioso, F., Arcelli, D., Marchesini, J., et al., 2003. Analysis of osteoblast-like MG63 cells' response to a rough implant surface by means of DNA microarray. *J. Oral Implantol.* 29 (5), 215–220.
- Chan, Y.K., Sy, K.H.S., Wong, C.Y., Man, P.K., Wong, D., Shum, H.C., 2015. In vitro modeling of emulsification of silicone oil as intraocular tamponade using microengineered eye-on-a-chip. *Investig. Ophthalmol. Vis. Sci.* 56 (5), 3314–3319.
- Chang, W.C., Sretavan, D.W., 2008. Novel high-resolution micropatterning for neuron culture using polylysine adsorption on a cell repellent, plasma-polymerized background. *Langmuir* 24 (22), 13048–13057.
- Chang, T.Y., Yadav, V.G., De Leo, S., Mohedas, A., Rajalingam, B., Chen, C.L., et al., 2007. Cell and protein compatibility of parylene-C surfaces. *Langmuir* 23 (23), 11718–11725.
- Charest, J.L., Eliason, M.T., Garcia, A.J., King, W.P., 2006. Combined microscale mechanical topography and chemical patterns on polymer cell culture substrates. *Biomaterials* 27 (11), 2487–2494.
- Chen, C.S., Mrksich, M., Huang, S., Whitesides, G.M., Ingber, D.E., 1997. Geometric control of cell life and death. *Science* 276 (5317), 1425–1428.
- Chen, C.S., Mrksich, M., Huang, S., Whitesides, G.M., Ingber, D.E., 1998. Micropatterned surfaces for control of cell shape, position, and function. *Biotechnol. Prog.* 14 (3), 356–363.
- Chen, S., Cao, Z., Jiang, S., 2009. Ultra-low fouling peptide surfaces derived from natural amino acids. *Biomaterials* 30 (29), 5892–5896.
- Cheng, X., Wang, Y., Hanein, Y., Bohringer, K.F., Ratner, B.D., 2004. Novel cell patterning using microheater-controlled thermoresponsive plasma films. *J. Biomed. Mater. Res. A* 70 (2), 159–168.
- Cheng, C.M., Steward Jr., R.L., LeDuc, P.R., 2009. Probing cell structure by controlling the mechanical environment with cell-substrate interactions. *J. Biomech.* 42 (2), 187–192.
- Chien, H.W., Chang, T.Y., Tsai, W.B., 2009. Spatial control of cellular adhesion using photo-crosslinked micropatterned polyelectrolyte multilayer films. *Biomaterials* 30 (12), 2209–2218.
- Chinn, J.A., Horbett, T.A., Ratner, B.D., 1994. Laboratory preparation of plasticware to support cell culture. *Methods Cell Sci.* 16 (3), 155–159.
- Chiu, D.T., Jeon, N.L., Huang, S., Kane, R.S., Wargo, C.J., Choi, I.S., Ingber, D.E., Whitesides, G.M., 2000. Patterned deposition of cells and proteins onto surfaces by using three-dimensional microfluidic systems. *Proc. Natl. Acad. Sci. U. S. A.* 97 (6), 2408–2413.
- Chollet, C., Chanseau, C., Remy, M., Guignandon, A., Bareille, R., Labrugere, C., et al., 2009. The effect of RGD density on osteoblast and endothelial cell behavior on RGD-grafted polyethylene terephthalate surfaces. *Biomaterials* 30 (5), 711–720.
- Claase, M.B., Olde Riekerink, M.B., de Bruijn, J.D., Grijpma, D.W., Engbers, G.H., Feijen, J., 2003. Enhanced bone marrow stromal cell adhesion and growth on segmented poly(ether ester)s based on poly(ethylene oxide) and poly(butylene terephthalate). *Biomacromolecules* 4 (1), 57–63.
- Clark, P., Connolly, P., Curtis, A.S., Dow, J.A., Wilkinson, C.D., 1987. Topographical control of cell behaviour. I. Simple step cues. *Development* 99 (3), 439–448.
- Clark, P., Connolly, P., Curtis, A.S., Dow, J.A., Wilkinson, C.D., 1990. Topographical control of cell behaviour: II. Multiple grooved substrata. *Development* 108 (4), 635–644.
- Clark, P., Connolly, P., Curtis, A.S., Dow, J.A., Wilkinson, C.D., 1991. Cell guidance by ultrafine topography in vitro. *J. Cell Sci.* 99 (Pt 1), 73–77.
- Cleveland, P.H., Koutz, P.J., 2005. Nanoliter dispensing for uHTS using pin tools. *Assay Drug Dev. Technol.* 3 (2), 213–225.
- Connelly, C.S., Fahl, W.E., Iannaccone, P.M., 1989. The role of transgenic animals in the analysis of various biological aspects of normal and pathologic states. *Exp. Cell Res.* 183 (2), 257–276.
- Curtis, A., Wilkinson, C., 1999. New depths in cell behaviour: reactions of cells to nanotopography. *Biochem. Soc. Symp.* 65, 15–26.
- Curtis, A.S., Forrester, J.V., McInnes, C., Lawrie, F., 1983. Adhesion of cells to polystyrene surfaces. *J. Cell Biol.* 97 (5 Pt 1), 1500–1506.

- Curtis, A.S., Gadegaard, N., Dalby, M.J., Riehle, M.O., Wilkinson, C.D., Aitchison, G., 2004. Cells react to nanoscale order and symmetry in their surroundings. *IEEE Trans. Nanobiosci.* 3 (1), 61–65.
- Cutler, S.M., Garcia, A.J., 2003. Engineering cell adhesive surfaces that direct integrin $\alpha 5 \beta 1$ binding using a recombinant fragment of fibronectin. *Biomaterials* 24 (10), 1759–1770.
- Dalby, M.J., Riehle, M.O., Johnstone, H., Affrossman, S., Curtis, A.S., 2002. In vitro reaction of endothelial cells to polymer demixed nanotopography. *Biomaterials* 23 (14), 2945–2954.
- Dalby, M.J., Riehle, M.O., Yarwood, S.J., Wilkinson, C.D., Curtis, A.S., 2003. Nucleus alignment and cell signaling in fibroblasts: response to a micro-grooved topography. *Exp. Cell Res.* 284 (2), 274–282.
- Dalby, M.J., Riehle, M.O., Sutherland, D.S., Agheli, H., Curtis, A.S., 2004. Changes in fibroblast morphology in response to nanocolumns produced by colloidal lithography. *Biomaterials* 25 (23), 5415–5422.
- Dehner, L.P., 1998. The evolution of the diagnosis and understanding of primitive and embryonic neoplasms in children: living through an epoch. *Mod. Pathol.* 11 (7), 669–685.
- Dike, L.E., Chen, C.S., Mrksich, M., Tien, J., Whitesides, G.M., Ingber, D.E., 1999. Geometric control of switching between growth, apoptosis, and differentiation during angiogenesis using micropatterned substrates. *In Vitro Cell. Dev. Biol. Anim.* 35 (8), 441–448.
- Du, Y., Shim, J., Vidula, M., Hancock, M.J., Lo, E., Chung, B.G., et al., 2009. Rapid generation of spatially and temporally controllable long-range concentration gradients in a microfluidic device. *Lab Chip* 9 (6), 761–767.
- Edaheji, J., Sumaru, K., Tada, Y., Ohi, K., Takagi, T., Kameda, M., et al., 2005. In situ control of cell adhesion using photoresponsive culture surface. *Biomacromolecules* 6 (2), 970–974.
- Eiges, R., Schuldiner, M., Drukker, M., Yanuka, O., Itskovitz-Eldor, J., Benvenisty, N., 2001. Establishment of human embryonic stem cell-transfected clones carrying a marker for undifferentiated cells. *Curr. Biol.* 11 (7), 514–518.
- Elloumi-Hannachi, I., Yamato, M., Okano, T., 2010. Cell sheet engineering: a unique nanotechnology for scaffold-free tissue reconstruction with clinical applications in regenerative medicine. *J. Intern. Med.* 267 (1), 54–70.
- Engler, A.J., Sen, S., Sweeney, H.L., Discher, D.E., 2006. Matrix elasticity directs stem cell lineage specification. *Cell* 126 (4), 677–689.
- Erickson, C.A., 1978. Contact behaviour and pattern formation of BHK and polyoma virus-transformed BHK fibroblasts in culture. *J. Cell Sci.* 33, 53–84.
- Ertel, S.I., Ratner, B.D., Horbett, T.A., 1990. Radiofrequency plasma deposition of oxygen-containing films on polystyrene and poly(ethylene terephthalate) substrates improves endothelial cell growth. *J. Biomed. Mater. Res.* 24 (12), 1637–1659.
- Falsey, J.R., Renil, M., Park, S., Li, S., Lam, K.S., 2001. Peptide and small molecule microarray for high throughput cell adhesion and functional assays. *Bioconjug. Chem.* 12 (3), 346–353.
- Fan, X., Lin, L., Messersmith, P.B., 2006. Cell fouling resistance of polymer brushes grafted from ti substrates by surface-initiated polymerization: effect of ethylene glycol side chain length. *Biomacromolecules* 7 (8), 2443–2448.
- Ferrell, N., Desai, R.R., Fleischman, A.J., Roy, S., Humes, H.D., Fissell, W.H., 2010. A microfluidic bioreactor with integrated trans-epithelial electrical resistance (TEER) measurement electrodes for evaluation of renal epithelial cells. *Biotechnol. Bioeng.* 107 (4), 707–716.
- Ferrell, N., Ricci, K.B., Groszek, J., Marmorstein, J.T., Fissell, W.H., 2012. Albumin handling by renal tubular epithelial cells in a microfluidic bioreactor. *Biotechnol. Bioeng.* 109 (3), 797–803.
- Fisher, P.E., Tickle, C., 1981. Differences in alignment of normal and transformed cells on glass fibres. *Exp. Cell Res.* 131 (2), 407–410.
- Flaim, C.J., Chien, S., Bhatia, S.N., 2005. An extracellular matrix microarray for probing cellular differentiation. *Nat. Methods* 2 (2), 119–125.
- Folch, A., Toner, M., 2000. Microengineering of cellular interactions. *Annu. Rev. Biomed. Eng.* 2, 227–256.
- Fratzl, P., 2008. Bone fracture: when the cracks begin to show. *Nat. Mater.* 7 (8), 610–612.
- Fredriksson, C., Khilman, S., Kasemo, B., Steel, D.M., 1998. In vitro real-time characterization of cell attachment and spreading. *J. Mater. Sci. Mater. Med.* 9 (12), 785–788.
- Frimat, J.P., Menne, H., Michels, A., Kittel, S., Kettler, R., Borgmann, S., et al., 2009. Plasma stencilling methods for cell patterning. *Anal. Bioanal. Chem.* 395 (3), 601–609.
- Gallant, N.D., Garcia, A.J., 2007. Model of integrin-mediated cell adhesion strengthening. *J. Biomech.* 40 (6), 1301–1309.
- Garcia, A.J., 2005. Get a grip: integrins in cell-biomaterial interactions. *Biomaterials* 26 (36), 7525–7529.
- Garrod, D.R., Steinberg, M.S., 1973. Tissue-specific sorting-out in two dimensions in relation to contact inhibition of cell movement. *Nature* 244 (5418), 568–569.
- Gerecht, S., Bettinger, C.J., Zhang, Z., Borenstein, J.T., Vunjak-Novakovic, G., Langer, R., 2007. The effect of actin disrupting agents on contact guidance of human embryonic stem cells. *Biomaterials* 28 (28), 4068–4077.
- Gobin, A.S., West, J.L., 2003. Val-ala-pro-gly, an elastin-derived non-integrin ligand: smooth muscle cell adhesion and specificity. *J. Biomed. Mater. Res. A* 67 (1), 255–259.
- Goessl, A., Gollidge, S.L., Hoffman, A.S., 2001. Plasma lithography – thin-film patterning of polymers by RF plasma polymerization II: study of differential binding using adsorption probes. *J. Biomater. Sci. Polym. Ed.* 12 (7), 739–753.
- Goldstein, S.A., 2002. Tissue engineering: functional assessment and clinical outcome. *Ann. N. Y. Acad. Sci.* 961, 183–192.
- Gomez, N., Chen, S., Schmidt, C.E., 2007. Polarization of hippocampal neurons with competitive surface stimuli: contact guidance cues are preferred over chemical ligands. *J. R. Soc. Interface* 4 (13), 223–233.
- Groger, S., Michel, J., Meyle, J., 2008. Establishment and characterization of immortalized human gingival keratinocyte cell lines. *J. Periodontol. Res.* 43 (6), 604–614.
- Hacking, S.A., Boby, J.D., Tanzer, M., Krygier, J.J., 1999. The osseous response to corundum blasted implant surfaces in a canine hip model. *Clin. Orthop. Relat. Res.* 364, 240–253.
- Hacking, S.A., Tanzer, M., Harvey, E.J., Krygier, J.J., Boby, J.D., 2002. Relative contributions of chemistry and topography to the osseointegration of hydroxyapatite coatings. *Clin. Orthop. Relat. Res.* (405), 24–38.
- Hacking, S.A., Harvey, E.J., Tanzer, M., Krygier, J.J., Boby, J.D., 2003. Acid-etched microtexture for enhancement of bone growth into porous-coated implants. *J. Bone Joint Surg. Br.* 85 (8), 1182–1189.
- Hacking, S.A., Zuraw, M., Harvey, E.J., Tanzer, M., Krygier, J.J., Boby, J.D., 2007. A physical vapor deposition method for controlled evaluation of biological response to biomaterial chemistry and topography. *J. Biomed. Mater. Res. A* 82 (1), 179–187.
- Hacking, S.A., Harvey, E., Roughley, P., Tanzer, M., Boby, J., 2008. The response of mineralizing culture systems to microtextured and polished titanium surfaces. *J. Orthop. Res.* 26 (10), 1347–1354.

- Haghighipour, N., Tafazzoli-Shadpour, M., Shokrgozar, M.A., Amini, S., Amanzadeh, A., Khorasani, M.T., 2007. Topological remodeling of cultured endothelial cells by characterized cyclic strains. *Mol. Cell. Biomech.* 4 (4), 189–199.
- Halldorsson, S., Lucumi, E., Gómez-Sjöberg, R., Fleming, R.M.T., 2015. Advantages and challenges of microfluidic cell culture in polydimethylsiloxane devices. *Biosens. Bioelectron.* 63, 218–231.
- Hamilton, D.W., Brunette, D.M., 2007. The effect of substratum topography on osteoblast adhesion mediated signal transduction and phosphorylation. *Biomaterials* 28 (10), 1806–1819.
- Hamilton, D.W., Wong, K.S., Brunette, D.M., 2006. Microfabricated discontinuous-edge surface topographies influence osteoblast adhesion, migration, cytoskeletal organization, and proliferation and enhance matrix and mineral deposition in vitro. *Calcif. Tissue Int.* 78 (5), 314–325.
- Hannafin, J.A., Attia, E.A., Henshaw, R., Warren, R.F., Bhargava, M.M., 2006. Effect of cyclic strain and plating matrix on cell proliferation and integrin expression by ligament fibroblasts. *J. Orthop. Res.* 24 (2), 149–158.
- Hanson, A.D., Marvel, S.W., Bernacki, S.H., Banes, A.J., van Aalst, J., Lobo, E.G., 2009. Osteogenic effects of rest inserted and continuous cyclic tensile strain on hASC lines with disparate osteodifferentiation capabilities. *Ann. Biomed. Eng.* 37 (5), 955–965.
- Hasan, A., Paul, A., Memic, A., Khademhosseini, A., 2015. A multilayered microfluidic blood vessel-like structure. *Biomed. Microdevices* 17 (5), 88.
- Hayflick, L., 1965. The limited in vitro lifetime of human diploid cell strains. *Exp. Cell Res.* 37, 614–636.
- Hayflick, L., 1985. The cell biology of aging. *Clin. Geriatr. Med.* 1 (1), 15–27.
- Heckman, C.A., 2009. Contact inhibition revisited. *J. Cell. Physiol.* 220 (3), 574–575.
- Henshaw, D.R., Attia, E., Bhargava, M., Hannafin, J.A., 2006. Canine ACL fibroblast integrin expression and cell alignment in response to cyclic tensile strain in three-dimensional collagen gels. *J. Orthop. Res.* 24 (3), 481–490.
- Higuchi, A., Hamamura, A., Shindo, Y., Kitamura, H., Yoon, B.O., Mori, T., et al., 2004. Photon-modulated changes of cell attachments on poly(spiropyran-co-methyl methacrylate) membranes. *Biomacromolecules* 5 (5), 1770–1774.
- Hubbell, J.A., Massia, S.P., Desai, N.P., Drumheller, P.D., 1991. Endothelial cell-selective materials for tissue engineering in the vascular graft via a new receptor. *Biotechnology* 9 (6), 568–572.
- Huh, D., Matthews, B.D., Mammoto, A., Montoya-Zavala, M., Hsin, H.Y., Ingber, D.E., 2010. Reconstituting organ-level lung functions on a chip. *Science* 328 (5986), 1662–1668.
- Hui, E.E., Bhatia, S.N., 2007. Microscale control of cell contact and spacing via three-component surface patterning. *Langmuir* 23 (8), 4103–4107. <https://doi.org/10.1021/la0630559>.
- Hynes, R.O., 2002. Integrins: bidirectional, allosteric signaling machines. *Cell* 110 (6), 673–687.
- Hyun, J., Zhu, Y.J., Liebmann-Vinson, A., Beebe, T.P., Chilkoti, A., 2001. Microstamping on an activated polymer surface: patterning biotin and streptavidin onto common polymeric biomaterials. *Langmuir* 17 (20), 6358–6367.
- Hyun, J., Chen, J., Setton, L.A., Chilkoti, A., 2006. Patterning cells in highly deformable microstructures: effect of plastic deformation of substrate on cellular phenotype and gene expression. *Biomaterials* 27 (8), 1444–1451.
- Inoue, S., Iida, Y., Otani, Y., Hirano, Y., Tabata, Y., 2009. Adhesion behavior of human adipo-stromal cells on self-assembled monolayers with different surface densities or gradients of RGD peptide. *J. Biomater. Sci. Polym. Ed.* 20 (4), 495–510.
- Jacobson, B.S., Ryan, U.S., 1982. Growth of endothelial and HeLa cells on a new multipurpose microcarrier that is positive, negative or collagen coated. *Tissue Cell* 14 (1), 69–83.
- Jameson, J., Loscalzo, J., 2010. *Harrison's Nephrology and Acid-Base Disorders*. McGraw-Hill Companies, Inc, New York.
- Jang, K.-J., Suh, K.-Y., 2010. A multi-layer microfluidic device for efficient culture and analysis of renal tubular cells. *Lap Chip* 10 (1), 36–42.
- Jang, K.-J., Mehr, A.P., Hamilton, G.A., McPartlin, L.A., Chung, S., Suh, K.-Y., Ingber, D.E., 2013. Human kidney proximal tubule-on-a-chip for drug transport and nephrotoxicity assessment. *Integr. Biol.* 5 (9), 1119–1129.
- Jensen, P.J., Koren, H.S., 1979. Depletion of NK by cellular immunoadsorption. *J. Immunol.* 123 (3), 1127–1132.
- Johnston, E.E., Bryers, J.D., Ratner, B.D., 2005. Plasma deposition and surface characterization of oligoglyme, dioxane, and crown ether nonfouling films. *Langmuir* 21 (3), 870–881.
- Joshi, S.D., Webb, K., 2008. Variation of cyclic strain parameters regulates development of elastic modulus in fibroblast/substrate constructs. *J. Orthop. Res.* 26 (8), 1105–1113.
- Kallrot, M., Edlund, U., Albertsson, A.C., 2006. Surface functionalization of degradable polymers by covalent grafting. *Biomaterials* 27 (9), 1788–1796.
- Kantawong, F., Burchmore, R., Gadegaard, N., Oreffo, R.O., Dalby, M.J., 2009. Proteomic analysis of human osteoprogenitor response to disordered nanotopography. *J. R. Soc. Interface* 6 (40), 1075–1086.
- Kasemo, B., Lausmaa, J., 1994. Material-tissue interfaces: the role of surface properties and processes. *Environ. Health Perspect.* 102 (Suppl. 5), 41–45.
- Kataropoulou, M., Henderson, C., Grant, M.H., 2005. Metabolic studies of hepatocytes cultured on collagen substrata modified to contain glycosaminoglycans. *Tissue Eng.* 11 (7–8), 1263–1273.
- Keselowsky, B.G., Collard, D.M., Garcia, A.J., 2003. Surface chemistry modulates fibronectin conformation and directs integrin binding and specificity to control cell adhesion. *J. Biomed. Mater. Res. A* 66 (2), 247–259.
- Khademhosseini, A., 2005. Chips to Hits: microarray and microfluidic technologies for high-throughput analysis and drug discovery. *Expert Rev. Mol. Diagn.* 5 (6), 843–846.
- Khademhosseini, A., Jon, S., Suh, K.Y., Tran, T.T., Eng, G., Yeh, J., et al., 2003. Direct patterning of protein and cell resistant polymeric monolayers and microstructures. *Adv. Mat.* 15 (23), 1995–2000.
- Khademhosseini, A., Suh, K.Y., Yang, J.M., Eng, G., Yeh, J., Levenberg, S., Langer, R., 2004. Layer-by-layer deposition of hyaluronic acid and poly-L-lysine for patterned cell co-cultures. *Biomaterials* 25 (17), 3583–3592.
- Khademhosseini, A., Langer, R., Borenstein, J., Vacanti, J.P., 2006. Microscale technologies for tissue engineering and biology. *Proc. Natl. Acad. Sci. U. S. A.* 103 (8), 2480–2487.
- Kikuchi, K., Sumaru, K., Eda, H., Oshima, Y., Sugiura, S., Takagi, T., Kanamori, T., 2009. Stepwise assembly of micropatterned co-cultures using photoresponsive culture surfaces and its application to hepatic tissue arrays. *Biotechnol. Bioeng.* 103 (3), 552–561.
- Kilinc, D., Peyrin, J.-M., Soubeyre, V., Magnifico, S., Saias, L., Viovy, J.-L., Brugg, B., 2011. Wallerian-like degeneration of central neurons after synchronized and geometrically registered mass axotomy in a three-compartmental microfluidic chip. *Neurotox. Res.* 19 (1), 149–161.

- Kim, H.J., Ingber, D.E., 2013. Gut-on-a-Chip microenvironment induces human intestinal cells to undergo villus differentiation. *Integr. Biol.* 5 (9), 1130–1140.
- Kim, D.H., Kim, P., Suh, K., Kyu Choi, S., Ho Lee, S., Kim, B., 2005. Modulation of adhesion and growth of cardiac myocytes by surface nanotopography. *Conf. Proc. IEEE Eng. Med. Biol. Soc.* 4, 4091–4094.
- Kim, H.J., Huh, D., Hamilton, G., Ingber, D.E., 2012. Human gut-on-a-chip inhabited by microbial flora that experiences intestinal peristalsis-like motions and flow. *Lab Chip* 12 (12), 2165–2174.
- Klein-Soyer, C., Hemmendinger, S., Cazenave, J.P., 1989. Culture of human vascular endothelial cells on a positively charged polystyrene surface, primaria: comparison with fibronectin-coated tissue culture grade polystyrene. *Biomaterials* 10 (2), 85–90.
- Koepsel, J.T., Murphy, W.L., 2009. Patterning discrete stem cell culture environments via localized self-assembled monolayer replacement. *Langmuir* 25 (21), 12825–12834.
- Koller, M.R., Palsson, M.A., Manchel, I., Maher, R.J., Palsson, B.O., 1998. Tissue culture surface characteristics influence the expansion of human bone marrow cells. *Biomaterials* 19 (21), 1963–1972.
- Kortsmits, J., Rutten, M., Wijlaars, M., Baaijens, F., 2009. Deformation controlled load application in heart valve tissue-engineering. *Tissue Eng. Part C Methods* 15 (4), 707–716.
- Kowalczyńska, H.M., Kaminski, J., 1991. Adhesion of L1210 cells to modified styrene copolymer surfaces in the presence of serum. *J. Cell Sci.* 99 (Pt 3), 587–593.
- Kunzler, T.P., Huwiler, C., Drobek, T., Voros, J., Spencer, N.D., 2007. Systematic study of osteoblast response to nanotopography by means of nanoparticle-density gradients. *Biomaterials* 28 (33), 5000–5006.
- Kurpinski, K., Chu, J., Hashi, C., Li, S., 2006. Anisotropic mechanosensing by mesenchymal stem cells. *Proc. Natl. Acad. Sci. U. S. A.* 103 (44), 16095–16100.
- Larson, B.J., Helgren, J.M., Manolache, S.O., Lau, A.Y., Lagally, M.G., Denes, F.S., 2005. Cold-plasma modification of oxide surfaces for covalent biomolecule attachment. *Biosens. Bioelectron.* 21 (5), 796–801.
- Lavanant, L., Pullin, B., Hubbell, J.A., Klok, H.A., 2010. A facile strategy for the modification of polyethylene substrates with non-fouling, bioactive poly(poly(ethylene glycol) methacrylate) brushes. *Macromol. Biosci.* 10 (1), 101–108.
- Lee, J.H., Jung, H.W., Kang, I.K., Lee, H.B., 1994. Cell behaviour on polymer surfaces with different functional groups. *Biomaterials* 15 (9), 705–711.
- Lee, J.H., Lee, J.W., Khang, G., Lee, H.B., 1997. Interaction of cells on chargeable functional group gradient surfaces. *Biomaterials* 18 (4), 351–358.
- Lee, S.J., Khang, G., Lee, Y.M., Lee, H.B., 2003. The effect of surface wettability on induction and growth of neurites from the PC-12 cell on a polymer surface. *J. Colloid Interface Sci.* 259 (2), 228–235.
- Li, L., Chen, S., Jiang, S., 2007. Protein interactions with oligo(ethylene glycol) (OEG) self-assembled monolayers: OEG stability, surface packing density and protein adsorption. *J. Biomater. Sci. Polym. Ed.* 18 (11), 1415–1427.
- Liliensiek, S.J., Murphy, C., Nealey, P.F., 2009. Characterization of endothelial basement membrane nanotopography in rhesus macaque as a guide for vessel tissue engineering. *Tissue Eng. Part A* 15 (9), 2643–2651.
- Lo, C.M., Wang, H.B., Dembo, M., Wang, Y.L., 2000. Cell movement is guided by the rigidity of the substrate. *Biophys. J.* 79 (1), 144–152.
- Loesberg, W.A., te Riet, J., van Delft, F.C., Schon, P., Figdor, C.G., Speller, S., et al., 2007. The threshold at which substrate nanogroove dimensions may influence fibroblast alignment and adhesion. *Biomaterials* 28 (27), 3944–3951.
- Lovmand, J., Justesen, J., Foss, M., Lauridsen, R.H., Lovmand, M., Modin, C., et al., 2009. The use of combinatorial topographical libraries for the screening of enhanced osteogenic expression and mineralization. *Biomaterials* 30 (11), 2015–2022.
- Mann, B.K., West, J.L., 2002. Cell adhesion peptides alter smooth muscle cell adhesion, proliferation, migration, and matrix protein synthesis on modified surfaces and in polymer scaffolds. *J. Biomed. Mater. Res.* 60 (1), 86–93.
- Maroudas, N.G., 1977. Sulphonated polystyrene as an optimal substratum for the adhesion and spreading of mesenchymal cells in monovalent and divalent saline solutions. *J. Cell. Physiol.* 90 (3), 511–519.
- Martinez, E., Lagunas, A., Mills, C.A., Rodriguez-Segui, S., Estevez, M., Oberhansl, S., et al., 2009. Stem cell differentiation by functionalized micro- and nanostructured surfaces. *Nanomedicine* 4 (1), 65–82.
- Massia, S.P., Hubbell, J.A., 1990a. Covalent surface immobilization of Arg-Gly-Asp- and Tyr-Ile-Gly-Ser-Arg-containing peptides to obtain well-defined cell-adhesive substrates. *Anal. Biochem.* 187 (2), 292–301.
- Massia, S.P., Hubbell, J.A., 1990b. Covalently attached GRGD on polymer surfaces promotes biospecific adhesion of mammalian cells. *Ann. N. Y. Acad. Sci.* 589, 261–270.
- Massia, S.P., Hubbell, J.A., 1991a. Human endothelial cell interactions with surface-coupled adhesion peptides on a nonadhesive glass substrate and two polymeric biomaterials. *J. Biomed. Mater. Res.* 25 (2), 223–242.
- Massia, S.P., Hubbell, J.A., 1991b. An RGD spacing of 440 nm is sufficient for integrin alpha V beta 3-mediated fibroblast spreading and 140 nm for focal contact and stress fiber formation. *J. Cell Biol.* 114 (5), 1089–1100.
- Matsuda, T., Chung, D.J., 1994. Microfabricated surface designs for cell culture and diagnosis. *ASAIO J* 40 (3), M594–M597.
- McBeath, R., Pirone, D.M., Nelson, C.M., Bhadriraju, K., Chen, C.S., 2004. Cell shape, cytoskeletal tension, and RhoA regulate stem cell lineage commitment. *Dev. Cell* 6 (4), 483–495.
- McCartney, M.D., Buck, R.C., 1981. Comparison of the degree of contact guidance between tumor cells and normal cells in vitro. *Cancer Res.* 41 (8), 3046–3051.
- Meredith, D.O., Riehle, M.O., Curtis, A.S., Richards, R.G., 2007. Is surface chemical composition important for orthopaedic implant materials? *J. Mater. Sci. Mater. Med.* 18 (2), 405–413.
- Mi, L., Bernards, M.T., Cheng, G., Yu, Q., Jiang, S., 2010. pH responsive properties of non-fouling mixed-charge polymer brushes based on quaternary amine and carboxylic acid monomers. *Biomaterials* 31 (10), 2919–2925.
- Monchaux, E., Vermette, P., 2007. Bioactive microarrays immobilized on low-fouling surfaces to study specific endothelial cell adhesion. *Biomacromolecules* 8 (11), 3668–3673.
- Mrksich, M., Whitesides, G.M., 1996. Using self-assembled monolayers to understand the interactions of man-made surfaces with proteins and cells. *Annu. Rev. Biophys. Biomol. Struct.* 25, 55–78.
- Muller, R., Ruhl, S., Hiller, K.A., Schmalz, G., Schweikl, H., 2008. Adhesion of eukaryotic cells and *Staphylococcus aureus* to silicon model surfaces. *J. Biomed. Mater. Res. A* 84 (3), 817–827.
- Nakamura, H.K., Butz, F., Saruwatari, L., Ogawa, T., 2007. A role for proteoglycans in mineralized tissue-titanium adhesion. *J. Dent. Res.* 86 (2), 147–152.

- Nakayama, Y., Matsuda, T., Irie, M., 1993. A novel surface photo-graft polymerization method for fabricated devices. *ASAIO J* 39 (3), M542–M544.
- Nandkumar, M.A., Yamato, M., Kushida, A., Konno, C., Hirose, M., Kikuchi, A., Okano, T., 2002. Two-dimensional cell sheet manipulation of heterotypically co-cultured lung cells utilizing temperature-responsive culture dishes results in long-term maintenance of differentiated epithelial cell functions. *Biomaterials* 23 (4), 1121–1130.
- Nge, P.N., Rogers, C.L., Woolley, A.T., 2013. Advances in microfluidic materials, functions, integration, and applications. *Chem. Rev.* 113 (4), 2550–2583.
- Niles, W.D., Coassin, P.J., 2005. Piezo- and solenoid valve-based liquid dispensing for miniaturized assays. *Assay Drug Dev. Technol.* 3 (2), 189–202.
- O'Neill, C., Jordan, P., Riddle, P., Ireland, G., 1990. Narrow linear strips of adhesive substratum are powerful inducers of both growth and total focal contact area. *J. Cell Sci.* 95 (Pt 4), 577–586.
- Oh, S., Brammer, K.S., Li, Y.S., Teng, D., Engler, A.J., Chien, S., Jin, S., 2009. Stem cell fate dictated solely by altered nanotube dimension. *Proc. Natl. Acad. Sci. U. S. A.* 106 (7), 2130–2135.
- Opas, M., 1994. Substratum mechanics and cell differentiation. *Int. Rev. Cytol.* 150, 119–137.
- Ostuni, E., Kane, R., Chen, C.S., Ingber, D.E., Whitesides, G.M., 2000. Patterning mammalian cells using elastomeric membranes. *Langmuir* 16 (20), 7811–7819.
- Park, J., Bauer, S., von der Mark, K., Schmuki, P., 2007. Nanosize and vitality: TiO₂ nanotube diameter directs cell fate. *Nano Lett.* 7 (6), 1686–1691.
- Pelham Jr., R.J., Wang, Y., 1997. Cell locomotion and focal adhesions are regulated by substrate flexibility. *Proc. Natl. Acad. Sci. U. S. A.* 94 (25), 13661–13665.
- Peter, X., Ma, J.H.E., 2006. *Scaffolding in Tissue Engineering*. CRC Press.
- Petrie, T.A., Raynor, J.E., Reyes, C.D., Burns, K.L., Collard, D.M., Garcia, A.J., 2008. The effect of integrin-specific bioactive coatings on tissue healing and implant osseointegration. *Biomaterials* 29 (19), 2849–2857.
- Prasad, K.N., Carvalho, E., Kentroti, S., Edwards-Prasad, J., Freed, C., Vernadakis, A., 1994. Establishment and characterization of immortalized clonal cell lines from fetal rat mesencephalic tissue. *In Vitro Cell. Dev. Biol. Anim.* 30A (9), 596–603.
- Preiss-Bloom, O., Mizrahi, J., Elisseff, J., Seliktar, D., 2009. Real-time monitoring of force response measured in mechanically stimulated tissue-engineered cartilage. *Artif. Organs* 33 (4), 318–327.
- Prime, K., Whitesides, G., 1991. Self-assembled organic monolayers: model systems for studying adsorption of proteins at surfaces. *Science* 252 (5009), 1164–1167.
- Priori, E.S., Wilbur, J.R., Allen, P.T., East, J.L., Dmochowski, L., 1975. Transformation of cells in human bone tumor cultures. *Bibl. Haematol.* 40, 185–196.
- Rhee, S.W., Taylor, A.M., Tu, C.H., Cribbs, D.H., Cotman, C.W., Jeon, N.L., 2005. Patterned cell culture inside microfluidic devices. *Lab Chip* 5 (1), 102–107.
- Riboh, J., Chong, A.K., Pham, H., Longaker, M., Jacobs, C., Chang, J., 2008. Optimization of flexor tendon tissue engineering with a cyclic strain bioreactor. *J. Hand Surg. [Am]* 33 (8), 1388–1396.
- Riches, A., Peddie, C., Rendell, S., Bryant, P., Zitzelsberger, H., Bruch, J., et al., 2001. Neoplastic transformation and cytogenetic changes after Gamma irradiation of human epithelial cells expressing telomerase. *Radiat. Res.* 155 (1 Pt 2), 222–229.
- Rodionova, N.V., Oganov, V.S., 2003. Changes of cell-vascular complex in zones of adaptive remodeling of the bone tissue under microgravity conditions. *Adv. Space Res.* 32 (8), 1477–1481.
- Roth, J., Albrecht, V., Nitschke, M., Bellmann, C., Simon, F., Zschoche, S., et al., 2008. Surface functionalization of silicone rubber for permanent adhesion improvement. *Langmuir* 24 (21), 12603–12611.
- Saha, K., Keung, A.J., Irwin, E.F., Li, Y., Little, L., Schaffer, D.V., Healy, K.E., 2008. Substrate modulus directs neural stem cell behavior. *Biophys. J.* 95 (9), 4426–4438.
- Scherer, W.F., Syverton, J.T., Gey, G.O., 1953. Studies on the propagation in vitro of poliomyelitis viruses. IV. Viral multiplication in a stable strain of human malignant epithelial cells (strain HeLa) derived from an epidermoid carcinoma of the cervix. *J. Exp. Med.* 97 (5), 695–710.
- Sciancalepore, A.G., Sallustio, F., Girardo, S., Gioia Passione, L., Camposeo, A., Mele, E., et al., 2014. A Bioartificial renal tubule device embedding human renal stem/progenitor cells. *PLoS One* 9 (1), e87496.
- Shen, M., Horbett, T.A., 2001. The effects of surface chemistry and adsorbed proteins on monocyte/macrophage adhesion to chemically modified polystyrene surfaces. *J. Biomed. Mater. Res.* 57 (3), 336–345.
- Shen, J., Li, Y., Zuo, Y., Zou, Q., Li, J., Huang, D., Wang, X., 2009. Characterization and cytocompatibility of surface modified polyamide66. *J. Biomed. Mater. Res. B Appl. Biomater.* 91 (2), 897–904.
- Shin, S.R., Kilic, T., Zhang, Y.S., Avci, H., Hu, N., Kim, D., et al., 2017. Label-free and regenerative electrochemical microfluidic biosensors for continual monitoring of cell secretomes. *Adv. Sci. (Weinh.)* 4 (5), 1600522.
- Sipehia, R., Chawla, A.S., Daka, J., Chang, T.M., 1988. Immobilization of enzymes on polypropylene bead surfaces by anhydrous ammonia gaseous plasma technique. *J. Biomed. Mater. Res.* 22 (5), 417–422.
- Sosale, G., Hacking, S.A., Srikar, V., 2008. Topography analysis of grit-blasted and grit-blasted-acid-etched titanium implant surfaces using multi-scale measurements and multi-parameter statistics. *J. Mater. Res.* 23 (10), 2704–2713.
- Staat, W.D., Fok, K.F., Zutter, M.M., Adams, S.P., Rodriguez, B.A., Santoro, S.A., 1991. Identification of a tetrapeptide recognition sequence for the alpha 2 beta 1 integrin in collagen. *J. Biol. Chem.* 266 (12), 7363–7367.
- Steele, J.G., Dalton, B.A., Underwood, P.A., Smith, G.J., 1991. Differences in adhesion to tissue culture plastic of clonally related transformed and control sublines from an epithelial cell strain. *J. Cell Sci.* 100 (Pt 1), 195–203.
- Steele, J.G., Dalton, B.A., Johnson, G., Underwood, P.A., 1993. Polystyrene chemistry affects vitronectin activity: an explanation for cell attachment to tissue culture polystyrene but not to unmodified polystyrene. *J. Biomed. Mater. Res.* 27 (7), 927–940.
- Strobl, C.J., von Guttenberg, Z., Wixforth, A., 2004. Nano- and pico-dispensing of fluids on planar substrates using SAW. *IEEE Trans. Ultrason. Ferroelectr. Freq. Control* 51 (11), 1432–1436.
- Takayama, S., McDonald, J.C., Ostuni, E., Liang, M.N., Kenis, P.J.A., Ismagilov, R.F., Whitesides, G.M., 1999. Patterning cells and their environments using multiple laminar fluid flows in capillary networks. *Proc. Natl. Acad. Sci. U. S. A.* 96 (10), 5545–5548.
- Takayama, S., Ostuni, E., LeDuc, P., Naruse, K., Ingber, D.E., Whitesides, G.M., 2001. Subcellular positioning of small molecules. *Nature* 411 (6841), 1016.
- Tan, J., Saltzman, W.M., 2002. Topographical control of human neutrophil motility on micropatterned materials with various surface chemistry. *Biomaterials* 23 (15), 3215–3225.

- Tashiro, K., Sephel, G.C., Weeks, B., Sasaki, M., Martin, G.R., Kleinman, H.K., Yamada, Y., 1989. A synthetic peptide containing the IKVAV sequence from the A chain of laminin mediates cell attachment, migration, and neurite outgrowth. *J. Biol. Chem.* 264 (27), 16174–16182.
- Teixeira, A.I., McKie, G.A., Foley, J.D., Bertics, P.J., Nealey, P.F., Murphy, C.J., 2006. The effect of environmental factors on the response of human corneal epithelial cells to nanoscale substrate topography. *Biomaterials* 27 (21), 3945–3954.
- Timpe, L., Martz, E., Steinberg, M.S., 1978. Cell movements in a confluent monolayer are not caused by gaps: evidence for direct contact inhibition of overlapping. *J. Cell Sci.* 30, 293–304.
- Tobasnick, G., Curtis, A.S., 2001. Chloride channels and the reactions of cells to topography. *Eur. Cells Mater.* 2, 49–61.
- Toyoda, T., Matsumoto, H., Fujikawa, K., Saito, S., Inoue, K., 1998. Tensile load and the metabolism of anterior cruciate ligament cells. *Clin. Orthop. Relat. Res.* 353, 247–255.
- van Griensven, M., Diederichs, S., Roeker, S., Boehm, S., Peterbauer, A., Wolbank, S., et al., 2009. Mechanical strain using 2D and 3D bioreactors induces osteogenesis: implications for bone tissue engineering. *Adv. Biochem. Eng. Biotechnol.* 112, 95–123.
- Weber, L.M., Anseth, K.S., 2008. Hydrogel encapsulation environments functionalized with extracellular matrix interactions increase islet insulin secretion. *Matrix Biol.* 27 (8), 667–673.
- Weber, L.M., Hayda, K.N., Haskins, K., Anseth, K.S., 2007. The effects of cell-matrix interactions on encapsulated beta-cell function within hydrogels functionalized with matrix-derived adhesive peptides. *Biomaterials* 28 (19), 3004–3011.
- Welle, A., Gottwald, E., Weibezahn, K.F., 2002. Patterned polymer surfaces for cell culture applications. *Biomed. Tech.* 47 (Suppl. 1 Pt 1), 401–403.
- Whitesides, G.M., 2006. The origins and the future of microfluidics. *Nature* 442, 368.
- Wipff, P.J., Majd, H., Acharya, C., Buscemi, L., Meister, J.J., Hinz, B., 2009. The covalent attachment of adhesion molecules to silicone membranes for cell stretching applications. *Biomaterials* 30 (9), 1781–1789.
- Wittelsberger, S.C., Kleene, K., Penman, S., 1981. Progressive loss of shape-responsive metabolic controls in cells with increasingly transformed phenotype. *Cell* 24 (3), 859–866.
- Wojciak-Stothard, B., Curtis, A.S., Monaghan, W., McGrath, M., Sommer, I., Wilkinson, C.D., 1995. Role of the cytoskeleton in the reaction of fibroblasts to multiple grooved substrata. *Cell Motil. Cytoskelet.* 31 (2), 147–158.
- Wong, J.Y., Velasco, A., Rajagopalan, P., Pham, Q., 2003. Directed movement of vascular smooth muscle cells on gradient-compliant hydrogels. *Langmuir* 19 (5), 1908–1913.
- Wood, A., 1988. Contact guidance on microfabricated substrata: the response of teleost fin mesenchyme cells to repeating topographical patterns. *J. Cell Sci.* 90 (Pt 4), 667–681.
- Wu, J.C., Merlino, G., Fausto, N., 1994. Establishment and characterization of differentiated, nontransformed hepatocyte cell lines derived from mice transgenic for transforming growth factor alpha. *Proc. Natl. Acad. Sci. U. S. A.* 91 (2), 674–678.
- Yasuda, T., Kanamori, M., Nogami, S., Hori, T., Oya, T., Suzuki, K., Kimura, T., 2009. Establishment of a new human osteosarcoma cell line, UTOS-1: cytogenetic characterization by array comparative genomic hybridization. *J. Exp. Clin. Cancer Res.* 28 (1), 26.
- Yoshii, F., Kaetsu, I., 1983. Cell culture on polymers prepared by radiation-induced grafting of various monomers. *Appl. Biochem. Biotechnol.* 8 (6), 505–513.
- Yu, J., Jin, F., Deng, Z., Li, Y., Tang, L., Shi, J., Jin, Y., 2008. Epithelial-mesenchymal cell ratios can determine the crown morphogenesis of dental pulp stem cells. *Stem Cells Dev.* 17 (3), 475–482.
- Yue, K., Trujillo de Santiago, G., Alvarez, M., Tamayol, A., Annabi, N., Khademhosseini, A., 2015. Synthesis, properties, and biomedical applications of gelatin methacryloyl (GelMA) hydrogels. *Biomaterials* 73, 254–271.
- Zemljic Jokhadar, S., Znidarcic, T., Svetina, S., Batista, U., 2007. The effect of substrate and adsorbed proteins on adhesion, growth and shape of CaCo-2 cells. *Cell Biol. Int.* 31 (10), 1097–1108.
- Zhang, Y.S., Aleman, J., Shin, S.R., Kilic, T., Kim, D., Mousavi Shaegh, S.A., et al., 2017. Multisensor-integrated organs-on-chips platform for automated and continual in situ monitoring of organoid behaviors. *Proc. Natl. Acad. Sci. U. S. A.* 114 (12), E2293–E2302.
- Zheng, F., Fu, F., Cheng, Y., Wang, C., Zhao, Y., Gu, Z., 2016. Organ-on-a-Chip systems: Microengineering to biomimic living systems. *Small* 12 (17), 2253–2282.
- Zhu, Y., Gao, C., Guan, J., Shen, J., 2004. Promoting the cytocompatibility of polyurethane scaffolds via surface photo-grafting polymerization of acrylamide. *J. Mater. Sci. Mater. Med.* 15 (3), 283–289.

2.1.4

Functional Tissue Architecture, Homeostasis, and Responses to Injury

RICHARD N. MITCHELL, FREDERICK J. SCHOEN

Department of Pathology/Brigham and Women's Hospital and Harvard Medical School, Boston, MA, United States

It is reasonable to ask why a chapter that covers concepts of tissue anatomy, physiology, and pathophysiology should be included in a book on biomaterials science. In the current era of sophisticated biomaterials development, there are at least three key reasons that merit emphasis:

1. The safety and effectiveness of biomaterials will be enhanced by design and testing informed by a deep understanding of the architecture, function, and dysfunction of the tissue ecosystem into which they are placed.
2. The surgical or other interventional procedure by which biomaterials are implanted into the body disrupt and induce some injury and associated physiological responses in the surrounding tissues. Consequently, inflammation and healing are superimposed on and may significantly influence biomaterials–tissue interactions.
3. Optimal development of increasingly interactive, regenerative and tissue-engineered biomaterials demands a knowledge of both functional tissue organization and how cell phenotypes and tissue adaptation and remodeling processes are controlled by their mechanical and biochemical environment.

Tissue Constituents, Organization, and Integration

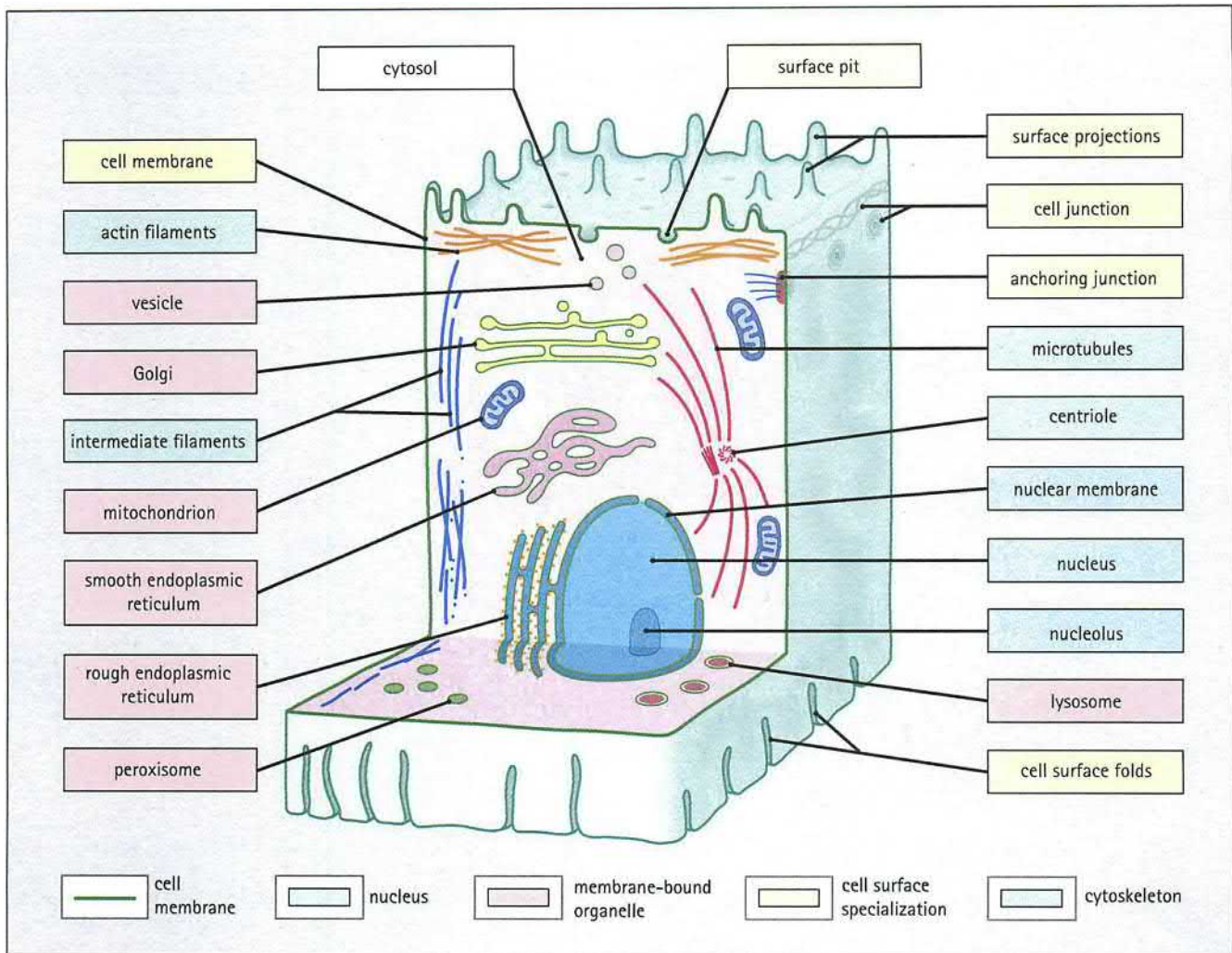
A major goal in this first section is to describe how *biological structure is adapted to perform physiologic function*. This general and overarching concept extends from cells (and their *subcellular* constituents) to the organization of tissues and organs. Beginning with the smallest subunits of cellular organization we will build to progressively more complex systems. We also provide an introduction to the physiologic responses to environmental stimuli, and the mechanisms of and responses to cell injury and tissue–biomaterials interactions. For additional detail, see [Lodish et al. \(2016\)](#).

The Essential Role of Cells

Cells constitute the basic structural building blocks of all living matter. Each cell is a structurally highly ordered and functionally integrated assembly of signal transduction molecules, enzymes, cytoskeletal proteins, and organelles—all of which are discrete, specialized structures within a cell. Virtually all cells share the same core functional attributes, including nutrient uptake, metabolism, waste removal, organelle turnover, and proliferation ([Fig. 2.1.4.1](#)).

Except for the circulating blood elements, cells are joined via cell–cell junctions to form *tissues* that comprise a handful of general types: *epithelium*, *connective tissue*, *muscle*, and *nerve*. *Hematopoietic and lymphoid tissues*—responsible for generating erythrocytes, granulocytes, monocytes, platelets, and lymphocytes—also exhibit similar features as they proliferate and differentiate into their final circulating progeny. *Organs* are assembled from the basic tissue types and are “glued” together within an *extracellular matrix* (ECM) composed of myriad proteins, glycoproteins, *mucopolysaccharides* (sugar polymers), and *proteoglycans* (polymeric sugars attached to a protein core) synthesized by the individual cells. For information on the specific constituents of the ECM, [Chapter 2.1.5](#). Organs are self-contained collections of several different types of tissues arranged into a functional unit with a specific vital function (e.g., the heart, liver, or a joint). Collectively, the organs—often grouped in physiologic systems (exemplified by the cardiovascular and respiratory systems, the gastrointestinal tract, the bones and joints, and the internal and external genitalia)—perform the various functions required by the intact living organism, including circulation, respiration, digestion, excretion, movement, and reproduction, respectively.

The basic functional attributes of cells include protection, signaling, nutrient absorption and assimilation, energy generation, macromolecule synthesis, growth, and reproduction. Without these basic activities, cells cannot live. However, most cells also exhibit specialization—that is, they have additional capabilities, such as irritability, conductivity, contraction, absorption, or



• **Figure 2.1.4.1** General schematic of a typical mammalian cell, demonstrating the overall organization and major organelles. (James, S.L., Peter, G.A., 2015. Stevens & Lowe's Human Histology, fourth ed.)

secretion of molecules. *Multicellular organisms are thus composed of individual cells with marked specialization of structure and function.* Differentiated cells allow a division of labor in the performance and coordination of complex functions carried out in architecturally distinct and organized tissues. It is also important to note that cells are not only the fundamental building blocks of the body, but that injury at the cellular level is the underlying basis of virtually all disease (see Rubin et al., 2014; Kumar et al., 2015).

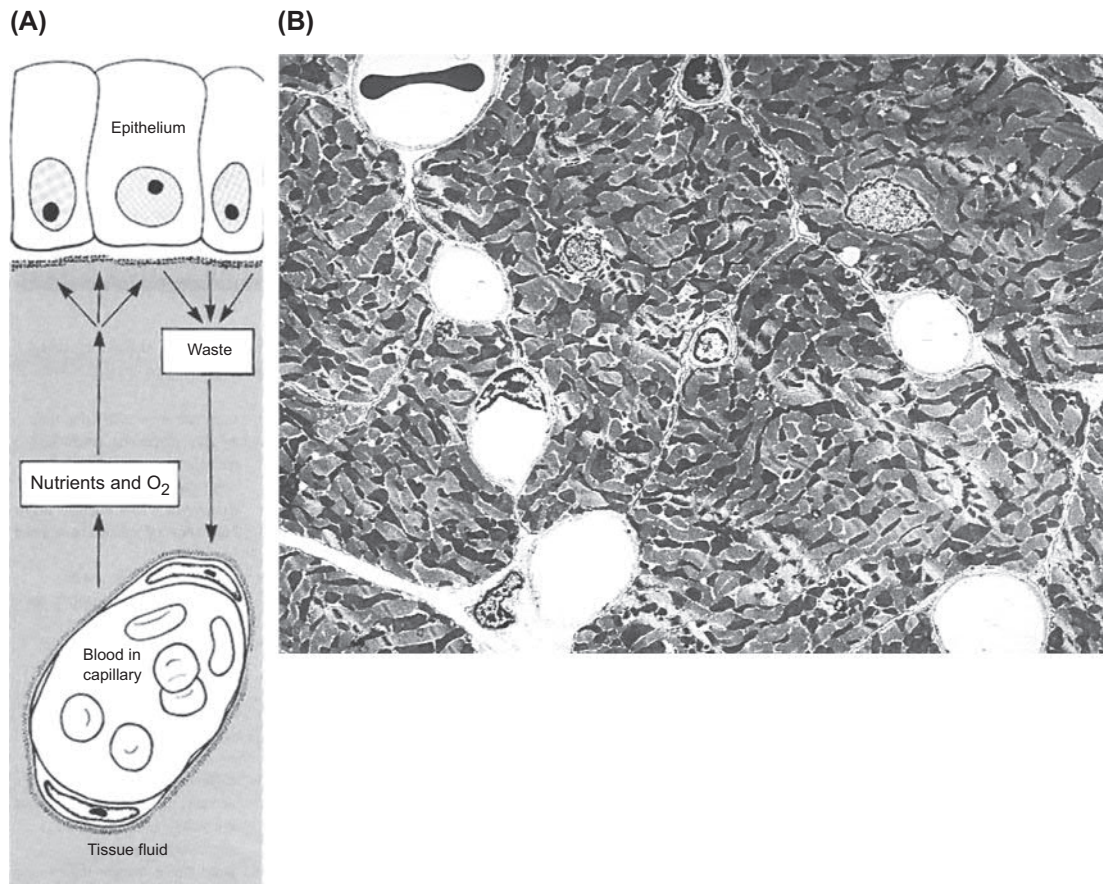
Parenchyma and Stroma

Organs are broadly organized into *parenchyma*—the cells that provide the specific function of a tissue (e.g., neurons in the brain, cardiac myocytes in the heart, hepatocytes in the liver, etc.), and the *stroma* (also called *mesenchyma*)—the surrounding support tissues. Stroma can be conceptualized as the maintenance core or infrastructure (support members, plumbing, electrical, communications, etc.) in a large building—while the parenchyma can be thought of as the specialized office

or living space. Like the structural support of a building, the stroma will also provide the framework for tissue reconstruction in the event of damage. Stroma in tissues characteristically includes the blood vessel vascular supply, as well as nerves, supportive fat (*adipose tissue*), and fibrous connective tissue (*including ECM*) synthesized by adipocytes and fibroblasts, respectively.

Vascular Supply: Tissue Perfusion

To maintain baseline cellular function (through ATP synthesis), as well as sustain the ongoing turnover of sub-cellular structures, cells require a continuous supply of oxygen and nutrients; in the setting of *increased demand* (e.g., exercise or increased cell proliferation), baseline oxygen consumption can increase 10- to 20-fold. In addition, metabolic by-products (e.g., CO_2) must be constantly removed to prevent tissue acidosis. Consequently, most tissues have a dense arborizing network of blood vessels (*vasculature*) to deliver oxygenated nutrient-rich arterial



• **Figure 2.1.4.2** Role of the vasculature in tissue function. (A) Schematic of the route by which cells in a tissue obtain nutrition and oxygenation by diffusion from underlying capillaries. Metabolic waste products diffuse in the reverse direction and are removed into the circulation. In each case, diffusion occurs through the fluid that permeates the extracellular matrix. (B) Myocardium, a highly metabolically active tissue, has a rich capillary network, as demonstrated by transmission electron microscopy. The six open round spaces are capillaries, with a red blood cell seen on cross-section in the capillary in the upper left corner. ((A) Reproduced by permission from Cormack, D.H., 1987. *Ham's Histology*, ninth ed. Lippincott, Philadelphia, PA.)

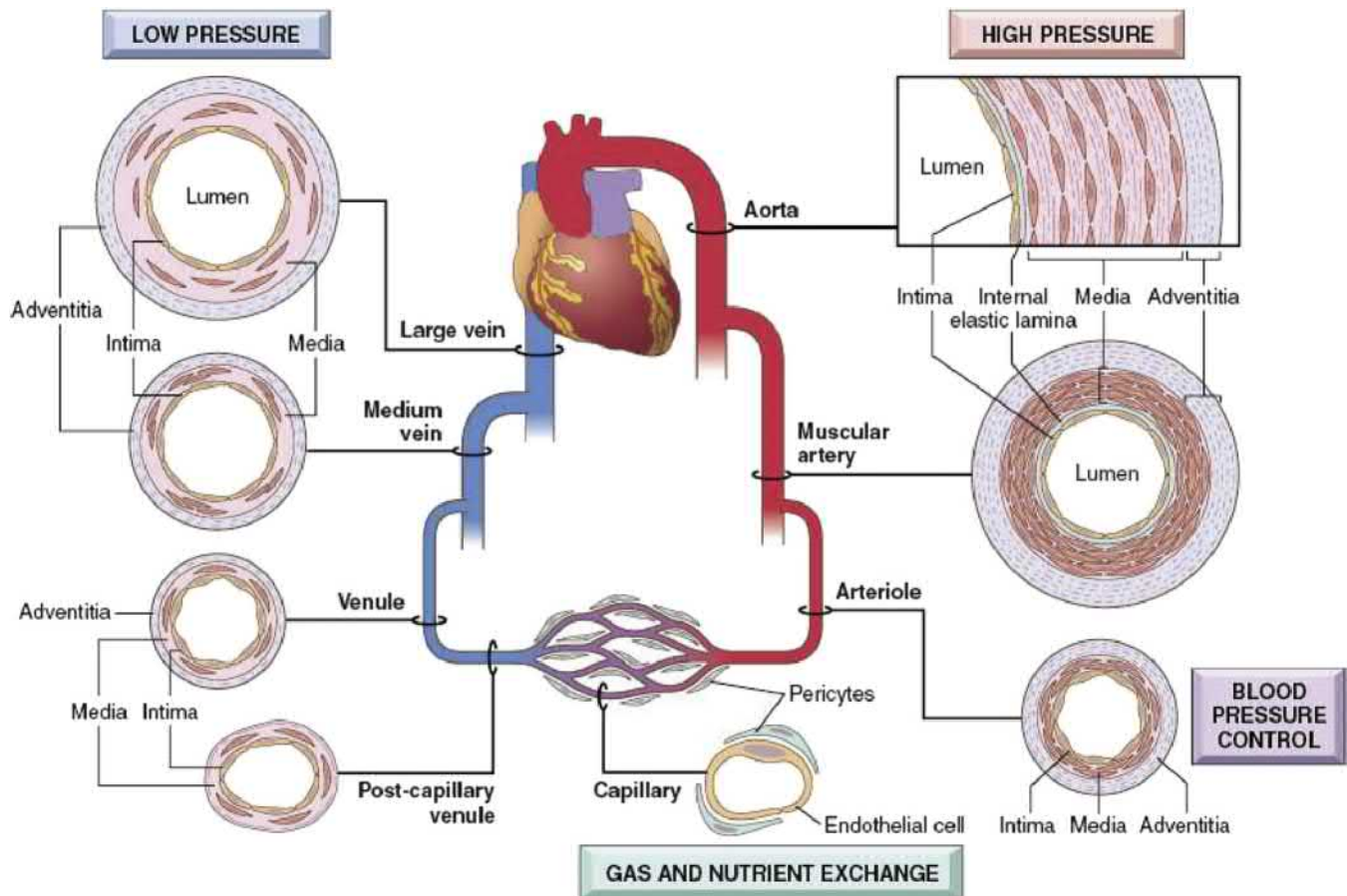
blood and remove depleted venous blood (Fig. 2.1.4.2). In virtually all tissues there is also a parallel series of *lymphatics*, responsible for draining excess water and electrolytes (as well as inflammatory cells) that have accumulated in the extravascular spaces.

Perfusion of (i.e., delivery of blood to) a tissue or an organ is accomplished through the cardiovascular system, composed of a pump (the *heart*) and a closed loop of distributing and collecting tubes in series: *arteries* → *arterioles* → *capillaries* → *venules* → *veins* (Fig. 2.1.4.3). The extensive system of thin-walled *capillaries* ultimately permits the efficient and rapid exchange of substances between the blood and the tissues. Since blood exits the heart at high pressure, the proximal vasculature (arteries and arterioles) must buffer pulsatile flow to ensure steady low-pressure flow within the capillaries. On the venous side, distensibility of the vasculature provides a high capacitance storage of excess volume. Other functions of the circulation include regulation of body temperature and the distribution of various regulating substances (e.g., hormones, inflammatory mediators, growth factors). Most of the time, the vasculature must maintain blood in a liquid

form; however, when vessels are injured, the vessel walls contribute to *hemostasis*—that is, preventing severe hemorrhage by a coordinated response of vasoconstriction, plugging vascular defects by platelet clumps, and activating the coagulation cascade. Moreover, the circulatory system distributes inflammatory cells to their sites of action. The regulation of coagulation, vascular pressure, and the egress of inflammatory cells and mediators is accomplished through the function of *endothelial cells* that line the entire cardiovascular system and interface with the circulating blood elements.

Extracellular Matrix (See also Chapter 2.1.5)

ECM comprises the biological material produced by, residing in between, and supporting cells; it is synthesized, remodeled, and otherwise maintained by the cells associated with the ECM. ECM, stromal, and parenchymal cells, capillaries and nerves are physically and functionally integrated in tissues and organs (Fig. 2.1.4.4). The ECM provides physical support and a matrix to which cells can adhere, signal each other, and interact. However, the ECM is more



• **Figure 2.1.4.3** Regional structural variations in the cardiovascular system. Although the basic organization of vessels is constant, the thickness and composition of the various layers differ as a functional response to varying hemodynamic forces and tissue metabolic requirements. (Reproduced by permission from Mitchell, R.N., Schoen, F.J., 2010. Blood Vessels. In: Kumar, V., Abbas, A.K., Fausto, N., Aster, J.C. (Eds.), Robbins and Cotran Pathologic Basis of Disease, eighth ed. Saunders, Philadelphia, PA.)

than a scaffold that maintains tissue and organ structure. Indeed, the ECM regulates many aspects of cell behavior:

- mechanical support for cell anchorage;
- determination of cell orientation (cell polarity, e.g., what is up and down);
- control of cell growth;
- cell differentiation;
- scaffolding for orderly tissue renewal;
- establishment of tissue microenvironments;
- sequestration, storage, and presentation of soluble regulatory molecules.

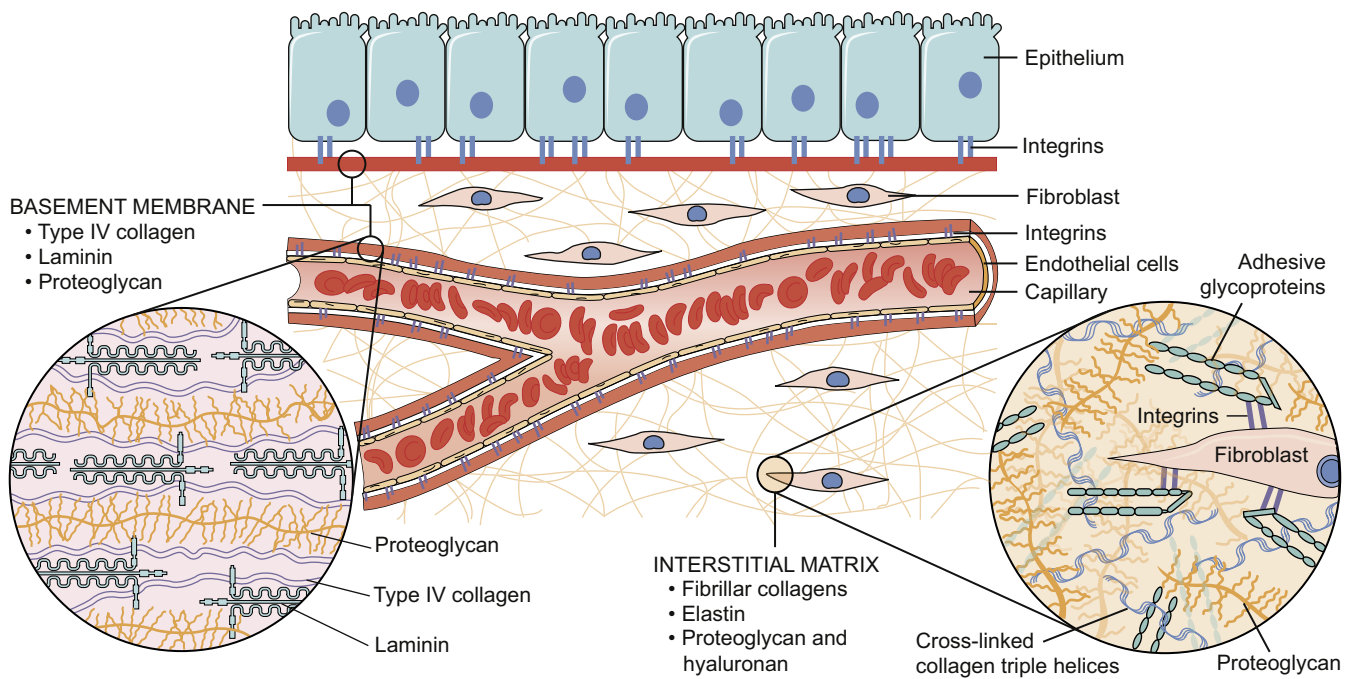
Some ECMs are also specialized for a particular function, such as strength (tendon), filtration (the basement membranes in the kidney glomerulus), or adhesion (basement membranes supporting most epithelia). To produce additional mechanical strength in bones and teeth, the ECM is calcified. Even in a tissue as “simple” as a heart valve leaflet, the coordinated interplay of several ECM components and the spatial and temporal dynamics of ECM interactions are critical to function. Importantly, the scaffolds used in tissue-engineering applications are intended to replicate the several functions of natural ECM.

ECM components are synthesized, secreted, and remodeled by cells in response to environmental cues. Virtually all cells secrete and degrade ECM to some extent (see later). Certain cell types (e.g., fibroblasts and smooth muscle cells) are particularly active in the production of interstitial ECM (i.e., the ECM between cells). Epithelial cells also synthesize the ECM of their basement membranes (Fig. 2.1.4.4).

The mechanical forces that cells experience from their surroundings markedly influence cellular phenotypes, including cell shape, orientation, and differentiated function; this occurs through the interaction of cell surface receptors (Kumar et al, 2017; Mammoto et al, 2013) (such as *integrins*) with ECM molecules (Fig. 2.1.4.5). The resultant changes in cytoskeletal organization and in the production of second messengers can modify gene expression (Fig. 2.1.4.6).

Organ Structure

Organs have a composite structure with epithelial, lymphoid or other specialized tissues, called *parenchyma*, performing specific functions of the organ, while *stroma* consists of connective tissue and blood vessels that provide support and nourishment



• **Figure 2.1.4.4** Main components of the extracellular matrix (ECM), including collagen, proteoglycans, and adhesive glycoproteins. Both epithelial cells and fibroblasts interact with ECM via integrins. Basement membranes and interstitial ECM have differing architecture and general composition, although there is some overlap between them. Some ECM components (e.g., elastin) are not included for the sake of simplification. (Reproduced by permission from Kumar, V., Abbas, A.K., Fausto, N., Aster, J.C., 2010. Robbins and Cotran Pathologic Basis of Disease, eighth ed. Saunders, Philadelphia, PA.)

to the specialized tissues (Figs. 2.1.4.7 and 2.1.4.8). Although parenchymal cells are generally more sensitive to chemical, physical, or ischemic (i.e., low blood flow) injury than is stroma, when an organ is injured, orderly repair and regrowth of parenchymal cells requires an intact underlying stroma.

There are two basic organ patterns: tubular (or hollow) and compact (or solid) organs. Tubular organs include the blood vessels and the digestive, urinary-genital, and respiratory tracts; they have similar architectures in that each is composed of layers of tissue arranged in a specific sequence. Each has an inner coat consisting of a lining of epithelium, a middle coat consisting of layers of muscle (usually smooth muscle) and connective tissue, and an external coat consisting of connective tissue typically covered by epithelium. Compact, solid organs (e.g., liver, lymph node or spleen) have an extensive connective tissue framework, surrounded by a dense, connective tissue capsule.

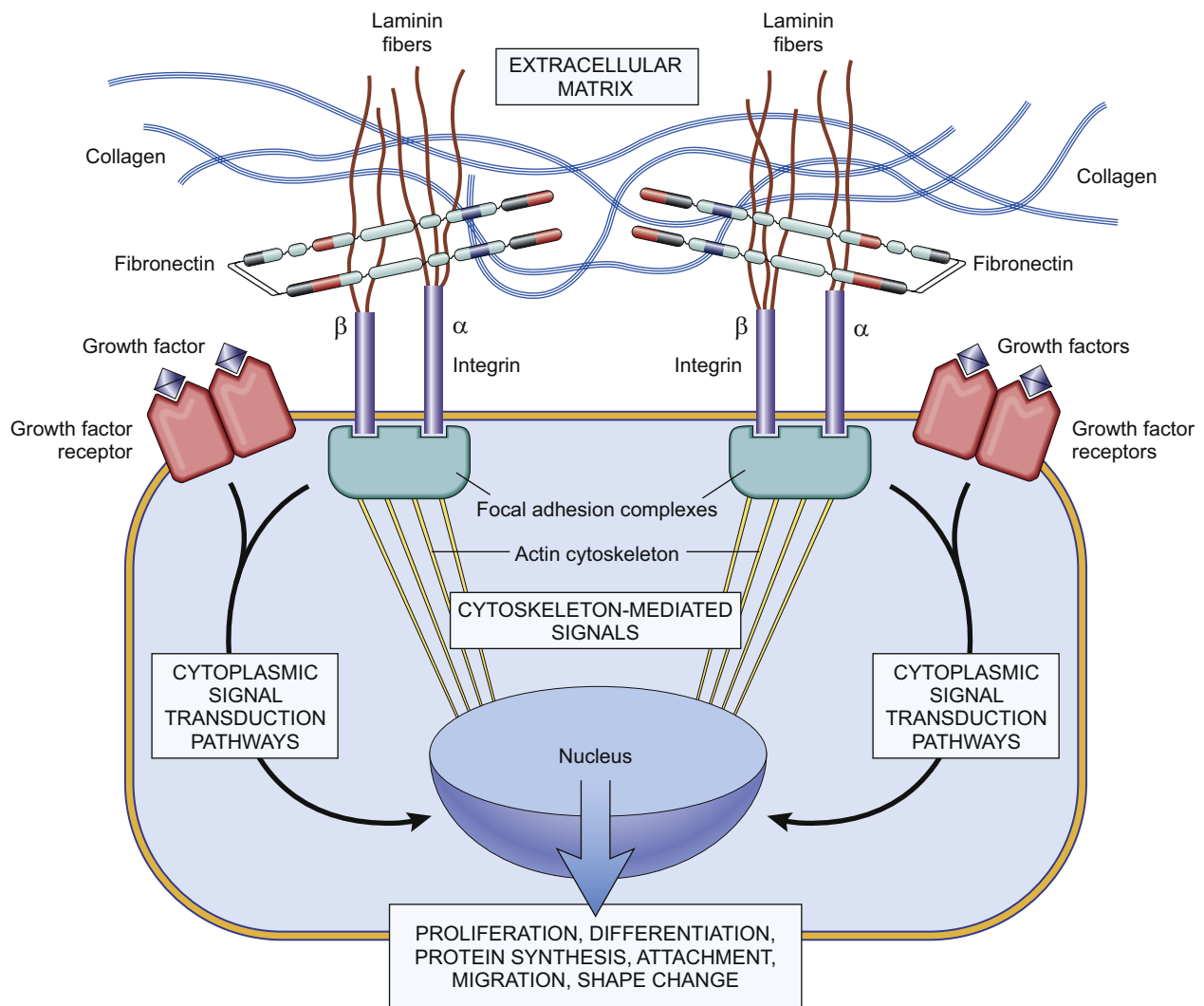
Blood vessels are also *organs*. Blood vessels have three layers: an *intima* (the *endothelium*, which is an epithelium), a *media* (primarily smooth muscle and elastin), and an *adventitia* on the outside (primarily collagen). The amounts and relative proportions of layers of the blood vessels are influenced by mechanical factors (especially blood pressure, which determines the amount and arrangement of muscular tissue), and metabolic factors (reflecting the local nutritional needs of the tissues). The histologic composition and organization as well as the thickness of these three layers varies characteristically with the specific physiologic functions performed by the different segments of the cardiovascular system (Fig. 2.1.4.3).

The blood supply of an organ comes from its outer aspect (Figs. 2.1.4.7 and 2.1.4.8). Compact organs have a hilus or area of thicker connective tissue where blood vessels and other conduits enter the organ. In tubular organs, large vessels penetrate the outer coat, perpendicular to it, and give off branches that run parallel to the tissue layers. These vessels divide yet again to give off penetrating branches that course through the muscular layer, and branch again in the connective tissue parallel to the layers. The small blood vessels have junctions (*anastomoses*) with one another in the connective tissue. These junctions may provide *collateral* pathways that can allow blood to bypass obstructions.

Cell and Tissue Differentiation, Phenotype, and Maintenance

Structure–Function Correlation

As cells differentiate, they become increasingly specialized, and develop well-defined structural and functional characteristics. For example, striated muscle cells have well-organized actin and myosin filaments that slide over one another, facilitating cellular contraction. Gastric (stomach) epithelial cells have large numbers of mitochondria to generate the ATP necessary to pump hydrogen ions out of the cell against a concentration gradient and acidify the stomach contents. Skin keratinocytes function as a protective barrier by undergoing autophagic programmed cell death and becoming scale-like structures composed of durable, nonliving keratin (an intermediate filament). Specialized phagocytic cells of the immune system detect infectious



• **Figure 2.1.4.5** Soluble and mechanotransduction pathways by which a variety of cell behaviors, e.g., proliferation, differentiation, protein synthesis, locomotion, or shape change, can be modified. Note that soluble mediators can act through plasma membrane receptors (or intracellular receptors, not shown) to affect changes in nuclear transcription. Extrinsic mechanical forces can also impact cellular phenotypes through protein–protein interactions linking ECM proteins (e.g., fibronectin and laminin) with cell surface integrins that are in turn connected to the nucleus through cytoskeletal elements such as actin microfilaments. Integrins are important components of *focal adhesion complexes*, which can provide secondary signaling (e.g., by driving protein phosphorylation) when external mechanical forces are applied to proteins connected to them. *EGF*, Epidermal growth factor; *IL-1/TNF*, interleukin-1/tumor necrosis factor; *PDGF*, platelet-derived growth factor; *TGF-β*, transforming growth factor-β; *TIMPs*, tissue inhibitors of metalloproteinases. (Reproduced by permission from Kumar, V., Abbas, A.K., Fausto, N., Aster, J.C., 2010. Robbins and Cotran Pathologic Basis of Disease, eighth ed. Saunders, Philadelphia, PA.)

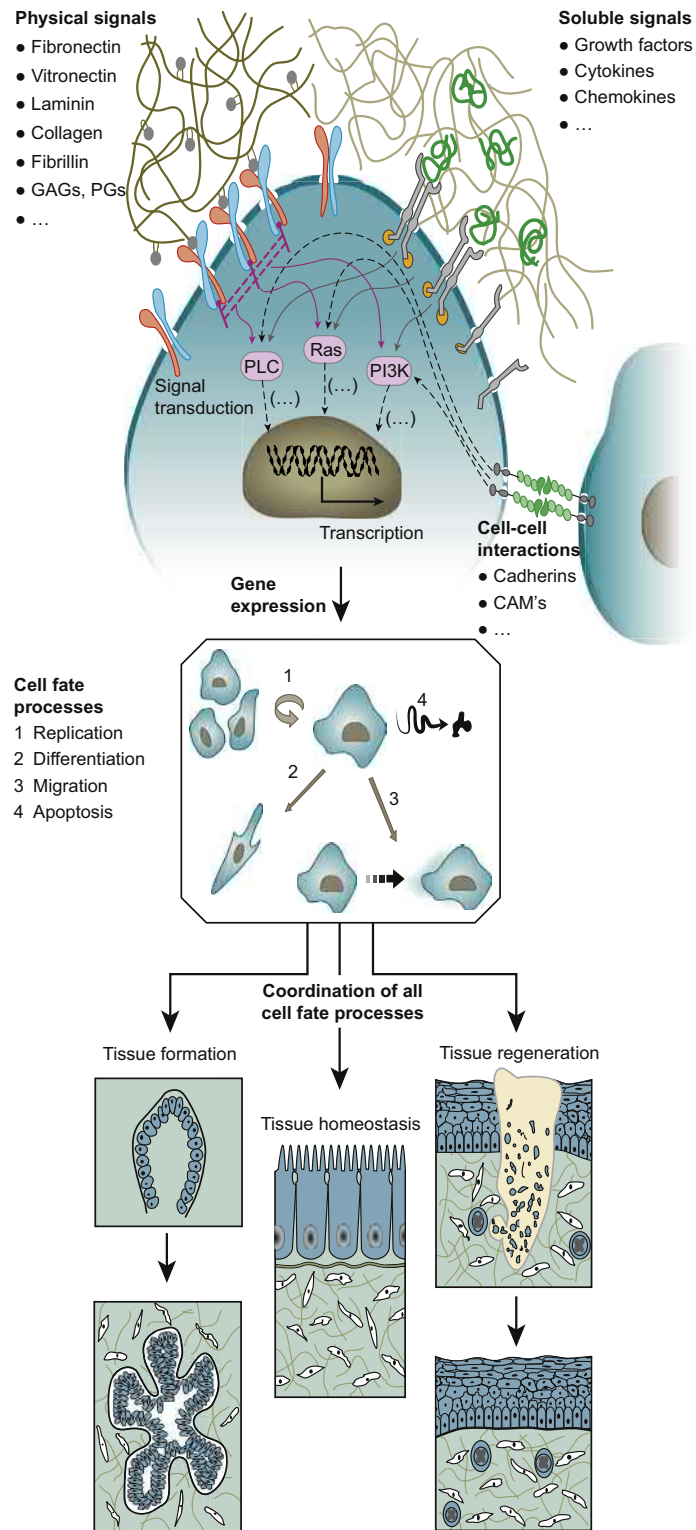
microorganisms (e.g., bacteria, parasites, and viruses), actively migrate to them, and then ingest and destroy them. *Polymorphonuclear leukocytes* (also called *PMNs* or *neutrophils*) are particularly active against bacteria, while *macrophages* react to other types of organisms and foreign material. B lymphocytes are not phagocytic but contribute to immunity by producing antibodies that can bind and neutralize infectious agents.

Stem Cells

Cells with the capacity to both divide and yield differentiated cells of one or more types are called *stem cells*. *Stemness*

can be functionally understood as the capacity for *asymmetric division*: one progeny cell maintains *totipotency* or *pluripotency* (it can still potentially become any [or many] cell type[s]), while the other daughter cell transcribes selected subsets of genes to become more differentiated.

Thus the stem cells in early embryos (found only rarely in adult cell populations) are totipotent with virtually limitless replicative capacity. As the fetus grows and develops, subsets of these totipotent cells *differentiate* and assume specific functions that will eventually lead to the formation of mature tissues, e.g., bone, muscle, liver, skin, and brain (Fig. 2.1.4.9).



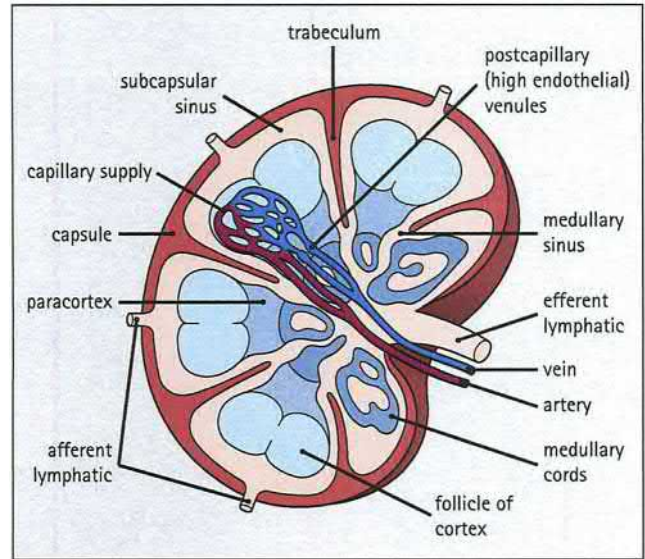
• **Figure 2.1.4.6** Individual cell behaviors and the dynamic states of multicellular tissues are regulated by reciprocal molecular interactions between cells and their environment. (Reproduced by permission from Lutolf, M.P., Hubbell, J.A., 2005. Synthetic biomaterials as instructive extracellular microenvironments for morphogenesis in tissue engineering. *Nat. Biotechnol.* 23, 47–55.)

As cells differentiate along particular specialization or tissue pathways, they lose the ability to interconvert and develop into all cell types, although they may be able to form most or all the cells of a particular tissue. Thus gastrointestinal stem cells in the small bowel can differentiate into absorptive epithelial cells, mucus-producing epithelial cells, and Paneth crypt cells that produce bacteriocidal proteins; however, they cannot differentiate into smooth muscle cells or even other types of epithelium. Stem cells in these lineages are said to be *pluri-* or *multipotential*; they may also have slightly limited replicative capacity. With further differentiation, cells may lose replicative capacity altogether.

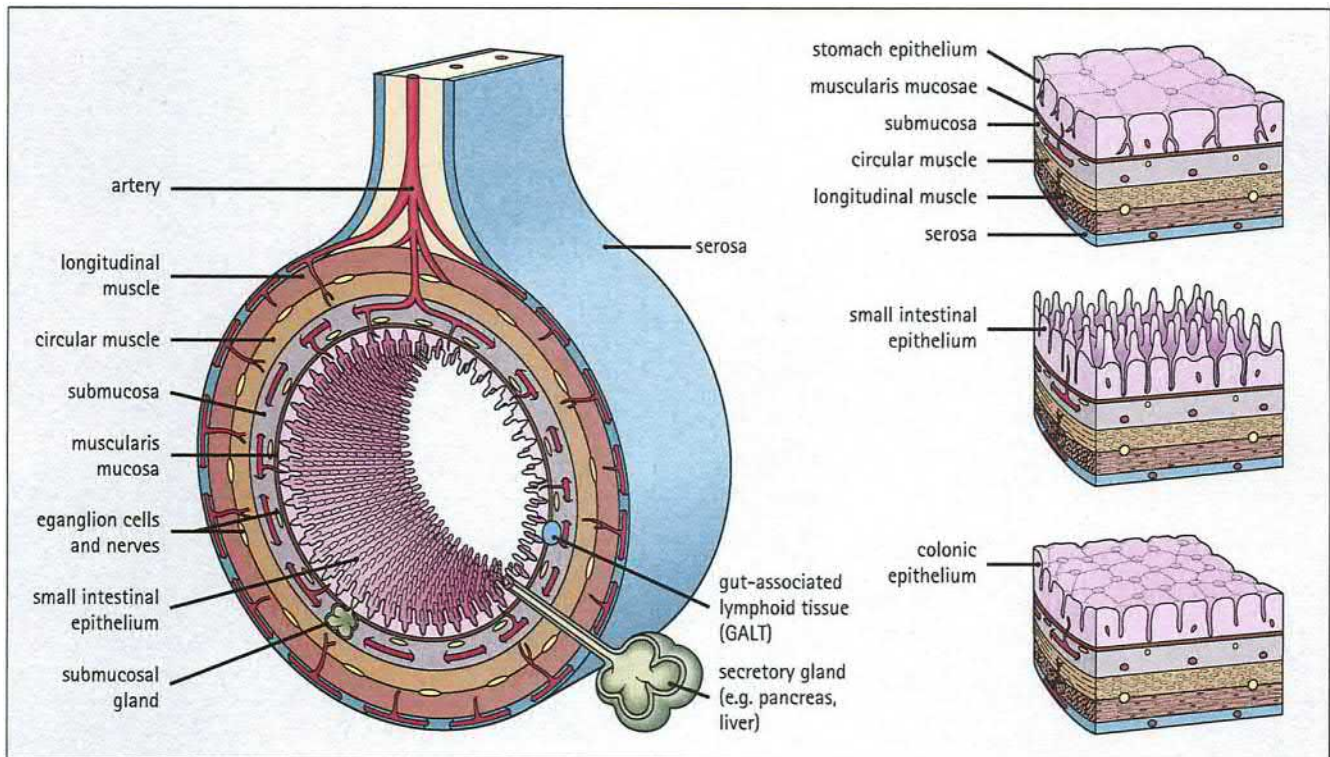
Therefore the various stem cell populations *downstream of the totipotent stem cells* are not all created equal; each type of stem cell has a repertoire of cells that it can potentially differentiate into. For example, pluripotent stem cells such as hematopoietic stem cells can form only circulating blood elements (red cells, platelets, leukocytes, etc.); with progressive maturation, even those lineages will develop into populations that become progressively more restricted in their differentiation capacity (i.e., capable of making only red cells or lymphocytes).

It is also important to recognize that differentiated cells cannot typically *transdifferentiate* into other cell types—that is transform from one mature somatic cell into another without an intermediate pluripotent or progenitor cell (also called *lineage reprogramming*). Thus a keratinocyte in the skin does not naturally become an absorptive epithelial cell like those in the gastrointestinal tract. An apparent exception to this is seen in certain tissues where one mature adult cell type is replaced with another (called *metaplasia*; see later in the chapter). In

reality, this occurs through a reprogramming of a precursor stem cell to generate a different cellular phenotype. Moreover, it is now possible to experimentally genetically reprogram mature, differentiated cells by the addition of certain transcription factors; this is the basis for generating inducible progenitor stem cells from adult end-stage cells.



• **Figure 2.1.4.8** Lymph node structure. Blood vessels enter and efferent lymphatics emerge from the hilum. Lymphoid follicles comprise the parenchyma. (Reproduced from James, S.L., Peter, G.A., 2015. Stevens & Lowe's Human Histology, fourth ed.)



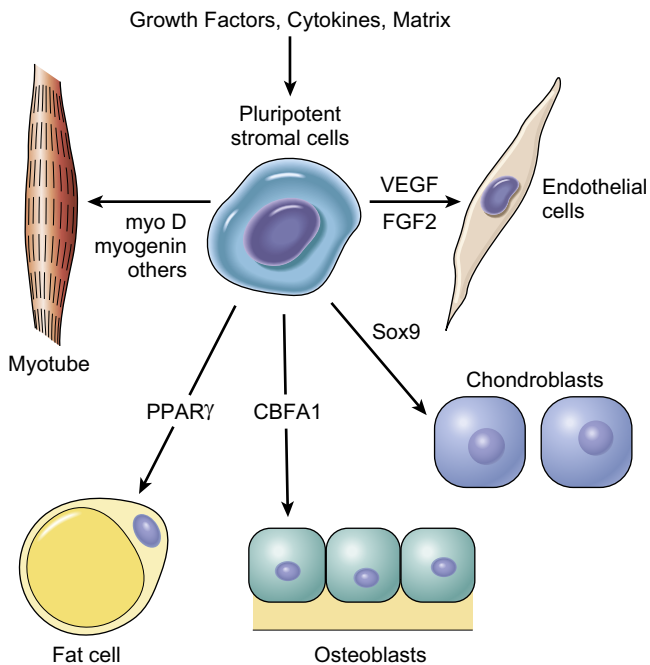
• **Figure 2.1.4.7** Vascolarization of a hollow organ, as exemplified by the digestive tract. The specialized epithelium differs from region to region (stomach, small intestine and colon, as indicated) but the essential wall architecture remains the same throughout, as in the cardiovascular system (recall Figure 2.1.4.3). (Reproduced from James, S.L., Peter, G.A., 2015. Stevens & Lowe's Human Histology, fourth ed.)

Cellular Differentiation and Gene Expression

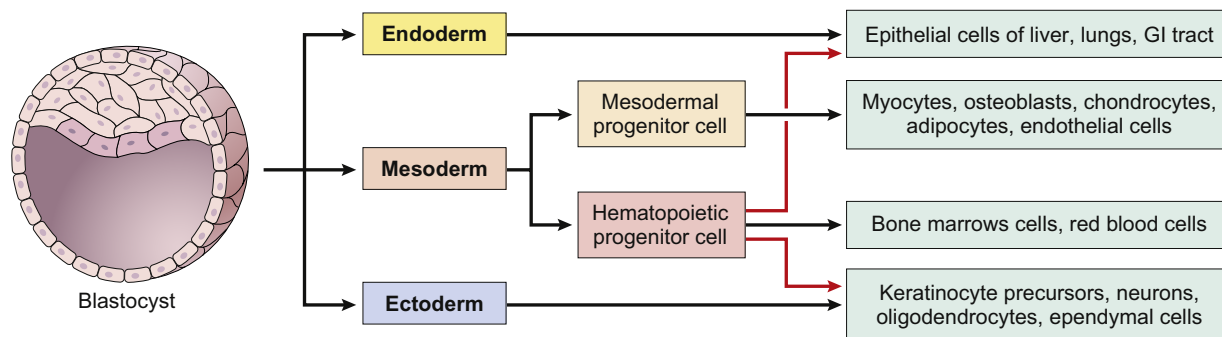
Every cell in the body has the same complement of genes (called the *genotype*). When selected subsets of genes are preferentially expressed, yielding a distinct biological profile (called the *phenotype*), progressive differentiation occurs. As cells progressively specialize, more and more of the “unnecessary” genes in the differentiating cell are turned off (usually irreversibly). Some genes are active at all times (*constitutively expressed*); others may be selectively activated or *modulated* depending on external influences (e.g., injury). Thus from one type of pluripotent cell, differential activations of specific genes can engender the development of endothelial cells, skeletal muscle, fat, bone, or cartilage (Fig. 2.1.4.10).

The specific function(s) of a given cell are reflected by the relative amount and types of organelles it contains. The relative predominance of specific types of organelles can often be inferred by examination of tissue sections prepared by standard histologic techniques and can be confirmed by transmission electron microscopy. For example, cells with substantial energy requirements need a significantly greater capacity to generate adenosine triphosphate (ATP), the energy currency of the cell. Thus kidney tubular epithelial cells (which reabsorb sodium and chloride against concentration gradients) and cardiac myocytes (which rhythmically contract 50–100 times per minute) have a generous complement of mitochondria. In comparison, cells specifically adapted to synthesize and export selected proteins (e.g., insulin in a pancreatic islet cell, or antibody produced by a plasma cell) have a well-developed rough endoplasmic reticulum (the key site of protein synthesis). A corollary to this general concept is that the nutritional and extracellular structural needs of a cell can also be inferred from the organellar constituents and the presumed cellular function. Thus cells with substantial energy demands but little in the way of

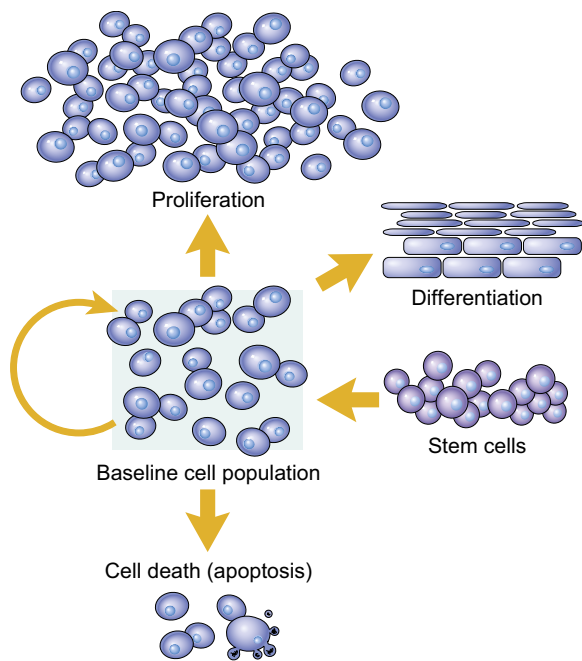
intracellular energy reserves (e.g., cardiac muscle cells) will need a continuous source of oxygen and glucose—provided by a dense capillary network with minimal diffusion distance from blood to cardiomyocyte mitochondria.



• **Figure 2.1.4.10** Differentiation of pluripotent mesodermal progenitor cells. The same stromal cell can differentiate in different developmental pathways depending on the activation of specific genes; this can occur through exogenous soluble factors or via mechanical cell–matrix interactions. Thus, vascular endothelial growth factor (VEGF) and fibroblast growth factor-2 (FGF-2) are two (of many) soluble signaling molecules that induce endothelial differentiation. Sox9, CBFA1, PPAR γ , and myoD are all intracellular transcription factors whose activities will induce the specific lineages shown. (Reproduced by permission from Kumar, V., Abbas, A.K., Fausto, N., 2005. Robbins and Cotran Pathologic Basis of Disease, Seventh ed. Saunders, Philadelphia, PA.)



• **Figure 2.1.4.9** Differentiation of mature cell lineages from the *totipotent* blastocyst. Cells in the early embryo have the capacity to proliferate and differentiate into all adult tissues. As the embryo expands, distinct layers (*endoderm*, *ectoderm*, and *mesoderm*) from the original sphere become three general *pluripotential* lineages—now with more limited cellular differentiation repertoires. Eventually, after multiple rounds of replication and additional differentiation, the final adult tissues develop. *Adult stem cells* derived from the original pluripotential lineages will persist within the organs they formed, with the capacity to regenerate cells specifically of that tissue. In addition, adult hematopoietic progenitors from the original mesoderm have the relatively unique capacity to generate tissues of the endoderm and ectoderm—in addition to making marrow-derived blood cells. (Reproduced by permission from Kumar, V., Abbas, A.K., Fausto, N., 2005. Robbins and Cotran Pathologic Basis of Disease, Seventh ed. Saunders, Philadelphia, PA.)



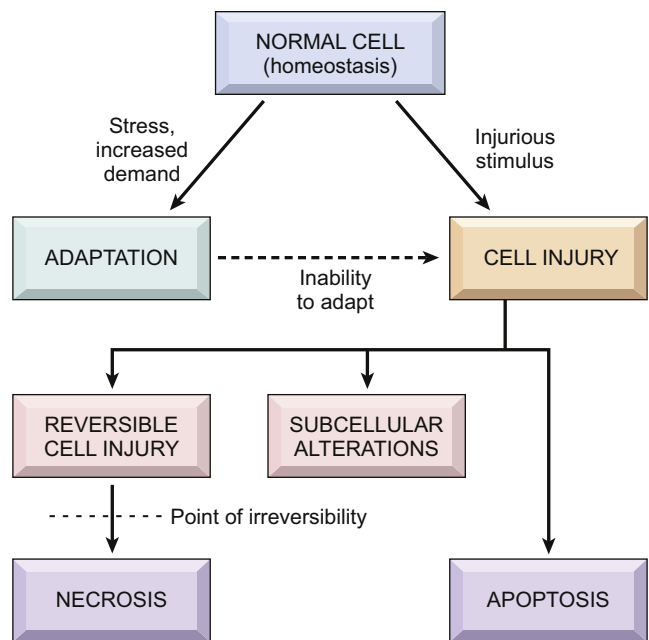
• **Figure 2.1.4.11** Achieving steady-state populations of cells. Total cell numbers in a baseline tissue population can be regulated by changes in stem cell output, loss of cells through programmed cell death (*apoptosis*), cellular proliferation, or differentiation. (Reproduced by permission from Kumar, V., Abbas, A.K., Fausto, N., 2005. *Robbins and Cotran Pathologic Basis of Disease*, Seventh ed. Saunders, Philadelphia, PA.)

Tissue Homeostasis

Tissues function best when maintained within certain physiologic ranges of pH, temperature, nutrition, pressure, etc. Reflecting that in reality, the body—and organs, tissues, and even individual cells—strives to achieve *homeostasis* (i.e., an optimal range of conditions) in the face of variations in the internal and external environments. This dynamic adaptation of biologic structure and function may require increased or decreased function, and requires signaling through soluble molecules (e.g., hormones, cytokines, etc.), as well as cell–cell and cell–ECM interactions (Fig. 2.1.4.5). Even extracellular mechanical forces (e.g., torsion or tension) can be translated into intracellular signaling or transcription events. Thus tissue homeostasis can also critically depend on cellular interactions with the surrounding ECM. (Smith et al, 2018)

Cell Turnover

A fundamental concept is that structural and functional specialization is typically associated with large-scale loss of the capacity for cellular replication; for example, neutrophils, cardiac myocytes, and neurons are all end-stage cells and cannot proliferate. In the small bowel, the terminally differentiated absorptive cells actually divide no further and undergo programmed cell death within 3–4 days of their genesis. Consequently, maintaining cell numbers or repairing sites of injury require multipotent stem cells to proliferate and differentiate. Thus, even in fully developed organisms, populations of multipotential cells capable of repopulating



• **Figure 2.1.4.12** General overview of potential cellular responses to stressors and injurious stimuli. (Reproduced by permission from Kumar, V., Abbas, A.K., Fausto, N., Aster, J.C., 2010. *Robbins and Cotran Pathologic Basis of Disease*, eighth ed. Saunders, Philadelphia, PA.)

adult tissues persist—providing the balance between cellular proliferation, programmed cell death (*apoptosis*), and *differentiation* into specialized end-stage cells that have lost the ability to reproduce (Fig. 2.1.4.11).

Matrix Remodeling

In most tissues, the ECM is constantly turning over and being remodeled in a coordinated, regulated manner. Although matrix turnover is generally quite low in normal mature (i.e., stable) tissues, rapid and extensive remodeling characterizes embryological development, adaptation to changing environmental conditions, and wound repair. Tissue remodeling is a major goal of many tissue-engineering approaches, and an understanding of cell–substrate interactions and matrix remodeling are central to the application of biomaterials technology, tissue engineering, and regenerative therapeutics.

Connective tissue remodeling, either physiological or pathological, is typically a highly organized process involving the coordinated action of a group of enzymes that can collectively degrade most proteins of the ECM. Called *matrix metalloproteinases* (MMPs), these are synthesized by macrophages, fibroblasts, and epithelial cells; 28 MMPs have been described, each with a distinct specificity for the various types of collagens and other ECM components. MMP enzymatic activities are counterregulated by *tissue inhibitors of metalloproteinases* (TIMPs); these are multifunctional proteins with both MMP inhibitor activity and cell growth modulating properties. Distortion of the balance between matrix synthesis and turnover may result in altered matrix composition amounts and organization. Particularly important in tissue remodeling are *myofibroblasts*, cells with features of both smooth muscle cells

(i.e., contractile proteins such as α -actin) and fibroblasts (i.e., synthesis of ECM proteins such as collagen).

Cell and Tissue Injury, Adaptation, and Other Responses (Fig. 2.1.4.12)

For more detail, see Rubin et al. (2014) and Kumar et al. (2015). As noted previously, cells and tissues attempt to maintain their milieu and function within a relatively narrow range of physiologic parameters (*homeostasis*). However, as cells and tissues encounter more challenging physiologic stresses or pathologic stimuli, they undergo more extensive changes (*adaptations*) designed to achieve a new steady state but in all cases to preserve viability. Usually, if the stressors recede, the cells and tissues will revert to their prestressed state. However, if the stressors persist and a cell's adaptive capability is exceeded, *cell injury* develops. Up to a point, cell injury itself is reversible, and with normalization of the stimulus, the cell returns to its baseline state. However, with severe or persistent stress, the cell suffers irreversible injury and dies. For example, when heart muscle cells are subjected to diminished blood flow due to an occluded coronary artery, there is an imbalance between blood supply and energy demand (a physiological condition called *ischemia*); fortunately, the cells may be only *reversibly injured* if the occlusion is incomplete or sufficiently brief. Alternatively, cardiac myocytes may undergo *irreversible injury* (i.e., cell death, also called *necrosis*, as in *myocardial infarction*) if there is complete or prolonged ischemia caused by arterial occlusion. Other types of responses may be initially adaptive and protective but eventually progress to pathologic states; as described later, these include *atrophy* (i.e., a decrease in organ or tissue size or function); *hypertrophy* (i.e., an increase in cell size and function); or *hyperplasia* (i.e., an increase in cell number).

Cell Regeneration and Proliferation

At a tissue level, the ability to regenerate is a function of the level of differentiation of the stem cells within that tissue and their overall replicative potential. These fall into three broad general categories: *labile*, *stable*, and *permanent* tissues.

Labile tissues have pluripotent stem cells that are constantly in cell cycle and thus constantly generating new cells that will differentiate into the final population comprising the parenchyma of that particular organ. As those final differentiated cells senesce, they typically undergo programmed cell death (*apoptosis*, discussed later); nevertheless, they are continuously being replaced by cells of the “next generation,” and thus the integrity of the tissue is maintained. These tissues include many epithelia that cover the skin, oral cavity, vagina, and cervix; the linings of the ducts draining exocrine organs (e.g., salivary glands, pancreas, biliary tract, gastrointestinal tract, uterus, fallopian tubes, and the urinary tract). The hematopoietic cells of the bone marrow are also continuously replenishing the circulating peripheral blood cell elements. As a corollary of

their ongoing proliferation, labile tissues typically repopulate sites of injury relatively quickly. However, they are also most sensitive to extrinsic insults such as radiation or chemotherapy for tumors—which is why patients being treated for cancer lose their hair (hair follicle epithelium), malabsorb food (gastrointestinal epithelium), and are anemic and prone to infections and bleeding (bone marrow).

Stable tissues have pluripotent stem cells that typically rest in a quiescent stage of the cell cycle and are not actively turning over. However, these cells have substantial regenerative capacity when stimulated by injury or surgical cell loss; these include the parenchymal cells of the liver and kidney, as well as endothelial cells, fibroblasts, and smooth muscle.

Permanent tissues include neurons and cardiac myocytes. Classically, cardiac muscle cells and neurons are considered as terminally differentiated cells without the ability to reproduce. Skeletal muscle has a limited regenerative capacity, largely due to the proliferation and transformation of a small population of stem cells. Moreover, we are also learning that terminally differentiated permanent cells—previously thought to be irreplaceable once destroyed (e.g., nerve and cardiac muscle)—may be potentially repopulated by bone marrow-derived stem cells or even small populations of tissue-endogenous stem cells. While exciting, the extent to which we can utilize this replacement process appears to be very limited; for all practical purposes (for now), dead permanent cells are repaired by scar formation (Buja, 2019; Talman and Ruskoaho, 2016). There is also accumulating evidence to suggest that cells of end-stage, highly differentiated tissues can, under very limited conditions (e.g., some forms of injury), dedifferentiate into multipotent stem cells (Ma et al, 2017; Brumbaugh et al, 2019).

These concepts have important ramifications not only for embryogenesis, but also for the tissue engineer. For applications that require large numbers of differentiated cells, expansion of terminally differentiated cell populations may work for some cell types (e.g., skin). However, cells such as heart or nerve will probably require directed differentiation from expanded stem cells.

Reversible versus Irreversible Injury

Whether a specific form of stress induces adaptation or causes reversible or irreversible injury depends not only on the type of injury, its duration, and the severity of the stress, but also on several other cell-specific variables, including vulnerability of the type of cell being injured, degree of differentiation, blood supply, nutrition, and the previous state of health of the cell. For example, skeletal muscle in the leg can tolerate complete ischemia for 2–3 h without suffering irreversible injury, while cardiac muscle will die after only 20–30 min, and central nervous system neurons are dead after 2–3 min. Within limits, cells can compensate for disturbance of any of these, and if the injurious stimulus abates, will return to normalcy. Persistent or excessive injury, however, causes cells to pass the threshold into *irreversible injury*. In other words, they die;

in pathology jargon, the cells are said to become *necrotic* or undergo *necrosis*. The specialized activities relating to cell function may shut down relatively early in the setting of injury, and in most cases long before there is any cell death. For example, myocardial cells become noncontractile after 1–2 min of ischemia, although they will not die until 20–30 min of ischemia have elapsed. Consequently, if the injury can be halted before cells become irretrievably damaged then restoration of function can be anticipated. Of course, lack of cardiac function may lead to death of other important structures (e.g., the brain) even before the heart cells themselves reach the “point of no return.”

Adaptation

As cells and tissues encounter more chronic physiologic stresses or pathologic stimuli, they undergo adaptations designed to achieve a new steady state, but in all cases to preserve tissue function. The principal significant adaptive responses are:

hypertrophy: an increase in size of individual cells;

hyperplasia: an increase in cell number;

atrophy: a decrease in size, without appreciable change in cell number;

metaplasia: transformation from one mature cell type to another.

For example, when heart muscle cells are subjected to persistent increased load (e.g., high blood pressure), the cells adapt by undergoing *hypertrophy* (enlargement of the individual myocytes and eventually the entire heart) to compensate for the higher pressures they must pump against. Conversely, in periods of prolonged starvation (as can happen in prolonged illness or with malignant tumors), all myocytes (and thus the heart) will undergo *atrophy*. Hypertrophy and hyperplasia are closely related and often develop concurrently in tissues, so that both may contribute to an overall increase in organ size in organs whose cells can proliferate (i.e., the gravid uterus).

Hyperplasia Can Be Physiologic or Pathologic

Physiologic hyperplasia is divided into (1) hormonal hyperplasia, exemplified by proliferation of the glandular epithelium of the female breast at puberty and during pregnancy, and (2) compensatory hyperplasia, that is, hyperplasia that occurs when a portion of the tissue is removed or diseased—driven by local growth factor expression. Hyperplasia is also a critical response of connective tissue cells in wound healing, by which growth factor-stimulated fibroblasts and blood vessels proliferate to facilitate repair.

Atrophy, Proteasomes, and Autophagy

Loss of cell substance will result in reduction in cell size—denoted as atrophy. When a sufficient number of cells are involved, the entire tissue or organ diminishes in size, becoming atrophic. It should be emphasized that *although atrophic cells may have diminished function, they are not*

dead. Atrophy represents a reduction in the structural elements of the cell; the biochemical mechanisms underlying this process are varied but ultimately affect the balance between synthesis and degradation. Causes of atrophy include decreased workload (for example, immobilization of a limb to permit healing of a fracture), loss of innervation, diminished blood supply, inadequate nutrition, loss of endocrine stimulation, and aging. Although some of these stimuli are physiologic (e.g., loss of hormone stimulation in menopause) and others pathologic (e.g., denervation), the fundamental cellular changes are identical. They represent a retreat by the cell to a smaller size at which survival is still possible; a new equilibrium is achieved between cell size and diminished blood supply, nutrition, or trophic stimulation.

Mammalian cells contain two systems that serve distinct degradative functions:

- The *ubiquitin–proteasome pathway* is responsible for the degradation of many cytosolic and nuclear proteins.
- *Lysosomes* contain proteases and other enzymes that degrade *endocytosed molecules* and *phagocytosed particles* from the extracellular environment, as well as catabolize cellular components such as *senescent organelles*.

Metaplasia

Metaplasia is a reversible change in which one adult cell type (epithelial or mesenchymal) is replaced by another adult cell type. This is a cellular adaptation whereby cells sensitive to a particular stress are replaced by other cell types putatively “better” able to withstand the adverse environment. Metaplasia is thought to arise by genetic *reprogramming* of stem cells.

Neoplasia

Beyond adaptive responses, environmental stimuli can also induce genetic changes that can trigger abnormal proliferation and differentiation. Such behavior is uncoordinated relative to normal tissues, has lost its responsiveness to normal growth controls, and persists after cessation of the stimuli that initiated it. This condition is called *neoplasia*; in its malignant form, it is more commonly called *cancer* (see Chapter 2.5.11).

Causes of Cell Injury

Hypoxia and Ischemia

The efficient production of ATP by mitochondria—and therefore the energy needed to run all cell activities—is critically dependent on oxygen. *Hypoxia* is decreased O₂ supply relative to the needs of a particular cell or tissue. *Anoxia* is the complete absence of oxygen. Tissue hypoxia can occur in any setting where there is reduced oxygen tension, including causes as diverse as high altitude, anemia, and carbon monoxide poisoning (the latter diminishes the oxygen-carrying capacity of hemoglobin). However, the most common cause of tissue hypoxia is diminished blood flow, called *ischemia*. Irreversible tissue injury (*necrosis*) due to ischemia is called *infarction*

(as already discussed). It is also important to note that diminished blood flow will also affect the ability to remove waste products from a metabolizing tissue, so that, all things considered, *ischemia is far worse than simple hypoxia*.

Toxic Injury and Trauma

Chemical agents include components of food, naturally occurring toxins, hormones, neurotransmitters, synthetic drugs, environmental pollutants, poisons, ethanol, tobacco, and even toxic biomaterials. Chemicals induce cell injury by one of two general mechanisms:

- By combining directly with a critical molecular component or cellular organelle and thereby inhibiting its normal activity.
- Chemicals that are not intrinsically biologically active may be converted to toxic metabolites during normal physiologic breakdown.

Injury can also result by direct mechanical force (trauma, pressure), temperature extremes (burn, frostbite), electric shock, or ionizing radiation.

Infection and Inflammation

Infectious agents run the gamut from virus and bacteria to fungi, protozoans, and helminths (worms). There is generally a preferred cell or tissue of invasion (called a *tropism*), and therefore each agent tends to have a defined spectrum of potential injury. *Viruses* multiply intracellularly, appropriating host biosynthetic machinery in the process; cell lysis may occur directly, or as a result of the immune system's recognition and destruction of infected cells. *Bacteria* have toxic cell wall constituents (e.g., endotoxin), and can release a variety of exotoxins. Moreover, the very process of eradicating infections by the host immune system can also cause injury—and in many cases constitutes the bulk of the pathology.

Pathogenesis of Cell Injury

There are three basic mechanisms of cell injury:

- *Loss of adequate ATP production.* Ischemia, hypoxia, or mitochondrial dysfunction will all cause a precipitous drop in ATP synthesis.
- *Oxygen and oxygen-derived free radicals.* Lack of oxygen (and loss of ATP production) obviously underlies the pathogenesis of ischemic cell injury. In addition, *partially reduced, activated oxygen species* are important mediators of cell death. *Free radicals* are chemical species with a single unpaired electron in an outer orbital; they are extremely unstable and readily react with inorganic or organic chemicals. When generated in cells, free radicals cause single-strand breaks in DNA, fragment lipids in membranes via lipid peroxidation, and fragment or cross-link proteins leading to accelerated degradation or loss of enzymatic activity.
- *Failure of intracellular calcium homeostatic mechanisms.* Cytosolic free calcium is normally maintained by

ATP-dependent calcium transporters at extremely low concentrations (less than $0.1\ \mu\text{M}$), while extracellular calcium and sequestered mitochondrial and endoplasmic reticulum calcium stores are typically at roughly 10^4 -fold higher concentrations. Consequently, any cell ischemia or injury potentially opens a floodgate of calcium. Increased cytosolic calcium in turn activates a variety of *phospholipases* (promoting membrane damage), *proteases* (catabolizing structural and membrane proteins), *ATPases* (accelerating ATP depletion), and *endonucleases* (fragmenting genetic material).

Ischemia-Reperfusion Injury

If cells are reversibly injured in ischemic circumstances, restoration of blood flow should theoretically result in cell recovery. However, in many cases, restoration of blood flow to ischemic but otherwise viable tissues results in paradoxically exacerbated and accelerated injury.

Cell Death

Necrosis

Two phenomena consistently characterize irreversible injury. The first is the *inability to reverse mitochondrial dysfunction* (lack of oxidative phosphorylation and ATP generation) even upon restoration of oxygen; the second is the development of *profound disturbances in membrane function*. Massive calcium influx into the cell occurs, particularly if ischemic tissue is reperfused after the point of irreversible injury, with broad activation of calcium-dependent catabolic enzymes. Precipitation of calcium salts in cells (*calcification*) is discussed in detail in [Chapter 2.4.4](#).

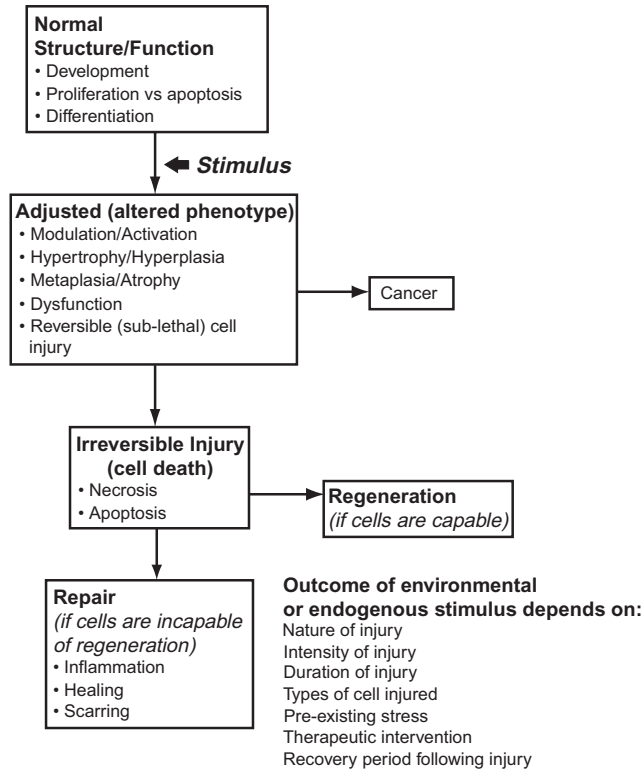
Since necrotic tissue is a potential nidus for secondary infections, the body rapidly mobilizes inflammatory cells to remove the resulting debris and initiates the process of either rebuilding the dead tissue or laying down a fibrous scar (see [Chapter 2.2.2](#)). As mentioned previously, the recruited inflammation can in itself be a cause of further local injury. Moreover, having to replace a specialized tissue with a nonfunctional matrix scar is also a less than optimal outcome.

Apoptosis

The cell death that has been thus far described is the consequence of irreversible injury; in a way, this can be thought of as cellular “homicide.” However, there is also an important form of controlled or *programmed* cell death that can be conceptualized as cellular “suicide.” Apoptosis is responsible for programmed cell death in several important physiologic (as well as pathologic) processes, including:

- the programmed destruction of cells during embryogenesis, including implantation, organogenesis, and developmental involution;
- hormone-dependent physiologic involution, such as the endometrium during the menstrual cycle, or the lactating breast after weaning; or pathologic atrophy, as in the prostate after castration;

- cell deletion in proliferating populations such as intestinal crypt epithelium, or cell death in tumors;
- deletion of autoreactive T cells in the thymus, cell death of cytokine-starved lymphocytes, or cell death induced by cytotoxic T cells;



• **Figure 2.1.4.13** Cellular mechanisms of disease, emphasizing the general concept that stressor stimuli induce altered cell behaviors (reversible cell injury with phenotypic alterations) to compensate and maintain viability; notably, such changes can also lead to malignancy. Failure to successfully adapt to stressors leads to irreversible cell injury (death) with the downstream outcomes of regeneration and/or scarring, depending on cell type and other variables.

- a variety of mild injurious stimuli (heat, radiation, cytotoxic cancer drugs, etc.) that cause irreparable DNA damage that in turn triggers cell suicide.

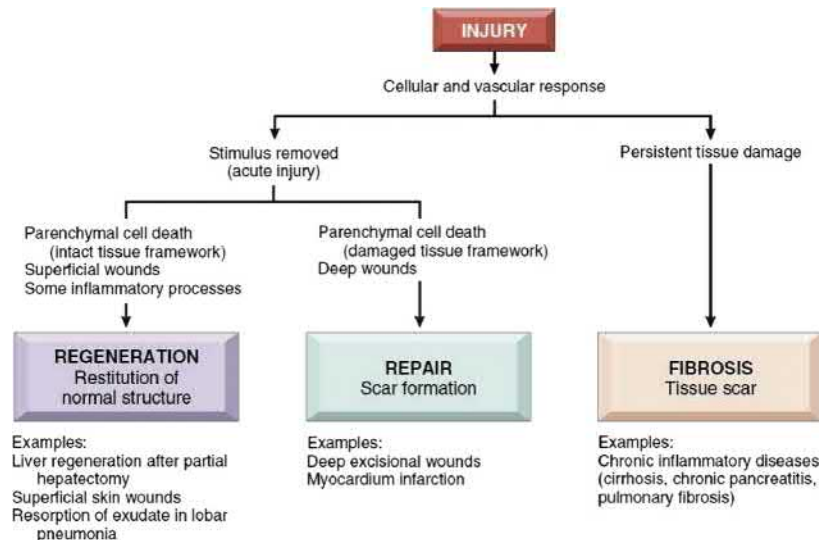
Apoptotic cells and their fragments have marker molecules on their surfaces that signal uptake and disposal by adjacent cells or phagocytes. This (and other) alterations allow the early recognition and phagocytosis of apoptotic cells without release of proinflammatory mediators. The process is so efficient that dead cells typically disappear without leaving a trace, and inflammation is virtually absent.

The general framework of cell injury (and subsequent responses to injury) is summarized in Fig. 2.1.4.13.

Response to Tissue Injury and Biomaterials

A key protective response of an organism is its ability to eliminate damaged tissues and foreign invaders, such as microbes or exogenous nonbiological materials (examples of the latter ranging from splinters to inhaled environmental particulate pollutants to therapeutic biomaterials). The goal of this response is to rid the organism of both the cause of injury (especially if it is microbial) and ameliorate potential adverse consequences (i.e., secondary infection). Without this protective process, tissue wounds would not heal and infections would go unchecked. However, inappropriately triggered or inadequately controlled inflammation can also be harmful. Inflammation usually is a highly coordinated sequence of events involving local and circulating proteins, leukocytes, and phagocytic cells (macrophages) that are recruited to a site of injury.

The outcome of tissue injury depends primarily on the tissue type and the extent and persistence of the injury (Fig. 2.1.4.14). When tissue injury is transient or short-lived, tissue destruction is small, the tissue is capable of regeneration, and the outcome is typically (and happily) restoration of normal structure and function. When an infection or foreign material cannot be eliminated, (Singer and Clark, 1999)



• **Figure 2.1.4.14** Regeneration, repair, and fibrosis after injury and inflammation. (Reproduced by permission from Kumar, V., Abbas, A.K., Fausto, N., Aster, J.C., 2010. Robbins and Cotran Pathologic Basis of Disease, eighth ed. Saunders, Philadelphia, PA.)

when the injury is extensive, or occurs in tissues that do not regenerate, inflammation and scarring occur. In those situations, the body often “controls” the foreign body or infection by creating a wall around it (see [Chapter 2.2.2](#)).

In the case of most “inert” materials, the late tissue reaction involves *encapsulation* by a fibrous tissue capsule (composed of collagen and fibroblasts). Encapsulation is largely a result of the healing of the wound engendered by the implantation of a biomaterial. If a superimposed infection occurs that cannot be easily eliminated, an abscess (i.e., localized collection of acute inflammation and infectious organisms) is the outcome, adding yet an additional component of injury.

Inflammation and Innate Immunity

As described earlier, inflammation and repair follow cell and tissue injury induced by various exogenous and endogenous stimuli, both eliminating (i.e., diluting, destroying, or isolating) the cause of the injury (e.g., microbes or toxins) and degrading necrotic cells and tissues that occur as a result of the injury. In doing so, the inflammatory response initiates the process that heals and reconstitutes the tissue, replacing the wound by native parenchymal cells, or by filling up the defect with fibroblastic scar tissue, or some combination of both. Although *lymphocytes* (*B and T cells*) may eventually be involved in responses to various forms of injury (so-called *antigen specific* or *adaptive immunity*), the initial response to cell and tissue damage is the cells of innate immunity, *neutrophils* and *macrophages*. In the vast majority of cases, these innate cells (and their mediators) are sufficient to resolve the original injury and drive the regenerative or scarring process. As described later, these cells lack the exquisite specificity of lymphocytes, but nevertheless do have a reasonable repertoire of receptors that allow them

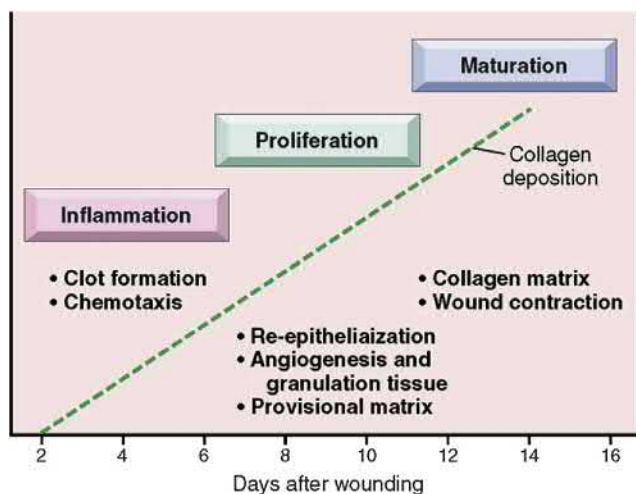
to recognize pathogens and damaged tissues (for additional information, see [Chapter 2.2.3](#)).

Inflammation and repair constitute an overlapping sequence of several processes ([Fig. 2.1.4.15](#)):

- Acute inflammation is the immediate early response to injury. It is of relatively short duration (usually 1–3 days) and is characterized by fluid and plasma protein exudation into the tissue, as well as by the accumulation of the innate immune cells called *neutrophils* (*PMNs*). Neutrophils are recruited to sites of inflammation through the increased adhesiveness of endothelium in the postcapillary venules at those sites, and by the local elaboration of several chemotactic mediators (*chemokines*).
- Chronic inflammation: This next phase (days to weeks after injury) involves macrophage recruitment (these are also cells of *innate immunity*), and later—in some cases—lymphocytes (cells of *adaptive immunity*); there is often concurrent tissue destruction. The chronic inflammatory response is responsible for driving the subsequent *repair* mechanisms, representing some combination of host tissue *regeneration* versus *scarring*.

A special type of chronic inflammation characterized by activated macrophages and often multinucleated giant cells is called a *granuloma* or *granulomatous inflammation*. Granulomatous inflammation characteristically occurs when the inciting agent cannot be degraded, including in the setting of implanted foreign bodies.

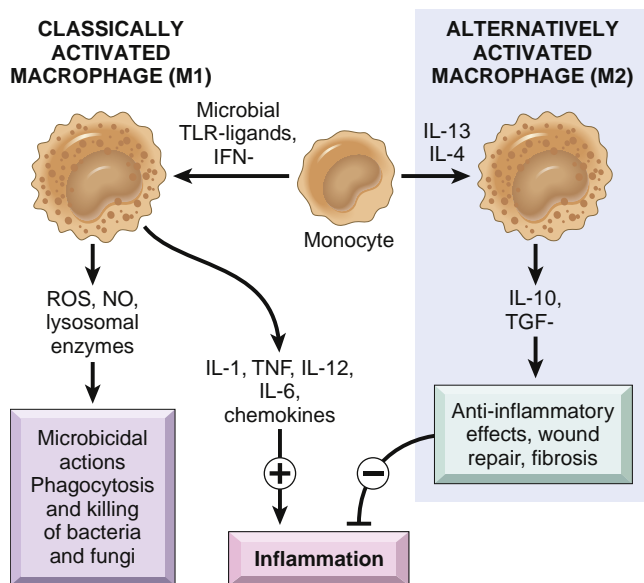
- Scarring: In situations where repair cannot be accomplished by complete tissue regeneration, scarring will ensue. This occurs through three sequential processes: (1) formation of new blood vessels (*angiogenesis*), (2) deposition of collagen (*fibrosis*), and (3) maturation and remodeling of the scar (*remodeling*). The early healing tissue—called *granulation tissue* (not to be confused with granuloma, above)—exhibits a dense network of new capillaries and proliferating fibroblasts (synthesizing new ECM). The ECM deposition in scarring is usually well developed by 4–6 weeks, although full scar remodeling may require much longer. ([Gurtner et al, 2008](#); [Rodriguez et al, 2019](#); [Wynn and Vannella, 2016](#)).



• **Figure 2.1.4.15** Phases of cutaneous wound healing: inflammation, proliferation, and maturation. (Reproduced by permission from Kumar, V., Abbas, A.K., Fausto, N., Aster, J.C., 2010. *Robbins and Cotran Pathologic Basis of Disease*, eighth ed. Saunders, Philadelphia, PA.)

Macrophage Recruitment and Polarization

Tissue macrophages—and their bone marrow-derived circulating precursors, ([Caputa et al, 2019](#); [Kim and Nair, 2019](#)) the *monocytes*—are the central figures in chronic inflammation. The half-life of circulating monocytes is about 1 day; they begin to emigrate at the site of injury within the first 24–48 h after onset of acute inflammation. However, once they have transmigrated into the tissues and assumed the identity of macrophages, these cells are impressively long-lived, and in fact may persist for the lifetime of the host organism. Transmigrated macrophages may become “activated,” a process resulting in increased cell size, increased content of lysosomal enzymes, more active metabolism, and greater ability to kill ingested organisms. Activation signals include cytokines secreted by sensitized T lymphocytes (in particular interferon- γ), bacterial endotoxins (lipopolysaccharide), various mediators produced during acute inflammation, and



• **Figure 2.1.4.16** Classical and alternative macrophage activation. Different stimuli activate monocytes/macrophages to develop into functionally distinct populations. Classically activated (M1) macrophages are induced by microbial products (via toll-like receptors [TLRs]) and cytokines, particularly interferon- γ (IFN- γ). M1 macrophages phagocytose and degrade microbes and necrotic material, as well as augment inflammatory reactions through the production of additional cytokines (e.g., interleukin [IL]-1, tumor necrosis factor [TNF], etc.) and mediators such as reactive oxygen species (ROSs), lysosomal enzymes, and nitric oxide (NO). Alternatively activated macrophages (M2) are induced by a different set of cytokines (e.g., IL-13 and IL-4); they are critical for coordinating tissue repair and the resolution of inflammation. *TGF- β* , Transforming growth factor- β . (Reproduced by permission from Kumar, V., Abbas, A.K., Aster, J.C. (Eds.), 2018. *Robbins Basic Pathology*, tenth ed. Elsevier, Philadelphia, PA.)

ECM proteins such as fibronectin. In the usual histologic preparations, “activated” macrophages are enlarged and have pale pink granular cytoplasm with indistinct cell boundaries, so-called *epithelioid* macrophages (because they resemble the cells that comprise squamous epithelium).

Following activation, *macrophages secrete a wide variety of biologically active products* important in mediating subsequent tissue destruction, angiogenesis, and the fibrosis characteristic of chronic inflammation. *Steroids* have their profound salutary effects on chronic inflammation and subsequent scarring largely due to their inhibition of macrophage activation.

Products synthesized by activated macrophages are:

- *Acid and neutral proteases*, which can digest and/or remodel the ECM.
- *Complement components and coagulation factors*. Although hepatocytes are the major source of these proteins in plasma, activated macrophages make locally significant amounts of these proteins in the ECM.
- *Reactive oxygen species and nitric oxide*.
- *Prostaglandins and leukotrienes*.
- *Cytokines*, such as interleukin-1 and tumor necrosis factor, as well as a variety of *growth factors* that influence proliferation and ECM production by smooth muscle cells and fibroblasts.

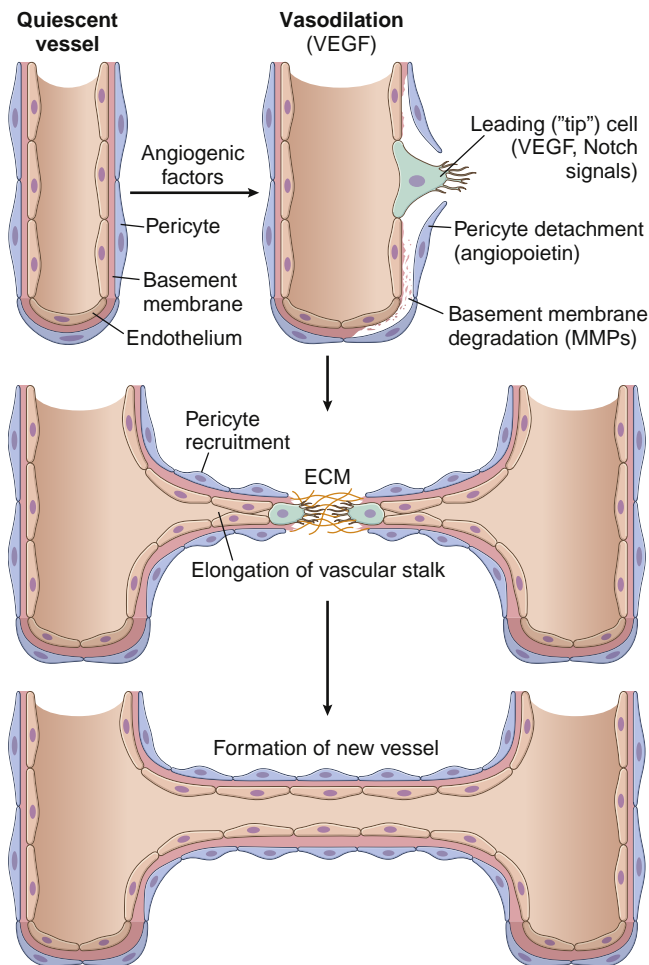
Macrophages comprise at least two distinct subsets with distinct functions, depending on the pathways by which they are activated (Fig. 2.1.4.16) (Adams et al, 2019). The classically activated M1 macrophage—induced by interferon- γ and toll-like receptor pathways—that is initially induced at a site of injury is typically proinflammatory; it not only recruits and activates additional inflammatory cells, but also exhibits increased cytotoxic features. Alternatively, the M2 macrophage subset (induced by interleukins-4 and -13, or by hemoglobin in sites of hemorrhage) develops later in the response to injury, and tends to turn off inflammation, producing cytokines and enzymes that drive fibrosis. Recent experiments suggest that M1 macrophages can differentiate into M2 macrophages (and vice versa), depending on the cytokine milieu, and that the gradual transition from predominantly M1 to M2 at the sites of wound healing are not necessarily due to differential recruitment of the two subsets.

Regeneration Versus Fibrosis (Scar)

In terms of healing and reparative potential, the mitotic capability of a cell population, *or* the capacity of immature precursor cells to divide and differentiate to fill an injured void, will ultimately decide the outcome of tissue destruction. As discussed previously, not all cells are equally capable of such proliferative expansion. In labile and stable cells capable of regeneration, the cell proliferation process is regulated by a combination of *cell-ECM interactions* and *growth factors* (Fig. 2.1.4.5). ECM provides a substratum for cell adhesion, and critically regulates the growth, movement, and differentiation of the cells living within it. Importantly, although labile and stable cells are capable of complete regeneration, *reconstitution of normal structure requires an intact ECM*. In particular, the basement membrane directs cell polarity and is required for the orderly renewal of an epithelial tissue; in the absence of an intact basement membrane, cells proliferate in a haphazard fashion, producing disorganized masses bearing no morphologic and—more importantly—no functional resemblance to the original tissue.

Growth Factors

For the most part, these are polypeptides that can act on a variety of cell types, or may have a rather circumscribed target population. Besides promoting growth, these mediators also influence cell locomotion, contractility, protein synthesis, and differentiation (i.e., almost *any* cellular activity), all of which can affect repair and wound healing. The various growth factors typically work via cell-to-cell communication over short distances. For example, wound healing and repair in connective tissues are most commonly achieved by one cell in a tissue secreting a factor that regulates the activities of adjacent cells (*paracrine pathways*). Cells that carry receptors for their own endogenously produced factors will also exhibit *autocrine stimulation*, important in compensatory epithelial hyperplasia at sites of injury (e.g., hepatic regeneration). In addition to specific signals that stimulate and positively regulate growth, cells and tissues are also maintained by a number of *negative growth inhibitory signals*.



• **Figure 2.1.4.17** Angiogenesis. In tissue repair, angiogenesis primarily occurs through the sprouting of new vessels, driven by vascular endothelial growth factor (VEGF) and other soluble mediators. The process involves basement membrane degradation, endothelial proliferation, chemotaxis, and differentiation, as well as the recruitment of pericytes to form mature vessels. (Reproduced by permission from Kumar, V., Abbas, A.K., Aster, J.C. (Eds.), 2018. Robbins Basic Pathology, tenth ed. Elsevier, Philadelphia, PA.)

When cells are not capable of complete proliferative regeneration or when the ECM is not entirely preserved, the outcome will be scar. This involves the progressive degradation of the originally damaged tissues, the generation of new blood vessels to provide a path for delivering nutrients and cells to make the scar, and eventually remodeling of the deposited matrix.

Vascular Response

New vessels in the evolving site of repair originate by budding from preexisting vessels, a process called *angiogenesis* or *neovascularization* (Fig. 2.1.4.17). There are several different proangiogenic mediators (many synthesized by activated macrophages), although *vascular endothelial growth factor* (VEGF) and *basic fibroblast growth factor* are probably the most important. These factors induce the following vasculogenic effects:

- proteolytic degradation of the parent vessel basement membrane allowing formation of a capillary sprout;

- migration of endothelial cells toward the angiogenic stimulus;
- proliferation of the endothelial cells behind the leading front of migrating cells;
- maturation of endothelial cells and organization into capillary tubes.

These new vessels have incompletely formed interendothelial junctions, resulting in the leakage of proteins and red cells into the extravascular space. VEGF also profoundly increases endothelial transcytosis, which will augment fluid leak across the vessel wall. Indeed, this leakiness explains why *granulation tissue is often edematous*, and accounts for much of the edema that persists in healing wounds long after the acute inflammatory response has resolved. Subsequent long-term vessel stabilization of the new vessels requires *angiopoietin-1* binding to Tie2 receptors on endothelial cells to induce perivascular *pericyte* (perivascular smooth muscle-like cells) recruitment.

Wound Healing in the Presence of Biomaterials

For biomaterials and medical device implantation, two sources of injury are important: that caused by the surgery itself, and that secondary to the implanted foreign body (for additional details, see chapter on inflammation, FBR and repair - Babensee). Regardless of the size, nature, and overall biocompatibility of an implant, some degree of tissue disruption, necrosis, and cell damage is unavoidable, even with minimally invasive insertion. By itself, this will induce some inflammation and fibrosis at the tissue–implant interface. In general, synthetic biomaterials are not immunogenic, and are therefore not “rejected” by adaptive immune cells like a transplanted organ. However, they typically elicit a *foreign body reaction* (FBR), a special form of nonimmune inflammation involving the innate immune system. To the extent that a foreign body reaction is elicited, the fibrotic process will be augmented. The nature of the reaction is largely dependent on the chemical and physical characteristics of the implant. Tissue interactions can be modified by changing the chemistry of the surface (e.g., by adding specific chemical groupings to stimulate adhesion or bone formation in orthopedic implants, or inadvertently by adding some toxic component), inducing roughness, complexity, or porosity to enhance physical binding to the surrounding tissues, incorporating a surface-active agent to chemically bond the tissue, or using a bioresorbable component to allow slow replacement by tissue to simulate natural healing properties (Nour et al, 2019).

The most prominent cells in the FBR are macrophages, activated to phagocytose the material; however, degradation in many cases is likely to be difficult, if not impossible (e.g., a titanium implant). As already described, these activated macrophages (Chu et al, 2020) will elaborate cytokines that stimulate inflammation or fibrosis. The more *biocompatible* the implant, the more quiescent the ultimate response. However, in the absence of perfect biocompatibility, there will always be some degree of fibrosis. Moreover, the macrophage-driven

inflammation can cause local tissue injury; the ability of inflammatory cells to adhere to but not phagocytose particles larger than a critical size (*frustrated phagocytosis*) can lead to release of enzymes (exocytosis) to the extracellular environment. In bone, the cytokines elaborated by the macrophages can also induce bone resorption. Thus inflammatory cell products that are critical in killing microorganisms in typical inflammation can damage tissue adjacent to foreign bodies (e.g., osteolysis adjacent to an implant in bone).

Complications and Defective Wound Healing

In wound healing, normal cell growth and fibrosis may be altered by a variety of influences, frequently reducing the quality and adequacy of the reparative process:

- *Infection* is the single most important cause of delay in healing, by prolonging the inflammation phase of the process, and potentially increasing the local tissue injury.
- *Nutrition* has profound effects on wound healing; protein deficiency, for example, and particularly vitamin C deficiency, inhibit collagen synthesis and retard healing.
- *Glucocorticoids* have antiinflammatory effects (largely by reducing macrophage activation) and cause poor wound strength due to diminished fibrosis and/or remodeling.
- *Mechanical factors* such as increased local tension may cause wounds to pull apart (*dehisce*).
- *Poor perfusion* (e.g., due to atherosclerosis or obstructed venous drainage) also impairs healing.
- Finally, *foreign bodies* such as fragments of steel, glass, or even bone act as foci for chronic inflammation and impede healing.

Acknowledgments

RNM and FJS would like to recognize the helpful discussions and thoughtful input of Dr. Cecelia Yates, Ph.D.,

Assistant Professor, Department of Health Promotion and Development, School of Nursing, University of Pittsburgh.

References

- Brown, B.N., Ratner, B.D., Goodman, S.B., Amar, S., Badylak, S.F., 2012. Macrophage polarization: An opportunity for improved outcomes in biomaterials and regenerative medicine. *Biomaterials* 33, 3792–3802.
- Carmeliet, P., 2003. Angiogenesis in health and disease. *Nature Med* 9, 653–660.
- Chen, C.S., 2008. Mechanotransduction: A field pulling together? *J. Cell Sci.* 121, 3285–3292.
- Duggal, S., Fronsdal, K.B., Szöke, K., Shahdadfar, A., Melvik, J.E., et al., 2009. Phenotype and gene expression of human mesenchymal stem cells in alginate scaffolds. *Tissue Eng. Part A* 15, 1763–1773.
- Hinz, B., Phan, S.H., Thannickal, V.J., Galli, A., Bochaton-Piallat, M.L., et al., 2007. The myofibroblast: One function, multiple origins. *Am. J. Pathol.* 170, 1807–1816.
- Lutolf, M.P., Hubbell, J.A., 2005. Synthetic biomaterials as instructive extracellular microenvironments for morphogenesis in tissue engineering. *Nat. Biotechnol.* 23, 47–55.
- Lutolf, M.P., Gilbert, P.M., Blau, H.M., 2009. Designing materials to direct stem-cell fate. *Nature* 26 (462), 433–441.
- Mosser, D.M., Edwards, J.P., 2008. Exploring the full spectrum of macrophage activation. *Nature* 8, 958–969.
- Yi, B.A., Wernet, O., Chien, K.R., 2010. Regenerative medicine: Developmental paradigms in the biology of cardiovascular regeneration. *J. Clin. Invest.* 120, 20–28.
- Ingber, D.E., 2003. Mechanosensation through integrins: Cells act locally but think globally. *Proc. Natl. Acad. Sci.* 100, 1472.
- Ingber, D.E., 2010a. Mechanical control of tissue and organ development. *Development* 137, 1407–1420.
- Ingber, D.E., 2010b. From cellular mechanotransduction to biologically inspired engineering. *Ann. Biomed. Eng.* 38, 1148–1161.

2.1.5

The Extracellular Matrix and Cell–Biomaterial Interactions

WOJIN M. HAN^{1,3}, YOUNG C. JANG^{2,3}, ANDRÉS J. GARCÍA^{1,3}

¹George W. Woodruff School of Mechanical Engineering, Georgia Institute of Technology, Atlanta, GA, United States

²School of Biological Sciences, Georgia Institute of Technology, Atlanta, GA, United States

³Parker H. Petit Institute of Bioengineering and Biological Science, Georgia Institute of Technology, Atlanta, GA, United States

Introduction

The extracellular matrix (ECM) serves as a microenvironmental niche providing both biophysical and biochemical signals in which cells reside and function within the body. Therefore, understanding the composition, structure, and functions of the native ECM is essential to engineering biomaterials for maintaining and/or directing cellular function for biomedical applications. This chapter summarizes compositions, properties, and functions of the native ECM, and how these inform the understanding and engineering of cell–biomaterial interactions. The following concepts are covered:

1. Definition, properties, and functions of the ECM
2. Cell–biomaterial interactions.

Extracellular Matrices

Extracellular matrices (ECMs) are heterogeneous mixtures of noncellular biological materials that, together with cells, constitute tissues and organs (Box 2.1.5.1). At a tissue-level, the ECM acts as scaffolding materials that provide structural and mechanical support. At a cellular-level, the ECM functions as a physical medium in which cells can adhere and function. Indeed, the ECM provides an array of biochemical and biophysical cues that regulate important cellular functions, including survival, proliferation, migration, self-renewal, and differentiation. Finally, the ECM also serves as a reservoir for growth factors and cytokines through sequestration; these signaling molecules are critical for modulating processes of tissue development, homeostasis, and regeneration (Fig. 2.1.5.1).

In many cases, the composition and structure of the ECM can permit highly specialized functions of a tissue. For example, in tendons, densely packed and aligned collagen fibers within the ECM grant high levels of tensile strength and elasticity (Benjamin et al., 2008). In the kidney, the glomerular basement membrane composed of a complex mixture of proteins, including type IV collagen, laminin, and proteoglycans, dictates selectively permeable filtration between the vasculature and the urinary space (Miner, 2012). Thus, variations in the ECM composition and structure can give rise to tissues with highly diverse forms and functions. Concurrently, tissue resident cells that interact with their ECM continuously process environmental cues to regulate tissue development, homeostasis, and regeneration.

The ECM is composed of cell-secreted proteins (Figs. 2.1.5.1 and 2.1.5.2A). The ECM is structurally dynamic and adaptive, as the cells constantly remodel (enzymatically and nonenzymatically) their surrounding microenvironment. Components of the ECM can be broadly classified into: (1) fibrillar, structural, and adhesive proteins (e.g., collagen, elastin, laminin, fibronectin, and vitronectin); (2) amorphous matrix macromolecules (e.g., proteoglycans, glycosaminoglycans, and hyaluronan); and (3) specialized soluble factors (e.g., growth factors, cytokines, and hormones). The ECM composition varies depending on the tissue type, developmental stage, age, and pathology. Details for these ECM components are discussed in the subsequent sections.

Properties of the Extracellular Matrix

The ECM provides a vast array of signaling cues for the cells to process and elicit downstream functions. Inherent ECM

properties define such signaling cues, which can be broadly categorized into biophysical and biochemical properties.

Biophysical properties of the ECM include stiffness, viscoelasticity, topography, and permeability (Fig. 2.1.5.2B). These properties dictate cellular functions in both direct and indirect manners. Mechanical properties of the ECM, such as stiffness and viscoelasticity, directly impact cellular phenotype and function through cell receptor-targeting ligands to which cells adhere. In response to the ECM mechanical properties, cells adapt their shape, cytoskeletal organization, and tension that result in changes to cellular function, such as migratory activity and gene expression. Structural properties of the ECM, such as topography, influence cellular shape, orientation, and alignment, which further contribute to determining tissue forms and function. The ECM instructs cells to regulate ECM composition and structure through an intricate feedback mechanism, a concept known as “dynamic reciprocity” (Bissell et al., 1982). Other biophysical properties, such as permeability, facilitate solute and nutrient transport. Thus, an assembly of biophysical properties of the ECM contributes to complex mechanisms

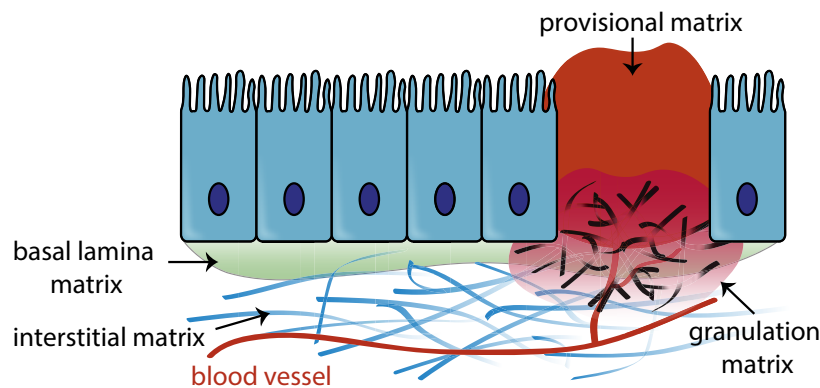
• BOX 2.1.5.1 Functions of the ECM

ECMs act as dynamic scaffolding materials that provide physical support and enable specialized functions of tissues. Furthermore, ECMs provide materials in which cells can adhere and function. The primary functions of ECMs include:

- Matrix for cell adhesion
- Regulation of cell morphology and orientation
- Regulation of cell proliferation
- Regulation of stem cell self-renewal and differentiation
- Sequestration and presentation of growth factors and cytokines.

governing tissue organogenesis, homeostasis, regeneration, and pathology in a cell- and tissue-specific manner.

Biochemical properties of the ECM include types of receptor-targeting ligands for cell adhesion, electrochemical potential, pH, protease sensitivity, and soluble signaling factors (Fig. 2.1.5.2B). Cells express a variety of receptors, including integrins, on their surface to bind to the ECM. The ECM proteins present targeted cell-binding sites that are specific to types of adhesion receptors (e.g., integrins) found on cell surface, which varies depending on the ECM composition (Fig. 2.1.5.2C). Engaging specific sets of adhesion receptors initiates critical cellular functions in a cell- and tissue-specific context, including cell survival, migration, proliferation, and stem cell self-renewal and differentiation. Interactions between receptors and the ECM also influence cellular anchorage to the ECM. Divalent cations, such as Ca^{2+} and Mg^{2+} , mediate the integrin–ligand binding event. Other ions present in the ECM, including Na^+ , Cl^- , K^+ , H^+ , and OH^- are critical for maintaining physiological ionic concentration gradients, osmolarity, pH, and cellular membrane potential. Furthermore, certain ECM components (e.g., anionic hyaluronan and heparan sulfate proteoglycans) play important roles in sequestering specialized soluble factors (e.g., cationic growth factors) through charge interactions. Sequestration enables the ECM to protect growth factors from degradation, modulate availability in a spatiotemporal manner, and potentially enhance their activity. In some specialized tissues, such as articular cartilage, negatively charged proteoglycans interact with positively charged ions to achieve internal tissue pressurization through a Donnan osmotic effect (Mow et al., 1984; Roughley, 2006). This swelling effect gives articular cartilage not only the ability to withstand high compressive loads, but also provides a cellular microenvironment with high levels of hydrostatic and osmotic pressure to regulate



Interstitial Matrix	Basal Lamina Matrix	Provisional Matrix	Granulation Matrix
<ul style="list-style-type: none"> ▪ Collagen type I-III ▪ Elastin ▪ Fibronectin ▪ Proteoglycans ▪ Growth factors 	<ul style="list-style-type: none"> ▪ Collagen IV ▪ Laminins ▪ Entactin/nidogen ▪ Proteoglycans ▪ Growth factors 	<ul style="list-style-type: none"> ▪ Fibrinogen/fibrin ▪ Fibronectin (plasma) ▪ Proteoglycans 	<ul style="list-style-type: none"> ▪ Collagen type I-III ▪ Fibronectin (cellular) ▪ Proteoglycans

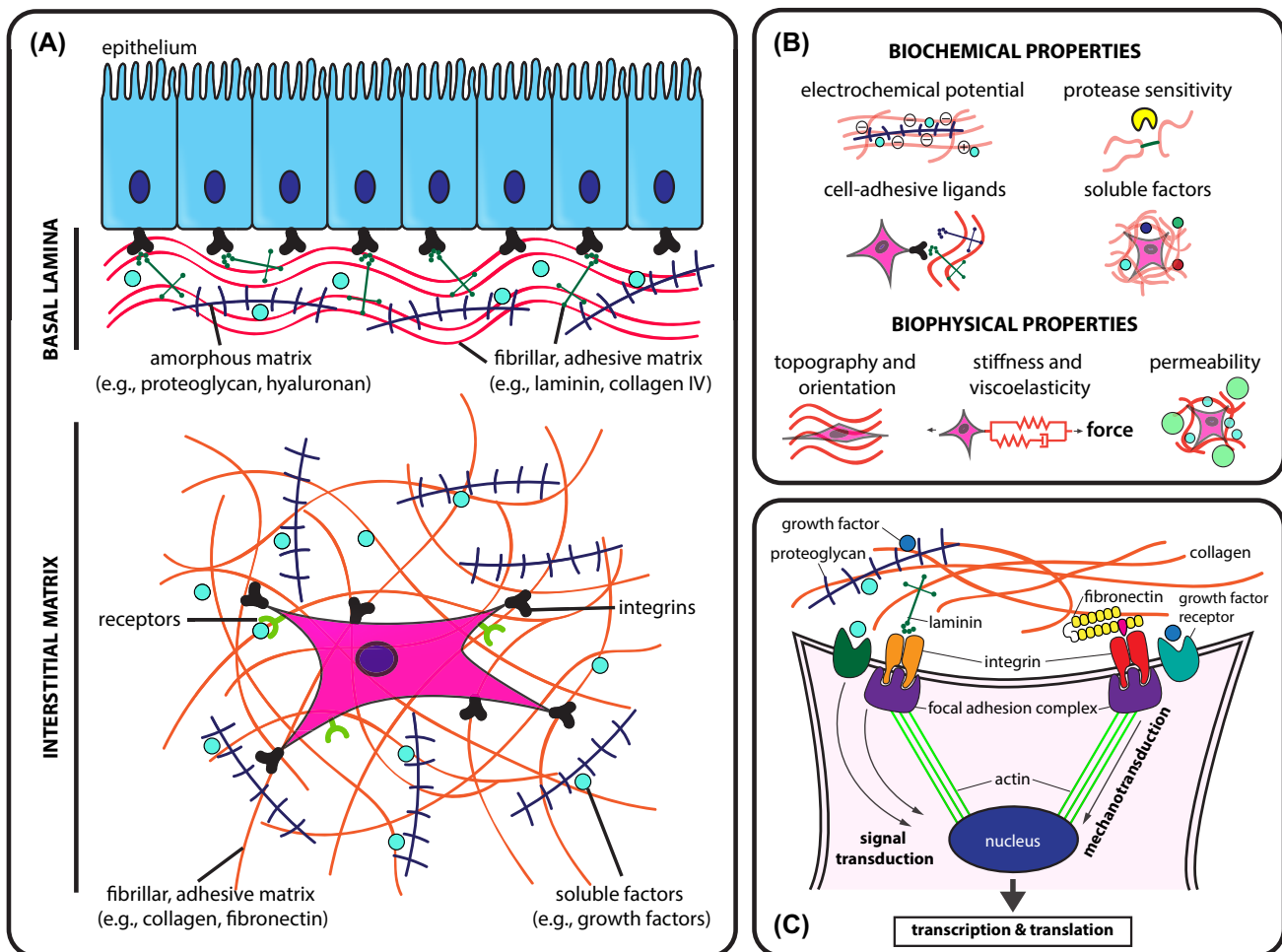
• **Figure 2.1.5.1** The composition of different ECM types: interstitial matrix, basal lamina matrix, provision (clot) matrix, and granulation matrix.

chondrocyte function. Finally, protease-sensitive domains found throughout various ECM proteins enable cells to readily degrade their surrounding matrix for remodeling and migration. Therefore, it is important to note that both biochemical and biophysical properties of the ECM collectively provide indispensable cell-instructive cues for regulating tissue development, homeostasis, and regeneration. ECM components that contribute to these properties are described below.

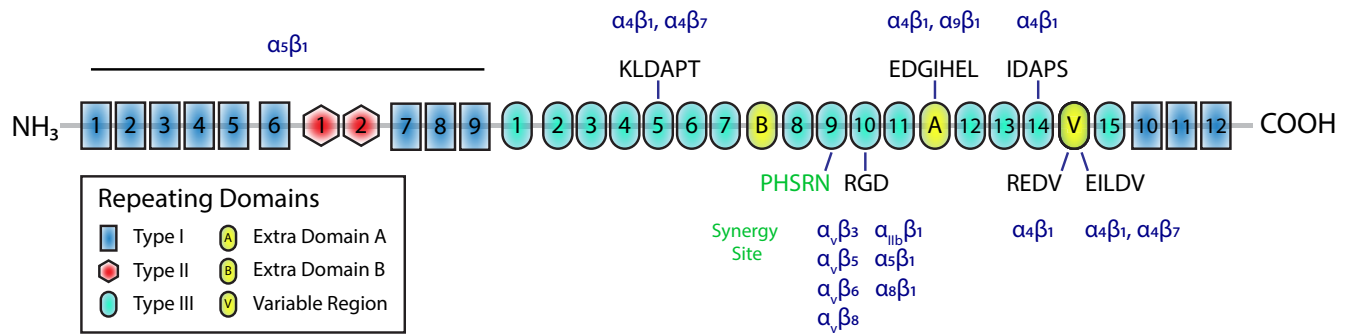
Collagens and Elastin

Collagen is a highly conserved family of proteins found throughout the body. In fact, collagen is one of the most common proteins in mammals, constituting approximately 25% of the whole-body protein composition. The primary function of collagen is to provide a structural framework for tissues and organs. In fibrous connective tissues, such

as tendons, collagen plays an indispensable role in enabling tensile strength of a tissue. Collagen consists of a highly organized group of tropocollagens—a triple helical structure consisting of three polypeptide chains tightly coiled together. To date, there are over 25 different subtypes of collagens identified. Generally, these subtypes of collagens can be categorized into groups according to the structure they form—fibrillar and nonfibrillar. Collagen types I, II, III, and V are fibrillar collagens that are the most abundant in the body. Type I collagen is a ubiquitous component of hard and soft tissues, including skin, tendons, bone, and vasculature. Type II collagen is most commonly found in cartilaginous tissues, including articular cartilage and intervertebral disks. Type III collagen is a major component of soft tissues, including the liver and bone marrow. It is also normally present in conjunction with type I collagen. Type V collagen is found in dermal–epidermal junctions (e.g., hair) and placental tissues, and similarly to type III collagen, it is also commonly



• **Figure 2.1.5.2** The extracellular matrix (ECM). (A) Main components of the ECM. Prominent ECM components include collagens, fibronectin, laminins, proteoglycans, and growth factors. Basal lamina and interstitial matrix have different composition and structure. (B) Key properties of the ECM can be classified into biophysical and biochemical properties. These properties regulate cell behavior in both direct and indirect manners. (C) Cell–ECM interactions. Cells adhere to the ECM primarily through integrin–ECM interactions. Cells process various ECM cues through integrin and receptors. Integrins modulate activities of focal adhesion complexes and cytoskeleton, which further generate downstream signaling to alter transcription and translation.



• **Figure 2.1.5.3** Schematic of fibronectin depicting its structure, binding sites, and target integrins.

found in tissues containing type I collagen. Collagen type IV is a nonfibrillar collagen that is universally present in basement membranes, which form the basal lamina for epithelial and endothelial tissues throughout the body. Collagen, as one of the most abundant proteins that constitute the ECM, plays a critical role in giving tissues their mechanical and structural integrity. Consequently, it is one of the most important ECM components that prescribe the various biophysical properties of the ECM, such as stiffness, viscoelasticity, topography, and porosity. Furthermore, collagen also contains numerous integrin-binding domains that the cells can directly interact with. For example, integrins $\alpha_1\beta_1$ and $\alpha_2\beta_1$ are common collagen-targeting integrins that directly bind to sites within types I, II, and IV collagens (Gullberg et al., 1990; Staatz et al., 1991; Vandenberg et al., 1991). These $\alpha_1\beta_1$ and $\alpha_2\beta_1$ integrin-binding sites consist of the six-residue polypeptide sequence *GFOGER* arranged in a triple-helical conformation located in the $\alpha_1(I)$ chain of collagen I and IV (Knight et al., 2000; Reyes and García, 2003).

Elastic fibers, composed of elastin proteins, are primarily responsible for the highly elastic properties of a tissue, which allow tissues to return to their original or resting state after being deformed. Therefore, elastin plays a critical role in tissues that are mechanically dynamic, such as the arteries, lungs, skin, bladder, and tendons. Elastin further contributes to the complexity of ECM biophysical properties through direct regulation of the local elasticity at the cellular level. In addition, elastin possesses domains that target several integrins and other receptors. For example, the polypeptide sequences *GRKRK* and *VGVAPG* found in tropoelastin monomers bind $\alpha_v\beta_3$ and $\alpha_v\beta_5$ integrins, as well as a receptor known as the 67-kDa elastin-binding protein in a synergistic manner (Bax et al., 2009; Blood et al., 1988; Floquet et al., 2004; Lee et al., 2014; Patel et al., 2011).

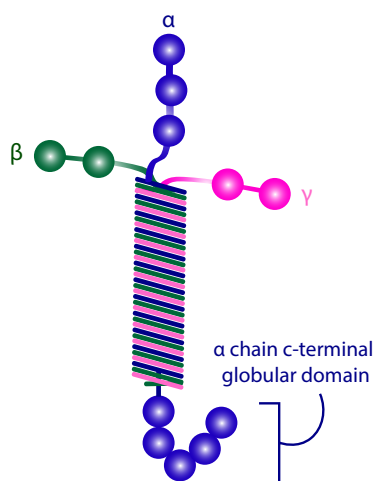
Fibronectin

Fibronectin is a glycoprotein that contains numerous binding sites for integrins as well as other ECM proteins, such as collagen, fibrin, and proteoglycans. Two types of fibronectin exist: soluble plasma fibronectin and insoluble cellular fibronectin. Soluble fibronectin is a dimeric protein, where two polypeptide subunits are covalently joined by disulfide bonds at the C-terminal ends. Fibronectin is also

synthesized and processed by cells to yield insoluble cellular fibronectin in the form of fibrils. The fibronectin molecule consists of three types of repeating domains: types I, II, and III (Fig. 2.1.5.3; Pankov and Yamada, 2002). These repeating domains present various binding sites for integrins and other ECM proteins as either exposed or cryptic forms (Fig. 2.1.5.3). Cryptic interaction sites, often found in type III domains, are normally inaccessible to binding due to their structure. However, these cryptic sites become accessible upon conformational change, such as cell-mediated mechanical unfolding of the protein, suggesting its dynamic nature. Here, it is important to highlight that fibronectin exists in different forms with differential adhesive properties due to alternative splicing that occurs prior to translation. Fibronectin harbors binding sites for more than 10 types of integrins, including $\alpha_5\beta_1$, $\alpha_4\beta_1$, $\alpha_5\beta_1$, and $\alpha_v\beta_3$, making it a ubiquitous and potent cell-adhesive protein found in the ECM (Pankov and Yamada, 2002). One of the most well-known binding sites, the *RGD* tripeptide sequence, is found in the type III domain of fibronectin. The *RGD* sequence alone recognizes a host of integrins, from $\alpha_5\beta_1$, $\alpha_8\beta_1$, $\alpha_v\beta_1$, $\alpha_v\beta_3$, $\alpha_v\beta_5$, $\alpha_v\beta_6$, $\alpha_v\beta_8$, to $\alpha_{IIb}\beta_3$ (Pankov and Yamada, 2002; Ruoslahti, 1996). Other integrin-binding sequences, such as *REDV*, *EILDV*, *IDAPS*, and *KLDAPT*, present within fibronectin bind integrins $\alpha_4\beta_1$ and $\alpha_4\beta_7$ (Pankov and Yamada, 2002). As a result, fibronectin is a vital ECM protein that regulates cellular functions in critical biological events, including embryogenesis, development, and wound healing.

Laminins

Laminins are a major constituent of the basement membrane. Laminins are large trimeric proteins consisting of α , β , and γ chains assembled in a coiled coil structure, which can give rise to at least distinct 15 isoforms (five variants of α , four variants of β , and three variants of γ ; Fig. 2.1.5.4). As a major constituent of basement membranes, laminins play important roles in interacting with proteoglycans, glycoproteins, and collagens (e.g., syndecan, agrin, heparin, collagen IV, and collagen VII) and in turn strengthening the ECM structure. Through a series of systematic screening assays using proteolytic fragments and synthetic peptides, multiple cell-binding sites have been identified throughout



• **Figure 2.1.5.4** Schematic of laminins. Laminins are trimeric proteins consisting of α , β , and γ chains assembled in a coiled coil structure.

the trimeric chains. For example, in the laminin-111 isoform, 45, 14, and 12 active peptide sequences that modulate cell adhesion are present in $\alpha 1$, $\beta 1$, and $\gamma 1$ chains, respectively (Kikkawa et al., 2013). Of note, *YIGSR* from $\beta 1$ chain (targets the 67-kDa laminin receptor) and *IKVAV* from $\alpha 1$ chain (targets $\alpha_3\beta_1$ and $\alpha_6\beta_1$ integrins) polypeptide sequences are implicated in various cellular and disease contexts, such as tumor adhesion, proliferation, and angiogenesis (Kikkawa et al., 2013).

Proteoglycans, Glycosaminoglycans, and Hyaluronic Acid

Glycosaminoglycans (GAGs) are highly polarized (charged) carbohydrates composed of repeating disaccharide units. GAGs are categorized into four groups based on their carbohydrate residues: hyaluronic acid, chondroitin/dermatan sulfate, heparan sulfate, and keratan sulfate. Highly sulfated GAG chains are coupled to core proteins to form proteoglycans that resemble a bottle brush. Hyaluronic acid is an exception, as it is the only type of GAG to lack sulfation, as well as lacking attachment to a core protein to form a proteoglycan. Diverse types of proteoglycans exist based on variation of the core protein and decorated GAGs. Small proteoglycans (<50 kDa) include decorin, biglycan, testican, fibromodulin, and lumican; large proteoglycans (>100 kDa) include versican, perlecan, aggrecan, neurocan, and brevican. Structurally, proteoglycans described as “filler” macromolecules that are amorphous. Despite the lack of defined structure, GAGs and proteoglycans impart important functions in the ECM. Proteoglycans attract and retain large volumes of water in the interstitial space through its polar nature. In certain tissues, such as the articular cartilage, GAGs and proteoglycans impart lubricating and shock-absorbing properties to the tissue (Mow et al., 1984; Roughley, 2006). Small proteoglycans participate in regulation of collagen fibril growth and organization (Chen and Birk, 2013; Kalamajski and Oldberg, 2010). Finally, cell membrane-bound proteoglycans, such as

syndecans, also play an important role in binding collagen and fibronectin in the ECM as well as growth factors (Elfenbein and Simons, 2013).

Growth Factor Sequestering Proteins and Motifs

Soluble factors, such as growth factors, cytokines, and hormones, are potent modulators of cellular functions. Within the ECM, dynamic biochemical interactions between the ECM and growth factors intricately control the stability, availability, and bioactivity of growth factors. For example, heparan sulfate proteoglycans present in the ECM can bind soluble factors, such as fibroblast growth factor 2 (FGF-2), and regulate spatiotemporal presentation of the growth factor to the cells through sequestration (Ornitz, 2000; Raman et al., 2003). Alternatively, heparan sulfate proteoglycans present on outer cell membranes bind soluble growth factors to temporally increase local concentration to accentuate their effects (Bernfield et al., 1999). Fibronectin also contains domains (e.g., 12th to 14th type III repeats, III12–14) that promiscuously bind growth factors with high affinity, including the vascular endothelial growth factor (VEGF), platelet-derived growth factor (PDGF), and transforming growth factor- β (TGF- β ; Martino and Hubbell, 2010). When this growth factor-binding domain is in proximity to an integrin-binding domain (e.g., presence of growth factor-binding III 12–14 and $\alpha_4\beta_1$ integrin-binding III 9–10 domains in the same polypeptide chain), a synergistic downstream response is produced through a cross-talk between the signals generated from the growth factor receptors and integrins (Martino et al., 2011). Similarly, multiple isoforms of laminin interact and bind growth factors through their α chain laminin-type G domains and accentuate the efficacy of growth factor-mediated responses (Ishihara et al., 2018). Thus, growth factor binding to the ECM sequesters growth factors from degradation, while increasing availability and bioactivity of growth factors in a spatiotemporal manner.

ECM Remodeling and Proteolysis

The ECM is structurally dynamic and adaptive, in which the cells continuously remodel through matrix degradation, synthesis, assembly, and modification. Regulation of ECM remodeling has direct implications on cell proliferation, migration, as well as release of sequestered growth factors, and it is essential for guiding important biological processes including morphogenesis, angiogenesis, development, and regeneration. In contrast, abnormal ECM remodeling is often associated with pathologic conditions. For instance, aberrant matrix deposition without adequate degradation causes fibrosis and matrix stiffening, which can further compromise normal cell function, tissue integrity, and aggravate disease progression (Bonnans et al., 2014). In fact, dysregulated ECM dynamics is a hallmark of cancer, where aberrant ECM promotes cellular mutation and metastasis (Lu et al., 2012).

Proteases mediate the breakdown of the ECM proteins. Three major families of proteases involved in degrading the ECM proteins are matrix metalloproteinases (MMPs), cathepsins, and a disintegrin and metalloproteinases with thrombospondin motifs (ADAMTS). There are over 20 members of MMPs that target a range of ECM proteins, including fibronectin, proteoglycans, collagen, and laminin (Nagase et al., 2006). Cathepsins are lysosomal proteases that are present in both intracellular and extracellular spaces and play critical roles in protein turnover. There are 11 types of cathepsins, which act as endopeptidases (types L, V, S, K, and F) or exopeptidases (types X, B, C, and H) to cleave peptide bonds at nonterminal and terminal ends of amino acid polypeptides, respectively. ADAMTS, consisting of 19 members, mostly target various types of proteoglycans. On the contrary, tissue inhibitors of metalloproteinases (TIMPs) regulate the enzymatic activity of MMPs through inhibition. Therefore, orchestrated activity of proteolytic enzymes, protease inhibitors, and protein synthesis and modifications dictate catabolic or anabolic outcomes of ECM remodeling.

Integrins and Adhesion Receptors

Cells interact with the ECM primarily through transmembrane adhesion receptors. A major class of such transmembrane proteins that mediate cell–ECM interactions are integrins. Integrins are heterodimers composed of two subunits of glycoproteins (α and β). In humans, there are at least 24 and 8 identified types of α and β subunits, respectively. Combinatory interactions of α and β subunits form diverse heterodimeric integrins, with each integrin type exhibiting differing ECM ligand-binding specificities. A list of human integrins and their respective target ECM ligands is summarized in Table 2.1.5.1 (Takada et al., 2007). Here, it is important to note that integrin–ECM ligand interactions (i.e., specificity and affinity) are dependent on extracellular divalent cations (Ca^{2+} and/or Mg^{2+}) as well as the conformational state of the extracellular portion of the integrins.

Two prominent functions of integrins are to provide anchoring forces to the ECM and to transduce signals from the ECM to the cell. During integrin-mediated adhesion, many adherent cell types form large cell adhesion complexes, known as focal adhesions, at the sites of integrin attachment. At focal adhesions, cytosolic proteins, such as vinculin, paxillin, tensin, and talin, cluster to form dynamic and multiprotein structures that provide a mechanical linkage between the ECM and cytoskeletal actin filaments. Cells process a variety of ECM-induced biophysical and/or biochemical signals through focal adhesion dynamics and signaling. Kinases, such as focal adhesion kinase (FAK) and Src kinases, regulate focal adhesion activity and its downstream functions. In many cases, growth factor receptors (e.g., epidermal growth factor receptor, EGFR) also localize to focal adhesions, and support integrin-mediated (e.g., $\alpha_2\beta_1$ and $\alpha_3\beta_1$) signaling through cross-talk signaling (Mainiero et al., 1996; Yu et al., 2000). Furthermore, emerging evidence

TABLE 2.1.5.1 List of Human Integrins and Their Known ECM Targets (Takada et al., 2007)

Integrins	ECM Target
$\alpha_1\beta_1$	Laminin, collagen
$\alpha_2\beta_1$	Laminin, collagen, thrombospondin, tenascin
$\alpha_3\beta_1$	Laminin, thrombospondin
$\alpha_4\beta_1$	Thrombospondin, fibronectin, osteopontin
$\alpha_5\beta_1$	Fibronectin, osteopontin, fibrillin, thrombospondin
$\alpha_6\beta_1$	Laminin, thrombospondin
$\alpha_7\beta_1$	Laminin
$\alpha_8\beta_1$	Tenascin, fibronectin, osteopontin, vitronectin
$\alpha_9\beta_1$	Tenascin, osteopontin
$\alpha_{10}\beta_1$	Laminin, collagen
$\alpha_{11}\beta_1$	Collagen
$\alpha_v\beta_1$	Fibronectin, osteopontin
$\alpha_v\beta_3$	Fibrinogen, vitronectin, thrombospondin, fibrillin, tenascin, fibronectin, osteopontin
$\alpha_{11b}\beta_3$	Fibrinogen, thrombospondin, fibronectin, vitronectin
$\alpha_6\beta_4$	Laminin
$\alpha_v\beta_5$	Osteopontin, vitronectin
$\alpha_v\beta_6$	Fibronectin, osteopontin
$\alpha_4\beta_7$	Fibronectin, osteopontin
$\alpha_D\beta_2$ (leukocytes)	Fibrinogen, fibronectin, vitronectin
$\alpha_M\beta_2$ (leukocytes)	Fibrinogen, heparin
$\alpha_X\beta_2$ (leukocytes)	Fibrinogen, heparin, collagen

implicates integrins in controlling cytoskeletal and nuclear structures in response to mechanical properties of the ECM. For example, mechanical signals (e.g., strain) may be transmitted from the ECM to the nucleus through integrin–actin–nuclear envelope connectivity and elicit alterations in the underlying chromatin structure to regulate gene expression, cellular phenotype, and function.

Integrin–ECM interactions are indispensable in governing critical biological functions in tissue- and cell-specific fashions. For instance, deletion of integrins (e.g., α_2 , α_4 , α_5 , and β_1 integrins) or ECM proteins (e.g., fibronectin, laminin α_5) results in embryonic lethality, underscoring the critical importance of integrin–ECM interactions during early embryogenesis (De Arcangelis and Georges-Labouesse, 2000; George et al., 1993; Miner et al., 1998). In many cell types, including fibroblasts, epithelial, and endothelial cells, loss of integrin-mediated

adhesion results in anoikis (anchorage-dependent apoptosis; Frisch and Ruoslahti, 1997). In bone, fibronectin-specific $\alpha_5\beta_1$ and collagen-specific $\alpha_2\beta_1$ integrins are essential for osteoblastic differentiation of bone marrow-derived mesenchymal stromal cells (Mizuno et al., 2000; Moursi et al., 1997). In skeletal muscle, laminin-specific $\alpha_7\beta_1$ integrin is necessary for maintaining the quiescence and self-renewal capacity of muscle satellite cells (Blanco-Bose et al., 2001; Rozo et al., 2016). In the immune system, leukocytes express $\alpha_M\beta_2$ integrin to mediate macrophage interaction with fibronectin and fibrinogen (Flick et al., 2004; Yakubenko et al., 2002). These examples highlight the vital role of integrin–ECM interactions in governing biological functions.

In addition to integrins, other types of receptors regulate ECM adhesion in a cell type-dependent manner. For example, fibroblasts, smooth muscle cells, neutrophils, and several types of cancer cells express the 67-kDa elastin-laminin receptor that primarily interacts with elastin and laminin with high affinity. Discoidin domain receptors (DDR) are collagen receptors expressed by both epithelial cells (DDR-1) and cells of mesenchymal origin (DDR-2), which also function as receptor tyrosine kinases. Syndecans, single transmembrane proteins decorated with heparan sulfate and chondroitin sulfate chains, also facilitate cell adhesion to the ECM, including collagen I, III, V, and fibronectin in a cell type-dependent manner. In certain contexts, syndecans act as coreceptors with integrins and growth factor receptors to potentiate downstream responses. In blood, leukocytes express P-selectin glycoprotein ligand-1 that interacts with P-selectin expressed on the activated platelets and endothelium, which facilitate the recruitment of leukocytes to the inflamed tissue. Thus, cells express a wide array of adhesion receptors to mediate binding and interactions with their surrounding ECM.

Cell–Biomaterial Interactions

Because of the pivotal importance of ECM–cell interactions in modulating cellular functions, incorporation of ECM-mimicking biophysical and biochemical properties that guide context-dependent cellular function is a central consideration in engineering biomaterials. To promote interactions between cells and biomaterials, purified ECM molecules and engineered ECM-mimetic adhesive peptides that target specific integrins and/or other receptors can be incorporated into the material. Broadly, this can be achieved through (1) adsorption from solution, (2) biochemical functionalization, and (3) cell-mediated ECM deposition. Furthermore, other ECM-mimetic features, such as material degradability and geometry, can be engineered to direct more complex cellular function using biomaterials. The subsequent sections highlight key strategies for engineering ECM-mimetic biomaterials designed to guide cell–biomaterial interactions and to achieve targeted cell and tissue responses.

Cell Interactions With Adsorbed Proteins on Biomaterials

Biomaterials can be coated with proteins through a process known as adsorption, the noncovalent deposition of macromolecules from solution onto a surface. Protein adsorption is controlled by three major determinants: (1) relative protein concentrations in solution, (2) diffusion of proteins, and (3) protein affinity for a biomaterial substrate. Protein properties (e.g., size, charge, hydrophobicity, structural stability) and material surface properties (e.g., charge, topography, hydrophobicity) influence these factors, and thus are important considerations in protein adsorption processes. Indeed, interactions between protein and surface physicochemical properties define the composition, quantity, affinity, and conformation of adsorbed proteins (and other biomacromolecules), and ultimately impact the cells through engagement of integrins and other receptors with varying degrees of specificity. For instance, protein conformational changes that occur following adsorption may expose cryptic binding sites that increase cell adhesion, or mask cell-binding ligands that reduce cell adhesion (Vogel et al., 2001). The importance of surface chemistry on cell responses has been illustrated in basic studies using self-assembled monolayers as model surfaces. In adsorbing full-length fibronectin to a substrate, surface chemistry ($-\text{CH}_3$, $-\text{OH}$, $-\text{COOH}$, and $-\text{NH}_2$) has profound effects on its conformational presentation on integrin-binding domains to cells (Keselowsky et al., 2003). Fibronectin adsorbed onto $-\text{OH}$ - and $-\text{NH}_2$ -modified surfaces exhibits selective binding affinity for $\alpha_5\beta_1$ integrin, whereas fibronectin adsorbed onto a $-\text{COOH}$ -modified surface exhibits high binding affinity for both $\alpha_5\beta_1$ and $\alpha_v\beta_3$ integrins (Keselowsky et al., 2003). Importantly, surface-directed modulation of fibronectin and its selective targeting of $\alpha_5\beta_1$ and $\alpha_v\beta_3$ integrins directly influences osteoblast adhesion, proliferation, and differentiation (Keselowsky et al., 2005). These studies highlight the importance of surface-dependent effects on ECM protein adsorption, bioactivity and integrin-binding specificity.

A major advantage of adsorbing a full-length ECM protein onto a surface is that it can support integrin-mediated cellular processes in a relatively simple manner with preservation of multiple bioactive sites. Physicochemical compatibility between the protein and substrate of interest is a predominant factor in controlling the presentation of these bioactive sites. However, the effects of specific integrins and growth factors are difficult to systematically investigate and control through adsorption of ECM proteins due to the presence of multiple integrin- and growth factor-binding sites. Additionally, adsorbed proteins can be out-competed or displaced by other macromolecules present in the biological environment. Furthermore, the possibility of transmitting a pathogen, eliciting a host immune response, and lot-to-lot variability of naturally derived matrices limit the use of such a methodology in the clinical setting (Box 2.1.5.2; Simon et al., 2003).

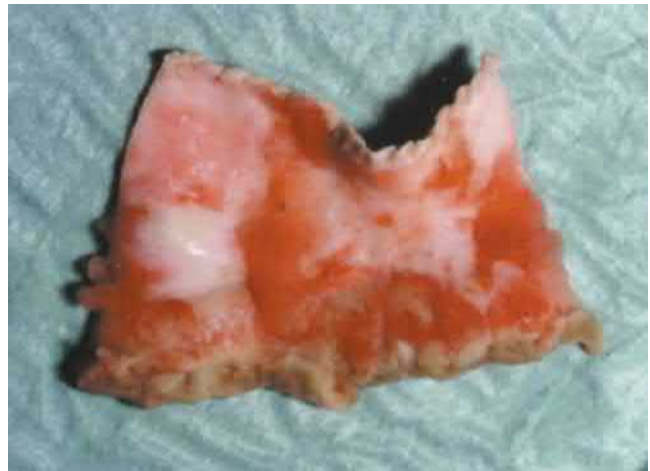
• BOX 2.1.5.2 Case Study—Safety Considerations in Manufacturing Naturally Derived Materials

Decellularized ECM scaffolds have been used in the clinical setting for over 10 years. A major advantage of decellularized ECM scaffolds is that they maintain bioactive sites and molecules. However, decellularized ECMs used in the clinic are typically derived from xenogeneic or allogeneic tissue sources, and therefore there is a possibility of transmitting pathogens and lot-to-lot variability. Furthermore, complete decellularization is difficult to achieve, and there is a significant risk of eliciting host immune responses. In 2001, xenogeneic collagen matrix-based decellularized porcine heart valves, Synergraft, were implanted in four pediatric patients (Simon et al., 2003). Unfortunately, three of the four patients died due to severe foreign body responses attributed to incomplete decellularization (Fig. 2.1.5.5). The fourth valve was prophylactically explanted from the patient 2 days after implantation (Fig. 2.1.5.5). Processing of naturally derived materials, thus, is an important safety consideration in clinical translation. These concerns also motivate the need for alternative *synthetic* approaches to regulate cell–biomaterial interactions in regenerative medicine, such as engineering receptor-targeting peptides, MMP-sensitive peptides, and synthetic peptide fibers that mimic the ECM structure.

Engineered Receptor-Targeting Peptide Sequences for Cell Adhesion

A strategy to systematically modulate integrin-specific cell functions is to functionalize biomaterial surfaces with short synthetic ECM-mimetic adhesive peptides derived from appropriate ECM proteins. ECM proteins possess domains that exhibit affinity for specific integrins and receptors. Prior work with proteolytically degraded protein fragments and screening for their specific integrin and receptor binding affinity led to the identification of numerous receptor-targeting domains. These ECM-derived cell-binding motifs are typically comprised of a short sequence of amino acids and establish the minimal amino acid sequences necessary to bind one or more integrin receptors. Integrin-targeting peptide sequences can easily be synthesized with high reproducibility and covalently functionalized onto biomaterial surfaces to promote cell adhesion. Furthermore, functionalization of peptide sequences to synthetic substrates enables the generation of fully synthetic biomaterials, which offer numerous advantages over naturally derived matrices, including minimal lot-to-lot variability and reduced risk of pathogen transmission.

The fibronectin-derived cell-binding tripeptide sequence *RGD* (arginine-glycine-aspartic acid) was first discovered by Pierschbacher and Ruoslahti in 1984 (Pierschbacher and Ruoslahti, 1984). The *RGD* sequence enables ubiquitous interactions with multiple integrins (Ruoslahti, 1996, Table 2.1.5.2). Although the *RGD* sequence was originally derived from fibronectin, the *RGD* motif is also found in other ECM proteins, including vitronectin, osteopontin, thrombospondin, and fibrinogen. As a potent binder of integrins, biomaterial substrates with the *RGD* peptides grafted onto the



• **Figure 2.1.5.5** An implant explanted 2-days post-implantation exhibits a severe inflammatory response and fibrotic sheath formation around the graft. (Adapted from Simon, P., Kasimir, M.T., Seebacher, G., Weigel, G., Ullrich, R., Salzer-Muhar, U., Rieder, E., Wolner, E., 2003. Early failure of the tissue engineered porcine heart valve SYNERGRAFT® in pediatric patients. *Eur. J. Cardiothorac. Surg.* 23, 1002–1006. [https://doi.org/10.1016/S1010-7940\(03\)00094-0](https://doi.org/10.1016/S1010-7940(03)00094-0).)

surface are widely investigated for various biomedical applications. *RGD* peptides immobilized onto an inert substrate retain their bioactivity and support cell adhesion (Massia and Hubbell, 1990). Furthermore, hydrogels consisting of naturally derived, synthetic, or natural-synthetic composite materials have emerged as powerful tools to engineer artificial ECMs that mimic many key features of the native ECM (Hern and Hubbell, 1998; Lutolf and Hubbell, 2005; Tibbitt and Anseth, 2009). For example, synthetic hydrogels functionalized with *RGD* peptides support human pluripotent stem cell-derived intestinal stem cell expansion and differentiation, giving rise to organoids analogous to native tissue (Cruz-Acuña et al., 2017; Gjorevski et al., 2016). In skeletal muscle, synthetic hydrogels functionalized with *RGD* peptides support muscle stem (satellite) cell survival, proliferation, and differentiation, and enable a biomaterial-mediated cell delivery strategy for treating muscle trauma and pathology (Han et al., 2018). Collectively, these studies demonstrate that *RGD*-functionalized synthetic hydrogels exhibit equal or better performance in supporting cellular functions compared to naturally derived matrices, such as collagen and Matrigel, and establish *RGD*-tethered biomaterials as potential alternatives for naturally derived ECM scaffolds (Cruz-Acuña et al., 2017; Gjorevski et al., 2016; Han et al., 2018; Lutolf and Hubbell, 2005). Biomaterials functionalized with *RGD* sequences have been used to direct cell adhesion, migration, and differentiation in diverse applications, including bone, neural, endothelial, liver, and cancer cells (as reviewed in Hersel et al., 2003).

Ligand density and clustering profoundly influence cellular functions in a cell type-dependent manner. For example, adhesion strength, proliferation, and mineralization potential of osteoblasts on *RGD*-functionalized surfaces positively correlate with *RGD* peptide density (Harbers and Healy, 2005). Dorsal root ganglia cells exhibit a biphasic

TABLE 2.1.5.2 List of Peptide Sequences and Their Known Integrin and Receptor Targets

Peptide Sequence	Parent ECM	Target Integrins and Receptors
RGD	Fibronectin	$\alpha_v\beta_3$, $\alpha_v\beta_5$, $\alpha_v\beta_6$, $\alpha_v\beta_8$, $\alpha_{IIb}\beta_1$, $\alpha_5\beta_1$, $\alpha_8\beta_1$
EILDV	Fibronectin	$\alpha_4\beta_1$, $\alpha_4\beta_7$
REDV	Fibronectin	$\alpha_4\beta_1$
KLDAPT	Fibronectin	$\alpha_4\beta_1$, $\alpha_4\beta_7$
EDGIHEL	Fibronectin	$\alpha_4\beta_1$, $\alpha_9\beta_7$
IDAPS	Fibronectin	$\alpha_4\beta_1$
PHSRN	Fibronectin	Synergy sequence for $\alpha_5\beta_1$
GFOGER	Collagen	$\alpha_1\beta_1$, $\alpha_2\beta_1$
GRKRK	Elastin	67-kDa elastin receptor, $\alpha_v\beta_3$, $\alpha_v\beta_5$
VGVAPG	Elastin	67-kDa elastin receptor, galectin-3 receptor, $\alpha_v\beta_3$
YIGSR	Laminin β_1 chain	67-kDa laminin receptor
IKVAV	Laminin α_1 chain	$\alpha_3\beta_1$, $\alpha_6\beta_1$
KAFDITYVRLKF (C16)	Laminin γ_1 chain	Syndecans, β_1
RKRLQVQLSIRT (AG73)	Laminin α_1 globular domain	Syndecans
SYWYRIEASRTG (A2G10)	Laminin α_2 globular domain	$\alpha_6\beta_1$

neurite outgrowth response as a function of the *RGD* peptide density in both two- and three-dimensional matrices, where the maximal neurite outgrowth is achieved at intermediate ligand densities and the neurite outgrowth is inhibited at higher ligand densities (Schense and Hubbell, 2000). Furthermore, fibroblast motility is directly dependent on *RGD* peptide density, and nanoscale clustering of the *RGD* peptides supports cell motility at significantly reduced overall ligand density (Maheshwari et al., 2000). These studies show that ligand density and clustering directly control the degree of integrin clustering, which ultimately influences cell adhesion, locomotion, and other cell-specific phenotypic changes through integrin-mediated signaling pathways.

Another factor that regulates integrin specificity of the biomimetic peptide sequence is the molecular structure that the peptide sequences form, i.e., secondary and tertiary

protein structures. As noted above, the linear *RGD* tripeptide sequence ubiquitously interacts with multitude of integrins. However, presentation of the tripeptide *RGD* in cyclic penta- and hexapeptide conformations further modulates its integrin specificity and affinity (Gurrath et al., 1992). For example, presentation of the *RGD* motif in cyclic forms, such as cyclo(*RGDFV*), significantly increases its binding specificity for $\alpha_v\beta_3$ integrin (Haubner et al., 1996). In the case of osteogenic cells, functionalization of the cyclic *RGD* on poly(methyl methacrylate) and poly(ethylene glycol)-poly(D,L-lactic acid) substrates promotes osteoblast adhesion, proliferation, and bone formation through selective engagement of $\alpha_v\beta_3$ and $\alpha_v\beta_5$ integrins (Kantlehner et al., 2000; Lieb et al., 2005). *GFOGER* is a hexapeptide sequence derived from the $\alpha_1(I)$ chain of collagen I and IV, where its mimicry of collagen's tertiary triple helical structure is critical for the recognition of $\alpha_1\beta_1$ and $\alpha_2\beta_1$ integrins (Knight et al., 2000; Reyes and García, 2003, 2004; Table 2.1.5.2). Indeed, the linear arrangement of the *GFOGER* sequence does not support effective binding of $\alpha_2\beta_1$ integrin in multiple cell types (Knight et al., 2000), highlighting the importance of the structure of integrin-targeting peptide sequences. In bone tissue engineering, *GFOGER*-functionalized hydrogels promote superior osteogenic differentiation and bone formation of human mesenchymal stromal cells compared to *RGD*-functionalized hydrogels both in vitro and in vivo (Shekaran et al., 2014). This further emphasizes the importance of targeting specific integrins in a context-dependent manner.

Other ECM-derived, integrin-targeting peptide sequences have been identified. Within fibronectin, other peptide sequences, such as *EILDV*, *REDV*, and *PHSRN*, are available. *EILDV* targets $\alpha_4\beta_1$ and $\alpha_4\beta_7$ integrins and plays a role in antimetastatic activity of tumors (Kaneda et al., 1997; Ukawala et al., 2011; Yamamoto et al., 1994, Table 2.1.5.2). *REDV* recognizes the $\alpha_4\beta_1$ integrin (Massia and Hubbell, 1992, Table 2.1.5.2). Fibronectin-derived *PHSRN* sequence acts as a synergistic motif with *RGD* in promoting $\alpha_5\beta_1$ binding to fibronectin and other $\alpha_5\beta_1$ -targeting peptide sequences when presented appropriately (Aota et al., 1994; Pankov and Yamada, 2002, Table 2.1.5.2). The synergistic binding affinity for $\alpha_5\beta_1$ integrin binding is further improved through a recombinant fibronectin fragment derived from type III repeats (FNIII₇₋₁₀; contains both *PHSRN* and *RGD* sequences) that recapitulates the native structure present in fibronectin, where cells exhibit superior adhesion strength and proliferation on a substrate functionalized with FNIII₇₋₁₀ than on a substrate functionalized with the *RGD-PHSRN* linear peptide (Petrie et al., 2006). Furthermore, FNIII₇₋₁₀-coated titanium improves implant integration and stability in vivo, highlighting the importance of protein tertiary structure in further modulating integrin specificity of peptide sequences arranged in a linear form (Petrie et al., 2008). Elastin-derived peptides *GRKRK* (Bax et al., 2009; Lee et al., 2014) and *VGVAPG* (Blanchevove et al., 2013; Blood et al., 1988; Floquet et al., 2004; Patel et al., 2011, Table 2.1.5.2) target $\alpha_v\beta_3$ and $\alpha_v\beta_5$ integrins, as

well as the 67-kDa elastin-binding protein in a synergistic manner. Finally, hundreds of adhesive peptide sequences are present within different isoforms of the laminin α , β , and γ chains (Hozumi et al., 2012, 2010; Katagiri et al., 2014, 2012; Kikkawa et al., 2013; Urushibata et al., 2010, 2009). Of note, *YIGSR* (β_1 chain-derived, targets 67 kDa receptor, Table 2.1.5.2) and *IKVAV* (α_1 chain-derived, targets $\alpha_3\beta_1$ and $\alpha_6\beta_1$ integrins, Table 2.1.5.2) sequences interact with different cell types, including cancer and mesenchymal stromal cells. Other laminin-derived peptide sequences and their respective targets are summarized in Table 2.1.5.2.

Engineered MMP-Sensitive Peptide Sequences for ECM Remodeling and Proteolysis

ECM remodeling is an important process that influences cellular activity (e.g., proliferation, migration) and tissue function (e.g., angiogenesis, regeneration) in native tissues. In designing biomaterials for regenerative medicine, material degradability is thus a major consideration in achieving the desired therapeutic outcomes. For example, when delivering stem cells using a hydrogel, the cells may need to degrade and remodel their surrounding matrix to survive, proliferate, migrate, and differentiate. It may also be necessary to engineer a biomaterial to degrade at a specific rate so that no material remains at the completion of therapy. To recapitulate cell-degradable properties, numerous proteolytically sensitive matrix metalloproteinase (MMP) and cathepsin substrate sequences have been identified and incorporated into biomaterials. For instance, these peptide sequences can be used to cross-link polymeric macromers to form a hydrogel, where the resulting hydrogel is endowed with a protease-sensitive property in which the cells can locally degrade as necessary. Incorporation of protease-sensitivity increases cell migration and proliferation within the material and provides a favorable condition for promoting an enhanced tissue-regenerative response in vivo (Lee et al., 2008, 2005; Lutolf et al., 2003, 2003b, 2003a; Phelps et al., 2010; West and Hubbell, 1999).

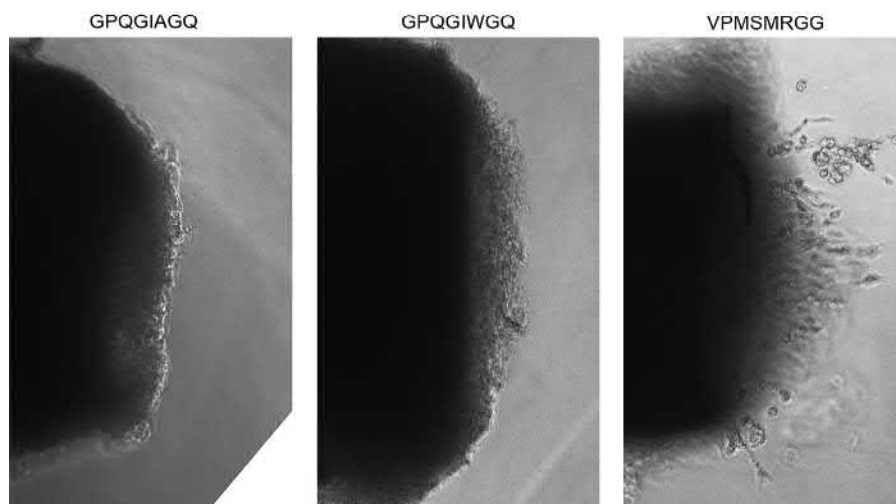
Early studies conducted to identify MMP-specific substrate sites using synthetic peptide sequences focused on protease-cleavable sites found in the α -chains of collagens (Dixit et al., 1979; Fields et al., 1987; Gross et al., 1974; Highberger et al., 1982; Miller et al., 1976; Nagai et al., 1976). It is now known that the peptide sequence *GPQG/ IAGQ* (glycine-proline-glutamine-glycine-isoleucine-alanine-glycine-glutamine; / indicates the cleavage site) found in the α -chains of collagens is MMP-active, and that a single amino acid substitution from A to W significantly increases its proteolytic susceptibility (Nagase and Fields, 1996). Indeed, synthesizing hydrogels with peptide sequences with a single amino acid substitution as polymer cross-linkers results in hydrogels that exhibit varying rates of degradation (Lutolf et al., 2003a). When used as a scaffold for bone healing, bone morphogenic protein-2 (BMP-2)-loaded

hydrogels that are more susceptible to proteolytic degradation support superior cellular invasion and bone formation in vivo degradation (Lutolf et al., 2003a). Similarly, superior vascularization is achieved when vascular endothelial growth factor (VEGF) is delivered using protease-sensitive hydrogels as opposed to nondegradable hydrogels, demonstrating that the protease-sensitivity is an essential property for promoting vascular invasion into the material (Phelps et al., 2010).

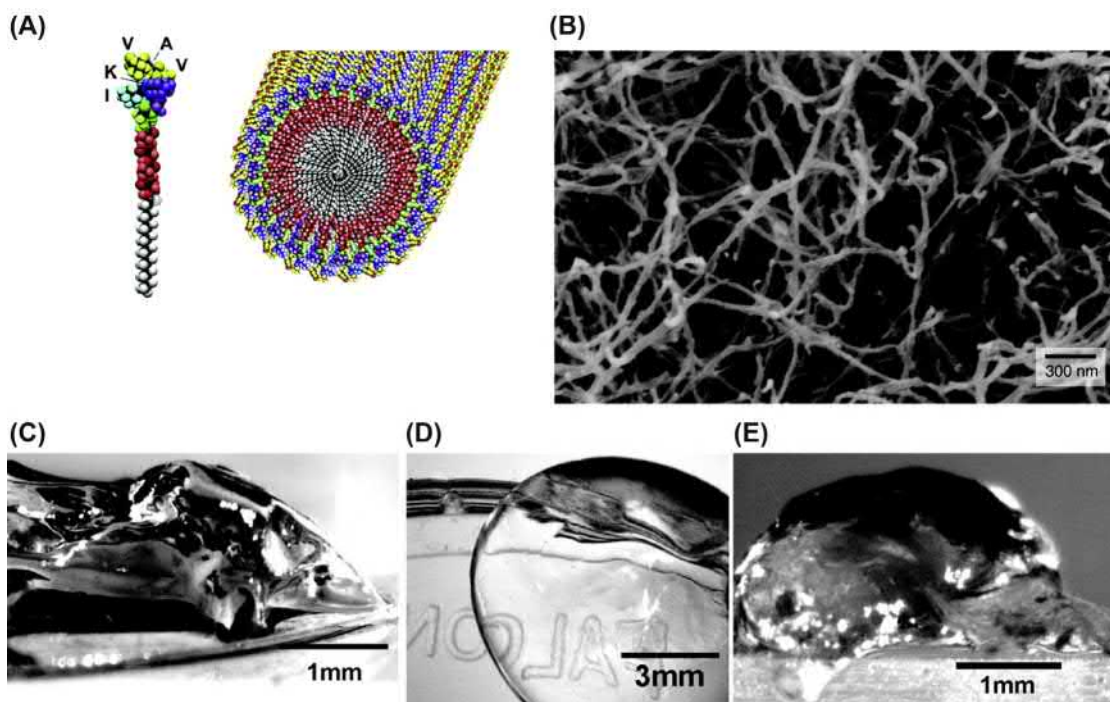
In addition to the collagen α -chains-derived *GPQG/ IAGQ* or *GPQG/IWGQ* sequences, many ECM-derived protease substrate sequences that exhibit specific affinity for different MMP types have been identified (Nagase and Fields, 1996; Patterson and Hubbell, 2010). Incorporation of protease-sensitive peptide sequences that exhibit differential sensitivity and specificity enables more precise tuning of hydrogel degradability. For example, the *VPMS/ MRGG* sequence exhibits increased sensitivity for MMP-1, 2, 3, 7, and 9 compared to the collagen α -chains-derived *GPQG/IAGQ* or *GPQG/IWGQ* sequences, and results in hydrogels that degrade more rapidly (Patterson and Hubbell, 2010). By tuning the hydrogel degradability, cellular functions, such as cell migration into the hydrogel, can be guided (Fig. 2.1.5.6, Patterson and Hubbell, 2010). *IPES/ LLAG* sequence, compared to the *VPMS/MRGG* sequence, exhibits reduced sensitivity for MMP-1, 3, and 9, but similar sensitivity for MMP-2 and 7, while its sensitivity for all MMP-1, 2, 3, 7, and 9 is higher than the collagen α -chains-derived *GPQG/IAGQ* or *GPQG/IWGQ* sequences (Patterson and Hubbell, 2010). As a result, hydrogels cross-linked with the *IPES/LLAG* sequence exhibit an intermediary degradation response, where they degrade at a higher rate than the *GPQG/IAGQ* or *GPQG/IWGQ* sequences but at a slower rate than the *VPMS/MRGG* sequence in response to MMP-1 and MMP-2 treatment (Patterson and Hubbell, 2010). Consequentially, cell spreading, proliferation, and migration of myofibroblasts encapsulated in these hydrogels can be controlled in a degradation rate-dependent manner (Patterson and Hubbell, 2010).

Engineered Peptide Fibers That Mimic the ECM Structure

The native ECM is composed of heterogeneous protein mixtures that are often fibrillar in form (e.g., collagens, elastin, fibronectin). The fibrillar structure plays an important role in regulating local mechanical properties, providing topographical cues for cellular alignment, and enhancing integrin-binding affinity (e.g., *GFOGER* peptide). To generate scaffolds that mimic the native ECM structure, self-assembled peptide amphiphiles (PAs) have been explored for synthesizing materials with fibrillar properties (Gore et al., 2001; Lin et al., 2012; Silva et al., 2004, Fig. 2.1.5.7). PAs are peptides conjugated with hydrophobic moieties, such as lipid tails (Berndt et al., 1995). Due to their amphiphilic properties, imparted by a hydrophobic tail and beta-sheet



• **Figure 2.1.5.6** Cell invasion into hydrogels can be guided by tuning the hydrogel degradability. Phase contrast micrographs of chick aortic rings encapsulated in the hydrogels after 48 h. Slow (GPQG/IAGQ), reference (GPQG/IWGQ), fast (VPMS/MRGG) degrading hydrogels, respectively. (Adapted from Patterson, J., Hubbell, J.A., 2010. Enhanced proteolytic degradation of molecularly engineered PEG hydrogels in response to MMP-1 and MMP-2. *Biomaterials* 31, 7836–7845. <https://doi.org/10.1016/j.biomaterials.2010.06.061>.)



• **Figure 2.1.5.7** (A) Schematic of IKVAV-presenting peptide amphiphile. (B) Scanning electron micrograph of nanofibrous network. (C–E) Photographs of the gels formed by adding IKVAV-presenting peptide amphiphiles in biological solutions (Silva et al., 2004).

forming amino acids, PAs self-assemble into aggregates of diverse structures in water. When physicochemical properties (e.g., charge, branching, tail length) are appropriately modulated, PAs self-assemble into a hydrogel with nanofibrous structure (Gore et al., 2001; Lin et al., 2012; Silva et al., 2004; Sleep et al., 2017). For instance, assembly of PA fibers that recapitulate the triple helical structure of a collagen fibril can be guided through controlling amphiphile

tail lengths (Gore et al., 2001). Encapsulation of neural progenitor cells in a hydrogel consisting of laminin-derived IKVAV-presenting nanofibrous network promotes selective and more rapid differentiation into neurons compared to laminin and soluble IKVAV peptides (Silva et al., 2004). Furthermore, myogenic precursor cells encapsulated in a PA hydrogel survive, proliferate, and differentiate into aligned myotubes (Sleep et al., 2017), suggesting that engineered

PAs can serve as a powerful system to introduce complex structural features in ECM-mimicking synthetic biomaterials for guiding cellular patterning and function. In addition to PAs, protein-based hydrogels consisting solely of artificially proteins, such as engineered elastin-like proteins, are also emerging as a strategy to generate bioscaffolds with precise control of structure and function (Sun et al., 2014; Wang et al., 2018) and present a tunable system for studying cell–matrix interactions.

Summary

The ECM is composed of a heterogeneous mixture of proteins and other macromolecules forming tissues and organs. The ECM provides both biophysical and biochemical signals to the resident cells, where the cell–ECM interactions are indispensable for many biological processes, including development, homeostasis, and regeneration. Therefore, recapitulating key aspects of the ECM is a critical consideration in engineering biomaterials. Notably, minimal peptide sequences that target specific integrins and other receptors enable systematic investigation of integrin-specific cell functions using biomaterials. Furthermore, peptide sequences that are sensitive to various types of proteases, as well as engineered peptide amphiphiles that self-assemble to form a nanofibrous network, increase the intricacy in mimicking structural dynamics of the native ECM, and enable engineering synthetic biomaterials for guiding cellular function and improving regenerative outcome in a context-dependent manner.

References

- Aota, S., Nomizu, M., Yamada, K.M., 1994. The short amino acid sequence Pro-His-Ser-Arg-Asn in human fibronectin enhances cell-adhesive function. *J. Biol. Chem.* 269, 24756–24761.
- Bax, D.V., Rodgers, U.R., Bilek, M.M.M., Weiss, A.S., 2009. Cell adhesion to tropoelastin is mediated via the C-terminal GRKRR motif and integrin alphaVbeta3. *J. Biol. Chem.* 284, 28616–28623. <https://doi.org/10.1074/jbc.M109.017525>.
- Benjamin, M., Kaiser, E., Milz, S., 2008. Structure-function relationships in tendons: a review. *J. Anat.* 212, 211–228. <https://doi.org/10.1111/j.1469-7580.2008.00864.x>.
- Berndt, P., Fields, G.B., Tirrell, M., 1995. Synthetic lipidation of peptides and amino acids: monolayer structure and properties. *J. Am. Chem. Soc.* 117, 9515–9522. <https://doi.org/10.1021/ja00142a019>.
- Bernfield, M., Götte, M., Park, P.W., Reizes, O., Fitzgerald, M.L., Lincecum, J., Zako, M., 1999. Functions of cell surface heparan sulfate proteoglycans. *Annu. Rev. Biochem.* 68, 729–777. <https://doi.org/10.1146/annurev.biochem.68.1.729>.
- Bissell, M.J., Hall, H.G., Parry, G., 1982. How does the extracellular matrix direct gene expression? *J. Theor. Biol.* 99, 31–68.
- Blanchevoye, C., Floquet, N., Scandola, A., Baud, S., Maurice, P., Bocquet, O., Blaise, S., Ghoneim, C., Cantarelli, B., Delacoux, F., Dauchez, M., Efreimov, R.G., Martiny, L., Duca, L., Debelle, L., 2013. Interaction between the elastin peptide VGVAPG and human elastin binding protein. *J. Biol. Chem.* 288, 1317–1328. <https://doi.org/10.1074/jbc.M112.419929>.
- Blanco-Bose, W.E., Yao, C.C., Kramer, R.H., Blau, H.M., 2001. Purification of mouse primary myoblasts based on alpha 7 integrin expression. *Exp. Cell Res.* 265, 212–220. <https://doi.org/10.1006/excr.2001.5191>.
- Blood, C.H., Sasse, J., Brodt, P., Zetter, B.R., 1988. Identification of a tumor cell receptor for VGVAPG, an elastin-derived chemotactic peptide. *J. Cell Biol.* 107, 1987–1993.
- Bonnans, C., Chou, J., Werb, Z., 2014. Remodelling the extracellular matrix in development and disease. *Nat. Rev. Mol. Cell Biol.* 15, 786–801. <https://doi.org/10.1038/nrm3904>.
- Chen, S., Birk, D.E., 2013. The regulatory roles of small leucine-rich proteoglycans in extracellular matrix assembly. *FEBS J.* 280, 2120–2137. <https://doi.org/10.1111/febs.12136>.
- Cruz-Acuña, R., Quirós, M., Farkas, A.E., Dedhia, P.H., Huang, S., Siuda, D., García-Hernández, V., Miller, A.J., Spence, J.R., Nusrat, A., García, A.J., 2017. Synthetic hydrogels for human intestinal organoid generation and colonic wound repair. *Nat. Cell Biol.* 19, 1326–1335. <https://doi.org/10.1038/ncb3632>.
- De Arcangelis, A., Georges-Labouesse, E., 2000. Integrin and ECM functions: roles in vertebrate development. *Trends Genet.* 16, 389–395.
- Dixit, S.N., Mainardi, C.L., Seyer, J.M., Kang, A.H., 1979. Covalent structure of collagen: amino acid sequence of alpha 2-CB5 of chick skin collagen containing the animal collagenase cleavage site. *Biochemistry* 18, 5416–5422.
- Elfenbein, A., Simons, M., 2013. Syndecan-4 signaling at a glance. *J. Cell Sci.* 126, 3799–3804. <https://doi.org/10.1242/jcs.124636>.
- Fields, G.B., Van Wart, H.E., Birkedal-Hansen, H., 1987. Sequence specificity of human skin fibroblast collagenase. Evidence for the role of collagen structure in determining the collagenase cleavage site. *J. Biol. Chem.* 262, 6221–6226.
- Flick, M.J., Du, X., Witte, D.P., Jirousková, M., Soloviev, D.A., Busuttill, S.J., Plow, E.F., Degen, J.L., 2004. Leukocyte engagement of fibrin(ogen) via the integrin receptor alphaMbeta2/Mac-1 is critical for host inflammatory response in vivo. *J. Clin. Investig.* 113, 1596–1606. <https://doi.org/10.1172/JCI20741>.
- Floquet, N., Héry-Huynh, S., Dauchez, M., Derreumaux, P., Tamburro, A.M., Alix, A.J.P., 2004. Structural characterization of VGVAPG, an elastin-derived peptide. *Biopolymers* 76, 266–280. <https://doi.org/10.1002/bip.20029>.
- Frisch, S.M., Ruoslahti, E., 1997. Integrins and anoikis. *Curr. Opin. Cell Biol.* 9, 701–706.
- George, E.L., Georges-Labouesse, E.N., Patel-King, R.S., Rayburn, H., Hynes, R.O., 1993. Defects in mesoderm, neural tube and vascular development in mouse embryos lacking fibronectin. *Development* 119, 1079–1091.
- Gjorevski, N., Sachs, N., Manfrin, A., Giger, S., Bragina, M.E., Ordóñez-Morán, P., Clevers, H., Lutolf, M.P., 2016. Designer matrices for intestinal stem cell and organoid culture. *Nature* 539, 560–564. <https://doi.org/10.1038/nature20168>.
- Gore, T., Dori, Y., Talmon, Y., Tirrell, M., Bianco-Peled, H., 2001. Self-assembly of model collagen peptide amphiphiles. *Langmuir* 17, 5352–5360. <https://doi.org/10.1021/la010223i>.
- Gross, J., Harper, E., Harris, E.D., McCroskery, P.A., Highberger, J.H., Corbett, C., Kang, A.H., 1974. Animal collagenases: specificity of action, and structures of the substrate cleavage site. *Biochem. Biophys. Res. Commun.* 61, 605–612.
- Gullberg, D., Turner, D.C., Borg, T.K., Terracio, L., Rubin, K., 1990. Different beta 1-integrin collagen receptors on rat hepatocytes and cardiac fibroblasts. *Exp. Cell Res.* 190, 254–264.
- Gurrath, M., Müller, G., Kessler, H., Aumailley, M., Timpl, R., 1992. Conformation/activity studies of rationally designed potent anti-adhesive RGD peptides. *Eur. J. Biochem.* 210, 911–921.

- Han, W.M., Anderson, S.E., Mohiuddin, M., Barros, D., Nakhai, S.A., Shin, E., Amaral, I.F., Pêgo, A.P., García, A.J., Jang, Y.C., 2018. Synthetic matrix enhances transplanted satellite cell engraftment in dystrophic and aged skeletal muscle with comorbid trauma. *Sci. Adv.* 4, eaar4008. <https://doi.org/10.1126/sciadv.aar4008>.
- Harbers, G.M., Healy, K.E., 2005. The effect of ligand type and density on osteoblast adhesion, proliferation, and matrix mineralization. *J. Biomed. Mater. Res. A* 75, 855–869. <https://doi.org/10.1002/jbm.a.30482>.
- Haubner, R., Gratiyas, R., Diefenbach, B., Goodman, S.L., Jonczyk, A., Kessler, H., 1996. Structural and functional aspects of RGD-containing cyclic pentapeptides as highly potent and selective integrin $\alpha V\beta 3$ antagonists. *J. Am. Chem. Soc.* 118, 7461–7472. <https://doi.org/10.1021/ja9603721>.
- Hern, D.L., Hubbell, J.A., 1998. Incorporation of adhesion peptides into nonadhesive hydrogels useful for tissue resurfacing. *J. Biomed. Mater. Res.* 39, 266–276.
- Hersel, U., Dahmen, C., Kessler, H., 2003. RGD modified polymers: biomaterials for stimulated cell adhesion and beyond. *Biomaterials* 24, 4385–4415.
- Highberger, J.H., Corbett, C., Dixit, S.N., Yu, W., Seyer, J.M., Kang, A.H., Gross, J., 1982. Amino acid sequence of chick skin collagen alpha 1(I)-CB8 and the complete primary structure of the helical portion of the chick skin collagen alpha 1(I) chain. *Biochemistry* 21, 2048–2055.
- Hozumi, K., Akizuki, T., Yamada, Y., Hara, T., Urushibata, S., Katagiri, F., Kikkawa, Y., Nomizu, M., 2010. Cell adhesive peptide screening of the mouse laminin $\alpha 1$ chain G domain. *Arch. Biochem. Biophys.* 503, 213–222. <https://doi.org/10.1016/j.abb.2010.08.012>.
- Hozumi, K., Ishikawa, M., Hayashi, T., Yamada, Y., Katagiri, F., Kikkawa, Y., Nomizu, M., 2012. Identification of cell adhesive sequences in the N-terminal region of the laminin $\alpha 2$ chain. *J. Biol. Chem.* 287, 25111–25122. <https://doi.org/10.1074/jbc.M112.348151>.
- Ishihara, J., Ishihara, A., Fukunaga, K., Sasaki, K., White, M.J.V., Briquez, P.S., Hubbell, J.A., 2018. Laminin heparin-binding peptides bind to several growth factors and enhance diabetic wound healing. *Nat. Commun.* 9, 2163. <https://doi.org/10.1038/s41467-018-04525-w>.
- Kalamajski, S., Oldberg, A., 2010. The role of small leucine-rich proteoglycans in collagen fibrillogenesis. *Matrix Biol.* 29, 248–253. <https://doi.org/10.1016/j.matbio.2010.01.001>.
- Kaneda, Y., Yamamoto, Y., Okada, N., Tsutsumi, Y., Nakagawa, S., Kakiuchi, M., Maeda, M., Kawasaki, K., Mayumi, T., 1997. Antimetastatic effect of synthetic Glu-Ile-Leu-Asp-Val peptide derivatives containing D-amino acids. *Anticancer Drugs* 8, 702–707.
- Kantlehner, M., Schaffner, P., Finsinger, D., Meyer, J., Jonczyk, A., Diefenbach, B., Nies, B., Hölzemann, G., Goodman, S.L., Kessler, H., 2000. Surface coating with cyclic RGD peptides stimulates osteoblast adhesion and proliferation as well as bone formation. *Chembiochem* 1, 107–114.
- Katagiri, F., Ishikawa, M., Yamada, Y., Hozumi, K., Kikkawa, Y., Nomizu, M., 2012. Screening of integrin-binding peptides from the laminin $\alpha 4$ and $\alpha 5$ chain G domain peptide library. *Arch. Biochem. Biophys.* 521, 32–42. <https://doi.org/10.1016/j.abb.2012.02.017>.
- Katagiri, F., Takagi, M., Nakamura, M., Tanaka, Y., Hozumi, K., Kikkawa, Y., Nomizu, M., 2014. Screening of integrin-binding peptides in a laminin peptide library derived from the mouse laminin β chain short arm regions. *Arch. Biochem. Biophys.* 550–551, 33–41. <https://doi.org/10.1016/j.abb.2014.04.008>.
- Keselowsky, B.G., Collard, D.M., García, A.J., 2005. Integrin binding specificity regulates biomaterial surface chemistry effects on cell differentiation. *Proc. Natl. Acad. Sci. U.S.A.* 102, 5953–5957. <https://doi.org/10.1073/pnas.0407356102>.
- Keselowsky, B.G., Collard, D.M., García, A.J., 2003. Surface chemistry modulates fibronectin conformation and directs integrin binding and specificity to control cell adhesion. *J. Biomed. Mater. Res. A* 66, 247–259. <https://doi.org/10.1002/jbm.a.10537>.
- Kikkawa, Y., Hozumi, K., Katagiri, F., Nomizu, M., Kleinman, H.K., Koblinski, J.E., 2013. Laminin-111-derived peptides and cancer. *Cell Adhes. Migrat.* 7, 150–256. <https://doi.org/10.4161/cam.22827>.
- Knight, C.G., Morton, L.F., Peachey, A.R., Tuckwell, D.S., Farndale, R.W., Barnes, M.J., 2000. The collagen-binding A-domains of integrins alpha(1)beta(1) and alpha(2)beta(1) recognize the same specific amino acid sequence, GFOGER, in native (triple-helical) collagens. *J. Biol. Chem.* 275, 35–40.
- Lee, P., Bax, D.V., Bilek, M.M.M., Weiss, A.S., 2014. A novel cell adhesion region in tropoelastin mediates attachment to integrin $\alpha V\beta 5$. *J. Biol. Chem.* 289, 1467–1477. <https://doi.org/10.1074/jbc.M113.518381>.
- Lee, S.-H., Miller, J.S., Moon, J.J., West, J.L., 2005. Proteolytically degradable hydrogels with a fluorogenic substrate for studies of cellular proteolytic activity and migration. *Biotechnol. Prog.* 21, 1736–1741. <https://doi.org/10.1021/bp0502429>.
- Lee, S.-H., Moon, J.J., West, J.L., 2008. Three-dimensional micropatterning of bioactive hydrogels via two-photon laser scanning photolithography for guided 3D cell migration. *Biomaterials* 29, 2962–2968. <https://doi.org/10.1016/j.biomaterials.2008.04.004>.
- Lieb, E., Hacker, M., Tessmar, J., Kunz-Schughart, L.A., Fiedler, J., Dahmen, C., Hersel, U., Kessler, H., Schulz, M.B., Göpferich, A., 2005. Mediating specific cell adhesion to low-adhesive diblock copolymers by instant modification with cyclic RGD peptides. *Biomaterials* 26, 2333–2341. <https://doi.org/10.1016/j.biomaterials.2004.07.010>.
- Lin, B.F., Megley, K.A., Viswanathan, N., Krogstad, D.V., Drews, L.B., Kade, M.J., Qian, Y., Tirrell, M.V., 2012. pH-responsive branched peptide amphiphile hydrogel designed for applications in regenerative medicine with potential as injectable tissue scaffolds. *J. Mater. Chem.* 22, 19447–19454. <https://doi.org/10.1039/C2JM31745A>.
- Lu, P., Weaver, V.M., Werb, Z., 2012. The extracellular matrix: a dynamic niche in cancer progression. *J. Cell Biol.* 196, 395–406. <https://doi.org/10.1083/jcb.201102147>.
- Lutolf, M.P., Hubbell, J.A., 2005. Synthetic biomaterials as instructive extracellular microenvironments for morphogenesis in tissue engineering. *Nat. Biotechnol.* 23, 47–55. <https://doi.org/10.1038/nbt1055>.
- Lutolf, M.P., Lauer-Fields, J.L., Schmoekel, H.G., Metters, A.T., Weber, F.E., Fields, G.B., Hubbell, J.A., 2003a. Synthetic matrix metalloproteinase-sensitive hydrogels for the conduction of tissue regeneration: engineering cell-invasion characteristics. *Proc. Natl. Acad. Sci. U.S.A.* 100, 5413–5418. <https://doi.org/10.1073/pnas.0737381100>.
- Lutolf, M.P., Raeber, G.P., Zisch, A.H., Tirelli, N., Hubbell, J.A., 2003. Cell-responsive synthetic hydrogels. *Adv. Mater.* 15, 888–892. <https://doi.org/10.1002/adma.200304621>.
- Lutolf, M.P., Weber, F.E., Schmoekel, H.G., Schense, J.C., Kohler, T., Müller, R., Hubbell, J.A., 2003. Repair of bone defects using synthetic mimetics of collagenous extracellular matrices. *Nat. Biotechnol.* 21, 513–518. <https://doi.org/10.1038/nbt818>.

- Maheshwari, G., Brown, G., Lauffenburger, D.A., Wells, A., Griffith, L.G., 2000. Cell adhesion and motility depend on nanoscale RGD clustering. *J. Cell Sci.* 113 (Pt 10), 1677–1686.
- Mainiero, F., Pepe, A., Yeon, M., Ren, Y., Giancotti, F.G., 1996. The intracellular functions of alpha6beta4 integrin are regulated by EGF. *J. Cell Biol.* 134, 241–253.
- Martino, M.M., Hubbell, J.A., 2010. The 12th–14th type III repeats of fibronectin function as a highly promiscuous growth factor-binding domain. *FASEB J.* 24, 4711–4721. <https://doi.org/10.1096/fj.09-151282>.
- Martino, M.M., Tortelli, F., Mochizuki, M., Traub, S., Ben-David, D., Kuhn, G.A., Müller, R., Livne, E., Eming, S.A., Hubbell, J.A., 2011. Engineering the growth factor microenvironment with fibronectin domains to promote wound and bone tissue healing. *Sci. Transl. Med.* 3, 100ra89. <https://doi.org/10.1126/scitranslmed.3002614>.
- Massia, S.P., Hubbell, J.A., 1992. Vascular endothelial cell adhesion and spreading promoted by the peptide REDV of the IIIICS region of plasma fibronectin is mediated by integrin alpha 4 beta 1. *J. Biol. Chem.* 267, 14019–14026.
- Massia, S.P., Hubbell, J.A., 1990. Covalent surface immobilization of Arg-Gly-Asp- and Tyr-Ile-Gly-Ser-Arg-containing peptides to obtain well-defined cell-adhesive substrates. *Anal. Biochem.* 187, 292–301.
- Miller, E.J., Harris, E.D., Chung, E., Finch, J.E., McCroskery, P.A., Butler, W.T., 1976. Cleavage of Type II and III collagens with mammalian collagenase: site of cleavage and primary structure at the NH2-terminal portion of the smaller fragment released from both collagens. *Biochemistry* 15, 787–792.
- Miner, J.H., 2012. The glomerular basement membrane. *Exp. Cell Res.* 318, 973–978. <https://doi.org/10.1016/j.yexcr.2012.02.031>.
- Míner, J.H., Cunningham, J., Sanes, J.R., 1998. Roles for laminin in embryogenesis: exencephaly, syndactyly, and placentopathy in mice lacking the laminin alpha5 chain. *J. Cell Biol.* 143, 1713–1723.
- Mizuno, M., Fujisawa, R., Kuboki, Y., 2000. Type I collagen-induced osteoblastic differentiation of bone-marrow cells mediated by collagen-alpha2beta1 integrin interaction. *J. Cell. Physiol.* 184, 207–213. [https://doi.org/10.1002/1097-4652\(200008\)184:2<207::AID-JCP8>3.0.CO;2-U](https://doi.org/10.1002/1097-4652(200008)184:2<207::AID-JCP8>3.0.CO;2-U).
- Moursi, A.M., Globus, R.K., Damsky, C.H., 1997. Interactions between integrin receptors and fibronectin are required for calvarial osteoblast differentiation in vitro. *J. Cell Sci.* 110 (Pt 18), 2187–2196.
- Mow, V.C., Holmes, M.H., Lai, W.M., 1984. Fluid transport and mechanical properties of articular cartilage: a review. *J. Biomech.* 17, 377–394.
- Nagai, Y., Masui, Y., Sakakibara, S., 1976. Substrate specificity of vertebrate collagenase. *Biochim. Biophys. Acta* 445, 521–524.
- Nagase, H., Fields, G.B., 1996. Human matrix metalloproteinase specificity studies using collagen sequence-based synthetic peptides. *Biopolymers* 40, 399–416. [https://doi.org/10.1002/\(SICI\)1097-0282\(1996\)40:4%3C399::AID-BIP5%3E3.0.CO;2-R](https://doi.org/10.1002/(SICI)1097-0282(1996)40:4%3C399::AID-BIP5%3E3.0.CO;2-R).
- Nagase, H., Visse, R., Murphy, G., 2006. Structure and function of matrix metalloproteinases and TIMPs. *Cardiovasc. Res.* 69, 562–573. <https://doi.org/10.1016/j.cardiores.2005.12.002>.
- Ornitz, D.M., 2000. FGFs, heparan sulfate and FGFRs: complex interactions essential for development. *Bioessays* 22, 108–112. [https://doi.org/10.1002/\(SICI\)1521-1878\(200002\)22:2<108::AID-BIES2>3.0.CO;2-M](https://doi.org/10.1002/(SICI)1521-1878(200002)22:2<108::AID-BIES2>3.0.CO;2-M).
- Pankov, R., Yamada, K.M., 2002. Fibronectin at a glance. *J. Cell Sci.* 115, 3861–3863.
- Patel, D., Menon, R., Taite, L.J., 2011. Self-assembly of elastin-based peptides into the ECM: the importance of integrins and the elastin binding protein in elastic fiber assembly. *Biomacromolecules* 12, 432–440. <https://doi.org/10.1021/bm101214f>.
- Patterson, J., Hubbell, J.A., 2010. Enhanced proteolytic degradation of molecularly engineered PEG hydrogels in response to MMP-1 and MMP-2. *Biomaterials* 31, 7836–7845. <https://doi.org/10.1016/j.biomaterials.2010.06.061>.
- Petrie, T.A., Capadona, J.R., Reyes, C.D., García, A.J., 2006. Integrin specificity and enhanced cellular activities associated with surfaces presenting a recombinant fibronectin fragment compared to RGD supports. *Biomaterials* 27, 5459–5470. <https://doi.org/10.1016/j.biomaterials.2006.06.027>.
- Petrie, T.A., Raynor, J.E., Reyes, C.D., Burns, K.L., Collard, D.M., García, A.J., 2008. The effect of integrin-specific bioactive coatings on tissue healing and implant osseointegration. *Biomaterials* 29, 2849–2857. <https://doi.org/10.1016/j.biomaterials.2008.03.036>.
- Phelps, E.A., Landázuri, N., Thulé, P.M., Taylor, W.R., García, A.J., 2010. Bioartificial matrices for therapeutic vascularization. *Proc. Natl. Acad. Sci. U.S.A.* 107, 3323–3328. <https://doi.org/10.1073/pnas.0905447107>.
- Pierschbacher, M.D., Ruoslahti, E., 1984. Cell attachment activity of fibronectin can be duplicated by small synthetic fragments of the molecule. *Nature* 309, 30–33.
- Raman, R., Venkataraman, G., Ernst, S., Sasisekharan, V., Sasisekharan, R., 2003. Structural specificity of heparin binding in the fibroblast growth factor family of proteins. *Proc. Natl. Acad. Sci. U.S.A.* 100, 2357–2362. <https://doi.org/10.1073/pnas.0437842100>.
- Reyes, C.D., García, A.J., 2004. Alpha2beta1 integrin-specific collagen-mimetic surfaces supporting osteoblastic differentiation. *J. Biomed. Mater. Res. A* 69, 591–600. <https://doi.org/10.1002/jbm.a.30034>.
- Reyes, C.D., García, A.J., 2003. Engineering integrin-specific surfaces with a triple-helical collagen-mimetic peptide. *J. Biomed. Mater. Res. A* 65, 511–523. <https://doi.org/10.1002/jbm.a.10550>.
- Roughley, P.J., 2006. The structure and function of cartilage proteoglycans. *Eur. Cells Mater.* 12, 92–101.
- Rozo, M., Li, L., Fan, C.-M., 2016. Targeting beta1-integrin signaling enhances regeneration in aged and dystrophic muscle in mice. *Nat. Med.* 22, 889–896. <https://doi.org/10.1038/nm.4116>.
- Ruoslahti, E., 1996. RGD and other recognition sequences for integrins. *Annu. Rev. Cell Dev. Biol.* 12, 697–715. <https://doi.org/10.1146/annurev.cellbio.12.1.697>.
- Schense, J.C., Hubbell, J.A., 2000. Three-dimensional migration of neurites is mediated by adhesion site density and affinity. *J. Biol. Chem.* 275, 6813–6818.
- Shekaran, A., García, J.R., Clark, A.Y., Kavanaugh, T.E., Lin, A.S., Guldberg, R.E., García, A.J., 2014. Bone regeneration using an alpha 2 beta 1 integrin-specific hydrogel as a BMP-2 delivery vehicle. *Biomaterials* 35, 5453–5461. <https://doi.org/10.1016/j.biomaterials.2014.03.055>.
- Silva, G.A., Czeisler, C., Niece, K.L., Beniash, E., Harrington, D.A., Kessler, J.A., Stupp, S.I., 2004. Selective differentiation of neural progenitor cells by high-epitope density nanofibers. *Science* 303, 1352–1355. <https://doi.org/10.1126/science.1093783>.
- Simon, P., Kasimir, M.T., Seebacher, G., Weigel, G., Ullrich, R., Salzer-Muhar, U., Rieder, E., Wolner, E., 2003. Early failure of the tissue engineered porcine heart valve SYNERGRAFT® in pediatric patients. *Eur. J. Cardiothorac. Surg.* 23, 1002–1006. [https://doi.org/10.1016/S1010-7940\(03\)00094-0](https://doi.org/10.1016/S1010-7940(03)00094-0).

- Sleep, E., Cosgrove, B.D., McClendon, M.T., Preslar, A.T., Chen, C.H., Sangji, M.H., Pérez, C.M.R., Haynes, R.D., Meade, T.J., Blau, H.M., Stupp, S.I., 2017. Injectable biomimetic liquid crystalline scaffolds enhance muscle stem cell transplantation. *Proc. Natl. Acad. Sci. U.S.A.* <https://doi.org/10.1073/pnas.1708142114>.
- Staat, W.D., Fok, K.F., Zutter, M.M., Adams, S.P., Rodriguez, B.A., Santoro, S.A., 1991. Identification of a tetrapeptide recognition sequence for the alpha 2 beta 1 integrin in collagen. *J. Biol. Chem.* 266, 7363–7367.
- Sun, F., Zhang, W.-B., Mahdavi, A., Arnold, F.H., Tirrell, D.A., 2014. Synthesis of bioactive protein hydrogels by genetically encoded SpyTag-SpyCatcher chemistry. *Proc. Natl. Acad. Sci. U.S.A.* 111, 11269–11274. <https://doi.org/10.1073/pnas.1401291111>.
- Takada, Y., Ye, X., Simon, S., 2007. The integrins. *Genome Biol.* 8, 215. <https://doi.org/10.1186/gb-2007-8-5-215>.
- Tibbitt, M.W., Anseth, K.S., 2009. Hydrogels as extracellular matrix mimics for 3D cell culture. *Biotechnol. Bioeng.* 103, 655–663. <https://doi.org/10.1002/bit.22361>.
- Ukawala, M., Rajyaguru, T., Chaudhari, K., Manjappa, A.S., Murthy, R.S.R., Gude, R., 2011. EILDV-conjugated, etoposide-loaded biodegradable polymeric micelles directing to tumor metastatic cells overexpressing $\alpha 4 \beta 1$ integrin. *Cancer Nanotechnol.* 2, 133–145. <https://doi.org/10.1007/s12645-011-0023-7>.
- Urushibata, S., Hozumi, K., Ishikawa, M., Katagiri, F., Kikkawa, Y., Nomizu, M., 2010. Identification of biologically active sequences in the laminin alpha2 chain G domain. *Arch. Biochem. Biophys.* 497, 43–54. <https://doi.org/10.1016/j.abb.2010.03.006>.
- Urushibata, S., Katagiri, F., Takaki, S., Yamada, Y., Fujimori, C., Hozumi, K., Kikkawa, Y., Kadoya, Y., Nomizu, M., 2009. Biologically active sequences in the mouse laminin alpha3 chain G domain. *Biochemistry* 48, 10522–10532. <https://doi.org/10.1021/bi901421t>.
- Vandenberg, P., Kern, A., Ries, A., Luckenbill-Edds, L., Mann, K., Köhn, K., 1991. Characterization of a type IV collagen major cell binding site with affinity to the alpha 1 beta 1 and the alpha 2 beta 1 integrins. *J. Cell Biol.* 113, 1475–1483.
- Vogel, V., Thomas, W.E., Craig, D.W., Krammer, A., Baneyx, G., 2001. Structural insights into the mechanical regulation of molecular recognition sites. *Trends Biotechnol.* 19, 416–423. [https://doi.org/10.1016/S0167-7799\(01\)01737-1](https://doi.org/10.1016/S0167-7799(01)01737-1).
- Wang, H., Paul, A., Nguyen, D., Enejder, A., Heilshorn, S.C., 2018. Tunable control of hydrogel microstructure by kinetic competition between self-assembly and crosslinking of elastin-like proteins. *ACS Appl. Mater. Interfaces* 10, 21808–21815. <https://doi.org/10.1021/acsami.8b02461>.
- West, J.L., Hubbell, J.A., 1999. Polymeric biomaterials with degradation sites for proteases involved in cell migration. *Macromolecules* 32, 241–244. <https://doi.org/10.1021/ma981296k>.
- Yakubenko, V.P., Lishko, V.K., Lam, S.C.-T., Ugarova, T.P., 2002. A molecular basis for integrin alphaMbeta 2 ligand binding promiscuity. *J. Biol. Chem.* 277, 48635–48642. <https://doi.org/10.1074/jbc.M208877200>.
- Yamamoto, S., Kaneda, Y., Okada, N., Nakagawa, S., Kubo, K., Inoue, S., Maeda, M., Yamashiro, Y., Kawasaki, K., Mayumi, T., 1994. Antimetastatic effects of synthetic peptides containing the core sequence of the type III connecting segment domain (IIICS) of fibronectin. *Anticancer Drugs* 5, 424–428.
- Yu, X., Miyamoto, S., Mekada, E., 2000. Integrin alpha 2 beta 1-dependent EGF receptor activation at cell-cell contact sites. *J. Cell Sci.* 113 (Pt 12), 2139–2147.

Chapter Exercises

- Describe key functions and properties of the extracellular matrix.
 - How do cells interact with their surrounding extracellular matrix?
 - What are some of the properties and factors that need to be considered when engineering a cell-instructive biomaterial?
- Describe a strategy to design a biomaterial that exhibits increased sequestration of growth factors, such as FGF2 and PDGF. Justify your proposed strategy.
 - What are some of the advantages and disadvantages of using naturally derived matrices for biomedical applications? What are some of the advantages and disadvantages of synthetic matrices?

2.1.6

Effects of Mechanical Forces on Cells and Tissues

AUSTIN VEITH¹, DAN CONWAY², LEI MEI¹, SUZANNE G. ESKIN³,
LARRY V. MCINTIRE³, AARON B. BAKER¹

¹Department of Biomedical Engineering, University of Texas at Austin, Austin, TX, United States

²Department of Biomedical Engineering, Virginia Commonwealth University, Richmond, VA, United States

³Wallace H. Coulter Department of Biomedical Engineering, Georgia Institute of Technology, Atlanta, GA, United States

Introduction

Mechanical forces are present throughout the body as a consequence of the normal motion and the physiological functioning of organs. These forces are key regulators of the body's interaction with biomaterials and it is essential to account for these mechanical factors in the design of biomaterials. The mechanical issues of biomaterial design can be divided into issues relating to the mechanical properties of biomaterials and issues of the mechanical forces experienced by the materials, cells, and tissue–material interfaces. This chapter reviews the basics of our understanding of how cells and tissues respond to mechanical forces and mechanical cues in their microenvironment. We first discuss the general aspects of how cells can sense their mechanical environment and then continue with a review of experimental techniques used to study mechanobiology and engineer-tailored mechanical environments in biomaterials. Finally, we examine the mechanical aspects of the vascular system and the bones, two organ systems that are highly regulated by mechanical forces.

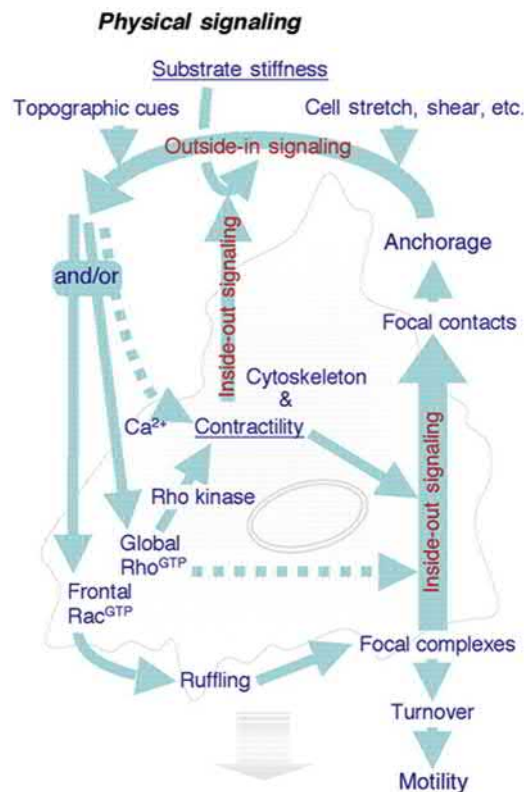
Molecular Mechanisms of Cellular Mechanotransduction

In work published in 1892, Julius Wolff described the structural remodeling of bone in response to mechanical forces (Wolff, 1892). The concept that mechanical forces could alter tissue remodeling was one of the first realizations of mechanosensing in biological systems and later became

known as Wolff's law. For several decades, it has also been known that forces from blood pressure and flow can induce remodeling in the vascular system. In fact, specific regions of the arterial system become prone to the formation of atherosclerosis based on the presence of low/oscillating shear stress (Koskinas et al., 2009). More recently, studies have found that the mechanical environment can alter the differentiation of stem cells and alter the behavior of cancer cells (Engler et al., 2006; Matthew et al., 2005). Fundamental to these processes is the mechanisms through which cells sense and respond to mechanical forces. Cellular mechanosensing can be roughly divided into three areas: (1) focal adhesion and mechanosensing at the extracellular matrix (ECM)/biomaterial interface, (2) cytoskeletal mechanotransduction, and (3) nuclear mechanotransduction.

Focal Adhesion and Mechanosensing at the ECM–Biomaterial Interface

Perhaps the most obvious place to search for mechanically sensitive molecules is at the location of attachment of the cell to its surrounding environment. Focal adhesions are complexes of proteins found at the cell membrane that provide physical attachment to the cell's extracellular environment. The dynamic regulation of focal adhesions plays a key role in cell migration, cytoskeletal remodeling, and cell survival (Parsons et al., 2010). Focal adhesions are integrin-containing, multiprotein architectures that form a mechanical link between the cell's cytoskeleton and the local microenvironment (Harburger and Calderwood,



• **Figure 2.1.6.1** Cellular motion is mediated by inside-out/outside-in integrin signaling. Integrins can be activated to bind ligands (“inside-out” signaling) or ligand binding can mediate cellular responses (“outside-in” signaling) (Discher et al., 2005).

2009; Hynes, 2002). Integrins are heterodimeric cell surface receptors that bind to the ECM and other receptors (Hynes, 1992). The two integrin subunits that form the integrin (e.g., $\alpha\text{v}\beta3$) determine the types of ECM or other molecules to which the integrin binds (Plow et al., 2000). Integrins function bidirectionally. Integrins can be activated to bind ligands (“inside-out” signaling) or ligand binding can mediate cellular responses (“outside-in” signaling) (Fig. 2.1.6.1) (Shen et al., 2012; Geiger et al., 2001). The importance of integrin signaling on cell survival and proliferation has made it of interest in designing biomaterials that need to interact directly with cells. A common strategy to enhance cellular adhesion to biomaterials and hydrogels is to conjugate RGD-containing peptides (Ruoslahti and Pierschbacher, 1987; Burdick and Anseth, 2002), allowing cells to attach and survive on the materials. The RGD sequence mimics adhesion motifs in many extracellular matrix proteins that bind to and activate integrins.

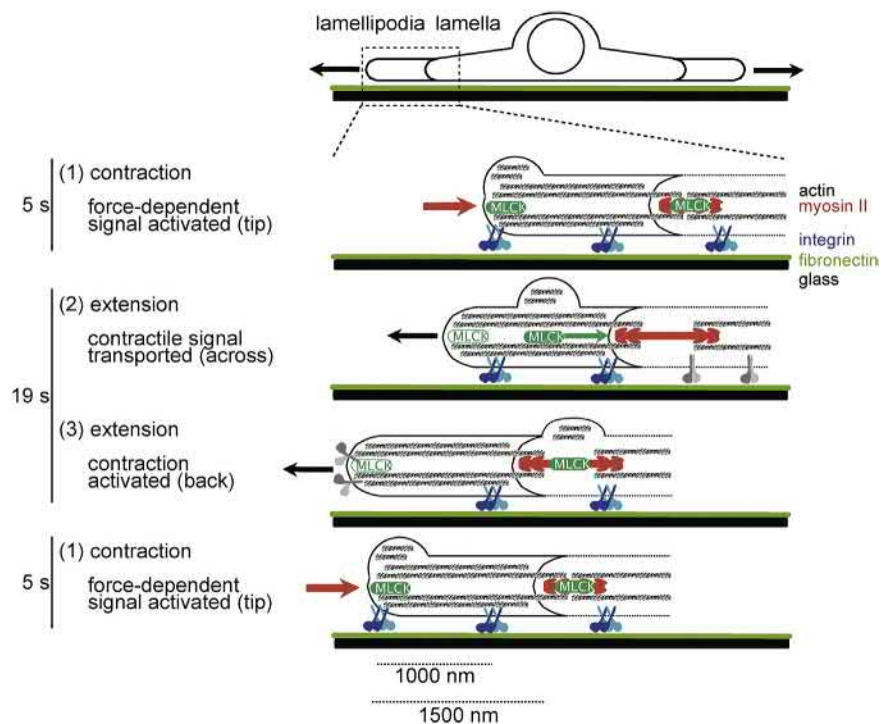
The canonical model of cell adhesion is that integrin activation leads to the rapid recruitment of focal adhesion-associated proteins including vinculin, talin, and paxillin. Talin can link directly to the actin cytoskeleton, allowing mechanical force to be applied to the linkage and slowing retrograde flow of actin subunits. Vinculin can also control the formation of focal adhesion through interactions with talin and other proteins (Humphries et al., 2007),

and directly senses mechanical tension across the focal adhesions (Grashoff et al., 2010). These nascent adhesion complexes lead to activation of focal adhesion kinase and subsequent recruitment of other scaffolding and signaling proteins as the focal adhesion matures. The focal adhesions can also alter cytoskeletal remodeling through multiple mechanisms. For example, integrin regulation of Src and focal adhesion kinase (FAK) activity can in turn regulate members of the Rho family of GTPases, such as Rac1 or RhoA, leading to reorganization of the actin cytoskeleton.

As cells move through their local microenvironment, they are continually sensing the local stiffness and adhesion of the surrounding matrix. During migration there is continual formation of new focal adhesions at the front of the lamellipodia. In one potential mechanism, cells can sense the stiffness of the material through cycles of contraction mediated by myosin II molecular motors (Fig. 2.1.6.2) (Giannone et al., 2004). Essentially, the cell pulls back on the adhesions during migration/cytoskeletal remodeling and based on mechanically sensitive signaling can assess the stiffness of the matrix. Mechanical tension applied by the cell to the underlying ECM can also lead to activation of transforming growth factor-beta ($\text{TGF-}\beta$), a growth factor involved in regulating fibrosis, proliferation, and many other processes (Shi et al., 2011). The cell synthesizes $\text{TGF-}\beta1$ as an inactive propeptide (latent $\text{TGF-}\beta$) that can deposit in the ECM. Latent $\text{TGF-}\beta$ can be activated by a number of factors including the application of mechanical force by cells through αv integrins. In myofibroblasts, substrate stiffness can regulate the $\text{TGF-}\beta$ pathway (Arora et al., 1999). On soft substrates, cell-generated tension on the $\text{TGF-}\beta$ latent complex results in deformation of the matrix and the latent complex remains inactive, keeping $\text{TGF-}\beta$ sequestered in the complex and preventing its release. On stiffer substrates, cell-generated tension deforms the $\text{TGF-}\beta$ latent complex, releasing $\text{TGF-}\beta$ where it can be activated (Wells and Discher, 2008). This bioactive $\text{TGF-}\beta$ binds its receptor and activates Smad-family transcription factors. Mechanically regulated $\text{TGF-}\beta$ signaling has been shown to mediate the communication between endothelial cells and vascular smooth muscle cells in the artery (Baker et al., 2008), cancer (Wei et al., 2015), and many other physiological processes (Horiguchi et al., 2012). While not reviewed extensively here, mechanical forces and cytoskeletal tension can also be sensed through cell–cell junctions and cell–cell adhesion molecules, including members of the cadherin family of proteins (Charras and Yap, 2018).

Cytoskeletal Mechanotransduction

Activation of focal adhesion complexes leads to the polymerization and organization of actin filaments and nonmuscle myosin II into stress fibers (Tojkander et al., 2012; Vicente-Manzanares et al., 2009). These actomyosin stress fibers form the major contractile structure in

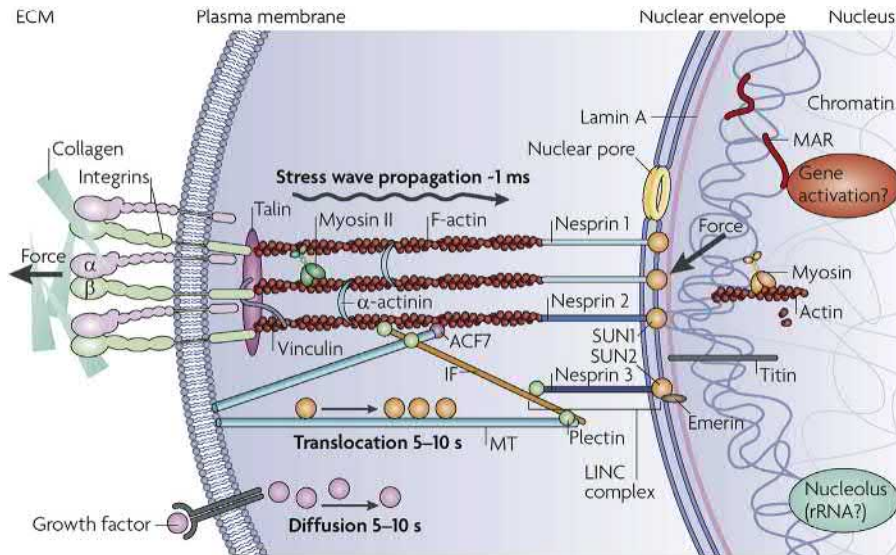


• **Figure 2.1.6.2** The cycle of contraction of myosin II molecular motors. (1) Lamellipodial contraction generates force that activates force-dependent MLCK signals (green ellipses) at the lamellipodial tip. This results in the formation of transient integrin/paxillin adhesion sites at the tip (blue). (2) The cell then extends after contraction. A wave of material (actin, α -actinin, MLCK) containing the contractile signal is transported rearward by actin flow. (3) When the contractile signal reaches the back of the lamellipodium, it stimulates the contractile machinery (myosin II, red) (Giannone et al., 2004).

most cells, powering cellular migration and the protrusion of lamellipodia and filopodia. Rho and Rac proteins are involved in the creation of focal adhesions (Buchsbau, 2007). Respectively, Rho is inhibited through Src activation of RhoGAP and Rac is activated through Vav signaling and other pathways (reviewed extensively elsewhere) (Sit and Manser, 2011; Hall, 1998). Combined, these proteins coordinate the formation of actomyosin stress fibers (Nobes and Hall, 1995) and transmit the required force to bring epithelial cells together into continuous tissues (Vasioukhin et al., 2000; Nusrat et al., 1995; Yonemura et al., 1995; Ridley and Hall, 1992). Proteins such as talin and vinculin mediate the link between focal adhesions and actomyosin complexes and play a key role in how cells sense tension and mature their adhesions (Parsons et al., 2010; Grashoff et al., 2010). Internally, talin and vinculin act as a molecular clutch (Mitchison and Kirschner, 1988; Case and Waterman, 2015). When these proteins are subjected to high tension (integrin binding on stiff substrates), the proteins are activated, converting the contractile force of the actomyosin stress bundles into movement. When these proteins are subjected to low tensions, they do not activate and as a result the cells may retract their adhesions. It has also been suggested that the actin filament itself functions as a tension sensor (Hayakawa et al., 2011). Tension on actin filaments prevents the fibers from being severed and disassembled by members of the cofilin family of actin-binding proteins.

Nuclear Mechanotransduction

The nucleus can also directly participate in mechanosensing in cells. The nucleus contains the majority of the cell's genetic material that is separated from the cytoplasm by the nuclear envelope. The nuclear envelope is composed of two lipid bilayers separated by the perinuclear space. Nuclear pore complexes allow the regulated transfer of proteins into the nucleus. The nuclear lamina lines the inside of the nuclear envelope, providing mechanical support for the nucleus, anchoring nuclear pore complexes, and interacting with chromatin (Wang et al., 2009). Forces applied at focal adhesions can be transmitted to the nucleus either through signal molecules or direct mechanical force transmission (Wang et al., 2009). Nuclear envelope spectrin repeat proteins (nesprins) are found on the outside of the nuclear envelope and can link actin filaments and microtubules to the nucleus (Haque et al., 2006; Zhang et al., 2001). Lamins are found on the inner side of the nuclear envelope and are a major structural protein in the nuclear lamina. Nesprins link to the proteins SUN-1 or SUN-2 through a highly conserved KASH domain, and SUN1/2 binds to lamins to cross the nuclear envelope. Thus, mechanical forces applied from the cytoskeleton can transmit directly to the chromatin (Fig. 2.1.6.3) (Sosa et al., 2012). These structures are collectively known as “linker of nucleoskeleton and cytoskeleton” (LINC) complexes, and disruption of LINC complexes prevents mechanically induced activation of genes. This, in turn, can lead to adverse effects on migration, membrane polarization,



• **Figure 2.1.6.3** Proteins involved in mechanotransduction from the ECM to the nucleus. A local force applied to integrins through the extracellular matrix (ECM) is concentrated at focal adhesions. This stress wave then propagates through stress fiber complexes, connected to the focal adhesions by molecular clutch proteins. Stress fibers then interact with the nuclear envelope through LINC proteins. At this interface, the force transferred from the cell surface can interact with chromatin structures (Wang et al., 2009).

and cellular structural development (Lombardi et al., 2011). The direct transmission of force from the extracellular environment in the form of tension or compression can affect chromatin opening and recombination, nuclear transport, and nuclear matrix distortion (Dahl et al., 2008; Wang et al., 2009). The absence of lamins, a key mediator of chromatin structures, has been shown to impair the cellular response to mechanical stress (Houben et al., 2007). Nuclei exposed to shear stress upregulate and redistribute lamins to change their nuclear shape (Philip and Dahl, 2008) and cells that do not contain lamin structures do not respond to shear stress. Lamins have also been shown to scale with tissue stiffness (Swift et al., 2013), where stiffer tissues contain more lamin proteins than softer tissues. Nuclear envelope distortion has also been shown to stimulate calcium entry through ion channels and alter gene transcription (Itano et al., 2003). Finally, stress and strain on nuclear scaffolds have also been shown to influence chromatin organization (Stein et al., 2007). One regulator of mechanically mediated signaling is the transcriptional regulators YAP and TAZ (YAP/TAZ), which are key molecules in the Hippo signaling pathway (Dupont, 2016; Dupont et al., 2011; Fischer et al., 2016). When cells are subjected to mechanical conditions with high tension, YAP/TAZ is localized to the nucleus where it affects a variety of cellular processes including proliferation. When cells experience low intracellular tension, YAP/TAZ is sequestered in the cytoplasm by proteins such as 14-3-3 ϵ or degraded. The nuclear deformation caused by tension on LINC proteins helps to promote YAP/TAZ nuclear entry and subsequent transcription (Totaro et al., 2018; Elosegui-Artola et al., 2017). Combined, these results indicate that mechanical forces acting on the nucleus may alter the cellular process through multiple mechanisms which remains an area of active research.

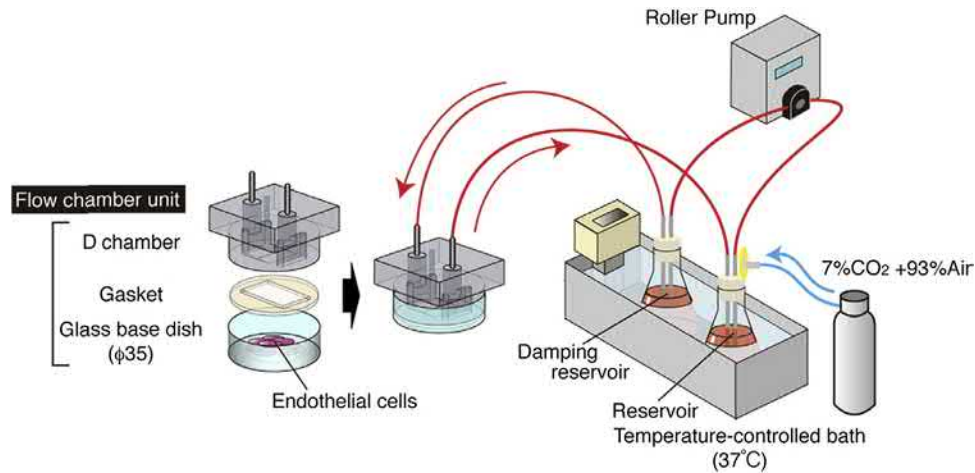
Techniques for Studying Mechanical Interactions of Cells

Shear Stress

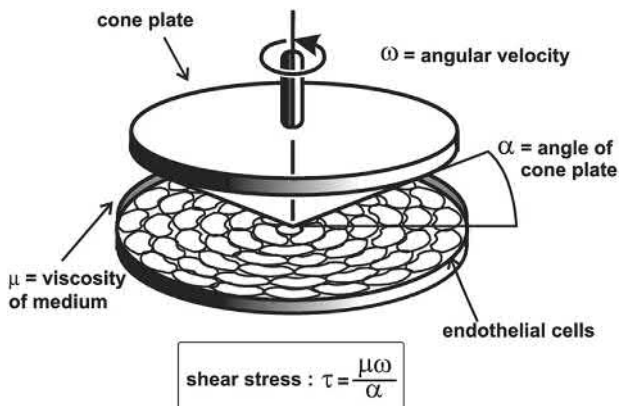
Two in vitro systems have been developed to characterize the response of endothelial cells to a variety of shear stresses: the parallel plate flow chamber (Fig. 2.1.6.4) and the cone and plate system (Fig. 2.1.6.5). In the parallel plate model, two glass slides are used to form a flow chamber with a thin gasket in between to provide accurate spacing (Frangos et al., 1988). This creates a very small gap width through which tissue culture medium can be circulated. The geometric dimensions are known, allowing for the calculation of the fluid shear stress from the flow rate. For a Newtonian fluid flowing through a parallel plate flow chamber with a rectangular cross section, under steady laminar flow yields a shear stress as follows:

$$\tau_w = \frac{6\mu Q}{bh^2}$$

in which τ_w = wall shear stress, μ = viscosity, Q = flow rate, b = channel width, and h = channel height. By varying the chamber geometry, the flow rate, or the viscosity, the entire physiological range of wall shear stresses can be investigated. The flow rate is varied using a syringe pump or gravity-driven system to provide the desired wall shear stress across the cells. The cone-and-plate system consists of a tissue culture dish as the plate, and a fixed-angle cone mounted to a motor that imparts an angular velocity. For small cone angles, the shear rate (and therefore the shear stress) is essentially constant throughout the flow field. Since the dimensions of this system are also characterized,



• **Figure 2.1.6.4** In vitro parallel plate systems for studying the effects of shear stress on cells. In the parallel plate system cells are grown on glass slides and mounted onto a parallel plate chamber. The gasket provides a known gap height. Fluid flows in the inlet, across the deck, and out the exit slot. Some systems may include a damping reservoir to mitigate the oscillatory effects of the roller pump (Yoshino et al., 2013).



• **Figure 2.1.6.5** Cone and plate systems for studying the effects of shear stress on cells. In the cone and plate system cells are grown on a circular dish, which forms a viscometer at the bottom. A small fixed angle cone is rotated at a constant angular velocity providing a constant shear stress across the cells. The degree of shear stress depends upon the viscosity of the medium, the angular velocity of the cone plate, and the angle of the cone (Morawietz et al., 2008).

the fluid shear stress can be calculated for a given angular velocity.

A common way to analyze the effects of shear stress in vitro is with a cone and plate apparatus. In these systems, cells are cultured on a substrate while being subjected to shear stress from a rotating cone. An advantage of this type of system is to be able to create complex shear stress waveforms that are found in the body (Blackman et al., 2002). For example, waveforms that model arterial shear stress have been used to evaluate the response in endothelial cells, and may give more accurate insight into how cells react in physiological conditions (Spencer and Baker, 2016b). Shear stress has been shown to change endothelial cell shape and affect cytoskeletal changes through Rac1 activation (Malek and Izumo, 1996; Tzima et al., 2002). It has also been shown to selectively upregulate specific adhesion proteins associated with focal adhesion sites (Nagel et al., 1994; Girard and Nerem, 1995).

Recently, a high-throughput system with 96 cone-tipped shafts was designed to allow drug screening and adhesion assay under flow in a 96-well format (Spencer et al., 2016; Spencer and Baker, 2016a). In order to analyze adhesion kinetics to biomaterials, methods such as the spinning disc assay have been employed (Reyes and Garcia, 2003; Garcia et al., 1997). In these assays, cells are cultured on biomaterials and subjected to high shear forces in a physiological solution. The resulting detachment patterns give an insight into the adhesive properties of the materials. Microfluidic devices have also been used to analyze the effects of shear stress in vitro (Lu et al., 2004; Polachek et al., 2013). These apparatuses range from the commercially available microfluidic chambers to custom human-on-a-chip apparatuses that mimic relevant tissue structures. Lung-on-a-chip and intestine-on-a-chip devices provide a more accurate in vitro model of the mechanical forces that act on the cells. Organotypic microfluidic devices for blood vessels have also been employed (Polachek et al., 2017). These systems use 3D gels that mimic the mechanical properties of blood vessels, to create more accurate representations of the organ system. As with the cone and plate systems, microfluidic devices have been created with higher throughput configurations (Voyvodic et al., 2012). In this device, Voyvodic et al. employed a pulse dampener to remove the pulsatility of the flow coming from the peristaltic pump. In this manner, they could then compare the effects of steady flow and pulsatile flow in the same apparatus.

Mechanical Stretch

Numerous devices have been devised to impart mechanical strain to cells and substrates (Brown, 2000). In general, cells are cultured on flexible membranes and these membranes are subjected to mechanical strains through deformation. Simple stretch machines employ one-directional

stress to their substrates. More complex biaxial and triaxial stretch devices have also been devised for both cell (Neidlinger-Wilke et al., 1994; Sellaro et al., 2007; Schürmann et al., 2016) and tissue applications (May-Newman and Yin, 1995). These multiaxial devices attempt to account for mechanical behavior that tissues experience in vivo (Sacks and Sun, 2003), by applying mechanical stretch in two and three dimensions. Substrate distension machines are also a popular method to impart mechanical strain to cells. Platen (Hasegawa et al., 1985), prong (Vandenburgh, 1988), vacuum (Banes et al., 1985), and fluid swelling (Winston et al., 1989) modalities have been employed to study mechanical strain. A review paper by Brown in 2000 provides a good starting point for those interested in designing and developing mechanical stretch devices. As with shear stress devices, the development of physiological waveforms has led to greater insights into the responses of cells to their mechanical environments (Orr et al., 2006). Mechanical stretch systems are commercially available, and high-throughput apparatuses have also been developed (Lee et al., 2013). In one such system, Lee et al. created a device that could apply mechanical stretch to six, six-well plates at the same time via a moveable platen. The linear motor that drives the motion of the plate can be programmed to apply arbitrary stretch waveforms, from simple sinusoidal waves to more complex biphasic waves.

Substrate Stiffness

Substrate stiffness plays a key role in regulating normal cell growth and apoptosis (Wang et al., 2000). Furthermore, the movement of cells is also guided by the rigidity of their extracellular environments (Lo et al., 2000). For example, a soft substrate is easier for cells to deform, which reduces the stress at the focal adhesions in the cell. Conversely, on a stiffer substrate, the actin cytoskeleton may increase the force to equilibrate through passive deformation and through changes in myosin motor activity (Chen, 2008). During the process of balancing the external–internal forces, cytoskeletal structure changes could be triggered and following downstream regulations could happen (Torsoni et al., 2005; Xiao-Han et al., 2007; Liu et al., 2007). It has been demonstrated that stiffness modulates mechanotransduction pathways by directing FAs and myosin-based contractility. FAs are found to be smaller in cells cultured on soft substrates and focal adhesion kinase (FAK) phosphorylation is decreased (Paszek and Weaver, 2004). RhoA activity was also shown to be decreased on soft substrates (Engler et al., 2006). Collagen-coated polyacrylamide sheets with a transition in rigidity from soft to stiff were developed to elucidate cell preference for matrix compliance. More recently, photoactivatable gels that change their stiffness with exposure to light have been used to understand the effects of substrate stiffness (Isenberg et al., 2009; Rowlands et al., 2008). In addition, gels with reversible photoactivatable groups or

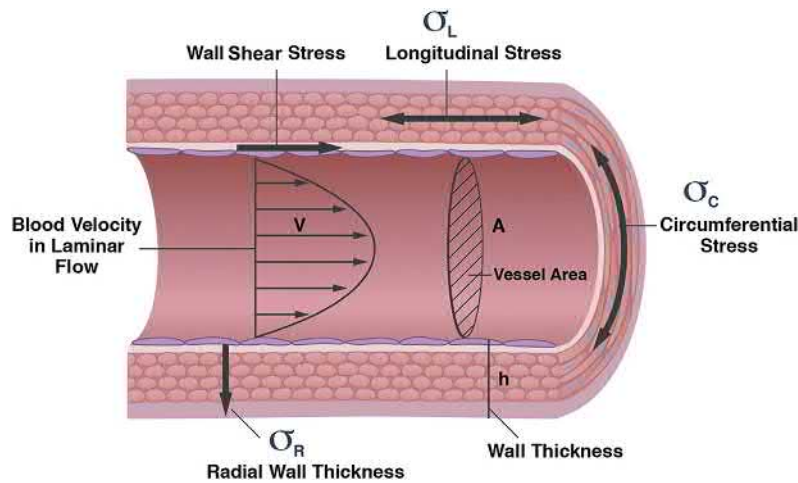
biomolecule hybridization can be used to change polymer chain conformation, altering the substrate stiffness (Rosales and Anseth, 2016). In these systems, researchers can selectively direct the stiffness state of the substrate allowing the in vitro matrix to mimic responses and changes experienced in vivo.

Micro- and Nanopatterning

Micropatterning and more recently nanopatterning have emerged as powerful techniques to direct cell growth and morphology by altering the cell's local mechanical environment (Chen et al., 1998; Arnold et al., 2004; Kim et al., 2012). Ultraviolet photolithography techniques are often employed to create islands of ECM with photopolymerizable polymers. PDMS stamping is another popular technique to deposit proteins on a substrate surface (Christman et al., 2006). Common topographies include grooves, aligned fibers, pillars, and pits. Gradients of these topographies also have been used to ascertain the effects of feature distance. These arrays also help inform haptotactic behavior in cells. Haptotaxis occurs in response to the concentration of ligands on an adhesive surface (Engler et al., 2004). At the most basic level, micro- and nanopatterning direct cell integrin function (Arnold et al., 2004). These changes lead to effects on cell motility (Yim et al., 2005) and cell spreading (Cavalcanti-Adam et al., 2007). The in vivo extracellular milieu is a textured matrix of micro- and nanostructured pores, fibers, and protrusions. As a result, topographic cues also appear to be important in mechanical-mediating pathways. A number of studies have revealed the properties of cell alignment and elongation with micro- and nanogrooved substrates via the guidance of microtubules, actin microfilaments, and the interplay between lamellipodium and ECM ligands (Wojciak-Stothard et al., 1995; Walboomers et al., 2000; Oakley and Brunette, 1993). More than the morphological changes, surface patterning has also been shown to mediate FA formation, cytoskeletal organization, cell migration (Dalton et al., 2001), gene expression (Lee et al., 2009), differentiation (Cai et al., 2012), and other cell processes. In the past decade, new biomaterials have been synthesized and fabricated into various shapes, compliances, and surface topographies. The effects of 3D nanotopographies have also been explored (Horwitz and Alan, 2010). These materials are excellent candidates to mimic in vivo mechanical environments and efficient tools for deeper understanding of mechanotransduction.

Mechanical Forces in the Vascular System

Large blood vessels are comprised of three major cell types: endothelial cells, vascular smooth muscle cells, and fibroblasts. A single cell thick layer of endothelial cells forms the endothelium that lines the lumen of blood vessels. The endothelium provides barrier function, and controls thrombosis and hemostasis by maintaining an active thromboresistant



• **Figure 2.1.6.6** Schematic representation of the hemodynamic forces acting on the artery wall. Cross-section through the artery, in which all layers are constantly subjected to tensile stress (cyclic strain) which arises from normal forces generated by the pulsatility of blood flow. Longitudinal section through the artery. Fluid flow profile (illustrated by the parabola) imparts tangential forces (shear stress) to the blood vessel wall. Endothelial cells lining the blood vessel wall respond first to this force (Whitlock and Hundley, 2015).

surface. Large arteries also include a middle layer, the media, which consists of smooth muscle cells with secreted extracellular matrix. The outermost layer, the adventitia, consists primarily of fibroblasts and extracellular matrix, and contains blood vessels and nerves supplying the artery itself. Vascular smooth muscle cells (vSMCs) in the medial layer contract, relax, proliferate, synthesize matrix, and migrate in response to shear stress, cyclic strain, and paracrine factors from endothelial cells. Vessels denuded of the endothelium expose the vSMCs to blood flow, resulting in the binding of platelets and thrombosis (Wagner and Frenette, 2008). Extensive studies that apply shear stress or cyclic strain to endothelial cells in vitro confirm that these cells actively participate in vascular physiology.

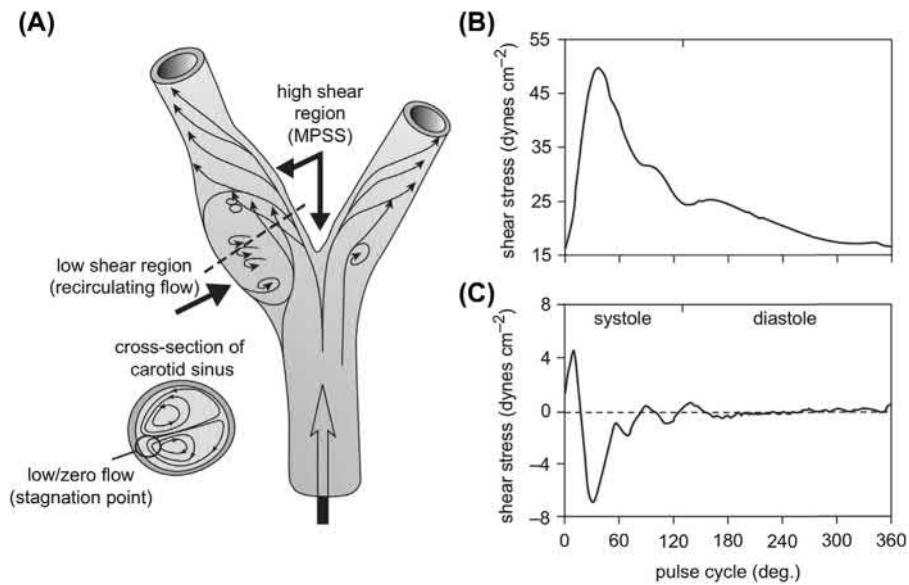
Mechanical forces resulting from blood flow directly affect cellular functions and morphology in the cardiovascular system (Davies, 2009). Over the cardiac cycle, blood vessels experience wall shear stress and circumferential strain (Fig. 2.1.6.6). These forces are essential for the homeostasis of vessels and altering these forces can lead to vessel remodeling to normalize these forces (Gibbons and Dzau, 1994). A key component of this is Murray's law that states the following,

$$r_p^3 = r_1^3 + r_2^3$$

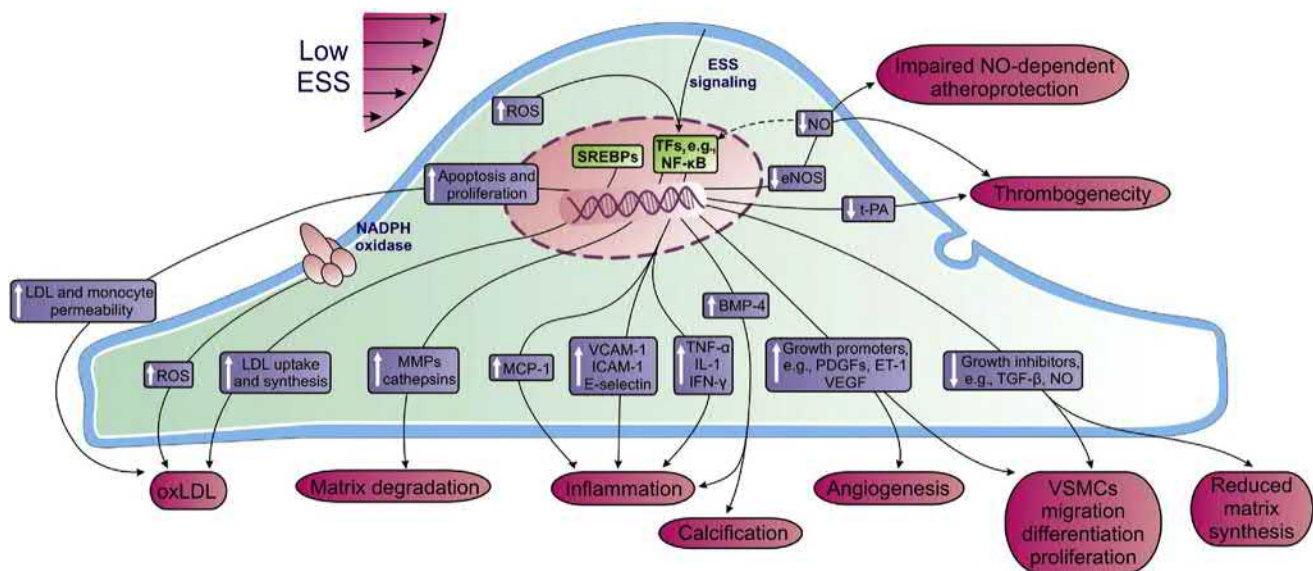
where, r_p is the parent vessel, and r_1 and r_2 are the daughter vessels (Williams et al., 2008). In this relationship, the cost of transport and maintenance is minimized. Disruption or distortion of hemodynamic forces can prime areas of the vasculature for the formation of atherosclerotic plaques (Glagov et al., 1988). Regions within vasculature that have low time-averaged shear stress, flow reversal, or spatial/temporal gradients in shear stress have increased probability for formation of vascular disease (Glagov et al., 1988; Davies, 2008). One reason for the profound effect of flow on vascular disease is the exquisite sensitivity of endothelial cells to

flow. Atheroprone flow induces a proinflammatory state in the endothelial cells, feeding the cycle of chronic inflammation that drives the development of atherosclerotic plaques. Virchow's triad delineates the factors important to the formation of thrombosis and includes vessel wall injury, hypercoagulability, and flow disturbance (stasis) (Watson et al., 2009). Consequently, alterations in flow can also alter the risk of formation of clotting in blood. Overall, disturbances in mechanical forces and flow due to implantation of medical devices in the vascular system can create new pathophysiological processes, including the proliferation of vSMCs, immune cell activation, and thrombosis.

Endothelial cells have been studied extensively for their ability to respond to changes in shear stress. Endothelial cells exposed to long-term (24 h or greater) steady shear stress at arterial levels (10–25 dyn/cm²), as well as pulsatile, nonreversing shear stress (Fig. 2.1.6.7A and B), have been shown to possess a more antiinflammatory and antiproliferative phenotype than when exposed to pulsatile, reversing conditions or low shear stress or to static culture (Fig. 2.1.6.7C) (McCormick et al., 2001; Dai et al., 2004; Chien, 2008; Yee et al., 2008). Acute responses to arterial shear stress include release of signaling molecules such as nitric oxide and prostacyclin, phosphorylation of membrane proteins, and activation of GTPases and tyrosine kinases (Frangos et al., 1985; White and Frangos, 2007). Released signaling molecules, such as prostacyclin and nitric oxide, can in turn act on smooth muscle cells to mediate vasorelaxation. The response of endothelial cells to arterial level shear stresses of 24 h or longer includes alignment of the actin cytoskeleton, movement of the microtubule organizing center toward the direction of flow, and cell elongation and alignment in the direction of flow (Eskin and McIntire, 1988; Orr et al., 2006).



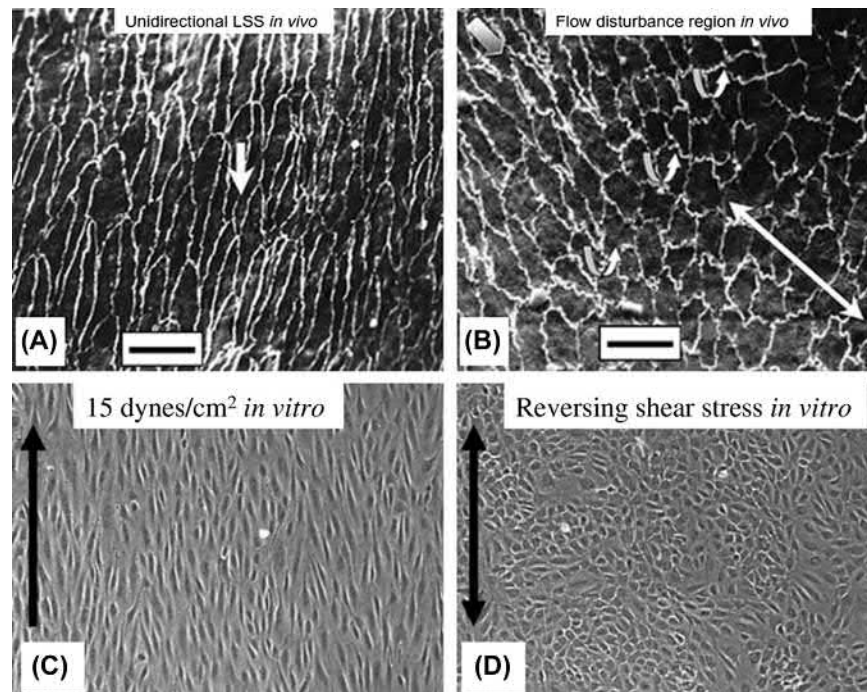
• **Figure 2.1.6.7** Representation of flow features at the carotid bifurcation. (A) Change in wall shear stress throughout the course of the cardiac cycle at two locations within the carotid bifurcation, low shear (including recirculating flow) and high shear regions (MPSS, mean positive shear stress). (B) Waveform of shear stress during one cardiac cycle (1 s) measured at the high shear stress region; (C) waveform of shear stress at the low shear stress region, showing reversing (recirculating) flow (White and Frangos, 2007).



• **Figure 2.1.6.8** Overview of molecular mechanisms in arteries under high and low shear stress conditions. (Chatzizisis, Y.S., Coskun, A.U., Elazer, M.J., Edelman, R., Feldman, C.L., Stone, P.H., June 2007. Role of endothelial shear stress in the natural history of coronary atherosclerosis and vascular remodeling. *J. Am. Coll. Cardiol.* 49 (25), 2379–2393.)

Endothelial cells respond differently to reversing or oscillatory shear stress as compared to nonreversing shear stress. Steady or nonreversing shear stress transiently induces proinflammatory and proliferative pathways, which are subsequently downregulated by long-term exposure to shear stress. However, oscillatory or reversing shear stress results in sustained activation of these pathways, leading to the hypothesis that under steady shear stress cells adapt and downregulate these pathways, whereas

under disturbed flow the continued changes in flow magnitude and direction lead to sustained activation (Dai et al., 2004; Orr et al., 2006; Chien, 2008). Fig. 2.1.6.8 shows a summary of the changes induced by reversing shear stress in comparison with nonreversing shear stress. The increases in cell proliferation, lipid metabolism, and inflammation observed in endothelial cells exposed to reversing shear stress in vitro suggest that in vivo disturbed hemodynamics may prime local sites for atherosclerosis.



• **Figure 2.1.6.9** Arterial endothelial cell alignment in vivo (porcine) and in vitro (human). (A) Endothelial cell alignment in undisturbed unidirectional laminar flow in the descending thoracic aorta (LSS, laminar shear stress), and (B) absence of transition from alignment in disturbed flow adjacent to a branch of the aorta. In (B), a region of cell alignment changes abruptly to polygonal cell morphology beyond a line of flow separation (curved arrows) that marks the boundary of a disturbed flow region in which oscillating, multidirectional flow typically occurs (double-headed arrow). Scale bar in each panel = 15 μm . (C) Endothelial cell alignment under in vitro steady shear stress (15 dyn/cm^2), and (D) reversing shear stress (modeled after the wall shear stress at the carotid sinus) is similar to in vivo alignment (Davies, 2009).

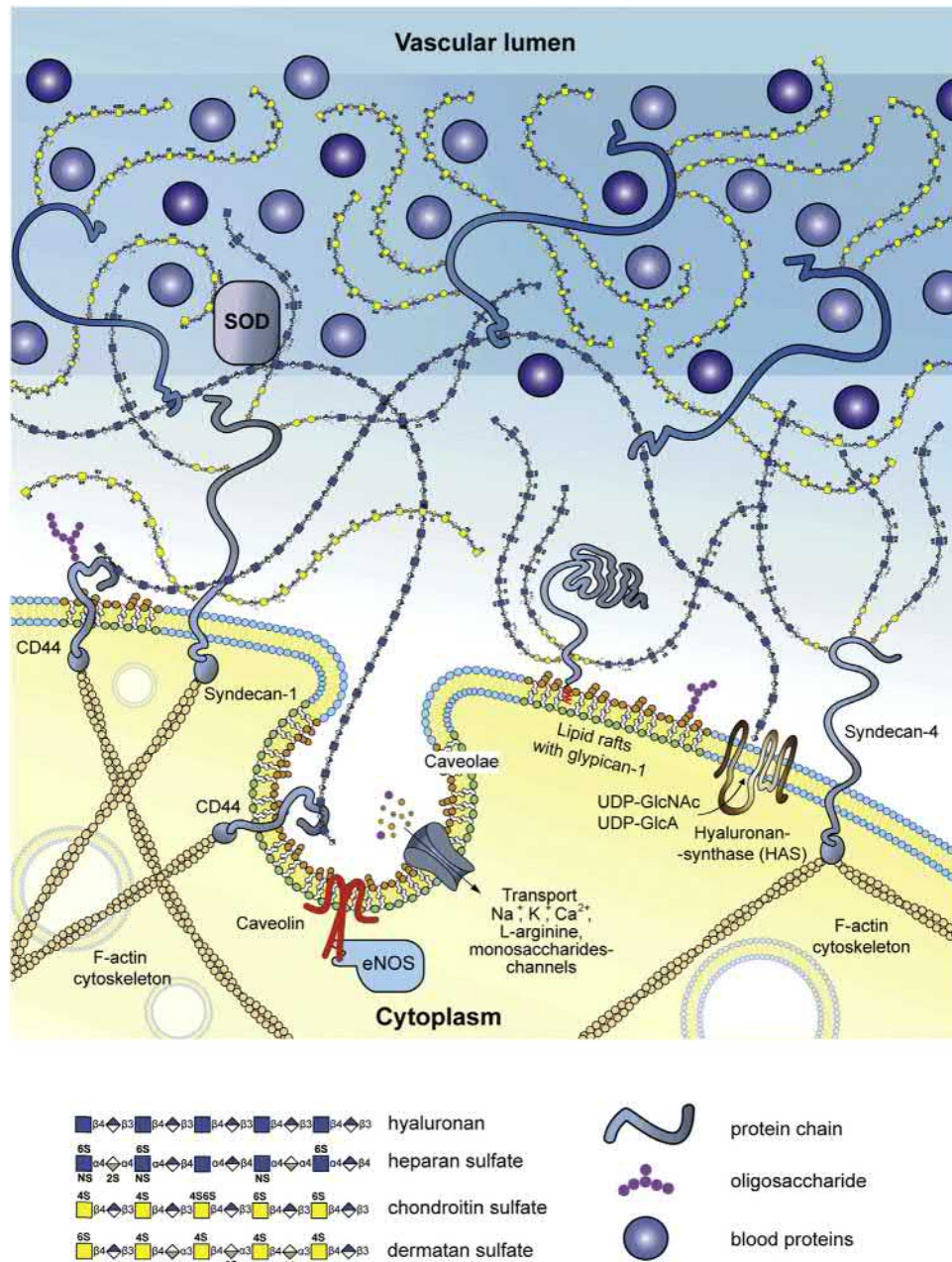
Consistent with biochemical differences, cells do not elongate or align in the direction of flow at sites of atherosclerosis (Fig. 2.1.6.9).

There is evidence that endothelial cells respond to shear stress within seconds. Rapid changes occur through the activation of ion channels, G-proteins, and stimulation of protein kinases (Davies et al., 2003; White and Frangos, 2007). Shear stress may act directly on the cell membrane to deform the cell surface and activate unknown sensor proteins. However, recent evidence has suggested that shear stress forces are transmitted by the cytoskeleton to intracellular locations where signaling can occur, such as intercellular junctions, focal adhesions, the nuclear membrane, and lipid-rich regions of the cell membrane known as caveolae (Stamatas and McIntire, 2001; Davies et al., 2003; Boyd et al., 2003). In addition to remodeling of the cytoskeleton in response to shear stress there is also evidence of focal adhesion remodeling and activation of proteins at these adhesion sites (Davies et al., 2003), supporting the hypothesis that the majority of shear stress sensing is directly coupled to the cytoskeleton.

More recently, the glycocalyx has reemerged as an important mechanosensor of shear stress in endothelial cells. The glycocalyx is an extracellular membrane-bound layer of glycoproteins and plasma proteins that has been shown to extend up to 500 μm from the endothelial cell membrane

(Fig. 2.1.6.10). In vivo, this structure is large enough to prevent cells and even large plasma proteins from reaching the surface of the cell. Removal of key glycocalyx molecules results in a reduced response to shear stress (reduction in nitric oxide production, absence of cell elongation in response to flow, and loss of shear stress-induced suppression of cell proliferation), suggesting that the glycocalyx is an important mechanosensor of fluid shear stress in endothelial cells (Tarbell and Pahakis, 2006). A reduction in the glycocalyx has also been observed in a number of disease states, including hypertension, inflammation, ischemia and reperfusion, hyperglycemia, and at known sites of atherosclerosis (internal carotid sinus). Furthermore, reduced glycocalyx expression has been correlated with increased leukocyte adhesion, suggesting that the glycocalyx may provide protection against atherogenesis (VanTeeffelen et al., 2007). Recently, it has been suggested that in vitro endothelial cells do not form a hemodynamically relevant glycocalyx, highlighting the need for a better understanding of the formation and regulation of this potentially important mechano-sensitive extracellular structure (Potter and Damiano, 2008).

Animal models have further validated data generated from in vitro systems. Suo et al. used computational fluid dynamics to model the wall shear stress in the mouse aortic arch (Suo et al., 2007). Although the mouse vasculature



• **Figure 2.1.6.10** A schematic of the endothelial glycocalyx (V Maksimenko, 2017).

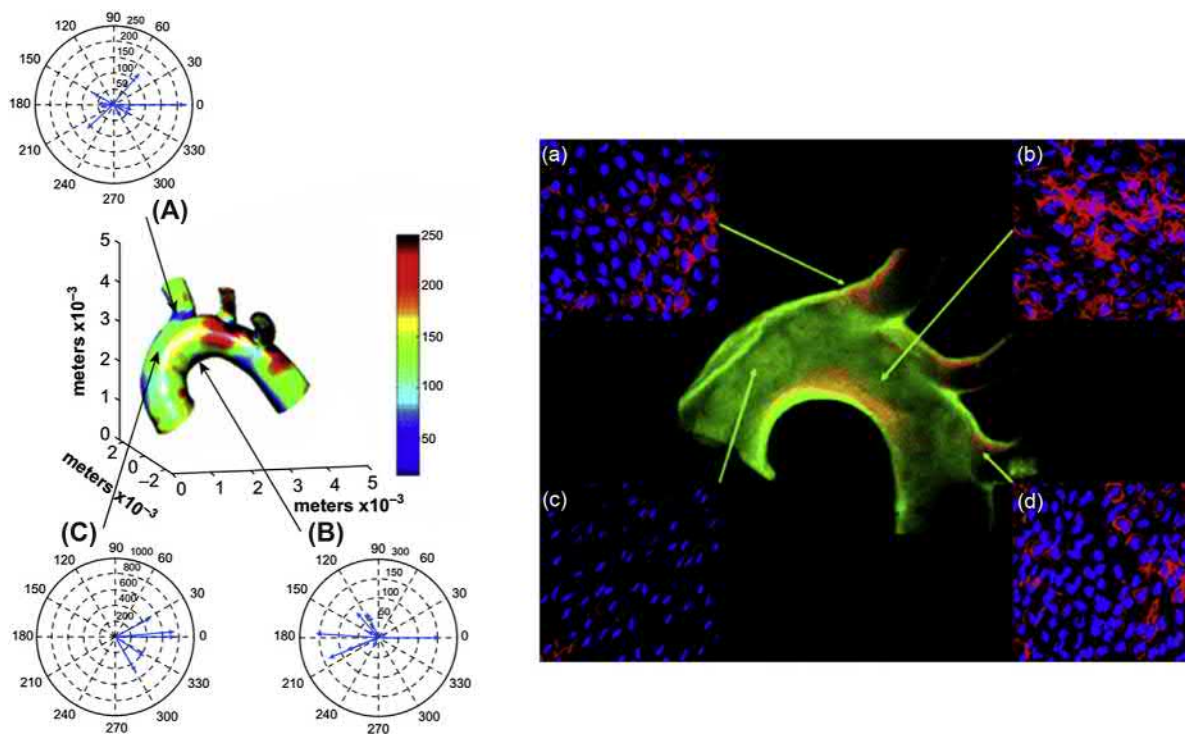
has higher overall shear stresses than the human vasculature, inflammatory markers, such as intracellular adhesion molecule-1 (ICAM-1) and vascular cell adhesion molecule-1 (VCAM-1), were upregulated at sites with low time-averaged shear stress and changes in shear stress direction (Fig. 2.1.6.11) (Suo et al., 2007). Microarray analysis of disturbed flow and undisturbed flow regions in the porcine aorta showed increased inflammatory cytokines and receptors in regions of disturbed flow (Passerini et al., 2004). These in vivo studies suggest that shear stress at sites of atherosclerosis may prime the endothelium toward an inflammatory state, which then may be exacerbated by additional risk factors (e.g., cholesterol, smoking, exercise).

Effect of Shear Stress on Blood Vessels

The flow of blood over the endothelium generates viscous drag forces in the direction of flow. The resulting tangential force exerted per unit area of vessel surface at the blood–endothelium surface defines shear stress. Mathematically, the product between the viscosity (μ) and the velocity gradient at the wall, also known as the wall shear rate ($\dot{\gamma}$), equates to wall shear stress (τ_w):

$$\tau_w = \mu \dot{\gamma}$$

With ventricular contraction, momentum propagates as waves down the aorta, but diminishes in amplitude on the arterial side of the circulation, with distance from the



• **Figure 2.1.6.11** Regional differences in wall shear stress in the mouse aortic arch correlates with regional differences in VCAM-1 expression. (Left) The computed, time-varying wall shear stress vectors are depicted at areas (A), (B), and (C) in one mouse aorta. The color coding indicates the mean wall shear stress distribution (defined as the wall shear stress magnitude averaged over the cardiac cycle). The vector diagrams indicate the time-varying changes in the direction and magnitude of wall shear stress throughout the cardiac cycle. There is a greater variation in the direction of the instantaneous wall shear stress vectors in areas (a) and (b), as can be seen in the polar plots of wall shear stress. Note that the relatively low mean wall shear stress zone at the inner curvature of the aortic arch (b) has instantaneous magnitudes of wall shear stress up to approximately 150 dyn/cm^2 , whereas values exceeding 600 dyn/cm^2 were found along the lateral wall of the ascending aorta (c). (Right) High expression of VCAM-1 protein correlates with areas of the aortic arch with low and time-varying shear stresses (a, b, and d), whereas VCAM-1 expression in the ascending aorta (c) is lower, consistent with unidirectional flow (Suo et al., 2007).

heart. Pulsatility is generated by the pumping action of the heart and gives rise to pulsatile shear stress and cyclic strain. Typical mean arterial values of shear stress range from 6 to 40 dyn/cm^2 , but can vary from close to 0 to well over 100 dyn/cm^2 elsewhere in the vasculature (Goldsmith and Turitto, 1986; Dobrin et al., 1989). While pulsing down the arterial tree, blood flow normally remains laminar throughout the vascular system with the exception of the ascending aorta, which can have turbulent regions. In regions of complexity, such as regions of arterial branching or tortuosity, there can be disturbed laminar flow with flow reversal and regions of recirculation (Fig. 2.1.6.7).

Effect of Cyclic Strain on Blood Vessels

Along with momentum, pressure propagates as waves down the arterial tree, leading to a periodic circumferential tensile stress in the vessel lumen (Fig. 2.1.6.6). In vivo, blood pressure measures the variation in force against the blood vessel wall as the blood is ejected from the heart during each heartbeat (each cardiac cycle). In measuring blood pressure in humans, the brachial artery is occluded by a pressure cuff (attached to a sphygmomanometer), while the sound of the

blood flow is measured downstream with a stethoscope. The pressure cuff is slowly loosened, allowing the pressure to decrease and the blood to flow downstream. The pressure at which the blood flow begins is the systolic pressure. As the pressure continues to decrease, the value at which the sound disappears is the diastolic pressure. Since the arterial wall is compliant, this periodic pressure difference gives rise to a cyclic wall strain. Since arteries and some synthetic substrates on which cells are cultured are elastic, cyclic strain can be measured as the percentage change in diameter between the systolic and diastolic pressures. In normal circulation, the internal diameter and, thus, circumference of large mammalian arteries, increases cyclically between 2% and 18% over the cardiac cycle at a frequency of approximately 1 Hz (60 cycles/min) (Dobrin, 1978). The arterial cyclic strain can increase by 15% in hypertension (Gupta and Grande-Allen, 2006). Typical systole/diastole values in large human arteries range from 90/60 mmHg to 120/80 mmHg.

To study cyclic strain effects in vitro, cells must be cultured on a deformable substrate, usually silicone rubber or segmented polyurethane coated with extracellular matrix proteins, then subjected to cyclic deformation at a rate similar to the heart rate (1 Hz). Most frequently, custom-built

uniaxial strain devices are driven mechanically by an eccentric cam, which imposes a nearly uniform strain along the substrate at a frequency simulating the heart rate (1 Hz) (Frye et al., 2005; Yung et al., 2009). Custom-built biaxial strain units have also been used (Kim et al., 1999). The mechanical forces generated in *in vitro* studies on uniaxial cyclic strain optimally include a “motion control” condition. “Motion control” controls for the reversing shear stress (less than 0.5 dyne/cm²) from fluid motion accompanying the cyclic strain of the membrane. Some endothelial cells are more responsive to motion control than to cyclic strain (Sung et al., 2007). Cultured cells have been exposed to cyclic strain in commercially available Flexercell Strain Units (Flexcell International, Corp.), which can deform in uniaxial or biaxial modes (Matheson et al., 2007). These units are driven by vacuum pressure beneath six-well plates with flexible elastomeric bottoms, on which cells are cultured, thus deforming substrate and cells (Haseneen et al., 2003). It should be noted that not only do the mechanical forces that impinge on a population of cultured cells alter their function, but also the substrate on which the cells are cultured may affect cell response. Cyclic strain has been shown to alter the phenotype of cultured smooth muscle cells on polymeric scaffolds (Kim et al., 1999), and to cause differentiation of embryonic stem cells into smooth muscle cells (Shimizu et al., 2008).

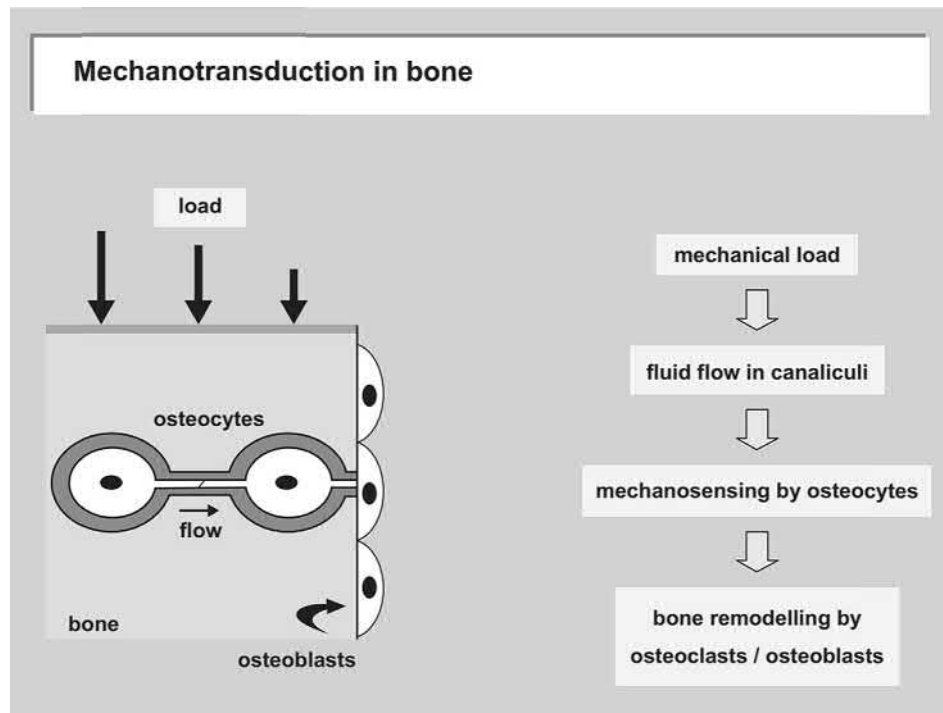
Although the effects of shear stress and cyclic strain are most frequently studied independently of each other, recent work has suggested that the synchronization of the two forces when applied simultaneously can affect gene expression and morphology (Owatverot et al., 2005). The stress phase angle has been defined as the temporal phase angle between cyclic strain and wall shear stress (Dancu et al., 2004). The stress phase angle has been shown to be most negative at sites prone to atherosclerosis when compared to other regions of the vasculature and can be made even more negative with hypertension (Dancu et al., 2004). Cells exposed to identical wall shear stress and cyclic strain, but at a stress phase angle of -180 degrees instead of 0 degrees, had reduced endothelial nitric oxide production and increased endothelin-1 production (Dancu et al., 2004), suggesting that asynchronous wall shear stress and cyclic strain could lead to endothelial cell dysfunction.

Bone and Cartilage

Bone is made up of three types of cells: osteocytes, osteoblasts, and osteoclasts. These cells maintain bone function, build new bone, and degrade bone, respectively. Furthermore, they reside in a matrix of collagen and hydroxyapatite, a complex tetracalcium phosphate, which is produced by osteoblasts. The osteocytes are mechanosensors, which release prostaglandins in response to mechanical forces, principally shear stress (Jiang et al., 2007). They transmit signals to other bone cells and the matrix through thin channels in the matrix to influence bone remodeling. Bone is a tissue that is constantly undergoing remodeling in

response to mechanical loading, forming new bone parallel to the loading direction, and losing density in unstressed regions. Bone loss from a sedentary lifestyle, limb paralysis, or microgravity during space flight has provided conclusive *in vivo* evidence for the positive effects of physiological loading of skeletal tissues (Orr et al., 2006). Mechanical loading generates fluid shear stress, hydrostatic compression, and stretch on bone cells. The dense bone matrix resists compressive forces, limiting the transfer of force to the cells (Orr et al., 2006). Physiological strains are only 0.04%–0.3%; however, *in vitro* it has been shown that strains must be 1%–10% to induce cellular responses (Orr et al., 2006). Unmineralized matrix around osteocytes is more permeable than mineralized bone, creating lacuno-canalicular porosities for interstitial fluid flow. As a result, compressive forces generate pressure gradients that drive interstitial fluid flow in the matrix; these shear stresses have been estimated to be 8–30 dyn/cm², similar to arterial wall shear stress (Orr et al., 2006). Interstitial fluid flow due to mechanical loading is thought to be the primary mechanism for action of mechanical forces on bone (Fig. 2.1.6.12) (Klein-Nulend et al., 2005). Although *in vitro* both osteoclasts and osteoblasts have been shown to respond to shear stress, the geometry of the lacuno-canalicular porosity suggests that interstitial fluid flow is preferentially sensed by the osteoclasts (Orr et al., 2006). Osteocytes respond to mechanical stimuli by secreting factors that can then, in turn, modulate both osteoblasts and osteoclasts (Klein-Nulend et al., 2005). Recent models, however, have suggested that the interstitial fluid flow applies drag forces to the pericellular matrix of the osteocyte that are 20 times larger than the fluid shear forces applied directly to the cell surface (Han et al., 2004). The fluid flow through the pericellular matrix induces strain on the actin filaments of the cytoskeleton, which results in strain amplification at the cellular level an order of magnitude greater than tissue-level strains. These recent models question the hypothesis that the regulatory mechanical force on osteocytes is fluid shear stress, and instead suggest that shear-induced strain may be the principal mechano-transducing force (Orr et al., 2006; Han et al., 2004).

Exercise-stimulated bone remodeling may be the response of osteoblasts to interstitial fluid flow (Reich et al., 1990; Hillsley and Frangos, 1994). Furthermore, temporal gradients in interstitial fluid flow, imposed by pulsatile shear stress (designed to simulate mechanical loading) stimulate osteoblast proliferation *in vitro* (Jiang et al., 2002), whereas steady shear stress does not stimulate osteoblast signal transduction or proliferation. Exposure of mouse osteocytes and mixed-population human bone cells to pulsating shear stress *in vitro* increased prostaglandin and nitric oxide release, similar to the effects of shear stress on vascular endothelial cells, suggesting that there may be some similar mechanisms for sensing fluid flow (Klein-Nulend et al., 2005). Strain rate has been shown to be more important than strain amplitude in inducing bone formation in response to loading, supporting the hypothesis that bone formation is stimulated by dynamic rather than static loads (Klein-Nulend et al., 2005).



• **Figure 2.1.6.12** Model for the transduction of mechanical strain to osteocytes in bone. (Left) The osteocyte-lining cell network of bone tissue under stress (large arrows). Loading results in flow of interstitial fluid in the canalicular nonmineralized matrix (horizontal arrow) (Klein-Nulend et al., 2005).

Cartilage, located on the articulating surfaces of joints, provides low friction for freely moving joints. In the growing embryo, cartilage is the precursor to bone. Cartilage cells (chondrocytes) secrete a matrix of collagen fibers embedded in mucopolysaccharide (e.g., chondroitin sulfate). Although cartilage is relatively avascular compared with bone, cartilage responds to mechanical loading similarly to bone. Increased load leads to increased matrix production, resulting in stronger tissue. Cartilage must withstand tensile and shear forces in addition to compression (Kim et al., 1994). Most of the work on cartilage loading focuses on compression and hydrostatic pressure. Cyclic compression of explants (0.1 Hz, 2%–3% compression) stimulated matrix synthesis by chondrocytes (Shieh and Athanasiou, 2003).

Summary

Nearly all mammalian cells and tissues are subject to mechanical forces. We began by highlighting the molecular mechanisms behind mechanotransduction, as well as the major protein architecture responsible for sensing and transducing mechanical forces. We have highlighted the cardiovascular and skeletal systems adapted specifically to mechanical forces, to variations in blood flow and pressure, and to loadbearing, respectively. In vitro models have been employed to study how isolated endothelial and smooth muscle cells from arteries and veins respond to conditions of controlled shear stress and cyclic strain. Gene expression is sensitively regulated by alterations in shear stress and cyclic strain, which translates to functional changes in the

cells. The elucidation of roles of different bone cell types has been clarified using in vitro models. We are just beginning to understand interstitial fluid flow in the lymphatic system, and the influence mechanical forces may have on cell migration and tumor growth.

In order to properly design biomaterials that successfully simulate native tissues, understanding the mechanical environment in which the biomaterial is implanted is important. Cells exposed to disturbed mechanical environments (e.g., reversing flow in blood vessels, compliance mismatch of blood vessel grafts, lack of weight bearing on bone) typically have reduced function, and may promote the development of a pathological condition. In designing a biomaterial, we must attempt to recreate the mechanical environment that is to receive the implant for maximum success and long-term viability.

References

- Arnold, M., Cavalcanti-Adam, E.A., Glass, R., Blummel, J., ECK, W., Kantelehner, M., Kessler, H., Spatz, J.P., 2004. Activation of integrin function by nanopatterned adhesive interfaces. *Chemp-hyschem* 5, 383–388.
- Arora, P.D., Narani, N., Mcculloch, C.A., 1999. The compliance of collagen gels regulates transforming growth factor-beta induction of alpha-smooth muscle actin in fibroblasts. *Am. J. Pathol.* 154, 871.
- Baker, A.B., Ettenson, D.S., Jonas, M., Nugent, M.A., Iozzo, R.V., Edelman, E.R., 2008. Endothelial cells provide feedback control for vascular remodeling through a mechanosensitive autocrine TGF-beta signaling pathway. *Circ. Res.* 103, 289–297.

- Banes, A.J., Gilbert, J., Taylor, D., Monbureau, O., 1985. A new vacuum-operated stress-providing instrument that applies static or variable duration cyclic tension or compression to cells in vitro. *J. Cell Sci.* 75, 35–42.
- Blackman, B.R., Garcia-Cardena, G., Gimbrone JR., M.A., 2002. A new in vitro model to evaluate differential responses of endothelial cells to simulated arterial shear stress waveforms. *J. Biomech. Eng.* 124, 397–407.
- Boyd, N.L., Park, H., Yi, H., Boo, Y.C., Sorescu, G.P., Sykes, M., Jo, H., 2003. Chronic shear induces caveolae formation and alters ERK and Akt responses in endothelial cells. *Am. J. Physiol. Heart Circ. Physiol.* 285, H1113–H1122.
- Brown, T.D., 2000. Techniques for mechanical stimulation of cells in vitro: a review. *J. Biomech.* 33, 3–14.
- Buchsbaum, R.J., 2007. Rho activation at a glance. *J. Cell Sci.* 120, 1149–1152.
- Burdick, J.A., Anseth, K.S., 2002. Photoencapsulation of osteoblasts in injectable RGD-modified PEG hydrogels for bone tissue engineering. *Biomaterials* 23, 4315–4323.
- Cai, L., Zhang, L., Dong, J., Wang, S., 2012. Photocured biodegradable polymer substrates of varying stiffness and microgroove dimensions for promoting nerve cell guidance and differentiation. *Langmuir* 28, 12557–12568.
- Case, L.B., Waterman, C.M., 2015. Integration of actin dynamics and cell adhesion by a three-dimensional, mechanosensitive molecular clutch. *Nat. Cell Biol.* 17, 955–963.
- Cavalcanti-Adam, E.A., Volberg, T., Micoulet, A., Kessler, H., Geiger, B., Spatz, J.P., 2007. Cell spreading and focal adhesion dynamics are regulated by spacing of integrin ligands. *Biophys. J.* 92 (8), 2964–2974.
- Charras, G., Yap, A.S., 2018. Tensile forces and mechanotransduction at cell-cell junctions. *Curr. Biol.* 28, R445–R457.
- Chatzizisis, Y.S., Coskun, A.U., Jonas, M., Edelman, E.R., Feldman, C.L., Stone, P.H., June 2007. Role of endothelial shear stress in the natural history of coronary atherosclerosis and vascular remodeling. *J. Am. Coll. Cardiol.* 49 (25), 2379–2393.
- Chen, C.S., 2008. Mechanotransduction – a field pulling together? *J. Cell Sci.* 121, 3285.
- Chen, C.S., Mrksich, M., Huang, S., Whitesides, G.M., Ingber, D.E., 1998. Micropatterned surfaces for control of cell shape, position, and function. *Biotechnol. Prog.* 14, 356–363.
- Chien, S., 2008. Effects of disturbed flow on endothelial cells. *Ann. Biomed. Eng.* 36, 554–562.
- Christman, K.L., Enriquez-Rios, V.D., Maynard, H.D., 2006. Nanopatterning proteins and peptides. *Soft Matter* 2, 928–939.
- Dahl, K.N., Ribeiro, A.J., Lammerding, J., 2008. Nuclear shape, mechanics, and mechanotransduction. *Circ. Res.* 102, 1307–1318.
- Dai, G., Kaazempur-Mofrad, M.R., Natarajan, S., Zhang, Y., Vaughn, S., Blackman, B.R., Kamm, R.D., Garcia-Cardena, G., Gimbrone JR., M.A., 2004. Distinct endothelial phenotypes evoked by arterial waveforms derived from atherosclerosis-susceptible and -resistant regions of human vasculature. *Proc. Natl. Acad. Sci. U. S. A.* 101, 14871–14876.
- Dalton, B.A., Walboomers, X.F., Dziegielewska, M., Evans, M.D., Taylor, S., Jansen, J.A., Steele, J.G., 2001. Modulation of epithelial tissue and cell migration by microgrooves. The Japanese Society for Biomaterials, and The Australian Society for Biomaterials and the Korean Society for Biomaterials *J. Biomed. Mater. Res.* 56, 195–207.
- Dancu, M.B., Berardi, D.E., Heuvel, J.P.V., Tarbell, J.M., 2004. Asynchronous shear stress and circumferential strain reduces endothelial NO synthase and cyclooxygenase-2 but induces endothelin-1 gene expression in endothelial cells. *Arterioscler. Thromb. Vasc. Biol.* 24, 2088–2094.
- Davies, P.F., 2008. Endothelial transcriptome profiles in vivo in complex arterial flow fields. *Ann. Biomed. Eng.* 36, 563–570.
- Davies, P.F., 2009. Hemodynamic shear stress and the endothelium in cardiovascular pathophysiology. *Nat. Clin. Pract. Cardiovasc. Med.* 6, 16–26.
- Davies, P.F., Zilberberg, J., Helmke, B.P., 2003. Spatial microstimuli in endothelial mechanosignaling. *Circ. Res.* 92, 359–370.
- Discher, D.E., Janmey, P., Wang, Y.L., 2005. Tissue cells feel and respond to the stiffness of their substrate. *Science* 310, 1139–1143.
- Dobrin, P.B., 1978. Mechanical properties of arteries. *Physiol. Rev.* 58, 397–460.
- Dobrin, P.B., Littooy, F.N., Endean, E.D., 1989. Mechanical factors predisposing to intimal hyperplasia and medial thickening in autogenous vein grafts. *Surgery* 105, 393–400.
- Dupont, S., 2016. Role of YAP/TAZ in cell-matrix adhesion-mediated signalling and mechanotransduction. *Exp. Cell Res.* 343, 42–53.
- Dupont, S., Morsut, L., Aragona, M., Enzo, E., Giulitti, S., Cordeonsi, M., Zanconato, F., LE Digabel, J., Forcato, M., Bicciato, S., Elvassore, N., Piccolo, S., 2011. Role of YAP/TAZ in mechanotransduction. *Nature* 474, 179–183.
- Elosegui-Artola, A., Andreu, I., Beedle, A.E.M., Lezamiz, A., Uroz, M., Kosmalska, A.J., Oria, R., Kechagia, J.Z., Rico-Lastres, P., Le Roux, A.L., Shanahan, C.M., TREPAT, X., Navajas, D., Garcia-Manyes, S., Roca-Cusachs, P., 2017. Force triggers YAP nuclear entry by regulating transport across nuclear pores. *Cell* 171, 1397–1410 e14.
- Engler, A., Bacakova, L., Newman, C., Hategan, A., Griffin, M., Discher, D., 2004. Substrate compliance versus ligand density in cell on gel responses. *Biophys. J.* 86, 617–628.
- Engler, A.J., Sen, S., Sweeney, H.L., Discher, D.E., 2006. Matrix elasticity directs stem cell lineage specification. *Cell* 126, 677–689.
- Eskin, S.G., Mcintire, L.V., 1988. Hemodynamic effects on atherosclerosis and thrombosis. *Semin. Thromb. Hemost.* 14, 170–174.
- Fischer, M., Rikeit, P., Knaus, P., Coirault, C., 2016. YAP-mediated mechanotransduction in skeletal muscle. *Front. Physiol.* 7, 41.
- Frangos, J.A., Eskin, S.G., Mcintire, L.V., Ives, C.L., 1985. Flow effects on prostacyclin production by cultured human endothelial cells. *Science* 227, 1477–1479.
- Frangos, J.A., Mcintire, L.V., Eskin, S.G., 1988. Shear stress induced stimulation of mammalian cell metabolism. *Biotechnol. Bioeng.* 32, 1053–1060.
- Frye, S.R., Yee, A., Eskin, S.G., Guerra, R., Cong, X., Mcintire, L.V., 2005. cDNA microarray analysis of endothelial cells subjected to cyclic mechanical strain: importance of motion control. *Physiol. Genom.* 21, 124–130.
- Garcia, A.J., Ducheyne, P., Boettiger, D., 1997. Quantification of cell adhesion using a spinning disc device and application to surface-reactive materials. *Biomaterials* 18, 1091–1098.
- Geiger, B., Bershadsky, A., Pankov, R., Yamada, K.M., 2001. Transmembrane crosstalk between the extracellular matrix-cytoskeleton crosstalk. *Nat. Rev. Mol. Cell Biol.* 2, 793–805.
- Giannone, G., Dubin-Thaler, B.J., Dobreiner, H.G., Kieffer, N., Bresnick, A.R., Sheetz, M.P., 2004. Periodic lamellipodial contractions correlate with rearward actin waves. *Cell* 116, 431–443.
- Gibbons, G.H., Dzau, V.J., 1994. The emerging concept of vascular remodeling. *N. Engl. J. Med.* 330, 1431–1438.
- Girard, P.R., Nerem, R.M., 1995. Shear stress modulates endothelial cell morphology and F-actin organization through the regulation of focal adhesion-associated proteins. *J. Cell. Physiol.* 163, 179–193.

- Glagov, S., Zarins, C., Giddens, D.P., Ku, D.N., 1988. Hemodynamics and atherosclerosis. Insights and perspectives gained from studies of human arteries. *Arch. Pathol. Lab Med.* 112, 1018–1031.
- Goldsmith, H.L., Turitto, V.T., 1986. Rheological aspects of thrombosis and haemostasis: basic principles and applications. ICTH-Report-Subcommittee on Rheology of the International Committee on Thrombosis and Haemostasis. *Thromb. Haemost.* 55, 415–435.
- Grashoff, C., Hoffman, B.D., Brenner, M.D., Zhou, R., Parsons, M., Yang, M.T., Mclean, M.A., Sligar, S.G., Chen, C.S., Ha, T., Schwartz, M.A., 2010. Measuring mechanical tension across vinculin reveals regulation of focal adhesion dynamics. *Nature* 466, 263–266.
- Gupta, V., Grande-Allen, K.J., 2006. Effects of static and cyclic loading in regulating extracellular matrix synthesis by cardiovascular cells. *Cardiovasc. Res.* 72, 375–383.
- Hall, A., 1998. Rho GTPases and the actin cytoskeleton. *Science* 279, 509–514.
- Han, Y., Cowin, S.C., Schaffler, M.B., Weinbaum, S., 2004. Mechanotransduction and strain amplification in osteocyte cell processes. *Proc. Natl. Acad. Sci. U. S. A.* 101, 16689–16694.
- Haque, F., Lloyd, D.J., Smallwood, D.T., Dent, C.L., Shanahan, C.M., Fry, A.M., Trembath, R.C., Shackleton, S., 2006. SUN1 interacts with nuclear lamin a and cytoplasmic nesprins to provide a physical connection between the nuclear lamina and the cytoskeleton. *Mol. Cell Biol.* 26, 3738–3751.
- Harburger, D.S., Calderwood, D.A., 2009. Integrin signalling at a glance. *J. Cell Sci.* 122, 159–163.
- Hasegawa, S., Sato, S., Saito, S., Suzuki, Y., Brunette, D.M., 1985. Mechanical stretching increases the number of cultured bone cells synthesizing DNA and alters their pattern of protein synthesis. *Calcif. Tissue Int.* 37, 431–436.
- Haseneen, N.A., Vaday, G.G., Zucker, S., Foda, H.D., 2003. Mechanical stretch induces MMP-2 release and activation in lung endothelium: role of EMMPRIN. *Am. J. Physiol. Lung Cell Mol. Physiol.* 284, L541–L547.
- Hayakawa, K., Tatsumi, H., Sokabe, M., 2011. Actin filaments function as a tension sensor by tension-dependent binding of cofilin to the filament. *J. Cell Biol.* 195, 721–727.
- Hillsley, M.V., Frangos, J.A., 1994. Bone tissue engineering - the role of interstitial fluid-flow - review. *Biotechnol. Bioeng.* 43, 573–581.
- Horiguchi, M., Ota, M., Rifkin, D.B., 2012. Matrix control of transforming growth factor-beta function. *J. Biochem.* 152, 321–329.
- Horwitz, K.E.K., Alan, R., 2010. Reducing background fluorescence reveals adhesions in 3D matrices. *Nat. Cell Biol.* 13, 3.
- Houben, F., Ramaekers, F.C., Snoeckx, L.H., Broers, J.L., 2007. Role of nuclear lamina-cytoskeleton interactions in the maintenance of cellular strength. *Biochim. Biophys. Acta* 1773, 675–686.
- Humphries, J.D., Wang, P., Streuli, C., Geiger, B., Humphries, M.J., Ballestrem, C., 2007. Vinculin controls focal adhesion formation by direct interactions with talin and actin. *J. Cell Biol.* 179, 1043–1057.
- Hynes, R.O., 1992. Integrins: versatility, modulation, and signaling in cell adhesion. *Cell* 69, 11–25.
- Hynes, R.O., 2002. Integrins: bidirectional, allosteric signaling machines. *Cell* 110, 673–687.
- Isenberg, B.C., Dimilla, P.A., Walker, M., Kim, S., Wong, J.Y., 2009. Vascular smooth muscle cell durotaxis depends on substrate stiffness gradient strength. *Biophys. J.* 97, 1313–1322.
- Itano, N., Okamoto, S., Zhang, D., Lipton, S.A., Ruoslahti, E., 2003. Cell spreading controls endoplasmic and nuclear calcium: a physical gene regulation pathway from the cell surface to the nucleus. *Proc. Natl. Acad. Sci. U. S. A.* 100, 5181–5186.
- Jiang, G.L., White, C.R., Stevens, H.Y., Frangos, J.A., 2002. Temporal gradients in shear stimulate osteoblastic proliferation via ERK1/2 and retinoblastoma protein. *Am. J. Physiol. Endocrinol. Metab.* 283, E383–E389.
- Jiang, J.X., Siller-Jackson, A.J., Burra, S., 2007. Roles of gap junctions and hemichannels in bone cell functions and in signal transmission of mechanical stress. *Front. Biosci.* 12, 1450–1462.
- Kim, B.S., Nikolovski, J., Bonadio, J., Mooney, D.J., 1999. Cyclic mechanical strain regulates the development of engineered smooth muscle tissue. *Nat. Biotechnol.* 17, 979–983.
- Kim, D.H., Provenzano, P.P., Smith, C.L., Levchenko, A., 2012. Matrix nanotopography as a regulator of cell function. *J. Cell Biol.* 197, 351–360.
- Kim, Y.J., Sah, R.L., Grodzinsky, A.J., Plaas, A.H., Sandy, J.D., 1994. Mechanical regulation of cartilage biosynthetic behavior: physical stimuli. *Arch. Biochem. Biophys.* 311, 1–12.
- Klein-Nulend, J., Bacabac, R.G., Mullender, M.G., 2005. Mechanobiology of bone tissue. *Pathol. Biol.* 53, 576–580.
- Koskinas, K.C., Chatzizisis, Y.S., Baker, A.B., Edelman, E.R., Stone, P.H., Feldman, C.L., 2009. The role of low endothelial shear stress in the conversion of atherosclerotic lesions from stable to unstable plaque. *Curr. Opin. Cardiol.* 24, 580–590.
- Lee, J., Wong, M., Smith, Q., Baker, A.B., 2013. A novel system for studying mechanical strain waveform-dependent responses in vascular smooth muscle cells. *Lab Chip* 13, 4573–4582.
- Lee, S.W., Kim, S.Y., Rhyu, I.C., Chung, W.Y., Leesungbok, R., Lee, K.W., 2009. Influence of microgroove dimension on cell behavior of human gingival fibroblasts cultured on titanium substrata. *Clin. Oral Implant. Res.* 20, 56–66.
- Liu, W.F., Nelson, C.M., Tan, J.L., Chen, C.S., 2007. Cadherins, RhoA, and Rac1 are differentially required for stretch-mediated proliferation in endothelial versus smooth muscle cells. *Circ. Res.* 101, e44.
- Lo, C.M., Wang, H.B., Dembo, M., Wang, Y.L., 2000. Cell movement is guided by the rigidity of the substrate. *Biophys. J.* 79, 144–152.
- Lombardi, M.L., Jaalouk, D.E., Shanahan, C.M., Burke, B., Roux, K.J., Lammerding, J., 2011. The interaction between nesprins and Sun proteins at the nuclear envelope is critical for force transmission between the nucleus and cytoskeleton. *J. Biol. Chem.* 286 (30), 26743–26753.
- Lu, H., Koo, L.Y., Wang, W.M., Lauffenburger, D.A., Griffith, L.G., Jensen, K.F., 2004. Microfluidic shear devices for quantitative analysis of cell adhesion. *Anal. Chem.* 76, 5257–5264.
- Malek, A.M., Alper, S.L., Izumo, S., 1999. Hemodynamic shear stress and its role in atherosclerosis. *JAMA* 282, 2035–2042.
- Malek, A.M., Izumo, S., 1996. Mechanism of endothelial cell shape change and cytoskeletal remodeling in response to fluid shear stress. *J. Cell Sci.* 109 (Pt 4), 713–726.
- Matheson, L.A., Maksym, G.N., Santerre, J.P., Labow, R.S., 2007. Differential effects of uniaxial and biaxial strain on U937 macrophage-like cell morphology: influence of extracellular matrix type proteins. *J. Biomed. Mater. Res. A* 81, 971–981.
- Paszek, M.J., Zahir, N., Johnson, K.R., Lakins, J.N., Rozenberg, G.I., Gefen, A., Reinhart-King, C.A., Margulies, S.S., Dembo, M., Boettiger, D., Hammer, D.A., Weaver, V.M., 2005. Tensional homeostasis and the malignant phenotype. *Cancer Cell* 8, 241–254.
- May-Newman, K., Yin, F.C., 1995. Biaxial mechanical behavior of excised porcine mitral valve leaflets. *Am. J. Physiol.* 269, H1319–H1327.
- Mccormick, S.M., Eskin, S.G., McIntire, L.V., Teng, C.L., Lu, C.M., Russell, C.G., Chittur, K.K., 2001. DNA microarray reveals changes in gene expression of shear stressed human umbilical vein endothelial cells. *Proc. Natl. Acad. Sci. U. S. A.* 98, 8955–8960.
- Mitchison, T., Kirschner, M., 1988. Cytoskeletal dynamics and nerve growth. *Neuron* 1, 761–772.

- Morawietz, H., Wagner, A.H., Hecker, M., Goetsch, W., 2008. Endothelin receptor B-mediated induction of c-jun and AP-1 in response to shear stress in human endothelial cells. *Can. J. Physiol. Pharmacol.* 86, 499–504.
- Nagel, T., Resnick, N., Atkinson, W.J., Dewey JR., C.F., Gimbrone JR., M.A., 1994. Shear stress selectively upregulates intercellular adhesion molecule-1 expression in cultured human vascular endothelial cells. *J. Clin. Investig.* 94, 885–891.
- Neidlinger-Wilke, C., Wilke, H.J., Claes, L., 1994. Cyclic stretching of human osteoblasts affects proliferation and metabolism: a new experimental method and its application. *J. Orthop. Res.* 12, 70–78.
- Nobes, C.D., Hall, A., 1995. Rho, rac, and cdc42 GTPases regulate the assembly of multimolecular focal complexes associated with actin stress fibers, lamellipodia, and filopodia. *Cell* 81, 53–62.
- Nusrat, A., Giry, M., Turner, J.R., Colgan, S.P., Parkos, C.A., Carnes, D., Lemichez, E., Boquet, P., Madara, J.L., 1995. Rho protein regulates tight junctions and perijunctional actin organization in polarized epithelia. *Proc. Natl. Acad. Sci. U. S. A.* 92, 10629–10633.
- Oakley, C., Brunette, D., 1993. The sequence of alignment of microtubules, focal contacts and actin filaments in fibroblasts spreading on smooth and grooved titanium substrata. *J. Cell Sci.* 106, 343–354.
- Orr, A.W., Helmke, B.P., Blackman, B.R., Schwartz, M.A., 2006. Mechanisms of mechanotransduction. *Dev. Cell* 10, 11–20.
- Owatverot, T.B., Oswald, S.J., Chen, Y., Wille, J.J., Yin, F.C., 2005. Effect of combined cyclic stretch and fluid shear stress on endothelial cell morphological responses. *J. Biomech. Eng.* 127, 374–382.
- Parsons, J.T., Horwitz, A.R., Schwartz, M.A., 2010. Cell adhesion: integrating cytoskeletal dynamics and cellular tension. *Nat. Rev. Mol. Cell Biol.* 11, 633–643.
- Passerini, A.G., Polacek, D.C., Shi, C., Francesco, N.M., Manduchi, E., Grant, G.R., Pritchard, W.F., Powell, S., Chang, G.Y., Stoekert JR., C.J., Davies, P.F., 2004. Coexisting proinflammatory and antioxidative endothelial transcription profiles in a disturbed flow region of the adult porcine aorta. *Proc. Natl. Acad. Sci. U. S. A.* 101, 2482–2487.
- Paszek, M.J., Weaver, V.M., 2004. The tension mounts: mechanics meets morphogenesis and malignancy. *J. Mammary Gland Biol. Neoplasia* 9, 325–342.
- Philip, J.T., Dahl, K.N., 2008. Nuclear mechanotransduction: response of the lamina to extracellular stress with implications in aging. *J. Biomech.* 41, 3164–3170.
- Plow, E.F., Haas, T.A., Zhang, L., Loftus, J., Smith, J.W., 2000. Ligand binding to integrins. *J. Biol. Chem.* 275, 21785–21788.
- Polacek, W.J., Kutys, M.L., Yang, J., Eyckmans, J., Wu, Y., Vasavada, H., Hirschi, K.K., Chen, C.S., 2017. A non-canonical Notch complex regulates adherens junctions and vascular barrier function. *Nature* 552, 258–262.
- Polacek, W.J., Li, R., Uzel, S.G., Kamm, R.D., 2013. Microfluidic platforms for mechanobiology. *Lab Chip* 13, 2252–2267.
- Potter, D.R., Damiano, E.R., 2008. The hydrodynamically relevant endothelial cell glycocalyx observed in vivo is absent in vitro. *Circ. Res.* 102, 770–776.
- Reich, K.M., Gay, C.V., Frangos, J.A., 1990. Fluid shear-stress as a mediator of osteoblast cyclic adenosine-monophosphate production. *J. Cell. Physiol.* 143, 100–104.
- Reyes, C.D., Garcia, A.J., 2003. A centrifugation cell adhesion assay for high-throughput screening of biomaterial surfaces. *J. Biomed. Mater. Res. A* 67, 328–333.
- Ridley, A.J., Hall, A., 1992. The small GTP-binding protein rho regulates the assembly of focal adhesions and actin stress fibers in response to growth factors. *Cell* 70, 389–399.
- Rosales, A.M., Anseth, K.S., 2016. The design of reversible hydrogels to capture extracellular matrix dynamics. *Nat. Rev. Mater.* 1.
- Rowlands, A.S., George, P.A., Cooper-White, J.J., 2008. Directing osteogenic and myogenic differentiation of MSCs: interplay of stiffness and adhesive ligand presentation. *Am. J. Physiol. Cell Physiol.* 295, C1037–C1044.
- Ruoslahti, E., Pierschbacher, M.D., 1987. New perspectives in cell adhesion: RGD and integrins. *Science* 238, 491–497.
- Sacks, M.S., Sun, W., 2003. Multiaxial mechanical behavior of biological materials. *Annu. Rev. Biomed. Eng.* 5, 251–284.
- Schurmann, S., Wagner, S., Herlitz, S., Fischer, C., Gumbrecht, S., Wirth-Hucking, A., Prolls, G., Lautscham, L.A., Fabry, B., Goldmann, W.H., Nikolova-Krsteveski, V., Martinac, B., Friedrich, O., 2016. The IsoStretcher: an isotropic cell stretch device to study mechanical biosensor pathways in living cells. *Biosens. Bioelectron.* 81, 363–372.
- Sellaro, T.L., Hildebrand, D., Lu, Q., Vyavahare, N., Scott, M., Sacks, M.S., 2007. Effects of collagen fiber orientation on the response of biologically derived soft tissue biomaterials to cyclic loading. *J. Biomed. Mater. Res. A* 80, 194–205.
- Shen, B., Delaney, M.K., Du, X., 2012. Inside-out, outside-in, and inside-outside-in: G protein signaling in integrin-mediated cell adhesion, spreading, and retraction. *Curr. Opin. Cell Biol.* 24, 600–606.
- Shi, M., Zhu, J., Wang, R., Chen, X., Mi, L., Walz, T., Springer, T.A., 2011. Latent TGF- β structure and activation. *Nature* 474, 343–349.
- Shieh, A.C., Athanasiou, K.A., 2003. Principles of cell mechanics for cartilage tissue engineering. *Ann. Biomed. Eng.* 31, 1–11.
- Shimizu, N., Yamamoto, K., Obi, S., Kumagaya, S., Masumura, T., Shimano, Y., Naruse, K., Yamashita, J.K., Igarashi, T., Ando, J., 2008. Cyclic strain induces mouse embryonic stem cell differentiation into vascular smooth muscle cells by activating PDGF receptor beta. *J. Appl. Physiol.* 104, 766–772.
- Sit, S.T., Manser, E., 2011. Rho GTPases and their role in organizing the actin cytoskeleton. *J. Cell Sci.* 124, 679–683.
- Sosa, B.A., Rothballe, A., Kutay, U., Schwartz, T.U., 2012. LINC complexes form by binding of three KASH peptides to domain interfaces of trimeric SUN proteins. *Cell* 149, 1035–1047.
- Spencer, A., Baker, A.B., 2016a. High throughput label free measurement of cancer cell adhesion kinetics under hemodynamic flow. *Sci. Rep.* 6.
- Spencer, A., Baker, A.B., 2016b. High throughput label free measurement of cancer cell adhesion kinetics under hemodynamic flow. *Sci. Rep.* 6.
- Spencer, A., Spruell, C., Nandi, S., Wong, M., Crexiell, M., Baker, A.B., 2016. A high-throughput mechanofluidic screening platform for investigating tumor cell adhesion during metastasis. *Lab Chip* 16, 142–152.
- Stamatas, G.N., Mcintire, L.V., 2001. Rapid flow-induced responses in endothelial cells. *Biotechnol. Prog.* 17, 383–402.
- Stein, G.S., Lian, J.B., Van Wijnen, A.J., Stein, J.L., Javed, A., Montecino, M., Choi, J.Y., Vradii, D., Zaidi, S.K., Pratap, J., Young, D., 2007. Organization of transcriptional regulatory machinery in nuclear microenvironments: implications for biological control and cancer. *Adv. Enzym. Regul.* 47, 242–250.
- Sung, H.J., Yee, A., Eskin, S.G., Mcintire, L.V., 2007. Cyclic strain and motion control produce opposite oxidative responses in two human endothelial cell types. *Am. J. Physiol. Cell Physiol.* 293, C87–C94.
- Suo, J., Ferrara, D.E., Sorescu, D., Guldberg, R.E., Taylor, W.R., Giddens, D.P., 2007. Hemodynamic shear stresses in mouse aortas: implications for atherogenesis. *Arterioscler. Thromb. Vasc. Biol.* 27, 346–351.

- Swift, J., Ivanovska, I.L., Buxboim, A., Harada, T., Dingal, P.C., Pinter, J., Pajeroski, J.D., Spinler, K.R., Shin, J.W., Tewari, M., Rehfeldt, F., Speicher, D.W., Discher, D.E., 2013. Nuclear lamin-A scales with tissue stiffness and enhances matrix-directed differentiation. *Science* 341, 1240104.
- Tarbell, J.M., Pahakis, M.Y., 2006. Mechanotransduction and the glycocalyx. *J. Intern. Med.* 259, 339–350.
- Tojkander, S., Gateva, G., Lappalainen, P., 2012. Actin stress fibers-assembly, dynamics and biological roles. *J. Cell Sci.* 125, 1855–1864.
- Torsoni, A.S., Marin, T.M., Velloso, L.A., Franchini, K.G., 2005. RhoA/ROCK signaling is critical to FAK activation by cyclic stretch in cardiac myocytes. *Am. J. Physiol. Heart Circ. Physiol.* 289, H1488.
- Totaro, A., Panciera, T., Piccolo, S., 2018. YAP/TAZ upstream signals and downstream responses. *Nat. Cell Biol.* 20, 888–899.
- Tzima, E., Del Pozo, M.A., Kiosses, W.B., Mohamed, S.A., Li, S., Chien, S., Schwartz, M.A., 2002. Activation of Rac1 by shear stress in endothelial cells mediates both cytoskeletal reorganization and effects on gene expression. *EMBO J.* 21, 6791–6800.
- V Maksimenko, A., 2017. Translational research into vascular wall function: regulatory effects of systemic and specific factors. *J. Transl. Sci.* 3.
- Vandenburgh, H.H., 1988. A computerized mechanical cell stimulator for tissue culture: effects on skeletal muscle organogenesis. *In Vitro Cell. Dev. Biol.* 24, 609–619.
- Vanteeffelen, J.W., Brands, J., Stroes, E.S., Vink, H., 2007. Endothelial glycocalyx: sweet shield of blood vessels. *Trends Cardiovasc. Med.* 17, 101–105.
- Vasioukhin, V., Bauer, C., Yin, M., Fuchs, E., 2000. Directed actin polymerization is the driving force for epithelial cell-cell adhesion. *Cell* 100, 209–219.
- Vicente-Manzanares, M., Ma, X., Adelstein, R.S., Horwitz, A.R., 2009. Non-muscle myosin II takes centre stage in cell adhesion and migration. *Nat. Rev. Mol. Cell Biol.* 10, 778–790.
- voyvodic, P.L., Min, D., Baker, A.B., 2012. A multichannel dampened flow system for studies on shear stress-mediated mechanotransduction. *Lab Chip* 12, 3322–3330.
- Wagner, D.D., Frenette, P.S., 2008. The vessel wall and its interactions. *Blood* 111, 5271–5281.
- Walboomers, X., Ginsel, L., Jansen, J., 2000. Early spreading events of fibroblasts on microgrooved substrates. The Japanese Society for Biomaterials, and The Australian Society for Biomaterials and the Korean Society for Biomaterials *J. Biomed. Mater. Res.* 51, 529–534.
- Wang, H.B., Dembo, M., Wang, Y.L., 2000. Substrate flexibility regulates growth and apoptosis of normal but not transformed cells. *Am. J. Physiol. Cell Physiol.* 279, C1345–C1350.
- Wang, N., Tytell, J.D., Ingber, D.E., 2009. Mechanotransduction at a distance: mechanically coupling the extracellular matrix with the nucleus. *Nat. Rev. Mol. Cell Biol.* 10, 75–82.
- Watson, T., Shantsila, E., Lip, G.Y., 2009. Mechanisms of thrombogenesis in atrial fibrillation: Virchow's triad revisited. *Lancet* 373, 155–166.
- Wei, S.C., Fattet, L., Tsai, J.H., Guo, Y., Pai, V.H., Majeski, H.E., Chen, A.C., Sah, R.L., Taylor, S.S., Engler, A.J., Yang, J., 2015. Matrix stiffness drives epithelial-mesenchymal transition and tumour metastasis through a TWIST1-G3BP2 mechanotransduction pathway. *Nat. Cell Biol.* 17, 678–688.
- Wells, R.G., Discher, D.E., 2008. Matrix elasticity, cytoskeletal tension, and TGF-beta: the insoluble and soluble meet. *Sci. Signal.* 1, pe13.
- White, C.R., Frangos, J.A., 2007. The shear stress of it all: the cell membrane and mechanochemical transduction. *Philos. Trans. R. Soc. Biol. Sci.* 362, 1459–1467.
- Whitlock, M.C., Hundley, W.G., 2015. Noninvasive imaging of flow and vascular function in disease of the aorta. *JACC Cardiovasc. Imaging* 8, 1094–1106.
- Williams, H., Trask, R., Weaver, P., Bond, I., 2008. Minimum mass vascular networks in multifunctional materials. *J. R. Soc. Interface* 55–65.
- Winston, F.K., Macarak, E.J., Gorfien, S.F., Thibault, L.E., 1989. A system to reproduce and quantify the biomechanical environment of the cell. *J. Appl. Physiol.* 67, 397–405.
- Wojciak-Stothard, B., Curtis, A., Mcgrath, M., Sommer, I., Wilkinson, C., Monaghan, W., 1995. Role of the cytoskeleton in the reaction of fibroblasts to multiple grooved substrata. *Cell Motil. Cytoskeleton* 31, 147–158.
- Wolff, J., 1892. *Das Gesetz der Transformation der Knochen*, Berlin, A. Hirschwald. *The Law of Bone Remodeling*.
- Xiao-Han, Z., Carol, L., Pam, A., Katalin, S., Andras, K., Mcculloch, C.A., 2007. Force activates smooth muscle alpha-actin promoter activity through the Rho signaling pathway. *J. Cell Sci.* 120, 1801–1809.
- Yee, A., Bosworth, K.A., Conway, D.E., Eskin, S.G., McIntire, L.V., 2008. Gene expression of endothelial cells under pulsatile non-reversing vs. steady shear stress; comparison of nitric oxide production. *Ann. Biomed. Eng.* 36, 571–579.
- Yim, E.K., Reano, R.M., Pang, S.W., Yee, A.F., Chen, C.S., Leong, K.W., 2005. Nanopattern-induced changes in morphology and motility of smooth muscle cells. *Biomaterials* 26, 5405–5413.
- Yonemura, S., Itoh, M., Nagafuchi, A., Tsukita, S., 1995. Cell-to-cell adherens junction formation and actin filament organization: similarities and differences between non-polarized fibroblasts and polarized epithelial cells. *J. Cell Sci.* 108 (Pt 1), 127–142.
- Yoshino, D., Sakamoto, N., Takahashi, K., Inoue, E., Sato, M., 2013. Development of novel flow chamber to study endothelial cell morphology: effects of shear flow with uniform spatial gradient on distribution of focal adhesion. *J. Biomech. Sci. Eng.* 8, 233–243.
- Yung, Y.C., Vandenburgh, H., Mooney, D.J., 2009. Cellular strain assessment tool (CSAT): precision-controlled cyclic uniaxial tensile loading. *J. Biomech.* 42, 178–182.
- Zhang, Q., Skepper, J.N., Yang, F., Davies, J.D., Hegyi, L., Roberts, R.G., Weissberg, P.L., Ellis, J.A., Shanahan, C.M., 2001. Nesprins: a novel family of spectrin-repeat-containing proteins that localize to the nuclear membrane in multiple tissues. *J. Cell Sci.* 114, 4485–4498.

2.2.1

Introduction to Biological Responses to Materials

SHELLY E. SAKIYAMA-ELBERT

Department of Biomedical Engineering, The University of Texas at Austin, Austin, TX, United States

Systemic and tissue-level responses to biomaterials and medical devices are largely driven by biomaterial–tissue interactions in the local environment where they are implanted. Particularly for devices that are not retrieved and are meant to be “permanently” implanted, their ability to function and alleviate the condition for which they were implanted is dependent on minimizing or quickly resolving undesirable interactions with host tissue. Key concepts and systems that mediate these host responses are described in the following chapters.

The first chapter focuses on inflammation, wound healing, and foreign body response to implanted materials. Inflammation is one of the most critical responses, which is required for healing but needs to be balanced and resolved over time to avoid chronic issues. The second chapter focuses on immune responses to materials, both innate and adaptive, including the key types of cells involved in each type of response. It also highlights key regulatory elements of immune responses, and how those can be potentially modulated with materials. The third chapter focuses on complement and how this key component of the innate immune response can play an important role in the response to biomaterial implants. It provides detail on the different activation pathways, signaling and key interaction with the coagulation cascade, as well as highlighting applications

where complications often arise due to complement activation. The fourth chapter focuses on systemic and immune-mediated toxicity of materials, which can be a source of failure for medical devices, particularly “permanent” implants. Key areas of discussion include metals, hypersensitivity and immunotoxicity, as well as localization of the response.

The fifth chapter focuses on coagulation and blood–material interactions. This is a critical topic for materials that are involved in vascular applications. Most if not all materials that are implanted surgically will come into contact with blood during implantation, so these issues are broadly important. Modification of material surfaces to alter the interactions with blood proteins and platelets have been a major focus of biomaterials research over the years. The sixth chapter focuses on the potential that implanted materials could cause or promote tumor growth. This chapter focuses on the pathobiology of tumor formation near biomaterials and also highlights concerns specific to the transplantation of stem cells with biomaterials. The final chapter in this section focuses on biofilms and device-related infections. Infections are a major source of failure for long-term biomaterial implants, and thus approaches that prevent bacterial adhesion and biofilm formation could reduce complications in many types of implants.

2.2.2

Inflammation, Wound Healing, the Foreign-Body Response, and Alternative Tissue Responses

JULIA E. BABENSEE

Wallace H. Coulter Department of Biomedical Engineering, Georgia Institute of Technology and Emory University, Atlanta, GA, United States

Biocompatibility and Implantation

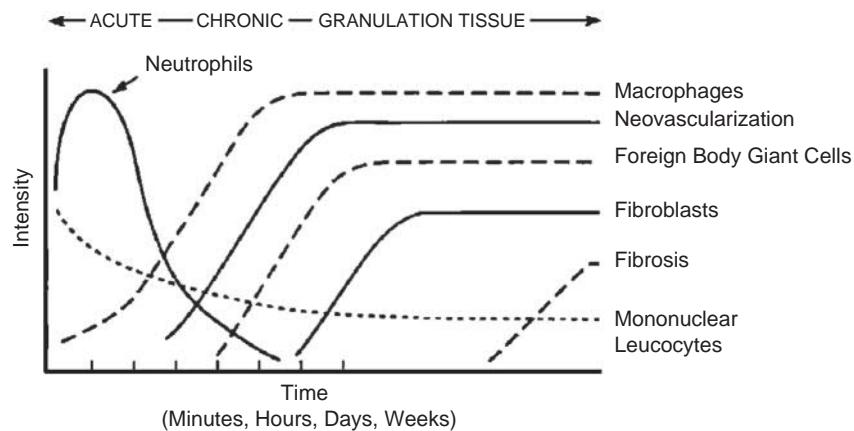
The surgical implantation of a biomaterial or introduction of an injectable biomaterial via a minimally invasive process, introduces the biomaterial into a physiological environment. The site or type of tissue into which the material is implanted will determine the chief biological processes which will predominate in the host response. For example, anastomosis of a vascular graft to replace a diseased vessel puts a material in contact with flowing blood, so clearly blood compatibility will be a key factor in determining the success of the biomaterial. However, the tissue response on the adventitial side will involve soft-tissue healing. The accepted definition of biocompatibility, proposed by D.F. Williams, is “the ability of a material to perform with an appropriate host response in a specific application” (Williams, 1999). From this definition, biocompatibility defines a particular host response that allows for the biomaterial to perform its intended function in a specific application context. The anatomical site into which the biomaterial is implanted and how the body will respond to that material macroscopically will also play a role in determining the host response.

The temporal sequence of events following implantation of a biomaterial is illustrated in Fig. 2.2.2.1. The properties of the biomaterials influence the host response, and hence the biocompatibility of materials. Material properties include biomaterial size, shape, roughness, topography, surface chemistry, and stiffness. Biomaterial properties may be responsible for variations in intensity and duration of the inflammatory and wound-healing process phases. Furthermore, the intensity and/or duration of the inflammatory reaction may characterize the biocompatibility of the biomaterial. The host response is proportional to the implant surface area that the body needs to respond to. Degradation

of biomaterials, either intended for the function or an unintended consequence of the environment, may produce degradation products or particulates which may stimulate inflammatory cells or have toxic effects to affect the biocompatibility of the material used in the device.

The host response to the biomaterial will determine the success or failure of a biomedical device. Examples of beneficial aspects of the tissue reaction to a biomaterial include a vascularized tissue reaction, a thin fibrous capsule, and integration of the material with the surrounding tissue to result in a seamless continuity within the tissue. Examples of deleterious consequences of an adverse tissue reaction include thick fibrous and avascular capsule, scar formation, and chronic inflammatory response.

As noted by the definition of biocompatibility, the aspects of the tissue reaction would need to be considered with respect to the intended application and how the tissue reaction hinders or supports the function of the device. For example, for biosensors that detect an analyte in the blood, the analyte needs to diffuse out of the blood vessel, through the tissue to the sensor. Thus, an avascular fibrous capsule would act as a diffusion barrier and could also be comprised of cells that consume the analyte, making the analyte reading by the biosensor inaccurate (Klueh et al., 2007). A vascularized tissue reaction would bring blood vessels closer to the biosensor–tissue interface to facilitate more accurate readings of blood levels of the analyte (Kenneth Ward et al., 2004). A similar case can be made for the necessity of close vascular structures and adequate functional vascularization of the tissue surrounding or incorporated into tissue-engineered constructs or regenerated tissue (Richardson et al., 2001). Scar-free healing, observed in embryonic/fetal wounds (Ferguson and O’Kane, 2004), is often a desirable host response and the unique features that facilitate this are often aimed to be recapitulated for this desirable host response. Scar-free healing



• **Figure 2.2.2.1** The temporal variation in the acute inflammatory response, chronic inflammatory response, granulation tissue development, and foreign-body reaction to implanted biomaterials. The intensity and time variables are dependent upon the extent of injury created in the implantation and the size, shape, topography, and chemical and physical properties of the biomaterial.

is distinct from adult wound healing, the former having a predominance of TGF- β 3 and hyaluronic acid (Ferguson and O’Kane, 2004).

Sequence of the Host Response Following Implantation of Medical Devices

The implantation of a biomedical device, if it involves surgical incision, will initiate a wound healing response. Wound healing involves hemostasis, inflammation, proliferation, and remodeling. Each phase is mediated by distinct cellular and molecular participants in an intensely directed response to the implant (Anderson, 2008). Cytokines initiate and orchestrate the manifold cellular activities which underscore inflammation and healing. Immediately upon insertion of a biomaterial, the cutting of blood vessels will initiate blood coagulation, involving platelet activation and deposition of a provisional fibrin matrix. Thus, the biomaterial will interact with these blood-derived coagulation factors and blood compatibility of the material will contribute to these initial host responses. During this early phase, plasma proteins will adsorb to the biomaterial, blood coagulation and complement activation would occur as directed by the biomaterial properties as well as the homeostatic response to the insertional injury. The adsorbed proteins will mediate all cellular responses with the material.

The second phase is the inflammatory phase in which phagocytic cells, first neutrophils followed by macrophages, migrate to the injury site in response to released chemotactic factors to clear the injury/implant site of cellular and tissue debris and any pathogens. The implanted biomaterial can activate tissue macrophages to release chemokines (Rodriguez et al., 2009) and components of the complement activation pathway in response to the biomaterial, releases chemotactic anaphylatoxins for chemotaxis of inflammatory cells to the tissue implant site (Nilsson et al., 2007). Fibrin degradation fragments, produced upon plasmin degradation of the early fibrin clot, are chemoattractants for leukocytes. Pathogen-derived fragments such as fMLP (*N*-formylmethionyl-leucyl-phenylalanine) from

bacteria are chemoattractants for leukocytes if there is any bacterial infection of the implant site. These cells release growth factors and cytokines to attract the next wave of reparative cells and affect the functions that they will perform. For example, macrophages release vascular endothelial cell growth factor (VEGF), which is a chemotactic and proliferative factor for endothelial cells, promoting new blood vessel formation in the injury site. Transforming growth factor released by platelets and neutrophils stimulates fibroblast migration to the injury site to restore normal tissue and deposit extracellular matrix (ECM).

Finally, there is a remodeling phase of the nascent tissue under the influence of enzymes such as matrix metalloproteinases (MMPs) or tissue inhibitor of metalloproteinase (TIMP). Wound healing is often presented as cutaneous wound healing and the proliferative phase focuses on reepithelization and keratinocyte proliferation to remake the skin barrier (Sun et al., 2014). The fibroblast proliferation and collagen formation are analogous to scar tissue formation. Remodeling can also be considered from the point of view of tissue or scar contraction. As with all of the biological processes considered in determining the host response to a biomaterial, careful control of the amount of inflammation or the extent of fibrous tissue formation is needed since excessive levels of these processes can lead to too much inflammation and deleterious consequences such as tissue damage or biomaterial damage. Excess fibroblast proliferation with associated collagen deposition can lead to excessive scar tissue or fibrous encapsulation. However, as wound healing is initiated, the first stage is inflammation, and one must go through the inflammatory stage, but a short-lived inflammatory stage is ideal to encourage the subsequent reparative phase of wound healing. Resolution of the proinflammatory phase to the prohealing phase is necessary for successful wound healing (Eming et al., 2007).

Wound Healing

Wound healing is a response to injury to return the system to homeostasis. Wound healing, whether initiated by trauma, microbes, or foreign materials, proceeds via an overlapping

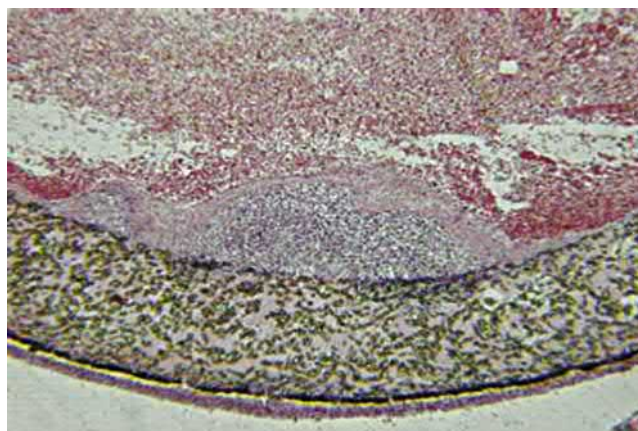
pattern of events including coagulation, inflammation, epithelialization, formation of granulation tissue, tissue formation, and matrix/tissue remodeling (Sun et al., 2014). Complex interplay between plasma protein-derived components, multiple cytokines/growth factors, cells, and extracellular matrix is central to the initiation, progression, and resolution of wounds.

During the homeostatic response to blood vessel cutting, coagulation occurs with a fibrin clot formation where platelets release biomolecules such as platelet-derived growth factor (PDGF) and transforming growth factor- β (TGF- β) to call in the inflammatory cells (Sun et al., 2014). Fibrinopeptides released upon plasminogen degradation of the clot are also chemoattractants. The first type of inflammatory cells to the injury site is the neutrophil, which also responds to chemokines released early in inflammation such as CX3CL1 and CCLs. Complement activation fragments such as C5a and C3a are chemoattractant for neutrophils.

Inflammation is an early necessary phase of the wound-healing response (Eming et al., 2007). Wounds do not heal without the initial inflammatory phase to bring in leukocytes which will clear the injury site of debris and pathogen during the pro-inflammatory phase. The inflammatory phase is characterized by the expression of proinflammatory cytokines such as tumor necrosis factor- α , interleukin-1 (IL-1), IL-6, and growth factors such as TGF- β and PDGF, and is directed to a large extent by macrophages (Eming et al., 2007). As fewer proinflammatory mediators are released and proregenerative mediators are generated, the wound healing will enter into a regenerative phase with the goal of restitution of the tissue structure and restoring of normal tissue function (Eming et al., 2007). Growth factors released by macrophages, endothelial cells, keratinocytes, and fibroblasts provide autocrine and paracrine signaling for reparative cell recruitment and proliferation for angiogenesis, tissue regeneration, or scar tissue formation. Factors released at the wound site that drive the process of inflammatory resolution include antiinflammatory cytokines such as IL-10, TGF- β isoforms, IL-1 receptor antagonist (IL-1Ra), and other mechanisms to reduce inflammation such as reconstitution of vascular permeability, receptor and transcription factor downregulation (e.g., NF- κ B), proteolysis of chemokines, and lymphatic drainage (Eming et al., 2007). The healed wound site can undergo subsequent remodeling under the influence of growth factors such as TGF- β , PDGF, and fibroblast growth factor-2 (FGF-2), and MMPs and TIMPs (Sun et al., 2014).

Host Response to Implanted Biomaterials

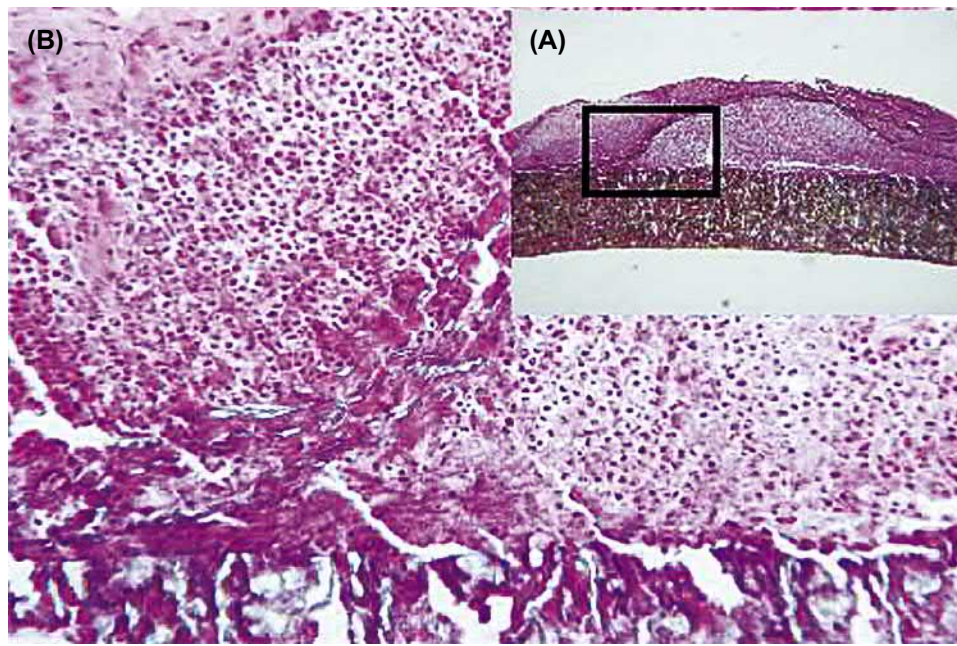
The implantation or introduction of a biomaterial into living tissue will initiate an inflammatory response to the material (Anderson, 2008). This occurs within the wound-healing context of any injury caused by the implantation of the biomaterial. However, there are distinct aspects and stages of the inflammatory response to a biomaterial which should be discussed. The inflammatory response is fundamentally a protective response, the ultimate goal being to rid the organisms of both the initial cause of cell injury (e.g., microbes, toxins) and the consequences of such inflammation. The inflammatory response is



• **Figure 2.2.2.2** Acute inflammation, secondary to infection, of an ePTFE (expanded poly tetrafluoroethylene) vascular graft. A focal zone of polymorphonuclear leukocytes is present at the luminal surface of the vascular graft, surrounded by a fibrin cap, on the blood-contacting surface of the ePTFE vascular graft. Hematoxylin and eosin stain. Original magnification 4 \times .

closely intertwined with the process of repair. Inflammation serves to destroy, dilute, or wall off the injurious agent, but it, in turn, sets into motion a series of events that, as far as possible, heal and reconstitute the damaged tissue (Anderson, 2008). The first phase of the inflammatory response to the implantation of a biomaterial is the response to injury, the cutting of blood vessels during insertion of the biomaterial, which initiates the coagulation cascade and platelet activation and degranulation resulting in clot formation and deposition of a provisional fibrin matrix. The platelets release biomolecules which are chemoattractant for leukocytes such as PDGF and TGF- β . The fibrin matrix provides a provisional matrix for leukocytes and other cells to use to migrate in the wound site, as the normal matrix may be damaged or destroyed. Fibrin degradation products are also chemotactic for leukocytes, aiding in their recruitment to participate in healing. The key cellular players of the inflammatory response and their morphological features for their identification in micrographs are discussed in Chapter 2.2.3 by B.G. Keselowsky.

The early phase of the inflammatory response is the acute inflammatory response (Anderson, 2008). This phase can last minutes to several days, as determined by the extent and persistence of an acute inflammatory stimulus such as bacteria or microparticles. Local hemodynamic changes, increased vascular permeability resulting in “leaky vessels” that allows the passage of a protein-rich exudate to the extravascular space, include a process known as exudation. With exudation, plasma proteins contact subendothelial tissue factor to initiate the extrinsic pathway of blood coagulation with fibrin deposition. Local neutrophil accumulation is the hallmark of acute inflammation (Fig. 2.2.2.2). Acute inflammation is a very stereotypical reaction. These leukocytes that circulate in flowing blood within the vasculature, sample the endothelium, until they encounter an inflamed activated endothelium that expresses cell surface molecules such as E-selectin and other unique glycoproteins, that capture flowing leukocytes and mediate their rolling as the L-selectin that they express,



• **Figure 2.2.2.3** Chronic inflammation, secondary to infection, of an ePTFE arteriovenous shunt for renal dialysis. (A) Low-magnification view of a focal zone of chronic inflammation. (B) High-magnification view of the outer surface with the presence of monocytes and lymphocytes at an area where the outer PTFE wrap had peeled away from the vascular graft. Hematoxylin and eosin stain. Original magnification (A) 4 \times , (B) 20 \times .

typically on projecting microvilli, interacts with its counterligand on the inflamed endothelium (Ley et al., 2007). As this leukocyte is rolling and interacting with the inflamed endothelium, it is activated by cytokines such as interleukin-8 (IL-8) that is released by the endothelial cells. Once activated, the integrin receptor that they express will change its conformation to an activated form such that it can bind to its counterreceptor intracellular adhesion molecule (ICAM-1) on endothelial cells to mediate firm adhesion of the leukocyte. Leukocytes (neutrophils, monocytes) roll, firmly adhere to, and transigrate through the endothelium and provisional fibrin clot and ECM to chemotactic stimulus. Integrins are the receptors used to bind to ECM motifs for migration through the tissue. Proteolytic degradation of the ECM by MMPs facilitates leukocyte movement through the tissue.

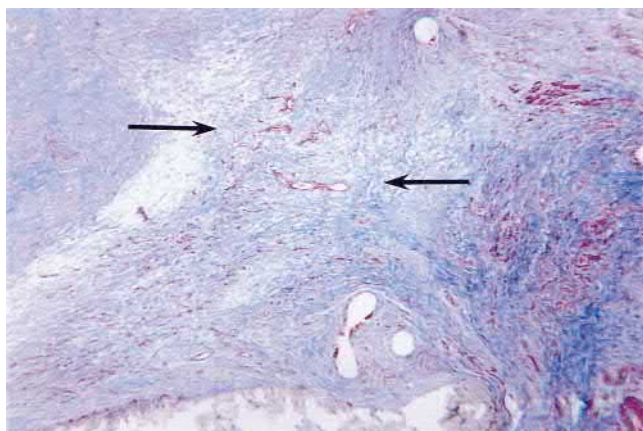
Once at the site of inflammation, leukocytes will clear the site of any cellular debris, bacteria, or foreign material by receptor-mediated phagocytosis and release toxic products (e.g., reactive oxygen species, lysosomal enzymes) to kill or destroy the foreign matter. Neutrophils also release growth factor mediators of tissue regeneration and recruitment of the second wave of inflammatory cells, the monocytes that differentiate in the tissue to macrophages. Neutrophils and macrophages interact with foreign surfaces through receptor-mediated binding to implant surface-adsorbed proteins to result in cell attachment and activation, which includes secretion of cytokines, release of reactive oxygen intermediates, and proteolytic enzymes, the latter two aiming to degrade the foreign material upon phagocytosis of the implant. Tissue-resident macrophages can also participate in directing the inflammatory response to an implant, sensing the foreign material or its biologically derived signals, to the call for recruitment of circulating leukocytes.

Tissue-resident macrophages can also proliferate in situ to add to the force of inflammatory cells reacting to the foreign entity (Ensan et al., 2016).

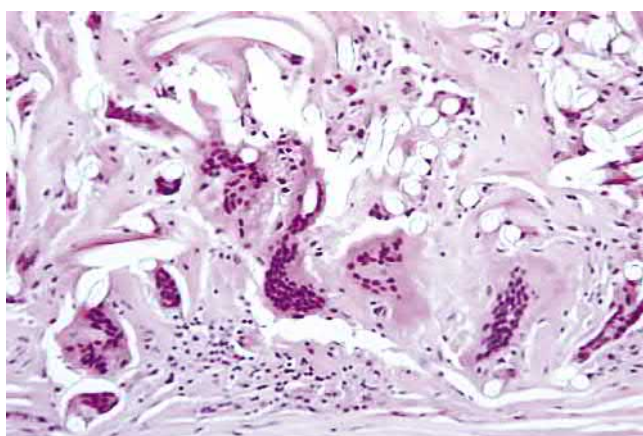
The next phase of the inflammatory response is chronic inflammation (Anderson, 2008). Persistence of an inflammatory stimulus leads to chronic inflammation, as do repeated bouts of acute inflammation, persistence of intracellular microorganisms, prolonged exposure to nondegradable substances, immune reactions, and micromotion of implants. The cellular profile is characterized by the presence of monocytes/macrophages and particularly lymphocytes and plasma cells (Fig. 2.2.2.3). During this stage, there is proliferation of blood vessels and fibroblasts, the latter to increase the presence of connective tissue. However, the chronic destructive nature of this stage of the inflammatory response will lead to tissue destruction that can then only be repaired by scarring. The chronic inflammatory response can also lead to biomaterial destruction, such as stress cracking of surfaces, particularly those associated with foreign body giant cells. This stage of the inflammatory response should resolve within a week or so, but with persistence of a stimulus it can last weeks to years. Thus, the reaction is much less stereotypical than acute inflammation.

Granulation tissue is the healing phase of inflammation and is initiated by the action of macrophages and their release of molecular factors (Anderson, 2008). This phase is characterized by the proliferation of fibroblasts, synthesis of collagen and proteoglycans, and angiogenesis (Fig. 2.2.2.4). Depending on the extent of injury, it can be seen as early as 3–5 days after injury.

This final stage of biomaterial inflammation, the foreign body reaction, is comprised of foreign body giant cells (FBGCs)/macrophages apposed to the biomaterial surface (Fig. 2.2.2.5),

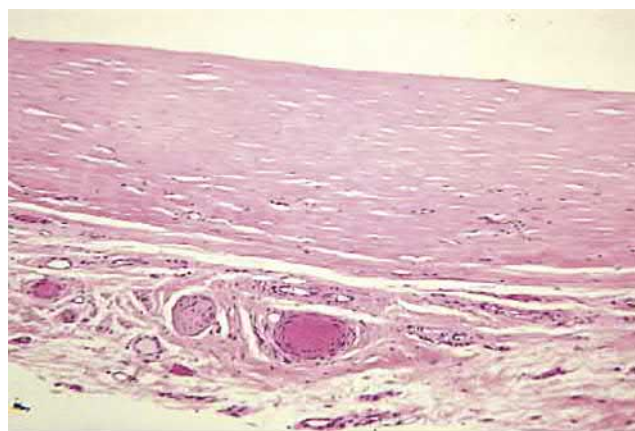


• **Figure 2.2.2.4** Granulation tissue in the anastomotic hyperplasia at the anastomosis of an ePTFE vascular graft. Capillary development (red slits) and fibroblast infiltration with collagen deposition (blue) from the artery form the granulation tissue (arrows). Masson's Trichrome stain. Original magnification 4 \times .



• **Figure 2.2.2.5** Foreign-body reaction with multinucleated foreign body giant cells and macrophages at the periadventitial (outer) surface of a Dacron vascular graft. Fibers from the Dacron vascular graft are identified as clear oval voids. Hematoxylin and eosin stain. Original magnification 20 \times .

surrounded by granulation tissue and/or fibrosis (Anderson, 2008). Blood vessels would be seen within the granulation tissue, but typically not in the fibrous capsule. Foreign body giant cells are formed by the fusion of multiple macrophages as they try to engulf a surface that is too large for them to phagocytose, so they undergo “frustrated phagocytosis” (Anderson, 2008). Foreign body cells are very large cells with abundant cytoplasm and as many as 10 nuclei of the macrophages are fused to form this cell. The presence of FBGCs at the surface of biomaterials, as with polyurethane pacemaker leads, is associated with stress cracking just beneath them on the biomaterial surface with subsequent device failure (Zhao et al., 1991). This suggests that these FBGCs have presumably formed to intensify their local inflammatory activity at the biomaterial site. Thus, in this sense they are viewed as bad as far as biomaterials are concerned (McNally and Anderson, 1995). However, other studies suggest that they may be a stable, quiescent, and thus less inflammatory cell than actively inflammatory macrophages (McNally and Anderson, 2002).



• **Figure 2.2.2.6** Fibrous capsule composed of dense, compacted collagen. This fibrous capsule had formed around a Mediport catheter reservoir. Loose connective tissue with small arteries, veins, and a nerve is identified below the acellular fibrous capsule.

Another type of final stage of biomaterial inflammation is fibrosis (Fig. 2.2.2.6). This response is characterized by a dense, aligned collagen produced by the interspersed fibroblasts. The response is characterized by mature fibroblasts and associated collagen that surround the material and wall it off from the rest of the native tissue. Fibroblasts can take on a myofibroblast phenotype to participate in the contraction of the fibrous capsule associated with the implant (Anderson, 2008). Other deleterious consequences of a foreign body reaction/fibrosis are its mass transfer barrier and consumption of nutrients for tissue-engineered cell/biomaterial constructs, encapsulated cells, or biosensors for an analyte in the blood. The foreign body reaction lasts for the lifetime of the device recipient, as long as the implant remains in the body (Anderson, 2008).

Tissue Remodeling and Biomaterial Integration—Alternative Tissue Responses

The wound-healing environment is becoming better understood by the scientific community, with a shift in the goal of biomaterial scientists to utilize this understanding to design biomaterials that integrate more naturally with the implant environment. Alternative host responses to the foreign body response and fibrosis were suggested in a J.M. Anderson review citing an angiogenic tissue response as a potential outcome (Anderson, 1993). One needs to understand the range of host responses that can be achieved in vivo and define new goals for a desirable tissue reaction. One also needs to consider the cell types and biological mediators of these alternative tissue reactions. Finally, one needs to understand the physicochemical and design features of biomaterials and devices that give rise to these alternative tissue responses.

A tissue response to implanted biomaterials that was deemed desirable is one that is well vascularized. This was first observed using a biomaterial system with a pillared biomaterial surface topology which allowed host cell infiltration into the membrane with close vascular structures (Picha and Drake, 1996). The work by J.H. Brauker at Baxter identified

the pore size of membranes as influencing inflammatory cell infiltration into pores with close vascular structures (Brauker et al., 1995). Baxter was interested in encapsulating cells with immunoisolation to facilitate cell transplantation without the need for immunosuppression as for allogeneic or xenogeneic cell transplantation. They recognized that not only did they need to keep immune cells and immune components from entry into the immunoisolation device, but they had another design criteria which was to have vascularization in the tissue surrounding these devices so that nutrients could be delivered to the encapsulated cells, and waste products removed, and also that the secreted product, which was the biologic drug target of the system, needed to be taken up by the bloodstream. They showed a pore size of about 5–8 μm as promoting vascularizing membranes (Brauker et al., 1995). They used a laminated membrane with an inner immunoisolating membrane and an outer vascularizing membrane.

Ratner followed up on these studies using membranes of a set pore size, prepared using a sphere templated porous hydrogel scaffold in which pores around 40 μm (Marshall et al., 2004) were optimal for close vascular structures or 60 μm for percutaneous porous biomaterial epithelial and dermal integration (Fukano et al., 2010). Concurrently, S.L. Badylak et al. were describing the unique tissue restorative capacity seen with a decellularized ECM, porcine small intestine submucosa (SIS) (Valentin et al., 2009). These authors showed constructive remodeling and tissue integration with noncross-linked decellularized matrices which were lost with cross-linking of ECM materials. See Chapter 1.3.6A by K.L. Christman for further discussion. Brown also demonstrated a tendency for reparative, wound-healing phenotype of M2 macrophages with these positive tissue reactions (Brown et al., 2012). Macrophage phenotype is thought to occur within a color wheel with three equidistant spoke locations of classical inflammatory (M1), regulatory macrophages, and wound-healing macrophage phenotypes (M2) (Mosser and Edwards, 2008). A caveat to the M1/M2 macrophage characterization/notation is the complex and dynamic in vivo environment of wound healing or tissue response to biomaterials wherein macrophages may shift their expression of phenotypic markers in response to the ever-changing microenvironmental signals, potentially expressing a range of M1/M2 markers (Brown et al., 2012). A solely biomaterial chemistry-based angiogenic response was observed with polyacrylate copolymers containing poly(methacrylic acid) (Butler and Sefton, 2007).

Alternatives to a fibrotic tissue response to a synthetic polymeric mesh of polypropylene used to treat hernias were demonstrated in two structural designs—one based on the pore size of the mesh and the other on the three-dimensional design of the device. Meshes with an in vivo effective pore size of <1 mm demonstrate a tissue reaction of granuloma and fibrosis around each fiber that merge and form bridging fibrosis around the mesh (Klinge et al., 2002). An alternative tissue response was observed for large pore size meshes >3 mm, wherein the mesh was integrated into a loose network of perifilamentary granulomas and fat tissue in the region between the widely placed

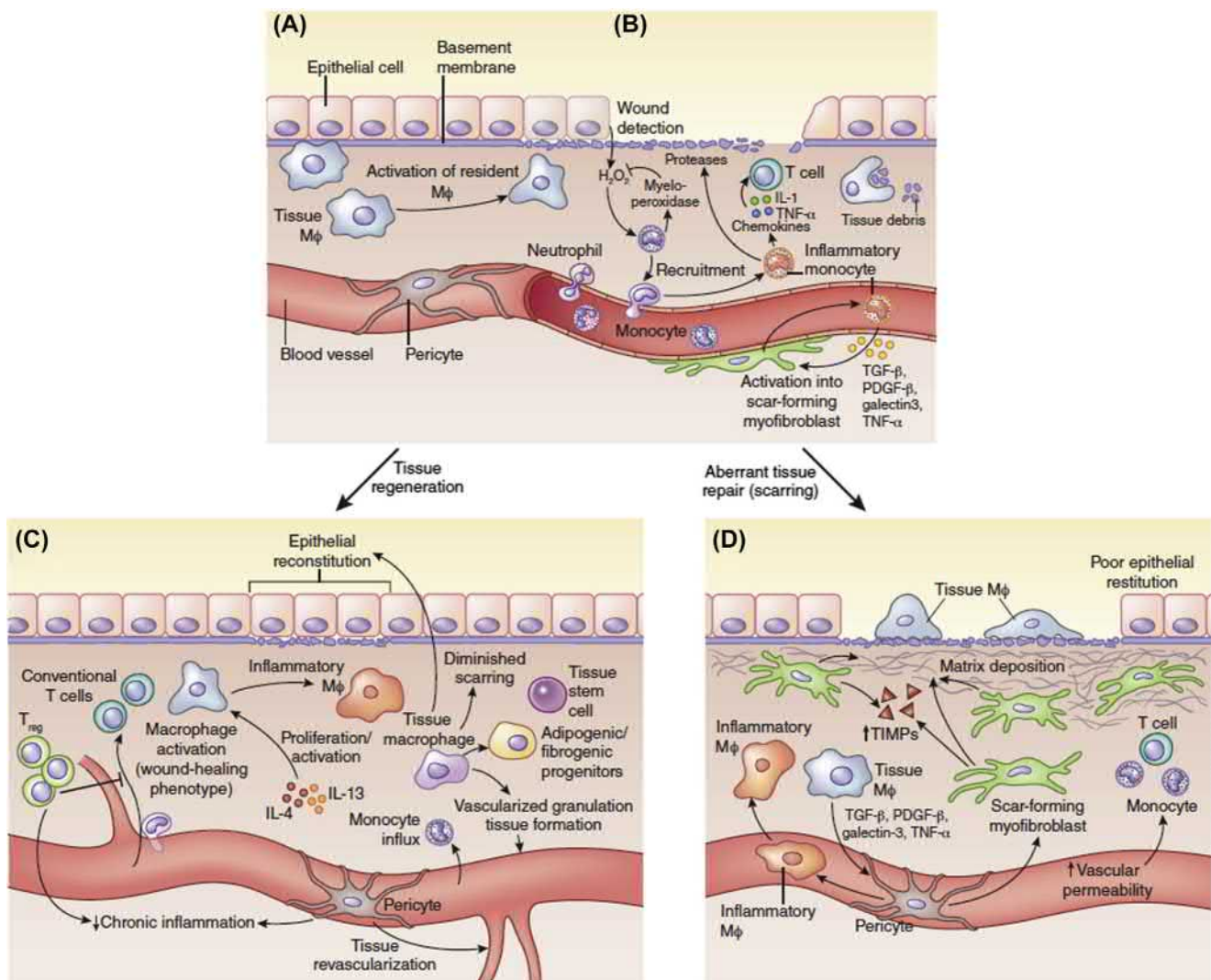
fibers (Muhl et al., 2008). A cellular/molecular basis for this alternative tissue reaction is based on the multipotential nature of circulating fibrocytes in their ability to differentiate into myofibroblasts (the cells that form the fibrous capsule around biomaterials) (Schmidt et al., 2003) as well as adipocytes (fat cells) (Hong et al., 2005). Tang et al., demonstrated the induction of adipogenic (fat) tissue associated with biomaterial implants when inhibiting transforming growth factor or infusing an adipogenic differentiation cocktail at the implant site (Baker et al., 2014).

Another example of an alternative to a fibrotic tissue response was observed for a large-pore, polypropylene mesh, that was multilamellar “flower”-shaped positioned on the outside of the peritoneum with a flat sheet on the other side of the peritoneal wall (Amato et al., 2014). This device is not strictly fixed at the implant site, and the movement of the device is meant to adapt to the movement of the implant site, but the design holds it in place. The flower shape of the device has an inherent outward recoil, which as opposed to cone-shaped plugs, has a tendency to collapse. A beneficial aspect of the host response to this 3D dynamic responsive prosthesis was noted with neotissue formation, myogenesis, lack of fibrosis, newly formed elastic fibers, angiogenesis, and neurogenesis (Amato et al., 2014).

Cellular and Molecular Mediators of Constructive Remodeling and Tissue Restoration

The wound-healing environment and key cellular and molecular players that determine constructive remodeling/tissue restoration as opposed to a scarring/fibrotic response have been described in a new paradigm by Forbes and Rosenthal (2014). The regenerative capacity of stem cells delivered to a site of degenerative diseases is greatly influenced by the cellular and signaling components of the local microenvironment to which they are seeded. This microenvironment is the “soil” to the “stem cell seed.” The inflammatory state of the implant site can affect the extent to which a stem cell therapy is successful. Endogenous healing of tissues such as liver and skeletal muscle are described in this chapter, including the conditions of key players in regeneration (Fig. 2.2.2.7). Situations that will lead to aberrant regeneration, scarring, and tissue death are clearly described.

Macrophage phenotype is a central player in determining the wound-healing outcome. Proinflammatory M1 macrophages release signals such as platelet-derived growth factor- β (PDGF- β), transforming growth factor- β (TGF- β), tissue necrosis factor- α (TNF- α), and galectin-3. Endothelium-encircling pericytes are affected by these factors to induce scar-forming myofibroblasts. In tissue restoration, macrophages are influenced by antiinflammatory molecules such as IL-4 and IL-13 to result in a wound-healing type of macrophage M2. The environmental signals that determine tissue regeneration or adherent healing and scarring are described in Rosenthal for the liver, gut, skin, kidney, skeletal muscle, and heart. Regulatory T cells (T_{regs}) are present in a regenerating

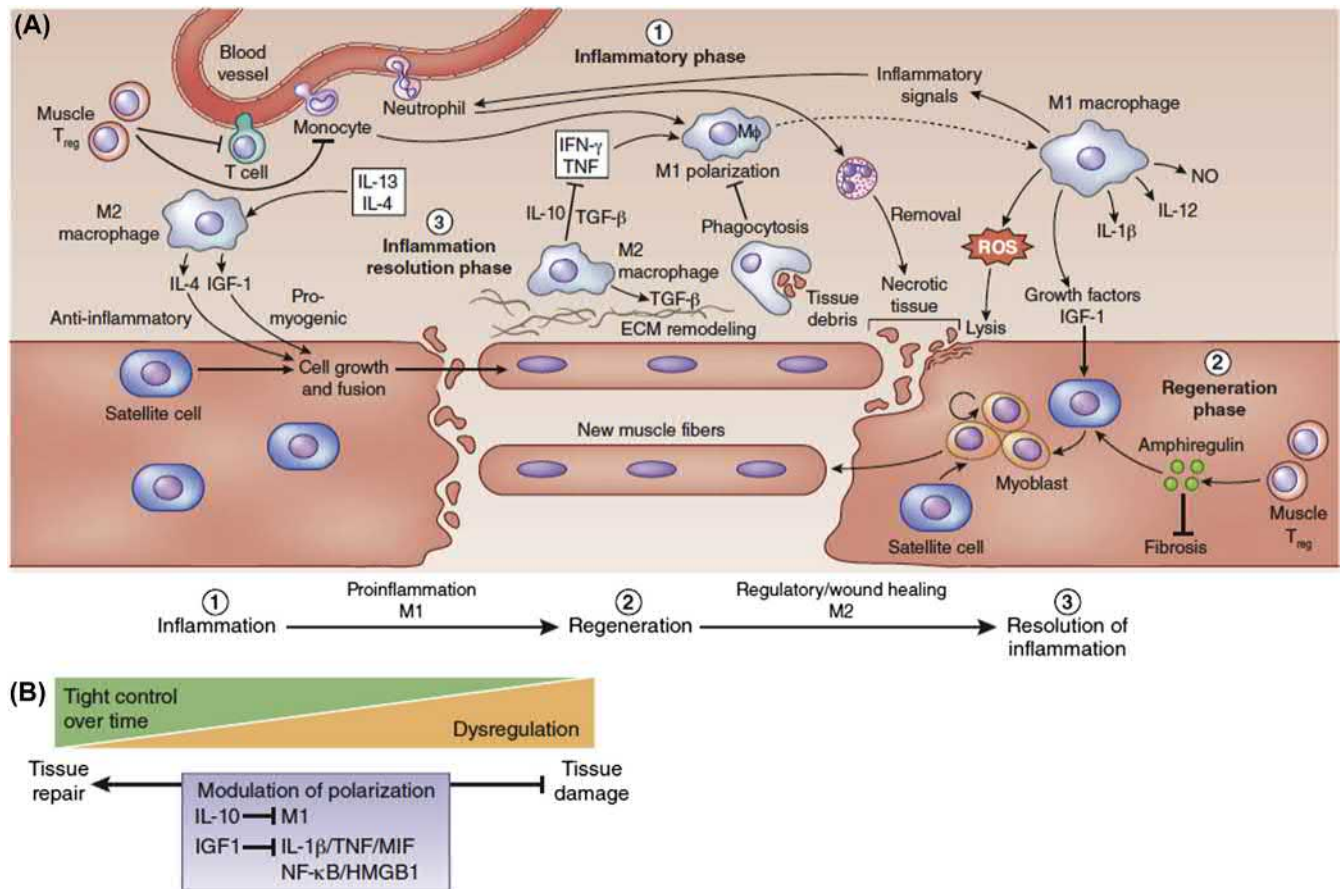


• **Figure 2.2.2.7** General model of tissue repair. (A) In healthy tissue, there is little monocyte trafficking or neutrophil efflux into tissues, an intact basement membrane and no scar tissue. (B) Upon tissue damage, there is loss of epithelia, neutrophil influx, activation of resident macrophages (M ϕ) and recruitment of inflammatory monocytes. In addition to release of inflammatory factors and activation of pericytes into myfibroblasts. (C) During tissue regeneration, there is epithelial proliferation for reconstitution, macrophage activation into a wound-healing phenotype and matrix remodeling. In addition, T_{reg} cells are recruited to decrease chronic inflammation. (D) During aberrant tissue repair, excessive scarring occurs as a result of continued activation of inflammatory cells and impaired epithelial regeneration. TIMPs, tissue inhibitor of metalloproteinases; PDGF- β , platelet-derived growth factor- β .

tissue to provide signals to inhibit chronic inflammation and activation of conventional T cells. A positive remodeling tissue environment supports endogenous tissue stem cells, adipogenesis/fibrogenic progenitors, and endothelial progenitors to participate in new tissue formation and tissue restitution. Another principle of tissue repair as opposed to tissue dysregulation is that tight control over the inflammatory response is needed (Fig. 2.2.2.8). A dysregulated inflammatory response will lead to tissue damage and scarring. Macrophage polarization is central in determining such outcomes of wound healing with immunosuppressive molecules such as IL-10 and insulin growth factor-1 (IGF-1), inhibiting proinflammatory M1 phenotype processes such as IL-1 β /TNF- α /macrophage infiltration factor (MIP), proinflammatory nuclear

factor-kappa B (NF- κ B)/high-molecular-weight group box 1 (HMGB1) pathways. As such, potential targets and mechanisms for enhancing a healing response to implanted biomaterials are suggested by such knowledge.

The central role of the immune system in adult tissue regeneration is also discussed in a relevant review by D.L. Mann et al., who present the immune cell profile in the resting, uninjured heart as including immune cells, primarily macrophages, sparse populations of dendritic cells, mast cells, and B cells and regulatory T cell subsets (Epelman et al., 2015). Neutrophils are recruited to the site upon injury or infection. Immune cells such as regulatory T cells, B cells, and dendritic cells support the role that adaptive immune cells can provide regulatory signals for tissue



• **Figure 2.2.2.8** Modulation of inflammation and cell replacement in muscle regeneration (A) Muscle injury disrupts capillaries and triggers inflammatory cascades, which result in neutrophil invasion for necrotic tissue removal and M1 macrophage activation by IFN- γ and TNF. M1 macrophages secrete proinflammatory factors and IGF-1 (1). Muscle regeneration depends on a precise balance between pro- and anti-inflammatory factors: wound repair initiates fibrosis and ECM remodeling replacing destroyed myofibers with connective tissue, but continued accumulation of fibrotic tissue compromises muscle function (2). Together with IL-4 and IL-13, IGF-1 promotes polarization of M2 macrophages, which control excess inflammation and promote regeneration through release of TGF- β (3). T_{reg} cells have also been recently shown to have a role in this process regenerative process by regulating macrophage activation and releasing amphiregulin for muscle repair, clearing the inflammation³³. (B) Macrophage polarization is promoted by cytokines (IL-10) and growth factors (IGF-1). The temporal control over the polarization process is crucial: dysregulation leads to excessive inflammation and disease. ROS, reactive oxygen species; MIF, macrophage migration inhibitory factor; NF- κ B, nuclear factor- κ B; HMGB1, high-mobility group box 1.

regeneration under the appropriate conditions. Along a similar argument, a recent study showed that the improved heart function upon intracardiac injection of cardiac stem cells to treat a heart ischemic injury was by inducing an acute sterile immune response, characterized by the temporal and regional induction of CCR2⁺ and CX3CR1⁺ macrophages, that led to functional regeneration of the heart without incorporation of delivered cardiac cells or production of new cardiomyocytes (Vagnozzi et al., 2020).

Biomaterials scientists, such as J.H. Elisseeff, have demonstrated adaptive immune cell participation in sterile inflammatory/tissue responses to biomaterials and tissue regeneration. Elisseeff demonstrated a clear role of adaptive immunity in driving the repair of a volumetric muscle loss murine model of traumatic injury using a tissue-derived decellularized ECM biomaterial (Sadtler et al., 2016). Specifically, a role for CD4⁺

T cells and a Th2 helper phenotype were shown to be regulatory through its secretion of IL-4 that influenced macrophages to an M2-like phenotype and the increased presence with time of CD4⁺FoxP3⁺ Tregs. The culmination of such a response is dependent on the immune cell recruitment and activation based on interaction with the ECM biomaterial-derived signals and communication between the different cells present. Another study showed infiltration and polarization of several immune subtypes including macrophages, dendritic cells, neutrophils, monocytes, B cells, and T cells in response to implanted tissue-derived ECM scaffolds (Sadtler et al., 2017).

Strategies to Control Host Responses

A recent study by O. Veisheh et al. explored the role of the geometry, shape, and size of biomaterial implants on the

extent of the foreign body reaction and fibrosis around the implant (Veiseh et al., 2015). They found that implanted spheres of 1.5 mm or above in diameter across a wide range of material types, including hydrogels, ceramics, metals, and plastics, significantly abrogated the foreign body reaction and fibrosis when compared to smaller spheres. This interesting result appears to contradict prior dogma wherein the amount of surface area of an implant is directly correlated with the extent of foreign body reaction and fibrosis—as the implant recipient has a greater surface area to respond to so the implant has a greater host response. Macrophages were shown to be key to the extent of foreign body reaction/fibrosis, with attenuation of these responses when this cell population was depleted in a transgenic model. Furthermore, gene expression profiles for classically activated (pro-inflammatory, M_{classic}), alternative activation (prohealing, M_{wound}), and regulatory activation (M_{Reg}) were analyzed for 1.5 or 0.5 mm capsules, wherein it was demonstrated that a lack of regulatory macrophage cell accumulation on large-sized spheres correlates with the truncated fibrosis responses. Presumably the geometry or curvature of the biomaterial surface on a microscale to which the host cells respond affects the macrophage phenotype, accounting for the results seen in this study.

In another study by this group, a combinatorial library of alginate microcapsules was screened in an in vivo whole-animal imaging system using a fluorescent probe for cathepsin activity at implant sites as an indicator of inflammatory response (Vegas et al., 2016). Unique microcapsule hydrogel chemistries were identified that showed thin fibrous capsules upon subcutaneous implantation in rodents or for at least 6 months in nonhuman primates. The unique chemistry moieties identified were triazole derivatives. While the mode of action of this chemistry on the inflammatory response to implanted microcapsules was not known, a small molecule triazole scaffold is being investigated as an immunomodulatory agent through its effects on T cells, not macrophages (Kharb and Sharma, 2011; Lindstedt et al., 2009).

Another interesting piece of the story of host response to biomaterials cited the central role of a chemokine receptor, colony-stimulating factor-1 receptor (CSF1R), for the foreign body response to biomaterial implants in rodents and nonhuman primates (Doloff et al., 2017). It was demonstrated that macrophages are required and responsible for downstream B-cell recruitment via the B-cell chemoattractant CXCL13, and that following their arrival B cells enhance fibrotic deposition. Inhibition of the macrophage-associated cytokine receptor CSF1R eliminated host-immune-mediated recognition and propagation of foreign body rejection responses to a broad range of materials. The attenuation of the host responses was not, however, done at the expense of other macrophage functions such as skin incision wound healing, macrophage phagocytic activity, and reactive oxygen species production. The result suggests a potentially highly specific target for abrogating the fibrotic response to implanted

biomaterials rather than generally suppressing the immune system to avoid a fibrotic response.

Immunotherapy technologies are beginning to be applied to the problem of fibrosis. For example, in a recent study, T cells were engineered using chimeric antigen receptors (CAR) T-cell technology to target pathogenic cardiac fibrosis (Aghajanian et al., 2019). The efficacy of redirected T-cell immunotherapy to specifically target pathological cardiac fibrosis in mice was demonstrated. It was found that cardiac fibroblasts expressing a xenogeneic antigen can be effectively targeted and ablated by adoptive transfer of antigen-specific CD8⁺ T cells. An endogenous target of cardiac fibroblasts was identified using expression analysis of the gene signatures of cardiac fibroblasts obtained from healthy and diseased human hearts, namely, fibroblast activation protein. Adoptive transfer of T cells that express a chimeric antigen receptor against fibroblast activation protein resulted in a significant reduction in cardiac fibrosis and restoration of function after injury in mice, suggesting a promising approach for clinical testing. Immunotherapy approaches are expected to be able to modulate aspects of the host response to biomaterials and regeneration.

References

- Aghajanian, H., et al., 2019. Targeting cardiac fibrosis with engineered T cells. *Nature* 573, 430.
- Amato, G., et al., 2014. Modified fixation free plug technique using a new 3D multilamellar implant for inguinal hernia repair: a retrospective study of a single operator case series. *Hernia* 18, 243–250.
- Anderson, J.M., 1993. Mechanisms of inflammation and infection with implanted devices. *Cardiovasc. Pathol.* 2 (3 (Suppl.)), 333–415.
- Anderson, J., 2008. Foreign body reaction to biomaterials. *Semin. Immunol.* 20, 86–100.
- Baker, D.W., et al., 2014. Alternative strategies to manipulate fibrocyte involvement in the fibrotic tissue response: pharmacokinetic inhibition and the feasibility of directed-adipogenic differentiation. *Acta Biomater.* 10, 3108–3116.
- Brauker, J.H., Carr-Brendel, V.E., Martinson, L.A., Crudele, J., Johnston, W.D., Johnson, R.C., 1995. Neovascularization of synthetic membranes directed by membrane microarchitecture. *J. Biomed. Mater. Res.* 29, 1517–1524.
- Brown, B.N., et al., 2012. Macrophage phenotype as a predictor of constructive remodeling following the implantation of biologically derived surgical mesh materials. *Acta Biomater.* 8, 978–987.
- Butler, M.J., Sefton, M.V., 2007. Poly(butyl methacrylate-co-methacrylic acid) tissue engineering scaffold with pro-angiogenic potential in vivo. *J. Biomed. Mater. Res. A* 82, 265–273.
- Doloff, J.C., et al., 2017. Colony stimulating factor-1 receptor is a central component of the foreign body response to biomaterial implants in rodents and non-human primates. *Nat. Mater.* 16, 671–680.
- Eming, S.A., et al., 2007. Inflammation in wound repair: molecular and cellular mechanisms. *J. Invest. Dermatol.* 127, 514–525.
- Ensan, S., et al., 2016. Self-renewing resident arterial macrophages arise from embryonic CX3CR1⁺ precursors and circulating monocytes immediately after birth. *Nat. Immunol.* 17, 159–168.
- Epelman, S., Liu, P., Mann, D., 2015. Role of innate and adaptive immune mechanisms in cardiac injury and repair. *Nat. Rev. Immunol.* 15, 117–129.

- Ferguson, M.W.J., O'Kane, S., 2004. Scar-free healing: from embryonic mechanisms to adult therapeutic intervention. *Philos. Trans. R. Soc. Lond. B* 359, 839–850.
- Forbes, S.J., Rosenthal, N., 2014. Preparing the ground for tissue regeneration: from mechanism to therapy. *Nat. Med.* 20, 857–869.
- Fukano, Y., Usui, M.L., Underwood, R.A., et al., 2010. Epidermal and dermal integration into sphere-templated porous poly(2-hydroxyethyl methacrylate) implants in mice. *J. Biomed. Mater. Res. A* 94, 1172–1186.
- Hong, K.M., et al., 2005. Characterization of human fibrocytes as circulating adipocyte progenitors and the formation of human adipose tissue in SCID mice. *FASEB J.* 19, 2029–2031.
- Kenneth Ward, W., Wood, M.D., Casey, H.M., Quinn, M.J., Federiuk, I.F., 2004. The effect of local subcutaneous delivery of vascular endothelial growth factor on the function of a chronically implanted amperometric glucose sensor. *Diabetes Technol. Ther.* 6 (2), 137–145.
- Kharb, R., Sharma, P.C., Yar, M.S., 2011. Pharmacological significance of triazole scaffold. *J. Enzym. Inhib. Med. Chem.* 26, 1–21.
- Klinge, U., et al., 2002. Impact of polymer pore size on the interface scar formation in a rat model. *J. Surg. Res.* 103, 208–214.
- Klueh, U., Kaur, M., Montrose, D.C., Kreutzer, D.L., 2007. Inflammation and glucose sensors: use of dexamethasone to extend glucose sensor function and life span in vivo. *J. Diabetes Sci. Technol.* 1 (4), 496–504.
- Ley, K., Laudanna, C., Cybulsky, M.I., Nourshargh, S., 2007. Getting to the site of inflammation: the leukocyte adhesion cascade updated. *Nat. Rev. Immunol.* 7, 678–689.
- Lindstedt, R., et al., 2009. The immunosuppressor st1959, a 3,5-diaryls-triazole derivative, inhibits T cell activation by reducing NFAT nuclear residency. *Int. J. Immunopathol. Pharmacol.* 22, 29–42.
- Marshall, A.J., Irvin, C.A., Barker, T., et al., 2004. Biomaterials with tightly controlled pore size that promote vascular in-growth. *ACS Polym. Prepr.* 45, 100–101.
- McNally, A.K., Anderson, J.M., 1995. Interleukin-induces foreign body giant cells from human monocytes/macrophages differential lymphokine regulation of macrophage fusion leads to morphological variants of multinucleated giant cells. *Am. J. Pathol.* 147, 1487–1499.
- McNally, A.K., Anderson, J.M., 2002. β 1 and β 2 integrins mediate adhesion during macrophage fusion and multinucleated foreign body giant cell formation. *Am. J. Pathol.* 160, 621–630.
- Mosser, D.M., Edwards, J.P., 2008. Exploring the full spectrum of macrophage activation. *Nat. Rev. Immunol.* 8, 958–969.
- Muhl, T., et al., 2008. New objective measurement to characterize the porosity of textile implants. *J. Biomed. Mater. Res. B Appl. Biomater.* 84, 176–183.
- Nilsson, B., Ekdahl, K.N., Mollnes, T.E., Lambris, J.D., 2007. The role of complement in biomaterial-induced inflammation. *Mol. Immunol.* 44, 82–94.
- Picha, G.J., Drake, R.F., 1996. Pillard-surface microstructure and soft-tissue implants: effect of implant site and fixation. *J. Biomed. Mater. Res.* 30, 305–312.
- Richardson, T.P., Peters, M.C., Ennett, A.B., Mooney, D.J., 2001. Polymeric system for dual growth factor delivery. *Nature* 19, 1029–1034.
- Rodriguez, A., Meyerson, H., Anderson, J.M., 2009. Quantitative in vivo cytokine analysis at synthetic biomaterial implant sites. *J. Biomed. Mater. Res. A* 89, 152–159.
- Sadtler, K., et al., 2016. Developing a pro-regenerative biomaterial scaffold microenvironment requires T helper 2 cells. *Science* 352, 366–370.
- Sadtler, K., et al., 2017. The scaffold immune microenvironment: biomaterial-mediated immune polarization in traumatic and non-traumatic applications. *Tissue Eng. A* 23, 1044–1053.
- Schmidt, M., et al., 2003. Identification of circulating fibrocytes as precursors of bronchial myofibroblasts in asthma. *J. Immunol.* 171, 380–389.
- Sun, B.K., et al., 2014. Advances in skin grafting and treatment of cutaneous wounds. *Science* 346, 941–945.
- Vagnozzi, R.J., Maillet, M., Sargent, M.A., Khalil, H., Johansen, A.K.Z., Schwanekamp, J.A., York, A.J., Huang, V., Nahrendorf, M., Sadayappan, S., Molkentin, J.D., 2020. An acute immune response underlies the benefit of cardiac stem cell therapy. *Nature* 566, 405.
- Valentin, J.E., Stewart-Akers, A.M., Gilbert, T.W., Badylak, S.F., 2009. Macrophage participation in the degradation and remodeling of extracellular matrix scaffolds. *Tissue Eng. A* 15 (7).
- Vegas, A.J., et al., 2016. Combinatorial hydrogel library enables identification of materials that mitigate the foreign body response in primates. *Nat. Biotechnol.* 34, 345–352.
- Veisoh, O., et al., 2015. Size- and shape-dependent foreign body immune response to materials implanted in rodents and non-human primates. *Nat. Mater.* 14, 643–651.
- Williams, D.F., 1999. *The Williams Dictionary of Biomaterials*. Liverpool University Press.
- Zhao, Q., et al., 1991. Foreign-body giant cells and polyurethane biostability: in vivo correlation of cell adhesion and surface cracking. *J. Biomed. Mater. Res.* 25, 177–183.

2.2.3

Innate and Adaptive Immunity: The Immune Response to Foreign Materials

BENJAMIN GEORGE KESELOWSKY¹, ABHINAV ACHARYA², JAMAL S. LEWIS³

¹Department of Biomedical Engineering, University of Florida, Gainesville, FL, United States

²School for Engineering of Matter, Transport and Energy, Biodesign Center for Immunotherapy, Vaccines and Virotherapy, Arizona State University, Tempe, AZ, United States

³Biomedical Engineering, University of California, Davis, CA, United States

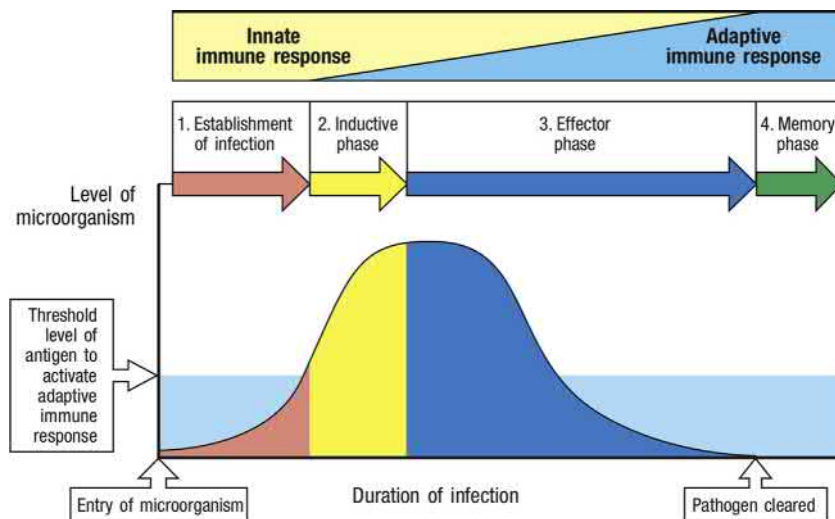
Overview

The intersection of immunology and biomaterials is a rich field for synergy. For example, early immunology work by Ilya Mechnikov in the late 1800s, remarkably relevant to modern biomaterials approaches to immune engineering, utilized readily available natural material as a tool to observe the process of phagocytosis. He inserted plant thorns composed primarily of the natural polymer cellulose (potentially along with microbial contaminants) into starfish larvae and observed an influx of interrogating cells. This line of inquiry and availability of materials-based tools subsequently uncovered the fundamental process of phagocytosis, the means by which immune cells engulf and degrade foreign material. Mechnikov's work earned him the Nobel Prize in Physiology or Medicine, shared with Paul Ehrlich in 1908. In keeping with the synergy between materials and immunology, the use of the material alum as a vaccine adjuvant began in the 1920s and has since been saving millions of lives annually. With these and many more such powerful examples in fundamental science and application as guideposts, a growing number of biomaterial scientists aim to continue this tradition, but often must first become acquainted with the basic principles of immunology.

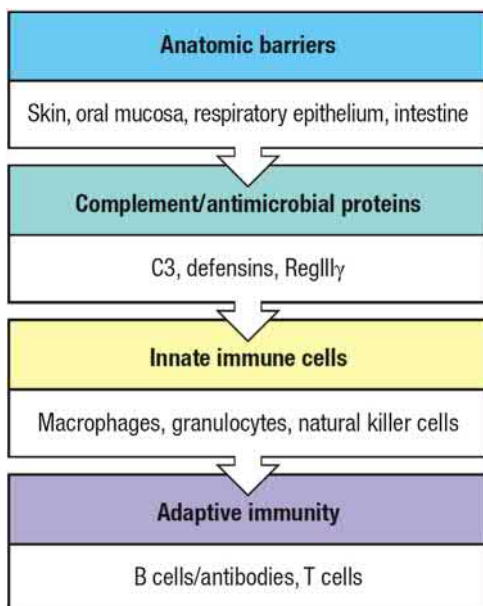
The immune system is the defense mechanism of the body that is responsible for protecting against damaging foreign pathogens, maintaining components of self, and permitting benign commensal microbes (Matzinger, 1994; Ridge et al., 1996; Janeway, 1989). It is notable that aspects of immunology are integral in enormously diverse topics in biology and medicine spanning conception to death. These topics include reproduction, development, wound healing, infection, vaccination, cancer, immunotherapy, autoimmunity, transplantation, and diagnostics. More extensive discussion of the immune system can be found in a number of excellent

basic immunology texts (Abbas and Pober, 2000; Travers et al., 2001). Emerging concepts are extending even further, as immunology is increasingly being understood as an integral component of the homeostatic health of many tissues, for example, through interactions with stem cells, localized metabolic regulation, and regulating the microbiome (Wood and Martin, 2017; Masopust D, 2019; Round and Palm, 2018; Immunity in the tissues, 2013; O'Neill et al., 2016).

Keeping in mind the intended biomaterials scientist readership, we discuss here the primary components and functions of classical immunology and how the immune system recognizes and eliminates or reacts to foreign bodies at an introductory level. Components of the immune system that differentiate between “self” and “nonself” along with mechanisms for elimination of the recognized threat are described. While the field of immunology is typically covered in multiple introductory and specialized courses, this overview chapter only introduces *innate* and *adaptive* immunity with the intent to provide a fundamental understanding of the body's response to the insertion of a foreign material. It is with these basic immunology concepts in mind that the reader can be better prepared to anticipate issues that arise at the biomaterials–tissue interface. This chapter therefore outlines the two main arms of the immune response, the interlinked innate and adaptive systems, with the innate immune response preceding, potentiating, and directing the adaptive response to the establishment of infection, followed by an induction phase, effector phase, and memory phase (Fig. 2.2.3.1). Each arm of immunology possesses multiple layers of defense with many interacting components (Fig. 2.2.3.2). Finally, areas of particular interest to biomaterials and biomaterials-centric applications are described. Note, the topic of the foreign body reaction to implanted synthetic materials is covered in detail in Chapter 2.2.2.



• **Figure 2.2.3.1** The innate and adaptive immune response act in concert to eliminate pathogens. (1) Pathogen establishes infection and induces the innate response upon detection. (2) As the antigen levels go above a threshold, they trigger the adaptive immune response. (3) After 4–7 days, adaptive immune response components clear the infection. (4) After the infection is cleared, long-term memory in the form of antibodies and cells is established (Travers et al., 2001). (Figure 11.1 Janeway's Immunobiology ninth edition).



• **Figure 2.2.3.2** Protection against pathogens relies on several levels of defense. The first is the anatomic barrier provided by the body's epithelial surfaces. In the second, various chemical and enzymatic systems, including complement, act as an immediate antimicrobial barrier near these epithelia. If epithelia are breached, nearby various innate lymphoid cells can coordinate a rapid cell-mediated defense. If the pathogen overcomes these barriers, the slower-acting defenses of the adaptive immune system are brought to bear (Travers et al., 2001). (Figure 1.5 Janeway's Immunobiology ninth edition).

Innate Immunity

Innate immunity encompasses the first phase of responses to foreign pathogen or injury (Medzhitov, 2007). The primary response of innate immunity is to recruit effector cells to the site of invasion or injury, and recognize nonspecific or broadly specific foreign body markers. These responses then

lead to effective removal of a foreign body or initiation of tissue remodeling and healing.

Innate immunity utilizes a range of biomolecules, including antimicrobial enzymes, antimicrobial peptides, complement systems, cytokines, and reactive oxygen and nitrogen species among others to neutralize the perceived “danger.” Additionally, innate immunity also has a range of different types of specialized cells such as macrophages, dendritic cells (DCs), natural killer (NK) cells, and $\gamma\delta$ T cells among others to neutralize the perceived “danger” (Travers et al., 2001). Notably, some cells of the innate immune system can recognize pathogen-associated molecular patterns (PAMPs) of different types of pathogens, setting in motion development of an immune response capable of eliminating the pathogen within minutes to hours (Iwasaki and Medzhitov, 2010; Janeway et al., 2002; Kumar et al., 2011). Only when the innate immune system fails to clear pathogens is the adaptive immunity (described later) activated, which then generates a “memory” response toward the pathogen. In the following sections we will discuss different components of the innate immune system, their function, and mechanisms.

First Barriers Against Danger

Epithelial layers of the body such as those in skin, gut, lungs, and oral cavity provide the first barrier against foreign bodies (Fig. 2.2.3.3). Epithelial cells are joined by tight junctions to provide mechanical tissue integrity. In addition to physically blocking pathogen entry, epithelia are also responsible for producing various chemicals and biomolecules that provide defense against pathogens. Specifically, these cells can produce lysozymes and phospholipases to dissolve the membrane of bacteria (Travers et al., 2001). If the pathogens survive this first barrier, the next line of defense, called the complement system, is activated (Travers et al., 2001).

	Skin	Gut	Lungs	Eyes/nose/oral cavity
Mechanical	Epithelial cells joined by tight junctions			
	Longitudinal flow of air or fluid	Longitudinal flow of air or fluid	Movement of mucus by cilia	Tears Nasal cilia
Chemical	Fatty acids	Low pH Enzymes (pepsin)	Pulmonary surfactant	Enzymes in tears and saliva (lysozyme)
	β -defensins Lamellar bodies Cathelicidin	α -defensins (cryptdins) RegIII (lecticidins) Cathelicidin	α -defensins Cathelicidin	Histatins β -defensins
Microbiological	Normal microbiota			

• **Figure 2.2.3.3** Many barriers prevent pathogens from crossing epithelia and colonizing tissues. Surface epithelia provide mechanical, chemical, and microbiological barriers to infection (Travers et al., 2001). (Figure 2.5 Janeway's Immunobiology ninth edition).

Complement System

The complement system is a large, diverse set of soluble proteins produced primarily in the liver, which are utilized by the innate immune system to complement antibody responses to recognize and eliminate a foreign body. The complement system can recognize a pathogen's molecular patterns and become activated, which can result in direct killing of the pathogen, enhanced phagocytosis, and production of local inflammatory responses. Notably, various natural and synthetic biomaterials can also engage and activate the complement system, increasing biomaterial-associated inflammation (Hubbell et al., 2009). The complement system is described in detail in Chapter 2.2.4.

Pattern Recognition by the Innate Immune System

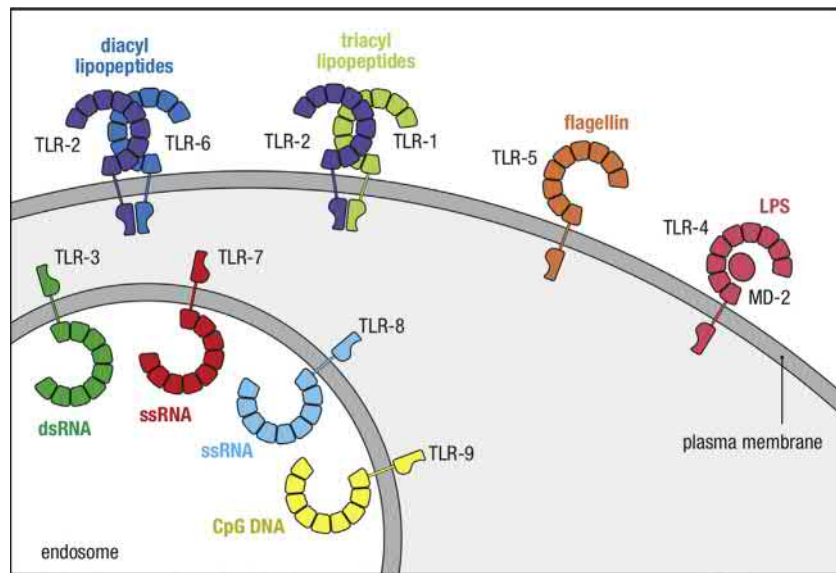
The innate immune system has evolved receptors that recognize specific patterns of foreign materials. This class of receptors is called pattern recognition receptors (PRRs) (Janeway et al., 2002). PRRs are divided into four main categories: (1) soluble complement receptors (discussed earlier), (2) membrane-bound phagocytic receptors, (3) membrane-bound signaling receptors, and (4) cytoplasmic signaling receptors.

Membrane-bound phagocytic receptors, such as mannose receptor, Dectin-1, lipid receptor, and scavenger receptors among others are utilized by cells of the innate immune system to phagocytose foreign materials (discussed in the section "Antigen Processing and Presentation"). On the other hand, membrane-bound signaling receptors such as toll-like receptors (TLRs) (Kumar et al., 2011; Acharya et al., 2016) are utilized to signal the presence of pathogen and induce an immune response. TLRs are ancient pathogen-recognizing receptors that can recognize different molecules expressed by pathogens. Since these molecules are

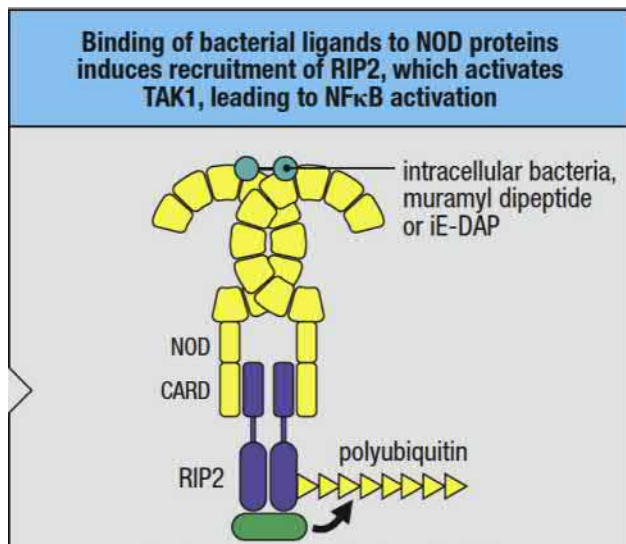
characteristic of the pathogens that are not found in host tissue, they are called PAMPs. There are several PAMPs such as lipopolysaccharide (expressed in the cell wall of Gram-negative bacteria), bacterial DNA, diacyl and triacyl lipopeptide, flagellin, and double- and single-stranded RNA, which are recognized by the innate immune system. To recognize these wide variety of molecules, TLRs (TLR1–TLR10 in humans; TLR1–TLR13 in mice) located either on the cell surface or in endosomal vesicles are utilized (Fig. 2.2.3.4). These TLRs are capable of activating MYD88 and TIR-domain-containing adapter-inducing interferon- β signaling pathways, which then lead to immune cell activation and functions such as phagocytosis and removal of pathogens.

Another group of receptors recognizing PAMPs in the cytosol of innate immune cells are called nucleotide-binding oligomerization domain (NOD)-like receptors (NLRs) (Inohara and Nuñez, 2001). Examples of NLRs include NOD-1 and NOD-2 (Fig. 2.2.3.5), which are responsible for detecting breakdown products of the peptidoglycans of bacteria. Another interesting subclass of NLRs is called NOD leucine-rich repeat and pyrin domain (NLRP). There are 14 different types of NLRPs expressed in humans, and although the activation of these is not clearly understood they can recognize extracellular ATP molecules.

A very important group of cytosolic RNA-detecting mechanisms of the innate immune system is called retinoic acid-inducible gene I (RIG-I)-like receptors (RLRs) (Takeuchi and Akira, 2008). RIG-I detect single-stranded RNA and induce the production of type I interferons. Similar to RIG-I, another RLR, MDA-5 (also called helicard) detects double-stranded RNA. Both RIG-I and MDA-5 are important receptors of intracellular viruses and for mounting an antiviral immune response (Fig. 2.2.3.6). Cytosolic DNA molecules such as cyclic-di-AMP, cyclic-di-GMP, etc. are detected by stimulator of interferon genes (STING) receptors (Archer et al., 2014). STING receptors are innate



• **Figure 2.2.3.4** The cellular locations of the mammalian toll-like receptors (TLRs). TLRs are transmembrane proteins whose extracellular region contains 18–25 copies of the leucine-rich repeat (LRR), but these cartoons depict only nine LRRs for simplicity. Some TLRs are located on the cell surface of dendritic cells, macrophages, and other cells, where they are able to detect extracellular pathogen molecules. TLRs are thought to act as dimers. Only those that form heterodimers are shown in dimeric form here; the rest act as homodimers. TLRs located intracellularly, in the walls of endosomes, can recognize microbial components, such as DNA, that are accessible only after the microbe has been broken down. The diacyl and triacyl lipopeptides recognized by the heterodimeric receptors TLR-6:TLR-2 and TLR-1:TLR-2, respectively, are derived from the lipoteichoic acid of Gram-positive bacterial cell walls and the lipoproteins of Gram-negative bacterial surfaces (Travers et al., 2001). (Figure 2.14 Janeway's Immunobiology ninth edition).



• **Figure 2.2.3.5** Intracellular nucleotide-binding oligomerization domain (NOD) proteins sense the presence of intracellular pathogens. NOD-like receptors reside in the cytoplasm, and are activated in the presence of various ligands (bacterial ligand shown here). NOD1 recognizes γ -glutamyl diaminopimelic acid (iE-DAP), a breakdown product of Gram-negative bacterial cell walls. The binding of these ligands to NOD1 or NOD2 induces aggregation, allowing caspase recruitment domain (CARD)-dependent recruitment of the serine–threonine kinase RIP2. RIP2 is then responsible for inducing nuclear factor kappa-light-chain-enhancer of activated B cells (NF κ B) production, which then leads to activation of the immune cells (Travers et al., 2001). (Adapted from Figure 3.17 Janeway's Immunobiology ninth edition).

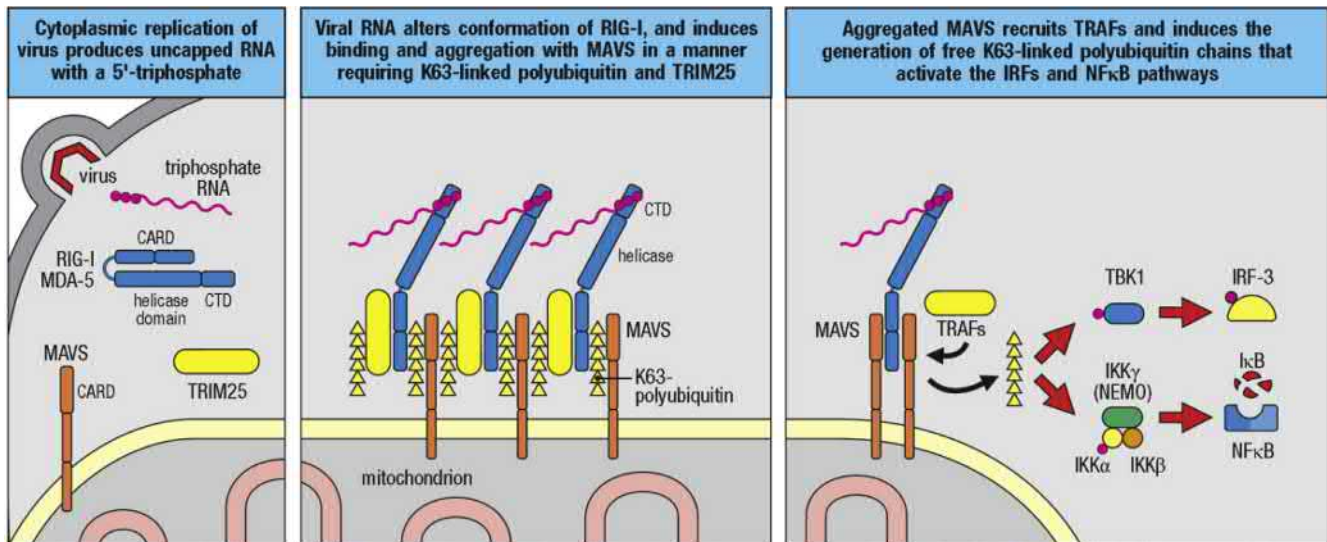
sensors of intracellular DNA fragments generated by viral or bacterial species (Fig. 2.2.3.7).

In sum, the innate immune system has multiple PRRs that can recognize a variety of different molecules from pathogens. Once these molecules are recognized, PRRs induce downstream signaling in innate immune cells for the production of cytokines, chemokines, and costimulatory molecules, which are essential for the function of adaptive immune responses. Furthermore, PRRs can also be activated by host molecules that can be generated from cellular infection, damage, stress, or transformation. Such host molecules have been termed damage-associated molecular patterns (DAMPs), and some of the molecules in this class can also be recognized by receptors involved in pathogen recognition, such as the TLRs. Upon recognition of DAMPs, innate immunity is activated leading to further immune responses.

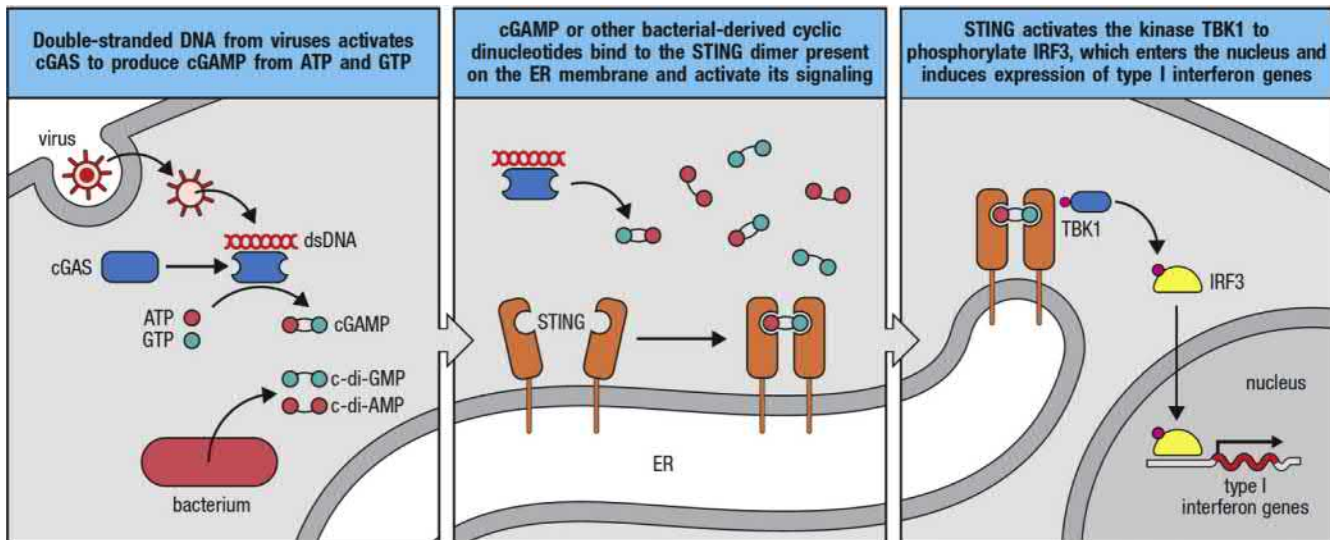
Cells of the Innate Immune System

To mount a robust immune response, the innate immune system utilizes several different types of immune cells such as innate lymphoid cells (ILCs, e.g., NK cells), mast cells, eosinophils, basophils, $\gamma\delta$ T cells, neutrophils, monocytes, macrophages, and DCs (Fig. 2.2.3.8). The function of each of these innate cells is outlined next:

Monocytes: Monocytes are one of the largest constituents of total white blood cells in terms of abundance (Travers et al., 2001). Monocytes are derived from hematopoietic



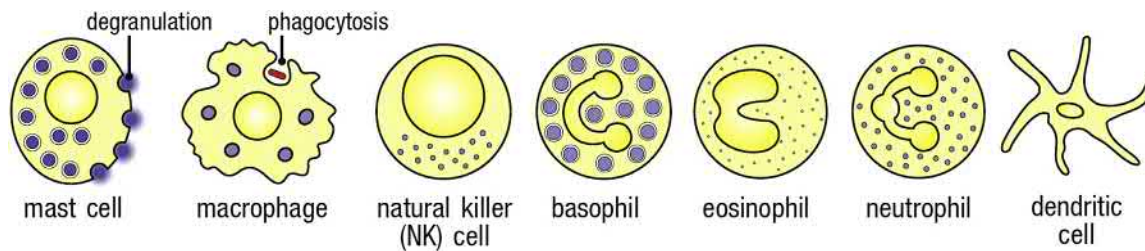
• **Figure 2.2.3.6** Retinoic acid-inducible gene I (RIG-I) and other RIG-I-like receptors are cytoplasmic sensors of viral RNA. Detection of uncapped 5'-triphosphate RNA by RIG-I, or viral dsRNA by MDA-5, changes the conformation of their caspase recruitment domain (CARD) domains to become free to interact with the aminoterminal CARD domain of the adaptor protein called mitochondrial antiviral signaling protein (MAVS), attached to the outer mitochondrial membrane. This interaction involves the generation of K63-linked polyubiquitin from the E3 ligases TRIM25 or Riplet. The K63 polyubiquitin is then able to upregulate interferon and nuclear factor kappa-light-chain-enhancer of activated B cells (NFκB) signaling leading to the activation of the immune cells (Travers et al., 2001). (Adapted from Figure 3.21 Janeway's Immunobiology ninth edition).



• **Figure 2.2.3.7** Stimulator of interferon gene (STING) recognizes cytosolic cyclic DNA (cDNA) and induces a type I interferon-mediated innate immune response against intracellular pathogens. *First panel:* cyclic GMP-AMP synthase (cGAS) resides in the cytoplasm and serves as a sensor of double-stranded DNA (dsDNA) from viruses. When cGAS binds dsDNA, its enzymatic activity is stimulated, leading to production of cyclic-GMP-AMP (cGAMP). Bacteria that infect cells produce second messengers such as cyclic dinucleotides, including cyclic diguanylate monophosphate (c-di-GMP) and cyclic diadenylate monophosphate (c-di-AMP). *Second panel:* cGAMP and other bacterial dinucleotides can bind and activate the STING dimer present on the endoplasmic reticulum (ER) membrane. *Third panel:* in this state, STING activates type I interferons through TBK1 and IRF3, although the details of this interaction are still unclear (Travers et al., 2001). (Adapted from Figure 3.22 Janeway's Immunobiology ninth edition).

stem cells, and although not terminally differentiated, play an important role in innate immunity. Monocytes typically circulate in the blood for 1–3 days, and in the presence of injury or infection are directed to enter peripheral tissue via extravasation through blood vessels as directed by

endothelial cell upregulation of adhesion (e.g., selectin) and chemoattractant molecules. Monocytes utilize adhesion molecules (e.g. carbohydrate ligands), to bind to endothelium and exit the blood stream. Cytokines produced by tissue-resident innate immune cells induce rolling monocytes



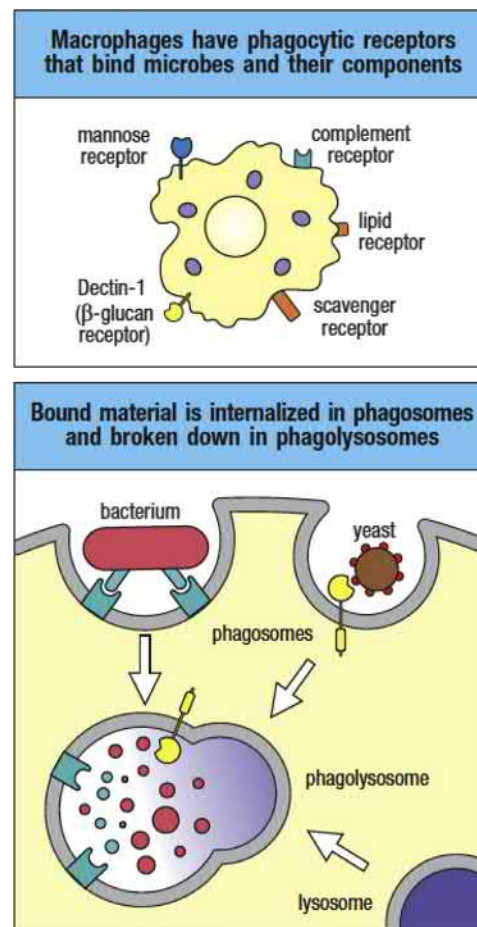
• **Figure 2.2.3.8** Cells of the innate immune system. Travers et al., 2001. (Adapted from the preface, “Icons used throughout the book”, Janeway’s Immunobiology ninth edition).

to activate integrin receptors that then tightly bind to the endothelial cells. A sequential step of cytoskeleton rearrangement then allows monocytes to extravasate between endothelial cells into tissues. Once in the tissue, monocytes terminally differentiate into DCs or macrophages.

Macrophages: Bone marrow-derived macrophages differentiate from monocytes and are a type of phagocytic cell (Travers et al., 2001). A major function of macrophages is to phagocytose cellular debris, pathogens, foreign particles, malignant cells, and other particulates, as illustrated in Fig. 2.2.3.9. Phagocytosis is initiated when specific receptors on the surface of the cell interact with the microbial-specific molecules present on the surface of the pathogen. The bound pathogen is first surrounded by the phagocyte plasma membrane and then internalized in a large membrane-enclosed endocytic vesicle known as a phagosome. The phagosome then fuses with another vesicle, the lysosome, to generate a phagolysosome, which has low pH (Abbas and Pober, 2000; Travers et al., 2001; Wood and Martin, 2017), digestive enzymes such as lysozyme and defensins, antimicrobial peptides, and increased levels of reactive oxygen species such as superoxide, as well as nitric oxide radicals. Once in the phagolysosome, ingested materials are degraded by their combined action, and pathogens are killed.

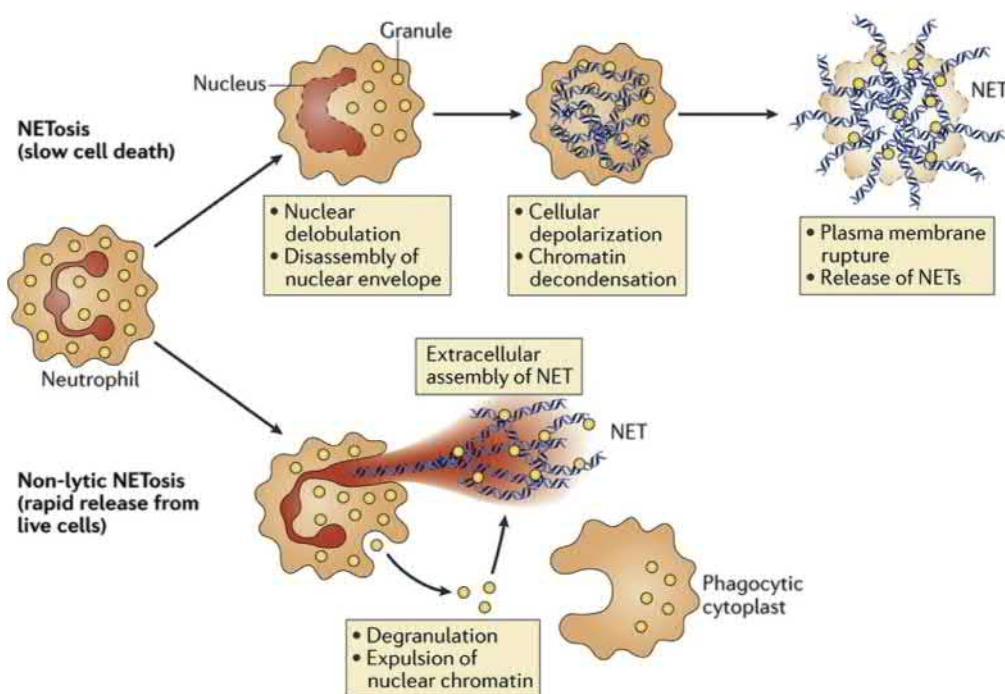
Interestingly, certain pathogens such as *Mycobacterium tuberculosis* have evolved with humans to survive within macrophages by preventing the fusion of phagosomes and lysosomes. Notably, in the presence of bulk materials (e.g., a biomaterial implant) or particulate too large to be phagocytosed by a single macrophage (greater than $\sim 10\ \mu\text{m}$), many macrophages will fuse together to form multinuclear foreign body giant cells (FBGCs). These cells either attempt to engulf the entire material or try to degrade it by releasing reactive oxygen species.

Dendritic cells (DCs): There are functionally two main types of DCs: plasmacytoid DCs (pDCs) and conventional DCs (or most often simply DCs), arising from distinct progenitors in the marrow. A major function of pDCs is production of type I interferons. On the other hand, DCs form the bridge between innate and adaptive immunity. In addition to producing cytokines in response to signaling through PRRs, DCs are specialized for particularly efficient antigen uptake, processing, and presentation (discussed further in the section “Antigen Uptake, Processing, and Presentation”) in a manner uniquely capable of initiating adaptive immune responses (Acharya et al., 2016; Acharya et al., 2009; Acharya et al., 2008; Acharya et al., 2011; Banchereau and Steinman, 1998; Palucka and Banchereau, 2012).



• **Figure 2.2.3.9** Macrophages express receptors that enable them to take up microbes by phagocytosis. Macrophages express receptors such as Dectin-1 (member of the C-type lectin family), complement receptor, lipid receptors, mannose receptors, and scavenger receptors for binding molecules on pathogen surfaces. The receptor-bound material is phagocytosed into intracellular phagosomes, which fuse with lysosomes to form an acidified phagolysosome in which the ingested material is broken down by lysosomal hydrolases (Travers et al., 2001). (Adapted from Figure 3.2 Janeway’s Immunobiology ninth edition).

DCs act as sentinels in the periphery and form an important part of gut-associated lymphatic tissue and epithelium lymphatic tissue. Specifically, DCs line the mucosal layers of the nose, intestine, lungs, stomach, and skin. In these and other peripheral tissues, DCs continuously sample the environment for the presence of foreign materials. DCs express an array of TLRs and other types of PRRs to recognize pathogens. Once foreign materials are recognized, DCs release an array of cytokines and chemokines, and then traffic toward secondary



Nature Reviews | Immunology

• **Figure 2.2.3.10** Neutrophil extracellular traps (NETs) protect against infection. Neutrophils undergo a slow cell death pathway termed NETosis that begins with nuclear delobulation and the disassembly of the nuclear envelope and continues with loss of cellular polarization, chromatin decondensation, and plasma membrane rupture. Moreover, neutrophils can also undergo a nonlytic form of NETosis. In this case, cell death is accompanied by secretion of nuclear chromatin and granule proteins through degranulation (Liongue et al., 2011). (Figure 1, Nat Rev Immunol. 2018 Feb;18(2):134–147. <https://doi.org/10.1038/nri.2017.105>).

lymphoid organs to initiate an adaptive immune response, aspects of which are discussed further in the sections “Antigen Processing and Presentation” and “Adaptive Immunity.”

Neutrophils: Neutrophils, also called polymorphonuclear neutrophils (PMNs), are the most abundant cells of the immune system in the bloodstream and are the hallmark of acute inflammation due to infection or injury (Travers et al., 2001). Neutrophils extravasate through the endothelium to reach the site of injury or infection in response to cytokines and chemokines. Once in injured or infected tissue, neutrophils perform the functions of phagocytosis of infectious agents, degranulation, release of soluble antimicrobials, and generation of neutrophil extracellular traps. Specifically, neutrophils are capable of phagocytosing foreign particles that are opsonized or coated with antibodies. Once phagocytosed, the foreign particles are exposed to reactive oxygen species in phagosomes, leading to their killing and elimination. Neutrophils are also capable of releasing granules that contain a powerful arsenal of molecules that can neutralize pathogens. For example, these granules contain myeloperoxidase that generates reactive oxygen species, defensins, proteases, elastase, collagenase, histaminase, and alkaline phosphatase among others. Interestingly, neutrophils also generate neutrophil extracellular traps (NETs) that are composed of chromatin (Fig. 2.2.3.10). These NETs are capable of trapping pathogens such as bacteria, thereby restricting them to the site of infection. Notably, formation of NETs has also been demonstrated to occur in response

to exposure to synthetic biomaterials (Sperling et al., 2017; Jhunjhunwala & et al., 2015).

Mast cells: Mast cells are large innate immune cells of the hemocytoblast lineage with granules filled with several inflammatory molecules (Travers et al., 2001). These cells become activated when multimeric antigen binds immunoglobulin E (IgE) antibody expressed on its surface. Multimeric antigens can come from parasites such as protozoa or helminths. Once activated, mast cells release granule contents, leading to chemoattraction of several adaptive immune cell types. Unfortunately, these inflammatory mediators (e.g., histamine and cytokines) are also involved in several immune disorders, including allergy, anaphylaxis, and autoimmunity.

Eosinophils: Eosinophils are derived from bone marrow from hemocytoblasts and like mast cells are filled with granules containing cytotoxic granule cationic proteins such as major basic protein, eosinophil cationic protein, and eosinophil peroxidase, which produce reactive oxygen species (Travers et al., 2001). After activation via recognition of antibody-coated parasites, eosinophils undergo cytolysis (cell death), releasing the granules. While inefficient phagocytes, eosinophils still play an important role in the killing of multicellular parasites too large to be phagocytosed.

Basophils: Similar to mast cells and eosinophils, basophils are a member of the phagocytes derived in the marrow from hemocytoblasts (Travers et al., 2001). Basophils are the rarest type of innate immune cells, and constitute less than 1% of the circulating leukocytes. Similar to mast cells, basophils

TABLE 2.2.3.1 Some of the Cytokines of the Innate Immune System and Their Targets

Cytokine	Principal Cell Sources	Principal Cellular Targets and Biologic Effect
TNF	Macrophage	Endothelial cell activation; neutrophil activation, apoptosis in different cells
IL-1	Macrophage, endothelial cells, epithelial cells	Endothelial cell activation
IL-12	Macrophage, dendritic cells	NK cell and T cell activation, increased cytolytic activity
Type 1 interferons	Macrophages, dendritic cells, fibroblasts	Antiviral activity in all cell types, increased MHC-I expression, activation of NK cells

IL, Interleukin; *MHC*, major histocompatibility complex; *NK*, natural killer; *TNF*, tumor necrosis factor.
Adapted from Appendix III—Cytokines and their receptors—Janeway's Immunobiology ninth edition.

have granules containing histamine, proteolytic enzymes, and inflammatory mediators. Additionally, basophils also have receptors for IgE-FcεRI receptors and are activated in the presence of neuropeptides, anaphylatoxins, f-Met-Leu-Phe, bacterial products/TLR ligands, and animal venom components.

Innate lymphoid cells: ILCs are similar in some ways to adaptive arm T cells as far as function and phenotype, in that their activation, expansion, and effector function mirror T cells (Travers et al., 2001). However, ILCs are activated in the presence of stress, microbial molecules, or cytokines in contrast to T cells, which require specific antigens for activation. Notably, ILCs are directly activated by tissue “danger” signals, and therefore are classified as part of the innate immune system. ILCs are divided into three subcategories, ILC1, ILC2, and ILC3, according to their function. ILC1 expands and secretes interferon (IFN)-γ in response to interleukin (IL)-12, IL-15, and IL-18, generated by intracellular microbe-infected cells. Activated ILC1 then leads to activation of macrophages, and induces cytotoxicity in infected cells. An important ILC closely related to but distinct from ILC1 is the NK cell, discussed next. ILC2 expands and secretes IL-4, IL-5, and IL-13 in response to IL-25, IL-33, thymic stroma lymphopoietin, basophil-derived IL-4, and products of the arachidonic acid pathway, in response to parasite infection, allergens, and epithelial injury. Activation of ILC2 leads to tissue repair, alternate macrophage activation, mucus production, and thermoregulation among other functions. ILC3 expands and secretes lymphotoxins, granulocyte-macrophage colony-stimulating factor (GM-CSF), IL-22, and IL-17 in the fetus, early after birth and during inflammation. Activation of ILC3 leads to epithelium survival, phagocytosis, and production of antimicrobial peptides.

Natural killer cells: NK cells are large lymphocyte-like cells with a granular cytoplasm. These cells originate from common lymphoid progenitor cells in the bone marrow and were first discovered due to their ability to kill specific types of cancer cells and cells infected with herpesviruses. NK cells perform this function immediately upon recognizing the absence of “self” marker major histocompatibility complex (MHC) I, uniquely without requiring any further activation signals. NK cells respond to cellular stress and to infections by releasing cytolytic granules, which then cause apoptosis

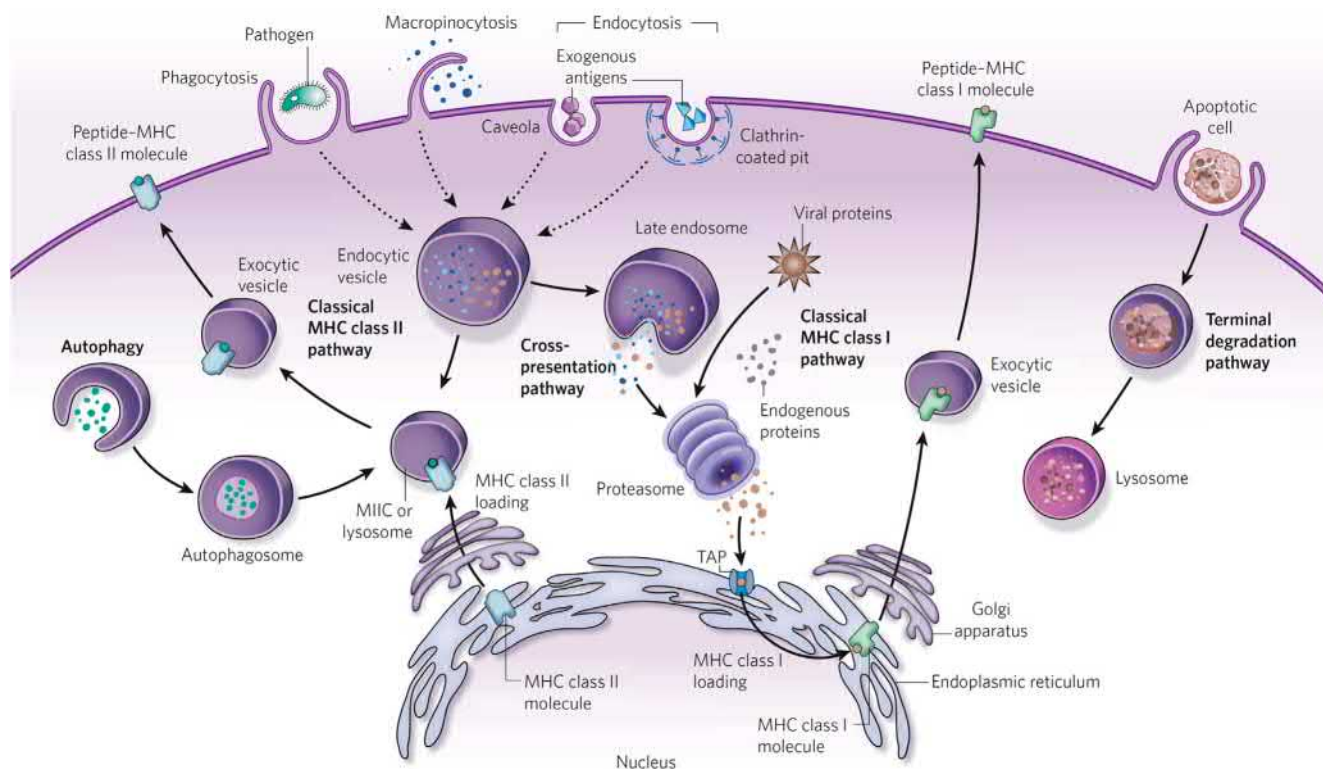
in infected cells. Moreover, NK cells can also release innate cytokines (Table 2.2.3.1), which then lead to activation of T lymphocytes and other NK cells. Importantly, NK cells are responsible for inducing early innate responses to viral infections before the adaptive immune responses are developed.

γδ T cells: γδ T cells are also called “unconventional” T cells, and are defined by expression of heterodimeric T cell receptors (TCRs) composed of γ and δ chains. Notably, γδ T cells recognize a broad array of infected or transformed cells. Moreover, once infected or transformed cells are recognized, γδ T cells produce cytokines such as IFN-γ, tumor necrosis factor (TNF)-α, and IL-17, produce chemokines such as RANTES, IP-10, and lymphotactin, and also cause the cytolysis of infected or transformed target cells using perforin, granzymes, and TRAIL. In addition to directly modulating the infected cells and initiating immune response, γδ T cells also interact with epithelial cells, monocytes, DCs, neutrophils, and B cells, and modulate their function.

Together, cells of the innate immune system act in concert to develop a robust innate immune response against pathogens. The innate immune response shapes the subsequent adaptive response. As mentioned, DCs act as a bridge between the innate and adaptive immune responses, being the key player in initiating and sustaining adaptive immune responses, where the distinguishing feature in this capacity is antigen processing and presentation.

Antigen Uptake, Processing, and Presentation

While there are multiple types of phagocytic cells, such as macrophages, monocytes, granulocytes (e.g., neutrophils, eosinophils, basophils), and multiple “professional” antigen-presenting cells (APCs) (DCs, macrophages, and B cells), DCs are the most efficient at antigen uptake, processing, and presentation. DCs sample antigenic sources from numerous compartments, utilizing multiple mechanisms such as phagocytosis, micropinocytosis, endocytosis, and autophagy, as illustrated in Fig. 2.2.3.11. Antigen components are degraded (e.g., proteins broken down to peptides and trimmed to appropriate lengths), then loaded onto MHCs I and II, and displayed on the APC surface (Yeung, 2012).



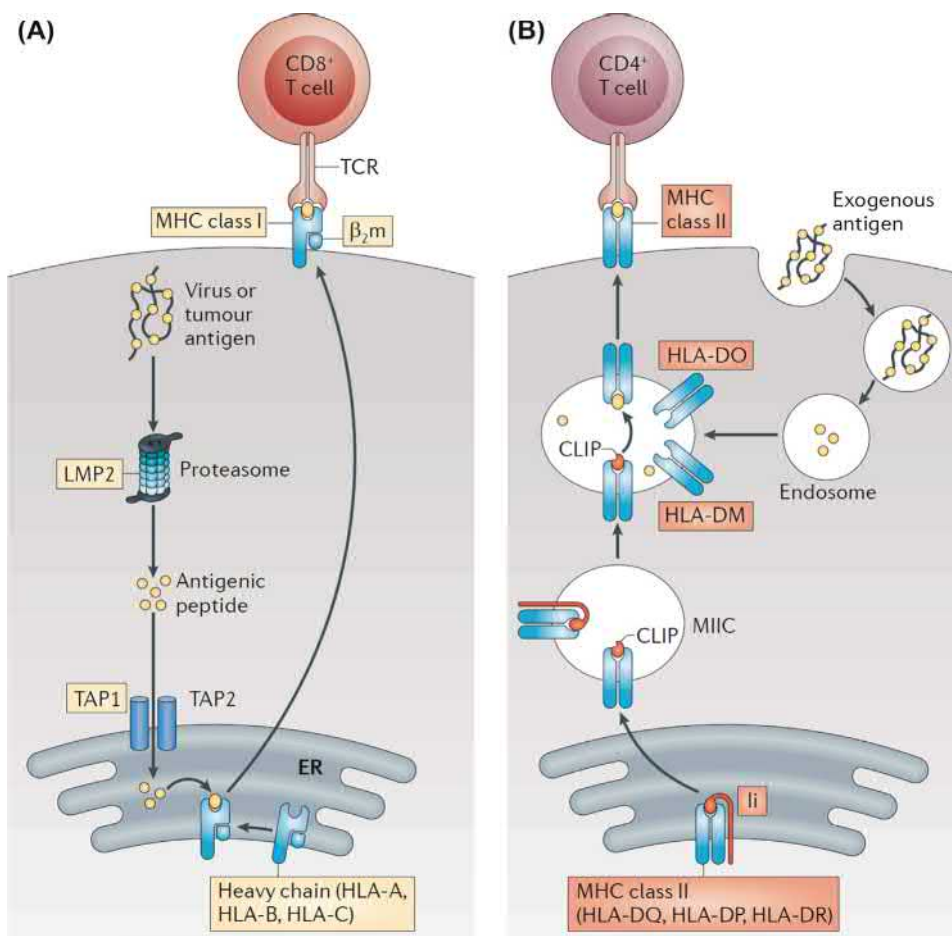
• **Figure 2.2.3.11** Intracellular pathways of dendritic cell antigen presentation. *Left*, exogenous particles, proteins, or pathogens can be taken into the cell through various pathways, including phagocytosis (for particles $>1\ \mu\text{m}$), macropinocytosis ($<1\ \mu\text{m}$), and endocytosis from caveolae ($\sim 60\ \text{nm}$) or clathrin-coated pits ($\sim 120\ \text{nm}$). Exogenous antigens are then processed in endocytic vesicles (phagosomes, endosomes, lysosomes, and/or endolysosomes; *dashed arrows* represent multiple vesicular steps). Processed antigen (peptide) is subsequently loaded onto major histocompatibility complex (MHC) class II molecules (which have been assembled in the endoplasmic reticulum, transported through the Golgi apparatus, and targeted to endocytic compartments) in a lysosome or MHC class II compartment. The peptide–MHC class II complexes then move through exocytic vesicles to the cell surface, where antigen presentation occurs. MHC class II loading of endogenous antigen provided by autophagy can also occur, particularly when the cell is under stress. *Right*, antigen can be loaded onto MHC class I molecules through two main pathways. In the classical pathway, endogenous or viral proteins in the cytosol are processed through the proteasome, transported into the endoplasmic reticulum through the molecule TAP (transporter associated with antigen processing), loaded onto MHC class I molecules, and then transported through the Golgi apparatus and exocytic vesicles to the cell surface for presentation. In addition, exogenous antigens that have been phagocytosed, macropinocytosed, or endocytosed can be cross-presented on MHC class I molecules by some subsets of dendritic cell. In this pathway, antigen either may be loaded in endocytic compartments (not shown) or may escape endosomes and arrive in the cytosol, where it is processed through the proteasome as usual, loaded onto MHC class I molecules, and transported to the surface. Finally, terminal degradation pathways can occur (for example, when apoptotic cells are internalized) (Acharya et al., 2016). (Nat Rev 2009 Nov; 462:26. <https://doi.org/10.1038/nature08604>).

In humans, the MHC gene cluster is located on chromosome 6 and the molecules are called the *human leukocyte antigens*. There are two major classes of MHC molecules, called *MHC class I (MHC I)* and *MHC class II (MHC II)*. Structurally, these two classes diverge, with MHC I having only one transmembrane stalk and MHC II having two. However, they both have an extracellular domain that contains an elongated groove where peptide can bind. Although the antigen-processing and delivery pathways differ, antigen presentation on these two molecules has similarities. The peptide becomes trapped in the groove of the MHC molecule, which is then transported to the surface membrane and displayed to either CD8^+ or CD4^+ T cells via MHC I or MHC II, respectively (Fig. 2.2.3.12). All nucleated cells

of the body possess MHC I molecules, whereas only professional APCs (DCs, B cells, and macrophages) express MHC II molecules. As such, it is primarily a distinct role of professional APCs to engage CD4^+ T cells to amplify immune responses (Germain, 1994).

Costimulatory Molecules

In addition to activating antigen processing and presentation functions, critically, activation of innate sensing pathways also leads to the induction of costimulatory molecules on APCs. For example, pathogen recognition via TLRs leads to expression of two important costimulatory molecules on the cell-surface proteins B7.1 (CD80) and B7.2 (CD86), which bind



• **Figure 2.2.3.12** Antigen presentation to T cells via the MHC class I and MHC class II antigen-presentation pathways. (A) Intracellular anti-gens, such as virus or tumour antigens, are processed into peptides by the immunoproteasome, which is composed of multiple subunits, including LMP2. Peptides are transported into the endoplasmic reticulum (ER), where they are loaded into the groove of the MHC class I complex, which is composed of a heavy chain and β 2-microglobulin (β 2m). MHC class I complexes present antigens on the cell surface to CD8+ T cells. Proteins in the MHC class I pathway that are encoded by genes regulated by the MHC class I transactivator NOD-, LRR- and CARD-containing 5 (NLRC5) are shown in yellow boxes. (B) Antigens from extracellular sources, such as bacterial antigens, are processed by endolysosomal enzymes into peptides. These peptides bind to the groove of the MHC class II complex by displacing the class II-associated invariant chain peptide (CLIP), which is derived from the MHC class II-associated invariant chain (Ii). HLA-DO and HLA-DM regulate the antigen-loading process. The MHC class II complex presents antigens to CD4+ T cells. Proteins in the MHC class II pathway that are encoded by genes regulated by the class II transactivator (CIITA) are shown in red boxes. *MIIC*, MHC class II compartment; *TAP*, transporter associated with antigen processing; *TCR*, T cell receptor. (Kobayashi et al., *Nature Reviews Immunology* volume 12, pages 813–820 (2012), Figure 1).

to the costimulatory coreceptors expressed on the surface of T cells. Both stimulation from antigen presentation and costimulation from APCs are necessary for T cell stimulation, and generation of adaptive immune responses (discussed later).

Chemokines and Cytokines

Chemokines and cytokines are important proteins that mediate the immune cell responses, which are produced by many cell types. For example, chemokines released by injured or infected cells (e.g., epithelial cells) are responsible for attracting innate immune cells (e.g., neutrophils) to the site of the infection. Examples of such chemokines include MIP1 α , RANTES, GRO α , GCP-2, and SDF-1 α/β (for a

comprehensive list of chemokines, refer to *Janeway's Immunobiology*, ninth edition—Appendix IV).

Cytokines also play a critical role in the development of an immune response against invading pathogens or a foreign material. Activated innate cells secrete cytokines to recruit other immune cells from the blood into the injured or infected tissues, a process known as inflammation. Cytokines are also released by epithelial cells that lead to vasodilation, and further infiltration of the cells at the site of the infection or injury (Table 2.2.3.1). Cytokines released by T-helper cells (see the section “Adaptive Immunity”) play a role in eliminating intracellular pathogens in macrophages. Ultimately, immune cell functions are broadly directed by different sets of cytokines that determine the final outcome of the immune response.

Adaptive Immunity

The secondary phase of the immune response is *adaptive* immunity, which is sometimes referred to as *specific* or *acquired* immunity. This is attributed to the fact that the response becomes adapted to specific antigens. An *antigen* is a molecule that induces a specific immune response. Antigens can be proteins, carbohydrates, lipids, as well as other smaller molecules (e.g., dinitrophenol) when coupled to a carrier. Antigens can be from a foreign source or derived from the host and referred to as a *self-antigen*. The breadth of potential antigens represents an overwhelming number of possibilities. Unlike the innate immune system, which utilizes receptors with broad specificity, the adaptive immune system is equipped to recognize an enormous diversity of antigens, primarily through cells bearing antigen receptors of a single specificity. This feature is believed to be crafted through evolution out of necessity and is also seminal for the development of long-term memory to newly encountered antigens. As such, adaptive immunity is characterized by an extraordinary repertoire of receptor molecules that arise from *somatic gene recombination* and *immunological memory*. The major components of adaptive immunity are *lymphocytes* and *soluble mediators*. *Lymphocytes* are cells with a diverse repertoire of molecules on their surfaces that are important for antigen recognition. This class of cells can be categorized as either *T or B lymphocytes* (cells). The other arm of adaptive immunity is called *humoral immunity*, derived from the Latin word *humor*, which means *fluid*. The humoral response encompasses soluble molecules that act by binding to either antigenic material or specific immune cells. These molecules include *antibodies*, or *antikorpers* as they were first coined by the German scientist Paul Ehrlich in 1891. The cellular and humoral immune systems each have an antigen recognition capacity of 10^9 – 10^{11} distinct antigenic *determinants*. With such a diverse repertoire of cell surface and soluble receptors, the distinctive beauty of the adaptive arm of the immune system is that it has the armamentarium to be highly effective in tailoring immune reactions toward a new pathogen, while reducing collateral damage to host tissue. Following recognition of an invader, specific T cells and B cells undergo a rapid expansion phase. Altogether, these processes are called *clonal selection* and *expansion*, where a few hundred cells bearing receptors for the pathogenic antigens proliferate into thousands of responding daughter cells in just a few days (Liongue et al., 2011; Shanker, 2010; Langefeld et al., 2009).

A component of adaptive immunity is *immunological memory* as a secondary but critical outcome of clonal selection and expansion. The capacity for long-lasting response capability provides protective immunity from subsequent challenge by the same pathogen (Farber et al., 2016). After responding to the pathogenic threat, most effector cells will die. However, a small fraction of the clonally expanded cells persists after antigen elimination. These cells, called *memory cells*, remain for decades after the initial antigen encounter and are able to provide a rapid response upon reexposure to the pathogenic material. This concept is the basis of vaccination, one of the most effective and impactful medical interventions devised, saving millions of lives every year.

Components of Adaptive Immunity

The primary components of the adaptive immune response are:

1. T lymphocytes (or T cells): lymphocytes that develop in the *thymus* prior to migration to peripheral or secondary lymphoid tissues (e.g., spleen, lymph nodes). They are functionally divided into two main classes: *helper T cells* and *cytotoxic T cells*. Helper T cells (*Th cells*) are specialized for the production of *cytokines*, which orchestrate the activities of other cells, including those of the innate immune system. Cytotoxic T-lymphocytes (*CTLs*) are capable of directly killing cells that are infected with viruses. T cells can also be divided based on the expression of special surface proteins that are integral for communication with APCs and result in immune signaling. The proteins typically associated with Th cells are designated as *CD4* (*CD* = *cluster of differentiation*), whereas *CD8* is expressed on CTLs. All T cells have CD3, a protein complex part of the TCR, which is critical for antigen recognition and T cell activation (Vallejo et al., 2004).
2. Cytokines of the adaptive immune system: soluble factors typically secreted by helper T cells, but which can also be produced by various innate immune cells, APCs, and B cells. These small proteins (5–20 kDa) are released by cells and have specific functional effects on their target cells that bear receptors for them. Typically, multiple cytokines synergize to influence the phenotype of a particular effector cell. Some critical cytokines of the adaptive immune system and their effects are listed in Table 2.2.3.2.
3. B lymphocytes (or B cells): similar in size and morphology to T lymphocytes, B cells are small, round cells with a large nucleus and very little cytoplasm, particularly in the inactive state. However, in contrast to T cells, B cells undergo development in the bone marrow. The prominent feature of B cells is the B cell surface receptor, which is essentially a membrane-bound antibody. Upon activation through the binding of antigen, B cells differentiate into *plasma cells* to secrete antibodies, a soluble version of the B cell receptor (BCR).
4. Antibodies: large, Y-shaped proteins (~250 kDa) secreted by plasma cells with high-affinity binding sites, which recognize three-dimensional features of specific antigens (Fig. 2.2.3.13), further described later.

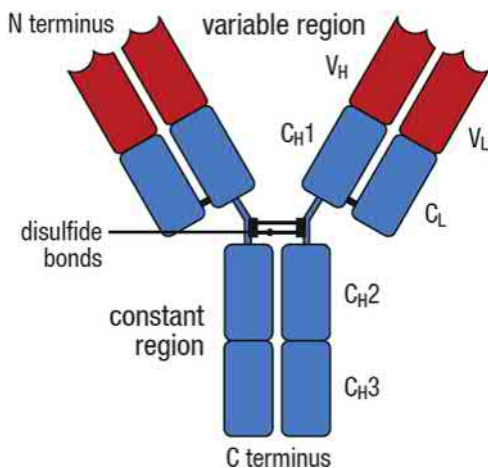
It should be noted that there is great complexity to the dynamics and kinetics of adaptive immune mediators. These effectors can work individually or collectively, synergistically or antagonistically at various phases to influence and dictate the outcome of an immune response to an antigen. For instance, in viral infections, early responses may be tilted toward the involvement of cytotoxic T cells. Later, B cells become important to produce neutralizing antibodies against extracellular viral particles to ward against the spread of infection from cells containing latent virus. Moreover, uncontrolled inflammation can lead to harmful collateral damage to host tissues, and must be kept in check. The adaptive immune system therefore has negative feedback

TABLE 2.2.3.2 The Cytokines of the Adaptive Immune System and Their Effects on Specific Immune Cells A (Travers et al., 2001)

Cytokine	T-Cell Source	Effects on					Other Tissue Cells	Effect of Gene Knockout
		B Cells	T Cells	Macrophages	Hematopoietic Cells			
Interleukin-2	Naïve, Th1, some CD8	Stimulates growth and J-chain synthesis	Growth and differentiation	–	Stimulates NK cell growth	–	Impaired Treg cell development and function	
Interferon- γ	Th1, Tfh, CTL	Differentiation IgG2a synthesis (mouse)	Inhibits Th2 and Th17 cell differentiation	Activation, 1MHC class I and class II	Activates NK cells	Antiviral 1MHC class I and class II	Susceptible to mycobacteria, some viruses	
Lymphotoxin- α (TNF- β)	Th1, some CTLs	Inhibits	Kills	Activates, induces NO production	Activates neutrophils	Kills fibroblasts and tumor cells	Absence of lymph nodes, disorganized spleen	
Interleukin-4	Th2, Tfh	Activation, growth IgG1, IgE 1MHC class II induction	Growth, survival	Promotes marginal zone macrophage activation	↑ Growth of mast cells	–	No Th2	
Interleukin-5	Th2	Mouse: differentiation IgA synthesis	–	–	↑ Eosinophil growth and differentiation	–	Reduced eosinophilia	
Interleukin-13	Th2	IgG1, IgE class switch	–	Promotes marginal zone macrophage	–	↑ Production of mucus (goblet cell)	Impaired helminth expulsion	
Interleukin-17	Th17	Promotes IgG2a, IgG2b, IgG3 (mouse)	–	–	Stimulates neutrophil recruitment (indirect)	Stimulates fibroblasts and epithelial cells to secrete chemokines	Impaired antibacterial defense	
Interleukin-22	Th17	–	–	–	–	Stimulates mucosal epithelium and skin to produce antimicrobial peptides	Impaired antibacterial defense	
Transforming growth factor- β	Treg	Inhibits growth IgA switch factor	Th17 and iTreg differentiation, inhibits Th1 and Th2	Inhibits activation	Activates neutrophils	Inhibits/stimulates cell growth	Impaired Treg cell development, multiorgan auto immunity, and death ~10 weeks	

Interleukin-10	Treg, some Th1, Th2, Th17, CTL	↑MHC class II	Inhibits Th1	Inhibits inflammatory cytokine release	Costimulates mast cell growth	–	IBD
Interleukin-3	Th1, Th2, Th17, some CTLs	–	–	–	Growth factor for progenitor hematopoietic cells (multicolony-stimulating factor)	–	–
Tumor necrosis factor- α	Th1, Th17, some Th2, some CTLs	–	–	Activates, induces NO production	–	Activates microvascular endothelium	Susceptibility to Gram-negative sepsis
Granulocyte-macrophage colony-stimulating factor	Th1, Th17, some Th2, some CTLs	Differentiation	Inhibits growth?	Activation, differentiation to dendritic cells	↑ Production of granulocytes and macrophages (myelopoiesis) and dendritic cells	–	–

CTLs, Cytotoxic T lymphocytes; *IBD*, inflammatory bowel disease; *NO*, nitric oxide; *MHC*, major histocompatibility complex; *TNF- β* , tumor necrosis factor beta; *Treg*, regulatory T cells. Janeway's Immunobiology, ninth edition; [Chapter 9](#), Figure 9.40.



• **Figure 2.2.3.13** General antibody structure and effector functions. Antibodies most often adopt a “Y”-shaped structure composed of two light chains and two heavy chains. The N-termini are the antigen binding fragments (Fab) and are contained in the variable regions that allow the necessary diversity. Fab regions recognize three-dimensional features on specific antigens. The C-termini are constant for any particular immunoglobulin isotype (called the Fc fragment) (Travers et al., 2001). (Janeway’s Immunobiology, ninth edition; Chapter 4, Figure 4.1c).

mechanisms to shut down inflammatory responses not long after their initiation. To a large extent, this inhibitory responsibility falls on a subset of helper T cells that produce biochemical messengers with regulatory effects.

Humoral Immunity

Soluble effectors of immunity found in bodily fluids, including antibodies, are collectively known as humoral immunity. Antibodies are a class of proteins known as *immunoglobulins* (Igs) that accounts for a significant portion of plasma proteins. In general, antibodies are “Y”-shaped molecules composed of four disulfide-linked polypeptide chains: two smaller (~25 kDa) light chains and two larger (~50 kDa) heavy chains (Fig. 2.2.3.13). The heavy chains in a given antibody are identical as are the light chains. The N-termini of a light and heavy chain combine to the *antigen-binding site*, which recognizes three-dimensional features on pathogens. Each antibody contains two identical antigen-binding sites that can result in pathogens with multiple antigenic regions such as viral surfaces to become cross-linked by multiple antibodies. The N-termini of different antibodies contain vast sequence variability and are the source of the immense antigen-binding capacity of the total antibody repertoire.

On the other hand, the C-termini of the polypeptide chains have relatively little sequence diversity and this portion of the two larger chains makes up the “body” of the Ig or the constant region, or the fragment crystallizable (Fc) region. This stem of the antibody has a critical role in interacting with other effector molecules and cells (Padlan, 1994). There are five different classes of Igs, based upon the variability in sequence, structure, and properties of the Fc region. These five major isotypes are IgM, IgD, IgG, IgA,

and IgE; IgG has five subtypes and IgA has two (Salfeld, 2007; Brerski and Georgiou, 2016). All the major isotypes are soluble proteins with the exception of IgD, which is only found in the membrane-bound form as the antigen receptor for B cells and is critical for B cell activation and differentiation. The constant region of the soluble antibody determines its engagement with effector mechanisms that help to dispose of antibody-bound antigen. The structure of the antibody is thus well suited to its function to protect against pathogens or their products. Antibodies accomplish this goal through three primary effector modalities: *neutralization*, *opsonization*, and *complement activation* (discussed in the section “Effector Pathways in Adaptive Immunity”).

Cell-Mediated Immunity

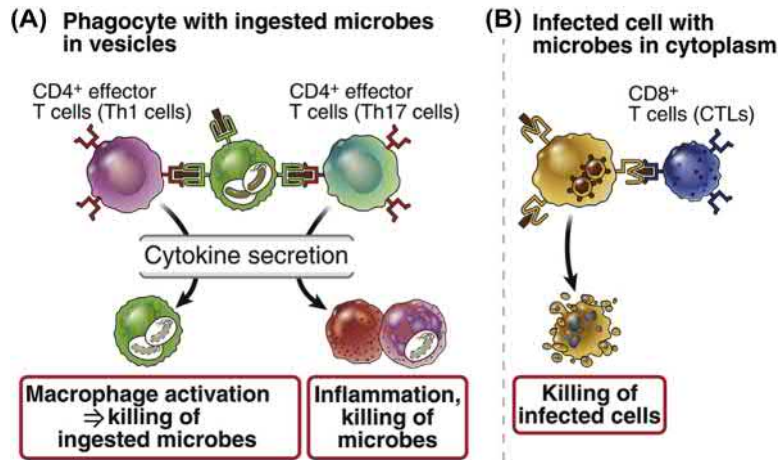
Antibodies are efficient at detecting and inducing removal of extracellular pathogenic material. Antibodies, however, lack access to intracellularly localized foreign agents (e.g., viruses and mycobacteria). In this case, other forms of immunity must be engaged. Cell-mediated immune responses, driven by T cells, are the primary catalysts behind mechanisms to rid the host of intracellular pathogens. Recall that there are two major functional classes of T lymphocytes: (1) cytotoxic T cells (CTLs) and (2) helper T cells (Sallusto et al., 1999).

Cytotoxic T Cells

Of the two major T cell classes, CTLs are the more direct in executing their antipathogen functions. These cells primarily express the CD8 coreceptor on their surfaces, and are critical for responding to cells that have been infected by viruses (Fig. 2.2.3.14). They recognize viral antigens on the surface of infected host cells presented via the MHC-I complex, which is found on all nucleated cells of the body. These CTLs bind to and directly kill virus-infected cells to control the infection through a number of effector mechanisms, including membrane pore formation, release of degradative enzymes, and apoptosis. Cytotoxic T cells can also secrete inflammatory cytokines (e.g., IFN- γ), which have direct and indirect actions that help to control the viral infection. For instance, IFN- γ inhibits viral replication directly while also promoting the expression of MHC-I and proteins important for the formation of the immunoproteasome, a modified form of the proteasome that efficiently generates small antigenic peptides to be loaded onto MHC-I molecules.

Helper T Cells

Helper T cells express and utilize the CD4 coreceptor. As the name suggests, the effector actions of these cells are indirect and often carried out by the cytokines they secrete (Fig. 2.2.3.14), serving to activate other immune cells. Helper T lymphocytes are integral to the control of bacterial infections, including intracellular mycobacteria that can proliferate in intracellular vacuoles of mammalian cells (Abbas et al., 1996). For example, *Mycobacterium tuberculosis* is the causative agent



• **Figure 2.2.3.14** T cell-mediated immunity. (A) CD8 T cells recruited to the site of infection/inflammation express surface molecules that are directly cytotoxic to infected target cells by inducing apoptosis and can also exert antiviral activity by secreting cytokines. (B) CD4 T cells are the earliest lymphocytes activated during an adaptive immune response. CD4 T cells are able to affect the behavior of other immune cells (thereby acting as “helpers”) by secreting cytokines, for example, in the case of a Th1 or Th17 phenotype, that promote macrophage activation and antimicrobial activity, as well as promoting local inflammation in general (Abbas and Pober, 2000). CTLs, Cytotoxic T lymphocytes. (Adapted from Abbas et al., Cellular and Molecular Immunology, seventh edition).

of tuberculosis. This pathogen grows in the macrophage intracellular vesicles where microorganisms are typically digested due to the caustic environment and the presence of enzymes and antimicrobial proteins. Such intracellular bacteria are able to flourish by inhibiting the fusion of these phagocytic vesicles with lysosomes containing the degradative elements. Controlling these intracellular pathogens requires the “help” of CD4 T cells, specifically the *Th1* subset, which induce the formation of the phagolysosome in macrophages through the release of activating cytokines (e.g., IFN- γ). Th1 cells also enhance macrophage functions such as respiratory burst and release of cytokines that boost local inflammation (e.g., TNF- α).

The *Tfh* subset of CD4 T cells, found in specialized regions in lymph nodes called germinal centers, is important for the activation of B cells, and therefore well suited for immunity to extracellular pathogens. While activation and differentiation of B cells into antibody-secreting cells is stimulated by antigen binding to the BCR, this process is greatly improved by the action of *Tfh* cells. Notably, however, Th1 and Th2 cells can also contribute to B cell activation, albeit to a lesser extent. The Th2 response is also important for responses to larger extracellular pathogens (e.g., hookworms) and a special class of polymeric antigens called allergens (e.g., tropomyosin from shellfish). Th2 cells secrete a particular host of cytokines, primarily IL-4, -5, -6, -10, and -13, which give rise to an array of actions in other cells, including increased antibody production from B cells, eosinophil activation, and inhibition of several macrophage functions, which provides a phagocyte-independent protective response (Zhu et al., 2010).

Another important helper T cell subset is the Th17 (Ouyang et al., 2008), which plays a critical role in responses to extracellular bacteria and is also involved in the induction of tissue inflammation by producing IL-17. The IL-17 cytokine induces

numerous immune and nonimmune tissue-resident cell types to secrete many other inflammatory cytokines. Overproduction of IL-17 has emerged as a particularly significant proinflammatory factor linked to pathological tissue destruction associated with many chronic immune-inflammatory and autoimmune diseases, including rheumatoid arthritis (RA), multiple sclerosis, inflammatory bowel disease, and inflammatory skin disorders. Th17 cells are typically generated in the context of IL-23 or transforming growth factor (TGF)- β 1 and IL-6 or IL-1, and Th17 cells are characterized by production of a specific cluster of cytokines, notably IL-17, IL-21, IL-22, and IL-26.

Having a shared lineage with Th17 cells are the *antiinflammatory, regulatory T cells (Tregs)*, which are critical for controlling undesired inflammatory reactions such as those observed in autoimmune diseases like RA. This subset of CD4 T cells is integral for maintenance of peripheral tolerance by actively suppressing antigen-specific responses as well as localized “bystander suppression,” typically through the secretion of the antiinflammatory cytokines TGF- β 1 and IL-10. Other modes of action by these cells include contact-mediated apoptosis, inhibition of DC maturation, and metabolic disruption, where Treg metabolism (e.g., ATP to AMP catabolism) results in the deprivation of critical factors for neighboring effector T cell proliferation and survival (e.g., IL-2). This CD4 subset can be further subdivided into three major classes: classical regulatory T cells (Tregs; FOXP3 and CD25 expression), Th3 cells (denoted by IL-4, IL-10, and TGF- β 1 production; localized in mucosal areas and responds to benign foreign antigen), and Tr1 cells (denoted by LAG-3 expression and IL-10 secretion) (Sakaguchi & et al., 2001; Sakaguchi, 2004; Weiner, 2001; Weiner et al., 2011). Induction or expansion of these regulatory T cell classes can lead to tolerance and reversal of autoimmune inflammation.

Recognition in Adaptive Immunity

A key principle in adaptive immunity is recognition of foreign material prior to activation and actuation of responses. To initiate an appropriate program of responses, proper recognition is critical to discern self from nonself tissue. It is believed that B cells, antibodies, and T cells can recognize up to 10^{11} different antigen epitopes and this receptor diversity is enabled by genetic processes, including somatic mutation and gene rearrangement (beyond the scope of this discussion). However, the basic tenets of how these immune elements recognize antigens is critical to our understanding of the interplay between the immune system and materials and is further discussed here.

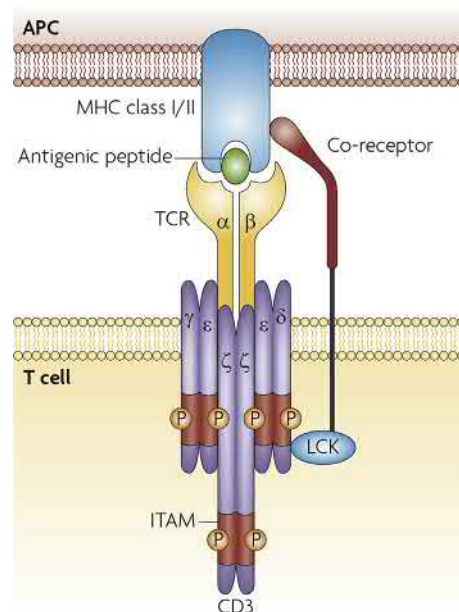
B Cell and Antibody Recognition

As already noted, antibodies, also known as Igs, are the antigen recognition apparatus of B cells. Antibodies are secreted by plasma cells, which are terminally differentiated B cells. Antibodies have a vast range of possible antigen specificities, with each individual B cell, or “clone,” producing antibodies of a single specificity. Moreover, each B cell has a single variant of membrane-bound Ig that serves as a receptor for antigen and is called the BCR. Immobilized or solubilized, these Igs can bind to specific antigens. The antibody and its respective antigen form a complex primarily based on their structural complementarity. In other words, the primary, secondary, and tertiary aspects of protein structures of both the antibody and antigen determine their association. The portion of the antigenic molecule that interacts with the antibody is called the epitope (determinant), and a single antigen can have multiple epitopes. This property can sometimes activate B cells without help from CD4 T cells, as multiple epitopes can induce clustering and cross-linking of BCRs and lead to the production of IgM. Certain determinants may be internally folded and initially inaccessible to the Ig. Exposure of these hidden epitopes to antibodies can be subsequently realized via denaturation or enzymatic degradation at sites of inflammation (Treanor, 2012).

T Cell Recognition

In contrast to B cells and antibodies, T cells recognize only small antigenic regions that are displayed on the surfaces of the body's own cells. These antigens can be derived from extracellular (e.g., bacteria), intracellular (e.g., viruses), or even cellular (e.g., senescent cytosolic protein) sources. The TCR can only interact with proteolytically degraded peptide fragments (“processed antigen”) presented in the context of being bound to the *major histocompatibility molecules* (MHC-I or MHC-II) displayed on the surface of APCs (both professional and nonprofessional), as illustrated in Fig. 2.2.3.15.

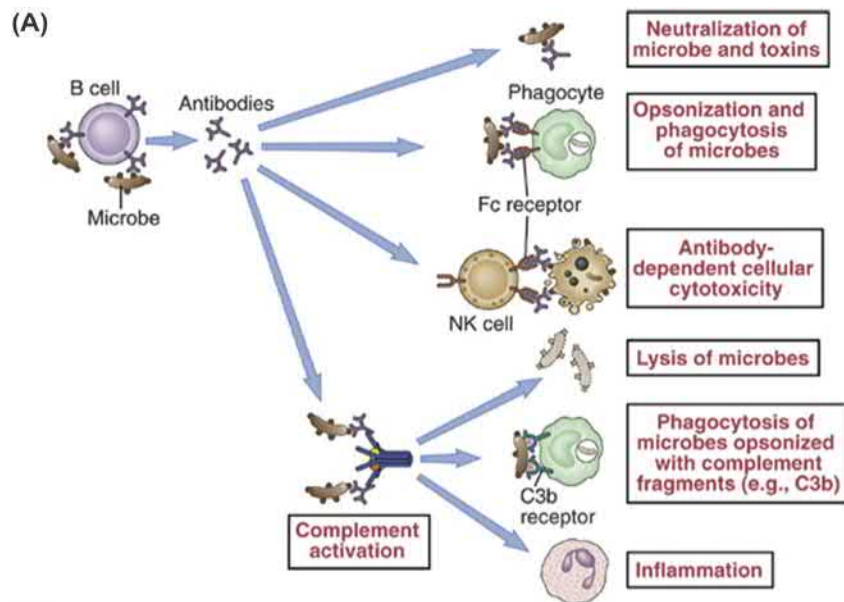
There is significant divergence on which classes of T cells are able to interact with the two different MHC molecules. The MHC I molecule presents peptide to CD8 T cells only,



• **Figure 2.2.3.15** The T cell receptor (TCR) interacts with peptide loaded onto the major histocompatibility complex (MHC). The coreceptor (CD4 or CD8) stabilizes this interaction by bringing the kinase LCK in the proximity of the TCR–CD3 complex. LCK can then phosphorylate the CD3-associated immunoreceptor tyrosine-based activation motifs (ITAMs) and engender intracellular signaling that leads to the generation of inflammatory mediators by the T cell (Kroczek et al., 2004). (Gascoigne, *Nature Reviews Immunology* 8, 895–900 (2008), Figure 1).

where the peptide is primarily cytosol derived. As such, any cell infected with virus can be detected and killed by CD8 T cells through their interaction with MHC I molecules. MHC I, along with the machinery for peptide processing and loading, is expressed in all nucleated cells of the body, and thus serves as a primary mechanism to defend against viral infection. In contrast, MHC II molecules are only expressed on the surfaces of “professional” APCs (discussed earlier): DCs, B cells, and macrophages. In the MHC II loading pathway, peptide typically originates from extracellular entities, such as bacteria that have been phagocytosed. *MHC restriction* also applies to this pathway in that only CD4 T cells can interact with MHC II molecules, including Th1, Th2, Th17, and regulatory T cells. It should be noted that there are instances where the MHC restriction rules have exceptions and extracellularly derived antigen is displayed on MHC I complexes, referred to as *cross-presentation* (Li et al., 2008; Kasturi and Pulendran, 2008).

Irrespective of the mechanism of communication, peptide–MHC complexation with T cells leads to *activation*. On T cells, the critical recognition molecule is the TCR, which is a multiprotein complex that spans the T cell membrane, and in which coreceptors (e.g., CD4) form an integral part. Furthermore, ligation of these coreceptor molecules to MHC is required for clonal expansion and differentiation. Antigen binding leads in conformational changes in the TCR complex that triggers intracellular signaling cascades and results in selective gene transcription (Zhong et al., 2011; Rappazzo and Birnbaum, 2017). Within this



• **Figure 2.2.3.16** Effector mechanisms of antibodies. (A) Antibodies can neutralize pathogens or toxins preventing infection of host cells. Antibodies can recruit other effector molecules such as complement, or activate effector cells via their fragment crystallizable (Fc) portion. Binding of the Fc region of an antibody to a specific Fc receptor expressed by innate cells can facilitate pathogen internalization and destruction by phagocytes (a process referred to as “opsonization”) (Davies et al., 2013). (B) A list of antibody isotype and their function is shown. *NK*, Natural killer. (Adapted from Abbas and Lichtman: Basic Immunology, third edition, Copyright © 2010 by Saunders, an imprint of Elsevier, Inc. All rights reserved).

molecular communication bridge between APC and T cell (or immune synapse), other molecules also play a role in enhancing intracellular signaling networks that lead to complete activation. These molecules are called *costimulators* (e.g., CD28 on T cells binding to CD86 on APCs). In their absence, there is insufficient stimulation of T cells resulting in a state of hyporesponsiveness to the antigen or *anergy* (Kroczek et al., 2004; McAdam et al., 1998; Suzuki et al., 1995). The ligation of CD28 on T cells by B7 molecules (e.g., CD86, CD80) is necessary for optimal clonal expansion as it induces the expression of IL-2, critical for T cell growth and division, and CD25 (the high-affinity receptor for IL-2). Other critical APC–T cell costimulatory complexes include: (1) CD70–CD27; (2) CD40–CD40L, and (3) OX40L–OX40. These costimulatory complexes all

enhance clonal expansion and differentiation. Finally, adhesion molecules (e.g., leukocyte functional antigen-1 and intracellular adhesion molecule-2) also play a role in mediating initial interactions between the APC and T cell, and stabilize those interactions if an antigen match is made.

Effector Pathways in Adaptive Immunity

From the discussion thus far, it should be evident that the adaptive immune system is a major effector wing of the immune system, tailored to specific antigens and that different elements are activated based on the nature of the threat to the host. Fig. 2.2.3.16 summarizes the mechanisms engaged by antibodies, as a B cell effector molecule, to respond to extracellular pathogens. These include *neutralization*,

opsonization, and *complement activation*. Neutralization is the case where antibodies bind to pathogenic material, restricting the potential interaction of these foreign agents with host cells and thereby limiting pathogenicity. This functionality of antibodies is particularly important for defense against viruses and bacterial toxins, and is a major feature elicited by most vaccines. Opsonization is the case where antibodies coating pathogens initiate phagocytosis by phagocytic cells bearing Fc receptors to bind the constant region of the antibody (Joller et al., 2011). The third major function of antibodies is complement activation. While complement activation can also occur independently of antibody involvement, the pathway is much more efficient when the antibody constant region acts as the platform for complement activation on the pathogen surface. Together, antibodies, complement proteins, and antimicrobial peptides comprise the major components of humoral immunity.

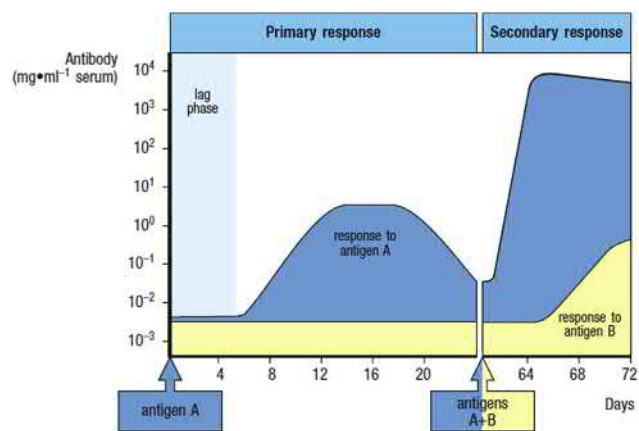
The fourth effector mechanism of antibodies depicted in this figure is *antibody-dependent cell-mediated cytotoxicity (ADCC)*, which is triggered when the Fc portion of antibodies bound to pathogen interacts with Fc receptors on NK cells. NK cell killing of the Ig-coated pathogen is executed through mechanisms similar to those used by CTLs, involving perforin-based membrane pore formation and secretion of proteolytic enzymes. ADCC is important in controlling viral infection, as well as tumor cell proliferation (Wang et al., 2015). Finally, it has been recently demonstrated that antibody structure, pharmacokinetics, affinity, and function can be influenced by posttranslational modification of *N*-glycosylation motifs in the constant and variable regions of some antibodies. For instance, lower glycosylation of the constant region, which interacts with Fc receptors, is thought to enhance ADCC.

Effector measures for T cells, on the other hand, include the cytotoxic mechanisms of CD8 CTLs and the indirect chemokine/cytokine-based actions of CD4 helper T cells that enhance the efficacy of other immune system elements to clear pathogenic material. These pathways were outlined in the sections “Cytotoxic T Cells” and “Helper T Cells” and illustrated in Fig. 2.2.3.14.

Immunological Memory

The final distinguishing facet of the adaptive immune system is its ability to generate immunological memory, which is critical in protecting mammalian hosts from repeated exposure to an infectious agent. This concept is the core principle of vaccines, which have eradicated a number of infectious diseases (e.g., smallpox) over the past two centuries. As such, vaccinology is one of the most critical fields in human health, and biomaterial scientists are now working in concert with immunologists to devise new and effective ways to address limitations in current vaccines to generate long-term protective immunity.

Immunological memory is a cell-based phenomenon and a result of the clonal selection and expansion that occurs when a naïve T cell interacts with its cognate antigen (as presented bound to MHC molecules). A small fraction of the lymphocytes

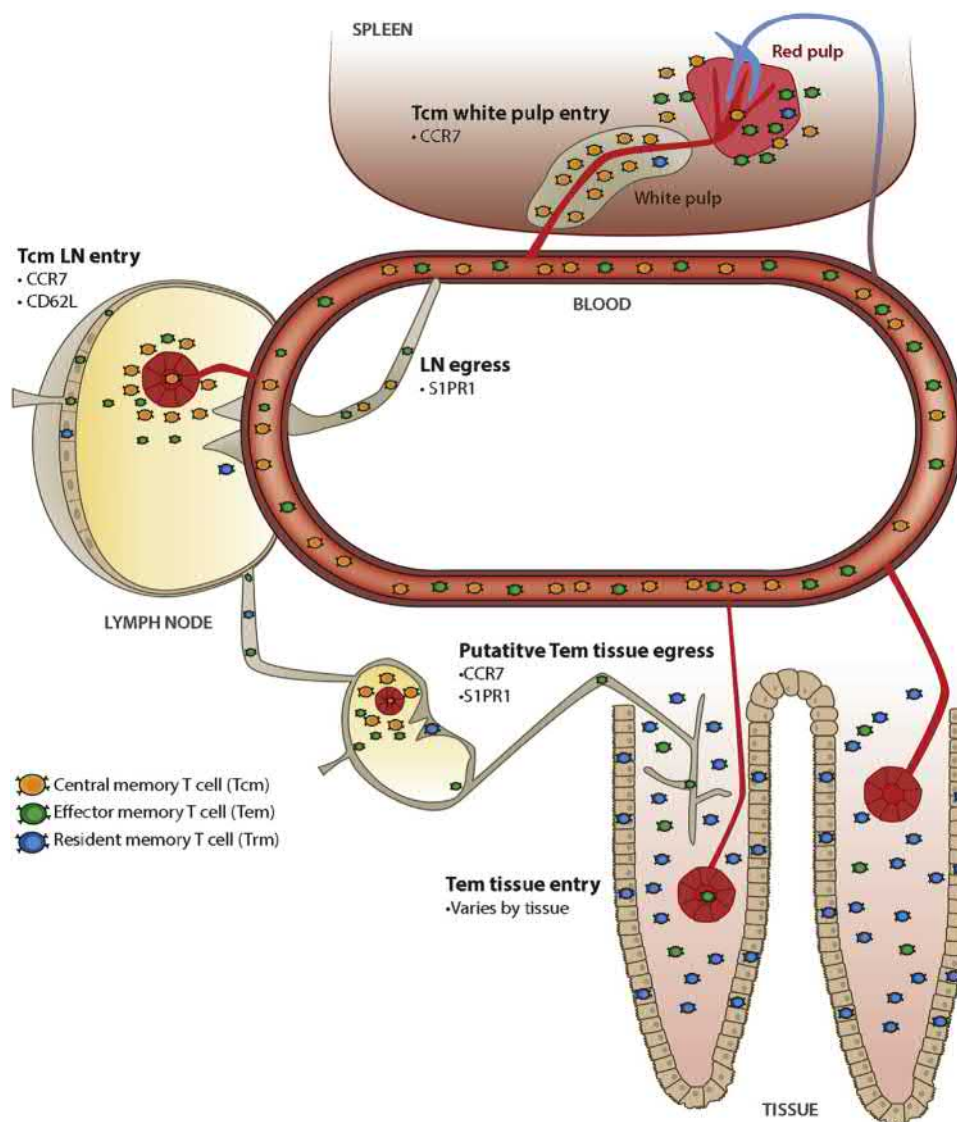


• **Figure 2.2.3.17** Immunological memory. A typical time course of production of immunoglobulins in response to antigen. When an animal is injected with antigen A, antibody is produced beginning around day 7 and peaking at about 14 days before declining. If the animal is reinjected 28 days later with the same antigen, there is a rapid and elevated production of immunoglobulin, indicating a secondary response (Travers et al., 2001). (Janeway's Immunobiology, ninth edition; Chapter 1, Figure 1.25).

generated by this event do not die after the pathogenic threat has been cleared. Instead, they persist for the lifetime of the host and can be reactivated much more quickly than naïve lymphocytes. Immunological memory is showcased by the antibody response to *primary* and *secondary (booster) immunization*, as illustrated in Fig. 2.2.3.17. The secondary antibody response is significantly quicker and a markedly higher titer is engendered (Ratajczak et al., 2018; Sprent, 2002).

In the secondary exposure to an antigen, memory B cells that had previously developed a high affinity for the antigen (undergone isotype switching and somatic mutation in germinal centers located in lymph nodes) now comprise a significant portion of the immune response. These cells are able to bind antigen with high avidity and respond rapidly via interaction with helper T cells to secrete high affinity IgG and IgA antibodies. This example illustrates the effector antibody response, but the same principles of memory generation and heightened and quicker responses hold true for T cells as well.

In pathogen reexposure events, memory T cells are also among the first responders. Memory T cells can be CD4⁺ or CD8⁺, and as such are typically divided into three major subsets: (1) central memory T cells—highly proliferative but poor effectors; (2) effector memory T cells—at-the-ready effectors, expressing the receptor S1PR1, enabling egress from lymph; and (3) tissue-resident memory T cells, which reside long term in peripheral tissues. The major differences among these subsets are centered on their migration patterns (Fig. 2.2.3.18). For instance, central memory T cells, expressing lymph-homing receptors CD62L as well as CCR7, exist primarily in secondary lymphoid tissues and in circulation. Effector memory T cells lack lymph node-homing receptor CD62L and express the receptor S1PR1, which drives egress from lymph, and are thus entirely found in circulation and peripheral tissues. Tissue-resident T cells have relatively low migratory capacity and exist in epithelial tissues without recirculating.

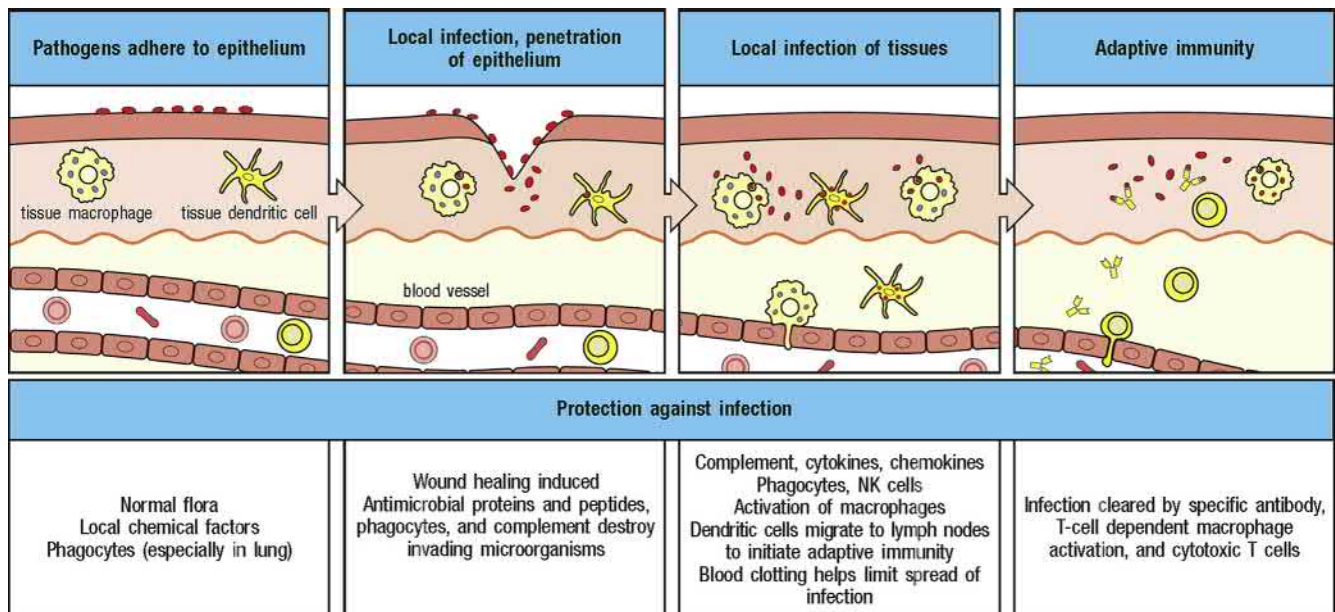


• **Figure 2.2.3.18** Memory T cell migration properties. Memory T cells can be classified into subsets based on their migration patterns. Central memory T (Tcm) cells recirculate through blood and constitutively migrate through lymph nodes (LNs) using high endothelial venules. Effector memory T (Tem) cells are also found in blood and exhibit diverse migration properties, but they do not enter uninflamed lymph nodes via high endothelial venules. Resident memory T (Trm) cells do not recirculate and remain local occupants of tissues during the steady state (Masopust D, 2019). Homing receptors: C–C chemokine receptor type 7 (CCR7) recognizes chemokines CCL19 and CCL21 produced in the lymph node; CD62L, or L-selectin, acts as a homing receptor for lymphocytes to enter secondary lymphoid tissues via recognizing ligands on high endothelial venules; sphingosine-1-phosphate receptor 1 (S1PR1) recognizes sphingosine-1-phosphate found in blood and is needed for the egress of immune cells from the lymphoid organs (Masopust D, 2019). (Figure 1 from *Annu. Rev. Immunol.* 2019. 37:521–546).

Overview of the Immune Response to Pathogens

Innate immunity is the first set of mechanisms deployed against pathogens. This immune response is rapid, occurring within minutes to hours and involves a number of effectors, including soluble proteins and phagocytes. The second line of defense, adaptive immunity, is prompted by intricate interplay between APCs, T cells, and B cells. Adaptive immune responses are highly coordinated based on the immune compartment of intercepted pathogenic

material, either extracellular or cytosolic (intracellular) (Figs. 2.2.3.11 and 2.2.3.12). Extracellular pathogens may be eliminated quickly by the innate immune system, largely through phagocytic and complement effector mechanisms. In the case of prolonged infection, support from helper T cell responses (Th2 type) and B cell activation and differentiation results in the generation of pathogen-specific antibodies that can bind, neutralize, and opsonize extracellular pathogens. These effector mechanisms greatly aid the innate immune system in removing extracellular pathogens and their secreted toxins. Helper T cells also play a significant



• **Figure 2.2.3.19** Infection and the immune response directed toward it can be divided into a series of stages. These stages are illustrated for a pathogen entering the wound in the skin. Both innate and adaptive immune cells are required to act in concert to eliminate the pathogen (Travers et al., 2001). NK, Natural killer. (Janeway's Immunobiology ninth edition, Figure 2.8).

role by secreting cytokines that recruit first responder cells and boost their phagocytic ability by provoking phagosome–lysosome fusion and production and release of reactive oxygen species and nitric oxide. Secretion of proinflammatory cytokines (e.g., TNF- α) by innate and adaptive immune cells is also critical for inducing local inflammatory responses that minimize the spread of pathogens to other areas in the host.

In the case where pathogens are present in cytosolic compartments, then antibodies, unable to traverse the plasma membrane, are ineffective. A different set of defensive measures are therefore employed to eliminate intracellular pathogens, including the activation of NK cells and CTLs. CD8 CTLs are effective saboteurs of virus-infected host cells and work in a coordinated fashion with helper T cell-activated macrophages to clear viral infections. Cytokines are also critical to this response, with IFN- γ perhaps the most important soluble mediator in responding to virally infected cells. IFN- β augments CTL activation, production of important molecules for immune cell recognition, interaction and activation (e.g., MHC-I, CD40), and formation of the immunoproteasome, which boosts presentation of viral antigens. Illustrated in Fig. 2.2.3.19 are representative stages and coordination between numerous components of the immune response toward infection.

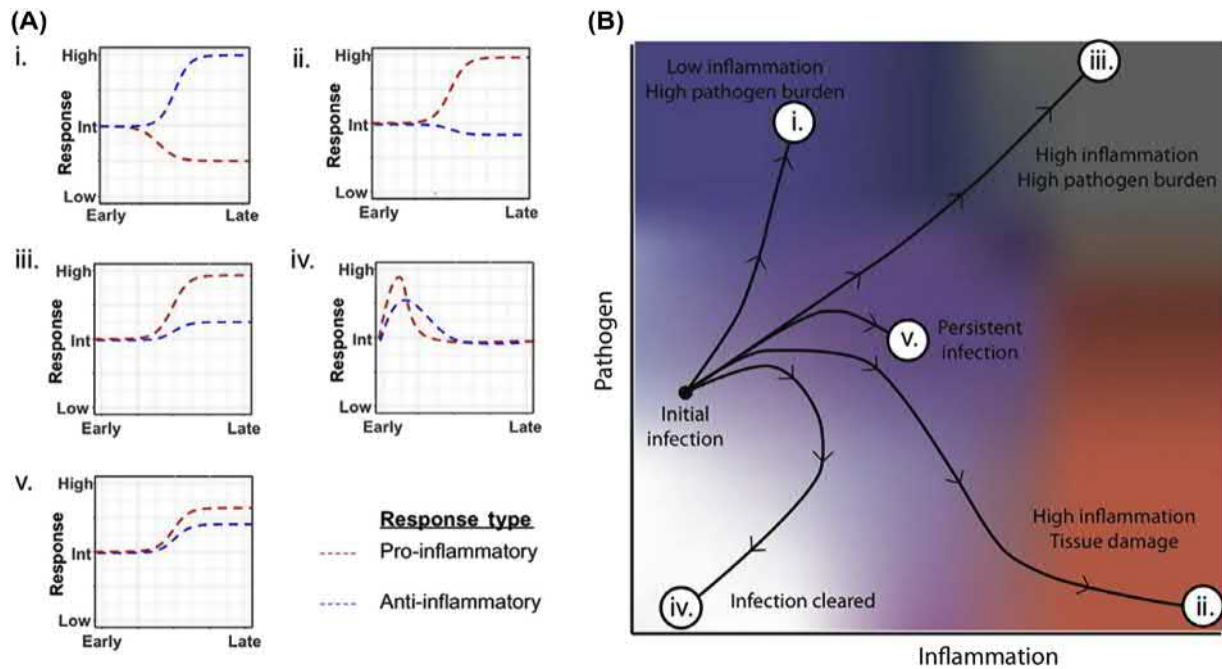
Overview of Immune Regulation and Tolerance

From the discussion so far, it is clear that the mammalian immune system has an impressive array of weapons to defend against the constant microbial threats from the external environment. However, these same protective

mechanisms can also become destructive against the host. It is imperative for an immune response to be commensurate to the danger. The inflammatory response includes indiscriminate degradative components damaging to host tissue, resulting in unnecessary collateral damage if left unchecked. The immune system therefore has built-in regulatory safeguards to turn inflammation off. For example, the same stimuli-triggering inflammatory signaling pathways often also initiate antiinflammatory signaling responses. These may be tuned to become fully engaged after an appropriate delay, and with complex dynamic interplay between interlinked pathways with feedback responses, the balance of which determines the outcome of pathogen clearance and host tissue sparing and healing responses, as illustrated in Fig. 2.2.3.20 (Cicchese et al., 2018). Most immune cell types display at least some regulatory activities in certain circumstances (Immunity in the tissues, 2013). Other immune regulatory mechanisms facilitate maintenance of healthy tissue homeostasis, such as the antiinflammatory clearance of apoptotic cells by macrophages, maintenance of stem cell populations, and promotion of wound healing by Tregs (Ali et al., 2017; Burzyn et al., 2013; Davies et al., 2013).

In some cases, the immune system is persistently destructive against host tissues in a targeted, self-antigen (autoantigen)-specific manner, described as a loss of *immune tolerance* and leading to *autoimmune disease*. Autoimmune diseases are characterized by chronic, dysregulated immune reactions and vary in their severity, tissue distribution, and mechanisms of tissue damage. Some common autoimmune diseases are listed in Table 2.2.3.3. The incidence of autoimmune diseases is below 5% in the developed world, although it is on the rise.

Mechanisms of tolerance inherent in the development and maintenance of the immune system aim to ward against



• **Figure 2.2.3.20** Dynamics of pro- and anti-inflammatory immune responses steer disease progression along various trajectories. Schematic of relative pro- and anti-inflammatory responses to a pathogen over time corresponding to various host outcomes (A). Schematic of disease trajectories corresponding to qualitative ratios of pro- and anti-inflammatory responses (B). The outcomes are (i) high pathogen burden (blue); (ii) severe tissue damage (red); (iii) high pathogen burden along with a large amount of tissue damage (gray); (iv) a cleared infection and return to base levels of inflammation (white); and (v) a dynamically balanced pro- and anti-inflammatory response to control pathogen growth and limit host pathology (purple) (Zaveri & et al., 2017). (Adapted from *Immunol. Rev.* (2018) September; 285(1): 147–167. <https://doi.org/10.1111/imr.12671>, Figure 1).

such attacks on self. The generation of autoimmunity can be partially attributed to the same mechanisms that are used to create the diversity of the adaptive immune system—somatic gene rearrangement. Pathogen exposure is also thought to be important, as autoimmune disease is prevented in various experimental models by infection with different bacteria, viruses, and parasites. During the development of the adaptive immune system, emergent lymphocytes may have receptors capable of binding to antigens from self-proteins. Such lymphocytes are typically removed from the repertoire or restrained by a number of mechanisms, collectively referred to as immune tolerance. Immune tolerance describes an inability to mount an inflammatory response against a self-antigen. This lack of response is vital for maintenance of immune homeostasis and is an accomplished mechanism that can be grouped into two categories: (1) *central tolerance*, which occurs during the development of adaptive immune cells from stem cells, and (2) *peripheral tolerance*, a continuous process of immune regulation throughout the host's lifetime.

Central immune tolerance is defined by the negative selection of T and B cells that have a high affinity to self-epitopes during lymphocyte development. Newly formed lymphocytes are quite sensitive to strong signaling through their membrane-bound antigen receptors and undergo cell death or inactivation upon strong recognition, culling

self-reactive clones. For T cells, this occurs in the thymus, and for B cells, in the bone marrow. Peripheral tolerance, on the other hand, is induced in lymphocytes that have already left the primary organs and utilize mechanisms such as anergy, apoptosis, ignorance, and receptor editing in peripheral tissue to mitigate autoimmune damage (Halverson et al., 2004). Anergy is defined as a state of functional inactivity. It arises due to incomplete T cell stimulation by APCs, where antigen may be presented but there is a lack of costimulation. This scenario can also result in deletion of engaged T cells through apoptosis, a process in which cells undergo programmed cell death and can also be induced through Fas/Fas ligand interactions found between T cells and thymic epithelial cells. Some self-reactive lymphocytes simply do not have access to their cognate antigen because it is in an immunologically privileged site (e.g., testis), and are termed ignorant. Such ignorant lymphocytes normally go unstimulated and can eventually undergo apoptosis. Persistence, however, can cause autoimmunity if antigen is released from privileged tissues undergoing damage. A recently discovered mechanism of tolerance is receptor editing where self-reactive receptors from the B cell repertoire are purged, by the same genetic process that drives affinity maturation, and replaced with inoffensive receptors.

A special subset of T cells, Tregs, exploit multiple tolerance mechanisms. Tregs are the immune system workhorse

TABLE 2.2.3.3 Autoimmune Diseases and Their Known Autoantigens (Acharya et al., 2017)

Organ-Specific Diseases		Nonorgan-Specific Diseases	
Disease	Antigen(s)	Disease	Antigen(s)
Addison's disease	Adrenal cortical cells ^a	Ankylosing spondylitis	Vertebral
Autoimmune hemolytic anemia	RBC membrane antigens	Chronic active hepatitis	Nuclei, DNA
Graves' disease	TSH receptor	Multiple sclerosis	Brain/myelin basic protein
Guillain-Barré syndrome	Peripheral nerves (gangliosides)	Rheumatoid arthritis	IgG (rheumatoid factor) connective tissues
Hashimoto's thyroiditis	Thyroid peroxidase thyroglobulin/T4	Scleroderma	Nuclei, elastin, nucleoli centromeres, topoisomerase 1
Insulin-dependent diabetes mellitus	β cells in the pancreas (GAD), tyrosine phosphatase	Sjögren's syndrome	Exocrine glands, kidney, liver, thyroid
Pemphigus	Desmosomal antigens in keratinocytes	Systemic lupus erythematosus	Double-stranded DNA, nuclear antigens
Pernicious anemia	Intrinsic factor	Wegener's granulomatosis	Proteinase 3
Polymyositis	Muscle (histidine tRNA synthetase)	Celiac disease	Small intestine
Primary biliary cirrhosis	Pyruvate dehydrogenase		
Several Organs Affected			
Goodpasture syndrome	Basement membrane of kidney and lung (type IV collagen)		
Polyendocrine	Multiple endocrine organs (hepatic cytochrome p450; intestinal tryptophan hydroxylase)		

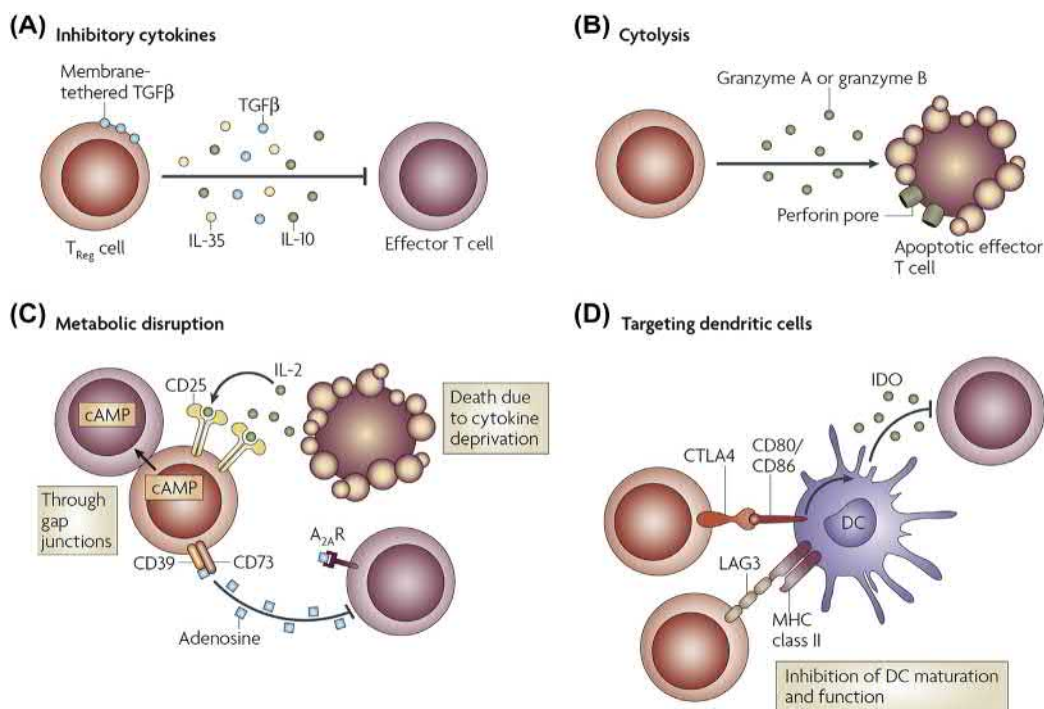
GAD, Glutamic acid decarboxylase; RBC, red blood cell; TSH, thyroid-stimulating hormone.
^aAdrenocorticotrophic hormone receptor; 17α- and 21-hydroxylases.
 Adapted from Instant notes in Immunology; Garland Science, 2011; Table L2.3.

for the maintenance of peripheral tolerance, keeping auto-reactive cells in check to avoid autoimmunity. Incidentally, Tregs arise during the negative selection process of central tolerance from TCR binding, which is too weak to provoke deletion but at an affinity too great for positive selection. Furthermore, Tregs can be induced from naïve T cells that recognize their antigen in the presence of certain antiinflammatory cytokines (e.g., TGF-β1). Tregs take a number of functionally distinct forms, including CD4⁺ CD25⁺ FoxP3-expressing Tregs and IL-10-producing Type 1 regulatory cells. The plurality of Treg types is representative of the multiplicity of mechanisms employed by these cells to inhibit autoimmune reactions (Fig. 2.2.3.21). These mechanisms range from modulation of APC stimulatory capacity, to inhibition of activation and cytolysis of naïve T cells, as well as metabolic disruption where Tregs “starve” effector cells of key nutrients or cytokines needed for survival. Moreover, activated Tregs secrete anti-inflammatory cytokines that act in an autocrine as well

as a paracrine manner on nearby bystander cells. In this way, all autoreactive cells, including those without the specific antigenicity of the secreting Treg, may be locally suppressed. This phenomenon can be referred to as *infectious tolerance* to a growing pool of antigens. These multiple mechanisms of regulation may act and in a complementary or synergistic manner.

Intersection of Biomaterials and Immunology

Whether or not the biomaterial scientist intends for a material or device to engage the immune system, it is clear that interactions with major components of the immune system are an inescapable reality for the vast majority of applications. This is true even in the case of implantation of what may be considered an inert synthetic material, as illustrated in Fig. 2.2.3.22. For example, implanted biomaterial surfaces induce adsorption



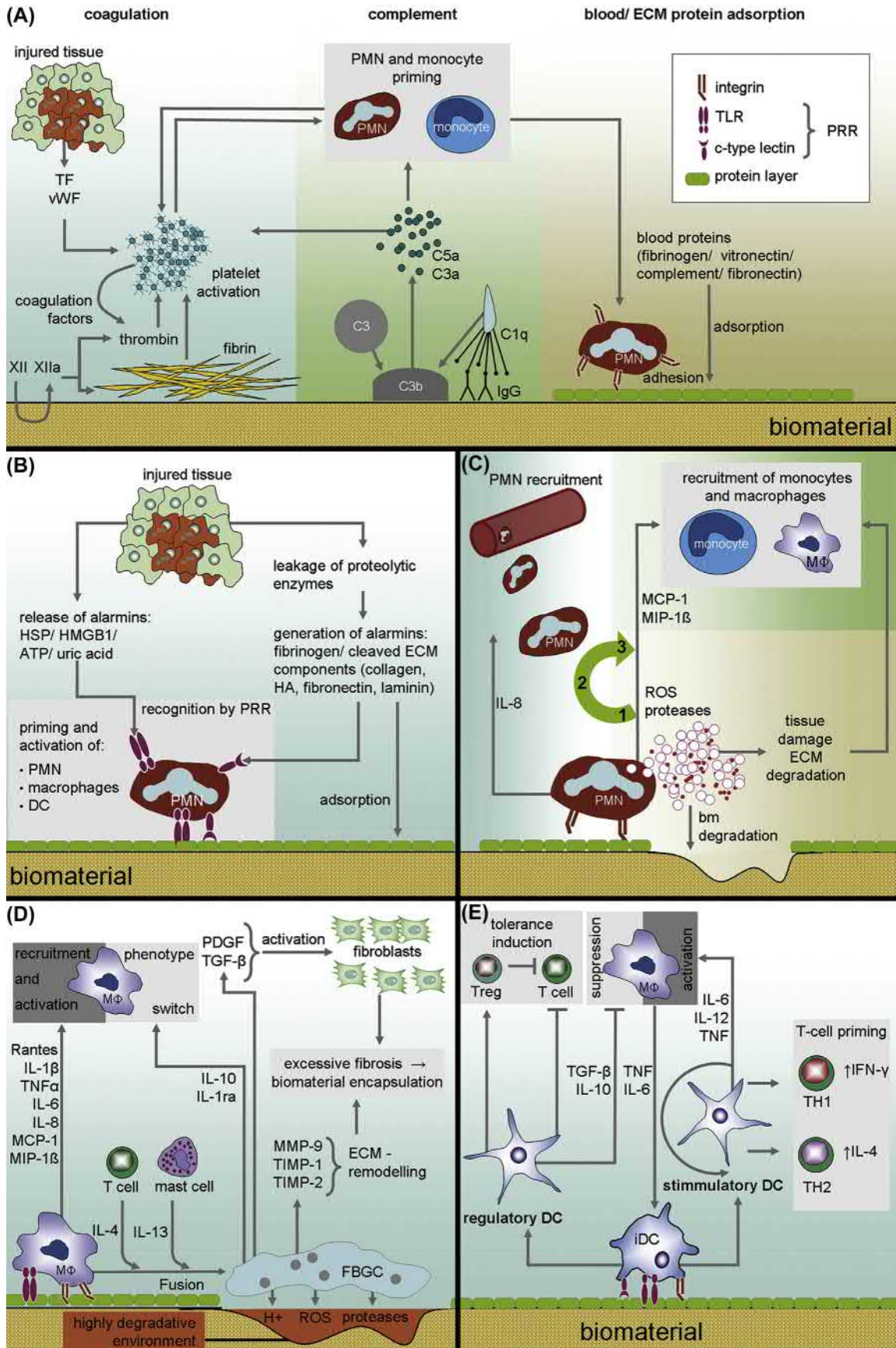
• **Figure 2.2.3.21** Effector mechanisms of regulatory T cells. Regulatory T cells exercise regulatory roles through various contact-dependent and -independent mechanisms, such as: (A) inhibiting effector T cell proliferation through inflammatory cytokine production, inducing effector T cell death by (B) granzyme secretion, and (C) metabolic disruption, as well as (D) inducing a suppressive phenotype of dendritic cells (DCs) to limit their capacity to activate effector T cells (Allen et al., 2018). *CD*, cluster of differentiation; *CTLA4*, cytotoxic T-lymphocyte-associated protein 4; *IDO*, indoleamine 2,3-dioxygenase; *IL*, interleukin; *LAG3*, Lymphocyte Activating gene 3; *MHC*, Major histocompatibility complex; *TGFβ*, Transforming growth factor beta. (Vignali et al., Nature Reviews Immunology 8, 523 – 532 (2008), Figure 1).

of blood proteins, activation of the coagulation cascade, and activation of complement and platelets resulting in the priming and activation of PMNs, monocytes, and macrophages (Zaveri et al., 2014; Zaveri et al., 2017; Keselowsky and Lewis, 2017; Lewis et al., 2015). These innate system components also employ adaptive system cells, which helps shape the overall immune response to the implanted biomaterial.

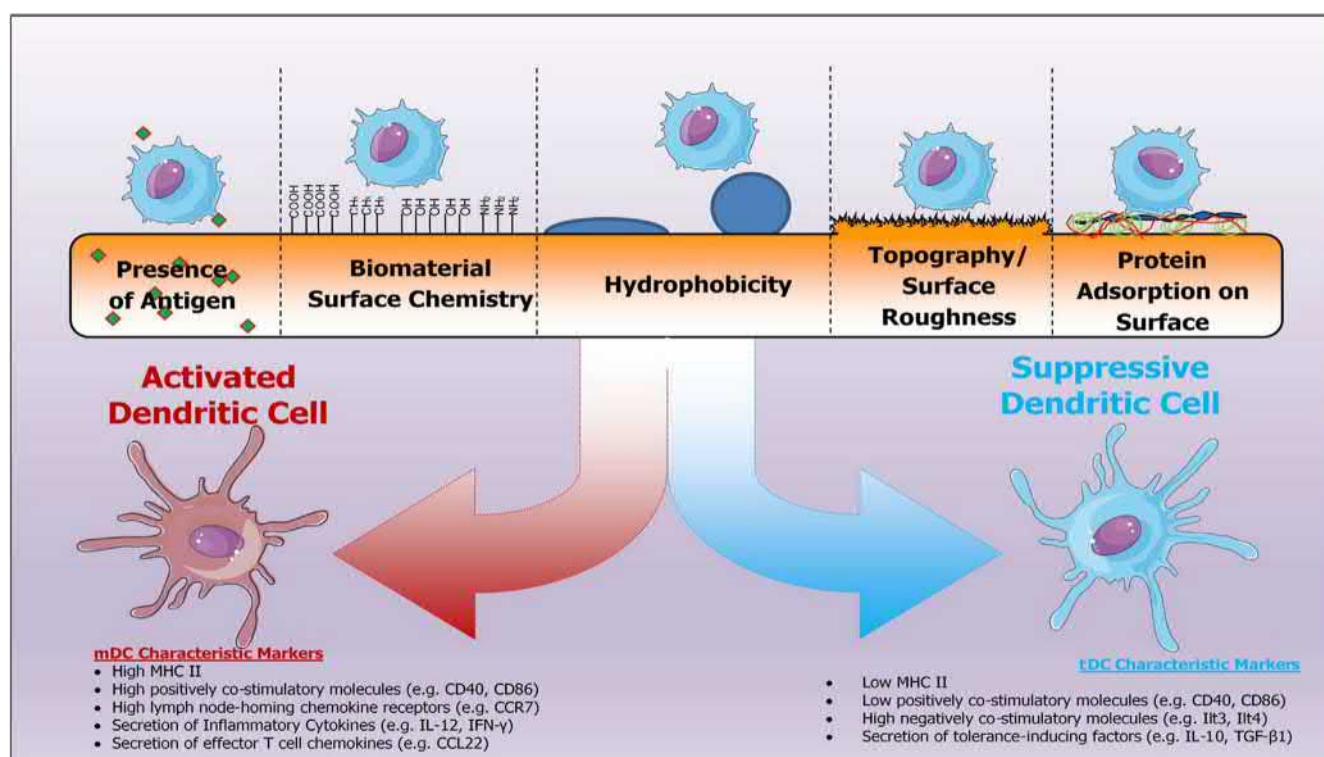
Adaptive immunity plays an even more active role in cases where the implanted material is of biological origin (e.g., silk, decellularized extracellular matrix), and when cells or tissues are incorporated, as is typical in tissue engineering, regenerative medicine, and immunoisolation applications. In these cases, the implants serve as a depot of foreign antigens, some of which may be capable of initiating specific immune responses. With this in mind, researchers are investigating the potential that immune responses can be skewed to enhance immune responses toward activation or suppression in the context of biomaterials, a conceptualization of which is illustrated in Fig. 2.2.3.23. For example, parameters such as the availability of antigen, biomaterial surface chemistry, surface topography/roughness (Kou et al., 2011), and protein adsorption can be modulated to skew toward either a pro- or antiinflammatory response.

Biomaterial scientists are also utilizing drug delivery capabilities as well as manipulating material properties to productively engage both the innate and adaptive immune

systems, as illustrated in Fig. 2.2.3.24, from a transplant and tissue-engineering perspective. For example, scaffolds housing a foreign islet transplant can also serve as a drug delivery depot to provide controlled release of agents that inhibit monocyte migration and/or macrophage maturation, repel macrophage infiltration, scavenge detrimental products from activated macrophages, or promote an M2-like macrophage phenotype. Release or surface presentation of factors to modulate adaptive immunity is also possible, where strategies such as promoting tolerogenic phenotypes, inhibiting T cell egress from the lymph node, and locally inducing immune cell apoptosis are all being investigated. Biomaterials are being utilized to act as immunoisolation devices, where material encapsulation of a foreign transplant serves to block direct antigen presentation pathways. This approach relies on a material pore size large enough to allow exchange of nutrients and metabolites, with pores being small enough to block cell ingress/egress. However, this approach still allows activation of indirect pathways, where soluble-shed antigens can pass through the material barrier, be taken up by host APCs, and stimulate antigen-specific responses, which are capable of directing cell killing of the transplant through release of soluble mediators. To address this unwanted activation of adaptive immunity, immunomodulatory agents can be incorporated within the biomaterial or tethered to the material surface for local modulation of APCs and/or



• **Figure 2.2.3.22** Immune response toward biomaterials. (A) Adsorption of blood proteins and activation of the coagulation cascade, complement, and platelets result in the priming and activation of polymorphonuclear neutrophils (PMNs), monocytes, and resident macrophages. (B) Danger signals (alarmins) released from damaged tissue additionally prime the immune cells for enhanced function via pattern recognition receptor (PRR) engagement. (C) The acute inflammatory response is dominated by the action of PMNs. PMNs secrete proteolytic enzymes and reactive oxygen species (ROS), corroding the biomaterial surface. IL-8 released from PMNs enhances PMN influx and priming. In the transition from acute to chronic inflammation, PMNs stop secreting IL-8 in favor of cytokines promoting migration and activation of monocytes and macrophages. (D) Macrophages are the driving force of chronic inflammation. Constant release of inflammatory mediators like TNF- β , IL-6, and MCP-1 results in permanent activation of macrophages. Fusion-inducing stimuli like IL-4 and IL-13 promote the fusion of macrophages to foreign body giant cells (FBGCs), which form a highly degradative environment on the biomaterial surface. Furthermore, FBGCs promote extracellular (ECM) remodeling and fibroblast activation resulting in excessive fibrosis and biomaterial encapsulation. (E) Macrophage-derived cytokines and PRR engagement activate dendritic cells (DCs) on the biomaterial surface. Depending on the nature of the stimulus, DCs mature to either immunogenic or tolerogenic subtypes, amplifying or suppressing the inflammatory response (Jewell et al., 2011). *bm*, Bone marrow; *HA*, hydroxyapatite; *PDGF*, platelet-derived growth factor; *TGF- β* , transforming growth factor beta; *TLR*, toll-like receptor. (Adapted from Biomaterials. (2011) Oct;32(28):6692–6709. <https://doi.org/10.1016/j.biomaterials.2011.05.078>; Figure 1).

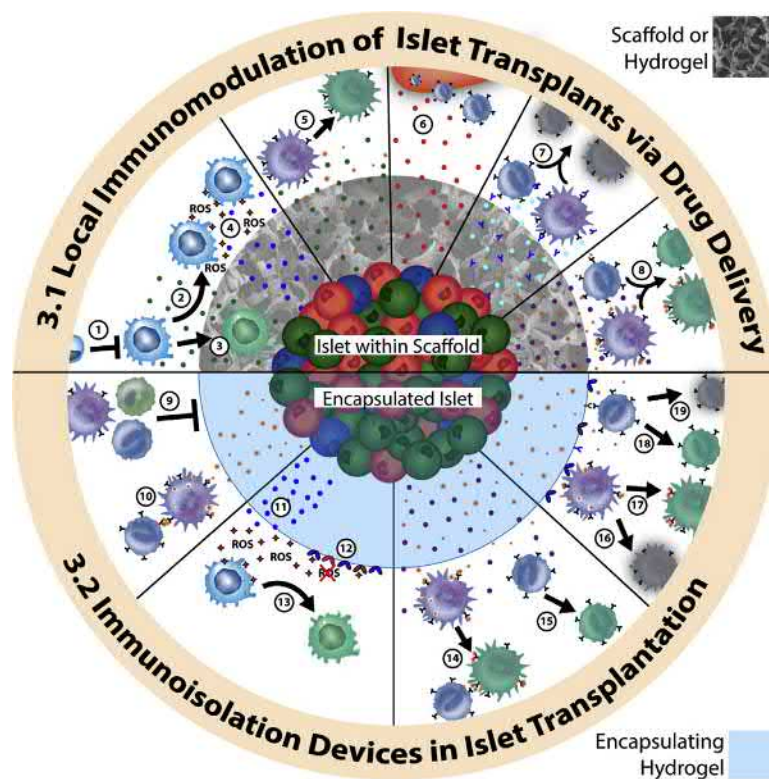


• **Figure 2.2.3.23** Implant material factors that influence the fate of local dendritic cell responses and shape the implant immune microenvironment. The surface properties of the implant can be modulated to skew the immune response of dendritic cells toward activation or suppression. This response is characterized by markers such as major histocompatibility complex (MHC)-II, CD86, interleukin (IL)-12, and IL-10, among others (Yoon & et al., 2015). (Semin Immunol. 2017 Feb;29:33–40. <https://doi.org/10.1016/j.smim.2017.04.002>, Figure 1).

T cells to instruct toward apoptotic or tolerogenic pathways, with local antigen delivery from the transplanted cells providing antigen specificity.

Taking a cue from the nanoscale features of alum as a vaccine adjuvant material, approaches using biomaterial nanoparticles and microparticles are actively being investigated in numerous compositions and forms to modulate immune functions, mimicking characteristics of pathogen internalization and processing by APCs (Acharya et al., 2017). Strategies illustrating biomaterial approaches

directing immune function, paying particular attention to particle-based systems, are illustrated in Fig. 2.2.3.25. For example, the size and shape of particles, along with material interfacial chemistry, ligand coupling (Lewis et al., 2012), and other physicochemical properties (Allen et al., 2018) and responsiveness can be readily tuned to impact delivery of factors to either cell surface receptors or intracellular compartments, drainage to lymphatics, interactions with APCs, and the intrinsic immunogenicity of many common polymers (Champion and Mitragotri, 2009; Doshi

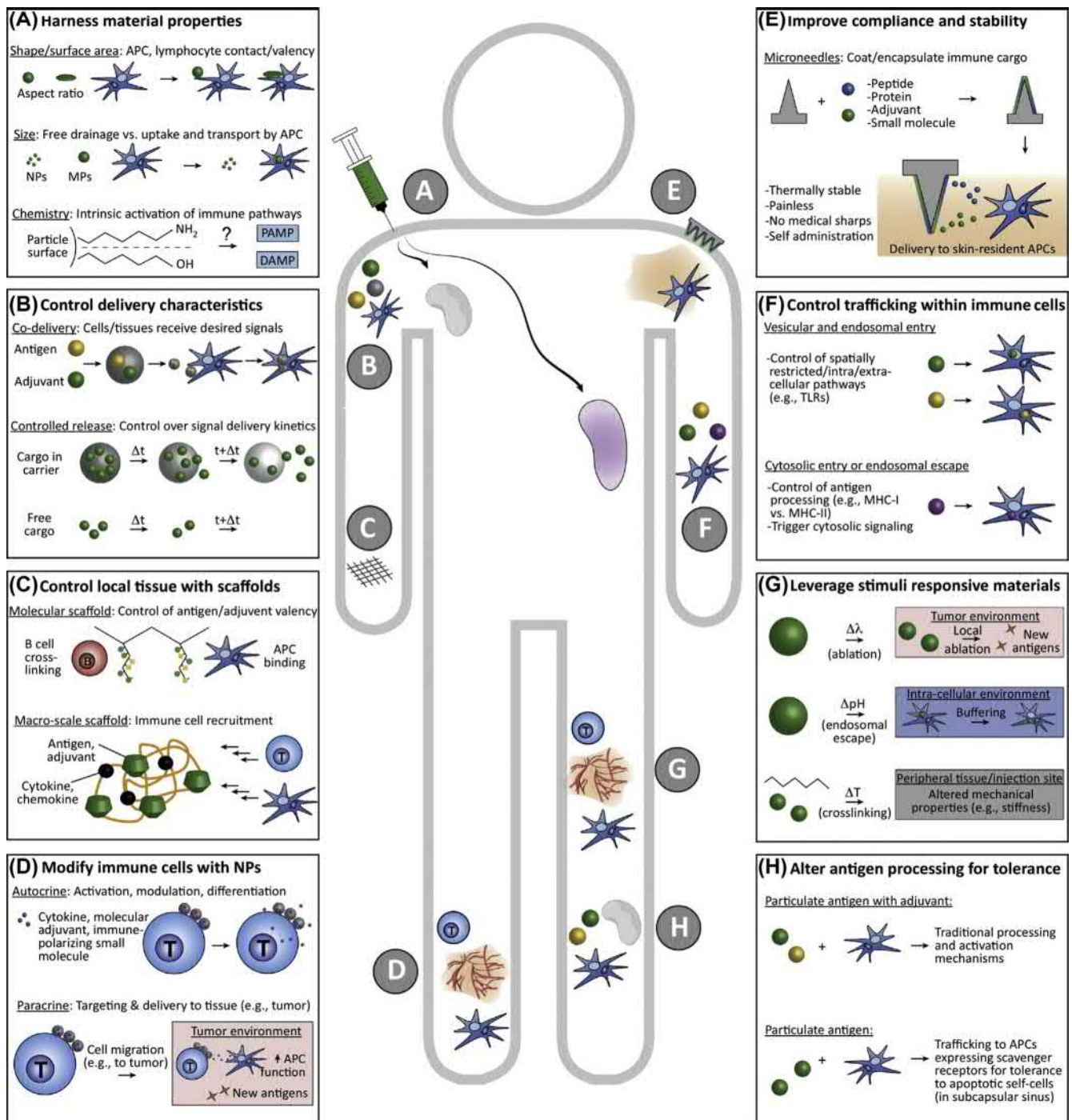


• **Figure 2.2.3.24** Immunomodulatory biomaterial approaches for islet and B cell transplantation. *Top*: Local immunomodulation via drug delivery. Scaffolds housing the foreign islet transplant can serve as a drug delivery depot. For modulation of inflammation, scaffolds can release agents that inhibit monocyte migration and/or macrophage maturation (1), repel macrophage infiltration (2), scavenge detrimental products from activated macrophages, such as reactive oxygen species (ROS) (3), and/or promote an M2-like macrophage phenotype (4). For modulation of adaptive immunity, drugs are released/presented to inhibit antigen uptake or promote a tolerogenic dendritic phenotype (5), inhibit activated T cell egress from the lymph node (6), induce immune cell apoptosis (7), and/or promote tolerogenic phenotype (8). The presence of the islet graft also provides antigen delivery (orange). *Bottom*: Immunoisolation devices. Encapsulation of the foreign transplant serves to block direct antigen presentation pathways (9) but indirect pathways (10) can still be activated. Drugs incorporated within the biomaterial (11) or tethered to the material surface (12) can serve to dampen inflammatory response to the material and cells via inhibition of macrophage activation, scavenging of detrimental agents, and/or promotion of an M2-like phenotype (13). To dampen adaptive immune responses, immunomodulatory agents can be incorporated into the encapsulating material and released for local modulation of antigen-presenting cell (14) and/or T cell (15) activation. Conjugation of immunomodulatory agents to the surface of the biomaterial can also serve to instruct immune cells toward apoptotic (16 and 18) and/or tolerogenic (17 and 19) pathways with local antigen delivery (from the transplanted cells) to provide antigen specificity (Sunshine et al., 2014). (Keselowsky et al., 2019 Nature Materials Reviews).

and Mitragotri, 2010). Biomaterial particle configurations can be used to control the combinations and relative concentrations (Yoon et al., 2015) of immune cargos (antigens, immunomodulatory factors) reaching APCs and lymphocytes, or, by designing polymers with a desired degradation rate, the cargo delivery kinetics (Acharya et al., 2016; Joshi et al., 2014; Jewell et al., 2011). In addition to APCs, T cells and other immune cells can also be targeted with nanoparticles incorporating immune signals (Sunshine et al., 2014; Fadel et al., 2014; Smith et al., 2017).

While explored to a lesser extent, biomaterial systems are also being utilized to develop immunosuppressive responses. For example, delivery of vitamin D₃, TGF- β 1, and GM-CSF in the presence of disease-relevant antigens showed marked improvement in type 1 diabetes, multiple sclerosis,

and rheumatoid arthritis mouse models (Lewis et al., 2015; Yoon et al., 2015; Allen et al., 2019; Lewis et al., 2019). Additionally, scaffolds can be used to deliver antigens and adjuvants, and as a local environment to recruit APCs or lymphocytes for either immune activation or tolerance (Ali et al., 2009; Verbeke & et al., 2017). Other material configurations such as microneedles incorporating immune cues are also being investigated (Sullivan & et al., 2010; Demuth & et al., 2013). Overall, biomaterials provide numerous precisely definable and facile tools to target specific immune cells, and modulate responses for pathologies ranging from cancer, autoimmune disease, and infections. Both biomaterials science and immunology stand to gain tremendously from the continued integration of these disparate but synergistic fields.



• **Figure 2.2.3.25** Strategies involving biomaterials for engineering immune function. (A) Material shape, size, chemistry, and other physicochemical properties impact drainage through lymphatics, interactions with antigen-presenting cells (APCs), and the intrinsic immunogenicity of many common polymers. (B) Biomaterials can be used to control the combinations and relative concentrations of immune cargos reaching APCs and lymphocytes, or, by designing polymers with a desired degradation rate, the cargo delivery kinetics. (C) Scaffolds can be used to control the context or density in which antigens and adjuvants are displayed, and as local environments to recruit APCs or lymphocytes (e.g., by incorporation of chemokines). (D) T cells, APCs, and other immune cells can be modified with nanoparticles (NPs) incorporating immune signals to exert autocrine effects on the modified cells, or to exert paracrine effects on target cells and tissue to which the modified cell will migrate (e.g., a tumor). (E) Microneedles coated with or incorporating immune cues increase safety and patient compliance by efficiently targeting skin-resident immune cells without pain, generation of medical sharps, or need for refrigeration. (F) Biomaterial carriers can be engineered with specific moieties to control cellular entry and intracellular trafficking for directing spatially restricted immune processes (e.g., toll-like receptor [TLR] signaling and antigen processing). (G) Stimuli responsive materials can exploit physiological (e.g., changes in pH or temperature) or external (e.g., ultraviolet light) cues to provide environment-specific control within cells, target tissues, or tumors (e.g., access to neoantigens during NP-enabled local ablation via photothermal exposure). (H) NPs and microparticles (MPs) can alter how antigens are processed to modulate responses away from proimmune and toward regulation. *DAMP*, Damage-associated molecular pattern; *MHC*, major histocompatibility complex; *PAMP*, pathogen-associated molecular pattern (Trends in Immunology, February 2018, Vol. 39, No. 2 <https://doi.org/10.1016/j.it.2017.10.002>, Figure 2).

References

- Abbas, A.L.A., Pober, J., 2000. Cellular and Molecular Immunology, fourth ed.
- Abbas, A.K., Murphy, K.M., Sher, A., 1996. Functional diversity of helper T lymphocytes. *Nature* 383, 787–793.
- Acharya, A.P., et al., 2016. A cell-based microarray to investigate combinatorial effects of microparticle-encapsulated adjuvants on dendritic cell activation. *J. Mater. Chem. B*. <https://doi.org/10.1039/c5tb01754h>.
- Acharya, A.P., et al., 2017. Localized multi-component delivery platform generates local and systemic anti-tumor immunity. *Adv. Funct. Mater.* <https://doi.org/10.1002/adfm.201604366>.
- Acharya, A.P., Dolgova, N.V., Clare-Salzler, M.J., Keselowsky, B.G., 2008. Adhesive substrate-modulation of adaptive immune responses. *Biomaterials*. <https://doi.org/10.1016/j.biomaterials.2008.08.040>.
- Acharya, A.P., Clare-Salzler, M.J., Keselowsky, B.G., 2009. A high-throughput microparticle microarray platform for dendritic cell-targeting vaccines. *Biomaterials*. <https://doi.org/10.1016/j.biomaterials.2009.04.032>.
- Acharya, A.P., Dolgova, N.V., Xia, C.Q., Clare-Salzler, M.J., Keselowsky, B.G., 2011. Adhesive substrates modulate the activation and stimulatory capacity of non-obese diabetic mouse-derived dendritic cells. *Acta Biomater.* <https://doi.org/10.1016/j.actbio.2010.08.026>.
- Ali, N., et al., 2017. Regulatory T cells in skin facilitate epithelial stem cell differentiation. *Cell*. <https://doi.org/10.1016/j.cell.2017.05.002>.
- Ali, O.A., Huebsch, N., Cao, L., Dranoff, G., Mooney, D.J., 2009. Infection-mimicking materials to program dendritic cells in situ. *Nat. Mater.* <https://doi.org/10.1038/nmat2357>.
- Allen, R.P., Bolandparvaz, A., Ma, J.A., Manickam, V.A., Lewis, J.S., 2018. Latent, immunosuppressive nature of poly(lactic-co-glycolic acid) microparticles. *ACS Biomater. Sci. Eng.* <https://doi.org/10.1021/acsbiomaterials.7b00831>.
- Allen, R., Chizari, S., Ma, J.A., Raychaudhuri, S., Lewis, J.S., 2019. Combinatorial, microparticle-based delivery of immune modulators reprograms the dendritic cell phenotype and promotes remission of collagen-induced arthritis in mice. *ACS Appl. Bio Mater.* <https://doi.org/10.1021/acsabm.9b00092>.
- Archer, K.A., Durack, J., Portnoy, D.A., 2014. STING-dependent type I IFN production inhibits cell-mediated immunity to *Listeria monocytogenes*. *PLoS Pathog.* <https://doi.org/10.1371/journal.ppat.1003861>.
- Banchereau, J., Steinman, R.M., 1998. Dendritic cells and the control of immunity. *Nature*. <https://doi.org/10.1038/32588>.
- Brerski, R.J., Georgiou, G., 2016. Immunoglobulin isotype knowledge and application to Fc engineering. *Curr. Opin. Immunol.* 40, 62–69.
- Burzyn, D., Benoist, C., Mathis, D., 2013. Regulatory T cells in nonlymphoid tissues. *Nat. Immunol.* <https://doi.org/10.1038/ni.2683>.
- Champion, J.A., Mitragotri, S., 2009. Shape induced inhibition of phagocytosis of polymer particles. *Pharm. Res.* <https://doi.org/10.1007/s11095-008-9626-z>.
- Cicchese, J.M., et al., 2018. Dynamic balance of pro- and anti-inflammatory signals controls disease and limits pathology. *Immunol. Rev.* <https://doi.org/10.1111/imr.12671>.
- Davies, L.C., Jenkins, S.J., Allen, J.E., Taylor, P.R., 2013. Tissue-resident macrophages. *Nat. Immunol.* <https://doi.org/10.1038/ni.2705>.
- Demuth, P.C., et al., 2013. Polymer multilayer tattooing for enhanced DNA vaccination. *Nat. Mater.* <https://doi.org/10.1038/nmat3550>.
- Doshi, N., Mitragotri, S., 2010. Macrophages recognize size and shape of their targets. *PLoS One*. <https://doi.org/10.1371/journal.pone.0010051>.
- Fadel, T.R., et al., 2014. A carbon nanotube-polymer composite for T-cell therapy. *Nat. Nanotechnol.* <https://doi.org/10.1038/nnano.2014.154>.
- Farber, D.L., Netea, M.G., Radbruch, A., Rajewsky, K., Zinkernagel, R.M., 2016. Immunological memory: lessons from the past and a look to the future. *Nat. Rev. Immunol.* 16, 124–128.
- Germain, R.N., 1994. MHC-dependent antigen-processing and peptide presentation - providing ligands for t-lymphocyte activation. *Cell* 76, 287–299.
- Halverson, R., Torres, R.M., Pelandra, R., 2004. Receptor editing is the main mechanism of B cell tolerance toward membrane antigens. *Nat. Immunol.* <https://doi.org/10.1038/ni1076>.
- Hubbell, J.A., Thomas, S.N., Swartz, M.A., 2009. Materials engineering for immunomodulation. *Nature*. <https://doi.org/10.1038/nature08604>.
- Immunity in the tissues. *Nat. Immunol.* 2013. <https://doi.org/10.1038/ni.2722>.
- Inohara, N., Nuñez, G., 2001. The NOD: a signaling module that regulates apoptosis and host defense against pathogens. *Oncogene*. <https://doi.org/10.1038/sj.onc.1204787>.
- Iwasaki, A., Medzhitov, R., 2010. Regulation of adaptive immunity by the innate immune system. *Science*. [https://doi.org/10.1126/science.1183021\(80-.\)](https://doi.org/10.1126/science.1183021(80-.)).
- Janeway, C. a, Medzhitov, R., Janeway Jr., C.A., Medzhitov, R., 2002. Innate immune recognition. *Annu. Rev. Immunol.* <https://doi.org/10.1146/annurev.immunol.20.083001.084359>.
- Janeway, C.A., 1989. Cold Spring Harbor Symposia on Quantitative Biology.
- Jewell, C.M., Bustamante Lopez, S.C., Irvine, D.J., 2011. In situ engineering of the lymph node microenvironment via intranodal injection of adjuvant-releasing polymer particles. *Proc. Natl. Acad. Sci.* <https://doi.org/10.1073/pnas.1105200108>.
- Jhunjunwala, S., et al., 2015. Neutrophil responses to sterile implant materials. *PLoS One*. <https://doi.org/10.1371/journal.pone.0137550>.
- Joller, N., Weber, S.S., Oxenius, A., 2011. Antibody - Fc receptor interactions in protection against intracellular pathogens. *Eur. J. Immunol.* 41, 889–897.
- Joshi, V.B., et al., 2014. Tumor lysate-loaded biodegradable microparticles as cancer vaccines. *Expert Rev. Vaccines*. <https://doi.org/10.1586/14760584.2014.851606>.
- Kasturi, S.P., Pulendran, B., 2008. Cross-presentation: avoiding trafficking chaos? *Nat. Immunol.* <https://doi.org/10.1038/ni0508-461>.
- Keselowsky, B.G., Lewis, J.S., 2017. Dendritic cells in the host response to implanted materials. *Semin. Immunol.* <https://doi.org/10.1016/j.smim.2017.04.002>.
- Kou, P.M., Schwartz, Z., Boyan, B.D., Babensee, J.E., 2011. Dendritic cell responses to surface properties of clinical titanium surfaces. *Acta Biomater.* <https://doi.org/10.1016/j.actbio.2010.10.020>.
- Kroczeck, R.A., Mages, H.W., Hutloff, A., 2004. Emerging paradigms of T-cell co-stimulation. *Curr. Opin. Immunol.* 16, 321–327.
- Kumar, H., Kawai, T., Akira, S., 2011. Pathogen recognition by the innate immune system. *Int. Rev. Immunol.* <https://doi.org/10.3109/08830185.2010.529976>.
- Langefeld, T.W., Muhling, J., Engel, J., Harbach, H., Chakraborty, T., 2009. Part 2: the acquired immune system. *Anesthesiol. Intensive Care*. 50, 29–35.

- Lewis, J.S., et al., 2015. A combination dual-sized microparticle system modulates dendritic cells and prevents type 1 diabetes in pre-diabetic NOD mice. *Clin. Immunol.* <https://doi.org/10.1016/j.clim.2015.03.023>.
- Lewis, J.S., et al., 2019. Dual-Sized microparticle system for generating suppressive dendritic cells prevents and reverses type 1 diabetes in the nonobese diabetic mouse model. *ACS Biomater. Sci. Eng.* <https://doi.org/10.1021/acsbomaterials.9b00332>.
- Lewis, J.S., Zaveri, T.D., Crooks, C.P., Keselowsky, B.G., 2012. Microparticle surface modifications targeting dendritic cells for non-activating applications. *Biomaterials.* <https://doi.org/10.1016/j.biomaterials.2012.06.049>.
- Li, Y., et al., 2008. Efficient cross-presentation depends on autophagy in tumor cells. *Cancer Res.* <https://doi.org/10.1158/0008-5472.CAN-08-0161>.
- Liongue, C., John, L.B., Ward, A.C., 2011. Origins of adaptive immunity. *Crit. Rev. Immunol.* 31, 61–71.
- Masopust D, S.A., 2019. Tissue-resident T cells and other resident leukocytes. *Annu. Rev. Immunol.* 37.
- Matzinger, P., 1994. Tolerance, danger, and the extended family. *Annu. Rev. Immunol.* <https://doi.org/10.1146/annurev.iy.12.040194.005015>.
- McAdam, A.J., Schweitzer, A.N., Sharpe, A.H., 1998. The role of B7 co-stimulation in activation and differentiation of CD4(+) and CD8(+) T cells. *Immunol. Rev.* 165, 231–247.
- Medzhitov, R., 2007. Recognition of microorganisms and activation of the immune response. *Nature.* <https://doi.org/10.1038/nature06246>.
- O'Neill, L.A.J., Kishton, R.J., Rathmell, J., 2016. A guide to immunometabolism for immunologists. *Nat. Rev. Immunol.* <https://doi.org/10.1038/nri.2016.70>.
- Ouyang, W.J., Kolls, J.K., Zheng, Y., 2008. The biological functions of T helper 17 cell effector cytokines in inflammation. *Immunity* 28, 454–467.
- Padlan, E.A., 1994. Anatomy OF the antibody molecule. *Mol. Immunol.* 31, 169–217.
- Palucka, K., Banchereau, J., 2012. Cancer immunotherapy via dendritic cells. *Nat. Rev. Cancer.* <https://doi.org/10.1038/nrc3258>.
- Rappazzo, C.G., Birnbaum, M.E., 2017. Tuning up T-cell receptors. *Nat. Biotechnol.* 35, 1145–1146.
- Ratajczak, W., Niedzwiedzka-Rystwej, P., Tokarz-Deptula, B., Deptula, W., 2018. Immunological memory cells. *Cent. Eur. J. Immunol.* 43, 194–203.
- Ridge, J.P., Fuchs, E.J., Matzinger, P., 1996. Neonatal tolerance revisited: turning on newborn T cells with dendritic cells. *Science.* <https://doi.org/10.1126/science.271.5256.1723>. (80-).
- Round, J.L., Palm, N.W., 2018. Causal effects of the microbiota on immune-mediated diseases. *Sci. Immunol.* <https://doi.org/10.1126/sciimmunol.aao1603>.
- Sakaguchi, S., et al., 2001. Immunologic tolerance maintained by CD25(+) CD4(+) regulatory T cells: their common role in controlling autoimmunity, tumor immunity, and transplantation tolerance. *Immunol. Rev.* 182, 18–32.
- Sakaguchi, S., 2004. Naturally arising CD4(+) regulatory T cells for immunologic self-tolerance and negative control of immune responses. *Annu. Rev. Immunol.* 22, 531–562.
- Salfeld, J.G., 2007. Isotype selection in antibody engineering. *Nat. Biotechnol.* 25, 1369–1372.
- Sallusto, F., Lenig, D., Forster, R., Lipp, M., Lanzavecchia, A., 1999. Two subsets of memory T lymphocytes with distinct homing potentials and effector functions. *Nature* 401, 708–712.
- Shanker, A., 2010. Adaptive control of innate immunity. *Immunol. Lett.* 131, 107–112.
- Smith, T.T., et al., 2017. In situ programming of leukaemia-specific t cells using synthetic DNA nanocarriers. *Nat. Nanotechnol.* <https://doi.org/10.1038/NNANO.2017.57>.
- Sperling, C., Fischer, M., Maitz, M.F., Werner, C., 2017. Neutrophil extracellular trap formation upon exposure of hydrophobic materials to human whole blood causes thrombogenic reactions. *Biomater. Sci.* <https://doi.org/10.1039/c7bm00458c>.
- Sprent, J., 2002. T memory cells: quality not quantity. *Curr. Biol.* 12, R174–R176.
- Sullivan, S.P., et al., 2010. Dissolving polymer microneedle patches for influenza vaccination. *Nat. Med.* <https://doi.org/10.1038/nm.2182>.
- Sunshine, J.C., Perica, K., Schneck, J.P., Green, J.J., 2014. Particle shape dependence of CD8+ T cell activation by artificial antigen presenting cells. *Biomaterials.* <https://doi.org/10.1016/j.biomaterials.2013.09.050>.
- Suzuki, G., Nomura, M., Uzawa, A., Akashi, M., Nakata, Y., 1995. Impaired CD28-MEDIATED CO-stimulation in anergic t-cells. *Int. Immunol.* 7, 37–43.
- Takeuchi, O., Akira, S., 2008. MDA5/RIG-I and virus recognition. *Curr. Opin. Immunol.* <https://doi.org/10.1016/j.coi.2008.01.002>.
- Janeway Jr., C.A., Travers, P., Walport, M., Shlomchik, M.J., 2001. *Immunobiology*, ninth ed.
- Treanor, B., 2012. B-cell receptor: from resting state to activate. *Immunology* 136, 21–27.
- Vallejo, A.N., Davila, E., Weyand, C.M., Goronzy, J.J., 2004. Biology of T lymphocytes. *Rheum. Dis. Clin. N. Am.* 30, 135.
- Verbeke, C.S., et al., 2017. Multicomponent injectable hydrogels for antigen-specific tolerogenic immune modulation. *Adv. Healthc. Mater.* <https://doi.org/10.1002/adhm.201600773>.
- Wang, W., Erbe, A.K., Hank, J.A., Morris, Z.S., Sondel, P.M., 2015. NK cell-mediated antibody-dependent cellular cytotoxicity in cancer immunotherapy. *Front. Immunol.* 6. <https://doi.org/10.3389/fimmu.2015.00368>.
- Weiner, H.L., da Cunha, A.P., Quintana, F., Wu, H., 2011. Oral tolerance. *Immunol. Rev.* 241, 241–259.
- Weiner, H.L., 2001. Induction and mechanism of action of transforming growth factor-beta-secreting Th3 regulatory cells. *Immunol. Rev.* 182, 207–214.
- Wood, W., Martin, P., 2017. Macrophage functions in tissue patterning and disease: new insights from the fly. *Dev. Cell.* <https://doi.org/10.1016/j.devcel.2017.01.001>.
- Yeung, M., 2012. *Transplantation Immunobiology*.
- Yoon, Y.M., et al., 2015. A combination hydrogel microparticle-based vaccine prevents type 1 diabetes in non-obese diabetic mice. *Sci. Rep.* <https://doi.org/10.1038/srep13155>.
- Zaveri, T.D., et al., 2017. Macrophage integrins modulate response to ultra-high molecular weight polyethylene particles and direct particle-induced osteolysis. *Biomaterials.* <https://doi.org/10.1016/j.biomaterials.2016.10.038>.
- Zaveri, T.D., Lewis, J.S., Dolgova, N.V., Clare-Salzler, M.J., Keselowsky, B.G., 2014. Integrin-directed modulation of macrophage responses to biomaterials. *Biomaterials.* <https://doi.org/10.1016/j.biomaterials.2014.01.007>.
- Zhong, X.P., et al., 2011. Receptor signaling in immune cell development and function. *Immunol. Res.* 49, 109–123.
- Zhu, J.F., Yamane, H., Paul, W.E., 2010. In: Paul, W.E., Littman, D.R., Yokoyama, W.M. (Eds.) *Annual Review of Immunology*, Vol 28, vol. 28, pp. 445–489.

Chapter Exercises

Innate Immunity

1. What is the first defense mechanism and what are its salient features?

Answer: Epithelial surfaces of the body provide the first line of defense against foreign materials. The salient features are (1) microbiota, (2) chemical—pH, enzymes, fatty acids, mucosa, surfactants, and cilia, and (3) mechanical—epithelial tight junctions, mucous flow, flow of air, and fluid.

2. What is the first protein complex in the classical pathway of complement activation?

Answer: C1.

3. Name three main pathogen recognition receptors?

Answer: TLRs, NLRs, and RLRs.

4. How many TLRs have been identified to date in humans and mice?

Answer: Humans TLR1–10 and mice TLR1–13.

5. What type of innate immune cells are activated by stress, microbial molecules, or cytokines and are responsible for chemokine-based attraction of APCs? What are their major classifications?

Answer: ILCs. ILC1—IFN γ producing proinflammatory phenotype; ILC2—IL-4 producing tissue repair phenotype; and ILC3—IL-17, IL-22, and GM-CSF producing chemoattractive cells.

Adaptive Immunity

1. What are the major constituents of the adaptive immune response?

Answer: T lymphocytes, adaptive immune cytokines, B lymphocytes, and antibodies comprise the major components of the adaptive immune response.

2. True or false: Antibodies, in general, have four polypeptide chains of similar size that are connected at the “hinge” by disulfide bonds.

Answer: False; antibodies have two light chains and two heavy chains, which are much larger than the former.

3. All of the following are effector mechanisms of antibodies except:

- Neutralization
- Opsonization
- ADCC
- Agglomeration

Answer: d. Agglomeration.

4. Briefly explain what is meant by the term “anergy.”

Answer: Within the molecular communication bridge between APC and T cell (or immune synapse), other molecules also play a role in enhancing intracellular signaling networks that lead to complete activation. These molecules are called costimulators (e.g., CD28 on T cells binding to CD86 on APCs). In their absence, there is insufficient stimulation of T cells resulting in a state of hyporesponsiveness to the antigen or anergy.

5. Outline five general biomaterial-based strategies employed to harness the function of the immune system.

Answer: Any explanation, including five of the following strategies is an acceptable response:

- Material shape, size, chemistry, and other physicochemical properties impact drainage through lymphatics, interactions with APCs, and the intrinsic immunogenicity of many common polymers.
- Biomaterials can be used to control the combinations and relative concentrations of immune cargos reaching APCs and lymphocytes, or, by designing polymers with a desired degradation rate, the cargo delivery kinetics.
- Scaffolds can be used to control the context or density in which antigens and adjuvants are displayed, and as local environments to recruit APCs or lymphocytes (e.g., by incorporation of chemokines).
- T cells, APCs, and other immune cells can be modified with nanoparticles incorporating immune signals to exert autocrine effects on the modified cells, or to exert paracrine effects on target cells and tissue to which the modified cell will migrate (e.g., a tumor).
- Microneedles coated with or incorporating immune cues increase safety and patient compliance by efficiently targeting skin-resident immune cells without pain, generation of medical sharps, or need for refrigeration.
- Biomaterial carriers can be engineered with specific moieties to control cellular entry and intracellular trafficking for directing spatially restricted immune processes (e.g., TLR signaling and antigen processing).
- Stimuli responsive materials can exploit physiological (e.g., changes in pH or temperature) or external (e.g., ultraviolet light) cues to provide environment-specific control within cells, target tissues, or tumors (e.g., access to neoantigens during nanoparticle-enabled local ablation via photothermal exposure).
- Nanoparticles and microparticles can alter how antigens are processed to modulate responses away from proimmune and toward regulation.

2.2.4

The Complement System

RICHARD J. JOHNSON

BioPhia Consulting, Lake Forest, IL, United States

As discussed in the previous chapter, the immune system acts to protect each of us from the constant exposure to pathogenic agents such as bacteria, fungi, viruses, and cancerous cells that pose a threat to our lives. The sheer multitude of structures that the immune system must recognize, differentiate from “self,” and mount an effective response against has driven the evolution of this system into a complex network of proteins, cells, and distinct organs. An immune response to any foreign element involves all of these components, acting in concert, to defend the host from intrusion. Historically, the immune system has been viewed from two perspectives: cellular or humoral. This is a somewhat subjective distinction, since most humoral components (such as antibodies, complement components, and cytokines) are made by the various cells of the immune system and, in turn, often function to regulate the activity of the multiple types of immune cells. The goal of this chapter will be to provide a basic understanding of the biochemistry and pathobiology of the complement system, including its interaction with both cells and the coagulation pathway, underscoring its relevance to biomaterials research and development.

Introduction

Complement is a term devised by Paul Ehrlich to refer to plasma components that were known to be necessary for antibody-mediated bactericidal activity (Ross, 1986). We now know that the complement system is composed of more than 30 distinct plasma- and membrane-bound proteins involving three separate pathways: classical, alternative, and lectin pathways. The complement system directly and indirectly contributes to both innate inflammatory reactions, as well as cellular (i.e., adaptive) immune responses (West et al., 2018). This array of effector functions is due to the activity of a number of complement components and their receptors on various cells. These activities are summarized in Table 2.2.4.1, along with the responsible complement protein(s). One of the principal functions of complement is to serve as a primitive self–nonself discriminatory defense system. This is accomplished by coating a foreign material

with complement fragments and recruiting phagocytic cells that attempt to destroy and digest the “intruder.” Although the system evolved to protect the host from the invasion of adventitious pathogens, the nonspecific and spontaneous nature of the alternative pathway (AP) permits activation by various biomaterial surfaces. The adsorption of proteins onto biomaterial surfaces, such as IgG or ficolins, drives activation of the classical and lectin pathways, respectively. Because complement activation can follow three distinct but interacting pathways, the various ways of activating the cascade will be outlined separately in the following.

One of the principal functions of complement is to serve as a primitive self–nonself discriminatory defense system. This is accomplished by coating a foreign material with complement fragments and recruiting phagocytic cells that attempt to destroy and digest the “intruder.” Although the system evolved to protect the host from the invasion of adventitious pathogens, the nonspecific and spontaneous nature of the alternative pathway (AP) permits activation by various biomaterial surfaces.

Classical Pathway

The classical pathway (CP) is activated primarily by immune complexes (ICs) composed of antigen and specific antibody, although other proteins, such as C-reactive protein, serum amyloid protein, and amyloid fibrils, as well as apoptotic bodies, can also activate the CP (Bohlsion et al., 2007; Cooper, 1985). The proteins of this pathway are C1, C2, C4, C1 inhibitor (C1-Inh), and C4 binding protein (C4bp). Some of their basic characteristics are summarized in Table 2.2.4.2.

Complement activation by the CP is illustrated in Fig. 2.2.4.1. This system is an example of an enzyme cascade in which each step in the series, from initiation to the final product, involves enzymatic reactions (in this case, proteolytic cleavage reactions) that result in some degree of amplification. Research with knockout mice (mice deficient in C1q, C2, C4, or IgG) has shown that the CP is in a state of continuous low-level activation, essentially primed to react vigorously in the presence of an IC (Manderson et al., 2001). When an IC forms, the cascade is initiated when

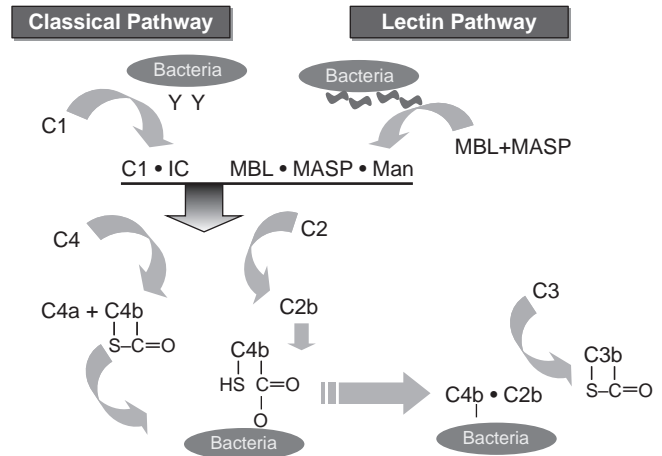
TABLE 2.2.4.1 Complement Activities

Activity	Complement Protein
Identification/opsonization of pathogens	C3, C4
Recruitment/activation of inflammatory cells	C3a, C5a
Lysis of pathogens/cytotoxicity	C5b-9 (MAC)
Clearing immune complexes and apoptotic cells	C1q, C3b, C4b
Augment cellular immune responses (T and B cells)	C3, C4, C3a, C5a, DAF(CD55)

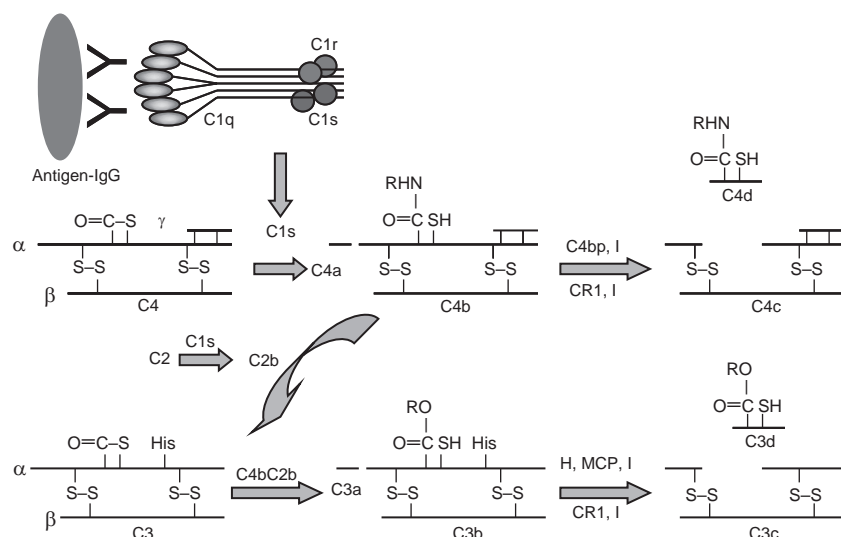
TABLE 2.2.4.2 Proteins of the Classical Pathway of Complement

Protein	Molecular Weight	Subunits	Plasma Concentration ($\mu\text{g/mL}$)
C1q	410,000	6A, 6B, 6C	70
C1r	85,000	1	35
C1s	85,000	1	35
C2	102,000	1	25
C4	200,000	α , β , γ	600
C1-Inh	104,000	1	200
C4bp	570,000	8	230

C1 binds to the Fc portion of an antigen–antibody complex. The C1 protein is composed of three different types of subunits called C1q, C1r, and C1s (Fig. 2.2.4.2). One end of C1q binds to an IC formed between an antigen and one molecule of (pentameric) immunoglobulin (Ig) M or several closely spaced IgG molecules. This interaction may produce a conformational change in the C1q that results in activation (i.e., autocatalytic proteolysis) of the two C1r



• **Figure 2.2.4.1** Complement activation by the classical pathway (CP). Upon binding to the Fc region of an immune complex, C1 is activated and cleaves C4, exposing its thioester, which permits covalent attachment of C4b to the activating surface. C2 is cleaved, producing C2b, which binds to C4b to form the CP C3 convertase. C2b is a serine protease that specifically acts on C3 to generate C3b and C3a. The lectin pathway is also illustrated. Mannose-binding lectin (MBL) recognizes certain sugar residues (mannose, *N*-acetylglucosamine) on the surface of an activator (bacteria). MBL-associated serine protease 1 (MASP-1) appears to activate MASP-2, which then cleaves both C4 and C2 of the CP, generating the CP C3 convertase.



• **Figure 2.2.4.2** Schematic illustration of C4 and C3 protein structures. O=C–S represents the reactive thioester bond that permits covalent attachment to surface nucleophiles (hydroxyl or amino groups). The pattern of proteolytic degradation and the resulting fragments are also shown. Although factor I is the relevant *in vivo* protease, some of these same fragments can be generated with trypsin, plasmin, and thrombin.

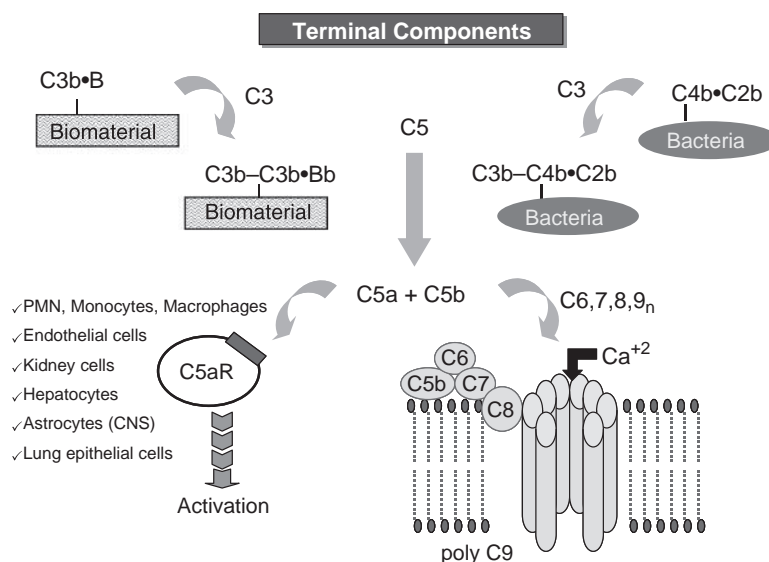
and then the two C1s subunits bound to the other end of the C1q protein. Recent work suggests that activation may also occur through intramolecular contact between two C1 molecules bound closely together (Mortensen et al., 2017), bringing the C1r proteins in close juxtaposition. Both C1r and C1s are zymogen serine proteases that are bound to the C1q in a calcium-dependent manner that is inhibited by calcium chelators such as citrate or ethylenediaminetetraacetic acid (EDTA). The proteolysis of C1s completes the activation of C1, which then proceeds to act on the next proteins in the cascade, C4 and C2.

C4 is composed of three separate chains, α , β , and γ (Fig. 2.2.4.2), bound together by disulfide bonds. Activated C1s cleaves C4 near the amino terminus of the α chain, yielding a 77-amino acid polypeptide called C4a and a much larger C4b fragment. The C4 protein contains a unique structural element called a thioester (Fig. 2.2.4.2), which has only been detected in two other plasma proteins, α 2-macroglobulin and C3. Upon cleavage of C4, the buried thioester becomes exposed and available to react with surface-containing amino or hydroxyl moieties. About 5% of the C4b molecules produced react through the thioester, and become covalently attached to the surface. This represents the first amplification step in the pathway, since each molecule of C1 produces a number of surface-bound C4b sites.

The C4b protein, attached to the surface, acts as a receptor for C2. After binding to C4b, C2 becomes a substrate for C1s. Cleavage of C2 yields two fragments: a smaller C2a portion diffuses into the plasma, while the larger C2b remains bound to the C4b. The C2b protein is another serine protease that, in association with C4b, represents the CP C3/C5 convertase.

As the name implies, the function of the C4b•C2b complex is to bind and cleave C3. The C3 protein sits at the juncture of the classical and alternative pathways, and represents one of the critical control points. Cleavage of C3 by C2b yields a 9 kDa C3a fragment and a 175 kDa C3b fragment that are very similar to C4b in both structure and function. Cleavage of C3 produces a conformational change in the C3b protein that results in exposure of its thioester group (Fig. 2.2.4.2). Condensation with surface nucleophiles (such as carbohydrates) results in covalent attachment of 10%–15% of the C3b to the surface of the activator. This is the second amplification step in the sequence, since as many as 200 molecules of C3b can become attached to the surface surrounding every C4b•C2b complex. Eventually one of the C3b molecules reacts with a site on the C4b protein, creating a C3b–C4b•C2b complex that acts as a C5 convertase (Fig. 2.2.4.3). The C4b•C2b complex can also cleave C5 at very low rates, but the addition of C3b to the complex increases the affinity for (and thus the turnover of) C5 by approximately 1000-fold (Rawal et al., 2008).

In contrast to C3, which can be cleaved in the fluid phase (see later discussion), proteolytic activation of C5 occurs only after it is bound to the C3b portion of the C5 convertase on the surface of an activator (e.g., the immune complex). Like C3, C5 is also cleaved by C2b to produce fragments designated C5a (16 kDa) and C5b (170 kDa). The C5b molecule combines with the proteins of the terminal components to form the membrane attack complex (MAC) described later. C5a is a potent inflammatory mediator, and is responsible for many of the adverse reactions normally attributed to complement activation in various clinical settings.



• **Figure 2.2.4.3** Conversion of C5 produces C5a and C5b, the latter leads to formation of the membrane attack complex. C5a binds to receptors on a variety of cells and results in numerous activities. C5b, formed by the classical pathway, lectin pathway, or the alternative pathway, binds C6 and C7 to form a complex that associates with the plasma membrane. This C5b67 multimer then binds C8, which results in the formation of a small hole in the lipid bilayer that allows small molecules to pass through. Association of multiple C9 proteins enlarges the pore, leading to loss of membrane integrity and cell death. *PMN*, polymorphonuclear neutrophil.

TABLE 2.2.4.3 Proteins of the Lectin Pathway of Complement

Protein	Molecular Weight	Subunits	Plasma Concentration ($\mu\text{g/mL}$)
MBL	270–650,000	18	1–3
MASP-1	93,000	2 (H,L)	6
MASP-2	76,000	2 (H,L)	0.4
MASP-3	110,000	2 (H,L)	

MASP, MBL-associated serine protease; MBL, mannose-binding lectin.

Lectin Pathway

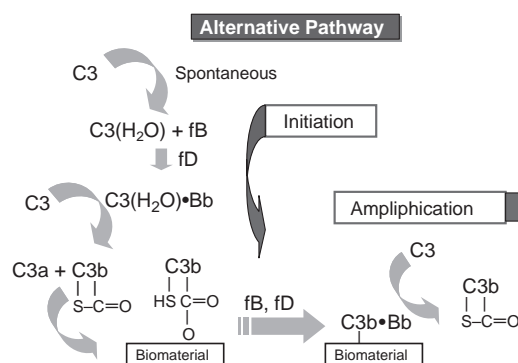
In the 1990s, investigators working with a protein called mannose-binding lectin (MBL) discovered a third pathway that leads to complement activation (Matsushita, 1996). This scheme is called the lectin pathway (LP), and is composed of lectins like MBL and three MBL-associated serine proteases or MASPs (Table 2.2.4.3). MBL is an acute-phase protein, so its concentration in plasma increases substantially during an infection. MBL binds to terminal mannose, *N*-acetyl-glucosamine, and *N*-acetyl-mannosamine residues in complex carbohydrate structures. MBL has long been recognized as an opsonin, i.e., a protein that facilitates phagocytosis of bacteria. Low concentrations of MBL in children are associated with recurrent bacterial infections. MBL is similar in structure to C1q, having an amino terminal domain with a collagen-like structure that binds the MASP proteins, followed by a globular carbohydrate recognition domain that binds to sugar residues. There are three MASP proteins, called MASP-1, MASP-2, and MASP-3, which are very similar in structure to C1r and C1s (Wong et al., 1999). MASP-2 can cleave both C4 and C2, forming a CP C3 convertase (Fig. 2.2.4.1), while MASP-1 cleaves MASP-2 to help accelerate convertase formation (Heja et al., 2012). MASP-3 competes with MASP-2 for binding to MBL, acting to slow LP activation, but also appears to be the primary activator of the AP protease, factor D, in resting human blood (Dobo et al., 2016). The LP can also be activated by other proteins, including ficolins (ficolin-1, -2, and -3) and collectin-11.

Alternative Pathway

The AP was originally discovered in the early 1950s by Pillemer et al. (1954). Pillemer's group studied the ability of a yeast cell wall preparation, called zymosan, to consume C3 without affecting the amount of C1, C2, or C4. A new protein, called properdin, was isolated and implicated in initiating C3 activation independent of the CP. This new scheme was called the properdin pathway. However, this work fell into disrepute when it was realized that plasma contains natural antibodies against zymosan, which implied CP involvement in Pillemer's experiments. The pathway was rediscovered in the late 1960s

TABLE 2.2.4.4 Proteins of the Alternative Pathway of Complement

Protein	Molecular Weight	Subunits	Plasma Concentration ($\mu\text{g/mL}$)
C3	185,000	α, β	1300
B	93,000	1	210
D	24,000	1	1
H	150,000	1	500
I	88,000	α, β	34
P	106–212,000	2–4	20

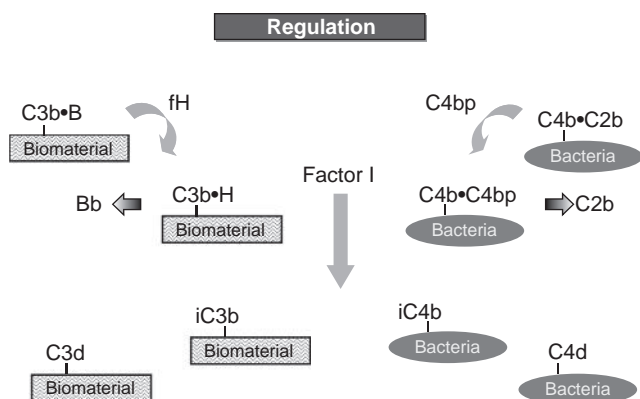


• **Figure 2.2.4.4** Complement activation by the alternative pathway. The spontaneous conversion of C3 to C3(H₂O) permits the continuous production of C3b from C3, a process called C3 tickover. In the presence of an activating surface, the C3b is covalently bound and becomes the focal point for subsequent interactions. The bound C3b is recognized by factor B, which is then cleaved by factor D to produce a surface-bound C3 convertase (C3b•Bb). This results in amplification of the original signal to produce more convertase.

with the study of complement activation by bacterial lipopolysaccharide (LPS), and with the discovery of a C4-deficient guinea pig. The 1970s witnessed the isolation and characterization of each of the proteins of this pathway until it was possible to completely reconstruct the entire AP by recombining each of the purified proteins (Schreiber et al., 1978). While some biomaterials can activate complement through either the CP (Andersson et al., 2005) or the LP (Banda et al., 2014), most biomaterials activate the AP, either directly or by recognizing surface-bound C3b produced during activation by the CP/LP.

While some biomaterials can activate complement through either the CP (Andersson et al., 2005) or the LP (Banda et al., 2014), most biomaterials activate the AP, either directly or by recognizing surface-bound C3b produced during activation by the CP/LP.

The proteins of this pathway are described in Table 2.2.4.4. Their actions can be conceptually divided into three phases: initiation, amplification, and regulation (Figs. 2.2.4.4 and 2.2.4.5). Initiation is a spontaneous process that



• **Figure 2.2.4.5** Control of complement activation by factors H, I, and C4 binding protein. The extent to which complement activation occurs on different surfaces is dependent on the ability of fH or C4BP to recognize C3b or C4b on the surface. Degradation by factor I results in irreversible inactivation and the production of C3 and C4 fragments recognized by various complement receptors on white blood cells.

is responsible for the nonselective nature of complement. During this stage, a small portion of the C3 molecules in plasma undergo a conformational change that results in hydrolysis of the thioester group, producing an activated form of C3 called C3(H₂O) (“C3-water”) that will bind to factor B. The C3(H₂O)•B complex is a substrate for factor D (a protease), which cleaves the B protein to form a solution-phase AP C3 convertase: C3(H₂O)•Bb. Analogous to C2b in the CP, Bb is a serine protease that (in association with C3(H₂O)) will cleave more C3 to form C3b. Under normal physiological conditions, most of the exposed thioester in the C3b produced is hydrolyzed and inactivated, a process that has been termed “C3 tickover.” C3 tickover is a continuous process that ensures a constant supply of reactive C3b molecules to deposit on foreign surfaces, such as cellulosic- or nylon-based biomaterials. Recognition of the C3b by factor B, cleavage by factor D, and generation of more C3 convertase leads to the amplification phase (Fig. 2.2.4.4). During this stage, many more C3b molecules are produced, bind to the surface, and in turn lead to additional C3b•Bb sites. Eventually, a C3b molecule attaches to one of the C3 convertase sites by direct attachment to the C3b protein component of the enzyme. This C3b–C3b•Bb complex is the AP C5 convertase and, in a manner reminiscent of the CP C5 convertase, converts C5 to C5b and C5a (Fig. 2.2.4.3).

Recent work with purified proteins and techniques to measure direct interactions with polymer surfaces has revealed an additional potential mechanism for AP activation (Andersson et al., 2002). Both C3b and C3 will adsorb to (not react with) polystyrene. A portion (about 10%) of the bound C3 or C3b binds factor B. This complex is recognized by factor D, which then catalyzes the formation of an AP C3 convertase. This process is facilitated by properdin, which increases the amount of convertase formed under these conditions. Interestingly, while the C3b•Bb convertase is controlled by factors H and I (see later), the surface-bound C3•Bb convertase is not. The adsorption of C3 does

TABLE 2.2.4.5 Proteins of the Membrane Attack Complex

Protein	Molecular Weight	Subunits	Plasma Concentration (μg/mL)
C5	190,000	α, β	70
C6	120,000	1	60
C7	105,000	1	60
C8	150,000	α, β	55
C9	75,000	1	55
S-protein	80,000	1	500

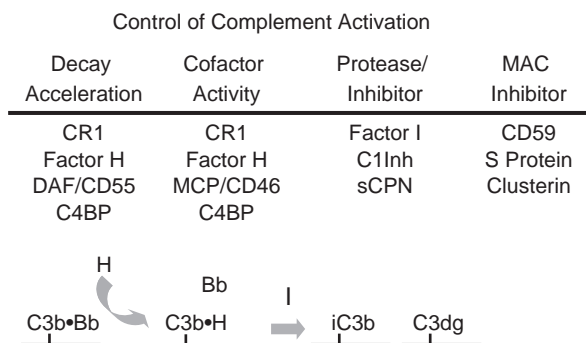
not occur if the polystyrene surface is precoated with fibrinogen, so the extent to which this occurs in whole blood, where many other proteins can compete with C3 for binding to a biomaterial surface, has not been demonstrated.

Membrane Attack Complex

All three pathways lead to a common point: cleavage of C5 to produce C5b and C5a. C5a is a potent inflammatory mediator and is discussed later in the context of receptor-mediated white blood cell (WBC) activation. The production of C5b initiates the formation of a macromolecular complex of proteins called the MAC that disrupts the cellular lipid bilayer, leading to cell death (Table 2.2.4.5). The sequence of events in MAC formation is outlined in Fig. 2.2.4.3.

Following cleavage of C5 by C5 convertase, the C5b remains weakly bound to C3b in an activated state in which it can bind C6 to form a stable complex called C5b6. This complex binds to C7 to form C5b67, which has amphiphilic properties that allow it to bind to, and partially insert into, lipid bilayers. The C5b67 complex then binds C8 and inserts itself into the lipid bilayer. The C5b678 complex disrupts the plasma membrane and produces small pores ($r \sim 1$ nm) that permit leakage of small molecules. The final step occurs when multiple copies of C9 bind to the C5b678 complex and insert into the membrane. This enlarges the pore to about 10 nm, and can lead to lysis and cell death. Even at sublytic levels, formation of MAC on host cells results in a number of activation responses (elevated Ca²⁺, arachidonic acid metabolism, cytokine production).

In addition to the usual means of generating C5b (i.e., through C5 convertase activity), several groups (Vogt, 1996; Vogt et al., 1992) have shown that C5 can be modified by a variety of oxidizing agents (H₂O₂, superoxide anion, and others) to convert C5 into a C5b-like structure that will bind C6. The oxidized C5•C6 complex can bind C7, C8, and C9 to form lytic MAC. This mechanism of MAC formation may be relevant at sites where neutrophils and macrophages attempt to phagocytize a biomaterial, producing a variety of reactive oxygen species, or in hypoxia/reperfusion settings (angioplasty, cardiopulmonary bypass [CPB], etc.).



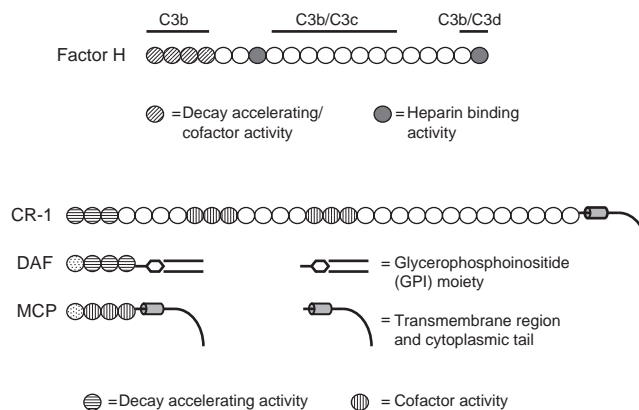
• **Figure 2.2.4.6** Control of complement activation occurs by various mechanisms, and is facilitated by a number of different proteins in the plasma (fH, fI, C1 Inh, C4BP, sCPN, S protein, and clusterin) or on cell surfaces (CR1s, DAF, MCP, and CD59). Decay acceleration refers to the increased rate of displacement of either C2b or fBb from classical pathway or alternative pathway convertases. Cofactor activity refers to the increased rate of factor I-mediated proteolysis facilitated by some proteins; MAC, membrane attack complex.

Control Mechanisms

Various types of control mechanisms have evolved to regulate the activity of the complement system at numerous points in the cascade (Liszewski et al., 1996; Bajic et al., 2015). These mechanisms are shown in Fig. 2.2.4.6 and include: (1) decay (dissociation) of convertase complexes; (2) proteolytic degradation of active components that is facilitated by several cofactors; (3) protease inhibitors; and (4) association of control proteins with terminal components that interfere with MAC formation. Without these important control elements, unregulated activation of the cascade results in overt inflammatory damage to various tissues, and has been demonstrated to contribute to the pathology of many diseases (discussed later). Some of these regulatory components have been leveraged to control complement activation by biomaterials (discussed later).

Starting at the top of the cascade, control of classical and lectin pathway activation is mediated by a protein called C1-Inh. C1-Inh acts by binding to activated C1r and C1s subunits in C1, as well as MASP proteases bound to MBL. C1-Inh actually forms a covalent bond with these proteases, thus irreversibly inactivating these proteins. The effectiveness of this interaction is illustrated by the short half-life of C1s under physiological conditions (13 s). The classical/lectin pathway C3/C5 convertase (C4b•C2b complex) spontaneously “decays” by dissociation of the C2b catalytic subunit. The rate of dissociation is increased by C4bp, which competes with C2 for a binding site on C4b. C4bp also acts as a cofactor for another control protein called factor I, which destroys the C4b by proteolytic degradation (Figs. 2.2.4.2 and 2.2.4.6).

The AP is also highly regulated by mechanisms that are very similar to the CP. The intrinsic instability of the C3b thioester bond (half-life = 60 μ s) ensures that most of the C3b (80%–90%) is inactivated in the fluid phase. Once formed, the C3 convertase (C3b•Bb complex) also spontaneously dissociates, and the rate of “decay” is increased by



• **Figure 2.2.4.7** Structure–activity relationships for complement control proteins. Each circle represents one short consensus repeat (SCR) domain, made up of about 60 amino acids. These SCR domains are strung together to create the different structures shown; CR-1, complement receptor 1; DAF, decay-accelerating factor; MCP, membrane cofactor protein.

factor H. Aside from accelerating the decay of C3 convertase activity, factor H also promotes the proteolytic degradation of C3b by factor I (Figs. 2.2.4.2 and 2.2.4.6). Factors H and I also combine to limit the amount of active C3(H₂O) produced in the fluid phase.

In addition to factor H, there are several cell membrane-bound proteins that have similar activities and structures (Fig. 2.2.4.7). These proteins act to limit complement-mediated damage to autologous bystander cells. Decay-accelerating factor, or DAF, displaces Bb from the C3 convertase and thus destroys the enzyme activity. DAF is found on all cells in the blood (bound to the plasma membrane through a unique glycosylphosphatidylinositol [GPI] lipid group), but is absent in a disease called paroxysmal nocturnal hemoglobinuria, which manifests a high spontaneous rate of red blood cell (RBC) lysis. In addition to DAF, there are two other cell-bound control proteins: membrane cofactor protein (MCP) and complement receptor 1 (CR1; see later discussion). MCP is found on all blood cells except erythrocytes, while CR1 is expressed on most blood cells as well as cells in tissues such as the kidney. Both of these proteins display cofactor activity for the factor I-mediated cleavage of C3b. CR1 also acts like factor H and DAF to displace Bb from the C3 convertase. A soluble recombinant form of CR1 (sCR1) was originally described by Weisman et al. (1990), and later produced commercially (Avant [now Celldex] Immunotherapeutics). A number of investigations have used sCR1 to limit complement activation in various disease models (Couser et al., 1995; Larsson et al., 1997).

In contrast to the inhibitory proteins already discussed, properdin functions by binding to surface-bound C3b and stabilizing the C3 and C5 convertase enzymes. Work from several labs has suggested that properdin can bind to a number of AP activators (rabbit erythrocytes, zymosan, LPS, and apoptotic and necrotic cells) independent of C3b. This has led to an alternative model for AP activation on some surfaces, where properdin plays the initial role in

TABLE 2.2.4.6 Receptors for Complement Proteins

Receptor Name/Ligand	Structure	Cellular Distribution/Response
CR1/C3b, C4b	200,000 Da single chain	RBC, PMN, monocytes, B, and T cells/clearance of immune complexes, phagocytosis, facilitates cleavage of C3b to C3dg by factor I
CR2/C3dg	140,000 Da single chain	B cells/regulate B cell proliferation
CR4	150,000 Da α chain 95,000 Da β chain	PMN, platelets, B cells/leukocyte—endothelial cell interaction
CR3/iC3b, ICAM-1, β -glucan, fibrinogen, factor Xa	185,000 Da α chain 95,000 Da β chain	PMN, monocyte/phagocytosis of microorganisms, respiratory burst activity
C5a/C5a _{des Arg}	40,000 Da	PMN, monocytes, mast cells, T cells, epithelial and endothelial cells, hepatocytes, CNS, fibroblasts/chemotaxis, degranulation, hyperadherence, respiratory burst, cytokine production (IL-6, IL-8)
C3a/C3a _{des Arg}	65,000 Da	Mast cells, eosinophils (various tissues)/histamine release, IL-6 production
C1q/C1q	70,000 Da	PMN, monocytes, B cells/respiratory burst activity
H/H	50,000 Da (three chains)	B cells, monocytes/secretion of factor I, respiratory burst activity

PMN, polymorphonuclear neutrophil; *RBC*, red blood cell.

surface recognition, binds C3b, facilitates factor B binding, and helps drive AP activation (Spitzer et al., 2007; Kimura et al., 2008). Saggu et al. (2013) demonstrated that purified and gel-filtered properdin binds to activated but not resting platelets and facilitates complement activation on the platelet surface providing a mechanism for local complement activation at sites of thrombosis. Using purified and gel-filtered properdin is important in assessing the relevance of these experiments as Harboe et al. (2017) has recently demonstrated that some AP activators (zymosan, *E. coli*, *Neisseria meningitidis*, and human umbilical vein endothelial cells [ECs]) do appear to require prior deposition of C3b to bind properdin.

As with the other stages of the cascade, there are several control mechanisms that operate to limit MAC formation and the potential for random lysis of “bystander” cells. The short half-life of the activated C5b (2 min), and the propensity of the C5b67 complex to self-aggregate into a nonlytic form, helps limit MAC formation. In addition, a MAC inhibitor, originally called S protein and subsequently shown to be identical to vitronectin, binds to C5b67 (also C5b678 and C5b6789) and prevents cell lysis. Another way to control MAC on the surface of the cell is through the action of CD59. Like DAF/CD55, CD59 is a GPI lipid-linked membrane protein. It is widely distributed and found on erythrocytes, WBCs, ECs, epithelial cells, and hepatocytes. CD59 functions by interacting with C8 and C9, preventing functional assembly of MAC complexes on the cell membrane. Finally, cells are also able to form outward vesicles or exosomes, releasing a portion of their plasma membrane. These microvesicles have been shown to contain MAC, and MAC has been shown to stimulate

vesicle formation, leading to the suggestion that this may be a mechanism used by cells to physically remove MAC from the plasma membrane.

Complement Receptors

Except for the cytotoxic action of the MAC, most of the biological responses elicited by complement proteins result from ligand–receptor-mediated cellular activation (Sengelov, 1995; Bajic et al., 2015). These ligands are listed in Table 2.2.4.6 and are discussed briefly here.

The ability of complement to function in the opsonization of foreign elements is accomplished in large part by a set of receptors that recognize various C3 and C4 fragments bound to these foreign surfaces. These receptors are called CR1, CR2, CR3, and CR4. CR1 is found on a variety of cells, including RBCs, neutrophils, monocytes, B cells, and some T cells, and recognizes a site within the C3c region of C3b (Fig. 2.2.4.2). On neutrophils and monocytes, activated CR1 will facilitate the phagocytosis of C3b- and C4b-coated particles. On RBCs, CR1 acts to transport C3b-immune complexes to the liver for metabolism. As discussed earlier, CR1 is also a complement regulatory protein. CR2 is structurally similar to CR1 (with 16 short consensus repeat [SCR] domains; see Fig. 2.2.4.7), but recognizes the C3d fragment of C3b that is bound to antigen. CR2 is expressed on antigen-presenting cells, such as follicular dendritic cells and B cells, where it facilitates the process of antigen-immune complex-driven B cell proliferation, providing a link between innate and adaptive immunity. CR3 represents another complement receptor that binds to iC3b and β -glucan structures found on zymosan (yeast cell wall).

Also, on activated monocytes, CR3 has been shown to bind fibrinogen and factor Xa (of the coagulation cascade). CR3 is a member ($\alpha_M\beta_2$) of the β_2 -integrin family of cell adhesion proteins that includes leukocyte functional antigen-1 (LFA-1) and CR4. LFA-1, CR3, and CR4 are routinely referred to as CD11a, CD11b, and CD11c, respectively. Each of these proteins associates with a molecule of CD18 to form an α - β heterodimer that is then transported and expressed on the cell surface. These proteins help mediate the cell–cell interactions necessary for activities such as chemotaxis and cytotoxic killing. A genetic deficiency in CR3/LFA proteins leads to recurrent life-threatening infections. CR4 is found on neutrophils and platelets, and binds C3d and iC3b. CR4 may facilitate the accumulation of neutrophils and platelets at sites of immune complex deposition.

In contrast to the ligands discussed earlier, which remain attached to activating surfaces, C3a, C4a, and C5a are small cationic polypeptides that diffuse into the surrounding medium to activate specific cells. These peptides are called anaphylatoxins because they stimulate histamine release from mast cells and cause smooth muscle contraction, which can produce increased vascular permeability and lead to a fatal form of shock called anaphylactic shock. These activities are lost when the peptides are converted to their des Arg analogs (i.e., with the loss of their carboxyl terminal arginine residue, referred to as C3a_{des Arg}, C5a_{des Arg}, etc.). This occurs rapidly in vivo (intravascularly) and is catalyzed by serum carboxypeptidase N (Mueller-Ortiz et al., 2009).

In addition to their anaphylatoxic properties, C5a and C5a_{des Arg} bind to specific receptors originally found on neutrophils and monocytes. The receptors for both C5a and C3a have been cloned and sequenced. C5aR (CD88) has been shown to be expressed on ECs, hepatocytes, epithelial cells (lung and kidney tubules), T cells, and cells in the CNS, as well as on the myeloid cell lines (Monk et al., 2007). In addition, expression levels of C5aRs are increased on ECs and hepatocytes by exposure to LPS and IL-6. In myeloid cells (neutrophils and monocytes), the C5a–receptor interaction leads to a variety of responses, including chemotaxis of these cells into an inflammatory locus; activation of the cells to release the contents of several types of secretory vesicles and produce reactive oxygen species that mediate cell killing; increased expression of CR1, CR3, and LFA-1, resulting in cellular hyperadherence; and the production of other mediators such as various arachidonic acid metabolites and cytokines, e.g., IL-1, -6, and -8. Many of the adverse reactions seen during extracorporeal therapies, such as hemodialysis, are directly attributable to C5a production. C3aRs are expressed on a variety of cell types, including eosinophils, neutrophils, monocytes, mast cells, and astrocytes (in the CNS), as well as γ -IFN-activated T cells. In eosinophils, C3a elicits responses similar to C5a, including intracellular calcium elevation, increased endothelial cell adhesion, and the generation of reactive oxygen intermediates. In contrast, C3a has been shown to limit migration of neutrophils from the bone marrow into the blood, suggesting it may have antiinflammatory activity in some settings (Coulthard and Woodruff, 2015).

Measurement of Complement Activation

There are numerous methods that have been developed over the decades to measure complement activation in biological fluids (Harboe et al., 2011). This discussion will be limited to those assays that are most common and commercially available, while also noting specific assays that have been suggested by regulatory authorities for use in characterizing the complement activating potential of materials used in medical devices. The oldest method to measure complement activation is the CH50 assay, which measures the residual hemolytic activity of complement in a plasma or serum sample. This assay was optimized in the early 1900s and utilizes a rabbit IgM antibody bound to sheep RBCs and largely measures the CP. A hemolytic assay for AP that uses rabbit RBCs is also available. These types of assays are not very sensitive and have been largely replaced by more sensitive and selective assays. These include enzyme-linked immunoassays (EIAs) for C4a, C3a, C5a, iC3b, SC5b-9, and other proteolytic split products generated during complement activation. The most commonly used assay is for C3a, which is an excellent marker for the early stages of complement activation, but does not distinguish between CP, LP, and AP activation mechanisms. Measuring C4a levels can help define pathway mechanisms, or, for in vitro experiments, measuring C3a levels with 5–10 mM EGTA-Mg (to bind excess calcium and inhibit CP/LP while permitting AP activation) can also be performed. EIAs for C5a and SC5b-9 are used to determine production of the C5a inflammatory mediator and activation of the terminal pathway. In whole blood samples, C5a is difficult to measure since it is rapidly bound up to cellular receptors and internalized. For this reason, many investigators prefer the SC5b-9 assay, which does not have this issue. However, in contrast to C5a, SC5b-9 has no biological activity, so some investigators prefer to measure biomaterial complement-activating potential in plasma samples where C5a can be assayed without the interference of C5a receptors. Regulatory groups such as the International Standards Organization (ISO) provide guidance on various aspects of measuring the suitability of medical plastics used in medical devices. ISO 10993-Part 4 defines methods for measuring blood–material interactions and suggests using the EIAs for C3a and SC5b-9 for this purpose.

Measurement of complement activity will depend on the type and dose of anticoagulant used in the study. For in vitro experiments using whole blood or plasma samples, heparin at 1–2 IU/mL is the preferred anticoagulant. Heparin or its analogs can also be used but is more expensive than heparin and not as clinically relevant. Citrate should be avoided as it will bind up calcium (and some magnesium) and, depending on the citrate concentration, will partially or completely inhibit complement activation (Huang et al., 2015). For clinical samples, for control in vitro samples, or for any sample where further complement activation is to be stopped, EDTA at 5–10 mM should be used.

TABLE 2.2.4.7 Complement–Coagulation Interactions

Complement Component(s)	Coagulation Component(s)	Type of Interaction
C3, C5, factor B	Thrombin	Proteolysis of C3, C5, FB by thrombin
C3, C5, C1s	Plasmin	Proteolysis of C3, C5, FB during fibrinolysis
C3, factor B	Kallikrein, thrombin	Kallikrein cleaves C3 and FB; C3 convertase (Bb) cleaves thrombin
C5a	Tissue factor	C5a stimulates TF production from platelets and endothelial cells
C5b-9	Platelets	Sublytic MAC activates platelets
C3, properdin	Platelets	Platelets act as a complement-activating surface

MAC, membrane attack complex; TF, tissue factor.

Complement–Coagulation System Interactions

Evidence accumulated over the last three decades has demonstrated numerous interactions between the complement and coagulation cascades (reviewed in [Oikonomopoulou et al., 2012](#)). The interactions can be classified into two distinct types: (1) protein–protein interactions and (2) protein–cell or platelet interactions. Some examples of this crosstalk between complement and coagulation are shown in [Table 2.2.4.7](#) and are discussed in more detail later.

A number of studies have shown that activated coagulation proteins can cleave both C3 and C5, generating active fragments that result in further complement activation and inflammatory responses. [Amara et al. \(2010\)](#) demonstrated that the order of efficiency in the cleavage of C3 by various coagulation proteases is: FXa > plasmin > thrombin > FIXa > FXIa. This activity is consistent with the long-standing observation that background values of C3a and C5a are 5–10-fold greater in serum compared to EDTA-anticoagulated plasma (see the section “Measurement of Complement”). Conversely, it has also been shown that C3 convertase (C3bBb) and MASP-1 and MASP-2 ([Fair et al., 1981](#); [La Bonte, 2012](#)) can cleave prothrombin to thrombin. Several reports ([Ritis et al., 2006](#); [Redecha et al., 2007](#)) have demonstrated that C5a can stimulate WBCs to express tissue factor (TF). TF can then activate prothrombin-to-thrombin conversion via the extrinsic pathway of coagulation. Hemodialysis on complement-activating membranes has been shown to correlate with increased expression of WBC TF and decreased prothrombin time values during clinical hemodialysis ([Kourtzelis et al., 2010](#)). Finally, C1 esterase inhibitor binds to FXIIa and activated kallikrein to inhibit their activity (in addition to its ability to inhibit C1r, C1s, and MASP proteases). A genetic deficiency of C1INH underlies the pathology of hereditary angioedema, a life-threatening condition where uncontrolled bradykinin production (generated from prokallikrein) can lead to severe edema in the airways.

The second type of interaction occurs when complement proteins bind to platelets, ECs, or WBCs. Stimulation of TF on WBCs by C5a was discussed earlier. Complement activation has also been shown to stimulate TF expression on ECs, involving both C5a and MAC ([Oikonomopoulou et al., 2012](#)). C1q has been shown to bind to a receptor on platelets and inhibit collagen-induced platelet aggregation. Factor D has been shown to compete with thrombin for binding to protease-activated receptors on platelets and inhibit thrombin-induced platelet aggregation. Binding of C5b-9 to platelets (at sublytic levels) has been shown to result in platelet activation (due to increased intracellular calcium concentrations), including degranulation of α -granules and release of microvesicles that are enriched in prothrombinase activity ([Sims and Wiedmer, 1991](#)). Activated platelets in turn have been demonstrated to promote complement activation on their surface ([Peerschke et al., 2010](#)).

Clinical Correlates

The normal function of complement is to mediate a localized inflammatory response to a foreign material. The complement system can become clinically relevant in situations where it either fails to function or where it is activated inappropriately; some of these settings are shown in [Table 2.2.4.8](#) ([Markiewski and Lambris, 2007](#); [Unsworth, 2008](#); [Nilsson et al., 2007](#)). In the first instance, a lack of activity due to a genetic deficiency in one or more complement proteins has been associated with increased incidence of recurrent infections (MBL deficiency in children), autoimmune disease (over 90% of C1-deficient patients develop systemic lupus erythematosus), and other pathologies (for example, a deficiency of C1 inhibitor is the cause of hereditary angioedema, as already noted). A recent genomic analysis has linked a mutation in factor H to various diseases. The strongest association has been made with the development of adult macular degeneration (AMD; [Klein et al., 2005](#)). The mutation has been shown to decrease the interaction of factor H with cell surface sugars, linking this loss in cell surface control of complement to the development of AMD and other diseases ([Schmidt et al., 2008](#)). This is

TABLE 2.2.4.8 Clinical Settings Involving Complement

Hemodialysis and Cardiopulmonary Bypass
Kidney disease (atypical hemolytic uremic syndrome, glomerulonephritis)
Ischemia/reperfusion injury (e.g., trauma, surgical settings)
Sepsis and adult respiratory distress syndrome
Recurrent infections
Transplantation
Rheumatoid arthritis
Systemic lupus erythematosus
Asthma
Alzheimer's disease
Hereditary angioedema
Adult macular degeneration

also an example of inappropriate activation, which can occur in a variety of circumstances. It is now recognized that ECs exposed to hypoxic conditions (ischemia due to angioplasty or a blocked artery due to atherosclerosis) activate complement following reperfusion of the blocked vessel. This results in further damage to the vessel wall, and eventually to the surrounding tissue. Activation of the CP by immune complexes occurs in various autoimmune diseases, such as systemic lupus erythematosus and rheumatoid arthritis. Glomerular deposition of immune complexes results in local inflammation that can contribute to a type of kidney damage called glomerulonephritis (GN). Quite a bit of experimental and clinical data have accumulated demonstrating that complement directly contributes to the initiation and/or progression of GN (Table 2.2.4.9), resulting in the development of end stage renal disease, and the necessity of hemodialysis therapy.

One of the major settings where complement has been implicated in adverse clinical reactions is during extracorporeal therapies such as hemodialysis, cardiopulmonary bypass, and apheresis therapy. The same nonspecific mechanism, which permits the AP to recognize microbes, results in complement activation by the various biomaterials found in different medical devices. The following discussion summarizes the clinical experience with hemodialysis and cardiopulmonary bypass, but many of the observations concerning complement activation and WBC activation are relevant to other medical biomaterial applications.

One of the major settings where complement has been implicated in adverse clinical reactions is during extracorporeal therapies such as hemodialysis, cardiopulmonary bypass, and apheresis therapy. The same nonspecific mechanism, which permits the AP to recognize microbes, results in complement activation by the various biomaterials found in different medical devices.

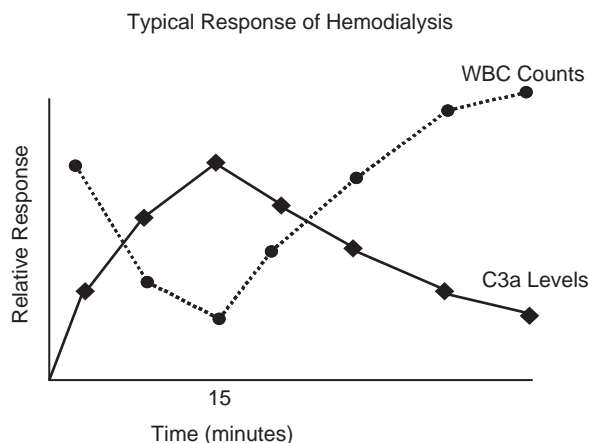
TABLE 2.2.4.9 Types of Studies Demonstrating a Role for Complement in Kidney Disease

Deficiency of loss of Complement Regulatory activity results in tissue damage
Mechanistic and knockout studies implicate complement and C5 in particular
Ongoing glomerular disease is associated with various indices of complement activation
Inhibition of complement activation attenuates tissue damage in model systems

TABLE 2.2.4.10 Clinical Symptoms Associated With Cuprophane-Induced Biocompatibility Reactions

Cardiopulmonary	Pulmonary hypertension, hypoxemia, respiratory distress (dyspnea), neutropenia (pulmonary leukosequestration), tachycardia, angina pectoris, cardiac arrest
Other	Nausea, vomiting, diarrhea, fever, chills, malaise, urticaria, pruritus, headache

One of the most investigated materials (from the perspective of complement activation) is the cellulosic Cuprophane membrane used extensively for hemodialysis. Some of the adverse reactions that occur during clinical use of a Cuprophane dialyzer are listed in Table 2.2.4.10. Craddock et al (1977) showed that some of these same manifestations (neutropenia, leukosequestration, and pulmonary hypertension) could be reproduced in rabbits and sheep when the animals were infused with autologous plasma that had been incubated in vitro with either Cuprophane or zymosan. This effect could be abrogated by treatment of the plasma to inhibit complement activation (heating to 56°C or addition of EDTA), thus linking these effects with complement. The development and use of specific radioimmunoassays to measure C3a and C5a by Dennis Chenoweth (1984) led to the identification of these complement components in the plasma of patients during dialysis therapy. A typical patient response to a Cuprophane membrane is shown schematically in Fig. 2.2.4.8. The C3a (and C5a) levels rise during the first 5–15 min, peaking between 10 and 20 min. For a Cuprophane membrane, typical peak C3a levels range from 4000 to 6000 ng/mL. During this period the WBCs become hyperadherent and are trapped in the lung, resulting in a peripheral loss of these cells (neutropenia). As complement activation is controlled (e.g., by factor H), the C3a and C5a levels decrease to baseline levels, and the WBC returns to the peripheral circulation, now in a more activated (primed) state. This is a very consistent response, and many authors have noted a direct correlation between the extent of complement

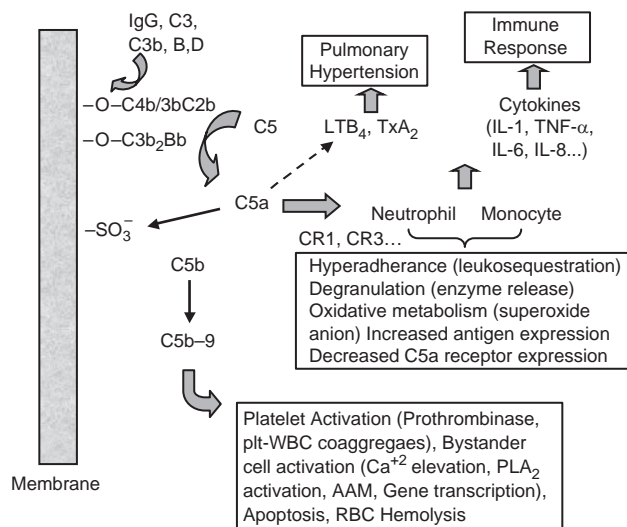


• **Figure 2.2.4.8** A typical response pattern to dialysis with a complement-activating hemodialysis membrane. Many investigators have noted that the extent of C3a production is directly proportional to the degree of neutropenia at the same time points; *WBC*, white blood cells.

activation and the degree of neutropenia (as well as other responses such as CR3 expression) seen with various dialysis membranes.

Based on our understanding of the biochemistry of complement and its biological actions, the following scenario can be drawn (Fig. 2.2.4.9). Contact by blood with the membrane results in initial protein deposition, including IgG, C3, and especially C3b, eventually leading to the formation of C3 and C5 convertase enzymes. Conversion of C5 results in C5a production, which leads to receptor-mediated neutrophil and monocyte activation. Production of C5b leads to MAC formation, which binds to bystander cells and results in subsequent activation of these cells through calcium-dependent mechanisms. Recognition of biomaterial-bound C3 and C4 fragments by WBC results in cell adherence and further activation of these cells. These various responses account for much of the pathophysiology seen clinically. The critical role of C5a in mediating many of these adverse reactions was confirmed in experiments employing purified sheep C5a. Infusion of this isolated peptide into sheep, in a manner that would simulate exposure to this molecule during hemodialysis, produced dose-dependent responses identical to those seen when the sheep are subjected to dialysis (Johnson et al., 1996). In addition, numerous *in vivo* and *in vitro* studies have documented the relationship between complement activation by biomaterials, the extent of WBC activation, and the resulting inflammatory response illustrated in Fig. 2.2.4.9 (Lewis and Van Epps, 1987; Gemmell et al., 1996; Larsson et al., 1997; Tang et al., 1998).

In the same timeframe that clinicians were linking complement with leukopenia in the hemodialysis setting, a number of cardiovascular scientists were demonstrating complement activation by the materials used to make cardiopulmonary bypass circuits. Typical levels of C3a produced in these procedures ranged from 300 to 2400 ng/mL. These investigations soon associated C3a and C5a production with a group of symptoms known as “postperfusion” or “postpump”



• **Figure 2.2.4.9** The biochemical basis for complement-mediated adverse reactions during extracorporeal therapy. Production of C5a leads to receptor-dependent white blood cell activation. This results in profound neutropenia, increased concentrations of degradative enzymes, and reactive oxygen species that ultimately may lead to tissue damage and dysfunction of these important immune cells. Generation of secondary mediators, such as arachidonic acid metabolites (TxA₂, LTB₄) and cytokines, can have profound consequences on whole organ systems. Finally, formation of the membrane attack complex (C5b-9) has been linked with increased hemolysis during cardiopulmonary bypass, formation of microparticles, and has been shown to increase platelet prothrombinase activity *in vitro*. This last observation suggests that surfaces that activate complement aggressively may be more thrombogenic; *RBC*, red blood cell; *WBC*, white blood cell.

TABLE 2.2.4.11 Postperfusion or Postpump Syndrome

Increased capillary permeability with accumulation of interstitial fluid
Blood loss requiring transfusions
Fever
Leukocytosis (increased white blood cell counts)
Organ dysfunction: heart, liver, kidney, brain, and gastrointestinal tract

syndrome (Table 2.2.4.11). Further analysis showed that complement was activated by the materials in the circuit (such as the polypropylene membranes and the nylon filters), but was also activated during neutralization of the heparin anticoagulant with the protamine sulfate that was given to each patient at the end of the operation. This was further exacerbated by complement activation that occurred in the ischemic vascular bed upon reperfusion of the tissue that also occurred at the end of the procedure. The importance of complement activation, and C5 conversion in particular, to the clinical outcome of CPB patients was clearly demonstrated in a study by Fitch et al. (1999). These investigators showed, using a single chain anti-C5 antibody fragment that inhibited C5a and MAC generation during the procedure, that this antibody fragment

lowered WBC activation, blood loss, cognitive deficits, and myocardial injury. Subsequent studies demonstrated that this complement inhibitor significantly reduced mortality in higher risk cardiac surgical patients (Haverich et al., 2006). These results are consistent with other studies (Velthuis et al., 1996; Hsu, 2001) using heparin-coated CPB circuits that demonstrate lower inflammatory indices (complement, cytokine, and elastase levels) that are associated with improved clinical outcomes (less blood loss, shorter ICU stays, and lower morbidity).

The CPB experience with heparin-coated devices demonstrates that modification of device materials (or the blood-contacting surfaces of those materials) can dramatically limit complement activation and the subsequent inflammatory response. Based in part on this and similar observations, hemodialyzer/membrane manufacturers began developing new membranes to produce more biocompatible (i.e., less complement-activating) devices. These new membranes tend to fall into two groups: moderately activating modified cellulose (such as cellulose acetate, hemophane, and cellulose triacetate) and low activating synthetics (such as polyacrylonitrile [AN69], polymethylmethacrylate, and polysulfone). Moderately activating modified cellulose produce C3a levels and neutropenic responses that are about 50% of Cuprophan levels, while the synthetic materials display 0%–20% activation compared to Cuprophan. Based on the known properties of complement, and the structures of these membranes, the reasons for the improved biocompatibility can be rationalized as follows. Most of these materials have a diminished level of surface nucleophiles. In theory, this should result in lower deposition of C3b, and in fact this has been verified experimentally. The diminished capacity to bind C3b results in lower levels of C3 and C5 convertase activity, and consequently a reduced production of C3a and C5a. Patient exposure to C5a is reduced even further by materials that allow for transport through the membrane to the dialysate (for example, high-flux membranes such as polysulfone will do this) or by absorbing the peptide back onto the surface (the negatively charged AN69 has been shown to have a high capacity for binding cationic C5a). Thus limiting C3b deposition and C5a exposure are two proven mechanisms of avoiding the clinical consequences of complement activation.

The same result can also be accomplished by facilitating the normal control of C3 convertase by factor H. Kazatchkine et al. (1979) have shown that heparin, coupled to either zymosan or Sepharose, limits the normal complement activation that occurs on these surfaces by augmenting C3b inactivation through factors H and I. Presumably, this accounts for the improved biocompatibility of heparin-coated circuits used in CPB described earlier. Mauzac et al. (1985) prepared heparin-like dextran derivatives that are extensively modified with carboxymethyl and benzylamine sulfonate groups. These researchers have shown that these modifications diminish complement activation by the dextran substrate. A simple modification of cellulose membranes (Cuprophan) with maleic anhydride has been

shown to limit the complement-activating potential of these materials by over 90% (Johnson et al., 1990). Again, increased binding of factor H to surface-bound C3b appears to account for the improved biocompatibility of maleated cellulose. Wu et al (2011) discovered peptides that displayed a high affinity for factor H. When these peptides were coupled to a biomaterial, the surface was protected from complement attack. Thus materials that limit complement activation through normal regulatory mechanisms are on hand, and may prove to be the next generation of complement-compatible materials. In addition, pharmaceutical control of complement is now possible with agents that are FDA approved (Alexion's Solaris) or now in clinical development (Ricklin et al., 2017).

Thus materials that limit complement activation through normal regulatory mechanisms are on hand, and may prove to be the next generation of complement-compatible materials. In addition, pharmaceutical control of complement is now possible with agents that are FDA approved (Alexion's Solaris) or now in clinical development (Ricklin et al., 2017).

Summary and Future Directions

The immune response to a biomaterial involves both humoral and cellular components. Activation of the complement cascade by either classical, lectin, or alternative pathways leads to the deposition of C4b and C3b proteins. Recognition of these molecules by receptors on granulocytes can cause activation of these cells, leading to the production of degradative enzymes and destructive oxygen metabolites. Recognition of C4b or C3b by other proteins in the cascade leads to enzyme formation (C3 and C5 convertases), which amplifies the response and can lead to the production of a potent inflammatory mediator, C5a. C5a binds to specific receptors found on polymorphonuclear leukocytes and monocytes. The interaction of C5a with these cells elicits a variety of responses, including hyperadherence, degranulation, superoxide production, chemotaxis, and cytokine production. Systemic exposure to C5a during extracorporeal therapies has been associated with neutropenia and cardiopulmonary manifestations (Tables 2.2.4.10 and 2.2.4.11) that can have pathologic consequences. The other portion of the C5 protein, C5b, leads to the formation of a MAC that activates cells at sublytic levels and has cytotoxic potential if produced in large amounts. The control of these processes is understood well enough to begin designing materials that are more biocompatible. Limiting C3b deposition (nucleophilicity), adsorbing C5a to negatively charged surface groups, and facilitating the role of factors H and I are three approaches that have been shown to be effective. Translating the last mechanism into commercial materials is one of the major challenges facing the development of truly complement-compatible membranes. Pharmacological control of complement activation is also possible with several inhibitors that are either FDA approved or are in late-stage clinical development.

References

- Ammara, U., Flierl, M.A., Rittirsch, D., Klos, A., Chen, H., Ackers, B., Bruckner, U.B., Nilsson, B., Gebhard, F., Lambris, J.D., Huber-Lang, M., 2010. Molecular inter-communication between complement and coagulation systems. *J. Immunol.* 185, 5628–5636.
- Andersson, J., Ekdahl, K.N., Lambris, J.D., Nilsson, B., 2005. Binding of C3 fragments on top of adsorbed plasma proteins during complement activation on a model biomaterial surface. *Biomaterials* 26, 1477–1485.
- Andersson, J., Ekdahl, K.N., Larson, R., Nilsson, U.R., Nilsson, B., 2002. C3 adsorbed to a polymer surface can form initiating alternative pathway convertase. *J. Immunol.* 168, 5786–5791.
- Bajic, G., Degn, S.E., Theil, S., Andersen, G.R., 2015. Complement activation, regulation and molecular basis for complement-related diseases. *EMBO J.* 34, 2735–2757.
- Banda, N.K., Mehta, G., Chao, Y., Wang, G., Inturi, S., Fossati-Jimack, L., Botto, M., Wu, L., Moghimi, S.M., Simberg, D., 2014. Mechanisms of complement activation by dextran-coated superparamagnetic iron oxide (SPIO) nanoworms in mouse versus human serum. *Part. Fibre Toxicol.* 11, 64–74.
- Bohlsion, S.S., Fraser, D.A., Tenner, A.J., 2007. Complement proteins C1q and MBL are pattern recognition molecules that signal immediate and long-term protective immune functions. *Mol. Immunol.* 44, 33–43.
- Chenoweth, D.E., 1984. Complement activation during hemodialysis: clinical observations, proposed mechanisms and theoretical implications. *Artif. Organs* 8, 231–287.
- Cooper, N.R., 1985. The classical complement pathway: activation and regulation of the first complement component. *Adv. Immunol.* 37, 151–216.
- Coulthard, L.G., Woodruff, T.M., 2015. Is the complement activation product C3a a proinflammatory molecule? Re-evaluating the evidence and myth. *J. Immunol.* 194, 3542–3548.
- Couser, W.G., Johnson, R.J., Young, B.A., Yeh, C.G., Toth, C.A., Rudolph, A.R., 1995. The effects of soluble complement receptor 1 on complement-dependent glomerulonephritis. *J. Am. Soc. Nephrol.* 5, 1888–1894.
- Craddock, P.R., Fehr, J., Brigham, K.L., Kronenberg, R.S., Jacob, H.S., 1977. Complement and leukocyte-mediated pulmonary dysfunction in hemodialysis. *N. Engl. J. Med.* 296, 769–774.
- Dobo, J., Szakacs, S., Oroszlan, G., Kortvely, E., Kiss, B., Boros, E., Szasz, R., Zavodszky, P., Gal, P., Pal, G., 2016. MASP-3 is the exclusive pro-factor D activator in resting blood: the lectin and the alternative complement pathway are fundamentally linked. *Sci. Rep.* 6, 31877.
- Fair, D.S., Sundsmo, J.S., Schwartz, B.S., Edgington, T.S., Muller-Eberhard, H.J., 1981. Prothrombin activation by factor B (Bb) of the alternative pathway of complement. *Thromb. Hemost.* 46, 301–309.
- Fitch, J.C.K., Rollins, S., Matis, L., Alford, B., Aranki, S., Collard, C.D., Dewar, M., Eleftheriades, J., Hines, R., Kopf, G., Kraker, P., Li, L., O'Hara, R., Rinder, C., Rinder, H., Shaw, R., Smith, B., Stahl, G., Shernan, S., 1999. Pharmacology and biological efficacy of a recombinant humanized, single-chain antibody C5 complement inhibitor in patients undergoing coronary artery bypass graft surgery with cardiopulmonary bypass. *Circulation* 100, 2499–2506.
- Gemmell, C.H., Black, J.P., Yeo, E.L., Sefton, M.V., 1996. Material-induced up-regulation of leukocyte CD11b during whole blood contact: material differences and a role for complement. *J. Biomed. Mater. Res.* 32, 29–35.
- Harboe, M., Johnson, C., Nymo, S., Ekholt, K., Schjalm, C., Lindstad, J.K., Pharo, A., Hellerud, B.C., Ekdahl, K.N., Mollnes, T.E., Nilsson, P.H., 2017. Properdin binding to complement activating surfaces depends on initial C3b deposition. *Proc. Natl. Acad. Sci. USA* 114, E534–E539.
- Harboe, M., Thorgersen, E.B., Mollnes, T.E., 2011. Advances in assay of complement function and activation. *Adv. Drug Deliv. Rev.* 63, 976–987.
- Haverich, A., Shernan, S., Levy, J.H., Chen, J.C., Carrier, M., Taylor, K.M., Van de Werf, F., Newman, M.F., Adams, P.X., Todaro, T.G., van der Laan, M., Verrier, E.D., 2006. Pexelizumab reduces death and myocardial infarction in higher risk cardiac surgical patients. *Ann. Thorac. Surg.* 82, 486–493.
- Heja, D., Kocsis, A., Dobo, J., Szilagyi, K., Szasz, R., Zavodszky, P., Pal, G., Gal, P., 2012. Revised mechanism of complement lectin-pathway activation revealing the role of serine protease MASP-1 as the exclusive activator of MASP-2. *Proc. Natl. Acad. Sci. U.S.A.* 109, 10498–10503.
- Hsu, L.-C., 2001. Heparin-coated cardiopulmonary bypass circuits: current status. *Perfusion* 16, 417–428.
- Huang, S., Sandholm, K., Jansson, N., Nilsson, A., Wieslander, A., Grundstrom, G., Hancock, V., Ekdahl, K.N., 2015. Low concentrations of citrate reduce complement and granulocyte activation in vitro in human blood. *Clin. Kidney J.* 8, 31–37.
- Johnson, R.J., Lelah, M.D., Sutliff, T.M., Boggs, D.R., 1990. A modification of cellulose that facilitates the control of complement activation. *Blood Purif.* 8, 318–328.
- Johnson, R.J., Burhop, K.E., Van Epps, D.E., 1996. Infusion of ovine C5a into sheep mimics the inflammatory response of hemodialysis. *J. Lab. Clin. Med.* 127, 456–469.
- Kazatchkine, M., Fearon, D.T., Silbert, J.E., Austen, K.F., 1979. Surface-associated heparin inhibits zymosan induced activation of the human alternative complement pathway by augmenting the regulatory action of control proteins. *J. Exp. Med.* 150, 1202–1215.
- Kimura, Y., Miwa, T., Zhou, L., Song, W.-C., 2008. Activator-specific requirement of properdin in the initiation and amplification of the alternative pathway complement. *Blood* 111, 732–740.
- Klein, R.L., Zeiss, C., Chew, E.Y., Tsai, J.-Y., Sackler, R.S., Haynes, C., Henning, A.K., SanGiovanni, J.P., Mane, S.M., Mayne, S.T., Bracken, M.B., Ferris, F.L., Ott, J., Barnstable, C., Hoh, J., 2005. Complement factor H polymorphism in age-related macular degeneration. *Science* 308, 385–389.
- Kourtzelis, I., Markiewski, M.M., Doumas, M., Rafail, S., Kambas, K., Mitroulis, I., Panagoutsos, S., Passadakis, P., Vargemzis, V., Magotti, P., Qu, H., Mollnes, T.E., Ritis, K., Lambris, J.D., 2010. Complement anaphylatoxin C5a contributes to hemodialysis-associated thrombosis. *Blood* 116, 631–639.
- La Bonte, L.R., Pavlov, V.I., Tan, Y.S., Takahashi, K., Takahashi, M., Banda, N.K., Zou, C., Fujita, T., Stahl, G., 2012. Mannose binding lectin-associated serine protease-1 is a significant contributor to coagulation in a murine model of occlusive thrombosis. *J. Immunol.* 188, 885–891.
- Larsson, R., Elgue, G., Larsson, A., Nilsson Ekdahl, K., Nilsson, U.R., Nilsson, B., 1997. Inhibition of complement activation by soluble recombinant CR1 under conditions resembling those in a cardiopulmonary circuit: upregulation of CD11b and complete abrogation of binding of PMN to the biomaterial surface. *Immunopharmacology* 38, 119–127.
- Lewis, S.L., Van Epps, D.E., 1987. Neutrophil and monocyte alterations in chronic dialysis patients. *Am. J. Kidney Dis.* 9, 381–395.
- Liszewski, M.K., Farries, T.C., Lubin, D.M., Rooney, I.A., Atkinson, J.P., 1996. Control of the complement system. *Adv. Immunol.* 61, 201–282.

- Manderson, A.P., Pickering, M.C., Botto, M., Walport, M.J., Parish, C.R., 2001. Continual low-level activation of the classical complement pathway. *J. Exp. Med.* 194, 747–756.
- Markiewski, M.M., Lambris, J.D., 2007. The role of complement in inflammatory diseases from behind the scenes into the spotlight. *Am. J. Pathol.* 171, 715–727.
- Matsushita, M., 1996. The lectin pathway of the complement system. *Microbiol. Immunol.* 40, 887–893.
- Mauzac, M., Maillat, F., Jozefonvicz, J., Kazatchkine, M., 1985. Anti-complementary activity of dextran derivatives. *Biomaterials* 6, 61–63.
- Monk, P.N., Scola, A.-M., Madala, P., Fairlie, D.P., 2007. Function, structure and therapeutic potential of complement C5a receptors. *Br. J. Pharmacol.* 152, 429–448.
- Mortensen, S.A., Sander, B., Jensen, R.K., Pedersen, J.S., Golas, M.M., Jensenius, J.C., Hansen, A.G., Thiel, S., Andersen, G.R., 2017. Structure and activation of C1, the complex initiating the classical pathway of the complement cascade. *Proc. Natl. Acad. Sci. U.S.A.* 114, 986–991.
- Mueller-Ortiz, S.L., Wang, D., Morales, J.E., Li, L., Chang, J.-Y., Wetsel, R., 2009. Targeted disruption of the gene encoding the murine small subunit of carboxypeptidase N (CPN1) causes susceptibility to C5a anaphylatoxin-mediated shock. *J. Immunol.* 182, 6533–6539.
- Nilsson, B., Nilsson Ekdahl, K., Mollnes, T.E., Lambris, J.D., 2007. The role of complement in biomaterial-induced inflammation. *Mol. Immunol.* 44, 82–94.
- Oikonomopoulou, K., Ricklin, D., Ward, P.A., Lambris, J.D., 2012. Interactions between coagulation and complement- their role in inflammation. *Semin. Immunopathol.* 34, 151–165.
- Peerschke, E.L., Yin, W., Ghebrehiwet, B., 2010. Complement activation on platelets: implications for vascular inflammation and thrombosis. *Mol. Immunol.* 47, 2170–2175.
- Pillemer, L., Blum, L., Lepow, I.H., Ross, O.A., Todd, E.W., Wardlaw, A.C., 1954. The properdin system and immunity. I. Demonstration and isolation of a new serum protein, properdin, and its role in immune phenomena. *Science* 120, 279–285.
- Rawal, N., Rajagopalan, R., Salvi, V.P., 2008. Activation of Complement Component C5; Comparison of the C5 convertases of the lectin and the classical pathway of complement. *J. Biol. Chem.* 283, 7853–7863.
- Redecha, P., Tilley, R., Tencat, M., Salmon, J., Kirchhofer, D., Machman, N., Giradi, G., 2007. Tissue factor: a link between C5a and neutrophil activation in anti-phospholipid antibody-induced fetal injury. *Blood* 110, 2423–2431.
- Ricklin, D., Barratt-Due, A., Mollnes, T.E., 2017. Complement in clinical medicine: clinical trials, case reports and therapy monitoring. *Mol. Immunol.* 89, 10–21.
- Ritis, K., Doumas, M., Mastellow, D., Micheli, A., Giaglis, S., Magotti, P., Raulf, S., Kartalis, G., Sidas, P., Lambris, J.D., 2006. A novel C5a-receptor-tissue factor cross-talk in neutrophils links innate immunity to coagulation pathway. *J. Immunol.* 177, 4794–4802.
- Ross, G.D., 1986. *Immunobiology of the Complement System*. Academic Press, New York.
- Schmidt, C.Q., Herbert, A.P., Hocking, H.G., Uhrin, D., Barlow, P.N., 2008. Translational mini-review series on complement factor H: structural and functional correlations for factor H. *Clin. Exp. Immunol.* 151, 14–24.
- Saggu, G., Cortes, C., Emch, H., Ramirez, G., Worth, R.G., Ferreira, V.P., 2013. Identification of a novel mode of complement activation on stimulated platelets mediated by properdin and C3(H₂O). *J. Immunol.* 190, 6457–6467.
- Schreiber, R.D., Pangburn, M.K., Lesaure, P.H., Muller-Eberhard, H.J., 1978. Initiation of the alternative pathway of complement: recognition of activators by bound C3b and assembly of the entire pathway from six isolated proteins. *Proc. Natl. Acad. Sci. U.S.A.* 75, 3948–3952.
- Sengelov, H., 1995. Complement receptors in neutrophils. *Crit. Rev. Immunol.* 15, 107–131.
- Sims, P., Wiedmer, T., 1991. The response of human platelets to activated components of the complement system. *Immunol. Today* 12, 338–342.
- Spitzer, D., Mitchell, L.M., Atkinson, J.P., Hourcade, D.E., 2007. Properdin can initiate complement activation by binding specific target surfaces and providing a platform for de novo convertase assembly. *J. Immunol.* 179, 2600–2608.
- Tang, L., Liu, L., Elwing, H.B., 1998. Complement activation and inflammation triggered by model biomaterial surfaces. *J. Biomed. Mater. Res.* 41, 333–340.
- Unsworth, D.J., 2008. Complement deficiencies and disease. *J. Clin. Pathol.* 61, 1013–1017.
- Velthuis, H., Jansen, P.G.M., Hack, E., Eijssman, L., Wildevuur, C.R.H., 1996. Specific complement inhibition with heparin-coated extracorporeal circuits. *Ann. Thorac. Surg.* 61, 1153–1157.
- Vogt, W., Zimmerman, B., Hesse, D., Nolte, R., 1992. Activation of the fifth component of human complement, C5, without cleavage, by methionine oxidizing agents. *Mol. Immunol.* 29, 251–256.
- Vogt, W., 1996. Complement activation by myeloperoxidase products released from stimulate human polymorphonuclear leukocytes. *Immunobiology* 195, 334–346.
- Weisman, H.F., Bartow, T., Leppo, M.K., Marsch Jr., H.C., Carson, G.R., Concino, M.F., Boyle, M.P., Roux, K.H., Weisfeldt, M.L., Fearon, D.T., 1990. Soluble human complement receptor type 1: in vivo inhibitor of complement suppressing post-ischemic myocardial inflammation and necrosis. *Science* 249, 146–151.
- West, E.E., Kolev, M., Kemper, C., 2018. Complement and the regulation of T cell responses. *Annu. Rev. Immunol.* 36, 309–338.
- Wong, N.K.H., Kojima, M., Dobo, J., Ambrus, G., Sim, R.B., 1999. Activities of the MBL-associated serine proteases (MASPs) and their regulation by natural inhibitors. *Mol. Immunol.* 36, 853–861.
- Wu, Y.-Q., Qu, H., Sfyroera, G., Tzekou, A., Kay, B.K., Nilson, B., Nilson-Ekdahl, K., Ricklin, D., Lambris, J.D., 2011. Protection of non-self surfaces from complement attack by factor H-binding peptides: implications for therapeutic medicine. *J. Immunol.* 186, 4269–4277.

Chapter Questions

1. Identify the typical activators of the (a) classical pathway, (b) lectin pathway, and (c) alternative pathway.
2. Name three approaches to limit complement activation by biomaterials.
3. ISO guidelines suggests two ways to monitor complement activation on blood-contacting materials, what are they?
4. Hemodialysis on complement-activating membranes produces a significant neutropenia within 15 min of initiating therapy. What complement component is responsible for this adverse event?
5. Explain why C3a and C5a levels are higher in serum compared to anticoagulated plasma.
6. Based on surface properties, rank these biomaterials in order of increasing potential to activate complement: Cuprophan hemodialysis (HD) membrane, cellulose triacetate HD membrane, polypropylene oxygenator membrane, nylon apheresis membrane, sulfonated nanomaterials.
7. Omeros is a biotechnology company developing inhibitors to MASP-2 and MASP-3 for the treatment of various pathologies. How would this help control AP activation?
8. During collection of plasma with an apheresis device containing a nylon membrane, both C3a and C5a levels are observed to increase modestly in both the collected plasma and in the blood returned to the donors. Citrate is the standard anticoagulant used in these procedures. Predict what would happen if heparin would be substituted for citrate in this clinical setting.
Answers to questions: 1. (a) Immune complexes, CRP; (b) mannose-containing polysaccharides, ficolins; (c) yeast or bacterial cell walls, biomaterials. 2. Limit surface nucleophiles for C3b attachment, remove C5a by filtration or binding to negatively charged groups, facilitate control by factor H (e.g., heparin coating), or pharmacologically. 3. C3a and SC5b-9 EIA methods. 4. C5a. 5. Thrombin produced during coagulation cleaves both C3 and C5 producing the anaphylatoxins. 6. Cuprophan > nylon membrane > cellulose triacetate > polypropylene oxygenator membrane > sulfonated materials. 7. MASP-3 cleaves profactor D to active factor D in blood, providing this important AP component. MASP-2 indirectly affects AP by activating C1, which forms the CP C3 convertase and produces C3b. C3b can then bind factor B and form the AP C3 convertase in an amplification loop. 8. Much higher levels of C3a and C5a would be produced since citrate partially inhibits complement activation.

2.2.5

Systemic and Immune Toxicity of Implanted Materials

AARON BARCHOWSKY

Department of Environmental and Occupational Health, University of Pittsburgh, Pittsburgh, PA, United States

Local adverse pathological effects, as well as distal organ and organ system effects, can result from absorption and distribution of materials leached from implanted devices and implant-associated compounds (e.g., cements and adhesives). Medical implants are composed of a large range of materials, including metals, metallic alloys, polymers, ceramics, hydrogels, and composites. In addition, the implants are often fixed into tissues with glues or cements that contain additional, potentially toxic compounds. Before they are clinically and commercially viable, all materials, devices, and degradation by-products must meet regulatory standards for biocompatibility and be proven to be nontoxic.

International and national regulatory agencies define biocompatibility for any sterile or nonsterile device that comes into direct or indirect contact with the human body as the potential for unacceptable adverse biological responses resulting from the contact. Biocompatibility endpoints that could be impacted by the materials in, on, or from an implanted device include cytotoxicity, sensitization, irritation or intracutaneous reactivity, acute, subchronic, and chronic systemic toxicity, material-mediated pyrogenicity, genotoxicity, hemocompatibility (hemolysis, complement activation, thrombosis), carcinogenicity, reproductive or developmental toxicity, and biodegradation (for absorbable materials). However, the expected duration of device contact and its expected permanence dictate which toxic endpoints might be expected and need to be confirmed not to occur. ISO 10993-1 guidelines triage toxicity testing by categorizing contact duration into three categories: limited (i.e., <24h), prolonged (i.e., >24h to 30 days), or permanent/long term (i.e., >30 days). Thus a device that is used for less than 30 days would not need to be tested for carcinogenicity and devices implanted in adults beyond developmental or reproductive age would not need to be tested for developmental and reproductive toxicity.

The fundamental principle of toxicology is that the dose makes the poison. The implication for implanted medical devices and associated materials is that, whether they are

designed to deliver bioactive compounds, degrade over time, or remain in place for a prolonged time or permanently, the materials they are made of must never be in a toxic concentration at the point of contact or be released from the device in a toxic concentration. This chapter will not discuss potential toxicities from drug delivery devices, but will discuss toxicities from materials released from implanted devices that are designed to degrade after providing benefit or that are permanently implanted. With the exception of pathologic calcification of certain polymer implants, the surface changes may not be significant for degrading the mechanical strength or intended use of the implant. However, the substances released have potential for biological incompatibilities in surrounding tissues and systemically in remote organs and in the immune system. The following discussion focuses on systemic toxic or hypersensitivity reactions caused by device-derived metals, chemicals, and composites.

Basic Principles of Systemic Distribution and Toxicity of Biomaterial Constituents

Conventionally, the major routes of exposure for toxic substances are the gastrointestinal tract (ingestion), the lungs (inhalation), and the skin (topical, percutaneous, or dermal). In contrast, exposure to the elemental and chemical constituents of implanted biomaterials results from absorption into local tissue and distribution systemically by blood and lymph vessels. Similar to conventional exposures, the elements and chemicals have to cross cell membranes and tissue layers for distribution through the body, for metabolism to either more toxic or less toxic compounds, and ultimately for excretion into urine, feces, sweat, hair, and nails. These are the basic kinetic principles of absorption, distribution, metabolism, and elimination for biological actions of device materials. Biomaterials would not be toxic if they were not absorbed or distributed to a target organ

in sufficient concentrations to elicit an adverse biological response. Nor would they be toxic if they were not metabolized to a more potent toxicant or eliminated rapidly enough to keep concentrations below toxic thresholds.

Simple diffusion of chemicals into surrounding tissues is possible, but is often limited by the chemical and physical properties of the released constituents. Small lipophilic chemicals readily cross the lipid bilayers of cells, but have limited solubility in the aqueous media of blood or lymph. In contrast, particulates, metals, and other charged molecules are not soluble in membranes and have limited access to cells. In both cases, distribution in aqueous media or across cell and organelle membranes is facilitated by binding to protein carriers, by transmembrane uptake mechanisms, or by channel proteins. Binding to serum proteins and lipid particles, especially albumin, globulins, and lipoproteins, allows systemic distribution of metals and lipophilic compounds in the blood and lymphatic system. Only the unbound or “free” fraction of the metals or chemicals is available for uptake into target cells and biological actions. In fact, many “free” endogenous and device-derived metal ions are toxic and it is extremely rare that metals have appreciable “free” fractions in the circulation or in cells, as they are chaperoned by carrier proteins and transported by relatively specific ion channels. As a defense mechanism that supplements elimination, metals or chemicals are stored away from biologic action by being deposited in bone, adipose tissues, and specialized storage proteins (e.g., metallothionein and ferritins). However, this deposition can ultimately be detrimental as the metal or chemical can have local effects in the deposits (e.g., stimulation of osteolysis in bone) or be a source of low-level chronic exposure (e.g., lead in bone, organic carcinogens in adipose tissues).

The blood and lymph flow in different tissues and organs varies greatly, which results in differences in both degradation pressure on the device and the volume of degradation by-products distributed away from the device. Physical or wear pressure can be substantial and result in catastrophic device failure with the release of both small and large particulate matter. There is a significant concern that distribution of large particles will cause life-threatening physical hazards of clogging capillaries or small blood vessels, especially in the lung (pulmonary embolism) and brain (stroke). However, it is more likely that due to their size or insolubility they will cause only local inflammation, foreign body reactions, and tissue necrosis. Small micron and submicron particulate matter can distribute systemically and be engulfed by cells through phagocytosis and endosomal processing. Lysosomal processing of the particles can liberate metal and chemical constituents within the cells if they are not eliminated through vesical release or secreted through channels.

The range of constituents and contaminants in biomaterials is immense given that devices are made from multiple classes of elements, alloys, chemicals, and composites. In turn, possible contaminants also include residual monomers, chemical initiators, plasticizers, antioxidants, bonding agents, and cements. Released constituents are subject to further metabolic oxidation, reduction, hydrolysis,

and conjugation reactions as the body attempts to utilize, detoxify, and eliminate the foreign compound. In general, highly lipophilic chemicals are oxidized by Phase I metabolizing enzymes (e.g., cytochrome p450 enzymes) to make them more reactive and soluble. The reactive metabolite can cause toxicity by covalently binding to proteins and nucleic acids (i.e., genotoxic). However, the reactive metabolite is more often reduced and conjugated by Phase II metabolism to produce aqueous soluble compounds for elimination. Reactive metabolites are generally not toxic unless they reach concentrations sufficient to overwhelm the Phase II metabolism. Even metals can be metabolized and most commonly are oxidized or reduced to form more or less reactive species. Ion channels that transport metals across cell membranes are highly charge specific and changing the charge or valence of the metal greatly affects cellular uptake and responses. Chromium is a prime example, as toxic hexavalent chromium(VI) is readily taken into the cell through sulfate and phosphate channels, while oxidation to chromium(III) creates an octahedral cation that does not cross the membrane (Standeven and Wetterhahn, 1989). Thus chromium(VI) is toxic and chromium(III) is relatively inert and nontoxic.

The key kinetic question is whether there is sufficient reactivity to implant constituents at point of contact to cause local toxicity or sufficient release of constituents to allow concentration-dependent toxic actions or immune responses in distal organs. Acute tissue injury and cell death are generally caused by much higher concentrations than morbidities or disease caused by chronic, low-level exposures. Carcinogenicity, for example, is generally promoted by low chronic levels of metals (e.g., chromium or tungsten), and it is more difficult to test for carcinogenicity given that there may be a latency period of years, even after removal of a device, before cancers appear. Acute release of constituents due to excessive wear or catastrophic device failure is the most common source of local and systemic toxicities.

Rapid degradation can result in physical tissue damage from acid/base reactions (e.g., metal oxides acting as Lewis acids) or creation of pockets of liberated gases. For example, in physiological medium, acute degradation of magnesium (Mg)-based degradable implants can release Mg^{2+} in sufficient quantities to release hydrogen to create gas pockets as the Mg reacts with water to form $Mg(OH)_2$. In turn, physiologic levels of chloride results in the formation of $MgCl_2$ from the $Mg(OH)_2$, and in the process releases hydroxide ions that increase local pH (Kamrani and Fleck, 2019).

Release of large amounts of metals and chemicals that are similar to essential metals or endogenous compounds can produce systemic injuries by mimicking or displacing the essential metals (e.g., nickel or cobalt inhibition of cardiac calcium channels, manganese toxicity in neural tissue) or creating tissue damage in metabolizing organs (e.g., liver toxicity). Chronic low-level release can affect cell-signaling pathways that regulate distal organ metabolism or function (e.g., chronic acrylamide and other type-2 alkene inhibitions of presynaptic membrane proteins in neurotransmission). Chronic low levels of certain metals (e.g., cobalt) and organic

compounds (e.g., plasticizers, bisphenol A, phthalates, acrylamide) disrupt endocrine systems to cause systemic metabolic and reproductive toxicities. Thus complete testing for biocompatibility must address both possible tissue damage in target organs (e.g., histological assessment of pathology) and markers of target organ or homeostatic dysfunction (e.g., abnormal heart function, neurological disturbance, disturbed motor function, reproductive effects, and abnormal blood metabolite levels). The ISO 10993-1 (ISO, 2018) guidelines provide a risk assessment and triage system to identify which types of toxicity testing must be done based on the nature, organ placement, and duration of the implanted device. Standardized toxicity testing for regulatory approval of materials and devices should be performed using the internationally accepted guidelines and is facilitated by focusing on regulatory agency recommendations (e.g., FDA, 2019a).

Metals and Metal Alloy Toxicity

Metals comprise a substantial portion of medical implant materials and pose unique systemic toxicities relative to organic chemical constituents. The US Food and Drug Administration (FDA) Center for Devices and Radiological Health recently released a comprehensive review of biological responses to metal implants (FDA, 2019a). This was the result of extensive postmarket reviews of data associated with specific metal-containing implants after safety concerns were raised for metal-on-metal (MoM) or metal-on-polyethylene total hip arthroplasty systems, as well as metal-based intrauterine devices. In addition to being concerned with metal wear debris being associated with local pseudotumors and aseptic loosening of the prosthesis with subsequent need for revision, the review was concerned with broad systemic effects and symptoms that reflect susceptibility of recipient immune systems to metals in and from the devices.

The most common metals used in durable implants are stainless steel (iron-based alloys), cobalt-based alloys, chromium alloys, pure titanium, and nickel–titanium-based alloys. Various refractory metals (metals that are difficult to fuse or corrode), such as molybdenum, tungsten, vanadium, and tantalum, have also been used as alloying elements in implantation materials. Noble metals, such as gold, silver, platinum, and iridium, are common in implants with electronic components. Recently developed implants designed to degrade after they provide benefit are primarily based on pure magnesium, or magnesium and/or zinc alloys containing alkaline and rare earth metals (e.g., strontium, yttrium, lanthanides, etc.) (see Chapter 1.3.3D).

Many metals used in implants are “essential” metals that in appropriate amounts are critical to the structure and function of numerous human proteins and enzymes. For example, zinc is the second most abundant transition metal in the body (iron is the first) and is essential in 100–300 enzymatic reactions. Magnesium is the fourth most abundant element in the body and the second most abundant intracellular cation. However, when in an excess free concentration or in an inappropriate oxidation or valence state, these essential metals become toxic. Free metal concentrations and their access

to intracellular compartments and proteins is tightly controlled by chaperoning proteins, transport proteins, and ion channels. For example, there are over 30 highly conserved transporters and channels that maintain functional zinc levels. Toxicity to zinc will occur when these transport and chaperone systems fail or are overwhelmed, leading to neurologic disorders (e.g., ataxia, lethargy), impaired absorption of other essential metals, and tissue destruction from high zinc oxide levels that act as a strong Lewis acid. Displacement of or competition for zinc by other metals in these channels and enzymes can result in potentially toxic-free zinc concentrations or toxicity from loss of zinc-dependent function.

The metal transporters can also provide the beneficial effects of the essential metals. An example would be the TRPM7 ion channel that, in addition to transporting magnesium, zinc, and calcium into cells, can act as a signaling enzyme and epigenetic regulator of DNA changes (Wrighton, 2014; Krapivinsky et al., 2014). In this manner, magnesium transport through and activation of the channel stimulates angiogenesis and cell motility that promotes wound healing. However, excess activity of the channel can provide growth advantages to dysplastic tissues and cancers (Trapani et al., 2013).

Table 2.2.5.1 lists essential metals used in medical devices and their potential systemic toxicities. The systemic toxicities of cobalt (Co) illustrate the concerns in evaluating systemic toxicity from metals, as well as potential mechanisms for metal-promoted toxicity. MoM or metal-on-polyethylene articulated implants represent the most prevalent nondietary and nonoccupational exposures to Co in the general population, with millions of articulations being implanted (Leyssens et al., 2017; Reich et al., 2019). Cobalt in trace amounts is an essential cofactor for vitamin B12 and lack of cobalt causes vitamin B12 deficiency. However, when cobalt levels rise above 300 µg/L in the blood of normal individuals, a syndrome of systemic toxicities, known as “arthroprosthetic cobaltism” syndrome, occurs (Leyssens et al., 2017). The blood levels needed to trigger the syndrome can be much less in susceptible individuals (FDA, 2019a; Leyssens et al., 2017; Reich et al., 2019). Co–chromium (Cr) is a common alloy for MoM implants due to resistance to corrosion and wear. Unfortunately, nanosized wear particles of CoCr can be liberated from the MoM implant. Although modern MoM implants are highly resistant to wear, particle release can be substantial in patients who received an MoM implant to replace a failed ceramic implant (i.e., more debris to grind the MoM implant), in patients with mixed manufacturers of MoM implants, and in poor placement or bilateral hip replacements (Leyssens et al., 2017; FDA, 2019a). Studies of periprosthetic tissues find insoluble Cr³⁺-containing nanoparticles, but the highly soluble Co²⁺ ions bind to synovial fluid proteins and adjacent tissue surfaces and are distributed in peripheral blood and lymph. There is a consensus that blood levels of 10 µg/L or less indicate normal implant wear and are not of concern. However, again this may not be protective of susceptible patients (Reich et al., 2019; Leyssens et al., 2017).

Ionized Co²⁺ is the primary toxic form for systemic toxicity and the free fraction of Co²⁺ ions is bioavailable for interaction with ion channels and cellular targets (Madl et al., 2015).

TABLE 2.2.5.1 Common Essential Metals in Implants (FDA, 2019a)

Metal	Major Physiological Roles of Proteins Utilizing the Metal	Potential Toxicities of Excess Metal
Chromium	Glucose metabolism/tolerance Lipid metabolism	Cr ³⁺ <ul style="list-style-type: none"> • Potential liver issues • Potential kidney issues Cr ⁶⁺ <ul style="list-style-type: none"> • Respiratory symptoms • Dermatitis/ulcerations • Gastrointestinal (GI) symptoms • Lung cancer
Cobalt	Metabolism of purines/pyrimidines amino acids, fatty acids, folate	Allergic contact dermatitis Cardiomyopathy Cardiac electrical abnormalities Polycythemia Neuropathy Altered thyroid function
Copper	Collagen cross-linking Bone formation Iron metabolism Hemostasis/thrombosis Neurotransmitter synthesis Free radical control	GI symptoms Hemolysis Cardiac failure Renal failure Hepatic dysfunction Alzheimer's Disease
Iron	Oxygen transport Oxygen storage DNA synthesis/repair RNA transcription Synthesis of collagen, neurotransmitters Energy metabolism Immune function	Free radical generation GI symptoms (acute) Hemochromatosis <ul style="list-style-type: none"> • Cardiomyopathy • Cirrhosis • Diabetes • Arthritis
Magnesium	Mitochondrial respiration Bone structure Vitamin D metabolism	GI symptoms (acute) Cardiac electrical abnormalities Neurotoxicity Local generation of H ₂ and hydroxide (high pH)
Manganese	Metabolism of carbohydrates, lipids Neurotransmitter synthesis Bone/cartilage formation Urea metabolism Control of free radicals	Headache Psychiatric symptoms GI symptoms Parkinson's-like signs/symptoms
Molybdenum	Metabolism of amino acids Metabolism of purine/nucleotides, uric acid Metabolism of drugs/prodrugs Metabolism of neurotransmitters	Elevated uric acid/gout Secondary copper deficiency Reduced testosterone
Zinc	Protein and carbohydrate metabolism Immune function Wound healing DNA synthesis and repair Control of free radicals Stabilization of protein structure Intracellular signaling	GI symptoms (acute) Copper deficiency Myeloneuropathy
Vanadium	Phosphate metabolism Insulin enhancement Lipid metabolism	GI symptoms Headache Weakness Tremor

A shift in the distribution of free versus bound cobalt toward a larger portion of free Co²⁺ ions can occur in various disease states, such as renal failure, iron deficiency, sepsis, malnutrition, alcoholism, or in response to certain medications. This may be why individual patients present with toxic responses

at a much lower total blood concentration. At the molecular level, high levels of Co²⁺ ions elicit pathological responses by generating reactive oxygen species (ROS), causing lipid peroxidation, interrupted mitochondrial respiration, and altered calcium and iron homeostasis (Madl et al., 2015; Leysens

et al., 2017). They can also trigger erythropoiesis, interrupt thyroid iodine uptake (goiterogenic), promote genotoxicity, and possibly impair DNA repair processes (Madl et al., 2015; Leyssens et al., 2017). The generation of ROS and lipid peroxides is worth noting as it occurs by catalyzing the Fenton reaction that is common to all metal cations that can undergo sequential two-electron reduction. Unpaired electrons are donated to oxygen or lipids to create protein and nucleic acid damaging free radical species.

Systemic Co or other MoM constituent toxicities are infrequent; however, the syndrome once elicited includes variable presentation of neurological, cardiovascular, immunological, and endocrine symptoms, depending on the systemic cobalt levels found in the blood or urine (Leyssens et al., 2017; Pacheco, 2019; Reich et al., 2019). Many endpoints that progress over the years with permanent implants reverse once the failing implant is replaced with one of a more compatible composition. This suggests that the device constituents cause the toxicities.

Co-related neurotoxicity can cause central and peripheral deficits with loss of hearing, balance, cognitive function, and sensory motor performance (Leyssens et al., 2017). Cardiovascular myopathies caused by Co have long been recognized and include both cardiac rhythm disturbances and destruction of cardiac tissues (Leyssens et al., 2017). These symptoms occur when free levels of Co in the heart tissue are very high and might be exacerbated by alcohol consumption or malnutrition (Barceloux, 1999). Unfortunately, injured cardiac tissue does not repair, although rhythm disturbances have reversed (Leyssens et al., 2017; Reich et al., 2019). Increased red blood cell counts (polycythemia) and hemoglobin levels are rare markers of systemic Co toxicity, and are reversible (Leyssens et al., 2017). Co interference with iodide uptake and synthesis of thyroid hormone (hypothyroidism) can have wide-ranging metabolic and cardiovascular effects, as well as affect homeostasis of other essential metals (e.g., calcium and iron) (Leyssens et al., 2017; Reich et al., 2019).

Immune responses can manifest as rheumatoid symptoms of muscle (polymyalgia) and joint (polyarthralgia) pain, low-grade fevers, dermatological rashes, and sensitization (Reich et al., 2019). Immune responses are also highly associated with implant loosening or failure, and a majority of individuals with failed prosthesis test positive in skin patch testing for metal sensitization or allergies (Pacheco, 2019). Fortunately, there is insufficient evidence from multiple large-scale patient studies to implicate MoM implants in increasing the overall risk of cancers (FDA, 2019a; Leyssens et al., 2017).

Table 2.2.5.2 presents metals used in medical devices that are not essential for human health, and may produce pathological responses in humans. It is important to note that most of the adverse effects have been investigated in therapeutic or occupational exposures other than from implants where concentrations may be higher (FDA, 2019a). A general principle is that nonessential metals have biological effects by mimicking or displacing essential metals. The ability to mimic or displace essential metals depends on the physical properties and valence of the nonessential metal. The immune system often recognizes nonessential metals as foreign, which is the basis

TABLE 2.2.5.2 Common Nonessential Metals in Implants (FDA, 2019a)

Metal	Potential Adverse Effects
Aluminum	Osteomalacia Hepatic dysfunction Anemia Dialysis encephalopathy (dementia, myoclonus) Weak association with Alzheimer's Disease
Gold	Bone marrow suppression Dermatitis Glomerulonephritis Vasculitis Hepatotoxicity Neuropathy
Iridium	Some salts may cause allergic reactions
Mercury	Neurotoxicity Neuropathy Renal toxicities
Nickel	Delayed hypersensitivity Acute: Gastrointestinal (GI) symptoms, headache, vertigo, vision changes Chronic: <ul style="list-style-type: none"> • Altered iron metabolism • Cardiovascular, respiratory or kidney disease • Alteration in hemostasis of calcium, magnesium, manganese, zinc
Palladium	Lip edema Itching Respiratory symptoms
Platinum	Certain platinum-containing compounds may cause respiratory symptoms, including kidney toxicity, hearing loss, bone marrow damage
Silver	Local argyria (blue-gray skin or organ discoloration)
Tin	Acute: GI symptoms, headache Altered metabolism of zinc, iron, copper Cholesterol metabolism
Titanium	Suppression of osteogenic differentiation Yellow nail syndrome
Tungsten	Certain compounds may antagonize molybdenum Immune suppression Enhances cobalt toxicity

for common delayed hypersensitivity reactions elicited by the metals (e.g., nickel allergy). Patch testing for metal sensitivity is a useful means of identifying sensitive individuals and determining which metal alloy might be biocompatible in their implant (Pacheco, 2019).

Mercury is a nonessential metal released from dental amalgams, and has long created public concern with health impacts to patients and practitioners. The European Commission (2014) and its Scientific Committee of Emerging and Newly Identified Health Risks, as well as the US FDA in a systematic review (FDA, 2019b), investigated possible adverse

effects of mercury-containing dental amalgams on neurological, renal, immunological, psychological, reproductive, and other potential systemic toxicities. Both agencies concluded that patients' blood mercury levels can be significantly elevated depending on the number of amalgam fillings, but that there is little epidemiological evidence to show that the levels of mercury released are sufficient to increase the risk of adverse effects or systemic diseases. The dose makes the poison.

Hypersensitivity and Immunotoxicity

While it is clear that the dose makes the poison, almost all foreign compounds and even essential metals can elicit a memory of exposure with acquired hypersensitivity or allergic reactions in susceptible individuals. Innate immune or inflammatory responses are an essential part of wound healing with potentials to become pathological foreign body reactions. This is critical to acute acceptance of the implant, but an excessive foreign body immune response can include local osteolysis, necrosis, pseudotumor formation, tissue granulation (e.g., giant cell formation), and fibrous capsule contractions. Immediately following implantation, host protein adsorption to the implant surface initiates the local inflammatory response. Injury to host tissues is rapidly followed by activation of coagulation and complement pathways and adsorption of proteins to the implant surface to form an encapsulating matrix of stress and structural proteins. This phase is followed by phagocytic and immune cell recruitment designed to eliminate or seal the offending material away from the body. However, if prolonged, normal surrounding tissues are injured and the device may be subject to degradation and liberation of more offending materials. In general, metal, plastic, or composite implants produce rapid inflammation and innate immune responses that resolve/heal within 1 to 2 weeks following implantation. This resolution is critical to limiting tissue pathology and precluding subsequent implant failure. Thus selection of materials for implants and manufacturing processes must be tested in advance for eliciting the foreign body reactions to ensure compatibility with normal wound healing and resolution to limit device failure. Procedures for premarket testing of hypersensitivity and immune responses to implanted materials are outlined in ISO 10993-20:2006 Biological evaluation of medical devices—Part 20: Principles and methods for immunotoxicology testing of medical devices (ISO, 2006).

Debris and wear particles taken into phagocytic cells can elicit inflammatory responses that produce systemic responses, such as aseptic low-grade fever or systemic histamine release. Current understanding of the mechanisms involved in the inflammatory and innate immune responses to metal and implant particles has been reviewed in the recent FDA white paper on Biological Responses to Metal Implants (FDA, 2019a). In brief, pattern recognition receptors in the innate immune cells, as well as contacted tissues, recognize particles as foreign and elicit release of inflammatory cytokines to recruit more inflammatory cells and responses to eliminate the particles. If persistent, this process may enhance local tissue destruction and device failure.

Acquired immune or delayed hypersensitivity responses or allergies require exposure to a foreign substance, but the response becomes disproportionate to the level of exposure through amplification of lymphocytes bearing antibodies that target the foreign substance. The response requires uptake and processing of nonself antigens by antigen-presenting cells to initiate cell-mediated and humoral responses by T and B lymphocytes, respectively. The most important allergens based on the large volumes of procedures are metals (e.g., nickel, cobalt, and chromium) and constituents of bone cement in orthopedic and dental implants. Metal allergies are among the most common contact hypersensitivities with nickel allergies being prevalent in approximately 40% of the general population. While there is concern with nickel-containing cardiovascular, neurological, and reproductive devices causing systemic delayed hypersensitivity reactions, there is a large amount of controversy regarding causative relationships between allergic reactions and adverse outcomes from metal implants (FDA, 2019a; Pacheco, 2019). The incidences of acquired immune and hypersensitivity reactions to surgical implants are relatively rare, since, in addition to exposure, the implant recipient must be genetically susceptible and the metals and cement constituents must form complexes with larger protein structures (i.e., hapten formation) to be recognized as allergens. Once the initial antibody-generating response occurs, however, the metal or small molecule itself can elicit a full systemic allergic reaction. Thus an individual who has sensitivity to nickel or cobalt due an exposure prior to receiving the implant might have a large allergic reaction to modest amounts of metal released from the implant. There are suggestions that patients be tested for allergies to device constituents prior to implantation to reduce the risk of hypersensitivity reactions or device failures (Pacheco, 2019; FDA, 2019a). However, this is complicated by the fact that not all those who test positive for allergies will have an immune response sufficient to require replacement (FDA, 2019a).

Delayed hypersensitivity or allergic reactions are categorized in four major types (Types I–IV) based on the formation of humoral antibodies initiated by B cells (Types I–III) or cell-mediated reactions caused by T lymphocytes (Type IV). Types II and III allergies comprise antigen–antibody encounters that include complement activation, cell lysis, release of vasoactive substances, inflammatory reaction, and tissue damage. However, they are very rare with surgical implants. Instead, Type I B cell and Type IV T cell reactions are the more important responses to consider.

The Type I reaction is based on an interaction between antigens and B cell-derived IgE and IgM immunoglobulins located on mast cells, basophils, eosinophils, and platelets. Antigen binding to IgE or IgM antibodies stimulates release of inflammatory mediators, such as histamine, prostaglandins, and other vasoactive substances within a short timeframe (e.g., minutes to hours). Again, these processes are part of the normal wound repair response. However, in pathological metal hip implant failures, elevated levels of B cells are consistently found in the tissues adjacent to MoM total hip replacement, and B cells isolated from patients

with metal implants activate in response to stimulation with metals (FDA, 2019a; Pacheco, 2019). While antibodies to haptized metal ions are also found in patients with stable cobalt–chromium or metal composite implants, there is a much higher incidence of patients with failed implants who have high antibody titers (Pacheco, 2019).

Type IV T cell-mediated hypersensitivity is referred to as delayed, since it requires more than 12 h and sometimes days to develop. The T cells initiating the response must be sensitized by prior encounter with the allergen to produce T cell recognition receptors. Activation occurs from cognate interaction between the T cell receptors and antigenic peptide (hapten) embedded in major histocompatibility proteins found on the surface of antigen-presenting cells. The interaction elicits release of inflammatory mediators, cytokines, and cytotoxic agents that cause tissue damage, as well as further production and attraction of T cells. The responses become systemic and the time delay involves cell expansion and recruitment of associated lymphocytes, macrophages, and mononuclear phagocytes. The predominance of lymphocytes in implant-associated ectopic lymphoid structures led to the categorization of these adverse cell-mediated responses as aseptic lymphocytic vasculitis-associated lesions (FDA, 2019a; Pacheco, 2019; Willert et al., 2005). While the prevalence of this reaction is low, the persistence or early reappearance of symptoms, including a marked joint effusion and the development of osteolysis, after primary implantation suggests that these reactions are a real concern (Willert et al., 2005; FDA, 2019a). Again, as the Type IV response requires prior exposure to the antigen or hapten formation, patient risk can be mitigated by screening for allergic reactions prior to device implantation. A large number of device and device cement constituents have been recognized as possible allergens and have been suggested to be included in dermal patch testing (Pacheco, 2019).

Organ Localization of Inflammatory and Immune Responses to Device Materials

Localized and tissue-specific responses to devices and device materials can inform the pathological pathways through which the materials, devices, and host responses interact. However, it is often difficult to prove there is an immune component to device failure or toxicity. Common symptoms of failure include pain, swelling, warmth, decreased range of motion, loosening or instability, and sometimes itching or burning. Dermatitis over the surgical site is a well-recognized indication of hypersensitivity to an implant, but this rarely occurs. It is important to note that these systemic toxicities may take years or even decades to develop and the implanted device is often not recognized as the source of a given adverse organ response by physicians treating the pathologic symptoms (Reich et al., 2019). Overall, the local tissue response may dictate the local and systemic effects of the implanted materials.

As orthopedic devices have largely been discussed, it is important to note the local, bone-specific effects of immune

responses to these devices. Aseptic loosening and instability can be triggered by local inflammatory responses caused by sensitization to metal or bone cement components, cement failure, or poor bone formation. Periprosthetic osteolysis (bone loss) may lead to loosening of the device, causing pain and possibly failure. Osteoclasts promote bone resorption, and the balance of osteoclastogenesis and osteogenesis by osteoblasts is a dynamic process that integrates inflammatory, metabolic, and immune inputs for maintenance of skeletal integrity. Osteoclasts couple production of pro-inflammatory cytokines and chemokines to corrosive oxidation and uptake of metal particulates that can promote delayed hypersensitivity. Implant metals and materials can be selected that suppress osteoclast inflammatory responses (e.g., gold and zinc) or are osteogenic (e.g., magnesium or calcium phosphate bone cements) (FDA, 2019a). According to the FDA, metal ions released by oxidative metal corrosion may not trigger osteolysis, but may instead serve as critical amplifiers of inflammatory pathways that contribute to osteoclastogenic development, programming of osteoclastic functions, and crosstalk with other immune and inflammatory mediators. Targeted inhibitors of osteoclastogenesis are under investigation for a variety of osteolytic disorders, including osteolysis associated with prosthetics (FDA, 2019a).

Neurological devices present a number of organ-specific challenges and toxicities. The large number of responsive cell types and structures in the brain and neural tissue are potential targets of implants and their materials. There are case reports of reactions to neurostimulators that include localized burning and itching and generation of rashes near implantation sites (FDA, 2019a; Pacheco, 2019). Nickel–titanium (Nitinol) has been used in a number of neurological applications, and adverse outcomes have occurred in nickel allergic patients. Triggering of oxidative responses in brain microglia may liberate nickel ions that can be disruptive to ion signaling, as well as being immunogenic (FDA, 2019a). These potentially toxic pathways are not restricted to neuronal tissues, but implantation in neural tissue results in unique toxicities in the anatomical compartment.

Due to their interface with blood, complications and adverse events associated with metallic cardiac and vascular implants result from coagulation cascade activation and thrombus formation. The endothelial cells lining blood vessels are sensitive to metals and their injury results in platelet activation, as well as recruitment of circulating leukocytes. Loss of endothelial function, increased leukocyte deposition, and stimulation of underlying smooth muscle hyperplasia result in stent failure and vessel restenosis. Thus effects of materials on the cells of the vessel walls should be tested in addition to testing materials for thrombogenicity. The proximity to the circulation also enhances occurrence of systemic effects from cardiovascular devices. There are reports of nickel allergies and dermal reaction being elicited by peripheral Nitinol stent failure (Pacheco, 2019). Cardiac and neurostimulators present a number of potential sensitization hazards as they are composed of many metal alloys, plastics,

resins, and glues. In addition to the structural metals, metals in wire leads also pose hazards that have been associated with local as well as systemic sensitization and immune responses (Pacheco, 2019). In most cases, symptoms resolve when the offending device is removed, which implicates aseptic responses to the device materials as the cause.

Summary and Conclusions

Failure of medical implants due to systemic toxicities and/or pathogenic immunological responses is relatively rare based on the low rate of adverse events found with the tens of millions of medical implantations performed globally (e.g., orthopedic, dental, neurological, cardiovascular implants). The low rates of toxicity and failures due to biological incompatibility are testaments to the rigorous premarket testing and postmarket reviews for biocompatibility of all implanted materials and devices. This testing follows international (e.g., ISO 10993) and national (e.g., FDA) standards and guidelines that outline cell-based and animal testing that must

be performed to ensure the safety of implanted devices and their complex list of metal and chemical constituents. Testing for both implantation site and systemic toxicities has greatly reduced, but has not eliminated, risks of adverse effects and device failures. The main concern is the dose of potentially toxic materials that are released locally and available for distribution to distant organs, which might be particularly sensitive to the toxic effects of the materials (i.e., systemic toxicities). In addition, given the nature of delayed or acquired immune responses, clinicians need to be vigilant not to implant an offending material in a susceptible individual, or should change the implant to a more compatible material when adverse immune responses arise. It is also important to consider not just the materials contained in a device, but also all of the materials involved in implanting devices, since adhesives, cements, and surgical materials can pose toxic risks. The intent of this overview is to increase student awareness of the potential hazards from implanted device constituents and incorporation of biocompatibility considerations in biomaterials and device systems design.

CASE STUDY: SYSTEMIC AND IMMUNE TOXICITY OF IMPLANTED MATERIALS

What Problem was Addressed?

Failure of medical implants due to systemic toxicities and/or pathogenic immunological responses to the metals and chemicals associated with the implants are relatively rare. However, they can be highly significant, debilitating, and life threatening for individual patients. An example is the case of a 45-year-old woman who had chronic systemic metal ion toxicity from wear on a revised cobalt–chromium trunnion (Reich et al., 2019). She had received total hip arthroplasty at age 22 and then revision surgery 11 years later due to developing acetabular osteolysis. Two years after the revision surgery, she developed a constellation of medical symptoms, including polymyalgia, polyarthralgia, oral ulcers, body aches, headaches, intermittent low-grade fevers, fatigue, and a malar rash. She had a family history of rheumatoid arthritis, Hashimoto's thyroiditis, and Grave's disease. She sought treatment from her primary physician and a rheumatologist. In addition, she saw a cardiologist for lightheadedness and syncope, and her tilt-table test was positive. She was diagnosed with systemic lupus erythematosus, mixed connective tissue disease, fibromyalgia, and postural orthostatic tachycardia syndrome (POTS). Despite drug treatments, her symptoms remained after 8 years (10 years after revision), and she had developed intermittent, disseminated, and pruritic facial, hand, and arm rash, as well as nondermatomal paresthesia in her upper and lower extremities and "brain fog." Extensive testing did not reveal the cause of her symptoms, but upon returning to her orthopedic surgeon for joint pain 12 years after revision, she was diagnosed with cobalt ion toxicity. She received a second revision, and the cobalt–chromium components were replaced with a titanium alloy stem and ceramic femoral head. Within 6 months, her cognitive abilities improved, and 15 months later, her POTS and dermatological symptoms resolved. However, while improved, not all systemic symptoms disappeared (Reich et al., 2019).

What Properties were Required of the Biomaterials?

The low rates of toxicity to implant materials and failures due to biological incompatibility were testament to rigorous

premarket testing and postmarket reviews for biocompatibility of all implanted materials and devices. This testing follows international (e.g., ISO 10993) and national (e.g., FDA) standards and testing guidelines that outline cell-based and animal testing that must be performed to ensure the safety of implanted devices and their complex list of metal and chemical constituents. Testing for both implantation site and systemic toxicities has greatly reduced, but has not eliminated, risks of adverse effects and device failures. The main concern is the dose of potentially toxic materials that are released locally and available for distribution to distant organs, which might be particularly sensitive to the toxic effects of the materials. Despite a strong safety record with the materials, this woman's case illustrates complications that might arise in susceptible individuals and that were enhanced by the selection of materials used in the original surgery and her revisions. Her family history and early need for replacement may have indicated that she would be susceptible. The mixed materials in her first revision increased wear debris from the trunnion. The long timeline for symptom development and misdiagnoses suggest the need for increased awareness of potential systemic toxic syndromes that might result from implant constituents, even when low levels of constituent metal ions are found in the blood.

What Approach and Biomaterials Could Be Used?

Diligent premarket testing for biocompatibility and implant material safety is essential to reduce risks of systemic pathologies and local device failures. ISO 10993-1 guidelines should be consulted for assessing the risks that should be addressed with toxicity testing appropriate to the device application. ISO 10993-20 guidelines specifically address tests for immunotoxicity. However, in the clinic, care should be taken when mixing manufacturers' components, since mixed components, as in revision of some but not all of the prostheses, may increase risk of generating wear debris or introducing chemical interactions that were not tested by the individual manufacturers. Also at the clinical level, care should be taken to identify patients who are susceptible to toxicities and to select materials that are compatible with the individual.

References

- Barceloux, D.G., 1999. Cobalt. *J. Toxicol. Clin. Toxicol.* 37, 201–206.
- European Commission, 2014. Scientific Committee on Health and Environmental Risks, Opinion on the environmental risks and indirect health effects of mercury from dental amalgam (update 2014), pp. 1–48. https://ec.europa.eu/health/sites/health/files/scientific_committees/environmental_risks/docs/scher_o_165.pdf.
- FDA, 2019a. Biological Responses to Metal Implants. United States Food and Drug Administration: Center for Device and Radiological Health, pp. 1–143. <https://www.fda.gov/media/131150/download>.
- FDA, 2019b. Epidemiological evidence on the adverse health effects reported in relation to mercury from dental amalgam: systematic literature review (2010–present). In: United States Food and Drug Administration: Center for Device and Radiological Health. <https://www.fda.gov/media/131151/download>.
- ISO, 2006. ISO/TS 10993-20:2006 Biological Evaluation of Medical Devices — Part 20: Principles and Methods for Immunotoxicology Testing of Medical Devices. International Organization for Standardization, pp. 1–17.
- ISO, 2018. ISO 10993-1:2018 Biological Evaluation of Medical Devices — Part 1: Evaluation and Testing within a Risk Management Process. International Organization for Standardization, pp. 1–41.
- Kamrani, S., Fleck, C., 2019. Biodegradable magnesium alloys as temporary orthopaedic implants: a review. *Biometals* 32, 185–193.
- Krapivinsky, G., Krapivinsky, L., Manasian, Y., Clapham, D.E., 2014. The TRPM7 channel is cleaved to release a chromatin-modifying kinase. *Cell* 157, 1061–1072.
- Leyssens, L., Vinck, B., Van Der Straeten, C., Wuyts, F., Maes, L., 2017. Cobalt toxicity in humans—A review of the potential sources and systemic health effects. *Toxicology* 387, 43–56.
- Madl, A.K., Liong, M., Kovichich, M., Finley, B.L., Paustenbach, D.J., Oberdorster, G., 2015. Toxicology of wear particles of cobalt-chromium alloy metal-on-metal hip implants part I: physicochemical properties in patient and simulator studies. *Nanomedicine* 11, 1201–1215.
- Pacheco, K.A., 2019. Allergy to surgical implants. *Clin. Rev. Allergy Immunol.* 56, 72–85.
- Reich, M.S., Javidan, P., Garg, V.K., Copp, S.N., 2019. Chronic systemic metal ion toxicity from wear on a revised cobalt-chromium trunnion. *J. Orthop. Case Rep.* 9, 48–51.
- Standeven, A.M., Wetterhahn, K.E., 1989. Chromium(VI) toxicity: uptake, reduction, and DNA damage. *J. Am. Coll. Toxicol.* 8, 1275–1283.
- Trapani, V., Arduini, D., Cittadini, A., Wolf, F.I., 2013. From magnesium to magnesium transporters in cancer: TRPM7, a novel signature in tumour development. *Magnes. Res.* 26, 149–155.
- Willert, H.G., Buchhorn, G.H., Fayyazi, A., Flury, R., Windler, M., Koster, G., Lohmann, C.H., 2005. Metal-on-metal bearings and hypersensitivity in patients with artificial hip joints. A clinical and histomorphological study. *J. Bone Joint Surg. Am.* 87, 28–36.
- Wrighton, K.H., 2014. Epigenetics: the TRPM7 ion channel modifies histones. *Nat. Rev. Mol. Cell Biol.* 15, 427.

Chapter Exercises

1. You are developing magnesium alloy-based orthopedic plates and screws designed to support healing of a bone fracture, which then degrades. This avoids the need for a second surgery to remove the plates and screws. The plates need to retain structural integrity for 6 weeks and then degrade over another 6 weeks to a year. What local and systemic toxicity testing would be required by the regulatory agencies to approve the safety of the magnesium alloy implants? What rationale would allow you to eliminate certain toxicity tests (e.g., carcinogenesis, reproductive toxicity) and provide patient selection recommendations instead?

Answer: Dissolution rate and cytotoxic dose response to local cell types; histological evaluation of local site for osteolysis/osteogenesis and gas pocket formation; blood ion level disturbance; histological evaluation of brain, liver, heart, and kidney tissues; immunological testing if alloy contains an allergenic metal or metal of unknown allergenicity; carcinogenesis if the alloy contains a potentially carcinogenic metal or metal of unknown carcinogenesis; etc.

The alloy would not need to be tested for carcinogenesis if it does not contain any potential carcinogenic metals. However, magnesium can promote tumor growth and a recommendation for concern with implanting the device in a cancer patient might be made. Magnesium is beneficial in pregnancy and development. However, if the alloy contains a metal with known reproductive effects, a recommendation might be made to avoid implantation in pregnant women. This is of course relevant to those who would still be pregnant when the device degrades.

2. You have optimized the design and manufacturing process for a novel trunnion for total hip arthroplasty, and have been highly diligent in testing for potential toxicities. The FDA gives approval for its use and you want to maintain an impeccable safety record to grow sales. What instructions would you provide clinicians to ensure that their selection of patients, placement of the trunnion, and postsurgery monitoring reduce risks of failure and/or systemic toxicity in the patient? Suggest a postimplantation monitoring program that allows you to provide postmarket safety data to the FDA (e.g., Phase III clinical trial data).

Answer: The surgeons might be advised to use the trunnion only with compatible components (e.g., stems and femoral heads) to avoid grinding and release of cobalt particles. Care should be taken in revision surgery where catastrophic failure of the original implants might leave debris that grind the trunnion. The surgeons also might be advised to use adhesives and cements that are compatible. They may be warned that patients with a history or family history of metal allergies, or susceptibility to potential cobalt toxicities (e.g., rheumatic disease, thyroid conditions, cardiac disease), might be prone to device failure and metal-induced disease. Patch testing

for metal allergies might be useful in identifying patients who should not receive the material or should be monitored for symptoms of metal disease. In addition to device failure, postmarket testing might include monitoring for cobalt levels in the blood, muscle and joint pain, neurological symptoms (ataxia, confusion), cardiac abnormalities, thyroid deficiency, and dermatological rashes.

3. Name four ways that metals like cobalt or nickel can cause systemic toxicity and identify the form of the metal that would likely result in toxicity.

Answer: Trace amounts of cobalt are essential cofactors for vitamin B12. However, above trace levels, cobalt can bind to proteins to generate allergenic haptens, can bind inappropriately to regulatory signaling molecules to cause cardiac tissue damage, and can cause electrical disturbance in the heart and brain by competing with ion uptake essential for normal electrical conduction and transduction. Nickel is a nonessential metal and, in addition to forming allergenic haptens and blocking calcium channels, can displace essential metals from their effector sites.

It is the free concentration of the elemental ionic form of the metal that is important.

4. What is required for an element like nickel to elicit sensitization that would result in an allergy to a nickel-based implant? When would a Nitinol implant elicit an allergic reaction?

Answer: Elemental nickel is a weak but highly prevalent allergen. For nickel allergy to occur, the patient must be genetically susceptible and exposed to elemental nickel ions (Ni^{2+}). The nickel ions must bind to proteins to form hapten complexes that are taken into antigen-processing cells and incorporated into major histocompatibility complexes (MHCs) on the surface of antigen-presenting cells. Reexposure results in T cells interacting with the Ni-hapten in the MHC, which stimulates differentiation into cytotoxic T cells and an allergic reaction promoting B cells. The Nitinol (nickel–titanium) alloys are not allergenic. However, if the implanted device corrodes or generates wear debris, nickel ions might be released and be available to elicit an allergic reaction in a susceptible individual.

5. Zinc is an essential metal, but can produce local and systemic toxicity when in excess and when depleted. What would be necessary for zinc from an implant to be toxic and what would cause another metal leached from an implant to cause zinc toxicity?

Answer: The levels of essential metals like zinc in the circulation and in cells are tightly controlled. The level of free zinc available for toxicity is very low and toxicity occurs only when the levels of zinc overwhelm the capacity of cellular compartments to maintain homeostatic zinc levels or when zinc levels are depleted. Other metals can promote zinc toxicity by displacing zinc from storage or protein-binding sites resulting in an excess of free zinc concentration. Toxicity can also result from the

metal preventing zinc access to essential sites of action, which simulates zinc deficiency. Finally, the metal may substitute for zinc in essential structural sites and disrupt protein function by changing the zinc-dependent protein structure.

6. You have designed and perfected a metal/ceramic/plastic composite dental implant and proven that each constituent, as well as the final manufactured implant, is biocompatible and safe. The FDA approves a clinical trial and several patients have severe allergic reactions to the implant. What would be the probable cause for these

allergic reactions when your premarket testing showed the implant was completely nonallergenic?

Answer: The most likely culprit would be that an allergenic adhesive or cement was used for the implantation. A suggestion might be to market the implant with adhesives and cements that have been tested not to generate an allergic reaction to your implant. A secondary culprit would be that mice are not men and all of the premarket testing in animals failed to reveal a human-specific response.

2.2.6

Blood Coagulation and Blood–Material Interactions

STEPHEN R. HANSON¹, ERIK I. TUCKER¹, ROBERT A. LATOUR²

¹Division of Biomedical Engineering, School of Medicine, Oregon Health & Science University, Portland, OR, United States

²Bioengineering Department, Clemson University, Clemson, SC, United States

Introduction

The hemostatic mechanism is designed to arrest bleeding from injured blood vessels. The same process may produce adverse consequences when artificial surfaces are placed in contact with blood. These events involve a complex set of interdependent reactions between: (1) the surface; (2) platelets; and (3) coagulation proteins, resulting in the formation of a clot or thrombus, which may subsequently undergo removal by (4) fibrinolysis. The process is localized at the surface by opposing activation and inhibition systems, which combine to maintain the fluidity of blood in the circulation. In this chapter, an overview of hemostatic mechanisms is first presented in Section [Platelet Adhesion and the Blood Coagulation Cascade—An Overview](#) to provide a general understanding of blood and blood coagulation processes. Following these generalized section, more specific content addressing blood–material interactions is presented in Section [Blood–Material Interactions](#). Although a great deal is known about blood responses to injured arteries and blood-contacting devices, important relationships remain to be defined in many instances. More detailed discussions of hemostasis, thrombosis, and blood–material interactions have been provided elsewhere ([Thompson et al., 2017](#); [Reviakine et al., 2017](#); [Jung and Braune, 2016](#); [Liu et al., 2015](#); [Jaffer et al., 2015](#); [Xu et al., 2014](#); [Li and Henry, 2011](#); [Ratner, 1993, 2007](#); [Colman et al., 2005](#); [Gorbet and Sefton, 2004](#); [Esmon, 2003](#); [Gresle et al., 2002](#); [Stamatoyannopoulos et al., 1994](#); [Forbes and Courtney, 1987](#)).

Platelet Adhesion and the Blood Coagulation Cascade—An Overview

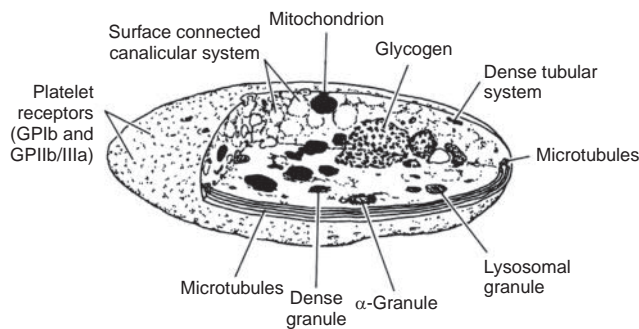
Cellular Composition of Blood

Erythrocytes (Red Cells)

Red cells are usually considered as passive participants in processes of hemostasis and thrombosis, although under some conditions (low shear or venous flows) red cells may comprise a large proportion of the total thrombus mass. The concentration and motion of red cells have important mechanical effects on the diffusive transport of blood elements. For example, in flowing blood through small blood vessels, red cells tend to be concentrated in the middle of the blood vessel and displace a layer of plasma along with platelets toward the wall of the blood vessels, which is referred to as the marginal zone effect ([Fournier, 2007](#)). This phenomenon substantially increases the concentration of the platelets along the wall of the blood vessel. Under some conditions, red cells may also contribute chemical factors that influence platelet reactivity ([Turitto and Weiss, 1980](#)).

Leukocytes (White Cells)

The various classes of white cells perform many functions in inflammation, infection, wound healing, and the blood response to foreign materials. White cell interactions with artificial surfaces may proceed through as yet poorly defined mechanisms related to activation of the complement, coagulation, fibrinolytic, and other enzyme systems, resulting in the expression by white cells of procoagulant, fibrinolytic, and inflammatory activities. For example, stimulated



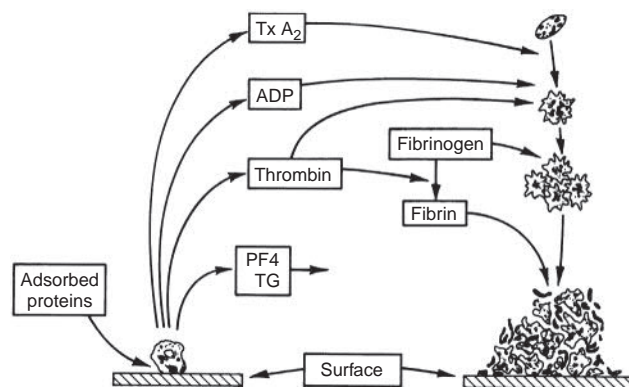
• **Figure 2.2.6.1** Platelet structure.

monocytes express tissue factor, which can initiate thrombus formation by the extrinsic coagulation cascade. Neutrophils may contribute to clot dissolution by releasing potent fibrinolytic enzymes (e.g., neutrophil elastase). White cell interactions with devices having large surface areas may be extensive (especially with surfaces that activate complement), resulting in their marked depletion from circulating blood. Activated white cells, through their enzymatic and other activities, may produce organ dysfunction in other parts of the body. In general, the role of white cell mechanisms of thrombosis and thrombolysis, in relation to other pathways, remains an area of considerable interest.

Platelets

Platelets (“little plates”) are nonnucleated, disk-shaped cells having a diameter of 2–3 μm , and an average volume of $10 \times 10^{-9} \text{mm}^3$ (Haley et al., 2011). Platelets are produced in the bone marrow, circulate at an average concentration of about 250,000 cells per microliter of whole blood, and occupy approximately 0.3% of the total blood volume. In contrast, red cells (erythrocytes) normally circulate at about 5×10^6 cells per microliter, and comprise 40%–50% of the total blood volume. Platelet functions are designed to: (1) initially arrest bleeding through the formation of platelet plugs; and (2) stabilize the initial platelet plugs by catalyzing coagulation reactions leading to the formation of fibrin.

Platelet structure provides a basis for understanding platelet function. In the normal (nonstimulated) state, the platelet discoid shape is maintained by a circumferential bundle (cytoskeleton) of microtubules (Fig. 2.2.6.1). The external surface coat of the platelet contains membrane-bound receptors [e.g., glycoproteins (GP) Ib, and IIb/IIIa] that mediate the contact reactions of adhesion (platelet–surface interactions) and aggregation (platelet–platelet interactions). The membrane also provides a phospholipid surface that accelerates important coagulation reactions and forms a spongy, canal-like (canalicular) open network that represents an expanded reactive surface to which plasma factors are selectively adsorbed. Platelets contain substantial quantities of muscle protein (e.g., actin, myosin) which allow for internal contraction when platelets are activated. Platelets also contain three types of cytoplasmic storage granules: (1) α -granules, which are numerous and contain the platelet-specific proteins platelet factor 4 (PF-4) and



• **Figure 2.2.6.2** Platelet reactions to artificial surfaces. Following protein adsorption to surfaces, platelets adhere and release α -granule contents, including platelet factor 4 (PF-4) and β -thromboglobulin (β -TG), and dense granule contents, including ADP. Thrombin is generated locally through coagulation reactions catalyzed by procoagulant platelet surface phospholipids. Thromboxane A_2 (TxA_2) is synthesized. ADP, TxA_2 , and thrombin recruit additional circulating platelets into an enlarging platelet aggregate. Thrombin-generated fibrin stabilizes the platelet mass.

β -thromboglobulin (β -TG), and proteins found in plasma (including fibrinogen, albumin, fibronectin, coagulation factors V and VIII); (2) dense granules which contain adenosine diphosphate (ADP), calcium ions (Ca^{2+}), and serotonin; and (3) lysosomal granules containing enzymes (acid hydrolases).

Platelets are extremely sensitive cells that may respond to minimal stimulation. Activation causes platelets to become sticky and change in shape to irregular spheres with spiny pseudopods. Activation is accompanied by internal contraction and extrusion of the storage granule contents into the extracellular environment. Secreted platelet products such as ADP stimulate other platelets, leading to irreversible platelet aggregation and the formation of a fused platelet thrombus (Fig. 2.2.6.2).

Platelet Adhesion

Platelets adhere to artificial surfaces and injured blood vessels. At sites of vessel injury, the adhesion process involves the interaction of platelet glycoprotein Ib (GP Ib) and connective tissue elements, which become exposed (e.g., collagen) and require plasma von Willebrand factor (vWF) as an essential cofactor. GP Ib (about 25,000 molecules per platelet) acts as the surface receptor for vWF (Colman et al., 2005). The hereditary absence of GP Ib or vWF results in defective platelet adhesion and serious abnormal bleeding.

Platelet adhesion to artificial surfaces, which is mediated by adsorbed proteins (see Chapter 2.1.2), may also be mediated through platelet glycoprotein IIb/IIIa (integrin $\alpha_{IIb}\beta_3$), as well as through the GP Ib–vWF interaction. GP IIb/IIIa (about 80,000 copies per resting platelet) is the platelet receptor for adhesive plasma proteins that support cell attachment, including fibrinogen, vWF, fibronectin, and vitronectin (Gresle et al., 2002). Resting platelets do not bind these adhesive glycoproteins in circulation, an event

TABLE 2.2.6.1 Properties of Human Clotting Factors

Clotting Factor	Apparent Molecular Weight (Number of Chains)	Approximate Normal Plasma Concentration ($\mu\text{g/mL}$)	Active Form
<u>Intrinsic Clotting System</u>			
Prekallikrein	86,000 (1)	50	Serine protease
High-molecular-weight kininogen	120,000 (1)	70–90	Cofactor
Factor XII	80,000 (1)	30–40	Serine protease
Factor XI	160,000 (2)	3–6	Serine protease
Factor IX	55,000 (1)	3–5	Serine protease
Factor VIII ^a	330,000 (1)	0.1–0.2	Cofactor
Von Willebrand factor ^a	250,000 (1)	10	Cofactor for platelet adhesion
<u>Extrinsic Clotting System</u>			
Tissue factor	47,000 (1)	0 ^b	Cofactor
Factor VII	50,000 (1)	0.5	Serine protease
<u>Common Pathway</u>			
Factor X	59,000 (2)	8–10	Serine protease
Factor V	330,000 (1)	5–12	Cofactor
Prothrombin	72,000 (1)	100–150	Serine protease
Fibrinogen	340,000 (6)	1500–4500	Fibrin polymer
Factor XIII	320,000 (4)	10	Transglutaminase

^aIn plasma, factor VIII is complexed with von Willebrand factor, which circulates as a series of multimers ranging in molecular weight from about 600,000 to 2×10^7 .
^bThe tissue factor concentration in cell-free plasma is absent or minimal since tissue factor is an integral cell membrane-associated protein expressed by vascular and inflammatory cells.

which normally occurs only after platelet activation causes a conformational change in GP IIb/IIIa. Platelets which have become activated near artificial surfaces (for example, by exposure to factors released from already adherent cells) adhere directly to surfaces through this mechanism (e.g., via GP IIb/IIIa binding to surface-adsorbed fibrinogen). Also, normally unactivated GP IIb/IIIa receptors can react with surface proteins that have undergone conformational changes as a result of the adsorption process (Savage and Ruggeri, 1991) (see Chapter 2.1.2). The enhanced adhesiveness of platelets toward surfaces preadsorbed with fibrinogen supports this view. Following adhesion, activation, and release reactions, the expression of functionally competent GP IIb/IIIa receptors may also support tight binding and platelet spreading through multiple focal contacts with fibrinogen and other surface-adsorbed adhesive proteins.

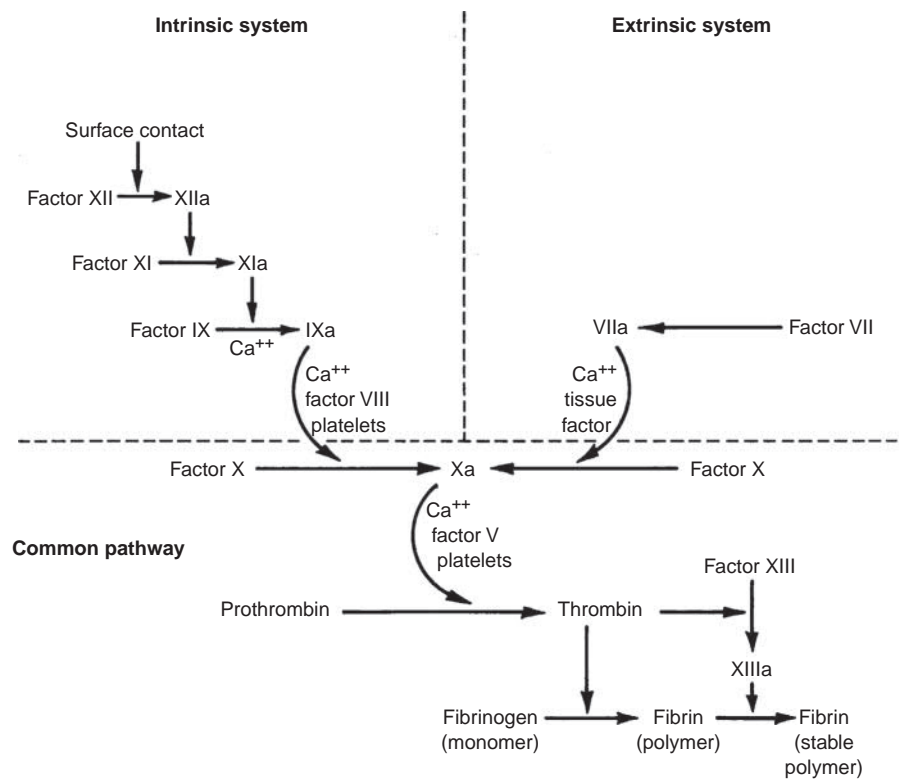
Platelet Aggregation

Following platelet adhesion, a complex series of reactions is initiated involving: (1) the release of dense granule ADP; (2) the formation of small amounts of thrombin (Fig. 2.2.6.2); and (3) the activation of platelet biochemical processes leading to the generation of thromboxane A_2 . The release of

ADP, thrombin formation, and generation of thromboxanes all act in concert to recruit platelets into the growing platelet aggregate (Fig. 2.2.6.2). Platelet stimulation by these agonists causes the expression on the platelet surface of activated GP IIb/IIIa, which then binds plasma proteins that support platelet aggregation. In normal blood, fibrinogen, owing to its relatively high concentration (Table 2.2.6.1), is the most important protein supporting platelet aggregation. The platelet–platelet interaction involves Ca^{2+} -dependent bridging of adjacent platelets by fibrinogen molecules (platelets will not aggregate in the absence of fibrinogen, GP IIb/IIIa, or Ca^{2+}). Thrombin binds directly to platelet thrombin receptors, and plays a key role in platelet aggregate formation by: (1) activating platelets, which then catalyze the production of more thrombin; (2) stimulating ADP release and thromboxane A_2 formation; and (3) stimulating the formation of fibrin, which stabilizes the platelet thrombus.

Platelet Release Reaction

The platelet release reaction is the secretory process by which substances stored in platelet granules are extruded from the platelet. ADP, collagen, epinephrine, and thrombin are physiologically important release-inducing agents, and interact



• **Figure 2.2.6.3** Mechanisms of clotting factor interactions. Clotting factors (proenzymes), identified by Roman numerals, interact in a sequential series of enzymatic activation reactions (coagulation cascade) leading to the amplified production of the enzyme thrombin, which in turn cleaves fibrinogen to form a fibrin polymer that stabilizes the clot or thrombus. Clotting is initiated by either an intrinsic or extrinsic pathway with subsequent factor interactions which converge upon a final, common path. The underlined factors are all activatable by the enzyme thrombin. The dotted lines indicate the divisions between the intrinsic, extrinsic, and common pathways.

with the platelet through specific receptors on the platelet surface. Alpha-granule contents (PF-4, β -TG, and other proteins) are readily released by relatively weak agonists such as ADP. Release of the dense granule contents (ADP, Ca^{2+} , and serotonin) requires platelet stimulation by a stronger agonist, such as thrombin. Agonist binding to platelets also initiates the formation of intermediates that cause activation of the contractile–secretory apparatus, production of thromboxane A_2 , and mobilization of calcium from intracellular storage sites. Elevated cytoplasmic calcium is probably the final mediator of platelet aggregation and release. As noted, substances which are released (ADP), synthesized [thromboxane A_2 (TxA_2)], and generated (thrombin), as a result of platelet stimulation and release, affect other platelets and actively promote their incorporation into growing platelet aggregates. In vivo, measurements of plasma levels of platelet-specific proteins (PF-4, β -TG) have been widely used as indirect measures of platelet activation and release.

Platelet Coagulant Activity

When platelets aggregate, platelet coagulant activity is initiated, including the expression of negatively charged membrane phospholipids (phosphatidyl serine) which accelerate two critical steps of the blood coagulation sequence: factor

X activation and the conversion of prothrombin to thrombin (Fig. 2.2.6.3). Platelets may also promote the proteolytic activation of factors XII and XI. The surface of the aggregated platelet mass thus serves as a site where thrombin can form rapidly in excess of the neutralizing capacity of blood anticoagulant mechanisms. Thrombin also activates platelets directly and generates polymerizing fibrin, which adheres to the surface of the platelet thrombus.

Platelet Consumption

Platelet consumption refers to the removal of platelets from the bloodstream by the liver and spleen, with the consumed platelets then normally replaced by new platelets freshly released from the bone marrow. As shown by radioisotope-labeling studies in humans, platelets are cleared from circulating blood in an approximately linear fashion over time, with an apparent lifespan of approximately 10 days. With ongoing or chronic thrombosis, which may be produced by cardiovascular devices, platelets may be removed from circulating blood at a more rapid rate. Thus steady-state elevations in the rate of platelet destruction, as reflected in a shortening of platelet lifespan, have been used as a measure of the thrombogenicity of artificial surfaces and prosthetic devices (Hanson et al., 1980, 1990).

Coagulation

In the test tube, at least 12 plasma proteins interact in a series of reactions leading to blood clotting. Their designation as Roman numerals was made in order of discovery, often before their role in the clotting scheme was fully understood. Their biochemical properties are summarized in [Table 2.2.6.1](#). Initiation of clotting occurs either intrinsically by surface-mediated reactions that occur within a blood vessel, or extrinsically due to blood contacting tissue external to the vasculature due to a disrupted blood vessel wall through factors derived from tissues (i.e., tissue factor). The two systems converge upon a final common pathway, which leads to the formation of thrombin and an insoluble fibrin gel when thrombin acts on fibrinogen.

Coagulation proceeds through a “cascade” of reactions by which normally inactive factors (e.g., factor XII) become enzymatically active following surface contact, or after proteolytic cleavage by other enzymes (e.g., surface contact activates factor XII to factor XIIa). The newly activated enzymes in turn activate other normally inactive precursor molecules (e.g., factor XIIa converts factor XI to factor XIa). Because this sequence involves a series of steps, and because one enzyme molecule can activate many substrate molecules, the reactions are quickly amplified so that significant amounts of thrombin are produced, resulting in platelet activation, fibrin formation, and the arrest of bleeding. The process is localized (i.e., widespread clotting does not occur) owing to dilution of activated factors by blood flow, the actions of inhibitors that are present or are generated in clotting blood, and because several reaction steps proceed at an effective rate only when catalyzed on the surface of activated platelets or at sites of tissue injury.

[Fig. 2.2.6.3](#) presents a scheme of the clotting factor interactions involved in both the intrinsic and extrinsic systems, and their common path. Except for the contact phase, calcium is required for most reactions and is the reason why chelators of calcium (e.g., citrate) are effective anticoagulants. It is also clear that the *in vitro* interactions of clotting factors, i.e., clotting, are not necessarily identical with coagulation *in vivo*, which may be triggered by artificial surfaces and by exposure of the cell-associated protein, tissue factor. There are also interrelationships between the intrinsic and extrinsic systems, such that under some conditions “cross-over” or reciprocal activation reactions may be important ([Bennett et al., 1987](#); [Colman et al., 2005](#)).

Mechanisms of Coagulation

In the intrinsic clotting system, contact activation refers to reactions following the adsorption of contact factors to a material surface. These interactions are addressed in detail in [Section Contact Activation of the Blood Coagulation Cascade](#). All of these contact reactions take place in the absence of calcium. Although extremely important for blood–material interactions, their pathologic significance in the absence of a biomaterial remains uncertain. For example, in

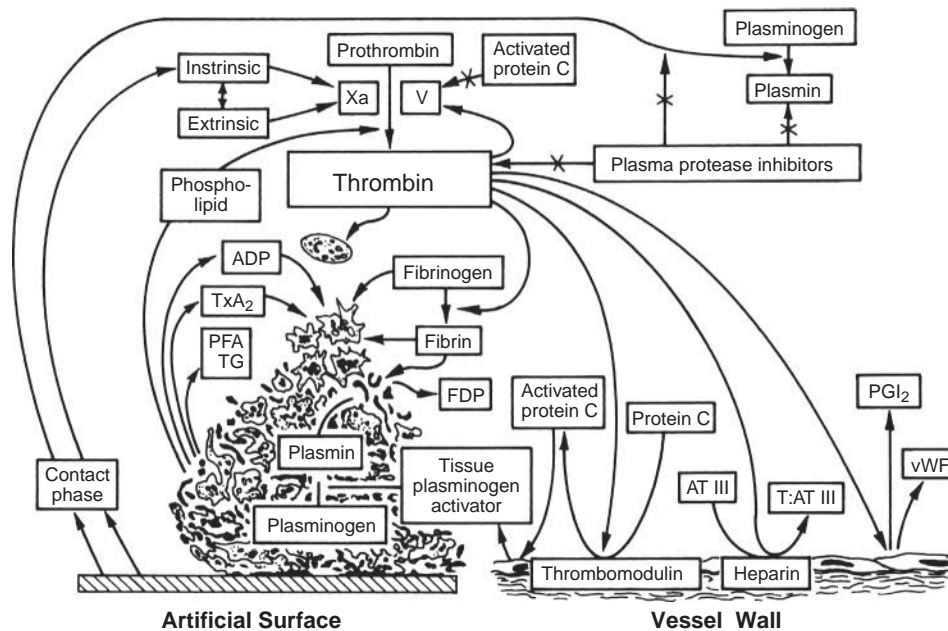
hereditary disorders, a deficiency of factor XII, which is the initiating factor in the intrinsic coagulation cascade, is not associated with an increased bleeding tendency, and only a marked deficiency of factor XI produces abnormal bleeding.

A middle phase of intrinsic clotting begins with the first calcium-dependent step, the activation of factor IX by factor XIa. Factor IXa subsequently activates factor X. Factor VIII is an essential cofactor in the intrinsic activation of factor X, and factor VIII first requires modification by an enzyme, such as thrombin, to exert its cofactor activity. In the presence of calcium, factors IXa and VIIIa form a complex (the “tenase” complex) on phospholipid surfaces (expressed on the surface of activated platelets) to activate factor X. This reaction proceeds slowly in the absence of an appropriate phospholipid surface, and serves to localize the clotting reactions to the surface (vs. bulk fluid) phase. The extrinsic system is initiated by the activation of factor VII. When factor VII interacts with tissue factor, a cell membrane protein that may also circulate in a soluble form, factor VIIa becomes an active enzyme which is the extrinsic factor X activator. Tissue factor is present in many body tissues, is expressed by stimulated white cells and endothelial cells, and becomes available when underlying vascular structures are exposed to flowing blood upon vessel injury.

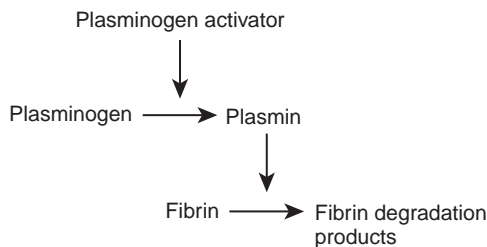
The common path begins when factor X is activated by either factor VIIa–tissue factor by or the factor IXa–VIIIa complex. After formation of factor Xa, the next step involves factor V, a cofactor, which (like factor VIII) has activity after modification by another enzyme, such as thrombin. Factor Xa–Va, in the presence of calcium and platelet phospholipids, forms a complex (“prothrombinase” complex) that converts prothrombin (factor II) to thrombin. Like the conversion of factor X, prothrombin activation is effectively surface catalyzed. The higher plasma concentration of prothrombin ([Table 2.2.6.1](#)), as well as the biological amplification of the clotting system, allows a few molecules of activated initiator to generate a large burst of thrombin activity. Thrombin, in addition to its ability to activate factors V and VIII and also platelets, acts on two substrates: fibrinogen and factor XIII. The action of thrombin on fibrinogen releases small peptides from fibrinogen (e.g., fibrinopeptide A), which can be assayed in plasma as evidence of thrombin activity. The fibrin monomers so formed polymerize to become a gel. Factor XIII is either trapped within the clot or provided by platelets, and is activated directly by thrombin. A tough, insoluble fibrin polymer is then formed by interaction of the fibrin polymer with factor XIIIa.

Control Mechanisms

Obviously, the blood and vasculature must have mechanisms for avoiding massive thrombus formation once coagulation is initiated. At least four types of mechanisms may be considered. First, blood flow may reduce the localized concentration of precursors and remove activated materials by dilution into a larger volume, with subsequent removal from the circulation following passage through the liver.



• **Figure 2.2.6.4** Integrated hemostatic reactions between a foreign surface and platelets, coagulation factors, the vessel endothelium, and the fibrinolytic system.



• **Figure 2.2.6.5** Fibrinolytic sequence. Plasminogen activators, such as tissue plasminogen activator (tPA) or urokinase, activate plasminogen to form plasmin. Plasmin enzymatically cleaves insoluble fibrin polymers into soluble degradation products (FDPs), thereby effecting the removal of unnecessary fibrin clot.

Second, the rate of several clotting reactions is fast only when the reaction is catalyzed by a surface. These reactions include the contact reactions, the activation of factor X by factor VII tissue factor at sites of tissue injury, and reactions which are accelerated by locally deposited platelet masses (activation of factor X and prothrombin). Third, there are naturally occurring inhibitors of coagulation enzymes, such as antithrombin III that are potent inhibitors of thrombin and other coagulation enzymes (plasma levels of thrombin–antithrombin III complex can also be assayed as a measure of thrombin production in vivo). Another example of a naturally occurring inhibitor is tissue factor pathway inhibitor (TFPI), a protein that, in association with factor Xa, inhibits the tissue factor–factor VII complex. Fourth, during the process of coagulation, enzymes are generated that not only activate coagulation factors, but also degrade cofactors. For example, the fibrinolytic enzyme plasmin (Figs. 2.2.6.4 and 2.2.6.5) degrades fibrinogen and fibrin monomers, and can inactivate cofactors V and VIII. Thrombin is also removed when it binds to thrombomodulin, a protein found on the surface of blood vessel endothelial cells.

The thrombin–thrombomodulin complex then converts another plasma protein, protein C, to an active form that can also degrade factors V and VIII. In vivo, the protein C pathway is a key physiologic anticoagulant mechanism (Esmon, 2003; Colman et al., 2005). In short, the platelet, coagulation, and endothelial systems interact in a number of ways that promote localized hemostasis while preventing generalized thrombosis. Fig. 2.2.6.4 depicts some of the relationships and inhibitory pathways that apply to blood reactions following contact with both natural and artificial surfaces.

Fibrinolysis

The fibrinolytic system removes unwanted fibrin deposits to improve blood flow following thrombus formation, and to facilitate the healing process after injury and inflammation. It is a multicomponent system composed of precursors, activators, cofactors, and inhibitors, and has been studied extensively (Forbes and Courtney, 1987; Colman et al., 2005). The fibrinolytic system also interacts with the coagulation system at the level of contact activation (Bennett et al., 1987). A simplified scheme of the fibrinolytic pathway is shown in Fig. 2.2.6.5.

The most well-studied fibrinolytic enzyme is plasmin, which circulates in an inactive form as the protein plasminogen. Plasminogen adheres to a fibrin clot, being incorporated into the mesh during polymerization. Plasminogen is activated to plasmin by the actions of plasminogen activators, which may be present in blood or released from tissues, or which may be administered therapeutically. Important plasminogen activators occurring naturally in humans include tissue plasminogen activator (tPA) and urokinase. Following activation, plasmin digests the fibrin clot,

releasing soluble fibrin–fibrinogen digestion products (FDP) into circulating blood, which may be assayed as markers of *in vivo* fibrinolysis (e.g., the fibrin D-D dimer fragment). Fibrinolysis is inhibited by plasminogen activator inhibitors (PAIs), and by a thrombin-activated fibrinolysis inhibitor (TAFI), which promotes the stabilization of fibrin and fibrin clots (Colman et al., 2005).

Complement

The complement system is primarily designed to induce a biological response to antigen–antibody reactions. Like the coagulation and fibrinolytic systems, complement proteins are activated enzymatically through a complex series of reaction steps (Bennett et al., 1987). Several proteins in the complement cascade function as inflammatory mediators. The end result of these activation steps is the generation of an enzymatic complex that causes irreversible damage (by lytic mechanisms) to the membrane of the antigen-carrying cell (e.g., bacteria).

Since there are a number of interactions between the complement, coagulation, and fibrinolytic systems, there has been considerable interest in the problem of complement activation by artificial surfaces, prompted in part by observations that devices having large surface areas (e.g., hemodialyzers) may cause: (1) reciprocal activation reactions between complement enzymes and white cells; and (2) complement activation, which may mediate both white cell and platelet adhesion to artificial surfaces. Further observations regarding the complement activation pathways involved in blood–materials interactions are likely to be of interest.

Blood–Material Interactions

Overview

The medical treatment of cardiovascular disease today incorporates the use of a wide range of devices that involve direct contact between blood and artificial materials. These devices include catheters, stents, vascular grafts, and cardiac-support systems such as artificial heart valves, ventricular assist devices, and the total artificial heart. In addition, blood undergoes contact with large surface areas of artificial materials in extracorporeal blood-treatment devices, such as the blood oxygenator, tubing, and blood pump that are used during heart–lung-bypass surgery; blood filtration systems used for hemodialysis; and blood component separation processes used during apheresis.

Unfortunately, while these applications are obviously intended to benefit the patient, the inherent response of blood when it comes in contact with an artificial material surface is to activate the body's natural defense systems (Reviakine et al., 2017; Liu et al., 2015; Jaffer et al., 2015). These responses lead to blood coagulation as well as the activation of the inflammation and complement systems—all of which, if unchecked, lead to the formation of thrombus and thromboemboli, with potentially life-threatening

consequences. In order to prevent or at least substantially suppress these natural responses for patients undergoing procedures involving blood–material interactions, the current approach implemented in medical practice relies on the use of anticoagulant and/or antiplatelet drugs in an attempt to inhibit the generation of material-contact-induced thrombus and thromboemboli (Reviakine et al., 2017; Liu et al., 2015; Jaffer et al., 2015). Despite these pharmacological treatments, thrombus formation is still a significant problem in essentially every device that is used for blood-contacting applications (Reviakine et al., 2017; Liu et al., 2015; Ratner, 2007). Furthermore, the use of these drugs, which cause the systemic suppression of blood coagulation, can lead to serious complications due to uncontrolled hemorrhaging, thus establishing the need for blood-compatible materials to minimize the use of these pharmacological agents. Although advances have been made over the past several decades of research in an attempt to develop materials that inhibit blood coagulation, thrombosis remains an unsolved problem for all synthetic materials used in blood-contact applications.

There are two primary mechanisms through which thrombus formation is initiated from contact between blood and artificial materials: (1) interaction between platelets with the material surface, which is mediated by adsorbed proteins, leading to platelet activation, and (2) contact-activation of the intrinsic clotting cascade directly by the material surface. These mechanisms are addressed in Section [Platelet–Material Interactions](#) and Section [Approaches to Improve the Blood Compatibility of Artificial Materials](#). Section [Platelet–Material Interactions](#) addresses the topic of platelet–material interactions and Section [Contact Activation of the Blood Coagulation Cascade](#) addresses contact activation. Section [Approaches to Improve the Blood Compatibility of Artificial Materials](#) then summarizes approaches that are currently being explored in an attempt to improve the blood compatibility of artificial materials that are used in blood-contact applications.

Platelet–Material Interactions

When an artificial material comes in contact with blood, the surface of the material is coated with an adsorbed layer of blood-plasma proteins within a matter of seconds (Horbett, 1993; Latour, 2008). This topic is covered in detail in [Chapter 2.1.2](#). This process is initially kinetically driven, which results in the surface being first coated with the fastest diffusing proteins, such as albumin, which is the protein with the highest concentration in blood plasma (about 40 mg/mL) in addition to being relatively low molecular weight (about 67 kDa). Depending on how strongly these proteins are adsorbed, the initially adsorbed layer of protein may subsequently be displaced by more strongly adsorbing proteins, such as fibrinogen, through the Vroman effect, which is controlled by thermodynamics (i.e., processes driven by lowering the free-energy state of the system) (Dee et al., 2002).

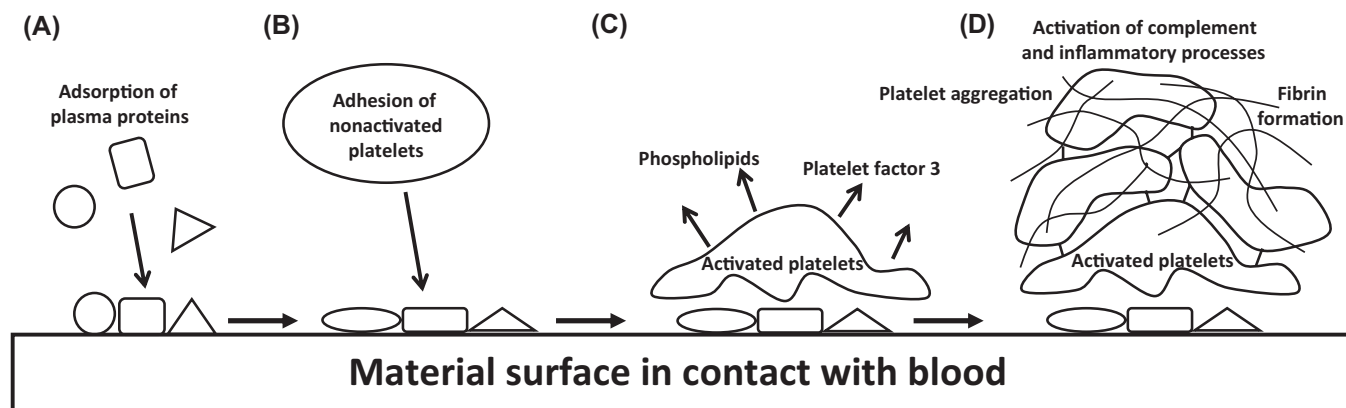
Although still not yet fully understood, nonactivated platelets in blood have the ability to detect this adsorbed layer of proteins as something abnormal, which causes platelets to adhere to the adsorbed proteins, leading to platelet activation (Savage and Ruggeri, 1991). Once activated, platelets release factors including various phospholipids and platelet factor 3 that directly activate the blood coagulation cascade and nearby circulating platelets, as well as complement and inflammatory processes. Platelet activation also results in greatly increased expression of the fibrinogen-binding integrin receptor, GP IIb/IIIa (also known as $\alpha_{IIb}\beta_3$), which strongly binds to fibrinogen. The bifunctionality of fibrinogen enables each fibrinogen protein to bind to two different platelets, resulting in platelet aggregation (Dee et al., 2002). Fig. 2.2.6.6 provides a schematic illustrating thrombus formation induced by platelet adhesion on a synthetic material surface.

Platelets remaining adherent to the protein-coated surface result in the growth of thrombus on the material surface, leading to the reduction or possible complete blockage of blood flow, or the possible loss of function of the implanted prosthesis, such as has occurred with artificial heart valves and ventricular assist devices (Jaffer et al., 2015; Affeld et al., 2016). Alternatively, if the activated platelets release from the surface, thromboemboli may be generated, which will travel downstream in the vasculature to become lodged in subsequent capillary beds of downstream organs (Affeld et al., 2016; Liu et al., 2015; Li and Henry, 2011; Cannegieter et al., 1994). If the thromboemboli occur in the venous system, they may result in pulmonary embolism. Or, if they occur in the arterial system, they may result in stroke, myocardial infarction, or the blockage of blood flow to other organs in the body leading to organ failure.

The fact that nonactivated platelets will adhere and activate against adsorbed proteins such as fibrinogen, but not undergo activation in flowing blood when they are constantly interacting with these same proteins in the blood plasma, indicates that the adsorption of proteins to material

surfaces must somehow alter their conformation in a manner for platelets to recognize them as something abnormal. Evidence of adsorption-induced conformational changes in adsorbed fibrinogen has been found through in vitro studies involving changes in the elutability of adsorbed fibrinogen with time (Bohnert and Horbett, 1986), changes in monoclonal antibody binding with time (Lindon et al., 1986; Horbett and Lew, 1994), and atomic force spectroscopy (Agnihotri and Siedlecki, 2004). Using circular dichroism spectropolarimetry to determine the secondary structure of fibrinogen before and after adsorption under a broad range of conditions, Sivaraman and Latour more recently directly showed that platelet adhesion to adsorbed fibrinogen is strongly correlated with the degree of adsorption-induced unfolding of the protein (Sivaraman and Latour, 2010a). Surprisingly, Sivaraman and Latour then also showed that platelets will even adhere to adsorbed albumin, which does not contain platelet-binding sites in its native structure, once the albumin unfolds beyond a critical degree (measured to be a loss of more than about 33% of albumin's α -helical structure) (Sivaraman and Latour, 2010b). Platelet adhesion to both of these proteins was found to be mediated by the GP IIb/IIIa platelet receptors (Sivaraman and Latour, 2011). Furthermore, an irreversibly adsorbed layer of albumin, which is initially resistant to platelet adhesion, may subsequently induce platelet adhesion and activation after undergoing aging-induced unfolding (Sivaraman and Latour, 2012), thus potentially providing an explanation for the occurrence of late thrombus formation on drug-eluting cardiovascular stents (McFadden et al., 2004; Virmani et al., 2004).

The adhesion and activation of platelets to adsorbed proteins has also been found to be influenced by the shear strain rate at the material surface (Affeld et al., 2016; Goto et al., 1998). Under wall shear strain rates above about 1000 s^{-1} , the adsorption of von Willebrand factor (vWf) is required for platelets to bind to the surface in a manner that is sufficiently strong to hold the platelets on the surface and



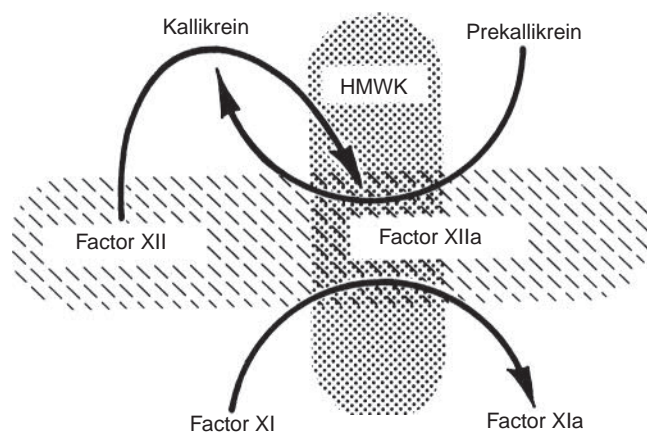
• **Figure 2.2.6.6** (A) Adsorption of plasma proteins to material surface. (B) Conformational changes in adsorbed proteins followed by the adhesion of nonactivated platelets from the blood stream. (C) Platelet activation leading to the release of activating factors. (D) Platelet aggregation and the activation of the blood coagulation cascade leading to thrombus formation, along with the subsequent activation of complement and inflammatory processes.

resist the tendency of the high shear stress along the wall to sweep the platelets downstream along with the flowing blood (Tronic et al., 2016; Goto et al., 1998). When vWf adsorbs to a material surface under these conditions, the high shear strain rate causes the protein to unfurl on the surface to expose otherwise hidden domains within the protein structure that bind to GP Ib receptors that are expressed by nonactivated platelets. Although this binding event does not tend to activate the adherent platelets, once the platelets bind securely to the adsorbed vWf, they are able to be activated through interactions of the platelet GP IIb/IIIa receptors to neighboring adsorbed adhesive proteins, such as fibrinogen, leading to the formation of thrombus and/or thromboemboli.

Contact Activation of the Blood Coagulation Cascade

The other primary mechanism that mediates thrombus formation against biomaterial surfaces that are used in blood-contact applications is referred to as contact activation. This pathway of thrombus formation was discovered by Margolius and Ratnoff in the 1950s (Margolius and Ratnoff, 1956). Margolius and Ratnoff observed that the blood from a patient named Hageman tended to clot unusually slowly in glass tubes. Further investigation determined that this patient lacked a certain factor that was involved with the initial stages of blood coagulation in response to material contact. The factor was initially called Hageman factor. Hageman factor was subsequently termed coagulation factor XII (FXII) and determined to be the first step of the intrinsic blood coagulation cascade.

As with platelet adhesion and activation, contact activation is mediated by the adsorption of plasma proteins on a



• **Figure 2.2.6.7** Contact activation. The initial event in vitro is the adsorption of factor XII to a negatively charged material surface (hatched, horizontal ovoid) where it is activated to form factor XIIa. Factor XIIa converts prekallikrein to kallikrein. Additional factor XIIa and kallikrein are then generated by reciprocal activation. Factor XIIa also activates factor XIa. Both prekallikrein and factor XI bind to a cofactor, high-molecular-weight kininogen (HMWK), which anchors them to the charged surface. Kallikrein is also responsible for the liberation of the vasoactive peptide bradykinin for HMWK, linking coagulation and inflammation.

material surface. This process primarily involves four plasma proteins that interact with material surfaces to activate the intrinsic blood coagulation cascade: FXII (Hageman factor), coagulation factor XI (FXI), prekallikrein (PKK), and high-molecular-weight kininogen (HMWK), which complexes with both FXI and PKK (Xu et al., 2014).

Although the specific mechanism has not yet been fully understood, the adsorption of FXII to material surfaces is believed to induce a conformational change that activates this protein to its enzymatic form of FXIIa, which is referred to as autoactivation (Griffin, 1978). Once activated, FXIIa interacts with adsorbed HMWK-PKK to cause the PKK to convert to kallikrein (KK), which subsequently acts to induce further conversion of FXII to FXIIa (Meier et al., 1977). This process is referred to as reciprocal activation. FXIIa then also activates HMWK-bound FXI to FXIa, which then continues to propagate the intrinsic blood coagulation cascade leading to thrombus generation (Vogler and Siedlecki, 2009; Miller et al., 1980). This overall process is illustrated in Fig. 2.2.6.7.

Numerous studies investigating the contact activation pathway have shown that it is influenced by the surface chemistry, surface energy, surface area, and surface topology of the contacting material (Bauer et al., 2017; Xu et al., 2014; Chatterjee et al., 2009; Sperling et al., 2009; Vogler et al., 1995). In particular, contact activation is induced most strongly on negatively charged hydrophilic surfaces (Griep et al., 1986; Mitropoulos, 1999) while essentially being suppressed on highly hydrophobic surfaces (Xu et al., 2014; Sperling et al., 2009). Siedlecki, Vogler, and coworkers have shown that both negatively charged hydrophilic and hydrophobic surfaces will actually induce the autoactivation of FXII to FXIIa in simple buffer solution, while only negatively charged hydrophilic surfaces appear to induce this reaction in blood plasma (Xu et al., 2014). The reason for this difference is believed to be that the much stronger adsorption of plasma proteins to hydrophobic surfaces compared to hydrophilic surfaces results in the strong adsorption of numerous other proteins that effectively interfere with the adsorption of FXII, thus limiting the autoactivation of FXII to FXIIa.

As shown by Sperling et al. (2009), the opposite response is found with platelet adhesion and activation on material surfaces, with greater platelet response typically occurring on hydrophobic versus hydrophilic materials. Interestingly, in their study they found that heterogeneous surfaces that combine both negatively charged hydrophilic groups and hydrophobic groups, thus inducing both platelet adhesion and contact activation, exhibit the greatest degree of thrombogenicity. These results indicate that a synergistic interaction occurs between platelet responses and contact activation, with the surface of the activated platelets also inducing the conversion of FXII to FXIIa to further amplify the contact activation pathway.

Recognition of the important role of the contact activation pathway to induce thrombus formation against biomaterial surfaces has led to attempts to use pharmaceutical

agents to block the activation of FXII to FXIIa or FXI to FXIa, thus inhibiting the initiation of the intrinsic blood coagulation cascade through these processes (Muller et al., 2011; Montfoort and Meijers, 2013; Kenna and Renne, 2014; Bane and Gailani, 2014).

Approaches to Improve the Blood Compatibility of Artificial Materials

Because thrombus formation against artificial surfaces by both platelet adhesion and contact activation is mediated by adsorbed proteins, one of the primary approaches in attempts to prevent thrombus formation has been the development of surface coatings that are strongly resistant to protein adsorption (Thompson et al., 2017; Liu et al., 2015; Jaffer et al., 2015; Li and Henry, 2011). These surface chemistries include polyHEMA, polyethylene glycol (PEG), phosphatidyl choline, and, more recently, zwitterionic molecules such as betaines [poly(carboxybetaine) (PCB) and poly(sulfobetaine) (PSB)]. However, while demonstrated to be highly effective *in vitro*, these surface chemistries have not been shown to be fully effective in eliminating protein adsorption and subsequent thrombus formation *in vivo* (Liu et al., 2015). Thus the development of protein-resistant surfaces continues as an ongoing area of research.

Other approaches to develop artificial materials that are resistant to thrombus formation include surface functionalization with bioactive molecules that inhibit thrombus formation and the coating of surfaces with endothelial cells in attempts to provide surfaces that resemble that of natural blood vessels (Thompson et al., 2017; Liu et al., 2015; Jaffer et al., 2015; Li and Henry, 2011).

Attempts to provide surface functionalization with biomolecules to inhibit thrombus formation have included the use of heparin and hirudin (Liu et al., 2015; Jaffer et al., 2015; Li and Henry, 2011), both of which are potent inhibitors of thrombin. Heparin is a natural polysaccharide, which, in combination with antithrombin III (ATIII), strongly binds and deactivates thrombin. Heparin–ATIII complexes can also inhibit other blood coagulation factors including XIa, Xa, and IXa (Holmer et al., 1981). Hirudin is a small protein composed of only 65 amino acids, which is derived from the medicinal leech. These types of strategies have been explored in *in vivo* studies as coatings for mechanical heart valves, stents, and artificial vascular grafts with varied levels of success, with the use of such bioactive coatings still representing an active area of research (Liu et al., 2015; Li and Henry, 2011).

Other approaches include polymer coatings that release nitric oxide (NO), which are strong inhibitors of thrombin formation (Goudie et al., 2017; Naghavi et al., 2013). One of the inherent limitations of this approach, however, is that once the NO release is diminished, prevention of thrombus formation is lost, thus potentially limiting this approach to short-term blood-contact applications. Another more recent approach is to apply coatings designed to bind to plasminogen, which upon activation by circulating plasminogen-activating

factor may result in the rapid breakdown of thrombus if it begins to form on the material surface (Liu et al., 2015).

The blood-contacting surface of the natural vasculature is lined with a layer of endothelial cells, which is, of course, nonthrombogenic. Thus the coating of blood-contacting artificial material surfaces with a layer of viable endothelial cells holds promise for providing long-term blood compatibility (Liu et al., 2015; Jaffer et al., 2015; Li and Henry, 2011). Unfortunately, thus far, this approach has proven to be extremely difficult to achieve. As a biological cell, endothelial cells used for surface coatings must be of autologous origin to prevent immunological reactions against these cells. Early attempts to accomplish the endothelialization of artificial vascular grafts have thus tried seeding the surfaces with autologous endothelial cells. However, under *in vivo* flow conditions, the cells tended to wash off from the surface, indicating a need for approaches to increase the strength of cell attachment to maintain complete coverage of the surface and cell viability. Attempts to overcome this problem have included preconditioning the endothelial cell-coated surfaces *in vitro* under moderate flow conditions or precoating the material surfaces with adhesive peptides to provide stronger focal adhesions between the endothelial cells and the underlying material surface.

Another approach to coat artificial material surfaces with endothelial cells that has been tried is by *in situ* endothelialization (Liu et al., 2015; Li and Henry, 2011). This approach requires functionalizing the surface with bioactive molecules designed to stimulate the migration and proliferation of endothelial cells from the adjacent vasculature, or to capture endothelial progenitor cells from the circulation and stimulate their maturation to form a firmly attached endothelial cell layer to completely cover the material surface. Attempts to accomplish this for vascular grafts and stents, however, have thus far also been unsuccessful and efforts to achieve this capability continue.

At this time, the development of a truly blood-compatible material remains an unreached goal. As summarized above, this capability requires material surfaces that are resistant to thrombus formation induced by both platelet adhesion and the contact-activation pathway. While successful treatments have been demonstrated *in vitro*, these same methods have not been proven to be as effective *in vivo*. It is thus apparent that the *in vitro* tests conducted thus far are not adequately representative of *in vivo* conditions. One of the possible explanations for these shortcomings is the “cross-talk” that occurs between blood coagulation and the activation of inflammation and complement processes, with the *in vitro* tests that have been performed thus far not being sufficiently complex to capture these types of interactions. The solution to this problem may thus require the implementation of more complex multifaceted *in vitro* test methods combined with *in vitro* test-method standardization (Braune et al., 2013) (see Chapter 2.3.5—Evaluation of Blood–Material Interactions).

While significant progress has been made over the past several decades of research, the development of blood-compatible materials still remains an unsolved issue and research continues toward the attainment of this long-sought-after goal.

Conclusions

Interrelated blood systems respond to tissue injury in order to rapidly minimize blood loss, and later to remove unneeded deposits after healing has occurred. When artificial surfaces are exposed, an imbalance between the processes of activation and inhibition of these systems can lead to excessive thrombus formation, and an exaggerated inflammatory response. While many of the key blood cells, proteins, and reaction steps have been identified, their reactions in association with artificial material surfaces have not been well defined in many instances. Therefore, blood reactions which might cause thrombosis continue to limit the potential usefulness of many cardiovascular devices for applications in humans (Reviakine et al., 2017; Liu et al., 2015; Jaffer et al., 2015; Li and Henry, 2011; Ratner, 2007; Gorbet and Sefton, 2004). Consequently, these devices still require anticoagulant and/or antiplatelet drugs to be used, which present an inherent bleeding risk due to the resulting systemic suppression of blood coagulation processes.

Acknowledgments

This work was supported by research grant HL-31469 and from the National Institutes of Health, U.S. Public Health Service, by the ERC Program of the National Science Foundation under Award EEC-9731643, and by an Institutional Development Award (IDeA) from the National Institute of General Medical Sciences of the National Institutes of Health under grant number 1P30GM131959.

References

- Agnihotri, A., Siedlecki, C.A., 2004. Time-dependent conformational changes in fibrinogen measured by atomic force microscopy. *Langmuir* 20, 8846–8852.
- Affeld, K., Schaller, J., Wölken, T., Krabatsch, T., Kertzsch, U., 2016. Role of flow for the deposition of platelets. *Biointerphases* 11, 1–9 Article 029804.
- Bane Jr., C.E., Gailani, D., 2014. Factor XI as a target for antithrombotic therapy. *Drug Discov. Today* 19, 1454–1458.
- Bauer, J.W., Xu, L.-C., Vogler, E.A., Siedlecki, C.A., 2017. Surface dependent contact activation of factor XII and blood plasma coagulation induced by mixed thiol surfaces. *Biointerphases* 12, 1–10 Article 02D410.
- Bennett, B., Booth, N.A., Ogston, D., 1987. Potential interactions between complement, coagulation, fibrinolysis, kinin-forming, and other enzyme systems. In: Bloom, A.L., Thomas, D.P. (Eds.), *Haemostasis and Thrombosis*, second ed. Churchill Livingstone, New York, NY, pp. 267–282.
- Bohnert, J.L., Horbett, T.A., 1986. Changes in adsorbed fibrinogen and albumin interactions with polymers indicated by decreases in detergent elutability. *J. Colloid Interface Sci.* 111, 363–377.
- Braune, S., Grunze, M., Straub, A., Jung, F., 2013. Are there sufficient standards for the in vitro hemocompatibility testing of biomaterials? *Biointerphases* 8 (33), 1–9.
- Canegijeter, S., Rosendaal, F., Briet, E., 1994. Thromboembolic and bleeding complications in patients with mechanical heart valve prostheses. *Circulation* 89, 635–641.
- Chatterjee, K., Guo, Z., Vogler, E.A., Siedlecki, C.A., 2009. Contributions of contact activation pathways of coagulation factor XII in plasma. *J. Biomed. Mater. Res.* 90A, 27–34.
- Colman, R.W., Marder, V.J., Clowes, A.W., George, J.N., Goldhaber, S.Z. (Eds.), 2005. *Hemostasis and Thrombosis*, fifth ed. Lippincott, New York, NY.
- Dee, K.C., Puleo, D.A., Bizios, R., 2002. Blood-biomaterial interactions and coagulation. In: *An Introduction to Tissue-Biomaterial Interactions*, pp. 53–88 Chapter 4.
- Esmon, C.T., 2003. The protein C pathway. *Chest* 124 (3 Suppl. 1), 26S–32S.
- Forbes, C.D., Courtney, J.M., 1987. Thrombosis and artificial surfaces. In: Bloom, A.L., Thomas, D.P. (Eds.), *Haemostasis and Thrombosis*, second ed. Churchill Livingstone, New York, NY, pp. 902–921.
- Fournier, R.L., 2007. Marginal zone theory. In: *Basic Transport Phenomenon in Biomedical Engineering*, second ed. Taylor & Francis, New York, pp. 132–134. Section 4.13.
- Gorbet, M.B., Sefton, M.S., 2004. Biomaterial-associated thrombosis: roles of coagulation factors, complement, platelets and leukocytes. *Biomaterials* 25, 5681–5703.
- Goto, S., Ikeda, Y., Saldivar, E., Ruggeri, Z.M., 1998. Distinct mechanisms of platelet aggregation as a consequence of different shearing flow conditions. *J. Clin. Investig.* 101, 479–486.
- Goudie, M.J., Pant, J., Handa, H., 2017. Liquid-infused nitric oxide-releasing (LINORel) silicone for decreased fouling, thrombosis, and infection of medical devices. *Sci. Rep.* 7, 1–13 Article 13623.
- Gresle, P., Page, C.P., Fuster, F., Vermynen, J., 2002. *Platelets in Thrombotic and Non-thrombotic Disorders*, first ed. Cambridge University Press, Cambridge.
- Griep, M.A., Fujikawa, K., Nelsestuen, G.L., 1986. Possible basis for the apparent surface selectivity of the contact activation of human blood coagulation factor XII. *Biochemistry* 25, 6688–6694.
- Griffin, J.H., 1978. Role of surface in surface-dependent activation of Hageman factor (blood coagulation factor XII). *Proc. Natl. Acad. Sci. U.S.A.* 75, 1998–2002.
- Haley, K.M., Loren, C.P., Phillips, K.G., McCarty, O.J.T., 2011. Characterization of single platelet mass, volume, and density in response to agonist stimulation. *Blood* 118, 5261.
- Hanson, S.R., Harker, L.A., Ratner, B.D., Hoffman, A.S., 1980. In vivo evaluation of artificial surfaces using a nonhuman primate model of arterial thrombosis. *J. Lab. Clin. Med.* 95, 289–304.
- Hanson, S.R., Kotze, H.F., Pieters, H., Heyns, A., du, P., 1990. Analysis of 111-Indium platelet kinetics and imaging in patients with aortic aneurysms and abdominal aortic grafts. *Arteriosclerosis* 10, 1037–1044.
- Holmer, E., Kurachi, K., Söderström, G., 1981. The molecular-weight dependence of the rate-enhancing effect of heparin on the inhibition of thrombin, factor Xa, factor IXa, factor XIa, factor XIIa and kallikrein by antithrombin. *Biochem. J.* 193, 395–400.
- Horbett, T.A., 1993. Principles underlying the role of adsorbed plasma proteins in blood interactions with foreign materials. *Cardiovasc. Pathol.* 2, 137S–148S.
- Horbett, T.A., Lew, K.R., 1994. Residence time effects on monoclonal antibody binding to adsorbed fibrinogen. *J. Biomater. Sci. Polym. Ed.* 6, 15–33.
- Jaffer, I.H., Fredenburgh, J.C., Hirsh, J., Weitz, J.I., 2015. Medical device-induced thrombosis: what causes it and how can we prevent it? *J. Thromb. Haemost.* 13 (Suppl. 1), S72–S81.

- Jung, F., Braune, S., 2016. Thrombogenicity and hemocompatibility of biomaterials. *Biointerphases* 11 (2), 1–3 Article 029601.
- Kenna, E., Renne, T., 2014. Factor XII: a drug target for safe interference with thrombosis and inflammation. *Drug Discov. Today* 19, 1459–1464.
- Latour, R.A., 2008. Biomaterials: protein–surface interactions. In: Wnek, G.E., Bowlin, G.L. (Eds.), *Encyclopedia of Biomaterials and Biomedical Engineering*, vol. 1. second ed. Informa Healthcare, New York, NY, pp. 270–284.
- Li, S., Henry, J.D., 2011. Nonthrombogenic approaches to cardiovascular bioengineering. *Annu. Rev. Biomed. Eng.* 13, 451–475.
- Lindon, J.N., McManama, G., Kushner, L., Merrill, E.W., Salzman, E.W., 1986. Does the conformation of adsorbed fibrinogen dictate platelet interactions with artificial surfaces? *Blood* 68, 355–362.
- Liu, X., Yuan, L., Li, D., Tang, Z., Wang, Y., Chen, G., Chen, H., Brash, J.L., 2015. Blood compatible materials: state of the art. *J. Mater. Chem. B* 35 (2), 5709–5926.
- Margolius, A., Ratnoff, O.D., 1956. Observations on the hereditary nature of Hageman trait. *Blood* 11, 565–569.
- McFadden, E.P., Stabile, E., Regar, E., Cheneau, E., Ong, A.T., Kinnaird, T., Suddath, W.O., Weissman, N.J., Torguson, R., Kent, K.M., Pichard, A.D., Satler, L.F., Waksman, R., Serruys, P.W., 2004. Late thrombosis in drug-eluting coronary stents after discontinuation of antiplatelet therapy. *Lancet* 364, 1519–1521.
- Meier, H.L., Pierce, J.V., Colman, R.W., Kaplan, A.P., 1977. Activation and function of human Hageman factor. The role of high molecular weight kininogen and prekallikrein. *J. Clin. Investig.* 60, 18–31.
- Miller, G., Silverberg, M., Kaplan, A.P., 1980. Autoactivatability of human Hageman factor (factor XII). *Biochem. Biophys. Res. Commun.* 92, 803–810.
- Mitropoulos, K.A., 1999. High affinity binding of factor XIIa to an electronegative surface controls the rates of factor XII and prekallikrein activation in vitro. *Thromb. Res.* 94, 117–129.
- Montfoort, M.L.V., Meijers, J.C.M., 2013. Anticoagulation beyond direct thrombin and factor Xa inhibitors: indications for targeting the intrinsic pathway? *Thromb. Haemost.* 110, 223–232.
- Muller, F., Gailani, D., Renne, T., 2011. Factor XI and XII as anti-thrombotic targets. *Curr. Opin. Hematol.* 18, 349–355.
- Naghavi, N., de Mel, A., Alavijeh, O.S., Cousins, B.G., Seifalian, A.M., 2013. Nitric oxide donors for cardiovascular implant applications. *Small* 9, 22–35.
- Ratner, B.D., 2007. The catastrophe revisited: blood compatibility in the 21st Century. *Biomaterials* 28, 5144–5147.
- Ratner, B.D., 1993. The blood compatibility catastrophe. *J. Biomed. Mater. Res.* 27, 283–287.
- Reviakine, I., Jung, F., Braune, S., Brash, J.L., Latour, R., Gorbet, M., Oeveren, 2017. Stirred, shaken, or stagnant: what goes on at the blood-biomaterial interface. *Blood Rev.* 31, 11–21.
- Savage, B., Ruggeri, Z.M., 1991. Selective recognition of adhesive sites in surface-bound fibrinogen by glycoprotein IIb-IIIa on non-activated platelets. *J. Biol. Chem.* 266, 11227–11233.
- Sivaraman, B., Latour, R.A., 2010a. The relationship between platelet adhesion on surfaces and the structure versus the amount of adsorbed fibrinogen. *Biomaterials* 31, 832–839.
- Sivaraman, B., Latour, R.A., 2010b. The adherence of platelets to adsorbed albumin by receptor-mediated recognition of binding sites exposed by adsorption-induced unfolding. *Biomaterials* 31, 1036–1044.
- Sivaraman, B., Latour, R.A., 2011. Delineating the roles of the GPIIb/IIIa and GP-Ib-IX-V platelet receptors in mediating platelet adhesion to adsorbed fibrinogen and albumin. *Biomaterials* 32, 5365–5370.
- Sivaraman, B., Latour, R.A., 2012. Time-dependent conformational changes in adsorbed albumin and its effect on platelet adhesion. *Langmuir* 28, 2745–2752.
- Sperling, C., Fischer, M., Maitz, M.F., Werner, C., 2009. Blood coagulation on biomaterials requires the combination of distinct activation processes. *Biomaterials* 30, 4447–4456.
- Stamatoyannopoulos, G., Nienhuis, A.W., Majerus, P.W., Varmus, H., 1994. *The Molecular Basis of Blood Diseases*, second ed. W.B. Saunders, Philadelphia, PA.
- Thompson, M., Blaszykowski, C., Sheikh, S., Rodriguez-Emmenegger, C., Pereira, A.D., 2017. Biological consequences of the blood-surface interaction. In: Thompson, M. (Ed.), *Biological Fluid-Surface Interactions in Detection and Medical Devices*. Royal Society of Chemistry, Cambridge, UK.
- Tronic, E.H., Yakovenko, O., Weinder, T., Baio, J.E., Penkala, R., Castner, D.G., Thomas, W.E., 2016. Differential surface activation of the A1 domain of von Willebrand factor. *Biointerphases* 11, 1–9 Article 029803.
- Turitto, V.T., Weiss, H.J., 1980. Red cells: their dual role in thrombus formation. *Science* 207, 541–544.
- Virmani, R., Guagliumi, G., Farb, A., Musumeci, G., Grieco, N., Motta, T., Mihalsik, L., Tespili, M., Valsecchi, O., Kolodgie, F.D., 2004. Localized hypersensitivity and late coronary thrombosis secondary to a sirolimus-eluting stent: should we be cautious? *Circulation* 109, 701–705.
- Vogler, E.A., Graper, J.C., Harper, G.R., Sugg, H.W., Lander, L.M., Brittain, W.J., 1995. Contact activation of the plasma coagulation cascade .1. Procoagulant surface-chemistry and energy. *J. Biomed. Mater. Res.* 29, 1005–1016.
- Vogler, E.A., Siedlecki, C.A., 2009. Contact activation of blood-plasma coagulation. *Biomaterials* 30, 1857–1869.
- Xu, L.-C., Bauer, J.W., Siedlecki, C.A., 2014. Proteins, platelets, and blood coagulation at biomaterial surfaces. *Colloids Surf. B* 124, 49–68.

Further Reading

- Reinthal, M., Braune, S., Lendlein, A., Landmesser, U., Jung, F., 2016. Platelets and coronary artery disease: interactions with the blood vessel wall and cardiovascular devices. *Biointerphases* 11 (2), 1–8 Article 029702.

Chapter Exercise Questions

Question 1

Cardiovascular stents are positioned at a site of arterial stenosis by inserting a catheter containing an undeployed stent at its tip into an artery in the arm or groin area, with the tip of the catheter then guided to the site of the stenosis for deployment of the stent under real-time imaging. Once the stent is deployed, the catheter is then removed with the stent remaining at the site of stenosis to hold the artery open at that location.

Part A. When a catheter is inserted into the artery, will the blood coagulation cascade primarily be activated via the extrinsic or intrinsic pathway at the site of catheter insertion?

Answer: At the site of insertion, the blood vessel wall will be cut, causing blood to be exposed to tissue external to the vasculature, with the blood then exposed to tissue factor. Exposure of the blood to tissue factor will initiate blood coagulation via the extrinsic pathway.

Part B. As the catheter is slid within the artery away from the insertion site, will the blood coagulation cascade primarily be activated by the catheter via the extrinsic or intrinsic pathway?

Answer: Away from the insertion site, the catheter will be exposed to blood within intact arteries without exposure to tissue outside of the vasculature, thus tending to activate the intrinsic blood coagulation pathway.

Question 2

Which blood protein is polymerized and cross-linked at the end of the common pathway of the blood coagulation cascade to form a stable insoluble blood clot?

Answer: Fibrinogen polymerization and cross-linking is the final phase of the common pathway of the blood coagulation cascade to form a stable insoluble fibrin blood clot.

Question 3

To prevent or at least minimize blood coagulation against medical devices that are used during cardiovascular procedures, patients are given either anticoagulant or antiplatelet drugs, or a combination of both. What are the differences in the physiological activities in these two different types of antithrombotic drugs?

Answer: Anticoagulant drugs inhibit the contact activation of the coagulation factors of the blood clotting cascade while antiplatelet drugs suppress platelet activation.

2.2.7

Tumorigenesis and Biomaterials

VICKIE Y. JO, FREDERICK J. SCHOEN

Department of Pathology, Brigham and Women's Hospital and Harvard Medical School, Boston, MA, United States

The possibility that implant materials could cause tumors or promote tumor growth has long been a concern of surgeons and biomaterials researchers. This chapter describes general concepts in neoplasia, the association of tumors with implants in human and animals, and the pathobiology of tumor formation adjacent to biomaterials. As therapies utilizing biomaterial stem cells are in brisk development and have begun to be investigated in clinical trials, the current understanding of stem cell-related tumorigenesis is also discussed.

General Concepts

Neoplasia, which literally means “new growth,” is the process of excessive and uncontrolled cell proliferation (Kumar et al., 2015). The new growth is called a *neoplasm* or *tumor* (i.e., a swelling), since most neoplasms are expansile, solid masses of abnormal tissue. Tumors are either *benign* (when their pathologic characteristics and clinical behavior are relatively innocent) or *malignant* (harmful, often deadly). Malignant tumors are collectively referred to as *cancers* (derived from the Latin word for crab, to emphasize their obstinate ability to adhere to adjacent structures and spread in many directions simultaneously). The characteristics of benign and malignant tumors are summarized in Table 2.2.7.1. Examples of malignant tumors are depicted in Fig. 2.2.7.1. Benign tumors do not penetrate (invade) adjacent tissues, nor do they spread to distant sites. They remain localized and surgical excision is curative in many cases. In contrast, malignant tumors show aggressive growth and have a propensity to invade contiguous tissues. Moreover, owing to their ability to gain entrance into blood and lymph vessels, cells from a malignant neoplasm can spread to distant sites, where subpopulations of malignant cells take up residence, grow, and again invade as satellite tumors (called *metastases*).

The primary descriptor of any tumor is the site of origin and the normal cell or tissue/organ that it recapitulates. For malignant tumors arising in epithelium, the suffix “carcinoma” is applied (e.g., squamous cell or adenocarcinoma,

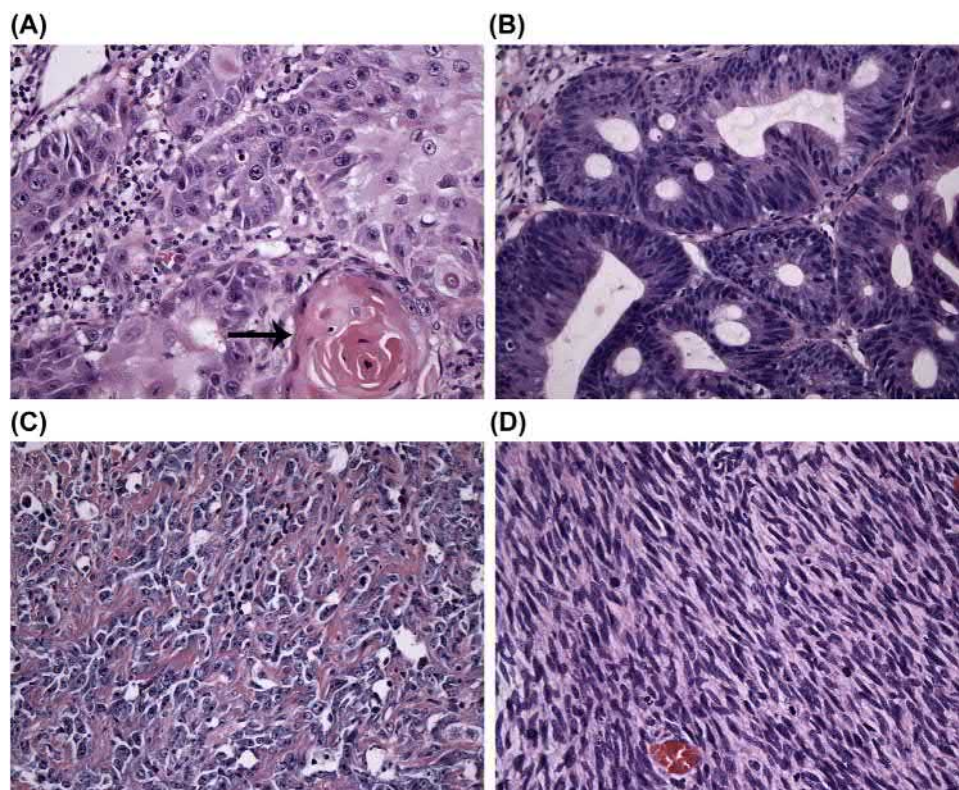
referring to protective and glandular epithelia, respectively), while the suffix “sarcoma” is used for mesenchymal malignancies (e.g., osteo- or chondrosarcoma, producing bone and cartilage, respectively). Malignant neoplasms of the hematopoietic system, in which the cancerous cells circulate in blood, are called leukemias; solid tumors arising from lymphoid tissue are called lymphomas. Neoplastic growth entails both abnormal cellular proliferation and modification of the structural and functional characteristics of the cell types involved. Tumor *grade* or differentiation refers to the degree to which a tumor resembles its counterpart normal cell or tissue type. Malignant cells are generally less differentiated than normal cells. The morphologic similarity of cancer cells to their normal counterparts enables specific *diagnosis* (source organ and cell type); moreover, the grade also predicts the *prognosis* of the patient (i.e., expected outcome based on biologic behavior of the cancer). Therefore, poorly differentiated tumors generally are more aggressive (i.e., display more malignant behavior) than those that are better differentiated. The extent of spread and other effects on the patient determine its *stage*. Both *grade* and *stage* are clinically useful indicators of prognosis.

Neoplastic growth occurs by evasion of normal regulatory cell and tissue functions. Neoplastic cell proliferation is therefore unrelated to the physiological requirements of the tissue, and once initiated is unaffected by removal of the stimulus which initially caused it. These characteristics differentiate neoplasms from (1) normal proliferations of cells during fetal development or postnatal growth, (2) normal wound healing following an injury, and (3) hyperplastic growth which adapts to a physiological need, but which ceases when the stimulus is removed.

All tumors, benign and malignant, have two basic components: (1) proliferating neoplastic cells that constitute their *parenchyma*, and (2) supportive *stroma* comprised of connective tissue and blood vessels. The parenchymal component is more readily recognizable as neoplasia (resembling normal cell and tissue counterparts). Tumor growth and evolution are critically dependent on the nonspecific stromal elements and inflammatory cells.

TABLE 2.2.7.1 Characteristics of Benign and Malignant Tumors

Characteristics	Benign	Malignant
Differentiation	Well defined; structure may closely resemble normal cell or tissue/organ counterpart	Less differentiated with pleomorphism and bizarre (anaplastic) cells; often atypical structure
Rate of growth	Usually progressive and slow; may come to a standstill or regress; cells in mitosis are rare	Erratic, and may be slow to rapid; mitoses may be absent to numerous with abnormal forms
Local invasion	Usually cohesive, expansile, well-demarcated masses that neither invade nor infiltrate the surrounding normal tissues	Locally invasive, infiltrating adjacent normal tissues
Metastasis	Absent	Frequently present; larger and more undifferentiated primary tumors are more likely to metastasize



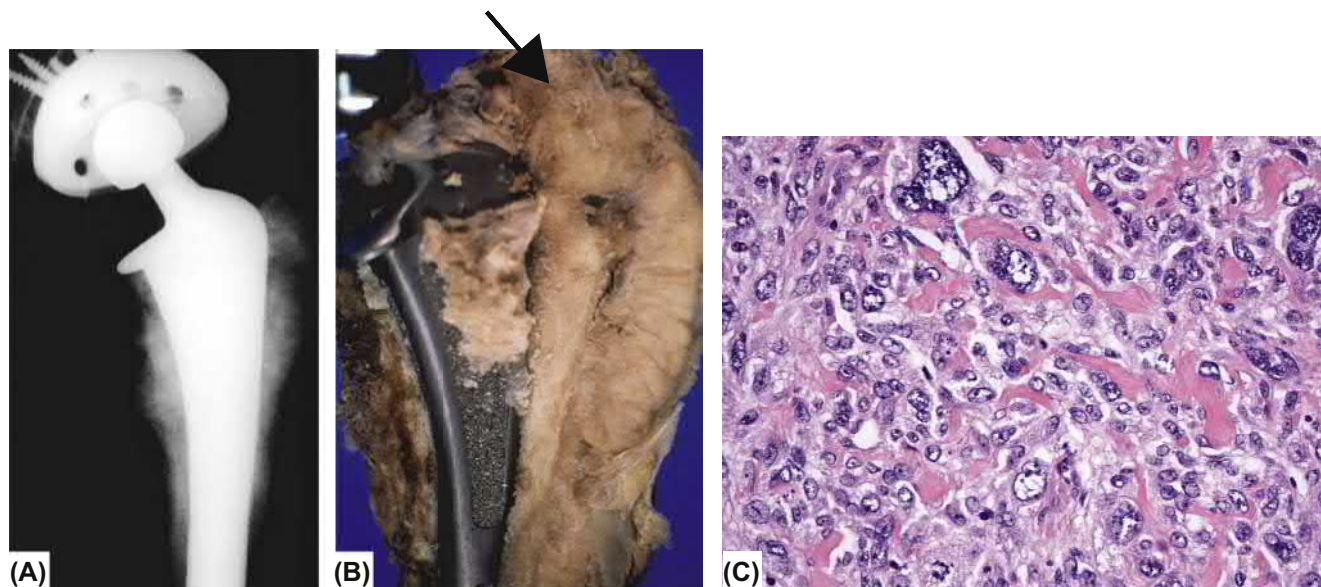
• **Figure 2.2.7.1** Examples of malignant tumor types. (A) Squamous cell carcinoma, with characteristic keratinization (*arrow*). (B) Adenocarcinoma, showing abnormal proliferation of back-to-back glands. (C) Angiosarcoma, with tumor cells forming vague slitlike spaces mimicking vascular channels. (D) Malignant peripheral nerve sheath tumor, an example of a high-grade spindle cell sarcoma. (All slides stained with hematoxylin and eosin.)

Association of Implants With Human and Animal Tumors

Neoplasms occurring at the site of implanted medical devices are rare, despite the large numbers of implants used clinically over an extended period of time. Nevertheless, cases of both human and veterinary implant-associated tumors have been reported (Balzer and Weiss, 2009; Black, 1988; Jennings et al., 1988; Pedley et al., 1981; Schoen, 1987; Visuri et al., 2006a,b). In all, approximately 100 cases of tumors associated with surgical implants have been reported, as well as other cases of tumors related to nontherapeutic foreign

materials (e.g., bullets, shrapnel, other metal fragments, sutures, bone wax, and surgical sponges) (Ebrahimzadeh et al., 2013). One comprehensive review cites 46 cases of reported malignant tumors at the site of total hip arthroplasty from 1974 to 2002 (Visuri et al., 2006a).

Implant-related tumors have been reported to arise in settings of both short- and long-term implantation. Over 25% of tumors associated with foreign material develop within 15 years, while over 50% arise within 25 years (Brand and Brand, 1980). The vast majority of malignant neoplasms associated with clinical fracture fixation devices, total joint replacements, mechanical heart valves, vascular grafts, breast implants and



• **Figure 2.2.7.2** Orthopedic implant-related osteosarcoma in a 68-year-old man, arising 3 years following total hip replacement. (A) Radiograph demonstrating the osteoblastic (i.e., bone-making) tumor surrounding the implant. (B) Resected tumor, showing its relationship to the implant and partially destroyed proximal femur. (C) Photomicrograph of tumor, demonstrating high-grade osteosarcoma. The cytologically malignant cells surround coarse lacelike neoplastic bone. ((A) and (B) reproduced and modified with permission from Keel, S.B. et al., 2001. Orthopedic implant-related sarcoma: a study of 12 cases. *Mod. Pathol.* 14, 969–977. (C) Courtesy of Rosenberg, A.E., Department of Pathology, University of Miami, Laser Institute of America, Miami, FL, United States of America.)

experimental foreign bodies in both animals and humans are sarcomas (i.e., mesenchymal tumors), and are characterized by rapid and locally infiltrative growth. While various histologic subtypes have been reported, including osteosarcoma, chondrosarcoma, and angiosarcoma, most of these sarcomas are unclassified (i.e., lacking evidence of a specific line of differentiation) (Keel et al., 2001). An osteosarcoma forming adjacent to a hip joint prosthesis is illustrated in Fig. 2.2.7.2. Carcinomas, reported in association with foreign bodies far less frequently, have usually been restricted to situations where an implant has been placed in the lumen of an epithelium-lined organ. Illustrative reported cases are noted in Table 2.2.7.2; descriptions of others are available (Goodfellow, 1992; Jacobs et al., 1992; Jennings et al., 1988). Lymphomas have been reported most commonly in association with the capsules surrounding breast implants (Balzer and Weiss, 2009; Gaudet et al., 2002; Keech and Creech, 1997; Mallick et al., 2009; Sahoo et al., 2003; Visuri et al., 2006a, de Jong et al., 2008; Miranda et al., 2014). Occasional cases of nonimplant-related primary tumors (i.e., a metastasis to an implant site) exist in the literature, such as a report of gastric cancer with a metastasis to a total knee replacement (Kolstad and Hgstopr, 1990).

Whether there is a causal role for implanted medical devices in local or distant malignancy remains controversial and a general association is unproven. In an individual case, caution is necessary in implicating the implant in the formation of a neoplasm; clearly, demonstration of a tumor occurring adjacent to an implant does not necessarily prove that the implant caused the tumor (Morgan and Elcock, 1995). Large-scale epidemiological studies and reviews of available data have concluded that there is no evidence in humans for increased tumorigenicity of nonmetallic and metallic surgical implants (McGregor et al.,

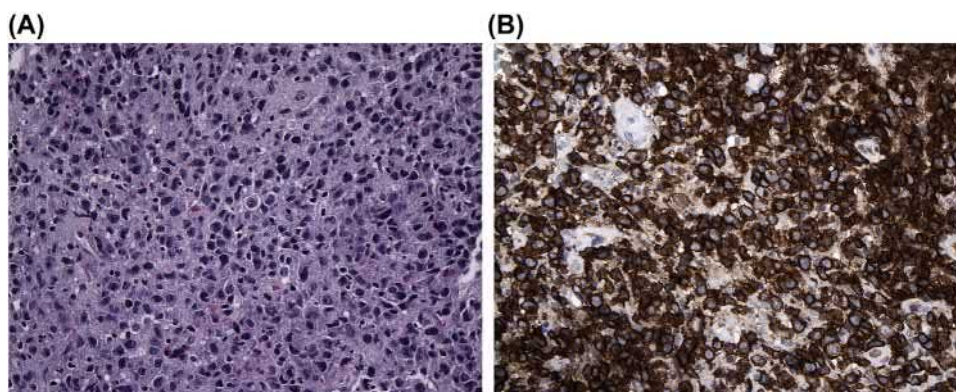
2000). Indeed, the risk in populations appears low, as exemplified by cohorts of patients with both total hip replacement and breast implants that demonstrated no detectable increases in tumors at the implant site (Berkel et al., 1992; Deapen and Brody, 1991; Mathiesen et al., 1995; Brinton and Brown, 1997; Visuri et al., 2006a). Although cancers at most other organ sites seem not to be increased, some studies suggest that there may be a slightly increased risk of hematopoietic cancers (i.e., leukemias and lymphomas). Such cancers occur in organs where exogenous elements and particles may accumulate; in this regard, one study suggests enhanced surveillance in total hip recipients with metal-on-metal articulations, in which the number of metallic particles is estimated to be much higher than with metal-on-plastic bearings (Visuri et al., 2006a), and the size of the particles smaller, with a correspondingly high reactive surface area. However, one population-based study of patients showed no overall differences in risk of cancer development between patients with metallic and nonmetallic hip replacements over a 4-year follow-up period (Mäkelä et al., 2012). Another clinical and experimental study suggested that the incidence of breast carcinoma may be decreased in women with breast implants (Su et al., 1995). Interestingly, breast implant-associated anaplastic large-cell lymphoma has been established as a distinct T-cell lymphoproliferative disorder that is postulated to evolve from malignant transformation of the normal, indolent chronic inflammatory response to the implant and local infection (Miranda et al., 2014; Leberfinger et al., 2017). This is the first observed robust association between a clinical implant and development of neoplasia, although the pathogenetic mechanism has yet to be established. Fig. 2.2.7.3 illustrates an example of an anaplastic large-cell lymphoma that arose in association with a breast implant. Most cases arise

TABLE 2.2.7.2 Tumors Associated With Implant Sites in Humans—Representative Reports and Series

Device (Adjacent Material) ^a	Tumor ^b	References	Postimplantation (Years)
Fracture Fixation			
Intramedullary rod (V)	L	McDonald (1980)	17
Smith-Petersen (V)	OS	Ward et al. (1987)	9
Unknown (SS)	ALCL	Palraj et al. (2010)	7
Total Hip			
Mittlemeier (Al ₂ O ₃)	STS	Ryu et al. (1987)	1+
Charnley-Mueller (UHMWPE)	OS	Martin et al. (1988)	10
Charnley-Mueller (SS, PMMA)	SS	Lamovec et al. (1988)	12
Unknown (porous Ti-cobalt alloy)	OS	Adams et al. (2003)	3
Ti6Al4V, hydroxyapatite coat	OS	Kavalari et al. (2016)	15
Varied (including three metal-polyethylene)	AS	Terrando et al. (2018)	11–30
Total Knee			
Unknown (V)	ES	Weber (1986)	4
Unknown (metallic)	AS	Drexler et al. (2010)	25
Stryker Triathlon (metallic, N/R)	DLBCL	Sanchez-Gonzalez B et al. (2013)	4
Breast			
Implant (S)	SCC	Olsen et al. (2017)	>25
Implant (S and saline)	ALCL	Miranda et al. (2014)	9 (median)
Implant (S)	ALCL	Doren et al. (2017)	10.7 (mean)
Vascular Graft			
Abdominal aortic graft (D)	AS	Fehrenbacher et al. (1981)	12
Abdominal aortic graft (PTFE)	AS	Milite et al. (2016)	<1
Heart Valve Prosthesis			
St. Jude Medical (Carbon, -Silzone coated Dacron Sewing Cuff)	RS	Grubitzsch et al. (2001)	<1

^aMaterials: *D*, Dacron; *N/R*, not reported; *PMMA*, poly(methacrylate) bone cement; *PTFE*, polytetrafluoroethylene; *S*, silicone; *SS*, stainless steel; *Ti*, titanium; *Ti6Al4V*, titanium aluminum vanadium alloy; *UHMWPE*, ultrahigh-molecular-weight polyethylene; *V*, vitallium.

^bTumor types: *ALCL*, anaplastic large cell lymphoma; *AS*, angiosarcoma; *ES*, epithelioid sarcoma; *L*, lymphoma; *OS*, osteosarcoma; *RS*, rhabdomyosarcoma; *SCC*, squamous cell carcinoma; *SS*, synovial sarcoma; *STS*, soft tissue sarcoma.



• **Figure 2.2.7.3** Breast implant-associated anaplastic large-cell lymphoma. (A) Cohesive population of large atypical cells with large irregular nuclei (hematoxylin and eosin stain). (B) Strong and uniform membranous staining for CD30 immunohistochemistry is a diagnostic feature.

secondary to a “textured” implant, presenting as an effusion or mass confined to the textured capsule, with a mean time to presentation of 9–10 years after placement (Quesada et al., 2019). To date the United States Food and Drug Administration (FDA) has received reports of approximately 400 cases of

breast implant-associated anaplastic large-cell lymphoma (U.S. FDA, 2018, <https://www.fda.gov/medicaldevices/productsandmedicalprocedures/implantsandprosthetics/breastimplants/ucm239995.htm>). While the relative risk of developing breast implant-associated anaplastic large-cell lymphoma is increased

in women with breast implants, the absolute risk remains extremely low (de Boer et al., 2018). Currently, the FDA recommends routine care for patients with breast implants, with special attention to patients who develop late-onset (greater than 7 years after implantation) periimplant seromas or masses. Based on available data, most cases have an excellent prognosis with explantation and complete surgical resection of disease, and do not require chemotherapy, although more aggressive behavior may be seen for mass-forming disease compared to effusions confined to the capsule (Quesada et al., 2019).

Moreover, some neoplasms are common in both humans and animals and can occur independently at the sites at which biomaterials are implanted. Sporadic human benign and malignant neoplasms in musculoskeletal sites are not unusual. Most clinical veterinary cases have been observed in dogs, a species with a relatively high natural frequency of osteosarcoma and other tumors at sites where orthopedic devices are implanted. However, since sarcomas arising in the aorta and other large arteries are rare, the association of primary vascular malignancies with clinical polymeric grafts may be stronger than that with orthopedic devices.

Clinically, benign but exuberant foreign body reactions may simulate neoplasms. For example, fibrohistiocytic proliferations resembling malignant tumors may occur as a reaction to silica, previously injected as a soft-tissue sclerosing agent (Weiss et al., 1978), and these exuberant fibrohistiocytic lesions have been observed in association with the capsules that form around breast implants (Balzer and Weiss, 2009) and a type of polytetraethylene sleeve used for lung cancer resections (Fernandez et al., 2008). Moreover, regional lymphadenopathy (i.e., enlargement of lymph nodes) may result from an exuberant foreign body reaction to material that has migrated from a prosthesis. This has been documented in cases of silicone emanating from both finger joints (Christie et al., 1977) and breast prostheses (Hausner et al., 1978), as well as with polymeric replacements of the temporomandibular joint and with conventional metallic, ceramic, and polymeric total replacements of large joints (Jacobs et al., 1995). Reactive fibrous lesions can arise secondarily to a foreign body reaction and simulate a neoplasm, often referred to as a *pseudotumor*; *gossypibomas* (derived from Latin “gossypium” for cotton), or *textilomas*, refer to large mass-forming foreign body reactions to inadvertently retained materials during surgery, such as surgical sponges (Malot and Meena, 2012). Interestingly, nodular fasciitis, a benign myofibroblastic entity that arises rapidly but spontaneously regresses, often mimics sarcoma but is known as a “transient neoplasm,” harboring recurrent *USP6-MYH9* fusion gene (Erickson-Johnson et al., 2011).

Pathobiology of Foreign Body Tumorigenesis

Considerable progress has been made over the last several decades in the understanding of the molecular basis of cancer (Kumar et al., 2015). These fundamental principles are well accepted: (1) Neoplasia is associated with

and often results from nonlethal genetic damage (or mutation), either inherited or acquired by the action of environmental agents such as physical effects [e.g., radiation, fibers or foreign bodies (Fry, 1989)], chemicals, or viruses. (2) The principal targets of the genetic damage are cellular regulatory genes (normally present and necessary for physiologic cell function, inducing cellular replication, growth and repair of damaged DNA). (3) The tumor mass evolves from the clonal expansion of a single progenitor cell which has incurred the genetic damage. (4) Tumorigenesis is a multistep process, generally owing to accumulation of successive genetic lesions. Once tumorigenesis has been initiated, the most important factors in tumor growth are the kinetics (i.e., balance of replication or loss) of cell number change and its blood supply. The formation of new vessels (*angiogenesis*) is also essential for enlargement of tumors and for their access to the vasculature and hence, metastasis (Carmeliet and Jain, 2000).

The pathogenesis of implant-induced tumors is not well understood, yet most experimental data indicate that there is an interplay of physical effects of the implant and subsequent tissue response (i.e., microenvironment). Most data indicate that the physical effects rather than the chemical characteristics of the foreign body are the principal determinants of tumorigenicity (Brand et al., 1975). Tumors can be induced experimentally by a wide array of materials of diverse composition, including those that could be considered essentially nonreactive, such as certain glasses, gold, or platinum, and other relatively pure metals and polymers. Indeed, one surgeon performed a much-maligned experiment in which dimes inserted in rats led to the development of sarcomas in 60% within 16 months (prompting the suggestion that dimes and probably all metallic coins were carcinogenic and should be discontinued!) (Moore and Palmer, 1997). Solid materials implanted in a configuration that maximizes surface area are most tumorigenic. Materials lose their tumorigenicity when implanted in pulverized, finely shredded, or woven form, or when surface continuity is interrupted by multiple perforations. This trend is often called the *Oppenheimer effect*. Thus, foreign body neoplasia is generally considered to be a transformation process mediated by the physical state of implants; it is largely independent of the composition of the materials, unless specific carcinogens are present.

Nanotechnology is an active area of research and has gained many applications in medicine, including disease diagnosis, molecular imaging, and target-specific drug delivery. Recent evidence suggests that tumor formation induced by nanoparticles is dependent on both the physical properties and chemical properties in a particle-dependent preneoplasia–neoplasia model (Hansen et al., 2006). In vivo studies in a rat model comparing bulk versus nanoparticulate implants have demonstrated that secondary sarcomas arose secondary to both nickel and cobalt nanoparticles; however, only bulk nickel implants were associated with sarcomas, while no malignancies developed with cobalt bulk implants (Hansen et al., 2006). Nanoparticles may accumulate both at the site of injection and easily translocate to

other organs and through cell walls; their migratory capability depends on their size, shape, and physical and chemical properties (Kumar and Dhawan, 2013). While nanoparticles may accumulate in organs and cells, their clearance from the body is slower. Solid-state tumorigenesis depends in part on the development of a fibrous capsule around the implant. Tumorigenicity corresponds directly to the extent and maturity of tissue encapsulation of a foreign body and inversely with the degree of active cellular inflammation. Thus, an active, persistent inflammatory response inhibits tumor formation in experimental systems. Host (especially genetic) factors also affect the propensity to form tumors as a response to foreign bodies. Humans are less susceptible to foreign body tumorigenesis than are rodents, the usual experimental model. In rodent systems, tumor frequency and latency depend on species, strain, sex, and age. Concern was initially raised over the possibility that foreign body neoplasia can be induced by the release of wear debris or needlelike elements from composites in a mechanism that is analogous to that of asbestos-related mesothelioma (Brown et al., 1990; Jurand, 1991)—see below. However, animal experiments suggest that only particles with very high length-to-diameter ratios (>100) produce this effect. Particles with this high aspect ratio are highly unlikely to arise as wear debris from orthopedic implants.

Nevertheless, cancer at foreign body sites may be mechanistically related diseases in which tissue fibrosis is a prominent feature, including asbestosis (i.e., lung damage caused by chronic inhalation of asbestos), lung or liver scarring, or chronic bone infections (Brand, 1982). Asbestos is well known as having a causal relationship with mesothelioma, and occurs with pulmonary ingestion specific to fiber shape. Interestingly, most cancers associated with tissue damage and scarring are epithelial, in contrast to the fact that most implant-related tumors are mesenchymal malignancies. Indeed, tissue and matrix stiffness has a role in cancer development. Cells engage in “tensional homeostasis” and increased tissue stiffness results in adaptations in cell behavior, leading to sustained changes in biochemical signaling and ultimately gene expression pathways that can induce malignant transformation (Butcher et al., 2009). Ex vivo studies have also implicated viscoelasticity of tissue and tissue porosity as additional physical properties that may promote neoplasia, which can lead to nuclear deformation and damage and aberrant DNA repair (Singh et al., 2018).

Chemical induction effects are also possible. With orthopedic implants, the stimulus for tumorigenesis could be metal particulates released by wear of the implant (Harris, 1994). Indeed, implants of chromium, nickel, cobalt, and some of their compounds, either as foils or debris, are carcinogenic in rodents (Swierenza et al., 1987), and the clearly demonstrated widespread dissemination of metal debris from implants (to lymph nodes, bone marrow, liver, and spleen, particularly in subjects with loose, worn joint prostheses) could cause both damage to distant organs and be associated with the induction of neoplasia (Case et al., 1994). Although unequivocal cases of metal particles

TABLE 2.2.7.3 Steps in Implant-Associated Tumorigenesis: A Hypothesis^a

1. Cellular foreign body reaction
2. Fibrous capsule formation
3. Preneoplastic cells contact implant surface during quiescent tissue reaction
4. Preneoplastic cell maturation and proliferation within a sequestered microenvironment
5. Tumor growth

^aAdapted from K. G. Brand and colleagues.

or elemental metals provoking the formation of malignant tumors are not available, continued vigilance and further study of the problem in animal models is warranted (Lewis and Sunderman, 1996).

“Nonbiodegradable” and “inert” implants have been shown to contain and/or release trace amounts of substances such as remnant monomers, catalysts, plasticizers, and anti-oxidants. Nevertheless, such substances injected in experimental animals at appropriate test sites (without implants) in quantities comparable to those found adjacent to implants, are generally not tumorigenic. Moreover, chemical carcinogens such as nitrosamines or those contained in tobacco smoke may potentiate scar-associated cancers.

A chemical effect has been considered in the potential carcinogenicity of polyurethane biomaterials (Pinchuk, 1994). Under certain conditions (i.e., high temperatures in the presence of strong bases), diamines called 2,4-toluene diamine (TDA) and 4,4'-methylene dianiline (MDA) can be produced from the aromatic isocyanates used in the synthesis of polyurethanes. TDA and MDA are carcinogenic in rodents. However, it is uncertain whether (1) TDA and MDA are formed in vivo, and (2) these compounds are indeed carcinogenic in humans, especially in the low dose rate provided by medical devices. Although attention has been focused on polyurethane foam-coated silicone gel-filled breast implants, one type of which contained the precursor to TDA, the risk is considered zero to negligible (Expert Panel, 1991).

Foreign body tumorigenesis is typically characterized by a long latency period, during which chronic exposure to the implant instigates tumor formation. Available data suggest the following sequence of essential developmental stages in foreign body tumorigenesis (summarized in Table 2.2.7.3): (1) cellular proliferation in conjunction with tissue inflammation associated with the foreign body reaction (specific susceptible preneoplastic cells may be present at this stage); (2) progressive formation of a well-demarcated fibrotic tissue capsule surrounding the implant; (3) quiescence of the surrounding tissue reaction (i.e., dormancy and phagocytic inactivity of macrophages attached to the foreign body), but direct contact of clonal preneoplastic cells with the foreign body surface and progression of tumor microenvironment; (4) final maturation of preneoplastic cells; and (5) sarcomatous proliferation. Primary support for this multistep hypothesis for foreign body tumorigenesis comes from an

experimental study by Kirkpatrick et al. (2000) in which premalignant lesions were frequently found in implant capsules. A spectrum of lesions was observed, from proliferative lesions without atypical cells to atypical proliferation to incipient sarcoma.

The essential hypothesis is that initial acquisition of neoplastic potential and the determination of specific tumor characteristics do not depend on direct physical or chemical interaction between susceptible cells and the foreign body, and, thus, the intrinsic properties of the foreign body itself probably do not initiate the tumor. However, although the critical initial event occurs early during the foreign body reaction, the final step to neoplastic autonomy (presumably a genetic event) is accomplished only when preneoplastic cells attach themselves to the foreign body surface. Subsequently, there is proliferation of abnormal mesenchymal cells in this sequestered microenvironment by the fibrous capsule, a situation not permitted with the prolonged active inflammation associated with less inert implants. The fibrous capsule acts to sequester the tumor microenvironment, creating an “immune-privileged microenvironment” that can selectively impart the immune system from recognizing tumor antigens that would normally lead to destruction of the cancerous cells (Kitamura et al., 2015). Interestingly one study using a model of biomaterial-induced sarcoma formation in which preneoplastic changes in both tumors and the foreign-body-induced fibrous capsule can be studied by contemporary histologic and molecular techniques (Kirkpatrick et al., 2000), suggested that biomaterial-associated tumorigenesis does not occur by a specific genetic insult, and thereby is different to spontaneous tumorigenesis (Weber et al., 2009). There is increased evidence supporting inflammatory mechanisms in carcinogenesis, with a role for the formation of reactive oxygen and nitrogen species in malignant progression; this is likely the basis for carcinogenesis by nanoparticles (Okada, 2007; Onuma et al., 2009). In vitro and in vivo experiments have shown that nanoparticles can induce DNA damage and mutations due to excessive oxidative stress and generation of free radicals having mutagenic potential (Kumar and Dhawan, 2013). Rodent studies of multiwalled carbon nanotubes have shown widespread development of mesotheliomas, both at the site of injection and elsewhere (Takagi et al., 2008; Sakamoto et al., 2009). Further research is necessary to clarify the malignancy risks in patients.

Thus, the critical factors in sarcomas induced by foreign bodies include implant configuration, fibrous capsule development and remodeling, and a period of latency long enough to allow progression to neoplasia in a susceptible host. The major role of the foreign body itself seems to be that of stimulating the formation of a fibrous capsule conducive to neoplastic cell maturation and proliferation by yet poorly understood mechanisms. The rarity of human foreign body-associated tumors suggests that cancer-prone cells are infrequent in the foreign body reactions to implanted human medical devices.

Stem Cell Therapies and Tumorigenesis

There have been many recent advances in stem cell-based regenerative therapies, which also raise specific considerations for tumorigenesis in these settings (among other controversies). Currently, stem cell therapies in most countries are in the stages of preclinical research and clinical trials, and one major obstacle to clinical implementation is the potential for tumorigenesis. Stem cells are pluripotent, meaning they have the potential to differentiate and mature into any kind of cell type (Kumar et al., 2015). Preclinical research has focused on human embryonic stem cells (collected from embryonic and fetal tissues) (hESC) and human-induced pluripotent stem cells (hiPSCs), which are engineered from adult cells using viral transfection to “genetically reprogram” pluripotent potential. Adult stem cells are normally present in certain tissues and divide to replenish damaged tissue, and are the basis for bone marrow transplants. While stem cells are an attractive source for tissue regeneration, hESCs and hiPSCs have the potential for unregulated growth after implantation, and in vivo animal studies show frequent development of teratomas (i.e., tumors comprised of varied and haphazard primitive tissues recapitulating fetal development) (Cooke et al., 2006; Shih et al., 2007; Blum and Benvenisty, 2008; Knoepfler, 2009; Cunningham et al., 2012). The tumorigenic potential between hESCs and hiPSCs varies; however, because adult stem cells are typically restricted and can only differentiate into certain lineages, they are rarely implicated in tumorigenesis. Research has indicated that the development of these malignancies occurs secondary to unique gene expression profiles that are permissive to tumorigenesis, as well as the acquisition of genetic mutations in culture (Blum et al., 2009). Furthermore, the behavior of stem cells is somewhat unpredictable outside of the intricate regulatory mechanisms of embryogenesis, which dictate specific patterns of differentiation and migration.

The issue of teratoma development has been a major barrier to clinical implementation of stem cell therapy and an area of active research. Ongoing clinical trials are investigating methods for treatment standardization and reducing the risk of tumorigenesis, including measured dosage administration and preimplantation induction of “partial” differentiation of stem cells (Fox et al., 2014; Mazzini et al., 2015). Studies in a macaque monkey model have shown that grafts of hESCs that are induced to differentiate into cardiomyocytes can enhance cardiac function (Liu et al., 2018). The residual “undifferentiated” pluripotent stem cells within a stem cell preparation are considered to be the source of tumorigenesis, and in vivo mouse studies have shown that selective inhibition of undifferentiated stem cells by a variety of methods mitigates against teratoma and tumor formation, such as targeting antiapoptotic pathways by small molecules (Lee et al., 2013), treatment by high-concentration L-alanine medium (Nagashima et al., 2018), and induced phototoxicity (Cho et al., 2015).

Currently, the U.S. FDA encourages patients to enroll only in regulated, approved clinical trials. Worldwide, several commercial exploitative stem cell operations with

limited or no regulation, employing unproven therapies, and reports of unusual, unclassifiable malignancies have been reported in these patients (Amariglio et al., 2009; Thirabanasak et al., 2010; Berkowitz et al., 2016).

Conclusions

Neoplasms associated with therapeutic clinical implants in humans are rare, and causality is difficult to demonstrate in any individual case. Experimental implant-related tumors are induced by a large spectrum of materials and biomaterials, dependent primarily on the physical and not the chemical configuration of the implant. However, specific considerations for tumorigenesis exist for the newer technologies of nanomedicine and stem cell therapy. The mechanism of experimental tumor formation, yet incompletely understood, appears related to the implant fibrous capsule, which sequesters an inflammatory response and immune-privileged tumor microenvironment. Although the mechanism is yet uncertain, the pattern of lymphomas occurring in the context of a breast implant appears to be the first established clinical situation of tumor clearly associated with, and likely directly causal to, a surgical implant.

References

- Adams, J.E., Jaffe, K.A., Lemons, J.E., Siegal, G.P., 2003. Prosthetic implant associated sarcomas: a case report emphasizing surface evaluation and spectroscopic trace metal analysis. *Ann. Diagn. Pathol.* 7, 35–46.
- Amariglio, N., Hirshberg, A., Scheithauer, B.W., Cohen, Y., Loewenthal, R., Trakhtenbrot, L., Paz, N., Koren-Michowitz, M., Waldman, D., Leider-Trejo, L., Toren, A., Constantini, S., Rechavi, G., 2009. Donor-derived brain tumor following neural stem cell transplantation in an ataxia telangiectasia patient. *PLoS Med.* 6, e1000029.
- Balzer, B.L., Weiss, S.W., 2009. Do biomaterials cause implant-associated mesenchymal tumors of the breast? Analysis of 8 new cases and review of the literature. *Hum. Pathol.* 40, 1564–1570.
- Berkel, H., Birdsall, D.C., Jenkins, H., 1992. Breast augmentation: a risk factor for breast cancer? *N. Engl. J. Med.* 326, 1649–1653.
- Berkowitz, A.L., Miller, M.B., Mir, S.A., Cagney, D., Chavakula, V., Guleria, I., Aizer, A., Ligon, K.L., Chi, J.H., 2016. Glioproliferative lesion of the spinal cord as a complication of “stem-cell tourism”. *N. Engl. J. Med.* 375, 196–198.
- Black, J., 1988. *Orthopedic Biomaterials in Research and Practice*. Churchill-Livingstone, New York, pp. 1–394.
- Blum, B., Bar-Nur, O., Golan-Lev, T., Benvenisty, N., 2009. The anti-apoptotic gene survivin contributes to teratoma formation by human embryonic stem cells. *Nat. Biotechnol.* 27, 281–287.
- Blum, B., Benvenisty, N., 2008. The tumorigenicity of human embryonic stem cells. *Adv. Cancer Res.* 100, 133–158.
- Brand, K.G., 1982. Cancer associated with asbestosis, schistosomiasis, foreign bodies and scars. In: Becker, F.F. (Ed.), *Cancer: A Comprehensive Treatise*, vol. I. second ed. Plenum Publ, New York, pp. 661–692.
- Brand, K.G., Buoen, L.C., Johnson, K.H., Brand, I., 1975. Etiological factors, stages, and the role of the foreign body in foreign body tumorigenesis: a review. *Cancer Res.* 35, 279–286.
- Brand, K.G., Brand, I., 1980. Risk assessment of carcinogenesis at implantation sites. *Plast. Reconstr. Surg.* 66, 591–595.
- Brinton, L.A., Brown, S.L., 1997. Breast implants and cancer. *J. Natl. Cancer Inst.* 17, 1341–1349.
- Brown, R.C., Hoskins, J.A., Miller, K., Mossman, B.T., 1990. Pathogenetic mechanisms of asbestos and other mineral fibres. *Mol. Asp. Med.* 11, 325–349.
- Butcher, D.T., Alliston, T., Weaver, V.M., 2009. A tense situation: forcing tumour progression. *Nat. Rev. Cancer* 9, 108–122.
- Carmeliet, P., Jain, R.K., 2000. Angiogenesis in cancer and other diseases. *Nature* 407, 249–257.
- Case, C.P., Langkamer, V.G., James, C., Palmer, M.R., Kemp, A.J., Heap, R.F., Solomon, L., 1994. Widespread dissemination of metal debris from implants. *J. Bone Joint Surg. Br.* 76-B, 701–712.
- Cho, S.J., Kim, S.Y., Jeong, H.C., Cheong, H., Kim, D., Park, S.J., Choi, J.J., Kim, H., Chung, H.M., Moon, S.H., Cha, H.J., 2015. Repair of ischemic injury by pluripotent stem cell based cell therapy without teratoma through selective photosensitivity. *Stem Cell Rep.* 5, 1067–1080.
- Christie, A.J., Weinberger, K.A., Dietrich, M., 1977. Silicone lymphadenopathy and synovitis. Complications of silicone elastomer finger joint prostheses. *JAMA* 237, 1463–1464.
- Cooke, M.J., Stojkovic, M., Przyborski, S.A., 2006. Growth of teratomas derived from human pluripotent stem cells is influenced by the graft site. *Stem Cells Dev.* 15, 254–259.
- Cunningham, J.J., Ulbright, T.M., Pera, M.F., Looijenga, L.H., 2012. Lessons from human teratomas to guide development of safe stem cell therapies. *Nat. Biotechnol.* 30, 849–857.
- de Boer, M., van Leeuwen, F.E., Hauptmann, M., Overbeek, L.I.H., de Boer, J.P., Hijmering, N.J., Sernee, A., Klazen, C.A.H., Lobbes, M.B.I., van der Hulst, R.R.W.J., Rakhorst, H.A., de Jong, D., 2018. Breast implants and the risk of anaplastic large-cell lymphoma in the breast. *JAMA Oncol* 4, 335–341.
- de Jong, D., Vasmel, W.L., de Boer, J.P., Verhave, G., Barbé, E., Casparie, M.K., van Leeuwen, F.E., 2008. Anaplastic large-cell lymphoma in women with breast implants. *JAMA* 300, 2030–2035.
- Deapen, D.M., Brody, G.S., 1991. Augmentation mammoplasty and breast cancer: a 5-year update of the Los Angeles study. *Mammoplast Breast Cancer* 89, 660–665.
- Doren, E.L., Miranda, R.N., Selber, J.C., Garvey, P.B., Liu, J., Medeiros, L.J., Butler, C.E., Clemens, M.W., 2017. U.S. epidemiology of breast implant-associated anaplastic large cell lymphoma. *Plast. Reconstr. Surg.* 139, 1042–1050.
- Drexler, M., Dolkart, O., Amar, E., Pritsch, T., Dekel, S., 2010. Late recurrent hemarthrosis following knee arthroplasty associated with epithelioid angiosarcoma of bone. *Knee.* 17, 365–376.
- Ebrahimzadeh, M.H., Vahedi, E., Ganji, R., Bozorgnia, S., 2013. Skeletal sarcoma on the site of retained war bullet fragments and a literature review on long term complications of retained war shells. *Arch. Bone Jt. Surg.* 1, 107–111.
- Erickson-Johnson, M.R., Chou, M.M., Evers, B.R., Roth, C.W., Seys, A.R., Jin, L., Ye, Y., Lau, A.W., Wang, X., Oliveira, A.M., 2011. Nodular fasciitis: a novel model of transient neoplasia induced by MYH9-USP6 gene fusion. *Lab. Investig.* 91, 1427–1433.
- Expert Panel on the Safety of Polyurethane-covered Breast Implants, 1991. Safety of polyurethane-covered breast implants. *Can. Med. Assoc. J.* 145, 1125–1128.
- Fernandez, S., de Castro, P.L., Tapia, G., Astudillo, J., 2008. Pseudotumor associated with polytetrafluoroethylene sleeves. *Eur. J. Cardio. Surg.* 33, 937–938.
- Fehrenbacher, J.W., Bowers, W., Strate, R., Pittman, J., 1981. Angiosarcoma of the aorta associated with a Dacron graft. *Ann. Thorac. Surg.* 32, 297–301.

- Fox, I.J., Daley, G.Q., Goldman, S.A., Huard, J., Kamp, T.J., Trucco, M., 2014. Stem cell therapy. Use of differentiated pluripotent stem cells as replacement therapy for treating disease. *Science* 345, 1247391.
- Fry, R.J.M., 1989. Principles of carcinogenesis: physical. In: DeVita, V. (Ed.), *Cancer. Principles and Practice of Oncology*, third ed., pp. 136–148.
- Gaudet, G., Friedberg, J.W., Weng, A., Pinkus, G.S., Freedman, A.S., 2002. Breast lymphoma associated with breast implants: two case-reports and a review of the literature. *Leuk. Lymphoma* 43, 115–119.
- Goodfellow, J., 1992. Malignancy and joint replacement. *J. Bone Jt. Surg.* 74B, 645.
- Grubitzsch, H., Wollert, H.G., Eckel, L., 2001. Sarcoma associated with silver coated mechanical heart valve prosthesis. *Ann. Thorac. Surg.* 72, 1730–1740.
- Hansen, T., Clermont, G., Alves, A., Eloy, R., Brochhausen, C., Boutrand, J.P., Gatti, A.M., Kirkpatrick, C.J., 2006. Biological tolerance of different materials in bulk and nanoparticulate form in a rat model: sarcoma development by nanoparticles. *J. R. Soc. Interface* 22, 767–775.
- Harris, W.H., 1994. Osteolysis and particle disease in hip replacement. *Acta Orthop. Scand.* 65, 113–123.
- Hausner, R.J., Schoen, F.J., Pierson, K.K., 1978. Foreign body reaction to silicone in axillary lymph nodes after prosthetic augmentation mammoplasty. *Plast. Reconstr. Surg.* 62, 381–384.
- Jacobs, J.J., Rosenbaum, D.H., Hay, R.M., Gitelis, S., Black, J., 1992. Early sarcomatous degeneration near a cementless hip replacement. *J. Bone Joint. Surg. Br.* 74B, 740–744.
- Jacobs, J.J., Urban, R.M., Wall, J., Black, J., Reid, J.D., Veneman, L., 1995. Unusual foreign-body reaction to a failed total knee replacement: simulation of a sarcoma clinically and a sarcoid histologically. *J. Bone Jt. Surg.* 77, 444–451.
- Jurand, M.C., 1991. Observations on the carcinogenicity of asbestos fibers. *Ann. N.Y. Acad. Sci.* 643, 258–270.
- Jennings, T.A., Peterson, L., Axiotis, C.A., Freidlander, G.E., Cooke, R.A., Rosai, J., 1988. Angiosarcoma associated with foreign body material. A report of three cases. *Cancer* 62, 2436–2444.
- Kavalar, R., Fokter, S.K., Lamovec, J., 2016. Total hip arthroplasty-related osteogenic osteosarcoma: case report and review of the literature. *Eur. J. Med. Res.* 21, 8.
- Keech Jr., J.A., Creech, B.J., 1997. Anaplastic T-cell lymphoma in proximity to a saline-filled breast implant. *Plast. Reconstr. Surg.* 100, 554–555.
- Keel, S.B., Jaffe, K.A., Petur Nielsen, G., Rosenberg, A.E., 2001. Orthopaedic implant-related sarcoma: a study of twelve cases. *Mod. Pathol.* 14, 969–977.
- Kirkpatrick, C.J., Alves, A., Kohler, H., Kriegsmann, J., Bittinger, F., Otto, M., Williams, D.F., Eloy, R., 2000. Biomaterial-induced sarcoma. *Am. J. Pathol.* 156, 1455–1467.
- Kitamura, T., Qian, B.Z., Pollard, J.W., 2015. Immune cell promotion of metastasis. *Nat. Rev. Immunol.* 15, 73–86.
- Knoepfler, P.S., 2009. Deconstructing stem cell tumorigenicity: a roadmap to safe regenerative medicine. *Stem Cells* 27, 1050–1056.
- Kolstad, K., Hgstorpe, H., 1990. Gastric carcinoma metastasis to a knee with a newly inserted prosthesis. *Acta Orthop. Scand.* 61, 369–370.
- Kumar, V., Abbas, A.K., Aster, J.C. (Eds.), 2015. *Cotran/Robbins Pathologic Basis of Disease*, ninth ed. Elsevier, Philadelphia, pp. 265–340.
- Kumar, A., Dhawan, A., 2013. Genotoxic and carcinogenic potential of engineered nanoparticles: an update. *Arch. Toxicol.* 87, 1883–1900.
- Lamovec, J., Zidar, A., Cucek-Plenicar, M., 1988. Synovial sarcoma associated with total hip replacement. *J. Bone Jt. Surg.* 70A, 1558–1560.
- Leberfinger, A.N., Behar, B.J., Williams, N.C., Rakszawski, K.L., Potochny, J.D., Mackay, D.R., Ravnic, D.J., 2017. Breast implant-associated anaplastic large cell lymphoma: a systematic review. *JAMA Surg* 152, 1161–1168.
- Lee, M.O., Moon, S.H., Jeong, H.C., Yi, J.Y., Lee, T.H., Shim, S.H., Rhee, Y.H., Lee, S.H., Oh, S.J., Lee, M.Y., Han, M.J., Cho, Y.S., Chung, H.M., Kim, K.S., Cha, H.J., 2013. Inhibition of pluripotent stem cell-derived teratoma formation by small molecules. *Proc. Natl. Acad. Sci. USA* 110, E3281–E3290.
- Lewis, C.G., Sunderman Jr., F.W., 1996. Metal carcinogenesis in total joint arthroplasty. *Clin. Orthop. Relat. Res.* 329S, S264–S268.
- Liu, Y.W., Chen, B., Yang, X., Fugate, J.A., Kalucki, F.A., Futakuchi-Tsuchida, A., Couture, L., Vogel, K.W., Astley, C.A., Baldessari, A., Ogle, J., Don, C.W., Steinberg, Z.L., Seslar, S.P., Tuck, S.A., Tsuchida, H., Naumova, A.V., Dupras, S.K., Lyu, M.S., Lee, J., Hailey, D.W., Reinecke, H., Pabon, L., Fryer, B.H., MacLellan, W.R., Thies, R.S., Murry, C.E., 2018. Human embryonic stem cell-derived cardiomyocytes restore function in infarcted hearts of non-human primates. *Nat. Biotechnol.* 36, 597–605.
- Mäkelä, K.T., Visuri, T., Pulkkinen, P., Eskelinen, A., Remes, V., Virolainen, P., Junnila, M., Pukkala, E., 2012. Risk of cancer with metal-on-metal hip replacements: population based study. *BMJ* 345, e4646.
- Mallick, A., Jain, S., Proctor, A., Pandey, R., 2009. Angiosarcoma around a revision total hip arthroplasty and review of literature. *J. Arthroplast.* 24, 323.
- Malot, R., Meena, D.S., 2012. Gossypiboma of the thigh mimicking soft tissue sarcoma: case report and review of literature. *J. Orthop. Case Rep.* 2, 21–24.
- Martin, A., Bauer, T.W., Manley, M.T., Marks, K.H., 1988. Osteosarcoma at the site of total hip replacement. *J. Bone Jt. Surg.* 70A, 1561–1567.
- Mathiesen, E.B., Ahlbom, A., Bermann, G., Lindsgren, J.U., 1995. Total hip replacement and cancer. A cohort study. *J. Bone Joint. Surg. Br.* 77B, 345–350.
- Mazzini, L., Gelati, M., Profico, D.C., Sgaravizzi, G., Progetti Pensi, M., Muzi, G., Ricciolini, C., Rota Nodari, L., Carletti, S., Giorgi, C., Spera, C., Domenico, F., Bersano, E., Petruzzelli, F., Cisari, C., Maglione, A., Sarnelli, M.F., Stecco, A., Querin, G., Masiero, S., Cantello, R., Ferrari, D., Zalfa, C., Binda, E., Visioli, A., Trombetta, D., Novelli, A., Torres, B., Bernardini, L., Carriero, A., Prandi, P., Servo, S., Cerino, A., Cima, V., Gaiani, A., Nasuelli, N., Massara, M., Glass, J., Sorarù, G., Boulis, N.M., Vescovi, A.L., 2015. Human neural stem cell transplantation in ALS: initial results from a phase I trial. *J. Transl. Med.* 13, 17.
- McDonald, W., 1980. Malignant lymphoma associated with internal fixation of a fractured tibia. *Cancer* 48, 1009–1011.
- McGregor, D.B., Baan, R.A., Partensky, C., Rice, J.M., Wilbourn, J.D., 2000. Evaluation of the carcinogenic risks to humans associated with surgical implants and other foreign bodies – a report of an IARC Monographs Programme Meeting. *Eur. J. Cancer* 36, 307–313.
- Milite, D., Pilon, F., Ferrari, A., Danieli, D., Desole, A., 2016. Aortic epithelioid angiosarcoma after endovascular aneurysm repair. *Ann. Vasc. Surg.* 35, e17–21.
- Miranda, R.N., Aladily, T.N., Prince, H.M., Kanagal-Shamanna, R., de Jong, D., Fayad, L.E., Amin, M.B., Haideri, N., Bhagat, G., Brooks, G.S., Shifrin, D.A., O'Malley, D.P., Cheah, C.Y., Bacchi, C.E., Gualco, G., Li, S., Keech Jr., J.A., Hochberg, E.P., Carty, M.J., Hanson, S.E., Mustafa, E., Sanchez,

- S., Manning Jr., J.T., Xu-Monette, Z.Y., Miranda, A.R., Fox, P., Bassett, R.L., Castillo, J.J., Beltran, B.E., de Boer, J.P., Chakhachiro, Z., Ye, D., Clark, D., Young, K.H., Medeiros, L.J., 2014. Breast implant-associated anaplastic large-cell lymphoma: long-term follow-up of 60 patients. *J. Clin. Oncol.* 32, 114–120.
- Moore, G.E., Palmer, Q.N., 1977. Money causes cancer. *Ban it. JAMA* 238, 397.
- Morgan, R.W., Elcock, M., 1995. Artificial implants and soft tissue sarcomas. *J. Clin. Epidemiol.* 48, 545–549.
- Nagashima, T., Shimizu, K., Matsumoto, R., Honda, H., 2018. Selective elimination of human pluripotent stem cells using medium with high concentration of L-alanine. *Sci. Rep.* 8, 12427.
- Okada, F., 2007. Beyond foreign-body-induced carcinogenesis: impact of reactive oxygen species derived from inflammatory cells in tumorigenic conversion and tumor progression. *Int. J. Cancer* 121, 2364–2372.
- Olsen, D.L., Keeney, G.L., Chen, B., Visscher, D.W., Carter, J.M., 2017. Breast implant capsule-associated squamous cell carcinoma: a report of 2 cases. *Hum. Pathol.* 67, 94–100.
- Onuma, K., Sato, Y., Ogawara, S., Shirasawa, N., Kobayashi, M., Yoshitake, J., Yoshimura, T., Iigo, M., Fujii, J., Okada, F., 2009. Nano-scaled particles of titanium dioxide convert benign mouse fibrosarcoma cells into aggressive tumor cells. *Am. J. Pathol.* 175, 2171–2183.
- Palraj, B., Paturi, A., Stone, R.G., Alvarez, H., Sebenik, M., Perez, M.T., Bush, L.M., 2010. Soft tissue anaplastic large T-cell lymphoma associated with a metallic orthopedic implant: case report and review of the current literature. *J. Foot Ankle Surg.* 49, 561–564.
- Pinchuk, L., 1994. A review of the biostability and carcinogenicity of polyurethanes in medicine and the new generation of ‘biostable’ polyurethanes. *J. Biomater. Sci. Polym. Ed.* 6, 225–267.
- Pedley, R.B., Meachim, G., Williams, D.F., 1981. Tumor induction by implant materials. In: Williams, D.F. (Ed.), *Fundamental Aspects of Biocompatibility*, vol. II. CRC Press, Boca Raton, FL, pp. 175–202.
- Quesada, A.E., Medeiros, L.J., Clemens, M.W., Ferrufino-Schmidt, M.C., Pina-Oviedo, S., Miranda, R.N., 2019. Breast implant-associated anaplastic large cell lymphoma: a review. *Mod. Pathol.* 32, 166–188.
- Ryu, R.K.N., Bovill Jr., E.G., Skinner, H.B., Murray, W.R., 1987. Soft tissue sarcoma associated with aluminum oxide ceramic total hip arthroplasty. A case report. *Clin. Orthop. Relat. Res.* 216, 207–212.
- Sahoo, S., Rosen, P.P., Feddersen, R.M., Viswanatha, D.S., Clark, D.A., 2003. Anaplastic large cell lymphoma arising in a silicone breast implant capsule: case report and review of the literature. *Arch. Pathol. Lab. Med.* 127, e115–e118.
- Sakamoto, Y., Nakae, D., Fukumori, N., Tayama, K., Maekawa, A., Imai, K., Hirose, A., Nishimura, T., Ohashi, N., Ogata, A., 2009. Induction of mesothelioma by a single intrascrotal administration of multi-wall carbon nanotube in intact male Fischer 344 rats. *J. Toxicol. Sci.* 34, 65–76.
- Sanchez-Gonzalez, B., Garcia, M., Montserrat, F., Sanchez, M., Angona, A., Solano, A., Salar, A., 2013. Diffuse large B-cell lymphoma associated with chronic inflammation in metallic implant. *J. Clin. Oncol.* 31, e148–e151.
- Schoen, F.J., 1987. Biomaterials-associated infection, tumorigenesis and calcification. *Trans. Am. Soc. Artif. Intern. Organs* 33, 8–18.
- Shih, C.C., Forman, S.J., Chu, P., Slovak, M., 2007. Human embryonic stem cells are prone to generate primitive, undifferentiated tumors in engrafted human fetal tissues in severe combined immunodeficient mice. *Stem Cells Dev.* 16, 893–902.
- Singh, A., Brito, I., Lammerding, J., 2018. Beyond tissue stiffness and bioadhesivity: advanced biomaterials to model tumor microenvironments and drug resistance. *Trends Cancer* 4, 281–291.
- Su, C.W., Dreyfuss, D.A., Krizek, T.J., Leoni, K.J., 1995. Silicone implants and the inhibition of cancer. *Plast. Reconstr. Surg.* 96, 513–520.
- Swierzena, S.H.H., Gilman, J.P.W., McLean, J.R., 1987. Cancer risk from inorganics. *Cancer Metastasis Rev.* 6, 113–154.
- Takagi, A., Hirose, A., Nishimura, T., Fukumori, N., Ogata, A., Ohashi, N., Kitajima, S., Kanno, J., 2008. Induction of mesothelioma in p53^{+/−} mouse by intraperitoneal application of multi-wall carbon nanotube. *J. Toxicol. Sci.* 33 (1), 105–116.
- Terrando, S., Sambri, A., Bianchi, G., Cevolani, L., Foschi, L., Gozzi, E., Pignatti, G., Donati, D.M., 2018. Angiosarcoma around total hip arthroplasty: case series and review of the literature. *Musculoskelet Surg* 102, 21–27.
- Thirabanasak, D., Tantiwongse, K., Thorner, P.S., 2010. Angiomyeloproliferative lesions following autologous stem cell therapy. *J. Am. Soc. Nephrol.* 21, 1218–1222.
- U.S. Food and Drug Administration, 2018. Breast Implant-Associated Anaplastic Large Cell Lymphoma (BIA-ALCL). <https://www.fda.gov/medicaldevices/productsandmedicalprocedures/implantsandprosthetics/breastimplants/ucm239995.htm>.
- Visuri, T.I., Pulkkinen, P., Paavolainen, P., 2006a. Malignant tumors at the site of total hip prosthesis. Analytic review of 46 cases. *J. Arthroplast.* 21, 311–323.
- Visuri, T.I., Pukkala, E., Pukkinen, P., Paavolainen, P., 2006b. Cancer incidence and causes of death among total hip replacement patients: a review based on Nordic cohorts with a special emphasis on metal-on-metal bearings. *Proc. Inst. Mech. Eng H* 220, 399–407.
- Ward, J.J., Dunham, W.K., Thornbury, D.D., Lemons, J.E., 1987. Metal-induced sarcoma. *Trans. Soc. Biomater.* 10, 106.
- Weber, P.C., 1986. Epithelioid sarcoma in association with total knee replacement. A case report. *J. Bone Jt. Surg.* 68B, 824–826.
- Weber, A., Strehl, A., Springer, E., Hansen, T., Schad, A., Kirkpatrick, C.J., 2009. Biomaterial-induced sarcomagenesis is not associated with microsatellite instability. *Virchows Arch.* 454, 195–201.
- Weiss, S.W., Enzinger, F.M., Johnson, F.B., 1978. Silica reaction simulating fibrous histiocytoma. *Cancer* 42, 2738–2743.

2.2.8

Biofilms, Biomaterials, and Device-Related Infections

IOLANDA FRANCOLINI¹, LUANNE HALL-STOODLEY², PAUL STOODLEY^{2,3,4,5}

¹Department of Chemistry, Sapienza University of Rome, Rome, Italy

²Department of Microbial Infection and Immunity, The Ohio State University, Columbus, OH, United States

³Departments of Orthopaedics and Microbiology, The Ohio State University, Columbus, OH, United States

⁴Campus Imaging and Microscopy Facility, Office of Research, The Ohio State University, Columbus, OH, United States

⁵National Centre for Advanced Tribology, Mechanical Engineering, University of Southampton, Southampton, United Kingdom

Introduction

The chapter “A History of Biomaterials” at the start of this book documents the development and design of indwelling materials for medical and dental purposes. The primary design criteria in the choice of materials were pragmatic and based on the necessary mechanical properties required to fashion a functional device. Orthopedic implants require strong materials for load bearing, articulating surfaces such as joints require durability and resistance to wear, stents and shunts require flexibility and patency, and sutures require a high tensile strength, yet must also be flexible enough for intricate manipulation.

Indwelling devices, however, increase the risk of infection. Catheter-associated urinary tract infection (CAUTI), the most common health care-associated infection, accounted for nearly 40% of all nosocomial infections worldwide (Hooton et al., 2010). Prolonged catheter use is the primary risk factor for developing CAUTI (www.cdc.gov/hai/ca_uti/uti.html). Additionally, the incidence of prosthetic joint (hip and knee) infections (PJIs) and cardiovascular implantable device (CID) infections is increasing dramatically (Xu et al., 2017). CIDs include cardiovascular implantable electronic devices and ventricular assist devices, and implantation is increasing with an aging population. Although estimates vary with the types of devices, host

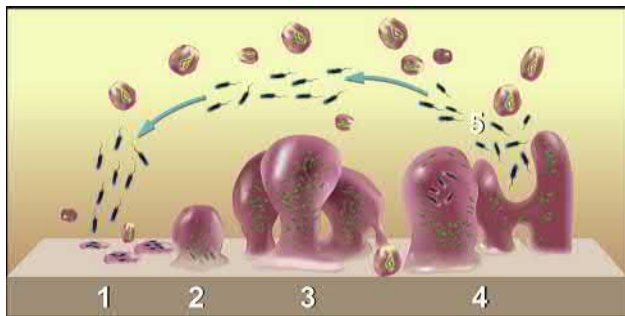
factors and underlying diseases, infection rates generally increase with duration.

While for some procedures, such as orthopedic joint arthroplasty, surgical-site infection rates are low (1%–2%) (Kurtz et al., 2012), the ever-growing number of patients undergoing these procedures translates to large numbers of infection each year. By 2020, estimates suggest that there will be 70,000 cases of infection in the United States alone (Kurtz et al., 2012). Infection of artificial joints is especially devastating, since oral or intravenous antibiotic therapy frequently fails to resolve the infection, leaving the only course of action to surgical debridement, or partial or total revision. The formation of microbial biofilms on these devices contributes significantly to device-related surgical site infections rendering these infections extremely difficult to treat with conventional topical or systemic antibiotic therapy.

Bacterial Biofilms

What Are Biofilms and Why Are They Problematic?

Bacterial biofilms are communities of bacteria that attach and subsequently grow on surfaces of abiotic materials as well as host tissues (Hall-Stoodley and Stoodley, 2009) (Fig. 2.2.8.1). Biofilms also exist as aggregates in fluid or mucus



• **Figure 2.2.8.1** Key processes in biofilm development. (1) Initial attachment of single cells and cell aggregates in the overlying fluid. (2) Initiation of microcolony formation where production of extracellular polymeric substances (EPS) more firmly adheres cells to the surface. (3) Early development of biofilm clusters by clonal expansion (mixed or single species). (4) Mature biofilm. (5) Dispersion of single cells and detachment of biofilm aggregates containing cells and EPS. (Redrawn from Stoodley, P., Sauer, K., Davies, D.G., Costerton, J.W., 2002. Biofilms as complex differentiated communities. *Annu. Rev. Microbiol.* 56, 187–209.)

layers adjacent to tissues (Dastgheyb et al., 2017). Once attached, bacteria embed themselves in a highly hydrated and protective material termed “extracellular polymeric substances” (EPS). While the EPS matrix consists of bacterially produced polymers, such as extracellular DNA (eDNA), polysaccharides, lipids, proteins (Flemming and Wingender, 2010), host materials can also be incorporated into the EPS. Numerous *in vitro* and *ex vivo* studies show that both Gram-negative and -positive pathogens can form biofilms on commonly used medical materials and devices such as surgical sutures and meshes (Engelsman et al., 2007), orthopedic implants and catheters (Jacobsen et al., 2008; Machado et al., 2009), and on host tissues (Hall-Stoodley et al., 2006; Malone et al., 2017a).

The Biofilm Microenvironment

Importantly, biofilms can modify their local environment (Benoit and Koo, 2016) largely because transport through the biofilm EPS is diffusion limited. Nutrients, such as oxygen, are consumed by bacterial cells respiring at the periphery of the biofilm more rapidly than they are able to diffuse into the biofilm. Similarly, acid fermentation deeper within biofilm structures can lead to anaerobic and acidic conditions at the base of the biofilm.

Antibiotic and Antimicrobial Tolerance of Bacteria in Biofilms

Bacteria in biofilms are more resistant to environmental stresses such as dehydration, metal toxicity, and ultraviolet (UV) light exposure than free-floating planktonic bacteria. These strategies, which likely evolved for survival in the natural environment, facilitate survival against attempts to eradicate them with modern materials, antibiotics, and antimicrobial agents. While the exact nature of biofilm tolerance is not fully understood, the most common mechanisms

involve (1) bacteria in the interior of the biofilm enter a dormant state due to nutrient depletion (Fux et al., 2004), (2) reaction of antimicrobial agents with the EPS through binding and/or degradation (Anderl et al., 2000), and (3) the development of recalcitrant populations, such as slow growing small colony variants or “persister” cells (Lewis, 2005). These mechanisms are referred to as “tolerance,” which is distinct from “resistance,” a genetically heritable trait. Recalcitrance to antibiotics and the multifactorial nature of biofilm development requires multitargeted strategies for control (Koo et al., 2017).

Biofilms and the Immune Response

Once formed, biofilms are difficult to eradicate by host immune effectors, including oxidative stress and low pH. Foreign materials alone may also suppress the efficacy of host immunity. Biofilm defense mechanisms include EPS matrix production, which protects bacteria within the biofilm from phagocytes due in part to physical size and viscoelastic properties (Davis-Fields et al., 2019), depending on the biofilm species and age (Guenther et al., 2009). The EPS matrix also reduces the ability of antibodies to penetrate the biofilm (De Beer et al., 1997). Thus biofilm formation facilitates evasion of host immune effectors, and many biofilm-associated infections (cystic fibrosis lung infection, chronic otitis media, gingivitis, and PJI) are associated with chronic inflammation (Hoiby et al., 2015). Paradoxically, such an inflammatory response fails to eradicate the biofilm but contributes to the pathology by damaging host tissue. In some infections, however, biofilms evade the immune system by eliciting a muted inflammatory response (Le et al., 2018). Growing evidence suggests that low-virulence organisms, such as *Staphylococcus epidermidis* and *Cutibacterium acnes*, survive in biofilms as “subclinical” infections.

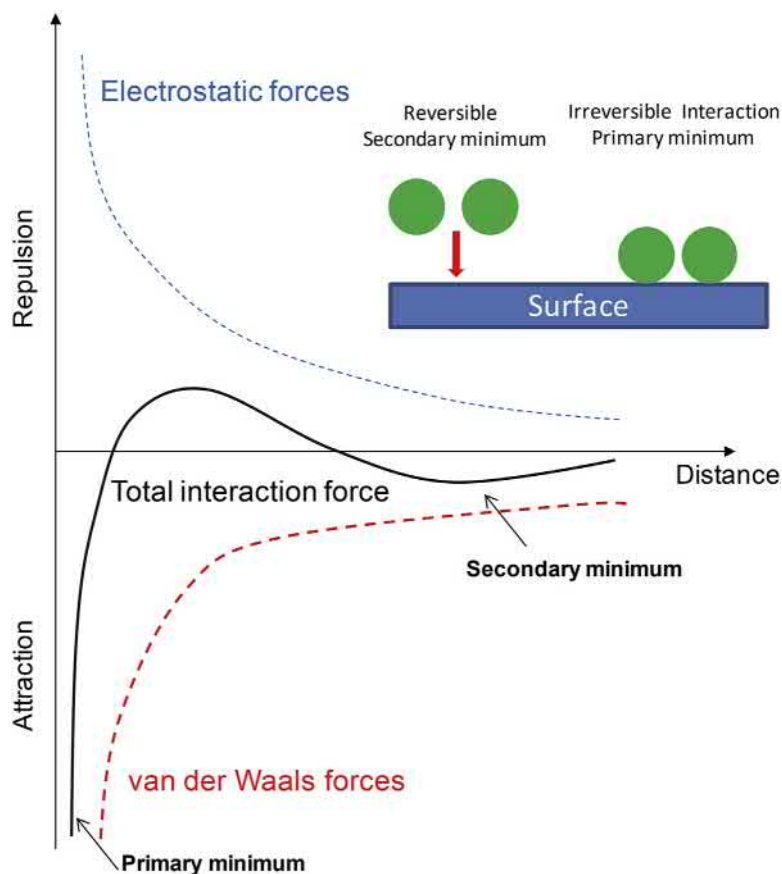
Bacterial Adhesion

Since bacteria become much more difficult to control once they have formed a biofilm, the ideal antibiofilm surface would prevent attachment in the first place. Such a surface would have surface properties that were inherently nonadherent to bacteria, yet were biocompatible.

The Process of Bacterial Adhesion to Surfaces

Bacterial adhesion is a process occurring in integrated phases, the first of which involves bacteria approaching and interacting with the biomaterial surface by long-range, nonspecific interactions like van der Waals or gravitational forces. Once in proximity to the surface (<5 nm), short-range interactions, such as hydrogen bonding and hydrophobic, ionic, and dipole interactions, can be established between the biomaterial surface and the bacterial cell.

Two approaches have been proposed to understand the forces acting between biomaterial surface and bacterial cell during the adhesion process: (1) Derjaguin, Landau,



• **Figure 2.2.8.2** The Derjaguin, Landau, Verwey, Overbeek theory prediction of bacterial cell adhesion (green spheres) on a flat surface.

Verwey, Overbeek (DLVO) theory and (2) the thermodynamic model. In both models, bacterial cells are considered abiotic colloid particles even if recent reports of rapid aggregation of staphylococci in synovial fluid (Dastgheyb et al., 2015) suggest that initial interactions of some species with surfaces might not be in the form of single cells, as commonly depicted in conceptual models, but might occur as aggregates of cells. These “protobiofilm” aggregates, which form rapidly through adhesive processes rather than growth, are tolerant to antibiotics and may provide protection even before bacterial proliferation and EPS production occurs on the surface.

DLVO Theory

DLVO theory considers that microorganisms approaching a surface are attracted or repelled depending on the resultant net interaction force deriving from the sum of van der Waals interactions (generally attractive) and Coulomb electrostatic interactions generated from the electrical double layer of the cell and the substratum (generally repulsive) as the driving force in bacterial adhesion (Van Loosdrecht et al., 1990) (Fig. 2.2.8.2).

DLVO theory has been shown to have limited application in the study of bacterial adhesion. Indeed, direct observations of planktonic bacteria using electron microscopy showed that planktonic bacterial cells are not

smooth-surfaced colloid particles (Fux et al., 2005). Rather, the entire surface of single bacterial cells is covered by protein appendages (i.e., flagella and pili) projecting as much as 2–6 μm from the cell, and a structured matrix of hydrophobic extracellular polymeric substances (EPS). This external “glycocalyx” is anchored to the polysaccharide O-antigen fibers that project from the lipopolysaccharide of the outer membrane of Gram-negative bacteria, and polysaccharide teichoic acid fibers that project from the cell wall of Gram-positive cells, such that the actual surface of planktonic bacterial cells capable of interacting with a surface consists of a 0.2–0.4- μm -thick layer of protein and polysaccharide fibers.

Thermodynamic Model

The thermodynamic model (Morra and Cassinelli, 1997) takes into account different types of cell/biomaterial interactions (e.g., van der Waals, ionic, and dipole interactions), which are expressed in terms of Gibbs free energy (G) through the determination of the surface tension of adhering bacterial cells, the surface, and the suspending liquid medium, according to:

$$\Delta G^{adh} = \gamma_{bs} + \gamma_{bl} + \gamma_{sl} \quad (2.2.8.1)$$

where ΔG^{adh} is the free energy of adhesion, γ_{bs} is the bacterium–substratum interfacial tension, γ_{bl} is the

bacterium–liquid interfacial tension, and γ_{sl} is the substratum–liquid interfacial tension. It is possible to obtain experimental data for the various interfacial tensions involving solid surfaces by the use of Young's equation:

$$\gamma_{sv} - \gamma_{sl} = \gamma_{lv} \cos \theta \quad (2.2.8.2)$$

where γ_{sv} , γ_{sl} , and γ_{lv} are, respectively, the surface tension (or surface free energy) of solid substratum S and vapor phase V , solid substratum S and the liquid L , and the liquid L and vapor phase V ; θ is the contact angle of the liquid on the solid (Fig. 2.2.8.3).

By thermodynamic consideration (Neumann et al., 1974), an equation state relation for the substrate and the liquid surface tension (γ_{sl}) has been formulated where γ_{sl} depends on γ_{lv} and γ_{sv} :

$$\gamma_{sl} = \frac{[(\gamma_{sv})^{0.5} - (\gamma_{lv})^{0.5}]^2}{1 - 0.015 (\gamma_{sv}\gamma_{lv})^{0.5}} \quad (2.2.8.3)$$

Combined with Young's equation this gives:

$$\cos \theta = \frac{(0.015 \gamma_{sv} - 2) (\gamma_{sv}\gamma_{lv})^{0.5} + \gamma_{lv}}{\gamma_{lv} [0.015 (\gamma_{sv}\gamma_{lv})^{0.5} - 1]} \quad (2.2.8.4)$$

which allows the determination of the unknown surface tension of the surface–vapor, γ_{sv} , through contact angle measurements and liquid–vapor surface tensions (γ_{lv}) data. Therefore for a specific liquid–surface couple, for which γ_{lv} and γ_{sv} are known, determination of the surface tension of the bacterial species (γ_{bv}) can be used to predict the extent of adhesion. Adhesion will be favored if the process itself causes a decrease in the interfacial free energy ΔG^{adh} . In this regard, two distinct situations are possible: (1) the surface tension of the bacterium is greater than that of the suspending medium ($\gamma_{lv} < \gamma_{bv}$), in this case ΔG^{adh} decreases with increasing γ_{sv} (bacterial adhesion is favored onto hydrophilic surfaces), or (2) the surface tension of a bacterium is lower than that of

the suspending medium ($\gamma_{lv} > \gamma_{bv}$), in which case ΔG^{adh} decreases with decreasing γ_{sv} . This thermodynamic approach was validated by studying the adhesion of bacterial strains onto various polymer surfaces with different concentrations of dimethylsulfoxide to vary liquid surface tension. The surface tension of various bacterial species was determined by evaluating the contact angle on layers of cells (Absolom et al., 1983). While this model describes only the equilibrium of adhesion and cannot be used to describe the kinetics, it helps illustrate why surface hydrophobicity generally induces the adhesion of bacteria, while surface hydration has the opposite effect.

Influence of Material Properties on Bacterial Adhesion

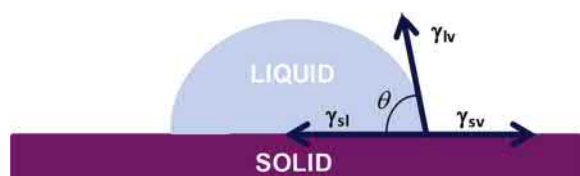
The biomaterial physicochemical properties have been shown to affect bacterial adhesion (Fig. 2.2.8.4). A combination of charge, roughness, hydrophobicity/hydrophilicity, and mechanical properties of the substratum surface may either encourage or discourage bacterial adhesion (Song et al., 2015).

Surface Free Energy (Wettability)

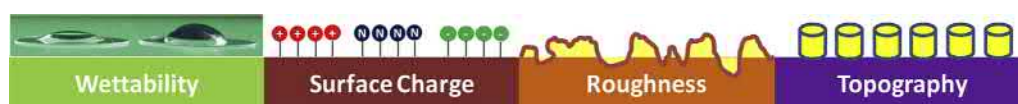
The surface free energy values and contact angles of common polymeric biomaterials are shown in Table 2.2.8.1. Material surfaces are classified as hydrophilic if the contact angle (θ) is less than 90 degrees and hydrophobic when higher than 90 degrees. The wetting features of materials depend on surface chemical compositions. Fluorinated compounds like polytetrafluoroethylene are the most hydrophobic, while oxygenated compounds like polyethyleneoxide are the most hydrophilic. In general, bacterial adhesion is more pronounced on hydrophobic surfaces. However, recent studies have shown that *superhydrophobic* (contact angles higher than 150 degrees) and *superhydrophilic* (very low contact angles) surfaces can both prevent biofilm formation. Although none of the currently used biomaterials exhibits extreme wetting features (Table 2.2.8.1), superhydrophobicity or superhydrophilicity can be obtained by combining surface composition with surface topography and roughness (Feng et al., 2002). Indeed, for rough surfaces the contact angle is described by the Wenzel equation:

$$\cos \theta^* = r \cos \theta$$

where θ^* is the apparent contact angle, θ is the intrinsic contact angle, and r is the roughness factor defined as the



• **Figure 2.2.8.3** Representation of the contact angle (θ) of the Young's equation.



• **Figure 2.2.8.4** Schematic illustration of the main material properties (wettability, surface charge, roughness, and topography) affecting bacterial adhesion.

ratio between actual and projected surface. This equation predicts an increase in apparent contact angle (increase in hydrophobicity) for rougher hydrophobic materials and the opposite behavior for hydrophilic materials.

Various mechanisms have been described to explain the resistance of superhydrophobic and superhydrophilic surfaces to bacterial fouling. Superhydrophilic surfaces are anti-fouling due to the formation of a dense layer of water (*water layer theory*) that weakens the interaction between bacterium and substrate. In contrast, superhydrophobic surfaces prevent wetting due to air trapped in the surface features (Zhang et al., 2012). According to the Cassie model, water droplets cannot penetrate into the surface roughness grooves and thus sit atop the surface protrusions (Fig. 2.2.8.5).

Consequently, the adhesion force between water droplets and material surface weakens and water droplets readily roll off providing easy-to-clean properties, i.e., the “lotus leaf effect.”

Roughness

Generally, an increase in surface roughness promotes bacterial adhesion, since bacteria have a larger surface available and are protected from shear forces (Boyd et al., 2002). Specifically, a small increase in surface roughness increases bacterial adhesion, while a large increase may decrease or have no effect as found for polymethyl methacrylate (PMMA) surfaces in which a small increase in the arithmetic average roughness ($R_a = 0.04\text{--}1.24\ \mu\text{m}$) promoted bacterial adhesion while higher R_a values ($R_a = 1.86\text{--}7.89\ \mu\text{m}$) had the opposite behavior (Taylor et al., 1998). However, the roughness threshold values will depend on the material, bacterial strain, and culture conditions, making it difficult to predict the extent of bacterial adhesion just on the basis of material roughness.

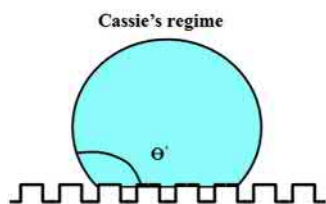
Environment Factors Influence Bacterial Adhesion

Bacterial adhesion is multifactorial, affected by bacterial density, flow conditions, and organic conditioning layers. Flow conditions are known to influence the extent of bacterial adhesion (Thomen et al., 2017), biofilm structure (Stoodley et al., 1998), and quorum sensing (QS) communication (Stoodley, 2016). *Escherichia coli* adhesion was studied under different shear stresses by a microfluidic system that allowed control of hydrodynamic conditions and real-time monitoring of biofilm development. A threshold value of shear stress was reported for biofilm settlement, where a shear stress of 10 MPa inhibited biofilm formation (Thomen et al., 2017). In addition, the shear stress values favoring bacterial attachment were significantly lower than those needed to cause bacterial detachment, suggesting that stronger interactions between the bacterium and the surface are established after initial adhesion (Ming et al., 1998).

A bioorganic conditioning layer on the material surface can also affect bacterial adhesion mediated via ligand/receptor interactions. Indeed, many bacterial strains like staphylococci can express multiple adhesins for host proteins and matrix polymers (Liesenborghs et al., 2018). Therefore the deposition of such molecules onto the biomaterial surface after implantation, which occurs as a typical foreign body reaction (FBR), can mask underlying surface properties and significantly affect bacterial adhesion. Interestingly, the effects of some surface device features, such as charge, roughness, and hydrophobicity, on FBR are similar to those reported for bacterial adhesion processes (Klopfleisch and Jung, 2017), suggesting it may be possible to develop a biomaterial well tolerated by the host and at the same time be resistant to bacterial adhesion.

TABLE 2.2.8.1 Surface Free Energy of Main Polymeric Biomaterials

Material	Surface Free Energy (20°C) (Dynes/cm)	Contact Angle (Degrees)	Notes
Water	72.8	–	
Polyethylene	27	93	Hydrophobic
Polypropylene	28	95	Hydrophobic
Polyvinyl chloride	27	103	Hydrophobic
Polydimethylsiloxane	20	114	Very Hydrophobic
Polytetrafluoroethylene	16	119	Very Hydrophobic
Polyethyleneterephthalate	43	75	Hydrophilic
Polyurethane	38	85	Hydrophilic
Polycarbonate	46	75	Hydrophilic
Polymethylmethacrylate	37	65	Very Hydrophilic
Polyethyleneoxide	43	63	Very Hydrophilic



• **Figure 2.2.8.5** Cassie model for rough surfaces.

Device-Related Infection

Medical and surgical practices rely on an increasing array of biomedical implants and tens of millions are implanted each year. Intravenous catheters, prosthetic heart valves, joint prostheses, orthopedic fixation hardware, peritoneal dialysis catheters, cardiac pacemakers, cerebrospinal fluid shunts, and endotracheal tubes save millions of lives, but all carry the risk of device-related infection, which is generally the first or second most common complication. Many types of catheters and fluid management devices, such as central venous catheters (CVCs), dialysis catheters, ventilators, neurosurgical shunts, and drains, are commonly associated with infection (Rolighed Thomsen et al., 2010). In the United States in 2002 surgical site infection accounted for 20% (244,000) of all healthcare-associated infections outside the ICU (Klevens et al., 2007). Although difficult to dissect exact numbers, many of these were likely associated with a foreign body. The same study reported that 36% of these infections (424,060) were urinary tract infections (UTIs) and the Centers for Disease Control reported that CAUTI accounts for 75% of UTIs (www.cdc.gov/hai/ca_uti/uti.html). Additionally, 250,000 catheter-related bloodstream infections occurred in the United States in 2002 (Daniels and Frei, 2013). In orthopedics, up to 70,000 cases of hip and knee arthroplasty infection are estimated by 2020, with hospital costs expected to reach \$1.62 billion (Kurtz et al., 2012).

Major Medical Devices, Materials, and Pathogens

There is a clear correlation between implanted devices and risk of surgical site infection. Any time the protective skin barrier is breached, the possibility exists of introducing bacterial pathogens by air or being drawn in during surgical incision. As early as 1956, Elek showed the inherent propensity of indwelling medical devices to serve as a source of microbial attachment and chronic infection (Elek, 1956). While an injection of 7.5×10^6 *Staphylococcus aureus* into the dermis of healthy volunteers was required to establish an infection (which uneventfully resolved), a 1 cm length of nondissolvable silk suture required only 100–10,000 cells to develop “severe local abscesses that required draining and vigorous antibiotic treatment” to resolve, illustrating that the presence of a foreign material could decrease the infectious dose by 500- to 10,000-fold. Table 2.2.8.2 lists some of the leading medical devices associated with biofilm infection as well as the material and common pathogens.

Evidence for Biofilms on Devices

Biofilm-associated infections are difficult to detect by conventional blood culture (Tzeng et al., 2015). Most clinical studies of biofilm infections on medical devices therefore rely on the recovery of bacteria from the device (Trampuz and Widmer, 2006), or the culture of strains positive for biofilm formation without directly showing aggregated bacteria (Arciola et al., 2006). Confocal microscopy can analyze hydrated specimens and is compatible with a wide range of fluorescent labeling techniques, including nucleic acid viability staining, antibody labeling, and fluorescent in situ hybridization probes to identify specific bacterial species that directly show viable aggregated bacteria on the device. Figs. 2.2.8.6 and 2.2.8.7 are ex vivo examples of biofilms growing on retrieved components from revision orthopedic surgery from a chronic infection. Typically, biofilms on retrieved implants are more heterogeneous than those grown in vitro and show small aggregates of cells. A combination of confocal microscopy, polymerase chain reaction (PCR), and quantitative reverse transcription PCR (RT-qPCR) provide the most robust evidence for the presence of active bacterial biofilms on implant materials (Nucci et al., 2005, Stoodley et al., 2010).

Control of Biofilm Formation

Control strategies can be divided into three main classes (Fig. 2.2.8.8): (1) antimicrobial approaches, (2) antifouling approaches, and (3) approaches that affect biofilm architecture. Antimicrobial approaches rely on biomaterials that kill microorganisms in proximity to or contacting the surface. Antifouling materials instead repel microbes by either physical or chemical modalities. Biomaterials affecting biofilm architecture do not necessarily kill microbes or prevent adhesion but rather target biofilm virulence.

Antimicrobial Approaches: Biomaterials With Antimicrobial Properties

The design of novel antimicrobial biomaterials is the major focus in preventing biofilm-associated medical device-related infections (Francolini et al., 2017; Koo et al., 2017). Most biomaterials in this category either display or release bioactive molecules, while others promote cell lysis by exposing functional groups that effectively interact with bacteria cell membranes.

Biomaterials Releasing Bioactive Molecules

A common approach in preventing biofilm formation entails surface modification with antibacterial agents, such as antibiotics, metal ions, and nitric oxide. These active compounds are applied to the biomaterial surface by different strategies, namely: (1) physical adsorption (Piozzi et al., 2004); (2) impregnation inside the biomaterial (Donelli

TABLE 2.2.8.2 Materials, Devices, and Common Infecting Pathogens

Device	Uses	Materials	Pathogens	References
Coronary stents	Treatment of coronary arteries suffering from stenosis	- Stainless steel - Chromium/cobalt (Cr-Co) alloy - Nitinol (Ni-Ti) alloy	<i>Staphylococcus aureus</i> (methicillin-resistant <i>Staphylococcus aureus</i> and methicillin-susceptible <i>Staphylococcus aureus</i>)	Elieson et al. (2012)
Central venous catheters (tunneled, nontunneled, or totally implanted ports)	Administration of medication or fluids; monitoring venous pressure; blood sampling	- Polyurethanes (Biomer, Pellethane, Corethane, and Tecoflex) - Polyvinyl chloride - Polyethylene - Silicone rubber	<i>S. aureus</i> <i>Staphylococcus epidermidis</i>	Mickley (2002)
Peripheral venous catheters	Administration of medication or fluids, blood sampling	- Polyurethane (Vialon) - Teflon - Polyvinylchloride - Silicone rubber	<i>S. aureus</i> , <i>S. epidermidis</i> , and <i>Enterobacter</i> spp. (60%) <i>Pseudomonas aeruginosa</i> and <i>Escherichia coli</i> (35%) <i>Candida</i> sp. (5%) Polymicrobial infections (25%)	Sato et al. (2017)
Vascular grafts	Redirect blood flow in a specific region of the body	Teflon Dacron (polyethyleneterephthalate)	<i>S. aureus</i> (20%–53%) Enterobacteriaceae (14%–41%), coagulase-negative staphylococci (15%) <i>P. aeruginosa</i> , <i>Streptococcus</i> sp., and <i>Enterococcus</i> sp. (10%–15%) Polymicrobial infections (20%), yeast 1%–2%	Revest et al. (2015)
Urinary catheters	Bladder draining	Silicone rubber Latex	<i>E. coli</i> (50%) <i>Enterococcus</i> spp. (30%) <i>Candida</i> spp. (20%)	Nicolle (2014)
Sutures	Wound closure to skin or other tissues	Not absorbable: - Polyethyleneterephthalate - Polyethylene - Polyamide Absorbable: - Polyglycolic acid - Polylactic-glycolic acid (65/35) - Polydioxanone	<i>S. epidermidis</i> (30%) <i>S. aureus</i> (15%) <i>Peptostreptococcus</i> spp. (13%) <i>E. coli</i> (5%) <i>Enterococcus</i> spp. (5%) <i>P. aeruginosa</i> (5%)	Edmiston et al. (2013)
Orthopedic prostheses	Replacing a missing joint/bone or supporting a damaged bone	- Stainless steel - Cobalt alloy - Titanium - Polymethylmethacrylate (bone cement) - Polyethylene (weightbearing surface of hip and knee arthroplasty)	<i>S. aureus</i> (20%–30%) Coagulase-negative staphylococci (20%–40%), <i>Streptococcus</i> spp. (1%–10%) <i>Enterococcus</i> spp. (3%–7%) <i>P. aeruginosa</i> (6%–10%) <i>Propionibacteria</i> and <i>Peptostreptococci</i> (rare)	Moriarty et al. (2016)

et al., 2006); (3) complexation (Francolini et al., 2013); and (4) conjugation (Woo et al., 2002). Physical adsorption is the simplest strategy applicable to many drugs but can suffer from uncontrolled release and short-term device durability. While drug complexation or conjugation may better control drug release, this approach requires a functionalization step to introduce chemical groups capable of binding the selected drugs. Drug-releasing approaches have been applied to different kinds of devices, including orthopedic implants, CVCs, and urinary catheters.

Antibiotics

In orthopedic applications, antibiotics are either impregnated in bone cements (usually PMMA) used for prosthesis fixation or adsorbed onto the titanium (Ti) surface of the prosthesis in cementless prostheses. A number of antibiotic-loaded (A-L) acrylic bone cements and spacers have been developed to prevent or treat PJIs (Table 2.2.8.3). Notably in the United States, the Food and Drug Administration approved the use of A-L cements only in the second stage of a two-stage total joint revision, while in Europe they are

approved also for use in primary total joint arthroplasty. Gentamicin is the most common drug for bone cement impregnation and a large number of gentamicin-loaded cements are available. Gentamicin is also combined with other antibiotics such as vancomycin.

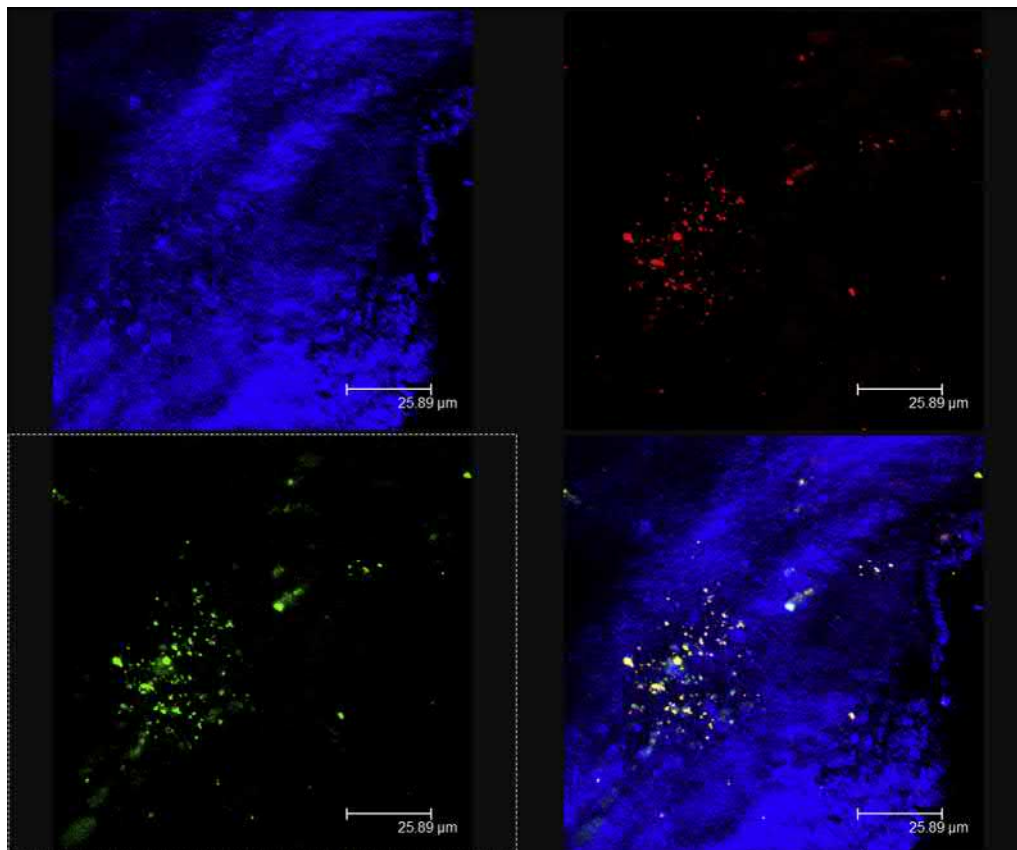
In cementless prostheses, an alternative approach involves coating the implant surface with biodegradable materials that release antibiotic in a controlled fashion. In these systems, the kinetics of antibiotic release strictly follows the kinetics of coating biodegradation. The biodegradable polylactic-*co*-glycolic acid (PLGA) copolymer (Aviv et al., 2007) and poly(D,L-lactide) (PDLLA) polymer (Vester et al., 2010) have been intensively used as coatings for Ti implants to deliver gentamicin. These systems significantly reduced infection rate and improved patient recovery. More recently, mesoporous materials, such as hydroxyapatite, due to their ability to promote osteogenesis, have been used alone or in combination with antimicrobial agents as coatings for dental and bone implants (Oliveira et al., 2017).

For CVCs, antimicrobial-CVCs coated with chlorhexidine/silver sulfadiazine (CH/SS) or minocycline-rifampin (M/R) were first approved for clinical trials in the mid-1990s. The in vivo efficacy of such CVCs was compared in a recent Cochrane analysis (Chong et al., 2017) and

indicated that M/R-CVCs reduced catheter colonization more robustly than CH/SS-CVCs. Both types of antimicrobial-CVCs, however, improved outcomes of catheter-related bloodstream infections. Notably, the routine use of M/R-CVCs in ICUs does not appear to increase antibiotic resistance (Turnbull et al., 2018). Rifampicin-miconazole-coated CVCs were developed to counteract CVC colonization by *Candida* spp. and showed reduced colonization with respect to uncoated CVCs (5% vs. 36%) over 7 days (Yucel et al., 2004). M/R were also adsorbed to silicone urinary catheters, but lacked antimicrobial efficacy against *E. coli* and *Pseudomonas aeruginosa* (Singha et al., 2017). In contrast, the adsorption of rifampin, sparfloxacin, and triclosan onto urinary catheters provided long-term broad-spectrum antibiofilm activity against *Proteus mirabilis*, *S. aureus*, and *E. coli*. The antibiotic-coated Nitrofurantoin-impregnated Foley catheter has been shown to be an effective urinary catheter in preventing biofilm formation compared to silver alloy-coated catheters (Johnson et al., 2012).

Silver

Silver (Ag) has raised much interest because of its long-lasting antimicrobial effect against Gram-positive and -negative bacteria, fungi, protozoa, and certain viruses. The active



• **Figure 2.2.8.6** Biofilm attached to orthopedic screws from a nonunion fracture case. The screw surface with associated invested tissue is blue imaged by reflected confocal microscopy. Staphylococci were stained red by fluorescent in situ hybridization using the Sau probe. All bacteria were stained green with the Eub338 probe. The overlay (*bottom right*) shows that the biofilm consisted primarily of staphylococci with other types of cocci. Scale bar = 25 μ m.

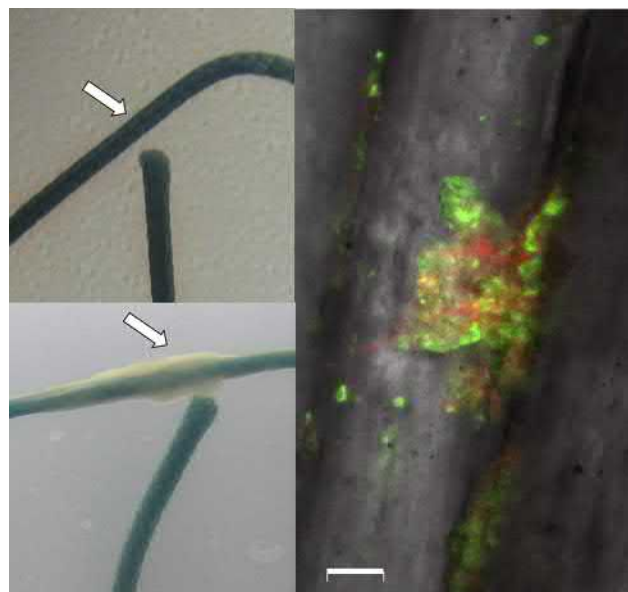
form of silver (Ag^+) accumulates at the cellular membrane and leads to membrane perforation (Brett, 2006). In addition to directly damaging cell membranes, Ag^+ appears to be able to interact with essential cell enzymes blocking electron transport chain function and promoting the generation of reactive oxygen species. Ag ions can be released from different formulations, including Ag salts, Ag oxide, metallic Ag, Ag alloy, or Ag nanoparticles. Ag nanoparticles are the most active form exerting antimicrobial activity at 10-fold lower concentrations than Ag ions (Lok et al., 2006).

Silver has been loaded into PLGA coatings for Ti implants and reduced the survival of either methicillin-resistant

Staphylococcus aureus (MRSA) or *P. aeruginosa* in a rabbit orthopedic implant infection model (Zeng et al., 2019). Three types of silver-CVCs have also been developed: (1) CH/SS, (2) silver-containing zeolites (AgIon technology), and (3) silver, platinum, and carbon black polyurethane (PU) catheters (oligon catheter). While the CH/SS-coated CVCs improved the outcomes of catheter-related bloodstream infections, their efficacy in vivo was lower than M/R-CVCs (Chong et al., 2017), presumably due to low activity of silver against Gram-positive bacteria. Also a metaanalysis found the efficacy of the other two types of silver-CVCs to be limited (Chen et al., 2014), raising questions about the utility of Ag.

Silver is also commonly used for urinary catheters (Johnson et al., 2012). Most clinical trials are focused on Ag alloy coatings due to poor solubility of silver salts. Generally, Ag alloy-coated urinary catheters were more effective in reducing CAUTI than Ag oxide-based coatings (Davenport and Keeley, 2005), but less effective than antimicrobial nitrofurantoin coatings (Pickard et al., 2012).

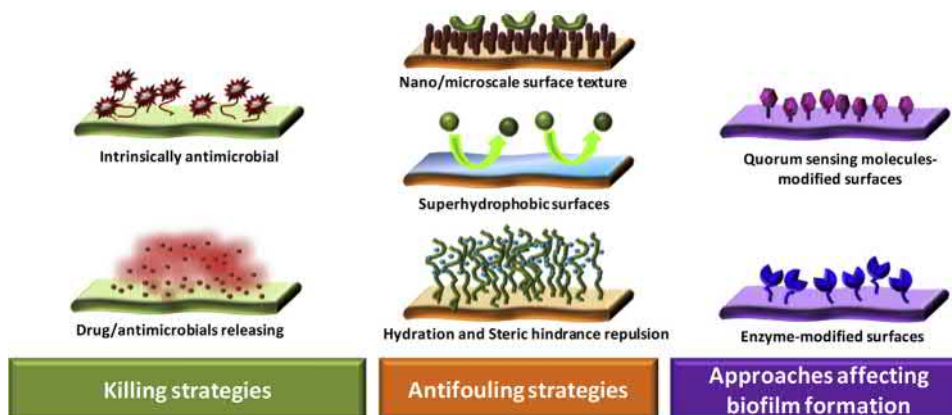
Silver is successfully used in wound-dressing materials. In a recent Cochrane systematic review analyzing dressings and topical agents for treating venous leg ulcers, silver dressings were among the most highly ranked treatments. Silver dressings increased healing of venous leg ulcers (Norman et al., 2018), and silver-treated polyethylene mesh or nylon hydrophobic materials exhibited prolonged efficacy with sustained Ag release compared to hydrophilic dressings (Kostenko et al., 2010), illustrating how material properties may influence the efficacy of an antimicrobial agent.



• **Figure 2.2.8.7** Biofilm aggregated attached to a braided permanent surgical suture associated with a knee arthroplasty revision (Swearingen et al., 2016). *Left panels:* Outgrowth of biofilm (white arrow) after 2 days from a section of the suture that was placed in nutrient agar immediately after explantation. No visual indication of biofilm presence was on the suture before incubation (top left, white arrow). *Right panel:* Confocal microscopy of biofilm on a suture from the same case. Bacterial cocci stained red with the nucleic acid probe Syto59 and surrounding EPS stained green with a lectin that labels poly-*N*-acetyl glucosamine, an EPS polymer of staphylococcal biofilms. PCR confirmed *Staphylococcus aureus*. Scale bar = 5 μm .

Low-Dose Nitric Oxide

While low-dose nitric oxide (NO) was first shown to modulate *c*-di-GMP levels in *P. aeruginosa*, which in turn led to biofilm dispersal, biofilm dispersal has subsequently been shown with multiple types of bacteria (Barraud et al., 2015). Since gaseous NO is highly labile, NO donors in a material are stabilized to selectively deliver NO. Nitroxides (sterically hindered NO analogs) that exert biological responses via NO-mimetic properties are being evaluated to address stability (De La Fuente-Núñez et al., 2013).



• **Figure 2.2.8.8** Approaches to control bacterial adhesion and biofilm formation onto biomaterials.

TABLE 2.2.8.3 Examples of Antibiotic Releasing Devices

Device	Product Type	Antibiotic
Orthopedic prosthesis	Bone cements	Gentamicin
		Tobramycin
		Gentamicin + Vancomycin
		Gentamicin and clindamycin
	Prosthesis coatings	Erythromycin and colistin
		PLGA + Gentamicin
		PDLLA + Gentamicin
Central venous catheters	Catheter coatings (both the internal and external surfaces are coated with antibiotics)	HA + gentamicin, tobramycin, vancomycin, or doxycycline
		Minocycline and rifampin- central venous catheter
Urinary catheters	Catheter coatings	Rifampin and miconazole-central venous catheter
		Minocycline-rifampin silicone catheters
		rifampin, sparfloxacin, and triclosan
		Nitrofurantoin

HA, Hydroxyapatite; PDLLA, poly(D,L-lactide); PLGA, polylactic-co-glycolic acid.

For example, carboxy-TEMPO induced *P. aeruginosa* and *E. coli* biofilm dispersal similar to NO as well as reduced biofilm tolerance to ciprofloxacin. Carboxy-TEMPO failed, however, to disperse MRSA biofilms, indicating that NO activity may be restricted to certain bacteria. Other strategies under development combine antibiotic activity with a donor compound (e.g., antibiotic–nitroxide conjugates), or target QS alongside NO pathway fimbrolide–NO donor hybrids (Kutty et al., 2013).

Intrinsically Bioactive Biomaterials: Cationic Materials

Many research groups have recently focused on intrinsically biocidal polymers because of their long lifetime and low propensity to induce antibiotic resistance (Munoz-Bonilla and Fernandez-Garcia, 2012). The best studied macromolecular biocides are cationic polymers with a net positive charge either in the backbone or side chain. Cationic polymers bind to the negatively charged components of the microbial cell membrane promoting membrane disassembly and leakage or lysis. Cationic polymers are extracted from natural sources or synthesized in the lab.

Natural Cationic Polymers

Chitosan. Chitosan is a polysaccharide composed of randomly distributed *N*-acetylglucosamine and *D*-glucosamine having low toxicity toward mammalian cells (Kumar et al., 2004) and antibacterial activity against many Gram-positive and -negative bacteria (Rabea et al., 2003). Chitosan can be processed to obtain a variety of products, including hydrogels, membranes, fibers, and coatings. In addition, its reactive functional groups can be functionalized to improve polymer solubility (Stepnova et al., 2007) and antimicrobial activity

(Amato et al., 2018). Chitosan is largely employed in wound dressings, drug formulations, and tissue engineering (Rajoka et al., 2019).

Covalent grafting of chitosan to Ti and Ti alloys was shown to prevent *S. aureus* biofilm formation (Tan et al., 2011). Similarly, chitosan covalently attached to various polymer surfaces (Popelka et al., 2012; Wang et al., 2012a) conferred plastics with antimicrobial properties against *E. coli*, *S. aureus*, and *P. mirabilis*.

Chitosan has also been combined with anionic polymers, such as heparin, hyaluronic acid, and alginate, to obtain antimicrobial self-assembled multilayered films. Chitosan/ κ -carrageenan films displayed better antiadhesive properties against enterococci than pure chitosan (Bratskaya et al., 2007). Chitosan/lentinan multilayered coatings on PU surfaces significantly inhibited *P. aeruginosa* (Wang et al., 2012b). Finally, hyaluronic acid/chitosan polyelectrolyte multilayers were successfully developed onto Ti-6Al-4V alloys for orthopedic applications (Valverde et al., 2019).

Antimicrobial Peptides. Antimicrobial peptides (AMPs) are produced as part of the first line of defense in innate immunity system. Typical AMPs are small cationic peptides (10–50 amino acids) with amphiphilic features to optimally interact with bacterial membranes. As polycations, AMPs interact with negatively charged moieties of cells and then cross or produce pores in the outer membrane or cell wall of bacteria. Several AMP antibiofilm mechanisms have been described, including: (1) degradation of the biofilm matrix; (2) interference with bacterial cell signaling systems; and (3) downregulation of genes responsible for biofilm formation (Yasir et al., 2018). Several

studies have focused on functionalization of biomaterials with AMPs. Self-assembling AMPs layered onto nanotubular titanium surfaces coated with calcium phosphate reduced the adhesion of *E. coli* and *S. mutans* with respect to control surface in vitro (Yazici et al., 2019). The AMP tachyplesin I (Tac), first linked to the polyhydroxyalkanoate granule-associated protein (PhaP) and further immobilized on poly(3-hydroxybutyrate-co-3-hydroxyvalerate) films via hydrophobic interaction, resulted in a coated film significantly inhibiting the growth of *E. coli*, *P. aeruginosa*, *S. aureus*, and *Bacillus cereus* in vitro and accelerating wound healing in a deep-wound mouse model (Xue et al., 2018). Temporin-SHa, a small hydrophobic and low cationic AMP, covalently immobilized on modified gold surfaces and displayed antibacterial activity (from 80% to 90% killing efficiency) of Gram-positive *Listeria ivanovii* (Oger et al., 2019). Finally, Moussa et al. (Moussa et al., 2019) synthesized an amphipathic antimicrobial peptide (GL13K) for usage in dental resin composite restorations to prevent dental caries (Moussa et al., 2019).

Synthetic Cationic Polymers

Polyethylenimine (PEI) represents one of the most investigated synthetic cationic polymers. PEI is a hyperbranched cationic polymer with a high density of positive charges, with activity against a number of Gram-positive and -negative bacteria and fungi (Barros et al., 2015). Due to cytotoxicity concerns, PEI derivatives with lower toxicity have been developed with even higher antimicrobial activity (Pasquier et al., 2008). For instance, the derivative *N,N*-dodecylmethyl-PEI has been applied to several surfaces, including glass (Haldar et al., 2007), titanium, and stainless steel for orthopedic applications (Schaer et al., 2012). Bromohexane-alkylated PEI chains linked to the surface of ureteral stents exhibited a brush-like structure with activity against multiple bacterial species without cytotoxic effects (Gultekinoglu et al., 2015). Similarly, quaternized polyethylenimine methacrylate applied to the surfaces of cylindrical catheters and cross-linked to obtain a stable, nonleachable coating achieved a 2-log reduction in MRSA growth and 94.51% reduction in vancomycin-resistant *Enterococcus faecalis* in a mouse catheter model (Zhou et al., 2017).

Other synthetic antimicrobial cationic materials include cationic PUs (Grapski and Cooper, 2001), cationic silicones (Gottenbos et al., 2002), and cationic acrylic polymers (Francolini et al., 2013).

Antifouling Approaches: Biomaterials That Repel Microbes

Antifouling materials effectively repel microbes, thereby impairing bacterial adhesion and biofilm formation. Different types of materials show antifouling properties and are classified as: (1) hydrophilic polymers; (2) superhydrophobic materials; and (3) materials with nano/microscale surface texture.

Hydrophilic Materials Based on Polyethylene Glycol

Polyethylene glycol (PEG) is the most relevant antifouling polymer in biomedical devices. PEG antifouling properties are thought to be related to surface hydration and steric hindrance effects (Chen et al., 2010). PEG chains linked to a material surface assume a brush-like configuration at the water/surface interface, limiting the approach to the surface by bacteria. Compression of the highly hydrated layer of PEG chains is unfavorable because it would involve a reduction in PEG chain mobility and removal of water molecules. Surface packing density and polymer chain length can be used to control PEG antifouling properties (Roosjen et al., 2004). PEG-functionalized PUs were developed by PEG introduction either in the polymer backbone (Corneillie et al., 1998) or polymer side chain (Francolini et al., 2019). Auto-oxidization in the presence of oxygen, metal ions, and enzymes able to oxidize PEG hydroxyl groups, however, may limit long-term effectiveness.

Superhydrophobic Materials

Since the discovery of the “lotus leaf effect,” research efforts have focused on developing superhydrophobic surfaces due to their unique self-cleaning and bacterial fouling-resistant properties (Zhang et al., 2012). Superhydrophobic materials can be obtained by combining hydrophobic moieties with proper micro/nanoscale topography. For example, superhydrophobic paper was obtained by deposition of fluorinated silica particles on cellulose surfaces with positive effects on *E. coli* adhesion reduction (Yang and Deng, 2008). Functionalization with fluoroalkyl silane of TiO₂ nanotubes formed in situ reduced *S. aureus* adhesion onto Ti surfaces (Tang et al., 2011). Antifouling Ti surfaces were also obtained by the formation of self-organized nanostructures (superhydrophobic lotus-like Ti), which dramatically increased the contact angle and prevented *P. aeruginosa* but not *S. aureus* adhesion, suggesting that the type of bacteria affects adhesion to nanostructured surfaces (Fadeeva et al., 2011).

Materials With Nano/Microscale Surface Texture

Physical methods are used to fabricate nano/microstructured surfaces (Jaggessar et al., 2017). Lithography or hydrothermal treatments permit nanostructured bioinspired geometries, including cicada wing, dragonfly wing, and Gecko skin patterns. Each of these structures has a specific geometry and peculiar nanodimensions, which affect selective interaction with Gram-negative and -positive bacteria (Jaggessar et al., 2017).

For soft polymeric materials, surface texture is usually obtained by applying various types of lithography, i.e., soft, nanoimprint, deep UV, electron beam, or X-ray lithography. Soft lithography is a polymer replication method that allows the transfer of micro- and nanostructures onto polymer surfaces by molding (Qin et al., 2010). Soft lithography applied to plastic surfaces (polystyrene, polycarbonate,

and polyethylene) and cast into a shrink-induced rough polydimethylsiloxane mold resulted in rough materials with large ~150-degree contact angles (Freschauf et al., 2012). The materials further exhibited a sliding angle (the angle between the substrate surface and the horizontal plane where a liquid drop slides off the surface by gravity) below 20 degrees, significantly lower than that of flat surfaces (~90 degrees), which significantly reduced *E. coli* adhesion.

For metallic surfaces (i.e., orthopedic implants), surface topographies can be obtained by hydrothermal treatment, a reaction carried out in the presence of water under high temperature and pressure. Hydrothermal treatment at 225°C of Ti implants resulted in a novel nanoflower topography without cytotoxicity, yet showed antimicrobial activity against *S. aureus* (Vishnu et al., 2019). Titanium surfaces with homogeneous spike-like structures prepared by hydrothermal reaction showed robust bactericidal activity against *E. coli* (Lorenzetti et al., 2015).

Biomaterials Affecting Biofilm Architecture

While failing to prevent microbial adhesion, some modified materials can affect biofilm architecture. Such materials can expose enzymes or QS molecules that modify biofilm structure and enhance biofilm removal by either physical methods or antibiotic treatments.

Biomaterials Modified With QS-Quenching Enzymes

Bacterial cell–cell communication in biofilms is regulated by the secretion of signaling molecules and concentration gradients of specific molecules in the local biofilm environment. Several QS signals have been identified (Jiang et al., 2019), including: (1) *N*-acyl-homoserine lactones (AHLs), (2) lipids, and (3) cyclic or linear peptides. Recently, QS-quenching enzymes have been isolated and AHL-lactonases and AHL-acylases affect biofilm architecture. The AHL lactonase AiiA, isolated from *Bacillus* and deposited on gold nanoparticles, reduced biofilm thickness of multidrug-resistant *Proteus* (Vinoj et al., 2015), while acylase-functionalized biomedical PUs reduced biofilm *P. aeruginosa* (Grover et al., 2016). A combination of acylase and esterases immobilized on medical plastics resulted in a 2-log reduction in *P. aeruginosa* biofilm formation on enzyme-treated silicone (Kisch et al., 2014). Silicone urinary catheters coated with a stable coating of alternating layers of acylase and the cationic polymer PEI also reduced *P. aeruginosa* biofilm formation in vitro (Ivanova et al., 2015).

Furanones produced by plants can inhibit bacterial adhesion and biofilm formation by interfering with QS pathways, including the AHL-regulatory system in Gram-negative bacteria and the alternative AI-2 signaling system in both Gram-negative and -positive bacteria (DE Nys et al., 2006). The benzofuranone usnic acid, when attached to PUs, was shown to kill adherent *S. aureus* cells and affect *P. aeruginosa* biofilm structure (Francolini et al., 2004). In contrast, the brominated furanone furanone-3 applied to a polyvinyl

chloride surface was ineffective against *S. aureus* biofilm (Yujie et al., 2013), but inhibited *E. coli* biofilms (Lianhua et al., 2013). Adsorbed 3-(1-bromohexyl)-5-dibromomethylene-2(5H)-furanone onto various biomaterials reduced *S. epidermidis* adhesion and EPS production (Baveja et al., 2004). Dichloro-5-hydroxy-2(5H)-furanone incorporated onto succinimidyl-functionalized polyvinylpyrrolidone and linked onto PU surfaces enhanced hydrophilicity and increased antibacterial activity against *S. aureus*, *S. epidermidis*, and *P. aeruginosa* (Xie et al., 2018). Finally, halogenated 4-bromo-5-(bromomethylene)-2(5H)-furanone embedded in biodegradable polylactide nanoparticles and applied to Ti implants resulted in localized inhibition of *S. aureus* throughout a 60-day study period, long enough to prevent implant-related infections in both the early and intermediate stages of device implantation (Cheng et al., 2015).

Biofilm Matrix-Degrading Enzymes

Two enzymes, dispersin-B (a poly-*N*-acetylglucosamine [*p*NAG] degrading enzyme) and DNase I (eDNA-degrading thermonuclease) can degrade *p*NAG or eDNA in the biofilm EPS matrix. Dispersin-B was isolated from the periodontopathogen *Aggregatibacter actinomycetemcomitans* and was shown to disperse preformed biofilms of multiple types of bacteria (Itoh et al., 2005). Layered hydrogels based on cross-linked poly(allylamine hydrochloride) and poly(methacrylic acid) loaded with dispersin-B prevented biofilm formation by *S. epidermidis* (Pavlukhina et al., 2012). Dispersin-B was also adsorbed onto PUs and inhibited *S. epidermidis* biofilm formation as well as exerting synergism with the antibiotic cefamandole nafate (Donelli et al., 2007).

DNase has also been adsorbed to materials and studied for its ability to affect biofilm formation by several pathogens. A DNaseI-functionalized PMMA coating was developed by using dopamine as linker (Swartjes et al., 2013). The resulting coating delayed *S. aureus* and *P. aeruginosa* biofilm formation. Using dopamine as an intermediate DNase I was also immobilized on a titanium surface, where it modified wettability of Ti substrate, increased its hydrophilicity, and inhibited *S. mutans* and *S. aureus* adhesion and biofilm formation over 24 h (Ye et al., 2017). Finally, Foley urinary catheters coated with DNase were able to restrict *P. aeruginosa* biofilm formation for up to 5 days (Ghanwate et al., 2014).

Methods for Testing Antibacterial and Antifouling Properties of Biomaterials

While thousands of strategies have been discussed in the literature for antibiofilm purposes, few have yet to make it to commercialization. One issue is that success in vitro and even small animal models are often not good predictors of therapeutic success in humans. A recent metaanalysis showed that the observed magnitude of biofilm killing in vitro was more dependent on the experimental setup than the active agents themselves (Stewart and Parker, 2019). While conventional

minimum inhibitory and biocidal concentration assays are generally good predictors of antibiotic efficacy against a broad range of bacterial species and antibiotics in acute infections, a comparable generic test for biofilms is lacking. This is due to the complexity of the biofilm–implant environment, the diversity of biofilm phenotypes, and the diverse nature of therapeutic strategies. The need for standard methods has been recognized (Coenye et al., 2018; Malone et al., 2017b) and EPA standard methods EPA MLB SOP MB-19, “Growing a Biofilm using the CDC Biofilm Reactor,” and EPA MLB SOP MB-20, “Single Tube Method for Determining the Efficacy of Disinfectants against Bacterial Biofilms,” are now available. At

least a 6-log reduction in colony forming units (CFUs) per CDC Biofilm Reactor coupon (~1 cm²) is recognized as a criterion for demonstrating probable efficacy. An important consideration, however, is that the method of removing cells from the surface (usually scraping, sonication, and/or vortexing) prior to enumerating CFUs must itself be validated. While these standards are being adopted as guidelines by regulatory agencies the log reduction required to clear a biofilm infection clinically is unclear and is likely highly contextual. Ideally, a reproducible low-cost, simple test could be designed with broad predictive value for many types of devices.

CASE STUDY I: CLINICAL EXAMPLE OF DIFFICULTY IN DIAGNOSING AND TREATING A DEVICE-RELATED BIOFILM INFECTION

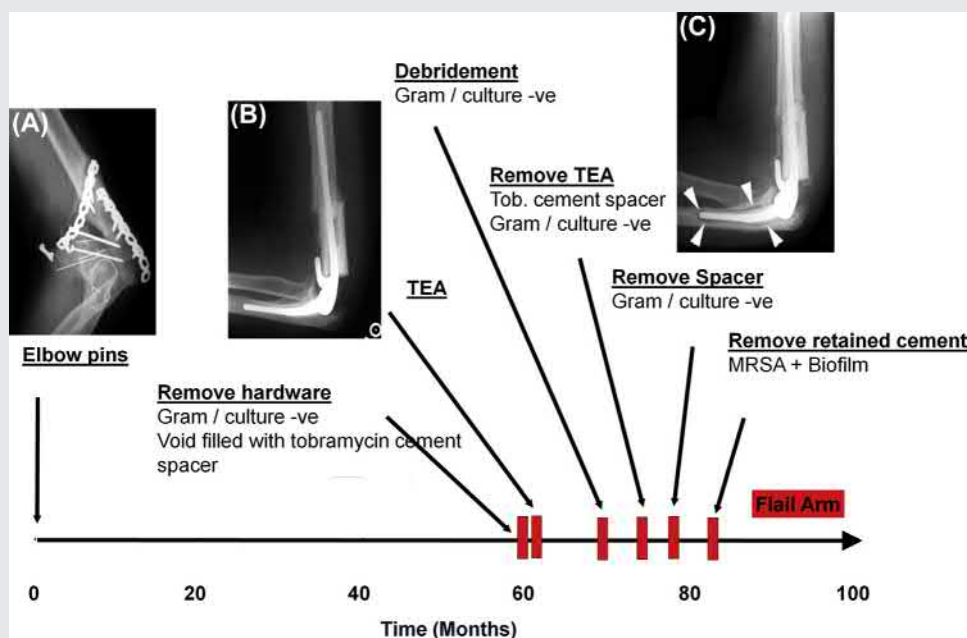
Internal metal plates and screws for fixing fractures and the first total joint arthroplasty were performed on knees and hips in the 1890s. Various materials were used and the implants fixed in place by screws and cements formulated from plaster of Paris, resins, and other additives. Early issues included corrosion, lack of mechanical strength, surface wear, osteolysis in response to shed wear particles, and infection. With improvements in materials and implant design, many of the mechanical issues have been resolved; however, infection remains a major complication. Here we present a case timeline illustrating issues with diagnosing and treating an orthopedic infection. The patient was a laborer who had fallen and shattered his elbow, which was subsequently repaired with internal fixation. Five years of discomfort and radiographic evidence of hardware failure led to the decision to perform a total elbow arthroplasty. There was no direct evidence of infection but a two-stage revision was performed to ensure the elbow was infection free prior to implantation. Eight months later the elbow was debrided due to pain. The patient then went through three other operations over 2 years and at each stage there was no direct

evidence of bacterial infection by culture or clinical microscopy. Finally, a piece of retained tobramycin-loaded PMMA cement was recovered and examined in a research lab by confocal microscopy and PCR. Live biofilm was found on the cement, despite multiple courses of antibiotics. The infection then resolved but the patient was left with a flail arm.

Learning Points

1. Despite multiple surgeries at great discomfort and cost the only way that the biofilm infection was resolved was removal of the foreign body.
2. Bacterial infection was suspected, but not definitively diagnosed, until the final surgery.
3. Even antibiotic-loaded cement was susceptible to biofilm although it is not known whether the antibiotics had eluted to below therapeutic levels prior to biofilm formation.

Stoodley et al. (2008). “Direct demonstration of viable *Staphylococcus aureus* biofilms in an infected total joint arthroplasty: a case report.” *The Journal of Bone and Joint Surgery. American volume*. 90(8):1751.



CASE STUDY II: SILVER ALLOY COATED URINARY CATHETERS

What Problem Was Addressed?

A 65–70-year-old woman suffering from neurogenic bladder disorder had been permanently catheterized with an indwelling catheter via the suprapubic route since 2006. Soon after, she experienced frequent symptomatic catheter-associated urinary tract infections (0.5–1 CAUTIs/month) requiring antibiotics (0.3–1 antibiotic treatments/month). CAUTIs recurred despite several prevention approaches, including prophylactic antibiotics and bladder rinsing with chlorhexidine.

Interventions

In 2009, the patient started using a silicone catheter, which is less prone to infection and hypersensitivity reactions than latex. In 2011, the patient changed to a silicone catheter coated with phosphate silver ion technology incorporated in a hydrogel coating. In 2013, a silver alloy (gold, silver, and palladium) and hydrogel-coated BIP Foley Catheter was inserted.

Catheters' Performance

While using control catheters, the patient experienced symptomatic CAUTIs requiring antibiotics almost every month

for 4 years. The silver-coated catheter had some positive effects. The patient was free from CAUTI for a short period but the symptoms reoccurred after 3 months. After 1 month with the silver alloy Foley catheter, the patient remained free of symptomatic CAUTIs and antibiotic treatment for the following 2.5 years, despite bacteriuria. The coating was stable, with no significant metal release into urine. The same levels of metals were found on both 1 month-used and unused catheters.

Learning Points

1. In long-term catheterization, coated catheters should be preferred to control catheters.
2. The coating technology affects performance of silver-coated catheters. Silver ion technology is less efficacious than silver alloy in long-term catheterization.
3. A nonreleasing mechanism of action ensures coating durability and is safe for patients.
Magnusson, B., et al., 2019. Long-term use of noble metal alloy coated urinary catheters reduces recurrent CAUTI and decreases proinflammatory markers. *Ther. Adv. Urol.* 11. <https://doi.org/10.1177/1756287219854915>.

Conclusions

Indwelling medical devices are increasingly used in patient management, whether temporarily for fluids exchange in the case of catheters, or as permanent implants to repair loss of function in the case of orthopedic joints, and cardiovascular stents to stabilize electrical function, or to monitor blood chemistry. Devices will also continue to become more complex in both function and materials. Vexingly, despite advancements in infection control, the rates of surgical site infections have not dropped. Of further concern is the increasing threat of antimicrobial resistance. Infection control engineered into medical devices therefore represents an important strategy to combat infection. A challenge to biomaterials engineers and surface scientists is to develop materials for manufacturing devices that are functional, biocompatible, resistant to infection, and do not promote the development of resistant microbes. While 100% biofilm-proof surfaces remain elusive, more research to better understand biofilm biology may lead to breakthroughs in therapeutic strategies. This formidable challenge offers great rewards with the potential to improve the quality of life of millions of people.

References

- Absolom, D., Lamberti, F.V., Policova, Z., Zingg, W., Van Oss, C.J., Neumann, A.W., 1983. Surface thermodynamics of bacterial adhesion. *Appl. Environ. Microbiol.* 46, 90–97.
- Amato, A., Migneco, L.M., Martinelli, A., Pietrelli, L., Piozzi, A., Francolini, I., 2018. Antimicrobial activity of catechol functionalized-chitosan versus *Staphylococcus epidermidis*. *Carbohydr. Polym.* 179, 273–281.
- Anderl, J.N., Franklin, M.J., Stewart, P.S., 2000. Role of antibiotic penetration limitation in *Klebsiella pneumoniae* biofilm resistance to ampicillin and ciprofloxacin. *Antimicrob. Agents Chemother.* 44, 1818–1824.
- Arciola, C.R., Campoccia, D., Baldassarri, L., Donati, M.E., Pirini, V., Gamberini, S., Montanaro, L., 2006. Detection of biofilm formation in *Staphylococcus epidermidis* from implant infections. Comparison of a PCR-method that recognizes the presence of *ica* genes with two classic phenotypic methods. *J. Biomed. Mater. Res. A* 76, 425–430.
- Aviv, M., Berdicevsky, I., Zilberman, M., 2007. Gentamicin-loaded bioresorbable films for prevention of bacterial infections associated with orthopedic implants. *J. Biomed. Mater. Res. A* 83A, 10–19.
- Barraud, N., Kelso, M.J., Rice, S.A., Kjelleberg, S., 2015. Nitric oxide: a key mediator of biofilm dispersal with applications in infectious diseases. *Curr. Pharmaceut. Des.* 21, 31–42.
- Barros, J., Dias, A., Rodrigues, M.A., Pina-Vaz, C., Lopes, M.A., Pina-Vaz, I., 2015. Antibiofilm and antimicrobial activity of poly-ethylenimine: an interesting compound for endodontic treatment. *J. Contemp. Dent. Pract.* 16, 427–432.
- Baveja, J.K., Wilcox, M.D.P., Hume, E.B.H., Kumar, N., Odell, R., Poole-Warren, L.A., 2004. Furanones as potential anti-bacterial coatings on biomaterials. *Biomaterials* 25, 5003–5012.
- Benoit, D.S., Koo, H., 2016. Targeted, triggered drug delivery to tumor and biofilm microenvironments. *Nanomedicine (Lond.)* 11(8), 873–879.
- Boyd, R., Verran, J., Jones, M., Bhakoo, M., 2002. Use of the atomic force microscope to determine the effect of substratum surface topography on bacterial adhesion. *Langmuir* 18, 2343–2346.
- Bratskaya, S., Marinin, D., Simon, F., Synytska, A., Zschoche, S., Busscher, H.J., Jager, D., Van der Mei, H.C., 2007. Adhesion and viability of two enterococcal strains on covalently grafted chitosan and chitosan/kappa-carrageenan multilayers. *Biomacromolecules* 8, 2960–2968.
- Brett, D.W., 2006. A discussion of silver as an antimicrobial agent: alleviating the confusion. *Ostomy/Wound Manag.* 52, 34–41.
- Chen, S.F., Li, L.Y., Zhao, C., Zheng, J., 2010. Surface hydration: principles and applications toward low-fouling/nonfouling biomaterials. *Polymer* 51, 5283–5293.
- Chen, Y.M., Dai, A.P., Shi, Y., Liu, Z.J., Gong, M.F., Yin, X.B., 2014. Effectiveness of silver-impregnated central venous catheters for preventing catheter-related blood stream infections: a meta-analysis. *Int. J. Infect. Dis.* 29, 279–286.

- Cheng, Y.C., Zhao, X.H., Liu, X.H., Sun, W.G., Ren, H.F., Gao, B., Wu, J., 2015. Antibacterial activity and biological performance of a novel antibacterial coating containing a halogenated furanone compound loaded poly(L-lactic acid) nanoparticles on microarc-oxidized titanium. *Int. J. Nanomed.* 10, 727–737.
- Chong, H.Y., Lai, N.M., Apisarnthanarak, A., Chaiyakunapruk, N., 2017. Comparative efficacy of antimicrobial central venous catheters in reducing catheter-related bloodstream infections in adults: abridged Cochrane systematic review and network meta-analysis. *Clin. Infect. Dis.* 64, S131–S140.
- Coenye, T., Goeres, D., Van Bambeke, F., Bjarnsholt, T., 2018. Should standardized susceptibility testing for microbial biofilms be introduced in clinical practice? *Clin. Microbiol. Infect.* 24, 570–572.
- Cornellie, S., Lan, P.N., Schacht, E., Davies, M., Shard, A., Green, R., Denyer, S., Wassall, M., Whitfield, H., Choong, S., 1998. Polyethylene glycol-containing polyurethanes for biomedical applications. *Polym. Int.* 46, 251–259.
- Daniels, K.R., Frei, C.R., 2013. The United States' progress toward eliminating catheter-related bloodstream infections: incidence, mortality, and hospital length of stay from 1996 to 2008. *Am. J. Infect. Contr.* 41, 118–121.
- Dastgheyb, S., Otto, M., Hickok, N., 2017. Biofilm on Bone Repair Devices. *Biofilms and Implantable Medical Devices*. Elsevier.
- Dastgheyb, S.S., Villaruz, A.E., Le, K.Y., Tan, V.Y., Duong, A.C., Chatterjee, S.S., Cheung, G.Y., Joo, H.-S., Hickok, N.J., Otto, M., 2015. Role of phenol-soluble modulins in formation of *Staphylococcus aureus* biofilms in synovial fluid. *Infect. Immun.* 83, 2966–2975.
- Davenport, K., Keeley, F.X., 2005. Evidence for the use of silver-alloy-coated urethral catheters. *J. Hosp. Infect.* 60, 298–303.
- Davis-Fields, M., Bakhtiari, L., Kovach, K., Gordon, V., 2019. Assaying How the Success of Phagocytosis Depends on the Mechanics of a Large Viscoelastic Target. *bioRxiv*, p. 545004.
- De La Fuente-Núñez, C., Reffuveille, F., Fairfull-Smith, K.E., Hancock, R.E., 2013. Effect of nitroxides on swarming motility and biofilm formation, multicellular behaviors in *Pseudomonas aeruginosa*. *Antimicrob. Agents Chemother.* 57, 4877–4881.
- DE Nys, R., Givskov, M., Kumar, N., Kjelleberg, S., Steinberg, P.D., 2006. Furanones. *Prog. Mol. Subcell. Biol.* 42, 55–86.
- De Beer, D., Stoodley, P., Lewandowski, Z., 1997. Measurement of local diffusion coefficients in biofilms by micro-injection and confocal microscopy. *Biotechnol. Bioeng.* 53, 151–158.
- Donelli, G., Francolini, I., Romoli, D., Guaglianone, E., Piozzi, A., Ragunath, C., Kaplan, J.B., 2007. Synergistic activity of dispersin B and cefamandole nafate in inhibition of staphylococcal biofilm growth on polyurethanes. *Antimicrob. Agents Chemother.* 51, 2733–2740.
- Donelli, G., Francolini, I., Ruggeri, V., Guaglianone, E., D'ilario, L., Piozzi, A., 2006. Pore formers promoted release of an antifungal drug from functionalized polyurethanes to inhibit *Candida* colonization. *J. Appl. Microbiol.* 100, 615–622.
- Edmiston, C.E., Krepel, C.J., Marks, R.M., Rossi, P.J., Sanger, J., Goldblatt, M., Graham, M.B., Rothenburger, S., Collier, J., Seabrook, G.R., 2013. Microbiology of explanted suture segments from infected and noninfected surgical patients. *J. Clin. Microbiol.* 51, 417–421.
- Elek, S.D., 1956. Experimental staphylococcal infections in the skin of man. *Ann. N.Y. Acad. Sci.* 65, 85–90.
- Elieson, M., Mixon, T., Carpenter, J., 2012. Coronary stent infections a case report and literature review. *Tex. Heart Inst. J.* 39, 884–889.
- Engelsman, A.F., Van Der Mei, H.C., Ploeg, R.J., Busscher, H.J., 2007. The phenomenon of infection with abdominal wall reconstruction. *Biomaterials* 28, 2314–2327.
- Fadeeva, E., Truong, V.K., Stiesch, M., Chichkov, B.N., Crawford, R.J., Wang, J., Ivanova, E.P., 2011. Bacterial retention on superhydrophobic titanium surfaces fabricated by femtosecond laser ablation. *Langmuir* 27, 3012–3019.
- Feng, L., Li, S., Li, Y., Li, H., Zhang, L., Zhai, J., Song, Y., Liu, B., Jiang, L., Zhu, D., 2002. Super-hydrophobic surfaces: from natural to artificial. *Adv. Mater.* 14, 1857–1860.
- Flemming, H.-C., Wingender, J., 2010. The biofilm matrix. *Nat. Rev. Microbiol.* 8, 623.
- Francolini, I., Norris, P., Piozzi, A., Donelli, G., Stoodley, P., 2004. Usnic acid, a natural antimicrobial agent able to inhibit bacterial biofilm formation on polymer surfaces. *Antimicrob. Agents Chemother.* 48, 4360–4365.
- Francolini, I., Silvestro, I., DI Lisio, V., Martinelli, A., Piozzi, A., 2019. Synthesis, characterization, and bacterial fouling-resistance properties of polyethylene glycol-grafted polyurethane elastomers. *Int. J. Mol. Sci.* 20.
- Francolini, I., Taresco, V., Crisante, F., Martinelli, A., D'ilario, L., Piozzi, A., 2013. Water soluble usnic acid-polyacrylamide complexes with enhanced antimicrobial activity against *Staphylococcus epidermidis*. *Int. J. Mol. Sci.* 14, 7356–7369.
- Francolini, I., Vuotto, C., Piozzi, A., Donelli, G., 2017. Antifouling and antimicrobial biomaterials: an overview. *Appl. Microbiol.* 125, 392–417.
- Freschauf, L.R., Mclane, J., Sharma, H., Khine, M., 2012. Shrink-induced superhydrophobic and antibacterial surfaces in consumer plastics. *PLoS One* 7.
- Fux, C.A., Shirliff, M., Stoodley, P., Costerton, J.W., 2005. Can laboratory reference strains mirror "real-world" pathogenesis? *Trends Microbiol.* 13, 58–63.
- Fux, C.A., Wilson, S., Stoodley, P., 2004. Detachment characteristics and oxacillin resistance of *Staphylococcus aureus* biofilm emboli in an in vitro catheter infection model. *J. Bacteriol.* 186, 4486–4491.
- Ghanwate, N., Thakare, P., Bhise, P.R., Tayde, S., 2014. Prevention of biofilm formation in urinary catheters by treatment with antibiofilm agents. *Int. J. Sci. Res.* 3, 714–717.
- Gottenbos, B., Van Der Mei, H.C., Klatter, F., Nieuwenhuis, P., Busscher, H.J., 2002. In vitro and in vivo antimicrobial activity of covalently coupled quaternary ammonium silane coatings on silicone rubber. *Biomaterials* 23, 1417–1423.
- Grapski, J.A., Cooper, S.L., 2001. Synthesis and characterization of non-leaching biocidal polyurethanes. *Biomaterials* 22, 2239–2246.
- Grover, N., Plaks, J.G., Summers, S.R., Chado, G.R., Schurr, M.J., Kaar, J.L., 2016. Acylase-containing polyurethane coatings with anti-biofilm activity. *Biotechnol. Bioeng.* 113, 2535–2543.
- Guenther, F., Stroh, P., Wagner, C., Obst, U., Hansch, G.M., 2009. Phagocytosis of staphylococci biofilms by polymorphonuclear neutrophils: *S. aureus* and *S. epidermidis* differ with regard to their susceptibility towards the host defense. *Int. J. Artif. Organs* 32, 565–573.
- Gultekinoglu, M., Sarisozen, Y.T., Erdogdu, C., Sagiroglu, M., Aksoy, E.A., Oh, Y.J., Hinterdorfer, P., Ulubayram, K., 2015. Designing of dynamic polyethyleneimine (PEI) brushes on polyurethane (PU) ureteral stents to prevent infections. *Acta Biomater.* 21, 44–54.
- Haldar, J., Weight, A.K., Klibanov, A.M., 2007. Preparation, application and testing of permanent antibacterial and antiviral coatings. *Nat. Protoc.* 2, 2412–2417.
- Hall-Stoodley, L., Hu, F.Z., Gieseke, A., Nistico, L., Nguyen, D., Hayes, J., Forbes, M., Greenberg, D.P., Dice, B., Burrows, A., 2006. Direct detection of bacterial biofilms on the middle-ear mucosa of children with chronic otitis media. *JAMA* 296, 202–211.
- Hall-Stoodley, L., Stoodley, P., 2009. Evolving concepts in biofilm infections. *Cell Microbiol.* 11, 1034–1043.

- Hoiby, N., Bjarsholt, T., Moser, C., Bassi, G.L., Coenye, T., Donelli, G., Hall-Stoodley, L., Hola, V., Imbert, C., Kirketerp-Moller, K., Lebeaux, D., Oliver, A., Ullmann, A.J., Williams, C., Biofilms, E.S.G., Consulting External Expert, W., 2015. ESCMID* guideline for the diagnosis and treatment of biofilm infections 2014. *Clin. Microbiol. Infect.* 21, S1–S25.
- Hooton, T.M., Bradley, S.F., Cardenas, D.D., Colgan, R., Geerlings, S.E., Rice, J.C., Saint, S., Schaeffer, A.J., Tambayh, P.A., Tenke, P., 2010. Diagnosis, prevention, and treatment of catheter-associated urinary tract infection in adults: 2009 international clinical practice guidelines from the infectious diseases society of America. *Clin. Infect. Dis.* 50, 625–663.
- Itoh, Y., Wang, X., Hinnebusch, B.J., Preston, J.F., Romeo, T., 2005. Depolymerization of beta-1,6-N-acetyl-D-glucosamine disrupts the integrity of diverse bacterial biofilms. *J. Bacteriol.* 187, 382–387.
- Ivanova, K., Fernandes, M.M., Mendoza, E., Tzanov, T., 2015. Enzyme multilayer coatings inhibit *Pseudomonas aeruginosa* biofilm formation on urinary catheters. *Appl. Microbiol. Biotechnol.* 99, 4373–4385.
- Jacobsen, S.M., Stickler, D.J., Mobley, H.L., Shirliff, M.E., 2008. Complicated catheter-associated urinary tract infections due to *Escherichia coli* and *Proteus mirabilis*. *Clin. Microbiol. Rev.* 21, 26–59.
- Jaggessar, A., Shahali, H., Mathew, A., Yarlagaadda, P., 2017. Biomimicking nano and micro-structured surface fabrication for antibacterial properties in medical implants. *J. Nanobiotechnol.* 15.
- Jiang, Q., Chen, J., Yang, C., Yin, Y., Yao, K., 2019. Quorum sensing: a prospective therapeutic target for bacterial diseases. *Biomed Res. Int.* 4.
- Johnson, J., Johnston, B., Kuskowski, M., 2012. In vitro comparison of nitrofurazone- and silver alloy-coated Foley catheters for contact-dependent and diffusible inhibition of urinary tract infection-associated microorganisms. *Antimicrob. Agents Chemother.* 56, 4969–4972.
- Kisch, J.M., Utpatel, C., Hilterhaus, L., Streit, W.R., Liese, A., 2014. *Pseudomonas aeruginosa* biofilm growth inhibition on medical plastic materials by immobilized esterases and acylase. *ChemBiochem* 15, 1911–1919.
- Klevens, R.M., Edwards, J.R., Richards Jr., C.L., Horan, T.C., Gaynes, R.P., Pollock, D.A., Cardo, D.M., 2002. 2007. Estimating health care-associated infections and deaths in US hospitals. *Public Health Rep.* 122, 160–166.
- Klopfleisch, R., Jung, F., 2017. The pathology of the foreign body reaction against biomaterials. *J. Biomed. Mater. Res. A* 105, 927–940.
- Koo, H., Allan, R.N., Howlin, R.P., Stoodley, P., Hall-Stoodley, L., 2017. Targeting microbial biofilms: current and prospective therapeutic strategies. *Nat. Rev. Microbiol.* 15, 740.
- Kostenko, V., Lyczak, J., Turner, K., Martinuzzi, R.J., 2010. Impact of silver-containing wound dressings on bacterial biofilm viability and susceptibility to antibiotics during prolonged treatment. *Antimicrob. Agents Chemother.* 54, 5120–5131.
- Kumar, M., Muzzarelli, R.A.A., Muzzarelli, C., Sashiwa, H., Domb, A.J., 2004. Chitosan chemistry and pharmaceutical perspectives. *Chem. Rev.* 104, 6017–6084.
- Kurtz, S.M., Lau, E., Watson, H., Schmier, J.K., Parvizi, J., 2012. Economic burden of periprosthetic joint infection in the United States. *J. Arthroplast.* 27, 61–65 e1.
- Kutty, S.K., Barraud, N., Pham, A., Iskander, G., Rice, S.A., Black, D.S., Kumar, N., 2013. Design, synthesis, and evaluation of fimbrolide–nitric oxide donor hybrids as antimicrobial agents. *J. Med. Chem.* 56, 9517–9529.
- Le, K.Y., Park, M.D., Otto, M., 2018. Immune evasion mechanisms of *Staphylococcus epidermidis* biofilm infection. *Front. Microbiol.* 9, 359.
- Lewis, K., 2005. Persister cells and the riddle of biofilm survival. *Biochemistry (Mosc.)* 70, 267–274.
- Lianhua, Y., Yunchao, H., Geng, X., Youquang, Z., Guangqiang, Z., Yujie, L., 2013. Effect of brominated furanones on the formation of biofilm by *Escherichia coli* on polyvinyl chloride materials. *Cell Biochem. Biophys.* 67, 893–897.
- Liesenborghs, L., Verhamme, P., Vanassche, T., 2018. *Staphylococcus aureus*, master manipulator of the human hemostatic system. *J. Thromb. Haemost.* 16, 441–454.
- Lok, C.N., Ho, C.M., Chen, R., He, Q.Y., Yu, W.Y., Sun, H.Z., Tam, P.K.H., Chiu, J.F., Che, C.M., 2006. Proteomic analysis of the mode of antibacterial action of silver nanoparticles. *J. Proteome Res.* 5, 916–924.
- Lorenzetti, M., Dogsa, I., Stosicki, T., Stopar, D., Kalin, M., Kobe, S., Novak, S., 2015. The influence of surface modification on bacterial adhesion to titanium-based substrates. *ACS Appl. Mater. Interfaces* 7, 1644–1651.
- Machado, J.D., Suen, V.M., Figueiredo, J.F., Marchini, J.S., 2009. Biofilms, infection, and parenteral nutrition therapy. *JPEN J. Parenter. Enter. Nutr.* 33, 397–403.
- Malone, M., Bjarsholt, T., McBain, A.J., James, G.A., Stoodley, P., Leaper, D., Tachi, M., Schultz, G., Swanson, T., Wolcott, R.D., 2017a. The prevalence of biofilms in chronic wounds: a systematic review and meta-analysis of published data. *J. Wound Care* 26, 20–25.
- Malone, M., Goeres, D.M., Gosbell, I., Vickery, K., Jensen, S., Stoodley, P., 2017b. Approaches to biofilm-associated infections: the need for standardized and relevant biofilm methods for clinical applications. *Expert Rev. Anti Infect. Ther.* 15, 147–156.
- Mickley, V., 2002. Central venous catheters: many questions, few answers. *Nephrol. Dial. Transplant.* 17, 1368–1373.
- Ming, F., Whish, W.J.D., Hubble, J., Eisenthal, R., 1998. Estimation of parameters for cell-surface interactions: maximum binding force and detachment constant. *Enzym. Microb. Technol.* 22, 94–99.
- Moriarty, T.F., Kuehl, R., Coenye, T., Metsemakers, W.J., Morgenstern, M., Schwarz, E.M., Riool, M., Zaat, S.A.J., Khana, N., Kates, S.L., Richards, R.G., 2016. Orthopaedic device-related infection: current and future interventions for improved prevention and treatment. *Efort Open Rev.* 1, 89–99.
- Morra, M., Cassinelli, C., 1997. Bacterial adhesion to polymer surfaces: a critical review of surface thermodynamic approaches. *J. Biomater. Sci. Polym. Ed.* 9, 55–74.
- Moussa, D.G., Fok, A., Aparicio, C., 2019. Hydrophobic and antimicrobial dentin: a peptide-based 2-tier protective system for dental resin composite restorations. *Acta Biomater.* 88, 251–265.
- Munoz-Bonilla, A., Fernandez-Garcia, M., 2012. Polymeric materials with antimicrobial activity. *Prog. Polym. Sci.* 37, 281–339.
- Neumann, A., Good, R., Hope, C., Sejpal, M., 1974. An equation-of-state approach to determine surface tensions of low-energy solids from contact angles. *J. Colloid Interface Sci.* 49, 291–304.
- Nicolle, L.E., 2014. Catheter associated urinary tract infections. *Antimicrob. Resist. Infect. Contr.* 3.
- Norman, G., Westby, M.J., Rithalia, A.D., Stubbs, N., Soares, M.O., Dumville, J.C., 2018. Dressings and topical agents for treating venous leg ulcers. *Cochrane Database Syst. Rev.* 15.
- Nucci, C., Artini, M., Pasmore, M., Missiroli, F., Costerton, J.W., Selan, L., 2005. A microbiological and confocal microscopy study documenting a slime-producing *Staphylococcus epidermidis* isolated from a nylon corneal suture of a patient with antibiotic-resistant endophthalmitis. *Graefes Arch. Clin. Exp. Ophthalmol.* 43, 951–954.
- Oger, P.C., Piesse, C., Ladram, A., Humblot, V., 2019. Engineering of antimicrobial surfaces by using temporin analogs to tune the biocidal/antiadhesive effect. *Molecules* 24.

- Oliveira, H.L., DA Rosa, W.L.O., Cuevas-Suarez, C.E., Carreno, N.L.V., Da Silva, A.F., Guim, T.N., Dellagostin, O.A., Piva, E., 2017. Histological evaluation of bone repair with hydroxyapatite: a systematic review. *Calcif. Tissue Int.* 101, 341–354.
- Pasquier, N., Keul, H., Heine, E., Moeller, M., Angelov, B., Linser, S., Willumeit, R., 2008. Amphiphilic branched polymers as antimicrobial agents. *Macromol. Biosci.* 8, 903–915.
- Pavluhina, S.V., Kaplan, J.B., Xu, L., Chang, W., Yu, X.J., Madhyastha, S., Yakandawala, N., Mentbayeva, A., Khan, B., Sukhishvili, S.A., 2012. Noneluting enzymatic antibiofilm coatings. *ACS Appl. Mater. Interfaces* 4, 4708–4716.
- Pickard, R., Lam, T., MacLennan, G., Starr, K., Kilonzo, M., Mcpherson, G., Gillies, K., McDonald, A., Walton, K., Buckley, B., Glazener, C., Boachie, C., Burr, J., Norrie, J., Vale, L., Grant, A., N'dow, J., 2012. Types of urethral catheter for reducing symptomatic urinary tract infections in hospitalised adults requiring short-term catheterisation: multicentre randomised controlled trial and economic evaluation of antimicrobial- and antiseptic-impregnated urethral catheters (the CATHETER trial). *Health Technol. Assess.* 16, 1.
- Piozzi, A., Francolini, I., Occhiperti, L., Venditti, M., Marconi, W., 2004. Antimicrobial activity of polyurethanes coated with antibiotics: a new approach to the realization of medical devices exempt from microbial colonization. *Int. J. Pharm.* 280, 173–183.
- Popelka, A., Novak, I., Lehocky, M., Junkar, I., Mozetic, M., Kleinova, A., Janigova, I., Slouf, M., Bilek, F., Chodak, I., 2012. A new route for chitosan immobilization onto polyethylene surface. *Carbohydr. Polym.* 90, 1501–1508.
- Qin, D., Xia, Y.N., Whitesides, G.M., 2010. Soft lithography for micro- and nanoscale patterning. *Nat. Protoc.* 5, 491–502.
- Rabea, E.I., Badawy, M.E.T., Stevens, C.V., Smagghe, G., Steurbaut, W., 2003. Chitosan as antimicrobial agent: applications and mode of action. *Biomacromolecules* 4, 1457–1465.
- Rajoka, M.S.R., Zhao, L.Q., Mehwish, H.M., Wu, Y.G., Mahmood, S., 2019. Chitosan and its derivatives: synthesis, biotechnological applications, and future challenges. *Appl. Microbiol. Biotechnol.* 103, 1557–1571.
- Revest, M., Camou, F., Senneville, E., Caillon, J., Laurent, F., Calvet, B., Feugier, P., Batt, M., Chidiac, C., Grp Reflexion Infect Protheses, V., 2015. Medical treatment of prosthetic vascular graft infections: review of the literature and proposals of a Working Group. *Int. J. Antimicrob. Agents* 46, 254–265.
- Rolighed Thomsen, T., Moser, C., Hall-Stoodley, L., Stoodley, P., 2010. The role of bacterial biofilms in infections of catheters and shunts. In: Bjarnsholt, T., Jensen, P.O., Moser, C., Hoiby, N. (Eds.), *Biofilm Infections*. Springer, New York.
- Roosjen, A., Van Der Mei, H.C., Busscher, H.J., Norde, W., 2004. Microbial adhesion to poly(ethylene oxide) brushes: influence of polymer chain length and temperature. *Langmuir* 20, 10949–10955.
- Sato, A., Nakamura, I., Fujita, H., Tsukimori, A., Kobayashi, T., Fukushima, S., Fujii, T., Matsumoto, T., 2017. Peripheral venous catheter-related bloodstream infection is associated with severe complications and potential death: a retrospective observational study. *BMC Infect. Dis.* 17.
- Schaer, T.P., Stewart, S., Hsu, B.B., Klibanov, A.M., 2012. Hydrophobic polycationic coatings that inhibit biofilms and support bone healing during infection. *Biomaterials* 33, 1245–1254.
- Singha, P., Locklin, J., Handa, H., 2017. A review of the recent advances in antimicrobial coatings for urinary catheters. *Acta Biomater.* 50, 20–40.
- Song, F., Koo, H., Ren, D., 2015. Effects of material properties on bacterial adhesion and biofilm formation. *J. Dent. Res.* 94, 1027–1034.
- Stepnova, E.A., Tikhonov, V.E., Babushkina, T.A., Klimova, T.P., Vorontsov, E.V., Babak, V.G., Lopatin, S.A., Yamskov, I.A., 2007. New approach to the quaternization of chitosan and its amphiphilic derivatives. *Eur. Polym. J.* 43, 2414–2421.
- Stewart, P.S., Parker, A.E., 2019. Measuring antimicrobial efficacy against biofilms: a meta-analysis. *Antimicrob. Agents Chemother.* 00020-19.
- Stoodley, P., 2016. Biofilms: flow disrupts communication. *Nat. Microbiol.* 1, 15012.
- Stoodley, P., Conti, S., Nistico, L., Kreft, R., Johnson, S., Darabi, A., Post, J.C., Ehrlich, G.D., Kathju, S., 2010. Demonstration of a mixed MRSA/MRSE biofilm in an infected total ankle arthroplasty by confocal microscopy, Ibis T5000, RT-PCR and culture. *FEMS Immunol. Med. Microbiol.* 62(1), 66–74.
- Stoodley, P., Dodds, I., Boyle, J.D., Lappin-Scott, H.M., 1998. Influence of hydrodynamics and nutrients on biofilm structure. *J. Appl. Microbiol.* 85 (Suppl. 1), 19S–28S.
- Stoodley, P., Nistico, L., Johnson, S., Carabin, L.-A., Baratz, M., Gahlot, V., Ehrlich, G.D., Kathju, S., 2008. Direct demonstration of viable *S. aureus* biofilms in an infected total joint arthroplasty. *JBJS.* 90, 1751–1758.
- Stoodley, P., Sauer, K., Davies, D.G., Costerton, J.W., 2002. Biofilms as complex differentiated communities. *Annu. Rev. Microbiol.* 56, 187–209.
- Swartjes, J., Das, T., Sharifi, S., Subbiahdoss, G., Sharma, P.K., Krom, B.P., Busscher, H.J., Van der Mei, H.C., 2013. A functional DNase I coating to prevent adhesion of bacteria and the formation of biofilm. *Adv. Funct. Mater.* 23, 2843–2849.
- Swearingen, M.C., Dibartola, A.C., Dusane, D., Granger, J., Stoodley, P., 2016. 16S rRNA analysis provides evidence of biofilms on all components of three infected periprosthetic knees including permanent braided suture. *Pathog. Dis.* 74.
- Tan, Y.L., Han, F., Ma, S., Yu, W.G., 2011. Carboxymethyl chitosan prevents formation of broad-spectrum biofilm. *Carbohydr. Polym.* 84, 1365–1370.
- Tang, P.F., Zhang, W., Wang, Y., Zhang, B.X., Wang, H., Lin, C.J., Zhang, L.H., 2011. Effect of superhydrophobic surface of titanium on *Staphylococcus aureus* adhesion. *J. Nanomater.*
- Taylor, R., Verran, J., Lees, G., Ward, A., 1998. The influence of substratum topography on bacterial adhesion to polymethyl methacrylate. *J. Mater. Sci. Mater. Med.* 9, 17–22.
- Thomen, P., Robert, J., Monmeyran, A., Bitbol, A., Douarche, C., Henry, N., 2017. Bacterial biofilm under flow: first a physical struggle to stay, then a matter of breathing. *PLoS One* 12.
- Trampuz, A., Widmer, A.F., 2006. Infections associated with orthopedic implants. *Curr. Opin. Infect. Dis.* 19, 349–356.
- Turnbull, I.R., Buckman, S.A., Horn, C.B., Bochicchio, G.V., Mazuski, J.E., 2018. Antibiotic-impregnated central venous catheters do not change antibiotic resistance patterns. *Surg. Infect.* 19, 40–47.
- Tzeng, A., Tzeng, T.H., Vasdev, S., Korth, K., Healey, T., Parvizi, J., Saleh, K.J., 2015. Treating periprosthetic joint infections as biofilms: key diagnosis and management strategies. *Diagn. Microbiol. Infect. Dis.* 81, 192–200.
- Valverde, A., Perez-Alvarez, L., Ruiz-Rubio, L., Olivenza, M.A.P., Blanco, M.B.G., Diaz-Fuentes, M., Vilas-Vilela, J.L., 2019. Antibacterial hyaluronic acid/chitosan multilayers onto smooth and micropatterned titanium surfaces. *Carbohydr. Polym.* 207, 824–833.
- Van Loosdrecht, M.C., Norde, W., Zehnder, A.J., 1990. Physical chemical description of bacterial adhesion. *J. Biomater. Appl.* 5, 91–106.
- Vester, H., Wildemann, B., Schmidmaier, G., Stockle, U., Lucke, M., 2010. Gentamycin delivered from a PDLLA coating of metallic implants in vivo and in vitro characterisation for local prophylaxis of implant-related osteomyelitis. *Injury* 41, 1053–1059.

- Vinoj, G., Pati, R., Sonawane, A., Vaseeharan, B., 2015. In vitro cytotoxic effects of gold nanoparticles coated with functional acyl homoserine lactone lactonase protein from *Bacillus licheniformis* and their antibiofilm activity against *Proteus* species. *Antimicrob. Agents Chemother.* 59, 763–771.
- Vishnu, J., Manivasagam, V.K., Gopal, V., Garcia, C.B., Hameed, P., Manivasagam, G., Webster, T.J., 2019. Hydrothermal treatment of etched titanium: a potential surface nano-modification technique for enhanced biocompatibility. *Nanomedicine* 102016.
- Wang, R., Neoh, K.G., Shi, Z.L., Kang, E.T., Tambyah, P.A., Chiong, E., 2012a. Inhibition of *Escherichia coli* and *Proteus mirabilis* adhesion and biofilm formation on medical grade silicone surface. *Biotechnol. Bioeng.* 109, 336–345.
- Wang, Y.F., Hong, Q.F., Chen, Y.J., Lian, X.X., Xiong, Y.F., 2012b. Surface properties of polyurethanes modified by bioactive polysaccharide-based polyelectrolyte multilayers. *Colloids Surfaces B Biointerfaces* 100, 77–83.
- Woo, G.L.Y., Yang, M.L., Yin, H.Q., Jaffer, F., Mittleman, M.W., Santerre, J.P., 2002. Biological characterization of a novel biodegradable antimicrobial polymer synthesized with fluoroquinolones. *J. Biomed. Mater. Res.* 59, 35–45.
- Xie, D., Howard, L., Almousa, R., 2018. Surface modification of polyurethane with a hydrophilic, antibacterial polymer for improved anti-fouling and antibacterial function. *J. Biomater. Appl.* 33, 340–351.
- Xu, Y., Larsen, L.H., Lorenzen, J., Hall-Stoodley, L., Kikhney, J., Moter, A., Thomsen, T.R., 2017. Microbiological diagnosis of device-related biofilm infections. *APMIS* 125, 289–303.
- Xue, Q., Liu, X.B., Lao, Y.H., Wu, L.P., Wang, D., Zuo, Z.Q., Chen, J.Y., Hou, J., Bei, Y.Y., Wu, X.F., Leong, K.W., Xiang, H., Han, J., 2018. Anti-infective biomaterials with surface-decorated tachyplesin I. *Biomaterials* 178, 351–362.
- Yang, H., Deng, Y., 2008. Preparation and physical properties of superhydrophobic papers. *J. Colloid Interface Sci.* 325, 588–593.
- Yasir, M., Willcox, M.D.P., Dutta, D., 2018. Action of antimicrobial peptides against bacterial biofilms. *Materials* 11.
- Yazici, H., Habib, G., Boone, K., Urgen, M., Utku, F.S., Tamerler, C., 2019. Self-assembling antimicrobial peptides on nanotubular titanium surfaces coated with calcium phosphate for local therapy. *Mater. Sci. Eng. C* 94, 333–343.
- Ye, J., Shao, C., Zhang, X., Guo, X.Y., Gao, P., Cen, Y.Z., Ma, S.Q., Liu, Y., 2017. Effects of DNase I coating of titanium on bacteria adhesion and biofilm formation. *Mater. Sci. Eng. C* 78, 738–747.
- Yucel, N., Lefering, R., Maegele, M., Max, M., Rossaint, R., Koch, A., Schwarz, R., Korenkov, M., Beuth, J., Bach, A., Schierholz, J., Pulverer, G., Neugebauer, E.A.M., 2004. Reduced colonization and infection with miconazole-rifampicin modified central venous catheters: a randomized controlled clinical trial. *J. Antimicrob. Chemother.* 54, 1109–1115.
- Yujie, L., Geng, X., Huang, Y.C., Li, Y., Yang, K., Ye, L., Chen, X., Zhao, G., Yin, C., 2013. The effect of brominated furanones on the formation of *Staphylococcus aureus* biofilm on PVC. *Cell Biochem. Biophys.* 67, 1501–1505.
- Zeng, X.M., Xiong, S.J., Zhuo, S.Y., Liu, C.P., Miao, J., Liu, D.X., Wang, H.X., Zhang, Y.Y., Wang, C.L., Liu, Y., 2019. Nanosilver/poly (DL-lactic-co-glycolic acid) on titanium implant surfaces for the enhancement of antibacterial properties and osteoinductivity (vol 14, pg 1849, 2019). *Int. J. Nanomed.* 14, 3469–3469.
- Zhang, Y.L., Xia, H., Kim, E., Sun, H.B., 2012. Recent developments in superhydrophobic surfaces with unique structural and functional properties. *Soft Matter* 8, 11217–11231.
- Zhou, C., Wu, Y., Thappeta, K.R.V., Subramanian, J.T.L., Pranantyo, D., Kang, E.T., Duan, H.W., Kline, K., Chan-Park, M.B., 2017. In vivo anti-biofilm and anti-bacterial non-leachable coating thermally polymerized on cylindrical catheter. *ACS Appl. Mater. Interfaces* 9, 36269–36280.

Chapter Questions

1. What are the main stages in bacterial biofilm formation and give examples of how three of these stages may require different approaches with respect to biofilm control?
2. What are three features of bacteria when they are growing as biofilms that make them much more difficult to kill than when they are growing rapidly as a planktonic culture?
3. Classify the different strategies of biofilm control on the basis of their effects on bacterial cells.
4. Given the following three types of medical devices (urinary catheters, orthopedic implants, and CVCs), identify and list materials used for fabrication of the device.
5. Explain how material surface texture (roughness, topography) affects bacterial adhesion.
6. List three antibiotics used for medical device coating to prevent device-related infections. What are three main challenges with coating strategies?

2.3.1

How Well Will It Work? Introduction to Testing Biomaterials

BUDDY D. RATNER

Bioengineering and Chemical Engineering, Director of University of Washington Engineered Biomaterials (UWEB), Seattle, WA, United States

When an engineer designs a suspension bridge over a river, he or she will start with a precise engineering drawing and then, based on well-established mathematical models, assess the strength of materials and corrosion resistance needed to ensure the structure will stand for some anticipated lifetime, e.g., 100 years. The strength of materials and corrosion resistance are compiled in widely accepted handbooks containing data obtained through rigorous testing. The engineer can confidently design the bridge from computer models and handbook data. The bridge will stand and function appropriately for 100 years. Moreover, such a bridge manufactured according to a given set of design criteria and specifications should perform approximately the same whether it crosses a river in Seattle, Birmingham, or Boston.

Now, consider an engineer who sets out to design a heart assist device or a hip prosthesis. This engineer will find the basic mechanical property data relevant to the materials used in handbooks, but little on specific biointeractions, biodurability, and the implications of these biological reactions for the ultimate performance of the complex device. Because of the limited amounts of validated and qualified data on how a given material will perform in the challenging in vivo environment, biomaterials scientists devise tests to observe the performance of materials (and devices) and assess potential biointeractions. These tests are often (but not always) focused on the mechanics and biology relevant to the specific application (orthopedic, cardiovascular, urological, etc.), and they do not consider the potential for different circumstances and possibly different biomaterials–tissue interactions in different patients. This section of the textbook focuses on useful tools and ideas for testing biomaterials.

After this introduction, the section leads off with a chapter titled “The Concept and Assessment of Biocompatibility” (Chapter 2.3.2). Biocompatibility is possibly the most central concept in understanding biomaterials, and you cannot test for biocompatibility until you understand what it is. Chapter 2.3.3 (“In Vitro Assessment of Cell and Tissue Compatibility”) and Chapter 2.3.4 (“In Vivo Assessment of Tissue Compatibility”) provide fine overviews of thinking circa early 21st century on testing for biocompatibility, primarily focused on toxicology (in vitro) and the foreign-body reaction (in vivo), and parallel the thinking by most national regulatory agencies (for example, the US Food and Drug Administration). So, why do we need a chapter on the concept of biocompatibility? There are new developments that will probably change the definition of biocompatibility. For example, Chapter 2.3.2 discusses a material (with no toxic leachables) fabricated as a solid film that heals with the classic foreign-body reaction, and the same material fabricated as a precise, porous structure that heals in a vascularized, afibrotic manner. Today’s definitions and regulatory climate are not structured to appreciate the significance of these differences. Furthermore, there are other strategies to shift the healing of today’s “biocompatible” biomaterials to a more tissue-integrated, vascularized reconstruction. In this fourth edition of the *Biomaterials Science* textbook, we introduce the issues and concerns stimulating new thinking on biocompatibility in Chapter 2.3.2. Chapter 2.2.2 (“Inflammation, Wound Healing, and the Foreign-Body Response”) provides essential background to understand the material in Chapters 2.3.2, 2.3.3, and 2.3.4.

Chapter 2.3.5, “Evaluation of Blood–Materials Interactions,” looks at another face of the biological reaction to synthetic materials. Millions of medical devices are interfaced

with the bloodstream each year. The reaction of blood with biomaterials is strikingly different from the reactions seen in soft tissue and bone in both kinetics (rapid) and outcomes (clot). Although blood compatibility assessment goes back to the 1930s, to this day we have no widely accepted list of biomaterials that are blood compatible. Indeed, there is little agreement about the structural/chemical/molecular characteristics of a material that engender blood compatibility. Why this lack of clarity and consensus? [Chapter 2.3.5](#) introduces the issues in blood compatibility assessment (the nature of blood, the impact of flow, and the nature of the biomaterial), and illustrates how simple assessment schemes can lead to erroneous conclusions. Accepted blood compatibility tests are introduced but, more importantly, the chapter provides guidelines for drawing conclusions from the results of these tests. Some thoughts on which materials might be blood compatible are offered in this chapter.

[Chapter 2.3.6](#) addresses the use of animals in biomaterials and medical device research. Animal implants (in vivo assessment) are usually required for preclinical testing of medical devices. Without animal testing, it is less likely that the research we perform will transition from laboratory bench to patient. The use of animals in testing is fraught with ethical issues—respect for the animal lives to be sacrificed and minimization of pain to the animal (see

[Chapter 3.1.11](#)). Also, a key issue is how significant are the results obtained in animals for understanding the performance of the medical device in humans? Humans are different genetically, biochemically, and biomechanically from animals. Also, humans are different genetically, biochemically, and biomechanically from each other. Can predictive models be developed? The answer is, in most cases, “yes,” but with some forethought and planning. Without careful consideration and understanding of specific animal models, animal lives will be sacrificed and research funds wasted, since the results obtained may not be useful for the human device. The biomechanics issue is particularly challenging. Almost any orthopedic device (spine, joints) will be subjected to different mechanical forces in the skeletal system of an animal walking on four legs versus an upright, bipedal human. Other considerations are: (1) should we go directly from in vitro testing to testing in human subjects, and (2) what about developing devices for veterinary use (for example, about 5000 intraocular lenses are implanted in dogs each year)? Biomaterials researchers are largely dependent on animal models, and understanding them is essential—[Chapter 2.3.6](#) provides an introduction to the regulatory, ethical, and practical implementation issues associated with common animal models used in the biomaterials community.

2.3.2

The Concept and Assessment of Biocompatibility

BUDDY D. RATNER¹, FREDERICK J. SCHOEN²

¹Bioengineering and Chemical Engineering, Director of University of Washington Engineered Biomaterials (UWEB), Seattle, WA, United States

²Department of Pathology/Brigham and Women's Hospital and Harvard Medical School, Boston, MA, United States

What do we mean when we say a biomaterial is biocompatible?

- Is biocompatibility simply a binary “yes” or “no,” or is there a continuum of biocompatibilities ranging from “good” to “bad?”
- How can we measure biocompatibility?
- How do we improve or enhance the biocompatibility of a biomaterial?

The *idea* of biocompatibility is central to what makes a material a biomaterial. Also, new developments and concepts in cell biology are shifting thinking about biocompatibility, and this chapter offers an opportunity of a glimpse into the future of biocompatible biomaterials.

Biocompatibility is so central to what makes a material a biomaterial, that a focused discussion of the subject is justified.

This chapter clarifies some of the issues in biocompatibility, and also raises questions that will likely impact the field in the coming years. In contrast to empirical approaches and practical considerations focused solely about the safety of implanted devices (for example, toxicology, the state of the art today), modern cell and molecular biology ideas may give us a useful “theory of biocompatibility” with quantifiable parameters, testable hypotheses, and validated engineering rules.

Biocompatibility Today

We start with an overview of the state of the art in biocompatibility today, i.e., in the first quintile of the 21st century.

A definition for biocompatibility, widely used in the biomaterials/medical device community, is:

“the ability of a material to perform with an appropriate host response in a specific application (Williams, 1987; Zhang and Williams, 2019).”

This definition, though accurate and quite useful in the design, development, and application of biomaterials in medicine, nevertheless offers no insights into the mechanisms of biocompatibility, how to test the biocompatibility of a material or how to optimize or enhance the biocompatibility of a material to improve clinical outcomes. This section of the textbook will expand the definition and explore the philosophical and scientific ideas surrounding biocompatibility.

Specific concepts impacting biocompatibility are elaborated upon in [Chapters 2.2.2, 2.3.3 and 2.3.4](#). Biocompatibility can be assessed using *in vitro* and *in vivo* assays. Although a variety of direct chemical and physical interactions may also be important, measurement of the consequences of leachable or secreted substances from biomaterials to cells in culture is the primary goal of *in vitro* biocompatibility assays. For example, cell proliferation inhibition or cell death are negative outcomes in such assays, and we assume that they would reflect characteristics of materials that are not biocompatible. The *in vivo* (implantation) response to a “biocompatible” biomaterial is generally described as a mild inflammatory reaction, which, after some 3–6 weeks, resolves itself into a thin fibrous capsule (essentially scar), to a large extent a consequence of the tissue trauma of implantation. Moreover, there may be an ongoing low-level *chronic* inflammatory response, characterized by a limited number of macrophages present at the implant surface even years after implantation, but the reaction site is relatively

quiescent, and with no other indication of adverse local or systemic response. Additionally, the presence of some multinucleated foreign-body giant cells (FBGCs) at the biomaterial–tissue interface is common and of no significant consequence, but a high density of macrophages and many FBGCs suggests that the biomaterial is exerting a persistent inflammatory stimulus. The composite reaction is termed the “foreign-body reaction,” or FBR.

Four factors impact that which we refer to as “biocompatibility.” These are:

1. Toxicology (the measurement and study of the effects of material leaching from biomaterials) (Chapters 2.3.3 and 3.1.3).
2. Reactions related to products from extrinsic microbiologic organisms colonizing the biomaterial (for example, endotoxin contamination; see Chapters 2.2.8 and 3.1.4).
3. Mechanical effects such as rubbing, irritation, compression, stress concentrations caused by high aspect ratio shapes, corners and modulus mismatch, and mechanical failure. Closely related are size-related effects, for example, if the implant is much larger than a macrophage, comparable in size to a macrophage, and capable of being phagocytosed, or much smaller than a macrophage, i.e., nano-size.
4. A broad range of interactions with the surrounding environment, including proteins, other soluble molecules and ions in extracellular fluid and blood, live microorganisms, and cells, inducing cell–biomaterial interactions (and tissue–biomaterial interactions) that might affect and, indeed, in some cases dominate longer term in vivo outcomes.

Four factors impact that which we refer to as “biocompatibility.” These are:

- toxicology
- extrinsic organisms
- mechanical effects
- various biological interactions with the environment, including cell–biomaterial interactions.

Points 1, 2, and 3, above, are well understood, and often applied in the design of biocompatible biomaterials—we understand the principles, have the ability to measure their impact, and we can design devices using clearly defined principles to achieve good outcomes. Point 4 is less well-developed and concerns are expanded upon below, and in other chapters in this textbook. It is important to understand that in contrast to living organ transplants, biomaterials are not generally “rejected.” The process of tissue or whole-organ rejection denotes an inflammatory process that results from a specific immune response (i.e., a response to defined antigens by antibodies and antigen-specific T cells), and which synthetic biomaterials typically do not generate. In the FBR (as discussed below), the nature of the reaction is largely dependent on the chemical and physical characteristics of the implant and is a non-specific (or “innate”) immune response.

Toxicology

Polymeric materials often contain extractable components, such as unreacted monomer, oligomers, initiator fragments, stabilizers, and other processing additives. Metals, glasses, and ceramics can release ions and other processing components. The type of reaction that will be considered from a toxicology standpoint is if these substances are released and negatively impact cells (in vitro) or adjacent tissues (in vivo), or if they affect an organism systemically. Biomaterials science, standards organizations, and allied fields have developed reliable methods to measure and identify leachates, and also sensitive and standardized methods to look at the reaction of tissues and cells to these leached substances. These methods are summarized in Chapter 2.3.3. The ISO 10993 standards provide many specific, defined tests for toxicity associated with leachables.

The Products of Extrinsic Organisms Colonizing the Biomaterial

Bacteria (whether viable or not) and their cell wall components are intense inflammatory activators. Fungi such as *Candida* are also inflammatory activators (Kojic and Darouiche, 2004). In the case of implants that are contaminated with fungi, bacteria, or bacterial cell-wall endotoxin (lipopolysaccharide), an intense and usually long-term biological reaction is seen, characterized by large numbers of white blood cells (mostly polymorphonuclear leukocytes [aka neutrophils] and macrophages, collectively called “pus”) in the vicinity of the implant. In humans, this reaction would be described by the patient as producing pain, redness, and heat. This response to the contaminated implant can lead to exceptionally thick foreign-body capsules. High concentrations of inflammatory cells (including FBGCs) and thick, dense foreign-body capsules are characteristics of poor biocompatibility. Such extreme reactions to devices with contaminating organisms have been documented with breast implants (Pajkos et al., 2003), and other implant devices. This is distinct from *infection* with live microbiologic organisms, such as bacteria or fungi, in which the organisms may multiply and cause ongoing local tissue destruction and potentially systemic effects. Although infection with live organisms shares some morphologic features with, and can occasionally look like, “poor biocompatibility,” the *acute* inflammatory reaction induced by active infection is generally dominated by neutrophils and morphologically distinct from FBR. Infection is generally not regarded as a biocompatibility issue, but rather owing to ineffective sterilization, intraoperative contamination, or seeding by microorganisms during in vivo function (see Chapter 3.1.4).

Mechanical Effects

If an implant is rubbing, abrading, or moving in contact with tissue, or has sharp corners, undesirable reactions that

are superficially classified as “nonbiocompatible” will be observed, irrespective of the material composition. Mechanical mismatch between a hard biomaterial and a soft tissue can lead to damage or irritation to the soft tissue. Cell and tissue responses to mechanical forces are well-known and usually quite significant (Stamenović; Ingber, 2009; Jan-son and Putnam, 2015; Kumar et al., 2017; Vining and Mooney, 2017; Murray, 2017). An excellent example of the mechanical effect on in vivo bioreaction was seen in 1976, when scientists implanted in rat muscle medical-grade “biocompatible” materials having circular, triangular, and pentagonal shapes (Matlaga et al., 1976). The degree of reaction increased in the order: circle (lowest reaction), pentagon, triangle. The effect was attributed to micromotion associated with the acute angle of the triangle leading to the greatest tissue irritation (induced by stress concentration). In general, it is the role of the implant designer to ensure that the device does not excessively rub or irritate tissue (rounded edges are better than sharp edges, for example). Wherever possible, a surgeon places and anchors a device into an implant site in a manner that minimizes rubbing and irritation.

Cell–Biomaterial Interactions

This topic dominates the literature in biomaterials science (see Chapter 2.1.3). It has been clear since the mid-19th century that living cells interact and attach to different materials in different ways, and the nature of that interaction may have immense influence on gene expression and thereby cell fate, including attachment, migration, spreading, proliferation, differentiation, activation, secretion, and detachment. It is also well established that an adsorbed protein film always precedes cell interaction with surfaces, and the nature of the protein layer directs and modulates the cell response (see Chapter 2.1.2). Since inflammatory cells, such as neutrophils and macrophages, “interrogate” implanted materials shortly after implantation, and since different surfaces interact in different ways with proteins and cells, we would expect the biomaterial to impact the cell-driven in vivo reaction. However, let’s examine this conclusion. In vitro, profound differences are seen in cell interactions between different materials. For example, a poly(2-hydroxyethyl methacrylate) (polyHEMA) hydrogel will not permit macrophages to adhere in cell culture, while a tissue culture polystyrene (TCPS) surface readily allows those same cells to adhere. Yet, if the polyHEMA and TCPS are implanted in vivo, both will heal similarly with an avascular, collagenous foreign-body capsule (again, both resulting from the dominant effect of healing of a surgical wound). In fact, all “biocompatible” materials, be they hydrophilic, hydrophobic, metallic, polymeric, or ceramic, will heal similarly with a classic (and largely quiescent) foreign-body reaction (FBR) if there are: (1) no leachables; (2) no products from extrinsic organisms; and (3) no mechanical irritation. The explanation for this striking difference between in vitro bioreaction and in vivo bioreaction has yet to be elucidated,

but does highlight the multicell complexity of the in vivo environment, in comparison to the relatively simple environment with one cell type in vitro.

Two additional phenomena are important in modulating the biomaterial–tissue interaction: (1) frustrated phagocytosis; and (2) cytokine release. Macrophages are functionally differentiated to engulf and digest foreign material, in a process called *phagocytosis* (literally, cell eating). Phagocytosis occurs after the adsorbed proteins on the foreign body interact with receptor proteins that are on the surface of the macrophage. The macrophage then stretches itself around the foreign body and, if possible, engulfs it. This traps the foreign particle in a compartment called a lysosome, into which the macrophage secretes a battery of chemicals that attempt to degrade the foreign material. Frustrated phagocytosis is the term used to describe the situation when the macrophage is incapable of “eating” a piece of biomaterial much larger than its size and certainly cannot engulf a macroscopic implant. In this situation the lysosomes (which may be in contact with the foreign material but open to the surroundings) may release their contents into (and themselves may be highly irritating to) the adjacent tissues, causing local tissue damage and inflammation. Moreover, to address a large surface, a macrophage can fuse with other macrophages to form multinucleated FBGCs, whose quantity is often used as a marker of the activity (i.e., aggressiveness) of the FBR (i.e., more FBGC indicative of less biocompatibility). Macrophages also release cytokines (diffusible signaling proteins) in response to biomaterials (Bonfield et al., 1992). Cytokines can be considered as proinflammatory (e.g., IL-1, TNF- α) or antiinflammatory (e.g., IL-4, IL-10) (Kim and Nair, 2019). A measurement of the cytokine shower from an implanted biomaterial may offer insights into its biocompatibility. The neutrophil and the macrophage, both cell types seen in the early phases of the reaction to implanted biomaterials, are considered elements of the innate immunity system. There is now evidence suggesting that T cells, usually thought of as components of the adaptive immune system, are also part of the reaction to biomaterials, particularly when proregenerative healing is noted (Sadtler et al. 2016).

For biodegradable materials used as implants, there are a few additional considerations. Most biodegradable materials degrade sufficiently slowly that a low-level FBR is observed. When the implanted degradable material ultimately disappears, the foreign-body capsule may largely recede. The magnitude of the FBR may be impacted by reaction to the low-molecular-weight degradation products. For example, consider poly(lactic glycolic acid) (PLGA). Though the degradation products are lactic acid and glycolic acid, metabolic molecules always seen in normal physiology, if the degradation is rapid, the high, local acid concentration could damage tissue and trigger an intensified FBR.

Summary of Ideas to This Point

Important points about biocompatibility as we understand it today are:

1. The biological reaction we call biocompatibility is negatively impacted by leachables, products of extrinsic organism surface contamination, and micromotion.
2. As long as leachables, extrinsic organism surface contamination, and micromotion are not impacting the reaction, all materials will give an approximately similar bioreaction *in vivo*, referred to as the “normal” (i.e., expected, low-level) FBR, composed of a thin fibrous capsule and minimal ongoing inflammation.
3. When the foreign body capsule is thin and the reaction site, after approximately 1 month or longer, is relatively quiescent, this is an acceptable (and indeed, usually unavoidable) FBR and we call the implant “biocompatible (or inert).”
4. Inert biomaterials lead to the reaction described in point 3 (above), and thus are called “biocompatible.”
5. The favorable long-term interface between a biomaterial and the surrounding tissues in most medical devices is characterized by a thin, dense, collagenous capsule that isolates the biomaterial implant from the body, and has a minimal, if any, inflammatory component.

New Developments Are Changing the Paradigm of Biocompatibility

Although millions of devices made of biocompatible biomaterials are implanted in humans every year, largely with successful outcomes, there are concerns with the way some implants heal (the FBR), and the fibrous capsule can cause defects in implant performance. For example, a dense fibrous capsule can inhibit diffusion of analytes to implanted sensors, interfere with release of drugs from implanted controlled drug release devices, and enhance the resistance of an electrical path, thereby blocking communication with tissues for implanted electrodes. Capsular contraction is a problem for some devices, such as breast implants, where the contraction of the fibrous capsule (i.e., not an unexpected consequence, since all scars contract) distorts the soft implant, tending to make it spherical. Moreover, a lack of vascularity near the implant–tissue interface can slow the body’s response to, and treatment of, an infection adjacent to a medical device. Certainly, the fibrous capsule associated with the FBR can create surgical problems for device removal and revision. In many cases, vascularized, integrated tissue (more resembling normal tissue structure) would be preferable to an avascular, dense capsule.

The potential for vascularized, nonfibrotic healing is now being realized. Such reconstructive healing can be achieved with extracellular matrix (ECM) components or with inert biomaterials with engineered porosity.

Decellularized ECM derived from a number of tissues, for example, small intestinal submucosa (SIS), has been found to heal into the body with little or no fibrosis, excellent vascularity, and general tissue reconstruction (Badyalak, 2007). SIS and other decellularized ECMs have been used in millions of human surgeries, largely with good results.

If the SIS is cross-linked, it will heal in a proinflammatory manner, with a capsule and a classical FBR. The excellent healing of SIS is attributed to the ability of macrophages to degrade the ECM to bioactive peptides that actively promote healing. Importantly, the ECM structure is heavily infused with macrophages in the early stage of healing, and those macrophages have been shown to be in a phenotype (also referred to as a polarization) conducive to healing (called M2), in contrast to the proinflammatory, fibrotic phenotype (designated M1) (Mantovani, 2006; Badyalak et al., 2008; Murray, 2017). There are also suggestions that soluble ECMs derived from neonatal cell culture might be used as coating for implants to aid in healing and integration (Naughton and Kellar, 2008).

Certain porous synthetic biomaterials will also heal in a minimally fibrotic, angiogenic fashion. Observations on the special characteristics of the healing of porous structures in the body go back to the early 1970s (Karp et al., 1973; Klawitter et al., 1976). Many studies demonstrate the importance of pore characteristics to biocompatibility and implant healing (Brauker et al., 1995; Golden et al., 1990). The concern with all these studies was that the materials used had a broad distribution of pore sizes, making it difficult to ascertain the effect on healing of a specific pore size. A method was developed to make materials with a single, consistent pore size, based on using solvent-soluble microspheres as templates to create uniform, interconnected pores. When such materials were implanted subcutaneously, it was noted that when pores were in the size range 30–40 microns, vascularized healing and reconstruction with little fibrosis were observed (Marshall et al., 2004; Madden et al., 2010). Also, these materials were heavily infused with macrophages during healing, and many of the macrophages were in the M2 phenotype (Madden et al., 2010; Sussman et al., 2014). These same materials with 30–40-micron pores healed well in skin percutaneous sites (with dermal and epidermal reconstruction) (Fukano et al., 2010), heart muscle, and other tissues. A further discussion of porous materials can be found in Chapter 1.4.7.

Other strategies have recently been described to manipulate the FBR and the healing response. Implanted spheres of sizes around 1.5 mm have demonstrated reduced FBR (Veiseh et al., 2015). Certain triazole analogs have also been observed to inhibit the FBR (Vegas et al., 2016). Exceptionally nonfouling zwitterionic gels will heal in with no capsule and good local vascularity (Zhang, 2013). Other strategies for modulating the FBR have involved the surface display of important proteins that steer the macrophage to a pro-healing state and delivery of cytokines (i.e., toward the M2 phenotype).

With relevance to biocompatibility, consider differences engendered solely as a result of physical factors. A synthetic hydrogel is fabricated as a solid slab or as a porous structure with 30–40-micron interconnected pores. The chemical compositions of both are identical. Also, they have similar mechanical properties, no leachables, and no endotoxin or bacteria. Yet one heals in a capsule with the classic FBR,

while the other heals in a vascularized, reconstructed manner with little fibrosis. It seems challenging to use the word “biocompatible” for both, given the sharp differences in *in vivo* biological reaction, despite identical chemistries.

A “biocompatible” material is fabricated as a porous structure or a solid slab. The porous structure heals in an avascular, proangiogenic manner. The solid slab is encapsulated with the classic FBR. How can we use the word “biocompatible” for two such different bioreactions?

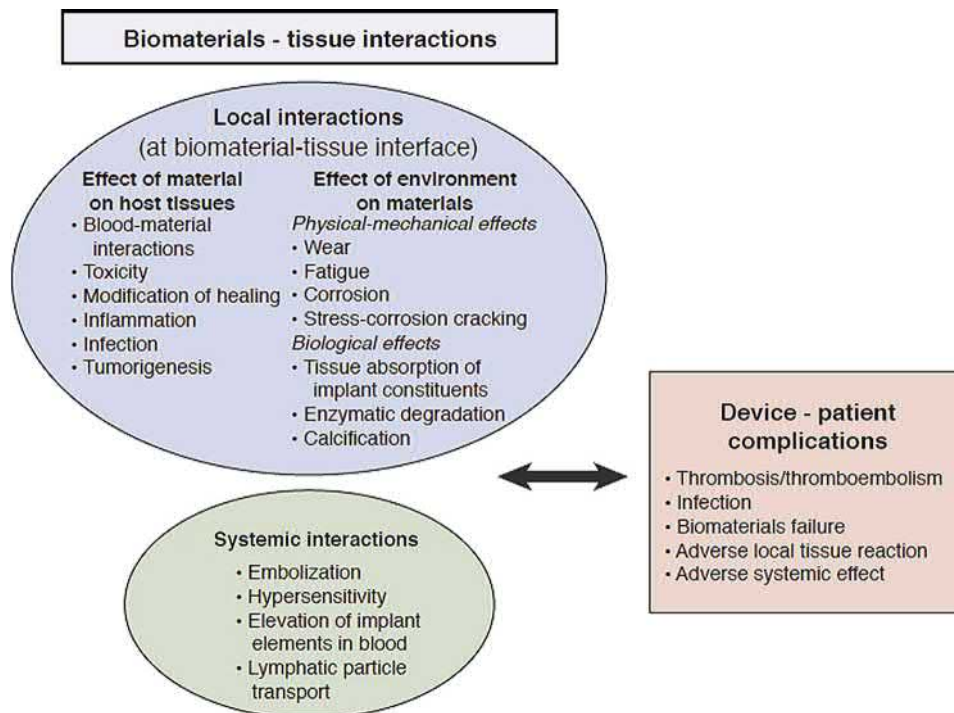
Clinical Significance of Biocompatibility

Most implants serve their recipients well for extended periods by alleviating the conditions for which they were implanted. However, some implants and extracorporeal devices ultimately develop complications (i.e., adverse interactions of the patient with the device or vice versa) which constitute device failure, and thereby may cause harm to or death of the patient. Complications generally result from biomaterial–tissue interactions. Moreover, complications are costly, both to patient outcomes (mortality and morbidity) and to the healthcare budget.

Complications of biomaterials and medical devices result largely as a consequence of biomaterial–tissue interactions, which all implants have with the environment into which they are placed. Although specific issues related to inflammatory

mechanisms were discussed in detail above, not all complications that might be considered problems with “biocompatibility” are primarily inflammatory. The broader view includes a wide range of effects of both the implant on the host tissues and the host on the implant (Fig. 2.3.2.1) including specific immunological reactions, systemic effects, blood–material interactions, tumor formation, and infection (discussed in Chapters 2.2.2, 2.2.5, 2.2.7, 2.2.8 and 2.3.5 respectively). To a great extent, these interactions arise from qualitative or quantitative alterations of physiological (normal) processes (e.g., inflammation, blood coagulation, etc.) comprising host defense mechanisms that function to protect an organism from deleterious external threats (such as bacteria and other microbiologic organisms, injury, and foreign materials).

Moreover, systemic and remote “biocompatibility” effects can occur. For example, biomaterial-related systemic toxicity and hypersensitivity reaction (through lymphatics and the bloodstream) in animals and patients with either stainless steel or cobalt-based orthopedic total joint replacement components, where elevations of metallic content occur in tissue (at both local and remote sites) and in serum and urine. Transport of particulates over large distances by macrophages to surround and damage the bone of a metal-on-metal hip joint to cause prosthetic joint loosening owing to “osteolysis” (Ebramzadeh et al., 2011; Gibon et al., 2017) or transport to regional lymph nodes and to the lungs and liver can occur. As a consequence, an enlarged, hard axillary lymph node in a woman who received a silicone-gel breast



• **Figure 2.3.2.1** Biomaterials–tissue interactions. (Reproduced from Schoen, F.J., Padera, R.F., 2012. Cardiovascular Pathology. In: *Cardiac Surgery in the Adult*, fourth ed., Cohn, L.H., Edmunds, L.H. (Eds.), McGraw-Hill, pp. 95–148.)

prosthesis for reconstruction following mastectomy for a carcinoma can be misdiagnosed as tumor (Hausner et al., 1978) and prosthetic hip joint or heart valve failure may lead to particulate matter in the liver (Peoc'h, 1996). "Metal allergy" is well recognized and is frequently associated in women with the use of cheap, high-nickel alloy costume jewelry or earrings, and can also occur in association with metallic implants (Hallab et al., 2001). By themselves, metal ions lack the structural complexity required to challenge the immune system. However, when combined with proteins, such as those available in the skin, connective tissues, and blood, a wide variety of metals induce immune responses, and this can have clinical effects. Cobalt, chromium, and nickel are included in this category, with nickel perhaps the most potent; at least 10% of a normal population will be sensitive by skin test to one or more of these metals, at some threshold level.

Conclusions

Since the introduction of "modern" biomaterials to medical practice in the late 1940s and early 1950s, we have seen an evolution in sophistication and functionality (Williams, 2008). *First-generation* biomaterials were simply inert (e.g., titanium, Teflon, polyethylene). *Second-generation* biomaterials (1970, 1980s) interacted with and changed the biological environment in a controlled manner. Such materials might be engineered for biodegradability, poly(lactic acid) for example, or engineered to integrate into bone and induce bone healing, such as bioactive glasses, or to induce a controlled thrombotic deposit, such as a textured polymer surface on the internal surface of a left ventricular assist device. *Third-generation* biomaterials (1990+) bio-specifically orchestrate biological processes, and can direct regeneration and restore functionality, and/or respond to the environment in a proactive manner to favorably influence a tissue reaction. Examples include engineered extracellular matrices (Lutolf and Hubbell, 2005), sphere templated biomaterials (Madden et al., 2010), SIS (Badylak, 2007), "smart" biomaterials (Reyes et al., 2007) and resorbable materials that may induce regeneration solely by harnessing the power of endogenous cells and mechanical signals (Hoerstrup et al., 2000; Wissing et al., 2017). Also, consider the published debate on the effectiveness of biomaterials guided by specific peptide signals (Williams, 2011). As biomaterials evolve, so too must the definition of biocompatibility.

Thus, the way we define biocompatibility may change over the next few years and beyond. Examples that challenge the present paradigm of biocompatibility are published, and materials that show unique healing are being applied in clinical medicine. Recent clarification on the diversity of macrophage phenotypes and understanding of resident tissue stem cell pools in the body may permit engineered "biocompatibility," with control of the extent, rate, and speed of integration. These new developments strengthen the science of biocompatibility, and bring biomaterials and

tissue engineering closer together. Precision control of biocompatibility can lead to new biomaterials-based therapies with profound advantages for patients.

For now, the medical device regulatory agencies subscribe almost exclusively to the definition of biocompatibility that we have been using since the first functionally successful implants in the 1950s. In learning the subject of biomaterials, it is important that one appreciates the accepted standards for biomaterials; standards that are used by the \$300 billion plus medical device industry worldwide and standards that impact millions of patients (see Chapter 3.1.5). Still, since we are on the cusp of a shift in thinking about this subject, it is useful for these newer ideas to be addressed and placed in the context of the word "biocompatibility."

The reader is also referred to complementary views on the subject of the evolving concept of biocompatibility (Bryers et al., 2012; Ratner, 2011; Veisoh and Vegas, 2019; Williams, 2016).

Understanding biocompatibility is central to understanding biomaterials and their clinical outcomes.

References

- Badylak, S.F., 2007. The extracellular matrix as a biologic scaffold material. *Biomaterials* 28 (25), 3587–3593.
- Badylak, S., Valentin, J., Ravindra, A., McCabe, G., Stewart-Akers, A., 2008. Macrophage phenotype as a determinant of biologic scaffold remodeling. *Tissue Eng. A* 14 (11), 1835–1842.
- Bonfield, T.L., Colton, E., Marchant, R.E., Anderson, J.M., 1992. Cytokine and growth factor production by monocyte/macrophages on protein preadsorbed polymers. *J. Biomed. Mater. Res.* 26, 837–850.
- Brauker, J.H., Carr-Brendel, V.E., Martinson, L.A., Crudele, J., Johnston, W.D., et al., 1995. Neovascularization of synthetic membranes directed by membrane microarchitecture. *J. Biomed. Mater. Res.* 29, 1517–1524.
- Bryers, J.D., Giachelli, C.M., Ratner, B.D., 2012. Engineering biomaterials to integrate and heal: the biocompatibility paradigm shifts. *Biotechnol. Bioeng.* 109 (8), 1898–1911.
- Ebramzadeh, E., Campbell, P.A., Takamura, K.M., Lu, Z., Sangiorgio, S.N., Kalma, J.J., De Smet, K.A., Amstutz, H.C., 2011. Failure modes of 433 Metal-on metal hip implants: how, why, and wear. *Orthop. Clin. N. Am.* 42 (Issue 2), 241–250.
- Fukano, Y., Usui, M.L., Underwood, R.A., Isenhath, S., Marshall, A.J., et al., 2010. Epidermal and dermal integration into sphere-templated porous poly(2-hydroxyethyl methacrylate) implants in mice. *J. Biomed. Mater. Res. A* 94 (4), 1172–1186.
- Gibon, E., Córdova, L.A., Lu, L., Lin, T., Yao, Z., Hamadouche, M., Goodman, S.B., 2017. The biological response to orthopedic implants for joint replacement. II: polyethylene, ceramics, PMMA, and the foreign body reaction. *J. Biomed. Mater. Res. B Appl. Biomater.* 105 (6), 1685–1691.
- Golden, M.A., Hanson, S.R., Kirkman, T.R., Schneider, P.A., Clowes, A.W., 1990. Healing of polytetrafluoroethylene arterial grafts is influenced by graft porosity. *J. Vasc. Surg.* 11 (6), 838–844.
- Hallab, N., Merritt, K., Jacobs, J.J., 2001. Metal sensitivity in patients with orthopaedic implants. *J. Bone Joint Surg. Am.* 83, 428–436.

- Hausner, R.J., Schoen, F.J., Pierson, K.K., 1978. Foreign body reaction to silicone in axillary lymph nodes after prosthetic augmentation mammoplasty. *Plast. Reconstr. Surg.* 62, 381–384.
- Hoerstrup, S.P., Sodian, R., Daebritz, S., Wang, J., Bacha, E.A., Martin, D.P., Moran, A.M., Guleserian, K.J., Sperling, J.S., Kaushal, S., Vacanti, J.P., Schoen, F.J., Mayer Jr., J.E., 2000. Functional living trileaflet heart valves grown in vitro. *Circulation* 102 (19 Suppl. 3), III44–III49 7.
- Janson, I.A., Putnam, A.J., 2015. Extracellular matrix elasticity and topography: material-based cues that affect cell function via conserved mechanisms. *J. Biomed. Mater. Res. A* 103 (3), 1246–1258.
- Karp, R.D., Johnson, K.H., Buoen, L.C., Ghobrial, H.K.G., Brand, I., et al., 1973. Tumorigenesis by millipore filters in mice: histology and ultrastructure of tissue reactions as related to pore size. *J. Natl. Cancer Inst.* 51 (4), 1275–1279.
- Kim, S.Y., Nair, M.G., 2019. Macrophages in wound healing: activation and plasticity. *Immunol. Cell Biol.* 97, 258–267.
- Klawitter, J.J., Bagwell, J.G., Weinstein, A.M., Sauer, B.W., Pruitt, J.R., 1976. An evaluation of bone growth into porous high density polyethylene. *J. Biomed. Mater. Res.* 10 (2), 311–323.
- Kojic, E.M., Darouiche, R.O., 2004. Candida infections of medical devices. *Clin. Microbiol. Rev.* 17 (2), 255–267.
- Kumar, A., Placone, J.K., Engler, A.J., 2017. Understanding the extracellular forces that determine cell fate and maintenance. *Development* 144 (23), 4261–4270.
- Lutolf, M.P., Hubbell, J.A., 2005. Synthetic biomaterials as instructive extracellular microenvironments for morphogenesis in tissue engineering. *Nat. Biotechnol.* 23 (1), 47–55.
- Madden, L.R., Mortisen, D.J., Sussman, E.M., Dupras, S.K., Fugate, J.A., et al., 2010. Proangiogenic scaffolds as functional templates for cardiac tissue engineering. *Proc. Natl. Acad. Sci. U.S.A.* 107 (34), 15211–15216.
- Mantovani, A., 2006. Macrophage diversity and polarization: in vivo veritas. *Blood* 108 (2), 408–409.
- Marshall, A.J., Irvin, C.A., Barker, T., Sage, E.H., Hauch, K.D., et al., 2004. Biomaterials with tightly controlled pore size that promote vascular in-growth. *ACS Polymer Preprints* 45 (2), 100–101.
- Matlaga, B.F., Yasenchak, L.P., Salthouse, T.N., 1976. Tissue response to implanted polymers: the significance of sample shape. *J. Biomed. Mater. Res.* 10 (3), 391–397.
- Murray, P.J., 2017. Macrophage polarization. *Annu. Rev. Physiol.* 10 (79), 541–566.
- Naughton, G., Kellar, R., 2008. Human ECM for devices and therapeutics. *May MD & DI* 102–109, May.
- Pajkos, A., Deva, A.K., Vickery, K., Cope, C., Chang, L., et al., 2003. Detection of subclinical infection in significant breast implant capsules. *Plast. Reconstr. Surg.* 111 (5), 1605–1611.
- Peoc'h, M., Moulin, C., Pasquier, B., 1996. Systemic granulomatous reaction to a foreign body after hip replacement. *N. Engl. J. Med.* 335, 133–134.
- Ratner, B.D., 2011. The biocompatibility manifesto: biocompatibility for the twenty-first century. *J. Cardiovasc. Translat. Res.* vol. 5 (5), 523–527.
- Reyes, C.D., Petrie, T.A., Burns, K.L., Schwartz, Z., García, A.J., 2007. Biomolecular surface coating to enhance orthopaedic tissue healing and integration. *Biomaterials* 28 (21), 3228–3235.
- Sadtler, K., Estrellas, K., Allen, B.W., Wolf, M.T., Fan, H., Tam, A.J., Patel, C.H., Lubber, B.S., Wang, H., Wagner, K.R., Powell, J.D., Housseau, F., Pardoll, D.M., Elisseeff, J.H., 2016. Developing a pro-regenerative biomaterial scaffold microenvironment requires T helper 2 cells. *Science* 352 (6283), 366–370.
- Stamenović, D., Ingber, D.E., 2009. Tensegrity-guided self assembly: from molecules to living cells. *Soft Matter* 5 (6), 1137–1145.
- Sussman, E.M., Halpin, M.C., Muster, J., Moon, R.T., Ratner, B.D., 2014. Porous implants modulate healing and induce shifts in local macrophage polarization in the foreign body reaction. *Ann. Biomed. Eng.* 42 (7), 1508–1516.
- Vegas, A.J., Veiseh, O., Doloff, J.C., Ma, M., Tam, H.H., Bratlie, K., Li, J., Bader, A.R., Langan, E., Olejnik, K., Fenton, P., Kang, J.W., Hollister-Locke, J., Bochenek, M.A., Chiu, A., Siebert, S., Tang, K., Jhunjhunwala, S., Aresta-Dasilva, S., Dholakia, N., Thakrar, R., Vietti, T., Chen, M., Cohen, J., Siniakowicz, K., Qi, M., McGarrigle, J., Lyle, S., Harlan, D.M., Greiner, D.L., Oberholzer, J., Weir, G.C., Langer, R., Anderson, D.G., 2016. Combinatorial hydrogel library enables identification of materials that mitigate the foreign body response in primates. *Nat. Biotechnol.* 34 (3), 345–352.
- Veiseh, O., Doloff, J.C., Ma, M., Vegas, A.J., Tam, H.H., Bader, A.R., Li, J., Langan, E., Wyckoff, J., Loo, W.S., Jhunjhunwala, S., Chiu, A., Siebert, S., Tang, K., Hollister-Lock, J., Aresta-Dasilva, S., Bochenek, M., Mendoza-Elias, J., Wang, Y., Qi, M., Lavin, D.M., Chen, M., Dholakia, N., Thakrar, R., Lacik, I., Weir, G.C., Oberholzer, J., Greiner, D.L., Langer, R., Anderson, D.G., 2015. Size- and shape-dependent foreign body immune response to materials implanted in rodents and non-human primates. *Nat. Mater.* 14 (6), 643–651.
- Veiseh, O., Vegas, A.J., 2019. Domesticating the foreign body response: recent advances and applications. *Adv. Drug Deliv. Rev.* 144, 148–161.
- Vining, K.H., Mooney, D.J., 2017. Mechanical forces direct stem cell behaviour in development and regeneration. *Nat. Rev. Mol. Cell Biol.* 18 (12), 728–742.
- Williams, D.F., 1987. Definitions in biomaterials. 72. In *Progress in Biomedical Engineering*, vol. 4. Elsevier, Amsterdam, p. 72. p 72.
- Williams, D.F., 2008. On the mechanisms of biocompatibility. *Biomaterials* 29 (20), 2941–2953.
- Williams, D.F., 2011. The role of short synthetic adhesion peptides in regenerative medicine: the debate. *Biomaterials* 32 (18), 4195–4197.
- Williams, D.F., 2016. Biocompatibility pathways: biomaterials-induced sterile inflammation, mechanotransduction, and principles of biocompatibility control. *ACS Biomater. Sci. Eng.* 3 (1), 2–35.
- Wissing, T.B., Bonito, V., Bouten, C.V.C., Smits, A.I.P.M., 2017. Biomaterial-driven in situ cardiovascular tissue engineering—a multi-disciplinary perspective. *NPJ Regen Med* 2, 18 2017 16.
- Zhang, L., Cao, Z., Bai, T., Carr, L., Ella-Menye, J.-R., Irvin, C., Ratner, B.D., Jiang, S., 2013. Zwitterionic hydrogels implanted in mice resist the foreign-body reaction. *Nat. Biotechnol.* 31 (6), 553–556.
- Zhang, X.D., Williams, D.F., 2019. Definitions of biomaterials for the twenty-first century. In: *Proceedings of Conference (Chengdu, China, June 2018)*. Elsevier, Amsterdam.

2.3.3

In Vitro Assessment of Cell and Tissue Compatibility

MICHAEL F. WOLF¹, KELLY P. COLEMAN², EDWARD A. RANKIN²,
GREGORY M. LEWERENZ²

¹Medtronic, Corporate Science and Technology, Minneapolis, MN, United States

²Medtronic, Physiological Research Laboratories, Minneapolis, MN, United States

Introduction

This chapter explains how in vitro methods may be used to assess the biological safety of medical device materials. While such methods unavoidably utilize simplified systems as compared to the complex in vivo milieu, they are valuable because they provide insight into potential in vivo tissue and cellular responses. Many in vitro methods have been standardized through a global harmonization process. These standardized tests serve a key role in the biological safety evaluation of medical devices and materials. In the following pages, the scientific basis for each test is examined. Also presented are examples of special in vitro techniques developed in response to a growing shift toward devices that combine drugs or biological agents to improve therapy. It should be noted that results of in vitro tests described in this chapter are often supported with additional in vivo testing (see [Chapter 2.3.4](#)).

Background Concepts

At the cellular and molecular level, the presence of a biomaterial has the potential to perturb the local surroundings, which may impact any number of proteins, genes, pathways, molecular modules and networks, and cells. The compatibility of such perturbations—that is, the particular response of a cell or tissue to the material and vice versa—is defined by the extent to which the response is deleterious to the microenvironment or the *material*. Adding to this complexity is the wide range of tissue interfaces and types of materials used in today's medical device applications.

Exogenous chemicals found inside the body are referred to as *xenobiotics*. Any chemical leaching from a device or material falls under this definition. Thus, assessing the cellular and tissue compatibility of a device/material often involves

examination of the potential xenobiotic chemicals that it may release. Whether these released chemicals trigger an unacceptable response in the host biological microenvironment is key to determining the biological safety of the device/material.

Exogenous chemicals found inside the body are referred to as xenobiotics. Any chemical leaching from a medical device or material falls under this definition. Thus, assessing the cellular and tissue compatibility of a device/material often involves examination of the potential xenobiotic chemicals that it may release.

Chemicals that possess potentially harmful or adverse properties are referred to as *toxicants*.¹ The response to a toxicant coming from a device/material is greatly influenced not only by the material itself, but also by the type of exposure. Exposure characteristics include the *route* and *site* of exposure (e.g., brain tissue vs. subcutaneous tissue, or skin contact vs. vascular tissue contact, direct or indirect circulating blood contact), *duration of exposure* (e.g., minutes to hours vs. permanent implantation), and the potential *frequency of exposure* over the treatment period or lifetime of the host. (Contrast, for example, the exposure a patient with degenerative heart disease receives from a single prosthetic valve implant to the exposure a diabetic individual receives from insulin pump infusion lines replaced every 72 h.) *Chemical reactivity* of a toxicant is an additional key factor that will impact the degree and type of response in the host (Casarett et al., 2003). A particular reaction may occur because of an agent's chemical reactivity, or it may be due to a more specific recognition or reactivity toward a molecular structure in the biological environment. The compatibility of a chemically reactive agent depends on whether or not it elicits undesirable cell responses or damages cellular structures.

¹These are substances that are produced by, or are a by-product of, anthropogenic (manmade) activities, as opposed to toxins that are made by biological systems (Casarett et al., 2003).

TABLE 2.3.3.1 International Organization for Standardization ISO 10993 *Biological Evaluation of Medical Devices* Standard by Parts Relevant to In Vitro Tests for Cell and Tissue Compatibility

Part ^a	Title (Publication Year: Status)	Focus	In Vitro Tests for Cell and Tissue Compatibility
3	Tests for genotoxicity (G), carcinogenicity (C), and reproductive toxicity (RT) (2014)	In vitro and in vivo tests	<ul style="list-style-type: none"> • Bacterial reverse mutation assay (G) • In vitro mouse lymphoma tk assay (G) • Chromosomal aberration in mammalian cells (G) • Syrian hamster embryo cell transformation assay (C) • Balb/c 3T3 focus transformation assay (C) • Embryonic stem cell test (RT)
4	Selection of tests for interactions with blood (2017)	In vitro and in vivo tests	<ul style="list-style-type: none"> • Hemolysis • General suggestions regarding testing for thrombosis, coagulation, platelet function, hematology, and immunology
5	Tests for in vitro cytotoxicity (2009: under revision)	In vitro tests	<ul style="list-style-type: none"> • Tests on extracts <ul style="list-style-type: none"> - L929 elution test - Neutral red uptake test (in Annex) - Colony formation test (in Annex) - Methylthiazol-tetrazolium and related tests (in Annex) • Direct contact test • Indirect contact tests <ul style="list-style-type: none"> - Agar diffusion test - Filter diffusion
10	Sensitization (2010: under revision in 2019)	In vitro and in vivo tests	DPPRA, KeratinoSens, LuSens, SENS-IS, IL-18 RhE assay, EpiSensA, SenCeeTox, h-CLAT, U-SENS, IL-8 Luc assay, and GARD
13, 14, 15	Identification and quantification of degradation products from polymeric medical devices (2010); from ceramics (2001); and from metals and alloys (2000: under revision), respectively	In vitro analytical tests	Information for material characterization and toxicological risk assessment
17	Establishment of allowable limits for leachable substances (2002)		
18	Chemical characterization of materials (2005)		
19	Physicochemical, morphological, and topographical characterization of materials (2006)		
23	Tests for Irritation (new standard being finalized in 2019)	In vitro and in vivo tests	Reconstituted human epidermis assay

^aParts 1, 2, 7, 9, and 12 are general guidance documents on use of the standard, animal welfare, sterilization residuals, degradation products, and sample preparation, respectively; Parts 4, 6, 10, 11, 16, and 20 are general guidance documents on in vivo testing relevant to local effects after implantation, irritation and delayed-type hypersensitivity, toxicokinetics study of degradation products and leachables, and principles of immunotoxicity testing, respectively. Part 8 was withdrawn and does not exist.

The *degree of response* in the host in relation to the amount of material or toxicant present defines its *dose–response* relationship. This relationship is extremely important in the characterization of toxicants, as it can often depict a threshold dose below which the probability of an adverse response occurring in the host is either very low (the lowest-observed adverse effect level, or LOAEL) or not measurable (the no-observed adverse effect level, or NOAEL). This threshold dose is of key interest when studying the dose–response effect of a device material and attempting to assess its compatibility with cells and tissues. A classic example of the latter is demonstrated in the

case of porcine bioprosthetic heart valves treated with glutaraldehyde to increase biostability and durability. Here, low levels of residual glutaraldehyde may produce negative responses in in vitro tests. Nonetheless, the device itself has proven to be safe and enormously beneficial in patients with cardiac valve disease.

Assessing cell and tissue biological safety has historically been evaluated with the in vitro tests described in this chapter. The focus has been on assays for DNA damage, cytotoxicity, cell proliferation, and quantification of specific proteins recognized to be an influential component or end product of a critical pathway or event (Table 2.3.3.1).

Use of Medical Device/Biomaterial Chemical Composition and Their Extracts for Toxicological Risk Assessment and In Vitro Testing

Medical devices are primarily composed of polymers, metals, ceramics, and to a lesser extent xenograft and allograft biological tissues and molecules. Assessing the in vitro cell and tissue compatibility of these solid multidimensional and often multicomponent devices presents significant challenges. Not surprisingly, these challenges have led to the development of international standards on device or test material evaluation and sample preparation methods (ISO 10993-1:2018 and ISO 10993-12:2012, respectively).

Challenges encountered in sample preparation include: (1) how to properly bring diverse material and device test samples into a standardized and appropriate level of contact with test systems; (2) how to treat composite materials and devices; (3) how to treat degradable materials and devices; (4) how to account for potential material interactions, given the frequency of composite devices; and (5) other confounding factors. Examples of the latter include device size, supplier variability and proprietary issues, tissue contact differences, implant duration diversity, potential manufacturing residues and contamination, and varying biological responses due to individual patient genetics, age, size, sex, and disease state. For in vitro testing, a simplifying premise is that compatibility is most readily verified by focusing on the impact of chemical constituents that may potentially be released, or actually are released as intended in the case of biodegradable materials, from the device/material in vivo. For example, while most polymers used in medical devices are made from clinically proven, relatively inert, high molecular weight materials, it is their low molecular weight leachable components (i.e., residual monomers, oligomers, catalysts, processing aids, additives, and contaminants) that often present a concern. The presence and extent of such leachables depends on a host of factors, such as the source of the material, differing manufacturing processes, and the intended function of the additive(s). In addition, new chemical species may be formed during secondary manufacturing processes, such as heat treatments, irradiation, welding, and sterilization. This is why standards emphasize testing of final finished devices to ensure that test samples have undergone all manufacturing processes (including packaging and sterilization) and are truly representative of what the patient will receive.

In devices composed of inorganic materials such as metals, alloys, and ceramics, the release of metal ions (e.g., through wear debris, corrosion, or leaching) may also be a cause for concern. Once free, metal ions have the potential to form complexes with proteins and/or DNA due to their structure and/or valence state. These complexes may, in turn, disrupt a number of biological processes (ISO 10993-3:2014; Shamsi and Krantz, 2013).

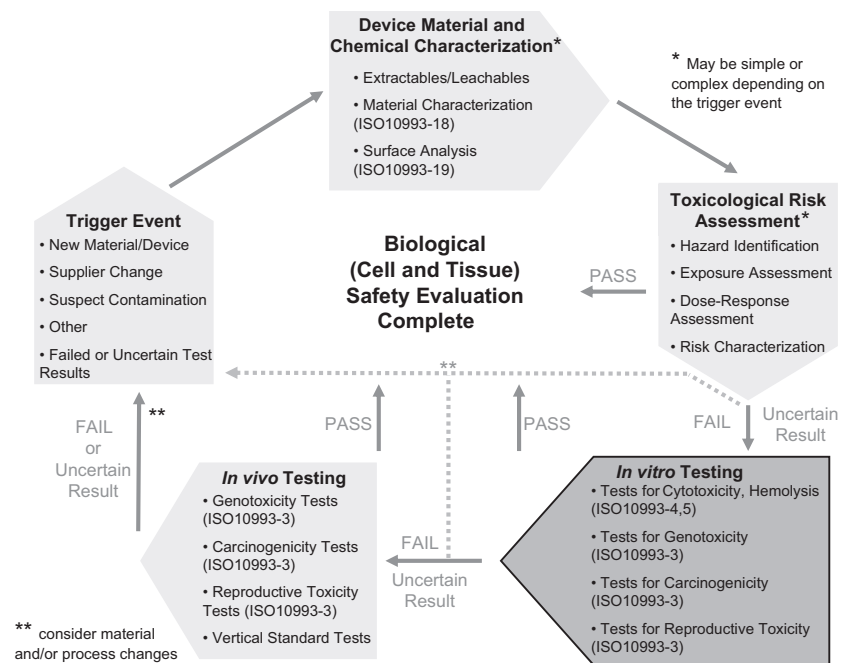
The potential toxicity of a device material is determined by a *toxicological risk assessment*. Such assessments involve: (1)

identifying hazardous chemicals present in medical devices; (2) assessing the extent of a patient's potential exposure to these chemicals; (3) determining the dose–response relationship of each chemical; and (4) combining this information to characterize the risk. Risk assessment calculations are based upon conservative worst-case exposure scenarios. Such scenarios often assume that all leachable chemical constituents will be released into the patient during the first 24 h to determine acute exposure risk, or over 31 days to determine chronic exposure risk. (In clinical practice this is unlikely to occur, but these are nevertheless common conservative assumptions designed to protect patients.) In these calculations, tolerable intakes (TIs) for chemicals of concern are determined using safe exposure level values (e.g., NOAEL or LOAEL), and uncertainty factors (UFs) to account for human genetic variation (UF₁), interspecies extrapolation from animals to humans (UF₂), and quality and relevance of the experimental data (UF₃). A margin of safety (MOS) is then calculated (TI divided by the worst-case exposure dose) to verify that exposure to the chemical of concern does not present a health risk (ISO 10993-17:2002). Supporting toxicity information is frequently found on free government websites or in proprietary commercial databases.² ISO 10993-1:2018 recommends that toxicological risk assessments be conducted as a precursor to biological testing (Fig. 2.3.3.1). The underlying rationale is that a well-thought-out and thorough risk assessment may negate the need for most or all expensive and time-consuming in vitro and in vivo biological testing.

The potential toxicity of a material is determined by a *toxicological risk assessment*. Such assessments involve: (1) identifying hazardous chemicals present in medical devices; (2) assessing the extent of a patient's potential exposure to these chemicals; (3) determining the dose–response relationship of each chemical; and (4) combining this information to characterize the risk. A well-thought-out and thorough risk assessment may negate the need for expensive and time-consuming in vitro and in vivo biological testing.

Detailed guidance for preparing in vitro testing samples is provided throughout ISO 10993 *Biological evaluation of medical devices*, Parts 1, 3, 4, 5, and 12 (ISO 10993-1:2018; ISO 10993-3:2014 Annex D, 10993-4:2017; 10993-5:2009; 10993-12:2012). Sample preparation for in vitro biological tests requires careful attention due to each test's volume and extractable percentage requirements. Extraction procedures should: (1) exaggerate the clinical conditions of use; (2) take into account the chemical characteristics of the test and control samples; (3) not cause significant changes in the physicochemical properties of the sample (e.g., degrade or dissolve the material); (4) test the device or material in its intended clinical use state (e.g., identically packaged and sterilized); (5) consider use of both a polar and a nonpolar extraction solvent to simulate the body's aqueous and lipophilic environments

²Free online sites include ToxNet, IPCS-InChem, ATSDR, ECHA, SIDS, ICE, NICNAS, and CICADS. Commercial databases include BIOSISToxicology, Toxfile, RTECS, ToxCenter, and ToxPlanet.



• **Figure 2.3.3.1** Schematic depicting the process that occurs to establish the preclinical biological safety of a medical device material. Material characterization and toxicological risk assessment precede in vitro testing for cell and tissue compatibility. In vivo testing may follow, but only if warranted based upon in vitro findings. Note: *structural alerts* refer to chemical structures of varying concern that may be linked to known toxicological mechanisms.

(Table 2.3.3.2); (6) understand potential impact to the in vitro test system; (7) be performed in chemically inert sterile closed containers; (8) be conducted for appropriate duration; and (9) be carried out at a suitable temperature, particularly when using cell culture media as an extraction vehicle. It is also mandatory to use and document the appropriate ratio of sample quantity (e.g., surface area or mass) to extract volume, the proper extract storage conditions, and proper/minimal time delay in testing samples in extractable/leachable studies.

In Vitro Assays to Assess Cell and Tissue Compatibility in Medical Device/Biomaterial Evaluation for Regulatory Purposes

The primary purpose of a preclinical biological safety evaluation of a material or device is to protect humans from potential biological risks arising from the use of the material or device (ISO 10993-1:2018). Standardizing this process safeguards consumers, but also provides industry and governments with a common and accepted scientific basis for evaluating new medical technologies. The most widely recognized guidance documents for this purpose are the ISO 10993 series of standards for the biological and clinical evaluation of medical devices developed by the International Organization for Standardization (ISO) Technical Committee 194 (for further information see <https://www.iso.org/committee/54508.html>).

Five of the ISO 10993 standards (Parts 3, 4, 5, 10, and 23) describe certain considerations and particular methodologies for in vitro assessment of material/device compatibility with cells and tissues (Table 2.3.3.1). These methods are discussed in further detail later. As benchtop material surface and chemical analytical tests focusing on the material characterization elements of the toxicological risk assessment (described earlier) are themselves indirect tests for cell and tissue compatibility, these ISO 10993 standards are included for reference (Parts 13, 14, 15, 17, 18, and 19). In addition, the in vivo approaches included in the 10993 standards, and many device-specific *vertical standards*, are also important to proper cell and tissue biocompatibility testing.

In Vitro Tests for Genotoxicity, Carcinogenicity, and Reproductive Toxicity: ISO 10993-3

Much of our understanding of cellular processes stems from the study of genetics and our ability to manipulate and characterize DNA and RNA (and the proteins they regulate). The ability to show the impact of these manipulations has been crucial as well. Such information has increased our understanding of how genetic anomalies lead to human disease and defects and has provided critical insight into the mechanisms of carcinogenesis. This awareness has also provided medical device material and component suppliers, device manufacturers, and regulatory bodies with

TABLE 2.3.3.2 In Vitro Tests Under ISO 10993 Part 3: Tests for Genotoxicity, Carcinogenicity, and Reproductive Toxicity

In vitro Test Category	Test ^a	Assay Basis	Information Gained
Genotoxicity	Bacterial reverse mutation assay (Ames test)	<i>Reverse mutation assay.</i> Small changes in prokaryotic DNA induced by a test material or extract thereof result in a quantifiable change in phenotypic expression of a target gene	Determines if a device material ^b has potential to react with DNA and cause altered DNA expression. Caveat: has potential for false positives.
Genotoxicity	In vitro mouse lymphoma tk assay	<i>Forward mutation assays</i> same as reverse mutation test above but assay utilizes a eukaryotic cell line	Same as above. Note: This test may be more predictive than tests using prokaryotic cell lines.
Genotoxicity	Chromosomal aberration	<i>Chromosome morphology analysis.</i> Quantification and categorization of mammalian cell chromosome aberrations	Determines if a device material ^b shows potential to interfere with normal DNA replication and/or division processes leading to changes in normal chromosome morphology
Carcinogenicity	Syrian hamster embryo cell transformation assays ^a	<i>Morphological transformation of normal karyotype primary cells.</i> Assay designed to mimic two-stage carcinogenesis model (initiation and promotion)	Determines if a device material ^b has potential to transform normal cells to cells with morphologies and behavior consistent with tumorigenic cells
Carcinogenicity	Balb/c 3T3 focus transformation assay ^a	<i>Macroscopic and microscopic morphological categorization of foci.</i> Assay uses immortalized aneuploid fibroblastic cell line; assay can mimic two-stage carcinogenesis model	Determines if a device material ^b has potential to transform cells into cells with morphologies consistent with tumorigenic cells; caveat: time consuming and mixed reproducibility.
Reproductive/developmental toxicity	Embryonic stem cell (ESC) test ^a	<i>Biostatistically derived, prediction-model equations</i> utilizing values for 50% inhibition of ESC differentiation, 50% inhibition of cell growth of ESC cells, and 50% inhibition of cell growth of BALB/c 3T3 cells	Determines if a device material ^b has potential to be embryotoxic (teratogenic); presumes (with its limitations) that demonstration of toxicity at this stage may be indicative of concern for impact at other stages of reproduction

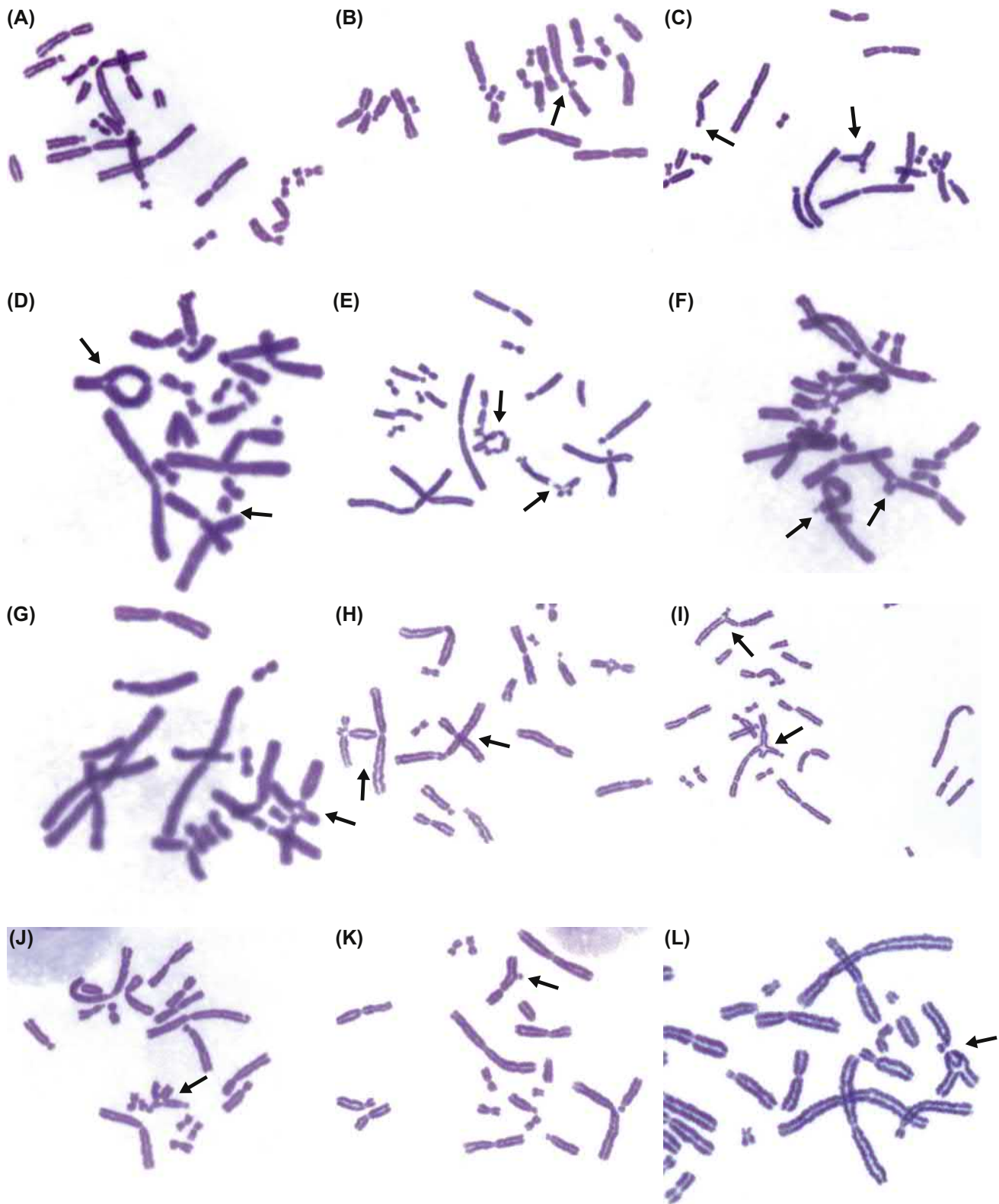
^aSee <https://www.elsevier.com/books-and-journals/book-companion/9780128161371> for assay details.

^bDevice material extract/leachable chemical(s), or a metabolic derivative(s) thereof.

increasingly sophisticated in vitro tools and standardized methods for screening materials and chemicals for potential health concerns falling under this category.

In the context of biomaterials science, genotoxicity refers to the potential of the solid device material, and/or its constituent chemicals, biodegradation products, metabolites, leachables, or contaminants, to induce a detrimental effect on DNA, or on the genetic processes of a host cell or tissue (ISO 10993-3:2014). To thoroughly screen the genotoxic potential of a new device or material, the Part 3 standard relies on well-established in vitro test methods that were modified for devices from historical Organization for Economic Cooperation and Development (OECD) guidelines for testing chemicals. These guidelines describe primary tests that look at gene mutations in prokaryote bacteria (see ISO 10993-33:2015 clause 6), cytogenetic evaluation of chromosomal damage in eukaryotic mammalian cells (i.e., chromosome aberration test [see ISO 10993-33:2015 clause 7; Fig. 2.3.3.2]), gene mutation in mouse lymphoma cells (ISO 10993-33:2015 clause 9), and formed micronuclei in human/mammalian peripheral blood lymphocytes

or certain rodent cells (see ISO 10993-33:2015 clause 8). A favored eukaryotic test is the mouse lymphoma tk assay, based on its ability to evaluate for both point mutations (ability to affect only one or a few nucleotides in a gene) and clastogenicity (inducing disruption or breakage of chromosomes leading to sections of the chromosome being deleted, added, or rearranged). These are the two main classes of genetic damage addressed in ISO 10993-3. Taken together, when each in vitro assay is negative, the results indicate a low potential for genotoxicity. When one or more of the tests give a positive result, the device or material is presumed to have a genotoxic potential. In the latter case, in vivo assays can be considered to further evaluate the genotoxicity of the device or material. The combined results of such testing can then be evaluated by weight of evidence or mode of action approaches (see ISO 10993-33:2015 clauses 10 and 11 for in vivo methods, and ISO 10993-3:2014 in general). See the Biomaterials Science textbook <https://www.elsevier.com/books-and-journals/book-companion/9780128161371> for details on the bacterial reverse mutation and chromosome aberration assays.



• **Figure 2.3.3.2** Some common chromosome aberrations seen after exposure of CHO cells to extracts from test materials and/or positive controls. (A) Normal spread; (B) chromosome break; (C) chromatid break and triradial; (D) double minute and ring; (E) complex rearrangements and many breaks; (F) complex rearrangements and triradial; (G) quadraradial; (H) quadraradials; (I) triradial; (J) quadraradial; (K) interstitial deletion; and (L) chromosomal interchange. Note: in this type of testing, chromatid gaps, isochromatid gaps, and uncoiled chromosomes are identified but are not computed in the analysis. Arrows point to each type of aberration. See <https://www.elsevier.com/books-and-journals/book-companion/9780128161371> for further details.

In the context of biomaterials science, genotoxicity refers to the potential of the solid device/material, and/or its constituent chemicals, biodegradation products, metabolites, leachables, or contaminants to cause an undesirable effect on DNA itself, or on the genetic processes of a host cell or tissue (ISO 10993-3:2014).

Along with tests for genotoxicity, carcinogenicity is also addressed in ISO 10993-3:2014. Although devices and materials indicating a genotoxic potential may be presumed to have a carcinogenic potential, a toxicological risk assessment focused on carcinogenic effects is strongly advised before proceeding to carcinogenicity testing. This is based on the predictive potential of the in vitro assays, the need to abide by stipulations in ISO 10993-1, ISO 10993-2, and ISO 10993-6 to eliminate unnecessary use of animals, and on the known mechanisms of carcinogenesis. These mechanisms have clearly shown that not all genotoxins are carcinogens, and vice versa. That is, some chemical carcinogens act through pathways that disrupt cellular metabolic processes (rather than DNA integrity) to induce uncontrolled cell division leading to tumor formation. Therefore careful consideration must be given to a material's history of safe clinical use and chemical characterization before proceeding to carcinogenicity studies.

Given the complex processes involved in carcinogenesis, standard carcinogenicity testing (when called for) requires time-consuming and costly in vivo models. As a result, several non-OECD in vitro alternatives designed to mimic stages of the complex multistep carcinogenic process have been developed for prescreening and are mentioned in the standard. The particular in vitro tests that have received the greatest attention are referred to as "cell transformation assays" (e.g., the Syrian Hamster Embryo Cell Transformation Assay and the BALB/c 3T3 Focus Transformation Assay—see the Biomaterials Science textbook <https://www.elsevier.com/books-and-journals/book-companion/9780128161371> for details). In these assays the transformed cells (resulting from exposure to test xenobiotics or device/material extracts) that have acquired the characteristics of malignant cells have also demonstrated the ability to induce tumors in susceptible animals. Other cellular features indicative of transformation to a tumorigenic phenotype include alteration of individual cell morphology, development of anchorage-independent replication, and formation of disordered patterns of colony growth.

The final topic covered in this section is reproductive and developmental toxicity. Careful review of a device's history of safe clinical use and a thorough toxicological risk assessment based on chemical characterization are necessary before in vivo or in vitro testing is considered. Here, attention is directed at the potential exposure of the material/device, or any of its constituents, to the host reproductive tissues, an embryo/fetus, or a potential nursing child. With sufficient and supportive toxicity data from absorption, distribution, metabolism, and excretion studies and the published literature, there is often no need for reproductive toxicity testing

(ISO 10993-3:2014). Furthermore, this type of testing is not required where a toxicological risk assessment has established steps to appropriately mitigate situations of reproductive and developmental toxicity concern.

Current testing for reproductive and developmental toxicology relies heavily upon established in vivo models, given the complexity of the phenomena being investigated (modified OECD standards indicated in ISO 10993-3:2014). However, a variety of alternatives to whole animal testing are becoming increasingly available. For example, the in vitro embryonic stem cell test (EST) has received particular attention due to its correlation to primary embryonic cells and whole embryos. Here, a validation study funded by the European Centre for the Validation of Alternative Methods (ECVAM) found a strong correlation between three in vitro embryotoxicity tests across a diverse group of chemicals presenting different embryotoxic potentials (ECVAM, 2009). Details of the EST test can be found on the Biomaterials Science textbook <https://www.elsevier.com/books-and-journals/book-companion/9780128161371>.

Medical devices/materials with circulating blood contact, no matter the duration, should be evaluated for reproductive/developmental toxicity, as even acute exposure to a teratogen could impact a developing fetus or embryo. In addition to blood-contacting devices, applications of concern include intrauterine devices, urinary catheters, and energy-releasing radioactive seeds used in oncology that may come into close or direct contact with reproductive tissues, an embryo, or fetus.

As discussed earlier, medical devices are typically composed of solid materials, which often must be extracted in vitro to mimic leaching that may occur in the body. The resultant extracts are often complex chemical mixtures, which are different from the single-chemical assessments upon which genotoxicity tests were developed. These complex mixtures then require several refined analytical chemistry techniques to identify specific agents of concern. In addition, analyses are further complicated by the fact that metabolic activation often plays a central role in the genotoxic potential of a material or chemical. To account for this, genotoxicity testing should include a parallel set of test extracts exposed to an in vitro metabolic activation system.³ This is done to capture chemicals called *promutagens* (compounds that are not mutagenic by themselves but may be activated into mutagens by metabolic processes). The most common activator used is the S9 fraction culled from rat livers. In the Bacterial Reverse Mutation Assay, for instance, the metabolic enzymes in prokaryotic cells differ from those of normal intact mammalian cells. Likewise, eukaryotic cells may present a metabolic deficiency or may lack normal metabolic enzymes. In vitro tests for genotoxicity, carcinogenicity, and reproductive/developmental toxicity must therefore include a mammalian

³An in vitro metabolic activation system is commonly derived from a mammalian tissue homogenate (usually liver). The most commonly employed metabolic activation system is referred to as S9. This is a standard rat liver metabolic-activating system that refers to the supernatant fraction of the homogenate obtained after a 9000g centrifugation (Malling and Frantz, 1974).

metabolic activator to detect the presence of metabolically activated promutagens and toxicants in the device extracts.

Table 2.3.3.2 briefly summarizes the *in vitro* tests for genotoxicity, carcinogenicity, and reproductive/developmental toxicity as mentioned in ISO 10993-3. Recall that the *in vitro* methods described in Table 2.3.3.2 are considered applicable *only* when the need to evaluate a medical device for potential genotoxicity, carcinogenicity, or reproductive/developmental toxicity has been established. This is determined through a toxicological risk assessment process based on material characterization data (Fig. 2.3.3.1, and ISO 10993-1, -17, and -18 [ISO/TC 194, 2018, 2002, and 2005, respectively]). When the risk assessment recommends *in vitro* testing, the limitations are that no single genotoxicity test is capable of detecting all relevant toxic agents, and that not all test methods are equally well developed or validated for the testing of medical devices or materials. Consequently, to effectively evaluate genotoxicity, a battery of tests is often performed.

The standard indicates that one prokaryotic test together with one eukaryotic test are sufficient for this initial battery.

In Vitro Tests for Interactions with Blood: ISO 10993-4

A significant proportion of today's medical devices contact blood. These devices span a variety of limited, prolonged, and permanent contact applications, and the nature of the blood contact varies widely. Important factors at the blood interface include the material, blood flow, surface area, blood anticoagulation and dilution, plus the presence of blood trauma and other tissues. Given the importance of this interface, and the range of blood-contacting device applications, this area of testing has a separate ISO 10993 standard (ISO 10993-4:2017). This subject is also given special treatment in Chapters 2.2.6 and 2.3.5. Table 2.3.3.3 identifies some of the most

TABLE 2.3.3.3 Commonly Applied In Vitro Tests by Key Category of Material/Device Compatibility With the Cellular and Protein Elements in Blood

In Vitro Test Area	Test	Assay Basis ^a	Information Gained
Thrombosis	Thrombus assessment	Assessment of extent and sites of thrombus formation using gross imaging, histology, and scanning electron microscopy	Thrombus presence may indicate material or flow-related thrombogenesis. Caveat: acute exposure and <i>in vitro</i> nature of human or animal blood studies may not give observations relevant to actual <i>in vivo</i> chronic performance.
Coagulation	Assays for coagulation proteins (examples include TAT and FPA)	<i>Enzyme-linked immunosorbent assay</i> for key coagulation factors. TAT is proportional to thrombin and FPA is proportional to fibrin.	Estimate of coagulation cascade activation. High levels may indicate extensive device or material-related thrombin activity and fibrin formation. Caveat: may also reflect surgical trauma and/or tissue injury; levels may be subject dependent; and levels are highly impacted by type and amount of anticoagulant present, such as heparin
Platelets and platelet function	Platelet counting and assays that assess platelet degranulation	<i>Electronic particle counting and enzyme-linked immunosorbent assay</i> for granule-release proteins, e.g., β TG or PF4	Estimates platelets being consumed or activated in response to a material or device. Caveat: platelet aggregation, activation and granule release are highly impacted by thrombin.
Hematology	Material-induced hemolysis Mechanical-induced hemolysis Differential cell blood count (CBC) analysis	<i>Colorimetric assay</i> for plasma-free hemoglobin (pfHb); <i>electronic particle counting</i> for CBC	pfHb indicates red blood cell damage in response to a material or device, either from extracts/leachants from the device material(s), or from physical forces from the device; CBC provides basic monitor of cell numbers
Immunology	Complement pathway activation via C3a and/or SC5b9 protein assessment	<i>Enzyme-linked immunosorbent assay</i> for key complement protein fragments	May indicate device material has potential to activate the alternative complement pathway (caveat: complement activation is surface area, surface chemistry, and anticoagulant dependent).

FPA, Fibrinopeptide A; PF4, platelet factor 4; pfHb, plasma-free hemoglobin; TAT, thrombin–antithrombin III complex; β TG, β -thromboglobulin. SC5b9 is the terminal component of the complement system. Note: TAT, FPA, β TG, PF4, and complement assays are commonly used in *in vitro* characterization studies, as well as in routine preclinical testing. Also, the meaningfulness of findings in *in vitro* studies is directly proportional to how well the *in vitro* model replicates actual clinical use conditions of blood flow and temperature, freshness of blood, device exposure surface area, anticoagulation, and other factors.

^aSamples from proper *in vitro* or *in vivo* simulated use.

commonly applied in vitro tests by the key categories of concern in material/device interaction with blood. These assays focus on evaluating the device or material for potential to bring about red blood cell damage and lysis, cause thrombosis, interact with platelets, and stimulate alternative pathway immune reactions (i.e., complement pathway activation).

Just as there are a host of unique blood-contacting considerations associated with each device application, in vitro testing for blood interaction requires unique models and carefully designed and controlled experiments. Models must be designed to mimic the conditions expected in clinical use (e.g., temperature, fresh/not aged blood (Leendert et al., 2016), blood flow, test material surface area:blood ratio (cm^2/mL blood), anticoagulant conditions, and contact duration). See also Münch et al. (2000), Tepe et al. (2002), Sinn et al. (2011), and Girdhar et al. (2018).

Despite the availability of various in vitro assays and models for characterization of materials with blood, lack of validation and questions on relevance to chronic in vivo responses have made such testing more common in acute blood exposure applications and feasibility studies, rather than as standard regulatory requirements (see Braune et al., 2013). An exception is the in vitro use of radiolabeled platelets for platelet stability studies on storage containers for transfusions (Holme et al., 1993; BEST Collaborative, 2006). Most often, a device in its final design is tested in an in vivo model, alongside a legally marketed comparator device, with a subsection of the study dedicated to specific tests or measurements that characterize blood material/device interactions.

For basic material characterization of blood interaction, the most common in vitro screening tests continue to be the direct and indirect hemolysis assays (ISO 10993-4:2017, ASTM F756). These particular assays may be viewed as special cytotoxicity tests where human or animal red blood cells are used rather than the mouse fibroblast cells used in standard cytotoxicity testing. The second most common in vitro hematological assay applied today is for complement pathway activation. Here, ELISA (enzyme-linked immunosorbent assays) for C3a and/or SC5b9 protein fragments are used to estimate a material's potential for activation of the alternative pathway complement system (see Chapter 2.2.4 of this textbook). The utility of such testing on small surface area devices is controversial because it is not certain if clinical adverse events mediated by complement activation occur on these devices.

In Vitro Tests for Cytotoxicity: ISO 10993-5

A general sequence of events is assumed to take place upon host exposure to a toxicant. First, the toxicant can remain locally or be transported systemically by a combination of active transport processes, for example, via entry into the vasculature and diffusion through tissues. The toxicant can then either: (1) alter the local biological environment causing a general molecular, organelle, cellular, or tissue/organ dysfunction, or (2) interact with specificity to a particular endogenous target molecule such as a protein, membrane component, or

DNA. Both scenarios can lead to perturbations in normal cell function and repair processes, leading to cytotoxicity.

The exposure of a single toxicant to a host presents a slightly different situation compared to exposure to a mixture of potential toxicants leaching from a medical device/material. Nevertheless, similar complex biological perturbations are believed to take place when toxicant exposure comes from a medical device material. Classic examples include chemicals that alter local pH and osmolality; solvents and detergents that disturb cell membranes and alter transmembrane gradients; elements that physically deter normal inter- or extracellular transport phenomena; chemicals that facilitate aberrant phosphorylation of proteins; xenobiotics that dysregulate electrically excitable cells; and agents that disrupt mitochondrial function (Chapter 2.3.2 of this textbook) (Gregus and Klaassen, 2003). Mediators of tissue inflammation and fibrosis, as well as agents causing necrosis and apoptosis, are other well-known examples. The phenomenon of fibrotic tissue encapsulation that is invariably associated with implanted medical devices is yet another feature that distinguishes, and potentially limits, toxicant exposure associated with device materials (Chapters 2.2.1 and 2.2.2 of this textbook).

Chemicals that possess potentially harmful or adverse properties are referred to as *toxicants*. When released from a medical device or material, toxicants can remain locally or be transported systemically by a combination of active transport processes, such as entry into the vasculature and diffusion through tissues. A toxicant can then either: (1) alter the local biological environment causing a general molecular, organelle, cellular, or tissue/organ dysfunction, or (2) interact with specificity to a particular endogenous target molecule, such as a protein, membrane component, or DNA. Both scenarios can lead to perturbations in normal cell function and repair processes leading to cytotoxicity.

Table 2.3.3.4 presents the most commonly used in vitro tests to assess medical devices or their component materials for cytotoxicity. It should be noted that these tests detect general toxicity pathways and mechanisms. Thus, the nature of the tests is not inclusive of all possible toxicity pathways. These tests have, however, demonstrated appropriate usefulness in human health risk assessment, which is the main objective of the ISO 10993 standards. As with any test, each has its limitations and criticisms. Typically, exposure is only of short duration, only a few toxicity pathways are tested, and false positives can occur. In addition, some tests utilize a subjective visual morphological scoring procedure (Fig. 2.3.3.3), whereas others use rapid analysis with colorimetric methods and numerical assessment. Finally, one should be aware that the 2009 version of ISO 10993-5 recommends quantitative cytotoxicity assessment over qualitative methods, and that quantitative methods have a more stringent pass/fail criteria. See Table 2.3.3.4 and <https://www.elsevier.com/books-and-journals/book-companion/9780128161371> for further details of each test.

**TABLE
2.3.3.4**

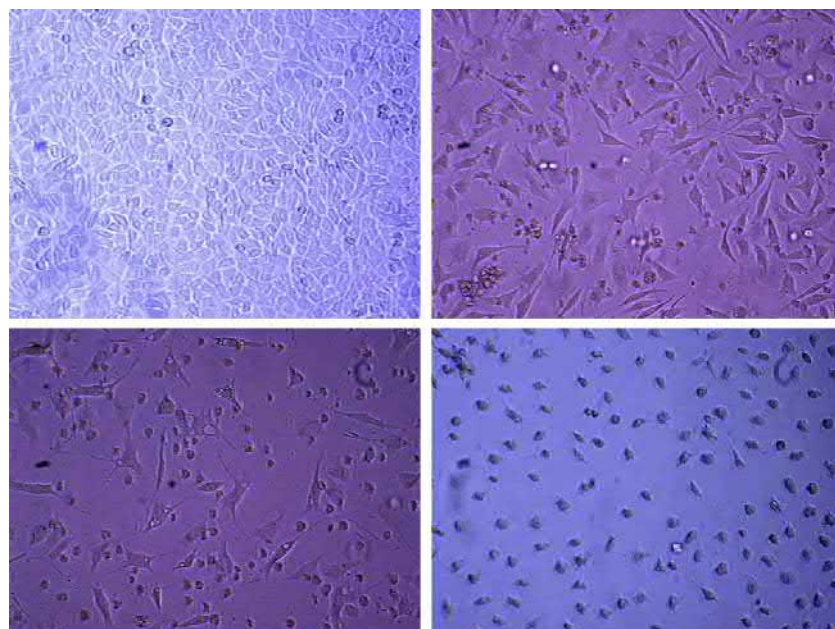
In Vitro Tests Under ISO 10993 Part 5: Tests for Cytotoxicity

Assessment	Test ^a	Assay Basis	Information Gained ^b
Qualitative	L929 elution test	<i>Light microscopy and cell morphology scoring using mouse L929 fibroblast cells.</i> Cells examined at 100× to evaluate cellular characteristics and the percent of apparent cell lysis according to a defined scoring system	Determines if a device material <i>extract</i> has potential to cause cell morphology changes and/or lysis
	Direct contact tests	<i>Light microscopy and cell morphology scoring following layering sample(s) onto mouse L929 fibroblast cell monolayers.</i> Cells examined to evaluate cellular characteristics and the percent of apparent cell lysis according to a defined scoring system.	Determines if a device material <i>itself</i> has potential to be cytotoxic. Caveat: care must be taken to avoid confounding impact of uncontrolled physical interactions.
	Indirect contact tests <i>Agar diffusion test</i> <i>Filter diffusion test</i>	Same as direct contact test but with test material physically separated from cell monolayer by a nominal 2mm agarose layer or 0.45 μm pore cellulose acetate filter paper, respectively. Same scoring system as direct contact.	Determines if a device material <i>itself</i> has potential to release agents that may be cytotoxic. Caveat: may only be relevant for leachables that can pass through agarose.
Quantitative ^c	Neutral red uptake (NRU) test	<i>Colorimetric assay of NR uptake in BALB/c 3T3 cells.</i> Neutral red (NR) acts via a noncytotoxic penetration into live cells and accumulation in intracellular lysosomes. Cells exposed to a cytotoxic xenobiotic(s) show loss of integrity and function and decreased NR uptake and binding.	Determines if a device material <i>extract</i> has potential to be cytotoxic. Numerical assessment makes NRU assay less subjective than L929 elution test.
	V79 colony formation assay	<i>Colony enumeration and calculation of plating (colony formation) efficiency using Chinese hamster lung cell (V79) culture system.</i> Plating efficiency of a test material is measured against the negative control group.	Determines if a device material <i>extract</i> has potential to be cytotoxic
	Methylthiazol-tetrazolium (MTT) and related tests	<i>Microculture tetrazolium assay (MTA).</i> Colorimetric assay using water-soluble MTT compound. Upon exposure to L929 cells, MTT is reduced enzymatically or through direct reaction with NADH or NADPH. A bright blue formazan product forms with intensity proportional to number of viable cells present.	Determines if a device material <i>extract</i> has potential to be cytotoxic. Note: other MTA tests that form similar formazan products are also used.

^aSee <https://www.elsevier.com/books-and-journals/book-companion/9780128161371> for assay details.

^bPositive results may require additional testing and justification to establish safe use.

^cCommon scoring criteria among the quantitative assessment methods determine noncytotoxicity for plating or viability values >70% of negative control. Potential cytotoxic values fall below the 70% threshold.



• **Figure 2.3.3.3** Representative light microscopic images of L929 cells in the L929 elution test. (A) and (D) represent the negative and positive controls showing no cell cytotoxicity and approximately 100% cytotoxicity, respectively. Images (B) and (C) represent approximately 50% and 80% cytotoxicity, respectively.

Application-Specific In Vitro Assays Considered in Proof-of-Concept Testing

Classically, assessing the cell or tissue compatibility of a material or device has centered on applying in vitro and in vivo methods to establish a low risk for adverse impact on the host. However, one area of biomaterials science that has been rapidly evolving is *bioactive materials*, which have been modified to impart desirable effects on certain proteins, cells, or tissues. Concepts of this nature typically target one or more specific protein, cellular, or tissue reactions recognized to play a role in how the device or material interacts with the host in a specific application. The following four case studies are intended to illustrate this point, and to show how contemporary in vitro testing technology has played a critical role in demonstrating the capacity of special composite medical device materials to improve certain cellular and tissue responses.

Classically, assessing the cell or tissue compatibility of a material or device has centered on applying in vitro and in vivo methods to establish a low risk for adverse impact on the host. Biomaterials science, however, has been rapidly evolving in the area of *bioactive materials*, which are materials that have been modified to impart desirable effects on certain proteins, cells, or tissues. Concepts of this nature typically target one or more specific protein, cellular, or tissue reactions recognized to play a role in how the device or material interacts with the host in a specific application.

Future Challenges in In Vitro Assessment of Cell and Tissue Compatibility

The task of regulatory agencies and device manufacturers is to select the appropriate combination of supporting information and testing that ensures product safety, device performance, and patient outcome. This task is becoming more complicated because of the expanding repertoire of device applications, specialty materials, and associated biological interfaces.

In light of this complexity, standard tests must be well designed, scientifically sound, and broadly applicable and predictive. As a result, preclinical safety testing faces challenges that include: (1) questions about predictive power; (2)

concerns with costs and completion times; (3) issues with the selection and design of appropriate animal models; (4) validation and acceptance of novel in vitro tests; and (5) lengthy development and approval timelines for new methods.

Thankfully, progress is being made in addressing these challenges. First, ISO 10993-1, which provides overall guidance for the biological evaluation of medical devices, was recently revised (2018). Like the previous standard, this version emphasizes that biological evaluation of medical devices or materials should follow a three-step process: (1) material characterization; (2) toxicological risk assessment; and (3) biological testing. Given the extensive information available today on medical device materials, including history of safe clinical use, the intent of the Part 1 standard is to focus on characterization and risk assessment to reduce the amount of biological testing required.

In cases where biological testing is indicated, ISO 10993-1:2018 states that validated and reliable in vitro test methods: “shall be considered for use in preference to in vivo tests,” and that: “whenever possible, in vitro screening shall be carried out before in vivo tests are commenced.” This guidance is clearly intended to minimize the use of in vivo testing.

A second area of progress involves the development of in vitro assays that are designed to replace in vivo methods. In recent years, news articles and published reports have pointed to a paradigm shift in toxicology testing involving in vitro cell-based assays (NRC, 2007; Schmidt, 2009; US EPA, 2009). In the United States, the TOX21 partnership between the Environmental Protection Agency, National Toxicology Program, National Institutes of Health, and the Food and Drug Administration is an example of this shift. TOX21 is focused on applying new scientific tools in computational, informational, and molecular science to identify and characterize chemicals on the basis of how they activate toxicity pathways inside cells (preferably of human origin). This move away from traditional whole animal toxicity testing to cell-based assays seeks to identify new mechanisms of chemical activity in cells, and to develop better predictive models of human response to toxicants. Results of these models will help regulators make more informed decisions based on actual human toxicity data instead of animal data, which is often suspect and controversial.

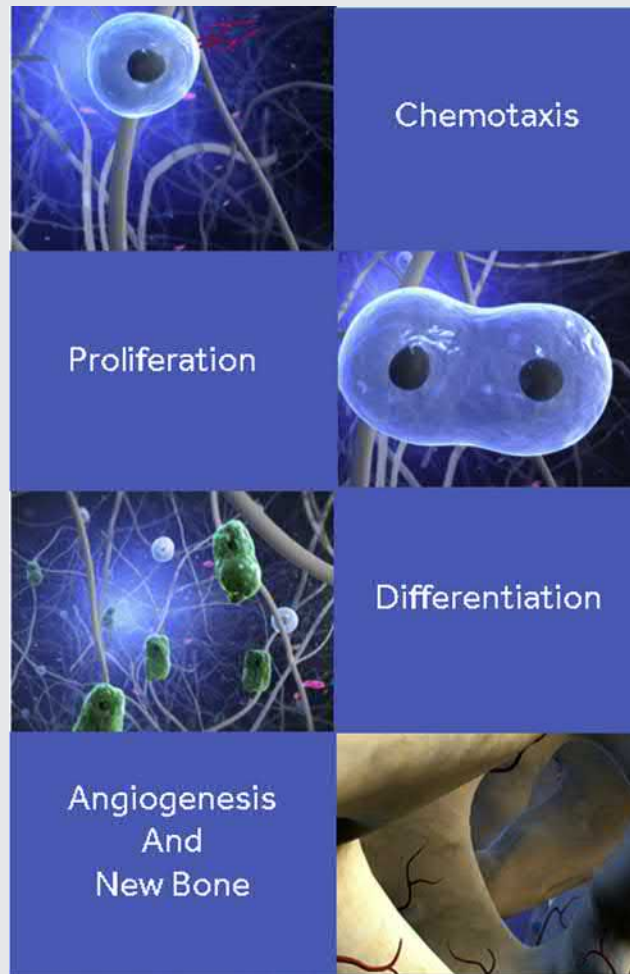
CASE 1 RECOMBINANT HUMAN BONE MORPHOGENETIC PROTEIN IN ABSORBABLE COLLAGEN SPONGE BONE GRAFTS

When bone becomes damaged through traumatic or degenerative processes, one form of therapy involves replacement of the compromised area with bone graft material. Autologous tissue is a common choice, with iliac crest bone the preferred material given its availability and degree of cellularity, which favors healing. Unfortunately, harvesting this bone graft often results in postoperative pain and increased morbidity. To reduce these complications, avoiding the use of iliac crest bone has become more common. Other graft options, such as local bone harvested during the surgical procedure, have been supplemented with either synthetic calcium phosphate ceramics or demineralized allograft bone. However, the quantity of local bone graft available is often limited and contains fewer live cells compared to iliac crest bone (Dempster et al., 1993).

Osteoinductive factors isolated from demineralized bone matrix (Urist and Strates, 1971), now known as bone morphogenetic proteins (BMPs), provide an alternative to autologous bone graft. When the human BMP-2 protein was recombinantly manufactured (recombinant human bone morphogenetic protein or rhBMP-2) and delivered on an absorbable collagen sponge (ACS) scaffold, it was found to induce new bone formation. This was first demonstrated using simple in vitro tests to gauge the bioactivity of the material. In demonstrating chemotactic properties, in vitro studies showed that rhBMP-2 stimulated specific chemotactic migration of bone-forming cells (Lind et al., 1996; Fiedler et al., 2002). In vitro studies also showed that rhBMP-2 could increase the proliferation of several pluripotent cell lines, which are capable of differentiating

(Continued)

CASE 1 RECOMBINANT HUMAN BONE MORPHOGENETIC PROTEIN IN ABSORBABLE COLLAGEN SPONGE BONE GRAFTS—CONT'D



• **Figure 2.3.3.4** Schematic showing the primary cell influences of bone morphogenetic protein (chemotaxis, proliferation, and differentiation) that together lead to angiogenesis and new trabecular bone generation.

into osteoblasts (Yamaguchi et al., 1991; Mayer et al., 1996; Puleo, 1997; Wilke et al., 2001; Akino et al., 2003). In addition, in vitro studies of rhBMP-2 demonstrated that rhBMP-2 binds to specific receptors on the surface of certain stem cells (e.g., mesenchymal stem cells), and causes them to differentiate into bone-forming cells (Schmitt et al., 1999; Wilke et al., 2001). Furthermore, rhBMP-2 indirectly stimulates angiogenesis through this increased availability of osteoblasts that secrete vascular endothelial growth factor (Deckers et al., 2002; Grosso et al., 2017). Together, these studies showed the crucial role

that BMP could have on new bone growth. Today, given the capacity of rhBMP-2 to induce alkaline phosphatase (AP) activity (Cheng et al., 2003; Luu et al., 2007), an in vitro AP activity test has been developed for quality control assessment of commercial product. This test uses controlled exposures of rhBMP-2 to the W20-17 bone marrow stromal cell line in combination with the synthetic AP substrate *p*-nitrophenol phosphate to assess inductive capacity. Clinically, rhBMP-2 combined with ACS is now used as an effective substitute to autologous bone in certain bone graft procedures (Fig. 2.3.3.4).

CASE 2 HEPARIN COATINGS IN BLOOD-CONTACTING MEDICAL DEVICE APPLICATIONS

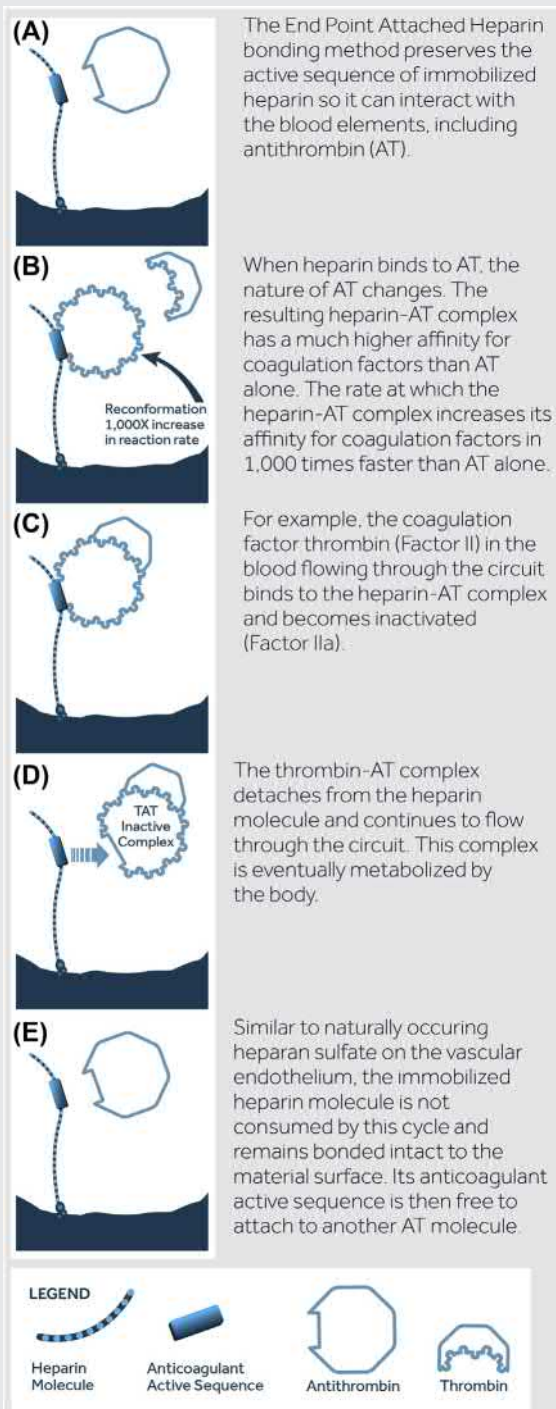
Recognizing that processes associated with coagulation play a major role in adverse events observed with blood-contacting devices, material scientists have focused on ways materials can be made to better mimic the hemostatic properties of native endothelium—the special cellular lining of the entire vasculature. One early observation was that endothelial cell surfaces have high negative charges, and this characteristic may impart a portion of their hemostatic properties (i.e., by repelling the negatively charged platelets) (Coleman, 2000). In addition, it was observed that *heparan* sulfate, a proteoglycan that is structurally and functionally similar to the anticoagulant heparin, is naturally present across the cell surface of vascular endothelium (Olsson et al., 2000). These molecules are chemically linked to the surface of endothelial cells in a manner that exposes the polysaccharide chains to protein molecules in blood. One particular

plasma protein, the serine protease inhibitor called antithrombin (AT), upon binding to a specific chemical sequence on the heparan sulfate molecule, develops a high specificity for deactivating key proteins in the coagulation process, namely thrombin and factor Xa (Marcum et al., 1984; Coleman, 2000). This is precisely the mechanism of action of heparin itself, a polysaccharide that is not naturally found in the circulatory system, but rather is ubiquitously present in connective tissue. Here, heparin binds to AT at a unique binding site; the AT molecular configuration is altered, increasing the rate of enzyme–inhibitor complex formation by a factor of 1000 or more (Rosenberg et al., 2001); then, the enzyme–inhibitor complex detaches from heparin leaving it available to interact with other AT molecules (Olsson et al., 2000). Heparin is not consumed in this process, but rather acts as a catalyst (Fig. 2.3.3.5).

CASE 2 HEPARIN COATINGS IN BLOOD-CONTACTING MEDICAL DEVICE APPLICATIONS—CONT'D

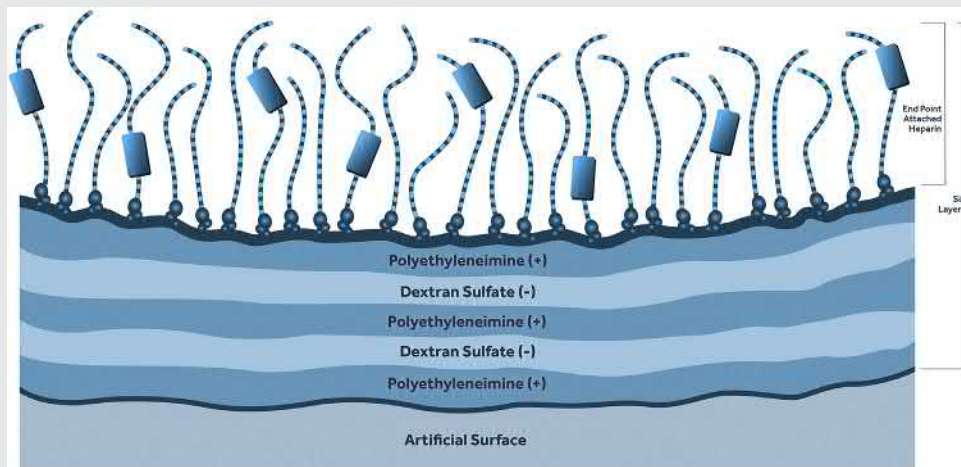
Pioneering work by [Larm et al. \(1983\)](#) first described a method of attaching heparin to solid materials through reactive aldehyde groups present at the ends of heparin molecules. Using this approach, the immobilized heparin mimics the orientation of

the heparan sulfate molecule on the vascular endothelium, with heparin's active sequence exposed and available to interact with blood elements. Importantly, the active AT binding region does not become involved in the surface attachment chemistry ([Fig. 2.3.3.6](#)).



• **Figure 2.3.3.5** (A) Heparin attached to a solid material is oriented so that its active sequence can interact with the blood elements. (B) When heparin binds to antithrombin (AT), its tertiary structure changes resulting in a heparin-AT complex that has a much greater affinity for coagulation factors than AT alone. The heparin-AT complex has a 1000-fold increased affinity for interaction with thrombin compared to AT alone. (C) For example, an active coagulation factor, Factor IIa (thrombin), in the blood flowing past the material binds to the heparin-AT complex and becomes inactivated. (D) The thrombin-AT complex detaches from the heparin molecule and is eventually metabolized by the body. (E) Similar to naturally occurring heparan sulfate on the vascular endothelium, immobilized heparin is not consumed by this cycle and remains available to attach to other AT molecules.

CASE 2 HEPARIN COATINGS IN BLOOD-CONTACTING MEDICAL DEVICE APPLICATIONS—CONT'D



• **Figure 2.3.3.6** Attachment of heparin to material surfaces uses a stable covalent bond to the end of the molecule and orients the heparin so that its anticoagulant active sequence is free to interaction with the blood.

Numerous *in vitro* approaches have been applied to establish the hematologic compatibility of such heparin-modified surfaces. The starting approach, however, is a demonstration in an *in vitro* system that the immobilized heparin applied to the surface retains its intended biological activity. Here, heparin-coated materials or devices are first exposed to an excess of AT. This saturates the AT binding sites on the immobilized heparin. The uptake of this biologically active inhibitor is then quantified by subsequent exposure to a known quantity of active thrombin. Assessment

of residual thrombin activity using a synthetic chromogenic substrate (e.g., S2238 or rhodamine 110, bis- $[\beta$ -tosyl-L-glycyl-L-prolyl-L-arginine amide]) and analysis using a kinetic microplate reader completes the test. Immobilized heparin bioactivity is reported in international units of thrombin (T) deactivated per square centimeter of test material (IUT_{deac}/cm^2). Using this particular *in vitro* analysis, specific heparin activity can be measured on the various material components in cardiopulmonary bypass equipment that are coated with immobilized heparin.

In light of the detailed information available today on medical device materials, often including extensive histories of clinical use, the ISO 10993-1 standard calls for evaluation of medical devices or materials to follow a three-step process: (1) material characterization; (2) toxicological risk assessment; and (3) biological testing. In the latter area, *in vivo* testing remains critical. However, technology and regulations are driving a move away from traditional whole animal toxicity models toward cell-based assays that identify actual mechanisms of chemical activity in cells. This, in turn, will lead to development of better predictive models of human response to toxicants. Results of these models will help regulators make more informed decisions based on actual human toxicity data instead of animal data, which is often suspect and controversial.

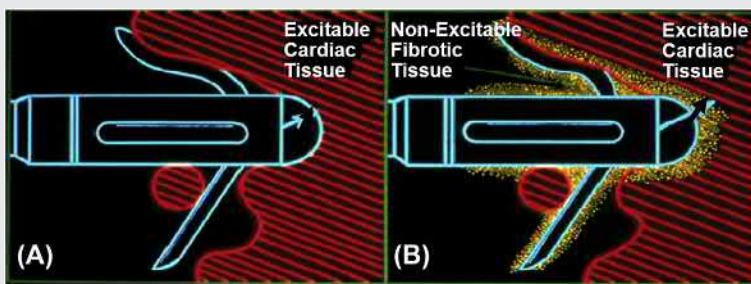
The ECVAM is one of the key leaders driving the development of *in vitro* methods. Over the past 20 years, ECVAM has validated or endorsed a variety of alternative methods. These include the EST for embryotoxicity, the reduced Local Lymph Node Assay for skin sensitization, the EpiSkin, EpiDerm, and SkinEthic RHE *in vitro* assays for skin irritation, the human Cell Line Activation Test, KeratinoSens assay, Direct Peptide Reactivity Assay, U937 cell line activation test (U-SENS), and the LuSens assay for assessing skin sensitization, plus the EpiOcular and SkinEthic HCE eye irritation tests (Spielmann et al., 2007; Grindon et al., 2008a,b; also see ECVAM's website: <https://ec.europa.eu/jrc/en/eurl/ecvam>).

Other governmental organizations dedicated to the validation of alternative methods include the Interagency Coordinating Committee on the Validation of Alternative Methods in the United States, the Japanese Center for the Validation of Alternative Methods, the Korean Center for the Validation of Alternative Methods, and the Canadian Centre for Validation of Alternative Methods. These groups are all part of a global consortium known as the International Cooperation on Alternative Test Methods, which seeks to expand and strengthen cooperation, collaboration, and communications among national validation organizations on the scientific validation and evaluation of new alternative testing methods proposed for regulatory health and safety assessments (ICATM, 2009).

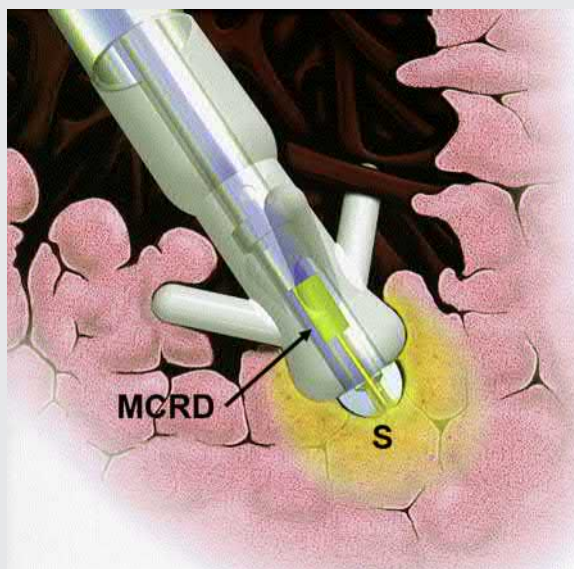
Efforts by these governmental organizations, along with work in academia and industry, will lead to the development and adoption of more sensitive and predictive human cell-based *in vitro* tests designed to replace *in vivo* methods (Basketter, 2008; Natsch and Emter, 2008).

For instance, in the medical device industry an idea has recently emerged concerning the most common *in vivo* tests in the ISO 10993 series: irritation and sensitization (ISO 10993-10:2010); systemic toxicity (ISO 10993-11:2017); material-mediated pyrogenicity (ISO 10993-11:2017); along with hemolysis and thrombogenicity (ISO 10993-4:2017). Replacing all of these tests with validated and reliable *in vitro* methods is being termed the "In Vitro Six-Pack" (Table 2.3.3.1). For example, the rabbit intracutaneous irritation assay will be replaced by reconstructed human epidermal assays (to that end

CASE 3 STEROID-ELUTING ELECTRODES IN PACEMAKER APPLICATIONS



• **Figure 2.3.3.7** Cross-section of typical tissue response at the interface of a cardiac pacing lead electrode and endocardial tissue: (A) immediately at implantation and (B) after 8 or more weeks after implantation. Nonelectrically excitable fibrotic tissue is seen around the electrode.



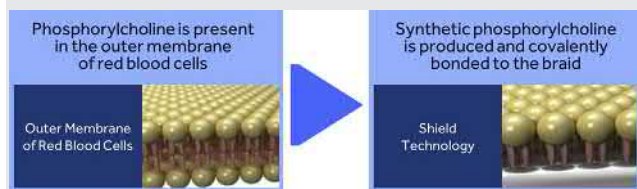
• **Figure 2.3.3.8** Depiction of a tined steroid-eluting pacing lead electrode positioned against cardiac tissue. The yellow zone represents steroid (S) eluting into the local tissue from a monolithic controlled release device (MCRD) consisting of drug in a silicone matrix.

One problem of early lead electrodes used in cardiac pacing was that the pacing threshold often increased over time. *Pacing threshold* is the minimum voltage that the electrode needs to deliver to cardiac tissue to consistently depolarize/excite the muscle into contraction. An increase in this threshold can cause pacing failure and/or escalate energy consumption on the battery—a factor that can ultimately reduce the longevity of the implanted device. Such an increase in pacing threshold was found to be associated with the inflammatory reaction at the electrode tip insertion site (Timmis et al., 1983; Benditt et al., 1989). It is the inflammatory response-induced tissue capsule formed around the electrode that results in an increase in impedance at the electrode–tissue interface (Fig. 2.3.3.7). To mitigate this problem a process for delivering antiinflammatory steroid drugs from the electrode tip was developed (Fig. 2.3.3.8). Through gradual elution, the steroid mitigates the foreign-body response at the electrode tip, and results in a minimal-to-zero threshold rise as a function of implant time (Benditt et al., 1989). Here, the drug-imparted control of the cell and tissue response at the minute tip of the pacing device

mitigates a deleterious response that shortens device life and triggers less accurate sensing.

A critical development in this technology was demonstrating an appropriate and nontoxic level of steroid delivered to the cardiac cells and tissues. To examine the delivery rate and prove this point, in vitro elution studies were conducted on test electrodes immersed in fresh pooled human plasma agitated at 37°C. Here the elution rate was seen to follow an exponential function that, when analyzed graphically, displayed a bimodal relationship. This is explained by considering the origin and path the steroid must follow to reach the tissue. Initially, steroid within the electrode pores and on the surface of the silicone-based monolithic controlled-release device (MCRD “plug”) located in the lead tip readily dissolves and diffuses across a concentration gradient to the host tissue. Then, upon acclimation to exposure to the blood plasma and moisture penetration into the MCRD, additional dissolved steroid from within the MCRD faces the extra barrier of passing through the silicone matrix. Importantly, throughout the elution time course, the amount of steroid released remains lower than the threshold of toxicological concern for the targeted patient population.

CASE 4 BIOMATERIAL SURFACE MADE TO RESEMBLE A CELL PHOSPHOLIPID BILAYER



• **Figure 2.3.3.9** Phosphorylcholine (PC) is present in the outer layer of the cell phospholipid bilayer of all cells, such as red blood cells. PC coating technology such as the Shield Technology presents the PC head groups on the blood-contacting surface of a device, thus mimicking the natural cell phospholipid membrane.

Phosphorylcholine (PC) is present in the outer layer of the cell phospholipid bilayer (Fig. 2.3.3.9, left). Due to its favorable biomimetic properties, PC has been attractive as a coating

on vascular devices such as stents to improve material thrombogenicity (Wijns et al., 2014). In one application involving an intraluminal flow diverter device for intracranial aneurysm treatment, covalent attachment of synthetic PC to the metallic surface (Fig. 2.3.3.9, right) results in a uniform atomic level (~3 nm thick) of PC on the surface. The reduction in material thrombogenicity due to the PC was subsequently confirmed in several in vitro studies with significant reduction in thrombus accumulation on the device together with thrombin generation and platelet activation measurements comparable to negative controls (Girdhar et al., 2015, 2018). Importantly, in vivo studies with direct visualization of the thrombus on the device (Clarencon et al., 2018) have corroborated these findings, along with an ex vivo shunt study in a nonhuman primate model that demonstrated the reduction in thrombogenicity with covalently bound PC to be similar to that obtained on the uncoated device in the presence of an antiplatelet drug (Hagen et al., 2017).

a new ISO 10993-23 standard has been developed that includes this in vitro irritation test) (De Jong et al., 2018), while the guinea pig maximization test for sensitization may be replaced with assays that measure certain marker genes. In addition, the US National Toxicology Program is actively evaluating for quantitative structure–activity relationship alternatives to the rodent acute systemic toxicity test. Plus, as a replacement for the rabbit pyrogenicity test, the monocyte activation test, may soon be validated for use in evaluating medical devices and materials for endotoxin and nonendotoxin-induced pyrogenicity. Also, testing labs have begun adapting the ASTM F756 hemolysis test for use with human blood rather than rabbit blood. Furthermore, as a replacement for the canine thrombogenicity test, experts have been developing simple and dynamic flow in vitro loop models using human blood to assess thrombogenicity risks from devices and materials (Münch et al., 2000; Tepe et al., 2002; Sinn et al., 2011; and Girdhar et al., 2015, 2018).

Lastly, as the ISO 10993 standards have been revised, they have recognized new bioanalytical techniques. One example is the inclusion of the methylthiazol-tetrazolium assay in ISO 10993-5 as a supplement or replacement for traditional categorical assessment cytotoxicity analysis. Also, ELISA assays for measuring factors indicative of material-related coagulation and thrombosis are more officially recognized (ISO 10993-4:2017).

Summary Remarks

This chapter has focused on current in vitro methods used to evaluate the biological compatibility of medical devices and materials. The methods were presented from two perspectives: (1) in vitro assays that are accepted internationally for preclinical biological safety evaluations and risk assessments, and (2) specialized material- and application-specific in vitro assays designed for certain cell and tissue responses. As the latter area is complex and growing at a pace that is much faster than typical method standardization, some contemporary case examples were presented that reflect this additional and increasingly

important type of in vitro test. These cases demonstrate that specifically designed in vitro assays have proven to be critical in moving new medical device therapies into clinical practice.

Today, materials in new device concepts do not often go through an *early* evaluation using the ISO 10993 process. Instead, engineers and material scientists often use other types of tests in proof-of-concept in vitro studies, in which the majority of device prototypes use well-characterized biocompatible materials with long histories of safe use. This approach is driven by the desire to bring new therapies to the market quickly, using new technologies that improve device performance via promoting improved cell and tissue interaction properties.

As the range of medical device materials and applications expands, the challenges faced by product engineers, materials scientists, regulatory agencies, and standards developers will certainly grow. Nevertheless, progress will no doubt continue to be made in the development and application of in vitro assays to support new therapies, improved medical materials, and advances in patient care.

References

- Akino, K., Mineta, T., Fukui, M., Fujii, T., Akita, S., 2003. Bone morphogenetic protein-2 regulates proliferation of human mesenchymal stem cells. *Wound Repair Regen.* 11, 354–360.
- ASTM F756, 2017. Standard practice for assessment of hemolytic properties of materials. *Am. Soc. Test. Mater* 13(1), 1–6.
- Basketter, D.A., 2008. Nonanimal alternatives for skin sensitization: a step forward? *Toxicol. Sci.* 102, 1–2.
- Benditt, D.G., Kriett, J.M., Ryberg, C., Gornick, C.C., Stokes, K.L., et al., 1989. Cellular electrophysiologic effects of dexamethasone sodium phosphate: implications for cardiac stimulation with steroid-eluting electrodes. *Int. J. Cardiol.* 22, 67–73.
- BEST, Collaborative, 2006. Platelet radiolabelling procedure: the biomedical excellence for safer transfusion (BEST) collaborative. *Transfusion* 46 (Suppl. 1), 59–66.
- Braune, S., Grunze, M., Straub, A., Jung, F., 2013. Are there sufficient standards for the in vitro hemocompatibility testing of biomaterials? *Biointerphases* 8, 33.

- Casarett, L.J., Klaassen, C.D., Watkins, J.B., 2003. Casarett and Doull's Essentials of Toxicology. McGraw-Hill/Medical Pub. Div, New York, NY.
- Cheng, H., Jiang, W., Phillips, F.M., Haydon, R.C., Peng, Y., et al., 2003. Osteogenic activity of the fourteen types of human bone morphogenetic proteins (BMPs). *J. Bone Joint Surg. Am.* 85-A, 1544–1552.
- Clarencon, F., Tamura, T., Wainwright, J.M., Gounis, M.J., Marosfoi, M., Puri, A.S., Marosfoi, M., Clarencon, F., Langan, E.T., King, R.M., et al., 2018. Acute thrombus formation on phosphorilcholine surface modified flow diverters. *J. Neurointerventional Surg.* 10 (4), 406–411.
- Coleman, R., 2000. Overview of hemostasis. In: Coleman, R., Clowes, A., George, J., Hirsh, J., Marder, V. (Eds.), *Hemostasis and Thrombosis: Basic Principles and Clinical Practice*, fourth ed. Lippincott Williams & Wilkins, Philadelphia, PA.
- Deckers, M.M., van Bezooijen, R.L., van der Horst, G., Hoogendam, J., van Der Bent, C., Papapoulos, S.E., Löwik, C.W., 2002. Bone morphogenetic proteins stimulate angiogenesis through osteoblast-derived vascular endothelial growth factor A. *Endocrinology* 143 (4), 1545–1553.
- Dempster, D.W., Ferguson-Pell, M.W., Mellish, R.W., Cochran, G.V., Xie, F., Fey, C., Horbert, W., Parisien, M., Lindsay, R., 1993. Relationships between bone structure in the iliac crest and bone structure and strength in the lumbar spine. *Osteoporos. Int.* 3 (2), 90–96.
- De Jong, W.H., Hoffmann, S., Lee, M., Kandárová, H., Pellevoisin, C., Haishima, Y., Rollins, B., Zdawczyk, A., Willoughby, J., Bachelor, M., Schatz, T., Skoog, S., Parker, S., Sawyer, A., Pescio, P., Fant, K., Kim, K.M., Kwon, J.S., Gehrke, H., Hofman-Hüther, H., Meloni, M., Julius, C., Briotet, D., Letasiova, S., Kato, R., Miyajima, A., De La Fonteyne, L.J.J., Videau, C., Tornier, C., Turley, A.P., Christiano, N., Rollins, T.S., Coleman, K.P., 2018. Round robin study to evaluate the reconstructed human epidermis (RhE) model as an in vitro skin irritation test for detection of irritant activity in medical device extracts. *Toxicol. In Vitro* 50, 439–449.
- ECVAM, 2009. European commission joint research centre. In: Institute for Health and Consumer Protection (IHCP) of the Joint Research Centre (JRC). European Centre for the Validation of Alternative Methods, Ispra, Italy.
- Fiedler, J., Roderer, G., Gunther, K.P., Brenner, R.E., 2002. BMP-2, BMP-4, and PDGF-bb stimulate chemotactic migration of primary human mesenchymal progenitor cells. *J. Cell. Biochem.* 87, 305–312.
- Genschow, E., Speilmann, H., et al., 2002. The ECVAM international validation study on in vitro embryotoxicity tests: results of the definitive phase and evaluation of prediction models. European centre for the validation of alternative methods. *Altern. Lab. Anim.* 30, 151–176.
- Girdhar, G., Li, J., Kostousov, L., Wainwright, J., Chandler, W.L., 2015. In-vitro thrombogenicity assessment of flow diversion and aneurysm bridging devices. *J. Thromb. Thrombolysis* 40 (4), 437–443.
- Girdhar, G., Andersen, A., Pangerl, E., Jahanbekam, R., Ubl, S., Nguyen, K., Wainwright, J., Wolf, M.F., 2018. Thrombogenicity assessment of Pipeline Flex, Pipeline Shield, and FRED flow diverters in an in vitro human blood physiological flow loop model. *J. Biomed. Mater. Res. A.* <https://doi.org/10.1002/jbm.a.36514>. wileyonlinelibrary.com.
- Gregus, Z., Klaassen, C.D., 2003. Mechanisms of toxicity. In: Klaassen, C.D., Watkins, J.B. (Eds.), *Essentials of Toxicity*. McGraw-Hill, New York, NY.
- Grindon, C., Combes, R., Cronin, M.T., Roberts, D.W., Garrod, J.F., 2008a. Integrated decision-tree testing strategies for skin corrosion and irritation with respect to the requirements of the EU REACH legislation. *Altern. Lab. Anim.* 36 (Suppl. 1), 65–74.
- Grindon, C., Combes, R., Cronin, M.T., Roberts, D.W., Garrod, J.F., 2008b. Integrated decision-tree testing strategy for skin sensitization with respect to the requirements of the EU REACH legislation. *Altern. Lab. Anim.* 36 (Suppl. 1), 75–89.
- Grosso, A., Burger, M.G., Lunger, A., Schaefer, D.J., Banfi, A., Di Maggio, N., 2017. It takes two to tango: coupling of angiogenesis and osteogenesis for bone regeneration. *Bioeng. Biotechnol.* 5, 68.
- Hagen, M.W., Girdhar, G., Wainwright, J., Hinds, M.T., 2017. Thrombogenicity of flow diverters in an ex vivo shunt model: effect of phosphorylcholine surface modification. *J. Neurointerventional Surg.* 9 (10), 1006–1011.
- Holme, S., Heaton, A., Roodt, J., 1993. Concurrent label method with ¹¹¹In and ⁵¹Cr allows accurate evaluation of platelet viability of stored concentrates. *Br. J. Haematol.* 84, 717–723.
- ICATM, 2009. Memorandum of Cooperation on International Cooperation on Alternative Test Methods (ICATM). http://iccva.m.niehs.nih.gov/docs/about_docs/ICATM-MOC.pdf.
- ISO 10993-1, 2018. Biological Evaluation of Medical Devices – Part 1: Evaluation and Testing. International Organization for Standardization, Geneva, Switzerland.
- ISO 10993-3, 2014. Biological Evaluation of Medical Devices – Part 3: Tests for Genotoxicity, Carcinogenicity and Reproductive Toxicity. International Organization for Standardization, Geneva, Switzerland.
- ISO 10993-4, 2017. Biological Evaluation of Medical Devices – Part 4: Selection of Tests for Interactions with Blood. International Organization for Standardization, Geneva, Switzerland.
- ISO 10993-5, 2009. Biological Evaluation of Medical Devices – Part 5: Tests for in Vitro Cytotoxicity. International Organization for Standardization, Geneva, Switzerland.
- ISO 10993-12, 2012. Biological Evaluation of Medical Devices – Part 12: Sample Preparation and Reference Materials. International Organization for Standardization, Geneva, Switzerland.
- ISO 10993-17, 2002. Biological Evaluation of Medical Devices – Part 17: Establishment of Allowable Limits for Leachable Substances. International Organization for Standardization, Geneva, Switzerland.
- ISO, 2009. International Standards for Business. Government and Society: International Organization for Standardization. <http://www.iso.org/iso/home.htm>.
- ISO/TC 194, 2004. TC 194: Biological Evaluation of Medical Devices – Business Plan. International Organization for Standardization, Geneva, Switzerland.
- Larm, O., Larsson, R., Olsson, P., 1983. A new non-thrombogenic surface prepared by selective covalent binding of heparin via a modified reducing terminal residue. *Biomater. Med. Devices Artif. Organs* 11, 161–173.
- Leendert, S., Blok, J., Engels, G.E., van Oeveren, W., 2016. In vitro hemocompatibility testing: the importance of fresh blood. *Biointerphases* 11, 029802. <https://doi.org/10.1116/1.4941850>.
- Lind, M., Eriksen, E.F., Bunger, C., 1996. Bone morphogenetic protein-2 but not bone morphogenetic protein-4 and -6 stimulates chemotactic migration of human osteoblasts, human marrow osteoblasts, and U2-OS cells. *Bone* 18, 53–57.
- Luu, H.H., Song, W.X., Luo, X., Manning, D., Luo, J., et al., 2007. Distinct roles of bone morphogenetic proteins in osteogenic differentiation of mesenchymal stem cells. *J. Orthop. Res.* 25, 665–677.
- Malling, H.V., Frantz, C.N., 1974. Metabolic activation of dimethylnitrosamine and diethyl-nitrosamine to mutagens. *Mutat. Res.* 25, 179–186.

- Marcum, J.A., McKenney, J.B., Rosenberg, R.D., 1984. Acceleration of thrombin-antithrombin complex formation in rat hindquarters via heparin like molecules bound to the endothelium. *J. Clin. Investig.* 74, 341–350.
- Mayer, H., Scutt, A.M., Ankenbauer, T., 1996. Subtle differences in the mitogenic effects of recombinant human bone morphogenetic proteins -2 to -7 on DNA synthesis on primary bone-forming cells and identification of BMP-2/4 receptor. *Calcif. Tissue Int.* 58, 249–255.
- Münch, K., Wolf, M.F., Fogt, E.J., Schroeder, P., Bergan, M., et al., 2000. Use of simple and complex in vitro models for multiparameter characterization of human blood-material/device interactions. *J. Biomater. Sci. Polym. Ed.* 11, 1147–1163.
- Natsch, A., Emter, R., 2008. Skin sensitizers induce antioxidant response element dependent genes: application to the in vitro testing of the sensitization potential of chemicals. *Toxicol. Sci.* 102, 110–119.
- NRC, 2007. Toxicity testing in the 21st century: a vision and a strategy. In: Committee on Toxicity Testing and Assessment of Environmental Agents: National Research Council & U.S. Environmental Protection Agency, The National Academies Press. The National Academies Press.
- Olsson, P., Sanchez, J., Mollnes, T.E., Riesenfeld, J., 2000. On the blood compatibility of end-point immobilized heparin. *J. Biomater. Sci. Polym. Ed.* 11, 1261–1273.
- Puleo, D.A., 1997. Dependence of mesenchymal cell responses on duration of exposure to bone morphogenetic protein-2 in vitro. *J. Cell. Physiol.* 173, 93–101.
- Rosenberg, R., Edelberg, J., Zhang, L., 2001. The heparin/antithrombin system: a natural anticoagulant mechanism. In: Coleman, R., Clowes, A., George, J., Hirsh, J., Marder, V. (Eds.), *Hemostasis and Thrombosis: Basic Principles and Clinical Practice*, fourth ed. Lippincott Williams & Wilkins, Philadelphia, PA.
- Schmidt, C.W., 2009. Tox 21: new dimensions of toxicity testing. *Environ. Health Perspect.* 117, A348–A353.
- Schmitt, J.M., Hwang, K., Winn, S.R., Hollinger, J.O., 1999. Bone morphogenetic proteins: an update on basic biology and clinical relevance. *J. Orthop. Res.* 17, 269–278.
- Shamsi, M.H., Kraatz, H.-B., 2013. Interactions of metal ions with DNA and some applications. *J. Inorg. Organomet. Polym. Mater.* 23, 4–23.
- Spielmann, H., Hoffmann, S., Liebsch, M., Botham, P., Fentem, J.H., et al., 2007. The ECVAM international validation study on in vitro tests for acute skin irritation: report on the validity of the EPISKIN and EpiDerm assays and on the skin integrity function test. *Altern. Lab. Anim.* 35, 559–601.
- Sinn, S., Scheuermann, T., Deichelbohrer, S., Ziemer, G., Wendel, H.P., 2011. A novel in vitro model for preclinical testing of the hemocompatibility of intravascular stents according to ISO 10993-4. *J. Mater. Sci. Mater. Med.* 22 (6), 1521–1528.
- Tepe, G., Wendel, H.P., Khorchidi, S., Schmehl, J., Wiskirchen, J., Pusich, B., Claussen, C.D., Duda, S.H., 2002. Thrombogenicity of various endovascularstent types: an in vitro evaluation. *J. Vasc. Interv. Radiol.* 13 (10), 1029–1035.
- Timmis, G., Gordon, S., Westveer, D., Stewart, J., Stokes, K., et al., 1983. A new steroid-eluting low-threshold pacemaker lead. In: Steinbach, K. (Ed.), *7th World Symposium on Cardiac Pacing*. Darmstadt. Steinkopff Verlag.
- Urist, M.R., Strates, B.S., 1971. Bone morphogenetic protein. *J. Dent. Res.* 50, 1392–1406.
- US EPA, 2009. Epa 100/k-09/001: the U.S. Environmental Protection Agency's Strategic Plan for Evaluating the Toxicity of Chemicals: Office of the Science Advisor Science Policy Council.
- Wilke, A., Traub, F., Kienapfel, H., Griss, P., 2001. Cell differentiation under the influence of rh-BMP-2. *Biochem. Biophys. Res. Commun.* 284, 1093–1097.
- Wijns, W., Steg, P.G., Mauri, L., Kurowski, V., Parikh, K., Gao, R., Bode, C., Greenwood, J.P., Lipsi, c E., Alamgir, F., et al., 2014. Endeavour zotarolimus-eluting stent reduces stent thrombosis and improves clinical outcomes compared with cypher sirolimus-eluting stent: 4-year results of the PROTECT randomized trial. *Eur. Heart J.* 35 (40), 2812–2820.
- Yamaguchi, A., Katagiri, T., Ikeda, T., Wozney, J.M., Rosen, V., et al., 1991. Recombinant human bone morphogenetic protein-2 stimulates osteoblastic maturation and inhibits myogenic differentiation in vitro. *J. Cell Biol.* 113, 681–687.

Chapter Questions

1. List the five ISO 10993 standards that discuss in vitro tests for cell and tissue compatibility.
2. In Part 3 of the ISO 10993 standards, the three areas of testing describe tests for genotoxicity, carcinogenicity, and reproductive toxicity. Name one type of in vitro test in each category and use one to three sentences to describe the basic scientific premise behind each test.
3. In one to three sentences describe Part 4 of the ISO 10993 standards and list the five categories of the type of testing done under this part of the standard.
4. Define toxicant and xenobiotic. What is the main distinction between these terms?
5. You have been asked to test a certain new medical device material for cytotoxicity, and for thoroughness you have been asked to perform two tests. Name two tests for cytotoxicity that you would apply and describe the scientific basis behind each test.
6. In vitro tests to establish cell and tissue compatibility can be broken down into two general areas of testing: (1) standardized screening tests such as those described in the ISO 10993 standards, and (2) specialized device-specific or material-specific tests that are often used to evaluate a special bioactive property of the material. In the latter, name one such bioactive material, the molecular/biochemical nature of the *bioactivity*, and describe the specific bioactive test performed to ascertain bioactivity.
7. What do the acronyms NOAEL, LOAEL, TI, and MOS stand for? Given that a TI for chemical X is 1.0 mg/kg and the worst-case exposure dose of chemical X is 0.0003 mg/kg, calculate the MOS for chemical X.
8. Draw the basic geometry of a normal chromosome, then draw a chromosome that presents an interstitial deletion. What category of in vitro test does this question describe?
9. Describe the molecular mechanism behind immobilized heparin applied to medical devices.
10. Describe two events that could trigger the need for an in vitro assessment of cell or tissue compatibility and describe two of the immediate next steps in the assessment.

2.3.4

In Vivo Assessment of Tissue Compatibility

JAMES M. ANDERSON¹, FREDERICK J. SCHOEN², NICHOLAS P. ZIATS¹

¹Department of Pathology, Case Western Reserve University, Cleveland, OH, United States

²Pathology and Health Sciences and Technology (HST), Harvard Medical School, Department of Pathology, Brigham and Women's Hospital, Boston, MA, United States

Introduction

The goal of in vivo assessment of tissue compatibility of a biomaterial, prosthesis, or medical device is to determine the biocompatibility (as a key component of safety) of the biomaterial, prosthesis, or medical device in a biological environment. Indeed, biocompatibility is a critical element in the performance of an implanted medical device, and many complications of clinical devices derive from inadequate biocompatibility. Moreover, the concept of biocompatibility has evolved in recent years as biomaterials technology has become more sophisticated, particularly in permitting the biomaterial to effect complex, and potentially beneficial, interactions with the surrounding tissues (Hench and Pollak, 2002; Williams, 2008, 2019; see Chapter 2.3.2). Thus, the contemporary definition of biocompatibility focuses on the ability of a medical device to perform with an appropriate host response in a specific application, and biocompatibility assessment serves as a measurement of the magnitude and duration of the pathophysiologic mechanisms that determine the host response. From a practical perspective, the in vivo assessment of tissue compatibility of medical devices is carried out to determine that the device performs as intended, and presents no significant harm to the patient or user simulating clinical use. In this chapter, the term “medical device” will be used to describe biomaterials, prostheses, artificial organs, and other medical devices, and the terms “tissue compatibility assessment,” “biocompatibility assessment,” and “safety assessment” will be considered to be synonymous.

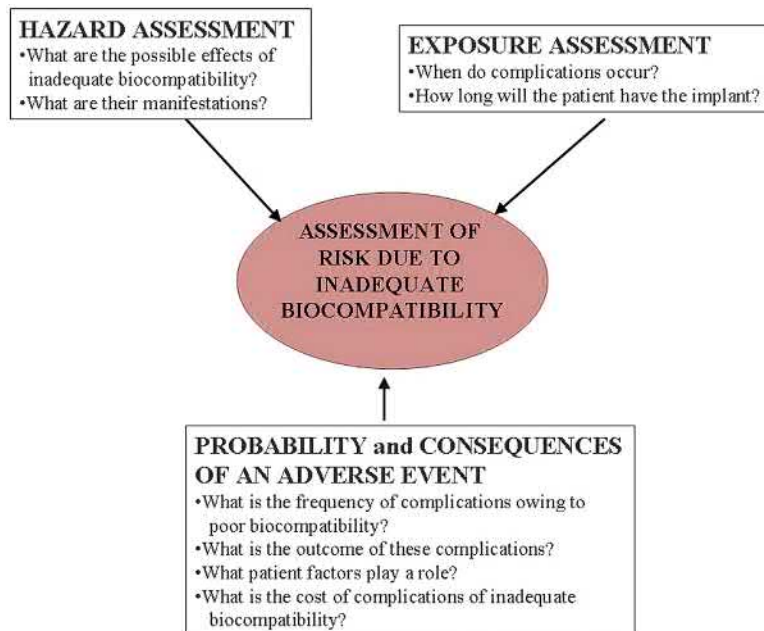
The in vivo assessment of tissue compatibility is necessary to establish the biocompatibility, safety, and function (efficacy) of a medical device and its components under conditions of intended use. Intended use conditions are also utilized to select in vitro tests and animal models that will provide essential information to determine biocompatibility.

Extensive efforts have been made by government regulatory agencies, e.g., the US Food and Drug Administration (FDA), and standards organizations, e.g., ASTM International (ASTM International, 2018 Annual Book of ASTM Standards, Volume 13.01), the International Organization for Standardization (ISO), and US Pharmacopeia (USP), to provide procedures, protocols, guidelines, and standards that may be used in the in vivo assessment of the tissue compatibility of medical devices. This chapter draws heavily on the ISO 10993 standard, Biological Evaluation of Medical Devices, in presenting a systematic approach to the in vivo assessment of tissue compatibility of medical devices.

The nature and extent of risk due to inadequate biocompatibility may be conceptualized as shown in Fig. 2.3.4.1. The first consideration in the selection of biomaterials to be used in device design should be the chemical, toxicological, physical, electrical, morphological, and mechanical properties of the biomaterial(s) to fulfill the intended use. Relevant to the overall in vivo assessment of tissue compatibility of a biomaterial or device is knowledge of the chemical composition of the materials, and the nature, degree, frequency, and duration of exposure of the device and its constituents to the tissues in which it will be utilized. Table 2.3.4.1 presents a list of biomaterial components and characteristics that may affect the overall biological responses of the medical device. The range of potential biological hazards is broad, and may include short-term effects, long-term effects, or specific toxic effects, which should be considered for every material and medical device. However, this does not imply that testing for all potential hazards will be necessary or practical.

Selection of in Vivo Tests According to Intended Use

As it is recognized that biomaterial–tissue interaction may vary with the anatomic site and duration of exposure, and



• **Figure 2.3.4.1** The risks associated with inadequate biocompatibility are a composite function of the exposure (i.e., nature and duration), the hazard (i.e., effects on the recipient), and the probability and consequences of complications.

TABLE 2.3.4.1 Biomaterials and Components Relevant to In Vivo Assessment of Tissue Compatibility

The material(s) of manufacture
Intended additives, process contaminants, and residues
Leachable substances
Degradation products
Other components and their interactions in the final product
The properties and characteristics of the final product

application-specific conditions, in vivo tests for assessment of tissue compatibility are chosen to simulate end-use applications. To facilitate the selection of appropriate tests, medical devices with their component biomaterials can be categorized by the nature of tissue contact of the medical device, and by its duration of contact. Table 2.3.4.2 presents medical device categorization by nature of tissue contact and contact duration. The tissue contact categories and subcategories, as well as the contact duration categories, have been derived from standards, protocols, and guidelines utilized in the past for safety evaluation of medical devices. Certain devices may fall into more than one category, in which case testing appropriate to each category should be considered.

Biomaterial and Device Perspectives in In Vivo Testing

Two perspectives may be considered in the in vivo assessment of tissue compatibility of biomaterials and medical devices.

TABLE 2.3.4.2 Medical Device Categorization by Tissue Contact and Contact Duration

Tissue Contact	
Surface devices	Skin Mucosal membranes Breached or compromised surfaces
External communicating devices	Blood path, indirect Tissue/bone/dentin communicating Circulating blood
Implant devices	Tissue/bone Blood
Contact Duration	
	Limited: ≤24 h Prolonged: >24h and <30 days Permanent: >30 days

The first perspective involves the utilization of in vivo tests to determine the general biocompatibility of newly developed biomaterials for which some knowledge of the tissue compatibility is necessary for further research and development. In this type of situation, manufacturing and other processes necessary to the development of a final product, i.e., the medical device, have not been carried out. However, the in vivo assessment of tissue compatibility at this early stage of development can provide additional information relating to the proposed design criteria in the production of a medical device. While it is generally recommended that the identification and quantification of extractable chemical entities of a medical device should precede biological evaluation, it is quite common to carry out preliminary in vivo assessments to determine if there may be unknown or as-yet unidentified chemical entities that

TABLE 2.3.4.3 In Vivo Tests for Tissue Compatibility

Sensitization
Irritation
Intracutaneous reactivity
Systemic toxicity (acute toxicity)
Subchronic toxicity (subacute toxicity)
Genotoxicity
Implantation
Hemocompatibility
Chronic toxicity
Carcinogenicity
Reproductive and developmental toxicity
Biodegradation
Immune responses

produce adverse biological reactions. Utilized in this fashion, early in vivo assessment of the tissue compatibility of a biomaterial may provide insight into the biocompatibility, and thereby may permit further development of this biomaterial into a medical device. Obviously, problems observed at this stage of development would require further efforts to improve the biocompatibility of the biomaterial, and to identify the agents and mechanisms responsible for the adverse reactions. As the in vivo assessment of tissue compatibility of a biomaterial or medical device is focused on the end-use application, it must be appreciated that a biomaterial considered compatible for one application may not be compatible for another.

The second perspective regarding the in vivo assessment of tissue compatibility of medical devices focuses on the biocompatibility of the final product, that is, the fabricated medical device in the condition in which it is to be implanted. Thus, issues related to desired fabrications, interactions between biomaterials, and to mechanical conductors, etc., may come into play. Although medical devices in their final form and condition are commonly implanted in carefully selected animal models to determine function, as well as biocompatibility, it may be inappropriate to carry out all of the recommended tests necessary for regulatory approval on the final device. In these situations, some tests may initially be carried out on biomaterial components of devices that have been prepared under manufacturing and sterilization conditions, and other processes utilized in the final product (see Table 2.3.4.3).

Specific Biological Properties Assessed by In Vivo Tests

In this section, brief perspectives on the general types of in vivo tests are presented. Details regarding these tests are found in the lists of standards provided at the end of this

chapter. ISO 10993 standards advise that the biological evaluation of all medical device materials include testing for cytotoxicity, sensitization, and irritation. (Cytotoxicity tests are considered in vitro tests.) Beyond these fundamentals, the selection of further tests for in vivo biocompatibility assessment is based on the characteristics and end-use application of the device or biomaterial under consideration.

Sensitization, Irritation, and Intracutaneous (Intradermal) Reactivity

Exposure to, or contact with, even minute amounts of potential leachables from medical devices or biomaterials can result in allergic or sensitization reactions. Sensitization tests estimate the potential for contact sensitization to medical devices, materials, and/or their extracts. Symptoms of sensitization are often seen in skin, and tests are often carried out topically in guinea pigs. Test design should reflect the intended route (skin, eye, mucosa) and nature, degree, frequency, duration, and conditions of exposure of the biomaterial in its intended clinical use. While sensitization reactions are immune system responses to contact with chemical substances, ISO guidelines suggest irritation to be a local tissue inflammation response to chemicals, without a systemic immunological component. The most severely irritating chemical leachables may be discovered prior to in vivo studies by careful material characterization and in vitro cytotoxicity tests. Irritant tests emphasize utilization of extracts of the biomaterials to determine the irritant effects of potential leachables. Intracutaneous (intradermal) reactivity tests determine the localized reaction of tissue to intracutaneous injection of extracts of medical devices, biomaterials, or prostheses in the final product form. Intracutaneous tests may be applicable where determination of irritation by dermal or mucosal tests is not appropriate. Albino rabbits are most commonly used, however newer ISO guidelines refer to determination of skin irritation using reconstructed human epidermis as an alternative to animal testing (ISO 10933-23).

Since these tests focus on determining the biological response of leachable constituents of biomaterials, their extracts in various solvents are utilized to prepare the injection solutions. Critical to the conduct of these tests is that the preparation of the test material and/or extract solution should be chosen to include testing for both water-soluble and fat-soluble leachables.

Systemic Toxicity: Acute, Subacute, and Subchronic Toxicity

Systemic toxicity tests estimate the potential harmful effects in vivo on target tissues and organs away from the point of contact (i.e., site of implantation) with either single or multiple exposures to medical devices, biomaterials, and/or their extracts. These tests evaluate the systemic toxicity potential of medical devices that release constituents into the body. These tests also include pyrogenicity testing, which assesses the induction of a systemic inflammatory response, often measured as fever.

In tests using extracts, the form and area of the material, the thickness, and the surface area to extraction vehicle volume are critical considerations in the testing protocol. Appropriate extraction vehicles, i.e., solvents, should be chosen to yield a maximum extraction of leachable materials for use in the testing. Mice, rats, or rabbits are the usual animals of choice for the conduct of these tests, and oral, dermal, inhalation, intravenous, intraperitoneal, or subcutaneous application of the test substance may be used, depending on the intended application of the biomaterial. Acute toxicity is considered to be the adverse effects that occur after administration of a single dose or multiple doses of a test sample given within 24 h. Subacute toxicity (repeat dose toxicity) focuses on adverse effects occurring after administration of a single dose or multiple doses of a test sample per day during a period of from 14 to 28 days. Subchronic toxicity is considered to be the adverse effects occurring after administration of a single dose or multiple doses of a test sample per day given during a part of the lifespan, usually 90 days but not exceeding 10% of the lifespan of the animal.

Pyrogenicity tests are also included in the system toxicity category to detect material-mediated fever-causing reactions to extracts of medical devices or material. Although the rabbit pyrogen test has been the standard, the Limulus amebocyte lysate (LAL) reagent test has been used increasingly in recent years and is considered an appropriate testing method. It is noteworthy that no single test can differentiate pyrogenic reactions that are material mediated per se from those due to endotoxin contamination.

Genotoxicity

In vivo genotoxicity tests are carried out if indicated by the chemistry and/or composition of the biomaterial (see [Table 2.3.4.1](#)) or if in vitro test results indicate potential genotoxicity [changes in deoxyribonucleic acid (DNA) that could lead to changes in cellular proliferation, differentiation, and/or function]. Initially, at least three in vitro assays should be used, and two of these assays should utilize mammalian cells. The initial in vitro assays should cover the three levels of genotoxic effects: DNA destruction; gene mutations; and chromosomal aberrations (as assessed by cytogenetic analysis). In vivo genotoxicity tests include the micronucleus test and the in vivo mammalian bone marrow cytogenetic tests—chromosomal analysis, the rodent dominant lethal tests, the mammalian germ cell cytogenetic assay, the mouse spot test, and the mouse heritable translocation assay. Not all of the in vivo genotoxicity tests need be performed; the most common test is the rodent micronucleus test. Genotoxicity tests are performed with appropriate extracts or dissolved materials using appropriate media, as suggested by the known composition of the biomaterial.

Implantation

Implantation tests assess the local pathological effects on the structure and function of living tissue induced by a

TABLE 2.3.4.4 Biological Response Parameters as Determined by Histological Assessment of Implants

Number and distribution of inflammatory cells as a function of distance from the material/tissue interface
Thickness and vascularity of fibrous capsule
Quality and quantity of tissue ingrowth (for porous materials)
Degeneration as determined by changes in tissue morphology
Presence of necrosis
Other parameters such as material debris, fatty infiltration, granuloma, dystrophic calcification, apoptosis, proliferation rate, biodegradation, thrombus formation, endothelialization, migration of biomaterials or degradation products

sample of a material or final product at the site where it is surgically implanted or placed into an implant site or tissue appropriate to the intended application of the biomaterial or medical device. In some cases, the anatomic site of implantation used for biocompatibility evaluation is not the same as the site of ultimate use, but has representative mechanisms and consequences of tissue–biomaterial interaction (e.g., subcutaneous implantation in rodents of bioprosthetic heart valve materials to study calcification that occurs as a major clinical limitation in humans; see [Chapter 2.4.5](#)). The most basic evaluation of the local pathological effects is carried out at both the gross level and the microscopic level. Histological (microscopic) evaluation is used to characterize various biological response parameters ([Table 2.3.4.4](#)). To address specific questions, more sophisticated studies may need to be done. Examples include immunohistochemical staining of histological sections to determine the types of cells present, and studies of collagen formation and destruction. For short-term implantation evaluation out to 12 weeks, mice, rats, guinea pigs, or rabbits are the most common animals utilized in these studies. For longer-term testing in subcutaneous tissue, muscle, or bone, animals such as rats, guinea pigs, rabbits, dogs, sheep, goats, pigs, and other animals with relatively long life expectancies are suitable. If a complete medical device is to be evaluated, larger species may be utilized so that human-sized devices may be used in the site of intended application. For example, substitute heart valves are usually tested as heart valve replacements in sheep, whereas calves are usually the animal of choice for ventricular assist devices and total artificial hearts.

In all aspects of biocompatibility testing, it is important to recognize that the effects of the material on the surrounding tissues are generally superimposed on the events occurring during physiological wound repair induced by the surgery of implantation. This is particularly important in shorter term experiments.

Hemocompatibility

Hemocompatibility tests evaluate effects on blood and/or blood components by blood-contacting medical devices or materials. In vivo hemocompatibility tests are usually designed to simulate the geometry, contact conditions, and flow dynamics of the device or material in its clinical application. From the ISO standards perspective, five test categories are indicated for hemocompatibility evaluation: thrombosis; coagulation; platelets; hematology; and immunology (complement and leukocytes). Two levels of evaluation are indicated: Level 1 (required); and Level 2 (optional). Regardless of blood contact duration, hemocompatibility testing is indicated for three categories of medical devices: (1) external communicating devices—blood path indirect; (2) external communicating devices—circulating blood; and (3) blood-contacting implant devices. [Chapter 2.3.5](#) gives further details on the testing of blood–material interactions.

Several issues are important in the selection of tests for hemocompatibility of medical devices or biomaterials. In particular, the hemocompatibility depends not only on the material's characteristics, but also on the fluid mechanics of the device (i.e., stasis promotes thrombus formation), and the coagulability of the blood. Thus, in vivo testing in animals may be convenient, but anatomic differences among species and species-related differences in blood reactivity must be considered, and these may limit the predictability of any given test in the human clinical situation. While blood values and reactivity between humans and nonhuman primates are very similar, European Community law prohibits the use of nonhuman primates for blood compatibility and medical device testing. Hemocompatibility evaluation in animals is complicated by the lack of appropriate and adequate test materials, for example, appropriate antibodies for immunoassays. Use of human blood in hemocompatibility evaluation implies in vitro testing, which usually requires the use of anticoagulants that are not generally present with the device in the clinical situation, except for perhaps the earliest implantation period. Although species differences may complicate hemocompatibility evaluation, the utilization of animals in short- and long-term testing is considered to be appropriate for evaluating thrombosis and tissue interaction.

Chronic Toxicity

Chronic toxicity tests determine the effects of either single or multiple exposures to medical devices, materials, and/or their extracts during a period of at least 10% of the lifespan of the test animal, e.g., over 90 days in rats. Chronic toxicity tests may be considered an extension of subchronic (subacute) toxicity testing, and both may be evaluated in an appropriate experimental protocol or study.

Carcinogenicity

Carcinogenicity tests determine the tumorigenic potential of medical devices, materials, and/or their extracts from either

single or multiple exposures or contacts over a period of the major portion of the lifespan of the test animal. Both carcinogenicity (tumorigenicity) and chronic toxicity may be studied in a single experimental study. With biomaterials, these studies focus on the potential for solid-state carcinogenicity, i.e., the Oppenheimer effect (see [Chapter 2.2.7](#)). Thus, in carcinogenicity testing, controls of a comparable form and shape should be included; polyethylene implants are a commonly used control material. The use of appropriate controls is imperative as animals may spontaneously develop tumors, and statistical comparison between the test biomaterial/device and the controls is necessary. To facilitate and reduce the time period for carcinogenicity testing of biomaterials, the FDA is exploring the use of transgenic mice carrying the human prototype c-Ha-ras gene as a bioassay model for rapid carcinogenicity testing.

Since tumors associated with clinical medical devices have been rare (see [Chapter 2.2.7](#)) carcinogenicity tests should be conducted only if data from other sources suggest a tendency for tumor induction. However, considerations of carcinogenicity may become important in some future applications in which pluripotential stem cells produced by any methodology are used.

Reproductive and Developmental Toxicity

These tests evaluate the potential effects of medical devices, materials, and/or their extracts on reproductive function, embryonic development (teratogenicity), and prenatal and early postnatal development. The application site of the device must be considered, and tests and/or bioassays should only be conducted when the device has a potential impact on the reproductive potential of the subject.

Biodegradation

Biodegradation tests determine the effects of a biodegradable material and its biodegradation products on the tissue response. They focus on the amount of degradation during a given period of time (the kinetics of biodegradation), the nature of the degradation products, the origin of the degradation products (e.g., impurities, additives, corrosion products, bulk polymer), and the qualitative and quantitative assessment of degradation products and leachables in adjacent tissues and in distant organs. The biodegradation of biomaterials may occur through a wide variety of mechanisms, which in part are biomaterial dependent, and all pertinent mechanisms related to the device and the end-use application of the device must be considered. Test materials comparable to degradation products may be prepared and studied to determine the biological response of degradation products anticipated in long-term implants. An example of this approach is the study of metallic and polymeric wear particles that may be present with long-term orthopedic joint prostheses. Moreover, for intentionally biodegradable scaffolds used in tissue engineering (see [Chapter 2.6.3](#)), biodegradation and the attendant tissue response are important to follow histologically. Further insights on biodegradation are available in [Chapters 1.3.2F](#), [1.3.3D](#) and [Section 2.4](#).

Immune Responses

Immune response evaluation is not a component of the standards currently available for *in vivo* tissue compatibility assessment. However, ASTM, ISO, and the FDA currently have working groups developing guidance documents for immune response evaluation where pertinent. Synthetic materials are not generally immunotoxic (see [Chapter 2.2.3](#)). However, immune response evaluation is necessary with modified natural tissue implants such as collagen, which has been utilized in a number of different types of implants and may elicit immunological responses. The Center for Devices and Radiological Health of the FDA released a draft immunotoxicity testing guidance document in 1998 ([Langone, 1998](#)), whose purpose is to provide a systematic approach for evaluating potential adverse immunological effects of medical devices and constituent materials. However, there have only been updated documents on pharmaceuticals and not medical devices (S8 Immunotoxicity Studies for Human Pharmaceuticals, 2005). Immunotoxicity is any adverse effect on the function or structure of the immune system or other systems as a result of an immune system dysfunction. Adverse or immunotoxic effects occur when humoral or cellular immunity needed by the host to defend itself against infections or neoplastic disease (immunosuppression) or unnecessary tissue damage (chronic inflammation, hypersensitivity, or autoimmunity) is compromised. Potential immunological effects and responses that may be associated with one or more of these effects are presented in [Table 2.3.4.5](#).

Representative tests for the evaluation of immune responses are given in [Table 2.3.4.6](#). [Table 2.3.4.6](#) is not all-inclusive, and other tests that specifically consider possible immunotoxic effects potentially generated by a given device or its components may be applicable. Examples presented in [Table 2.3.4.6](#) are only representative of the large number of tests that are currently available. However, direct and indirect markers of immune responses may be validated and their predictive value documented, thus providing new

tests for immunotoxicity in the future. Direct measures of immune system activity by functional assays are the most important types of tests for immunotoxicity. Functional assays are generally more important than tests for soluble mediators, which are more important than phenotyping. Signs of illness may be important in *in vivo* experiments,

TABLE 2.3.4.5 Potential Immunological Effects and Responses

Effects
Hypersensitivity
Type I— anaphylactic
Type II— cytotoxic
Type III— immune complex
Type IV— cell-mediated (delayed)
Chronic inflammation
Immunosuppression
Immunostimulation
Autoimmunity
Responses
Histopathological changes
Humoral responses
Host resistance
Clinical symptoms
Cellular responses
T cells
Natural killer cells
Macrophages
Granulocytes

TABLE 2.3.4.6 Representative Tests for the Evaluation of Immune Responses

Functional Assays	Phenotyping	Soluble Mediators	Signs of Illness
Skin testing	Cell surface markers	Antibodies	Allergy
Immunoassays (e.g., ELISA)	MHC markers	Complement	Skin rash
Lymphocyte proliferation	Chemokines	Immune complexes	Urticaria
Plaque-forming cells	Basoactive amines	Cytokine patterns(T-cell subsets)	Edema
Local lymph node assay	—	Cytokines (IL-1, IL-1ra, TNF α , IL-6, TGF- β , IL-4, IL-13)	Lymphadenopathy
Mixed lymphocyte reaction	—	—	—
Tumor cytotoxicity	—	—	—
Antigen presentation	—	—	—
Phagocytosis	—	—	—

but symptoms may also have a significant role in studies of immune function in clinical trials and postmarket studies.

Combination devices where drugs (or cells) are utilized within medical devices should also be considered for immune response evaluation. Hypersensitivity reactions have been reported with drug-eluting coronary stents (DES). With DES, concomitantly prescribed medications such as clopidogrel (platelet inhibitor) have been considered the causative agent for hypersensitivity, as well as the DES itself (Nebeker et al., 2006).

Selection of Animal Models for In Vivo Tests

Animal models are used to predict the clinical behavior, safety, and biocompatibility of medical devices in humans (Table 2.3.4.7). The selection of animal models for the in vivo assessment of tissue compatibility must consider the advantages and disadvantages of the animal model for human clinical application. Several examples follow, which exemplify the advantages and disadvantages of animal models in predicting clinical behavior in humans.

Preclinical testing in animal models is an important part of the regulatory process, used to determine the safety and efficacy of devices prior to human clinical trials. The choice of the animal model and the selection of in vitro tests should be made according to the intended use of the respective medical device, prosthesis, or biomaterial.

A single test animal may not assess all pertinent clinically important complications. For example, as described earlier, sheep are commonly used for the evaluation of heart valves (see Chapter 2.5.2A). This is based on size considerations, and also the propensity to calcify tissue components of bioprosthetic heart valves and thereby be a sensitive model for this complication. Thus, the choice of this animal model for bioprosthetic heart valve evaluation is made on the basis of accelerated calcification, the major clinical problem, assessed in rapidly growing animals which has its clinical correlation in young and adolescent humans. Nevertheless, normal sheep may not provide a sensitive assessment of the propensity of a valve to thrombosis, which may be potentiated by the reduced flow seen in abnormal subjects, but diminished by the specific coagulation profile of sheep.

The in vivo assessment of tissue responses to vascular graft materials is an example in which animal models present a particularly misleading picture of what generally occurs in humans. Virtually all animal models, including nonhuman primates, heal rapidly and completely with an endothelial blood-contacting surface. Humans, on the other hand, do not show extensive endothelialization of vascular graft materials, and the resultant pseudointima from the healing response in humans has potential thrombogenicity. Consequently, despite favorable results in animals, small-diameter vascular grafts (less than 4 mm in internal diameter) usually yield early thrombosis in humans, the major mechanism of failure which is secondary to the lack of endothelialization in the luminal surface-healing response.

Originally, the porcine coronary artery model was considered the model of choice for the evaluation of arterial stents. More recently, the rabbit iliac artery model for the evaluation of drug-eluting stents has been considered to be more realistic, as endothelialization is slower in the rabbit model than in the porcine model, and inflammation is not as extensive in the rabbit (Nakazawa et al., 2008). Thus, endothelialization, healing, and inflammation in the rabbit iliac artery model may be closer to these responses in humans than the porcine coronary artery model.

The use of appropriate animal models is an important consideration in the safety evaluation of medical devices that may contain potential immunoreactive materials. The in vivo evaluation of recombinant human growth hormone in poly(lactic-co-glycolic acid) (PLGA) microspheres demonstrates the appropriate use of various animal models to evaluate biological responses and the potential for immunotoxicity. Utilizing biodegradable PLGA microspheres containing recombinant human growth hormone (rhGH, Cleland et al., 1997) used Rhesus monkeys, transgenic mice expressing hGH, and normal control (Balb/C) mice in their in vivo evaluation studies. Rhesus monkeys were utilized for serum assays in the pharmacokinetic studies of rhGH release, as well as tissue responses to the injected microcapsule formulation. Placebo injection sites were also utilized, and a comparison of the injection sites from rhGH PLGA microspheres and placebo PLGA microspheres demonstrated a normal inflammatory and wound-healing response

TABLE 2.3.4.7 Animal Models for the In Vivo Assessment of Medical Devices

Device Classification	Animal
Cardiovascular	
Heart valves	Sheep
Vascular grafts	Dog, pig
Stents	Pig, rabbit, dog
Ventricular assist devices	Calf
Artificial hearts	Calf
Ex vivo shunts	Baboon, dog
Orthopedic/Bone	
Bone regeneration/ Substitutes	Rabbit, dog, pig, mouse, rat Dog, goat, nonhuman primate
Total joints—hips, knees	Sheep, goat, baboon
Vertebral implants	Rabbit, pig, dog, nonhuman primate
Craniofacial implants	Rabbit, dog
Cartilage	Dog, sheep
Tendon and ligament substitutes	Goat
Neurological	
Peripheral nerve regeneration	Rat, cat, nonhuman primate
Electrical stimulation	Rat, cat, nonhuman primate
Ophthalmological	
Contact lens	Rabbit
Intraocular lens	Rabbit, monkey

with a normal focal foreign-body reaction. To further examine the tissue response, transgenic mice were utilized to assess the immunogenicity of the rhGH PLGA formulation. Transgenic mice expressing a heterologous protein have been previously used for assessing the immunogenicity of structural mutant proteins. With the transgenic animals, no detectable antibody response to rhGH was found. In contrast, the Balb/C control mice had a rapid onset of high-titer antibody response to the rhGH PLGA formulation. This study points out the appropriate utilization of animal models to not only evaluate biological responses, but also one type of immunotoxicity (immunogenicity).

Future Perspectives on In Vivo Medical Device Testing

As presented earlier in this chapter, the in vivo assessment of tissue compatibility of biomaterials and medical devices is dependent on the end-use application of the biomaterial or medical device. In this sense, the development and utilization of new biomaterials and medical devices will dictate the development of new test protocols and procedures for evaluating these new products. Furthermore, it must be understood that the in vivo assessment of tissue compatibility of biomaterials and medical devices is open ended, and new end-use applications will require new tests.

The future development of medical devices is anticipated to provide more complexity to the composition and construction of these devices and, thus, to the array of potential biomaterial–tissue interactions. Future assessments will require a more sophisticated approach to test protocols and methodologies that must clearly identify biocompatibility and function. In this regard, new tests, methods, and animal models may have to be developed to adequately and appropriately characterize the biocompatibility and function of these new devices. Therefore, the development of guidelines and standards is dynamic and constantly evolving, driven by the complexity of new devices developed for application in tissue engineering, regenerative medicine, and nanomedicine.

Over the past half-century, medical devices and biomaterials have generally been “passive” in their tissue interactions. That is, a mechanistic approach to biomaterial–tissue interactions has rarely been used in the development of biomaterials or medical devices. Heparinized biomaterials are an exception to this, but considering the five subcategories of hemocompatibility, these approaches have a minimal impact on the development of blood-compatible materials.

In the past decade, increased emphasis has been placed on bioactivity and tissue engineering in the development of biomaterials and medical devices for potential clinical application. Rather than a “passive” approach to tissue interactions, bioactive and tissue-engineered devices have focused on an “active” approach in which biological or tissue components, i.e., growth factors, cytokines, drugs, enzymes, proteins, extracellular matrix components, and cells that may or may not be genetically modified, are used

in combinations with synthetic, i.e., passive, materials to produce devices that control or modulate a desired tissue response. Obviously, in vivo assessment of the targeted biological response of a tissue-engineered device will play a significant role in the research and development of that device, as well as in its safety assessment. It is clear that scientists working on the development of tissue-engineered devices will contribute significantly to the development of in vivo tests for biocompatibility assessment, as these tests will also be utilized to study the targeted biological responses in the research phase of the device development.

Regarding tissue-engineered devices, it must be appreciated that biological components may induce varied effects on tissue in the in vivo setting. For example, a simplistic view of the potentially complex problems that might result from a device releasing a growth factor to enhance cell proliferation is presented. The presence of a growth factor may result in markedly different cell proliferation, differentiation, protein synthesis, attachment, migration, shape change, etc., which would be cell-type dependent. Thus, different cell-type dependent responses in an implant site, reacting to the presence of a single exogenous growth factor, may result in inappropriate, inadequate, or adverse tissue responses. These perspectives must be integrated into the planned program for in vivo assessment of tissue compatibility of tissue-engineered devices. Moreover, a major challenge to the in vivo assessment of tissue compatibility of tissue-engineered devices is the use of animal tissue components in the early phase of device development, whereas the ultimate goal is the utilization of human tissue components in the final device for end-use application. Novel and innovative approaches to the in vivo tissue compatibility of tissue-engineered devices must be developed to address these significant issues. Finally, the development of clinically useful tissue-engineered devices will require enhanced understanding of the influence of the patient and biomechanical factors on the structure and function of healed and remodeled tissues. It will also require new methodology for assessment of biocompatibility, and the dynamic progression of remodeling in vivo (Mendelson and Schoen, 2006).

Careful studies of retrieved implants to establish biomarkers and mechanisms of structural evolution will be critical (see Chapter 2.1.5).

References

- An, Y.H., Friedman, R.J., 1999. *Animal Models in Orthopaedic Research*. CRC Press, Boca Raton, FL.
- Association for the Advancement of Medical Instrumentation, 1998. *AAMI standards and recommended practices, vol. 4. Biol. Eval. Med. Dev. 4S (Suppl.)* 1997.
- Chapekar, M.S., 1996. Regulatory concerns in the development of biologic–biomaterial combinations. *J. Biomed. Mater. Res. Appl. Biomater.* 33, 199–203.
- Cleland, J.L., Duenas, E., Daugherty, A., Marian, M., Yang, J., et al., 1997. Recombinant human growth hormone poly(lactic-co-glycolic acid) (PLGA) microspheres provide a long lasting effect. *J. Control. Release* 49, 193–205.

- FDA (US Food and Drug Administration), 1995. Blue Book Memorandum G95-1: FDA-Modified Version of ISO 10993-Part 1, Biological Evaluation of Medical Devices – Part 1. Evaluation and Testing.
- Hench, L.L., Pollak, J.M., 2002. Third-generation biomedical materials. *Biomaterials* 29, 1014–1017.
- Langone, J.J., 1998. Immunotoxicity Testing Guidance. Draft Document, Office of Science and Technology. Center for Devices and Radiological Health, Food and Drug Administration.
- Mendelson, K., Schoen, F.J., 2006. Heart valve tissue engineering: concepts, approaches, progress, and challenges. *Ann. Biomed. Eng.* 34, 1799–1819.
- Nakazawa, G., Finn, A.V., Ladich, E., Ribichini, F., Coleman, L., et al., 2008. Drug-eluting stent safety: findings from preclinical studies. *Expert Rev. Cardiovasc. Ther.* 6 (10), 1379–1391.
- Nebeker, J.R., Virmani, R., Bennett, C.L., Hoffman, J.M., Samore, M.H., et al., 2006. Hypersensitivity cases associated with drug-eluting coronary stents. *J. Am. Coll. Cardiol.* 47, 175–181.
- Williams, D.F., 2008. On the mechanisms of biocompatibility. *Biomaterials* 29, 2941–2953.
- Williams, D.F., 2019. The language of biomaterials-based technologies. *Regen. Eng. Transl. Med.* 5, 53–60.
- Yamamoto, S., Urano, K., Koizumi, H., Wakana, S., Hioki, K., et al., 1998. Validation of transgenic mice carrying the human prototype c-Ha-ras gene as a bioassay model for rapid carcinogenicity testing. *Environ. Health Perspect.* 106 (Suppl. 1), 57–69.

ISO Standards

- ISO 10993, Biological Evaluation of Medical Devices. International Standards Organization, Geneva, Switzerland.
- ISO 10993-1 Evaluation and Testing within a Risk Management System. (2018).
- ISO 10993-2, Animal Welfare Requirements.
- ISO 10993-3, Tests for Genotoxicity, Carcinogenicity, and Reproductive Toxicity.
- ISO 10993-4, Selection of Tests for Interactions with Blood.
- ISO 10993-5, Tests for in Vitro Cytotoxicity.
- ISO 10993-6, Tests for Local Effects after Implantation.
- ISO 10993-7, Ethylene Oxide Sterilization Residuals.
- ISO 10993-9, Framework for the Identification and Quantification of Potential Degradation Products.
- ISO 10993-10, Tests for Irritation and Delayed-type Hypersensitivity.
- ISO 10993-11, Tests for Systemic Toxicity.
- ISO 10993-12, Sample Preparation and Reference Materials.
- ISO 10993-13, Identification and Quantification of Degradation Products from Polymeric Medical Devices.
- ISO 10993-14, Identification and Quantification of Degradation Products from Ceramics.
- ISO 10993-15, Identification and Quantification of Degradation Products from Metals and Alloys.
- ISO 10993-16, Toxicokinetic Study Design for Degradation Products and Leachables.
- ISO 10993-17, Method for the Establishment of Allowable Limits for Leachable Substances.
- ISO 10993-18, Chemical Characterization of Materials.
- ISO 10993-19, Physico-Chemical Morphological and Topographical Characterization of Materials.
- ISO-10993-20, Principles and Methods for Immunotoxicology Testing of Medical Devices.

- ISO-10993-23, Determination of Skin Irritation of Medical Device Extracts Using Reconstructed Human Epidermis (RhE).
- ISO 14971, Medical Devices – Application of Risk Management to Medical Devices.

ASTM International, 2018 Annual Book of ASTM Standards, Volume 13.01

- F 895, Agar Diffusion Cell Culture Screening for Cytotoxicity.
- F 2382, Assessment of Intravascular Medical Device Materials on Partial Thromboplastin Time (PTT).
- E 1397, In Vitro Rat Hepatocyte DNA Repair Assay.
- E 1398 In Vivo Rat Hepatocyte DNA Repair Assay.
- F 1983, Assessment of Compatibility of Absorbable/Resorbable Biomaterials for Implant Applications.
- F 981, Assessment of Compatibility of Biomaterials for Surgical Implants with Respect to Effect of Materials on Muscle and Bone.
- F 756, Assessment of Hemolytic Properties of Materials.
- F 1027, Assessment of Tissue and Cell Compatibility of Orofacial Prosthetic Materials and Devices.
- F 1877, Characterization of Particles.
- F 813, Direct Contact Cell Culture Evaluation of Materials for Medical Devices.
- F 749, Evaluating Material Extracts by Intracutaneous Injection in the Rabbit.
- F 750, Evaluating Material Extracts by Systemic Injection in the Rabbit.
- F 2148, Evaluation of Delayed Contact Hypersensitivity Using the Murine Local Lymph Node Assay (LLNA).
- F 1906, Evaluation of Immune Responses in Biocompatibility Testing Using ELISA Tests, Lymphocyte Proliferation, and Cell Migration.
- F 619, Extraction of Medical Plastics.
- F 2147, Guinea Pig: Split Adjuvant and Closed Patch Testing for Contact Allergens.
- F 748, Selecting Generic Biological Test Methods for Materials and Devices.
- F 1905, Selecting Tests for Determining the Propensity of Materials to Cause Immunotoxicity.
- F 763, Short-Term Screening of Implant Materials.
- F 1408, Subcutaneous Screening Test for Implant Materials.
- F 719, Testing Biomaterials in Rabbits for Primary Skin Irritation.
- F 1903, Testing for Biological Responses to Particles In Vitro.
- F 720, Testing Guinea Pigs for Contact Allergens: Guinea Pig Maximization Test.
- F 2065, Testing for Alternative Pathway Complement Activation in Serum by Solid Materials.
- F 2567, Testing for Classical Pathway Complement Activation in Serum by Solid Materials.
- F 1984, Testing for Whole Complement Activation in Serum by Solid Materials.
- F 1904, Testing the Biological Responses to Particles In Vivo.
- E 1263, Conduct of Micronucleus Assays in Mammalian Bone Marrow Erythrocytes.
- E 1202, Development of Micronucleus Assay Standards.
- E 1262, Performance of Chinese Hamster Ovary Cell/Hypoxanthine Guanine Phosphoribosyl Transferase Gene Mutation Assay.
- F 1439, Performance of Lifetime Bioassay for the Tumorigenic Potential of Implant Materials.
- E 1280, Performing the Mouse Lymphoma Assay for Mammalian Cell Mutagenicity.

2.3.5

Evaluation of Blood–Materials Interactions

BUDDY D. RATNER¹, THOMAS A. HORBETT², WILLIAM R. WAGNER³

¹Bioengineering and Chemical Engineering, Director of University of Washington Engineered Biomaterials (UWEB), Seattle, WA, United States

²Bioengineering and Chemical Engineering, University of Washington, Seattle, WA, United States

³Departments of Surgery, Bioengineering & Chemical Engineering, McGowan Institute for Regenerative Medicine, University of Pittsburgh, Pittsburgh, PA, United States

Introduction

Thousands of devices fabricated from synthetic materials or processed natural materials are interfaced with blood for a wide range of medical procedures (see Section 2.5, particularly [Chapters 2.5.2 and 2.5.3](#)). Blood-contacting materials have a unique set of requirements, and most are quite different from implants in soft tissue or bone. The most obvious complication is the undesirable formation of a thrombus or clot, but many other reactions can impact performance when a synthetic material is interfaced with blood. How can the biomaterials engineer know which materials might be best used in the fabrication of a blood-contacting device? It would be ideal if this chapter could end with a definitive list of “blood-compatible” biomaterials that might be used in blood-contacting medical devices (note that generalized suggestions are offered near the end of this chapter). The considerations driving the interpretation of blood interaction tests are sufficiently complex that such a list of materials cannot be presented. The reader should appreciate this point after working through this chapter.

This chapter outlines methods and concerns in evaluating the blood compatibility of biomaterials and medical devices. It does not automatically follow that if the materials comprising a device are blood compatible, then a device fabricated from those materials will also be blood compatible. This important point should be clear by the end of this chapter. Before considering the evaluation of materials and devices, the reader should be familiar with the protein and cellular reactions of blood coagulation, platelet responses, and fibrinolysis, as discussed in [Chapter 2.2.6](#). The history of methods to assess blood compatibility is addressed in [Ratner \(2000\)](#).

Background and Principles of Blood–Materials Interactions Assessment

What Is Blood Compatibility?

Blood-compatibility assessment would be straightforward if, following the introductory paragraph, there were a list of standard tests that might be performed to evaluate blood compatibility. By simply performing the tests outlined in such a list, a material could be rated “blood compatible” or “not blood compatible.” Unfortunately, no widely recognized, standard list of blood-compatibility tests exists. Due to the complexity of blood–materials interactions (BMI), there is a basic body of ideas that must be mastered to appreciate what blood interaction tests actually measure. This section introduces the rationale for BMI testing, and addresses a few important measurement schemes.

“Blood compatibility” can be defined as the property of a material or device that permits it to function in contact with blood without inducing adverse reactions. But this simple definition offers little insight into what a blood-compatible material is. More useful definitions become increasingly complex. This is because there are many mechanisms for the body to respond to material intrusions into the blood. A material that will not trigger one response mechanism may be highly active in triggering an alternative pathway. The mechanisms by which blood responds to materials have been discussed in [Chapter 2.2.6](#). This chapter will integrate many of these ideas, and provide a framework for BMI (and blood-compatibility) assessment. A unique collection of discussions and commentary on the state of knowledge regarding the phenomena related to blood compatibility provides

supplemental depth to many of the considerations raised here (Jaffer and Weitz, 2019; Brash et al., 2019; Gorbet et al., 2019; Maitz et al., 2019).

Blood compatibility is impacted by the biochemistry of coagulation, the mechanisms of blood–materials interactions (BMI), and the design and function of a device in the bloodstream. This chapter will integrate many of these ideas and provide a framework for BMI and blood-compatibility assessment.

Blood compatibility can also be viewed from a different perspective, i.e., by considering a material that is *not* blood compatible (a thrombogenic material). Such a material would produce specific adverse reactions when placed in contact with blood: formation of clot or thrombus composed of various blood elements; shedding of thromboemboli (detached thrombus); destruction of circulating blood components; activation of the complement system; and other immunologic pathways (Salzman and Merrill, 1987). Most often, in designing blood-contacting materials and devices, our aim is to minimize these generally undesirable blood reactions. Are these reactions always undesirable? Consider the case of a hemostatic device that is designed to rapidly induce clotting.

Why Measure Blood Compatibility?

Many devices and materials are presently used in humans to treat, or to facilitate treatment of, health problems. Such devices include the extracorporeal pump-oxygenator (heart–lung machine) used in many surgical procedures, hollow fiber hemodialyzers for treatment of kidney failure, catheters for blood access and blood vessel manipulation (e.g., angioplasty), heart assist devices, stents for lumenally supporting blood vessels, and devices for the permanent replacement of diseased heart valves (prosthetic heart valves) and arteries (vascular grafts). Since these and other blood-contacting devices have been successfully used in patients for 40 or more years, and are judged to be therapeutically beneficial, it is reasonable to ask: (1) is there a continued need for assessing BMI, and (2) are there important problems that remain to be addressed? The answer in both cases is an emphatic “yes.”

To address point 1, the ongoing need for BMI measurement, consider that existing devices are frequently modified by incorporation of new design features or materials primarily intended to improve durability and physical and mechanical characteristics, i.e., devices may be modified to improve characteristics other than BMI. However, since these changes may also affect blood responses, and since BMI are not entirely predictable based on knowledge of device composition and configuration, blood-compatibility testing is nearly always required to document safety.

There are substantial problems with devices used today in the bloodstream (point 2). The performance of many existing devices is frequently less than optimal (Jaffer and Weitz, 2019; Baumann Kreuziger and Massicotte, 2015; Byrne and Joner, 2015; Ratner, 1993a, 2000, 2007). For example,

prolonged cardiopulmonary bypass and membrane oxygenation can produce a severe bleeding tendency. Mechanical heart valves occasionally shed emboli to the brain, leading to stroke. Angiographic catheters can also generate strokes. Synthetic vascular grafts perform less well than grafts derived from natural arteries or veins; graft failure due to thrombosis can lead to ischemia (lack of oxygen) and death of downstream tissue beds; small diameter synthetic vascular grafts (<4 mm i.d.) perform so poorly that they are rarely used. Thus while performance characteristics have been judged to be acceptable in many instances (i.e., the benefit/risk ratio is high), certain existing devices could be improved to extend their period of safe operation (e.g., oxygenators) and to reduce adverse BMI long term (e.g., heart valves). Furthermore, many devices are only “safe” when anticoagulating drugs are used (e.g., oxygenators, mechanical heart valves, hemodialyzers). Device improvements that would reduce adverse BMI, and thereby minimize the need for anticoagulant therapy, would have important implications both for health (fewer bleeding complications due to drug effects) and cost (complications can be expensive to treat). The reusability of devices that can undergo repeated blood exposure in individual patients (e.g., dialyzers) is also an important economic consideration.

For certain applications there are no devices presently available that perform adequately (due to adverse BMI), even when antithrombotic drugs are used. Thus there are needs for devices that could provide long-term oxygenation for respiratory failure, complete cardiac support, and intravascular measurement of physiologic parameters and metabolites (O₂, CO₂, pH, glucose). Also, there are demands for long-term, small diameter vascular grafts (<5 mm i.d.) and other conduits (e.g., stents and stent grafts) for reconstruction of diseased arteries and veins. Overall, there is a compelling need for continued and improved methods for evaluating BMI.

What Is Thrombogenicity?

A thrombogenic device may cause a localized accumulation of protein and cellular blood elements. Cardiovascular devices may also induce regions of disturbed flow or stasis that lead to the formation of blood clots. These accumulations or clots may compromise device functions, such as flow of blood through artificial blood vessels, mechanical motions of heart valves, gas exchange through oxygenators, removal of metabolic waste products through dialysis membranes, etc. Local blood reactions may also impact other parts of the host organism, i.e., systemic effects might be noted. Thus thrombi may detach from a surface (embolize) and be carried downstream, eventually occluding a blood vessel of comparable size and impairing blood flow distal to the site of occlusion. When the tissue dependent on this blood flow becomes necrotic, it is termed an infarct. Chronic devices may produce steady-state destruction or “consumption” of circulating blood elements (e.g., mechanical destruction of red cells by heart prostheses producing anemia or removal of platelets due to ongoing thrombus

formation or platelet activation), with a concomitant rise in plasma levels of factors released from those blood elements (e.g., plasma hemoglobin, platelet factor 4). This consumption may lower the concentration in blood of that component or be masked by increased production. Mediators of inflammatory responses and vessel tone may also be produced or released from cells (e.g., platelets, white cells, the complement pathway) following blood–surface interactions that can affect hemodynamics and organ functions at other sites. Thus “thrombogenicity” may be broadly defined as the extent to which a device, when employed in its intended use configuration, induces the adverse responses outlined earlier. While all artificial surfaces will interact with blood, an acceptably nonthrombogenic device can be defined as one that would produce neither local nor systemic effects with significant health consequence to the host organism.

Thrombogenicity may be broadly defined as the extent to which a device, when employed in its intended use configuration, induces adverse responses.

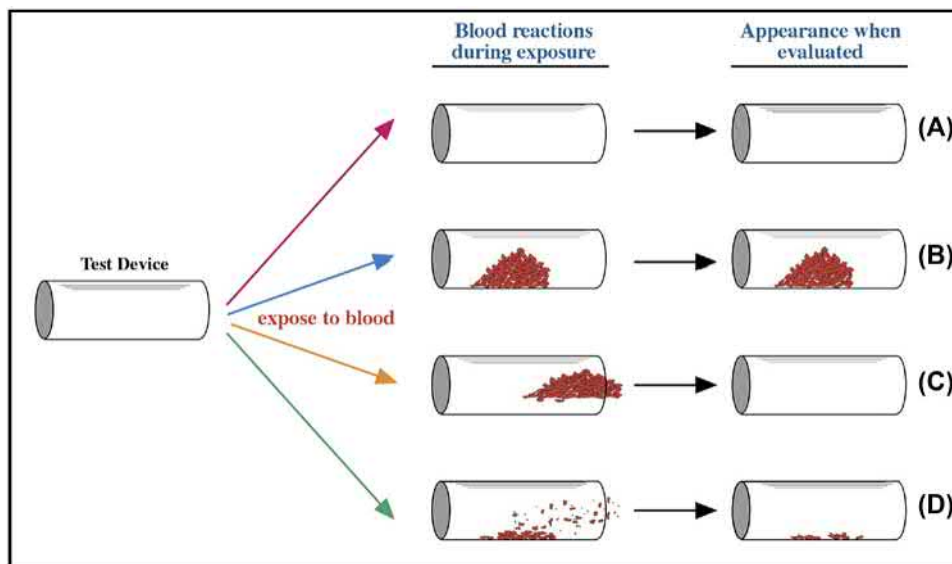
With “thrombogenicity” now defined as adverse outcomes associated with device usage, the obvious goal is to design and improve devices using materials that are blood compatible (nonthrombogenic) for specific applications. Ideally, the biomaterials engineer would like to consult a handbook for a list of materials useful in the fabrication of a blood-contacting device. Unfortunately, there is little consensus as to the materials that are blood compatible (Ratner, 1984). Because of this lack of consensus, there is no “official” list of blood-compatible materials. As a result, in the construction of a

new blood-contacting device the biomaterials engineer generally consults published studies or directly performs blood-compatibility assessment studies on candidate materials.

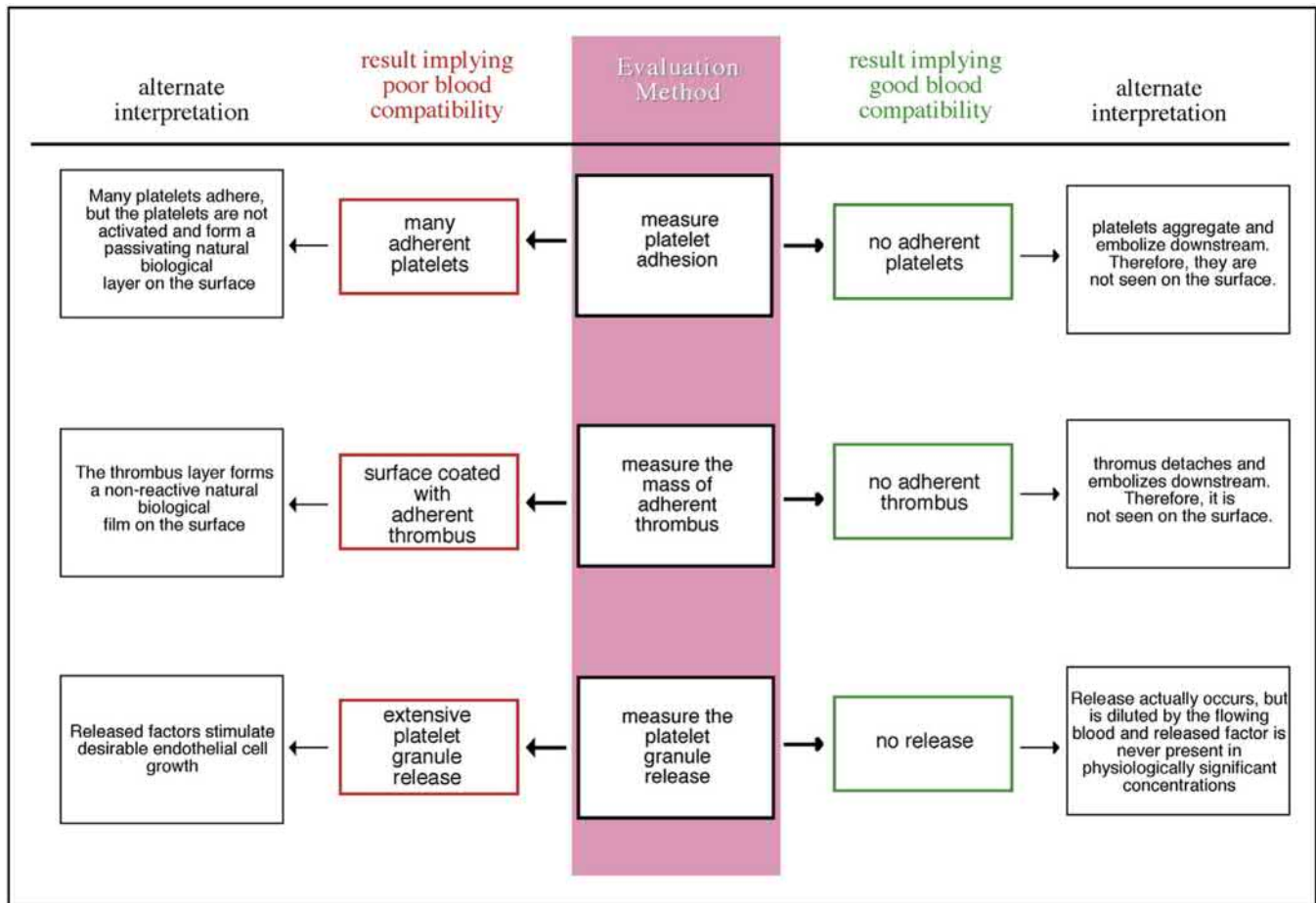
Understanding the blood compatibility of specific materials used in blood-contacting devices is complex because:

- (1) The types of blood-contacting devices used are numerous (see Chapters 2.5.2 and 2.5.3), and the device design will impact the apparent thrombogenicity of materials used in those devices.
- (2) Blood-contacting devices are commercially manufactured, and manufacturers are, for competitive reasons, reluctant to discuss specific chemical compositions or changes made to raw materials in the device design.
- (3) The possible blood responses are numerous, complex, dynamic, and often not fully understood.
- (4) It is difficult and expensive to measure device thrombogenicity (clinically significant local thrombosis or systemic effects) in a systematic way, in either experimental animals or humans.

Most tests purported to measure blood compatibility in fact evaluate certain BMI, which are the events that occur (and observations that are made) when blood contacts a material. Fig. 2.3.5.1 illustrates how alternate interpretations can be applied to data from “blood-compatibility” tests. This concept is further expanded upon in Fig. 2.3.5.2. These alternate interpretations often invalidate or modify conclusions drawn from such tests. For accuracy, the term “BMI assessment” will be used for the remainder of this chapter, instead of “blood-compatibility test.” Based upon the characteristics of the evaluation method (i.e., what is really being measured) the biomaterials scientist must relate



• **Figure 2.3.5.1** Possible scenarios for blood–materials interactions and alternate interpretations of testing outcome. This example points out limitations of evaluating only local thrombus formation at fixed time points. (A) The device remains free of thrombus after exposure to blood; (B) a large thrombus forms and adheres tightly, as is observed at the endpoint; (C) a large thrombus forms but detaches (embolizes); (D) the surface is highly reactive toward blood but deposited material is quickly removed through micro-embolism and/or lysis. Inspection of devices (C) and (D) could lead to the incorrect conclusion that these surfaces are blood compatible.



• **Figure 2.3.5.2** Alternate scenarios that can be applied for interpreting results of blood–materials interaction assays.

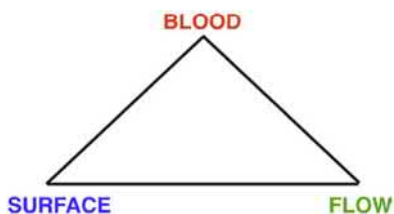
the significance of the events being observed (the BMI) to the blood compatibility of the material or device. A solid understanding of the physical and biological mechanisms of blood–materials interactions is required to make this connection in a rational way.

Most tests purported to measure blood compatibility in fact evaluate BMI, which are the events that occur when blood contacts a material. For example, is a material that adheres platelets not blood compatible? [Figs. 2.3.5.1 and 2.3.5.2](#) demonstrate alternate interpretations of such data.

In more specific terms, BMI are the interactions (reversible and irreversible) between surfaces and blood solutes, proteins, and cells (e.g., adsorption, absorption, adhesion, denaturation, activation, spreading) that occur under defined conditions of exposure time, blood composition, and blood flow. Since each of these variables influence BMI, we generally cannot: (1) extrapolate results obtained under one set of test conditions to another set of conditions; (2) use short-term testing to predict long-term results; and (3) predict in vivo device performance based on BMI testing of materials per se in idealized flow geometries. Nonetheless, such tests have provided important insights into the mechanisms of thrombus formation in general, and the

relationships between BMI and blood compatibility. These studies also permit some general guidelines for device construction and, to a limited extent, may allow prediction of device performance in humans. These points are addressed in subsequent sections of this chapter.

The foregoing considerations suggest that no material may be simply “blood compatible” or “nonthrombogenic,” since this assessment will depend strongly on details of the test system or usage configuration. In fact, under conditions of sluggish (low shear) blood flow or stasis, most if not all artificial materials may become associated with localized blood clotting and thus be considered “thrombogenic.” This is because synthetic materials, unlike the vascular endothelium (the perfect “blood-compatible material” that lines all blood vessels), cannot actively inhibit thrombosis and clotting by directly producing and releasing inhibitors or by inactivating procoagulant substances. The possibility that there may be no “biomaterials solution” for certain situations or that device performance could be improved by emulating strategies found in nature has led some investigators to consider coating devices with endothelial cells, antithrombotic drugs, or anticoagulating enzymes. These “antithrombogenic” approaches appear promising, and are being widely explored ([Maitz et al., 2019](#)). As for conventional synthetic materials



• **Figure 2.3.5.3** Virchow's triad.

and devices, establishing the usefulness of biologic surfaces and drug delivery devices requires appropriate methods for evaluating their blood interactions. An important point is that we use millions of devices in contact with blood each year in patients with generally good outcomes. It is not that the problem of blood compatibility is impossible to solve, but outcomes can often be improved by optimizing BMI.

We use millions of devices in contact with blood each year in patients with generally good outcomes. The problem of blood compatibility is complex, but outcomes can often be improved by optimizing BMI.

Key Considerations for BMI Assessment

In 1856, Rudolph Virchow implied that three factors contribute to the coagulation of blood: blood chemistry, blood-contacting surface, and flow regime (commonly referred to as Virchow's triad—[Fig. 2.3.5.3](#)).

This assessment is still valid and provides a framework for more formally introducing the variables important in any system intended to evaluate BMI. Also, the interaction time of blood with materials (ranging from seconds to years) has an impact on BMI. As described in the following paragraphs, these variables may each profoundly influence the results and interpretation of BMI testing. It is assumed that the reader has reviewed the mechanisms of blood response to artificial surfaces, as outlined in [Chapter 2.2.6](#).

Blood: A Fragile Fluid That Is Readily Compromised

The source of the blood and methods for its handling can strongly influence BMI. Human blood and blood from various animal species have been employed in BMI assessment in vitro and in vivo, both in the presence and absence of anticoagulants. Blood reactivity is also influenced by manipulations in vitro, the surface-to-volume ratio of blood in extracorporeal circuits, and the use of pumps for blood recirculation. These aspects are discussed later and summarized in [Table 2.3.5.1](#).

Although there are general similarities in the blood chemistry of all mammals, there are also differences characteristic of each species. In particular, blood may vary with respect to blood proteins (concentrations and functionality), and cells that participate in coagulation, thrombosis, and fibrinolysis ([Chapter 2.2.6](#)). The size of blood-formed elements may also differ. A comparison of blood chemistry between humans and the more commonly used animal species has been published ([McIntire et al., 1985](#)). While human blood

TABLE 2.3.5.1 Factors Important in the Acquisition and Handling of Blood for Blood–Materials Interactions (BMI) Experiments

- Species of the blood donor
- Health, gender, and age of the blood donor
- Blood reactivity of the donor (individual physiological differences)
- Time interval between blood draw and BMI experiment
- Care with which the puncture for the blood draw was made or if drawn from an indwelling catheter
- Temperature (for blood storage and testing)
- Anticoagulation
- Drugs and anesthetics present in the blood
- Cellular activation or damage due to centrifugation and separation operations
- Activation due to contact with foreign surfaces prior to the BMI experiment (syringe, needle, blood bag, bottles, tubing, etc.)
- Blood damage due to the air–blood interface
- Blood damage due to pumping and recirculation

is obviously preferable for BMI, it is often impossible to use human blood in certain experiments. In addition, there are significant health concerns in experimenting with human blood, and animals are commonly used for both in vitro and in vivo studies. Unfortunately, most investigations have employed a single animal species or blood source. There have been few comparisons between human and animal blood responses for evaluating BMI in particular test situations (also see [Chapter 2.3.6](#)). Differences between human and animal blood responses can be large, and such differences should lead to caution in directly interpreting experimental results. Furthermore, the variation is generally not simply a “less” or “more” reactive consideration; rather, some species may have less platelet reactivity offset by more coagulation or fibrinolytic activity. Activation may be more sensitive to some agonists and less for others. Similarly, the animal response to anticoagulants and antiplatelet agents may vary substantially from humans. Following the implantation of chronic blood-contacting devices (e.g., vascular grafts) there may be large differences between humans and other animal species in terms of device healing, which will be reflected as differences in the *time course* of BMI. Furthermore, while laboratory animals serving as blood donors for BMI experiments may represent a relatively homogeneous population in terms of age, health status, blood responses, etc., the human donors of blood for research (and recipients of blood-contacting devices) may vary considerably in terms of these parameters. Consider, for example, human diet, drug use (e.g., aspirin, alcohol), overall health, and even donor sex (males and females were found to have different platelet responses in experiments in our laboratory). Thus the

results obtained with animal species must be viewed with caution if conclusions are to be drawn as to the significance of the results for humans. Even the blood drawn from one human can give misleading results when generalizations to all humans are attempted.

Despite these limitations, animal testing has been helpful in defining *mechanisms* of BMI and thrombus formation, and the interdependence of blood biochemical pathways, the nature of the surface, and the blood flow regime. In addition, while results of animal testing may not quantitatively predict results in humans, in many cases results can be qualitatively similar and allow for relative comparisons between materials and devices. These aspects are discussed further later. In general, studies in lower animal species, such as the rabbit, rat, and guinea pig, may be useful to screen for profound differences between materials, for example, by incorporation of an antithrombotic drug delivery system into an otherwise thrombogenic device. Short-term screening to identify markedly reactive materials, and longer-term studies to evaluate healing and its impact on BMI can also be performed in species such as sheep and pig. When differences in BMI are likely to be modest (for example, as a consequence of subtle changes in surface chemistry or device configuration) the ranking of materials based on tests with lower animal species may be different from results that would be obtained in humans.

In vitro testing generally requires anticoagulation of the blood that can have a profound effect on BMI. In vivo testing and the use of extracorporeal circuits are also commonly performed with anticoagulants. Two anticoagulants are frequently used: sodium citrate, a calcium ion chelator required for certain reactions of platelets and coagulation proteins, and heparin, a natural polysaccharide used to block the action of the coagulation protease thrombin (Chapter 2.2.6). Both can markedly affect BMI. In particular, the removal of calcium ions may profoundly depress platelet–surface reactions, and the capacity of platelets to aggregate and form thrombi. Thus the relationship between BMI in the presence of citrate anticoagulant and “thrombogenicity” in the absence of anticoagulant is questionable. Similar concerns apply to heparin anticoagulation. Although this agent is less likely to interfere with the earliest platelet reactions, thrombus formation may be impaired by inhibition of thrombin activity. The use of heparin is appropriate for evaluation of devices where heparinization is used clinically (e.g., oxygenators, dialyzers). In general, results with anticoagulated blood cannot be used to predict performance in the absence of anticoagulants. A discussion of anticoagulants in the context of BMI has been presented (McIntire et al., 1985).

Blood is a fragile fluid that begins to change from the moment it is removed from the body. It may become more active (activated) or less active (refractory). Thus BMI evaluations with blood externalized from the normal circulatory system for more than a few hours are questionable. If purified blood components or cells are used (e.g., platelets, fibrinogen), studies must be performed to ensure that they

remain functionally normal. In most cases the volume of blood used, relative to test surface area, should be large. Similarly, the area of nontest surfaces, including exposure to air interfaces, should be minimized. Changes in blood temperature, test surface temperature, or exposure to bright light sources (Haycox et al., 1991) can also produce artifactual results. When blood is pumped, the recirculation rate (fraction of total blood volume pumped per unit time) should be minimized, since blood pumping alone can induce platelet and red cell damage, platelet release reactions, and platelet refractoriness (Haycox and Ratner, 1993). If care is taken to ensure that critical experimental variables are well controlled, a recent multicenter study has indicated that concordant results and conclusions can be reached in measuring acute platelet adhesion and activation by selected biomaterials between laboratories and within a study (Braune et al., 2017). Although the complexity of this assessment was low, only looking at platelet adhesion from plasma, similar attempts to control variability in other BMI assessment processes may allow more comparative data to be considered as candidate materials are considered for a given application.

Blood is a complex, fragile fluid, and outcomes of BMI studies will be strongly impacted by the animal species (or human donor), blood-handling protocols, and storage time.

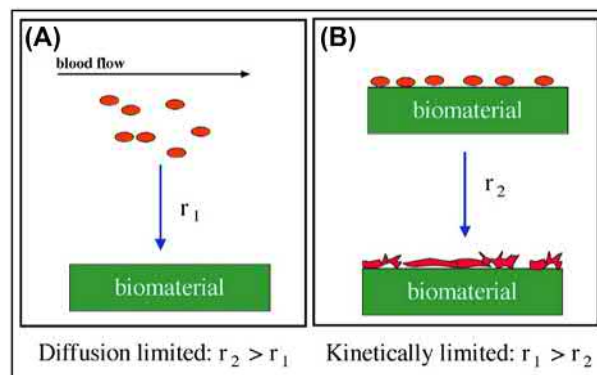
Flow: Blood Interactions Dictated by Shear and Mass Transport

Blood flow controls the rate of transport (by diffusion and convection) of proteins, cells, and thrombi in the vicinity of artificial surfaces and thus plays a critical role in the multistep process of thrombus growth. This subject has been reviewed (Brass and Diamond, 2016; Pantelev et al., 2015; and Chapter 2.1.6). Platelet diffusion in flowing blood, and early platelet attachment to surfaces, may be increased 50–100-fold by the presence of red blood cells that greatly enhance the movement of platelets across parallel streamlines. While physiological blood shear forces probably do not damage or activate platelets directly, such forces can dislodge platelet aggregates and thrombi (embolization) to distal circulatory beds. At supraphysiologic shear stresses, as might occur in stenoses or in the flow paths of some devices, shear activation of platelets can be a concern. Similarly, red cells may also be subject to mechanical damage and release chemical factors enhancing platelet reactivity (Turitto and Baumgartner, 1987).

A number of studies using well-characterized flow geometries have suggested that the initial attachment of platelets to artificial surfaces increases with increasing blood flow or, more specifically, with increasing wall shear rate (the slope of the velocity profile at the surface). Under conditions of low wall shear rate flow (less than $\sim 1000/s$), early platelet adhesion (over the first minutes of exposure) may depend more upon the platelet arrival rate (i.e., platelet availability) than on substrate surface properties (Friedman et al., 1970). Under these conditions the platelet–surface reaction rate is said to be *diffusion controlled*. At higher shear rates, platelet

adhesion may depend less upon platelet transport to the surface, and more on the reactions triggered by surface properties (*reaction controlled*, Schaub et al., 2000); thus studies designed to assess the role of surface properties are best performed under flow conditions where platelet transport is not limiting. Following initial platelet adhesion, subsequent processes of platelet aggregation and in vivo thrombus formation (over minutes to hours) are predominantly *reaction controlled*. For example, platelet accumulation on highly thrombogenic artificial surfaces (e.g., fabric vascular grafts) or biologic surfaces (e.g., collagen) may be rapid, and dependent on both the substrate reactivity and factors influencing platelet availability (shear rate, hematocrit, and platelet content of blood) (Harker et al., 1991). Under other circumstances, the rate of platelet–surface interactions may be almost entirely reaction controlled. For example, with smooth-walled artificial surfaces that repeatedly embolize small platelet aggregates continuously over days, the overall rate of platelet destruction depends strongly on material properties, but not on blood flow rate or circulating platelet numbers over wide ranges of these variables (Hanson et al., 1980). These concepts of diffusion and reaction control are further explained in Fig. 2.3.5.4.

It has been observed that under arterial flow conditions (high wall shear rate), thrombus that forms in vivo may be largely composed of platelets (“white thrombus”), while thrombus that forms under venous flow conditions (low shear rate) may contain mostly red cells entrapped in a fibrin mesh (“red thrombus”). The process of platelet thrombus formation may not be affected by administration of heparin (i.e., arterial thrombosis may be heparin resistant), while venous thrombosis is effectively treated with heparin. This insensitivity of platelet reaction to heparin in high shear blood flow is somewhat surprising, since the procoagulant enzyme thrombin, one of the most potent activators of platelets, is strongly inhibited by heparin. These observations have been incorrectly interpreted to mean that arterial thrombosis and venous thrombosis are separable processes, with the former depending only on platelet reactions, and the latter depending only on surface protein-triggered coagulation events. However, while platelet-dependent (arterial) thrombosis may be little affected by heparin, it is blocked quite effectively by other inhibitors of thrombin (Hanson and Harker, 1988; Wagner and Hubbell, 1990), indicating that heparin is limited in its capacity to block the thrombin enzyme when thrombin is produced locally in high concentrations through reactions that may be catalyzed on the platelet surface (Chapter 2.2.6). The formation of fibrin, due to the action of thrombin on fibrinogen, is also important for thrombus formation and stabilization since: (1) fibrinolytic enzymes can reduce platelet thrombus formation, and (2) arterial thrombi are often composed of alternating layers of platelets and fibrin. Thus in most circumstances, thrombin is a key promotor of *local* platelet and fibrin accumulation (on surfaces) under both high shear and low shear conditions. Thrombi may differ in appearance, because under high flow conditions, thrombin and precursor procoagulant

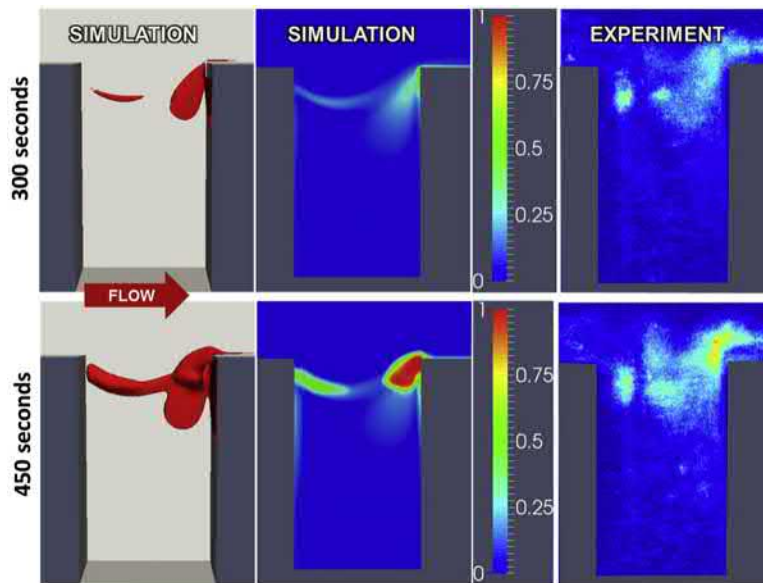


• **Figure 2.3.5.4** The effects of flow and material surface properties on platelet transport to, and reaction with, surfaces. One can define two rate processes: r_1 , the rate of platelet transport from blood to the surface (higher in rapidly flowing blood), and r_2 , the rate of reaction of a platelet with the surface. (A) In low wall shear rate blood flow, platelets can be slow to reach the surface and r_1 dominates the kinetics of the reaction—for reactive surfaces, the surface can be “starved” of platelets for reaction. (B) In high wall shear rate blood flow, platelets are transported to the surface much more rapidly than they can react with the surface, and the intrinsic reactivity of the surface, r_2 , can be observed.

enzymes (e.g., Factor Xa) may be diluted sufficiently to prevent *bulk phase* clotting and trapping of red cells.

Modeling of the coupled effects of flow and surface-associated reactions on biomaterial thrombosis has been the subject of growing interest as the power of numerical simulations and computational processing have increased. The potential future benefit of such approaches is apparent. By selecting parameters that reflect the activation status and reactivity of a typical patient’s blood, by defining a geometry and boundary conditions for a device blood flow path, and by inputting parameters that reflect a given biomaterial surface’s propensity to support platelet adhesion, activation, and coagulation cascade activation, a simulation could predict whether and where thrombus was likely to form. Using such a simulation, parameters could be altered to minimize the risk for such deposition. In particular, the flow path could be altered to improve transport and minimize risk in some parts of the device, or a less activating material or surface treatment could be applied in an area at high risk.

Despite important advances, such coupled models are not yet routine, although computational fluid dynamics models are commonly applied to cardiovascular device design to minimize “hot spots” of high shear stress, recirculation, or stagnation (Bluestein, 2017). From a biomaterials perspective, the challenge in defining the needed surface activation parameters to use in coupled simulations is highlighted in this chapter. The blood parameters are also challenging to define for a patient population, as would be the effect of anticoagulant therapy. An example of the current state of thrombosis modeling of relevance to biomaterial and device design is shown in Fig. 2.3.5.5 (Wu et al., 2017). For a disturbed flow situation introduced by a crevice in the wall of the flow path, the modeling captures some of the characteristics of the experimentally observed



• **Figure 2.3.5.5** Modeling of thrombus deposition from blood flowing over a crevice (similar to what might be found at a seam or joint within a blood pump). The computational simulation (*left and middle panels*) is shown to generally predict the nonintuitive regions of platelet deposition versus flow chamber experiments with fluorescently labeled platelets flowing in whole blood over a crevice with a Ti6Al4V alloy surface at $t=300$ and 450 s and a crevice length of $L_c=0.075$ mm. *Center and right panels* indicate volume fraction of platelets in the near-wall region of the channel. (From Wu, W.T., Jamiolkowski, M.A., Wagner, W.R., Aubry, N., Massoudi, M., Antaki, J.F., 2017. Multi-constituent simulation of thrombus deposition. *Sci. Rep.* 7, 42720.)

early platelet deposition. Experimental studies with similar disturbed flow path geometries and biomaterial surfaces of different thrombogenicity have shown the relative effects of changing the flow disturbance (crevice size) versus employing less thrombogenic materials (Jamiolkowski et al., 2016), although the contact times for both the simulations and experiments noted are short.

In summary, thrombus formation requires the transport by flow of platelets and coagulation proteins to surfaces. Fibrin polymerization, as well as local platelet activation and recruitment into growing thrombi, requires conversion of prothrombin to thrombin, the end product of a sequential series of coagulation reactions that are also catalyzed by platelets, and may be amplified or inhibited by various feedback mechanisms (Chapter 2.2.6). Blood flow regulates each reaction step, such that under low (venous) flow conditions fibrin formation is abundant; thrombi may resemble coagulated whole blood with many entrapped red cells. Under high (arterial) flows, platelets stabilized by much smaller amounts of fibrin may comprise the greater proportion of total thrombus mass. Modeling of flow-related effects in thrombosis is rapidly advancing and may offer a means to better design blood biocompatible devices in the future.

Thrombus formation requires the transport by flow of platelets and coagulation proteins to (and from) surfaces. Absence of flow, low shear flow, and high shear flow can each give dramatically different BMI results.

Surfaces: Actively Studied, but Least Well Defined, of the BMI Variables

Many different artificial surfaces, in various device applications, are used in contact with blood. It is well documented that surface physicochemical properties of materials can influence early events, for example, on protein adsorption (Chapter 2.1.2) and platelet adhesion—yet how these effects relate to subsequent thrombus formation remains uncertain.

When placed in contact with blood, most, if not all, artificial surfaces first acquire a layer of adsorbed blood proteins whose composition and mass may vary with time in a complex manner depending on substrate surface type (Chapter 2.1.2). This layer mediates the subsequent attachment of platelets and other blood cells that can lead to the development of thrombi. The relationship between material properties, the protein layer, and the propensity of a material or device to accumulate thrombus is not well understood because: (1) protein–surface reactions involve complex, dynamic processes of competitive adsorption, denaturation, and activation; (2) cell–surface interactions may modify the protein layer, i.e., cells may deposit lipid and protein “footprints” derived from the cell membrane; (3) the importance of specific adsorbed proteins for subsequent cell interactions, especially in vivo, is not well defined; and (4) there have been few *relevant* tests in which both protein adsorption and later thrombus formation have been assessed. Under conditions of low blood shear, the capacity of negatively charged surfaces (such as glass)

to activate intrinsic coagulation (via Factor XII) can lead to thrombin production, with subsequent platelet deposition and fibrin clot formation. Under other circumstances the availability on surfaces of adhesive plasma proteins, such as fibrinogen, will be important for regulating cell attachment and subsequent thrombus formation (Brash et al., 2019; Sivaraman and Latour, 2010).

With anticoagulated blood, initial platelet attachment to a variety of surfaces may be comparable and limited to a partial platelet monolayer, suggesting that surface properties may be “inconsequential” for early platelet adhesion, especially where platelet transport to the surface may be rate limiting (Friedman et al., 1970). In the absence of anticoagulants, initial platelet attachment may vary, but no general relationship to substrate surface properties has been demonstrated. In attempts to establish such relationships, thrombus formation has been studied using devices implanted in animals and composed of various materials, including polymers, metals, carbons, charged surfaces, and hydrogels. Correlations have been sought between the blood response and surface properties, such as charge (anionic–cationic), hydrophilicity, hydrophobicity, polarity, contact angle, wettability, and critical surface tension (Kaelble and Moacanin, 1977; McIntire et al., 1985; Salzman and Merrill, 1987; Williams, 1987). These parameters have not proven satisfactory for predicting device performance even in idealized test situations, reflecting the complexity of the phenomena being investigated, the limitations of animal experiments and, in some cases, the inadequate characterization of material surface properties (see Chapters 1.2.4 and 3.1.9, and Ratner, 1993a).

In many cases, material properties are constrained by the specific mechanical and morphological needs of the intended blood-contacting device application. For example, vascular grafts and the sewing ring of prosthetic heart valves are composed of fabric or porous materials to permit healing and tissue anchoring. Other materials must be permeable to blood solutes and gases (dialysis and oxygenator membranes) or distensible (pump ventricles, balloon catheters). These design constraints often necessitate complex flow geometries. In general, devices with flow geometries that cause regions of flow recirculation and stasis tend to produce localized clotting in the absence of heparin anticoagulation. On a microscopic scale, surface imperfections and crevices may serve as foci to initiate thrombus formation, as noted earlier. While surface smoothness is usually desirable, many devices having a fabric or microporous surface (e.g., vascular grafts) function well if the layer of thrombus that forms is not thick enough to interfere with device function and does not embolize.

The lack of consensus on the blood compatibility of materials was pointed out by Ratner (1984). This is a consequence of the complex, multifactorial nature of BMI. Assigning a label of “blood compatible” or ranking materials as to their suitability for use in blood is still fraught with uncertainty, and at best would need to be specifically qualified with the device and operating conditions considered.

Blood Interaction Times With Materials and Devices

Different events may occur at short and long BMI times. Consider the case of a patient supported by a ventricular assist device where a thromboembolic event (stroke) occurs after several months of uneventful support. What changed at this late time point to trigger the event? Blood chemistry will certainly vary as a patient’s health changes, for instance, with an infection, or with health changes due to the device action (e.g., improved diet and exercise resulting in more robust immune and hemostatic systems). Anticoagulation and antiplatelet medications need to be managed. The device may change as it interacts with the blood and nearby tissue. The embolus that triggered the event may be one of a long series of shed emboli that statistically happened to be of a large enough size this time, and followed a path to a region of the cerebrovasculature where an infarct would be noticed and had adequate mechanical properties not to break down. Clearly, many variables are in play, and BMI may present an ongoing risk. A test performed where blood contacts a device for seconds or minutes may yield a result that will have limited meaning for devices used for hours or days, or which may be implanted chronically. Thus measurements of protein adsorption (an early event) can, in some cases, predict levels of platelet adhesion. But platelet adhesion alone is not an adequate measure of thrombogenicity, and it does not predict local or systemic thrombogenic effects that could be harmful. Still, several studies indicate that an early maximum in platelet thrombus accumulation may be seen within hours of device exposure, and this can be sufficient to produce device failure (e.g., small diameter vascular graft occlusion) (Harker et al., 1991). Therefore short-term testing (over hours) may be appropriate for predicting the clinical usefulness of devices that can produce an acute, severe thrombotic response.

Evaluation of BMI

A summary of some (or historically important) *in vitro* and *in vivo* testing procedures commonly used to evaluate BMI is presented in this section. A few relevant case studies with commentary are included. We emphasize that a thorough characterization of surface properties is critical for the interpretation of these tests (Chapters 1.2.4 and 1.4.2, and Ratner, 1993b), since the surface composition of materials is often significantly different from “as received and labeled.” A few specific tests that have been historically influential and tests that are used today are summarized in Table 2.3.5.2.

BMI can be evaluated *in vitro* and *in vivo*. Also, we can look at the BMI of either the biomaterials in isolation in a test configuration or the blood interactions of real devices. There are typically unique systems and geometries for *in vitro*, *in vivo*, and device-based assays. However, there are commonalities in the measurements of blood parameters. For example, blood can be circulated through a tube *in vitro*, circulated through an implanted biomaterial shunt *in vivo*, or circulated through a hemodialyzer (*in vivo*

TABLE 2.3.5.2 A Partial List of Blood–Materials Interactions Tests

- Qualitative assessment (look at the thrombus)
- Count adherent blood elements
- Observe and categorize platelet morphology
- Measure platelet release molecules
- Clotting times and related coagulation assays
- Measure soluble products of thrombosis
- Platelet consumption
- Flow cytometry to measure activation of cells in the bulk phase
- Microparticles or microaggregates (flow cytometry)
- Embolus measurement

or in vitro). In all cases, the blood emerging from the test system might be assessed by a partial thromboplastin time test, measurement of soluble by-products of thrombotic reactions, or a flow cytometric analysis of activated platelets. Thus the methods for contacting blood with biomaterials, and the methods for assessing blood change, can often be considered independently.

In Vitro Tests

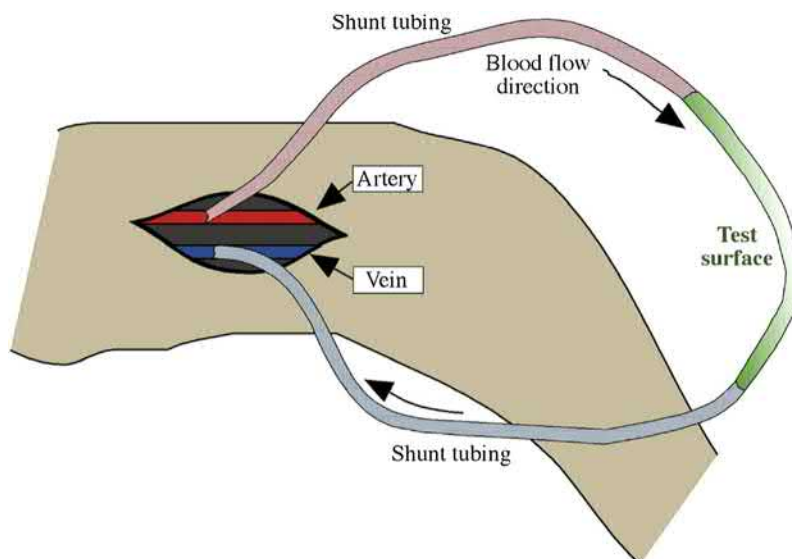
In vitro BMI tests involve placing blood or plasma in a container composed of a test material, in a container containing the test material, or recirculating blood through a flow system in which test materials contact blood under well-defined flow regimes that simulate physiologic flow conditions. Many flow geometries have been studied, including tubes, parallel plates, packed beds, annular flows, rotating probes, and spinning disks. The historical (but still relevant) literature on these test methods has been reviewed (McIntire et al., 1985; Turitto and Baumgartner, 1987), and has yielded considerable insight into how proteins and platelets are transported to, and react with, artificial surfaces. Such studies provided a wealth of morphologic information at the cellular level regarding details of platelet–surface and platelet–platelet interactions (Sakariassen et al., 1989). However, as discussed earlier, these tests are usually of short duration, and are strongly influenced by the blood source, handling methods, and use of anticoagulants. Thus, in vitro test results generally cannot be used to predict longer-term BMI and in vivo outcomes, and can provide only the most general guidelines for the selection of materials for particular devices. However, in vitro tests may be useful for screening materials that are highly reactive toward blood.

Tests of the whole blood clotting time and variations thereof involve placing nonanticoagulated whole blood (or blood anticoagulated with sodium citrate, which is then

recalcified) into containers of test material (or adding the test material to the container) and measuring the time for a visible clot to form. Materials that quickly activate intrinsic coagulation and cause blood to clot within a few minutes (like glass surfaces) are probably unsuitable for use in devices with low shear blood flow or in the absence of anticoagulants. These tests are known by names such as whole blood clotting time, activated partial thromboplastin time, and whole blood recalcification time. An older variant of these tests, frequently mentioned in the early biomaterials literature, is the Lee–White clotting time test.

Possibly the most commonly performed assay for BMI involves quantifying platelets deposited onto surfaces and visualizing platelet reaction to surfaces. The limitations of these tests have been discussed and are reiterated in this section. Still, these assessments are so commonly performed that some discussion is appropriate. The limitations of these platelet attachment tests are important to consider up front: (1) are the platelets mass transport limited in arriving at the surface?; (2) are dynamic events such as transient adhesion, release, and/or emboli formation being missed due to limited time points for observation?; (3) are the platelets active or refractory (unresponsive)?; (4) can species differences in platelet adhesiveness have large effects on the observed numbers of platelets?; (5) can platelets spread into extremely thin surface films be difficult to observe or count (Haycox and Ratner, 1993)?; and (6) are platelet deposition studies typically short term, and thus generally have limited meaning for devices that reside for longer periods of time in blood? A promising approach to address the significance of surface adherent platelets for blood compatibility is to consider not only platelet number, but also platelet morphology (Waples et al., 1996). Platelets on surfaces can appear discoid without dendrites (unactivated), and then might show various degrees of activation (spread, mildly dendritic, highly dendritic, etc.). Such platelet morphologies can be assessed using light microscopy, fluorescent methods, or scanning electron microscopy. It is also possible to assess the activity of the deposited platelets in terms of their support of coagulation reactions by annexin V binding (Nechipurenko et al., 2019). Nonadherent platelets may be assessed in the bulk phase with flow cytometric techniques to quantify activation status (Ye et al., 2010; Blit et al., 2011) to allow further consideration of the scenarios indicated in Fig. 2.3.5.1.

Recirculation of heparinized blood or citrated blood through tubular devices and materials may lead to platelet activation and/or platelet deposition onto highly thrombogenic materials, with the appearance in plasma of proteins released from platelets (Kottke-Marchant et al., 1985; Haycox and Ratner, 1993). Thus these and similar methods may identify materials that might cause rapid platelet accumulation in vivo over short time periods, and therefore be unsuitable for certain applications such as small diameter vascular grafts or blood conduits. Both recirculation tests and in vitro clotting assays can be



• **Figure 2.3.5.6** Illustration of an arteriovenous (A-V) shunt placed between the femoral artery and vein (in the leg) of an experimental animal. Materials to be tested (in this case a tubular device) are interposed between inlet and outlet segments of the shunt.

considered for preliminary screening and identification of materials that could be highly thrombogenic. Most artificial surfaces in common use in blood-contacting devices would probably “pass” these tests. Since small differences in test results are of little significance for predicting material performance in actual use applications, these tests are not appropriate for optimizing or refining material properties. *In vivo* testing is more appropriate for discerning finer distinctions in blood reactivity, and such tests are discussed next.

In Vivo Tests of BMI

Many studies have been performed in which test materials, in the form of rings, tubes, and patches, are inserted for short or long time periods into the arteries or veins of experimental animals (McIntire et al., 1985; Salzman and Merrill, 1987; Williams, 1987). Here are a few concerns and considerations for such tests:

- (1) The timing and type of measurements may be such that important blood responses are unrecognized. In particular, the measurement of gross thrombus formation at a single point in time may lead to incorrect conclusions about local thrombus formation (e.g., Fig. 2.3.5.1), and does not provide assessment of systemic effects of thrombosis such as embolization and blood element consumption.
- (2) With more commonly used animal species (e.g., sheep, dogs), blood responses may differ from humans both quantitatively and qualitatively.
- (3) The blood flow conditions of the model may not be controlled or measured, and in fact may not even be relevant for actual implant device geometries.

- (4) There may be variable blood vessel trauma and tissue injury that can cause local thrombus formation through the extrinsic pathway of blood coagulation (Chapter 2.2.6).

Evaluations of BMI may be performed in animals having arteriovenous (A-V) or arterioarterial shunts, i.e., tubular blood conduits placed between an artery and vein or between an artery and artery. A-V shunts have been studied in a variety of animals, including baboons, dogs, pigs, and rabbits (McIntire et al., 1985). Qualitatively similar results have been obtained with shunts in dogs and baboons (Hanson et al., 1980; Sefton et al., 2000). An A-V shunt system is illustrated in Fig. 2.3.5.6. Once surgically established, shunts may remain patent (not occluded) for long periods of time (months) without the use of anticoagulants. Test materials or devices are simply inserted as extension segments or between inlet and outlet portions of the chronic shunt. These systems have many advantages: (1) blood flow is easily controlled and measured; (2) native or anticoagulated blood can be employed; (3) the animal’s physiology removes damaged blood elements and makes new blood with each circulation through the body; and (4) both short-term and long-term BMI, including both local and systemic effects, can be evaluated. The downsides of these tests are demanding surgery, high expense, and ethical issues associated with chronic shunting of larger animals.

As an example, consider the A-V shunt model in baboons—baboons are used because they are hematologically similar to humans. The blood responses to tubular biomaterials and vascular grafts have been quantitatively compared with respect to: (1) localized thrombus accumulation; (2) consumption of circulating platelets and

fibrinogen; (3) plasma levels of factors released by platelets and coagulation proteins during thrombosis; and (4) embolization of microthrombi to downstream circulatory beds (Harker et al., 1991). These studies in primates are consistent with observations in humans that certain commonly used polymers (e.g., polytetrafluoroethylene, polyethylene, plasticized poly(vinyl chloride), silicone rubbers) and some vascular grafts (e.g., polytetrafluoroethylene) are relatively nonthrombogenic in extracorporeal circuits and arteries. Thus results with shunt models, particularly in higher animal species, may be predictive of BMI in humans when employed under comparable flow conditions (laminar unidirectional flow with arterial shear rates). Since extracorporeal shunts exclude modulating effects of blood vessel cells and tissue injury, results with these models may be less relevant to the behavior of devices that are placed surgically or whose responses may be mediated by interactions with the vessel wall as well as the blood (e.g., heart valves, grafts, indwelling catheters, and sensors). It is further noted that

due to the expense and ethical considerations associated with the use of primates that BMI testing in this model is increasingly limited to latter stage assessments with device configurations.

In Vivo Evaluation of Devices

Since the blood response to devices is complex and not well predicted by testing of materials per se in idealized configurations, animal testing, and ultimately clinical testing, of functioning devices is required to establish safety and efficacy. Broad guidelines, based on the type of device being considered, are given next and apply to both animal and clinical testing. A summary of in vivo blood responses to devices, and of commonly used methods that have proven useful for evaluating those responses, is given in Table 2.3.5.3. Table 2.3.5.4 lists the wide range of screens that have been used in one group to understand blood interaction with devices, specifically ventricular assist devices (Wagner et al., 2000).

TABLE 2.3.5.3 Some Blood–Material Responses and Their Evaluation

Blood Components	Blood Response	Assessment ^a
Thrombus	Clot	Direct visual and histologic evaluation; noninvasive imaging (angiography, ultrasound, radioisotope, magnetic resonance); evidence of device dysfunction or blood path blockage.
	Thromboembolism	Emboli detection (ultrasound, laser); evidence of organ/limb ischemia; assessment of infarcts in organs; stroke.
Platelets	Consumption	Increased removal of labeled cells; reduced blood platelet count.
	Dysfunction ^b	Reduced platelet aggregation or responsiveness to agonist by FACS in vitro; prolonged bleeding time; altered thromboelastogram
	Activation	Increased plasma levels of platelet factor 4 and β -thromboglobulin; platelet membrane alterations (e.g., by FACS).
Red cells ^b	Destruction	Decreased red cell count; increased plasma hemoglobin.
White cells ^b	Consumption/activation	Decreased counts of white cell populations; increased white cell plasma enzymes (e.g., neutrophil elastase); expression of activation markers (by FACS)
Coagulation factors	Consumption ^b	Reduced plasma fibrinogen or other coagulation factors
	Thrombin generation	Increased plasma levels of prothrombin fragment 1.2 and thrombin:antithrombin III complex.
	Fibrin formation	Increased plasma level of fibrinopeptide A.
	Dysfunction ^b	Prolonged plasma clotting times.
Fibrinolytic proteins	Consumption ^b	Reduced plasma plasminogen level.
	Plasmin generation	Increased plasma level of plasmin:antiplasmin complex.
	Fibrinolysis	Increased plasma level of fibrin D-dimer fragment.
Complement proteins ^b	Activation	Increased plasma levels of complement proteins C3a, C3b, C5a, C5b-9.

FACS, Fluorescence-activated cell sorting.

^aMonoclonal antibody-based assays for immunoassay kits or flow cytometry may not be available or applicable for detection of nonhuman proteins.

^bTests that may be particularly important with long-term and/or large surface area devices.

Devices that have relatively small surface areas and are exposed for short periods of time (hours to days) include catheters, guidewires, sensors, and some components of extracorporeal circuits. With these devices, the primary concern is the formation of significant thrombus that could interfere with device function, e.g., thrombus blocks the diffusion of an analyte to a sensor, occludes the blood vessel, embolizes spontaneously, or is stripped from the device surface when it is removed from the body (e.g., during catheter withdrawal through a vessel insertion site) producing occlusion of distal vessels and tissue ischemia. Devices exposed for short periods that have large surface areas (dialyzers) and complex circuitries (pump-oxygenators) may, in addition, produce: (1) a marked depletion of circulating blood cells and proteins (e.g., platelets and coagulation factors); (2) an immune/inflammatory response through activation of complement proteins and white cells; and (3) organ dysfunction mediated by hemodynamic, hematologic, and inflammatory reactions. Mechanical devices that are used for long periods of time (heart assist devices, extracorporeal membrane oxygenators) may produce profound systemic

effects and organ dysfunction such that their use in humans remains challenging.

With both long-term and short-term device applications, thrombus formation can be assessed directly and indirectly. Important indirect assessments include depletion from circulating blood of cells and proteins consumed in the process of thrombus formation, and the appearance in plasma of proteins generated in the process of thrombus formation (e.g., fibrinopeptide A, platelet factor 4) as well as the detection of circulating activated blood cells by flow cytometry (Snyder et al., 2002). For some common devices, thrombosis is inferred through an increase in torque (power consumption) for rotary blood pumps (Scandroglia et al., 2016), decreased gas transfer or increased pressure drop across hollow fiber membrane bundles of blood oxygenators (Kaesler et al., 2019), regurgitant flow by Doppler flow measurements in prosthetic valves, and hemolysis in devices where a high velocity blood flow path is being constricted by putative thrombus to elevate shear stress and damage erythrocytes. Direct assessment of blood flow rate, flow geometry, and extent of flow channel occlusion can in many cases be achieved using sophisticated methods, including angiography, ultrasound imaging, and magnetic resonance imaging. Devices that are removed from the circulation should be visually inspected at the macroscopic and microscopic levels to assess whether thrombus has formed at particular sites or on certain materials. Emboli in flowing blood may be detected using ultrasound-based techniques (e.g., in cerebral arteries by Wilhelm et al., 1999), although these methods are not used widely in preclinical device assessment because of their complexity and translation to some animal models where skull thickness creates challenges. Thrombus formation and rates of platelet destruction by both acutely placed and chronically implanted devices can be determined quantitatively by measurements of platelet lifespan and scintillation camera imaging of radioisotopically labeled blood elements (McIntire et al., 1985; Hanson et al., 1990; Snyder et al., 2002).

While it was noted earlier that there are techniques available to detect thromboemboli when they are being transported in the bloodstream during the implant period, it is much more common in preclinical testing to examine the animal at the conclusion of the study for evidence of thromboembolic damage. In accordance with Figs. 2.3.5.1 and 2.3.5.2, a device may have little to no thrombotic deposition, yet clear evidence of thromboembolism at distal sites can be found. With many devices, such as cardiac valves, some vascular grafts, and circulatory support devices, it is the phenomenon of thromboembolism that is responsible for much of the morbidity and mortality associated with device implantation. As a result, *in vivo* preclinical testing of these devices routinely involves the assessment of organs where thromboemboli may travel and cause tissue ischemia. A downstream organ that is readily assessed is the kidney,

TABLE 2.3.5.4 Parameters Measured in the Assessment of Blood Interactions With Ventricular Assist Devices

Flow Assessment

Power consumption or torque generation by rotary pump, direct visualization (for some extracorporeal devices), ultrasound and fluorescent image tracking velocimetry

Coagulation

Prothrombin fragment F1.2, thrombin–antithrombin, clotting times

Embolism

Infarcts in end organs (e.g., kidneys, liver), neurologic symptoms, transcranial Doppler ultrasound, flow cytometric assays for the quantification of circulating platelet-containing microaggregates

Fibrinolysis

D-Dimer

Platelet Activation and Deposition

Platelet factor 4, beta thromboglobulin, flow cytometric detection of circulating platelet activation level and agonist responsiveness (e.g., p-selectin expression), platelet deposition (microscopy)

Complement

C3a, C5b-9

Leukocyte Activation

Flow cytometric detection of monocyte tissue factor expression, leukocyte–platelet microaggregates, leukocyte surface activation markers

where thromboembolism results in clear infarcts that can be measured and quantified.

Finally, it is important to emphasize that thrombosis occurs dynamically, such that thrombi continuously undergo processes of both formation and dissolution. Device failure and morbid events represent the imbalance of these processes. Older thrombi may also be reorganized considerably by the enzymatic and lytic mechanisms of white cells. Although thrombotic complications with most devices tend to occur early in the implant period, new thrombus growth may occur at later time points leading to a clinical event (occlusion or thromboembolic stroke) several weeks, months, or even years after implantation and an otherwise unremarkable implant period. While the initial consequences of surgical device placement include tissue injury, thrombosis due to tissue injury, and foreign-body reactions, the flow surface of long-term implants may become covered with a stable lining of cells (e.g., ingrowth of vascular wall endothelial and smooth muscle cells onto and into vascular grafts) or blood-derived materials (e.g., compacted fibrin). Certain reactions of blood elements (e.g., platelets, thrombin) may also stimulate the healing response. Ultimately, long-term devices, such as the small caliber graft, may fail due to excessive tissue ingrowth that could be largely unrelated to biomaterials properties or may be stimulated by the biomaterials.

We summarize this section on device testing by recognizing that many of the device applications just described, as well as laboratory and clinical methods for evaluating their biologic responses, will be unfamiliar to the bioengineer. However, it is important to appreciate that: (1) each device may elicit a unique set of blood responses, both short term and long term; (2) methods are available to assess systemic changes in the blood and host organism that indirectly reflect thrombus formation; and (3) localized thrombus formation can often be measured directly and quantitatively. Whenever possible, serial and dynamic studies should be performed to establish the time course of ongoing thrombus formation and dissolution. These measurements will ultimately predict device performance and allow for both better patient management strategies as well as the rational selection of biomaterials that will minimize adverse blood-device interactions.

Contemporary Concepts in BMI Evaluation

A general trend in the literature in recent years has been the increasing application of specific molecular detection technologies (e.g., monoclonal antibodies, peptides) to provide a more detailed and temporal interrogation of BMI. Two such applications, flow cytometry and targeted thrombus imaging, will be highlighted here and in three case studies.

The use of flow cytometry to analyze activation of blood elements can be an effective method of measuring blood

cell reactions and isolating specific pools of cells that have or have not undergone reaction. The basic technology behind flow cytometry (sometimes called fluorescence-activated cell sorting, FACS) involves the laser separation of fluorescently labeled cells from a narrow flowing stream of cells. The fluorescently labeled cells can be diverted from the flow stream to another flow channel where they are counted and harvested, or the fluorescence and light scattering can simply be recorded for each cell to give a precise count of cells exhibiting defined ranges of certain characteristics. One of the earliest studies using flow cytometry for blood-compatibility studies showed that in contact with blood-activating synthetic materials, thrombotic membrane fragments called microparticles are released (Gemmell et al., 1995). Since that important study, flow cytometry has been widely used to look at the upregulation of platelet P-selectin (CD62P), a consequence of α -granule release, monocyte and neutrophil CD11b (Mac-1 receptor) upregulation (Gemmell, 2000), platelet activation by annexin V binding to the negative phospholipid found on activated platelets (Wagner et al., 2000), and a number of other markers relating to platelet activation, white cell activation, and platelet aggregate formation. The power of the flow cytometry method resides in its ability to pinpoint and count selected features in a large pool of cells that can be identified by a fluorescently labeled targeting molecule, such as a monoclonal antibody. The method is applicable to blood that has been contacted with synthetic materials *in vitro* or *in vivo*.

While flow cytometry allows interrogation of cells in the bulk phase, the power of labeled targeting molecules can also be leveraged in imaging methods to define regions of thrombotic deposition and the amount of deposition in complex medical device flow paths. On a microscale this can be done with perfusion channels compatible with direct observation of flow and thrombus growth dynamics (Nechipurenko et al., 2019). Using targeted imaging agents, the researcher may look for specific features in the thrombotic process such as fibrin or activated platelets. Such imaging techniques remain limited by expense when performing whole animal imaging or using monoclonal antibodies. In these cases, less expensive targeting agents such as peptides or naturally selective binding molecules (e.g., annexin V for activated platelets) are employed.

Examples of BMI Evaluation

Three case studies will now be presented that place many of the concepts discussed to this point in the context of real-world BMI testing, moving from a well-defined *in vitro* test system to more complex *in vivo* testing with a blood-contacting device and targeted imaging applied to devices following clinical use.

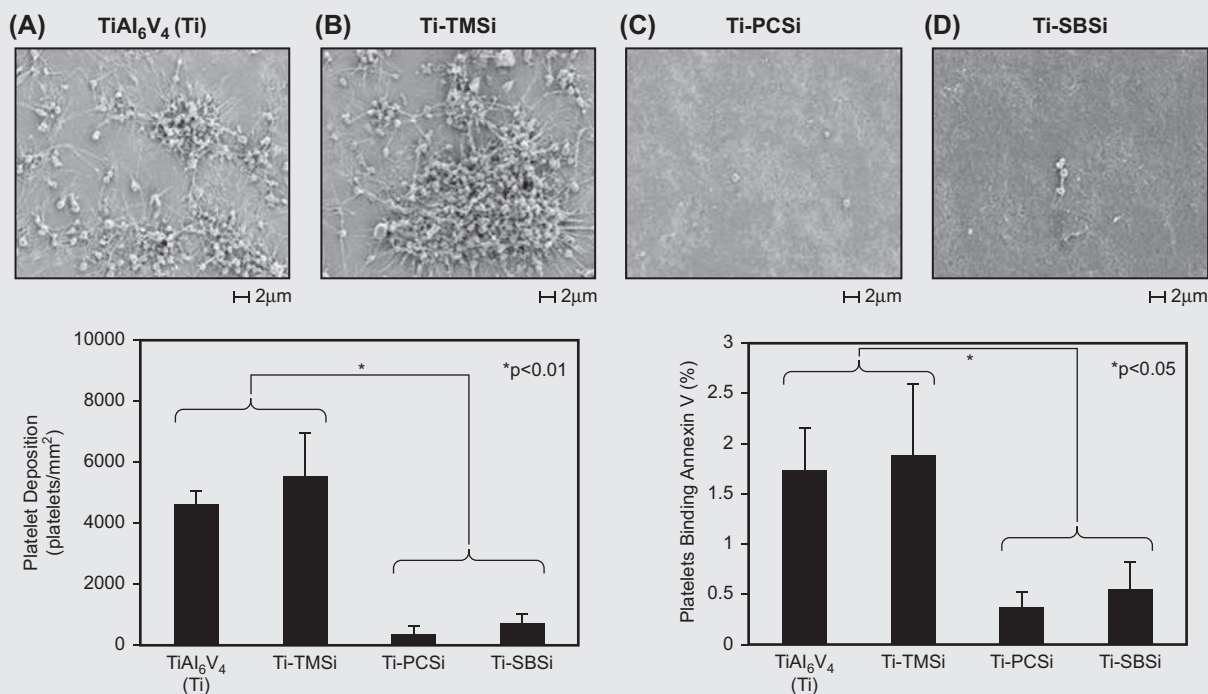
CASE STUDY I

Platelet Deposition and Platelet Activation Measured *in Vitro* (Ye et al., 2010)

Despite the limits of short-term blood contact studies *in vitro*, such studies can have value as a first-level assessment of relative thrombogenicity and, particularly, to assess if a surface modification is exhibiting a hypothesized reduction in platelet deposition and bulk-phase activation. Such results can then justify progression to more expensive *in vivo* testing. Fig. 2.3.5.7 shows results from an acute blood contact study of Ti6Al4V (Ti) alloy surfaces with and without zwitterionic surface modifications. This alloy is a commonly used metal in blood contacting devices where high strength and stiffness are required (e.g., blood pumps). For a broader discussion of zwitterionic surface modification, see Chapter 1.4.3A. The surfaces studied were cleaned and oxidized Ti6Al4V (Ti) alloy, trimethoxysilane modified alloy (Ti-TMSi, a non-zwitterionic control) and alloy with one of two types of covalently attached zwitterionic silanating modifiers based on phosphorylcholine (Ti-PCSi) or sulfobetaine (Ti-SBSi).

Heparin-anticoagulated ovine blood was contacted with test surfaces under rocking for 2 h after which platelet deposition

was measured quantitatively using a lactate dehydrogenase assay, and deposited platelet morphology was observed with scanning electron microscopy. Activation of platelets that were not deposited on the surface but were present in the bulk phase of contacting blood was measured using flow cytometry with fluorescent annexin V binding. This protein adheres to platelets that have activated and are expressing a membrane surface supportive of coagulation reactions. In Fig. 2.3.5.7, one can see formed platelet aggregates on the surfaces without the zwitterionic modification and these platelets have the classic appearance of activation with numerous extended pseudopodia. Few platelets are seen on the zwitterionic-modified surfaces. The quantified platelet deposition supports the visual results. Flow cytometry results showed that platelets not deposited on the surfaces were also less activated with the zwitterionic surfaces. Not shown in the figure are results that found lower levels of fibrinogen adsorption from a pure protein solution with the zwitterionic materials. The study provides an example of an *in vitro* evaluation combining assessments of platelet deposition and flow cytometric measurements of platelet activation.



• **Figure 2.3.5.7** (Top) Scanning electron micrographs of (A) TiAl₆V₄ (Ti), (B) Ti-TMSi, (C) Ti-PCSi, and (D) Ti-SBSi surfaces after contact with fresh, heparinized ovine blood under mixing for 2 h at 37°C. The right two surfaces have been modified with zwitterionic molecules. Note the platelet aggregates and individual platelets with extended pseudopodia indicating activation on the nonzwitterionic surfaces. (Bottom left) Platelet deposition on the same surfaces quantified with a lactate dehydrogenase assay. (Bottom right) Platelet activation in the bulk phase of blood contacted with the surfaces where fewer activated platelets are seen after zwitterionic surface contact. (From Ye, S.H., Johnson, C.A. Jr, Woolley, J.R., Murata, H., Gamble, L.J., Ishihara, K., Wagner, W.R., 2010. Simple surface modification of a titanium alloy with silanated zwitterionic phosphorylcholine or sulfobetaine modifiers to reduce thrombogenicity. *Colloids Surf. B Biointerfaces*. 79 (2), 357–364.)

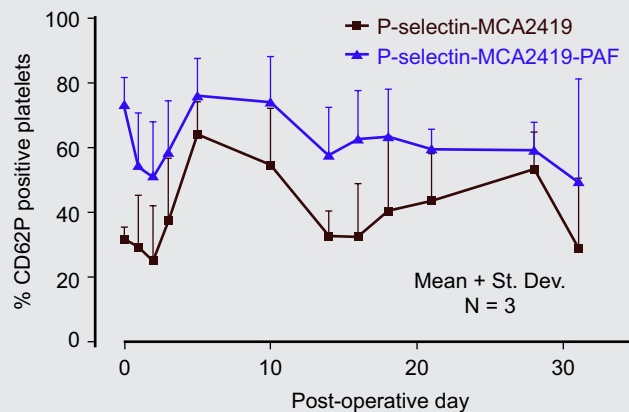
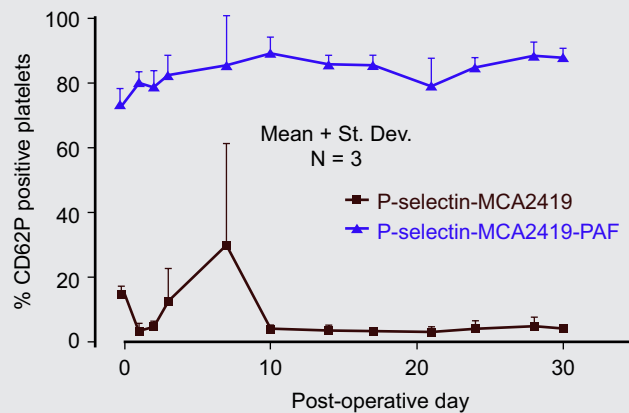
Device Thrombogenicity With Circulating Activated Platelets, Platelet Responsiveness, and Thromboembolic Effects Measured (Johnson et al., 2011)

One of the attractive features of using flow cytometric techniques to assess platelet activation is that it allows the researcher to monitor the status of circulating platelets over the course of a device implant directly, as opposed to only evaluating thrombotic effects at the time of device recovery. As an example of this technique, Johnson et al. (2011) evaluated an extracorporeal, magnetically levitated pediatric circulatory support device and specifically compared different candidate cannula designs. The cannulae are conduits that are placed within the vasculature to serve as inlet and outlet blood paths for this rotary blood pump (Fig. 2.3.5.8). Using an ovine model, the device was connected and functioned for a 30-day period. During the support period, blood was collected and flow cytometry applied to measure CD62P expression on platelet membranes. CD62P, also called p-selectin, is found in the α -granules of platelets. Upon platelet activation the granule fuses with the outer membrane and the CD62P can be detected with an antibody (in this study the antibody is MCA-2419, which cross-reacts with human and sheep CD62P). Flow cytometry is used to determine the percent of platelets that are above a background threshold level of antibody binding. Separate aliquots of the collected blood were stimulated with a potent platelet agonist, platelet-activating factor (PAF), to measure whether the circulating platelet population was responsive or had reduced responsiveness due to ongoing damage from the device. For a less thrombogenic device, one would expect to see low levels of circulating activated platelets, but high levels of platelet activation following PAF stimulation. For a thrombogenic device, higher levels of activated platelets would be observed and the response to PAF would be muted.

In Fig. 2.3.5.8 the temporal results for unstimulated and PAF-stimulated blood are shown for two groups of sheep that had two different cannula designs. At the time of study completion, the kidneys were assessed for infarcts (attributable to thromboembolism) and the device surfaces were assessed for obvious thrombotic deposition. With one type of cannulae (top Fig. 2.3.5.8) platelet activation rose early in the implant period, but then returned to low levels. The relative elevation of the preoperative blood sample at day 0 is attributable to its collection by venipuncture versus latter blood collection through indwelling lines after the implant surgery. Platelet responsiveness to PAF was high throughout the implant period, no thrombi were found on the devices, and few (<4) or no infarcts were found in the kidneys.

In contrast, the second cohort of sheep (bottom Fig. 2.3.5.8), which represented a subset of animals receiving a different cannula design, had a different course of platelet activation. The unstimulated, circulating activated platelet levels were elevated throughout the implant period. Stimulation with PAF showed responsiveness, but the levels attainable were reduced and the gap between unstimulated and stimulated was narrowed versus the other animal group. Furthermore, thrombus deposition was found in the cannula of one animal and all animals had >4 kidney infarcts.

In interpreting these data, the caveats noted earlier in this chapter regarding differences between animal and human blood apply. Also, this device was being developed for the pediatric population, where unique differences exist between human adult and neonatal/pediatric hemostatic systems. Furthermore, the number of animals is low (a common economic constraint), limiting statistical power. However, one can see that such results could provide guidance regarding the selection of a cannula design to consider advancing to subsequent preclinical testing and development based on blood biocompatibility assessed with these methods.



• **Figure 2.3.5.8** (Top) Example of inflow and outflow cannulae that connect the vasculature to a pediatric blood pump. (Middle) Circulating activated platelets reflected in CD62P expression with (platelet activating factor, PAF) or without agonist stimulation during a 30-day implant period in ovine model. In this animal group the postoperative course was not remarkable, few infarcts were found in the kidneys, and there was no gross thrombus on the device. Circulating activated platelet levels were low and platelets responded strongly to PAF. (Bottom) With a different cannula design, a subset of sheep had higher levels of circulating activated platelets and less responsiveness to PAF. At explant, one animal had device thrombus and all animals had >4 kidney infarcts. (From Johnson et al., 2011.)

Imaging Thrombotic Deposition in a Complex Device (Cui et al., 2018)

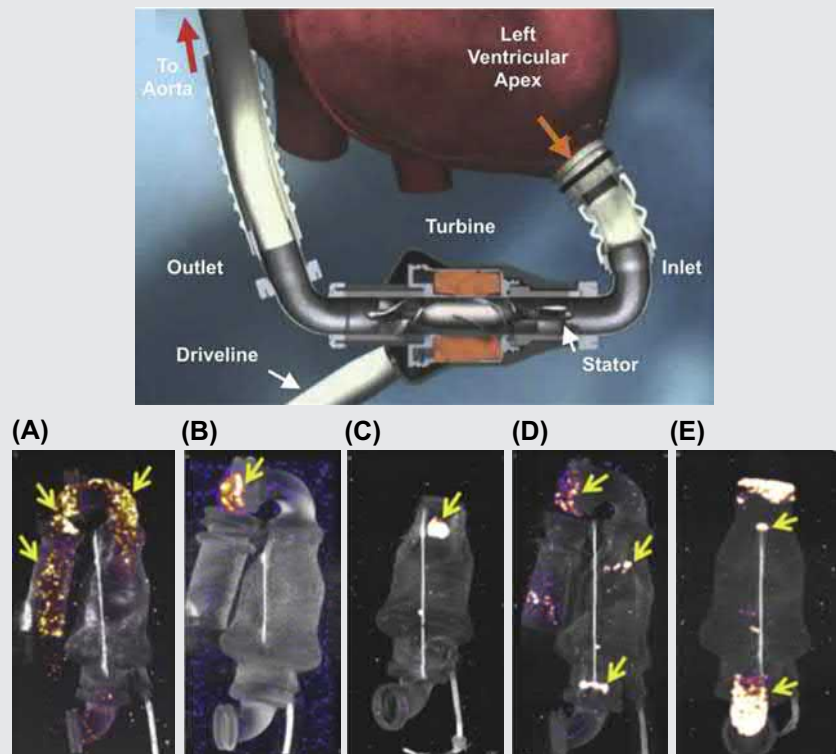
For many blood-contacting devices, thrombotic deposition can be detected and assessed with ultrasound and angiography. These techniques are commonly applied with vascular grafts and prosthetic valves and are utilized in the diagnosis and management of clinical thrombosis. There are also several secondary measures well correlated with thrombotic deposition that can trigger diagnostic imaging or intervention. For oxygenators, the pressure drop across the fiber bundle is such a critical measurement. For rotary blood pumps, power consumption, flow rates, and hemolysis are used clinically with increasing sophistication to assess and address risks to the patient (Scandroglio et al., 2016). In cardiovascular device development these same techniques are employed as surrogates for more direct measurements in animal models during the implant period.

For both clinical and preclinical assessment of device thrombogenicity it would be useful to be able to utilize targeted imaging, where the imaging agent binds specifically to a given marker, such as an activated platelet or fibrin. It would also be desirable if this imaging could be done in regions where simpler imaging methods are not feasible. For example, within and near metallic blood pumps, ultrasound imaging is not possible. Cui et al. (2018) developed a high-avidity fibrin imaging probe incorporating the radiolabel ^{99m}Tc for gamma imaging and using a fibrin-binding peptide sequence as a tetramer. The probe (^{99m}Tc -F4A) was shown to be capable of binding to aged thrombi under high shear and in the presence of anticoagulation. All of these factors have historically been challenging for thrombus-targeted probes.

Furthermore, with this imaging modality, the attenuation from the metal pump housing was minor and did not preclude high sensitivity and quantitative image collection.

The probe was used to evaluate thrombus deposition in a commonly applied rotary blood pump (Fig. 2.3.5.9) in a series of patients who had their pumps removed either for heart transplantation or pump exchange. The imaging results in Fig. 2.3.5.9 show areas of fibrin deposition that vary for the different cases. All patients except that for image C had evidence of pump thrombosis at some point during the implantation period by hemolysis or ischemic stroke. In images C, D, and E the areas of the inlet and outlet bearings for the pump have fibrin deposition (yellow arrows). This has been a common risk area for thrombosis in this device.

While this experiment was done on explanted pumps, the probe may be expected to be compatible with future preclinical and clinical studies. Such imaging can help to better map regions at elevated risk (and potentially confirm future predictive models as in Fig. 2.3.5.5 or justify specific design changes) and also be used to better manage individual patient thrombotic risk by guiding anticoagulation management or indicating a need for device exchange. It is important to point out that when devices enter the clinic, the need for thrombogenicity assessment continues. While device design changes at this stage are expensive and time consuming, it is at the clinical stage where all of the caveats noted in this chapter about the limits of in vitro and preclinical testing come to bear impact. By following devices from preclinical through clinical testing, the design engineer gains important insight where in vitro and in vivo testing provided useful guidance or a false sense of security regarding blood biocompatibility.



• **Figure 2.3.5.9** (Top) Schematic for a clinically utilized axial flow ventricular assist device, the HeartMate II. Note the architecture that is reproduced in explanted devices imaged in parts A–E in the lower section of the figure. (Bottom, A–E) Targeted imaging of fibrin with ^{99m}Tc -F4A from five explanted devices after clinical support. The arrows indicate areas of distinct fibrin-rich thrombi. For A and B, deposition is primarily in the inflow region of the device, prior to the rotor. In C, D, and E the bearing areas at the front and back of the rotor are noted regions of fibrin deposition. (From Cui, G., Akers, W.J., Scott, M.J., Nassif, M., Allen, J.S., Schmieder, A.H., Paranandi, K.S., Itoh, A., Beyder, D.D., Achilefu, S., Ewald, G.A., Lanza, G.M., 2018. Diagnosis of LVAD thrombus using a high-avidity fibrin-specific ^{99m}Tc probe. *Theranostics* 8 (4), 1168–1179.)

What Materials Are Blood Compatible?

The biomaterials community still awaits clear guidelines as to which materials are blood compatible. But, from the perspective of one author of this chapter (Ratner), here are a few guidelines that you might use. First, the important distinction must be made that materials will perform differently in low wall shear rate blood flow (venous flow or static blood) and high wall shear rate blood flow (arterial flow). For low wall shear rate materials, heparinized surfaces are often good (although their period of performance may be limited), and hydrogels seem good. Excellent nonfouling surfaces are also promising (see Chapter 1.4.3). For arterial blood flows, highly hydrophobic materials often show promise (silicones, fluoropolymers, and materials with surface-localized, long *n*-alkyl chains). Also, the exceptional nonfouling materials seem promising—these include good-quality poly(ethylene glycol) surfaces, phosphatidyl choline-based surfaces, sulfobetaines, and carboxybetaines (see Chapter 1.4.3). In all cases, the choice of materials will be dictated by the nature of the flow(s) in the actual device in the bloodstream, the mechanical properties required, the length of time in contact with the blood, the use of anticoagulants and antiplatelet agents, and the consequences of embolization at the specific anatomical site. Trial-and-error optimization of suitable candidate materials may be needed to achieve performance appropriate to the specific application.

Conclusions

The most blood-compatible material known is the natural, healthy, living lining of our blood vessels. This “material” functions well by a combination of appropriate surface chemistries, good blood flow characteristics, and active biochemical processes involving removal of prothrombotic substances and secretion of natural anticoagulants. It seems unlikely that we will ever match this performance in a synthetic material or device, although attempts to imitate aspects of the natural system represent a promising strategy for developing a new generation of blood-compatible devices (for example, see Chapters 1.4.3 and 2.2.6). At present, however, synthetic materials that perform less well than the vessel wall, but still satisfactorily, are needed. This chapter provided only a brief outline of the issues involved in evaluating materials and devices to find those that are minimally damaging or activating toward blood. The subject of blood-compatibility testing is complex, and advanced study of the subject is required before considering experiments intended to elucidate basic mechanisms or improve human health. Further discussion elaborating upon the complexity of the issues involved in BMI testing can be found in Ratner (1984, 1993a, 2000) and Gorbet et al. (2019). Detailed discussion on the characterization of materials for biomaterials application and on BMI testing can also be found in a publication coordinated by the Device and

Technology Branch of the National Heart, Lung and Blood Institute, National Institutes of Health (Harker et al., 1993). Also, see ISO standard 10993-4 (Biological evaluation of medical devices—Part 4: Selection of tests for interactions with blood). The importance of ISO standards is elaborated upon in Chapter 2.3.3.

A 2020 Google Scholar search of the term “blood compatibility” has yielded 8400 references since 2016. The majority of these studies compared biomaterials and then concluded one material was better than another. With such levels of effort exploring this subject, one might assume we would have sound knowledge of what are truly blood-compatible biomaterials. Such a knowledge is still incomplete. This chapter has provided a nuanced view of this subject and should help you the reader to better understand the numerous complexities in pronouncing a biomaterial or device as “blood compatible.”

References

- Baumann Kreuziger, L., Massicotte, M.P., 2015. Mechanical circulatory support: balancing bleeding and clotting in high-risk patients. *Hematology Am. Soc. Hematol. Educ. Program* 2015, 61–68.
- Blit, P.H., McClung, W.G., Brash, J.L., Woodhouse, K.A., Santerre, J.P., 2011. Platelet inhibition and endothelial cell adhesion on elastin-like polypeptide surface modified materials. *Biomaterials* 32 (25), 5790–5800.
- Bluestein, D., 2017. Utilizing computational fluid dynamics in cardiovascular engineering and medicine—what you need to know. Its translation to the clinic/bedside. *Artif. Organs* 41 (2), 117–121.
- Brash, J.L., Horbett, T.A., Latour, R.A., Tengvall, P., 2019. The blood compatibility challenge. Part 2: protein adsorption phenomena governing blood reactivity. *Acta Biomater.* 94, 11–24.
- Braune, S., Sperling, C., Maitz, M.F., Steinseifer, U., Clauser, J., Hiebl, B., Krajewski, S., Wendel, H.P., Jung, F., 2017. Evaluation of platelet adhesion and activation on polymers: Round-robin study to assess inter-center variability. *Colloids Surf. B: Biointerfaces* 158, 416–422.
- Brass, L.F., Diamond, S.L., 2016. Transport physics and biorheology in the setting of hemostasis and thrombosis. *J. Thromb. Haemostasis* 14 (5), 906–917.
- Byrne, R.A., Joner, M., 2015. Kastrati A Stent thrombosis and restenosis: what have we learned and where are we going? *Eur. Heart J.* 36 (47), 3320–3331.
- Cui, G., Akers, W.J., Scott, M.J., Nassif, M., Allen, J.S., Schmieder, A.H., Paranandi, K.S., Itoh, A., Beyder, D.D., Achilefu, S., Ewald, G.A., Lanza, G.M., 2018. Diagnosis of LVAD thrombus using a high-avidity fibrin-specific ^{99m}Tc probe. *Theranostics* 8 (4), 1168–1179.
- Friedman, L.L., Liem, H., Grabowski, E.F., Leonard, E.F., McCord, C.W., 1970. Inconsequentiality of surface properties for initial platelet adhesion. *Trans. Am. Soc. Artif. Intern. Organs* 16, 63–70.
- Gemmell, C.H., 2000. Flow cytometric evaluation of material-induced platelet and complement activation. *J. Biomater. Sci. Polym. Ed.* 11 (11), 1197–1210.
- Gemmell, C.H., Ramirez, S.M., Yeo, E.L., Sefton, M.V., 1995. Platelet activation in whole blood by artificial surfaces: identification of platelet-derived microparticles and activated platelet binding to leukocytes as material induced activation events. *J. Lab. Clin. Med.* 125, 276.

- Gorbet, M., Sperling, C., Maitz, M.F., Siedlecki, C.A., Werner, C., Sefton, M.V., 2019. The blood compatibility challenge. Part 3: material associated activation of blood cascades and cells. *Acta Biomater.* 94, 25–32.
- Hanson, S.R., Harker, L.A., 1988. Interruption of acute platelet-dependent thrombosis by the synthetic antithrombin D-phenylalanyl-L-prolyl-L-arginyl chloromethylketone. *Proc. Natl. Acad. Sci. U.S.A.* 85, 3184–3188.
- Hanson, S.R., Harker, L.A., Ratner, B.D., Hoffman, A.S., 1980. In vivo evaluation of artificial surfaces using a nonhuman primate model of arterial thrombosis. *J. Lab. Clin. Med.* 95, 289–304.
- Hanson, S.R., Kotze, H.F., Pieters, H., Heyns, A. duP., 1990. Analysis of 111-Indium platelet kinetics and imaging in patients with aortic aneurysms and abdominal aortic grafts. *Arteriosclerosis* 10, 1037–1044.
- Harker, L.A., Kelly, A.B., Hanson, S.R., 1991. Experimental arterial thrombosis in non-human primates. *Circulation* 83 (6) IV-41–IV-55.
- Harker, L.A., Ratner, B.D., Didisheim, P., 1993. Cardiovascular biomaterials and biocompatibility: a guide to the study of blood–material interaction. *Cardiovasc. Pathol.* 2 (Suppl. 3).
- Haycox, C.L., Ratner, B.D., 1993. In vitro platelet interactions in whole human blood exposed to biomaterial surfaces: insights on blood compatibility. *J. Biomed. Mater. Res.* 27, 1181–1193.
- Haycox, C.L., Ratner, B.D., Horbett, T.A., 1991. Photoenhancement of platelet adhesion to biomaterial surfaces observed with epi-fluorescent video microscopy (EVM). *J. Biomed. Mater. Res.* 25, 1317–1320.
- Jaffer, I.H., Weitz, J.I., 2019. The blood compatibility challenge. Part 1: blood-contacting medical devices: the scope of the problem. *Acta Biomater.* 94, 2–10.
- Jamiolkowski, M.A., Pedersen, D.D., Wu, W.T., Antaki, J.F., Wagner, W.R., 2016. Visualization and analysis of biomaterial-centered thrombus formation within a defined crevice under flow. *Biomaterials* 96, 72–83.
- Johnson, C.A. Jr, Shankarraman, V., Wearden, P.D., Kocyildirim, E., Maul, T.M., Marks, J.D., Richardson, J.S., Gellman, B.N., Borovetz, H.S., Dasse, K.A., Wagner, W.R., Platelet activation after implantation of the Levitronix PediVAS in the ovine model. *ASAIO J* 57, 2011. 516–521.
- Kaelble, D.H., Moacanin, J., 1977. A surface energy analysis of bioadhesion. *Polymer* 18, 475–482.
- Kaesler, A., Hesselmann, F., Zander, M.O., Schlanstein, P.C., Wagner, G., Bruners, P., Schmitz-Rode, T., Steineseifer, U., Arens, J., 2019. Technical indicators to evaluate the degree of large clot formation inside the membrane fiber bundle of an oxygenator in an in vitro setup. *Artif. Organs* 43 (2), 159–166.
- Kottke-Marchant, K., Anderson, J.M., Rabinowitch, A., Huskey, R.A., Herzig, R., 1985. The effect of heparin vs. citrate on the interaction of platelets with vascular graft materials. *Thromb. Haemostasis* 54, 842–849.
- Maitz, M.F., Martins, M.C.L., Grabow, N., Matschegewski, C., Huang, N., Chaikof, E.L., Barbosa, M.A., Werner, C., Sperling, C., 2019. The blood compatibility challenge. Part 4: surface modification for hemocompatible materials: passive and active approaches to guide blood–material interactions. *Acta Biomater.* 94, 33–43.
- McIntire, L.V., Addonizio, V.P., Coleman, D.L., Eskin, S.G., Harker, L.A., et al., 1985. Guidelines for Blood–Material Interactions – Devices and Technology Branch, Division of Heart and Vascular Diseases, National Heart, Lung and Blood Institute. NIH Publication No. 85–2185, Revised July, 1985, U.S. Department of Health and Human Services, Washington, DC. NIH Publication No. 85–2185, revised July, 1985, U.S.
- Nechipurenko, D.Y., Receveur, N., Yakimenko, A.O., Shepelyuk, T.O., Yakusheva, A.A., Kerimov, R.R., Obydenyy, S.I., Eckly, A., Léon, C., Gachet, C., Grishchuk, E.L., Ataullakhanov, F.I., Mangin, P.H., Pantelev, M.A., 2019. Clot contraction drives the translocation of procoagulant platelets to thrombus surface. *Arterioscler. Thromb. Vasc. Biol.* 39 (1), 37–47.
- Pantelev, M.A., Dashkevich, N.M., Ataullakhanov, F.I., 2015. Hemostasis and thrombosis beyond biochemistry: roles of geometry, flow and diffusion. *Thromb. Res.* 136 (4), 699–711.
- Ratner, B.D., 1984. Evaluation of the blood compatibility of synthetic polymers: consensus and significance. In: Boretos, J.W., Eden, M. (Eds.), *Contemporary Biomaterials: Materials and Host Response, Clinical Applications, New Technology and Legal Aspects*. Noyes Publications, Park Ridge, NJ, pp. 193–204.
- Ratner, B.D., 1993a. The blood compatibility catastrophe. *J. Biomed. Mater. Res.* 27, 283–287.
- Ratner, B.D., 1993b. Characterization of biomaterial surfaces. *Cardiovasc. Pathol.* 2 (Suppl. 3), 87S–100S.
- Ratner, B.D., 2000. Blood compatibility – a perspective. *J. Biomater. Sci. Polym. Ed.* 11 (11), 1107–1119.
- Ratner, B.D., 2007. The catastrophe revisited: blood compatibility in the 21st century. *Biomaterials* 28 (34), 5144–5147.
- Sakariassen, K.S., Muggli, R., Baumgartner, H.R., 1989. Measurements of platelet interaction with components of the vessel wall in flowing blood. *Methods Enzymol.* 169, 37–70.
- Salzman, E.W., Merrill, E.D., 1987. Interaction of blood with artificial surfaces. In: Colman, R.W., Hirsh, J., Marder, V.J., Salzman, E.W. (Eds.), *Hemostasis and Thrombosis*, second ed. JB Lippincott, Philadelphia, PA, pp. 1335–1347.
- Scandroglio, A.M., Kaufmann, F., Pieri, M., Kretzschmar, A., Müller, M., Pergantis, P., Dreysse, S., Falk, V., Krabatsch, T., Potapov, E.V., 2016. Diagnosis and treatment algorithm for blood flow obstructions in patients with left ventricular assist device. *J. Am. Coll. Cardiol.* 67 (23), 2758–2768.
- Schaub, R.D., Kameneva, M.V., Borovetz, H.S., Wagner, W.R., 2000. Assessing acute platelet adhesion on opaque metallic and polymeric biomaterials with fiber optic microscopy. *J. Biomed. Mater. Res.* 49, 460–468.
- Sefton, M.V., Gemmell, C.H., Gorbett, M.B., 2000. What really is blood compatibility? *J. Biomater. Sci. Polym. Ed.* 11 (11), 1165–1182.
- Sivaraman, B., Latour, R.A., 2010. The relationship between platelet adhesion on surfaces and the structure versus the amount of adsorbed fibrinogen. *Biomaterials* 31 (5), 832–839.
- Snyder, T.A., Watach, M.J., Litwak, K.N., Wagner, W.R., 2002. Platelet activation, aggregation, and life span in calves implanted with axial flow ventricular assist devices. *Ann. Thorac. Surg.* 73 (6), 1933–1938.
- Turitto, V.T., Baumgartner, H.R., 1987. Platelet–surface interactions. In: Colman, R.W., Hirsh, J., Marder, V.J., Salzman, E.W. (Eds.), *Hemostasis and Thrombosis*, second ed. JB Lippincott, Philadelphia, PA, pp. 555–571.
- Wagner, W.R., Hubbell, J.A., 1990. Local thrombin synthesis and fibrin formation in an in vitro thrombosis model result in platelet recruitment and thrombus stabilization on collagen in heparinized blood. *J. Lab. Clin. Med.* 116, 636–650.
- Wagner, W.R., Schaub, R.D., Sorensen, E.N., Snyder, T.A., Wilhelm, C.R., et al., 2000. Blood biocompatibility analysis in the setting of ventricular assist devices. *J. Biomater. Sci. Polym. Ed.* 11 (11), 1239–1259.

- Waples, L.M., Olorundare, O.E., Goodman, S.L., Lai, Q.J., Albrecht, R.M., 1996. Platelet-polymer interactions: morphologic and intracellular free calcium studies of individual human platelets. *J. Biomed. Mater. Res.* 32, 65–76.
- Wilhelm, C.R., Ristich, J., Knepper, L.E., Holubkov, R., Wisniewski, S.R., Kormos, R.L., Wagner, W.R., 1999. Measurement of hemostatic indexes in conjunction with transcranial doppler sonography in patients with ventricular assist devices. *Stroke.* 30, 2554–2561.
- Williams, D., 1987. *Blood Compatibility*. CRC Press, Boca Raton, FL.
- Wu, W.T., Jamiolkowski, M.A., Wagner, W.R., Aubry, N., Massoudi, M., Antaki, J.F., 2017. Multi-constituent simulation of thrombus deposition. *Sci. Rep.* 7 42720.
- Ye, S.H., Johnson Jr., C.A., Woolley, J.R., Murata, H., Gamble, L.J., Ishihara, K., Wagner, W.R., 2010. Simple surface modification of a titanium alloy with silanated zwitterionic phosphorylcholine or sulfobetaine modifiers to reduce thrombogenicity. *Colloids Surf. B Biointerfaces* 79 (2), 357–364.

2.3.6

Animal Surgery and Care of Animals

MICHAEL Y. ESMAIL¹, DAVID LEE-PARRITZ²

¹Tufts Comparative Medicine Services, Tufts University, Boston, MA, United States

²Department of Environmental and Population Health, Tufts University Cummings School of Veterinary Medicine, North Grafton, MA, United States

Introduction

The appropriate use of animal models in biomaterials research allows prospective, controlled evaluation of disease processes and candidate therapeutics in a manner that is impossible or unethical in human patients or volunteers. Investigators must consider scientific, practical, and humane issues when developing studies that use animals. High-quality research requires close collaboration between veterinary and research professionals to guide model selection and development, minimize animal pain and distress, and advance the scientific goals of the project. This chapter briefly reviews ethical and regulatory issues, describes available information resources, and discusses the design of surgical facilities, animal selection, anesthesia, and analgesia.

Ethical and Regulatory Overview

Investigators and research institutions have an ethical and legal responsibility to consider animal welfare concerns in research using animals. Russell and Burch expressed the most widely understood ethical principles governing humane design of experiments using animals, summarized in the concept of the “three Rs”: replacement, reduction, and refinement (Russell and Burch, 1959).

The first principle, replacement, states that nonanimal models should be used instead of animals to the maximum extent possible. While regulatory agencies require in vivo animal model testing for safety and efficacy of new drugs and devices, in vitro and ex vivo biocompatibility and efficacy screening methods are increasingly common in biomedical research, including the use of “organ on chips” allowing for the study of molecular- and cellular-scale activities in specific human tissues (Fujibayashi et al., 2003; James Kirkpatrick et al., 2007; Pariente et al., 2000; Zhang et al., 2018). These techniques reduce the total number of animals used and allow significant savings in time and resources compared to experimental animal models.

The principle of reduction states that investigators should use the minimum number of animals to allow statistically valid inferences to be drawn from the data. In this context, it is as important to avoid using too few animals as it is too many. Important considerations in determining the statistical power of an animal experiment include inherent variability of the model and expected efficacy of the test therapeutic (Bate and Clark, 2014; Fitts, 2011; Parker and Browne, 2014). Consultation with a biostatistician should be conducted prior to starting animal studies.

Regulatory agencies and institutional review committees require justification of the numbers of animals used in an experiment (National Research Council, 2011; US Congress, 1985a; Silverman et al., 2014). Suggested strategies to reduce animal usage include “(1) rational selection of group size (pilot study, power analysis); (2) careful experimental design; (3) maximizing the use of each animal; (4) minimizing loss of animals; and (5) statistical analysis (maximum information from minimum number of animals)” (Fitts, 2011).

The most important of the “three Rs” is the principle of refinement, which states that investigators should use the least invasive and most modern techniques possible to minimize animal pain and distress (Orlans et al., 1996). Continuous refinement and improvement in animal husbandry and the diagnosis and control of infectious disease has greatly reduced nonexperimental morbidity and mortality in modern research facilities. Surgical models in particular have benefited from advances in veterinary anesthesia, instrumentation (e.g., laparoscopic procedures), and monitoring, which have allowed further reduction and refinement of research animal use.

Governmental Regulations

Widespread acceptance of the “three Rs” and continued public scrutiny of biomedical research oblige investigators and institutions to comply with strict regulatory standards

governing all aspects of research animal use. In the United States, the United States Department of Agriculture (USDA), the Public Health Service (PHS), and the Food and Drug Administration (FDA) are the primary agencies that regulate animal research.

United States Department of Agriculture

The specific focus of animal welfare regulations varies by agency. Well-publicized incidents (Phinizy, 1965; Wayman, 1966) of pet theft and their subsequent mistreatment in research laboratories prompted the US Congress to enact the Animal Welfare Act (AWA) in 1966 (Congress, 2013). The AWA regulates all warm-blooded animals, with some exceptions, such as rats, mice, or birds bred for research. The Animal Welfare Act Regulations (AWAR) are the interpretation of the federal AWA law and contain enforceable standards. In many institutions, the term “regulated species” refers to animals subject to the AWA (e.g., guinea pigs, rabbits, pigs, sheep, nonhuman primates). The USDA enforces the AWA through the Animal and Plant Health Inspection Service. Registered facilities file annual reports of animal usage with the USDA and are subject to unannounced inspection.

Public Health Service

The PHS, through the National Institutes of Health (NIH), is the largest single sponsor of biomedical research using animals and has adopted regulations to ensure humane and scientifically valid use of animals. The Health Research Extension Act of 1985 provides the legislative mandate for the Public Health Service Policy on Human Care and Use of Laboratory Animals (US Congress, 1985b, 1985a). The NIH Office of Laboratory Animal Welfare (OLAW) develops and implements standards for animal care and use at recipient institutions, as described in the Guide for the Care and Use of Laboratory Animals, commonly referred to as “The Guide” (National Research Council, 2011). Institutions receiving PHS support (e.g., funding from the NIH, FDA) must file an “Animal Welfare Assurance” with OLAW indicating sufficient institutional resources to provide proper husbandry and veterinary care. Institutions must also indicate how they will approve and monitor research to ensure scientific integrity and prevent inhumane treatment of animals. Assurances are approved for 5 years, after which a new application must be submitted. The PHS Policy applies to all vertebrate animals, including those not regulated by the AWA (US Congress, 1985a).

Food and Drug Administration

In the United States, the development of new drugs and devices must undergo a rigorous oversight process. The US Federal Food, Drug and Cosmetic Act, initially passed in 1938, authorizes the FDA to oversee the safety of food, drugs, medical devices, and cosmetics. In 1987, passage of the Good Laboratory Practices (GLP) Act (21 CFR 58.90) required the FDA to regulate preclinical research conducted in direct support of new drugs or medical devices (US Congress, 1987).

The GLP regulations ensure reproducibility and integrity of data used to support new drug or device applications. These regulations include minimum basic requirements for study conduct, personnel, facilities, equipment, written protocols, operating procedures, study reports, and the system of quality assurance oversight for each study. The GLP regulations govern nonclinical studies, including controlled in vivo and in vitro experiments to evaluate the safety of test articles (e.g., new drug or device) in validated animal and laboratory test systems (US Congress, 1987). These studies do not include clinical or field studies with human or animal subjects or basic exploratory studies.

The FDA approval process differs for drugs and devices. Clinical testing of a new drug in humans requires FDA approval of an Investigational New Drug (IND) application. The IND application contains data from nonclinical/preclinical laboratory studies, including toxicity testing, pharmacology, and pharmacodynamic studies. Nonclinical studies must include data from more than one species, typically one rodent and one nonrodent (e.g., rabbits, dogs, nonhuman primates) (21 USC, Section 314 and 316) (US Congress, 2019). Testing of the new drug in human volunteers and patients occurs only after approval of the IND and if successful is followed by submission of a New Drug Application (NDA) to request FDA approval of the new pharmaceutical for sale or marketing in the United States. The NDA includes data from preclinical studies and clinical Phase I, Phase II, and Phase III trials.

The approval process for new medical devices differs significantly from that for new drugs (US Congress, 2019). The FDA classifies medical devices by a risk-based system, with higher classes receiving increased regulatory control. Class I devices pose the least risk to consumers (e.g., oxygen masks, surgical tools) and require only the use of good manufacturing practices. Class II devices (e.g., wheelchairs, some pregnancy tests) pose more risk to consumers than Class I and require specific testing to assure safety and performance. Class III devices support or sustain life, are implanted in the body, or have the potential for significant risk of illness or injury (e.g., pacemakers, implanted defibrillators, heart devices) if defective or improperly used. Some implanted devices, e.g., orthopedic fracture fixation devices and joint replacement devices, are sometimes determined by the FDA to be classified as Class II. Class III devices require premarket application (PMA) approval to provide scientific evidence that the benefits to human health outweigh risks and that the device will significantly help a large portion of the target population.

Sponsors submit one of three types of applications for new medical devices. Class III devices require PMA approval unless they are similar to current marketed devices. The PMA must contain nonclinical GLP study results. The less-restrictive premarket notification or 501(k) requirement applies to Class I and Class II devices as well as to Class III devices similar to others on the market. Lastly, devices can be submitted under humanitarian device exemption where devices are used to treat or diagnosis a disease or condition that affects fewer than 4000 people (21 USC Part 314)

(US Congress, 2019). Additional information on medical device development and regulatory concerns can be found in Part 3 of this book.

Institutional Responsibilities

Productive and humane research animal care and use requires close coordination and support from multiple institutional entities. The three key components of the program are the Institutional Animal Care and Use Committee (IACUC), the attending veterinarian (AV), and the principal investigator (PI). The separate and interrelated roles of these entities are legally defined and described next.

Institutional Animal Care and Use Committee

The AWAR and the PHS Policy assign primary responsibility for an animal research program to the IACUC (US Congress, 2013, 1985b). The regulations require a minimum of three (AWAR) or five (PHS) members and must minimally include a veterinarian, a scientist, a nonscientist, and an unaffiliated member. The IACUC reviews and approves in advance all animal research protocols to ensure compliance with the relevant regulatory requirements. In addition, the IACUC regularly inspects the animal research facility, reviews the animal care and use program, designs and implements institutional policies, and investigates allegations of animal mistreatment.

Attending Veterinarian

The AV must have training/experience in the care and management of species used at the institution and has direct or delegated authority for animal activities at the facility (National Research Council, 2011; US Congress, 2013). Veterinarians offer important expertise to investigators using animals. Laboratory animal medicine is a subspecialty of veterinary medicine that involves additional training and acquisition of skills in the diagnosis and treatment of laboratory animal diseases, development of new experimental techniques, and provision of specialized preoperative, intraoperative, and postoperative care. Most large research institutions have at least one staff veterinarian trained and experienced in laboratory animal medicine. Smaller institutions may use consultant veterinarians. Other veterinary specialties of potential value in a biomaterials research program include surgery, anesthesia, pathology, and internal medicine.

Principal Investigator

The PI is responsible for proposing, designing, conducting, and/or implementing research involving animals. The PI must obtain advanced approval for all research procedures and assure proper training, oversight, and safety of laboratory members in the conduct of these studies. These study details are typically contained in the IACUC protocol. The PI must assure the IACUC that (1) procedures causing discomfort, distress, and pain are minimized, (2) alternatives to procedures that may cause pain or distress

have been considered, (3) activities do not unnecessarily duplicate previous experiments, (4) procedures causing pain and distress will be alleviated with sedatives, analgesics, or anesthetics, except when they must be omitted for scientific reasons, (5) personnel conducting procedures are adequately trained, (6) no animal will undergo more than one major operative procedure without scientific justification, and (7) a veterinarian is consulted in the generation of the animal care protocol (National Research Council, 2011; US Congress, 2013).

Surgical Facility Design

Minimum functional components of the survival surgery suite include dedicated areas for surgery, animal preparation, surgeon's scrub, postoperative recovery, and surgical support. In the United States, federal regulations require the use of dedicated surgical suites for major survival surgery on USDA-regulated species other than rats, mice, and birds. Surgical suites must allow aseptic surgery, animal preparation, and surgeon scrub to occur in separate dedicated rooms, arranged to facilitate entry and exit of animals and staff and minimize unnecessary traffic. Animal recovery may occur in the same room as anesthesia induction and preparation. Institutions receiving federal funding (e.g., NIH) may permit rodent survival surgery in any procedure space provided necessary conditions for asepsis are present (National Research Council, 1980).

Many research institutions maintain centralized experimental surgery suites to maximize economies of scale and efficient use of equipment and skilled support staff. Support spaces in large surgical suites may be configured to allow two or more operating rooms to run simultaneously from shared animal and surgeon preparation rooms. Specialized facilities may be appropriate to accommodate unique experimental requirements such as imaging, cardiopulmonary bypass, specimen preparation, or postoperative intensive care and monitoring. Principles of research animal operating room design have been described (Hessler and Lehner, 2009; National Research Council, 1980).

Other functional areas commonly required in, at, or near the experimental surgery suite are: a pharmacy, including secure controlled substance storage; instrument cleaning and sterilization; and record keeping. Secure data collection and storage require network connections, and possibly other information technology capabilities. Radiography and other imaging modalities are often necessary in experimental surgical studies and may be conveniently located within or adjacent to the surgery suite.

Model Selection

A wide variety of animal models are used in biomedical research. Nonanimal models are an integral part of drug and device development, and include in vitro systems, computer simulations, and mathematical models. By definition,

a model serves as a surrogate and is rarely identical to the subject being modeled. Desired features of an animal model include (National Research Council, 1998):

1. The model is appropriate for its intended use, in that the specific disease model faithfully mimics the human disease AND/OR the model system is appropriate for the human system being modeled.
2. The model can be developed, maintained, and provided at reasonable cost in relation to the perceived or potential scientific values that will accrue from it.
3. The model is of value for more than one limited kind of research.
4. The model is reproducible and reliable, so results can be confirmed.
5. The model is reasonably available and accessible.

The essential characteristic of a useful animal model is that it has been validated through a formal, hypothesis-driven process to determine that significant similarities exist between the model and what is being modeled (Shapiro, 1998). For this reason, choice of the proper animal model is critical to successful development of novel technologies and scientific discoveries.

Cardiovascular Devices

Virtually all traditional research species have been used in cardiovascular research, including zebrafish, mice, rats, rabbits, dogs, sheep, pigs, and nonhuman primates. Each species differs in its specific advantages and disadvantages, including size, cost, ability to use genetic engineering, and similarity to human anatomy and physiology. However, due to similarity to humans, swine and sheep models are more commonly used for the testing of biomedical devices and cardiovascular tissue engineering.

Heart Valve Replacement

Heart valve repair historically has focused on replacing the defective or diseased heart valve with a mechanical or animal tissue-derived artificial valve. Valve repair via tissue engineering has been an active area of research but has not been clinically realized yet (Cheung et al., 2015; Kheradvar et al., 2015; Rashid et al., 2004; Sodian et al., 2000a,b; Stassen et al., 2017; Vesely, 2005). Research behind heart valve devices and replacements is covered in Section 2.5 of this book. Pigs, sheep, and dogs are typically used for preclinical safety and efficacy studies of novel prosthetic heart valves. The benefits to using these species include similarities in size, anatomy, and physiology of the heart. However, differences between pigs, sheep, and dogs must be considered when choosing an animal model. The following sections provide a brief overview of these animal models. For animal models of spontaneous and induced heart valve disease, readers are encouraged to review Kheradvar et al. (2017).

Swine heart valves are remarkably similar to those of humans with respect to mitral valve size, leaflets, and chordae tendineae configuration (Crick et al., 1998; Lelovas et al., 2014). The tricuspid valve of pigs has three leaflets,

unlike the two leaflets of dogs (Evans and de LaHunta, 2010; Lelovas et al., 2014). The semilunar (aortic and pulmonary) valves of pigs also share significant similarities to those of humans. As with humans and unlike sheep and calves, pigs have a fibrous attachment to the noncoronary cusp of the aortic valve (Sands et al., 1969), although the fibrous continuity between mitral and aortic valve leaflets is less pronounced in humans (Crick et al., 1998; Lelovas et al., 2014). However, the relative geometry and size of the three aortic valve cusps to each other differ between pigs and humans (Sim et al., 2003).

The use of pigs in implantable heart or intravascular devices research requires careful consideration of the study goals and duration, as the growth of the cardiovascular system is rapid and substantial in many breeds of pigs, especially those bred for meat production (e.g., Yorkshire, Landrace). The growth of the swine heart from birth to sexual maturity at 4.5 months of age is analogous to the growth of the human heart from birth to mid-teenage years (Swindle et al., 2013). Therefore the use of animals whose adult body size is comparable to humans, like miniature pigs or sheep, is preferable for nonacute implantable cardiovascular device studies (Kheradvar et al., 2017). For example, one study demonstrates relatively long-term survival (20 weeks) of Bama miniature pigs implanted with prosthetic heart valves (Li et al., 2007).

Another challenge to the use of pigs in cardiac studies includes the sensitivity of the heart to anesthesia and surgical manipulation, which can cause intraoperative and postsurgical complications, including arrhythmia and death (Kheradvar et al., 2017; Swindle and Smith, 2016). In addition, maintaining safe levels of the anticoagulant warfarin is challenging in swine mechanical heart studies as warfarin is associated with a high incidence of hemorrhagic complications (Grehan et al., 2000).

Given that pigs are unable to reliably maintain chronic implants, sheep are the accepted gold standard model for regulatory and investigative valve replacement studies (Ahlberg et al., 2013; Gallegos et al., 2005; Kheradvar et al., 2017). The size and anatomy of heart valves and valve orifices of adult sheep are similar to those of humans (DiVincenti et al., 2014; Sands et al., 1969). Standardization requires the use of animals of similar age and weight. The relatively large left and right atria of the sheep facilitate the surgical approach to the valves. In addition, normal cardiovascular physiological parameters of sheep approximate normal human values for blood pressure, heart rate, cardiac output, and intracardiac pressure (Barnhart et al., 1982; Gallegos et al., 2005).

Historically, dogs were common in cardiac valve research due to their slow growth, cooperative temperament, and similarity to human cardiac anatomy and adult body size. Imaging and cardiac monitoring are also simpler in dogs compared to pigs and sheep. However, dog tricuspid valves have two leaflets, as opposed to three in humans, pigs, and sheep (Evans and de LaHunta, 2010). In addition, dogs exhibit variability in the number and position of papillary

muscles (Ahlberg et al., 2013; Kheradvar et al., 2017). These factors and public sensitivity to the use of dogs in biomedical research have reduced the use of this model for cardiac valve research and development.

Ventricular Assist Devices

For patients in end-stage heart failure or suffering from acute myocardial infarction, ventricular assist devices (VADs) are a useful bridge-to-transplant therapy when donor hearts for transplantation are unavailable. Recent advances have expanded the role of VADs to provide long-term, chronic support (Monreal et al., 2014). The VAD is a blood pump system designed to palliate severe congestive heart failure and is composed of inflow and outflow cannulae, connectors, and controllers.

VAD technology has been advanced by a variety of animal models. Preclinical testing of VADs typically uses healthy large animals. However, the human recipients of VADs are almost always in end-stage heart failure, making the healthy animal an imperfect model. There are multiple experimental models of heart failure. Sustained rapid pacing produces severe biventricular systolic dysfunction (Shinbane et al., 1997). Myocardial infarction can be performed in a minimally invasive manner by catheter-induced coronary embolization or by coronary artery ligation via thoracotomy (reviewed in Monreal et al., 2014). Additional large animal models of heart failure are reviewed in Dixon and Spinale (2009), Gallegos et al. (2005), and Chapter 10 in Gross (2009).

The calf (juvenile cow or bull) is the most commonly used VAD model (Litwak et al., 2008). Calves are used to study the function, biocompatibility, and efficacy of VAD. The bovine blood-contacting surfaces are procoagulant and activate blood clotting, therefore a device that resists thrombosis in a calf model will reduce the possibility of adverse events in human trials. The calf model also allows simulation of common clinical complications such as thrombosis, obstructions, or kinks, and mechanical, electrical, or software failures. The large thoracic cavity and large peripheral vessels facilitate vascular access and further contribute to the value of the calf model. Four- to six-month-old calves (70–100 kg) model average human body size. Much like swine, calves grow rapidly to a size not suited to long-term studies (Monreal et al., 2014).

Sheep are also common in VAD research. Sheep do not have a significant coronary collateral network, and in this respect are similar to humans and pigs (DiVincenti et al., 2014; Schaper et al., 1972). This characteristic makes sheep useful as a model in myocardial infarction. However, unlike right-side dominant humans and pigs, sheep hearts receive blood from the left coronary artery (DiVincenti et al., 2014). Adult sheep are compatible in body size and temperament for long-term studies.

Orthopedic Devices

Orthopedic devices and implants are very diverse, including wires, pins, screws, plates, spinal fixation devices, internal

and external fixation, bone grafts, and joint replacements. These devices treat a variety of orthopedic injuries and diseases, including fractures, bone loss, and immune-related or degenerative joint conditions. Virtually every major laboratory animal species has been used in orthopedic research, including zebrafish, mice, rats, rabbits, guinea pigs, goats, sheep, dogs, cats, pigs, and horses. Dogs, sheep, and pigs are the most commonly used models for preclinical testing.

Animal model choice must weigh several factors, including, but not limited to, the nature of the device/implant, study timeline, species-specific bone characteristics (microstructure, bone composition, bone modeling/remodeling characteristics, etc.), animal size, and regulatory requirements (Pearce et al., 2007). Scientists interested in reviewing the bone differences between species and the appropriateness of common disease models should consult Nunamaker (1998), Pearce et al. (2007), Li et al. (2015), and Wancket (2015).

However, some innate characteristics of animals pose challenges in translating orthopedic animal studies to humans. All mammalian research animals except nonhuman primates are quadrupeds. The resulting differences in weight bearing and mechanical load on the musculoskeletal system will alter the load that orthopedic devices and implants experience, as compared to humans. In addition, the inability to control weight bearing and joint motion postoperatively pose additional challenges (Rodeo, 2017). For example, sheep and dogs that undergo rotator cuff repair will uniformly retear in the early postoperative period unlike humans undergoing the same procedure (Derwin et al., 2007, 2018; Rodeo et al., 2007).

Bone Defect Models

Bone grafts are one of the most commonly used surgical methods to augment bone regeneration. There are four common induced bone defect animal models: calvarial defect, long bone or segmental defect, partial cortical defect, and cancellous bone defect (reviewed in Bigham-Sadegh and Oryan, 2015; McGovern et al., 2018). Important in all bone defect animal models is the size of the defect.

An important but controversial concept in bone defect research is that of the “critical size defect.” The purpose of the critical size defect is to create a reliable, repeatable, and translatable model that represents a “stringent test of a material’s ability to induce or augment bone growth.” ASTM International (2014), an organization that develops recognized standard consensus for preclinical testing, defines critical size defect “as the minimum defect dimension that the animal is incapable of repairing without intervention. The dimensions of critical defects generally differ for each species and should be considered carefully when designing the implant dimensions and method of fixation.” The length of the defect should at least be equal to 1.5 times the diameter of the selected bone but may exceed 2.5 times this diameter (Gugala et al., 2007; Lindsey et al., 2006). The recommended critical size defect will vary based on species, strain, bone used, age, weight, and metabolic condition of

the animal (Bigham-Sadegh and Oryan, 2015; Lammens et al., 2017). Since the interaction of these variables is complex and the dimensions are often not reported in publications, some consider critical size defect models unreliable for translational studies (Cooper et al., 2010; Lammens et al., 2017; Reichert et al., 2009b).

The rat calvaria model is one of the most common pre-clinical bone defect models. After incising the skin, the surgeon uses a trephine to create a standardized full thickness circular bone defect between 5 and 8 mm in diameter, using saline irrigation to prevent thermal damage to surrounding bone (Cooper et al., 2010; Vajgel et al., 2014). Experimental tissue-engineered materials in scaffold are then applied to the bone defect (Bigham-Sadegh and Oryan, 2015; McGovern et al., 2018).

The sheep tibia is the most common model for segmental long bone defects (McGovern et al., 2018). Some of the advantages of using sheep include body size, bone dimensions, and healing characteristics similar to adult humans (Pearce et al., 2007; Reichert et al., 2009a; Wancket, 2015). In addition, the mechanical loading in sheep hind limbs is well documented and approximately half that in humans during the walking phase (Taylor et al., 2006). Reported sheep critical size defects range from 2 to 3 times the diameter of the bone (Christou et al., 2014; Gugala et al., 2007; Lammens et al., 2017; Lindsey et al., 2006). Sheep cortical bone is primarily plexiform through 7–9 years of age, unlike human cortical bone, which is lamellar (Wancket, 2015). In addition, during winter, sheep undergo seasonable bone loss, which may impact bone healing (Bonucci and Ballanti, 2014). Adult sheep trabecular bone tends to be stronger and more dense than human bone. Immature sheep, however, have weaker, low-density trabecular bone that is highly flexible (Nafei et al., 2000; Wancket, 2015).

Vascular

Animal models are used in vascular biomaterials research to investigate biocompatibility and strategies to increase resistance to stenosis and thrombosis. Considerations for animal model selection include size, availability, and specific biological requirements of the model, including size and accessibility of the vasculature. The regulatory requirements for preclinical assessment of synthetic vascular conduits have been described and require consideration of the diameter and length of the target vessel and intended clinical application (Byrom et al., 2010).

The unique biological characteristics of a particular species should guide model selection and interpretation (Byrom et al., 2010). In some cases, a more stringent model is indicated to provide a better margin for safety in translating results to the human clinical application. For example, pigs and dogs are relatively hypercoagulable compared to humans, so a vascular conduit resistant to thrombosis in these species may be more likely to resist thrombosis in humans. Of the common laboratory animal species, the coagulation systems of the rabbit and baboon

coagulation systems are considered the most similar to humans (Byrom et al., 2010).

Large animal models in vascular biomaterials research include sheep, swine, dogs, and baboons (Ahmed et al., 2014; Brennan et al., 2008; Bhattacharya et al., 2000; Byrom et al., 2010). Small animal models include mice, rats, and rabbits. Swine are widely preferred for the development and assessment of intravascular stents, because of their size and the ability to assess devices in the setting of common human comorbid conditions such as atherosclerosis, which is easily induced in this species (Swindle et al., 2012). Rapidly growing animals such as juvenile sheep (Brennan et al., 2008) and swine (Robotin-Johnson et al., 1998) have been used to evaluate the ability of grafts to grow with the host. Aged sheep have been used to assess tolerability of vascular grafts in the senescent model (Ahmed et al., 2014).

Anesthetic and analgesic management of animals in these studies is comparable to other applications. Since thrombosis prevention by modification of the luminal surface or the use of drug-eluting grafts is often a key scientific goal of the study, supplemental antithrombotic drugs are not common. In other cases, antithrombotic medications such as aspirin are appropriate (Bélanger and Marois, 2000). Care is required to prevent prolonged ischemia when inserting interposition grafts to avoid neuromuscular damage and paralysis. Rabbits are relatively susceptible to this complication following abdominal aorta interposition grafts, whereas sheep are relatively resistant following common carotid artery grafts (Byrom et al., 2010).

Ophthalmology

Animal models serve an important role in the development of ocular biomaterials. The eye is sensitive to painful stimuli, prone to inflammation, and most procedures require specialized skill and instrumentation. Failure or infection of an implant may cause chronic pain or blindness. Therefore all implants must demonstrate biocompatibility and durability in an animal model before being applied to humans. Animal models allow the additional advantage of histologic assessment of implants for stability and biocompatibility.

The pig and rabbit are the most commonly used animal model species for ocular research. Both species are readily available and have globes of comparable size to humans. The rabbit eye is especially prone to inflammation, which may complicate experimental manipulation but provides an important indicator of biocompatibility. Although the large size of the rabbit eye makes it attractive for surgical and drug therapy trials, important differences include a thinner cornea, larger lens, and relatively poorly vascularized retina. The rabbit is the model of choice for the assessment of intraocular lenses and other ophthalmic devices and solutions (Werner et al., 2006). Cats and nonhuman primates are less commonly used in ophthalmologic model studies but may have value for certain applications (Steinert and Jain, 2013).

Anesthesia for ocular animal model research is similar to other procedures, with several important caveats. The

oculocardiac vagal response is pronounced in many species, leading to potentially fatal profound bradycardia or asystole during surgical manipulation of the globe. Monitoring of the heart rate is therefore essential during ocular procedures. This effect is less common during ketamine anesthesia compared to propofol and can be largely prevented with the use of topical proparacaine (Singh et al., 2010). Systemic glycopyrrolate effectively treats vagal bradycardia. However, routine preoperative use of anticholinergic agents may predispose to arrhythmias and is not advised.

The eye often deviates away from the central position under general anesthesia. Neuromuscular blocking agents may be a useful aid to proper positioning of the globe for intraocular procedures. Mydriasis is often required for procedures on the lens and to prevent postoperative adhesions. Effective mydriasis can be achieved with topical 1% cyclopentolate hydrochloride and 2.5% phenylephrine; 0.3% scopolamine combined with 10% phenylephrine; 1% atropine; or a combination of 1% atropine and 10% phenylephrine (Gelatt, 2011a; Werner et al., 2006). Since eye position and pupil size are important indicators of anesthetic depth, the surgeon must assure adequate anesthetic depth when using these agents. Instrumentation for intraocular surgery has been described in Gelatt (2011b).

Skin

Rodents and swine are the most commonly used experimental models for wound healing and biomaterial studies. Rodents are inexpensive and readily available in well-defined inbred and transgenic strains and outbred stocks. Limitations to the use of rodents include small size, limiting the size of implants, opportunity for sequential biopsy, dense fur coat, and thin dermis and epidermis. Swine are more comparable to humans because of sparse body hair, and similar epidermal thickness, microscopic anatomy, and collagen composition. Pigs further resemble humans because both species lack the panniculus carnosus present in most loose-skinned animals. As a result, cutaneous wounds in pigs heal primarily through reepithelization rather than by contraction as occurs in rodents (Sullivan et al., 2001).

Anesthetic and analgesic requirements for wound healing and biomaterials studies in rodent and swine models are similar to those for other applications. Procedures are typically brief and lend themselves to injectable anesthetic technique. The potential for pain following excisional procedures or subcutaneous implantation through a skin incision is minor and can be readily treated with short-term systemic nonsteroidal antiinflammatory agents or opioid analgesics. Extensive wounds or partial thickness injuries have greater potential for pain and typically require analgesic treatment for several days.

Dressing of cutaneous wounds requires special care and ingenuity to prevent infection and physical disruption of the healing wound through scratching and grooming by cage or pen mates. Adhesive dressings should be applied so as not to impair mobility or access to food and water, and to facilitate removal and wound inspection.

Animal Management and Care of Animals

The remainder of the chapter will review species-specific considerations for rodents, ruminants, swine, and rabbits, including animal selection, anesthesia, analgesia, and preoperative and operative considerations. While PIs must consult a veterinarian in the design of animal studies, it is common for investigators and animal users to perform procedures without continuous veterinary support. Therefore it is important for animal users to be familiar with these considerations.

Rodent

Animal Selection and Preoperative Preparation

Specific pathogen-free (SPF) rodents should be used for all surgical procedures to reduce experimental variability and morbidity and mortality from chronic respiratory disease. Infectious agents may cause severe clinical disease and mortality, or even when subclinical may alter immune function, impair detoxification of anesthetic or experimental drugs, or introduce other experimental variables.

Many institutions will implement a stringent rodent health program and restrict the sources of animals to approved vendors. Several commercial vendors supply common strains and stocks of laboratory rodents free from the majority of rodent infectious agents. These are known as SPF rodents. The specific panel of excluded agents may vary according to the vendor. Animals sourced from academic or other institutions may harbor excluded agents. Animals from these suppliers commonly require quarantine or rederivation before entry to the clean vivarium. SPF animals introduced to rooms with enzootic viral infection may rapidly acquire and succumb to severe clinical disease. A conditioning period of at least 3 days after purchase is advised to assure animals have recovered from dehydration and other shipping stress.

General Anesthesia

Most surgical procedures in rodents are brief. Small body size and limited vascular access complicate anesthesia and intraoperative support of rodents. Nevertheless, skilled operators with appropriate instrumentation can accomplish delicate vascular surgery and other procedures in rats and mice with minimal postoperative mortality. Endotracheal intubation and positive pressure ventilation are also possible and require the use of customized equipment (Gaertner et al., 2008).

Rodents do not vomit, and preoperative fasting is not recommended. When fasting is required the duration should be kept to a minimum (2–3 h) to avoid hypoglycemia and shock (Flecknell et al., 2015).

Several anesthetic combinations are appropriate for brief, noninvasive procedures in rodents. Intraperitoneal (IP) injection of ketamine (40–100 mg/kg) and xylazine (3–10 mg/kg) provides 20–60 min of surgical anesthesia with good muscle relaxation in most rodents. Medetomidine (1 mg/kg IP) may be substituted for xylazine. Anesthetic duration

varies in a dose-dependent manner. If necessary, supplemental administration of half doses of ketamine will prolong anesthesia. Ketamine volumes commonly required for rats and mice require division of an intramuscular (IM) dose between two or more sites if the IP route is contraindicated. Atipamezole (1 mg/kg IP) will reverse medetomidine or xylazine-associated sedation and speed recovery from anesthesia but will also likely reverse residual xylazine-induced analgesia (Janssen et al., 2017). Side effects of general anesthesia in rodents may include hypercarbia, hypoxemia, and hypotension although these effects are less evident with ketamine and xylazine in comparison with older agents such as sodium pentobarbital.

Isoflurane provides safe and effective anesthesia in rats and mice. This agent is suitable both for brief restraint and for procedures of up to several hours' duration. Isoflurane requires the use of a precision vaporizer to maintain consistent anesthetic concentration. The "drop method" of placing a rodent in a closed chamber with an isoflurane-soaked gauze is strongly discouraged for survival surgery because the unregulated and large resulting anesthetic dose may cause unacceptably high mortality. Rapid induction of anesthesia follows placement of animals into an induction chamber containing 3%–4% isoflurane in oxygen. Most animals awaken 1–2 min after removal from the chamber, which is sufficient time for blood sampling or tail biopsy. To maintain anesthesia for longer periods, place the animal's head and nose into a customized nose cone connected to a nonbreathing anesthetic circuit and scavenger. Concentrations of 2%–3% isoflurane are commonly used for maintenance. The absence of the pedal withdrawal reflex confirms adequate anesthetic depth. Rodent nose cones are easily fashioned from funnels or disposable syringe barrels. For procedures requiring positive pressure ventilation, endotracheal intubation is easily accomplished. Techniques for endotracheal intubation for rodents have been described (Gaertner et al., 2008).

Analgesia

Buprenorphine is the most widely used opioid analgesic in rodents. Buprenorphine is a mixed mu agonist/antagonist and a kappa receptor agonist with approximately 25–40 times the analgesic potency of morphine. The relative activity at each receptor may be dose dependent. The standard buprenorphine hydrochloride formulation agent provides safe and effective analgesia for 4–8 h after dosing. The current recommended dose of buprenorphine hydrochloride for most rodent indications is 0.03–0.05 mg/kg IP or subcutaneous (SQ) (Lee-Parritz, 2007; Curtin et al., 2009). Sustained-release buprenorphine (SR-Lab, <https://wildpharm.com/>) provides effective analgesia up to 72 h after a single administration (1.0–1.2 mg/kg SQ rat; 0.5–1.0 mg/kg mouse).

For procedures under isoflurane, buprenorphine is given at least 1 h before incision. The anesthetist should be aware of the anesthesia-sparing effects of buprenorphine and be prepared to reduce the isoflurane vaporizer

setting by 30%–50% as necessary or reduce the amount of injectable anesthetic needed (Brunson, 2008). Preoperative administration of buprenorphine or other narcotics at standard ketamine/medetomidine or xylazine doses may cause unpredictable increases in anesthetic depth (Roughan et al., 1999; Lee-Parritz, 2007). Local infusion of the surgical site with lidocaine (up to 1 mL/kg of 1.0% lidocaine or 0.25% bupivacaine) before incision will provide additional intraoperative and postoperative analgesia (Lee-Parritz, 2007; Wenger, 2012).

Clinically significant side effects of buprenorphine include consumption of bedding (pica), and excessive licking or biting of the limbs and cage, which may also be directed to the surgical incision. These effects are more common in rats that receive high doses (0.1–0.3 mg/kg) and can often be managed through temporarily placing animals on a wire grid during surgical recovery or substitution of a synthetic for a natural bedding substrate. A generalized increase in activity and a reduction of ventral grooming may also occur. These effects most likely represent a direct effect of the drug, and do not necessarily indicate the presence or absence of pain (Lee-Parritz, 2007).

The nonsteroidal antiinflammatory drugs (NSAIDs) ketoprofen, carprofen, and meloxicam are the next most widely used analgesics. These drugs block the formation of inflammatory mediators associated with surgical injury, and also act centrally to inhibit secondary allodynia. The current recommended dose for meloxicam is 1 mg/kg PO (per os or orally) or SQ in rats, and up to 10 mg/kg in mice. The dose for ketoprofen and carprofen in rats is 5 mg/kg SQ. The dose interval for these agents has not been critically evaluated in rodents but is 12–24 h in other species. Sustained-release meloxicam protects against mechanical hypersensitivity but thermal hypersensitivity up to 96 h after administration in the rat (Seymour et al., 2016). NSAIDs are highly effective preemptive analgesics when administered 1 h or more before surgery, and isoflurane vaporizer settings or injectable anesthetic doses typically do not require adjustment (Lee-Parritz, 2007).

There are few reported adverse side effects associated with NSAIDs in rodents. Diffuse intestinal ulceration may occur at high doses, especially in animals with concurrent disease. Most NSAIDs inactivate platelet function to some extent through cyclooxygenase-mediated inactivation of thromboxane. This may slightly prolong the bleeding time, but rarely causes adverse clinical effects in humans even when administered preoperatively (Lee-Parritz, 2007).

Ruminants (Sheep, Goats, Calves)

Animal Selection and Preoperative Preparation

Sheep and goats are desirable research animals, because the adult body weight is comparable to humans and they are hardy, inexpensive, and have a calm disposition. Calves (immature cattle) are also readily available and of suitable size and disposition when young. Sheep are particularly useful for reproductive research because investigators may

easily obtain cohorts of pregnant animals with known gestational age and hysterotomy, and fetal manipulation is possible with a low postoperative abortion rate.

The quality of sheep and goats used in research often depends on the source. Surgical and transportation stress will reduce resistance to disease. A conditioning and quarantine period after arrival allows recovery from shipping stress, acclimation to the facility, and reduces transmission of infectious diseases to resident animals (Underwood et al., 2015).

Facilities should adopt measures to prevent transmission of zoonoses from sheep and goats. Silent infection with *Coxiella burnetii*, the causative agent of human Q fever, is common in sheep. Fetal membranes and amniotic fluid from infected animals carry large numbers of hardy organisms. Human infection occurs from direct contact with infected materials or from fomites. Signs of Q fever infection in humans range from subclinical disease to severe flu-like symptoms, pneumonia, endocarditis, and death. Diagnosis of subclinical infection in sheep is difficult and false-negative results are common because animals may shed large numbers of organisms in the absence of detectable antibody. Contagious ecthyma (“orf”) is a poxvirus-induced papular disease of sheep and goats. Infected animals frequently have lesions on the mucocutaneous junctions of the head, which can spread to humans by direct contact. Affected animals and humans develop long-lasting immunity and usually recover in 10–14 days. Effective vaccines for sheep and goats are available but provide only short-term protection and pose some hazard to humans. No human vaccine is available (Fox et al., 2015). For these reasons, researchers should always wear gloves and other personal protective equipment and report unexpected illness to a physician familiar with specific occupational risks associated with animals.

Careful preoperative preparation of the rumen is required for safe anesthesia of sheep and goats. Adult animals require withdrawal of food and water for at least 8–12 h and no longer than 24 h before surgery to reduce rumen size and digestive activity. Rumen distension and hypoventilation are common when positioning animals in dorsal or lateral recumbency. Preoperative passage of a 1–2 cm diameter thick-walled stomach tube into the rumen allows intraoperative decompression and aspiration of gas if required. Removal of large amounts of fluid is typically unnecessary and may impair return of normal gut motility. Placement of a cuffed endotracheal tube should immediately follow anesthetic induction to prevent aspiration pneumonia. Aspiration pneumonia can be fatal after regurgitation because rumen fluid contains numerous anaerobic bacteria. Infant ruminants (<30 days of age) lack a functional rumen and should not be fasted longer than 8–12 h if at all (Flecknell et al., 2015).

Most anesthetic and analgesic drugs are used off-label in small ruminant species. Therefore animals that receive these drugs in research may not enter the food supply through rehoming, slaughter, or compost (Flecknell et al., 2015).

Brief Restraint

Sheep and goats are docile and rarely require sedation for blood sampling, dressing changes, or other routine procedures. For more invasive procedures, animals may be sedated for 10–20 min with a low dose of xylazine (0.02–0.04 mg/kg intravenous [IV] or IM) or medetomidine (0.01–0.02 mg/kg IV). Atipamezole (0.02–0.06 mg/kg IM) reverses xylazine or medetomidine sedation when necessary. Research staff should be mindful of the much lower xylazine dose required for ruminants compared to other species. By contrast, the dose of medetomidine in ruminants is similar in most laboratory animal species. Animals in late pregnancy should not receive xylazine to avoid fetal hypooxygenation secondary to depressed maternal cardiac output. The benzodiazepines diazepam (0.25 mg/kg IV) and midazolam (1.3 mg/kg IV) produce muscle relaxation and sedation in sheep and goats, with less depression of cardiac output than is seen with medetomidine (Flecknell et al., 2015).

General Anesthesia

Isoflurane is the anesthetic of choice for general anesthesia of sheep and goats. Anesthesia is induced by premedication with a low dose of xylazine (0.03 mg/kg IM) followed 10–15 min later by ketamine (5 mg/kg) and diazepam (0.3–0.5 mg/kg IV to effect) to produce light anesthesia of 10–20 min duration suitable for endotracheal intubation (Flecknell et al., 2015). Propofol (4.0–6.0 mg/kg IV to effect) is a suitable induction agent and may be suitable as a sole agent for brief procedures, or by continuous rate infusion (0.5 mg/kg/min) for longer procedures (Flecknell et al., 2015).

Profuse salivation follows the administration of most anesthetic drugs in ruminants. Administration of anticholinergic drugs is not recommended in ruminants, because these agents may increase salivary viscosity and impair gastrointestinal motility. Anesthetized ruminants should be positioned with the head down to encourage drainage of saliva away from the airway (Flecknell et al., 2015).

Endotracheal intubation requires a laryngoscope with a 20–30 cm blade. Vinyl- or silicone-cuffed tubes 10–16 mm in diameter are suitable for most sheep and goats. An assistant positions the animal in sternal recumbency, extends the neck, and holds the mouth open. The anesthetist visualizes the epiglottis with the laryngoscope and intubates the trachea during inspiration. Prior application of 2% lidocaine spray to the vocal cords prevents laryngospasm. The use of a stylet may help deflect the tip of the tube into the larynx. A mouth gag is often necessary to prevent damage to the tube by sharp molar teeth. After inflation of the cuff, secure the tube with gauze to the mandible. Isoflurane vaporizer settings of 0.75%–1.0% are often sufficient to maintain general anesthesia in sheep and goats. Absence of chewing motions and the palpebral reflex in response to stimulation indicates an adequate surgical plane. Eye position is not a reliable indicator of anesthetic depth in sheep and goats. Intermittent positive pressure ventilation

is recommended to prevent hypoventilation from positioning and pressure from abdominal viscera (Flecknell et al., 2015).

Analgesia

Signs of pain in ruminants may be subtle and limited to lethargy, reduced appetite, and rumination. Signs of severe pain include rolling, moaning, grunting, and grinding of the teeth (bruxism). The general anesthetics isoflurane and propofol provide minimal analgesia, therefore effective pre-emptive and postoperative analgesia is essential.

NSAIDs are highly effective in small ruminants and recommended for first-line treatment unless scientifically contraindicated. Flunixin (1.1–2.2 mg/kg), ketoprofen (2–3 mg/kg), carprofen (4 mg/kg), and meloxicam (0.5 mg/kg IV or 1 mg/kg PO) provide effective analgesia for up to 24 h after dosing. All NSAIDs should be administered parenterally in small ruminants. The intravenous route is preferred for animals with severe acute pain, but the subcutaneous and intramuscular routes have been widely reported.

Opioid analgesics may be indicated as a supplement or as primary analgesics in some cases. The epidural space is easily accessed in small ruminants. Epidural morphine (0.1 mg/kg diluted in sterile saline) administered in the lumbosacral or sacrocaudal spaces provides up to 12 h of analgesia (Riebold, 2017). The transdermal fentanyl patch (50 µg/h) produces effective blood levels in sheep for up to 72 h, but may be unpredictable in goats. Buprenorphine (0.005–0.01 mg/kg) is effective in calves and sheep but requires administration every 4–6 h for effective analgesia. Buprenorphine causes excitation in goats and is not recommended (Flecknell et al., 2015).

Local anesthetics are effective agents in multimodal analgesic protocols for thoracotomy and other painful procedures. The long-acting local anesthetic bupivacaine may be administered by diffusion catheter at the incision site (0.25%, 5–12 mL q8h). Ruminants are more sensitive to systemic effects of local anesthetics than other species. The maximum suggested dose of lidocaine for sheep and goats is 0.5 mL/kg of a 2% solution. For wide infiltration, 2% lidocaine may be diluted to 1%. Signs of systemic local anesthetic overdose include seizures, respiratory depression, bradycardia, hypotension, and collapse (Flecknell et al., 2015).

Rabbit

Animal Selection and Preoperative Preparation

The most common respiratory pathogen in conventional rabbits is *Pasteurella multocida*; however, most laboratory animal vendors provide animals free of this agent. *P. multocida* infection may be clinically inapparent or cause severe mucopurulent nasal discharge (“snuffles”) and/or middle ear disease resulting in head tilt. Rabbits do not vomit, and aspiration pneumonia is therefore not a concern. Adult rabbits will tolerate an overnight fast without difficulty, and the resulting reduction in stomach contents may help maintain

adequate oxygenation during spontaneous respiration under anesthesia. Rabbits weighing less than 2 kg should not be fasted, as hypoglycemia and metabolic acidosis may be significant (Lipman et al., 2008). Prolonged fasting may cause dehydration and subsequent intestinal motility disorders (Flecknell et al., 2015; Lipman et al., 2008). Traumatic lower-back fracture is common when inexperienced staff handle rabbits. The best way to handle rabbits is to grasp the scruff of the neck with one hand while supporting the rump and hind legs with the other. Sudden onset of flaccid paraplegia in rabbits is almost always the result of lower-back fracture and warrants immediate euthanasia for humane reasons (Nowland et al., 2015). Never lift, move, or restrain rabbits by the ears.

Brief Procedures

Combined administration of ketamine (35–50 mg/kg IM) and xylazine (5–10 mg/kg IM) provides excellent anesthesia for a variety of applications in the rabbit. General anesthesia lasts for 30–60 min and provides adequate analgesia and restraint for procedures of moderate intensity. Supplemental use of a narcotic analgesic such as buprenorphine (0.05 mg/kg IM) prolongs anesthesia and improves analgesia. Propofol administered by intravenous bolus or constant rate infusion produces light anesthesia suitable only for intubation or nonpainful procedures such as imaging. Telazol should not be used for survival procedures in rabbits, because renal tubular damage is a common complication even at standard anesthetic dosages (Flecknell et al., 2015; Lipman et al., 2008).

General Anesthesia

The intramuscular ketamine/xylazine combination suggested for brief procedures is also an excellent induction agent prior to endotracheal intubation for inhalation anesthesia. Intravenous administration of ketamine and xylazine through the ear vein will achieve rapid induction, but care is required to minimize skin irritation from perivascular infiltration. Mask induction is rarely indicated because apnea, breath holding, bradycardia, and struggling are common when unsedated rabbits are exposed to isoflurane, and because operator exposure to waste anesthetic is difficult to avoid in this setting (Flecknell et al., 2015).

Propofol (10–20 mg/kg IV) is an effective rabbit anesthetic induction agent that produces significantly faster postoperative recovery than ketamine/xylazine in animals maintained on sevoflurane or isoflurane. By contrast, anesthetic recovery following ketamine/xylazine or ketamine/medetomidine may require up to 120 min. Animals should receive preoperative analgesics and be preoxygenated by mask before propofol administration.

The initial propofol dose of 10 mg/kg should be administered slowly over 60 s (~0.17 mg/kg/s), with additional small increments as required to allow endotracheal intubation. Respiratory arrest may occur, particularly following rapid infusion (>0.25 mg/kg/s) (Allweiler et al., 2010).

Endotracheal intubation of the rabbit may be difficult because of several distinctive anatomic features. Prominent incisor teeth, a long oropharynx, and limited mobility of the temporomandibular joint hinder direct visualization of the larynx from the front. Lidocaine spray on the vocal cords is necessary to prevent further narrowing of the larynx through laryngospasm. Benzocaine spray (Cetacaine) produces methemoglobinemia in rabbits and should be avoided. Supine, prone, or lateral positions are all suitable for endotracheal intubation. Hyperextension of the neck will straighten the larynx and facilitate proper tube placement. Blind intubation of the trachea is easily accomplished with practice. Studies have shown that using supraglottic airway devices (e.g., v-gel) offers some benefits over blind intubation, including faster placement and less trauma to the airway (Engbers et al., 2017; Zeeland and Schoemaker, 2012).

Anesthetic maintenance with isoflurane usually requires a vaporizer setting of 1%–4%. Absence of the pinna withdrawal reflex is the best indicator of a surgical anesthetic plane in the rabbit. Many rabbits retain the corneal and pedal withdrawal reflexes even under very deep anesthesia (Flecknell et al., 2015; Lipman et al., 2008).

If an anticholinergic agent is required, investigators should be aware that approximately 50% of rabbits produce atropinesterase (AtrE) as a genetically determined trait. Glycopyrrolate resists AtrE and is therefore recommended over atropine for rabbits. Glycopyrrolate prevents xylazine-associated bradycardia in rabbits (Flecknell et al., 2015; Lipman et al., 2008).

Analgesia

The most frequently recognized signs of pain and discomfort in rabbits include anorexia, an unkempt appearance due to failure to groom, and reduced activity. Untreated anorexia can create serious secondary disease, including generalized gastrointestinal stasis, rapid weight loss, and fatal hepatic lipidosis (Flecknell et al., 2015; Lipman et al., 2008). The recent validation of a facial grimace score, which assesses orbital tightening, cheek flattening, nose shape, and changes in whiskers, has facilitated the diagnosis and management of pain in rabbits (Hampshire and Robertson, 2015; Keating et al., 2012).

The best indicator of gastrointestinal health in the rabbit is the quantity and consistency of fecal pellets. Dehydration and anorexia result in a reduced number of firm dry pellets. Treatment of anorexic postoperative rabbits should be directed to relief of underlying pain if present and toward restoration of normal gastrointestinal function. A high-fiber supplement such as Oxbow Critical Care or blenderized rabbit chow is preferred over low-fiber nutritional gels such as Nutrical to restore normal gut motility. Aggressive analgesia, fluid therapy, and force feeding may be necessary in some cases.

Narcotic analgesics are preferred for the treatment of moderate to severe postoperative pain in rabbits. Buprenorphine (0.01–0.05 mg/kg SQ twice or three times a day) is

the narcotic of choice, because it provides effective analgesia at a convenient dosing interval and is generally well tolerated. The fentanyl patch (25 µg/h) is an alternative narcotic analgesic option that provides continuous analgesia up to 72 h without the requirement for regular injections (Flecknell et al., 2015).

NSAIDs are also highly effective in rabbits, particularly for musculoskeletal pain or coadministered with narcotics for multimodal analgesia. Flunixin (1.1 mg/kg SQ q24h), carprofen (4 mg/kg SQ q24h), and meloxicam (0.3 mg/kg PO q24h) all demonstrate good clinical efficacy in rabbits (Lipman et al., 2008). Meloxicam oral suspension (Metacam, 1.5 mg/mL) has recently undergone pharmacokinetic evaluation in rabbits. Oral administration of 0.3 mg/kg once a day produced blood levels comparable to those shown to be clinically effective in other species for up to 24 h. Although rabbits demonstrate more rapid metabolism of meloxicam than other species, delayed gastrointestinal absorption of the drug allows maintenance of effective blood levels throughout the dose period (Carpenter et al., 2009; Fredholm et al., 2013; Turner et al., 2006).

Swine

Animal Selection and Preoperative Preparation

Swine are commonly used in experimental surgery because of many anatomic and physiologic similarities to humans. Advantages to the use of pigs in the laboratory include low cost, ready availability, and ease of acclimation to the laboratory. Disadvantages include the uncooperative nature of pigs with respect to most clinical procedures, limited number of intravenous access sites, and relative difficulty of endotracheal intubation.

Because animals larger than 100 kg are difficult to handle in the laboratory, selective breeding has produced several types of miniature swine for research. The Gottingen minipigs and the Yucatan micropigs achieve a maximum bodyweight of 35–55 kg at 2 years of age. The Hanford and Yucatan minipigs are somewhat larger and weigh 70–90 kg at 2 years of age. By contrast, adult crossbred farm pigs weigh 90–110 kg at 6 months of age, and 200–300 kg at 2 years of age (Bollen Hansen et al., 2000; Swindle and Smith, 2016). Juvenile crossbred farm pigs are less expensive than minipigs or micropigs, and are often used for short-term surgical studies. Juvenile farm pigs gain 2–4 kg/week and require larger pens as they grow to maintain facility compliance with the Guide (National Research Council, 2011).

Careful evaluation of the vendor health program is required to reduce experimental morbidity from unrelated clinical conditions. Chronic respiratory disease is common in commercial swine operations. Although subclinical infections are common, transportation, anesthesia, and surgery may activate latent infections and result in excess morbidity and mortality. Many commercial breeders of laboratory minipigs and micropigs maintain specific SPF herds free from infection with common pathogens.

Malignant hyperthermia (MH) is an autosomal recessive trait that causes affected animals to develop marked

hyperthermia (rectal temperature $>41^{\circ}\text{C}$), and extensor muscle rigidity and necrosis after exposure to environmental extremes or halothane or isoflurane anesthesia. The disease has been described only in farm animals bred for rapid growth, including but not limited to the Landrace, Yorkshire, Duroc, Pietrain, and Poland China breeds. MH is increasingly rare as commercial breeders identify and cull carrier pigs but may still be encountered sporadically when farm pigs are used for experimental surgery. The condition has not been described in minipigs or micropigs or other species. Treatment of animals that develop MH during an experimental procedure requires immediate termination of anesthesia and supply of 100% oxygen, whole body cooling, and administration of corticosteroids, sodium bicarbonate, and dantrolene sodium (3–5 mg/kg IV) (Helke et al., 2015; Swindle and Smith, 2016; Swindle et al., 2012).

Food and contact bedding must be removed 6–8 h prior to general anesthesia. Water may be offered until 2 h before anesthesia. The presence of food in the stomach frequently results in gastric distension, hypoventilation, and tachycardia during prolonged general anesthesia, requiring prompt decompression through orogastric intubation (Swindle and Smith, 2016).

Brief Restraint

Pigs may be easily trained to accept handling for physical examination, blood collection through a vascular access port, and dressing changes. The acclimation period following arrival to the facility before study initiation is an appropriate training time. Uncooperative pigs may require chemical restraint for minor clinical procedures. Slings and hammocks are available that will allow restraint of calm pigs up to 50 kg for up to several hours (Swindle and Smith, 2016). The Panepinto sling was specifically designed for veterinary practice and laboratory environments and is easy to operate and sanitize. Sedation may be necessary to facilitate initial placement of animals into the sling. Azaperone (4 mg/kg IM) is a useful agent for this purpose. For more invasive procedures, a mixture of Telazol (4.4–6.6 mg/kg IM), xylazine (2.2 mg/kg IM), and atropine (0.05 mg/kg) provides approximately 30 min of anesthesia suitable for minor surgery, followed by smooth recovery. Endotracheal intubation for subsequent maintenance on isoflurane is also possible after Telazol and xylazine induction (Bollen Hansen et al., 2000; Swindle and Smith, 2016).

General Anesthesia

Prolonged or invasive procedures are best conducted under isoflurane anesthesia. Endotracheal intubation is warranted for general anesthesia in swine to protect the airway and allow for controlled ventilation when required. Endotracheal intubation is possible with the pig in dorsal, ventral, or lateral recumbency. Two anatomic characteristics can complicate the procedure. First, the soft palate is long and must be displaced dorsally for visualization of the larynx. Second, the laryngeal diverticulum distal to the larynx may “trap” the tip of the endotracheal tube unless the tube is

TABLE 2.3.6.1 Recommendations of Animal Models by Clinical Application (Byrom et al., 2010)

Species	Indication
Sheep	Vascular conduits 4–6 mm diameter
Baboon	Thrombogenicity Tissue-engineered conduits
Rabbit	Vascular conduits 1–4 mm diameter

gently twisted as it passes over the epiglottis. After intubation, maintenance anesthesia usually requires an isoflurane vaporizer setting of 1.5%–2.5% in oxygen. The actual concentration of isoflurane will vary according to the anesthetic induction regimen, type of procedure, and concurrent use of other narcotic and sedative agents. Administration of Telazol and xylazine for anesthetic induction has a substantial isoflurane-sparing effect that may last for the first 30–60 min of anesthesia. Adequate surgical anesthesia is indicated by the absence of the pedal withdrawal reflex, minimal jaw tone, and stable heart rate and blood pressure (Flecknell et al., 2015; Smith and Swindle, 2008).

Analgesia

Diagnosis of pain in swine may be challenging. Pain scoring systems reported by some investigators have not been validated in large-scale studies. Withdrawal to palpation of painful areas, for example, is the most obvious sign of pain in pigs. Although an indirect measure, depressed appetite is a common indicator of pain in postoperative pigs. In addition, depending on the nature of the pain, pigs may exhibit reduced or increased activity and depressed attitude compared to normal pigs (Flecknell et al., 2015; Ison et al., 2016).

Narcotics are commonly used postoperative analgesics in swine. Buprenorphine is the most widely used narcotic and provides excellent analgesia at a convenient dose interval with few side effects. The fentanyl patch (5 $\mu\text{g}/\text{kg}/\text{h}$) is effective in swine and reduces the need to handle animals during the immediate postoperative period, when struggling may increase pain at the incision line or predispose to dehiscence. Fentanyl patches should be applied in the dorsal midscapular region to prevent accidental dislodgement and ensure consistent absorption (Harvey-Clark, 2000; Malavasi et al., 2005; Osorio Lujan et al., 2017). Group-housed pigs may remove and consume patches applied to cage mates and develop acute narcotic overdose.

NSAIDs are highly effective analgesics in swine. Carprofen (2 mg/kg SQ or PO q24h), meloxicam (0.4 mg/kg SQ q24h), and flunixin (1–4 mg/kg SQ or IM q24h) have been used as sole agents or in combination with opioid local anesthetics. Gastric irritation has not been reported following short-term use, but may be a concern in animals that require chronic therapy (Smith and Swindle, 2008; Swindle and Smith, 2016) (Table 2.3.6.1).

CASE STUDY

You are a biomaterials engineer for a large pharmaceutical company. You wish to evaluate a novel material in an animal model for use in the repair of large segmental long bone defects. The test material contains human-origin stem cells in a proprietary matrix. You propose to use 100 nonhuman primates for the study. During protocol prereview, the attending veterinarian suggested you clarify the following questions in your IACUC protocol before submission for full committee review:

1. Provide scientific justification to use nonhuman primates for this model. Your answer should identify at least two other animal models in common use (species and bone):
 - a. *Scientific justification:*
 - i. *Nonhuman primates are bipedal, therefore mechanical loading is more similar to humans.*
 - ii. *Human-origin stem cells may be more likely to engraft in a nonhuman primate species than in other species.*
 - b. *Common models:*
 - i. *Sheep tibia*
 - ii. *Rat calvarium*
2. What are the advantages and disadvantages of the common models over the nonhuman primate model?
 - a. *Advantages:*
 - i. *Lower cost and increased availability, reduced bio-hazard concern.*
 - ii. *Large experience base and consensus acceptance of these species as standard models compared to primates.*
 - b. *Disadvantages:*
 - i. *Quadrupedal locomotion.*
 - ii. *Different microscopic anatomy.*
 - iii. *Rapid rejection of xenogeneic tissue.*
3. What postoperative complications should you be prepared for (provide at least two) and what would you do to detect and treat these if they occur?
 - a. *Complications:*
 - i. *Pain from creation of the defect.*
 - ii. *Infection or inflammation associated with the implant.*
 - iii. *Collapse or pathologic fracture of the bone.*
 - b. *Detection and treatment:*
 - i. *Postoperative monitoring for poor appetite, increased attention to wound, redness, swelling, or discharge.*

- ii. *Treatment.*
 1. *NSAID and/or narcotic analgesic for at least 3 days or longer as needed.*
 2. *Consultation with facility veterinarian:*
 - a. *Warm compresses, antibiotics, analgesics, or other treatments as directed.*
 - b. *Euthanasia if complication causes untreatable pain or disability or if treatment will introduce unacceptable study variables.*
4. Clarify, reevaluate, and revise your protocol considering the “three Rs” (replacement, reduction, refinement) as an ethical imperative. For example, replacement is demonstrated by replacing animals with a computer model.
 - a. *Replacement:*
 - i. *Evaluate potential of embryonic stem cells to stimulate bone formation in an in vitro model (cells in culture, “organ on a chip,” ex vivo model).*
 - ii. *Before proceeding to nonhuman primate studies, demonstrate proof of concept in a smaller number of rodents using the rodent calvarium model with either rodent-origin stem cells or in an immune-compromised rodent (nude rat, severe combined immunodeficient mouse) with human-origin cells. This is also an example of refinement since the calvarium model is arguably less painful than a segmental defect model because the calvarium is not weight bearing.*
 - b. *Reduction:*
 - i. *Perform power analysis to justify animal numbers used by fully describing control and treatment groups, expected treatment effect, and inherent variability of the animal model.*
 - ii. *Consider using one control group for multiple treatment groups.*
 - c. *Refinement:*
 - i. *Evaluate and optimize an analgesic, surgical, and postoperative care regimen in a small pilot study before proceeding to full 100 primate study.*
 - ii. *Assure adequate staffing and budget to provide needed monitoring and care.*

References

- Ahlberg, S., Bateman, M., Eggen, M., Quill, J., Richardson, E., Iaizzo, P., 2013. Animal models for cardiac valve research. In: Iaizzo, P., Bianco, R., Hill, A., St Louis, J. (Eds.), *Heart Valves: From Design to Clinical Implantation*. Springer, New York, NY, pp. 343–359. <https://doi.org/10.1016/B978-012370615-7/50044-5>.
- Ahmed, M., Hamilton, G., Seifalian, A.M., 2014. The performance of a small-calibre graft for vascular reconstructions in a senescent sheep model. *Biomaterials* 35, 9033–9040. <https://doi.org/10.1016/j.biomaterials.2014.07.008>.
- Allweiler, S., Leach, M.C., Flecknell, P.A., 2010. The use of propofol and sevoflurane for surgical anaesthesia in New Zealand White rabbits. *Lab. Anim.* 44, 113–117. <https://doi.org/10.1258/la.2009.009036>.
- ASTM International, 2014. Standard Guide for Preclinical In Vivo Evaluation in Critical Size Segmental Bone Defects. <https://doi.org/10.1520/F2721-09R14.1>. Designation: F2721-09.
- Barnhart, G., Jones, M., Ishihara, T., Chavez, A., 1982. Bioprosthetic valvular failure. Clinical and pathological observations in an experimental animal model. *J. Thorac. Cardiovasc. Surg.*
- Bate, S.T., Clark, R.A., 2014. *The Design and Statistical Analysis of Animal Experiments*. Cambridge University Press, Cambridge, UK.
- Bélanger, M.C., Marois, Y., 2001. Hemocompatibility, biocompatibility, inflammatory and in vivo studies of primary reference materials low-density polyethylene and polydimethylsiloxane: a review. *J. Biomed. Mater. Res.* 58, 467–477. <https://doi.org/10.1002/jbm.1043>.
- Bhattacharya, V., Mcsweeney, P.A., Shi, Q., Bruno, B., Ishida, A., Nash, R., Storb, R.F., Sauvage, L.R., Hammond, W.P., Hong, M., Wu, D., 2000. Enhanced endothelialization and microvessel formation in polyester grafts seeded with CD34⁺ bone marrow cells. *Blood* 95, 581–585.
- Bigham-Sadegh, A., Oryan, A., 2015. Selection of animal models for pre-clinical strategies in evaluating the fracture healing, bone graft substitutes and bone tissue regeneration and engineering. *Connect. Tissue Res.* 56 (3), 175–194. <https://doi.org/10.3109/03008207.2015.1027341>.
- Bollen, P.J.A., Hansen, A.K., Rasmussen, H.J., 2000. The laboratory swine. In: *Lab. Anim. Pocket Ref. Ser.* CRC Press, New York.

- Bonucci, E., Ballanti, P., 2014. Osteoporosis—bone remodeling and animal models. *Toxicol. Pathol.* 42, 957–969. <https://doi.org/10.1177/0192623313512428>.
- Byrom, M.J., Bannon, P.G., White, G.H., Ng, M.K.C., 2010. Animal models for the assessment of novel vascular conduits. *J. Vasc. Surg.* 52, 176–195. <https://doi.org/10.1016/j.jvs.2009.10.080>.
- Carpenter, J.W., Pollock, C.G., Koch, D.E., Hunter, R.P., 2009. Single and multiple-dose pharmacokinetics of meloxicam after oral administration to the rabbit (*Oryctolagus cuniculus*). *J. Zoo Wildl. Med.* 40, 601–606. <https://doi.org/10.1638/2007-0115.1>.
- Cheung, D.Y., Duan, B., Butcher, J.T., 2015. Current progress in tissue engineering of heart valves: multiscale problems, multiscale solutions. *Expert Opin. Biol. Ther.* 15, 1155–1172. <https://doi.org/10.1517/14712598.2015.1051527>.
- Christou, C., Oliver, R.A., Pelletier, M.H., Walsh, W.R., 2014. Ovine model for critical-size tibial segmental defects. *Comp. Med.* 64, 377–385.
- Congress, U., 2013. Animal Welfare Act, Transportation, Sale, and Handling of Certain Animals, as Amended. Congress, Washington, DC.
- Cooper, G., Mooney, M., Gosain, A., Campbell, P., Losee, J.E., Huard, J., 2010. Testing the “critical-size” in calvarial bone defects: revisiting the concept of a critical-sized defect (CSD). *Plast. Reconstr. Surg.* 125, 1685–1692. <https://doi.org/10.1016/j.cgh.2008.07.016.Cytokeratin>.
- Crick, S.J., Sheppard, M.N., Ho, S.Y., Gebstein, L., Anderson, R.H., 1998. Anatomy of the pig heart: comparisons with normal human cardiac structure. In: L.I.O.R.G.E.B.S.T.E., On, a N.D.R.O.B.E.R.T.H. a N.D.E.R.S., Crick, S.J., Sheppard, M.N., Ho, S.Y., Gebstein, L., Anderson, R.H. *J. Anat.* 193 (Pt 1), 105–119. <https://doi.org/10.1046/j.1469-7580.1998.19310105.x>.
- Curtin, L.I., Grakowsky, J.A., Suarez, M., Thompson, A.C., DiPirro, J.M., Martin, L.B., Kristal, M.B., 2009. Evaluation of buprenorphine in a postoperative pain model in rats. *Comp. Med.* 59, 60–71.
- Derwin, K.A., Baker, A.R., Codsí, M.J., Iannotti, J.P., 2007. Assessment of the canine model of rotator cuff injury and repair. *J. Shoulder Elb. Surg.* 16, 140–148. <https://doi.org/10.1016/j.jse.2007.04.002>.
- Derwin, K.A., Galatz, L.M., Ratcliffe, A., Thomopoulos, S., 2018. Enthesis repair: challenges and opportunities for effective tendon-to-bone healing. *J. Bone Jt. Surg.* 100, 109–110. <https://doi.org/10.2106/JBJS.18.00200>.
- DiVincenti, L., Westcott, R., Lee, C., 2014. Sheep (*Ovis aries*) as a model for cardiovascular surgery and management before, during, and after cardiopulmonary bypass. *J. Am. Assoc. Lab. Anim. Sci.* 53, 439–448.
- Dixon, J.A., Spinale, F.G., 2009. Large animal models of heart failure; A critical link in the translation of basic science to clinical practice. *Circ. Hear. Fail.* 2, 262–271. <https://doi.org/10.1161/CIRCHEARTFAILURE.108.814459>.
- Engbers, S., Larkin, A., Rousset, N., Prebble, M., Jonnalagadda, M., Knight, C.G., Pang, D.S.J., 2017. Comparison of a supraglottic airway device (v-gel®) with blind orotracheal intubation in rabbits. *Front. Vet. Sci.* 4. <https://doi.org/10.3389/fvets.2017.00049>.
- Evans, H., de LaHunta, A., 2010. Guide to the Dissection of the Dog, seventh ed. Saunders Elsevier, St. Louis, MO.
- Flecknell, P., Lofgren, J.L.S., Dyson, M.C., Marini, R.R., Swindle, M.M., Wilson, R.P., 2015. Preanesthesia, anesthesia, analgesia, and euthanasia. In: Fox, J., Anderson, L., Otto, G., Pritchett-Corning, K., Whary, M. (Eds.), *Laboratory Animal Medicine*. Elsevier, Oxford, UK, pp. 1135–1200.
- Fitts, D.A., 2011. Minimizing animal numbers: the variable-criteria sequential stopping rule. *Comp. Med.* 61, 206–218.
- Fox, J.G., Otto, G., Colby, L.A., 2015. Chapter 28 – selected zoonoses. In: *Laboratory Animal Medicine*. <https://doi.org/10.1016/B978-0-12-409527-4.00028-6>.
- Fredholm, D.V., Carpenter, J.W., KuKanich, B., Kohles, M., 2013. Pharmacokinetics of meloxicam in rabbits after oral administration of single and multiple doses. *Am. J. Vet. Res.* 74, 636–641. <https://doi.org/10.2460/ajvr.74.4.636>.
- Fujibayashi, S., Neo, M., Kim, H., Kokubo, T., Nakamura, T., 2003. A comparative study between in vivo bone ingrowth and in vitro apatite formation on Na₂O-CaO-SiO₂ glasses. *Biomaterials* 24, 1349–1356.
- Gallegos, R., Rivard, A., Bianco, R., 2005. Animal models for cardiac research. In: Iazzo, P. (Ed.), *Handbook of Cardiac Anatomy, Physiology, and Devices*. Humana Press, Totawa, NJ, pp. 343–357. https://doi.org/10.1007/978-1-4614-6144-9_14.
- Gaertner, D.J., Hallman, T.M., Hankenson, F.C., Batchelder, M., 2008. Anesthesia and analgesia for laboratory rodents. In: Fish, R.E., Brown, M.J., Danneman, P.J., Karas, A.Z. (Eds.), *Anesthesia and Analgesia in Laboratory Animals*. Academic Press, London, UK, pp. 239–298.
- Gelatt, K., 2011a. Anesthesia for ophthalmic surgery. In: *Veterinary Ophthalmic Surgery*. W.B. Saunders, pp. 37–49. <https://doi.org/10.1016/B978-0-7020-3429-9.00003-1>.
- Gelatt, K., 2011b. Surgical instrumentation. In: *Veterinary Ophthalmic Surgery*. W.B. Saunders, pp. 1–15. <https://doi.org/10.1016/B978-0-7020-3429-9.00001-8>.
- Grehan, J.F., Hilbert, S.L., Ferrans, V.J., Droel, J.S., Salerno, C.T., Bianco, R.W., 2000. Development and evaluation of a swine model to assess the preclinical safety of mechanical heart valves. *J. Heart Valve Dis.* 9 710–9; discussion 719–20.
- Gross, D., 2009. *Animal Models in Cardiovascular Research*, third ed. Springer, New York, NY. https://doi.org/10.1007/978-0-387-95962-7_6.
- Gugala, Z., Lindsey, R.W., Gogolewski, S., 2007. New approaches in the treatment of critical-size segmental defects in long bones. *Macromol. Symp.* 253, 147–161. <https://doi.org/10.1002/masy.200750722>.
- Hampshire, V., Robertson, S., 2015. Using the facial grimace scale to evaluate rabbit wellness in post-procedural monitoring. *Lab. Anim.* 44, 259–260.
- Helke, K., Ezell, P., Duran-Struuck, R., Swindle, M., 2015. Biology and diseases of swine – Biology and diseases of swine. In: Fox, J., Anderson, L., Otto, G., Pritchett-Corning, K., Whary, M. (Eds.), *Laboratory Animal Medicine*. Elsevier, Oxford, UK, pp. 616–665.
- Hessler, J.R., Lehner, N.D.M., 2009. *Planning and Designing Research Animal Facilities*. Elsevier/Academic Press, London, UK.
- Ison, S.H., Clutton, R.E., Di Giminianni, P., Rutherford, K.M.D., 2016. A review of pain assessment in pigs. *Front. Vet. Sci.* 3, 1–16. <https://doi.org/10.3389/fvets.2016.00108>.
- James Kirkpatrick, C., Fuchs, S., Iris Hermanns, M., Peters, K., Unger, R.E., 2007. Cell culture models of higher complexity in tissue engineering and regenerative medicine. *Biomaterials* 28, 5193–5198. <https://doi.org/10.1016/j.biomaterials.2007.08.012>.
- Janssen, C.F., Maiello, P., Wright, M.J., Kracinovsky, K.B., Newsome, J.T., 2017. Comparison of atipamezole with yohimbine for antagonism of xylazine in mice anesthetized with ketamine and xylazine. *J. Am. Assoc. Lab. Anim. Sci.* 56, 142–147.
- Kheradvar, A., Zareian, R., Kawauchi, S., Goodwin, R.L., Rugonyi, S., 2017. Animal models for heart valve research and development. *Drug Discov. Today Dis. Model.* 24, 55–62. <https://doi.org/10.1016/j.ddmod.2018.04.001>.
- Keating, S.C.J., Thomas, A.A., Flecknell, P.A., Leach, M.C., 2012. Evaluation of EMLA cream for preventing pain during tattooing

- of rabbits: changes in physiological, behavioural and facial expression responses. *PLoS One* 7, 1–11. <https://doi.org/10.1371/journal.pone.0044437>.
- Kheradvar, A., Groves, E.M., Dasi, L.P., Alavi, S.H., Tranquillo, R., Grande-Allen, K.J., Simmons, C.A., Griffith, B., Falahatpisheh, A., Goergen, C.J., Mofrad, M.R.K., Baaijens, F., Little, S.H., Canic, S., 2015. Emerging trends in heart valve engineering: Part I. Solutions for future. *Ann. Biomed. Eng.* 43, 833–843. <https://doi.org/10.1007/s10439-014-1209-z>.
- Lammens, J., Maréchal, M., Geris, L., Van der Aa, J., Van Hauwermeiren, H., Luyten, F.P., Delpont, H., 2017. Warning about the use of critical-size defects for the translational study of bone repair: analysis of a sheep tibial model. *Tissue Eng. C Methods* 23, 694–699. <https://doi.org/10.1089/ten.tec.2017.0147>.
- Lee-Parriz, D., 2007. Analgesia for rodent experimental surgery. *Isr. J. Vet. Med.* 62, 74–78.
- Lelovas, P.P., Kostomitsopoulos, N.G., Xanthos, T.T., 2014. A comparative anatomic and physiologic overview of the porcine heart. *J. Am. Assoc. Lab. Anim. Sci.* 53, 432–438.
- Li, D., Ren, B.H., Shen, Y., Wu, H., Wang, C., Zhang, L., Zhu, J., Jing, H., 2007. A swine model for long-term evaluation of prosthetic heart valves. *ANZ J. Surg.* 77, 654–658. <https://doi.org/10.1111/j.1445-2197.2007.04180.x>.
- Li, Y., Chen, S.K., Li, L., Qin, L., Wang, X.L., Lai, Y.X., 2015. Bone defect animal models for testing efficacy of bone substitute biomaterials. *J. Orthop. Transl.* 3, 95–104. <https://doi.org/10.1016/j.jot.2015.05.002>.
- Lindsey, R., Gugala, Z., Milne, E., Sun, M., Gannon, F., Latta, L., 2006. The efficacy of cylindrical titanium mesh cage for the reconstruction of a critical-size canine segmental femoral diaphyseal defect. *J. Orthop. Res.* <https://doi.org/10.1002/jor>.
- Lipman, N., Marini, R., Flecknell, P., 2008. Anesthesia and analgesia in rabbits. In: Fish, R., Brown, M., Danneman, P., Karas, A. (Eds.), *Anesthesia and Analgesia in Laboratory Animals*. Elsevier.
- Litwak, K.N., Unger, L.S., Fukamachi, K., Saeed, D., 2008. Retrospective analysis of adverse events in preclinical ventricular assist device experiments. *ASAIO J* 54, 347–350. <https://doi.org/10.1097/MAT.0b013e31817d92a8>.
- Malavasi, L.M., Augustsson, H., Jensen-Waern, M., Nyman, G., 2005. The effect of transdermal delivery of fentanyl on activity in growing pigs. *Acta Vet. Scand.* 46, 149–157. <https://doi.org/10.1186/1751-0147-46-149>.
- McGovern, J.A., Griffin, M., Hutmacher, D.W., 2018. Animal models for bone tissue engineering and modelling disease. *Dis. Model. Mech.* 11. <https://doi.org/10.1242/dmm.033084>. dmm033084.
- Monreal, G., Sherwood, L.C., Sobieski, M.A., Giridharan, G.A., Slaughter, M.S., Koenig, S.C., 2014. Large animal models for left ventricular assist device research and development. *ASAIO J.* 60, 2–8. <https://doi.org/10.1097/MAT.0000000000000005>.
- Nafei, A., Danielsen, C.C., Linde, F., Hvid, I., 2000. Properties of growing trabecular ovine bone, part I: mechanical and physical properties. *J. Bone Jt. Surg.* 82-B, 910–920.
- National Research Council, 1980. Criteria for selecting experimental animals. In: *Laboratory Animal Management – Rodents*, pp. 16–35. https://doi.org/10.1007/978-90-481-9962-4_2. Washington, DC.
- National Research Council, 1998. *Biomedical Models and Resources: Current Needs and Future Opportunities*. The National Academies Press, Washington, DC. <https://doi.org/10.17226/6066>.
- National Research Council, 2011. *Guide for the Care and Use of Laboratory Animals*, eighth ed. National Academy Press, Washington, DC. https://doi.org/10.1163/1573-3912_islam_DUM_3825.
- Nowland, M., Brammer, D., Garcia, A., Rush, H., 2015. Biology and diseases of rabbits. In: Fox, J., Anderson, L., Otto, G., Pritchett-Corning, K., Whary, M. (Eds.), *Laboratory Animal Medicine*. Elsevier, Oxford, UK, pp. 329–364. <https://doi.org/10.1016/b978-012263951-7/50012-0>.
- Nunamaker, D.M., 1998. Experimental models of fracture repair. *Clin. Orthop. Relat. Res.* 56–65. <https://doi.org/10.1097/00003086-199810001-00007>.
- Orlans, F.B., Beauchamp, T.L., Dresser, R., Morton, D.B., Gluck, J.P., 1996. *The Human Use of Animals: Case Studies in Ethical Choice*. Oxford University Press, New York, NY.
- Osorio Lujan, S., Habre, W., Daali, Y., Pan, Z., Kronen, P.W., 2017. Plasma concentrations of transdermal fentanyl and buprenorphine in pigs (*Sus scrofa* domesticus). *Vet. Anaesth. Analg.* 44, 665–675. <https://doi.org/10.1016/j.vaa.2016.09.002>.
- Pariante, J.L., Bordenave, L., Bareille, R., Baquey, C., Le Guillou, M., 2000. Cultured differentiated human urothelial cells in the biomaterials field. *Biomaterials* 21, 835–839. [https://doi.org/10.1016/S0142-9612\(99\)00253-7](https://doi.org/10.1016/S0142-9612(99)00253-7).
- Parker, R.M.A., Browne, W.J., 2014. The place of experimental design and statistics in the 3Rs. *ILAR J.* 55, 477–485. <https://doi.org/10.1093/ilar/ilu044>.
- Pearce, A.I., Richards, R.G., Milz, S., Schneider, E., Pearce, S.G., 2007. Animal models for implant biomaterial research in bone: a review. *Eur. Cells Mater.* 13, 1–10. <https://doi.org/10.22203/eCM.v013a01>.
- Phinzy, C., 1965. The lost pets that stray to the labs. *Sports Illus.* 36–49.
- Rashid, S.T., Salacinski, H.J., Hamilton, G., Seifalian, A.M., 2004. The use of animal models in developing the discipline of cardiovascular tissue engineering: a review. *Biomaterials* 25, 1627–1637. [https://doi.org/10.1016/S0142-9612\(03\)00522-2](https://doi.org/10.1016/S0142-9612(03)00522-2).
- Reichert, J.C., Epari, D.R., Wullschleger, M.E., Saifzadeh, S., Steck, R., Lienau, J., Sommerville, S., Dickinson, I.C., Schütz, M.A., Duda, G.N., Hutmacher, D.W., 2009a. Establishment of a preclinical ovine model for tibial segmental bone defect repair by applying bone tissue engineering strategies. *Tissue Eng. B Rev.* 16, 93–104. <https://doi.org/10.1089/ten.teb.2009.0455>.
- Reichert, J.C., Saifzadeh, S., Wullschleger, M.E., Epari, D.R., Schütz, M.A., Duda, G.N., Schell, H., van Griensven, M., Redl, H., Hutmacher, D.W., 2009b. The challenge of establishing preclinical models for segmental bone defect research. *Biomaterials* 30, 2149–2163. <https://doi.org/10.1016/j.biomaterials.2008.12.050>.
- Riebold, T.W., 2017. Ruminants. In: Tranquilli, W.J., Thurmon, J.C., Grimm, K.A. (Eds.), *Veterinary Anesthesia and Analgesia*. John Wiley & Sons, Ltd, Chichester, UK, pp. 912–927. <https://doi.org/10.1002/9781119421375.ch49>.
- Robotin-Johnson, M.C., Swanson, P.E., Johnson, D.C., Schuessler, R.B., Cox, J.L., Kennedy, J.H., Chachques, J.C., Crawford, J., Verrier, E.D., 1998. An experimental model of small intestinal submucosa as a growing vascular graft. *J. Thorac. Cardiovasc. Surg.* [https://doi.org/10.1016/S0022-5223\(98\)00436-X](https://doi.org/10.1016/S0022-5223(98)00436-X).
- Rodeo, S.A., 2017. Translational animal models in orthopaedic research. *Am. J. Sports Med.* 45, 1487–1489. <https://doi.org/10.1177/0363546517710641>.
- Rodeo, S.A., Potter, H.G., Kawamura, S., Turner, A.S., Kim, H.J., Atkinson, B.L., 2007. Biologic augmentation of rotator cuff tendon-healing with use of a mixture of osteoinductive growth factors. *J. Bone Jt. Surg.* 89, 2485. <https://doi.org/10.2106/JBJS.C.01627>.

- Roughan, J.V., Ojeda, O.B., Flecknell, P.A., 1999. The influence of pre-anesthetic administration of buprenorphine on the anaesthetic effects of ketamine/medetomidine and pentobarbitone in rats and the consequences of repeated anaesthesia. *Lab. Anim.* 33, 234–242. <https://doi.org/10.1258/002367799780578183>.
- Russell, W.M.S., Burch, R.L., 1959. *The Principles of Humane Experimental Technique*. Methuen and Co, London.
- Sands, M.P., Rittenhouse, E.A., Mohri, H., Merendino, K.A., 1969. An anatomical comparison of human, pig, calf, and sheep aortic valves. *Ann. Thorac. Surg.* 8, 407–414. [https://doi.org/10.1016/S0003-4975\(10\)66071-7](https://doi.org/10.1016/S0003-4975(10)66071-7).
- Schaper, W., Flameng, W., De Brabander, M., 1972. Comparative aspects of coronary collateral circulation. In: Bloor, C. (Ed.), *Comparative Pathophysiology of Circulatory Disturbances*. Advances in Experimental Medicine and Biology. Springer, Boston, MA, pp. 267–276. https://doi.org/10.1007/978-1-4684-3213-8_15.
- Seymour, T.L., Adams, S.C., Felt, S.A., Jampachaisri, K., Yeomans, D.C., Pacharinsak, C., 2016. Postoperative analgesia due to sustained-release buprenorphine, sustained-release meloxicam, and carprofen gel in a model of incisional pain in rats (*Rattus norvegicus*). *Jaalas* 55, 300–305.
- Shapiro, K., 1998. Looking at animal models: both sides of the debate. Assessing animal models of human disorders: Validity vs. “productive generativity.” *Lab Anim. (NY)* 27, 26–30.
- Shinbane, J.S., Wood, M.A., Jensen, D.N., Ellenbogen, K.A., Fitzpatrick, A.P., Scheinman, M.M., 1997. Tachycardia-induced cardiomyopathy: a review of animal models and clinical studies. *J. Am. Coll. Cardiol.* 29, 709–715. [https://doi.org/10.1016/S0735-1097\(96\)00592-X](https://doi.org/10.1016/S0735-1097(96)00592-X).
- Silverman, J., Suckow, M.A., Murthy, S., 2014. The IACUC handbook. In: *The IACUC Handbook*. CRC Press, Boca Raton, FL. <https://doi.org/10.1201/b12106>.
- Sim, E.K.W., Muskawad, S., Lim, C.S., Yeo, J.H., Lim, K.H., Grignani, R.T., Durrani, A., Lau, G., Duran, C., 2003. Comparison of human and porcine aortic valves. *Clin. Anat.* 16, 193–196. <https://doi.org/10.1002/ca.10149>.
- Singh, J., Roy, S., Mukherjee, P., Konar, D., Konar, A., Hazra, S., 2010. Influence of topical anesthetics on oculocardiac reflex and corneal healing in rabbits. *Int. J. Ophthalmol.* 3, 14–18. <https://doi.org/10.3980/j.issn.2222-3959.2010.01.04>.
- Smith, A.C., Swindle, M.M., 2008. Chapter 15 – anesthesia and analgesia in swine. In: *Anesthesia and Analgesia in Laboratory Animals*. Elsevier Inc. <https://doi.org/10.1016/B978-0-12373898-1.50019-X>.
- Sodian, R., Hoerstrup, S.P., Sperling, J.S., Daebritz, S., Martin, D.P., Moran, A.M., Kim, B.S., Schoen, F.J., Vacanti, J.P., Mayer, J.E., 2000a. Early in vivo experience with tissue-engineered trileaflet heart valves. *Circulation* 102. https://doi.org/10.1161/circ.102.suppl_3.III-22. Iii-22-Iii-29.
- Sodian, R., Hoerstrup, S.P., Sperling, J.S., Daebritz, S.H., Martin, D.P., Schoen, F.J., Vacanti, J.P., Mayer, J.E., 2000b. Tissue engineering of heart valves: in vitro experiences. *Ann. Thorac. Surg.* 70, 140–144. [https://doi.org/10.1016/S0003-4975\(00\)01255-8](https://doi.org/10.1016/S0003-4975(00)01255-8).
- Stassen, O.M.J.A., Muylaert, D.E.P., Bouten, C.V.C., Hjortnaes, J., 2017. Current challenges in translating tissue-engineered heart valves. *Curr. Treat. Options Cardiovasc. Med.* 19. <https://doi.org/10.1007/s11936-017-0566-y>.
- Steinert, R., Jain, R., 2013. Ophthalmologic applications: introduction. In: *Biomaterials Science: An Introduction to Materials*, pp. 905–957. <https://doi.org/10.1016/B978-0-08-087780-8.00076-0>.
- Sullivan, T.P., Eaglstein, W.H., Davis, S.C., Mertz, P., 2001. The pig as a model for human wound healing. *Wound Repair Regen.* 9, 66–76. <https://doi.org/10.1046/j.1524-475X.2001.00066.x>.
- Swindle, M., Smith, A., 2016. *Swine in the Laboratory: Surgery, Anesthesia, Imaging, and Experimental Techniques*, third ed. CRC Press, Boca Raton, FL.
- Swindle, M.M., Makin, a., Herron, a.J., Clubb, F.J., Frazier, K.S., 2012. Swine as models in biomedical research and toxicology testing. *Vet. Pathol.* 49, 344–356. <https://doi.org/10.1177/0300985811402846>.
- Swindle, M.M., Smith, A.C., Helke, K., 2013. Recommendations for medical device implantation in swine. *Isr. J. Vet. Med.* 68, 3–11.
- Taylor, W.R., Ehrig, R.M., Heller, M.O., Schell, H., Seebeck, P., Duda, G.N., 2006. Tibio-femoral joint contact forces in sheep. *J. Biomech.* 39, 791–798. <https://doi.org/10.1016/j.jbiomech.2005.02.006>.
- Turner, P.V., Cheng Chen, H., Taylor, W.M., 2006. Pharmacokinetics of meloxicam in rabbits after oral administration of single single and repeat oral dosing. *Am. J. Vet. Res.* 56, 63–67. <https://doi.org/10.2460/ajvr.74.4.636>.
- Underwood, W.J., Blauwiekel, R., Delano, M.L., Gillesby, R., Mischler, S.A., Schoell, A., 2015. Chapter 15 – Biology and diseases of ruminants (sheep, goats, and cattle). In: *Laboratory Animal Medicine*. <https://doi.org/10.1016/B978-0-12-409527-4.00015-8>.
- US Congress, 1985a. Public Health Service Policy on Humane Care and Use of Laboratory Animals. (Washington, DC).
- US Congress, 1985b. Health Research Extension Act, “Animals in Research.” Congress. (Washington, DC).
- US Congress, 1987. 21 USC: Food and Drugs; Part 58 – Good Laboratory Practice for Nonclinical Laboratory Studies.
- US Congress, 2013. Animal Welfare Regulations. (USA).
- US Congress, 2019. 21 USC: Federal Food, Drug, and Cosmetic Act, as Amended. https://doi.org/10.1007/978-94-011-7373-5_36. USA.
- Vajgel, A., Mardas, N., Farias, B.C., Petrie, A., Cimões, R., Donos, N., 2014. A systematic review on the critical size defect model. *Clin. Oral Implant. Res.* 25, 879–893. <https://doi.org/10.1111/clr.12194>.
- Vesely, I., 2005. Heart valve tissue engineering. *Circ. Res.* 97, 743–755. <https://doi.org/10.1161/01.RES.0000185326.04010.9f>.
- Wancket, L.M., 2015. Animal models for evaluation of bone implants and devices. *Vet. Pathol.* 52, 842–850. <https://doi.org/10.1177/0300985815593124>.
- Wayman, S., 1966. Concentration Camps for Dogs. *Life* 22–29.
- Wenger, S., 2012. Anesthesia and analgesia in rabbits and rodents. In: *Journal of Exotic Pet Medicine*. Elsevier Inc. <https://doi.org/10.1053/j.jepm.2011.11.010>.
- Werner, L., Chew, J., Mamalis, N., 2006. Experimental evaluation of ophthalmic devices and solutions using rabbit models. *Vet. Ophthalmol.* 9, 281–291. <https://doi.org/10.1111/j.1463-5224.2006.00495.x>.
- Zeeland, Y.R.A., Schoemaker, N.J., 2012. A new supraglottic device as alternative for rabbit endotracheal. *Assoc. Exot. Mammal Vet.* 11th Annu. Conf. 67–68.
- Zhang, B., Korolj, A., Lai, B.F.L., Radisic, M., 2018. Advances in organ-on-a-chip engineering. *Nat. Rev. Mater.* 3, 257–278. <https://doi.org/10.1038/s41578-018-0034-7>.

Further Reading

- Ahern, B.J., Soma, L.R., Boston, R.C., Schaar, T.P., 2009. Comparison of the analgesic properties of transdermally administered fentanyl and intramuscularly administered buprenorphine during and following experimental orthopedic surgery in sheep. *Am. J. Vet. Res.* 70, 418–422. <https://doi.org/10.2460/ajvr.70.3.418>.

- Burkholder, T.H., Linton, G., Hoyt, R.F., Young, R., 2012. The rabbit as an experimental model. In: *The Laboratory Rabbit, Guinea Pig, Hamster, and Other Rodents*, first ed. Elsevier Inc. <https://doi.org/10.1016/B978-0-12-380920-9.00018-3>.
- Delong, D., 2012. Bacterial diseases. In: *The Laboratory Rabbit, Guinea Pig, Hamster, and Other Rodents*. Elsevier, pp. 69–118. <https://doi.org/10.1201/9781351075428>.
- Harvey-Clark, C., Gillespie, K., Riggs, K., 2000. Transdermal fentanyl compared with parenteral buprenorphine in post-surgical pain in swine: a case study. *Lab. Anim.* 34, 386–398.
- International Organization for Standardization, 2009. ISO 10993-1: biological evaluation of medical devices — Part 1: evaluation and testing within a risk management process. *Int. Stand.* 1–28. <https://doi.org/10.1109/IEEESTD.2007.4288250>.
- Ko, J.C., Williams, B.L., Smith, V.L., McGrath, C.J., Jacobson, J.D., 1993. Comparison of Telazol, Telazol-ketamine, Telazol-xylazine, and Telazol-ketamine-xylazine as chemical restraint and anesthetic induction combination in swine. *Lab. Anim. Sci.*
- Leader, R.W., Padgett, G.A., 1980. The genesis and validation of animal models. *Am. J. Pathol.* 101, S11–S16.
- Maurer, K., Quimby, F., 2015. Animal models in biomedical research. In: Fox, J., Anderson, L., Otto, G., Pritchett-Corning, K., Whary, M. (Eds.), *Laboratory Animal Medicine*. Elsevier, Oxford, UK, pp. 1497–1535.
- Whary, M., Baumgarth, N., Fox, J.G., Barthold, S., 2015. Biology and diseases of mice. In: *Laboratory Animal Medicine*. Academic Press, pp. 43–149. <https://doi.org/10.1016/B978-0-12-409527-4.00003-1>.

Chapter Study Questions

- 1 What characteristic of coronary circulation of the pig heart makes it a better cardiac animal model than dogs and sheep?
 - a Answer: Pigs' hearts are supplied primarily by the right coronary artery, much like humans. Sheep and dogs are supplied primarily by the left coronary artery.
- 2 What are the four common bone defect models in animals and which is most commonly performed in rodents? Which is the most common in sheep?
 - a Answer: Calvarial defect (rodent most common), long bone or segmental defect, partial cortical defect, and cancellous bone defect.
 - b Answer: The sheep tibia is the most common segmental long bone defect model.
- 3 A new graduate student in your lab is responsible for handling rabbits on your studies. The student has experience with mice and was briefly trained on rabbit care by the outgoing graduate student. The facility veterinarian notifies you that one of your rabbits has complete paralysis in the back legs. The student acknowledged the rabbit struggled and kicked during the previous day's physical examination. What is the likely diagnosis and treatment? What could have prevented this from occurring?
 - a Answer: It is likely that this rabbit experienced lower back fracture during handling by the inexperienced researcher. The seventh lumbar vertebra is considered the most frequent site of fracture. This occurs when the hindquarters of the rabbit are not supported, allowing for the powerful hind limb muscles to damage the relatively light and fragile skeleton. Radiologic examination can confirm the diagnosis; however, these clinical signs are characteristic. The injury is painful and not treatable. The animal requires emergency euthanasia for humane reasons.
 - b Answer: Training and a calm unhurried approach are critical for successful handling of any animal in research. Although the facility veterinary staff typically provides training and technical support by request, the PI is ultimately responsible to assure all staff have training and experience in research procedures, including handling and restraint.
- 4 What nerve mediates the oculocardiac reflex, which can cause bradycardia and death during surgical procedures on the eye? What drugs are recommended for prevention and treatment?
 - a Answer: The vagus nerve mediates the oculocardiac reflex.
 - b Answer: Topical proparacaine reduces the incidence and severity of the reflex. Glycopyrrolate is effective for treatment.
5. What injectable anesthetic combination is recommended for short-term surgical procedures in rats? What drug is recommended to speed recovery by antagonizing one of the drugs in the combination?
 - a Answer: Ketamine combined with either xylazine or medetomidine provides 15–30 min of surgical anesthesia.
 - b Answer: Atipamezole reverses xylazine or dexmedetomidine.
6. Which injectable analgesic provides 72 h of postoperative pain control in rats?
 - a Answer: Sustained-release buprenorphine.
7. Which opioid analgesic provides effective pain control for 48–72 h when applied as a topical patch?
 - a Answer: Fentanyl.
8. What are the three separate functional components required to perform survival aseptic surgery in dogs, pigs, and other USDA "regulated species"?
 - a Answer: Animal preparation.
 - b Answer: Surgeon preparation.
 - c Answer: Surgery room.
9. Which common research animal resembles the human because it lacks the panniculus carnosus causing cutaneous wounds to heal by reepithelialization rather than by contraction?
 - a Answer: Swine.
10. What anatomic features complicate endotracheal intubation in the pig?
 - a Answer: Long soft palate.
 - b Answer: Laryngeal diverticulum.

2.4.1

Introduction: The Body Fights Back— Degradation of Materials in the Biological Environment

BUDDY D. RATNER¹, WILLIAM R. WAGNER²

¹Bioengineering and Chemical Engineering, Director of University of Washington Engineered Biomaterials (UWEB), Seattle, WA, United States

²Departments of Surgery, Bioengineering & Chemical Engineering, McGowan Institute for Regenerative Medicine, University of Pittsburgh, Pittsburgh, PA, United States

The biological environment, seemingly a mild, aqueous salt solution at 37°C, is, in fact, surprisingly aggressive and can lead to rapid or gradual breakdown of many materials. Some mechanisms of biodegradation have evolved over millennia specifically to rid the living organism of invading foreign substances—these same mechanisms now attack our contemporary biomaterials. Other breakdown mechanisms have their basis in well-understood chemical and physical principles and will occur in a living organism or in a beaker on a laboratory bench. After this introduction, four chapters (2.4.2–2.4.5) directly address degradation, where the emphasis is on processes working against the intent of the material or device design. The first three of these chapters consider breakdown in the biological environment for polymers, metals, and ceramics, respectively. These chapters build upon the fundamental principles associated with these broad classes of materials as covered in [Section 2.3](#). Not specifically addressed in this section is the range of biodegradation processes for biologically derived materials. In some cases, these biological materials will not be modified or processed to resist natural degradation mechanisms (as is the case with decellularized tissues) and the principles of wound healing and tissue remodeling apply. In other cases where there has been cross-linking or fixation of the material, the intent is often to reduce immunogenicity and impart degradation resistance. An example of such processing occurs with commercial bioprosthetic

heart valves. For these processed tissues a common concern is another type of degradation, calcification, which can lead to device failure and can exacerbate other degradation mechanisms. [Chapter 2.4.4](#) describes the issue of pathological calcification in detail.

In addition to the chapters of [Section 2.4](#), several textbook chapters address biomaterial degradation in other contexts. [Chapter 1.3.2F](#) reviews the chemistry of polymers designed to be biodegradable, while [Chapter 1.3.3D](#) addresses the rapidly growing area of intentionally degradable metallic materials. [Chapter 2.6.3](#) on scaffolds for tissue engineering demonstrates how degradation processes can be engineered into more complex systems intended to provide improved tissue-based outcomes. [Chapter 3.1.9](#) addresses device failure, with multiple examples where unintentional degradation or mechanical failure occurred clinically, and many of the device-focused chapters of [Section 2.5](#) consider degradation issues.

Careful consideration of the working environment for many implanted medical devices highlights why degradation is a fundamental biomaterial design consideration. The biomaterials of medical devices are usually exposed to varying degrees of cyclic or periodic stress (humans ambulate and the cardiovascular system pumps). Abrasion and flexure may also take place. Particularly challenging are designs where biomaterials must cyclically articulate with one another, or surrounding tissue, under high loads (e.g., hip

and knee prostheses). Such mechanical loading occurs in an aqueous, ionic environment that can be electrochemically active to metals and plasticizing (softening) to polymers. It is well known that a material under mechanical stress will degrade more rapidly than the same material that is not under load.

Specific biological mechanisms are also invoked. Proteins adsorb to the material and can enhance the corrosion rate of metals. Cells (especially macrophages) adhere to materials via interfacial proteins, and can be activated to secrete powerful oxidizing agents and enzymes intended to digest or dissolve the material. The secreted, potent degradative agents are concentrated in the space between the adherent cell and the biomaterial upon which they act, undiluted by the surrounding aqueous medium. Also, bacteria, bacterial biofilms (Chapter 2.2.8), and yeast, and the local immune response to these infections, can markedly enhance degradation and corrosion rates.

To understand the biological degradation of implant materials, synergistic pathways must be considered. For example, cracks associated with stress crazing in polymers open up fresh surface areas to reaction. Swelling and water uptake can similarly increase the number of sites for reaction, and provide an access route for degradative agents into the bulk of the biomaterial. Amorphous material at metal grain boundaries can degrade more rapidly, leading to increases in surface area and localized stresses. Degradation products can alter the local pH, catalyzing further reaction. Hydrolysis of hydrophobic polymers can generate hydrophilic species, leading to polymer swelling and an increased propensity for degradation reactions. Cracks might also serve as sites for the initiation of calcification.

Biodegradation is a term that is used in many contexts. It can be used for reactions that occur over minutes or over years. It can be engineered to happen at a specific time after implantation or it can be an unexpected long-term consequence of the severity of the biological environment. Implant materials can solubilize, crumble, tear, become rubbery, or become rigid with time. The products of degradation may be toxic or irritating to the body or they may be designed to stimulate a desirable local cellular response.

Calcification, a process we strive for in bone healing, is undesirable in most soft tissue contexts. Calcific mineral can interfere with the mechanical function of devices, induce cracking in polymers and tissues, and embolize, leading to complications downstream. Implants based on natural tissue are particularly subject to calcification, but calcification is reasonably common in synthetic polymer devices.

Below are some comments and questions on biomaterial degradation issues that are meant to stimulate further thinking on this subject in conjunction with the chapters in this section:

- Consider strategies used to create materials that degrade at controlled rates versus strategies for synthesizing biostable materials intended for long-term performance in the body.
- Consider the degradation of materials commonly used in medicine that do not have well-defined breakdown mechanisms. Some examples include poly(ethylene glycol), hydroxyapatite, and some polysaccharides. How does the body deal with these common materials?
- Classes of biomaterials have been designed that degrade on cue. The cue might be thermal, photonic, or enzymatic. Ingenious chemical design principles are being applied to create such materials, but how might the body react to the products generated by a sudden breakdown of the structure?
- Learn about new strategies to stabilize materials against degradation. For example, for orthopedic polymers the loading of vitamin E or the development of new types of cross-linked materials for articulating surfaces. For elastomers, the incorporation of polyisobutylene or other degradation-resistant segments into block copolymer designs.
- Endovascular stents are among the most widely used of all medical devices (Chapter 2.5.2B). New designs of biodegradable stents have entered clinical testing and been approved in some regions. Some have been removed from the market. Whether these degradable devices will take substantial market share from non-degradable stents is not yet clear. Consider the biocompatibility concerns associated with biodegradable poly(lactic acid) or magnesium, iron, or zinc (Chapter 1.3.3D) in the complex intravascular environment.
- For a medical device intended for years of service, especially a device where failure can lead to death, how can we test and qualify the device for the expected period of service? Are there useful *in vitro* tests? What accelerants might be brought to bear? Are there relevant and justified animal models?
- Consider medical device failure, past and present, associated with degradation, and how these unintended complications will lead to better medical devices. A few examples include the degradation of polyurethane pacemaker leads, the breakdown of a protective sheath on the tailstring of the Dalkon Shield intrauterine device, and the wear debris associated with the oxidation of ultrahigh molecular weight polyethylene in hip prostheses or the failure of metal-on-metal hip designs (see Chapter 3.1.9).

Degradation in biological environments is seen with metals, polymers, ceramics, and natural materials. Undesired degradation is observed to some degree in most long-term implants, and even in some medium- and short-term implants. Often, its initiation, mechanisms, and consequences are incompletely defined. Biodegradation as a subject is broad in scope, and critical to device performance. It rightfully should command considerable attention for the biomaterials scientist. The intent of this section is to provide a basis for further study and insight into this complex but essential subject.

2.4.2

Chemical and Biochemical Degradation of Polymers Intended to Be Biostable

ARTHUR J. COURY

Northeastern University, Boston, MA, United States

Introduction

Biodegradation is the chemical breakdown of materials by the action of living organisms that leads to changes in physical properties. It is a concept of vast scope, ranging from decomposition of environmental waste involving microorganisms to host-induced deterioration of biomaterials in implanted medical devices. It is a precise term, implying that specific biological processes are required to effect such changes (Williams, 1989). This chapter, while grounded in biodegradation, addresses other processes that contribute to the often-complex mechanisms of polymer degradation even before communicating with tissue (see Table 2.4.2.1). While minor attention is paid to physical breakdown, its focus is the unintended chemical breakdown in the body of synthetic, solid-phase polymers. (See Chapter 1.3.2F for a description of systems designed to break down in the body). The factors impacting the undesired biodegradation of polymeric implants are largely well-defined, moreover, some recent progress (to be noted) has been made in mitigating such degradation.

Polymeric components of implantable devices are designed to be reliable for their intended lifetimes. Careful selection and extensive preclinical testing of the compositions, fabricated components, and devices generally establish functionality and durability. However, with chronic, indwelling devices, it is not feasible during qualification (typically short-term testing) to match all implant conditions in real time for years or decades of use.

The accelerated in vitro aging, animal implants, limited clinical trials and statistical projections employed cannot expose all of the variables that may cause premature deterioration of performance. The ultimate measure of the acceptability of a material for a medical device is its acceptable performance for the device's intended lifetime

as ascertained in human postimplant surveillance (Coury, 1999). No polymer is totally impervious to the chemical processes and mechanical action of the body. Generally, polymeric biomaterials degrade because body constituents attack the biomaterials directly or through other device components, sometimes with the intervention of external factors. The seeds for biodegradation may be sown prior to implantation by compositional or processing issues.

Polymer Degradation Processes

Preimplant Degradation

Numerous operations are performed on a polymer from the time of its synthesis to its use in the body (see Table 2.4.2.2). Table 2.4.2.2 lists states and stages in the history of a polymeric biomaterial leading to its implantation which, alone or in concert, may predispose it to degradation when implanted (Brauman et al., 1981; Greisser et al., 1994; Ling et al., 1998). A prominent example of biomaterial degradation caused by preimplant processing is the gamma irradiation sterilization of ultrahigh-molecular-weight polyethylene used in total joint prostheses. The process generates free radicals within the material that react with oxygen to produce undesirable oxidation products. Chain oxidation, scission, and cross-linking can occur for periods of months to years, causing loss of strength and embrittlement with limited shelf-life (Furman and Li, 1995; McKellop et al., 1995; Weaver et al., 1995; Daly and Yin, 1998; Blanchet and Burroughs, 2001; Kurtz et al., 2005; Rimmnac and Pruitt, 2008). Recent attempts to mitigate degradation effects by gamma sterilization in inert atmospheres instead of air and the use of antioxidants such as vitamin E have provided some improvement in the long-term in vivo performance of polyethylene joint components (Booth, 1995; Medel et al., 2009; Crowninshield and

TABLE 2.4.2.1 Mechanisms Leading to Degradation of Polymer Properties^a

Physical	Chemical
Sorption	Thermolysis
Swelling	Radical scission
Softening	Depolymerization
Dissolution	Oxidation
Mineralization	Chemical
Extraction	Thermooxidative
Crystallization	Solvolysis
Decrystallization	Hydrolysis
Stress cracking	Alcoholysis
Fatigue fracture	Aminolysis, etc.
Impact fracture	Photolysis
	Visible
	Ultraviolet
	Radiolysis
	Gamma rays
	X-rays
	Electron beam
	Fracture-induced radical reactions

^aSome degradation processes may involve combinations of two or more individual mechanisms.

TABLE 2.4.2.2 Typical Operations on an Injection-Moldable Polymer Biomaterial

Polymer: Synthesis, extrusion, pelletizing
Pellets: Packaging, storage, transfer, drying
Components: Injection-molding, postmold finishing, cleaning, inspecting, packaging, storage
Device: Fabrication, storage (presterilization), cleaning, inspecting, packaging, storage (packaged), sterilization, storage (sterile), shipment, storage (preimplant), implantation, operation in body

Muratoglu, 2008). Polypropylene and polytetrafluoroethylene are also notable as polymers that are predominately, but not entirely (Liebert et al., 1976), chemically stable in the body, but can be severely degraded during processing by sterilization with ionizing radiation (Williams, 1982; Portnoy, 1997). Gamma irradiation may also cause optical changes such as darkening of poly(methyl methacrylate) intraocular lenses (Hoffman, 1999). It is crucially important, therefore, that appropriate and rigorous processing and characterization protocols be followed for all operations (Coury et al., 1988; Shen et al., 1999).

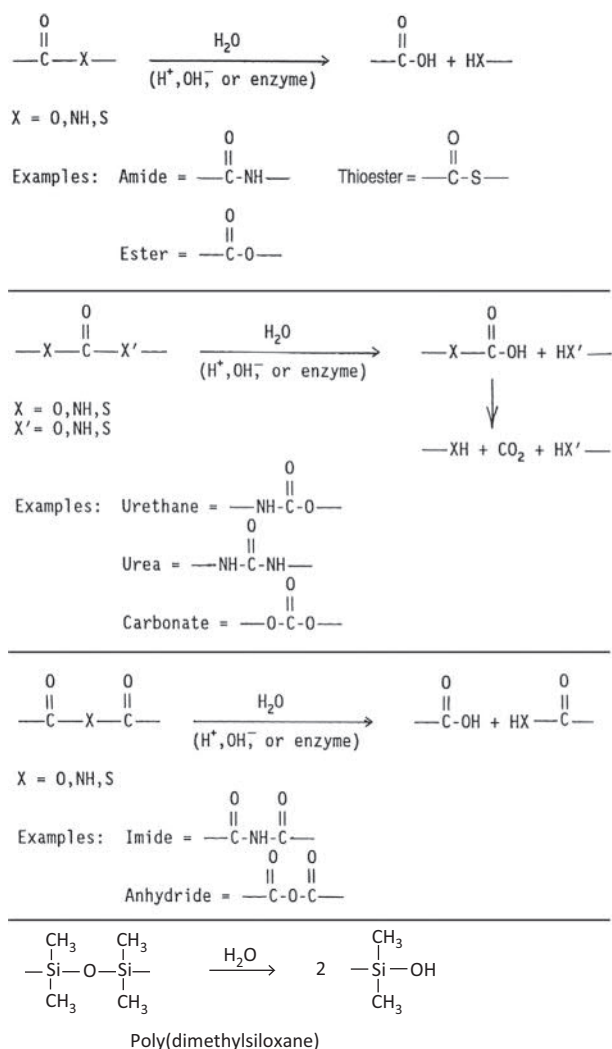
Postimplant Degradation Forces

After a device has been implanted, adsorption and absorption processes occur. Polymeric surfaces in contact with body fluids immediately adsorb proteinaceous components, and the bulk begins to absorb soluble components such as water, ions, proteins, and lipids. Cellular elements subsequently attach to the surfaces and initiate chemical processes. With biostable components, this complex interplay of factors is of little functional consequence. At equilibrium fluid absorption, there may be some polymer plasticization causing dimensional and mechanical property changes (Coury et al., 1988). On the surface, a powerful acute attack by cells and humoral chemical agents, including oxidants and enzymes, will have been substantially withstood, although inconsequential, superficial changes may occur. Over days to weeks, with the resolution of this acute inflammatory phase, a fibrous capsule will likely have formed over the device, and the rate of release of powerful chemicals from activated cells will have markedly decreased. For those polymers subjected to chemical degradation in vivo, few if any reports have comprehensively described the sequential processes and interactions that produce the deleterious effects. Rather, explant analysis and occasionally metabolite evaluation are used to infer reaction pathways. Analysis of chemically degraded polymers has almost always implicated either hydrolysis or oxidation as an essential component of the process. Device fouling by mineralization and thrombosis is not addressed within the scope of this chapter, but the processes are covered in Cauch-Rodriguez et al. (2013) and in Chapters 2.3.5 and 1.4.3A, B. Regarding rates of degradation of polymers used in implantable devices, a publication by Lyu and Untereker (2009) elegantly describes propensities and rate equations for predominant polymer hydrolytic and oxidative degradation mechanisms which have high predictive values for choosing polymer biomaterials.

Hydrolytic Biodegradation

Structures of Hydrolyzable Polymers

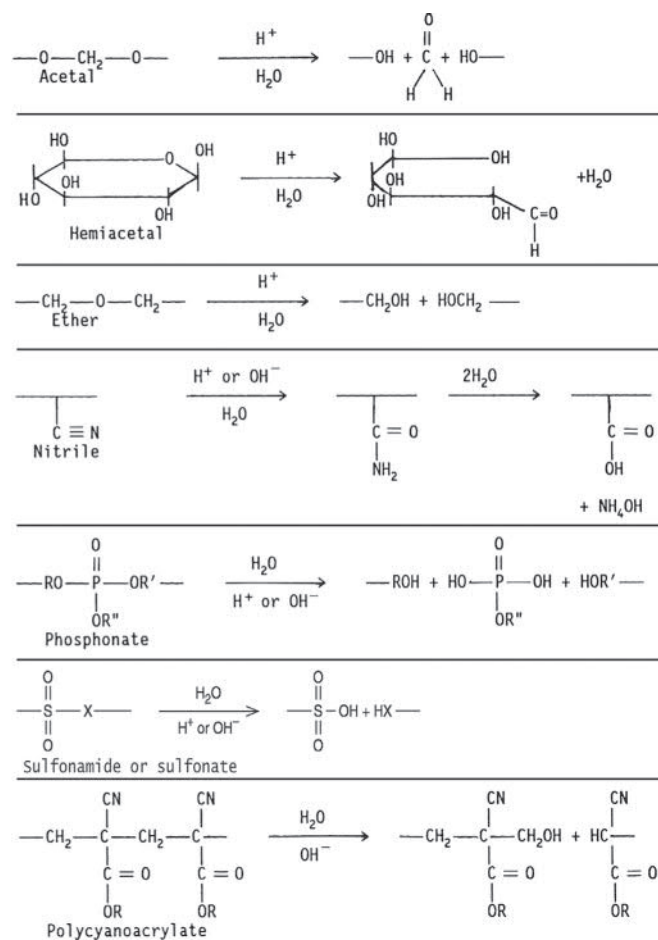
Hydrolysis is the scission of susceptible molecular functional groups by aqueous attack. Hydrolysis may be catalyzed by acids, bases, salts, or enzymes. It is a single-step process in which the rate of chain scission is directly proportional to the rate of initiation of the reaction (Schnabel, 1981). A polymer's susceptibility to hydrolysis is the result of its chemical structure, its morphology, its mass and dimensions and the body's environment. In a commonly used category of hydrolyzable polymeric biomaterials, functional groups consist of carbonyls bonded to heterochain elements (O, N, S). Examples include esters, amides, urethanes, carbonates, and anhydrides (Fig. 2.4.2.1). Other polymers containing groups such as ether, acetal, nitrile, phosphonate, sulfonate, sulfonamide, or active methylenes hydrolyze under certain conditions (Fig. 2.4.2.1). Hydrolytically susceptible groups exhibit differing rates of degradation which are dependent



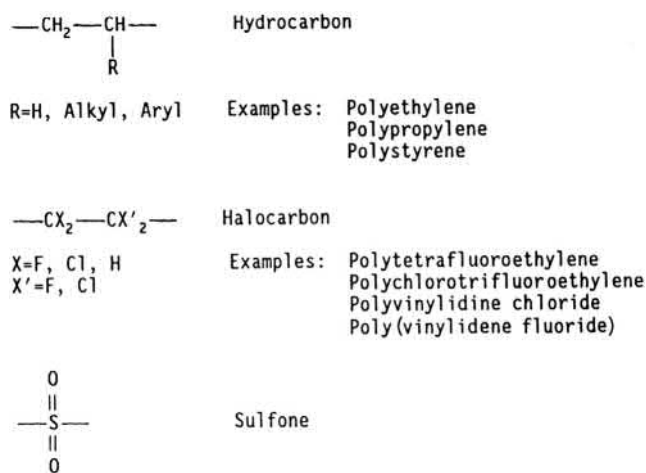
• **Figure 2.4.2.1** Hydrolyzable groups in polymer.

on the intrinsic properties of the functional group and on other molecular and morphological characteristics. Among carbonyl polymers with oxygen heteroatoms attached, anhydrides display the highest hydrolysis rates followed, in order, by esters and carbonates. Polymers containing such groups, in fact, comprise many of the intentionally resorbable devices (Chapter 1.3.2F). Other carbonyl-containing groups such as urethane, imide, amide, and urea can demonstrate long-term stability in vivo if contained in a hydrophobic backbone or highly crystalline morphologic structure. Groups that are normally very stable to hydrolysis are indicated in Fig. 2.4.2.2.

The rate of hydrolytic degradation tends to increase with one or more of the following: a high proportion of hydrolyzable groups in the main or side chain; other polar groups which enhance hydrophilicity; low crystallinity; low or negligible cross-link density; a high ratio of exposed surface area to volume; and, in some cases, mechanical stress. Porous hydrolyzable structures undergo rapid property loss relative to monolithic structures, because of their large surface area. Factors that tend to suppress hydrolysis rate include hydrophobic molecular moieties (e.g., hydrocarbon



• **Figure 2.4.2.2** Groups highly stable to hydrolysis.



or fluorocarbon); cross-linking; high crystallinity due to chain order, thermal annealing or orientation; low stress and compact shape (low surface-to-volume ratio). While the molecular weight of linear polymers per se may not have a great effect on the hydrolysis-induced degradation rate,

physical property losses may be retarded for a given number of chain cleavage events with relatively high-molecular-weight polymers. Property loss caused by chain cleavage is more pronounced in polymers with weak intermolecular bonding forces.

Host-Induced Hydrolytic Processes

The body is normally a highly controlled reaction medium. Through homeostasis, the normal environment of most implants is maintained at isothermal (37°C), ~neutral (pH 7.4), aseptic, and photo-protected aqueous steady state. By *in vitro* standards, these conditions may appear mild. However, complex interactions of humoral and cellular components of body fluids involving activators, receptors, inhibitors, etc., produce aggressive responses to any foreign bodies through the processes of cell adhesion, cell activation, chemical attack, and particulate transport.

Several scenarios leading to hydrolysis in the host can be considered. For all scenarios, hydrolysis can only occur at a site other than the surface of a polymer mass after water permeates to the site. The first scenario considers water at pH 7. Water is capable of hydrolyzing certain polymers (e.g., polyglycolic acid), intended to degrade, at a significant rate (Chapter 1.3.2F and Zaikov, 1985). However, this simple hydrolysis mechanism is unlikely to be significant in polymer compositions selected for long-term *in vivo* biostability.

Next, ion-catalyzed hydrolysis offers a likely scenario in body fluids. Extracellular fluids contain ions such as: H⁺, OH⁻, Na⁺, Cl⁻, HCO₃⁻, PO₄³⁻, K⁺, Mg²⁺, Ca²⁺, and SO₄²⁻. Organic acids, proteins, lipids, lipoproteins, etc., also circulate as soluble or colloidal components. It has been shown that certain ions (e.g., PO₄³⁻) are effective hydrolysis catalysts, enhancing, for example, reaction rates of polyesters by several orders of magnitude (Zaikov, 1985). Ion catalysis may be a surface effect or a combined surface–bulk effect, depending on the hydrophilicity of the polymer. Very hydrophobic polymers (e.g., those containing <2% water of saturation) absorb negligible concentrations of ions. Hydrogels, on the other hand, which can absorb large amounts of water (>15% by weight) are essentially “sieves,” allowing significant levels of ions to permeate and be absorbed with consequent bulk hydrolysis via acid, base, or salt catalysis.

Localized pH changes in the vicinity of the implanted device, which usually occur during acute inflammation or infection, can cause catalytic rate enhancement of hydrolysis (Zaikov, 1985). Organic components, such as lipoproteins, circulating in the bloodstream or in extracellular fluid, appear to be capable of transporting catalytic inorganic ions into the polymer bulk by poorly defined mechanisms.

Enzymes generally serve a classic catalytic function, altering the reaction rate (via ion or charge transfer) without being consumed by modifying activation energy, but not thermodynamic equilibrium. While enzymes function in extracellular fluids, they are most effectively transferred onto target substrates by direct cell contact (e.g., during

phagocytosis). Hydrolytic enzymes or hydrolases (e.g., proteases, esterases, lipases, glycosidases) are named for the molecular structures they affect. They are cell-derived proteins which act as highly specific catalysts for the scission of water-labile functional groups.

Enzymes contain molecular chain structures and develop conformations that allow “recognition” of chain sequences (receptors) predominately found on biopolymers. Complexes form between chain segments of the enzyme and the biopolymer substrate which result in enhanced bond cleavage rates. Lacking the recognition sequences of susceptible natural polymers, most synthetic polymers are more resistant to enzymatic degradation than natural polymers. Nevertheless, comparative studies have shown some enhancement of hydrolysis rates by enzymes, particularly with synthetic polyesters and polyamides (Kopecek and Ulbrich, 1983; Zaikov, 1985; Smith et al., 1987). Apparently, the enzymes can recognize and interact with structural segments of the polymers, or more accurately, of the polymers coated with serum proteins, to initiate their catalytic action *in vivo* (Pitt, 1992).

Enzymes with demonstrated effects on hydrolysis rates can be quite selective in the presence of several hydrolyzable functional groups. For example, poly(ether urethane ureas) and poly(ester urethane ureas) exposed to hydrolytic enzymes (an esterase, cholesterol esterase, and a protease, elastase) were observed for rate of hydrolysis and hydrolytic site. Enzyme catalysis was clearly observed for the ester groups, while the hydrolytically susceptible urea, urethane, and ether groups did not show significant hydrolysis, as indicated by release of radiolabeled degradation products (Santerre et al., 1994; Labow et al., 1995, 2002a).

Many enzymes exert predominantly a surface effect because of their molecular size, which prevents absorption. Even hydrogels [e.g., cross-linked poly(acrylamide)], which are capable of absorbing certain proteins, have molecular weight cut-offs for absorption, and can exclude large enzymes. However, as the degrading surface becomes roughened or fragmented, enzymatic action may be enhanced as a result of increased surface area if the substrates remain accessible to phagocytic cells that express the active enzymes. Implanted devices that are in continuous motion relative to neighboring tissue can provoke inflammation, stimulating enzyme release.

Hydrolysis: Preclinical and Clinical Experience

A discussion of *in vivo* responses of several prominent polymer compositions known to be susceptible to hydrolysis follows. The structures of these polymers are described in Chapter 1.3.2.

Polyesters. Poly(ethylene terephthalate) (PET), in woven, velour, or knitted fiber configurations, remains a primary choice of cardiovascular surgeons for large-diameter vascular prostheses, arterial patches, valve sewing rings, etc. In extruded, drawn form, it is a strong, flexible polymer, stabilized by high crystallinity as a result of chain rigidity and

orientation, and is often considered to be biostable. Yet, over several decades, there have been numerous reports of long-term degeneration of PET devices in vivo, owing to breakage of fibers and device dilation. Proposed causes have been structural defects, processing techniques, handling procedures, and hydrolytic degradation (Cardia and Regina, 1989).

Systematic studies of PET implants in healthy dogs have shown slow degradation rates, which were estimated to be equivalent to those in humans. For woven patches implanted subcutaneously, a mean total absorption time by the body of 30 ± 7 years, with 50% deterioration of fiber strength in 10 ± 2 years was projected. In infections in dogs, however, where localized pH dropped to as low as 4.8, degradation was enhanced exponentially, with complete loss of properties within a few months (Zaikov, 1985). Human implant retrieval studies have shown significant evidence of graft infection (Gumargalieva et al., 1982; Vinard et al., 1991). Besides the obvious pathological consequences of infection, the enhanced risk of polymer degradation due to local pH and, perhaps, cell-derived oxidative agents is a cause for concern.

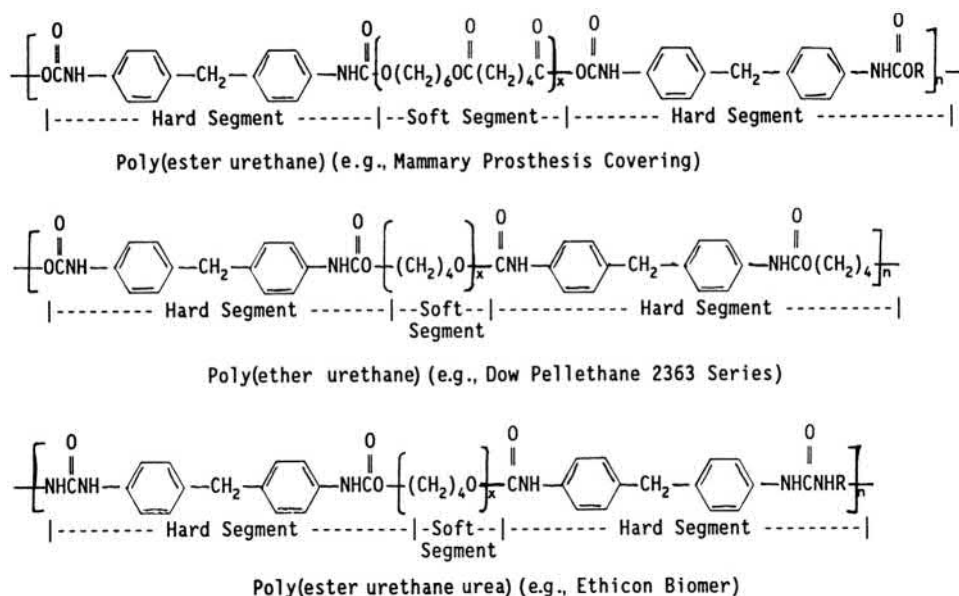
Aliphatic polyesters are most often intended for use as biodegradable polymers, with polycaprolactone, for example, undergoing a significant decrease in molecular weight, as indicated by a drop of 80%–90% in relative viscosity within 120 weeks of implant (Kopecek and Ulbrich, 1983).

Poly(Ester Urethanes). As an introduction to segmented polyurethanes in general, aromatic hard segments offer advantages over aliphatic ones for their higher physical properties and resistance to chemical degradation, and aromatic polyurethanes constitute the majority of polyurethanes used in long-term implants (Lamba et al., 1998). Whatever degradation is stated for aromatic polyurethanes, with the exception of discoloration, would be exceeded in the same tests for aliphatic polyurethanes.

The earliest reported implants of polyurethanes, dating back to the 1950s, were cross-linked, aromatic poly(ester urethane) foam compositions (Bloch and Hastings, 1972; Blais, 1990). Their use in plastic and orthopedic reconstructive surgery initially yielded promising results. Acute inflammation was low. Tissue ingrowth promoted thin fibrous capsules. However, within months they were degraded and fragmented, producing unsatisfactory chronic effects (Bloch and Hastings, 1972). Foci of initial degradation of those polymers are generally considered to be the polyadipate ester soft segments that undergo hydrolysis (Fig. 2.4.2.3). By comparison, corresponding poly(ether urethanes) are very resistant to hydrolysis, although more susceptible to oxidation (see Section Oxidative Biodegradation). Whether such hydrolytically degraded poly(ester urethanes) subsequently produce meaningful levels of aromatic amines (suspected carcinogens) by hydrolysis of urethane functions in vivo is an unresolved subject (Blais, 1990; Szycher and Siciliano, 1991).

An excellent analysis of historical references to the consideration of the carcinogenicity of aromatic polyurethanes was published by Pinchuk (1994). His literature search demonstrated that, among the few suspected human cases of device-related carcinogenicity at that time (Schoen, 1987), none were assigned to polyurethanes. However, “solid state tumors” can be induced preclinically as described in the following paragraph.

Several other points are noted. First, implantation of polyurethanes and other polymers in rodents leads to the formation of tumors as functions of their physical characteristics (size, shape, surface characteristics). Tumorigenesis, in such cases, is independent of the compositions of the polymers, as long as they reside in situ long enough to stimulate that response. Second, this effect, called the “Oppenheimer effect” (Oppenheimer et al., 1961) or “solid-state



• **Figure 2.4.2.3** Structure of implantable poly(ester urethane), poly(ether urethane), and poly(ester urethane urea).

tumorigenesis,” which occurs in rodents, has not been shown to correlate with human implant studies. Finally, even studies of workers in polyurethane foam manufacturing plants experienced nonsignificant development of several types of neoplasms, all attributable to the free isocyanates (hydrolyzable to aromatic amines) with which they were working (Hagmar et al., 1993).

Therefore, the extensive use of aromatic polyurethanes in chronic implants continues with low concern for or observation of polyurethane carcinogenicity. It is noteworthy that poly(ester urethane) foam-coated silicone mammary implants had survived as commercial products for decades (Blais, 1990), despite the polyurethane's known propensity to degrade. Apparently, the type of fibrous capsules formed, initially by ingrowth into the degradable foam, was favored by some clinicians over those caused by smooth-walled silicone implants. In large devices not stabilized by tissue ingrowth, the frictional effects of sliding may cause increased capsule thickness and contraction (Snow et al., 1981), along with extensive chronic inflammation.

However, an important consideration recently published for mammary prostheses deserves brief mention. The FDA first published a warning of rare cancer incidence with textured implants above those of smooth implants in 2011 and updated it in 2019 (U.S. FDA, 2019). This update confirmed the greater, but not exclusive, occurrence of the rare lymphoma within the fibrous capsules of textured implants. It was noted that physical structure, not chemical composition, was the important variable.

Polysiloxane/Urethane Soft Segment Issues. This family of polymers is covered in the section on hydrolysis, as hydrolysis is postulated to be the major chemical mechanism of biodegradation. In 2006, the first new polyurethane biomaterial composition in decades was introduced as pacemaker/defibrillator lead insulation with improved biostability. It is an aromatic polyurethane with soft segments of mixed polysiloxane/polyether composition and a compatibilizing amount of poly(hexamethylene oxide) (Simmons et al., 2004; Padsalgikar, 2015). It demonstrated physical properties superior to silicone elastomers (Parmar, 2012). Some studies showed improved, but not total, degradation resistance of this polymer family when compared to softer (Shore 80 A hardness) poly(ether urethanes) formerly introduced as pacing lead insulation (St. Jude Medical, Inc., 2012). Consequently, since cardiac leads can be implanted for decades, a history of commercial use is being accumulated.

Literature of the marketer (formerly St. Jude Medical, now Abbott) of this “silicone/urethane” copolymer indicates that longevity performance of leads insulated with this copolymer in human implants is comparable to the highest performing poly(ether urethanes) (Shore 55D hardness) in similar applications (St. Jude Medical, 2012). These harder poly(ether urethanes), although considered by some as being stiffer than optimal for use in endocardial pacing leads, have been well adapted by design innovations for such purposes. Abbott's (2019) product performance publication indicates

satisfactory survival probability for its silicone/urethane-based bradycardia and defibrillator leads. The latter, having insulation more susceptible to degradation, demonstrates a 10-year survival probability range of 78%–98% (Abbott, 2019).

Regarding the mechanisms of failure of the silicone/urethane pacing lead insulation, two hypotheses have been presented, one based on physical, the other based on chemical, degradation. Articles published by cardiologists indicate that abrasion of the insulation leads to breaches and failures (Hauser et al., 2013). This may be due to the “hybrid” structure of silicone/urethanes, incorporating components of both low (silicones) and high (polyurethanes) abrasion resistance where intermediate abrasion resistance and, therefore, toughness, may be hypothesized. The second hypothesis of failure of silicone/urethanes is susceptibility of linear poly(dimethyl siloxane), i.e., silicone, moieties to hydrolysis. Studies involving accelerated aging of the silicone/urethanes in aqueous environments indicated such a mechanism (Chaffin et al., 2012). This phenomenon is known for linear silicones' environmental degradation (Griessbach and Lehmann, 1999; Graiver et al., 2003). The hydrolysis mechanism seems rational since, as, for other hydrolyzable functional groups stated above, siloxanes are formed by the dehydration of silanols which should be reversible by hydrolysis. To conclude this subsection, silicone/urethane copolymers constitute a viable alternative to other polyurethane compositions, but, for defibrillator lead insulation in particular, they display some characteristics that allow some level of biodegradation. That said, all major pacemaker manufacturers have experienced defibrillator lead recalls for various reasons (Thomas, 2012), emphasizing the ongoing and specifically serious biodegradation problems for this important device component.

Polyamides. Nylon 6 (polycaproamide) and nylon 6,6 [poly(hexamethylene adipamide)] contain a hydrolyzable amide connecting groups, as do proteins. A significant use for polyamides is as “nonabsorbable” sutures (Chen et al., 1993). These synthetic polymers can absorb 9%–11% water, by weight, at saturation. It is predictable, then, that they degrade by ion-catalyzed surface and bulk hydrolysis (Fig. 2.4.2.1). In addition, hydrolysis due to enzymatic catalysis leads to surface erosion (Zaikov, 1985). Quantitatively, nylon 6,6 lost 25% of its tensile strength after 89 days, and 83% after 726 days in dogs (Kopecek and Ulbrich, 1983). An example of polyamide degradation of particular consequence involved the *in vivo* fragmentation of the nylon 6 tail string of an intrauterine contraceptive device. This string consisted of a nylon 6-sheath around nylon 6 multifilaments. The combination of fluid absorption (>10%) and hydrolysis was claimed to produce environmental stress cracking. The cracked coating allegedly provided a pathway for bacteria to travel from the vagina into the uterus along the filaments, resulting in significant pelvic inflammatory disease (Hudson and Crugnola, 1987).

Degradation of a poly(arylamide) intended for orthopedic use (the fiber-reinforced polyamide from *m*-xylylene

diamine and adipic acid) was also shown in a rabbit implant study. Although the material provoked a foreign body reaction comparable to a polyethylene control, surface pitting associated with resolving macrophages was noted at 4 weeks and became more pronounced by 12 weeks. This result was not predicted, since poly(arylamides) are very resistant to solvents and heat (Finck et al., 1994).

Polyamides with long aliphatic hydrocarbon chain segments [e.g., poly(dodecanamide), Nylon 12] (Duke Extrusion.com, Copyright, 2019) such as that used for intraarterial balloon catheters are more hydrolytically stable than shorter-chain nylons, and correspondingly degrade slower in vivo.

Poly(Alkyl Cyanoacrylates). This class of polymers used as tissue adhesives is noteworthy as a rare case in which carbon–carbon bonds are cleaved by hydrolysis (Fig. 2.4.2.1). This occurs because the methylene ($-\text{CH}_2-$) hydrogen in the polymer is highly activated inductively by electron-withdrawing neighboring groups. Formation of the polymer adhesive from monomers is base catalyzed, with adsorbed water on the adherend being basic enough to initiate the reaction.

Catalysts for equilibrium reactions affect the reverse, as well as the forward, reaction. Therefore, water associated with tissue can induce poly(cyanoacrylate) hydrolysis by a “reverse Knoevenagel” reaction (Fig. 2.4.2.1). More basic conditions and (as suggested by in vitro cell culture or implant studies) enzymatic processes are much more effective at inducing hydrolysis. In chick embryo liver culture (a rich source of a variety of enzymes), poly(methyl cyanoacrylate) degraded much faster than in cell culture medium alone. In animal implants, poly(methyl cyanoacrylate) was extensively degraded within 4–6 months (Kopecek and Ulbrich, 1983). Higher alkyl (e.g., butyl) homologs degraded slower than the methyl homolog, and were less cytotoxic (Hegyeli, 1973; Vauthier et al., 2003). Octyl cyanoacrylate polymer, introduced to the device field as a dermal tissue adhesive (Singer et al., 2008), promises to be the most stable cyanoacrylate device composition to date, based on increased hydrophobicity. Preclinical and clinical studies have yielded promising results with the use of octyl cyanoacrylate as a surgical sealant (Barbarini Ferraz et al., 2009; Carr, 2011), and, more recently, a composition containing the monomers octyl cyanoacrylate and butyl lactoyl cyanoacrylate was FDA (US Food and Drug Administration) approved as a blood vessel anastomotic sealant (US FDA, 2010).

Polymers Containing Hydrolyzable Pendant Groups

Certain polymers intended for long-term implantation consist of biostable main chain sequences and hydrolyzable pendant groups. Poly(methyl methacrylate) (PMMA) used in bone cements and intraocular lenses is an example of a hydrophobic polymer with a stable hydrocarbon main chain and hydrolyzable ester side groups. It has been proven,

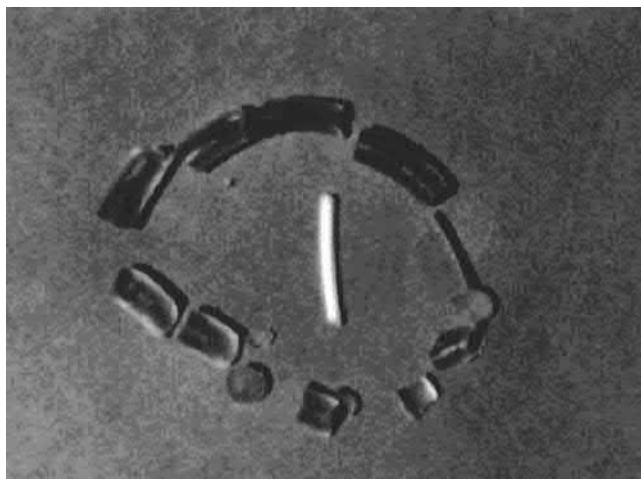
over decades of use, to provide reliable, stable service, with hydrolysis rates being so slow as to be inconsequential.

Another polymer system with a hydrocarbon backbone, poly(methyl acrylate-*co*-2-hydroxyethyl acrylate) also contains hydrolyzable ester side groups. This polymer, which forms hydrogels in an aqueous environment, has been used as a “scleral buckling” device for retinal detachment surgery. Basically, the dry polymer, shaped as a band or ring, placed as a “belt” around the sclera, expands through hydration to create an indentation in the zone of the retinal detachment to reestablish retinal contact. The device is left in place as a permanent implant (or “explant” as it is sometimes called because it is external to the sclera) (Braunstein and Winnick, 2002). This hydrogel device, introduced into clinical practice in the 1980s (Refojo and Leong, 1981; Colthurst et al., 2000), apparently performed satisfactorily for years as an approved product. However, in the 1990s, reports of long-term complications of these hydrogel scleral buckles began to surface (Hwang and Lim, 1997; Roldan-Pallares et al., 1999). The hydrogel structures resumed swelling, sometimes with fragmentation, after maintaining stable dimensions for years. One report described a difficult explantation 13 years after implantation (Braunstein and Winnick, 2002). An article described three unique complications from hydrogel scleral buckle use: orbital cellulitis mimicry; fornical shortening with orbital prosthetic intolerance; and orbital pseudotumor (Bernardino et al., 2006). Those buckles remained in place for 7–15 years, with a mean time of 10.7 years. In a study of 15 patients with 17 scleral buckles, all reported complications within 4–14 years (Figs. 2.4.2.4–2.4.2.6). Removal of the buckles was technically difficult and post-operative complications were significant, although immediate palliative relief was experienced after surgery. Pressure applied to the eye by the swelling has led to blindness and loss of the eyeball. Hydrogel scleral buckles are no longer used in retinal surgery (Watt, 2001).



• **Figure 2.4.2.4** A subconjunctival and subpalpebral hydrogel explant interferes with ocular motility, especially on attempted gaze up and to the right. (From Kearney, J.J., Lahey, J.M., Borirakchanyavat, S., Schwartz, D.M., Wilson, D., et al., 2004. Complications of hydrogel explants used in scleral buckling surgery. *Am. J. Ophthalmol.* 137 (1), 96–100.)

Very little speculation has been provided in published articles about the mechanism of failure of acrylate scleral buckling devices other than that chemical degradation has occurred (Roldan-Pallares et al., 1999). I suggest that a likely mechanism involves hydrolysis of the ester side groups enhanced by the hydrophilic nature of the polymer (as contrasted to hydrophobic polymers such as PMMA). Hydrolysis of either of the two acrylate esters in the polymer chain provides an acrylic acid moiety. Linear poly(acrylic acid) is fully water soluble, and each hydrolytic event renders the polymer more hydrophilic and subject to enhanced swelling. This process is slow but inexorable in the case of the scleral buckling device. The valuable lesson is that devices with intrinsically susceptible groups can eventually degrade by predictable mechanisms. This may take longer than is required for pivotal preclinical qualification studies (typically two-year animal implants). In fact, Bernardino et al. (2006), in discussing long-term hydrogel implants, warn: “Patients with newer uses of hydrogel, such as orbital expanders, should also be observed for long-term



• **Figure 2.4.2.5** A washed 4-mm hydrogel explant showing multiple fragments of a swollen explant and a 3-mm silicone sponge explant for comparison. The sponge was removed at the same surgical sitting as the hydrogel explant. (From Kearney, J.J., Lahey, J.M., Borirakchanyavat, S., Schwartz, D.M., Wilson, D., et al., 2004. Complications of hydrogel explants used in scleral buckling surgery. *Am. J. Ophthalmol.* 137 (1), 96–100.)

complications.” If late degradation is suspected, therefore, accelerated aging studies should be performed in vitro with correlations made to in vivo studies. Such efforts give valuable, if not completely trustworthy, information (see Section [Polymer Degradation Processes](#)).

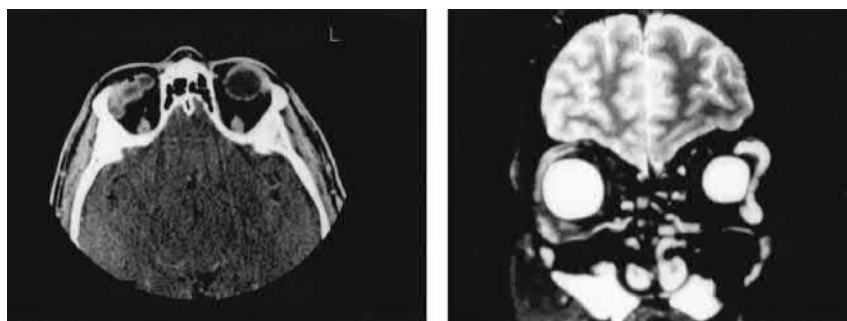
Oxidative Biodegradation

Oxidation Reaction Mechanisms and Polymer Structures

While much is known about the structures and reaction products of polymers susceptible to oxidative biodegradation, confirmation of the individual reaction steps has not yet been demonstrated analytically. Still, mechanistic inferences are possible from extensive knowledge of physiological oxidation processes and polymer oxidation in vitro.

The polymer oxidation processes to be discussed may be consistent with a homolytic chain reaction or a heterolytic mechanism. Species such as carbonyl, hydroxyl, and chain scission products are detectable in these types of processes. Classic initiation, propagation, and termination events for homolysis and ionic heterolytic processes are detailed in [Fig. 2.4.2.7](#).

The principles of polymer degradation resistance stated in the section on hydrolyzable polymers (e.g., group frequency, crystallinity, hydrophobicity) are valid for predicting relative oxidation resistance of polymers, except where particularly oxidation-susceptible groups are present. Sites favored for initial oxidative attack, consistent with a homolytic or heterolytic pathway, are those that allow abstraction of an atom or ion and provide resonance stabilization of the resultant radical or ion. [Fig. 2.4.2.8](#) provides a selection of readily oxidized groups and the atom at which initial attack occurs. In [Fig. 2.4.2.9](#), examples of radical and ion stabilization by resonance in ether and branched hydrocarbon structures are provided. Peroxy, carbonyl, and other radical intermediates are stabilized by similar resonance delocalization of electrons from the elements C, O, H, or N. Within [Fig. 2.4.2.9](#), a coupling reaction which can lead to polymer cross-linking as a consequence of oxidative degradation is shown. [Fig. 2.4.2.10](#)



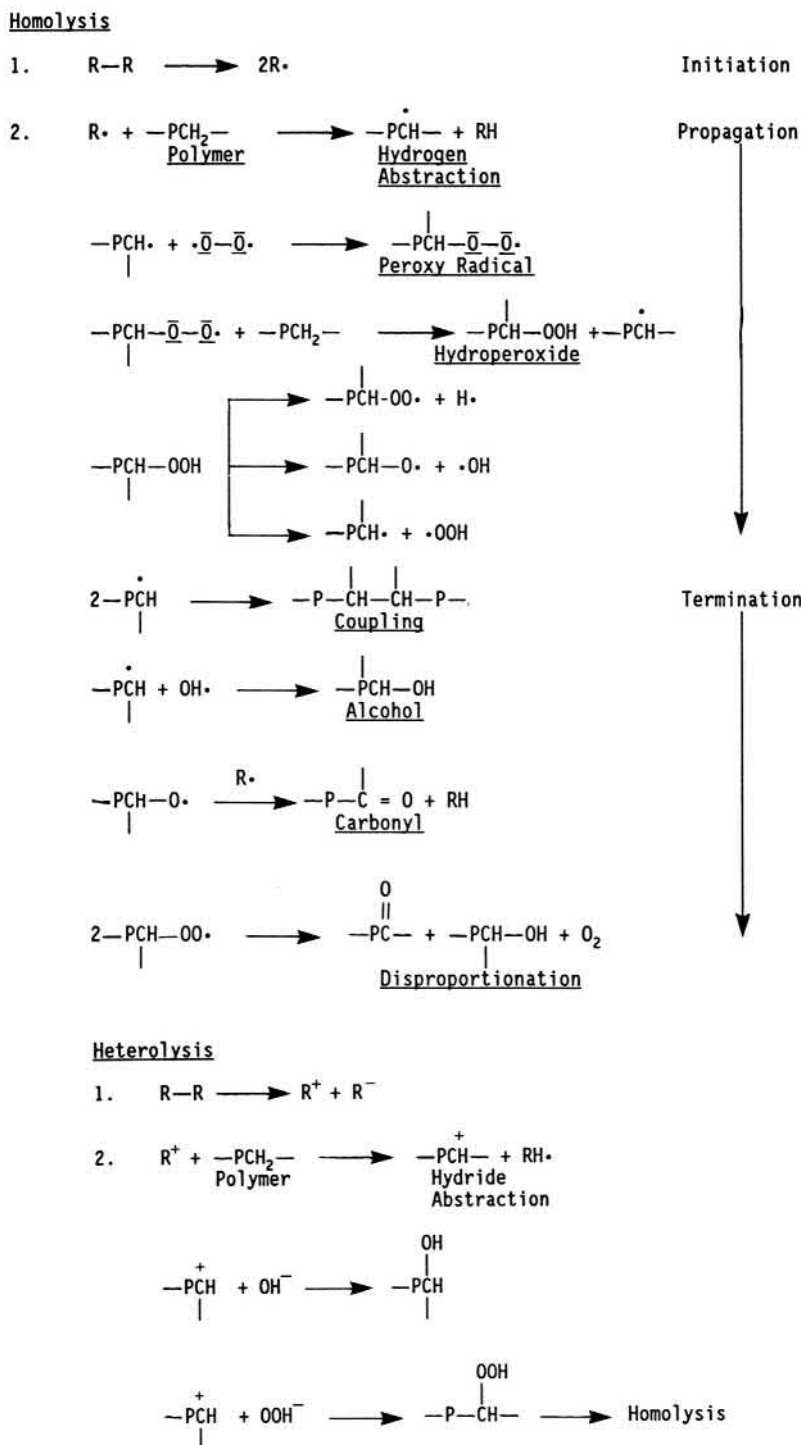
• **Figure 2.4.2.6** (Left panel) Computed tomography scan showing a hydrogel implant in the anterior orbit of the right eye. (Right panel) Magnetic resonance image of the left orbit shows an expanded hydrogel explant. (From Kearney, J.J., Lahey, J.M., Borirakchanyavat, S., Schwartz, D.M., Wilson, D., et al., 2004. Complications of hydrogel explants used in scleral buckling surgery. *Am. J. Ophthalmol.* 137 (1), 96–100.)

incorporates the points made in the previous three figures and illustrates the general sequence of oxidative degradation of an ether function by cleavage at the carbon–oxygen bond which would lead to chain scission of polyether-containing polymers.

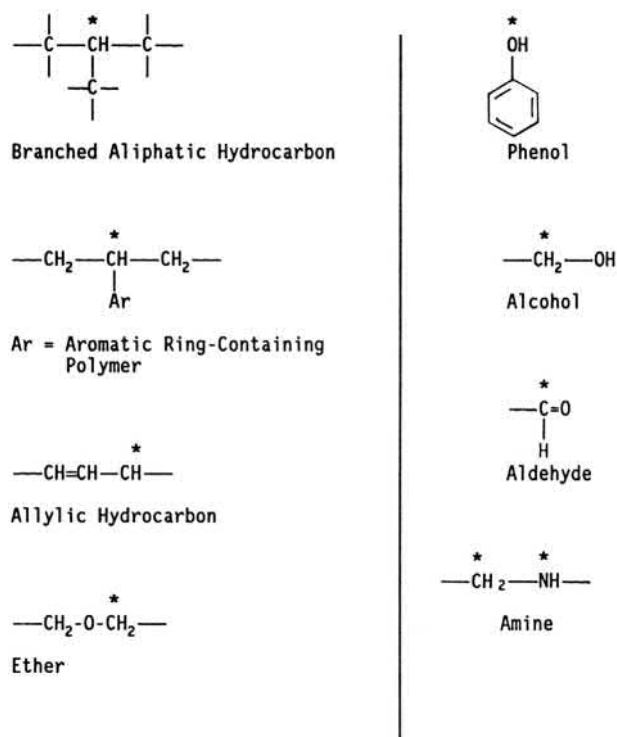
Two general categories of oxidative biodegradation, based on the source of initiation of the process, are direct oxidation by the host and external environment-mediated oxidation.

Direct Oxidation by Host

In these circumstances, host-generated molecular species effect or potentiate oxidative processes directly on the polymer. Current thinking, based on solid analytical evidence, is that such reactive molecules are derived from activated phagocytic cells responding to the injury and the properties of the foreign body at the implant site (Zhao et al., 1991). The two major types of these cells are the neutrophils



• **Figure 2.4.2.7** Proposed homolytic chain reaction and heterolytic oxidation mechanisms.



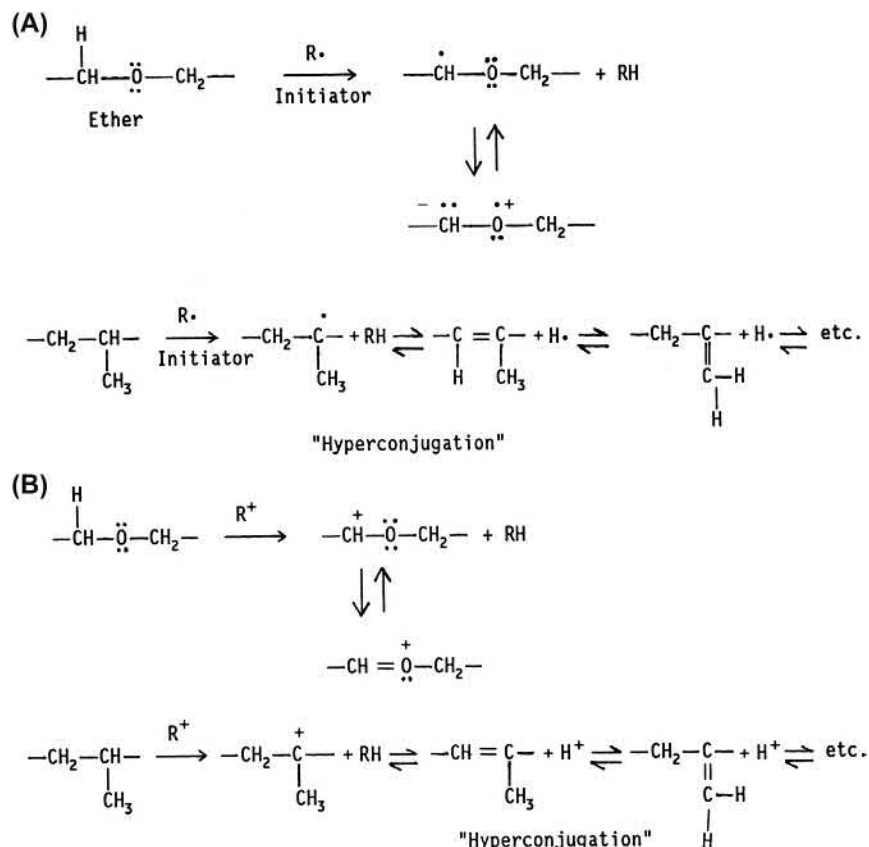
• **Figure 2.4.2.8** Readily oxidizable functional groups (* is the site of homolysis or heterolysis).

(polymorphonuclear leukocytes, PMNs) and the monocytes. The latter, which are found in circulation, can differentiate upon attachment to tissue and divide into macrophage and foreign-body giant cell (FBGC) phenotypes (see [Chapter 2.2.2](#)) ([Ziats, 1988](#)).

Much work is under way to elucidate the sequence of events leading to phagocytic oxidation. Certain important processes of wound healing in the presence of biologically derived foreign bodies such as bacteria and parasites have shown some relevance to biomaterial implants ([Northup, 1987](#)).

Neutrophils, responding to chemical mediators at the wound site, mount a powerful but transient chemical attack within the first few days of injury ([Test and Weiss, 1986](#); [Northup, 1987](#)). Chemically susceptible biomaterials may be affected if they are in close apposition to the wound site ([Sutherland et al., 1993](#)). Activated macrophages subsequently multiply and subside within days at a benign wound site or in weeks if stimulants such as toxins or particulates are released at the site. Their fusion products (FBGCs) can survive for months to years on the implant surface. Macrophages also remain resident in the collagenous foreign-body capsule for extended periods.

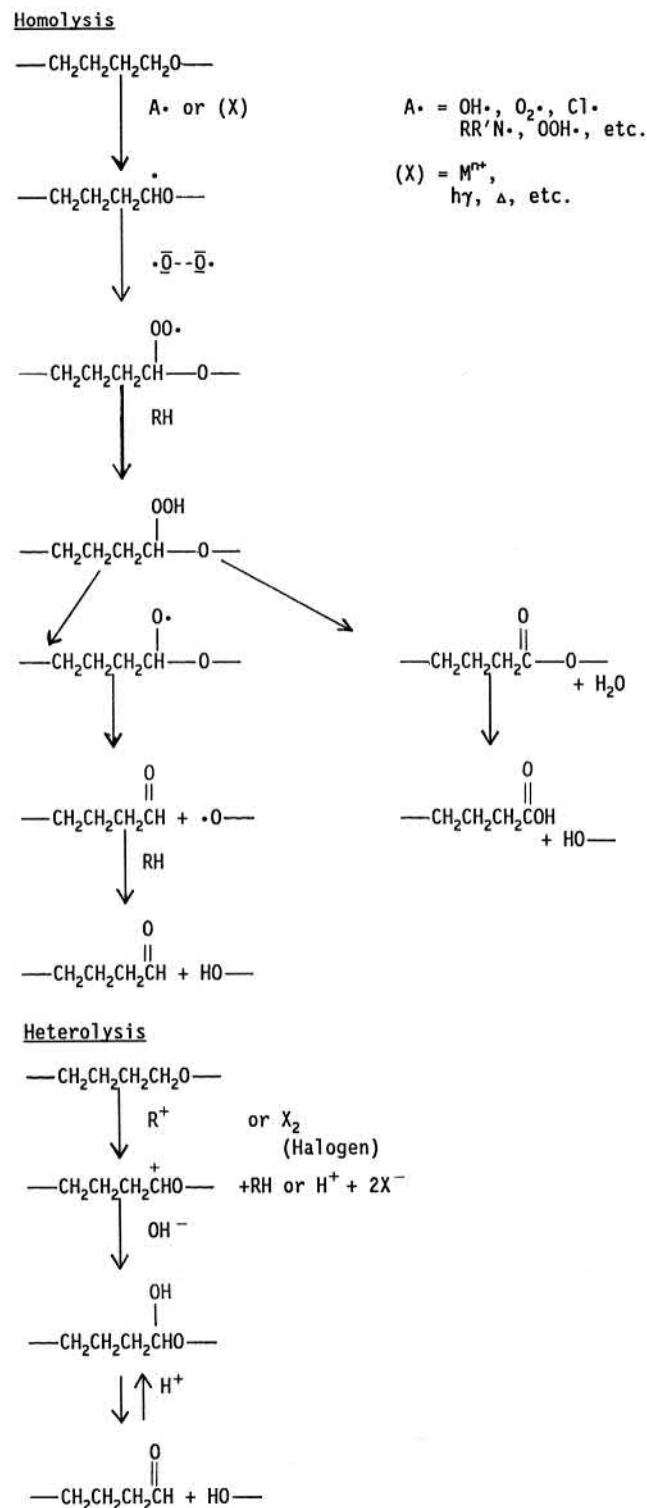
While it is recognized that the complete mechanism of cellular attack and oxidation of biomaterials is as yet



• **Figure 2.4.2.9** (A) Resonance stabilization of ether and hydrocarbon radicals; (B) resonance stabilization of ether and hydrocarbon cations.

unconfirmed, the following discussion attempts to provide logical biological pathways to powerful oxidants capable of producing known degradation products.

Both PMNs and macrophages metabolize oxygen to form a superoxide anion ($O_2^{\bullet -}$). This intermediate can undergo transformation to more powerful oxidants, and conceivably can initiate homolytic reactions on the polymer. Superoxide



• **Figure 2.4.2.10** Pathways for oxidative fragmentation of polyethers.

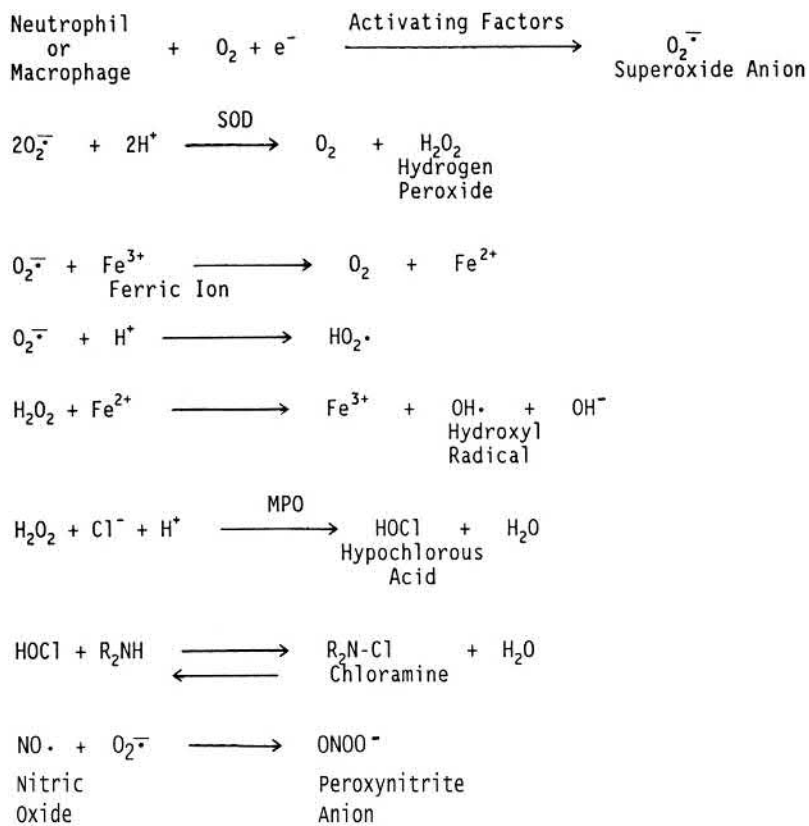
dismutase (SOD), a ubiquitous peroxidase enzyme, can catalyze the conversion of superoxide to hydrogen peroxide which, in the presence of myeloperoxidase (MPO) derived from PMNs, is converted to hypochlorous acid (HOCl). A potent biomaterial oxidant in its own right (Coury et al., 1987), hypochlorite (ClO^-) can oxidize free amine functionality (e.g., in proteins) to chloramines which can perform as long-lived sources of chlorine oxidant (Test and Weiss, 1986; Figs. 2.4.2.11 and 2.4.2.12). Hypochlorite can oxidize other substituted nitrogen functional groups (amides, ureas, urethanes, etc.) with potential chain cleavage of these groups.

The following paragraphs describe potential cooperative reactions involving acquired peroxidase and free ferrous ions. Macrophages contain essentially no MPO, so their hydrogen peroxide is not normally converted to HOCl. However, PMN-derived MPO can bind securely to foreign-body surfaces (Locksley et al., 1982), and serve as a catalyst reservoir for macrophage- or FBGC-derived HOCl production. If free ferrous ion, which is normally present in negligible quantities in the host, is released to the implant site by hemolysis or other injury, it can catalyze the formation of the powerfully oxidizing hydroxyl radical via the Haber–Weiss cycle (Klebanoff, 1982; Fig. 2.4.2.10).

Fig. 2.4.2.11 shows radical and ionic intermediates of HOCl that may initiate biomaterial oxidation. Fig. 2.4.2.12 is a diagram showing a leukocyte phagocytic process that employs endogenous MPO catalysis of HOCl formation. In a more general sense, the MPO may come from within or outside of the cell.

The foregoing discussion of sources of direct oxidation is focused primarily on acute implant periods in which bursts of PMN activity followed by macrophage activity normally resolve within weeks. However, since the foreign body subsequently remains implanted, a sustained if futile attempt to phagocytose an implanted device provides a prolonged release of chemicals onto the biomaterial. This phenomenon, called exocytosis, occurs over months to possibly years (Zhao et al., 1990), and results primarily from the macrophage-FBGC line. It can contribute to long-term chemical degradation of the polymer. The oxidation processes induced by phagocytes are the result of oxidants produced by the general foreign-body response (innate immune response), not direct receptor–ligand catalysis by oxidase enzyme (adaptive immune response). Attempts to degrade oxidatively susceptible polymers by direct contact with oxidase enzymes have produced short-range or limited effects (Sutherland et al., 1993; Santerre et al., 1994).

Macrophages mediate other processes, such as fibrous capsule formation, around the device. Their release of cellular regulatory factors stimulates fibroblasts to populate the implant site and produce the collagenous sheath. Any knowledge of the effects of factors such as fibroblasts or fibrous capsules on rates and mechanisms of polymer degradation is, at this time, incompletely understood.

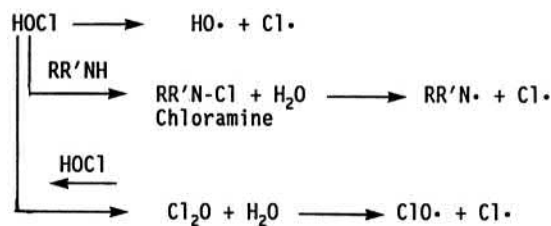


• **Figure 2.4.2.11** Generation of potential oxidants by phagocytic processes.

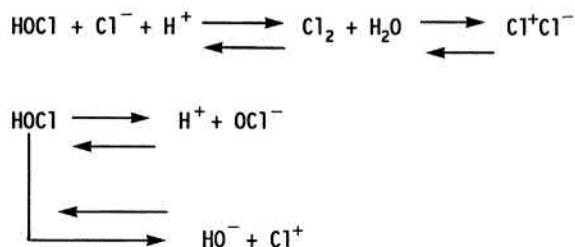
Equilibrium Products



Radical Intermediates



Ionic Intermediates



• **Figure 2.4.2.12** Hypochlorous acid: formation and potential reaction intermediates.

Stress Cracking

An important category of host-induced biodegradation with an oxidative component is stress cracking as manifested in poly(ether urethane) elastomer implants. It differs from classic environmental stress cracking (ESC), which involves a susceptible material at a critical level of stress in a medium that may permeate and swell the polymer but does not dissolve the polymer. Classic ESC is not accompanied by significant chemical degradation (Stokes, 1988). In contrast, stress cracking of polyurethanes is characterized by surface attack of the polymer, and by chemical changes induced by relatively specific *in vivo* or *in vitro* oxidizing conditions. Conditions relevant to stress cracking of certain poly(ether urethane) compositions are stated in Table 2.4.2.3.

Experimental information on the stress cracking of poly(ether urethanes) and poly(ether urethane ureas) (e.g.,

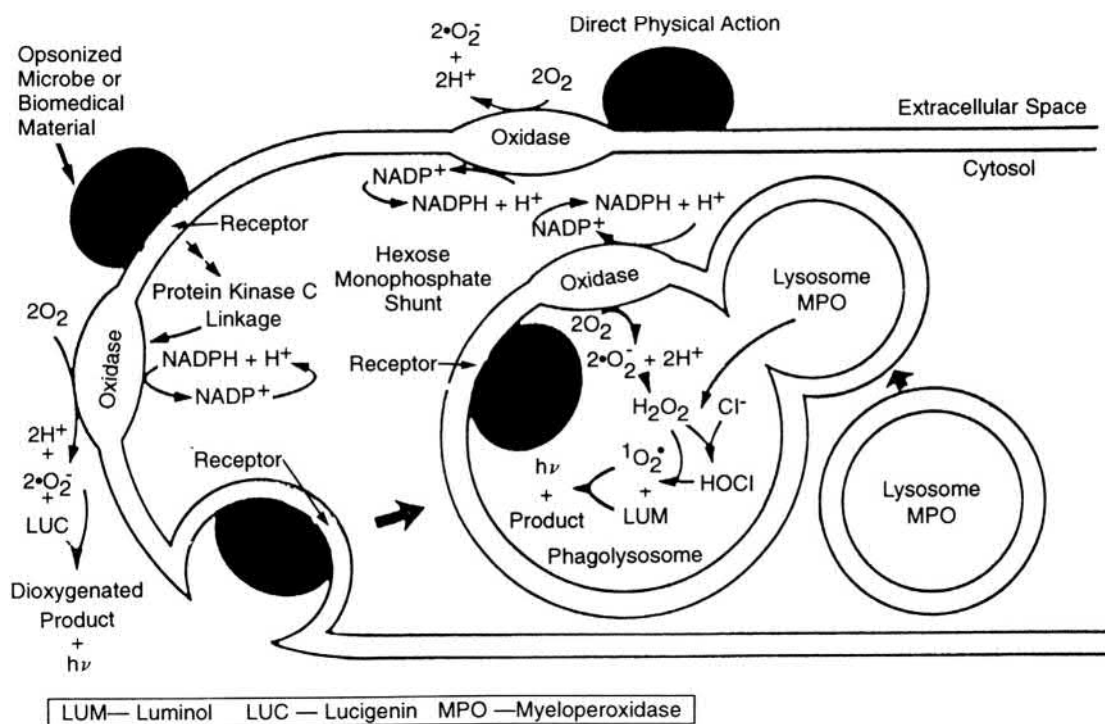
TABLE 2.4.2.3 Characteristics of Poly(Ether Urethanes) That Cracked In Vivo

Components contained residual processing and/or applied mechanical stresses/strains
Components were exposed to a medium of viable cellular and extracellular body constituents
Polymers had oxidatively susceptible (aliphatic ether) groups
Analysis of polymers showed surface oxidation products

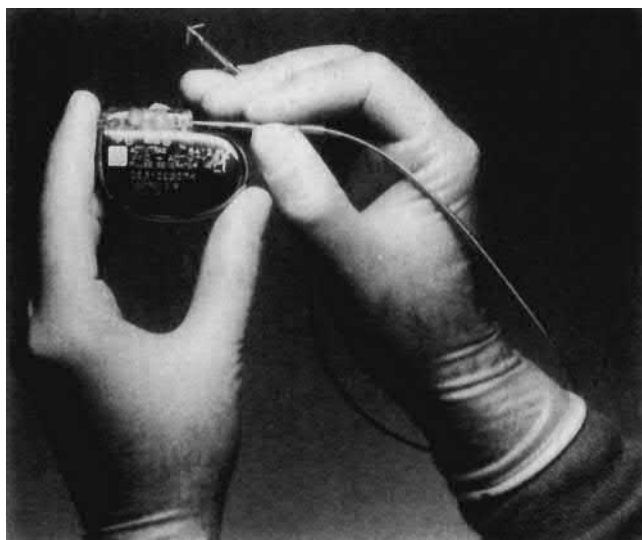
the polymers described in Fig. 2.4.2.3) has provided insights which may be valid for these and other compositions that can be oxidized, for example, polypropylene (Liebert et al., 1976; Altman et al., 1986) or polyethylenes (Wasserbauer et al., 1990; Zhao et al., 1995).

Poly(ether urethane) compositions containing low poly-ether content, which are resistant to degradation *in vivo*, are used as connectors (also called “headers”), insulators, and adhesives for cardiac pacemakers and neurological stimulators (Fig. 2.4.2.13). They have performed with high reliability in chronic clinical applications since 1975. Certain poly(ether urethane) pacing leads have displayed surface cracks in their insulation after residence times *in vivo* of months to years. These cracks are directly related in frequency and depth to the amount of residual stress (Figs. 2.4.2.14 and 2.4.2.15) and the ether (soft segment) content of the polyurethane (Coury et al., 1987; Martin et al., 2001).

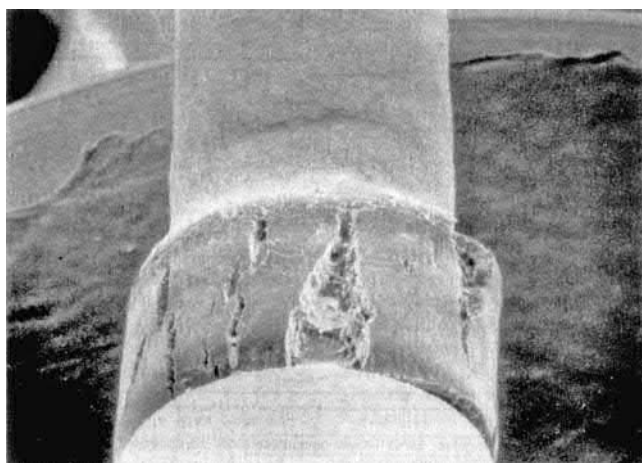
Morphologically, the rough-walled cracks display regular patterns predominately normal to the force vectors, occasionally with “tie fibers” bridging the gaps, indicative of ductile rather than brittle fracture (Figs. 2.4.2.16 and 2.4.2.17). Infrared (IR) analysis indicates that oxidation does not take place detectably in the bulk, but only on the surface where extensive loss of ether functionality (as seen in the ether IR stretch, 1110 cm^{-1}) and enhanced absorption in the hydroxyl and carbonyl regions are observed (Stokes et al., 1987). Possible mechanisms for the oxidative degradation of ethers are



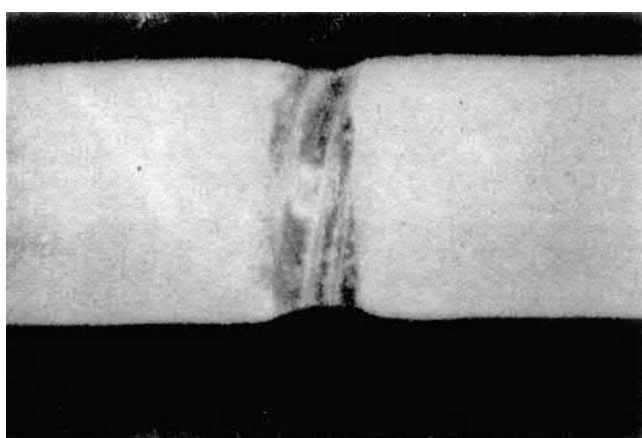
• **Figure 2.4.2.13** Activation of phagocyte redox metabolism: chemiluminogenic probing with luminol and lucigenin. (From Allen, R.C., 1991. Activation of Phagocyte Redox Metabolism: Chemiluminogenic Probing with Luminol and Lucigenin. Drawing provided (Personal communication).)



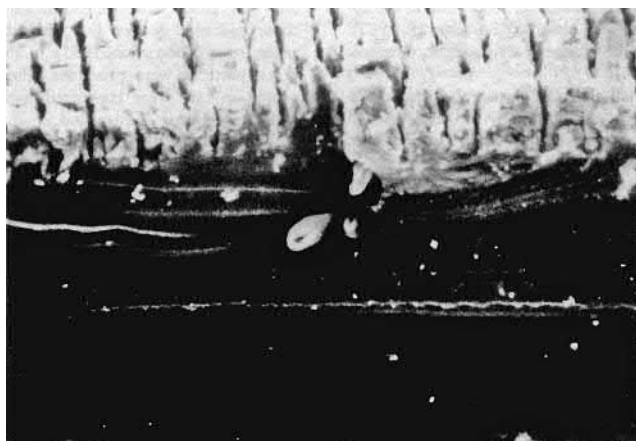
• **Figure 2.4.2.14** Cardiac pacemaker with polyurethane lead insulation, tine, and connector. (Courtesy of Medtronic, Inc.)



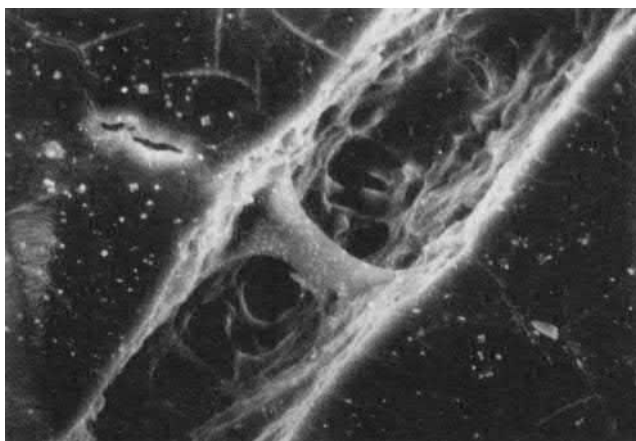
• **Figure 2.4.2.15** Pellethane 2463-80A pacemaker lead tubing with high applied radial stress showing total breach.



• **Figure 2.4.2.16** Pellethane 2363-80A pacemaker lead tubing showing "frosting" due to stress from tight ligature.



• **Figure 2.4.2.17** Stress crack pattern (frosting) near tight ligature ($\times 14$).



• **Figure 2.4.2.18** Single stress crack in pacemaker lead tubing with rough walls and "tie fibers" indicative of ductile fracture ($\times 700$).

presented in [Fig. 2.4.2.18](#). The participation of molecular oxygen in the degradation mechanism is supported by studies which showed that poly(ether urethane urea) degradation in vitro correlated with oxygen diffusion into the polymer bulk after surface oxidation was initiated by hydrogen peroxide/cobalt chloride ([Schubert et al., 1997a,b](#)).

In a seminal study, [Zhao et al. \(1990\)](#) placed polyurethane tubing under strain in cages permeable to fluids and cells (therefore under high initial stress, which was subject to subsequent stress relaxation), and implanted them in rats. In certain cases, antiinflammatory steroids or cytotoxic polymers were coimplanted in the cages. Implants of up to 15 weeks were retrieved. The only prestressed samples to crack were those that did not reside in the cages with the cytotoxic coimplants. The authors concluded that adherent cells caused the stress cracking, and cell necrosis or deactivation inhibited crack induction.

Subsequently, viable phagocytic cells were implicated as a cause of crack initiation in vivo ([Zhao et al., 1991](#)). By removing adherent foreign-body giant cells after 10-week implantation of a curved poly(ether urethane urea) film in a wire cage, exposed foreign-body cell "footprints" showed localized surface cracking in the order of several microns deep and wide.

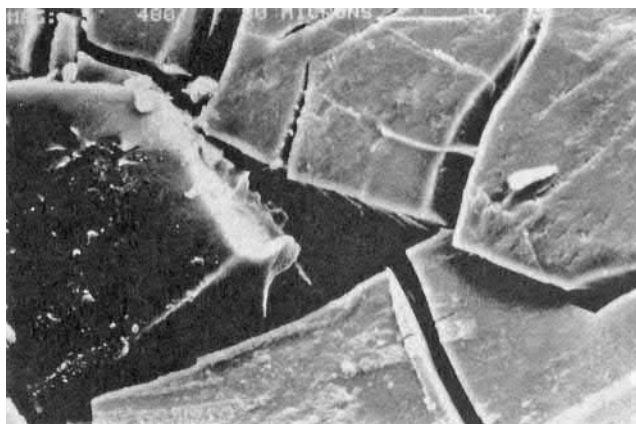
Adjacent areas of polymer which were devoid of attached cells were not cracked. Owing to relatively low stresses in the implanted film, deep crack propagation was not observed.

In vitro studies of strained (Stokes, 1988) and unstrained poly(ether urethane) films (Phua et al., 1987; Ratner et al., 1988; Bouvier et al., 1991; Wiggins et al., 2003) using oxidants, enzymes, etc., have sought to duplicate in vivo stress cracking. Although some surface chemical degradation with products similar to those seen in vivo was demonstrated, stress crack morphology was most closely matched in vitro in two studies. A test which involves immersing stressed poly(ether urethane) tubing in a medium of glass wool, hydrogen peroxide, and cobalt chloride produces cracks which duplicate those produced in vivo, but with rate acceleration of up to seven times (Zhao et al., 1995). These investigators also showed that human plasma proteins, particularly alpha-2-macroglobulin and ceruloplasmin, enhance in vitro stress cracking by oxidants in patterns morphologically similar to those observed in vivo (Zhao et al., 1993). The potential of macrophages to contribute to stress cracking of poly(ether urethanes) was verified in an in vitro study which succeeded in potentiating macrophage oxidative effects with ferrous chloride, and inhibiting them with the antiinflammatory steroid dexamethasone (Casas et al., 1999). In another study, comparable crack patterns were produced when specimens of stressed tubing in rats were compared with those incubated with PMNs in culture (Sutherland et al., 1993). Moreover, this study revealed a difference in chemical degradation products with time of implants which correlated with products from oxidants generated primarily by PMNs (HOCl) and macrophages (ONOO⁻). Early implant times, activated PMNs, and HOCl caused a preferential decrease in the urethane oxygen stretch peak, while longer implant times and ONOO⁻ caused selective loss of the aliphatic ether stretch peak (by infrared spectroscopy).

Taken together, the foregoing observations are consistent with a hypothesized two-step mechanism for stress cracking in vivo. In the first step, surface oxidation induces very shallow, brittle microcracks. The second step involves propagation of the cracks in which specific body fluid components act on the formed cracks to enhance their depth and width, without inducing major detectable bulk chemical reactions. Should this hypothesis prove correct, the term “oxidation-initiated stress cracking” would be reasonably descriptive.

The above description of stress cracking has generally considered static stress, such as that entrained in polymers during the cooling of molten parts, or the assembly of components. Dynamic stresses and strains such as those occurring during cooling with stretching as with extruded tubing or by the operation of diaphragm or bladder heart pumps or artificial joints can cause related cracking in areas of high flex. The cracking has been purported to increase with time of device operation, but to display only minor surface chemical changes (Tomita et al., 1999; Wu et al., 1999).

The stress cracking related to entrained stress in the polymer has been controlled by reducing residual stress,



• **Figure 2.4.2.19** Random crack pattern of Pellethane 2363-80A lead insulation caused by metal ion-induced oxidation ($\times 480$).

isolating the polymer from cell contact (Tang et al., 1994), protecting the polymer from stress-cracking media, or using stress crack-resistant polymers (e.g., in the case of polyurethanes, ether-free compositions) (Coury et al., 1990; Takahara et al., 1994; Tanzi et al., 1997), and use of antioxidants such as hindered phenols (e.g., vitamin E, Monsanto Santowhite powder) (Schubert et al., 1997a,b). Stress cracking is next compared with another type of degradation, metal ion-induced oxidation.

Particularly alpha-2-macroglobulin and ceruloplasmin, enhance in vitro stress cracking by oxidants in patterns morphologically similar to those observed in vivo (Zhao et al., 1993).

Device- or Environment-Mediated Oxidation

Metal Ion-Induced Oxidation. A process of oxidative degradation that has, thus far, primarily been reported clinically for poly(ether urethane) pacemaker leads, requires, as does stress cracking, a very specific set of conditions. The enabling variables and fracture morphology are quite different from stress cracking, although oxidative degradation products are similar. Biodegradation of implanted devices through stress cracking always occurs on polymer surfaces exposed to living cells and provides characteristic rough-walled fissures (indicative of ductile fracture) oriented perpendicular to the stress vector (Figs. 2.4.2.14–2.4.2.17). Metal ion-induced oxidation initiates on the enclosed inner surfaces of pacing lead insulation near corroded metallic components and their entrapped corrosion products. Smooth crack walls and microscopically random crack orientation is indicative of brittle fracture (Figs. 2.4.2.19 and 2.4.2.20). Macroscopically, crack patterns that track metal component configurations may be present (Fig. 2.4.2.21). Degradation products that may be found deeper in the bulk than with stress cracking are again indicative of brittle fracture.

This phenomenon, called metal ion-induced oxidation (MIO), has been confirmed by in vitro studies, in which poly(ether urethanes) were aged in metal ion solutions of



• **Figure 2.4.2.20** Smooth crack wall indicative of brittle fracture caused by metal ion-induced oxidation ($\times 830$).



• **Figure 2.4.2.21** Crack pattern on inner lumen of poly(ether urethane) lead insulation tracking coil imprint indicative of metal ion-induced oxidation ($\times 100$).

different standard oxidation potentials. Above an oxidation potential of about +0.77, chemical degradation was severe. Below that oxidation potential, changes in the polymer that are characteristic of simple plasticization were seen (Coury et al., 1987, Table 2.4.2.4). This technique also showed that metal ion-induced oxidation was proportional to the ether content of the polyurethane (Table 2.4.2.5).

The effect of various metals on oxidation in vitro and in vivo has also been studied. Different metallic components of pacing lead conductors were sealed in poly(ether urethane) (Dow Pellethane 2363-80A) tubing and immersed in 3% hydrogen peroxide at 37°C for up to 6 months (Stokes et al., 1987) or implanted in rabbits for up to 2 years (Stokes et al., 1990). Both techniques resulted in corroded metals and degraded tubing lumen surfaces under certain conditions within 30 days. In particular, the in vivo interaction of body fluids with cobalt and its alloys resulted in oxidative cracking of the polymer.

The metal ion-induced oxidation process clearly involves corrosion of metallic elements to their ions, and subsequent oxidation of the polymer. In operating devices, the metal ion may be formed by solvation, galvanic or electrolytic corrosion, or chemical or biochemical oxidation (Fig. 2.4.2.22).

TABLE 2.4.2.4 Effect of Metal Ion Oxidation Potential on Properties of Poly(Ether Urethane) (Pellethane 2363-80A)^a

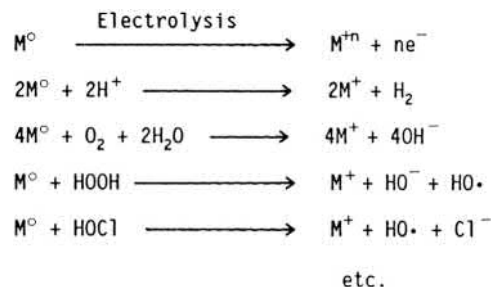
Aqueous Solution	Standard Oxidation Potential	Change in Tensile Strength (%)	Change in Elongation (%)
PtCl ₂	~ +1.2	-87	-77
AgNO ₃	+0.799	-54	-42
FeCl ₃	+0.771	-79	-10
Cu ₂ Cl ₂	+0.521	-6	+11
Cu ₂ (OAc) ₂	+0.153	-11	+22
Ni(OAc) ₂	-0.250	-5	+13
Co(OAc) ₂	-0.277	+1	+13

^aConditions: 0.1 M solutions/90°C/35 days versus controls aged in deionized water; ASTM (D-1708) microtensile specimens; specimens were tested wet.

TABLE 2.4.2.5 Effect of Ether Content of Poly(Ether Urethane) on Susceptibility to Metal Ion-Induced Oxidation^a

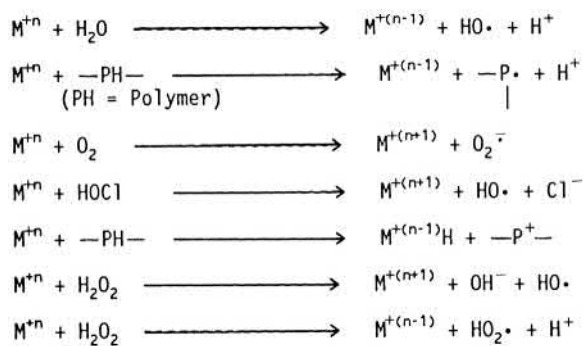
Poly(Ether Urethane)	Polyether Content	Change in Tensile Strength (%)	Change in Elongation (%)
Pellethane 2363-80A	High	-54	-42
Pellethane 2363-55D	Low	-23	-10
Model segmented polyurethane	None	+9	+3

^aConditions: 0.1 M AgNO₃/90°C/35 days versus controls aged in deionized water; ASTM (D-1708) microtensile specimens.



• **Figure 2.4.2.22** Formation of metal ion from metal.

In turn, these metal ions develop oxidation potentials that may well be enhanced in body fluids over their standard half-cell potentials. As strong oxidants, they produce intermediates or attack the polymer to initiate the chain reaction (Fig. 2.4.2.23). Metal ion-induced oxidation is, therefore,



• **Figure 2.4.2.23** Initiation of oxidation pathways by metal ions.

the result of a highly complex interaction of the device, the polymer, and the body.

Should metal ion-induced oxidation, specifically, be a possibility in an implanted device, several approaches are available to control this problem. They are not universally applicable, however, and should be incorporated only if functionality and biocompatibility are retained. Potentially useful techniques include using corrosion-resistant metals, “flushing” corrosive ions away from the susceptible polymer, isolating the metals and polymer from electrolyte solutions, incorporating appropriate antioxidants, and using oxidation-resistant polymers.

Chemical Structure Strategies to Combat Oxidation

To address oxidation susceptibility, polyurethane elastomers with enhanced oxidation stability have been developed. They should be ester-free and ether-free or deficient, and generally contain unconventional soft segments, including, for example, hydrogenated polybutadiene, polyisobutylene, polydimethylsiloxane (subject to hydrolytic consideration, above), polycarbonate, and dimerized fatty acid derivatives (Coury et al., 1990; Pinchuk et al., 1991; Takahara et al., 1991, 1994; Kato et al., 1995; Mathur et al., 1997; Hernandez et al., 2007; Kang et al., 2010; Desai et al., 2011). In implant tests, they have shown reduced tendency to stress crack oxidatively, and some have shown high resistance to metal ion oxidants in vitro. Early attempts to stabilize polyurethanes by laminating more biostable polymers (such as silicone rubbers) to tissue-facing surfaces have met with limited success in dynamic applications, due to the delamination tendencies Pinchuk (1992).

Other approaches to stabilizing polyurethanes to oxidative attack in situ have involved the use of surface modifying (“blooming”) macromolecules (SMMs) (Santerre et al., 2000), surface-modifying end groups (SMEs) (Ward et al., 1995, 1998), and, more recently, self-assembling monolayer end groups (SAMEs) (Ward, 2008). SMMs, typically fluorocarbon-based polymers, are blended with the polyurethanes during processing, and migrate to the surface prior to implantation. SMEs are moieties (typically polysiloxane) bonded to polyurethane as end groups. SAMEs are formed from molecules appended to the backbone of polymers

during synthesis. Such molecules consist of three components: a chemically reactive group for conjugation to the polymer as it is being made; typically, a hydrophobic spacer chain, to provide self-assembly at the surface of the formed article; and a head group from a variety of surface chemistries to provide specific bioactivity. One potential function is to stabilize the polymer against biodegradation (Ward, 2008).

The covalently modified polyurethanes may be used in bulk or as additives to conventional polyurethanes. Both approaches have provided enhanced in vivo stability for polyurethane implants; however, the long-term effects of these treatments are not, as yet, confirmed. SMMs have been covalently modified with bioactive agents, such as antioxidants, to provide further degradation resistance (Ernsting et al., 2002).

All of the “barrier” strategies to protecting polyurethanes described above appear to have validity, at least for protecting polyurethanes in the short term. The long-term (multi-year) benefits of these approaches remain to be seen in light of issues such as surface dynamics, interfacial interactions, and coating durability.

All of these polyurethane modifications, while potentially providing enhanced resistance to biodegradation, still allow susceptibility to attack by biological components, often at a slow rate.

Oxidative Degradation Induced by External Environment

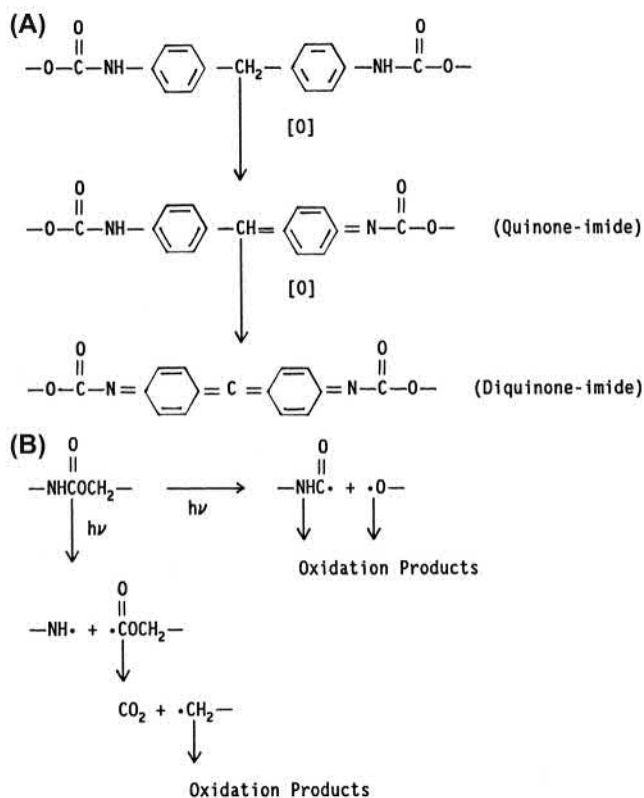
Under very limited circumstances, the body can transmit electromagnetic radiation that may affect the integrity of implanted polymers. For example, the cornea and vitreous humor of the eye, as well as superficial skin layers, allow the passage of long-wave (320–400 nm) “ultraviolet A” radiation. Absorption of ultraviolet radiation causes electron excitation that can lead to photooxidative degradation. This process has been suggested in the breakdown of polypropylene components of intraocular lenses (Altman et al., 1986; Jongbloed and Worst, 1986).

In maxillofacial exo- and very likely endoprostheses, elastomers may undergo undesirable changes in color and physical properties as a consequence of exposure to natural sunlight-frequency radiation (Craig et al., 1980). Photooxidation mechanisms involving the aromatic units and the urethane of aromatic poly(ether urethanes) or poly(ester urethanes) are shown in Fig. 2.4.2.24. Antioxidants and ultraviolet absorbers provide limited protection for these materials.

Emerging Long-Term Elastomer Applications

Polyurethanes

Three polyurethane families are now elaborated, the first for its broad-based popularity as an alternative to poly(ether



• **Figure 2.4.2.24** Photooxidative reactions of aromatic polyurethanes. (A) Formation of quinone-imide from aromatic polyurethane. (B) Photolytic cleavage of urethane link. (From Coury, A.J., Slaikeu, P.C., Cahalan, P.T., Stokes, K.B., Hobot, C.M., 1988. Factors and interactions affecting the performance of polyurethane elastomers in medical devices. *J. Biomater. Appl.* 3, 130–179. (B) From Brauman, S.K., Mayorga, G.D., Heller, J., 1981. Light stability and discoloration of segmented polyether urethanes. *Ann. Biomed. Eng.* 9, 45–58.)

urethanes), sometimes perhaps, unwarranted. The second is one that uses a large proportion of hydrocarbon soft segment with a lesser amount of polyether soft segment. The third elastomer family comprises polymers and copolymers that are completely hydrocarbon-based. Poly(carbonate urethanes) are specially elaborated in this section because their *in vivo* use has both oxidative and hydrolytic implications. Their mechanical properties rival the best poly(ether urethanes) and are favorite compositions for short-term implantable catheters with consideration for chronic use (Wright, 2006). In some studies, they have shown superior oxidation resistance to poly(ether urethanes) in several studies (Mathur et al., 1997; Tanzi et al., 1997). In other studies, however, these compositions were shown to be susceptible to oxidation (Christenson et al., 2004). Additionally, in aqueous media *in vitro* and *in vivo*, slow degradation attributable to simple hydrolysis was also detected (Zhang et al., 1997). The body fluid environment provides a relatively stable long-term hydrolytic medium, generally less subject to cellular “respiratory bursts” that strongly enhance oxidative processes. Although phagocytic processes may also produce hydrolytic enzymes, their effects on synthetic polymers are specific and limited (Labow et al., 2002a). Simple hydrolysis, therefore, may be expected to take place continuously,

in the body buffer, with poly(carbonate urethane) integrity also susceptible to a combination of mechanical stress and vigorous oxidizing conditions (Faré et al., 1999; Labow et al., 2002b). A 3-year implantation study indicated detectable degradation (Seifalian et al., 2003). Only long-term implant studies (e.g., 5 years or greater) would ascertain the acceptability of poly(carbonate urethanes) or, for that matter, other new polymers having potentially susceptible groups. Unfortunately, financial constraints dictate that these extended studies would only be feasible as postmarket surveillance.

One of the most promising polyurethane families for use as tough, biostable polyurethane elastomers is in development by Boston Scientific Corporation, Formerly Cardiac Pacemakers, Inc., now Abbott Corporation (Desai et al., 2014, 2015). This polyurethane family employs poly(isobutylene diol) as a major soft segment component along with a lesser, reinforcing amount of poly(ether diol) soft segment and conventional methylene dianiline diisocyanate/short chain diol hard segment. Studies predictive of high biostability have been executed (Cozzens et al., 2010).

Hydrocarbon Elastomers

In 1987, Carl McMillin published a pioneering article on a set of elastomers intended for long-term flex fatigue resistance in medical devices such as artificial heart diaphragms (McMillin, 1987a,b). For simple flex life in an *in vitro* setup, Hexsyn [cross-linked poly(1-hexene)] rubber stood out. It was used in early artificial heart designs under the name of “Bion” rubber. A communication from Dr. McMillin indicated that its lack of adequate tear strength inhibited its successful use, but it may be a very valuable material for dynamic use not subject to cuts and abrasions.

A final very promising hydrocarbon rubber enjoying clinical use is the triblock copolymer, poly(styrene-isobutylene-styrene) (SIBS), spearheaded by (Pinchuk et al., 2007). It is reported to be stable in the body without degradation, long term, and causes a minimal host response. Its early use was as a drug carrier for the Boston Scientific TAXUS coronary artery stent. An advanced current clinical application is as a glaucoma drainage conduit (Pinchuk et al., 2015). The previous two uses were basically static implants. For dynamic applications, it is noted that SIBS is not as tough as polyurethanes and has not been reported for pacemaker lead insulation. In animal studies for heart valve leaflets, the leaflets failed, from “material failure and calcification” (Wang et al., 2010). However, subsequent studies of these copolymers, in cross-linked form to enhance toughness, have shown indications of greater durability while maintaining favorable host response for synthetic heart valves (Sheriff et al., 2015).

Conclusions

Polymers that are carefully chosen for use in implanted devices generally serve effectively for their intended lifetimes if they are properly selected, processed, and

device–material–host interactions are adequately addressed. In certain limited circumstances, excessive hydrolytic or oxidative biodegradation occurs. This may be induced by direct attack by the host or by nonbiological factors in the environment surrounding the implant. With susceptible polymers, protective measures can be taken to ensure extended efficacy, although new, biodegradation-resistant polymers that are on the horizon may require less protection. Knowledge of biodegradation mechanisms and the employment of appropriate countermeasures such as proper material selection or modification, optimal component design, protection from environmental attack, and careful processing, handling, and implantation procedures will promote continued progress in the development of polymers as long-term implantable biomaterials.

Acknowledgments

The author is very grateful to Dr. R.C. Allen for providing the drawing on activated phagocyte redox metabolism. For their technical advice and contributions, I sincerely thank James Anderson, Ken Stokes, Jonathan Sears, John Eaton, Allan Hoffman, John Mahoney, Maurice Kreevoy, Grace Picciolo, Buddy Ratner, Bob Ward, SuPing Lyu, Darrel Untereker, and Len Pinchuk. For the preparation of the original manuscript, I am deeply indebted to my “computer wizard,” Mrs. Jayne McCaughey. For help in updating original literature sources, I thank Ms. Mari Ferentinos.

References

- Abbott, 2019. Product Performance Report, first ed., pp. 162–194. Cardiac Arrhythmia and Heart Failure.
- Allen, R.C., 1991. Activation of Phagocyte Redox Metabolism: Chemiluminescent Probing with Luminol and Lucigenin. Drawing provided.
- Altman, J.J., Gorn, R.A., Craft, J., Albert, D.M., 1986. The breakdown of polypropylene in the human eye: is it clinically significant? *Ann. Ophthalmol.* 18, 182–185.
- ASTM D1708 – 10, 2010. Standard Test Method for Tensile Properties of Plastics by Use of Microtensile Specimens. <http://www.astm.org/Standards/D1708.htm>.
- Barbarini Ferraz, L.C., Schellini, S.A., Wludarski, S.L., Padovani, R., Selva, D., et al., 2009. Extraocular muscle fixation to porous polyethylene orbital implants using 2-octyl cyanoacrylate. *Eur. J. Ophthalmol.* 19 (4), 527–529.
- Bernardino, C.R., Mihora, L.D., Fav, A.M., Rubin, P.A., 2006. Orbital complications of hydrogel scleral buckles. *Ophthalmic Plast. Reconstr. Surg.* 22 (3), 206–208.
- Blais, P., 1990. Letter to the editor. *J. Appl. Biomater.* 1, 197.
- Blanchet, T.A., Burroughs, B.R., 2001. Numerical oxidation model for gamma radiation-sterilized UHMWPE: consideration of dose-depth profile. *J. Biomed. Mater. Res.* 58 (6), 684–693.
- Bloch, B., Hastings, G., 1972. *Plastics Materials in Surgery*, second ed. Charles C. Thomas, Springfield, IL, pp. 97–98.
- Booth, A.E., February 1995. Industrial sterilization technologies: new and old trends shape manufacturer choices. *Med. Dev. Diagn. Ind.* 64–72.
- Bouvier, M., Chawla, A.S., Hinberg, L., 1991. *In vitro* of a poly(ether urethane) by trypsin. *J. Biomed. Mater. Res.* 25, 773–789.
- Brauman, S.K., Mayorga, G.D., Heller, J., 1981. Light stability and discoloration of segmented polyether urethanes. *Ann. Biomed. Eng.* 9, 45–58.
- Braunstein, R.A., Winnick, M., 2002. Complications of Mira-gel-pseudotumor. *Arch. Ophthalmol.* 120, 228–229.
- Cardia, G., Regina, G., 1989. Degenerative Dacron graft changes: is there a biological component in this textile defect? A case report. *Vasc. Surg.* 23 (3), 245–247.
- Carr, J., 2011. The intracorporeal use of 2-octyl cyanoacrylate resin to control air leaks after lung resection. *Eur. J. Cardiothorac. Surg.* 39 (4), 579–583.
- Casas, J., Donovan, M., Schroeder, P., Stokes, K., Untereker, D., 1999. *In vitro* modulation of macrophage phenotype and inhibition of polymer degradation by dexamethasone in a human macrophage/Fe/stress system. *J. Biomed. Mater. Res.* 46, 475–484.
- Cauich-Rodríguez, J.V., Chan-Chan, L.H., Hernandez-Sánchez, F., Cervantes-Uc, J.M., March 27, 2013. Degradation of polyurethanes for cardiovascular applications. In: Pignatello, R. (Ed.), *Advances in Biomaterials Science and Biomedical Applications*. IntechOpen.
- Chaffin, K.A., Buckalew, A.J., Schley, J.L., Chen, X., et al., 2012. Influence of water on the structure and properties of PDMS-containing multiblock polyurethanes. *Macromolecules* 45 (22), 9110–9120.
- Chen, L.E., Seaber, A.V., Urbaniak, 1993. Comparison of 10-0 polypropylene with 10-0 nylon sutures in rat arterial anastomoses. *Microsurgery* 14 (5), 328–333.
- Christenson, E.M., Anderson, J.M., Hiltner, A., 2004. Oxidative mechanisms of poly(carbonate urethane) and poly(ether urethane) biodegradation: *In vivo* and *in vitro* correlations. *J. Biomed. Mater. Res. Part A.* 70, 245–255.
- Cipriani, E., Bracco, P., Kurtz, S.M., Costa, L., Zanetti, M., 2013. *In-vivo* degradation of poly(carbonate-urethane) based spine implants. *Polym. Degrad. Stab.* 98 (6), 1225–1235.
- Colthurst, M.J., Williams, R.L., Hiscott, P.S., Grierson, I., 2000. Biomaterials used in the posterior segment of the eye. *Biomaterials* 21, 649–665.
- Coury, A.J., Slaikeu, P.C., Cahalan, P.T., Stokes, K.B., 1987. Medical applications of implantable polyurethanes: current issues. *Prog. Rubber Plast. Technol.* 3 (4), 24–37.
- Coury, A.J., Slaikeu, P.C., Cahalan, P.T., Stokes, K.B., Hobot, C.M., 1988. Factors and interactions affecting the performance of polyurethane elastomers in medical devices. *J. Biomater. Appl.* 3, 130–179.
- Coury, A.J., Hobot, C.M., Slaikeu, P.C., Stokes, K.B., Cahalan, P.T., 1990. A new family of implantable biostable polyurethanes. In: *Trans. 16th Annual Meeting Soc. for Biomater.*, May 20–23, p. 158.
- Coury, A.J., 1999. Biostable polymers as durable scaffolds for tissue engineered vascular prostheses. In: Zilla, P., Greisler, H. (Eds.), *Tissue Engineering of Vascular Prosthetic Grafts*, vol. 43. R.G. Landes Company, Austin, TX, pp. 469–480.
- Cozzens, D., Ojha, U., Kulkarni, P., Faust, R., Desai, S., 2010. Long term *in vitro* biostability of segmented polyisobutylene-based segmented, thermoplastic polyurethanes. *J. Biomed. Mater. Res.* 95 (3), 774–782.
- Craig, R.G., Koran, A., Yus, R., April 1980. Elastomers for maxillofacial applications. *Biomaterials* 1, 112–117.
- Crowninshield, R., Muratoglu, O., 2008. How have new sterilization techniques and new forms of polyethylene influenced wear in total joint replacement? *J. Am. Acad. Orthop. Surg.* 16 (Suppl. 1), S80–S85.
- Daly, B.M., Yin, J., 1998. Subsurface oxidation of polyethylene. *J. Biomed. Mater. Res.* 42, 523–529.

- Desai, S., Boden, M., January 6, 2015. U.S. Patent 8,927,660, Cross-linkable Polyisobutylene-Based Polymers and Medical Devices Containing the Same.
- Desai, S., Boden, M., DeRoche, S., Foster, A., Reddy, S., March 3, 2011. US Patent Application 20110054580. Polyisobutylene Urethane Urea and Urethane/Urea Copolymers and Medical Leads Containing the Same.
- Desai, S., Boden, M., DeRoche, S., et al., December 2, 2014. U.S. Patent 8,903,507, Polyisobutylene Urethane, Urea and Urethane/Urea Copolymers and Medical Devices Containing the Same.
- Duke Extrusion.com (Copyright, 2019). <https://www.dukeextrusion.com/materials/nylon-medical-extrusion>.
- Ernsting, M.J., Santerre, J.P., Labow, R.S., 2002. Surface modification of a polycarbonate-urethane using a Vitamin E derivatized fluoroalkyl surface modifier. In: Trans. 28th Annual Meeting Soc. Biomater., April 24–27, p. 16.
- Faré, S., Petrini, P., Motta, A., Cigada, A., Tanzi, M.C., 1999. Synergistic efforts of oxidative environments and mechanical stress on *in vitro* stability of polyetherurethanes and polycarbonateurethanes. J. Biomed. Mater. Res. 45, 62–74.
- Finck, K.M., Grosse-Siestrup, C., Bisson, S., Rinck, M., Gross, U., 1994. Experimental *in vivo* degradation of polyarylamide. In: Trans. 20th Annual Meeting Soc. for Biomater., April 5–9, p. 210.
- Furman, B., Li, S., 1995. The effect of long-term shelf life aging of ultra high molecular weight polyethylene. In: Trans. 21st Annual Meeting Soc. for Biomater., March 18–22, p. 114.
- Graiver, D., Farminer, K.W., Narayan, R., 2003. A review of the fate and effects of silicones in the environment. J. Polym. Environ. 11, 129–136.
- Griessbach, E.F., Lehmann, R.G., 1999. Degradation of polydimethylsiloxane fluids in the environment—a review. Chemosphere 38 (6), 1461–1468.
- Greisser, H.J., Gengenbach, T.R., Chatelier, R.C., 1994. Longterm changes in the surface composition of polymers intended for biomedical applications. Trans. 20th Annual Meeting Soc. for Biomater. 19, 5–9.
- Gumargalieva, K.Z., Moiseev, Y.V., Daurova, T.T., Voronkova, O.S., 1982. Effect of infections on the degradation of polyethylene terephthalate implants. Biomaterials 3 (3), 177–180.
- Hagmar, L., Welinder, H., Mikoczy, Z., 1993. Cancer incidence and mortality in the Swedish polyurethane foam manufacturing industry. Br. J. Ind. Med. 50, 537–543.
- Hauser, R.G., Abdelhadi, R.H., McGriff, D.M., Kallinen Retel, L., 2013. Failure of a novel silicone-polyurethane copolymer (Optim™) to prevent implantable cardioverter-defibrillator lead insulation abrasions. Europace 15 (2), 278–283.
- Hegyeli, A., 1973. Use of organ cultures to evaluate biodegradation of polymer implant materials. J. Biomed. Mater. Res. 7, 205–214.
- Hernandez, R., Weksler, J., Padsalgikar, A., Runt, J., 2007. *In vitro* oxidation of high polydimethylsiloxane content bio-medical polyurethanes: correlation with the microstructure. J. Biomed. Mater. Res. 87 (2), 546–556.
- Hoffman, A., 1999. Personal Communication.
- Hudson, J., Crugnola, A., 1987. The *in vivo* biodegradation of nylon 6 utilized in a particular IUD. J. Biomater. Appl. 1, 487–501.
- Hwang, K.I., Lim, J.I., 1997. Hydrogel explant fragmentation 10 years after scleral buckling surgery. Arch. Ophthalmol. 115, 1205–1206.
- Jongebloed, W.L., Worst, J.F.G., 1986. Degradation of polypropylene in the human eye: a SEM-study. Doc. Ophthalmol. 64, 143–152.
- Kang, J., Erdodi, G., Brendel, C.M., Ely, D., Kennedy, J.P., 2010. Polyisobutylene-based polyurethanes. V. Oxidative- hydrolytic stability and biocompatibility. J. Polym. Sci. A 48 (10), 2194–2203.
- Kato, Y.P., Dereume, J.P., Kontges, H., Frid, N., Martin, J.B., et al., 1995. Preliminary mechanical evaluation of a novel endoluminal graft. In: Trans. 21st Annual Meeting Soc. for Biomater., March 18–22, p. 81.
- Kearney, J.J., Lahey, J.M., Borirakchanyavat, S., Schwartz, D.M., Wilson, D., et al., 2004. Complications of hydrogel explants used in scleral buckling surgery. Am. J. Ophthalmol. 137 (1), 96–100.
- Klebanoff, S., 1982. Iodination catalyzed by the xanthine oxidase system: role of hydroxyl radicals. Biochemistry 21, 4110–4116.
- Kopecek, J., Ulbrich, K., 1983. Biodegradation of biomedical polymers. Prog. Polym. Sci. 9, 1–58.
- Kurtz, S.M., Rimnac, C.M., Hozack, W.J., Turner, J., Marcolongo, M., et al., 2005. *In vivo* degradation of polyethylene liners after gamma sterilization in air. J. Bone Jt. Surg. 87, 815–823.
- Labow, R.S., Erfle, D.J., Santerre, J.P., 1995. Neutrophil-mediated degradation of segmented polyurethanes. Biomaterials 16, 51–59.
- Labow, R.S., Tang, Y., McCloskey, C.B., Santerre, J.P., 2002a. The effect of oxidation on the enzyme-catalyzed hydrolytic degradation of polyurethanes. Can. J. Biomater. Sci. Polym. Ed. 13 (6), 651–665.
- Labow, R.S., Meek, E., Matherson, L.A., Santerre, J.P., 2002b. Human macrophage-mediated biodegradation of polyurethanes: assessment of candidate enzyme activities. Biomaterials 23 (19), 3969–3975.
- Lamba, K., Woodhouse, K.A., Cooper, S.L., Lelah, M.D., 1998. Polyurethanes in Biomedical Applications. CRC Press, Boca Raton.
- Liebert, T.C., Chartoff, R.P., Cosgrove, S.L., McCuskey, R.S., 1976. Subcutaneous implants of polypropylene filaments. J. Biomed. Mater. Res. 10 (6), 939–951.
- Ling, M.T.K., Westphal, S.P., Qin, S., Ding, S., Woo, L., 1998. Medical plastics failures from heterogeneous contamination. Med. Plast. Biomater. 5 (2), 45–49.
- Locksley, R., Wilson, C., Klebanoff, S., May 1982. Role of endogenous and acquired peroxidase in the toxoplasmicidal activity of murine and human mononuclear phagocytes. J. Clin. Investig. 69, 1099–1111.
- Lyu, S., Untereker, D., 2009. Degradability of polymers for implantable medical devices. Int. J. Mol. Sci. 10 (9), 4033–4065.
- Martin, D.J., Poole Warren, L.A., Gunatillake, P.A., McCarthy, S.J., Meijs, G.F., et al., 2001. New methods for the assessment of *in vitro* and *in vivo* stress cracking in biomedical polyurethanes. Biomaterials 22 (9), 973–978.
- Mathur, A.B., Collier, T.O., Kao, W.J., Wiggins, M., Schubert, M.A., et al., 1997. *In vivo* biocompatibility and biostability of modified polyurethanes. J. Biomed. Mater. Res. 36, 246–257.
- McKellop, H., Yeom, B., Campbell, P., Salovey, R., 1995. Radiation induced oxidation of machined or molded UHMWPE after seventeen years. In: Trans. 21st Annual Meeting Soc. Biomater., March 18–22, p. 54.
- McMillin, C., 1987a. Development of tests to evaluate candidate elastomers for artificial heart diaphragms. Artif. Organs 11 (5), 395–404.
- McMillin, C., 1987b. Characterization of Hexsyn, a polyolefin rubber. J. Biomater. Appl. 2 (1), 3–100.
- Medel, F.J., Kurtz, S.M., Hozack, W.J., Parvizi, J., Purtill, J.J., et al., 2009. Gamma inert sterilization: a solution to polyethylene oxidation? J. Bone Jt. Surg. 91, 839–849.
- Northup, S., 1987. Strategies for biological testing of biomaterials. J. Biomater. Appl. 2, 132–147.
- Oppenheimer, E.T., Willhite, M., Danishefsky, I., Stout, A.P., January 1961. Observations on the effects of powdered polymer in the carcinogenic process. Cancer Res. 21, 132–134.

- Padsalgikar, A., Gallagher, G., Cosgriff-Hernandez, Runt, J., 2015. Polyurethanes in cardiac device leads – effect of morphology on performance. *PU Mag.* 12 (2).
- Parmar, A., January 24, 2012. Who makes the secret sauce in St. Jude's Optim technology? *MedCity News*. <https://medcitynews.com/2012/01/who-makes-the-secret-sauce-in-st-judes-highly-touted-optim-technology-another-mn-company/>.
- Phua, S.K., Castillo, E., Anderson, J.M., Hiltner, A., 1987. Biodegradation of a polyurethane *in vitro*. *J. Biomed. Mater. Res.* 21, 231–246.
- Pinchuk, L., Esquivel, M.C., Martin, J.B., Wilson, G.J., 1991. Cor-ethane: A new replacement for polyether urethanes for longterm implant applications. In: *Trans. 17th Annual Meeting Soc. Biomater.*, May 1–5, p. 98.
- Pinchuk, L., Wilson, G., Barry, J., Schoepfoerster, R., Parel, J.-M., Kennedy, J., 2007. Medical applications of poly(styrene-block-isobutylene-block-styrene) (“SIBS”). *Biomaterials* 2–13 Accepted, September.
- Pinchuk, L., Riss, I., Battle, J.F., et al., August 2015. The development of a micro-shunt made from poly(styrene-block-isobutylene-block-styrene) to treat glaucoma. *J. Biomed. Mater. Res. Part B* 1–11.
- Pinchuk, L., September 15, 1992. Adhesiveless Bonding of Silicone Rubber to Polyurethanes and the Use of Bonded Materials. *US Patent*, 5, 147, 725.
- Pinchuk, L., 1994. A review of the biostability and carcinogenicity of polyurethanes in medicine and the new generation of 'biostable' polyurethanes. *J. Biomater. Sci. Polym. Ed.* 6 (3), 225–267.
- Pitt, C.G., 1992. Non-microbial degradation of polyesters: mechanisms and modifications. In: Vert, M., Feijin, J., Albertson, A., Scott, G., Chiellini, E. (Eds.), *Biodegradable Polymers and Plastics*. R. Soc. Chem., Cambridge, UK, pp. 1–19.
- Portnoy, R., 1997. Clear, radiation-tolerant autoclavable polypropylene. *Med. Plast. Biomater.* 4 (1), 40–48.
- Ratner, B.D., Gladhill, K.W., Horbett, T.A., 1988. Analysis of *in vitro* enzymatic and oxidative degradation of polyurethanes. *J. Biomed. Mater. Res.* 22, 509–527.
- Refojo, M.F., Leong, F.L., 1981. Poly(methylacrylate-co-hydroxyethyl acrylate) hydrogel implant material of strength and softness. *J. Biomed. Mater. Res.* 15, 497–509.
- Rimnac, C., Pruitt, L., 2008. How do material properties influence wear and fracture mechanisms? *Am. Acad. Orthop. Surg.* 16 (Suppl. 1), S94–S100.
- Roldan-Pallares, M., del Castillo, J.L., Awad-El Susi, S., Refojo, M.F., 1999. Long-term complications of silicone and hydrogel explants in retinal reattachment surgery. *Arch. Ophthalmol.* 177, 197–201.
- Santerre, J.P., Labow, R.S., Duguay, D.G., Erfle, D., Adams, G.A., 1994. Biodegradation evaluation of polyether- and polyester-urethanes with oxidative and hydrolytic enzymes. *J. Biomed. Mater. Res.* 28, 1187–1199.
- Santerre, J.P., Meek, E., Tang, Y.W., Labow, R.S., 2000. Use of fluorinated surface modifying macromolecules to inhibit the degradation of polycarbonate-urethanes by human macrophages. In: *Trans. 6th World Biomaterials Congress*, p. 77.
- Schnabel, W., 1981. *Polymer Degradation Principles and Practical Applications*. Macmillan, New York, NY. pp. 15–17, 179–185.
- Schoen, F.J., 1987. Biomaterial-associated infection, neoplasia and calcification. Clinicopathologic features and pathophysiologic concepts. *Trans. Am. Soc. Artif. Intern. Organs* 33 (1), 8–18.
- Schubert, M.A., Wiggins, M.J., Anderson, J.M., Hiltner, A., 1997a. Comparison of two antioxidants for poly(etherurethane urea) in an accelerated *in vitro* biodegradation system. *J. Biomed. Mater. Res.* 34, 493–505.
- Schubert, M.A., Wiggins, M.J., Anderson, J.M., Hiltner, A., 1997b. Role of oxygen in biodegradation of poly(etherurethane urea) elastomers. *J. Biomed. Mater. Res.* 34, 519–530.
- Seifalian, A.M., Salacinski, H.J., Tiwari, A., Edwards, E., Bowald, S., et al., 2003. *In vivo* biostability of a poly(carbonate urea) urethane graft. *Biomaterials* 24 (14), 2549–2557.
- Shen, F.W., Yu, Y.J., McKellop, H., 1999. Potential errors in FTIR measurement of oxidation in ultra-high molecular weight polyethylene implants. *J. Biomed. Mater. Res.* 48, 203–210.
- Sheriff, J., Claiborne, T.E., Tran, P.T., Pinchuk, M., Slepian, M.J., Blues-tein, D., et al., 2015. Physical characterization and platelet interactions under shear flows of a novel thermoset polyisobutylene-based copolymer. *ACS Appl. Mater. Interfaces* 7 (39), 22058–22066.
- Simmons, A., Hyvarinen, J., O'Dell, R., Martin, D., et al., 2004. Long-term *in vivo* biostability of poly(dimethylsiloxane)/poly(hexamethylene oxide) mixed macrodiol-based polyurethane elastomers. *Biomaterials* 25, 4887–4900.
- Singer, A.J., Quinn, J.V., Hollander, J.E., 2008. The cyanoacrylate topical skin adhesives. *Am. J. Emerg. Med.* 26 (4), 490–496.
- Smith, R., Oliver, C., Williams, D.F., 1987. The enzymatic degradation of polymers *in vitro*. *J. Biomed. Mater. Res.* 21, 991–1003.
- Snow, J., Harasaki, H., Kasick, J., Whalen, R., Kiraly, R., et al., 1981. Promising results with a new textured surface intrathoracic variable volume device for LVAS. *Trans. Am. Soc. Artif. Intern. Organs XXVII*, 485–489.
- St. Jude Medical, Inc., 2012. Optim® Insulation, A New Material for a New Generation of Cardiac Leads. Product Information. <http://www.sjmprofessional.com/Products/US/CRT-Systems/Optim-Insulation.aspx>.
- Stokes, K., Coury, A., Urbanski, P., April 1987. Autooxidative degradation of implanted polyether polyurethane devices. *J. Biomater. Appl.* 1, 412–448.
- Stokes, K., Urbanski, P., Upton, J., 1990. The *in vivo* autooxidation of polyether polyurethane by metal ions. *J. Biomater. Sci. Polym. Ed.* 1 (3), 207–230.
- Stokes, K., October 1988. Polyether polyurethanes: biostable or not? *J. Biomater. Appl.* 3, 228–259.
- Sutherland, K., Mahoney, J.R., II, Coury, A.J., Eaton, J.W., 1993. Degradation of biomaterials by phagocyte-derived oxidants. *J. Clin. Investig.* 92, 2360–2367.
- Szycher, M., Siciliano, A., 1991. An assessment of 2,4-TDA formation from Surgitek polyurethane foam under stimulated physiological conditions. *J. Biomater. Appl.* 5, 323–336.
- Takahara, A., Coury, A.J., Hergenrother, R.W., Cooper, S.L., 1991. Effect of soft segment chemistry on the biostability of segmented polyurethanes. I. *In vitro* oxidation. *J. Biomed. Mater. Res.* 25, 341–356.
- Takahara, A., Coury, A.J., Cooper, S.L., 1994. Molecular design of biologically stable polyurethanes. In: *Trans. 20th Annual Meeting Soc. Biomater.*, April 5–9, p. 44.
- Tang, W.W., Santerre, J.P., Labow, R.S., Waghay, G., Taylor, D., 1994. The use of surface modifying macromolecules to inhibit biodegradation of segmented polyurethanes. In: *Trans. 20th Annual Meeting Soc. Biomater.*, April 5–9, p. 62.
- Tanzi, M.C., Mantovani, D., Petrini, P., Guidoin, R., Laroche, G., 1997. Chemical stability of polyether urethanes versus polycarbonate urethanes. *J. Biomed. Mater. Res.* 36, 550–559.
- Test, S., Weiss, S., 1986. The generation of utilization of chlorinated oxidants by human neutrophils. *Adv. Free Radical Biol. Med.* 2, 91–116.
- Thomas, C., August 23, 2012. ICD Warning: Defective Defibrillator Leads Recalled, Heart Sisters for Women with Heart Disease. <http://myheartsisters.org/2012/08/23/icd-warning-defective-defibrillator-leads-recalled/>.

- Tomita, N., Kitakura, T., Onmori, N., Ikada, Y., Aoyama, E., 1999. Prevention of fatigue cracks in ultra-high molecular weight polyethylene joint components by the addition of vitamin E. *J. Biomed. Mater. Res.* 48, 474–478.
- US FDA (Food and Drug Administration) Document: Medical Devices, 2010. Device Approvals: <http://www.fda.gov/medical-devices/productsandmedicalprocedures/deviceapprovalsand-clearances/recently-approved-devices/ucm215106.htm> 2010.
- US FDA, February 6, 2019. Breast Implant Associated-Anaplastic Large Cell Lymphoma (BIA-ALCL) – Letter to Health Care Providers. <https://www.fda.gov/medical-devices/letters-health-care-providers/breast-implant-associated-anaplastic-large-cell-lymphoma-bia-alcl-letter-health-care-providers>.
- Vauthier, C., Dubernet, C., Fattal, E., Pinto-Alphandary, H., Couvreur, P., 2003. Poly (alkylcyanoacrylates) as biodegradable materials for biomedical applications. *Adv. Drug Deliv. Rev.* 55 (4), 519–548.
- Vinard, E., Eloy, R., Descotes, J., Brudon, J.R., Giudicelli, H., et al., 1991. Human vascular graft failure and frequency of infection. *J. Biomed. Mater. Res.* 25, 499–513.
- Wang, Q., McGoron, A.J., Bianco, R.W., Kato, Y., Pinchuk, L., Schoepfoerster, R.T., 2010. In-vivo assessment of a novel polymer (SIBS) trileaflet heart valve. *J. Heart Valve Dis.* 19 (4), 499–505.
- Ward, R.S., White, K.A., Gill, R.S., Wolcott, C.A., 1995. Development of biostable thermoplastic polyurethanes with oligomeric polydimethylsiloxane end groups. In: *Trans. 21st Annual Meeting Soc. Biomater.*, March 18–22, p. 268.
- Ward, R.S., Tian, Y., White, K.A., 1998. Improved polymer biostability via oligomeric end groups incorporated during synthesis. *Polym. Mater. Sci. Eng.* 79, 526–527.
- Ward, R.S., 2008. New horizons for biomedical polymers. *Med. Des. Tech.* 19 (5), 26–28 30–31.
- Wasserbauer, R., Beranova, M., Vancurova, D., Dolezel, B., January 1990. Biodegradation of polyethylene foils by bacterial and liver homogenates. *Biomaterials* 11, 36–40.
- Watt, D.R., 2001. Miragel Sponge Complications. www.retina-doc.com/scripts/retina.pl?function=viewquestions&forum=retina,11/07/012001.
- Weaver, K.D., Sauer, W.L., Beals, N.B., 1995. Sterilization induced effects on UHMWPE oxidation and fatigue strength. In: *Trans. 21st Annual Meeting Soc. Biomater.*, March 18–22, p. 114.
- Wiggins, M.J., Anderson, J.M., Hiltner, A., 2003. Biodegradation of polyurethane under fatigue loading. *J. Biomed. Mater. Res. Part A* 65A (4), 524–535.
- Williams, D.F., 1982. Review: biodegradation of surgical polymers. *J. Mater. Sci.* 17, 1233–1237.
- Williams, D.F., 1989. *Definitions in Biomaterials*. Amsterdam Elsevier.
- Wright, J.I., March 1, 2006. Using Polyurethanes in Medical Applications, Medical Device and Diagnostics Industry. QMed. <https://www.mddionline.com/using-polyurethanes-medical-applications>.
- Wu, L., Weisberg, D.M., Runt, J., Felder III, G., Snyder, A.J., et al., 1999. An investigation of the *in vivo* stability of poly(ether urethane urea) blood sacs. *J. Biomed. Mater. Res.* 44, 371–380.
- Zaikov, G.E., 1985. Quantitative aspects of polymer degradation in the living body. *JMS Rev. Macromol. Chem. Phys.* C25 (4), 551–597.
- Zhang, Z., Marois, Y., Guidoin, R., Bull, P., Marois, M., et al., 1997. Vascugraft® polyurethane arterial prosthesis as femoro-popliteal and femoro-peroneal bypass in humans: pathological, structural and chemical analyses of four excised grafts. *Biomaterials* 18, 113–124.
- Zhao, Q., Agger, M., Fitzpatrick, M., Anderson, J., Hiltner, A., et al., 1990. Cellular interactions with biomaterials: *In vivo* cracking of pre-stressed pellethane 2363-80A. *J. Biomed. Mater. Res.* 24, 621–637.
- Zhao, Q., Topham, N., Anderson, J.M., Hiltner, A., Lodoen, G., et al., 1991. Foreign-body giant cells and polyurethane biostability: *In vivo* correlation of cell adhesion and surface cracking. *J. Biomed. Mater. Res.* 25, 177–183.
- Zhao, Q.H., McNally, A.K., Rubin, K.R., Renier, M., Wu, Z., et al., 1993. Human plasma α 2-macroglobulin promotes *in vitro* oxidative stress cracking of Pellethane 2363-80A. *Biomed. Mater. Res.* 27, 379–389.
- Zhao, Q., Casas-Bejar, C., Urbanski, P., Stokes, K., 1995. Glass wool-H₂O₂/COCl₂ for *in vitro* evaluation of biodegradative stress cracking in polyurethane elastomers. *J. Biomed. Mater. Res.* 29, 467–475.
- Ziats, N., Miller, K., Anderson, J., January 1988. *In vitro* and *in vivo* interactions of cells with Biomaterials. *Biomaterials* 9, 5–13.

Chapter Questions

- Hydrophobic polymer biomaterials designed both to degrade and to be stable in vivo may produce sub-micron particles during use. What are issues with the host responses that are common to the degradation of both types of polymers?
- Consider the degradation of materials commonly used in medicine that do not have well-defined breakdown mechanisms. Some examples include poly(ethylene glycol), hydroxyapatite, and some polysaccharides. How does the body deal with these common materials?
- A new class of biomaterials is now under development that degrades on cue. The cue might be thermal, photonic, or enzymatic. Ingenious chemical design principles are being applied to create such materials, but how might the body react to the products generated by a sudden breakdown of the structure?
- Learn about new strategies to stabilize materials against degradation, for example, vitamin E loading of orthopedic polymers, and incorporation of poly-isobutylene segments into elastomers.
- Endovascular stents are among the most widely used of all medical devices (Chapter 2.5.2B). A new generation of biodegradable stents is expected to have a huge impact on cardiovascular therapies. Consider how biodegradable poly(lactic acid) or magnesium or iron will perform in the complex intravascular environment.
- For a medical device intended for years of service, especially a device where failure can lead to death, how can we test and qualify the device for the expected period of service? Are there useful in vitro tests? Are there relevant and justified animal models?
- Henry Petroski and other authors have discussed the important role of failure in advancing engineering design. Consider medical device failure, past and present, associated with degradation, and how these unintended complications will lead to better medical devices. A few examples include the degradation of polyurethane pacemaker leads, the breakdown of a protective sheath on the tailstring of the Dalkon Shield IUD, and the wear debris associated with the oxidation of ultrahigh-molecular-weight polyethylene in hip prostheses.

2.4.3

Metallic Degradation and the Biological Environment

JEREMY L. GILBERT

Department of Bioengineering, Clemson University, Charleston, SC, United States

Introduction

Metallic biomaterials experience degradation in the biological environment with a rate, form, and extent of damage accumulation that depends on the alloy, its surface structure and properties, and the mechanical, chemical, and biological processes ongoing adjacent to the alloy surface. Some alloys (e.g., magnesium alloys) degrade rapidly and are under consideration as “biodegradable” alloys where the implant is designed to be temporary and is removed by electrochemical processes over time, while other alloys (e.g., stainless steel, titanium, and cobalt–chromium–molybdenum alloys) are not intended to degrade and are meant to survive for the life of the patient. Such distinctions are important to understand and consider when making medical devices out of medical alloys. Alloys intended for degradation, including magnesium, zinc, and others, are rapidly corroding metals, while those intended for lifetime performance in the human body are highly corrosion resistant. The materials factors dictating such differences in performance include the basic concepts of electrochemistry where both the thermodynamics of oxidation (i.e., the driving force for oxidation) and the kinetics of oxidation governed primarily by the presence of passive oxide films on the surface are important.

Generally, metal alloys are used in the body to provide mechanical support and to resist fatigue, wear, and corrosion processes in various medical device applications. In some circumstances, metals serve an electrical or electrochemical role (e.g., as an electrode). When considering degradation of metals in the body, the processes of most concern typically relate to tribology (wear processes), corrosion, and fatigue (Gilbert, 2017). This chapter will focus on the tribology–corrosion–biology interactions that may arise in a range of medical device applications where metals are used.

The biological system affects the potential forms of metal alloy degradation (tribology and corrosion) and is

variable with location (skeletal tissue, cardiovascular, etc.). The effects of degradation on the biological system and the effects of the biological system on degradation are both important and central to the complex interplay that often results in failure of a medical device. The basic mechanisms of degradation of metal surfaces will be discussed and the conjoint interaction between processes, and the interplay between the biological system and the degrading alloy will be discussed in this chapter.

The Severe Biological Environment (Fatigue, Tribology, Corrosion, and Biology)

Metallic biomaterials are used in a wide range of applications where high cyclic stresses, tribological interactions, and exposure to body solutions, biological molecules, tissues, and cells are all present. This combination of factors is most easily recognized in total hip prostheses, where tribology, corrosion, and fatigue are experienced in a biological environment that can be inflamed and reactive. Typical hip implants used in the recent past (Fig. 2.4.3.1) have been comprised primarily of Ti–6Al–4V hip stems, CoCrMo necks and heads, CoCrMo acetabular liners, and Ti–6Al–4V acetabular shells. The combination of harsh body environment, comprised of local biological solutions, inflammation and inflammatory cells, and a range of proteins, enzymes, cytokines, etc., the large mechanical stresses due to activities of daily living, and the wear and corrosion mechanisms that arise can lead to large-scale, severe tribologically based and corrosion-based damage. In most cases these two combine to form a conjoint degradation mechanism known as mechanically assisted corrosion (MAC) and tribocorrosion (Gilbert et al., 1993; Swaminathan and Gilbert, 2012; Cao and Mischler, 2018; Mischler and Debaud, 1998).

the solution, resulting in currents (electronic and ionic) through both phases.

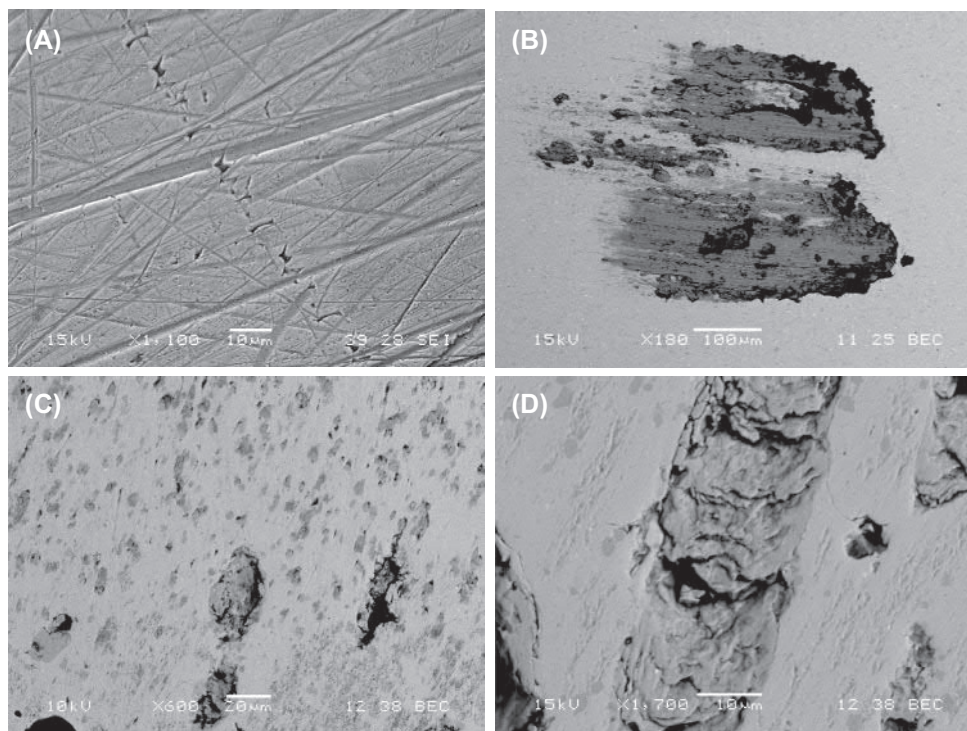
Corrosion, in and of itself, does not define failure of the metallic implant. Failure, clinically, is more appropriately defined as the need to remove the device (metal) due to a clinically defined failure mode (e.g., pain, loosening, infection, adverse biological reaction, etc.). Thus while corrosion may be associated with failure, it is likely that other biologically based processes (e.g., adverse local tissue reactions) lead to the clinical conditions for revision. It is often difficult to determine the causal relationships between materials-based damage modes and biological processes leading to inflammation, pain, and ultimately revision. However, corrosion is a nearly universal observation in metallic biomaterials (i.e., all metals corrode to some extent). It is often the case that these metals, even though they are corroding, can perform their function and not lead to clinically significant failure modes. Indeed, biocompatibility is not the absence of degradation and even with such degradation processes (which are inevitable), the biomaterials can perform their function with an appropriate host response, making them biocompatible.

The biological environment adjacent to the metallic biomaterial may change with time from implantation, where highly inflammatory wound-healing mechanisms are at play, to chronic inflammatory conditions often associated with ongoing degradation processes. That is, there are feedback

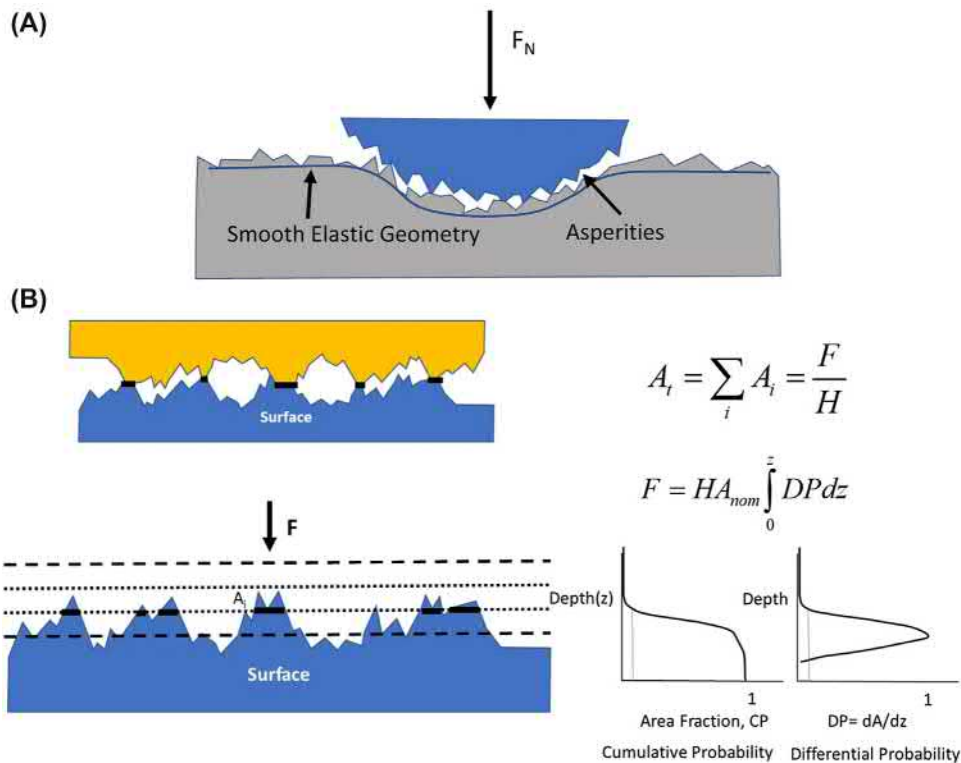
systems that may develop between the immune system response and the degradation mechanisms that can accelerate degradation of the metal and/or amplify the immune reaction. Such positive feedback systems and conditions are currently under active investigation for metallic biomaterial interactions with the living system (FDA, 2019).

Tribological Aspects of Metal-Hard Contact Degradation

From a tribological perspective, the contact and movement of metallic biomaterial surfaces relative to other surfaces can lead to wear processes of the metal (oxide) surface that include adhesive, abrasive (second and third body), and fatigue wear mechanisms (discussed in Chapter 1.2.4 of this text). Examples of CoCrMo alloy surfaces from retrieved total hip metal-on-metal implants, Fig. 2.4.3.3, show examples of abrasive, adhesive, and fatigue wear damage. When metals make contact with other metals or other hard contacting surfaces, the tribological interaction has a number of unique elements that require special consideration. This includes the fact that hard second-phase particles (e.g., oxides and carbides) may become free and serve as third body wear particles. These may roll or slide across the interface and imprint or scratch the surface (Fig. 2.4.3.3A). Adhesive wear interactions between CoCrMo and Ti-6Al-4V (Fig. 2.4.3.3B) are also possible where the



• **Figure 2.4.3.3** (A) Evidence of abrasive wear damage on a CoCrMo head-bearing surface. (B) Adhesive wear of Ti-6Al-4V debris (darker gray) onto CoCrMo femoral head (lighter gray). (C) and (D) Fatigue wear of CoCrMo metal-on-metal acetabular-bearing surfaces from retrieved total hip replacements. Note, evidence of abrasive wear (scratching) and of rolling hard particle imprinting in (A). In (B), the Ti alloy debris is a reacted oxide debris that came from entrainment of Ti alloy into the bearing surface from other components of the implant. In (C) and (D), fatigue wear arose from the high cyclic contact stresses near the edge of the acetabular component, the debris oxidized and partially refilled the region where the fatigue fracture occurred.



• **Figure 2.4.3.4** Schematic of an asperity–asperity contact between two hard surfaces. While the nominal stresses that arise may fall within the elastic range, the stresses at the asperity contact points rapidly reach the hardness or surface yield strength of the material and plastically deform.

titanium alloy and its degradation products can adhere to the CoCrMo surface in an oxidized form. Fatigue wear results from high cyclic contact stresses inducing fatigue fracture of the metal in the subsurface region and loss of alloy particles from the surface (Fig. 2.4.3.3C,D). The remnant holes can be partially refilled with oxidized tribocorrosion debris. In all wear cases that breach the oxide film in the body, there is a corresponding oxidation reaction that accompanies the wear damage resulting in repassivation of the oxide. Thus wear of these metals in the body is always associated with corrosion processes. It is important to note that not all tribological interactions of a metal surface result in breaching of the oxide film. It is only when the metal surface is abraded such that plastic deformation of the surface occurs that oxide films are disrupted. Thus wear against materials softer than the metal will not typically induce oxide film disruption. However, if there are hard particles (as hard as or harder than the metal surface) embedded within softer (polymeric) materials, then such third body particles can induce oxide film disruption and repassivation reactions on the alloy surface.

The three main nonbiodegradable alloy systems (titanium, cobalt–chromium–molybdenum, and stainless steel) are all passive oxide film-covered alloys. As such, contact of the metal surface involves these few nanometer-thick oxides and the immediately adjacent metallic grains contacting the opposing surface in an asperity–asperity contact condition. Even the smallest (nanometer or smaller) topographies give rise to localized asperities of the metal oxide surface, which will influence the contact conditions across the interface

(Fig. 2.4.3.4). Thus the stress developed at these asperities quickly rises to the level of the yield stress (or hardness) of the surface and can induce localized plastic deformation. While the overall stress distribution may be nominally elastic, these local asperities experience plastic deformation and may cause disruption of the oxide film on these surfaces due to the local plastic deformation at and near the contacting asperities.

Metal-on-Metal (Hard) Surface Mechanics

In many circumstances, metal surfaces within the body come into contact with other hard surfaces (metals, ceramics, etc.). These metal–hard contact regions have several unique mechanical aspects to them that need to be clearly understood in terms of the contacting conditions and the associated corrosion and tribocorrosion processes that may arise. First, it has been generally acknowledged that the contact mechanics of metal–hard surfaces can be, to first approximation, modeled in terms of Hertzian elastic contact where geometrically smooth surfaces are in contact (e.g., sphere on sphere, flat on sphere, etc.). For two elastic spheres of radius R_1 and R_2 , in contact with a force, F , there is elastic deformation of both spheres to develop a circular contact area, A , with radius of contact, a , where a is

$$a = \left(\frac{3FR}{4E^*} \right)^{1/3} \quad (2.4.3.1)$$

where the effective radius, R , is

$$\frac{1}{R} = \frac{1}{R_1} + \frac{1}{R_2} \quad (2.4.3.2)$$

and the reduced modulus for the two materials is

$$\frac{1}{E^*} = \frac{1 - \nu_1^2}{E_1} + \frac{1 - \nu_2^2}{E_2} \quad (2.4.3.3)$$

The average stress, $\sigma = F/A$, and the stress across the contact is distributed as

$$\sigma = \sigma^{\max} \left(1 - \left(\frac{r}{a} \right)^2 \right)^{1/2} \quad \text{and} \quad \sigma^{\max} = \frac{3F}{2A} \quad \text{where} \quad A = \pi a^2 \quad (2.4.3.4)$$

It is commonly thought that such analyses apply to metal–metal, or metal–hard contacts, and while the overall stress interaction is typically elastic when metals are in contact, there is an important role played by asperities (small-scale protruding features on the metal and other surfaces, see Fig. 2.4.3.4) that modify this conceptual framework. As shown in Fig. 2.4.3.4, when a hard sphere with asperities comes into contact with a metal surface also with small asperities present, the overall geometric deformation follows Hertzian contact; however, the local stresses at the peak asperities are more severe. At these asperities, the stresses quickly rise to the hardness (H) or yield stress of the metal surface and induce plastic deformation (dislocation motion) at and near the surface (Popov, 2010). When considering metal–hard surfaces, the true area of contact is dictated not by the Hertzian analysis, but rather by this asperity–asperity yielding process. This is shown schematically in Fig. 2.4.3.4B (bottom), where a smooth flat hypothetical surface is brought into contact with a random asperity-based surface. In this case, the highest asperities contact first and the contact stress in these asperities rises to the yield point, deforming the asperities plastically and allowing the next highest asperities to come into contact. This continues, with each asperity quickly reaching the yield stress of the surface, until the true area of contact is just the amount of asperity area needed to carry the applied load, F . That is, the true area of contact is given by $A = F/H$, where H is the hardness of the alloy that is yielding. Typically, the true area of contact of metal–hard surfaces is only a small fraction of the nominal (or even the Hertzian-based) contact area. The distribution of asperity heights in the surface can be defined by the cumulative probability (CP) function as the fraction of the area at a particular height, z , that is occupied by the material of the surface. This distribution varies from 0 to 1. The differential probability is simply the derivative of the CP and shows the height-based distribution of asperities. This differential probability function describes the area contact of two hard asperity–asperity contacting conditions (Fig. 2.4.3.4).

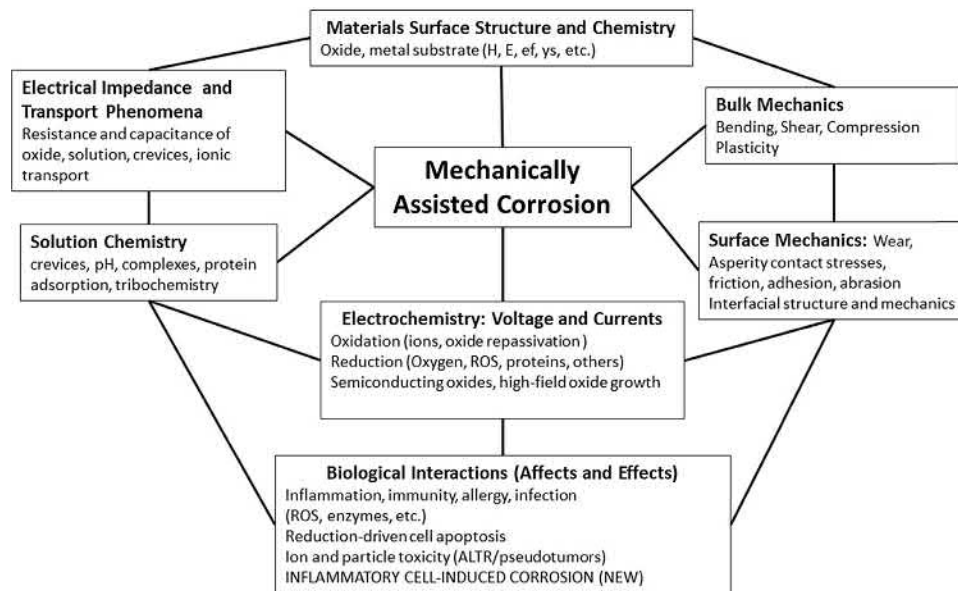
When tribological events occur (e.g., sliding of the two surfaces), it is the interaction of asperities that dominates the overall wear processes with the highest contacting regions experiencing damage and degradation. The oxide films on these interacting asperities will be disrupted by plastic deformation processes and the sliding will expose fresh metal to oxidation (releasing ions and repassivating the surface) and to generation of oxidized particles of debris.

Clinically Observed Mechanically Assisted Crevice Corrosion (Fretting Crevice Corrosion) In Vivo

One of the most studied and clearly identified degradation mechanisms associated with metallic biomaterials is a process known as mechanically assisted crevice corrosion (MACC, see Fig. 2.4.3.5 for a description of the complex multifactorial processes associated with this conjoint degradation mechanism). This term arose from the study of modular tapered junctions in total hip implants in the 1990s up to the present time. It is a degradation process that combines mechanical processes, particularly fretting, with corrosion processes and often involves crevice-like geometries where the local solution chemistry can be dramatically altered from the bulk environment by reactions at the surface. The biological system, its reaction to the alloy degradation, and its affect upon the degradation is also a critical aspect of this conjoint process.

MACC was first identified in modular tapered total hip replacements where the head of the prosthesis is attached to the stem by way of a conical tapered section called a modular taper junction. The surgeon assembles these parts during implantation surgery by impacting the head on to the neck. The junction between these two parts results in a crevice geometry into which body fluids can penetrate and fretting within the junction causes oxide abrasion/disruption at the asperity–asperity contacts leading to a tribocorrosion process. Such fretting crevice corrosion processes are also observed in other orthopedic implants, fracture fixation devices, dental implants, and any other cases where metal–metal contact is possible. The asperity–asperity nature of metal–metal junctions, described earlier, results in only a few percent of the nominal taper contact area being in actual contact, and the remaining space results in a crevice geometry into which solution can penetrate. During loading, high cyclic stresses induce fretting motion, asperity–asperity sliding, and fretting crevice corrosion.

Modular tapers often consist of different alloys coming into contact and concerns have been raised about the possibility of galvanic effects between, for example, Ti–6Al–4V and CoCrMo. However, these concerns are overstated. Typically, galvanic interactions occur between two alloys with significantly different electrode potentials (open circuit potential, OCP), where the more active (negative) potential alloy will experience an increased rate of corrosion, while the more noble (positive) potential alloy will be protected



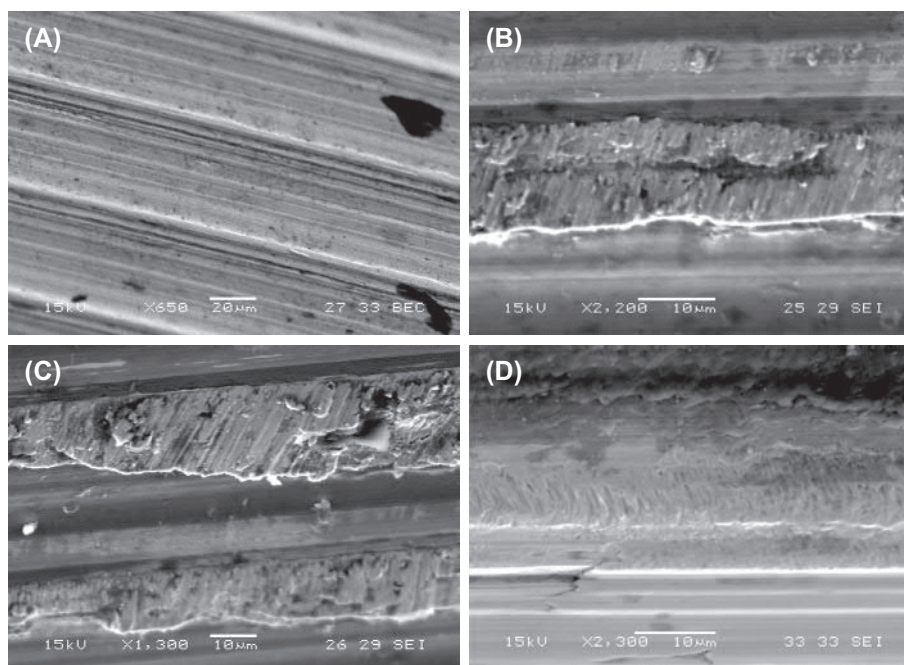
• **Figure 2.4.3.5** Schematic description of the interdisciplinary nature of mechanically assisted corrosion of metallic biomaterials. Knowledge across a range of disciplines is required to understand the *in vivo* interactions of metal surfaces, wear and corrosion-based degradation, and the biological environment. It includes materials science, bulk and surface mechanics, electrical and transport phenomena, and electrochemistry, all within a biological system that is both reactive to the degradation and contributing to the accelerated attack possible. *ALTR*, Adverse local tissue reaction; *ROS*, reactive oxygen species; *H*, hardness; *E*, Modulus; *ef*, fracture strain; *ys*, yield stress. (Used with permission from Gilbert, J.L., Sivan, S., Mali, S., 2015. Corrosion of modular tapers in total joint replacements: a critical assessment of design, materials, surfaces structure, mechanics, electrochemistry and biology. In: Greenwald, K., Lemons, M. (Eds.), ASTM Special Technical Publication on Implant Modularity, STP 1591. ASTM Int, 192–223.)

and will see a decreased rate of corrosion. Titanium and CoCrMo alloys, with passive oxide films intact, have very similar OCPs, thus little galvanic potential exists for increasing corrosion. In addition, if any difference in OCP exists, it is typically that Ti is more active and CoCrMo is more noble, thus it would be the titanium that would be accelerated in its corrosion. The passive oxide films also serve as a kinetic barrier to corrosion and limit galvanic effects (Jacobs et al., 1998). When modular tapers of Ti–6Al–4V and CoCrMo are examined, both the titanium and the CoCrMo are corroded and there is no evidence that either protects the other. Finally, MACC is observed in all possible alloy combinations and thus is not dependent on any galvanic effects. Therefore galvanic corrosion, while a mechanism that may play out in some circumstances (e.g., corrosion near carbides vs. bulk alloy, for example), does not contribute significantly to the MACC mechanism.

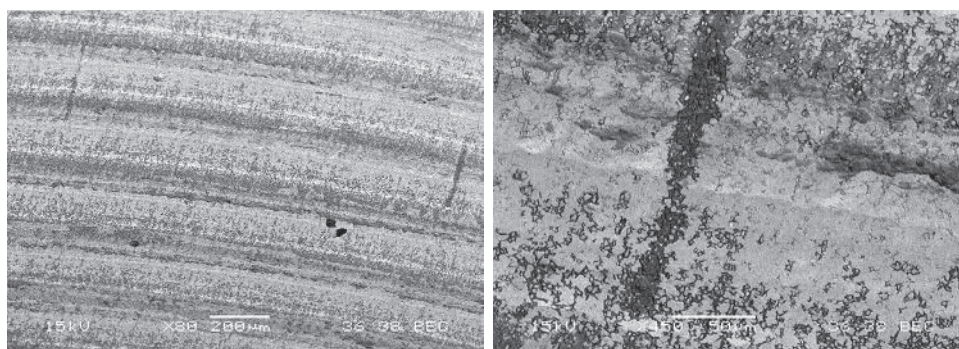
Examples of the type of damage resulting from MACC are shown in Figs. 2.4.3.6–2.4.3.8, where fretting damage, intergranular corrosion, direct oxide conversion, and pitting of CoCrMo and/or Ti–6Al–4V are all observed. Fig. 2.4.3.6 demonstrates the basic fretting damage that results in small parallel abrasion patterns due to asperity–asperity contact and cyclic micromotion. Examples of more severe fretting corrosion damage in Fig. 2.4.3.6 show generation of oxide debris that accumulates within the taper region. Fig. 2.4.3.6A is an undamaged region of a CoCrMo head taper after retrieval. Fig. 2.4.3.6B–D are examples demonstrating

minor fretting damage resulting primarily from contact and motion.

Fig. 2.4.3.7 shows an example of the more severe corrosion that can arise in CoCrMo alloy modular tapers resulting from MACC where fretting corrosion within the crevice led to intergranular corrosion that is affiliated with the imprinting of the male trunnion. Intergranular corrosion at the grain boundaries of this high-carbon CoCrMo alloy surface is evident. Examples of corrosion damage in Ti–6Al–4V alloy modular taper junctions, Fig. 2.4.3.8, show the severe damage possible *in vivo* for these alloy systems. Fig. 2.4.3.8A is a scanning electron micrograph of a retrieved Ti–6Al–4V acetabular shell taper region (CoCrMo alloy was on the other side). Note the pitting and dissolution of the surface. Fig. 2.4.3.8B–D are scanning electron micrography (SEM) micrographs of sectioned regions through the taper junction of Ti–6Al–4V alloy modular body tapers (where Ti–6Al–4V was on both sides of the taper). These micrographs show the corrosion reaction leading to several hundred micron-thick oxide corrosion products (Fig. 2.4.3.8B), a sectioned region through a large (200 μm) pit in Ti–6Al–4V filled with oxide, and a section through a Ti–6Al–4V/Ti–6Al–4V alloy junction still intact (Fig. 2.4.3.8D), where about 10 μm of oxide formation has occurred at the taper junction. These images show that Ti alloys are susceptible to severe corrosion damage under MACC circumstances. The fretting corrosion aspects of MACC have been extensively



• **Figure 2.4.3.6** Evidence of fretting crevice corrosion in retrieved modular head/neck tapers of total hip replacements. (A) Undamaged machining ridges in a retrieved modular CoCrMo head taper. (B)–(D) Examples of minor fretting damage seen in retrieved CoCrMo head components.



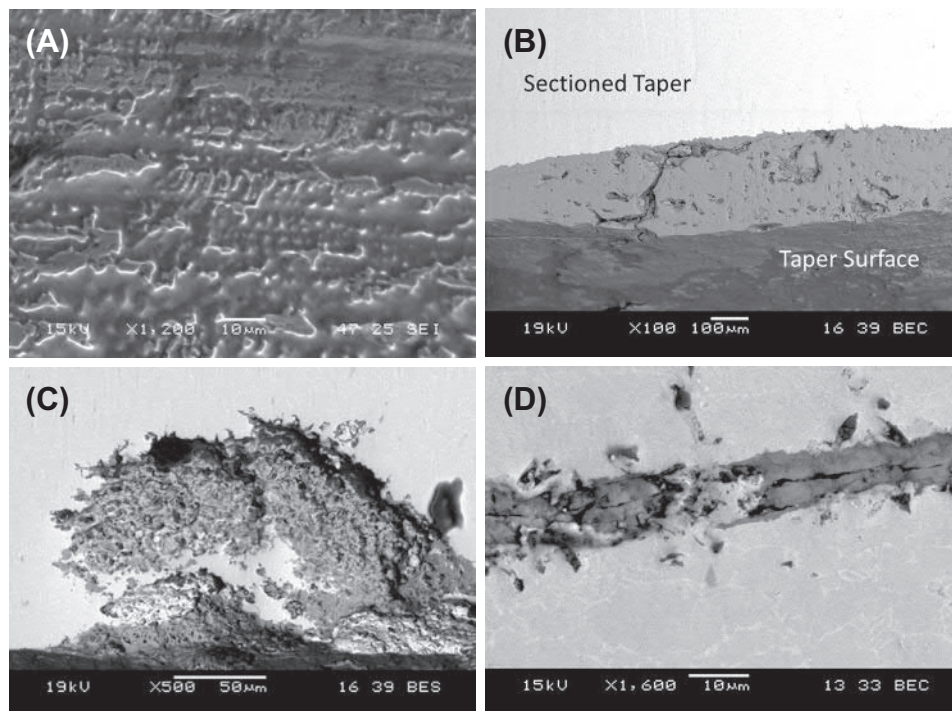
• **Figure 2.4.3.7** Retrieved CoCrMo head taper with extensive intergranular corrosion damage associated with mechanically assisted crevice corrosion. Corrosion damage around the grain boundaries and between the alloy and the second-phase particles is evident and associated with the fretting-based imprinting from the countersurface.

studied and reproduced in device and basic pin-on-disk tests. However, the severe corrosion damage of both CoCrMo and Ti–6Al–4V alloys seen in these retrievals (e.g., intergranular corrosion of CoCrMo, thick oxide formation, and pitting in Ti–6Al–4V) has not been reproduced in any in vitro laboratory tests to date that represent the in vivo conditions, and the detailed conditions and mechanisms of generation of this type of damage are still under investigation.

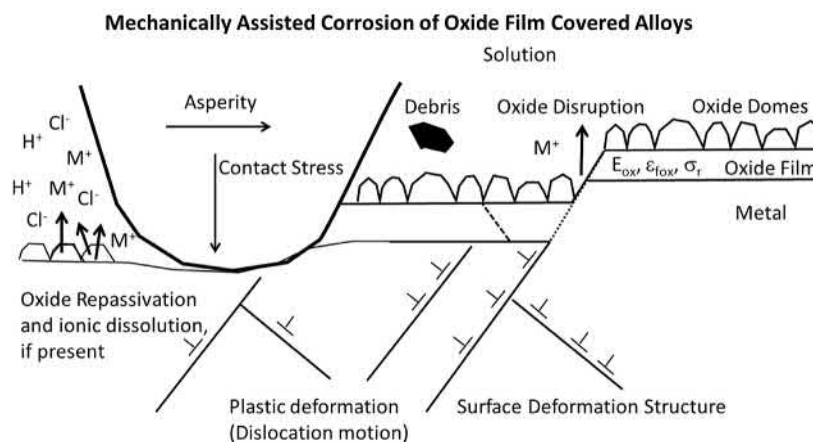
Mechanically Assisted Corrosion Basics for CoCrMo and Ti–6Al–4V Alloys

MACC is a conjoint degradation process (Fig. 2.4.3.9) that combines mechanics, materials, surfaces, chemistry, and biology. A hard asperity makes contact with the metal

oxide passive film-covered surface where the contact stresses reach the yield point of the substrate. This results in disruption (removal) of the oxide film covering the surface and generates oxide-based debris that can be released from the surface. Metal ions may be released into the solution from the regions where the oxide film has been removed; however, these regions rapidly repassivate (within milliseconds) and return the surface to a passive state. Because the contact stresses reach or exceed yielding, the substrate alloy undergoes plastic deformation (dislocation motion) of the near-surface region, which can work harden the outer alloy layer and develop very high dislocation densities. The corrosion reactions present are associated with both the ionic release of metal and the reaction of metal with oxygen and water for form metal oxides (repassivation). These reactions, because they involve the liberation of electrons, result in currents that can be detected and used to monitor the



• **Figure 2.4.3.8** Examples of corrosion damage in retrieved Ti-6Al-4V alloy components. (A) Ti-6Al-4V shell taper from a retrieved acetabular component. (B)–(D) examples of retrieved, sectioned Ti-6Al-4V alloy-corroded taper regions that show thick oxide formation (B), pitting (C), and direct conversion of the alloy (bright regions) to oxide (darker gray region in center). All examples were from retrieved components demonstrating in vivo corrosion damage. (Fig. 2.4.3.8B,C are used with permission from Gilbert, J.L., Mali, S.A., Urban, R.M., Silverton, C.D., Jacobs, J.J., 2012. In-vivo oxide-induced stress corrosion cracking of Ti-6Al-4V in a neck-stem modular taper: emergent behavior in a new mechanism of in-vivo corrosion. *J. Biomed. Mater. Res. B Appl. Biomat.* 100B(2), 584–594.)

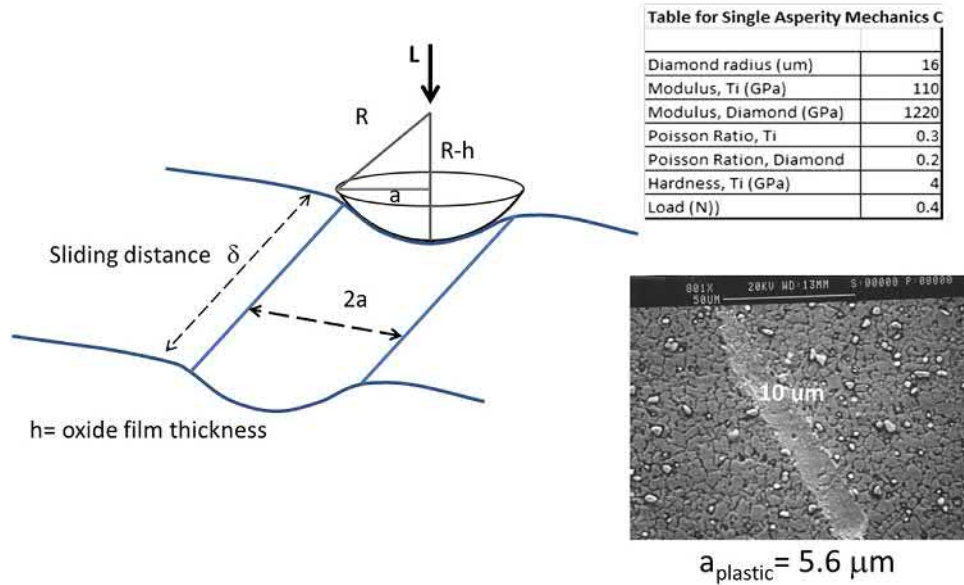


• **Figure 2.4.3.9** Schematic of mechanically assisted crevice corrosion. (Reprinted with permission. Adapted from Gilbert, J.L., Sivan, S., Mali, S., 2015. Corrosion of modular tapers in total joint replacements: a critical assessment of design, materials, surfaces structure, mechanics, electrochemistry and biology. In: Greenwald, K., Lemons, M. (Eds.), *ASTM Special Technical Publication on Implant Modularity*, STP 1591. ASTM Int, 192–223 and Gilbert, J.L., Mali, S., 2012. Medical implant corrosion: electrochemistry at metallic biomaterial surfaces, *Degradation of Implant Materials*. In: Eliaz, N. (Ed.), Springer Press, New York, NY.)

corrosion processes arising from mechanical disruption of the surface. Reduction reactions are also present, but can be remote from the site of abrasion.

Much has been learned about MACC from retrievals, but also from fundamental studies of oxide film disruption and repassivation tests that include high-speed single

asperity scratch tests (Gilbert et al., 1996; Goldberg et al., 1997; Goldberg and Gilbert, 2004), to pin-on-disk fretting corrosion tests (Swaminathan and Gilbert, 2012, 2013), and in vitro implant tests (Goldberg and Gilbert, 2003; Gilbert et al., 2009 Jan; Mali and Gilbert, 2015). These tests have, for example, shown that during oxide



• **Figure 2.4.3.10** Schematic of the area abraded analysis based on plastic deformation. Scanning electron micrography micrograph is of a 16 μm radius diamond stylus scratching a high-carbon CoCrMo alloy surface under a controlled load (0.4N). The width of the permanent scratch is determined by the hardness (4 GPa) and the normal load applied.

disruption, the corrosion reactions release free electrons into the metal (due to oxidation), which accumulate within the metal electrode and cause a negative excursion in potential. These electrons are eventually consumed in reduction reactions; however, it is well known that the open circuit potential of alloys engaged in MAC can drop significantly. The potential drop is limited by the potential where metal oxide films will begin to form (passivation potential). For titanium this potential is -1 V versus Ag/AgCl, while it is about -0.5 to -0.8 V for CoCrMo. The amount the potential drops in these cases depends on the rate of oxide abraded (and repassivated), the amount of available area for the reduction reactions to take place, and the kinetics of the reduction reaction. These effects are also reflective in the changes in impedance of the electrode where larger area electrodes have lower resistances and higher capacitances that will affect the extent of voltage change (Gilbert et al., 2016). In addition, the thickness of passive oxide film that repassivates depends primarily on the electrode potential above the passivation potential. This thickness is linearly dependent on the electrode potential difference (when within the passive range of the oxide). Thus the potential of the metal changes with MACC and the changing potential affects the repassivation processes, and these effects may have significant impacts on the nature of the corrosion damage observed (Figs. 2.4.3.6–2.4.3.8).

There are a number of models under development to describe the tribocorrosion behavior of passive film-covered alloys. These rely on the processes of oxide disruption and current arising from film growth (repassivation) and ionic dissolution (Gilbert et al., 1996; Goldberg et al., 1997). The mechanics of abrasion relate to asperity contact and sliding mechanics (Swaminathan and Gilbert, 2012). Here, a hard

(rigid) spherical single asperity of some radius, R , indenting into a surface will penetrate to some load-dependent depth and will result in a contact area (Fig. 2.4.3.10) of

$$A_{\text{contact}} = \pi a^2 = \left(\frac{L}{H}\right) \quad \text{or} \quad a_{\text{contact}} = \left(\frac{L}{\pi H}\right)^{1/2} \quad (2.4.3.5)$$

where a is the contact radius, L is the normal load, and H is the hardness of the metal. When this asperity slides some distance, δ , then the area abraded is twice the contact radius times the sliding distance:

$$A_{\text{abraded}} = 2a\delta = 2\delta \left(\frac{L}{\pi H}\right)^{1/2} \quad (2.4.3.6)$$

and the volume of oxide abraded (and repassivated) is

$$V_{\text{abraded}} = A_{\text{abraded}}h = 2\delta \left(\frac{L}{\pi H}\right)^{1/2} h \quad (2.4.3.7)$$

Since the repassivation rate is typically much faster than the rates of abrasion of the oxide, the sliding abrasion is the rate limiting step in the generation of currents resulting from MACC. The current due to film formation can be found by determining the volume of oxide film disrupted per unit time (which corresponds to the volume reformed) times the charge per unit volume of oxide created by the oxidation reactions. The volume of oxide abraded (disrupted) depends on the true contact area diameter times the sliding distance per unit time times the oxide film thickness:

$$I(t) = \frac{\rho n F d V}{M w dt} \quad (2.4.3.8)$$

TABLE 2.4.3.1 Physical Properties for TiO₂, CoCrMo, and 316L SS Oxides (Based on Alloy Composition)

	TiO ₂	CoCrMo Oxide	316L SS	Units
ρ	4.45	6.06	5.81	g/cm ³
n	4	2.37	2.9	
M_w	79.9	76.91	130.09	g/mol
m	1.8	2.0	2.0	nm/V
E_o	-1,000	-500	-100	mV
$\rho n F / M_w$	21,498	18,020	12,498	C/cm ³

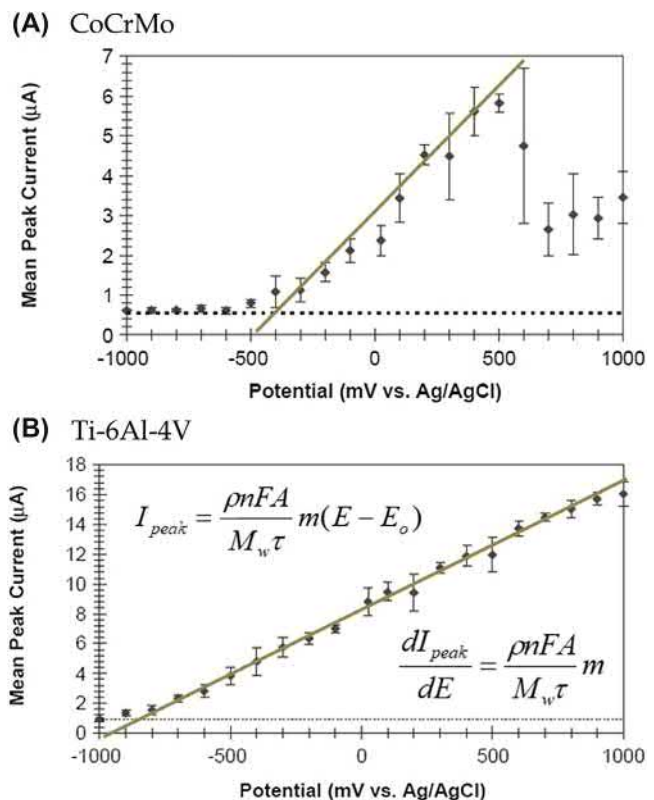
where:

$$\frac{dV}{dt} = h \frac{dA}{dt} = 2h \sqrt{\frac{L}{\pi H}} \frac{d\delta}{dt} \quad (2.4.3.9)$$

Here, δ is the sliding distance, L is the normal load, H is the hardness of the alloy, and h is the thickness of the oxide film. The film thickness, h , varies linearly with potential above the passivation potential by about 2 nm/V (known as m , the anodization rate, see Table 2.4.3.1) and with these, one can obtain the current that arises from oxide film abrasion. Table 2.4.3.1 summarizes the various physical properties of the oxides of Ti, CoCrMo, and 316L SS used in the estimation of currents arising from tribocorrosion processes.

For example, if 1 mm² of oxide (2 nm thick) is abraded and reformed on titanium in 1 s, the associated currents would be about 43 μ A of current. This analysis ignores the currents arising from ionic dissolution reactions as these currents are typically much smaller than the film currents (Gilbert et al., 1996; Goldberg et al., 1997). As a comparison, the currents typically measured in fretting corrosion tests of modular tapers are on the order of 1–10 μ A, or about 0.1 mm² abraded area per second. This shows that currents that result from MAC can be highly sensitive to the rate of the area abraded, that the true contact area undergoing oxide disruption is only a small fraction of the nominal area, and that monitoring of these currents is an excellent means for assessing the damage process in experimental setups.

The thickness of oxide film reformed depends on the potential. It must be above the passivating potential to form oxide and for CoCrMo and 316L SS must be below the breakdown potential for the alloy (about +500 mV vs. Ag/AgCl). If the potential exceeds this latter potential, then the passive film is no longer passive and this analysis does not hold. The variation of single asperity scratch current with potential can be seen in Fig. 2.4.3.11A,B, which are the results of single diamond asperity high-speed scratch tests (Gilbert et al., 1996; Goldberg et al., 1997; Goldberg and Gilbert, 2004) on both CoCrMo and Ti-6Al-4V alloy surfaces. Using controlled loads and scratch distances, the current response as a function of applied potential shows that

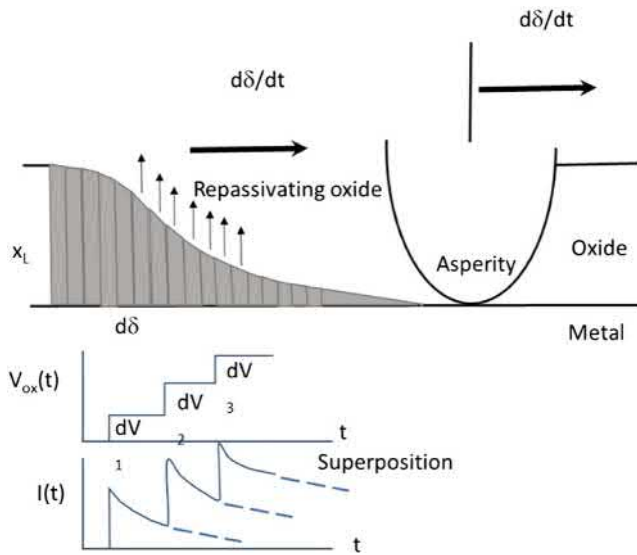


• **Figure 2.4.3.11** Single asperity high-speed scratch test peak currents plotted against applied potential. These plots show the passivation potential for the two alloys and how the peak scratch current varies linearly with potential over the passive range of the alloy. (Adapted with permission from Goldberg, J.R., Gilbert, J.L., 2004. The electrochemical and mechanical behavior of passivated and TiN/AlN-coated CoCrMo and Ti6Al4V alloys *Biomaterials* 25 (5), 851–864.)

there is a lower scratch current with more negative potentials that approach zero at unique potentials (–1 V for Ti-6Al-4V and –0.5 V for CoCrMo), which are the onset potentials or passivating potentials for the respective oxides (primarily TiO₂, Cr₂O₃). The linear increase of current above the passivation potential relates to the linear dependence of the oxide film thickness with potential.

Because MAC processes include tribological factors and electrochemical factors, the details of these interactions are important to study. Test methods, including electrochemical fretting pin-on-disk tests, have been developed to explore the range of interactions present (Swaminathan and Gilbert, 2012, 2013). These studies have shown, for example, that there are effects of potential on the fretting coefficient of friction (Swaminathan and Gilbert, 2012, 2013; Liu and Gilbert, 2017) and that the currents generated during fretting corrosion scale directly with the work of fretting (i.e., the energy dissipated per cycle of fretting motion).

Fretting corrosion currents generated by oxide film disruption and repassivation can be modeled using a heredity integral approach based on the idea (Fig. 2.4.3.12) that an asperity abrasion process can be thought of as consisting of infinitesimal increments of oxide disruption, dV , and repassivation, and that each increment in oxide disruption



• **Figure 2.4.3.12** Schematic of an asperity removing oxide film and the film regrowing where each infinitesimal volume of oxide removal and regrowth results in a current spike and decay transient. The overall current response is the sum (integral) of each of these infinitesimal processes over time and is related to the sliding speed. (Used with permission from Gilbert, J.L., Zhu, D., October, 2019. A tribocorrosion model linking fretting mechanics, currents and potentials: model development and experimental comparison. *J. Biomed. Mat. Res. B Appl. Biomat.* (In Review).)

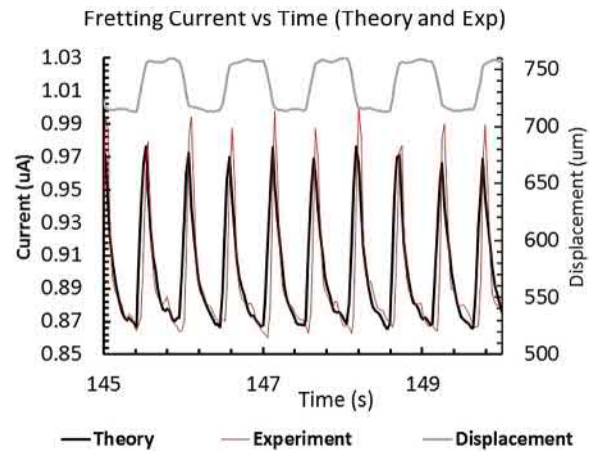
and repassivation results in current transient responses that can be superimposed and summed over time to obtain the full current response. This is similar to the approach of Boltzmann superposition used in viscoelastic theory to predict stresses in a viscoelastic material in response to an arbitrary strain path over time. Here, the currents can be determined from the integral over time of the current transient response of each infinitesimal oxide disruption event. The equation that describes this behavior, known as a Dumahel integral, is

$$I(t) = A^T(t) V(0) + \int_{\lambda=0}^t A^T(t-\lambda) \frac{dV}{d\lambda} d\lambda \quad (2.4.3.10)$$

where V is the oxide volume abraded (and repassivated), λ is a dummy variable in time, and $A^T(t-\lambda)$ is the tribocorrosion admittance (or transfer function) relating currents to volume abraded. This function is

$$A^T(t-\lambda) = \frac{I_0}{V} e^{-\frac{t-\lambda}{\tau}} = \left(\frac{\rho n F}{M_w \tau} + \frac{i_0}{h} e^{\frac{\eta}{\beta_a}} \right) e^{-\frac{t-\lambda}{\tau}} \approx \frac{\rho n F}{M_w \tau} e^{-\frac{t-\lambda}{\tau}} \quad (2.4.3.11)$$

where ρ is the oxide density, n is the valence of the cation, F is Faraday's constant (96,485 C/mol), M_w is the molecular weight of the oxide, h is the oxide thickness, i_0 is the exchange current density for ionic release through bare metal, β_a is the anodic Tafel slope for ionic release, τ is the time constant for the current transient, and η is the overpotential for ionic release. This equation shows that the



• **Figure 2.4.3.13** Comparison of predicted currents and experimental currents resulting from a pin-on-disk fretting corrosion experiment of CoCrMo alloy in phosphate-buffered saline. Tribocorrosion currents can be modeled theoretically with this approach when the potential remains fixed.

current transient that results from an instantaneous removal and repassivation of oxide film will result in an exponential decay of the current and has been developed previously from single asperity high-speed scratch tests of titanium and CoCrMo alloy surfaces in physiologically representative solutions (Gilbert et al., 1996; Goldberg et al., 1997; Goldberg and Gilbert, 2004).

Eq. (2.4.3A.10) describes how the current will vary over time, depending on the rate of volume abraded over time.

This equation predicts the tribocorrosion currents for any arbitrary sliding distance time response and has been verified experimentally (Fig. 2.4.3.13) where step-like displacements of pin-on-disk coupled to CoCrMo/CoCrMo were tested and comparison of the experimental currents with the theoretical currents shows high similarity.

These studies demonstrated that when mechanical disruption of the passive oxide film on titanium and CoCrMo alloys occurs, the resulting corrosion reactions are generated by the repassivation reaction and ionic release and these can be measured and calculated such that the degradation response can be modeled and assessed systematically.

Tribocorrosion Layer and Surface Damage on Metallic Biomaterials Surfaces

Studies of the resultant damage to metal surfaces experiencing tribocorrosion processes have identified a mixed tribocorrosion layer that may form within the top few nanometers of the surface wherein the oxide debris mixes with the alloy to result in a layer of mixed metal, metal oxide, and adsorbed protein (Wimmer et al., 2003, 2010). This tribocorrosion layer may alter the properties of the surface (hardness, corrosion response) and affect subsequent tribocorrosion processes. Other studies have investigated the plastic deformation damage observed in the near-surface alloy grains resulting from fretting contacts. Here, highly deformed surface grains may be induced to undergo strain-induced transformation and/or develop

highly deformed dislocation substructures that appear to be similar to nanocrystalline regions. Such fine crystalline zones may well egress from the surface and be a source of metal particulates released into the surrounding tissues (Oladokun et al., 2019).

Biology and Corrosion: Additional Insights

Starting in the 1970s and 1980s, Hans Willert et al. (1990, 2005) and Jasty and Harris (Jasty et al., 1994) recognized that particulates from a range of biomaterials can induce significant adverse biological reactions. These reactions may be chronic inflammatory reactions, dominated by macrophages, lymphocytes, and foreign body giant cells within granulomatous tissues (Davies et al., 2005), or may result in osteolysis (bone destruction) or soft tissue inflammation. For metallic biomaterials, the effects of tribocorrosion on local tissue responses have only more recently been identified as a result of the introduction of metal-on-metal hip implants. Here, metallic or metal oxide debris generated from tribocorrosion processes may be released into the joint fluid and surrounding joint tissues and be associated with significant adverse local tissue reactions. While the specific causal relationships and mechanisms of interaction are still not well understood, there appears to be an effect of CoCrMo degradation products on the local tissue reaction that is the result of an immunological response to the alloy degradation products (Davies et al., 2005). These effects are described in more detail in other sections of this text (Chapter 2.4.3) and will not be focused on here. However, there are certain interactions between the biological system and metallic biomaterials that merit further attention.

In particular, the biological system can affect the corrosion behavior of these alloys and the electrochemical behavior of the alloys can affect the local biology in ways that have not been fully appreciated. This feedback interaction may be a significant factor in why some people are more reactive to metallic degradation debris than others and why some implants show much more severe corrosion damage than others.

Reduction Reactions Affect Cells

The first new insight has to do with how cells respond to metal surfaces that are held to different electrochemical potentials. Work by Ehrensberger and Gilbert (Ehrensberger et al., 2010), Kalbacova et al. (2007), and Haeri et al. (2012) have shown that preosteoblast-like cells (e.g., MC3T3-E1 preosteoblasts) cultured on titanium and CoCrMo surfaces are highly sensitive to the electrode potential of the metal and, in particular, that cathodic potentials (wherein reduction reactions are taking place) can induce cell death (by an apoptotic process) within a few hours. That is, reduction reactions involving the reduction of oxygen and water induce the killing of cells on or near to the metal surface. It is thought that this killing effect may be the result of

consumption of oxygen, shifting of the near-surface solution to higher pH, and/or the generation of reactive oxygen intermediates (ROS) from the reduction process.

As shown in Fig. 2.4.3.2, reduction of oxygen and water can create small fractions of ROS and these chemistries can have significant effects on cells cultured on the surface (Wiegand et al., 2019). This is true regardless of the alloy. The killing effect occurs for both mammalian cells and bacteria (Ehrensberger et al., 2015). This approach is now being adopted for the possible control of cancer cells (Kim and Gilbert, 2018) or bacterial biofilms on metallic implant surfaces (Ehrensberger et al., 2015). Reduction reactions can be induced on metallic medical devices, and such reactions can kill bacteria on the surface. These observations represent a new and potentially significant means for treating infection. In addition, tribocorrosion processes can induce large drops in potential and the increased associated reduction reactions have also been shown to induce cell killing on the surface (Kubacki et al., 2017). Thus redox reactions not specifically associated with metal ion release or oxide film formation can result in significant cellular effects that are as yet unrecognized and/or understudied.

Recent work (Wiegand et al., 2018) has sought to identify an “electrochemical zone of viability,” which is defined as the electrode potential range wherein cells can remain viable and outside of which cells die. For titanium, cells can remain viable on the surface up to at least +1 V versus Ag/AgCl, but that by -0.4 V and lower, cells will rapidly die. For CoCrMo, the zone of viability is limited to +0.3 V where cells on CoCrMo above this potential rapidly die by necrosis and metal ion toxicity, while below -0.4 V cells die by reduction-induced apoptosis. These zones of viability may also be dependent of cell type (Wiegand et al., 2018) where it has been shown that macrophage-like cells can survive for longer periods to more negative potentials than preosteoblast-like cells. This is likely due to their increased ability to control their redox homeostasis in the presence of ROS generated by the electrode surface. Such electrochemical effects on cells may induce a wider range of responses than have been previously understood, and possible sensing and control of systems by electrochemical means remain a potentially important area of study.

Reactive Oxygen Species May Enhance Corrosion Reactions

In addition to the fact that reduction reactions affect biological systems, the effect of immune cell responses on the corrosion of metallic biomaterials is also a new area of focus. In these circumstances, it is hypothesized that the respiratory burst processes associated with a range of phagocytic cells can release a range of ROS and reactive nitrogen species molecules into the near implant space. These oxidizing species, if they come into contact with the alloy surface, have been shown to have significantly deleterious effects on the corrosion resistance, particularly

in CoCrMo alloys (Liu and Gilbert, 2018; Kubacki and Gilbert, 2018). That is, chemistry that includes hydrogen peroxide or hypochlorous acid, or other oxidizing species, lowers the impedance of the oxide films on CoCrMo and titanium alloys and can shift the electrode potential of the metal such that this combined effect can raise the rate of corrosion significantly and alter tribocorrosion processes (Liu and Gilbert, 2017). Such effects may play a significant role in the corrosion behavior of these alloys in vivo and additional work is needed to better understand this corrosion–biology interplay.

Summary

This chapter has outlined the principal means by which metallic biomaterial surfaces undergo degradation in the body. The central role of passive oxide films on these alloys and how mechanical disruption in conjunction with corrosion and biological environments can lead to severe degradation mechanisms. Degradation by corrosion can increase reduction reactions as well and has been shown to have killing effects on nearby cells. Inflammatory species (e.g., ROS) can increase the corrosion response of titanium, CoCrMo, and 316L SS alloys. In all, metal degradation in the biological environment is a complex interplay of conjoint mechanisms and can result in a wide range of damage modes and potential biological outcomes. Our understanding of the tribocorrosion processes present in many metallic implant systems and the physics, chemistry, and mechanics at play will assist in designing metal-based implants for the future.

Acknowledgments

There were many students and colleagues that participated in the development of this work and shared in the efforts to document and characterize the degradation of metals in the body. These include: Joshua J. Jacobs, Robert Urban, Jay Goldberg, Christine Buckley, Mark Ehrensberger, Viswanathan Swaminathan, Shiril Sivan, Jua Kim, Sachin Mali, Greg Kubacki, Yangping Liu, Morteza Haeri, and Michael Wiegand. Their efforts and contributions are greatly appreciated by the author.

References

- Cao, S., Mischler, S., 2018. “Modeling tribocorrosion of passive metals – a review”. *Curr. Opin. Solid State Mater. Sci.* 22, 127–141.
- Davies, A.P., Willer, H.G., Capbell, P.A., Learmonth, I.D., Case, C.P., 2005. An unusual lymphocytic perivascular infiltration in tissues around contemporary metal-on-metal joint replacements. *J. Bone Jt. Surg.* 87A (1), 18–27.
- Ehrensberger, M., Sivan, S., Gilbert, J.L., 2010. “Titanium is NOT “the most biocompatible metal” under cathodic potentials: the relationship between voltage and MC3T3 pre-osteoblast behavior on electrically polarized cpTi surfaces”. *J. Biomed. Mat. Res. A* 93A (4), 1500–1509.
- Ehrensberger, M.T., Tobias, M.E., Nodzo, S.R., Hansen, L.A., Luke-Marshall, N.R., Cole, R.F., Wild, L.M., Campagnari, A.A., 2015. Cathodic voltage-controlled electrical stimulation of titanium implants as treatment for methicillin-resistant *Staphylococcus Aureus* periprosthetic infections. *Biomaterials* 41, 97–105.
- Biological Responses to Metal Implants, US FDA. , September 2019. Center for Devices and Radiological Health. <https://www.fda.gov/media/131150/download>.
- Gilbert, J.L., 2017. Corrosion in the human body: metallic implants in the complex body environment. *Corrosion* 73 (12), 1478–1495.
- Gilbert, J.L., Kubacki, G.W., 2015. “Oxidative stress, inflammation and the corrosion of metallic biomaterials: corrosion causes biology and biology causes corrosion”. In: Dziubla, T.D., Butterfield, D.A. (Eds.), *Oxidative Stress and Biomaterials*. Elsevier Press (Chapter 3).
- Gilbert, J.L., Mali, S., 2012. “Medical implant corrosion: electrochemistry at metallic biomaterial surfaces”. In: Eliaz, N. (Ed.), *Degradation of Implant Materials*. Springer Press, New York, NY.
- Gilbert, J.L., Zhu, D., October, 2019. “A tribocorrosion model linking fretting mechanics, currents and potentials: model development and experimental comparison”. *J. Biomed. Mat. Res. B Appl. Biomat.* In Review.
- Gilbert, J.L., Buckley, C.A., Jacobs, J.J., 1993. In-vivo corrosion of modular hip prosthesis components in mixed and similar metal combinations: the effect of crevice, stress, motion and alloy coupling. *J. Biomed. Mater. Res.* 27 (12), 1533–1544.
- Gilbert, J.L., Buckley, C.A., Lautenschlager, E.P., 1996. “Titanium Oxide Film Fracture and Repassivation: The Effect of Potential, pH and Aeration”, *Medical Applications of Titanium and its Alloys the Materials and Biological Issues*. ASTM Special Technical Publication 1272, American Society for Testing and Materials, Philadelphia, PA, pp. 199–215.
- Gilbert, J.L., Mehta, M., Pinder, B., January 2009. In-vitro fretting crevice corrosion of stainless steel-cobalt chrome modular hip stems: effect of material, assembly and offset. *J. Biomed. Mater. Res. B* 88B (1), 162–173.
- Gilbert, J.L., Mali, S.A., Urban, R.M., Silverton, C.D., Jacobs, J.J., 2012. “In-vivo oxide-induced stress corrosion cracking of Ti-6Al-4V in a neck-stem modular taper: emergent behavior in a new mechanism of in-vivo corrosion”. *J. Biomed. Mater. Res. B Appl. Biomat.* 100B (2), 584–594.
- Gilbert, J.L., Sivan, S., Mali, S., 2015. “Corrosion of modular tapers in total joint replacements: a critical assessment of design, materials, surfaces structure, mechanics, electrochemistry and biology”. In: Greenwald, K., Lemons, M. (Eds.), *ASTM Special Technical Publication on Implant Modularity, STP 1591*. ASTM Int, pp. 192–223.
- Gilbert, J.L., Mali, S.A., Liu, Y., 2016. Area-dependent impedance based voltage shifts during tribocorrosion of Ti-6Al-4V biomaterials: theory and experiment. In: *IOP Surface Topography: Metrology and Properties, Special Topic Issue: Surfaces and Interfaces in Bioengineering Systems* 034002; 1–18.
- Goldberg, J.R., Gilbert, J.L., 2003. In-vitro corrosion testing of modular hip tapers. *Appl. Biomater.* 64B (2), 78–93.
- Goldberg, J.R., Gilbert, J.L., 2004. The electrochemical and mechanical behavior of passivated and TiN/AlN-coated CoCrMo and Ti6Al4V alloys. *Biomaterials* 25 (5), 851–864.
- Goldberg, J.R., Lautenschlager, E.P., Gilbert, J.L., 1997. Electrochemical response of CoCrMo to high speed fracture of its metal oxide using an electrochemical scratch test method. *J. Biomed. Mater. Res.* 37 (2), 421–433.

- Goldberg, J., Gilbert, J.L., Jacobs, J.J., 2002. "A multicenter retrieval analysis of taper fretting-crevice corrosion of modular femoral total hip prostheses". *Clin. Orthop. Relat. Res.* 401, 149–161.
- Haeri, M., Wollert, T., Langford, G.M., Gilbert, J.L., 2012. Electrochemical control of cell death by reduction-induced intrinsic apoptosis and oxidation-induced necrosis on CoCrMo alloy in vitro. *Biomaterials* 33, 6295–6304.
- Jacobs, J.J., Gilbert, J.L., Urban, R.M., 1998. Current concepts review, "corrosion of metal orthopaedic implants". *J. Bone Jt. Surg.* 80-A (2), 268–282.
- Jasty, M., Bragdon, C., Jiranek, W., Chandler, H., Mahoney, W., Harris, W.H., 1994. Etiology of osteolysis around porous-coated cementless total hip arthroplasties. *Clin. Orthop. Relat. Res.* 308, 111–126.
- Kalbacova, M., Roessler, S., Hempel, U., Tsaryk, R., Peters, K., Scharnweber, D., Kirkpatrick, J., Dieter, P., 2007. The effect of electrochemically simulated titanium cathodic corrosion products on ROS production and metabolic activity of osteoblasts and monocytes/macrophages. *Biomaterials* 28, 3263–3272.
- Kim, J., Gilbert, J.L., 2018. In-vitro cytotoxicity of galvanically coupled magnesium-titanium particles on human osteosarcoma SAOS2 cells: a potential cancer therapy. *J. Biomed. Mater. Res. B* 107B, 178–189.
- Kubacki, G.W., Gilbert, J.L., 2018. The effect of the inflammatory species hypochlorous acid on the corrosion and surface damage of Ti-6Al-4V and CoCrMo alloys. *J. Biomed. Mater. Res. A* 106A, 3185–3194.
- Kubacki, G.M., Hui, T., Gilbert, J.L., 2017. Voltage and wear debris from Ti-6Al-4V interact to affect cell viability during in-vitro fretting corrosion. *J. Biomed. Mater. Res. A* 106A, 160–167.
- Liu, Y., Gilbert, J.L., 2017. The effect of simulated inflammatory conditions and pH on fretting corrosion of CoCrMo alloy surfaces. *Wear* 390–391, 302–311.
- Liu, Y., Gilbert, J.L., 2018. The effect of simulated inflammatory solutions and fenton chemistry on the electrochemistry of CoCrMo alloy. *J. Biomed. Mater. Res. B Appl. Biomat.* 106B, 209–220.
- Mali, S., Gilbert, J.L., 2015. "Correlating fretting corrosion and micromotions in modular tapers: test method development and assessment". In: Greenwald, K., Lemons, M. (Eds.), *ASTM Special Technical Publication 1591 on Implant Modularity*. ASTM International, W., Conshohocken, PA, pp. 259–282.
- Mischler, S., Debaud, S., 1998. Landolt, "wear-accelerated corrosion of passive metals in tribocorrosion systems". *J. Electrochem. Soc.* 145 (3), 750–758.
- Oladokun, A., Hall, R.M., Neville, A., Bryant, M.G., 2019. The evolution of subsurface microstructure and tribochemical processes in CoCrMo-Ti-6Al04V fretting corrosion contacts: what lies at and below the surface? *Wear* 440–441 203095.
- Popov, V.L., 2010. *Contact Mechanics and Friction*. Springer Press, New York, NY.
- Swaminathan, V., Gilbert, J.L., 2012. Fretting corrosion of CoCrMo and Ti6Al4V interfaces. *Biomaterials* 33, 5487–5503.
- Swaminathan, V., Gilbert, J.L., 2013. Potential and frequency effects on fretting corrosion of Ti6Al4V and CoCrMo surfaces. *J. Biomed. Mater. Res. A* 101A (9), 2602–2612.
- Wiegand, M.J., Kubacki, G.W., Gilbert, J.L., September, 2018. Electrochemical potential zone of viability on CoCrMo surfaces is affected by cell type: macrophages under cathodic bias are more resistant to killing. *J. Biomed. Mater. Res. A* 107A, 526–534 2019.
- Wiegand, M.J., Benton, T., Gilbert, J.L., 2019. A fluorescent approach for detection and measuring reduction reaction byproducts near a cathodically-biased metallic surface: reactive oxygen species production and quantification. *J. Bioelectrochem.* 129, 235–241.
- Willert, H.G., Bertram, H., Buchhorn, G.H., 1990. Osteolysis in Alloarthroplasty of the Hip: the role of ultrahigh molecular weight polyethylene wear particles. *Clin. Orthop. Relat. Res.* 258, 95–107.
- Willert, H.G., Buchhorn, G.H., Fayyazi, A., Flurry, R., Windler, M., Koster, G., Lohmann, C.H., 2005. Metal-on-Metal bearings and hypersensitivity in patients with artificial hip joints: a clinical and histomorphological study. *J. Bone Jt. Surg.* 87-A (1), 28–36.
- Wimmer, M.A., Sprecher, C., Hauert, R., Tager, G., Fischer, A., 2003. Tribochemical reaction on metal-on-metal hip joint bearings: a comparison between in-vitro and in-vivo. *Wear* 225, 1007–1014.
- Wimmer, M.A., Fischer, A., Buscher, R., Porsal, R., Sprecher, C., Hauert, R., Jacobs, J.J., 2010. *Wear Mechanisms in Metal-on-Metal Bearings: the important of tribochemical reaction layers*. *J. Orthop. Res.* 28, 436–443.

2.4.4

Degradative Effects of the Biological Environment on Ceramic Biomaterials

MARIA VALLET REGI, PEDRO ESBRIT, ANTONIO J. SALINAS

Chemical Department of Pharmaceutical Sciences, Faculty of Pharmacy, Universidad Complutense of Madrid, Spain

Introduction

Ceramic materials are important sources of biomaterials for clinical applications. In this field, they are usually denoted as bioceramics and continue to be used to regenerate and repair ill or damaged tissues mainly in orthopedics and dentistry. Ceramics are inorganic materials exhibiting a combination of ionic and covalent bonding that show high melting temperatures, low conduction of electricity and heat, and high hardness. In addition, ceramics show high wetting degrees and surface tensions, which favor the adhesion of proteins and cells. Moreover, ceramics show great compression but low tensile strengths, stiffness and little plastic deformation. Bioceramics as implants are often manufactured with interconnected hierarchical porosity, which decreases the mechanical properties but allows ingrowth of cells and the necessary blood vessels.

The biological environment is both very aggressive and susceptible to material-provoked adverse reactions (Williams, 2008). Thus implanted bioceramics might suffer surface modifications and degradation during their required lifespan. Plasma is an aqueous medium containing anions (bicarbonate, chloride, phosphate, sulfate), cations (calcium, magnesium, potassium, sodium), as well as more than 20 different types of proteins: albumin, immunoglobulins, and fibrinogen being the most abundant. It also contains dissolved gases, mainly oxygen, carbon dioxide, and nitrogen. Finally, blood also includes red blood cells, white blood cells (neutrophils, eosinophils, basophils, lymphocytes, and monocytes), and platelets. This set of blood components is normally buffered at pH in the range 7.35–7.45, at a temperature of 37°C. Other biological fluids, such as cerebrospinal fluid, synovial fluid, saliva, tears, and lymph present some variations with respect to the components of blood but they are as complex and aggressive as blood itself on any material in contact with them.

Many of the blood components are extremely corrosive such as chlorine ions—present at a concentration that is one-third of that of sea water—or oxygen concentration in venous blood, a quarter of that in air. In addition, the presence of proteins is known to have a significant influence on the corrosive nature of the body fluids (Black and Hastings, 1998). Also of note, in inflammatory or infectious conditions, the biological medium pH can be acidified for short periods, reaching values of 4 or 5.

Reactivity of Bioceramics

When bioceramics are in contact with the biological fluids, three types of behavior can be expected. Whereas some ceramics, named *bioinert*, remain almost unchanged, others end up being reabsorbed after a certain period of time, and so are named *resorbable*; a third group of ceramics, called *bioactive*, undergo a set of reactions on their surface promoting binding to bone and, occasionally, soft tissues. Based on this different behavior, bioceramics are normally classified according to three subdivisions, which are described in depth in other chapters of this book:

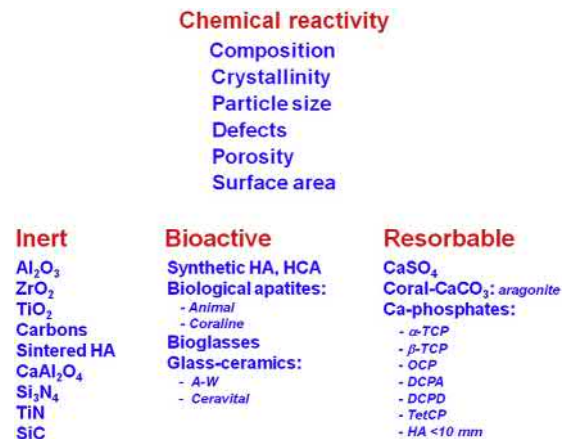
1. *Inert (or almost inert)* ceramics.
2. *Resorbable* ceramics
3. Ceramics with surface reactivity, i.e., *bioactive* ceramics.

Bioinert ceramics, namely Al_2O_3 , ZrO_2 , TiO_2 , or TiN , which exclusively contain covalent bonds that require a high energy to break, are very stable in the biological environmental, as observed in clinical practice. However, these bioceramics are also denoted as “almost inert” (Hench, 1991), since in contact with biological fluids they are usually covered with water, proteins, and other biological components. The former concept of “aging” of inert ceramics, which decreases their mechanical properties, appears to be more associated with an incorrect way of their preparation (Chevalier, 2006). As an example, zirconia, ZrO_2 , like

most of this type of ceramics, is brittle but when used to design implant components, it is prepared in a polymorphic phase with great toughness. The stability of this polymorph was achieved with addition of yttria (Y_2O_3) to reach partially stabilized zirconia (PSZ). However, incorrect thermal treatment of this material could cause the deterioration of mechanical properties of zirconia.

Resorbable bioceramics are ceramic materials containing ionic bonds that are stable in the air but dissolve in aqueous media. From their chemical structure, it is possible to identify their potential to produce bioceramics with a controlled degradation rate when implanted. Since any material that degrades in the body will release its constituents to the surrounding tissues, it is necessary to select as constituents of bioceramics cations and anions that are harmlessly incorporated in the metabolic processes. Ionic compounds containing sodium or calcium, including calcium phosphates and calcium carbonates, are widely used in this respect. The degradation rate of these bioceramics depends on their chemical composition and microstructure (Bohner, 2000). Hence, tricalcium phosphate [TCP, $Ca_3(PO_4)_2$] degrades quite rapidly, while hydroxyapatite [HA, $Ca_{10}(PO_4)_6(OH)_2$] is relatively stable. However, these compounds present variations in this regard: the α polymorphic form of [$Ca_3(PO_4)_2$] is more soluble than the β form. For this reason, α -TCP is frequently used as an ingredient of calcium phosphate cements, whereas β -TCP is used in bone grafts, pure, or as a component of biphasic calcium phosphates, containing HA and β -TCP. HA-based ceramics exhibit different solubility degrees depending on various factors. In general, HA can only be considered a resorbable material when obtained with a particle size smaller than $10\ \mu\text{m}$. Moreover, porosity highly affects ceramic solubility. Therefore dense ceramic materials will degrade slowly, while a porous material will be susceptible to a more rapid degradation. It is considered that dissolution rates in vivo can be predicted from their behavior in simple aqueous solutions mimicking the biological fluid, although there are some differences within the body in this regard, especially in the rate of degradation observed at the different implantation sites. It is possible that cell activity, related to phagocytosis or the release of free radicals, could be responsible for such variations.

Between the two extremes in terms of stability, represented by the (almost) inert and resorbable ceramics, there is a relatively small group of ceramics that exhibits a limited reactivity. This is particularly observed with a number of silica-based glasses and glass-ceramics mainly containing Si, Ca, Na, and P. In these ceramics, a selective dissolution of the surface takes place, involving the release of Ca and P, until a SiO_2 layer is formed. This is of considerable interest due to the ability of such surface layer to attract calcium and phosphate ions from the body fluids forming a calcium phosphate layer that makes possible the binding to bone, as discussed in other parts of this book. This bone-bonding ability was also reported for HA. In fact, in spite of some controversy regarding HA surface reactivity when soaked in simulated biological solutions, this ceramic is the best-known example



• **Figure 2.4.4.1** Factors governing the reactivity of ceramics and a classification of bioceramics according to their in vivo reactivity.

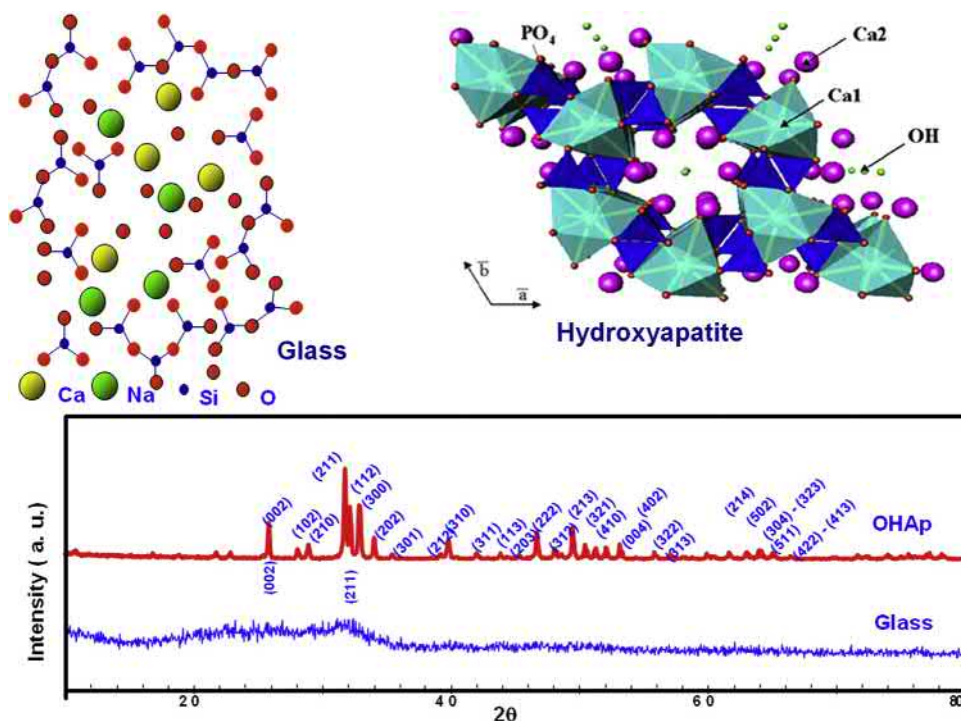
of *bioactive* ceramics. These implanted bioceramics are characterized by the absence of a fibrous tissue layer formation isolating them from the surrounding tissues, as occurs with inert ceramics as implants. A common method to evaluate the bioactivity of a ceramic under in vitro conditions is based on the use of a simulated body fluid (SBF), proposed by Kokubo (Kokubo et al., 1990). SBF is an aqueous acellular solution with a composition of inorganic ions almost equal to that of human plasma. In this assay, the formation of a layer of hydroxycarbonate apatite (HCA) nanocrystals on the material surface indicates an expected positive bioactive response in vivo (Vallet-Regí, 2001).

Fig. 2.4.4.1 shows representative examples of these three categories of bioceramics, including the family of carbon-based materials, which exhibit many ceramic-like properties.

Factors Influencing the Degradation of Bioceramics

The stability of ceramics in different environments displays a variable behavior depending on their chemical reactivity. In this regard, it is critical to bear in mind that selection of a particular bioceramic would be governed by a combination of its mechanical and physicochemical properties, depending on the intended application (e.g., as long-term or short-term implants). For a ceramic to be used as an implant for bone arthroplasty, inert ceramics are often used due to their very low friction coefficient that produces a minimum amount of wear particles. However, for those implant parts in contact with bone, a bioactive or biodegradable ceramic is mandatory to contribute to the process of bone regeneration, since inert ceramics cannot do that task.

Besides composition, other factors are known to affect bioceramic reactivity affecting their dissolution behavior in the biological medium (Fig. 2.4.4.1). Among them, the size of the crystalline domains (crystallinity), the particle size, or the presence of crystalline defects are critical. Thus decreasing the crystallinity and grain size augments the presence of



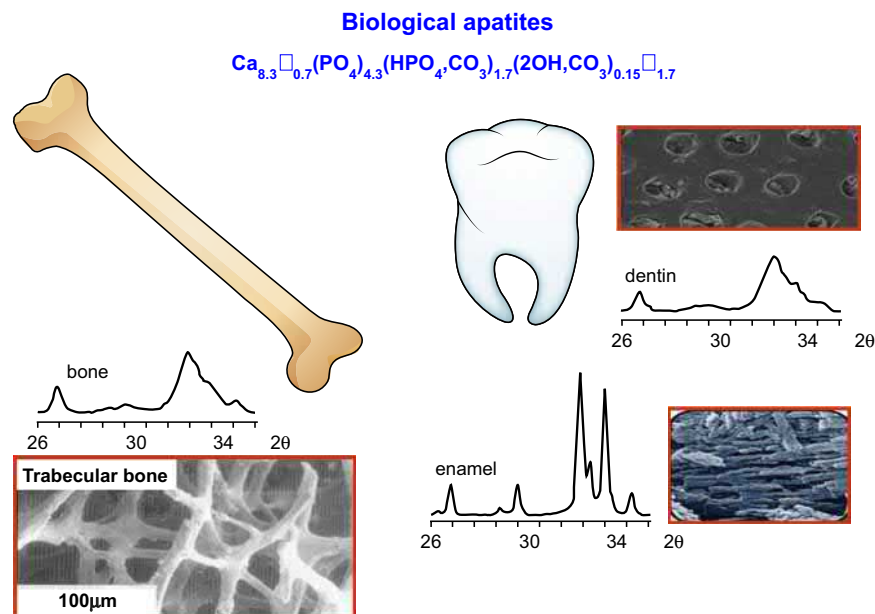
• **Figure 2.4.4.2** Comparison between the structure of a silica-based glass (disordered) and hydroxyapatite (ordered). The corresponding X-ray diffraction patterns are shown at the bottom.

network defects, which increase ceramic solubility. In addition, an increase in the surface area and porosity also promotes the latter. Fig. 2.4.4.2 shows in a comparative manner the different crystallinities exhibited by bioceramics, exemplified by the characteristic disordered structure of a silica-based glass containing a small proportion of phosphorus, calcium, and sodium as network modifiers, and the ordered crystalline structure of HA. These different structures produce very different X-ray diffraction patterns.

Increasing the crystallinity of a ceramic such as HA also tends to diminish its reactivity and, consequently, its bioactivity. However, since crystallinity is not the only factor responsible for ceramic reactivity, HA and other crystalline ceramics might exhibit a surface reactivity that makes them capable of binding to bone, i.e., to be bioactive. On the other hand, most of the available compositions of glasses behave as inert compounds when implanted. In fact, in traditional glasses obtained by quenching of a melt, the SiO_2 content should not exceed 60 mol%, and must contain over 10%–15% of monovalent oxides, such as Na_2O or K_2O , and divalent oxides, such as CaO or MgO , to be bioactive. The method of glass synthesis producing materials with radically different textural properties will also have a marked influence on their reactivity. Thus glasses obtained by wet methods, such as the sol–gel route, have high specific surface and porosity, which allow them to display bioactivity even with a SiO_2 content of 90 mol%. Likewise, glasses with compositions that make them totally degradable in the biological environment can also be obtained. Concerning the influence of particle size on ceramic bioactivity, glasses with a composition within the bioactivity window and a

particle size of less than $90\ \mu\text{m}$ can be completely degraded in vivo. Equally, by sintering at high temperatures, HA may reach a large particle size, which promotes formation of a thick fibrous nonadherent layer around the implanted material, thus preventing its bioactivity. In contrast, HA can be obtained by wet methods with very small particle size. This fact together with the presence of crystalline defects or ionic substitutions favors the release of reactive substances in the biological medium and its degradation. The complex behavior of a ceramic as determined by different structural variables justifies that HA was included in the three ceramic categories depicted in Fig. 2.4.4.1.

Considering the foregoing, reactivity has turned out to be a more suitable criterion than chemical composition or crystallinity for classifying bioceramics. Therefore slight differences in glass composition give rise to a bioinert, bioactive, or resorbable behavior (Hench and Anderson, 1993). In addition, it is possible to find glasses with identical composition behaving as bioinert or bioactive ceramics when synthesized by either melting or a sol–gel method (Vallet-Regi et al., 2003a; Salinas and Vallet-Regi, 2017). Moreover, some glass compositions considered bioactive can be completely resorbed when used as particles under a certain size limit, namely $90\ \mu\text{m}$ for Bioglass 45S5 (Hench and Polak, 2002; Salinas et al., 2018). Similarly, in the case of crystalline ceramics the in vivo reactivity of HA can range from almost bioinert, when it is sintered at high temperatures as dense monoliths, to resorbable (Kumta, 2006), when having a particle size under $10\ \mu\text{m}$, and in between we have the bioactive character generally attributed to HA (Vallet-Regi and Gonzalez-Calbet, 2004).



• **Figure 2.4.4.3** Biological apatites present in bone and in tooth enamel and dentin.

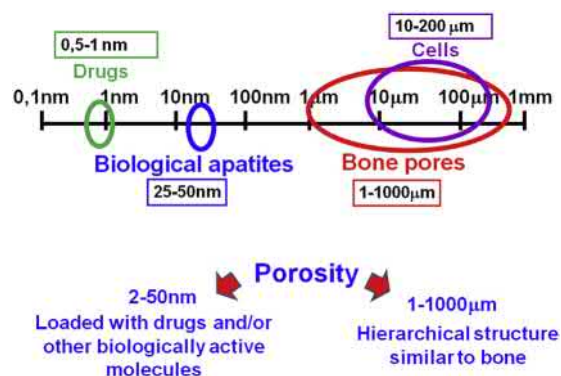
An implanted bioceramic may induce extracellular and/or intracellular responses in vivo. Implant biocompatibility ensures that these responses are not only harmless but indeed promote the function of target host tissues. In addition, degradability of bioceramics, which in part depends on their physicochemical structure, is also an important aspect to define their biocompatibility in vivo. In general, their predominant ionic bonds and chemical stability make bioceramics highly biocompatible materials for a range of clinical applications.

Reactivity and Degradation of Natural Apatites

A good example for understanding the complexity of factors that influence the reactivity and degradation of bioceramics can be provided by the three types of natural apatites present in tooth enamel, dentin, and bone (Fig. 2.4.4.3).

Bones of vertebrates are made of organic–inorganic composite materials whose structure includes an inorganic component made of carbonated and calcium-deficient nonstoichiometric HA. These biological apatite crystals, in the range of 25–50 nm (Vallet-Regi and Arcos-Navarrete, 2008; LeGeros, 1991), grow at the mineralization sites of the collagen molecules, which are grouped together forming collagen fibers. Furthermore, a certain hierarchical bone porosity is needed to accomplish bone physiological functions (Frieb and Warner, 2002). The order of magnitude of biological apatites and bone pores is shown in Fig. 2.4.4.4.

Bone remodeling, involving a coordinated process of bone degradation and new bone formation, is required for both bone repair and mineral homeostasis. For this reason,



• **Figure 2.4.4.4** Layout of different orders of magnitude in biological apatite and bone pores.

bone mineral contains nanometric pores and many crystallographic vacancies in the structure (i.e., empty positions in which there should be ions), which produces a calcium-deficient nonstoichiometric apatite. Likewise, this apatite structure can accommodate numerous types of extra ions in the three sublattices: Ca^{2+} , $(\text{PO}_4)^{3-}$, and OH^- ; specifically, carbonate groups that are flat in shape and replace tetrahedral phosphate groups. Their presence in a proportion higher than 4% in bone apatite is very important since it produces structure stresses and increases apatite solubility. Therefore bone apatite is based on nanometric calcium-deficient carbonate HA. All these characteristics give them a high reactivity and ability to readily dissolve during bone remodeling.

However, in dentin and especially in enamel, mechanical behavior is most important; thus enamel contains much larger apatite crystals but lower defects, ion substitutions, and nonstoichiometry, compared to bone (Fig. 2.4.4.3).

Evolution in the Use of Bioceramics for Bone Repair

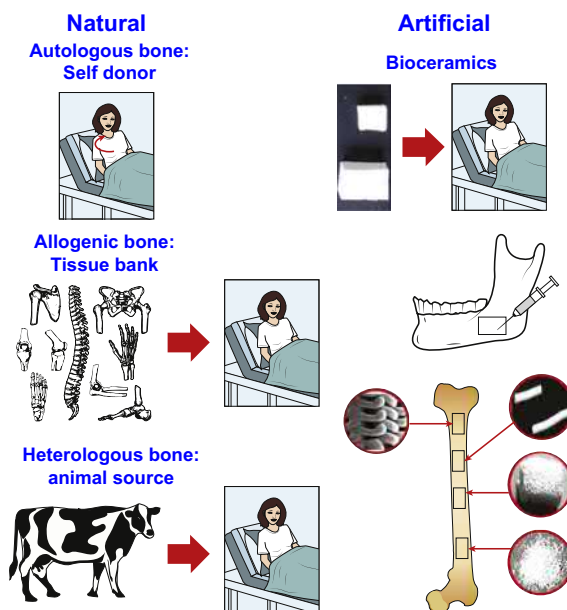
By the 1950s, inert ceramics like alumina, Al_2O_3 , began to be used for structural applications in bone replacement due to their *in vivo* biocompatibility and excellent mechanical features. In the 1980s, ceramics based on calcium phosphates or calcium sulfates, bioactive glasses, and glass-ceramics started to be used as bone grafts or metallic implant coatings due to their degradation pattern and bioactive behavior. Current developments focus on new porous ceramics designed as scaffolds for hosting cells and bioactive molecules to help drive bone tissue regeneration. New advanced bioceramics, namely mesoporous silica-based materials, ordered glasses, and organic–inorganic hybrids, as well as mesoporous nanoparticles, are under investigation.

The field of bioceramics is an excellent example of translational biomedicine, since the synthesized material by chemists and engineers must be functionally validated as an implant into the host. The interaction of bioceramics with living tissues controls the biological behavior and degradation of the implanted materials, which requires the cross-over of various clinical specialties and experimental sciences.

The development of a bioceramic implant for a specific clinical need in this field involves various stages, including *in vitro* and *in vivo* biocompatibility tests and other preclinical testing discussed elsewhere in this text. Regarding their mechanical behavior, ceramics exhibit great compression and low tensile strengths; they are stiff and brittle materials wherein failure takes place without plastic deformation. In addition, ceramics show high wetting degrees in a variety of forms: powder, porous pieces, dense pieces, injectable mixtures and cements, or as coatings. Ceramic surface tension favors the adhesion of proteins, cells, and other biological moieties, and the surface might exhibit antibacterial properties after appropriate treatment. However, recently developed ceramics with interconnected porosity show a significant decrease of their mechanical features.

Until recently, the most popular solutions in bone repair involved the use of natural materials, using autologous bone or bone allografts from a donor bank, or animal bone. This approach presents some drawbacks such as the need for two surgical interventions (autologous implant) and the risk of infection. Alternative inert, resorbable, or bioactive materials (ceramics) have found promising applications in this respect (Fig. 2.4.4.5).

The outcome of different ceramics as implants for bone repair and bone regeneration can be summarized as follows: *inert ceramics* induce the formation of an acellular collagen capsule, which isolates the material from the host tissue, and thus the artificial nature of the material prevails; *bioactive ceramics* react with the biological environment giving rise to bony apatite that, in concert with osteogenic cells, promotes new bone formation. These ceramics have excellent biocompatibility and bioactivity, but their mechanical properties are poor, rendering them unsuitable for the



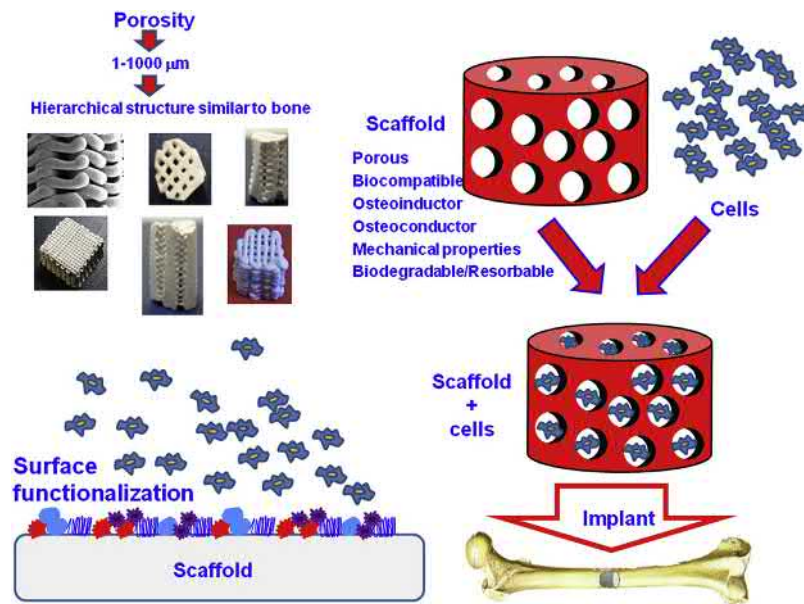
• **Figure 2.4.4.5** Natural bone and artificial bioceramics for human bone repair.

repair of large osseous defects. However, they are excellent for the filling of small defects. Glass-ceramics exhibiting improved mechanical properties with respect to the parent glass can be obtained by thermal treatments. Furthermore, organic–inorganic hybrid materials containing bioactive glasses as the inorganic component can also be manufactured. These hybrid materials have mechanical features like natural bone and are bioactive. The present technology allows design of bioactive ceramics with mechanical properties matching those of bone tissue in bone repair applications.

As mentioned earlier, ceramics with a hierarchical porous structure are now being investigated for putative use as scaffolds in bone tissue engineering. Pores, in the range of 2–50 nm (mesopores), enable the loading and release of biological molecules. Moreover, they must exhibit interconnected porosity with macropores and channels in the 2–1000 μm range, which allow cell interaction and vascularization when implanted (Fig. 2.4.4.4). This is an important point because the reactivity of ceramics begins at their surface in contact with a wet medium and in the presence of cells and proteins. This porosity though implies a certain sacrifice of their mechanical properties.

The pathway to reach third-generation bioceramics based on porous ceramic scaffolds as implants is depicted in Fig. 2.4.4.6. All of the ceramics mentioned earlier could be conformed into pieces with interconnected and hierarchical porosity within the micron range. Some sort of “smart” behavior is also required, so that these materials can modify their behavior in response to external or internal stimuli or to variations in the environment.

The possible ceramic degradation *in vivo* is an important issue to consider when designing a bioceramic as an implant. This applies to the so-called “traditional”



• **Figure 2.4.4.6** Requirements to be met by scaffolds for bone tissue engineering.

bioceramics of well-proven use in the clinic, and also to the *novel* bioceramics, whose development is at the forefront of knowledge and currently in progress. This aspect will be dealt with in more detail later on in this chapter.

As an example of these *new* bioceramics, silica-based mesoporous nanoparticles are currently at a preliminary research stage for putative cancer therapy. For this application their small size allows their incorporation into the bloodstream to carry antitumor drugs where necessary and deliver this cargo only where needed after receiving a stimulus that can be internal or external.

Bioceramic Interactions With the Biological Environment

When implanted, bioceramics trigger various cell and tissue responses, including acute and/or chronic inflammation, formation of granulation tissue, and fibrous encapsulation, which depend on the ceramic chemical composition and its structural features.

In [Table 2.4.4.1](#), the most important bioceramics used clinically are shown.

Inert Ceramics: First-Generation Bioceramics

The most widely used near bioinert ceramics are alumina (Al_2O_3), zirconia (ZrO_2), TiO_2 , and diverse forms of carbon, such as the low-temperature isotropic (LTI) form of pyrolytic carbon (PyC), glassy (vitreous) carbon, the ultralow temperature isotropic (ULTI) form of PyC and carbon fibers, carbon nanotubes, and graphene.

Applications of alumina and zirconia as load-bearing prosthetics in orthopedics and dentistry are similar, based

on their excellent mechanical features such as wear resistance, high strength, and smooth surface; zirconia being superior to alumina for its higher toughness ([Chevalier, 2006](#)). Moreover, titanium and its alloys, first used as dental implants, have been subsequently and continuously used as long-lasting implants for their excellent biocompatibility and resistance to corrosion. Carbons are mainly used as coatings for improving the physicochemical and biological (e.g., antithrombogenic and antibacterial) properties of implants ([Hu et al., 2010](#); [Fan et al., 2010](#); [Allen et al., 1994](#); [Zhu et al., 2007](#); [Bloomfield et al., 1991](#)) or as fibers in reinforced composites.

Despite an almost bioinert character, first-generation ceramics can elicit a foreign body reaction, involving the recruitment of macrophages and the secretion of inflammatory cytokines ([Rodrigo et al., 2006](#)), and ultimately the formation of an acellular collagenous capsule isolating the implant from the host tissue ([Ratner and Castner, 2002](#)). This provokes interfacial micromovements that might eventually lead to implant failure. However, for most medical applications of these nearly bioinert ceramics, this foreign body reaction is rarely an issue.

The first applications of alumina as bone substitute ([Smith, 1963](#)) and dental implant were reported in the 1960s ([Sandhaus, 1967](#)). In addition, the first bioceramic couple (alumina–alumina), with enhanced wear resistance, was implanted in 1970 ([Boutin, 1971](#)). Alumina has been extensively used as an implant material for hip and knee arthroplasty ([Oonishi et al., 1981](#)) and as single crystal alumina bone screws and in dental applications since the 1980s ([Kawahara, 1981](#)). The mechanical properties (toughness and wear resistance) of alumina were improved by decreasing the grain size of alumina from 10 to 2 μm, increasing purity, lowering porosity, and using hot isostatic pressure as a processing method. Current research studies are focused

TABLE 2.4.4.1 First, Second, and Third-Generation Bioceramics

Type of Bioceramic	In Vivo Reactivity	Examples
<p>First Generation:</p> <p>Bioinert nonabsorbable</p>	Isolated by a nonadherent fibrous capsule	<p>Alumina: Al_2O_3</p> <p>Zirconia: ZrO_2</p> <p>Carbons, mainly pyrolytic and as fibers in composites</p>
<p>Second Generation:</p> <p>Biodegradable resorbable</p>	Dissolved after a specific time	<p>Calcium phosphates</p> <p>Calcium sulfate</p> <p>Calcium phosphates and sulfates + ZnO, Al_2O_3, Fe_2O_3</p> <p>Coralline: CaCO_3</p>
<p>Bioactive surface reactive</p>	Tightly bonded to the living tissues through a surface reaction	<p>Hydroxyapatite, pure and substituted</p> <p>Hydroxycarbonate apatite</p> <p>Glasses: by melting and sol-gel</p> <p>Glass ceramics: apatite/wollastonite glass-ceramic and Ceravital</p>
<p>Third Generation:</p> <p>Scaffolds of biologically active molecules</p>	Stimulating living tissue regeneration	<p>Bioglass: in particulate form</p> <p>Porous bioactive and biodegradable ceramics</p> <p>Advanced bioceramics: Mesoporous materials, organic-inorganic hybrids</p>

on reducing the alumina ball size to make it more appropriate for patients shorter in height; ZrO_2 -based prostheses being more efficient in this respect. Postoperative failure of alumina, and other bioinert ceramic implants, is mainly a consequence of crack propagation (due to fabrication flaws or corrosion) under loading conditions (Morrell et al., 2012). Alumina has been used in dentistry for root analogs, endosteal screws, blades, and pin-type dental implants, and even ceramic crowns (Li and Hastings, 1998). However, mechanical tests showed functional limitations in some of these long-term devices. In this regard, single crystalline alumina showed mechanical strength superior to polycrystalline alumina as high-load devices. Alumina ceramics have also been used for total knee prosthesis, middle ear implants, and in ophthalmology (Schulte, 1990; Polack and Heimke, 1980).

Partially stabilized (with MgO or Y_2O_3) zirconia has been gaining market in orthopedics and dentistry as an option to alumina because of its enhanced mechanical properties, mainly toughness (Christel et al., 1988; Afzal, 2014; Akagawa et al., 1993). Moreover, in dentistry, compared to conventional titanium implants, the white color of zirconia makes it more similar to natural teeth. Large volume variations of around 5% take place when zirconia transforms from tetragonal to monoclinic polyform, which leads to an increase in the risk of cracking. Thus zirconia is usually stabilized by adding small amounts of oxides such as calcia (CaO), magnesia (MgO), or yttria (Y_2O_3), leading to PSZ or tetragonal zirconia polycrystals, which are partially or totally in tetragonal phase, respectively. PSZ zirconia

represents the main form of modern medical-grade zirconia. This material also presents advantages over alumina in terms of lower friction and wear resistance. However, the use of zirconia as a bioceramic elicits adverse outcomes produced by surface degradation releasing particles and also radioactive impurities. Degradation is a major drawback in this respect, due to the phase transformation accelerated with material aging in the aqueous body environment, particularly under dynamic loads. Although surface degradation of zirconia balls due to phase transformation does not seem to be significant, and particulate debris is chemically stable and biocompatible, femoral head zirconia prostheses have a relatively short history and further investigation is required. Putative improvements of these bioinert ceramics might come from the preparation of alumina/zirconia composites (Kurtz et al., 2014).

Titanium and its alloys have been used as orthopedic and dental implants for more than 40 years (Elias et al., 2008). Upon air exposure, the formed outer TiO_2 layer prevents corrosion and greatly improves the biocompatibility of titanium by adsorbing proteins of the host environment (Liu et al., 2004). Attempts to further improve the biocompatibility of Ti-based biomaterials by HA coating and adsorption of osteogenic peptides have been carried out (Khorasani et al., 2015; Van der Stok et al., 2015).

Several carbon allotropes, including nanocrystalline glassy carbon, graphene, diamond-like carbon, and PyC, are widely used as implant coatings, since they show optimal adherence to both metallic and polymeric substrates and are not degraded in vivo. The most common form of carbon

TABLE 2.4.4.2 Clinical Applications of First- and Second-Generation Bioceramics

Ceramic	Clinical Application	Examples
Bioinert	Coatings for tissue ingrowth: orthopedic, dental, maxillofacial	Al ₂ O ₃
	Orthopedic load-bearing applications	Al ₂ O ₃ , ZrO ₂ , PE–HA composite
	Artificial heart valves	Pyrolytic carbon coatings
	Artificial tendon and ligament	PLA–carbon fiber composites
Bioactive	Coatings for prosthesis fixation: orthopedic, dental, maxillofacial	HA, bioactive glasses, and glass-ceramics
	Percutaneous devices	Bioactive glasses, bioactive composites
	Periodontal pocket elimination	HA, HA–PLA composite, sodium phosphate, calcium phosphates, bioactive glasses
	Spinal surgery	Bioactive glass-ceramics, HA
Bioinert and bioactive	Dental implants	Al ₂ O ₃ , HA, bioactive glasses
	Alveolar ridge augmentations	Al ₂ O ₃ , HA, HA–autogenous bone, bioactive glasses
	Maxillofacial reconstruction	Al ₂ O ₃ , HA, HA–PLA composite, bioactive glasses
	Otolaryngological applications	Al ₂ O ₃ , HA, glasses, glass-ceramics
	Orthopedic fixation devices	PLA–carbon fibers, PLAc/a/p glass fibers
Resorbable	Temporary bone spacers, fillers	Calcium phosphates (α - and β -TCP, etc.), calcium sulfate

HA, Hydroxyapatite; PE, polyethylene; PLA, poly(lactic acid); TCP, tricalcium phosphate.

used in this regard is PyC, presented in two forms: LTI and ULTI (Dauskardt and Ritchie, 1993). The former material presents excellent biocompatibility with the cell and protein components of blood and soft tissues, and it has received special attention related to its nonthrombogenic behavior which has led to its wide use in prosthetic heart valves. Moreover, LTI carbon shows no degradation and excellent strength and resistance to wear and fatigue in vivo. At present, over 90% of mechanical heart valve prostheses use LTI–PyC as a coating on a polycrystalline substrate or as a monolithic material. PyC can also be used in small orthopedic joints such as fingers and as spinal inserts. However, current efforts are being addressed to eliminate the traces of silicon carbide in PyC, due to its thrombogenicity, and to improve PyC mechanical properties.

Future improvements of almost bioinert ceramics could be derived from manufacturing alumina/zirconia composites or, alternatively, from research on nonoxide bioinert ceramics, namely nitrides and carbides like Si₃N₄ or SiC.

Table 2.4.4.2 shows important clinical applications of bioinert ceramics and second-generation ceramics that will be described in the next section.

Resorbable and Bioactive Ceramics: Second-Generation Bioceramics

Bioactive ceramics denote those ceramics whose surface is able to form a strong bond with soft and hard tissues (Hench

et al., 1971), making them suitable for many clinical applications. As mentioned in another section of this chapter, typical examples of bioactive ceramics are HA and some compositions of glasses and glass-ceramics (Vallet-Regi et al., 2006; Hench and Wilson, 1984; Yuan et al., 1999; Vallet-Regi et al., 1999; Livingston et al., 2002; Kokubo et al., 2003). In contact with biological fluids, dissolution products of these ceramics cause the formation of an HA-like layer on their surface, whereby they can promote cell attachment and cell differentiation (Kokubo, 1998; Sanders and Hench, 1973; Xynos et al., 2001). The apatite particles on the surface of bioactive ceramics are easily recognizable by scanning electron microscopy because they have a needle-like shape of around 500 nm in length, agglomerated in pseudospherical particles of 10 μ m in diameter. These bioceramics are osteoinductive materials, so that they activate bone tissue regeneration (Hench and Polak, 2002). They have excellent features in terms of biocompatibility and bioactivity, which are strongly associated with ion release from their surface into the surrounding tissue (Hoppe et al., 2011). Furthermore, these implanted bioceramics induce no deleterious effects related to tissue inflammation. However, prepared as dense monoliths, they are brittle, which renders them unsuitable for repairing large osseous defects.

These bioceramics are available in different formats: powder, porous pieces, dense pieces, injectable mixtures, and coatings, dependent on the intended application. Thus a bioactive glass shaped as a porous piece exhibits a

fast bioactive response. In this form, the biological fluid can reach the inner structure of the glass more effectively, thus improving its reactivity. These bioceramics are excellent for the filling of small bone defects, where the rate of bone regeneration is the main concern, but the mechanical properties are a secondary aspect. In addition, glasses can also be used for the production of glass-ceramics (see later) by thermal treatment (Roman et al., 2003), which exhibit a somewhat lower bioactivity than glasses but mechanical properties closer to natural bone. In addition, both bioactive glasses and glass-ceramics can be used to design magnetic materials for promoting bone regeneration and, simultaneously, killing bone cancer cells by hyperthermia (Del Real et al., 2002).

Biodegradable ceramics are designed to fulfill a specific function for a certain period of time to help tissue regeneration, and they are resorbed thereafter. In this manner, possible deleterious effects associated with a prolonged permanence of a synthetic biomaterial in the host can be avoided. Calcium phosphates and calcium sulfates are typically considered major members of degradable ceramics (Elliott, 1994; De Groot, 1991; Dorozhkin and Epple, 2002; Pietrzak and Ronk, 2000). In vivo ceramic degradation usually occurs by passive dissolution of ions and/or by cell-mediated resorption in the biological environment (i.e., by enzymatic activities and pH changes). Host monocytes/macrophages and even osteoclasts from the bone marrow rapidly invade the bioceramic implant surface and play a key role in material degradation (Rae, 1986). Thus phagocytosis by monocytes/macrophages or acidification by osteoclasts causes the resorption of the bioceramic implant (Heymann et al., 1999). In addition, osteoblasts and other mesenchymal cells present at the implantation site have been shown to be able to phagocytose calcium phosphate (Heymann et al., 1999; Gregoire et al., 1990). As mentioned earlier in this chapter, decreasing the particle size or increasing the hydrophilic character can promote bioceramic degradation (Vallet-Regi et al., 2001; Colilla et al., 2006). Moreover, the loss of mechanical integrity of these ceramics during degradation might contribute to material disintegration (Tamimi et al., 2012; LeGeros, 1993). The latter generates particles that can adversely affect extracellular matrix production by osteoblasts and may result in periimplant osteolysis (Grover et al., 2003). Hence, a critical aspect in designing resorbable ceramics will be to adjust the ceramic degradation rate, which is usually faster than the process of tissue healing, to a specific biomedical application.

Present research is focused on the development of porous and new advanced bioceramics as scaffolds for hosting cells and bioactive molecules (growth factors, small peptides) to be released into the biological environment in a controlled manner for tissue-engineering applications (Langer and Vacanti, 1993; Salinas et al., 2013). This is discussed in detail in other sections of this chapter.

Calcium phosphates. Most of the second-generation ceramics used for bone regeneration are based on calcium

phosphates Zhang et al. (2007); Dorozhkin (2010); Lew et al. (2012); Daculsi et al. (2014); Wang et al. (2014); Habraken et al. (2016). These include: synthetic apatites, pure and substituted biphasic mixtures of calcium phosphates, and calcium cements, containing calcium phosphates and calcium sulfate.

Synthetic apatites. HA and type B HCA are the most investigated calcium phosphate bioceramics due to similarities with the inorganic component of bone (Elliott, 1994). Submicrometric particles of HA can be obtained by aerosol pyrolysis (Vallet-Regi et al., 1994), precipitation (Naasaraju and Phebe, 1996; Vallet-Regi et al., 1997), or the liquid mix technique (Pechini, 1967; Peña and Vallet-Regi, 2003). The biological type B HCA, where CO_3^{2-} are located in the PO_4^{3-} positions, is synthesized using moderate temperatures (Doi et al., 1998). At higher temperatures a high CO_3^{2-} content is included in the structure but located in the OH^- sublattice; in this way a nonbiological type A HCA is obtained (LeGeros, 1991).

HA structure can accept many compositional variations in the Ca^{2+} , PO_4^{3-} , or OH^- sublattices. Thus apatite crystals usually included ions such as Na^+ , K^+ , Mg^{2+} , Sr^{2+} , Cl^- , F^- , or HPO_4^{2-} (Jha et al., 1997). The migration of these extra ions toward the surrounding tissues produces an increase in the crystal size, decreasing the solubility of the bioceramic. This effect has positive physiological consequences in the rapidly growing young—and less crystalline—bone. Ion substitutions in the HA structure turn bone into an important system to quench toxic heavy metals in the biological milieu. In addition, the ability to host ions allows the design of synthetic calcium phosphates with improved properties for specific biomedical applications. The ionic substitutions can modify the surface structure and electric charge of HA, with potential influence on the biological environments. In addition, while carbonate and strontium ions facilitate apatite dissolution, the release of certain chemical elements, namely strontium, zinc, or silicate, during resorption facilitates bone formation. Silicates in the network increase the mechanical strength of HA, and accelerate its bioactive response (Vallet-Regi and Arcos, 2005; Gibson et al., 1999). Thus the current trend is to obtain synthetic calcium phosphates partially substituted with different ions for use as implants.

Biphasic mixtures of calcium phosphates. The most popular materials of this type are based on HA and β -TCP, β - $\text{Ca}_3(\text{PO}_4)_2$, mixtures (Daculsi, 1998; Tancred et al., 1998; Kivrak and Tas, 1998; Sanchez-Salcedo et al., 2008a), which can evolve to HCA in the biological environment. This process involves the gradual dissolution of the mixture, releasing Ca^{2+} and PO_4^{3-} to the local environment, thus providing a source of newly formed bone minerals. This material can be injected and used as a coating or as bulk in bone replacement. Moreover, other biphasic mixtures have been investigated, including calcium phosphates together with other second-generation ceramics, namely bioactive glasses and calcium sulfates (Ramila et al., 2002; Cabañas et al., 2002).

Bone cements. Cements based on calcium phosphates, calcium carbonates, or calcium sulfates have attracted much attention due to their excellent biocompatibility. Most of the injectable calcium phosphate cements evolved to either a calcium apatite or octacalcium phosphate during the setting reaction. Physical–chemical properties of these materials, such as the setting time, porosity, and mechanical behavior, depend on the cement formulation and the presence of additives (Ginebra et al., 2004; Otsuka et al., 1995; Nilsson et al., 2002). These cements cured in field are biocompatible and they slowly resorb, while newly formed bone grows and replaces the cement in vivo. Research is under way on shortening the curing time in contact with blood and improving the mechanical toughness.

Calcium phosphate coatings. HA and other calcium phosphates are also used as coatings to protect the surface of metals (i.e., titanium alloys, Ti6Al4V, and commercially pure Ti) from the biological environment. Commercial implants with such coatings are produced by plasma spray at high temperature (Koch et al., 1990; García-Sanz et al., 1997; Sun et al., 2001), which is advantageous in terms of a rapid deposition rate and a relatively low cost. However, the formation of resorbable amorphous calcium phosphate (ACP) in the coating by this method compromises implant integrity. Other unresolved issues related to these coatings are the adherence to substrate and instability of HA at high temperatures or the phase transition of titanium at 1156 K. Alternative techniques to obtain the coatings at lower temperature, including physical vapor deposition (PVD) (Park et al., 2005), chemical vapor deposition (CVD) (Cabañas et al., 2003), magnetron sputtering (Wolke et al., 1998), electrophoretic deposition (Kannan et al., 2002), pulsed laser deposition (PLD) (Arias et al., 2003), and sol–gel-based dip coating (Hijon et al., 2006), allow a higher control of the coating thickness and crystallinity of phases.

Glasses. Specific compositions of glasses react with body fluids forming an HCA layer, which favors the generation of a bone matrix and bone growth. These glasses are used for filling osseous cavities, substitution of ear ossicles, maxillofacial reconstruction, and dental applications (Vallet-Regi et al., 2003a,b). Those glasses exhibiting a high bioactivity are eligible as bioactivity accelerators of mineral apatites or as bioactivity inductors of magnetic materials for hyperthermia treatment of osseous tumors.

Melt glasses. The first bioactive glasses, prepared by quenching of a melt, contained SiO_2 and P_2O_5 as network formers, and CaO and Na_2O as network modifiers (Hench et al., 1971). By using the SBF test, the silica-rich layer formed on the glass surface by the ionic exchange of calcium and sodium ions in the glass and protons in the solution were initially found to attract calcium, phosphate, and carbonate ions in the surrounding fluid to form ACP. This then crystallizes into a biologically active HCA layer that promotes new bone formation (Vallet-Regi, 2001). Those glasses with the highest bioactivity, as tested by this method, were able to bond to both hard and soft tissues. To explain these differences in reactivity, in 1994 Hench defined two

classes of bioactivity: class A (osteoproducer) and class B (osteoconductor) (Hench, 1994, 2016).

The high bioactivity of sol–gel glasses (SGGs) makes them excellent candidates to be used in coatings, mixed materials, or as porous scaffolds in third-generation biomaterials, which will be described later on in this chapter.

Sol–gel glasses. The sol–gel synthesis of bioactive glasses produces materials (fibers and highly porous monoliths, or coatings) with high textural properties and excellent biocompatibility in both cell cultures (Olmo et al., 2003) and animal models (Gil-Albarova et al., 2005). The sol–gel route is more time consuming than the traditional quenching of a melt, but it requires noticeably lower temperatures. The $\text{CaO-P}_2\text{O}_5\text{-SiO}_2$ system has been the most studied type of SGGs (Li et al., 1991; Pereira et al., 1994; Peltola et al., 1999; Salinas et al., 2001), containing additions such as MgO , ZnO , or removing P_2O_5 , to modify the mechanical properties, the resorption rate, or the interaction with osteoblasts (Perez-Pariente et al., 1999; Du and Chang, 2004; Oki et al., 2004). CaO plays an essential role in the texture and bioactive response of SGGs (Martinez et al., 2000); Ca^{2+} ions released to the medium increase exposure of the silanol (Si-OH) groups on the glass surface, which favors the formation of the HCA layer. Of note, formation of the latter depends on the presence of P_2O_5 in the glass (Salinas et al., 2002). CaO-SiO_2 glasses exhibit higher reactivity. In contrast, in $\text{CaO-P}_2\text{O}_5\text{-SiO}_2$ glasses, ACP formation is slower but evolves more rapidly to HCA nanocrystals than CaO-SiO_2 glasses.

Mesoporous bioactive glasses. (MBGs), first synthesized by Zhao et al. in 2004 (Yan et al., 2004), have more controlled and reproducible textural properties than SGGs. They also exhibit twofold higher surface areas and pore volumes than those of SGG analogs with identical composition (Izquierdo-Barba et al., 2013), consistent with the observed faster bioactivity kinetics than the latter glasses. Also, in contrast to SGGs, MBGs exhibit ordered mesopores with a pore diameter between 2 and 10 nm in a very narrow pore size distribution. MBGs also have abundant silanol groups on their surface that allow their functionalization as required and facilitate an excellent performance in SBF (Vallet-Regi and Salinas, 2017). The large surface area of MBGs is thought to be responsible for the high reactivity in SBF medium reaching a pH of 6.7 on the surface during the first stages of the assay, instead of a pH of 7.4 commonly observed in these assays for bioactive melt and SGGs in this assay (Vallet-Regi and Salinas, 2018). This lower pH made possible the formation of octacalcium phosphate as an intermediate phase between ACP and calcium-deficient HA (CDHA), as reported to occur during bone maturation in vivo. All these characteristics make MBGs excellent candidates for bone tissue-engineering applications.

As for the SGGs, most of the investigated MBGs belong to the $\text{SiO}_2\text{-CaO-P}_2\text{O}_5$ system synthesized by the evaporation-induced self-assembly method (Brinker et al., 1999). The CaO content and the temperature used for the aging of gel during the process of synthesis influence the

order of mesopores obtained (García et al., 2009). Analysis of the mesostructure of MBGs and SGGs by high-resolution transmission electron microscopy allowed a better understanding of the role of the P_2O_5 content in the behavior of these glasses in SBF medium (Vallet-Regi et al., 2005b; Vallet-Regi and Salinas, 2018). In both types of glasses, P_2O_5 binds to calcium to form calcium phosphate nuclei, removing calcium ions from the glass network and, as a consequence, retarding ACP formation in the in vitro assay. On the other hand, the formation of CDHA identical to that of biological apatite is accelerated. In vitro studies using SBF assay showed the different bioactive responses of two SGGs and two MBGs, with or without P in their composition, respectively. The presence of P was quite important for SGGs and minimal for MBGs.

There is now a growing tendency to include small amounts of other oxides with biological activity, such as CeO_2 , Ga_2O_3 , ZnO , CuO , SrO , CoO , or Ag_2O , for improving the biological performance of MBGs (Salinas et al., 2011; Kargozar et al., 2018; Sanchez-Salcedo et al., 2018). Surfactants are a necessary addition during MBG syntheses for self-assembly in aqueous solution to produce mesophases acting as structure-directing agents of the glass network. The most common mesoporous arrangements obtained for MBGs are 2D hexagonal, spatial group (SG) P6mm, and 3D cubic bicontinuous SG Ia-3d.

Bioactive glass coatings. As previously mentioned for calcium phosphate, many techniques can be used to obtain ceramic coatings on metallic substrates, including PLD, PVD, CVD, plasma spray, and dip coating. The latter method controls the porosity, roughness, and composition of the bioactive film formed on the metal surface. As an example of the stability of such coatings, a bioactive glass composed of 20%CaO–80%SiO₂ (mol%) coating the Ti6Al4V surface completely dissolved in 14 days in the SBF assay (Izquierdo-Barba et al., 2003). However, in the presence of osteoblasts, this coating not only remained stable in the culture medium, but it promoted cell adhesion, proliferation, and differentiation (Izquierdo-Barba et al., 2006). The influence of the substrate on the behavior of SGG coatings is well illustrated by using 316L stainless steel as substrate. In this case, silicon in the glass bonds to chromium in the substrate during the dip-coating synthesis, subsequently increasing the corrosion of this metallic alloy (Vallet-Regi et al., 2003b).

Mixed materials containing bioactive SGGs. Mixed materials, including bioactive SGGs, have been investigated, including: SGG–polymer–drug, SGG–magnetic component, and SGG–HA. *SGG–polymer–drug materials* were designed to obtain systems with controlled release of bioactive drugs. In this case, bone integration is improved, and the drug release is favored by the ionic exchange between the glass and the biological medium. *SGG–magnetic glass–ceramics* have been designed for treating bone tumors, based on the higher sensitivity of cancer cells to hyperthermia (Arcos et al., 2003). The in vitro

biocompatibility of these mixed ceramics has been established (Serrano et al., 2008). SGG–HA materials have also been designed to ameliorate the bioactivity of HA. Thus a 30%CaO–70%SiO₂ glass/HA mixture was found to be covered with an HCA layer after 12 h in SBF, whereas HA alone was not modified in this regard after 45 days. The highest reactivity in this in vitro setting was achieved with biphasic HA and dried-gel glass mixtures with an average particle size of 30 μ m.

Glass-ceramics. This family of compounds is obtained by the thermal treatment of glasses that produced the formation of crystalline phases inside the glass matrix. The synthesis of a glass-ceramic requires the stages of nucleation and growth. The former is favored by the addition of nucleating agents. Further annealing causes uniform crystal growth. Thus glass-ceramics behave as composites with the crystalline phases strengthening the glassy matrix. Consequently, they exhibit superior mechanical properties compared to the parent glass, and also to sintered crystalline ceramics, but without matching those of cortical bone (Vallet-Regi et al., 2005a,b). Glass-ceramics with rapid bioactive response were synthesized by thermal treatment of SGGs (Padilla et al., 2005; Boccardi et al., 2017). However, glass-ceramics present a poorer bioactive response than glasses due to a lower abundance of Si–OH groups on their surface and a decreased release of calcium ions from the crystalline phases. The bioactive response, expressed as the bioactivity index $I_B = 100/t_{0,5bb}$ (day^{-1}) ($t_{0,5bb}$ days required for 50% bioceramic surface bonding to bone) varied for different ceramics between 0 for alumina and other bioinert ceramics; 2.3 for HA; 3.2 for apatite/wollastonite glass-ceramic; and 12.5 for Bioglass 45S5 (Hench, 1998).

Table 2.4.4.3 shows important bioactive and resorbable bioceramics and their clinical applications.

Third-Generation Ceramics

Third-generation bioceramics are based on resorbable or bioactive materials obtained in a porous form that allows them to act as scaffolds for cells and inducing molecules to drive tissue regeneration. This category includes bioceramics based on porous second-generation bioceramics, like nanometric apatites, shaped as pieces with interconnected porosity, and new advanced bioceramics like silica mesoporous materials, mesoporous ordered glasses, or organic–inorganic hybrids. Manufacturing of these ceramic scaffolds for tissue engineering requires the use of conformation methods that yield pieces with interconnected porosity and pores in the 2–400 μ m range (Sanchez-Salcedo et al., 2008b). Several of these methods proceed at room temperature (Roman et al., 2008), which makes it possible to include molecules with biological activity.

Silica-based mesoporous materials. These materials were initially proposed for use as drug delivery systems in biomedical applications (Vallet-Regi et al., 2001), and thereafter as bioactive ceramics (Vallet-Regi et al., 2006).

TABLE 2.4.4.3 Bioactive and Resorbable Bioceramics and Their Uses as Implants

Ceramic	Form	Application	Function
Calcium phosphates	Bulk	Bone graft substitutes, cell scaffolds	Replace the bone loss
	Coatings	Surface coatings on total joint prosthesis	Provide bioactive bonding to bone
Glasses	Bulk	Endosseous alveolar ridge maintenance	Space filling and tissue bonding
		Middle ear prosthesis	Replacement of part of the ossicular chain
		Orbital floor prosthesis	Repair damaged bone supporting eye
	Powder	Fixation or revision arthroplasty	Restore bone after prostheses loss
		Filler in periodontal defects	Periodontal disease treatment
Glass-ceramics	Bulk	Vertebral prostheses	Replace vertebrae removed by surgery
		Iliac crest prostheses	Substitute bone removed for autogenous graft
	Coatings	Fixation of hip prosthesis	Provide bioactive bonding
Calcium sulfate	Bulk and powder	Bone graft substitutes	Repairing osseous tissues

They are synthesized with surfactants acting as templates to obtain materials with ordered porosity—in the nanometer range—and amorphous silica pore walls. Previously described MBGs obtained in this manner as powder can be processed to form scaffolds enabling decoration with osteogenic substances (Perez et al., 2018). Moreover, bioactive glass microspheres with accelerated deposition of HCA have shown to exhibit hemostatic efficacy (Ostomel et al., 2006) and magnetic silica microspheres for drug targeting have been reported (Ruiz-Hernandez et al., 2008).

Organic–inorganic hybrid materials. These materials are synthesized at room temperature to preserve the organic component as bulk, coatings, and fibers. Organic–inorganic hybrids containing SiO_2 –CaO glasses as the inorganic component and several biocompatible polymers as the organic component have been investigated with regard to their mechanical features comparable to bone (Vallet-Regi and Arcos, 2006). In some hybrid systems, only weak physical interactions exist between inorganic and organic domains with several containing poly(vinyl alcohol) (PVA) (Pereira et al., 2000; Martin et al., 2005) or poly(hydroxyethyl methacrylate) (Schiraldi et al., 2004). In other cases, chemical links between both components are formed, as occurs with hybrids containing poly(methyl methacrylate) (Rhee and Choi, 2002), poly(ϵ -caprolactone) (Rhee, 2004), or gelatin (Ren et al., 2002; Coradin et al., 2004). To improve the bioactive response of these hybrids, inorganic components such as TiO_2 were added to hybrids with poly(dimethylsiloxane) (PDMS) (Chen et al., 2000; Manzano et al., 2006a) or poly(tetramethylene oxide) (Miyata et al., 2004). Examples

of hybrid systems investigated for bone repair include: (1) CaO – SiO_2 –PDMS, obtained as bioactive coatings (Hijon et al., 2005) or as bioactive monoliths with or without P additions to improve bioactivity (Salinas et al., 2007; Manzano et al., 2006b); (2) CaO – SiO_2 – P_2O_5 –PVA, synthesized as transparent films (Pereira et al., 2000) or as bioactive and degradable monoliths (Martin et al., 2005); and (3) CaO – SiO_2 -based hybrids with organic polymers containing methacryloxy and amino groups (Colilla et al., 2006), designed with tailored bioactivity and degradability proposed for time release of bioencapsulates (Gonzalez et al., 2008). Components of bioactive organic–inorganic hybrids are based on the so-called star gels, a family of materials that exhibit remarkable mechanical properties (Michalczyk and Sharp, 1995). These materials have a unique structure made of an organic core surrounded by flexible arms that yield materials with a mechanical behavior between that of glasses and rubbers (Sharp, 1998). Addition of Ca^{2+} ions conferred bioactivity in SBF to the star gels (Manzano et al., 2006a,b). Notably, these hybrids exhibit fracture toughness comparable to that of the human tibia.

Organic–inorganic hybrid materials were also synthesized as porous scaffolds (Tsuru et al., 2008) with interconnected pore structure. Thus SiO_2 –PDMS with 90% porosity and pore size between 200 and 500 μm , obtained using sieved sucrose particles as a template (Yabuta et al., 2003), were evaluated in a bioreactor and implanted in vivo into brain defects. Gelatin-siloxane (3-glicidopropyltrimethoxysilane, GPTMS) hybrid scaffolds with different orders of porosity (5–10, 30–50, and 300–500 μm), obtained by freeze drying wet hybrid gels (Ren et al., 2002), were also assessed after

CASE STUDY: BIPHASIC CALCIUM PHOSPHATES

What Problem Was Addressed?

The treatment of bone defects resulting from surgery, trauma, or disease requires the use of biomaterials to achieve faster and better healing outcomes. Indeed, the use of biomaterials is an essential requirement to treat critical bone defects where their size is too large to heal on their own. Autografts and allografts are the gold standard to be used in this respect. However, these approaches have important drawbacks, including the limited supply of donor bone grafts, secondary trauma in harvesting autografts, and the immune response and/or the possibility of disease transmission for allografts. These facts stimulated interest in the development of new synthetic materials with similar properties to native bone for bone replacement and regeneration.

What Properties Were Required of the Material?

In the context of bone regeneration, the design of new biocompatible, osteoconductive, and osteoinductive materials is an important challenge. With this aim, calcium phosphate bioceramics are processed as porous materials, which makes tissue ingrowth possible. Moreover, they exhibit a bioactive surface that facilitates cell attachment, proliferation, and differentiation. With this application, a family of compounds designated biphasic calcium phosphates (BCPs) is a promising alternative for bone reconstruction. BCPs are formed by two phases: one is more stable, which contributes to its bioactive and osteoconductive surface; the other degrades with time and releases phosphate and calcium ions to the medium enabling new bone formation and causing an increase in material porosity, which facilitates tissue ingrowth. The partial degradation of BCP allows the maintenance of sufficient mechanical properties of the implanted biomaterial until new bone is formed.

What Partially Degradable Bioceramic Was Used?

BCPs are a combination between the more stable bioactive phase of hydroxyapatite ($\text{Ca}_{10}(\text{PO}_4)_6(\text{OH})_2$, HA) and the more soluble β -tricalcium phosphate ($\text{Ca}_3(\text{PO}_4)_2$, β -TCP), thus allowing control of the material dissolution rate and the tailoring of mechanical properties. BCPs were first elaborated in 1986 by LeGeros, although some of the materials previously implanted as HA were actually a mixture of HA and β -TCP. The most common way to prepare BCPs is the thermal treatment of calcium-deficient apatites obtained by precipitation. When the calcium deficiency is small, that is, the Ca/P molar ratio is close to 1.67, the amount of β -TCP formed after calcination is very small. However, when the deficiency in calcium increases to Ca/P values close to 1.50, the amount of β -TCP in the BCP becomes increasingly high. Therefore by varying the calcium deficiency of the precursor hydroxyapatite, BCPs with the desired proportion of HA and β -TCP can be obtained. Currently, there are over 30 commercially available BCPs as bone substitutes for various orthopedic and maxillofacial applications. At present, there is no general agreement on the optimum proportions of HA and β -TCP in BCP. The majority of these commercial products contain a 60:40 ratio of HA: β -TCP, but there are also several products with other ratio values: 20:80, 65:35, or even 96:4. Variations of pH, temperature, and duration of the sintering process produce unique materials with different chemical and physical properties that lead to different tissue responses. Furthermore, BCP has been used as either a carrier or delivery system for therapeutic drugs (antibiotics, hormones, and growth factors) in bone tissue engineering. Despite the many BCPs in use, much research must be done concerning the optimum features for specific applications, including composition and grain size, to improve the desirable osteoinductive behavior of these materials.

implantation in brain defects where no inflammation was observed (Deguchi et al., 2006). Moreover, in vitro biocompatibility of chitosan–GPTMS hybrids, with or without calcium addition, with 90% porosity and 100 μm pores, prepared by freeze-drying methods, were proven in cell cultures (Shirosaki et al., 2008). Taken together, these data point to organic–inorganic hybrids as promising candidates to be used as scaffolds in tissue engineering.

Summary and Future Perspectives

Ceramics are widely used for bone repair and bone regeneration in orthopedics and dentistry. This chapter described the key role played by the interactions of these materials with the biological environment in bioceramic efficiency when implanted. Specifically, ceramic degradation behavior allows classification of bioceramics into three categories. Inert (or almost inert) ceramics have no tendency to degrade in vivo. Resorbable ceramics, on the contrary, are degradable to various degrees. The degradation products of these ceramics are directly phagocytosed by inflammatory cells, osteoclasts, or even mesenchymal cells of the host, or chemically disintegrated (i.e., by local cell-mediated pH

changes) after implantation. A third category of bioceramics, usually referred to as bioactive ceramics, shows a surface affinity for bone binding. Inert and second-generation (bioactive and resorbable) ceramics are currently used as implants and other medical devices for bone repair. The degradation rate of these implanted bioceramics should match or at least approximate the osteogenic rate. In addition, resorbable and bioactive bioceramics, obtained as porous forms, are used for manufacturing scaffolds susceptible to hosting osteogenic cells and molecules for bone tissue-engineering applications. Incorporation of small peptides (osteostatin) or inorganic compounds (i.e., Sr, Cu, Zn) influencing bone growth and function into these ceramics appears to be an attractive approach in this context. It is obvious that despite extensive research carried out in the field, the perfect bioceramic implant is still not available. In this regard, third-generation bioceramics, which refer to those actively driving tissue regeneration and displaying optimal controlled degradability, are currently under investigation. Likewise, bioceramic nanoparticles might be envisioned as easily functionalized materials for intravenous injection or integrated into polymeric scaffolds to specifically target damaged tissues.

References

- Afzal, A., 2014. Implantable zirconia bioceramics for bone repair and replacement: a chronological review. *Materials Express* 4, 1–12.
- Akagawa, Y., Ichikawa, Y., Nikai, H., Tsuru, H., 1993. Interface histology of unloaded and early loaded partially-stabilized zirconia endosseous implant in initial bone healing. *J. Prosthet. Dent.* 69, 599–604.
- Allen, M., Law, F., Rushton, N., 1994. The effects of diamond-like carbon coatings on macrophages, fibroblasts and osteoblast-like cells in vitro. *Clin. Mater.* 17, 1–10.
- Arcos, D., del Real, R.P., Vallet-Regí, M., 2003. Biphasic materials for bone grafting and hyperthermia treatment of cancer. *J. Biomed. Mater. Res.* 65A, 71–78.
- Arias, J.L., Mayor, M.B., Pou, J., Leng, Y., León, B., Pérez-Amor, M., 2003. Micro- and nano-testing of calcium phosphate coatings produced by pulsed laser deposition. *Biomaterials* 24, 3403–3408.
- Black, J., Hastings, G. (Eds.), 1998. *Handbook of Biomaterial Properties*. Chapman & Hall, New York, NY, pp. 114–124.
- Bloomfield, P., Wheatley, D.J., Prescott, R.J., Miller, H.C., 1991. Twelve-year comparison of a Bjork–Shiley mechanical heart valve with porcine bioprostheses. *N. Engl. J. Med.* 324, 573–579.
- Boccardi, E., Ciraldo, F.E., Boccaccini, A.R., 2017. Bioactive glass-ceramic scaffolds: processing and properties. *MRS Bull.* 42, 226–232.
- Bohner, M., 2000. Calcium orthophosphates in medicine: from ceramics to calcium phosphate cements. *Injury* 31 (S-4), 37–47.
- Boutin, P., 1971. Alumina and its use in surgery of the hip. *Presse Med.* 79, 639–640.
- Brinker, C.J., Lu, Y., Sellinger, A., Fan, H., 1999. Evaporation-induced self-assembly: nanostructures made easy. *Adv. Mater.* 11, 579–601.
- Cabañas, M.V., Vallet-Regí, M., 2003. Calcium phosphate coatings deposited by aerosol chemical vapour deposition. *J. Mater. Chem.* 13, 1104–1107.
- Cabañas, M.V., Rodríguez-Lorenzo, L.M., Vallet-Regí, M., 2002. Setting behavior and in vitro bioactivity of hydroxyapatite/calcium sulphate cements. *Chem. Mater.* 14, 3550–3555.
- Chen, Q., Miyaji, F., Kokubo, T., Nakamura, T., 2000. Bioactivity and mechanical properties of PDMS-modified CaO-SiO₂-TiO₂ hybrids prepared by sol-gel process. *J. Biomed. Mater. Res.* 51, 605–611.
- Chevalier, J., 2006. What future for zirconia as a biomaterial? *Biomaterials* 27 (4), 535–543.
- Christel, P., Meunier, A., Dorlot, J.M., Crolet, J.M., Witvoet, J., Sedel, L., Boutin, P., 1988. Biomechanical compatibility and design of ceramic implants for orthopaedic surgery. *Bioceramics: material characteristics versus in vivo behaviour*. *Ann. NY Acad. Sci.* 523, 234–256.
- Colilla, M., Salinas, A.J., Vallet-Regí, M., 2006. Amino-polysiloxane hybrid materials for bone reconstruction. *Chem. Mater.* 18, 5676–5683.
- Coradin, T., Bah, S., Livage, J., 2004. Gelatine/silicate interactions: from nanoparticles to composite gels. *Colloids Surf. B* 35, 53–58.
- Daculsi, G., 1998. Biphasic calcium phosphate concept applied to artificial bone, implant coating and injectable bone substitute. *Biomaterials* 19, 1473–1478.
- Daculsi, G., Fellah, B.H., Miramond, T., 2014. The essential role of calcium phosphate bioceramics in bone regeneration. In: Ben-Nissan, B. (Ed.). *Springer Series in Biomaterials Science and Engineering*, vol. 2. Springer, Berlin, Heidelberg.
- Dauskardt, R.H., Ritchie, R.O., 1993. Pyrolytic carbon coatings. In: Hench, L.L., Wilson, J. (Eds.), *An Introduction to Bioceramics*. World Scientific, Singapore, pp. 261–280.
- De Groot, K., 1991. Bioceramics consisting of calcium phosphate salts. *Biomaterials* 1, 47–50.
- Deguchi, K., Tsuru, K., Hayashi, T., Takaishi, M., Nagahara, M., Nagotani, S., Sebara, Y., Jin, G., Zhang, H., Hayakawa, S., Shoji, M., Miyazaki, M., Osaka, A., Huh, N.-H., Abe, K., 2006. Implantation of a new porous gelatin-siloxane hybrid into a brain lesion as a potential scaffold for tissue regeneration. *J. Cereb. Blood Flow Metab.* 26, 1263–1273.
- Del Real, R.P., Arcos, D., Vallet-Regí, M., 2002. Implantable magnetic glass-ceramic based on (Fe, Ca) SiO₃ solid solutions. *Chem. Mater.* 14, 64–70.
- Doi, Y., Shibutani, T., Moriwaki, Y., Kajimoto, T., Iwayama, Y.J., 1998. Sintered carbonate apatites as bioresorbable bone substitutes. *J. Biomed. Mater. Res.* 39, 603–610.
- Dorozhkin, S.V., 2010. Bioceramics of calcium orthophosphates. *Biomaterials* 31, 1465–1485.
- Dorozhkin, S.V., Epple, M., 2002. Biological and medical significance of calcium phosphates. *Angew. Chem. Int. Ed.* 41, 3130–3146.
- Du, R.L., Chang, J., 2004. Preparation and characterization of Zn and Mg doped bioactive glasses. *J. Inorg. Mater.* 19, 1353–1358.
- Elias, C.N., Lima, J.H.C., Valiev, R., Meyers, M.A., 2008. Biomedical applications of titanium and its alloys. *JOM J. Miner. Metals Mater. Soc.* 60 (3), 46–49.
- Elliott, J.C., 1994. *Structure and Chemistry of the Apatites and Other Calcium Orthophosphates*. Elsevier, London.
- Fan, H., Wang, L., Zhao, K., Li, N., Shi, Z., Ge, Z., Jin, Z., 2010. Fabrication, mechanical properties, and biocompatibility of graphene-reinforced chitosan composites. *Biomacromolecules* 11, 2345–2351.
- Frieb, W., Warner, J., 2002. Biomedical applications. In: Schuth, F., Sing, K.S.W., Weitkamp, J. (Eds.), *Handbook of Porous Solids*. Wiley-VCH, Weinheim, pp. 2923–2970.
- García, A., Cicuendez, M., Izquierdo-Barba, I., Arcos, D., Vallet-Regí, M., 2009. Essential role of calcium phosphate heterogeneities in 2D-hexagonal and 3D-cubic SiO₂-CaO-P₂O₅ mesoporous bioactive glasses. *Chem. Mater.* 21, 5474–5484.
- García-Sanz, F.J., Mayor, M.B., Arias, J.L., Pou, J., Leon, B., Perez-Amor, M., 1997. Hydroxyapatite coatings: a comparative study between plasma-spray and pulsed laser deposition techniques. *J. Mater. Sci. Mater. Med.* 8, 861–865.
- Gibson, I.R., Best, S.M., Bonfield, W., 1999. Chemical characterization of silicon substituted hydroxyapatite. *J. Biomed. Mater. Res.* 44, 422–428.
- Gil-Albarova, J., Salinas, A.J., Bueno-Lozano, A.L., Román, J., Aldini-Nicolo, N., García-Barea, A., Giavaresi, G., Fini, M., Giardini, R., Vallet-Regí, M., 2005. The in vivo behaviour of a sol-gel glass and a glass-ceramic during critical diaphyseal bone defects healing. *Biomaterials* 26, 4374–4382.
- Ginebra, M.P., Driessens, F.C.M., Planell, J.A., 2004. Effect of the particle size on the micro and nanostructural features of a calcium phosphate cement: a kinetic analysis. *Biomaterials* 25, 3453–3462.
- González, B., Colilla, M., Vallet-Regí, M., 2008. Time-delayed release of bioencapsulates: a novel controlled delivery concept for bone implant technology. *Chem. Mater.* 20, 4826–4834.
- Gregoire, M., Orly, I., Menanteau, J., 1990. The influence of calcium phosphate biomaterials on human bone cell activities. An in vitro approach. *J. Biomed. Mater. Res.* 24, 165–177.

- Grover, L.M., Knowles, J.C., Fleming, G.J.P., Barralet, J.E., 2003. In vitro ageing of brushite calcium phosphate cement. *Biomaterials* 24, 4133–4141.
- Habraken, W., Habibovic, P., Epple, M., Bohner, M., 2016. Calcium phosphates in biomedical applications: materials for the future? *Mater. Today* 19, 69–87.
- Hench, L.L., 1991. Bioceramics: from concept to clinic. *J. Am. Ceram. Soc.* 74, 1487–1510.
- Hench, L.L., 1994. Bioactive ceramics: theory and clinical applications. In: Anderson, Ö.H., Happonen, R.-P., Yli-Urpo, A. (Eds.), *Bioceramics 7*. Butterworth-Heinemann Ltd, Oxford, pp. 3–14.
- Hench, L.L., 1998. Bioceramics. *J. Am. Ceram. Soc.* 81, 1705–1728.
- Hench, L.L., 2016. Bioglass: 10 milestones from concept to commerce. *J. Non-cryst. Solids* 432, 2–8.
- Hench, L.L., Anderson, O., 1993. Bioactive glasses. In: Hench, L.L., Wilson, J. (Eds.), *An Introduction to Bioceramics*. World Scientific, Singapore, pp. 41–62.
- Hench, L.L., Polak, J.M., 2002. Third-generation biomedical materials. *Science* 295, 1014–1017.
- Hench, L.L., Wilson, J., 1984. Surface-active biomaterials. *Science* 226, 630–636.
- Hench, L.L., Splinter, R.J., Allen, W.C., Greenlee, T.K., 1971. Bonding mechanisms at the interface of ceramic prosthetic materials. *J. Biomed. Mater. Res.* 2, 117–4.
- Heymann, D., Pradal, G., Benahmed, M., 1999. Cellular mechanisms of calcium phosphate ceramic degradation. *Histol. Histo-pathol.* 14, 871–877.
- Hijon, N., Manzano, M., Salinas, A.J., Vallet-Regí, M., 2005. Bioactive CaO-SiO₂-PDMS coatings onto Ti6Al4V substrates. *Chem. Mater.* 17, 1591–1596.
- Hijon, N., Cabañas, M.V., Izquierdo-Barba, I., García, M.A., Vallet-Regí, M., 2006. Nanocrystalline bioactive apatite coatings. *Solid State Sci.* 8, 685–689.
- Hoppe, A., Güldal, N.S., Boccaccini, A.R., 2011. A review of the biological response to ionic dissolution products from bioactive glasses and glass-ceramics. *Biomaterials* 32, 2757–2774.
- Hu, W., Peng, C., Luo, W., Lv, M., Li, X., Li, D., Huang, Q., Fan, C., 2010. Graphene-based antibacterial paper. *ACS Nano* 4, 4317–4323.
- Izquierdo-Barba, I., Asenjo, A., Esquivias, L., Vallet-Regí, M., 2003. SiO₂-CaO vitreous films deposited onto Ti6Al4V Substrates. *Eur. J. Inorg. Chem.* 1608–1613.
- Izquierdo-Barba, I., Conde, E., Olmo, N., Lizarbe, M.A., García, M.A., Vallet-Regí, M., 2006. Vitreous SiO₂-CaO coatings onto Ti6Al4V alloys: reactivity in a cellular solution vs osteoblast cell culture. *Acta Biomater.* 2, 445–455.
- Izquierdo-Barba, I., Salinas, A.J., Vallet-Regí, M., 2013. Bioactive glasses: from macro to nano. *Int. J. Appl. Glass Sci.* 4, 149–16.
- Jha, L.J., Best, S.M., Knowles, J.C., Rehman, I., Santos, J.D., Bonfield, W., 1997. Preparation and characterization of fluoride-substituted apatites. *J. Mater. Sci. Mater. Med.* 8, 185–191.
- Kannan, S., Balamurugan, A., Rajeswari, S., 2002. Development of calcium phosphate coatings on type 316L SS and their in-vitro response. *Trends Biomater. Artif. Organs* 16, 8–11.
- Kargozar, S., Baino, F., Hamzehlou, S., Hill, R.G., Mozafari, M., 2018. Bioactive glasses: sprouting angiogenesis in tissue engineering. *Trends Biotechnol.* 36, 430–444.
- Kawahara, H., 1981. Implant biomaterial and ceramics. *Orthopaedic Ceramic Implants* 1, 1–10.
- Khorasani, A.M., Goldberg, M., Döeven, E.H., Littlefair, G., 2015. Titanium in biomedical applications—properties and fabrication: a review. *J. Biomater. Tissue Eng.* 5 (8), 593–619.
- Kivrak, N., Tas, A.C., 1998. Synthesis of calcium hydroxyapatite-tricalcium phosphate (HA-TCP) composite bioceramic powders and their sintering behavior. *J. Am. Ceram. Soc.* 82, 2245–2252.
- Koch, B., Wolke, J.G., de Groot, K., 1990. X-ray diffraction studies on plasma-sprayed calcium phosphate-coated implants. *J. Biomed. Mater. Res.* 24, 655–667.
- Kokubo, T., 1998. Apatite formation on surfaces of ceramics, metals and polymers in body environment. *Acta Mater.* 46, 2519–2527.
- Kokubo, T., Kushitani, H., Sakka, S., Kitsugi, T., Yamamuro, T., 1990. Solutions able to reproduce in vivo surface-structure changes in bioactive glass-ceramic A-W. *J. Biomed. Mater. Res.* 24, 721–734.
- Kokubo, T., Kim, H.M., Kawashita, M., 2003. Novel bioactive materials with different mechanical properties. *Biomaterials* 24, 2161–2175.
- Kumta, P.N., 2006. In: Guelcher, S.A., Hollinger, J. (Eds.), *Ceramic Biomaterials: An Introduction to Biomaterials*. CRC Taylor & Francis, Boca Raton, pp. 311–340.
- Kurtz, S.M., Kocagöz, S., Arnholt, C., Huet, R., Ueno, M., Walter, W.L., 2014. Advances in zirconia toughened alumina biomaterials for total joint replacement. *J. Mech. Behav. Biomed. Mater.* 31, 107–116.
- Langer, R., Vacanti, J.P., 1993. Tissue engineering. *Science* 260, 920–926.
- LeGeros, R.Z., 1991. Calcium phosphates in oral biology and medicine. In: Myers, H.M. (Ed.), *Monographs in Oral Science*, vol. 15. S. Karger, Basel.
- LeGeros, R.Z., 1993. Biodegradation and bioresorption of calcium phosphate ceramics. *Clin. Mater.* 14, 65–88.
- Lew, K.S., Othman, R., Ishikawa, K., Yeoh, F.Y., 2012. Macroporous bioceramics: a remarkable material for bone regeneration. *J. Biomater. Appl.* 27, 345–358.
- Li, J., Hastings, G.W., 1998. Oxide bioceramics: inert ceramic materials in medicine and dentistry. In: Black, J., Hastings, G. (Eds.), *Handbook of Biomaterial Properties*. Chapman Hall, Oxford, pp. 340–354.
- Li, R., Clark, A.E., Hench, L.L., 1991. An investigation of bioactive glass powders by sol-gel processing. *J. Appl. Biomater.* 2, 231–239.
- Liu, X., Chu, P.K., Ding, C., 2004. Surface modification of titanium, titanium alloys, and related materials for biomedical applications. *Mater. Sci. Eng. R Rep.* 47 (3), 49–121.
- Livingston, T., Ducheyne, P., Garino, J., 2002. In vivo evaluation of a bioactive scaffold for bone tissue engineering. *J. Biomed. Mater. Res.* 62, 1–13.
- Manzano, M., Arcos, D., Delgado, M.R., Ruiz, E., Gil, F.J., Vallet-Regí, M., 2006a. Bioactive star gels. *Chem. Mater.* 18, 5696–5703.
- Manzano, M., Salinas, A.J., Vallet-Regí, M., 2006b. P-containing ormosils for bone reconstruction. *Prog. Solid State Chem.* 34, 267–277.
- Martin, A.I., Salinas, A.J., Vallet-Regí, M., 2005. Bioactive and degradable organic-inorganic hybrids. *J. Eur. Ceram. Soc.* 25, 3533–3538.
- Martínez, A., Izquierdo-Barba, I., Vallet-Regí, M., 2000. 'Bioactivity of a CaO-SiO₂ binary glasses system'. *Chem. Mater.* 12, 3080–3088.
- Michalczyk, M.J., Sharp, K.G., 1995. US Patent 5378790.
- Miyata, N., Fuke, K., Chen, Q., Kawashita, M., Kokubo, T., Nakamura, T., 2004. Apatite-forming ability and mechanical properties of PTMO-modified CaO-SiO₂-TiO₂ hybrids derived from sol-gel processing. *Biomaterials* 25, 1–7.
- Morrell, R., Danzer, R., Milosev, I., Trebse, R., 2012. An assessment of in vivo failures of alumina ceramic total hip joint replacements. *J. Eur. Ceram. Soc.* 32, 3073–3084.

- Narasaraju, T.S.B., Phebe, D.E., 1996. Some physico-chemical aspects of hydroxyapatite. *J. Mater. Sci.* 31, 1–21.
- Nilsson, M., Fernández, E., Sarda, S., Lidgren, L., Planell, J.A., 2002. Characterization of a novel calcium phosphate/sulphate bone cement. *J. Biomed. Mater. Res.* 61, 600–607.
- Oki, A., Parveen, B., Hossain, S., Adeniji, A., Donahue, H., 2004. Preparation and *in vitro* bioactivity of zinc containing sol-gel-derived bioglass materials. *J. Biomed. Mater. Res.* 69A, 216–221.
- Olmo, N., Martín, A.I., Salinas, A.J., Turnay, J., Vallet-Regí, M., Lizarbe, M.A., 2003. Bioactive sol-gel glasses with and without a hydroxycarbonate apatite layer as substrates for osteoblast cell adhesion and proliferation. *Biomaterials* 24, 3383–3393.
- Onishi, H., Okabe, N., Hamaguchi, T., Nabeshima, T., 1981. Cementless alumina ceramic total knee prosthesis. *Orthopaedic Ceramic Implants* 1, 11–18.
- Ostomel, T.A., Shi, Q.H., Tsung, C.K., Liang, H.J., Stucky, G.D., 2006. Spherical bioactive glass with enhanced rates of hydroxyapatite deposition and hemostatic activity. *Small* 2, 1261–1265.
- Otsuka, M., Matsuda, Y., Suwa, Y., Fox, J.L., Higuchi, W., 1995. Effect of particle size of metastable calcium phosphates on mechanical strength of a novel self-setting bioactive calcium phosphate cement. *J. Biomed. Mater. Res.* 29, 25–32.
- Padilla, S., Roman, J., Carenas, A., Vallet-Regí, M., 2005. Influence of the phosphorus content on the bioactivity in sol-gel glass ceramics. *Biomaterials* 26, 475–483.
- Park, Y.S., Yi, K.Y., Lee, I.S., Han, C.H., Jung, Y.C., 2005. The effects of ion beam-assisted deposition of hydroxyapatite on the grit-blasted surface of endosseous implants in rabbit tibiae'. *Int. J. Oral Maxillofac. Implant.* 20, 31–38.
- Pechini, M.P., July 11, 1967. U. S. Patent 3 330,697.
- Peltola, T., Jokinen, M., Rahiala, H., Levänen, E., Rosenhold, J.B., Kangasniemi, I., Yli-Urpo, A., 1999. Calcium phosphate formation on porous sol-gel-derived SiO₂ and CaO-P₂O₅-SiO₂ substrates *in vitro*. *J. Biomed. Mater. Res.* 44, 12–21.
- Peña, J., Vallet-Regí, M., 2003. Hydroxyapatite, tricalcium phosphate and biphasic materials prepared by a liquid mix technique. *J. Eur. Ceram. Soc.* 23, 1687–1696.
- Pereira, M.M., Clark, A.E., Hench, L.L., 1994. Calcium-phosphate formation on sol-gel-derived bioactive glasses *in-vitro*. *J. Biomed. Mater. Res.* 28, 693–698.
- Pereira, A.P.V., Vasconcelos, W.L., Oréfice, R.K., 2000. Novel multicomponent silicate-poly(vinyl alcohol) hybrids with controlled reactivity. *J. Non-cryst. Solids* 273, 180–185.
- Pérez-Pariente, J., Balas, F., Román, J., Salinas, A.J., Vallet-Regí, 1999. Influence of composition and surface characteristics on the *in vitro* bioactivity of SiO₂-CaO-P₂O₅-MgO sol-gel glasses. *J. Biomed. Mater. Res.* 47, 170–175.
- Perez, P., Sanchez-Salcedo, S., Lozano, D., Heras, C., Esbrit, P., Vallet-Regí, M., Salinas, A.J., 2018. Osteogenic effect of ZnO-mesoporous glasses loaded with osteostatin. *Nanomaterials* 8 (8).
- Pietrzak, W.S., Ronk, R., 2000. Calcium sulphate bone void filler: a review and a look ahead. *J. Craniofac. Surg.* 11, 327–334.
- Polack, F.M., Heimke, G., 1980. Ceramic kerato-prostheses. *Ophthalmology* 87, 693–698.
- Rae, T., 1986. The macrophage response to implant materials-with special reference to those used in orthopedics. *CRC Crit. Rev. Biocompat.* 2, 97–126.
- Ramila, A., Padilla, S., Muñoz, B., Vallet-Regí, M., 2002. A new hydroxyapatite/glass biphasic material: *in vitro* bioactivity'. *Chem. Mater.* 14, 2439–2943.
- Ratner, B.D., Castner, D.G., 2002. Biomedical surface science: foundations to frontiers. *Surf. Sci.* 500, 28–60.
- Ren, L., Tsuru, K., Hayakawa, S., Osaka, A., 2002. Novel approach to fabricate porous gelatin-siloxane hybrids for bone tissue engineering. *Biomaterials* 23, 4765–4773.
- Rhee, S.H., 2004. Bone-like apatite-forming ability and mechanical properties of poly(ϵ -caprolactone)/silica hybrid as a function of poly(ϵ -caprolactone) content. *Biomaterials* 25, 1167–1175.
- Rhee, S., Choi, J., 2002. Preparation of a bioactive poly(methyl methacrylate)/silica nanocomposite. *J. Am. Ceram. Soc.* 85, 1318–1320.
- Rodrigo, A., Valles, G., Saldaña, L., Rodríguez, M., Martínez, M.E., Munuera, L., Vilaboa, N., 2006. Alumina particles influence the interactions of cocultured osteoblasts and macrophages. *J. Orthop. Res.* 24, 46–54.
- Roman, J., Padilla, S., Vallet-Regí, M., 2003. Sol-gel glasses as precursors of bioactive glass-ceramics. *Chem. Mater.* 15, 798–806.
- Román, J., Cabañas, M.V., Peña, J., Doadrio, J.C., Vallet-Regí, M., 2008. An optimised β -tricalcium phosphate and agarose scaffold fabrication technique. *J. Biomed. Mater. Res. A* 84A, 99–107.
- Ruiz-Hernández, E., López-Noriega, A., Arcos, D., Vallet-Regí, M., 2008. Mesoporous magnetic microspheres for drug targeting. *Solid State Sci.* 10, 421–426.
- Salinas, A.J., Vallet-Regí, M., 2017. Sol-gel silica-based biomaterials and bone tissue regeneration. In: Klein, L., Aparicio, M., Jitianu, A. (Eds.), *Handbook of Sol-Gel Science and Technology*, second ed. The Springer, pp. 3597–3618.
- Salinas, A.J., Vallet-Regí, M., Izquierdo-Barba, I., 2001. Biomimetic apatite deposition on calcium silicate gel glasses. *J. Sol. Gel Sci. Technol.* 21, 13–25.
- Salinas, A.J., Martín, A.I., Vallet-Regí, M., 2002. Bioactivity of three CaO-P₂O₅-SiO₂ sol-gel glasses. *J. Biomed. Mater. Res.* 61, 524–532.
- Salinas, A.J., Merino, J.M., Gil, F.J., Babonneau, F., Vallet-Regí, M., 2007. Microstructure and macroscopic properties of CaO-SiO₂-PDMS hybrids for use in implants. *J. Biomed. Mater. Res. B* 81B, 274–282.
- Salinas, A.J., Shruti, S., Malavasi, G., Menabue, L., Vallet-Regí, M., 2011. Substitutions of cerium, gallium and zinc in ordered mesoporous bioactive glasses. *Acta Biomater.* 7, 3452–3458.
- Salinas, A.J., Esbrit, P., Vallet-Regí, M., 2013. A tissue engineering approach based on the use of bioceramics for bone repair. *Biomater. Sci.* 1, 40–51.
- Salinas, A.J., Vallet-Regí, M., Heikkilä, J., 2018. Use of bioactive glasses as bone substitutes in orthopedics and traumatology. In: *Bioactive Glasses, Materials, Properties and Applications*. Woodhead Publishing Series in Biomaterials, pp. 337–364.
- Sánchez-Salcedo, S., Nieto, A., Vallet-Regí, M., 2008a. Hydroxyapatite/ β -tricalcium phosphate/agarose macroporous scaffolds for bone tissue engineering. *Chem. Eng. J.* 137, 62–71.
- Sanchez-Salcedo, S., Werner, J., Vallet-Regí, M., 2008b. Hierarchical pore structure of calcium phosphate scaffolds by combination of the gel casting and multiple tape casting methods. *Acta Biomater.* 4, 913–922.
- Sanchez-Salcedo, S., Malavasi, G., Salinas, A.J., Lusvardi, G., Rigamonti, L., Menabue, L., Vallet-Regí, M., 2018. Highly-bioreactive silica-based mesoporous bioactive glasses enriched with gallium(III). *Materials* 11, 367.
- Sanders, D., Hench, L., 1973. Mechanisms of glass corrosion. *J. Am. Ceram. Soc.* 56, 373–377.
- Sandhaus, S., 1967. Bone Implants and Drills and Taps for Bone Surgery. British Patent 1083769.
- Schiraldi, C., D'Agostino, A., Oliva, A., Flamma, F., De la Rosa, A., Apicella, A., Aversa, R., De la Rosa, M., 2004. Development of hybrid materials based on hydroxyethylmethacrylate as supports for improving cell adhesion and proliferation. *Biomaterials* 25, 3645–3653.

- Schulte, W., 1990. The Frialit Tuebingen implant system. In: Heimke, G. (Ed.), *Osseointegrated Implants Volume II. Implants in Oral and ENT Surgery*. CRC Press, Boca Raton, pp. 1–34.
- Serrano, M.C., Portolés, M.T., Pagani, R., Sáez de Guinoa, J., Ruíz-Hernández, E., Arcos, D., Vallet-Regí, M., 2008. In vitro positive biocompatibility evaluation of glass-glass ceramic thermoseeds for hyperthermic treatment of bone tumors. *Tissue Eng. A* 14, 617–627.
- Sharp, K.G., 1998. Inorganic/organic hybrid materials. *Adv. Mater.* 10, 1243–1248.
- Shirosaki, Y., Tsuru, K., Hayakawa, S., Osaka, A., 2008. Biodegradable chitosan-silicate porous hybrids for drug delivery. *Key Eng. Mater.* 361–363, 1219–1222 (Switzerland, Trans Tech Publications).
- Smith, L., 1963. Ceramic plastic material as a bone substitute. *Arch. Surg.* 87, 653–661.
- Sun, L.M., Berndt, C.C., Gross, K.A., Kucuk, A., 2001. Material fundamentals and clinical performance of plasma-sprayed hydroxyapatite coatings: a review. *J. Biomed. Mater. Res.* 58, 570–592.
- Tamimi, F., Sheikh, Z., Barralet, J., 2012. Dicalcium phosphate cements: brushite and monetite. *Acta Biomater.* 8, 474–487.
- Tancred, D.C., McCormack, B.A.O., Carr, A.J., 1998. A synthetic bone implant macroscopically identical to cancellous bone. *Biomaterials* 19, 2303–2311.
- Tsuru, K., Hayakawa, S., Osaka, A., 2008. Cell proliferation and tissue compatibility of organic-inorganic hybrid materials. *Key Eng. Mater.* 377, 167–180 *Progress in Bioceramics*, Vallet-Regí, M. (ed), Switzerland, Trans Tech Publications.
- Vallet-Regí, M., 2001. Ceramics for medical applications. *J. Chem. Soc., Dalton Trans.* 97–108.
- Vallet-Regí, M., 2006. Revisiting ceramics for medical applications. *Dalton Trans.* 5211–5220.
- Vallet-Regí, M., Arcos, D., 2005. Silicon substituted hydroxyapatites. A method to upgrade calcium phosphate based implants. *J. Mater. Chem.* 15, 1509–1516.
- Vallet-Regí, M., Arcos, D., 2006. Nanostructured hybrid materials for bone tissue regeneration. *Curr. Nanosci.* 2, 179–189.
- Vallet-Regí, M., Arcos-Navarrete, D., 2008. *Biomimetic Nanoceramics in Clinical Use: From Materials to Applications*. Royal Society of Chemistry, Cambridge.
- Vallet-Regí, M., González-Calbet, J., 2004. Calcium phosphates in the substitution of bone tissue. *Prog. Solid State Chem.* 32, 1–31.
- Vallet-Regí, M., Salinas, A.J., 2017. Mesoporous bioactive glasses in tissue engineering and drug delivery. In: Boccaccini, A.R., Brauer, D.S., Hupa, L. (Eds.), *Bioactive Glasses: Fundamentals, Technology and Applications*. The Royal Society of Chemistry, London, UK, pp. 393–419.
- Vallet-Regí, M., Salinas, A.J., 2018. Role of the short distance order in glass reactivity. *Materials* 11, 415.
- Vallet-Regí, M., Gutiérrez-Ríos, M.T., Alonso, M.P., de Frutos, M.I., Nicolopoulos, S., 1994. Hydroxyapatite particles synthesized by pyrolysis of an aerosol. *J. Solid State Chem.* 112, 58–64.
- Vallet-Regí, M., Rodríguez-Lorenzo, L.M., Salinas, A.J., 1997. Synthesis and characterisation of calcium deficient apatite. *Solid State Ion.* 101–103, 1279–1285.
- Vallet-Regí, M., Romero, A.M., Ragel, C.V., LeGeros, R.Z., 1999. XRD, SEM-EDS and FTIR studies of in vitro growth of an apatite-like layer on sol-gel glasses. *J. Biomed. Mater. Res.* 44, 416–421.
- Vallet-Regí, M., Rámila, A., del Real, R.P., Pérez-Pariente, J., 2001. A new property of MCM-41: drug delivery system. *Chem. Mater.* 13, 308–311.
- Vallet-Regí, M., Ragel, C.V., Salinas, A.J., 2003a. Glasses with medical applications. *Eur. J. Inorg. Chem.* (6) 1029–1042.
- Vallet-Regí, M., Izquierdo-Barba, I., Gil, F.J., 2003b. Localized corrosion of 316L Stainless Steel with SiO₂-CaO films obtained by means of sol-gel treatment. *J. Biomed. Mater. Res.* 67A, 674–678.
- Vallet-Regí, M., Román, J., Padilla, S., Doadrio, J.C., Gil, F.J., 2005a. Bioactivity and mechanical properties of SiO₂-CaO-P₂O₅ glass-ceramics. *J. Mater. Chem.* 15, 1353–1359.
- Vallet-Regí, M., Salinas, A.J., Ramírez-Castellanos, J., González-Calbet, J.M., 2005b. Nanostructure of bioactive sol-gel glasses and organic inorganic hybrids. *Chem. Mater.* 17, 1874–1879.
- Vallet-Regí, M., Ruiz-González, M.L., Izquierdo-Barba, I., González-Calbet, J.M., 2006. Revisiting silica based ordered mesoporous materials: medical applications. *J. Mater. Chem.* 16, 26–31.
- Van der Stok, J., Lozano, D., Chai, Y.C., Yavari, S.A., Bastidas Coral, A.P., Verhaar, J.A.N., Gomez-Barrena, E., Schrooten, J., Jahr, H., Zadpoor, A.A., Esbrit, P., Weinans, H., 2015. *Tissue Eng. A* 21, 1495–1506.
- Wang, G.C., Lu, Z.F., Zreiqat, H., 2014. Bioceramics for skeletal bone regeneration. In: *Bone Substitute Biomaterials*. Woodhead Publishing Series in Biomaterials, pp. 180–186. 187e-190e, 187-216.
- Williams, D.F., 2008. On the mechanisms of biocompatibility. *Biomaterials* 29, 2041–2953.
- Wolke, J.G.C., de Groot, K., Jansen, J.A., 1998. Subperiosteal implantation of various RF magnetron sputtered Ca-P coatings in goats. *J. Biomed. Mater. Res.* 43, 270–276.
- Xynos, I.D., et al., 2001. Gene-expression profiling of human osteoblasts following treatment with the ionic products of Bioglass® 45S5 dissolution. *J. Biomed. Mater. Res.* 55 (2), 151–157.
- Yabuta, T., Bescher, E.P., Mackenzie, J.D., Tsuru, K., Hayakawa, S., Osaka, A., 2003. Synthesis of PDMS-based porous materials for biomedical applications. *J. Sol. Gel Sci. Technol.* 26, 1219–1222.
- Yan, X., Yu, C., Zhou, H., Tang, J., Zhao, D., 2004. Highly ordered mesoporous bioactive glasses with superior in vitro bone-forming bioactivities. *Angew. Chem. Int. Ed.* 43, 5980–5984.
- Yuan, H.P., Kurashina, K., de Bruijn, J.D., Li, Y.B., de Groot, K., Zhang, X.D., 1999. A preliminary study on osteoinduction of two kinds of calcium phosphate ceramics. *Biomaterials* 20, 1799–1806.
- Zhang, F., Chang, J., Lu, J., Lin, K., Ning, C., 2007. Bioinspired structure of bioceramics for bone regeneration in load-bearing sites. *Acta Biomater.* 3, 896–904.
- Zhu, L., Chang, D.W., Dai, L., Hong, Y., 2007. DNA damage induced by multiwalled carbon nanotubes in mouse embryonic stem cells. *Nano Lett.* 7, 3592–3597.

2.4.5

Pathological Calcification of Biomaterials

FREDERICK J. SCHOEN¹, ROBERT J. LEVY², HOBEY TAM³, NAREN VYAVAHARE⁵

¹Department of Pathology, Brigham and Women's Hospital, and Harvard Medical School, Boston, MA, United States

²Department of Pediatrics, The Childrens' Hospital of Philadelphia, The Perelman School of Medicine at the University of Pennsylvania, Philadelphia, PA, United States

³Department of Bioengineering, Rhodes Engineering Research Center, Clemson University, Clemson, SC, United States

Calcification of biomaterial implants is an important pathologic process affecting a variety of tissue-derived biomaterials, as well as synthetic polymers in various functional configurations. The pathophysiology has been partially characterized by some useful animal models; common features are the involvement of devitalized cells and cellular debris and often extracellular matrix proteins, and oxidative damage to the extracellular matrix and/or other reactive sites within the implant. Calcification of biomaterials often contributes to deleterious outcomes. Clinically useful preventive approaches based on modifying biomaterials appear to be promising in some contexts.

The formation of nodular deposits of calcium phosphate or other calcium-containing compounds may occur on biomaterials and prosthetic devices used in the circulatory system and at other sites. This process, known as *calcification* or *mineralization*, has been encountered in association with both synthetic and biologically derived biomaterials in diverse experimental and clinical settings, including chemically treated tissue (*bioprosthetic*), homografts, and polymeric cardiac valve substitutes (Mitchell et al., 1998; Schoen and Levy, 1999, 2005; Claiborne et al., 2012), blood pumps used as cardiac assist devices (Schoen and Edwards, 2001), breast implants (Peters et al., 1998; Legrand et al., 2005), intrauterine contraceptive devices (Patai et al., 1998), urological stents (Vanderbrink et al., 2008), intraocular lenses (Neuhann et al., 2008; Nakanome et al., 2008; Rimmer et al., 2010; Rahimi et al., 2018), and scleral buckling materials (Brockhurst et al., 1993; Yu et al., 2005). Vascular access grafts for hemodialysis and synthetic vascular replacements composed of Dacron or expanded polytetrafluoroethylene

(e-PTFE) also calcify in some patients (Tomizawa et al., 1998; Schlieper et al., 2008). Importantly, calcification can lead to important clinical complications of implanted biomaterials and medical devices, examples of which are stiffening and/or tearing of tissue heart valve substitutes, encrustation with blockage of a urinary stent or clouding of intraocular lenses (Table 2.4.5.1).

Deposition of mineral salts of calcium (as calcium phosphates, especially calcium hydroxyapatite) occurs normally in bones and teeth and is a critical determinant of their mechanical and biological properties (called *physiologic* mineralization). Mineralization of skeletal tissues is both controlled and restricted to specific anatomic sites. The mature mineral phase of bone is a poorly crystalline calcium phosphate known as calcium hydroxyapatite, which has the chemical formula $\text{Ca}_{10}(\text{PO}_4)_6(\text{OH})_2$. Mineralization of some implant biomaterials is desirable for proper function, e.g., osteoinductive materials used for orthopedic or dental applications (Habibovic and de Groot, 2007), and materials used to engineer skeletal and dental tissues (Kretlow and Mikos, 2007; Bueno and Glowacki, 2009). However, severe consequences can occur if mineralization occurs in regions that do not normally calcify (*pathologic* or *ectopic* mineralization) (Kirsch, 2008).

Because the biomaterials used in medical devices outside of the musculoskeletal and dental systems are not intended to calcify, calcification of these biomaterials is *pathologic*. The mature mineral phase of biomaterial-related and other forms of pathologic calcification is a poorly crystalline calcium phosphate that closely resembles the calcium hydroxyapatite present in bones and teeth. Indeed, as we

TABLE 2.4.5.1 Representative Prostheses and Devices With Clinical Consequences due to Biomaterials Calcification

Configuration	Biomaterial	Clinical Consequence
Cardiac valve prostheses	Glutaraldehyde-pretreated porcine aortic valve or bovine pericardium, and allograft aortic/pulmonary valves	Valve obstruction or incompetency
Cardiac ventricular assist bladders	Polyurethane	Dysfunction by stiffening or cracking
Vascular grafts	Dacron® grafts and aortic allografts	Graft obstruction or stiffening
Soft contact lens	Hydrogels	Opacification
Intrauterine contraceptive devices	Silicone rubber, polyurethane or copper	Birth control failure by dysfunction or expulsion
Urinary prostheses	Silicone rubber or polyurethane	Incontinence and/or infection
Breast implants	Silicone	Implant contracture

will see later, biomaterials-related calcification shares many features with other conditions of pathologic calcification and physiologic mineralization. Pathologic calcification of natural structures is also a common feature of important disease processes; for example, in native arteries and heart valves, calcification occurs as an important feature of disease processes such as atherosclerosis and calcific aortic stenosis (Mitchell and Schoen, 2010; Schoen and Mitchell, 2010; Andrews et al., 2018; Pawade et al., 2015).

Pathologic calcification is further classified as either *dystrophic* or *metastatic*, depending on its setting (Kumar et al., 2015). In dystrophic calcification the deposition of calcium salts (usually calcium phosphates) occurs in damaged or diseased tissues or in or related to biomaterials; moreover, dystrophic calcification usually occurs in the setting of normal systemic calcium metabolism (generally defined by a product of the serum levels of calcium and phosphorus within the physiologic range). In contrast, metastatic calcification comprises the deposition of calcium salts in otherwise normal tissues in individuals who have deranged mineral metabolism, usually with markedly elevated blood calcium or phosphorus levels. Conditions favoring dystrophic and metastatic calcification can act synergistically. Thus, the rate and extent of dystrophic mineralization within abnormal tissues are accelerated when calcium and/or phosphorus serum levels are high, for example, in kidney failure or calcium supplementation (Umana et al., 2003; Peacock, 2010), and in osteoporosis (Hofbauer et al., 2007; Hjortnaes et al., 2010). Moreover, the ability to form physiologic mineral (e.g., in bone) is regulated through adjustment of enhancing and inhibiting substances, many of which circulate in the blood (Weissen-Planz et al., 2008). In young individuals (especially into early adulthood) the balance appropriately favors bone formation; moreover, the biochemical environment that favors physiologic bone formation in children also promotes calcification of biomaterials (Bass and Chan, 2006; Peacock, 2010).

Additionally, calcification of an implanted biomaterial can occur either within the material (*intrinsic* calcification)

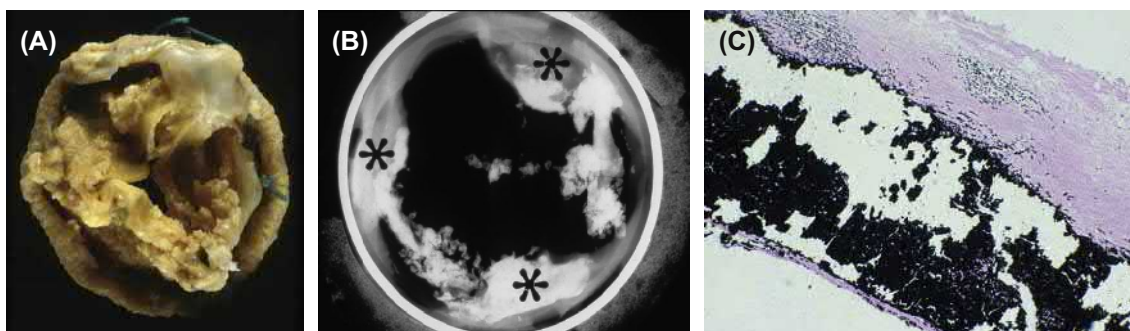
or at the surface, usually associated with attached cells and proteins or in the implant fibrous capsule (*extrinsic* calcification). A notable instance of extrinsic calcification is that associated with prosthetic valve infection (also called prosthetic valve endocarditis) or thrombi.

The Spectrum of Pathologic Biomaterial and Medical Device Calcification

Bioprosthetic Heart Valves

Calcific degeneration of bioprosthetic heart valves composed of glutaraldehyde-pretreated heterograft materials, typically either porcine aortic valves or bovine pericardium (Fig. 2.4.5.1) is the most prevalent clinically significant and well-characterized dysfunction of a medical device due to biomaterials calcification (Schoen and Levy, 1999, 2005). The predominant pathologic process is intrinsic calcification of the valve cusps, largely initiated in the deep interstitial cells of the tissue from which the valve was fabricated and often involves collagen and elastin. Calcification leads to valve failure most commonly by causing tissue tears or tissue stiffening, and rarely by inducing distant emboli. Overall, approximately half of contemporary bioprostheses fail within 15–20 years.

Calcification is more rapid and aggressive in younger recipients; to exemplify, the rate of failure of bioprostheses is approximately 10% in 10 years in elderly recipients but is nearly uniform in less than 4 years in most adolescent and preadolescent children (Chan et al., 2006). In some young individuals with congenital cardiac defects or acquired aortic valve disease, human *allograft/homograft* aortic or pulmonary valves surrounded by a sleeve of the aorta or pulmonary artery, respectively, are used. Allograft valves are valves removed from a person who has died and transplanted to another individual; the tissue is usually cryopreserved (and thawed immediately prior to implantation), but not chemically cross-linked. Allograft vascular segments (without a valve) can be used to replace a large blood vessel.



• **Figure 2.4.5.1** Calcification of a pericardial bioprosthetic heart valve, implanted in a person for many years: (A) gross photograph, demonstrating marked thickening of cusps by nodular calcific deposits; (B) radiograph of another long-term valve, demonstrating predominant deposits at commissures; (C) photomicrograph demonstrating calcific nodule deeply embedded within cuspal tissue; von Kossa stain (calcium phosphates black) 100 \times .

Allograft vascular tissue, whether containing an aortic valve or not, can undergo severe calcification in the wall; calcification can lead to allograft valve dysfunction or deterioration (Mitchell et al., 1998).

Transcatheter (or Percutaneous) Cardiac Valve Replacements

Transcatheter aortic valve replacement (TAVR, also known as transcatheter aortic valve implantation [TAVI]) has emerged over the past decade as a widely used minimally invasive therapeutic option for patients with symptomatic severe aortic stenosis who are ineligible for or at excessive risk for conventional surgical aortic valve replacement (Baumgartner et al., 2017). In this procedure, the diseased valve is not removed; instead, it is simply pushed out of the flow stream by the expanded replacement valve. Transcatheter valves are usually fabricated from bovine pericardium and mounted on a self-expanding or balloon-expandable stent crimped into and deployed via a catheter inserted through the femoral artery and threaded retrograde through the aorta to the heart, or across the apex of the ventricle into the heart.

Although this procedure was initially preferred for people who have severe valve disease but are not suitable for open-heart surgery, recent demonstration of favorable outcomes (relatively to open surgery) in intermediate- and low-risk patients suggests that the use of transcatheter valve replacement may be expanding. These valve replacements are also deployed after a failure of a bioprosthetic heart valve implant in a *valve-in-valve* procedure. The old replacement valve is *left inside the patient*, and the TAVR is deployed inside of the old valve, thereby pushing open the old valve and opening up a smaller but unblocked/functional valve with effective orifice area. The overall long-term durability of transcatheter replacement valves is yet uncertain; nevertheless, calcification has been observed in some cases (Zareian et al., 2019; Kataruka and Otto, 2018). Furthermore, studies have shown that crimping is associated with higher level of passive tissue calcification (Ramin et al., 2019; Munnely et al.,

2012). Most of the TAVRs currently used are treated with proprietary anticalcification treatments.

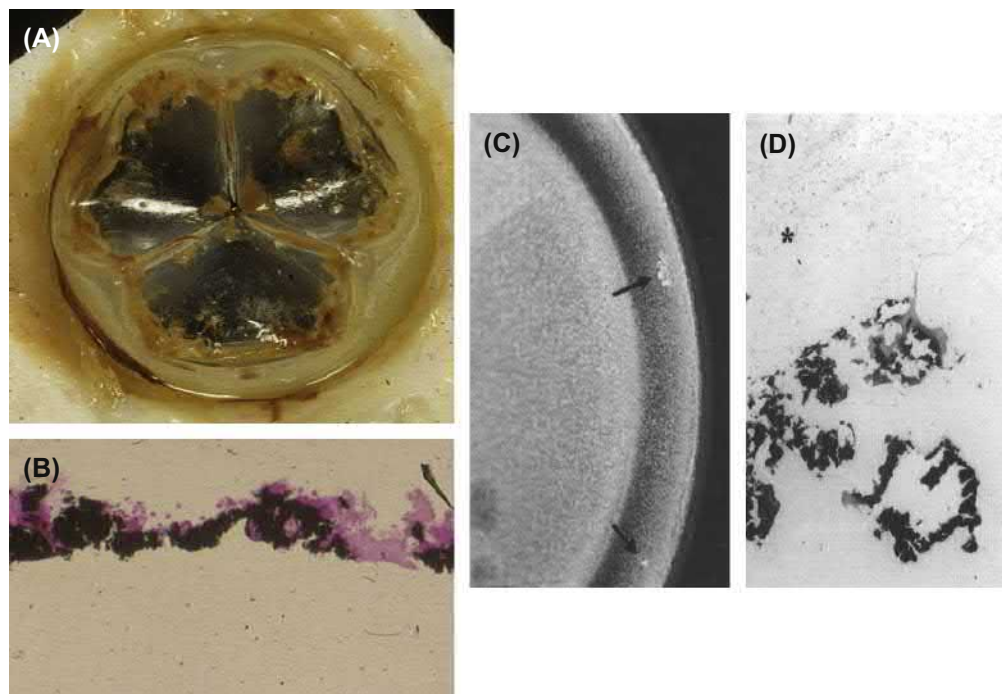
Polymeric Heart Valves and Blood Pump Bladders

Calcification has also complicated the use of heart valves and artificial mitral valve *chordae tendineae* composed of polymers (e.g., polyurethane) (Fukunaga et al., 2010; Hilbert et al., 1987; Schoen et al., 1992a; Schoen and Levy, 1999; Wang et al., 2010) and the flexing bladder surfaces of blood pumps used as ventricular assist devices or total artificial hearts (Schoen and Edwards, 2001) (Fig. 2.4.5.2). Massive deposition of mineral leading to failure of cardiac assist devices has been noted in experimental animals, but only a lesser degree of calcification has been encountered following extended human implantation. Mineral deposits can result in deterioration of pump or valve performance through loss of bladder pliability or the initiation of tears. Blood pump calcification, regardless of the type of polyurethane used, generally predominates along the flexing margins of the diaphragm, emphasizing the important potentiating role of mechanical factors in this system (Coleman et al., 1981; Harasaki et al., 1987; Kantrowitz et al., 1995).

Calcific deposits associated with a polymeric heart valve or blood pump components can occur either within the adherent layer of deposited thrombus, proteins, and cells on the blood-contacting surface (a form of extrinsic mineralization) or below the surface (a form of intrinsic calcification) (Joshi et al., 1996). In some cases, calcific deposits are associated with microscopic surface defects, originating either during bladder fabrication or resulting from cracking during the function.

Breast Implants

Calcification of silicone-gel breast implant capsules occurs as discrete calcified plaques at the interface of the inner fibrous capsule with the implant surface (Peters et al., 1998; Gumus, 2009). Capsular calcification has also been encountered with breast implants in patients with silicone envelopes filled with saline. Calcification could interfere with effective



• **Figure 2.4.5.2** Calcification of an experimental polymeric (polyurethane) heart valve: (A) gross photograph of valve; (B) photomicrograph of calcified material at surface of polymer (polymer at bottom of photo); and calcification of the flexing bladder of a ventricular assist pump removed from a person after 257 days. (C) Gross photograph. Calcific masses are noted by arrows; (D) photomicrograph. (B) and (D) von Kossa stain (calcium phosphates black) 100 \times .

tumor detection and diagnosis, which could potentially delay treatment, particularly during monitoring for recurrence in patients who have breast implants following reconstructive surgery for breast cancer. In a study of breast implants removed predominantly for capsular contraction, 16% overall demonstrated calcific deposits, including 26% of implants inserted for 11–20 years, and all those inserted for more than 23 years (Peters and Smith, 1995). Another study demonstrated calcification associated with virtually all implants examined after more than 20 years (Legrand et al., 2005).

Ivalon (polyvinyl alcohol) sponge prostheses, used quite extensively during the 1950s, were also frequently associated with calcification. In Japan, where augmentation mammoplasty was frequently performed using an injection of foreign material (liquid paraffin from approximately 1950 until 1964, and primarily liquid silicone injections thereafter), the incidence of calcification has been much higher. One study showed calcification in 45% of breast augmentations which were done by injection (Koide and Katayama, 1979).

Intrauterine Contraceptive Devices

Intrauterine contraceptive devices (IUDs) are composed of plastic or metal and placed in a woman's uterus chronically to prevent implantation of a fertilized egg. Device dysfunction due to calcific deposits can be manifested as a contraceptive failure or device expulsion. For example, accumulation of calcific plaque could prevent the release of the active contraception-preventing agent—either ionic copper from

copper-containing IUDs or an active agent from hormone-releasing polymer IUD systems. Studies of explanted IUDs using transmission and electron microscopy coupled with X-ray microprobe analysis have shown that surface calcium deposition is virtually ubiquitous, but highly variable among patients (Khan and Wilkinson, 1985; Patai et al., 1998).

Urinary Stents and Prostheses

Mineral crusts form on the surfaces of urinary stents and nephrostomy tubes, which are used extensively in urology to alleviate a urinary obstruction or incontinence (Goldfarb et al., 1989; Vanderbrink et al., 2008). Observed in both male and female urethral implants and artificial ureters, this calcification can lead to obstruction and device failure. The mineral crust typically consists of either calcium oxalate or calcium phosphate mineral such as hydroxyapatite or struvite, ammonium- and magnesium-containing phosphate mineral derived from urine. There is some evidence that encrustation may both result from and predispose to bacterial infection.

Intraocular and Soft Contact Lenses and Scleral Buckles

Calcium phosphate deposits can opacify intraocular and soft contact lenses, typically composed of poly-2-hydroxyethyl-methacrylate polymers (pHEMA) (Bucher et al., 1995; Nakanome et al., 2008; Neuhann et al., 2008; Rimmer et al., 2010; MacLean et al., 2015; Phogat et al., 2017).

TABLE 2.4.5.2 Methods for Assessing Calcification

Technique	Sample Preparation	Analytical Results
Morphologic Procedures		
Gross examination	Gross specimen	Overall morphology
Radiographs	Gross specimen	Calcific deposit distribution
Microcomputed tomography	Gross specimen	Three-dimensional reconstruction of calcific deposit morphology, localization, and quantification
Light microscopy—von kossa or alizarin red stains	Formalin or glutaraldehyde fixed	Microscopic phosphate or calcium distribution, respectively
Transmission electron microscopy	Glutaraldehyde fixed	Mineral ultrastructure
Scanning electron microscopy with electron microprobe	Glutaraldehyde fixed	Elemental localization and quantitation
Electron energy loss spectroscopy	Glutaraldehyde fixed or rapidly frozen	Elemental localization and quantitation (high sensitivity)
Chemical Procedures		
Atomic absorption	Ash or acid hydrolysate	Bulk calcium
Colorimetric phosphate analysis	Ash or acid hydrolysate	Bulk phosphorus
X-ray diffraction	Powder	Nature of crystal phase
Infrared spectroscopy	Powder	Carbonate mineral phase

Tear fluid provides the source of the calcium in the deposits found on HEMA contact lens, and calcification may be potentiated in patients with systemic and ocular conditions associated with elevated tear calcium levels (Klintworth et al., 1977). Encircling scleral bands, used in surgery for retinal detachment, and composed of silicone or hydrogel materials, also can calcify (Lane et al., 2001).

Assessment of Biomaterial Calcification

Calcific deposits are investigated using morphologic and chemical techniques (Table 2.4.5.2). Morphologic techniques facilitate detection and characterization of the microscopic and ultrastructural sites and distribution of calcific deposits, and their relationship to tissue or biomaterials structural details. Such analyses directly yield important qualitative (but not quantitative) information. In contrast, chemical techniques, which require destruction of the tissue specimen, permit identification and quantitation of both bulk elemental composition and determination of crystalline mineral phases. However, such techniques generally cannot relate the location of the mineral to the details of the underlying tissue structure. The most comprehensive studies use several analytical modalities to simultaneously characterize both morphologic and chemical aspects of calcification.

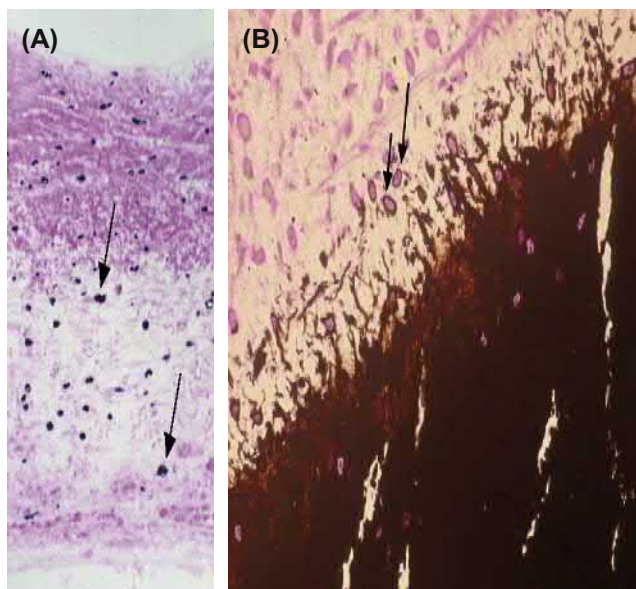
Moreover, newer techniques are available for non-destructive and potentially noninvasive characterizing of calcification, both in specimens (microcomputed tomography [micro-CT]) (Ford-Hutchinson et al., 2003; Rousselle et al., 2019; Neues and Epple, 2008), and in vivo using molecular imaging (Aikawa et al.,

2007). Micro-CT has been used extensively in studies of bone-regenerative biomaterials (Jiang et al., 2009). Molecular imaging, which probes *biomarkers* of particular targets or pathways of the cellular and molecular mechanisms of calcification, is particularly exciting in this context to enable the visualization of the ongoing and dynamic process of calcification, potentially quantitatively and repetitively in living organisms (New and Aikawa, 2011).

Morphologic Evaluation

Morphologic assessment of calcification is done using several readily available and well-established techniques that range from macroscopic (gross) examination and radiographs (X-rays) of explanted prostheses to more sophisticated analytical techniques such as electron energy loss spectroscopy. Each method has advantages and limitations; several techniques are often used in combination to obtain an understanding of the structure, composition, and mechanism of each type of calcification.

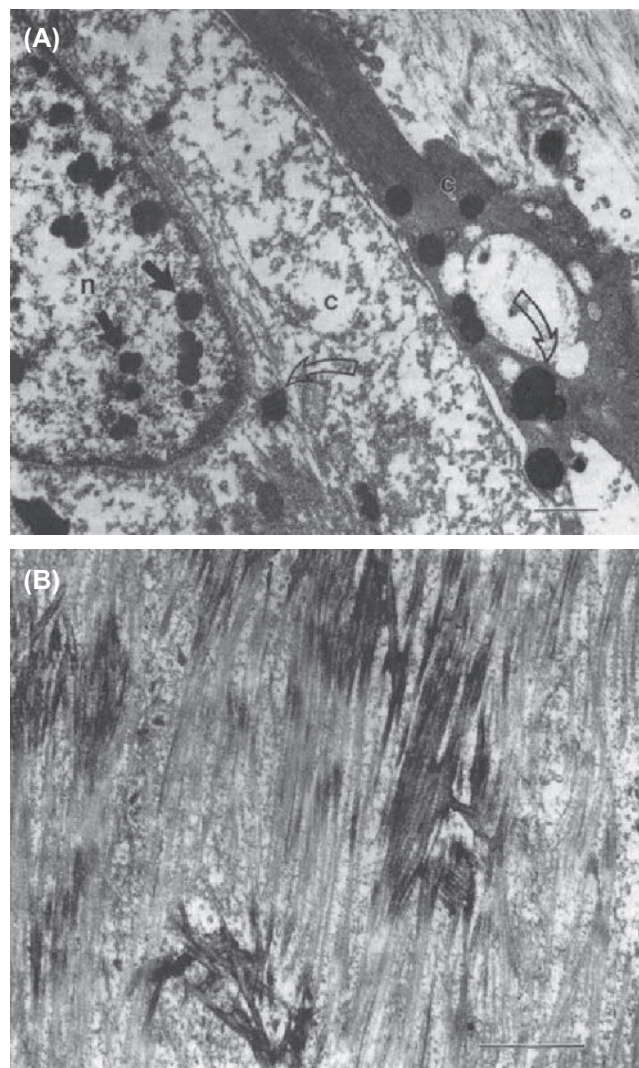
Careful visual examination of the specimen, often under a dissecting (low-power) microscope and radiography assess the distribution of mineral. Specimen radiography typically involves placing the explanted prosthesis on an X-ray film plate and exposing to an X-ray beam in a special device used for small samples (e.g., Faxitron, Hewlett-Packard, McMinnville, CA, with an energy level of 35 keV for 1 min for valves). Deposits of mineral appear as bright densities which have locally blocked the beam from exposing the film (see Fig. 2.4.5.1B).



• **Figure 2.4.5.3** Light microscopic appearance of calcification of experimental porcine aortic heart valve tissue. Note cell-based orientation of initial deposits (arrows). (A) Implanted subcutaneously in 3-week-old rats for 72h; (B) implanted in growing sheep for 5 months, demonstrating predominant site of growing edge of calcification in cells of the residual porcine valve matrix (arrows). ((B) Reproduced by permission from Schoen, F. J. (2001). Pathology of heart valve substitution with mechanical and tissue prostheses, In: Cardiovascular Pathology, third ed., Silver, M. D., Gotlieb, A. I. and Schoen, F. J. (Eds.). W. B. Saunders: Philadelphia, PA, pp. 629–677.)

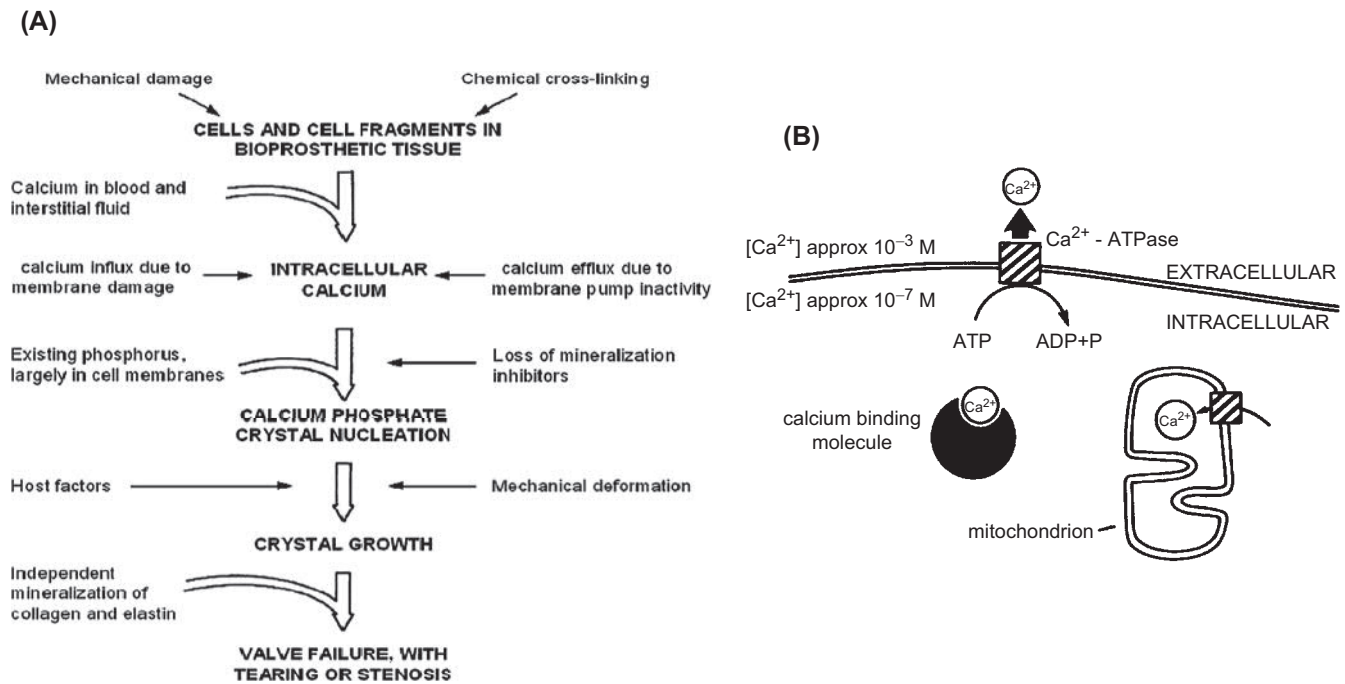
Light microscopy of calcified tissues is widely used. Identification of calcium-phosphate mineral is facilitated through the use of either calcium- or phosphorus-specific stains, such as alizarin red (which stains calcium red) or von Kossa (which stains phosphates brown-black) (Figs. 2.4.5.2B and 2.4.5.3). The von Kossa stain generally permits the most discrete localization of the mineral deposits. Staining for alkaline phosphatase, an enzyme involved in the pathogenesis of some forms of calcification, can also be useful in some contexts (Maranto and Schoen, 1988; Levy et al., 1991). These histologic stains are readily available, can be easily applied to tissue sections embedded in either paraffin or plastic, and are most useful for confirming and characterizing suspected calcified areas which have been noted by routine hematoxylin and eosin staining techniques. Sectioning of calcified tissue which has been embedded in paraffin often leads to considerable artifacts due to fragmentation; embedding of tissue with calcific deposits in a harder medium such as glycolmethacrylate polymer can yield superior section quality. On light microscopic sections, the extent of calcification can be semiquantitatively graded, and its locations described relative to key landmarks of the implant (Bennink et al., 2018).

Transmission electron microscopy may facilitate determination of early sites of calcific deposits. In TEM, an electron beam traverses an ultra-thin (0.05 μm) section of tissue (Fig. 2.4.5.4); observation of the ultrastructure (i.e., submicron tissue features) of calcification by TEM may contribute to an understanding of the mechanisms by which calcific



• **Figure 2.4.5.4** Transmission electron microscopy of calcification of experimental porcine aortic heart valve implanted subcutaneously in 3-week-old rats. (A) 48-hour implant demonstrating focal calcific deposits in nucleus of one cell (closed arrows) and cytoplasm of two cells (open arrows), n, nucleus; c, cytoplasm. (B) 21-day implant demonstrating collagen calcification. Bar=2 μm . Ultrathin sections stained with uranyl acetate and lead citrate. ((A) Reproduced with permission from Schoen, F.J., Levy, R.J., Nelson, A.C., Bernhard, W.F., Nashef, A., et al. (1985). Onset and progression of experimental bioprosthetic heart valve calcification. *Lab. Investig.*, 52, 523–532.)

crystals form. Scanning electron microscopy (SEM) images the specimen surface and can be coupled with elemental localization by energy-dispersive X-ray analysis (EDXA), allowing a semiquantitative evaluation of the local progression of calcium and phosphate deposition in a site-specific manner. Electron energy loss spectroscopy (EELS) couples transmission electron microscopy with highly sensitive elemental analyses to provide a most powerful localization of incipient nucleation sites and early mineralization (Webb et al., 1991). In general, the more highly sensitive and sophisticated morphologic techniques require more demanding and expensive preparation of specimens to avoid unwanted artifacts, which may complicate interpretation of high-resolution morphologic information. Since choice



• **Figure 2.4.5** Extended hypothetical model for the calcification of bioprosthetic tissue. (A) Overall model, which considers host factors, implant factors, and mechanical damage, and relates initial sites of mineral nucleation to increased intracellular calcium in residual cells and cell fragments in bioprosthetic tissue. The ultimate result of calcification is valve failure, with tearing or stenosis. The key contributory role of existing phosphorus in membrane phospholipids and nucleic acids in determining the initial sites of crystal nucleation is emphasized, and a possible role for the independent mineralization of collagen is acknowledged. Mechanical deformation probably contributes to both nucleation and growth of calcific crystals. (B) Events at the cell membrane and other calcium-binding structures. There is a substantial physiologic (normal) gradient of free calcium across the cell membrane (10^{-3} M outside, 10^{-7} M inside) which is maintained as an energy-dependent process. With cell death or membrane dysfunction, calcium phosphate formation can be initiated at the membranous cellular structures. ((A) Reproduced by permission from Schoen, F. J. and Levy, R. J. (2005). Calcification of tissue heart valve substitutes: Progress toward understanding and prevention. *Ann. Thorac. Surg.*, 79, 1072–1080. (B) Reproduced by permission from Schoen, F. J. et al. (1988). Biomaterials-associated calcification: Pathology, mechanisms, and strategies for prevention. *J. Appl. Biomater.*, 22, 11–36.)

of analytical methodology involves trade-offs, forethought about, and careful planning, specimen handling optimizes the yield provided by the array of available techniques and allows multiple approaches to be used on specimens from a particular experiment.

Chemical Assessment

Quantitation of calcium and phosphorus in biomaterial calcifications permits characterization of the progression of deposition, comparison of severity of deposition among specimens, and determination of the effectiveness of preventive measures (Levy et al., 1983a, 1985a; Schoen et al., 1985, 1986, 1987; Schoen and Levy, 1999). However, such techniques destroy the specimen (and hence obliterate any spatial information) during preparation. A widely used technique for quantitation of calcium is atomic absorption spectroscopy of acid-hydrolyzed or ashed samples. Phosphorus is usually quantitated as phosphate, using a molybdate complexation technique with spectrophotometric detection. The degree of calcification associated with a gross explant specimen can also be semiquantitatively graded by specimen

radiographs (Schoen et al., 1987). The specific crystalline form of the mineral phase can be determined by X-ray diffraction. Carbonate-containing mineral phases may also be analyzed by infrared spectroscopy.

Mechanisms of Biomaterial Calcification

Regulation of Pathologic Calcification

Three factors regulate biomaterial mineralization: (1) biological factors (local environment of function and recipients systemic metabolic state and circulating regulatory factors); (2) biomaterial factors (the structure and chemistry of the substrate biomaterial); and (3) biomechanical factors (degree and locations of stress and strain). (see Fig. 2.4.5.5).

Role of Biological Factors

The most important host metabolic factors relate to young age, with more rapid calcification taking place in younger patients or experimental animals (Levy et al., 1983a), and pathologic alterations of mineral concentrations in the

circulating blood. Although the relationship with age is well-established and incontrovertible, the mechanisms accounting for this “physiologic” effect of age are uncertain but may be related to a more active mineral metabolism that exists at a young age to create and strengthen the skeleton. Other factors that can change blood chemistry such as comorbidities (e.g., chronic kidney impairment or diabetes) may aggravate the mineral deposition process. Local tissue factors such as oxidative potential and pH alteration due to inflammation can also stimulate material degradation and calcification.

Dystrophic pathologic calcification has typically been considered a passive, unregulated, and degenerative process. However, the observations of matrix vesicles, hydroxyapatite mineral, and bone-related morphogenetic and noncollagenous proteins in situations of pathological calcification have suggested that the mechanisms responsible for pathologic calcification may be at least partially regulated, similarly to physiologic mineralization of bone and other hard tissues. Moreover, some of the mechanisms regulating biomaterial-associated calcification may be shared with other pathological process that have calcification as a prominent feature, such as atherosclerosis and calcific aortic valve disease (Johnson et al., 2006; Demer and Tintut, 2008; Pery and D’Haese, 2009). In healthy blood vessels and valves, inhibitory mechanisms outweigh procalcification-inductive mechanisms; in contrast, in bone and pathologic tissues, inductive mechanisms dominate. Naturally occurring inhibitors to crystal nucleation and growth (of which many have been identified) may also play a role in biomaterial and other cardiovascular calcification (Weissen-Plenz et al., 2008). Specific inhibitors in this context include osteopontin (Steitz et al., 2002) and phosphocitrate (Tew et al., 1980). Naturally occurring mineralization cofactors, such as inorganic phosphate (Jono et al., 2000), bone morphogenetic protein (a member of the transforming growth factor [TGF] beta family) (Bostrom et al., 1993), pro-inflammatory lipids (Demer, 2002), and other substances (e.g., cytokines) may also play a role in pathologic calcification. The noncollagenous proteins osteopontin, TGF-beta1, and tenascin-C involved in bone matrix formation and tissue remodeling have been demonstrated in clinical calcified bioprosthetic heart valves, natural valves, and atherosclerosis, suggesting that they play a regulatory role in these forms of pathologic calcification in humans (Srivasta et al., 1997; Bini et al., 1999; Jian et al., 2001, 2003), but a direct mechanistic relationship has not yet been demonstrated.

Role of Biomaterial Factors

Biomaterial structural and chemical properties play a significant role in the propensity of calcification. An important implant factor for calcification of bioprosthetic tissue is pretreatment with glutaraldehyde, done to preserve the tissue (Golomb et al., 1987; Grabenwoger et al., 1996). It has been hypothesized that the cross-linking agent glutaraldehyde stabilizes and perhaps modifies phosphorous-rich calcifiable structures in the bioprosthetic tissue. These sites seem to be capable of mineralization upon implantation when exposed to the comparatively high calcium levels of extracellular fluid. Calcification of the two principal types of tissue used

in bioprostheses—glutaraldehyde-pretreated porcine aortic valve or glutaraldehyde-pretreated bovine pericardium—is similar in extent, morphology, and mechanisms (Schoen and Levy, 2005). Glutaraldehyde also has been shown to be an inefficient cross-linker for other tissue-based materials.

Nevertheless, the elastin and glycosaminoglycans present in the tissue are not stabilized, and degradation and leaching of those components can create voids and a site for additional calcification (Lovekamp et al., 2006). Thus stabilizing those components in the biological tissue has been shown to improve calcification resistance (Tripi and Vyavahare, 2014). Degraded elastin fibers can also be calcification-prone sites (Bailey et al., 2003).

Calcification mechanisms of synthetic polymers are different from those of tissue-based materials and mostly occur on the surface of the materials, a feature generally considered to be related to protein and platelet attachment (Bernacca et al., 1997). Surface properties of the materials play a significant role in material calcification. Segmented polyether urethanes are prone to oxidation, and that can cause surface cracking that would provide sites for mineralization (Stachelek et al., 2006). Increasing hydrophilicity of degradable polyurethanes has been shown to increase the extent of calcification (Gorna and Gogolewski, 2002). Surface modification of synthetic polymers has been extensively investigated to prevent calcification (Bernacca and Wheatley, 1998).

Role of Biomechanical Factors

Mechanical factors also regulate calcification. Both intrinsic and extrinsic mineralization of a biomaterial are generally enhanced at the sites of intense mechanical deformations generated by motion, such as the points of flexion in heart valves (Thubrikar et al., 1983; Schoen and Levy, 1999). The mechanisms underlying mechanical potentiation of calcification associated with biomaterials are incompletely understood, but the effect mimics the well-known Wolf’s law in bone, in which formation and adaptation occurs in response to the mechanical forces that it experiences (Chen et al., 2009). Moreover, enhancement of mineral deposition is seen in systems where static but not dynamic mechanical strain is applied (Levy, 1983a), and in systems where live stem cells are subjected to a spectrum of mechanical environments (Yip et al., 2009). Furthermore, long-term cyclic wear on materials has been demonstrated to cause permanent geometric deformations that are due to ECM degradation in tissue-based valves, specifically the collagen triple helix unraveling (Sun et al., 2004). Recently, it has been suggested that preimplantation crimping of the pericardium in transcatheter aortic valves can lead to material damage that promotes calcification (Zareian et al., 2019).

Experimental Models for Biomaterial Calcification

Animal models have been developed for the investigation of the calcification of bioprosthetic heart valves, aortic homografts, cardiac assist devices, and trileaflet polymeric valves

TABLE 2.4.5.3 Experimental Models of Calcification and Typical Durations

Type	System	Typical Duration
Calcification of bioprosthetic or other tissue heart valve	In vitro incubation of tissue fragment or flexing valves	Days to weeks
	Rat subdermal implant of tissue fragment	3 weeks
	Calf or sheep orthotopic valve replacement	3–5 months
	Rat or sheep descending aorta	1–5 months
Calcification of polyurethane	Rat subdermal implant of material sample after induction of calciphylaxis	1–3 months
	Calf or sheep artificial heart implant	5 months
	Trileaflet polymeric valve implant in calf or sheep	5 months
Calcification of hydrogel	Rat subdermal implant of material sample	3 weeks
Calcification of collagen or elastin	Rat subdermal implant of material sample	3 weeks
Urinary encrustation	In vitro incubation	Hours to days
	In vivo bladder implants (rats and rabbits)	10 weeks

(Table 2.4.5.3). The most widely used experimental models are used as a preclinical screen in the development of new or modified materials and design configurations, and to investigate the pathophysiology of bioprosthetic tissue calcification. They include orthotopic valve replacements (in the tricuspid, pulmonary, mitral, or aortic positions) or conduit-mounted valves in sheep or calves, and isolated tissue (i.e., not in a valve) samples implanted subcutaneously in mice, rabbits, or rats (Levy et al., 1983a; Schoen et al., 1985, 1986). In both circulatory and noncirculatory models, bioprosthetic tissue calcifies progressively with a morphology similar to that observed in clinical specimens, but with markedly accelerated kinetics. In vitro models of biomaterial calcification have been investigated, but have not yielded useful information in studying mechanisms or preventive strategies (Schoen et al., 1992a; Mako and Vesely, 1997).

Compared with the several years normally required for calcification of clinical bioprostheses, valve replacements in sheep or calves calcify extensively in 3–6 months (Schoen et al., 1985, 1986, 1994). However, these models are expensive, limiting the number of subjects, and they are technically complex, demanding a high level of surgical expertise, postoperative care, and stringent housing and management procedures. Also, the available large animal models grow rapidly, have differences in anatomy from that of humans, and are without the pathologic substrate into which human implants are placed, and often yield results that vary among subjects treated similarly. These limitations stimulated the development of subdermal (synonym, *subcutaneous*—under the skin) implant models. Subdermal bioprosthetic implants in rats, rabbits, and mice provide the following useful features: (1) a markedly accelerated rate of calcification in a morphology comparable to that seen in circulatory explants; (2) sufficient economies that permit many specimens to be studied with a given set of experimental conditions, thereby

allowing quantitative characterization and statistical comparisons; and (3) quick retrieval of specimens from the experimental animals, which facilitates the careful manipulation and rapid processing required for detailed analyses (Levy et al., 1983a,b; Schoen et al., 1985, 1986). Moreover, controls are easily generated so that specific factors that may place a role in calcification can be isolated, and hypothetical mechanisms studied in detail. Moreover, these models provide a data set to which inhibitory approaches can be screened.

Polymer calcification has also been studied with subdermal implants in rats (Joshi et al., 1996). Calcification of a synthetic polymer such as polyurethane mostly occurs on the surface due to the hydrophobic nature of the materials, and it is therefore much more difficult to assess. Changes in surface or bulk properties or topology of the polymer due to these degradation processes or adherent biological material may promote extrinsic calcification. Oxidation of polymer chains may promote polymer degradation. For example, polyether urethanes calcify more than polycarbonate urethanes due to susceptibility of ether bonds to oxidation (Bernacca et al., 1997; Joshi et al., 1996). These degradation and subsequent calcification processes often mechanically weaken the polymer (surface cracking and tearing) and enhance vulnerability to failure in a dynamic setting of cardiovascular applications. Aggravated calcification animal models such as calciphylaxis are often needed to accelerate and augment calcification of polymers (Joshi et al., 1996).

Thus, the subcutaneous model provides a technically convenient and economically advantageous vehicle for investigating host and implant determinants and mechanisms of mineralization, as well as for an initial screening of potential strategies for its inhibition (*anticalcification*). Promising approaches may be investigated further in a large animal valve implant model. Large animal implants

as valve replacements are also used: (1) to elucidate further the processes accounting for clinical failures; (2) to evaluate the performance of design and biomaterial modifications in valve development studies; (3) to assess the importance of blood–surface interactions; and (4) to provide data required for approval by regulatory agencies (Schoen et al., 1992b, 1994). Indeed, regulatory guidelines require such large animal implants and prescribe many of the parameters of these animal studies and postexplant analysis (Gallegos et al., 2005; Zhang et al., 2019).

Data from valve explants from patients and subdermal and circulatory experiments in animal models using bioprosthetic heart valve tissue have elucidated the pathophysiology of this significant clinical problem and enhanced our understanding of pathologic biomaterial calcification more generally (Fig. 2.4.5.4). The similarities of calcification in the different experimental models and clinical bioprostheses suggest common mechanisms, independent of the implant site (across vascular and extravascular locations). Indeed, calcification of bioprosthetic tissue appears to depend on exposure of a susceptible substrate to calcium-containing extracellular fluid; other local implant-related or circulating substances may play a regulatory role. Residual phosphorus in cell-related membranes localizes the Ca–P mineral nucleation sites. Consistent with a dystrophic mechanism, and encountered in other situations (Cardoso and Weinbaum, 2018), the initial calcification sites in bioprosthetic tissue are predominantly dead cells and cell membrane fragments (Levy et al., 1983a; Schoen et al., 1985, 1986; Schoen and Levy, 1999) (see Fig. 2.4.5.4).

Role of Cells

Normally, extracellular calcium concentration in tissues is approximately 1 mg/mL (10^{-3} M). In contrast, the intracellular concentration of calcium (in the cytoplasm) is 1000–10,000 times lower (approximately 10^{-7} M). This steep calcium gradient is maintained in healthy cells because mechanisms in their intact membranes pump calcium to the exterior using calcium ATP-ases and other vehicles for extrusion. In cells which have been rendered nonviable by glutaraldehyde fixation, the physiologic cellular handling of calcium ions is disabled. The cell membranes and other intercellular structures are high in phosphorus (as phospholipids, especially phosphatidyl serine, which can bind calcium); such sites can serve as nucleators. Glutaraldehyde pretreatment also stabilizes these phosphorous stores. Other susceptible sites can include collagen and elastic fibers of the extracellular matrix, denatured proteins, phosphoproteins, fatty acids, blood platelets and, in the case of infection, bacteria.

Moreover, since the morphology and extent of calcification in subcutaneous implants is analogous to that observed in clinical and experimental circulatory implants, despite the lack of dynamic mechanical activity characteristic of the circulatory environment, it is clear that dynamic stress promotes, but is not prerequisite for, calcification of

bioprosthetic tissue. In the subcutaneous model, calcification is enhanced in areas of tissue folds, bends, and areas of shear, suggesting that static mechanical deformation also potentiates mineralization (Levy et al., 1983a). Also, long-term bioprosthetic valve function is accompanied by collagen degradation in the most highly stressed regions (Sun et al., 2004; Vyavahare et al., 1997; Sacks and Schoen, 2002); highly stressed regions typically manifest the earliest and most substantial calcification. Nevertheless, although these data suggest that local tissue disruption mediates the mechanical effect, the precise mechanisms by which mechanical factors influence calcification are uncertain.

Role of Collagen and Elastin

Calcification of the extracellular matrix structural proteins collagen and elastin has been observed in clinical and experimental implants of bioprosthetic and homograft valvular and vascular tissue and has been studied using a rat subdermal model. Collagen-containing implants are widely used in various surgical applications, such as tendon prostheses and surgical absorptive sponges, but their usefulness is compromised owing to calcium phosphate deposits and the resultant stiffening. Cross-linking by either glutaraldehyde or formaldehyde promotes the calcification of collagen sponge implants made of purified collagen, but the extent of calcification does not correlate with the degree of cross-linking (Levy et al., 1986). Elastin calcification has also been studied (Vyavahare et al., 1999; Lee et al., 2006). As mentioned previously, elastin is not stabilized by glutaraldehyde cross-linking in bioprosthetic valves and its degradation, in particular in an aortic portion of the valve, can lead to elastin-specific calcification (Isenburg et al., 2005).

Role of Glutaraldehyde

The role of glutaraldehyde (GA) in promoting calcification is well established and strong (Golomb et al., 1987). Two key processes, not yet fully understood, yet both directly related to the chemical effects of GA, are believed to dominate: (1) the reaction between the residual phosphorus and associated phospholipids with calcium in the surrounding fluid to yield calcium-phosphate mineral associated with the cells of the tissue devitalized by GA (as described above), and (2) chemical reactions related to the presence of active residual-free aldehyde functional groups induced by GA fixation (Simionescu, 2004). Collagen and elastic fibers can also serve as calcium-phosphate nucleation sites, independent of cellular components, perhaps through reactive aldehyde-related mechanisms. It is unknown whether these several mechanisms are independent or interrelated.

In addition to cellular devitalization and stabilizing phosphorus in the tissue, glutaraldehyde treatment produces functional group residuals (i.e., aldehydes, various carbon-yls, Schiff bases, etc.) by which not only cells, but potentially

matrix glycosaminoglycans and structural proteins, such as collagen and elastin, may also bind calcium. Tissue levels of reactive functional group residuals can be directly correlated to bioprosthetic tissue calcification (Manji et al., 2006; Zilla et al., 1997a,b; Cunanan et al., 2001; Tod and Dove, 2016). Indeed, tissue levels of calcification correlate with aldehyde content. The close association between aldehyde content and the calcification of bovine pericardial tissue suggests that processing of bioprosthetic valves to reduce the content or reactivity of reactive residual aldehydes may offer a significant advantage in terms of reducing the potential for long-term bioprosthetic valve calcification (Webb et al., 1988; Shang et al., 2017; Christian et al., 2015; Everaerts et al., 2006). Oxidative mechanisms may also play a role (Christian et al., 2014; Lee et al., 2017).

Role of Immunologic Factors

A potential role for inflammatory and immune processes has been postulated by some investigators (Love, 1993; Human and Zilla, 2001a,b), since (1) experimental animals can be sensitized to both fresh and cross-linked bioprosthetic valve tissues; (2) antibodies to valve components can be detected in some patients following valve dysfunction; and (3) some failed tissue valves have brisk mononuclear inflammation. However, no definite evidence for a role of immunologic mechanisms in calcification has been demonstrated, and many lines of evidence suggest that neither nonspecific inflammation nor specific immunologic responses appear to favor bioprosthetic tissue calcification. Specific evidence against a contributory role of immunologic process is as follows: (1) calcification in either circulatory or subcutaneous locations is not usually associated with inflammation, and (2) in experiments in which valve cusps were enclosed in filter chambers that prevent host cell contact with tissue, but allow free diffusion of extracellular fluid and implantation of valve tissue in congenitally athymic (“nude”) mice who have essentially no T-cell function, calcification morphology, and extent were unchanged (Levy et al., 1983a,b). Clinical and experimental data detecting antibodies to valve tissue after failure might reflect a secondary response to valve damage, rather than a cause of failure.

Calcification of the adjacent aortic wall portion of glutaraldehyde-pretreated porcine aortic valves, and valvular allografts and vascular segments, is also observed clinically and experimentally. Mineral deposition occurs throughout the vascular cross-section but is accentuated in the dense bands at the inner and outer media, and cells and elastin (itself not a prominent site of mineralization in cusps) are the major sites. In nonstented porcine aortic valves which have higher portions of the aortic wall exposed to blood than in currently used stented valves, calcification of the aortic wall could stiffen the root, altering hemodynamic efficiency, causing nodular calcific obstruction, potentiating wall rupture or providing a nidus for emboli. Some anticalcification agents, including 2-amino-oleic acid (AOA) and ethanol, prevent experimental cuspal but not aortic wall calcification (Chen et al., 1994a,b).

Prevention of Calcification

The major strategy for preventing calcification of biomaterial implants has been biomaterial modifications, whether by removal of a calcifiable component, the addition of an exogenous agent, or chemical alteration. The principles are well-illustrated by the work done with bioprosthetic heart valves, in which the subcutaneous model has been used to screen potential strategies for calcification inhibition (*anticalcification* or *antimineralization*). Promising approaches have been investigated further in a large animal valve implant model. However, some strategies that appeared efficacious in subcutaneous implants have not proven favorable when used on valves implanted into the circulation.

Analogous to any new or modified drug or device, a potential antimineralization treatment must be effective and safe. The treatment should not impede valve performance such as hemodynamics or durability. Investigations of an anticalcification strategy must demonstrate not only the effectiveness of the therapy but also the absence of adverse effects (Schoen et al., 1992b). Adverse effects in this setting could include systemic or local toxicity, a tendency toward thrombosis or infection, induction of immunological effects, or accelerated structural degradation, with either immediate loss of mechanical properties or premature deterioration and failure. Indeed, there are several examples whereby an antimineralization treatment contributed to an unacceptable degradation of the tissue (Jones et al., 1989; Gott et al., 1992; Schoen, 1998). As summarized in more detail in Table 2.4.5.4, a rational approach for preventing bioprosthetic calcification must integrate safety and efficacy considerations with the scientific basis for inhibition of calcium-phosphate crystal formation. This will of necessity involve the steps summarized in Table 2.4.5.5, before appropriate clinical trials can be undertaken (Schoen et al., 1992b; Vyavahare et al., 1997a).

Experimental studies have demonstrated that adequate doses of systemic agents used to treat clinical metabolic bone

TABLE 2.4.5.4 Criteria for Efficacy and Safety of Antimineralization Treatments

Efficacy

- Effective and sustained calcification inhibition

Safety

- Adequate valve performance (i.e., unimpaired hemodynamics and durability)
- Does not cause adverse blood–surface interactions (e.g., hemolysis, platelet adhesion, coagulation protein activation, complement activation, inflammatory cell activation, binding of vital serum factors)
- Does not enhance local or systemic inflammation (e.g., foreign body reaction, immunologic reactivity, hypersensitivity)
- Does not cause local or systemic toxicity
- Does not potentiate infection

Modified from Schoen F.J. et al. (1992). Antimineralization treatments for bioprosthetic heart valves. Assessment of efficacy and safety. *J. Thorac. Cardiovasc. Surg.*, 104, 1285–1288.

TABLE 2.4.5.5 Preclinical Efficacy and Safety Testing of Antimineralization Treatments

Type of Study	Information Derived
Subcutaneous implantation in rats	<ul style="list-style-type: none"> Initial efficacy screen Mechanisms Dose–response Toxicity
Biomechanical evaluation	<ul style="list-style-type: none"> Hemodynamics Accelerated wear
Morphologic studies of unimplanted valves	<ul style="list-style-type: none"> Structural degradation assessed by light and transmission electron microscopy Scanning electron microscopy
Circulatory implants in large animals	<ul style="list-style-type: none"> Device configuration, surgical technique, in vivo hemodynamics, explant valve pathology Durability, thrombi, thromboembolism, hemolysis, cardiac and systemic pathology

Modified from Schoen F.J. et al. (1992). Antimineralization treatments for bioprosthetic heart valves. Assessment of efficacy and safety. *J. Thorac. Cardiovasc. Surg.*, 104, 1285–1288.

disease, including calcium chelators (e.g., diphosphonates such as ethane hydroxybisphosphonate [EHBP]), can dramatically lower the calcification potential of bioprosthetic tissue implanted subcutaneously in rats (Levy et al., 1987). However, systemic therapy is unlikely to be safe, because such chemicals generally also interfere with physiologic calcification (i.e., bone growth), causing growth retardation. To avoid this difficulty, coimplants of a drug-delivery system adjacent to the prosthesis, in which the effective drug concentration would be confined to the site where it is needed (i.e., the implant), were investigated, in the hope that systemic side-effects would be prevented (Levy et al., 1985b). A localized anticalcification effect would be particularly attractive in young people. Although studies incorporating EHBP in non-degradable polymers, such as ethylene-vinyl acetate (EVA), polydimethylsiloxane (silicone), silastic, and polyurethanes showed effectiveness of this strategy in animal models, this approach has been challenging to implement clinically.

Thus, modification of the substrate, either by removing or altering a calcifiable component or binding an inhibitor has been an area of focus. Forefront strategies should also consider: (1) a possible synergism provided by multiple anticalcification agents and approaches used simultaneously; (2) new materials; and (3) the possibility of tissue-engineered heart valve replacements. The agents most widely studied, for efficacy, mechanisms, lack of adverse effects, and potential clinical utility are summarized below and in Table 2.4.5.6. Combination therapies using multiple agents may provide a synergy of beneficial effects (Levy et al., 2003). The paragraphs below describe some of the approaches that have been investigated in preclinical studies; several have achieved regulatory approval and proven successful in clinical bioprosthetic valves.

TABLE 2.4.5.6 Prototypical Agents for Mechanism-Based Prevention of Calcification in Bioprosthetic Heart Valves

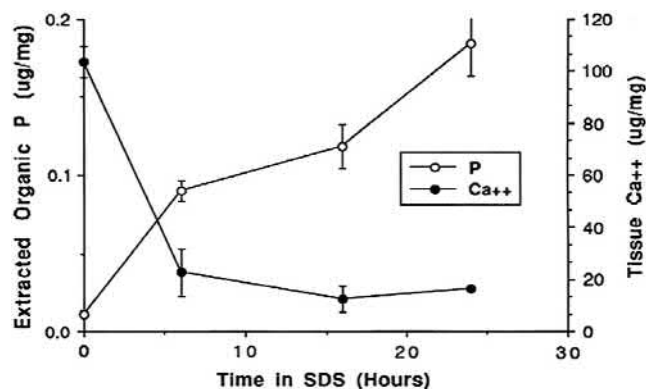
Mechanisms	Strategy/Agent
Inhibition of hydroxyapatite formation	Ethane hydroxybisphosphonate (EHBP)
Inhibition of calcium uptake	2-Alpha-amino-oleic acid (AOA™)
Inhibition of Ca–P crystal growth; inhibition of alkaline phosphate; chemical modification of elastin	Ferric/aluminum chloride exposure
Phospholipid extraction	Sodium dodecyl sulfate (SDS)
Phospholipid extraction and collagen conformation modification	Ethanol exposure
Binding of agents that prevent calcification	Osteopontin, EDTA, heparin
Eliminate glutaraldehyde potentiation of calcification:	Modification of (alternatives to) glutaraldehyde fixation
<ul style="list-style-type: none"> Amino acid neutralization of glutaraldehyde residues Polyepoxide (polyglycidal ether), acyl azide, carbodiimide, cyanamide and glycerol cross-linking Dye-mediated photooxidation Natural cross-linkergenipin, tannic acid Polymerization of aldehydes by thermal treatment 	

Inhibitors of Hydroxyapatite Formation *Bisphosphonates*

Ethane hydroxybisphosphonate (EHBP) has been approved by the FDA for human use to inhibit pathologic calcification, and to treat hypercalcemia of malignancy. Compounds of this type probably inhibit calcification by poisoning the growth of calcific crystal by chelation. As discussed above, either cuspal pretreatment or systemic or local therapy of the host with diphosphonate compounds inhibits experimental bioprosthetic valve calcification (Levy et al., 1985a,b, 1987; Johnston et al., 1993). Recently, controlled clinical trials which have orally administered bisphosphonates have demonstrated the ability to stabilize osteoporosis.

Trivalent Metal Ions

Pretreatment of bioprosthetic tissue with iron and aluminum (e.g., FeCl₃ and AlCl₃) inhibited calcification of subdermal implants with glutaraldehyde-pretreated porcine cusps or



• **Figure 2.4.5.6** Reduction of calcification of bioprosthetic tissue by preincubation in 1% SDS demonstrated in a rat subcutaneous model of glutaraldehyde cross-linked porcine aortic valve. These results support the concept that phospholipid extraction is an important but perhaps not the only mechanism of SDS efficacy. (Reproduced by permission from Schoen, F. J., Levy, R. J. and Piehler, H. R. (1992). Pathological considerations in replacement cardiac valves. *Cardiovasc. Pathol.*, 1, 29–52.)

pericardium (Webb et al., 1991; Carpentier et al., 1997). Such compounds are hypothesized to act through complexation of the cation (Fe or Al) with phosphate, thereby preventing calcium phosphate formation. Both ferric ion and the trivalent aluminum ion inhibit alkaline phosphatase, an important enzyme in bone formation. This may be related to their mechanism for preventing the initiation of calcification. Furthermore, research from our laboratories has demonstrated that aluminum chloride prevents elastin calcification through a permanent structural alteration of the elastin molecule (Vyavahare et al., 1999). These compounds are also active when released from polymeric controlled-release implants.

Calcium Diffusion Inhibitor

2-Alpha-amino-oleic acid (AOA, Biomedical Designs, Inc., Atlanta, GA) bonds covalently to bioprosthetic tissue through an amino linkage to residual aldehyde functions, and inhibits calcium flux through bioprosthetic cusps (Chen et al., 1994a,b). AOA is effective in mitigating cusp, but not aortic wall, calcification in rat subdermal and cardiovascular implants. This compound is used in FDA-approved porcine aortic valves (Fyfe and Schoen, 1999; Celiento et al., 2012; El-Hamamsy et al., 2010).

Removal/Modification of Calcifiable Material Surfactants

Incubation of bioprosthetic tissue with sodium dodecyl sulfate (SDS) and other detergents extracts the majority of acidic phospholipids (Hirsch et al., 1993); this is associated with reduced mineralization, probably resulting from suppression of the initial cell-membrane-oriented calcification (Fig. 2.4.5.6). This compound is used in an FDA-approved porcine aortic valve bioprosthesis (David et al., 1998; Bottio et al., 2003).

Alcohol Treatments

Ethanol preincubation of glutaraldehyde cross-linked porcine aortic valve bioprostheses prevents calcification of the valve cusps in both rat subdermal implants, and sheep mitral valve replacements (Vyavahare et al., 1997b, 1998). Eighty percent ethanol pretreatment: (1) extracts almost all phospholipids and cholesterol from glutaraldehyde cross-linked cusps; (2) causes a permanent alteration in collagen conformation as assessed by attenuated total reflectance-Fourier transform infrared spectroscopy (ATR-FTIR); (3) affects cuspal interactions with water and lipids; and (4) enhances cuspal resistance to collagenase. Ethanol is in clinical use as a porcine valve cuspal pretreatment in both Europe and the United States, and use in combination with aluminum treatment of the aortic wall of a stentless valve is under consideration. Other alcohols that have shown promise to remove phospholipids include methanol, isopropanol, and 1,2 octanediol (Vyavahare et al., 2000; Pettenazzo et al., 2008).

Glutaraldehyde Neutralization

As glutaraldehyde cross-linking itself has been shown to aggravate tissue calcification (Levy, 1994; Gong et al., 1991), several approaches have been suggested to neutralize remnant aldehyde residues in the tissue after glutaraldehyde cross-linking. Several amino acids, amines, and natural compounds such as taurine have been used to bind to unreacted glutaraldehyde residues (Jorge-Herrero et al., 1996; Meuris et al., 2018). These treatments have shown promise in preventing tissue calcification in rodent subcutaneous models and sheep heart valve replacement models. Storage of tissues in glutaraldehyde after the anticalcification treatment has shown a partial return of calcification for the tissues. Thus, other storage conditions without glutaraldehyde have been investigated. One product where the bioprosthetic valve is stored in dry conditions after glycerol treatment is now clinically available (Inspiris Resilia by Edwards Lifesciences, Irvine, California). New methods where the combination of multiple treatments such as removing phospholipids and glutaraldehyde neutralization followed by storage in glutaraldehyde free solutions have shown promise in animal studies to prevent calcification (Meuris et al., 2018).

Decellularization

Since the initial mineralization sites are devitalized connective cells of bioprosthetic tissue, these cells may be removed from the tissue, with the intent of making the bioprosthetic matrix less prone to calcification (Courtman et al., 1994; Wilson et al., 1995). Decellularized tissues have been used as scaffolds for tissue-engineered heart valves that would be populated with host cells and would grow with patients and hopefully not calcify. In vivo animal studies have seen some success for patency of a functional valve (Dohmen et al., 2006; Baraki et al., 2009). However, clinical experiments have shown valve failure due to inflammation and calcification (Simon et al., 2003). It is clear from these studies that extracellular matrix in the tissue (collagen and elastin) can degrade and create sites for calcification. Physical stabilization of collagen and elastin by pentagalloyl glucose

TABLE 2.4.5.7 Currently Used Anticalcification Treatments for Bioprosthetic Heart Valves

Heart Valve Producer	Anticalcification Trade Name	Anticalcification Method
Edwards Lifesciences	Thermaflox™	Proprietary annealing process developed internally to increase the durability of the material and rid excess aldehyde residues
Edwards Lifesciences	Inspiris Resilia	Dehydration of the tissue and reduction in lipid content, dry storage
Medtronic	AOA™	Alpha-oleic-acid treatment to decrease high-affinity sites of calcification, neutralizes residual glutaraldehyde
Abbott (formerly St. Jude Medical)	Linx™	Ethanol treatment to decrease high-affinity sites of calcification combined with a proprietary method to rid excess aldehyde residues

has been shown to reduce valvular calcification (Deborde et al., 2016). CorMatrix, a decellularized porcine intestinal submucosa, is also being investigated for cardiovascular implants (Zaidi et al., 2014).

Modification of Glutaraldehyde Fixation and Other Tissue Fixatives

Since previous studies have demonstrated that conventional glutaraldehyde fixation is conducive to calcification of bioprosthetic tissue, several studies have investigated modifications of, and alternatives to, conventional glutaraldehyde pretreatment. For example, and paradoxically, fixation of bioprosthetic tissue by extraordinarily high concentrations of glutaraldehyde (5–10× those normally used) appear to inhibit calcification (Zilla et al., 1997a,b, 2000). Moreover, residual glutaraldehyde residues in bioprosthetic tissue can be neutralized (“detoxified”) by treatment with lysine or diamine, which inhibits calcification of subdermal implants (Grabenwoger et al., 1992; Zilla et al., 2000, 2005; Trantina-Yates et al., 2003). Removing phospholipids or neutralizing aldehyde residues by end capping with amines, reduction with borohydride, or using high-temperature fixation strategies have been now clinically used for preventing tissue calcification (Table 2.4.5.7) Nonglutaraldehyde cross-linking of bioprosthetic tissue with epoxides, carbodiimides, acyl azides, and other compounds reduces their calcification in rat subdermal implant studies (Xi et al., 1992; Myers et al., 1995), and with triglycidylamine (TGA), an epoxy cross-linker (Connolly et al., 2005).

Additionally, alternative cross-linking chemistries (i.e., carbodiimide, triglycidylamine, or epoxies; Connolly et al., 2011), and photooxidative preservatives in sheep implants (Moore and Phillips, 1997) with tissue still embedded with devitalized cells results in a marked reduction of calcification (Tam et al., 2017). This further supports the notion that glutaraldehyde products themselves, in conjunction with devitalized cells, may serve as high-affinity sites for calcification. It is also known that glutaraldehyde does not stabilize many components in the tissue such as glycosaminoglycans and elastin. The degradation and depletion of those components can create voids and

high-affinity calcium-binding sites that can aggravate calcification (Isenbarg et al., 2005; Raghavan et al., 2010).

Novel methods of material fabrication can also include combining methods in more irreversible cross-linking chemistries to produce a more chemically resilient material to biological and chemical insult. Moreover, the discussion above emphasizes that mechanisms of calcification can be complex. Indeed, several material factors can work in concert to cause calcification, and inhibition of one factor alone is not likely to prevent long-term calcification. For instance, carbodiimide can be used with a network extender to provide a more stable, irreversible cross-linking mesh in a tissue-based material than carbodiimide or glutaraldehyde can do alone (Leong et al., 2013). Other current approaches include combination of decellularization/delipidation, end-capping aldehydes, storage in nonglutaraldehyde-based conditions so that calcification of the valve materials could be completely prevented (Meuris et al., 2018). Additives like pentagalloyl glucose that have been shown to physically stabilize elastin and collagen as well as prevent calcification can be imparted into the implants and stacked together in these fixation techniques (Tedder et al., 2009; Chuang et al., 2009). These different additives that modularly protect different parts of the base tissue material ECM are being combined to produce superior biomaterials that resist calcification and cyclic wear while maintaining native-like biomechanics (Tam et al., 2017).

Alternative Materials

Synthetic polymers have been investigated as possible candidates for heart valve leaflets. Polyurethane trileaflet valves have been fabricated and studied as a reasonable alternative to bioprostheses or mechanical valve prostheses (Ghanbari et al., 2009). Despite versatile properties, such as superior abrasion resistance, hydrolytic stability, high flexural endurance, excellent physical strength, and acceptable blood compatibility, the use of polymers has been hampered by calcification, thrombosis, tearing, and biodegradation. Although the exact mechanism of polyurethane calcification is as yet unclear, it is

TABLE 2.4.5.8 Design Considerations for Preventing Calcification of Biomaterials

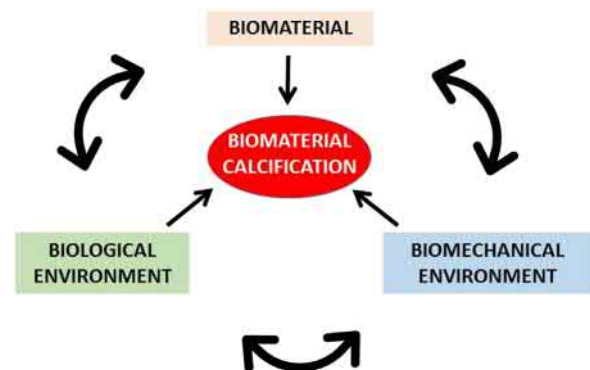
Material Considerations	Biomechanical Environment Considerations	Biological Environment Considerations
<ul style="list-style-type: none"> Principal chemical bond stability Chemical bond oxidation potential High-affinity binding sites for calcium phosphates Toxicity of residuals and leachables Surface texture and topography 	Structural degradation leading to creation of voids, new nucleation sites, or fragmentation of material during cyclic wear and shear flow	Patient factors <ul style="list-style-type: none"> Age Metabolism Comorbidities Local factors <ul style="list-style-type: none"> pH Oxidative potential
Material Characterization Techniques	Biomechanical Testing Conditions	Biological Testing Conditions
<ul style="list-style-type: none"> In vitro aqueous hydrolytic degradation Water and lipid swelling study In vitro oxidative stress testing Incubation in supersaturated Ca:P solution SEM for surface characterization Uniaxial/biaxial testing SFDI imaging analysis 	<ul style="list-style-type: none"> Prolonged static or dynamic strain/stress to study creep/stress relaxation; determines material's ability to resist permanent geometric deformations^a Cyclic fatigue for >500M cycles to determine long-term material durability^b 	<ul style="list-style-type: none"> In vitro enzymatic challenges that can degrade the material Cytotoxicity testing with leachables In vitro/in vivo hemocompatibility testing Implantation in rodents and small animals as a subcutaneous implant in either healthy animals or under harsher conditions like calciphylaxis or diabetes Large animal model device implantation

^aThese tests can be done in biological testing conditions for more robust model.
^bIn vitro/in vivo calcification studies can be performed on fatigued material.

believed that several physical, chemical, and biologic factors (directly or indirectly) play an important role in initiating this pathologic disease process (Schoen et al., 1992; Joshi et al., 1996; Hyde et al., 1999). A new generation of polyurethanes and other materials are showing promise as an alternative for fabrication of calcification-resistant bioprosthetic heart valves (Bezuidenhout et al., 2015).

Design Considerations and Selection of Materials to Avoid Calcification

Preclinical studies comprise in vitro (i.e., engineering and materials characterization) and in vivo components (i.e., animal models). For example, in the United States, animal model testing of heart valve substitutes is guided by document ISO-5840 from the International Standards Organization, supplemented by appropriate FDA guidance documents, which identifies the goals of preclinical in vivo assessment in evaluation of performance characteristics not amenable to be assessed by in vitro testing (Zhang et al., 2019). Selecting a material candidate appropriate for heart valve replacements remains to this day a difficult task because of the inherent mechanical requirements (hundreds of millions of cycles with high flexural pressure) as well as the short- and long-term failure modes it must resist—namely calcification and/or noncalcific structural deterioration, manifest in vivo as leaflet stiffening and/or tearing. These two failure modes are not mutually exclusive and have covariate factors that are illustrated in Table 2.4.5.8. This table illustrates the design considerations from material



• **Figure 2.4.5.7** Biomaterials calcification triad. The pathophysiology of calcification involves three interrelated factors:

(column 1), biomechanical (column 2), and biological (column 3) perspectives as well as the associated tests used to assess material characteristics. Finding the ideal material candidate for heart valve replacements involves designing around a multitude of criteria that could very quickly narrow down the list of suitable materials that merit further development. The animal model for in vivo studies must be carefully considered, for example, it is well known that juvenile animals of some species (e.g., sheep) have accelerated calcification of tissue heart valve and other biomaterials in device configurations. The design considerations discussed above must be applied to any candidate material that, using appropriate tests, shows it is not likely to calcify. This should be done before investing substantial amounts of resources for further verification or validation testing of new materials in novel configurations (Fig. 2.4.5.7).

Conclusions

Calcification of biomaterial implants is an important pathologic process affecting a variety of tissue-derived biomaterials, as well as synthetic polymers in various functional configurations. The pathophysiology has been partially characterized through the judicious use of animal models. Common features of biomaterial calcification in several clinical applications includes the involvement of devitalized cells and cellular debris, extracellular matrix degradation, and oxidative degradation of materials. Preventive approaches based on modifying biomaterials to make them resistant to degradation due either to biological insult or biomechanical factors appear to be promising. Several anticalcification strategies are already used clinically, particularly for extending the functional lifetime of bioprosthetic heart valves. The long-term data suggest that these new technologies may be efficacious and safe. Further materials development based on the principles described in this chapter may be beneficial and translatable to the clinic.

References

- Aikawa, E., Nahrendorf, M., Figueiredo, J.L., Swirski, F.K., Shtatland, T., et al., 2007. Osteogenesis associates with inflammation in early-stage atherosclerosis evaluated by molecular imaging in vivo. *Circulation* 116, 2841–2850.
- Andrews, J., Psaltis, P.J., Bartolo, B.A.D., Nicholls, S.J., Puri, R., 2018. Coronary arterial calcification: a review of mechanisms, promoters and imaging. *Trends Cardiovasc. Med.* 28, 491–501.
- Bailey, M.T., Pillarisetti, S., Xiao, H., Vyavahare, N.R., 2003. Role of elastin in pathologic calcification of xenograft heart valves. *J. Biomed. Mater. Res. A* 66, 93–102.
- Baraki, H., Tudorache, I., Braun, M., Höffler, K., Görler, A., Lichtenberg, A., et al., 2009. Orthotopic replacement of the aortic valve with decellularized allograft in a sheep model. *Biomaterials* 30, 6240–6.
- Bass, J.K., Chan, G.M., 2006. Calcium nutrition and metabolism during infancy. *Nutrition* 22, 1057–1066.
- Baumgartner, H., Falk, V., Bax, J.J., et al., 2017. ESC/EACTS guidelines for the management of valvular heart disease. *Eur. Heart J.* 38, 2739–2791.
- Bennink, G., Torii, S., Brugmans, M., Cox, M., Svanidze, O., Ladich, E., Carrel, T., Virmani, R., 2018. A novel restorative pulmonary valved conduit in a chronic sheep model: mid-term hemodynamic function and histologic assessment. *J. Thorac. Cardiovasc. Surg.* 155 (6), 2591–2601.
- Bernacca, G.M., Mackay, T.G., Wilkinson, R., Wheatley, D.J., 1997. Polyurethane heart valves: fatigue failure, calcification, and polyurethane structure. *J. Biomed. Mater. Res.* 34, 371–379.
- Bernacca, G.M., Wheatley, D.J., 1998. Surface modification of polyurethane heart valves: effects on fatigue life and calcification. *Int. J. Artif. Organs* 21, 814–819.
- Bini, A., Mann, K.G., Kudryk, B.J., Schoen, F.J., 1999. Non-collagenous bone proteins, calcification and thrombosis in carcinoid artery atherosclerosis. *Arterio Sci. Thromb. Vasc. Biol.* 19, 1852–1861.
- Bezuidenhout, D., Williams, D.F., Zilla, P., 2015. Polymeric heart valves for surgical implantation, catheter-based technologies and heart assist devices. *Biomaterials* 36, 6–25.
- Bostrom, K., Watson, K.E., Horn, S., Wortham, C., Herman, I.M., et al., 1993. Bone morphogenetic protein expression in human atherosclerotic lesions. *J. Clin. Investig.* 91, 1800–1809.
- Bottio, T., Thiene, G., Pettenazzo, E., Ius, P., Bortolotti, U., et al., 2003. Hancock II bioprostheses: a glance at the microscope in mid-long-term explants. *J. Thorac. Cardiovasc. Surg.* 126, 99–105.
- Brockhurst, R.J., Ward, P.C., Lou, P., Ormerod, D., Albert, D., 1993. Dystrophic calcification of silicone scleral buckling implant materials. *Am. J. Ophthalmol.* 115, 524–529.
- Bucher, P.J., Buchi, E.R., Daicker, B.C., 1995. Dystrophic calcification of an implanted hydroxyethylmethacrylate intraocular lens. *Arch. Ophthalmol.* 113, 1431–1435.
- Bueno, E.M., Glowacki, J., 2009. Cell-free and cell-based approaches for bone regeneration. *Nat. Rev. Rheumatol.* 5, 685–697.
- Cardoso, L., Weinbaum, S., 2018. Microcalcifications, their genesis, growth, and biomechanical stability in fibrous cap rupture. *Adv. Exp. Med. Biol.* 1097, 129–155. https://doi.org/10.1007/978-3-319-96445-4_7. Review.
- Carpentier, S.M., Carpentier, A.F., Chen, L., Shen, M., Quintero, L.J., et al., 1997. Calcium mitigation in bioprosthetic tissues by iron pretreatment: the challenge of iron leaching. *Ann. Thorac. Surg.* 63, 1514–1515.
- Celiento, M., Ravenni, G., Milano, A.D., Pratali, S., Scioti, G., Nardi, C., et al., 2012. Aortic valve replacement with Medtronic Mosaic bioprosthesis: a 13-year follow-up. *Ann. Thorac. Surg.* 93, 510–515.
- Chan, V., Jamieson, W.R., Germann, E., Chan, F., Miyagishima, R.T., et al., 2006. Performance of bioprostheses and mechanical prostheses assessed by composites of valve-related complications to 15 years after aortic valve replacement. *J. Thorac. Cardiovasc. Surg.* 131, 1267–1273.
- Chen, W., Kim, J.D., Schoen, F.J., Levy, R.J., 1994a. Effect of 2-amino oleic acid exposure conditions on the inhibition of calcification of glutaraldehyde crosslinked porcine aortic valves. *J. Biomed. Mater. Res.* 28, 1485–1495.
- Chen, W., Schoen, F.J., Levy, R.J., 1994b. Mechanism of efficacy of 2-amino oleic acid for inhibition of calcification of glutaraldehyde-pretreated porcine bioprosthetic valves. *Circulation* 90, 323–329.
- Chen, J.-H., Liu, C., You, L., Simmons, C.A., 2009. Boning up on Wolff's Law: mechanical regulation of the cells that make and maintain bone. *J. Biomech.* 43, 108–118.
- Christian, A.J., Lin, H., Alferiev, I.S., Connolly, J.M., Ferrari, G., Hazen, S.L., Ischiropoulos, H., Levy, R.J., 2014. The susceptibility of bioprosthetic heart valve leaflets to oxidation. *Biomaterials* 35, 2097–2102.
- Christian, A.J., Alferiev, I.S., Connolly, J.M., et al., 2015. The effects of the covalent attachment of 3-(4-hydroxy-3,5-di-tert-butylphenyl)propyl amine to glutaraldehyde pre-treated bovine pericardium on structural degeneration, oxidative modification and calcification of rat subdermal implants. *J. Biomed. Mater. Res.* 103, 2441–2448.
- Chuang, T.H., Stabler, C., Simionescu, A., Simionescu, D.T., 2009. Polyphenol-stabilized tubular elastin scaffolds for tissue engineered vascular grafts. *Tissue Eng. A* 15, 2837–2851.
- Claiborne, T.E., Slepian, M.J., Hossainy, S., Bluestein, D., 2012. Polymeric trileaflet prosthetic heart valves: evolution and path to clinical reality. *Expert Rev. Med. Devices* 9, 577–594.
- Coleman, D., Lim, D., Kessler, T., Andrade, J.D., 1981. Calcification of nontextured implantable blood pumps. *Trans. Am. Soc. Artif. Intern. Organs* 27, 97–103.

- Connolly, J.M., Alferiev, I., Clark-Gruel, J.N., Eidelman, N., Sacks, M., Palmatory, E., Kronsteiner, A., Defelice, S., Xu, J., Ohri, R., Narula, N., Vyavahare, N., Levy, R.J., 2005. Triglycidylamine crosslinking of porcine aortic valve cusps or bovine pericardium results in improved biocompatibility, biomechanics, and calcification resistance: chemical and biological mechanisms. *Am. J. Pathol.* 166 (1), 1–13.
- Connolly, J.M., Bakay, M.A., Alferiev, I.S., Gorman, R.C., Gorman, J.H., Kruth, H.S., Ashworth, P.E., Kutty, J.K., Schoen, F.J., Bianco, R.W., Levy, R.J., 2011. Triglycidylamine cross-linking combined with ethanol inhibits bioprosthetic heart valve calcification. *Ann. Thorac. Surg.* 92, 858–865.
- Courtman, D.W., Pereira, C.A., Kashef, V., McComb, D., Lee, J.M., et al., 1994. Development of a pericardial acellular matrix biomaterial: biochemical and mechanical effects of cell extraction. *J. Biomed. Mater. Res.* 28, 655–666.
- Cunanan, C.M., Cabiling, C.M., Dinh, T.T., et al., 2001. Tissue characterization and calcification potential of commercial bioprosthetic heart valves. *Ann. Thorac. Surg.* 71, S417–S421.
- David, T.E., Armstrong, S., Sun, Z., 1998. The Hancock II bioprosthesis at 12 years. *Ann. Thorac. Surg.* 66, S95–S98.
- Deborde, C., Simionescu, D.T., Wright, C., Liao, J., Sierad, L.N., Simionescu, A., 2016. Stabilized collagen and elastin-based scaffolds for mitral valve tissue engineering. *Tissue Eng. A* 22, 1241–1251.
- Demer, L.L., 2002. Vascular calcification and osteoporosis: inflammatory responses to oxidized lipids. *Int. J. Epidemiol.* 31, 737–741.
- Demer, L.L., Tintut, Y., 2008. Vascular calcification: pathobiology of a multifaceted disease. *Circulation* 117, 2938–2948.
- Dohmen, P.M., da Costa, F., Holinski, S., Lopes, S.V., Yoshi, S., et al., 2006. Is there a possibility for a glutaraldehyde-free porcine heart valve to grow? *Eur. Surg. Res.* 38, 54–61.
- El-Hamamsy, I., Clark, L., Stevens, L.M., Sarang, Z., Melina, G., Takkenberg, J.J., et al., 2010. Late outcomes following freestyle versus homograft aortic root replacement: results from a prospective randomized trial. *J. Am. Coll. Cardiol.* 55, 368–376.
- Everaerts, F., Gillissen, M., Torrianni, M., et al., 2006. Reduction of calcification of carbodiimide-processed heart valve tissue by prior blocking of amine groups with monoaldehydes. *J. Heart Valve Dis.* 15, 269–277.
- Ford-Hutchinson, A.F., Cooper, D.M., Hallgrímsson, B., Jirik, F.R., 2003. Imaging skeletal pathology in mutant mice by microcomputed tomography. *J. Rheumatol.* 30, 2659–2665.
- Fukunaga, S., Tomoeda, H., Ueda, T., Mori, R., Aovagi, S., Kato, S., 2010. Recurrent mitral regurgitation due to calcified synthetic chordae. *Ann. Thorac. Surg.* 89, 955–957.
- Fyfe, B., Schoen, F.J., 1999. Pathologic analysis of removed non-stented Medtronic Freestyle™ aortic root bioprostheses treated with amino oleic acid (AOA). *Semin. Thorac. Cardiovasc. Surg.* 11 (4), 151–156.
- Gallegos, R.P., Nockel, P.J., Rivard, A.L., Bianco, R.W., 2005. The current state of in-vivo pre-clinical models for heart valve evaluation. *J. Heart Valve Dis.* 14, 423–432.
- Ghanbari, H., Viatge, H., Kidane, A.G., Burriesci, G., Tavakoli, M., et al., 2009. Polymeric heart valves: new materials, emerging hopes. *Trends Biotechnol.* 27, 359–367.
- Goldfarb, R.A., Neerhus, G.J., Lederer, E., 1989. Management of acute hydronephrosis of pregnancy by urethral stenting: risk of stone formation. *J. Urol.* 141, 921–922.
- Golomb, G., Schoen, F.J., Smith, M.S., Linden, J., Dixon, M., et al., 1987. The role of glutaraldehyde-induced crosslinks in calcification of bovine pericardium used in cardiac valve bioprostheses. *Am. J. Pathol.* 127, 122–130.
- Gong, G., Ling, Z., Seifert, E., Factor, S.M., Frater, R.W., 1991. Aldehyde tanning: the villain in bioprosthetic calcification. *Eur. J. Cardiothorac. Surg.* 5, 288–299.
- Gott, J.P., Chih, P., Dorsey, L.M., Jay, J.L., Jett, G.K., et al., 1992. Calcification of porcine valves: a successful new method of anti-mineralization. *Ann. Thorac. Surg.* 53, 207–216.
- Gorna, K., Gogolewski, S., 2002. Biodegradable polyurethanes for implants. II. In vitro degradation and calcification of materials from poly(ε-caprolactone)–poly(ethylene oxide) diols and various chain extenders. *J. Biomed. Mater. Res.* 60, 592–606.
- Grabenwoger, M., Grimm, M., Ebyl, E., Leukauf, C., Müller, M.M., et al., 1992. Decreased tissue reaction to bioprosthetic heart valve material after L-glutamic acid treatment. A morphological study. *J. Biomed. Mater. Res.* 26, 1231–1240.
- Grabenwoger, M., Sider, J., Fitzal, F., Zelenka, C., Windberger, U., et al., 1996. Impact of glutaraldehyde on calcification of pericardial bioprosthetic heart valve material. *Ann. Thorac. Surg.* 62, 772–777.
- Gümüş, N., 2009. Capsular calcification may be an important factor for the failure of breast implant. *Plast. Reconstr. Aesthet. Surg.* 62, e606–e608.
- Habibovic, P., de Groot, K., 2007. Osteoinductive biomaterials – properties and relevance in bone repair. *J. Tissue Eng. Regenat. Med.* 1, 25–32.
- Harasaki, H., Moritz, A., Uchida, N., Chen, J.F., McMahon, J.T., et al., 1987. Initiation and growth of calcification in a polyurethane coated blood pump. *Trans. Am. Soc. Artif. Intern. Organs* 33, 643–649.
- Hilbert, S.L., Ferrans, V.J., Tomita, Y., Eidbo, E.E., Jones, M., 1987. Evaluation of explanted polyurethane trileaflet cardiac valve prostheses. *J. Thorac. Cardiovasc. Surg.* 94, 419–429.
- Hirsch, D., Drader, J., Thomas, T.J., Schoen, F.J., Levy, J.T., et al., 1993. Inhibition of calcification of glutaraldehyde pretreated porcine aortic valve cusps with sodium dodecyl sulfate: preincubation and controlled release studies. *J. Biomed. Mater. Res.* 27, 1477–1484.
- Hjortnaes, J., Butcher, J., Figueiredo, J.-H., Riccio, M., Kohler, R.H., et al., 2010. Arterial and aortic valve calcification inversely correlates with osteoporotic bone remodeling: a role for inflammation. *Eur. Heart J.* 31, 1975–1984.
- Hofbauer, L.C., Brueck, C.C., Shanahan, C.M., Schoppet, M., Dobnig, H., 2007. Vascular calcification and osteoporosis – clinical observation towards molecular understanding. *Osteoporos. Int.* 18, 251–259.
- Human, P., Zilla, P., 2001a. Inflammatory and immune processes: the neglected villain of bioprosthetic degeneration? *J. Long Term Eff. Med. Implant.* 11, 199–220.
- Human, P., Zilla, P., 2001b. The possible role of immune responses in bioprosthetic heart valve failure. *J. Heart Valve Dis.* 10, 460–466.
- Hyde, J.A., Chinn, J.A., Phillips Jr., R.E., 1999. Polymer heart valves. *J. Heart Valve Dis.* 8, 331–339.
- Isenburg, J.C., Simionescu, D.T., Vyavahare, N.R., 2005. Tannic acid treatment enhances biostability and reduces calcification of glutaraldehyde fixed aortic wall. *Biomaterials* 26, 1237–1245.
- Jian, B., Jones, P.L., Li, Q., Mohler 3rd, E.R., Schoen, F.J., et al., 2001. Matrix metalloproteinase-2 is associated with tenascin-C in calcific aortic stenosis. *Am. J. Pathol.* 159, 321–327.
- Jian, B., Narula, N., Li, Q.Y., Mohler 3rd, E.R., Levy, R.J., 2003. Progression of aortic valve stenosis: TGF-beta 1 is present in calcified aortic valve cusps and promotes aortic valve interstitial cell calcification via apoptosis. *Ann. Thorac. Surg.* 75, 457–465.
- Jiang, X., Zhao, J., Wang, S., Sun, X., Zhang, X., et al., 2009. Mandibular repair in rats with premineralized silk scaffolds and BMP-2 modified bMSCs. *Biomaterials* 30, 4522–4532.

- Johnson, R.C., Leopold, J.A., Loscalzo, J., 2006. Vascular calcification. Pathobiological mechanisms and clinical implications. *Circ. Res.* 99, 1044–1059.
- Johnston, T.P., Webb, C.L., Schoen, F.J., Levy, R.J., 1993. Site-specific delivery of ethanedihydroxy diphosphonate from refillable polyurethane reservoirs to inhibit bioprosthetic tissue calcification. *J. Control. Release* 25, 227–240.
- Jones, M., Eidbo, E.E., Hilbert, S.L., Ferrans, V.J., Clark, R.E., 1989. Anticalcification treatments of bioprosthetic heart valves: in vivo studies in sheep. *J. Card. Surg.* 4, 69–73.
- Jono, S., McKee, M.D., Murry, C.E., Shiroi, A., Nishizawa, Y., et al., 2000. Phosphate regulation of vascular smooth muscle cell calcification. *Circ. Res.* 87, e10–e17.
- Jorge-Herrero, E., Fernández, P., Escudero, C., García-Páez, J.M., Castillo-Olivares, J.L., 1996. Calcification of pericardial tissue pretreated with different amino acids. *Biomaterials* 17, 571–575.
- Joshi, R.R., Underwood, T., Frautschi, J.R., Phillips Jr., R.E., Schoen, F.J., et al., 1996. Calcification of polyurethanes implanted subdermally in rats is enhanced by calciphylaxis. *J. Biomed. Mater. Res.* 31, 201–231 207.
- Kantrowitz, A., Freed, P.S., Zhou, Y., Mandell, G., DeDecker, P., Riddle, J., et al., 1995. A mechanical auxiliary ventricle. Histologic responses to long-term, intermittent pumping in calves. *AS70 J* 41, M340–M345.
- Kataruka, A., Otto, C.M., 2018. Valve durability after transcatheter aortic valve implantation. *J. Thorac. Dis.* 10 (Suppl. 30), S3629–S3636.
- Khan, S.R., Wilkinson, E.J., 1985. Scanning electron microscopy, X-ray diffraction, and electron microprobe analysis of calcific deposits on intrauterine contraceptive devices. *Hum. Pathol.* 16, 732–738.
- Kirsch, T., 2008. Determinants of pathologic mineralization. *Crit. Rev. Eukaryot. Gene Expr.* 18, 1–9.
- Klintworth, G.K., Reed, J.W., Hawkins, H.K., Ingram, P., 1977. Calcification of soft contact lenses in patient with dry eye and elevated calcium concentration in tears. *Investig. Ophthalmol. Vis. Sci.* 16, 158–161.
- Koide, T., Katayama, H., 1979. Calcification in augmentation mammoplasty. *Radiology* 130, 337–338.
- Kretlow, J.D., Mikos, A.G., 2007. Mineralization of synthetic polymer scaffolds for bone tissue engineering. *Tissue Eng.* 13, 927–938.
- Kumar, V., Abbas, A., Aster, J.C., 2015. Robbins/Cotran Pathologic Basis of Disease, ninth ed. W. B. Saunders, Philadelphia, PA.
- Lane, J.I., Randall, J.G., Campeau, N.G., Overland, P.K., McCannell, C.A., Matsko, T.A., et al., 2001. Imaging of hydrogel episclearal buckle fragmentation as a late complication after retinal reattachment surgery. *Am. J. Neuroradiol.* 22, 1199–1202.
- Lee, J.S., Basalyga, D.M., Simionescu, A., Isenburg, J.C., Simionescu, D.T., et al., 2006. Elastin calcification in the rat subdermal model is accompanied by up-regulation of degradative and osteogenic cellular responses. *Am. J. Pathol.* 168, 490–498.
- Lee, S., Levy, R.J., Christian, A.J., Hazen, S.L., Frick, N.E., Lai, E.K., Grau, J.B., Bavaria, J.E., Ferrari, G., 2017. Calcification and oxidative modifications are associated with progressive bioprosthetic heart valve dysfunction. *J. Am. Heart Assoc.* 8, 6.
- Legrand, A.P., Marinov, G., Pavlov, S., Guidoin, M.E., Famery, R., et al., 2005. Degenerative mineralization in the fibrous capsule of silicone breast implants. *J. Mater. Sci. Mater. Med.* 16, 477–485.
- Leong, J., Munnely, A., Liberio, B., Cochrane, L., Vyavahare, N., 2013. Neomycin and carbodiimide crosslinking as an alternative to glutaraldehyde for enhanced durability of bioprosthetic heart valves. *J. Biomater. Appl.* 27, 948–960.
- Levy, R.J., Schoen, R.J., Levy, J.T., Nelson, A.C., Howard, S.L., et al., 1983a. Biologic determinants of dystrophic calcification and osteocalcin deposition in glutaraldehyde-reserved porcine aortic valve leaflets implanted subcutaneously in rats. *Am. J. Pathol.* 113, 142–155.
- Levy, R.J., Schoen, F.J., Howard, S.L., 1983b. Mechanism of calcification of porcine aortic valve cusps: role of T-lymphocytes. *Am. J. Cardiol.* 52, 629–631.
- Levy, R.J., Hawley, M.A., Schoen, F.J., Lund, S.A., Liu, P.Y., 1985a. Inhibition by diphosphonate compounds of calcification of porcine bioprosthetic heart valve cusps implanted subcutaneously in rats. *Circulation* 71, 349–356.
- Levy, R.J., Wolfrum, J., Schoen, F.J., Hawley, M.A., Lund, S.A., et al., 1985b. Inhibition of calcification of bioprosthetic heart valves by local controlled-released diphosphonate. *Science* 229, 190–192.
- Levy, R.J., Schoen, F.J., Sherman, F.S., Nichols, J., Hawley, M.A., et al., 1986. Calcification of subcutaneously implanted type I collagen sponges: effects of glutaraldehyde and formaldehyde pretreatments. *Am. J. Pathol.* 122, 71–82.
- Levy, R.J., Schoen, F.J., Lund, S.A., Smith, M.S., 1987. Prevention of leaflet calcification of bioprosthetic heart valves with diphosphonate injection therapy. Experimental studies of optimal dosages and therapeutic durations. *J. Thorac. Cardiovasc. Surg.* 94, 551–557.
- Levy, R.J., 1994. Glutaraldehyde and the calcification mechanism of bioprosthetic heart valves. *J. Heart Valve Dis.* 3, 101–104.
- Levy, R.J., Schoen, F.J., Flowers, W.B., Staelin, S.T., 1991. Initiation of mineralization in bioprosthetic heart valves: studies of alkaline phosphatase activity and its inhibition by AlCl₃ or FeCl₃ preincubations. *J. Biomed. Mater. Res.* 25, 905–935.
- Levy, R.J., Vyavahare, N., Ogle, M., Ashworth, P., Bianco, R., et al., 2003. Inhibition of cusp and aortic wall calcification in ethanol- and aluminum-treated bioprosthetic heart valves in sheep: background, mechanisms, and synergism. *J. Heart Valve Dis.* 12, 209–216.
- Love, J.W., 1993. Autologous Tissue Heart Valves. R. G. Landes, Austin, TX.
- Lovekamp, J.J., Simionescu, D.T., Mercuri, J.J., Zubiate, B., Sacks, M.S., Vyavahare, N.R., 2006. Stability and function of glycosaminoglycans in porcine bioprosthetic heart valves. *Biomaterials* 27, 1507–1518.
- MacLean, K.D., Apel, A., Wilson, J., Werner, L., 2015. Calcification of hydrophilic acrylic intraocular lenses associated with intracameral air injection following DMEK. *J. Chem. Res., Synop.* 41, 1310–1314.
- Mako, W.J., Vesely, I., 1997. In vivo and in vitro models of calcification in porcine aortic valve cusps. *J. Heart Valve Dis.* 6, 316–323.
- Manji, R.A., Zhu, L.F., Nijjar, N.K., et al., 2006. Glutaraldehyde-fixed bioprosthetic heart valve conduits calcify and fail from xenograft rejection. *Circulation* 114, 318–327.
- Maranto, A.R., Schoen, F.J., 1988. Alkaline phosphatase activity of glutaraldehyde-treated bovine pericardium used in bioprosthetic heart valves. *Circ. Res.* 63, 844–848.
- Meuris, B., De Praetere, H., Strasly, M., Trabucco, P., Lai, J.C., et al., 2018. A novel tissue treatment to reduce mineralization of bovine pericardial heart valves. *J. Thorac. Cardiovasc. Surg.* 156, 197–206.
- Mitchell, R.N., Jonas, R.A., Schoen, F.J., 1998. Pathology of explanted cryopreserved allograft heart valves: comparison with aortic valves from orthotopic heart transplants. *J. Thorac. Cardiovasc. Surg.* 115, 118–127.
- Mitchell, R.N., Schoen, F.J., 2010. Blood vessels. In: Kumar, V., Fausto, N., Aster, J.C., Abbas, A. (Eds.), Robbins/Cotran Pathologic Basis of Disease, eighth ed. W.B. Saunders, Philadelphia, pp. 487–528.
- Moore, Phillips, R.E., 1997. Biocompatibility and immunologic properties of pericardial tissue stabilized by dye-mediated photo-oxidation. *J. Heart Valve Dis.* 6, 307–315.

- Munnely, A.E., Cochrane, L., Leong, J., Vyavahare, N.R., 2012. Porcine vena cava as an alternative to bovine pericardium in bioprosthetic percutaneous heart valves. *Biomaterials* 33, 1–8.
- Myers, D.J., Nakaya, G., Girardot, G.M., Christie, G.W., 1995. A comparison between glutaraldehyde and diepoxide-fixed stentless porcine aortic valves: biochemical and mechanical characterization and resistance to mineralization. *J. Heart Valve Dis.* 4, S98–S101.
- Nakanome, S., Watanabe, H., Tanaka, K., Tochikubo, T., 2008. Calcification of Hydroview H60M intraocular lenses: aqueous humor analysis and comparisons with other intraocular lens materials. *J. Cataract Refract. Surg.* 34, 80–86.
- Neues, F., Epple, M., 2008. X-ray microcomputer tomography for the study of biomineralized endo- and exoskeletons of animals. *Chem. Rev.* 108, 4734–4741.
- Neuhann, M., Kleinmann, G., Apple, D.J., 2008. A new classification of calcification of intraocular lenses. *Ophthalmology* 115, 73–79.
- New, S.E., Aikawa, E., 2011. Molecular imaging insights into early inflammatory stages of arterial and aortic valve calcification. *Circ. Res.* 108, 1381–1391.
- Patai, K., Berényi, M., Sipos, M., Noszál, B., 1998. Characterization of calcified deposits on contraceptive intrauterine devices. *Contraception* 58, 305–308.
- Pawade, T.A., Newby, D.E., Dweck, M.R., 2015. Calcification in aortic stenosis: the skeleton key. *J. Am. Coll. Cardiol.* 66, 561–577.
- Peacock, M., 2010. Calcium metabolism in health and disease. *Clin. J. Am. Soc. Nephrol.* 5, S23–S30.
- Persy, V., D’Haese, P., 2009. Vascular calcification and bone disease: the calcification paradox. *Trends Mol. Med.* 15, 405–416.
- Peters, W., Pritzker, K., Smith, D., Fornasier, V., Holmyard, D., et al., 1998. Capsular calcification associated with silicone breast implants: incidence, determinants, and characterization. *Ann. Plast. Surg.* 41, 348–360.
- Peters, W., Smith, D., 1995. Calcification of breast implant capsules: incidence, diagnosis, and contributing factors. *Ann. Plast. Surg.* 34, 8–11.
- Pettenazzo, E., Valente, M., Thiene, G., 2008. Octanediol treatment of glutaraldehyde fixed bovine pericardium: evidence of anticalcification efficacy in the subcutaneous rat model. *Eur. J. Cardiothorac. Surg.* 34, 418–422.
- Phogat, J., Rathi, M., Verma, R., Marwah, N., Sachdeva, S., et al., 2017. Calcification of hydrophilic intraocular lenses: laboratory analysis and surgical technique for intraocular lens exchange. *MSJCRS Online Case Reports* 5, 64–66.
- Raghavan, D., Shah, S.R., Vyavahare, N.R., 2010. Neomycin fixation followed by ethanol pretreatment leads to reduced buckling and inhibition of calcification in bioprosthetic valves. *J. Biomed. Mater. Res. Part B, Appl. Biomater.* 92, 168–177.
- Rahimi, M., Azimi, A., Hosseinzadeh, M., 2018. Intraocular lens calcification: clinico-pathological report of two cases and literature review. *J. Ophthalmic Vis. Res.* 13, 195–199.
- Ramin, Z., Jen-Chieh, T., Robert, F., Jeffrey, M., et al., 2019. Effect of stent crimping on calcification of transcatheter aortic valves. *Interact. Cardiovasc. Thorac. Surg.* 29(1), 64–73.
- Rimmer, T., Hawkesworth, N., Kirkpatrick, N., Price, N., Manners, R., et al., 2010. Calcification of Hydroview lenses implanted in the United Kingdom during 2000 and 2001. *Eye* 24, 199–200.
- Rousselle, S.D., Wicks, J.R., Tabb, B.C., Price, N., Tellez, A.O’Brien, M., 2019. Histology strategies for medical implants and interventional device studies. *Toxicol Pathol* 47, 235–249.
- Sacks, M.S., Schoen, F.J., 2002. Collagen fiber disruption occurs independent of calcification in clinically explanted bioprosthetic heart valves. *J. Biomed. Mater. Res.* 62, 359–371.
- Schlieper, G., Krüger, T., Djuric, Z., Damjanovic, T., Markovic, N., et al., 2008. Vascular access calcification predicts mortality in hemodialysis patients. *Kidney Int.* 74, 1582–1587.
- Schoen, F.J., 1998. Pathologic findings in explanted clinical bioprosthetic valves fabricated from photooxidized bovine pericardium. *J. Heart Valve Dis.* 7, 174–179.
- Schoen, F.J., Edwards, W.D., 2001. Pathology of cardiovascular interventions, including endovascular therapies, revascularization, vascular replacement, cardiac assist/replacement, arrhythmia control and repaired congenital heart disease. In: Silver, M.D., Gotlieb, A.I., Schoen, F.J. (Eds.), *Cardiovascular Pathology*, third ed. W. B. Saunders, Philadelphia, PA, pp. 678–723.
- Schoen, F.J., Kujovich, J., Webb, C.L., Levy, R.J., 1987. Chemically determined mineral content of explanted porcine aortic valve bioprostheses: Correlation with radiographic assessment of calcification and clinical data. *Circulation* 76, 1061–1066.
- Schoen, F.J., Levy, R.J., 1999. Tissue heart valves: current challenges and future research perspectives. *J. Biomed. Mater. Res.* 47, 439–465.
- Schoen, F.J., Levy, R.J., 2005. Calcification of tissue heart valve substitutes: progress toward understanding and prevention. *Ann. Thorac. Surg.* 79, 1072–1080.
- Schoen, F.J., Levy, R.J., Nelson, A.C., Bernhard, W.F., Nashef, A., et al., 1985. Onset and progression of experimental bioprosthetic heart valve calcification. *Lab. Investig.* 52, 523–532.
- Schoen, F.J., Tsao, J.W., Levy, R.J., 1986. Calcification of bovine pericardium used in cardiac valve bioprostheses. Implications for mechanisms of bioprosthetic tissue mineralization. *Am. J. Pathol.* 123, 143–154.
- Schoen, F.J., Golomb, G., Levy, R.J., 1992a. Calcification of bioprosthetic heart valves: a perspective on models. *J. Heart Valve Dis.* 1, 110–114.
- Schoen, F.J., Levy, R.J., Hilbert, S.L., Bianco, R.W., 1992b. Antimineralization treatments for bioprosthetic heart valves. Assessment of efficacy and safety. *J. Thorac. Cardiovasc. Surg.* 104, 1285–1288.
- Schoen, F.J., Levy, R.J., Piehler, H.R., 1992c. Pathological considerations in replacement cardiac valves. *Cardiovasc. Pathol.* 1, 29–52.
- Schoen, F.J., Hirsch, D., Bianco, R.W., Levy, R.J., 1994. Onset and progression of calcification in porcine aortic bioprosthetic valves implanted as orthotopic mitral valve replacements in juvenile sheep. *J. Thorac. Cardiovasc. Surg.* 108, 880–887.
- Shang, H., Claessens, S.M., Tian, B., et al., 2017. Aldehyde reduction in a novel pericardial tissue reduces calcification using rabbit intramuscular model. *J. Mater. Sci. Mater. Sci.* 28, 16.
- Simon, P., Kasimir, M.T., Seebacher, G., Weigel, G., Ullrich, R., et al., 2003. Early failure of the tissue engineered porcine heart valve SYNERGRAFT in pediatric patients. *Eur. J. Cardiothorac. Surg.* 23, 1002–1006.
- Simionescu, D., 2004. Prevention of calcification in bioprosthetic heart valves: challenges and perspectives. *Biol. Ther.* 4, 1971–1985.
- Srivasta, S.S., Maercklein, P.B., Veinot, J., Edwards, W.D., Johnson, C.M., et al., 1997. Increased cellular expression of matrix proteins that regulate mineralization is associated with calcification of native human and porcine xenograft bioprosthetic heart valves. *J. Clin. Investig.* 5, 996–1009.
- Stachelek, S.J., Alferiev, I., Choi, H., Chan, C.W., Zubiato, B., et al., 2006. Prevention of oxidative degradation of polyurethane by covalent attachment of di-tert-butylphenol residues. *J. Biomed. Mater. Res. A* 78, 653–661.
- Steitz, S.A., Speer, M.Y., McKee, M.D., Liaw, L., Almeida, M., et al., 2002. Osteopontin inhibits mineral deposition and promotes regression of ectopic calcification. *Am. J. Pathol.* 161, 2035–2046.

- Sun, W., Sacks, M., Fulchiero, G., Lovekamp, J., Vyavahare, N., et al., 2004. Response of heterograft heart valve biomaterials to moderate cyclic loading. *J. Biomed. Mater. Res. A* 69, 658–669.
- Tam, H., Zhang, W., Infante, D., Parchment, N., Sacks, M., Vyavahare, N., 2017. Fixation of bovine pericardium-based tissue biomaterial with irreversible chemistry improves biochemical and biomechanical properties. *J. Cardiovasc. Transl. Res.* 10, 194–205.
- Tedder, M.E., Liao, J., Weed, B., Stabler, C., Zhang, H., Simionescu, A., et al., 2009. Stabilized collagen scaffolds for heart valve tissue engineering. *Tissue Eng. A* 15, 1257–1268.
- Tew, W.P., Mahle, C., Benavides, J., Howard, J.E., Lehninger, A.L., 1980. Synthesis and characterization of phosphocitric acid, a potent inhibitor of hydroxylapatite crystal growth. *Biochemistry* 19, 1983–1988.
- Thubrikar, M.J., Deck, J.D., Aouad, J., Nolan, S.P., 1983. Role of mechanical stress in calcification of aortic bioprosthetic valves. *J. Thorac. Cardiovasc. Surg.* 86, 115–125.
- Tod, T.J., Dove, J.S., 2016. The association of bound aldehyde content with bioprosthetic tissue calcification. *J. Mater. Sci. Mater. Med.* 27, 8.
- Tomizawa, Y., Takanashi, Y., Noishiki, Y., Nishida, H., Endo, M., et al., 1998. Evaluation of small caliber vascular prostheses implanted in small children: activated angiogenesis and accelerated calcification. *Am. Soc. Artif. Intern. Organs J.* 44, M496–M500.
- Trantina-Yates, A.E., Human, P., Zilla, P., 2003. Detoxification on top of enhanced, diamine-extended glutaraldehyde fixation significantly reduces bioprosthetic root calcification in the sheep model. *J. Heart Valve Dis.* 12, 93–100.
- Tripi, D.R., Vyavahare, N.R., 2014. Neomycin and pentagalloyl glucose enhanced cross-linking for elastin and glycosaminoglycans preservation in bioprosthetic heart valves. *J. Biomater. Appl.* 28, 757–766.
- Umaña, E., Ahmed, W., Alpert, M.A., 2003. Valvular and perivalvular abnormalities in end-stage renal disease. *Am. J. Med. Sci.* 325, 237–242.
- Vanderbrink, B.A., Rastinehad, A.R., Ost, M.C., Smith, A.D., 2008. Encrusted urinary stents: evaluation and endourologist management. *J. Endocrinol.* 22, 905–912.
- Vyavahare, N.R., Chen, W., Joshi, R., Lee, C.-H., Hirsch, D., et al., 1997a. Current progress in anticalcification for bioprosthetic and polymeric heart valves. *Cardiovasc. Pathol.* 6, 219–229.
- Vyavahare, N., Hirsch, D., Lerner, E., Baskin, J.Z., Schoen, F.J., et al., 1997b. Prevention of bioprosthetic heart valve calcification by ethanol preincubation. Efficacy and mechanism. *Circulation* 95, 479–488.
- Vyavahare, N.R., Hirsch, D., Lerner, E., Baskin, J.Z., Zand, R., et al., 1998. Prevention of calcification of glutaraldehyde-crosslinked porcine aortic cusps by ethanol preincubation: mechanistic studies of protein structure and water–biomaterial relationships. *J. Biomed. Mater. Res.* 40, 577–585.
- Vyavahare, N., Ogle, M., Schoen, F.J., Levy, R.J., 1999. Elastin calcification and its prevention with aluminum chloride pretreatment. *Am. J. Pathol.* 155, 973–982.
- Vyavahare, N.R., Jones, P.L., Hirsch, D., Schoen, F.J., Levy, R.J., 2000. Prevention of glutaraldehyde-fixed bioprosthetic heart valve calcification by alcohol pretreatment: further mechanistic studies. *J. Heart Valve Dis.* 9, 561–566.
- Wang, Q., McGoron, A.J., Bianco, R., Kato, Y., Pinchuk, L., Schoephoerster, R.T., 2010. In-vivo assessment of a novel polymer (SIBS) trileaflet heart valve. *J. Heart Valve Dis.* 19, 499–505.
- Weissen-Plenz, G., Nitschke, Y., Rutsch, F., 2008. Mechanisms of arterial calcification: spotlight on the inhibitors. *Adv. Clin. Chem.* 46, 263–293.
- Webb, C.L., Benedict, J.J., Schoen, F.J., Linden, J.A., Levy, R.J., 1988. Inhibition of bioprosthetic heart valve calcification with aminodiphosphonate covalently bound to residual aldehyde groups. *Ann. Thorac. Surg.* 46, 309–316.
- Webb, C.L., Schoen, F.J., Flowers, W.E., Alfrey, A.C., Horton, C., et al., 1991. Inhibition of mineralization of glutaraldehyde-pretreated bovine pericardium by AlCl₃. Mechanisms and comparisons with FeCl₃ LaCl₃ and Ga(NO₃)₃ in rat subdermal model studies. *Am. J. Pathol.* 138, 971–981.
- Wilson, G.J., Courtman, D.W., Klement, P., Lee, J.M., Yeager, H., 1995. Acellular matrix: a biomaterials approach for coronary artery and heart valve replacement. *Ann. Thorac. Surg.* 60, S353–S358.
- Xi, T., Ma, J., Tian, W., Lei, X., Long, S., et al., 1992. Prevention of tissue calcification on bioprosthetic heart valve by using epoxy compounds: a study of calcification tests in vitro and in vivo. *J. Biomed. Mater. Res.* 26, 1241–1251.
- Yip, C.Y.Y., Chen, J.-H., Zhao, R., Simmons, C.A., 2009. Calcification by valve interstitial cells is regulated by the stiffness of the extracellular matrix. *Arterioscler. Thromb. Vasc. Biol.* 29, 936–942.
- Yu, S.-Y., Viola, F., Christoforidis, J.B., D’Amico, D.J., 2005. Dystrophic calcification of the fibrous capsule around a hydrogel explant 13 years after scleral buckling surgery: capsular calcification of a hydrogel explant. *Retina* 25, 1104–1107.
- Zaidi, A.H., Nathan, M., Emani, S., Baird, C., del Nido, P.J., Gauvreau, K., Harris, M., Sanders, S.P., Padera, R.F., 2014. Preliminary experience with porcine intestinal submucosa (CorMatrix) for valve reconstruction in congenital heart disease: histologic evaluation of explanted valves. *J. Thorac. Cardiovasc. Surg.* 148 2216–4.
- Zareian, R., Tseng, J.C., Fraser, R., Meganck, J., Kilduff, M., Sarraf, M., Dvir, D., Kheradvar, A., 2019. Effect of stent crimping on calcification of transcatheter aortic valves. *Interact. Cardiovasc. Thorac. Surg.* 1–10.
- Zhang, B., Bianco, R.W., Schoen, F.J., 2019. Preclinical assessment of cardiac valve substitutes. Current Status and considerations for engineered tissue heart valves. *Front. Cardiovasc. Med.* (in press).
- Zilla, P., Weissenstein, C., Bracher, M., Zhang, Y., Koen, W., et al., 1997a. High glutaraldehyde concentrations reduce rather than increase the calcification of aortic wall tissue. *J. Heart Valve Dis.* 6, 490–491.
- Zilla, P., Fullard, L., Trescony, P., et al., 1997b. Glutaraldehyde detoxification of aortic wall tissue: a promising perspective for emerging bioprosthetic valve concepts. *J. Heart Valve Dis.* 6, 510–520.
- Zilla, P., Weissenstein, C., Human, P., Dower, T., von Oppell, U.O., 2000. High glutaraldehyde concentrations mitigate bioprosthetic root calcification in the sheep model. *Ann. Thorac. Surg.* 70, 2091–2095.
- Zilla, P., Bezuidenhout, D., Torrianni, M., Hendriks, M., Human, P., 2005. Diamine-extended glutaraldehyde- and carbodiimide crosslinks act synergistically in mitigating bioprosthetic aortic wall calcification. *J. Heart Valve Dis.* 14, 538–545.

Further Reading

- Anderson, H.C., 1988. Mechanisms of pathologic calcification. *Rheum. Dis. Clin. N. Am.* 14, 303–319.
- Anderson, H.C., 1989. Mechanism of mineral formation in bone. *Lab. Investig.* 60, 320–330.
- Arora, S., Ramm, C.J., Misenheimer, J.A., Vavalle, J.P., 2017. Early transcatheter valve prosthesis degeneration and future ramifications. *Cardiovasc. Diagn. Ther.* 7, 1–3.
- Barrere, F., van Blitterswijk, C.A., de Groot, K., 2006. Bone regeneration: molecular and cellular interactions with calcium phosphate ceramics. *Int. J. Nanomed.* 1, 317–332.

- Bechtel, J.F., Muller-Steinhardt, M., Schmidtke, C., Bruswik, A., Stierle, U., et al., 2003. Evaluation of the decellularized pulmonary valve homograft (SynerGraft). *J. Heart Valve Dis.* 12, 734–739.
- Bonucci, E., 1987. Is there a calcification factor common to all calcifying matrices? *Scanning Microsc.* 1, 1089–1102.
- Cheng, P.T., 1988. Pathologic calcium phosphate deposition in model systems. *Rheum. Dis. Clin. N. Am.* 14, 341–351.
- Courtman, D.W., Pereira, C.A., Omar, S., Langdon, S.E., Lee, J.M., et al., 1995. Biomechanical and ultrastructural comparison of cryopreservation and a novel cellular extraction of porcine aortic valve leaflets. *J. Biomed. Mater. Res.* 29, 1507–1516.
- Deutsch, M.-A., Mayr, N.P., Assmann, G., Will, A., Krane, M., Piazza, N., et al., 2015. Structural valve deterioration 4 years after transcatheter aortic valve replacement. *Circulation* 131, 682.
- Discher, D.E., Mooney, D.J., Zandstra, P.W., 2009. Growth factors, matrices, and forces combine and control stem cells. *Science* 324, 1673–1677.
- Everaerts, F., Torrianni, M., van Luyn, M.J., Van Wachem, P.B., Feijen, J., et al., 2004. Reduced calcification of bioprostheses, cross-linked via an improved carbodiimide based method. *Biomaterials* 25, 5523–5530.
- Flameng, W., Ozaki, S., Meuris, B., Herijgers, P., Yperman, J., et al., 2001. Antimineralization treatments in stentless porcine bioprostheses. An experimental study. *J. Heart Valve Dis.* 10, 489–494.
- Fradet, G., Bleese, N., Busse, E., Jamieson, E., Raudkivi, P., et al., 2004. The mosaic valve clinical performance at seven years: results from a multicenter prospective clinical trial. *J. Heart Valve Dis.* 13, 239–247.
- Gertz, S.D., Kurgan, A., Eisenberg, D., 1988. Aneurysm of the rabbit common carotid artery induced by periarterial application of calcium chloride in vivo. *J. Clin. Investig.* 81, 649–656.
- Giachelli, C.M., 1999. Ectopic calcification: gathering hard facts about soft tissue mineralization. *Am. J. Pathol.* 154, 671–675.
- Gott, J.P., Girardot, M.N., Girardot, J.M., Hall, J.D., Whitlark, J.D., et al., 1997. Refinement of the alpha aminooleic acid bioprosthetic valve anticalcification technique. *Ann. Thorac. Surg.* 64, 50–58.
- Grunkemeier, G.L., Jamieson, W.R., Miller, D.C., Starr, A., 1994. Actuarial versus actual risk of porcine structural valve deterioration. *J. Thorac. Cardiovasc. Surg.* 108, 709–718.
- Harbaoui, B., Courand, P.-Y., Schmitt, Z., Farhat, F., Dauphin, R., Lantelme, P., 2016. Early Edwards SAPIEN valve degeneration after transcatheter aortic valve replacement. *JACC Cardiovasc. Interv.* 9, 198.
- Hendriks, M., Eveaerts, F., Verhoeven, M., 2001. Alternative fixation of bioprostheses. *J. Long Term Eff. Med. Implant.* 11, 163–183.
- Human, P., Bezuidenhout, D., Torrianni, M., Hendriks, M., Zilla, P., 2002. Optimization of diamine bridges in glutaraldehyde treated bioprosthetic aortic wall tissue. *Biomaterials* 23, 2099–2103.
- Johnston, T.P., Webb, C.L., Schoen, F.J., Levy, R.J., 1992. Assessment of the in vitro transport parameters for ethanehydroxy diphosphate through a polyurethane membrane. A potential refillable reservoir drug delivery device. *Am. Soc. Artif. Intern. Organs Trans.* 38, M611–M616.
- Langer, R., Vacanti, J.P., 1993. Tissue engineering. *Science* 260, 920–926.
- Lentz, D.L., Pollock, E.M., Olsen, D.B., Andrews, E.J., 1982. Prevention of intrinsic calcification in porcine and bovine xenograft materials. *Trans. Am. Soc. Artif. Intern. Organs* 28, 494–497.
- Luo, G., Ducey, P., McKee, M.D., Pinero, G.J., Loyer, E., et al., 1997. Spontaneous calcification of arteries and cartilage in mice lacking matrix GLA protein. *Nature* 386, 78–81.
- Mayer Jr., J.E., Shin'oka, T., Shum-Tim, D., 1997. Tissue engineering of cardiovascular structures. *Curr. Opin. Cardiol.* 12, 528–532.
- McGonagle-Wolff, K., Schoen, F.J., 1992. Morphologic findings in explanted Mitroflow pericardial bioprosthetic valves. *Am. J. Cardiol.* 70, 263–264.
- Meuris, B., Phillips, R., Moore, M.A., Flameng, W., 2003. Porcine stentless bioprostheses: prevention of aortic wall calcification by dye-mediated photooxidation. *Artif. Organs* 27, 537–543.
- Ogle, M.F., Kelly, S.J., Bianco, R.W., Levy, R.J., 2003. Calcification resistance with aluminum-ethanol treated porcine aortic valve bioprostheses in juvenile sheep. *Ann. Thorac. Surg.* 75, 1267–1273.
- Ong, S.H., Mueller, R., Iversen, S., 2011. Early calcific degeneration of a CoreValve transcatheter aortic bioprosthesis. *Eur. Heart J.* 33, 586.
- Parhami, F., Basseri, B., Hwang, J., Tintut, Y., Demer, L.L., 2002. High-density lipoprotein regulates calcification of vascular cells. *Circ. Res.* 91, 570–576.
- Pascual, I., Avanzas, P., Mori's, C., 2017. Degenerative pattern of a percutaneous aortic valve. *Rev. Esp. Cardiol.* 70, 772.
- Piatti, F., Sturla, F., Marom, G., Sheriff, J., Claiborne, T.E., et al., 2015. Hemodynamic and thrombogenic analysis of a trileaflet polymeric valve using a fluid-structure interaction approach. *J. Biomech.* 48, 3641–3649.
- Richardt, D., Hanke, T., Sievers, H.H., 2015. Two cases of heart failure after implantation of a CoreValve prosthesis. *N. Engl. J. Med.* 372, 1079–1081.
- Schoen, F.J., 2001. Pathology of heart valve substitution with mechanical and tissue prosthesis. In: Silver, M.D., Gotlieb, A.I., Schoen, F.J. (Eds.), *Cardiovascular Pathology*, third ed. W. B. Saunders, Philadelphia, PA, pp. 629–677.
- Schoen, F.J., Mitchell, R.N., 2015. The heart. In: Kumar, V., Abbas, A., Aster, J.C. (Eds.), *Robbins/Cotran Pathologic Basis of Disease*, ninth ed. W.B. Saunders, Philadelphia, pp. 523–578.
- Schoen, F.J., 1988. Biomaterials-associated calcification: pathology, mechanisms, and strategies for prevention. *J. Appl. Biomater.* 22, 11–36.
- Shinoka, T., Ma, P.X., Shum-Tim, D., Breuer, C.K., Cusick, R.A., et al., 1996. Tissue-engineered heart valves. Autologous valve leaflet replacement study in a lamb model. *Circulation* 94 II-164–II-168.
- Speer, M.Y., Giachelli, C.M., 2004. Regulation of vascular calcification. *Cardiovasc. Pathol.* 13, 63–70.
- Speer, M.Y., McKee, M.D., Guldberg, R.E., Liaw, L., Yang, H.-Y., et al., 2002. Inactivation of the osteopontin gene enhances vascular calcification of matrix Gla protein-deficient mice: evidence for osteopontin as an inducible inhibitor of vascular calcification in vivo. *J. Exp. Med.* 196, 1047–1055.
- Stock, U.A., Nagashima, M., Khalil, P.N., Nollert, G.D., Herden, T., et al., 1999. Tissue engineered valved conduits in the pulmonary circulation. *J. Thorac. Cardiovasc. Surg.* 119, 732–740.
- Thoma, R.J., Phillips, R.E., 1995. The role of material surface chemistry in implant device calcification: a hypothesis. *J. Heart Valve Dis.* 4, 214–221.
- van Steenberghe, M., de Vasconcelos, C.-Y., Delay, D., Niclauss, L., Kirsch, M., 2016. Early transcatheter aortic valve degeneration in the young. *Int. J. Cardiol.* 222, 786–787.
- Van Wachem, P.B., Brouwer, L.A., Zeeman, R., Dijkstra, P.J., Feijen, J., et al., 2000. In vivo behavior of epoxy-crosslinked porcine heart valve cusps and walls. *J. Biomed. Mater. Res.* 53, 18–27.

- Van Wachem, P.B., Brouwer, L.A., Zeeman, R., Dijkstra, P.J., Feijen, J., et al., 2001. Tissue reactions to epoxy-crosslinked porcine heart valves post-treated with detergents or a dicarboxylic acid. *J. Biomed. Mater. Res.* 55, 415–423.
- Wada, T., McKee, M.D., Steitz, S., Giachelli, C.M., 1999. Calcification of vascular smooth muscle cell cultures. Inhibition by osteopontin. *Circ. Res.* 84, 166–178.
- Webb, J.G., Dvir, D., 2015. Is transcatheter aortic valve replacement a durable therapeutic strategy? *JACC Cardiovasc. Interv.* 8, 1092.
- Zilla, P., Weissenstein, C., Bracher, M., Human, P., 2001. The anticalcific effect of glutaraldehyde detoxification on bioprosthetic aortic wall tissue in the sheep model. *J. Card. Surg.* 16, 467–472.

2.5.1

Introduction to Applications of Biomaterials

MICHAEL J. YASZEMSKI¹, FREDERICK J. SCHOEN², JACK E. LEMONS³

¹Orthopaedic Surgery and Biomedical Engineering, Mayo Clinic College of Medicine, Rochester, MN, United States

²Department of Pathology, Brigham and Women's Hospital and Harvard Medical School, Boston, MA, United States

³Schools of Dentistry, Medicine and Engineering, University of Alabama at Birmingham, Birmingham, AL, United States

Most students of biomaterials have a strong interest in medical, surgical, or dental applications. Biomaterials are used for the construction of components in an extensive array of devices across a wide range of biomedical disciplines. When considering the applications of biomaterials as a section in *Biomaterials Science, Fourth Edition: An Introduction to Materials in Medicine*, the primary consideration is on outcomes of treatments. Outcomes are evaluated in terms of the medical discipline involved and the specific biomaterial properties needed for a targeted application to improve the outcomes of patients with specific clinical problems. For example, a total joint replacement has very different considerations than a tooth root replacement, although both anchor in bone for function. Similarly, requirements for a heart valve are very different compared to a vessel replacement or an endovascular stent, although all have extensive blood contact and some biomaterial properties are in common. A central theme is the generation and use of design criteria based on desired functionality, potentially deleterious biomaterials–tissue interaction mechanisms, pathologies of the underlying conditions for which the implant is needed, and the basic properties of the various biomaterials available or needing to be developed. It should not be surprising that considerable research and development has led to clinically used devices with active mechanical, electrical, biologic, or mass exchange functions.

Most implants serve their recipients well for extended periods by alleviating the conditions for which they were implanted. Considerable effort is expended in understanding biomaterials–tissue interactions and eliminating patient–device complications (the clinically important manifestations of biomaterials–tissue interactions). Moreover, many patients receive substantial and extended benefit, despite complications. For example, heart valve disease is a serious medical problem affecting over 100,000 people per year in the United States. Patients with aortic stenosis (the most common form of heart valve disease) have a 50% chance of dying within approximately 3 years without surgery. Surgical replacement of a diseased valve leads to an expected survival of 70% at 10 years, a substantial improvement over the natural course. However, of these patients whose longevity and quality of life have clearly been enhanced, approximately 60% will suffer a serious valve-related complication within 10 years after the operation. Thus long-term failure of biomaterials leading to a clinically significant event does not preclude clinical success for a significant duration. The estimated annual expenditure for implanted medical devices in the United States is 100 billion dollars, and the worldwide expenditure is 300 billion dollars.

The following chapters that constitute [Section 2.5](#) present a broad spectrum of biomaterials applications and the key properties needed for specific physiological environments.

Section 2.5 begins with Chapter 2.5.2A, “Cardiovascular Medical Devices: Heart Valves, Pacemakers and Defibrillators, Mechanical Circulatory Support and Other Intracardiac devices,” by Robert F. Padera and Frederick J. Schoen and Chapter 2.5.2B “Cardiovascular medical devices: stents, grafts, stent-grafts” by Michael A. Seidman, Robert F. Padera and Frederick J. Schoen. Multifunction endovascular implants, for example, an aortic stent that includes an aortic valve, can significantly lessen the procedural risk in treating aortic valvular disease when compared to open valve replacement in patients who often have multiple comorbidities.

Chapter 2.5.3, “Extracorporeal Artificial Organs and Therapeutic Devices,” by Rei Ukita, Alastair Campbell Richie, Angela Lai and Keith E. Cook, discusses the role of functional biomaterials that provide bodily functions that no longer exist because of disease or trauma.

Chapter 2.5.4, “Orthopedic Applications,” by Joshua J. Jacobs and Nadim James Hallab, presents the spectrum of biomaterials that replace musculoskeletal functions, which include joints, cartilaginous surfaces, tendons, ligaments, and bones.

Chapter 2.5.5, “Dental Applications,” by David H. Kohn and Jack E. Lemons, discusses the hard and soft tissues whose function is replaced by biomaterials when those tissues’ functions are absent because of normal wear, disease, or trauma.

Chapter 2.5.6, “Ophthalmologic Applications,” by Heather Sheardown, Emily Anne Hicks, Ben Muirhead, and Aftab Taiyab, gives an introductory overview on biomaterials used to treat diseases of the eye.

Chapter 2.5.7, “Bioelectronic and Neural Implants,” by Jeffrey R. Capadona and Andrew J. Shoffstall, presents the fundamentals of these devices, including the materials used, their selection criteria, the neuroinflammatory response to them, and the brain–computer interface.

Chapter 2.5.8, “Burn Dressings and Skin Substitutes,” by Steven T. Boyce, Petra M. Warner, and Philip Hyungjin Chang, discusses the sequence of treatment for burn patients, beginning with debridement/escharotomy, selection of wound dressings, including subatmospheric (“negative”) pressure dressings, management of microbial contamination, fluid balance, and temporary and/or permanent skin substitutes (some of which are polymeric biomaterials), all leading to wound closure. As an example of the advances made in this area by Dr. Boyce’s team, Dr. Yannas’ team and other colleagues working in this field, my medical/surgical colleagues and I treated a wounded soldier with an 81% body surface area burn in a middle east theater hospital. After escharotomy and temporary wound coverage with a degradable polymeric dressing, he was flown directly, nonstop, from the combat zone to the US Army Institute of Surgical Research Burn Center at the San Antonio Military Medical Center for his definitive treatment. He survived; an engineered skin substitute with which he was treated at the Burn Center, and the temporary biodegradable wound

dressings applied at the field hospital, played significant roles in his survival.

Chapter 2.5.9, “Description and Definition of Adhesives, and Related Terminology,” by Bryan K. Lawson and Darshan Shah, discusses three distinct and yet related biomaterial categories. Adhesives effect a bond between tissues or between a tissue and a biomaterial that is the same or different from the adhesive biomaterial. In addition, the adhesive biomaterials may link hard tissues together, soft tissues together, or a hard tissue to a soft tissue. Hard tissue adhesives find many applications in both dental and bone applications. Sealants find uses in minimizing blood loss during surgery, after trauma, and/or after surgery. Sutures keep wound edges apposed as the wound, whether it be surgical or traumatic, heals to a point that it can resist failure without the presence of the sutures. Lawson and Shah discuss natural and synthetic sutures, degradable and nondegradable sutures, polymeric and metallic sutures, and the appropriate uses for these myriad biomaterials.

Chapter 2.5.10, “Biomaterials for Immunoengineering,” by Susan Thomas, Margaret P. Manspeaker, and Paul A. Archer, describes interactions between the immune system and biomaterials with the goal of inducing the immune system to behave in a desired manner to treat disease. The sections of this chapter include biomaterial use in vaccine development, vaccine efficacy, and increased vaccine performance via biomaterial adjuvants. The chapter also covers biomaterial use for B cell activation and to effect an increased humoral response. Finally, the authors discuss biomaterials use in the targeting and modulation of T cell therapies.

Chapter 2.5.11, “Biomaterials-based model systems to study tumor-microenvironment interactions,” by Claudia Fischbach-Teschl, Brittany Elizabeth Schutrum, and Matthew A. Whitman, presents the tumor microenvironment and its importance in understanding cancer behavior. The authors then discuss the development of biomaterial systems to model the function of the tumor microenvironment to learn how best to alter the cancer’s natural behavior in a way that is optimal for the patient.

Chapter 2.5.12, “Drug Delivery Systems,” by Danielle Benoit, Marian Adriana Ackun-Farmmer, Kenneth R. Sims Jr., and Clyde Thomas Overby III, discusses the history of controlled drug delivery, and presents the design factors that are important for the development of drug delivery systems. These include pharmacokinetics, targeting, solubility behavior, delivery routes, biomaterial properties, and biomaterial stability.

Chapter 2.5.13, “Responsive Polymers in the Fabrication of Enzyme-Based Biosensors,” by John R. Aggas and Anthony Guiseppi-Elie, presents the role of polymers in the design of enzyme-based biosensors: bioconjugation, bioimmobilization, biohosting, biocompatibility, and active transduction. Examples of polymers that fulfill these roles include inherently conductive polymers, responsive hydrogels, polymeric redox mediators, and ferroelectric, piezoelectric, and pyroelectric polymers.

The range of tolerable risks of adverse effects varies directly with the medical benefit obtained by the therapy. Benefit and risk go hand in hand, and clinical decisions are made to maximize the ratio of benefit to risk. The tolerable benefit–risk ratio may depend on the type of implant and the medical problem it addresses. Thus more risk can be tolerated with a heart assist device (a life-sustaining implant) than with a prosthetic hip joint (an implant that relieves pain and disability and enhances function), or with a breast implant (an implant with predominantly cosmetic benefit). As an example, total hip arthroplasties (THAs) with metal-on-metal (MoM), or more correctly cobalt alloy-on-cobalt alloy articulating surfaces (the metal stem trunion–metal femoral head junction, and the metal femoral head–metal acetabular component junction) have been used clinically since the 1950s. The history of implant innovation is replete with examples of implants that performed well during the *in vitro* and *in vivo* phases of their development, and performed well during the Food and Drug Administration (FDA) clinical studies to determine safety and effectiveness, only to have something unexpected occur after FDA marketing approval and subsequent widespread clinical use. MoM THAs were introduced to general clinical use in the 2000–02 timeframe. After being in use for about 5–7 years after FDA marketing approval, concerns arose regarding both foreign body

reactions to metallic wear debris that produced benign “pseudotumors” and neurologic illnesses from cobalt toxicity. Both the United Kingdom and the United States performed product recalls, and warned patients about these previously unknown responses to the cobalt metal debris. Further information regarding this specific topic can be found on the following FDA Website: <http://www.fda.gov/MedicalDevices/ProductsandMedicalProcedures/ImplantsandProsthetics/MetalonMetalHipImplants/default.htm>. The message for us is that we must constantly be on the lookout for potential complications that may arise both before and after FDA approval to market a new biomaterial implant. We must expect that something unexpected may occur even after a thorough evaluation of an implant leading to marketing approval. MoM THAs, once thought to herald the arrival of the ultimate THA implant, have disappeared (correctly so) from the armamentarium of the total joint reconstructive surgeon.

In summary, Section 2.5 explores the most widely used applications of materials in medicine, biology, and artificial organs. The progress made in many of these areas has been substantial. In most cases, the individual chapters describe a device category from the perspective of the clinical need, the spectrum of devices available to the practitioner, the results and complications, and the challenges to the field that must be addressed and solved to optimize success.

2.5.2A

Cardiovascular Medical Devices: Heart Valves, Pacemakers and Defibrillators, Mechanical Circulatory Support, and Other Intracardiac Devices

ROBERT F. PADERA, FREDERICK J. SCHOEN

Department of Pathology, Brigham and Women's Hospital and Harvard Medical School, Boston, MA, United States

Introduction

Cardiovascular disease continues to be the leading cause of mortality and morbidity in the Western world, resulting in over 800,000 (nearly one-third of) deaths in the United States each year. Moreover, as the leading cause of death globally, cardiovascular disease kills more than 17 million individuals per year, a number that is expected to grow to more than 23 million by 2030. The most important subtype is coronary heart disease accounting for more than 1 in 7 deaths, killing over 360,000 people a year in the United States. Additionally, over 25,000 persons per year in the United States succumb to valvular heart disease, of which 17,000 have aortic valve disease, a number which is expected to double by 2040 and triple by 2060 (Benjamin et al., 2019).

The good news is that the past several decades have witnessed a virtual explosion in the number and scope of innovative surgical and interventional diagnostic and therapeutic procedures for patients with cardiovascular diseases. Data from the National Center for Health Statistics and the American Heart Association indicate that approximately 8 million major cardiac and vascular operations are performed annually in the United States. Concurrent with and integral to the broad application of these surgical and interventional procedures is the use of various prostheses and medical devices composed of highly advanced biomaterials. Data from 2014 show 475,000 percutaneous

coronary interventions (almost all using endovascular bare-metal or drug-eluting stents), 371,000 coronary artery bypass graft procedures, 156,000 cardiac valve procedures, pacemakers, leads, and cardioverter-defibrillators (420,000), and use of many cardiac assist devices, vascular grafts, umbrellas, patches, and other devices (D'Agostino et al., 2018; Benjamin et al., 2019).

Thus cardiovascular prostheses and medical devices, and their constituent biomaterials, are of critical importance to the practices of interventional cardiologists and cardiac and vascular surgeons. The number and complexity of devices permit choices among surgical or catheter-based interventional options that optimize short- and long-term patient management. The recognition and understanding of complications of these devices, many of them related to the biomaterials that comprise them, has led to iterative efforts to improve their performance and safety through biomaterials and device research and development. The result has been highly significant improvements, which have been translated into better patient care. The nature, frequency, and pathologic anatomy of their complications, as well as the responsible blood–tissue–biomaterials interaction mechanisms, have been published for widely used devices used for many years, but are less well appreciated for recently introduced or modified devices and those currently in development (Schoen and Gotlieb, 2016; Buja and Schoen, 2016).

This chapter and the one following summarize key considerations in cardiovascular medical devices, including the

underlying pathology of the conditions they are designed for and used to treat, relevant biomaterials information, and the most important complications that need to be circumvented. The first chapter emphasizes biomaterials and engineering design issues relevant to cardiac valve prostheses, which have been used extensively for approximately six decades and are clinically important; the outcomes and pathological descriptions of complications encountered with many different types of valve prostheses are well known. The chapter also discusses pacemakers and implantable cardioverter-defibrillators (ICDs), implantable cardiac assist devices and artificial hearts, and miscellaneous intracardiac devices, including percutaneous catheter-based techniques to treat cardiovascular disease in a minimally invasive manner, such as septal defect closure devices, and left atrial occlusion devices. The second chapter discusses devices used for vascular repair and replacement (including vascular grafts and endovascular stents and stent grafts), filters to prevent pulmonary embolism, and other catheters and cardiovascular devices that reside outside the heart.

Heart Valve Function and Valvular Heart Disease

The four intracardiac valves play a critical role in assuring unidirectional forward blood flow through the heart. The tricuspid valve allows one-way flow from the right atrium to the right ventricle, and correspondingly the pulmonary valve from the right ventricle to the pulmonary artery, the mitral valve from the left atrium to the left ventricle, and the aortic valve from the left ventricle to the aorta. The heart valves open and close with each cardiac cycle, i.e., approximately once per second, which equates to approximately 40 million times per year and 3 billion times in a 75-year lifetime.

Disorders of heart valves can cause stenosis (i.e., obstruction to flow) or regurgitation (i.e., reverse flow across the valve) (Schoen and Mitchell, 2015; Schoen and Butany, 2016). Sometimes, both stenosis and regurgitation are present in the same valve. Some disease processes such as infective endocarditis (infection of a heart valve) can cause rapid (in days) destruction of the affected valve and lead to abrupt heart failure and death, while others such as calcific aortic stenosis can take many decades to develop clinical manifestations. Progress has been made in recent years toward elucidating a conceptual framework that integrates the dynamic functional structure of heart valves from macro- to micro- to ultrastructure, the biomechanical properties, and the pathobiological behavior of the cardiac valves (Ayoub et al., 2017).

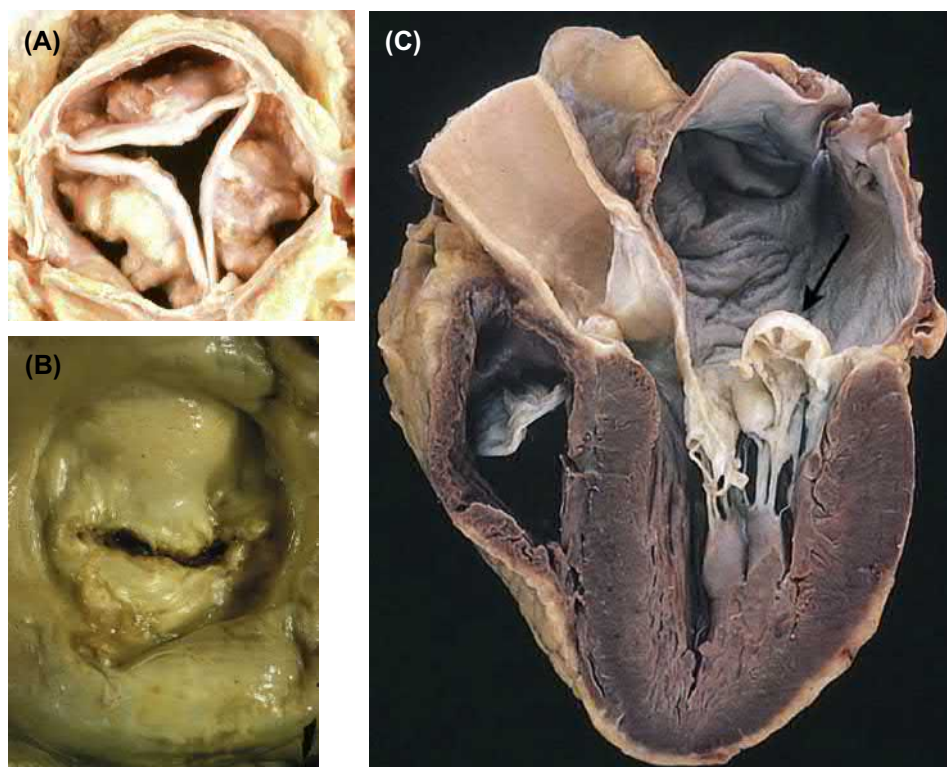
There are several major forms of valvular heart disease; most involve the aortic and/or the mitral valve. The most common type of valve disease and most frequent indication for valve replacement overall is calcific aortic stenosis—obstruction at the aortic valve secondary to age-related calcification of the cusps of a valve that was previously anatomically normal

(Fig. 2.5.2A.1A) (Carabello and Paulus, 2009). Elucidating the precise mechanisms of calcification of the aortic valve has been elusive, but recent insights have been gained through the study of the effects of continuous and cyclical mechanical forces on the behavior of the valvular interstitial cells and the associated inflammatory cytokine milieu within the valve tissue (Merryman and Schoen, 2013). Calcific nodules form in the valve cusps, which do not allow the valve to fully open, resulting in pressure overload of the left ventricle, which induces hypertrophy (enlargement of the mass) of the walls of this chamber. This condition takes decades to develop and typically produces symptoms in approximately the seventh and eighth decades of life.

Although the normal aortic valve has three cusps, 1%–2% of all individuals are born with a bicuspid aortic valve (i.e., with only two cusps), a condition called congenital bicuspid aortic valve (Mathieu et al., 2015). A congenitally bicuspid valve generally functions well initially and into adulthood, but persons who have this condition develop valve dysfunction and thereby symptoms at relatively younger ages—approximately 10 years earlier than in a patient having a valve with three cusps.

Aortic regurgitation (also known as insufficiency) is a less frequent but nevertheless important problem, most often caused by dilation of the aortic root. This prevents complete and effective closure of the cusps, allowing backflow across the valve and leading to volume overload of the left ventricle (Goldberg and Halperin, 2008). Mitral stenosis (Fig. 2.5.2A.1B) has a single predominant cause—chronic rheumatic heart disease—which leads to scarring and stiffening of the mitral leaflets. This condition usually becomes clinically manifest many years or even decades following an episode of acute rheumatic fever secondary to streptococcal pharyngitis (a common form of childhood throat infection) (Chandrasekhar et al., 2009). Mitral regurgitation, on the other hand, results from many different conditions; the most frequent is myxomatous valve degeneration (also known as floppy mitral valve), in which the strength of the mitral valve tissue is deficient, thereby causing the valve leaflets to deform excessively (Carabello, 2008) (Fig. 2.5.2A.1C). Conditions in which the left ventricle is abnormally dilated and/or scarred and consequently the valve is not supported properly, and infective endocarditis (i.e., infection of the valve), are among the other major causes of mitral regurgitation.

Diseases of the right-sided valves (tricuspid and pulmonary) are much less common than those of the left-sided valves. However, in children with congenital heart disease, there is a need for valves in the pulmonary position (in addition to left-sided valves); replacement of valves for congenital anomalies account for approximately 5% of valve replacements (Barnett and Ad, 2009). The major clinical complication of valvular heart disease is cardiac failure secondary to changes in the myocardium induced by pressure or volume overload of the chambers either upstream or downstream of the diseased valve.



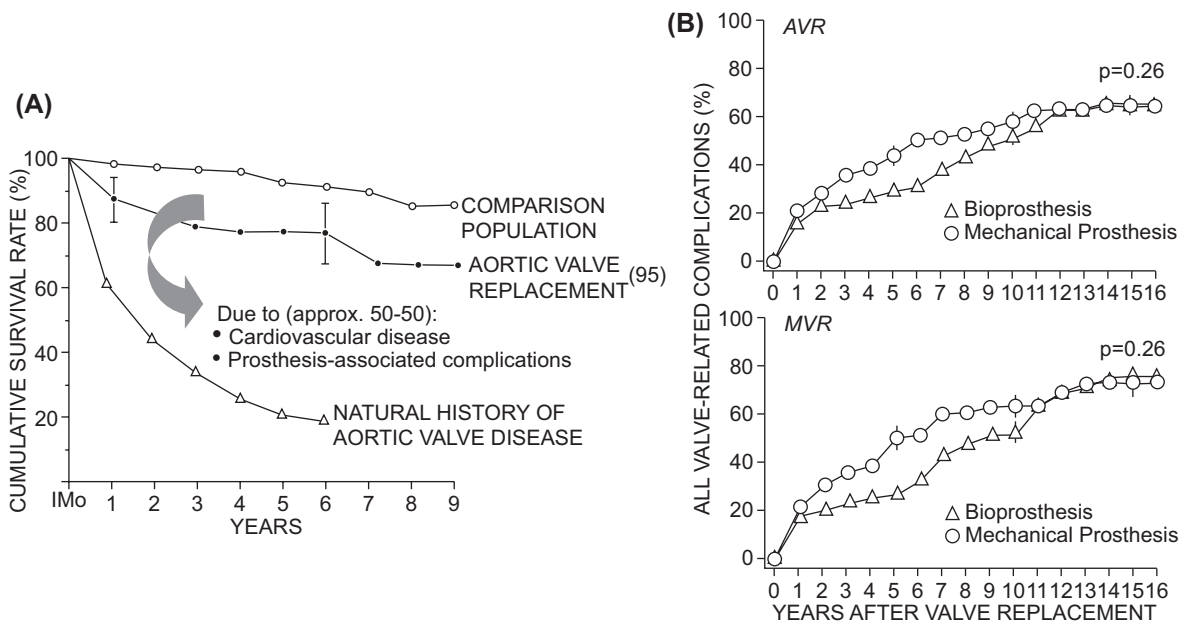
• **Figure 2.5.2A.1** Types of heart valve disease. (A) Severe degenerative calcification of a previously anatomically normal tricuspid aortic valve, the predominant cause of aortic stenosis, and the leading form of valvular heart disease. (B) Chronic rheumatic heart disease, manifest as mitral stenosis, viewed from the left atrium. (C) Myxomatous degeneration of the mitral valve, demonstrating hoarding with prolapse of the posterior mitral leaflet into the left atrium (*arrow*). ((A, B) Reproduced by permission from Schoen, F.J., Edwards, W.D., 2001. Valvular heart disease: General principles and stenosis. In: Silver, M.D., Gotlieb, A.I., Schoen, F.J. (Eds.), *Cardiovascular Pathology*, third ed. Churchill Livingstone, New York. (C) Reproduced by permission from Schoen, F.J., Mitchell, R.N., 2015. The heart. In: Kumar, V., et al., (Eds.), *Robbins Pathologic Basis of Disease*, ninth ed. W.B. Saunders, Philadelphia.)

Heart valve disease is common and serious, and individuals with its various forms have significant mortality and morbidity. For example, the mortality of nonsurgically treated critical aortic stenosis, the most deleterious functional abnormality, is approximately 50% at 2–3 years following the onset of symptoms (Fig. 2.5.2A.2A); thus this natural history is more severe than that of many cancers. Valve replacement is a highly beneficial therapy for such patients; survival following valve replacement is 50%–70% and serious complication-free survival is approximately 30%–50% at 10–15 years (Rahimtoola, 2003). Operative mortality for aortic and mitral valve replacement is 3% and 6%, respectively. While valve replacement thus provides a substantial improvement over the natural history of disease, patients with artificial valves can suffer complications related to the device (Fig. 2.5.2A.2A).

The surgical treatments available for valvular heart disease include replacement of the valve with a prosthesis and repair of the existing abnormal valve tissue to make it functional (Fedak et al., 2008). According to estimates derived from data collected by the Healthcare Cost and Utilization Project, Agency for Healthcare Research and Quality, in 2005, 36,678 individuals had aortic or mitral valve replacement in the United States and 8669 had valve repairs (Barnett and Ad, 2009). Reconstructive/repair procedures to eliminate

mitral insufficiency and to minimize the severity of rheumatic mitral stenosis are now highly effective and commonplace. A recent survey of practice in the United States showed that 69% of mitral valve operations for mitral regurgitation currently use repair rather than replacement (Gammie et al., 2009). Whenever possible, repair of a valve is preferable over replacement; advantages of repair relate to the elimination of both the risk of prosthesis-related complications and the need for chronic anticoagulation that is required in many patients with substitute valves, and mandatory in patients with mechanical valves. Surgical valve repair is often accompanied by stabilization of the annulus with or without implantation of a prosthetic annuloplasty ring. Unfortunately, repair is usually not possible for most forms of aortic valve disease.

When repair is not possible, severe symptomatic valvular heart disease is treated by surgical valve replacement, which comprises excision of part or all of the diseased valve and replacement by a functional substitute. From a design standpoint, the ideal replacement valve would be nonthrombogenic, nonhemolytic, infection resistant, chemically inert, durable, and easily inserted. It would open fully and close quickly and completely, heal appropriately in place, and not be noticed by the patient (for example, it would be noise free) (Harken et al., 1962; Sapirstein and Smith, 2001).



• **Figure 2.5.2A.2** Outcome following cardiac valve replacement. (A) Survival curves for patients with untreated aortic valve stenosis (natural history of valve disease) and aortic valve stenosis corrected by valve replacement, as compared with an age-matched control population without a history of aortic valve stenosis. The numbers presented in this figure for survival following valve replacement nearly four decades ago remain accurate today. This reflects the fact that improvements in valve substitutes and patient management have been balanced by a progressive trend toward operations on older and sicker patients with associated medical illnesses. (B) Frequency of valve-related complications and tissue valves following mitral valve replacement (MVR) and aortic valve replacement (AVR). ((A) Reproduced by permission from Roberts, L., et al., 1976. Long-term survival following aortic valve replacement. *Am. Heart J.* 91, 311–317. (B) Reproduced by permission from Hammermeister, K., et al., 2000. Outcomes 15 years after valve replacement with a mechanical versus a bioprosthetic valve: Final report of the Veterans Affairs Randomized Trial. *J. Am. Coll. Cardiol.* 36, 1152–1158.)

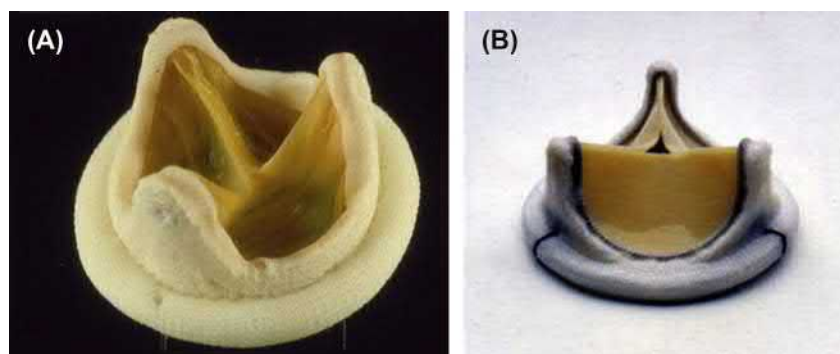
Surgical Bioprosthetic and Mechanical Heart Valves

The evolution of prosthetic heart valves and related cardiovascular surgical technology was enabled during the first half of the 20th century by multiple key developments, including cardiac catheterization, innovative surgical techniques, cardiopulmonary bypass machines, and the anti-coagulant heparin (Chaikoff, 2007). In the late 1950s, stimulated by collaborations established between surgeons and biomedical engineers, innovative procedures and device technology matured in the surgical research laboratory were translated to clinical practice. These developments fostered new opportunities to replace dysfunctional cardiovascular components with biologic or synthetic prostheses. A key step in modern valve replacement technology was the Hufnagel ball valve, designed to be implanted rapidly into the descending thoracic aorta with the use of proximal and distal fixation rings in patients with aortic regurgitation (Butany et al., 2002). However, with this valve, regurgitant flow from the lower body was prevented, but cardiac work was only partially relieved and coronary flow was not improved. Subsequently, cardiac surgeon Dr. Albert Starr and his colleagues, along with a mechanical engineer, Lowell Edwards, fabricated a valve consisting of a stainless-steel cage, a heat-cured Silastic

ball, and a base surrounded by a Teflon fabric sewing cuff, the latter component permitting the surgeon to suture the valve in place orthotopically (i.e., in the anatomically appropriate location within the heart). The three generic components just described, moving part (either synthetic or biologic), superstructure to guide the motion of the moving occluder, and sewing cuff (anchored at the anastomotic site), comprise the key parts of all previous and present surgical heart valve prostheses. Now used extensively for more than a half century, cardiac valve prostheses are a clinically important achievement of biomaterials science and biomedical engineering. Indeed, the prestigious 2007 Lasker Award for Clinical Medical Research was granted to Drs. Albert Starr and Alain Carpentier to recognize the importance of cardiac valve replacement as a major clinical success (Chaikoff, 2007; Lifton, 2007). Starr performed the first successful valve replacement in the heart in 1960 by implanting a caged-ball mechanical valve prosthesis in the mitral position (Starr, 2007). Carpentier fabricated a “bioprosthesis,” combining chemically treated biologic tissue and a mechanical structure to create a tissue-based (though nonliving) heart valve replacement (Carpentier, 2007). Relevant outcome data and pathological descriptions of complications of many different types of valve prostheses are well known (Vongpatanasin et al., 1996; Bonow et al., 2006; Schoen and Butany, 2016).



• **Figure 2.5.2A.3** Mechanical prosthetic heart valves. (A) Starr-Edwards caged-ball valve. (B) Bjork-Shiley tilting disk valve. (C) St. Jude Medical bileaflet tilting disk heart valve. (Reproduced by permission from Schoen, F.J., 2001. Pathology of heart valve substitution with mechanical and tissue prostheses. In: Silver, M.D., Gotlieb, A.I., Schoen, F.J. (Eds.), Cardiovascular Pathology, third ed. Churchill Livingstone, New York.)



• **Figure 2.5.2A.4** Tissue heart valve replacement devices. (A) Hancock porcine valve. (B) Carpentier-Edwards bovine pericardial valve. (Reproduced by permission from Schoen, F.J., 2001. Pathology of heart valve substitution with mechanical and tissue prostheses. In: Silver, M.D., Gotlieb, A.I., Schoen, F.J. (Eds.), Cardiovascular Pathology, third ed. Churchill Livingstone, New York.)

The achievements of Starr and Carpentier provided the foundation on which the clinical success of heart valve replacement is built. Today, more than 80,000 valves are replaced each year in the United States and more than 275,000 worldwide. Moreover, devices and techniques for minimally invasive and percutaneous (catheter-based) valve replacement and repair and other interventional techniques are undergoing rapid innovation and development, and there has been exciting progress toward the creation of a living tissue-engineered heart valve replacement.

Hundreds of designs of substitute heart valve replacement devices have been explored experimentally and in patients; most have been abandoned because of design and materials deficiencies that manifest in complications that became apparent only in clinical use (Dewall et al., 2000; Edmunds, 2001; Schoen and Butany, 2016). The opening and closing of a prosthetic valve are purely passive, with the moving parts (occluder or disk[s]) responding to changes in pressure and blood flow within the chambers of the heart and great vessels. Today's cardiac valvular substitutes are of two generic types: mechanical valves and biological tissue valves. The choice of which valve to use in a particular patient is often difficult (Rahimtulla, 2003; Head et al., 2017; Hirji et al., 2018), even though the overall complication rates for mechanical versus bioprosthetic valves is similar over time in both the aortic and mitral positions (Fig. 2.5.2A.2B).

Mechanical prosthetic heart valves (Fig. 2.5.2A.3) are composed of nonphysiologic biomaterials that employ rigid, mobile occluders in a metallic cage (cobalt-chrome or titanium alloy) as in the Bjork-Shiley, Hall-Medtronic, and OmniScience valves, or two carbon hemidisks in a carbon housing as in the St. Jude Medical (the most widely used), CarboMedics CPHV, Medical Carbon Research Institute, or On-X prostheses. Visually, mechanical valves do not resemble the natural heart valves. Today, all mechanical valve occluders are fabricated from pyrolytic carbon. Pyrolytic carbon has high strength, fatigue and wear resistance, and exceptional biocompatibility, including relative thromboresistance. Patients receiving mechanical valves must be treated with lifelong anticoagulation to reduce the risk of thrombosis and thromboembolic events.

Having a trileaflet configuration with a central orifice, tissue valves (Fig. 2.5.2A.4) resemble natural valves. The term “bioprosthesis” describes a special type of tissue valve composed of three cusps of tissue derived from animals—most frequently either a porcine (pig) aortic valve or bovine (cow) pericardium—each treated with glutaraldehyde. Glutaraldehyde fixation preserves the tissue, decreases its (already relatively low) immunological reactivity, and kills the cells within the valve tissue. No immunosuppression is required for these xenografts as is required for whole organ transplants (e.g., kidney, liver, or heart). However, since

these valves no longer contain viable cells, the cusps themselves cannot remodel or respond to injury as does normal tissue. Fabricated tissue valve cusps are usually mounted on a metal or plastic stent with three posts (or struts) to simulate the geometry of a native semilunar valve. As with mechanical valves, the base ring is covered by a Dacron- or Teflon-covered sewing cuff to facilitate surgical implantation and healing. The most widely used valve type is the Carpentier-Edwards pericardial valve.

Also used occasionally are tissue valves derived from human cadaveric aortic or pulmonary valves with or without the associated vascular conduit (called allografts, or homografts). These valves have good hemodynamic profiles, a low incidence of thromboembolic complications without chronic anticoagulation, and a low reinfection rate following valve replacement for endocarditis (O'Brien et al., 2001). Several decades ago, when the use of valve allografts began, they were sterilized and/or preserved with chemicals or irradiation; such valves suffered a high rate of leaflet calcification and rupture. Subsequent technical developments have led to the current practice—allografts that are cryopreserved rather than chemically preserved. Freezing is performed with protection from ice crystal formation using dimethyl-sulfoxide. The valves are subsequently stored until use at -196°C in liquid nitrogen. Contemporary allograft valves yield freedom from degeneration and tissue failure equal to or better than those of conventional porcine bioprosthetic valves, but their use is limited by availability, difficulty in obtaining the proper size, and a more complex surgical procedure for implantation.

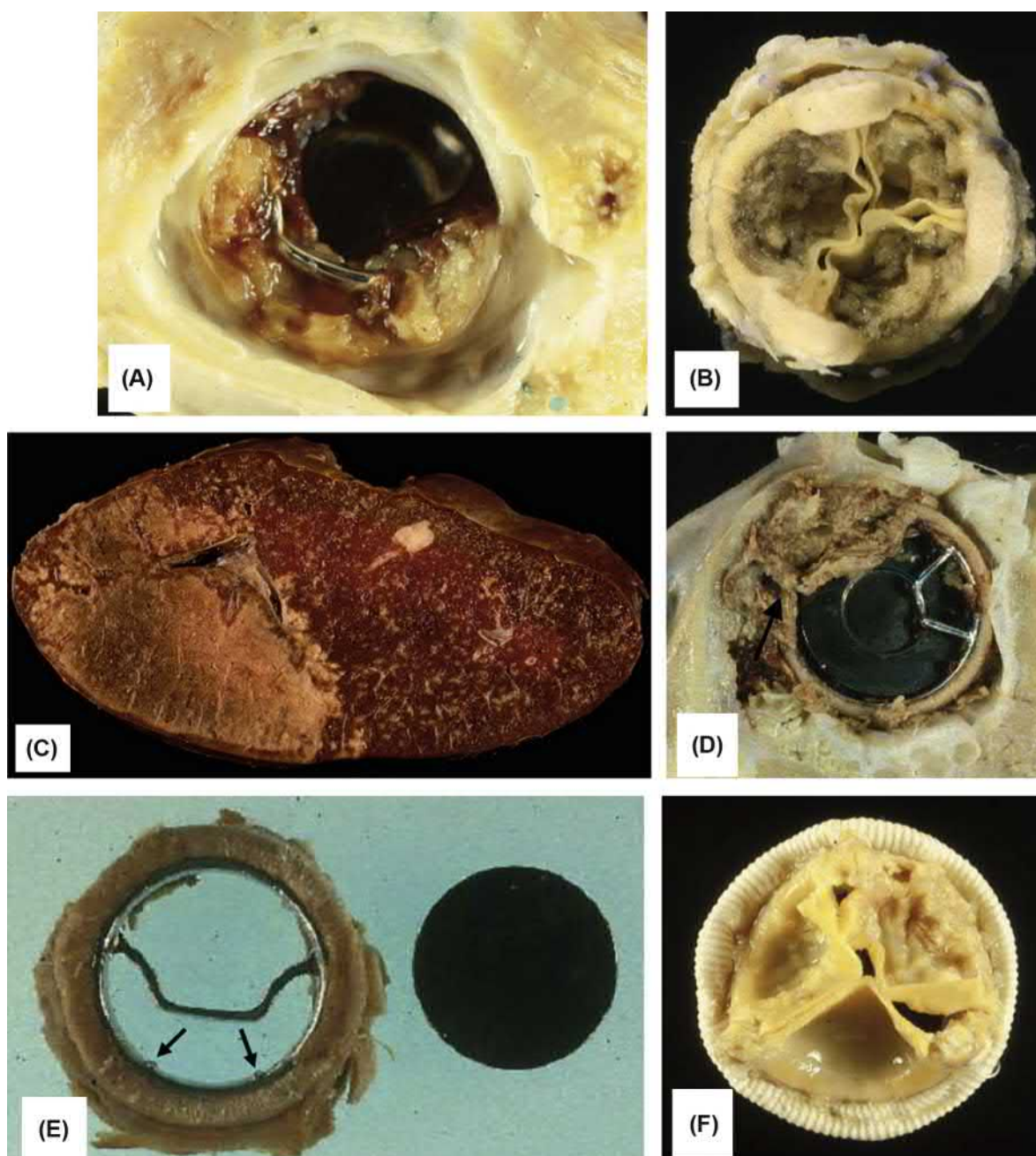
The reliability of a valve prosthesis and its interactions with the host and local tissues play a major role in patient outcome. Four categories of valve-related complications have been most important in limiting success (Fig. 2.5.2A.5): thrombosis and thromboembolism, infection, structural dysfunction (i.e., failure or degeneration of the biomaterials comprising a prosthesis), and nonstructural dysfunction (i.e., miscellaneous complications and modes of failure not encompassed in the previous groups). The major advantages of tissue valves compared to mechanical prostheses are their pseudoanatomic central flow and relative nonthrombogenicity (see later); consequently, patients with tissue valves usually do not require anticoagulant therapy unless they have atrial fibrillation (AF) or another specific propensity to thrombose the valve.

Thromboembolic complications are the major cause of mortality and morbidity after cardiac valve replacement with mechanical valves. No synthetic or modified biological surface is as resistant to thrombosis (*thromboresistant*) as normal unperturbed endothelium. As in the cardiovascular system in general, Virchow's triad (surface thrombogenicity, hypercoagulability, and locally static blood flow) largely predicts the relative propensity of a device to thrombus formation and location of thrombotic deposits with cardiovascular prostheses (Bennett et al., 2009). Exposure of blood to an artificial surface can induce thrombosis, embolization, and consumption of platelets and plasma coagulation factors, as well as

the systemic effects of activated coagulation, complement products, and platelets. Thus patients who have received mechanical substitute heart valves require lifetime therapeutic anticoagulation with warfarin derivatives, which induces a risk of hemorrhage, is potentially serious, and in some cases is fatal (Vahanian, 2008). Thrombotic deposits forming on valve prostheses can immobilize the occluder or shed emboli to downstream arterial beds (Fig. 2.5.2A.5A–C).

Prosthetic valve infection (endocarditis) occurs in 3%–6% of recipients of substitute valves (Fig. 2.5.2A.5D). When endocarditis was the reason for the original valve replacement, the risk is markedly increased. Rates of infection of bioprostheses and mechanical valves are similar. However, since mechanical valve biomaterials cannot themselves become infected, endocarditis on mechanical valves is localized to the prosthesis/tissue junction at the sewing ring, with accompanying tissue destruction in this area (Piper et al., 2001). While bioprosthetic valve endocarditis can also be localized to the host tissue/prosthesis junction, biological tissue (despite being chemically fixed) can support growth of bacteria and other microorganisms, and thus the cusps are involved in some cases. The most frequent portals of entry include the mouth via dental procedures, urologic infections and interventions, and indwelling catheters; all comprise breaches of a natural mucosal or cutaneous barrier that may release organisms into the blood. Prosthetic valve endocarditis can occur either early (less than 60 days postoperatively) or late (can be years). The microbial etiology of early prosthetic valve endocarditis is dominated by the staphylococcal species *Staphylococcus epidermidis* and *Staphylococcus aureus*, even though prophylactic antibiotic regimens used routinely at the time of implantation are targeted against these microorganisms. The clinical course of early prosthetic valve endocarditis tends to be fulminant. The most common organisms in late prosthetic valve endocarditis are *S. epidermidis*, *S. aureus*, *Streptococcus viridans*, and *Enterococci*. Prosthetic valve endocarditis is very difficult to eradicate by antibiotics alone, and thus usually necessitates surgical reintervention.

Prosthetic valve dysfunction because of materials degradation can necessitate reoperation or cause prosthesis-associated death. Many valve models have been withdrawn from clinical use because of poor durability. Durability considerations vary widely for mechanical valves and bioprostheses, for specific types of each, for different models of a particular prosthesis utilizing different materials or having different design features, and even for the same model prosthesis placed in the aortic rather than the mitral position. Fractures of metallic or carbon components of mechanical valve prostheses are usually catastrophic but are fortunately rare (Fig. 2.5.2A.5E). Contemporary single-leaflet or bileaflet tilting disk valves with pyrolytic carbon occluders and either metallic struts or carbon housing have generally favorable durability. Fractures related to past design defects are noteworthy in two valve cohorts. In one instance, the Bjork-Shiley single-leaflet tilting disk valve was redesigned with the intention of enhancing disk opening and



• **Figure 2.5.2A.5** Complications of prosthetic heart valve. (A) Thrombosis on a Bjork-Shiley tilting disk aortic valve prosthesis, localized to outflow strut near minor orifice, a point of flow stasis. (B) Thrombosis of Hancock porcine bioprosthesis. (C) Thromboembolic infarct of the spleen (light area on left) secondary to embolus from valve prosthesis. (D) Prosthetic valve endocarditis with large ring abscess (*arrow*), viewed from the ventricular aspect of an aortic Bjork-Shiley tilting disk aortic valve. (E) Strut fracture of Bjork-Shiley valve, showing valve housing with single remaining strut and adjacent disk. Sites of prior attachment of missing fractured strut designated by *arrows*. (F) Structural valve dysfunction (manifest as calcific degeneration with cuspal tear) of porcine valve. ((D) Reproduced by permission from Schoen, F.J., 1987. Cardiac valve prostheses: pathological and bioengineering considerations. *J. Card. Surg.* 2 (65). (A and E) Reproduced by permission from Schoen, F.J., Levy, R.J., Piehler, H.R., 1992. Pathological considerations in replacement cardiac valves. *Cardiovasc. Pathol.* 1 (29).)

relieving obstruction and thromboembolic complications that occurred with the original and widely used model. The resultant Bjork-Shiley 60- and 70-degree convexo-concave tilting disk valves suffered fractures of the welded metallic outlet strut and separation from the valve, leading

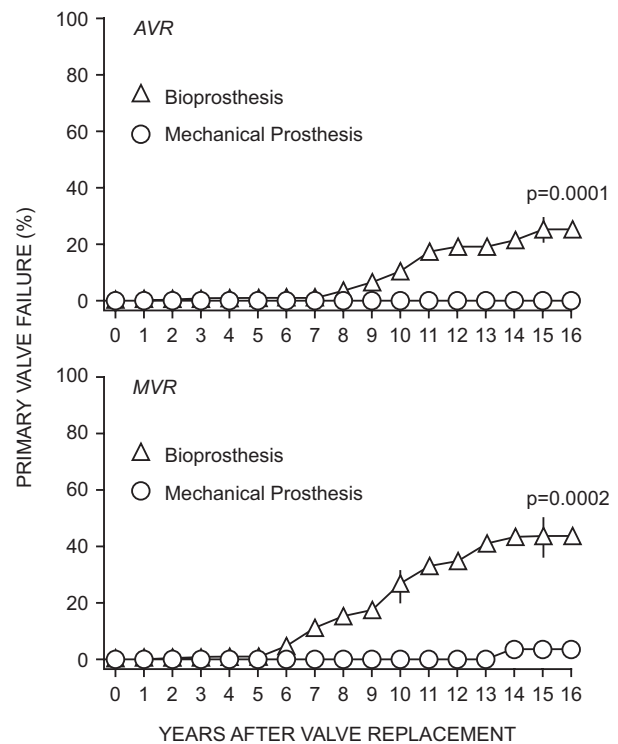
to frequently fatal disk escape (Blot et al., 2005; Harrison et al., 2013). Over 80,000 valves of this model were implanted and at least 600 fractured in this manner. The underlying problem was due to the unanticipated consequence of disk closure at a higher velocity and force, causing

the overrotation and an excessively hard contact with the metallic outlet strut. When the outlet strut stress exceeded its endurance limit, fatigue fracture occurred, most frequently in the region of the welds anchoring this strut to the housing. In another instance, fractures of carbon valve components (hemidisk or housing) occurred in implanted Edwards (previously Hemex)-Duromedics bileaflet tilting disk valves. At least 46 valves of this type failed in this manner (Mastroroberto et al., 2000). Studies of these explants suggest that valve fracture with leaflet escape resulted from variable combinations of five factors: (1) microporosity in the pyrolytic carbon coating in the leaflets, (2) cavitation bubbles impacting on the carbon surfaces during function, (3) unusual combinations of dimensional tolerances, (4) poor shock-absorbing qualities of the annular tissues in some patients (perhaps due to calcification-induced rigidity), and (5) structural defects in the valve prosthesis induced by fabrication or surgical mishandling. Fractures of carbon components have been encountered only rarely with other carbon bileaflet tilting disk valves, such as the St. Jude Medical valve.

In contrast, structural valve failure with dysfunction is frequent and is the major cause of failure of the most widely used bioprostheses (Fig. 2.5.2A.5F). Bioprosthetic valve structural tissue failure usually results in progressive symptomatic deterioration, which requires reoperation (Schoen and Levy, 2005). Within 15 years following implantation, 30%–50% of porcine aortic valves implanted as either mitral or aortic valve replacements require replacement because of primary tissue failure (Fig. 2.5.2A.6). Cuspal calcification (see Chapter 2.4.5) is the major responsible pathologic mechanism, with regurgitation through tears the most frequent failure mode in porcine valves. The more frequently used contemporary bovine pericardial valves also suffer design-related tearing and/or calcification. Calcification is markedly accelerated in younger patients, with children and adolescents having an especially accelerated course (Saleeb et al., 2014).

Within the group of complications causing nonstructural failure are those that relate to healing of the valve in the site of implantation, either too little or too much. Inadequate healing can cause paravalvular leaks, which permit reverse flow usually through a relatively small defect at the junction of prosthesis and host tissue when the valve is closed. Paravalvular leaks may be clinically inconsequential, may cause hemolysis (i.e., destruction of red blood cells through mechanical destruction of their membranes by the high shear stresses engendered by blood being forced at high velocity through small spaces), or may cause heart failure through regurgitation. In contrast, overexuberant healing, called tissue overgrowth (or pannus), can block occluder motion or lead to secondary thrombus.

Various incremental improvements to valve prostheses are being investigated in preclinical studies and clinical research and implementation. For example, methods are being actively studied and some are being used clinically to prevent calcification of bioprosthetic valves. The confidence engendered by early data that these methods may have extended the durable



• **Figure 2.5.2A.6** Frequency of primary valve failure (nonthrombotic valve obstruction or central valvular regurgitation) for mechanical and tissue valves following mitral valve replacement (MVR) and aortic valve replacement (AVR). Cuspal mineralization is the major responsible pathologic mechanism with regurgitation through tears the most frequent failure mode. (Reproduced by permission from Hammermeister, K., et al., 2000. Outcomes 15 years after valve replacement with a mechanical versus a bioprosthetic valve: Final report of the Veterans Affairs Randomized Trial. *J. Am. Coll. Cardiol.* 36, 1152–1158.)

lifetime of bioprosthetic valves has led to a dramatic resurgence of their use. Thus as reflected in overall heart valve replacement industry data, innovations in tissue valve technologies and design have stimulated this segment of the market to grow disproportionately in the last decade by expanding indications for tissue valve use and potentially enhanced durability. Thus there has been a trend toward an increasing fraction of tissue valves implanted relative to mechanical valves. Tissue valve use continues to expand, and studies estimate that tissue valves now represent as much as 80% of all substitute heart valves used in some countries (Mohr, 2014; Isaacs et al., 2015; Goldstone et al., 2017). The trend toward increasing use of bioprostheses (relative to mechanical valves) is especially high in older recipients, who generally have diminished rates of calcific failure and in whom anticoagulation carries increased risk of serious hemorrhage.

The advent of so-called sutureless valves for aortic valve disease has allowed for quicker implantations using a more minimally invasive surgical approach (Zannis et al., 2012). The surgery involves removing the diseased aortic cusps and deploying the sutureless valve device. While the valves are implanted surgically, they incorporate several design features discussed later for percutaneous transcatheter valves. The 3f Enable valve (Medtronic, Inc., Minneapolis, MN) consists of three equal pieces of equine pericardium mounted

on a self-expanding Nitinol frame, which contains a polyester flange on the inflow aspect to prevent migration and minimize paravalvular leak. The Perceval S valve (LivaNova, London, UK) contains bovine pericardial cusps mounted within a Nitinol frame. The frame consists of proximal and distal segments with connecting elements to support the valve cusps and allow anchoring to the aortic root. Both of these valves have shown promise clinically for selected patient populations (Chauvette et al., 2018; Fuzellier et al., 2016).

Other approaches to provide improved valves include modifications of bioprosthetic valve stent design and tissue-mounting techniques to reduce cuspal stresses, tissue treatment modifying or an alternative to conventional glutaraldehyde pretreatment to enhance durability and post-implantation biocompatibility, and minimally cross-linked autologous pericardial valves. Near-anatomic configuration, central flow trileaflet prostheses using three flexible synthetic polymeric leaflets in an anatomy that resemble the natural aortic valve, may be facilitated by major developments in the technology of polymeric materials, particularly in the thermoplastic polyurethanes (Bezuidenhout et al., 2015). Although a polymer valve has been used clinically in a cardiac assist device (Leat and Fisher, 1993), durability limitations have been the major concern in an orthotopic (in the natural site) flexible polymeric valve replacement, with preclinical valve failures being marked by thrombosis, tearing, and/or calcification of the cusps (Fishbein et al., 1975; Claiborne et al., 2012). Sutureless valves provide the opportunity in minimally invasive and conventional aortic valve surgery to minimize aortic cross-clamp time and maximize effective valve area. Performance and safety have been demonstrated for up to 5 years (Meuris et al., 2015; Di Eusanio and Phan, 2015).

Scientific and technological progress has stimulated the goal of generating a living valve replacement that would obviate the complications of conventional valve replacement, adapt to changing environmental conditions in the recipient, and potentially grow with a growing patient (Schoen, 2011; Rippel et al., 2012; Bouten et al., 2012; Emmert et al., 2014). The long-term success of a tissue-engineered (living) valve replacement will depend on the ability of its viable cellular components (particularly valvular interstitial cells) to assume normal function with the capacity to repair structural injury, remodel the extracellular matrix, and potentially grow in a growing patient. Translational challenges are substantial (Rabkin et al., 2002; Stassen et al., 2017; Zhang et al. 2019).

Tissue-engineered heart valves grown as valved conduits from autologous cells (either vascular wall cells or bone marrow-derived mesenchymal stem cells) seeded on biodegradable synthetic polymers (e.g., polyglycolic acid mesh coated in poly-4-hydroxybutyrate) grown in vitro have functioned in the pulmonary circulation of growing lambs for up to 5 months (Hoerstrup et al., 2000; Rabkin et al., 2002). In some studies, these grafts evolved in vivo to a specialized layered structure that resembled that of a native semilunar valve. Pulmonary vascular walls fabricated from vascular

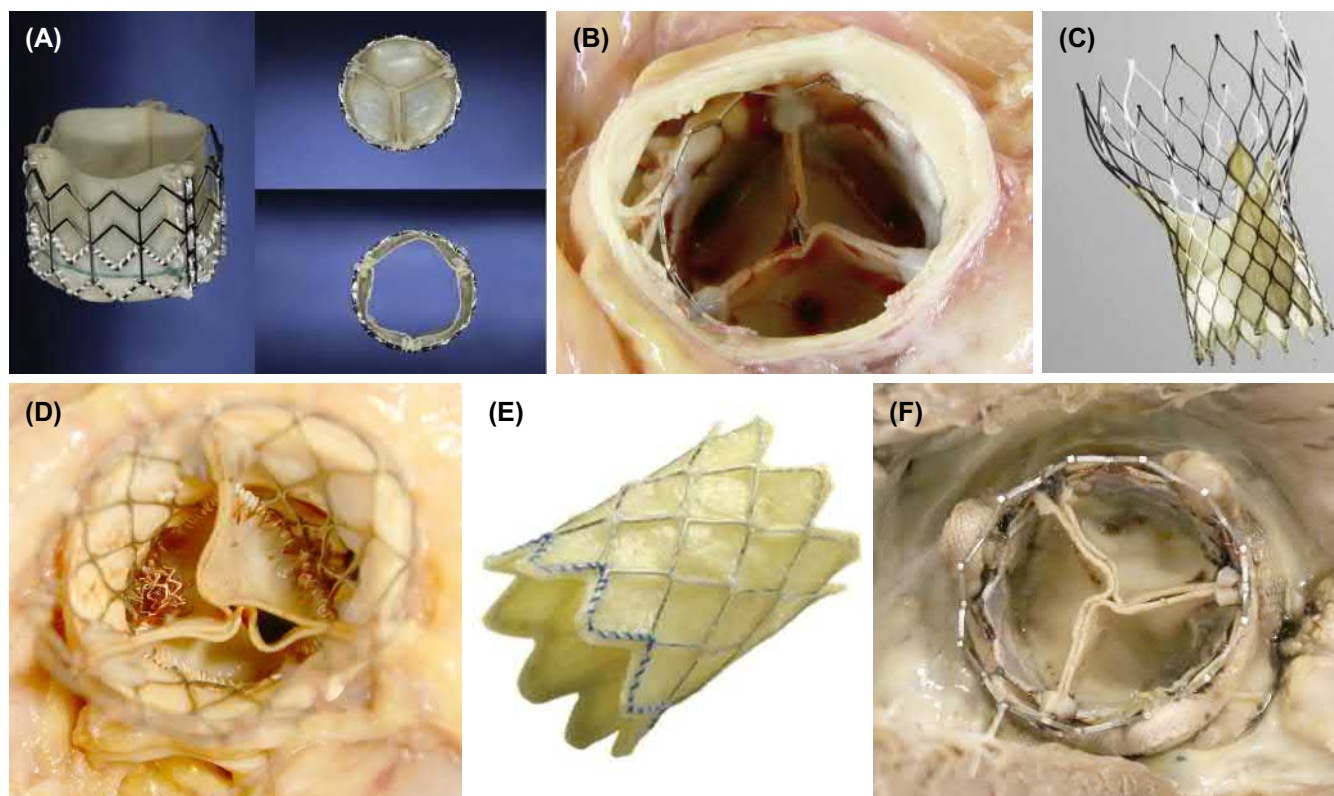
wall cells and biodegradable polymer and implanted into very young lambs enlarged proportionally to overall animal growth over a 2-year period (Hoerstrup et al., 2006). Innovative heart valve tissue approaches may be enabled by emerging biomaterials technologies, including 3D bioprinting, multilayer biomaterials, metal mesh scaffolds, and decellularized valves (Cheung et al., 2015; Lueders et al., 2014; Zhang et al., 2015; Alavi and Kheradvar, 2015; Masoumi et al., 2014).

To eliminate the need for in vitro cell seeding and culture steps, an alternative tissue-engineering strategy has used a scaffold of either decellularized naturally derived biomaterial (such as animal xenograft or human allograft valve, decellularized sheep intestinal submucosa) or a porous polymer matrix implanted without prior seeding but with the intent of harnessing intrinsic circulating cells to populate and potentially remodel the scaffold (Matheny et al., 2000; Ghazanfari et al., 2015; Boroumand et al., 2018). Tissue-derived scaffolds must possess desirable three-dimensional architecture, mechanical properties, and potential adhesion/migration sites for cell attachment and ingrowth. Nevertheless, decellularized porcine valves implanted in humans had a strong inflammatory response and suffered structural failure (Simon et al., 2003). Work is also being done on cell-seeded, engineered tissue valves for transcatheter implantation (Driessen-Mol et al., 2014).

Percutaneous Transcatheter Valves and Other Devices

Surgical implantation of bioprosthetic and mechanical valves (discussed previously) has a long and proven track record of success, with symptom and quality of life improvements, and enhanced survival. However, a substantial fraction of patients with aortic stenosis, estimated to be 30%–40% overall, is deemed unsuitable for surgical aortic valve replacement because of advanced age, frailty, and often multiple comorbidities (Goldberg et al., 2007). However, a highly significant development over the past several decades is a minimally invasive alternative to conventional aortic valve replacement, called *transcatheter aortic valve implantation* (TAVI), which was initially used clinically in 2002, and has extended the opportunity for effective mechanical correction of valve disease to a potentially large population of otherwise untreatable individuals (Rodes-Cabau, 2012; Genereux et al., 2012; Hamm et al., 2016). Thus TAVI, with its associated novel valve replacement devices, has rapidly become the new standard of care for many (especially elderly) patients who would otherwise be deemed inoperable.

In contrast to classical open surgical treatment of heart valve disease, catheter-based valve implantation uses peripheral arterial access into the femoral artery via a catheter passed retrograde up the aorta to the aortic valve where a novel type of valve device is deployed (i.e., expanded); thus this procedure avoids opening the chest. Alternatively, the device can be deployed in the heart via an antegrade and minimally invasive surgical approach that exposes the apex



• **Figure 2.5.2A.7** Percutaneous valve replacement technology. (A) The Edwards-Sapien balloon-expandable aortic valve replacement designed for percutaneous implantation, constructed from bovine pericardium attached to a stainless-steel stent. A fabric sealing cuff covers the ventricular aspect to prevent leaks between the prosthesis and surrounding tissues. The valve is mechanically crimped onto a valvuloplasty balloon catheter and expanded within the aortic annulus to displace and exclude the stenotic native valve from the circulation. (B) The Sapien valve in situ, which has been deployed within the aortic valve to treat aortic stenosis, viewed from the ascending aorta. (C) Corevalve aortic bioprosthesis, constructed of bovine pericardium attached to a self-expanding nickel-titanium alloy (Nitinol) stent. The ventricular portion has a high radial force to compress the native valve. The midportion is tapered to avoid interference with the coronary arteries. The aortic portion is flared to provide additional fixation against the wall of the ascending aorta. Nitinol can be made soft at cold temperatures allowing the stent to be tightly compressed within a delivery sheath. Once positioned within the native valve the sheath is withdrawn allowing the stent to assume its predetermined shape. There is adequate radial force to compress the native valve. (D) The Corevalve in situ, which has been deployed within the aortic valve to treat aortic stenosis viewed from the ascending aorta. A coronary artery stent that was placed in the left main coronary artery can be seen peeking through the Nitinol stent of the Corevalve at the left of the image. (E) The Melody pulmonary valve is constructed from a bovine jugular venous valve attached with sutures to a platinum-iridium alloy stent. The relatively delicate venous valve functions well in the pulmonary circulation but is too fragile for use in the systemic circulation. Although often referred to as a pulmonary valve, its maximum expanded diameter of 22 mm largely limits its use for surgically constructed right ventricular to pulmonary artery conduits in the pediatric population. (F) A Sapien valve has been deployed within a failing surgically placed bioprosthesis in the mitral position in a “valve-in-valve” application, viewed from the left ventricle. ((A) and (C) reproduced by permission from Schoen, F.J., Webb, J.G., 2008. Prosthetics and the Heart. In: McManus, B.M., Braunwald, E. (Eds.), Atlas of Cardiovascular Pathology for the Clinician, Current Medicine, Philadelphia, 241–256.)

of the left ventricle (called *transapical implantation*). This approach is favored in patients in whom manipulation of catheters through severely atherosclerotic sites in the femoral artery and aorta might dislodge debris leading to emboli. The delivery strategy involves collapsing the device and placing it within a catheter-based sheath; for balloon expandable devices, they must be collapsed over a balloon. In the case of aortic stenosis, the valve device is deployed between the cusps of the calcified aortic valve, pushing the diseased cusps out of the flow stream (i.e., in contrast to

open surgery, the diseased valve tissue is not removed during TAVI—Fig. 2.5.2A.7B). During TAVI, delivery, positioning, and permanent fixation in the optimal location are critical to procedural success and usually guided by a combination of external imaging modalities.

Clinical experience with TAVI is growing rapidly; since the first clinical implantations in 2002, an estimated 300,000+ TAVI procedures have been performed worldwide. Randomized and observational clinical trials from different countries, including observational studies and

randomized trials, have compared TAVI to classical aortic valve replacement (Smith et al., 2011; Kodali et al., 2012; Kim et al., 2014). The consensus of these studies is that TAVI is at least as good as classical aortic valve replacement in terms of procedure “success” regarding morbidity and mortality in high-risk patients to at least 2 years (Tice et al., 2014; Reardon et al., 2015). TAVI and surgical valve replacement are comparable hemodynamically. Recent data suggest that TAVI may also be an excellent alternative to open surgery in patients with intermediate or lower surgical risk (Reardon et al., 2017; Mack et al., 2019; Popma et al., 2019).

The devices used in transcatheter valve implantation have an outer stent-like structure that contains leaflets. The stent holds open a valve annulus and resists the tendency of a valve annulus or diseased native leaflets to recoil following balloon dilation, supports the valve leaflets, and provides the means for seating the prosthesis in the annulus. Tissues used for the valve component include bovine, equine, or porcine pericardium and bovine jugular venous valves. The stents are made from self-expandable stainless steel, platinum-iridium, or other alloys, or shape-memory materials such as nickel-titanium alloys (e.g., Nitinol).

Several catheter-based devices are currently in various stages of development and clinical use in the aortic and pulmonary position. The two transcatheter aortic valves with the largest clinical experience are the Edwards-Sapien family of devices (Edwards LifeSciences) and the CoreValve ReValving system (Medtronic). The Sapien device is composed of a balloon-expandable stainless-steel stent that houses a bovine pericardial trileaflet valve (Fig. 2.5.2A.7A and B). There is a polymer skirt circumferentially attached to the stent to reduce paravalvular leaks. The CoreValve device is composed of a self-expandable Nitinol stent that houses a porcine pericardial trileaflet valve (Fig. 2.5.2A.7C and D). For children with failed right-ventricular to pulmonary artery devices used to correct certain types of congenital heart defects, the Medtronic Melody transcatheter pulmonary valve, composed of a balloon-expandable platinum-iridium alloy stent that houses a segment of bovine jugular vein with its native venous valve, is threaded from the femoral vein to the inferior vena cava through the right side of the heart (Fig. 2.5.2A.7E) (Lurz et al., 2009). Catheter-based valves may also play a role in the treatment of surgically implanted bioprosthetic valves that are failing due to stenosis or regurgitation in a so-called “valve-in-valve” application in which a new prosthesis is inserted directly into a prior one (Fig. 2.5.2A.7F).

Transcatheter valve implantation presents novel challenges (Fishbein et al., 2014). Valved stents are significantly larger than most existing percutaneous cardiac catheters and devices, and thus vascular access is difficult, potential damage along the course of the catheter passage is possible, and dislodging debris that can become emboli is a significant risk. In the aortic position, there is the potential to impede coronary flow, or interfere with anterior mitral leaflet mobility, the conduction system, or the native diseased

leaflets. Stent architecture may also preclude future catheter access to the coronaries for possible interventions. Secure seating within the aortic annulus or a pulmonary conduit and long-term durability of both the stent and the valve tissue are also major challenges. Surgical complications include most frequently paravalvular leak, vascular injury with hemorrhage, and embolic stroke (Fassa et al., 2013; Van Mieghem et al., 2015). Transcatheter heart valves are also likely susceptible to prosthesis-associated failure modes typical of surgical bioprostheses and unique to their specific design; prosthetic valve endocarditis (Mylotte et al., 2015; Neraqi-Miandoab et al., 2015; Amat-Santos et al., 2015) and structural valve failure due to leaflet calcification and thrombosis are the most frequent complications. A critical unknown in the expanding use of transcatheter techniques is the durability of the prostheses.

Many patients with mitral valve disease also are in need of less invasive transcatheter therapies. The first transcatheter mitral valve replacement (TMVR) in a native valve was performed in 2012. However, the complexities and variability of the mitral valve anatomy and its relationship to neighboring structures have resulted in slower progress with this new therapy compared to the rapid uptake that has occurred with transcatheter aortic valve implantation (Patel and Bapat, 2017; Wyler von Ballmoos et al., 2018). TMVR can be applied to degenerated prosthetic valves and annuloplasty rings or to a wide variety of native mitral valve diseases. In cases of degenerated bioprosthetic valves, annuloplasty ring, and native valve mitral annular calcification, transcatheter heart valves designed for the aortic position can be implanted with high procedural safety and success rates. In the case of native valve mitral regurgitation, the complexities have led to the development of several TMVR systems for native valve disease with different anchoring mechanisms and geometry; all are currently investigational and none are Food and Drug Administration (FDA) approved at this time. Percutaneous mitral valve replacement has been investigated using a device similar to that used for TAVI (Webb et al., 2019).

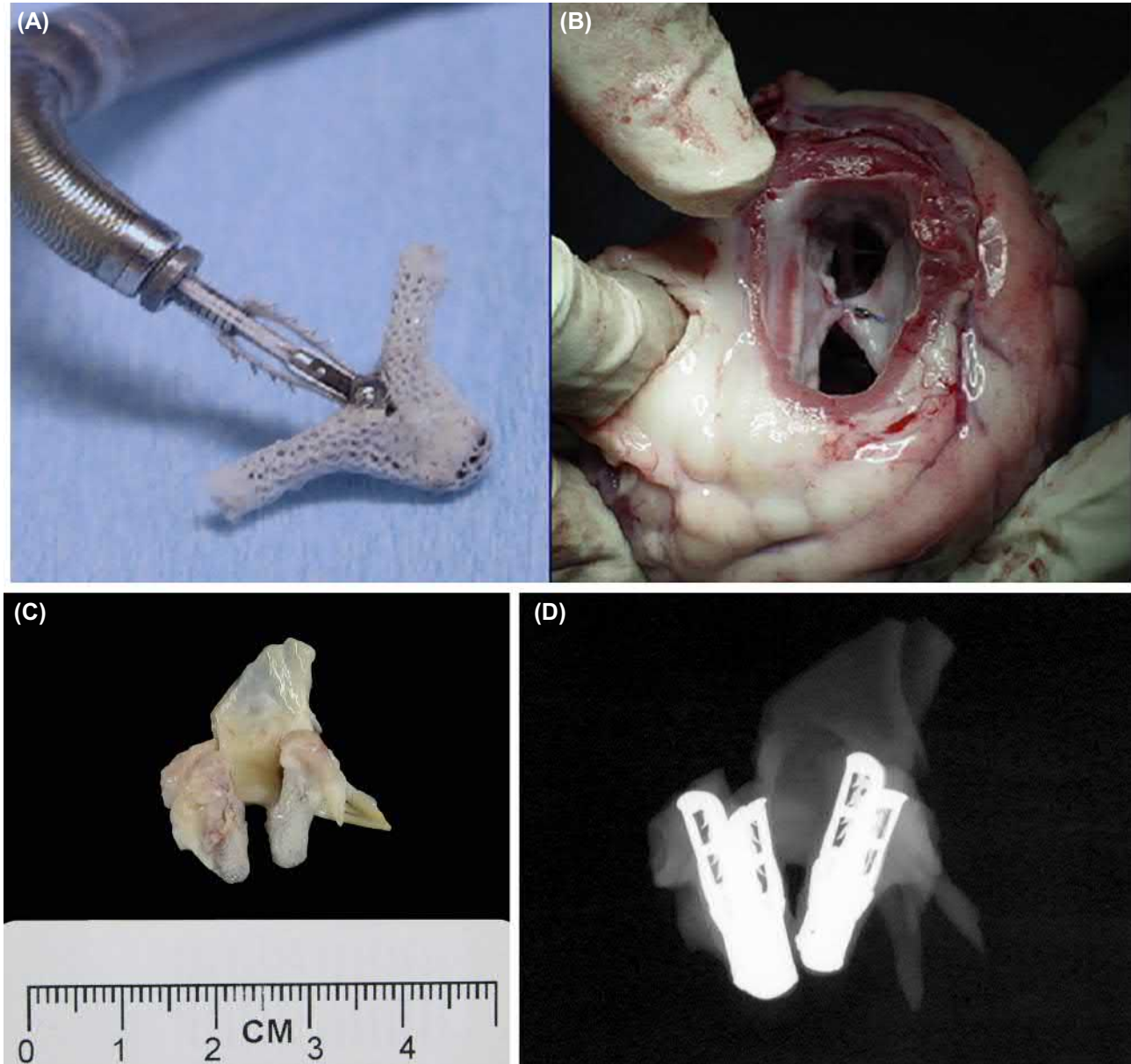
Other percutaneous devices for the treatment of mitral regurgitation are under development or in clinical use. The MitraClip device (Abbott Laboratories, Abbott Park, IL) is a transcatheter-delivered device that reduces mitral regurgitation by fastening the anterior and posterior leaflets together in an edge-to-edge fashion (Panaich and Eleid, 2018). Approved in 2013 by the FDA, the device is composed of a polyester-covered implant that consists of two cobalt-chromium metallic arms that can be opened and closed to capture the edges of the anterior and posterior leaflets of the mitral valve (Fig. 2.5.2A.8). When the arms are closed, the leaflets are held together and the valve orifice approximates a “Fig. 2.5.2A.8” with two openings, rather than the single opening of the native valve. The polyester is macroporous, allowing for tissue ingrowth with the goal both of anchoring the device and preventing thrombosis on the foreign material. Clinical studies have been done; a recent clinical trial

of MitraClip versus medical therapy demonstrated safety and efficacy of the device in patients with heart failure due to moderate-to-severe or severe mitral regurgitation (Stone et al., 2018).

Cardiac Arrhythmias

The normal cardiac electrical cycle (Fig. 2.5.2A.9A) begins with an impulse initiated by the sinoatrial (SA) node, the

heart's natural pacemaker, which is located in the right atrium near the junction with the superior vena cava. The impulse spreads through the muscle of both left and right atrial walls, causing depolarization of the cardiac myocytes that results in atrial contraction. The impulse arrives at the atrioventricular (AV) node, which is located in the posterior right atrium enclosed by the ostium of the coronary sinus, the septal leaflet of the tricuspid valve, and the membranous portion of the interatrial septum (called the

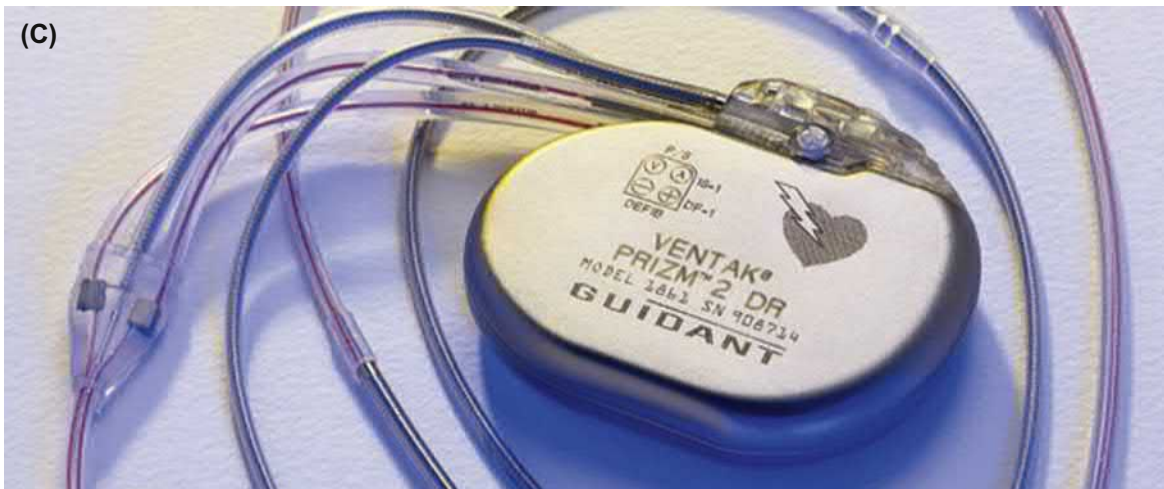
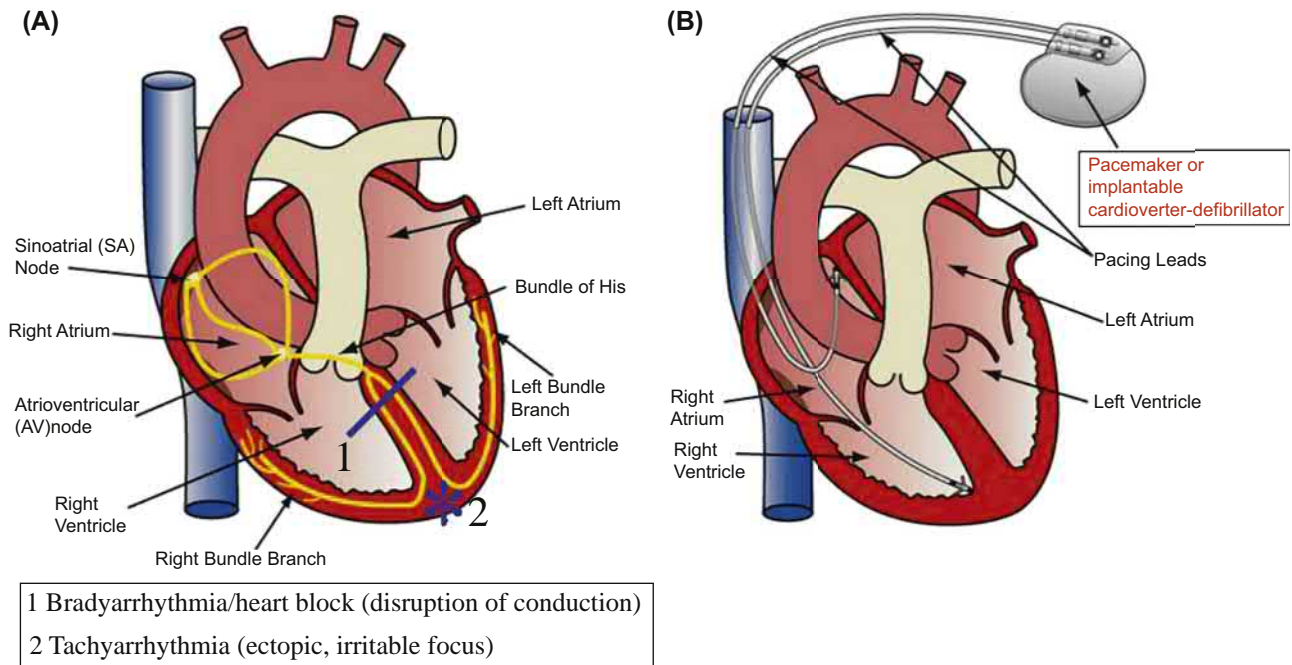


• **Figure 2.5.2A.8** The MitraClip device for mitral regurgitation. (A) MitraClip device on delivery apparatus. (B) Edge-to-edge approximation of the anterior and posterior leaflets of the mitral valve is achieved by deployment of the MitraClip device that is analogous to an Alfieri stitch, thereby creating a double orifice with improved leaflet coaptation. (C) Two MitraClip devices are seen attached to a portion of the mitral valve. The portion of valve and devices were removed surgically during a valve replacement necessitated by worsening mitral regurgitation. The cloth covering has facilitated tissue ingrowth into the device to help passivate the blood-contacting surface and minimize thrombosis. (D) A specimen radiograph shows the structure of the two cobalt-chromium metallic arms in the closed position. ((A) and (B) reproduced with permission from Schoen, F.J., Butany, J., 2016. Cardiac valve replacement and related interventions. In: Buja, L.M., Butany, J. (Eds.), *Cardiovascular Pathology*, fourth ed. Elsevier, 529–576.)

triangle of Koch). After a short delay within the AV node, the impulse passes to the bundle of His and into the left and right bundle branches, located in the intraventricular septum. The impulse spreads through the right and left ventricular myocardium causing a wave of myocyte depolarization and thereby coordinated ventricular contraction. The SA and AV nodes and the bundles of His and its right and

left bundle branches are composed of cardiac muscle cells specialized for conduction.

Cardiac arrhythmias (Huikuri et al., 2001) reflect disturbances of either impulse initiation or impulse conduction. Foci of impulse-generating (automatic) cells outside the SA node, called ectopic foci, may initiate cardiac impulses that generate suboptimal ventricular



• **Figure 2.5.2A.9** Cardiac arrhythmias and device therapy. (A) The normal cardiac electrical cycle showing schematically sites of both conduction blocks and ectopic foci of impulse generation. (B) Schematic demonstrating implantable cardioverter-defibrillator (ICD) lead placement in the right ventricle. (C) Guidant Prizm II DR ICD, introduced to the US market in 2000, and withdrawn in 2005. (D) Transvenous pacing lead placed in right ventricle demonstrating fibrosis of the distal portion of the lead (*arrow*). (E) Fibrous capsule surrounding pacemaker electrode in the right ventricle. Low-power photomicrograph demonstrating the space previously occupied by the electrode (e), fibrous tissue separating electrode from blood in the right ventricular chamber (*between arrows*) and extending around the electrode to separate it from myocardium (m), potentially creating a barrier to conduction of the pacing impulse. (F) Micra Transcatheter Pacing System capsule, which is meant to be implanted in the right ventricle as a leadless pacemaker. (G) Photograph depicting failure of the polymer insulation surrounding the wires (blue) of an ICD, allowing the wires to directly contact the myocardium in areas away from the lead tip. ((E) Reproduced by permission from Schoen, F.J., Webb, J.G., 2008. Prosthetics and the Heart. In: McManus, B.M., Braunwald, E. (Eds.), Atlas of Cardiovascular Pathology for the Clinician, Current Medicine, Philadelphia, 241–256.)

(Continued)

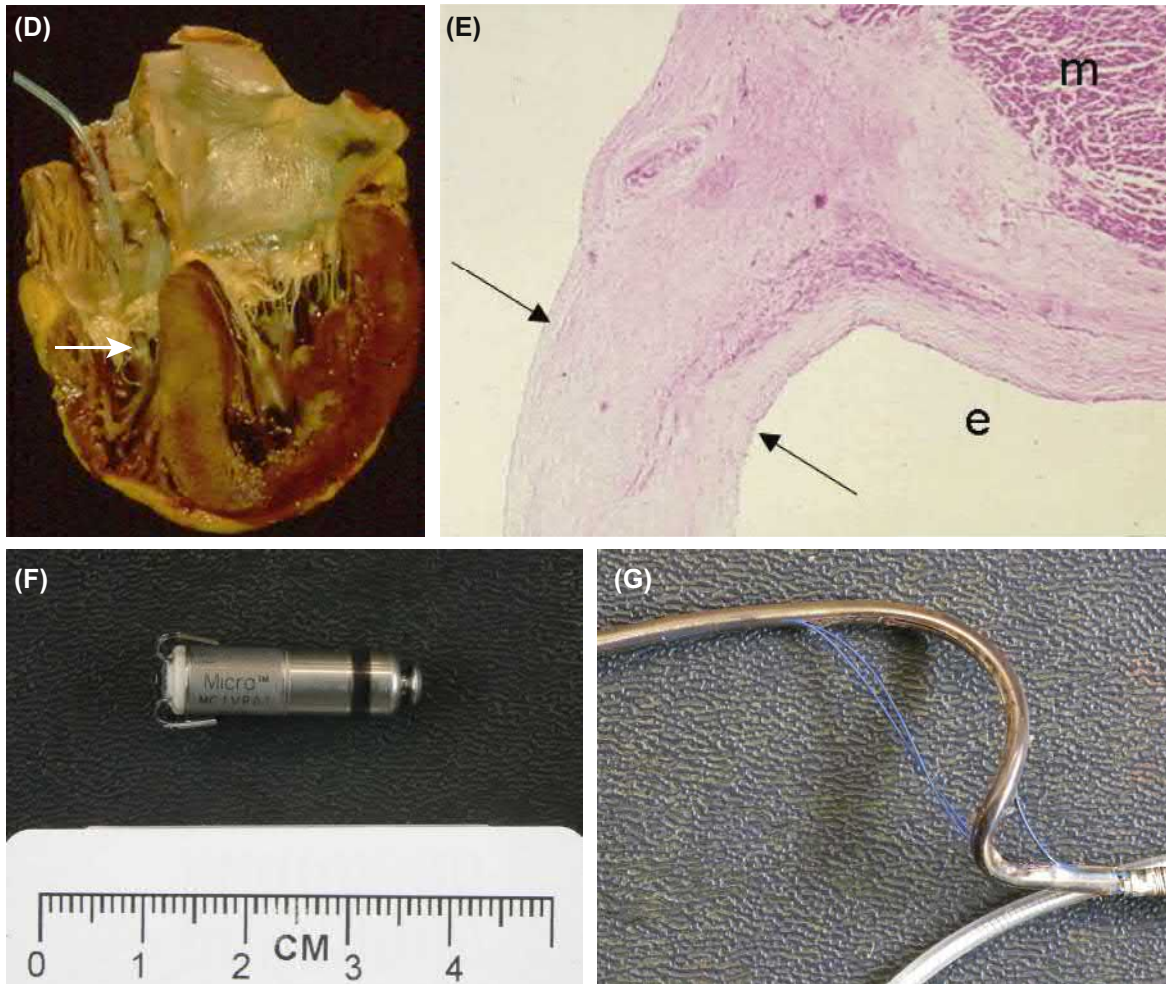


Figure 2.5.2A.9 cont'd

contractions. These arrhythmias are usually fast, i.e., tachyarrhythmias, and can result in ventricular fibrillation, which can be fatal. Intrinsic SA node dysfunction also can account for disturbances of impulse initiation. In contrast, disturbances of impulse conduction mainly consist of conduction blocks or reentry. Conduction blocks constitute a failure of propagation of the usual impulse through the specialized muscle as a result of a disease process (such as ischemia or inflammation) or certain drugs. Blocks can be complete (no impulse propagation) or incomplete (impulse propagates more slowly than normal), and can be permanent or transient. Reentry is said to occur when a cardiac impulse traverses a loop of cardiac fibers and reexcites previously excited tissue without a second impulse from the SA node. For patients in whom these cardiac arrhythmias cannot be controlled pharmacologically by antiarrhythmic drugs, two therapeutic options are available: (1) electrical therapy to control the cardiac rhythm, such as direct current cardioversion or implantable devices such as pacemakers and ICDs, and (2) interventional/surgical therapy to remove the affected tissue or interrupt the abnormal pathway such as endocardial resection, cryoablation, or radiofrequency ablation (Halbfass et al., 2018).

Cardiac Pacemakers

Cardiac pacemakers are medical devices that provide impulses to the conduction system to initiate contraction. The first cardiac pacemaker was implanted (Atlee and Bernstein, 2001) in 1958 and since then cardiac pacing has become a well-established therapeutic tool. The first pacemakers were large (40–200 cm³) by today's standards (9–45 cm³) and contained few of the features that are standard in current devices. Over a million patients in the United States currently have pacemakers (Fig. 2.5.2A.9B and C) and over 250,000 new permanent pacemakers are implanted each year; pacemaker placement, revision or removal is a commonly performed procedure. Most cardiac pacemakers are implanted in patients over 60 years old but they are also used in children, including infants, when necessary. The most common indications for permanent cardiac pacing are various types of conduction block. Some conduction blocks lead to bradycardia (abnormally low heart rate), while others, predominantly in the left or right bundles, will result in ventricular dyssynchrony and inefficient ventricular contraction in the setting of a normal heart rate. These conduction blocks can result in decreased cardiac output and the signs and symptoms of congestive heart failure, but can be well treated by cardiac pacing.

Modern cardiac pacing (Kusumoto and Goldschlager, 2002), either temporary or permanent, is achieved by a system of interconnected components consisting of (1) a pulse generator, which includes a power source and circuitry to initiate the electric stimulus and to sense cardiac electrical activity; (2) one or more electrically insulated conductors leading from the pulse generator to the heart, with a bipolar electrode at the distal end of each; and (3) a tissue, or blood and tissue, interface between electrode and adjacent myocardial cells. The pacemaker delivers a small current (2–4 mA) to the myocardium via the electrodes, resulting in depolarization and contraction of the heart.

Temporary pacing is most frequently used for patients with acute myocardial infarction that is complicated by cardiac conduction system disturbances that could progress to complete heart block. Leads for temporary cardiac pacing are generally directed transvenously into the apex of the right ventricle and the pulse generator is located outside the body. In the context of cardiac surgery when the epicardium is already exposed, temporary pacing is achieved by placing insulated wires with bare ends to the epicardial surfaces of the atria or ventricles with the leads emerging transthoracically from the anterior chest to permit easy withdrawal. Ultimately, the temporary pacemaker is either replaced by a permanent device or discontinued.

Permanent cardiac pacing involves long-term implantation of both pulse generator and electrode leads. The generator, usually made of a titanium alloy, is placed in a tissue pocket beneath the skin on the left anterior chest with the leads advanced transvenously through the left subclavian vein to terminate at the endocardial surface of the heart. The conducting elements are typically made of MP-35N (an alloy of nickel, cobalt, chromium, and molybdenum with excellent strength and corrosion resistance) in a composite with higher electrical conductance materials such as silver or stainless steel; these are typically insulated with an outer coating of silicone and/or urethane. The tips of the electrodes are typically placed within the right atrium and/or right ventricle depending on the pacing modality.

A single chamber pacemaker delivers a stimulus based on a programmed timing interval. The pacemaker also senses intrinsic cardiac activity and can be inhibited from providing unnecessary or inappropriate stimuli. This “demand” pacing is valuable in a patient whose problem is intermittent. A dual-chamber pacemaker with electrodes in both the atrium and ventricle delivers the sequential atrial and ventricular signals to approximate the timing of the normal heartbeat. This device also senses intrinsic atrial and ventricular depolarizations and delivers stimuli at the appropriate time to maintain proper synchrony of the chambers.

Patients with ventricular conduction delays such as left bundle branch block may suffer from heart failure due to dyssynchrony of ventricular contraction, where the right and left ventricles do not contract simultaneously. Cardiac resynchronization therapy via biventricular pacing is an intervention in which pacing electrodes are placed in the right atrium, right ventricle, and coronary sinus. The

coronary sinus electrode stimulates the lateral wall of the left ventricle to allow for simultaneous excitation of the right and left ventricles, and for more uniform contraction of the entire left ventricle. Cardiac resynchronization therapy has been shown to significantly improve cardiac function in these patients (McAlister et al., 2007).

Permanent implantable pacemakers are powered by lithium-iodide batteries with a finite lifespan of 5–8 years, requiring removal and reimplantation of a new device when the battery is exhausted. In fact, the first patient to receive an implantable pacemaker in 1958 required 22 different pulse generators until his death in 2001 at the age of 86. Improving battery technology to allow for longer lifespan would minimize the number of reimplantations that a patient would require and the complications that arise from these procedures.

The interface between the electrode and depolarizable myocardial tissue is of critical importance in the proper functioning of the pacemaker (Fig. 2.5.2A.9D). Typically, a layer of nonexcitable fibrous tissue induced by the electrode forms around the tip of the electrode, which is undesirable as it increases the strength of the threshold pacing stimulus required to initiate myocyte depolarization (Fig. 2.5.2A.9E). Strategies to reduce this fibrosis include improved lead designs, and the use of slow, local release of corticosteroids to minimize the thickness of fibrous tissue formed after lead implantation (Mond and Grenz, 2004). The practical point is that, if pulse generator output is not set sufficiently high in the early postimplantation phase, loss of pacing with potentially fatal consequences can result. By contrast, maintaining output at such high levels once thresholds have stabilized greatly shortens battery life. Thus pacemakers with adjustable variations in output have been developed.

An ideal endocardial pacing lead should provide stable fixation immediately from the time of implantation, achieve and maintain a minimal threshold for stimulation, maximize sensing, and function reliably for many years. Electrode fixation to the endocardium may be active or passive. In active fixation, the electrode is designed to grasp the endocardial surface to achieve immediate fixation at implantation. A very effective aid to passive fixation is the addition of projecting “tines,” or fins, in the region of the electrode tip. A different approach to improving fixation has been the development of electrodes with porous metal surfaces to foster tissue ingrowth. An endocardial pacemaker lead may require a special design if it is implanted at a particular site. One example is the J-shaped atrial lead, which is curved to facilitate placing the electrode tip in the right atrial appendage, inherently the most stable site for fixation.

“Leadless” pacemaker therapy (Della Rocca et al., 2018) is a new technology that has been introduced into clinical practice in the form of two novel devices: the Nanostim Leadless Pacing System (St. Jude Medical) and the Micra Transcatheter Pacing System (Medtronic, Inc.). These devices (Fig. 2.5.2A.9F) consist of a single capsule-like module that contains all of the functions of a traditional single-chamber pacemaker, but is implanted entirely within

the apical aspect of the right ventricle and attached to the interventricular septum via a primary fixation method involving a helical coil or tines. Implantation is performed percutaneously via a transvenous route under fluoroscopic guidance; the devices have a design feature at their proximal end such that they can be recaptured for repositioning during implantation or removal at a later date. The aim of these devices is to provide the same pacing function as a traditional transvenous pacemaker, but without the complications discussed later associated with a large subcutaneous generator pocket and associated long leads traversing the cardiac chambers and valves.

Implantable Cardioverter-Defibrillators

The first implantable cardioverter defibrillator (ICD) was placed in 1980; currently, more than 100,000 ICDs are implanted annually in the United States. The goal of ICDs is to prevent sudden death in patients with certain life-threatening arrhythmias by resetting the heart's electrical activity and stimulating a normal cardiac rhythm. ICDs have been shown to revert sustained ventricular tachycardia (abnormally high ventricular rate) and ventricular fibrillation (uncoordinated electrical/myocardial activity) in multiple prospective clinical trials. Benefit in overall mortality has been well documented (*The Antiarrhythmics versus Implantable Defibrillators (AVID) Investigators, 1997*).

A transvenous ICD consists of similar components to a pacemaker, namely a pulse generator and leads for tachy-dysrhythmia detection and therapy. The pulse generator is a self-powered, self-contained computer with one or two 3.2 V lithium-silver vanadium oxide batteries used to power all components of the system, including aluminum electrolytic storage capacitors. The devices have a service life of 3–5 years, at which point they require removal and implantation of a new device. The lead is generally placed in the right ventricle through a transvenous approach. ICD leads typically contained several coaxial conducting elements that can sense as well as deliver an appropriate shock, each conducting element may be coated in an insulator such as polytetrafluoroethylene, with all of the elements encased within silicone and coated with an outer layer of urethane insulation. The ICD constantly monitors the ventricular rate, and when the rate exceeds a certain value, provides therapy. Current devices will initially provide a short burst of rapid ventricular pacing that terminates some types of ventricular tachyarrhythmias without providing a large shock. This approach can terminate up to 96% of episodes of ventricular tachycardia without the need for a shock. If this pacing fails to break the arrhythmia, the ICD delivers a shock of 10–30 J between the electrode in the right ventricle and the surface of the pulse generator to terminate the dysrhythmic episode. These devices also keep a running record of arrhythmias and treatment results. ICDs are indicated in patients at high risk for ventricular arrhythmias (primary prevention) and in patients who have already had an episode of aborted sudden cardiac death (secondary prevention).

In contrast to the transvenous ICD, a type of ICD termed a subcutaneous ICD (S-ICD) has been developed and is in clinical use for the detection and termination of malignant arrhythmias (*Willcox et al., 2016*). The S-ICD uses an extravascular lead that is implanted in the subcutaneous tissue parallel to the sternum just to the left of midline in most cases. The lead is connected to the generator, which is implanted in the midaxillary line on the left side of the thorax. The lead senses a “far field” signal from the electrical activity of the heart in a manner similar to a surface electrocardiogram, and the shock is delivered by the generator in the subcutaneous tissue overlying the heart in a way similar to an external defibrillator. The S-ICD is therefore not in contact with the heart and blood and is in a more stable mechanical environment, with the hope that some of the complications noted later will be reduced.

Complications of Pacemakers and ICDs

These devices share many of the same complications, many of them requiring device removal and replacement. Like many cardiovascular devices, these are life-sustaining technologies and the implications of device failure can be fatal due to a lack of appropriate cardiac pacing (for pacemakers) or inability to sense or deliver appropriate therapy for a lethal arrhythmia (for ICDs). While normal device end-of-service from a depleted battery may not be technically considered a device malfunction, it certainly requires device replacement, and may happen prematurely due to increased fibrosis at the lead–tissue interface requiring a higher stimulus threshold. Failures of the hardware, including the battery/capacitor and charge circuit, connectors, and leads, are the most common device malfunctions, with software problems being less prevalent. Some mechanical failures include electrode dislodgment, lead fractures, electrode corrosion, and insulation failure (*Fig. 2.5.2A.9G*) (*Zeitler et al., 2015*). Complications of leads may be related to the body of the lead, as distinct from the lead–device pack interface or the electrodes. Several devices and components have been recalled in recent years for these modes of failure (*Amin and Ellenbogen, 2010*). Lead improvements over the years have included helical coil and multifilament designs to decrease electrical resistance and enhance flexibility and durability (*Haqqani and Mond, 2009*). In the past, many reports appeared on interference with pacemaker function by devices ranging from electric razors, toothbrushes, and microwave ovens at home to electrosurgical and diathermy apparatus in hospitals. Fortunately, recent generations of cardiac pacemakers have been greatly improved with regard to their resistance to electromagnetic interference.

Many complications relate to the interaction of the device biomaterials with the host tissue. These include infection, thrombosis and thromboembolism, myocardial penetration or perforation, pressure necrosis of the skin overlying the pulse generator, and migration or rotation of the pulse generator. Infection is a dreaded complication of implantable devices in general, and this is certainly true for

pacemakers and ICDs (Joy et al., 2017). The infection may originate in the subcutaneous pocket and track along the lead, which acts as a contaminated foreign body. Alternatively, it may occur by implantation of bacteria on traumatized endocardium or thrombus contiguous with the lead. The most common organisms responsible for these infections are coagulase-negative *Staphylococcus* species such as *S. epidermidis*. Septicemia may develop and septic pulmonary emboli may occur. The fundamental therapeutic principle in device-related endocarditis is treatment of the infection with antibiotics followed by removal of at least the lead and, when the pacemaker pocket is involved, the entire pacing system (Baddour et al., 2010).

ICDs contain more extensive hardware than pacemakers, and this may contribute an increased relative frequency of complications. Several additional considerations are specific to ICDs. The consequences of repeated defibrillations can cause the following effects: (1) direct effect of repeated discharges on the myocardium and vascular structures, and (2) possible thrombogenic potential of the indwelling intravascular electrodes. Another major complication of ICDs from the standpoint of the patient, other than the inability to sense or terminate an arrhythmia leading to sudden death, is an inappropriate shock. In addition to being startling and quite painful at the time of the shock, patients receiving multiple inappropriate shocks have been known to develop posttraumatic stress disorder symptoms.

As mentioned earlier, the leads are designed to optimize their interactions with the adjacent myocardium; this can be problematic when a complication arises in which the leads must be removed. Some leads can be removed by prolonged gentle traction, but many require additional tools and techniques to free them from the venous wall through which the body of the lead travels and from the myocardium to which they are often tenaciously adherent (Krainski et al., 2018). Recourse to cardiotomy with cardiopulmonary bypass may be needed if the lead is densely incarcerated in fibrous tissue.

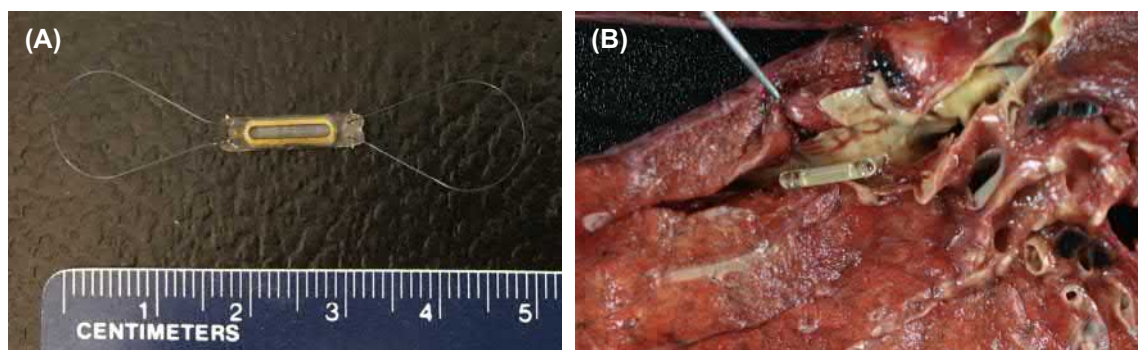
Congestive Heart Failure

Congestive heart failure (Jessup and Brozena, 2003) is a deficiency of the pumping function of the heart and is an extremely common condition, affecting approximately 6.2

million Americans. Each year in the United States, congestive heart failure is the principal cause of death in 60,000 individuals, a contributing factor in over 280,000 deaths, and the primary discharge diagnosis in over 1.1 million hospitalizations, all increases over previous years. Cardiac transplantation is a potential solution for some of these patients (Mancini and Lietz, 2010). However, the increasing discrepancy between the number of acceptable donor hearts (only 2500 per year) and the number of patients who might benefit from cardiac transplantation (estimated at greater than 100,000 per year) has prompted efforts toward the development of mechanical devices to augment or replace cardiac function (Baughman and Jarcho, 2007; Boilson et al., 2010; Krishnamani et al., 2010).

Congestive heart failure is the final common pathway of many specific cardiac conditions, including valvular heart disease, coronary artery atherosclerosis with resultant ischemic heart disease, and diseases that affect the cardiac muscle directly (termed cardiomyopathies). Heart failure can occur precipitously, as in myocardial infarction or viral myocarditis, or it can be a slow, progressive worsening of exercise tolerance and shortness of breath over many months or years because of ongoing deterioration of the heart muscle. It can manifest itself in the postoperative period after both cardiac surgery (e.g., valve replacement, cardiac transplantation) and noncardiac surgery (e.g., abdominal aortic aneurysm repair).

When the left ventricle is failing of whatever etiology, blood backs up into the pulmonary circulation raising the pulmonary vascular resistance and increasing the pulmonary arterial pressure necessary to overcome that resistance. Hence, the pulmonary arterial pressure can be a surrogate marker of the degree of left heart failure in patients with chronic congestive heart failure. The CardioMEMS HF System (Micro-Electrico-Mechanical HF System, Abbott Medical, Inc., Abbott Park, IL) provides hemodynamic information that can be used for the monitoring and management of heart failure (Ayyadurai et al., 2019). The device consists of a wireless sensor that is implanted in the distal pulmonary artery (Fig. 2.5.2A.10) generally via a catheter-based procedure. The sensor consists of a three-dimensional coil and pressure-sensitive capacitor encased between two wafers of fused silica, which is further encased in silicone.



• **Figure 2.5.2A.10** CardioMEMS device. (A) Unimplanted CardioMEMS pressure sensor. (B) In situ view of a CardioMEMS pressure sensor implanted in a branch of the pulmonary artery within the lung.

The coil electromagnetically couples the pressure-sensitive capacitor to the electronics system, allowing the measurement of the resonant frequency of the circuit without the need for an implanted battery. The resonant frequency is continuously converted to a pressure measurement, and the pressure waveform (including systolic, diastolic, and mean arterial pressures) and heart rate are transmitted to a receiver either in the hospital or the patient's home if they are ambulatory. The treating physician can access the data remotely and in real time to evaluate the patient and make any changes to the medical regimen. This strategy can be beneficial in certain patient groups or when used in structured programs (Dickinson et al., 2018).

As one might expect therefore, the natural history of heart failure depends on the cause and progression of the underlying disease process. For example, patients with heart failure after cardiac surgery (called postcardiotomy shock) often recover the vast majority of their cardiac function after a short period of time if they are otherwise sustained by mechanical circulatory support. In contrast, patients with dilated cardiomyopathy, one of the most common indications for cardiac transplantation, often need long-term mechanical support; studies have shown that at least 50% of such individuals would die in 3–5 years from their disease without it. One must take these clinical considerations into account when designing mechanical support systems, as different devices may best serve patients with different problems (DiGiorgi et al., 2003).

Cardiopulmonary Bypass

First used in 1953 by Dr. John H. Gibbon, cardiopulmonary bypass devices pump blood external to the body and thereby permit complex cardiac surgical procedures to be done safely and effectively. Bypass machines are useful in extracorporeal membrane oxygenation (ECMO) to assist in the transport of oxygen and carbon dioxide for patients (especially neonates and infants) with pulmonary diseases such as the respiratory distress syndrome (Alpard and Zwischenberger, 2002).

The basic operating principles of the current heart–lung machines are quite straightforward and have changed little in the past half century. Deoxygenated blood returning from the systemic circulation into the right atrium is withdrawn by gravity siphon into a cardiotomy reservoir and is then pumped into an oxygenator. The most common type of oxygenator is a membrane oxygenator, where oxygen is passed through the tube side of a shell-and-tube-type device while the blood passes through the shell side. Oxygen and carbon dioxide are exchanged via diffusion through synthetic membranes (usually polypropylene or silicone) with high permeability to these respiratory gases. The oxygenated blood is then passed through a heat exchanger to adjust the temperature of the blood and the blood is returned to the systemic circulation via the aorta. At the beginning of the procedure, the patient is anticoagulated with heparin to reduce the risk of thrombosis within the device; as the patient is weaned from bypass, the anticoagulation can be quickly reversed by the use of a drug called protamine.

During an operation, the heat exchanger lowers the temperature of the blood and therefore the core body temperature, decreasing the metabolic requirements of the body and protecting the organs (including the heart) against ischemic damage. At the end of the operation, the blood can be warmed to normal physiologic temperature as the patient is weaned from the bypass machine.

A specially trained perfusionist controls the operation of the heart–lung machine, allowing the surgeon and anesthesiologist to concentrate on their respective tasks. This device therefore provides the function of both the heart (maintaining systemic blood flow and pressure) and the lungs (oxygenating blood and removing carbon dioxide), allowing the heart to be effectively stopped for delicate surgical procedures that would be more difficult or impossible to perform on a beating, moving heart. Many improvements to the original design of cardiopulmonary bypass machines have been made since their inception. One of the problems with the original heart–lung machines was the trauma that they would cause to the blood cells. Hemolysis of red blood cells would lead to functional anemia and loss of oxygen-carrying capacity of the blood; damage to platelets would lead to thrombocytopenia (low numbers of or dysfunctional platelets), resulting in bleeding problems. The problem of blood cell damage has been largely overcome with advanced pump designs and the use of the membrane oxygenators. Roller pumps and centrifugal pumps are commonly used because they cause a lesser degree of hemolysis and shear forces; it is important in the design of these pumps to determine the optimum balance between pumping function and hemolysis/shear stress to the formed blood elements. Bubble oxygenators, which directly pass bubbles of oxygen gas through the blood, cause more hemolysis, protein denaturation, and platelet dysfunction than membrane oxygenators and are currently less frequently used. In addition, newer devices allow blood that has escaped the circulation within the sterile operating field around the heart to be processed and returned to the patient, reducing the need for blood transfusion during the procedure.

Cardiopulmonary bypass can result in many pathophysiologic changes, including complement activation from the prolonged interaction of blood with synthetic surfaces, platelet and neutrophil activation and aggregation, changes in systemic vascular resistance, and expression of other pro-inflammatory mediators (Levy and Tanaka, 2003). When these changes are severe, the use of the heart–lung machine can result in complications, including confusion, renal insufficiency, pulmonary dysfunction, low-grade hepatic dysfunction, and increased susceptibility to infection. Together, these manifestations are termed the postperfusion syndrome. The last decade has seen development of mini extracorporeal circuit (MECC) cardiopulmonary bypass systems (Curtis et al., 2010) with a goal of providing cardiopulmonary bypass with a reduction in this harmful systemic inflammatory response. The MECC has a greatly reduced tubing length, smaller priming volumes, reduction in the blood–air interface, and fewer components than the standard bypass systems, and utilizes heparin-coated components and centrifugal blood

pumps. These systems show a reduction in postoperative cytokine levels, organ damage, postoperative complications, and the need for blood transfusions compared to standard circuits (Vohra et al., 2009).

Percutaneous Mechanical Circulatory Support Devices

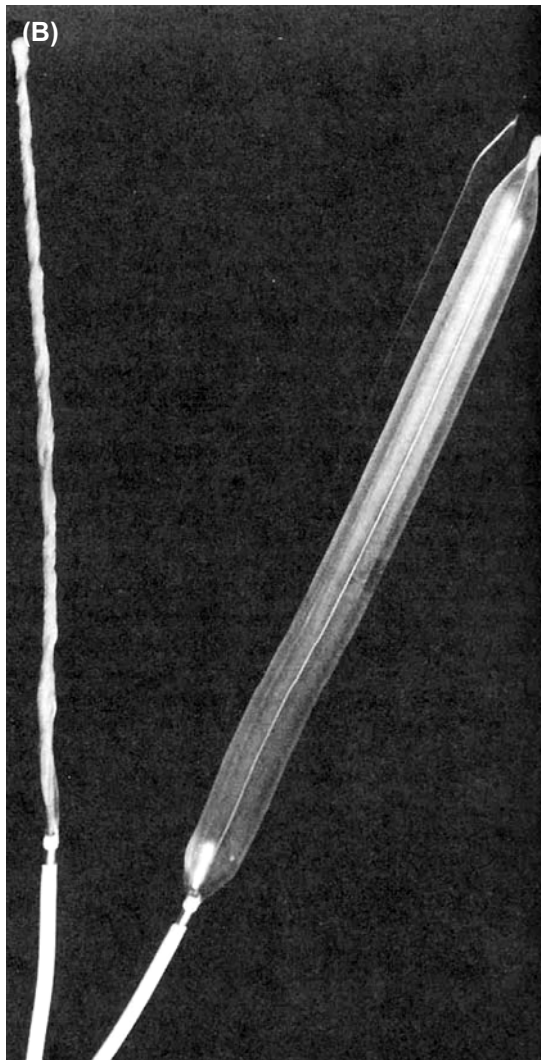
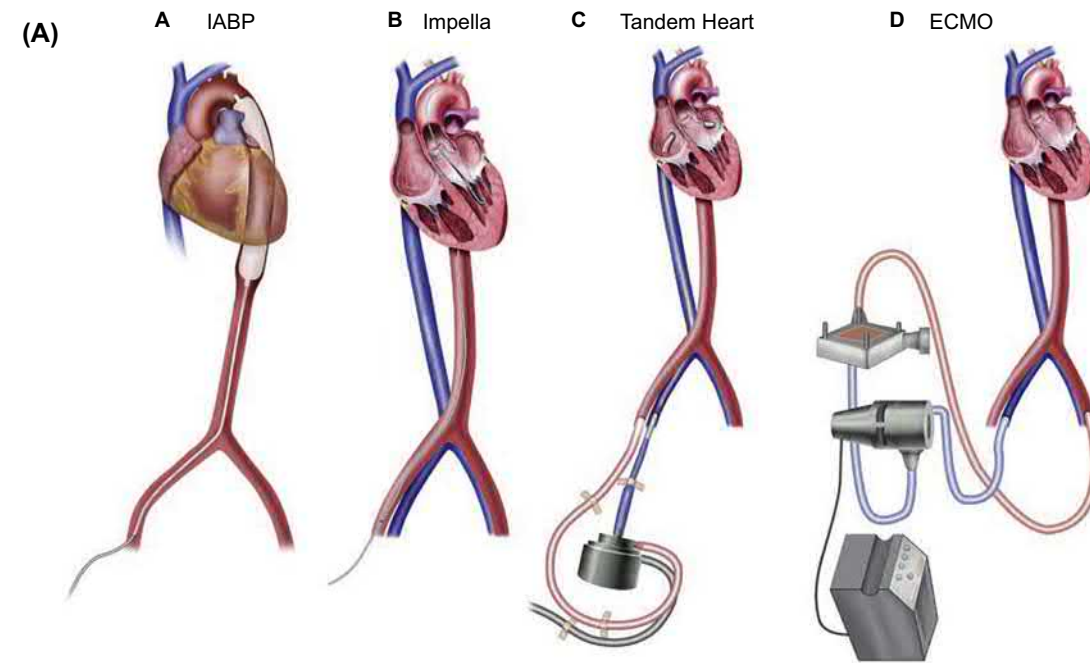
Percutaneous ventricular assist devices (VADs) (Mandawat and Rao, 2017; Miller et al., 2017) are used primarily for potentially reversible acute heart failure or cardiogenic shock, in which cardiac function is likely to recover with cardiac rest (e.g., postcardiotomy shock), or in cases of acute heart failure in which the patient needs to be stabilized quickly so that the possibilities for additional life-saving therapies (e.g., coronary artery bypass surgery, valve surgery, durable VAD placement, heart transplantation) can be assessed (“bridge-to decision”). The typical patient is critically ill with acute cardiogenic shock, mechanical complications of myocardial infarction such as ventricular septal or papillary muscle rupture, unrelenting ventricular arrhythmias, or advanced heart failure. Also, patients undergoing high-risk cardiac surgical procedures or percutaneous revascularization may benefit from the use of devices in the periprocedure period to reduce myocardial oxygen demand. Percutaneous devices (Fig. 2.5.2A.11A) used in these situations include the intraaortic balloon pump (IABP), TandemHeart (Cardiac Assist, Inc., Pittsburgh, PA), Impella (ABIOMED, Inc., Danvers, MA), and ECMO.

Since the original use of the IABP in 1968 by Kantrowitz, the basic design and function of the current device has remained relatively similar during the ensuing decades. IABPs (Fig. 2.5.2A.11B) are catheter-based polyethylene or polyurethane balloons with volumes of 25–50 mL, although smaller devices are used in the pediatric population. Helium is most often used as the inflating gas; its low viscosity allows for rapid inflation and deflation and it is rapidly dissolved in the bloodstream in the event of inadvertent balloon rupture. IABPs (Baskett et al., 2002; De Sousa et al., 2010) are generally positioned under fluoroscopic guidance in the descending thoracic aorta after percutaneous insertion via the femoral artery. They are timed to inflate during diastole (ventricular filling) and deflate during systole (ventricular contraction) using the patient’s electrocardiogram or arterial pressure curve for synchronization; the devices discussed later do not have this requirement. This is termed counterpulsation (Trost and Hillis, 2006), which is out of phase with the patient’s heartbeat, and causes volume displacement of blood proximally and distally within the aorta. Several beneficial effects serve to improve cardiac function. Coronary blood flow (the majority of which occurs in diastole) is increased by the rise in diastolic pressure, delivering more oxygenated blood to the myocardium. In addition, left ventricular afterload (the pressure the myocardium must attain to pump blood into the aorta) is decreased, reducing the workload and therefore the oxygen requirement of the myocardium. The combination of these two hemodynamic

factors therefore improves the balance between myocardial oxygen supply and demand, and results in improved cardiac performance. The device also directly improves systemic circulation to a modest degree (approximately 10%). IABP therapy permits the heart to rest and recover enough function to support adequate circulation after the device has been removed, usually after only a few days. The major contraindications for IABP use include severe peripheral vascular disease, including aneurysms, aortic valve regurgitation, and aortic dissection (because of the need to thread the balloon through peripheral arteries and the aorta). Complications, which occurred in approximately 7% of patients with IABPs in a registry study, include limb ischemia from insertion site problems, bleeding, thrombosis with embolization, aortic dissection, balloon rupture, and sepsis.

The TandemHeart (Fig. 2.5.2A.11C) is a percutaneous VAD that supports the systemic circulation by withdrawing blood from the left atrium and reinjecting it into the abdominal aorta or iliac artery. The device has been commercially available since 2004. The pump, which sits in an extracorporeal location, is a continuous flow centrifugal pump that can provide up to 4–5 L/min of blood flow. The inflow cannula (usually 21-Fr in size) is typically inserted into a femoral vein, advanced into the right atrium and then pushed across the interatrial septum via transseptal puncture into the left atrium; when the device is withdrawn at the end of use, a small atrial septal defect remains. The outflow cannula (usually 15- to 17-Fr in size) is typically inserted into a femoral artery and advanced into the iliac artery or abdominal aorta. TandemHeart has been successfully used in a wide variety of clinical scenarios, including during high-risk percutaneous coronary interventions, bridge-to-recovery, bridge-to-decision, and bridge-to-transplant for patients with acute and advanced heart failure (Tempelhof et al., 2011; Kar et al., 2006). A modification of the TandemHeart allows it also to be used as a right VAD; a dual lumen cannula sits such that the inflow cannula of the device resides in the right atrium while the outflow cannula sits in the pulmonary artery distal to the pulmonic valve. One complication of the left-sided TandemHeart is the migration of the inflow cannula (meant to be in the left atrium) back into the right atrium. When this occurs, deoxygenated blood from the systemic venous return is drawn into the pump and returned into the systemic circulation, resulting in a right-to-left shunt. In addition, this steals blood from the right heart resulting in decreased pulmonary arterial flow leading to hypoxic respiratory failure. The most common complication with the TandemHeart is bleeding at the cannula insertion site(s), exacerbated by the need for anticoagulation to prevent pump thrombosis.

The Impella device (Fig. 2.5.2A.11D) is a continuous, non-pulsatile axial flow pump that employs an Archimedes-screw impeller that draws blood from the left ventricular cavity and expels blood into the ascending aorta distal to the aortic valve. There are currently three versions of the device for left-sided support. The Impella 2.5 provides 2.5 L/min of flow, the Impella CP provides 3.7 L/min, and the Impella 5.0 provides



• **Figure 2.5.2A.11** Percutaneous mechanical circulatory support devices. (A) The intraaortic balloon pump (IABP) is inserted through the femoral artery and resides within the aorta. The Impella is inserted through the femoral artery and passed retrograde across the aortic valve, with the pump inflow within the left ventricle and the outflow in the ascending aorta. The TandemHeart pump is extracorporeal, with the inflow cannula tip in the left atrium and the outflow in the iliac artery or abdominal aorta. Extracorporeal membrane oxygenation (ECMO) consists of both a pump and oxygenator, drawing deoxygenated blood from the systemic venous system and returning newly oxygenated blood to the systemic arterial circulation, similar in principle to cardiopulmonary bypass. (B) Percutaneous IABP. *Left*, balloon deflated for insertion. *Right*, balloon inflated. (C) Tandem Heart pump, with the central inflow port and peripheral outflow port. (D) Impella device with the inflow (*yellow arrow*) and outflow (*red arrow*) areas that would sit in the left ventricle and ascending aorta, respectively. The motor is housed in the gray area adjacent to the outflow area. ((B) Courtesy S. Volvek, Datascope Corp., Oakland, NJ.)

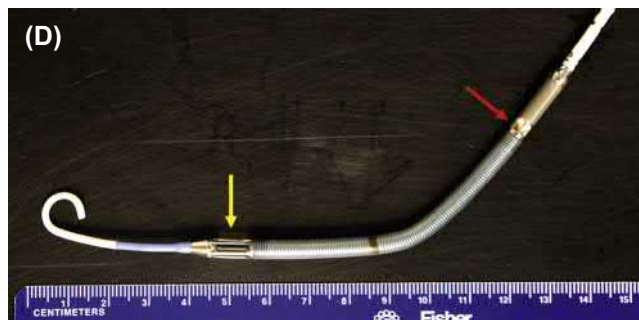


Figure 2.5.2A.11 cont'd

5.0L/min. The device is typically inserted into the femoral or axillary artery and advanced retrograde across the aortic valve so the device inlet rests in the left ventricular cavity and the outlet sits distal to the aortic valve. While the first two devices can generally be inserted purely in a percutaneous fashion, the Impella 5.0 is large enough that it often requires a surgical cut down at the arterial insertion site. By virtue of its position in the left ventricle, the Impella unloads the left ventricular pressure as well as unloading volume, which is advantageous for reducing ventricular oxygen consumption and demand. In contrast, the left atrial inlet cannula position of the TandemHeart only unloads volume without significantly changing left ventricular pressure directly. Impella devices have been extensively used for patients undergoing high-risk percutaneous coronary interventions and for patients in cardiogenic shock secondary to acute myocardial infarction. They have also been investigated as a bridge-to-decision and even as a bridge-to-transplant in appropriate patients (Cheng et al., 2018). They are contraindicated in patients who have mechanical aortic valves or left ventricular thrombi. The more common complications of the device include device migration, thrombosis/thromboembolism, bleeding, hemolysis, and damage to left ventricular cardiac structures such as the aortic and mitral valves. The Impella RP is a similar device designed for right heart failure, which is inserted in the systemic venous circulation and sits such that the device inflow is in the right heart and the outflow is in the pulmonary artery distal to the pulmonic valve.

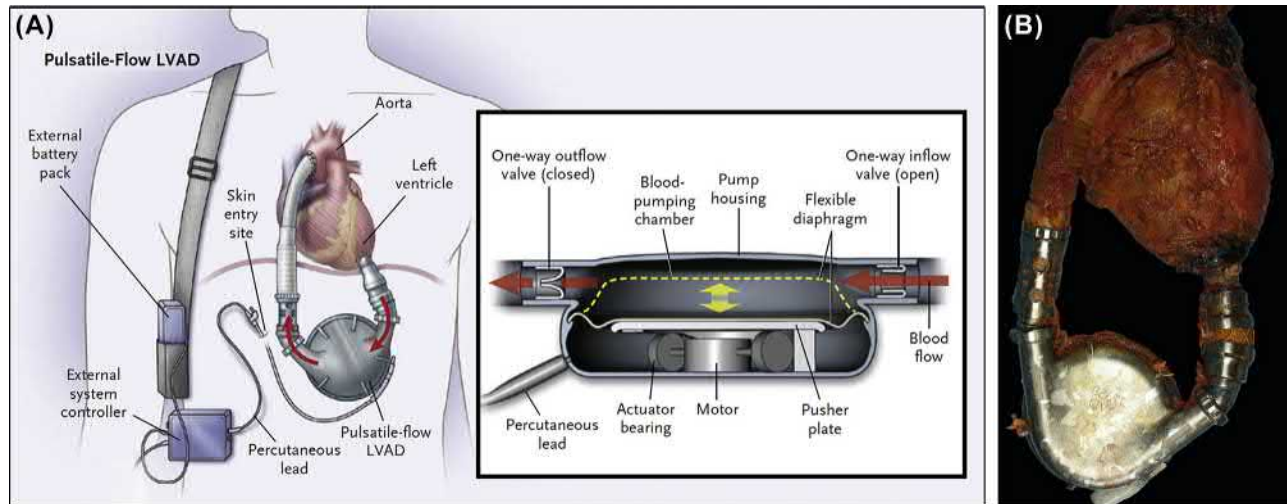
ECMO, in contrast to the other percutaneous devices, provides the functions of both the heart (blood pressure and flow) and lungs (gas exchange) and is increasingly being used for patients with both acute cardiovascular and pulmonary diseases. The ECMO circuit is analogous to cardiopulmonary bypass in the operating room, but in a system that can be utilized at the bedside. The usual configuration is venoarterial (VA-ECMO) where systemic venous blood is removed from the patient, and passed through a continuous flow centrifugal pump, a heat exchanger, and a membrane oxygenator to provide full biventricular support and gas exchange. Cannulation can occur peripherally and percutaneously using the femoral vein and artery, or can use a surgical approach with cannulation of the right atrium and aorta in an open procedure. Just as with cardiopulmonary bypass, it is critical to have an experienced multidisciplinary team ensuring adequate functioning of the device and monitoring of the patient.

Durable Ventricular Assist Devices and Total Artificial Hearts

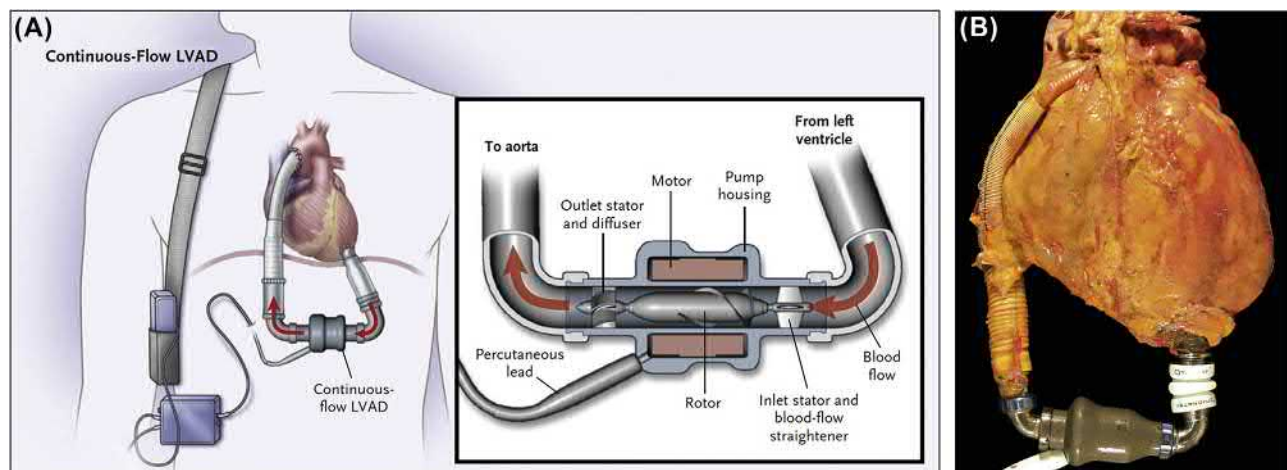
Durable VADs, first successfully employed by DeBakey in 1963, can replace ventricular function for extended periods, in contrast to the short-term duration of cardiopulmonary bypass, IABP, and percutaneous VADs. Durable VADs are currently used primarily in three settings: (1) for end-stage cardiac failure not likely to recover and where mechanical support will provide a “bridge-to-transplantation”; (2) for long-term cardiac support for patients with end-stage congestive heart failure that are not transplant candidates (“destination therapy”) (Christiansen et al., 2008); and (3) for chronic congestive heart failure where the unloading of the left ventricle may induce myocardial changes that might lead to normalization of cardiac function and eventually allow device removal (“bridge-to-recovery”). Research in this latter area focuses on the mechanisms of cardiac recovery, identification of patients who could achieve recovery, and specifics such as the timing and duration of therapy (Maybaum et al., 2008; Birks, 2010).

The first generation of durable VADs used as bridge-to-transplant or destination therapy (Hunt and Frazier, 1998) were large, pulsatile systems, with the inflow cannula of the device generally connected to the left ventricular apex and the outflow cannula connected to the ascending aorta. The pump itself would either be implanted in the peritoneal cavity with a driveline traversing the skin to provide power and controller functions, or would remain extracorporeal with the inflow and outflow cannulae each traversing the skin. Examples of first-generation pulsatile left ventricular assist devices (LVADs) included Thoratec HeartMate XVE (Fig. 2.5.2A.12) (Rose et al., 2001) and Novacor Ventricular Assist System (Dagenais et al., 2001); the Thoratec PVAD (Farrar et al., 1990) is an example of a paracorporeal VAD. These devices generally consisted of a flexible polymer pumping bladder or diaphragm actuated by a pusher plate to allow filling and emptying of the pumping chamber. Valves on the inflow and outflow aspect of the pump ensured unidirectional flow of blood. These devices were very large and posed many challenges; nevertheless, these devices were critical in bridging patients to transplant from the 1980s into the mid-2000s. While the Thoratec PVAD is still occasionally used, the other devices are obsolete.

The second generation of durable VADs consists of implantable continuous axial flow devices, where the long



• **Figure 2.5.2A.12** (A) Diagram of the HeartMate XVE pulsatile ventricular assist device. (B) Photograph of HeartMate XVE and heart after removal from a patient at autopsy. ((A) Reproduced with permission from Slaughter, M.S., Rogers, J.G., Milano, C.A., Russell, S.D., Conte, J.V., Feldman, D., Sun, B., Tatooles, A.J., Delgado, R.M., Long, J.W., Wozniak, T.C., Ghumman, W., Farrar, D.J., Frazier, O.H., 2009. Advanced heart failure treated with continuous-flow left ventricular assist device. *N. Engl. J. Med.* 361, 2241–2251.)

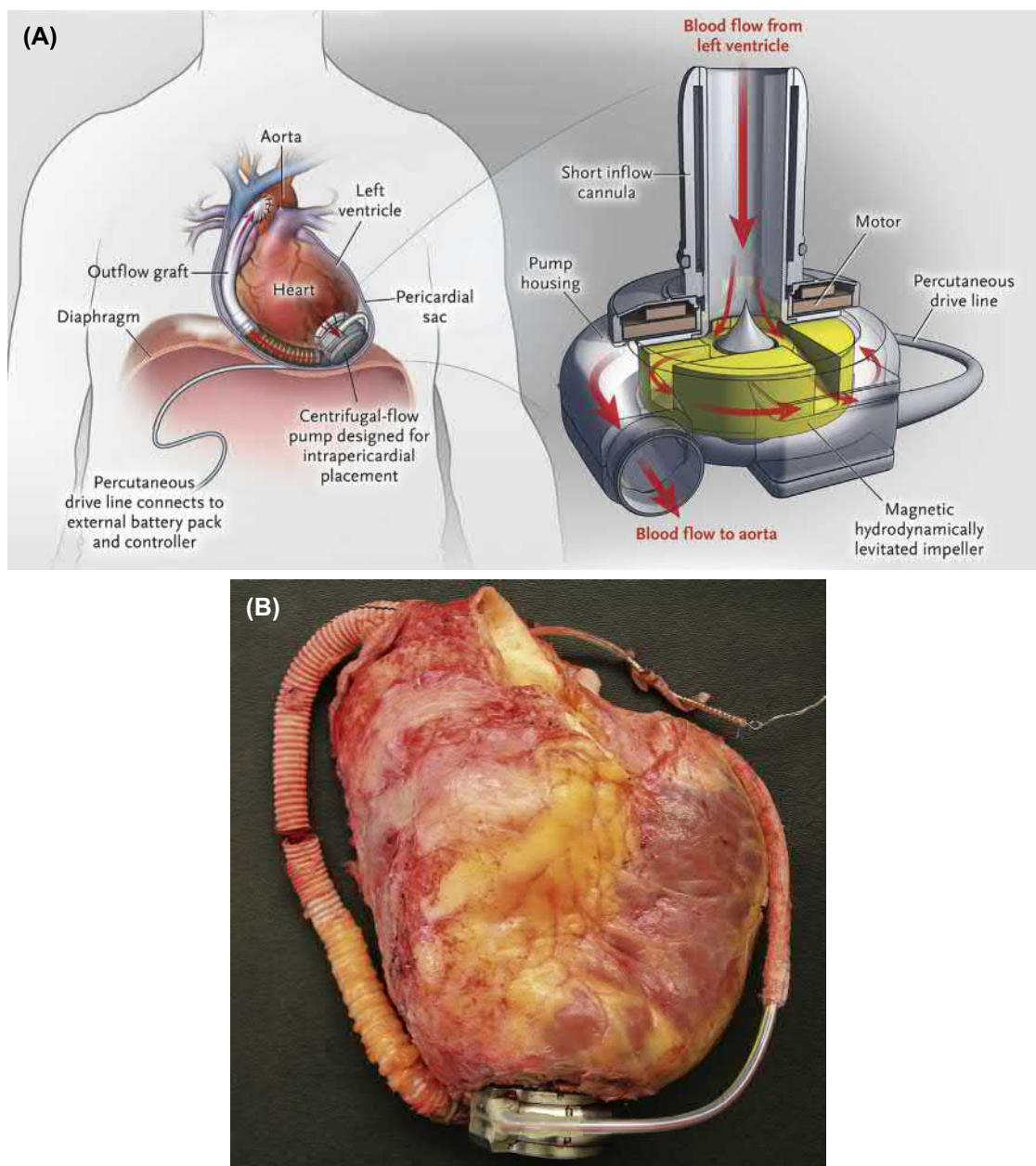


• **Figure 2.5.2A.13** (A) Diagram of the HeartMate II continuous axial flow ventricular assist device. (B) Photograph of HeartMate II and heart after removal from patient at autopsy. ((A) Reproduced with permission from Slaughter, M.S., Rogers, J.G., Milano, C.A., Russell, S.D., Conte, J.V., Feldman, D., Sun, B., Tatooles, A.J., Delgado, R.M., Long, J.W., Wozniak, T.C., Ghumman, W., Farrar, D.J., Frazier, O.H., 2009. Advanced heart failure treated with continuous-flow left ventricular assist device. *N. Engl. J. Med.* 361, 2241–2251.)

axis of the impeller is parallel to the direction of blood flow. Examples of such devices include Thoratec HeartMate II (Fig. 2.5.2A.13) (Slaughter et al., 2009), BerlinHeart INCOR (Schmid et al., 2005) (pumps reside within the peritoneal cavity), and Jarvik 2000 FlowMaker (Sorensen et al., 2012) (the pump is intraventricular). These second-generation devices are connected in much the same way as the implantable first-generation devices but are much smaller, making implantation easier and allowing smaller patients to receive them; they are also more durable than the first-generation devices. Since these are all continuous flow devices, the pumps themselves do not impart pulsatility to the blood resulting in reduced pulse pressure for the patient;

this reduction of pulse pressure does not seem to have significant clinical effects. Data demonstrate lower complication rates and improved outcomes over this time, especially with newer continuous flow LVADs as compared to the first-generation pulsatile devices (Kirklin et al., 2017).

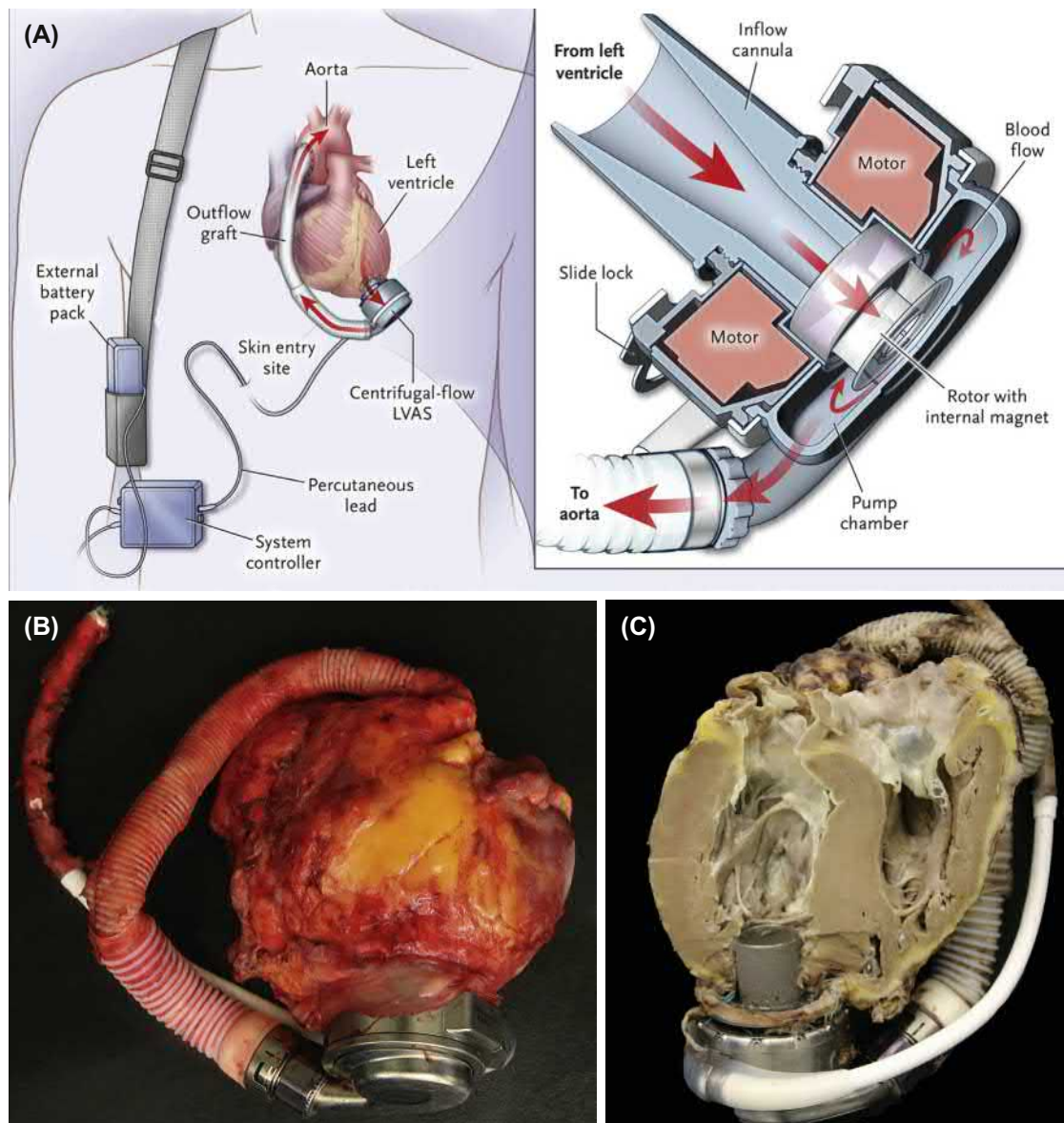
The third generation of VADs consists of implantable continuous centrifugal flow devices, where the impeller creates a centrifugal force to add kinetic energy to the flowing blood. Examples of such devices include HeartWare HVAD (Aaronson et al., 2012), Thoratec HeartMate 3 (Schmitto et al., 2015), and Evaheart LVAS (Saito et al., 2014). The use of these devices is accelerating, with a respective decline in the use of the second-generation VADs.



• **Figure 2.5.2A.14** (A) Diagram of the HeartWare Ventricular Assist Device (HVAD), a continuous flow centrifugal pump. (B) Photograph of HVAD and heart after surgical explantation from a patient who was bridged to cardiac transplantation with this device. ((A) Reproduced with permission from Rogers, J.G., Pagani, F.D., Tatooles, A.J., Bhat, G., Slaughter, M.S., Birks, E.J., Boyce, S.W., Najjar, S.S., Jeevanandam, V., Anderson, A.S., Gregoric, I.D., Mallidi, H., Leadley, K., Aaronson, K.D., Frazier, O.H., Milano, C.A., 2017. Intrapericardial left ventricular assist device for advanced heart failure. *N. Engl. J. Med.* 376, 451–460.)

The HeartWare Ventricular Assist Device (HVAD, Medtronic, Inc., Minneapolis, MN) was the first implantable third-generation centrifugal flow device available in the United States, with important design differences from the commercially available axial flow devices (Larose et al., 2010); it received CE Mark approval in 2008 followed by FDA approval in 2012. The pump is smaller and resides directly on the epicardial surface of the left ventricle (Fig. 2.5.2A.14), with the inflow cannula residing within the left ventricular cavity. The rotor produces continuous, centrifugal flow with a magnetically levitated impeller rather than

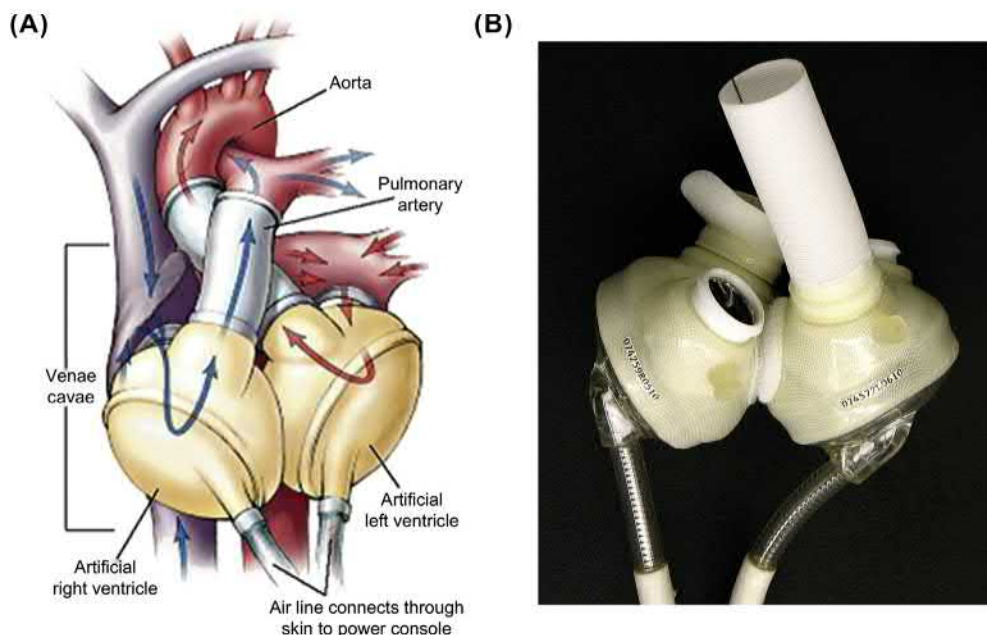
the axial flow system of the Thoratec HeartMate II, for example, which requires inflow and outflow bearings to support and align the impeller. The smaller pump size and driveline, intrathoracic positioning, and flow characteristics of the HVAD are thought to be advantageous in reducing common device complications such as infection, thrombosis, and bleeding. The HVAD ADVANCE trial demonstrated noninferiority (91% patient survival at 6 months) to other commercially available devices in a bridge-to-transplant setting, and there are longer follow-up data in a postmarket registry (Streuber et al., 2014). The original HVAD inflow



• **Figure 2.5.2A.15** (A) Diagram of the HeartMate 3 Ventricular Assist Device, a continuous flow centrifugal pump. (B and C) Photograph of HeartMate 3 and heart after surgical explantation from a patient who was bridged to cardiac transplantation with this device. (A) Reproduced with permission from Mehra, M.R., Naka, Y., Uriel, N., Goldstein, D.J., Cleveland, J.C., Colombo, P.C., Walsh, M.N., Milano, C.A., Patel, C.B., Jorde, U.P., Pagani, F.D., Aaronson, K.D., Dean, D.A., McCants, K., Itoh, A., Ewald, G.A., Horstmannshof, D., Long, J.W., Salerno, C., 2017. A fully magnetically levitated circulatory pump for advanced heart failure. *N. Engl. J. Med.* 376, 440–450.)

cannula had a smooth, polished titanium outer surface, which raised concerns about the increased risk of cerebrovascular accidents secondary to device-related thromboemboli (Najjar et al., 2014). A change in the HVAD inflow cannula design was therefore implemented in an attempt to promote nonthrombotic passivating tissue overgrowth by replacing the smooth, polished titanium surface with one incorporating a collar of sintered titanium microspheres (Soltani S, 2015). However, this created a discontinuity at the smooth-sintered interface on the outer aspect of the inflow cannula that appears to serve as a nidus for thrombus formation (Glass et al., 2019). The HeartMate 3 (Fig. 2.5.2A.15) is the latest third-generation centrifugal flow pump with a fully magnetically levitated motor along with active magnetic

mounting (Chatterjee et al., 2018). It was first implanted in humans in 2014 by a group in Germany (Schmitto et al., 2015). The motor incorporates a contactless bearing technology and consists of the rotor with passive magnets for drive and bearing, the stator with electromagnetic coils for drive and levitation, along with distance sensors and a microcontroller. This pump is approximately one-third the size of the HeartMate I and is implanted in the pericardial space rather than in the abdominal cavity. The inflow cannula is fully sintered and resides within the left ventricular chamber, with the outflow graft anastomosed to the ascending aorta. It can deliver up to 10 L/min of flow, and can also generate an “artificial pulse” by periodically increasing and decreasing the pump speed mimicking a pulse rate of



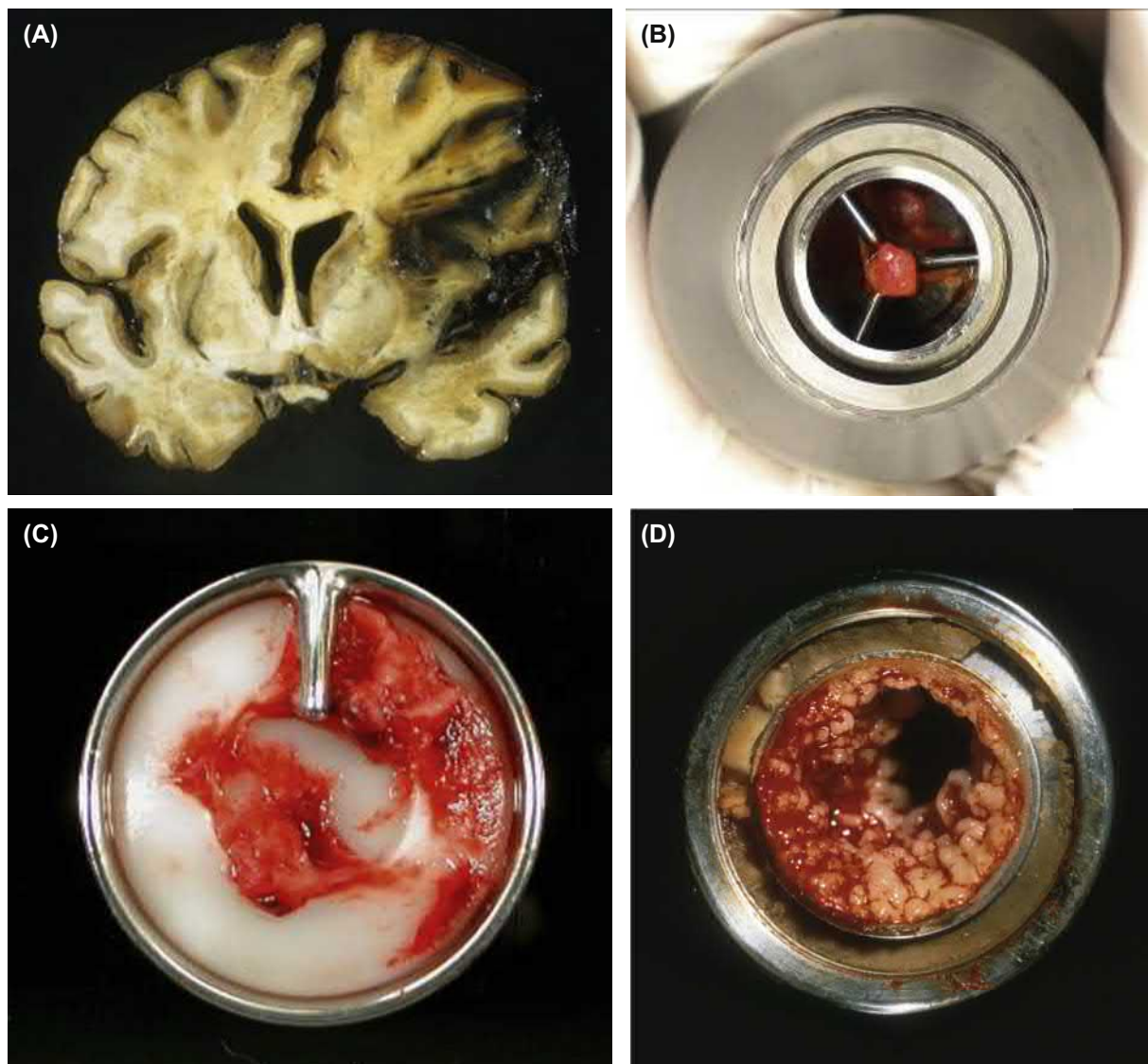
• **Figure 2.5.2A.16** (A) Diagram of the SynCardia Total Artificial Heart. (B) Photograph of an unimplanted SynCardia Total Artificial Heart. ((A) Reproduced with permission from Copeland, J.G., Smith, R.G., Arabia, F.A., Nolan, P.E., Sethi, G.K., Tsau, P.H., McClellan, D., Slepian, M.J., 2004. Cardiac replacement with a total artificial heart as a bridge to transplantation. *N. Engl. J. Med.* 351, 859–867.)

30 beats per minute. The MOMENTUM 3 clinical trial was designed to compare the centrifugal flow HeartMate 3 with the axial flow HeartMate II in patients with advanced heart failure. The HeartMate 3 showed lower rates of pump thrombosis, stroke, and reoperation to remove or replace a malfunctioning pump compared to the HeartMate II at 2-year follow-up (Mehra et al., 2018).

In contrast to VADs where the native heart remains in place, a total artificial heart is composed of two pumping chambers that together replace the entire heart and provide both right and left ventricular function, analogous to heart transplantation (Fig. 2.5.2A.16). The SynCardia Total Artificial Heart (SynCardia Systems, Inc.; Tucson, AZ) has been implanted worldwide in more than 1000 patients with biventricular heart disease (Copeland et al., 2003; Copeland et al., 2012). The device was approved by the FDA in 2004 and has proven to be an effective and reliable device for successful bridge-to-transplant. The clinical indications for implantation have included biventricular failure, left ventricular failure with prior mechanical heart valves, left ventricular failure with severe anatomical damage (ventricular septal defect, AV disruption), intractable malignant arrhythmias, massive ventricular thrombus, cardiac allograft failure, hypertrophic or restrictive cardiomyopathy, and complex congenital heart disease. The device is an implantable, pneumatically driven pulsatile pair of pumps consisting of polyurethane ventricles, whose inflows are anastomosed to the left and right atria and whose outflows are anastomosed to the ascending aorta and pulmonary artery after complete removal of the native cardiac ventricles and all four valves. Medtronic-Hall mechanical valves on the inflow and outflow aspects of the pump ensure unidirectional flow.

Systemic infection and thromboembolic or hemorrhagic events have been reported as the most common complications that prevent successful bridge-to-transplant.

The major complications of cardiac assist devices are hemorrhage, thrombosis/thromboembolism, infection, interactions with host tissue, and device component failure, including the pump and peripheral electrical systems (Fig. 2.5.2A.17). Hemorrhage continues to be a problem in device recipients, although the risk of major hemorrhage has been decreasing with improved devices, therapies, patient selection, and surgical methods. Many factors predispose to perioperative hemorrhage, including (1) anticoagulation therapy and its management along with coagulopathy secondary to liver dysfunction and poor nutritional status, (2) contact of the blood with the device resulting in intrinsic platelet dysfunction and acquired von Willebrand disease, and (3) the extensive nature of the required surgery. Nonthrombogenic blood-contacting surfaces are essential for a clinically useful cardiac assist device or artificial heart. Indeed, thromboembolism occurred in most patients having long-term implantation of the Jarvik-7 artificial heart and is a major design consideration for current devices. In the absence of adequate anticoagulation and despite the development of minimally thrombogenic blood-contacting surfaces and appropriate blood flow characteristics, thrombi can form in areas of disturbed blood flow such as connections of conduits and other components to each other and to the natural heart. The current generation of continuous flow LVADs is carefully designed to minimize thrombosis, but oral anticoagulation is still required. Pump thrombosis in the continuous axial flow HeartMate II LVAD at the inflow bearing was one of the major sources of morbidity and mortality for patients with this device. Thrombi also may form outside the



• **Figure 2.5.2A.17** Complications of cardiac assist devices. (A) Hemorrhage into the brain in a patient with a left ventricular assist device (LVAD). (B) Thrombus on the inflow flow straightener and inflow bearing of the impeller of the HeartMate II LVAD. (C) Thrombus on the inflow valve of a Thoratec PVAD. (D) Fungal infection in LVAD outflow graft. ((A) and (C) Reproduced with permission from Padera, R.F., 2008. Pathology of ventricular assist devices. In: McManus, B.M., Braunwald, E. (Eds.), *Atlas of Cardiovascular Pathology for the Clinician*, second ed. Current Medicine Group LLC, Philadelphia. (D) Reproduced by permission from Schoen, F.J., Edwards, W.D., 2001. Pathology of cardiovascular interventions. In: Silver, M.D., Gotlieb, A.I., Schoen, F.J. (Eds.), *Cardiovascular Pathology*, third ed. Churchill Livingstone, New York.)

LVAD, often in association with crevices and voids as in the HeartWare HVAD discussed earlier, and in areas of disturbed blood flow such as near connections of conduits and other components to the native heart. These thrombi can detach and lead to catastrophic embolic events such as ischemic stroke. Accounting for significant morbidity and mortality following the prolonged use of cardiac assist devices, infection can occur either within the device or associated with percutaneous drive lines (Padera, 2006). Susceptibility to infection is potentiated not only by the usual prosthesis-associated factors, but also by the multisystem organ damage from the underlying disease, the periprosthetic culture medium provided by postoperative hemorrhage, and by prolonged hospitalization with the associated risk of nosocomial infections. Assist device-associated infections are often resistant to antibiotic therapy and host defenses,

but are generally considered not an absolute contraindication to subsequent cardiac transplantation. Novel device designs, including alternative sites for driveline placement and the elimination of the driveline altogether with transcutaneous energy transmission technology, may play a role in further decreasing infection.

Atrial Septal Defects and Other Intracardiac Defects

In prenatal life, circulation is different than it is in postnatal life (Schoen and Mitchell, 2015). The lungs of the fetus are not providing gas exchange, so oxygenation of fetal blood is provided via the placenta and maternal circulation. This

requires two important shunts that need to close immediately after birth to separate the circulation into the pulmonary and the systemic arms. The foramen ovale, a hole in the fetal intraatrial septum, allows oxygenated blood returning to the right atrium from the placenta to preferentially pass into the left atrium. This blood passes through the mitral valve into the left ventricle and is pumped out through the aorta into the systemic circulation. The ductus arteriosus, present between the pulmonary artery and aorta, allows deoxygenated blood pumped from the right ventricle to bypass the lungs and directly reenter the systemic circulation, as the prenatal pulmonary circulation has a high vascular resistance (because of the nonexpanded lungs). After birth, these functional shunts should close to completely separate the right and left circulations; failure to do so results in a patent foramen ovale (PFO) or patent ductus arteriosus (PDA) that can allow inappropriate shunting of blood in the postnatal circulation. In addition, atrial septal defects (ASDs) or ventricular septal defects (VSDs) can also result from abnormal formation of the atrial septum or ventricular septum. While these defects can be closed via an open surgical procedure (sutures and/or fabric patches for PFO, ASD, or VSD, ligation for PDA), efforts have been made to allow closure of these defects using a minimally invasive approach. The decision to close a PFO, ASD, VSD, or PDA depends on the size of the shunt and the symptoms of the patient; the choice of technique (surgical vs. percutaneous) depends on the anatomy and structure of the defect.

Closure Devices

The first catheter-based closure of a PDA was performed in 1967 by Porstmann using an Ivalon plug to occlude flow through the ductus arteriosus. Of the many PDA closure devices that have been developed over the years, most are metal-based devices that work by causing thrombosis of the PDA with subsequent organization and fibrosis, permanently preventing flow through the residual ductus arteriosus. Three of the more commonly used devices are the Gianturco coil (stainless-steel coil containing polyester fibers to promote thrombosis), the Amplatzer Duct Occluder (ADO, a conical device consisting of Nitinol wires and a polyester fiber patch to promote thrombosis and tissue integration), and the next-generation ADO II (Baruteau et al., 2014).

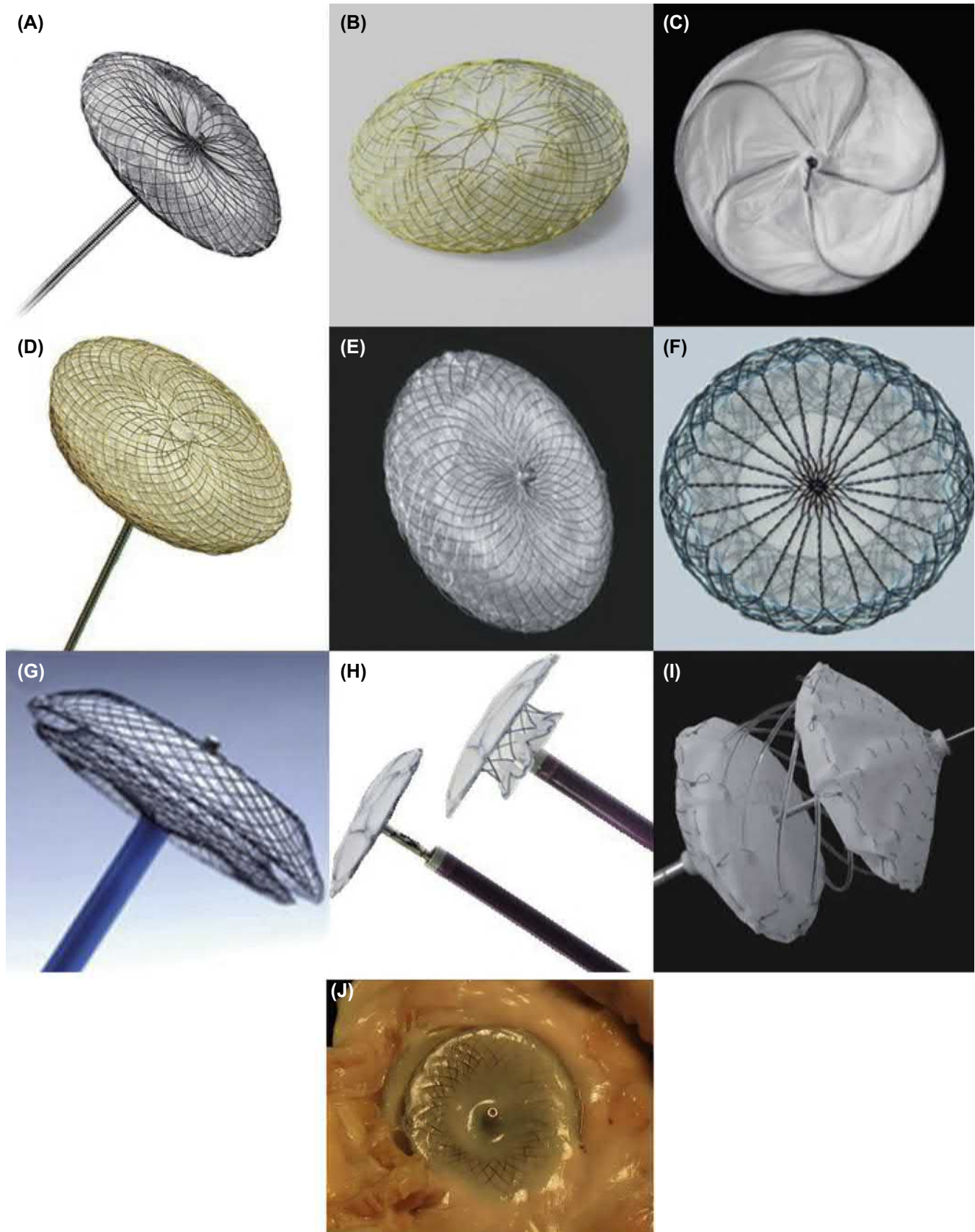
Mills and King reported the first transcatheter closure of an ASD in 1976 using a double umbrella device that covered the opening from both the right and left atrial sides. Their occlusion device consisted of a skeleton of expanded polytetrafluoroethylene (ePTFE)-coated wire supporting an occluder of Dacron fabric delivered through a catheter. Improvements over the years include better device fixation methods and smaller caliber introducers. Several designs (Fig. 2.5.2A.18) of PFO/ASD closure devices are currently in use (Jung and Choi, 2018). The Amplatzer device (St. Jude Medical, St. Paul, MN) is a self-centering device that consists of double Nitinol disks filled with polyester patches

connected by a small waist; the waist sits within the defect to connect the disks, which sit on either side of and are selected to be larger than the defect. The Gore Cardioform Septal Occluder (W.L. Gore and Associates, Flagstaff, AZ) is a nonself-centering device composed of a platinum-filled Nitinol wire framework, which is covered by an ePTFE patch designed to promote endothelialization. Advantages of nonsurgical closure devices such as these include shorter hospital stay, more rapid recovery, and no residual thoracotomy scar. With the experience gained in the transcatheter closure of PFOs and ASDs, this interventional technology is being extended to the closure of some VSDs, particularly in patients thought to be poor operative risks.

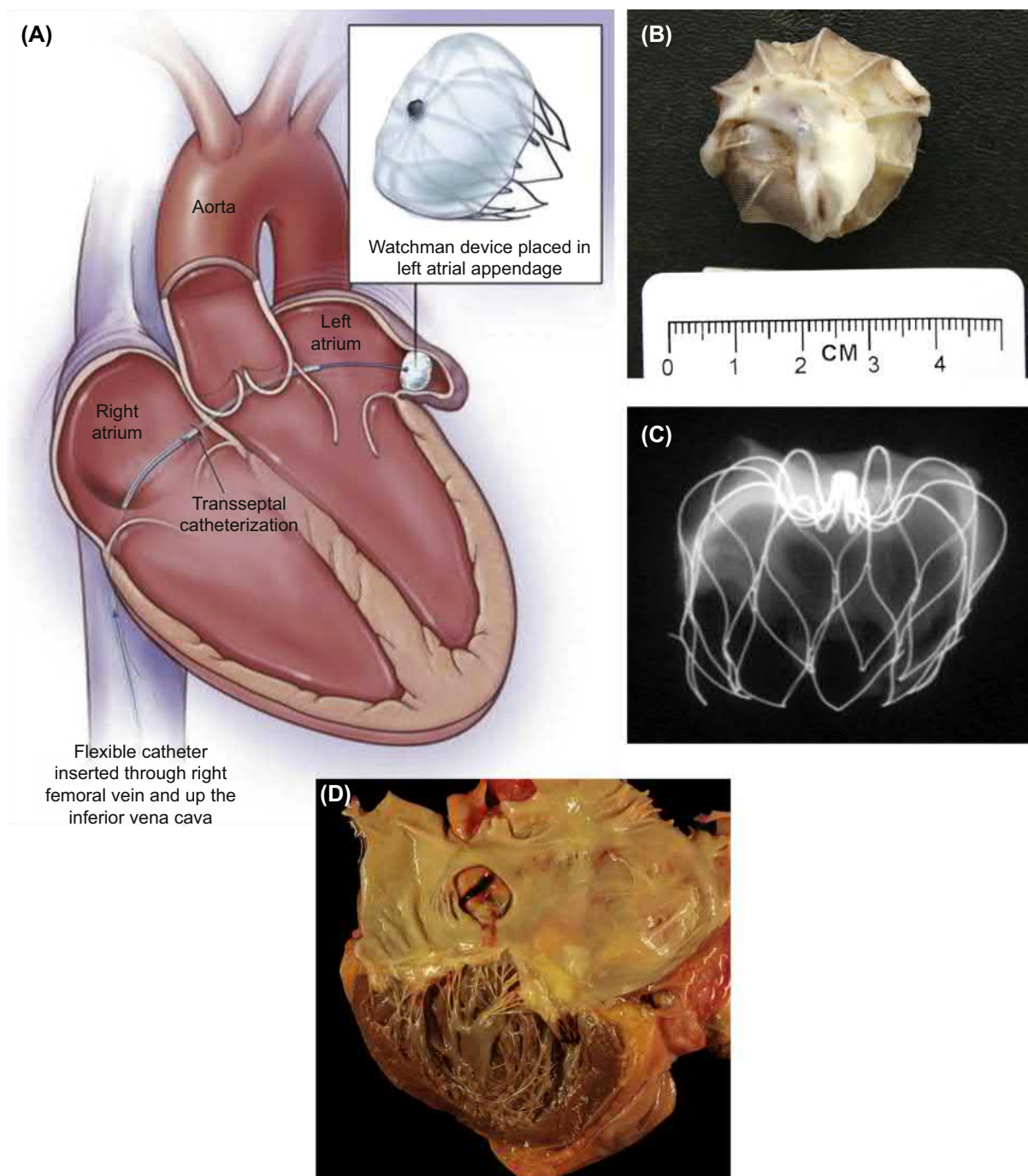
Several types of complications have been reported for closure devices. The most straightforward is the failure to fully close the defect resulting in residual shunting. Erosion of the device through the interatrial septum occurs in some patients with perforation and device embolization; this is thought to be secondary to the specific anatomy of the defect, but the stiffness of the device may also play a role. Inadequate fixation of the device within the defect or a device-defect size mismatch can also result in device embolization. Closure devices are effective in closing defects at least in part via thrombosis; if the thrombosis extends beyond the defect on the device, thromboemboli may result. Fractures of various device components, air embolism at the time of device deployment, infection, and development of new arrhythmias have also been reported. A number of devices are in development, with the trends being defect-specific design and minimization of the amount of foreign material left in the patient, including the use of biodegradable components (O'Byrne and Levi, 2019).

Atrial Fibrillation

AF affects more than 3 million individuals in the United States, making it the most common cardiac arrhythmia. Instead of orderly atrial contraction initiated by the SA node, rapid disorganized electrical activity in the atria causes these upper chambers of the heart to quiver or fibrillate resulting in poor contractile function and irregular flow within the chamber. As would be predicted by Virchow's triad, thrombosis may occur due to these flow abnormalities within the atria, especially within the atrial appendage. Atrial appendage thrombi are an important source of thromboemboli, explaining why patients with AF are at a fivefold greater risk for embolic stroke than individuals in sinus rhythm. Anticoagulation is effective in reducing the risk of atrial thrombosis and stroke, but this therapy has many drawbacks, including a narrow therapeutic window, variability in metabolism of the drug, interactions with other drugs and metabolites, need for frequent monitoring by blood drawing, poor patient compliance, and, most importantly, the risk of life-threatening bleeding. These side effects are reduced in a class of drugs called nonvitamin K antagonist oral anticoagulants when compared to the established vitamin K antagonists such as warfarin (Granger et al., 2011), but there is still a



• **Figure 2.5.2A.18** Closure devices for intraatrial septal defects. (A) Amplatzer Septal Occluder; (B) Occlutech Figulla Flex II device; (C) Gore Cardioform Septal Occluder; (D) Cocoon Septal Occluder; (E) CeraFlex ASD device; (F) Nit Occlud ASD-R device; (G) Cardi-O-Fix Septal Occluder; (H) Ultrarecept II ASD Occluder; (I) Carag Bioresorbable Septal Occluder; (J) Amplatzer Septal Occluder after 2 years with fibrous tissue overgrowth. ((A–I) Reproduced with permission from Jung, S.Y., Choi, J.Y., 2018. Transcatheter closure of atrial septal defect: principles and available devices. *J. Thorac. Dis.* 10, S2909–S2922.)



• **Figure 2.5.2A.19** The Watchman left atrial appendage occluder device. (A) Diagrammatic. (B) Photograph of Watchman device showing coverage by host tissue. (C) Specimen radiograph of Watchman device showing metallic framework. (D) Photograph of heart at autopsy with Watchman device successfully occluding the left atrial appendage. ((A) Reproduced with permission from Maisel, W.H., 2009. Left atrial appendage occlusion – closure or just the beginning? *N. Engl. J. Med.* 360, 2601–2603.)

bleeding risk with these newer medications. An approach for reducing the risk of thromboembolic stroke in patients with AF is to remove or ligate the left atrial appendage, first proposed in the 1930s and first performed in 1949 via a surgical approach. This approach is typically used when a patient is undergoing a concomitant cardiac surgical procedure such as valve replacement or bypass surgery.

Left Atrial Appendage Occlusion Devices

Nonsurgical device-based approaches to close the left atrial appendage have been developed, including several devices that can be deployed percutaneously to occlude the opening to the appendage and isolate it from the blood in the left atrium (Pacha et al., 2019). The Watchman (Fig. 2.5.2A.19)

left atrial appendage system (Boston Scientific, Marlborough, MA) is an FDA-approved, percutaneously deployed parachute-shaped device consisting of a Nitinol cage with a polyethylene terephthalate membrane on its surface and fixation barbs along the perimeter, which allows it to anchor in the atrial appendage. This device has been shown to be noninferior to standard warfarin therapy for prevention of embolic stroke and systemic embolization, and superior to warfarin for prevention of cardiovascular death and hemorrhagic stroke in recent clinical trials (Holmes et al., 2009; Reddy et al., 2017). The Amplatzer Amulet (St. Jude Medical, Minneapolis, MN) device is another current generation percutaneously deployed left atrial occlusion device that is currently in clinical trials (Kleinecke et al., 2017) prior to FDA approval. The Atriclip Device System (Atricure, Inc., West Chester, OH) is an occlusion device applied on the epicardial surface at the base of the left atrial appendage to close the entrance to the left atrial appendage by external compression (Ailawadi et al., 2011). The device consists of two parallel rigid titanium tubes with elastic Nitinol springs that hold the device closed.

References

- Aaronson, K.D., Slaughter, M.S., Miller, L.W., McGee, E.C., Cotts, W.G., Acker, M.A., et al., 2012. Use of an intrapericardial, continuous-flow, centrifugal pump in patients awaiting heart transplantation. *Circulation* 125, 3191–3200.
- Ailawadi, G., Gerdisch, M.W., Harvey, R.L., Hooker, R.L., Damiano, R.J., Salamon, T., Mack, M.J., 2011. Exclusion of the left atrial appendage with a novel device: early results of a multicenter study. *J. Thorac. Cardiovasc. Surg.* 142, 1002–1009.
- Alavi, S.H., Kheradvar, A., 2015. A hybrid tissue-engineered heart valve. *Ann. Thorac. Surg.* 99, 2183–2187.
- Alpard, S.K., Zwischenberger, J.B., 2002. Extracorporeal membrane oxygenation for severe respiratory failure. *Chest Surg. Clin. N. Am.* 12, 355–378.
- Amat-Santos, I.J., Ribeiro, H.B., Urena, M., et al., 2015. Prosthetic valve endocarditis after transcatheter valve replacement: a systemic review. *JACC Cardiovasc. Interv.* 8, 334–336.
- Amin, M.S., Ellenbogen, K.A., 2010. The effect of device advisories on implantable cardioverter-defibrillator therapy. *Curr. Cardiol. Rep.* 12, 361–366.
- Atlee, J.L., Bernstein, A.D., 2001. Cardiac rhythm management devices (part I): indications, device selection, and function. *Anesthesiology* 95, 1265–1280.
- Ayoub, S., Ferrari, G., Gorman, R.C., Gorman III, J.H., Schoen, F.J., Sacks, M.S., 2017. Heart valve biomechanics and underlying mechanobiology. *Compr. Physiol.* 6, 1743–1780.
- Ayyadurai, P., Alkhwam, H., Saad, M., Al-Sadawi, M.A., Shah, N.N., Kosmas, C.E., Vittorio, T.J., 2019. An update on the CardioMEMS pulmonary artery pressure sensor. *Ther. Adv. Cardiovasc. Dis* 13, 1–11.
- Baddour, L.M., Epstein, A.E., Erickson, C.C., Knight, B.P., Levison, M.E., Lockhart, P.B., Masoudi, F.A., Okum, E.J., Wilson, W.R., Beerman, L.B., Bolger, A.F., Estes 3rd, N.A., Gewitz, M., Newburger, J.W., Schron, E.B., Taubert, K.A., 2010. Update on cardiovascular implantable electronic device infections and their management: a scientific statement from the American Heart Association. *Circulation* 121, 458–477.
- Barnett, S.C., Ad, N., 2009. Surgery for aortic and mitral valve disease in the United States: a trend of change in surgical practice between 1998 and 2005. *J. Thorac. Cardiovasc. Surg.* 137, 1422–1429.
- Baruteau, A.-E., Hascoet, S., Baruteau, J., Boudjemline, Y., Lambert, V., Angel, C.-Y., Belli, E., Petit, J., Pass, R., 2014. Transcatheter closure of patent ductus arteriosus: past, present and future. *Arch. Cardiovasc. Dis.* 107, 122–132.
- Baskett, R.J.F., Ghali, W.A., Maitland, A., Hirsch, G.M., 2002. The intraaortic balloon pump in cardiac surgery. *Ann. Thorac. Surg.* 74, 1276–1287.
- Baughman, K.L., Jarcho, J.A., 2007. Bridge to life – cardiac mechanical support. *N. Engl. J. Med.* 357, 846–849.
- Benjamin, E.J., Munter, P., Alonso, A., 2019. Heart disease and stroke statistics-2019 update. *Circulation* 139 (10), e56–e528.
- Bennett, P.C., Silverman, S.H., Gill, P.S., Lip, G.Y., 2009. Peripheral arterial disease and Virchow's triad. *Thromb. Haemost.* 101, 1032–1040.
- Bezuidenhout, D., Williams, D.F., Zilla, P., 2015. Polymeric heart valves for surgical implantation, catheter-based technologies and heart assist devices. *Biomaterials* 36, 6–25.
- Birks, E.J., 2010. Myocardial recovery in patients with chronic heart failure: is it real? *J. Card. Surg.* 25, 472–477.
- Blot, W.J., Ibrahim, M.A., Ivey, T.D., Acheson, D.E., Brookmeyer, R., Weyman, A., Defauw, J., Smith, J.K., Harrison, D., 2005. Twenty-five year experience with the Bjork-Shiley convexoconcave heart valve: a continuing clinical concern. *Circulation* 111, 2850–2857.
- Boilson, B.A., Raichlin, E., Park, S.J., Kushwaha, S.S., 2010. Device therapy and cardiac transplantation for end-stage heart failure. *Curr. Probl. Cardiol.* 35, 8–64.
- Bonow, R.O., Carabello, B.A., Kanu, C., et al., 2006. ACC/AHA 2006 guidelines for the management of patients with valvular heart disease: a report of the American College of cardiology/American heart association task force on practice guidelines (writing committee to revise the 1998 guidelines for the management of patients with valvular heart disease): developed in collaboration with the Society of cardiovascular anesthesiologists: endorsed by the Society for cardiovascular angiography and interventions and the Society of thoracic surgeons. *Circulation* 114, e84–e231.
- Boroumand, S., Asadpour, S., Akbarzadeh, A., Faridi-Majidi, R., Ghanbari, H., 2018. Heart valve tissue engineering: an overview of heart valve decellularization processes. *Regen. Med.* 13, 41–54.
- Bouten, C.V., Driessen-Mol, A., Baaijens, F.P., 2012. In situ heart valve tissue engineering: simple devices, smart materials, complex knowledge. *Expert Rev. Med. Devices* 9, 453–457.
- Buja, L.M., Schoen, F.J., 2016. The pathology of cardiovascular interventions and devices for coronary artery disease, vascular disease, heart failure, and arrhythmias. In: Buja, L.M., Butany, J. (Eds.), *Cardiovascular Pathology*, fourth edition. Elsevier, pp. 577–610.
- Butany, J., Ahluwalia, M.S., Payet, C., et al., 2002. Hufnagel valve: the first prosthetic mechanical valve. *Cardiovasc. Pathol.* 11, 351–353.
- Carabello, B.A., 2008. The current therapy for mitral regurgitation. *J. Am. Coll. Cardiol.* 52, 319–326.
- Carabello, B.A., Paulus, W.J., 2009. Aortic stenosis. *Lancet* 373, 956–966.
- Carpentier, A., 2007. Lasker Clinical Research Award. The surprising rise of nonthrombogenic valvular surgery. *Nat. Med.* 13, 1165–1168.
- Chaikoff, E.L., 2007. The development of prosthetic heart valves – lessons in form and function. *N. Engl. J. Med.* 357, 1368–1371.
- Chandrashekar, Y., Westaby, S., Narula, J., 2009. Mitral stenosis. *Lancet* 374, 1271–1283.

- Chatterjee, A., Feldman, C., Hanke, J.S., Ricklefs, M., Shrestha, M., Dogan, G., Haverich, A., Schmitto, J.D., 2018. The momentum of HeartMate 3: a novel active magnetically levitated centrifugal left ventricular assist device. *J. Thorac. Dis.* 10, S1790–S1793.
- Chauvette, V., Mazine, A., Bouchard, D., 2018. Ten-year experience with the Perceval S sutureless prosthesis: lessons learned and future perspectives. *J. Vis. Surg.* May 3; 4, 87. <https://doi.org/10.21037/jovs.2018.03.10>.
- Cheng, R., Tank, R., Ramzy, D., Azarbai, B., Chung, J., Esmailian, F., Kobashigawa, J.A., Moriguchi, J., Arabia, F.A., 2018. Clinical outcomes of Impella microaxial devices used to salvage cardiogenic shock as a bridge to durable circulatory support or cardiac transplantation. *ASAIO J.* 65, 642–648.
- Cheung, D.Y., Duan, B., Butcher, J.T., 2015. Current progress in tissue engineering of heart valves: multiscale problems, multiscale solutions. *Expert Opin. Biol. Ther.* 15, 1155.
- Christiansen, S., Kolcke, A., Autschback, R., 2008. Past, present and future of long-term mechanical circulatory support in adults. *J. Card. Surg.* 23, 664–676.
- Claiborne, T.E., Slepian, M.J., Hossainy, S., Bluestein, D., 2012. Polymeric trileaflet prosthetic heart valves: evolution and path to clinical reality. *Expert Rev. Med. Devices* 9, 577–594.
- Copeland, J.G., Arabia, F.A., Tsau, P.H., Nolan, P.E., McClellan, D., Smith, R.G., Slepian, M.J., 2003. Total artificial hearts: bridge to transplantation. *Cardiol. Clin.* 21, 101–113.
- Copeland, J.G., Copeland, H., Gustafson, M., Mineburg, N., Covington, D., Smith, R.G., Friedman, M., 2012. Experience with more than 100 total artificial heart implants. *J. Thorac. Cardiovasc. Surg.* 143, 727–734.
- Curtis, N., Vohra, H.A., Ohri, S.K., 2010. Mini extracorporeal circuit cardiopulmonary bypass system: a review. *Perfusion* 25, 115–124.
- Dagenais, F., Portner, P.M., Robbins, R.C., Oyer, P.E., 2001. The Novacor left ventricular assist system: clinical experience from the Novacor registry. *J. Card. Surg.* 16, 267–271.
- De Sousa, C.F., Brito, F.D., de Lima, V.C., Carvalho, A.C., 2010. Percutaneous mechanical assistance for the failing heart. *J. Interv. Cardiol.* 23, 195–202.
- Della Rocca, D.G., Gianni, C., Di Base, L., Natale, A., Al-Ahmad, A., 2018. Leadless pacemakers: state of the art and future perspectives. *Card. Electrophysiol. Clin.* 10, 17–29.
- DeWall, R.A., Qasim, N., Carr, L., 2000. Evolution of mechanical heart valves. *Ann. Thorac. Surg.* 69, 1612–1621.
- Di Eusanio, M., Phan, K., 2015. Sutureless aortic valve replacement. *Am. Cardiothorac. Surg.* 4, 123–130.
- Dickinson, M.G., Allen, L.A., Albert, N.A., Disalvo, T., Ewald, G.A., Vest, A.R., Whellan, D.J., Zile, M.R., Givertz, M.M., 2018. Remote monitoring of patients with heart failure: a white paper from the heart failure society of America scientific statements committee. *J. Card. Fail.* 24, 682–694.
- DiGiorgi, P.L., Rao, V., Naka, Y., Oz, M.C., 2003. Which patient, which pump? *J. Heart Lung Transplant.* 22, 221–235.
- Driessen-Mol, A., Emmert, M.Y., Dijkman, P.E., et al., 2014. Transcatheter implantation of homologous “off-the-shelf” tissue-engineered heart valves with self-repair capacity: long-term functionality and rapid in vivo remodeling in sheep. *J. Am. Coll. Cardiol.* 63, 1320–1329.
- D’Agostino, R.S., Jacobs, J.P., Bodhwar, V., Fernandez, F.G., Paone, G., Wormuth, D.W., Shahian, D.M., 2018. The Society of thoracic surgeons adult cardiac surgery database: 2018 update on outcomes and quality. *Ann. Thorac. Surg.* 105, 15–23.
- Edmunds Jr., L.H., 2001. Evolution of prosthetic heart valves. *Am. Heart J.* 141, 849–855.
- Emmert, M.Y., Weber, B., Falk, V., Hoerstrup, S.P., 2014. Transcatheter tissue engineered heart valves. *Expert Rev. Med. Devices* 11, 15–21.
- Farrar, D.J., Lawson, J.H., Litwak, P., Cederwall, G., 1990. Thoratec VAD system as a bridge to heart transplantation. *J. Heart Lung Transplant.* 9, 415–422.
- Fassa, A.A., Himbert, D., Vahanian, A., 2013. Mechanisms and management of TAVR-related complications. *Nat. Rev. Cardiol.* 10, 685–695.
- Fedak, P.W., McCarthy, P.M., Bonow, R.O., 2008. Evolving concepts and technologies in mitral valve repair. *Circulation* 117, 963–974.
- Fishbein, M.C., Roberts, W.C., Golden, A., Hufnagel, C.A., 1975. Cardiac pathology after aortic valve replacement using Hufnagel trileaflet prostheses: a study of 20 necropsy patients. *Am. Heart J.* 89, 443–448.
- Fishbein, G.A., Schoen, F.J., Fishbein, M.C., 2014. Transcatheter aortic valve implantation: status and challenges. *Cardiovasc. Pathol.* 23, 65.
- Fuzellier, J.F., Campisi, S., Gerbay, A., Haber, B., Ruggieri, V.G., Vola, M., 2016. Two hundred consecutive implantation of the sutureless 3f Enable aortic valve: what we have learned. *Ann. Thorac. Surg.* 101, 1716–1723.
- Gammie, J.S., Sheng, S., Griffith, B.P., et al., 2009. Trends in mitral valve surgery in the United States: results from the Society of thoracic surgeons adult cardiac surgery database. *Ann. Thorac. Surg.* 87, 1431–1437.
- Généreux, P., Head, S.J., Wood, D.A., et al., 2012. Transcatheter aortic valve implantation 10-year anniversary: review of current evidence and clinical implications. *Eur. Heart J.* 33, 2399–2402.
- Ghazanfari, S., Driessen-Mol, A., Sanders, B., et al., 2015. In vivo collagen remodeling in the vascular wall of decellularized stented tissue-engineered heart valves. *Tissue Eng. A* 21, 2206–2215.
- Glass, C.H., Christakis, A., Fishbein, G.A., Watkins, J.C., Strickland, K.C., Mitchell, R.N., Padera, R.F., 2019. Thrombus on the inflow cannula of the HeartWare HVAD: an update. *Cardiovasc. Pathol.* 38, 14–20.
- Goldberg, S.H., Halperin, J.L., 2008. Aortic regurgitation: disease progression and management. *Nat. Clin. Pract. Cardiovasc. Med.* 5, 269–279.
- Goldberg, S.H., Elmariah, S., Miller, M.A., Fuster, V., 2007. Insights into degenerative aortic valve disease. *J. Am. Coll. Cardiol.* 50, 1205.
- Goldstone, A.B., Chiu, P., Baiocchi, M., Lingala, B., Patrick, W.L., Fischbein, M.P., Woo, Y.J., 2017. Mechanical or biologic prosthesis for aortic valve and mitral valve replacement. *N. Engl. J. Med.* 377, 1847–1857.
- Granger, C.B., Alexander, J.H., McMurray, J.J., Lopes, R.D., Hylek, E.M., Hanna, M., Al-Khalidi, H.R., Ansell, J., Atar, D., Avezum, A., Bahit, M.C., Diaz, R., Easton, J.D., Ezekowitz, J.A., Flaker, G., Garcia, D., Geraldes, M., Gersh, B.J., Golitsyn, S., Goto, S., Hermosillo, A.G., Hohnloser, S.H., Horowitz, J., Mohan, P., Jansky, P., Lewis, B.S., Lopez-Sendon, J.L., Pais, P., Parkhomenko, A., Verheugt, F.W., Zhu, J., Wallentin, L., 2011. Apixaban versus warfarin in patients with atrial fibrillation. *N. Engl. J. Med.* 365, 981–992.
- Halbfass, P., Sonne, K., Nentwich, K., Ene, E., Deneke, T., 2018. Current developments in cardiac rhythm management devices. *Clin. Res. Cardiol.* 107, S100–S104.
- Hamm, C.W., Arsalan, M., Mack, M.J., 2016. The future of transcatheter aortic valve implantation. *Eur. Heart J.* 37, 203–210.
- Haqqani, H.M., Mond, H.G., 2009. The implantable cardioverter-defibrillator lead: principles, progress and promises. *Pacing Clin. Electrophysiol.* 32, 1336–1353.

- Harken, D.F., Taylor, W.J., LeFemine, A.A., et al., 1962. Aortic valve replacement with a caged ball valve. *Am. J. Cardiol.* 9, 292–299.
- Harrison, D.C., Ibrahim, M.A., Weyman, A.E., Kuller, L.H., Blot, W.J., Miller, D.E., 2013. The Bjork-Shiley convexo-concave heart valve experience from the perspective of the supervisory panel. *Am. J. Cardiol.* 112, 1921–1931.
- Head, S.J., Celik, M., Kappetein, A.P., 2017. Mechanical versus bioprosthetic aortic valve replacement. *Eur. Heart J.* 38, 2183–2191.
- Hirji, S.A., Kolkailah, A.A., Ramirez-Del Val, R., Lee, J., McGurk, S., Pelletier, M., Singh, S., Mallidi, H.R., Aranki, S., Shekar, P., Kaneko, T., 2018. Mechanical versus bioprosthetic aortic valve replacement in patients aged 50 years and younger. *Ann. Thorac. Surg.* 106, 1113–1120.
- Hoerstrup, S.P., Sodian, R., Daebritz, S., et al., 2000. Functional living trileaflet heart valves grown in-vitro. *Circulation* 102, III 44–III 49.
- Hoerstrup, S.P., Cummings, I., Lachat, M., et al., 2006. Functional growth in tissue engineered living vascular grafts: follow up at 100 weeks in a large animal model. *Circulation* 114, I159–I166.
- Holmes, D.R., Reddy, V.Y., Turi, Z.G., Doshi, S.K., Sievert, H., Buchbinder, M., Mullin, C.M., Sick, P., 2009. Percutaneous closure of the left atrial appendage versus warfarin therapy for prevention of stroke in patients with atrial fibrillation: a randomized non-inferiority trial. *Lancet* 374, 534–542.
- Huikuri, H.V., Castellanos, A., Myerburg, R.J., 2001. Sudden death due to cardiac arrhythmias. *N. Engl. J. Med.* 345, 1473–1482.
- Hunt, S.A., Frazier, O.H., 1998. Mechanical circulatory support and cardiac transplantation. *Circulation* 97, 2079–2090.
- Isaacs, A.J., Shuhaiber, J., Salemi, A., Isom, O.W., Sekraky, A., 2015. National trends in utilization and in-hospital outcomes of mechanical versus bioprosthetic aortic valve replacements. *J. Thorac. Cardiovasc. Surg.* 149, 1262–1269.
- Jessup, M., Brozena, S., 2003. Heart failure. *N. Engl. J. Med.* 348, 2007–2018.
- Joy, P.S., Kumar, G., Poole, J.E., London, B., Olshansky, B., 2017. Cardiac implantable electronic device infections: who is at greatest risk? *Heart Rhythm* 14, 839–845.
- Jung, S.Y., Choi, J.Y., 2018. Transcatheter closure of atrial septal defect: principles and available devices. *J. Thorac. Dis.* 10, S2909–S2922.
- Kar, B., Adkins, L.E., Civitello, A.B., Loyalka, P., Palanichamy, N., Bemmato, C.J., Myers, T.J., Gregoric, I.D., Delgado 3rd, R.M., 2006. Clinical experience with the TandemHeart percutaneous ventricular assist device. *Tex. Heart Inst. J.* 33, 111–115.
- Kim, S.J., Samad, Z., Bloomfield, G.S., Douglas, P.S., 2014. A critical review of hemodynamic changes and left ventricular remodeling after surgical aortic valve replacement and percutaneous aortic valve replacement. *Am. Heart J.* 168, 150–159.
- Kirklin, J.K., Pagani, F.D., Kormos, R.L., Stevenson, L.W., Blume, E.D., Myers, S.L., et al., 2017. Eighth annual INTERMACS report: special focus on framing the impact of adverse events. *J. Heart Lung Transplant.* 36, 1080–1086.
- Kleinecke, C., Park, J.W., Godde, M., Zintl, K., Schnupp, S., Brachmann, J., 2017. Twelve-month follow-up of left atrial appendage occlusion with Amplatzer Amulet. *Cardiol. J.* 24, 131–138.
- Kodali, S.K., Williams, M.R., Smith, C.R., Svensson, L.G., Webb, J.G., Makkar, R.R., et al., 2012. Two-year outcomes after transcatheter or surgical aortic-valve replacement. *N. Engl. J. Med.* 366, 1686–1695.
- Krainski, F., Pretorius, V., Birgersdotter-Green, U., 2018. A practical approach to lead removal: transvenous tools and techniques. *Card. Electrophysiol. Clin.* 10, 637–650.
- Krishnamani, R., DeNofrio, D., Konstam, M.A., 2010. Emerging ventricular assist devices for long-term cardiac support. *Nat. Rev. Cardiol.* 7, 71–76.
- Kusumoto, F.M., Goldschlager, N., 2002. Device therapy for cardiac arrhythmias. *JAMA* 287, 1848–1852.
- Larose, J.A., Tamez, D., Ashenuga, M., Reyes, C., 2010. Design concepts and principle of operation of the HeartWare ventricular assist system. *ASAIO J.* 56, 285–289.
- Leat, M.E., Fisher, J., 1993. Comparative study of the function of the Abiomed polyurethane heart valve for use in left ventricular assist devices. *J. Biomed. Eng.* 15, 516–520.
- Levy, J.H., Tanaka, K.A., 2003. Inflammatory response to cardiopulmonary bypass. *Ann. Thorac. Surg.* 75, S715–S720.
- Lifton, R.P., 2007. Lasker Award to heart valve pioneers. *Cell* 130, 971–974.
- Lueders, C., Jastram, B., Hetzer, R., Schwandt, H., 2014. Rapid manufacturing techniques for the tissue engineering of human heart valves. *Eur. J. Cardiothorac. Surg.* 46, 593–601.
- Lurz, P., Bonhoeffer, P., Taylor, A.M., 2009. Percutaneous pulmonary valve implantation: an update. *Expert Rev. Cardiovasc. Ther.* 7, 823–833.
- Mack, M.J., Leon, M.B., Thourani, V.H., Makkar, R., Kodali, S.K., Russo, M., Kapadia, S.R., Malaisrie, S.C., Cohen, D.J., Pibarot, P., Leipsic, J., Hahn, R.T., Blanke, P., Williams, M.R., McCabe, J.M., Brown, D.L., Babaliaros, V., Goldman, S., Szeto, W.Y., Genereux, P., Pershad, A., Pocock, S.J., Alu, M.C., Webb, J.G., Smith, C.R., PARTNER 3 Investigators., 2019. Transcatheter aortic valve replacement with a balloon-expandable valve in low-risk patients. *N. Engl. J. Med.* 380, 1695–1705.
- Mancini, D., Lietz, K., 2010. Selection of cardiac transplantation candidates in 2010. *Circulation* 122, 173–183.
- Mandawat, A., Rao, S.V., 2017. Percutaneous mechanical circulatory support devices in cardiogenic shock. *Circ. Cardiovasc. Interv.* 10 (5), e004337.
- Masoumi, N., Annabi, N., Assmann, A., et al., 2014. Tri-layered elastomeric scaffolds for engineering heart valve leaflets. *Biomaterials* 35, 7774–7785.
- Mastroloberto, P., Chello, M., Bevacqua, E., Cirillo, F., Covino, E., 2000. Duromedics original prosthesis: what do we really know about diagnosis and mechanism of leaflet escape? *Can. J. Cardiol.* 16, 1269–1272.
- Matheny, R.G., Hutchison, M.L., Dryden, P.E., Hiles, M.D., Shaar, C.J., 2000. Porcine small intestine submucosa as a pulmonary valve leaflet substitute. *J. Heart Valve Dis.* 9, 769.
- Mathieu, P., Bosse, Y., Huggins, G.S., Della Corte, A., Pibarot, P., Michelena, H.I., Limongelli, G., Boulanger, M.-C., Evangelista, A., Bedard, E., Citro, R., Body, S.C., Nemer, M., Schoen, F.J., 2015. The pathology and pathobiology of bicuspid aortic valve: state of the art and novel research perspectives. *J. Pathol.: Clin. Res.* 1, 195–206.
- Maybaum, S., Kamalakannan, G., Murthy, S., 2008. Cardiac recovery during mechanical assist device support. *Semin. Thorac. Cardiovasc. Surg.* 20, 234–246.
- McAlister, F.A., Ezekowitz, J., Hooton, N., Vandermeer, B., Spooner, C., Dryden, D.M., Page, R.L., Hlatky, M.A., Rowe, B.H., 2007. Cardiac resynchronization therapy for patients with left ventricular systolic dysfunction: a systematic review. *JAMA* 297, 2502–2514.
- Mehra, M.R., Goldstein, D.J., Uriel, N., Cleveland, J.C., Yuzefpolskaya, M., Salerno, C., Walsh, M.N., Milano, C.A., Patel, C.B., Ewald, G.A., Itoh, A., Dean, D., Krishnamoorthy, A., Cotts, W.G., Tatroles, A.J., Jorde, U.P., Bruckner, B.A., Estep, J.D.,

- Jeevanandam, V., Sayer, G., Horstmanshof, D., Long, J.W., Gulati, S., Skipper, E.R., O'Connell, J.B., Heatley, G., Sood, P., Naka, Y., For the MOMENTUM 3 Investigators, 2018. Two-year outcomes with a magnetically levitated cardiac pump in heart failure. *N. Engl. J. Med.* 378, 1386–1395.
- Merryman, W.D., Schoen, F.J., 2013. Mechanisms of calcification in aortic valve disease: role of mechanokinetics and mechanodynamics. *Curr. Cardiol. Rep.* 15 (5) 355.
- Meuris, B., Flameng, W.J., Laborde, F., et al., 2015. Five-year results of the pilot trial of a stentless valve. *J. Thorac. Cardiovasc. Surg.* 150, 84.
- Miller, P.E., Solomon, M.A., McAreevey, D., 2017. Advanced percutaneous mechanical circulatory support devices for cardiogenic shock. *Crit. Care Med.* 45, 1922–1929.
- Mohr, F.W., 2014. Decade in review – valvular disease: current perspectives on treatment of valvular heart disease. *Nat. Rev. Cardiol.* 11, 637–638.
- Mond, H.G., Grenz, D., 2004. Implantable transvenous pacing leads: the shape of things to come. *Pacing Clin. Electrophysiol.* 27, 887–893.
- Mylotte, D., Andalib, A., Theriault-Lauzier, P., et al., 2015. Transcatheter heart valve failure: a systematic review. *Eur. Heart J.* 36, 1306–1327.
- Najjar, S.S., Slaughter, M.S., Pagani, F.D., Starling, R.C., McGee, E.C., Eckman, P., et al., 2014. An analysis of pump thrombus events in patients in the HeartWare ADVANCE bridge to transplant and continued access protocol trial. *J. Heart Lung Transplant.* 33, 23–34.
- Neraqi-Miandoab, S., Ewstbrook, B., Flynn, J., Blakely, J., Baribeau, Y., 2015. Prosthetic valve endocarditis five months following transcatheter aortic valve implantation and review of literature. *Heart Surg. Forum* 18, E20–E22.
- O'Byrne, M.L., Levi, D.S., 2019. State-of-the-art atrial septal defect closure devices for congenital heart. *Interv. Cardiol. Clin.* 8, 11–21.
- O'Brien, M.F., Harrocks, S., Stafford, E.G., et al., 2001. The homograft aortic valve: a 29-year, 99.3% follow up of 1022 valve replacements. *J. Heart Valve Dis.* 10, 334–344.
- Pacha, H.M., Al-khadra, Y., Soud, M., Darmoch, F., Pacha, A.M., Alraies, M.C., 2019. Percutaneous devices for left atrial appendage occlusion: a contemporary review. *World J. Cardiol.* 11, 57–70.
- Padera, R.F., 2006. Infection in ventricular assist devices: the role of biofilm. *Cardiovasc. Pathol.* 15, 264–270.
- Panaich, S.S., Eleid, M.F., 2018. Current status of MitraClip for patients with mitral and tricuspid regurgitation. *Trends Cardiovasc. Med.* 28, 200–209.
- Patel, A., Bapat, V., 2017. Transcatheter mitral valve replacement: device landscape and early results. *Eurointervention* 13, AA31–AA39.
- Piper, C., Korfer, R., Horstkotte, D., 2001. Prosthetic valve endocarditis. *Heart* 85, 590–593.
- Popma, J.J., Deeb, G.M., Yakubov, S.J., Mumtaz, M., Gada, H., O'Hair, D., Bajwa, T., Heiser, J.C., Merhi, W., Kleiman, N.S., Askew, J., Sorajja, P., Rovin, J., Chetcuti, S.J., Adams, D.H., Teirstein, P.S., Zorn 3rd, G.L., Forrest, J.K., Tchétché, D., Resar, J., Walton, A., Piazza, N., Ramlawi, B., Robinson, N., Petrossian, G., Gleason, T.G., Oh, J.K., Boulware, M.J., Qiao, H., Mugglin, A.S., Reardon, M.J., Evolut Low Risk Trial Investigators, 2019. Transcatheter aortic valve replacement with a self-expanding valve in low-risk patients. *N. Engl. J. Med.* 380, 1706–1715.
- Rabkin, E., Hoerstrup, S.P., Aikawa, M., et al., 2002. Evolution of cell phenotype and extracellular matrix in tissue-engineered heart valves during in-vitro maturation and in-vivo remodeling. *J. Heart Valve Dis.* 11, 308–314.
- Rahimtulla, S.H., 2003. Choice of prosthetic heart valve for adult patients. *J. Am. Coll. Cardiol.* 41, 893–904.
- Reardon, M.J., Adams, D.H., Kleiman, N.S., et al., 2015. 2-year outcomes in patients undergoing surgical or self-expanding transcatheter aortic valve replacement. *J. Am. Coll. Cardiol.* 66, 113–121 ([Epub]).
- Reardon, M.J., Van Mieghem, N.M., Popma, J.J., Kleiman, N.S., Søndergaard, L., Mumtaz, M., Adams, D.H., Deeb, G.M., Maini, B., Gada, H., Chetcuti, S., Gleason, T., Heiser, J., Lange, R., Merhi, W., Oh, J.K., Olsen, P.S., Piazza, N., Williams, M., Windecker, S., Yakubov, S.J., Grube, E., Makkar, R., Lee, J.S., Conte, J., Vang, E., Nguyen, H., Chang, Y., Mugglin, A.S., Serruys, P.W., Kappetein, A.P., SURTAVI Investigators, 2017. Surgical or transcatheter aortic valve replacement in intermediate-risk patients. *N. Engl. J. Med.* 376, 1321–1331.
- Reddy, V.Y., Doshi, S.K., Kar, S., Gibson, D.N., Price, M.J., Huber, K., Horton, R.P., Buchfinder, M., Neuzil, P., Gordon, N.T., Holmes, D.R., PREVAIL and PROTECT AF Investigators, 2017. 5-year outcomes after left atrial appendage closure: from the PREVAIL and PROTECT AF trials. *J. Am. Coll. Cardiol.* 70, 2964–2975.
- Rippel, R.A., Ghanbari, H., Seifalian, A.M., 2012. Tissue-engineered heart valve; future of cardiac surgery. *World J. Surg.* 36, 1581–1591.
- Rodés-Cabau, J., 2012. Transcatheter aortic valve implantation: current and future approaches. *Nat. Rev. Cardiol.* 9, 15–29.
- Rose, E.A., Gelijns, A.C., Moskowitz, A.J., Heitjan, D.F., Stevenson, L.W., Dembitsky, W., et al., 2001. Long-term use of a left ventricular assist device for end-stage heart failure. *N. Engl. J. Med.* 345, 1435–1443.
- Saito, S., Yamazaki, K., Nishinaka, T., Ichihara, Y., Ono, M., Kyo, S., et al., 2014. Post-approval study of a highly pulsed, low-shear-rate, continuous-flow, left ventricular assist device, EVAHEART: a Japanese multicenter study using J-MACS. *J. Heart Lung Transplant.* 33, 599–608.
- Salieb, S.F., Newburger, J.W., Geva, T., Baird, C.W., Gauvreau, K., Padera, R.F., Del Nido, P.J., Borisuk, M.J., Sanders, S.P., Mayer, J.E., 2014. Accelerated degeneration of a bovine pericardial bioprosthetic aortic valve in children and young adults. *Circulation* 130, 51–60.
- Sapirstein, J.S., Smith, P.K., 2001. The “ideal” replacement heart valve. *Am. Heart J.* 141, 856–860.
- Schmid, C., Tjan, T.D., Etz, C., Schmidt, C., Wenzelburger, F., Wilhelm, M., et al., 2005. First clinical experience with the Incor left ventricular assist device. *J. Heart Lung Transplant.* 24, 1188–1194.
- Schmitto, J.D., Hanke, J.S., Rosa, S.V., Asvar, M., Haverich, A., 2015. First implantation in man of a new magnetically levitated left ventricular assist device (HeartMate 3). *J. Heart Lung Transplant.* 34, 858–860.
- Schoen, F.J., 2011. Heart valve tissue engineering: quo vadis? *Curr. Opin. Biotechnol.* 22, 698–705 ([Epub ahead of print]).
- Schoen, F.J., Butany, J., 2016. Cardiac valve replacement and related interventions. In: Buja, L.M., Butany, J. (Eds.), *Cardiovascular Pathology*, fourth ed. Elsevier, pp. 529–576.
- Schoen, F.J., Gotlieb, A.I., 2016. Heart valve health, disease, replacement and repair: a 25-year cardiovascular pathology perspective. *Cardiovasc. Pathol.* 25, 341–352.
- Schoen, F.J., Levy, R.J., 2005. Calcification of tissue heart valve substitutes: progress toward understanding and prevention. *Ann. Thorac. Surg.* 79, 1072–1080.
- Schoen, F.J., Mitchell, R.N., 2015. The heart. In: Kumar, V., Abbas, A.K., Aster, J.C. (Eds.), *Robbins and Cotran Pathologic Basis of Disease*, ninth ed. W.B. Saunders, Philadelphia, PA, pp. 523–578.

- Schoen, F.J., Webb, J.G., 2008. Prosthetics and the heart. In: McManus, B.M., Braunwald, E. (Eds.), *Atlas of Cardiovascular Pathology for the Clinician*, pp. 241–256 Current Medicine, Philadelphia.
- Simon, P., Kasimir, M.T., Seebacher, G., et al., 2003. Early failure of the tissue engineered porcine heart valve SYNERGRAFT in pediatric patients. *Eur. J. Cardiothorac. Surg.* 23, 1002–1006.
- Slaughter, M.S., Rogers, J.G., Milano, C.A., Russell, S.D., Conte, J.V., Feldman, D., et al., 2009. Advanced heart failure treated with continuous-flow left ventricular assist device. *N. Engl. J. Med.* 361, 2241–2251.
- Smith, C., Leon, M., Mack, M., et al., 2011. Transcatheter versus surgical aortic-valve replacement in high-risk patients. *N. Engl. J. Med.* 364, 2187–2198.
- Soltani, S., Kaufmann, F., Vierecke, J., Kretzschmar, A., Hennig, E., Stein, J., et al., 2015. Design changes in continuous-flow left ventricular assist devices and life-threatening pump malfunction. *Eur. J. Cardiothorac. Surg.* 47, 984–989.
- Sorensen, E.N., Pierson 3rd, R.N., Feller, E.D., Griffith, B.P., 2012. University of Maryland surgical experience with the Jarvik 2000 axial flow ventricular assist device. *Ann. Thorac. Surg.* 93, 133–140.
- Sarr, A., 2007. Lasker clinical medical research award. The artificial heart valve. *Nat. Med.* 10, 1160–1164.
- Stassen, O.M.J.A., Muylaert, D.E.P., Bouten, C.V.C., Hjortnaes, J., 2017. Current challenges in translating tissue-engineered heart valves. *Curr. Treat. Options Cardiovasc. Med.* 19 (9), 71.
- Stone, G.W., Lindenfeld, J., Abraham, W.T., Kar, S., Lim, D.S., Mishell, J.M., Whisenant, B., Grayburn, P.A., Rinaldi, M., Kapadia, S.R., Rajagopal, V., Sarembock, I.J., Briekke, A., Marx, S.O., Cohen, D.J., Weissman, N.J., Mack, M.J., COAPT Investigators, 2018. Transcatheter mitral valve repair in patients with heart failure. *N. Engl. J. Med.* 379, 2307–2318.
- Strueber, M., Larbalestier, R., Jansz, P., Zimpfer, D., Fiane, A.E., Tsui, S., Simon, A., Schmitto, J.D., Khaghani, A., Wieselthaler, G.M., Najarian, K., Schueler, S., 2014. Results of the postmarket registry to evaluate the HeartWare left ventricular assist system (ReVOLVE). *J. Heart Lung Transplant.* 33, 486–491.
- Tempelhof, M.W., Klein, L., Cotts, W.G., Benzuly, K.H., Davidson, C.J., Meyers, S.N., McCarthy, P.M., Malaisrie, C.S., McGee, E.C., Beohar, N., 2011. Clinical experience and patient outcomes associated with the TandemHeart percutaneous transseptal assist device among a heterogeneous patient population. *Am. Soc. Artif. Intern. Organs J.* 57, 254–261.
- The Antiarrhythmics versus Implantable Defibrillators (AVID) Investigators, 1997. A comparison of antiarrhythmic-drug therapy with implantable defibrillators in patients resuscitated from near-fatal ventricular arrhythmias. *N. Engl. J. Med.* 337, 1576–1583.
- Tice, J.A., Sellke, F.W., Schaff, H.V., 2014. Transcatheter aortic valve replacement in patients with severe aortic stenosis who are at high risk for surgical complications: Summary assessment of the California Technology Assessment Forum. *J. Thorac. Cardiovasc. Surg.* 148, 482–491.
- Trost, J.C., Hillis, L.D., 2006. Intra-aortic balloon counterpulsation. *Am. J. Cardiol.* 97, 1391–1398.
- Vahanian, A., 2008. Antithrombotic therapy for patients with valvular heart disease. *Herz* 33, 44–51.
- Van Mieghem, N.M., El Faquir, N., Rahhab, Z., et al., 2015. Incidence and predictors of debris embolizing to the brain during transcatheter aortic valve implantation. *JACC Cardiovasc. Interv.* 8, 718.
- Vohra, H.A., Whistance, R., Modi, A., Ohri, S.K., 2009. The inflammatory response to miniaturised extracorporeal circulation: a review of the literature. *Mediat. Inflamm.* 2009, 2009, 707042.
- Vongpatanasin, W., Hillis, L.D., Lange, R.A., 1996. Prosthetic heart valves. *N. Engl. J. Med.* 335, 407–416.
- Webb, J.G., Murdoch, D.J., Boone, R.H., Moss, R., Attinger-Toller, A., Blanke, P., Cheung, A., Hensey, M., Leipsic, J., Ong, K., Sathanathan, J., Wood, D.A., Ye, J., Tartara, P., 2019. Percutaneous transcatheter mitral valve replacement: first-in-human experience with a new transseptal system. *J. Am. Coll. Cardiol.* 73, 1239–1246.
- Willcox, M.E., Prutkin, J.M., Bardy, G.H., 2016. Recent developments in the subcutaneous ICD. *Trends Cardiovasc. Med.* 26, 526–535.
- Wyler von Ballmoos, M.C., Kalra, A., Reardon, M.J., 2018. Complexities of transcatheter mitral valve replacement (TMVR) and why it is not transcatheter aortic valve replacement (TAVR). *Ann. Cardiothorac. Surg.* 7, 724–730.
- Zannis, K., Folliguet, T., Laborde, F., 2012. New sutureless aortic valve prosthesis: another tool in less invasive aortic valve replacement. *Curr. Opin. Cardiol.* 27, 125–129.
- Zeitler, E.P., Pokorney, S.D., Zhou, K., Lewis, R.K., Greenfield, R.A., Daubert, J.P., Matchar, D.B., Piccini, J.P., 2015. Cable externalization and electrical failure of the Riata family of implantable cardioverter-defibrillator leads: a systematic review and meta-analysis. *Heart Rhythm* 12, 1233–1240.
- Zhang, X., Xu, B., Puperi, D.S., et al., 2015. Integrating valve-inspired design features into poly(ethylene glycol) hydrogel scaffolds for heart valve tissue engineering. *Acta Biomater.* 14, 11–21.
- Zhang, B.L., Bianco, R.W., Schoen, F.J., 2019. Preclinical assessment of cardiac valve substitutes: current status and considerations for engineered tissue heart valves. *Front. Cardiovasc. Med.* 6, 72.

2.5.2B

Cardiovascular Medical Devices: Stents, Grafts, Stent-Grafts and Other Endovascular Devices

MICHAEL A. SEIDMAN^a, ROBERT F. PADERA, FREDERICK J. SCHOEN

Department of Pathology, Brigham and Women's Hospital and Harvard Medical School, Boston, MA, United States

Vascular disorders and their downstream sequelae are responsible for more morbidity and mortality than any other category of human disease. The top two causes of death worldwide, ischemic heart disease and stroke, collectively comprising approximately 13 million persons annually, more than one-quarter of all deaths in both men and women (Lozano et al., 2012), are both manifestations of vascular pathology. Additionally, aortic aneurysms and related pathologies are associated with over 175,000 deaths a year globally (GBD 2013 Mortality and Causes of Death Collaborators, 2015). Thus, the vasculature has been a longstanding and important target for both open surgical procedures and endovascular interventions using biomaterials and associated devices. The devices that have facilitated these procedures are highly specialized to the anatomic site and functional role of the segment of vascular bed targeted, and to the specific pathological processes the procedures and devices are intended to manage.

This chapter focuses on the biomaterials and devices used to manage vascular disease. However, before discussing specific device categories, we provide a brief overview of the vascular system and the key pathologic processes that affect it.

Key Concepts in Vascular Structure and Function

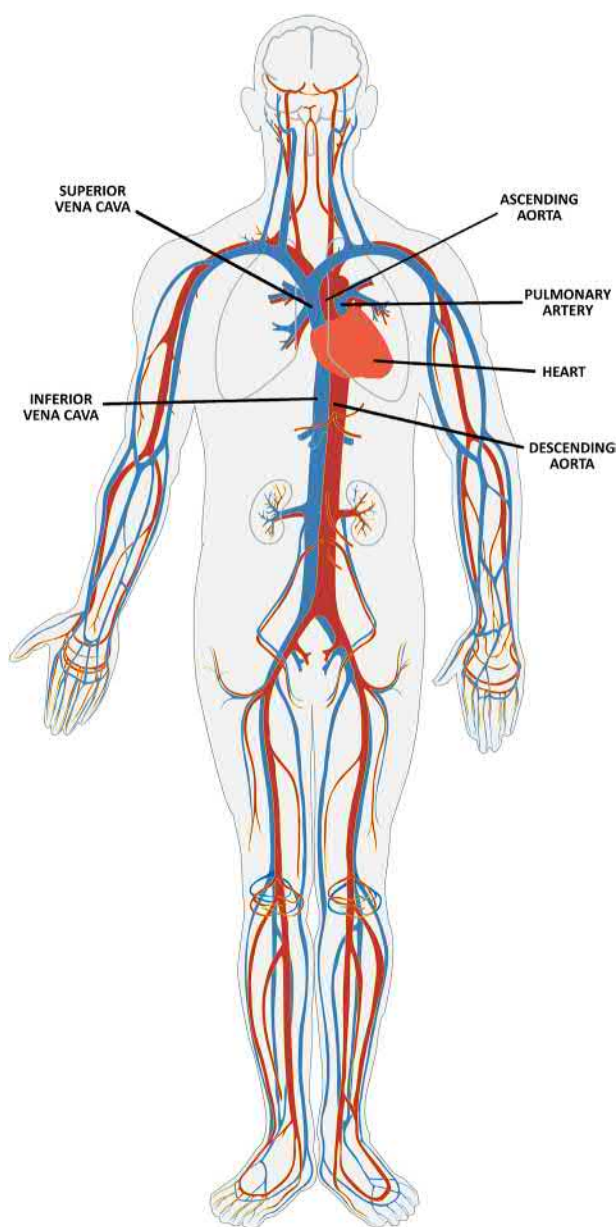
Architecture of the Circulation

The circulation (a.k.a. the *cardiovascular system*) transports and distributes essential substances throughout the body and

helps eliminate waste products. The cardiovascular system is composed of a pump, a series of distributing and collecting tubes that carry blood away from the heart (*arteries*), vessels that carry blood toward the heart (*veins*), and an extensive network of thin-walled vessels (*capillaries*) that provide nutrient and gas exchange to the tissues and remove byproducts of metabolism (i.e., oxygen and nutrients in; carbon dioxide and other waste products out). To accomplish these functions, the cardiovascular system must regulate blood pressure and volume at all levels of the vasculature, buffer pulsatile flow in order to ensure steady and slow velocity flow in the capillaries, maintain circulatory continuity while permitting free and bidirectional exchange of substances between blood and the extravascular compartments, and control *hemostasis*, i.e., prevent clots (*thrombi*) when the circulation is intact, and prevent hemorrhage when the vessel is injured. Other functions of the circulation include regulation of body temperature, and systemic distribution of various regulating substances (e.g., hormones, inflammatory mediators, growth factors, and therapeutic substances). Moreover, the circulatory system distributes immune and inflammatory cells, and the lining cells of the circulatory system (*endothelial cells*) facilitate egress of the immune cells from the blood to the tissues in which they are needed.

The human circulation is composed of two parallel circuits with this generalized configuration (Fig. 2.5.2B.1). The *systemic circulation* originates at the aortic valve of the heart; the single lead artery, the aorta, branches into successively smaller arteries until ultimately reaching the capillaries, the level of the circulatory system at which metabolic exchange with the tissues occurs. The capillaries then “coalesce” into small and progressively larger veins, ultimately returning to the right side of the heart via the largest veins, the inferior and superior venae cavae. Similarly, and

^aDr. Seidman is presently affiliated with the University Health Network and the University of Toronto, Toronto, Canada.



• **Figure 2.5.2B.1** The cardiovascular system. Large and medium-sized vessels carrying oxygenated (red) and deoxygenated (blue) blood are shown with respect to the heart (orange). The ascending aorta (red) and pulmonary artery (blue) carry blood away from the heart, the superior and inferior vena cavae (blue) carry blood back to the heart (the pulmonary veins, in red behind the pulmonary artery, also return blood to the heart). The descending aorta passes behind the heart but does not anastomose with it. (Reproduced from <https://commons.wikimedia.org/w/index.php?curid=10005587>. (Accessed 3 September 2019).)

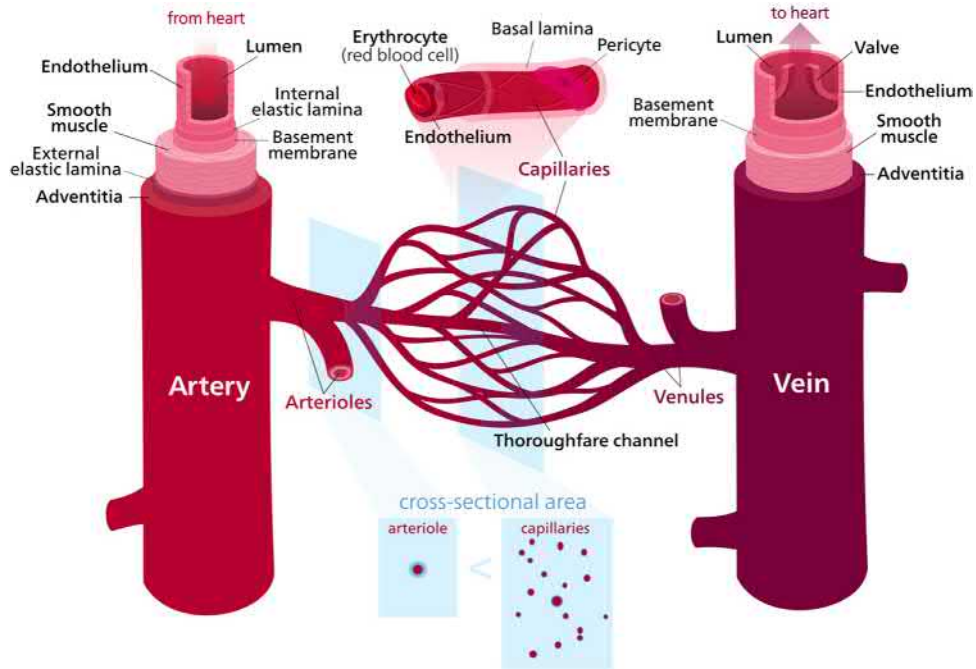
in parallel, the *pulmonary circulation* begins at the pulmonary valve, from which arises the main pulmonary artery (the only large artery in the body which carries blood which has not yet been oxygenated). In the lung, the pulmonary artery branches successively into smaller arteries, then capillaries, and collects oxygenated blood into successively larger veins, returning blood to the left atrium via the pulmonary veins. In most organs and tissues, one or a few larger arteries bring blood in, then branch into capillaries in a manner

that creates *vascular beds* within each organ. The branching structure dramatically increases the surface area available for gas and nutrient exchange at the capillary level.

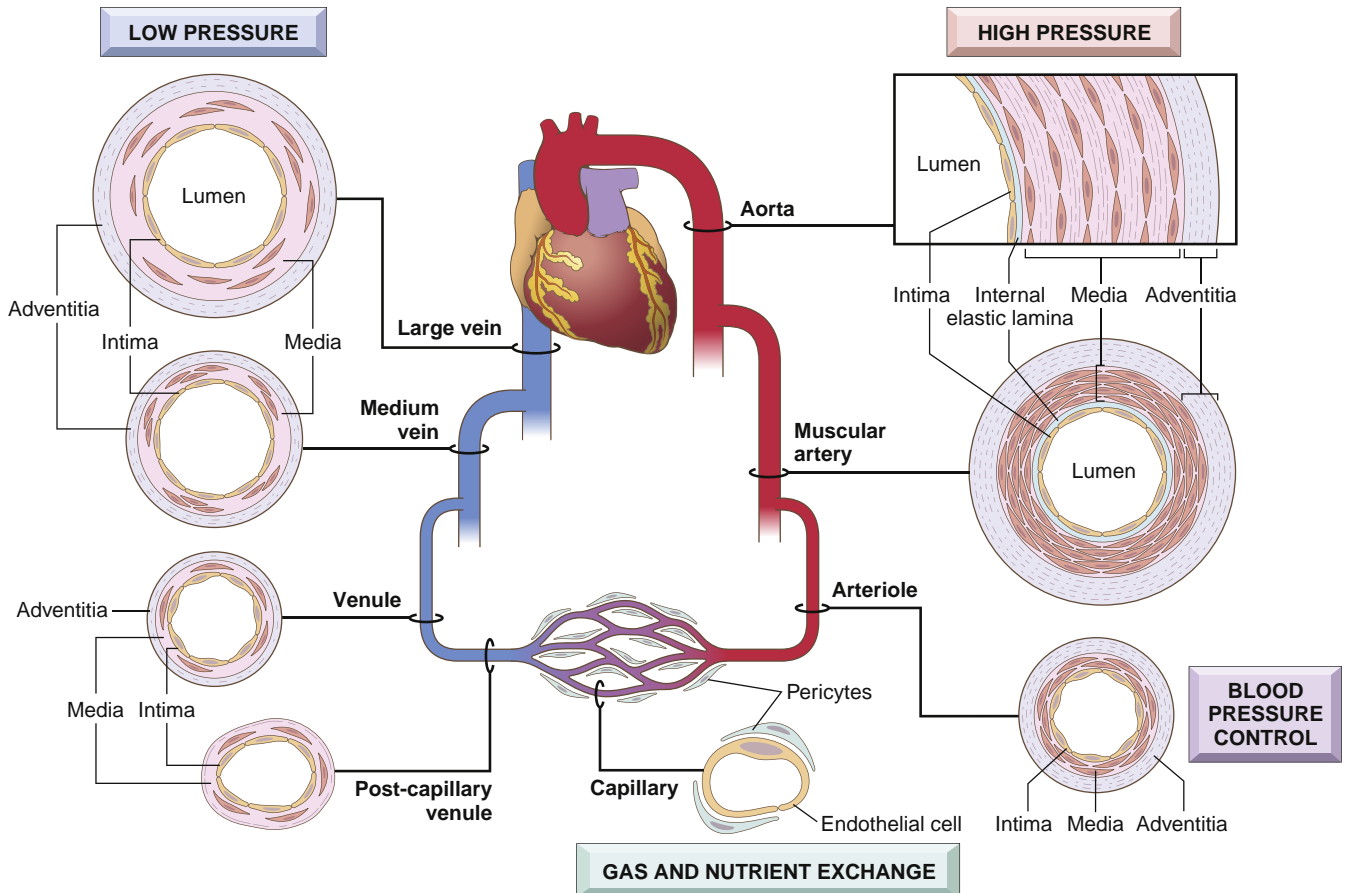
The entire cardiovascular system follows a consistent architectural paradigm with regional differences (Figs. 2.5.2B.2 and 2.5.2B.3). Three basic structural constituents comprise the walls of blood vessels: endothelium, muscular tissue, and extracellular matrix (ECM), including collagen and elastic elements. These tissues are arranged in concentric layers (called *tunica*, meaning coats): (1) the *intima*—consisting of endothelial cells (ECs), subendothelial connective tissue and the internal elastic lamina; (2) the *media*—consisting of smooth muscle cells (SMCs) and elastic laminae, including the external elastic lamina; and (3) *adventitia*—collagenous connective tissue. The histologic composition and organization, as well as the thickness of these three layers, vary characteristically with the physiologic functions performed by specific segments of the vascular system (see Fig. 2.5.2B.3). The layered structure of the blood vessels progressively undergoes segmental differentiation and adaptation to local factors, both mechanical (especially blood pressure, which determines the amount and arrangement of muscular tissue), and metabolic (reflecting the local nutritional needs of the tissues).

As emphasized above, the structure of vessels varies with their functional role. Arteries are usually divided into three major categories. In sequential order from the heart they are: *elastic arteries* (large or conducting arteries), *muscular arteries* (medium or distributing arteries), and *arterioles* (smallest arteries, <200 μm). The elastic arteries include the aorta and its largest primary branches (e.g., common carotid and common iliac arteries). The elastic components of the aorta allow it to expand during ventricular contraction (a phase called *systole*), thereby storing some of the energy of each heart contraction. Between heart beats (*diastole*), elastic recoil of the vascular wall (especially in the aorta) propels blood through the vascular system. Since diffusion of oxygen and other crucial substances from the lumen to the outer layers of the media is inadequate in all but the thinnest walled arteries, small arterioles called *vasa vasorum* course through the adventitia and send capillary twigs into the media. These small vessels provide *perfusion* (i.e., blood flow) to the vascular wall itself. The wall of an artery is generally thicker than that of the wall of a corresponding vein, in order to withstand the higher blood pressures within arteries compared with veins. Veins typically have a larger overall diameter, a larger lumen, and a thinner wall than corresponding arteries with which they course.

Although the circulation must provide high hydrostatic pressure to distribute sufficient blood throughout the body, blood in capillary beds must be delivered under low pressure to protect the capillary walls (which are necessarily thin for exchange) and low flow (to maximize residence time). These conditions of blood flow into capillary beds are facilitated by the high resistance in the arterioles (i.e., the *resistance vessels*). Arterioles are the smallest branches of the arteries, generally between 20 and 100 μm in diameter. They have a



• **Figure 2.5.2B.2** Structure of arteries and veins. Shown are the layers of an artery and vein of approximately equal size. The artery demonstrates the intima (endothelium and internal elastic lamina), media (smooth muscle and external elastic lamina), and adventitia. The vein structure is similar but lacking elastic laminae. Also shown is a cross section of an arteriole and of capillaries (bottom) to demonstrate size and structure, as well as a schematic (on a magnified scale) of a capillary structure (top). (Reproduced from <https://commons.wikimedia.org/w/index.php?curid=65695195>. (Accessed 3 September 2019).)



• **Figure 2.5.2B.3** Schematic of the cardiovascular system with respect to arteries and veins, demonstrating schematically regional progression of vessel sizes, composition, relationships, and different functions. (Reproduced from Mitchell, R., 2015. Blood vessels. In: Kumar, V., Abbas, A., Aster, J. (Eds.), Robbins and Cotran Pathologic Basis of Disease, ninth ed. Elsevier.)

small lumen, and a circular muscular coat with the ability to adjust the degree of contraction of such, thereby restricting lumen diameter and generating high resistance that lowers arterial blood pressure and dampens pulsatility in the downstream vessel. Therefore the capillary microcirculation experiences near-continuous low-pressure blood flow. Subsequently, postcapillary blood flows slowly into the veins, with large lumens and thin walls. Rich in connective tissue, veins are distensible and play an important role as a variable blood reservoir (*capacitance vessels*). Most of the blood volume is contained in the low-pressure circulation (i.e., approximately 75% veins, 20% arteries and 5% capillaries).

Moreover, in this conception of the cardiovascular system, the heart is considered to be a highly specialized blood vessel, i.e., a segment of the circulation, functionally adapted to pump blood, with its media represented by the *myocardium*, containing muscle specialized for rhythmic, strong contractions (*cardiac myocytes*); the *endocardium* as the intima; and the *epicardium* as the adventitia. The *coronary arteries* provide perfusion of blood to the myocardium. They comprise the vasa vasorum of the heart.

Vascular Pathology

Vascular pathology results in disease primarily via one of two principal mechanisms: (1) narrowing (*stenosis*) or complete obstruction of vessel lumens, either progressively (e.g., by intimal hyperplasia or atherosclerosis, see below) or precipitously (e.g., by either thrombosis directly or fragmentation of thrombus with downstream vessel blockage, called *embolism*); and (2) weakening of vessel walls, leading to dilation or rupture. Other forms of embolism include fat (most commonly as a result of massive tissue damage forcing extravascular tissue into the vasculature), atherosclerotic (portions of plaque dislodging from the original site and traveling downstream), mycotic (dislodging of material from a site of infection), and foreign material (e.g., from intravascular procedures or devices).

Vascular Injury and Healing

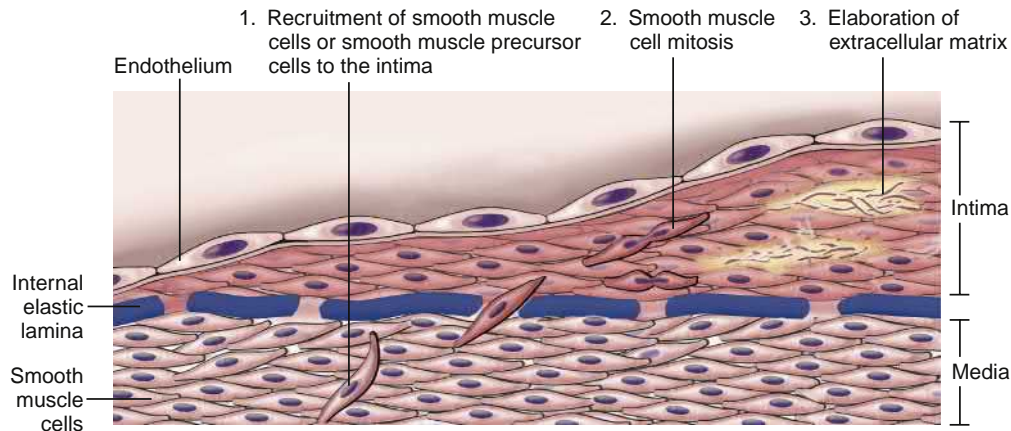
The integrated function of the cells of the vascular walls, endothelial cells (ECs) and smooth muscle cells (SMCs), is critical to the mechanisms by which the vasculature develops and responds to hemodynamic and biochemical stimuli. ECs play a role in the maintenance of a nonthrombogenic blood–tissue interface, the modulation of blood flow and vascular resistance, the metabolism of hormones, the regulation of immune and inflammatory reactions, and the growth regulation of other cell types, particularly SMCs. ECs have substantial phenotypic variability based on anatomic site and dynamic adaptation to local chemical and mechanical cues (e.g., cytokines and shear stress; Gimbrone and García-Cardena, 2013). Thus, healthy ECs can respond to various pathophysiologic stimuli by modulating their usual (*constitutive*) functions and by expressing newly acquired (*inducible*) properties, such as expression of adhesion molecules, procoagulant and anticoagulant moieties,

and major histocompatibility complex molecules, and synthesis and release of cytokines and chemokines, growth factors, vasoactive, and a variety of other biologically active products. Through the production of both relaxing factors (e.g., nitric oxide) and contracting factors (e.g., endothelin), ECs influence the vasoreactivity of the underlying smooth muscle cells. Normal endothelial function is characterized by a balance of these factors and the ability of the vessel to respond appropriately to various pharmacologic stimuli. In contrast, *endothelial dysfunction*, defined as a significantly altered (and indeed pathologic) phenotype that impairs vasoreactivity, induces a surface that is thrombogenic, or is abnormally adhesive to inflammatory cells, and thereby contributes significantly to the initiation of thrombus formation, atherosclerosis, and other vascular lesions, such as intimal hyperplasia (see below). Dysfunctional endothelium may appear normal morphologically (i.e., by conventional microscopy or scanning electron microscopy). Thus, the presence of a histologically observed structurally intact endothelium on the luminal surface of either a native vessel or a vascular replacement does not ensure that the cells comprise healthy and properly functional endothelial cells. Moreover, the demonstration of endothelial dysfunction requires functional analysis demonstrating failure to perform essential endothelial functions (most typically vasodilation and hemostasis), or by demonstration of abnormal gene expression.

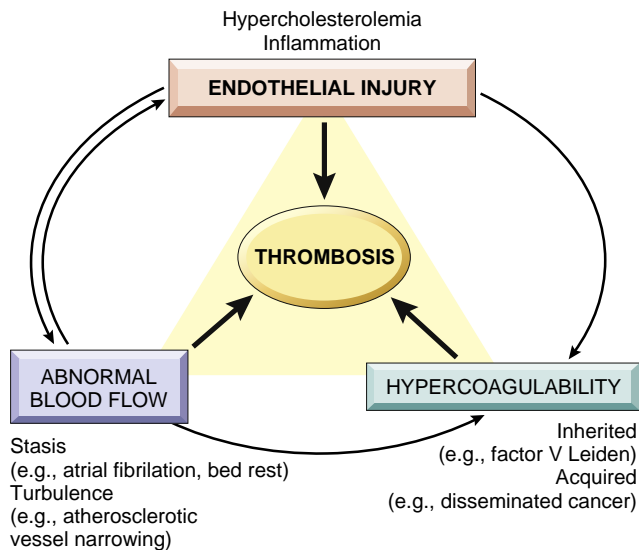
Importantly, vascular injury (whether endothelial denudation, where cells are lost from the luminal surface, or endothelial dysfunction with otherwise structurally intact cells) can stimulate SMC growth by disrupting the physiologic balance between inhibition and stimulation. This process occurs in many adult arteries, and is associated with ongoing mild vascular damage such as turbulent flow, systemic hypertension, and diabetes. Following minor vessel injury, reconstitution of the damaged vascular wall includes the formation of a neointima in which SMCs (1) migrate from the media to the intima, (2) multiply as intimal SMCs, and (3) synthesize and deposit ECM (Fig. 2.5.2B.4), causing intimal thickening. An exaggerated healing response leads to intimal hyperplasia, which, when excessive, can cause stenosis or occlusion of small and medium-sized blood vessels or grafts. Such processes contribute to clinically significant vascular pathology, as in atherosclerosis, in the coronary arteries of heart transplants, and at the junction of a vascular prosthetic graft with the natural vessel to which it is attached.

Thrombosis

Thrombosis is intravascular clot formation. Current thinking considers that the propensity to thrombosis depends on a complex interaction of three key factors, which comprise “Virchow's triad” (Fig. 2.5.2B.5): (1) the nature of the vascular luminal surface (healthy endothelium vs. endothelial injury vs. synthetic biomaterial, with or without attached biological material), (2) the quality of blood flow (laminar vs. turbulent vs. static), and (3) blood coagulation status



• **Figure 2.5.2B.4** Intimal hyperplasia following vascular injury. Smooth muscle cells (SMCs) reconstitute the damaged vascular wall by (1) migrating from the media to the intima, (2) multiplying as intimal SMCs, and (3) synthesizing and depositing extracellular matrix (ECM). The new intimal cells are shown in a different color to emphasize that they have a proliferative, synthetic, and noncontractile phenotype, distinct from medial smooth muscle cells. (Reproduced from Mitchell, R., 2015. Blood vessels. In: Kumar, V., Abbas, A., Aster, J. (Eds.), Robbins and Cotran Pathologic Basis of Disease, ninth ed. Elsevier.)



• **Figure 2.5.2B.5** Virchow's triad. The interactions of endothelial injury, abnormal blood flow, and systemic hypercoagulability in thrombus formation. (Reproduced from Kumar, V., Abbas, A., Aster, J., 2015. Hemodynamic disorders, thromboembolic disease, and shock. In: Kumar, V., Abbas, A., Aster, J. (Eds.), Robbins and Cotran Pathologic Basis of Disease, ninth ed. Elsevier.)

(normal vs. hypercoagulable vs. anticoagulated). Of note, vascular biomaterials are variably thrombogenic due to surface properties, and may alter the quality of local blood flow. These features are of less concern in large grafts (see below), such as in the aorta, where the surface thrombogenicity of the graft may be mitigated by brisk flow. However, in smaller grafts, where the anastomosis to the native circulation may promote turbulent flow, the smaller lumen is more susceptible to obstruction from thrombosis (hence patients with these devices being on long-term anticoagulation medications), and are more prone to obstruction of outflow (*run-off*).

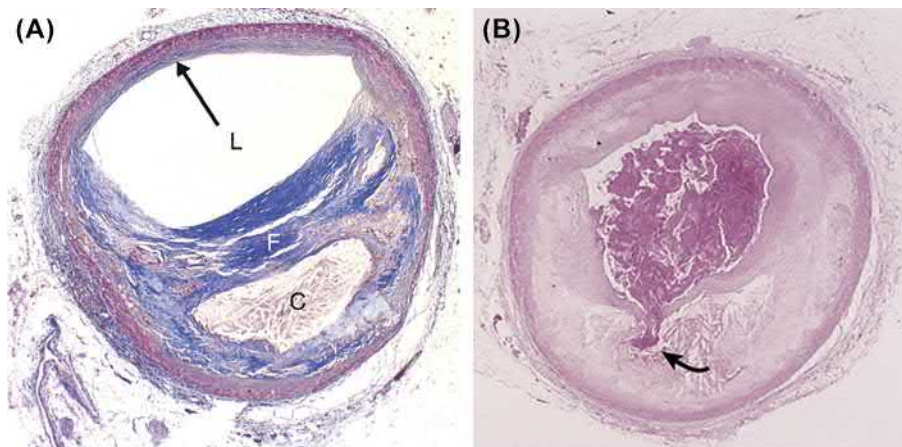
Atherosclerosis

Atherosclerosis, the most common clinically significant vascular pathology, begins in and preferentially affects the intimal layer of arteries. Atherosclerotic lesions (called *plaques*) protrude into and obstruct vascular lumens and/or weaken the underlying media to cause aneurysmal dilation, and/or thrombosis, and/or embolism (Fig. 2.5.2B.6). The early lesions of atherosclerosis comprise a thickening of the intima associated with subendothelial intimal accumulation of lipids; endothelial dysregulation of thrombosis, inflammation, vascular tone, and other functions; and inflammation, a process facilitating additional intimal thickening (Geovanini and Libby, 2018). As the plaque progresses in thickness, or if a thrombus forms, most often due to acute plaque rupture into the lumen or erosion of the overlying endothelium, downstream tissues may receive inadequate oxygen supply (*ischemia*). Ischemia of substantial degree and/or duration may result in *infarction*, i.e., ischemic death, of downstream tissue.

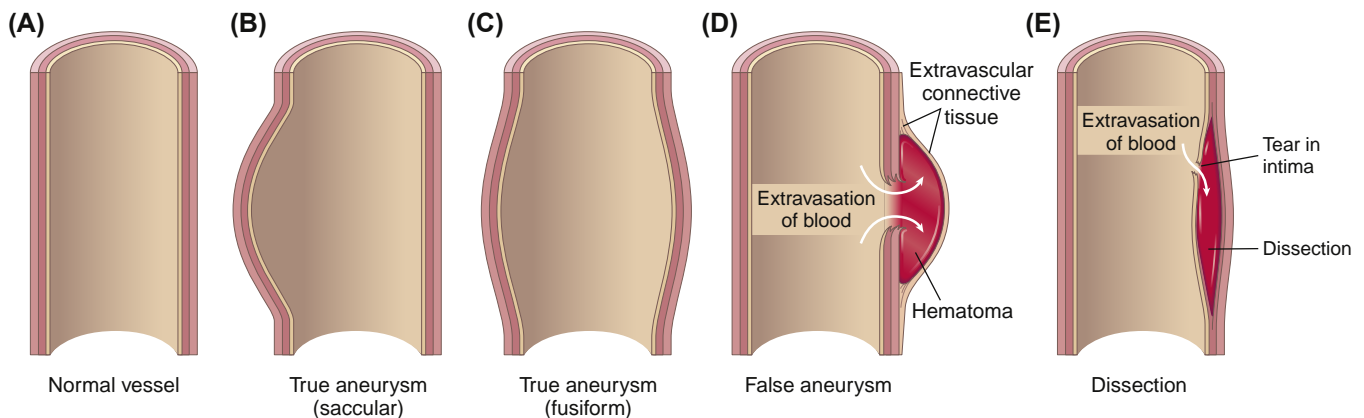
Atherosclerotic plaques develop primarily in elastic arteries (e.g., aorta, carotid, and iliac arteries) and large and medium-sized muscular arteries (e.g., coronary, renal, and popliteal arteries). As such, common clinically relevant sites include the heart (causing coronary artery disease, associated with myocardial infarction or “heart attack”), brain (causing cerebrovascular disease, associated with cerebral infarction or “stroke”), aorta (causing abdominal aortic aneurysm, creating a risk of rupture), kidneys (often resulting in systemic hypertension due to hormonal feedback), and lower extremities (causing peripheral vascular disease).

Aneurysms and Dissections

Aneurysms and dissection are illustrated schematically in Fig. 2.5.2B.7. An aneurysm is an abnormal dilation of a blood vessel that can promote abnormal blood flow and thrombosis. When an aneurysm is bounded by all arterial



• **Figure 2.5.2B.6** Atherosclerotic plaque in the coronary artery. (A) Overall architecture demonstrating a fibrous cap (F) and a central lipid core (C). The lumen (L) has been moderately narrowed. Note the plaque-free segment of the wall (*arrow*). In this section, collagen has been stained blue (Masson trichrome stain). (B) Coronary thrombosis superimposed on an atherosclerotic plaque with focal disruption of the fibrous cap (*arrow*), triggering fatal myocardial infarction. ((A) Reproduced from Mitchell, R., 2015. Blood vessels. In: Kumar, V., Abbas, A., Aster, J. (Eds.), Robbins and Cotran Pathologic Basis of Disease, ninth ed. Elsevier. (B) Reproduced from Schoen, F.J., 1989. Interventional and Surgical Cardiovascular Pathology: Clinical Correlations and Basic Principles. WB Saunders, p. 61.)



• **Figure 2.5.2B.7** Patterns of vessel wall weakening. (A) Normal vessel. (B) and (C) Types of true aneurysm, where the wall bulges outward and may be attenuated but is otherwise intact. (D) False aneurysm, where the wall is ruptured, and there is a collection of blood (hematoma) that is bounded externally by adherent extravascular tissues. (E) Dissection, where blood has entered (dissected) the media of the vessel wall; although this is shown as occurring through a tear in the lumen, dissections can also occur by rupture of the vessels of the vasa vasorum within the media. (Reproduced from Mitchell, R., 2015. Blood vessels. In: Kumar, V., Abbas, A., Aster, J. (Eds.), Robbins and Cotran Pathologic Basis of Disease, ninth ed. Elsevier.)

wall components on all sides it is called a true aneurysm. In contrast, a false aneurysm (also called *pseudoaneurysm*) is a breach in the vascular wall leading to an extravascular *hematoma* (i.e., collection of blood) that communicates with the intravascular space (“pulsating hematoma”) but is contained within the extravascular tissue. This is in subtle contrast to *rupture*, where the blood continues to flow outside of the vessel wall into adjacent tissue.

A *dissection* occurs when blood enters the wall of the artery with the formation of a blood-filled channel within the artery wall, called a *false lumen*, a space where the blood remains under pressure but does not usually contribute to downstream circulation. Dissections are frequently initiated by an intimal tear providing passage to the media. Dissections can also rupture.

Aneurysms and dissections typically have the greatest clinical impact when they involve the aorta. Aortic aneurysms result in about 175,000 deaths a year globally (GBD 2013 Mortality and Causes of Death Collaborators, 2015). Aortic dissections affect an estimated 2.0–3.5 people per every 100,000 every year, with incidence possibly rising (Olsson et al., 2006). Although aortic dissections are more common in men, dissections in women can occur during pregnancy (Wanga et al., 2016) and sometimes thereafter.

Atherosclerotic aneurysms occur most frequently in the abdominal aorta (*abdominal aortic aneurysm*, often abbreviated to AAA). The most important clinical consequence of an AAA is rupture, causing hemorrhage into the abdomen caused by aneurysm. The risk of rupture is directly related to the size of the aneurysm, varying from zero for a small AAA

(less than approximately 4 cm in diameter), to 33% per year for those larger than 7 cm (Sakalihasan et al., 2018). The treatment of abdominal and thoracic aortic aneurysms has been largely open surgery with a tubular textile graft. Treatment is evolving toward endoluminal approaches using stent grafts (see below) for many patients.

In contrast, aneurysms in the ascending/thoracic aorta and in many visceral sites are associated with hereditary predisposition to wall weakening through aberrant extracellular matrix metabolism or smooth muscle cell dysfunction, such as in Marfan syndrome (affecting up to 1 in 5000 individuals; National Organization for Rare Disorders, 2017), Loays-Dietz syndrome, Ehlers-Danlos syndrome, or other forms of fibromuscular dysplasia. Ascending aortic aneurysms are also associated with bicuspid aortic valve, vascular inflammation (*vasculitis*), and prior surgery. Treatment again largely relies on surgical repair, frequently involving placement of a textile graft.

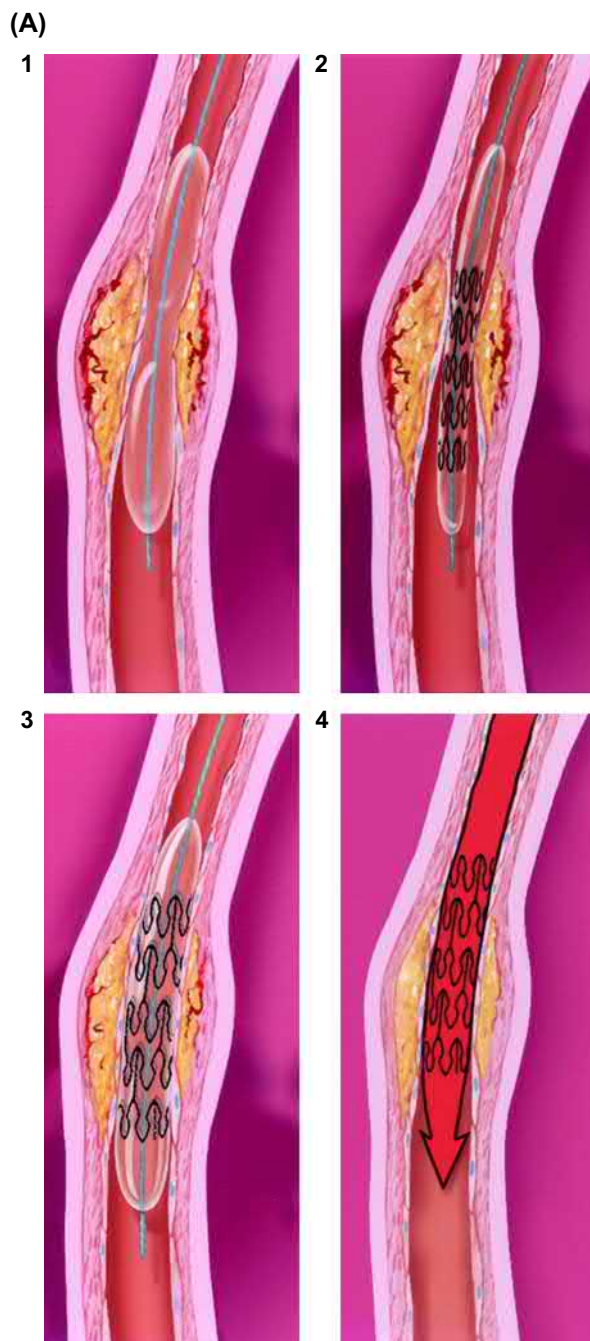
Vascular Devices and Biomaterials

To address the pathologies discussed above, a number of devices and biomaterials have been developed to restore a state that approximates normal. Many of these have focused on coronary artery disease, given the significant epidemiologic burden, but uses in other vessels are expanding rapidly.

Angioplasty and Endovascular Stents

Percutaneous transluminal coronary angioplasty (PTCA) and endovascular stents are used to restore blood flow through a diseased portion of the coronary circulation in patients with acute (typically due to thrombus) or chronic (typically due to progressive atherosclerosis) occlusion causing *stable angina* (chest pain due to cardiac ischemia occurring during exercise and resolving at rest), *unstable angina* (similar chest pain but also occurring at rest), or acute myocardial infarction (heart attack) (see Fig. 2.5.2B.8A). In PTCA, a procedure developed and implemented first by Andreas Grüntzig in the 1970s (Grüntzig and Hopff, 1974; Barton et al., 2014), a long catheter is passed retrograde from within the femoral artery up the aorta to the openings of the coronary arteries that arise from the aorta immediately distal to the aortic valve cusps. Using radio-opaque dye and fluoroscopy, areas of stenosis can be identified (called a coronary catheterization, or “cath,” study). A deflated balloon is passed over a guide-wire to a site of stenosis, where the balloon is inflated using progressive and substantial expansile force (~10 atm). PTCA-induced enlargement of the lumen and increased blood flow occurs by plaque reduction via compression, embolization, or redistribution of the plaque contents and by overall mechanical expansion of the vessel wall (Virmani et al., 1994).

In a minority of patients, short-term failure of this procedure (i.e., closure of the treated vessel within hours to days) occurs via one or more of several mechanisms, including



• **Figure 2.5.2B.8** Catheter-based interventions for opening occluded coronary arteries. (A) Balloon angioplasty and endovascular stenting: (1) percutaneous transluminal coronary angioplasty (PTCA); (2) stent placement at a site of prior PTCA; (3) balloon-mediated expansion of the stent; (4), balloon deflated and removed. (B) Metallic stents on expanded balloons. ((A) Reproduced by permission from Michaels, A. D. and Chatterjee, K. (2002). Cardiology patient pages. Angioplasty versus bypass surgery for coronary artery disease. *Circulation* 106: e187-190. (B) Reproduced by permission from Al Suwaidi, J., Berger, P.B., Holmes, D.R., 2000. Coronary artery stents. *JAMA* 284, 1828-1836.)

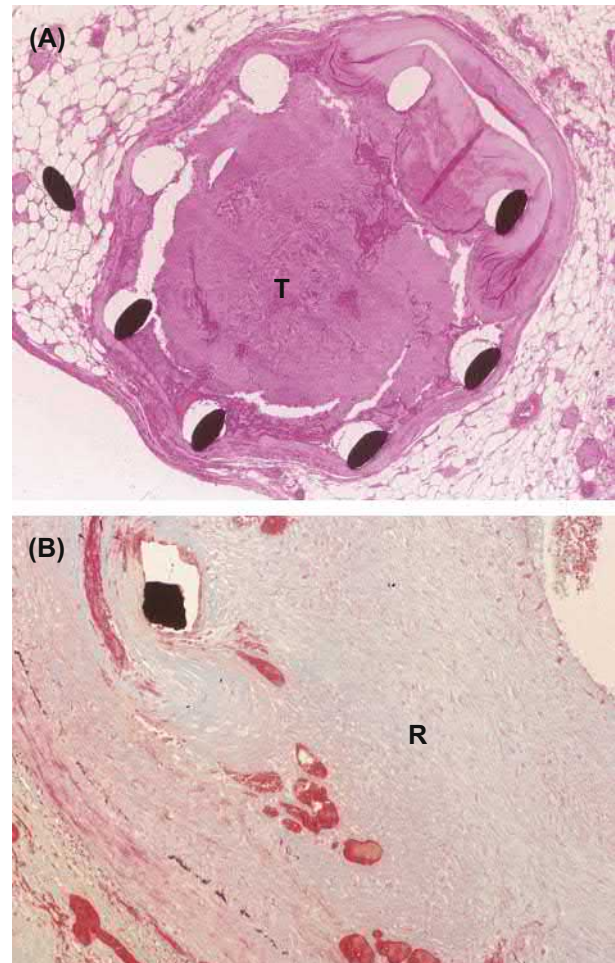
elastic recoil of the vessel wall stretched by the balloon, thrombosis at the site of angioplasty, and acute dissection (i.e., blood within the vessel wall itself) at the site of angioplasty. The major problem, however, is progressive, proliferative restenosis due to intimal hyperplasia, which occurs in 30%–40% of patients, most frequently within the first 4–6 months (Haudenschild, 1993).

In current practice, virtually all patients undergoing PTCA also receive a stent, an expandable tube of metallic mesh that splints open the vessel wall (Fig. 2.5.2B.8). Stents have been used in patients since the late 1980s. Stents preserve luminal patency by limiting elastic recoil and mechanically preventing vascular spasm. They provide a scaffold to support the disrupted vascular wall and increase blood flow, thus minimizing thrombus formation and restenosis. Endoluminal stents also provide a means of delivering any localized therapy intended to reduce restenosis, such as a pharmacologic agent or radiation (Daemen et al., 2007a,b).

Available stents range from 2.5 to 6 mm in diameter and from 8 to 50 mm in length. Deployment of a stent involves circumferential expansion of the stent in apposition to the inside surface of the coronary artery. To accomplish this, the stent is positioned across a stenotic lesion, which has usually been predilated with a balloon, with the aid of coronary catheterization. The first coronary stents developed for clinical use were bare-metal stents (BMS), composed of 316L stainless steel, which required balloon expansion, or nitinol, an alloy of nickel and titanium that is self-expanding by virtue of its “shape memory” characteristics (i.e., the stent is compressed into the delivering catheter at room temperature, and then spontaneously recovers its original, undeformed, expanded stent shape upon removal of the delivery sheath at body temperature).

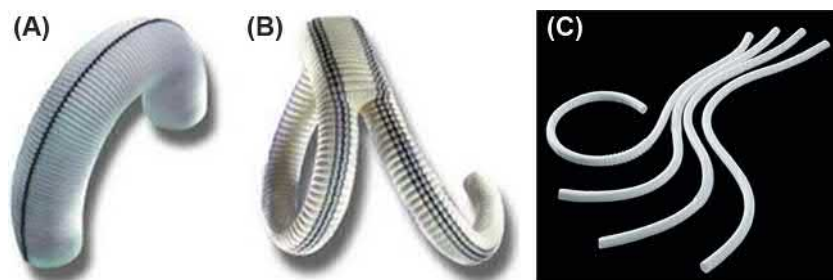
Development has focused on permitting stents to become more flexible and more easily delivered and deployed to a target site, allowing the treatment of a greater number and complexity of lesions. The choice of stent is based on several factors, including the characteristics of a given plaque, such as diameter, length, and location within the coronary anatomy, and the experience of the interventional cardiologist with a particular stent. The use of BMS demonstrated that the most important early complication of stenting is thrombosis, which occurs in 1%–3% of patients within 7–10 days of the procedure (Fig. 2.5.2B.9A). This complication has largely been overcome by aggressive multidrug treatment inhibiting platelet and soluble clotting factor function. In this context, the major long-term complication of bare-metal stenting is in-stent proliferative restenosis (Fig. 2.5.2B.9B), again a form of exaggerated tissue healing and intimal hyperplasia, which occurs in as many as 50% of patients within 6 months of receiving a BMS (Virmani and Farb, 1999).

Thus, the proliferative restenosis that frequently occurs after PTCA alone was found not to be prevented by stenting with BMS. With the goal of eliminating this intimal thickening, drug-eluting stents (DESs) were developed. The first generation of DESs were stents coated with a



• **Figure 2.5.2B.9** Stent complications. (A) Early thrombosis (T) associated with a metallic coronary artery stent. (B) Late proliferative restenosis with fibrous tissue (R) filling the lumen inside of the stent. Black is stent wire cross sections in the histologic sections. (Reproduced by permission from Schoen, F.J., Edwards, W.D., 2001. Pathology of cardiovascular interventions. In: Silver, M.D., Gotlieb, A.I., Schoen, F.J. (Eds.) Cardiovascular Pathology, third ed. Churchill Livingstone.)

polymer containing either rapamycin (sirolimus) or paclitaxel. Rapamycin, a drug used for immunosuppression in solid organ transplant recipients, inhibits proliferation, migration, and growth of fibroblasts and smooth muscle cells, and blocks extracellular matrix synthesis. Along with its antiinflammatory properties, this drug targets the major mechanisms of restenosis. Paclitaxel, a drug used in the chemotherapeutic regimens for several types of cancer, also has similar anti-smooth muscle cell activities. These drugs are embedded in a polymer matrix (such as a copolymer of poly-n-butyl methacrylate and polyethylene-vinyl acetate or a gelatin-chondroitin sulfate coacervate film) that is coated onto the stent. The drug is released by diffusion and/or polymer degradation over varying periods of time that can be engineered by the specifics of the polymer–drug system. Drug-eluting stents have virtually eliminated restenosis over time periods of 2 years and longer, and represent a major breakthrough in the treatment of coronary artery disease. Although early DES had a problem with late thrombotic



• **Figure 2.5.2B.10** Different types of synthetic vascular grafts. (A) Dacron aortic interposition graft (Terumo). (B) Dacron aorto-iliac graft (Terumo). (C) ePTFE small vessel grafts (Gore).

stenosis, newer generations of stents use thinner struts and improved polymers to significantly decrease this risk of thrombosis, while reducing the need for long-term anticoagulant medications (Torii et al., 2020). Also being investigated is the use of drug-eluting balloons in combination with bare metal stents to combine the advantages of both strategies (Richelsen et al., 2016).

Another development is resorbable/biodegradable stents (RBSs; Hytönen et al., 2018; Lee and de la Torre Hernandez, 2018). In contrast to the permanent presence of a foreign body in BMSs and DESs, RBSs provide a scaffold to support vessel expansion and then ultimately disappear by resorption of the foreign material that may potentiate a thrombotic event. RBS designs may also incorporate the controlled release of antiproliferative agents. The eventual disappearance of RBSs obviates interference of the device on noninvasive radiologic diagnostic imaging such as cardiac magnetic resonance imaging (MRI) and computed tomography (CT). Since RBSs may potentially mitigate the problems of late thrombosis, vessel distortion, and interference with surgical coronary arterial revascularization, they have been the subject of extensive research and development efforts in recent years. Clinical trials and even regulatory approval have occurred with both degradable polymeric (e.g., poly-L-lactide) and metallic (Mg alloy) stents. One of the former stent systems (Abbott's Absorb bioresorbable vascular scaffold) has been removed from the market after regulatory approval due to low clinical adoption.

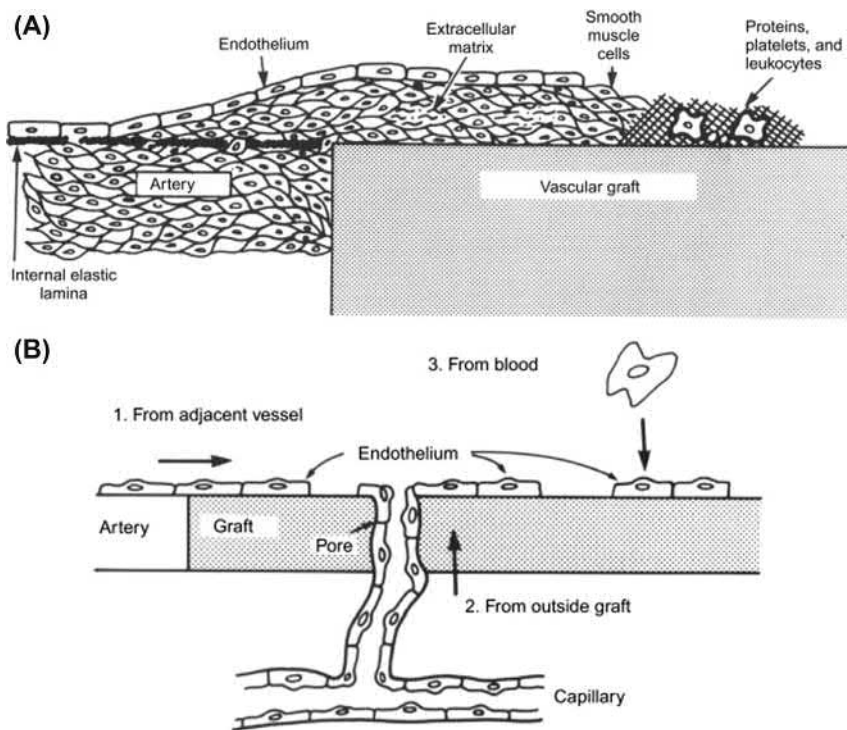
Stents are also used to manage stenosis in other arterial sites, such as the carotid artery, with many of the same principles (Morr, 2014). These approaches include use in large branch vessels of the aorta, such as the renal, celiac, and mesenteric arteries, as well as smaller vessels such as the femoral arteries in the legs. Over 1.8 million stents are placed annually in the United States alone, with over half of these being for coronary artery disease (iData Research, 2018).

Vascular Grafts

Vascular grafts provide new conduits to otherwise compromised components of the vasculature. The most important roles of such grafts are in aneurysm or dissection, particularly in the aorta; bypass of obstructed vessels, such as in the coronary or peripheral arteries; and to permit repetitive vascular access for hemodialysis. The clinical performance of

a vascular graft depends primarily on its type, biomaterial, anatomic location, and diameter. In general, large-diameter (12–18 mm) synthetic fabric grafts currently used in high-flow, low-resistance locations such as the aorta, the iliac and proximal femoral arteries, and aorto-femoral bypass generally have good clinical outcomes, with 5–10-year patency rates of 90% (Clagett, 2002). In contrast, small-diameter synthetic vascular grafts (less than 6–8 mm in diameter) generally perform less well with 5-year patency less than 50%. Moreover, tissue grafts (especially autologous tissue) generally outperform synthetic grafts in small-diameter locations. The tissue graft most frequently used is a saphenous vein from the patient needing the bypass, which is surgically moved to the site needed to bypass blockages, for example, for coronary artery bypass grafting or in the extremities for femoropopliteal bypass grafting. Other natural vessels such as the internal mammary artery may be used to bypass some blockages in the coronary circulation (typically vessels <4 mm), with good results (approximately 90% patent at 10 years postoperatively).

Contemporary synthetic vascular grafts are typically fabricated from polyethylene terephthalate (PET; Dacron, DuPont), typical for larger grafts, or polytetrafluoroethylene (PTFE; Teflon, Chemours) or expanded polytetrafluoroethylene (ePTFE, Gore-Tex, Gore), typical for grafts <8 mm diameter (Fig. 2.5.2B.10). When being used to bypass a stenosis, the graft is sewn onto the native circulation proximally and distally to the blockage, creating a new branch “vessel” and providing an intact, alternate path for blood. In aneurysm and dissection, the graft is sewn proximally and distally to the pathologic segment on the inside of the vessel and passed endoluminally, limiting the flow of blood to a lumen approximating physiologic size. In the case of aneurysm, a large portion of the dilated space is now excluded from the blood flow, creating a space for hematoma, seroma, and/or infection outside the graft (see below). In the case of dissection, the graft ideally excludes further blood flow into the false lumen and/or supports the aortic wall at the site of the dissection, reducing pressure in the rupture-prone false lumen and again directing blood flow through a space approximating physiologic size. The excluded space in this event is primarily the false lumen, which will typically heal and form scar tissue in the original vessel wall. As many of these grafts are placed into large vessels such as the aorta, it is necessary to also ensure blood flow to multiple branch



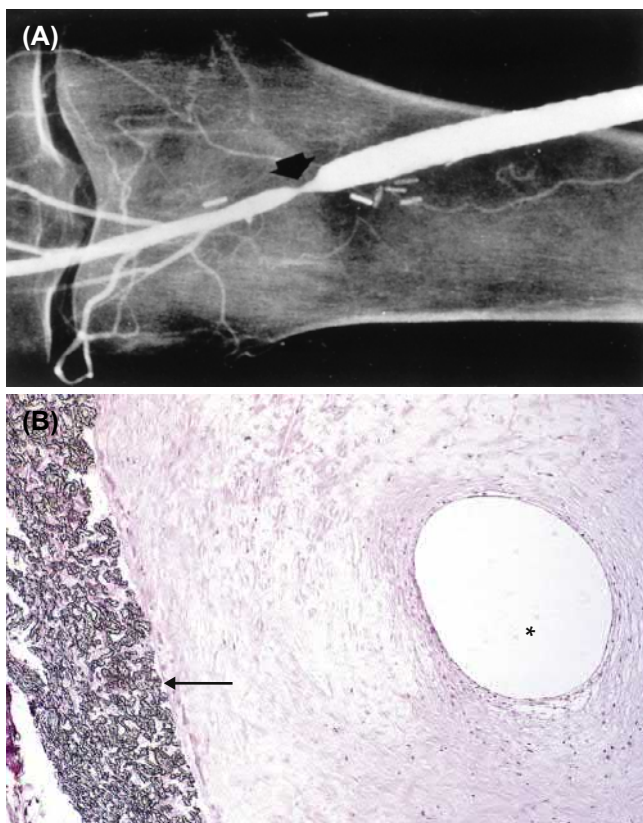
• **Figure 2.5.2B.11** Vascular graft incorporation. (A) Schematic diagram of pseudointima (platelet-fibrin aggregate, right) and neointima (smooth muscle cells and endothelial cells, left) formation at the site of anastomosis between a native artery and a graft. (B) Possible sources of endothelium on the blood-contacting surface of a microporous vascular graft. ((A) and (B) Reproduced by permission from Schoen, F.J., 1989. *Interventional and Surgical Cardiovascular Pathology: Clinical Correlations and Basic Principles*, WB Saunders; Philadelphia, PA.)

vessels. This is accomplished by sewing the branch vessels directly into the graft at appropriate anatomic locations, or by bridging these anastomoses with additional smaller grafts (Kuo and Han, 2017).

To ensure a high likelihood of clinical success and long-term patency, vascular grafts must have mechanical compliance consistent with that of the normal and diseased vessels to which they will be anastomosed, be resistant to thrombus to prevent occlusion, resistant to tissue overgrowth causing intimal hyperplasia (particularly at an anastomosis), have a sufficient level of suturability to facilitate placement, and be fatigue resistant (i.e., durable). When a synthetic graft is implanted and exposed to the blood, the luminal surface of the graft becomes coated with a film of plasma proteins and subsequent deposition of cellular elements and products of the coagulation cascade, as discussed in detail in other chapters of this book. With extended time *in vivo*, the deposition develops into a platelet-fibrin-rich layer termed a *pseudointima*. Over time, endothelial cells may coat this layer, serving as a nonthrombogenic surface, creating a *neointima* (Fig. 2.5.2B.11A). Humans have limited ability to endothelialize vascular grafts, however, with confluent endothelium covering only a 10–15 mm zone adjacent to the anastomosis in typical grafts, while the remainder of the graft will be covered only in pseudointima even after long-term implantation. A graft covered completely on its internal surface by endothelium is said to be “healed.” Species differences in

regenerative capacity to provide luminal tissue coverage of vascular grafts have also been identified, something that is of high importance for the selection of appropriate animal models (Zilla et al., 2007).

One method to address lack of extensive neointima formation within most of the graft has been to create fabric grafts that have sufficient transwall porosity to foster entry of endothelial cells from surrounding small vessels in external tissues of the recipient into the entirety of the lumen (Fig. 2.5.2B.11B). To prevent early hemorrhage through these pores, however, highly porous grafts may be impregnated during fabrication with connective tissue proteins to aid clotting, or are precoated with the patient's own blood prior to implantation. However, many clinical vascular grafts are impervious in order to obviate hemorrhage (for example, the widely used ePTFE grafts typically have a limited porosity that is insufficient to permit cellular ingrowth). Thus, direct endothelial seeding of vascular grafts has been used, with some success, and there is considerable current interest in designing grafts that can best utilize the potential of circulating endothelial cell precursors to cover grafts, but this has not yet been realized (Zhang et al., 2014). Another approach is vascular tissue engineering, where *ex vivo* sources of cells are being explored to seed or entirely construct vascular grafts, or a porous absorbable polymer graft is implanted with the intent that endogenous (recipient) cells would replace the polymer by layered vascular structural



• **Figure 2.5.2B.12** Anastomotic intimal hyperplasia of a synthetic graft. (A) Angiogram demonstrating constriction (*arrow*). (B) Photomicrograph demonstrating ePTFE graft (*arrow*) with prominent intimal proliferation and very small residual lumen (*). (Reproduced by permission from Mitchell, R., 2015. Blood vessels. In: Kumar, V., Abbas, A., Aster, J. (Eds.), Robbins and Cotran Pathologic Basis of Disease, Ninth ed. Elsevier; (A) Original courtesy of Antony D. Whittemore, Brigham and Women's Hospital, Boston, MA.)

elements (Pashneh-Tala, 2016; Wissing, 2017; Song, 2018; Stowell and Wang, 2018).

The tissue reaction to synthetic vascular grafts may include the formation of exuberant fibrous tissue in the lumen of the anastomotic site as an overactive physiologic repair response (Fig. 2.5.2B.12). This reaction, called *intimal hyperplasia*, occurs in clinical and experimental vascular grafts, especially those less than 8 mm in diameter. Intimal hyperplasia results primarily from smooth muscle cell migration, proliferation, and extracellular matrix elaboration following and possibly mediated by acute or ongoing endothelial cell injury. Contributing factors include: (1) surface thrombogenesis, (2) delayed or incomplete endothelialization of the fabric, (3) disturbed flow across the anastomosis, and (4) mechanical factors (i.e., compliance mismatch) at the junction of implant and host tissues. Intimal hyperplasia tends to develop predominantly at or near anastomoses, particularly at the distal site in both synthetic and tissue vascular prostheses. In tissue grafts, intimal hyperplasia is often diffuse, leading to progressive luminal reduction of the entire graft.

An implanted graft becomes encapsulated in the surrounding connective tissue and elicits a typical foreign body

reaction, which consists of a layer of foreign body inflammation containing giant cells adjacent to the material, covered by collagen, fibroblasts, blood vessels, and other cellular and extracellular connective tissue elements. This response can be exuberant, resulting in scar tissue extending into and possibly disrupting surrounding structures, inflammation eroding into surrounding structures or a space being created that can become filled with blood (hematoma) or fluid (seroma). A similar healing response can also be seen in the space excluded from an aneurysm during repair (see above), which again can develop hematoma and/or seroma. Both hematomas and seromas create sites predisposed to infection.

Prophylactic perioperative systemic antibiotics limit infection of implanted vascular prostheses generally to 6% of patients or less, and grafts are sometimes impregnated with antibiotics to further prevent infection. Early infections are typically related to contamination that occurs during the surgical procedure itself or to perioperative complications such as wound infection. Late infections usually occur secondary to seeding from the blood of the synthetic material in patients with low-grade bacteremia, often secondary to dental or gastrointestinal procedures. Since the anastomotic suture line is usually involved, an infected vascular graft may have a partially disrupted connection to the natural artery; thus, rupture with hemorrhage at the graft site may bring the patient to clinical attention. Surgical removal of an infected graft is usually necessary to address a graft infection.

Progressive deterioration of a synthetic vascular graft can cause mechanical disruption at the anastomotic site or within the body of the prosthesis leading to aneurysm formation or the formation of an external collection of blood due to rupture (called a false aneurysm; see Fig. 2.5.2B.7). The incidence of long-term graft deterioration is small but unknown. Delayed failure is associated with chemical, thermal, or mechanical damage to polymeric yarn materials during manufacture, fabric defects induced during manufacture (e.g., dropped stitches) or during insertion (even “atraumatic” vascular clamps can damage yarn fibers), and potentially postoperative biodegradation of graft material.

Worthy of a separate mention, grafts are also used in hemodialysis, which helps maintain a majority of patients with end-stage renal disease. This requires repeated access to the patient's circulation (Scott and Glickman, 2007; Lee and Misra, 2016). In the United States alone, an estimated 468,000 patients were on dialysis in 2016 (National Institute of Diabetes and Digestive and Kidney Diseases, 2016). The major approaches to repetitive vascular access are the biological arteriovenous fistula (AVF) or the synthetic arteriovenous graft (AVG). Owing to high rates of AVF maturation failure and recurrent stenosis of AVGs (owing to thrombosis, intimal hyperplasia, or infection), as well as the paucity of effective therapies for these two major problems, vascular access dysfunction remains a major cause of morbidity and mortality in hemodialysis patients, often resulting in subsequent surgery to repair the site. Hemodialysis is also discussed in Chapters 2.5.3 and 2.6.6.



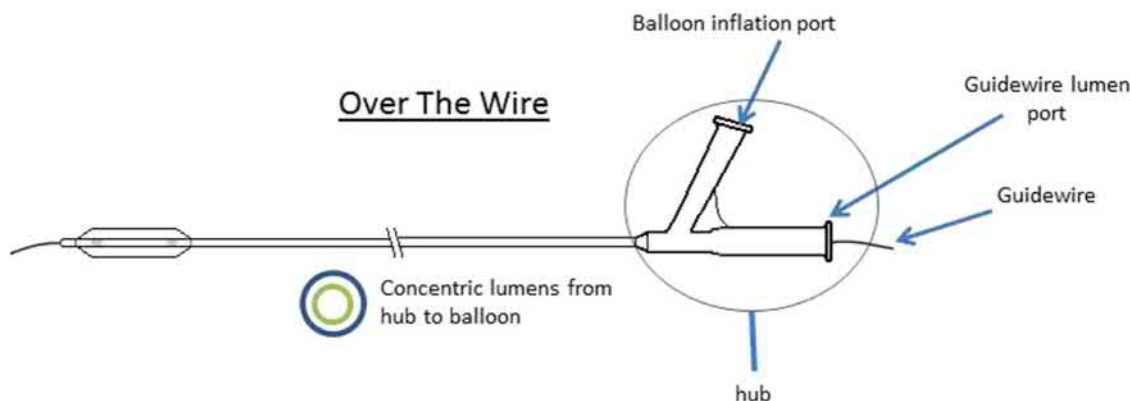
• **Figure 2.5.2B.13** Stent grafts. (A and B) Modular bifurcated stent grafts with a nitinol exoskeleton and polyester or ePTFE linings; (A) relies on radial force to fix the device and (B) has proximal barbs to anchor the graft. (C) PTFE graft with an internal cobalt chromium alloy stent. (D) Multiple segment graft with external stainless steel frame. (E) High-power photomicrograph of a cross section of a well-healed experimental stent graft device explanted from a dog aorta; the lumen is widely patent, and the fabric and metal components are visible. ((A–D) Reproduced by permission from Baril, D.T., 2007. *Surgery insight: advances in endovascular repair of abdominal aortic aneurysms*. *Nat. Clin. Pract. Cardiovasc. Med.* 4, 206. (E) Original courtesy of Jagdish Butany, MD, University of Toronto.)

Endovascular Stent-Grafts

Mortality rates of abdominal aortic aneurysm surgery vary from less than 10% for nonruptured aneurysms and up to 80% for leaking or ruptured aneurysms. This high mortality led to the development of less invasive methods for treatment of aortic aneurysms and other aortic abnormalities, especially for patients who are not good candidates for conventional open surgery. Endovascular aneurysm repair (EVAR) performed through percutaneous vascular access can provide effective and durable repair, improved morbidity and mortality relative to open surgical correction, and reduced hospital costs, particularly for intact aneurysms

(Patel, 2016). Originally developed for treatment of abdominal aortic aneurysms, EVAR has been extended to thoracic endovascular aortic graft repair.

EVAR uses an endovascular device, often called a stent-graft, which consists of a metallic stent covered by a cloth sleeve that resembles a vascular graft (Fig. 2.5.2B.13). These stent-grafts are generally constructed of a stainless steel or nitinol frame covered by polyester or ePTFE, either on the luminal or abluminal (outside) aspect of the metallic stent. Stent grafts are deployed endovascularly either as self-expanding units or over an inflatable balloon. The stent used for a given application is selected by the diameter, length, and geometry of the lesion and location of side



• **Figure 2.5.2B.14** Over-the-wire balloon catheter structure. The guide wire passes through the center of the catheter lumen, and the balloon is passed over the wire, still within the catheter lumen. (Image adapted from https://commons.wikimedia.org/wiki/File:OTW_Vs._Rx.jpg.)

braches or branch points. These stents hold the graft in place via tension against the vessel wall and/or by metallic hooks that become embedded into the vessel wall, removing the requirement for sutures. The fabric provides a mechanical barrier to prevent intravascular pressure from being transmitted to the weakened wall of the aneurysm, thus excluding the aneurysm from the flow of blood, just as with surgically implanted grafts. Stent-grafts may be straight, typically with both ends anchored to the aorta; bifurcated, with the proximal end typically attached to the aorta and the graft limbs fastened to the iliac arteries; or branched in more complex fashion using carefully placed fenestrations and iterative placement of stent-grafts (Kuo and Han, 2017; Pearce et al., 2017; Lindström et al., 2019).

Although EVAR has been a significant advance in aneurysm management for some patients, complications continue to occur and EVAR technology development is ongoing (Belvroy, 2018). Complications related to the device include (1) thrombosis; (2) obstruction owing to device twisting, kinking, or oversizing; (3) infection; (4) graft dilation or structural failure with tear or fracture; (5) device migration or change in alignment; (6) erosion of the graft into/through the arterial wall; and/or (7) aneurysm expansion or rupture. These complications may be further associated with *endoleak*, the persistence of blood flow outside the lumen of the endoluminal graft but within the aneurysm sac. This may result from an incomplete “seal” between the endograft and the wall of the aorta, inadequate connection between components of modular prostheses (i.e., failed prosthesis-to-prosthesis anastomosis), fabric defects or porosity, or retrograde blood flow from patent aortic side-branches. This may further promote aneurysm enlargement, graft damage, and graft migration. Many of these can warrant immediate or delayed conversion to an open surgical repair, with the further risks and complications of that procedure.

Other Vascular Devices

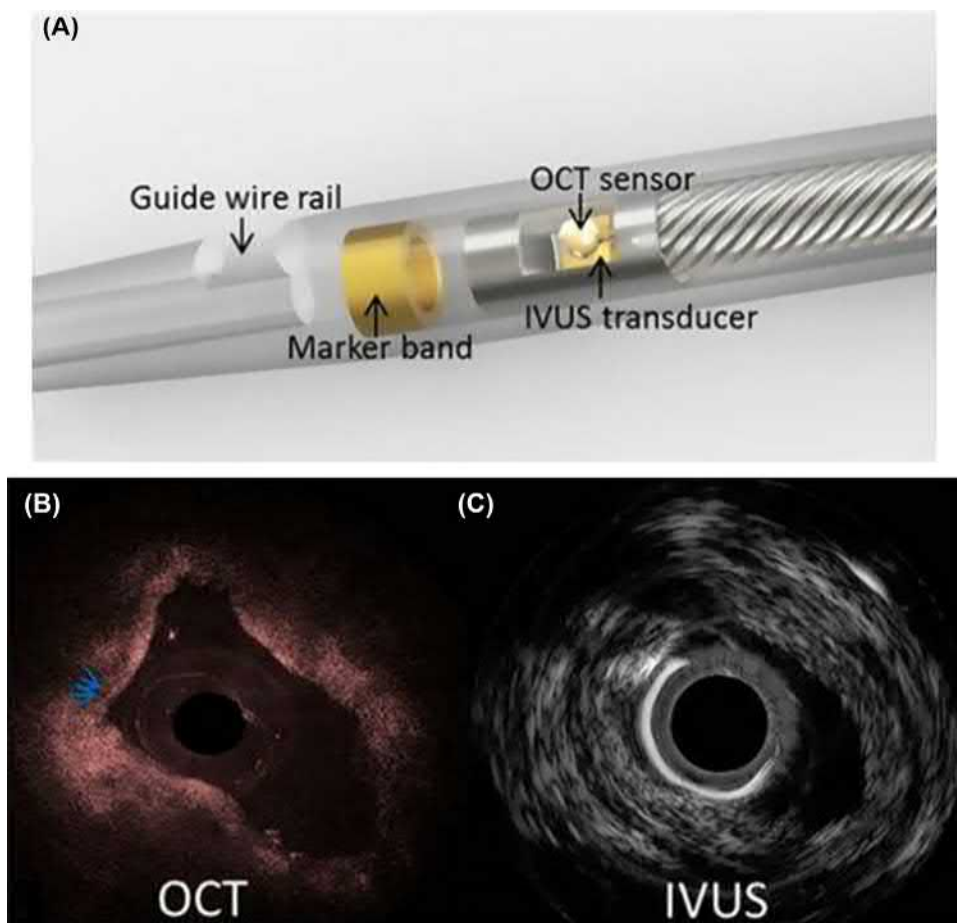
Endovascular Catheters

Perhaps the most ubiquitous vascular medical device, catheters, mentioned numerous times above and in other

chapters, are tubes of various types, in this context specifically for communicating with the vascular space. As such, they are small-diameter, typically flexible devices, generally made of polymers, most commonly polyurethanes or silicone. They are often passed through an outer sheath to facilitate entry into the vasculature, and are typically guided by a steerable wire, or *guide wire*, passed through the catheter lumen (Fig. 2.5.2B.14). As needed, this guide wire can be removed while leaving the catheter in place. The inner lumen, where the guide wire is or was, can be used to deliver varying materials, such as nutritional or metabolic (e.g., salt) support, medications (such as agents to promote thrombus regression or vascular dilation), other medical substances, or additional devices. These catheters are typically left in the body for only a very short duration (minutes to days), except in critically ill patients in whom central venous lines may be indwelling for longer duration. The major complication in such patients is catheter-based infection (Bell, 2017).

Diagnostic Catheters

Catheters may be used in combination with sensors as diagnostic devices, such as to measure blood pressure, temperature, or oxygenation of sites not directly accessible by ex vivo devices. Catheters can also be used to deliver radio-contrast agents to facilitate improved visualization of vascular structures; as vessel wall thickness is typically below the resolution of ex vivo imaging techniques, these contrast agents facilitate detailed imaging of the vessel lumen. Common techniques include fluoroscopy (a continuous real-time X-ray-based technique), computed tomography (CT, an X-ray technique to visualize in three dimensions), or magnetic resonance imaging (MRI, a radiofrequency technique also used to image in three dimensions). When specifically applied to vessels, terminology for these techniques is often adapted to use the term angiography, such as with CT angiography (CTA) or magnetic resonance angiography (MRA). These techniques allow for vessel lumens to be assessed for absence of flow into expected regions (e.g., occlusions or narrowing of vessel lumens) as well as to identify blood passage into inappropriate sites,



• **Figure 2.5.2B.15** Combined optical coherence tomography (OCT)/intravascular ultrasound (IVUS) catheter. (A) Magnified view of the catheter probe. (B) OCT image generated from the device. (C) IVUS image generated from the device. (Reproduced by permission from Li, J., et al., 2015. Ultrafast optical-ultrasonic system and miniaturized catheter for imaging and characterizing atherosclerotic plaques in vivo. *Sci. Rep.*, 18406.)

such as extravascular space. These techniques are the basis for diagnostic coronary catheterization, cerebrovascular imaging, and other diagnostic procedures. Although more often administered peripherally, radioactive tracers can also be delivered in a similar manner.

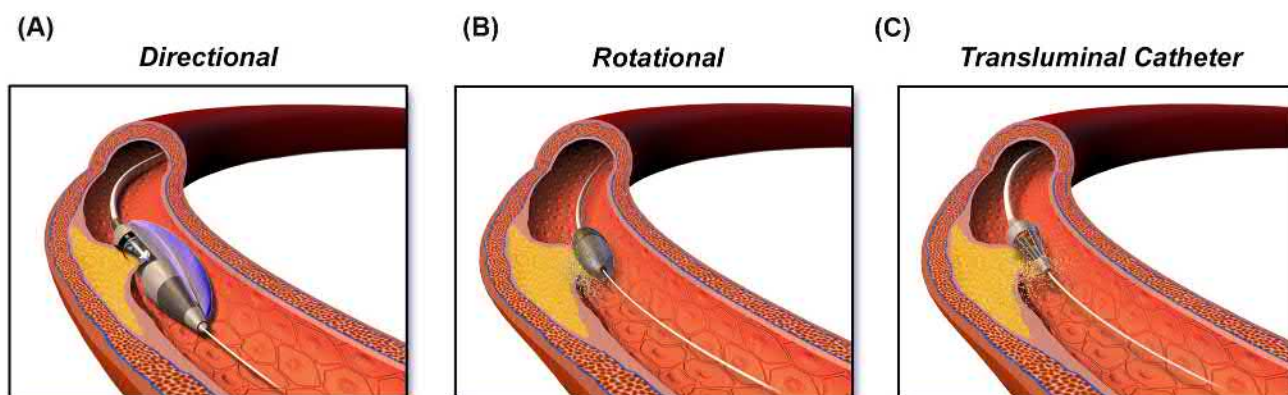
Coronary imaging has started routine use of more advanced intravascular imaging, where the imaging device itself is passed through the catheter (Fig. 2.5.2B.15), but these are also starting to see use in other vascular beds. As blood itself is opaque to visible light, preventing direct visualization of vessel walls, the two most common techniques that have emerged are intravascular ultrasound (IVUS) and optical coherence tomography (OCT). In IVUS, the catheter is adapted to have an ultrasound probe on the tip that is designed to provide circumferential radial imaging. This allows ultrasonic assessment of the vessel wall that, as the catheter is passed through the course of the vessel, can be used to construct a three-dimensional image of a short vascular segment. The depth of penetration of the IVUS image is up to 200 μm into the vessel wall, albeit with relatively low resolution. In contrast, OCT catheters are infrared light-based probes, including both source and sensor,

typically based through the catheter lumen. These only have penetration of up to 20 μm , and thus typically only capture one side of the vessel wall, but provide higher resolution imaging (with adaptations, called micro-OCT, being developed with cellular level resolution). Combined IVUS-OCT devices exist to facilitate combined imaging.

Therapeutic Catheters

Therapeutically, catheters can be used, as mentioned above, to deliver medical therapies systemically or locally. In fact, intravenous access sites are, in effect, simply short catheters. Similarly, “central lines” are catheters designed to deliver medications to the large vessel circulation rather than peripherally. Hemodialysis catheters, absent fistula or graft sites (described above), are paired catheters, inserted at a single, typically large-vessel site that includes one port to remove blood from the patient to the dialysis machine, and one catheter to return the filtered blood. Catheters can also be used to aspirate thrombus from obstructed vessels.

Some medical devices have been specifically developed to provide intravascular therapy in combination with catheters. One of the simplest types of these is inflatable



• **Figure 2.5.2B.16** Atherectomy devices. (A) Directional atherectomy, utilizing repeated passages of the device over the plaque. (B) Rotational atherectomy, using a high-speed rotational bore. (C) Transluminal atherectomy, using a smaller and slower rotational bore design, typically combined with suction to capture dislodged fragments. (Adapted by permission from https://en.wikipedia.org/wiki/File:Blausen_0064_Atherectomy.png.)

balloons, as described above, often constructed of polyethylene terephthalate (PET) or nylon. Devices have also been designed to remove atherosclerotic plaque (*atherectomy*) without surgical intervention (Figs. 2.5.2B.16A; Chambers et al., 2016). *Directional atherectomy* uses a device that is repeatedly passed over the plaque to scrape away material. *Rotational atherectomy* uses a rotational device (often over 100,000 rpm) to bore through plaque, which, while requiring fewer passes of the catheter to obtain a larger end lumen diameter, does result in small fragments of plaque that may cause clinically relevant downstream embolism and occlusion. Similar risk exists with *ultrasonic atherectomy* using ultrasonic waves instead of mechanical force. *Transluminal atherectomy* modifies the rotational technique using a smaller bore and lower speed rotational device (approximately 2000 rpm) associated with suction to retrieve the resulting plaque fragments. *Laser atherectomy* uses a laser (typically 355 nm) to burn away plaque, resulting in less embolization risk.

Transcatheter lasers have also been employed to burn away fibrous adhesions between other intravascular devices and the vessel wall. One of the most common applications of this technique is when electrophysiology leads become adherent to the superior vena cava but require extraction. The laser is used to carefully burn away the pathologic fibrous tissue, but this does carry a risk of perforating the vessel wall. A similar tissue dissolution process may be used for destroying other pathologic tissues sites, for example in ablating foci of aberrant electrical activity (i.e., arrhythmia) in the heart atria.

Endovascular Coils

One catheter-delivered strategy that warrants special mention is the use of metallic coils and related devices used to ablate small vascular spaces, typically small aneurysms (such as so-called *berry aneurysms* of the cerebrovascular circulation) or inappropriate vascular connections (e.g., patent ductus arteriosus) (Jia, 2018; Agrawal, 2019). As

an alternative to open surgical obliteration of the structures, these metallic coils (radio-opaque for visualization and often made from platinum) are specifically intended to induce a clotting reaction, with the thrombus that forms occluding the space. Over time, this thrombus will organize and form durable fibrous tissue to close off the space. There are also similar techniques combining metal and fabric components. Of note, coiling can be utilized to occlude blood vessels serving tumors (typically benign ones), resulting in a way to specifically infarct the pathologic tissue, potentially negating the need to remove the lesion surgically.

Vascular Filters

Venous thromboembolic disease is a significant cause of morbidity and mortality, largely due to the potential complication of pulmonary embolism (PE). The most common scenario is for a thrombus to form in the deep venous system of the lower extremities (so-called deep venous thrombus, DVT), become detached from the wall of the vein, travel through the inferior vena cava to the right side of the heart and lodge as an embolus in one of the large branches of the pulmonary artery. Therapy for patients with DVT or PE usually involves anticoagulation with warfarin and/or low-molecular-weight heparin. However, when anticoagulation is contraindicated due to active or threatened bleeding, or when there is recurrent DVT/PE despite adequate anticoagulation, placement of an inferior vena cava (IVC) filter is indicated.

Prior to the development of these devices, surgical ligation of the IVC during an open abdominal operation was performed. Following a period when filters were placed surgically, interventional radiologists began to place filters using a minimally invasive percutaneous approach in the 1980s. There are five types of filters commonly used in current clinical practice whose common design elements include metallic wires in a configuration to catch emboli in the bloodstream, a mechanism to anchor the device securely to the wall of the IVC and an ability to be deployed through a catheter

percutaneously (Fig. 2.5.2B.17). These devices are made variably from titanium, stainless steel, nitinol, and other metal alloys (Ha and Rectenwald, 2018). Complications of these devices include thrombosis at the insertion site, thrombi forming on the filter itself, thrombosis and obstruction of the IVC, migration or tilting of the device, and penetration of the IVC wall. Many of these complications are rare and/or without clinical consequence. As these devices have become safer and more effective, the indications for their use have expanded. Current research involves creating devices with a lower profile to make insertion easier and reduce insertion site thrombosis, designing removable devices and continuing to evolve the devices with the goal of catching potentially lethal emboli while maintaining adequate vena caval blood flow (Magnowski, 2017; Kaufman, 2018).

A similar concept is used in catheter-based interventions where there is a likelihood of creating embolic particles, such as cerebral emboli with transcatheter valve technologies (Nombela-Franco, 2018). In these settings, a cage-like device is deployed through the catheter to a position distal to the treatment site, facilitating capture of the most clinically relevant emboli.

Vascular Closure Devices (VCDs)

The very nature of nonsurgical vascular interventions necessitates that a vascular wall has been punctured to pass the device into the circulation. In small entries, particularly in the low-pressure venous circulation, these will close and heal without further medical intervention, although possibly associated with a small hematoma that typically resolves. Larger interventions require at a minimum that pressure and bandaging be applied to ensure proper closure of the vessel site. In the case of access to a large artery by a large-bore device, such as with many of these transcatheter technologies described above, surgical ligation had been the standard of care. However, percutaneous VCD, typically utilizing the same catheter as the original intervention, has been developed to close the defect at the end of the intervention (Bechara et al., 2010; van Wiechen et al., 2019).

A number of strategies for these VCDs have been developed. Devices such as Prostar XL and ProGlide (Abbott Vascular) utilize precise suturing methods. Others utilize titanium or nitinol clips or discs, such as the StarClose (Abbott Vascular), Angiolink EVS (Medtronic), and Boomerang (Cordiva). A third strategy is the use of biological collagen plugs to seal the access site, such as with the MANTA (Essential Medical) and the Angio-Seal (St. Jude Medical). The InSeal VCD (InSeal Medical) membrane-based device consists of a nitinol frame, a biodegradable patch, and a polyglycolic acid (PGA) tether. The PerQseal (Vivasure Medical) D consists of a bioresorbable patch and scaffold.

Unintended Embolic Biomaterials

One additional complication of virtually all endovascular procedures is the possibility for small fragments of foreign material to break off the device and travel through the

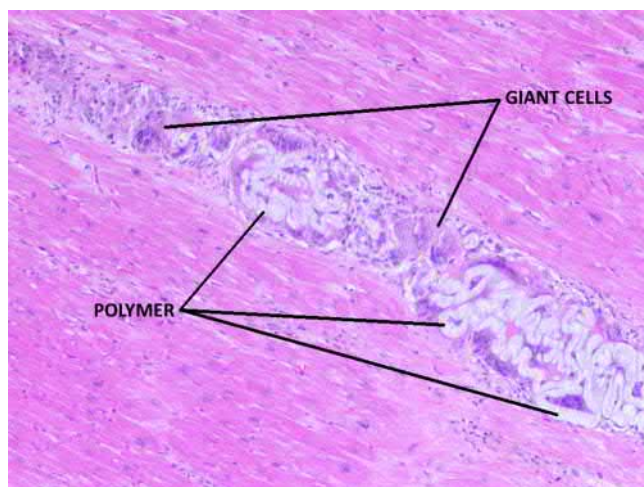


• **Figure 2.5.2B.17** Vena cava filter with clot.

vasculature. Although metallic devices are rarely associated with such failures, degeneration of other materials, particularly plastics, has been described to have such long-term complications. Furthermore, catheter delivery systems rely on the use of polymer lubricants such as compounds including polyethylene glycol, hydroxyethyl cellulose, and hydroxypropyl methylcellulose, to ensure smooth passage of the various components, and these gel-like substances are emerging as a source of embolic material found throughout the systemic vasculature (Fig. 2.5.2B.18; Chopra et al., 2017). At this time, the clinical significance of these emboli is uncertain, but ongoing research is evaluating the relative risk as several cases have been correlated with ischemic events.

Ex Vivo Evaluation

To facilitate quality assurance, quality control, and quality improvement, any vascular device that is recovered must be



• **Figure 2.5.2B.18** Intravascular foreign material (pale blue) in the heart of a patient that received an intravascular procedure, consistent with hydrophilic polymer emboli (HPE). There is an associated foreign-body inflammatory reaction characterized by multinucleated giant cells.

evaluated properly. Removal might be encountered in the context of device explant (typically removed due to mechanical failure or infection), organ or large-tissue resections containing the device (for example, heart explant at the time of transplantation), or autopsy. In fact, quality control of this type and device retrieval is one of the most compelling arguments for performance of a medical autopsy. Relevant findings may be primary mechanical device failure, overgrowth of tissue onto the device surface restricting function (pannus), occlusive thrombosis, dehiscence (detachment of the device from the biologic substrate), and infection.

The evaluation of these devices upon recovery requires cooperation between individuals with expertise both in the tissue biology and evaluation, such as pathologists, as well as individuals that are expert in the appropriate engineering principles, most notably biomedical engineers. This facilitates a precise understanding of the intrinsic human pathology, the device functioning after being exposed to the human environment, and the events stimulated by the interaction of the device with the human. Proper evaluation is best facilitated by a combination of *ex vivo* imaging of the device and tissue (e.g., device X-ray, CT, or MRI), expert dissection, and device functional evaluation. Some of the techniques used by pathologists for this evaluation include electroelution of stents (Bradshaw et al., 2009), plastic embedding and diamond cutting of tissue with the device in site, novel imaging techniques (many of which are also being applied *in vivo*, such as microprobe ultrasound and OCT), and devices such as borescopes to visualize the internal aspects of devices and vascular lumens.

Conclusions

The core principles evident in this chapter for developing endovascular biomaterials are maintenance of the vascular integrity, prevention of thrombus and excessive tissue

healing, and resistance to device-centered infection. Future advances will focus on improving these features in existing applications, and will almost certainly see new devices for solving additional biological challenges, focusing on the same principles.

References

- Agrawal, H., Waller, B.R., Surendan, S., Sathanandam, S., 2019. New patent ductus arteriosus closure devices and techniques. *Interv. Cardiol. Clin.* 8, 23–32.
- Barton, M., Grüntzig, J., Husmann, M., Rösch, J., 2014. Balloon angioplasty – the legacy of Andreas Grüntzig, M.D. (1939–1985). *Front. Cardiovasc. Med.* 1, 15.
- Bechara, C.F., Annambhotla, S., Lin, P.H., 2010. Access site management with vascular closure devices for percutaneous transarterial procedures. *J. Vasc. Surg.* 52, 1682–1696.
- Bell, T., O'Grady, N.P., 2017. Prevention of central line-associated bloodstream infections. *Infect. Dis. Clin. N. Am.* 31, 551–559.
- Belvroy, V.M., Houben, I.B., Trimarchi, S., Patel, H.J., Moll, F.L., Van Herwaarden, J.A., 2018. Identifying and addressing the limitations of EVAR technology. *Expert Rev. Med. Devices* 15, 541–554.
- Bradshaw, S.H., Kennedy, L., Dexter, D.F., Veinot, J.P., 2009. A practical method to rapidly dissolve metallic stents. *Cardiovasc. Pathol.* 18, 127–133.
- Chambers, J.W., Behrens, A.N., Martinsen, B.J., 2016. Atherectomy devices for the treatment of calcified coronary lesions. *Interv. Cardiol. Clin.* 5, 143–151.
- Chopra, A.M., Mehta, M., Bismuth, J., Shapiro, M., Fishbein, M.C., Bridges, A.G., et al., 2017. Polymer coating embolism from intravascular medical devices - a clinical literature review. *Cardiovasc. Pathol.* 30, 45–54.
- Clagett, G.P., 2002. What's new in vascular surgery. *J. Am. Coll. Surg.* 194, 165–201.
- Daemen, J., Serruys, P.W., 2007a. Drug-eluting stent update 2007: part I. A survey of current and future generation drug-eluting stents: meaningful advances or more of the same? *Circulation* 116, 316–328.
- Daemen, J., Serruys, P.W., 2007b. Drug-eluting stent update 2007: part II: unsettled issues. *Circulation* 116, 961–968.
- GBD 2013 Mortality and Causes of Death Collaborators, 2015. Global, regional, and national age-sex specific all-cause and cause-specific mortality for 240 causes of death, 1990–2013: a systematic analysis for the global burden of disease study 2013. *Lancet* 385, 117–171.
- Geovanini, G.R., Libby, P., 2018. Atherosclerosis and inflammation: overview and updates. *Clin. Sci.* 132, 1243–1252.
- Gimbrone, M.A., García-Cardena, G., 2013. Vascular endothelium, hemodynamics, and the pathobiology of atherosclerosis. *Cardiovasc. Pathol.* 22, 9–15.
- Grüntzig, A., Hopff, H., 1974. [Percutaneous recanalization after chronic arterial occlusion with a new dilator-catheter (modification of the dotter technique) (author's transl)]. *Dtsch. Med. Wochenschr.* 99, 250–2510, 2511.
- Ha, C.P., Rectenwald, J.E., 2018. Inferior vena cava filters: current indications, techniques, and recommendations. *Surg. Clin. N. Am.* 98, 293–319.
- Haudenschild, C.C., 1993. Pathobiology of restenosis after angioplasty. *Am. J. Med.* 94, 40S–44S.
- Hytönen, J.P., Taavitsainen, J., Tarvainen, S., Ylä-Herttua, S., 2018. Biodegradable coronary scaffolds: their future and clinical and technological challenges. *Cardiovasc. Res.* 114, 1063–1072.

- iData Research, 2018. Over 1.8 Million Stents Implanted Per Year in the U.S. Retrieved from: <https://idataresearch.com/over-1-8-million-stents-implanted-per-year-in-the-u-s/>.
- Jia, Z.Y., Shi, H.B., Miyachi, S., Hwang, S.M., Sheen, J.J., Song, Y.S., et al., 2018. Development of new endovascular devices for aneurysm treatment. *J. Stroke* 20, 46–56.
- Kaufman, J.A., 2018. Inferior vena cava filters: current and future concepts. *Interv. Cardiol. Clin.* 7, 129–135.
- Kim, M.S., Klein, A.J., Carroll, J.D., 2007. Transcatheter closure of intracardiac defects in adults. *J. Interv. Cardiol.* 20, 524–545.
- Kuo, E.C., Han, S.M., 2017. Treatment of complex thoracoabdominal aortic disease. *Cardiol. Clin.* 35, 411–429.
- Lee, D., de la Torre Hernandez, J.M., 2018. The newest generation of drug-eluting stents and beyond. *Eur. Cardiol.* 13, 54–59.
- Lee, T., Misra, S., 2016. New insights into dialysis vascular access: molecular targets in arteriovenous fistula and arteriovenous graft failure and their potential to improve vascular access outcomes. *Clin. J. Am. Soc. Nephrol.* 11, 1504–1512.
- Lindström, D., Mani, K., Lundberg, G., Wanhainen, A., 2019. Bridging stent grafts in fenestrated and branched endovascular aortic repair: current practice and possible complications. *J. Cardiovasc. Surg.* 60, 476–484.
- Lozano, R., Naghavi, M., Foreman, K., Lim, S., Shibuya, K., Aboyans, V., et al., 2012. Global and regional mortality from 235 causes of death for 20 age groups in 1990 and 2010: a systematic analysis for the global burden of disease study 2010. *Lancet* 380, 2095–2128.
- Magnowski, A., Brown, M., Schramm, K., Lindquist, J., Rochon, P.J., Johnson, D.T., et al., 2017. The law of unintended consequences: current design challenges in inferior vena cava filters. *Expert Rev. Med. Devices* 14, 805–810.
- Morr, S., Lin, N., Siddiqui, A.H., 2014. Carotid artery stenting: current and emerging options. *Med. Devices* 7, 343–355.
- National Organization for Rare Disorders, 2017. Marfan Syndrome. Retrieved from: <https://rarediseases.org/rare-diseases/marfan-syndrome/>.
- National Institute for Diabetes and Digestive and Kidney Diseases, 2016. Kidney Disease Statistics for the United States | NIDDK. Retrieved from: <https://www.niddk.nih.gov/health-information/health-statistics/kidney-disease>.
- Nombela-Franco, L., Armijo, G., Tirado-Conte, G., 2018. Cerebral embolic protection devices during transcatheter aortic valve implantation: clinical versus silent embolism. *J. Thorac. Dis.* 10, S3604–S3613.
- Olsson, C., Thelin, S., Ståhle, E., Ekbom, A., Granath, F., 2006. Thoracic aortic aneurysm and dissection: increasing prevalence and improved outcomes reported in a nationwide population-based study of more than 14,000 cases from 1987 to 2002. *Circulation* 114, 2611–2618.
- Pashneh-Tala, S., MacNeil, S., Claeysens, F., 2016. The tissue-engineered vascular graft—past, present, and future. *Tissue Eng. B Rev.* 22, 68–100.
- Patel, R., Sweeting, M.J., Powell, J.T., Greenhalgh, R.M., 2016. Endovascular versus open repair of abdominal aortic aneurysm in 15-years' follow-up of the UK endovascular aneurysm repair trial 1 (EVAR trial 1): a randomised controlled trial. *Lancet* 388, 2366–2374.
- Pearce, B.J., Scali, S.T., Beck, A.W., 2017. The role of surgeon modified fenestrated stent grafts in the treatment of aneurysms involving the branched visceral aorta. *J. Cardiovasc. Surg.* 58, 861–869.
- Richelsen, R.K.B., Overvad, T.F., Jensen, S.E., 2016. Drug-eluting balloons in the treatment of coronary de novo lesions: a comprehensive review. *Cardiol. Ther.* 5, 133–160.
- Sakalihan, N., Michel, J., Katsargyris, A., Kuivaniemi, H., Defraigne, J., Nchimi, A., et al., 2018. Abdominal aortic aneurysms. *Nat. Rev. Dis. Primers* 4, 34.
- Scott, E.C., Glickman, M.H., 2007. Conduits for hemodialysis access. *Semin. Vasc. Surg.* 20, 158–163.
- Song, H.G., Rumma, R.T., Ozaki, C.K., Edelman, E.R., Chen, C.S., 2018. Vascular tissue engineering: progress, challenges, and clinical promise. *Cell Stem Cell* 22, 340–354.
- Stowell, C.E.T., Wang, Y., 2018. Quickening: translational design of resorbable synthetic vascular grafts. *Biomaterials* 173, 71–86.
- Torii, S., Jinnouchi, H., Sakamoto, A., Kutyna, M., Cornelissen, A., Kuntz, S., et al., 2020. Drug-eluting coronary stents: insights from preclinical and pathology studies. *Nat. Rev. Cardiol.* 17, 37–51.
- van Wiechen, M.P., Lighthart, J.M., Van Mieghem, N.M., 2019. Large-bore vascular closure: new devices and techniques. *Interv. Cardiol.* 14, 17–21.
- Virmani, R., Farb, A., 1999. Pathology of in-stent restenosis. *Curr. Opin. Lipidol.* 10, 499–506.
- Virmani, R., Farb, A., Burke, A.P., 1994. Coronary angioplasty from the perspective of atherosclerotic plaque: morphologic predictors of immediate success and restenosis. *Am. Heart J.* 127, 163–179.
- Wanga, S., Silversides, C., Dore, A., de Waard, V., Mulder, B., 2016. Pregnancy and thoracic aortic disease: managing the risks. *Can. J. Cardiol.* 32, 78–85.
- Wissing, T.B., Bonito, V., Bouten, C.V.C., Smits, A.I.P.M., 2017. Biomaterial-driven in situ cardiovascular tissue engineering—a multi-disciplinary perspective. *NPJ Regen. Med.* 2, 18.
- Zhang, M., Malik, A.B., Rehman, J., 2014. Endothelial progenitor cells and vascular repair. *Curr. Opin. Hematol.* 21, 224–228.
- Zilla, P., Bezuidenhout, D., Human, P., 2007. Prosthetic vascular grafts: wrong models, wrong questions and no healing. *Biomaterials* 28, 5009–5027.

2.5.3

Extracorporeal Artificial Organs and Therapeutic Devices

REI UKITA¹, ALASTAIR CAMPBELL RITCHIE², ANGELA LAI¹, KEITH E. COOK¹

¹Department of Biomedical Engineering, Carnegie Mellon University, Pittsburgh, PA, United States

²Department of Mechanical, Materials and Manufacturing Engineering, University of Nottingham, Nottingham, United Kingdom

Introduction

Artificial lungs and kidneys are commonly used for short-term support during either acute organ failure or chronic organ dysfunction. When using both devices, blood is pumped from major blood vessels, through the artificial organ and back to the patient. For efficient mass transfer, both artificial lungs and kidneys utilize densely packed bundles of hollow fibers to transfer nutrients to and wastes from blood. As a result, both feature a high degree of blood–biomaterial interaction, protein adsorption, cellular adhesion, and activation of inflammation and coagulation. On the other hand, artificial lungs and kidneys transfer different substances and have different periods of use, and thus use different base materials for mass transfer and different approaches to reducing activation of coagulation and inflammation. Artificial lungs are expected to act continuously for several days to months at a time, while artificial kidneys are typically used for less than 6 h. As such, blood–biomaterial interactions in artificial lungs are sustained, and the biomaterials requirements are more stringent. Thus, the area of extracorporeal respiratory support has been a more fertile ground for device and biomaterials innovation recently.

Extracorporeal Respiratory Support

Pulmonary Disease—Incidence, Causes, and Mortality

More than 190,000 people in the United States suffer from adult respiratory distress syndrome (ARDS) each year (Matthay and Zemans, 2011). Typical causes of ARDS are sepsis, pneumonia, aspiration of gastric contents, and major trauma (Rubenfeld et al., 2005). These diverse causes all lead to

damage to the alveolar capillary membrane, typically through a neutrophil-mediated inflammatory reaction, causing increased pulmonary vascular permeability and leakage of proteinaceous exudate into the alveoli. This fluid leakage leads to increased diffusional resistance between alveolar gas and capillary blood, increased alveolar surface tension, alveolar collapse, and ultimately reduced oxygen and carbon dioxide transfer in the lungs. Most clinicians in this setting try to overcome the gas transfer deficit by increasing inspired oxygen fractions and alveolar recruitment with increased tidal volumes and airway pressures. Despite short-term gains in gas exchange, these ventilator settings can further damage the lung over the long run, worsening long-term gas exchange, systemic inflammation, and thus increasing mortality. For these reasons, low tidal volumes (<6 mL/kg) and low airway pressures (<30 cm H₂O) are desired. While these settings have decreased ARDS mortality rates to around 30%–40% (ARDS Network et al., 2000; Li et al., 2011), sufficient gas exchange may not be possible for patients with severe ARDS without support via artificial lungs.

Over 12 million Americans also suffer from chronic lung diseases such as chronic obstructive pulmonary disease (COPD), cystic fibrosis (CF), and interstitial lung disease (ILD) (American Lung Association 2008). Patients with COPD, CF, and ILD all experience a gradual decline in respiratory function over a period of years coupled with acute exacerbations that lead to a transient, but dangerous, worsening of dyspnea, hypoxia, and hypercapnia (Hyzy et al., 2007), hospitalization within the ICU, and death. In the United States, there are over 6.9 million emergency room visits (CDC, 2014), 700,000 hospital discharges per year and approximately 180,000 deaths. Lung transplantation is the only restorative treatment for these patients, but there are only approximately 2300 transplants in the United States

each year (Valapour et al., 2018). As a result, the vast majority of these patients will suffer for years with life-threatening exacerbations and will never receive a lung transplant.

Chronic lung disease patients undergoing acute exacerbations receive oxygen therapy in a form of noninvasive or invasive ventilation. Noninvasive ventilation (NIV) uses a facemask, positive pressure, and elevated inspiratory oxygen fractions to improve lung ventilation and gas exchange. If NIV cannot provide sufficient gas exchange, invasive mechanical ventilation with endotracheal (ET) intubation is required. Like ARDS, however, invasive ventilation is associated with many serious health risks, including ventilator-induced lung injury, lower respiratory tract infection, and diaphragmatic atrophy (Powers et al., 2002). As a result, prolonged duration of mechanical ventilation is also associated with higher hospital mortality (Loss et al., 2015), and it is not well-suited for long-term support.

Extracorporeal Membrane Oxygenation (ECMO)

Due to the insufficient, often harmful nature of prolonged mechanical ventilation, extracorporeal membrane oxygenation (ECMO) was developed. The goal of ECMO is to supply the majority of a patient's oxygen requirements and remove nearly all of their carbon dioxide (CO_2) production using a blood-processing extracorporeal circuit. This should allow patients with respiratory dysfunction to be supported on either gentle mechanical ventilation, noninvasive ventilation, or better yet, normal respiration.

During routine ECMO, cannulas are inserted into two major blood vessels for blood drainage and blood reinfusion. Venous blood is then pumped from the body, through the ECMO circuit, and then back to the patient at flow rates typically ranging from 60 to 100 mL/kg/min for adults. Typical ECMO circuits consist of drainage and reinfusion cannulas, the oxygenator, a pump, medical-grade Tygon tubing (S-50-HL), and polycarbonate connectors to connect everything together (Fig. 2.5.3.1). Modern circuits typically employ a centrifugal pump with a spinning, plastic, impeller to drive blood flow. However, roller pumps can still be used. In these devices, the circuit tubing is placed within the pump raceway, where rollers compress the tubing to peristaltically drive blood flow.

ECMO gas exchangers are typically called oxygenators. However, these devices are also highly efficient at transferring CO_2 and would more accurately be called artificial lungs. Early ECMO oxygenators utilized flat sheets of silicone rubber as the gas transfer membranes, but modern oxygenators all utilize bundles of polymethylpentene (PMP) hollow fibers (Fig. 2.5.3.2). These fibers have micropores throughout the fiber wall for excellent gas diffusion, and a 1–2 μm , solid outer skin to eliminate any leakage of plasma through the fiber wall. All current devices employ 380 μm outer diameter (OD) fibers that are woven together in gauzy fiber mats using multiple strands of polyethylene terephthalate (PET) filaments. Fiber mats are then wound around cores

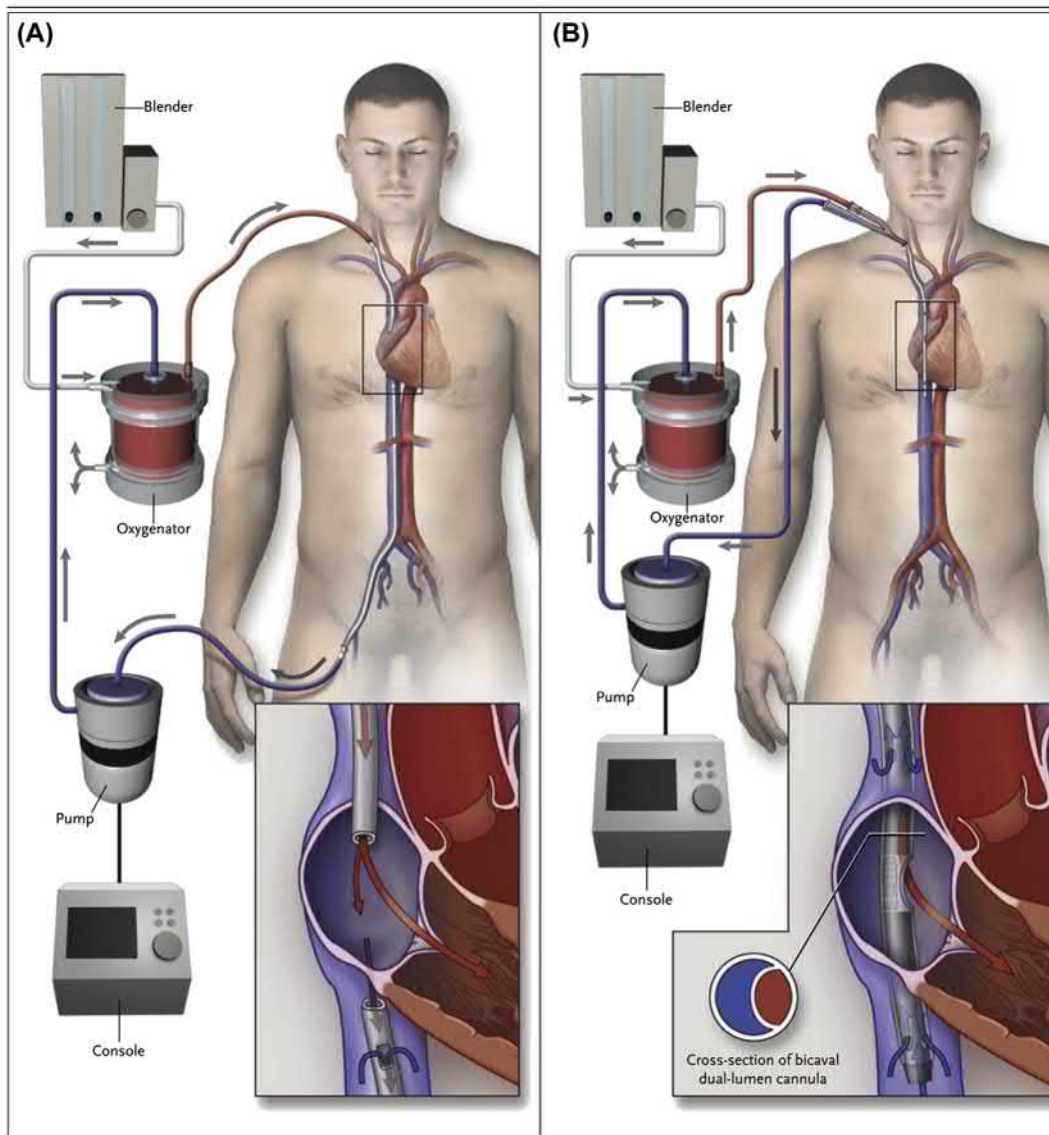
into fiber bundles and fixed within polycarbonate housings using polyurethane potting material. Typical fiber bundle surface areas are around 1.8 m^2 for adult oxygenators, representing over 90% of the total blood-contacting surface area of the ECMO circuit. Other fiber materials, such as solid PDMS or PDMS-coated porous polypropylene have been tested but have been largely used in experimental devices.

The most common ECMO attachment modes are veno-venous (VV) and veno-arterial (VA). During veno-venous ECMO, blood is drained from a large vein and returned to another large vein (Fig. 2.5.3.1). The drainage cannula is typically inserted in the jugular vein and down into the larger vena cava near the right atrium for easier blood drainage. In an earlier era of ECMO, during which patients were sedated and bed-bound, femoral vessels were frequently used for drainage and reinfusion. During more modern, ambulatory ECMO, a single, dual-lumen catheter is typically used to drain blood from the inferior and superior vena cava and reinfuse it directly into the right atrium. This keeps drainage away from the femoral vessels and allows for greater patient mobility. Veno-arterial ECMO also drains blood from the vena cava but returns oxygenated blood to a large artery, typically the carotid artery. By pumping blood around the heart and into the arterial system, VA ECMO thus provides both respiratory and cardiac support. However, pumping blood into the high-pressure arterial system requires higher pump speeds, leading to greater blood shear stress, red blood cell damage, and platelet activation, and a greater risk of bleeding from the arterial cannulation site (Lukito et al., 2016). It is thus utilized only in patients who require cardiac support.

Regardless of support mode or system, ECMO patients must be supported in the intensive care unit. This is due primarily to the respiratory deficits of the patients. However, once appropriate respiratory support is established, continuing biocompatibility issues such as systemic inflammation, bleeding and thrombotic complications, and multiorgan dysfunction continue to plague the patient requiring continuous, close care and monitoring (see Oxygenator Biocompatibility Challenges: Coagulation and Inflammation).

AMBULATORY ECMO

During its initial application, all ECMO patients were sedated and bed-bound. However, it has been recognized that patients recover more effectively if they can be mobilized, and unique dual-lumen cannulas have been invented that allow veno-venous ECMO via the jugular vein. This eliminates femoral cannulation that can interfere with walking. Now, ambulatory ECMO is being applied when possible to allow patients to walk while being supported during ECMO, particularly when ECMO is used as a bridge to lung transplantation (Lehr et al., 2015; Garcia et al., 2010). The circuits utilized during ambulatory ECMO are still cumbersome, however, and there is a trend toward creating more compact ECMO systems that allow patients to walk. Additionally, circuits are now being attached via vascular grafts during VA ECMO for greater safety when long-term support is envisioned. Further refinements, including better biomaterials, may allow these patients to leave the ICU altogether.



• **Figure 2.5.3.1** Venovenous (VV) extracorporeal membrane oxygenation (ECMO) using either (A) jugular and femoral access or (B) a single dual-lumen cannula. (Reproduced from Brodie D, Bacchetta M. 2011. Extracorporeal Membrane Oxygenation for ARDS in Adults. *N. Engl. J. Med.* 365, 1905–1914.)

Alternative Extracorporeal Gas Exchange Devices

Although ECMO is the mainstay for clinical respiratory support, a number of other devices are currently under development to support patients with acute or chronic lung disease. These devices offer different means of generating blood flow or gas exchange, leading to specific advantages such as smaller circuits and greater mobility, less blood damage and activation, simpler deployment, or better unloading of the right ventricle.

The desire to allow patients to live more normally while on ECMO, including ambulation, has motivated the development of various combined pump-lung systems (Fig. 2.5.3.3). Circuit modifications may be as simple as closely connecting the pump, pump console, and oxygenator to reduce circuit volume, as in the clinical Maquet



• **Figure 2.5.3.2** Artificial lung fiber bundle prior to incorporation into a full device.

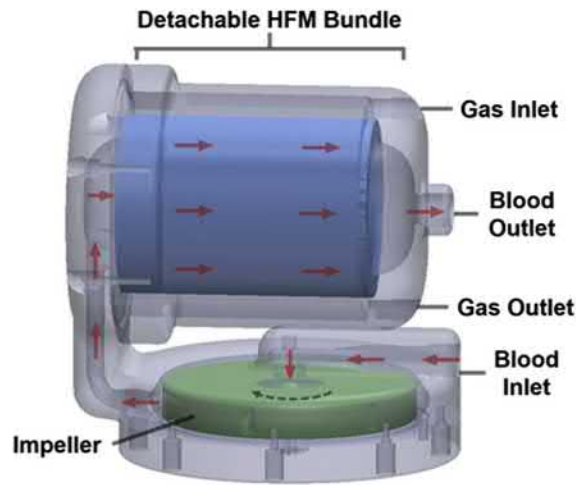


• **Figure 2.5.3.3** ModELAS pump-lung, showing the full device as well as the blood flow paths in the gas exchanger and pump.

Quadrox system, or actually combining the pump impeller and the oxygenator fibers within one housing, as with the University of Maryland (Wu et al., 2012b; Wei et al., 2016) and University of Pittsburgh pump-lungs (Madhani et al., 2017c). In either case, these systems are smaller and lighter than traditional ECMO systems and thus offer greater portability.

Extracorporeal carbon dioxide removal, or ECCO₂R, also attempts to reduce circuit size and complexity by focusing support solely on CO₂ removal. ECCO₂R can be performed using a smaller membrane oxygenator and blood flow rates of 0.5–1.0 L/min because CO₂ is 20 times more blood-soluble than O₂ and thus far easier to transfer. ECCO₂R is ideal in situations where CO₂ transfer is the primary problem, such as acute exacerbations of COPD. Because of the lower blood flow requirement, the device can even be attached without a pump in an arteriovenous configuration. Novalung's interventional lung assist (iLA) device is the only commercial device specifically designed for this purpose and is used clinically during arteriovenous carbon dioxide removal (AVCO₂R) via femoral artery and femoral vein cannulation (Zimmermann et al., 2009). A pumped, veno-venous ECCO₂R system, Alung Technology's Hemolung Respiratory Assist System, has also been developed and is currently undergoing clinical trials. This ultralow-flow system is frequently referred to as "respiratory dialysis."

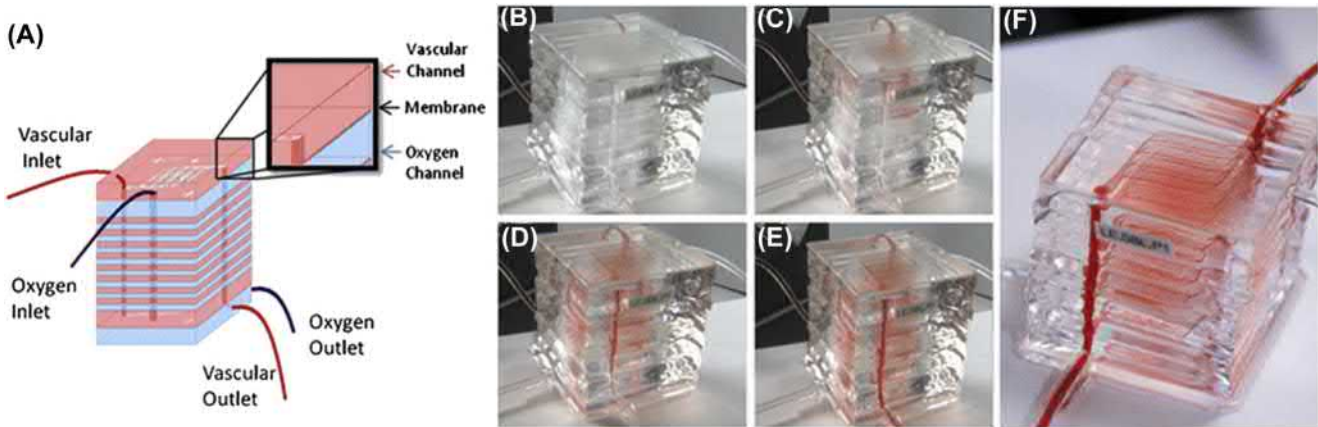
Thoracic artificial lungs (TALs) are also under development as either a bridge to lung transplantation or as permanent respiratory support for patients with chronic lung disease (Fig. 2.5.3.4) (Schewe et al., 2012a; Skoog et al., 2017). TALs attach to the pulmonary circulation, with blood flow coming from the proximal pulmonary artery (PA) and returning to the left atrium. The right ventricle (RV) drives blood flow through the TAL, and thus no mechanical pump is necessary. As a result, like AVCO₂R, the TAL circuit is compact. In addition to providing respiratory support, the TAL can eliminate



• **Figure 2.5.3.4** Compliant thoracic artificial lung (cTAL). (Reproduced from Schewe RE, Khanafer KM, Arab A, Mitchell JA, Skoog DJ, Cook KE. 2012. Design and In Vitro Assessment of an Improved, Low-Resistance Compliant Thoracic Artificial Lung. *ASAIO. J.* 58, 583–589.)

pulmonary hypertension (PH) and improve RV function by creating a second, low-resistance pathway around the diseased natural lungs (Akay et al., 2010). However, to accomplish this, a TAL must be designed with a very low resistance, similar to that of a healthy natural lung. The low blood-flow resistance, low shear stresses, and the lack of a pump, heat exchanger, and reservoir cause a reduction in coagulation, inflammation, and damage to formed elements in blood as compared to ECMO (Cook and Mockros, 2002). Thus, unlike ECMO, no blood products need to be given during use (Skoog et al., 2017), and devices such as the MC3 Biolung and the compliant TAL (cTAL) caused no significant hematological, hemodynamic, or organ function deficits during 14–30 days of testing (Skoog et al., 2017).

Lastly, there are growing efforts to design oxygenators that utilize thin 20–200 μm -tall channel gas transfer membranes, known as microchannel lungs (Fig. 2.5.3.5) (Thompson et al., 2017; Shin et al., 2004; Potkay, 2014; Kovach et al., 2015; Hoganson et al., 2011, 2010; Burgess et al., 2009). These devices are fabricated with soft lithography using PDMS, which has high gas permeability. To increase gas exchange efficiency, these channels are thin, have short diffusional distances, and high surface area to blood volume ratios. Therefore, they have the

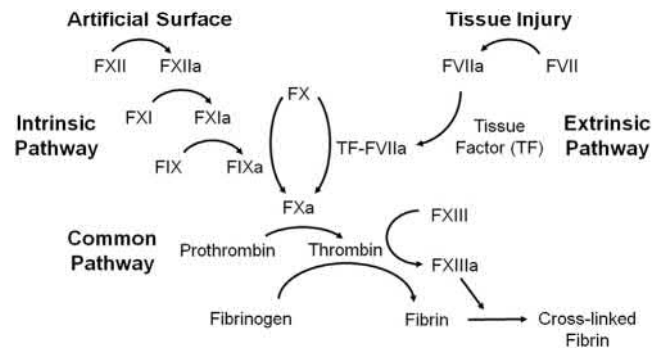


• **Figure 2.5.3.5** Microchannel artificial lung featuring multiple, interconnected layers of microchannel networks (A). Sequential images (B–F) demonstrate the blood entering the layers during priming. (Reproduced from Kniazeva T, Hsiao JC, Charest JL, Borenstein JT. 2011. A microfluidic respiratory assist device with high gas permeance for artificial lung applications. *Biomed Microdevices* 13, 315–323.)

potential to have higher gas exchange efficiencies than conventional hollow fiber devices and smaller device sizes. However, these small channels create new design challenges. First, blood flow must be distributed from a single, large feeder tube such as a vascular graft or cannula down to the small microchannels and back without numerous generations of branching channels, large amounts of additional device volume, or abrupt shifts in channel dimensions that lead to flow recirculation, accelerated clot formation, and increased blood flow resistance. Second, these devices have useful lifetimes of a few hours, using standard clinical anticoagulation protocols prior to occluding due to thrombus formation. The high surface area to volume ratio and small channel heights lead to rapid clot formation, as it only takes a small amount of clot to plug the entire channel. Thus, previous *in vitro* and *in vivo* whole-blood microchannel studies used higher levels of anticoagulation than ECMO (activated clotting time, ACT > 500 s) (Plegue et al., 2018; Kovach et al., 2015), and these devices will not be practical until less thrombogenic surfaces are developed. Current development focuses on using various surface coatings to reduce thrombosis (Kovach et al., 2015; Plegue et al., 2018). A possible solution to this issue may be the use of microchannel lungs constructed from biological tissue (Comber et al., 2019). These devices are endothelialized to reduce clot formation with their collagen-based structures promoting normal endothelial cell growth and function. Although promising, these devices will require several years of development to achieve full-scale designs suitable for preclinical testing.

Oxygenator Biocompatibility Challenges: Coagulation and Inflammation

All artificial lungs are composed of a variety of hydrophobic materials including polypropylene (PP), polymethylpentene (PMP), and polydimethylsiloxane (PDMS) gas exchange



• **Figure 2.5.3.6** Coagulation cascade demonstrating the intrinsic pathway, which is activated by artificial surface contact; the extrinsic pathway, which is activated by tissue factor; and the common coagulation pathway.

fibers, polyvinyl chloride (PVC) in tubing, polycarbonate housings, and polyurethane “potting” that separates the blood and gas space. The fiber bundle is the predominant site of clot formation in artificial lungs due to its large, densely packed surface area (Fig. 2.5.3.2). Coagulation and inflammation are initiated by protein adsorption onto their hydrophobic surfaces, changing protein conformations and exposing either binding or active sites that lead to further procoagulant reactions (Cook and Mockros, 2002). Adsorption of two proteins is predominantly responsible for clot formation. First, FXII adsorption to the biomaterial surface causes its activation to FXIIa, leading to activation of the intrinsic branch of the coagulation cascade (Fig. 2.5.3.6). This leads to generation of proinflammatory molecules via the kallikrein–kinin system and thrombin by the common coagulation pathway (Renne et al., 2012). Thrombin formation then causes conversion of fibrinogen to fibrin, thus forming the solid clot, and platelet activation, which accelerates the process. The second pathway causing clot formation is direct platelet binding to proteins adsorbed on the biomaterial surface. The predominant protein causing this is fibrinogen, which undergoes a conformational change upon

adsorption, allowing platelet binding via its GpIIb/IIIa ($\alpha_{IIb}\beta_3$ integrin) receptor. Platelet binding initiates activation, releasing numerous procoagulants and causing platelet aggregation and acceleration of clot formation (Cook and Mockros, 2002).

The gold standard for reducing clot formation in artificial lungs is continuous, intravenous (IV) infusion of unfractionated heparin. Heparin is a carbohydrate with molecular weights ranging from 3 to 30 kDa. Heparin is cleared from the systemic circulation by the kidney and has a half-life of 60–90 min, so it must be continuously administered during ECMO to maintain anticoagulation. When in plasma, heparin inhibits the common coagulation cascade (Fig. 2.5.3.6) by forming a complex with antithrombin III (ATIII) and inactivating Factor Xa (FXa) and thrombin. Thus, heparin inhibits coagulation initiated by both the intrinsic and extrinsic branches within the artificial lung and the patient, respectively, and serious bleeding issues can occur during ECMO even with careful anticoagulant management. These complications are further exacerbated by platelet and coagulation factor consumption by the artificial surfaces and pump.

In a study of pediatric ECMO, bleeding complications occurred in 33% of neonates and 45% of pediatric patients. Thrombotic complications occurred in 29% of neonates and 33% of pediatric patients (Dalton et al., 2015). As a result, bleeding and thrombosis complications were associated with a 40% and 33% decrease in survival, respectively. In another recent study (Mazzeffi et al., 2016), serious bleeding events occurred in 56.1% of adult patients, causing a 2.22 crude odds ratio for in-hospital mortality. Thus, both thrombosis and bleeding are significant risks during ECMO.

Alternative approaches to systemic anticoagulation have been examined in an attempt to reduce these complications. These include use of direct thrombin (Jyoti et al., 2014) and FX inhibitors (Weitz and Gross, 2012) and various types of platelet inhibitors, particularly aspirin (He et al., 2014; Staudacher et al., 2016; Esper et al., 2015). Like heparin, these inhibitors all inhibit coagulation at artificial surfaces and in the tissues, so their benefits to reducing bleeding and thrombotic complications are minimal. An anticoagulation approach gaining promise is to selectively inhibit the intrinsic pathway alone. The rationale is to focus on the upstream portion of the intrinsic branch while leaving the extrinsic branch unaffected to minimize bleeding complications. A complete lack of intrinsic branch activity is safe naturally; a genetic deficiency in plasma FXII or prekallikrein does not lead to an increase in spontaneous or injury-related bleeding in tissues (Renne et al., 2012; Schloesser et al., 1997). Therefore, a highly selective intrinsic branch inhibitor could significantly reduce clot formation at artificial surfaces while having little to no effect on clot formation within the patient's tissues. Moreover, an overdose of this inhibitor would not cause bleeding complications, and thus one could err on the high end of inhibition and

reduce monitoring requirements. These inhibitors, therefore, might allow for safer and simpler management of anticoagulation.

This approach is not new (Wachtfogel et al., 1998). The challenge, however, has been finding an intrinsic branch inhibitor that is both potent and highly selective. This is a significant challenge, as FXIIa is a trypsin-like serine protease, and plasmin and most coagulation factors are also serine proteases. Thus, FXIIa inhibitors found in plants, insects, and bacteria also significantly inhibit trypsin, the extrinsic or common coagulation cascade, and plasmin. One synthetic, kallikrein inhibitor, nafamostat mesilate, has been tested during ECMO. However, a large, well-controlled study demonstrated that nafamostat has a bleeding complications rate that is significantly *greater* than that of heparin (Lim et al., 2016), presumably due to its concurrent inhibition of thrombin, plasmin, and ADP-induced platelet aggregation (Sundaram et al., 1996). Poor selectivity has thus motivated the development of a new generation of synthetic, highly selective inhibitors. This includes RNA aptamers (Woodruff et al., 2013), FXIIa antibodies (Worm et al., 2015; Larsson et al., 2014), and bicyclic peptides (Middendorp et al., 2017; Zorzi et al., 2017). Their applications in artificial lungs have so far been at a preclinical stage but have shown promising results.

Blood contact with the artificial surfaces of artificial lungs also activates the immune system, leading to a “whole body inflammatory response.” The predominant causes are surface-activated contact factors and complement fragments. Neutrophil and monocyte binding to adsorbed proteins on the extracorporeal circuit may also contribute to their activation. Studies of leukocyte activation during ECMO are quite limited, but they suggest significant inflammation during the first 24 h of extracorporeal circulation, at which point activation subsides (Fortenberry et al., 1996). This indicates that, while coagulation in artificial lungs is progressive, surface-induced inflammation subsides over time and is a lesser concern during use of artificial lungs.

NATURAL ORGAN VERSUS ARTIFICIAL ORGAN ANTICOAGULATION

The blood vessels in our bodies are all lined with endothelial cells that actively anticoagulate blood under normal conditions using multiple, cooperative means of anticoagulation that primarily act at the endothelial surface (van Hinsbergh, 2012). This includes a benign surface that does not activate the clotting cascade and multiple types of platelet and coagulation cascade inhibitors. Our historic approach with artificial organs, however, has typically featured large, systemic doses of the coagulation cascade inhibitor, heparin, creating patient-wide anticoagulation. This approach is changing, however, through the combined application of surfaces that both passively and actively inhibit local clot formation coupled with lower doses of systemic anticoagulants (Wu et al., 2007; Amoako et al., 2016).

Organs coated with endothelial cells have been examined as well, although maintaining cells on artificial surfaces for long periods poses significant challenges (Wiegmann et al., 2016; Pflaum et al., 2017; Polk et al., 2010).

Surface Coatings

Two general types of surface coatings have been designed with a primary goal of reducing artificial surface coagulation: surface immobilization of anticoagulant molecules and surfaces that repel nonspecific protein adsorption and ensuing activation of thrombosis. Table 2.5.3.1 outlines the specific types of commercial coatings and their polymeric compositions. In assessing the value of these coatings, one must be extremely careful to examine the conditions under which the testing occurs, including the substrate for the coating (an idealized surface versus hydrophobic polymers commonly used in artificial lungs), the geometric complexity of the test device (flat surface versus full artificial lung), the test media (single protein solution versus whole blood), the test setting (in vitro versus in vivo), and lastly the duration of testing.

We will focus our discussion of these coatings when they are applied to the densely packed, hydrophobic surfaces of full artificial lungs and exposed to whole blood. Together, this represents perhaps the most challenging setting for these coatings. If possible, we would prefer to discuss their use during long-term use of artificial lungs during ECMO, but there are few to no data in this setting. Thus, the majority of this discussion of coatings will focus on animal or clinical cardiopulmonary bypass (CPB). In analyzing these results, one must keep in mind that CPB only lasts on the order of hours and is a far more complex setting than ECMO, with several factors that confound the ability of the coating to reduce clotting and inflammation. These include significant soft- and hard-tissue trauma from the surgery itself, blood damage and activation by the pump, and the air–blood interface in an open-air blood reservoir. The effect of coating may, therefore, be too small compared to the extent of the other sources of blood activation during the procedure, and this could cause an underestimation of the true effect of the coating.

Heparin Coatings: Heparin coatings have the longest history as cardiovascular coatings and are most commonly used today. The initial rationale for surface heparin coating was to immobilize heparin for localized inhibition of FXa and thrombin. However, their long, flexible carbohydrate chains also exert a steric hindrance effect and repel protein adsorption (Weber et al., 2002; Amiji and Park, 1993), and this can be further enhanced by adding hydrophilic spacer groups, such as polyethylene oxide, between the surface and the heparin molecule (Amiji and Park, 1993; Byun et al., 1995).

Heparinized coatings were first applied using ionic attachment, but these bonds were found to be unstable, and these coatings leach heparin over long-term use (Noishiki and Miyata, 1985). Hence, covalent grafting supplanted this due to its higher stability. Heparin could either be attached at a single point (end-point) or at multiple points along the chain (multipoint), but end-point grafting has better bioactivity compared to the multipoint (Larsson et al., 1987) and is the more common method of heparin coating (Weber et al., 2002). Some of the notable examples of commercial coatings making use of end-point grafting are Carmeda BioActive Surface (CBAS) from Medtronic and Maquet's Bioline. CBAS consists of depolymerized, lower molecular weight heparin covalently grafted to surfaces by aminating the base matrix, which consists of positively charged polyethyleneimine and negatively charged dextran sulfate (Biran and Pond, 2017). Bioline coating is a combination of heparin and albumin with both ionic and covalent linkages to the surface.

Studies have shown that the Bioline and CBAS heparin coatings can reduce inflammatory responses during short-term artificial lung use, as occurs during CPB (Sohn et al., 2009). However, the ability of these coatings to reduce coagulation is likely poor, with studies indicating an inability to slow thrombin or fibrin formation. It is thus hypothesized that surface-bound heparin has a limited

TABLE 2.5.3.1 Commercial Oxygenator Coating Materials and Their Mechanisms

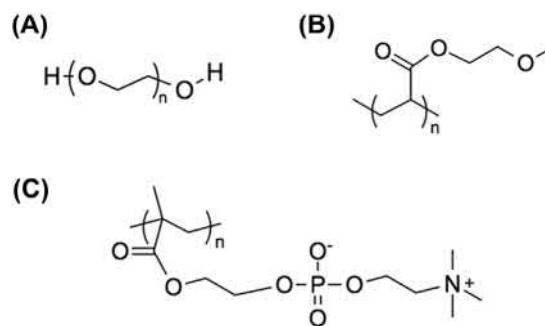
Polymer Type	Mechanism	Commercial Brand (Company)
Heparin	Inhibition of FXa and thrombin, antiadsorptive (Liu and Pedersen, 2007; Weber et al., 2002; Amiji and Park, 1993)	Carmeda Bioactive Surface (Medtronic), BIOLINE (Maquet), Duraflo II (Baxter), Trilium (Medtronic)
Albumin	Bioinert surface, antiadsorptive (Amiji and Park, 1993)	Safeline (Maquet), BIOLINE (Maquet)
Polyethylene glycol (PEG)	Hydration layer (hydrogen bonding) antiadsorptive (Jeon et al., 1991; Alcantar et al., 2000)	Trilium (Medtronic)
PMEA	Hydration layer (hydrogen bonding), antiadsorptive (Tanaka et al., 2000b, 2002; Chen et al., 2010)	X-coating (Terumo)
Phosphorylcholine	Hydration layer (electrostatics), antiadsorptive (Ishihara, 2000; Hatakeyama et al., 2010)	P.h.i.s.i.o. (Sorins), Agile (Eurosets)
Carboxybetaine & sulfobetaine	Hydration layer (electrostatics), antiadsorptive (Cao and Jiang, 2012)	None

bioavailability relative to its soluble counterpart and only provides mild benefit in reducing coagulation via inhibition of thrombin or FXa (Savannah et al., 2014). Rather, the efficacy of heparinized coating may be due to changes in protein adsorption and conformational changes (Weber et al., 2002).

Albumin Coatings: Albumin solutions have long been used to prime CPB and ECMO circuits in order to preadsorb relatively benign albumin, limit fibrinogen adsorption, and in theory, reduce thrombus formation (Mulvihill et al., 1990). After initiating blood flow through the circuit, however, IgG and fibrinogen will displace albumin and bind to the surface (Vroman and Adams, 1986). Thus surface passivation with albumin is only a short-lasting solution and not sufficient for long-term artificial lung use (Vroman and Adams, 1986). Different approaches have thus been taken to more stably anchor albumin using covalent grafting (Kasálková et al., 2014; Kamath and Park, 1994), irradiation (Kamath and Park, 1994; Sivaraman and Latour, 2010), and cross-linking (Amiji et al., 1992). Albumin has thus been incorporated into commercial coatings such as Safeline and, as discussed previously, Bioline. Safeline utilizes covalently attached human albumin, while Bioline contains both heparin and albumin in the coating. The effectiveness of Bioline was discussed previously, and studies comparing the two suggest they have similar, limited effectiveness (Zimmermann et al., 2007).

Polyethylene Glycol (PEG) Coatings: Polyethylene glycol (PEG), also referred to as polyethylene oxide (PEO), is commonly used as a biocompatible material in various biological applications including low-fouling coatings (Alcantar et al., 2000; Kovach et al., 2014; Ding et al., 2012), biomolecule stabilization (Roberts et al., 2002), and stealth particles (Jokerst et al., 2011). The polymer commonly is a linear polyether chain (Fig. 2.5.3.7). When there are about 10 or fewer repeat units, it is referred to as oligo-ethylene glycol (OEG).

The effects of PEG on reducing protein adsorption and platelet fouling have been demonstrated in vitro mainly by exposing surfaces to single-protein solutions or plasma (Alcantar et al., 2000; Ma et al., 2004; Prime and Whitesides, 1993). While these results were promising, the in vivo results have been mixed. Kidane et al. coated polyethylene, silicone rubber, and expanded polytetrafluoroethylene tube surfaces with triblock PEG copolymer coatings and exposed them to a fibrinogen solution and platelet-rich plasma in vitro (Kidane et al., 1999). The same coating that reduced fibrinogen by 70% in vitro did not significantly reduce platelet adhesion in an ex vivo canine shunt model. Similarly, plasma-deposited PEG on a fluorinated ethylene propylene surface reduced fibrinogen adsorption from a single protein solution to $<10 \text{ ng/cm}^2$, and yet the coated surface had more polymorphonuclear leukocyte adhesion relative to the uncoated control when exposed to whole blood or plasma (Shen et al., 2002). When the same coated materials were also implanted subcutaneously in rats, there were signs



• **Figure 2.5.3.7** (A) Polyethylene glycol (PEG), (B) 1,2-polymethoxyethyl acrylate (PMEA), and (C) 2-methacryloyloxyethyl phosphorylcholine (MPC).

of surface degradation after 1-day and 4-week implantation, and the authors suggested that the degradation was due to reactive oxygen species secreted by the leukocytes (Shen et al., 2002). Other studies have reported that PEG may not be stable for long-term in vivo applications, as discussed in other chapters in this book. PEG can be metabolized by the body and broken down into organic acids (Herold et al., 1989). Additionally, PEG can undergo oxidative degradation in the presence of oxygen or transition metal catalysts (Ulbricht et al., 2014).

The most well-known commercial PEG coating is Medtronic's Trillium, which combines PEG, heparin, and sulfonate groups. In short-term CPB settings, the coating has demonstrated anywhere from mild to no benefits compared to no coating. Trillium showed a similar benefit in preserving platelet counts as the heparin CBAS coating or albumin precoating via the prime (Palanzo et al., 1999, 2001). However, others have shown no difference in adhered platelets, leukocytes, or fibrin (van den Goor et al., 2006), or inflammatory response and blood loss compared to an uncoated control during CPB (Ereth et al., 2001). This may have been caused, in part, by the lack of coating in the rest of the circuit (Ereth et al., 2001; van den Goor et al., 2006). The reports on PEG's in vivo hemocompatibility in the setting of oxygenators are thus mixed, and there is clearly a discrepancy between its promising in vitro results and mixed in vivo results. The sum of these results suggest that this material is unlikely to be of significant benefit to long-term artificial lungs. There is, to date, no long-term study demonstrating a reduction in clot formation or inflammation.

1,2-Polymethoxyethyl Acrylate (PMEA) Coatings: PMEA consists of a hydrophobic alkyl carbon backbone with pendant hydrophilic groups (Fig. 2.5.3.7). It has primarily been explored as an antithrombogenic coating for cardiovascular devices, including membrane oxygenators, by the Terumo Corporation branded as Xcoating. The low-fouling property of PMEA is attributed to high bound water content near the surface that is stabilized by hydrogen bonds with the polymer chains (Tanaka et al., 2000a,b, 2002; Tanaka and Mochizuki, 2010).

In vitro blood circulation studies show that platelet adhesion, activation, and fibrin deposition were reduced

with PMEA coating compared to uncoated polypropylene (Gupta et al., 2014) and PVC surfaces (Yoshizaki et al., 2005). Several CPB studies concluded that PMEA coating offered benefits by preserving platelet count and reducing platelet activation and blood loss compared to its uncoated control (Zimmermann et al., 2004). On the other hand, there are contradictory results regarding PMEA's ability to reduce coagulation relative to heparin coatings during CPB or simulated CPB (Veysel et al., 2006), and a general trend toward similar or greater activation of complement and inflammation with PMEA (Veysel et al., 2006). Unfortunately, the limited number of studies and the variability in the type of heparin coating and test methods make these results difficult to interpret. Furthermore, the long-term benefit of PMEA coating are completely untested.

Phosphorylcholine Coatings: Current research on phospholipid-like coatings began with interesting observations about cell surfaces: their phospholipid composition was asymmetric across the membrane, such the inner membrane was largely made up of negatively charged species like phosphatidylserines and the outer part was made up of species like phosphatidylcholines that have a balanced, overall neutral charge (Zwaal et al., 1977). Furthermore, the charged inner layer was highly thrombogenic, whereas the outer, neutral layer was much more thromboresistant (Zwaal et al., 1977; Zwaal and Hemker, 1982). This led to the development of the phospholipid-like antithrombogenic coating known as phosphorylcholine (PC), characterized by the negative phosphate group and the positive ammonium group. The balanced positive and negative charges categorize PC as a zwitterionic polymer. Commonly, 2-methacryloyloxyethyl phosphorylcholine (MPC, Fig. 2.5.3.7) is used as the monomer for a coating (Wang et al., 2014; Tateishi et al., 2014). Poly-MPC chains consist of an acrylate backbone with PC branches. Because MPC is highly water-soluble, it is common practice to copolymerize it with a hydrophobic moiety, such as n-butyl methacrylate, for better adsorption to surfaces (Ishihara, 2000; Ishihara et al., 1992). Currently, the Ph.i.s.i.o. PC coating from Sorin is the only commercially available zwitterionic coating for oxygenators for CPB and ECMO in the United States. In Europe, EUROSETS.A.L.ONE from Italy is also commercially available.

The mechanism for PC's low-fouling property is like that of PEG and other hydrophilic coatings. The charged moieties present in the polymer electrostatically attract water molecules to create a hydration layer. Because these charge interactions are stronger than hydrogen bonding, the hydration layer is much stronger and harder to disrupt by protein adsorption (Hatakeyama et al., 2010; Morisaku et al., 2008).

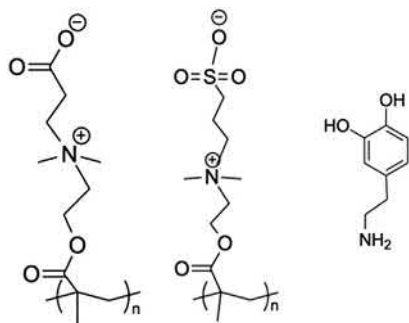
In vitro PC coating has been applied to various surface types including polyethylene (Ishihara et al., 1991), magnesium alloy (Ye et al., 2013), gold (Emmenegger et al., 2009), and PDMS (Goda et al., 2006). These reports generally show success in reducing protein and platelet fouling when tested in single-protein solutions and platelet-rich plasma (Tateishi

et al., 2014). Animal and clinical studies of PC-coated oxygenators have shown good biocompatibility, though the amount of available data is small. A 2-hour canine extracorporeal study with cross-linkable PC coating on PP hollow-fiber membrane oxygenators demonstrated reduced platelet activation and clot formation (Wang et al., 2016). Clinical PC studies also showed reduced platelet activation but no reduction in thrombin activation or overall clot formation (De et al., 2002). On the other hand, one adult CPB study reported that the PC-coated oxygenator from Sorin had a lower increase in transoxygenator pressure drop compared to the uncoated control, indicating decreased thrombus formation (Lorusso et al., 2009). Therefore, PC coating of clinical CPB circuits had mixed results in comparison to its successes in vitro, but the long-term efficacy on artificial lungs is still under investigation. One downside that may limit application is that MPC synthesis is challenging due to the sensitivity to moisture, which may cause variations in batch quality (Zhang et al., 2006).

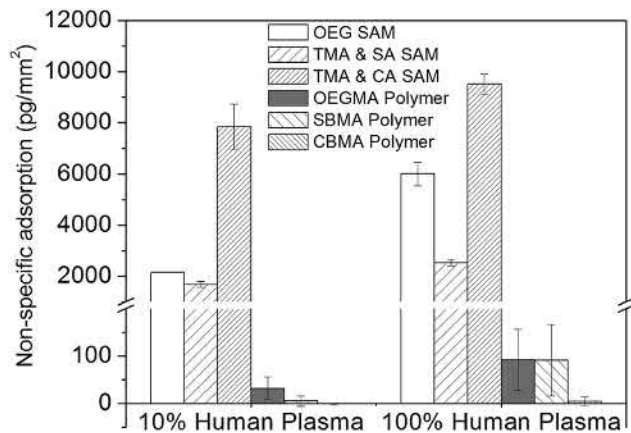
Sulfobetaines and Carboxybetaine Coatings: Recently, other types of zwitterionic polymers have been developed and tested. Polycarboxybetaine (pCB) and polysulfobetaine (pSB) have been the most successful examples (Fig. 2.5.3.8), and thus represent one of the most active areas of investigation for nonfouling coatings. These polymers bear similar structure to PC, but their negative moieties are different; carboxybetaine has a carboxylate group, and sulfobetaine has a sulfonate group. Furthermore, both pSB and pCB, much like PC, are bioinspired materials. SB is similar in structure to taurine, which is an amino acid abundantly present in the body (Zhang et al., 2006), while CB structurally resembles glycine betaine, a molecule that is believed to have osmoregulatory and protein-stabilizing functions in many species including humans (Papageorgiou and Murata, 1995).

Evidence suggests that pCB and pSB coatings create a waterlike layer that both repels proteins while maintaining their conformations (Keefe and Jiang, 2012; Abraham et al., 2011). Both pCB and pSB have been tested to examine the extent of protein adsorption, and pCB has particularly shown excellent in vitro performance. Ladd et al. reported a protein fouling study with surface plasmon resonance (SPR) that compared the efficacy of various polymer brushes over a gold substrate, including poly-oligo-ethylene methacrylate (pOEGMA), polysulfobetaine methacrylate (pSBMA), and polycarboxybetaine methacrylate (pCBMA). When 100% plasma flowed over the surface, only pCBMA showed protein fouling of <10 pg/mm² versus ~ 100 pg/mm² for pOEGMA and pSBMA (Fig. 2.5.3.9) (Ladd et al., 2008). Another SPR study demonstrated that only pCB coating had protein adsorption below the detection limit of 6 pg/mm² when exposed to 33% human plasma for 30 min, whereas PEG, pSB, and PC all had measurable amounts of 1200, 3200, and 4600 pg/mm², respectively (Emmenegger et al., 2009). Thus, pCB is currently the least fouling material tested and has great potential toward long-term artificial lung applications.

Many approaches to pCB and pSB coating have been examined. Like PEG and PC coating, copolymerizing pCB and pSB with hydrophobic or amphiphilic moieties is a simple yet effective graft-to approach (Li et al., 2012). The loss of stability and leaching are the main points of concern for this approach. Another common graft-to approach makes use of 3,4-dihydroxyphenylalanine (DOPA), a bioinspired



• **Figure 2.5.3.8** Polycarboxybetaine (PCB), polysulfobetaine (PSB), and 3,4-dihydroxyphenylalanine (DOPA).

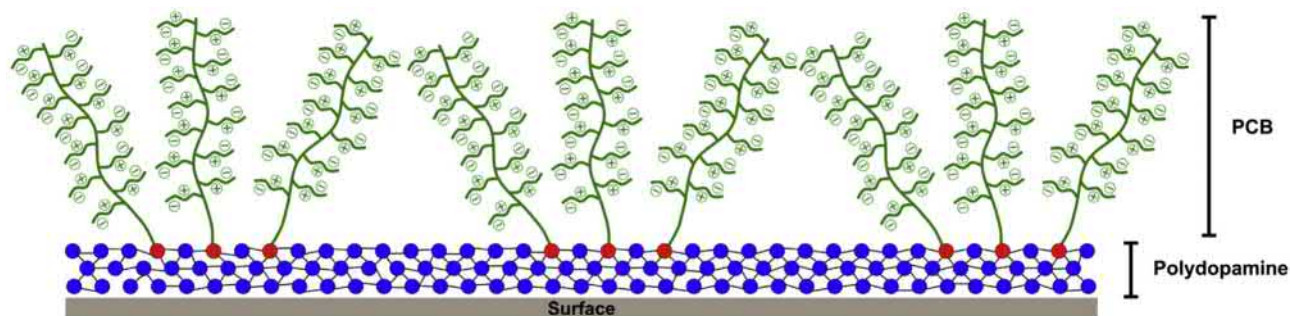


• **Figure 2.5.3.9** Protein adsorption levels on a variety of antiadsorptive surface coatings, including poly(oligoethylene methacrylate) (pOEGMA), polysulfobetaine methacrylate (pSBMA), and polycarboxybetaine methacrylate (pCBMA). (Reproduced from Ladd J, Zhang Z, Chen S, Hower JC, Jiang S. 2008. Zwitterionic polymers exhibiting high resistance to nonspecific protein adsorption from human serum and plasma Biomacromolecules 9, 1357–1361.)

adhesive molecule found naturally in byssal threads of mussels (Fig. 2.5.3.8). These threads can attach securely to various types of surfaces in a wet, tidal environment because of DOPA's unique chemistry (Herbert, 1983). On organic surfaces, the hydroxyl groups present on DOPA are oxidized and covalently attach themselves to the surface, whereas the same hydroxyls can attach via hydrogen-bonding to inorganic surfaces (Lee et al., 2006). DOPA is hence a versatile and powerful adhesive over a wide range of surface types. Sundaram et al. utilized DOPA's property to design a simple, one-step dip-coating or wash-through methodology for grafting pCB polymers to a variety of surfaces including PDMS, PVC, and PP (Fig. 2.5.3.10) (Sundaram et al., 2014). The simple approach and broad application across polymers make this an attractive option for the diverse materials within artificial lungs and ECMO circuits. The challenge with this approach is that a high grafting density may not be achieved due to the steric effects imposed by the long, bulky polymer chains.

Graft-from approaches have also been investigated. This approach, however, requires premodification of the surface with an initiator for polymerization but, theoretically, allows for greater grafting density. Surface-initiated atom transfer radical polymerization (SI-ATRP) of pCB on PDMS (Hong et al., 2017), SI-ATRP of pSB on polysulfone membranes (Yue et al., 2013), and single electron transfer-living radical polymerization of SB and CB brushes over a flat polymethylpentene sheet have all been demonstrated (Obstals et al., 2018). Mussel-derived peptides were also used as initiators for polymerizing pSBMA over metal oxides, gold, and polycarbonate (Kuang and Messersmith, 2012). Higher grafting density should yield reduced fouling; however, the scalability of this approach for larger specimen, such as full-scale artificial lungs, remains a challenge (Sun et al., 2017).

All of these approaches are currently being examined for application to artificial lungs. A DOPA-pCB coating on PDMS sheet demonstrated a 77% reduction in platelet binding over the control following 8 h of in vitro citrated platelet-rich plasma recirculation (Amoako et al., 2016), while an identical study using PMEA coatings demonstrated only a 17% reduction (Gupta et al., 2014). A pSB



• **Figure 2.5.3.10** Polycarboxybetaine (pCB) coating using 3,4-dihydroxyphenylalanine (DOPA) to attach pCB to the device surface. (Reproduced from Sundaram HS, Han X, Nowinski AK, Brault ND, Li Y, Ella-Menye, J-R, Amoako, KA, Cook, KE, Marek, P, Senecal, K, Jiang, S. 2014. Achieving One-Step Surface Coating of Highly Hydrophilic Poly(Carboxybetaine Methacrylate) Polymers on Hydrophobic and Hydrophilic. Surfaces Adv Mater Interfaces 1(6), 2014.)

copolymer-coated PMP hollow-fiber membrane achieved an 80%–95% reduction in platelet deposition from citrated whole blood following a 3h incubation (Malkin et al., 2018). Ultimately, however, the true test of pCB and pSB coatings is their long-term function in contact with whole blood. A lightly cross-linked pCBMA hydrogel was used to coat glucose sensors, and the sensors showed high measurement sensitivity and accuracy after 42 days, while the control failed after 2 days (Yang et al., 2012). This suggests an elimination of bulk clot formation. Studies demonstrating that pCB coatings can be applied to full-scale artificial lungs and reduce coagulation during long-term testing are only now emerging but have been promising. A sheep VV-ECMO study was conducted by Ukita et al. to determine the optimal grafting method for pCB coating in a miniature artificial lung (Ukita et al., 2019). The parallel, head-to-head testing demonstrated that DOPA-pCB was the most effective grafting strategy over SI-ATRP or copolymerization approaches. Moreover, the same DOPA-pCB approach was used to coat a small artificial lung circuit tip-to-tip and was tested in a rabbit VV-ECMO model for 4 hours. This model demonstrated that the coating reduced clot formation by 59%.

Nitric Oxide Surface Flux

Another approach to reducing thrombosis is to actively provide anti-platelet activity at the material surface via surface nitric oxide (NO) flux. Nitric oxide is normally produced by endothelium in the vasculature, causing both vasodilation and platelet inhibition. Nitric oxide is small, lipophilic, and is thus able to diffuse easily through platelet membranes. Inside the platelet, it activates guanylyl cyclase, inhibits phosphoinositide 2-kinase, impairs calcium influx, reduces binding to platelet agonists such as thrombin, ADP, and thromboxane, and reduces GpIIb/IIIa receptor expression. Nitric oxide thus limits platelet activation, adhesion, and aggregation. Importantly, the robust antiplatelet effect of NO is localized to where it is released due to its short, 0.05–2 ms half-life in whole blood (Thomas et al., 2001). Thus, NO can be used to create localized anti-thrombotic activity at a biomaterial surface, including those of artificial lungs. When released from or generated at a biomaterial surface, NO inhibits platelets near the surface, but those same platelets return to normal function while flowing back to the patient. Therefore, NO flux in extracorporeal devices does not cause bleeding like systemic anticoagulants. On the other hand, binding of NO to hemoglobin in red blood cells results in methemoglobin (MetHb) formation. MetHb is a form of hemoglobin that cannot effectively deliver oxygen. Therefore, at high concentrations, MetHb will decrease oxygenator efficiency and cause tissue hypoxia (Stepuro and Zinchuk, 2006). As a result, NO flux rates must be limited.

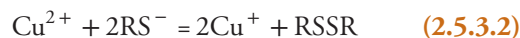
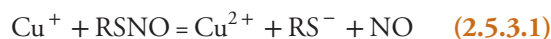
NO has been used as a surface anti-platelet agent in three ways: (1) release from NO donors located within circuit polymeric materials (NOrel), (2) generation from endogenous donors in blood (NOgen), and (3) NO

delivery via the artificial lung sweep gas. In general, surfaces with NO flux rates greater than the endothelium ($>0.5 \times 10^{-10}$ mol/min/cm²) reduce platelet consumption and clot formation, and this inhibition is linearly related to NO flux during short-term (<4h) in vitro or in vivo (Amoako and Cook, 2011). Blood clotting time at a PDMS surface, for example, is 2–4 times normal at NO flux rates of $1.4\text{--}3.6 \times 10^{-10}$ mol/min/cm².

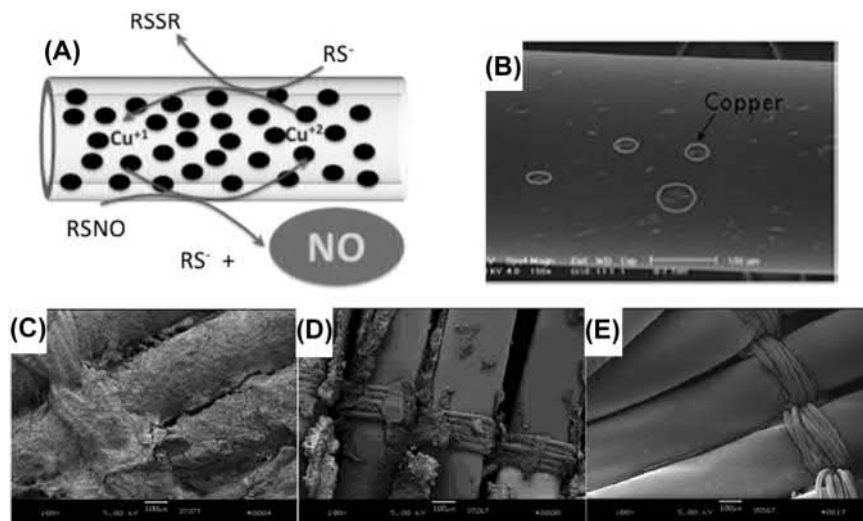
NO release is not the best choice for an artificial lung, as artificial lung fibers are thin, and the NO payload would not be sufficient for long-term use. On the other hand, NO release has been tested extensively in the polymer tubing used to connect devices in the ECMO circuit. Platelet losses are typically reduced from 60% to 25% when NO is released from Tygon tubing during short-term (4h) in vivo extracorporeal circulation studies using tubing-only circuits (Zhang et al., 2003; Major et al., 2010; Handa et al., 2013; Amoako et al., 2012). Unfortunately, tubing represents <10% of the typical surface area of artificial lung circuits, is less thrombogenic than the oxygenator, and is thus a lesser player in circuit coagulation.

The simpler and more common mode of NO delivery in oxygenators is via the artificial lung sweep gas. Published studies using less than 100 ppm in the sweep gas demonstrate either small or no platelet inhibition (Keh et al., 1999), while use of 500–1000 ppm significantly reduced platelet adhesion to the oxygenator (Sly et al., 1996). Unfortunately, these higher concentrations also increased metHb to almost 9%. The ideal range is thus likely between 100 and 500 ppm. Concentrations of 100 and 200 ppm do not increase metHb levels significantly, but 500 ppm increases their levels to approximately 5% (Demarest, 2017). The benefit to platelet binding, however, is small in this range (Amoako et al., 2016; Demarest, 2017) in part due to conversion of NO to nitrates when delivered with oxygen in the sweep gas.

The last means of supplying NO is generating it from donors that are already in blood and/or supplied intravenously. This method can provide a constant supply of surface NO that is less diminished by formation of nitrates and nitrites. The most common method for NO generation is incorporating copper (Cu) particles in the biomaterial surface as a catalyst to decompose NO donors in the blood (Noble et al., 1999; Wang et al., 2002). As a stoichiometric reaction (Eqs. 2.5.3.1 and 2.5.3.2), the rate of NO release can be controlled with the availability of NO donor and how much Cu is exposed to the donor:



This reduction–oxidation reaction can cycle indefinitely if there is a supply of NO donors. For artificial lung fibers, this has been accomplished by incorporating Cu nanoparticles in polydimethylsiloxane (PDMS; Fig. 2.5.3.11) (Amoako et al., 2013; Amoako and Cook, 2011; Lai et al., 2019).



• **Figure 2.5.3.11** Nitric oxide (NO) generating polydimethylsiloxane (PDMS) surface applied to artificial lung hollow fibers, including (A) mechanism of NO generation, (B) copper nanoparticles in the fiber wall, (C), (D) typical clot formation on control fibers without copper, and (E) typical clot formation on NO-generating fibers. (Reproduced from Amoako K A., Montoya PJ, Major TC, et al. 2013. Fabrication and in vivo thrombogenicity testing of nitric oxide generating artificial lungs *J Biomed Mater Res Part A* 101, 3511–3519.)

Surface NO generation was catalyzed via copper nanoparticles within PDMS gas exchange fibers in a 4-h, pumpless arteriovenous ECMO rabbit model using a continuous infusion of S-Nitroso-N-acetylpenicillamine (SNAP) as the NO donor (Amoako et al., 2013). This study demonstrated a markedly lower increase in blood flow resistance and less clot formation on NO-generating hollow fibers. Additionally, the surface-generated NO did not create an increase in metHb over the 4 hours. NO-generating fibers also showed significantly reduced blood flow resistance, increased device lifespan, and reduced clot formation on the hollow fibers when compared to standard PMP fibers in a 72-hour, pumped veno-venous ECMO sheep model (Lai et al., 2019). However, this method is limited in two ways: (1) copper leaches off fibers into the vasculature, and this could lead to excessive copper delivery and resulting toxicity, and (2) the copper is likely to reduce the gas permeability and gas transfer. Despite these negatives, this method of NO delivery has the most experimentally demonstrated benefit.

Renal Replacement Therapies and Therapeutic Apheresis

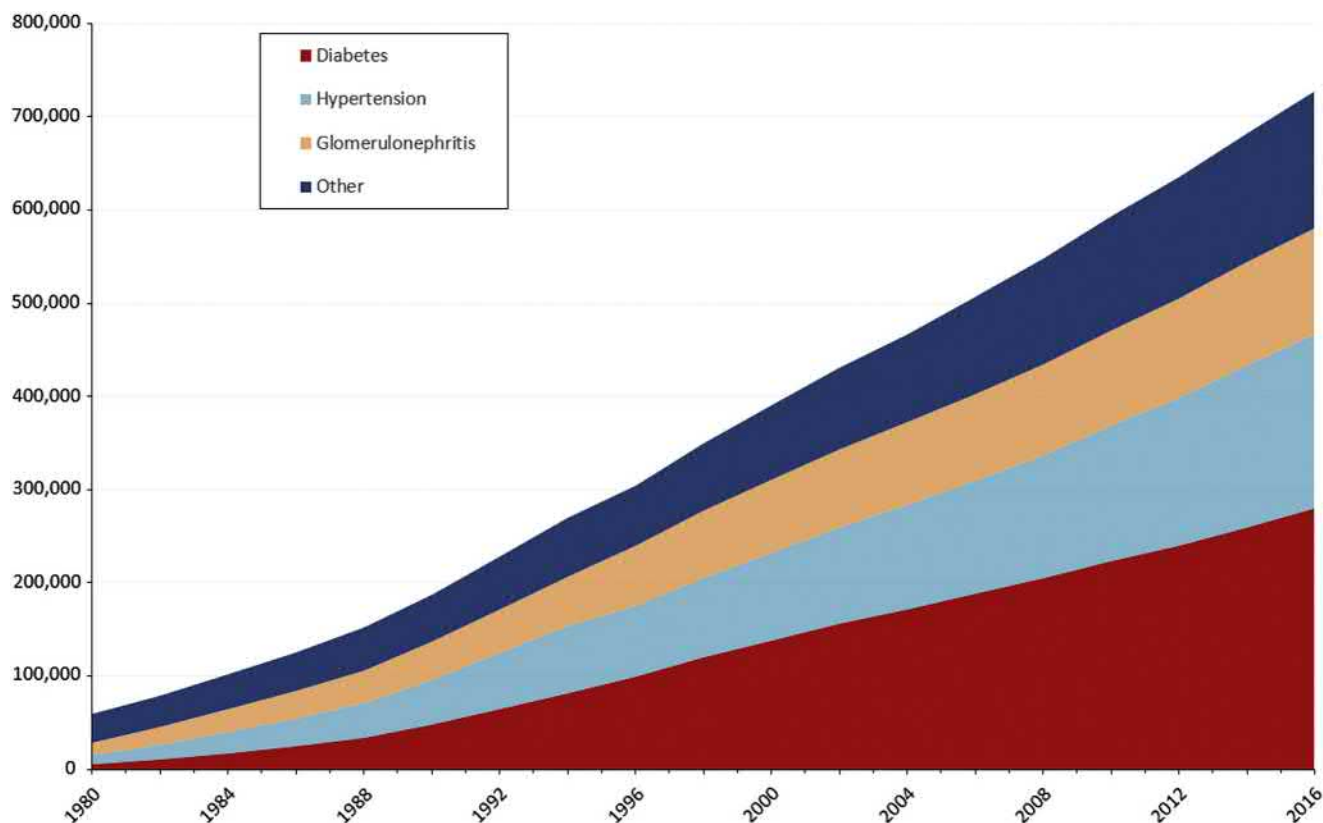
Introduction

The purpose of renal replacement therapies and therapeutic apheresis is to remove toxins and metabolic waste products from the blood and to maintain the volumetric and osmotic balance of the patient. The vast majority of these procedures are performed intermittently, or as a temporary partial or total replacement. All these procedures involve the contact of blood with biomaterials, mechanical pumping of the blood, and mass transfer to and from the blood. As with artificial lungs, blood-biomaterial compatibility is essential to the success or failure of a procedure.

Renal Replacement Therapy

Renal replacement therapy describes treatments such as peritoneal dialysis, hemodialysis, and hemofiltration, used to detoxify blood in cases of renal insufficiency. Renal insufficiency may be caused by: acute renal failure, typically of rapid onset and due to external causes; or chronic renal failure, usually due to damage to the tissues of the kidneys. Chronic renal failure may be caused by infection, toxins, or hypertension, and may also arise as a complication in diabetes mellitus. The number of prevalent (i.e., alive and receiving treatment) patients with end-stage renal disease in the United States between 1980 and 2016 is given in Fig. 2.5.3.12 (USRDS, 2009, 2018). As can be seen from the graph, the incidence of chronic renal failure has risen steadily since 1980, and diabetes has become the prominent cause of renal failure, accounting for some 38.5% of all cases in 2016, followed by hypertension, and glomerulonephritis. Of the 726,331 surviving ESRD patients listed by the United States Renal Data System in that year (USRDS, 2009, 2018), 215,061 (29.6% of the total) had received a transplant that was still functioning. The other patients were dependent upon renal replacement therapy.

In 2016, there were 511,270 patients receiving renal replacement therapy in the United States, of whom 89.6% received hemodialysis treatment. Blood may be treated by extracorporeal hemodialysis (famously known as dialysis), peritoneal dialysis, and extracorporeal hemofiltration (a form of plasmapheresis). Fig. 2.5.3.13 shows the numbers of patients treated by blood purification therapies in the United States between 1980 and 2016 (USRDS, 2009, 2018). As can be seen, as the patient population has increased, the number and proportion of patients treated by hemodialysis has increased similarly. The number of patients treated by peritoneal dialysis has remained at around 10% of the total, with 51,057 in 2016. The proportion



• **Figure 2.5.3.12** Prevalence and causes of chronic renal failure in the USA, 1980-2016. Source: United States Renal Data System (USRDS) Annual Data Reports, 2009 and 2018. Data is as at December 31st of stated year.¹

of patients treated by hemofiltration is very small, as this is predominantly used in intensive care medicine, particularly in the treatment of multiple organ failure (Coles and El Nahas, 2000).¹

Function of the Kidney

The kidney is responsible for maintaining the osmotic and water balance of the body; for detoxification and the removal of metabolic waste; and endocrine functions. It operates by a combination of filtration, selective reabsorption, and active secretion. The functional unit of the kidney is the nephron, of which there are approximately one million in each kidney. Fig. 2.5.3.14 shows a schematic representation of a nephron, and its associated specialized blood vessels.

In the glomerulus, the whole blood is filtered. The filtrate contains water and solutes with a molecular weight below 60,000 (small proteins, amino acids, glucose, urea, and ionic solutes), of similar composition to blood plasma. Approximately 10% of the blood volume entering the glomerulus is filtered here. The remaining blood passes into the peritubular capillaries and vasa recta while the filtrate enters the proximal convoluted tubule. Within the remaining structures of the kidneys, water, small proteins, and solutes are reabsorbed

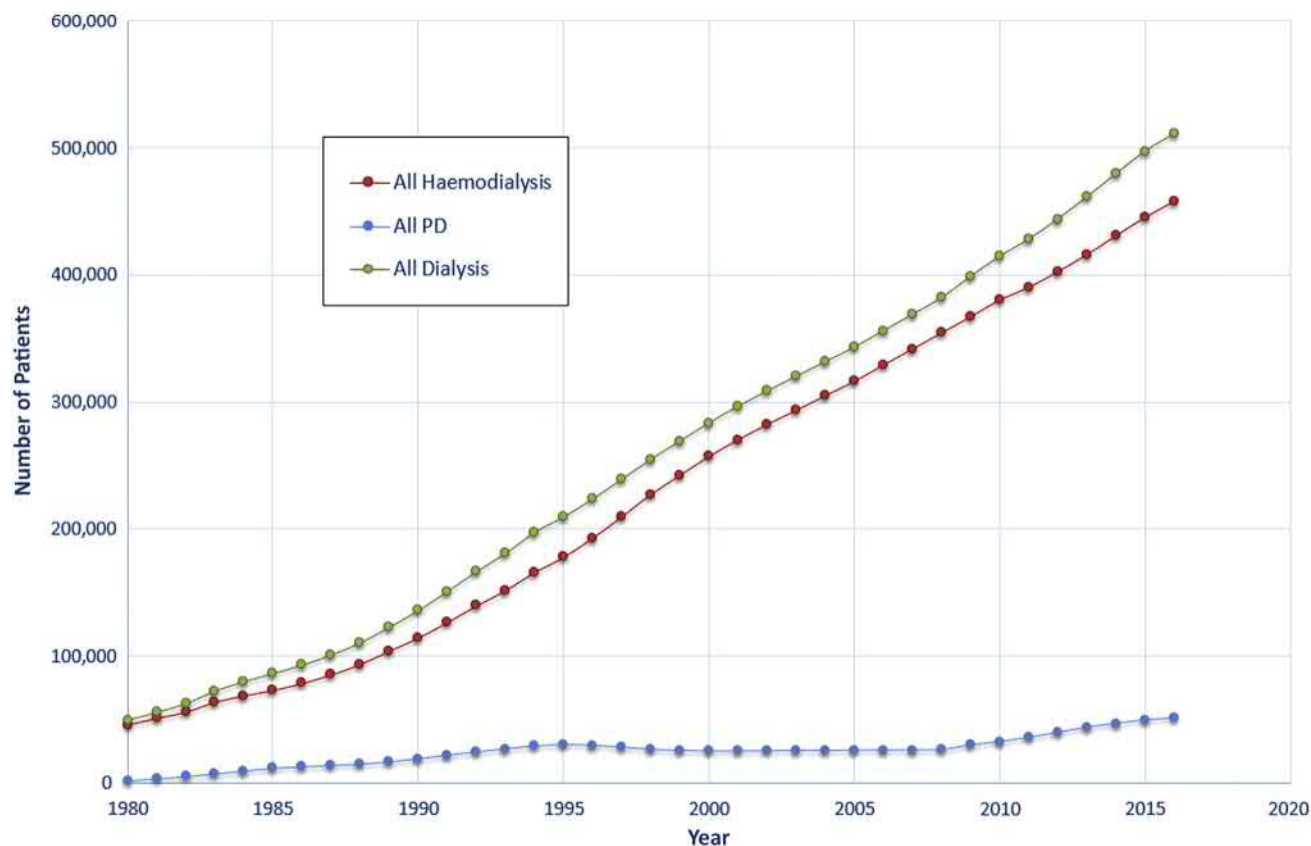
by active and passive processes, while certain metabolites are secreted directly into the tubular fluid. These processes result in a net reabsorption of approximately 98%–99% of the water filtered, and total reabsorption of glucose, proteins, and amino acids from the filtrate. A healthy individual will excrete 1–2 L of concentrated urine per day, on average.

In addition to its excretory function, the kidney also has regulatory and endocrine functions. It controls the acid–base balance of the blood, and the water balance of the body, through selective secretion of H^+ into the urine to control pH, and the action of antidiuretic hormone, which controls the urine concentration. The kidney plays a role in the regulation of blood pressure through secretion of renin and tissue hormones (prostaglandins). The kidney also secretes erythropoietin, which promotes red blood cell formation in the bone marrow.

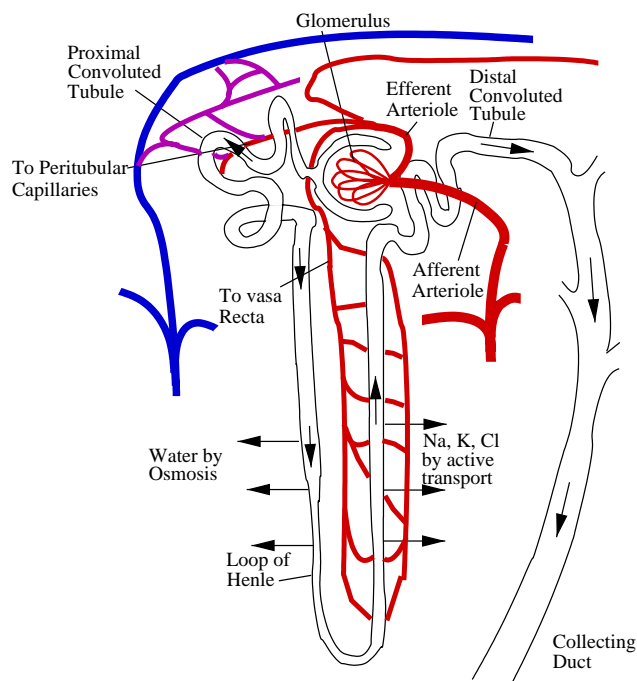
Treatment of Renal Failure

In its initial stages, chronic renal failure (end-stage renal disease, or ESRD) is treated conservatively. As the disease progresses, blood purification is needed to remove toxins from the blood (Wing and Jones, 2000). The severity of chronic renal failure may be reduced by restricting a patient's protein, potassium (K^+), and water intake through carefully managed diets, and the administration of bicarbonate supplements to maintain a healthy blood pH. Erythropoietin supplements are given to maintain the patient's hematocrit (Coles and El Nahas, 2000). As the disease progresses, some form of renal replacement therapy becomes necessary.

¹The data reported here have been supplied by the United States Renal Data System (USRDS). The interpretation and reporting of these data are the responsibility of the author(s) and in no way should be seen as an official policy or interpretation of the U.S. government.



• **Figure 2.5.3.13** Number of patients receiving regular dialysis (hemodialysis and peritoneal dialysis) in the USA, 1980–2016. Source: United States Renal Data System (USRDS) Annual Data Reports, 2009 and 2018.

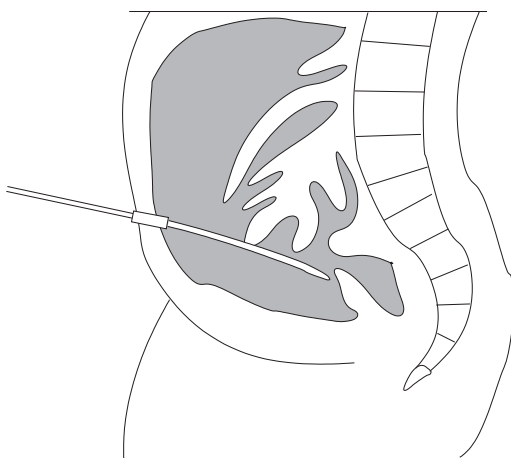


• **Figure 2.5.3.14** Structure of a renal nephron.

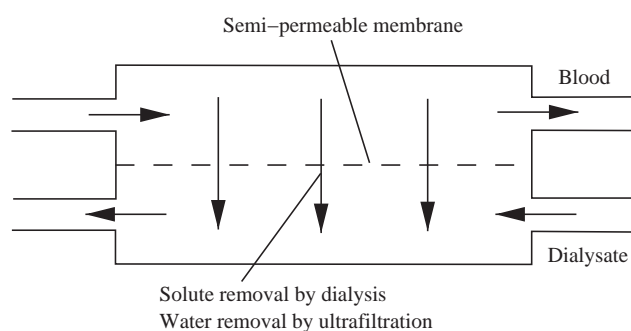
Peritoneal Dialysis

Peritoneal dialysis uses the peritoneum, the membrane lining the walls of the abdominal cavity, and the abdominal organs for mass exchange. Dialysate is introduced into the peritoneal cavity through a catheter, as shown in Fig. 2.5.3.15. While

in the peritoneal cavity, metabolic wastes such as urea and creatinine, toxins, and excess solutes (K^+ , for example) are transferred from the blood into the dialysate by dialysis, while water is removed by osmosis (Sargent and Gotch, 1996). Used dialysate is then removed.



• **Figure 2.5.3.15** Positioning of catheter in peritoneal cavity for peritoneal dialysis.



• **Figure 2.5.3.16** Principle of dialysis.

Peritoneal dialysis is dependent on a number of factors. The rate of solute removal is dependent on the blood flow in the capillaries of the peritoneum and its permeability, as well as on concentration gradients between the blood and the dialysate. In addition, the suitability of a patient for treatment by peritoneal dialysis is often dependent on the amount of residual renal function.

There are two principal forms of peritoneal dialysis therapy. *Continuous ambulatory peritoneal dialysis* (CAPD) is the most commonly used form, particularly in younger patients who can manage their own therapy. In this treatment method, the dialysate is infused into the peritoneal cavity, allowed to dwell for a set length of time, then drained and replaced with fresh dialysate. Typically, a patient would perform between five and six exchanges per day (Malchesky, 2004). It has the advantage that it offers patients a certain amount of independence, as they are not tied to any equipment for the majority of the time.

In *automated peritoneal dialysis* (APD), also known as continuous cycler-assisted peritoneal dialysis (CCPD), a machine (cycler) performs the exchanges, usually at night while the patient is sleeping. APD can increase the clearance of metabolites considerably, particularly in patients with rapid rates of exchange between the peritoneum and the dialysate (high or fast transporters). In APD treatment, the cycler will perform several complete exchanges in a night, with a complete cycle of infusion, dwell, and drainage being completed in 30 min or less, and treatment for 8–12 h in

total. APD is sometimes referred to as *intermittent peritoneal dialysis*, if the APD is only performed at night. Many patients use a combination of CAPD during the day and APD at night.

Toxin removal in peritoneal dialysis is the sum of the patient's residual renal function and the toxin removal by hemodialysis. The overall removal of toxins, metabolites, and water must be sufficient to keep the patient healthy. As water removal is dependent on the osmotic pressure of the dialysate, dialysate is supplied in three different strengths: 3.86% glucose, 2.27% glucose, and 1.36% glucose. All three strengths are hypertonic and will result in water transfer to the dialysate, the rate of transfer is dependent on the osmotic gradient. A more concentrated dialysate will increase the ultrafiltration rate, and hence the removal of solutes as well as water will be enhanced; however, the stronger dialysate concentrations are only used when necessary, and most transfers are performed using the standard (1.36%) dialysate strength.

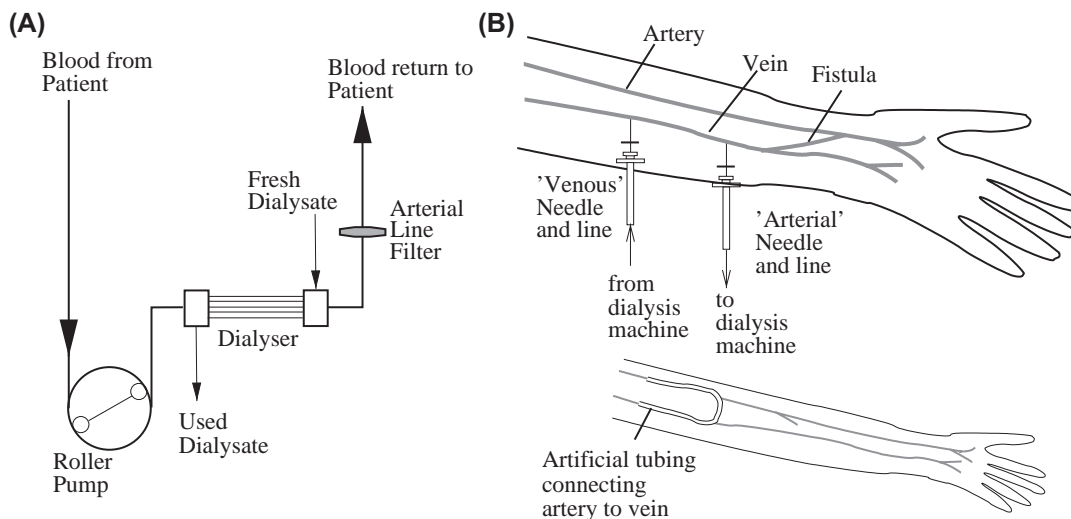
Peritoneal dialysis has the advantage that the patient's blood does not come into contact with any artificial surfaces, hence there is no need for anticoagulation. It has the disadvantage that the dialysate has to be infused into a body cavity, with the attendant risk of infection (Malchesky, 2004). It is vital to ensure the sterility of the dialyzing solutions and to prevent infections at the access site. The most common complication of peritoneal dialysis is peritonitis, and this is also the most common reason for the discontinuation of PD. In most cases where peritoneal dialysis has to be discontinued, patients will begin treatment by hemodialysis.

Hemodialysis

Dialysis is the process of solute transfer across a semipermeable membrane, and is similar in principle to diffusion. It is a passive process, with solute molecules that are small enough to pass through the membrane traveling from an area of high solute concentration to an area of low solute concentration. Typical hemodialyzers use membranes with a molecular weight cut-off between 5000 (low-flux membranes) and 20,000 (high-flux membranes) (Boure and Vanholder, 2004) and a surface area of between 0.5 and 2.1 m².

In the hemodialyzer, blood flows through membrane hollow fibers, with dialysate flowing in countercurrent fashion, as shown in Fig. 2.5.3.16. Metabolic wastes such as urea and creatinine are transferred from the blood into the dialysate, due to the concentration gradient. The dialysate must be carefully formulated to ensure that normal concentrations of glucose and blood solutes are maintained. The blood and dialysate are osmotically balanced, hence any solute removal is by ultrafiltration, due to the differential pressure ($P_B - P_D$) between the blood and dialysate compartments.

Hemodialysis is an intermittent therapy, and is typically administered every 48 h, with sessions lasting up to 6 hours at a time (Malchesky, 2004). The limiting factor for hemodialysis session duration is the rate of water removal, as water can only be drawn out of the blood plasma, and rates of fluid transfer from the intracellular fluid and interstitial



• **Figure 2.5.3.17** (A) Circuit for hemodialysis. (B) Hemodialysis access from arteriovenous fistula (top) and from a graft (bottom) (Wing and Jones, 2000).



• **Figure 2.5.3.18** Hollow fiber dialyzer (Terumo Clirans C061) with end cap removed to show arrangement of hollow fibers.

fluid pools to the plasma (plasma refilling) must be sufficient to maintain normal blood pressure.

Fig. 2.5.3.17A shows a typical hemodialysis circuit, incorporating a blood pump, dialyzer, and arterial line filter. Blood is drawn from a dialysis access (Fig. 2.5.3.17B), usually located in the arm, and pumped through the dialyzer (Fig. 2.5.3.18) at rates varying between 50 and 400 mL/min, depending on the condition of the patient, particularly the blood flow and blood pressure within the access vessel and the required solute clearance and ultrafiltration rates. The dialysate is either prepared in batches, or continuously, typically by mixing concentrate and processed mains water. Dialysate flow rates vary within the range of 300–800 mL/min, with most procedures performed at 500 mL/min. A higher dialysate flow rate will increase the clearance of solutes from

the blood, but this increase in performance has to be balanced against the increased cost of the dialysate used.

Dialyzer Materials and Coatings

Dialyzer materials are chosen based on two main characteristics: waste clearance and biocompatibility. The ideal fiber has well controlled pore sizes to create a sharp drop in the permeability at a specific molecular weight. Low-flux dialyzers remove low-molecular-weight solutes (<500 Da), including urea (60 Da), creatinine (113 Da), and phosphate (134 Da). High-flux dialyzers are designed to also allow the loss of middle- to high-molecular-weight solutes (500–15,000 Da) and protein-bound uremic toxins (>15,000 Da) (National Kidney Foundation, 2013). In an attempt to mimic the human kidney, the Japanese Society of Dialysis Therapy (JSdT) recommends that pore sizes allow less than 3g of albumin (66,000 Da) lost per session with a blood flow rate of 200 mL/min and a dialysate flow rate of 500 mL/min (Saito, 2011).

The first dialyzers utilized cellulose membranes, but these are no longer used due to issues with biocompatibility. In particular, the cellulose surface contains hydroxyl groups that bind complement fragment C3b, slowing its inactivation by plasma inhibitors. This allows activation of the alternative complement pathway, neutrophil and monocyte activation, and inflammation (Cook and Mockros, 2002). As a result, cellulose was chemically modified to replace the hydroxyl group with acetate to form cellulose acetate, diacetate, or triacetate. Despite this improvement, greater flux and biocompatibility were desired, leading to the development of other hollow-fiber materials. Current dialyzers thus utilize polysulfone (PS), polyethersulfone (PES), polyester polymer alloy (PEPA), polyacrylonitrile (PAN), and polymethylmethacrylate (PMMA) fibers (National Kidney Foundation, 2013; Ahmad et al., 2014). The PS, PES, and PEPA membranes are hydrophobic and thus are all mixed with polyvinylpyrrolidone (PVP) to achieve surface hydrophilicity. This improves waste transport and filtration during hemofiltration, and reduces protein adsorption and platelet adhesion (Kokubo et al., 2015a,b).

The AN69 PAN membrane possesses a significantly negative charge, and this leads to increased activation of FXII, the contact system, and generation of bradykinin. Bradykinin is known to cause increased capillary permeability and blood vessel vasodilation. Under normal circumstances, bradykinin is deactivated by angiotensin-converting enzyme (ACE). However, in patients taking ACE inhibitors to control blood pressure, bradykinin deactivation is insufficient and patients can develop a dangerous anaphylactic-like response leading to severe hypotension. In order to remedy this, the AN69ST fiber utilized a polyethylenimine (PEI) polycation spacer molecule. The addition of this polycation thus changes the adsorptive character of this surface, resulting in significant increases in the adsorption of cytokines (Shiga et al., 2014), fibroblast growth factor (Yamato et al., 2016), and anticoagulants such as heparin and nafamostat mesilate (Hirayama et al., 2017; Nakamura et al., 2017).

The ability of AN69ST to adsorb heparin has been used in an attempt to reduce or eliminate systemic heparin when dialyzing patients with a history of bleeding issues. In initial studies, the circuit was prerinsed with a heparin solution to adsorb the heparin and then used normally. Unfortunately, studies examining the frequency of circuit failure due to clot formation showed no significant improvement over polysulfone fibers (Brunet et al., 2011). One small study, however, has demonstrated the ability to reduce rather than eliminate systemic anticoagulation (Sanchez-Canel et al., 2012). Subsequently, heparin has begun to be preadsorbed during the manufacturing process, leading to the HeprAN membrane (Thomas et al., 2011). A study of 45 dialysis patients demonstrated that the HeprAN fiber allowed for a reduction in systemic heparin anticoagulation in 67% of patients (Kessler et al., 2013).

Heparin coating has also been employed on unmodified cellulose fibers (Lee et al., 2004) and, more recently, polysulfone fibers. The poor biocompatibility of cellulose fibers likely halted further research on their surface coating (Kessler et al., 2015); the polysulfone coatings appear promising (Ren et al., 2013), but there has been no evaluation of their clinical benefits.

Vitamin E coatings are also applied to dialysis membranes. One of the complications of dialysis over long-term treatment is amyloidosis and atherosclerosis. Both are thought to be caused by repeated oxidative stress imposed over time by hemodialysis. To combat this, vitamin E-coated PS membranes have been developed. In small studies, these membranes have demonstrated reduced oxidative stress (Satoh et al., 2001; Clermont et al., 2001), reduced activation of the contact system of the coagulation cascade, and platelet surface binding (Sasaki, 2006).

In addition to the membranes of the hemodialyzer, the blood will also come into contact with the tubing and connectors used in the extracorporeal circuit. Commonly used materials for blood tubing include poly(vinyl chloride) (PVC), polyurethane, and silicone rubber (PDMS, polydimethyl siloxane). However, the area of these materials, and the exposure time, is much lower than for the functional membrane surface.

Coagulation and Inflammation During Hemodialysis

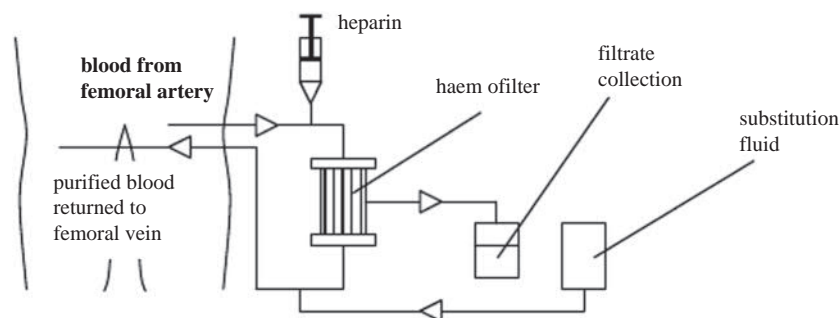
Much like artificial lungs, the large, densely packed artificial surfaces of dialyzers cause significant protein adsorption, direct activation of the coagulation cascade and complement, platelet adhesion and activation, and white cell activation. As a result, clot forms rapidly on the dialyzer surface unless significant anticoagulation is used, and the patient is exposed to repeated systemic activation of coagulation and inflammation during each treatment. All blood returning to the patient is filtered to ensure that thromboemboli cannot enter the patient's bloodstream.

To combat coagulation, heparin is the anticoagulant of choice. In the United States, unfractionated heparin is typically used, whereas in Europe, low-molecular-weight heparin is recommended by the European Best Practice Guidelines (Kessler et al., 2015). Unlike ECMO, there is no "typical" heparin dose: heparin doses are tailored based on experience with patients' bleeding propensity during hemodialysis and vary widely from dialysis facility to facility (Davenport et al., 2014). Heparin is delivered as an initial bolus and may then be followed by either a continuous drip, hourly heparin boluses, or no additional heparin at all. Although there is no standard, an example of the former method would be to deliver an initial bolus of 2000 U, followed by 1200 U/h. When repeated boluses are given, 500–750 U may be given hourly (Davenport et al., 2014). In places that reuse dialyzers, heparin doses are increased to limit the formation of clot and loss in dialyzer function. Unlike ECMO, the degree of anticoagulation is typically not monitored due to the short duration, relatively low bleeding complication rate during hemodialysis, and cost.

In addition to heparin, several other anticoagulants have been attempted to decrease the relative risks of dialyzer coagulation and patient bleeding. These include direct platelet inhibitors (prostacyclin) and other systemic inhibitors of the coagulation cascade, such as heparinoids (danaparoid, fondaparinux), direct thrombin inhibitors (hirudin, argatroban, melagatran, lepirudin, bivalirudin), and the broad-spectrum serine protease inhibitor nafamostat mesilate. Like heparin, these anticoagulants inhibit both surface-induced coagulation as well as tissue-based coagulation and thus offer little advantage over heparin. One attempted solution to this problem is regional citrate anticoagulation (RCA). In this method, citrate is used to chelate calcium and thus anticoagulate blood just prior to the dialyzer blood inlet. Calcium is then added back to the blood prior to it returning to the patient. Although offering some potential benefits, this method is cumbersome, complicated, and thus costly to employ (Kessler et al., 2015). Therefore, this also has not supplanted heparin use.

Extracorporeal Hemofiltration

Extracorporeal hemofiltration is mostly used in the treatment of acute renal failure, particularly where renal failure is accompanied by fluid overload. The toxins and excess water are removed by ultrafiltration, and fluid balance is maintained by addition of an isotonic substitution fluid "downstream" of the filter (see Fig. 2.5.3.19). This method is particularly effective in the removal of toxins, although as the substitution fluid is mixed directly with the blood,



• **Figure 2.5.3.19** Schematic showing access and extracorporeal circuit for hemofiltration.

and hence enters the body directly, it is very expensive to prepare. Its principal advantage over dialysis is the enhanced removal of solutes from the blood, of particular importance in cases of poisoning and multiple organ failure.

The most modern hemofiltration techniques use pure hemofiltration (convective transfer) in combination with dialysis (diffusive transfer) to achieve the desired blood purification. This technique is usually referred to as hemodiafiltration or high-flux dialysis; the set up is similar to that for conventional dialysis, although the vascular access is still arterio-venous (Malchesky, 2004).

Hemoperfusion

The term hemoperfusion applies to the direct perfusion of whole blood over a sorbent bed or reactor. The sorbent used may be activated charcoal, nonionic or ionic resins, or immunosorbents, while reactors may contain enzymes, cells, or tissues. The purpose of the treatment is either to remove specific toxins or metabolites, or to carry out specific biochemical reactions. Issues with biocompatibility, safety, and immunological isolation have limited the application of hemoperfusion to the use of charcoal and resins as sorbents (Kambic and Nose, 1993).

Sorption of the solute into the sorbent is based on chemical affinity, rather than molecular size. Due to the nature of the sorbent granules, the surface area for sorption is very high, but it also makes it possible for particulates to be released from the reactor into the blood. The nonspecific nature of charcoal sorption can also lead to the removal of beneficial compounds from the blood. For these reasons, hemoperfusion has largely been superseded by plasma treatment (plasma perfusion) and sorbent dialysis, which will have a similar therapeutic effect with fewer potential hazards. The very large surface area of sorbents also leads to extensive blood–biomaterial contact, resulting in complement activation and initiation of the coagulation cascade. These events will cause a reduction in leukocyte and platelet levels in the blood.

Therapeutic Apheresis

“Apheresis” describes any technique in which a fraction of the blood (platelets, plasma, red blood cells, leukocytes) is removed, and the remaining blood is returned to the donor. This can be divided into “donor apheresis,” in which volunteers give blood fractions for the treatment of

others, and “therapeutic apheresis,” where blood fractions are selectively removed to achieve a therapeutic result.

Therapeutic apheresis can be used to treat diseases where abnormal blood proteins or cells are present in the bloodstream, and these proteins or cells are implicated in the condition’s progression. In plasmapheresis, the plasma is separated and either replaced (plasma exchange), or treated prior to recombination with the blood (plasma treatment). In cytapheeresis, one or more of the cellular components of the blood is selectively removed. Cytapheeresis is overwhelmingly used as a donation procedure, for collection of blood proteins, platelets, and immune cells, with only 0.8% of the 1562 patient cases (13 cases) studied in the 2007 International Apheresis Registry² treated with therapeutic cytapheeresis.

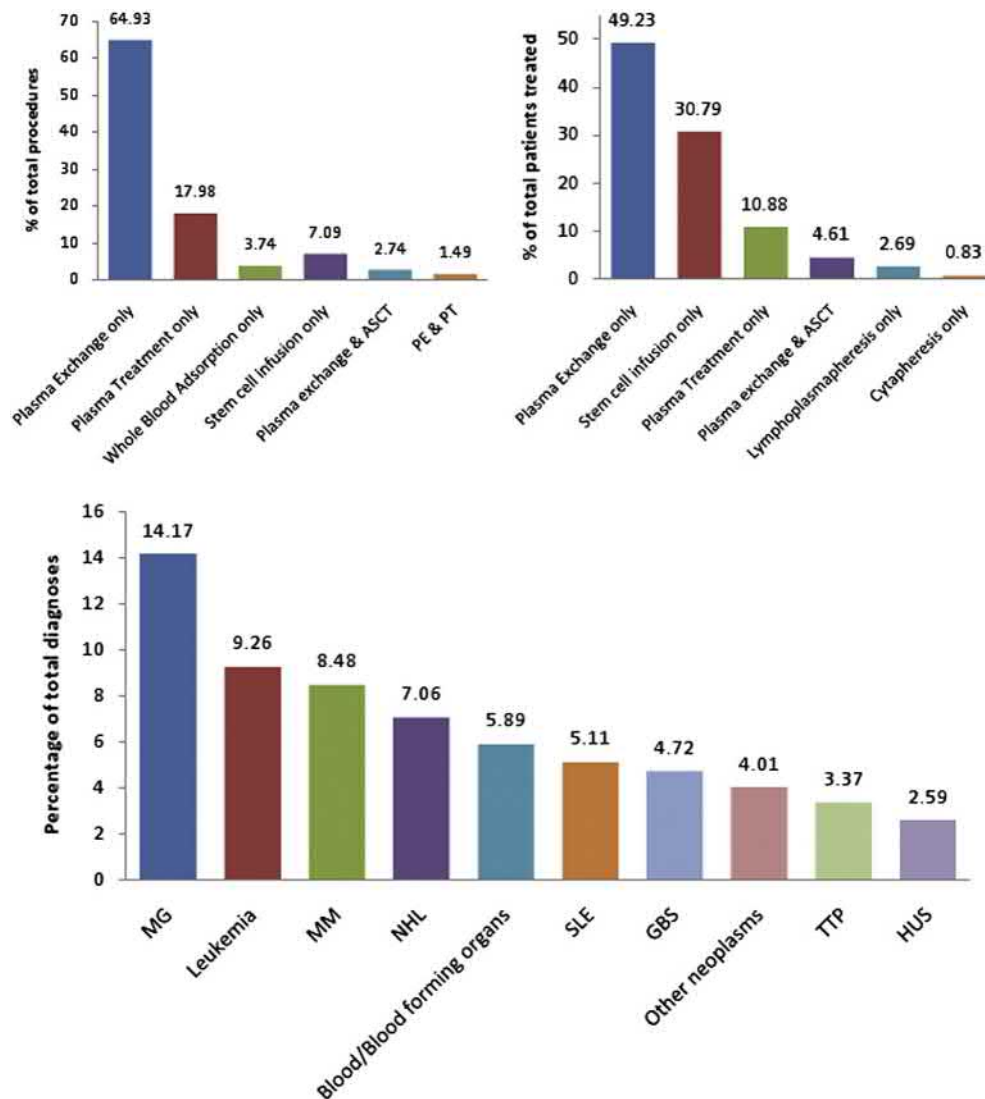
Plasmapheresis

Plasmapheresis has been used with considerable success in the treatment of a number of conditions, notably myasthenia gravis, leukemia, multiple myeloma, non-Hodgkins lymphoma, and other disorders affecting the blood and blood-forming organs (Kambic and Nose, 1993). Plasmapheresis is also used in the management of possible rejection of transplanted tissue due to ABO mismatch. Fig. 2.5.3.20 gives a breakdown of the number of treatments, number of patients treated by therapeutic apheresis, and the type of treatment used in the 2007 International Apheresis registry (Malchesky et al., 2009). Note that stem cell infusion was recorded in the survey although it is not an apheresis technique. Myasthenia gravis was the most common condition treated, both in terms of the number of patients and the number of treatments (it is a chronic condition, hence repeated treatments would be necessary), followed by leukemia (this figure does not include Hodgkins disease and non-Hodgkins lymphoma), multiple myeloma, and non-Hodgkins lymphoma.

Plasma Separation

Plasma separation can be achieved by centrifugal or membrane methods. Centrifugal methods can be batch or continuous. In a batch method, anticoagulated blood is removed from the patient, and then centrifuged to separate the plasma, red blood cells, and buffy coat (lymphocytes and platelets). In a continuous process, shown schematically in Fig. 2.5.3.21, blood is fed

²The 2007 International Apheresis registry is drawn from 20 participating centers offering apheresis treatment; these numbers should not be taken as estimates of the total number of patients worldwide.



• **Figure 2.5.3.20** Modes of treatment and conditions treated by apheresis, from the 2007 International Apheresis Registry (Malchesky et al., 2009). ASCT = Autologous Stem Cell Therapy; GBS = Guillan-Barre Syndrome; HUS = Hemolytic Uremic Syndrome; MG = Myasthenia Gravis; MM = Multiple Myeloma; NHL = Non-Hodgkins lymphoma; PE & PT = Plasma Exchange and Plasma Treatment; SLE = Systemic Lupus erythematosus; TTP = Thrombotic thrombocytopenic purpura.

into the center of a rotating bowl and centrifugal forces (in the order of $100 \times g$) cause separation into three distinct streams of red blood cells, buffy coat, and plasma (Malchesky, 2004). Table 2.5.3.2 gives the concentration, cell diameter, density and sedimentation coefficient for the constituents of whole blood. The most dense element of the blood is the red blood cells, and hence these will be most affected by the centrifugal forces, followed by the white blood cells, and then the platelets. One-stage separation can isolate the red blood cells, buffy coat, and the plasma, but two or more stages are required if concentration of specific white blood cell types is to be achieved. As the velocities used in the separation must not be too high, to prevent damage to the cells, it is usual for the plasma fraction to contain some cells—usually platelets.

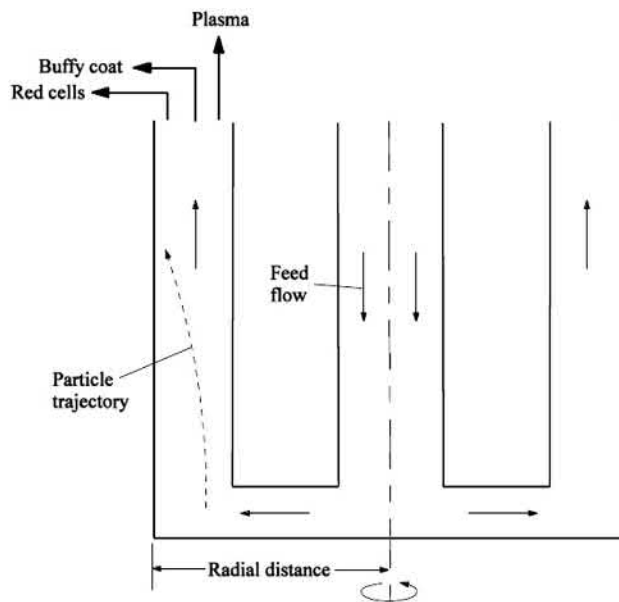
Membrane plasma separation is dependent on the pore size of the membrane and it is usual to use pore sizes much smaller than the cells to prevent sieving. Fig. 2.5.3.22 shows

the principle of membrane separation. If the pressure on the blood side is higher than the pressure on the plasma side, then there will be ultrafiltration of water and solutes with a molecular weight lower than the membrane cut off. Due to the nature of the process, the separated plasma will not contain any cells, and the concentration of macromolecular solutes in the filtrate will be almost identical to the concentration in the plasma.

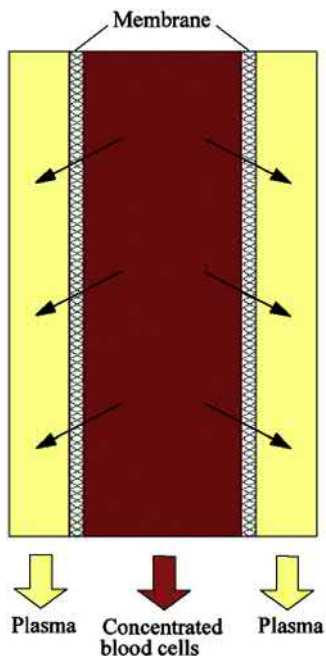
The production of particulate-free filtrate by membrane plasma separation is considered to be a key advantage of this process over centrifugal plasma separation. The absence of these particulates is particularly important if the plasma is to be treated, and then returned to the patient, as the particulates may interfere with the treatment process.

Plasma Exchange

Plasma exchange has already been introduced in the section on hemofiltration. It is the most used form of plasmapheresis, and



• **Figure 2.5.3.21** Centrifugal separation of blood into plasma, buffy coat, and red cells (adapted from Malchesky, 2004).



• **Figure 2.5.3.22** Membrane plasma separation (adapted from Malchesky, 2004).

is very effective in the removal of toxins from the bloodstream. However, it has the disadvantage that it is indiscriminate—in addition to the toxins and metabolites removed, large quantities of beneficial or physiological proteins including albumin, immunoglobulins, and clotting factors will be removed as well. This limits the volume of plasma that can be removed in a single session, and the infusion of substitution fluids carries the risk of allergic reactions or viral infections. Plasma exchange would usually be used when the specific pathogenic factors in the plasma are unknown, or where a specific technique to remove these factors is not available (Malchesky, 2004). It could also be used if a combination of factors is to be removed and plasma exchange is the simplest and most effective method

to achieve this. The substitution fluid typically contains ionic solutes and albumin, but in some cases donated whole plasma or reconstituted plasma containing plasma fractions such as immunoglobulins can be used.

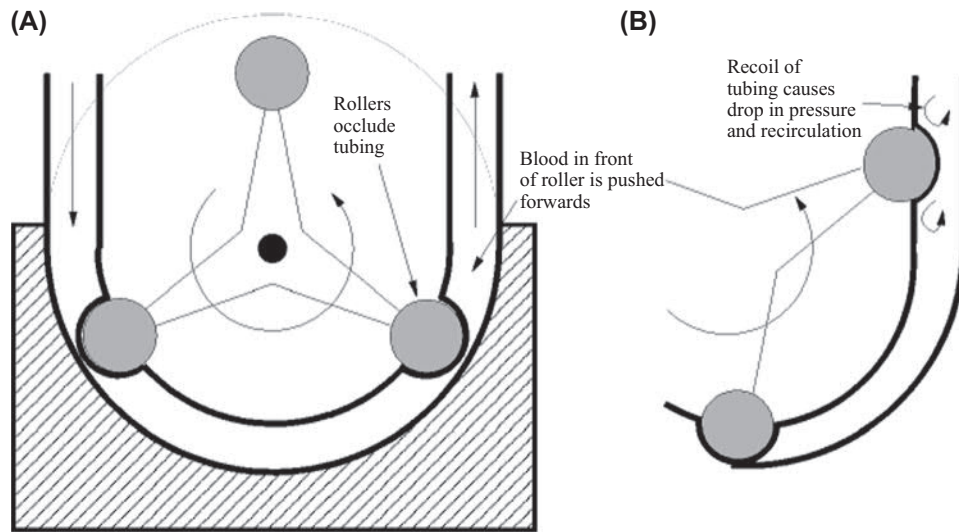
Plasma Treatment

Plasma may be treated by dialysis, membrane filtration, sorption, and processing by enzyme or biological reactions. Dialysis of fractionated plasma is similar to the dialysis of whole blood, and achieves the same result—removal of small solutes with a molecular weight below the membrane's cut-off. In membrane filtration, the plasma is filtered through one or more membranes following separation from the blood. The membrane cut-off of these membranes would be larger than a dialysis membrane, but smaller than the cut-off of the membrane plasma separator, so that larger molecules in the plasma would be filtered out. It is also possible to perform membrane filtration at temperatures below physiological levels (cryofiltration) and above physiological levels (thermofiltration). Cryofiltration is used to remove serum solutes which aggregate at lower temperatures, while thermofiltration is used to selectively remove low-density lipoproteins (LDL) in the treatment of hyperlipidemia.

The principle of plasma treatment by sorption is similar to hemoperfusion over a sorbent column. The plasma is perfused through a sorbent column to remove the targeted solutes, then recombined with the concentrated cell fraction and returned to the patient. Sorption has been used to treat poisoning, drug overdose, uremia, liver insufficiency, autoimmune disorders, and familial hypercholesterolemia.

Sorbent Dialysis

The main area of application for sorbent dialysis is the treatment of acute liver failure, a condition for which the medical prognosis is usually poor (Bosch, 2005; Galletti and Jau-regui, 2006). Improvement in patient condition has been



• **Figure 2.5.3.23** Principle of operation of a roller pump.

shown as a result of treatment by albumin dialysis (molecular adsorbent recirculating system, or MARS) and by fractionated plasma separation and adsorption (Prometheus), a form of plasmapheresis, discussed above.

The MARS system passes the patient's blood through a high-flux dialyzer, and albumin-bound toxins in the patient's blood diffuse through the membrane to bind with albumin recirculating in the primary dialysate compartment. The dialysate coming out of the dialyzer is regenerated in a series of sorbent columns (typically activated charcoal and anion exchange resin) which will remove toxins from the albumin, and a low-flux dialyzer which removes water soluble toxins. Prospective randomized controlled trials of MARS treatment in acute-on-chronic hepatic failure have shown significantly improved patient survival compared to the control group (patients receiving conventional ICU care). A meta-analysis of MARS trials has shown that further studies are needed before a final judgment can be made regarding the superiority of the MARS treatment (Bosch, 2005).

Blood Pumps in Extracorporeal Circulation

The common factor in the extracorporeal circuits described in this chapter is the need for a pump to move the blood through the circuit. In apheresis and hemodialysis, roller pumps are used, as blood flow rates are relatively small and the flexible tubing required for pumping can be easily incorporated into a single-use tubing kit.

While a full discussion of the operating principles and efficiency of the pumps used in extracorporeal circulation lies beyond the scope of this chapter, mechanical pumping of the blood will have an effect on its condition, and may add to the complications of the procedure.

Roller Pumps

In a roller pump, a section of flexible tubing is mounted against a rigid outer support, as shown in Fig. 2.5.3.23. The rollers compress a section of tubing, preventing backflow, and pushing the blood forwards. The flow from a roller pump is pulsatile, which can have a beneficial effect on mass

transfer, and if the rollers occlude the tubing completely, the flow rate is dependent on the speed of rotation of the roller head, and relatively independent of the back-pressure due to the flow resistance of the extracorporeal circuit.

The roller pump is very versatile, and flow can be reversed if this is desired. It has the disadvantage that it can damage the blood, due to high shear rates induced in the vicinity of the rollers during occlusion and particularly during the reopening of the tubing once the roller has passed. During reopening, there may be momentary backflows with very high velocities. High shear on the cell membranes can lead to premature aging of the red blood cells, which leads to aggregation and in extreme cases, to hemolysis of the red blood cells, releasing hemoglobin into the plasma.

Platelets and leukocytes are more susceptible to shear damage than red blood cells, and hence the mechanical trauma of pumping will add to the effects of blood–biomaterial contact, particularly platelet activation and leukopenia. The degree of trauma is considerably increased when high flow rates are needed—hence the roller pump is most often used in applications where flow rates are low, such as dialysis and apheresis.

Summary

Artificial lungs and kidneys save millions of lives each year via their treatment of acute and chronic organ failure. Their effectiveness is limited, however, by the negative interactions between blood and the artificial materials used to provide mass transfer within these devices. This results in clotting, inflammation, and increases in patient morbidity and mortality. These negative interactions have been significantly improved by new biomaterials that provide similar levels of mass transfer but a lesser degree of coagulation and inflammation. Despite this, a significant degree of innovation must occur before kidney dialysis has similar long-term outcomes as kidney transplantation and artificial lungs are capable of years of continuous support for patients with chronic lung diseases.

References

- Abraham, S., So, A., Unsworth, L.D., 2011. Poly(carboxybetaine methacrylamide)-modified nanoparticles: a model system for studying the effect of chain chemistry on film properties, adsorbed protein conformation, and clot formation kinetics. *Biomacromolecules* 12, 3567–3580.
- Ahmad, S., Misra, M., Hoenich, N., Daugirdas, J.T., 2014. Hemodialysis apparatus. In: Daugirdas, J.T., Blake, P.G., Ing, T.S. (Eds.), *Handbook of Dialysis*. Wolter Kluwers Health.
- Akay, B., Reoma, J.L., Camboni, D., Pohlmann, J.R., Albert, J.M., Kawatra, A., Gouch, A.D., Bartlett, R.H., Cook, K.E., 2010. In-parallel artificial lung attachment at high flows in normal and pulmonary hypertension models. *Ann. Thorac. Surg.* 90, 259–265.
- Alcantar, N.A., Aydil, E.S., Israealchvili, J.N., 2000. Polyethylene glycol-coated biocompatible surfaces. *J. Biomed. Mater. Res.* 51, 343–351.
- American Lung Association, 2008. Lung disease data: 2008. Focus: Clean Air and Lung Disease. American Lung Association. Retrieved from: <http://www.lungusa.org>.
- Amiji, M., Park, K., 1993. Surface modification of polymeric biomaterials with poly (ethylene oxide), albumin, and heparin for reduced thrombogenicity. *J. Biomater. Sci. Polym. Ed.* 4, 217–234.
- Amiji, M., Park, H., Park, K., 1992. Study on the prevention of surface-induced platelet activation by albumin coating. *J. Biomater. Sci. Polym. Ed.* 3, 375–388.
- Amoako, K., Cook, K.E., 2011. Nitric oxide-generating silicone as a blood-contacting biomaterial. *Am. Soc. Artif. Intern. Organs J.* 57, 539–544.
- Amoako, K.A., Archangeli, C., Handa, H., Major, T., Meyerhoff, M.E., Annich, G.M., Bartlett, R.H., 2012. Thromboresistance characterization of extruded nitric oxide-releasing silicone catheters. *ASAIO J.* 58, 238–246.
- Amoako, K.A., Montoya, P.J., Major, T.C., Suhaib, A.B., Handa, H., Brant, D.O., Meyerhoff, M.E., Bartlett, R.H., Cook, K.E., 2013. Fabrication and in vivo thrombogenicity testing of nitric oxide generating artificial lungs. *J. Biomed. Mater. Res. A* 101, 3511–3519.
- Amoako, K.A., Sundaram, H.S., Suhaib, A., Jiang, S.Y., Cook, K.E., 2016. Multimodal, biomaterial-focused anticoagulation via super-low fouling zwitterionic functional groups coupled with anti-platelet nitric oxide release. *Adv. Mater. Interfaces* 3.
- ARDS Network, Brower, R.G., Matthay, M.A., Morris, A., Schoenfeld, D., Thompson, B.T., Wheeler, A., 2000. Ventilation with lower tidal volumes as compared with traditional tidal volumes for acute lung injury and the acute respiratory distress syndrome. *N. Engl. J. Med.* 342, 1301–1308.
- Biran, R., Pond, D., 2017. Heparin coatings for improving blood compatibility of medical devices. *Adv. Drug Deliv. Rev.* 112, 12–23.
- Bosch, T., 2005. Therapeutic apheresis – state of the art in the year 2005. *Ther. Apher. Dial.* 9, 459.
- Boure, T., Vanholder, R., 2004. Which dialyser membrane to choose? (Editorial comment). *Nephrol. Dial. Transplant.* 19, 293.
- Brunet, P., Frances, J., Vacher-Coponat, H., Jaubert, D., Lebrun, G., Gondouin, B., Duval, A., Berland, Y., 2011. Hemodialysis without heparin: a randomized, controlled, crossover study of two dialysis membranes (AN69ST and polysulfone F60). *Int. J. Artif. Organs* 34, 1165–1171.
- Burgess, K.A., Hu, H.H., Wagner, W.R., Federspiel, W.J., 2009. Towards microfabricated biohybrid artificial lung modules for chronic respiratory support. *Biomed. Microdevices* 11, 117–127.
- Byun, Y., Jacobs, H.A., Kim, S.W., 1995. Heparin surface immobilization through hydrophilic spacers: thrombin and antithrombin III binding kinetics. *J. Biomater. Sci. Polym. Ed.* 6, 1–13.
- Cao, Z., Jiang, S., 2012. Super-Hydrophilic Zwitterionic Poly (Carboxybetaine) and Amphiphilic Non-ionic Poly (Ethylene Glycol) for Stealth Nanoparticles, pp. 404–413.
- Centers for Disease Control, 2014. National Hospital Ambulatory Medical Care Survey: 2014 Emergency Department Summary Tables.
- Chen, S., Li, L., Zhao, C., Zheng, J., 2010. Surface hydration: principles and applications toward low-fouling/nonfouling biomaterials. *Polymer* 51, 5283–5293.
- Clermont, G., Lecour, S., Cabanne, J.F., Motte, G., Guiland, J.C., Chevet, D., Rochette, L., 2001. Vitamin E-coated dialyzer reduces oxidative stress in hemodialysis patients. *Free Radic. Biol. Med.* 31, 233–241.
- Coles, G.A., El Nahas, A.M., 2000. Mechanisms and clinical management of chronic renal failure. In: El Nahas, A.M. (Ed.), *Mechanisms and Clinical Management of Chronic Renal Failure*, second ed. Oxford University Press, Oxford.
- Comber, E.M., Palchesko, R.N., Ng, W.H., Ren, X., Cook, K.E., 2019. De novo lung biofabrication: clinical need, construction methods, and design strategy. *Transl. Res.*
- Cook, K.E., Mockros, L.F., 2002. Biocompatibility of artificial lungs. In: Vaslef, S.N., Anderson, R.W. (Eds.), *The Artificial Lung*. Landes Bioscience, Austin, TX.
- Dalton, H.J., GARCIA-Filion, P., Holubkov, R., Moler, F.W., Shanley, T., Heidemann, S., Meert, K., Berg, R.A., Berger, J., Carcillo, J., Newth, C., Harrison, R., Doctor, A., Rycus, P., Dean, J.M., Jenkins, T., Nicholson, C., Eunice Kennedy Shriver National Institute Of Child, H., Human Development Collaborative Pediatric Critical Care Research, N, 2015. Association of bleeding and thrombosis with outcome in extracorporeal life support. *Pediatr. Crit. Care Med.* 16, 167–174.
- Davenport, A., Lai, K.N., Hertel, J., Caruana, R.J., 2014. Anticoagulation. In: Daugirdas, J.T., Blake, P.G., Ing, T.S. (Eds.), *Handbook of Dialysis*. Wolter Kluwers Health.
- De, S.F., Van, B.Y., Caes, F., François, K., Arnout, J., Bossuyt, X., Taeymans, Y., Van, N.G., 2002. Phosphorylcholine coating offers natural platelet preservation during cardiopulmonary bypass. *Perfusion* 17, 39–44.
- Demarest, C.T., 2017. Prolonging the Useful Lifetime of Artificial Lungs. Phd. Carnegie Mellon University.
- Ding, X., Yang, C., Lim, T.P., Hsu, L.Y., Engler, A.C., Hedrick, J.L., Yang, Y.-Y., 2012. Antibacterial and antifouling catheter coatings using surface grafted PEG-b-cationic polycarbonate diblock copolymers. *Biomaterials* 33, 6593–6603.
- Emmenegger, C.R., Brynda, E., Riedel, T., Sedlakova, Z., Houska, M., Alles, A.B., 2009. Interaction of blood plasma with antifouling surfaces. *Langmuir* 25, 6328–6333.
- Ereth, M.H., Nuttall, G.A., Clarke, S.H., Dearani, J.A., Fiechtner, B.K., Rishavy, C.R., Buda, D.A., Shaw, T.A., Orszulak, T.A., Oliver Jr, W.C., 2001. Biocompatibility of trillium biopassive surface-coated oxygenator versus uncoated oxygenator during cardiopulmonary bypass. *J. Cardiothorac. Vasc. Anesth.* 15, 545–550.
- Esper, S.A., Bermudez, C., Dueweke, E.J., Kormos, R., Subramanian, K., Mulukutla, S., Sappington, P., Waters, J., Khandhar, S.J., 2015. Extracorporeal membrane oxygenation support in acute coronary syndromes complicated by cardiogenic shock. *Cathet. Cardiovasc. Interv.* 86, S45–S50.
- Fortenberry, J.D., Bhardwaj, V., Niemer, P., Cornish, J.D., Wright, J.A., Bland, L., 1996. Neutrophil and cytokine activation with neonatal extracorporeal membrane oxygenation. *J. Pediatr.* 128, 670–678.

- Galletti, P.M., Jauregui, H.O., 2006. Liver support systems. In: Bronzino, J.D. (Ed.), *The Biomedical Engineering Handbook: Tissue Engineering and Artificial Organs*, third ed. CRC Press, Boca Raton, FL.
- Garcia, J.P., Iacono, A., Kon, Z.N., Griffith, B.P., 2010. Ambulatory extracorporeal membrane oxygenation: a new approach for bridge-to-lung transplantation. *J. Thorac. Cardiovasc. Surg.* 139, e137–e139.
- Goda, T., Konno, T., Takai, M., Moro, T., Ishihara, K., 2006. Biomimetic phosphorylcholine polymer grafting from polydimethylsiloxane surface using photo-induced polymerization. *Biomaterials* 27, 5151–5160.
- Gupta, S., Amoako, K.A., Suhaib, A., Cook, K.E., 2014. Multimodal, surface-focused anticoagulation using poly-2-methoxyethylacrylate polymer grafts and surface nitric oxide release. *Adv. Mater. Interfaces* 1, 1400012.
- Handa, H., Brisbois, E.J., Major, T.C., Refahiyat, L., Amoako, K.A., Annich, G.M., Bartlett, R.H., Meyerhoff, M.E., 2013. In vitro and in vivo study of sustained nitric oxide release coating using diazeniumdiolate-oped poly(vinyl chloride) matrix with poly(lactide-co-glycolide) additive. *J. Mater. Chem. B* 1, 3578–3587.
- Hatakeyama, T., Tanaka, M., Hatakeyama, H., 2010. Studies on bound water restrained by poly(2-methacryloyloxyethyl phosphorylcholine): comparison with polysaccharide-water systems. *Acta Biomater.* 6, 2077–2082.
- He, H.-W., Zhou, X., Long, Y., Wang, X.-T., Zhang, Q., Zhao, H., Zhang, H.-M., Chai, W.-Z., Liu, D.-W., 2014. Using anti-platelet therapy to prevent extracorporeal membrane oxygenator thrombosis without heparin resistance and with thrombocytopenia. *Crit. Care* 18 595–595.
- Herbert, W.J., 1983. Adhesion in byssally attached bivalves. *Biol. Rev.* 58, 209–231.
- Herold, D.A., Keil, K., Bruns, D.E., 1989. Oxidation of polyethylene glycols by alcohol dehydrogenase. *Biochem. Pharmacol.* 38, 73–76.
- Hirayama, T., Nosaka, N., Okawa, Y., Ushio, S., Kitamura, Y., Sendo, T., Ugawa, T., Nakao, A., 2017. AN69ST membranes adsorb nafamostat mesylate and affect the management of anticoagulant therapy: a retrospective study. *J. Intensive Care* 5, 46.
- Hoganson, D.M., Anderson, J.L., Weinberg, E.F., Swart, E., Orrick, B.K., Borenstein, J.T., Vacanti, J.P., 2010. Branched vascular network architecture: a new approach to lung assist device technology. *J. Thorac. Cardiovasc. Surg.* 140, 990–995.
- Hoganson, D.M., Pryor 2nd, H.I., Bassett, E.K., Spool, I.D., Vacanti, J.P., 2011. Lung assist device technology with physiologic blood flow developed on a tissue engineered scaffold platform. *Lab Chip* 11, 700–707.
- Hong, D., Hung, H.C., Wu, K., Lin, X., Sun, F., Zhang, P., Liu, S., Cook, K.E., Jiang, S., 2017. Achieving ultralow fouling under ambient conditions via surface-initiated ARGET ATRP of carboxybetaine. *ACS Appl. Mater. Interfaces* 9, 9255–9259.
- Hyzy, R., Huang, S., Myers, J., Flaherty, K., Martinez, F., 2007. Acute exacerbation of idiopathic pulmonary fibrosis. *CHEST J.* 132, 1652–1658.
- Ishihara, K., 2000. Bioinspired phospholipid polymer biomaterials for making high performance artificial organs. *Sci. Technol. Adv. Mater.* 1, 131–138.
- Ishihara, K., Oshida, H., Endo, Y., Ueda, T., Watanabe, A., Nakabayashi, N., 1992. Hemocompatibility of human whole blood on polymers with a phospholipid polar group and its mechanism. *J. Biomed. Mater. Res.* 26, 1543–1552.
- Ishihara, K., Ziats, N.P., Tierney, B.P., Nakabayashi, N., Anderson, J.M., 1991. Protein adsorption from human plasma is reduced on phospholipid polymers. *J. Biomed. Mater. Res.* 25, 1397–1407.
- Jeon, S.I., Lee, J.H., Andrade, J.D., DE Gennes, P.G., 1991. Protein—surface interactions in the presence of polyethylene oxide: I. Simplified theory. *J. Colloid Interface Sci.* 142, 149–158.
- Jokerst, J.V., Lobovkina, T., Zare, R.N., Gambhir, S.S., 2011. Nanoparticle PEGylation for imaging and therapy. *Nanomedicine (Lond.)* 6, 715–728.
- Jyoti, A., Maheshwari, A., Daniel, E., Motihar, A., Bhatihwal, R.S., Sharma, D., 2014. Bivalirudin in venovenous extracorporeal membrane oxygenation. *J. Extra-Corporeal Technol.* 46 94–97 4p.
- Kamath, K.R., Park, K., 1994. Surface modification of polymeric biomaterials by albumin grafting using γ -irradiation. *J. Appl. Biomater.* 5, 163–173.
- Kambic, H.E., Nose, Y., 1993. Plasmapheresis: historical perspective, therapeutic applications, and new frontiers. *Artif. Organs* 17, 850.
- Kasálková, N.S., Slepíčka, P., Kolská, Z., Hodačová, P., Kučková, Š., Švorčík, V., 2014. Grafting of bovine serum albumin proteins on plasma-modified polymers for potential application in tissue engineering. *Nanoscale Res. Lett.* 9, 161.
- Keefe, A.J., Jiang, S., 2012. Poly(zwitterionic)protein conjugates offer increased stability without sacrificing binding affinity or bioactivity. *Nat. Chem.* 4, 59–63.
- Keh, D., Gerlach, M., Kurer, I., Spielmann, S., Kerner, T., Busch, T., Hansen, R., Falke, K., Gerlach, H., 1999. Nitric oxide diffusion across membrane lungs protects platelets during simulated extracorporeal circulation. *Eur. J. Clin. Invest.* 29, 344–350.
- Kessler, M., Gangemi, C., Gutierrez Martones, A., Lacombe, J.L., Krier-Coudert, M.J., Galland, R., Kielstein, J.T., Moureau, F., Loughraieb, N., 2013. Heparin-grafted dialysis membrane allows minimal systemic anticoagulation in regular hemodialysis patients: a prospective proof-of-concept study. *Hemodial. Int.* 17, 282–293.
- Kessler, M., Moureau, F., Nguyen, P., 2015. Anticoagulation in chronic hemodialysis: progress toward an optimal approach. *Semin. Dial.* 28, 474–489.
- Kidane, A., Lantz, G.C., Jo, S., Park, K., 1999. Surface modification with PEO-containing triblock copolymer for improved biocompatibility: in vitro and ex vivo studies. *J. Biomater. Sci. Polym. Ed.* 10, 1089–1105.
- Kokubo, K., Kurihara, Y., Kobayashi, K., Tsukao, H., Kobayashi, H., 2015a. Evaluation of the biocompatibility of dialysis membranes. *Blood Purif.* 40, 293–297.
- Kokubo, K., Kurihara, Y., Tsukao, H., Maruyama, N., Kobayashi, K., Shinbo, T., Hirose, M., Kobayashi, H., 2015b. Effects of increased surface coverage of polyvinylpyrrolidone over a polysulfone hemofilter membrane on permeability and cell adhesion during continuous hemofiltration. *J. Artif. Organs* 18, 257–263.
- Kovach, K.M., Capadona, J.R., Sen Gupta, A., Potkay, J.A., 2014. The effects of PEG-based surface modification of PDMS microchannels on long-term hemocompatibility. *J. Biomed. Mater. Res. A* 102, 4195–4205.
- Kovach, K.M., Labarbera, M.A., Moyer, M.C., Cmolik, B.L., Van Lunteren, E., Sen Gupta, A., Capadona, J.R., Potkay, J.A., 2015. In vitro evaluation and in vivo demonstration of a biomimetic, hemocompatible, microfluidic artificial lung. *Lab Chip* 15, 1366–1375.
- Kuang, J., Messersmith, P.B., 2012. Universal surface-initiated polymerization of antifouling zwitterionic brushes using a mussel-mimetic peptide initiator. *Langmuir* 28, 7258–7266.
- Ladd, J., Zhang, Z., Chen, S., Hower, J.C., Jiang, S., 2008. Zwitterionic polymers exhibiting high resistance to nonspecific protein adsorption from human serum and plasma. *Biomacromolecules* 9, 1357–1361.

- Lai, A., Demarest, C.T., Do-Nguyen, C.C., Ukita, R., Skoog, D.J., Carleton, N.M., Amoako, K.A., Montoya, P.J., Cook, K.E., 2019. 72-Hour in vivo evaluation of nitric oxide generating artificial lung gas exchange fibers in sheep. *Acta Biomater.* 90, 122–131.
- Larsson, R., Larm, O., Olsson, P., 1987. The search for thromboresistance using immobilized heparin. *Ann. N.Y. Acad. Sci.* 516, 102–115.
- Larsson, M., Rayzman, V., Nolte, M.W., Nickel, K.F., Björkqvist, J., Jämsä, A., Hardy, M.P., Fries, M., Schmidbauer, S., Hedenqvist, P., 2014. A factor XIIa inhibitory antibody provides thromboprotection in extracorporeal circulation without increasing bleeding risk. *Sci. Transl. Med.* 6 222ra17-222ra17.
- Lee, K.B., Kim, B., Lee, Y.H., Yoon, S.J., Kang, W.H., Huh, W., Kim, D.J., Oh, H.Y., Kim, Y.G., 2004. Hemodialysis using heparin-bound Hemophan in patients at risk of bleeding. *Nephron Clin. Pract.* 97, c5–10.
- Lee, H., Scherer, N.F., Messersmith, P.B., 2006. Single-molecule mechanics of mussel adhesion. *Proc. Natl. Acad. Sci. USA* 103 12999 LP-13003.
- Lehr, C.J., Zaas, D.W., Cheifetz, I.M., Turner, D.A., 2015. Ambulatory extracorporeal membrane oxygenation as a bridge to lung transplantation: walking while waiting. *Chest* 147, 1213–1218.
- Li, G., Malinchoc, M., Cartin-Ceba, R., Venkata, C.V., Kor, D.J., Peters, S.G., Hubmayr, R.D., Gajic, O., 2011. Eight-year trend of acute respiratory distress syndrome: a population-based study in Olmsted County, Minnesota. *Am. J. Respir. Crit. Care Med.* 183, 59–66.
- Li, Y., Keefe, A.J., Giarmarco, M., Brault, N.D., Jiang, S., 2012. Simple and robust approach for passivating and functionalizing surfaces for use in complex media. *Langmuir* 28, 9707–9713.
- Lim, J.Y., Kim, J.B., Choo, S.J., Chung, C.H., Lee, J.W., Jung, S.H., 2016. Anticoagulation during extracorporeal membrane oxygenation; nafamostat mesilate versus heparin. *Ann. Thorac. Surg.* 102, 534–539.
- Liu, J., Pedersen, L.C., 2007. Anticoagulant heparan sulfate: structural specificity and biosynthesis. *Appl. Microbiol. Biotechnol.* 74, 263–272.
- Lorusso, R., De Cicco, G., Totaro, P., Gelsomino, S., 2009. Effects of phosphorylcholine coating on extracorporeal circulation management and postoperative outcome: a double-blind randomized study. *Interact. Cardiovasc. Thorac. Surg.* 8, 7–11.
- Loss, S.H., De Oliveira, R.P., Maccari, J.G., Savi, A., Boniatti, M.M., Hetzel, M.P., Dallegrave, D.M., Balzano, P.D.C., Oliveira, E.S., Höher, J.A., Torelly, A.P., Teixeira, C., 2015. The reality of patients requiring prolonged mechanical ventilation: a multicenter study. *Rev. Bras. Ter. Intensiva* 27, 26–35.
- Lukito, P., Wong, A., Jing, J., Arthur, J.F., Marasco, S.F., Murphy, D.A., Bergin, P.J., Shaw, J.A., Collett, M., Andrews, R.K., Gardiner, E.E., Davis, A.K., 2016. Mechanical circulatory support is associated with loss of platelet receptors glycoprotein Ibalpha and glycoprotein VI. *J. Thromb. Haemost.* 14, 2253–2260.
- Ma, H., Hyun, J., Stiller, P., Chilkoti, A., 2004. “Non-fouling” oligo(ethylene glycol)-functionalized polymer brushes synthesized by surface-initiated atom transfer radical polymerization. *Adv. Mater.* 16, 338–341.
- Madhani, S.P., Frankowski, B.J., Ye, S.H., Burgreen, G.W., Wagner, W.R., Kormos, R., D’cunha, J., Federspiel, W.J., 2017c. In vivo 5 Day animal studies of a compact, wearable pumping artificial lung. *ASAIO J.*
- Major, T.C., Brant, D.O., Reynolds, M.M., Bartlett, R.H., Meyerhoff, M.E., Handa, H., Annich, G.M., 2010. The attenuation of platelet and monocyte activation in a rabbit model of extracorporeal circulation by a nitric oxide releasing polymer. *Biomaterials* 31, 2736–2745.
- Malchesky, P.S., 2004. Extracorporeal artificial organs. In: Ratner, B.D., Hoffman, A.S., Schoen, F.J., Lemons, J.E. (Eds.), *Biomaterials Science: An Introduction to Materials in Medicine*, second ed. Academic Press, San Diego, CA.
- Malchesky, P.S., Koo, A.P., Skibinski, C.I., Hadsell, A.T., Rybicki, L.A., 2009. Apheresis technologies and clinical applications: the 2007 international apheresis registry. *Ther. Apher. Dial.* Published Online: August 11 2009.
- Malkin, A.D., Ye, S.H., Lee, E.J., Yang, X., Zhu, Y., Gamble, L.J., Federspiel, W.J., Wagner, W.R., 2018. Development of zwitterionic sulfobetaine block copolymer conjugation strategies for reduced platelet deposition in respiratory assist devices. *J. Biomed. Mater. Res. B Appl. Biomater.* 106, 2681–2692.
- Matthay, M.A., Zemans, R.L., 2011. The acute respiratory distress syndrome: pathogenesis and treatment. *Annu. Rev. Pathol.* 6, 147–163.
- Mazzeffi, M., Greenwood, J., Tanaka, K., Menaker, J., Rector, R., Herr, D., Kon, Z., Lee, J., Griffith, B., Rajagopal, K., Pham, S., 2016. Bleeding, transfusion, and mortality on extracorporeal life support: ECLS working group on thrombosis and hemostasis. *Ann. Thorac. Surg.* 101, 682–689.
- Middendorp, S.J., Wilbs, J., Quarroz, C., Calzavarini, S., Angelillo-Scherrer, A., Heinis, C., 2017. Peptide macrocycle inhibitor of coagulation factor XII with subnanomolar affinity and high target selectivity. *J. Med. Chem.* 60, 1151–1158.
- Morisaku, T., Watanabe, J., Konno, T., Takai, M., Ishihara, K., 2008. Hydration of phosphorylcholine groups attached to highly swollen polymer hydrogels studied by thermal analysis. *Polymer* 49, 4652–4657.
- Mulvihill, J.N., Faradji, A., Oberling, F., Cazenave, J., 1990. Surface passivation by human albumin of plasmapheresis circuits reduces platelet accumulation and thrombus formation. *Experimental and clinical studies. J. Biomed. Mater. Res.* 24, 155–163.
- Nakamura, Y., Hara, S., Hatamoto, H., Yamasaki, S., Nakano, T., Miyazaki, M., Matsumoto, N., Irie, Y., Ishikura, H., 2017. Adsorption of nafamostat mesilate on AN69ST membranes: a single-center retrospective and in vitro study. *Ther. Apher. Dial.* 21, 620–627.
- National Kidney Foundation, 2013. *A Clinical Update on Dialyzer Membranes: State-of-the-Art Considerations for Optimal Care in Hemodialysis.* National Kidney Foundation.
- Noble, D.R., Swift, H.R., Williams, D.L.H., 1999. Nitric oxide release from S-nitrosoglutathione (GSNO). *Chem. Commun.* 2317–2318.
- Noishiki, Y., Miyata, T., 1985. Successful animal study of small caliber heparin-protamine-collagen vascular grafts. *Am. Soc. Artif. Intern. Organs J.* 31.
- Obstals, F., Vorobii, M., Riedel, T., Los Santos Pereira, A., Bruns, M., Singh, S., Rodriguez-Emmenegger, C., 2018. Improving hemocompatibility of membranes for extracorporeal membrane oxygenators by grafting nonthrombogenic polymer brushes. *Macromol. Biosci.* 18, 1700359.
- Palanzo, D.A., Zarro, D.L., Montesano, R.M., Manley, N.J., Quinn, M., Elmore, B.-A., Gustafson, P.A., Castagna, J.M., 1999. Effect of Trillium™ Biopassive surface coating of the oxygenator on platelet count drop during cardiopulmonary bypass. *Perfusion* 14, 473–479.
- Palanzo, D.A., Zarro, D.L., Manley, N.J., Montesano, R.M., Quinn, M., Elmore, B.-A., Gustafson, P.A., Castagna, J.M., 2001. Effect of Carmeda® BioActive surface coating versus Trillium™ Biopassive surface coating of the oxygenator on circulating platelet count drop during cardiopulmonary bypass. *Perfusion* 16, 279–283.
- Papageorgiou, G., Murata, N., 1995. The unusually strong stabilizing effect of glycine betaine on the structure and function of the oxygen-evolving PSII complex. *Photosynth. Res.* 44, 243–252.

- Pflaum, M., Kuhn-Kauffeldt, M., Schmeckebier, S., Dipresa, D., Chauhan, K., Wiegmann, B., Haug, R.J., Schein, J., Haverich, A., Korossis, S., 2017. Endothelialization and characterization of titanium dioxide-coated gas-exchange membranes for application in the bioartificial lung. *Acta Biomater.* 50, 510–521.
- Plegue, T.J., Kovach, K.M., Thompson, A.J., Potkay, J.A., 2018. Stability of polyethylene glycol and zwitterionic surface modifications in PDMS microfluidic flow chambers. *Langmuir* 34, 492–502.
- Polk, A.A., Maul, T.M., Mckeel, D.T., Snyder, T.A., Lehocky, C.A., Pitt, B., Stolz, D.B., Federspiel, W.J., Wagner, W.R., 2010. A biohybrid artificial lung prototype with active mixing of endothelialized microporous hollow fibers. *Biotechnol. Bioeng.* 106, 490–500.
- Potkay, J.A., 2014. The promise of microfluidic artificial lungs. *Lab Chip* 14, 4122–4138.
- Powers, S.K., Shanely, R.A., Coombes, J.S., Koesterer, T.J., Mckenzie, M., Van Gammeren, D., Cicale, M., Dodd, S.L., 2002. Mechanical ventilation results in progressive contractile dysfunction in the diaphragm. *J. Appl. Physiol.* 92, 1851–1858.
- Prime, K.L., Whitesides, G.M., 1993. Adsorption of proteins onto surfaces containing end-attached oligo(ethylene oxide): a model system using self-assembled monolayers. *J. Am. Chem. Soc.* 115, 10714–10721.
- Ren, X., Xu, L., Xu, J., Zhu, P., Zuo, L., Wei, S., 2013. Immobilized heparin and its anti-coagulation effect on polysulfone membrane surface. *J. Biomater. Sci. Polym. Ed.* 24, 1707–1720.
- Renne, T., Schmaier, A.H., Nickel, K.F., Blomback, M., Maas, C., 2012. In vivo roles of factor XII. *Blood* 120, 4296–4303.
- Roberts, M.J., Bentley, M.D., Harris, J.M., 2002. Chemistry for peptide and protein PEGylation. *Adv. Drug Deliv. Rev.* 54, 459–476.
- Rubinfeld, G.D., Caldwell, E., Peabody, E., Weaver, J., Martin, D.P., Neff, M., Stern, E.J., Hudson, L.D., 2005. Incidence and outcomes of acute lung injury. *N. Engl. J. Med.* 353, 1685–1693.
- Saito, A., 2011. Definition of high-performance membranes - from the clinical point of view. *Contrib. Nephrol.* 173, 1–10.
- Sanchez-Canel, J.J., Pons-Prades, R., Salvetti, M.L., Seores, A., Vazquez, M., Perez-Alba, A., Tamarit, E., Calvo-Gordo, C., Villatoro, J., 2012. Evaluation of coagulation and anti-Xa factor when using a heparin-coated AN69ST(R) dialyser. *Nefrologia* 32, 605–612.
- Sargent, J.A., Gotch, F.A., 1996. Principles and biophysics of dialysis. In: Jacobs, C., Kjellstrand, C.M., Koch, K.M., Winchester, J.F. (Eds.), *Replacement of Renal Function by Dialysis*, fourth ed. Springer, Netherlands.
- Sasaki, M., 2006. Development of vitamin E-modified polysulfone membrane dialyzers. *J. Artif. Organs* 9, 50–60.
- Satoh, M., Yamasaki, Y., Nagake, Y., Kasahara, J., Hashimoto, M., Nakaniishi, N., Makino, H., 2001. Oxidative stress is reduced by the long-term use of vitamin E-coated dialysis filters. *Kidney Int.* 59, 1943–1950.
- Savannah, G., Jonas, A., Roy, B., Clayton, U., Johan, R., 2014. Heparin surfaces: impact of immobilization chemistry on hemocompatibility and protein adsorption. *J. Biomed. Mater. Res. B Appl. Biomater.* 102, 1817–1824.
- Schewe, R.E., Khanafer, K.M., Arab, A., Mitchell, J.A., Skoog, D.J., Cook, K.E., 2012a. Design and in vitro assessment of an improved, low-resistance compliant thoracic artificial lung. *Am. Soc. Artif. Intern. Organs J.* 58, 583–589.
- Schloesser, M., Zeerleder, S., Lutze, G., Halbmayer, W.M., Hof-ferbert, S., Hinney, B., Koestering, H., Lammle, B., Pindur, G., Thies, K., Kohler, M., Engel, W., 1997. Mutations in the human factor XII gene. *Blood* 90, 3967–3977.
- Shen, M., Martinson, L., Wagner, M.S., Castner, D.G., Ratner, B.D., Horbett, T.A., 2002. PEO-like plasma polymerized tetraglyme surface interactions with leukocytes and proteins: in vitro and in vivo studies. *J. Biomater. Sci. Polym. Ed.* 13, 367–390.
- Shiga, H., Hirasawa, H., Nishida, O., Oda, S., Nakamura, M., Mashiko, K., Matsuda, K., Kitamura, N., Kikuchi, Y., Fuke, N., 2014. Continuous hemodiafiltration with a cytokine-adsorbing hemofilter in patients with septic shock: a preliminary report. *Blood Purif.* 38, 211–218.
- Shin, M., Matsuda, K., Ishii, O., Terai, H., Kaazempur-Mofrad, M., Borenstein, J., Detmar, M., Vacanti, J.P., 2004. Endothelialized networks with a vascular geometry in microfabricated poly(dimethyl siloxane). *Biomed. Microdevices* 6, 269–278.
- Sivaraman, B., Latour, R.A., 2010. The Adherence of platelets to adsorbed albumin by receptor-mediated recognition of binding sites exposed by adsorption-induced unfolding. *Biomaterials* 31 1036–1036.
- Skoog, D.J., Pohlmann, J.R., Demos, D.S., Scipione, C.N., Iyengar, A., Schewe, R.E., Suhaib, A.B., Koch, K.L., Cook, K.E., 2017. Fourteen day in vivo testing of a compliant thoracic artificial lung. *Am. Soc. Artif. Intern. Organs J.* 63, 644–649.
- Sly, M.K., Prager, M.D., Li, J., Harris, F.B., Shastri, P., Bhujle, R., Chao, R., Kulkarni, P.V., Constantinescu, A., Jessen, M.E., Eberhart, R.C., 1996. Platelet and neutrophil distributions in pump oxygenator circuits. III. Influence of nitric oxide gas infusion. *ASAIO J.* 42, M494–M499.
- Sohn, N., Marcoux, J., Mycyk, T., Krahn, J., Meng, Q., 2009. The impact of different biocompatible coated cardiopulmonary bypass circuits on inflammatory response and oxidative stress. *Perfusion* 24, 231–237.
- Staudacher, D.L., Biever, P.M., Benk, C., Ahrens, I., Bode, C., Wengenmayer, T., 2016. Dual antiplatelet therapy (DAPT) versus no antiplatelet therapy and incidence of major bleeding in patients on venoarterial extracorporeal membrane oxygenation. *PLoS One* 11, e0159973.
- Stepuro, T.L., Zinchuk, V.V., 2006. Nitric oxide effect on the hemoglobin-oxygen affinity. *J. Physiol. Pharmacol.* 57, 29–38.
- Sun, F., Wu, K., Hung, H.C., Zhang, P., Che, X., Smith, J., Lin, X., Li, B., Jain, P., Yu, Q., Jiang, S., 2017. Paper sensor coated with a poly(carboxybetaine)-multiple DOPA conjugate via dip-coating for biosensing in complex media. *Anal. Chem.* 89, 10999–11004.
- Sundaram, S., Gikakis, N., Hack, C.E., Niewiarowski, S., Edmunds Jr., L.H., Koneti Rao, A., Sun, L., Cooper, S.L., Colman, R.W., 1996. Nafamostat mesilate, a broad spectrum protease inhibitor, modulates platelet, neutrophil and contact activation in simulated extracorporeal circulation. *Thromb. Haemost.* 75, 76–82.
- Sundaram, H.S., Han, X., Nowinski, A.K., Brault, N.D., Li, Y., Ella-Menye, J.-R., Amoako, K.A., Cook, K.E., Marek, P., Senecal, K., Jiang, S., 2014. Achieving one-step surface coating of highly hydrophilic poly(carboxybetaine methacrylate) polymers on hydrophobic and hydrophilic surfaces. *Adv. Mater. Interfaces* 1 n/a-n/a).
- Tanaka, M., Mochizuki, A., 2010. Clarification of the blood compatibility mechanism by controlling the water structure at the blood–poly(meth)acrylate interface. *J. Biomater. Sci. Polym. Ed.* 21, 1849–1863.
- Tanaka, M., Motomura, T., Ishii, N., Shimura, K., Onishi, M., Mochizuki, A., Hatakeyama, T., 2000a. Cold crystallization of water in hydrated poly(2-methoxyethyl acrylate) (PMEA). *Polym. Int.* 49, 1709–1713.
- Tanaka, M., Motomura, T., Kawada, M., Anzai, T., Yuu, K., Shiroya, T., Shimura, K., Onishi, M., Akira, M., 2000b. Blood compatible aspects of poly(2-methoxyethylacrylate) (PMEA)-relationship between protein adsorption and platelet adhesion on PMEA surface. *Biomaterials* 21, 1471–1481.
- Tanaka, M., Mochizuki, A., Ishii, N., Motomura, T., Hatakeyama, T., 2002. Study of blood compatibility with poly(2-methoxyethyl acrylate). Relationship between water structure and platelet compatibility in poly(2-methoxyethylacrylate-co-2-hydroxyethylmethacrylate). *Biomacromolecules* 3, 36–41.
- Tateishi, T., Kyomoto, M., Kakinoki, S., Yamaoka, T., Ishihara, K., 2014. Reduced platelets and bacteria adhesion on poly(ether ether

- ketone) by photoinduced and self-initiated graft polymerization of 2-methacryloyloxyethyl phosphorylcholine. *J. Biomed. Mater. Res. A* 102, 1342–1349.
- Thomas, D.D., Liu, X., Kantrow, S.P., Lancaster, J.R., 2001. The biological lifetime of nitric oxide: implications for the perivascular dynamics of NO and O₂. *Proc. Natl. Acad. Sci. USA* 98, 355–360.
- Thomas, M., Moriyama, K., Ledebro, I., 2011. AN69: evolution of the world's first high permeability membrane. *Contrib. Nephrol.* 173, 119–129.
- Thompson, A.J., Marks, L.H., Goudie, M.J., Rojas-Pena, A., Handa, H., Potkay, J.A., 2017. A small-scale, rolled-membrane microfluidic artificial lung designed towards future large area manufacturing. *Biomicrofluidics* 11, 024113.
- U.S. Renal Data System, USRDS 2009 and 2018 Annual Data Reports: Atlas of End-Stage Renal Disease in the United States, National Institutes of Health, National Institute of Diabetes and Digestive and Kidney Diseases, Bethesda, MD, 2009, 2018. The data reported here have been supplied by the United States Renal Data System (USRDS). The interpretation and reporting of these data are the responsibility of the author and in no way should be seen as an official policy or interpretation of the US government.
- Ukita, R., Wu, K., Lin, X., Carleton, N.M., Naito, N., Lai, A., Do-Nguyen, C.C., Demarest, C.T., Jiang, S., Cook, K.E., 2019. Zwitterionic poly-carboxybetaine coating reduces artificial lung thrombosis in sheep and rabbits. *Acta Biomater.* 92, 71–81.
- Ulbricht, J., Jordan, R., Luxenhofer, R., 2014. On the biodegradability of polyethylene glycol, polypeptides and poly(2-oxazolines). *Biomaterials* 35, 4848–4861.
- United States Renal Data System, 2018. USRDS annual data report: Epidemiology of kidney disease in the United States. National Institutes of Health, National Institute of Diabetes and Digestive and Kidney Diseases, Bethesda, MD, 2018.
- United States Renal Data System, 2009. USRDS Annual Data Report: Atlas of End-Stage Renal Disease in the United States. National Institutes of Health, National Institute of Diabetes and Digestive and Kidney Diseases, Bethesda, MD, 2009.
- Valapour, M., Lehr, C.J., Skeans, M.A., Smith, J.M., Carrico, R., Uccellini, K., Lehman, R., Robinson, A., Israni, A.K., Snyder, J.J., Kasiske, B.L., 2018. OPTN/SRTR 2016 annual data report: lung. *Am. J. Transplant.* 18, 363–433.
- Van Den Goor, J.M., Van Oeveren, W., Rutten, P.M., Tijssen, J.G., Eijssman, L., 2006. Adhesion of thrombotic components to the surface of a clinically used oxygenator is not affected by Trillium coating. *Perfusion* 21, 165–172.
- Van Hinsbergh, V.W., 2012. Endothelium—role in regulation of coagulation and inflammation. *Semin. Immunopathol.* 34, 93–106.
- Veysel, K., Tevfik, N., Sedat, O., Yasin, M., Hasan, E., Cevat, Y., 2006. Biocompatibility of heparin-coated cardiopulmonary bypass circuits in coronary patients with left ventricular dysfunction is superior to PMEA-coated circuits. *J. Card. Surg.* 21, 572–577.
- Vroman, L., Adams, A.L., 1986. Adsorption of proteins out of plasma and solutions in narrow spaces. *J. Colloid Interface Sci.* 111, 391–402.
- Wachtfogel, Y.T., Kettner, C., Hack, C.E., Nuijens, J.H., Reilly, T.M., Knabb, R.M., Kucich, U., Niewiarowski, S., Edmunds Jr., L.H., Colman, R.W., 1998. Thrombin and human plasma kallikrein inhibition during simulated extracorporeal circulation block platelet and neutrophil activation. *Thromb. Haemost.* 80, 686–691.
- Wang, P.G., Xian, M., Tang, X., Wu, X., Wen, Z., Cai, T., Janczuk, A.J., 2002. Nitric oxide donors: chemical activities and biological applications. *Chem. Rev.* 102, 1091–1134.
- Wang, Y.B., Gong, M., Yang, S., Nakashima, K., Gong, Y.K., 2014. Hemocompatibility and film stability improvement of crosslinkable MPC copolymer coated polypropylene hollow fiber membrane. *J. Membr. Sci.* 452, 29–36.
- Wang, Y.B., Shi, K.H., Jiang, H.L., Gong, Y.K., 2016. Significantly reduced adsorption and activation of blood components in a membrane oxygenator system coated with crosslinkable zwitterionic copolymer. *Acta Biomater.* 40, 153–161.
- Weber, N., Wendel, H.P., Ziemer, G., 2002. Hemocompatibility of heparin-coated surfaces and the role of selective plasma protein adsorption. *Biomaterials* 23, 429–439.
- Wei, X., Sanchez, P.G., Liu, Y., Claire Watkins, A., Li, T., Griffith, B.P., Wu, Z.J., 2016. Extracorporeal respiratory support with a miniature integrated pediatric pump-lung device in an acute ovine respiratory failure model. *Artif. Organs* 40, 1046–1053.
- Weitz, J.I., Gross, P.L., 2012. New oral anticoagulants: which one should my patient use? *Hematology Am. Soc. Hematol. Educ. Program* 2012, 536–540.
- Wiegmann, B., Von Seggern, H., Hoffler, K., Korossis, S., Dipresa, D., Pflaum, M., Schmeckeber, S., Seume, J., Haverich, A., 2016. Developing a biohybrid lung – sufficient endothelialization of poly-4-methyl-1-pentene gas exchange hollow-fiber membranes. *J. Mech. Behav. Biomed. Mater.* 60, 301–311.
- Wing, A.J., Jones, E., 2000. Epidemiology of end-stage failure: a global perspective. In: El Nahas, A.M. (Ed.), *Mechanisms and Clinical Management of Chronic Renal Failure*, second ed. Oxford University Press, Oxford.
- Woodruff, R., Xu, Y., Layzer, J., Wu, W., Ogletree, M., Sullenger, B., 2013. Inhibiting the intrinsic pathway of coagulation with a factor XII-targeting RNA aptamer. *J. Thromb. Haemost.* 11, 1364–1373.
- Worm, M., Köhler, E.C., Panda, R., Long, A., Butler, L.M., Stavrou, E.X., Nickel, K.F., Fuchs, T.A., Renné, T., 2015. The factor XIIa blocking antibody 3F7: a safe anticoagulant with anti-inflammatory activities. *Ann. Transl. Med.* 3.
- Wu, B., Gerlitz, B., Grinnell, B.W., Meyerhoff, M.E., 2007. Polymeric coatings that mimic the endothelium: combining nitric oxide release with surface-bound active thrombomodulin and heparin. *Biomaterials* 28, 4047–4055.
- Wu, Z.J., Zhang, T., Bianchi, G., Wei, X., Son, H.S., Zhou, K., Sanchez, P.G., Garcia, J., Griffith, B.P., 2012b. Thirty-day in-vivo performance of a wearable artificial pump-lung for ambulatory respiratory support. *Ann. Thorac. Surg.* 93, 274–281.
- Yamato, M., Minematsu, Y., Ikemiya, Y., Shibata, J., Fujii, J., Minato, T., Miyagawa, S., Takaori, K., Tomiyama, Y., Nagayama, I., Wada, A., Ito, T., Iwatani, H., 2016. Continuous hemodiafiltration with an AN69ST hemofilter (AN69ST-CHDF) as FGF-23-lowering therapy. *Clin. Lab.* 62, 2349–2354.
- Yang, W., Bai, T., Carr, L.R., Keefe, A.J., Xu, J., Xue, H., Irvin, C.A., Chen, S., Wang, J., Jiang, S., 2012. The effect of lightly cross-linked poly(carboxybetaine) hydrogel coating on the performance of sensors in whole blood. *Biomaterials* 33, 7945–7951.
- Ye, S.H., Jang, Y.S., Yun, Y.H., Shankarraman, V., Woolley, J.R., Hong, Y., Gamble, L.J., Ishihara, K., Wagner, W.R., 2013. Surface modification of a biodegradable magnesium alloy with phosphorylcholine (PC) and sulfobetaine (SB) functional macromolecules for reduced thrombogenicity and acute corrosion resistance. *Langmuir* 29, 8320–8327.
- Yoshizaki, T., Tabuchi, N., Van Oeveren, W., Shibamiya, A., Koyama, T., Sunamori, M., 2005. PMEA polymer-coated PVC tubing maintains anti-thrombogenic properties during in vitro whole blood circulation. *Int. J. Artif. Organs* 28, 834–840.
- Yue, W.-W., Li, H.-J., Xiang, T., Qin, H., Sun, S.-D., Zhao, C.-S., 2013. Grafting of zwitterion from polysulfone membrane via surface-initiated ATRP with enhanced antifouling property and biocompatibility. *J. Membr. Sci.* 446, 79–91.

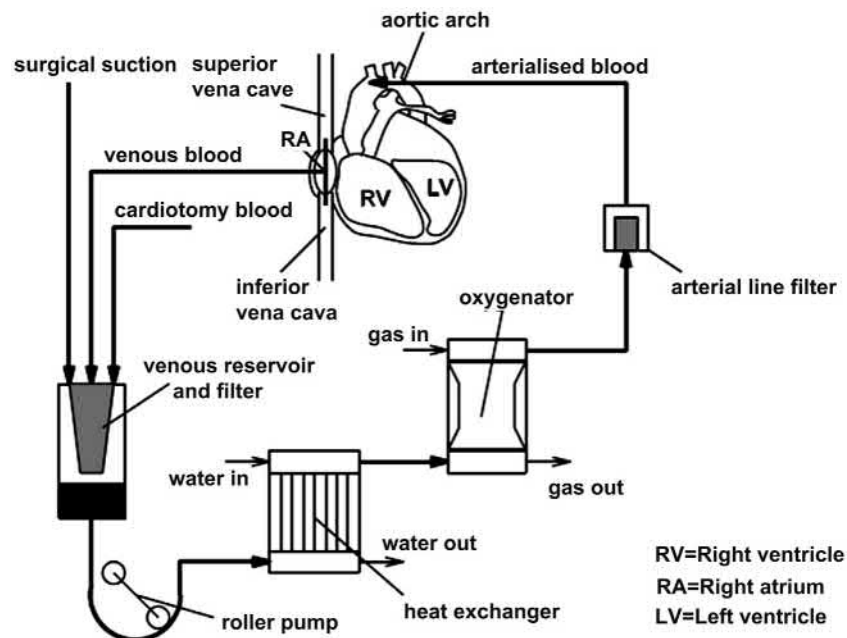
- Zhang, H., Annich, G.M., Miskulin, J., Stankiewicz, K., Osterholzer, K., Merz, S.I., Bartlett, R.H., Meyerhoff, M.E., 2003. Nitric oxide-releasing fumed silica particles: synthesis, characterization, and biomedical application. *J. Am. Chem. Soc.* 125, 5015–5024.
- Zhang, Z., Chao, T., Chen, S., Jiang, S., 2006. Superlow fouling sulfobetaine and carboxybetaine polymers on glass slides. *Langmuir* 22, 10072–10077.
- Zimmermann, A.K., Aebert, H., Reiz, A., Freitag, M., Husseini, M., Ziemer, G., Wendel, H.P., 2004. Hemocompatibility of PMEA coated oxygenators used for extracorporeal circulation procedures. *Am. Soc. Artif. Intern. Organs J.* 50, 193–199.
- Zimmermann, A.K., Weber, N., Aebert, H., Ziemer, G., Wendel, H.P., 2007. Effect of biopassive and bioactive surface-coatings on the hemocompatibility of membrane oxygenators. *J. Biomed. Mater. Res. B Appl. Biomater.* 80, 433–439.
- Zimmermann, M., Bein, T., Arlt, M., Philipp, A., Rupprecht, L., Mueller, T., Lubnow, M., Graf, B.M., Schlitt, H.J., 2009. Pumpless extracorporeal interventional lung assist in patients with acute respiratory distress syndrome: a prospective pilot study. *Crit. Care* 13, R10.
- Zorzi, A., Middendorp, S.J., Wilbs, J., Deyle, K., Heinis, C., 2017. Acylated heptapeptide binds albumin with high affinity and application as tag furnishes long-acting peptides. *Nat. Commun.* 8, 16092.
- Zwaal, R.F.A., Hemker, H.C., 1982. Blood cell membranes and haemostasis. *Pathophysiol. Haemostasis Thrombosis* 11, 12–39.
- Zwaal, R.F.A., Comfurius, P., Van Deenen, L.L.M., 1977. Membrane asymmetry and blood coagulation. *Nature* 268 358–358.
- Anaesthesia. Greenwich Medical Media, Cambridge, pp. 253–258.
- Hanson, S.R., 2004. Blood coagulation and blood-materials interactions. In: Ratner, B.D., Hoffman, A.S., Schoen, F.J., Lemons, J.E. (Eds.), *Biomaterials Science: An Introduction to Materials in Medicine*, second ed. Academic Press, San Diego, CA.
- Kay, N.E., Raij, L., 1987. Differential effect of hemodialysis membranes on human lymphocyte natural killer function. *Artif. Organs* 11, 165.
- Kitano, H., Mori, T., Takeuchi, Y., Tada, S., Gemmei-Ide, M., Yokoyama, Y., Tanaka, M., 2005. Structure of water incorporated in sulfobetaine polymer films as studied by ATR-FTIR. *Macromol. Biosci.* 5, 314–321.
- Kung, M.C., Lee, J.K., Kung, H.H., Mockros, L.F., 2008. Micro-channel technologies for artificial lungs: (2) screen-filled wide rectangular channels. *ASAIO J.* 54, 383–389.
- Lever, M.J., 2005. Artificial exchange systems. In: Hench, L.L., Jones, J.R. (Eds.), *Biomaterials, Artificial Organs and Tissue Engineering*. Woodhead, Cambridge.
- Mackay, J.H., Arrowsmith, J.E., 2004. Coagulopathy during cardiopulmonary bypass. In: Mackay, J.H., Arrowsmith, J.E. (Eds.), *Core Topics in Cardiac Anaesthesia*. Greenwich Medical Media, Cambridge.
- Mulholland, J.W., 2008. Cardiopulmonary bypass. *Surgery* 26 (12), 486–488.
- Murphy, G.J., Bryan, A.J., 2004. Cardiopulmonary bypass. *Surgery* 22 (6), 126–128.
- Nishinaka, T., Nishida, H., Endo, M., Miyagishima, M., Ohtsuka, G., Koyanagi, H., 1996. Less blood damage in the impeller centrifugal pump: a comparative study with the roller pump in open heart surgery. *Artif. Organs* 20, 707.
- Organisation for Economic Co-operation and Development, 2005. *Health at a Glance – OECD Indicators 2005*. OECD Publishing.
- Shao, Q., He, Y., White, A.D., Jiang, S., 2012. Different effects of zwitterion and ethylene glycol on proteins. *J. Chem. Phys.* 136 225101–225101.

Further Reading

- Broers, H., 2006. *Inventor for Life – the Story of W.J. Kolff, Father of Artificial Organs*. trans. K. Ashton. B&V Media Publishers, Kampen, The Netherlands.
- Extracorporeal Life Support Organization (ELSO) Anticoagulation Guideline, 2014. (Ann Arbor, MI).
- Gifford, D., Gray, S.J., 2004. Cardiopulmonary equipment. In: Mackay, J.H., Arrowsmith, J.E. (Eds.), *Core Topics in Cardiac*

Chapter Exercises

1. What are the common disease states that might require the use of an artificial lung? What conditions require the most challenging requirements for respiratory support or blood–biomaterial interactions?
2. What is the dominant cause of coagulation in an ECMO circuit? Why is this the primary cause? What are some other causes?
3. Below is the schematic of the extracorporeal circuit used during cardiopulmonary bypass (CPB) when the heart is stopped to allow for surgical correction of cardiac defects (Fig. 2.5.3.24). This circuit is often described as a “heart–lung machine.”
 - a. What are the similarities and differences between CPB and ECMO surgeries and circuits?
 - b. How will these differences increase or decrease activation of coagulation and inflammation?
 - c. The vast majority of publications test commercial anti-coagulant surface coatings during CPB or simulated CPB. Discuss the confounding factors present during CPB and how this might lead to misconceptions about the effectiveness of the coatings during ECMO?
4. In the study by Ladd et al., (2008) they evaluated hydrophilic and zwitterionic coatings on a gold surface using four types of biological media: (1) 10% serum, (2) 100% serum, (3) 10% plasma, and (4) 100% plasma (see Fig. 2.5.3.9).
 - a. What is the fundamental difference between serum and plasma? How might this cause changes in the results?
 - b. Is 10% plasma sufficient for evaluating these coatings? How might blood present additional challenges?
 - c. Speculate on what these results say about surface coatings tested to examine the adsorption of single dilute proteins, such as albumin or fibrinogen?
5. What would be the total rate of nitric oxide delivery to the bloodstream in mL/min if it is delivered at a flux rate sufficient to significantly inhibit clot formation through a typical oxygenator?
6. Speculate on biocompatibility differences between peritoneal dialysis and hemodialysis. From your reading, what might be the differences in how these two treatment modes affect activation of coagulation and inflammation?
7. The typical hemodialysis blood flow rates were described as 200–400 mL/min through a dialyzer with a surface area of 0.8–2.5 m². Discuss how both the process of hemodialysis and the dialyzer design might be adjusted to reduce the duration of dialysis. What are the mitigating, negative consequences of these changes?
8. Discuss the similarities and differences between hemodialysis and ECMO and how these might affect the extent of coagulation and inflammation and their effects on the patients using these support modes.



• **Figure 2.5.3.24** Schematic showing cardiopulmonary bypass circuit for Exercise 3. (Campbell Ritchie, 2012).

2.5.4

Orthopedic Applications

NADIM JAMES HALLAB, JOSHUA J. JACOBS

Department of Orthopedic Surgery, Rush University Medical Center, Chicago, IL, United States

Orthopedic biomaterials are enormously successful in restoring mobility and quality of life to millions of individuals each year. Orthopedic implants include reconstructive implants, fracture management products, spinal products, rehabilitation products, arthroscopy products, electrical stimulation products, and casting products. These products are generally used for fracture fixation enhancement, joint replacement, or dynamic stabilization. More specific orthopedic applications within these categories are listed below.

- (1) Fracture fixation devices
 - Spinal fixation devices
 - Fracture plates
 - Wires, pins, and screws
 - Intramedullary devices
 - Artificial ligaments
- (2) Joint replacement (Fig. 2.5.4.1)
 - Hip arthroplasty
 - Knee arthroplasty
 - Spine arthroplasty
 - Ankle arthroplasty
 - Shoulder arthroplasty
 - Elbow arthroplasty
 - Wrist arthroplasty
 - Finger arthroplasty
- (3) Dynamic stabilization devices (new)
 - Spine stabilization devices

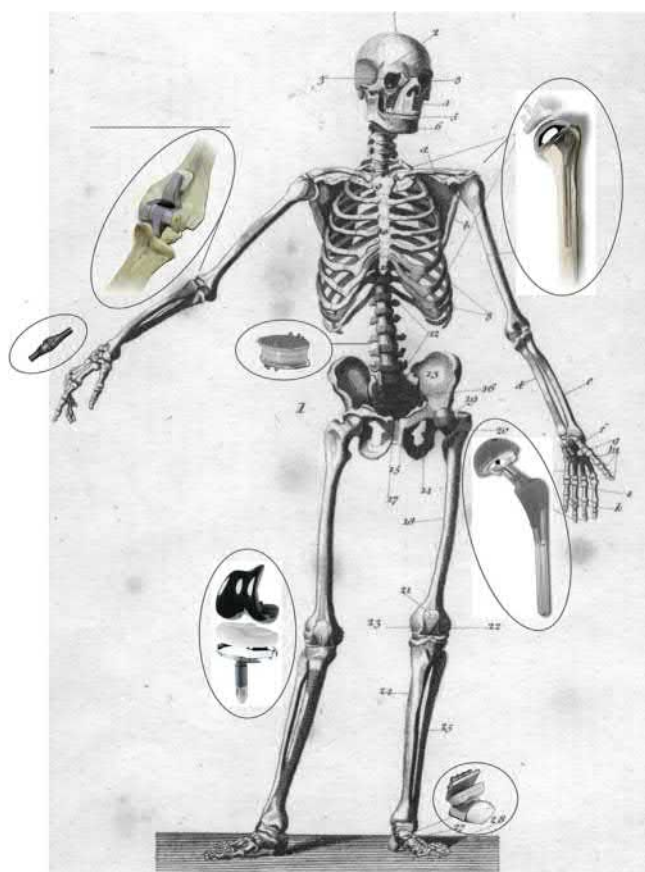
Orthopedic Biomaterials Market: The overwhelming success of orthopedic biomaterials is exemplified by their worldwide market, dominating biomaterial sales at approximately \$24 billion in 2007 with an expected growth rate of 7%–9% annually. Global sales of trauma fracture management products only totaled approximately \$3.7 billion in 2007, whereas \$10 billion was spent on knee and hip joint replacements (Fig. 2.5.4.1). Global sales of knee implant products equaled approximately \$5.8 billion in 2007, representing approximately 1.5 million knee replacement surgeries which include first-time joint replacement procedures and revision procedures for replacement, repair, or enhancement of an implant product or component from a previous procedure. Revision

procedures are growing at an accelerated rate of approximately 60% in the United States.

Orthopedic Biomaterials: Orthopedic biomaterials are generally limited to those materials that withstand cyclic load-bearing applications. While metals, polymers, and ceramics are used in orthopedics, it remains metals, which have over the years uniquely provided appropriate material properties such as high strength, ductility, fracture toughness, hardness, corrosion resistance, formability, and biocompatibility necessary for most load-bearing roles required in fracture fixation and total joint arthroplasty (TJA). The use of orthopedic biomaterials generally falls into one of three surgical specialty categories: upper extremity, spine, or lower extremity, and each specialty is typically divided into three general categories: pediatric, trauma, and reconstruction. Despite these numerous specialties and the hundreds of orthopedic applications there are only a few orthopedic metals, ceramics, and polymers which dominate all implants. Knowing the general properties, uses, and limitations of the “primary” orthopedic biomaterials is requisite to understanding what is required to improve the performance of current implant materials and why only a few dominate the industry. A summary of seven more prevalent orthopedic biomaterials and their primary use(s) are listed in Table 2.5.4.1.

Orthopedic Biomaterials Design: New biomaterials for orthopedic purposes face the same concerns present in current implants: (1) the material must not adversely affect its biological environment and (2) in return the material must not be adversely affected by the surrounding host tissues and fluids. (3) New materials must exceed the performance of present materials. Thus, understanding the interrelationship between the structure and properties of the natural tissues that are being replaced is important. An appreciation of the “form–function” relationship in calcified tissues will help provide insight into critical factors determining implant design as well as deciding which materials best meet a specific orthopedic need.

Structure and Properties of Calcified Tissues: There are several different calcified tissues in the human body and several different ways of categorizing them. All calcified



• **Figure 2.5.4.1** Total joint arthroplasties (TJAs) are currently used to replace hip, knee, shoulder, etc. (Courtesy of BioEngineering Solutions Inc.)

tissues have one thing in common: in addition to the principal protein component, collagen, and small amounts of other organic phases, they all have an inorganic component hydroxyapatite [abbreviated as OHAp, HA, or $\text{Ca}_{10}(\text{PO}_4)_6(\text{OH})_2$]. In the case of long bones such as the tibia or femur, an understanding of the organization of these two principal components is central to characterization. It has been convenient to treat the structure of compact cortical bone (e.g., the dense bone tissue found in the shafts of long bones) using four levels of organization.

The first level or molecular level of organization is the collagen triple helical structure (tropocollagen) and OHAp crystallography. It forms a hexagonal unit cell with space group symmetry $P 6_3/m$ and lattice constants $a = 9.880 \text{ \AA}$ and $c = 6.418 \text{ \AA}$, containing two molecular units, $\text{Ca}_5(\text{PO}_4)_3\text{OH}$, per unit cell. How cells produce this mineral phase and whether it is the first calcium phosphate laid down are subjects of considerable research at present. Because of its small crystallite size in bone (approximately $2 \text{ nm} \times 20 \text{ nm} \times 40 \text{ nm}$), the X-ray diffraction pattern of bone exhibits considerable line broadening, compounding the difficulty of identifying additional phases. A Ca-bearing inorganic compound in one of the components of calcified tissues has led to the development of a whole class of ceramic and glass-ceramic materials that are osteophilic within the body (i.e., they present surfaces that bone

TABLE 2.5.4.1 Most Common Orthopedic Biomaterials

Material	Primary Use(s)
Metals	
Ti alloy (Ti–6%Al –4%V)	Plates, screws, TJA components (nonbearing surface)
Co–Cr–Mo alloy	TJA components
Stainless steel	TJA components, screws, plates, cabling
Polymers	
Polymethylmethacrylate (PMMA)	Bone cement
Ultra-high-molecular-weight-polyethylene (UHMWPE)	Low-friction inserts for bearing surfaces in TJA
Ceramics	
Alumina (Al_2O_3)	Bearing surface TJA components
Zirconia (ZrO_2)	Bearing surface TJA components

chemically attaches to). As yet, we do not know fully how the two components, collagen and OHAp, are arranged and held together at this molecular level. Whatever the arrangement, when it is interfered with (as is apparently the case in certain bone pathologies in which the collagen structure is altered during formation), the result is a bone that is formed or remodeled with seriously compromised physical properties.

The second or ultrastructural level may be loosely defined as the structural level observed with transmission electron microscopy (TEM) or high-magnification scanning electron microscopy (SEM). Here too, we have not yet achieved a full understanding of the collagen–OHAp organization. It appears that the OHAp can be found both inter- and intrafibrillarly within the collagen. At this level, we can model the elastic properties of this essentially two-component system by resorting to some sort of linear superposition of the elastic moduli of each component, weighted by the percent volume concentration of each.

The third or microstructural level of organization is where these fibrillar composites form larger structures, fibers, and fiber bundles, which then pack into lamellar-type units that can be observed with both SEM and optical microscopy. The straight lamellar units forming the plexiform (lamellar) bone are found generally in young quadruped animals the size of cats and larger. This is the structural level that is described when the term “bone tissue” is used or when histology is generally being discussed. At this level, composite analysis can also be used to model the elastic properties of the tissue, thus providing an understanding of the macroscopic properties of bone. Unfortunately, this modeling is very complex and a complete description lies beyond the

scope of this chapter (and the authors). Interested readers are referred to some of the original sources (Katz, 1980a,b).

The fourth level is that of each of the macroscopic levels of each bone sample or large section of bone.

Since a significant portion of bone is composed of collagen, it is not surprising to find that in addition to being anisotropic and inhomogeneous, bone is also viscoelastic like all other biological tissues. Duplicating such properties with long-lasting synthetic biomaterials remains an unrealized goal of orthopedic biomaterials, where the history of implant development has been characterized by the elimination of available candidate materials based on their poor performance rather than production of biocompatible synthetic bone-mimetic materials.

Perhaps the best example of how orthopedic biomaterials have undergone implant design improvements over the past 100 years resulting in widespread success is total hip replacement (THR) or total hip arthroplasty (THA). While newer types of total joint arthroplasties such as those currently used for disc replacements (total disc arthroplasty, TDA) have benefitted from the arduous history of the total joint arthroplasty. Many if not all of the biomaterial-related issues (both mechanical and biological) that impact the performance of the THRs are applicable to other orthopedic implants. Therefore this chapter details the characteristics of where we come from using the total hip arthroplasty, and where we are using the example of current total disc arthroplasty designs, general current orthopedic materials technology, and future developments as a proxy of clinical concerns of orthopedic biomaterial development and current technology. The history of total hip arthroplasty is particularly pertinent to biomaterials science because it is one of the best illustrations of how an implant first used over a century ago has evolved to the highly successful status it has, primarily because of advances in biomaterials.

Biomaterials Development: A History of Total Hip Arthroplasty

The earliest attempts to restore mobility to painful and deformed hip joints took place in the 1820s (Dr Charles White in 1822 and John Rhea Barton of Philadelphia in 1826 conducted the first osteotomy on patients with post-traumatic ankylosis) and centered on simply removing the affected femoral and acetabular bone involved. This evolved in the 1830–80s into ghastly attempts to restore mobility using interpositional membranes between the femoral head and acetabulum, where such materials as wooden blocks and animal (e.g., pig) soft tissue were tried. The first prosthetic hip replacement is dated to 1890, when Gluck published a description of a carved ivory femoral head replacement using bone-cement-like materials such as pumice and plaster of Paris to secure the implants in place (Walker, 1978; Stillwell, 1987).

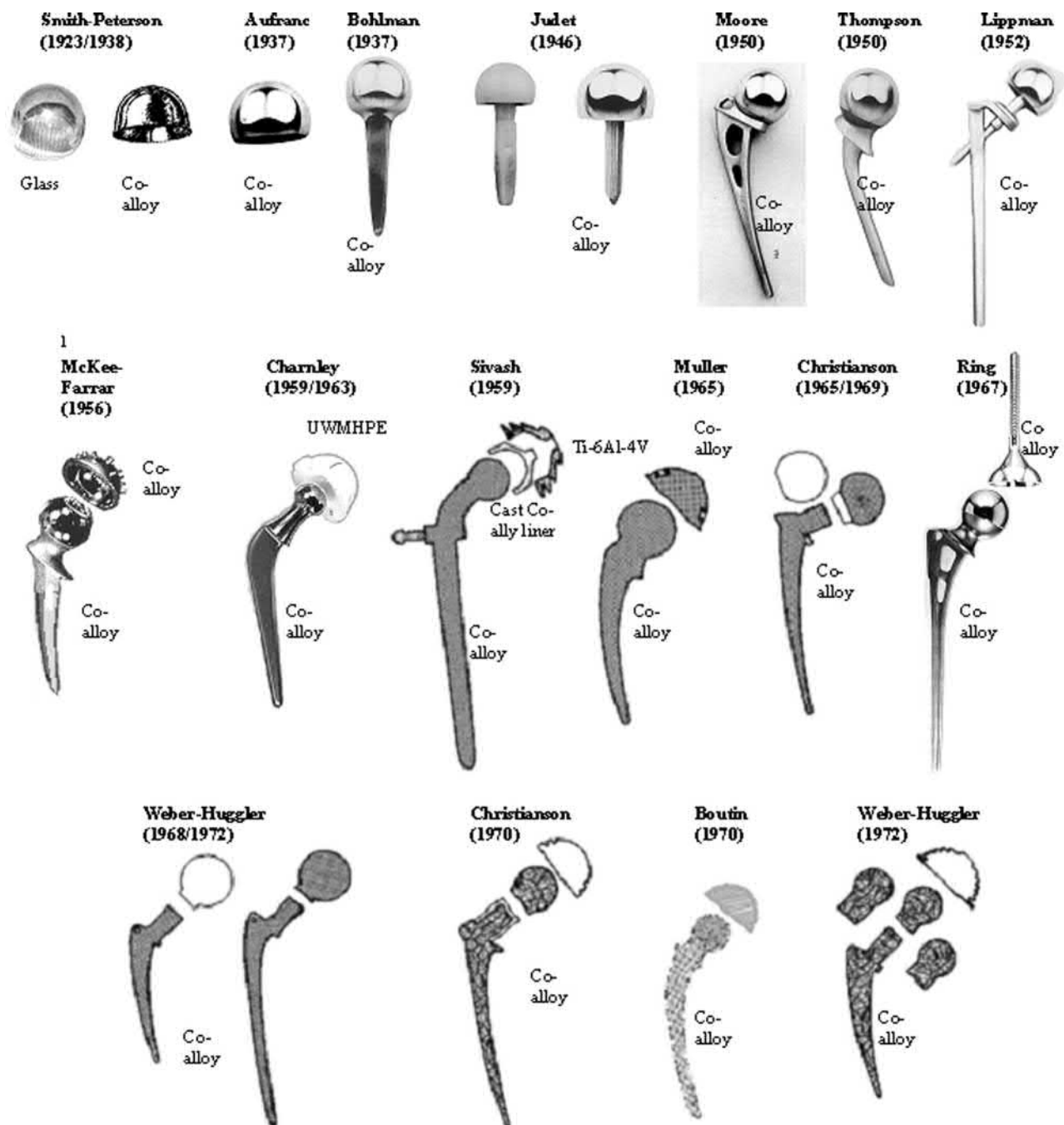
The interpositional membrane strategy continued from the 19th into the 20th century where the use of new implant materials in the early 1900s (1900–20) included organic materials (e.g., pig bladders and periimplant soft tissues)

and inorganic materials such as gold foil. The use of the individual's own soft tissues was the most popular method of interpositional membrane hip surgery. The limited success of this procedure prevented widespread use and thus the treatment of painful, disfigured, and “frozen” (ankylosed) hip joints remained commonplace into the 1920s.

Mold Arthroplasty: It was not until 1923 when Marius Smith-Peterson was credited with ushering in the modern era of total joint replacement with his development of the “mold” arthroplasty (Fig. 2.5.4.2), made of glass, inspired by a shard of glass found in a patient's back with a benign synovial-like membrane around it. This mold or cup arthroplasty was designed as a cup that fit in between the femoral head and the acetabular cup and articulated on both surfaces prompting a “tissue-engineered” synovial/cartilage-like layer. This was the first widespread attempt to develop a better interpositional membrane, a technique that had been in practice for the previous 100 years. The efforts of Smith-Peterson and his colleagues over the years from 1923 to 38 were spent improving the fracture resistance of the glass mold arthroplasty cup design using materials such as early polymers (e.g., celluloid or phenol-formaldehyde Bakelite or Formica) and improved glass, e.g., Pyrex. But it was not until 1939 when the first metal, a cobalt alloy termed Vitallium, was available and used by Venable, Stuck, and Beach that the corrosion resistance of the hip arthroplasty provided sufficient biocompatibility and performance (Fig. 2.5.4.2).

In 1937, Venable, Stuck, and Beach published a landmark article that was the first to analyze in a systematic fashion the electrolytic effects of various metals on bone and tissues (e.g., aluminum, copper, iron, nickel, lead, gold, magnesium, silver, stainless steel, and other alloys) and arrived at the conclusion that Vitallium (a cobalt–chromium alloy) was superior to the other metals in corrosion resistance and mechanical properties required for an implant (Charnley, 1979; Venable et al., 1937). By observing the effects of corrosion and proposing guidelines for performance Venable, Stuck, and Beach set the standard by which future metallic alloys were selected for use in hip and other types of implants.

The superior material properties of the Vitallium alloy facilitated further design modifications of the mold arthroplasty by Otto E. Aufranc (Fig. 2.5.4.2) where the rim of the Smith-Peterson mold was removed (which often was the cause of adhesions and cup “freezing,” and subsequent pain and immobility) and matching curves on the inner and outer surface were machined to meet at the rounded outer edge. Despite the high short-term success rates (<4 years) reported by Aufranc (>82%), the overall failure rate remained high (>50%). Another design modification of the mold arthroplasty in the 1940s–50s was the fixation of the mold to the acetabulum rim with screws, by such physicians as Albee-Pearson and Gaenslen. Although used in only four cases, Gaenslen reported using a cobalt alloy mold fixed to the acetabulum and another fixed to the femoral head creating a metal-on-metal total hip replacement. The popularity of mold arthroplasties endured into the 1970s when they



• **Figure 2.5.4.2** The history of total hip arthroplasty is particularly pertinent to biomaterials science because it is one of the best illustrations of how an implant first used over a century ago has evolved to the highly successful status it has, primarily because of advances in biomaterials.

remained touted as the treatment of choice for traumatic arthritis of the hip by leading orthopedic surgeons (Harris, 1969). However back in the 1930s the natural progress in THA development was the progression from mold arthroplasty to short-stem prostheses.

Femoral Head Prostheses/Short-Stem Prostheses: Femoral head prosthetics were first made of such materials as ivory (Dr. Themistocles Gluck in 1890 Berlin) and rubber (French surgeon Dr. Pierre Delbet in 1919) and were cemented (using a plaster-like cement) for stability (Walker, 1978; Stillwell, 1987). At about the same time these replacement heads were

first fitted with a short stem by Earnest Hey Groves who used an ivory nail to replace the articular surface of the femur. These types of implants were rare and remained unpopular compared to mold arthroplasties until 1937 when Harold Bohlman, using the work of Venable and Stuck, designed a corrosion resistant cobalt–chrome alloy femoral head replacement with a short stem. This design was popularized by the Judet brothers in Paris in 1946, who used polymethylmethacrylate (PMMA), which was presumed biologically inert in vivo, to manufacture short-stemmed prostheses (Fig. 2.5.4.2). Initial good results were soon replaced with

problems of implant fracture and excessive wear debris, and by the early 1950s these implants were losing favor and being removed by surgeons. Vitallium (cobalt–chrome alloy) eventually replaced acrylic in several other short-stem designs. However, there were sound short-stem designs as early as 1938 when Wiles introduced the cobalt alloy femoral shell attached to the femur with a central nail. This design was later popularized by Peterson in 1950, when he used a similar Vitallium shell design with a central nail and a plate attached to the nail for added stability. Others adopted and adapted the Judet brothers' design using Vitallium, such as J. Thompson (1951) and Rossignal (1950). Rossignal designed large threads onto the stem to aid in fixation. These short-stem designs were subject to what was deemed high shear stress and resulted in early loosening and failure in some patients. Short-stem designs were gradually replaced by longer stem designs that provided less stress concentration.

Long-Stem Prostheses: Long-stem prostheses continued the trend established by short-stemmed prostheses, that is, more and more weight-bearing forces were transferred to the femur through an intramedullary stem. The pattern for a long-stem prosthesis was established in 1940 by Bohlman in collaboration with Austin T. Moore in which they implanted a 12-inch Vitallium prosthesis that replaced the femoral head and had long supports that were screwed into the outside of the femoral shaft (Moore, 1943). And while there were innovations in long-stem design in the 1940s, such as the door knob design of Earl McBride, where a threaded stem was screwed into the intramedullary canal of the femur for fixation and load transferral, these designs were not popular. It was not until 1950 with the designs of Frederick R. Thompson and Austin T. Moore that long-stemmed prostheses became popular (Fig. 2.5.4.2). These designs were cast in Vitallium (cobalt–chrome alloy) and required the removal of the femoral head but only part of the neck. The design of Moore differed from that of Thompson in that it had fenestrations through the implant to allow bone growth and it had a rear vane to enhance rotational stability. Initially these implants were used without bone cement. Evidence for the successful designs of the Thompson and Moore prostheses is proved by their continued use with only slight variations from the original. Despite the excellent design of these early long-stemmed prostheses they were primarily successful when used in place of diseased femoral heads and did not work well when acetabular reaming was required. Therefore, this inadequacy prompted the development of the total hip replacement arthroplasty.

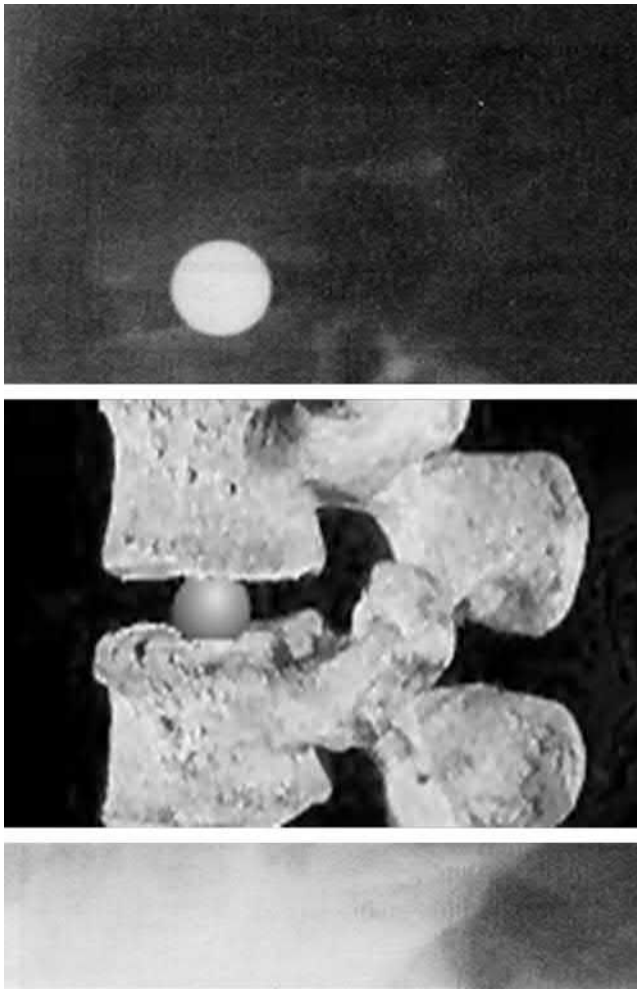
Total Hip Replacement Arthroplasty: Philip Wiles is credited with the first total hip arthroplasty in 1938 when he used a stainless steel ball secured to the femur with a bolt and a stainless acetabular liner secured with screws (Wiles, 1953). The results of this design were disappointing because of the poor corrosion resistance of early stainless steel in vivo, and the high stress concentrations of short-stemmed prostheses. An adaptation of this design that proved successful was developed by G.K. McKee and J. Watson-Farrar in 1951. They used a stainless steel cup and long-stemmed

prosthesis (Thompson stem) which failed rapidly due to the poor corrosion resistance of the stainless steel, and was then changed to cobalt–chrome alloy with greater success. The McKee-Farrar prosthesis evolved quickly to incorporate a true spherical femoral head that was undercut at the neck to reduce the impingement of the head on the rim of the acetabular prosthesis and provide for a greater range of mobility (Fig. 2.5.4.2) (McKee and Watson-Farrar, 1943).

The next milestone in the evolution of modern total hip arthroplasty was the advent/popularization of acrylic dental bone cement, first used by Sven Kiar in 1950 to attach a plastic prosthesis to bone (Charnley, 1964). Later that year the Hospital for Joint Diseases in New York used polymethylmethacrylate (acrylic) bone cement as a means of fixation in total hip arthroplasties (Wilson and Scales, 1970; Charnley, 1960). The development of acrylic bone cement dramatically reduced the rates of loosening associated with metal–metal total hip arthroplasty. The Stanmore metal–metal design, which used a horseshoe-shaped cup, was popular but led to excessive wear and was replaced by a complete cup. McKee and Watson-Farrar adapted their design to facilitate bone cement with a land-mine-like studded acetabular cup intended to maximize mechanical fixation.

The 1950s marked the introduction and popularization of the total hip arthroplasty when it became simple and reliable enough to be practiced on a wide scale by the average orthopedic surgeon. However, the squeaking reported to occur in Judet and some later metal prostheses was identified by Charnley to be a result of the relatively high frictional forces in the joint. These high torque and frictional forces resulted in the generation of significant metallic debris which purportedly resulted in early loosening. In 1960, Charnley developed a “low-friction arthroplasty” device using shells of polytetrafluoroethylene (PTFE; commonly called Teflon in related publications) on the femoral and acetabular sides, which resulted in early/immediate failures because of the massive debonding and wear debris. This was quickly followed by a thick-walled Teflon acetabular component articulating on a small head designed to reduce the shearing forces and torque. However, this design also generated excessive wear debris, which produced immediate and severe inflammation and failure of the prosthesis. Charnley then replaced the Teflon with high-density polyethylene which was not as friction-free as Teflon but was 1000 times more wear resistant. This prototype of total hip arthroplasty developed in 1962 was the basis for future designs, which remain the most popular form of total hip arthroplasty performed today (Fig. 2.5.4.2).

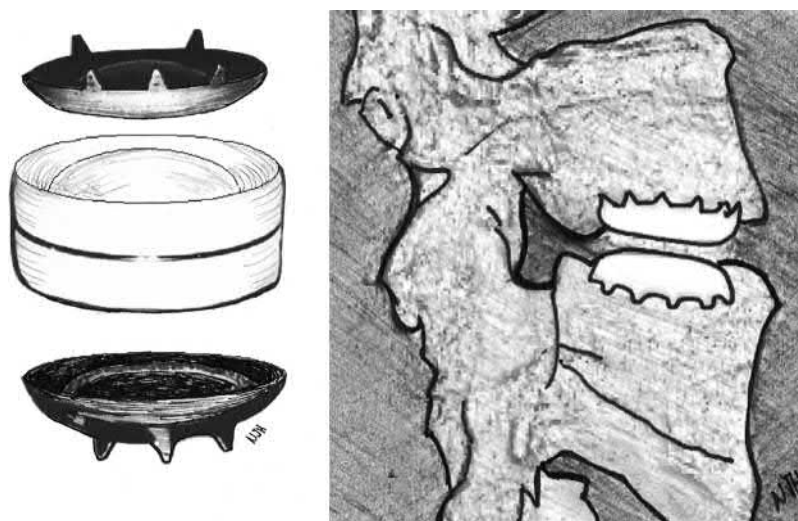
The basic design of Charnley was modified by Muller with variable neck sizes and larger heads. At the same period metal-on-metal designs by Smith, Ring, and others (Ring, 1968) were unsuccessful challengers to the basic Charnley metal-on-polymer design. Other currently adopted design modifications were developed by Ling, Aufranc, Turner, Amstutz, Harris, and Galante, which include such innovations as femoral prosthesis geometrical modification for increases in stability and mobility, modular components for increased customization, porous coatings, surface texturing/coating to



• **Figure 2.5.4.3** Fernström ball implants (stainless steel metal spheres) were the first disc arthroplasties. (Courtesy of BioEngineering Solutions Inc.)

increase fixation and bone ingrowth, etc. Charnley is often deified in orthopedic literature as the metaphorical spark that lit the flames of innovation in prosthetic design. This is a typical surgeon-centered overglorification. For one thing other implant designs which predate Charnley, such as the all-metal McKee-Farrar THA implant, have enjoyed similar success rates to those reported by Charnley. More importantly, total hip arthroplasty is, perhaps, the best example of how orthopedic biomaterials and implant success have evolved over the last century through the innovation and hard work of many scientists and physicians and advances in areas of materials technology, biomechanics, biochemistry, immunology, infectious diseases, thrombosis, and pharmacology to name a few.

In contrast to THA, total disc arthroplasty (TDA) is a relatively recent development and, despite clinical use over the past 10 years, it has yet to become a mainstream option for treating disc degeneration when compared with fusion. Spinal fixation device usage is steadily increasing, where the number of cervical and lumbar fusions increased 111% from 1993 to 2003 to roughly 105 fusions per 100,000 people in the United States, which is about 305,000 fusions per year (Cowan Jr. et al., 2006). The ultimate goal of intervertebral disc replacement technology is to replace spine fusion, eliminate pain, and restore structure and mobility. The first disc arthroplasties were cobalt-alloy spheres implanted as early as 1957 between vertebrae without any method of fixation (Harmon, 1963). A decade later stainless steel metal spheres termed Fernström balls (Fig. 2.5.4.3) were used in 103 patients starting in 1969 (McKenzie Alvin, 1995; Fernstrom, 1966). Other clinicians around the same time tried using polymer balls made of polymethyl methacrylate but the results were disastrous (Hamby and Glaser, 1959). The era of modern disc arthroplasty began in 1982, the first functional artificial intervertebral disc, the SB Charité, at the Charité hospital in Berlin (Fig. 2.5.4.4) (Büttner-Janz, 1992). This design was that using the low-friction

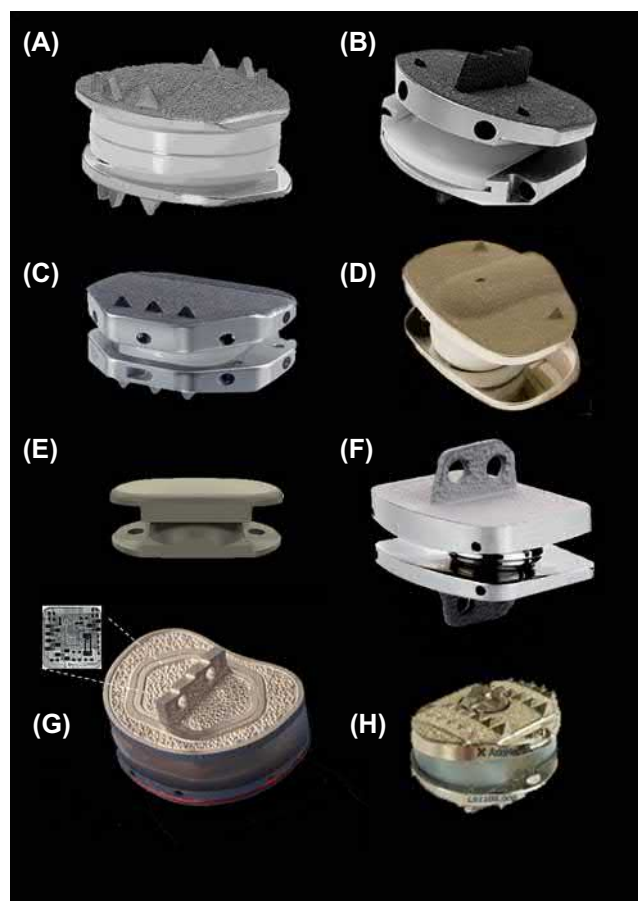


• **Figure 2.5.4.4** In 1982, Schellnack and Büttner-Janz developed the SB Charité artificial disc, which consisted of a UHMWPE sliding core articulating unconstrained between two highly polished stainless steel metal endplates. (Courtesy of Bioengineering Solutions Inc., Oak Park, IL.)

arthroplasty principle of John Charnley's, which by that time was successful used in total hip replacement for over 20 years. The Charité TDA consisted of a UHMWPE sliding core, which articulates between two metal endplates with multiple teeth-like projections for fixation to the vertebral endplates (Fig. 2.5.4.4). In general, current TDA designs have a TKA-like primary articulation (or motion) using polymer-on-metal, polymer-on-polymer, metal-on-metal, or some form of an all-elastic core technology. The long-term clinical success of many current total disc arthroplasty designs with motion-preserving properties remains under close evaluation (Fig. 2.5.4.5).

Current Biomaterials in Total Arthroplasty

Today, the archetype of the total hip implant remains much as it was in the 1970s, albeit with more variety of implant materials and geometries. Current THA is typically constructed of a titanium or cobalt–chromium alloy femoral stem (cemented with polymethylmethacrylate, PMMA, or press fit into place, connected to a “modular” cobalt–chromium alloy or ceramic head that articulates on an ultrahigh-molecular-weight polyethylene (UHMWPE) or ceramic acetabular cup fitted into a titanium or cobalt–chromium cup liner which is cemented, screwed, or press-fit into place. Despite this simple archetype of the total hip replacement there exist hundreds of variations on this theme offered to today's orthopedic surgeons, with little in terms of absolute guidelines as to which type of implant is (or which of the over 10 major manufacturers has) the best for well-defined orthopedic disease states. However, there are some general guidelines. Typically, implants in older individuals (>80 years of age) are cemented into place with PMMA bone cement, because the chance for revision is minimal when compared to younger individuals (<60 years) and removing bone cement is both technically challenging and may compromise the availability of bone stock. Generally, there are choices of surface roughness, coatings, geometry, material composition, etc. and each manufacturer claims that its product is superior to the rest. This, in combination with little to no publicly available information tracking the performance of each type of implant in patients, precludes accurate scientific analysis of which implant materials and design perform best. Additionally, competition between manufacturers and the requisite attention to marketing required to compete in the marketplace has resulted in a dizzying array of new implants released each year claiming to be improved over the previous year's model. These claims are suspect, because the typical total hip replacement enjoys a success rate of over 90% at 7 years, therefore, in most cases a minimum of 7–10 years must transpire before such claims can be substantiated, and even then proof of superior performance is compromised by a myriad of external factors such as surgeon, region of the country, average activity of patient populations, etc. This conflict between science, marketing, and market share may (in the opinion of this author) represent the single biggest obstacle to the scientific



• **Figure 2.5.4.5** Lumbar total disc replacements include metal-on-polymer, metal-on-metal, polymer-on-polymer, and flexible core technologies. (A) Metal-on-polymer articulation: the *LINK SB Charité III* (DePuy Spine) cobalt chrome alloy endplates articulate on a mobile bearing ultrahigh-molecular-weight polyethylene core. The endplates are covered with an osteoconductive surface of titanium/calcium-phosphate double coating under the trade name “TiCaP” (B) Metal-on-polymer articulation: The Prodisc (Synthes) lumbar TDR is composed of cobalt–chrome–molybdenum alloy and covered with a porous titanium alloy and articulates on a central core of UHMWPE. (C) Metal-on-polymer articulation: ActivL (Aesculap) uses a polymeric center core intended to allow both translation and rotation and to more closely approximate physiological motion. (D) Metal-on-polymer articulation: Dynardi (Zimmer) is a disc replacement implant with two opposing Co-alloy (Co–Cr–Mo) endplates coated with porous pure titanium for bone ingrowth, that articulate on a semiconstrained UHMWPE core. (E) Polymer-on-polymer articulation: NUBAC (Pioneer Surgical) is a polymer-on-polymer disc arthroplasty device and the first polyetheretherketone (PEEK)-on-PEEK articulated disc arthroplasty device. (F) Metal-on-metal articulation: The Maverick Disc (Medtronic) uses metal-on-metal articulation where the end plates are constructed of Co-alloy. (G) Elastic core articulation: The Theken eDisc (Theken Disc) represents another step in the evolution of orthopedic implant devices, in that as well as containing an elastic polyurethane-based core it provides measured in vivo load information to the surgeon and patient via electronic sensors and transmitters. (H) Elastic core articulation: The Freedom Lumbar Disc (Axiomed) uses a viscoelastic polymer (like polyurethane) to replicate the native function of a natural disc. The elastic core in combination with the implant design provides a three-dimensional motion that functions within the natural biomechanics of the spine. (Courtesy of DePuy Spine Inc, Medtronic, Spine Solutions Inc., and BioEngineering Solutions Inc.)



• **Figure 2.5.4.6** Examples of the three types of bearing couples using in modern TJA. From top to bottom: metal-on-polymer, ceramic-on-ceramic, and metal-on-metal (Lineage line from Wright Medical Technology, Inc. Arlington TN).

determination of superior implant design and progress. The unenviable responsibility rests with the FDA to prevent the zeal of economic pressure from undermining implant design in a regressive fashion. Today optimal implant selection is moving toward which material couple may best suit the individual from a biocompatibility standpoint (as described later) (Fig. 2.5.4.6).

Polymers: Polymers are most commonly used in orthopedics as articulating bearing surfaces of joint replacements (Fig. 2.5.4.3) and as an interpositional cementing material between the implant surface and bone (Fig. 2.5.4.4). Polymers used as articulating surfaces must have low coefficients of friction and low wear rates when in articulating contact with the opposing surface, which is usually made of metal. Initially, John Charnley used Teflon (PTFE) for the acetabular component of his total hip arthroplasty (Fig. 2.5.4.2). However, its accelerated creep and poor stress corrosion (for the material he used) caused it to fail *in vivo*, requiring replacement with his ultimate choice, ultrahigh-molecular-weight polyethylene (UHMWPE).

Polymers used for fixation as a structural interface between the implant component and bone tissue require appropriate mechanical properties of a polymer, which

can be molded into shape and cured *in vivo*. The first type to be used, polymethylmethacrylate (PMMA), was again popularized by Charnley's who borrowed from the field of dentistry. He adapted dental PMMA as a "grouting" material to fix both the stem of the femoral component and the acetabular component in place, and thus distribute the loads more uniformly from the implants to the bone. Since high interfacial stresses result from the accommodation of a high-modulus prosthesis within the much lower modulus bone, the use of a lower modulus interpositional material has been a goal of alternatives seeking to improve upon PMMA fixation. Thus, polymers such as polysulfone have been tried as porous coatings on the implant's metallic core to permit mechanical interlocking through bone and/or soft tissue ingrowth into the pores. However, to date, PMMA remains the method of choice for orthopedic surgeons. This requires that polymers have surfaces that resist creep under the stresses found in clinical situations and have high enough yield strengths to minimize plastic deformation. As indicated earlier, the important mechanical properties of orthopedic polymers are yield stress, creep resistance, and wear rate. These factors are controlled by such parameters as molecular chain structure, molecular weight, and degree of branching or (conversely) of chain linearity.

One of the more prevalent polymeric used in orthopedics today is a highly cross-linked UHMWPE, which is typically used in total joint arthroplasty as a load-bearing articulating surface, designed to provide low-friction load-bearing articulation. Polyethylene is available commercially in three different grades: low-density, high-density, and UHMWPE. The better packing of linear chains within UHMWPE results in increased crystallinity and provides improved mechanical properties required for orthopedic use even though there is a decrease in both ductility and fracture toughness. In total hip arthroplasty applications, an acetabular cup of UHMWPE typically articulates against a femoral ball of cobalt–chromium alloy. The predominant problem presented by these metal–polymer articulating surfaces is the production of wear particles, *i.e.*, polymer debris. The resultant wear of the polyethylene bearing purportedly produces billions of submicron-sized wear particles annually, in the <1–10 micron range. Producing greater cross-linking of polyethylene, using chemical and radiation techniques, has only recently improved its wear resistance in orthopedic applications. Wear tests have shown that the wear resistance of UHMWPE is improved by cross-linking with gamma irradiation at 2.5–5.0 Mrad and below as evidenced by simulator studies, however this can negatively affect such physical properties as tensile strength (McKellop *et al.*, 2000). Therefore, care must be taken to minimize any negative oxidative effects, while preserving high wear characteristics. Although newer more highly cross-linked polyethylene has generally been accepted as superior to previous implant UHMWPE, there remains incomplete data regarding its ultimate long-term performance. In order to maximize the performance characteristics of polyethylene it is cross-linked prior to fabrication into its final form, *e.g.*, an

acetabular cup. Typically, an extruded bar of polyethylene is cross-linked using conventional gamma irradiation and then heat treated to reduce residual free radicals.

Ceramics: In recent years, ceramics and glass ceramics have played an increasingly important role in implants. Although used in Europe for over a quarter century, only relatively recently (February 3, 2003), has the FDA approved the first ceramic-on-ceramic bearing hip implant to be used in total hip replacement procedures (Fig. 2.5.4.5). The primary reason for the introduction of this alternative bearing surface is the superior wear resistance of ceramics when compared to metal–metal or metal–polymer bearing surfaces. This and other improved properties such as resistance to further oxidation (implying inertness within the body), high stiffness, and low friction require the use of full-density, controlled, small, uniform grain size (usually less than 5 μm) ceramic materials. The small grain size and full density are important since these are the two principal bulk parameters controlling the ceramic's mechanical properties. Any voids within the ceramic's body will increase stress, degrading the mechanical properties. Grain size controls the magnitude of the internal stresses produced by thermal contractions during cooling. In ceramics, such thermal contraction stresses are critical because they cannot be dissipated as they can in ductile materials via plastic deformation.

Alumina (Al_2O_3) and zirconia (ZrO_2) ceramics have been used in orthopedic THA for the past 30 years. The first ceramic couple (alumina/alumina) was implanted in 1970 by Pierre Boutin. Since the outset the theoretical advantage of hard-on-hard articulating surfaces was low wear. Ceramics, because of their ionic bonds and chemical stability, are also relatively biocompatible. Initial concerns about fracture toughness and wear have been addressed by lowering grain size, increasing purity, lowering porosity, and improving manufacturing techniques (e.g., hot isostatic pressing, HIP). Early failures of these couples were plagued with both material-related and surgical errors. The very low wear rates combined with steadily decreasing rates of fracture (now estimated to occur to one in 2000 over 10 years) have resulted in the growing popularity of all ceramic bearings.

Zirconia was introduced in 1985, as a material alternative to Al_2O_3 for ceramic femoral heads, and was gaining market share because of its demonstrable enhanced mechanical properties in the laboratory when compared to alumina. Femoral heads of zirconia can typically withstand 250 kN (or 25 tons), a value generally exceeding that possible with alumina or metal femoral heads. However, the mechanical integrity of all ceramic components is extremely dependent on manufacturing quality controls as evidenced in the recall of thousands of zirconia ceramic femoral heads, by their manufacturer St. Gobain Desmarquest in 2001. This was because of in vivo fracture of some components due to a slight unintended variation in the manufacturing sintering process caused when the company bought a newer high-throughput assembly line type oven. In general ceramic particulate debris is chemically stable and biocompatible and causes untoward biologic responses at high concentrations.

There have been recent attempts to take advantage of the osteophilic surface of certain ceramics and glass ceramics. These materials provide an interface of such biological compatibility with osteoblasts (bone-forming cells) that these cells lay down bone in direct apposition to the material in some form of direct chemico-physical bond. Special compositions of glass ceramics, termed bioglasses, have been used for implant applications in orthopedics. The model proposed for the “chemical” bond formed between glass and bone is that the former undergoes a controlled surface degradation, producing an SiO-rich layer and a Ca,P-rich layer at the interface. Originally amorphous, the Ca,P-rich layer eventually crystallizes as a mixed hydroxycarbonate apatite structurally integrated with collagen, which permits subsequent bonding by newly formed mineralized tissues. There is still an entirely different series of inorganic compounds that also have been shown to be osteophilic. These include OHAp, which is the form of the naturally occurring inorganic component of calcified tissues, and calcite, CaCO_3 , and its Mg analog, dolomite, among others being studied. The most extensive applications in both orthopedics and dentistry have involved OHAp. This has been used as a cladding for metal prostheses for the former, and in dense, particulate form for the latter. The elastic properties of OHAp and related compounds are compared with those of bone, dentin, and enamel in Table 2.5.4.2. The use of both OHAp and the glass ceramics as claddings on the metallic stems of hip prostheses is yet another method of providing fixation instead of using PMMA. In these cases, the fixation is via the direct bonding of bone to the cladding surface.

Metals: Since the principal function of the long bones of the lower body is to act as load-bearing members, it was reasonable that the initial materials introduced to replace joints, such as artificial hips, were metals. Both stainless steel, such as 316L, and Co–Cr alloys became the early materials of choice, because of their relatively good corrosion resistance and reasonable fatigue life within the human body. Of course, their stiffness, rigidity, and strength, exceeded those of bone considerably. However, in certain applications, owing to size restrictions and design limitations (e.g., in rods used to straighten the spine in scoliosis), fatigue failures did occur. Metals remain the central material component of state-of-the-art total hip arthroplasties. Metals provide appropriate material properties such as high strength, ductility, fracture toughness, hardness, corrosion resistance, formability, and biocompatibility necessary for use in load-bearing roles required in fracture fixation and total joint arthroplasty (TJA). Implant alloys were originally developed for maritime and aviation uses where mechanical properties such as high strength and corrosion resistance are paramount. There are three principal metal alloys used in orthopedics and particularly in total joint replacement: (1) titanium-based alloys, (2) cobalt-based alloys, and (3) stainless steel alloys. Alloy-specific differences in strength, ductility, and hardness generally determine which of these three alloys is used for a particular application or implant component. However it is the high corrosion resistance of

TABLE 2.5.4.2 Mechanical Properties of Dominant Orthopedic Biomaterials

Orthopedic Biomaterial	ASTM Designation	Trade Name and Company(Examples)	Elastic modulus (Young's Modulus) (GPa)	Yield strength (Elastic Limit) (MPa)	Ultimate Strength (MPa)	Fatigue Strength (Endurance Limit) (MPa)	Hardness HVN	Elongation at Fracture(%)
Cortical Bone^{\$}								
Low strain			15.2	114t	150c/90t	30–45	–	–
High strain			40.8	–	400c–270t	–	–	–
Polymers								
UHMWPE			0.5–1.3	20–30	30–40t	13–20	60–90 (Mpa)	130–500
PMMA			1.8–3.3	35–70	38–80t	19–39	100–200 (Mpa)	2.5–6
Ceramics								
Al ₂ O ₃			366	–	3790c 310t		20–30 (Gpa)	–
ZrO ₂			201	–	7500c 420t	–	12 (Gpa)	–
Metals								
Stainless steels	ASTM F138	Protusul S30-Sulzer	190	792	930t	241–820	130–180	43–45
Co–Cr Alloys								
	ASTM F75	Alivium-Biomet CoCrMo-Biomet Endocast SIL-Krupp Francobal-Benoist Girard Orthochrome- DePuy Protosul 2-Sultzter Vinertia-Deloro Vitallium C-Howmedica VitalliumFHS- Howmedica Zimalloy-Zimmer Zimalloy Micrograin	210–253	448–841	655–1277t	207–950	300–400	4–14
	ASTM F90	Vitallium W-Howmedica	210	448–1606	1896t	586–1220	300–400	10–22
	ASTM F562	HS25I-Haynes Stellite MP35N-Std pressed Steel Corp.	200–230	300–2000	800–2068t	340–520	8–50 (RC)	10–40
	ASTM 1537	TJA 1537-Allvac Metasul-Sulzer	200–300	960	1300t	200–300	41 (RC)	20
Ti Alloys								
CPTi	ASTM F67	CSTi-Sulzer	110	485	760t	300	120–200	14–18
Ti–6Al–4V	ASTM 136	Isotan-Aesculap Werke Protosul 64WF-Sulzer Tilastan-Waldemar link Tivaloy 12-Biomet Tivanium-Zimmer	116	897–1034	965–1103t	620–689	310	8

^{\$}, cortical bone is both anisotropic and viscoelastic, thus properties listed are generalized; c, compression; t, tension; *, No current ASTM standard; RC, Rockwell Hardness Scale; HVN, Vickers Hardness Number, kg/mm.

all three alloys, more than anything, which has led to their widespread use as load-bearing implant materials. These material properties of metals (Table 2.5.4.2) are due to the miraculous nature of the metallic bond, molecular microstructure, and elemental composition of metals.

Stainless Steel Alloys: Stainless steels were the first metals to be used in orthopedics in 1926. However, it was not until 1943 when ASTM 304 was recommended as a standard implant alloy material that steels were reliable as an implant alloy. All steels are comprised of iron and carbon and may typically contain chromium, nickel, and molybdenum. Trace elements such as manganese, phosphorous, sulfur, and silicon are also present. Carbon and the other alloy elements affect the mechanical properties of steel through alteration of its microstructure.

The form of stainless steel most commonly used in orthopedic practice is designated 316LV (American Society for Testing and Materials F138, ASTM F138 others include F139, F899, F1586, F621 etc). “316” classifies the material as austenitic, and the “L” denotes the low carbon content and “V” the vacuum under which it is formed. The carbon content must be kept at a low level to prevent carbide (chromium-carbon) accumulation at the grain boundaries.

Although the mechanical properties of stainless steels are generally less desirable than those of the other implant alloys (lower strength and corrosion resistance), stainless steels do possess greater ductility indicated quantitatively by a threefold greater “percentage of elongation at fracture” when compared to other implant metals (Table 2.5.4.2). This aspect of stainless steel has allowed it to remain popular as a material for cable fixation components in total knee arthroplasty, and a low-cost alternative to Ti and Co alloys.

Cobalt–Chromium Alloys: Of the many Co–Cr alloys available, there are currently only two predominantly used as implant alloys (Table 2.5.4.3). These two are (1) cobalt–chromium–molybdenum (CoCrMo), which is designated ASTM F-75 and F-76 and (2) cobalt–nickel–chromium–molybdenum (CoNiCrMo) designated as ASTM F-562. Other Co-alloys approved for implant use include one which incorporates tungsten (W) (CoCrNiW, ASTM F-90) and another with iron (CoNiCrMoWFe, ASTM F-563). Co–Ni–Cr–Mo alloys, which contain large percentages of Ni (25%–37%), promise increased corrosion resistance, yet raise concerns of possible toxicity and/or immunogenic reactivity (discussed later) from released Ni. The biologic reactivity of released Ni from Co–Ni–Cr alloys is cause for concern under static conditions, and due to their poor frictional (wear) properties Co–Ni–Cr alloys are also inappropriate for use in articulating components. Therefore, the dominant implant alloy used for total joint components is Co–Cr–Mo (ASTM F-75).

Cobalt alloys are generally cast into their final shape because they are susceptible to work-hardening at room temperatures. That is, the improvements in strength and hardness gained by cold working are not worth the loss in fracture toughness. Thus Co–Cr–Mo alloy hip implant components are predominantly manufactured using lost wax (investment) casting methods.

Although Co–Cr–Mo alloys are the strongest, hardest, and most fatigue resistant of the metals used for joint replacement components, care must be taken to maintain these properties because the use of finishing treatments can also function to reduce these same properties (Table 2.5.4.2). For example, sintering of porous coatings onto femoral or tibial TJA Co–Cr–Mo stems can decrease the fatigue strength of the alloy from 200–250 to 150 MPa after heating (annealing) the implant at 1225°C.

Titanium Alloys: Titanium alloys were developed in the mid 1940s for the aviation industry and were first used in orthopedics around the same time. Two post-World War II alloys, commercially pure titanium (CPTi) and Ti–6Al–4V, remain the two dominant titanium alloys used in implants. Commercially pure titanium (CPTi, ASTM F67) is 98%–99.6% pure titanium. While CPTi is most commonly used in dental applications, the stability of the oxide layer formed on CPTi (and consequently its high corrosion resistance; Table 2.5.4.4) and its relatively higher ductility (i.e., the ability to be cold worked) compared to Ti–6Al–4V, has led to the use of CPTi in porous coatings (e.g., fiber metal) of TJA components. Generally, joint replacement components (i.e., TJA stems) are made of Ti–6Al–4V (ASTM F-136) rather than CPTi, because of its superior mechanical properties (Table 2.5.4.2).

Titanium alloys are particularly good for THA components because of their high corrosion resistance compared with stainless steel and Co–Cr–Mo alloys. A passive oxide film (primarily of TiO₂) protects both Ti–6Al–4V and CPTi alloys. Generally Ti–6Al–4V has mechanical properties that exceed those of stainless steel, with a flexural rigidity less than stainless steel and Co–Cr–Mo alloys. The torsional and axial stiffness (moduli) of Ti alloys are closer to those of bone and theoretically provide less stress shielding than do Co alloys and stainless steel. However, titanium alloys are particularly sensitive to geometrical factors, in particular notch sensitivity. This reduces the effective strength of a component by increasing the material’s susceptibility to crack propagation through the component. Therefore, care is taken both in the design geometry and in the fabrication of Ti alloy components. Perhaps the greatest drawback to Ti alloys is their relative softness compared to Co–Cr–Mo alloys (Table 2.5.4.2) and their relatively poor wear and frictional properties. Ti–6Al–4V is >15% softer than Co–Cr–Mo alloys and also results in significantly more wear than Co–Cr–Mo when used in applications requiring articulation, e.g., TKA or THA femoral heads. Thus Ti alloys are seldom used as materials where hardness or resistance to wear is the primary concern.

Zirconium and Tantalum Alloys: Zirconium (Zr) and tantalum (Ta) are characterized as refractory metals (others include molybdenum and tungsten) because of their relative chemical stability (passive oxide layer) and high melting points. Because of its high strength, chemical stability, and resistance to wear, alloys, such as Zr (e.g., Oxinium), are likely to gain popularity as orthopedic biomaterials. Because of their surface oxide layer’s stability, Zr and Ta are highly corrosion resistant. Corrosion resistance generally correlates with biocompatibility (although not always)

TABLE 2.5.4.3 Approximate Weight Percent of Different Metals Within Popular Orthopedic Alloys

Alloy	Ni	N	Co	Cr	Ti	Mo	Al	Fe	Mn	Cu	W	C	Si	V
Stainless steel (ASTM F138)	10–15.5	<0.5	*	17–19	*	2–4	*	61–68	*	<0.5	<2.0	<0.06	<1.0	*
CoCrMo alloys (ASTM F75)	<2.0	*	61–66	27–30	*	4.5–7.0	*	<1.5	<1.0	*	*	<0.35	<1.0	*
(ASTM F90)	9–11	*	46–51	19–20	*	*	*	<3.0	<2.5	*	14–16	<0.15	<1.0	*
(ASTM F562)	33–37	*	35	19–21	<1	9.0–11	*	<1	<0.15	*	*	*	<0.15	*
Ti alloys														
CPTi (ASTM F67)	*	*	*	*	99	*	*	0.2–0.5	*	*	*	<0.1	*	*
Ti–6Al–4V (ASTM F136)	*	*	*	*	89–91	*	5.5–6.5	*	*	*	*	<0.08	*	3.5–4.5
45TiNi	55	*	*	*	45	*	*	*	*	*	*	*	*	*
Zr alloy (95% Zr, 5% Nb)	*	*	*	*	*	*	*	*	*	*	*	*	*	*

* Indicates less than 0.05%. Note: Alloy compositions are standardized by the American Society for Testing and Materials (ASTM vol. 13.01).

TABLE
2.5.4.4

Electrochemical Properties of Implant Metals (Corrosion Resistance) in 0.1 M NaCl at pH=7

Alloy	ASTM Designation	Density (g/cm ³)	Corrosion Potential (vs. Calomel) (mVolts)	Passive Current Density (mAmps/cm ²)	Breakdown Potential (mVolts)
Stainless Steel					
	ASTM F138	8.0	-400	0.56	200-770
Co-Cr-Mo Alloys					
	ASTM F75	8.3	-390	1.36	420
Ti Alloys					
CPTi	ASTM F67	4.5	-90 to -630	0.72-9.0	>2000
Ti-6Al-4V	ASTM 136	4.43	-180 to -510	0.9-2.0	>1500
Ti5Al2.5Fe	**	4.45	-530	0.68	>1500
Ni45Ti	**	6.4-6.5	-430	0.44	890

** No current ASTM standard; The corrosion potential represents the Open Circuit Potential (OCP) between the metal and a calomel electrode. The more negative the OCP, the more chemically reactive and thus the less corrosion resistance. Generally low current density indicates greater corrosion resistance. The higher the breakdown potential the better (i.e., the more elevated the breakdown potential, the more stable the protective layer).



• **Figure 2.5.4.7** Examples of new THA and TKA oxidized zirconium components currently gaining popularity because of enhanced mechanical and biocompatibility properties (Oxinium, Smith and Nephew Inc., Memphis, TN). (Courtesy of Smith and Nephew Inc.)

because more stable metal oxides tend to be less chemically active and/or biologically available and are thus less participatory in biologic processes. This enhanced biocompatibility is produced by the relatively thick surface oxide layer (approximately 5 μm) and the ability to extend ceramic-like

material properties (i.e., hardness) into the material through techniques such as oxygen enrichment has resulted in the production of new implant components using these alloys (Fig. 2.5.4.7; e.g., Oxidized Zirconium TKA femoral components, Smith and Nephew Inc.). Although Zr alloys such

as Oxinium generally possess high levels of hardness (12 Gpa) and wear resistance (approximately 10-fold that of Co and Ti alloys, using abrasion testing), which makes them well suited for bearing surface applications, they are costly to manufacture and currently are sought after in special circumstances where issues such as a metal-allergy (or more accurately metal-hypersensitivity) require particular attention to biocompatibility. As difficulties associated with the cost of forming and machining these metals are overcome the use of these materials is expected to grow (Black, 1992).

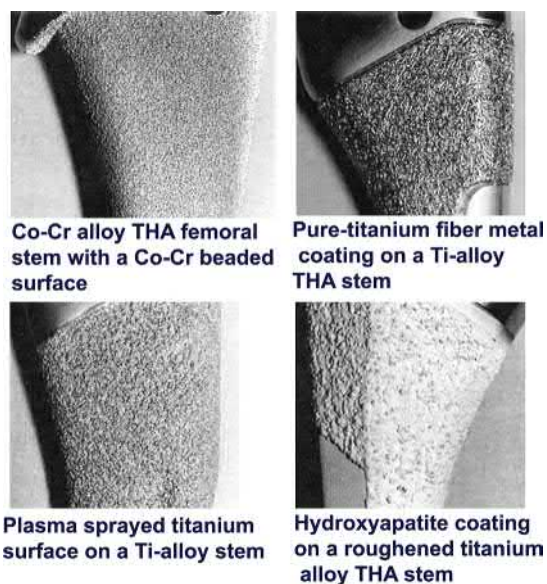
Surfaces and Coatings: A variety of surface coatings are currently used to enhance the short- and long-term performance of implants by encouraging bone ingrowth and providing enhanced fixation. These different surfaces include roughened titanium, porous coatings made of cobalt chromium or titanium beads, titanium wire mesh (fiber mesh), plasma-sprayed titanium, and bioactive nonmetallic materials such as hydroxyapatite or other calcium phosphate compositions (Fig. 2.5.4.8). Currently, osteoconductive and osteoinductive growth factors such as transforming growth factor beta (TGF-beta) are being developed for use as osteogenic surface coating treatments to enhance orthopedic implant fixation.

Orthopedic Biomaterials: Clinical Concerns

Implant biocompatibility/performance is dependent on the type and amount of degradation produced by wear and electrochemical corrosion. The host response to orthopedic implants debris is central to clinical performance (Willert and Semlitsch, 1977). Implant loosening due to aseptic osteolysis accounts for over 75% of TJA implant failure and is the predominant factor limiting the longevity of current total joint arthroplasties; other reasons include infection (7%), recurrent dislocation (6%), periprosthetic fracture (5%), and surgical error (3%) (Holt et al., 2007). Properly

positioned implants tend to wear at predictable rates. However, there are variable amounts of debris-induced bone loss around implants in patients with similar rates of implant wear (i.e., debris generation). It is commonly noted that some individuals with severely worn components can demonstrate little periprosthetic bone loss, while others with modest amounts of wear can demonstrate extensive osteolysis and implant loosening (Harris, 1995; Jacobs et al., 1992; Jasty et al., 1994; Huk et al., 1994; Schmalzried et al., 1994; Granchi et al., 1998b; Thompson and Puleo, 1995; Jones et al., 1999; Yao et al., 1995; Goodman et al., 1998; Huo et al., 1992; von Knoch et al., 2000; Willert et al., 1990). Debris-induced immune reactivity, aseptic inflammation, and subsequent early failure can be as high as 4%–5% at 6–7 years post op in current-generation metal-on-metal total hip arthroplasties (Jacobs and Hallab, 2006; Korovesis et al., 2006; Milosev et al., 2006). The benefits provided to patients by orthopedic implants in terms of pain, mobility, and quality of life are immeasurable. Therefore, the following sections which focus on the problems associated with implants seeks to provide the student of biomaterials a foundation for understanding the relevant issues for orthopedic research and is not intended to serve as an indictment of orthopedic materials.

Despite their overwhelming success over the long term (>7 years), orthopedic biomaterials have been associated with adverse local and remote tissue responses. It is generally the degradation products of orthopedic biomaterials (generated by wear and electrochemical corrosion) which mediate these adverse effects. This debris may be present as particulate wear, colloidal nanometer size complexes (specifically or nonspecifically bound by protein), free metallic ions, inorganic metal salts/oxides, or in an organic storage form such as hemosiderin. Clinical aspects of biocompatibility regarding polymer and metal release from orthopedic prosthetic devices have taken on an increasing sense of urgency due to the escalating rates of people receiving implants and the recognition of extensive implant debris within local and remote tissues. Particulate debris has enormous specific surface areas available for interaction with the surroundings and chronic elevations in serum metal content. Clinical issues associated with biomaterial degradation can be broken down into four basic questions: (1) How much material is released from the implant? (2) Where is the material transported and in what quantity? (3) What is the chemical form of the released degradation products (e.g., inorganic precipitate vs. soluble organometallic complex)? and (4) What are the pathophysiological interactions and consequences of such degradation? The answers to these questions, over the long term, remain largely unknown. There is a growing body of literature addressing the issues associated with the first two questions. However, little is currently known with regard to the latter two questions. The remainder of this chapter will focus on that which is known (and of orthopedic clinical concern) regarding biomaterial degradation (through wear and electrochemical corrosion), dissemination of debris, and consequent local/systemic effects.



• **Figure 2.5.4.8** Examples of currently used surface coatings on stems of THA to enhance both short- and long-term fixation.

Orthopedic Biomaterial Wear

The generation of wear debris, and the subsequent tissue reaction to such debris, is central to the longevity of total joint replacements. In fact, particulate debris is currently extolled as the primary factor affecting the long-term performance of joint replacement prostheses, and the primary source of orthopedic biomaterial degradation (based on overall implant mass or volume lost). Particulate debris generated by wear, fretting, or fragmentation induces the formation of an inflammatory reaction, which at a certain point promotes a foreign-body granulation tissue response that has the ability to invade the bone–implant interface. This commonly results in progressive, local bone loss that threatens the fixation of both cemented and cementless devices alike (Jacobs, 1995; Jacobs et al., 2001a, 1994a).

Mechanisms of Wear Debris Generation: Wear involves the loss of material in particulate form as a consequence of relative motion between two surfaces. Two materials placed together under load will only contact over a small area of the higher peaks or asperities. Electro-repulsive and atomic binding interactions occur at the individual contacts and, when the two surfaces slide relative to one another, these interactions are disrupted. This results in the release of material in the form of particles (wear debris). The particles may be lost from the system, transferred to the counterface, or remain between the sliding surfaces. There are primarily three processes which can cause wear: (1) abrasion—by which a harder surface “plows” grooves in the softer material; (2) adhesion—by which a softer material is smeared onto a harder countersurface forming a transfer film; and (3) fatigue—by which alternating episodes of loading and unloading result in the formation of subsurface cracks which propagate to form particles that are shed from the surface.

Wear Rates: During an initial “wearing in” period, the relative motion of surfaces causes a large number of asperities to break, resulting in a high wear rate. After this initial period, the actual contact area increases and the two surfaces can be said to have adapted to one other. Over time, the wear rates decrease and eventually become linearly dependent on the contact force and sliding distance represented by the steady-state wear equation:

$$V = KFx \quad (2.5.4.10)$$

where V is volumetric wear (mm^3/year), K is a material constant of the material couple, F is the contact force (N), and x is the distance of relative travel (mm).

Different types of orthopedic materials and couples produce different amounts and kinds of wear debris. Hard-on-hard material couples such as metal-on-metal articulations generally produce less wear (weight loss) than metal-on-polymer (see Fig. 2.5.4.9). There is a great deal of variability associated with in vivo wear rates of orthopedic biomaterials, which are generally measured by radiographic follow-up studies. Radiographic wear measurements are expressed as linear wear rates, whereas in vitro studies generally report

volumetric wear. Volumetric wear can be directly related to the number of wear particles released into periprosthetic fluids (typically on the order of 1×10^9 of particles per year). The most common wear couple for hip and knee arthroplasty currently in use in the United States is a cobalt–base alloy head (most commonly a Co–Cr–Mo alloy ASTM F-75) bearing on a UHMWPE cup or liner. The wear rates of this couple are generally on the order of 0.1 mm/year, with particulate generation as high as 1×10^6 particles per step or per cycle. Clinically, implant wear rates have been found to increase with the following: (1) physical activity, (2) weight of the patient, (3) size of the femoral head (32 vs. 28 mm), (4) roughness of the metallic counterface, and (5) oxidation of the polyethylene (Jacobs, 1995; Jacobs et al., 1994a, 2001).

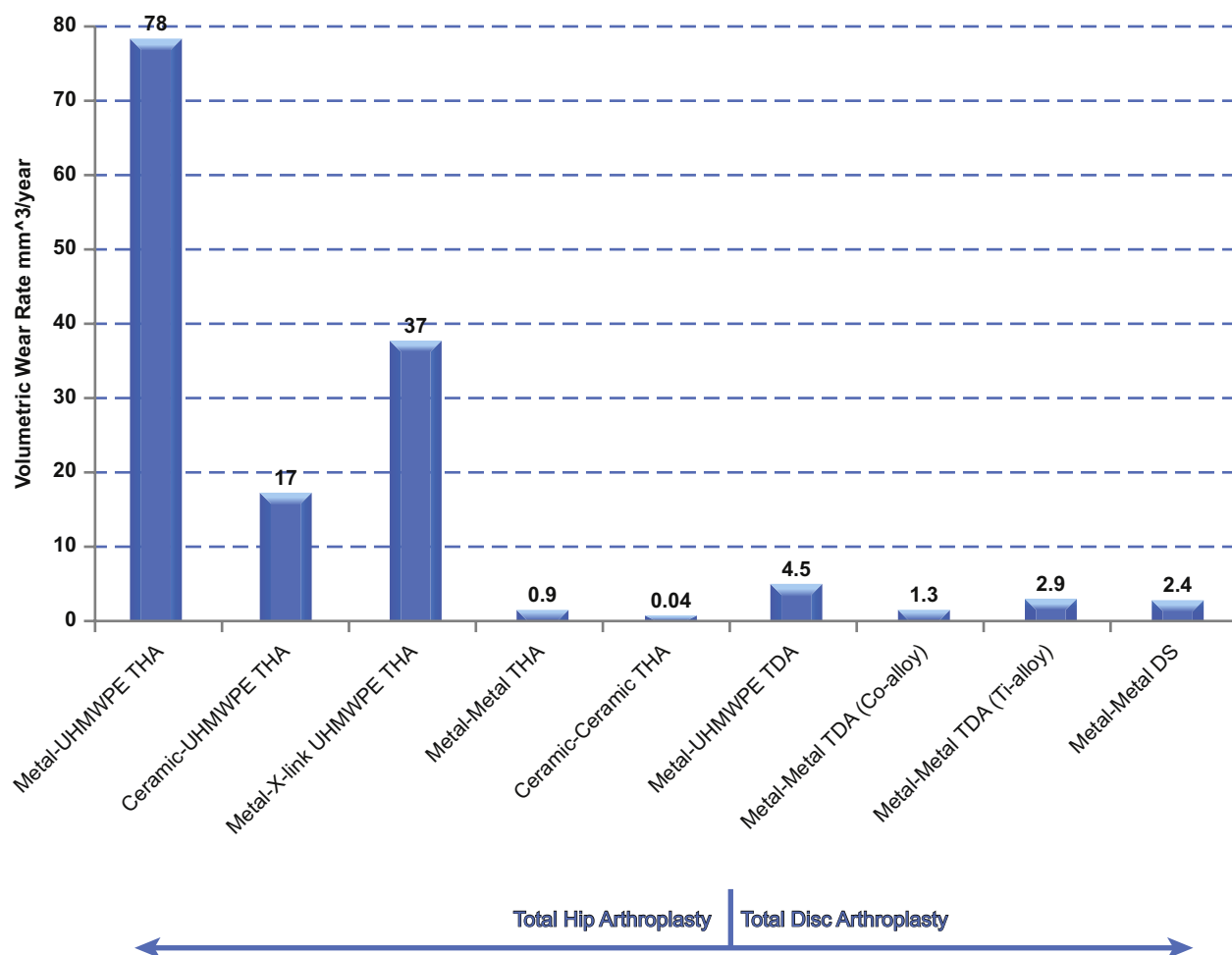
Although well established in the hip and knee, newer spinal implants are now undergoing the same types of analysis to try to assess which types of implant work best. These two basic types of articulating bearing designs are available in spine, knee, and hip arthroplasties.

Metal-on-polymer Spine Arthroplasty Wear: In vitro analysis of wear has demonstrated wear rates of metal-on-polymer bearing lumbar total disc arthroplasty devices range from 2 to 20.8 mm^3 per million cycles (Popoola et al., 2007; Pare et al., 2007), where the size of the wear debris generally ranges from 0.1 to 100 microns in diameter UHMWPE (Popoola et al., 2007; van et al., 2007; Anderson et al., 2003; Hallab et al., 2008). This amount of debris is 10-fold less wear than THAs and TKAs that are composed of metal on highly cross-linked polyethylene (x-UHMWPE)-bearing surfaces (Kurtz et al., 2005; Greenwald and Garino, 2001).

Metal-on-metal Spinal Arthroplasty Wear: In general the wear of metal-on-metal TJA is well below that of metal-on-polymer (Fig. 2.5.4.9) (Kurtz et al., 2005; Callaghan et al., 2007; Minoda et al., 2005; Heisel et al., 2004; Wroblewski et al., 1996; Saikko et al., 2002; Catelas et al., 2004; Tipper et al., 2002). The few published reports on the wear rates of metal-on-metal disc arthroplasty prostheses indicate a wear rate of 0.93–1.26 mm^3 per million cycles (cobalt-alloy) (Pare et al., 2007; Firkins et al., 2001). Another study of an all titanium–6%Al–4%V alloy disc arthroplasty found wear rates to be as high as 3 mm^3 per million cycles (Hellier et al., 1992). These values are similar to those reported for metal-on-metal hip replacements, which have been shown to range from approximately 0.05–6 mm^3 per million cycles (cobalt-alloy) (Catelas et al., 2004; Clarke et al., 2000; McKellop et al., 1996). Long-term follow-up of patients undergoing total disc arthroplasty is required to assess how intimately wear will correlate with inflammation and poor implant performance.

Orthopedic Biomaterial Corrosion

Electrochemical corrosion occurs to some extent on all metallic surfaces including implants. This is undesirable for two primary reasons: (1) the degradative process may reduce the structural integrity of the implant, and (2) the



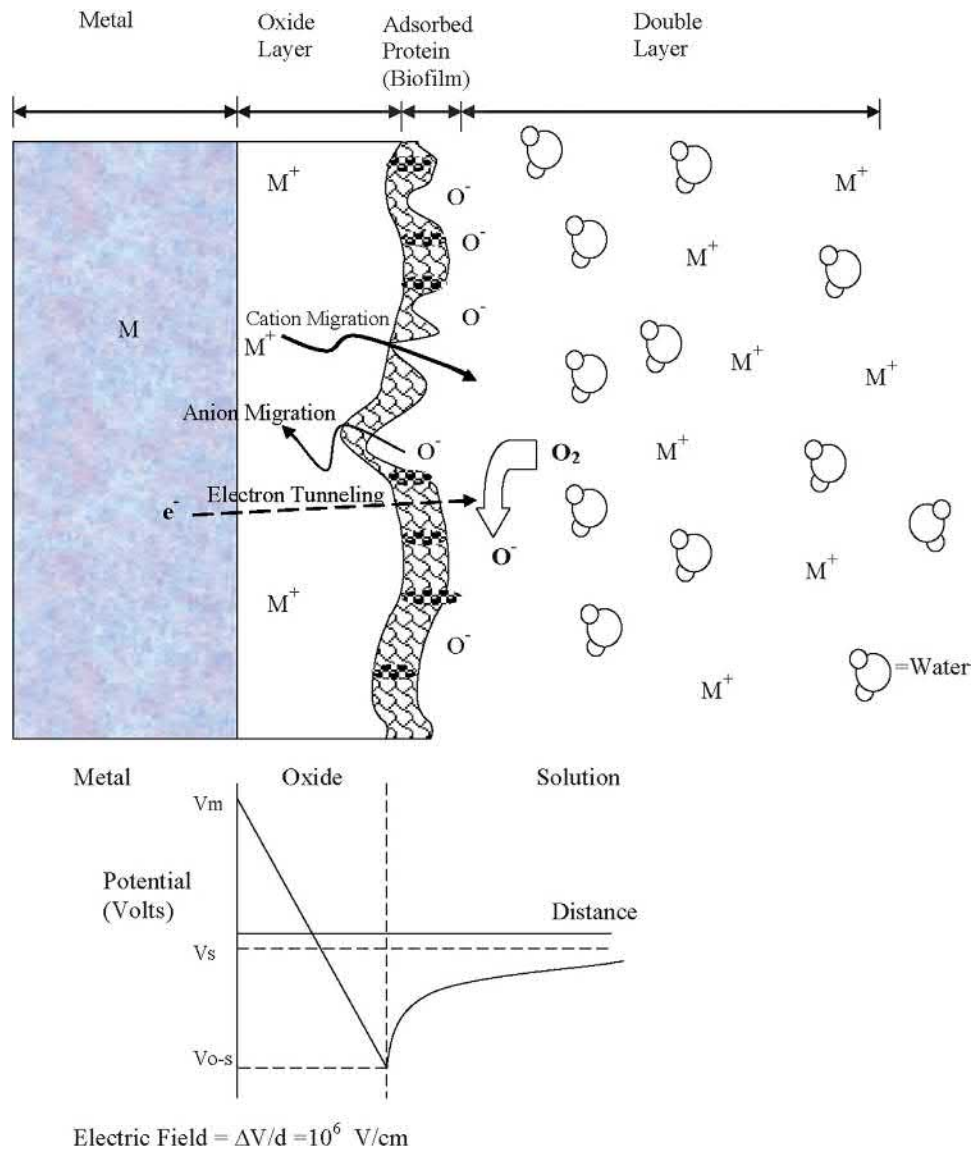
• **Figure 2.5.4.9** A comparison of the amount of wear debris generated from different types of total joint arthroplasties. There is relatively less (10x) polymeric debris generated by a total disc arthroplasty with a metal-on-polymer articulation. Note: Figure references: Metal–Poly (Callaghan et al., 2007); Ceramic–Poly (Minoda et al., 2005), Metal–X-linked Poly (Kurtz et al., 2005); Metal–X-linked Poly (Heisel et al., 2004), Metal–X-linked Poly (Wroblewski et al., 1996), Metal–X-linked Poly (Saikko et al., 2002), Metal–Metal (Catelas et al., 2004), Ceramic–Ceramic (Tipper et al., 2002), Metal–UHMWPE TDA (Popoola et al., 2007), Metal–Metal TDA (Pare et al., 2007).

release of products of degradation is potentially toxic to the host. Metallic biomaterial degradation may result from electrochemical dissolution phenomena or wear, but most commonly occurs through a synergistic combination of the two. Electrochemical processes include generalized corrosion uniformly affecting an entire surface, and localized corrosion affecting either areas of a device relatively shielded from the environment (crevice corrosion), or seemingly random sites on the surface (pitting corrosion). Additionally, these electrochemical and other mechanical processes interact, potentially causing premature structural failure and/or accelerated metal release (e.g., stress corrosion cracking, corrosion fatigue, and fretting corrosion) (Brown et al., 1992; Brown and Merritt, 1981; Bundy et al., 1991; Collier et al., 1992b; Cook et al., 1983; Gilbert and Jacobs, 1997).

Metallic corrosion happens through a series of reduction–oxidation reactions, similar to those of a battery. Note: The terms oxidation and reduction are complex and will be used as sparingly as possible in the following discussions.

A “high-energy” material, metal oxidizes to a lower energy state when corroded and acts as the anode, i.e., the metal is oxidized, forming metal ions and free electrons. The free electrons “reduce” the oxygen which often forms hydroxides, phosphates, etc., and provides a complimentary cathodic reaction. Thus, the dissolution (oxidizing) metal at the anode has basically two possible outcomes; the metal ions can go into solution, becoming hydrated, or the metal ions can form a compound which can form as solids collecting on the surface. When metal ions are forming, further oxidation of the metal ions can occur and an open pit can form. When the solid compounds collect on the surface, a protective barrier typically forms where the accumulation of solid material inhibits further corrosion. The basic underlying reaction which occurs during corrosion is increasing of the valence state (i.e., loss of electrons) of the metal atom to form an ion.

Again this metal corrosion (oxidation) event (loss of electrons and increased valence) may result in free ions in



• **Figure 2.5.4.10** Schematic of the interface of a passivating alloy surface in contact with a biological environment.

solution which can migrate away from the metal surface, or may result in other reactions such as the formation of metal-oxides, metal chlorides, organo-metallic compounds, or other species that typically precipitate out to form solid phases. The solid phases or oxidation products may be subdivided into (1) those which form adherent compact oxide films and (2) those which form nonadherent oxide (or other) particles which can migrate away from the metal surface.

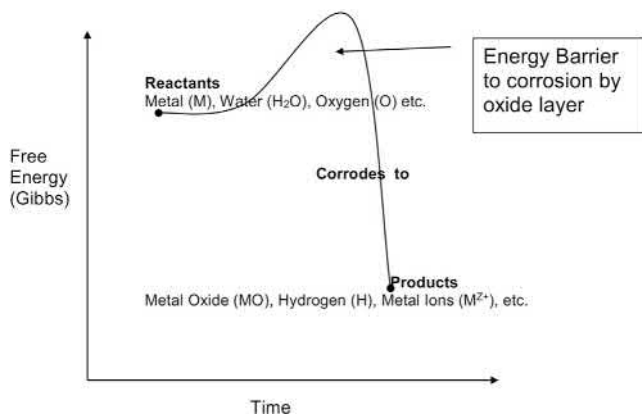
Corrosion Mechanisms: Corrosion of orthopedic biomaterials is a multifactorial phenomenon and is dependent on five primary factors: (1) geometric variables (e.g., taper crevices in modular component hip prostheses), (2) metallurgical variables (e.g., surface microstructure, oxide structure, and composition), (3) mechanical variables (e.g., stress and/or relative motion), (4) solution variables (e.g., pH, solution proteins, enzymes), and (5) the mechanical loading environment (e.g., degree of movement, contact forces, etc.). Current investigational efforts to minimize the

corrosion of orthopedic biomaterials deal directly with the complex interactions of these factors.

There are two essential features associated with how and why a metal corrodes. The first has to do with thermodynamic driving forces, which cause corrosion (oxidation/reduction) reactions. In general, whether or not corrosion will take place under the conditions of interest depends on the chemical driving force (ΔG), and the charge separation. This separation contributes to what is known as the electrical double layer (Fig. 2.5.4.10) which creates an electrical potential across the metal–solution interface (much like a capacitor):

$$\Delta G = -nF \Delta E \quad (2.5.4.11)$$

where n is the valence of the ion, F is the Faraday constant (95,000 coulombs/mole electrons), and E is the voltage across the metal–solution interface. This potential is a



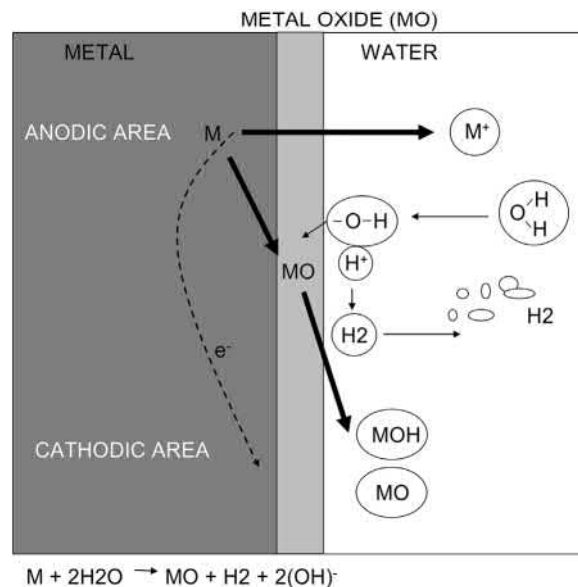
• **Figure 2.5.4.11** Metal-oxide passive films on metal surfaces are the typical example of a kinetic limitation to corrosion. In general, kinetic barriers to corrosion prevent either the migration of metallic ions from the metal to the solution, the migration of anions from solution to metal, or the migration of electrons across the metal–solution interface. Passive oxide films are the most common form of kinetic barrier in orthopedic implant corrosion, but other kinetic barriers exist including polymeric coatings.

measure of the reactivity of the metals or the driving force for metal oxidation. Therefore, the more negative the potential of a metal in solution, the more reactive it will tend to be (i.e., the greater is ΔG for reduction) (Fig. 2.5.4.11).

The second factor governing the corrosion process of metallic biomaterials is the kinetic barrier to corrosion (e.g., surface oxide layer). Kinetic barriers prevent corrosion not by energetic considerations but by physically limiting the rate at which oxidation or reduction processes can take place. The well-known process of passivation or the formation of a metal-oxide passive film on a metal surface is one example of a kinetic limitation to corrosion. In general, kinetic barriers to corrosion prevent either the migration of metallic ions from the metal to the solution, the migration of anions from solution to metal, or the migration of electrons across the metal–solution interface. Passive oxide films are the most well-known forms of kinetic barriers in corrosion, but other kinetic barriers exist, including polymeric coatings (Fig. 2.5.4.12) (Gilbert and Jacobs, 1997; Jacobs et al., 1998b).

Passivating Oxide Films: Most alloys used in orthopedic appliances rely on the formation of passive films to prevent significant oxidation from taking place. These films consist of metal oxides, which form spontaneously on the surface of the metal in such a way that they prevent further transport of metallic ions and/or electrons across the film. Passive films must have certain characteristics to be able to limit further oxidation. The films must be compact and fully cover the metal surface, they must have an atomic structure which limits the migration of ions and/or electrons across the metal–oxide–solution interface, and they must be able to remain on the surface of these alloys even with the mechanical stressing and abrasion which can be expected with orthopedic devices.

Passivating oxide films, which spontaneously grow on the surface of metals, have five primary structural and physical



• **Figure 2.5.4.12** All orthopedic alloys rely on the formation of passive films to prevent significant oxidation (corrosion) from taking place. These spontaneously formed films consist of metal oxides (ceramic films) that have an atomic structure which limits the migration of ions and/or electrons across the metal–oxide–solution interface; and are able to remain intact on the surface of these alloys, or reform rapidly during mechanical stressing or abrasion, expected with orthopedic devices.

characteristics, which are particularly relevant to implant degradation processes:

1. First, these oxide films are very thin, typically on the order of 5–70 Å, which depends on the potential across the interface as well as solution variables (e.g., pH). Furthermore, the oxide structure may be amorphous or crystalline. Since the potential across the metal solution interface for these reactive metals is typically 1–2 V, the electric field across the oxide is very high, on the order of 10^6 – 10^7 V/cm. One of the more widely accepted models is based on the theory of Mott and Cabrera, which states that oxide film growth depends on the electric field across the oxide. If the potential across the metal–oxide–solution interface is decreased (i.e., made closer to the electrochemical series potential), then the film thickness will decrease by reductive dissolution processes at the oxide. If the interfacial potential is made sufficiently negative or the pH of the solution is made low enough, then these oxide films will no longer be thermodynamically stable and will undergo reductive dissolution, without which corrosion will increase (Gilbert and Jacobs, 1997; Jacobs et al., 1998a).
2. Second, oxide films have the characteristics of semiconductors with an atomic defect structure, which determines the ability for ionic and electronic transport across films. Metal cations and oxygen anions require the presence of cationic or anionic vacancies (respectively) in the oxide for transport of these species across the film. If there is a deficit of metal ions in the oxide film (i.e., there are cationic vacancies), for example, then metal ion transport

is possible, and these oxides are known as p-type semiconductors. Chromium oxide (Cr_2O_3) is such a metal-deficit oxide. On the other hand, if there is an excess of metal ions in the oxide (or a deficit of anions) then cation transport is limited but anion transport can occur. These oxides will also have excess electrons and are known as n-type semiconductors. TiO_2 spontaneously formed on titanium alloy implant (Ti–6Al–4V) surfaces is one such n-type semiconductor. The greater the number of defects (vacancies or other valence species) the less able is the oxide film to prevent migration of ionic species and the lower is the kinetic barrier to corrosion. TiO_2 is very close to being stoichiometric (chemically homogeneous) and hence does not have many ionic defects resulting in an increased resistance to ionic transport. Other defects may be present in these passive oxide films which may alter their ability to limit corrosion. For instance, the addition of other metal ions with valence states, which are different from the native metal ions, can alter both the electronic and ionic transport of charge across the interface. These additions may enhance or degrade the ability of the oxide to prevent corrosion depending on the nature of the oxide. One example of improved corrosion resistance from mixed oxides comes from what is known as a spinel. Spinel is typically mixed oxides of the form $(\text{A}_2\text{O}_3)\text{BO}$, where A and B are +3 and +2 valence metal ions. In Co–Cr alloys, for instance, a spinel of $(\text{Cr}_2\text{O}_3)\text{CoO}$ can form on the surface. Spinel is typically known to have higher strengths and better resistance to diffusion of ions compared to single metal ion oxides. Therefore, a high concentration of spinels in the oxide layer will act to resist dissolution of a metal implant (Gilbert and Jacobs, 1997; Jacobs et al., 1998a).

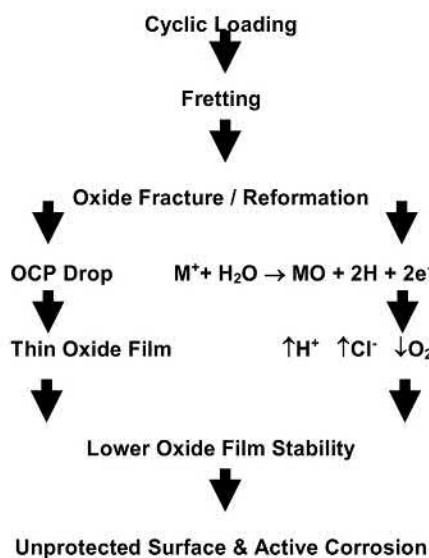
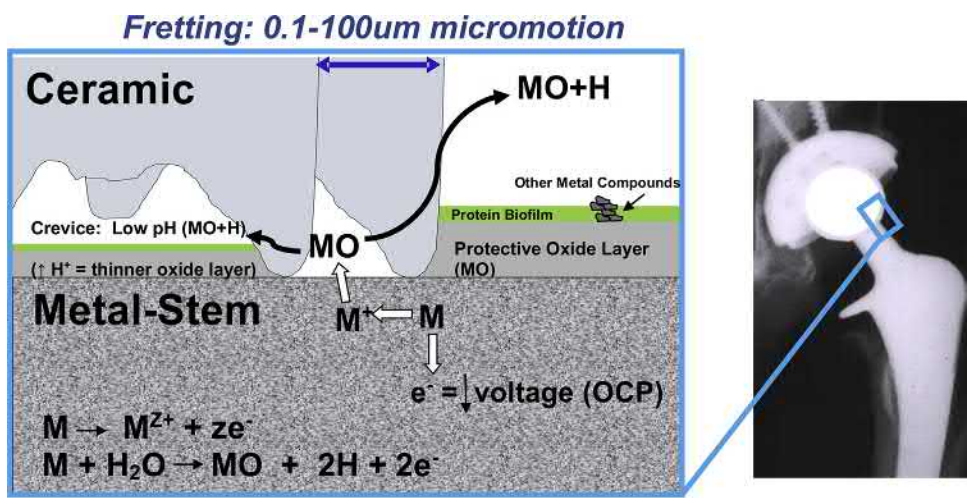
3. Third, the ratio of the “oxide specific volume” to metal alloy specific volume (i.e., Pilling Bedworth ratio) will determine if the oxide will adhere to the metal or not. If there is too great a mismatch between the metal and oxide lattice parameters then consequential stresses will be generated between the two. The magnitude of the internal stress will vary with the thickness of the oxide. Too great an oxide thickness will thus result in spontaneous fracture or spalling of the oxide, lowering the kinetic barrier effect of the oxide to corrosion (Gilbert and Jacobs, 1997; Jacobs et al., 1998a).
4. Fourth, the morphology of these oxide films is not one of a smooth, flat, continuous sheet of adherent oxide covering the metal. Transmission electron microscopy (TEM) and atomic force microscopy (AFM) techniques have shown that oxides of titanium, for instance, consist of needle or dome shapes. The size and shape of these oxide domes change with applied potential when immersed in oxalic and other acids (Gilbert and Jacobs, 1997; Jacobs et al., 1998a).
5. Finally, mechanical factors such as fretting, micromotion, or applied stresses may abrade or fracture oxide films. When an oxide film is ruptured from the metal substrate, fresh unoxidized metal is exposed to solution. When

these films reform or repassivate, the magnitude of the repassivation currents, which are subsequently generated, may be large. This is because large driving forces exist for oxidation and when the kinetic barrier is removed these large driving forces can operate to cause oxidation. However, the extent and duration of the oxidation currents will depend on the repassivation kinetics for oxide film formation. Hence, the mechanical stability of the oxide films as well as the nature of their repassivation process are central to the performance of oxide films in orthopedic applications (Gilbert and Jacobs, 1997; Jacobs et al., 1998a).

Corrosion at Modular Interfaces of Joint Replacements: One issue associated with orthopedic alloys is the corrosion observed in the taper connections of retrieved modular joint replacement components. With the growing number of total joint designs which use metal-on-metal conical tapers as modular connectors between components, the effects of crevices, stress, and motion take on increasing importance. Severe corrosion attack can take place in the crevices formed by these tapers in vivo.

Fretting Corrosion or Mechanically Assisted Crevice Corrosion (MACC)

Fretting corrosion or MACC, occurs at junctions or connections of implant components. It is caused by small-scale (1–100 μm) relative motion between implant components from cyclic loading (normal use). This type of corrosion occurs in all types of alloys regardless of material couple (e.g., stainless steel (SS)/stainless steel, Co-alloy/Co-alloy, Co-alloy/titanium, titanium/titanium, etc.). These corrosion products are bioreactive and cause local inflammation that results in local bone loss (osteolysis), pain, and ultimately implant loosening. Inflammation from corrosion debris is proportional to the amount of debris and thus can occur slowly over time (decades) with little debris or can occur within months. Stainless steel intermedullary rods used for femur fracture demonstrated aggressive corrosion in the modular taper resulting in rapid bone loss and ultimately recall of the implants (Jones et al., 2001). Fretting corrosion is dependent on the amount of micromotion, the designs of modular connections, the alloy combination, and other factors that affect the mechanical or chemical environment of the implant, including surgical factors. Fretting corrosion is typically mechanically assisted corrosion within a crevice where the mechanical abrasion of the oxide layer radically alters the chemistry within the crevice solution in a negative way further enhancing corrosion (it has also been termed MACC, mechanically assisted crevice corrosion). This process is driven by the reduction in free energy associated with metal-oxide formation that results in the sequestration of O_2 from any available source (primarily H_2O). Repassivation of a metal surface within the crevice environment results in a buildup of H^+ and Cl^- , and lowers the pH. This MACC (Gilbert and Jacobs, 1997; Gilbert et al., 2009) model of modular junction fretting corrosion is schematically represented in Fig. 2.5.4.13. The ultimate result of this



• **Figure 2.5.4.13** Fretting corrosion or mechanically assisted crevice corrosion (MACC). Fretting corrosion or MACC occurs at modular junctions or connections of implant components and is produced by small-scale (1–100 μm) relative motion between implant components induced by cyclic loading (normal use). This type of corrosion occurs in all types alloys regardless of material couple (e.g., stainless steel (SS)/stainless steel, Co-alloy/Co-alloy, Co-alloy/titanium, titanium/titanium, etc.).

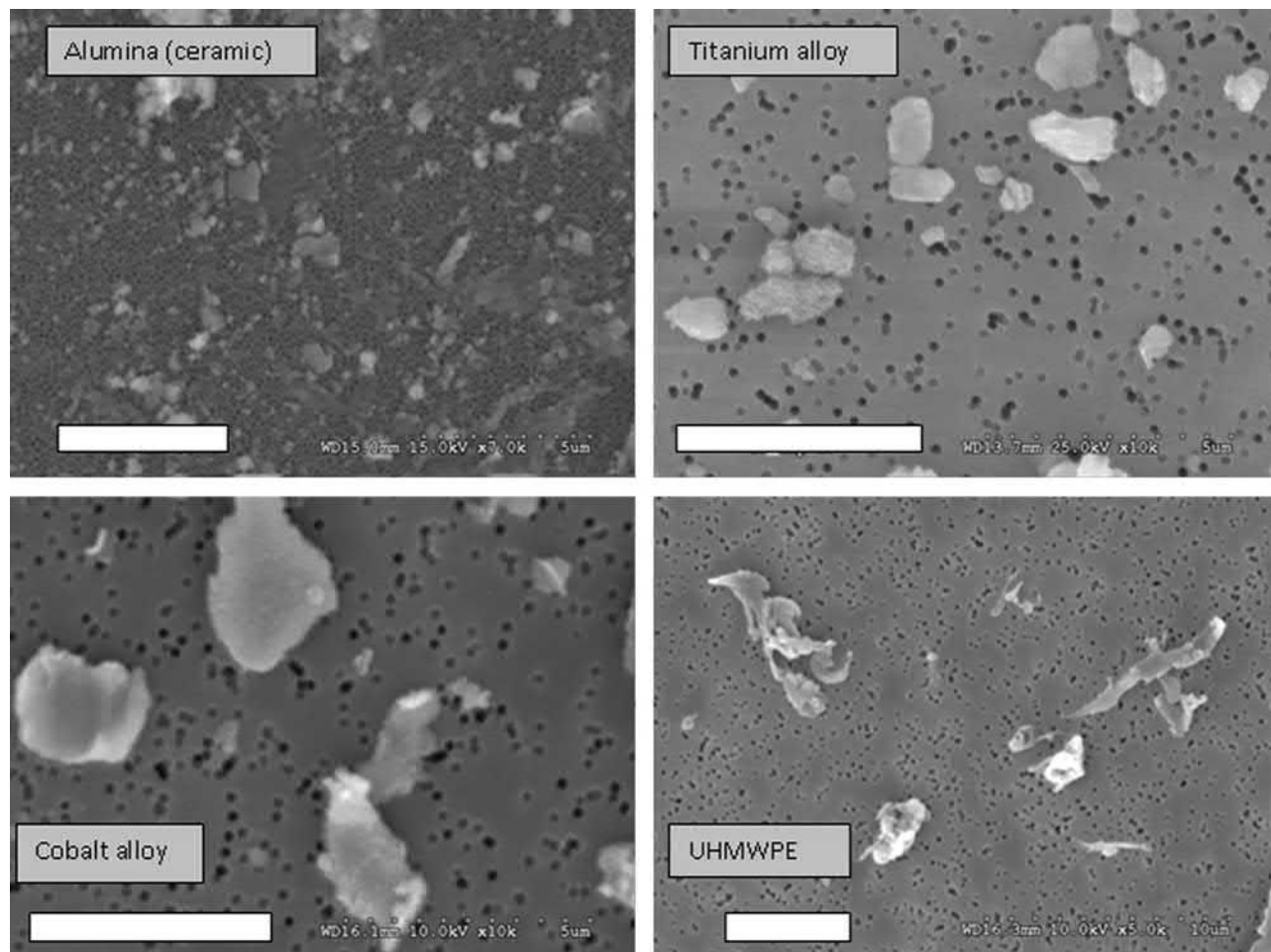
process is a loss of the oxide film and its kinetic barrier effect and an increase in the rate of corrosive attack in the taper region. The corrosion processes in the Co–Cr alloys have been observed to consist of intergranular corrosion, etching, selective dissolution of cobalt, and the formation of Cr-rich particles. In isolated cases, this occurs to such an extent that intergranular corrosion caused fatigue failure in the neck of a Co–Cr stem. Corrosion attack of titanium alloy stems has also been observed in some cases.

Very little is known about the mechanical stability of passive oxide films and the electrochemical reactions (e.g., ion and particle release) which occur when the oxide film is fractured. What is known is that when the oxide films of these orthopedic alloys are abraded or removed from the surface by rubbing, the open circuit potential can decrease to as low as –500 mV (vs. standard calomel electrode). These voltage potentials may be significant and prolonged

enough to cause changes in the oxide structure and stability by bringing the interface potential into the active corrosion range of the alloy, thereby dramatically accelerating the corrosion rate and decreasing implant performance (Brown et al., 1992, 1995; Bobyn et al., 1994; Collier et al., 1992a; Gilbert et al., 1993).

Implant Debris Types: Particles and Ions

The degradation products of all orthopedic implants are one of two basic types: particles or soluble debris (metal ions). While there is a large distinction between the two (ions vs. particles) the difference between them blurs as the size of particles decreases into the nanometer range and become essentially “in solution.” Typically, particulate wear debris (metal, ceramic, or polymer) exists from the submicron size up to thousands of microns (mm), while so-called “soluble



• **Figure 2.5.4.14** Implant debris from four types of materials are shown where the metal (cobalt alloy and titanium) and ceramic (alumina) debris are more rounded versus the polymeric (UHMWPE) debris which is more elongated in shape. Note: scale bars = 5 μm .

debris” is limited to metal ions (or nanoparticles that are too small to be distinguished from ions) that are bound to plasma proteins.

Particulate Debris

Different types of joint arthroplasty designs not only produce different amounts and kinds of wear debris, but also different sizes and shapes of debris that are specific to the type of implant materials used for the bearing interfaces. For instance, hard-on-hard material couples such as metal-on-metal articulations generally produce smaller sized (submicron), fairly round debris, whereas traditional metal-on-polymer bearings produce larger (micron-sized) debris that is more elongated in shape (see Fig. 2.5.4.14).

As is evident in Fig. 2.5.4.14, hard-on-hard material couples (e.g., metal-on-metal) produce smaller debris than do hard-on-soft material couples (e.g., metal on polyethylene). The particles produced from the articulating bearing in any metal-on-poly bearing implants are dominated by polymer particles, with little metallic debris unless there are other sources of metal release such as corrosion at metal-metal connections. Polymeric particles produced from implants

generally fall into the range of 0.23–1 μm (Fig. 2.5.4.14). Past investigations, primarily of UHMWPE wear debris in periimplant tissues, have shown that 70%–90% of recovered particulates were submicron, with the mean size being approximately 0.5 μm (Jacobs et al., 1994a; Campbell et al., 1995; Maloney et al., 1993). Metal and ceramic particles have generally been characterized as an order of magnitude smaller than polymer particles (at approximately 0.05 μm in diameter).

Histological Identification of Particles in vivo: The tissues surrounding modern implants may include areas of osseointegration, fibrous encapsulation, and a variable presence of the foreign-body response to polyethylene and cement debris in joint replacement devices. Absent is any specific histologic evidence of the slow release of metallic species that is known to occur with all metallic implants. However, accelerated corrosion and a tissue response that can be directly related to identifiable corrosion products can be demonstrated in the tissues surrounding multipart devices (Urban et al., 2000).

(1) *Stainless Steels:* Histological sections of the tissues surrounding stainless steel internal-fixation devices generally show encapsulation by a fibrous membrane with

little or no inflammation over most of the device. At screw-plate junctions, however, the membranes often contain macrophages, foreign-body giant cells, and a variable number of lymphocytes in association with two types of corrosion products. The first consists of iron-containing granules. The second, termed microplates, consists of relatively larger particles of a chromium compound. Microplates are found within the tissues as closely packed, plate-like particle aggregates ranging in size from 0.5 to 5.0 mm.

Hemosiderin-like granules often surround the collections of microplates, but the granules are found alone as well. The granules are yellow-brown, mainly spherical, and 0.1–3 or more micrometers in diameter. They are predominantly intracellular, most often in macrophages, but may also be found in other periprosthetic cells (e.g., fibroblasts). X-ray diffraction has indicated that the granules consist of a mixture of two or more of the iron oxides, $\alpha\text{Fe}_2\text{O}_3$ and $\sigma\text{Fe}_2\text{O}_3$, and the hydrated iron oxides, $\alpha\text{Fe}_2\text{O}_3\cdot\text{H}_2\text{O}$ and $\sigma\text{Fe}_2\text{O}_3\cdot\text{H}_2\text{O}$.

- (2) **Cobalt-Base Alloys:** The nature of corrosion at modular connections is similar whether modular heads are mated with cobalt-chromium alloy or Ti-6Al-4V alloy femoral stems. The principal corrosion product identified by electron microprobe energy-dispersive X-ray analysis and Fourier-transform infrared microprobe spectroscopy is a chromium-phosphate ($\text{Cr}(\text{PO}_4)_4\text{H}_2\text{O}$) hydrate-rich material termed “orthophosphate.” This corrosion product can be found at the modular head-neck junction and as particles within the joint capsules, at the bone-implant interfacial membranes and at sites of femoral osteolytic lesions. Particles of the orthophosphate material have been found at the bearing surface of the UHMWPE acetabular liners suggesting their participation in three-body wear and an increased production of polyethylene debris. Particles of the chromium orthophosphate hydrate-rich corrosion product found in the tissues ranged in size from submicron to aggregates of particles up to 500 μm .
- (3) **Titanium-Base Alloys:** The degradation products observed in histologic sections of tissues adjacent to titanium base alloys are of a different nature than the precipitates associated with stainless steel and cobalt base alloys. Despite the remarkable corrosion resistance of titanium base alloys, there have been persistent reports of tissue discoloration due to metallic debris in the periprosthetic tissues. These particulates observed in local tissues surrounding titanium alloy implants have the same elemental composition as the parent alloy as opposed to precipitated corrosion products which occur with stainless steel and cobalt-chromium alloys (Fig. 2.5.4.15). However, wear debris presents an enormous surface area for electrochemical dissolution, which, in all likelihood, is a major factor contributing to observed systemic elevations in titanium of patients with titanium implants (Urban et al., 1996b, 1997).

Particle Characterization: Traditionally, particle characterization uses methods such as scanning electron microscopy (SEM) or transmission electron microscopy (TEM), both of which are number-based counting methods. These methods have indicated that the majority of the wear (mass loss) from an implant is comprised of particles in the nanometer to submicron range. This understanding stems from the relatively low numbers of particles (e.g., 100s to 1000s) that are counted using image-based analysis techniques such as SEM. Newer analytical techniques, such as low-angle laser diffraction (LALLS) have the capability of sampling millions to billions of particles, counted as they pass in front of and scatter a laser light beam proportionally to their size. Thus, as millions of particles flow by LALLS analysis can detect the one-in-a-million large particle that comprises a significant portion of the total mass loss (i.e., total debris). This brings up the confusing concept that particle size of any given distribution depends on the method of evaluation. There is no one particle size. For example, the average size of 500 marbles and five basketballs is approximately the size of the marbles on a number basis and approximately the size of the basketball on a volume basis. Thus, when asking “what is the average size of particles that comprises approximately 50% of the total volume of particles?” is another way of asking what the mean size is (or average size) on a volume basis. Asking “what is the average size of the particles that comprises 50% of the total number of particles?” is the average size based on number basis. The stark differences between a volume- and number-based analysis of implant debris are shown in Fig. 2.5.4.16. When comparing the volume and number distributions in this figure the dominant contribution of larger particles to the total debris mass (volume) is evident and yet is insignificant to the total number of particles (Fig. 2.5.4.16).

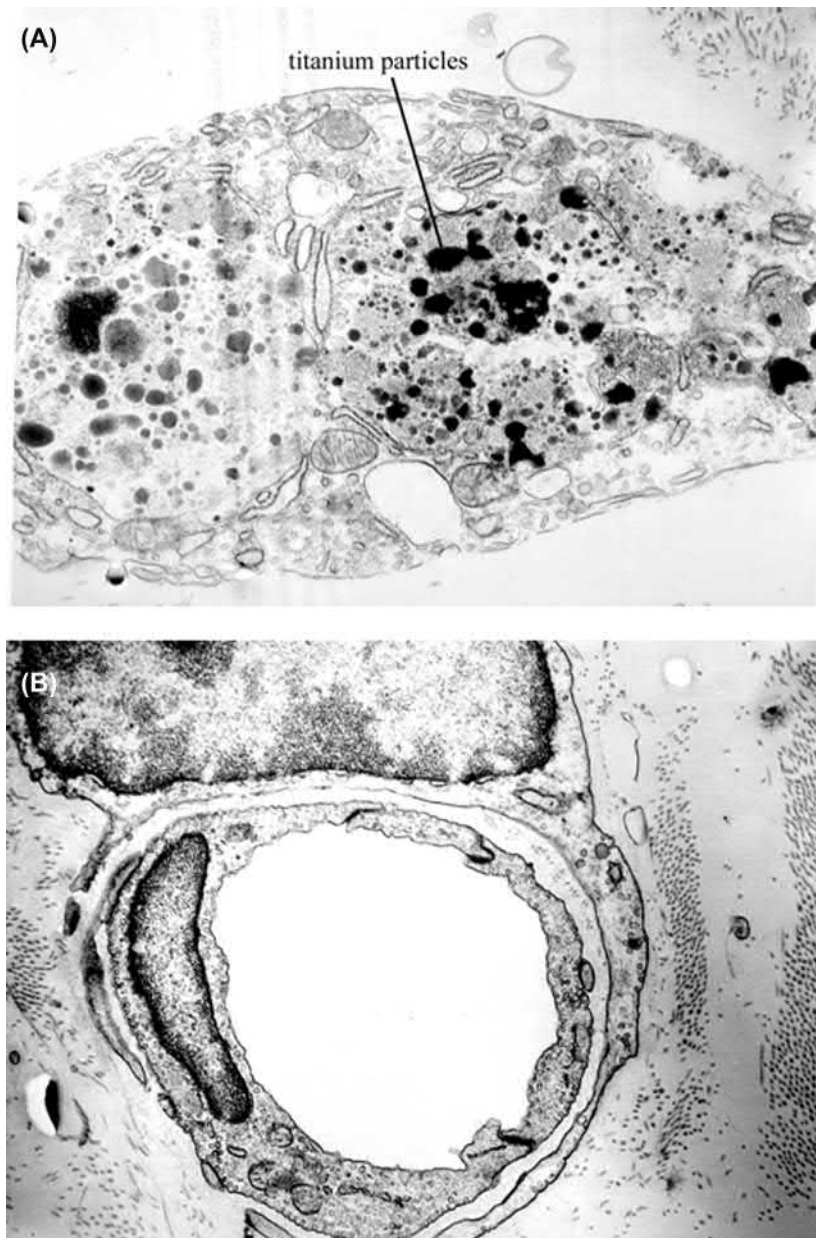
The ability to comprehensively characterize implant debris is important to the new designs and bearing surfaces used in new spinal implants. This multianalysis approach is necessary because a given amount of wear debris (weight loss from the implant) after a year of use could be attributed to the loss of a relatively few large particles, or hundreds of millions of small particles (e.g., approximately 0.2 mm^3 volume loss after a million cycles of use could be from approximately 400 particles of 100 microns diameter or 400 million particles only 1 micron in diameter). The bias of techniques limited to number analysis is that very similar number-based distributions can look very different from a volume perspective. This phenomenon is illustrated in Fig. 2.5.4.16 when comparing samples, A and B, where different samples of particles look like very different volume-based distributions, however they look like very similar number-based distributions. This shows how important it is to have both number- and volume-based distributions of the same particles to fully characterize the types of particles in the mix, if there is enough particulate mass (>0.05 mg of particles) for an LALLS type analysis. Unfortunately, in implant debris analysis there is usually less than 0.05 mg of debris

required for obtaining an accurate volume distribution and thus historically SEM and TEM analyses have been used to characterize debris.

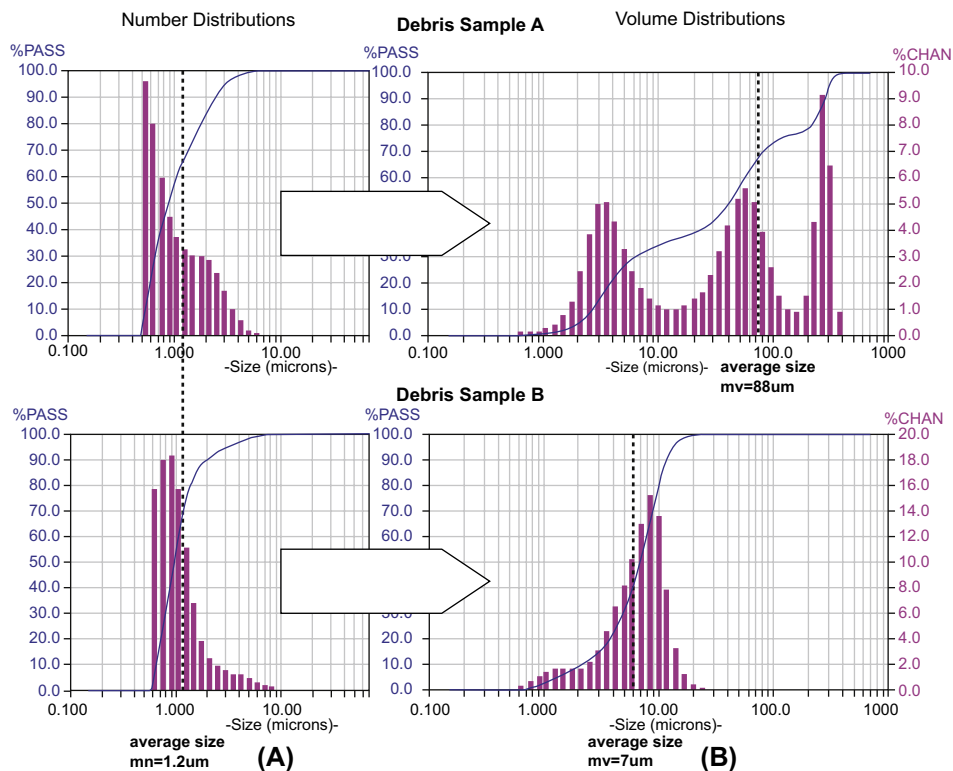
Particulate Debris Reactivity Characterization: Macrophages are immune cells that are involved in the phagocytosis of implant debris and the resulting inflammatory responses. Once debris is ingested by macrophages a host of biologic reactions can occur such as activation of T cells through antigen presentation (Hallab et al., 2001), release of proinflammatory mediators (Glant and Jacobs, 1994; Shanbhag et al., 1994; Matthews et al., 2000; Ingham et al., 2000; Cunningham et al., 2002), cytotoxicity (Hallab et al., 2005a), DNA damage (Hallab et al., 2005a; Savarino et al.,

2000; Nagaya et al., 1989), and oxidative stress (Soloviev et al., 2005). Macrophage reactions to debris are responsible for mediating debris-induced inflammation that is the leading cause of implant loosening over time.

Despite the large number of studies on metal, polymer, and ceramic particles effects on periimplant cells (e.g., macrophages, fibroblasts, osteoblasts, and osteoclasts), there are surprisingly few guidelines on what type of debris is most deleterious or bioreactive. However, there are a few general particle characteristics on which local inflammation has been shown to depend: (1) particle load (which depends on both particle size and total volume), (2) aspect ratio (the shape of the particles), and (3) chemical reactivity (the



• **Figure 2.5.4.15** Transmission electron photomicrographs. (A) Macrophage containing phagocytized titanium particles. (B) Endothelial cell lining with embedded titanium debris. These specimens were obtained from a tissue sample overlying the posterolateral fusion mass (16-week autograft + titanium) (TEM magnification = 20,000 \times).



• **Figure 2.5.4.16** These graphs demonstrate that the analysis of two sets of particles (debris) show very similar (A) “number” distributions (left panels), but very different (B) “volume” distributions (right panels) because the large particles that take up a dominant share of the total volume of debris are very few in number. Note: The x-axis is particle diameter and the y-axis is (i) percentage of total number of particles in each size range and (ii) the percentage of total mass in each size range. (Courtesy of BioEngineering Solutions Inc.)

chemical composition). Thus, theoretically a bioreactivity index of particulate would take the mathematical form:

$$\text{Particle Pro-inflammatory Index} \times K_{\text{Load}} (\text{particle load}) \times K_{\text{Shape}} (\text{aspect ratio}) \times K_{\text{Material}} (\text{material type}) \quad (2.5.4.1)$$

where: Ks are constants that depend on the testing environment, particle load is a function of both particle size and total debris volume.

(1) **Greater particle load: (size and volume) increases inflammation.** An inflammatory response in vivo is proportional to the particle load (the concentration of phagocytosable particles per tissue volume, which is characterized by both the size and total volume) (Matthews et al., 2000; González et al., 1996). While this seems obvious, the ramifications and the conditions under which this remains true are important and not so obvious. If a given amount of debris (mass loss from an implant) is comprised of small-diameter particles there will far greater numbers than if that same mass of debris was composed of larger diameter particles (Matthews et al., 2000). The degree to which equal numbers (doses) of large particles (e.g., 10 micron diameter) and smaller particle (1 micron diameter) induce a proinflammatory response has not been thoroughly investigated and remains unknown.

(2) **Aspect ratio: elongated (fibers) particles are more proinflammatory than round particles** (Laquerriere et al., 2003; Sieving et al., 2003). That fibers are more reactive than round debris has been well established over 30 years ago, with studies of asbestos fibers (Bruch, 1974). However, it remains unknown at what aspect ratio (aspect ratio: length/width) in the transition from round particles to fibers that elevated inflammation is generally initiated, and thus to date there is no “guideline” aspect ratio for implant debris particles to remain below.

(3) **More chemically reactive particles are more proinflammatory:** There is a growing consensus that metal particles are more proinflammatory when compared to other materials such as polymers (Ramachandran et al., 2006). However, this is not a unanimous opinion, others have concluded that polymers are more proinflammatory than metals (von Knoch et al., 2000). And other reports have shown no differences between similar metal and polymer particles (Baumann et al., 2004, 2005, 2006). Despite these reports to the contrary, there is a growing consensus that metallic particles are more proinflammatory because they are capable of corroding and releasing ions that have been associated with hypersensitivity responses, cytotoxicity, and DNA damage (Hallab et al., 2001, 2005; Caicedo et al., 2007b).

Controversial Particle Characteristics: Does particle size matter? Absolutely. In vitro inflammatory responses generally require particles <10 microns diameter to be phagocytosed. Thus, to produce an in vitro inflammatory response particles need to be less than 10 μm , that is, within a phagocytosable range. Purportedly, particles with a mean size of 0.2–10 μm are the most proinflammatory. Within this range there is no consensus as to which specific size(s) and/or dose of particles (particles/cell or particles/tissue volume) are maximally inflammatory (Matthews et al., 2000; Ingram et al., 2002; Rader et al., 1999; Shanbhag et al., 1995).

The effects of bacteria products (or endotoxin) on implant debris particles are presumably important because it has been found in periprosthetic tissue of failed implants, even in the absence of clinical signs of infection (Nalepka et al., 2006). Furthermore, even bacteria that is present at below clinically detectable levels have been shown to affect implant performance because antibiotic-eluting bone cement and systemically administered antibiotics reportedly reduce the frequency of long-term failure, i.e., aseptic loosening (Espehaug et al., 1997).

Metal Ions (Soluble Debris)

There is continuing concern regarding the release of chemically active metal ions, which bind to proteins and remain in solution from which they can then disseminate into the surrounding tissues, bloodstream, and remote organs. Particulate metallic wear debris presents an enormous surface area for electrochemical dissolution, which, in all likelihood, is a major factor contributing to observed systemic elevations in metals of patients with titanium implants (Jacobs et al., 1998a; Urban et al., 1996a, 1997, 1998, 2000). Normal human serum levels of prominent implant metals are approximately: 1–10 ng/mL Al, 0.15 ng/mL Cr, <0.01 ng/mL V, 0.1–0.2 ng/mL Co, and <4.1 ng/mL Ti. Following total joint arthroplasty, levels of circulating metal have been shown to increase (Jacobs et al., 1998a; Urban et al., 1996, 1997, 1998, 2000).

Metal Ion Release: In the long clinical experience of permanent and temporary metallic implants there has always been concern with local tissue reactions. Multiple studies have demonstrated chronic elevations in serum and urine Co and Cr following successful primary total joint replacement. In addition, transient elevations of urine and serum Ni have been noted immediately following surgery. This hypernickemia/hypernickeluria may be unrelated to the implant itself since there is such a small percentage of Ni within these implant alloys. Rather, this may be related to the use of stainless-steel surgical instruments or the metabolic changes associated with the surgery itself.

Chronic elevations in serum Ti and Cr concentrations are found in subjects with well-functioning Ti- and/or Cr-containing THR components without measurable differences in urine and serum Al concentrations. Vanadium concentrations have not been found to be greatly elevated in patients with TJA (Jacobs et al., 1994b, 1998a; Dorr et al., 1990; Michel et al., 1984; Stulberg et al., 1994).

Metal ion levels within serum and urine of TJA patients can be affected by a variety of factors. For example, patients with total knee replacement components containing Ti-base alloy and carbon fiber-reinforced polyethylene wear couples demonstrated 10-fold elevations in serum Ti concentrations at an average of 4 years after implantation. Up to 100 times higher than normal control values of serum Ti elevations have also been reported in patients with failed metal-backed patellar components where unintended metal/metal articulation was possible. However, even among these TJA patients, there was no elevation in serum or urine Al, serum or urine V levels, or urine Ti levels. Mechanically assisted crevice corrosion in patients with modular femoral stems from total hip arthroplasty has been associated with elevations in serum Co and urine Cr. It has been previously assumed that extensively porous coated cementless stems would give rise to higher serum and urine chromium concentrations due to the larger surface area available for passive dissolution. Recent studies suggest that disseminated Cr can predominantly come from fretting corrosion of the modular head/neck junction. However, wear of the articulating surface remains the purported predominant source of metallic implant debris (Jacobs et al., 1998a,b; Jacobs et al., 1999).

Metal-on-Metal Bearings: Metal-on-metal (MoM) bearing hip replacements (with a metal head and metal cup) are known to release metal ions through mechanical wear of their metallic bearings. For cobalt-alloy MOM bearings, wear results in the release of primarily Co and Cr ions and, to a lesser degree, Mo and Ni ions, which then results in ion elevations and ultimately excretion. A systemic level of metal ions reached steady state where excretion matches production and for MoM implants it is in the range of one–three parts per billion for both Co and Cr (ppb or $\mu\text{g/L}$) (Jacobs et al., 2001a,b; Campbell et al., 2014; Levine et al., 2013; Hallab et al., 2013). The acceptable level of serum Co and Cr ions is hotly debated. The current consensus statement by the American Association of Hip and Knee Surgeons, suggests that levels below 3 ppb (<3 $\mu\text{g/L}$) are considered low risk (and are associated with well performing implants over the long term), levels between 3 and 10 ppb are considered intermediate risk, and levels greater than 10 ppb are considered high risk and have been associated with implant performance issues such as THA cup–neck impingement and subsequent ALTR (Kwon et al., 2014a).

Corrosion at Modular Junctions: Corrosion at modular junctions in all orthopedic implants (e.g., modular necks, spinal scoliosis screw–rod connections, etc.) occurs through the process of MACC (Fig. 2.5.4.17). Head–neck corrosion causes a differential elevation of Co:Cr as most of the released Cr ions are presumed to precipitate locally on the taper in the form of chromium orthophosphate, resulting in a systemic ratio of Co:Cr > 5–10:1. This is in contrast to the ratio of Co:Cr in the bulk metal of the implant, which is approximately 3:1. Reference values have not yet been established for assessing the risk of head–neck corrosion, however past studies have suggested that the serum Co level in a well-functioning MoP THA should be <1 ppb (Levine et al., 2013).



• **Figure 2.5.4.17** Modular junction taper connection of a total hip arthroplasty showing corrosion of the taper connections. Macrograph of deposits of CrPO_4 corrosion particles products on the rim a modular cobalt–chromium femoral head.

When corrosion occurs at the modular junctions of implant component, there is typically a two- to fivefold differential elevation of serum Co:Cr ratio. Cr is sequestered into a more chemically stable oxide form (e.g., orthophosphate) on the implant surface and builds up locally as a precipitate. Cobalt, however, does not form a precipitate as easily and is transported away. Thus, although cobalt is three times more prominent in the parent alloy it is not typically released at higher concentrations than Cr when there are mild corrosion conditions. When there are aggressive corrosion conditions, Co begins to be released more substantially and thus aggressive corrosion can be detected diagnostically by a higher serum Co:Cr ratio. The current consensus statement by the American Association of Hip and Knee Surgeons suggests that levels below 1 ppb and a Co:Cr ratio <1 can be considered low risk, levels of 1–5 ppb with a ratio of one to five are considered moderate risk, and levels >5 ppb with a Co:Cr ratio >5 are considered high risk (Kwon et al., 2014a) and a sign of aggressive corrosion likely to lead to early device failure or local excessive inflammation.

When is High too High: A “safe” threshold level has not been established, due to the complexity of patient-, implant-, and environment-dependent situations. Levels of 5–10 ppb (parts per billion, $\mu\text{g/L}$ or ng/mL) have been generally accepted as guidelines for metal ion level limits that are indications for further analysis, surveillance, and/or action in the United States for orthopedic clinicians (Campbell et al., 2014; Kwon et al., 2014b). A lower threshold of 7 ppb for cobalt or chromium for all types of MoM hip implants was put forward by the British Medicines and Healthcare Products Regulatory Agency as an indication for cross-sectional imaging (<http://www.mhra.gov.uk/home/groups/dtsbs/documents/medicaldevicealert/con079162.pdf>).

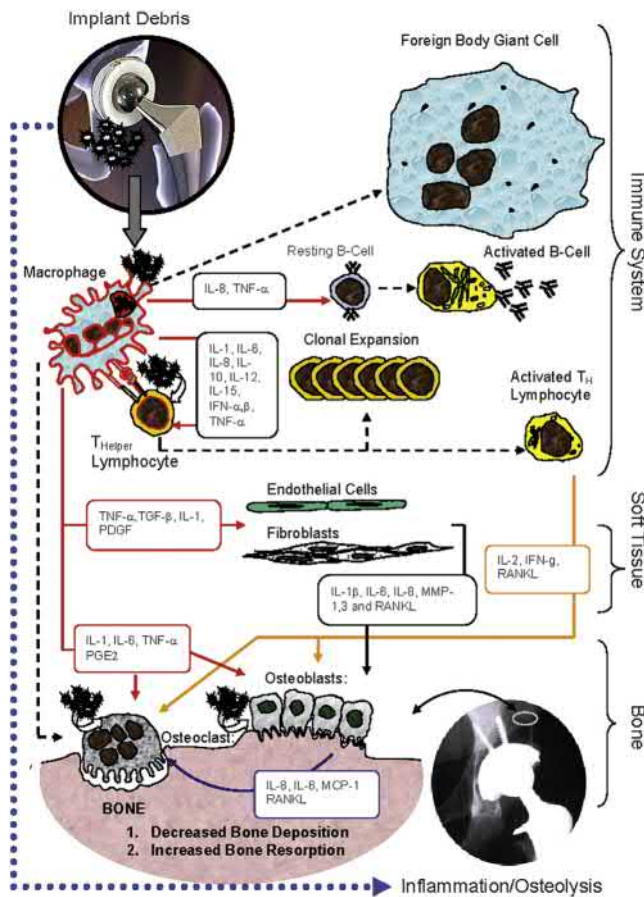
There have been some reports of metal ion referable systemic toxicity at levels of >100 ppb (Zywił et al., 2016). Established systemic effects have been limited to delayed-type hypersensitivity immune responses to metals (Amini et al., 2014; Kwon et al., 2010; Ricciardi et al., 2016). In the past very high levels of environmental cobalt exposure and toxicity have been reported connected with forms of blindness, hearing loss, tinnitus, cognitive decline, peripheral neuropathy, hypothyroidism, and cardiac dysfunction (Zywił et al., 2016; Jacobs et al., 2009). Implant-referable toxicity has not been definitively established in any orthopedic populations (Ricciardi et al., 2016; Jacobs et al., 2009).

Metal Ion Summary: The recognition that metal ion release from orthopedic implants can be pathogenic is well established. The measurement of systemic (whole blood or serum) Co and Cr levels is a minimally invasive tool in the armamentarium of doctors and is growing in popularity and reliability to implant performance and assess patients that have a painful implant. The clinical ramifications of metal ion release are discussed further in the next few sections.

Local Tissue Effects of Wear and Corrosion

Implant debris limits the long-term performance of total joint replacement by causing a local inflammatory response that leads to bone erosion and implant loosening. Normal bone maintenance relies on the balance of bone formation and bone resorption, which mainly involves the coordinated function of osteoblasts and osteoclasts. Thus, either a decrease in osteoblastic bone formation or an increase in osteoclastic bone resorption can result in net bone loss and osteolysis. Bone loss (i.e., osteolysis) around an implant is the primary concern associated with the local effects of orthopedic implant degradation. This osteolysis-causing implant debris occurs through both wear and corrosion mechanisms. Osteolysis is observed either as diffuse cortical thinning or as a focal cyst-like lesion. It was initially thought that reaction to particulate polymethylmethacrylate (PMMA) bone cement produced osteolytic lesions based on histological studies demonstrating cement debris associated with macrophages, giant cells, and a vascular granulation tissue. Recently, however, osteolysis has been recognized in association with loose and well-fixed uncemented implants, demonstrating that the absence of acrylic cement does not preclude the occurrence of osteolysis (Jacobs et al., 2001a; Vermes et al., 2001b).

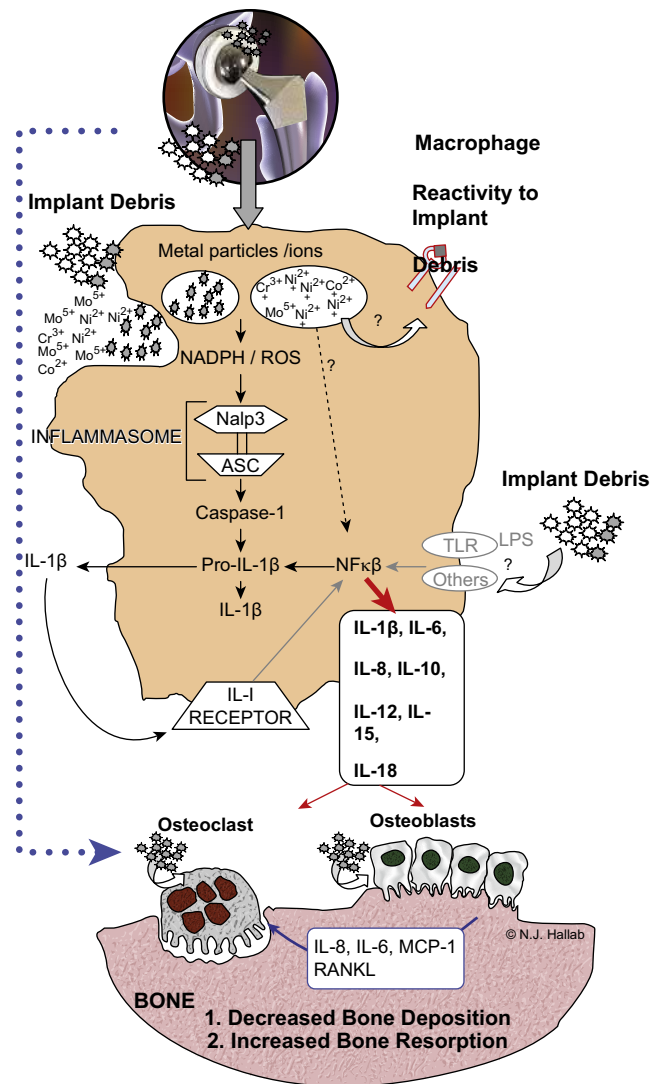
Implant debris causes low-grade inflammation that ultimately leads to implant failure. Exactly how this happens remains unclear. Over the past 40 years implant debris-induced inflammation has been characterized as aseptic, where debris-induced localized inflammation is caused in large part by macrophages which upregulate $\text{NF-}\kappa\text{B}$ and secrete inflammatory cytokines like $\text{IL-1}\beta$, $\text{TNF}\alpha$, IL-6 , and IL-8 (Jacobs et al., 2001a) (Fig. 2.5.4.18). Other anti-inflammatory cytokines such as IL-10 modulate the inflammatory process. Other factors involved with bone resorption include the enzymes responsible for catabolism of the



• **Figure 2.5.4.18** This schematic shows the numerous proinflammatory mediators produced by perimplant tissue and immune cells reacting to implant debris, which can negatively affect bone turnover. The proinflammatory cytokines IL-1, IL-6, and TNF-alpha are thought to be some of the most potent cytokines in this cascade of signaling. These cytokines produced by cells reacting to implant debris act through a variety of pathways to negatively affect bone turnover.

organic component of bone. These include matrix metalloproteinases, collagenase, and stromelysin. Prostaglandins, in particular PGE_2 , also are known to be important intercellular messengers in the osteolytic cascade produced by implant debris. More recently, several mediators known to be involved in stimulation or inhibition of osteoclast differentiation and maturation, such as RANKL (also referred to as osteoclast differentiation factor) and osteoprotegerin, respectively, have been suggested as key factors in the development and progression of bone loss (osteolytic lesions) produced from implant debris. Over the past 30 years we understand these mediators act to promote inflammation that decreases bone remodeling and are associated with the pathogenesis of osteolysis. However, we are only beginning to understand how implant debris could actually induce this immune system response at the cellular level.

Implant debris is typically sterile, relatively inert, and does not “look” like a pathogen in any molecularly recognizable way. How then can implant debris provoke an inflammatory response? That is, how do intracellular mechanisms sense and respond to sterile nonbiological challenge



• **Figure 2.5.4.19** The inflammasome pathway within cells such as macrophages has recently been reported to be central to implant debris-mediated proinflammatory reactivity. (Courtesy of BioEngineering Solutions Inc.)

agents such as implant debris? This question has remained unanswered for the past 40 years. But recently progress has implicated the “inflammasome,” a danger-signaling pathway (Fig. 2.5.4.19) (Caicedo et al., 2010).

In 1996, the discovery of specific pattern recognition receptors (PRRs) in the membrane and cytosol of human immune cells, such as macrophages, identified toll-like receptors (Taguchi et al., 1996) and their role in recognizing specific bacterial glycoproteins, now called “pathogen-associated molecular patterns” or PAMPs. We now understand that these receptors to highly conserved pathogen-associated molecular patterns (Mariathasan and Monack, 2007) now include toll-like receptors (TLRs), mannose receptors (MRs), and NOD-like receptors (NLRs) (Mariathasan and Monack, 2007). Upon pathogen/cell contact these PRRs initiate a downstream cascade of events that activate the cell and induce the secretion of proinflammatory cytokines leading to a broader inflammatory response.

In 2005, danger signal pathways were discovered where nonpathogenic derived stimuli were found to activate immune cells, similarly to PAMPs. Key components in this pathway were named the “inflammasome” and the activating stimuli were termed “danger-associated molecular patterns”, or DAMPs (Martinon et al., 2006). The paradigm for immune system activation, now includes reliance on specific receptors that recognize both PAMPs and DAMPs (Medzhitov, 2008; Ting et al., 2008). The inflammasome complex of proteins was the first pathway to explain how cells transduce sterile, nonpathogen-derived stimuli (e.g., cell stress and cell necrosis), into an inflammatory response (Mariathasan and Monack, 2007; Mariathasan et al., 2004). Nonpathogen-derived dangers include such nonbiological stimuli as UV light, particulate adjuvants present in modern vaccines (Dostert et al., 2008; Hornung et al., 2008) and, as it turns out, implant debris (Caicedo et al., 2009).

When the inflammasome pathway is activated it causes the release of IL-1 β , IL-18, IL-33, and other cytokines. This happens is as follows:

Debris \rightarrow phagocytosis \rightarrow lysosome damage \rightarrow ROS (reactive oxygen species) \rightarrow inflammasome (NALP3/ASC) \rightarrow caspase 1 \rightarrow IL-1 β (and other IL-1-family) cytokines (Fig. 2.5.4.18).

Once ingested by immune cells, DAMPs, such as asbestos and implant debris, etc. (i.e., macrophages) induce some degree of lysosomal destabilization. This causes an increase in NADPH (nicotinamide adenine dinucleotide phosphate-oxidase), and an increase in reactive oxygen species (ROS). This is not surprising given the protease- and acid-rich extreme environment inside lysosomes, used to digest and breakdown ingested particles/bacteria, etc. The release of these intracellular contents is sensed by the intracellular multiprotein inflammasome complex which is composed of NALP3 (NACHT-, LRR-, and pyrin domain-containing protein 3). NALP3 protein, in association with ASC (apoptosis-associated speck-like protein containing a CARD domain) is termed the inflammasome (Mariathasan and Monack, 2007; Petrilli et al., 2007). Activation of the inflammasome (NALPs–ASC complex) leads to the cleavage

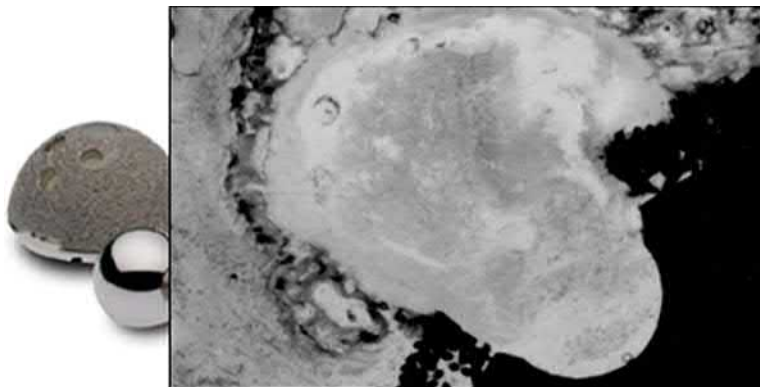
of procaspase-1 into active caspase-1. Active caspase-1 is required for the processing and subsequent release of active proinflammatory cytokines such as IL-1 β and IL-18 (and others) by cleaving intracellular pro-IL-1 β , pro-IL-18, etc. into their mature forms, IL-1 β and IL-18 etc.

How different implant debris can cause different immune responses through specific mechanisms, such as the inflammasome, remains unknown and is currently under study. These new understandings facilitate both direct targeting for drugs and can enhance diagnostic measurement for improving, measuring, and predicting when implant debris will result in loose total joint arthroplasties.

Goldring et al. (1983) were among the first to describe the synovial-like character of the bone–implant interface in patients with loose total hip replacements and determine that the cells within the membrane have the capacity to produce large amounts of bone-resorbing factors PGE₂ and collagenase. However, since studies typically can only document the end stage of the loosening process, rather than those initiating processes, pharmacologic interventions have been limited.

Osteolysis associated with total knee arthroplasty has been reported less frequently than that associated with total hip arthroplasty. It is unclear why. However, in addition to obvious factors such as implant/bone mechanical loading environments, other more subtle differential mechanisms of hip and knee wear, and differences in interfacial barriers to migration of debris have been postulated to account for this apparent disparity.

Although polyethylene particles are generally recognized as the most prevalent particles in the periprosthetic milieu, metallic and ceramic particulate species are also present in variable amounts and may have important repercussions. The bulk of this debris originates from the articular surface and has easy access to local bone. When present in sufficient amounts, particulates generated by wear, corrosion, or a combination of these processes can induce the formation of an inflammatory, foreign-body granulation tissue with the ability to invade the bone–implant interface (Fig. 2.5.4.20). Localized osteolytic lesions in these areas are common, but their clinical significance is limited unless large granulomatous lesions develop.



• **Figure 2.5.4.20** Photomicrograph (5 \times) of a section through an acetabular section of a femoral stem retrieved at autopsy, 89 months after implantation. Note the periprosthetic cavity surrounding development of a granuloma emanating from an unfilled screw hole.

The common observance of particle-induced osteolysis remote from the articulation surfaces has shown there is substantial particle migration between the joint space and the distal regions of the THA implant space. Autopsy specimens of retrieved implants have demonstrated the presence of connective tissue macrophages (histiocytes) in cavities surrounding regions of the femoral component. While the overall incidence of femoral osteolysis associated with THA tends to be proximal in the initial stages, over time it tends to progress distally. The volume of debris generated from THA polyethylene is related to a number of variables, including the smoothness of the concave metallic surface of the acetabular component, the tolerance between polyethylene and metal shell, and the relative stability of the insert (LaBerge, 1998; Shanbhag et al., 1998; Wimmer et al., 1998).

Sex Differences in Reactivity: Recent studies indicate that CoCrMo implant debris induces significantly increased osteolysis in females over that of males using a murine model of particle-induced osteolysis (Landgraeber et al., 2018). However, not all implant debris types have demonstrated sex-based differences in animal models of osteolysis in that UHMWPE particles did not induce sex-based differences in either particle-induced soft-tissue inflammation or osteolysis. Clinical observations have reported that women can suffer higher failure rates of some metal-on-metal THA designs under conditions of elevated metal release (Bornert et al., 2015). There are many possible mechanisms that account for this phenomenon. Metals such as CoCrMo and polyethylene particles can elicit different types of immune responses in vitro (Zhang et al., 2015; Endres et al., 2008; Masui et al., 2005), due to the pleotropic effects of cobalt-alloy implant debris such as induced hypoxia or hypoxia-like effects (Samelko et al., 2013), as well as innate (Caicedo et al., 2009, 2010, 2013) and adaptive immune reactivity (Hallab et al., 2001, 2005b, 2013). UHMWPE implant particles do not induce similar toxicity and immune responses, yet they do elicit innate immune reactivity inflammatory responses through inflammasome danger signaling (Zhang et al., 2015; Endres et al., 2008; Chen et al., 2015; Cunningham et al., 2013; Hallab et al., 2012). Thus the data at present support a complex picture where toxicity (e.g., hypoxia, pyroptosis, necrosis, DNA damage, etc.) and/or adaptive immune reactivity (such as lymphocyte-mediated metal hypersensitivity) (Hallab et al., 2001, 2005, 2013; Samelko et al., 2013) may alone, or in concert, produce greater downstream particle-induced osteolysis responses in women than in men. For central mechanisms of innate reactivity alone there does not appear, as yet, to be sex-based differences in innate immune reactivity alone (such as NLRP3 inflammasome, TLR signaling, costimulatory molecule expression, cytokine expression, etc.).

Remote and Systemic Effects of Wear and Corrosion

Implant surfaces and wear debris generated from the implant may release chemically active metal ions into the

surrounding tissues. While these ions may stay bound to local tissues, there is an increasing recognition that released metal products bind to specific protein moieties and are transported in the bloodstream and/or lymphatics to remote organs. The concern about the release and distribution of metallic degradation products is justified by the known potential toxicities of the elements used in modern orthopedic implant alloys: titanium, aluminum, vanadium, cobalt, chromium, and nickel. In general terms, metal toxicity may occur through (1) metabolic alterations, (2) alterations in host–parasite interactions, (3) immunologic interactions of metal moieties by virtue of their ability to act as haptens (specific immunological activation) or antichemotactic agents (nonspecific immunological suppression), and (4) by chemical carcinogenesis (Hartwig, 1998; Britton, 1996; Goering and Klaasen, 1995; Beyersmann, 1994; Luckey and Venugopal, 1979).

Cobalt, chromium, and possibly nickel and vanadium are essential trace metals in that they are required for certain enzymatic reactions. In excessive amounts, however, these elements may be toxic. Excessive cobalt may lead to polycythemia, hypothyroidism, cardiomyopathy, and carcinogenesis. Excessive chromium can lead to nephropathy, hypersensitivity, and carcinogenesis. Nickel can lead to eczematous dermatitis, hypersensitivity, and carcinogenesis. Vanadium can lead to cardiac and renal dysfunction, and has been associated with hypertension and depressive psychosis.

Biologically nonessential metallic elements also possess specific toxicities. Titanium, although generally regarded as inert, has been associated with pulmonary disease in patients with occupational exposure and with platelet suppression in animal models. Aluminum toxicity is well documented in renal failure and has been associated with anemia, osteomalacia, and neurological dysfunction, possibly including Alzheimer's disease. However, when considering the variety of documented toxicities of these elements, it is important to keep in mind that the toxicities generally apply to soluble forms of these elements and may not apply to the chemical species that result from prosthetic implant degradation.

At this time, the association of metal release from orthopedic implants with any metabolic, bacteriologic, immunologic, or carcinogenic toxicity is conjectural since cause and effect have not been well established in human subjects. However, this is due in large part to the difficulty of observation in that most symptoms attributable to systemic and remote toxicity can be expected to occur in any population of orthopedic patients (Jacobs et al., 1999).

Homogenates of remote organs and tissue obtained postmortem from subjects with Co base alloy total joint replacement components have indicated that significant increases in Co and Cr concentrations occur in the heart, liver, kidney, spleen, and lymphatic tissue (Table 2.5.4.5). Similarly, patients with Ti-base alloy implants demonstrated elevated Ti, Al, and V levels in joint pseudocapsules

TABLE 2.5.4.5 Concentrations of Metal in Body Tissue of Humans With and Without Total Joint Replacements ($\mu\text{g}/\text{G}$)

		Cr	Co	Ti	Al	V
Skeletal muscle	Normal	<12	<12	*	*	*
	TJA	570	160	*	*	*
Liver	Normal	<14	120	100	890	14
	TJA	1130	15,200	560	680	22
Lung	Normal	*	*	710	9830	26
	TJA	*	*	980	8740	23
Spleen	Normal	10	30	70	800	<9
	TJA	180	1600	1280	1070	12
Pseudocapsule	Normal	150	50	<65	120	<9
	TJA	3820	5490	39,400	460	121
Kidney	Normal	<40	30	*	*	*
	TJA	<40	60	*	*	*
Lymphatic Tissue	Normal	690	10	*	*	*
	TJA	690	390	*	*	*
Heart	Normal	30	30	*	*	*
	TJA	90	280	*	*	*

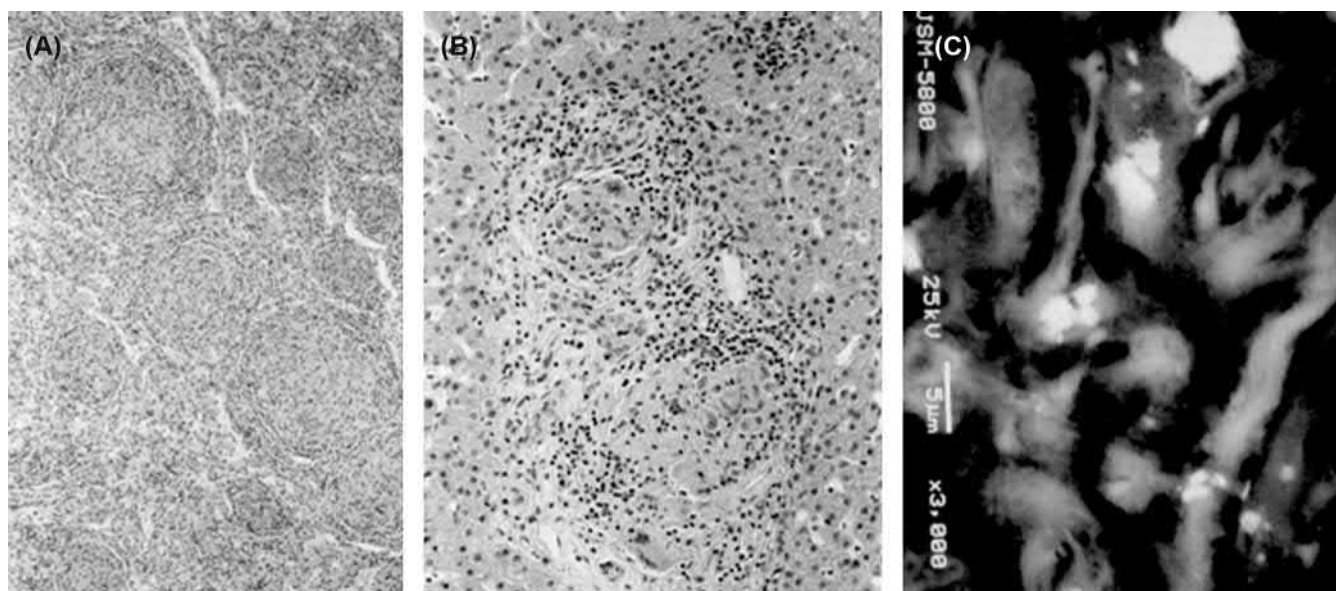
TJA, Subjects with well-functioning total joint arthroplasty; * Not tested.

(with up to 200 ppm of Ti six orders of magnitude greater than that of controls, 880 ppb of Al, and 250 ppb of V). Spleen Al levels and liver Ti concentrations can also be markedly elevated in patients with failed titanium-alloy implants (Jacobs et al., 1994c).

Systemic Particle Distribution: Variables influencing accumulation of wear debris in remote organs are not clearly identified. When the magnitude of particulate debris generated by a prosthetic device is increased, it seems likely that a corresponding elevation in both the local and systemic burdens of particles may be expected. Thus, component loosening, duration of implantation, and the modular designs of contemporary hip and knee replacement prostheses provide the potential for increased generation of metallic and polymeric debris. Wear particles found disseminated beyond the periprosthetic tissue are primarily in the submicron size range. Numerous case reports document the presence of metallic, ceramic, or polymeric wear debris from hip and knee prostheses in regional and pelvic lymph nodes (Fig. 2.5.4.21) along with the findings of lymphadenopathy, gross pigmentation due to metallic debris, fibrosis (buildup of fibrous tissue), lymph node necrosis, and histiocytosis (abnormal function of tissue macrophages), including complete effacement of nodal architecture. The inflammatory response to metallic and polymeric debris in lymph nodes has been demonstrated to include immune activation of macrophages and associated production of cytokines. Metallic wear particles have been detected in the

para-aortic lymph nodes in up to 70% of patients with total joint replacement components.

Lymphatic transport is thought to be a major route for dissemination of wear debris. Wear particles may migrate via perivascular lymph channels as free or phagocytosed particles within macrophages. Within the abdominal para-aortic lymph nodes the majority of disseminated particles are submicron in size, however metallic particles as large as 50 μm and polyethylene particles as large as 30 μm have also been identified. These particles may further disseminate to the liver or spleen where they are found within macrophages or, in some cases, as epithelioid granulomas throughout the organs. Within liver and spleen, the maximum size of metallic wear particles is nearly an order of magnitude less than that in lymph nodes, indicating there may be additional stages of filtration preceding the lymphatic system or alternate routes of particle migration. In the liver and spleen, as in the lymph nodes, cells of the mononuclear-phagocyte system may accumulate small amounts of a variety of foreign materials without apparent clinical significance. However, accumulation of exogenous particles can induce granulomas or granulomatoid lesions in the liver and spleen (Fig. 2.5.4.21). It is likely that the inflammatory reaction to particles in the liver, spleen, and lymph nodes is modulated, as it is in other tissues by (1) material composition, (2) the number of particles, (3) their rate of accumulation, (4) the duration that they are present, and (5) the biologic reactivity of cells to these particles. Metallic particles in the



• **Figure 2.5.4.21** Epithelioid granulomas (A) within the portal tract of the liver (40 \times) and, (B) within the splenic parenchyma (15 \times) in a patient with a failed titanium-alloy total hip replacement and symptomatic hepatitis. (C) Backscattered SEM of a granuloma in the spleen (3000 \times) demonstrating titanium alloy particles.

liver or spleen have been more prevalent in subjects with previously failed arthroplasties when compared with cases of well-functioning primary joint replacements. Metal particles, unlike polyethylene debris, can be characterized using an electron microprobe, which allows identification of individual, submicron metallic wear particles against a background of particulates from environmental or sources other than the prosthetic components. Overall, the smallest identifiable disseminated particles using the microprobe are approximately 0.1 μm in diameter. However, metallic wear debris may extend into the nanometer range, suggesting that additional methods of specimen preparation and analytic instrumentation may be required to more fully define the high burden of metallic wear particles in remote tissues (Urban et al., 1995, 2000).

Polyethylene particles comprise a substantial fraction of the disseminated wear particles both in subjects with revision and primary TJAs. While the presence of these polyethylene particles in lymph nodes can be confirmed by Fourier transform infrared spectroscopy microanalyses, polyethylene particulates in liver and spleen have so far precluded unequivocal identification. In these sites, the size of wear particles may be much smaller than 0.1 μm , making differentiation impossible by polarized light microscopy or infrared spectroscopy.

Diseases which cause obstruction of lymph flow through lymph nodes, such as metastatic tumor, or which cause generalized disturbances of circulation, such as chronic heart disease or diabetes, may be expected to decrease particle migration to remote organs. Other diseases, such as acute or chronic active inflammation in the periprosthetic tissues may increase particle migration (Jacobs et al., 1999, 2001; Vermes et al., 2001a).

Hypersensitivity

Some adverse responses to orthopedic biomaterials are subtle and continue to foster debate and investigation. One of these responses is “metal allergy” or hypersensitivity to metallic biomaterials. Released ions, while not sensitizers on their own, can activate the immune system by forming complexes with native proteins. These metal–protein complexes are considered to be candidate antigens (or allergens) in human clinical applications. Polymeric wear debris is not easily chemically degraded *in vivo* and has not been implicated as a source of allergic-type immune responses. This is presumably due to the relatively large degradation products associated with the mechanical wear of polymers *in vivo*, which may be large enough to prevent the formation of polymer–protein haptenic complexes with human antibodies (Hallab et al., 2000a,b, 2001a,b).

Metal hypersensitivity is a well-established phenomenon. Moreover, dermal hypersensitivity to metal is common, affecting about 10%–15% of the population. Dermal contact and ingestion of metals have been reported to cause immune reactions which most typically manifest as skin hives, eczema, redness, and itching. Although little is known about the short- and long-term pharmacodynamics and bioavailability of circulating metal degradation products *in vivo*, there have been many reports of immunologic-type responses temporally associated with implantation of metal components. Individual case reports link hypersensitivity immune reactions with adverse performance of metallic clinical cardiovascular, orthopedic, and plastic surgical and dental implants.

Metals accepted as sensitizers (haptenic moieties in antigens) include beryllium, nickel, cobalt, and chromium,

while occasional responses have been reported to tantalum, titanium, and vanadium. Nickel is the most common metal sensitizer in humans followed by cobalt and chromium. Cross-sensitivity reactions between metals are common. Nickel and cobalt are, reportedly, the most frequently cross-reactive. The amounts of these metals found in medical-grade alloys are shown in [Table 2.5.4.5](#).

Type IV delayed type hypersensitivity (DTH) is a cell-mediated type of response with which orthopedic implant-associated hypersensitivity reactions (metal sensitivity or metal allergy) are generally associated. Metal-antigen-sensitized T-DTH lymphocytes release various cytokines which result in the accumulation and activation of macrophages. The majority of DTH-participating cells are macrophages. Only 5% of the participating cells are antigen-specific T lymphocytes (T-DTH cells), within a fully developed DTH response. The effector phase of a DTH response is initiated by contact of sensitized T cells with antigen. In this phase T cells, which are antigen-activated, are termed T-DTH cells and secrete a variety of cytokines that recruit and activate macrophages, monocytes, neutrophils, and other inflammatory cells. These released cytokines include: IL-3 and GM-CSF, which promote hematopoiesis of granulocytes; monocyte chemotactic activating factor (MCAF), which promotes chemotaxis of monocytes toward areas of DTH activation; INF- γ and TNF- β , which produce a number of effects on local endothelial cells facilitating infiltration; and migration inhibitory factor (MIF), which inhibits the migration of macrophages away from the site of a DTH reaction. Activation, infiltration, and eventual migration inhibition of macrophages is the final phase of the DTH response. Activated macrophages, because of their increased ability to present class II MHC and IL-2, can trigger the activation of more T-DTH cells, which in turn activates more macrophages, which activates more T-DTH cells, and so on. This DTH self-perpetuating response can create extensive tissue damage.

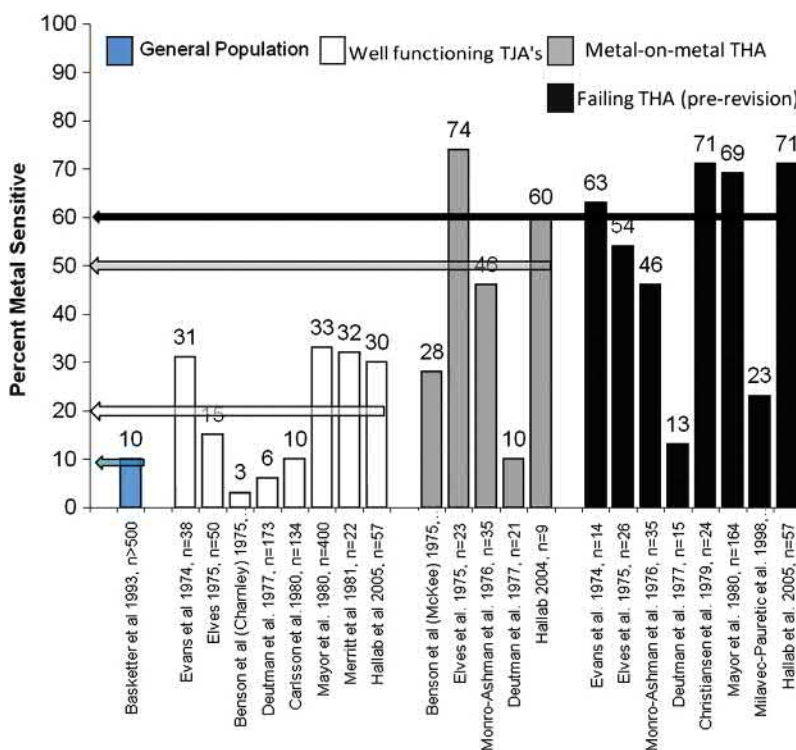
The first apparent correlation of eczematous dermatitis to metallic orthopedic implants was reported in 1966 by Foussereau and Laugier ([Foussereau and Laugier, 1966](#)), where nickel was associated with hypersensitivity responses. Over the past 20 years growing numbers of case reports link immunogenic reactions with adverse performance of metallic cardiovascular orthopedic and plastic surgical and dental implants. In some instances, clinical immunological symptoms have led directly to device removal. In these cases reactions of severe dermatitis (inflammation of the skin), urticaria (intensely sensitive and itching red round wheals on the skin), and/or vasculitis (patch inflammation of the walls of small blood vessels) have been linked with the relatively more general phenomena of metallosis (metallic staining of the surrounding tissue), excessive periprosthetic fibrosis, and muscular necrosis. The temporal and physical evidence leaves little doubt that the phenomenon of hypersensitivity to metal released from orthopedic implants does occur in some patients. These cases of severe metal sensitivity raise great concern.

Incidence of Hypersensitivity Responses Among Patients with Metal Implants: The incidence of metal sensitivity among patients with both well and poorly functioning implants is roughly twice as high as that of the general population, at approximately 25% ([Fig. 2.5.4.22](#)). Furthermore, the average incidence of metal sensitivity among patients with a “failed” implant (in need of revision surgery) is approximately 50%–60% ([Fig. 2.5.4.22](#)). This is greater than five times the incidence of metal sensitivity found in the general population and two to three times that of patients with metal implants. This increased prevalence of metal sensitivity among patients with a loose prosthesis has prompted the speculation that immunological processes may be a factor in implant loosening.

Specific types of implants with greater propensity to release metal in vivo may be more prone to induce metal sensitivity. Failures of total hip prostheses with metal-on-metal bearing surfaces were associated with greater incidence of metal allergy than similar designs with metal-on-ultrahigh molecular weight polyethylene bearing surfaces. Alternatively, several published reports have indicated that after total joint replacement with metallic components some patients show an induction of metal tolerance; that is, previously diagnosed metal sensitivity abated after implantation of a metallic prosthetic.

Confounding to any clear connection between metal sensitivity and implant failure is the lack of any reported correlation between incidence of metal sensitivity and implant residence time, infection, reason for removal, or pain. This lack of causal evidence implicating cell-mediated immune responses has prompted some to conclude that implantation of cemented metal-to-plastic joint prosthesis is safe, even in the case of a preexisting metal allergy. However, this is not a consensus opinion. At this time, however, it is unclear whether metal sensitivity causes implant loosening or whether implant loosening results in the development of metal sensitivity.

The majority of investigations conclude that metal sensitivity can be a contributing factor to implant failure. Such cases include instances in which clinical immunological symptoms lead directly to the need for device removal. In these or similar cases there have been reported reactions of severe dermatitis, urticaria, and/or vasculitis, all presumably linked to what has been reported as metallosis, excessive periprosthetic fibrosis, and muscular necrosis. The clinical observation of apparent immune sensitivity to metallic implants is not limited to orthopedic surgery. Some case reports suggest metal sensitivity to pacemakers, heart valves, reconstructive, dental, and general surgical devices. The temporal and physical evidence associated with such cases leaves little doubt that the phenomenon of metal-induced hypersensitivity does occur in some cases, currently accepted within the orthopedic community to be <1% of patients. However, it is currently unclear whether metal sensitivity exists only as an unusual complication in a few susceptible patients, or is a more subtle and common phenomenon, which over time plays a significant role in implant failure.



• **Figure 2.5.4.22** A compilation of investigations showing the averaged percentages of metal sensitivity among the general population for nickel, cobalt, and chromium, among patients after receiving a metal-containing implant, and among patient populations with failed implants. All subjects were tested by means of a patch or metal-LTT (lymphocyte transformation test).

It is likely that cases involving implant-related metal sensitivity have been underreported because alternate causes were attributed to failure of the implant. Mechanisms by which in vivo metal sensitivity occurs have not been well characterized. Thus, the degree to which a precondition of metal hypersensitivity may elicit an overaggressive immune response in a patient receiving an implant remains unpredictable. Continuing improvements in immunologic testing methods will likely enhance future assessment of patients susceptible to hypersensitivity responses (Hallab et al., 2000a,b, 2001a,b).

Testing for Metal Sensitivity. Implant debris-related DTH responses are bad enough to require revision arthroplasty in approximately 1%–2% of all orthopedic patients. There are only two accepted testing methods for diagnosing metal allergy, including skin testing (i.e., so-called patch testing) and cell culture blood testing called metal lymphocyte transformation testing (metal-LTT). Patch testing commercial kits exist for some metals (Hensten-Pettersen, 1993; Rooker and Wilkinson, 1980), however there is continuing concern about sensitizing patients using this type of patch testing (by placing high-concentration metal salt solutions in petroleum jelly on the skin for 48 h) (Merritt and Brown, 1980). Other problems associated with patch testing include disagreement as to how representative the skin is (with unique dermal antigen-presenting cells, i.e., Langerhans cells) as a proxy of periimplant antigen-presenting cells (Kuby, 1991; Korenblat, 1992). In vitro metal allergy testing, called lymphocyte proliferation testing (also known as LTT), involves

measuring the proliferative response of lymphocytes after they are activated by an antigen. A radioactive marker is used to precisely measure the amount of cell division over a set time period by measuring the amount of radioactive [^3H]-thymidine that is incorporated into the cellular DNA upon cell division after 4–6 days of exposure to antigen. [^3H]-thymidine uptake is measured using liquid scintillation, and the amount of immune response (proliferation factor or stimulation index) is calculated using measured radiation counts per minute (cpm):

$$\text{Proliferation Factor} = \frac{(\text{cpm with treatment})}{(\text{cpm without treatment})}$$

The use of proliferation testing to measure metal allergy was developed from similar methods to assess general drug sensitivity and has been well established as a method of testing DTH responses in a variety of clinical settings (Veien and Svejgaard, 1978; Veien et al., 1979; Svejgaard et al., 1978; Secher et al., 1977; Everness et al., 1990). The use of LTT for implant-related metal sensitivity is increasing given that it has been shown to have diagnostic efficacy, particularly in the area of metal-on-metal implants, which have led to higher rates of metal sensitivity responses (Granchi et al., 1998, 1999; Carando et al., 1985). Several investigations indicate that metal allergy can be more readily detected by LTT than by dermal patch testing (Carando et al., 1985; Granchi et al., 1996, 1998a). Thus, given the growing number of studies using the highly quantitative nature of LTT testing in orthopedics, it is likely better

suiting for the testing of implant-related sensitivity than dermal patch testing (Veien and Svejgaard, 1978; Veien et al., 1979; Svejgaard et al., 1978; Secher et al., 1977; Everness et al., 1990; Carando et al., 1985; Granchi et al., 1995, 2003).

As we learn more about the subtleties of immune response to implant debris, the adaptive immune system may be involved to a much larger degree in debris-induced inflammation than what has been previously attributed to the innate immune system via macrophages reactivity.

Carcinogenesis

The carcinogenic potential of implant debris remains an area of concern. Animal studies have documented that implant metals can act as carcinogens. Small increases in rat sarcomas were found to correlate with high levels of serum cobalt, chromium, or nickel content produced by metal implants. Additionally, lymphomas with some form of bone involvement were also more commonly found in rat animal models with metallic implants. Although not common, implant site tumors in dogs and cats—primarily osteosarcoma and fibrosarcoma—have been associated with stainless steel internal fixation devices.

Some epidemiological studies implicate orthopedic implants in causing cancer 10–20 years after total hip replacement. However, more recently larger studies have found no significant increase in cancers such as leukemia or lymphoma, although these studies did not include people with high amounts of metal, such as those with a metal-on-metal prosthesis. The many differences in the populations with and without implants that do not depend on the implant itself confounds the interpretation of any epidemiological investigations.

It remains unknown if metal release from orthopedic implants is carcinogenic because causality has not been established in human subjects, and in fact, testing by the authors found that periimplant cells became toxic prior to any DNA strand breaks when tested with increasing concentrations of metal ions found in implants (Caicedo et al., 2007a; Hallab et al., 2002). The actual number of cases of tumors associated with orthopedic implants is likely underreported due to the frequency of tumors in the population demographic receiving metal implants. However, compared to the number of devices implanted on a yearly basis (over one million) the incidence of cancer at the site of implantation is relatively rare. Continued monitoring and large long epidemiological studies are required to fully understand this risk (Nyren et al., 1995; Matheisen et al., 1995; Visuri and Koskenvuo, 1991; Gillespie et al., 1988).

Preventive Strategies and Future Directions

Current strategies designed to address the problem of biomaterial-related implant failure are primarily aimed at decreasing the amount of periprosthetic particulate burden and any subsequent effects. Recently there has been a great deal of

innovation regarding stronger, more wear-resistant polyethylene. These more highly cross-linked UHMWPE polymers are currently in various phases of clinical trial. However, initial results show a demonstrable decrease in polyethylene wear with potential for less particulate-induced bioreactivity/osteolysis and therefore greater implant performance. In the same vein, femoral heads with diameters of 32 mm have been associated with increased volumetric polyethylene wear; to combat this, smaller 28 mm heads are currently extolled as more biocompatible. Manufacturing flaws such as fusion defects and foreign body inclusions have also been suggested to contribute to adverse polyethylene wear properties. The elimination of polyethylene is another approach being investigated clinically in various centers. With the realization that early problems may have been related to the design and not the articulation, there has been renewed interest in the application of metal–metal and ceramic–ceramic bearings. Future designs which attempt to reduce wear include improved tolerances between polyethylene inserts and their metal backing, improved surface finish on the metallic concave surfaces, secure locking mechanisms, and the avoidance of holes on the convex portion of the acetabular prosthesis.

Metallic wear is also being addressed through techniques such as nitriding and nitrogen ion implantation to decrease the potential for abrasive wear and fretting in titanium alloy and cobalt alloy stems. Fabrication of metallic bearing surfaces with extremely low roughness can be expected to decrease articular wear rates. A polished metal head can be made as smooth as a ceramic head. Polishing of the stem will remove surface asperities and decrease particle generation from stem/bone fretting. In addition, polishing will minimize silicate contamination.

New metallic biomaterials are being proposed which attempt to improve load transfer to the bone and reduce the incidence of loosening and thigh pain. Currently used alloys (Co–Cr–Mo alloy, $E = 227$ GPa and Ti–6Al–4V alloy, $E = 115$ GPa) have relatively high elastic moduli, which limit smooth transfer of load to the surrounding bone in THA. Designs to improve load transfer can use a reduced cross-sectional area to increase flexibility, but at the expense of adequate stability of the implant within the bone. Additionally, the stresses may exceed the relatively low fatigue strength of Co–Cr–Mo implant alloy. Lower-modulus, more corrosion-resistant implant alloys are being developed. A Ti–13Nb–13Zr ($E = 79$ GPa) alloy is one such alloy which contains fewer elements of questionable cell response (i.e., Co, Cr, Mo, Ni, Fe, Al, V), and which possesses comparable strength and toughness to existing Ti–6Al–4V implant alloy. The Nb and Zr constituents seek to improve bone biocompatibility and corrosion resistance. Additionally, novel surface treatments on implant alloys such as the diffusion hardening (DH) treatment can produce a hardened surface with wear resistance superior to that of Co–Cr–Mo alloy, currently the industry leader for TKAs. These enhanced surface properties may lead to an improvement in the resistance to microfretting occurring within femoral head–neck taper regions and modular interfaces of current implant designs.

Electrochemical corrosion of orthopedic implants remains a significant clinical concern. Although the freely corroding implants used in the past have been replaced with modern corrosion-resistant “superalloys” deleterious corrosion processes have been observed in certain clinical settings. Attention to metallurgical processing variables, tolerances of modular connections, surface processing modalities, and appropriate material selection can diminish corrosion rates and minimize the potential for adverse clinical outcomes. For example, nitriding can reportedly significantly reduce the magnitude of fretting corrosion of Ti–6Al–4V devices. A need to further investigate the mechanical–electrochemical interactions of metal oxide surfaces in implants persists. Characterization of the stresses and motion needed to fracture passivating oxide films as well as the effects of repeated oxide abrasion on the electrochemical behavior of the interface and ultimately the implant remain avenues of active investigation.

The clinical significance of elevated metal content in body fluids and remote organs of patients with metallic implants needs to be further elucidated. Considerably more work will be required to discern the specific chemical forms and distribution of metal degradation products associated with the various forms of implant degradation. Continued efforts to better understand the constituents of orthopedic implant degradation and their biological effects is necessary to ultimately determine threshold levels of debris and circulating metal ions and measures of biologic reactivity (e.g., metal-LTT testing) that can be used to clinically determine when intervention is required to fix a downward spiral before too much bone loss and inflammation occur. The importance of this evaluation of orthopedic biomaterial performance is growing as the use of orthopedic biomaterials is increasing, as new orthopedic implants are being developed and as expectations of implant durability and performance increase (Jacobs et al., 1996; Black, 1996).

References

- Anderson, P.A., Rouleau, J.P., Bryan, V.E., Carlson, C.S., October 15, 2003. Wear analysis of the Bryan cervical disc prosthesis. *Spine* 28 (20), S186–S194.
- Amini, M., Mayes, W.H., Tzeng, A., Tzeng, T.H., Saleh, K.J., Mihalko, W.M., 2014. Evaluation and management of metal hypersensitivity in total joint arthroplasty: a systematic review. *J. Long Term Eff. Med. Implant.* 24 (1), 25–36.
- Baumann, B., Rader, C.P., Seufert, J., Noth, U., Rolf, O., Eulert, J., et al., June 2004. Effects of polyethylene and TiAlV wear particles on expression of RANK, RANKL and OPG mRNA. *Acta Orthop. Scand.* 75 (3), 295–302.
- Baumann, B., Seufert, J., Jakob, F., Noth, U., Rolf, O., Eulert, J., et al., November 2005. Activation of NF-kappaB signalling and TNFalpha-expression in THP-1 macrophages by TiAlV- and polyethylene-wear particles. *J. Orthop. Res.* 23 (6), 1241–1248.
- Baumann, B., Rolf, O., Jakob, F., Goebel, S., Sterner, T., Eulert, J., et al., 2006. Synergistic effects of mixed TiAlV and polyethylene wear particles on TNFalpha response in THP-1 macrophages. *Biomed. Tech.* 51 (5–6), 360–366.
- Beyersmann, D., June 1994. Interactions in metal carcinogenicity. *Toxicol. Lett.* 72 (1–3), 333–338.
- Black, J., 1992. *Biomaterials*, second ed. Marcel Dekker, Inc., New York.
- Black, J., 1996. *Prosthetic Materials*. VCH Publishers, Inc., New York.
- Bobyn, J.D., Tanzer, M., Krygier, J.J., Dujovne, A.R., Brooks, C.E., January 1994. Concerns with modularity in total hip arthroplasty. *Clin. Orthop.* (298), 27–36.
- Bornert, S., Lutzner, J., Beyer, F., Gunther, K.P., Hartmann, A., December 2015. Revision rate and patient-reported outcome after hip resurfacing arthroplasty: a concise follow-up of 1064 cases. *J. Arthroplast.* 30 (12), 2190–2195.
- Britton, R.S., 1996. Metal-induced hepatotoxicity. *Semin. Liver Dis.* 16 (1), 3–12.
- Brown, S.A., Merritt, K., July 1981. Fretting corrosion in saline and serum. *J. Biomed. Mater. Res.* 15 (4), 479–488.
- Brown, S.A., Flemming, C.A.C., Kawalc, J.S., Vassaux, C.J., Payer, J.H., Kraay, M.J., et al., 1992. Fretting accelerated crevice corrosion of modular hips. In: *Trans Soc Biomater Implant retrieval Symposium*, 15, p. 59.
- Brown, S.A., Flemming, C.A., Kawalc, J.S., Placko, H.E., Vassaux, C., Merritt, K., et al., 1995. Fretting corrosion accelerates crevice corrosion of modular hip tapers. *J. Appl. Biomater.* 6 (1), 19–26.
- Bruch, J., December 1974. Response of cell cultures to asbestos fibers. *Environ. Health Perspect.* 9, 253–254.
- Bundy, K.J., Williams, C.J., Luedemann, R.E., September 1991. Stress-enhanced ion release—the effect of static loading. *Biomaterials* 12 (7), 627–639.
- Büttner - Janz, K., 1992. *The Development of the Artificial Disc SB Charité*. Hundley & Associates.
- Caicedo, M., Jacobs, J.J., Reddy, A., Hallab, N.J., November 29, 2007a. Analysis of metal ion-induced DNA damage, apoptosis, and necrosis in human (Jurkat) T-cells demonstrates Ni(2+) and V(3+) are more toxic than other metals: Al(3+), Be(2+), Co(2+), Cr(3+), Cu(2+), Fe(3+), Mo(5+), Nb(5+), Zr(2+). *J. Biomed. Mater. Res. A* 86, 905–913.
- Caicedo, M., Reddy, A., Samee, I., Jacobs, J.J., Hallab, N., 2007b. Cobalt ions and Co-Cr-Mo alloy particles induce human monocyte co-stimulatory molecules CD-86, ICAM-1 and the cytokine IL-8: implications for innate activation of adaptive immune responses. In: *6th Combined Meeting of the Orthopaedic Research Societies*, 6, p. 535.
- Caicedo, M.S., Desai, R., McAllister, K., Reddy, A., Jacobs, J.J., Hallab, N.J., July 2009. Soluble and particulate Co-Cr-Mo alloy implant metals activate the inflammasome danger signaling pathway in human macrophages: a novel mechanism for implant debris reactivity. *J. Orthop. Res.* 27 (7), 847–854.
- Caicedo, M.S., Pennekamp, P.H., McAllister, K., Jacobs, J.J., Hallab, N.J., June 15, 2010. Soluble ions more than particulate cobalt-alloy implant debris induce monocyte costimulatory molecule expression and release of proinflammatory cytokines critical to metal-induced lymphocyte reactivity. *J. Biomed. Mater. Res. A* 93 (4), 1312–1321.
- Caicedo, M.S., Samelko, L., McAllister, K., Jacobs, J.J., Hallab, N.J., October 2013. Increasing both CoCrMo-alloy particle size and surface irregularity induces increased macrophage inflammasome activation in vitro potentially through lysosomal destabilization mechanisms. *J. Orthop. Res.* 31 (10), 1633–1642.
- Callaghan, J.J., Rosenberg, A., Rubash, H., 2007. *The Adult Hip*. Lippincott Williams & Wilkins, New York.
- Campbell, P., Ma, S., Yeom, B., McKellop, H., Schmalzried, T.P., Amstutz, H.C., January 1995. Isolation of predominantly submicron-sized UHMWPE wear particles from periprosthetic tissues. *J. Biomed. Mater. Res.* 29 (1), 127–131.

- Campbell, P.A., Kung, M.S., Hsu, A.R., Jacobs, J.J., December 2014. Do retrieval analysis and blood metal measurements contribute to our understanding of adverse local tissue reactions? *Clin. Orthop. Relat. Res.* 472 (12), 3718–3727.
- Carando, S., Cannas, M., Rossi, P., Portigliatti-Barbos, M., December 1985. The lymphocytic transformation test (L.T.T.) in the evaluation of intolerance in prosthetic implants. *Ital. J. Orthop. Traumatol.* 11 (4), 475–481.
- Catelas, I., Medley, J.B., Campbell, P.A., Huk, O.L., Boby, J.D., August 15, 2004. Comparison of in vitro with in vivo characteristics of wear particles from metal-metal hip implants. *J. Biomed. Mater. Res. B Appl. Biomater.* 70 (2), 167–178.
- Charnley, J., 1960. Anchorage of the femoral head prosthesis to the shaft of the femur. *J. Bone Joint Surg. Br.* 42, 28.
- Charnley, J., 1964. The bonding of prosthesis to bone by cement. *J. Bone Joint Surg. Br.* 46, 518.
- Charnley, J., 1979. *Low Friction Arthroplasty of the Hip, Theory and Practice.* Springer-Verlag, Berlin.
- Chen, Y., Hallab, N.J., Liao, Y.S., Narayan, V., Schwarz, E.M., Xie, C., May 2016. Antioxidant impregnated ultra-high molecular weight polyethylene wear debris particles display increased bone remodeling and a superior osteogenic: osteolytic profile vs. conventional UHMWPE particles in a murine calvaria model. *J. Orthop. Res.* 34 (5), 845–851.
- Clarke, I.C., Good, V., Williams, P., Schroeder, D., Anissian, L., Stark, A., et al., 2000. Ultra-low wear rates for rigid-on-rigid bearings in total hip replacements. *Proc. Inst. Mech. Eng. H* 214 (4), 331–347.
- Collier, J.P., Mayor, M.B., Jensen, R.E., Surprenant, V.A., Surprenant, H.P., McNamar, J.L., et al., December 1992. Mechanisms of failure of modular prostheses. *Clin. Orthop.* (285), 129–139.
- Collier, J.P., Surprenant, V.A., Jensen, R.E., Mayor, M.B., Surprenant, H.P., 1992b. Corrosion between the components of modular femoral hip prostheses. *J. Bone Joint Surg. Am.* 74-B, 511–517.
- Cook, S.D., Gianoli, G.J., Clemow, A.J., Haddad, R.J.J., August 1983. Fretting corrosion in orthopaedic alloys. *Biomater. Med. Devices Artif. Organs* 11 (4), 281–292.
- Cowan Jr., J.A., Dimick, J.B., Wainess, R., Upchurch Jr., G.R., Chandler, W.F., La, M.F., July 2006. Changes in the utilization of spinal fusion in the United States. *Neurosurgery* 59 (1), 15–20.
- Cunningham, B.W., Orbegoso, C.M., Dmitriev, A.E., Hallab, N.J., Seftor, J.C., McAfee, P.C., September 15, 2002. The effect of titanium particulate on development and maintenance of a posterolateral spinal arthrodesis: an in vivo rabbit model. *Spine* 27 (18), 1971–1981.
- Cunningham, B.W., Hallab, N.J., Hu, N., McAfee, P.C., September 2013. Epidural application of spinal instrumentation particulate wear debris: a comprehensive evaluation of neurotoxicity using an in vivo animal model. *J. Neurosurg. Spine* 19 (3), 336–350.
- Dorr, L.D., Bloebaum, R., Emmanuel, J., Meldrum, R., 1990. Histologic, biochemical and ion analysis of tissue and fluids retrieved during total hip arthroplasty. *Clin. Orthop. Relat. Res.* 261, 82–95.
- Dostert, C., Petrilli, V., Van, B.R., Steele, C., Mossman, B.T., Tschopp, J., May 2, 2008. Innate immune activation through Nalp3 inflammasome sensing of asbestos and silica. *Science* 320 (5876), 674–677.
- Endres, S., Bartsch, I., Sturz, S., Kratz, M., Wilke, A., March 2008. Polyethylene and cobalt-chromium molybdenum particles elicit a different immune response in vitro. *J. Mater. Sci. Mater. Med.* 19 (3), 1209–1214.
- Espehaug, B., Engesaeter, L.B., Vollset, S.E., Havelin, L.I., Langeland, N., July 1997. Antibiotic prophylaxis in total hip arthroplasty. Review of 10,905 primary cemented total hip replacements reported to the Norwegian arthroplasty register, 1987 to 1995. *J. Bone Joint Surg. Br.* 79 (4), 590–595.
- Everness, K.M., Gawkrödger, D.J., Botham, P.A., Hunter, J.A., March 1990. The discrimination between nickel-sensitive and non-nickel-sensitive subjects by an in vitro lymphocyte transformation test. *Br. J. Dermatol.* 122 (3), 293–298.
- Fernstrom, U., 1966. Arthroplasty with intercorporeal endoprosthesis in herniated disc and in painful disc. *Acta Chir. Scand. Suppl.* 357, 154–159.
- Firkins, P.J., Tipper, J.L., Saadatzadeh, M.R., Ingham, E., Stone, M.H., Farrar, R., et al., 2001. Quantitative analysis of wear and wear debris from metal-on-metal hip prostheses tested in a physiological hip joint simulator. *Bio Med. Mater. Eng.* 11 (2), 143–157.
- Foussereau, J., Laugier, 1966. Allergic eczemas from metallic foreign bodies. *Trans. St. John's Hosp. Dermatol. Soc.* 52, 220–225.
- Gilbert, J.L., Jacobs, J., 1997. The mechanical and electrochemical processes associated with taper fretting crevice corrosion: a review. In: *ASTM STP 1301 Modularity of Orthopedic Implants.* ASTM, Philadelphia, pp. 45–59.
- Gilbert, J.L., Buckley, C.A., Jacobs, J.J., December 1993. In vivo corrosion of modular hip prosthesis components in mixed and similar metal combinations. The effect of crevice, stress, motion, and alloy coupling. *J. Biomed. Mater. Res.* 27 (12), 1533–1544.
- Gilbert, J.L., Mehta, M., Pinder, B., January 2009. Fretting crevice corrosion of stainless steel stem-CoCr femoral head connections: comparisons of materials, initial moisture, and offset length. *J. Biomed. Mater. Res. B Appl. Biomater.* 88 (1), 162–173.
- Gillespie, W.J., Frampton, C.M., Henderson, R.J., Ryan, P.M., August 1988. The incidence of cancer following total hip replacement. *J. Bone Joint Surg. Br.* 70 (4), 539–542.
- Glant, T.T., Jacobs, J.J., 1994. Response of three murine macrophage populations to particulate debris: bone resorption in organ cultures. *J. Orthop. Res.* 12, 720–732.
- Goering, P.L., Klaasen, C.D., 1995. *Hepatotoxicity of Metals.* Academic Press, New York.
- Goldring, S.R., Schiller, A.L., Roelke, M., Rourke, C.M., O'Neill, D.A., Harris, W.H., 1983. The synovial-like membrane at the bone-cement interface in loose total hip replacements and its proposed role in bone lysis. *J. Bone Jt. Surg.* 65A, 575–584.
- González, O., Smith, R.L., Goodman, S.B., 1996. Effect of size, concentration, surface area, and volume of polymethylmethacrylate particles on human macrophages *in vitro*. *J. Biomed. Mater. Res.* 30, 463–473.
- Goodman, S.B., Lind, M., Song, Y., Smith, R.L., July 1998. In vitro, in vivo, and tissue retrieval studies on particulate debris. *Clin. Orthop.* 352, 25–34.
- Granchi, D., Ciapetti, G., Stea, S., Cavedagna, D., Bettini, N., Bianco, T., et al., October 1995. Evaluation of several immunological parameters in patients with aseptic loosening of hip arthroplasty. *Chir. Organi Mov.* 80 (4), 399–408.
- Granchi, D., Ciapetti, G., Savarino, L., Cavedagna, D., Donati, M.E., Pizzoferrato, A., June 1996. Assessment of metal extract toxicity on human lymphocytes cultured in vitro. *J. Biomed. Mater. Res.* 31 (2), 183–191.
- Granchi, D., Verri, E., Ciapetti, G., Savarino, L., Cenni, E., Gori, A., et al., January 1998. Effects of chromium extract on cytokine release by mononuclear cells. *Biomaterials* 19 (1–3), 283–291.

- Granchi, D., Verri, E., Ciapetti, G., Stea, S., Savarino, L., Sudanese, A., et al., September 1998. Bone-resorbing cytokines in serum of patients with aseptic loosening of hip prostheses. *J. Bone Joint Surg. Br.* 80 (5), 912–917.
- Granchi, D., Ciapetti, G., Stea, S., Savarino, L., Filippini, F., Sudanese, A., et al., June 1999. Cytokine release in mononuclear cells of patients with Co-Cr hip prosthesis. *Biomaterials* 20 (12), 1079–1086.
- Granchi, D., Savarino, L., Ciapetti, G., Cenni, E., Rotini, R., Mieti, M., et al., July 2003. Immunological changes in patients with primary osteoarthritis of the hip after total joint replacement. *J. Bone Joint Surg. Br.* 85 (5), 758–764.
- Greenwald, A.S., Garino, J.P., 2001. Alternative bearing surfaces: the good, the bad, and the ugly. *J. Bone Joint Surg. Am.* 83-A (Suppl. 2 Pt 2), 68–72.
- Hallab, N.J., Mikecz, K., Jacobs, J.J., September 2000. A triple assay technique for the evaluation of metal-induced, delayed-type hypersensitivity responses in patients with or receiving total joint arthroplasty. *J. Biomed. Mater. Res.* 53 (5), 480–489.
- Hallab, N.J., Jacobs, J.J., Skipor, A., Black, J., Mikecz, K., Galante, J.O., 2000b. Systemic metal-protein binding associated with total joint replacement arthroplasty. *J. Biomed. Mater. Res.* 49 (3), 353–361.
- Hallab, N., Merritt, K., Jacobs, J.J., March 2001a. Metal sensitivity in patients with orthopaedic implants. *J. Bone Joint Surg. Am.* 83-A (3), 428–436.
- Hallab, N.J., Mikecz, K., Vermes, C., Skipor, A., Jacobs, J.J., September 5, 2001b. Differential lymphocyte reactivity to serum-derived metal-protein complexes produced from cobalt-based and titanium-based implant alloy degradation. *J. Biomed. Mater. Res.* 56 (3), 427–436.
- Hallab, N.J., Vermes, C., Messina, C., Roebuck, K.A., Glant, T.T., Jacobs, J.J., June 5, 2002. Concentration- and composition-dependent effects of metal ions on human MG-63 osteoblasts. *J. Biomed. Mater. Res.* 60 (3), 420–433.
- Hallab, N.J., Anderson, S., Caicedo, M., Brasher, A., Mikecz, K., Jacobs, J.J., June 3, 2005. Effects of soluble metals on human peri-implant cells. *J. Biomed. Mater. Res. A* 74 (1), 124–140.
- Hallab, N.J., Anderson, S., Stafford, T., Glant, T., Jacobs, J.J., March 2005. Lymphocyte responses in patients with total hip arthroplasty. *J. Orthop. Res.* 23 (2), 384–391.
- Hallab, N.J., Khandha, A., Malcolmson, G., Timm, J.P., December 1, 2008. In vitro assessment of serum-saline ratios for fluid simulator testing of highly modular spinal implants with articulating surfaces. *SAS J.* 2 (4), 171–183.
- Hallab, N.J., McAllister, K., Brady, M., Jarman-Smith, M., February 2012. Macrophage reactivity to different polymers demonstrates particle size- and material-specific reactivity: PEEK-OPTIMA((R)) particles versus UHMWPE particles in the submicron, micron, and 10 micron size ranges. *J. Biomed. Mater. Res. B Appl. Biomater* 100 (2), 480–492.
- Hallab, N.J., Caicedo, M., McAllister, K., Skipor, A., Amstutz, H., Jacobs, J.J., February 2013. Asymptomatic prospective and retrospective cohorts with metal-on-metal hip arthroplasty indicate acquired lymphocyte reactivity varies with metal ion levels on a group basis. *J. Orthop. Res.* 31 (2), 173–182.
- Hamby, W.B., Glaser, H.T., 1959. Replacement of spinal intervertebral discs with locally polymerizing methyl methacrylate. *J. Neurosurg.* 16, 311–313.
- Harmon, P.H., 1963. Anterior excision and vertebral body fusion operation for intervertebral disc syndromes of the lower lumbar spine. *Clin. Orthop.* 26, 107–111.
- Harris, W.H., June 1969. Traumatic arthritis of the hip after dislocation and acetabular fractures: treatment by mold arthroplasty. An end-result study using a new method of result evaluation. *J. Bone Joint Surg. Am.* 51 (4), 737–755.
- Harris, W.H., 1995. The problem is osteolysis. *Clin. Orthop.* 311, 46–53.
- Hartwig, A., December 28, 1998. Carcinogenicity of metal compounds: possible role of DNA repair inhibition. *Toxicol. Lett.* 102–103, 235–239.
- Heisel, C., Silva, M., la Rosa, M.A., Schmalzried, T.P., April 2004. Short-term in vivo wear of cross-linked polyethylene. *J. Bone Joint Surg. Am.* 86-A (4), 748–751.
- Hellier, W.G., Hedman, T.P., Kostuik, J.P., June 1992. Wear studies for development of an intervertebral disc prosthesis. *Spine* 17 (6 Suppl. 1), S86–S96.
- Hensten-Pettersen, A., 1993. Allergy and hypersensitivity. In: Morrey, B.F. (Ed.), *Biological, Material, and Mechanical Considerations of Joint Replacements*. Raven Press, New York, pp. 353–360.
- Holt, G., Murnaghan, C., Reilly, J., Meek, R.M., July 2007. The biology of aseptic osteolysis. *Clin. Orthop. Relat. Res.* 460, 240–252.
- Hornung, V., Bauernfeind, F., Halle, A., Samstad, E.O., Kono, H., Rock, K.L., et al., August 2008. Silica crystals and aluminum salts activate the NALP3 inflammasome through phagosomal destabilization. *Nat. Immunol.* 9 (8), 847–856.
- Huk, O.L., Bansal, M., Betts, F., Rinnac, C.M., Lieberman, J.R., Huo, M.H., et al., July 1994. Polyethylene and metal debris generated by non-articulating surfaces of modular acetabular components. *J. Bone Joint Surg. Br.* 76 (4), 568–574.
- Huo, M.H., Salvati, E.A., Lieberman, J.R., Betts, F., Bansal, M., March 1992. Metallic debris in femoral endosteolysis in failed cemented total hip arthroplasties. *Clin. Orthop.* 276, 157–168.
- Ingham, E., Green, T.R., Stone, M.H., Kowalski, R., Watkins, N., Fisher, J., May 2000. Production of TNF-alpha and bone resorbing activity by macrophages in response to different types of bone cement particles. *Biomaterials* 21 (10), 1005–1013.
- Ingram, J., Matthews, J.B., Tipper, J., Stone, M., Fisher, J., Ingham, E., 2002. Comparison of the biological activity of grade GUR 1120 and GUR 415HP UHMWPE wear debris. *Bio Med. Mater. Eng.* 12 (2), 177–188.
- Jacobs, J.J., 1995. Particulate wear. *J. Am. Med. Assoc.* 273, 1950–1956.
- Jacobs, J.J., Hallab, N.J., June 2006. Loosening and osteolysis associated with metal-on-metal bearings: a local effect of metal hypersensitivity? *J. Bone Joint Surg. Am.* 88 (6), 1171–1172.
- Jacobs, J.J., Urban, R.M., Schajowicz, F., Gavriloic, J., Galante, J.O., 1992. Particulate-associated endosteal osteolysis in titanium-base alloy cementless total hip replacement. *Particulate Debris from Medical Implants. Am. Soc. Test. Mater.* 1992 (1992), 52–60.
- Jacobs, J.J., Shanbhag, A., Glant, T.T., Black, J., Galante, J.O., July 1994. Wear debris in total joint replacements. *J. Am. Acad. Orthop. Surg.* 2 (4), 212–220.
- Jacobs, J.J., Skipor, A.K., Urban, R.M., Black, J., Manion, L.M., Starr, A., et al., 1994b. Systemic distribution of metal degradation products from titanium alloy total hip replacements: an autopsy study. *Trans. Orthop. Res. Soc.* 838 New Orleans.
- Jacobs, J.J., Gilbert, J.L., Urban, R.M., 1994c. Corrosion of metallic implants. In: Stauffer, R.N. (Ed.), *Advances in Orthopaedic Surgery*, vol. 2. Mosby, St. Louis, pp. 279–319.
- Jacobs, J.J., Skipor, A.K., Doorn, P.F., Campbell, P., Schmalzried, T.P., Black, J., et al., August 1996. Cobalt and chromium concentrations in patients with metal on metal total hip replacements. *Clin. Orthop.* (329 Suppl. 1), S256–S263.

- Jacobs, J.J., Gilbert, J.L., Urban, R.M., February 1998. Corrosion of metal orthopaedic implants. *J. Bone Joint Surg. Am.* 80 (2), 268–282.
- Jacobs, J.J., Skipor, A.K., Patterson, L.M., Hallab, N.J., Paprosky, W.G., Black, J., et al., October 1998. Metal release in patients who have had a primary total hip arthroplasty. A prospective, controlled, longitudinal study. *J. Bone Joint Surg. Am.* 80 (10), 1447–1458.
- Jacobs, J.J., Silvertown, C., Hallab, N.J., Skipor, A.K., Patterson, L., Black, J., et al., January 1999. Metal release and excretion from cementless titanium alloy total knee replacements. *Clin. Orthop.* 358, 173–180.
- Jacobs, J., Goodman, S., Sumner, D.R., Hallab, N., 1999. Biologic response to orthopedic implants. In: *Orthopedic Basic Science*. American Academy of Orthopedic Surgeons, Chicago, pp. 402–426.
- Jacobs, J.J., Roebuck, K.A., Archibeck, M., Hallab, N.J., Glant, T.T., December 2001. Osteolysis: basic science. *Clin. Orthop.* (393), 71–77.
- Jacobs, J.J., Skipor, A.K., Patterson, L.M., Paprosky, W.G., Black, J., Galante, J.O., 2001b. A prospective, controlled, longitudinal study of metal release in patients undergoing primary total hip arthroplasty. *J. Bone Jt. Surg.*
- Jacobs, J.J., Urban, R.M., Hallab, N.J., Skipor, A.K., Fischer, A., Wimmer, M.A., February 2009. Metal-on-metal bearing surfaces. *J. Am. Acad. Orthop. Surg.* 17 (2), 69–76.
- Jasty, M., Bragdon, C., Jiranek, W., Chandler, H., Maloney, W., Harris, W.H., November 1994. Etiology of osteolysis around porous-coated cementless total hip arthroplasties. *Clin. Orthop.* (308), 111–126.
- Jones, L.C., Frondoza, C., Hungerford, D.S., 1999. Immunohistochemical evaluation of interface membranes from failed cemented and uncemented acetabular components. *J. Biomed. Mater. Res.* 48 (6), 889–898.
- Jones, D.M., Marsh, J.L., Nepola, J.V., Jacobs, J.J., Skipor, A.K., Urban, R.M., et al., April 2001. Focal osteolysis at the junctions of a modular stainless-steel femoral intramedullary nail. *J. Bone Joint Surg. Am.* 83-A (4), 537–548.
- Katz, J.L., January 3, 1980. Anisotropy of Young's modulus of bone. *Nature* 283 (5742), 106–107.
- Katz, J.L., 1980b. The structure and biomechanics of bone. *Symp. Soc. Exp. Biol.* 34, 137–168.
- Korenblat, P.E., 1992. *Contact Dermatitis*, second ed. W.B. Saunders Company, Philadelphia.
- Korovessis, P., Petsinis, G., Repanti, M., Repantis, T., June 2006. Metallosis after contemporary metal-on-metal total hip arthroplasty. Five to nine-year follow-up. *J. Bone Joint Surg. Am.* 88 (6), 1183–1191.
- Kuby, J., 1991. *Immunology*, second ed. W.H. Freeman and Company, New York.
- Kurtz, S.M., Hozack, W., Turner, J., Purtill, J., MacDonald, D., Sharkey, P., et al., October 2005. Mechanical properties of retrieved highly cross-linked crossfire liners after short-term implantation. *J. Arthroplast.* 20 (7), 840–849.
- Kwon, Y.M., Thomas, P., Summer, B., Pandit, H., Taylor, A., Beard, D., et al., April 2010. Lymphocyte proliferation responses in patients with pseudotumors following metal-on-metal hip resurfacing arthroplasty. *J. Orthop. Res.* 28 (4), 444–450.
- Kwon, Y.M., Lombardi, A.V., Jacobs, J.J., Fehring, T.K., Lewis, C.G., Cabanela, M.E., January 1, 2014. Risk stratification algorithm for management of patients with metal-on-metal hip arthroplasty: consensus statement of the American Association of Hip and Knee Surgeons, the American Academy of Orthopaedic Surgeons, and the Hip Society. *J. Bone Joint Surg. Am.* 96 (1), e4.
- Kwon, Y.M., Fehring, T.K., Lombardi, A.V., Barnes, C.L., Cabanela, M.E., Jacobs, J.J., November 2014. Risk stratification algorithm for management of patients with dual modular taper total hip arthroplasty: consensus statement of the American Association of Hip and Knee Surgeons, the American Academy of Orthopaedic Surgeons and the Hip Society. *J. Arthroplast.* 29 (11), 2060–2064.
- LaBerge, M., 1998. *Wear*. In: Black, J., Hastings, M.C. (Eds.), *Biomaterial Properties*. Chapman & Hall, London, pp. 364–405.
- Landgraaber, S., Samelko, L., McAllister, K., Putz, S., Jacobs, J.J., Hallab, N.J., 2018. CoCrMo alloy vs. UHMWPE particulate implant debris induces sex dependent aseptic osteolysis responses in vivo using a murine model. *Open Orthop. J.* 12, 115–124.
- Laquerriere, P., Grandjean-Laquerriere, A., Jallot, E., Balossier, G., Frayssinet, P., Guenounou, M., July 2003. Importance of hydroxyapatite particles characteristics on cytokines production by human monocytes in vitro. *Biomaterials* 24 (16), 2739–2747.
- Levine, B.R., Hsu, A.R., Skipor, A.K., Hallab, N.J., Paprosky, W.G., Galante, J.O., et al., March 20, 2013. Ten-year outcome of serum metal ion levels after primary total hip arthroplasty: a concise follow-up of a previous report*. *J. Bone Joint Surg. Am.* 95 (6), 512–518.
- Luckey, T.D., Venugopal, B., 1979. *Metal Toxicity in Mammals*. Plenum, NY.
- Maloney, W.J., Smith, R.L., Castro, F., Schurman, D.J., June 1993. Fibroblast response to metallic debris in vitro. Enzyme induction cell proliferation, and toxicity. *J. Bone Joint Surg. Am.* 75 (6), 835–844.
- Mariathasan, S., Monack, D.M., January 2007. Inflammasome adaptors and sensors: intracellular regulators of infection and inflammation. *Nat. Rev. Immunol.* 7 (1), 31–40.
- Mariathasan, S., Newton, K., Monack, D.M., Vucic, D., French, D.M., Lee, W.P., et al., July 8, 2004. Differential activation of the inflammasome by caspase-1 adaptors ASC and IPAF. *Nature* 430 (6996), 213–218.
- Martinon, F., Petrilli, V., Mayor, A., Tardivel, A., Tschopp, J., March 9, 2006. Gout-associated uric acid crystals activate the NALP3 inflammasome. *Nature* 440 (7081), 237–241.
- Masui, T., Sakano, S., Hasegawa, Y., Warashina, H., Ishiguro, N., May 2005. Expression of inflammatory cytokines, RANKL and OPG induced by titanium, cobalt-chromium and polyethylene particles. *Biomaterials* 26 (14), 1695–1702.
- Matheisen, E.B., Ahlbom, A., Bermann, G., Lindgren, J.U., 1995. Total hip replacement and cancer. *J. Bone Joint Surg. Br.* 77-B (3), 345–350.
- Matthews, J.B., Besong, A.A., Green, T.R., Stone, M.H., Wroblewski, B.M., Fisher, J., et al., November 2000. Evaluation of the response of primary human peripheral blood mononuclear phagocytes to challenge with in vitro generated clinically relevant UHMWPE particles of known size and dose. *J. Biomed. Mater. Res.* 52 (2), 296–307.
- McKee, G.K., Watson-Farrar, J., 1943. Replacement of the arthritic hips to the McKee-Farrar replacement. *J. Bone Joint Surg. Br.* 48, 245.
- McKellop, H., Park, S.H., Chiesa, R., Doorn, P., Lu, B., Normand, P., et al., August 1996. In vivo wear of three types of metal on metal hip prostheses during two decades of use. *Clin. Orthop.* (329 Suppl. 1), S128–S140.
- McKellop, H., Shen, F.W., Lu, B., Campbell, P., Salovey, R., December 2000. Effect of sterilization method and other modifications on the wear resistance of acetabular cups made of ultra-high molecular weight polyethylene. A hip-simulator study. *J. Bone Joint Surg. Am.* 82-A (12), 1708–1725.

- McKenzie Alvin, H., 1995. Fernström intervertebral disc arthroplasty: a long-term evaluation. *Orthod. Int. Ed.* 3B, 313–324.
- Medzhitov, R., July 24, 2008. Origin and physiological roles of inflammation. *Nature* 454 (7203), 428–435.
- Merritt, K., Brown, S., 1980. Tissue reaction and metal sensitivity. *Acta Orthop. Scand.* 51, 403–4111.
- Michel, R., Hoffman, J., Loer, F., Zilkens, J., 1984. Trace element burdening of human tissue due to corrosion of hip-joint prostheses made of cobalt-chromium alloys. *Arch. Orthop. Trauma Surg.* 103, 85–95.
- Milosev, I., Trebse, R., Kovac, S., Cor, A., Pisot, V., June 2006. Survivorship and retrieval analysis of Sikomet metal-on-metal total hip replacements at a mean of seven years. *J. Bone Joint Surg. Am.* 88 (6), 1173–1182.
- Minoda, Y., Kobayashi, A., Iwaki, H., Miyaguchi, M., Kadoya, Y., Ohashi, H., et al., October 2005. Polyethylene wear particle generation in vivo in an alumina medial pivot total knee prosthesis. *Biomaterials* 26 (30), 6034–6040.
- Moore, A.T., 1943. Metal hip joint : a case report. *J. Bone Joint Surg. Am.* 25, 688.
- Nagaya, T., Ishikawa, N., Hata, H., January 1989. Sister chromatid exchange analysis in lymphocytes of workers exposed to hexavalent chromium. *Br. J. Ind. Med.* 46 (1), 48–51.
- Nalepka, J.L., Lee, M.J., Kraay, M.J., Marcus, R.E., Goldberg, V.M., Chen, X., et al., October 2006. Lipopolysaccharide found in aseptic loosening of patients with inflammatory arthritis. *Clin. Orthop. Relat. Res.* 451, 229–235.
- Nyren, O., McLaughlin, J.K., Anders-Ekbom, G.G., Johnell, O., Fraumeni, A.H., 1995. Cancer risk after hip replacement with metal implants: a population-based cohort study in Sweden. *J. Natl. Cancer Inst.* 87, 28–33.
- Pare, P.E., Chan, F., Powell, M.L., Mathews, H.H., May 14, 2007. Wear characterization of the MAVERICK total disc replacement. In: *Trans 7th Annual Meeting Spine Arthroplasty Society*, p. 59.
- Petrilli, V., Dostert, C., Muruve, D.A., Tschopp, J., December 2007. The inflammasome: a danger sensing complex triggering innate immunity. *Curr. Opin. Immunol.* 19 (6), 615–622.
- Popoola, O.O., Shen, M., Heller, M., Seebeck, J., May 14, 2007. In vitro wear of UHMWPE inlays in Dynardi and Prodisc spine disc replacement implants. In: *Trans 7th Annual Meeting Spine Arthroplasty Society*, p. 49 Berlin.
- Rader, C.P., Sterner, T., Jakob, F., Schutze, N., Eulert, J., October 1999. Cytokine response of human macrophage-like cells after contact with polyethylene and pure titanium particles. *J. Arthroplast.* 14 (7), 840–848.
- Ramachandran, R., Goodman, S.B., Smith, R.L., June 1, 2006. The effects of titanium and polymethylmethacrylate particles on osteoblast phenotypic stability. *J. Biomed. Mater. Res. A* 77 (3), 512–517.
- Ricciardi, B.F., Nocon, A.A., Jerabek, S.A., Wilner, G., Kaplowitz, E., Goldring, S.R., et al., 2016. Histopathological characterization of corrosion product associated adverse local tissue reaction in hip implants: a study of 285 cases. *BMC Clin. Pathol.* 16, 3.
- Ring, P.A., 1968. Complete replacement arthroplasty of the hip by the Ring prosthesis. *J. Bone Joint Surg. Br.* 50, 720.
- Rooker, G.D., Wilkinson, J.D., 1980. Metal sensitivity in patients undergoing hip replacement. A prospective study. *J. Bone Jr. Surg.* 62-B (4), 502–505.
- Saikko, V., Caloni, O., Keranen, J., 2002. Wear of conventional and cross-linked ultra-high-molecular-weight polyethylene acetabular cups against polished and roughened CoCr femoral heads in a biaxial hip simulator. *J. Biomed. Mater. Res.* 63 (6), 848–853.
- Samelko, L., Caicedo, M.S., Lim, S.J., la-Valle, C., Jacobs, J., Hallab, N.J., 2013. Cobalt-alloy implant debris induce HIF-1alpha hypoxia associated responses: a mechanism for metal-specific orthopedic implant failure. *PLoS One* 8 (6), e67127.
- Savarino, L., Stea, S., Granchi, D., Visentin, M., Ciapetti, G., Donati, M.E., et al., 2000. Sister chromatid exchanges and ion release in patients wearing fracture fixation devices. *J. Biomed. Mater. Res.* 50 (1), 21–26.
- Schmalzried, T.P., Wessinger, S.J., Hill, G.E., Harris, W.H., June 1994. The Harris-Galante porous acetabular component press-fit without screw fixation. Five-year radiographic analysis of primary cases. *J. Arthroplast.* 9 (3), 235–242.
- Secher, L., Svejgaard, E., Hansen, G.S., November 1977. T and B lymphocytes in contact and atopic dermatitis. *Br. J. Dermatol.* 97 (5), 537–541.
- Shanbhag, A.S., Jacobs, J.J., Black, J., Galante, J.O., Glant, T.T., 1994. Macrophage/particle interactions. Effect of size, composition and surface area. *J. Biomed. Mater. Res.* 28, 81–90.
- Shanbhag, A.S., Jacobs, J.J., Black, J., Galante, J.O., Glant, T.T., 1995. Human monocyte response to particulate biomaterials generated in vivo and in vitro. *J. Orthop. Res.* 13, 792–801.
- Shanbhag, A.S., Hasselman, C.T., Jacobs, J.J., Rubash, H.E., 1998. Biological response to wear debris. In: *Callaghan, J.J., Rosenberg, A.G., Rubash, H. (Eds.), The Adult Hip*. Lippincott-Raven Publishers, Philadelphia, pp. 279–288.
- Sieving, A., Wu, B., Mayton, L., Nasser, S., Wooley, P.H., March 1, 2003. Morphological characteristics of total joint arthroplasty-derived ultra-high molecular weight polyethylene (UHMWPE) wear debris that provoke inflammation in a murine model of inflammation. *J. Biomed. Mater. Res.* 64A (3), 457–464.
- Soloviev, A., Schwarz, E.M., Darowish, M., O'Keefe, R.J., November 2005. Sphingomyelinase mediates macrophage activation by titanium particles independent of phagocytosis: a role for free radicals, NFkappaB, and TNFalpha. *J. Orthop. Res.* 23 (6), 1258–1265.
- Stillwell, W.T., 1987. *The Art or Total Hip Arthroplasty*. Grune & Stratton, Inc., Orlando.
- Stulberg, B.N., Merritt, K., Bauer, T., 1994. Metallic wear debris in metal-backed patellar failure. *J. Biomed. Mat. Res. Appl. Biomater.* 5, 9–16.
- Svejgaard, E., Morling, N., Svejgaard, A., Veien, N.K., 1978. Lymphocyte transformation induced by nickel sulphate: an in vitro study of subjects with and without a positive nickel patch test. *Acta Derm. Venereol.* 58 (3), 245–250.
- Taguchi, T., Mitcham, J.L., Dower, S.K., Sims, J.E., Testa, J.R., March 15, 1996. Chromosomal localization of TIL, a gene encoding a protein related to the Drosophila transmembrane receptor Toll, to human chromosome 4p14. *Genomics* 32 (3), 486–488.
- Thompson, G.J., Puleo, D.A., 1995. Effects of sublethal metal ion concentrations on osteogenic cells derived from bone marrow stromal cells. *J. Appl. Biomater.* 6 (4), 249–258.
- Ting, J.P., Willingham, S.B., Bergstralh, D.T., May 2008. NLRs at the intersection of cell death and immunity. *Nat. Rev. Immunol.* 8 (5), 372–379.
- Tipper, J.L., Hatton, A., Nevelos, J.E., Ingham, E., Doyle, C., Streicher, R., et al., August 2002. Alumina-alumina artificial hip joints. Part II: characterisation of the wear debris from in vitro hip joint simulations. *Biomaterials* 23 (16), 3441–3448.
- Urban, R.M., Jacobs, J.J., Tomlinson, M.J., Gavrilovic, J., Andersen, M., 1995. *Migration of Corrosion Products from the Modular Head Junction to the Polyethylene Bearing Surface and Interface Membranes of Hip Prostheses*. Raven Press, New York.

- Urban, R.M., Jacobs, J.J., Sumner, D.R., Peters, C.L., Voss, F.R., Galante, J.O., 1996a. The bone-implant interface of femoral stems with non-circumferential porous coating: a study of specimens retrieved at autopsy. *J. Bone Joint Surg. Am.* 78-A (7), 1068–1081.
- Urban, R.M., Jacobs, J.J., Tomlinson, M.J., Black, J., Turner, T.M., Sauer, P.A., et al., 1996b. Particles of metal alloys and their corrosion products in the liver, spleen and para-aortic lymph nodes of patients with total hip replacement prosthesis. *Orthop. Trans.* 19, 1107–1108.
- Urban, R.M., Jacobs, J., Gilbert, J.L., Rice, S.B., Jasty, M., Bragdon, C.R., et al., 1997. Characterization of solid products of corrosion generated by modular-head femoral stems of different designs and materials. In: Marlowe, D.E., Parr, J.E., Mayor, M.B. (Eds.), *STP 1301 Modularity of Orthopedic Implants*. ASTM, Philadelphia, pp. 33–44.
- Urban, R.M., Hall, D.J., Sapienza, C.I., Jacobs, J.J., Sumner, D.R., Rosenberg, A.G., et al., 1998. A comparative study of interface tissues in cemented vs. cementless total knee replacement tibial components retrieved at autopsy. *Trans. SFB* 21.
- Urban, R.M., Jacobs, J.J., Tomlinson, M.J., Gavrilovic, J., Black, J., Peoc'h, M., April 2000. Dissemination of wear particles to the liver, spleen, and abdominal lymph nodes of patients with hip or knee replacement. *J. Bone Joint Surg. Am.* 82 (4), 457–476.
- van, O.A., Kurtz, S.M., Stessels, F., Noten, H., van Rhijn, L., January 15, 2007. Polyethylene wear debris and long-term clinical failure of the Charite disc prosthesis: a study of 4 patients. *Spine* 32 (2), 223–229.
- Veien, N.K., Svejgaard, E., August 1978. Lymphocyte transformation in patients with cobalt dermatitis. *Br. J. Dermatol.* 99 (2), 191–196.
- Veien, N.K., Svejgaard, E., Menne, T., 1979. In vitro lymphocyte transformation to nickel: a study of nickel-sensitive patients before and after epicutaneous and oral challenge with nickel. *Acta Derm. Venereol.* 59 (5), 447–451.
- Venable, C.S., Stuck, W.G., Beach, A., 1937. The effects on bone of the presence of metals; based upon electrolysis. An experimental study. *Ann. Surg.* 105, 917.
- Vermes, C., Glant, T.T., Hallab, N.J., Fritz, E.A., Roebuck, K.A., Jacobs, J.J., December 2001. The potential role of the osteoblast in the development of periprosthetic osteolysis: review of in vitro osteoblast responses to wear debris, corrosion products, and cytokines and growth factors. *J. Arthroplast.* 16 (8 Suppl. 1), 95–100.
- Vermes, C., Chandrasekaran, R., Jacobs, J.J., Galante, J.O., Roebuck, K.A., Glant, T.T., February 2001. The effects of particulate wear debris, cytokines, and growth factors on the functions of MG-63 osteoblasts. *J. Bone Joint Surg. Am.* 83 (2), 201–211.
- Visuri, T., Koskenvuo, M., 1991. Cancer risk after Mckee-Farrar total hip replacement. *Orthopedics* 14, 137–142.
- von Knoch, M., Engh, C.A.S., Sychterz, C.J., Engh, C.A.J., Willert, H.G., January 2000. Migration of polyethylene wear debris in one type of uncemented femoral component with circumferential porous coating: an autopsy study of 5 femurs. *J. Arthroplast.* 15 (1) 72–815(1):72-8.
- Walker, P.S., 1978. *Human Joints and Their Artificial Replacements*. Charles C Thomas, Springfield.
- Wiles, P., 1953. The surgery of the osteoarthritic hip. *Br. J. Surg.* 45, 488.
- Willert, H.G., Semlitsch, M., 1977. Reactions of the articular capsule to wear products of artificial joint prostheses. *J. Biomed. Mater. Res.* 11, 157–164.
- Willert, H.G., Bertram, H., Buchhorn, G.H., September 1990. Osteolysis in alloarthroplasty of the hip. The role of ultra-high molecular weight polyethylene wear particles. *Clin. Orthop.* (258), 95–107.
- Wilson, J.N., Scales, J.T., September 1970. Loosening of total hip replacements with cement fixation. Clinical findings and laboratory studies. *Clin. Orthop.* 72, 145–160.
- Wimmer, M., Berzins, A., Kuhn, H., Bluhm, A., Nassutt, R., Schneider, E., et al., 1998. Presence of multiple wear directions in autopsy retrieved acetabular components. *Trans. ORS* 23.
- Wroblewski, B.M., Siney, P.D., Dowson, D., Collins, S.N., March 1996. Prospective clinical and joint simulator studies of a new total hip arthroplasty using alumina ceramic heads and cross-linked polyethylene cups. *J. Bone Joint Surg. Br.* 78 (2), 280–285.
- Yao, J., Glant, T.T., Lark, M.W., Mikecz, K., Jacobs, J.J., Hutchinson, N.I., et al., September 1995. The potential role of fibroblasts in periprosthetic osteolysis: fibroblast response to titanium particles. *J. Bone Miner. Res.* 10 (9), 1417–1427.
- Zhang, K., Yang, S.Y., Yang, S., Bai, L., Li, P., Liu, D., et al., January 2015. Different influence of Ti, PMMA, UHMWPE, and Co-Cr particles on peripheral blood monocytes during periprosthetic inflammation. *J. Biomed. Mater. Res. A* 103 (1), 358–364.
- Zywiel, M.G., Cherian, J.J., Banerjee, S., Cheung, A.C., Wong, F., Butany, J., et al., January 2016. Systemic cobalt toxicity from total hip arthroplasties: review of a rare condition Part 2. measurement, risk factors, and step-wise approach to treatment. *Bone Joint Lett.* J. 98-B (1), 14–20.

Chapter Study Questions

- (1) What are the general mechanical property qualifications for orthopedic biomaterials and what are the major categories of orthopedic implants?

Answer: Generally orthopedic implants must be capable of high strength, fracture toughness, and most importantly corrosion resistance. The two major kinds of orthopedic implants are bone fixation or total joint arthroplasty (to a less extent new kinds of dynamic stabilization devices with articulating components are slowly making their way into the market).

- (2) (A) What is the primary problem associated with the longevity of current total joint replacement implants and why? (B) How could this be solved by improved biomaterials?

Answer: (A) Particle and wear debris generation at the articulating surfaces of total joint replacements causes aseptic loosening of the implants through the induction of inflammation around the implant (macrophage-particle overload) which causes a decreased production of new bone and increased bone resorption. (B) More wear-resistant materials at the articulating surface while maintaining current available levels of other mechanical properties.

- (3) What are the primary cytokines associated with particle-induced osteolysis and what is the primary cell type involved in this process.

Answer: The primary cytokines associated with osteolysis are TNF-alpha, IL-6, IL-1beta, prostaglandin E₂, etc. produced by macrophage interaction with particulate debris from implants.

- (4) Name six of the primary orthopedic implant biomaterials?

Answer: (A) Co-base alloys, Ti-base alloys, stainless steel, PMMA, UHMWPE, and alumina.

- (5) Name one new orthopedic biomaterial and why it was introduced (i.e., what specific problem/deficit is it attempting to solve?).

Answer: Zirconium alloy was introduced to decrease the amount of metallic wear debris being generated at the bearing surface and as an alternative metal less likely to induce hypersensitivity reactions because of its corrosion resistance and less common presence environmentally.

- (6) What is one way in which current designs of orthopedic implants are creating more challenging conditions for biomaterials to overcome and why?

Answer: Orthopedic implant component modularity (more components that fit together in vivo) is creating more interfacial surfaces from which implant debris can be generated through fretting corrosion (micromotion) that interact both locally and systemically.

2.5.5

Dental Applications

DAVID H. KOHN¹, JACK E. LEMONS²

¹Departments of Biologic and Materials Sciences, and Biomedical Engineering, The University of Michigan, Ann Arbor, MI, United States

²Schools of Dentistry, Medicine and Engineering University of Alabama at Birmingham, Birmingham, AL, United States

Overview

The mouth is the gateway to the body. Links between oral and systemic health are widely accepted and compromises in general health are correlated with loss of oral dentition. Almost 20% of the US population older than 65 years is totally edentulous. A substantial number of other patients are partially edentulous, having an average of 10 missing teeth, and 50% of adults ages 20–64 has at least one missing tooth (Dye et al., 2015). In addition, 15% of the US population has periodontal disease severe enough to warrant surgery, 15 million people experience temporomandibular joint (TMJ) disorders, 30,000 patients a year undergo craniofacial resection surgery, and 4 million suffer from salivary gland disorders (Scheller et al., 2009). Collectively, more than 85% of the world's population requires repair or replacement of a dental, oral, or craniofacial (DOC) tissue.

Defects in DOC tissues resulting from disease, trauma, congenital abnormalities, or tumor resection present a challenge to clinicians, and replacement or restoration of these tissues is a subject of clinical, basic science and engineering concern. In addition to leaving patients with aesthetic deformities, defects in DOC tissues may be uncomfortable to the patient and affect function. Therefore structure, function, aesthetics, and pain must be managed and present challenges to biomaterial design that can be more complex than in other parts of the body.

Biomaterials scientists and engineers working in the DOC space have developed a wide range of solutions to manage loss of DOC tissue structure and function. In this chapter, we will start with a discussion of some of the unique needs in managing DOC problems and designing materials for DOC use. We will then provide an overview of restorative materials, followed by more in-depth discussions of dental implants and tissue-engineered medical products used in dentistry, two areas most relevant to biomedical engineers working in dentistry. Lastly, we will

discuss how biomaterials in dentistry have informed other areas of biomaterials and have played a central role in their discipline.

Unique Needs in Developing Biomaterials for DOC Procedures

Replacement, reconstruction, and regeneration of DOC tissues require the synthesis of engineering, biology, and clinical sciences. The tissues of the DOC region are complex and developing biomaterials for functional replacement of these tissues presents many unique design challenges. In the DOC region, maintaining or restoring aesthetics, in addition to restoring structure and function, presents a more complex design problem than in other regions of the body. In designing biomaterials for use in the oral microenvironment, it is also necessary to consider the microbial environment and the potentially altered host immune response. It is rare that a single DOC tissue needs to be replaced; rather, multiple tissues are usually in need of replacement. The tooth, for example, consists of multiple mineralized tissues (enamel and dentin) surrounding a pulpal cavity that contains vasculature and innervation. Within the mineralized tissue compartment of the tooth, there is an elegant functionally graded transition from enamel to dentin (the dentin–enamel junction). There are also important developmental differences between the craniofacial and axial skeleton; the craniofacial bones are formed by intramembranous ossification, whereas bones of the axial skeleton are formed via endochondral ossification. Thus tissue-engineering strategies that seek to mimic aspects of developmental biology may need to be optimized specifically for DOC applications.

Restorative Materials

Restorative dental materials, or materials used to reconstruct all or part of teeth, have played a prominent role in health

care for several thousand years and the development of dental materials has progressed more rapidly than other areas of biomaterials. The oral environment is one of the harshest environments in the body and is subjected to high and varying forces, fluctuating pH and temperature, and bacteria. Knowledge of biomaterials science and engineering is therefore critical for the selection, processing, and function of restorative materials.

Restorative materials may be direct (restoration is inserted directly into the tooth) or indirect (restoration is fabricated outside of the mouth). A wide range of materials falls under the umbrella of restorative dental materials, including amalgams, composites, cements, crowns, bridges, inlays, liners, varnishes, orthodontic materials, dentures, impressions, and investment materials. Specific classes of materials used for these applications include metals (silver–mercury amalgam alloys, noble metal inlays and crowns, base metal alloy partial dentures and crowns), ceramics (porcelain denture teeth, gypsum investments), polymers (acrylics for dentures, alginates for impressions), and composites (methacrylates reinforced with silica). About 75% of a general dentist's practice involves the use of restorative materials and there are many textbooks dedicated solely to restorative materials (Sakaguchi et al., 2018).

Composite materials, consisting of inorganic particulate fillers dispersed in a cross-linked polymeric continuous phase, have displaced amalgams as primary restorative materials because of their improved aesthetic properties and mercury-centered toxicity concerns associated with amalgams. Composite restoratives are typically processed in situ by photopolymerization whereby a filled resin (typically a methacrylate) is placed in the patient's mouth and irradiated with visible light, generating reactive species that initiate polymerization and harden the material. Filler particles are manufactured from silica (quartz, glass, fumed or colloidal silica) and range in size from 20 nm to 10 μm . The volume fraction of particles ranges from 50% to 85% and influences mechanical properties (stiffness, strength, fracture toughness, and wear), polymerization shrinkage, and the handling characteristics of the composite, an important factor in a composite's acceptance by clinicians.

Polymerization is accompanied by a significant amount of volumetric shrinkage and associated shrinkage stress, leading to localized debonding from the tooth, marginal gap formation, tooth deflection, and tooth cracking. Mitigation of polymerization-induced shrinkage and/or the concomitant stress is a primary area of research in dental biomaterials, and has been explored using an array of approaches, including low shrinkage ring-opening polymerization chemistries, modification of the in situ processing, polymerization-induced phase separation, thiol–ene-based polymerization, and allyl sulfide-based addition–fragmentation chain transfer (Cramer et al., 2011).

In addition to reducing shrinkage, other key research needs are reducing wear and increasing the longevity of the bond between the hydrophobic biomaterial and hydrophilic tooth structure. As the population ages, restorations for exposed

root surfaces are on the rise. With an aging population, chronic diseases are increasing and medically compromised patients present additional challenges. Nanotechnology and biofabrication may help overcome these challenges.

Dental Implants

Although removable dentures and fixed partial dentures offer effective treatments for many edentulous patients, those who have lost substantial tooth-bearing portions of bone and cannot manage prostheses or chew properly can improve their oral function through the use of dental implants. There are now 5 million dental implants inserted each year. Dental implants provide long-term (15 years) support for restorations. To design clinically effective dental implants, an understanding of the parameters governing the long-term success of the biomaterial/tissue composite system is needed. A requirement for dental implants to be successful is adequate bone (width, height, length, contour, and density) to support the implant.

Dental implants are classified into three categories:

1. Endosseous implants are embedded in mandibular or maxillary bone and project through the oral mucosa covering the edentulous ridge.
2. Subperiosteal implants rest on the surface of the bone beneath the periosteum.
3. Transosseous implants penetrate the inferior mandibular border and also project through the oral mucosa covering the edentulous ridge.

Root-form endosseous implants are the most common implants in clinical practice (Figs. 2.5.5.1 and 2.5.5.2). Early dental implants were primarily uniblock (single piece) systems combined with removable, fixed, or fixed–removable intra-oral prosthetics. Many implant biomaterials and designs have been studied; however, the larger numbers of applications have now become root-form designs placed, restored, and maintained for function through osseointegrated interfaces with



• Figure 2.5.5.1 Root-form type designs.

bone. The most common root-form implant is the two-stage endosteal screw-type implant. The implant is inserted first and the abutment and prosthetic components are assembled after a controlled period of postsurgical healing of bone and soft tissues. Access to the oral regions and the number of teeth per individual result in larger numbers of dental implants in use compared to other types of implant-based treatments for musculoskeletal disorders, such as hip and knee replacements. The biomaterials are now mostly titanium and alloys with a wide range of surface modifications for influencing interfacial tissue regions. Surface modifications include compositional (primarily oxides, calcium phosphates, and fluoride) and microtopographical features (degrees of roughness). These concepts also extend to the gingival and mucosal soft tissue to



• **Figure 2.5.5.2** Radiograph of root-form implants supporting intraoral bridge reconstructions.

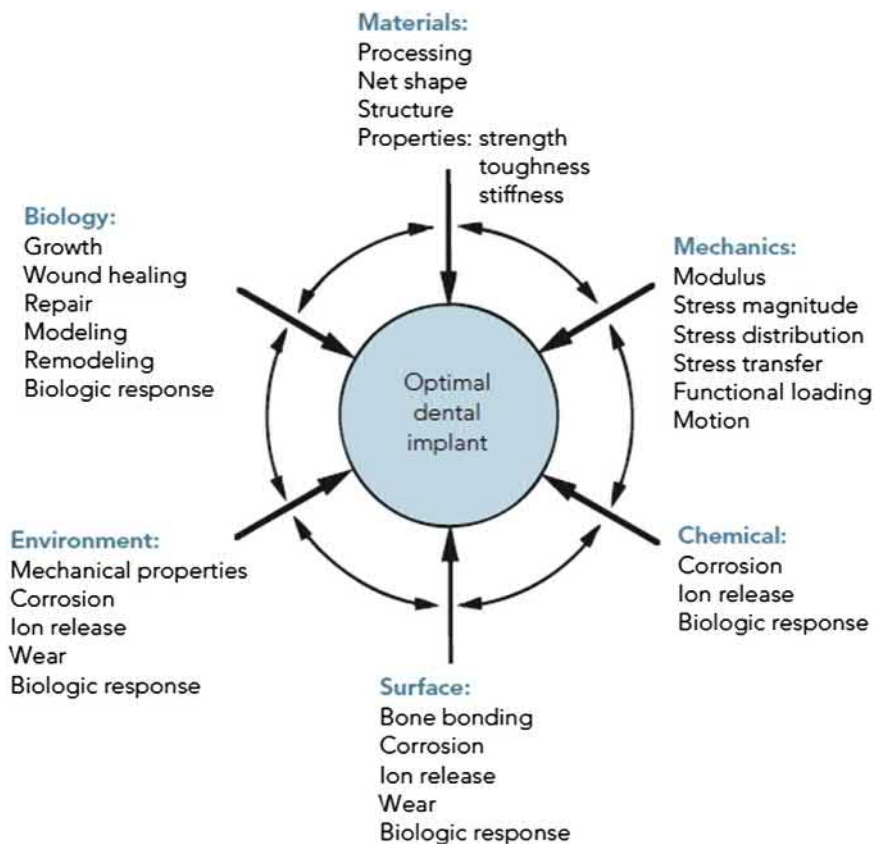
implant interfacial systems. Success rates for implants placed in the mandible are approximately 95% at 5 years and greater than 85% at 15 years. For maxillary implants, success rates are approximately 85%–90% at 5 years and 80% at 15 years (Kohn, 2008).

Criteria for Successful Implant Function

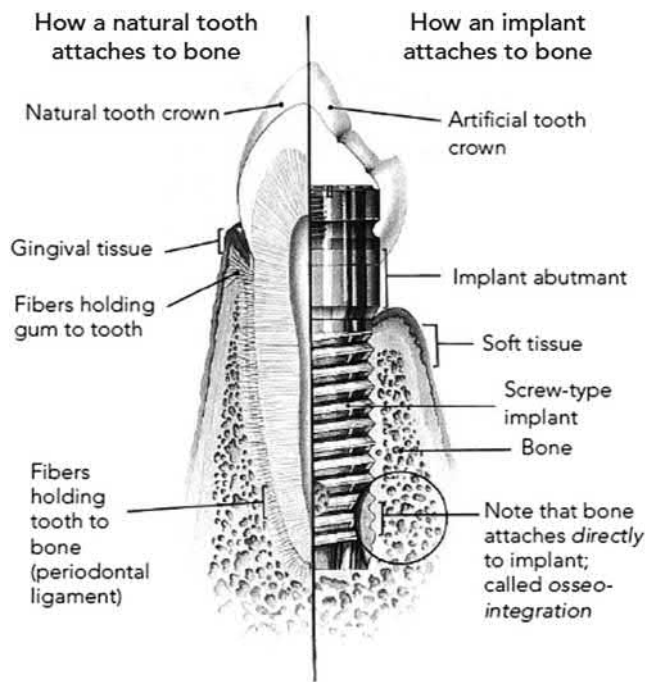
A clinically successful implant is guided by: (1) the implant material(s), (2) healing and remodeling of the adjacent tissues, and (3) the interfacial zone between the implant and tissue. In a well-functioning, stable implant, the interfacial zone is composed of a thin (<100 μm) layer of metal oxide, proteins, and connective tissue. The thickness of the interfacial zone affects interfacial integrity. Mechanical stability and integrity of the implant–tissue interface depend on material, mechanical, chemical, surface, biologic, and local environmental factors, all of which change as functions of time in vivo (Fig. 2.5.5.3). Implant success also depends on the patient's overall medical and dental status, surgical techniques, and the extent and kinetics of healing.

Osseointegration and Accelerating Healing and Attachment to Tissue

Unlike many biomaterials, which replace as much of a tissue's natural structure and function as possible, dental



• **Figure 2.5.5.3** Interdependent biomaterials factors that affect the success of dental implants. (Reprinted with permission from Kohn, D.H., 2008. Implant and bone augmentation materials. In: O'Brien, W.J. (Ed.), *Dental Materials and Their Selection*, fourth ed. pp. 300–312. Quintessence.)



• **Figure 2.5.5.4** Schematic of natural tooth versus implant attachment to bone. (Reprinted with permission from Taylor, T.D., 1990. *Dental Implants: Are They for Me?* Quintessence.)

implants do not restore function by mimicking the function of the periodontal ligament (PDL), which attaches the tooth to bone and absorbs forces of mastication (Fig. 2.5.5.4). Instead, osseointegration, or the direct structural and functional connection between ordered, living bone and the surface of a load-carrying implant, is what occurs with a well-functioning implant. This definition was originally based on retrospective radiographic and light microscopic observations of retrieved implants, and has since been modified based on scanning and transmission electron microscopic analyses and observations across multiple length scales (Palmquist, 2018).

Examination of implant/tissue interfaces from a wide range of implant materials, including steel, gold, platinum, and cobalt alloys, showed fibrous soft tissue (scar-like) at the interfaces where higher magnitude loads were transferred (Lemons, 1999). These zones were relatively dense collagenous structures that contained limited numbers of cells and blood vessels. In contrast, implants fabricated from higher purity aluminum oxides (alumina and sapphire forms), carbons, calcium phosphate compounds, and reactive group metals and alloys (primarily titanium) demonstrated a mixture of direct bone-to-implant contact and soft tissues when evaluated histologically by optical microscopy methods. These interfacial conditions were described as osseointegrated, and material and fabrication methods to routinely achieve osseointegration were developed.

The current definition of osseointegration is fundamentally the same: host bone responds in a safe, predictable, and versatile manner to surgical placement of an implant in a sterile wound, with healing sequelae leading to interfacial osteogenesis and mechanical stability of the implant.

In a well-functioning implant, following these short-term (4–6 months) events, a stable marginal bone level is maintained. In comparison, poorly differentiated connective tissue adjacent to an implant leads to mobility and implant failure.

To function appropriately, a dental implant must carry occlusal stresses, transfer the stresses across the implant–tissue interface, and transmit them to the adjacent bone. Stresses should be of a “correct” orientation and magnitude so that they mimic physiologic stresses and allow tissue viability to be maintained. The ability to transmit stress from implant to bone depends on achieving interfacial fixation. Thus two design goals are to stabilize the interface in as short a time postoperatively as possible and have the interface remain stable for as long a time as possible. “Stability” is defined as the maximum allowable displacement at an implant–tissue interface that will still result in osseointegration and bone maintenance, and motion of an implant less than 100–200 μm is considered most conducive to creating and maintaining osseointegration. Because a stable interface must be developed before loading, it is desirable to accelerate tissue apposition to implant surfaces. Material developments that have been implemented in clinical practice include the use of surface-roughened implants, nanostructured surfaces, bioactive ceramic coatings, bone grafting, recombinant growth factors, platelet-rich plasma, antimicrobial coatings, and bisphosphonate- and other drug-eluting coatings (Kohn, 2018; Rasouli et al., 2018; Qin et al., 2018; Alenezi et al., 2018; Kellesarian et al., 2017).

Analysis of the interface zone at nano-, micro-, and macro-levels of resolution demonstrates the importance of controlling implant bulk and surface properties, surgical methods, site dimensions, times and conditions of intraoral abutment and restoration placement, and maintenance (cleaning) of the percutaneous transition zone. As an example of the importance of biomaterial properties, if unit area of implant, bone, and force are modeled, the interfacial strain magnitude will depend on the magnitude and direction of applied forces, the roughness of the contact zone, attachment (bonding), and the elastic moduli of the implant and bone. Most ceramics, such as alumina, zirconia, and titania, and most surface-oxidized metals have contact with bone, but minimal or no chemical bonding. Roughening the implant surface, which leads to an increase in surface area, provides conditions for accelerating early healing (blood clotting, fibrin deposition, integrin binding) and microscopic interdigitation with bone, leading to increased force transfer and resistance to microscopic shear at the interface. If the interface is noninterdigitated and nonchemically bonded, stress magnitudes of each constituent in the contact zone will be proportional to the elastic modulus of the constituent. Relative to compact bone, alumina and zirconia have moduli more than 10 \times , metals 5–10 \times , with unalloyed titanium having the lower magnitude and calcium phosphates about 0.5–2 \times .

Surface Topology and Chemistry

A variety of implant surface configurations can improve the cohesiveness of the implant–tissue interface. Alterations in surface topology can decrease relative motion and fibrous integration in the short term, increasing transfer of occlusal loads to tissue, which can help minimize loosening in the long term. Implant surfaces may be smooth, textured, screw threaded, or coated. Textured surfaces can be created by adding (plasma spraying) or subtracting surface layers (acid etching, grit blasting). Osseointegration around screw-threaded implants occurs through tissue ongrowth, or apposition of tissue to the implant surface. Tissue ingrowth into roughened or 3D surface layers yields higher bone–implant shear strength than other types of fixation. Increased interfacial shear strength results in a better stress transfer from the implant to the surrounding bone, a more uniform stress distribution between the implant and bone, and lower stresses in the implant.

Understanding implant surface chemistry is important to ensure that the biomaterials do not adversely affect local and systemic tissues and organs, and that the *in vivo* environment does not degrade the biomaterial and compromise its function. The success of any implant depends on its bulk and surface properties. The surface of a biomaterial is frequently different in chemical composition and morphology than the bulk material. These differences arise from the molecular arrangement, surface reactions, and contamination at the surface. For metal implants, interface chemistry is determined by the properties of the metal oxide, not by the metal itself. Metallic oxides dictate interactions between cells and proteins and the implant surface, and are continually altered by the diffusion of oxygen and metal ions. The surface potential of the implant also affects osseointegration; metal oxides with low dielectric constants promote the migration of cells to an implant surface.

Metals are more susceptible to electrochemical degradation than ceramics. Therefore a fundamental criterion for choosing a metallic implant material is that it elicits a minimal biologic response. Titanium-based materials are well tolerated by the body because of their passive oxide layers, and alloying elements can be tolerated by the body in trace amounts. Larger concentrations of many metal ions usually cannot be tolerated. Therefore minimizing mechanical and chemical breakdown of implant biomaterials is a primary design criterion, and is achieved by material selection and design. Anodization is an electrochemical process in which current is applied to the implant while immersed in an electrolyte, resulting in a thickened oxide layer. Laser treatment of implant surfaces serves as a secondary means of sterilization and altering surface energy.

Mechanical Parameters and Implant Design

Mechanical properties important in designing implant materials include stiffness, yield, ultimate and fatigue strengths, and fracture toughness. Stiffness (modulus) dictates the ability of the implant to transmit stresses to the adjacent tissue. Selecting materials with high static and fatigue strength is important to avoid material failure. Fracture toughness

is a measure of the energy needed to cause fracture in the presence of a defect and is a critical parameter in designing biomaterials with surface topologies that could serve as sites of stress concentration.

Material failure of implants, generally by fatigue, does occur. Fatigue of implants is clinically important and fatigue properties of implant materials should be included in implant design. The stress distribution in an implant and surrounding tissue depends on the section size of the implant and the elastic moduli of the implant material and tissue. Use of larger, stiffer implants can reduce the probability of mechanical failure, but may compromise stress transfer to the tissue.

The design of dental implants is based on several factors, including the geometry of the implant (length, diameter, macroscopic and microscopic shapes), how the geometry affects mechanical properties, stress distribution, and the initial and long-term stability of the implant–tissue interface. Implants can be designed to: (1) maximize strength, (2) maximize interfacial stability, or (3) maximize load transfer, with each of these criteria a function of material and interfacial properties. Two goals of any implant design are to maximize initial stability to achieve osseointegration in as short a time as possible following implant placement, and minimize loosening (maintain osseointegration for as long a time as possible following achievement of stability).

Dental implants are subjected to axial, shear, bending, and torsional forces in service. In addition to the magnitude of the force, the direction must also be considered in the design process. Given the complex loading patterns a dental implant is subjected to and range of displacements that are considered “stable,” the time at which an implant can begin to undergo loading is implant and location specific. Quantifying stresses and strains in implants, tissues, and implant–tissue interfaces is therefore important for implant design and understanding adaptation of tissue around an implant. Implant geometry, elastic properties, loading, boundary conditions, interface conditions, and local stresses and strains are all important in this regard.

Materials Used in Dental Implants

Two classes of materials—metals and ceramics—are used to manufacture dental implants, either alone or in hybrid fashion. Metallic implant materials are largely titanium based, either commercially pure titanium (CPTi) or Ti-6Al-4V alloy. The synergistic relationship among processing, composition, structure, and properties of both the bulk materials and their surfaces provides clinicians with implants having an array of properties. Processing conditions, such as casting, forging, and machining of metal implants, densification of ceramics, deposition of ceramic and metal coatings onto metal implants, as well as cleaning and sterilization procedures, can all alter the microstructure, surface chemistry, and properties. Biomaterials used for the construction of dental implant systems are summarized in [Tables 2.5.5.1–2.5.5.3](#). This summary includes the nominal bulk compositions, mechanical properties, and surface conditions as described in national and international standards.

TABLE 2.5.5.1 Engineering Properties of Metals and Alloys Used for Surgical Implants^a

Material	Nominal Composition (w/o)	Modulus of Elasticity GPa	Ultimate Tensile MPa	Elongation to Fracture (%)	Surface
Titanium	99 ⁺ Ti	100	240–550	>15	Ti oxide
Titanium–aluminum–vanadium	90Ti–6Al–4V	120	860–930	>8	Ti oxide
Cobalt–chromium–molybdenum (casting)	66Co–28Cr–6Mo	235	520–1170	>8	Cr oxide
Stainless steel (316L)	70Fe–18Cr–12Ni	190	480–1000	>30	Cr oxide
Zirconium	99 ⁺ Zr	100	450–550	>15	Zr oxide
Tantalum	99 ⁺ Ta	–	170–520	<30	Ta oxide
Gold	99 ⁺ Au	100	210–310	>30	Au
Platinum	99 ⁺ Pt	165	130	40	Pt

w/o, weight percent.

^aMinimum values from the American Society for Testing and Materials Committee F4 documents are provided. Selected products provide a range of properties.**TABLE 2.5.5.2** Engineering Properties of Inert Ceramics Used as Biomaterials^a

Material	Modulus of Elasticity GPa	Ultimate Bending Strength MPa	Surface
Aluminum oxide			
Poly-crystalline	370	300–550	Al ₂ O ₃
Single crystal (sapphire)	390	640	Al ₂ O ₃
Zirconium oxide (partially stabilized zirconia)	150–240	500–650	ZrO ₂
Titanium oxide (titania)	280	70–100	TiO ₂
Carbon	25–40 (4–6)	150–250 (22–36)	C
Carbon–silicon (LTI)	25–40 (4–6)	200–700 (29–101)	CSi

^aThese high ceramics have 0% permanent elongation at fracture.**TABLE 2.5.5.3** Engineering Properties of Bioactive and Biodegradable Ceramics^a

Material	Modulus of Elasticity GPa	Ultimate Bending Strength MPa	Surface
Hydroxyapatite	10–120	15–300	Ca ₁₀ (PO ₄) ₆ (OH) ₂
Tricalcium phosphate	30–120	15–120	Ca ₃ (PO ₄) ₂
Bioglass or Ceravital	40–140	20–350	CaPO ₄
Apatite–Wollastonite ceramic	125	215	CaPO ₄ + F

^aThese ceramics have 0% permanent elongation at fracture.

Metals

Metallic implants used in clinical dentistry today are almost exclusively manufactured from titanium and its alloys. The strength of titanium is due to its hexagonal close-packed crystal lattice and crystallographic orientation, whereas its biocompatibility (corrosion resistance) is attributed to its stable, passive oxide layer. Titanium implants are in a passive state (their oxide is chemically stable) in a normal physiological microenvironment. Both CPTi and Ti-6Al-4V possess excellent corrosion resistance for a full range of oxide states and pH levels. The coherent oxide layer and ability of titanium to repassivate results in corrosion resistance. Titanium ions are released from transient chemical dissolution of the oxide. However, the low dissolution rate and relative nonreactivity of titanium dissolution products allow bone to thrive and osseointegrate with titanium.

The mechanical properties of titanium-based materials are well established. Microstructures with small (<20 μm) grain sizes have the highest fatigue strength (~500–700 MPa). Surface roughening results in a reduced fatigue strength compared with smooth-surfaced implants. The Ti-6Al-4V alloy has a 60% greater strength than pure titanium, but it is more expensive. Both CPTi and Ti-6Al-4V alloy have complex, heterogeneous surface oxides. There may be differences in cell adhesion, and tissues may be in closer proximity to pure titanium surfaces than to alloy surfaces; however, there is no difference in implant function between the two types of titanium.

Ceramics

Ceramic implants were introduced because of their relative biologic inertness compared to metals. Ceramics are fully oxidized materials and therefore chemically stable and less likely to elicit an adverse biologic response than metals, which only oxidize at their surface. Ceramics promote osseointegration by the nature of their osteoconductivity (a biomaterial that is conducive to bone growth on its surface or into its pores).

“Inert” ceramics include alumina (Al_2O_3) and zirconia (ZrO_2), which are used as bulk implants. Bioactive and bioresorbable ceramics are used as coatings to accelerate osseointegration. Bioactive ceramics elicit tissue formation, can bond with bone, and be replaced by bone over time. Bioactive ceramics are partially soluble, enabling ion transfer and the formation of a direct bond between implant and bone. Bioactive ceramics are primarily used as scaffold materials or as coatings on more structurally robust substrates. Bioresorbable or biodegradable ceramics have a higher degree of solubility than bioactive ceramics, gradually resorb and integrate into the surrounding tissue, and are used as bone augmentation materials.

The concept of bioactivity was originally introduced with respect to bioactive glasses via the following hypothesis: the biocompatibility of an implant material is optimal if the material elicits the formation of normal tissues at its surface,

and, in addition, if it establishes a contiguous interface capable of supporting the loads that normally occur at the site of implantation (Madsen and Kohn, 2019). Examples of bioactive materials are bioactive glasses, glass ceramics, and calcium phosphate ceramics. Bioactive glasses and glass ceramics include bioglass, which is synthesized from several glasses containing mixtures of silica, phosphate, calcia, and soda; Ceravital, which has a different alkali oxide concentration from that of bioglass; and apatite-wollastonite glass ceramic, a glass ceramic containing crystalline oxyapatite and fluorapatite [$\text{Ca}_{10}(\text{PO}_4)_6(\text{O},\text{F}_2)$] and β -wollastonite (SiO_2 -CaO) in an MgO-CaO-SiO₂ glassy matrix. Calcium phosphate ceramics are a group of biomaterials with varying calcium-to-phosphate ratios, depending on processing-induced physical and chemical changes. Among the calcium phosphates, the apatites have the largest use in implantology.

The impetus for using synthetic hydroxyapatite (HA) as a biomaterial stems from the perceived advantage of using a material similar to the mineral phase in bone and teeth for replacing these materials and the expectation that better tissue bonding can be achieved. Additional advantages of bioactive ceramics include elastic properties similar to those of bone when not fully dense, control of degradation rates through control of material properties (e.g., crystallinity and Ca/P ratio), and the potential for the ceramic to function as a barrier to corrosion when coated onto a metal implant.

Reactions (ion exchange) at the ceramic surface that dictate mechanical, chemical, physical, and biological properties depend on processing techniques, time, temperature, and atmosphere. Processing techniques used to bond Ca-P powders to implants include plasma and thermal spraying, sintering, ion beam and other sputter techniques, electrophoretic deposition, sol-gel techniques, pulsed laser deposition, and chemical vapor deposition (Madsen and Kohn, 2019). Different structures, compositions, and dissolution rates result from different processing approaches, and modulate biological reactions. For example, increased Ca/P ratios, fluorine and carbonate content, and crystallinity lead to greater stability. Ca/P ratios in the range 1.5–1.67 yield the most beneficial tissue response. Most synthetic HAs contain substitutions for the PO_4^{3-} and/or OH^- groups and vary from the absolute stoichiometry and Ca/P ratios of HA. Oxyhydroxyapatite, tricalcium phosphate (TCP), tetracalcium phosphate, and octocalcium phosphate have all been detected in commercially available apatite implants (Table 2.5.5.3, Madsen and Kohn, 2019). Understanding the processing–composition–structure–processing synergy for calcium phosphates is therefore critical to understanding the in vivo function of these materials.

Each calcium phosphate is defined by a unique set of chemical and physical properties. Physical parameters and properties of importance to the clinical function of calcium phosphate ceramics are summarized in Table 2.5.5.4, along with the functional and biological relevance and techniques used to characterize each parameter.

TABLE 2.5.5.4 Physical and Chemical Properties Important to the Function of Calcium Phosphate Bioceramics

Material Parameter(s)	Functional and Biological Relevance	Technique(s) to Characterize
Particle size, shape, distribution	Strength	Sifting, quantitative stereology
Pore size, shape, distribution	Strength, bioreactivity	Stereology, scanning electron microscopy (SEM)
Specific surface area	Dissolution, precipitation reactions	Brunauer–Emmett–Teller
Phases	Dissolution, protein adsorption	X-ray diffraction, Fourier transform infrared spectroscopy
Crystal structure, grain size, density	Strength, toughness, protein adsorption	Optical microscopy, SEM, transmission electron microscopy
Composition	Solubility	Auger electron spectroscopy, X-ray photoelectron spectroscopy (XPS)
Chemical stability, surface activity	Solubility, dissolution, cell adhesion	XPS, ionic flux, zeta potential
Thickness, hardness, roughness	Cell, protein adsorption	SEM, nanoindentation, profilometry

Adapted from Madsen, E.J., Kohn, D.H., 2019. Bioceramics. In: Kutz, M. (Ed.), *Biomedical Engineer's Handbook*, third ed. McGraw-Hill.

Future Directions

Advances in materials synthesis and processing, surgical technique, and clinical protocols have enabled dental implants to have excellent clinical success. Nonetheless, clinical failures occur at rates of approximately 2%–5% per year. Causes of failure and current problems with dental implants include:

1. Early loosening, stemming from a lack of initial osseointegration;
2. Late loosening, or loss of osseointegration;
3. Bone resorption;
4. Inflammation and infection;
5. Fracture of the implant and/or abutment and delamination of coatings from the bulk implant.

The most common failure mechanism with endosseous implants is alveolar crest resorption, leading to decreased volume of supporting tissues and ultimately implant loosening. Bone resorption can be mechanically mediated due, in part, to the elastic mismatch between implant and bone. Bone resorption can also occur secondary to peri-implantitis, an inflammatory process affecting hard and soft tissues surrounding an implant, leading to progressive periodontal lesions and loss of supporting bone.

Biomaterials advances include an increased use of implants made from zirconia for improved aesthetics (Roehling et al., 2019), additive manufacturing of implants via digital technologies and computer aided design for custom fitting and more rapid fabrication (Katkar et al., 2018), interfacing manufacturing with imaging for fabrication before tooth extraction and immediate insertion into sockets (Saeidi Pour et al., 2019), nanoscale modifications of implant surfaces, including patterning, functionalization, and molecular grafting (Rasouli et al., 2018), antibacterial coatings, both passive (kills bacteria in contact with biomaterial surface) and active (releases antibacterial agents to kill bacteria at some diffusion distance) (Qin et al., 2018), and

drug-eluting implant coatings, including technologies for the controlled release of bisphosphonates and bone morphogenetic proteins (BMPs) (Alenezi et al., 2018).

While these and other strategies have expanded the population of patients that can be treated with an implant, inadequate initial bone stock or loss of bone following implant placement necessitates alternative approaches to treat inflammation and/or regenerate bone. These approaches are discussed in the next section.

Tissue Engineering in Dentistry

Need for Tissue Engineering in Dentistry

Gold standard treatments for the repair of DOC tissues are similar to therapies used elsewhere in the body and include synthetic materials, autografts, and allografts. Each of these reconstructive strategies has limitations and lacks clinical predictability. Only a minimal amount of tissue can be harvested for autografts, the harvesting procedure may lead to donor site discomfort and morbidity, and it may be difficult to form this tissue into desired shapes (Scheerlinck et al., 2013), a problem that is particularly important in the craniofacial region. Autografting, the current “gold standard” for craniofacial bone regeneration, has failure rates as high as 30% (Scheller et al., 2009). Allografts have the potential to transfer pathogens. Freeze drying, demineralization, and irradiation reduce immunogenic potential, but can reduce structural integrity, leading to graft fracture. Use of growth factors relies on the presence of a sufficient population of undifferentiated progenitor cells capable of responding to the inductive cues provided by the growth factor. Such a population may not be available in aged or compromised patients. Complications with synthetic biomaterials include stress shielding, loosening, and mechanical breakdown. These limitations with current therapies have motivated tissue engineering as a solution to DOC problems.

Regeneration of DOC tissues presents a formidable challenge that requires synthesis of engineering, basic science, and clinical expertise. Identification of appropriate scaffolds, cell sources, and spatial and temporal signals (the tissue-engineering triad) is necessary to optimize development of single DOC tissues, hybrid tissues, and graded interfaces between tissues. Dental tissue engineers are interested in the regeneration of teeth, oral mucosa, salivary glands, craniofacial bone, cranial sutures, periodontium, muscle, and the TMJ.

Materials for Engineering DOC Tissue Structure and Function

Regeneration of DOC tissues can be pursued by one or a combination of the three general tissue-engineering strategies: conduction, induction, and cell transplantation. In a conductive approach, a biomaterial provides an appropriate microenvironment for host cells to attach, grow, and differentiate, leading to the formation of new tissue within the material. Conductive materials are the most clinically prevalent in dentistry. In an inductive approach, biologic agents, typically growth factors, induce host cells to form new tissue. Cell-based therapies involve transplantation of uncommitted or differentiated cells, and also genetically manipulated cells, and can be used in combination with a supporting biomaterial (conductive) and inductive agents. Biomaterials used for DOC tissue engineering include synthetic polymers, ceramics and composites, natural materials, and tissue derivatives.

Tissue-engineered products for DOC applications should satisfy the following design requirements (Scheller et al., 2009):

1. Biocompatibility;
2. Conductivity to guide attachment and proliferation of cells and secretion of new extracellular matrix (ECM);
3. Ability to incorporate inductive factors to direct and enhance new tissue growth;
4. Support of vascular ingrowth for oxygen and biomolecule transport;
5. Mechanical integrity to support loads at the graft site;
6. Controlled, predictable, reproducible rate of degradation into nontoxic species that are easily metabolized or excreted;
7. Easy and cost-effective processing into irregular 3D shapes of sufficient size to fill clinically relevant defects.

Integrating all of these criteria into a single biomaterial presents design challenges that require more complexity than simplified ECM mimics can provide.

Synthetic and natural biomaterials that mimic structural and/or functional aspects of natural ECMs and satisfy at least some of these design requirements include both organic and inorganic biomaterials: copolymers of poly(lactic-*co*-glycolic acid) (PLGA), polycaprolactone (PCL), polyethylene glycol (PEG), polyurethanes, poly(propylene fumarate), collagen, starch-based materials, alginate, silk, bioactive glasses and glass ceramics, calcium phosphate ceramics, calcium phosphate/collagen blends, and calcium phosphate/synthetic

polymer composites. Varying parameters of the biomaterial, such as composition, topology, and crystallinity, can significantly affect the amount and rate of tissue formation, and intensity or duration of inflammatory response (Madsen and Kohn, 2019; James et al., 1999).

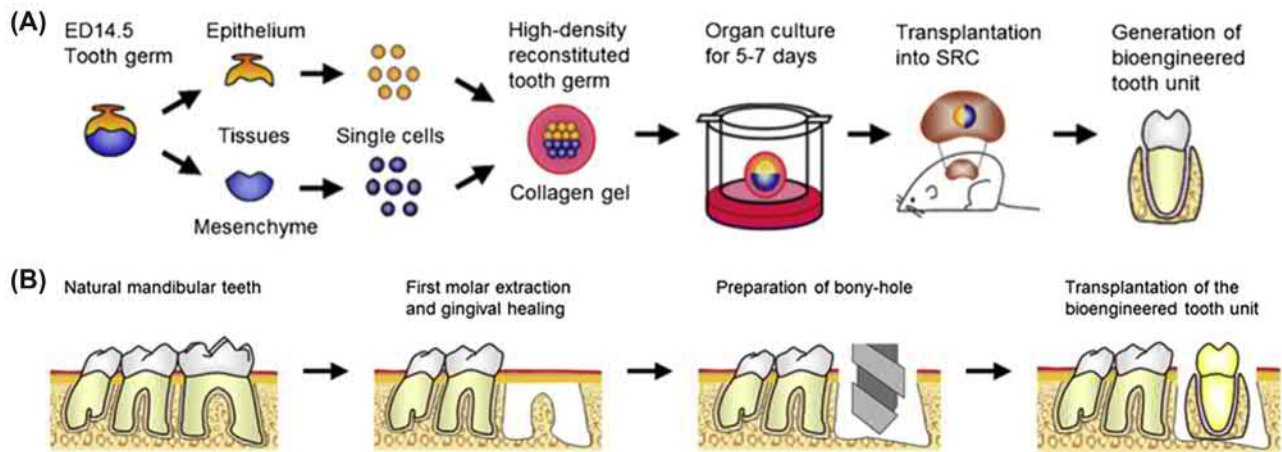
To satisfy a larger number of the design criteria listed in the previous paragraph, biomaterial modification can take on different levels of complexity, resulting in increasing levels of physiological “mimicry” and functionality. In addition to using natural ECMs, surface and bulk chemical modifications of synthetic materials can enhance the ability of a biomaterial to respond to physiological cues. Material modifications include changes in hydrophilicity, surface functionalization with charged groups, incorporation of insoluble ligands and peptide cell recognition sequences, attachment of larger proteins, supramolecular self-assembly, and development of materials that bind and release soluble factors (Mao and Mooney, 2015). Strategies based on physical cues include the reproduction of nanoscale topology, superposition of mechanical cues, and control of degradation. Designing biological recognition into a biomaterial may also obviate the need for therapies based on delivery of cells or recombinant growth factors, which are subject to regulatory constraints.

DOC Tissue-Engineering Applications Teeth

The tooth is composed of four distinct tissues: pulp, dentin, cementum, and enamel. The tooth root is supported by a PDL and encased in alveolar bone. The diversity in tissue types coupled with the need for the tooth to withstand forces of mastication makes engineering a tooth complex. Some groups focus on regenerating one or two of the subtissues for targeted repair, while others aim to engineer an intact tooth and alveolus simultaneously (Nakao et al., 2007).

Complete tooth regeneration is complicated by the fact that regrowth of a tooth is desired at a site where a tooth no longer exists. Thus unlike engineering bone and mucosa, where scaffolds and signals can draw on cues and cells present in the surrounding host tissue, an engineered tooth must be self-reliant. Autologous stem cells are used for whole tooth engineering due to the complex signaling required for shape morphogenesis and tooth eruption. Before eruption of a new tooth, a population of primitive stem cells in the tooth bud is capable of providing the instructions necessary for growth of the entire tooth (Oshima et al., 2011, Fig. 2.5.5.5). Non-stem cell-based approaches are used for regeneration and repair of single DOC dental tissues, including pulp, dentin, cementum, and enamel. Dental pulp stem cells are a unique mesenchymal stem cell (MSC) population that is present in the pulp. A second tooth-associated MSC population has been isolated from the PDL, periodontal ligament stem cells (PDLSCs). Dental pulp stem cells and PDLSCs transplanted on HA, TCP, and other scaffolds can regenerate a vascularized dentin/pulp-like complex.

Biomaterials that guide the engineering of whole teeth or individual tissues parallel those used in engineering other



• **Figure 2.5.5.5** Generation of a bioengineered tooth unit. Schematic representations of: (A) the regenerative technology of bioengineered tooth unit; (B) protocol used to transplant a bioengineered tooth unit in a murine tooth loss model. (Reprinted with permission from Oshima et al. (2011)).

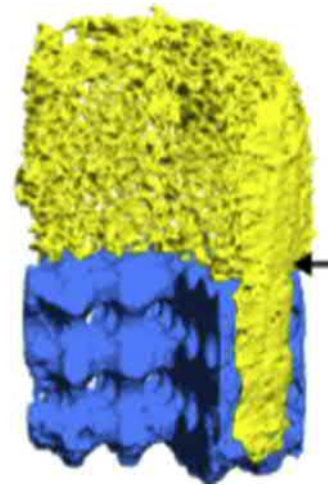
mineralized tissues and include: collagen, poly(glycolic acid), self-assembling peptides, gelatin–chondroitin–hyaluronan tripolymer, and silk. The success of *in vivo* tooth regeneration in rodents and rabbits is 20%–50% with implanted cell/scaffold combinations, with success defined as regeneration of at least three histologically intact structures, including enamel, dentin, pulp, cementum, and PDL (Scheller et al., 2009).

The acellular nature of enamel enables material-centric approaches to remineralization. Self-assembling peptides or peptide amphiphiles are based on principles of protein–protein interactions and protein folding. By understanding how supramolecular structures are assembled in nature, these processes can be exploited in the design of synthetic materials. In this regard, self-assembling peptides have been used to promote enamel remineralization by providing a biomimetic scaffold capable of HA nucleation, and injectable self-assembling peptide gels applied to carious lesions promote enamel remineralization in humans (Brunton et al., 2013).

Temporomandibular Joint

To overcome drawbacks in surgical methods of TMJ treatment, alternative methods have been developed, such as osteochondral allografts and autografts and delivery of chondrocytes (e.g., Carticel). Chondrocytes seeded on biomaterials like PLGA and collagen develop cartilage-like structures that express markers of chondrocyte differentiation and have compositions similar to normal articular cartilage. While MSCs can be differentiated into chondrocytes in cartilage defects, the regenerated cartilage rarely matches the structure and function of mature endogenous cartilage. Expression of growth factors such as basic fibroblast growth factor, transforming growth factor- β , and Sox9 is necessary for cartilage regeneration. Direct delivery of these factors, as well as *in vivo* injection and *ex vivo* delivery of viruses encoding these genes to chondrocytes, can enhance repair of cartilage and osteochondral defects.

Engineering a functional osteochondral graft requires the regeneration of both bone and cartilage with a defined interface.

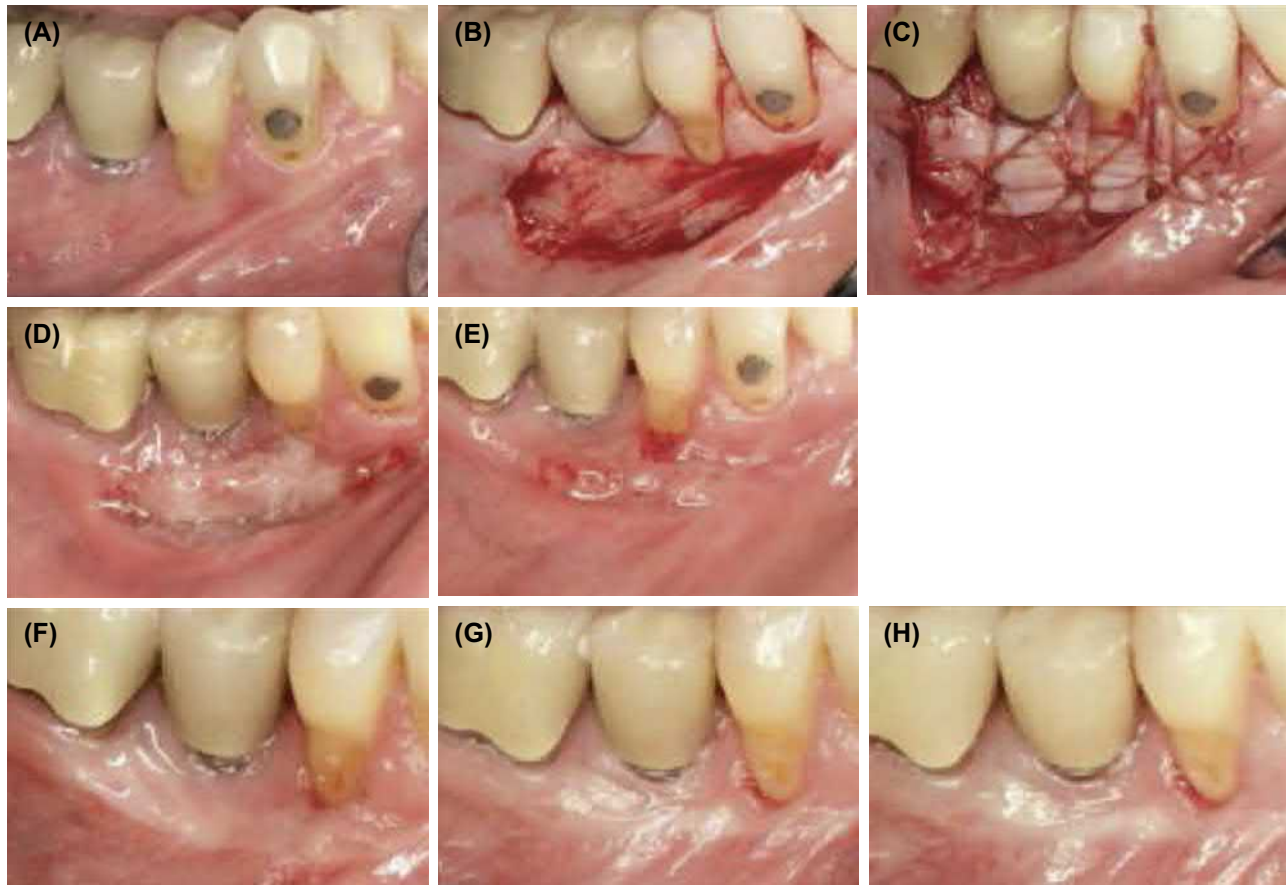


• **Figure 2.5.5.6** 3D reconstruction of computed tomography data showing the polymer phase (*top*), the hydroxyapatite phase (*bottom*), and the polymer struts that transverse both phases (*arrow*). A pie slice portion of the scaffold has been removed from the image to reveal the pore architecture of the scaffold. (Reprinted with permission from Schek, R.M., Taboas, J.M., Segvich, S.J., Hollister, S.J., Krebsbach, P.H., 2004. Engineered osteochondral grafts using biphasic composite solid free-form fabricated scaffolds. *Tissue Eng.* 10, 1376–1385.)

Strides have been made in engineering these tissues separately and simultaneous formation of bone and cartilage with a mineralized interface has been achieved in animals. Image-based design followed by solid freeform fabrication to control scaffold size and shape has been used to generate a biphasic scaffold (e.g., poly(L-lactide) /HA composite) in which chondrogenic and osteogenic cells are seeded onto the polymer and ceramic, respectively (Fig. 2.5.5.6). Marrow-containing vascularized bone, mature cartilage, and a defined mineralized interface can be engineered via this strategy (Yousefi et al., 2015).

Oral Mucosa

Oral mucosa is a highly specialized tissue made of stratified epithelium overlying a supportive lamina propria. Engineered



• **Figure 2.5.5.7** Clinical views of a patient in the study on intraoral grafting of tissue-engineered human oral mucosa. (A) Preoperative appearance, (B) supraperiosteal recipient site, (C) ex vivo-produced oral mucosa equivalent grafted in place, and appearances at (D) 7 days, (E) 14 days, (F) 30 days, (G) 90 days, (H) 180 days. (Reprinted with permission from Izumi, K., Neiva, R.F., Feinberg, S.E., 2013. Intraoral grafting of tissue-engineered human oral mucosa. *Int. J. Oral Maxillofac. Implants* 28, e295–e303.)

oral mucosa should reproduce the full-thickness tissue consisting of three distinct layers: the lamina propria, basement membrane, and stratified squamous epithelium. Layered differentiation can be mimicked by culturing keratinocytes with keratinocyte growth factors. Multilayer culture of gingival keratinocytes has met with some clinical success. Commercially available products for mucosal engineering include MatTek's gingival epithelium and keratinized stratified squamous epithelial products EpiOral™ and EpiGingival™.

To move beyond current gingival epithelium products, engineering a full-thickness mucosa with intact lamina propria requires scaffolds capable of supporting fibroblast infiltration with minimum shrinkage and controlled biodegradation. Scaffolds used for mucosal reconstruction include natural derivatives, such as acellular dermis, ECM protein-based scaffolds, synthetic materials, and hybrid scaffolds of both natural and synthetic matrices (Moharamzadeh et al., 2007).

Tissue-engineered human ex vivo-produced oral mucosa equivalents (EVPOMEs) have undergone first-in-human studies in patients with a lack of keratinized gingiva. A punch biopsy of the hard palate is taken to acquire oral keratinocytes, which are expanded, seeded, and cultured on an acellular dermal matrix. EVPOME grafts are applied over

an intact periosteal bed and secured in place. Six months postsurgery, keratinized tissue around teeth was augmented by 1 mm (Izumi et al., 2013, Fig. 2.5.5.7).

Salivary Glands

Loss of salivary gland function can result as a pharmacological side effect, from radiation therapy, or as a consequence of autoimmune diseases. Saliva is a complex hypotonic solution that carries water, electrolytes, proteins, and peptides into the oral cavity. Loss of salivary flow (xerostomia) significantly impacts quality of life and predisposes affected individuals to caries, dysphagia (difficulty swallowing), and mucosal infection. Tissue engineering a salivary gland substitute is one way to treat these patients. To accomplish this complex task, three objectives must be satisfied: identification of a cell population capable of differentiation and fluid movement, optimization of scaffold material properties, and definition of ideal culture conditions and ECM components.

Salivary glands are made up of highly specialized cells capable of fluid secretion, modification, and directional movement. The challenge of culturing and implanting cells capable of all of these functions is a primary focus of salivary gland tissue engineers. A human ductal epithelial salivary

gland cell line (human submandibular gland) can form gland monolayers on poly(L-lactide) scaffolds and generate osmotic gradients for saliva formation.

Scaffold design for an artificial salivary gland consists of an end tube made from a porous, biodegradable material (Aframian and Palmon, 2008) coated with matrix components on the inner surface of the tube to promote formation of polarized epithelial cell ducts capable of unidirectional fluid movement (secretion of fluids and salts into the oral cavity). Scaffold selection for salivary gland replacement takes cues from materials used to engineer replacements for other tubular structures such as intestine and blood vessels. Scaffolds designed from poly(L-lactide), PLGA, PEG-terephthalate/poly(butylene terephthalate), chitosan, and collagen have been investigated (Scheller et al., 2009).

Salivation occurs in response to agonists that generate an increase in intracellular Ca^{2+} concentration and is facilitated by osmotic gradient-directed fluid movement through water channels in the apical membrane known as aquaporins (AQPs). Isolated ductal epithelial cells lack expression of AQP and cannot mediate fluid movement. Reintroduction of transient AQP expression using adenoviral transduction has been successful in rat and minipig salivary gland tissue in vivo and was the subject of a recent clinical trial using AQP1 (Baum et al., 2012). The trial demonstrated successful outcomes to increase saliva production after irradiation without major side effects.

Bone and Periodontium

Strategies to engineer craniofacial bone and periodontium follow strategies used for the engineering of long bones, and include a variety of conductive, inductive, and cell therapy approaches. For periodontal therapies, treatment of inflammation often occurs in conjunction with regeneration. Biomaterials advances in the engineering of these two mineralized tissues focus on organic and inorganic nanomaterials and delivery of signals via peptides, proteins, and cell–cell communication.

A variety of cell functions are regulated by topology. Creation of nanofibrous materials from ECM constituents or blends of synthetic and natural polymers can provide a material with both the physical scale necessary to influence biological function and a biochemical composition that is similar to the ECM environment that cells interact with in vivo. Use of nanoscale surface topology to enhance cell adhesion and osseointegration has established itself in polymer scaffolds for periodontal and craniofacial defects. Large periodontal osseous defects in humans have been treated with patient-specific polymer scaffolds that are designed to form multiple tissues (bone–ligament–cementum) (Rasperini et al., 2015). Using 3D printing of PCL scaffolds to capture nanoscopic details of the root surface and PDL, scaffolds can be manufactured to precisely fit the defect and guide PDL formation along with mineralized tissue (Fig. 2.5.5.8). Advances in nanoscale inorganic biomimetic materials also impact bone and periodontium engineering. The self-assembly of nanoscale mineral

within the pores of a scaffold enhances cell adhesion, proliferation, and osteogenic differentiation, and modulates cytoskeletal organization and cell motility, leading to larger and more spatially uniform volumes of bone regenerated in vivo (Rossello and Kohn, 2014).

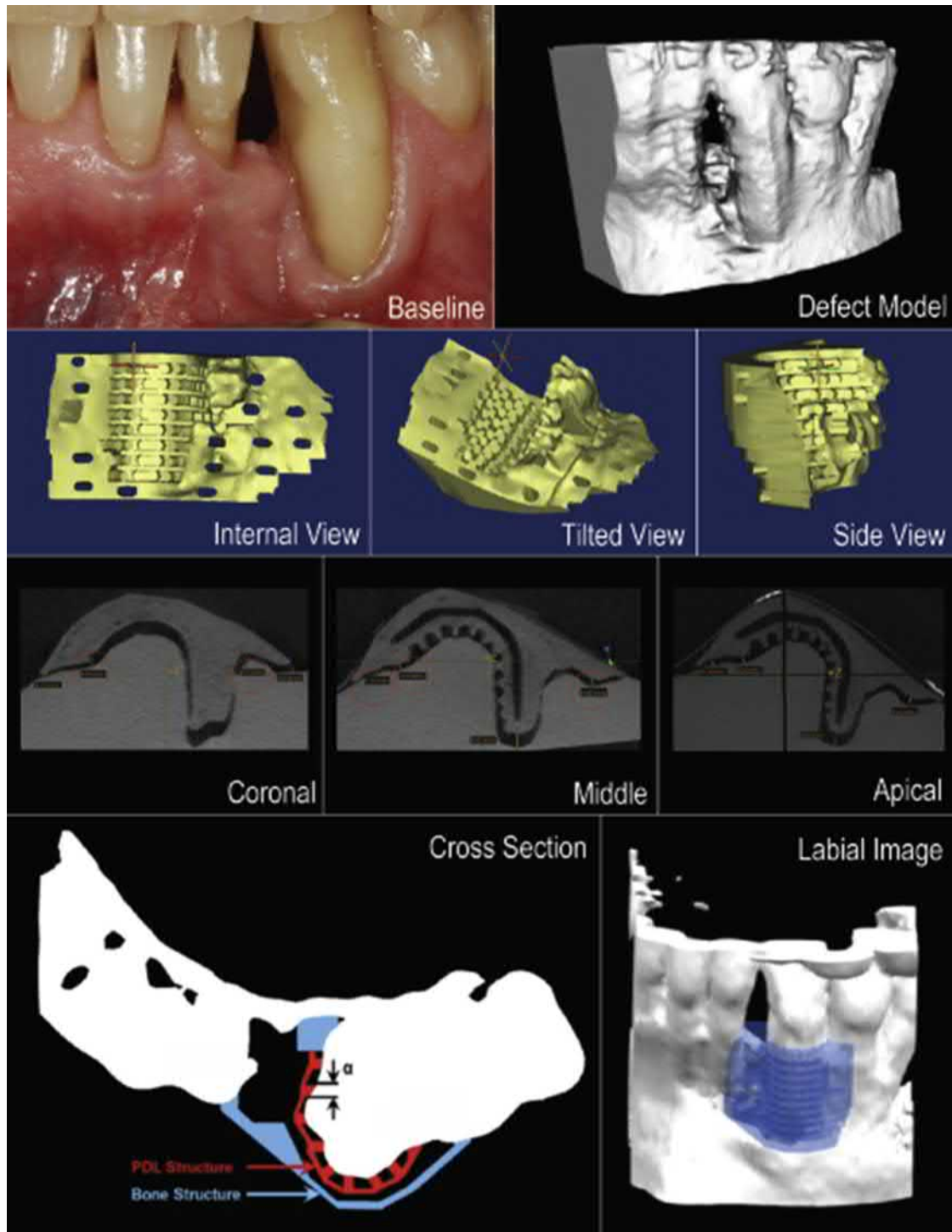
In addition to its structural role, the ECM provides adhesive ligands that direct cell function. Reproduction of these signals on engineered scaffolds can allow a more precise regulation of cell function and tissue formation. Peptide sequences that mimic sections of collagen and noncollagenous proteins, including laminin, bone sialoprotein, osteopontin, statherin, elastin, and osteonectin, increase cell adhesion, proliferation, and differentiation of osteoblasts and promote the function of cells that can form mineralized tissues of the oral cavity.

Inductive properties can be integrated into a material using methods to immobilize proteins, such as adsorption, entrapment, cross-linking, or covalent binding. Controlled release of a growth factor can be achieved by incorporating the factor into the bulk of a scaffold or hydrogel during polymerization and designing a release profile based on drug diffusion and/or material degradation. Adsorbing or covalently binding a drug to each layer of a material created by layer-by-layer assembly can provide temporal control over its delivery. This technology is most widely recognized in dentistry for delivering antibiotics to periodontal pockets.

Direct growth factor delivery and growth factor-containing scaffolds have been used for periodontal regeneration and have progressed to human clinical trials and commercialization. Delivery of recombinant BMPs (BMP-2 and BMP-7), platelet-derived growth factor (PDGF), insulin-like growth factor (IGF-1), and fibroblast growth factor enhance the repair of periodontal alveolar bone defects when delivered locally with defect healing equivalent or better than autografting. In humans, delivery of recombinant human (rh) BMP-2 on the xenogenic bone substitute Bio-Oss™ to alveolar ridge defects regenerates vertical defects. The first human clinical trial for periodontal disease used rhPDGF/rhIGF-1 in a methylcellulose vehicle and revealed twice as large osseous defect fill compared to vehicle controls (Giannobile, 1996). GEM-21S is now a commercial product, consisting of hPDGF in a TCP vehicle (Lynch Biologics).

Summary and How Experience From Dental Biomaterials has Brought Value to Other Areas of Biomaterials

The history of biomaterials in dentistry dates back several thousand years. Many areas of biomaterials have been influenced by materials developed for DOC applications. Dental implant treatments have, in part, contributed to changes in the philosophy of orthopedic and other implant-based therapies. Early reports of tissue integration for dental implants were complicated by nonstandardized clinical placement and time between placement and restoration/loading. Most implants were immediately (hours to weeks) subjected to biomechanical function. Immediate intraoral restoration



• **Figure 2.5.5.8** A customized scaffold was 3D printed using polycaprolactone to fit a periosseous defect using a prototyped model of the defect from a patient's cone beam computed tomography scan. The scaffold's internal region consisted of extended pegs for the support and guidance of periodontal ligament formation, perforations for fixation, and an internal compartment for delivery of recombinant human platelet-derived growth factor -BB, as shown in the cross-sectional view. Microcomputed tomography scans of the polycaprolactone scaffold fitted into the prototyped defect model (see coronal, middle, apical views) were used to determine the topographic adaptation of the scaffold to the root surface. *PDL*, Periodontal ligament. (Reprinted with permission from Rasperini, G., Pillipchuk, S.P., Flanagan, C.L., Park, C.H., Pagni, G., Hollister, S.J., Giannobile, W.V., 2015. 3D-printed bioresorbable scaffold for periodontal repair. *J. Dent. Res.* 94 (9 Suppl.), 153S–157S.)

CASE STUDY

What Problem Was Addressed?

Examination of implant/tissue interfaces from early implant materials retrieved from humans showed fibrous soft tissue (dense collagenous scar tissue with limited numbers of cells and blood vessels), but no osseointegration. One of the contributing factors was that abutments and prosthetics were attached and implants were loaded immediately before bone could heal. This observation led to a two-stage procedure in which implants were inserted and allowed to heal for 4–6 months prior to attachment of prosthetics, which, in turn, motivated the development of strategies to accelerate healing and reduce the 4–6-month wait time.

What Properties Were Required in a Material?

A material that is both bioactive and can also deliver biological factors would be desirable. A limiting factor in developing such a material is that most processes used to bond bioactive coatings to an implant require high temperatures, resulting in degradation of the biological agent.

What Material Solution Was Developed?

Low-temperature, low-pressure processes in which bioactive coatings are “biomimetically” formed on an implant surface were developed. Bone-like mineral was formed in vitro at standard temperature and pressure. Synthesis of bone-like mineral is based on principles of biomineralization, in which organisms use macromolecules to control mineral nucleation and growth. Macromolecules usually contain functional groups that are negatively charged at the crystallization pH, enabling them to chelate ions present in the surrounding media, which stimulate mineral crystal nucleation. By adding a biological agent to the ionic solution that the implant is immersed in the biological agent can be incorporated into the biomimetic apatite layer that is thermodynamically driven onto the implant surface. By altering the concentrations and times at which protein is added to the simulated body fluid, spatial control over protein location is achieved. Controlling the loading quantity and localization of the protein through the mineral thickness allows control over its release profile. Thus proteins encapsulated near the surface can be used when a burst is desired, and proteins encapsulated throughout the thickness of the mineral can be used when a sustained release is desired.

resulted in force transfer between the implant body and the supporting tissues during the period of initial tissue healing. The concepts of tissue integration of dental implants evolved to include both biomaterial and biomechanical aspects of device function. The learning curve about how preparation of the surgical bed, precision of insertion, bulk, and surface properties of the implant affect osseointegration provided strategies for the design of implants for other parts of the body.

Accessibility of the oral environment and ability to create minimally invasive models of hybrid tissues render oral tissues convenient platforms for testing tissue-engineered prototypes. Oral and craniofacial tissue engineering can have a twofold impact that extends beyond dentistry. First, advances initially made in dentistry because of the relatively simple surgical models can be translated into other organ systems. Second, technologies developed outside of dentistry can be tested in oral models. One of the common screening tools for bone tissue engineering is the critical size calvarial defect model. The hybrid tissue systems of the periodontium, TMJ, cranial suture, and mineralized tissues of the tooth can provide insight into how to design a composite tissue consisting of multiple cell types. Oral and craniofacial-derived stem cells from the dental pulp, PDL, and cranial sutures have utility in nondental and noncraniofacial applications. The impact of synergy between engineering oral tissues and engineering tissues elsewhere in the body is that oral and craniofacial tissue engineering is an integral component of the larger field of tissue engineering and should not be viewed as dental researchers solving dental problems in isolation.

References

- Aframian, D.J., Palmon, A., 2008. Current status of the development of an artificial salivary gland. *Tissue Eng.* 14, 187–198.
- Alenezi, A., Chrcanovic, B., Wennerberg, A., 2018. Effects of local drug and chemical compound delivery on bone regeneration around dental implants in animal models: a systematic review and meta-analysis. *Int. J. Oral Maxillofac. Implant.* 33, e1–e18.
- Baum, B.J., et al., 2012. Early responses to adenoviral-mediated transfer of the aquaporin-1 cDNA for radiation-induced salivary hypofunction. *Proc. Natl. Acad. Sci. USA* 109, 19403–19407.
- Brunton, P.A., Davies, R.P.W., Burke, J.L., Smith, A., Aggeli, A., Brookes, S.J., Kirkham, J., 2013. Treatment of early caries lesions using biomimetic self-assembling peptides – a clinical safety trial. *Br. Dent. J.* 215, E6.
- Cramer, N.B., Stansbury, J.W., Bowman, C.N., 2011. Recent advances and developments in composite dental restorative materials. *J. Dent. Res.* 90, 402–416.
- Dye, B.A., Thornton-Evans, G., Li, X., Iafolla, T.J., 2015. Dental caries and tooth loss in adults in the United States, 2011–2012. In: National Center for Health Statistics Data Brief No. 197. Data from the National Health and Nutrition Examination Survey, 2011–2012.
- Giannobile, W.V., 1996. Periodontal tissue engineering by growth factors. *Bone* 19, 23S–37S.
- Izumi, K., Neiva, R.F., Feinberg, S.E., 2013. Intraoral grafting of tissue-engineered human oral mucosa. *Int. J. Oral Maxillofac. Implant.* 28, e295–303.
- James, K., Levene, H., Parson, J.R., Kohn, J., 1999. Small changes in polymer chemistry have a large effect on the bone-implant interface: evaluation of a series of degradable tyrosine-derived polycarbonates in bone defects. *Biomaterials* 20, 2203–2212.
- Katkar, R.A., Taft, R.M., Grant, G.T., 2018. 3D volume rendering and 3D printing (additive manufacturing). *Dent. Clin. N. Am.* 62, 393–402.

- Kellesarian, S.V., Abduljabbar, T., Vohra, F., Malignaggi, V.R., Malmstrom, H., Romanos, G.E., Javed, F., 2017. Role of local alendronate delivery on the osseointegration of implants: a systematic review and meta-analysis. *Int. J. Oral Maxillofac. Surg.* 46, 912–921.
- Kohn, D.H., 2008. Implant and bone augmentation materials. In: O'Brien, W.J. (Ed.), *Dental Materials and Their Selection*, fourth ed., pp. 300–312 (Quintessence).
- Lemons, J., 1999. Biomaterials for dental implants. In: Misch, C.E. (Ed.), *Contemporary Implant Dentistry*, third ed. Mosby Elsevier, St. Louis, MA. Ch24.
- Madsen, E.J., Kohn, D.H., 2019. Bioceramics. In: Kutz, M. (Ed.), *Biomedical Engineer's Handbook*, third ed. McGraw-Hill.
- Mao, A.S., Mooney, D.J., 2015. Regenerative medicine: current therapies and future directions. *Proc. Natl. Acad. Sci. USA* 112, 14452–14459.
- Moharamzadeh, K., Brook, I.M., Van Noort, R., Scutt, A.M., Thornhill, M.H., 2007. Tissue-engineered oral mucosa: a review of the scientific literature. *J. Dent. Res.* 86, 115–124.
- Nakao, K., Morita, R., Saji, Y., Ishida, K., Tomita, Y., Ogawa, M., et al., 2007. The development of a bioengineered organ germ method. *Nat. Methods* 4, 227–230.
- Oshima, M., Mizuno, M., Imamura, A., Ogawa, M., Yasukawa, M., Yamazaki, H., Morita, R., Ikeda, E., Nakao, K., Takano-Yamamoto, T., Kasugai, S., Saito, M., Tsuji, T., 2011. Functional tooth regeneration using a bioengineered tooth unit as a mature organ replacement regenerative therapy. *PLoS One* 6, e21531.
- Palmquist, A., 2018. A multiscale analytical approach to evaluate osseointegration. *J. Mater. Sci. Mater. Med.* 29, 60.
- Qin, S., Xu, K., Nie, B., Ji, F., Zhang, H., 2018. Approaches based on passive and active antibacterial coating on titanium to achieve antibacterial activity. *J. Biomed. Mater. Res. A* 106, 2531–2539.
- Rasouli, R., Barhoum, A., Uludag, H., 2018. A review of nanostructured surfaces and materials for dental implants: surface coating, patterning and functionalization for improved performance. *Biomater. Sci.* 6, 1312–1338.
- Rasperini, G., Pilipchuk, S.P., Flanagan, C.L., Park, C.H., Pagni, G., Hollister, S.J., Giannobile, W.V., 2015. 3D-printed bioresorbable scaffold for periodontal repair. *J. Dent. Res.* 94 (9 Suppl.), 153S–157S.
- Roehling, S., Schlegel, K.A., Woelfler, H., Gahlert, M., 2019. Zirconia compared to titanium dental implants in preclinical studies—A systematic review and meta-analysis. *Clin. Oral Implant. Res.* 30, 365–395.
- Rossello, R.A., Kohn, D.H., 2014. Enhanced volume of stem cell-based regenerated tissue achieved by altering microenvironment and cell seeding strategies. *J. Tissue Sci. Eng.* S1, 005. <https://doi.org/10.4172/2157-7552.S1-005>.
- Saeidi Pour, R., Freitas Rafael, C., Engler, M.L.P.D., Edelhoff, D., Klaus, G., Prandtner, O., Berthold, M., Liebermann, A., 2019. Historical development of root analogue implants: a review of published papers. *Br. J. Oral Maxillofac. Surg.* <https://doi.org/10.1016/j.bjoms.2019.01.021>. (Epub ahead of print).
- Sakaguchi, R., Ferracane, J., Powers, J., 2018. In: *Craig's Restorative Dental Materials*, fourteenth ed. Elsevier.
- Scheerlinck, L.M.E., et al., 2013. Donor site complications in bone grafting: comparison of iliac crest, calvarial, and mandibular ramus bone. *Int. J. Oral Maxillofac. Implant.* 28, 222–227.
- Schek, R.M., Taboas, J.M., Segvich, S.J., Hollister, S.J., Krebsbach, P.H., 2004. Engineered osteochondral grafts using biphasic composite solid free-form fabricated scaffolds. *Tissue Eng.* 10, 1376–1385.
- Scheller, E.L., Krebsbach, P.H., Kohn, D.H., 2009. Tissue engineering: state of the art in oral rehabilitation. *J. Oral Rehabil.* 36, 368–389.
- Taylor, T.D., 1990. *Dental Implants: Are They for Me?* Quintessence.
- Yousefi, A.M., Hoque, M.E., Prasad, R.G., Uth, N., 2015. Current strategies in multiphasic scaffold design for osteochondral tissue engineering: a review. *J. Biomed. Mater. Res. A* 103, 2460–2481.

Chapter Exercises

1. What factors dictate the effectiveness of osseointegration? Who/what controls each of these factors?

Surgical technique—clinician.

Patient's medical and dental status—patient's physiology.

Bone quality—patient's physiology, with decisions on whether degree of bone quality in an individual patient is a contraindication made by the clinician.

Extent and kinetics of healing—patient's physiology, biomaterial (manufacturer).

Implant design factors—geometry, length, diameter, macroscopic and microscopic shapes of implant (manufacturer).

Minimization of interfacial motion—a large number of biomaterial factors, including material choice, mechanical properties of implant, surface topology, chemistry (manufacturer + clinician's choice of specific implant).

Biomechanics—loading patterns, bone quality/properties, loading (patient's physiology, implant material, design determined by manufacturer, time at which prosthesis is attached and patient can begin loading is determined by clinician).

2. What is the difference between an osteoconductive biomaterial and an osteoinductive biomaterial, and how can you demonstrate that a biomaterial is osteoinductive?

An osteoconductive biomaterial is a material that acts as a scaffold for new bone formation by providing an appropriate environment for attachment, proliferation and function of osteoblasts or their progenitor cells, leading to the formation of new bone matrix.

An osteoinductive biomaterial is a material (or biologic agent) that causes the conversion of nonlineage-committed cells preferentially to bone progenitor cells.

The key to demonstrating that a biomaterial is osteoinductive is to show that bone will form in a site that normally does not form bone (i.e., it is the material that triggers bone formation, not factors from the environment). Experiments conducted in a bony site cannot effectively demonstrate that a material is osteoinductive.

3. It is qualitatively understood that excessive micromotion (relative motion between an endosseous implant and adjacent bone) compromises osseointegration. However, few studies have quantified the effect of micromotion on osseointegration. Design an experiment to determine if there is a threshold in motion for osseointegration.

Key to experiments is designing a system in which motion is controlled, such as by creating a standard sized defect in an animal model and inserting different sized implants, and measuring the relative motion when subjected to a controlled load. Relative motion can then be related to histological findings or contact area to create a calibration curve between displacement and % bone contact or thickness of fibrous tissue as metrics for osseointegration.

4. You are starting a job at a new biomaterials startup company. Your first project is to scale up the technologies from an academic project on engineering craniofacial bone using 3D printed ceramic scaffolds and stem cells in a small animal. What are the considerations for scaleup that you should consider?

There are two components to scaleup: from small animal to human and from a small number of samples to a large number of samples.

In scaling from animal to human, the dimensions of your system needed to engineer larger volumes of tissue (size of scaffold, increased number of cells), does scaffold design need to change or just scale proportionally? Will transport considerations and ability to induce vasculature change? Will Good Laboratory Practice manufacturing be required and, if so, will any changes to the processes be needed?

In scaling from lab experiment to mass production, some considerations include: the cost of raw materials, space, and time requirements for manufacturing a much larger number of devices and cells, potential need to redesign bioreactors.

5. Recombinant growth factors are a means of stimulating oral tissue regeneration, and several have advanced to in-human studies and commercial products. What do you think are the advantages and disadvantages of using recombinant factors? What do you think are the key issues that must be thought through/experimentally tested if this application is to achieve greater clinical reality?

Advantages: Potentially unlimited supply; avoidance of transplanting cells/cell culture issues; avoidance of issues of transplant survival; no rejection.

Potential disadvantages/critical issues: safety; efficacy; means of delivery (carrier, implantation); retention of activity upon delivery; specificity of activity to targeted need; off-target effects; off-target effects; functionality/stability of new tissue; cost.

2.5.6

Ophthalmologic Applications: Introduction

HEATHER SHEARDOWN, EMILY ANNE HICKS, AFTAB TAYAB, BEN MUIRHEAD

Department of Chemical Engineering, McMaster University, Hamilton, ON, Canada

Overview of the Anatomy of the Eye

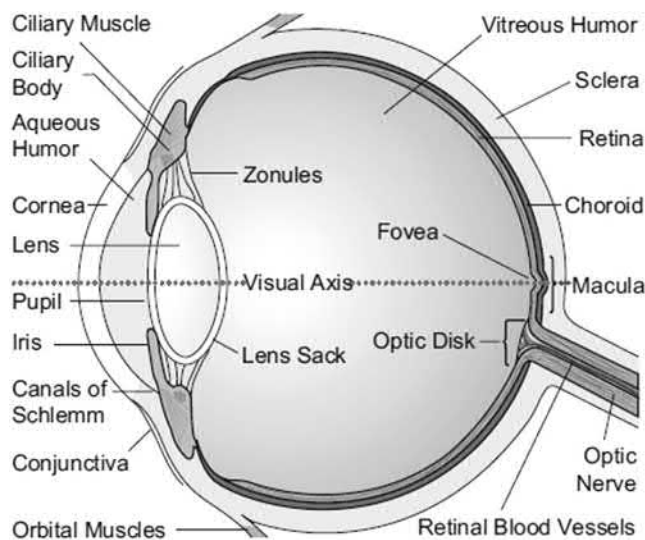
The purpose of the eye is to generate images from reflected or emitted light, focusing the light, and subsequently converting the images to electrical signals which are transmitted to the brain via the optic nerve. Performing these functions requires the interaction of a complex array of cellular components. The eye itself can be described as a globe within a globe (see [Fig. 2.5.6.1](#)), the dimensions of which are summarized in [Table 2.5.6.1](#).

Light enters the eye through the transparent window of the eye, the cornea. With a diameter that typically ranges between 10.5 and 12.5 mm, the cornea serves as both a protective barrier as well as performing a refractive function, providing ~80% of the focusing power of the eye. It has a refractive index of approximately 1.34 and is comprised of five structurally distinct layers. Covering the anterior surface of the cornea are five to six layers of corneal epithelial cells which serve mainly a protective role. The epithelial basement membrane, or Bowman's layer, is comprised mainly of collagen and is thought to represent a transition between the stromal and epithelial layers. The stroma, comprising approximately 90% of the thickness of the cornea, is made up mainly of hydrated (80% water) collagen with interspersed keratocyte cells that produce and repair the collagen matrix as well as producing other components (glycosaminoglycans for example). Descemet's membrane, the basement membrane of the corneal endothelium is comprised mainly of type IV and type VIII collagen. The endothelium is a single layer of quiescent cells which do not regenerate if damaged. It has the important function of maintaining stromal hydration, pumping water to the aqueous layer, while providing nutrients to the keratocytes. The lack of a blood supply to the cornea means that this transport is essential to maintaining corneal health and function. The transparency of the cornea is due to a combination of factors including the organization of the collagen in the stromal layer, the maintenance of hydration due to

the endothelial pump, the presence of glycosaminoglycans which reduce light scattering, and the lack of blood vessels in the eye. The structure and layers of the cornea are depicted in [Fig. 2.5.6.1](#).

The iris, responsible for controlling the amount of light that passes through to the retina by varying the size of the pupillary opening, is a vascularized, pigmented tissue. It separates the anterior and posterior chambers of the eye. The ciliary body, also a vascularized pigmented tissue, consists of the ciliary muscle and the ciliary process and has two major functions—the production of aqueous humor and accommodation. The aqueous humor, a clear fluid with a composition similar to blood plasma, that resides in the aqueous chamber, provides nutrients to the crystalline lens and the cornea, neither of which has a direct blood supply. The aqueous humor travels around the lens, through the pupil, and is ultimately drained into Schlemm's canal through the trabecular meshwork. The intraocular pressure of the eye is partially maintained by the balance of aqueous humor production by the ciliary processes and aqueous humor drainage through the trabecular meshwork. Typically, in the human, the intraocular pressure (IOP) is between 10 and 20 mmHg.

The crystalline lens sits in the posterior chamber, behind the iris and the pupil. The structure is shown in [Fig. 2.5.6.1](#). The center of the lens is comprised of a nucleus which is surrounded by lens fiber cells. These cells synthesize crystallin proteins which maintain the refractive index of the lens at approximately 1.42. The lens is connected to the ciliary body by fine suspending ligaments or zonules, which are critical to accommodation. Accommodation is the ability to change the focus of the lens to allow for visualization of both near and distant objects. The ability of the natural crystalline lens to accommodate decreases with age. When the ciliary muscle contracts, the zonule fibers relax their natural state of tension on the lens periphery, which changes the focal length of the lens. Surrounding the natural crystalline lens is a thin collagen membrane known as the capsular



• **Figure 2.5.6.1** Schematic representation of the cross-section of the eye (www.99main.com/~charlief/Blindness.htm).

TABLE 2.5.6.1 Approximate Dimensions of Globe and Ocular Structures

Measurement	Length, Thickness or Diameter (mm)
Axial length of globe	23–26
Corneal diameter (white-to-white)	10.5–12.5
Equatorial diameter	23–26
Anterior chamber depth (ACD)	3–4
Anterior chamber diameter	12.0–12.5
Sulcus diameter	11.0–11.7
Natural crystalline lens diameter	9.0–10.2
Natural crystalline lens thickness	3.5–4.5
Capsular bag diameter after lens extraction	9.2–10.5
Capsular thickness	0.004–0.014
Retinal thickness	0.2–0.25

bag. In the noncataractous lens, the anterior portion of the capsule is coated with a layer of lens epithelial cells; no cells are located on the posterior surface of the lens. With cataract formation, a layer of nontransparent epithelial cells can be generated on the anterior surface of the capsule.

At the posterior of the eye, the retina is up to 10 layers thick and is responsible for capture of the visual image and its translation via the optic nerve. It has a complex structure and consists of numerous cell types. The choroid is the vascular layer behind the retina, supplying oxygen and nutrients to the cellular layers of the retina. The retinal pigmented epithelial layer (RPE), forms a tight junction epithelial layer immediately apical to the choroid. The pigmented nature of these cells means that the absorption of light is among its primary functions. Critical to retinal health, the RPE layer also must provide

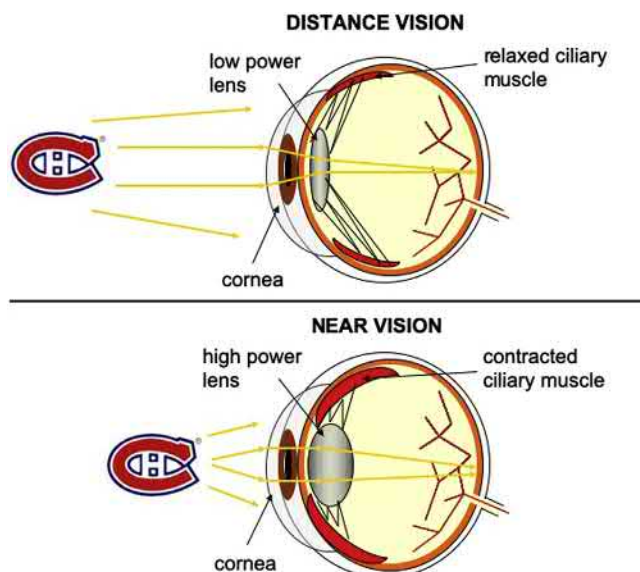
efficient defense against free radicals, light energy, and photo-oxidative exposure. The tight junctions suggest that the RPE layer also plays a role as part of the blood–retinal barrier and in the immune privilege of the eye. Two types of photoreceptors, rods and cones, sit next to the RPE layer. The cones are concentrated in the macula, the central region of the retina, while the rods are more dominant in the peripheral retina. Cones are responsible for central vision as well as for daytime vision; rods play a greater role in peripheral and dim light vision.

Eye-related Conditions and Statistics

The National Eye Institute in the United States has estimated that there are currently 2.9 million Americans living with low vision, defined as best corrected visual acuity <20/40. This number is expected to increase by 72% by 2030. Approximately one million of these patients are characterized as blind (Varma et al., 2016). Internationally, the World Health Organization estimates that there are more than 1.3 billion people living with some kind of vision impairment and 36 million of these are blind (Bourne et al., 2017, 2019).

The vast majority of vision issues occur in patients older than 50. In the United States, age-related diseases including cataract, glaucoma, and age-related macular degeneration account for almost 80% of all cases of vision-associated disorders (Varma et al., 2016). Diabetic retinopathy, the main vision issue of the working age population, accounts for the other 20% of cases. The economic burden of vision issues in the United States alone has been estimated at more than \$139 billion. Correctable and more common vision issues, including myopia, hyperopia, astigmatism, and presbyopia, arise from refractive errors. Myopia, more commonly known as near-sightedness, in which the patient cannot focus on an object in the distance, has reached epidemic proportions in children, particularly in the Far East (Brennan and Cheng, 2019; Greene and Greene, 2018). This is thought to be partly the result of screen time and a lack of outdoor play in children. Hyperopia, or far-sightedness, occurs when one can focus on objects in the distance but not on objects that are close. A schematic of image formation in the myopic and hyperopic eye is shown in Fig. 2.5.6.2. Presbyopia, a condition of aging, occurs as a result of the loss of accommodation in the lens. It typically becomes symptomatic between the ages of 40 and 50 and results in the need for reading glasses to allow for focusing on near objects. Astigmatism, estimated to affect as many as 30% of Americans, occurs when the cornea is no longer spherical.

Cataract, the leading cause of low vision in the United States, refers to clouding or opacification of the lens, typically as a result of aging. However, cataracts can also be due to trauma or injury, congenital, or can result from underlying pathologies or medications. They are highly treatable; affecting more than 20.5 million patients in the United States over the age of 40, more than two million surgeries, involving the replacement of the diseased lens with an artificial intraocular lens, are performed annually. The success



• **Figure 2.5.6.2** Depiction of lens changes during accommodation for distance.

rate is typically greater than 90%, with posterior capsule opacification (PCO) being the most common complication. PCO can be effectively treated with a secondary laser procedure.

Glaucoma, including primary open-angle glaucoma, angle closure glaucoma, and congenital glaucoma, is typically characterized by increased intraocular pressure, changes in the optic nerve head, specifically increased cupping, and/or loss of visual field. Vision loss is ultimately the result of the death of the nerve cells and as such is not reversible. Typically, the treatment strategy is initially pharmacological, with a goal of lowering the intraocular pressure (IOP). However, if the IOP cannot be managed pharmacologically, laser treatment or surgery to implant a glaucoma shunt or a stent is performed. Laser treatments, including argon laser trabeculoplasty or selective laser trabeculoplasty, have the goal of creating space in the trabecular meshwork to facilitate aqueous humor outflow. A glaucoma shunt consists of a plate, which resides in the subconjunctival space, and a tube, which is placed in the anterior chamber of the eye. The shunt aids in aqueous humor drainage by creating another outflow pathway, allowing the flow of aqueous humor out through a sieve into the tissues, where it is absorbed.

Age-related macular degeneration (AMD) is the most common cause of blindness in the aged population (Zhao et al., 2019; Rudnicka et al., 2015). Dry AMD, the most common form, accounts for approximately 90% of all cases and is characterized by the presence of small yellow deposits known as drusen, which accumulate in the retinal pigmented epithelial cells adjacent to the macula. Progression of the dry form to the wet form, which accounts for approximately 10% of all cases of AMD, leads to ~90% of AMD-associated vision loss. Wet AMD is characterized by the growth of abnormal blood vessels, known as choroidal neovascularization (CNV). These blood vessels originate

in the choroid under the macula, invading the retinal tissue and leading to major cellular damage and central vision loss. Treatment for wet AMD involves monthly injection of anti-VEGF molecules into the globe of the eye.

Diabetic retinopathy (DR) is the leading cause of blindness among the working age population (Groeneveld et al., 2019). Affecting approximately 7.7 million Americans, a number which is projected to increase to 11.3 million Americans by 2030, DR is associated with both types 1 and 2 diabetes. There are two types of DR—nonproliferative and proliferative. Nonproliferative DR is less severe, and leads to blurred vision as a result of the leakage of edema fluid from the blood vessels into the retina. Proliferative DR is usually more severe and results in neovascularization on the surface of the retina; these vessels can at times reach into the vitreous. These new, poorly formed vessels are leaky, leading to hemorrhage and profound vision loss. As with AMD, approved treatments include injections of anti-VEGF drugs into the back of the eye or in some cases laser treatment of the hypoxic retina.

Considerations for Ophthalmic Materials

Similar to materials used in other areas of the body, biocompatibility, stability, degradation, sterilizability, and manufacturability all must be considered. However, unique to materials to be used in ophthalmic applications, considerations around the optical properties must be taken into account. Optical properties are particularly critical for contact lens materials, corneal inlays or onlays, as well as intraocular lenses. The materials must be transparent, with a refractive index that is equal to or greater than the tissue that is being replaced. In some cases, UV-blocking agents are incorporated into these materials in order to protect the delicate retina from UV light exposure. In addition, any material used in the cornea, such as a contact lens or a corneal inlay, must have sufficient oxygen and nutrient permeability to allow for the maintenance of corneal health due to the lack of vascularization of this tissue. Biomaterials commonly used in ophthalmic applications are outlined in Table 2.5.6.2.

Biomaterials: Contact Lenses

In order to overcome variations in eye length, which can affect the ability of the refractive elements of the eye, the cornea and lens, to focus the image correctly on the retina, lenses, including spectacles and contact lenses, are placed in front of the cornea in order to adjust light refraction. Currently, it is estimated that 45 million Americans wear contact lenses; two-thirds of these wearers are female (Chalmers and Gleason, 2013). The decision to wear contact lenses over spectacles is affected by various factors but it is most often the practicality of lenses or their physical appearance that wearers consider. They are made from a variety of biomaterials, and because they are in intimate contact with the ocular tissues, they are subject to the same federal regulations that govern implant materials.

TABLE 2.5.6.2 Biomaterials Commonly Used in Ophthalmology

Ophthalmic Implants	Materials Commonly Used
Contact lenses	Poly(methyl methacrylate) (PMMA), 2-hydroxyethyl methacrylate (HEMA) copolymers, silicone hydrogels
Inlays or onlays	Hydrogels, collagen, permeable membranes
Intraocular lenses	Optic: PMMA, hydrophobic acrylic, silicone, hydrophilic acrylic; Haptic: polypropylene, PMMA, polyimide, polyvinylidene fluoride (PVDF)
Ophthalmic viscosurgical device (OVD)	Chondroitin sulfate, sodium hyaluronate, hyaluronic acid, hydroxypropyl methylcellulose (HPMS), polyacrylamide, collagen, or combinations of these materials
Glaucoma shunts	Plates: silicone (impregnated with barium), polypropylene; Tubing: silicone
Vitreous replacements	Silicone oil, gases

Materials used in contact lens applications must meet a number of requirements to be suitable. As optical devices, light transmission is paramount; the ability to transmit close to 100% of visible light is a key determinant in whether a material will be useful in contact lens applications. The ability to maintain a highly wettable surface is a key criterion in order to maintain the structure of the tear film. Surface properties that minimize fouling with tear components such as lipids and proteins are desirable since it has been suggested that the deposition of these molecules can impact optical properties, wearer comfort, and even the permeability of the lens materials.

Hydrogel materials, which are typically used in lens applications, have an inherently wettable surface, particularly when fully hydrated. However, when placed on the eye, thermodynamic factors can impact the surface properties. Water loss, particularly under adverse environmental conditions such as low humidity, high wind, or high temperatures can lead to wearer discomfort. Furthermore, polymer chain reorientation may occur, depending on such factors as polymer structure, cross-linking and the presence of bulky side groups. When in contact with the aqueous layer of the tears, typically the more hydrophilic groups will migrate to the surface. However, upon exposure to the tear film lipids or an air environment, the more hydrophilic groups are driven into the bulk of the material, exposing the more hydrophobic groups on the surface and leading to changes in biofouling and material performance which can affect eye performance.

Since the cornea is an avascular tissue, it receives oxygen from the ambient air during open eye conditions and from the palpebral conjunctival vessels during closed eye conditions. Diffusion of oxygen through the tear layer occurs with both of these sources. Therefore, contact lenses represent a significant barrier to oxygen transmission. In order to improve oxygen delivery to the cornea, it is necessary to either improve diffusive oxygen transmission through the lens or alter the convective tear exchange under the lens. Oxygen permeability through a contact lens is typically represented as Dk where D is the diffusion coefficient of oxygen in the material in cm^2/s and k is the Henry's law solubility coefficient with units of $\text{cm}^3 (\text{O}_2\text{STP})/[\text{cm}^3 (\text{polymer}) \text{mmHg}]$. Often the lens material oxygen transmissibility is normalized for the thickness of the lens (Dk/L), although companies typically report the Dk value for their lenses.

Lack of oxygen to the cornea has been shown to lead to corneal hypoxia, characterized by corneal swelling as well as other conditions including limbal hyperemia, neovascularization, corneal acidosis, epithelial keratitis, and endothelial polymegethism (McKay et al., 2017). Holden and Mertz determined that the oxygen transmissibility necessary to avoid corneal edema for daily wear is $24.1 \pm 2.7 \times 10^{-9}$ ($\text{cm} \times \text{mL O}_2/(\text{s} \times \text{mL} \times \text{mmHg})$) and $87.0 \pm 3.3 \times 10^{-9}$ ($\text{cm} \times \text{mL O}_2/(\text{s} \times \text{mL} \times \text{mmHg})$), although more recent experiments have suggested it may be higher than this (Fink et al., 2006; Gardner et al., 2005; Pilskalns et al., 2007; Harvitt and Bonanno, 1999; Ostrem et al., 1996).

Contact Lens Materials

There are two main categories of contact lenses that are grouped by their basic mechanical properties. Hard contact lenses, more commonly referred to as rigid gas-permeable lenses, are rigid materials with a high modulus, generally containing either silicone or fluorine derivatives to allow for oxygen permeation. Soft contact lenses are hydrogel materials with a low modulus and higher water content. Within this category, silicone hydrogels are newer materials that contain a hydrophobic but oxygen-permeable siloxane component, while conventional materials are typically made of more hydrophilic monomers.

Hard Contact Lenses

Originally made from poly(methyl methacrylate) (PMMA), hard contact lenses are now copolymers of PMMA functionalized with silicone- and fluorine-containing macromers. One of the first monomers to be discovered was methacryloxy propyl tris(trimethylsiloxy) silane (TRIS) (see Fig. 2.5.6.3), which significantly increases the oxygen permeability of these materials. Subtle changes in the chemical composition of the lens can impact clinical performance. For example, while silanes are effective at increasing oxygen permeation, their lipophilicity can lead to increased biofouling. Fluorinated polymers can

also improve oxygen permeability but are more resistant to fouling. Therefore currently marketed RGP lenses mainly consist of perfluoroalkyl-siloxanylalkyl-methyl methacrylate type materials which have both a high Dk and good surface properties (Chalmers and Gleason, 2013). While they make up a small fraction of contact lenses currently marketed (currently approximately 14% of all fits in the United States), hard contact lenses are particularly good for patients with significant corneal astigmatism or non-spherical corneal surfaces, and will therefore continue to have a market. However, materials developments in these materials are virtually nonexistent; wearable biosensors are one area where these materials might see revitalization (Ruan et al., 2017).

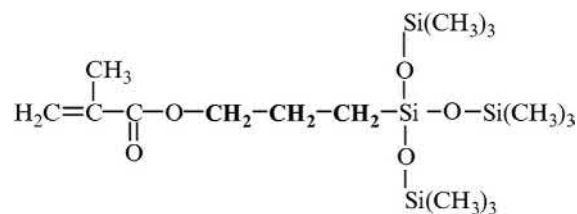
Soft Hydrogel Contact Lenses

Due to the water content of hydrogels, and their resulting low modulus, soft contact lenses have a high degree of comfort that allows them to be worn by a majority of the population. The first commercial contact lens material, poly 2-hydroxyethylmethacrylate (PHEMA), was developed by Wichterle and Lim in 1959. It has a water content of approximately 40% and has such advantages over previously developed materials related to stability to pH, temperature, and osmolarity as are found under physiological conditions. To increase the water content of these materials, a variety of other monomers have been used or incorporated. N-vinyl pyrrolidone (NVP), n,n-dimethyl acrylamide (DMA), vinyl acetate, post hydrolyzed to vinyl alcohol units as well as methacrylic acid (MAA) have proven to be particularly successful.

The Dk of conventional hydrogel materials increases exponentially with water content as delivery of oxygen is through the aqueous component of the lens. Therefore, the oxygen permeability limit of these hydrogels approaches that of the permeability of pure water to oxygen (Dk of water = 125 barrer). However, higher water-content materials, such as those with a water content over 50%, while possessing better O₂ permeability, suffer from a greater degree of dehydration and are more fragile due to low modulus. Decreasing the thickness of these materials can also be used to increase oxygen transmission but, again, mechanical properties suffer with this approach. Typically the Dk of conventional lenses ranges between 8 and 44 barrers (Chhabra et al., 2007; Compan et al., 2004).

Silicone Hydrogel Contact Lenses

As a result of their moderate oxygen transmissibility, conventional hydrogel materials are limited in terms of their ability to be worn overnight or for an extended period, with the risk of adverse effects increasing more than four-fold with extended wear. To overcome the limitations of these materials while maintaining comfort, the contact



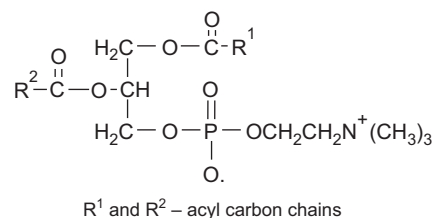
• **Figure 2.5.6.3** The structure of TRIS, used in contact lens manufacture.

lens industry developed siloxane-containing hydrogel materials. These lenses are prepared by copolymerizing typical hydrogel monomers with methacrylate or vinyl end capped polydimethylsiloxanes, novel comonomers, and/or hydrophilically modified TRIS. This leads to compatibilization with the more hydrophilic components of the hydrogel. Depending on the composition, the oxygen permeability of these siloxane-containing hydrogel materials ranges between 60 and 160 barrers (Chhabra et al., 2007; Compan et al., 2004) and, unlike conventional materials, there is an inverse relationship between O₂ permeability and equilibrium water content, since oxygen permeation occurs primarily through the siloxane-rich components of the material. However, as described in Nicolson and Vogt (2001), water and ion permeability are also essential in these materials to allow for lens-on-eye movement.

The presence of the mobile siloxane groups in these materials increases their surface hydrophobicity and decreases their wettability, leading to increased biofouling and the need for surface modification to alter the surface properties.

Surface Modification

The inherent hydrophilicity of conventional hydrogel materials originally led to the belief that no surface modification was necessary. It was found however, that certain bulk side-chain moieties led to the enhancement of surface properties, resulting in the development of materials with surface-active side groups, surface-modifying endcaps, or interpenetrating networks. The first material of this genre to be approved by the FDA was Omafilcon A (Proclear) lenses which contain a hydrophilic methacrylate monomer containing a zwitterionic side group, modeled after phosphatidyl choline (Fig. 2.5.6.3) that is thought to preferentially hold water on the surface.



Silicone hydrogel materials, due to the hydrophobic and mobile nature of the siloxane groups, require surface

modification to generate sufficiently wettable surfaces. The first silicone hydrogels on the market were plasma treated to alter the surface properties without adversely affecting the bulk. Balafilcon A (Pure Vision, Bausch, and Lomb) is plasma oxidized, creating glassy silicate islands on the lens surface. The properties of these islands are such that a hydrophilic surface is generated without altering the bulk properties of the material. Lotrafilcon A and B (Night and Day, O₂ Optix, CIBA Vision) has a plasma coating of a hydrophilic polymer approximately 25 nm thick. In both cases, these coatings are designed to lower the mobility of the underlying silicone layer, minimizing the reorientation of the silicones to the surface. However, the lack of chain mobility in these materials increases the lens modulus, leading to stiffer materials.

To overcome patent issues and issues with the use of plasma as a modification tool, Vistakon's first silicone hydrogel materials, galyfilcon A (Acuvue Advance) and senofilcon A (Acuvue Oasys) contain high-molecular-weight poly(vinyl pyrrolidone) (PVP) as an internal wetting agent, creating a wettable, lubricious surface without the need for subsequent surface treatment. Galyfilcon A is packaged with PVP in the packing solution; senofilcon A lenses have the PVP incorporated as polymeric end caps which preferentially migrate to the lens surface. In both cases, the increased wettability does not lead to compromised mechanical properties.

Comfilcon A (Biofinity, Coopervision) deviates from the expected oxygen permeability/water content curve, with a high water content at 48% and an unexpectedly high Dk, presumably the result of the presence of longer siloxane chains. It has no surface treatment or internal wetting agent and is produced by polymerization of two siloxy macromers of different sizes, one of which has only one vinyl polymerization site along with vinyl amides such as n-methyl-n-vinyl acetamide.

Contact Lens Solutions

Depending on the nature of the contact lens, effective daily disinfection and cleaning of the lens is necessary. Among the most popular systems currently are those based on hydrogel peroxide, although other chemically based systems are also common. Multipurpose cleaning solutions perform a myriad of functions including removal of deposits such as protein and lipid that are adsorbed from the tear film, disinfection, and prevention of future biofouling. Product efficacy varies depending on the composition of the solution as well as the lens that is paired with the solution. Most of these systems use hydrophilic polymers to increase cleaning efficiency and to improve lens surface hydration. Some of the polymers used, such as Poloxamer 407, act on the surface of the bacteria and not on the lens. Issues have arisen with lens cleaning solutions however, specifically related to topping up the solution resulting in a decrease in the efficacy of the killing of bacteria.

Intraocular Lens Implants

Introduction to Intraocular Lens Implants, the Optics of the Eye, and Cataracts

Cataracts are the leading cause of preventable blindness in the world (Flaxman et al., 2017). With the aging of the population, the incidence of cataracts is increasing globally, leading to the implantation of more than 10 million lenses annually. The cloudy, cataractous lens removed during surgery is replaced by a polymeric intraocular lens (IOLs) to restore visual acuity. Between 1990 and 2010, the rate of cataract surgeries more than tripled (Wang et al., 2017), making IOLs among the most commonly implanted biomaterials. With technical advancements and the demand for treatment solutions growing, creation of new biomaterials, designs, and applications is becoming increasingly important.

The physiological process of vision is complex. The refractive power of the cornea represents about 70% of the total refractive power of the eye and is fixed at approximately 43 diopters; the lens then provides the remaining variable refraction. The natural lens consists of a cortex-surrounded nucleus within a capsular bag attached to the ciliary muscle by ligaments, called zonules (Fig. 2.5.6.1). When relaxed, the zonules place the lens under tension, providing 20 diopters of refractive power for distant vision. For close-up vision, the ciliary muscle contracts, the zonules relax, resulting in a change in the lens shape which increases refractive power in a process called accommodation. With age, as the lens grows, the ability for accommodation gradually decreases to less than the 3 diopters necessary for reading distance and the eye is considered presbyopic.

Further aging of the lens can result in loss of optical clarity due to cataract formation. Cataract surgery involves the removal of the cataractous lens and the implantation of an intraocular lens. Prior to IOL implantation, thick spectacles were needed to restore the function of the removed natural lens, which had a significantly reduced field of vision and resulted in severe astigmatism from the large incision required for cataract surgery. The size and optic of the modern IOL and its intraocular location have eliminated these setbacks.

IOL Biomaterials and Design

Biomaterials selected for lens production must have such design objectives as targeted incision size for insertion and mechanical fixation, typically via haptics as well as transparency. In 1949, Sir Harold Ridley implanted the first IOL made of Perspex, a PMMA material, after shards of cockpit canopies made from the same material did not elicit the inflammatory response in the eyes of Royal Air Force pilots (Ridley, 1976). The original bulky PMMA lenses were rigid, requiring a large incision for insertion, making them difficult to surgically fix within the eye, and leading to serious post-op complications and ultimately discontinuation of their use. PMMA continued to be the material of choice

when smaller optics and fixation means were being designed (Apple, 1986).

Advances in surgical technique were critical to the development of current IOL materials. Currently, extracapsular cataract extraction (ECCE) removes the opacified lens, while preserving the intact capsular bag, excluding the anterior capsule face (Amon, 2001). However, residual lens epithelial cells (LECs) near the lens equator can undergo epithelial to mesenchymal transition, with a reduction in their transparency resulting in PCO and fibrotic contraction of the capsular bag (Kruger et al., 2001). PCO reduces optical clarity, resulting in the formation of a “secondary cataract.” An Nd-YAG laser can be used to create an optically transparent path in the posterior capsule, but there are several disadvantages including cost, damage to the IOL, and retinal detachment (Karahan et al., 2014). To prevent PCO, recent advances have led to changes in the optic shape and haptics to achieve complete contact of the PC-IOL to the posterior capsule, which minimizes epithelial migration and secondary cataract formation (Findl et al., 2010; Matsushima et al., 2008; Nibourg et al., 2015).

The introduction of ultrasonic phacoemulsification, a process providing both irrigation of the eye to prevent anterior chamber collapse and aspiration of the fragmented lens, decreased the rate of surgically induced astigmatism through the use of a smaller incision while producing a limited inflammatory response (Gills and Sanders, 1991). The 3-mm incision made during this process is self-healing, which eliminates the need for stitches, but introduced a need for a soft, foldable biomaterial that could fit through the small wound. The first foldable IOL, made of transparent polysiloxane introduced by Staar Surgical (Mazzocco, 1985), was followed by several formulations with different mechanical properties and refractive indices from other companies. In 1994, Alcon introduced the first acrylic foldable IOL, AcrySof, a copolymer of phenylethyl acrylate and phenylethyl methacrylate with a cross-linking agent and a bound UV-chromophore (Madrid-Costa et al., 2010). The AcrySof IOL soon became the most widely used foldable IOL, reaching over 100 million implanted by 2017, with satisfactory outcomes.

Newer generations of silicone foldable IOLs and hydrophobic, as well as hydrophilic, foldable acrylates continue to be developed (Table 2.5.6.2). The success of these IOLs requires favorable short-term postoperative results, as well as long-term reduction of PCO formation, with <5% capsulotomy rate for Alcon's AcrySof IOL (Madrid-Costa et al., 2010). PCO and laser capsulotomy rates are influenced by both the IOL biomaterial and optic edge design, with the best outcomes observed in hydrophobic IOLs with sharp edges, while haptic design and optic size also influence PCO formation (Perez-Vives, 2018).

The history of IOL materials can therefore be broken down into nonfoldable or foldable categories, based on flexibility. While nonfoldable PMMA IOLs are seldom used in the developed world due to advancements in surgical techniques, these lenses play an important role in countries

where ECCE with manual expression of the lens remains standard practice (Tabin et al., 2008). Foldable IOLs can further be broken down into silicone or acrylate materials. Hydrophobic and hydrophilic acrylic IOLs are currently the most commonly used materials with high refractive indexes and strong biocompatibility (Perez-Vives, 2018).

Current designs in modern IOLs show that the majority of implants are fixated within a capsular bag, as a single-piece IOL of homogeneous material or multipiece IOL with the optic and haptic made from different materials. Common haptic materials include PMMA, polypropylene, polyimide, and poly(vinylidene) fluoride (PVDF) (Izak et al., 2002). Haptic design is an important consideration for maintaining the IOL in a fixed position. Two factors contribute to good haptic design: loop rigidity and memory. Loop rigidity determines the resistance of the haptics to external forces acting to bend the loops centrally, such as the force from fibrotic capsular bag contraction, while memory is the ability of the haptics to reexpand to their original configuration after implantation (Izak et al., 2002).

IOLs With Variations of Optical Function

Traditional spherical IOLs are not mimetic of the asphericity of the natural lens. IOLs with appropriate aspheric optics can more closely match the optical quality of the natural lens and account for corneal aberrations. The first FDA-approved aspheric IOL was the Tecnis IOL by AMO (acquired by Johnson & Johnson Vision, Inc.) followed by AcrySof IQ made by Alcon, and SofPort AO made by Bausch & Lomb. Comparative evaluations are ongoing to determine the advantages and disadvantages of each design (Jia and Li, 2014). However, due to differences in surgical technique and materials, it is often difficult to directly compare different IOL compositions.

Using the same biomaterials as monofocal IOLs, toric IOLs offer an alternative for precise correction of preexisting corneal astigmatism. The first toric IOL was a non-foldable three-piece PMMA IOL, which required a large incision for implantation (Shimizu et al., 1994). Shortly after, the first foldable, one-piece silicone toric IOL was developed, which required a much smaller incision. Post-operative rotation of toric IOLs significantly compromises the optical objective. The FDA-approved AcrySof IQ Toric, made by Alcon, a single-piece optic with somewhat flexible haptics, has been shown to have good results without significant rotation. TecnisToric, by Johnson & Johnson Vision (previously AMO) and Bausch & Lomb TruLign Tori, is also FDA-approved.

Multifocal IOLs

With the use of computers and screens, satisfactory intermediate distance vision has become as much a requirement as near vision following cataract surgery. Multifocal IOL implantation aims to achieve complete spectacle independence for all viewing distances. Utilizing the same

biomaterials as monofocal IOLs, several designs have been investigated for optical imaging at different focal planes. The first concept of a truly multifocal IOL was conceived by Hoffer in 1983 (Hoffer, 1991) and the first bifocal IOL was implanted in 1986 (Keates et al., 1987).

Multifocal IOLs have distinct focal points and can be provided with various focal lengths. Lenses can be bifocal, trifocal, or the focus can be extended longitudinally with a far focus reaching intermediate distances also known as an extended depth of focus (EDOF) IOL. These IOLs are based on refractive and diffractive optic principles rather than on materials properties. The FDA-approved Array Multifocal IOL, introduced by AMO, had a radial array of alternation variable optical powers, providing distant and near vision (Steinert et al., 1999). A redesign of this IOL, with improvements for night-time driving and halos, is currently on the market as ReZOOM. TECNIS Multifocal (Johnson & Johnson Vision) has a diffractive optic design, which had similar halo effects with night-time driving as the Array Multifocal. A unique optical design combining central apodized diffractive optical zones with refractive optics beyond was introduced by Alcon as the AcrySoftReSTOR (Kohnen et al., 2006).

Newer multifocal IOLs include trifocal IOLs, with the generation of a third focal point. These IOLs have shown excellent levels of corrected distant, intermediate, and near visual acuities and good contrast sensitivity (Kretz et al., 2015a,b). The first EDOF IOL, Johnson & Johnson Vision's Symphony, was approved by the FDA in 2016. Other EDOF IOLs being investigated include LENTIS Mplus (Oculentis) and LenstecMiniwell IOL.

In certain presbyopic, hyperopic, or myopic patients, multifocal IOLs can be used to correct optical refractive errors. Combining different IOLs via bilateral multifocal IOL implantation can improve binocular vision at different distances. Multifocal IOLs provide overall spectacle independence for both distant and near vision in approximately 83% of patients compared to 10% in monofocal IOLs (Alio et al., 2017). Despite negative subjective phenomena, such as glares and halos, overall satisfaction and quality of life after multifocal implantation is generally high.

Phakic IOLs are an alternative to LASIK and photorefractive keratectomy procedures for correcting moderate to severe myopia, in some cases providing better and more predictable visual outcomes (Barsam and Allan, 2014). Currently the two FDA-approved phakic IOLs on the market are Visian ICL (implantable collamer lens) from Staar Surgical and Verisyse from AMO (now Johnson & Johnson Vision). Verisyse, an iris-fixated, rigid PMMA IOL offers a larger optic zone than LASIK, potentially causing less glare with large pupils. Visian ICL, a PC-IOL made of collagen copolymer (collamer), is a foldable implant, highly elastic in nature, and is reported to have fewer complications than its anterior counterpart (Sanders et al., 2004). Both phakic IOLs are capable of treating a wider range of myopic conditions than laser refractive procedures with better contract sensitivity, less visual distortions, and a higher level of satisfaction.

Accommodative IOLs

Providing true accommodation after cataract surgery as well as treating refractive errors with a safe and effective accommodative IOL has been of interest for several years. Single-optic accommodating IOLs, with flexible supporting elements, transmit the contraction of ciliary muscle into a change in anterior displacement of the optic, increasing power for near vision. Several single-optic IOLs are currently being investigated, including the 1CU (Human Optics), Tetraflex KH3500 (LensTec), and Crystalens AT-45 and Crystalens HD (Bausch & Lomb). A major drawback to single-optic accommodating designs is the limited amplitude of accommodation which declines following capsular fibrosis (Liang and Jia, 2018).

Dual-optic accommodating IOLs have a fixed, high-powered positive anterior optic and a negative posterior optic coupled by spring haptics designed to occupy the complete capsular bag to take advantage of natural accommodative mechanisms (Alio et al., 2017). Recent developments of dual-optic accommodating lenses include Visiogen's Synchrony and Bausch & Lomb's Sarfarazi IOL. Similar to single-optic accommodating IOLs, maintaining the elasticity of the capsular bag remains a challenge (McLeod et al., 2007, 2008).

NuLens (NuLens, Ltd.) is an example of a deformable surface-accommodating IOL made with a flexible gel contained in a small chamber made up of a PMMA anterior reference plane with a central hole, and a posterior piston (Alio et al., 2009). As the ciliary muscle contracts, the capsular bag displaces the gel component, resulting in a change in refractive power. Other early-stage accommodative IOLs include magnetic-driven shift utilizing the repulsive forces of magnets implanted under the superior and inferior rectus muscles driving the lens forward during accommodation (Sheppard et al., 2010). In the Fluid Vision IOL (Power Vision Inc.), with hollow optic and haptics, fluid displacement during muscle contraction or relaxation changes the surface curvature of the optic, thereby changing the refractive power (Kohl et al., 2014). Smart IOL (Medennium Inc.) is a thermoplastic hydrophilic acrylic implant that expands from rod-shaped at room temperature to its original shape at body temperature after implantation (Alfonso et al., 2016).

Adjustable-Power IOLs

Errors in IOL power selection from mathematical formulas and deviation in the axial position of the IOL result in postoperative residual refractive error (Werner et al., 2017). Spectacle correction of this error is acceptable, however in some cases explantation of the IOL is necessary. Postoperative adjustable power IOLs have been investigated, although the necessity for surgical reentry is of concern. Approved by the FDA in 2017, RxSight (previously Calhoun Vision, Inc.) created a unique biomaterial-based light-adjustable IOL (Tham et al., 2014). This IOL is implanted as a polymerized silicone matrix

containing nonpolymerized silicone macromers with an attached photoinitiator dispersed throughout for subsequent staged photopolymerization (Brubaker, 1991). Postoperatively, depending upon the sign and magnitude of refractive error, the IOL is judiciously exposed to long UV radiation from a slit-lamp-based LAL light delivery instrument, leading to partial photopolymerization. Exposing the central optical zone increases the power of the IOL, while exposure of the periphery decreases the power of the optic. Adjustments are made until targeted refraction is achieved, at which point the entire optic is exposed to UV radiation to lock-in the shape of the IOL. The procedure has been shown to be well tolerated by patients (Yalvac et al., 2004).

Perfect Lens LLS has developed a femtosecond laser system, Perfector, to adjust the refractive power of any commercially available acrylic IOL (Werner et al., 2017). Using green light (520 nm) at a power level below the threshold for ablation or cuts, the laser induces a chemical reaction in a targeted area of the optic, increasing hydrophilicity and decreasing refractive index (Bille et al., 2017). An in vivo animal model had promising postoperative outcomes without significant inflammatory reaction in the eye or damage to the IOL and showed good uveal and capsular biocompatibility, warranting further evaluations of this technology with clinical assessment (Werner et al., 2017).

Summary and Future of IOLs

While the need for IOLs to meet the demand of the aging population continues to grow, the development of more specialized materials and systems to create specific, functional outcomes along with evolving surgical techniques, has driven the creation of IOLs with optical and mechanical designs to meet these challenges. Development of multifocal and truly accommodative IOLs, mimicking the physiological function of the natural lens, has seen an acceleration along with improving phakic IOLs for correction of refractive errors. The modern IOL has the potential to replace spectacles, contact lenses, and corneal refractive surgeries, allowing for the achievement excellent vision. With improved understanding of the optical needs necessary for outstanding vision, customary IOLs may continue to evolve to target specific functional needs of aphakic and phakic eyes. The success IOLs have achieved in improving vision worldwide, with their continued advancement, will lead to better patient treatments and better outcomes in the future.

Glaucoma Drainage Devices

The World Health Organization (WHO) has identified glaucoma as the second largest cause of blindness in the world, affecting more than 70 million patients worldwide. Popularly known as a “silent disease,” due to the absence of noticeable symptoms, glaucoma is the leading cause of

visual disability in the United States. There is increasing incidence in Asia and Africa (Quigley and Broman, 2006; Tham et al., 2014), which has been attributed to disproportionate prevalence in Asian and African countries of improper documentation of the disease and a lack of available medical facilities. Glaucoma is often classified into two types, primary open-angle glaucoma (POAG) and primary angle-closure glaucoma (PACG).

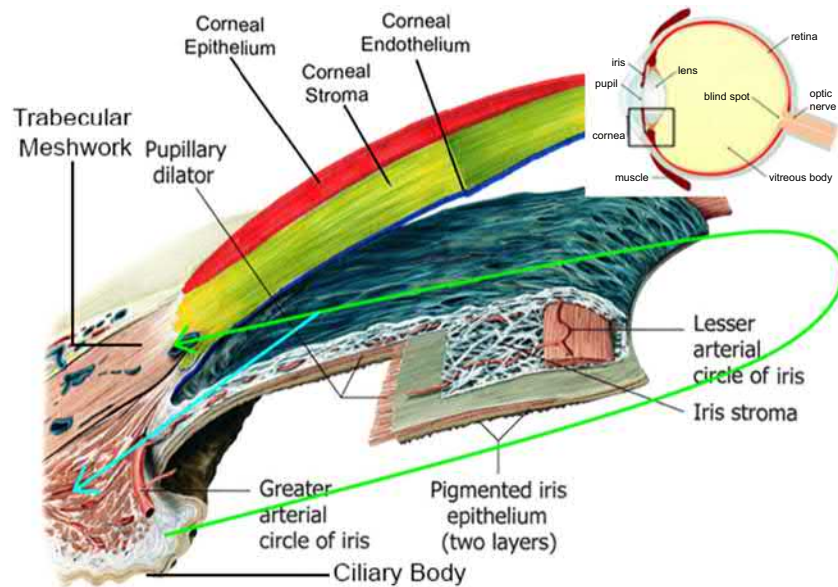
Aqueous Humor Production and Drainage

The development of POAG has been attributed to multiple structures in the anterior segment including the cornea, iris, lens, ciliary body, as well as the ocular drainage structures that make the anterior angle, such as the trabecular meshwork (TM) and Schlemm’s canal (SC). The movement of both the aqueous humor (AH), and the nourishing fluid of the anterior chamber, produced by the ciliary body at a rate of about 2.75 $\mu\text{L}/\text{min}$ (Brubaker, 1991) is shown in Fig. 2.5.6.4. The resistance in the outflow pathway, mostly the anterior angle, results in the blockade of the AH outflow leading to accumulation of AH and an increase in IOP. This increased IOP in the anterior chamber exerts pressure on the posterior chamber, leading to pressure-induced death of the retinal ganglion cells (Fig. 2.5.6.5), which are responsible for collecting visual signals. However, approximately 25% of glaucoma patients experience a loss of vision without indicating an elevation of IOP, called normal-pressure glaucoma (NPG). Regardless, the focus of glaucoma treatment has revolved around relieving IOP, thus reducing the pressure on the posterior segment of the eye.

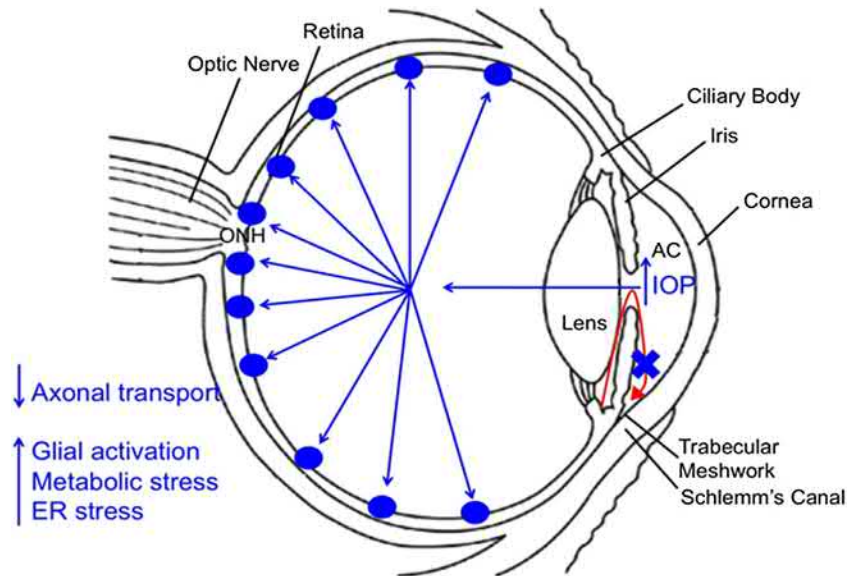
The methods for IOP management involve the following techniques: (1) topical drugs, (2) laser trabeculoplasty, or (3) drainage devices. Administration of IOP-lowering topical drugs is by far the most commonly used treatment method. These drugs typically work by increasing uveoscleral outflow and suppressing aqueous humor production. However, the efficiency of topical drugs wears off after the initial stage of efficacy, requiring increased drug dosage or an increase in the number of medications to try to control the IOP.

The most commonly practiced surgical method for lowering IOPs is argon laser trabeculoplasty (ALT) or selective laser trabeculoplasty (SLT), requiring at least two sessions to manage IOP. However, approximately 80% of glaucoma patients require continuation of topical medications within 5 years of treatment. A more invasive surgical method known as trabeculectomy, that redirects outflow drainage through a hole punched directly through the sclera, is necessary in approximately 5% of patients, although in many cases IOP is not managed just 3 years post surgery (Yalvac et al., 2004).

With the failure of pharmacological treatments and trabeculectomy to maintain the IOP, aqueous shunts or implants that are placed in the anterior segment using glaucoma surgery were developed. These implants enhance the aqueous



• **Figure 2.5.6.4** General anatomy of the eye. (A) A schematic depicting the anatomical structures of the mammalian eye. The area within the square is magnified in (B). (B) The green arrow traces the pathway of aqueous humor as it is produced by the ciliary body, travels between the lens and the iris to enter the anterior chamber, and continues to the iridocorneal angle where it will drain out of the trabecular meshwork and Schlemm's canal or the uveoscleral pathway (aqua arrow). In the event that either of these pathways is disrupted, an increase in IOP is caused that could lead to glaucomatous features. (Modified and Adapted from Atlas of Anatomy, 2015.)



• **Figure 2.5.6.5** Schematic depicting theories of the relationship between increased IOP and the development of glaucoma. When an impediment of the aqueous outflow pathway (red arrow) occurs (blue X) the pressure within the anterior chamber increases, also known as increased IOP. This increased pressure translates to the back of the eye where it will exert itself upon the retina, particularly at the optic nerve head (ONH). As a result it is thought that axonal transport of trophic factors is decreased, and/or there is an increase of glial activation, metabolic, and ER stress.

outflow by maintaining a patent, surgically created opening and preventing healing. All devices work by increasing the outflow of aqueous humor from the anterior chamber either by directly accessing Schlemm's canal or shunting aqueous humor to the suprachoroidal or subconjunctival space. The first-generation implants that utilized traditional glaucoma

surgery were large and bulky, with increased incidence of declining vision and complications. Recent advancements in the biomedical device industry have led to the development of implant devices that are of acceptable size and that can be implanted using an improved glaucoma surgery methodology, microinvasive glaucoma surgery (MIGS).

MIGS is minimally invasive and is known to avoid the complications typically encountered post glaucoma filtration surgery including hypotony, hyphema, infections, and endophthalmitis.

New-generation Microinvasive Glaucoma Surgery (MIGS) Implantation Devices

The Glaukos iStent Series

The **iStent** (Glaukos Inc.) is the first-generation trabecular bypass device that connects the anterior chamber with the Schlemm's canal, approved by the FDA in 2012. The product has a size of 1.0×0.3 mm, and is made from heparin-coated, nonmagnetic titanium and is provided preloaded in the inserter. The **iStent Inject** is a much smaller second-generation model. The mechanism of action of iStent inject is the same as the first-generation iStent. The iStent inject stents are delivered in an injector system which injects stents automatically into Schlemm's canal through a stainless-steel insertion tube. The procedure usually includes a clear corneal incision using topical anesthesia followed by a month of topical antiinflammatory and antiseptic medication. The **iStent supra** is a suprachoroidal implant made up of polyethersulfone and titanium that facilitates the transport of aqueous humor from the anterior chamber to the suprachoroidal space.

The **Hydrus** microstent is another trabecular stent that is manufactured by Ivantis Inc., currently in phase IV clinical trials. This 8 mm long stent is made up of nickel–titanium alloy (nitinol). It is inserted into Schlemm's canal, dilating Schlemm's canal in the complete nasal quadrant, thus facilitating aqueous outflow through multiple collector channels and bypassing the trabecular outflow facility. The Hydrus microstent decreased the baseline IOP by 20% in 80% of patients after 24 months following combined surgery using Hydrus microstent and PE/IOL (Pfeiffer et al., 2015). More trials are being conducted to prove the efficacy of the Hydrus microstent.

The Alcon **Cypass** micro polyamide stent creates a controlled cyclodialysis with stented outflow to the suprachoroidal space. The CE-mark was granted in 2008 and the FDA approved its usage in 2016. The Cypass is implanted through a clear corneal incision and requires the surgeon to load the implant in the injector. In a study conducted by Hoeh et al. an approximately 40% decrease in the IOP was noted after 12 months of implantation surgery (Hoeh et al., 2016). The most frequent side-effects involve hypotony, cataract progression, and transient hyphema.

The **XEN** (Allergan) is a subconjunctival gel stent made of porcine collagen cross-linked with glutaraldehyde. XEN was granted the CE-mark in 2013 and has been approved by the FDA for patients suffering from refractory glaucoma where previous surgery had failed and the patient became unresponsive to the maximum tolerated topical drug therapy. The stent facilitates aqueous outflow from

the anterior to the subconjunctival space. The implantation of this device results in the formation of a bleb that might lead to scar formation, which is controlled by administration of mitomycin C (MMC). The IOP was observed to be decreased by about 29% after 12 months of implantation surgery (Perez-Torregrosa et al., 2016). On-going studies are focused on ascertaining the side-effects.

Summary

The current management of glaucoma includes such methods as medication, laser, and surgery, with a focus on lowering the IOP. The new-generation glaucoma treatment strategies involving less invasive MIGS seem to be promising. The development of new intraocular pressure-relieving medical devices such as iStent inject and Hydrus have shown promising results. The developments in the field of material science and engineering are also facilitating the development of improved versions of glaucoma implants.

Retinal Implants

The idea of manipulating the eye using electricity was described in 1755, when Charles Le Roy, a French physician, induced an electric current across the ocular surface of a blind patient who reported visual precepts or “phosphenes.” Working directly on the brain, in the late 1920s, Otrifrid Foerster, a German neurosurgeon, generated a similar subjective experience of phosphenes through external electrical stimulation of the occipital pole where the primary visual cortex is located (Bloch et al., 2019). In 1968, Brindley and Lewin further explored this discovery using an 80-electrode prosthesis to stimulate the visual cortex in a deliberate, grid-like way. Their experiments confirmed a retinotopic map which had been generated after localized head injuries resulting from war (Brindley and Lewin, 1968). The final piece of this puzzle fell into place when it was discovered that electric current across the globe of the eye in blind patients could elicit a downstream effect in the visual cortex that could be recorded using electrodes (Potts and Inoue, 1969). With these experiments, it became clear that electrically stimulating the retina, even in blind patients, could produce both the subjective experience of vision, as well as activate the visual cortex, thus setting the stage for retinal prosthetics which attempt to restore sight by deliberately activating a dysfunctional retina.

Both hereditary diseases, such as retinitis pigmentosa (RP), and acquired degenerative diseases, such as age-related macular degeneration (AMD), can lead to dysfunction or death of light-sensitive photoreceptor (PR) cells, while leaving the remaining retinal circuitry intact. While there are no currently available treatments for late-stage inherited or acquired PR loss, visual information can often be at least partially restored via electrical stimulation of the remaining retinal neurons. The signal transduction cascade necessary

for vision can be recapitulated artificially to an extent; cells can be polarized in an electric field, causing voltage-sensitive ion channels on the depolarized side of the cell to open, thereby increasing cell potentiation and generating an action potential in appropriate neurons. Recent advances in biotechnology have seen extensive human trials and in some cases market approval of retinal prostheses (da Cruz et al., 2016; Stingl et al., 2017).

Current retinal implants are typically classified based on anatomical placement as either epiretinal, subretinal, or suprachoroidal. Epiretinal devices stimulate the RGCs directly through their placement directly on top of the retinal surface (Ahuja et al., 2013). Placing the device in this manner has some obvious advantages and disadvantages. Signals produced by photoreceptors are meant to be regulated and processed to a certain degree by other neural cell types in the retina, particularly horizontal cells, amacrine cells, and bipolar cells. By stimulating RGCs directly, other cells in the neural retina are bypassed. Further, different subtypes of RGCs have different roles when reporting an image (i.e., brightness, outlines, direction of motion, etc.) and require different types of induction signals to activate (Jepson et al., 2013). Identification and selective activation of these RGC subtypes remain a significant challenge, particularly in a dysfunctional retina where cells may not respond as expected. The GCL also contains the axonal processes from millions of RGCs all over the retina in a fibrous layer. It is nearly impossible to stimulate specific RGCs without also activating axons from potentially distant cells which happen to run near the site of electrical stimulation. Taken together, in human trials, patients have reported elongated, distorted visual forms instead of discrete, round spots of light as intended (Nanduri et al., 2012). However, epiretinal arrays can be implanted without extensive surgical effort, and can also be removed in cases of postsurgical complication or device failure.

In a subretinal implant, electrodes occupy the location of degenerated or missing photoreceptors. Unlike with an epiretinal device, electrical stimulation induced in the inner retinal neurons is transmitted through the retinal circuitry to the RGL, preserving as much as possible a healthy retinal signaling process. Consequently, several quirks of human vision are preserved, including flicker fusion (Lorach et al., 2015), edge detection, and contrast enhancements through center-surround antagonism (Ho et al., 2018), nonlinearity, and fine-scale heterogeneity of RGCs (Lorach et al., 2015), as well as ON and OFF responses (Ho et al., 2018). Unfortunately, implantation or removal in the subretinal space is much more difficult than mounting a device on the retinal surface, which may present a barrier to adoption.

The suprachoroidal approach places the implant behind the choroid in contact with the scleral wall. In this position, the system does not necessitate intraocular surgery and may therefore be less invasive and more easily accessible for subsequent repair or replacement. The suprachoroidal space is

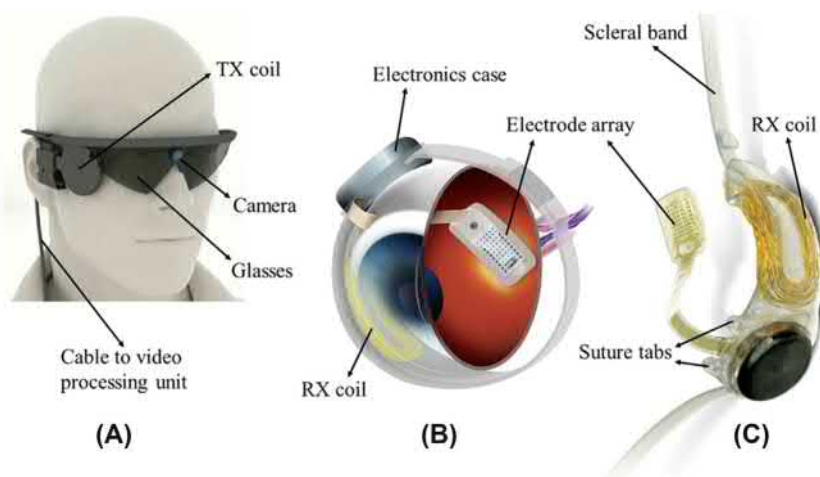
extremely vascularized, which creates a significant risk of hemorrhage. Further, the immunoprivileged nature of the eye does not extend to the choroid, increasing the risk of fibrosis or other complications stemming from the foreign body response. Unlike devices in other tissue microenvironments, these implants are mainly purposed to supplement declining peripheral vision. Peripheral vision loss is a symptom in several ocular pathologies, and, while often not blinding, can result in decreased quality of life as normal activities such as driving become impossible or dangerous. Because these implants are meant to help with low-resolution scotopic vision, the relatively large distance between stimulating electrodes and retinal neurons may be acceptable. Implantation into the suprachoroidal space, however, will certainly produce the worst spatial resolution of the three approaches discussed due to current spread (Ayton et al., 2014).

To date, only four devices have been approved for use in humans in any major regulatory environment: Retina Implant Alpha IMS (first-generation device, Retina Implant AG, Reutlingen, Germany), Retina Implant Alpha AMS (second-generation device, Retina Implant AG), Argus II Retinal Prosthesis System (Second Sight Medical Products Inc, Sylmar, CA), and IRIS II (Pixium Vision, Paris, France). The major difference between the Alpha devices and the Argus II and IRIS II systems is that the former has placed a photodiode array subretinally, whereas the latter two are epiretinal (Zrenner, 2013).

Epiretinal Devices

Argus II

The Argus II (Second Sight, Inc, Sylmar, CA), also known as the “Bionic Eye,” is a retinal prosthesis approved for use in retinitis pigmentosa in several jurisdictions, including the United States. It uses information from a head-mounted camera which is transferred along with power to a radiofrequency antenna to the implant (Ahuja et al., 2013). Image information is processed and encoded extracocularly before transmission to a 6×10 electrode array through a transscleral cable. A flexible foil with an array of $200\text{-}\mu\text{m}$ diameter electrodes spaced by $575\ \mu\text{m}$ is physically attached to the outer retinal surface (Fig. 2.5.6.4). The Argus II has thus far been implanted in over 200 patients with some success. The best visual acuity score the Argus II has produced is 20/1,260, which, while low, can nevertheless greatly improve the mobility and quality of life of someone who is totally blind (Ho et al., 2015). It has been observed that a lack of physical connection between the camera and eye movements creates perceptual confusion where the brain expects an image to shift. Eye-tracking algorithms may offer a solution in the near future. In 2019, the Argus II will reach the end of its 10-year phase II multicenter trial which involves 30 subjects to evaluate safety and functional visual and real-world task performance. At 5 years postimplantation, there were 24



reported serious adverse events in 12 patients (40% of the trial population) including conjunctival erosion, dehiscence, and hypotony (da Cruz et al., 2016).

The Intelligent Retinal Implant System II (IRIS II)

Similar to the Argus II, the IRIS II is characterized by a glasses-mounted camera transmitting to an external “pocket processor,” which transmits data to an extra- and intraocular implanted component containing a 150-microelectrode array (Fig. 2.5.6.6). Unlike the Argus II, the IRIS II uses a neuromorphic image sensor to more closely recapitulate how human eyes actually see, providing both the coordinates of changing pixels and their light intensities. The way the IRIS II encodes data, by dividing dynamic images into transient or sustained components, can be algorithmically processed to reduce any scene into its most relevant elements. Further, data generated by the pocket processor travel are transferred optically via infrared (IR) directly to the implant, permitting higher transfer rates and a smaller footprint than the Argus II. Data transfer rates are the typical bottleneck for stimulating greater numbers of electrodes at higher refresh rates, both of which are essential for improvements to visual acuity (Zhang et al., 2015). Power is supplied through a separate transmitter coil using radio frequency transmission, similar to the Argus II. Perhaps most importantly, the IRIS II emphasizes the importance of data processing over raw telemetry of information, and includes a learning retinal encoder, which allows for individualized customization to assign areas as excitatory or inhibitory, thereby mimicking the retinal ON/OFF pathways (Damle et al., 2017).

The IRIS II obtained approval for a clinical trial in 2016 and data for the initial 10 subjects implanted reported improvements demonstrated in square localization, direction of motion, picture recognition, and visual field testing, with a rate of 0.4 serious adverse events per recipient. The

unprecedented short lifespan of the device in vivo, however, has led to a postponement of further development.

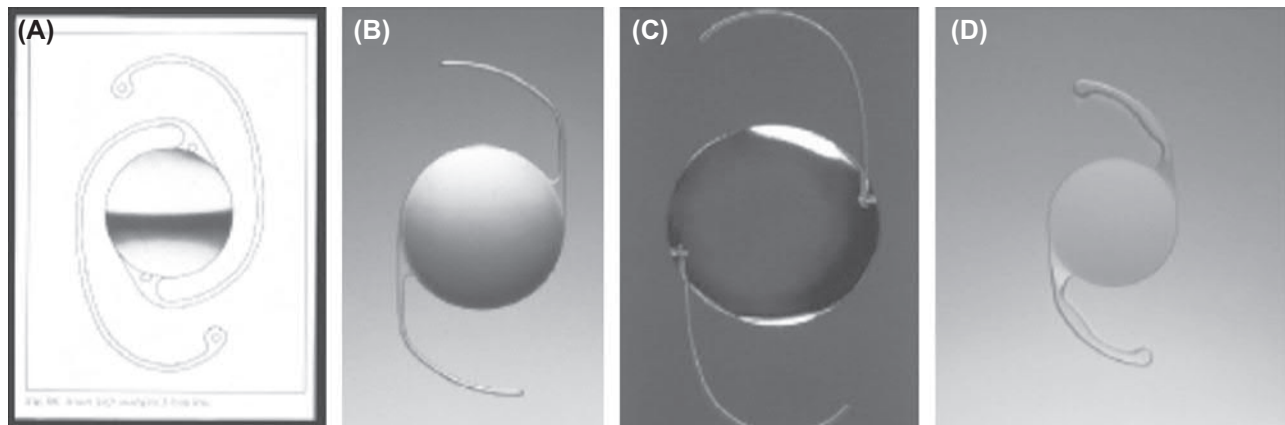
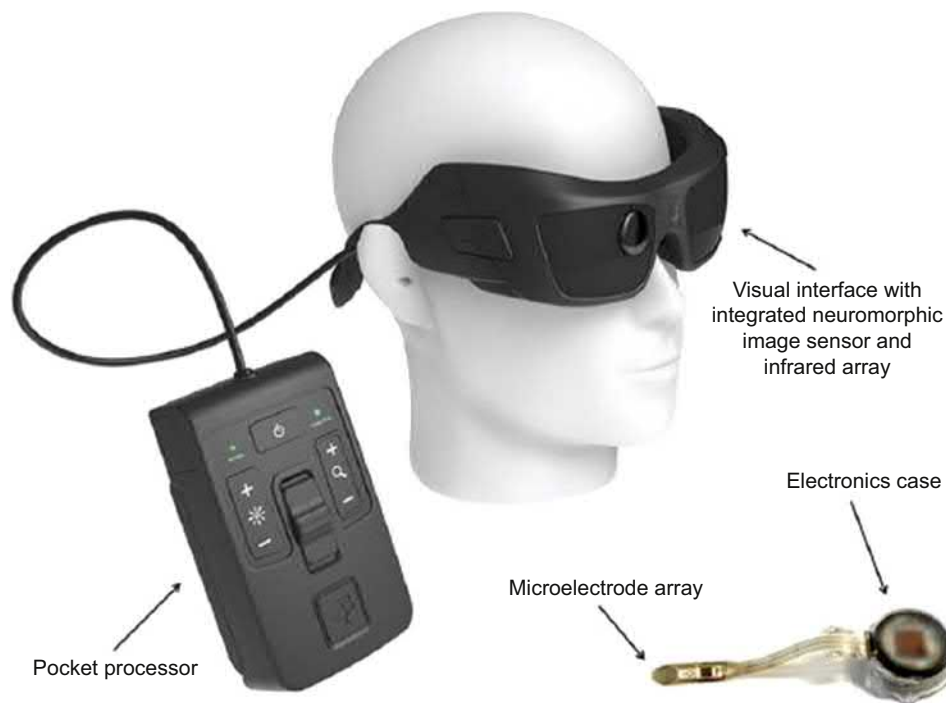
EPI-RET3 Retinal Implant System

The EPI-RET3 differs from other epiretinal devices by localizing all of its components within the eye. Its receiver coil and chip are placed inside the capsular bag, similar to an intraocular lens after cataract surgery, and is connected to the epiretinal electrode array via wire. By housing the entire device inside the eye, transscleral cabling is no longer required, greatly reducing the risk of infection or tissue erosion. The device is powered inductively when needed. As with other epiretinal devices, the EPI-RET3 requires an external camera and visual processor, which transmit stimulation pulses to the internal components. In a phase I clinical trial, a 25-electrode system was implanted into six patients for 4 weeks and then removed. All six subjects reported patterned phosphenes in regions corresponding to the stimulated retina. A much larger version of the electrode is currently being evaluated for human trials (Klauke et al., 2011).

Subretinal Devices

Alpha IMS/AMS

The Alpha IMS (Retina Implant AG, Reutlingen, Germany) is the only subretinal implant to obtain regulatory approval for human use. It incorporates a photovoltaic array, termed a “multiphotodiode array” (MPDA), which comprises a 3-mm (Bourne et al., 2019) microchip containing 1500 independent photodiode–amplifier–electrode units, each of which will convert ambient luminance into a useable electrical signal (Kuehlewein et al., 2017). It is powered by a subdermal coil, fixed under the temporalis muscle. A removable external coil magnetically attaches to the subdermal coil, allowing electromagnetic power induction and control of contrast sensitivity and brightness from a handheld unit (Stingl et al., 2017). Due

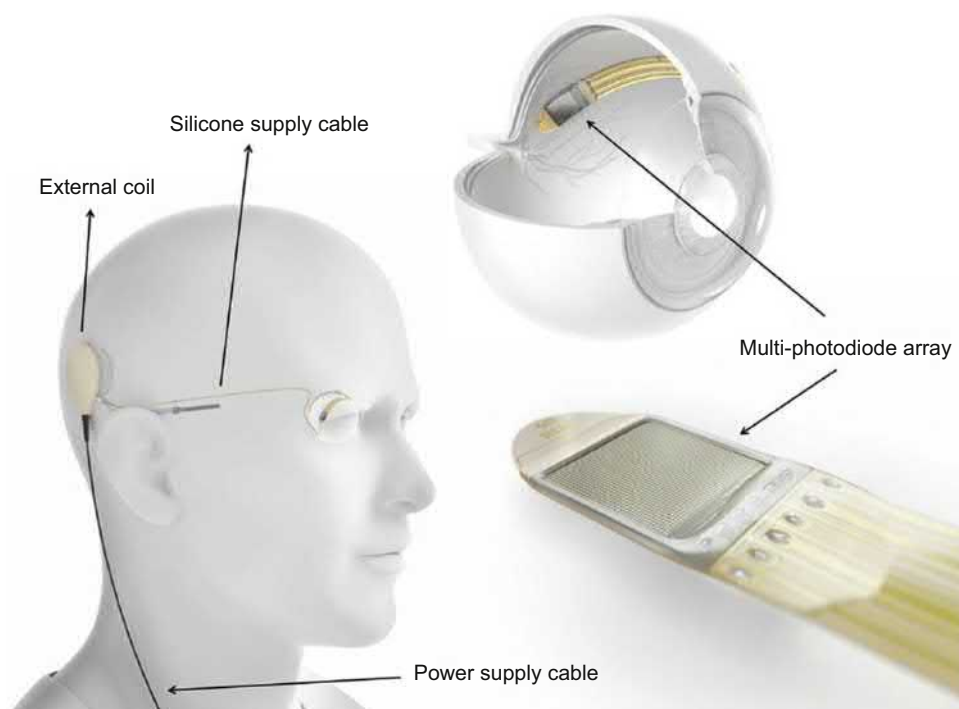


• **Figure 2.5.6.6** The IRIS II system. (A) Past three-piece PMMA IOL; (B) current single-piece PMMA IOL; (C) past three-piece foldable IOL; (D) current single-piece foldable IOL.

to the distal placement of the power coil and the intraocular placement of the MPDA, cooperation between medical teams is required for installation, increasing the costs and complexity of this approach. Furthermore, the delicacy of the subretinal space has been linked to premature device failure, as implants may need to be repositioned or replaced as a result of surgical or postoperative externalities (Kitiratschky et al., 2015).

The Alpha AMS is the second device in the Alpha line, replacing the Alpha IMS. Several vital changes were introduced into the Alpha AMS to improve its clinical efficacy and prolong its functional lifespan. In short, the AMS variant switched from a monophasic to a biphasic pulse, increased the size of the implant to include 1600 stimulation units compared with the 1500 found on the IMS. A huge potential advantage of the Alpha implants over their

competition is that they perform both light detection and charge transfer to the overlying inner retina, whereas the Argus II and IRIS II use a head-mounted digital camera to detect incident light that is then transmitted wirelessly to the implant. As discussed above, the Alpha devices eliminate the decoupling of eye movement with camera position, as the device itself is light sensitive, and is implanted where photoreceptors would normally exist (Edwards et al., 2018). The implant is powered through a transscleral cable connected to a radio frequency power receiver positioned behind the ear similar to a cochlear implant (Zrenner et al., 2011). The placement of this device results in greater visual acuity than that of its competitors; typical patients have 20/1200 after successful implantation, with a few demonstrating scores up to 20/550 (Stingl et al., 2015).



Photovoltaic Retinal Implant (PRIMA) Bionic Vision System

In the PRIMA system (Pixium Vision), images captured by an external camera are projected onto the retina using pulsed near-infrared (~ 880 nm) light. The PRIMA system represents perhaps the most modern approach to retinal prostheses. The implant itself is a modular array of a 1-mm-wide hexagonal chips containing 142 pixel cells each. Each pixel uses the pulsed near-infrared light being transmitted by a pair specially constructed glasses to stimulate phototransduction. Energy from the glasses activates a stimulating electrode, which in turn activates a return electrode, each connected to multiple photodiodes. These photodiodes generate an appropriate electrical current that stimulates proximal neural retina. The modular conformation makes it possible to produce arbitrarily sized implants which maintain spatial fidelity and require no extraneous circuitry or power source, regardless of size (Lee et al., 2016).

Preclinical studies with 70 and 55- μm pixels have been encouraging. Visual-evoked potential (VEP) testing after implantation in Royal College of Surgeons rats produced a similar shape and amplitude to VEPs in wild-type rats. The amplitude of the VEP was also responsive to light intensity or pulse duration (Lorach et al., 2015). It has been suggested that if these results transfer, an equivalent spatial resolution in humans may produce a visual acuity score of 20/250; far better than any other retinal prosthesis currently available (Lorach et al., 2015). Further, with plans to reduce pixel size and increase density, it is possible this prosthesis could surpass the threshold of legal blindness (20/200).

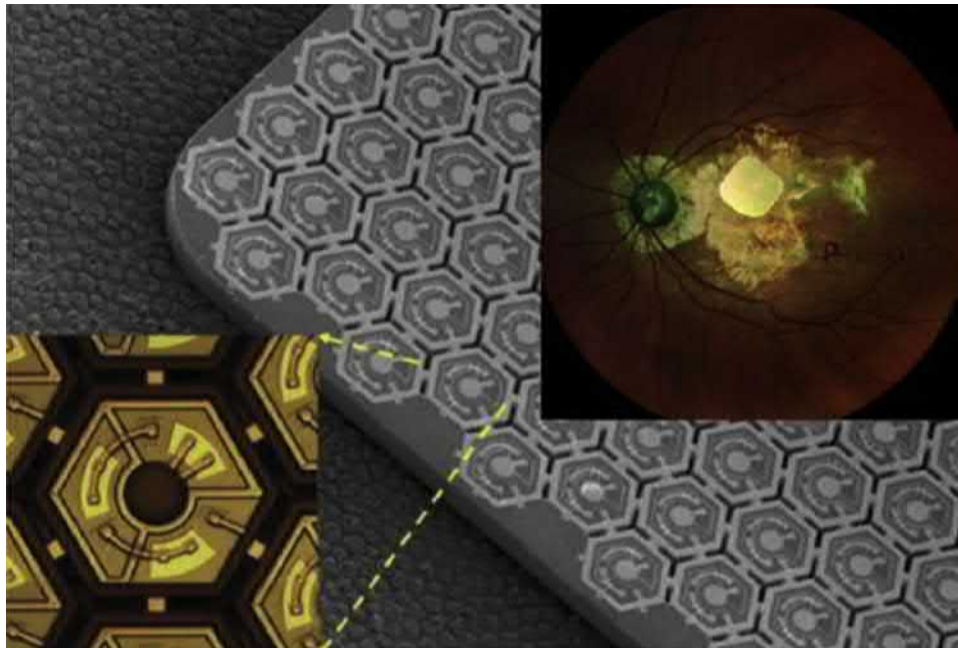
Clinical study began in France (2018) with subretinal implantation of a 2-mm wide 30- μm thick chip in five people with geographic atrophy, with five more Americans added later that year. This safety and feasibility study will last for 36 months, with preliminary results expected in 2019.

Suprachoroidal Devices

Bionic Vision Australia (BVA) Team

The Bionic Vision Australia (BVA) team is a consortium of Australian universities which have produced a number of suprachoroidal implant prototypes over the past 10 years, now being commercialized by Bionic Vision Technologies (BVT). The first of these was a 24-channel system, consisting of 20 stimulation channels and four return electrodes. Similar to the Alpha system, these implants require the dissection of the temporalis muscle for attachment of a transcutaneous module into bone. The array itself, connected by wire to the control module, requires that the lateral muscle is temporarily disinserted to allow for placement of the array into the suprachoroidal space (Saunders et al., 2014). Like the epiretinal devices, this prototype has no photoactive properties, relying on a head-mounted camera and image processor to provide appropriate information to the electrode.

Three subjects with blinding RP were implanted for 2 years as a pilot study in 2012. As expected, all subjects developed hemorrhages in the choroidal and subretinal space following implantation (Ayton et al., 2014). While light localization was better than random chance in all three participants, only one subject was able to complete a



visual acuity assignment, averaging 20/839. By the end of this study, electrical stimulation remained possible, despite the formation of a fibrotic capsule around the implants of all three patients (Saunders et al., 2014). As described, the most significant limitation of suprachoroidal implants is their distance from target tissues being electrically stimulated. A new device is being designed to address this issue, by incorporating a dual monopolar and hexapolar stimulation pattern which is meant to reduce retinotopic discrimination and high stimulation thresholds (Petoe et al., 2017).

Suprachoroidal–Transretinal Stimulation (STS)

A Japanese group in partnership with Nidek Inc. has created a similar device to the BVA system. Similar to BVA's approach, the STS requires a temporalis incision and tunneled connection between a decoder, an internal coil and a stimulating electrode array, and return electrode. Incident light is detected on a head-mounted camera and processed by a computer inside the arm of the spectacle component, which sends the signal to an external coil. This external coil relays the signal to a secondary implanted coil, which in turn generates the biphasic pulses needed to activate array electrodes. Unlike the BVA system, the electrodes on the STS protrude from the array by 0.3 mm, which places them slightly closer to the neural retina than the nonstimulating parts of the implant (Endo et al., 2018).

Following successful implantation of both single and dual 49-electrode arrays in animal models, three human

patients were given the device. While the safety profile of the device seemed better than the BVA system, with no significant adverse effects after 1 year, the performance of the implant was less convincing. Subjects were able to walk along a high-contrast white line and recognize some everyday objects better than chance, but without statistical significance over several time points (Fujikado et al., 2016). Clearly, larger studies are needed for both the STS device and the BVA devices to produce firmer conclusions, but with the evidence available so far placing devices across the sclera from the neural retina is fundamentally less effective than episcleral or subretinal localization.

Conclusions and Future Directions

While retinal prostheses can be grouped based on the tissue microenvironment in which they are meant to function, all devices currently in development face their own set of challenges. All devices are trying to replace the function of the retina by capturing light and transducing this signal into a subjective experience of vision. The density of rods or cones, particularly in the foveal pit where focal vision is produced, exceeds 150,000 cells per mm^2 . This pixel pitch far exceeds even the most ambitious electrode array, which is only capable of producing a coarse approximation of real vision. Existing electrode arrays are thought to have a theoretical maximum resolution that is at least 12 times less than that of the normal retina (Zrenner, 2013). As with most electronics, head dissipation is a physical bottleneck toward increasing electrode density arbitrarily. Even if it were possible to recapitulate the sensory density of healthy photoreceptors, generating useable signals which are able

to propagate through the neural retina to the visual cortex remains an unsolved challenge.

Regardless, the past decade has seen enormous progress in materials science, image processing and accompanying algorithms, data transfer rates, and miniaturization, which continue to drive the field forward toward genuine visual restoration. Unlike stem cell or genetic therapies, retinal prostheses hold the promise of producing meaningful impact in the near future. It is likely that the future will see combination devices which include a biological component along with a bioengineered substrate to break through the inherent limitations of completely artificial prosthetics.

References

- Ahuja, A.K., Yeoh, J., Dorn, J.D., Caspi, A., Wuyyuru, V., McMahon, M.J., Humayun, M.S., Greenberg, R.J., Dacruz, L., 2013. *Transl. Vision Sci. Technol.* 2, 1.
- Alfonso, J.F., Cueto, L.F.V., Belda-Salmeron, L., Montes-Mico, R., Fernandez-Vega, L., 2016. *Eur. J. Ophthalmol.* 26, 405.
- Alio, J.L., Ben-Nun, J., Rodriguez-Prats, J.L., Plaza, A.B., 2009. *J. Cataract Refract. Surg.* 35, 1671.
- Alio, J.L., Plaza-Puche, A.B., Fernandez-Buenaga, R., Pikkell, J., Maldonado, M., 2017. *Surv. Ophthalmol.* 62, 611.
- Amon, M., 2001. *J. Cataract Refract. Surg.* 27, 178.
- Apple, D., 1986. *J. Arch. Ophthalmol.* 104, 1150.
- Ayton, L.N., Blamey, P.J., Guymier, R.H., Luu, C.D., Nayagam, D.A., Sinclair, N.C., Shivdasani, M.N., Yeoh, J., McCombe, M.F., Briggs, R.J., Opie, N.L., Villalobos, J., Dimitrov, P.N., Varsamidis, M., Petoe, M.A., McCarthy, C.D., Walker, J.G., Barnes, N., Burkitt, A.N., Williams, C.E., Shepherd, R.K., Allen, P.J., Bionic Vision Australia Research, C., 2014. *PLoS One* 9, e115239.
- Barsam, A., Allan, B.D.S., 2014. *Cochrane Database Syst. Rev.*
- Bille, J.F., Engelhardt, J., Volpp, H.R., Laghouissa, A., Motzkus, M., Jiang, Z.X., Sahler, R., 2017. *Biomed. Opt. Express* 8, 1390.
- Bloch, E., Luo, Y., da Cruz, L., 2019. *Ther. Adv. Ophthalmol.* 11 2515841418817501.
- Bourne, R.R.A., Flaxman, S.R., Braithwaite, T., Cicinelli, M.V., Das, A., Jonas, J.B., Keeffe, J., Kempen, J.H., Leasher, J., Limburg, H., Naidoo, K., Pesudovs, K., Resnikoff, S., Silvester, A., Stevens, G.A., Tahhan, N., Wong, T.Y., Taylor, H.R., Vision Loss Expert, G., 2017. *Lancet Global Health* 5, E888.
- Bourne, R.R.A., Jonas, J.B., Resnikoff, S., 2019. *JAMA Ophthalmol.* 137, 158.
- Brennan, N.A., Cheng, X., 2019. *Eye Contact Lens* 45, 215.
- Brindley, G.S., Lewin, W.S., 1968. *J. Physiol.* 196, 479.
- Brubaker, R.F., 1991. *Investig. Ophthalmol. Vis. Sci.* 32, 3145.
- Chalmers, R.L., Gleason, W., 2013. *Eye Contact Lens* 39, 109.
- Chhabra, M., Prausnitz, J.M., Radke, C.J., 2007. *Biomaterials* 28, 4331.
- Compan, V., Lopez-Aleman, A., Riande, E., Refojo, M.F., 2004. *Biomaterials* 25, 359.
- da Cruz, L., Dorn, J.D., Humayun, M.S., Dagnelie, G., Handa, J., Barale, P.O., Sahel, J.A., Stanga, P.E., Hafezi, F., Safran, A.B., Salzmann, J., Santos, A., Birch, D., Spencer, R., Cideciyan, A.V., de Juan, E., Duncan, J.L., Elliott, D., Fawzi, A., Olmos de Koo, L.C., Ho, A.C., Brown, G., Haller, J., Regillo, C., Del Priore, L.V., Ardit, A., Greenberg, R.J., Argus, I.I.S.G., 2016. *Ophthalmology* 123, 2248.
- Damle, S., Lo, Y.H., Freeman, W.R., 2017. *Retina* 37, 1423.
- Edwards, T.L., Cottrill, C.L., Xue, K., Simunovic, M.P., Ramsden, J.D., Zrenner, E., MacLaren, R.E., 2018. *Ophthalmology* 125, 432.
- Endo, T., Fujikado, T., Hirota, M., Kanda, H., Morimoto, T., Nishida, K., 2018. Graefe's archive for clinical and experimental ophthalmology = Albrecht von Graefes. *Archiv. Klin. Exp. Ophthalmol.* 256, 1563.
- Findl, O., Buehl, W., Bauer, P., Sycha, T., 2010. *Cochrane Database Syst. Rev.*
- Fink, B.A., Mitchell, G.L., Hill, R.M., 2006. *Optom. Vis. Sci.* 83, 740.
- Flaxman, S.R., Bourne, R.R.A., Resnikoff, S., Ackland, P., Braithwaite, T., Cicinelli, M.V., Das, A., Jonas, J.B., Keeffe, J., Kempen, J.H., Leasher, J., Limburg, H., Naidoo, K., Pesudovs, K., Silvester, A., Stevens, G.A., Tahhan, N., Wong, T.Y., Taylor, H.R., 2017. Vision loss expert Grp global, B. *Lancet Global Health* 5, E1221.
- Fujikado, T., Kamei, M., Sakaguchi, H., Kanda, H., Endo, T., Hirota, M., Morimoto, T., Nishida, K., Kishima, H., Terasawa, Y., Oosawa, K., Ozawa, M., Nishida, K., 2016. *Investig. Ophthalmol. Vis. Sci.* 57, 6147.
- Gardner, H.P., Fink, B.A., Mitchell, L.G., Hill, R.M., 2005. *Optom. Vis. Sci.* 82, 459.
- Gills, J.P., Sanders, D.R., 1991. *J. Cataract Refract. Surg.* 17, 740.
- Greene, P.R., Greene, J.M., 2018. *Int. Ophthalmol.* 38, 869.
- Groeneveld, Y., Tavenier, D., Blom, J.W., Polak, B.C.P., 2019. *Diabet. Med.* 36, 1199.
- Harvitt, D.M., Bonanno, J.A., 1999. *Optom. Vis. Sci.* 76, 712.
- Ho, A.C., Humayun, M.S., Dorn, J.D., da Cruz, L., Dagnelie, G., Handa, J., Barale, P.O., Sahel, J.A., Stanga, P.E., Hafezi, F., Safran, A.B., Salzmann, J., Santos, A., Birch, D., Spencer, R., Cideciyan, A.V., de Juan, E., Duncan, J.L., Elliott, D., Fawzi, A., Olmos de Koo, L.C., Brown, G.C., Haller, J.A., Regillo, C.D., Del Priore, L.V., Ardit, A., Geruschat, D.R., Greenberg, R.J., Argus, I.I.S.G., 2015. *Ophthalmology* 122, 1547.
- Ho, E., Lorach, H., Goetz, G., Laszlo, F., Lei, X., Kamins, T., Mariani, J.C., Sher, A., Palanker, D., 2018. *Sci. Rep.* 8, 3145.
- Ho, E., Smith, R., Goetz, G., Lei, X., Galambos, L., Kamins, T.I., Harris, J., Mathieson, K., Palanker, D., Sher, A., 2018. *J. Neurophysiol.* 119, 389.
- Hoeh, H., Vold, S.D., Ahmed, I.K., Anton, A., Rau, M., Singh, K., Chang, D.F., Shingleton, B.J., Ianchulev, T., 2016. *J. Glaucoma* 25, 106.
- Hoffer, K., 1991. *J. Arch. Ophthalmol.* 109, 316.
- Izak, A.M., Werner, L., Apple, D.J., Macky, T.A., Trivedi, R.H., Pandey, S.K., 2002. *J. Cataract Refract. Surg.* 28, 1229.
- Jepson, L.H., Hottowy, P., Mathieson, K., Gunning, D.E., Dabrowski, W., Litke, A.M., Chichilnisky, E.J., 2013. *J. Neurosci.* 33, 7194.
- Jia, L.X., Li, Z.H., 2014. *Int. J. Ophthalmol.* 7, 816.
- Karahan, E., Tuncer, I., Zengin, M.O., 2014. *J. Ophthalmol.* 846385.
- Keates, R.H., Pearce, J.L., Schneider, R.T., 1987. *J. Cataract Refract. Surg.* 13, 557.
- Kitiratschky, V.B., Stingl, K., Wilhelm, B., Peters, T., Besch, D., Sachs, H., Gekeler, F., Bartz-Schmidt, K.U., Zrenner, E., 2015. Graefe's archive for clinical and experimental ophthalmology = Albrecht von Graefes. *Arch. Klin. Exp. Ophthalmol.* 253, 381.
- Klauke, S., Goertz, M., Rein, S., Hoehl, D., Thomas, U., Eckhorn, R., Bremmer, F., Wachtler, T., 2011. *Investig. Ophthalmol. Vis. Sci.* 52, 449.
- Kohl, J.C., Werner, L., Ford, J.R., Cole, S.C., Vasavada, S.A., Gardiner, G.L., Noristani, R., Mamalis, N., 2014. *J. Cataract Refract. Surg.* 40, 2113.

- Kohnen, T., Allen, D., Boureau, C., Dublineau, P., Hartmann, C., Mehdorn, E., Rozot, P., Tassinari, G., 2006. *Ophthalmology* 113, 578.
- Kretz, F.T.A., Attia, M.A.S., Linz, K., Auffarth, G.U., 2015a. *Klin. Monatsblätter Augenheilkd.* 232, 947.
- Kretz, F.T.A., Breyer, D., Klabe, K., Hagen, P., Kaymak, H., Koss, M.J., Gerl, M., Mueller, M., Gerl, R.H., Auffarth, G.U., 2015b. *J. Refract. Surg.* 31, 504.
- Kruger, A.J., Amon, M., Schauersberger, J., Abela-Formanek, C., Schild, G., Kolodjaschna, J., 2001. *J. Cataract Refract. Surg.* 27, 1987.
- Kuehlewein, L., Kitiratschky, V., Gosheva, M., Edwards, T.L., MacLaren, R.E., Groppe, M., Kusnyerik, A., Soare, C., Jackson, T.L., Sun, C.H., Chee, C., Sachs, H., Stingl, K., Wilhelm, B., Gekeler, F., Bartz-Schmidt, K.U., Zrenner, E., Stingl, K., 2017. *Ophthalmic Surg. Lasers Imag. Retina* 48, 993.
- Lee, D.Y., Lorach, H., Huie, P., Palanker, D., 2016. *Ophthalmic Surg. Lasers Imag. Retina* 47, 171.
- Liang, Y.L., Jia, S.B., 2018. *Int. J. Ophthalmol.* 11, 1028.
- Lorach, H., Goetz, G., Mandel, Y., Lei, X., Galambos, L., Kamins, T.I., Mathieson, K., Huie, P., Dalal, R., Harris, J.S., Palanker, D., 2015. *Vis. Res.* 111, 142.
- Lorach, H., Goetz, G., Smith, R., Lei, X., Mandel, Y., Kamins, T., Mathieson, K., Huie, P., Harris, J., Sher, A., Palanker, D., 2015. *Nat. Med.* 21, 476.
- Madrid-Costa, D., Cervino, A., Ferrer-Blasco, T., Garcia-Lazaro, S., Montes-Mico, R., 2010. *Clin. Exp. Optom.* 93, 426.
- Matsushima, H., Iwamoto, H., Mukai, K., Katsuki, Y., Nagata, M., Senoo, T., 2008. *Expert Rev. Med. Devices* 5, 197.
- Mazzocco, T.R., 1985. *Trans. Ophthalmol. Soc. U.K.* 104, 578.
- McKay, T.B., Hjortdal, J., Priyadarsini, S., Karamichos, D., 2017. *PLoS One* 12.
- McLeod, S.D., Vargas, L.G., Portney, V., Ting, A., 2007. *J. Cataract Refract. Surg.* 33, 37.
- McLeod, S.D., Trager, M.J., Vargas, L.G., Portney, V., 2008. *J. Cataract Refract. Surg.* 34, 9.
- Nanduri, D., Fine, I., Horsager, A., Boynton, G.M., Humayun, M.S., Greenberg, R.J., Weiland, J.D., 2012. *Investig. Ophthalmol. Vis. Sci.* 53, 205.
- Nibourg, L.M., Gelens, E., Kuijer, R., Hooymans, J.M.M., van Kooten, T.G., Koopmans, S.A., 2015. *Exp. Eye Res.* 136, 100.
- Nicolson, P.C., Vogt, J., 2001. *Soft contact lens polymers: an evolution. Biomaterials* 22 (24), 3273–3283.
- Ostrem, E.D., Fink, B.A., Hill, R.M., 1996. *Optom. Vis. Sci.* 73, 159.
- Perez-Torregrosa, V.T., Olate-Perez, A., Cerda-Ibanez, M., Gargallo-Benedicto, A., Osorio-Alayo, V., Barreiro-Rego, A., Duch-Samper, A., 2016. *Arch. Soc. Esp. Oftalmol.* 91, 415.
- Perez-Vives, C., 2018. *J. Ophthalmol.* 2687385.
- Petoe, M.A., McCarthy, C.D., Shivdasani, M.N., Sinclair, N.C., Scott, A.F., Ayton, L.N., Barnes, N.M., Guymer, R.H., Allen, P.J., Blamey, P.J., Bionic Vision Australia, C., 2017. *Investig. Ophthalmol. Vis. Sci.* 58, 3231.
- Pfeiffer, N., Garcia-Feijoo, J., Martinez-de-la-Casa, J.M., Larrosa, J.M., Fea, A., Lemij, H., Gandolfi, S., Schwenn, O., Lorenz, K., Samuelson, T.W., 2015. *Ophthalmology* 122, 1283.
- Piskalns, B., Fink, B.A., Hill, R.M., 2007. *Optom. Vis. Sci.* 84, 334.
- Potts, A.M., Inoue, J., 1969. *Investig. Ophthalmol.* 8, 605.
- Quigley, H.A., Broman, A.T., 2006. *Br. J. Ophthalmol.* 90, 262.
- Ridley, H., 1976. *Trans. Am. Acad. Ophthalmol. Otolaryngol.* 81, OP65.
- Ruan, J.L., Chen, C., Shen, J.H., Zhao, X.L., Qian, S.H., Zhu, Z.G., 2017. *Polymers* 9.
- Rudnicka, A.R., Kapetanakis, V.V., Jarrar, Z., Wathern, A.K., Wormald, R., Fletcher, A.E., Cook, D.G., Owen, C.G., 2015. *Am. J. Ophthalmol.* 160, 85.
- Sanders, D.R., Doney, K., Poco, M., Vukich, J.A., Barnett, R., Dulaney, D., Perkins, S., Rowen, S.L., Steel, D., Berkeley, R., Caplan, M., Mann, P., Bylsma, S., Martin, R.G., Brown, D.C., Grabow, H., Williamson, C.H., Shepherd, J.R., Fine, I.H., Kraff, M., Fabricant, R., Berg, A., Lamielle, H., Smith, D., Edelhauser, H., Grp, I.C.L.T.M.S., 2004. *Ophthalmology* 111, 1683.
- Saunders, A.L., Williams, C.E., Heriot, W., Briggs, R., Yeoh, J., Naya-gam, D.A., McCombe, M., Villalobos, J., Burns, O., Luu, C.D., Ayton, L.N., McPhedran, M., Opie, N.L., McGowan, C., Shepherd, R.K., Guymer, R., Allen, P.J., 2014. *Clin. Exp. Ophthalmol.* 42, 665.
- Sheppard, A.L., Bashir, A., Wolffsohn, J.S., Davies, L.N., 2010. *Clin. Exp. Optom.* 93, 441.
- Shimizu, K., Misawa, A., Suzuki, Y., 1994. *J. Cataract Refract. Surg.* 20, 523.
- Steinert, R.F., Aker, B.L., Trentacost, D.J., Smith, P.J., Tarantino, N., 1999. *Ophthalmology* 106, 1243.
- Stingl, K., Bartz-Schmidt, K.U., Besch, D., Chee, C.K., Cottrill, C.L., Gekeler, F., Groppe, M., Jackson, T.L., MacLaren, R.E., Koitschev, A., Kusnyerik, A., Neffendorf, J., Nemeth, J., Naeem, M.A., Peters, T., Ramsden, J.D., Sachs, H., Simpson, A., Singh, M.S., Wilhelm, B., Wong, D., Zrenner, E., 2015. *Vis. Res.* 111, 149.
- Stingl, K., Schippert, R., Bartz-Schmidt, K.U., Besch, D., Cottrill, C.L., Edwards, T.L., Gekeler, F., Greppmaier, U., Kiel, K., Koitschev, A., Kuehlewein, L., MacLaren, R.E., Ramsden, J.D., Roeder, J., Rothermel, A., Sachs, H., Schroder, G.S., Tode, J., Troelenberg, N., Zrenner, E., 2017. *Front. Neurosci.* 11, 445.
- Tabin, G., Chen, M., Espandar, L., 2008. *Curr. Opin. Ophthalmol.* 19, 55.
- Tham, Y.C., Li, X., Wong, T.Y., Quigley, H.A., Aung, T., Cheng, C.Y., 2014. *Ophthalmology* 121, 2081.
- Varma, R., Vajaranant, T.S., Burkemper, B., Wu, S., Torres, M., Hsu, C.Y., Choudhury, F., McKean-Cowdin, R., 2016. *JAMA Ophthalmol.* 134, 802.
- Wang, S.Y., Stem, M.S., Oren, G., Shtein, R., Lichter, P.R., 2017. *Eur. J. Ophthalmol.* 27, 387.
- Werner, L., Ludlow, J., Nguyen, J., Aliancy, J., Ha, L., Masino, B., Enright, S., Alley, R.K., Sahler, R., Mamalis, N., 2017. *J. Cataract Refract. Surg.* 43, 1100.
- Yalvac, I.S., Sahin, M., Eksioğlu, U., Midillioglu, I.K., Aslan, B.S., Duman, S., 2004. *J. Cataract Refract. Surg.* 30, 2050.
- Zhang, Y., Xiao, S., Feng, H., Zhang, L., Zhou, Z., Hu, W., 2015. *Opt. Express* 23, 33205.
- Zhao, S., Lan, X.W., Wu, J.Y., Yue, S., Zhang, H., Wu, Q., Zhang, G.S., Liu, L., 2019. *Medicine* 98.
- Zrenner, E., 2013. *Sci. Transl. Med.* 5 210ps16.
- Zrenner, E., Bartz-Schmidt, K.U., Benav, H., Besch, D., Bruckmann, A., Gabel, V.P., Gekeler, F., Greppmaier, U., Harscher, A., Kibbel, S., Koch, J., Kusnyerik, A., Peters, T., Stingl, K., Sachs, H., Stett, A., Szurman, P., Wilhelm, B., Wilke, R., 2011. *Proc. Biol. Sci.* 278, 1489.

2.5.7

Bioelectronic Neural Implants

ANDREW J. SHOFFSTALL^{1,2}, JEFFREY R. CAPADONA^{1,2}

¹Department of Biomedical Engineering, Case Western Reserve University, Cleveland, OH, United States

²Advanced Platform Technology Center, Rehabilitation Research and Development, Louis Stokes Cleveland VA Medical Center, Cleveland, OH, United States

Introduction

It has been reported that 38.3M Americans have a severe disability of some kind. Over 22.4M individuals have physical disabilities (i.e., a condition that substantially limits one or more basic physical activities such as walking, climbing stairs, reaching, lifting, or carrying), and 14.9M individuals have sensory disabilities (i.e., blindness, deafness, or a severe vision or hearing impairment) (Brault, 2012). Disabilities of this kind can have a significant impact on one's daily activities. For example, 10.1M limit their ability to go outside the home alone, even for basic needs. Additionally, another 9.4M Americans report on limitations in an activity of daily living, such as bathing, dressing, or eating.

Conventional treatments are, in many cases, ineffective, leaving many disabled individuals highly dependent on full-time caregivers for even simple daily activities. Requiring a full-time caregiver results in enormous costs to society for daily care and lost productivity. The causes of many movement disabilities are neurological disorders such as spinal cord injury, stroke, Parkinson's disease, epilepsy, and others. Such disorders can often be mitigated by the careful application of electrical stimulation to specific neural structures.

Bioelectronic neural devices (or implants) were originally conceived as basic science tools. Such devices have been used extensively to enhance our understanding of how the nervous system works in both normal and diseased states. However, for nearly 50 years, clinicians, scientists, and engineers around the world have been developing and applying technologies to manipulate the nervous system for therapeutic and rehabilitative purposes. As the sophistication of available neural stimulation technology continues to increase, the opportunities for increasing functional performance and targeted applications also increases. Despite this, the Research Plan for the National Center for Medical Rehabilitation Research specifically states that a shortage of appropriately trained engineers and scientists is a primary

obstacle to improving the effectiveness and efficiency of rehabilitation.

Therefore the focus of this chapter is to introduce readers (students) to the fundamentals to bioelectronic neural devices, with an emphasis on what materials are being used for an application, the neuroinflammatory response to the implants, evaluation criteria for materials selection, why historic devices have failed, and how one with an understanding of biomaterials science can develop solutions to enable this promising technology. The goal is that readers establish a base knowledge that can be supplemented with more in-depth readings provided in the references. Much of the background content will be fundamental to applications of bioelectronic neural devices regardless of the targeted tissue (see the Sections "Bioelectronic Devices" and "Technologies"). After some fundamentals are explained, we will briefly introduce several applications of the technology, followed by a more in-depth description of the current failure modes for the devices (see the Section "Applications") and biomaterials-based approaches to mitigate and overcome the most common failure modes (see the Section "Failure Modes"). The content in "Applications" and "Failure Modes" will be delivered in the context of brain-dwelling bioelectronic neural devices due to the more dominant nature of the problems, the research activity of biomaterials engineers to overcome these limitations, and the timeliness of the growth of the brain-computer interfacing field and commercial industries.

Bioelectronic Devices

Electrode Materials

Factors That Influence Materials Selection

The factors that influence materials selection are informed by the intended use within the system. For complex devices with multiple components (e.g., leads, wires, battery/circuitry, etc.), implanted medical devices typically involve

the use of several classes and types of materials to achieve different objectives. Some of the most common factors for consideration include:

- Electrical requirements (conductivity, capacitance)
- Location of use in the body/local anatomy (internal/external, flexibility, size, geometry)
- Duration of use and biocompatibility (temporary, implanted ± 30 days)
- Manufacturability and packaging (including sterilization)
- Costs

Since electrodes serve two primary purposes in the body, electrical stimulation and recording electrophysiology, one of the first material properties for consideration is their ability to carry (or impede) electrical current, i.e., whether they should be an electrical conductor or insulator. Some examples of common choices are described in more detail next.

Conducting/Capacitive Materials

The conductive components of electrodes have historically been made of metals and their alloys: platinum, platinum/iridium, gold, tungsten, stainless steel, and others. While functional and used in the mainstay of clinically used devices, these common metals have a number of drawbacks, including their inherent stiffness and their propensity to form reactive species during electrical stimulation. Material stiffness creates a mechanical mismatch between the tissue and the device, which is thought to exacerbate the inflammation in surrounding tissues (discussed in more detail in the Section “Biological” later) (Goldstein and Salcman, 1973; Harris and et al., 2011; Hess et al.; Subbaroyan et al., 2005). Many new materials have been investigated to overcome the limitations of the traditional metals. Ultrasmall carbon fibers, shape memory polymers, and conductive polymers have been investigated to establish softer, and in some cases, ionically conductive materials to serve as electrode conductors (Stocking et al., 2019; Patel et al., 2016; Kolarcik et al., 2015). Carbon is particularly attractive as it is very cheap, easy to manufacture at scale, and is thought to have low reactivity in the body under stimulation.

The formation of reactive species when voltages are exceeded above the so-called “water window,” a threshold above which hydrogen/oxygen gas is formed, is thought to contribute to neural damage near the electrode site (Kovach et al., 2016). The amount of damage that occurs is a function of the amount of charge that is injected through the electrode as well as its surface area. The higher the “charge density,” the more likely neural damage will be incurred (Shannon, 1992). Shannon (1992) helped to define the safe level of charge/charge density that can be applied through a platinum electrode. While the Shannon plots should not be overextrapolated, particularly to metals other than platinum, they do provide a framework for evaluating the safety of stimulating electrodes (Hudak et al., 2017; Kumsa et al., 2017; Cogan et al., 2016). Cogan additionally provides a detailed framework for evaluating neural stimulation electrodes on the benchtop with electrochemistry (cyclic voltammetry, electrochemical impedance spectroscopy, and voltage

transient analysis) (Cogan, 2008). Novel materials that have been tested to attempt to increase the charge injection limits include iridium oxide, titanium nitride, tantalum oxide, carbon, rough Pt/Pt-Ir, poly(3,4-ethylenedioxythiophene) (PEDOT), polypyrrole, and conductive hydrogels (Hudak et al., 2017; Kumsa et al., 2017; Ludwig et al., 2006).

Insulating Materials

The insulator is typically chosen based on the fabrication technique used to make the electrode. The most common insulators include polyimide, parylene-C, polydimethylsiloxane (PDMS), SU-8, and liquid crystalline polymer (Hassler et al., 2011). Wire-based electrodes have typically comprised extruded or dip-coated polymers for insulation: polytetrafluoroethylene, parylene-C, polyimide, poly(methyl methacrylate), epoxy, glass, and isonel. Micro-machined electrodes have included silicon oxynitride, glass, parylene-C, polyimide, and silicones (Szostak et al., 2017). Polymer-based electrodes have included silicon, polyimide, benzocyclobutene, SU-8, parylene-C, liquid crystal polymers, and shape memory polymers (Szostak et al., 2017; Ware et al., 2012).

Total insulation impedance is a function of the material resistivity, as well as the insulation thickness and signal properties, amplitude, and frequency. In most cases the dielectric breakdown voltages are not exceeded for common insulations chosen for in-body applications. However, with very thin material coatings particularly used to manufacture miniature devices, it may be an important consideration. Furthermore, at very high frequencies, most insulating materials pass more current. Therefore insulation requirements may be different for a 30 Hz, 100 μ s pulse versus the very high MHz frequencies used in radiofrequency heating and ablation applications.

Unfortunately, materials implanted in the body for long durations are vulnerable to hydrolytic, oxidative, and enzymatic degradation, similar to biological molecules. Naturally, such activity is important for tissue remodeling and tissue repair, and dominates the chronic foreign body response activated upon device implantation. Therefore the degradation of bioelectronics implants is due in part to the chronic foreign body response that is elicited upon implantation, as well as simply the normal aqueous/saline environment of the body (Hassler et al., 2011; Jorfi et al., 2015). Once insulation materials begin to break down, fluid ingress into the insulation can dramatically alter the function and lifespan of a bioelectronic neural electrode.

Equivalent Circuit Models

The first description of the chemistry of the electrode–electrolyte surface was provided by Helmholtz in 1879. At that time, Helmholtz also described the first equivalent circuit model for the electrode–electrolyte surface as a parallel plate capacitor. This oversimplified model described the electrode as positively or negatively charged due to an excess or lack of electrons. Likewise, the countercharge in the electrolyte

is due to the excess of charged ions in close proximity to the electrode surface. The alignment of charges at the electrode–electrolyte surface is known as the electrical double layer. Over the next 100 years, many other groups contributed to the further development of the equivalent circuit models, each focusing on different specific conditions.

Bioelectronic devices can interact with the body through either charge transfer faradaic processes or nonfaradaic adsorption and desorption events. An electrode can behave as either a polarizable or a nonpolarizable electrode under specific conditions at the interface, based on the materials used for the specific electrode design. However, most materials will also exhibit a minimal amount of the other process during use. A more detailed description of the electrode–electrolyte interface can be found in earlier editions of this book (see Chapter 11.5.10 Bioelectrodes by Venugopalan and Ideker). Within their chapter, Venugopalan and Ideker led readers to a detailed analysis of different types of recording and stimulation electrodes, and corresponding equivalent circuits discussed by Geddes and Baker (1989) and a review article by Geddes (1997).

Technologies

A typical implanted stimulation system includes an implantable pulse generator (IPG) containing a battery and circuitry, insulated lead wires, and electrodes with uninsulated metal contacts that inject charge into the body. Recording electrode systems are typically very similar in terms of electrode contacts and lead wires. In some cases, the recording lead wires are tunneled either to a percutaneous port to be fed to an amplifier and recording system, or they are connected to a telemetry system that performs signal conditioning and wirelessly transmits information to a receiver.

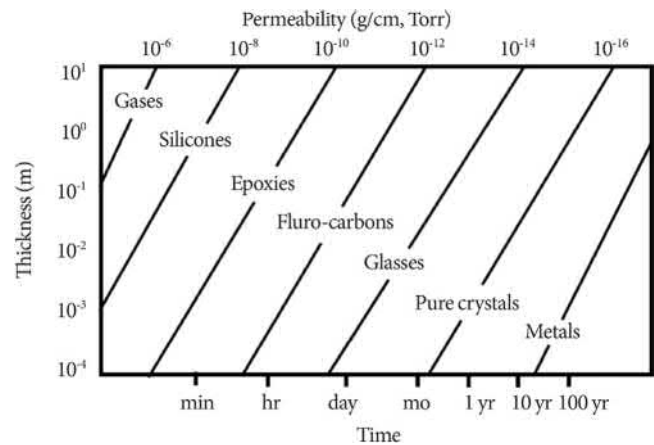
In both cases, several common key material challenges include reducing fluid ingress into protected circuitry and wires, maintaining electrical insulation integrity, preventing lead breakage, and optimizing the electrode–neural tissue interface, e.g., minimizing foreign body response and fibrosis through material selection. The latter challenge, the electrode–tissue interface, is the subject of extensive research. The “last-mile” connection is an important one that can determine the function of the overall system.

Each element in the system has different material requirements to achieve functional long-term performance. General descriptions of the system components and their material considerations are discussed next.

Battery, IPG

For implanted neural stimulation systems, there is typically an IPG, resembling a pacemaker. The IPG houses the battery and any circuitry required to control the device. The major material considerations for the IPG include:

- Battery composition
- Hermeticity
- Size and geometry
- Biocompatibility



• **Figure 2.5.7.1** Permeability of various materials used in bioelectronics device design. (Figure originally published in <https://www.ncbi.nlm.nih.gov/pmc/articles/PMC3797898/#!po=4.54545>, reproduced with permission.)

The primary purpose of the battery is to power the device and provide electrical impulses to the body. The design consideration is to allow maximal energy storage, recharging performance, and longevity. Current high-energy density IPG batteries are rechargeable lithium-ion (lithium-iodine polyvinylpyridine, lithium-carbon monofluoride, or lithium-polycarbon fluoride) (Joung, 2013).

As the lithium in the batteries is highly reactive with water, it is important to maintain a perfectly hermetically sealed device. The circuitry may also contain volatile or toxic (e.g., lead) compounds, which are important to isolate from the body. This is often accomplished by either encapsulating the device in silicones, epoxies, or other materials, or most effectively by laser welding the metal can together (Joung, 2013). The graph reproduced from Joung (Fig. 2.5.7.1) provides a qualitative/directional insight into the water permeability of various classes of materials as a function of thickness. Most existing pacemakers on the market today consist of a welded titanium package.

Leads and Interconnects

Typical lead architectures include single or multifilar wire arrangements that can be helically wound into strands and/or coils, which may include fluoropolymer insulation and an outer silicone tube. Material selection for the wire varies according to application and ranges from stainless steel and cobalt-chromium alloys to metallic composites (i.e., drawn filled tubes) and shape memory alloys (Gbur and Lewandowski, 2016). Additional considerations for material selection in neural electrode applications are discussed by Geddes and Roeder (Geddes and Roeder, 2003). The electrodes should be small and flexible, biocompatible, and demonstrate long-term reliability without degradation of the protective tubing or insulating layers. They must be able to undergo many mechanical fatigue cycles as would be endured in the body. A comprehensive review of materials used in biomedical applications and their mechanical testing

TABLE 2.5.7.1 Common Peripheral Nerve Stimulation Electrode Types per Application

Application	Electrode Types
Neuromuscular stimulation	Epimysial Intramuscular Nerve cuff Miniature radiofrequency coil
Spinal cord stimulation	Percutaneous Paddle
Peripheral nerve stimulation	Percutaneous Paddle Cuff In-body curing/conformal
Cranial nerve stimulation	Cuff (Huntington)
Genitourinary nerve stimulation	Disk Book Cuff Percutaneous

methods is provided by Gbur et al. (Gbur and Lewandowski, 2016).

The primary role of an interconnect is to allow for connection of the leads to the IPG during implantation. To allow for interchangeability, the leads are typically not soldered and therefore rely on mechanical contact. One standard connector used in neural prostheses is the inline “Letechia” connector (Letechia et al., 1991). Material considerations for interconnects include allowing electrical connection between the two contacts while maintaining an electrically and fluid isolated environment. Fluid ingress, in particular, leads to oxidation and rapid corrosion of the contacts.

Electrode Contacts

The last-mile connection to the nerve and central nervous system tissue can be very challenging. The ideal electrode for most applications is one that remains as close as possible to the target, induces little inflammatory response, minimizes mechanical strain on the tissue, and is easily deployable during surgery. Because the ideal interface is a challenge, there have been dozens of electrode designs specialized for each individual application (Table 2.5.7.1). The reader is referred to other resources for a more in-depth discussion, including the previous editions of this book (Tyler, 2018; Peckham and Ackermann, 2018; Peckham et al., 2013; Russell et al., 2019; Kim et al., 2019).

In general, the material constraints are informed by the anatomy with which the electrode is to interface. For example, for spinal cord stimulation, electrodes are implanted through surgical placement within the spinal column or around spinal roots exiting the foramen. Tight small spaces and a high degree of selectivity are required to achieve the desired effect without stimulating other nerves in proximity that may cause undesired side effects.

In selecting an electrode, there is an inherent tradeoff between invasiveness, safety, selectivity, and interface robustness. Current peripheral nerve stimulation (PNS) devices broadly fall along a spectrum of invasiveness, each with specific tradeoffs in safety versus sustained efficacy and robustness (Fig. 2.5.7.2).

Transcutaneous electric nerve stimulation is potentially the least invasive form of PNS, consisting of externally placed skin electrodes that stimulate superficial nerves (Fig. 2.5.7.2B). Fully implanted systems with cuff or intrafascicular electrodes are likely the most invasive, requiring full surgical access and freeing of the nerve from surrounding tissues to allow placement (Fig. 2.5.7.2F). Other systems that are available include: percutaneous systems (Fig. 2.5.7.2C), wirelessly coupled permanent implants (Fig. 2.5.7.2D), and fully implanted systems (Fig. 2.5.7.2E,F). The pros, cons, and other considerations for each approach are heavily debated among the field and are discussed in detail elsewhere. Practically speaking, stimulation device selection currently involves a balancing act between tradeoffs in safety, including implantation invasiveness, efficacy, and robustness. There remains an unmet need for implantable devices capable of maintaining robust connection with peripheral nerves while not requiring invasive surgery. To this end, a number of groups have attempted to develop miniaturized or otherwise injectable electrodes (Liu et al., 2015; Loeb et al., 2006; Seo et al., 2016; Trevathan et al., 2019).

Applications

The FDA does not approve materials as a wholesale class. Instead, they approve finished medical devices on the basis of safety and efficacy within a specific application for an intended use. Therefore it is important to carefully consider the application in which a neural implant is going to be used. There are dozens of clinical indications that already utilize electrical stimulation, with dozens more in preclinical development and/or undergoing commercialization (Fig. 2.5.7.3). While the breadth and depth of applications cannot be fully covered in this chapter alone, the following are a few applications of bioelectronic neural implants, which are briefly discussed.

Research

Neural electrodes play a role in basic neuroscience, electrophysiology, and biophysics. Common biopotentials measured in the body include:

- Muscle (electromyography)
- Nerve (electroneurography)
- Scalp/brain (electroencephalography)
- Cardio (electrocardiography)
- Intraocular and retinal (electrooculography and electroretinography)
- Cortical (electrocorticography and intracortical microelectrodes)

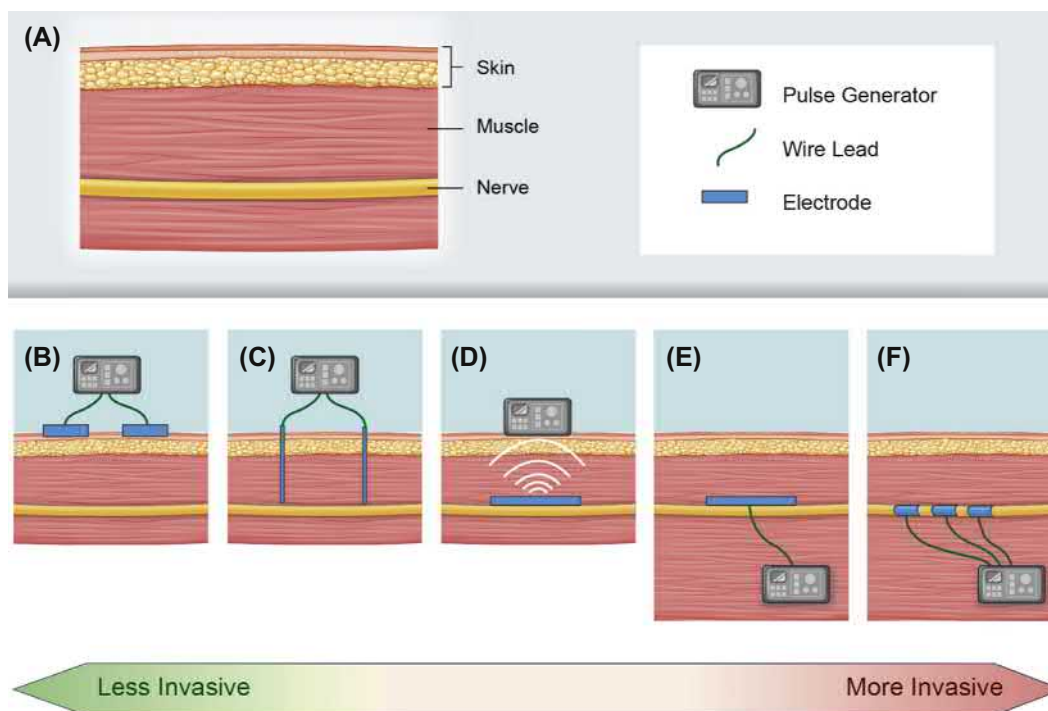
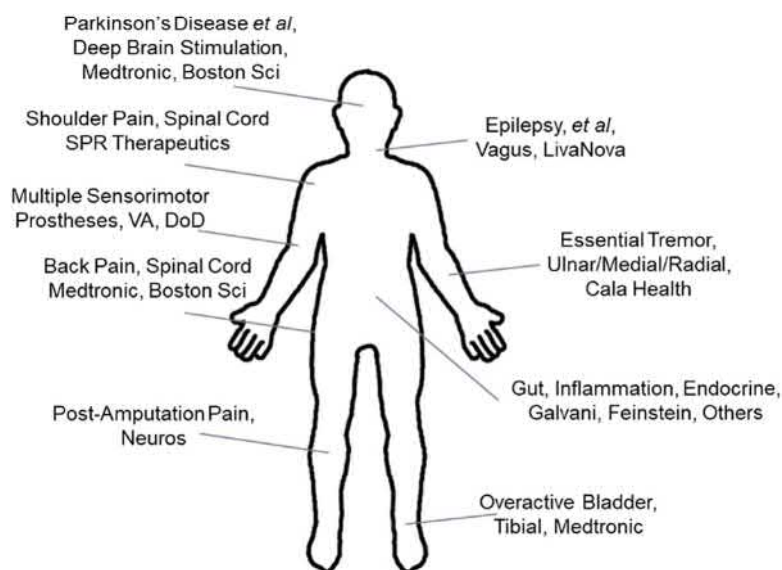


Illustration by Cleveland FES Center

- **Figure 2.5.7.2** Peripheral nerve stimulation electrode types from least to most invasive, left-to-right. (A) Simplified tissue schematic showing distinct layers of the skin, muscle, and nerve, (B) transcutaneous electric nerve stimulation, (C) percutaneous electric nerve stimulation, (D) injected wireless stimulator (e.g., BION device), (E) implanted nerve stimulator (e.g., spinal cord paddle electrode), (F) implanted cuff electrodes (e.g., vagus nerve stimulator). (Figure originally published in <https://www.biorxiv.org/content/10.1101/584995v1?rss=1>, reproduced with permission. Trevathan, J.K., et al., 2019. A truly injectable neural stimulation electrode made from an in-body curing polymer/metal composite. *bioRxiv*, 584995. <https://doi.org/10.1101/584995>.)



- **Figure 2.5.7.3** Small sample of marketed and in-development indications for therapeutic electrical stimulation of neural targets. (Compiled from references and cited company websites. Güemes and Georgiou (2018), Bonaz (2018), Pavlov and Tracey (2012), Koopman et al. (2016), Heiduschka and Thanos (1998), Tracey (2014), Humayun et al. (2016), Famm et al. (2013).)

Such signals can be used to interpret the status of the patient or subject, and can be used to interpret disease state, serve as objective outcome measures, or provide other feedback. The material considerations vary by application, e.g., whether the electrode is external or internal, and whether the electrode must be implanted over long duration. In general, an ideal recording electrode is one that (1) does not extensively disturb the existing biological systems they are intended to measure or stimulate, and (2) maintains performance over long periods of time for chronic applications.

Stimulating electrodes can be used in research to evoke a particular pathway or neural circuit. The combination of stimulating and recording electrodes makes a powerful basic science tool to investigate neuropathology and physiology.

Rehabilitation

Sensory Restoration

Sensory information is transduced by receptors and organs into neural signals that are transmitted along nerves, and interpreted and acted upon by the central nervous system. When these highways of sensory information are damaged, it results in significant disability. In some cases, the sensory system can be augmented or partially rehabilitated through the use of neural recording and stimulation electrodes.

Visual

An in-depth case study is presented by Humayan et al. in the previous version of this textbook, which the reader is referred to for more information (Humayan et al., 2013). A brief overview is provided here.

Light is transmitted through the lens of the eye and interacts with the retina, which acts as a transducer of the light to neural signals. The neural information is then transmitted through the optic nerve to the visual cortex where it is processed, interpreted, and acted upon by the brain. A visual prosthesis provides the concept where a digital camera is used to record the environment and convert the pixels into neural stimulation signals, which are projected as a pixel array on the retina. The number of electrodes and their density dictates the pixel resolution of the image the person is able to see. The Argus II implant, in development by Second Sight Medical Products, Sylmar, CA, is comprised of 60 electrodes that can be independently stimulated (Dagnelie et al., 2017; Stronks and Dagnelie, 2014).

To interface with the visual system, the options include implanting an electrode in the retina, the optic nerve, or the visual cortex. Several types of visual prostheses have been made. Due to the location and challenge with interfacing with the optic nerve, the two primary targets that have been investigated have been the retina and the visual cortex. In both cases, the tissue–electrode interface is a substantial materials challenge. The proximity of the interface to the retinal cells is important to maintain a low-impedance connection and reduce current spread. However, over time, the arrays become encapsulated with fibrous scar tissue leading to the spread of current, which limits the pixel resolution of the retinal prosthesis.

A substantial need in retinal prosthesis is the search for smaller, higher density arrays that adhere closely to the retina with limited fibrosis.

Tactile

While advanced prostheses can improve function for those with lost limbs, the prostheses are still identified as being unnatural or not fully integrated with the human body. Substantial progress has been made toward restoring the sensation of touch by using electrical neural stimulation (Tan et al., 2014; Graczyk et al., 2016). The prostheses incorporate pressure sensors to measure the forces experienced by the prosthesis, and then convert those into neural signals that can be felt by the user with applied electrical stimulation via nerve cuff electrodes implanted in the stump (Graczyk et al., 2018).

While the materials currently in use with the peripheral nerve interface have been adequate to restore significant function to the people receiving them, there is still progress that can be made. The overarching goal is to develop a prosthetic that fully integrates with the wearer. To achieve this task, there is a need for higher density and bidirectional arrays capable of producing prosthetics with even finer resolution tactile feedback.

Auditory

The cochlear implant is one of the best established and widely used neural prosthetic devices on the market. It involves the implantation of a small stimulator in the scala tympani of the cochlea and is controlled by a sensor and IPG located above or behind the ear. A more comprehensive case study of the material considerations with the cochlear implant can be found in an earlier edition of this book in a chapter by Spelman (2013).

The auditory system is complex and involves an intricate organ (the cochlea) to convert sounds of differing frequencies into neural signals. The conversion relies on small hairs as transducers whose small deflections originate the neural signal. Different frequencies cause different hairs along the organ to vibrate. The stimulating electrode is inserted into the scala tympani, and has multiple stimulation contact sites that each correspond to a region sensitive to different sound frequencies. The interleaved stimulation of these different contacts is able to reproduce sounds recorded by the microphone.

The materials used in the IPG, lead wires, and electrode have all been relatively well established; however, there are always opportunities for improvement (e.g., higher density arrays, lower power consumption, etc.) (Clopton and Spelman, 2003). The development of the cochlear prosthesis is widely regarded as “*the case study*” in the development of a neural prosthesis.

Genitourinary, Bladder Dysfunction

The lower urinary tract has two major functions: to store and void urine, referred to as continence and micturition, respectively. Smooth muscle in the bladder wall is

innervated by parasympathetic neurons stemming from the sacral spinal segments S2–S4. For the bladder to effectively empty, simultaneous contraction of the bladder and relaxation of the urethral sphincter must occur. However, in spinal cord injury, other neurological disorders can disrupt the co-occurrence of these events, leading to a condition called “bladder dyssynergia.” Currently, the clinical management of bladder dyssynergia relies on patients emptying their bladders through catheterization. Electrical stimulation (or inhibition) of these pathways has the potential to restore bladder control.

Disk, book, cuff, and percutaneous electrodes have all been used to treat bladder dysfunction. One of the primary approaches is to stimulate the sacral roots, the pudendal nerve, and/or the external urethral sphincter. The Medtronic peroneal tibial nerve stimulation (PTNS) system for the treatment of an overactive bladder is potentially one of the most widely used, and works by stimulating a spinal reflex that inhibits bladder voiding. PTNS currently relies on the use of a temporary percutaneous lead to provide stimulation. While this is not ideal, it has thus far been challenging to develop a fully implanted system due to the mechanical and space constraints of the anatomy. Ultrasmall, flexible, or other novel electrode designs may be able to address this challenge.

Motor Function

Motor function has been augmented through the use of “functional electrical stimulation” systems, and has been largely aimed at restoring function to those with paralysis or amputations. For example, trunk control, upper and lower limb, gait, and other neuromuscular stimulations have been applied to restore patient control of the muscular system. In most cases it is easier to stimulate large nerve fibers that innervate muscles rather than directly stimulating muscles or neuromuscular junctions. Therefore it is desirable to have electrodes that have high specificity that can engage specific groups of nerve fibers within a nerve trunk. For this purpose, the flat interface nerve cuff electrode has been developed from pliant PDMS-based structures. These enable greater specificity by reshaping the nerve within the cuff and provide access to individual fascicles with increased spatial resolution. Penetrating intrafascicular electrodes, which puncture the epineurium, has also been investigated. These electrodes have even greater material requirements as they must be stiff enough to pierce and be inserted through the thick epineurium, but soft enough not to overly stress the very low stiffness and easily damaged nerve tissue, and can be made from encapsulating microwires within silicone tubes.

Brain–Computer Interface

Intracortical microelectrodes for brain–machine interfacing have significant implications for reducing the burden associated with paralysis and limb loss. Notably, achievements have led to advanced control of prosthetics, which feel more natural and integrated with patients’ bodies. By bypassing

damaged regions of the nervous system, brain–computer interfaces (BCIs) offer the promise of reducing the burden of injury and enabling injured individuals to live more full and interactive lives (Pancrazio and Peckham, 2009). Unfortunately, implantable microelectrode arrays used in BCIs do not demonstrate long-term robustness, an observation that has been hypothesized to be due in large part to inflammation and neurodegeneration of brain tissue surrounding the implant (Goldstein and Salzman, 1973; Subbaroyan et al., 2005; Harris et al., 2011).

Common failure modes of intracortical microelectrodes for BCI and new materials-based approaches to improve the performance of BCIs are described later in the Sections “Failure Modes” and “Biomaterial-Based Strategies to Enable Neural Implants”.

Bioelectronic Medicine, “Electroceuticals”

The field of bioelectronic medicine has received a substantial amount of attention. Compared to pharmaceutical agents that travel throughout the entire body via the bloodstream, electrical stimulation of nerves has the potential to more directly treat certain pathologies in the body at the specific time and location it is needed (Sanjuan-Alberte et al., 2018). The stimulation may also be turned off at will, yielding some degree of reversibility of the treatment. As a result of their potential benefits, so-called “bioelectronic medicines” or “electroceuticals” are being studied and explored for numerous indications by commercial and government agencies (Tracey, 2014; Famm et al., 2013; Reardon, 2014; Koroshetz et al., 2018; French et al., 2018).

There are dozens of clinical indications currently being pursued with a nerve stimulation approach, some in pre-clinical stage and others already en route to commercialization (Fig. 2.5.7.3). Autonomic nerve stimulation (e.g., vagus nerve stimulation [VNS]) is a major player in the development of bioelectronic medicine technology. VNS has been proposed to produce benefits for a number of conditions (epilepsy, sepsis, lung injury, rheumatoid arthritis, stroke, traumatic brain injury, obesity, diabetes, cardiovascular control, pain management, and others) (Johnson and Wilson, 2018). Other peripheral nerve stimulation approaches have been used successfully to treat pain, develop motor and sensory prostheses, and restore bladder control (Heiduschka and Thanos, 1998; Humayun et al., 2016; Dones and Levi, 2018). Emerging areas of research include the use of therapeutic electrical stimulation to treat inflammation, metabolism, and endocrine disorders (Güemes and Georgiou, 2018; Bonaz, 2018; Pavlov and Tracey, 2012; Koopman et al., 2016). The indications are numerous and may help address otherwise challenging-to-treat conditions (Tracey, 2014; Sanjuan-Alberte et al., 2018).

In terms of material considerations for bioelectronic medicine applications, there is a substantial unmet need for electrode designs capable of interfacing with a broad range of targets. Given the many unique anatomical targets under consideration, it would be extremely valuable to have

a class of electrodes that is capable of interfacing with multiple conformations. This may come in the form of either flexible thin films (e.g., shape memory polymer electrodes) (Ware et al., 2012, 2013), highly conformable, injectable electrodes (Trevathan et al., 2019), or other novel concepts (Capadona et al., 2019; Wirdatmadja et al., 2016).

Regeneration

It has long been thought that electrical signals from nerve innervation play a role in growth, development, and the wound-healing process (Jaffe and Vanable, 1984; *Electrical Stimulation for Pressure Injuries: A Health Technology Assessment*, 2017). The most widely available of such approaches is the stimulation of bone growth (Kuzyk and Schemitsch, 2009; Zhou et al., 2019). While the efficacy of such treatments is debated (Aleem et al., 2016; Mollon et al., 2008), the applications are FDA approved and continue to be used to a certain extent in the United States and other countries. The devices rely on the application of low-intensity electric fields, including DC, high-frequency (>20 kHz), and low-frequency pulsed electromagnetic fields. While bone regeneration is one such example of the use of electric fields to direct or improve tissue regeneration, there are other examples (Yao and Li, 2016).

In terms of material considerations for regenerative stimulation, one can consider whether the electrode must be permanent, or whether it can be transient or allow itself to be remodeled as the growth occurs. At the cellular and molecular levels, everything within the body is in a permanent state of flux and remodeling. Dynamically changing materials and systems may therefore have an advantage in their interaction with living neural tissue.

The ultimate electrode for tissue regeneration purposes may incorporate actual living elements, or simply allow the body to remodel them as the scaffolding degrades. At the very least, osteointegrated electrodes appear to have some advantages: mechanical stability, insulation from other tissues, and a tight association with tissues (Dingle et al.). Additionally, cells attached to the electrode surface or incorporated into a scaffold have the advantage of being able to dynamically respond to changes in the local environment. Goding et al. developed a construct for seeding cells onto extracellular matrix components (Goding et al., 2017). Cui's group developed PEDOT/graphene oxide materials that may improve the stability of neural stem cells during transplantation (Weaver and Cui, 2015). While the study was performed for a different purpose, the substrate may also be used for camouflaging implanted microelectrodes or providing sustained release of factors from an attached layer of mesenchymal stem cells. Macroporous nanowire nanoelectronic scaffolds allow for the ingrowth of tissues (Tan et al., 2015; Tian et al., 2012), such that after the device is implanted it becomes tightly incorporated in the tissue environment. Having the biology interface well with the device opens up possibilities for introducing therapeutic cells (e.g.,

stem cells) or engineered cells as well as physiological recording with minimal disturbance to the tissues (Zhou et al., 2019; Leppik et al., 2018). A challenge for dynamic or integrated electrodes that will have to be grappled with is the possible complication of the device needing to be removed.

Failure Modes

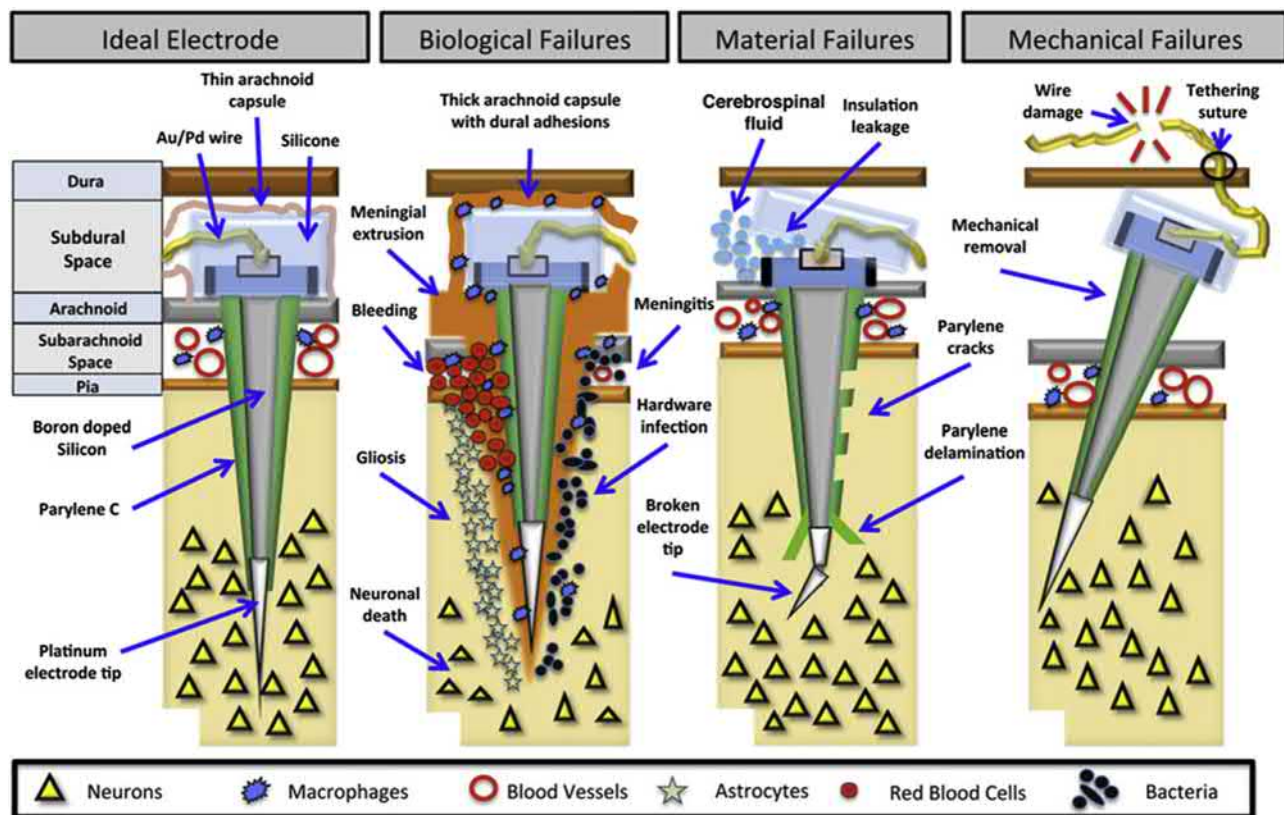
Bioelectronic neural implants can be placed in numerous locations in the body, see Table 2.5.7.1 for examples. Regardless of the location, the devices will eventually fail for one or a combination of reasons. In peripheral nerve electrode systems, the most common hardware failure modes are lead migration, lead fracture and malfunction, and battery failure (Eldabe et al., 2016). They also often suffer from other complications such as pain related to device components, infection, and skin breakdown. More rarely, complications include skin erosion, dural puncture, or other neurological injury related to insertion or postimplantation trauma (Eldabe et al., 2016).

However, the application that is the least stable, and has thus had the most focused research into understanding and combating failure modes, is intracortical microelectrodes for brain–computer interfacing applications. Therefore this section will describe failure modes for intracortical microelectrodes implanted into cortical brain tissue.

Intracortical microelectrodes have shown chronic cortical recording to be inconsistent in a variety of species and with multiple electrode types (Jorfi et al., 2015). In 2013, John Donoghue and his team published a retrospective analysis of the failure modes of several decades' worth of silicon-based intracortical microelectrode arrays implanted in nonhuman primates (Barrese et al., 2013). The team led by Donoghue converged on three main failure modes: mechanical, materials, and biological (Fig. 2.5.7.4). Two years later, the Capadona lab discussed subgroupings within these three groups to more specifically identify methods for preventing microelectrode failure (Jorfi et al., 2015). Here, due to the limited scope of this chapter, we will briefly discuss the major and minor failure mode classifications, and encourage readers to seek more detailed descriptions within the references and listed reviews.

Mechanical

Mechanical damage is defined as physical damage to the implants themselves, not the tissue. Mechanical damage to the tissue is grouped with biological response to the implant (see later). Traditional intracortical microelectrodes are derived from historically brittle materials: silicon-based materials, for example. Therefore it is not surprising that several studies have indicated that mechanical damage during or following insertion can lead to microelectrode failure. In 2009, Ward et al. implanted several different types of intracortical microelectrodes into rats and found mechanical failure in seven of 19 devices (Ward et al., 2009).



• **Figure 2.5.7.4** A summary of major failure modes to intracortical microelectrodes found by the Donoghue group's retrospective analysis from nonhuman primate studies. (Figure originally published in Barrese, J.C., et al., 2013. Failure mode analysis of silicon-based intracortical microelectrode arrays in non-human primates. *J. Neural Eng.* 10, 066014. <https://doi.org/10.1088/1741-2560/10/6/066014>, reproduced with permission.)

Interestingly, of all the mechanical failures described by Ward, only one failure of the implant shank was documented, meaning that the devices were failing in other places in higher numbers (Ward et al., 2009). Other groups have also reported on mechanical failures of the nonpenetrating components of the microelectrode array systems (Barrese et al., 2013; Prasad et al., 2012, 2014). In a summary of decades of nonhuman primate work, the Donoghue group found more than twice as many mechanical failures in the acute phase than biological or materials-based failures combined. Thus improvements in the mechanical stability of the entire system is an important area of research. Finally, as the field is driving toward smaller and smaller devices, the vulnerability of the implants to damage from improper handling, implantation into the neural tissue, or by the animal after implantation is increasingly important to consider.

Materials

The explanation of bioelectronics devices clearly demonstrates that the materials used are imperfect at preventing all damage to the device. Damage is typically more severe for stimulating devices than for recording devices. This is most evident in the evaluation of intracortical microelectrodes. Intracortical microelectrodes suffer a variable amount of

damage to the materials that comprise the device, depending on the choice of materials and the extent of the biological response to the implant. The connection between materials failure and biological-mediated failure will be further explored in the next section. Here, we describe materials damage to the microelectrode components as either corrosion of the electrical contacts, or damage to the insulating coatings. Electrode recording sites and/or the passivation layers and insulating coatings commonly incorporated into microelectrodes may degrade over time, which could reduce an electrode's ability to detect local ionic signals (Jorfi et al., 2015).

Corrosion to the electrical contacts is exacerbated when charge is injected into the materials. However, the same materials may experience faradaic charge transfer and corrosion over time (Merrill, 2010). A sequence of studies by the Sanchez group demonstrated that recording site deterioration is metal specific (Prasad et al., 2012, 2014). For example, tungsten microwires displayed progressively more severe structural changes with time of implantation (Prasad et al., 2012), while platinum/iridium (Pt/Ir)-based devices showed little structural changes to the metal recording site (Prasad et al., 2014). However, both studies demonstrated evidence that polyimide insulation was peeled away from the recording site and had signs of cracking.

The rate of corrosion and peeling/cracking of insulating layers is likely environment and material specific. In fact, several groups have demonstrated just that. For example, while bare tungsten and gold-plated tungsten wires corrode readily in phosphate-buffered saline, corrosion rates are accelerated in the presence of reactive oxygen species (ROS) (Patrick et al., 2011). Metals that form natural passivation layers are naturally more resistant to oxidative corrosion and have begun to be developed into microelectrode arrays (McCarthy et al., 2011). While accelerated aging methods are being developed for high-throughput in vitro/ex vivo evaluation of electrode materials (Takmakov et al., 2015), information regarding the corrosion rates of many common microelectrode materials under nonstimulating conditions is not readily available (Jorfi et al., 2015).

A number of mechanisms may influence the degradation of traditional insulating layers used as electrode materials: mechanical stress, film defects, as well as chemical or electrochemical reactions. For example, traditional passivation layers of silicon (Wang et al., 2007), silicon oxide (Hammerle et al., 2002), and silicon oxide/nitride stacks (Maloney and Baldwin) degrade within days (Wang et al., 2007) to months (Hammerle et al., 2002) of implantation, as fast as 1 mm/year (Maloney and Baldwin). Due to the chemical vulnerability of dielectric passivation layers originally designed for other industries, further encapsulation of microelectrodes with insulating polymers has become common practice (Schmidt et al., 1988; Hsu et al., 2009; Loeb et al., 1977). While the incorporation of polymer coatings has little impact on the neuroinflammatory response (compared to traditional passivation layers), several studies have demonstrated in vivo deterioration, resulting in compromised recording qualities (Prasad et al., 2012, 2014).

Among the most promising solutions is the development of amorphous silicon carbide (a-SiC) dielectric film for microelectrodes (Cogan et al., 2003). A-SiC has a dissolution rate of only 0.1 nm/h at 90°C (1/20th that of silicon nitride)—most importantly with no measurable dissolution at 37°C. More recently, in vivo evaluation of a-SiC intracortical microelectrodes suggests that a-SiC may provide a stable biocompatible substrate for the chronic recording and stimulation of neural structures (Deku et al., 2018; Knaack et al., 2016).

Biological

Several studies have demonstrated the connection between neuroinflammation and penetrating microelectrode performance, regardless of the materials used or the design of the implant (Kellis et al., 2010; Nolta et al., 2015; Prasad and Sanchez, 2012; Saxena et al., 2013). However, the exact mechanism or feature of the inflammatory response that is the most connected to device performance is still under debate. For decades, many labs have performed histological evaluation of the inflammatory response to devices placed into or near neural tissue structures. It has become increasingly clear that the brain's response consists of an

interconnected network of molecular and cellular components. Ultimately, the persistent presence of the implant in the brain tissue results in a self-perpetuation of the response (Potter et al., 2013) and prevention of device integration into the surrounding tissue, while the initial trauma from device implantation has been shown to heal (Potter et al., 2012; Hampton et al., 2004). For detailed reviews of the events following microelectrode implantation into neural tissue, in the context of the brain, readers are referred to the previous reviews of the topic (Jorfi et al., 2015; Tresco and Winslow, 2011; Michelson et al., 2018; Pancrazio et al.).

One of the leading theories for the prolonged proinflammatory state surrounding neural devices that penetrate neural tissue is repetitive motion-induced damage (Goldstein and Salcman, 1973; Harris et al., 2011; Hess et al.; Subbaroyan et al., 2005; Ware et al., 2012; Mahi and Rodrigue, 2012; Kim et al., 2004; Hess et al., 2011). The original idea can be traced back to Goldstein and Salcman's work in 1973 (Goldstein and Salcman, 1973), suggesting that motion of the brain with respect to the microelectrode may induce damage to the surrounding tissue. Approaches to overcome this theory are discussed later. Alternatively, in 1999, Norman suggested that the proximity of an implant in relation to the blood vessels can affect the foreign body response (Normann et al., 1999). A brief history of approaches to minimize damage to the blood–brain barrier will be presented later.

The final overarching mechanism discussed here is the impact that inflammatory-mediated oxidative events have in both materials degradation and tissue viability. The accumulation of oxidative stress events at the device–tissue interface has been suggested to occur as early as 2 weeks after implantation through the accumulation of ROS in activated macrophages responding to the implant (McConnell et al., 2009), and exist as long as the device is implanted (Prasad et al., 2012, 2014; Prasad and Sanchez, 2012). The in vivo evidence was extrapolated to suggest the correlation between oxidative events and corrosion of both insulating and conductive microelectrode material components. Takmakov et al. took the idea that oxidative stress causes damage and developed an accelerated aging method with hydrogen peroxide to study electrode degradation. They found that hydrogen peroxide-rich environments are especially damaging to polymer insulating layers, causing structural damage and changes in electrical properties in all types of electrodes (Takmakov et al., 2015), suggesting confirmation of the early in vivo studies in a more controlled setting.

The release of ROS around implanted intracortical microelectrodes can be caused by both material and biological sources. First, as a result of being in an aqueous environment, electrochemical reactions on the surface of the electrode can attribute to the conversion of water to hydroxyl radicals (Schmitt et al., 1999). In the case of electrical contacts (e.g., gold), chemical redox reactions at the surface can result in the oxidation of the electrode surface. The oxidation reactions can result in corrosive materials breakdown (Schmitt et al., 1999) seen in vivo (Prasad et al., 2012, 2014) and in vitro (Takmakov et al., 2015).

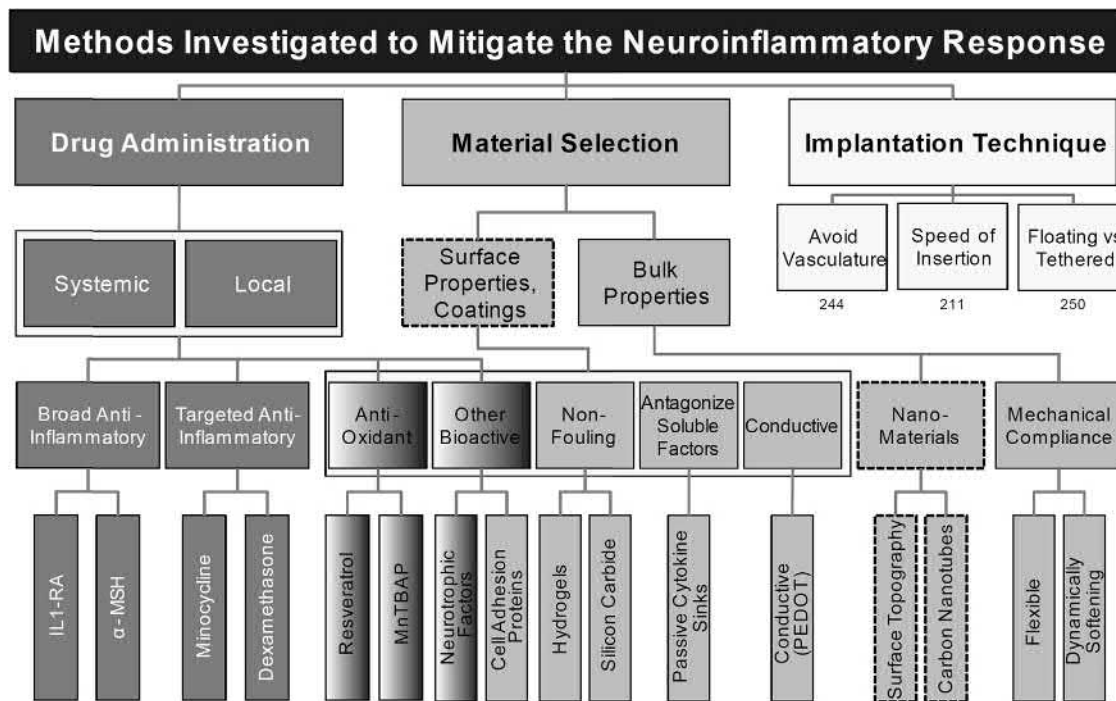
Additionally, the extent of inflammatory response occurring after implantation is strongly correlated to the formation of ROS around the device (He and Bellamkonda, 2008). ROS is released from cells due to an imbalance in the redox state of the cell (Balaban et al., 2005; Ray et al., 2012; Turrens, 2003). A simplified progression of the formation of ROS can be described as superoxide anion \rightarrow hydrogen peroxide \rightarrow hydroxyl anion that occurs during the conversion of oxygen to water. Particularly, mitochondrial dysfunction and heavy metals (e.g., copper and iron) within the cell are key contributors to driving the formation of ROS (Melo et al., 2011). Thus since all cells possess metal ions and mitochondria, unlike other proinflammatory molecules, ROS can be released by any cell type, not only inflammatory cells (Melo et al., 2011). To that end, several groups have confirmed that multiple cell types within the brain are capable of releasing ROS and other proinflammatory molecules (Abbott et al., 2006; Kettenmann, 2007; Kettenmann et al., 2011). Therefore an understanding of the series of cellular and molecular events involved in the inflammatory response is key to designing engineering strategies to combat failure modes caused by the formation and accumulation of ROS.

As the failure modes of intracortical microelectrodes are further elucidated, one mechanism that has been suggested to play a key role in several failure modes is oxidative stress and/or Fenton chemical reactions (iron-catalyzed peroxide formation) at the microelectrode–tissue interface (Barrese et al., 2013; Prasad et al., 2014; Prasad et al., 2012; Ereifej et al.,

2018). Specifically, oxidative stress can (1) facilitate corrosion and delamination of the microelectrode surface, (2) perpetuate the foreign body response to the implanted device through disruption of the blood–brain barrier, which is directly and indirectly linked to microelectrode performance (Nolta et al., 2015; Saxena et al., 2013), and (3) directly facilitate neuronal death and viability. Therefore oxidative events are directly or indirectly a part of most, if not all, events following neural electrode implantation into neural tissues.

Biomaterial-Based Strategies to Enable Neural Implants

There is increasing consensus that poor materials quality in conjunction with neuroinflammatory response to intracortical microelectrodes is a primary hurdle preventing neural technologies from reaching their full potential. Therefore improving the understanding of the neuroinflammatory response that develops following device implantation into neural tissues and developing strategies to reduce its impact are critical to achieving the promise to enable longer recording durations for basic science experiments and clinical applications. Many attempts at reducing the implications of the neuroinflammatory response on neural device performance can be grouped categorically by approach (Fig. 2.5.7.5) (Shoffstall and Capadona, 2018). For a more in-depth discussion on each, see Shoffstall and Capadona (2018). Here, we will briefly introduce attempts



• **Figure 2.5.7.5** Summary of leading methods to mitigate the biologically driven failure modes of an intracortical microelectrode. α -MSH, alpha-Melanocyte-stimulating hormone; IL-1-RA (interleukin-1 receptor antagonist); *MnTBAP*, Mn(III)tetrakis(4-benzoic acid)porphyrin; *PEDOT*, poly(3,4-ethylenedioxythiophene). (Figure originally published in Shoffstall, A., Capadona, J.R., 2018. In: Neuromodulation. Academic Press, pp. 393–413, reprinted with permission.)

to reduce the role of micromotion (one of the longest-standing hypotheses) and antioxidative strategies (in our opinion, among the most comprehensive approaches to mitigating tissue and device damage).

Micromotion and Tissue Mechanics

As discussed earlier, traditional microelectrodes have been composed of extremely stiff materials such as metals or silicon. The high stiffness has facilitated microelectrode implantation into the cortical tissue (Bjornsson et al., 2006) without the need for external insertion guides (Shoffstall et al., 2018). In silico modeling has suggested that creating neural devices from materials that more closely match the stiffness of neural tissue will relieve tissue strain caused during brain and device micromotion (Subbaroyan et al., 2005). However, simply making softer implantable neural devices has proved difficult for many reasons. First, softer devices are more difficult to implant with insertion aids (Shoffstall et al., 2018). Often, insertion aids are not translatable from single shank devices to multishank arrays used in clinical models. Additionally, traditional lithography techniques have taken over a decade to adapt to the materials of interest for neural applications (Ware et al., 2013; Hess et al., 2011; Yang et al., 2019), and many of the current device configurations are unlikely to translate well into clinical use due to poor device stability or the inability to retrieve the implant without damage to surrounding tissue. Therefore while “off-the-shelf” polymers are currently gaining the most attention (Capadona et al., 2019), they are unlikely to win out in the end for devices that dwell within the tissue. Consequently, the persistence to develop specialized materials for applications may provide the long-term solution to minimizing tissue and device damage due to compliance mismatch (Ware et al., 2013; Capadona et al., 2008).

Antioxidative Strategies

Given the role oxidative stress plays in several failure modes of intracortical microelectrodes, one group has been among the first to elucidate the role of oxidative stress events occurring around implanted microelectrodes (Dagnelie et al., 2017; Stronks and Dagnelie, 2014; Tan et al., 2014). As a proof of principle, their first strategy demonstrated that a two-dose intraperitoneal injection regime of antioxidant (resveratrol) at the time of implantation was capable of mitigating oxidative stress events, neuronal degeneration, and neuronal cell loss up to 4 weeks after implantation (Dagnelie et al., 2017). However, short-term antioxidant administration was unable to provide sustained neuroprotection (>4 weeks) around implanted devices. They hypothesized that the lack of sustained neuroprotection was based on fast clearance rates and low bioavailability (Geddes and Roeder,

2003; Letechipia et al., 1991; Tyler, 2018). Thus their next approach was to deliver the antioxidant treatment daily for 4 months (Potter-Baker et al., 2015). While regular administration of resveratrol provided neuroprotection, repetitive systemic administration resulted in side effects (Potter-Baker et al., 2015).

In an attempt to combat the limitations of systemic antioxidant delivery, multiple groups have demonstrated the success of immobilized antioxidative approaches in mitigating inflammatory pathways following device implantation (Jorfi et al., 2015; Potter-Baker and Capadona, 2015). While many natural and synthetic antioxidants are available for attachment to biomedical device substrates, it is important that the appropriate chemistry be available within the chemical structure of the antioxidant itself. One synthetic antioxidative molecule that has gained attention for its ability to be covalently bound to surfaces is Mn(III) tetrakis(4-benzoic acid)porphyrin (MnTBAP). MnTBAP was developed as a synthetic antioxidant mimetic enzyme to superoxide dismutase (SOD) (Batinic-Haberle et al., 2009).

To date, the development of a sustained antioxidative coating for intracortical microelectrode applications based on the immobilization of the MnTBAP SOD mimetic has only been reported in vitro (Potter-Baker et al., 2014). Their initial system utilized a coating of covalently immobilized MnTBAP (or SOD mimetic) designed to provide a sustained immobilized layer of antioxidant. Surfaces coated with the antioxidant demonstrated a significant reduction in accumulation of intracellular and extracellular ROS produced by adherent microglia (Potter-Baker et al., 2014). Results indicated that antioxidant-modified surfaces maintain beneficial levels of antioxidative activity (Potter-Baker et al., 2014). Based on these results, other groups are now also developing antioxidative coatings from melatonin, curcumin, estrogen, and other naturally derived antioxidants.

Conclusions and Future Directions

Again, the focus of this chapter was to introduce readers (students) to the fundamentals to bioelectronic neural devices. Here, our goal was to place an emphasis on the role of biomaterials in device design and performance. When the field of neural interfacing began around 50 years ago, the role of materials in neuroelectronic device performance was downplayed, especially as it related to the neuroinflammatory response. Over the last few decades, however, the bioelectronics field has grown to appreciate the importance of understanding mechanistically how materials interact with the neural environment under passive and active conditions. Therefore there is an increasing demand for individuals with a deep understanding and appreciation for biomaterials in the growing field of bioelectronics.

References

- Aleem, I.S., et al., 2016. Efficacy of electrical stimulators for bone healing: a meta-analysis of randomized sham-controlled trials. *Sci. Rep.* 6, 31724. <https://doi.org/10.1038/srep31724> [pii].
- Abbott, N.J., Ronnback, L., Hansson, E., 2006. Astrocyte–endothelial interactions at the blood–brain barrier. *Nat. Rev. Neurosci.* 7, 41–53.
- Balaban, R.S., Nemoto, S., Finkel, T., 2005. Mitochondria, oxidants, and aging. *Cell* 120, 483–495. <https://doi.org/10.1016/j.cell.2005.02.001>.
- Barrese, J.C., et al., 2013. Failure mode analysis of silicon-based intracortical microelectrode arrays in non-human primates. *J. Neural Eng.* 10, 066014. <https://doi.org/10.1088/1741-2560/10/6/066014>.
- Batinic-Haberle, I., et al., 2009. Pure MnTBAP selectively scavenges peroxynitrite over superoxide: comparison of pure and commercial MnTBAP samples to MnTE-2-PyP in two models of oxidative stress injury, an SOD-specific *Escherichia coli* model and carrageenan-induced pleurisy. *Free Radic. Biol. Med.* 46, 192–201. <https://doi.org/10.1016/j.freeradbiomed.2008.09.042>.
- Bjornsson, C.S., et al., 2006. Effects of insertion conditions on tissue strain and vascular damage during neuroprosthetic device insertion. *J. Neural Eng.* 3, 196–207.
- Bonaz, B., 2018. Is there a place for vagus nerve stimulation in inflammatory bowel diseases? *Bioelectron. Med.* 4, 4. <https://doi.org/10.1186/s42234-018-0004-9>.
- Brault, M.W., 2012. Americans with Disabilities: 2010. Household Economic Studies.
- Capadona, J.R., Shanmuganathan, K., Tyler, D.J., Rowan, S.J., Weder, C., 2008. Stimuli-responsive polymer nanocomposites inspired by the sea cucumber dermis. *Science* 319, 1370.
- Capadona, J.R., Shoffstall, A.J., Pancrazio, J.J., 2019. Neuron-like neural probes. *Nat. Mater.* <https://doi.org/10.1038/s41563-019-0312-9>.
- Clopton, B.M., Spelman, F.A., 2003. Technology and the future of cochlear implants. *Ann. Otol. Rhinol. Laryngol.* 112, 26–32. <https://doi.org/10.1177/00034894031120s906>.
- Cogan, S.F., 2008. Neural stimulation and recording electrodes. *Annu. Rev. Biomed. Eng.* 10, 275–309.
- Cogan, S.F., Ludwig, K.A., Welle, C.G., Takmakov, P., 2016. Tissue damage thresholds during therapeutic electrical stimulation. *J. Neural Eng.* 13, 021001. <https://doi.org/10.1088/1741-2560/13/2/021001>.
- Cogan, S.F., Edell, D., Guzelian, A.A., Ping Liu, Y., Edell, R., 2003. Plasma-enhanced chemical vapor deposited silicon carbide as an implantable dielectric coating. *J. Biomed. Mater. Res. A* 67, 856–867.
- Dagnelie, G., et al., 2017. Performance of real-world functional vision tasks by blind subjects improves after implantation with the Argus(R) II retinal prosthesis system. *Clin. Exp. Ophthalmol.* 45, 152–159. <https://doi.org/10.1111/ceo.12812>.
- Deku, F., et al., 2018. Amorphous silicon carbide ultramicroelectrode arrays for neural stimulation and recording. *J. Neural Eng.* 15.
- Dingle, A.M., et al. In: 2019 9th International IEEE/EMBS Conference on Neural Engineering (NER). pp. 782–786.
- Dones, I., Levi, V., 2018. Spinal cord stimulation for neuropathic pain: current trends and future applications. *Brain Sci.* 8 doi:E138 [pii] 10.3390/brainsci8080138 brainsci8080138 [pii].
- Eldabe, S., Buchser, E., Duarte, R.V., 2016. Complications of spinal cord stimulation and peripheral nerve stimulation techniques: a review of the literature. *Pain Med.* 17, 325–336 pnv025 [pii] 10.1093/pm/pnv025.
- Electrical stimulation for pressure injuries: a health technology assessment. *Ont. Health Technol. Assess. Ser.* 17, 2017, 1–106.
- Ereifej, E.S., et al., 2018. Implantation of neural probes in the brain elicits oxidative stress. *Front. Bioeng. Biotechnol.* 6, 1–12. <https://doi.org/10.3389/fbioe.2018.0000>.
- Famm, K., Litt, B., Tracey, K.J., Boyden, E.S., Slaoui, M., 2013. Drug discovery: a jump-start for electroceuticals. *Nature* 496, 159–161. <https://doi.org/10.1038/496159a>. 496159a [pii].
- French, J., et al., 2018. The need for understanding and engaging the patient as consumer of products developed by neural engineering. *J. Neural Eng.* 15, 040201.
- Gbur, J.L., Lewandowski, J.J., 2016. Fatigue and fracture of wires and cables for biomedical applications. *Int. Mater. Rev.* 61, 231–314. <https://doi.org/10.1080/09506608.2016.1152347>.
- Geddes, L.A., 1997. Historical evolution of circuit models for the electrode-electrolyte interface. *Ann. Biomed. Eng.* 25(1), 1–4.
- Geddes L.A., Baker L.E., 1989. Principles of Applied Biomedical Instrumentation, 3rd edition, ISBN 0-471-60899-8.
- Geddes, L.A., Roeder, R., 2003. Criteria for the selection of materials for implanted electrodes. *Ann. Biomed. Eng.* 31, 879–890.
- Goding, J., et al., 2017. A living electrode construct for incorporation of cells into bionic devices. *MRS Commun.* 7, 487–495. <https://doi.org/10.1557/mrc.2017.44>.
- Goldstein, S.R., Salcman, M., 1973. Mechanical factors in the design of chronic recording intracortical microelectrodes. *IEEE Trans. Biomed. Eng.* 20, 260–269.
- Graczyk, E.L., et al., 2016. The neural basis of perceived intensity in natural and artificial touch. *Sci. Transl. Med.* 8, 362ra142 8/362/362ra142 [pii] 10.1126/scitranslmed.aaf5187.
- Graczyk, E.L., Resnik, L., Schiefer, M.A., Schmitt, M.S., Tyler, D.J., 2018. Home use of a neural-connected sensory prosthesis provides the functional and psychosocial experience of having a hand again. *Sci. Rep.* 8, 9866. <https://doi.org/10.1038/s41598-018-26952-x>.
- Güemes, A., Georgiou, P., 2018. Review of the role of the nervous system in glucose homeostasis and future perspectives towards the management of diabetes. *Bioelectron. Med.* 4, 9. <https://doi.org/10.1186/s42234-018-0009-4>.
- Hammerle, H., et al., 2002. Biostability of micro-photodiode arrays for subretinal implantation. *Biomaterials* 23, 797–804.
- Hampton, D.W., Rhodes, K.E., Zhao, C., Franklin, R.J., Fawcett, J.W., 2004. The responses of oligodendrocyte precursor cells, astrocytes and microglia to a cortical stab injury, in the brain. *Neuroscience* 127, 813–820.
- Harris, J.P., et al., 2011a. In vivo deployment of mechanically adaptive nanocomposites for intracortical microelectrodes. *J. Neural Eng.* 8, 046010.
- Harris, J.P., et al., 2011b. Mechanically adaptive intracortical implants improve the proximity of neuronal cell bodies. *J. Neural Eng.* 8, 066011.
- Hassler, C., Boretius, T., Stieglitz, T., 2011. Polymers for neural implants. *J. Polym. Sci. B Polym. Phys.* 49, 18–33. <https://doi.org/10.1002/polb.22169>.
- He, W., Bellamkonda, R.V., 2008. In: Reichert, W.M. (Ed.), *Indwelling Neural Implants: Strategies for Contending with the In Vivo Environment*. CRC Press. Ch. 6.
- Heiduschka, P., Thanos, S., 1998. Implantable bioelectronic interfaces for lost nerve functions. *Prog. Neurobiol.* 55, 433–461. [https://doi.org/10.1016/S0301-0082\(98\)00013-6](https://doi.org/10.1016/S0301-0082(98)00013-6).
- Hess, A. et al. In: *Solid-State Sensors, Actuators and Microsystems Conference*. pp. 224–227.

- Hess, A.E., et al., 2011. Development of a stimuli-responsive polymer nanocomposite toward biologically optimized, MEMS-based neural probes. *J. Micromech. Microeng.* 21, 054009. <https://doi.org/10.1088/0960-1317/21/5/054009>.
- Hsu, J.M., Rieth, L., Normann, R.A., Tathireddy, P., Solzbacher, F., 2009. Encapsulation of an integrated neural interface device with Parylene C. *IEEE Trans. Biomed. Eng.* 56, 23–29. <https://doi.org/10.1109/TBME.2008.2002155>.
- Hudak, E.M., Kumsa, D.W., Martin, H.B., Mortimer, J.T., 2017. Electron transfer processes occurring on platinum neural stimulating electrodes: calculated charge-storage capacities are inaccessible during applied stimulation. *J. Neural Eng.* 14, 046012. <https://doi.org/10.1088/1741-2552/aa6945>.
- Humayun, M.S., Rowley, A.P., Whalen, J.J., Weiland, J.D., Tanguay, A.R., 2013. In: Ratner, B.D., Hoffman, A.S., Schoen, F.J., Lemons, J.E. (Eds.), *Biomaterials Science*, third ed. Academic Press, pp. 946–957.
- Humayun, M.S., de Juan, E., Dagnelie, G., 2016. The bionic eye: a quarter century of retinal prosthesis research and development. *Ophthalmology* 123, S89–S97. <https://doi.org/10.1016/j.ophtha.2016.06.044>.
- Jaffe, L.F., Vanable, J.W., 1984. Electric fields and wound healing. *Clin. Dermatol.* 2, 34–44. [https://doi.org/10.1016/0738-081X\(84\)90025-7](https://doi.org/10.1016/0738-081X(84)90025-7).
- Johnson, R.L., Wilson, C.G., 2018. A review of vagus nerve stimulation as a therapeutic intervention. *J. Inflamm. Res.* 11, 203–213. <https://doi.org/10.2147/JIR.S163248>. jir-11-203 [pii].
- Jorfi, M., Skousen, J.L., Weder, C., Capadona, J.R., 2015. Progress towards biocompatible intracortical microelectrodes for neural interfacing applications. *J. Neural Eng.* 12, 011001. <https://doi.org/10.1088/1741-2560/12/1/011001>.
- Joung, Y.H., 2013. Development of implantable medical devices: from an engineering perspective. *Int. Neurourol. J.* 17, 98–106. <https://doi.org/10.5213/inj.2013.17.3.98>.
- Kellis, S., et al., 2010. Classification of spoken words using surface local field potentials. *Conf. Proc. IEEE Eng. Med. Biol. Soc.* 2010, 3827–3830. <https://doi.org/10.1109/IEMBS.2010.5627682>.
- Kettenmann, H., 2007. The brain's garbage men. *Nature* 446, 987–988.
- Kettenmann, H., Hanisch, U.-K., Noda, M., Verkhratsky, A., 2011. Physiology of microglia. *Physiol. Rev.* 91, 461–553. <https://doi.org/10.1152/physrev.00011.2010.-Microglial>.
- Kim, D.H., Abidian, M., Martin, D.C., 2004. Conducting polymers grown in hydrogel scaffolds coated on neural prosthetic devices. *J. Biomed. Mater. Res. A* 71, 577–585.
- Kim, C., Jeong, J., Kim, S.J., 2019. Recent progress on non-conventional microfabricated probes for the chronic recording of cortical neural activity. *Sensors* 19, 1069.
- Knaack, G.L., et al., 2016. In vivo characterization of amorphous silicon carbide as a biomaterial for chronic neural interfaces. *Front. Neurosci.* 10, 301. <https://doi.org/10.3389/fnins.2016.00301>.
- Kolarcik, C.L., et al., 2015. Evaluation of poly(3,4-ethylenedioxythiophene)/carbon nanotube neural electrode coatings for stimulation in the dorsal root ganglion. *J. Neural Eng.* 12, 016008. <https://doi.org/10.1088/1741-2560/12/1/016008>.
- Koopman, F.A., et al., 2016. Vagus nerve stimulation inhibits cytokine production and attenuates disease severity in rheumatoid arthritis. *Proc. Natl. Acad. Sci. USA* 113, 8284.
- Koroshetz, W., et al., 2018. The state of the NIH BRAIN initiative. *J. Neurosci.* 38, 6427–6438. <https://doi.org/10.1523/JNEUROSCI.3174-17.2018>. JNEUROSCI.3174-17.2018 [pii].
- Kovach, K.M., et al., 2016. High-throughput in vitro assay to evaluate the cytotoxicity of liberated platinum compounds for stimulating neural electrodes. *J. Neurosci. Methods* 273, 1–9.
- Kumsa, D.W., Bhadra, N., Hudak, E.M., Mortimer, J.T., 2017. Electron transfer processes occurring on platinum neural stimulating electrodes: pulsing experiments for cathodic-first, charge-balanced, biphasic pulses for 0.566 k 2.3 in rat subcutaneous tissues. *J. Neural Eng.* 14, 056003. <https://doi.org/10.1088/1741-2552/aa7a4a>.
- Kuzyk, P.R., Schemitsch, E.H., 2009. The science of electrical stimulation therapy for fracture healing. *Indian J. Orthop.* 43, 127–131. <https://doi.org/10.4103/0019-5413.50846>.
- Leppik, L., et al., 2018. Combining electrical stimulation and tissue engineering to treat large bone defects in a rat model. *Sci. Rep.* 8, 6307. <https://doi.org/10.1038/s41598-018-24892-0>. 10.1038/s41598-018-24892-0 [pii].
- Letchipia, J.E., Peckham, P.H., Gazzdik, M., Smith, B., 1991. In-line lead connector for use with implanted neuroprosthesis. *IEEE Trans. Biomed. Eng.* 38, 707–709. <https://doi.org/10.1109/10.83572>.
- Liu, J., et al., 2015. Syringe-injectable electronics. *Nat. Nanotechnol.* 10, 629. 10.1038/nnano.2015.115 <https://www.nature.com/articles/nnano.2015.115#supplementary-information>.
- Loeb, G.E., Bak, M.J., Salzman, M., Schmidt, E.M., 1977. Parylene as a chronically stable, reproducible microelectrode insulator. *IEEE Trans. Biomed. Eng.* 24, 121–128. <https://doi.org/10.1109/TBME.1977.326115>.
- Loeb, G.E., Richmond, F.J.R., Baker, L.L., 2006. The BION devices: injectable interfaces with peripheral nerves and muscles. *Neurosurg. Focus* 20, E2.
- Ludwig, K.A., Uram, J.D., Yang, J., Martin, D.C., Kipke, D.R., 2006. Chronic neural recordings using silicon microelectrode arrays electrochemically deposited with a poly(3,4-ethylenedioxythiophene) (PEDOT) film. *J. Neural Eng.* 3, 59–70.
- Mahi, H., Rodrigue, D., 2012. Linear and non-linear viscoelastic properties of ethylene vinyl acetate/nano-crystalline cellulose composites. *Rheol. Acta* 51, 127–142. <https://doi.org/10.1007/s00397-011-0603-9>.
- Maloney, J.M., L. S., Baldwin, S.P., 2005. In Vivo Biostability of CVD Silicon Oxide and Silicon Nitride Films. In: *Mater. Res. Soc. Symp. Proc.* 872.
- McCarthy, P.T., Otto, K.J., Rao, M.P., 2011. Robust penetrating microelectrodes for neural interfaces realized by titanium micro-machining. *Biomed. Microdevices* 13, 503–515. <https://doi.org/10.1007/s10544-011-9519-5>.
- McConnell, G.C., et al., 2009. Implanted neural electrodes cause chronic, local inflammation that is correlated with local neurodegeneration. *J. Neural Eng.* 6, 056003. <https://doi.org/10.1088/1741-2560/6/5/056003>.
- Melo, A., et al., 2011. Oxidative stress in neurodegenerative diseases: mechanisms and therapeutic perspectives. *Oxid. Med. Cell Longev.* 467180.
- Merrill, D.R., 2010. The Electrochemistry of Charge Injection at the Electrode/Tissue Interface, pp. 85–138. https://doi.org/10.1007/978-0-387-98120-8_4.
- Michelson, N.J., et al., 2018. Multi-scale, multi-modal analysis uncovers complex relationship at the brain tissue-implant neural interface: new emphasis on the biological interface. *J. Neural Eng.* 15, 033001. <https://doi.org/10.1088/1741-2552/aa9dae>.
- Mollon, B., da Silva, V., Busse, J.W., Einhorn, T.A., Bhandari, M., 2008. Electrical stimulation for long-bone fracture-healing: a meta-analysis of randomized controlled trials. *J. Bone Joint Surg. Am.* 90, 2322–2330. <https://doi.org/10.2106/JBJS.H.00111>. 90/11/2322 [pii].

- Nolta, N.F., Christensen, M.B., Crane, P.D., Skousen, J.L., Tresco, P.A., 2015. BBB leakage, astrogliosis, and tissue loss correlate with silicon microelectrode array recording performance. *Biomaterials* 53, 753–762. <https://doi.org/10.1016/j.biomaterials.2015.02.081>.
- Normann, R.A., Maynard, E.M., Rousche, P.J., Warren, D.J., 1999. A neural interface for a cortical vision prosthesis. *Vis. Res.* 39, 2577–2587.
- Pancrazio, J.J., Peckham, P.H., 2009. Neuroprosthetic devices: how far are we from recovering movement in paralyzed patients? *Expert Rev. Neurother.* 9, 427–430. <https://doi.org/10.1586/ern.09.12>.
- Pancrazio, J. J., Voit, W. E. & Capadona, J. R. in Meeting Abstracts. 2298-2298 (The Electrochemical Society).
- Patel, P.R., et al., 2016. Chronic in vivo stability assessment of carbon fiber microelectrode arrays. *J. Neural Eng.* 13, 066002. <https://doi.org/10.1088/1741-2560/13/6/066002>.
- Patrick, E., Orazem, M.E., Sanchez, J.C., Nishida, T., 2011. Corrosion of tungsten microelectrodes used in neural recording applications. *J. Neurosci. Methods* 198, 158–171. <https://doi.org/10.1016/j.jneumeth.2011.03.012>.
- Pavlov, V.A., Tracey, K.J., 2012. The vagus nerve and the inflammatory reflex—linking immunity and metabolism. *Nat. Rev. Endocrinol.* 8, 743. <https://doi.org/10.1038/nrendo.2012.189>.
- Peckham, P.H., Ackermann, D.M., 2018. In: Krames, E.S., Peckham, P.H., Rezai, A.R. (Eds.), *Neuromodulation*, second ed. Academic Press, pp. 275–287.
- Peckham, P.H., Ackermann, D.M., Moss, C.W., 2013. In: Ratner, B.D., Hoffman, A.S., Schoen, F.J., Lemons, J.E. (Eds.), *Biomaterials Science*, third ed. Academic Press, pp. 981–996.
- Potter, K.A., et al., 2013. The effect of resveratrol on neurodegeneration and blood brain barrier stability surrounding intracortical microelectrodes. *Biomaterials* 34, 7001–7015. <https://doi.org/10.1016/j.biomaterials.2013.05.035>.
- Potter, K.A., Buck, A.C., Self, W.K., Capadona, J.R., 2012. Stab injury and device implantation within the brain results in inversely multiphasic neuroinflammatory and neurodegenerative responses. *J. Neural Eng.* 9, 046020.
- Potter-Baker, K.A., Capadona, J.R., 2015. Reducing the “stress”: antioxidative therapeutic and material approaches may prevent intracortical microelectrode failure. *ACS Macro Lett.* 275–279. <https://doi.org/10.1021/mz500743a>.
- Potter-Baker, K.A., et al., 2014. Development of superoxide dismutase mimetic surfaces to reduce accumulation of reactive oxygen species surrounding intracortical microelectrodes. *J. Mater. Chem. B* 2, 2248–2258.
- Potter-Baker, K.A., et al., 2015. Implications of chronic daily antioxidant administration on the inflammatory response to intracortical microelectrodes. *J. Neural Eng.* 12, 046002. <https://doi.org/10.1088/1741-2560/12/4/046002>.
- Prasad, A., et al., 2012. Comprehensive characterization and failure modes of tungsten microwire arrays in chronic neural implants. *J. Neural Eng.* 9, 056015. <https://doi.org/10.1088/1741-2560/9/5/056015>.
- Prasad, A., et al., 2014. Abiotic-biotic characterization of Pt/Ir microelectrode arrays in chronic implants. *Front. Neuroeng.* 7, 2. <https://doi.org/10.3389/fneng.2014.00002>.
- Prasad, A., Sanchez, J.C., 2012. Quantifying long-term microelectrode array functionality using chronic in vivo impedance testing. *J. Neural Eng.* 9, 026028.
- Ray, P.D., Huang, B.W., Tsuji, Y., 2012. Reactive oxygen species (ROS) homeostasis and redox regulation in cellular signaling. *Cell. Signal.* 24, 981–990.
- Reardon, S., 2014. Electroceuticals spark interest. *Nature* 511, 18.
- Russell, C., Roche, A.D., Chakrabarty, S., 2019. Peripheral nerve bionic interface: a review of electrodes. *Int. J. Intell. Robot. Appl.* 3, 11–18. <https://doi.org/10.1007/s41315-019-00086-3>.
- Sanjuan-Alberte, P., Alexander, M.R., Hague, R.J.M., Rawson, F.J., 2018. Electrochemically stimulating developments in bioelectronic medicine. *Bioelectron. Med.* 4, 1. <https://doi.org/10.1186/s42234-018-0001-z>.
- Saxena, T., et al., 2013. The impact of chronic blood–brain barrier breach on intracortical electrode function. *Biomaterials* 34, 4703–4713. <https://doi.org/10.1016/j.biomaterials.2013.03.007>.
- Schmidt, E.M., McIntosh, J.S., Bak, M.J., 1988. Long-term implants of Parylene-C coated microelectrodes. *Med. Biol. Eng. Comput.* 26, 96–101.
- Schmitt, G., et al., 1999. Passivation and corrosion of microelectrode arrays. *Electrochim. Acta* 44, 3865–3883.
- Seo, D., et al., 2016. Wireless recording in the peripheral nervous system with ultrasonic neural dust. *Neuron* 91, 529–539. <https://doi.org/10.1016/j.neuron.2016.06.034>. S0896-6273(16)30344-0 [pii].
- Shannon, R.V., 1992. A model of safe levels for electrical stimulation. *IEEE Trans. Biomed. Eng.* 39, 424–426. <https://doi.org/10.1109/10.126616>.
- Shoffstall, A., Capadona, J.R., 2018. *Neuromodulation*. Academic Press, pp. 393–413.
- Shoffstall, A.J., et al., 2018. A mosquito inspired strategy to implant microprobes into the brain. *Sci. Rep.* 8. <https://doi.org/10.1038/s41598-017-18522-4>.
- Spelman, F.A., 2013. In: Ratner, B.D., Hoffman, A.S., Schoen, F.J., Lemons, J.E. (Eds.), *Biomaterials Science*, third ed. Academic Press, pp. 967–980.
- Stocking, K.C., Vazquez, A.L., Kozai, T., 2019. Intracortical neural stimulation with untethered, ultrasmall carbon fiber electrodes mediated by the photoelectric effect. *IEEE Trans. Biomed. Eng.* <https://doi.org/10.1109/TBME.2018.2889832>.
- Stronks, H.C., Dagnelie, G., 2014. The functional performance of the Argus II retinal prosthesis. *Expert Rev. Med. Devices* 11, 23–30. <https://doi.org/10.1586/17434440.2014.862494>.
- Subbaroyan, J., Martin, D.C., Kipke, D.R., 2005. A finite-element model of the mechanical effects of implantable microelectrodes in the cerebral cortex. *J. Neural Eng.* 2, 103–113.
- Szostak, K.M., Grand, L., Constandinou, T.G., 2017. Neural interfaces for intracortical recording: requirements, fabrication methods, and characteristics. *Front. Neurosci.* 11, 665. <https://doi.org/10.3389/fnins.2017.00665>.
- Takmakov, P., et al., 2015. Rapid evaluation of the durability of cortical neural implants using accelerated aging with reactive oxygen species. *J. Neural Eng.* 12, 026003.
- Takmakov, P.R.K., Scott Phillips, K., Isayeva, I.S., Krauthamer, V., Welle, C.G., 2015. Rapid evaluation of the durability of cortical neural implants using accelerated aging with reactive oxygen species. *J. Neural Eng.* 12, 026003.
- Tan, D.W., et al., 2014. A neural interface provides long-term stable natural touch perception. *Sci. Transl. Med.* 6, 257ra138. <https://doi.org/10.1126/scitranslmed.3008669>. 6/257/257ra138 [pii].
- Tan, Y., et al., 2015. Silicon nanowire-induced maturation of cardiomyocytes derived from human induced pluripotent stem cells. *Nano Lett.* 15, 2765–2772. <https://doi.org/10.1021/nl502227a>.
- Tian, B., et al., 2012. Macroporous nanowire nanoelectronic scaffolds for synthetic tissues. *Nat. Mater.* 11, 986–994. <https://doi.org/10.1038/nmat3404>. nmat3404 [pii].
- Tracey, K.J., 2014. The revolutionary future of bioelectronic medicine. *Bioelectron. Med.* 1. <https://doi.org/10.15424/bioelectronmed.2014.00001>. 1-1.

- Tresco, P.A., Winslow, B.D., 2011. The challenge of integrating devices into the central nervous system. *Crit. Rev. Biomed. Eng.* 39, 29–44.
- Trevathan, J.K., et al., 2019. A truly injectable neural stimulation electrode made from an in-body curing polymer/metal composite. bioRxiv 584995. <https://doi.org/10.1101/584995>.
- Trevathan, J.K., et al., 2019. A truly injectable neural stimulation electrode made from an in-body curing polymer/metal composite. bioRxiv 584995.
- Turrens, J.F., 2003. Mitochondrial formation of reactive oxygen species. *J. Physiol.* 552, 335–344.
- Tyler, D.J., 2018. In: Krames, E.S., Peckham, P.H., Rezai, A.R. (Eds.), *Neuromodulation*, second ed. Academic Press, pp. 239–274.
- Wang, A., et al., 2007. Stability of and inflammatory response to silicon coated with a fluoroalkyl self-assembled monolayer in the central nervous system. *J. Biomed. Mater. Res. A* 81, 363–372. <https://doi.org/10.1002/jbm.a.31034>.
- Ward, M.P., Rajdev, P., Ellison, C., Irazoqui, P.P., 2009. Toward a comparison of microelectrodes for acute and chronic recordings. *Brain Res.* 1282, 183–200.
- Ware, T., et al., 2012. Fabrication of responsive, softening neural interfaces. *Adv. Funct. Mater.* 22, 3470–3479. <https://doi.org/10.1002/adfm.201200200>.
- Ware, T., Simon, D., Rennaker, R.L., Voit, W., 2013. Smart polymers for neural interfaces. *Polym. Rev.* 53, 108–129. <https://doi.org/10.1080/15583724.2012.751924>.
- Weaver, C.L., Cui, X.T., 2015. Directed neural stem cell differentiation with a functionalized graphene oxide nanocomposite. *Adv. Healthc. Mater.* 4, 1408–1416. <https://doi.org/10.1002/adhm.201500056>.
- Wirdatmadja, S.A., Balasubramaniam, S., Koucheryavy, Y., Jornet, J.M., 2016. 2016 IEEE 18th International Conference on E-Health Networking, Applications and Services (Healthcom), pp. 1–6.
- Yang, X., Zhou, T., Zwang, T.J., Hong, G., Zhao, Y., Viveros, R.D., Fu, T.-M., Gao, T., Lieber, C.M., 2019. Bioinspired neuron-like electronics. *Nat. Mater.* 18, 510–517.
- Yao, L., Li, Y., 2016. The role of direct current electric field-guided stem cell migration in neural regeneration. *Stem Cell Rev.* 12, 365–375. <https://doi.org/10.1007/s12015-016-9654-8>. 10.1007/s12015-016-9654-8 [pii].
- Zhou, P., He, F., Liu, B., Wei, S., 2019. Nerve electrical stimulation enhances osseointegration of implants in the beagle. *Sci. Rep.* 9, 4916. <https://doi.org/10.1038/s41598-019-41471-z>. 10.1038/s41598-019-41471-z [pii].

2.5.8

Burn Dressings and Skin Substitutes

STEVEN BOYCE, PHILIP CHANG, PETRA WARNER

Department of Surgery, University of Cincinnati and Shriners Hospitals for Children – Cincinnati, Cincinnati, OH, United States

Burn Wounds

Burn injuries to the skin have several causes including physical (i.e., flame, scald, electrical radiation, friction, frostbite) or chemical (i.e., strong acids or alkalis) agents, and may result in skin loss extending to superficial, partial-thickness, or full-thickness depths. Superficial burns (e.g., severe sunburn) tend to regenerate a functional epidermal barrier in a few days, and often require limited protection from infection and fluid loss (Herndon, 2012; Jan et al., 2018). In addition, skin loss involving sloughing of the interfollicular epidermis may occur after the immune response to infectious organisms, or to reactions to drugs or chemical toxins (Rogers et al., 2017; McCullough et al., 2017). These kinds of conditions have been treated effectively as partial-thickness burns that will often reepithelialize in less than 3 weeks with few long-term complications from scar because the anatomy of the dermis is well preserved. Partial-thickness burns involve the external epidermis and varying depths of dermis, but retain viable sources of cutaneous epithelial cells and melanocytes which will migrate and proliferate to restore the epidermal barrier and pigmentation to the surface of the wound. Until the epidermal barrier is restored, partial-thickness wounds will produce granulation tissue which promotes formation of scar. Some partial-thickness burns may also progress to full-thickness burns if vascular perfusion in the deep dermis becomes compromised. In that event, or if the burn destroys most or all of the epithelial sources at the site, then the epithelium must be restored by conventional grafting of split-thickness skin, or application of autologous epithelial cells as part of a skin substitute. Donor sites for autologous split-thickness skin grafts qualify as partial-thickness surgical wounds because they have some injury to the dermis, and retain sources of epithelial cells (Sidebar 2.5.8.1).

Surgical Planning for Wound Care

Clinical objectives for skin wound closure include, but are not limited to: (a) survival; (b) the earliest possible wound

closure; (c) the least amount of donor skin harvesting; (d) minimum scar; and (e) the best functional and cosmetic outcomes. Accomplishment of these goals requires careful planning after initial assessment of cutaneous burn injuries. The initial assessment identifies the magnitude, depth, and distribution of the wounds, availability of donor sites, as well as comorbid conditions that may delay or compromise healing. Important distinctions can be made for different anatomic sites. For example, the face, hands, feet, and perineum usually have the highest priority due to their functional and cosmetic importance to burn survivors. In many cases, the greatest absolute area involves the anterior and posterior torso, and extremities over the long bones. Part of the plan may require grafting of the back, which may involve prone positioning of the patient which may be complicated if support of the patient includes mechanical ventilation. Grafting over joints may require immobilization to minimize graft loss from shear during patient positioning and early physical therapy. In addition, the capacity of the patient to heal may be impacted negatively if there is lung injury with compromise of pulmonary function.

After this assessment is completed, an approach to permanent, stable wound closure should be specified, and timelines estimated. Because early excision of burn eschar has become a prevailing standard of care, full-thickness and deep partial-thickness wounds are excised to viable tissue, and partial-thickness wounds are debrided to remove necrotic tissue as early as possible after hospital admission. Together with excision and/or debridement, selection of wound dressings and skin substitutes must be determined.

Ideal Properties of Dressings and Skin Substitutes

The ideal properties for wound dressings and skin substitutes have been understood for many years (Pruitt and Levine, 1984; Yannas and Burke, 1980), but differ somewhat for dressings which provide temporary protection to the wound, and therapies which contain or recruit

SIDEBAR 2.5.8.1

Burn injuries vary greatly in etiology, magnitude anatomic location, and depth. Most burns are small in area, and superficial or partial-thickness in depth. These wounds can reepithelialize from the uninjured parts of epidermal glands and follicles, and often do not require hospitalization. Full-thickness burns lack epithelial sources, and usually require grafting of split-thickness skin, or engineered epithelium to accomplish wound closure. Deep burns are known to form thicker scar, which may require reconstructive surgery and additional therapy subsequently to acute hospitalization (American Burn Association, 2017; Stone li et al., 2018).

TABLE 2.5.8.1 Ideal Properties of Burn Dressings and Skin Substitutes

Ideal Qualities of Burn Dressings and Skin Substitutes

- Inexpensive
- Single application
- Bacterial barrier/microbicidal
- Semipermeable to water vapor
- Conformable and elastic
- Easy to apply (and remove)
- Reduces pain
- Nonimmunogenic and nontoxic
- Extended shelf life
- Maintains moisture and limits drainage
- Promotes tissue restoration and limits scar

Adapted from Helm, D.L., Orgill, B.D., Ogawa, R., Orgill, D.P., 2013. Burn dressings and skin substitutes. In: Ratner, B., Schoen, F., Hoffman, A., Lemons, J. (Eds.), *Biomaterials Science: An Introduction to Materials in Medicine*, third ed. Elsevier.

autologous cells and may persist indefinitely. These properties are listed in Table 2.5.8.1, and include: (a) provision of a barrier to environmental microorganisms and fluid loss; (b) adherence; (c) durability to mechanical loading and shear; (d) biocompatibility (i.e., nonimmunogenic, nontoxic); (e) resistance to microbial infection; (f) ease of application and/or removal; (g) reduction of pain; (h) ease of storage and extended shelf life; and (i) cost-effectiveness (Helm et al., 2013; Kempf et al., 2011). Although all dressings and skin substitutes may be considered to stimulate a reaction from the wound, materials containing allogeneic or autologous cells have been shown to deliver biologically active compounds, including growth factors, cytokines, and extracellular matrix peptides. These compounds may stimulate responses that are beneficial to wound healing, such as vascularization and epithelialization, and may inhibit negative responses, such as excessive granulation tissue and scar. In addition, if the dressing or engineered graft is intended to incorporate into the wound, it must also have sufficient

porosity and pore fraction to allow rapid vascularization of the material. The variety of materials that are currently available (see Tables 2.5.8.2 and 2.5.8.3) provide a broad spectrum of approaches to wound management from excision and debridement to final closure, restoration of function, and improvement of cosmesis.

Topical Microbial Management

By definition, burn wounds are not sterile, and may be anticipated to become contaminated over time with multiple strains of Gram-negative (e.g., *Pseudomonas* sp.), Gram-positive (e.g., *Staphylococcus* sp.), yeast (e.g., *Candida* sp.), and fungal (e.g., *Aspergillus* sp.) organisms. If microbial contamination develops, it may lead progressively to infection, invasion of the circulatory system, bacteremia, and sepsis. Clinical contamination of burn wounds is defined as 1×10^5 organisms per gram of tissue (Monafo and West, 1990; Pruitt et al., 1998), but virulence of the organisms must also be considered (Gallagher et al., 2012; Church et al., 2006). With these risks, alternatives for topical antimicrobials must be readily available, have broad microbicidal activity and low toxicity to wound tissue, and be relatively cost effective (Sidebar 2.5.8.2). Simultaneous antimicrobial activity and low toxicity to wound tissue will promote more rapid wound closure, and restoration of tissue integrity (Boyce et al., 1995, 1999a,b, 2006, 2017). Silver-containing compounds, such as silver-sulfadiazine cream and silver nitrate solutions have provided a prevailing standard of care for conventional treatment of bacterial and fungal organisms in burn wounds. In addition, mafenide acetate solution (5% Sulfamylon) has high antibacterial activity against Gram-negative bacteria. However, both ionic silver and mafenide acetate have been shown to be highly cytotoxic to skin substitutes that contain cultured cells (Cooper et al., 1991; Boyce et al., 1995, 1999a,b, 2006, 2017). By comparison, dressings that incorporate and release elemental, nanocrystalline silver exhibit lower cytotoxicity, with retention of antimicrobial activity against selected bacterial and fungal organisms. These types of dressings have an advantage that they require less nursing care because they can remain in place without changes for up to 1 week. Limited testing of one of those dressings (Acticoat) showed lower toxicity to engineered skin substitutes with cultured cells, and no impact on engraftment in full-thickness surgical wounds in preclinical studies (Supp et al., 2005).

Simple, inexpensive topical antimicrobials, such as dilute sodium hypochlorite (i.e., 0.5% Dakin's solution) (Lewandowski et al., 2013; Hegggers et al., 1991), or dilute hypochlorous acid (0.033% Vashe solution) (Day et al., 2017; Nerandzic et al., 2013) provide broad-spectrum antimicrobial activity with limited cytotoxicity to wounds. These agents act principally by delivery of bacteriocidal concentrations of chlorine to suppress microbial growth. Because these agents are in aqueous solutions, applications must be repeated or dressings changed periodically, but they are widely available. Naturopathic compounds, such

TABLE 2.5.8.2 Dressings and Temporary Skin Substitutes

Model	Composition	Indications for Use
Biobrane (Leshner et al., 2011; Arevalo and Lorente, 1999)	Nylon mesh on silicone sheet with collagen coating	Partial-thickness burns and donor sites
Suprathel (Rahmanian-Schwarz et al., 2011; Hundeshagen et al., 2018)	Poly-lactic acid fabric	Superficial and deep dermal partial-thickness burns
Mepitel (Campenella et al., 2011; Gotschall et al., 1998)	Poly-amide net with a soft silicone layer	Partial-thickness burns and grafted full-thickness burns
ActiCoat (Honari et al., 2001; Verbelen et al., 2014)	Nanocrystalline silver on poly-ethylene fabric	Partial-thickness burns, skin graft donor sites, skin graft application sites
Mepilex Ag (Hundeshagen et al., 2018; Barrett, 2009)	Nanocrystalline silver on an absorbent foam fabric	Partial-thickness burns, pressure ulcers, leg and foot ulcers
Aquacel Ag (Haith et al., 2015; Verbelen et al., 2014)	Ionic silver in carboxy-methyl cellulose with an absorbant foam and water-proof surface	Partial-thickness burns, skin graft donor sites, chronic wounds
Cadaver allograft (Kagan et al., 2005; May and Declement, 1981)	Human split-thickness skin, unfrozen or cryopreserved	Partial- and full-thickness burns, reconstructive surgery
Human amnio-chorionic membrane (Reilly et al., 2017; Tenenhaus, 2017)	Dehydrated amnio-chorionic membrane	Partial-thickness burns, chronic wounds and ophthalmic injuries
Porcine xenograft (Hermans, 2014; Burkey et al., 2016)	Porcine split-thickness skin, cryopreserved or lyophilized	Burns, reconstructive surgery
Piscine xenograft (Magnusson et al., 2017; Kerecis, 2018)	Fish skin from cod or tilapia	Partial-thickness burns, skin graft donor sites, excised full-thickness burns
Apligraf (Carlson et al., 2011; Bett, 2005)	Allo hF in collagen gel plus stratified allo hK	Diabetic foot ulcers
StrataGraft (Schurr et al., 2009; Centanni et al., 2011)	Allo hF in collagen gel plus stratified allo hK	Deep partial-thickness burns
DermaGraft (Stuart, 2008; Harding et al., 2013)	Allo hF on poly-galactin mesh	Diabetic foot ulcers

TABLE 2.5.8.3 Grafts and Permanent Skin Substitutes

Model	Composition	Indications for Use
Integra dermal regeneration template (Heimbach et al., 1988, 2003)	Lyophilized bovine collagen and chondroitin-sulfate with a silicone outer layer	Excised, full-thickness burns, reconstructive surgery
NovoSorb biodegradable temporizing matrix (Greenwood and Dearman, 2012a,b)	Bilaminar (film on foam) degradable polyurethane	Excised, full-thickness burns, reconstructive surgery
AlloDerm (Jansen et al., 2013; Ellis and Kulber, 2012)	Decellularized cadaveric skin	Reconstructive surgery
MatriDerm (Ryssel et al., 2010a,b)	Native collagen and elastin	Full-thickness burns and skin wounds (not available in United States)
EpiCel (Gallico et al., 1984; Sood et al., 2010)	Sheets of cultured autologous epidermal keratinocytes	Excised full-thickness burns of 30% TBSA or greater
ReCell (Gravante et al., 2007; Wood et al., 2012)	Suspensions of autologous keratinocytes, isolated and sprayed intraoperatively	Partial thickness burns
SkinTE (PolarityTE.com, 2018)	Disaggregated full-thickness autologous skin	Excised, full-thickness burns; and recalcitrant chronic wounds
Autologous engineered skin substitute (Boyce et al., 1995, 1999a,b, 2006, 2017)	Autologous fibroblasts and keratinocytes attached to a degradable collagen-glycosaminoglycan scaffold	Excised, full-thickness burns of 40% TBSA or greater (investigative)
Composite cultured skin (Dearman et al., 2013, 2014)	Autologous fibroblasts and keratinocytes attached to a degradable poly-urethane scaffold	Excised, full-thickness burns (investigative)
Reconstructed skin (Germain et al., 2018; Duranceau et al., 2014)	Autologous fibroblasts and keratinocytes combined without a degradable scaffold	Excised, full-thickness burns (investigative)

SIDEBAR 2.5.8.2

Management of microbial contamination in wounds is pivotal to the accomplishment of timely, stable wound closure. Topical compounds are known to reduce microbial loads, but may also inhibit the beneficial activities of wound healing. Optimal antimicrobial agents deliver specific inhibitory or microbicidal activities that penetrate the wound tissue, and have low cytotoxicity to fibrovascular and epithelial tissues that promote wound closure (Van Langeveld et al., 2017; Gallagher, 2012).

as Manuka honey, have been described as having antimicrobial activity for partial-thickness burns or skin wounds, and activity against organisms that are resistant to conventional antimicrobials (Ranzato et al., 2013; Mullai and Menon, 2007; Cooper et al., 2002). Another mixture of natural ingredients (honey, lanolin, olive oil, wheat germ oil, marshmallow root, aloe vera gel, wormwood, comfrey root, white oak bark, lobelia inflata, glycerin, bees wax, and myrrh) has been formulated by the Amish community as a burn wound ointment (Rieman et al., 2014; Kolacz et al., 2014). Claims of this ointment's medicinal benefits are balanced with disclaimers that the compound "... has not been evaluated by the US Food and Drug Administration ...," and that it is "... not intended to diagnose, treat, cure or prevent any disease" Therefore, use of these kinds of naturopathic compounds for hospital inpatients requires a physician's order.

Application of topical antimicrobials, such as equal parts Neosporin, Bactroban, and Nystatin ointments, and/or parenteral antimicrobials as topical solutions, such as ciprofloxacin (Boyce et al., 1995, 1999a,b, 2006, 2017), satisfy the requirements for low toxicity to grafts with cultured cells, but are off-label uses, and introduce risks of promoting resistant strains of organisms. This important issue deserves additional attention as the field of cellular therapy for burn care continues to advance.

Negative-Pressure Dressings

Wound treatment with subatmospheric pressure has been in practice for more than 20 years, and has demonstrated benefits for inhibition of burn depth progression from partial- to full-thickness wounds (Morykwas et al., 1999; Banwell, 1999). Negative-pressure wound therapy (NPWT) has been reported to facilitate and improve closure of chronic wounds of diabetic, venous stasis, and decubitus origins. More recently, NPWT has been shown to promote healing and early closure of partial-thickness burns, and to secure split-thickness skin grafts to increase engraftment over large wound areas (Kamolz et al., 2014; Nuutila et al., 2018). Although metastudies have suggested no conclusive benefits for closure of partial-thickness burns, it was noted that there have been insufficient numbers of controlled, randomized, prospective clinical trials from which to develop conclusions (Dumville et al., 2014). A more recent review of NPWT in treatment of burns supported the use of negative pressure for securing split-thickness skin grafts in large burns. As

more uniform protocols develop for the use and assessment of NPWT in burn care, it is likely that the reported benefits of more rapid healing and less frequent dressing changes may occur with greater frequency in burn care.

Degradable Polymers

As the culture of human epidermal keratinocytes (hK) became practical (Karasek and Charlton, 1971; Rheinwald and Green, 1975; Peehl and Ham, 1980; Boyce and Ham, 1983), it was recognized that combining hK with a dermal substitute might facilitate transplantation of hK for wound closure (Hansbrough and Boyce, 1984). Beginning in the 1970s in Boston, two models of dermal substitutes using xenogeneic collagen were developed (Bell et al., 1981; Yannas and Burke, 1980). As transplantation of hK began to be studied more actively in the 1980s, other biopolymers, such as fibrin, derivatized hyaluronic acid, and elastin from xenogeneic or allogeneic sources became more prevalent (Ter Horst et al., 2018; Idrus et al., 2014; Myers et al., 1997, 2007) in experimental models. These early studies identified the high compatibility of biologically derived polymers, but also identified the limitations of lot-to-lot variability in composition and performance, inconsistent availability due to biologic sources, and degradation by enzymatic mechanisms from tissue inflammation and microbial contamination. Despite these limitations, collagen-based and hyaluronic acid-derived polymers have become commercialized for multiple applications in wound care.

In response to these limitations, fully synthetic biopolymers were studied for cellular transplantation. These included FDA-approved polymers, such as poly-glycolic acid/poly-lactic acid (PGA/PLA) (Harding et al., 2013), poly-caprolactone (PCL) (Mahjour et al., 2015; Augustine et al., 2015), polyethylene-oxide/polybutylene terephthalate (PEO/PBT) (Beumer et al., 1993, 1994), and more recently, poly-urethane (PUR) (Greenwood and Dearman, 2012a,b; Dearman et al., 2013). These materials addressed effectively the variability from biologic sources, and offered degradation by chemical hydrolysis rather than by enzymes that reduce degradation by microbial and cellular activities. However, other limitations, including release of acid from PGA/PLA copolymers, and protracted degradation times of PCL and PUR, have reduced the broad adoption of these kinds of polymers as scaffolds for cell transplantation.

Currently, the number of commercial uses for degradable polymers continues to increase. For treatment of partial-thickness wounds, degradable polymers in combination with allogeneic skin cells have been shown to promote reepithelialization of wounds without the need for excision (Schurr et al., 2009). For excised full-thickness burns, acellular scaffolds of collagen-glycosaminoglycan (i.e., Integra Dermal Regeneration Template), or poly-urethane (Novosorb Biodegradable Temporizing Matrix) can act to attract and guide the development of fibrovascular tissue as a vascularized dermal tissue in preparation for grafting of split-thickness skin autograft (Sidebar 2.5.8.3). It may

SIDEBAR 2.5.8.3

Degradable polymers are often combined with skin cells for delivery to sites of tissue injury or necrosis. Polymer properties that impact survival and integration of transplanted cells include the abilities to vascularize within a few days, and be fully degraded within a few months of transplantation. Current and investigational skin substitutes have been reported to contain degradable polymers from biologic or synthetic sources (Shevchenko et al., 2010; Ulery et al., 2011; Boyce and Lalley, 2018).

be expected that advanced synthetic, or synthetic/biologic blends of polymers (Powell and Boyce, 2009; Kim et al., 2017), will continue to be developed until an optimal composition for temporary or permanent skin substitutes is tested and approved for burns and/or other skin wounds.

Temporary Skin Substitutes

A broad spectrum of materials has become available for partial- and full-thickness burns after consideration of the requirements for optimal wound closure. These materials may be categorized generally into acellular and cellular types with multiple examples in each category. Acellular materials are represented by those without delivery of silver, such as Biobrane, Suprathel, or Mepitel, which have been shown to provide effective protection during reepithelialization of debrided, partial-thickness wounds or donor sites for skin grafts, or as a temporizing dressing for coverage after excision of full-thickness burns (Lal et al., 2000; Rahmanian-Schwarz et al., 2011; Campanella et al., 2011). Biobrane is a nylon mesh bonded to a silicone sheet that is coated with porcine collagen peptides. It is either shed as epithelialization proceeds, or is removed prior to grafting. It is available in nonperforated or perforated formats, the latter to allow drainage, and to avoid suppuration. Suprathel is a poly-lactic acid sheet indicated for partial-thickness burns and donor sites for skin autografts. In a comparative study with OmniDerm, Suprathel recorded lower pain scores, better adherence to wounds, fewer dressing changes, and no differences in time to epithelialization. Mepitel is a silicone rubber dressing that is reported to reduce pain and promote healing of partial-thickness burns in comparison to silver sulfadiazine (Gotschall et al., 1998; Campanella et al., 2011). These kinds of materials can be effective in wounds with low levels of microbial contamination, or clean, surgical wounds.

For partial-thickness wounds that are colonized with microorganisms, silver-containing dressings are often used to limit the progression of wound contamination and to promote epithelial healing. Examples of these kinds of dressings include ActiCoat, Mepitel Ag, and Aquacel Ag (Honari et al., 2001; Choi et al., 2018; Verbelen et al., 2014). Silver-containing materials offer comparable antimicrobial activity to silver sulfadiazine, but with less toxicity to wound tissue and inhibition of wound repair. Advantages of silver-releasing dressings include broad-spectrum coverage,

fast-acting reductions of microbial contaminations, and few dressing changes with some silver dressings able to release monocationic silver for up to 7 days. These advantages have contributed to the cost-effectiveness of silver-releasing dressings, and to their increased adoption in burn care.

Although these kinds of advanced dressings have found utility in developed countries, they are not always available or affordable in many developing countries. In those kinds of environments xenogeneic skin substitutes are often more abundant and less costly than banked human skin, or than medicated dressings. Examples of xenografts that have been reported as temporary covers, include but are not limited to porcine xenograft (Hermans, 2014; Busby et al., 2014), fish-derived skin from tilapia or cod (Magnusson et al., 2017; Kerecis, 2018; News, 2017), or banked skin from other animals (e.g., frogs, rabbits, or sheep). Animal xenografts may also present risks of pathogen transfer, such as endogenous retrovirus (Kimsa-Dudek et al., 2015). Potato skins have also been used as a temporary cover for scald injuries (Keswani et al., 1990). In more developed countries, banked cadaveric human split-thickness skin is often available (Kagan et al., 2005; Kagan, 2000), and is used as an effective cover until split-thickness skin autograft is available. Several reports describe the use of human amniochorionic membrane as a temporary skin wound cover, or for wounds with critical impacts such as the eyes (Reilly et al., 2017; Tenenhaus, 2017; Magnusson et al., 2017). Because collection and distribution of human amnion may transmit disease, pathogen testing or sterilization during processing is required to maintain safety for transplantation to vulnerable patients with extensive burns. These kinds of biological dressings are known to deliver growth factors, matrix molecules, and essential nutrients to wounds to promote wound closure, and may have extended benefits if living cells are preserved.

In analogy, engineered skin allografts (i.e., StrataGraft; Apligraf; DermaGraft) offer days to weeks of wound protection for large TBSA partial-thickness burns (Schurr et al., 2009; Cavallaro et al., 1994), or small TBSA full-thickness chronic wounds (Edmonds, 2009; Harding et al., 2013). Engineered allografts may be generated from sterile scaffold materials and cell banks that are tested and determined to be disease free. During fabrication, immune cells and vascular elements from the donor are depleted from these materials which renders them less immunogenic. Although the allogeneic epidermal keratinocytes are immunogenic, they are usually not sufficient to stimulate a robust T-cell-mediated rejection, such as host-versus-graft disease (Hu et al., 2006; Centanni et al., 2011). Rather, these less immunogenic materials either degrade on the wound, or are exfoliated by migrating keratinocytes during reepithelialization of the wound within a few weeks. Definitive advantages of these materials include continuous availability, and consistency of composition due to their fabrication *in vitro*. These advantages are offset by high cost, needs for multiple applications, and limited benefits in long-term outcomes.

Permanent Skin Substitutes

Long-term durability of wound closure after full-thickness burns requires both restoration of dermal connective tissue, and autologous keratinocytes to restore the natural epidermal barrier. This may be accomplished by several approaches. Conventional treatment of small total body surface area (TBSA), full-thickness burns (e.g., less than 30% TBSA) with split-thickness skin autograft may be accomplished promptly and effectively, but requires harvesting of autologous donor skin. As the wound area increases, donor skin availability decreases, which requires larger expansion ratios for skin autografts up to a typical limit of approximately 1:4. Because open wounds generate granulation tissue which leads to scar (Robson et al., 1992; Porres-Reyes et al., 1991), the time to reepithelialization should be minimized to reduce scar. To address the needs for restoration of dermal connective tissue, and stable epidermal barrier, three categories of permanent skin substitutes have emerged.

Acellular dermal scaffolds have been commercialized to promote the development of a uniform layer of fibrovascular tissue to support and stabilize epidermal substitutes. Manufactured dermal substitutes may be composed of bovine collagen and glycosaminoglycan with a silicone cover (i.e., Integra Dermal Regeneration Template) (Heimbach et al., 2003; Boyce et al., 1995, 1999a,b, 2006, 2017), and recently, degradable poly-urethane (i.e., Biodegradable Temporizing Matrix) (Greenwood and Dearman, 2012a,b; Wagstaff et al., 2017). These materials may be applied to excised burn wounds at the time of excision of eschar to reduce the release of inflammatory cytokines, and the progression of microbial contamination and infection. They require 2 weeks or more to become vascularized sufficiently to support a thin, split-thickness skin graft. Favorable outcomes with these materials have been reported that may reduce long-term morbidity, such as wound contractures, and needs for scar reconstruction. Simultaneous application of a scaffold consisting of bovine collagen and elastin (i.e., MatriDerm) with split-thickness skin autograft has shown improved range of motion and smoother appearance than with meshed and expanded autograft alone (Bottcher-Haberzeth et al., 2012; Ryssel et al. 2010a,b). Similarly, decellularized human dermis (i.e., AlloDerm) or fetal bovine dermis (i.e., PriMatrix) have been described as dermal substitutes together with split-thickness skin autograft for burn reconstruction, and other soft tissue augmentation (Wainwright, 1995; Strong et al., 2016).

Because these acellular scaffolds recruit cells from the recipient wound bed, are slowly degraded, and replaced with recipient extracellular matrix, they may be categorized as “autologous” and “permanent” because the tissue restoration is of indefinite duration. Also, because the tissue restoration is guided by each of these scaffolds in a context of granulation tissue, the resulting anatomy of the fibrovascular tissue is not identical in the uninjured dermis. Therefore, the use of these kinds of dermal substitutes reduces variability of the tissue formation compared to granulation of the

wound, and confers a regulatory function that increases the predictability of the outcomes.

After restoration of a highly viable, vascularized wound bed, restoration of the epidermis is required to close the wounds long term. Widely meshed (i.e., 1:6) split-thickness skin autograft was covered with narrowly meshed (i.e., 1:1.5) cadaver skin allograft to protect and promote epithelial coverage, and conserve autologous donor skin (Alexander et al., 1981). For more than 30 years, cultured epithelial autografts (i.e., EpiCel) have been available for wound closure. However, those grafts are known to repeatedly blister and ulcerate, which predisposes them to high morbidity and risks of development of squamous cell carcinoma (Woodley et al., 1988; Kowal-Vern and Criswell, 2005). Suspensions of autologous epidermal keratinocytes (i.e., ReCell) may be prepared intraoperatively, and sprayed on deep, partial-thickness burns, or in combination with meshed, split-thickness skin autograft on excised, full-thickness burns. This approach has shown favorable outcomes, but is limited by the absolute numbers of viable keratinocytes that can be isolated intraoperatively, and by the random distribution of cells by the spraying process (Wood et al., 2012; Gravante et al., 2007). In a similar approach, the population of keratinocytes was increased by expansion in culture, and was applied with a pressurized pneumatic sprayer to facilitate surgical application (Schlabe et al., 2008; Hartmann et al., 2007). Because the culture process may expose the keratinocytes to hazardous compounds or procedures, a more complex path to regulatory approval can result. A recent approach has become available in which a small biopsy of full-thickness skin is collected, sent to a central laboratory, morselized, combined with a viscous vehicle (SkinTE), returned to the hospital in 1–3 days, and applied to prepared, full-thickness acute or chronic wounds (PolarityTE.com, 2018). Because the starting biopsy is full-thickness skin, this model claims to restore all of the anatomy and physiology of uninjured skin. This claim has not yet been well-substantiated, and the approach is also limited in its absolute ability to expand the biopsy. Due to an expedited regulatory pathway, this technology is being commercialized, but has not yet been compared to any standard-of-care treatment in prospective, multicenter studies (PolarityTE.com, 2018).

Autologous dermal–epidermal skin substitutes comprise combinations of dermal fibroblasts and epidermal keratinocytes with or without a degradable scaffold. Similarly to allogeneic models described above (see Temporary Skin Substitutes), skin substitutes containing mesenchymal and epithelial cells can organize into a stratified, keratinized epidermal component, can develop a basement membrane to form a biological bond between the epidermal and dermal substitutes, and a dermal component that can vascularize rapidly due to its porous structure and delivery of angiogenic factors to the wound. These models utilize culture in vitro to expand the cell populations to sufficient numbers to cover skin wounds up to 99% TBSA. This is the essential advantage provided by cultured epithelial autografts, but

this is improved by including a dermal substitute to promote formation of basement membrane, increase the mechanical strength of the material, and facilitate transplantation and attachment to the wound with staples or sutures. Autologous, bilayered models of engineered skin have been described in preclinical (Dearman et al., 2014) and clinical trials (Boyce et al., 1995, 1999a,b, 2006, 2017; Germain et al., 2018), but none is yet available commercially. Outcomes from clinical trials have been favorable in the accomplishment of stable, long-term wound closure, lower mortality in pediatric subjects compared with corresponding populations in the National Burn Repository, and functional range of motion. Similarly to split-thickness skin autograft, the resulting skin does not develop epidermal appendages (hair, sebaceous, or sweat glands), and pigmentation is deficient. These results offer reductions in requirements for donor skin, less long-term morbidity, and improved quality of life in comparison with widely meshed, split-thickness skin autografts. Ongoing research is addressing these deficiencies, and continued progress is expected toward a model of autologous engineered skin with the anatomy and physiology of uninjured skin. Beyond that long-term goal, experimental models that express specific genes or correct gene defects (Dakiw Piaceski et al., 2018; Comer et al., 2014) are under development to restore or enhance normal properties of the skin.

Cost Considerations

In addition to medical and surgical considerations, the relatively high cost of cell therapies requires careful consideration. Depending on the composition and labor intensity of the therapy, unit costs (i.e., per cm²) for cell therapies can range between US\$10–100. If the patient is an adult, and the total body surface area (TBSA) is extensive (e.g., greater than 50%), the total costs for skin substitutes can rise to more than US\$100,000. To justify these costs, there must be sufficient reductions in medical risks, such as requirements for time in intensive care, and/or long-term benefits, such as reductions in morbidity, needs for reconstructive surgery, or greater quality of life. These determinations of the cost effectiveness of burn dressings or skin substitutes appear only infrequently in the literature, but may contribute to planning of specifications for wound care, and priorities for long-term outcomes. Two studies (Schiavon et al., 2016; Hop et al., 2014) evaluated the total cost of acute care after use of acellular dermal substitutes, and found no differences in total costs for acute care of burns, but had wide ranges of costs that may have obscured differences attributable to the skin substitutes. Economic considerations must include not only costs for acquisition of the materials, but also procedural time for their application and care until completion of wound closure. Because of the multiple factors that contribute to total cost for use and care of cellular and non-cellular burn dressings and skin substitutes, performance of prospective studies and collection of conclusive data are difficult. Together with the fact that cost effectiveness is not required to receive marketing approval or reimbursement,

determination of cost effectiveness becomes a secondary priority behind the more immediate needs of patients during acute care of burn wounds.

Regulatory Considerations

The safety and efficacy of skin substitutes are regulated in the United States by the US Food and Drug Administration (FDA). Wound dressings and biologic skin substitutes have increased in complexity from models that protect wounds and release antimicrobials to those that: replace either dermis or epidermis; to dermal–epidermal models; to delivery of combinations of biopolymer scaffolds, multiple cell types or multiple cell sources; to expression of gene products for therapeutic improvements in wound healing (Boyce and Lalley, 2018). This spectrum of unprecedented materials presented questions regarding the regulatory framework within which each model would be evaluated for consideration of permission to market. Traditionally, the FDA has consisted of three centers for evaluation of human therapeutics: the Center for Devices and Radiologic Health (CDRH), the Center for Biologics Evaluation and Research (CBER), and the Center for Drug Evaluation and Research (CDER). Availability of cadaveric allograft has been provided under regulations for tissue banking, which are administered by CBER. As the spectrum of research models of skin substitutes broadened during the 1980s and 1990s, several investigative therapies had components that required review by multiple centers at the FDA. The agency responded proactively with two initiatives that have contributed to greater clarity of the regulatory process, and with Guidances to Industry (US FDA, 1996, 1998, 2006, 2011) on how to propose a path to market.

An early initiative was the FDA's participation in the establishment of definitions and standards for Tissue Engineered Medical Products (TEMPs) through formation of Division IV of Committee F04 for medical devices through the American Society for Testing and (ASTM, 2007) (ASTM) (Materials). Beginning in 1997, this organization has had members from academic institutions, government, and industry participating in a consensus process for composing definitions of materials, and provision of methods for calibration and testing of the materials. With regard to skin substitutes, the ASTM process has resulted in a Standard Guide for Classification of Therapeutic Skin Substitutes (ASTM, 2009), providing consensus definitions and nomenclature. The second initiative was the FDA's establishment in 2002 of the Office of Combination Products, by which investigative therapies are reviewed initially for their *primary mode of action*. This office confers with the Centers for Human Therapeutics to designate new therapies at a lead center at the FDA with participation from other centers as appropriate. Together, these initiatives have added clarity to the assignment of novel therapeutics to a designated regulatory path (Witten et al., 2015). In addition to providing a framework for innovative investigative therapies, the FDA provides “expanded access” or “compassionate use” permissions for treatment of selected conditions

that present high risks of mortality or morbidity to patients (US FDA, 2014c, 2017a).

More recently, the 21st Century Cures Act (Cures Act) was signed into law in the United States in December 2016. As the name implies, this law is intended to facilitate and expedite the availability of novel therapies to patients with serious, or potentially life-threatening, conditions. The Cures Act provides for expedited therapeutic development programs including the Regenerative Medicine Advanced Therapy (RMAT) designation for eligible biologics products, and the Breakthrough Devices program which is designed to facilitate the review of certain innovative medical devices (US FDA, 2016). These new designations by FDA are in addition to previous expedited regulatory pathways of Fast Track development (US FDA, 2017b), Breakthrough Therapy designation (US FDA, 2014a), Accelerated Approval (US FDA, 2014b), and Priority Review designation for drugs (US FDA, 2014d). Together, these alternative pathways to provisional or full marketing are likely to increase access to the most advanced therapies by patient populations with the greatest medical needs.

Conclusions and Future Directions

Future prospects for burn dressings and biologic skin substitutes are extensive and diverse. Advances in the use and regulation of stem cells in skin are highly likely to lead to autologous skin substitutes with greater homology to uninjured skin by providing restoration of skin pigmentation, epidermal appendages (hair, sebaceous and sweat glands), a vascular plexus, nerve, and subcutaneous tissues (Boyce and Supp, 2016; Boyce and Lalley, 2018). Genetic modification of autologous cells opens tremendous opportunities for regulation of wound closure, reductions in scar formation, and correction of congenital diseases (Hirsch et al., 2017; Siprashvili et al., 2016). Balancing with these exciting prospects are economic considerations that often constrain decisions, and favor low-cost alternatives over high-cost technologies. Because these advanced technologies have high costs of product development and acquisition, the relatively small size of the burn market may not be sufficient to support all of these products. Therefore, successful delivery of these kinds of novel therapeutics will be more likely in broader applications than burns alone, or by companies with additional products to subsidize revenue from burns. With effective management of these economic considerations, translation of advanced burn dressings and biologic skin substitutes into clinical care can be predicted with confidence to lead to reductions in morbidity from traumatic injuries and congenital diseases of the skin.

Acknowledgments, Disclosures and Disclaimer

This contribution was supported by grants #85200 and #84050 to Dr. Boyce from the Shriners Hospitals for

Children. Dr. Boyce performs paid consulting services that are reviewed and approved by the University of Cincinnati Office of Research. Dr. Boyce is employed by the University of Cincinnati, and has multiple patents that are licensed for development, and may generate royalties or other payments prospectively. Drs. Chang and Warner declare no financial conflicts of interest. Descriptions of commercially available products by the authors are based on published literature, and do not constitute a recommendation for whether or not any of the products are appropriate for specific uses. For medical indications or intended uses of the products, refer to their package inserts.

References

- Alexander, J.W., Macmillan, B.G., Law, E., Kittur, D.S., 1981. Treatment of severe burns with widely meshed skin autograft, and meshed skin allograft overlay. *J. Trauma* 21 (6), 433–438.
- American Burn Association, 2017. National Burn Repository.
- American Society For Testing And Materials, 2007. Standard Guide for Preservation of Tissue Engineered Medical Products. ASTM International.
- American Society For Testing And Materials, 2009. In: Cahn, F. (Ed.), Standard Guide for Classification of Therapeutic Skin Substitutes. ASTM International, West Conshohocken, PA.
- Arealo, J.M., Lorente, J.A., 1999. Skin coverage with Biobrane biomaterial for the treatment of patients with toxic epidermal necrolysis. *J. Burn Care Rehabil.* 20, 406–410.
- Augustine, R., Dominic, E.A., Reju, I., Kaimal, B., Kalarikkal, N., Thomas, S., 2015. Electrospun poly(epsilon-caprolactone)-based skin substitutes: in vivo evaluation of wound healing and the mechanism of cell proliferation. *J. Biomed. Mater. Res. B Appl. Biomater.* 103, 1445–1454.
- Banwell, P.E., 1999. Topical negative pressure therapy in wound care. *J. Wound Care* 8, 79–84.
- Barrett, S., 2009. Mepilex Ag: an antimicrobial, absorbent foam dressing with Safetac technology. *Br. J. Nurs.* 18 (S28), s30–s36.
- Bell, E., Ehrlich, H.P., Sher, S., Merrill, C., Sarber, R., Hull, B., 1981. Development and use of a living skin equivalent. *Plast. Reconstr. Surg.* 67, 386–392.
- Bett, B.J., 2005. Large or multiple congenital melanocytic nevi: occurrence of cutaneous melanoma in 1008 persons. *J. Am. Acad. Dermatol.* 52, 793–797.
- Beumer, G.J., Van Blitterswijk, C.A., Bakker, D., Ponc, M., 1993. Cell-seeding and in vitro biocompatibility evaluation of polymeric matrices of PEO/PBT copolymers and PLLA. *Biomaterials* 14, 598–604.
- Beumer, G.J., Van Blitterswijk, C.A., Ponc, M., 1994. Biocompatibility of a biodegradable matrix used as a skin substitute: an in vivo evaluation. *J. Biomed. Mater. Res.* 28, 545–552.
- Botcher-Haberzeth, S., Biedermann, T., Schiestl, C., Hartmann-Fritsch, F., Schneider, J., Reichmann, E., Meuli, M., 2012. Matriderm(R) 1 mm versus Integra(R) Single Layer 1.3 mm for one-step closure of full thickness skin defects: a comparative experimental study in rats. *Pediatr. Surg. Int.* 28, 171–177.
- Boyce, S.T., Ham, R.G., 1983. Calcium-regulated differentiation of normal human epidermal keratinocytes in chemically defined clonal culture and serum-free serial culture. *J. Investig. Dermatol.* 81, 33s–40s.
- Boyce, S.T., Lalley, A.L., 2018. Tissue engineering of skin and regenerative medicine for wound care. *Burns Trauma* 6, 4.

- Boyce, S.T., Supp, D.M., 2016. Biologic skin substitutes. In: Albanna, M.Z., Holmes, J.H. (Eds.), *Skin Tissue Engineering and Regenerative Medicine*. Academic Press/Elsevier, New York.
- Boyce, S.T., Warden, G.D., Holder, I.A., 1995. Non-cytotoxic combinations of topical antimicrobial agents for use with cultured skin. *Antimicrob. Agents Chemother.* 39 (6), 1324–1328.
- Boyce, S.T., Kagan, R.J., Meyer, N.A., Yakuboff, K.P., Warden, G.D., 1999a. The 1999 Clinical Research Award. Cultured skin substitutes combined with Integra to replace native skin autograft and allograft for closure of full-thickness burns. *J. Burn Care Rehabil.* 20, 453–461.
- Boyce, S.T., Supp, A.P., Swope, V.B., Warden, G.D., 1999b. Topical sulfamylon reduces engraftment of cultured skin substitutes on athymic mice. *J. Burn Care Rehabil.* 20, 33–36.
- Boyce, S.T., Kagan, R.J., Greenhalgh, D.G., Warner, P., Yakuboff, K.P., Palmieri, T., Warden, G.D., 2006. Cultured skin substitutes reduce requirements for harvesting of skin autograft for closure of excised, full-thickness burns. *J. Trauma* 60, 821–829.
- Boyce, S.T., Simpson, P.S., Rieman, M.T., Warner, P.M., Yakuboff, K.P., Kevin, B.J., Nelson, J.K., Fowler, L.A., Kagan, R.J., 2017. Randomized, paired-site comparison of autologous engineered skin substitutes and split-thickness skin graft for closure of extensive, full-thickness burns. *J. Burn Care Res.* 38, 61–70.
- Burkey, B., Davis III, W., Glat, P.M., 2016. Porcine xenograft treatment of superficial partial-thickness burns in paediatric patients. *J. Wound Care* 25, S10–S15.
- Busby, S.A., Robb, A., Lang, S., Takeuchi, Y., Vesely, P., Scobie, L., 2014. Antibiotic susceptibility and resistance of *Staphylococcus aureus* isolated from fresh porcine skin xenografts: risk to recipients with thermal injury. *Burns* 40, 288–294.
- Campanella, S.D., Rapley, P., Ramelet, A.S., 2011. A randomised controlled pilot study comparing Mepitel((R)) and SurfaSoft((R)) on paediatric donor sites treated with Recell((R)). *Burns* 37, 1334–1342.
- Carlson, M., Faria, K., Shamis, Y., Leman, J., Ronfard, V., Garlick, J., 2011. Epidermal stem cells are preserved during commercial-scale manufacture of a bilayered, living cellular construct (Apligraf(R)). *Tissue Eng. A* 17, 487–493.
- Cavallaro, J.F., Kemp, P.D., Kraus, K.H., 1994. Collagen fabrics as biomaterials. *Biotechnol. Bioeng.* 43, 781–791.
- Centanni, J.M., Straseski, J.A., Wicks, A., Hank, J.A., Rasmussen, C.A., Lokuta, M.A., Schurr, M.J., Foster, K.N., Faucher, L.D., Caruso, D.M., Comer, A.R., Len-Hoffmann, B.L., 2011. StrataGraft skin substitute is well-tolerated and is not acutely immunogenic in patients with traumatic wounds: results from a prospective, randomized, controlled dose escalation trial. *Ann. Surg.* 253, 672–683.
- Choi, Y.M., Campbell, K., Levek, C., Recicar, J., Moulton, S., 2018. Antibiotic ointment versus a silver-based dressing for children with extremity burns: a randomized controlled study. *J. Pediatr. Surg.* <https://doi.org/10.1016/j.jpedsurg.2018.06.011>. (Epub ahead of print).
- Church, D., Elsayed, S., Reid, O., Winston, B., Lindsay, R., 2006. Burn wound infections. *Clin. Microbiol. Rev.* 19, 403–434.
- Comer, A.R., Rasmussen, C.A., Thomas-Virnig, C.L., Lokuta, M.A., Shaughnessy, L.M., Schlosser, S.J., Johnston, C.E., Bauer, R.L., Clevon, T.D., Wiczorek, N.C., Allen-Hoffmann, B.L., 2014. Preclinical development and planned clinical evaluation of a human skin substitute engineered to secrete elevated levels of a host defense peptide. In: *Proceedings of the Innovations in Wound Healing Conference*.
- Cooper, M.L., Laxer, J.A., Hansbrough, J.F., 1991. The cytotoxic effects of commonly used topical antimicrobial agents on human fibroblasts and keratinocytes. *J. Trauma* 31, 775–782.
- Cooper, R.A., Halas, E., Molan, P.C., 2002. The efficacy of honey in inhibiting strains of *Pseudomonas aeruginosa* from infected burns. *J. Burn Care Rehabil.* 23, 366–370.
- Dakiw Piacieski, A., Larouche, D., Ghani, K., Bisson, F., Cortez Ghio, S., Larochelle, S., Moulin, V.J., Caruso, M., Germain, L., 2018. Translating the combination of gene therapy and tissue engineering for treating recessive dystrophic epidermolysis bullosa. *Eur. Cells Mater.* 35, 73–86.
- Day, A., Alkhalil, A., Carney, B.C., Hoffman, H.N., Moffatt, L.T., Shupp, J.W., 2017. Disruption of biofilms and neutralization of bacteria using hypochlorous acid solution: an in vivo and in vitro evaluation. *Adv. Skin Wound Care* 30, 543–551.
- Dearman, B.L., Stefani, K., Li, A., Greenwood, J.E., 2013. "Take" of a polymer-based autologous cultured composite "skin" on an integrated temporizing dermal matrix: proof of concept. *J. Burn Care Res.* 34, 151–160.
- Dearman, B.L., Li, A., Greenwood, J.E., 2014. Optimization of a polyurethane dermal matrix and experience with a polymer-based cultured composite skin. *J. Burn Care Res.* 35, 437–448.
- Dumville, J.C., Munson, C., Christie, J., 2014. Negative pressure wound therapy for partial-thickness burns. *Cochrane Database Syst. Rev.* 12, CD006215. <https://doi.org/10.1002/14651858.CD006215.pub3>. CD006215.
- Duranceau, L., Genest, H., Bortoluzzi, P., Moulin, V., Auger, F.A., Germain, L., 2014. Successful grafting of a novel autologous tissue-engineered skin substitutes (dermis and epidermis) on twelve burn patients. *J. Burn Care Res.* 35, S121.
- Edmonds, M., 2009. Apligraf in the treatment of neuropathic diabetic foot ulcers. *Int. J. Low. Extrem. Wounds* 8, 11–18.
- Ellis, C.V., Kulber, D.A., 2012. Acellular dermal matrices in hand reconstruction. *Plast. Reconstr. Surg.* 130, 256S–269S.
- Gallagher, J.J., 2012. Treatment of infection in burns. In: Herndon, D.N. (Ed.), *Total Burn Care*, fourth ed. Saunders-Elsevier, New York, NY.
- Gallagher, J.J., Branski, L.K., Williams-Bouyer, N., Villareal, C., Herndon, D.N., 2012. Treatment of infection in burns. In: Herndon, D.N. (Ed.), *Total Burn Care*. Saunders-Elsevier.
- Gallico III, G.G., O'connor, N.E., Compton, C.C., Kehinde, O., Green, H., 1984. Permanent coverage of large burn wounds with autologous cultured human epithelium. *N. Engl. J. Med.* 311, 448–451.
- Germain, L., Larouche, D., Nedelec, B., Perreault, I., Duranceau, L., Bortoluzzi, P., Beaudoin Cloutier, C., Genest, H., Caouette-Laberge, L., Dumas, A., Bussiere, A., Boghossian, E., Kanavsky, J., Leclerc, Y., Lee, J., Nguyen, M.T., Bernier, V., Knoppers, B.M., Moulin, V.J., Auger, F.A., 2018. Autologous bilayered self-assembled skin substitutes (SASSs) as permanent grafts: a case series of 14 severely burned patients indicating clinical effectiveness. *Eur. Cells Mater.* 36, 128–141.
- Gotschall, C.S., Morrison, M.I., Eichelberger, M.R., 1998. Prospective, randomized study of the efficacy of Mepitel on children with partial-thickness scalds. *J. Burn Care Rehabil.* 19, 279–283.
- Gravante, G., Di Fede, M.C., Araco, A., Grimaldi, M., De, A.B., Arpino, A., Cervelli, V., Montone, A., 2007. A randomized trial comparing ReCell system of epidermal cells delivery versus classic skin grafts for the treatment of deep partial thickness burns. *Burns* 33, 966–972.
- Greenwood, J.E., Dearman, B.L., 2012a. Comparison of a sealed, polymer foam biodegradable temporizing matrix against Integra(R) dermal regeneration template in a porcine wound model. *J. Burn Care Res.* 33, 163–173.
- Greenwood, J.E., Dearman, B.L., 2012b. Split skin graft application over an integrating, biodegradable temporizing polymer matrix: immediate and delayed. *J. Burn Care Res.* 33, 7–19.

- Haith, L.R., Stair-Buchmann, M.E., Ackerman, B.H., Herder, D., Reigart, C.L., Stoering, M., Guilday, R.E., Patton, M.L., Ross, K.M., 2015. Evaluation of Aquacel Ag for autogenous skin donor sites. *J. Burn Care Res.* 36, 602–606.
- Hansbrough, J.F., Boyce, S.T., 1984. What criteria should be used for designing artificial skin replacement and how well do the current materials meet these criteria. *J. Trauma* 24, 31s–35s.
- Harding, K., Sumner, M., Cardinal, M., 2013. A prospective, multi-centre, randomised controlled study of human fibroblast-derived dermal substitute (Dermagraft) in patients with venous leg ulcers. *Int. Wound J.* 10, 132–137.
- Hartmann, B., Ekkernkamp, A., Johnen, C., Gerlach, J.C., Belfekroun, C., Kuntscher, M.V., 2007. Sprayed cultured epithelial autografts for deep dermal burns of the face and neck. *Ann. Plast. Surg.* 58, 70–73.
- Heggers, J.P., Sazy, J.A., Stenberg, B.D., Strock, L.L., Mccauley, R.L., Herndon, D.N., Robson, M.C., 1991. Bactericidal and wound-healing properties of sodium hypochlorite solutions: the 1991 Lindberg Award. *J. Burn Care Rehabil.* 12, 420–424.
- Heimbach, D., Luterman, A., Burke, J.F., Cram, A., Herndon, D., Hunt, J., Jordon, M., Mcmanus, W., Solem, L., Warden, G., Zawacki, B., 1988. Artificial dermis for major burns; a multi-center randomized clinical trial. *Ann. Surg.* 208, 313–320.
- Heimbach, D.M., Warden, G.D., Luterman, A., Jordan, M.H., Ozobia, N., Ryan, C.M., Voigt, D.W., Hickerson, W.L., Saffle, J.R., Declement, F.A., Sheridan, R.L., Dimick, A.R., 2003. Multicenter postapproval clinical trial of Integra dermal regeneration template for burn treatment. *J. Burn Care Rehabil.* 24, 42–48.
- Helm, D.L., Orgill, B.D., Ogawa, R., Orgill, D.P., 2013. Burn dressings and skin substitutes. In: Ratner, B., Schoen, F., Hoffman, A., Lemons, J. (Eds.), *Biomaterials Science: An Introduction to Materials in Medicine*, third ed. Elsevier.
- Hermans, M.H., 2014. Porcine xenografts vs. (cryopreserved) allografts in the management of partial thickness burns: is there a clinical difference? *Burns* 40, 408–415.
- Herndon, D.N., 2012. *Total Burn Care*. W.B. Saunders, Philadelphia, PA.
- Hirsch, T., Rothoef, T., Teig, N., Bauer, J.W., Pellegrini, G., DE Rosa, L., Scaglione, D., Reichelt, J., Klausegger, A., Kneisz, D., Romano, O., Secone Seconetti, A., Contin, R., Enzo, E., Jurman, I., Carulli, S., Jacobsen, F., Luecke, T., Lehnhardt, M., Fischer, M., Kueckelhaus, M., Quagliano, D., Morgante, M., Bicciato, S., Bondanza, S., DE Luca, M., 2017. Regeneration of the entire human epidermis using transgenic stem cells. *Nature* 551, 327–332.
- Honari, S., Gibran, N.S., Engrav, L.H., Carlson, A.R., Heimbach, D.M., 2001. Clinical benefits and cost effectiveness of Acticoat as a dressing for donor sites. *J. Burn Care Rehabil.* 22, S74.
- Hop, M.J., Bloemen, M.C., Van Baar, M.E., Nieuwenhuis, M.K., Van Zuijlen, P.P., Polinder, S., Middelkoop, E., 2014. Cost study of dermal substitutes and topical negative pressure in the surgical treatment of burns. *Burns* 40, 388–396.
- Hu, S., Kirsner, R.S., Falanga, V., Phillips, T., Eaglstein, W.H., 2006. Evaluation of Apligraf persistence and basement membrane restoration in donor site wounds: a pilot study. *Wound Repair Regen.* 14, 427–433.
- Hundeshagen, G., Collins, V.N., Wurzer, P., Sherman, W., Voigt, C.D., Cambiaso-Daniel, J., Nunez Lopez, O., Sheaffer, J., Herndon, D.N., Finnerty, C.C., Branski, L.K., 2018. A prospective, randomized, controlled trial comparing the outpatient treatment of pediatric and adult partial-thickness burns with Suprathel or Mepilex Ag. *J. Burn Care Res.* 39, 261–267.
- Idrus, R.B., Rameli, M.A., Low, K.C., Law, J.X., Chua, K.H., Latiff, M.B., Saim, A.B., 2014. Full-thickness skin wound healing using autologous keratinocytes and dermal fibroblasts with fibrin: bilayered versus single-layered substitute. *Adv. Skin Wound Care* 27, 171–180.
- Jan, S.N., Khan, F.A., Bashir, M.M., Nasir, M., Ansari, H.H., Shami, H.B., Nazir, U., Hanif, A., Sohail, M., 2018. Comparison of Laser Doppler Imaging (LDI) and clinical assessment in differentiating between superficial and deep partial thickness burn wounds. *Burns* 44, 405–413.
- Jansen, L.A., De, C.P., Guay, N.A., Lineaweaver, W.C., Shokrollahi, K., 2013. The evidence base for the acellular dermal matrix AlloDerm: a systematic review. *Ann. Plast. Surg.* 70, 587–594.
- Kagan, R.J., 2000. FDA regulation of human tissue: implications for skin banks and burn centers. *J. Burn Care Rehabil.* 21, 353–357.
- Kagan, R.J., Robb, E.C., Plessinger, R.T., 2005. Human skin banking. *Clin. Lab. Med.* 25, 587–605.
- Kamolz, L.P., Lumenta, D.B., Parvizi, D., Wiedner, M., Justich, I., Keck, M., Pfurtscheller, K., Schintler, M., 2014. Skin graft fixation in severe burns: use of topical negative pressure. *Ann Burns Fire Disasters* 27, 141–145.
- Karasek, M.A., Charlton, M.E., 1971. Growth of post-embryonic skin epithelial cells on collagen gels. *J. Invest. Dermatol.* 51, 247–252.
- Kempf, M., Kimble, R.M., Cuttle, L., 2011. Cytotoxicity testing of burn wound dressings, ointments and creams: a method using polycarbonate cell culture inserts on a cell culture system. *Burns* 37, 994–1000.
- Kerecis, 2018. Fish-Skin Wound Treatment from the Pure Waters of Iceland. [Online]. Kerecis. Available from <https://www.kerecis.com/>.
- Keswani, M.H., Vartak, A.M., Patil, A., Davies, J.W., 1990. Histological and bacteriological studies of burn wounds treated with boiled potato peel dressings. *Burns* 16, 137–143.
- Kim, B.S., Lee, J.S., Gao, G., Cho, D.W., 2017. Direct 3D cell-printing of human skin with functional transwell system. *Biofabrication* 9, 025034.
- Kimsa-Dudek, M., Strzalka-Mrozik, B., Kimsa, M.W., Blecharz, I., Gola, J., Skowronek, B., Janiszewski, A., Lipinski, D., Zeyland, J., Szalata, M., Slomski, R., Mazurek, U., 2015. Screening pigs for xenotransplantation: expression of porcine endogenous retroviruses in transgenic pig skin. *Transgenic Res.* 24, 529–536.
- Kolacz, N.M., Jaroch, M.T., Bear, M.L., Hess, R.F., 2014. The effect of Burns & Wounds (B&W)/burdock leaf therapy on burn-injured Amish patients: a pilot study measuring pain levels, infection rates, and healing times. *J. Holist. Nurs.* 32, 327–340.
- Kowal-Vern, A., Criswell, B.K., 2005. Burn scar neoplasms: a literature review and statistical analysis. *Burns* 31, 403–413.
- Lal, S., Barrow, R.E., Wolf, S.E., Chinkes, D.L., Hart, D.W., Heggers, J.P., Herndon, D.N., 2000. Biobrane improves wound healing in burned children without increased risk of infection. *Shock* 14, 314–318.
- Leshner, A.P., Curry, R.H., Evans, J., Smith, V.A., Fitzgerald, M.T., Cina, R.A., Streck, C.J., Hebra, A.V., 2011. Effectiveness of Biobrane for treatment of partial-thickness burns in children. *J. Pediatr. Surg.* 46, 1759–1763.
- Lewandowski, L., Purcell, R., Fleming, M., Gordon, W.T., 2013. The use of dilute Dakin's solution for the treatment of angioinvasive fungal infection in the combat wounded: a case series. *Mil. Med.* 178, e503–e507.
- Magnusson, S., Baldursson, B.T., Kjartansson, H., Rolfsson, O., Sigurjonsson, G.F., 2017. Regenerative and antibacterial properties of acellular fish skin grafts and human amnion/chorion membrane: implications for tissue preservation in combat casualty care. *Mil. Med.* 182, 383–388.

- Mahjour, S.B., Fu, X., Yang, X., Fong, J., Sefat, F., Wang, H., 2015. Rapid creation of skin substitutes from human skin cells and biomimetic nanofibers for acute full-thickness wound repair. *Burns* 41, 1764–1774.
- May, S.R., Declément, F., 1981. Skin banking. Part I. Procurement of transplantable cadaveric allograft skin for burn wound coverage. *J. Burn Care Rehabil.* 2, 7–23.
- McCullough, M., Burg, M., Lin, E., Peng, D., Garner, W., 2017. Steven Johnson syndrome and toxic epidermal necrolysis in a burn unit: a 15-year experience. *Burns* 43, 200–205.
- Monafo, W.W., West, M.A., 1990. Current treatment recommendations for topical burn therapy. *Drugs* 40, 364–373.
- Morykwas, M.J., David, L.R., Schneider, A.M., Whang, C., Jennings, D.A., Canty, C., Parker, D., White, W.L., Argenta, L.C., 1999. Use of subatmospheric pressure to prevent progression of partial-thickness burns in a swine model. *J. Burn Care Rehabil.* 20, 15–21.
- Mullai, V., Menon, T., 2007. Bactericidal activity of different types of honey against clinical and environmental isolates of *Pseudomonas aeruginosa*. *J. Altern. Complement. Med.* 13, 439–441.
- Myers, S.R., Grady, J., Soranzo, C., Sanders, R., Green, C., Leigh, I.M., Navsaria, H.A., 1997. A hyaluronic acid membrane delivery system for cultured keratinocytes: clinical "take" rates in the porcine kerato-dermal model. *J. Burn Care Rehabil.* 18, 214–222.
- Myers, S.R., Partha, V.N., Soranzo, C., Price, R.D., Navsaria, H.A., 2007. Hyalomatrix: a temporary epidermal barrier, hyaluronan delivery, and neodermis induction system for keratinocyte stem cell therapy. *Tissue Eng.* 13, 2733–2741.
- Nerandzic, M.M., Rackaityte, E., Jury, L.A., Eckart, K., Donskey, C.J., 2013. Novel strategies for enhanced removal of persistent *Bacillus anthracis* surrogates and *Clostridium difficile* spores from skin. *PLoS One* 8, e68706.
- News, S., 2017. Can Tilapia Skin be Used to Bandage Burns? [Online]. Available from <https://www.statnews.com/2017/03/02/brazil-tilapia-skin-burns/>.
- Nuutila, K., Yang, L., Broomhead, M., Proppe, K., Eriksson, E., 2018. PWD: treatment platform for both prolonged field care and definitive treatment of burn-injured warfighters. Sep 25 Mil. Med. <https://doi.org/10.1093/milmed/usy242>. (Epub ahead of print).
- Peehl, D.M., Ham, R.G., 1980. Growth and differentiation of human keratinocytes without a feeder layer or conditioned medium. *In Vitro* 16, 516–525.
- PolarityTE.com, 2018. SkinTE Patient Information. [Online] PolarityTE, Salt Lake City, UT. Available from <https://www.polarityTE.com/products/skinTE-patients>.
- Porres-Reyes, B.H., Blair, H.C., Jeffery, J.J., Mustoe, T.A., 1991. Collagenase production at the border of granulation tissue in a healing wound: macrophage and mesenchymal collagenase production in vivo. *Connect. Tissue Res.* 27, 63–71.
- Powell, H.M., Boyce, S.T., 2009. Engineered human skin fabricated using electrospun collagen-PCL blends: morphogenesis and mechanical properties. *Tissue Eng. A* 15, 2177–2187.
- Pruitt Jr., B.A., Levine, S., 1984. Characteristics and uses of biologic dressings and skin substitutes. *Arch. Surg.* 199, 312–322.
- Pruitt Jr., B.A., Mcmanus, A.T., Kim, S.H., Goodwin, C.W., 1998. Burn wound infections: current status. *World J. Surg.* 22, 135–145.
- Rahmanian-Schwarz, A., Beiderwieden, A., Willkomm, L.M., Amr, A., Schaller, H.E., Lotter, O., 2011. A clinical evaluation of Biobrane((R)) and Suprathel((R)) in acute burns and reconstructive surgery. *Burns* 37, 1343–1348.
- Ranzato, E., Martinotti, S., Burlando, B., 2013. Honey exposure stimulates wound repair of human dermal fibroblasts. *Burns Trauma* 1, 32–38.
- Reilly, D.A., Hickey, S., Glat, P., Lineaweaver, W.C., Goverman, J., 2017. Clinical experience: using dehydrated human amnion/chorion membrane allografts for acute and reconstructive burn care. *Ann. Plast. Surg.* 78, S19–s26.
- Rheinwald, J.G., Green, H., 1975. Serial cultivation of strains of human epidermal keratinocytes: the formation of keratinizing colonies from single cells. *Cell* 6, 331–343.
- Rieman, M.T., Neely, A.N., Boyce, S.T., Kossensjans, W.J., Durkee, P.J., Zembrodt, J.M., Puthoff, B.K., Kagan, R.J., 2014. Amish burn ointment and burdock leaf dressings: assessments of antimicrobial and cytotoxic activities. *J. Burn Care Res.* 35, e217–e223.
- Robson, M.C., Barnett, R.A., Leitch, I.O.W., Hayward, P.G., 1992. Prevention and treatment of postburn scars and contracture. *World J. Surg.* 16, 87–96.
- Rogers, A.D., Blackport, E., Cartotto, R., 2017. The use of Biobrane((R)) for wound coverage in Stevens-Johnson syndrome and toxic epidermal necrolysis. *Burns* 43, 1464–1472.
- Ryssel, H., Germann, G., Kloeters, O., Gazyakan, E., Radu, C.A., 2010a. Dermal substitution with Matriderm((R)) in burns on the dorsum of the hand. *Burns* 36, 1248–1253.
- Ryssel, H., Radu, C.A., Germann, G., Otte, M., Gazyakan, E., 2010b. Single-stage Matriderm(R) and skin grafting as an alternative reconstruction in high-voltage injuries. *Int. Wound J.* 7, 385–392.
- Schiavon, M., Francescon, M., Drigo, D., Salloum, G., Baraziol, R., Tesei, J., Fraccalanza, E., Barbone, F., 2016. The use of Integra dermal regeneration template versus flaps for reconstruction of full-thickness scalp defects involving the calvaria: a cost-benefit analysis. *Aesthet. Plast. Surg.* 40, 901–907.
- Schlabe, J., Johnen, C., Schwartlander, R., Moser, V., Hartmann, B., Gerlach, J.C., Kuntscher, M.V., 2008. Isolation and culture of different epidermal and dermal cell types from human scalp suitable for the development of a therapeutical cell spray. *Burns* 34, 376–384.
- Schurr, M.J., Foster, K.N., Centanni, J.M., Comer, A.R., Wicks, A., Gibson, A.L., Thomas-Virnig, C.L., Schlosser, S.J., Faucher, L.D., Lokuta, M.A., Len-Hoffmann, B.L., 2009. Phase I/II clinical evaluation of StrataGraft: a consistent, pathogen-free human skin substitute. *J. Trauma* 66, 866–873.
- Shevchenko, R.V., James, S.L., James, S.E., 2010. A review of tissue-engineered skin bioconstructs available for skin reconstruction. *J. R. Soc. Interface* 7, 229–258.
- Siprashvili, Z., Nguyen, N.T., Gorell, E.S., Loutit, K., Khuu, P., Furukawa, L.K., Lorenz, H.P., Leung, T.H., Keene, D.R., Rieger, K.E., Khavari, P., Lane, A.T., Tang, J.Y., Marinkovich, M.P., 2016. Safety and wound outcomes following genetically corrected autologous epidermal grafts in patients with recessive dystrophic epidermolysis bullosa. *JAMA* 316, 1808–1817.
- Sood, R., Roggy, D., Zieger, M., Balledux, J., Chaudhari, S., Koumanis, D.J., Mir, H.S., Cohen, A., Knipe, C., Gabehart, K., Coleman, J.J., 2010. Cultured epithelial autografts for coverage of large burn wounds in eighty-eight patients: the Indiana University experience. *J. Burn Care Res.* 31, 559–568.
- Stone II, R., Natesan, S., Kowalczewski, C.J., Mangum, L.H., Clay, N.E., Clohessy, R.M., Carlsson, A.H., Tassin, D.H., Chan, R.K., Rizzo, J.A., Christy, R.J., 2018. Advancements in regenerative strategies through the continuum of burn care. *Front. Pharmacol.* 9, 672.

- Strong, A.L., Bennett, D.K., Spreen, E.B., Adhvaryu, D.V., Littleton, J.C., Mencer, E.J., 2016. Fetal bovine collagen matrix in the treatment of a full thickness burn wound: a case report with long-term follow-up. *J. Burn Care Res.* 37, e292–e297.
- Stuart, M., 2008. *The Rebirth of DermaGraft*, vol. 13. Start-Up.
- Supp, A.P., Neely, A.N., Supp, D.M., Warden, G.D., Boyce, S.T., 2005. Evaluation of cytotoxicity and antimicrobial activity of Acticoat Burn Dressing for management of microbial contamination in cultured skin substitutes grafted to athymic mice. *J. Burn Care Rehabil.* 26, 238–246.
- Tenenhaus, M., 2017. The use of dehydrated human amnion/chorion membranes in the treatment of burns and complex wounds: current and future applications. *Ann. Plast. Surg.* 78, S11–s13.
- Ter Horst, B., Chouhan, G., Moiemien, N.S., Grover, L.M., 2018. Advances in keratinocyte delivery in burn wound care. *Adv. Drug Deliv. Rev.* 123, 18–32.
- Ulery, B.D., Nair, L.S., Laurencin, C.T., 2011. Biomedical applications of biodegradable polymers. *J. Polym. Sci. B Polym. Phys.* 49, 832–864.
- US Food And Drug Administration, 2014a. Accelerated Approval. [Online]. Available from: <https://www.fda.gov/ForPatients/Approvals/Fast/ucm405447.htm>.
- US Food And Drug Administration, 2014b. Breakthrough Therapy. [Online]. Available from <https://www.fda.gov/ForPatients/Approvals/Fast/ucm405397.htm>.
- US Food and Administration, 2014c. Expanded Access for Medical Devices. [Online]. Available from <http://www.fda.gov/medicaldevices/deviceregulationandguidance/howtomarketyourdevice/investigationaldeviceex>.
- US Food And Drug Administration, 2014d. Priority Review. [Online]. Available from <https://www.fda.gov/ForPatients/Approvals/Fast/ucm405405.htm>.
- US Food And Drug Administration, 2017a. Expanded Access (Compassionate Use). [Online]. Available from <https://www.fda.gov/NewsEvents/PublicHealthFocus/ExpandedAccessCompassionateUse/default.htm>.
- US Food And Drug Administration, 2017b. Fast Track. [Online]. Available from <https://www.fda.gov/ForPatients/Approvals/Fast/ucm405399.htm>.
- US Food and Drug Administration, 1996. Guidance on applications for products comprised of living autologous cells manipulated ex vivo and intended for structural repair or reconstruction. Fed. Regist. 61, 26523–26524.
- US Food and Drug Administration, 1998. Guidance for industry: guidance for human somatic cell therapy and gene therapy. Fed. Regist. 63, 36413.
- US Food and Drug Administration, 2006. Guidance for industry: chronic cutaneous ulcer and burn wounds – developing products for treatment. Fed. Regist. 65, 39912.
- US Food And Drug Administration, 2011. Guidance for Industry: How to Write a Request for Designation.
- US Food And Drug Administration, 2016. 21st Century Cures Act. [Online]. Available from <https://www.fda.gov/RegulatoryInformation/LawsEnforcedbyFDA/SignificantAmendmentsstotheFDCAct/21stCentu>.
- Van Langeveld, I., Gagnon, R.C., Conrad, P.F., Gamelli, R.L., Martin, B., Choudhry, M.A., Mosier, M.J., 2017. Multiple-drug resistance in burn patients: a retrospective study on the impact of antibiotic resistance on survival and length of stay. *J. Burn Care Res.* 38, 99–105.
- Verbelen, J., Hoeksema, H., Heyneman, A., Pirayesh, A., Monstrey, S., 2014. Aquacel(R) Ag dressing versus Acticoat dressing in partial thickness burns: a prospective, randomized, controlled study in 100 patients. Part 1: burn wound healing. *Burns* 40, 416–427.
- Wagstaff, M.J., Caplash, Y., Greenwood, J.E., 2017. Reconstruction of an anterior cervical necrotizing fasciitis defect using a biodegradable polyurethane dermal substitute. *Eplasty* 17, e3.
- Wainwright, D.J., 1995. Use of an acellular allograft dermal matrix (AlloDerm) in the management of full-thickness burns. *Burns* 21, 243–248.
- Witten, C.M., Mcfarland, R.D., Simek, S.L., 2015. Concise review: the U.S. Food and Drug Administration and regenerative medicine. *Stem Cells Transl. Med.* 4, 1495–1499.
- Wood, F.M., Giles, N., Stevenson, A., Rea, S., Fear, M., 2012. Characterisation of the cell suspension harvested from the dermal epidermal junction using a ReCell(R) kit. *Burns* 38, 44–51.
- Woodley, D.T., Peterson, H.D., Herzog, S.R., Sriklin, G.P., Bureson, R.E., Briggaman, R.A., Cronce, D.J., O'keefe, E.J., 1988. Burn wounds resurfaced by cultured epidermal autografts show abnormal reconstitution of anchoring fibrils. *JAMA* 259, 2566–2671.
- Yannas, I.V., Burke, J.F., 1980. Design of an artificial skin. I Basic design principles. *J. Biomed. Mater. Res.* 14, 65–81.

Chapter Exercises

1. Based on developments in wound dressings and skin substitutes during the past 30 years, what kinds of new products would you expect to see in the next 30 years? Write a one-page summary.
2. Perform one or more literature reviews to extend your perspective beyond this chapter's references. Consider presentation of the review(s) in a journal club or study group.
3. Perform lab exercises (e.g., antimicrobial testing, cell growth, and tissue morphogenesis) to gain experience with basic procedures related to the topics presented in this chapter.
4. Consider arranging a clinical shadowing assignment, independent study course, or internship to gain first-person experience with the subject matter of this chapter.
5. Register for an elective course related to the subject matter of this chapter that is outside of, but complementary to, your major field of study.

2.5.9

Description and Definition of Adhesives, and Related Terminology

DARSHAN S. SHAH, M.D.¹, BRYAN K. LAWSON, M.D.², MICHAEL YASZEMSKI, M.D., PH.D.³

¹Department of Orthopaedic Surgery, San Antonio Military Medical Center, Ft Sam Houston, TX, United States

²Department of Orthopaedic Surgery, Mike O'Callaghan Military Medical Center, Nellis AFB, NV, United States

³Department of Orthopaedic Surgery, Mayo Clinic, Rochester, MN, United States

Introduction

Description and Definition of Adhesives, and Related Terminology

In the context of biomaterials, adhesion science and technology assume high importance. It is useful to commence with the slightly wider concept of *bonding*. It is evident that many biomaterial devices are structured from multiple components, and these need to retain their mutual integrity during clinical service.

The most challenging issue is the creation of a durable interfacial bond between a biomaterial and its host tissue. In addition to the function of bonding, per se, an adhesive biomaterial may be required to fulfill a *space-filling* role—replacing some or all of any lost natural tissue. A further ideal function of an adhesive is that of *sealing*; that is, the prevention of ingress of other substances through the bonded zone.

Adhesive is a general term, and in specific contexts may be replaced by designations such as cement, glue, paste, fixative, and bonding agent. Some adhesives may be designed to exhibit further functions, such as antibacterial action, delivery of drugs or beneficial ions, such as the antibacterial ion Ag⁺ or fluoride (F⁻).

The aim of this chapter is to give a sound introduction to the physicochemical and materials science aspects of adhesives, sealants, and sutures, together with a description of current systems utilized in a range of surgical practice. It does not attempt a detailed study of the molecular biological interactions of adhesives.

The Logic of Adhesion Procedures

Our starting point is the existence of *electromagnetic forces* between and within molecules. In addition to the *primary* bond types, *secondary* intermolecular forces include hydrogen bonds and van der Waals bonds, both dipolar and dispersion types. There is a wide variation in the relative strength of these bonds; even weak bonds can have a massive cumulative effect if they are present in a high enough density.

Nevertheless, there is a further topological factor: macroscopically smooth surfaces are often microscopically rough. The actual contact regions between the two solids are restricted to the “mountain peaks,” and a major proportion of each total solid area is not in contact and is held apart *beyond* the distance zone over which the interaction energies are significant. The *effective intimate contact area* between the two surfaces is then too small to *directly* realize the potential of the intermolecular forces. It follows that rigid contact between the two solids fails to deliver an appreciable net interaction force. However, there are some exceptions to this outcome when one or more of the contacting solids exhibits plastic flow under mechanical stress. For example, pieces of gold foil may become self-adherent under compressive stress. Similarly, waxes can mutually bond when temperature is raised slightly.

To achieve adhesive bonding in the general case of two rigid solids, such as a tooth enamel surface and an orthodontic bracket, it is necessary to apply a fluid adhesive between them. Moreover, the fluid must be of appropriate chemical formulation to initially wet both surfaces, exhibiting a low *contact angle*. One or both surfaces may have been subjected to some form of pretreatment or *conditioning* with

an *etchant* or *primer* that, inter alia, may have modified the surfaces' porosity. In this case, the adhesive fluid may be drawn into the solid surface layers by capillary action. Capillarity is the process by which fluid and bacteria are carried into the interstices of multifilament fibers.

The presence of a suitable fluid between two solids greatly enhances the potential for intermolecular force interactions at each solid–fluid boundary.

To achieve an adhesive bond zone that is stable against shear forces, it is imperative to convert the adhesive agent from a fluid to a solid. In this process, it is desirable for the adhesive agent to exhibit high dimensional stability in relation to the interface with one or more adherends. There are several physicochemical mechanisms available for achieving adhesive solidification, or *setting*, including:

- Phase transformation on cooling;
- Solvent evaporation;
- Polymerization (and cross-linking) of fluid monomers or oligomers;
- Acid–base reaction.

Phase transformation has not been applied with biomedical adhesives, as the requisite temperatures (normally above 100°C) are beyond the biologically tolerable range. Polymerization of monomer systems is the most widely used approach. However, this is susceptible to *polymerization shrinkage phenomena* and thus stress-development. Acid–base reactions are present in the setting of polycarboxylate and glass–ionomer cements.

The resultant interfacial bonds, generated by the above adhesion strategy, can be analyzed into different micro- or nanostructural contributions. These may include *micromechanical bonds* created by the interlocking of solidified adhesive “tags” (extensions) into surface porosity or roughness of the adherend. Where the microadaptation of the solid adhesive and the adherend remains molecularly intimate, the intermolecular forces can contribute; and where specific primary bonds are generated, especially with metallic adherends, their contribution is significant.

Given the foregoing general scheme of how adhesive bonds can be generated, many of the factors that can weaken or compromise these bonds will be obvious. These include air voids, contaminants, and weak boundary layers.

Hard-Tissue Adhesives: Bone and Tooth Cements

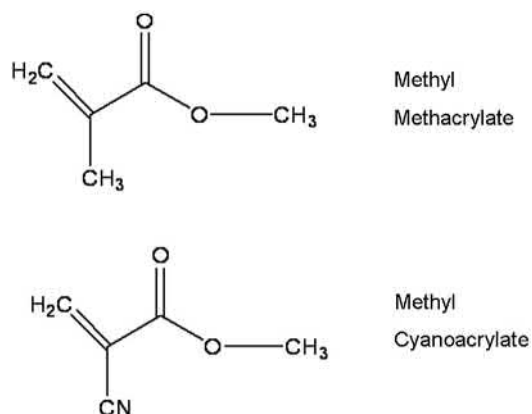
Autopolymerizing PMMA Bone Cement

Historical Background

In 1936 it was noted that mixing ground polymethylmethacrylate (PMMA) powder with its monomer, methyl methacrylate (MMA), produced a doughy material which could be manipulated and molded. Hence, it became one of the first biomaterials (Weber and Chapman, 1984; Donkerwolcke et al., 1998; Kühn, 2000; Webb and Spencer, 2007). The major breakthrough in the use of PMMA/MMA bone cement in total hip replacement (THR) was its use for secure fixation of the acetabular and femoral components to bone, and to transfer loads to bone (Charnley, 1960, 1970) (Fig. 2.5.9.1).



• **Figure 2.5.9.1** Cross-section of femur and interlocking bone cement showing good adaptation of the cement to the prosthesis (now removed), and a zone of interaction with the inner surface of the compact bone. (Courtesy of J. Charnley, personal communication.)



• **Figure 2.5.9.2** Methyl methacrylate and methyl cyanoacrylate.

Mechanism of Setting of PMMA/MMA Dough

MMA liquid (Fig. 2.5.9.2) is rapidly absorbed into PMMA powder, creating a tacky material that progresses to a non-tacky dough stage. These can be considered merely *physical* changes. However, benzoyl peroxide (BPO) initiator, mixed in with the powder, can be chemically activated to form free radicals, either by heating to above 60°C or by the incorporation of a suitable amine activator into the monomer, to enable room temperature autopolymerization or “cold-cure.” As activation generates free radicals from BPO, these start to react with the MMA molecules. The free radical polymerization reaction thus continues through the *propagation* stage—where chain growth occurs from multiple radical initiation sites—until this reaches the *termination* stage, where polymerization is either fully complete or the free radicals are consumed. MMA polymerization is a highly exothermic process, arising from the conversion of C=C bonds. Hence, in the constrained intrafemoral environment there is normally a significant temperature rise, which autoaccelerates the setting process, peaking above 56°C for 2–3 min in vivo. Sometimes higher temperatures

TABLE 2.5.9.1 Classification and Composition of Tissue Adhesives

Type	Components	Setting Mechanism
Hard-Tissue Adhesives		
Bone		
Acrylic bone cement	Methyl methacrylate and polymethylmethacrylate	Peroxide-amine initiated polymerization
Teeth		
Dental cements: zinc phosphate	Zinc oxide powder, phosphoric acid liquid	Acid–base reactions; Zn complexation
Zinc polycarboxylate	Zinc oxide powder, aqueous poly(acrylic acid)	Acid–base reactions; Zn complexation
Glass ionomer (polyalkenoate)	Ca, Sr, Al silicate glass powder aqueous poly(acrylic acid-itaconic acid)	Acid–base reactions; metal ion complexation
Resin modified glass ionomer	Dimethacrylate monomers. Aqueous poly(acrylic acid-methacrylate) comonomers. Silicate or other glass fillers	Peroxide-amine or photo-initiated polymerization
Resin-based	Aromatic or urethane dimethacrylates, HEMA	Photoinitiated addition polymerization
Dentin adhesive	Etchant: phosphoric acid (aq.). Primer: HEMA in ethanol or acetone bond. Resin: dimethacrylate monomers	Photoinitiated addition polymerization
Soft-Tissue Adhesives		
Cyanoacrylate	Butyl or isobutyl cyanoacrylate	Addition polymerization
Fibrin sealants	A. Fibrinogen, factor XIII B. Thrombin, CaCl ₂	Fibrin clot formation
GRF glue	Gelatin, resorcinol, formaldehyde	Condensation polymerization
Hydrogel	Block copolymers of PEG, poly(lactic acid) and acrylate esters	Photoinitiated addition polymerization

are reached, up to 90°C, which can volatilize unreacted monomer (the boiling point of MMA is 101°C). This creates voids that can later lead to mechanical failure.

Mechanism of “Bonding” or Grouting

As the cement flows under pressure to penetrate the interstices of cancellous bone and adapts to the surface of the femoral stem, it can achieve microinterlock with the bone when solidified. Nevertheless, PMMA bone cement undergoes a degree of shrinkage on polymerization. Hence another benefit of pressurized injection is partial compensation for this effect. Shrinkage is a potential major source of porosity (Gilbert et al., 2000).

Alternative Bone Cements: Calcium Phosphate

In orthopedic surgery there are some alternatives to PMMA bone cement, and there is also the option of cementless fixation. Inorganic cements, notably from the Ca–P system, include hydroxyapatite (HA) [Ca₁₀(PO₄)₆OH₂] and tricalcium phosphate (TCP) [Ca₃(PO₄)₂]. The biocompatibility of HA and its similarities to bone mineral have led to the study of dense HA for the augmentation of osseous defects.

Classical and Modern Dental-Bonding Cements: Conventional Acid–Base Cements

Dental cements are, traditionally, fast-setting pastes obtained by mixing solid and liquid components. Most of these materials set by an acid–base reaction, and subsequently developed resin cements harden by polymerization (Smith, 1971,

1991, 1998). The composition of these materials is shown in Table 2.5.9.1. The classes and typical mechanical properties are given in Table 2.5.9.2. The relationship between principal categories is illustrated in Fig. 2.5.9.3.

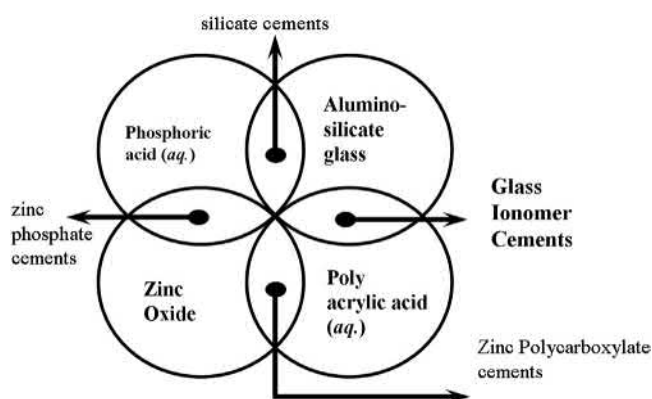
Zinc phosphate cement is the traditional standard. This material is composed primarily of zinc oxide powder and a 50% phosphoric acid solution containing aluminum and zinc. The mixed material sets to a hard, rigid cement (Table 2.5.9.1) by formation of an amorphous zinc phosphate binder. Although the cement is gradually soluble in oral fluids and can cause pulpal irritation, it is clinically effective over 10–20-year periods. The bonding arises entirely from penetration into mechanically produced irregularities on the surface of the prepared tooth and the fabricated restorative material. Some interfacial leakage occurs because of cement porosity and imperfect adaptation, but this is usually acceptable since the film thickness is generally below 100 μm.

Polyelectrolyte Cements: Zinc Polycarboxylates and Glass Ionomers

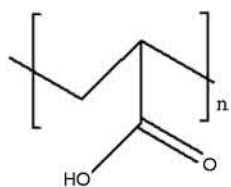
Poly(carboxylic acid) cements were developed in 1967 (Smith, 1967, 1998) to provide materials with properties comparable to those of phosphate cements, but with adhesive properties similar to those of calcified tissues. Zinc polyacrylate (polycarboxylate) cements are formed from zinc oxide and aqueous poly(acrylic acid) solution (Fig. 2.5.9.4). The metal ion cross-links the polymer structure via carboxyl groups, and other carboxyl groups form

TABLE 2.5.9.2 Properties of Dental Cements and Sealants

Dental Cement/Sealant	Strength			
	Compressive (MPa)	Tensile (MPa)	Elastic Modulus (GPa)	Fracture Toughness (MN ^{-1.5})
Zinc phosphate	80–100	5–7	13	~0.2
Zinc polycarboxylate	55–85	8–12	5–6	0.4–0.5
Glass ionomer	70–200	6–7	7–8	0.3–0.4
Dimethacrylate sealant unfilled	90–100	20–25	2	0.3–0.4
Dimethacrylate sealant filled	150	30	5	–
Dimethacrylate cement	100–200	30–40	4–6	–
Dimethacrylate composite	350–400	45–70	15–20	1.6



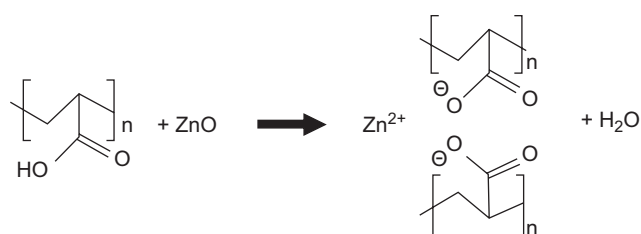
• **Figure 2.5.9.3** Classification of major types of acid-base dental cement based upon the combinations of basic powders of either zinc oxide or aluminosilicate glass with two aqueous acidic liquids.



• **Figure 2.5.9.4** Structure of the polyelectrolyte:poly(acrylic acid), as present in aqueous solution, in polycarboxylate and glass ionomer cements. The carboxyl anions COO⁻ are bridged by divalent or trivalent metal ions during the setting process, forming a salt matrix.

complexes with calcium ions on the surface of the tissue (Fig. 2.5.9.5). The zinc polycarboxylate cements have adequate physical properties, excellent biocompatibility with teeth, and proven adhesion to enamel and dentin (Smith, 1991), but they are opaque. The need for a translucent material led to the development of the glass-ionomer cements (GIC).

GICs are also based on poly(acrylic acid) or its copolymers with itaconic or maleic acids, but utilize a calcium aluminosilicate glass powder instead of zinc oxide. GICs set by cross-linking of the polyacid with calcium and aluminum ions from the glass, together with formations of

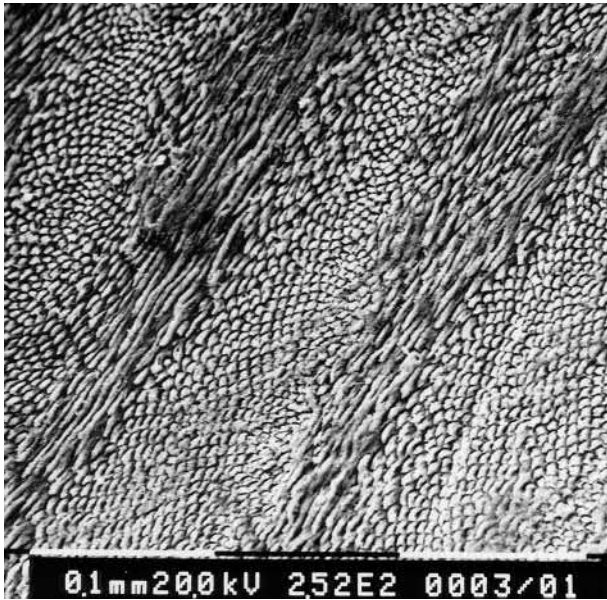


• **Figure 2.5.9.5** Neutralization of poly(acrylic acid) by zinc oxide to form zinc polycarboxylate cement, in which Zn²⁺ functions as a bridging ion between pairs of carboxylate groups, concurrently with ionic salt bridges with metal ions derived from an ion-leachable glass.

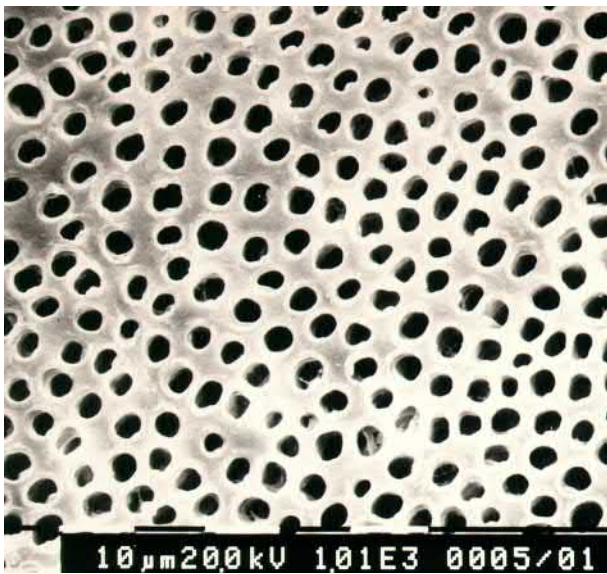
a silicate gel structure. The set structure and the residual glass particles form a stronger, more rigid cement (Table 2.5.9.1), but with similar adhesive properties to the zinc polyacrylate cements. Both cements are widely used clinically.

Acid-Etch Bonding to Enamel

Dental enamel is a hard, stiff substrate of generally uniform chemical composition. Bonding to enamel is required either in conjunction with bonding to dentin, for cavity restoration, or for bonding veneers or orthodontic brackets directly to the enamel of teeth in the upper or lower dental arch. In both cases, the modern approach was pioneered by Buonocore (Roulet and Degrange, 2000; Eliades et al., 2005). This involves conditioning with an aqueous phosphoric acid etchant for about 60 s. Subsequent water-rinsing and air-drying leaves a visibly matte surface on the enamel that is now differentially etched, with either the enamel-prism cores or the prism peripheries exposed (Fig. 2.5.9.6). Application of an unfilled resin (monomer mixture) or a moderate-viscosity resin-composite allows this to flow across the enamel, penetrating surface porosity. Subsequent hardening of the resin results in its retention via a multitude of microscopic tag-like resin extensions into the enamel surface.



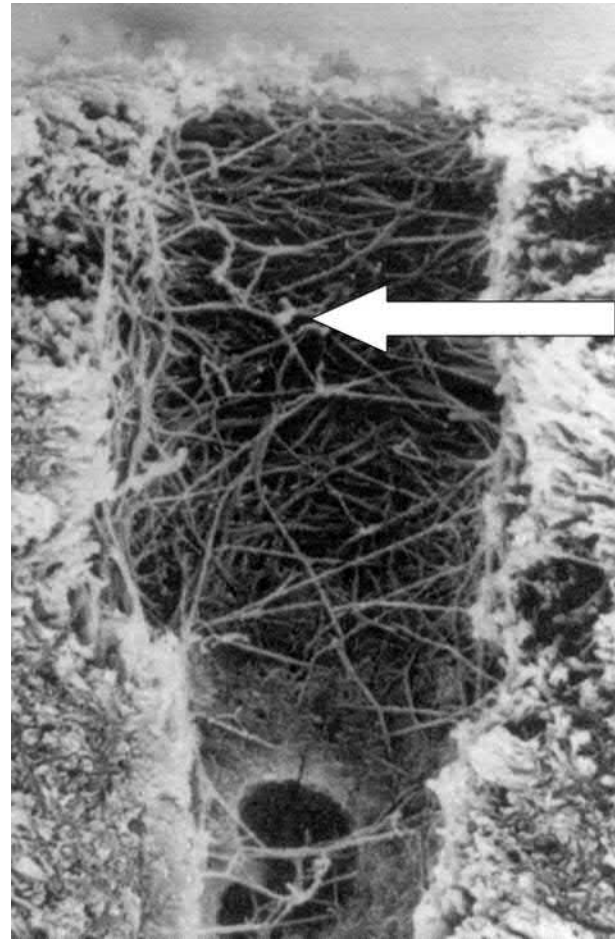
• **Figure 2.5.9.6** Surface of acid-etched dental enamel. In this image, there are alternating regions where the bundles of prism structures are viewed: (1) transversely (end-on); or (2) semilongitudinally. In the case of the transverse prisms, the prism peripheries have been preferentially etched, leaving the prism cores visible.



• **Figure 2.5.9.7** Dentin surface following etching with phosphoric acid solution. The dentin tubules are clearly visible.

Chemistry of Etchants, Primers, and Bonding Agents

Modern effective dentin bonding systems can be considered as incorporating a threefold set of agents, although two or even three of these functions may be combined in a simplified system. The *etchant* or *conditioner* function is provided by either an aqueous phosphoric acid gel or by acidic monomers. The *primer* function is classically achieved by a solution of a hydrophilic monomer, such as hydroxyethyl methacrylate (HEMA), in a solvent such as acetone



• **Figure 2.5.9.8** Cross-section of acid-etched and demineralized dentin. The collagen fibrils are visible (arrowed) within a tubule.

or ethanol. Subsequently, a “*bonding agent*” consisting of unfilled resin monomers is applied to the dentin.

Hybrid-Layer Creation Via A Three-Stage Approach: Etch, Prime, Bond

The optimal approach is to use a separate acid etchant, and to apply this to the dentin for about 10 s, which removes the smear layer (Fig. 2.5.9.7). This demineralizes the outer dentin layers, leaving residual type I collagen fibrils and proteoglycans. Washing the dentin removes the acid and salt residues. However, drying results in collapse or compaction of the collagen. The second agent, the primer, has the role of reexpanding the collagen, thereby restoring its porosity (Fig. 2.5.9.8). This permits the third agent—unfilled hydrophobic “bond” monomers—to permeate and seal the collagen. When these are photo-cured they form an entangled interpenetrating polymer network (IPN) with the collagen fibers. The resultant interfacial IPN region, typically 4 μm in thickness, is known as the hybrid zone. Effectively, the polymerized resin is taking the place of the original mineral phase in this region. The strength of this bonding zone depends on the continuing integrity of its component elements, principally the collagen fibrils and the polymerized monomers.

Aging and Stability of the Bonded Interface

When properly applied, good adaptation and bonding of the adhesive and restorative material to dentin can be achieved in the short and medium term. Also, a good initial seal of the interfacial zone can be achieved. However, a number of potential weaknesses have been identified (Breschi et al., 2008).

1. *Insufficient resin impregnation of dentin:* There are circumstances where the demineralized collagen is not fully supported by infiltrated resin, leaving a mechanically weak zone.
2. *High permeability of the bonded interface:* The hybrid zone is susceptible to “nano-leakage” by small molecules and ions, which may provide a pathway for degradation reactions over time.
3. *Suboptimal polymerization:* The efficiency of polymerization of the infiltrated monomer may be compromised by the presence of water and dissolved oxygen, thereby weakening the IPN structure.
4. *Phase separation:* Monomer mixtures in situ of varying hydrophilicity may spontaneously phase separate upon polymerization.
5. *Activation of endogenous collagenolytic enzymes:* Recent studies have revealed that dentin matrices may be slowly degraded over time by dentin-derived proteolytic enzymes, particularly matrix metalloproteinases (MMPs). Collagen integrity within the hybrid layers may be promoted by incorporation of chlorhexidine, an antibacterial agent with MMP-inhibiting properties.

Inhibitors for the Preservation of the Hybrid Interfacial Zone Between Adhesives and Human Dentin

The outstanding resistance of the collagenous dentin matrix against thermal and proteolytic disruption has been attributed to the high degree of intermolecular cross-linking and tight mechanical weave of this specialized connective tissue. However, great attention to the potential proteolytic activity of dentin has been raised since complexed and active forms of matrix metalloproteinases (MMPs) were identified in either nonmineralized or mineralized compartments of human dentin. MMPs belong to a group of zinc- and calcium-dependent enzymes that have been shown to be able to cleave native collagenous tissues at neutral pH in the metabolism of all connective tissues. Galardin is a synthetic MMP-inhibitor with potent activity against MMP-1, -2, -3, -8, and -9. It also partially preserved the mechanical integrity of the hybrid layer created by a two-step etch-and-rinse adhesive after artificial aging (Breschi et al., 2010).

Soft-Tissue Adhesives and Sealants

Performance Requirements

Most soft-tissue adhesives are intended to be temporary. On wound surfaces that are wet with tissue fluid or blood, the adhesive must be able to be spread easily on such a surface,

provide adequate working time, develop and maintain adhesion, preferably provide hemostasis, facilitate wound healing, and maintain biocompatibility. Positive antimicrobial action would be an additional advantage (Ikada, 1997).

Historical Overview

Few, if any, systems comply with all these requirements. Currently, there are two principal systems in widespread clinical use: cyanoacrylate esters and fibrin tissue adhesives. An important development by Messersmith and co-workers (Brubaker et al., 2010) has led to the synthesis of branched polyethylene glycol (PEG) cores with end groups derivatized with catechol, a functional group abundant in mussel adhesive proteins.

The Relationship Between Soft-Tissue Adhesion and Drug Delivery

Soft-tissue adhesives are not only required for surgical wound healing, but also for the controlled delivery of drugs to specific sites, of which the mucosal membranes are particularly suitable. The process of mucoadhesion involving a polymeric drug-delivery platform is a complex one that includes wetting, adsorption, and interpenetration of polymer chains among various other processes. The success and degree of mucoadhesion bonding are influenced by various polymer-based properties, such as the degree of cross-linking, chain length, and the presence of various functional groupings. The evolution of mucoadhesive formulations has developed from first-generation charged hydrophilic polymer networks to more specific second-generation systems based on lectin, thiol, and various other adhesive functional groups (Andrews et al., 2009).

Cyanoacrylate Esters

Chemistry

These esters are fluid, water-white monomers that polymerize rapidly by an anionic mechanism in the presence of weak bases such as water or NH_2 groups. Initially, methyl (Fig. 2.5.9.2), isobutyl, and n-butyl were used. However, 2-octyl cyanoacrylate gained FDA approval in the United States in 1998 (FDA, 1998). Prior formulations of cyanoacrylates such as n-butyl had shorter chain polymers and as a result were more brittle compared to the longer and more flexible polymer chains of 2-octyl cyanoacrylate (Singer et al., 2008; Bouten et al., 2014). The higher chain length cyanoacrylates spread more rapidly on wound surfaces, and polymerize more rapidly in the presence of blood. Furthermore, they degrade more slowly over several weeks, in contrast to methyl esters, which hydrolyze rapidly and yield formaldehyde. This process causes an acute inflammatory response.

Performance

These materials achieve rapid hemostasis, as well as a strong bond to tissue. However, the polymer film is somewhat brittle even in its newest formulations and can be dislodged on mobile tissue. To help reinforce the

wound–adhesive interface, polymer meshes have been used to increase the stability and strength of the wound closure (Ethicon, 2017).

The current uses of these cyanoacrylate ester materials are as a surface wound dressing in nearly all areas of surgery, especially in periodontics, and in life-threatening applications such as brain arteriovenous malformations. Reports of sarcomas in laboratory animals (Reiter, 1987) and evidence of in vitro cytotoxicity (Ciapetti et al., 1994) blocked N-butyl cyanoacrylate and prior formulations from regulatory approval, but 2-octyl cyanoacrylate has been approved for use in the United States via its improved toxicity profile (FDA, 1998).

Fibrin Sealants

Formulation, Presentation, and Setting Processes

Fibrin sealants involve the production of a synthetic fibrin clot as an adhesive and wound-covering agent. The concept of using fibrin dates back to 1909; the first available commercial materials consisted of two solutions that are mixed immediately before application to provide a controlled fibrin deposition (Matras, 1972). Later a “ready-to-use” formulation (Tisseel Duo) was introduced (Schlag and Redl, 1987). The essential components of these solutions are as follows:

Solution A:

Fibrinogen
Factor XIII

Solution B:

Thrombin
CaCl₂

The fibrinogen concentration in these sealants is much higher (~70 mg/mL) than that in human plasma. On mixing the two solutions, using a device such as a twin syringe with a mixing nozzle, a reaction similar to that of the final stages of blood clotting occurs. Polymerization of the fibrinogen to fibrin monomers and a white fibrin clot is initiated under the action of thrombin and CaCl₂. Aprotinin, an inhibitor of fibrinolysis, may also be included in solution A. The composition may be adjusted to promote hemostasis, for example, or to minimize persistence of the clot to avoid fibrosis.

Advantages and Applications

Originally developed during World War II to stop bleeding from battle injuries, fibrin sealants are presently used during surgery for several different purposes:

- to control bleeding in the area where the surgeon is operating;
- to speed wound healing;
- to seal off hollow body organs or cover holes made by standard sutures;
- to provide slow-release delivery of medication to tissues exposed during surgery.

The adhesive strength is not as high as that of cyanoacrylates, but it is adequate for many clinical situations. Thorough mixing of the ingredients, and application techniques or devices that allow uniform spreading, are both essential to success.

These materials have been used in a wide variety of surgical techniques for hemostasis and sealing; trauma, thoracic, cardiovascular, general, neurosurgical, orthopedic, plastic,

TABLE 2.5.9.3 Characteristics of Soft-Tissue Adhesives

Property	Cyanoacrylate	Fibrin Glue	GRF
Ease of application	Poor	Excellent	Poor
Set time	Short	Medium	Medium
Tissue bonding	Good	Poor	Excellent
Pliability	Poor	Excellent	Poor
Toxicity	Medium	Low	High
Resorbability	Poor	Good	Poor
Cell infiltration	Poor	Excellent	Poor

After Ikada, Y., 1997. Tissue adhesives. In Chu, C.C., von Fraunhofer, J.A., Greisler, H.P. (Eds.), *Wound Closure Biomaterials and Devices*. CRC Press, Boca Raton, FL, pp. 317–346.

and ophthalmic surgery, and as a biodegradable adhesive scaffold for meshed skin grafts in burn patients (Sierra and Salz, 1996; Ikada, 1997; Feldman et al., 1999).

Attempts to modify fibrin sealants have been directed toward: (1) improvements in their ease of application and control of setting by use of a one-component light-activated product (Scardino et al., 1999); (2) improvements in strength and performance by addition of fibrillar collagen (Sierra and Salz, 1996); and (3) development of a formulation containing gelatin (Ikada, 1997). A summary of sealant characteristics appears in Table 2.5.9.3 (Ikada, 1997). Gelatine-Resorcine-Formaline (GRF) adhesives show excellent tissue bonding, but their ease of application, resorbability and cell infiltration are poor and their toxicity is high.

Bioadhesives

Bioadhesives are involved in cell-to-cell adhesion, adhesion between living and nonliving parts of an organism, and adhesion between an organism and foreign surfaces. Adhesives produced by marine organisms, such as the barnacle and the mussel, have been extensively investigated over the past 40 years because of their apparent stable adhesion to a variety of surfaces under adverse aqueous conditions. Studies have shown that these organisms secrete a liquid acidic protein adhesive that is cross-linked by a simultaneously secreted enzyme system. The bonding likely involves hydrogen bonding and ionic bonding from the acidic groups (Waite, 1989).

The adhesive from the mussel has been identified as a polyphenolic protein, molecular mass about 130,000 Da, which is cross-linked by a catechol oxidase system in about 3 min. The basic unit of the polyphenolic protein has been identified as a specific decapeptide (Waite, 1989; Green, 1996). Recombinant DNA technology and peptide synthesis have been used in attempts to produce an affordable adhesive with superior properties.

Hydrogel Sealants

Hydrogels are formed by in situ deposition of aqueous formulations based on specialized dendritic macromolecules, followed by photopolymerization to highly cross-linked structures.

The macromers are reactive block copolymers consisting of a water-soluble core, such as polyoxyethylene, flanking biodegradable oligomers such as poly(lactic acid) or poly(trimethylene carbonate), and polymerizable end caps such as acrylate esters (Sawhney et al., 1993). Control of the physical properties and degradation rates is achieved by specifying the molecular structures and concentration of the reactants in the formulation (Dai et al., 2011). Photopolymerization can be effected by ultraviolet or visible light using appropriate photoinitiators. Typically, the initiator system eosin Y spirit-soluble (EYss)/triethanolamine (TEA) is employed with visible illumination in the 450–550 nm range.

In most applications for these hydrogels, strong bonding to tissue is required. This is achieved by use of a two-part sealant system consisting of primer and topcoat. Strong, durable bonding to a wide variety of internal tissues has been demonstrated (Coury et al., 1999).

New Research Directions: Biomimetic Approaches

Where relatively temporary (less than 30 days) adhesion is required, as in wound healing, systems based on natural models that allow biodegradation of the adhesive and interface, and subsequent normal tissue remodeling, appear to merit further development.

For longer term (years) durability in both soft and hard tissues, hydrophilic monomers and polymers of low toxicity that can both diffuse into the tissue surface, and form ionic bonds across the interface, seem to be a promising approach. The need for hydrophobic–hydrophilic balance in adhesive monomer systems has been demonstrated (Nakabayashi and Pashley, 1998), and the use of hydrophilic monomers such as hydroxyethyl methacrylate in commercial materials has facilitated surface penetration.

A promising development for hydrogels inspired by mussel adhesives has been described by the Messersmith group (Brubaker et al., 2010). Rather than using natural polypeptides, the synthesis of catechol-terminated polyethylene glycol (cPEG) solutions allows a hydrogel to be formed in about 30 s. Upon implantation, the cPEG adhesive elicited minimal acute or chronic inflammatory responses in C57BL6 mice, and maintained an intact interface with supporting tissue for up to 1 year. In situ cPEG adhesive formation was shown to efficiently immobilize transplanted islets at the epididymal fat pad and external liver surfaces, permitting normoglycemic recovery and graft revascularization. These findings establish the use of synthetic, biologically inspired adhesives for islet transplantation at extrahepatic sites. Another significant development has been the use of

PEG-based structures to make smart functional biomaterials (Tirelli et al., 2002; Park et al., 2003).

Finally, a major biomimetic initiative is the creation of self-healing polymer composites (Trask et al., 2007). Many materials in nature are themselves self-healing composite materials. So far this research has been mainly directed toward structural materials (Brown et al., 2005a,b), but it is a short step to apply these concepts and designs to the structural adhesives being designed for hard-tissue bonding.

Sutures

Genesis and Common Uses

A suture, by definition, is any strand of material that is used to ligate (tie) blood vessels or approximate tissue. The word suture, derived from the Latin *sutura*, means *to sew*. The earliest examples of this technology can be traced back thousands of years, when Egyptians, Indians, and other early suture developers used readily available materials, such as silk, linen, cotton, horsehair, and animal tendons and intestines. Currently, sutures comprise the largest portion of wound closure technologies, with the yearly market for sutures approaching a billion dollars in the United States alone.

The suture device is comprised of: (1) the suture strand; (2) the surgical needle; and (3) the packaging material used to protect the suture and needle during storage.

Description of Surgical Sutures

The suture is comprised of three distinct components: suture, needle, and packaging. Table 2.5.9.4 further describes each component, along with example permutations. The major distinguishing factor in suture strands is the absorbability of the suture. Absorbable (occasionally denoted resorbable, biodegradable, or erodible) materials are those which undergo a chemical degradation. In suture materials, this is most commonly the result of hydrolysis or enzymatic degradation. Currently, absorbable sutures maintain measurable strength for 6 months or longer. Absorbable sutures lose strength long before losing mass; it may take months or years after the suture loses strength to fully absorb.

Suture is manufactured in many sizes, and is selected by the surgeon based on a number of factors, including: surgical site; patient age and weight; immune history and response; presence of disease or infection; and personal history with suture materials (Ethicon, 2001). Size is based on diameter, as defined in the *United States Pharmacopeia* (USP) (Table 2.5.9.5), and often materials will exhibit slightly different performance characteristics based on size. Monofilament sutures exhibit lower tissue drag compared to braided multifilament sutures. However, many materials having high modulus and stiffness are not compliant enough to be useful as monofilament. Also, any defect caused during handling can create a weak region in the suture strand. For these reasons, multifilament braided

TABLE 2.5.9.4 Components and Permutations of the Suture Device

Component	Description and Permutations
Suture strand	Component of device that provides securement, only part of device that remains in tissue after implantation: <ul style="list-style-type: none"> • absorbable or nonabsorbable • sized according to USP^a or EU^b guidelines • braided or monofilament • coated or uncoated • natural or dyed
Needle	Component of device that pulls suture through tissue: <ul style="list-style-type: none"> • size is based on suture diameter • taper point, cutting, spatula, specialty • straight, ¼ circle, 3/8 circle, ½ circle, 5/8 circle, compound curved • coated or uncoated • swaged or rolled
Packaging	Component that provides a sterile barrier for storage and maintains storage conditions: <ul style="list-style-type: none"> • Tyvek[®] or foil • single suture or multipack • dry or with plasticizing fluid • plastic or paper folder

^aUnited States Pharmacopeia.
^bEuropean Union.

TABLE 2.5.9.5 Suture Diameter Requirements for Commonly Used Sutures^a

USP Suture Size	Collagen Suture Maximum Diameter (mm)	Synthetic Suture Maximum Diameter (mm)
6-0	0.10	0.07
5-0	0.15	0.10
4-0	0.20	0.15
3-0	0.30	0.20
2-0	0.35	0.30
0	0.40	0.35
1	0.50	0.40
2	0.60	0.50

^aUnited States Pharmacopeia (2008).

sutures were created. As a combination of fibers with much smaller diameter, relatively stiff materials in a composite structure have a perceived compliance much lower than material properties would suggest. Although multifilament technology allows the creation of suture from relatively stiff materials, there are possible drawbacks to this design. Void space in the braid creates capillarity, and thus potential

areas to harbor bacteria. Increased surface roughness associated with a braided construction can cause damage to the implant site due to increased tissue drag. To counteract this tissue drag and to increase lubricity, almost all braided and a few monofilament sutures are coated. Additionally, sutures are supplied as either natural or dyed to increase visual contrast. Table 2.5.9.6 identifies many of the most common sutures and examples of manufacturers.

Needles are supplied in a variety of shapes, each of which is suited to certain applications. Needle and suture are connected at the end of the needle, which can be attached mechanically by swaging, or attached using an eyed needle. The basic needle description includes shape and point geometry (Table 2.5.9.7 and Fig. 2.5.9.9). Needle shapes include straight, curved (described as a fraction of a circle), and compound curved. Fig. 2.5.9.10 provides an illustration of a curved needle, along with pertinent dimensional descriptions. The ideal needle is inert, as slim as possible without compromising strength, stable when held in the needle holder, sharp enough to penetrate tissue with minimum material resistance, rigid enough to not allow bending, ductile enough to not break during use, sterile, and corrosion resistant (Ethicon, 2001).

The primary purpose of the suture package is to maintain sterility during storage.

Surgical Gut Sutures

Gut sutures are primarily derived from bovine intestinal serosa, but also from the submucosa of sheep or goat intestine. The base material is primarily collagen, and requires purification and strengthening before it is suitable as a suture. After harvesting, the material is cleaned, cut into ribbons, and processed with a dilute formaldehyde solution. This increases strength and slows the degradation rate by modifying the activity of the end groups of the collagen (Chu, 1997a). The fibers are ground and polished to create the final suture diameter. Natural (or plain) gut suture is now ready for packaging. Chromic gut sutures are further processed by tanning in the presence of chromium salts, which slows the rate of degradation (Chu, 1997a).

The suture is sized by centerless grinding, in which two grinding wheels remove material around the diameter of the suture. Due to the grinding process, fibrils at the strand surface can be damaged, which can lead to weak points and inconsistent strength. Also, the fiber is easily frayed during tying (Benicewicz and Hopper, 1990). Since gut sutures are a naturally derived material, there are slight inconsistencies in performance, including initial strength and strength retention profile. Coating gut sutures to lower their friction coefficient and propensity to fray was described by Totakura and Shalaby (1997a,b). Gut sutures can be sterilized by irradiation or ethylene oxide gas permeation.

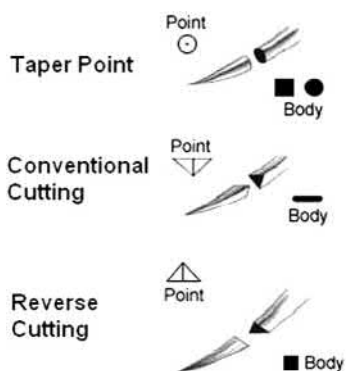
TABLE 2.5.9.6 Common Sutures and Materials Used

Material	Origin/Composition	Form ^a	Ultimate Strength, Straight (MPa)	Ultimate Strength, Knot (MPa)	Ultimate Elongation (%)	Young's Modulus (GPa)	Functionality	Clinical Applications	Example Devices
Nonabsorbable									
Silk	p-Gomore silk worm	B	370–570	240–290	9–31	8.4–12.9	1 ± years	General suturing, ligation	Ethicon Permahand™
Cotton	Plant-based	Tw	280–390	160–320	3–6	5.6–10.9	2 ± years	Not commonly used	Cotton
PET	Synthetic polyester	B	510–1060	300–390	8–42	1.2–6.5	Permanent	Heart valves, vascular prostheses, general	Ethicon Ethibond™ Teleflex Tevdek
PP	Synthetic polypropylene	M	410–760	300–570	30–60	2.1–4.1	Permanent	General, vascular	Ethicon Prolene™Covidien Surgipro™
Nylon	Synthetic Nylon-6,6 or Nylon-6	M	460–710	300–330	17–65	1.8–4.5	Permanent	Skin	EthiconCovidien Monosof™
Stainless steel	300-Series stainless steel	M, B	540–780	420–710	29–65	200	Permanent	Sternal closure, tendon repair, orthopedic	Ethicon Ethisteel™ Covidien Flexon™
UHMWPE	Synthetic polyethylene	B	1130–1590	680–908	<10	1.4–4.8	Permanent	Orthopedic	Teleflex Force Fiber Arthrex FiberWire
Absorbable									
PGA	Glycolide	B	760–920	310–590	18–25	7–14	2–4 weeks	Subcutaneous, peritoneal	Teleflex Bondek
PGLA	90/10 Glycolide/lactide	B	570–910	300–400	18–25	7–14	3–4 weeks	General, subcutaneous	Ethicon Vicryl™
PGLA (continued)	90/10 Glycolide/lactide	B	570–910	300–400	18–25	7–14	2 weeks	General, subcutaneous, skin	Ethicon Vicryl™ Rapide
PGLA (continued)	88/12 Lactide/glycolide	B	410–760	200–400	30–50	1.4–4.1	4–6 months	Orthopedic	Biomet Osteoprene
PDO	p-Dioxanone	M	450–560	240–340	30–38	1.2–1.7	4–6 weeks	General, cardiovascular, ophthalmic	Ethicon PDS™ IIAngiotech PDO
PG-CI	75/25 Glycolide/caprolactone	M	628	315	39	0.8	2–3 weeks	General	Ethicon Monocryl™ Angiotech Monosorb
PG-TMC	67/33 Glycolide/TMC	M	540–610	280–480	26–38	3.0–3.4	6 weeks	General, cardiovascular	Covidien Maxon™
Natural gut	Bovine serosa or submucosa of sheep or goat intestine	Tw M	310–380	110–210	15–35	2.4	1–2 weeks	General, subcutaneous	Ethicon Plain Gut
Chromic gut	Bovine serosa or submucosa of sheep or goat intestine treated in chromium solution	Tw M	310–380	110–210	15–35	2.4	2–3 weeks	General, subcutaneous	Ethicon Chromic Gut

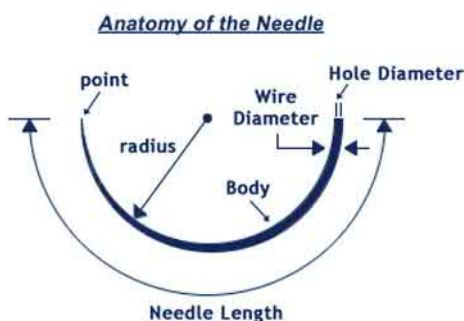
^aB = Braid, M = Monofilament, Tw = Twisted fiber.

TABLE 2.5.9.7 Common Suture Needles

Type and Description
Taper point: Circular cross-section gradually increasing in diameter from the point to the needle body
Conventional cutting: Triangular cross-section at the needle tip to provide cutting edges, allowing easy penetration into the tissue, which gradually transitions to a square needle body. One cutting edge is on the inside curvature of the needle
Reverse cutting: Triangular cross-section at the needle tip to provide cutting edges. Flat surface on the inside curvature of the needle to minimize risk of needle tearing through the tissue
Hemo seal: Tapered suture at needle-suture interface allows for thinner needle. Decreased size of needle and 1 to 1 ratio of needle to suture allows for decreased blood loss due to trauma of needle insertion.



• **Figure 2.5.9.9** Cross-section and point shape of common suture needles.



• **Figure 2.5.9.10** Anatomy of a curved suture needle.

Silk Sutures

Silk suture is a protein fiber typically derived from the *Bombyx mori* silkworm (Chu, 1997a). The silk is stripped of its natural waxes and gums, and braided or twisted to construct the suture thread. As with all braided sutures, it is coated. Typically, this is in the form of a beeswax-based coating or, in some cases, a siloxane-based coating. Successful efforts to substitute the highly tissue-reactive beeswax-based suture with practically nonreactive synthetic polyesters led to the development

TABLE 2.5.9.8 Repeat Units for Common Synthetic Nonabsorbable Sutures

Monomer Names	Repeat Unit Structure	Homopolymer
Ethylene	$[\text{CH}_2-\text{CH}_2]_n$	Polyethylene (PE)
Propylene	$[\text{CH}(\text{CH}_3)-\text{CH}_2]_n$	Polypropylene (PP)
Hexamethylene diamine and adipic acid	$[\text{CO}-(\text{CH}_2)_4-\text{CO}-\text{NH}-(\text{CH}_2)_6-\text{NH}]_n$	Nylon-6,6
Caprolactam	$[\text{CO}-(\text{CH}_2)_5-\text{NH}]_n$	Nylon-6
Ethylene terephthalate	$[\text{CO}-\text{C}_6\text{H}_4-\text{CO}-\text{O}-\text{CH}_2-\text{CH}_2-\text{O}]_n$	Polyethylene terephthalate (PET)

of a low-reactivity silk suture which can be made antimicrobial (Nagatomi et al., 2008). Although silk is not considered an absorbable suture, the strand loses strength and mass after implantation (Van Winkle and Hastings, 1972; Stashak and Yurraspe, 1978; Benicewicz and Hopper, 1990). This material is broken down by proteolysis, and is typically undetectable after 2 years (Lai et al., 2009). Silk sutures can be sterilized by irradiation and/or ethylene oxide gas permeation.

Polyester Sutures

Nonabsorbable polyester sutures are made from polymers such as poly(ethylene terephthalate) (PET), which is produced by a condensation reaction. This involves condensation of a dialcohol and terephthalic acid or an ester of terephthalic acid. The repeat unit of PET is shown in Table 2.5.9.8. PET is extruded into multifilament fibers and braided into suture. Polyester sutures are sterilized mostly by gamma irradiation.

Nylon Sutures

The polyamides Nylon-6 and Nylon-6,6 are both used as suture materials. Structures for both repeat units are shown in Table 2.5.9.8. Nylon sutures are made into braided or monofilament sutures, although the monofilament sutures may not tie as well, and require additional knots to secure them (Stashak and Yurraspe, 1978; Bellenger, 1982; Guttman and Guttman, 1994). To counteract this, monofilaments can be packaged with a plasticizing fluid to soften them for improved handling (Capperauld and Bucknall, 1984). Although nylon is a nonabsorbable suture, the amide bond is susceptible to hydrolysis and can lose strength over time (Chu, 1997a). Nylon sutures are sterilized by gamma irradiation.

Polypropylene Sutures

Polypropylene can be made with an atactic, isotactic, or syndiotactic chain conformation. Material used for suture

applications is practically isotactic, with an intermediate density. Polymerization is accomplished by polymerization from propylene monomer using a Zeigler-Natta catalyst; the repeat unit can be seen in Table 2.5.9.8. Polypropylene sutures elicit very low tissue response, and are not susceptible to hydrolysis. These sutures can also be difficult to tie securely, due to the smoothness and lubricity of the suture strand (Stashak and Yturraspe, 1978; Bellenger, 1982; Guttman and Guttman, 1994). Polypropylene is easily melt-extruded into monofilament or multifilament yarn, and is well-suited for the production of monofilament suture. Polypropylene sutures are usually sterilized by ethylene oxide, and occasionally by high-energy radiation.

Ultrahigh-Molecular-Weight Polyethylene (UHMWPE) Sutures

Ultrahigh-molecular-weight polyethylene (UHMWPE) suture (structure seen in Table 2.5.9.8) was introduced in the early 2000s; these ultrastrong sutures are 10–100 times stronger by weight than steel. As opposed to other synthetic suture materials, which exhibit about 40% crystallinity, UHMWPE can obtain crystallinity of greater than 85%, and can be highly oriented. The high molecular weight prevents the use of melt extrusion. Therefore, gel spinning techniques are employed to create the multifilament fibers. Gamma irradiation weakens this suture; for this reason they are sterilized by ethylene oxide (Deng et al., 1996).

Ultrahigh-strength sutures are much stronger than standard ones, and a smaller size will have a similar breaking load to that of a larger size standard suture. This allows the surgeon to use a smaller diameter suture for the same application, leaving less foreign material in the implant site. The inherent lubricity of the material results in increased tendency to slip compared to polyester sutures (Barber et al., 2009).

In addition to sutures made of only UHMWPE, there are several composite sutures that are prepared by braiding UHMWPE with PET, nylon, or other materials. Textures imparted by combining different materials allow for more secure tying, which can be a problem with inherently lubricious UHMWPE sutures (Burkart, 2004).

Stainless Steel Sutures

For surgical procedures requiring high-strength materials, such as sternal fixation and tendon repair, stainless steel is a common selection. These sutures are most often prepared from 300-series stainless steels (316L is a common variety and is used in Covidien STEEL sutures, for example). Stainless steel sutures are inert, do not exhibit capillarity, and are very strong. The high modulus of stainless steel, however, can cause irritation at the free end of the suture. These sutures are also prone to kinks, and surgeons must use extra caution during handling (Bellenger, 1982; Capperauld and Bucknall, 1984; Guttman and Guttman, 1994). Stainless steel sutures are available as a braid or monofilament (for small sizes).

TABLE 2.5.9.9 Repeat Units for Common Synthetic Absorbable Sutures

Monomer Names	Repeat Unit Structure	Homopolymer
<i>p</i> -Dioxanone	$[\text{O}-\text{CH}_2-\text{CH}_2-\text{O}-\text{CH}_2-\text{CO}]_n$	Polydioxanone (PDO)
Glycolide	$[\text{CH}_2-\text{COO}-\text{CH}_2-\text{COO}]_n$	Polyglycolide (PGA)
<i>L</i> -Lactide	$[\text{CH}(\text{CH}_3)-\text{COO}-\text{CH}(\text{CH}_3)-\text{COO}]_n$	Poly(lactide) (PLA)
ϵ -caprolactone	$[\text{O}-(\text{CH}_2)_5-\text{CO}]_n$	Polycaprolactone (PCL)
Trimethylene carbonate	$[(\text{CH}_2)_3-\text{O}-\text{CO}-\text{O}]_n$	Poly(trimethylene carbonate) (PTMC)
Ethylene oxide	$[\text{CH}_2-\text{CH}_2-\text{O}]_n$	Poly(ethylene glycol) (PEG, used as polyether-ester constituent in copolymers)

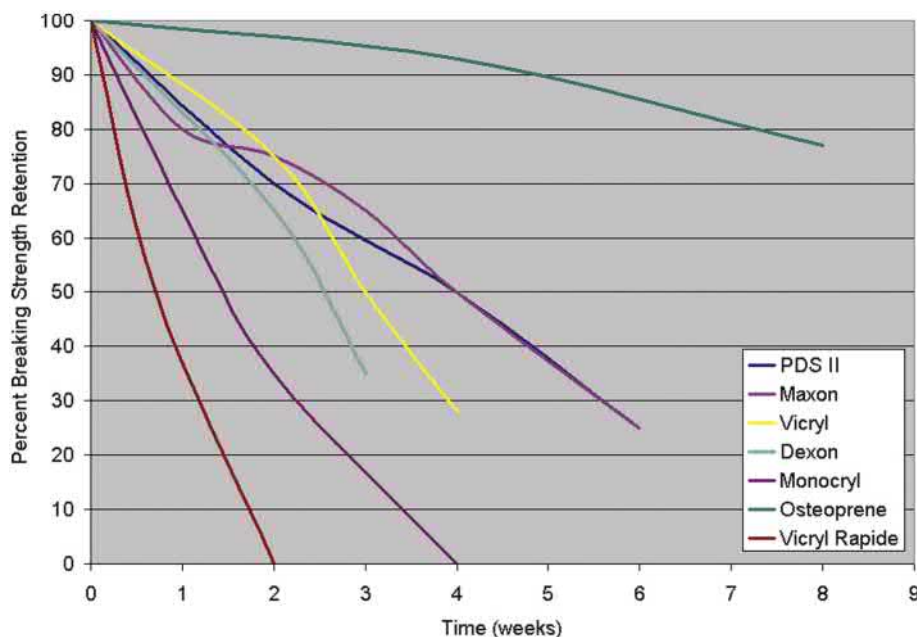
Synthetic Absorbable Sutures

Monomers and Preparation of Polymers

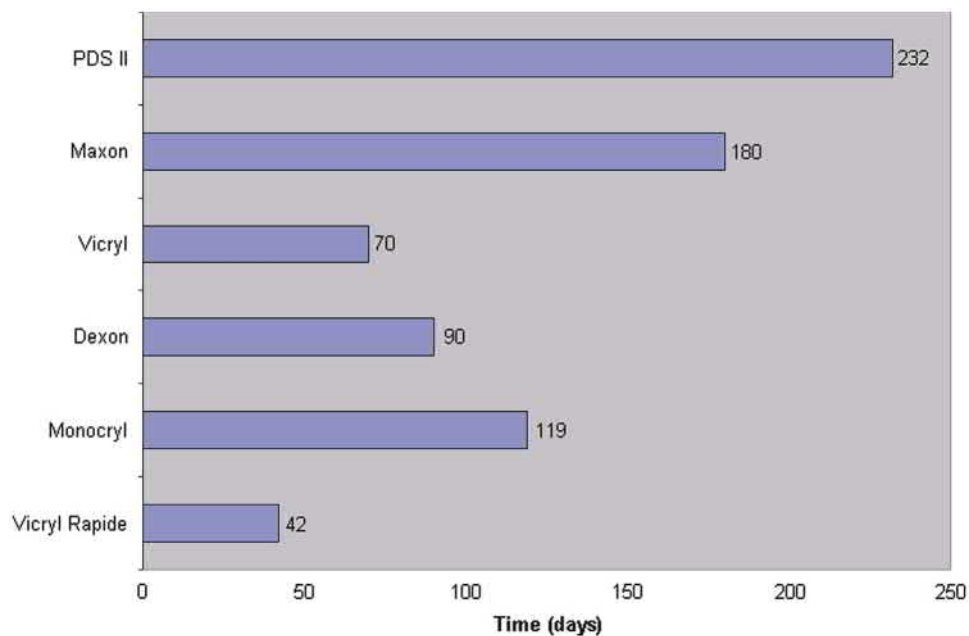
Natural and synthetic nonabsorbable sutures are made from materials which are polymerized from a select group of constituent monomers. These can be combined in a vast array of configurations exhibiting unique properties. These monomers include glycolide, lactide (*d*-, *l*-, and *dl*-), *p*-dioxanone, trimethylene carbonate (TMC), ϵ -caprolactone, and poly(ethylene glycol) (PEG), which become repeat units in the final polymer. Table 2.5.9.9 includes the repeat unit structure of commonly used absorbable polymers, all of which degrade by hydrolysis of ester bonds.

Polyglycolide and predominantly glycolide-based copolymers are highly crystalline, stiff materials which are very susceptible to hydrolysis, leading to a faster absorption profile. Lactide-based polymers can be crystalline, but are slightly softer than glycolide-based ones, and are not as susceptible to hydrolysis. The *p*-dioxanone polymers are crystalline, but are softer than most of the glycolide- or lactide-based polymers, and are between glycolide and lactide in sensitivity to hydrolysis. These three provide the major constituents for all synthetic absorbable sutures. TMC, ϵ -caprolactone, and PEG represent minor constituents in a number of sutures, and serve to alter the material properties to improve some aspect of suture performance. For example, many monofilaments are prepared from copolymers made primarily with glycolide as a hard segment and TMC or caprolactone as a softer segment, making the copolymer more flexible, while retaining strength.

Ethylene oxide is the standard method for sterilization of absorbable sutures due to the tendency of the copolymer chains to undergo scission when irradiated. Synthetic absorbable polymers degrade by hydrolysis, and are therefore sensitive to moisture.



• **Figure 2.5.9.11** Breaking strength retention profiles of several common synthetic absorbable sutures (Ethicon, 2001, 2008; Covidien, 2009a,b; Taylor, 2010).



• **Figure 2.5.9.12** Maximum time for sutures to be essentially absorbed (Ethicon, 2001, 2008; Covidien, 2009a,b).

Absorbable sutures are described primarily by their strength retention profile, then by their absorption profile. The strength retention profile indicates the useful life of the device, and is the primary factor for selection in a particular application. The strength retention and absorption profiles for several common sutures are shown in Figs. 2.5.9.11 and 2.5.9.12, respectively.

Poly(Glycolic Acid) (PGA)

Dexon, the first synthetic absorbable suture, is prepared from a homopolymer made of glycolic acid, and was released in 1971 by Davis & Geck, which is now Covidien

(Benicewicz and Hopper, 1990). PGA suture is available in braided form, and is coated to improve its handling properties. Current PGA sutures exhibit about 30%–50% crystallinity and retain about 65% of the initial strength after 2 weeks implantation, and 35% after 3 weeks. Absorption is essentially complete after 60–90 days (Covidien, 2005).

Poly(Dioxanone) (PDO) Sutures

PDSII (PolyDioxanoneSuture), the most recent iteration of *p-dioxanone* (PDO) by Ethicon, retains 25% of its initial strength after 6 weeks, making it the longest lasting

TABLE 2.5.9.10 Effect of Block Structure on PGA-co-TMC Copolymer Properties^a

Block Type	Glycolide Content (wt.%)	Melting Peak (°C)	Tensile Strength (kpsi)	Tensile Modulus (kpsi)	In vivo BSR ^b at 3 Weeks (%)	In vivo Absorption (Days)
Homopolymer	100	227	122	2100	20	<90
Random	88	209	65	970	3	<90
Block	65	216	42	610	53	<180
Modified block	65	213	61	260	69	<180

^aRoby et al. (1997).
^bBreaking strength retention.

commonly used suture currently available, allowing it to be used in slow-healing tissue that previously required nonabsorbable sutures (Ethicon, 2001; Capperauld and Bucknall, 1984).

High-Glycolide Copolymeric Sutures

The most well-known synthetic absorbable suture is braided Vicryl, which is a random copolymer containing 90% glycolide and 10% lactide (Guttman and Guttman, 1994). Braided Vicryl retains up to 25% of its initial strength for 4 weeks, and absorption is essentially complete in 56–70 days (Ethicon, 2001). An alternate version of Vicryl, named Vicryl Rapide, was introduced as a faster-absorbing version of the same material. This was accomplished by reducing the molecular weight of the fiber through a radiation sterilization process. Vicryl Rapide was designed as an alternative to Plain Gut suture, and loses strength within 2 weeks of implantation (Ethicon, 2008).

Most customization in this class of synthetic absorbable sutures has been in the area of monofilament sutures. Maxon suture, introduced in 1985 by Davis & Geck (now Covidien) is a triblock copolymer prepared from 67.5% glycolide and 32.5% TMC (Benicewicz and Hopper, 1991). The central block is composed of a random copolymeric initiator made of 85% TMC and 15% glycolide, while the two end grafts are primarily glycolide (Casey and Roby, 1984). This composition and structure resulted from a study comparing various block structures and ratios of the constituent monomers, the results of which can be seen in Table 2.5.9.10. This work highlights the sensitivity of the copolymers to structure, as well as to monomer composition. Increased TMC in the central chain reduces the tensile modulus, extends the strength retention profile, and increases the time required for absorption. The small amount of glycolide in the middle block is necessary because TMC absorbs very slowly; the glycolide allows the material to degrade into short segments that can be metabolized. Maxon suture retains 25% of its initial strength up to 6 weeks post-implantation, and essentially absorbs by 6 months.

To fill the need for a shorter term monofilament, Ethicon developed Monocryl suture. This material was developed as an alternative to gut suture (Bezwada et al., 1995), and is a triblock copolymer containing 75% glycolide and 25% caprolactone. The initiator is reported to be a random copolymer containing 55% glycolide and 45% caprolactone, while the end blocks are primarily made of glycolide (Bezwada et al., 1995). Monocryl suture retains 30%–40% of its initial strength after 2 weeks of implantation, and is essentially absorbed between 91 and 119 days.

This is not inclusive of all sutures currently available, but is an example of a few technologies. Major suture manufacturers are continuing development of other high-glycolide copolymers.

Dyes

Sutures are provided in *natural* or *dyed* colors. The natural color of suture materials is most often white to light tan. When sutures are placed in tissue, the contrast between the suture and host tissue is low. This effect is magnified when in the presence of blood, which can make differentiation between the suture and tissue difficult. For this reason, dyed sutures are often preferred. The US Food and Drug Administration (FDA) regulates the use of colorants, and the approval process is quite stringent. The current approved colors are seen in Table 2.5.9.11. Synthetic sutures are dyed during the extrusion process by adding a small amount of powdered colorant to the polymer just prior to extrusion. Natural materials are dyed in a color solution. Processing conditions and associated requirements may also place limitations on the use of some dyes in the suture strand.

Coatings

Braided and monofilament sutures have been coated with a wide variety of materials for the primary purpose of reducing tissue drag. Coatings also fill void space, thus reducing capillarity and the tendency to wick, and can act as carriers for antimicrobial agents such as triclosan.

TABLE 2.5.9.11 FDA-Approved Dyes for Use in Sutures^a

FDA-Approved Dye	Color	Used in Sutures Containing
Pyrogallol/ferric ammonium citrate	Blue	Gut
Logwood extract	Black	Silk, nylon
Chromium-cobalt-aluminum oxide	Blue-green	Polyethylene
D&C Blue No. 9	Blue	Cotton, silk
D&C Green No. 5	Green	Nylon
[Phthalocyaninato(2-)] Copper	Blue	Polybutester, polybutylene terephthalate, poly(vinylidene fluoride), poly(vinylidene fluoride-co-hexafluoropropylene)
FD&C Blue No. 2	Blue	Nylon
D&C Blue No. 6	Blue	Various
D&C Green No. 6	Green	Various
D&C Violet No. 2	Violet	PDO, PGA, glycolide copolymers

^aFDA (2007): 21 CFR Parts 73 and 74.

Early coatings were comprised of beeswax and other natural waxes. Other coating materials for nonabsorbable sutures include silicone and poly(tetrafluoroethylene) (PTFE, Teflon) based systems, as used on Deknatel's Tevdek and Polydek polyester sutures. Coatings for absorbable sutures are typically based on absorbable copolymers, and can include polyurethanes, PEG, caprolactone copolymers, and lactide/glycolide copolymers (Mattei, 1980; Bichon et al., 1984; Ethicon, 2001). Calcium stearate and other lubricants may also be included to improve friction properties.

Needles and Attachment

Suture needles are made from high-quality stainless steel. Typically, needles are prepared from 400-series stainless steel, though some specialties prefer 300-series needles (Hu-Friedy Mfg. Co., Inc., 2007). Needles are permanently attached by a swaging process. Monofilament sutures are placed directly into the drilled end for swaging, but braided sutures require tipping to harden the end of the strand so the swaging process holds firmly onto the end of the suture. Tipping is performed with a cyanoacrylate-based adhesive on the last ½ inch of the suture strand. Also, for small-size sutures, epoxy and cyanoacrylate are commonly used for needle attachment.

Packaging

Sutures are sold sterile in individual or multipacks. Packaging for nonabsorbable sutures can be in Tyvek packaging; however, synthetic absorbable sutures are always packaged in hermetically sealed foil packaging. The sealed foil maintains a sterile barrier, as well as protecting the suture from oxygen and moisture which would initiate the degradation of the suture. This is known as a *hermetically sealed package*.

Physical Properties

The function of the suture strand is to provide a holding force while maintaining a stable position in the implant location. There are, however, many aspects to tissue securement. The *United States Pharmacopeia* (USP) is a list of standards and requirements for the testing and production of medical devices, including several guidance documents pertaining to sutures.

Suture is defined by USP size, which is defined numerically on a scale from size 7 (largest) to 11–0 (smallest).

There are three basic strengths tested by the USP: unknotted tensile strength, knotted tensile strength (typically 60%–80% of unknotted), and needle attachment strength. These are critical as the suture must have enough tensile strength to hold the tissue in place under strain and while in a knot. Additionally, the suture must remain on the needle while being pulled through the tissue.

In Vitro and In Vivo Performance

For absorbable sutures, the strength retention profile is the key to material functionality. There are two methods for determining the strength loss profile. In vivo strength is typically analyzed by implanting strands of the suture subcutaneously in Sprague–Dawley rats. In vitro analysis involves placing suture in a physiologic buffered solution, e.g., 7.4 pH phosphate-buffered saline solution (PBS) at 37°C. At predetermined time points, samples are collected and tested for ultimate tensile strength. Information is reported as a percentage of the initial load. In vitro analysis must always be followed up with at least limited in vivo analysis, due to the difficulty of directly correlating performance between the two degradation conditions.

The suture strand must remain securely in place after implantation. To accomplish this, the knot needs to be stable. A single surgeon's knot is typically not sufficient to hold the suture securely, particularly in coated sutures. Additional knots are tied to increase the holding power of the knot. An important contributing factor to knot stability is the frictional property profile of the suture strand. For this reason, friction is another important performance parameter.

The ideal suture provides not only tissue securement, but is also sterile and biocompatible. Medical devices must meet stringent requirements for safety, with guidance by the International Standards Organization (ISO) standard 10993-1



• **Figure 2.5.9.13** Image of spiral cut barbs in Quill SRS suture, marketed by Angiotech Pharmaceuticals.

(ISO, 2009). According to this document, the suture strand must be tested for cytotoxicity, genotoxicity, sensitization, irritation, systemic toxicity, and subchronic toxicity. This represents an extensive set of in vitro and in vivo analyses. For absorbable sutures, the hydrolysis byproducts, along with the polymeric material, are tested.

Newer Trends and Future Developments

In the early 2000s, Ethicon released the first of their *Plus* line of sutures that contain a small amount of the antibiotic/antifungal agent Irgacare, a brand name for triclosan. Since this time, other agents have been incorporated into sutures and explored for antimicrobial effectiveness, including chlorhexidine and octenidine (Matl et al., 2009). Also, various coating polymers have been applied to improve or extend the length of triclosan release from the suture (Nagatomi et al., 2007). Therapeutic release applications have not been limited to antimicrobials, and drug release from the suture coating could be applied to a wide variety of soluble drugs and other active agents (Zhukovsky, 2003). Modified sutures have also been used as carriers in nontraditional applications. An instance of this includes the use of suture strands to position radioactive brachytherapy seeds to treat the cancerous margins after lung resection (Fernando et al., 2005).

New extrusion techniques are allowing for design of nontraditional surgical threads. Multicomponent coextrusion is making it possible to manufacture filaments with “*island in the sea*” and other geometries that could provide enhanced properties. In one instance, a PDO polymer was coextruded with a softer copolymer containing *p*-dioxanone, trimethylene carbonate, and caprolactone, the fibers of which exhibited a much higher knot security compared to a standard PDO suture (Im et al., 2007). Also of interest is the creation of ultrahigh-strength absorbable sutures. Currently, high-lactide copolymers are being investigated for this use, with proposed applications in orthopedic areas.

While traditional sutures depend on knots to secure placement of the suture strand, a novel technique involves the use of a suture with an integral securement mechanism, or barb, as seen in Fig. 2.5.9.13. Quill SRS (Self-Retaining System) barbed suture, marketed by Angiotech, was approved for use in 2004, and is gaining popularity in many soft-tissue procedures. This alternative approach to wound closure provides a faster method of approximation, and avoids extraneous foreign material in the wound due to the bulk of a surgical knot (Angiotech Pharmaceuticals, 2009). The downside to the Quill suture is that the barb is cut directly into the monofilament, which creates a natural weak point in the fiber. Newly released Stratafix is a barbed suture marketed by Ethicon. The barbs are made during the molding process rather than by cutting the already-manufactured monofilament (Ethicon, 2014). This provides the added benefit of a knotless suture without decreasing the strength of the filament.

References

- Andrews, G.P., Laverty, T.P., Jones, D.S., 2009. Mucoadhesive polymeric platforms for controlled drug delivery. *Eur. J. Pharm. Biopharm.* 71, 505–518.
- Angiotech Pharmaceuticals, 2009. Quill™ SRS Manual.
- Barber, F.A., Herbert, M.A., Beavis, R.C., 2009. Cyclic load and failure behavior of arthroscopic knots and high strength sutures. *Arthroscopy* 25, 192–199.
- Bellenger, C.R., 1982. Sutures. Part I: the purpose of sutures and available suture materials. *Comp. Ed. Pract. Vet.* 4, 507–515.
- Benicewicz, B.C., Hopper, P.K., 1990. Polymers for absorbable surgical sutures: Part I. *J. Bioactive Compat. Polymers* 5, 453–472.
- Benicewicz, B.C., Hopper, P.K., 1991. Polymers for absorbable surgical sutures: Part II. *J. Bioact. Compat. Polym.* 6, 64–94.
- Bezwada, R.S., Jamiolkowski, D.D., Lee, I.Y., Agarwal, V., Persivale, J., et al., 1995. Monocryl suture, a new ultrapliable absorbable monofilament suture. *Biomaterials* 16 (15), 1141–1148.
- Bichon, D., Borloz, W., Cassano-Zoppi, A.L., 1984. *In vivo* evaluation of a new polyurethane coated catgut suture. *Biomaterials* 5, 255–263.
- Bouten, P.J., Zonjee, M., Bender, J., Van Goor, H., van Hest, J.C.M., Hoogenboom, R., 2014. The chemistry of tissue adhesive materials. *Prog. Polym. Sci.* 39, 1375–1405.
- Breschi, L., Mazzoni, A., Ruggeri, A., Cadenaro, M., Di Lenarda, R., et al., 2008. Dental adhesion review: aging and stability of the bonded interface. *Dent. Mater.* 24, 90–101.
- Breschi, L., Martin, P., Mazzoni, A., Nato, F., Carrilho, M., et al., 2010. Use of a specific MMP-inhibitor (galardin) for preservation of hybrid layer. *Dent. Mater.* 26, 571–578.
- Brown, E.N., White, S.R., Sottos, N.R., 2005a. Retardation and repair of fatigue cracks in a microcapsule toughened epoxy composite. Part I: manual infiltration. *Compos. Sci. Technol.* 65, 2466–2473.
- Brown, E.N., White, S.R., Sottos, N.R., 2005b. Retardation and repair of fatigue cracks in a microcapsule toughened epoxy composite. Part II: *In situ* self-healing. *Compos. Sci. Technol.* 65, 2474–2480.

- Brubaker, C.E., Kissler, H., Wang, L.-J., Kaufman, D.B., Messersmith, P.B., 2010. Biological performance of mussel-inspired adhesive in extrahepatic islet transplantation. *Biomaterials* 31, 420–427.
- Burkart, S.S., 2004. Arthroscopic knots: the optimal balance of loop security and knot security. *Arthroscopy* 20, 489–502.
- Capperauld, I., Bucknall, T.E., 1984. Sutures and dressings. In: Bucknall, T.E., Ellis, H. (Eds.), *Wound Healing for Surgeons*. Bailliere Tindall, Eastbourne, UK, pp. 75–93.
- Casey, D.J., Roby, M.S., 1984. Synthetic Copolymer Surgical Articles and Method of Manufacturing the Same. U.S. Patent No. 4,429,080 (to American Cyanamid Co.).
- Charnley, J., 1960. Anchorage of the femoral head prosthesis to the shaft of the femur. *J. Bone Jt. Surg.* 42, 28–30.
- Charnley, J., 1970. *Acrylic Cement in Orthopedic Surgery*. E. S. Livingstone, Edinburgh, UK.
- Chu, C.C., 1997a. Chemical structure and manufacturing processes. Chapter 5. In: Chu, C.C., Von Fraunhofer, J., Greisler, H.P. (Eds.), *Wound Closure Biomaterials and Devices*. CRC Press, Boca Raton, FL, pp. 65–106.
- Ciapetti, G., Stea, S., Cenni, E., Sudanese, A., Marraro, D., et al., 1994. Toxicity of cyanoacrylates *in vitro* using extract dilution assay on cell cultures. *Biomaterials* 15, 92–96.
- Coury, A., Hebida, P., Mao, J., Medalie, D., Barman, S., et al., 1999. *In vivo* bonding efficacy of PEG-based hydrogels to a variety of internal tissues. *Trans. Soc. Biomater.* 25, 45.
- Covidien, 2005. IFU for Dexon™ II Coated, Braided Synthetic Absorbable Sutures.
- Covidien, 2009a. Dexon™ S suture. <http://www.covidien.com/imaGeServer.aspx?contentID=14356&contenttype=application/pdf>. [Accessed 5 May 2010].
- Covidien, 2009b. Maxons™ Suture. <http://www.covidien.com/imaGeServer.aspx?contentID=14354&contenttype=application/pdf>. [Accessed 5 May 2010].
- Dai, X., Chen, X., Yang, L., Foster, S., Coury, A.J., Jozefiak, T.H., 2011. Free radical polymerization of poly(ethylene glycol) diacrylate macromers: impact of macromer hydrophobicity and initiator chemistry on polymerization efficiency. *Acta Biomater.* 7 (5), 1965–1972.
- Deng, M., Tian, Y., Latour Jr., R.A., Shalaby, S.W., 1996. Effects of gamma irradiation on ultrahigh molecular weight polyethylene fibers. *Proc. Fifth World Biomater. Cong.* 2, 352.
- Donkerwolcke, M., Burny, F., Muster, D., 1998. Tissues and bone adhesives: historical aspects. *Biomaterials* 19, 1461–1466.
- Eliades, G., Watts, D.C., Eliades, T., 2005. *Dental Hard Tissues and Bonding: Interfacial Phenomena and Related Properties*. Springer-Verlag, Berlin.
- Ethicon, 2001. *Ethicon Wound Closure Manual*.
- Ethicon, 2008. IFU for Vicryl Rapide™ Sterile Synthetic Absorbable Suture.
- Ethicon, 2014. Performance Testing of STRATAFIX SYMMETRIC PDS PLUS 3-0, 0, and 1-Initiation Strength in Porcine Tissue AST 2013-0603.
- Ethicon, 2017. IFU for DERMABOND™ PRINEO™ Skin Closure System.
- FDA (US Food and Drug Administration), 2007. Summary of Color Additives for use in United States in foods, Drugs, cosmetics, and Medical Devices, vol. 21, CFR Parts 73 and 74.
- FDA(US Food and Drug Administration), 1998. Tissue Adhesive for the Topical Approximation of Skin.
- Feldman, D.S., Barker, T.H., Blum, B.E., Kilpadi, D.V., Reddon, R.A., 1999. Fibrin as a tissue adhesive and scaffold for meshed skin grafts in burn patients. *Trans. Soc. Biomater.* 25, 42.
- Fernando, C., Santos, R.S., Benfield, J.R., Grannis, F.W., Keenan, R.J., et al., 2005. Lobar and sublobar resection with and without brachytherapy for small stage 1A and non-small cell lung cancer. *J. Thorac. Cardiovasc. Surg.* 129, 261–267.
- Gilbert, J.L., Hasenwinkel, J.M., Wixson, R.L., Lautenschlager, E.P., 2000. A theoretical and experimental analysis of polymerization shrinkage of bone cement: a potential major source of porosity. *J. Biomed. Mater. Res.* 52, 210–218.
- Green, K., 1996. Mussel adhesive protein. In: Sierra, D.H., Salz, R. (Eds.), *Surgical Adhesives and Sealants*. Technomic Publishing, Lancaster, PA, pp. 19–28.
- Guttman, B., Guttman, H., 1994. Sutures: properties, uses and clinical investigation. In: Dumitriu, S. (Ed.), *Polymeric Biomaterials*. Marcel Dekker, New York, NY, pp. 325–346.
- Hu-Friedy Mfg Co, Inc, 2007. Perma Sharp® sutures. <http://www.hu-friedy.com/resource/viewResource.aspx?ResourceID=277>. [Accessed 5 May 2010].
- Ikada, Y., 1997. Tissue adhesives. In: Chu, C.C., von Fraunhofer, J.A., Greisler, H.P. (Eds.), *Wound Closure Biomaterials and Devices*. CRC Press, Boca Raton, FL, pp. 317–346.
- Im, J.N., Kim, J.K., Kim, H.K., Lee, K.Y., Park, W.H., 2007. Characteristics of novel monofilament sutures prepared by conjugate spinning. *J. Biomed. Mater. Res. B: App. Biomater.* 83B, 499–504.
- ISO (International Standards Organization), 2009. ISO 10993–1:2009. Biological Evaluation of Medical Devices—Part 1.
- Kühn, K.-D., 2000. *Bone Cements*. Springer-Verlag, Berlin.
- Lai, S., Becker, D., Edlich, R., 2009. Sutures and Needles. <http://emedicine.medscape.com/article/884838-overview>. [Accessed 12 February 2009].
- Matl, F.D., Zlotnyk, J., Obermeier, A., Friess, W., Vogt, S., et al., 2009. New anti-infective coatings of surgical sutures based on a combination of antiseptics and fatty acids. *J. Bio Sci.* 20, 1439–1449.
- Matras, H., 1972. Suture-free interfascicular nerve transplantation in animal experiments. *Wien. Med. Wochenschr.* 122, 517–523.
- Mattei, F.V., 1980. Absorbable Coating Composition for Sutures. U.S. Patent No. 4,201,216 (to Ethicon, Inc.).
- Nagatomi, S.D., Tate, P.L., Linden, D.E., Hucks, M.A., Shalaby, S.W., 2007. Antimicrobial absorbable multifilament braided sutures: a preliminary report. *Trans. Soc. Biomater.* 30, 182.
- Nagatomi, S., Linden, D., Vaughn, M., Corbett, J., Shalaby, M., et al., 2008. New Composite Silk Braids (Ligaprene Silk) as Low-Reactivity and Antimicrobial Sutures. 8th World Biomaterials Congress.
- Nakabayashi, N., Pashley, D.H., 1998. *Hybridization of Dental Hard Tissues*. Quintessence Publishing Co, Ltd, Tokyo.
- Park, Y.D., Tirelli, N., Hubbell, J.A., 2003. Photopolymerized hyaluronic acid-based hydrogels and interpenetrating networks. *Biomaterials* 24, 893–900.
- Reiter, A., 1987. Induction of sarcomas by the tissue-binding substance Histoacryl-blau in the rat. *Z. für Exper. Chirg. Transpl. Kunsliche Organe* 20, 55–60.
- Roby, M.S., Bennett, S., Kokish, M., Jiang, Y., April 30–May 4, 1997. A new synthetic monofilament absorbable suture from block copolymers of trimethylene carbonate, dioxanone and glycolide. Part I: synthesis and Processing. *Trans. 23rd Annual Meeting Soc. for Biomater.* 338.
- Roulet, J.-F., Degrange, M. (Eds.), 2000. *Adhesion: The Silent Revolution in Dentistry*. Quintessence Publishing Company, Inc, Chicago, IL.
- Sawhney, A.S., Pathak, C.P., Hubbell, J.A., 1993. Bioerodible hydrogels based on photopolymerized poly(ethylene glycol)-copoly(x-hydroxy acid) diacrylate macromers. *Macromolecules* 26, 581–587.
- Scardino, M.S., Swain, S.F., Morse, G.S., Sartin, E.A., Wright, J.C., et al., 1999. Evaluation of fibrin sealants in cutaneous wound closure. *J. Biomed. Mater. Res.* 48, 315–321.

- Schlag, G., Redl, H., 1987. Fibrin Sealant in Operative Medicine. Plastic Surgery, Maxillo Facial and Dental Surgery, vol. 4. Springer Verlag, Berlin.
- Sierra, D.H., Salz, R. (Eds.), 1996. Surgical Adhesives and Sealants. Technomic Publishing, Lancaster, PA.
- Singer, A.J., Perry, L.C., Allen, R.L., 2008. In vivo study of wound bursting strength and compliance of topical skin adhesives. *Acad. Emerg. Med.* 15, 1290–1294.
- Smith, D.C., 1967. A new dental cement. *Br. Dent. J.* 123, 540–541.
- Smith, D.C., 1971. Medical and dental applications of cements. *J. Biomed. Mater. Res. Symp.* 1, 189–205.
- Smith, D.C., 1991. Dental cements. *Curr. Opin. Dent.* 1, 228–234.
- Smith, D.C., 1998. Development of glass-ionomer cement systems. *Biomaterials* 19, 467–478.
- Stashak, E.S., Yturraspe, D.J., 1978. Considerations for selection of suture materials. *J. Vet. Surg.* 7, 48–55.
- Taylor, M.S., 2010. USLG and Osteoprene *In Vitro* and *In Vivo* Studies. Poly-Med, Inc. Internal Memorandum.
- Tirelli, N., Lutolf, M.P., Napoli, A., Hubbell, J.A., 2002. Poly(ethylene glycol) block copolymers. *Rev. Mol. Biotechnol.* 90, 3–15.
- Totakura, N., Shalaby, S.W., 1997a. Polymeric Compositions. U.S. Patent No. 5,607,866 (to U.S. Surgical).
- Totakura, N., Shalaby, S.W., 1997b. Suture Coating and Tubing Fluid. U.S. Patent No. 5,584,857 (to U.S. Surgical).
- Trask, R.S., Williams, H.R., Bond, I.P., 2007. Self-healing polymer composites: mimicking nature to enhance performance. *Bioinspiration Biomim.* 2 (1), 1–9.
- United States Pharmacopeia, 2008. United States Pharmacopeia and National Formulary (USP 31-NF 26). United States Pharmacopeia Convention. 3 volumes, 3, 788 pages.
- Waite, J.H., 1989. The glue protein of ribbed mussels (*Genkenskadenissa*): a natural adhesive with some features of collagen. *J. Comp. Physiol.*, MI 159 (5), 517–525.
- Webb, J.C.J., Spencer, R.F., 2007. The role of polymethylmethacrylate bone cement in modern orthopedic surgery. *J. Bone Jt. Surg.* 89-B (7), 851–857.
- Weber, S.C., Chapman, M.W., 1984. Adhesives in orthopedic surgery. *Clin. Orthop. Relat. Res.* 191, 249–261.
- Van Winkle Jr., W., Hastings, J.C., 1972. Considerations in the choice of suture material for various tissues. *Surg. Gynecol. Obstet.* 135, 113–126.
- Zhukovsky, V., 2003. Bioactive surgical sutures. *Autex Res. J.* 3, 41–45.

Further Reading

- ASTM, 2011. ASTM F1980-07 (2011): Standard Guide for Accelerated Aging of Sterile Barrier Systems for Medical Devices. ASTM International.
- Burg, K.J.L., Shalaby, S.W., 1999. Absorbable materials and pertinent devices. Chapter 6. In: Von Recum, A.F. (Ed.), *Handbook of Biomaterials Evaluation: Scientific, Technical, and Clinical Testing of Implant Materials*, second ed. Taylor & Francis, Philadelphia, PA, pp. 99–110.
- Carpenter, K.A., Shalaby, S.W., 2002. Dioxanone- and dioxepanone-based absorbable polymers. In: Atala, A., Lanza, R. (Eds.), *Methods for Tissue Engineering*. Academic Press, New York, NY, p. 591.
- Chu, C.C., 1997b. New emerging materials for wound closure. Chapter 2. In: Chu, C.C., Von Fraunhofer, J., Greisler, H.P. (Eds.), *Wound Closure Biomaterials and Devices*. CRC Press, Boca Raton, FL, pp. 347–384.
- FDA (US Food and Drug Administration), 2014. Stratafix Symmetric PDS Plus Knotless Tissue Control Devices.
- Moszner, N., Salz, U., 2007. Recent developments of new components for dental adhesives and composites. *Macromol. Mater. Eng.* 292, 245–271.
- Roby, M.S., Kennedy, J., 2004. Sutures. Chapter 7.13. In: Ratner, B.D., Hoffman, A.S., Schoen, F.J., Lemons, J.E. (Eds.), *Biomaterials Science, an Introduction to Materials in Medicine*, second ed. Elsevier Academic Press, San Diego, CA, pp. 615–627.
- Yoshihara, K., Yoshida, Y., Nagaoka, N., Fukegawa, D., Hayakawa, S., Mine, A., Nakamura, M., Minagi, S., Osaka, A., Suzuki, K., Van Meerbeek, B., 2010. Nano-controlled molecular interaction at adhesive interfaces for hard tissue reconstruction. *Acta Biomater.* 6 (9), 3573–3582. <https://doi.org/10.1016/j.actbio.2010.03.024>.

2.5.10

Biomaterials for Immunoengineering

SUSAN N. THOMAS^{1,2}, PAUL A. ARCHER^{1,3}, MARGARET P. MANSPEAKER^{1,3}

¹Parker H. Petit Institute for Bioengineering and Bioscience, Georgia Institute of Technology, Atlanta, GA, United States

²George W. Woodruff School of Mechanical Engineering, Georgia Institute of Technology, Atlanta, GA, United States

³School of Chemical and Biomolecular Engineering, Georgia Institute of Technology, Atlanta, GA, United States

Use of Biomaterials in Vaccine Development

Introduction

Vaccine-based therapies for the treatment of disease were first described over two centuries ago with the successful application of a smallpox vaccine by Edward Jenner in 1796 ([World Health Organization, 2009](#)). Since then, scientists have formulated vaccines against a wide variety of pathogens, including but not limited to measles, pertussis, tetanus, poliomyelitis, and cholera. These diseases, which used to be among the most significant threats to human health and causes of infant mortality, have been largely contained or even eradicated in developed countries and are rapidly declining worldwide ([World Health Organization, 2009](#)).

Vaccines work by introducing a killed or weakened whole pathogen or a subunit(s) of the pathogen to the immune system without the disease itself being active and harming the individual to cause a B cell (humoral) and/or T cell (cell-mediated) response. The magnitude and type of response depends on the specific treatment schedule as well as dose, antigen, adjuvant, etc. delivered in the vaccine. The effect of vaccination in most scenarios is ideally a lasting memory response to epitopes of the pathogen-associated antigen. Thus if the pathogen expressing those particular epitopes is subsequently encountered, antibodies already developed in response to the vaccine will bind and mark the pathogen for death (humoral response) to prevent infection. Cellular immunity can also be elicited by the vaccine to result in pathogen reexposure triggering direct cell-mediated lytic or cytokine responses. This allows for the prevention of

infection or pathogen clearance in vaccinated individuals ([U.S. Dept. of Health and Human Services, 2017](#)).

While vaccines have drastically improved the human lifespan, there is still room for improvement—many vaccines require a booster years after the initial inoculation, which is costly and can lead to a lapse in immunity and allow spreading of disease. Live-attenuated vaccines often cannot be tolerated by immunocompromised individuals due to their potency, leaving a subset of susceptible people at risk. Additionally, there are still pathogens that scientists have not been able to develop vaccines against due to their virulence, ability to rapidly mutate and evolve, the presence of many different subtypes with varying characteristic epitopes, or their inability to induce a strong immune response in subunit form. These pathogens include human immunodeficiency virus, hepatitis C, and malaria, though they have been investigated extensively in the medical research community ([Rappuoli et al., 2011](#)). Aside from the need to develop new and more effective vaccines, significant challenges in vaccine research exist in regard to their accessibility in developing countries. One major hurdle is breaking the “cold-chain,” or the need for refrigeration of vaccines and other medicines, which is not always available in rural or impoverished areas. This makes access to vaccines very difficult for a large portion of the global population, continuing the spread of preventable diseases that have been mostly eradicated in developed areas ([World Health Organization, 2015](#)).

The field of biomaterials has presented a variety of elegant solutions to medical problems throughout history, and thus has been a large part of vaccine research and the attempt to mitigate the drawbacks of currently approved vaccines. This

includes both making more effective vaccines that prevent a wider array of diseases or the need for additional boosters, and more stable formulations that allow for alternate administration routes and enhanced global accessibility. The following sections will review broad biomaterials-based strategies for improving vaccines in the aforementioned areas.

Biomaterials for Improving Vaccine Efficacy

Mounting a powerful, long-lasting immune response to a vaccine can be accomplished using two important components: (1) adjuvants, present in most vaccines, which provide additional immune stimulation, and (2) antigen that can be efficiently presented by antigen-presenting cells (APCs), which result in the priming of antigen-specific T cells that have direct cell-killing functions or can provide “help” through cytokine production that, for example, aids in the development of mature antibody (humoral) responses by B cells. In the last few decades, a large number of biomaterial systems have been characterized that specifically enhance different aspects of this process. Some important criteria for vaccine biomaterials are illustrated in Fig. 2.5.10.1.

Dendritic cells (DCs), macrophages, and B cells are known as professional APCs. Each of these cell types plays diverse and specialized roles in the immune response to vaccination, and thus represents a desirable therapeutic target with which biomaterials can be designed to interact. In this section, we consider the use of biomaterials to deliver adjuvants to APCs, but focus the discussion on DCs and macrophages. B cells are discussed separately and more specifically in the Section “Activation of B Cells and Humoral Immunity.”

Use of Biomaterials to Adjuvant the Immune System

While some vaccines are naturally potent or able to induce a lasting, protective immune response, others rely on a class of materials called adjuvants, which aim to amplify the efficacy of vaccines by providing additional immune stimulation.

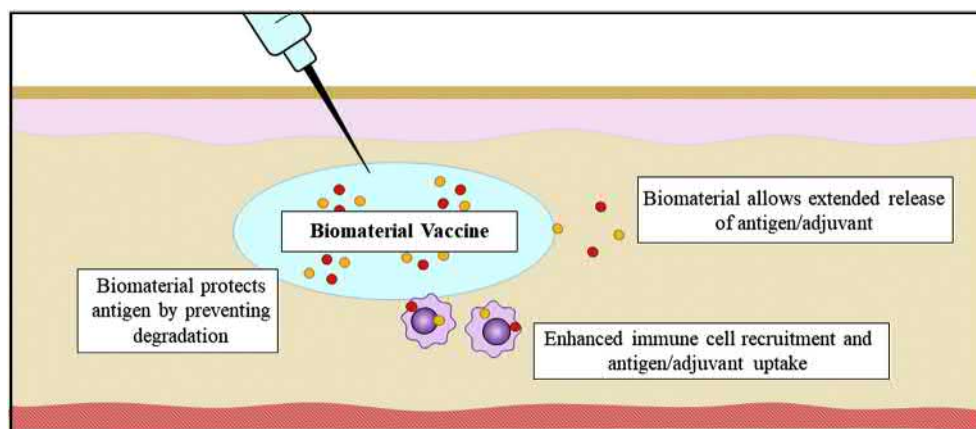
Traditional adjuvants aim to accomplish the following goals (European Medicines Agency, 2003):

1. Protect antigen from being degraded and increasing its bioavailability;
2. Distribute antigen to target specific cells and improve its presentation;
3. Direct stimulation of target immune cells.

Biocompatible materials have been used as adjuvants for almost a century (Marrack et al., 2009), beginning with the use of insoluble aluminum salts (most commonly known as “alum”) to enhance the efficacy of a diphtheria vaccine. Since its original discovery, alum has been used in a wide variety of vaccines and was the only approved vaccine adjuvant for many years. Despite its widespread use, the mechanism by which alum exerts an adjuvant effect is not fully elaborated.

Originally, alum derivatives were thought to adsorb antigen and form a depot in vivo, facilitating slow release of the antigen over time and leading to efficient amplification of antibody titer (Glenny et al., 1926), though formation of a depot has also been reported not to affect the adjuvanticity of alum (Hutchison et al., 2012). Similarly, other Food and Drug Administration (FDA)-approved adjuvants include oil-in-water emulsions such as Montanide or squalene-containing MF59. These operate in a similar manner by protecting and releasing antigen for long periods of time after immunization and have proven safer and more effective than previous iterations, including Freund’s adjuvant (Herbert, 1968). Other proposed mechanisms of action for the traditional adjuvants alum and oil-in-water emulsions include their propensity to attract innate immune cells (Calabro et al., 2011) and induce local inflammatory cascades that lead to cytokine release and enhanced types 1 and 2 helper T cell response (Grun and Maurer, 1989). Despite the widespread use of these traditional adjuvants, they have failed to enhance the efficacy for all types of immunization, leading to an increased interest in adjuvants that elicit a direct mechanistic effect.

Some of the principal cellular targets of this newly investigated class of adjuvant are DCs and macrophages, which are



• **Figure 2.5.10.1** Mechanisms of action of biomaterial-incorporated vaccines. Biomaterials can confer extended release, protection, or enhanced immune cell uptake of vaccine antigen and adjuvant.

important in the immune response for sampling their environment and detecting pathogen-associated molecular patterns (PAMPs) indicative of infection (Mosser and Edwards, 2008). These patterns are typically related to bacterial or viral structural and genetic components, such as lipopolysaccharide in bacterial cell membranes or double-stranded viral RNA, which they detect using pattern-recognition receptors such as Toll-like receptors (TLRs). Once PAMPs engage their appropriate receptor, they elicit a signaling cascade that leads to a state of enhanced antigen processing and presentation called maturation, the process by which these cells become “licensed” to activate naïve lymphocytes into effector cells (see Chapter 2.3.2). These TLR ligands are being heavily investigated as vaccine adjuvants that mimic PAMPs to elicit this heightened immune response. One such adjuvant is a TLR4 agonist monophosphoryl lipid A (MPLA), a less toxic form of lipopolysaccharide found in bacteria and is approved in an alum-containing formulation (AS04) or in a liposomal formulation (AS01B) (Center for Disease Control, 2018a,b).

Other heavily investigated experimental TLR ligands include the TLR9 agonist cytosine-phosphate-guanine (CpG), which mimics bacterial and viral DNA, which has been widely researched in the context of both traditional vaccines (Campbell, 2017) and cancer vaccines, the latter particularly due to its ability to enhance the CD8 T cell response (Kochenderfer et al., 2007). Additionally, other molecules such as imidazoquinoline compounds imiquimod and resiquimod have been investigated for their ability to agonize TLR7/8, which typically responds to single-stranded RNA, a viral component (Hemmi et al., 2002). Imiquimod and resiquimod have been shown to cause an antiviral response and are used to treat viral infection (Edwards et al., 1998) and some forms of cancer (Beutner et al., 1999) topically, and thus have been researched for their application to cancer vaccines in particular (Adams et al., 2008). However, to achieve the maximum effect of these adjuvants and reduce systemic immune overactivation, biomaterials have been investigated in the context of direct adjuvant delivery to APCs. These strategies for general adjuvant delivery are outlined in the following section.

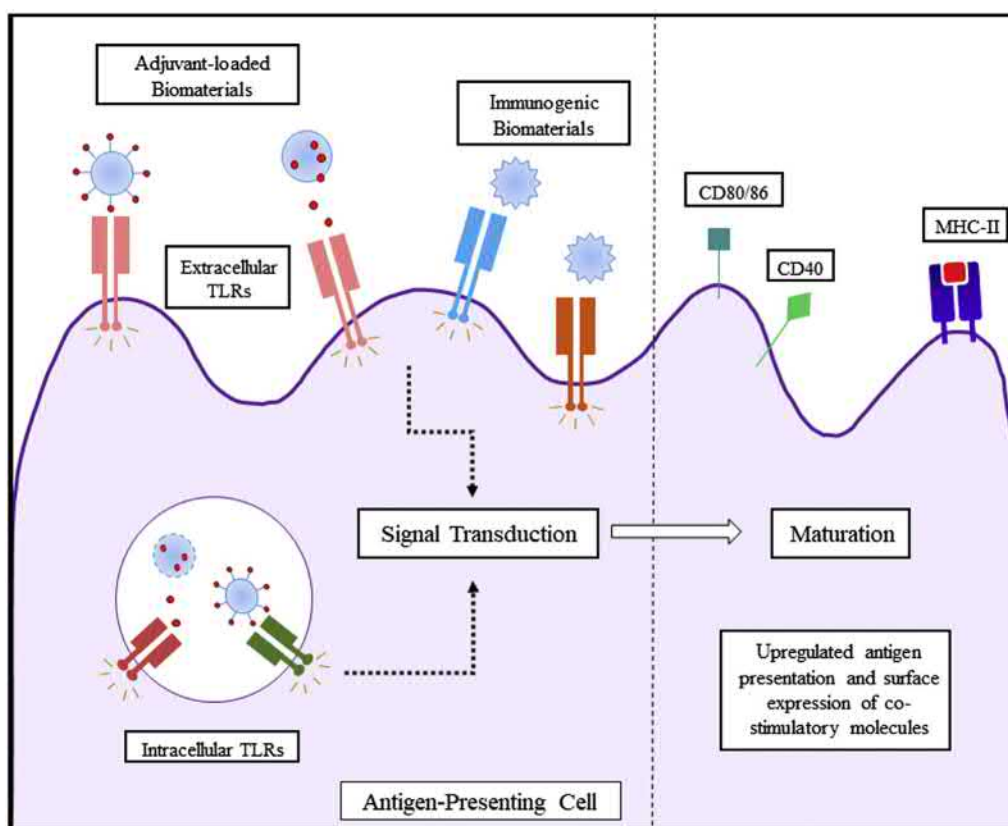
Biomaterials have been investigated both for their ability to deliver adjuvant to APCs in a targeted manner, and for their ability to directly adjuvant immune cells in the case of immunogenic materials. Though a wide variety of biomaterial formulations have been reported for the purpose of delivering adjuvant to APCs, several main trends emerge. In terms of the material carrier, poly(lactic-co-glycolic acid) (PLGA) is often used for its tunability and well-characterized in vivo response (Varypataki et al., 2016; Ali et al., 2009; Lynn et al., 2015), as well as other common FDA-approved biocompatible polymers, or supramolecular structures made from modified antigen and adjuvant. Overall, spherical carriers for the codelivery of antigen and adjuvant are the most commonly used strategy, with particle sizes ranging from tens of nanometers to target lymph node-resident APCs to hundreds of nanometers to enhance phagocytosis by APCs

(Manolova et al., 2008). TLR ligand can be conjugated or adsorbed to the material surface, or encapsulated within it depending on the receptor’s location on the extracellular or intracellular/vesicular membrane of the APC, respectively. Examples of this include CpG conjugated to small nanoparticles to activate extracellular TLR9 (Thomas et al., 2014) or MPLA-encapsulated lipid vesicles to adjuvant intracellular TLR4 signaling (Moon et al., 2011). Another non-particle approach to adjuvanting includes injectable gels or polymeric matrices that present stimulating factors for the purpose of attracting and maturing APCs (Ali et al., 2009). Because adjuvant-loaded materials are typically designed for codelivery with antigen, further criteria for the design of these materials will be considered in the Section “Use of Biomaterials to Improve Delivery of Antigen to APCs.”

Naturally immunogenic biomaterials have also been explored for their ability to adjuvant immune cells, and may provide an advantage over materials requiring conjugation or encapsulation of adjuvants as their efficacy can be hindered by loading efficiency. Several well-researched biomaterial adjuvants include organic materials like alginate, a block copolymer polysaccharide derived from algae, or its monomers mannuronic and guluronic acid (Yang and Jones, 2009). Additionally, inorganic materials have also been shown to elicit an adjuvant effect, including the mineral hydroxyapatite ($\text{Ca}_{10}(\text{PO}_4)_6(\text{OH})_2$) (Grandjean-Laquerriere et al., 2007). In both of these cases, the surface of the material mediates immune-stimulation via association with TLRs. Aside from this function, biomaterials can also be engineered to activate the complement cascade, which often results in the material being opsonized or flagged for phagocytosis by APCs. Nucleophilic chemical moieties, namely hydroxyl and amino groups, facilitate the deposition of complement proteins onto the material (Toda et al., 2008). This information has allowed for the design of hydroxyl-functionalized materials for adjuvanting the immune system via complement activation, leading to enhanced vaccine efficacy (Thomas et al., 2011). A summary of the biomaterial strategies for delivery of adjuvant to APCs and their mechanism of action can be visualized in Fig. 2.5.10.2.

Use of Biomaterials to Improve Delivery of Antigen to APCs

Once an antigen is encountered, DCs and macrophages undergo maturation and upregulate expression of major histocompatibility complex (MHC) I and II, which allows presentation of short antigenic peptide sequences to engage with the T cell receptors on CD8⁺ and CD4⁺ T cells, respectively. Antigen presentation occurs when a pathogen is phagocytosed from the extracellular space and then destroyed by the highly acidic and reductive environment within phagolysosomes, and antigenic peptide sequences are cleaved (see Chapter 2.3.2). Then, either the endosome fuses with an MHC II-containing vesicle and peptide fragments are loaded, or fragments escape the endosome and are loaded onto MHC I and transported to the cell surface



• **Figure 2.5.10.2** Mechanisms of action of adjuvant delivery via biomaterials. Adjuvant-loaded and/or immunogenic biomaterials access APCs, where they engage PRRs such as TLRs (left). The effect is APC maturation (right).

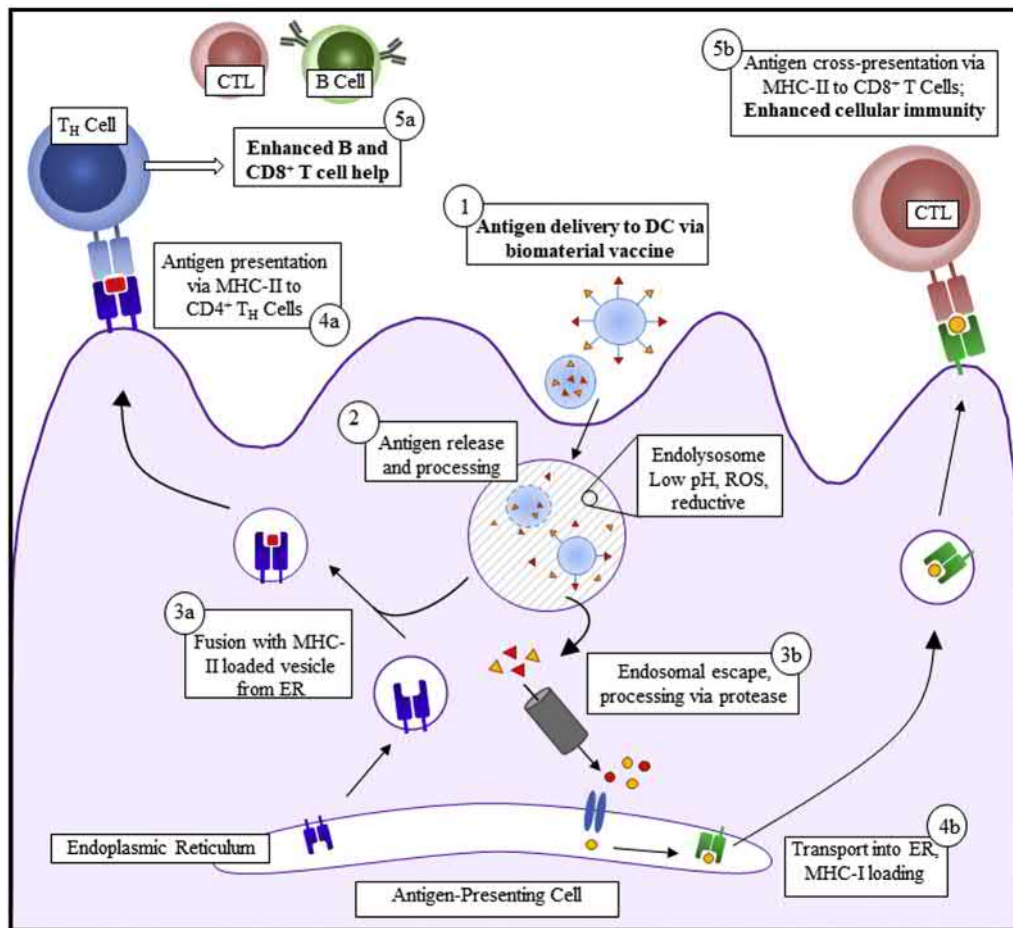
for expression (Joffre et al., 2012), a process termed cross-presentation. Because antigen escape from these phagolysosomes can lead to presentation via either type of MHC molecule, there is significant crosstalk between both pathways leading to antibody production and cytotoxic T cell expansion in response to many types of pathogens depending on the immunological context (Joffre et al., 2012). Biomaterials are utilized in this application because they can be engineered to improve both cell-mediated and humoral responses through designs that support endosomal escape to cause MHC presentation and cross-presentation.

One strategy for enhanced antigen presentation is incorporation into a nanocarrier that enables release into endolysosomal vesicles and efficient endosomal escape, leading to cross-presentation. This has been accomplished mainly by the use of materials that degrade at lysosomal pH, including PLGA (Shen et al., 2006), poly(dimethylaminoethyl methacrylate) (Foster et al., 2010), poly(glycidol) (Yuba et al., 2010), and poly(propylene sulfide) (Hirosue et al., 2010). Additionally, materials that degrade via enzymatic action, such as liposome formulations that are cleaved via endolysosomal lipases, have been considered (Moon et al., 2011). This formulation strategy also provides the benefit of extended release, where antigen is being freed from the endosomal compartment in a continual manner, allowing for persistent cross-presentation. Conjugation of peptide

antigen to nanocarriers via cleavable conjugation is also an effective strategy for antigen escape into the cytosol, including the use of reducible disulfide linkages (Hirosue et al., 2010). Besides endosomal escape, cell-penetrating peptides have been used as a mechanism for direct entry of antigen or nanocarrier-associated antigen to efficiently induce potent cytotoxic T cell responses (Nakamura et al., 2008). A summary of the biomaterial strategies for delivery of antigen to APCs and their mechanisms of action can be visualized in Fig. 2.5.10.3.

Activation of B Cells and Humoral Immunity

B cells mediate humoral immunity, which is particularly effective at neutralizing extracellular pathogens before they have a chance to damage host cells. Most existing vaccines are successful as a result of their ability to stimulate B cells and incite an antibody response that mediates prophylactic immunity (Lachmann, 2012). Many pathogens commonly vaccinated against such as polio, tetanus, and diphtheria can rapidly damage tissues if the body is unprepared upon initial contact, so it is critical for preexisting antibodies to be present to quickly neutralize the threat (Lachmann, 2012; Bachmann and Jennings, 2010). The importance of humoral immunity to vaccine efficacy makes methods of increasing B cell activation of great interest in vaccine design, and with



• **Figure 2.5.10.3** Mechanisms of action of antigen delivery via biomaterials. Antigen-loaded biomaterials access APCs (1) and are phagocytosed, leading to antigen release from the biomaterial due to pH, ROS, or reduction-sensitive conjugation schemes or biomaterial composition (2). Antigen then can either be presented via MHC-II (3a, 4a, 5a), or cross-presented via MHC-I (3b, 4b, 5b).

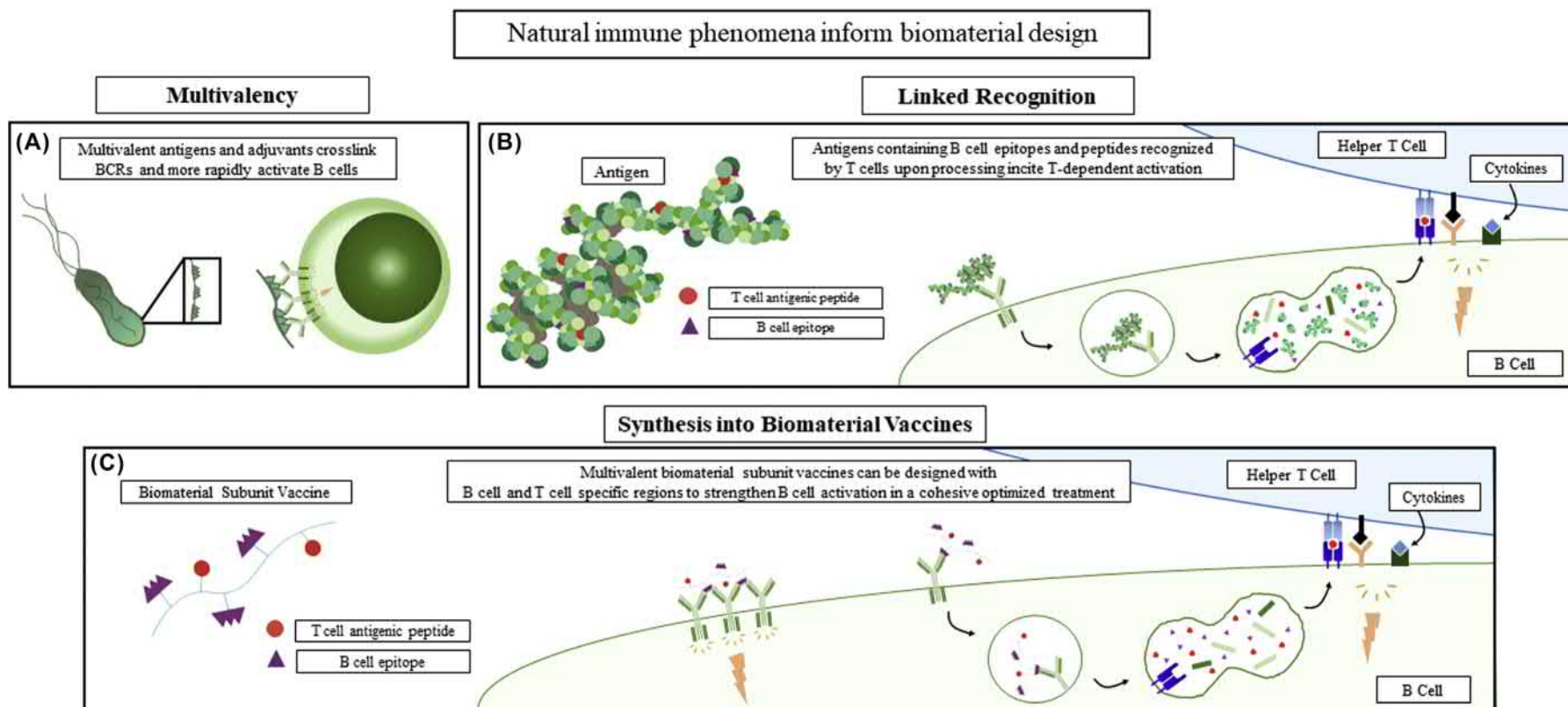
an understanding of the B cell activation process, unique strategies to modulate B cell responses with biomaterials can be rationally designed.

Overview of the B Cell Activation Process

At a fundamental level, B cell activation can be separated into either T cell-dependent or T cell-independent action, and this distinction is dependent upon the characteristics of the antigen causing the response. Central to both activation pathways is the B cell receptor (BCR), which is an immunoglobulin receptor on the B cell's surface that will bind to a specific region of an antigen. However, B cells cannot be fully activated solely by antigen recognition within a single BCR. Instead, their full activation depends on either the crosslinking of multiple BCRs and a secondary signal from an immune stimulant, or on the assistance of a concurrently activated helper T cell (Vos et al., 2000). Crosslinking of multiple BCRs can occur in response to antigens presented to the B cell at high local surface density, which can result in high multivalency, and can enable B cell activation without the need for T cell support (Fig. 2.5.10.4A). Even without sufficient multivalency to activate a B cell entirely, multivalency supports

the T cell-dependent pathway as well because it lowers the threshold for activation, therefore benefiting B cell activation in either case and making antigen multivalency a key feature in induction of a humoral response (Bennett et al., 2015).

T cell-dependent activation is more common and occurs through antigen binding at low surface density, frequently in the form of a free protein antigen that binds one BCR at a time (Cruse et al., 2004). BCR binding triggers an endocytosis and signaling cascade that results in internalization of the BCR-bound antigen within an endosome where it is degraded and processed, and some of its component peptides are shuttled back to the B cell's surface within MHC II proteins that the B cell will use to interact with helper T cells (Yuseff et al., 2013; Lanzavecchia, 1985; Harwood and Batista, 2010). As a result, these helper T cells can be specific to epitopes other than those directly recognized by the BCR, so while both the T cell and B cell may recognize different epitopes, their specificity is linked to the same pathogen (Harwood and Batista, 2010; see Chapter 2.3.2). This concept is known as linked recognition, and it is an important consideration in subunit vaccine design that can be leveraged using biomaterials to stimulate potent humoral responses (Fig. 2.5.10.4B).



• **Figure 2.5.10.4** Natural immune phenomena inform biomaterial design. (A) Strength of natural B cell activation is increased by multivalent antigens and adjuvants that crosslink BCRs, (B) Antigens containing B cell epitopes as well as component peptides recognized by T cells incite T-dependent activation with improved strength and immune memory, (C) Biomaterial subunit vaccines can be designed that synthesize both of these natural potent immune activation criteria and strengthen humoral response to a target antigen.

T cell-independent activation has the potential to be much faster, as it only requires the B cell to come into contact with a multivalent antigen and receive a secondary signal that can come from either the foreign substance itself through TLR signaling, or from cytokines released by innate immune cells in the vicinity (Vos et al., 2000). From a biomaterial standpoint, this form of activation may readily be achievable using a multivalent antigen and one of the many adjuvant strategies discussed in the previous section to activate APCs. However, a serious disadvantage of this method of activation is that it also tends to result in low-affinity antibody production, and either less effective immune memory function or none at all (Toellner et al., 2002). In contrast, T cell-dependent activation proceeds more slowly because it is limited by the full timescale of the adaptive immune response, but it also displays sustained immune memory and antibody class switching upon antigen rechallenge. Both mechanisms of B cell activation may be leveraged in vaccine design to increase the efficacy of humoral response, and this may be particularly achievable using biomaterials because of their highly controllable nature.

Biomaterial Design for Enhancing the Humoral Response

Potent humoral immune responses can generally be achieved with vaccines that incorporate multivalent antigens and include linked B and T cell epitopes specific to a target pathogen (Arsiwala et al., 2019; Wen and Collier, 2015; Renaudet et al., 2008) (Fig. 2.5.10.4C). While some vaccines have been successful at achieving strong humoral responses, precise amounts of B and T cell antigens and their specific degree of multivalency can influence immune responses significantly, so vaccine design can benefit from engineered platforms with greater control over these parameters (Wen and Collier, 2015; Purcell et al., 2007). To address this need, multivalent materials containing distinct quantities of B and T cell antigens, termed multiple antigen peptide systems or MAPs, have been an area of research since the 1980s (Tam, 1988). In early experiments, varied ratios of synthetic high-density malaria antigens designed to activate B cells and T cells were tested in mice. Results confirmed that multivalency boosted immune responses and also suggested that equimolar amounts of each antigen were optimal to induce the strongest humoral response to combat the disease (Tam et al., 1990). Decreased peptide density and exclusion of either the B cell-specific or T cell-specific antigen reduced or negated the immune response entirely (Tam et al., 1990). While both B cell and T cell antigen types are included in these vaccines, it is only B cell antigens that directly benefit from multivalency because of its relevance in B cell activation (Bennett et al., 2015). Importantly, in these first experiments, alum was coadministered to adjuvant the response, but subsequent work has shown that in many cases, biomaterial peptide nanocarriers can be designed to be immunogenic enough to serve as their own adjuvants, and can even outperform industry standards

such as alum and CpG (Tam et al., 1990; Chen et al., 2013; Rudra et al., 2012). Subsequent research has shown that many different approaches can be implemented to create biomaterials with highly multivalent surface antigens, including synthetic protein nanofibers and a variety of antigen-loaded lipid and polymer nanoparticles (Tam et al., 1990; Bennett et al., 2015; Moon et al., 2012). Recent protein nanofiber designs are particularly versatile because they can be built from a protein backbone linked by controllable quantities of customized epitopes, giving them potential as a platform for vaccination against diverse diseases (Hudalla et al., 2014). An interesting aspect of the protein nanofiber approach is that the nanofiber carrier acts as an adjuvant, which can be valuable in vaccine design because administration of traditional adjuvants unattached to a target antigen can result in less control over the subsequent immune response (Wen and Collier, 2015; Hudalla et al., 2013). Also promising is the use of multilayered lipid nanoparticles designed to both encapsulate target antigen in their core and present it at high multivalency on each layer of their lipid surfaces (Moon et al., 2011). This approach is interesting because it incorporates antigen designed to stimulate both B cells and T cells in a manner favorable to a response in both cell types, and does so in a delivery vehicle that is more efficiently taken up than soluble antigen by APCs (Yuseff et al., 2013). This lipid nanoparticle treatment has been tested with monophosphoryl lipid A as an adjuvant, and shown to prompt a superior antibody response at significantly reduced adjuvant levels than would be needed if the antigen were administered in its soluble, nonbiomaterial form (Moon et al., 2012). In addition, adjuvant can actually be loaded into the lipid vessels with antigen rather than just coadministered in the same injection, and achieve a very strong response (Moon et al., 2011). Other biomaterial designs have also enhanced humoral responses by manipulating surface peptide organization, including additional adjuvants on the material surface, and using complex synthetic antigen carriers designed to be cleaved within B cells at select sites to enable efficient release of T cell-specific antigen upon endocytosis (Bennett et al., 2015; Moon et al., 2012; Jegerlehner et al., 2002). For consideration in biomaterial design, studies of B cell surface features have shown that surface Ig receptors on resting B cells are separated by about 40 nm, and that a strong B cell activation signal requires the crosslinking of 10–20 surface receptors in a cluster (Vos et al., 2000). Antigens displayed with repeat epitope patterns spaced by 5–10 nm have shown great success at initiating B cell activation in an increasingly T-independent manner, so the precise control over antigen spacing offered by biomaterials can have great impacts on multiple different aspects of B cell activation (Bachmann et al., 1995). In addition to multivalency, one of the newer directions in B cell modulation by biomaterials is to control the stiffness of the substrate upon which antigens are presented, because studies have shown that a B cell exposed to the same antigen on a different surface

may react differently, both in the potency of its activation and in the types of antibodies it produces in response (Zeng et al., 2015; Wan et al., 2015). This is particularly true when comparing the strength of B cell responses to membrane-bound antigen as opposed to antigen in its free soluble form, as membrane-bound antigen is able to activate B cells orders of magnitude more effectively (Batista et al., 2001).

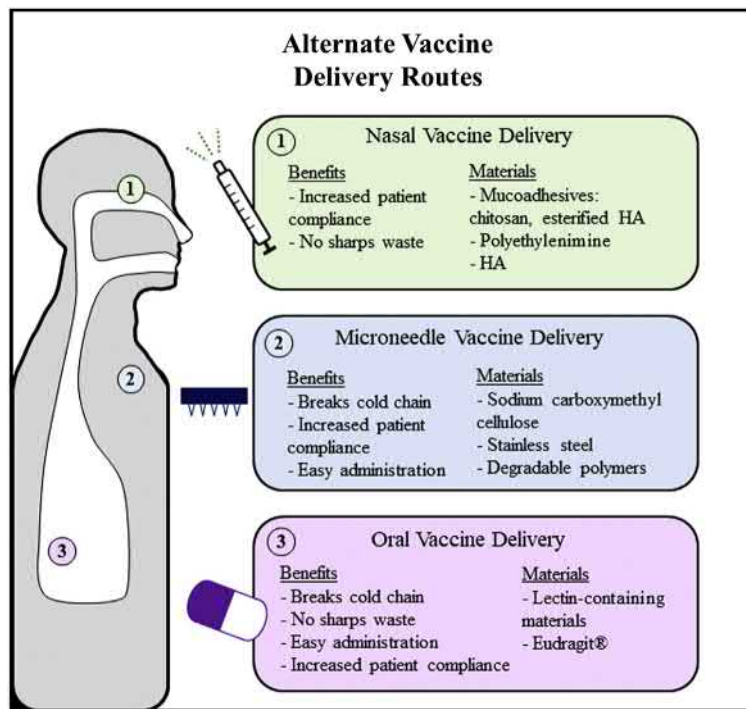
Although surface interactions between B cells and their target antigens are very important to biomaterial design, perhaps equally important is the ability of the biomaterial to actually deliver a vaccine to its target cell. Lymphocytes that survive their rigorous selection and maturation process migrate to secondary lymphoid tissues such as the lymph nodes, where they are housed in specific zones with highly regulated accessibility. It is therefore important for immunomodulatory biomaterials to be designed such that they can access lymph nodes in high concentrations, and for vaccines targeting humoral response to be designed with B cell follicle access in mind. Biomaterial approaches can aid in this process in many ways, including improving activation of DCs and macrophages in the periphery to enhance trafficking of antigen to the lymph node or acting as lymphatic draining carriers for antigen–adjuvant cargo, as discussed previously. However, if interested in specifically improving humoral response, biomaterials optimally sized for lymphatic drainage may offer advantages over free antigen vaccine formulations (Reddy et al., 2007; Mueller et al., 2015). B cells are housed within the lymph node follicles, where they have access to antigens that are either small enough to have passively drained there or have been shuttled there by macrophages and DCs, then transferred to follicular DCs present throughout the follicle (Bachmann and Jennings, 2010; Heesters et al., 2016). Important to this antigen-trafficking process is the subcapsular sinus macrophage (SSM), which lines the lymph node periphery and can mediate antigen transport to B cell follicles, so biomaterial strategies that elevate antigen–adjuvant interactions with SSMs can improve humoral responses to vaccines (Junt et al., 2007). This effect has been shown through experiments testing synthetic TLR4 agonist glucopyranosyl lipid adjuvant (GLA) injected in a squalene emulsion (GLA-SE), which is an adjuvant currently under investigation for inclusion in tuberculosis vaccination (Desbien et al., 2016). While GLA-SE improves both humoral and cell-mediated immunity, the humoral branch of its efficacy has been shown to depend heavily on SSM uptake within the lymph node, which it effectively achieves due to its favorable lymphatic drainage upon intramuscular injection and unique properties of squalene that strengthen the immune response (Desbien et al., 2016; Orr et al., 2013). Better control over B cell follicle access is achievable using biomaterial vaccine platforms, so these engineered approaches represent a promising way to improve humoral immune responses.

Biomaterials for Alternative Vaccine Administration Routes

Another important consideration in vaccine design is administration route. Currently, most vaccines are delivered by injecting directly into the subcutaneous or intramuscular space, allowing antigen and adjuvants to directly interface with the required immune cells. Some vaccines, such as FluMist (AstraZeneca), are delivered via alternate routes, including intranasal (FluMist), oral, or transdermal. This poses an advantage over traditional vaccine delivery requiring hypodermic needles in terms of patient compliance, cost of needles and biohazard disposal, and overall risk of disease spreading through improperly disposed needles. Biomaterials provide a highly useful strategy for this purpose as they can be formulated to optimize delivery to gut- and mucosal-associated lymphoid tissues (Fig. 2.5.10.5).

Among the noninvasive (nonneedle) delivery routes, oral administration would allow for the highest level of patient compliance, as pills and liquid suspensions are highly common drug formulations for other types of medication. However, the extremely low pH and enzymatic activity in the stomach and upper gastrointestinal tract has stunted most research in oral vaccine delivery as these conditions favor degradation of protein antigen before it is able to be taken up and presented by APCs (Russell-Jones, 2000). Here, biomaterials can be engineered to assume a protective role for the antigen or pathogen, preventing its degradation. One class of polymers that have been shown to enhance the stability of orally administered vaccines is acrylic and methacrylic acid copolymers, sold as excipients under the trade name Eudragit (Evonik). These materials offer delayed release kinetics, allowing delivery to the small and large intestines, and have been used heavily in oral vaccine research to deliver smaller antigen-containing particles into Peyer's patches, a collection of lymphoid tissues in the intestinal tract that play an important role in the mucosal immune system (Dea-Ayuela et al., 2006; Mercier et al., 2007; Xu et al., 2018; Zhu et al., 2012). Other strategies to directly target Peyer's patches include active targeting via lectin-containing biomaterials, which leverage the affinity of specialized epithelial "M" cells that coat Peyer's patches for specific lectin (glycoprotein) domains, as well as optimal size for uptake by M cells (5–10 μm) (Van Der Lubben et al., 2001; Artursson et al., 1994; Eldridge et al., 1990).

Similarly, intranasal vaccine delivery presents a promising strategy, and has already been employed in the clinic for the live-attenuated influenza vaccine under the trade-name FluMist (MedImmune). Though FluMist potentiates strong immune protection without the incorporation of biomaterials, few antigens are immunogenic enough to cause this type of response. This is partially due to rapid clearance by the mucociliary escalator, which functions to remove particles and pathogens before they arrive at



• **Figure 2.5.10.5** Current biomaterial approaches to alternate vaccine delivery routes, such as intranasal (1), microneedle (2), and oral vaccine delivery (3).

the lungs, insufficient uptake into nasal-associated lymphoid tissues (NALTs), and a lack of adjuvants specifically designed to enhance mucosal immunity (Zaman et al., 2013). Thus a variety of biomaterial adjuvants aimed to protect and deliver antigen to the NALT have been identified, including but not limited to polyethylenimine and hyaluronic acid, which exhibit a cationic surface allowing for increased endocytosis via mucosal tissue-resident APCs (Fan et al., 2015; Wegmann et al., 2012). An additional strategy is the use of mucoadhesive materials such as chitosan and esterified hyaluronic acid, which have been shown to adhere to mucus and exhibit an enhanced retention time before clearance by the mucociliary escalator, allowing for more APC processing and immune recognition (Singh et al., 2001; Primard et al., 2013).

Lastly, microneedles (MNs) present a highly promising strategy to combat all of the unfavorable aspects of traditional vaccination, not only including cost and patient compliance but also breaking the cold-chain and enhancing stability during dissemination through underdeveloped countries (Arya and Prausnitz, 2016). MNs consist of a patch containing an array of micron-scale needles that can deliver vaccines or other medication transdermally without the use of an injection. Many different MN formulations have been investigated for the application of vaccines, including hollow or coated metal needles as well as degradable polymer needles that break off after pressing into skin, which have each been widely investigated for vaccine delivery to improve patient compliance and reduce sharps waste (Choi et al., 2013; Holland et al., 2008; Kim et al., 2010; Kommareddy et al., 2012).

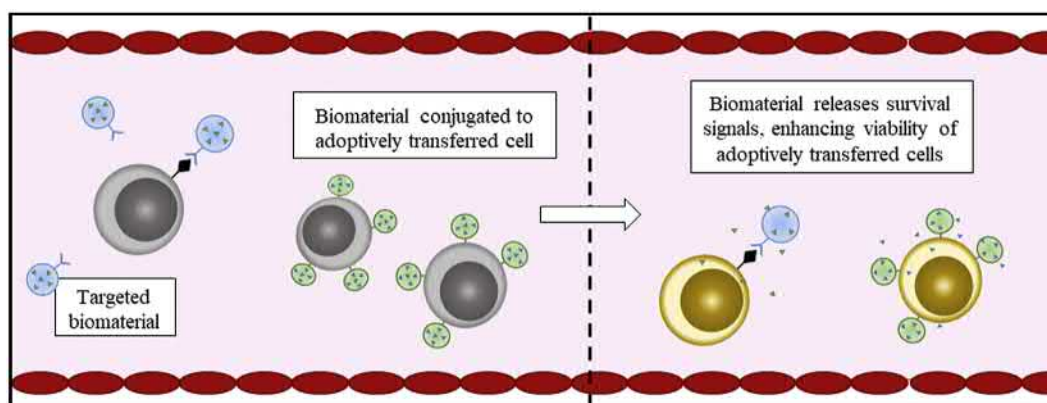
Biomaterials for Improved Vaccine Manufacturing and Accessibility

Biomaterials have been investigated for their potential to allow for long-distance shipping of stable, nonrefrigerated vaccines that would enhance global access to vaccination and lead to eradication of diseases already rare in first-world countries. Additionally, MN formulations (discussed earlier) may also play a huge role in breaking the cold-chain, and have shown safety and immunogenicity in early clinical trials (Rouphael et al., 2017; Kim et al., 2010).

In addition to enhancing vaccine stability, biomaterials are also being researched for the application of streamlined manufacturing, including formulations that could allow for the manufacturing of vaccines on demand as in the case of immediate worldwide need (Kanthamneni et al., 2012; Chen et al., 2011).

Conclusion/Future Directions

From this section, it was clear that effective vaccination is an important aspect of current and future medical challenges. Though vaccines have revolutionized medicine in the last century, boosters are still required for many vaccinations and a host of dangerous pathogens currently have no available prophylactic treatment available. Biomaterials have proven useful in many areas of medicine, particularly drug delivery, indicating their potential application to the field of vaccinology. Accordingly, many biomaterials have been engineered to enhance antigen and adjuvant exposure to lymphoid tissues from a variety of administration routes and increase



• **Figure 2.5.10.6** One strategy for biomaterial delivery to adoptively-transferred T cells *in vivo*. Biomaterial containing necessary growth and survival signals can be conjugated to a ligand that targets the adoptively transferred cells, or to cells themselves, leading to enhanced viability.

APC maturation, antigen uptake, and cross-presentation, leading to robust T and B cell responses and effective protection against pathogens of interest. Additionally, humoral immunity is of particular importance because it can facilitate prophylactic responses before host cells are infected, and the highly customizable nature of biomaterial approaches offers many advantages over traditional vaccines in this area. Both B and T cell epitopes against a target pathogen may readily be incorporated into biomaterial vaccine designs, and control over multivalency of B cell-specific epitopes in dense, repetitive patterns strengthens humoral response. Biomaterials are also being explored for previously ineffective routes of vaccine administration, which could enable safer, more thermostable, and more cost-effective vaccinations worldwide. This has led to a large database of biomaterial formulations that demonstrate success in preclinical small animal models, many of which are in the process of human clinical investigation.

Use of Biomaterials in T Cell Modulation

Introduction

T cells play a critical role in the immune response to virtually all types of disease, including but not limited to autoimmune conditions, bacterial and viral infections, and cancer. However, therapies that modulate T cells directly are underexplored. This makes the use of biomaterials for T cell targeting and direct modulation a promising solution that has been increasingly explored over the last several years. Though many therapies for a variety of applications have been shown to modulate T cell phenotype or populations via the targeting of APCs or other immune cell subtypes, this is not a form of direct T cell modulation, and will not be discussed here.

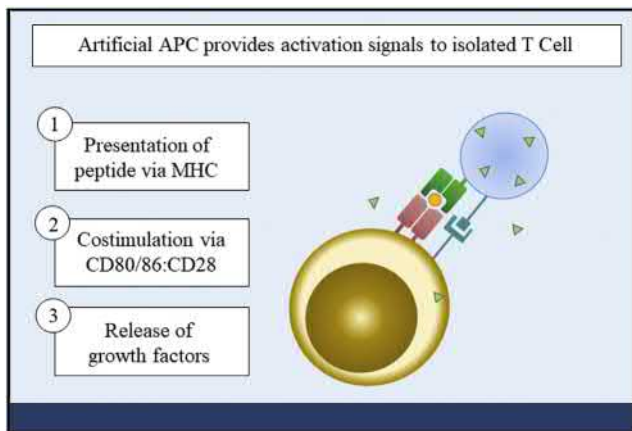
Biomaterials for Targeting and Modulation of T Cell Therapies

Despite the success of new T cell-based immunotherapies such as adoptively transferred or chimeric antigen receptor (CAR) T cells, these therapies are still not entirely effective

due to eventual cell death or exhaustion. Adoptively transferred T cells suffer from loss of effector function after reintroduction *in vivo* due to the immunosuppressive nature of the tumor microenvironment that T cells are ideally being trafficked to, and because of this both therapies often require coadministration of free cytokines, such as interleukin 2 (IL-2) (Dudley et al., 2005), to allow for improved survival. However, freely administered cytokines usually cause harsh systemic overactivation of other immune cells, leading to autoimmune-like side effects (Lerner et al., 1999; Vial and Descotes, 1992). Biomaterials have been investigated as a strategy to mitigate this current limitation to ensure higher efficacy and safety of adoptively transferred and CAR T cells *in vivo* (Fig. 2.5.10.6).

One strategy to accomplish this is to first incorporate a targeting molecule into the adoptively transferred or CAR T cell upon genetic modification to specifically deliver cytokines once the cells have been reintroduced into the patient *in vivo*. Then, a targeting antibody against the incorporated ligand can be conjugated to biomaterial liposomes containing a survival cytokine, such that free cytokine administration is not required and only the T cells of interest receive stimulation (Zheng et al., 2013). This concept could also be applied to the elimination of adoptively transferred cells that have successfully treated the tumor or other antigenic target of interest, and are presently causing symptoms of immune overactivation, as is an issue with remaining CAR T cells postcancer treatment. Though not widely studied, this concept has implications for general cell-targeted drug delivery via biomaterials.

Another more specialized strategy to modulate CAR- or adoptively transferred T cells *in vivo* is to physically conjugate a biomaterial to the T cell surface that provides an individual reservoir for cytokine survival signals such that they do not have to be freely administered. These materials have been made from the assembled protein cytokines themselves, and in some applications, disassemble and locally release to the T cell based on changing redox potential after activation (Tang et al., 2018), though this work is in a nascent stage of development thus far.



• **Figure 2.5.10.7** Mechanism of action of some *in vitro* biomaterial-based artificial APC systems. The biomaterial-based artificial APC provides peptide-MHC presentation as well as co-stimulation and growth factors to isolated T cells, allowing activation and survival.

Biomaterials for Enhanced T Cell Manufacturing

In addition to improving the *in vivo* efficacy of adoptively transferred or CAR T cells, some work has been done in improving the ability of these cells to be manufactured. Throughout the process of isolation, activation, expansion, and/or genetic modification, many of these T cells die, which introduces specific manufacturing constraints that drive up costs and make the therapy prohibitively expensive for many patients. Biomaterials have been used for *in vitro* culture and directed differentiation of a variety of other cell types (Engler et al., 2006; Pierschbacher and Ruoslahti, 1984), and thus show promise in being applied to the problem of T cell manufacturing. Though this field is in an early stage, some work has been done to improve the ability of T cells to be manufactured in a more efficient or cost-effective manner.

T cell activation depends on a specific interaction with APCs in which the T cell receptor interacts with its cognate peptide antigen bound to MHC presented by the APC, which provides activation signals, and CD28 interacts with CD80/86 on the APC, which provides survival signals. The process of T cell activation is important not only for our immune response to disease, but also especially in the case of adoptive cell therapy in which a patient's circulating T cells are taken from blood and activated and expanded *ex vivo*, which is extremely cost effective due to the difficult nature of the process. Therefore, artificial activation of T cells via biomaterials is a promising strategy to increase the efficiency of T cell manufacturing and decrease cost.

Artificial APCs have been investigated in recent literature for *ex vivo* activation and expansion of tumor-specific T cells in particular, though the concept could be used to expand any desired population of effector cells (Fig. 2.5.10.7). These artificial APCs usually consist of a combination of the peptide antigen of interest bound to MHC

for activation and anti-CD28 for survival, and have been made from common synthetic polymers such as PLGA (Steenblock et al., 2011), as well as inorganic metal formulations, including gold (Matic et al., 2013) and iron (Perica et al., 2014, 2015). In several works, magnetic particles are used to artificially cluster anti-CD3 on the particle bound to CD3 on the T cell when a magnetic field is applied, thus inducing activation, and in other applications a magnetic field is used to separate out bound and therefore activated T cells (Perica et al., 2014, 2015). Additionally, other proliferation signals such as IL-2 are artificially delivered to T cells *ex vivo* in extended release formulations to increase survival over the course of several days (Steenblock et al., 2011).

Conclusions/Future Directions

Overall, though the field of T cell modulation is still actively growing, the wide variety of diseases for which treatment requires T cell modulation as well as the thorough characterization of biomaterials for other applications will allow for rapid development of new therapies to emerge, particularly in the autoimmune disease space, and improve the safety and efficacy of current T cell cancer treatments. The ability to perform targeted modulation of any particular cell type has broader implications in the field of biomaterial-assisted drug delivery, and is being actively investigated by biomaterials researchers. Additionally, biomaterials are expected to have a large role in improving current manufacturing processes for *ex vivo* T cell expansion and genetic modification due to their current, promising role in 3D scaffolds for cell culture and differentiation, for example. In the coming years, biomaterial-based technologies for rapid, cheap, and even bedside isolation and expansion of patient-derived T cells are expected to drastically improve the accessibility of these therapies.

Use of Biomaterials to Induce Tolerance

Introduction

Previous sections of this chapter have focused on amplifying immune effector responses to antigens, but there are also many situations in which we would prefer to use biomaterials to induce immune tolerance to an antigen, rather than immunity. Controlling immune tolerance is of great interest in the treatment of autoimmune disorders such as diabetes, multiple sclerosis, and lupus, which can significantly diminish quality of life and even be fatal (Graham et al., 2013; Look et al., 2013). Current treatment options for autoimmune diseases require long-term systemic immune suppression, which can be effective, but can also cause serious side effects and weaken the body's defenses against all pathogens. Biomaterial approaches offer an alternative to systemic treatments and have the potential for much more fine-tuned and effective outcomes, many of which will be discussed in the following sections.

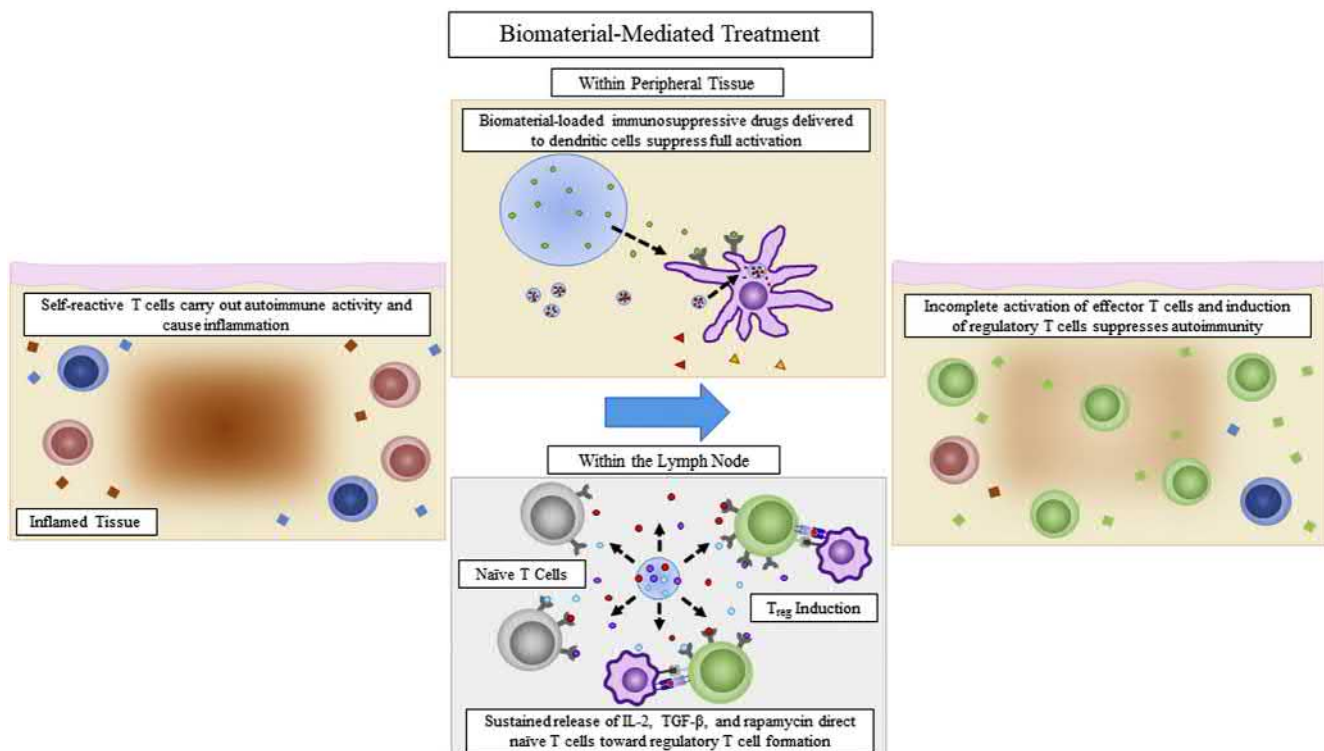
Induction of Tolerance in Autoimmune Disorders

Autoimmune diseases can be mediated through many different mechanisms of action, but are generally helper T cell controlled (Noack and Miossec, 2014; Azar et al., 1999). Helper T cells are implicated in these diseases because in the properly functioning immune system they are required to fully activate cytotoxic T cells and B cells in the majority of cases, and a subset of helper T cells known as regulatory T cells (Tregs) plays a very important role in suppression of self-reactive T cells (Kim et al., 2007). Aberrant lymphocyte behavior occurs occasionally and causes improper effector function against self-antigens, but biomaterial strategies can be used to combat this. In general, tolerance can be induced through T cell anergy or deletion, elevated Treg activity, or suppression of B cell activation to a specific antigen (Lewis and Allen, 2016). A summary of the following concepts is illustrated in Fig. 2.5.10.8.

T Cell Anergy and Deletion Through Incomplete Dendritic Cell Activation

Full activation of a T cell requires a multistep surface peptide interaction sequence with a mature DC. Critical steps in this process are the interaction of an MHC-bound antigen with the T cell receptor, and a secondary costimulatory interaction between the B7 and CD28 ligands on the DC and T cell, respectively. However, if this secondary signal is

not presented, full activation of the T cell cannot occur and the T cell can enter into an unresponsive, or anergic state as a natural tolerance mechanism (Mueller et al., 1989). DCs will only express B7 if fully activated upon their initial antigen encounter, which implicates incomplete DC activation against a target self-antigen as a potential therapeutic pathway for treatment of autoimmune diseases. This concept has been demonstrated using PLGA microparticles with surface anti-CD11c and anti-DEC205 antibodies (Lewis et al., 2012). These surface features specifically bind DC surface proteins, enabling significantly enhanced DC interactions and uptake. A series of in vitro and in vivo studies have shown that these biomaterials increase uptake and trafficking to the lymph node without causing the DC to release normal activation cytokines (Lewis et al., 2012). Biomaterial designs such as this one can be used to suppress function of specific autoreactive lymphocytes if administered at the same time as a target antigen because the antigen will be picked up by DCs in a tolerance-inducing environment (Iberg et al., 2017). A further study using microparticles encapsulating immunosuppressive drugs such as rapamycin and retinoic acid showed that DCs that took up these particles displayed reduced activation markers and resisted activation upon exposure to lipopolysaccharide, a known immune stimulant (Lewis et al., 2014). In addition, these DCs suppressed T cell activation in vitro, indicating a meaningful impact of the DC treatment on T cell effector function. These studies enable localized induction of



• **Figure 2.5.10.8** Biomaterial-mediated treatment of autoimmunity. Biomaterials loaded with immunosuppressive cytokines or drugs can take action within the lymph node to induce regulatory T cell formation or within peripheral tissue to suppress antigen presenting cell activation.

tolerance through T cell suppression, with the potential to be applied to targeted self-antigen tolerance to treat autoimmune diseases.

An alternative approach to targeted incomplete DC activation builds upon the observation that when a cell undergoes apoptosis, it releases antiinflammatory signals that suppress DC activation. This occurs as a safety mechanism in the body to prevent autoimmune activity against self-antigens released in the apoptosis process. Strategies to induce tolerance have been designed around this phenomenon by mixing self-peptides known to be involved in autoimmune disease with cells *ex vivo*, inducing apoptosis of these cells, and then injecting this solution of antiinflammatory signals with the self-peptide of interest into the body (Liu *et al.*, 2002). This technique is currently in clinical trials, but because it requires whole cells, effective scaleup is uncertain (Kontos *et al.*, 2012). An alternative acellular biomaterial strategy proposed for this problem is to instead design a fusion protein between the self-antigen of interest and a red blood cell surface-binding motif to bind the self-peptide to red blood cells already within the body and trigger DC uptake when these cells naturally go through apoptosis (Kontos *et al.*, 2012). In the human body, 1% of red blood cells naturally go through apoptosis on a daily basis, so tolerance induction of peptide bound to any given red blood cell's surface can occur fairly quickly. DCs that take up the self-antigen of interest among the lysed red blood cell debris do so in antiinflammatory signaling conditions, resulting in incomplete activation, and T cell deletion or anergy upon presentation to the self-antigen specific T cells causing the autoimmune disease (Kontos *et al.*, 2012). As this example suggests, biomaterial solutions can provide simple yet effective improvements over existing treatment options under consideration.

Elevation of Treg Activity to Induce Tolerance

Another natural tolerance mechanism in the body occurs through Treg action. These specialized T cells suppress activation and function of other cells, and as a result, reduced Treg activity is associated with decreased immune regulation, increased incidence of autoimmune disease, and transplant rejection (Cao, 2010). Options for Treg-mediated treatment include *ex vivo* expansion of Tregs followed by injection back into the body and *in situ* induction of naïve T cells toward a Treg phenotype using cytokine signaling. Of these two options, *ex vivo* expansion is more costly and time consuming, making *in situ* induction more appealing (Riley *et al.*, 2010). Still, inducing a Treg phenotype has its own challenges and requires the controlled and sustained presence of the cytokines IL-2, transforming growth factor (TGF) beta, and rapamycin, making this naturally conducive to a biomaterial approach. Successful induction of Tregs from naïve T cells has in fact been achieved *in vitro* using PLGA microparticles encapsulating IL-2, TGF-beta, and rapamycin with controlled release rates over

a 5-week period (Jhunjunwala *et al.*, 2012; McHugh *et al.*, 2015). This platform is promising because the chosen particle size causes subcutaneously injected particles to remain at the injection site, offering localized and targeted immunosuppression. In fact, additional studies have shown that these microparticles can be used to treat allergic contact dermatitis following subcutaneous microparticle injection at a skin site that has come in contact with an allergen (Balmert *et al.*, 2017). This is still a fairly new area of study and *in vivo* studies are not yet fully optimized, but *in situ* Treg control strategies made possible by biomaterials are on the horizon.

Suppression of B Cell Activation

Though much of the discussion to this point has dealt with controlling autoreactive T cells, humoral-mediated autoimmunity can also be controlled directly from the B cell source (Goodnow *et al.*, 2005). Much like DCs and T cells, B cells also have natural tolerance induction mechanisms that may be exploited through biomaterial strategies (Crocker and Varki, 2011). B cells express many suppressive surface ligands of the SIGLEC family, including CD22, that engage at later stages of B cell activation to prevent overstimulation (Crocker and Yasukawa, 2011). Experiments have shown that when a BCR and CD22 ligand are forcibly held together, CD22 effectively inhibits activation, making this an interesting therapeutic approach (Duong *et al.*, 2009). Polymers used to tether CD22 ligand and T cell-independent antigens were able to completely prevent antibody production against the antigen and even suppressed response upon free antigen rechallenge until an adjuvant was added (Duong *et al.*, 2009). This effect has also been observed for T cell-dependent antigens. Liposomal nanoparticles coated with CD22 ligand and autoreactive self-antigens implicated in hemophilia are capable of completely suppressing production of self-antigen-specific antibodies and show functional improvement in treated mice being able to form blood clots (Macauley *et al.*, 2013).

Concluding Remarks

Biomaterials find diverse applications in the induction of immune tolerance because they offer precise control over interactions between immune cells and specific antigens, and this makes them very effective at leveraging the many natural regulatory mechanisms the immune system has to offer. Successful tolerance-inducing strategies include induction of anergy or deletion in self-reactive lymphocytes, and in directing helper T cell activation toward the regulatory pathway to suppress unwanted effector function of other T cells. As was true in vaccine design, biomaterials enable engineered solutions to complex biological problems, and show promise to reshape our ability to reliably treat aberrant immune activity and autoimmune diseases in the future

References

- Adams, S., O'Neill, D.W., Nonaka, D., et al., 2008. Adjuvant using TLR7 agonist imiquimod as vaccine patients with full-length NY-ESO-1 protein immunization of malignant melanoma. *J. Immunol.* 181 (1), 776–784. <https://doi.org/10.4049/jimmunol.181.1.776>.
- Ali, O.A., Huebsch, N., Cao, L., Dranoff, G., Mooney, D.J., 2009. Infection-mimicking materials to program dendritic cells in situ. *Nat. Mater.* 8 (2), 151–158. <https://doi.org/10.1038/nmat2357>.
- Arsiwala, A., Castro, A., Frey, S., Stathos, M., Kane, R.S., 2019. Designing multivalent ligands to control biological interactions: from vaccines and cellular effectors to targeted drug delivery. *Chem. Asian J.* 14 (2), 244–255. <https://doi.org/10.1002/asia.201801677>.
- Artursson, P., Lindmark, T., Davis, S., Illum, L., 1994. Effect of chitosan on the permeability of monolayers of intestinal epithelial cells. *Pharm. Res.* 11.
- Arya, J., Prausnitz, M.R., 2016. Microneedle patches for vaccination in developing countries. *J. Control. Release* 240, 135–141. <https://doi.org/10.1016/j.jconrel.2015.11.019>.
- Azar, S.T., Tamim, H., Beyhum, H.N., et al., 1999. Type I (insulin-dependent) diabetes is a Th1- and Th2-mediated autoimmune disease. *Clin. Diagn. Lab. Immunol.* 6 (3), 2–7.
- Bachmann, M.F., Jennings, G.T., 2010. Vaccine delivery: a matter of size, geometry, kinetics and molecular patterns. *Nat. Rev. Immunol.* 10 (11), 787–796. <https://doi.org/10.1038/nri2868>.
- Bachmann, M.F., Hengartner, H., Zinkernagel, R.M., 1995. T helper cell-independent neutralizing B cell response against vesicular stomatitis virus: role of antigen patterns in B cell induction? *Eur. J. Immunol.* 25 (12), 3445–3451. <https://doi.org/10.1002/eji.1830251236>.
- Balmert, S.C., Donahue, C., Vu, J.R., Erdos, G., Falo, L.D., Little, S.R., July 2017. In vivo induction of regulatory T cells promotes allergen tolerance and suppresses allergic contact dermatitis. *J. Control. Release* 261, 223–233. <https://doi.org/10.1016/j.jconrel.2017.07.006>.
- Batista, F.D., Iber, D., Neuberger, M.S., 2001. B cells acquire antigen from target cells after synapse formation. *Nature* 411 (6836), 489–494. <https://doi.org/10.1038/35078099>.
- Bennett, N.R., Zwick, D.B., Courtney, A.H., Kiessling, L.L., 2015. Multivalent antigens for promoting B and T cell activation. *ACS Chem. Biol.* 10 (8), 1817–1824. <https://doi.org/10.1021/acscmbio.5b00239>.
- Beutner, K.R., Geisse, J.K., Helman, D., Fox, T.L., Ginkeld, A., Owens, M.L., 1999. Therapeutic response of basal cell carcinoma to the immune response modifier imiquimod 5% cream. *J. Am. Acad. Dermatol.* 41 (6), 1002–1007. [https://doi.org/10.1016/S0190-9622\(99\)70261-6](https://doi.org/10.1016/S0190-9622(99)70261-6).
- Calabro, S., Tortoli, M., Baudner, B.C., et al., 2011. Vaccine adjuvants alum and MF59 induce rapid recruitment of neutrophils and monocytes that participate in antigen transport to draining lymph nodes. *Vaccine* 29 (9), 1812–1823. <https://doi.org/10.1016/j.vaccine.2010.12.090>.
- Campbell, J.D., 2017. Development of the CpG adjuvant 1018: a case study. In: Fox, C. (Ed.), *Vaccine Adjuvants. Methods in Molecular Biology*, 1494, Humana Press, New York, NY, pp. 15–27.
- Cao, X., 2010. Regulatory T cells and immune tolerance to tumors. *Immunol. Res.* 46 (1–3), 79–93. <https://doi.org/10.1007/s12026-009-8124-7>.
- Center for Disease Control, 2018a. Excipients Included in. U.S. Vaccines.
- Center for Disease Control, 2018b. Adjuvants Help Vaccines Work Better.
- Chen, X., Fernando, G.J., Crichton, M.L., et al., 2011. Improving the reach of vaccines to low-resource regions, with a needle-free vaccine delivery device and long-term thermostabilization. *J. Control. Release* 152 (3), 349–355. <https://doi.org/10.1016/j.jconrel.2011.02.026>.
- Chen, J., Pompano, R.R., Santiago, F.W., et al., 2013. The use of self-adjuvanting nanofiber vaccines to elicit high-affinity B cell responses to peptide antigens without inflammation. *Biomaterials* 34 (34), 8776–8785. <https://doi.org/10.1016/j.biomaterials.2013.07.063>.
- Choi, H.-J., Bondy, B.J., Yoo, D.-G., Compans, R.W., Kang, S.-M., Prausnitz, M.R., 2013. Stability of whole inactivated influenza virus vaccine during coating onto metal microneedles. *J. Control. Release* 166 (2), 159–171. <https://doi.org/10.1016/j.jconrel.2012.12.002>.
- Crocker, P.R., Yasukawa, S., 2011. CD33-Related siglecs in the immune system. *Trends Glycosci. Glycotechnol.* 16 (91), 357–370. <https://doi.org/10.4052/tigg.16.357>.
- Cruse, J., Lewis, R., Wang, H., 2004. *Immunology Guidebook*, pp. 1568–1571. <https://doi.org/10.1016/B978-0-12-198382-6.50033-9>.
- Dea-Ayuela, M.A., Rama-Iñiguez, S., Torrado-Santiago, S., Bolas-Fernandez, F., 2006. Microcapsules formulated in the enteric coating copolymer Eudragit L100 as delivery systems for oral vaccination against infections by gastrointestinal nematode parasites. *J. Drug Target.* 14 (8), 567–575. <https://doi.org/10.1080/10611860600849464>.
- Desbien, A.L., Cauwelaert, N.D., Reed, S.J., et al., 2016. IL-18 and subcapsular lymph node macrophages are essential for enhanced B cell responses with TLR4 agonist adjuvants. *J. Immunol.* 197 (11), 4351–4359. <https://doi.org/10.4049/jimmunol.1600993>.
- Dudley, M.E., Wunderlich, J.R., Yang, J.C., et al., 2005. Adoptive cell transfer therapy following non-myeloablative but lymphodepleting chemotherapy for the treatment of patients with refractory metastatic melanoma. *J. Clin. Oncol.* 23 (10), 2346–2357. <https://doi.org/10.1200/JCO.2005.00.240>.
- Duong, B.H., Tian, H., Ota, T., et al., 2009. Decoration of T-independent antigen with ligands for CD22 and Siglec-G can suppress immunity and induce B cell tolerance in vivo. *J. Exp. Med.* 207 (1), 173–187. <https://doi.org/10.1084/jem.20091873>.
- Edwards, L., Ferenczy, A., Eron, L., et al., 1998. Self-administered topical 5% imiquimod cream for external anogenital warts. *Arch. Dermatol.* 134 (1), 25–30. <https://doi.org/10.1001/archderm.134.1.25>.
- Eldridge, J.H., Hammond, C.J., Meulbroeck, J.A., Staas, J.K., Gilley, R.M., Tice, T.R., 1990. Controlled vaccine release in the gut-associated lymphoid tissues. I. Orally administered biodegradable microspheres target the peyer's patches. *J. Control. Release* 11 (1–3), 205–214. [https://doi.org/10.1016/0168-3659\(90\)90133-E](https://doi.org/10.1016/0168-3659(90)90133-E).
- Engler, A.J., Sen, S., Sweeney, H.L., Discher, D.E., 2006. Matrix elasticity directs stem cell lineage specification. *Cell* 126 (4), 677–689. <https://doi.org/10.1016/j.cell.2006.06.044>.
- European Medicines Agency, 2003. Committee for Medicinal Products for Human Use (CHMP) Guideline on Adjuvants in Vaccines for Human Use Date for Coming into Operation.
- Fan, Y., Sahdev, P., Ochyl, L.J., Akerberg, J., Moon, J.J., 2015. Cationic liposome-hyaluronic acid hybrid nanoparticles for intranasal vaccination with subunit antigens. *J. Control. Release* 208, 121–129. <https://doi.org/10.1016/j.jconrel.2015.04.010>.

- Foster, S., Duvall, C.L., Crownover, E.F., Hoffman, A.S., Stayton, P.S., 2010. Intracellular delivery of a protein antigen with an endosomal-releasing polymer enhances CD8 T-cell production and prophylactic vaccine efficacy. *Bioconjug. Chem.* 21 (12), 2205–2212. <https://doi.org/10.1021/bc100204m>.
- Glenny, A.T., Pope, C.G., Waddington, H., Wallace, U., 1926. Immunological notes. XVII-XXIV. *J. Pathol. Bacteriol.* 29 (1), 31–40. <https://doi.org/10.1002/path.1700290106>.
- Goodnow, C.C., Sprent, J., Fazekas de St Groth, B., Vinuesa, C.G., 2005. Cellular and genetic mechanisms of self tolerance and autoimmunity. *Nature.* 435, 590–597. <https://doi.org/10.1038/nature03724>.
- Graham, J.G., Zhang, X., Goodman, A., et al., 2013. PLG scaffold delivered antigen-specific regulatory T cells induce systemic tolerance in autoimmune. *Tissue Eng. A.* 19 (11–12), 1465–1475. <https://doi.org/10.1089/ten.tea.2012.0643>.
- Grandjean-Laquerriere, A., Tabary, O., Jacquot, J., et al., 2007. Involvement of toll-like receptor 4 in the inflammatory reaction induced by hydroxyapatite particles. *Biomaterials* 28 (3), 400–404. <https://doi.org/10.1016/j.biomaterials.2006.09.015>.
- Grun, J.L., Maurer, P.H., 1989. Different T helper cell subsets elicited in mice utilizing two different adjuvant vehicles: the role of endogenous interleukin 1 in proliferative responses. *Cell. Immunol.* 121 (1), 134–145. [https://doi.org/10.1016/0008-8749\(89\)90011-7](https://doi.org/10.1016/0008-8749(89)90011-7).
- Harwood, N.E., Batista, F.D., 2010. Early Events in B Cell Activation 28, pp. 185–210. <https://doi.org/10.1146/annurev-immunol-030409-101216>.
- Heesters, B.A., van der Poel, C.E., Das, A., Carroll, M.C., 2016. Antigen presentation to B cells. *Trends Immunol.* 37 (12), 844–854. <https://doi.org/10.1016/j.it.2016.10.003>.
- Hemmi, H., Kaisho, T., Takeuchi, O., et al., 2002. Small anti-viral compounds activate immune cells via the TLR7 MyD88-dependent signaling pathway. *Nat. Immunol.* 3 (2), 196–200. <https://doi.org/10.1038/ni758>.
- Herbert, W.J., 1968. The mode of action of mineral-oil emulsion adjuvants on antibody production in mice. *Immunology* 14 (3), 301–318.
- Hirosue, S., Kourtis, I.C., van der Vlies, A.J., Hubbell, J.A., Swartz, M.A., 2010. Antigen delivery to dendritic cells by poly(propylene sulfide) nanoparticles with disulfide conjugated peptides: cross-presentation and T cell activation. *Vaccine* 28 (50), 7897–7906. <https://doi.org/10.1016/j.vaccine.2010.09.077>.
- Holland, D., Booy, R., Looze, F.D., et al., 2008. Intradermal influenza vaccine administered using a new microinjection system produces superior immunogenicity in elderly adults: a randomized controlled trial. *J. Infect. Dis.* 198 (5), 650–658. <https://doi.org/10.1086/590434>.
- Hudalla, G.A., Modica, J.A., Tian, Y.F., et al., 2013. A self-adjuvanting supramolecular vaccine carrying a folded protein antigen. *Adv. Healthc. Mater.* 2 (8), 1114–1119. <https://doi.org/10.1002/adhm.201200435>.
- Hudalla, G.A., Sun, T., Gasiorowski, J.Z., et al., 2014. Graded assembly of multiple proteins into supramolecular nanomaterials. *Nat. Mater.* 13 (8), 829–836. <https://doi.org/10.1038/nmat3998>.
- Hutchison, S., Benson, R.A., Gibson, V.B., Pollock, A.H., Garside, P., Brewer, J.M., 2012. Antigen depot is not required for alum adjuvanticity. *FASEB J.* 26 (3), 1272–1279. <https://doi.org/10.1096/fj.11-184556>.
- Iberg, C.A., Jones, A., Hawiger, D., 2017. Dendritic cells as inducers of peripheral tolerance. *Trends Immunol.* 38 (11), 793–804. <https://doi.org/10.1016/j.it.2017.07.007>.
- Jegerlehner, A., Storni, T., Lipowsky, G., Schmid, M., Pumpens, P., Bachmann, M.F., 2002. Regulation of IgG antibody responses by epitope density and CD21-mediated costimulation. *Eur. J. Immunol.* 32 (11), 3305–3314. [https://doi.org/10.1002/1521-4141\(200211\)32:11<3305::AID-IMMU3305>3.0.CO;2-J](https://doi.org/10.1002/1521-4141(200211)32:11<3305::AID-IMMU3305>3.0.CO;2-J).
- Jhunjunwala, S., Balmert, S.C., Raimondi, G., et al., 2012. Controlled release formulations of IL-2, TGF- β 1 and rapamycin for the induction of regulatory T cells. *J. Control. Release* 159 (1), 78–84. <https://doi.org/10.1016/j.jconrel.2012.01.013>.
- Joffre, O.P., Segura, E., Savina, A., Amigorena, S., 2012. Cross-presentation by dendritic cells. *Nat. Rev. Immunol.* 12, 557–569. <https://doi.org/10.1038/nri3254>.
- Junt, T., Moseman, E.A., Iannacone, M., et al., 2007. Subcapsular sinus macrophages in lymph nodes clear lymph-borne viruses and present them to antiviral B cells. *Nature* 450 (7166), 110–114. <https://doi.org/10.1038/nature06287>.
- Kanthamneni, N., Sharma, S., Meenach, S.A., et al., 2012. Enhanced stability of horseradish peroxidase encapsulated in acetalated dextran microparticles stored outside cold chain conditions. *Int. J. Pharm.* 431 (1–2), 101–110. <https://doi.org/10.1016/J.IJPHARM.2012.04.043>.
- Kim, J.M., Rasmussen, J.P., Rudensky, A.Y., 2007. Regulatory T cells prevent catastrophic autoimmunity throughout the lifespan of mice. *Nat. Immunol.* 8 (2), 191–197. <https://doi.org/10.1038/ni1428>.
- Kim, Y.C., Quan, F.S., Yoo, D.G., Compans, R.W., Kang, S.M., Prausnitz, M.R., 2010. Enhanced memory responses to seasonal H1N1 influenza vaccination of the skin with the use of vaccine-coated microneedles. *J. Infect. Dis.* 201 (2), 190–198. <https://doi.org/10.1086/649228>.
- Kim, Y.C., Quan, F.S., Compans, R.W., Kang, S.M., Prausnitz, M.R., 2010. Formulation and coating of microneedles with inactivated influenza virus to improve vaccine stability and immunogenicity. *J. Control. Release* 142 (2), 187–195. <https://doi.org/10.1016/J.JCONREL.2009.10.013>.
- Kochenderfer, J.N., Chien, C.D., Simpson, J.L., Gress, R.E., 2007. Maximizing CD8+ T cell responses elicited by peptide vaccines containing CpG oligodeoxynucleotides. *Clin. Immunol.* 124 (2), 119–130. <https://doi.org/10.1016/j.clim.2007.04.003>.
- Kommareddy, S., Baudner, B.C., Oh, S., Kwon, S., Singh, M., O'hagan, D.T., 2012. Dissolvable microneedle patches for the delivery of cell-culture-derived influenza vaccine antigens. *J. Pharm. Sci.* 101 (3), 1021–1027. <https://doi.org/10.1002/JPS.23019>.
- Kontos, S., Kourtis, I.C., Dane, K.Y., Hubbell, J.A., 2012. Engineering antigens for in situ erythrocyte binding induces T-cell deletion. *Proc. Natl. Acad. Sci. USA* 110 (1), E60–E68. <https://doi.org/10.1073/pnas.1216353110>.
- Lachmann, P.J., 2012. The use of antibodies in the prophylaxis and treatment of infections. *Emerg. Microb. Infect.* 1 (8), 1–5. <https://doi.org/10.1038/emi.2012.2>.
- Lanzavecchia, A., 1985. Antigen-specific interaction between T and B cells. *Nature.* 314 (6011), 537–539. <https://doi.org/10.1038/314537a0>.
- Lerner, D.M., Stoudemire, A., Rosenstein, D.L., 1999. Neuropsychiatric toxicity associated with cytokine therapies. *Psychosomatics* 40 (5), 428–435. [https://doi.org/10.1016/S0033-3182\(99\)71208-9](https://doi.org/10.1016/S0033-3182(99)71208-9).
- Lewis, J.S., Allen, R.P., 2016. An introduction to biomaterial-based strategies for curbing autoimmunity. *Exp. Biol. Med.* 241 (10), 1107–1115. <https://doi.org/10.1177/1535370216650294>.
- Lewis, J.S., Zaveri, T.D., Crooks, C.P., Keselowsky, B.G., 2012. Microparticle surface modifications targeting dendritic cells for non-activating applications. *Biomaterials* 33 (29), 7221–7232. <https://doi.org/10.1016/j.biomaterials.2012.06.049>.

- Lewis, J.S., Roche, C., Zhang, Y., et al., 2014. Combinatorial delivery of immunosuppressive factors to dendritic cells using dual-sized microspheres. *J. Mater. Chem. B* 2 (17), 2562–2574. <https://doi.org/10.1039/c3tb21460e>.
- Liu, K., Iyoda, T., Saternus, M., Kimura, Y., Inaba, K., Steinman, R.M., 2002. Immune tolerance after delivery of dying cells to dendritic cells in situ. *J. Exp. Med.* 196 (8), 1091–1097. <https://doi.org/10.1084/jem.20021215>.
- Look, M., Stern, E., Wang, Q.A., et al., 2013. Nanogel-based delivery of mycophenolic acid ameliorates systemic lupus erythematosus in mice. *J. Clin. Investig.* 123 (4), 1741–1749. <https://doi.org/10.1172/jci65907>.
- Lynn, G.M., Laga, R., Darrah, P.A., et al., 2015. In vivo characterization of the physicochemical properties of polymer-linked TLR agonists that enhance vaccine immunogenicity. *Nat. Biotechnol.* 33 (11), 1201–1210. <https://doi.org/10.1038/nbt.3371>.
- Macauley, M.S., Pfrengle, F., Rademacher, C., et al., 2013. Antigenic liposomes displaying CD22 ligands induce antigen-specific B cell apoptosis. *J. Clin. Investig.* 123 (7), 3074–3083. <https://doi.org/10.1172/JCI69187>.
- Manolova, V., Flace, A., Bauer, M., Schwarz, K., Saudan, P., Bachmann, M.F., 2008. Nanoparticles target distinct dendritic cell populations according to their size. *Eur. J. Immunol.* 38 (5), 1404–1413. <https://doi.org/10.1002/eji.200737984>.
- Marrack, P., McKee, A.S., Munks, M.W., 2009. Towards an understanding of the adjuvant action of aluminium. *Nat. Rev. Immunol.* 9 (4), 287–293. <https://doi.org/10.1038/nri2510>.
- Matic, J., Deeg, J., Scheffold, A., Goldstein, I., Spatz, J.P., 2013. Fine tuning and efficient T cell activation with stimulatory aCD3 nanoarrays. *Nano Lett.* 13 (11), 5090–5097. <https://doi.org/10.1021/nl4022623>.
- McHugh, M.D., Park, J., Urich, R., Gao, W., Horwitz, D.A., Fahmy, T.M., 2015. Paracrine co-delivery of TGF- β and IL-2 using CD4-targeted nanoparticles for induction and maintenance of regulatory T cells. *Biomaterials* 59, 172–181. <https://doi.org/10.1016/j.biomaterials.2015.04.003>.
- Mercier, G.T., Nehete, P.N., Passeri, M.F., et al., 2007. Oral immunization of rhesus macaques with adenoviral HIV vaccines using enteric-coated capsules. *Vaccine* 25 (52), 8687–8701. <https://doi.org/10.1016/j.vaccine.2007.10.030>.
- Moon, J.J., Suh, H., Bershteyn, A., et al., 2011. Interbilayer-cross-linked multilamellar vesicles as synthetic vaccines for potent humoral and cellular immune responses. *Nat. Mater.* 10, 243–251. <https://doi.org/10.1038/nmat2960>.
- Moon, J.J., Suh, H., Li, A.V., et al., 2012. Enhancing humoral responses to a malaria antigen with nanoparticle vaccines that expand Tfh cells and promote germinal center induction. *Proc. Natl. Acad. Sci. USA* 109 (4), 1080–1085. <https://doi.org/10.1073/pnas.1112648109>.
- Mosser, D.M., Edwards, J.P., 2008. Exploring the full spectrum of macrophage activation. *Nat. Rev. Immunol.* 8 (12), 958–969. <https://doi.org/10.1038/nri2448>.
- Mueller, D.L., Jenkins, M.K., Schwartz, R.H., 1989. Clonal expansion versus functional clonal inactivation: a costimulatory signaling pathway determines the outcome of T cell antigen receptor occupancy. *Annu. Rev. Immunol.* 7 (1), 445–480. <https://doi.org/10.1146/annurev.iy.07.040189.002305>.
- Mueller, S.N., Tian, S., DeSimone, J.M., 2015. Rapid and persistent delivery of antigen by lymph node targeting PRINT nanoparticle vaccine carrier to promote humoral immunity. *Mol. Pharm.* 12 (5), 1356–1365. <https://doi.org/10.1021/mp500589c>.
- Nakamura, T., Moriguchi, R., Kogure, K., Shastri, N., Harashima, H., 2008. Efficient MHC class I presentation by controlled intracellular trafficking of antigens in octarginine-modified liposomes. *Mol. Ther.* 16 (8), 1507–1514. <https://doi.org/10.1038/mt.2008.122>.
- Noack, M., Miossec, P., 2014. Th17 and regulatory T cell balance in autoimmune and inflammatory diseases. *Autoimmun. Rev.* 13 (6), 668–677. <https://doi.org/10.1016/j.autrev.2013.12.004>.
- Orr, M.T., Fox, C.B., Baldwin, S.L., et al., 2013. Adjuvant formulation structure and composition are critical for the development of an effective vaccine against tuberculosis. 172 (1), 190–200. <https://doi.org/10.1016/j.jconrel.2013.07.030>. (Adjuvant).
- Perica, K., Tu, A., Richter, A., Bieler, J.G., Edidin, M., Schneck, J.P., 2014. Magnetic field-induced T cell receptor clustering by nanoparticles enhances T cell activation and stimulates antitumor activity. *ACS Nano* 8 (3), 2252–2260. <https://doi.org/10.1021/nn405520d>.
- Perica, K., Bieler, J.G., Schütz, C., et al., 2015. Enrichment and expansion with nanoscale artificial antigen presenting cells for adoptive immunotherapy. *ACS Nano* 9 (7), 6861–6871. <https://doi.org/10.1021/acsnano.5b02829>.
- Pierschbacher, M.D., Ruoslahti, E., 1984. Cell attachment activity of fibronectin can be duplicated by small synthetic fragments of the molecule. *Nature*. 309, 30–33. <https://doi.org/10.1038/309030a0>.
- Primard, C., Poecheim, J., Heuking, S., Sublet, E., Esmaeili, F., Borchard, G., 2013. Multifunctional PLGA-based nanoparticles encapsulating simultaneously hydrophilic antigen and hydrophobic immunomodulator for mucosal immunization. *Mol. Pharm.* 10 (8), 2996–3004. <https://doi.org/10.1021/mp400092y>.
- Purcell, A.W., McCluskey, J., Rossjohn, J., 2007. More than one reason to rethink the use of peptides in vaccine design. *Nat. Rev. Drug Discov.* 6 (5), 404–414. <https://doi.org/10.1038/nrd2224>.
- Rappuoli, R., Mandl, C.W., Black, S., De Gregorio, E., 2011. Vaccines for the twenty-first century society. *Nat. Rev. Immunol.* 11 (12). <https://doi.org/10.1038/nri3085>.
- Reddy, S.T., Van Der Vlies, A.J., Simeoni, E., et al., 2007. Exploiting lymphatic transport and complement activation in nanoparticle vaccines. *Nat. Biotechnol.* 25 (10), 1159–1164. <https://doi.org/10.1038/nbt1332>.
- Renaudet, O., BenMohamed, L., Dasgupta, G., Bettahi, I., Dumy, P., 2008. Towards a self-adjuvanting multivalent B and T cell epitope containing synthetic glycolipopeptide cancer vaccine. *ChemMedChem* 3 (5), 737–741. <https://doi.org/10.1002/cmdc.200700315>.
- Riley, J.L., June, C.H., Blazar, B.R., 2010. Human T regulatory cell therapy: take a billion or so and call me in the morning. *Immunity* 30 (5), 656–665. <https://doi.org/10.1016/j.immuni.2009.04.006>.
- Rouphael, N.G., Paine, M., Mosley, R., et al., 2017. The safety, immunogenicity, and acceptability of inactivated influenza vaccine delivered by microneedle patch (TIV-MNP 2015): a randomised, partly blinded, placebo-controlled, phase 1 trial. *Lancet* 390 (10095), 649–658. [https://doi.org/10.1016/S0140-6736\(17\)30575-5](https://doi.org/10.1016/S0140-6736(17)30575-5).
- Rudra, J.S., Mishra, S., Chong, A.S., et al., 2012. Self-assembled peptide nanofibers raising durable antibody responses against a malaria epitope. *Biomaterials* 33 (27), 6476–6484. <https://doi.org/10.1016/j.biomaterials.2012.05.041>.
- Russell-Jones, G.J., 2000. Oral vaccine delivery. *J. Control Release* 65 (1–2), 46–54. [https://doi.org/10.1016/S0168-3659\(99\)00231-X](https://doi.org/10.1016/S0168-3659(99)00231-X).

- Shen, H., Ackerman, A.L., Cody, V., et al., 2006. Enhanced and prolonged cross-presentation following endosomal escape of exogenous antigens encapsulated in biodegradable nanoparticles. *Immunology* 117 (1), 78–88. <https://doi.org/10.1111/j.1365-2567.2005.02268.x>.
- Singh, M., Briones, M., O'Hagan, D.T., 2001. A novel bioadhesive intranasal delivery system for inactivated influenza vaccines. *J. Control. Release* 70 (3), 267–276. [https://doi.org/10.1016/s0168-3659\(00\)00330-8](https://doi.org/10.1016/s0168-3659(00)00330-8).
- Steenblock, E.R., Fadel, T., Labowsky, M., Pober, J.S., Fahmy, T.M., 2011. An artificial antigen-presenting cell with paracrine delivery of IL-2 impacts the magnitude and direction of the T cell response. *J. Biol. Chem.* 286 (40), 34883–34892. <https://doi.org/10.1074/jbc.M111.276329>.
- Tam, J.P., 1988. Synthetic peptide vaccine design: synthesis and properties of a high-density multiple antigenic peptide system (solid-phase peptide synthesis/peptide antigen/antipeptide antibody). *Proc. Natl. Acad. Sci. USA.* 85, 5409–5413. <https://doi.org/10.1073/pnas.85.15.5409>.
- Tam, J.P., Clavijo, P., Lu, Y., Nussenzweig, V., Nussenzweig, R., Zavala, F., 1990. Incorporation of T and B epitopes of the circumsporozoite protein in a chemically defined synthetic vaccine against malaria. *J. Exp. Med.* 171 (1), 299–306. <https://doi.org/10.1084/jem.171.1.299>.
- Tang, L., Zheng, Y., Melo, M.B., et al., 2018. Enhancing T cell therapy through TCR-signaling-responsive nanoparticle drug delivery. *Nat. Biotechnol.* 36 (8), 707–716. <https://doi.org/10.1038/nbt.4181>.
- Thomas, S.N., van der Vlies, A.J., O'Neil, C.P., et al., 2011. Engineering complement activation on polypropylene sulfide vaccine nanoparticles. *Biomaterials* 32 (8), 2194–2203. <https://doi.org/10.1016/j.biomaterials.2010.11.037>.
- Thomas, S.N., Vokali, E., Lund, A.W., Hubbell, J.A., Swartz, M.A., 2014. Targeting the tumor-draining lymph node with adjuvanted nanoparticles reshapes the anti-tumor immune response. *Biomaterials* 35 (2), 814–824. <https://doi.org/10.1016/j.biomaterials.2013.10.003>.
- Toda, M., Kitazawa, T., Hirata, I., Hirano, Y., Iwata, H., 2008. Complement activation on surfaces carrying amino groups. *Biomaterials* 29 (4), 407–417. <https://doi.org/10.1016/j.biomaterials.2007.10.005>.
- Toellner, K.M., Jenkinson, W.E., Taylor, D.R., et al., 2002. Low-level hypermutation in T cell-independent germinal centers compared with high mutation rates associated with T cell-dependent germinal centers. *J. Exp. Med.* 195 (3), 383–389. <https://doi.org/10.1084/jem.20011112>.
- U.S. Dept. of Health and Human Services, 2017.
- Van Der Lubben, I.M., Verhoef, J.C., Van Aelst, A.C., Borchard, G., Junginger, H.E., 2001. Chitosan microparticles for oral vaccination: preparation, characterization and preliminary in vivo uptake studies in Murine Peyer's patches. *Biomaterials* 22 (7), 687–694. [https://doi.org/10.1016/S0142-9612\(00\)00231-3](https://doi.org/10.1016/S0142-9612(00)00231-3).
- Varypataki, E.M., Silva, A.L., Barnier-Quer, C., Collin, N., Ossendorp, F., Jiskoot, W., 2016. Synthetic long peptide-based vaccine formulations for induction of cell mediated immunity: a comparative study of cationic liposomes and PLGA nanoparticles. *J. Control. Release* 226, 98–106. <https://doi.org/10.1016/j.jconrel.2016.02.018>.
- Vial, T., Descotes, J., 1992. Clinical toxicity of interleukin-2. *Drug Saf.* 7 (6), 417–433. <https://doi.org/10.2165/00002018-199207060-00004>.
- Vos, Q., Lees, A., Wu, Z.Q., Snapper, C.M., Mond, J.J., 2000. B-cell activation by T-cell-independent type 2 antigens as an integral part of the humoral immune response to pathogenic microorganisms. *Immunol. Rev.* 176 (1), 154–170. <https://doi.org/10.1034/j.1600-065X.2000.00607.x>.
- Wan, Z., Chen, X., Chen, H., et al., 2015. The activation of IgM- or isotype-switched IgG- and IgE-BCR exhibits distinct mechanical force sensitivity and threshold. *Elife* 4, 1–24. <https://doi.org/10.7554/elife.06925>.
- Wegmann, F., Gartlan, K.H., Harandi, A.M., et al., 2012. Polyethyleneimine is a potent mucosal adjuvant for viral glycoprotein antigens. *Nat. Biotechnol.* 30 (9), 883–888. <https://doi.org/10.1038/nbt.2344>.
- Wen, Y., Collier, J.H., 2015. Supramolecular peptide vaccines: tuning adaptive immunity. *Curr. Opin. Immunol.* 35, 73–79. <https://doi.org/10.1016/j.coi.2015.06.007>.
- World Health Organization, 2009. State of the World's Vaccines and Immunization. http://vaccine-safety-training.org/tl_files/vs/pdf/who_ivb_09_10_eng.pdf.
- World Health Organization, 2015. Immunization in practice: The Vaccine Cold Chain. https://www.who.int/immunization/documents/IIP2015_Module2.pdf.
- Xu, B., Zhang, W., Chen, Y., Xu, Y., Wang, B., Zong, L., 2018. Eudragit® L100-coated mannosylated chitosan nanoparticles for oral protein vaccine delivery. *Int. J. Biol. Macromol.* 113, 534–542. <https://doi.org/10.1016/j.ijbiomac.2018.02.016>.
- Yang, D., Jones, K.S., 2009. Effect of alginate on innate immune activation of macrophages. *J. Biomed. Mater. Res. A* 90A (2), 411–418. <https://doi.org/10.1002/jbm.a.32096>.
- Yuba, E., Kojima, C., Harada, A., Tana, C., Watarai, S., Kono, K., 2010. pH-Sensitive fusogenic polymer-modified liposomes as a carrier of antigenic proteins for activation of cellular immunity. *Biomaterials* 31 (5), 943–951. <https://doi.org/10.1016/j.biomaterials.2009.10.006>.
- Yuseff, M-I., Pierobon, P., Reversat, A., Lennon-Dumenil, A.-M., 2013. How B cells capture, process and present antigens: a crucial role for cell polarity. *Nat. Rev. Imm.* 13 (7), 475–486. <https://doi.org/10.1038/nri3469>.
- Zaman, M., Chandrudu, S., Toth, I., 2013. Strategies for intranasal delivery of vaccines. *Drug Deliv. Transl. Res.* 3 (1), 100–109. <https://doi.org/10.1007/s13346-012-0085-z>.
- Zeng, Y., Yi, J., Wan, Z., et al., 2015. Substrate stiffness regulates B-cell activation, proliferation, class switch, and T-cell-independent antibody responses in vivo. *Eur. J. Immunol.* 45 (6), 1621–1634. <https://doi.org/10.1002/eji.201444777>.
- Zheng, Y., Stephan, M.T., Gai, S.A., Abraham, W., Shearer, A., Irvine, D.J., 2013. In vivo targeting of adoptively transferred T-cells with antibody- and cytokine-conjugated liposomes. *J. Control. Release* 172 (2), 426–435. <https://doi.org/10.1016/j.jconrel.2013.05.037>.
- Zhu, Q., Talton, J., Zhang, G., et al., 2012. Large intestine-targeted, nanoparticle-releasing oral vaccine to control genitoretal viral infection. *Nat. Med.* 18, 1291–1296. <https://doi.org/10.1038/nm.2866>.

Exercises

1. The antigen included in a vaccine for Virus A is a protein present on the virus' surface. What "type" of vaccine is it? List the advantages and disadvantages of this kind of vaccine, and list several reasons why other types of vaccines may be unsuitable for immunizing against Virus A.
 - The vaccine is likely a subunit vaccine, which only include a component of the original pathogen (protein, polysaccharide) as the antigen. Other types of vaccines mentioned in the text are live/attenuated and inactivated whole pathogen, and toxoid vaccines, which include either the whole pathogen or a toxic byproduct as antigen.
 - These other vaccine subtypes may be unsuitable if Virus A is too virulent to be included in live-attenuated form, or if it does not produce a toxic byproduct that can be immunized against.
 - Advantages: Subunit vaccines are very safe, meaning they may be administered to the elderly and immunocompromised versus other vaccine types. Additionally, they immunize against a specific epitope, meaning that the resulting immune response can be more carefully controlled.
 - Disadvantages: Immune responses with subunit vaccines tend to be shorter-lived and can require additional boosters.
2. List several of the ways in which Alum improves the efficacy of currently approved vaccines as an adjuvant, and suggest an alternate biomaterial strategy for each.
 - Extended release of adsorbed antigen: Strategies may include conjugation or adsorption of antigen to the surface of or encapsulation within a biomaterial particle or surface, such as a nano/microparticle, or to/within a depot-forming biomaterial substrate. Additional strategies could include degradable biomaterial formulations, linkages, etc.
 - Protection of antigen: Strategies listed above and below could accomplish protection of antigen, particularly encapsulation of antigen in biomaterial particle or depot.
 - Formation of depot (controversial, though is a valid answer): Injectable gels or polymeric matrices are strategies that would allow formation of a depot at the injection site.
 - Attraction of immune cells to site of injection: Use of immunogenic biomaterials such as alginate or hydroxyapatite (mentioned in the text) to induce a local immune response and attract additional immune cells.
3. Below are several components of a currently approved vaccine. For each of these components, list a biomaterial design that could enhance the safety or efficacy of the vaccine. Please use information from the chapter, or cite if obtained from an outside source.
 - a. Whole inactivated virus (antigen)
 - b. Adjuvant
 - c. Stabilizing agents and preservatives
 - Answers may vary, this question is designed to be open-ended.
 - Antigen: More control could be exerted over an inactivated vaccine in terms of antigen presentation by incorporating a subunit from the pathogen into a biomaterial nanoparticle, provided that the pathogen has an immunogenic characteristic peptide. Additionally, this antigen could be conjugated to a biomaterial for enhanced delivery to APCs, or encapsulated within for added protection from proteases. Use of materials that degrade in the endosomal environment (low pH, ROS, reductive) could allow for enhanced antigen presentation and cross-presentation. Additionally, antigen could be incorporated within a depot-forming material for slow release from the injection site.
 - Adjuvant: Similarly, adjuvant could be incorporated into the same biomaterial nanocarrier as the antigen for co-delivery to the same APC in order to further enhance maturation and presentation/cross-presentation, or incorporated into the depot-forming material for extended release.
 - Stabilizing agents and preservatives: Typical vaccines are comprised of several excipients that extend the life of the antigen. Incorporating a biomaterial into the vaccine that protects or encapsulates the antigen could allow for stabilization such that fewer preservatives are needed, improving the safety of the vaccine as well as the efficacy as the antigen or pathogen is protected until it reaches its cellular target.
4. Your lab aims to design a vaccine that eliminates the need for multiple doses. List several broad strategies that could be utilized to accomplish this.
 - Stronger activation of immune system by targeted delivery to APCs. This can be accomplished using depot-forming materials, or nano/micro-particulate carriers to protect and co-deliver antigen and adjuvant.
 - Use of biomaterial that adjuvants the immune system itself.
 - Extended release formulation. This can be accomplished with depot-forming materials, slow-degrading polymers that allow protection of antigen for long periods of time.
 - Other answers may be acceptable provided they are reasonable or discussed in the chapter.
5. An existing vaccine is needed in an underdeveloped nation without adequate refrigeration or access to medical professionals, and thus needs to be reformulated in order ensure stability in a new environment.
 - a. List three engineering constraints of this new vaccine, and how biomaterials could provide a solution.
 - b. Design a formulation using specific biomaterials listed in this Chapter or in the literature (please cite if obtained from an outside source).

- 1) The vaccine needs to be stable without refrigeration, meaning it must be formulated to allow the antigen to be stable in a range of temperatures. Biomaterials could be used to stabilize the antigen by encapsulating it and thus protecting it from its environment, potentially allowing a lyophilized version to be utilized until delivering to patients. A microneedle strategy could be employed here for the above reasons.
 - 2) The vaccine should be formulated in a manner that avoids the use of medical professionals. Biomaterials can help with this by potentially allowing for oral administration in pill form, which is easy and highly portable. It also allows breaking of the cold chain.
 - 3) The vaccine should be long-lasting so that patients do not have to travel long distances for additional boosters. This can be accomplished by extended release formulations, biomaterials that protect antigen from degradation, or materials that allow for direct delivery to APCs.
 - Design a formulation using specific biomaterials listed in the Chapter: Answers will vary, this question is designed to be open-ended.
6. Say you are looking to engineer a biomaterial therapy that eliminates adoptively transferred T cells in a patient's body after they are cured. Using strategies outlined in the chapter or in literature, hypothesize a biomaterial strategy that could accomplish this.
- Similar to providing growth/survival factors to adoptively transferred cells *ex vivo*, the cells could be altered to express a unique marker that is targetable. At the desired time, one could administer a biomaterial containing 1) factors that would deplete the cells and 2) a targeting domain that is specific for the unique marker. However, there may be a variety of answers.
7. You are developing a new prophylactic vaccine in a mouse model and performing tests to assess its efficacy. Experiments show that your vaccine is not very effective in its current formulation. You check antibody titers in the blood and discover that insufficient quantities of antibody that can bind your pathogen are being produced.
- a. Why are antibody levels in the blood of interest when investigating prophylactic immunity?
 - b. How might you modify your vaccine formulation to increase its potential to induce antibody production?
- Prophylactic immunity is intended to prevent damage from a pathogen before it even begins, which can be achieved if the pathogen is neutralized before it has the ability to harm cells and is still within the extracellular space. The best way to achieve effective prophylactic immunity against a pathogen is to have B cells that have already been exposed to it producing antibodies that bind to specific epitopes on that pathogen so that it can be neutralized. These antibodies circulate through the body and initiate neutralization of the pathogen very quickly upon encountering it.
- Your vaccine can be designed to increase its potential to activate B cells by building antigenic components of you target pathogen into a biomaterial with multivalency of B cell epitopes and incorporation of T cell-specific antigens also associated with that pathogen to engage helper T cells in B cell activation. Including an adjuvant or using a different type of adjuvant if already using one may also be valuable.
8. Describe how biomaterials may be engineered to bias immune activation toward a humoral response or toward a cytotoxic T cell (cell-mediated) response.
- Biomaterial vaccines designed with antigen multivalency and antigens associated with linked recognition may help stimulate B cell activation and increase humoral response. Designs with biomaterial carriers that degrade at endosomal pH or in the presence of endolysosomal lipases can increase the incidence of endosomal escape, resulting in more cross presentation by APCs and enhanced activation of cytotoxic T cells.
9. List the methods of tolerance induction discussed in this chapter. Would any of these treatments be compatible in combination with each other? Why or why not?
- Incomplete dendritic cell activation causing T cell anergy or deletion
 - Elevation of Treg activity
 - Suppression of B cell activation
 - Yes, some of these treatments could be used in combination with each other because they act upon different stages of the adaptive immune response and on different cell types. For example, biomaterials administered to suppress full activation of dendritic cells could reduce the priming of new self-antigen specific effector T cells, while simultaneous treatment with biomaterials releasing IL-2, TGF-beta, and rapamycin could further direct T cells in the lymph node toward Treg function.
10. Look up an autoimmune disease of your choice and identify the mechanism of action for this disease (what is the biological cause of the disease or its symptoms?). What current treatment options are available? How might you design a biomaterial to induce tolerance in a way that improves upon these treatments?
- Answers will vary – this is meant to be open ended to stimulate independent study of ways biomaterials can improve the current state of medical treatment.

2.5.11

Biomaterials-Based Model Systems to Study Tumor–Microenvironment Interactions

BRITTANY E. SCHUTRUM^{1,*}, MATTHEW A. WHITMAN^{1,*}, CLAUDIA FISCHBACH^{1,2}

¹Nancy E. and Peter C. Meinig School of Biomedical Engineering, Cornell University, Ithaca, NY, United States

²Kavli Institute at Cornell for Nanoscale Science, Cornell University, Ithaca, NY, United States

Introduction

Cancer is the second leading cause of death, but treatment options remain limited. Statistically, each individual has a 38% chance of developing some form of cancer in his/her lifetime (Noone et al., 2018), and 18 million new cases were diagnosed worldwide in 2018 alone (Bray et al., 2018). In addition, cancer is associated with a significant economic burden and costs \$1.16 trillion per year globally (WHO, 2018). These numbers become even more alarming considering that the incidence of cancer significantly increases with aging and that the number of Americans ages 65 and older is projected to more than double within the next 50 years (Mather et al., 2015). Despite significant research into the mechanisms underlying cancer, clinical outcomes have improved only slightly over the past decades, which is in contrast to other medical conditions where an increase in knowledge has more directly advanced patient prognosis (Benjamin et al., 2017; Cronin et al., 2018).

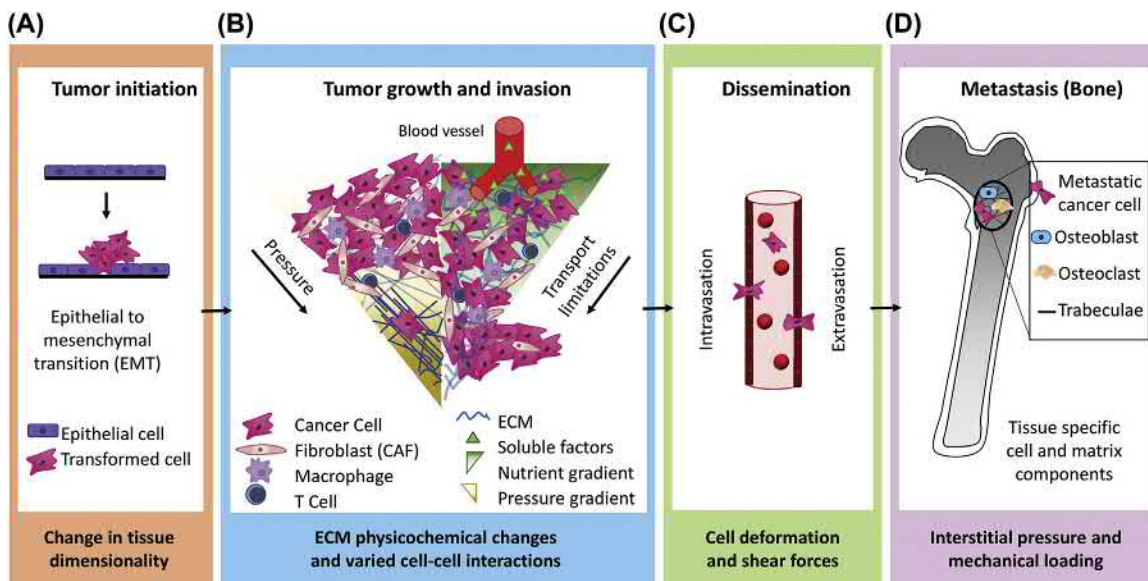
Cancer is traditionally thought to be caused by genetic abnormalities, but it is now clear that changes to the cells' microenvironment are equally important. Indeed, biochemical and biophysical perturbations of the tumor microenvironment (TME) including altered cell–cell and cell–extracellular matrix (ECM) interactions as well as perturbed transport and mechanical properties promote tumorigenesis by altering both the cells' phenotype and genotype (Bissell, 2007). For example, interactions of tumor cells with their surrounding ECM have been found to influence DNA damage responses with functional implications

for DNA repair and thus, disease development (Hodkinson et al., 2006; Lewis et al., 2002).

Despite increasing appreciation of the microenvironment's role in regulating cancer development and progression, most in vitro studies still utilize 2D cell culture techniques originally pioneered in the early 20th century (Weigelt et al., 2014). The traditional approach of growing immortalized cancer cell lines as a monolayer on a Petri dish is often preferred as an easy way to expand, harvest, genotype, image, or treat a large number of cells with therapeutics. However, reducing the complexity of tumor models overlooks the importance of microenvironmental conditions and their impact on tumor heterogeneity, in regulating the pathogenesis, and therapeutic response of cancer. These shortcomings and the fact that cancers and the TME evolve over time may help explain why many anticancer compounds show promise in vitro, but often fail in vivo (Breslin and O'Driscoll, 2013).

Biomaterials are now increasingly used in combination with tissue engineering, microfabrication, or 3D printing technologies to create physiologically relevant model systems for cancer studies. For example, various types of biomaterials from natural and synthetic origins, and modifications thereof, not only allow recapitulating cancer-specific ECM composition, structure, and mechanics, but also readily permit coculture with heterogeneous cell populations and incorporation of vascular conduits. Furthermore, utilizing biomaterials together with biomanufacturing and body-on-a-chip approaches provides emerging opportunities to mimic both local phenomena and systemic signaling that can influence cancer development, progression, and therapy response. As such, biomaterials-based, engineered model systems provide

*These authors contributed equally.



• **Figure 2.5.11.1** Microenvironmental changes during different stages of tumorigenesis. Carcinomas including breast, prostate, skin, and lung cancer all initiate in epithelial tissues. (A, B) Primary tumor development involves uncontrolled growth that leads to changes in tissue dimensionality and epithelial-to-mesenchymal transition (EMT) as well as stromal cell recruitment [e.g., cancer-associated fibroblasts (CAFs) and various immune cells (e.g., macrophages and T-cells)] and ECM remodeling. (B) These collective changes modulate blood vessel functions and increase intratumoral pressure both contributing to varied mass transport and, thus, gradients of nutrients and soluble factors. During invasion tumor cells migrate into adjacent healthy tissues using both single and collective cell migration modes. (C) Following intravasation into blood or lymphatic vessels, tumor cells travel through the circulation where they are exposed to shear forces. (D) After extravasation and dissemination to distant metastatic sites such as the bone, lungs, or the brain they may remain dormant for variable periods of time allowing them to evade therapy. However, local changes to their microenvironment (e.g., cellular composition or mechanical stimuli) can activate dormant tumor cells and enable the growth of metastatic tumors at these distant sites.

relevant platforms for basic and translational research and offer potential for patient-specific analysis of cancer malignancy and drug response in precision medicine settings.

This chapter will outline the biological, physical, and chemical changes intrinsic to the cancer microenvironment motivating critical design parameters for physiologically relevant tumor models. Subsequently, it will describe specific examples of natural and (semi-)synthetic materials and their respective advantages and disadvantages for tumor engineering. Finally, specific examples of biomaterials-based, state-of-the-art model systems will be described as well as opportunities for advanced applications of such systems in cancer research and drug testing.

Biological Design Considerations

Cancer is a group of diseases classified by an overproliferation of cells that ultimately results in their invasion of surrounding normal host tissue and spreading to distant sites in a process called metastasis (Fig. 2.5.11.1). This chapter focuses on carcinomas, which arise from epithelial tissues and are the most commonly diagnosed cancer type, but much of its content can be applied more broadly.

Tissue Dimensionality

The most fundamental biological adaptation in cancer cells is sustained proliferation, i.e., the ability of cells to divide

independent of the presence of signaling molecules required for normal cell growth (Hanahan and Weinberg, 2011). Due to the resulting increase in volume, tumors lose many physical, epithelial monolayer-associated growth constraints and experience a disruption of their basement membrane during a process involving epithelial-to-mesenchymal transition (EMT) (Fig. 2.5.11.1A) (Kalluri and Weinberg, 2009). Dimensional changes to a cell's environment, as in the change from a 2D epithelial sheet to a 3D tumor, have profound effects on cell behavior, signaling, response to therapy, and cause phenotypic changes in the tumor cells themselves (Bissell, 2007; dit Faute et al., 2002; Fischbach et al., 2009).

Transport Phenomena and Interstitial Pressure

Because of the proliferation-induced change in tissue dimensionality and rapid increase in size, many tumors quickly outgrow the nutritive capacity of existing vasculature (Fig. 2.5.11.1B). The resulting deficit in nutrients and oxygen supply and accumulation of metabolic byproducts exposes cancer cells to hypoxic, acidic, and stressful conditions (Vaupelet et al., 1989). Consequently, they often undergo a metabolic shift, known as the Warburg effect, where glycolysis is used to generate energy even in the presence of oxygen, in turn lowering microenvironmental pH through production of lactic acid (Hsu and Sabatini, 2008). Limited

• BOX 2.5.11.1 Tumor-Associated ECM Remodeling

Stromal cells are the primary mediators of protumorigenic ECM remodeling by altering both the biological and physical properties of the ECM (Lee et al., 2011). In particular, CAFs deposit increased amounts of collagen I, II, III, V, and IX, fibronectin, and heparan sulfate proteoglycans (Chandler et al., 2011; Lu et al., 2012) altering the composition of the ECM during tumor progression. They also release growth factors and cytokines and ECM remodeling enzymes including matrix-metalloproteinases (MMPs) (Gaggioli et al., 2007; Kalluri, 2016). CAFs are highly contractile cells that exert forces on the ECM. These forces contribute to the alignment of tumor-associated collagen fibers perpendicularly to the tumor boundary in invasive tumors (Conklin et al., 2011). CAFs can pull, stretch, and soften the basement membrane, enabling primary tumor invasion in an MMP-independent manner (Glentis et al., 2017). When CAFs exert tension on fibronectin fibers they can expose cryptic binding sites that modulate signaling directly or via differential sequestration of cytokines and growth factors (Arnoldini et al., 2017; Ortiz Franyuti et al., 2018).

vascularization also increases fluid pressure within a tumor, which in turn can alter cell malignancy and responsiveness to therapeutics (Nathan et al., 2005). Increased interstitial pressure can also limit solute transport via compression of blood and lymphatic vessels further fueling tumor progression and therapy resistance (Martin et al., 2016).

ECM Physicochemical Properties

Cancer-associated changes in ECM composition, structure, and mechanical properties are primarily mediated by stromal cells (Naba et al., 2012). Myofibroblasts—often referred to as cancer-associated fibroblasts (CAFs)—deposit fibrillar networks of ECM proteins, which they modify by proteolytic remodeling and force-mediated tension (Box 2.5.11.1; Fig. 2.5.11.1B). The resulting increase in ECM fiber thickness, alignment, and stiffness correlates with a more malignant and invasive tumor phenotype (Conklin et al., 2011; Levental et al., 2009). Indeed, changes in collagen fiber alignment and tumor stiffness direct tumor cell invasion by modulating cellular mechanosignaling (Provenzano et al., 2006; Wang et al., 2014) and can be useful prognostically (Conklin et al., 2011). Tumor-associated, ECM-dependent differences in tissue density and stiffness can be detected clinically via mammography and/or elastography and promote tumor cell malignancy independent of other factors (Fischer et al., 2013; Li et al., 2005; Paszek et al., 2005). While the mechanical properties of tumors are often described by their elastic moduli, tissues and their ECM are not linearly elastic but rather behave like viscoelastic materials, a difference that impacts disease progression and thus, should be considered in model design (Chaudhuri et al., 2016; Gong et al., 2018).

Immunological Changes

Typically, a properly functioning immune system is well prepared to protect against the development of cancer.

However, many cancers have evolved alternative mechanisms that allow them to avoid immune destruction and even hijack the body's natural defense mechanisms, such as inflammatory or immunomodulatory signals, to enhance tumorigenesis (Grivennikov et al., 2010). For example, some immune cells secrete factors that promote invasion or angiogenesis, whereas others suppress the cytotoxic activity of other immune cells or upregulate enzymes that degrade the matrix and promote tumor spreading. A prominent example is M2-type macrophages, which, unlike their M1 counterparts, are involved in wound healing and increase tumor progression by remodeling ECM, inhibiting inflammation, and stimulating vasculogenesis (Mantovani et al., 1992; Pollard, 2004). Importantly, changes in substrate structure and mechanical properties can directly influence macrophage phenotype (Gruber et al., 2018; McWhorter et al., 2013; Springer and Fischbach, 2016). Furthermore, increased ECM density and intratumoral pressure serve as physical barriers to immune cell invasion, thus linking tumor-associated microenvironmental changes with immune suppression (Nyga et al., 2016). As collagen alignment has a promigratory effect on CD8+ T-cells, a change in the directionality of fiber alignment with respect to the tumor can promote or prevent T-cell infiltration depending on whether it is parallel or perpendicular to the tumor (Pruitt et al., 2019).

Biomaterials to Study the Tumor Microenvironment

As the ECM is centrally involved in regulating the aberrant interplay between many of the above-described biochemical and biophysical factors, engineered tumor models are mostly based on natural or synthetic biomaterials that mimic aspects of healthy and tumor-associated ECM (Table 2.5.11.1). Naturally derived biomaterials are intrinsically cytocompatible and—in most cases—present cell adhesion sites. However, they are subject to batch-to-batch variations and can be costly. In contrast, synthetic biomaterials can be produced in large quantities, are relatively cost-efficient, and allow for the establishment of models with tunable biological and physical properties including mechanics, adhesion receptor-binding sites, degradability, soluble factor sequestration, and introduction of moieties that enable dynamic modification during the culture period (Mabry et al., 2015; Tse and Engler, 2010). Nevertheless, while synthetic materials allow for more control over material properties, they do so at the cost of reduced in vivo-like biologic interactions.

Natural Biomaterials

Protein-Based Materials

Matrigel is one of the most commonly used, naturally derived materials for tumor modeling (Lee et al., 2007). As it contains tumor-derived morphogens including basement membrane components laminin, collagen IV, and entactin as well as growth factors, cytokines, enzymes, and proteoglycans, it

TABLE
2.5.11.1

Natural and Synthetic Biomaterials for Cancer Research With Select Application Examples and Available Commercial Products

Class	Material	Material Origin	Advantages	Disadvantages	References	
Natural	Matrigel	<ul style="list-style-type: none"> - Mixture of basement membrane proteins - Isolated from Engelbreth-Holm-Swarm (EHS) mouse sarcoma 	<ul style="list-style-type: none"> - Inherent ease of use - Contains many different morphogens - Contains many different ECM components 	<ul style="list-style-type: none"> - Large batch-to-batch variability - High cost - inability to tune structural and mechanical properties 	<ul style="list-style-type: none"> Lee et al. (2007) Drost et al. (2016) Poincloux et al. (2011) Corning (2019) 	
	MaxGel		<ul style="list-style-type: none"> - Cells can remodel and degrade - Supports the growth and invasion of many different cell types 	<ul style="list-style-type: none"> - contains tumor-derived morphogens that prevent isolating ECM effects - Low stiffness prevents use in certain biomanufacturing applications 	<ul style="list-style-type: none"> Millipore Sigma (2019a) 	
	Collagen I	<ul style="list-style-type: none"> - Most abundant ECM component - Isolated from bovine skin and tendons, or porcine skin 	<ul style="list-style-type: none"> - Forms hydrogels with fibrillar structure - Possible to control fiber diameter, pore size, and density by adjusting gelation conditions - Contains natural integrin-binding sites - Cells can remodel and degrade 	<ul style="list-style-type: none"> - Lacks complexity of native ECM - Limited range of mechanical properties 	<ul style="list-style-type: none"> Wolf et al. (2009) Jeon et al. (2013) Polacheck et al. (2011) Choi et al. (2019) 	
	SpongeCol PureCol				<ul style="list-style-type: none"> Millipore Sigma (2019b) Advanced BioMatrix (2019) 	
	Hyaluronic acid (HA)	<ul style="list-style-type: none"> - Polysaccharide composed of repeating units of β-1,4-D-glucuronic acid - β-1,3-N-acetyl-D-glucosamine 	<ul style="list-style-type: none"> - Enzymatically degradable by hyaluronidase - contains binding sites for cell adhesion receptors including CD44 and CD168 - Can be modified to enable synthetic control of materials properties - chemical modifications permit control over mechanical and degradation features 	<ul style="list-style-type: none"> - Limited mechanical tunability if unmodified - Requires chemical modification for cell binding via integrins - CD44-binding site can interfere with cellular functions - Functionalization may interfere with cell binding sites 	<ul style="list-style-type: none"> Xiao et al. (2018) Xu et al. (2012) Gurski et al. (2009) Lou et al. (2018) 	
	HyStem	<ul style="list-style-type: none"> - Isolated from bovine testicles or rooster combs or produced recombinantly 				<ul style="list-style-type: none"> Millipore Sigma (2019c)
	Alginate	<ul style="list-style-type: none"> - Block copolymer comprised of guluronate and mannuronate - Derived from brown algae 	<ul style="list-style-type: none"> - ionic cross-linking using bivalent cations is cell-compatible - Stiffness and architecture can be independently modified 	<ul style="list-style-type: none"> - Nonadhesive to cells - Integrin-binding sites must be chemically introduced - Lacks fibrillar structure 	<ul style="list-style-type: none"> Fischbach et al. (2009); Wisdom et al. (2018) Stowers et al. (2017) Xu et al. (2013) 	
	AlgiMatrix 3D				<ul style="list-style-type: none"> (ThermoFisher, n.d.) 	
	Agarose	<ul style="list-style-type: none"> - Polysaccharide comprised of D-galactose and 3,6-anhydro-alpha-L-galactopyranose isolated from red algae 	<ul style="list-style-type: none"> - Nonadherent for cells allowing for attachment-free culture such as spheroid generation - Historically used in colony formation assays to determine tumorigenicity of cells 	<ul style="list-style-type: none"> - Lacks physiologically relevant microstructures 	<ul style="list-style-type: none"> Vidavsky et al. (2018) Friedrich et al. (2009) 	
	Cell-derived matrices (CDM)	<ul style="list-style-type: none"> - Matrix deposited by cells seeded on coverslips in vitro 	<ul style="list-style-type: none"> - cellularly derived matrices have properties unique to the cell type of origin - Preserves native ECM protein and proteoglycan composition - Retains microscale structural features of ECM 	<ul style="list-style-type: none"> - Time and labor intensive to produce - Cells can only be seeded on top - Naturally heterogeneous with batch-to-batch variability - Mechanical properties cannot be tuned readily 	<ul style="list-style-type: none"> Serebriiskii et al. (2008) Seo et al. (2015) 	
Whole-tissue decellularization	<ul style="list-style-type: none"> - Cells removed from a whole tissue keeping the large-scale structure and matrix composition intact 	<ul style="list-style-type: none"> - Preserves native 3D architecture and large-scale structure - Larger size and thickness allows for a true 3D cell culture unlike CDMs - Preserves native ECM protein and proteoglycan composition 	<ul style="list-style-type: none"> - Difficult to produce - May require perfusion setup - Low throughput due to time- and skill-intensive setup 	<ul style="list-style-type: none"> Tian et al. (2018) Marturano-Kruik et al. (2018) Piccoli et al. (2018) 		

Synthetic	Polyacrylamide (PA)	<ul style="list-style-type: none"> - Acrylamide monomers cross-linked with bis-acrylamide 	<ul style="list-style-type: none"> - Can be modified with different cell adhesion ligands - Wide stiffness range - independent control of stiffness and cell adhesion motifs possible 	<ul style="list-style-type: none"> - Cannot be used for cell encapsulation due to monomer toxicity - Nondegradable - Static stiffness 	<p>Labernadie et al. (2017) Pathak and Kumar (2012) Nasrollahi et al. (2017)</p>
	Poly (ethylene glycol) (PEG)	<ul style="list-style-type: none"> - Comprised of repeating units of ethylene glycol of varying lengths - Terminally functionalized and polymerized via many chemistries 	<ul style="list-style-type: none"> - Can be chemically modified to allow for different reaction chemistries, mechanical properties, degradation mechanisms, and cellular interactions - Easily modified affording the resulting hydrogels a broad range of materials properties - chemical modification can yield a dynamic material 	<ul style="list-style-type: none"> - Lacks inherent degradability - modification with cell adhesion sites is necessary for cellular interactions - Lack of ECM complexity and fibrillar structure - Reliance on UV-mediated cross-linking may bring harm to cells 	<p>Lohmann et al. (2017) Gill et al. (2012) Sieh et al. (2012)</p>
	Poly (lactic-co-glycolic acid) (PLGA)	Linear copolymer made of lactic acid (LA) and glycolic acid (GA)	<ul style="list-style-type: none"> - Can be fabricated into porous or fibrous in substrates - Biodegradable with precisely tunable degradation rates by varying the molecular ratio of LA and GA - Can be surface modified to promote cell-material interactions 	<ul style="list-style-type: none"> - Decreases the pH around cells during degradation - Limited tunability of mechanical properties - Substrates are typically stiffer than native ECM 	<p>Pathi et al. (2011) Fischbach et al. (2007) Kim et al. (2011)</p>

readily supports the growth and invasion of many tumor cell types without further manipulation or materials modification. However, large batch-to-batch variability, high cost, and an inability to mimic the structural and mechanical properties of the ECM in human tumors are primary disadvantages of its use (Debnath and Brugge, 2005). Included tumor-derived morphogens may prevent isolating the independent effect of specific biomolecules on tumor growth. Finally, Matrigel is a very soft material and, thus, cannot be used in certain biomanufactured culture models. For example, it is not readily possible to pattern microfluidic conduits into Matrigel to mimic blood vessel-mediated transport properties.

Given its high abundance in tumor-associated ECM, collagen is another ECM component that is frequently used to create 3D culture models of cancer. As the most abundant and easy to process, type I collagen is the primary type used for cancer studies. Type I collagen consists of proteins with a triple helical structure that self-assemble into aggregates called fibrils and then larger collagen fibers (Parenteau-Bareil et al., 2010). In vitro fibrillar architecture and biochemical composition can vary depending on the source of collagen (Wolf et al., 2013). It is possible to adjust biophysical properties by modifying gelation conditions and/or introducing additional physical or chemical cross-links. For example, highly tunable gels with controlled fiber structure and porosity can be formed by adjusting the gelation temperature, the ionic strength of the gelation medium, and/or the pH of the collagen solution (Sapudom et al., 2015; Wolf et al., 2009). Furthermore, fiber alignment can be achieved by casting collagen into pre-stretched molds that are relaxed following gelation (Brownfield et al., 2013; McCoy et al., 2018). Collagen is biodegradable, biocompatible, remodelable, and contains intrinsic cell adhesion sites. However, collagen only allows limited variation of mechanical properties. While procedures such as nonenzymatic glycation can be used to cover a wider range of rigidities, they are often not suitable to recreate mechanical properties of hard tissues relevant to cancer (e.g., bones) and may also cause secondary, stiffness-independent effects in cells, e.g., through activation of RAGE receptors (Roy et al., 2009; Sharaf et al., 2015). Introducing cross-links with chemicals such as aldehydes, carbodiimides, or isocyanates can yield a broader range of stiffnesses, but may be toxic to cells (Parenteau-Bareil et al., 2010). Finally, structural features of the collagen fibers produced in vitro differ from those produced in vivo. In vitro, many thin disorganized fibers spontaneously form, while thick cross-linked fibers form as a result of enzymatic lysyl oxidase (LOX) activity in vivo (Pawelec et al., 2016).

Carbohydrate-Based Materials

Hyaluronic acid (HA) is most abundant in the brain and, thus, is frequently used for studies of brain cancer (Chen et al., 2018). Nevertheless, HA is also present in the ECM of a desmoplastic ECM in tumors (Bertrand et al., 1992). Consequently, HA produced using recombinant technologies or isolated from bovine testicles or rooster combs is increasingly used for engineering models of the tumor microenvironment. In addition, HA is cell-remodelable

through enzymatic degradation by hyaluronidase and readily binds to cell adhesion receptors including CD44 and CD168; to allow for interactions via integrins, integrin-binding ligands such as RGD can be introduced chemically (Park et al., 2003). HA can be modified with many functional groups to enable polymerization into a hydrogel via addition/condensation reactions or through photochemically induced radical polymerization (Burdick and Prestwich, 2011). These chemical modifications can also be used to control mechanical and degradative features of the material (Burdick and Prestwich, 2011). However, varying the physicochemical properties of HA through chemical modifications can interfere with available cell adhesion domains.

Carbohydrate-based alginate is frequently used to study tumor cells in both 2D and 3D culture formats. Its cross-linking density and thus, stiffness, can be controlled via adjusting the density of ionic cross-links through modulating the concentration of bivalent cations such as Ca^{2+} , varying the molecular weight or ratio of guluronic to mannuronic acid monomers, and/or introducing chemical cross-links (Lee and Mooney, 2012). Alginate is typically nonadhesive to cells but can be readily modified with adhesion ligands such as RGD to enable integrin engagement. Hence, alginate substrates can be used to compare cell behavior under 2D and 3D culture conditions with and without integrin engagement (Fischbach et al., 2009). Furthermore, cross-linking alginate in the presence of collagen can be used to produce interpenetrated networks that offer independent control over mechanical properties, gel structures, and adhesive ligand presentation (Branco da Cunha et al., 2014).

Agarose is commonly used for colony formation assays that test a cell's ability to survive under anchorage-independent conditions, an indicator of their tumorigenicity (Borowicz et al., 2014). Agarose is biocompatible, undergoes thermoreversible self-gelation, and can be chemically modified for a multitude of applications (Zarrintaj et al., 2018). When combined with collagen, agarose can be used to increase the elasticity of 3D collagen networks over two orders of magnitude with negligible effects on collagen fiber organization (Ulrich et al., 2010). Such platforms enable studies of cell migration as a function of cell-induced stress dissipation via individual ECM fibers versus deformation of the continuum network.

Cell- and Tissue-Derived Materials

To preserve the composition, structure, and mechanical properties of native ECM, decellularized scaffold systems have been developed (Crapo et al., 2011). So-called cell-derived matrices (CDMs) are produced by letting a monolayer of cells grow and deposit ECM. Subsequent removal of these cells using detergent-based protocols leaves behind matrices that contain both protein- and carbohydrate-based ECM components. The stability, mechanical properties, or biochemical composition of CDMs can be altered by modifying the culture protocol. For example, supplementing ascorbic acid to the cell culture medium increases collagen production, while varied glucose concentrations can be used to modulate

deposition of fibronectin and collagen IV (Miller et al., 2014). Alterations can also be made by chemically cross-linking cell-free matrices (Franco-Barraza et al., 2016). To study the behavior of premalignant or cancer cells as a function of varied ECM characteristics, CDMs can be prepared from normal or tumor-associated stromal cells or from stromal cells residing in tissues known to control tumorigenesis (e.g., adipose stromal cells) (Beachley et al., 2015; Franco-Barraza et al., 2016; Seo et al., 2015). While CDMs are suitable to mimic microscale features of the ECM in vitro, the resulting substrates are relatively thin (approx. 10–20 μm) and do not recapitulate macroscale features of the ECM. Furthermore, cellular ECM deposition depends on the underlying substrates (Kubow et al., 2009; Loebel et al., 2019). Hence, culturing cells on plastic for CDM generation may induce artifacts. Whole-organ and tissue-level decellularization may be used to circumvent these limitations while preserving the native 3D architecture and complexity of tissues and organs (Mayorca-Guiliani et al., 2017). Indeed, decellularized tissues and organs, which are formed through perfusion of mild detergents, salt solutions, and cell culture media, have been used as model systems for research as well as in clinical applications (Faulk et al., 2014). In addition to presenting macroscale tissue architecture, decellularized tissues and organs retain microscale features such as blood vessels and/or spatial variations of specific matrix niches. These features allow for studying cells in 3D matrix microenvironments with compositional and structural features most like what is seen in vivo. Tissue or organ decellularization methods are subject to diffusional constraints of decellularization fluids and thus, often require perfusion setups. Furthermore, limits on the number of tissues and the time needed to prepare such platforms reduces the throughput achievable with this approach.

Synthetic Biomaterials

Synthetic Hydrogels

Polyacrylamide (PA) is widely used to study cell behavior on hydrogel surfaces of varying stiffness (Wang and Pelham, 1998). PA hydrogels are composed of acrylamide monomers cross-linked with bis-acrylamide in different ratios to control the mechanical properties of the resulting gels. These hydrogels are typically formed on aminosilane functionalized coverslips and the gel surface can be modified with cell adhesion ligands. By conjugating different types or concentrations of cell adhesion ligands onto PA gels of different stiffnesses it becomes possible to study the individual versus combined effects of substrate chemistry and mechanics on cell behavior (Caliari and Burdick, 2016; Peyton and Putnam, 2005). A significant drawback of PA-based platforms is that cells cannot be encapsulated inside the gels due to toxicity of the hydrogel precursors. This prompted the need to develop biocompatible hydrogel materials for 3D culture applications.

Due to highly tunable chemistries, mechanical properties, degradation mechanisms, and cellular interactions, poly(ethylene glycol) (PEG) is commonly used (Cushing and Anseth, 2007; Lin and Anseth, 2009). PEG's broad utility is demonstrated by its use for photoencapsulation

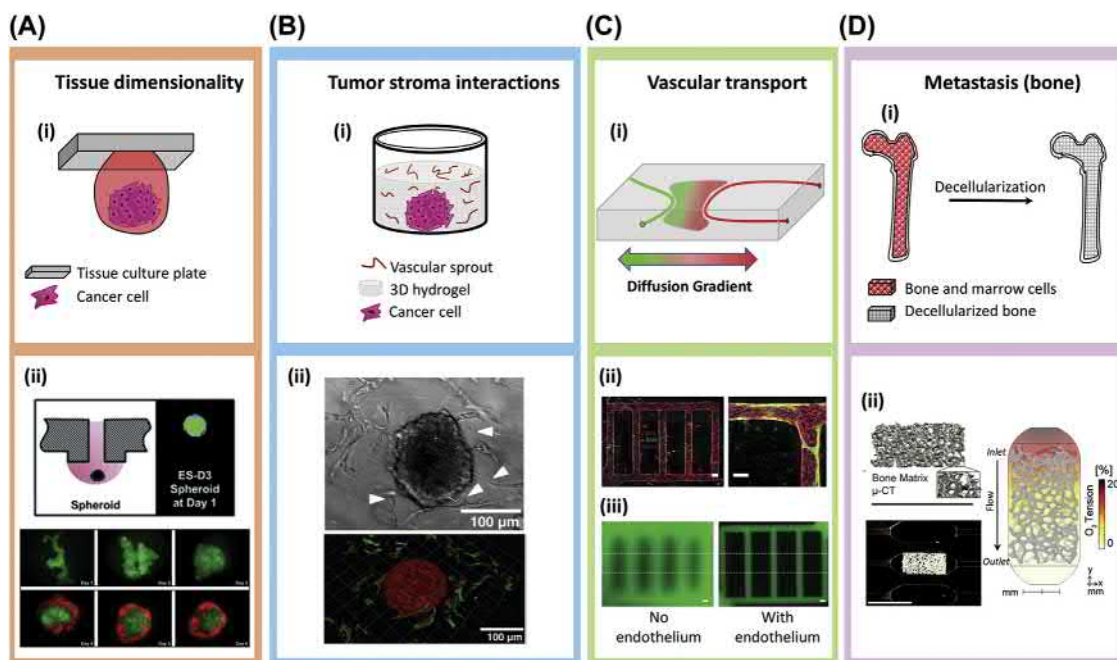
of osteoblasts (Burdick and Anseth, 2002), as an MMP-degradable hydrogel for the study of stromal or tumor cells (Lutolf et al., 2003), and as a vehicle for controlled release of biomolecules (Lin and Anseth, 2009). PEG's lack of complexity and fibrillar structure, and reliance on cross-linking techniques which may bring harm to cells are notable drawbacks. In particular, cross-linking via photopolymerization uses UV light and a photoinitiator to start the cross-linking can affect cell viability and activate DNA damage response pathways, influencing tumorigenesis confounding results (Fedorovich et al., 2009; Smith et al., 1995).

Polyesters

Biodegradable polyesters like polylactic acid (PLA), polyglycolic acid (PGA), and poly(lactic-co-glycolic) acid (PLGA) can be processed into cell culture scaffolds with different porosities (e.g., by gas-foaming particulate leaching) or fibrillar architectures (e.g., by electrospinning) to mimic the structural properties of the ECM (Brown et al., 2012; Fischbach et al., 2007). While cellular interactions with such scaffolds are typically enabled via adsorbed serum proteins, surface modification with defined adhesion ligands is also possible (Hersel et al., 2003). Polyester-based scaffolds have limited tunability of mechanical properties and decrease local pH with acidic degradation products (Fu et al., 2000). Decreased tumor pH has been associated with selective survival of cancer cells, inhibition of DNA repair leading to further mutations and transformations, and stimulation of invasion (Gatenby and Gillies, 2004). Thus, decoupling scaffold from tumor-induced changes in pH when using PGA, PLA, or PLGA scaffolds for cancer research is essential.

Composite Materials

Materials composed of both natural and synthetic biomaterials take advantage of the well-defined nature and sophisticated tunability of synthetic components while providing the functionality and complexity of native ECM molecules. For instance, functionalized PEG can be cross-linked to modified heparin molecules in various ratios to achieve independent control of stiffness, cell binding, and growth factor sequestration (Lohmann et al., 2017). Other groups take the opposite approach and modify natural ECM components like HA with synthetic moieties (Rosales et al., 2018). Direct chemical modification of HA can preserve its native cell-binding sites and cytocompatibility and expand the range and dynamics of the physical properties of HA. Natural inorganic components can also be combined with synthetic polymers. Both bone powder and nanoparticles of the bone mineral hydroxyapatite have been incorporated into PLGA scaffolds to study tumor–mineral interactions that may be relevant to bone metastasis (Lynch et al., 2016; Pathi et al., 2010). Finally, other materials draw inspiration from natural components and chemistry such as glutamine-to-lysine peptide bridge formation during fibrin clot formation to create PEG hydrogels with fibrin-like characteristics that can be cross-linked by the addition of factor XIIIa (Ehrbar et al., 2007).



• **Figure 2.5.11.2** Examples of biomaterials-based model systems to analyze tumor-microenvironment interactions. (A) Tissue dimensionality: (i) Multicellular spheroids simulating 3D cell-cell and cell-ECM interactions can be formed on a tissue culture plate using the hanging drop method. (ii) To generate uniformly sized and complex spheroids injection molded polystyrene plates with microfluidic channels that open at the bottom may be used. This approach enables multistage cell seeding to produce concentric layers of one or more cell types. (B) Tumor stroma interactions: (i) Encapsulating tumor spheroids into hydrogels containing different stromal cell types (e.g., endothelial cells) mimics aspects of tumor-stroma interactions. (ii) Hepatocarcinoma spheroids coembedded with endothelial cells into peptide-modified, growth factor-sequestering starPEG-heparin hydrogels stimulate vascular sprout formation (green: CD31; red: F-actin). (C) Vascular transport: (i) Microfluidic platforms allow for intricate arrangements of channels that can simulate mass transport through tumors. (ii) Perfusable and pericyte (green)-associated vascular networks can be established using microfabricated collagen-I hydrogels. (iii) Perfusion of FITC-labeled dextran through vessels without (left) and with endothelial cell coating (right) demonstrate the importance of endothelialization for modeling diffusivity of molecules into surrounding matrix. (D) Metastasis (bone): (i) Decellularized organs and tissues such as bone can provide culture substrates that preserve organic matrix structure and naturally occurring soluble factors that may not be effectively modeled by synthetic systems. (ii) μ -Computed tomography (μ -CT) shows that decellularized bone maintains its mineral content and structure. When embedded into microfluidic devices and seeded with endothelial cells and bone marrow-derived MSCs, decellularized bone serves to establish culture environments with varied oxygen tension for studies of bone metastasis. ((A) (ii) Images reproduced from Tung, Y.-C., Hsiao, A.Y., Allen, S.G., Torisawa, Y., Ho, M., Takayama, S., 2011. High-throughput 3D spheroid culture and drug testing using a 384 hanging drop array. *Analyst* 136, 473–478 with permission from Royal Society of Chemistry. (B) (ii). Images reproduced from Chwalek, K., Bray, L.J., Werner, C., 2014. Tissue-engineered 3D tumor angiogenesis models: potential technologies for anti-cancer drug discovery. *Adv. Drug Deliv. Rev.* 79–80, 30–39 with permission from *Advanced Drug Delivery Reviews*. (C) (iii). Images reproduced from Morgan, J.P., Delnero, P.F., Zheng, Y., Verbridge, S.S., Chen, J., Craven, M., Choi, N.W., Diaz-Santana, A., Kermani, P., Hempstead, B., López, J.A., Corso, T.N., Fischbach, C., Stroock, A.D., 2013. Formation of microvascular networks in vitro. *Nat. Protoc.* 8, 1820–1836 with permission from *Nature Methods*. (D) (ii). Images reproduced from Marturano-Kruik, A., Nava, M.M., Yeager, K., Chramiec, A., Hao, L., Robinson, S., Guo, E., Raimondi, M.T., Vunjak-Novakovic, G., 2018. Human bone perivascular niche-on-a-chip for studying metastatic colonization. *Proc. Natl. Acad. Sci.* 115, 1256–1261 with permission from PNAS.)

Applications of Biomaterials-Based Tumor Models

Analyzing the Effect of Tissue Dimensionality

By enabling 3D cell-cell and cell-ECM interactions, multicellular spheroids recapitulate many important characteristics of 3D tumors including changes in cell morphology, tissue-scale structural features, and mass transport dynamics (Tung et al.,

2011). Spheroids can be formed via the hanging drop method, which involves simply pipetting small volumes of cell suspension onto a polystyrene (PS) surface, inverting it, and placing it in an incubator to encourage the formation of cell aggregates (Fig. 2.5.11.2Ai). However, the resulting spheroids are in a low volume of culture medium per droplet and tend to be irregularly shaped. Circumventing some of these limitations, droplets of culture medium and cancer cells can be suspended vertically from a specially made PS plate (Fig. 2.5.11.2Aii) (Tung et al., 2011)

resulting in uniformly shaped spheroids that can be produced in different sizes, enabling testing of drug and nutrient diffusion as a function of tumor growth. Spheroids can also be generated in 96-well plates coated with low-melt agarose gel, which prevents cell adhesion (Friedrich et al., 2009; Vidavsky et al., 2018; Yuhás et al., 1977), using commercially available ultralow attachment culture surfaces, or by growing cells in pyramidal microwells (Strathern and Rothernberg, 2012; Ungrin et al., 2008).

Instead of inducing cell–cell contacts by physically aggregating cells, 3D cellular interactions can also be mimicked by seeding tumor cells into polymeric scaffolds or hydrogels. For example, tumor cells seeded into porous PLGA scaffolds form 3D histological structures that resemble those of tumors formed by the same cells implanted into mice (Fischbach et al., 2007). Exposing cancer cells to 3D tissue contexts significantly changes their signaling (Fischbach et al., 2009) and gene expression (Bissell, 2007) due to a variety of mechanisms including differential integrin engagement, cell–cell contact, as well as responses to tumor-intrinsic microenvironmental cues including hypoxia (Del-Nero et al., 2015; Fischbach et al., 2009; Tan et al., 2009).

To more directly identify the molecular mechanisms by which changes in direct cell–cell contact may influence cell behavior, it is possible to covalently couple adhesion molecules normally expressed on a cell's membrane onto a PDMS stamped micropatterned PEG hydrogel designed for single-cell culture (Lutolf et al., 2009). For example, PEG hydrogel microwells can be surface-modified with intercellular adhesion proteins such as N-cadherin, VE-cadherin, I-CAM, V-CAM, P-Sel, and Jag-1. Single cells seeded into the modified microwells interact with these proteins as if they were expressed by other cells. Such a system allows for isolation and direct study of cell–cell contacts via interaction of specific protein-binding pairs. This has identified how single-cell division kinetics are impacted by intercellular adhesion proteins and how these correlate to *in vivo* function (Lutolf et al., 2009). Furthermore, modification of the mechanical properties of PEG in this platform allows for studies of cellular interactions as a function of both adhesion domains and substrate mechanics.

Modeling Tumor–Stroma Interactions

To determine the impact of nontumor cells such as vascular cells, fibroblasts and immune cells on tumorigenesis, 3D coculture models have been developed. Perhaps most simplistically, incorporation of stromal cells such as CAFs into tumor spheroids permits studying how interactions between both cell types influence cancer cell behavior and has revealed increased expression of alpha-smooth muscle actin, epidermal growth factor receptor, and reduced expression of beta-catenin and E-cadherin, consistent with EMT phenotypes (Kim et al., 2015). While coculture spheroids can be studied in isolation, they can also be combined with artificial ECMs. For example, seeding coculture spheroids onto PA gels of varied stiffness elucidated that mechanically active heterotypic adhesion between CAFs and tumor cells can drive cancer cell invasion (Labernadie et al., 2017). Nevertheless, during initial stages of

tumor development, stromal cells primarily grow peripherally to a newly forming tumor rather than inside. Thus, seeding individual stromal cells and cancer spheroids separately into hydrogels may more closely simulate this early-stage cancer scenario (Fig. 2.5.11.2Bi). Indeed, culturing endothelial cells and mesenchymal stem cells (MSCs), together with tumor cells in peptide-modified, MMP-degradable PEG-heparin hydrogels recapitulates processes such as tumor-associated angiogenesis and stromal remodeling (Fig. 2.5.11.2Bii). Furthermore, such a platform can help identify the role of specific ECM-binding motifs in driving tumor cell invasion as a function of varied stromal compositions (Taubenberger et al., 2016).

Given the central role of the immune system in regulating cancer progression, dendritic cells, T cells, macrophages, natural killer cells, and lymphocytes have all been combined with cancer cells in coculture models (Nyga et al., 2016). The goal of such coculture models is to generate humanized immunocompetent cancer models for *in vitro* studies of tumor evasion of immune responses. For example, Algimatrix, a commercially available porous alginate scaffold, permitted coculture of breast cancer cells, fibroblasts, and macrophages, and revealed that spheroid formation was promoted with the triple coculture but reduced in the absence of macrophages (Rama-Esendagli et al., 2014). Incorporating regulatory T cells and natural killer cells into biomaterial cultures has been accomplished in Matrigel, and showed that NK cells alone reduced cancer cell growth, while regulatory T cells alone did not significantly reduce the size of the cancer aggregates, suggesting an important role for NK cells in cancer control (Augustine et al., 2015).

Platforms to Interrogate Cell–ECM Interactions

To study the effect of cell–ECM interactions on various processes contributing to tumor malignancy, nonadhesive hydrogels can be covalently modified with full-length ECM proteins or specific peptide sequences of these ECM proteins (Fischbach et al., 2009; Tibbitt and Anseth, 2009). For example, coupling RGD (fibronectin), IKVAV (laminin), and GFOGER (collagen type 1) into synthetic or composite materials at varying concentrations allows isolating the effect of varied integrin clustering and signaling on cell behavior (Taubenberger et al., 2016). Such studies can be performed in isolation and/or in the presence of altered hydrogel mechanical properties, which permits elucidating the integrated effects of tumor-associated changes in ECM composition and mechanics on cellular phenotypes (Hogrebe et al., 2018; Peyton et al., 2006). One specific example enabling such studies includes alginate hydrogels. Their mechanical properties can be readily adjusted by varying the cross-linking density, while integrin ligation (Box 2.5.11.2) can be modified by changing adhesion peptide presentation and/or mixing with Matrigel to form alginate-based interpenetrated networks (Chaudhuri et al., 2016, 2014). Similar studies can be performed with PEG hydrogels (Kyburz and Anseth, 2013; Zhu, 2010), but PEG-based hydrogels do not recapitulate the fibrillar features of native tumor ECM.

• BOX 2.5.11.2 Integrins

Cells sense and interact with their ECM environment through integrins, which are transmembrane heterodimers that consist of different alpha and beta subunits. Integrins link the ECM to the cytoskeleton and regulate cell signaling through many different pathways including growth factor receptor signaling and mechanotransduction (Alberts et al., 2002). In addition to this outside-in signaling, integrins are also involved in inside-out signaling where changes in cell signaling mediate differences in ECM remodeling (Hynes, 2002; Miranti and Brugge, 2002).

To mimic the structural properties of ECM *in vitro*, methacrylated dextran can be electrospun to produce substrates with fibrillar microarchitecture whose bulk and fiber elastic moduli may be tuned separately (Baker et al., 2015). Studies using this system revealed that cells adhering to matrices with soft fibers spread more than cells adhering to matrices with stiff fibers, but similar bulk stiffness. These experiments identified a new mechanism for how cells probe and respond to fibrillar ECM and suggested that bulk mechanical properties are not the only regulator of mechanosignaling (Baker et al., 2015).

In addition to varied fiber characteristics, pore size also changes in tumor-associated ECM and plays a role in determining whether tumor cells use individual or collective cell migration modes to invade interstitial spaces *in vivo* (Friedl et al., 2012a,b). Enabling such studies are, for example, collagen gels whose pore size can be adjusted by varying the gelation temperature or pH (Wolf et al., 2009). However, varying the pore size of collagen simultaneously changes fiber thickness, which may independently influence cell behavior (Liu et al., 2019). To separate pore size-dependent differences in cell confinement from substrate stiffness, micropatterned PA gels with independent control over channel size and material stiffness may be used (Pathak and Kumar, 2012). Experiments using such a 3D platform revealed that within similarly stiff substrates, cells migrate faster in small channels than in wide channels or on 2D controls. Additionally channels formed within stiffer substrates promoted cell migration speed, whereas high substrate stiffnesses may reduce cell migration speed in 2D culture (Peyton and Putnam, 2005). Despite the many insights that may be generated with the above models it has to be noted that fibers contained in tumor ECM not only vary in their microscale structure, but may additionally exhibit conformational changes (Arnoldini et al., 2017; Chandler et al., 2011; Wang et al., 2015). To more fully understand the effect of nano-, micro-, and macroscale matrix properties on tumorigenesis, experimental platforms will be needed that allow assessing the interactions between cells and tumor-associated ECM across multiple length scales.

While most commonly used hydrogels to study cell–ECM interactions exhibit purely elastic behavior and, thus, can be used to estimate differences in cellular mechanosignaling using traction force microscopy (TFM) (Box 2.5.11.3), biological tissues and ECMs behave like viscoelastic materials

• BOX 2.5.11.3 Traction Force Microscopy (TFM)

To measure the forces cells exert on an underlying substrate and gain clues about mechanosignaling, researchers use TFM. In this technique, fluorescent beads are embedded into PA gels of varying stiffness. Following modification of the gel surface with ECM adhesion molecules, cells are seeded on top and images are captured to mark the locations of the beads under tension from the cell. Next, trypsin, an enzyme, is used to remove the cells from the gel surface and images are acquired of the relaxed gel (Dembo and Wang, 1999). The forces the cell exerts on the gel are calculated from the displacement of the beads (Munevar et al., 2001; Plotnikov et al., 2014). These same principles can be applied to 3D systems through encapsulation of cells within MMP-degradable, fluorescent bead-containing PEG hydrogels (Legant et al., 2010). However, determining 3D traction forces is computationally challenging and requires special expertise, limiting its usability by nonexpert labs (Polacheck and Chen, 2016). Furthermore, the temporal and spatial resolution of confocal-based TFM is limited. Therefore, alternative TFM methods have been developed employing other imaging techniques such as optical coherence microscopy (Mulligan et al., 2017).

with functional consequences on cell behavior (Chaudhuri et al., 2016). Unlike in purely elastic materials, which recover from stress rapidly, the cell–material response of a viscoelastic material depends on both the timing of the molecular response within the cell and the rate of relaxation of the material (Gong et al., 2018). To account for these differences and study cell behavior as a function of ECM viscoelasticity, alternative materials systems have been developed. For example, alginate covalently bound to PEG spacers and ionically cross-linked via Ca^{2+} ions responds to stress viscoelastically (Chaudhuri et al., 2016; Nam et al., 2019). Stress relaxation rates in this system can be tuned by adjusting the molecular weight of alginate and concentrations of the PEG. Cells encapsulated within an alginate–PEG hydrogel differentiate, spread, and proliferate differently than cells in elastic materials. Entrapping linear, high-molecular-weight PA chains into cross-linked PA networks may also be used to characterize the effect of substrate viscous dissipation on cellular mechanosignaling (Charrier et al., 2018). Indeed, studies using such a platform revealed that cells adhering to viscoelastic matrices develop lower traction forces due to substrate-dependent energy dissipation. While both the above materials systems can be used to recapitulate ECM viscoelastic properties, they lack the fibrillar structure of native ECM. As an alternative, HA–collagen interpenetrating networks merge structure with viscoelasticity and were found to promote focal adhesion formation and matrix remodeling (Lou et al., 2018).

Dynamic Materials Systems for Studies of Mechanical Memory

The tumor microenvironment is not static but is subject to constant changes that can mediate the selection and transformation of specific tumor and stromal cell types. To study the

underlying mechanisms, a variety of sequential cell culture approaches or dynamic model systems may be used. For example, preconditioning cancerous and noncancerous epithelial cells on stiff PA gels mediates their transition to a more migratory phenotype that is maintained even after cells are transferred to softer gels (Nasrollahi et al., 2017). Similarly, fibroblasts cultured on 2D silicone substrates with tumorlike stiffness undergo a phenotypic shift to myofibroblasts. This phenotypic switching is time-dependent, as myofibroblast differentiation on stiff substrates for short culture periods is reversible, but irreversible after long culture periods (Balestrini et al., 2012). A time-dependent mechanical memory was also demonstrated in hMSCs precultured on PEG gels or silicone substrates of varying stiffness (Yang et al., 2014) and was attributable to microRNAs that preserved a mechanically induced fibrotic response phenotype (Li et al., 2017). Collectively, these results suggest that both tumor and stromal cells have a memory of their past mechanical environment and that these changes may contribute to tumor-associated fibrotic remodeling.

To more directly test dynamic effects of material degradation or mechanical properties on encapsulated cells, delayed secondary cross-linking approaches can be utilized (Khetan et al., 2013; Lutolf et al., 2003; Mabry et al., 2015; Moon et al., 2010; Rosales et al., 2018). Incorporating MMP-degradable peptide sequences into HA or other hydrogels enables cells to drive secondary modification via MMP-mediated degradation and remodeling (Lutolf et al., 2003; Moon et al., 2010). A secondary cross-linking reaction later during the culture period inhibits additional enzymatic degradation and isolates the effect of degradation-induced changes on cell phenotype (Khetan et al., 2013). To model MMP-independent, reversible changes in substrate mechanical properties, cells may be encapsulated within HA-based hydrogels that contain supramolecular cross-links formed via azobenzene bound to β -cyclodextrin (Rosales et al., 2018). Exposing these systems to either 400–500 or 365 nm light can be used to reversibly stiffen or soften these materials in a spatially and temporally controlled manner. Dynamic stiffening can also be accomplished with PEG-based systems using delayed thiolene polymerization (Mabry et al., 2015). Experiments using such systems suggest that myofibroblast differentiation in 3D MMP-degradable environments depends on cell spreading rather than substrate stiffness as soft hydrogels not only promoted cell spreading, but also myofibroblast differentiation. In contrast, delayed stiffening of soft, myofibroblast-incorporating hydrogels led to fibroblast deactivation. These results complement the above-described 2D studies on substrate-mediated dynamic changes of myofibroblast differentiation and highlight the importance of culture dimensionality in driving not only tumor, but also stromal cell, behavior.

Analyzing the Effect of Local and Systemic Transport Phenomena

As perturbed vascularization is the primary mediator of diffusional constraints and increased interstitial pressure in tumors, several approaches have been developed to mimic

blood vessels by integrating microfluidic channels into polymeric systems. One technique to create channels into PEG diacrylate (PEGDA) hydrogels uses laser ablation to cause local polymer structure breakdown (Heintz et al., 2016). Alternatively, it is possible to integrate vascular structures into hydrogel scaffolds by patterning cell adhesion peptides into otherwise nonadhesive materials using two-photon laser scanning photolithography (Culver et al., 2012). Soft-lithography can also be used to define networks of endothelialized microchannels within natural hydrogel matrices to study various tumor vascularization phenomena in long-term (1–2 weeks) cultures (Fig. 2.5.11.2C) (Morgan et al., 2013; Zheng et al., 2012). Instead of patterning the channels directly, it is possible to predefine channels for subsequent coating with endothelial cells by embedding a needle that creates a lumen upon removal (Chrobak et al., 2006) or by encasing fibers of a sacrificial material, such as polysaccharides, that leave behind a lumen upon dissolution (Bellan et al., 2009; Miller et al., 2012). Many of these lithographic approaches yield channel diameters of 75–750 μm , while capillaries are an order of magnitude smaller. This limitation can be circumvented using polydimethylsiloxane (PDMS)-based, microfluidic devices in which endothelial cells are seeded into a central, ECM-filled chamber and allowed to form perfusable vessels spontaneously (Fig. 2.5.11.2C) (Moya et al., 2013; Shin et al., 2012).

Three-dimensional (3D) bioprinting may be an alternative to technically challenging microfabrication approaches. Indeed, 3D printing can be used to design complex tissue macrostructures that incorporate parenchymal and stromal elements with microscale detail. In one such application, cells were suspended in inks composed of gelatin methacrylate, cell-culture media, and photoinitiator (Kolesky et al., 2014). After printing, gels were cross-linked with UV light, sacrificial materials were dissolved, and the channels were lined with endothelial cells. This resulted in intertwined patterns of defined regions of fibroblasts and vasculature all encapsulated in GelMA—methacrylate-modified denatured collagen. Importantly, systems like this allow for investigations of cell–vascular interactions in a spatially defined manner that would be very informative in tumor stroma studies.

In addition to altering mass transport, perturbed vessel function also modulates tumor interstitial fluid flow and pressure, which can independently affect tumorigenesis (Munson and Shieh, 2014). Indeed, collagen-embedded cancer cells subjected to interstitial flow conditions within a microfluidic device migrate either against or with direction of flow in a cell density, flow strength, and CCR7 activation-dependent manner (Munson et al., 2013; Polacheck et al., 2011). To better understand the role of interstitial flow and pressure on other cell types in the tumor microenvironment, fibronectin-coated PDMS-based microfluidic devices have also been used. With such models it has been shown, for example, that interstitial flow and shear stress impact endothelial cell sprouting, i.e., a key step in both lymph- and vascular angiogenesis (Song and Munn, 2011). As increased fluid pressure within a tumor impairs effective drug delivery by creating a fluid flow gradient

that works opposite to drug diffusion, similar models may be designed to more broadly study tumor cell responsiveness to therapeutics (Nathan et al., 2005).

Metastasis

Advanced cancers commonly spread to the lungs, liver, brain, and bones, and the specific microenvironmental conditions of these organs determine whether metastases form or not. One key difference between these metastatic sites is their ECM composition. For example, bone ECM contains high levels of collagen I, while brain ECM contains fibronectin, vitronectin, tenascin C, and laminin (Barney et al., 2015). To test the effect of particular ECM components on the metastatic capability of tumor cells, glass coverslips can be surface-treated with silane chemistry, coated with ECM components representative of these tissues, and then used to study the organ tropism of cancer cells (Barney et al., 2015). The effect of organ-specific ECM compositions can also be examined by isolating matrix from decellularized tissues, which not only preserves the ECM composition, but also bound signaling molecules. In one study, organ-specific metastasis models were created by pulverizing the decellularized tissue, reconstituting it, and allowing it to self-polymerize onto cell culture plates (Tian et al., 2018). Colorectal cancer cells seeded on top of these substrates formed large spheroids not seen on plastic. Additionally, these metastasis modeling substrates supported growth of cellular aggregates that were histologically similar to in vivo metastases and responded to treatments differently than when they were grown on plastic. While this particular method does not preserve geometry, structure, or mechanical properties of the metastatic tissues, whole-tissue decellularization can maintain these features. Indeed, decellularized tissues have been used to compare cancer cell behavior on healthy versus tumor matrix, but could also be useful in the study of

metastasis-associated cell–matrix interactions (Piccoli et al., 2018; Villasante et al., 2014). When combined with host cells and appropriate mechanical stimuli such as interstitial flow conditions, decellularized tissue models will enable many important insights such as the role of perivascular niche conditions in the chemotherapeutic resistance of disseminated tumor cells (Fig. 2.5.11.2D) (Marturano-Kruik et al., 2018).

An even greater level of complexity can be achieved with microfabricated tissue and organ models. To engineer a fully functional bone marrow compartment for studies of bone metastasis, collagen I is cast into microfabricated PDMS molds together with demineralized bone powder, and growth factors important for bone development (Torisawa et al., 2014). Implantation of the resulting collagen constructs into mice yields bonelike tissue containing a marrow-rich region with hematopoietic cells and some adipocytes. By placing the explanted tissue into a microfluidic device, the viability of these constructs can be maintained for at least 1 week, making it possible to study metastasis-associated interactions of tumor cells in the context of whole-bone complexity (Torisawa et al., 2014). To recapitulate organ-level function of the lung that may be implicated in metastasis, multifunctional microdevices can be created that possess structural, functional, and mechanical properties of the alveolar–capillary interface (Huh et al., 2010). This interfacial region is responsible for the gas exchange function of the lung and, thus, is an essential element when modeling lung tissue and its potential role in metastasis. Previously engineered lung-mimetic devices consist of vertically opposing microchannels separated by a stretchable PDMS membrane. Human endothelial cells and alveolar epithelial cells can be seeded on either side of the membrane, which is subsequently stretched to simulate lung movement. In toxicology studies, the artificial lung responded to toxins and inflammatory cytokines similarly to native lung, suggesting its potential value in studies of lung metastasis.

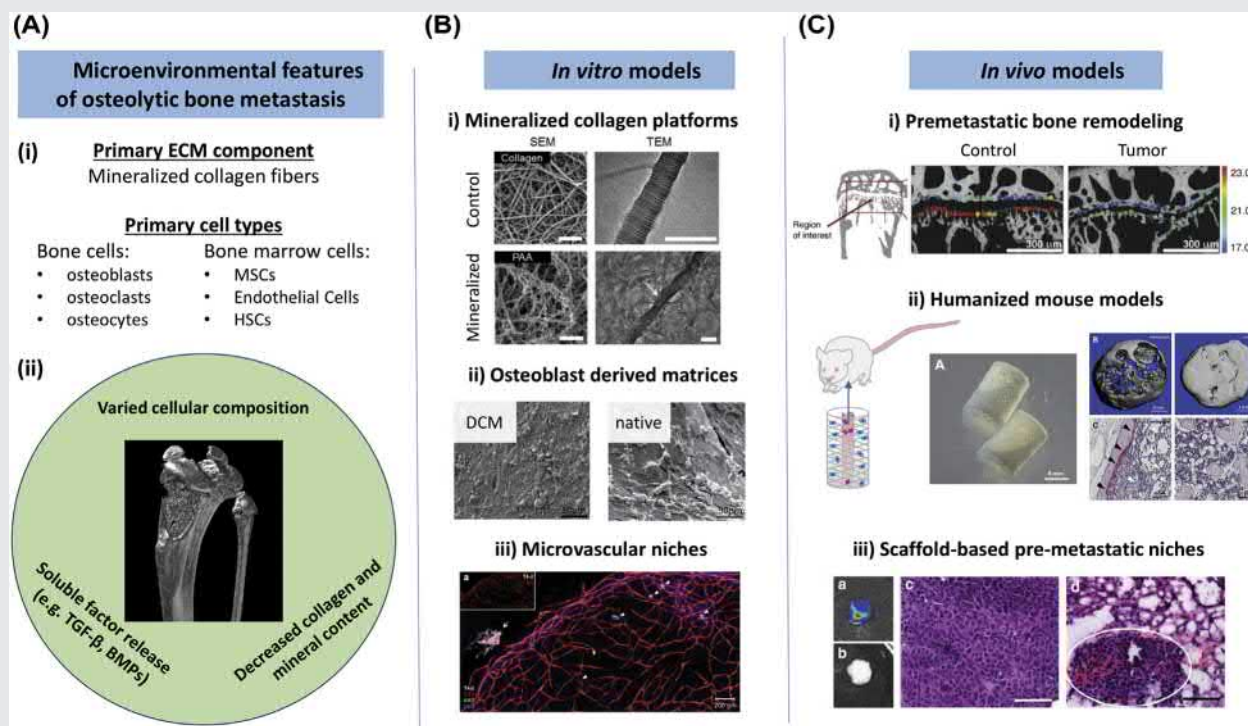
CASE STUDY: BONE METASTASIS

Approximately 85 percent of advanced breast cancer patients develop skeletal metastases in their lifetime (Coleman and Rubens, 1987). Bone metastases are characterized by painful, often osteolytic, lesions that increase fracture risk, decrease quality of life, and have no cure (Kozlow and Guise, 2005). Tumor cells activate osteolysis by releasing factors that stimulate osteoclastogenesis and inhibit osteogenesis (Fig. 2.5.11.3A). The resulting osteolytic bone degradation leads to the release of otherwise sequestered growth factors and cytokines that increase tumor cell proliferation, thereby activating the vicious cycle of osteolytic metastasis that is challenging to treat.

From a biomaterials perspective, bone is a hierarchical material composed of collagen fibers reinforced with hydroxyapatite endowing bone with its unique biomechanical properties (Fratzl and Weinkamer, 2007). As a result, the fibrillar structure and mineralization of bone ECM are critical design parameters for in vitro models of bone metastasis. To study the effect of bone mineralization on tumor cell behavior in vitro, bone ECM can be modeled using osteoblast-derived ECMs (Mastro et al., 2004; Taubenberger et al., 2013), mineral-containing culture models (Pathi et al., 2011; Suárez-González et al., 2010; Choi

et al., 2015), or mineralized collagen systems (Choi et al., 2019) (Fig. 2.5.11.3Bi, ii). For example, casting collagen into PDMS microwells and incubating these substrates in a calcium phosphate solution containing polyaspartic acid yields collagen scaffolds with biomimetic intrafibrillar mineralization (Choi et al., 2019). Studying breast cancer cell interactions with these substrates demonstrated mineral-mediated differences in cell contractility, focal adhesion formation, and cell traction forces that may be relevant to metastasis. Nevertheless, tumor cell dissemination to bone is also critically determined by interactions with bone marrow niches and the integrated vascular structures (Carlson et al., 2019; Croucher et al., 2016). To mimic tumor cell–endothelial cell interactions and their role in regulating tumor cell dormancy and therapy response, microvascular niches can be engineered by coculturing endothelial cells with bone marrow-derived MSCs, which supports the formation of interconnected vascular networks (Fig. 2.5.11.3Biii). When breast cancer cells were seeded on top of the endothelial networks it was found that dormancy is maintained by thrombospondin-1 (TSP-1) associated with stable vascular regions, whereas reduced levels of TSP-1 at sprouting neovascular tips activated tumor cells to escape from dormancy.

CASE STUDY: BONE METASTASIS—CONT'D



• **Figure 2.5.11.3** Bone metastasis case study. (A) (i) Metastasis-relevant bone microenvironmental conditions are determined by mineralized ECM and stromal cells located in bone and bone marrow. (ii) Bone homeostasis is perturbed during metastasis and characterized by increased osteoclast (e.g., breast cancer, shown here) or osteoblast (e.g., prostate cancer) activity. Osteolysis leads to release of soluble factors that promote osteoclastogenesis further decreasing collagen and mineral content. (B) (i) Intrafibrillar mineralization of collagen can be used to mineralize collagen networks in a biomimetic manner. (ii) Osteoblast-derived, decellularized matrices (DCM) replicate the organic and mineral components of native bone ECM. (iii) To model perivascular niches within bone marrow, microvascular networks can be created by culturing endothelial cells on top of bone marrow stromal cells. (C) (i) Synchrotron-based analysis of mineral nanostructure in regions prone to bone metastasis revealed that primary tumors remodel bone mineral even prior to secondary tumor formation. (ii) Implantable, tissue-engineered models of humanized bone based on electrospun PCL scaffolds allow studies of tumor-mediated bone destruction under relevant human conditions. (iii) Implantation of PLG scaffolds into tumor-bearing immunocompetent mice leads to spontaneous tumor cell dissemination to the scaffolds and can be used to study the importance of immune cells during metastasis. (A) explanted scaffold from mouse with tumor versus (B) control. (C) H&E staining of the primary tumor and (D) a metastatic lesion within the scaffold. ((A) Image courtesy of murine tibia with osteolytic metastasis: Frank He, Fischbach lab. (B) (i). Images reproduced from Choi, S., Friedrichs, J., Song, Y.H., Werner, C., Estroff, L.A., Fischbach, C., 2019. Intrafibrillar, bone-mimetic collagen mineralization regulates breast cancer cell adhesion and migration. *Biomaterials* 198, 95–106 with permission from Biomaterials. (B) (ii). Images reproduced from Taubenberger, A.V., Quent, V.M., Thibaudeau, L., Clements, J.A., Huttmacher, D.W., 2013. Delineating breast cancer cell interactions with engineered bone microenvironments. *J. Bone Miner. Res.* 28, 1399–1411 with permission from Journal of Bone and Mineral Research. (B) (iii). Images reproduced from Ghajar, C.M., Peinado, H., Mori, H., Matei, I.R., Evason, K.J., Brazier, H., Almeida, D., Koller, A., Hajjar, K.A., Stainier, D.Y.R., Chen, E.I., Lyden, D., Bissell, M.J., 2013. The perivascular niche regulates breast tumour dormancy. *Nat. Cell Biol.* 15, 807–817 with permission from Nature Cell Biology. (C) (i). Images reproduced from He, F., Chiou, A.E., Loh, H.C., Lynch, M., Seo, B.R., Song, Y.H., Lee, M.J., Hoerth, R., Bortel, E.L., Willie, B.M., Duda, G.N., Estroff, L.A., Masic, A., Wagermaier, W., Fratzl, P., Fischbach, C., 2017. Multiscale characterization of the mineral phase at skeletal sites of breast cancer metastasis. *Proc. Natl. Acad. Sci.* 114, 10542–10547 with permission from PNAS. (C) (ii). Images reproduced from Holzappel, B.M., Wagner, F., Loessner, D., Holzappel, N.P., Thibaudeau, L., Crawford, R., Ling, M.-T., Clements, J.A., Russell, P.J., Huttmacher, D.W., 2014. Species-specific homing mechanisms of human prostate cancer metastasis in tissue engineered bone. *Biomaterials* 35, 4108–4115 with permission from Biomaterials. (D) Images reproduced from Azarin, S.M., Yi, J., Gower, R.M., Aguado, B.A., Sullivan, M.E., Goodman, A.G., Jiang, E.J., Rao, S.S., Ren, Y., Tucker, S.L., Backman, V., Jeruss, J.S., Shea, L.D., 2015. In vivo capture and label-free detection of early metastatic cells. *Nat. Commun.* 6, 8094 with permission from Nature Communications.)

(Continued)

CASE STUDY: BONE METASTASIS—CONT'D

Typical *in vivo* studies of bone metastasis involve intracardiac injection of human tumor cells into immunocompromised mice as metastases in mice do not form spontaneously (Esposito et al., 2018). Interestingly, the regions that tumor cells target during bone metastasis are not only characterized by distinct cellular composition, but also contain less mature mineral that further changes during premetastatic remodeling (Fig. 2.5.11.3Ci) (He et al., 2017). Given that mineral properties can directly influence tumor cell behavior, studies of bone metastasis should not only consider tumor-associated changes of bone organic ECM components and the related cellular and molecular changes, but also the role of minerals in these processes (Choi et al., 2015; Pathi et al., 2011). To more closely mimic the importance of human microenvironmental components in driving bone metastasis, humanized mouse models of bone metastasis have been engineered. For example, humanized bone can be developed using polycaprolactone (PCL) scaffolds coated with calcium phosphate and cultured with primary human osteoblastic cells in the presence of recombinant human bone morphogenic protein (BMP)-7 (Holzapfel et al., 2014; Martine et al., 2017) (Fig. 2.5.11.3Cii). Following implantation into immunocompromised mice, the cell-seeded constructs develop into humanized ossicles complete with many structural and

biochemical features of native bone including mineralized collagen I and II and a bone marrow space containing osteoclasts, osteoblasts, and hematopoietic cells. When breast cancer cells were injected intracardially, bone metastases developed in the implant regions. The benefits of such systems are the reproducible formation of bone metastasis with similarities to those in humans (Dondossola et al., 2018; Tatosian and Shuler, 2009). However, these studies depend on the use of immunocompromised mice, which cannot recapitulate the full immunologic responses that are known to play a role in bone metastasis. Indeed, scaffold-based premetastatic niches implanted into immunocompetent mice have helped reveal the importance of specific immune cell populations in driving tumor cell dissemination (Fig. 2.5.11.3Ciii) (Azarin et al., 2015; Rao et al., 2016). More specifically, implantation of microporous PLGA or PCL scaffolds leads to the recruitment of different immune cell types generating a microenvironment that promotes recruitment of metastatic cells relative to neighboring sites with scaffold degradation kinetics appearing to play a role in this process. Hence, complementary *in vivo* approaches will be needed to elucidate the independent and combined effects of human conditions and the immune system in bone metastasis.

Conclusions

Biomaterials-based models of the tumor microenvironment contribute to a better understanding of cancer development, progression, and treatment. While previous and current approaches primarily focus on local phenomena, systemic effects broadly impact many aspects of tumor growth and therapeutic response. As such, more integrated approaches will be needed. In particular, microphysiological systems platforms in which models of varied tissues and organs are interconnected using fluidic conduits allow for mimicry of systemic interactions and can be used for analyzing treatment responses (Bhatia and Ingber, 2014; Tatosian and Shuler, 2009). Such systems are particularly useful in cancer drug screenings because a drug can be tested simultaneously for efficacy in killing the cancer cells and for side effects on other cell types. Furthermore, using such platforms in combination with patient-derived cells or organoids as well as *in vivo* studies will be critical to enable precision medicine applications that are poised to greatly improve clinical outcomes for patients in the future (DelNero et al., 2018).

Acknowledgments

Financial support was provided by the National Cancer Institute through the Center on the Physics of Cancer Metabolism (1U54CA210184), the Human Science Frontiers Program (RGP0016/2017), and NSF (Graduate Research Fellowships to Brittany Schutrum and Matthew Whitman).

References

- Advanced BioMatrix, 2019. PureCol [WWW Document]. <https://www.advancedbiomatrix.com/collagen-type-i/purecol-bovine-collagen-product-3-mgml/>.
- Alberts, B., Johnson, A., Lewis, J., et al., 2002. Integrins. In: Alberts, B., Johnson, A., Lewis, J., Raff, M., Roberts, K., W, P. (Eds.), *Molecular Biology of the Cell*. Garland Science, New York.
- Arnoldini, S., Moscaroli, A., Chabria, M., Hilbert, M., Hertig, S., Schibli, R., Béhé, M., Vogel, V., 2017. Novel peptide probes to assess the tensional state of fibronectin fibers in cancer. *Nat. Commun.* 8, 1793.
- Augustine, T.N., Dix-Peek, T., Duarte, R., Candy, G.P., 2015. Establishment of a heterotypic 3D culture system to evaluate the interaction of TREG lymphocytes and NK cells with breast cancer. *J. Immunol. Methods* 426, 1–13.
- Azarin, S.M., Yi, J., Gower, R.M., Aguado, B.A., Sullivan, M.E., Goodman, A.G., Jiang, E.J., Rao, S.S., Ren, Y., Tucker, S.L., Backman, V., Jeruss, J.S., Shea, L.D., 2015. *In vivo* capture and label-free detection of early metastatic cells. *Nat. Commun.* 6, 8094.
- Baker, B.M., Trappmann, B., Wang, W.Y., Sakar, M.S., Kim, I.L., Shenoy, V.B., Burdick, J.A., Chen, C.S., 2015. Cell-mediated fibre recruitment drives extracellular matrix mechanosensing in engineered fibrillar microenvironments. *Nat. Mater.* 14, 1262–1268.
- Balestrini, J.L., Chaudhry, S., Sarrazy, V., Koehler, A., Hinz, B., 2012. The mechanical memory of lung myofibroblasts. *Integr. Biol.* 4, 410.
- Barney, L.E., Dandley, E.C., Jansen, L.E., Reich, N.G., Mercurio, A.M., Peyton, S.R., 2015. A cell-ECM screening method to predict breast cancer metastasis. *Integr. Biol. (Camb.)* 7, 198–212.
- Beachley, V.Z., Wolf, M.T., Sadtler, K., Manda, S.S., Jacobs, H., Blatchley, M.R., Bader, J.S., Pandey, A., Pardoll, D., Elisseff, J.H., 2015. Tissue matrix arrays for high-throughput screening and systems analysis of cell function. *Nat. Methods* 12, 1197–1204.

- Bellan, L.M., Singh, S.P., Henderson, P.W., Porri, T.J., Craighead, H.G., Spector, J.A., 2009. Fabrication of an artificial 3-dimensional vascular network using sacrificial sugar structures. *Soft Matter* 5, 1354.
- Benjamin, E.J., Blaha, M.J., Chiuve, S.E., Cushman, M., Das, S.R., Deo, R., Ferranti, S.D., de Floyd, J., Fornage, M., Gillespie, C., Isasi, C.R., Jiménez, M.C., Jordan, L.C., Judd, S.E., Lackland, D., Lichtman, J.H., Lisabeth, L., Liu, S., Longenecker, C.T., Mackey, R.H., Matsushita, K., Mozaffarian, D., Mussolino, M.E., Nasir, K., Neumar, R.W., Palaniappan, L., Pandey, D.K., Thiagarajan, R.R., Reeves, M.J., Ritchey, M., Rodriguez, C.J., Roth, G.A., Rosamond, W.D., Sasson, C., Towfighi, A., Tsao, C.W., Turner, M.B., Virani, S.S., Voeks, J.H., Willey, J.Z., Wilkins, J.T., Wu, J.H., Alger, H.M., Wong, S.S., Muntner, P., 2017. Heart disease and stroke statistics—2017 update: a report from the American heart Association. *Circulation* 135 e146.
- Bertrand, P., Girard, N., Delpech, B., Duval, C., D'Anjou, J., Dauce, J.P., 1992. Hyaluronan (hyaluronic acid) and hyaluronectin in the extracellular matrix of human breast carcinomas: comparison between invasive and non-invasive areas. *Int. J. Cancer* 52, 1–6.
- Bhatia, S.N., Ingber, D.E., 2014. Microfluidic organs-on-chips. *Nat. Biotechnol.* 32, 760–772.
- Bissell, M.J., 2007. Architecture is the message: the role of extracellular matrix and 3-D structure in tissue-specific gene expression and breast cancer. *Pezcoller Found. J.* 16, 2–17.
- Borowicz, S., Van Scoyk, M., Avasarala, S., Karuppusamy Rathinam, M.K., Tauler, J., Bikkavilli, R.K., Winn, R.A., 2014. The soft agar colony formation assay. *J. Vis. Exp.* e51998.
- Branco da Cunha, C., Klumpers, D.D., Li, W.A., Koshy, S.T., Weaver, J.C., Chaudhuri, O., Granja, P.L., Mooney, D.J., 2014. Influence of the stiffness of three-dimensional alginate/collagen-I interpenetrating networks on fibroblast biology. *Biomaterials* 35, 8927–8936.
- Bray, F., Ferlay, J., Soerjomataram, I., Siegel, R.L., Torre, L.A., Jemal, A., 2018. Global cancer statistics 2018: GLOBOCAN estimates of incidence and mortality worldwide for 36 cancers in 185 countries. *CA. Cancer J. Clin.* 68, 394–424.
- Breslin, S., O'Driscoll, L., 2013. Three-dimensional cell culture: the missing link in drug discovery. *Drug Discov. Today* 18, 240–249.
- Brown, T.D., Slososch, A., Thibaudeau, L., Taubenberger, A., Loessner, D., Vaquette, C., Dalton, P.D., Hutmacher, D.W., 2012. Design and fabrication of tubular scaffolds via direct writing in a melt electrospinning mode. *Biointerphases* 7, 13.
- Brownfield, D.G., Venugopalan, G., Lo, A., Mori, H., Tanner, K., Fletcher, D.A., Bissell, M.J., 2013. Patterned collagen fibers orient branching mammary epithelium through distinct signaling modules. *Curr. Biol.* 23, 703–709.
- Burdick, J.A., Anseth, K.S., 2002. Photoencapsulation of osteoblasts in injectable RGD-modified PEG hydrogels for bone tissue engineering. *Biomaterials* 23, 4315–4323.
- Burdick, J.A., Prestwich, G.D., 2011. Hyaluronic acid hydrogels for biomedical applications. *Adv. Mater.* 23, H41–H56.
- Caliari, S.R., Burdick, J.A., 2016. A practical guide to hydrogels for cell culture. *Nat. Methods* 13, 405–414.
- Carlson, P., Dasgupta, A., Grzelak, C.A., Kim, J., Barrett, A., Coleman, I.M., Shor, R.E., Goddard, E.T., Dai, J., Schweitzer, E.M., Lim, A.R., Crist, S.B., Cheresh, D.A., Nelson, P.S., Hansen, K.C., Ghajar, C.M., 2019. Targeting the perivascular niche sensitizes disseminated tumour cells to chemotherapy. *Nat. Cell Biol.* 21, 238–250.
- Chandler, E.M., Saunders, M.P., Yoon, C.J., Gourdon, D., Fischbach, C., 2011. Adipose progenitor cells increase fibronectin matrix strain and unfolding in breast tumors. *Phys. Biol.* 8, 015008.
- Charrier, E.E., Pogoda, K., Wells, R.G., Janmey, P.A., 2018. Control of cell morphology and differentiation by substrates with independently tunable elasticity and viscous dissipation. *Nat. Commun.* 9, 449.
- Chaudhuri, O., Gu, L., Klumpers, D., Darnell, M., Bencherif, S.A., Weaver, J.C., Huebsch, N., Lee, H., Lippens, E., Duda, G.N., Mooney, D.J., 2016. Hydrogels with tunable stress relaxation regulate stem cell fate and activity. *Nat. Mater.* 15, 326–334.
- Chaudhuri, O., Koshy, S.T., Branco Da Cunha, C., Shin, J.W., Verbeke, C.S., Allison, K.H., Mooney, D.J., 2014. Extracellular matrix stiffness and composition jointly regulate the induction of malignant phenotypes in mammary epithelium. *Nat. Mater.* 13, 970–978.
- Chen, J.-W.E., Pedron, S., Shyu, P., Hu, Y., Sarkaria, J.N., Harley, B.A.C., 2018. Influence of hyaluronic acid transitions in tumor microenvironment on glioblastoma malignancy and invasive behavior. *Front. Mater.* 5, 39.
- Choi, S., Coonrod, S., Estroff, L., Fischbach, C., 2015. Chemical and physical properties of carbonated hydroxyapatite affect breast cancer cell behavior. *Acta Biomater.* 24, 333–342.
- Choi, S., Friedrichs, J., Song, Y.H., Werner, C., Estroff, L.A., Fischbach, C., 2019. Intrafibrillar, bone-mimetic collagen mineralization regulates breast cancer cell adhesion and migration. *Biomaterials* 198, 95–106.
- Chrobak, K.M., Potter, D.R., Tien, J., 2006. Formation of perfused, functional microvascular tubes in vitro. *Microvasc. Res.* 71, 185–196.
- Chwalek, K., Bray, L.J., Werner, C., 2014. Tissue-engineered 3D tumor angiogenesis models: potential technologies for anti-cancer drug discovery. *Adv. Drug Deliv. Rev.* 79–80, 30–39.
- Coleman, R.E., Rubens, R.D., 1987. The clinical course of bone metastases from breast cancer. *Br. J. Cancer* 55, 61–66.
- Conklin, M.W., Eickhoff, J.C., Riching, K.M., Pehlke, C.A., Eliceiri, K.W., Provenzano, P.P., Friedl, A., Keely, P.J., 2011. Aligned collagen is a prognostic signature for survival in human breast carcinoma. *Am. J. Pathol.* 178, 1221–1232.
- Corning, 2019. Corning® Matrigel® Matrix. ([WWW Document]).
- Crapo, P.M., Gilbert, T.W., Badylak, S.F., 2011. An overview of tissue and whole organ decellularization processes. *Biomaterials* 32, 3233–3243.
- Cronin, K.A., Lake, A.J., Scott, S., Sherman, R.L., Noone, A.-M., Howlader, N., Henley, S.J., Anderson, R.N., Firth, A.U., Ma, J., Kohler, B.A., Jemal, A., 2018. Annual report to the nation on the status of cancer, part I: national cancer statistics. *Cancer* 124, 2785–2800.
- Croucher, P.I., McDonald, M.M., Martin, T.J., 2016. Bone metastasis: the importance of the neighbourhood. *Nat. Rev. Cancer* 16, 373–386.
- Culver, J.C., Hoffmann, J.C., Poché, R.A., Slater, J.H., West, J.L., Dickinson, M.E., 2012. Three-dimensional biomimetic patterning in hydrogels to guide cellular organization. *Adv. Mater.* 24, 2344–2348.
- Cushing, M.C., Anseth, K.S., 2007. Materials science: hydrogel cell cultures. *Science* (80) 316, 1133–1134.
- Debnath, J., Brugge, J.S., 2005. Modelling glandular epithelial cancers in three-dimensional cultures. *Nat. Rev. Cancer* 5, 675–688.
- DelNero, P., Hopkins, B.D., Cantley, L.C., Fischbach, C., 2018. Cancer metabolism gets physical. *Sci. Transl. Med.* 10 eaaq1011.
- DelNero, P., Lane, M., Verbridge, S.S., Kwee, B., Kermani, P., Hempstead, B., Stroock, A., Fischbach, C., 2015. 3D culture broadly regulates tumor cell hypoxia response and angiogenesis via pro-inflammatory pathways. *Biomaterials* 55, 110–118.

- Dembo, M., Wang, Y.-L., 1999. Stresses at the cell-to-substrate interface during locomotion of fibroblasts. *Biophys. J.* 76, 2307–2316.
- dit Faute, M.A., Laurent, L., Ploton, D., Poupon, M.-F., Jardillier, J.-C., Bobichon, H., 2002. Distinctive alterations of invasiveness, drug resistance and cell-cell organization in 3D-cultures of MCF-7, a human breast cancer cell line, and its multidrug resistant variant. *Clin. Exp. Metastasis* 19, 161–168.
- Dondossola, E., Alexander, S., Holzapfel, B.M., Filippini, S., Starbuck, M.W., Hoffman, R.M., Navone, N., De-Juan-Pardo, E.M., Logothetis, C.J., Hutmacher, D.W., Friedl, P., 2018. Intravital microscopy of osteolytic progression and therapy response of cancer lesions in the bone. *Sci. Transl. Med.* 10 eaa05726.
- Drost, J., Karthaus, W.R., Gao, D., Driehuis, E., Sawyers, C.L., Chen, Y., Clevers, H., 2016. Organoid culture systems for prostate epithelial and cancer tissue. *Nat. Protoc.* 11, 347–358.
- Ehrbar, M., Rizzi, S.C., Hlushchuk, R., Djonov, V., Zisch, A.H., Hubbell, J.A., Weber, F.E., Lutolf, M.P., 2007. Enzymatic formation of modular cell-instructive fibrin analogs for tissue engineering. *Biomaterials* 28, 3856–3866.
- Esposito, M., Guise, T., Kang, Y., 2018. The biology of bone metastasis. *Cold Spring Harb. Perspect. Med.* 8.
- Faulk, D.M., Johnson, S.A., Zhang, L., Badylak, S.F., 2014. Role of the extracellular matrix in whole organ engineering. *J. Cell. Physiol.* 229, 984–989.
- Fedorovich, N.E., Oudshoorn, M.H., van Geemen, D., Hennink, W.E., Alblas, J., Dhert, W.J.A., 2009. The effect of photopolymerization on stem cells embedded in hydrogels. *Biomaterials* 30, 344–353.
- Fischbach, C., Chen, R., Matsumoto, T., Schmelzle, T., Brugge, J.S., Polverini, P.J., Mooney, D.J., 2007. Engineering tumors with 3D scaffolds. *Nat. Methods* 4, 855–860.
- Fischbach, C., Kong, H.J., Hsiong, S.X., Evangelista, M.B., Yuen, W., Mooney, D.J., 2009. Cancer cell angiogenic capability is regulated by 3D culture and integrin engagement. *Proc. Natl. Acad. Sci.* 106, 399–404.
- Fischer, T., Sack, I., Thomas, A., 2013. Characterization of focal breast lesions by means of elastography. *RöFo – Fortschritte auf dem Gebiet der Röntgenstrahlen und der Bildgeb. Verfahrenstechnik* 185, 816–823.
- Franco-Barraza, J., Beacham, D.A., Amatangelo, M.D., Cukierman, E., 2016. Preparation of extracellular matrices produced by cultured and primary fibroblasts. In: *Current Protocols in Cell Biology*. John Wiley & Sons, Inc., Hoboken, NJ, USA, pp. 10.9.1–10.9.34.
- Fratzl, P., Weinkamer, R., 2007. Nature's hierarchical materials. *Prog. Mater. Sci.* 52, 1263–1334.
- Friedl, P., Locker, J., Sahai, E., Segall, J.E., 2012a. Classifying collective cancer cell invasion. *Nat. Cell Biol.* 14, 777–783.
- Friedl, P., Sahai, E., Weiss, S., Yamada, K.M., 2012b. New dimensions in cell migration. *Nat. Rev. Mol. Cell Biol.* 13, 743–747.
- Friedrich, J., Seidel, C., Ebner, R., Kunz-Schughart, L.A., 2009. Spheroid-based drug screen: considerations and practical approach. *Nat. Protoc.* 4, 309–324.
- Fu, K., Pack, D.W., Klibanov, A.M., Langer, R., 2000. Visual evidence of acidic environment within degrading poly(lactic-co-glycolic acid) (PLGA) microspheres. *Pharm. Res.* 17, 100–106.
- Gaggioli, C., Hooper, S., Hidalgo-Carcedo, C., Grosse, R., Marshall, J.F., Harrington, K., Sahai, E., 2007. Fibroblast-led collective invasion of carcinoma cells with differing roles for RhoGTPases in leading and following cells. *Nat. Cell Biol.* 9, 1392–1400.
- Gatenby, R.A., Gillies, R.J., 2004. Why do cancers have high aerobic glycolysis? *Nat. Rev. Cancer* 4, 891–899.
- Ghajar, C.M., Peinado, H., Mori, H., Matei, I.R., Evason, K.J., Brazier, H., Almeida, D., Koller, A., Hajjar, K.A., Stainier, D.Y.R., Chen, E.I., Lyden, D., Bissell, M.J., 2013. The perivascular niche regulates breast tumour dormancy. *Nat. Cell Biol.* 15, 807–817.
- Gill, B.J., Gibbons, D.L., Roudsari, L.C., Saik, J.E., Rizvi, Z.H., Roybal, J.D., Kurie, J.M., West, J.L., 2012. A synthetic matrix with independently tunable biochemistry and mechanical properties to study epithelial morphogenesis and EMT in a lung adenocarcinoma model. *Cancer Res.* 72, 6013–6023.
- Glentis, A., Oertle, P., Mariani, P., Chikina, A., El Marjou, F., Attieh, Y., Zaccarini, F., Lae, M., Loew, D., Dingli, E., Sirven, P., Schoumacher, M., Gurchenkov, B.G., Plodinec, M., Vignjevic, D.M., 2017. Cancer-associated fibroblasts induce metalloprotease-independent cancer cell invasion of the basement membrane. *Nat. Commun.* 8, 924.
- Gong, Z., Szczesny, S.E., Caliri, S.R., Charrier, E.E., Chaudhuri, O., Cao, X., Lin, Y., Mauck, R.L., Janmey, P.A., Burdick, J.A., Shenoy, V.B., 2018. Matching material and cellular timescales maximizes cell spreading on viscoelastic substrates. *Proc. Natl. Acad. Sci.* 115, E2686–E2695.
- Grivennikov, S.I., Greten, F.R., Karin, M., 2010. Immunity, inflammation, and cancer. *Cell* 140, 883–899.
- Gruber, E., Heyward, C., Cameron, J., Leifer, C., 2018. Toll-like receptor signaling in macrophages is regulated by extracellular substrate stiffness and Rho-associated coiled-coil kinase (ROCK1/2). *Int. Immunol.* 30, 267–278.
- Gurski, L.A., Jha, A.K., Zhang, C., Jia, X., Farach-Carson, M.C., 2009. Hyaluronic acid-based hydrogels as 3D matrices for in vitro evaluation of chemotherapeutic drugs using poorly adherent prostate cancer cells. *Biomaterials* 30, 6076–6085.
- Hanahan, D., Weinberg, R.A., 2011. Hallmarks of cancer: the next generation. *Cell* 144, 646–674.
- He, F., Chiou, A.E., Loh, H.C., Lynch, M., Seo, B.R., Song, Y.H., Lee, M.J., Hoerth, R., Bortel, E.L., Willie, B.M., Duda, G.N., Estroff, L.A., Masic, A., Wagermaier, W., Fratzl, P., Fischbach, C., 2017. Multiscale characterization of the mineral phase at skeletal sites of breast cancer metastasis. *Proc. Natl. Acad. Sci.* 114, 10542–10547.
- Heintz, K.A., Bregenzler, M.E., Mantle, J.L., Lee, K.H., West, J.L., Slater, J.H., 2016. Fabrication of 3D biomimetic microfluidic networks in hydrogels. *Adv. Healthc. Mater.* 5, 2153–2160.
- Hersel, U., Dahmen, C., Kessler, H., 2003. RGD modified polymers: biomaterials for stimulated cell adhesion and beyond. *Biomaterials* 24, 4385–4415.
- Hodkinson, P.S., Elliott, T., Wong, W.S., Rintoul, R.C., Mackinnon, A.C., Haslett, C., Sethi, T., 2006. ECM overrides DNA damage-induced cell cycle arrest and apoptosis in small-cell lung cancer cells through $\beta 1$ integrin-dependent activation of PI3-kinase. *Cell Death Differ.* 13, 1776–1788.
- Hogrebe, N.J., Reinhardt, J.W., Tram, N.K., Debski, A.C., Agarwal, G., Reilly, M.A., Gooch, K.J., 2018. Independent control of matrix adhesiveness and stiffness within a 3D self-assembling peptide hydrogel. *Acta Biomater.* 70, 110–119.
- Holzapfel, B.M., Wagner, F., Loessner, D., Holzapfel, N.P., Thibaudeau, L., Crawford, R., Ling, M.-T., Clements, J.A., Russell, P.J., Hutmacher, D.W., 2014. Species-specific homing mechanisms of human prostate cancer metastasis in tissue engineered bone. *Biomaterials* 35, 4108–4115.
- Hsu, P.P., Sabatini, D.M., 2008. Cancer cell metabolism: Warburg and beyond. *Cell* 134, 703–707.
- Huh, D., Matthews, B.D., Mammoto, A., Montoya-Zavala, M., Hsin, H.Y., Ingber, D.E., 2010. Reconstituting organ-level lung functions on a chip. *Science* (80) 328, 1662–1668.

- Hynes, R.O., 2002. Integrins: bidirectional, allosteric signaling machines. *Cell* 110, 673–687.
- Jeon, J.S., Zervantonakis, I.K., Chung, S., Kamm, R.D., Charest, J.L., 2013. In vitro model of tumor cell extravasation. *PLoS One* 8, e56910.
- Kalluri, R., 2016. The biology and function of fibroblasts in cancer. *Nat. Rev. Cancer* 16, 582–598.
- Kalluri, R., Weinberg, R.A., 2009. The basics of epithelial-mesenchymal transition. *J. Clin. Investig.* 119, 1420–1428.
- Khetan, S., Guvendiren, M., Legant, W.R., Cohen, D.M., Chen, C.S., Burdick, J.A., 2013. Degradation-mediated cellular traction directs stem cell fate in covalently crosslinked three-dimensional hydrogels. *Nat. Mater.* 12, 458–465.
- Kim, J.W., Ho, W.J., Wu, B.M., 2011. The role of the 3D environment in hypoxia-induced drug and apoptosis resistance. *Anticancer Res.* 31, 3237–3245.
- Kim, S.-A., Lee, E.K., Kuh, H.-J., 2015. Co-culture of 3D tumor spheroids with fibroblasts as a model for epithelial–mesenchymal transition in vitro. *Exp. Cell Res.* 335, 187–196.
- Kolesky, D.B., Truby, R.L., Gladman, A.S., Busbee, T.A., Homan, K.A., Lewis, J.A., 2014. 3D bioprinting of vascularized, heterogeneous cell-laden tissue constructs. *Adv. Mater.* 26, 3124–3130.
- Kozlow, W., Guise, T.A., 2005. Breast cancer metastasis to bone: mechanisms of osteolysis and implications for therapy. *J. Mammary Gland Biol. Neoplasia* 10, 169–180.
- Kubow, K.E., Klotzsch, E., Smith, M.L., Gourdon, D., Little, W.C., Vogel, V., 2009. Crosslinking of cell-derived 3D scaffolds up-regulates the stretching and unfolding of new extracellular matrix assembled by reseeded cells. *Integr. Biol.* 1, 635.
- Kyburz, K.A., Anseth, K.S., 2013. Three-dimensional hMSC motility within peptide-functionalized PEG-based hydrogels of varying adhesivity and crosslinking density. *Acta Biomater.* 9, 6381–6392.
- Labernadie, A., Kato, T., Brugués, A., Serra-Picamal, X., Derzsi, S., Arwert, E., Weston, A., González-Tarragó, V., Elosegui-Artola, A., Albertazzi, L., Alcaraz, J., Roca-Cusachs, P., Sahai, E., Trepats, X., 2017. A mechanically active heterotypic E-cadherin/N-cadherin adhesion enables fibroblasts to drive cancer cell invasion. *Nat. Cell Biol.* 19, 224–237.
- Lee, G.Y., Kenny, P.A., Lee, E.H., Bissell, M.J., 2007. Three-dimensional culture models of normal and malignant breast epithelial cells. *Nat. Methods* 4, 359–365.
- Lee, H.-O., Mullins, S.R., Franco-Barraza, J., Valianou, M., Cukierman, E., Cheng, J.D., 2011. FAP-overexpressing fibroblasts produce an extracellular matrix that enhances invasive velocity and directionality of pancreatic cancer cells. *BMC Cancer* 11, 245.
- Lee, K.Y., Mooney, D.J., 2012. Alginate: properties and biomedical applications. *Prog. Polym. Sci.* 37, 106–126.
- Legant, W.R., Miller, J.S., Blakely, B.L., Cohen, D.M., Genin, G.M., Chen, C.S., 2010. Measurement of mechanical tractions exerted by cells in three-dimensional matrices. *Nat. Methods* 7, 969–971.
- Levental, K.R., Yu, H., Kass, L., Lakins, J.N., Egeblad, M., Erler, J.T., Fong, S.F.T., Csizsar, K., Giaccia, A., Weninger, W., Yamauchi, M., Gasser, D.L., Weaver, V.M., 2009. Matrix crosslinking forces tumor progression by enhancing integrin signaling. *Cell* 139, 891–906.
- Lewis, J.M., Truong, T.N., Schwartz, M.A., 2002. Integrins regulate the apoptotic response to DNA damage through modulation of p53. *Proc. Natl. Acad. Sci. USA* 99, 3627–3632.
- Li, C.X., Talele, N.P., Boo, S., Koehler, A., Knee-Walden, E., Balestrini, J.L., Speight, P., Kapus, A., Hinz, B., 2017. MicroRNA-21 preserves the fibrotic mechanical memory of mesenchymal stem cells. *Nat. Mater.* 16, 379–389.
- Li, T., Sun, L., Miller, N., Nicklee, T., Woo, J., Hulse-Smith, L., Tsao, M.-S., Khokha, R., Martin, L., Boyd, N., 2005. The association of measured breast tissue characteristics with mammographic density and other risk factors for breast cancer. *Cancer Epidemiol. Biomark. Prev.* 14, 343–349.
- Lin, C.-C., Anseth, K.S., 2009. PEG hydrogels for the controlled release of biomolecules in regenerative medicine. *Pharm. Res.* 26, 631–643.
- Liu, C., Chiang, B., Lewin Meija, D., Luker, K.E., Luker, G.D., Lee, A., 2019. Mammary fibroblasts remodel fibrillar collagen microstructure in a biomimetic nanocomposite hydrogel. *Acta Biomater.* 83, 221–232.
- Loebel, C., Mauck, R.L., Burdick, J.A., 2019. Local nascent protein deposition and remodelling guide mesenchymal stromal cell mechanosensing and fate in three-dimensional hydrogels. *Nat. Mater.* 1.
- Lohmann, N., Schirmer, L., Atallah, P., Wandel, E., Ferrer, R.A., Werner, C., Simon, J.C., Franz, S., Freudenberger, U., 2017. Glycosaminoglycan-based hydrogels capture inflammatory chemokines and rescue defective wound healing in mice. *Sci. Transl. Med.* 9, eaai9044.
- Lou, J., Stowers, R., Nam, S., Xia, Y., Chaudhuri, O., 2018. Stress relaxing hyaluronic acid-collagen hydrogels promote cell spreading, fiber remodeling, and focal adhesion formation in 3D cell culture. *Biomaterials* 154, 213–222.
- Lu, P., Weaver, V.M., Werb, Z., 2012. The extracellular matrix: a dynamic niche in cancer progression. *J. Cell Biol.* 196, 395–406.
- Lutolf, M.P., Doyonnas, R., Havenstrite, K., Koleckar, K., Blau, H.M., 2009. Perturbation of single hematopoietic stem cell fates in artificial niches. *Integr. Biol. (Camb)* 1, 59–69.
- Lutolf, M.P., Lauer-Fields, J.L., Schmoekel, H.G., Metters, A.T., Weber, F.E., Fields, G.B., Hubbell, J.A., 2003. Synthetic matrix metalloproteinase-sensitive hydrogels for the conduction of tissue regeneration: engineering cell-invasion characteristics. *Proc. Natl. Acad. Sci.* 100, 5413–5418.
- Lynch, M.E., Chiou, A.E., Lee, M.J., Marcott, S.C., Polamraju, P.V., Lee, Y., Fischbach, C., 2016. Three-dimensional mechanical loading modulates the osteogenic response of mesenchymal stem cells to tumor-derived soluble signals. *Tissue Eng Part A* 22, 1006–1015.
- Mabry, K.M., Lawrence, R.L., Anseth, K.S., 2015. Dynamic stiffening of poly(ethylene glycol)-based hydrogels to direct valvular interstitial cell phenotype in a three-dimensional environment. *Biomaterials* 49, 47–56.
- Mantovani, A., Bottazzi, B., Colotta, F., Sozzani, S., Ruco, L., 1992. The origin and function of tumor-associated macrophages. *Immunol. Today* 13, 265–270.
- Martin, J.D., Fukumura, D., Duda, D.G., Boucher, Y., Jain, R.K., 2016. Reengineering the tumor microenvironment to alleviate hypoxia and overcome cancer heterogeneity. *Cold Spring Harb. Perspect. Med.* 6.
- Martine, L.C., Holzapfel, B.M., McGovern, J.A., Wagner, F., Quent, V.M., Hesami, P., Wunner, F.M., Vaquette, C., De-Juan-Pardo, E.M., Brown, T.D., Nowlan, B., Wu, D.J., Huttmacher, C.O., Moi, D., Oussenko, T., Piccinini, E., Zandstra, P.W., Mazzieri, R., Lévesque, J.-P., Dalton, P.D., Taubenberger, A.V., Huttmacher, D.W., 2017. Engineering a humanized bone organ model in mice to study bone metastases. *Nat. Protoc.* 12, 639–663.
- Marturano-Kruik, A., Nava, M.M., Yeager, K., Chramiec, A., Hao, L., Robinson, S., Guo, E., Raimondi, M.T., Vunjak-Novakovic, G., 2018. Human bone perivascular niche-on-a-chip for studying metastatic colonization. *Proc. Natl. Acad. Sci.* 115, 1256–1261.

- Mastro, A.M., Gay, C.V., Welch, D.R., Donahue, H.J., Jewell, J., Mercer, R., DiGirolamo, D., Chislock, E.M., Guttridge, K., 2004. Breast cancer cells induce osteoblast apoptosis: a possible contributor to bone degradation. *J. Cell. Biochem.* 91, 265–276.
- Mather, M., Jacobsen, L.A., Pollard, K.M., 2015. *Population Bulletin*. Washington, DC.
- Mayorca-Guiliani, A.E., Madsen, C.D., Cox, T.R., Horton, E.R., Venning, F.A., Erler, J.T., 2017. ISDoT: in situ decellularization of tissues for high-resolution imaging and proteomic analysis of native extracellular matrix. *Nat. Med.* 23, 890–898.
- McCoy, M.G., Wei, J.M., Choi, S., Goerger, J.P., Zipfel, W., Fischbach, C., 2018. Collagen fiber orientation regulates 3D vascular network formation and alignment. *ACS Biomater. Sci. Eng.* 4, 2967–2976.
- McWhorter, F.Y., Wang, T., Nguyen, P., Chung, T., Liu, W.F., 2013. Modulation of macrophage phenotype by cell shape. *Proc. Natl. Acad. Sci.* 110, 17253–17258.
- Miller, C.G., Pozzi, A., Zent, R., Schwarzbauer, J.E., 2014. Effects of high glucose on integrin activity and fibronectin matrix assembly by mesangial cells. *Mol. Biol. Cell* 25, 2342–2350.
- Miller, J.S., Stevens, K.R., Yang, M.T., Baker, B.M., Nguyen, D.-H.T., Cohen, D.M., Toro, E., Chen, A.A., Galie, P.A., Yu, X., Chaturvedi, R., Bhatia, S.N., Chen, C.S., 2012. Rapid casting of patterned vascular networks for perfusable engineered three-dimensional tissues. *Nat. Mater.* 11, 768–774.
- Millipore Sigma, 2019a. MaxGel™ ECM Hydrogel: An in Vitro Human Cell Derived Basement Membrane Extract for 3D Cell Culture Applications. [WWW Document]. <https://www.sigmaaldrich.com/life-science/stem-cell-biology/3d-stem-cell-culture/maxgel-human-ecm.html>.
- Millipore Sigma, 2019b. SpongeCol. [WWW Document]. <https://www.sigmaaldrich.com/catalog/product/sigma/5135?lang=en®ion=US>.
- Millipore Sigma, 2019c. HyStem™ Hyaluronic Acid Based Hydrogels for 3D Cell Culture Applications. [WWW Document]. <https://www.sigmaaldrich.com/technical-documents/articles/biology/hystem-3d-hydrogels.html>.
- Miranti, C.K., Brugge, J.S., 2002. Sensing the environment: a historical perspective on integrin signal transduction. *Nat. Cell Biol.* 4, E83–E90.
- Moon, J.J., Saik, J.E., Poché, R.A., Leslie-Barbick, J.E., Lee, S.-H., Smith, A.A., Dickinson, M.E., West, J.L., 2010. Biomimetic hydrogels with pro-angiogenic properties. *Biomaterials* 31, 3840–3847.
- Morgan, J.P., Delnero, P.F., Zheng, Y., Verbridge, S.S., Chen, J., Craven, M., Choi, N.W., Diaz-Santana, A., Kermani, P., Hempstead, B., López, J.A., Corso, T.N., Fischbach, C., Stroock, A.D., 2013. Formation of microvascular networks in vitro. *Nat. Protoc.* 8, 1820–1836.
- Moya, M.L., Hsu, Y.-H., Lee, A.P., Hughes, C.C.W., George, S.C., 2013. In vitro perfused human capillary networks. *Tissue Eng. C Methods* 19, 730–737.
- Mulligan, J.A., Bordeleau, F., Reinhart-King, C.A., Adie, S.G., 2017. Measurement of dynamic cell-induced 3D displacement fields in vitro for traction force optical coherence microscopy. *Biomed. Opt. Express* 8, 1152.
- Munavar, S., Wang, Y., Dembo, M., 2001. Traction force microscopy of migrating normal and H-ras transformed 3T3 fibroblasts. *Biophys. J.* 80, 1744–1757.
- Munson, J.M., Bellamkonda, R.V., Swartz, M.A., 2013. Interstitial flow in a 3D microenvironment increases glioma invasion by a CXCR4-dependent mechanism. *Cancer Res.* 73, 1536–1546.
- Munson, J.M., Shieh, A.C., 2014. Interstitial fluid flow in cancer: implications for disease progression and treatment. *Cancer Manag. Res.* 6, 317–328.
- Naba, A., Clauser, K.R., Hoersch, S., Liu, H., Carr, S.A., Hynes, R.O., 2012. The matrisome: in silico definition and in vivo characterization by proteomics of normal and tumor extracellular matrices. *Mol. Cell. Proteom.* 11.
- Nam, S., Stowers, R., Lou, J., Xia, Y., Chaudhuri, O., 2019. Varying PEG density to control stress relaxation in alginate-PEG hydrogels for 3D cell culture studies. *Biomaterials* 200, 15–24.
- Nasrollahi, S., Walter, C., Loza, A.J., Schimizzi, G.V., Longmore, G.D., Pathak, A., 2017. Past matrix stiffness primes epithelial cells and regulates their future collective migration through a mechanical memory. *Biomaterials* 146, 146–155.
- Nathan, S.S., DiResta, G.R., Casas-Ganem, J.E., Hoang, B.H., Sowers, R., Yang, R., Huvos, A.G., Gorlick, R., Healey, J.H., 2005. Elevated physiologic tumor pressure promotes proliferation and chemosensitivity in human osteosarcoma. *Clin. Cancer Res.* 11, 2389–2397.
- Noone, A., Howlader, N., Krapcho, M., Miller, D., Brest, A., Yu, M., Ruhl, J., Tatalovich, Z., Mariotto, A., Lewis, D., Chen, H., Feuer, E., Cronin, K. (Eds.), 2018. *SEER Cancer Statistics Review*. Bethesda, MD.
- Nyga, A., Neves, J., Stamati, K., Loizidou, M., Emberton, M., Cheema, U., 2016. The next level of 3D tumour models: immunocompetence the complexity of the tumour microenvironment encompasses interactions between cancer and stromal cells. Moving from 2D cell culture methods into 3D models enables more-accurate investigation of those interactions. *Current 3D cancer models focus on cancer spheroid interaction with stromal cells.* *Drug Discov. Today* 21, 1421–1428.
- Ortiz Franyuti, D., Mitsi, M., Vogel, V., 2018. Mechanical stretching of fibronectin fibers upregulates binding of interleukin-7. *Nano Lett.* 18, 15–25.
- Parenteau-Bareil, R., Gauvin, R., Berthod, F., 2010. Collagen-based biomaterials for tissue engineering applications. *Materials* 3, 1863–1887.
- Park, Y.D., Tirelli, N., Hubbell, J.A., 2003. Photopolymerized hyaluronic acid-based hydrogels and interpenetrating networks. *Biomaterials* 24, 893–900.
- Paszek, M.J., Zahir, N., Johnson, K.R., Lakins, J.N., Rozenberg, G.I., Gefen, A., Reinhart-King, C.A., Margulies, S.S., Dembo, M., Boettiger, D., Hammer, D.A., Weaver, V.M., 2005. Tensional homeostasis and the malignant phenotype. *Cancer Cell* 8, 241–254.
- Pathak, A., Kumar, S., 2012. Independent regulation of tumor cell migration by matrix stiffness and confinement. *Proc. Natl. Acad. Sci.* 109, 10334–10339.
- Pathi, S.P., Kowalczewski, C., Tadipatri, R., Fischbach, C., 2010. A novel 3-D mineralized tumor model to study breast cancer bone metastasis. *PLoS One* 5, e8849.
- Pathi, S.P., Lin, D.D.W., Dorvee, J.R., Estroff, L.A., Fischbach, C., 2011. Hydroxyapatite nanoparticle-containing scaffolds for the study of breast cancer bone metastasis. *Biomaterials* 32, 5112–5122.
- Pawelec, K.M., Best, S.M., Cameron, R.E., 2016. Collagen: a network for regenerative medicine. *J. Mater. Chem. B* 4, 6484–6496.
- Peyton, S.R., Putnam, A.J., 2005. Extracellular matrix rigidity governs smooth muscle cell motility in a biphasic fashion. *J. Cell. Physiol.* 204, 198–209.
- Peyton, S.R., Raub, C.B., Keschrums, V.P., Putnam, A.J., 2006. The use of poly(ethylene glycol) hydrogels to investigate the impact of ECM chemistry and mechanics on smooth muscle cells. *Biomaterials* 27, 4881–4893.

- Piccoli, M., D'Angelo, E., Crotti, S., Sensi, F., Urbani, L., Maghin, E., Burns, A., De Coppi, P., Fassan, M., Rugge, M., Rizzolio, F., Giordano, A., Pilati, P., Mammato, E., Pucciarelli, S., Agostini, M., 2018. Decellularized colorectal cancer matrix as bioactive microenvironment for in vitro 3D cancer research. *J. Cell. Physiol.* 233, 5937–5948.
- Plotnikov, S.V., Sabass, B., Schwarz, U.S., Waterman, C.M., 2014. High-resolution traction force microscopy. In: *Methods in Cell Biology*, pp. 367–394.
- Poincloux, R., Collin, O., Lizárraga, F., Romao, M., Debray, M., Piel, M., Chavrier, P., 2011. Contractility of the cell rear drives invasion of breast tumor cells in 3D Matrigel. *Proc. Natl. Acad. Sci.* 108, 1943–1948.
- Polacheck, W.J., Charest, J.L., Kamm, R.D., 2011. Interstitial flow influences direction of tumor cell migration through competing mechanisms. *Proc. Natl. Acad. Sci.* 108, 11115–11120.
- Polacheck, W.J., Chen, C.S., 2016. Measuring cell-generated forces: a guide to the available tools. *Nat. Methods* 13, 415–423.
- Pollard, J.W., 2004. Tumour-educated macrophages promote tumour progression and metastasis. *Nat. Rev. Cancer* 4, 71–78.
- Provenzano, P.P., Eliceiri, K.W., Campbell, J.M., Inman, D.R., White, J.G., Keely, P.J., 2006. Collagen reorganization at the tumor-stromal interface facilitates local invasion. *BMC Med.* 4, 38.
- Pruitt, H.C., Lewis, D., Ciccaglione, M., Connor, S., Smith, Q., Hickey, J.W., Schneck, J.P., Gerecht, S., 2019. Collagen fiber structure guides 3D motility of cytotoxic T lymphocytes. *Matrix Biol.*
- Rama-Esendagli, D., Esendagli, G., Yilmaz, G., Guc, D., 2014. Spheroid formation and invasion capacity are differentially influenced by co-cultures of fibroblast and macrophage cells in breast cancer. *Mol. Biol. Rep.* 41, 2885–2892.
- Rao, S.S., Bushnell, G.G., Azarin, S.M., Spicer, G., Aguado, B.A., Stoehr, J.R., Jiang, E.J., Backman, V., Shea, L.D., Jeruss, J.S., 2016. Enhanced survival with implantable scaffolds that capture metastatic breast cancer cells in vivo. *Cancer Res.* 76, 5209–5218.
- Rosales, A.M., Rodell, C.B., Chen, M.H., Morrow, M.G., Anseth, K.S., Burdick, J.A., 2018. Reversible control of network properties in azobenzene-containing hyaluronic acid-based hydrogels. *Bioconjug. Chem.* 29, 905–913.
- Roy, R., Boskey, A., Bonassar, L.J., 2009. Processing of type I collagen gels using nonenzymatic glycation. *J. Biomed. Mater. Res. A* 9999A, (NA-NA).
- Sapudom, J., Rubner, S., Martin, S., Kurth, T., Riedel, S., Mierke, C.T., Pompe, T., 2015. The phenotype of cancer cell invasion controlled by fibril diameter and pore size of 3D collagen networks. *Biomaterials* 52, 367–375.
- Seo, B.R., Bhardwaj, P., Choi, S., Gonzalez, J., Andresen Eguiluz, R.C., Wang, K., Mohanan, S., Morris, P.G., Du, B., Zhou, X.K., Vahdat, L.T., Verma, A., Elemento, O., Hudis, C.A., Williams, R.M., Gourdon, D., Dannenberg, A.J., Fischbach, C., 2015. Obesity-dependent changes in interstitial ECM mechanics promote breast tumorigenesis. *Sci. Transl. Med.* 7, 301ra130.
- Serebriiskii, I., Castelló-Cros, R., Lamb, A., Golemis, E.A., Cukierman, E., 2008. Fibroblast-derived 3D matrix differentially regulates the growth and drug-responsiveness of human cancer cells. *Matrix Biol.* 27, 573–585.
- Sharaf, H., Matou-Nasri, S., Wang, Q., Rabhan, Z., Al-Eidi, H., Al Abdulrahman, A., Ahmed, N., 2015. Advanced glycation end-products increase proliferation, migration and invasion of the breast cancer cell line MDA-MB-231. *Biochim. Biophys. Acta – Mol. Basis Dis.* 1852, 429–441.
- Shin, Y., Han, S., Jeon, J.S., Yamamoto, K., Zervantonakis, I.K., Sudo, R., Kamm, R.D., Chung, S., 2012. Microfluidic assay for simultaneous culture of multiple cell types on surfaces or within hydrogels. *Nat. Protoc.* 7, 1247–1259.
- Sieh, S., Taubenberger, A.V., Rizzi, S.C., Sadowski, M., Lehman, M.L., Rockstroh, A., An, J., Clements, J.A., Nelson, C.C., Huttmacher, D.W., 2012. Phenotypic characterization of prostate cancer LNCaP cells cultured within a bioengineered microenvironment. *PLoS One* 7, e40217.
- Smith, M.L., Chen, I.T., Zhan, Q., O'Connor, P.M., Fornace, A.J., 1995. Involvement of the p53 tumor suppressor in repair of u.v.-type DNA damage. *Oncogene* 10, 1053–1059.
- Song, J.W., Munn, L.L., 2011. Fluid forces control endothelial sprouting. *Proc. Natl. Acad. Sci.* 108, 15342–15347.
- Springer, N.L., Fischbach, C., 2016. Biomaterials approaches to modeling macrophage–extracellular matrix interactions in the tumor microenvironment. *Curr. Opin. Biotechnol.* 40, 16–23.
- Stowers, R.S., Allen, S.C., Sanchez, K., Davis, C.L., Ebel, N.D., Van Den Berg, C., Suggs, L.J., 2017. Extracellular matrix stiffening induces a malignant phenotypic transition in breast epithelial cells. *Cell. Mol. Bioeng.* 10, 114–123.
- Strathearn, K., Rothernberg, M., 2012. Corning Ultra-Low Attachment Surface Promotes Spheroid Formation in MCF-7 Human Breast Cancer Cell Line. (Kennebunk).
- Suárez-González, D., Barnhart, K., Saito, E., Vanderby, R., Hollister, S.J., Murphy, W.L., Murphy, W.L., 2010. Controlled nucleation of hydroxyapatite on alginate scaffolds for stem cell-based bone tissue engineering. *J. Biomed. Mater. Res. A* 95, 222–234.
- Tan, C.P., Ri Seo, B., Brooks, D.J., Chandler, E.M., Craighead, H.G., Fischbach, C., 2009. Parylene peel-off arrays to probe the role of cell–cell interactions in tumour angiogenesis. *Integr. Biol.* 1, 587.
- Tatosian, D.A., Shuler, M.L., 2009. A novel system for evaluation of drug mixtures for potential efficacy in treating multidrug resistant cancers. *Biotechnol. Bioeng.* 103, 187–198.
- Taubenberger, A.V., Bray, L.J., Haller, B., Shaposhnykov, A., Binner, M., Freudenberg, U., Guck, J., Werner, C., 2016. 3D extracellular matrix interactions modulate tumour cell growth, invasion and angiogenesis in engineered tumour microenvironments. *Acta Biomater.* 36, 73–85.
- Taubenberger, A.V., Quent, V.M., Thibaudeau, L., Clements, J.A., Huttmacher, D.W., 2013. Delineating breast cancer cell interactions with engineered bone microenvironments. *J. Bone Miner. Res.* 28, 1399–1411.
- ThermoFisher, n.d. AlgiMatrix 3D Cell Culture System [WWW Document]. <https://www.thermofisher.com/us/en/home/life-science/cell-culture/organoids-spheroids-3d-cell-culture/extracellular-matrices-ecm/algimatrix-3d-cell-culture-system.html>.
- Tian, X., Werner, M.E., Roche, K.C., Hanson, A.D., Foote, H.P., Yu, S.K., Warner, S.B., Copp, J.A., Lara, H., Wauthier, E.L., Caster, J.M., Herring, L.E., Zhang, L., Tepper, J.E., Hsu, D.S., Zhang, T., Reid, L.M., Wang, A.Z., 2018. Organ-specific metastases obtained by culturing colorectal cancer cells on tissue-specific decellularized scaffolds. *Nat. Biomed. Eng.* 2, 443–452.
- Tibbitt, M.W., Anseth, K.S., 2009. Hydrogels as extracellular matrix mimics for 3D cell culture. *Biotechnol. Bioeng.*
- Torisawa, Y., Spina, C.S., Mammoto, T., Mammoto, A., Weaver, J.C., Tat, T., Collins, J.J., Ingber, D.E., 2014. Bone marrow-on-a-chip replicates hematopoietic niche physiology in vitro. *Nat. Methods* 11, 663–669.
- Tse, J.R., Engler, A.J., 2010. Preparation of hydrogel substrates with tunable mechanical properties. *Curr. Protoc. Cell Biol.* 47 10.16.1-10.16.16.

- Tung, Y.-C., Hsiao, A.Y., Allen, S.G., Torisawa, Y., Ho, M., Takayama, S., 2011. High-throughput 3D spheroid culture and drug testing using a 384 hanging drop array. *Analyst* 136, 473–478.
- Ulrich, T.A., Jain, A., Tanner, K., MacKay, J.L., Kumar, S., 2010. Probing cellular mechanobiology in three-dimensional culture with collagen–agarose matrices. *Biomaterials* 31, 1875–1884.
- Ungrin, M.D., Joshi, C., Nica, A., Bauwens, C., Zandstra, P.W., 2008. Reproducible, ultra high-throughput formation of multicellular organization from single cell suspension-derived human embryonic stem cell aggregates. *PLoS One* 3, e1565.
- Vaupel, P., Kallinowski, F., Okunieff, P., 1989. Blood flow, oxygen and nutrient supply, and metabolic microenvironment of human tumors: a review. *Cancer Res.* 49, 6449–6465.
- Vidavsky, N., Kunitake, J.A.M.R., Chiou, A.E., Northrup, P.A., Porri, T.J., Ling, L., Fischbach, C., Estroff, L.A., 2018. Studying biomineralization pathways in a 3D culture model of breast cancer microcalcifications. *Biomaterials* 179, 71–82.
- Villasante, A., Marturano-Kruik, A., Vunjak-Novakovic, G., 2014. Bioengineered human tumor within a bone niche. *Biomaterials* 35, 5785–5794.
- Wang, H., Abhilash, A.S., Chen, C.S., Wells, R.G., Shenoy, V.B., 2014. Long-range force transmission in fibrous matrices enabled by tension-driven alignment of fibers. *Biophys. J.* 107, 2592–2603.
- Wang, K., Andresen Eguiluz, R.C., Wu, F., Seo, B.R., Fischbach, C., Gourdon, D., 2015. Stiffening and unfolding of early deposited-fibronectin increase proangiogenic factor secretion by breast cancer-associated stromal cells. *Biomaterials* 54, 63–71.
- Wang, Y.-L., Pelham, R.J., 1998. Preparation of a flexible, porous polyacrylamide substrate for mechanical studies of cultured cells. *Methods Enzymol.* 298, 489–496.
- Weigelt, B., Ghajar, C.M., Bissell, M.J., 2014. The need for complex 3D culture models to unravel novel pathways and identify accurate biomarkers in breast cancer. *Adv. Drug Deliv. Rev.* 69–70, 42–51.
- WHO, 2018. Cancer.
- Wisdom, K.M., Adebowale, K., Chang, J., Lee, J.Y., Nam, S., Desai, R., Rossen, N.S., Rafat, M., West, R.B., Hodgson, L., Chaudhuri, O., 2018. Matrix mechanical plasticity regulates cancer cell migration through confining microenvironments. *Nat. Commun.* 9, 4144.
- Wolf, K., Alexander, S., Schacht, V., Coussens, L.M., von Andrian, U.H., van Rheenen, J., Deryugina, E., Friedl, P., 2009. Collagen-based cell migration models in vitro and in vivo. *Semin. Cell Dev. Biol.* 20, 931–941.
- Wolf, K., Te Lindert, M., Krause, M., Alexander, S., Te Riet, J., Willis, A.L., Hoffman, R.M., Figdor, C.G., Weiss, S.J., Friedl, P., 2013. Physical limits of cell migration: control by ECM space and nuclear deformation and tuning by proteolysis and traction force. *J. Cell Biol.* 201, 1069–1084.
- Xiao, W., Zhang, R., Sohrabi, A., Ehsanipour, A., Sun, S., Liang, J., Walthers, C.M., Ta, L., Nathanson, D.A., Seidlits, S.K., 2018. Brain-mimetic 3D culture platforms allow investigation of cooperative effects of extracellular matrix features on therapeutic resistance in glioblastoma. *Cancer Res.* 78, 1358–1370.
- Xu, X., Gurski, L.A., Zhang, C., Harrington, D.A., Farach-Carson, M.C., Jia, X., 2012. Recreating the tumor microenvironment in a bilayer, hyaluronic acid hydrogel construct for the growth of prostate cancer spheroids. *Biomaterials* 33, 9049–9060.
- Xu, X., Liu, C., Liu, Y., Li, N., Guo, X., Wang, S., Sun, G., Wang, W., Ma, X., 2013. Encapsulated human hepatocellular carcinoma cells by alginate gel beads as an in vitro metastasis model. *Exp. Cell Res.* 319, 2135–2144.
- Yang, C., Tibbitt, M.W., Basta, L., Anseth, K.S., 2014. Mechanical memory and dosing influence stem cell fate. *Nat. Mater.* 13, 645–652.
- Yuh, J.M., Li, A.P., Martinez, A.O., Ladman, A.J., 1977. A simplified method for production and growth of multicellular tumor spheroids. *Cancer Res.* 37, 3639–3643.
- Zarrintaj, P., Manouchehri, S., Ahmadi, Z., Saeb, M.R., Urbanska, A.M., Kaplan, D.L., Mozafari, M., 2018. Agarose-based biomaterials for tissue engineering. *Carbohydr. Polym.* 187, 66–84.
- Zheng, Y., Chen, J., Craven, M., Choi, N.W., Totorica, S., Diaz-Santana, A., Kermani, P., Hempstead, B., Fischbach-Teschl, C., Lopez, J.A., Stroock, A.D., 2012. In vitro microvessels for the study of angiogenesis and thrombosis. *Proc. Natl. Acad. Sci.* 109, 9342–9347.
- Zhu, J., 2010. Bioactive modification of poly(ethylene glycol) hydrogels for tissue engineering. *Biomaterials* 31, 4639–4656.

Chapter Exercises With (Guided) Solutions

Question 1: List four important biological design considerations for engineered tumor models.

Answer:

1. Tissue dimensionality
2. Mass and fluid transport/transport phenomena
3. ECM physicochemical properties/changes to stiffness, structure, chemical composition in malignancy, e.g., remodeling by stromal cells
4. Immunological considerations such as incorporation of immune cell types or immunocompetent animal models

Question 2: Describe three model systems that serve to replicate changes in tissue dimensionality during tumorigenesis. Explain how they are manufactured and which specific aspects of the tumor microenvironment they can recapitulate.

Answer:

1. Spheroids
 - (i) Formed via hanging drop, agarose-coated plates, or specialized plates (pyramidal microwells or plates with vertical channels)
 - (ii) Promote cell–cell contacts in three dimensions, provide mass transport dynamics seen in tissues, and tissue-like structural features
2. Scaffolds
 - (i) Encapsulation in polymeric scaffolds, hydrogels (both natural and synthetic)
 - (ii) Cells get cues from their surroundings, adopt morphology different from 2D, changes to signaling and gene expression due to a variety of mechanisms including differential integrin engagement, cell–cell contact, as well as responses to tumor-intrinsic microenvironmental cues including hypoxia
3. Patterned hydrogels
 - (i) Covalently couple adhesion molecules normally expressed on a cell's membrane onto a PDMS stamped micropatterned PEG hydrogel; examples include N-cadherin, VE-cadherin, I-CAM, V-CAM, P-Sel, and Jag-1
 - (ii) This system allows for isolation and direct study of cell–cell contacts via interaction of specific protein binding pairs. These are also mechanically tunable allowing to compare effects of cell–cell adhesion in the presence and absence of varied substrate mechanical properties. This has identified how single cell division kinetics are impacted by intercellular adhesion proteins and how these correlate to in vivo function

Question 3: Describe how changes in ECM dynamics can be recapitulated with hydrogel systems using examples from the text and explain the benefit of such systems to cancer research.

Answer: The tumor microenvironment is not static, but constantly changing. For example, spatial and temporal changes of ECM mechanical properties can be modulated by cell-mediated degradation. Studying the impact of

such changes can be achieved by incorporating specifically engineered cross-links into hydrogel systems. For example, covalent coupling of MMP degradable sequences enables cell-mediated degradation of the material and consequential changes in cell behavior. Additional chemistry can be incorporated to cause a secondary cross-linking reaction later during the culture period that inhibits additional enzymatic degradation. Mechanical properties can also be changed in a reversible manner through light-dependent stiffening or softening of materials. For example, reversible stiffening/softening of hyaluronic acid-based hydrogels can be achieved through incorporation of supramolecular cross-links formed via azobenzene bound to β -cyclodextrin where exposure to 365 nm light will soften and 400–500 nm light will stiffen the gels. PEG gels can also undergo delayed secondary cross-link reactions via thiol-ene polymerization. Such dynamic systems allow for cell-mediated remodeling, isolation of initial stiffness from another value, and separating the effect of morphology changes from those mediated by varied substrate mechanical properties.

Question 4: Which experimental technique is routinely used to measure the adhesive forces of cells on materials-based ECM mimics? Explain how this technique is performed.

Answer: Traction force microscopy. Fluorescent beads are embedded into polyacrylamide hydrogels. Cells are seeded on top and images are acquired of the cells as they exert a force on the underlying substrate. An enzyme called trypsin is then added to detach the cells from the gel. More images are taken in the same field of view of the gel in the relaxed state. The difference in the positions of the fluorescent beads is used to computationally determine the forces the cells were exerting.

Question 5: What are some immune-related changes that happen in cancer? To create a tumor model with functional immune response, what types of immune cells would you incorporate?

Answer:

A. Changes:

- (1) Hijack inflammatory and immunomodulatory signals to enhance tumorigenesis
- (2) Suppressed cytotoxic activity of other immune cells
- (3) Increased remodeling due to upregulation of enzymes to degrade matrix
- (4) Changes to matrix mechanics and structure (intratumoral pressure, ECM density, fiber alignment).

B. Cell types:

Dendritic cells, T cells (CD4+ and/or CD8+), macrophages (M1, M2), natural killer cells, lymphocytes. Other stromal cells such as endothelial cells or fibroblasts could also be useful.

Question 6: Many cancers metastasize to the brain and much is still unknown about what happens when they arrive there. Explain how model systems for the study of brain metastases will differ from the models in the case study on bone metastasis. Consider the properties of brain tissue that

would differ from bone and how these would affect your choice of materials.

Answer: Differences include mechanical properties, cell types, and ECM proteins present. Brain tissue is much softer than bone and thus, the materials used to model brain must have a lower Young's modulus than those used for bone. There are also compositional differences between the bone and brain ECM. Whereas the bone is composed predominantly of mineralized collagen, the brain contains fibronectin, vitronectin, tenascin C, laminin, and HA. The cellular composition of the brain and bone also vary and cocultures of brain cells with cancer cells would be very different from those used in bone. Finally, the interstitial pressure developing within the brain is significantly different given the space constraints mediated by the skull.

Question 7: What role does vasculature play in cancer? List four materials and methods that could be used to model vasculature. What could be improved on existing models to more accurately model tumor vasculature?

Answer: Vasculature transports oxygen, nutrients, metabolic waste products, cells (e.g., metastatic cancer cells, immune cells), and drugs. Tumors must develop new vasculature as they grow to support the increased number of cells and the oxygen and nutrients they require. Often tumors outgrow the blood supply and develop a hypoxic necrotic core. When new vessels are created, they are often dysfunctional and leaky leading to impaired mass transport kinetics and the development of interstitial pressure.

A. Example model systems include:

- Laser ablation of channels into PEGDA gels
- Patterning vascular structures into hydrogel scaffolds using photolithography-based coupling of cell-adhesion peptides
- Creating microfluidic networks within natural hydrogel matrices using soft lithography approaches
- Using sacrificial materials to pattern channels into hydrogels
- Performing vasculogenesis (i.e., individual endothelial cells forming vascular networks within hydrogel) within a microfluidic device
- 3D printing in GelMA

B. Improvements: Answers may vary, examples include: simulating leaky vessels, incorporating spheroid models with vascular models etc.

Question 8: A drug company has developed a new candidate drug that appears to target cellular adhesion mechanisms of cancer cells in solid tumors. When they tested the drug on prostate cancer cells seeded on a Petri dish, it was remarkably effective, but did not harm normal cells. However, investors are concerned that this experiment is not enough to justify the cost of preclinical animal testing. Outline and justify a series of experimental systems to test the drug's efficacy, first in a precisely controlled environment, then in a more biologically complex system. Consider the advantages of natural and synthetic materials as well as the clarity of the data produced by different systems. Consider also additional factors that may impact or confound your data.

Answer:

1. Controlled environments could utilize a synthetic hydrogel material like PEG conjugated with one or more specific adhesion sequences that are thought to play a role in the drug's mechanism of action (e.g., RGD from fibronectin). The lack of biological complexity will help focus the experiment on adhesion while still enabling 3D culture that is more faithful to tumor characteristics.
2. A more complex system could be a synthetic material that contains multiple peptide sequences, a composite material containing collagen or fibronectin, or a natural material. An experiment utilizing multiple cell types would be a closer approximation of a tumor. Embedding individual cells in a 3D gel or matrix would make the system less cumbersome to use, while embedding a spheroid into a hydrogel adds more complexity and cost.
3. Confounding factors: material porosity, pH, stiffness, viscoelasticity, fiber alignment, and/or size. For gels: mass transfer and diffusion from culture medium.

Question 9: Researchers are studying cancer progression in two groups of mice. One group of mice forms large aggressive tumors while the other group does not. The researchers hypothesize that it may have something to do with differences in the ECM properties between the two groups.

- a. Describe how this hypothesis could be studied using a cell-derived matrix model.
- b. Additional testing shows that the group of mice with larger tumors has stiffer ECM to start with. Design a model using synthetic biomaterials to test whether differences in ECM mechanics could be responsible for differences in tumor growth between the two groups of mice. Explain why you chose the material you did.

Answer:

1. Stromal cells can be isolated from each group of mice and cultured to produce matrices. The cultures can be decellularized to produce CDMs with unique properties to each group of mice. Cancer cells can be seeded on top of the matrices and analyzed for proliferation, morphology, migration, cluster formation, etc.
2. Many answers are possible. The main focus is on a material that has tunable mechanical properties. Other considerations include 2D versus 3D ability (PA versus PEG), the inclusion of cell-adhesive ligands (RGD), and degradable properties of the material

Question 10: Several immune cell types have previously been grown in coculture systems with cancer cells, but model systems that accurately model the role of the immune system in systemic regulation of cancer progression are still needed. Define the design criteria for a body-on-a-chip system that is comprised of three or more organoid systems relevant to cancer development, control, or metastasis. Your system should contain multiple cell types and consider physiological conditions necessary for cells to function normally (as in the lung-on-a-chip and endothelialized microvessel devices from the text).

Answer:

Possible design features—a primary tumor compartment with stromal cells of the primary site connected to other compartments by microfluidics or vascularized microvessels. Possible other compartments include common metastatic sites (liver, lung, brain, bone) as well as a lymphoid

compartment (lymph node, lymph vessels, skin, bone marrow, thymus, spleen, and liver). Physical design features will depend on the organs modeled, but mechanics, diffusion, and flow as well as multiple cell types relevant to the model designed should be considered.

2.5.12

Drug Delivery Systems

DANIELLE S.W. BENOIT^{1,2,3,4,5,6}, CLYDE T. OVERBY^{1,2}, KENNETH R. SIMS JR.^{1,6},
MARIAN A. ACKUN-FARMER^{1,2}

¹Department of Biomedical Engineering, University of Rochester, Rochester, NY, United States

²Department of Orthopaedics and Center for Musculoskeletal Research, University of Rochester, Rochester, NY, United States

³Materials Science Program, University of Rochester, Rochester, NY, United States

⁴Department of Chemical Engineering, University of Rochester, Rochester, NY, United States

⁵Department of Biomedical Genetics and Center for Oral Biology, University of Rochester, Rochester, NY, United States

⁶Translational Biomedical Science Program, University of Rochester, Rochester, NY, United States

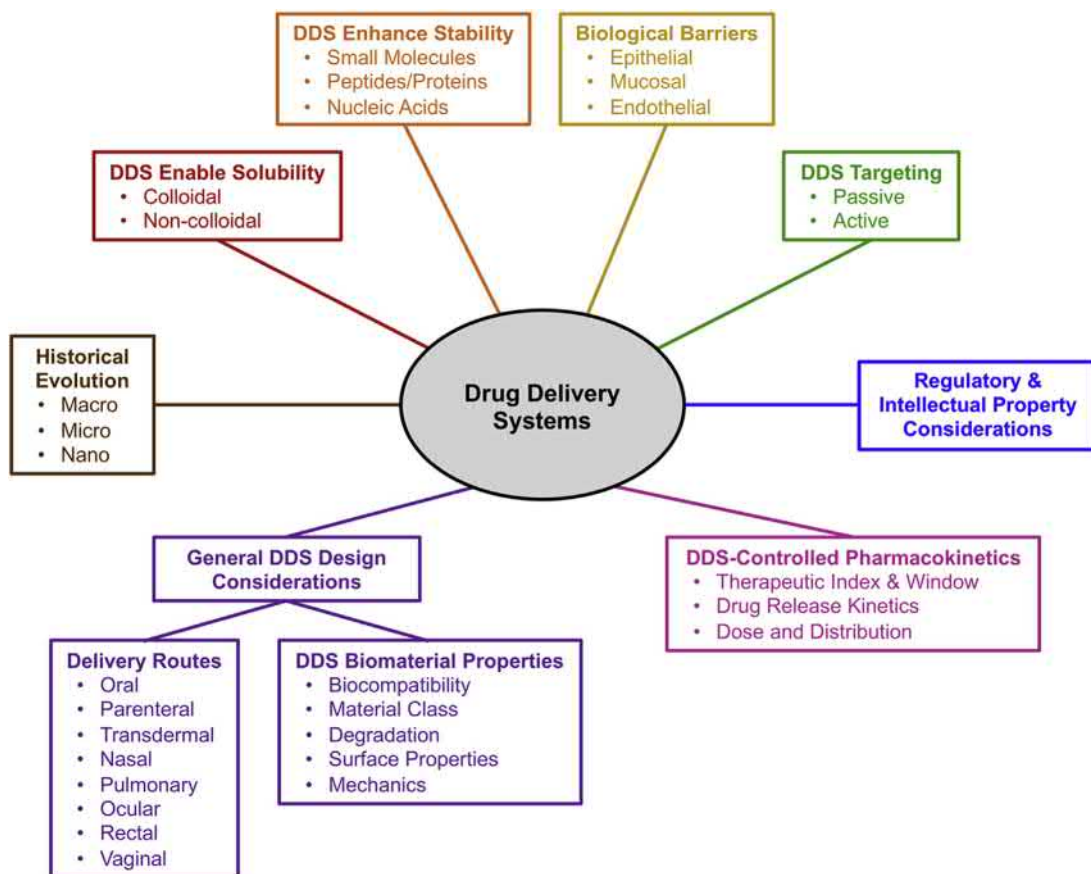
Biomaterials are outstanding platforms to ensure controlled, reproducible drug delivery. Furthermore, biomaterials play a critical role in enhancing or enabling drug efficacy for both traditional small molecule drugs and new classes of drugs, such as nucleic acids and proteins, that suffer from delivery challenges associated with instability and poor tissue localization. This chapter overviews drug delivery challenges as well as subsequent design and use of biomaterial drug delivery systems (DDSs) to overcome these hurdles. Fig. 2.5.12.1 summarizes the key aspects of DDS development from basic research to clinical applications that are discussed in this chapter. Although highly sophisticated, targeted, bioresponsive DDSs have only recently started delivering on ambitious promises, the concepts and approaches being developed are rooted in longstanding historical motivations. Therefore a brief overview of DDS history from its origins to today is first presented to provide a framework for understanding current biomaterial DDS design. For additional information on drug formulation and DDSs, please see these excellent in-depth reviews (Bader et al., 2014; Galaev and Mattiasson, 2010; Hilery et al., 2001; Hillery et al., 2002; Holowka and Bhatia, 2016; Mahato and Narang, 2018; Saltzman, 2001; Sinko, 2017).

History of DDS Development

Routine, periodic drug administration to achieve therapeutic efficacy has been used for more than 150 years. In the

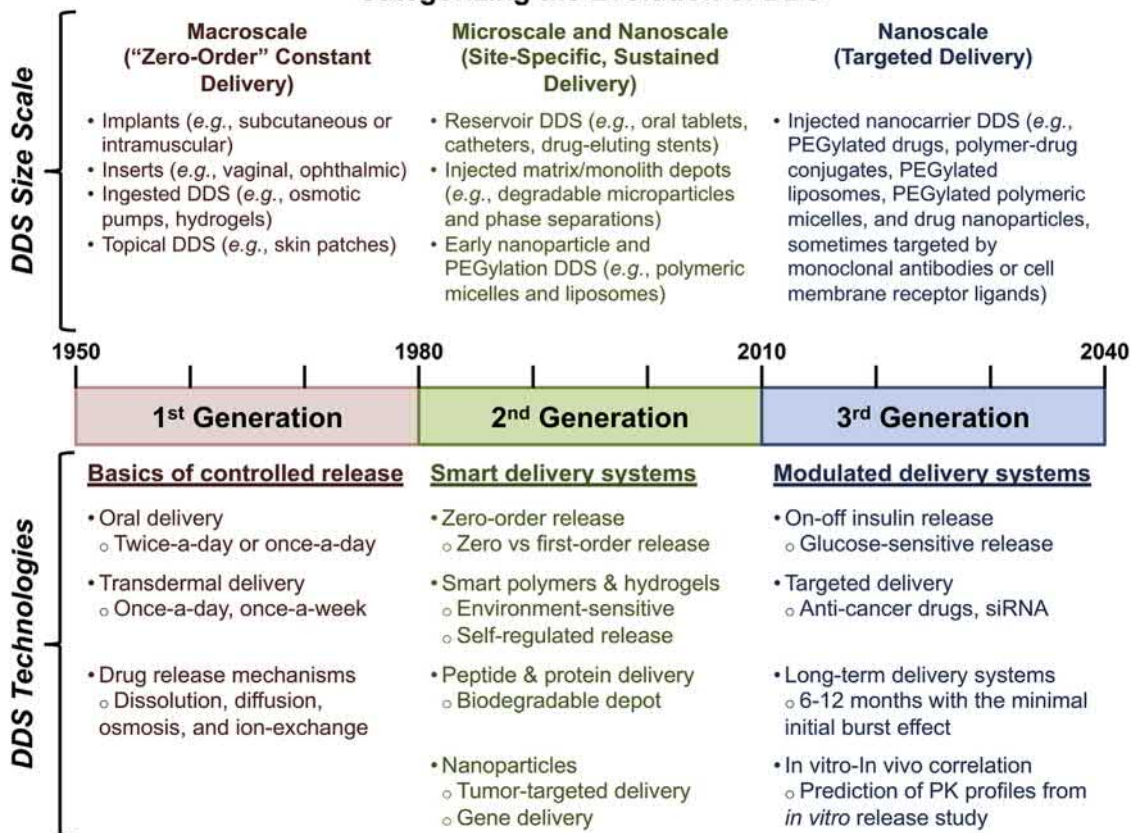
1850s, John Snow documented how periodic chloroform inhalation maintained anesthetizing effects throughout surgical procedures (Snow, 1858). In the early 1920s, Frederick Banting, Charles Best, and John Macleod identified that well-controlled, routine administration of insulin was necessary to treat diabetes (Herring, 1924; Banting and Best, 1922). These findings led to an early understanding of the typical “peak and trough” pharmacokinetics (PK) curve of drugs (see the section “DDSs to Improve Drug Pharmacokinetics”), which preceded the great advances in DDS development during the 20th century.

Pharmaceutical formulations capable of prolonging drug activity and reducing dosing frequency entered the market in the early 1950s (Fig. 2.5.12.2). In 1952, Smith Kline & French introduced the first commercial controlled-release formulation product, known as Dexedrine Spansules (Park, 2014). This product consisted of microspheres coated with a “wax-fat” layer (e.g., a mixture of glyceryl monostearate and bees wax), a formulation now commonly known as a reservoir, of varying thickness to control capsule dissolution and drug release (Blythe, 1956). However, the PK of such products varied greatly from patient to patient. In 1956, Riker Laboratories, Inc. introduced the first Food and Drug Administration (FDA)-approved pulmonary DDS, the pressurized metered dose inhaler, and dramatically advanced the therapeutic aerosol industry (Stein and Thiel, 2017; Anselmo and Mitragotri, 2014). These events marked the beginning of what has been defined as the first



• **Figure 2.5.12.1** Overview drug delivery system (DDS) development. (Adapted from Park, K., 2014. Controlled drug delivery systems: past forward and future back. *J. Control. Release* 190, 3–8.)

Categorizing the Evolution of DDS



• **Figure 2.5.12.2** Evolution of drug delivery systems (DDS) since 1950. (Adapted from Park, K., 2014. Controlled drug delivery systems: past forward and future back. *J. Control. Release* 190, 3–8; Yun, Y.H., Lee, B.K., Park, K., 2015. Controlled drug delivery: historical perspective for the next generation. *J. Control. Release* 219, 2–7). *PK*, Pharmacokinetics.

TABLE 2.5.12.1 Early Macroscopic Drug Delivery Systems Developed by Alza Corp

Product	Material	Purpose	Drug	Year Approved
Ocusert	Poly(ethylene-co-vinyl acetate)	Antiglaucoma ophthalmic insert	Pilocarpine	1974
Progestesert	Poly(ethylene-co-vinyl acetate)	Contraceptive intrauterine device	Progesterone	1976
Transderm Scop	Polypropylene	Antimotion sickness skin patch	Scopolamine	1979

generation of drug delivery (i.e., 1950–80) (Fig. 2.5.12.2) (Park, 2014).

In the mid-1960s, Alejandro Zaffaroni, inspired by his biochemistry and endocrinology training, envisioned DDSs that would release drugs with reproducible and predictable kinetics, independent of the patient (Hoffman, 2008; Urquhart, 2000; Zaffaroni, 1991). Simultaneously, Judah Folkman showed that a capsule made of silicone rubber (later termed “Silastic”) filled with drug, e.g., a reservoir, enabled sustained release (Folkman and Long, 1964). This concept led to the first zero-order reservoir DDS (Hoffman, 2008). Zaffaroni founded the first company dedicated to the concept of controlled drug delivery in 1968, Alza Corp., and Folkman was enlisted to head the Scientific Advisory Board (Hoffman, 2008). In 1971, Alza Corp. defined the key components of a DDS as “a drug delivery module comprising the drug, rate controller, and energy source” that were housed in a “platform” (Zaffaroni, 1991). The first controlled DDS products based on this definition were macroscopic designs with reservoirs of constant drug concentration enclosed in rate-controlling membranes made of polymers, such as Silastic or poly(ethylene-co-vinyl acetate) (Table 2.5.12.1). These first-generation DDSs employed different release mechanisms, including dissolution-, diffusion-, osmosis-, and ion exchange-based mechanisms, to produce devices that exhibited zero-order release rates to maintain constant drug plasma concentrations (Park, 2014). As such, this period established the basic understanding of DDSs and is characterized by the macroscopic size scale of DDSs developed (Fig. 2.5.12.2) (Park, 2014; Hoffman, 2008).

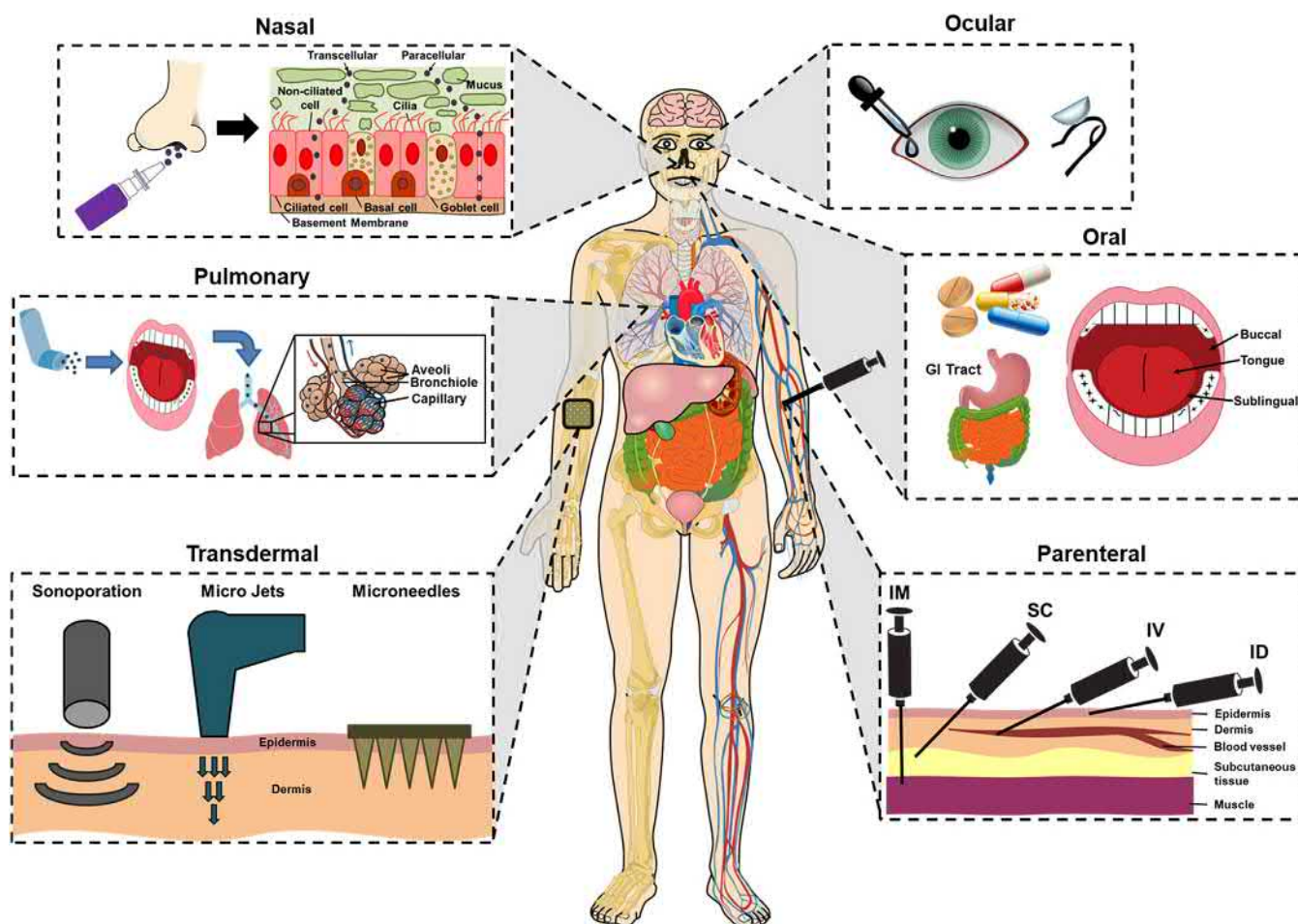
The second generation of drug delivery (1980–2010) included both micro- (~1980s) and nano- (~1990–2000s) sized DDS as well as “smart” DDS technologies (Fig. 2.5.12.2) (Park, 2014; Hoffman, 2008). The new technologies included depot DDSs using polymer microparticles, hydrogels, or phase-separated formulations (Park, 2014; Binauld and Stenzel, 2013). Many of these DDSs, such as the first FDA-approved matrix/monolithic depot DDS, Zoladex and Lupron introduced in 1989 (Park, 2014; Anselmo and Mitragotri, 2014; Zhang et al., 2013), were based on polyesters, such as poly(lactic acid) and poly(lactic-co-glycolic acid) (PLGA) that had been used previously in degradable sutures (Hoffman, 2008; Ulery et al., 2011). These degradable DDSs exhibited first-order release kinetics and were micron-sized particles. Furthermore, “smart” or environmentally triggered chemistries were

developed to enable drug delivery in response to an external stimulus, such as pH or temperature (Park, 2014; Binauld and Stenzel, 2013).

During the late 1980s and 1990s, interest and activity rapidly grew in the development of injectable nanocarriers, which are discussed in the section “DDSs to Enhance Stability.” This interest stemmed largely from two advances. First, the concept of poly(ethylene glycol) (PEG) conjugation to proteins to increase drug circulation times and decrease immunogenicity was spearheaded by Enzon Pharmaceuticals, Inc. in 1981 (Hoffman, 2016). Second, the discovery of the enhanced permeability and retention (EPR) effect in 1984 (Matsumura and Maeda, 1986; Maeda et al., 1985) provided strong rationale and motivation for the development of nanocarriers that passively target solid tumors, leading to the development of Doxil, a PEGylated liposomal doxorubicin approved in 1995 (Hoffman, 2008; Barenholz, 2012). Both PEGylation and the EPR effect contributed to the idea of passive targeting discussed further in the section “DDS Targeting.” Altogether, these advances aided in the development of site-specific and smart DDSs during the second generation of drug delivery (Fig. 2.5.12.2).

The third generation of drug delivery (i.e., 2010–present) (Fig. 2.5.12.2) has sought to modulate DDSs and understand how they behave in vivo to streamline development for licensure. Active targeting has also become a major focus in the field during this period and is discussed in more detail in the section “DDS Targeting.” Global nanoscale DDS research and development has increased steadily since the United States pioneered the use of national funds for such efforts with the announcement of the National Nanotechnology Initiative in 2000 and the passage of the 21st Century Nanotechnology Research and Development Act in 2003 (Bobo et al., 2016; Jia, 2005). For example, the number of FDA investigational new drug approvals for nanoscale DDS products has increased since 2003 despite increasingly stringent FDA regulations and escalating costs for new drug formulation licenses to more than US\$2.6 billion per drug (DiMasi et al., 2016). However, translation of actively targeted DDSs into the clinic has been slow and no targeted DDS has been approved to date.

Although many of the early DDS developments were focused on small molecule delivery, another recent focus has been on DDSs for macromolecular drug candidates, including peptides, proteins, and nucleic acids (e.g., DNA and siRNA). Onpattro (e.g., patisiran), which was developed by Alnylam Pharmaceuticals, Inc. as a lipid nanoparticle DDS,



• **Figure 2.5.12.3** Summary of typical drug delivery routes. Additional drug delivery routes include topical, rectal, vaginal, and intrathecal (not shown). *GI*, Gastrointestinal tract; *ID*, intradermal; *IM*, intramuscular; *IV*, intravenous; *SC*, subcutaneous.

became the first FDA-approved RNAi drug in 2018 (Mullard, 2018). Ultimately, the third generation will be defined by the success of these innovative modulated and targeted DDSs in clinical applications (Abdelwahed et al., 2006).

The remainder of this chapter focuses on the biomaterials used in DDSs as well as the design challenges and approaches to overcome these hurdles, including pertinent examples in use and under development. For a more detailed overview of the interesting history of the DDS field from its origins until today, the reader is referred to several review articles (Park, 2014; Hoffman, 2008; Urquhart, 2000; Zaffaroni, 1991; Zhang et al., 2013; Bobo et al., 2016).

General Considerations in DDS Design

Routes of Drug Delivery

Common routes of drug delivery for conventional drugs are oral, parenteral, transdermal, nasal, ocular, pulmonary, rectal, vaginal, and intrathecal (Fig. 2.5.12.3). Oral administration has excellent patient compliance and ~90% of current conventional drugs are administered via this route. In fact, tens of billions of pills are annually consumed worldwide

for aspirin alone (Anselmo and Mitragotri, 2014). However, oral delivery suffers from challenges associated with the harsh environments of the oral cavity, stomach, and intestines, as well as poor transport across the epithelial mucosal layer of the intestine, which is discussed further in this chapter (see the section “DDS Design to Overcome Biological Barriers”). Moreover, after systemic adsorption, orally delivered drugs are subject to first-pass metabolism by intestinal and liver enzymes, which results in drug degradation upon initial administration, thereby reducing unaltered drug concentration in the blood. Parenteral administration, accounting for more than 10 billion annual drug administrations worldwide (Kermode, 2004), includes intravenous, subcutaneous, and intramuscular injections. The parenteral route ensures that effective drug concentrations are rapidly achieved but suffers from poor patient compliance due to injection site pain (Spain et al., 2016; Rubin et al., 2009; Zambanini et al., 1999; Deacon and Abramowitz, 2006). Transdermal delivery has excellent patient compliance but has traditionally been limited to drugs that are small and lipophilic. Nasal, pulmonary, and vaginal routes are also of interest due to high epithelial surface area, leading to rapid drug efficacy; however, due to challenges associated with delivery across the epithelial mucosa,

these routes are also limited to small, lipophilic compounds. DDS designs seek to enhance drug efficacy and/or enable new routes of administration that avoid adverse side effects, address low patient compliance, or overcome biological barriers as discussed in the section “DDS to Overcome Biological Barriers.”

DDS Biomaterials Design Considerations

As highlighted previously in [Chapter 1.1.1](#), a biomaterial is “a material intended to interface with biological systems to evaluate, treat, augment, or replace any tissue, organ or function in the body,” with a focus on “treat” for DDSs. All biomaterials, including DDSs, must be biocompatible, that is, perform as designed without adverse effects. Thus DDSs should deliver drugs at the intended concentration, with appropriate kinetics, and to the target tissue. Behavior deviating from this expectation could result in adverse events or even death. Therefore understanding how biomaterials interact with the body is critical for DDS design. DDS biomaterials have the potential to interact with target and off-target tissues, adsorb proteins, and potentiate immune reactions. Biocompatibility is highly dependent upon DDS route of delivery; systemic introduction has significantly different expected interactions than transdermal, oral, or even depot-based delivery systems. Although many biomaterial properties are already highlighted in this textbook (see [Section 1.2](#)), this section will focus on the important aspects of biomaterials design with respect to DDS development.

Biomaterials Used in DDSs

Of the three main classes of biomaterials (metals, ceramics, and polymers), polymers are the most common platform for DDSs. Polymers have many advantages over other classes. Polymers can be fabricated into complex shapes and structures with a wide range of bulk compositions and physical properties. Furthermore, polymers have tunable chemistries, including controllable, responsive properties (e.g., stimuli responsive), yet allow for robust and flexible conjugation or incorporation of various drug classes. Synthetic rather than natural materials are often utilized as they are amenable to formation by controlled processes, which lead to highly reproducible structure–function relationships. The reader is encouraged to review [Chapter 1.3.2](#) for details about synthesis and characterization of polymeric biomaterials ([Cabral et al., 2018](#)).

DDS Biomaterial Properties

Degradation

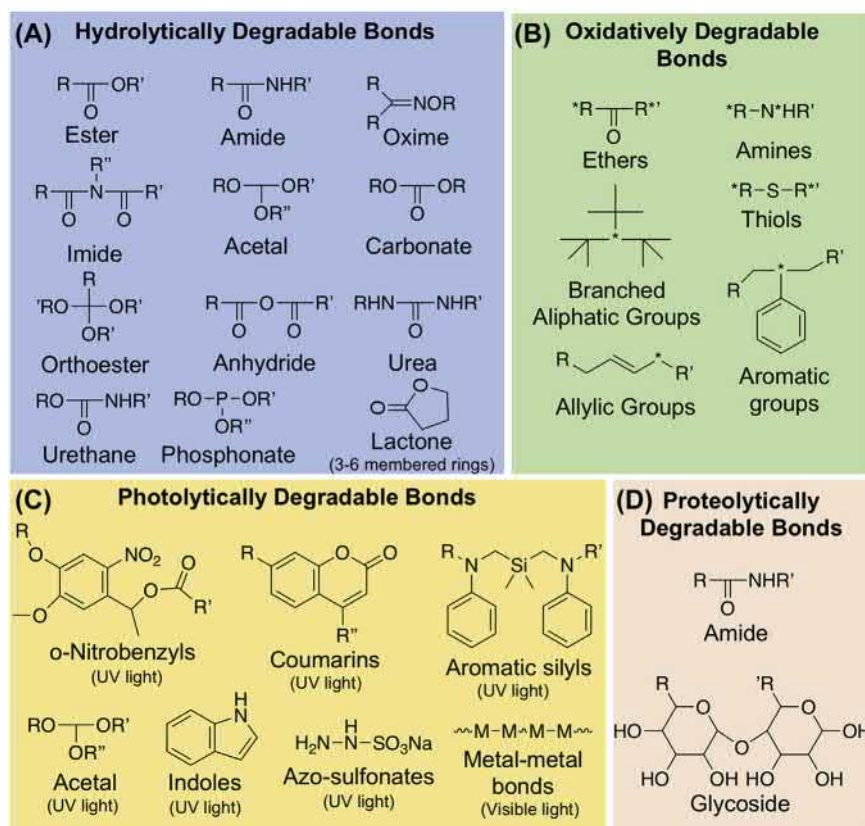
DDSs can be designed from both nondegradable and degradable materials to align with the intended application. For implanted DDSs, degradable materials can be used to control drug release, which is discussed in greater detail within the section “[DDSs to Improve Drug Pharmacokinetics](#),” and avoid secondary retrieval surgeries and outcomes associated with long-term biomaterial persistence. As discussed in [Chapter 1.3.2](#), degradation can be

controlled or uncontrolled (unintended) but falls into one of four classes: hydrolysis, oxidation, photolysis, and proteolysis. Briefly, hydrolytic degradation requires electrophiles susceptible to nucleophilic attack by the hydroxyl oxygen of water. Hydrolytically degradable groups include esters, amides, oximes, urethanes, urea, carbonate, acetal, phosphonate, anhydride, lactones, and imides ([Fig. 2.5.12.4A](#)). Oxidation is an inherently uncontrolled degradation mechanism that occurs when free radicals, resulting from inflammatory reactions, abstract hydrogens from branched aliphatic hydrocarbons, phenols, or other aromatic groups, thiols, amines, ethers, and carbon–carbon double bonds, causing polymer chain scission ([Fig. 2.5.12.4B](#)). Although photolysis or photodegradation is common for drugs, only recently has it been exploited to controllably degrade/alter biomaterials ([Pasparakis et al., 2012](#); [Watanabe and Ohtsuki, 2016](#)). Light-sensitive functional groups include nitrobenzyl derivatives, coumarins, azo sulfonates, metal–metal bonds, indoles, vinyl ketones, and aromatic silyl derivatives ([Pasparakis et al., 2012](#); [Watanabe and Ohtsuki, 2016](#)). Chemical structures and requisite wavelength ranges mediating photoreaction of these chemical moieties are shown in [Fig. 2.5.12.4C](#). Finally, proteolysis of natural materials, including carbohydrate, glycoprotein, protein, and proteoglycans, occurs when enzymes attack amides and glycosidic linkages ([Fig. 2.5.12.4D](#)).

DDS degradation depends on the relative rates of degradation and diffusion by the reactant (e.g., water, radicals, photons, or enzymes). This rate is a function of biomaterial hydrophilicity, crystallinity, surface area to volume, and pore size, as discussed in [Chapter 1.3.2](#). For example, the highly crystalline anhydride-based polymers that comprise the biodegradable polymer Gliadel undergo surface degradation, while less crystalline PLGA-based polymers typically bulk degrade ([Shoichet, 2009](#)). Both nondegradable and degradable materials may succumb to biological responses, such as inflammation, that can cause either unexpected or expedited degradation. If the biological environment deviates significantly due to atypical inflammatory responses (e.g., excessively acidic pH or increased reactive oxygen/nitrogen species generation), degradation, and therefore drug release rates, may be increased ([Helle et al., 2002](#); [Heller, 1990](#); [Heller et al., 2000, 2002](#)).

Surface Properties

As with any biomaterial, surface properties are a key design parameter for DDSs. Surface properties are particularly important for systemically delivered DDSs and implantable systems since surface interactions will control cell–material behaviors that affect drug delivery. Surface properties, such as hydrophilicity, roughness/curvature, and surface chemistry, lead to different levels of protein adsorption (as discussed in [Chapter 1.2.4](#)). If a permanent implant or depot is used, the repertoire of cells at the implant site can interact directly with the biomaterial or adsorbed proteins, leading to acute and possibly chronic inflammation or a foreign body reaction (FBR) (see [Chapter 2.2.2](#)). These reactions may



• **Figure 2.5.12.4** (A) Hydrolytically, (B) oxidatively, (C) photolytically, and (D) proteolytically degradable groups found within biomaterials and drugs that are susceptible to controlled or uncontrolled degradation. *Indicates group susceptible to radical attack during oxidation, R, R', R'' are generic hydrocarbon groups (Mahato and Narang, 2018; Pasparakis et al., 2012; Temenoff and Mikos, 2009). UV, Ultraviolet.

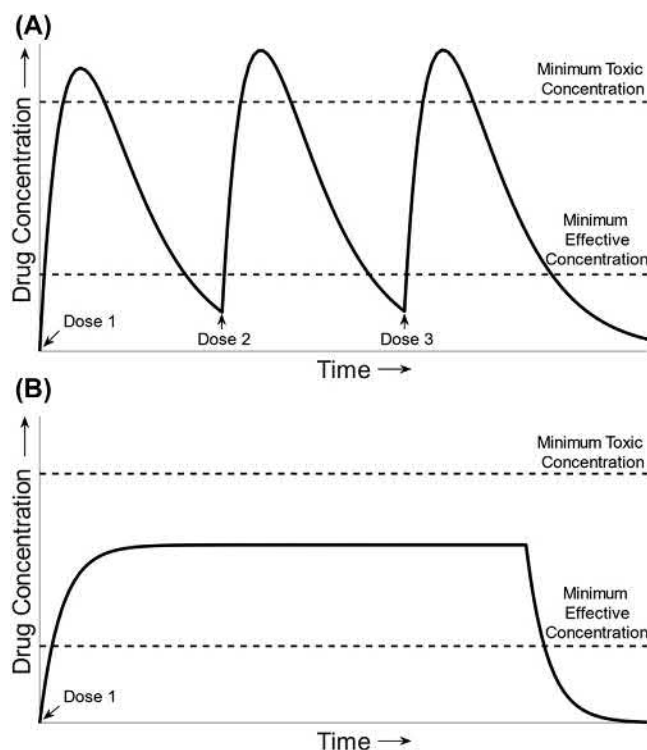
compromise controlled drug release. For example, inflammatory responses include reactive oxygen and nitrogen species and enzyme production. These reactants can expedite material degradation or cause uncontrolled degradation, which will lead to dramatic changes in drug release kinetics. Note, uncontrolled degradation of polymers is discussed in depth within [Chapter 1.3.2](#). The FBR is characterized by collagenous capsule formation around foreign materials that is a diffusional hindrance to drug release. This effect can be seen even with inert, unreactive biomaterials commonly used in DDSs, such as poly(tetrafluoroethylene) (Teflon), poly(urethanes), and poly(dimethylsiloxanes) (PDMSs), where capsules of $\sim 100 \mu\text{m}$ thick have been described (Ratner, 2002). Fibrous encapsulation due to FBR has been credited for inadequate control over steroid release from Norplant, an implantable device formed from PDMS-based Silastic (Ratner, 2002). Furthermore, FBR-related inconsistencies with drug delivery may also underpin the predominance of implantable depot applications within immune privileged tissues, such as the eye, brain, and prostate (e.g., eye: Ocusert, Vitrasert, Restisert, Ozurdex; brain: Gliadel; prostate: Vantas, Viadur).

For parenteral DDS, protein adsorption can also occur (Cedervall et al., 2007; Monopoli et al., 2012) and dramatically change naïve biomaterial surface properties, which may impact circulation time and/or biodistribution. Biomaterial

geometry, size, charge, and surface chemistry influence the protein–corona composition and adsorbed protein structure, and as many as 300 different proteins have been shown to be bound to nanoparticle surfaces irrespective of material class, charge, or hydrophilicity after 30-s incubations in serum (Tenzer et al., 2013; Huhn et al., 2013; Lundqvist et al., 2008; Fleischer and Payne, 2014; Parveen et al., 2017). Protein adsorption can then result in nonspecific cellular uptake by immune cells in the mononuclear phagocytic system (MPS) residing in the liver, spleen, and lymph nodes (Blanco et al., 2015).

Mechanics

The mechanical properties of implantable or transdermal DDSs can also impact drug delivery success. The relative crystallinity and elastomeric nature of polymeric systems (see [Chapter 1.3.2](#)) can affect resistance to mechanical forces exerted during placement (Temenoff and Mikos, 2009). If the material cracks or breaks during placement or duration of use, the increased surface area can lead to significant alterations in drug release due to a greater surface area-to-volume ratio and decreased biocompatibility due to an amplified FBR (Temenoff and Mikos, 2009). Altered inflammatory and/or FBR reactions can also result from tissue mechanical damage due to mismatched biomaterial depot and tissue properties (Temenoff and Mikos, 2009).



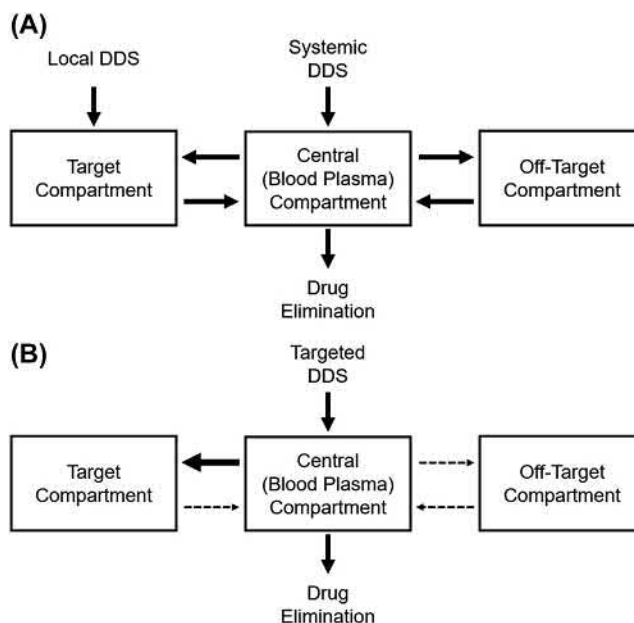
• **Figure 2.5.12.5** Pharmacokinetics (PK) curves of plasma concentration of a drug versus time for two types of delivery systems: (A) typical bolus PK for multiple dosing with oral tablets or injections; (B) zero-order PK for one dose of controlled drug delivery from a specific formulation or device.

DDSs to Improve Drug Pharmacokinetics

Pharmacokinetics

One of the primary motivations for the development of DDSs is to improve the therapeutic window (TW) of drug-based therapies. The TW is the range of drug concentrations that produce therapeutic benefit without causing intolerable harm. This concept is related to the therapeutic index (TI), which is the ratio of the minimum toxic concentration divided by the minimum effective concentration. Drugs with a narrow TI are more difficult to use clinically and correlate with increased complication rates compared with wider TI drugs (Blix et al., 2010). Typically, TI is intrinsic to a drug; however, DDSs can be used to dramatically improve its apparent TW. The effects of DDSs on TI are generally PK and consist of release rate modulation, dosage control, and localization.

The relationship between PK, the TW, and drug delivery is demonstrated in Fig. 2.5.12.5. Administration of a single large dose follows typical first-order PK (e.g., oral delivery) producing a spike in blood plasma drug concentration where the desired therapeutic concentration is achieved only for a short period of the time postadministration. This rise and fall follows the *LADME* sequence. *LADME* stands for *Liberation* of the drug from the formulation, *Absorption* of the drug into the blood, *Distribution* of the drug throughout the body, including action of the drug at various



• **Figure 2.5.12.6** A basic pharmacokinetics compartment model showing the interactions between blood plasma, target tissues, and off-target tissues. (A) Typical systemic drug delivery delivers to blood plasma either directly (i.e., intravenous injection) or indirectly (i.e., oral pills), which is transported to the target and off-target tissue. Accumulation in other compartments occurs through transport processes that typically follow first-order kinetics. Elimination of most drugs ultimately occurs by excretion by the kidneys, and hence is dependent on drug plasma concentration. Local delivery in the target tissue bypasses compartmental transport into the target but does not affect transport kinetics out of the target compartment and into others. (B) Targeted drug delivery systems (DDSs) alter the transport kinetics by increasing the affinity for the target compartment, which is described in the section “DDS Targeting”.

sites—especially at and within cells, *Metabolism* of the drug, usually in the liver, and finally *Elimination* of the drug from the body, usually by excretion through the kidneys in the urine. Elimination rate is typically described in terms of a first-order half-life ($t_{1/2}$), which is the time required for maximal blood plasma drug concentration to decrease by half. Note that in the absence of a drug delivery vehicle or excipients in a formulation, the “L” can be disregarded. Zero-order release maintains constant drug concentration in the blood plasma, ideally within the TW, after an initial equilibration period. The area under the PK curve (AUC) of drug concentration is used to quantify drug exposure. Higher AUC indicates greater drug exposure over time and is a useful comparison for different DDS systems. Additionally, the DDS can be used to localize drug concentrations to specific PK compartments, concentrating drug in target tissues rather than off-target tissues (Fig. 2.5.12.6). DDSs can also improve bioavailability, defined as the proportion of unaltered drug after administration, by reducing drug–serum protein binding and premature enzymatic degradation.

Many DDS strategies improve AUC by reducing elimination rate to increase $t_{1/2}$. Conjugation of drugs, including proteins and small molecules, and DDSs to hydrophilic

PEG (“PEGylation”) improve the circulation time by reducing elimination in the kidneys through increased solubility and physical size (Veronese and Pasut, 2005). PEGylation is particularly useful for drugs that are rapidly eliminated and has been shown to enhance therapeutic utility of antibody therapeutics and chemotherapy agents, such as Taxol and doxorubicin (Pasut and Veronese, 2009). Albumin-functionalized conjugates, such as paclitaxel-based Abraxane, have similar circulatory PK effects to PEGylation with benefits that include reduced drug chemistry modification and improved bioavailability (Green et al., 2006). However, albumin conjugates suffer from preferential liver and tumor biodistribution (Kratz, 2008). Nanocarrier systems, such as liposomes, polymeric nanoparticles, and others (see the section “DDSs to Improve Drug Solubility”) increase circulation time of drugs as they are too large (>4–6 nm) to pass through the glomeruli of the kidneys (Wilhelm et al., 2016). In cases where drug elimination is similar to or faster than absorption or pharmacodynamic effects, a DDS can be critical for the clinical application of a drug candidate.

Dosage and Distribution Control

DDSs allow better control of dosage to match the TI. Control can come via feedback (i.e., electrical control via sensors or from physical interactions with the body) or simple rate-limited release to improve convenience or better match the therapeutic concentration of a drug with a narrow TI. As an example, insulin is a hormone with a narrow and rapidly changing therapeutic concentration that is dependent upon food intake and composition, activity level, and blood glucose concentration. A fully integrated glucose sensor coupled with insulin release could act as an artificial pancreas and remove the burden of constant monitoring and calculation of insulin dosages, providing improved quality of life and reduced risk of hypo- or hyperglycemia. Current insulin delivery pumps, such as wearable modules that deliver insulin through a persistent subcutaneous injection site, offer excellent control over blood glucose levels and improve patient compliance, but still require user input despite attempts at automation (Bergenstal et al., 2010). One biomaterial DDS solution under development is the use of phenylboronic acid, a glucose-responsive moiety, as a sensor for insulin release from systemically delivered mesoporous silica nanoparticles (Zhao et al., 2009). DDSs designed for convenience include extended-release oral capsules, transdermal delivery patches, and implanted depots, which are covered in the section “DDSs to Overcome Biological Barriers.”

Controlling Drug Release Kinetics

Modifying drug delivery rate can be sufficient to ensure maintenance of the TW. Drug release rate from a DDS can be controlled via several mechanisms, including diffusion, dissolution, affinity, swelling, and ion exchange (Fig. 2.5.12.7). Table 2.5.12.2 lists examples of FDA-approved DDSs that exploit these delivery mechanisms. Diffusion from DDSs

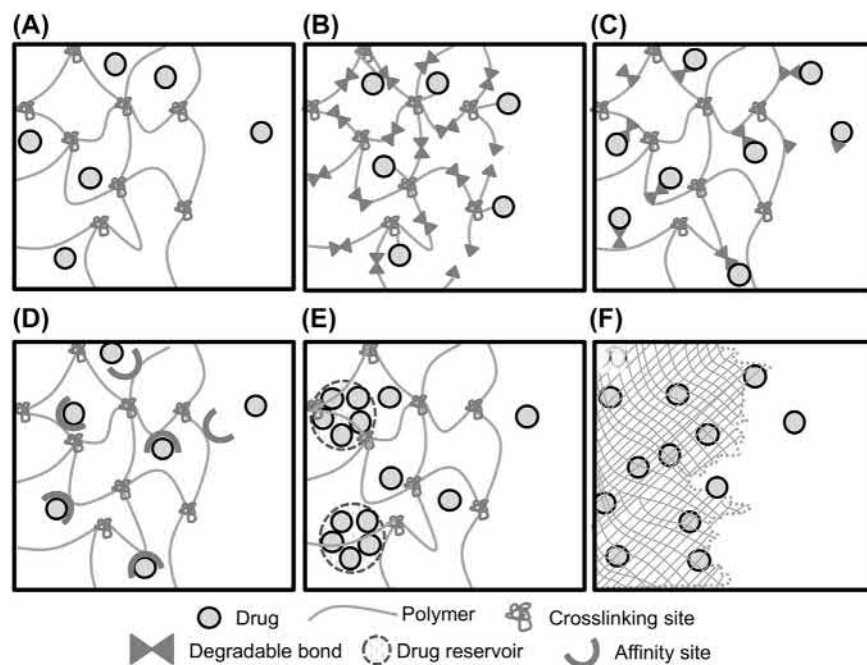
is common and driven by concentration gradients. The general categories for these DDSs are matrix or reservoir-type systems. Matrix-based systems, which are also known as monoliths, contain drug uniformly dispersed within the material and are commonly accompanied by an initial “burst” release of drug upon placement due to rapid diffusion of surface-localized drug. If the material is hydrophilic, swelling mediates diffusion-controlled release. If the material is hydrophobic, drug releases after water penetration enables a diffusive path. In addition to “burst” release, diffusive release from matrix devices inherently follows first-order kinetics and requires coupling with degradable DDS materials to modify the release profile. Reservoir systems contain drug within an inner core surrounded by a permeable membrane layer that controls release and can achieve zero-order release with appropriately designed membrane–drug combinations.

Dissolution is liberation of matrix-entrapped drug as a function of matrix degradation or dissolution rate (Fig. 2.5.12.7). The kinetics of drug delivery by dissolution is controlled by DDS properties, including pore size, degradable bonds, and hydrophobicity, rather than drug solubility and mobility, as in diffusion. However, drug release is often dependent upon both drug diffusion and dissolution, as dissolution or degradation alters the DDS pore size, thus liberating greater amounts of drug over time.

Affinity-based systems exploit noncovalent interactions, including electrostatic, van der Waals, hydrophobic, and hydrogen-bonding interactions between drug and DDS to control drug release rate (Fig. 2.5.12.7). Affinity-based DDS release rates are tunable and based on the association constant of drug–ligand interactions, which allow for release of multiple drugs with various kinetics. However, a priori identification of affinity ligands is necessary for affinity-based release. Several ligands have been identified; these include cyclodextrin, heparin, albumin, and various cationic DDSs to release a variety of drugs, including small molecule antibiotics, proteins, and nucleic acids (Bader et al., 2014; Fu et al., 2011; Oss-Ronen and Seliktar, 2011; Rivera-Delgado et al., 2016; Vulic and Shoichet, 2014; Wang and von Recum, 2011).

Charged drug molecules can be loaded into an ion exchange resin to provide control over release rate as a function of the ionic environment. Ion exchange is particularly suitable for enteral delivery routes, as ion exchange resins are typically inert, functionalized poly(styrene) derivatives formed into micron- or millimeter-scale beads that pass through the digestive tract safely (Guo et al., 2009). These resins have found commercial success in many over-the-counter extended release formulations (Table 2.5.12.2).

Swelling of osmotic pumps can control mechanical dispensing systems to achieve variable drug release (Table 2.5.12.2). An osmotic pump is a compartment surrounded by a semipermeable membrane typically composed of cellulose acetate. The membrane controls diffusion of water into the osmogen: a material with high osmotic pressure, such as sugars or salts, embedded into a carrier such as poly(ethylene oxide) or poly(hydroxypropyl methylcellulose). The influx



• **Figure 2.5.12.7** Mechanisms of drug release from drug delivery systems (DDSs). Release of drugs from DDSs can be controlled by a number of mechanisms. (A) Drug is encapsulated within a DDS with mesh/pore size to allow for diffusive release of the encapsulated drug with optional diffusional membrane barrier. (B) Drug is tethered to a DDS that degrades hydrolytically, oxidatively, photolytically, or proteolytically to control release. (C) Drug is tethered to the DDS by a degradable tether, and released upon linker cleavage via hydrolysis, oxidation, photolysis, or proteolysis. (D) Diffusive release of encapsulated drug is controlled by affinity interactions between the DDS and the drug. (E) Diffusive release of encapsulated drug is prolonged by delayed release of the drug from a matrix or reservoir. (F) Drug is encapsulated within a degradable DDS and released by dissolution as the material degrades. Not to scale. (Adapted from Van Hove, A.H., Benoit, D.S., 2015. Depot-based delivery systems for pro-angiogenic peptides: a review. *Front. Bioeng. Biotechnol.* 3, 102.)

of water to the osmogen increases the pressure inside the container, forcing the drug or drug carrier through micro-drilled pores within the membrane. There are many variations of osmotic pumps, from the single-component elementary osmotic pump (Theeuwes, 1975) to multistage, multichamber systems, all of which can range from ingestible pills to implantable devices. Release kinetics can be tuned from zero-order to complex profiles simulating multiple separate doses (Malaterre et al., 2009). More detailed reviews of osmotic pumps can be found within Malaterre et al. (2009) and Herrlich et al. (2012).

DDSs to Improve Drug Solubility

Drug solubility is vital for successful delivery. Dose variations, poor and unknown absorption profiles, low bioavailability, and subpar therapeutic efficacy are limitations associated with systemically delivered, poorly soluble, small molecule drugs. The intrinsic link between solubility and drug efficacy is described by Lipinski's rule of 5, which predicts that compounds with molecular weight <500 Da, H-bond donors ≤ 5 , H-bond acceptors ≤ 10 , and octanol-water partition coefficient ($\log P$) < 5 are more likely to succeed clinically due to better absorption and distribution (Choy and Prausnitz, 2011). However, approximately 40% of approved small molecule drugs and 70%–90%

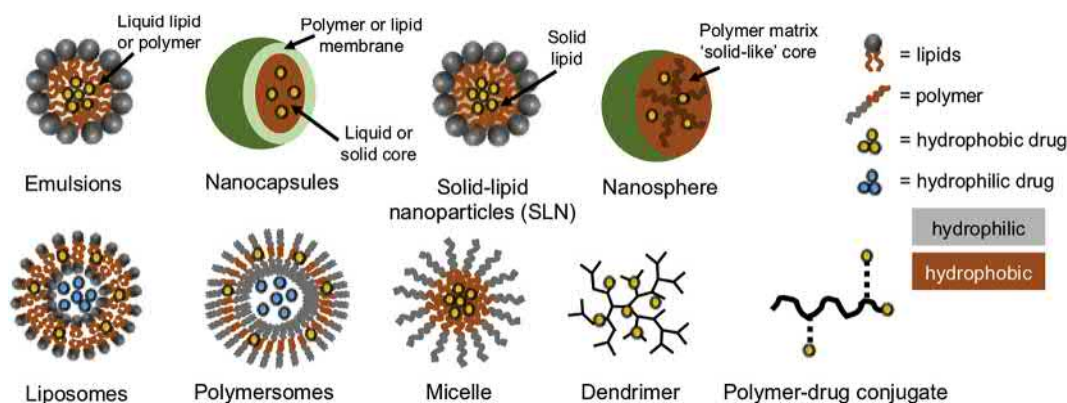
of pipeline agents are poorly soluble ($<100 \mu\text{g/mL}$) (e.g., do not follow Lipinski's rule of 5) (Kalepu and Nekkanti, 2015). Conventional approaches to improve drug solubility include salt formation, pH adjustments, and prodrug formulations. Unfortunately, these conventional strategies are not applicable for all drug candidates. Therefore colloidal and noncolloidal DDSs have been developed to enhance drug solubility. Many of these approaches also have the added benefit of improving drug stability, biodistribution, and cell uptake. However, for simplicity this section will focus only on improved solubility. Drugs can be dissolved, entrapped, encapsulated, chemically bonded, or adsorbed on DDSs and released by diffusion, dissolution, or swelling (Fig. 2.5.12.8). A brief introduction to these DDSs follows and highlights examples of solubility-enhancing DDSs with their routes of delivery, advantages and disadvantages, and the biomaterials employed (Table 2.5.12.3). While this section only focuses on nanoscale DDSs due to space constraints, there are similar approaches to enhance drug solubility using both micro- and macroscale formulations, such as tablets and capsules. For more comprehensive reviews, the interested reader may reference Chapter 1.3.8 and Cabral et al. (2018), Cerpnjak et al. (2013), Callender et al. (2017), Prasad et al. (2018), Date et al. (2010), Narvekar et al. (2014), Stegemann et al. (2007), and Letchford and Burt (2007).

TABLE 2.5.12.2 Sample of Clinically Approved Drug Delivery Systems (DDSs) With Various Release Mechanisms

Clinically Approved DDS	Release Mechanism	Polymer	Degradable Bond	Drug(s)	References
Gliadel	Dissolution	Bis(<i>p</i> -carboxyphenoxy) propane- <i>co</i> -sebacic acid	Anhydride	Carmustine, temozolomide	Zhang et al. (2013); Bock et al. (2010); Lawson et al. (2007)
Zoladex, Lupron Depot, Sandostatin LAR, Neutropin depot, Trelstar, Eligard, Risperdal, Consta, Vivitrol, Somatuline, Ozurdex	Diffusion and Dissolution	Poly(lactic- <i>co</i> -glycolic acid)	Ester	Goserelin acetate, Leuprolide acetate, polifeprosan 20/ carmustine, glucose/ octreotide acetate, recombinant human growth hormone, triptorelin pamoate, minocycline, Leuprolide acetate, risperidone, naltrexone lanreotide, dexamethasone	Zhang et al. (2013)
Atridox	Diffusion and Dissolution	Poly(lactic acid)	Ester	Doxycycline hyclate	Zhang et al. (2013)
Capronor	Diffusion and Dissolution	Poly(caprolactone)	Ester	Levonorgestrel	Ulery et al. (2011)
Implanon, Nexplanon, Probuaphine, Ocusert, Vitrasert	Diffusion	Ethylene- <i>co</i> -vinyl acetate	ND	Etonogestrel, buprenorphine, pilocarpine, ganciclovir	Major et al. (2016); Schneider et al. (2017)
Norplant, Jadelle, Mirena, Skyla, Liletta, Kyleena	Diffusion	Silastic	ND	Levonorgestrel	Major et al. (2016)
Onpattro	Affinity	Cholesterol and poly(ethylene glycol)-conjugated lipid nanoparticle complex	ND	siRNA	Mullard (2018); Hoy (2018); Morrison (2018)
Delsym, Tuzistra XR, Betoptic S	Ion Exchange	Poly(styrene) sulfonate	ND	Dextromethorphan, codeine, chlorpheniramine, betaxolol	Guo et al. (2009); Jani et al. (1994); Yoshida et al. (2013); Raghunathan et al. (1981)
Osmosin, Acutrim, Procardia XL, Ritalin SR, Xanax XR	Osmotic pump	Hydroxypropyl methylcellulose, poly(ethylene oxide), Cellulose acetate, other cellulose derivatives	ND	Indomethacin, phenylpropanolamine, nifedipine, methylphenidate, alprazolam	Malaterre et al. (2009); Herrlich et al. (2012); Keraliya et al. (2012)

ND, Nondegradable.

For additional information beyond referenced works, see Van Hove, A.H., Benoit, D.S., 2015. Depot-based delivery systems for pro-angiogenic peptides: a review. *Front. Bioeng. Biotechnol.* 3, 102; Liechty, W.B., et al., 2010. Polymers for drug delivery systems. *Annu. Rev. Chem. Biomol. Eng.* 1, 149–173; Mishra, S., De, A., Mozumdar, S., 2014. Synthesis of thermoresponsive polymers for drug delivery. *Methods Mol. Biol.* 1141, 77–101.



• **Figure 2.5.12.8** Schematic showing different drug delivery system platforms discussed herein.

Colloidal DDSs

Colloidal DDSs include a variety of nanoscale carriers that improve drug solubility by incorporating drug within a reservoir or matrix. Emulsions are early examples of colloidal DDSs. Because of their long-standing use in a variety of industries, including cosmetics, food, and agriculture, emulsions inevitably evolved into DDSs. Emulsions (Fig. 2.5.12.8) are heterogeneous dispersions of oil and water that improve drug solubility by increasing the surface area of the drug. The idea that increasing drug surface area improves drug solubility subsequently propelled the development of more advanced nanocarriers, including nanospheres, solid-lipid nanoparticles (SLNs), nanocapsules, micelles, polymersomes, and liposomes.

Nanospheres and SLNs are composed of a solid lipid or polymer matrix core that loads a variety of hydrophobic drugs (Fig. 2.5.12.8). Despite being formulated with different materials (i.e., lipids, polymers), drug loading in nanospheres and SLNs is achieved by selecting a core material with excellent drug solubility. Additional information can be found in Table 2.5.12.3.

Nanocapsules, micelles, polymersomes, and liposomes (Fig. 2.5.12.8) can be broadly categorized as reservoir DDSs. Specifically, nanocapsules have hydrophobic liquid or solid cores surrounded by a single layer of polymer or lipid corona, while micelles form a hydrophobic core and hydrophilic corona through the self-assembly of amphiphilic polymers (Fig. 2.5.12.8) (Letchford and Burt, 2007). The core of nanocapsules and micelles may also serve as a reservoir for hydrophobic drugs that can also enhance drug stability. In these carriers, the size of the hydrophobic region and drug–core interactions control loading capacity. A major advantage of nanocapsules and micelles is their stable core, which reduces premature drug loss. Specifically, micelles are thermodynamically stable, and are associated with low critical micelle concentration, allowing for maintenance of loaded material for long periods of time.

Polymersomes (Fig. 2.5.12.8) are amphiphilic copolymers, while liposomes are amphiphilic lipids that self-assemble into bilayered structures (Fig. 2.5.12.8). Polymersome formulations are complex and depend on the weight fraction of the hydrophilic block to ensure uniform distribution

(Letchford and Burt, 2007; Discher et al., 2007; Rideau et al., 2018). Both polymersomes and liposomes enable the delivery of various molecules, including small molecule hydrophobic drugs within the bilayer and, in contrast to other carriers, hydrophilic molecules (e.g., nucleic acids or proteins) within the core (Rideau et al., 2018). Similar to the other carriers, polymersome and liposome drug loading are highly dependent on drug interactions with the carrier's bilayer or core. To reduce rapid clearance of liposomes, PEG was introduced as a surface modification on Doxil, the first colloidal DDS approved by the FDA in 1995 (Lian and Ho, 2001). Since then, additional liposomal formulations have adapted PEG surface modifications resulting in various marketed DDSs, as listed in Table 2.5.12.3.

Colloidal DDSs range from core-based carriers to more complex bilayered structures. Regardless of the carrier type, drug loading and drug release kinetics are dictated by the lipid/polymer composition, drug–carrier interactions, and nanoparticle size (Prasad et al., 2018; Allen and Cullis, 2013; Kataoka et al., 2001; Mukherjee et al., 2009).

Noncolloidal DDSs

Dendrimers are highly branched polymer chains that are stable and easy to modify (Table 2.5.12.3) (Prasad et al., 2018; Marx, 2008; Boas and Heegaard, 2004; Morgan et al., 2006). Dendrimers have evolved over time from simple structures that enable covalent or electrostatic drug loading to more complex hydrophobic-to-hydrophilic structures that enable core encapsulation of hydrophobic drugs (Marx, 2008; Boas and Heegaard, 2004; Duncan and Izzo, 2005; Li et al., 2007). Examples of dendrimers, including the most prominent, poly(amidoamine) (PAMAM) (Duncan and Izzo, 2005; Esfand and Tomalia, 2001), are provided in Table 2.5.12.3, and information about the various biomaterials used for dendrimer formulations can be found in the following references (Buhleier et al., 1978; Hawker and Fréchet, 1990; Turnbull and Stoddart, 2002).

Polymer–drug conjugates (PDCs) are made of three components: the polymer, a linker, and the drug, as shown in Fig. 2.5.12.8. PDCs can achieve high drug loading via covalent linkages and exhibit tunable properties through

TABLE 2.5.12.3 Summary of Drug Delivery Systems (DDSs) That Address Poor Aqueous Solubility With Associated Advantages, Disadvantages, and Examples

DDS Type	Advantages	Disadvantages	Examples	Material	Delivery Routes	References
Emulsions	Liquid formulations facilitate faster absorption, adaptable for hydrophobic and hydrophilic drugs	Toxic excipients, phase separation over time, rapid clearance	TOCOSOL paclitaxel, Norvir, Restasis, cyclosporine A	Soybean, cottonseed, and safflower oils, Tween, Pluronics, etc.	Oral, parenteral, transdermal, ocular	Prasad et al. (2018); Narvekar et al. (2014)
Nanocapsules	Chemically stable, biocompatible, and reproducible	Delayed release of active drugs, loading capacity dictated by size of reservoir	SOLUDOTS-PTX	Ploxamer	Parenteral	Kothamasu et al. (2012)
Solid-Lipid Nanoparticle (SLN)	Easy scale-up, high lipid content, affordable, biocompatible lipids used	Limited drug loading potential, contains a mixture of colloidal structures, rapid clearance	Ciprofloxacin-loaded SLNs	Triglycerides, fatty acids, steroids, waxes, etc.	Oral, parenteral, topical	Zhang et al. (2013); Mukherjee et al. (2009)
Nanosphere	Flexibility in how drug is incorporated, tunable polymer	Rapid clearance, poor reproducibility	Eligard	MePEG- <i>b</i> -PLA, PEG- <i>b</i> -PDLLA, PEG-PCL, etc.	Parenteral	Ventola (2017)
Micelles	Thermodynamically stable, high drug loading, controllable release kinetics	Complex polymer chemistry	Estrasorb, Genexol-PM ^a	PLGA, MePEG- <i>b</i> -PDLLA, MePEG- <i>b</i> -PCL, MePEG- <i>b</i> -PLDA, etc.	Topical, parenteral	Yokoyama (2011)
Liposomes, polymersomes	Adaptable for hydrophobic and hydrophilic drugs (both), stable and less permeability (polymersomes)	Immunogenicity, toxicity, and cellular uptake, poor circulation time (liposomes)	Doxil/Caelyx, Marqibo, Onivyde	Phospholipids, PEO- <i>b</i> -PBD, etc.	Parenteral	Discher et al. (2007); Lian and Ho (2001); Allen and Cullis (2013)
Dendrimer	Enables incorporation of diverse drugs, stable, size is controllable, easy to modify	Low yield, complex synthesis	VivaGel ^b	PAMAM, PPI	Transdermal, oral, ocular, and pulmonary	Esfand and Tomalia (2001); Larson and Ghandehari (2012)
PDC	Selective delivery due to linker chemistry, can tune PK via conjugate molecular weight	Complex design, steric hindrance during drug incorporation	SMANCS, Oncaspar, Plegridy, Krystexxa	PEG, HPMA	Parenteral, topical	Larson Ghandehari (2012)

HPMA, Poly(*N*-(2-hydroxypropyl) methacrylamide); MePEG, methoxy(poly(ethylene glycol)); MePEG-*b*-PLA, methoxy(poly(ethylene glycol))-block-poly(D,L-lactic acid); MePEG-*b*-PLDA, methoxy(poly(ethylene glycol))-block-poly(D,L-lactide); PAMAM, poly(amidoamine); PDC, polymer-drug conjugate; PEG, poly(ethylene glycol); PEG-*b*-PDLLA, poly(ethylene glycol)-block-poly(D,L-lactide); PEG-PCL, poly(ethylene glycol)-poly(ϵ -caprolactone); PEO-*b*-PBD, poly(ethylene oxide)-*b*-poly(butadiene); PLGA, poly lactic-co-glycolic acid; PPI, polypropylenimine; SMANCS, poly(styrene-co-maleic acid)-neocarzinostatin.

^aDenotes European Medicines Agency approval.

^bDenotes clinical trials.

linker selection and molecular weight. However, PDCs can also diminish drug efficacy due to steric hindrance of conjugations close to or at drug active sites (Duncan, 2003; Ulbrich and Subr, 2010; Xu et al., 2015). Various biomaterials have been explored to develop PDCs, including PEG and poly(*N*-(2-hydroxypropyl) methacrylamide) (Table 2.5.12.3) (Ulbrich and Subr, 2010; Xu et al., 2015; Larson and Ghandehari, 2012).

Biomaterial DDSs Can Enhance Drug Stability

For various therapeutic compounds and biomaterial DDSs, instability can be a major hurdle to clinical success. The consequences of unexpected drug or DDS degradation—physically or chemically—are dire. These consequences include loss of potency, formation of toxic by-products, and for DDSs, loss of controlled delivery that may cause drug concentrations outside of the TW (subtherapeutic or toxic). Drug degradation mechanisms are similar to those discussed for DDSs (e.g., hydrolysis, oxidation, photolysis, and proteolysis), which can occur for all drug classes: small molecules, proteins/peptides, or nucleic acids. Use of DDSs has been shown to protect drugs from the various modes of degradation (Silva et al., 2018; Opanasopit et al., 2005), as detailed herein (Chono et al., 2008).

Small Molecule Drugs

Several small molecule drug candidates perceived to have excellent and selective therapeutic efficacy are unstable due to inclusive degradable groups. For example, esters and lactones are susceptible to hydrolysis and/or proteolysis by enzymes in the gastrointestinal (GI) (oral delivery) and serum proteins, such as albumin, in systemic circulation (Fig. 2.5.12.4) (Silva et al., 2018; Opanasopit et al., 2005; Dube et al., 2011; Di Martino et al., 2017; Ramezanli et al., 2017; Heredia et al., 2016; Montanari et al., 2016). For example, camptothecin and topotecan are potent chemotherapeutic drugs but include lactone rings making them susceptible to hydrolysis (Fig. 2.5.12.4A). Various approaches to protect these drugs include pH-responsive nanospheres of poly(2-hydroxyethyl methacrylate), liposomes, and SLNs (Silva et al., 2018; Iglesias et al., 2018). Another example is vitamin D₃, which is a steroid that can undergo oxidation (Fig. 2.5.12.4B) or photolysis-mediated isomerization (Fig. 2.5.12.4C), thus hindering its biological efficacy (Ramezanli et al., 2017). Micelles comprised of PEG, desaminotyrosyl-tyrosine octyl ester, and suberic acid triblock copolymers have been exploited to protect vitamin D₃ (Ramezanli et al., 2017).

Protein/Peptide Drugs

Protein and peptide therapeutics are a growing category of drug entities and have special requirements for stability.

Protein therapeutics, such as antibodies and cytokines, as well as peptide therapeutics, can suffer from sequence-specific enzymatic degradation of amide bonds as well as nonspecific enzymatic activity. Additionally, the amino acid functional groups of histidine, tryptophan, methionine, and cysteine are subject to oxidation (Fig. 2.5.12.4B) and tryptophan can photodegrade (Fig. 2.5.12.4C). Various DDSs (i.e., PLGA microspheres, amphiphilic anhydrides, silicone elastomer reservoirs, hydrogel-based systems, and ethylene-*co*-vinyl acetate polymer matrices, etc.) have been explored to protect and controllably delivery proteins/peptides (Van Hove and Benoit, 2015; Patel et al., 2014). Hydrogel-based depot systems are the most commonly used DDSs for protein and peptide delivery with mechanisms of release summarized in Fig. 2.5.12.7.

Nucleic Acid Drugs

Effective delivery of nucleic acid drugs, including DNA, small RNAs, ribozymes, aptamers, and even CRISPR-Cas9, is of immense interest due to their ability to drug the “undruggable.” Through mechanisms subverted from biology, nucleic acid drugs can inhibit, degrade, or alter DNA and/or RNA in ways not possible through traditional low molecular weight drugs or antibodies. However, nucleic acid drugs have significant stability challenges. While some nucleic acid base chemical modifications are protective (Behlke, 2008), generally, nucleic acids are susceptible to degradation by extracellular nucleases and exhibit short half-lives due to renal clearance. For this reason, the majority of nucleic acid-based drugs to undergo clinical trials have only been successfully developed for local delivery (Ozcan et al., 2015), and the development of DDSs to enable systemic delivery for nucleic acid drugs is of high priority (Giang et al., 2014).

Cationic DDSs are predominately used for nucleic acid delivery. Electrostatic interactions of cationic DDSs with anionic nucleic acids protect against enzymatic degradation and achieve nanoparticle formation, which triggers nonspecific intracellular uptake. After nanoparticle DDS uptake, intracellular trafficking through endolysosomes exposes the therapeutic to significant variations in pH (7.4–5) and degradative lysosomal enzymes. This pH gradient provides an environmental stimulus that can be exploited by DDS to escape lysosomal fate. Cationic polymers containing proton-accepting amine groups facilitate endosomal release by osmotic disruption through the “proton sponge” effect (Behr, 1996; Behr, 1997; Boussif et al., 1995; Lynn and Langer, 2000; Pack et al., 2000), which was first proposed by Behr and coworkers (Behr, 1996, 1997). By accepting protons during endosomal acidification, cationic polymers neutralize endosomes and inhibit the typical reduction in pH, resulting in a continued influx of protons and counterions (typically Cl⁻). This proton influx causes the osmotic pressure inside the vesicle to increase, resulting in greater water influx, swelling, endosomal membrane disruption, and finally the release of the endocytosed cargo. There

are many examples of amine-containing “proton sponge” DDSs, including poly(dimethylaminoethyl methacrylate) (DMAEMA), poly(diethylaminoethyl methacrylate), poly(ethylenimine), chitosan, poly(lysine), PAMAM, peptides, and cyclodextrin (Ozcan et al., 2015; Xiao et al., 2019; Sun et al., 2018; Smith, 2018; Li et al., 2018; Hong et al., 2018; Zhang and Wagner, 2017; Shi et al., 2017; Palmerston Mendes et al., 2017; Leiro et al., 2017; Ahmed, 2017; Pandey and Sawant, 2016; Miyata, 2016; Ho et al., 2016).

Polymers that are inert under physiological conditions and membrane disruptive at endolysosomal trafficking pH have also been used to prevent nucleic acid drug lysosomal degradation. Mechanistically, protonation of membrane-disruptive polymers causes a hydrophobic transition from an extended, soluble conformation into a compact, membrane interactive globule (Thomas and Tirrell, 1992; Thomas et al., 1994; Borden et al., 1987; Eum et al., 1989; Chen and Thomas, 1979). Membrane-disruptive DDSs include several polymeric and lipid-based formulations, including poly(propylacrylic acid) (PPAA), combinations of PPAA, butyl methacrylate, DMAEMA, and alkylamine-modified poly(styrene-alt-maleic anhydride) (Sun et al., 2018; Zhang and Wagner, 2017; Shi et al., 2017; Miyata, 2016; Buse and El-Aneedy, 2010; Jabr-Milane et al., 2008; MacEwan et al., 2010; Sebiakin Iu and Budanova, 2006).

In a landmark achievement in drug delivery, Alnylam Pharmaceuticals’ Onpattro (e.g., patisiran) received FDA approval in 2018, making it the first RNAi-based drug brought to market (Mullard, 2018; Hoy, 2018; Morrison, 2018). Developed to treat transthyretin-mediated liver amyloidosis, which is a rare but deadly genetic disease, patisiran is a particle formulation comprised of cholesterol and PEG-conjugated lipids. The lipid moieties contain ionizable amines that complex and protect the siRNA and trigger the proton sponge effect to escape lysosomal degradation upon cell uptake (Whitehead et al., 2014; Jayaraman et al., 2012; Akinc et al., 2008; Wolfrum et al., 2007). In addition to patisiran, numerous other nucleic acid drugs are currently in the developmental pipeline. Of the DDSs employed for systemic delivery of nucleic acids, nearly all are cationic and lipid-based nanocarriers (Ozcan et al., 2015). Continual improvements in rational design of DDSs, especially in controlled synthetic approaches enabling careful structure–function analyses, have the potential to ensure development of highly effective and safe nucleic acid-based therapeutics for clinical applications.

DDS Design to Overcome Biological Barriers

Many natural barriers exist to prevent free exchange of drugs within tissues and organs. The chemistry and function of these barriers vary among the protective outer epithelial layers, the water- and gas-permeable mucosal membranes, and the tightly interconnected phospholipid membranes of

endothelial cells. This section briefly discusses these biological barriers and the ways in which DDSs have been designed to overcome them.

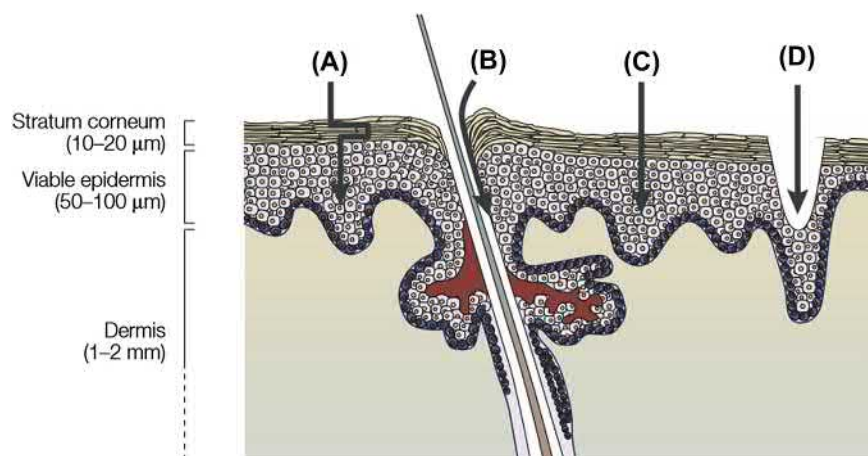
As already introduced in the section “General Considerations for DDS Design—Routes of Drug Delivery,” drug delivery routes include oral (e.g., buccal, sublingual, gastric, enteric), parenteral injection (e.g., intradermal, intramuscular, intravenous, and subcutaneous), transdermal, nasal (e.g., insufflation), rectal, vaginal, and intrathecal (Fig. 2.5.12.3) (Vaidhya, 2013; Tiwari et al., 2012; Ensign et al., 2012; Prausnitz, 2004; Naik et al., 2000). The most commonly used methods are parenteral injections due to high drug absorption (i.e., bioavailability) and oral delivery due to patient convenience and compliance. However, all routes have limitations due to known anatomical, physiological, chemical, pharmacological, or psychological barriers. The primary limitations associated with parenteral drug delivery are trypanophobia (i.e., fear of needles) and the requirement of skilled expertise for proper administration. The key limitations of oral drug delivery include poor drug solubility, stability, and bioavailability due to “first-pass metabolism” effects (Ensign et al., 2012). Therefore interest in additional drug delivery routes, most notably transdermal and mucosal approaches, has grown rapidly in recent years. A closer examination of the various drug delivery routes with respect to the epithelial, mucosal, and endothelial barriers is presented next.

Epithelial Barriers

The epithelium is the outermost of the body’s barriers and consists of the epidermis, various mucosal tissues (e.g., pulmonary, corneal, rectal, vaginal, etc.), and the alimentary canal (i.e., GI tract) tissues. These epithelia are the first barriers through which all drugs must pass before reaching target tissues. The primary drug delivery routes used to bypass epithelial barriers are parenteral and transdermal administration, as described next.

Parenteral Administration

The stratum corneum is the top layer of the epidermis and outermost skin layer that serves as the primary protective barrier to the body due to its unique mechanical and chemical protection (Fig. 2.5.12.9) (Landmann, 1988; Proksch et al., 2008). The stratum corneum consists of dead keratinocytes and intracellular spaces filled with continuous lipid layers (e.g., ceramides, free fatty acids, and cholesterol) measuring approximately 10–15 μm thick (Fig. 2.5.12.9) (Landmann, 1988). Although some small molecule drugs can penetrate the skin, the stratum corneum is impermeable to molecules larger than 500 Da (Bos and Meinardi, 2000), thus limiting drug delivery of higher molecular weight compounds. Mechanical penetration, such as intravenous (IV) injections using hypodermic needles, is a common option for bypassing this barrier and enabling maximal drug delivery to the bloodstream (Fig. 2.5.12.3). Additionally, subcutaneous and intramuscular administrations are the most



• **Figure 2.5.12.9** Schematic representation of a cross-section through human skin and potential routes for drug delivery. The stratum corneum provides nearly all of the barrier functions of the skin by keeping foreign substances out of the body while retaining moisture. Hair interrupts the stratum corneum, but lipid-containing sebum around the hair maintains barrier function. For transdermal DDSs, (A) diffusion, potentially with a chemical enhancer, (B) iontophoresis can enable transport through hair follicles or sweat glands, (C) electroporation can disrupt lipid bilayers, increasing transdermal transport, (D) microneedles puncture skin to enable delivery. (Used with permission from Prausnitz, M.R., Mitragotri, S., Langer, R., 2004. Current status and future potential of transdermal drug delivery. *Nat. Rev. Drug Discov.* 3 (2), 115–124.)

frequently used parenteral routes after IV (Fig. 2.5.12.3). Drugs delivered intramuscularly are absorbed faster than those delivered subcutaneously due to greater vascularity and volumetric capacity of muscle versus subcutaneous tissue (Guerra and Kitabchi, 1976; Turner et al., 2011). Parenteral administration is useful for any drugs or biologics that are sterile, fast acting, stable in serum, and not inherently suited for oral delivery without advanced DDSs. However, this delivery route is painful, typically requires trained personnel, and may cause difficult-to-control adverse events, including overdose.

Transdermal DDSs

Besides bypassing the skin through parenteral injection, various transdermal delivery systems provide direct drug administration through the epidermis. Transdermal DDSs are often considered more convenient than parenteral injections and improve patient compliance (Prausnitz and Langer, 2008). Some small molecule drugs can pass through the epidermis and typically follow a “Lipinski-like” rule set: <500 Da, log P between 2 and 3, and measurable solubility in both oil and water (Wiedersberg and Guy, 2014). For these skin-penetrating drugs, a topical patch or cream can be sufficient for delivery and have gained widespread regulatory approval (Prausnitz and Langer, 2008). However, for drugs with hindered diffusion through the skin, several active delivery systems exist (Prausnitz, 2004; Naik et al., 2000). Active transdermal systems transport the drug across the stratum corneum via mechanical, electrostatic, or chemical means, allowing hydrophilic drugs or larger molecules such as proteins to be delivered. Table 2.5.12.4 provides an overview of these techniques.

Prominent transdermal DDSs include microneedle arrays (Prausnitz, 2004), transdermal jets (Prausnitz and Langer,

2008; McAllister et al., 2014), thermal ablation (Arora et al., 2008), and ultrasonic sonophoresis (Park et al., 2014). These DDSs function by physically transporting drug through the stratum corneum by penetration or electroporation of the lipid layers. Electrostatic techniques include iontophoresis, where charged drug molecules are electrophoretically transported through the stratum corneum, and electroporation, where the stratum corneum (i.e., lipid layers) is disrupted by alternating current. Chemical enhancers improve the transport of drugs across the stratum corneum by acting as a solvent or surfactant to disrupt epidermal cell membranes, increasing drug penetration depths and rates. Enhancers are often used in combination with other active and passive techniques. The reader is directed to reviews of transdermal DDSs for more information (Prausnitz and Langer, 2008; Arora et al., 2008).

Mucosal DDSs

Mucosal membranes are the other major external barrier tissue found in the body. Mucous membranes are present in the eyes, oral cavity, nasal passages, pulmonary tract, stomach, intestines, urethra, vagina, and anus. These tissues vary in structure and function, but all secrete mucus (Bansil and Turner, 2018). The composition of mucus varies by tissue, but it is an omnipresent hydrogel composed of various mucins expressed by goblet cells in the outer mucosal layers and is well distributed on mucosal surfaces due to its shear-thinning properties and constant production (Bansil and Turner, 2018). Mucus dramatically reduces the local diffusion rate of entrapped compounds through a combination of its hydrogel mesh and lipid-binding properties (Bansil and Turner, 2018). However, mucosal barriers can be overcome with careful DDS design.

Important DDS design parameters that affect the ability to cross mucosa include hydrophobicity, electrostatic interactions, van der Waals interactions, size, osmotic solution

TABLE 2.5.12.4 Summary of Transdermal Drug Delivery Systems (DDS)

Delivery Mechanism	Description	Materials	Drugs	References
Topical Delivery (passive)	Drug or DDS diffuses through intact skin while a carrier acts as a depot	Vinyl acetate, poly(acrylic acid), poly(vinyl alcohol), Cyclodextrins	Methylphenidate, nicotine, buprenorphine, scopolamine, nitroglycerin	Naik et al. (2000); Prausnitz and Langer (2008)
Chemical Enhancers	Solvent disrupts integrity of lipids in stratum corneum, improving drug diffusion	Sodium laurel sulfate, phenyl piperazine, Cell penetrating peptides, Liposomes, Dendrimers	Insulin, testosterone, triamcinolone acetonide	Prausnitz and Langer (2008); Mitragotri (2000); Alkilani et al. (2015)
Iontophoresis and electrophoresis	Electrophoretic transport of charged drug molecules or disruption of stratum corneum	Metals (electrodes), poly(vinyl alcohol), poly(vinyl pyrrolidone), poly(acrylic acid)	Lidocaine, fentanyl, acyclovir	Prausnitz and Langer (2008); Ariura et al. (1984)
Microneedles	Submillimeter needles penetrate stratum corneum to carry drug through	Silicon, polycarbonate, titanium, poly(lactic acid)	Vaccines, parathyroid hormone, naltrexone	Prausnitz Langer (2008)
Thermal Ablation	Heat creates micropores in stratum corneum to allow drug diffusion	Metals	Human growth hormone, interferon α -2b, Insulin	Arora et al. (2008)
Transdermal MicroJets	High-velocity jet of liquid or microparticles penetrates stratum corneum by momentum	N/A	Influenza Vaccines (FDA approved)	McAllister et al. (2014)
Sonophoresis	Ultrasonic transducer cavitates lipids in stratum corneum along with gel medium	Poly(ethylene glycol), isopropyl trioleate, glycerol trioleate, linoleic acid	Dexamethasone, Insulin, erythropoietin, Heparin	Mitragotri (2000); Prausnitz et al. (2004); Park et al. (2014)

FDA, Food and Drug Administration; N/A, not applicable.

conditions, and mucoadhesion (Ensign et al., 2012). These parameters directly affect mucosal contact time, permeability, enzyme inhibition, and uptake rate by specialized mucosal regions, such as Peyer's patches, as described for DDSs in Table 2.5.12.5 (Ensign et al., 2012; Kumar et al., 2016; Rathbone et al., 2015; Aungst, 2000; Shaji and Patole, 2008; Saini and Singh, 2015; Lam et al., 2014). Moreover, mucosal permeation enhancers, similar to transdermal systems, increase mucosa permeability to increase drug diffusion (Ensign et al., 2012; Kumar et al., 2016; Rathbone et al., 2015; Aungst, 2000). Together, increased mucosal contact time, permeability, and enzyme inhibition allow for DDS transport across the mucosal barrier via paracellular (i.e., around cells) or transcellular (i.e., through cells) pathways (Ensign et al., 2012; Kumar et al., 2016; Rathbone et al., 2015).

Oral DDSs

Oral drug delivery is the most common and most convenient delivery route. However, many drugs are difficult to formulate for oral delivery due to low solubility, poor stability, and low absorption within the GI tract (Ensign

et al., 2012). As shown in Table 2.5.12.6, variations in epithelial cell type, mucus consistency, surface area, residence time, and pH within the GI tract make oral drug delivery particularly difficult. However, the development of smart DDS that can undergo relatively large and abrupt physical or chemical changes in response to small external changes in environmental conditions has overcome these challenges (Binauld and Stenzel, 2013; Perkins et al., 1999; Liu et al., 2016; Kumar et al., 2017). For example, enteric coatings are polymeric layers that protect drugs against the harsh acidic gastric environment, ensuring drug release in the small intestines. Additionally, DDSs have been designed to be responsive to environmental changes, such as fluctuations in temperature, pH, electric fields, magnetic fields, ultraviolet light exposure, and ionic strength (Binauld and Stenzel, 2013; Schmaljohann, 2006; Gao et al., 2010; Linsley and Wu, 2017; Bear et al., 2016; Mura et al., 2013; Zhao and Moore, 2001; Sood et al., 2016; Hoffman, 2013; Knipe and Peppas, 2014; Koetting et al., 2015), to deliver the right amount of drug to the right place within the GI tract at the right time. Some of these DDSs even release drugs

TABLE 2.5.12.5 Summary of Mucosal Drug Delivery System (DDS) Design Parameters

Mucosal Design Parameter	Description	Drug Delivery Mechanism	Examples	FDA-Approved DDS Examples	References
Mucosal Contact time	Maintains contact between drug or DDS and mucosal absorption surface for prolonged periods of time	Mucoadhesives, sustained Drug Release	Carrageenan, Chitosan, CMC, CP, Eudragit, HEC, HPC, HPMC, PIB, PIP, POE, pullulan, PVA, PVP, sodium alginate	Actiq (lozenge), NiQuitin (lozenge), Nitroguard (buccal tablet), Onsolis (buccal dissolvable film), Orabase (oral paste), Suboxone (sublingual tablet), Striant (buccal tablet)	Saini and Singh (2015); Lam et al. (2014); Hearnden et al. (2012); Shojaei (1998); Silva et al. (2015)
Permeability	The flux of drugs or DDS through the mucosa	Permeability Enhancers	Glycerol monooleate, lauryl lactate, LCC, PCC, propylene glycol, sodium caprate, sodium caprylate, bile salts (e.g., sodium chenodeoxycholate, sodium glycodeoxycholate, sodium lauryl sulfate, sodium taurocholate, sodium taurodeoxycholate, sodium ursodeoxycholate)	Oral-lyn (oral spray containing bile salts to improve buccal permeability)	Aungst (2000); Shaji and Patole (2008); Hearnden et al. (2012); Shojaei (1998); McCartney et al. (2016)
Enzyme Inhibition	Prevents enzyme degradation of drug or DDS	Enzyme Inhibitors	Aprotinin, bestatin, Chitosan, CP, deoxycholic acid, glutathione, Isabgol, soybean trypsin inhibitor, PEG, poly(acrylates), polycarbophil, puromycin, thiomers	Trasylol (IV injection)	Hearnden et al. (2012); Shojaei (1998); Semwal et al. (2014); Karsdal et al. (2015)

CMC, Sodium carboxymethyl cellulose; *CP*, Carbopol 934P; *HEC*, poly(hydroxy ethyl cellulose); *HPC*, poly(hydroxypropyl cellulose); *HPMC*, poly(hydroxypropyl methylcellulose); *HPMC/PVP*, poly(hydroxypropyl methylcellulose)/poly(vinyl pyrrolidone); *IV*, intravenous; *LCC*, lauryl carnitine chloride; *PCC*, palmitoyl carnitine chloride; *PEG*, poly(ethylene glycol); *PIB*, poly(isobutylene); *PIP*, poly(isoprene); *POE*, poly(oxyethylene); *PVA*, poly(vinyl alcohol); *PVP*, poly(vinyl pyrrolidone).

according to circadian rhythms (Jain et al., 2011). However, as previously mentioned, poor drug bioavailability due to “first-pass metabolism” effects within the GI tract or liver markedly limits oral DDS effectiveness (Ensign et al., 2012; Lam et al., 2014). Therefore alternative drug delivery routes capable of reducing or bypassing “first-pass effects” altogether have been widely investigated.

Additional transmucosal drug delivery routes capable of bypassing “first-pass effects” include nasal, sublingual, buccal, ocular, rectal, and vaginal approaches. Sublingual and buccal DDS approaches are two examples that have gained interest recently and have been reviewed elsewhere (see Kumar et al., 2016; Lam et al., 2014; Shojaei, 1998; Silva et al., 2015; Boateng et al., 2015; Mrsny, 2009; Goswami et al., 2008).

Endothelial Barriers

Once a DDS has crossed the epithelia or mucosa and is absorbed into the bloodstream after administration, a host of new endothelial and cell-associated barriers must be

overcome to reach most targets. Endothelial barriers consist of four main components: endothelial cell membranes, tight junctions between cells, the apical surface glycocalyx, and the basement membrane. The endothelial lumen glycocalyx is a thick layer of glycoproteins with embedded proteases. This glycoprotein network inhibits diffusion locally, serving as a barrier for nanoparticles and protein therapeutics (Frey et al., 1996; Aoki et al., 2005). Endothelial cell lipid bilayers prevent free diffusion of most water-soluble compounds over 500 Da due to robust tight junctions, composed of claudins, relegating transport of these molecules to endothelial transcytosis (Lipinski et al., 1997). The basement membrane consists of interconnected laminin and collagen fibers that restrict diffusion of particles greater than 10 nm (Vllasaliu et al., 2014). However, endothelial cell transcytosis can transport nanoparticles up to at least 100 nm in a charge-dependent manner (Bannunah et al., 2014). More detailed reviews of endothelial barriers and their transport mechanisms can be found in Lum et al. (1994), Minshall et al. (2002), and Abbott et al. (2010).

TABLE 2.5.12.6 Characteristics of Gastrointestinal (GI) Tract Segments

GI Tract Segment	Epithelial Cell Type	Mucus Type	Surface Area	Segment Length	Residence Time	pH	Temperature
Oral cavity	Stratified squamous	Dilute	100–220 cm ²	8–9 cm	Seconds to minutes	6.2–7.3	34–37°C
Esophagus	Stratified squamous	Salivary	200 cm ²	23–25 cm	4–8 s	~7.0	36–38°C
Stomach	Secretory columnar	Thick, adherent	3.5 m ²	0.25 m	90 min	1–2	36–38°C
Duodenum	Simple columnar	Thin, adherent	1.9 m ²	0.35 m	30–40 min	4–5.5	36–38°C
Jejunum	Simple columnar	Thin, adherent	184 m ²	2.8 m	1.5–2 h	5.5–7.0	36–38°C
Ileum	Simple columnar	Thin, adherent	276 m ²	4.2 m	5–7 h	7.0–7.5	36–38°C
Colon and rectum	Columnar dominated	Thick, increasing	1.3 m ²	1.5 m	1–60 h (35–38 h avg)	7.0–7.5	34–37°C

Biomaterial DDSs for Drug Targeting

Tissue targeting of DDSs can ameliorate many side effects, including off-target tissue toxicity, by increasing the width of the TW. Tissue targeting is especially critical for delivery of cytotoxic cancer treatments; the chemotherapeutic drug doxorubicin is dose limited due to off-target cardiotoxicity (Barenholz, 2012). Nanoscale DDSs can be used to passively target tissues based on the carrier physicochemical properties or modified with active targeting ligands to enhance tissue accumulation (Fig. 2.5.12.10). Recent advances in both passive and active targeting are shown in Table 2.5.12.7 and additional information can be found in Chapter 1.3.8.

Passive Targeting

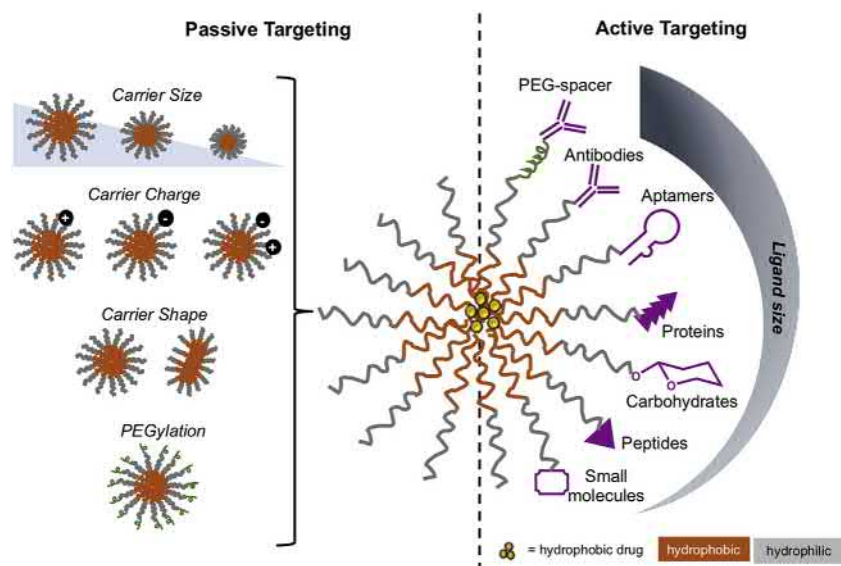
Passive targeting describes tissue accumulation of DDSs based on physicochemical properties and target tissue physiology (Fig. 2.5.12.10). In the 1980s, Maeda et al. observed preferential tumor accumulation of poly(styrene-*co*-maleic acid)-neocarzinostatin drug-polymer conjugates and coined the process as the enhanced permeability and retention (EPR) effect (Matsumura and Maeda, 1986; Maeda et al., 1985). The EPR effect describes the phenomena in which leaky vasculature of the tumor environment is coupled with poor lymphatic drainage, resulting in increased extravasation of macromolecular and nanoparticles into the interstitial space (Accardo and Morelli, 2015). EPR has been subsequently described as a consequence of tissue inflammation, including injury and infection. Passive targeting has evolved since the discovery of EPR, and the evolution has highlighted the importance of DDS physicochemical properties, including size, surface charge, shape, modulus, hydrophobicity, and PEGylation to achieve preferential targeting, as depicted in Fig. 2.5.12.10 (Blanco et al., 2015; Duncan, 2003; Chen et al., 2015; Perry et al., 2011; Merkel et al., 2011; Christian et al., 2009; Cai et al., 2007; Decuzzi

et al., 2010; Kolhar et al., 2013; Barua et al., 2013; Banerjee et al., 2016; Beletskii et al., 2014).

A unique advantage of passive targeting is that it requires little to no DDS modification and therefore is relatively simple, which leads directly to lower costs and easier translation (Muro, 2012). Passive targeting is a straightforward approach to achieve tissue-specific accumulation; however, it relies upon EPR. Unfortunately, the EPR effect applies predominantly to inflamed tissues and is not guaranteed to widen the TW to sufficiently limit off-target toxicity for all drugs. In addition to the EPR effect, when a DDS is injected systemically, it undergoes interactions with plasma proteins and subsequent immune cell recognition and uptake within the liver, spleen, and lymph nodes, the MPS (Lucas et al., 2017; Petschauer et al., 2015). MPS can be taken advantage of for passive targeting by altering DDS size, shape, surface modification, surface charge, and particle dose to dramatically impact their distribution (Lucas et al., 2017). For more information regarding the effect of other physicochemical properties of carriers on passive targeting, please refer to the following publications (Blanco et al., 2015; Chen et al., 2015; Perry et al., 2011; Decuzzi et al., 2010; Muro, 2012).

Active Targeting

The concept of the “magic bullet” (e.g., target-specific drug delivery) was first proposed by Paul Ehrlich (Strebhardt and Ullrich, 2008; Ehrlich, 1900). Although still not a reality due to the body’s inherent ability to recognize and clear foreign substances, active targeting has been attempted for a variety of DDSs, targets, and drugs to enhance tissue-specific accumulation (Hoffman, 2008). Active targeting involves direct coupling or adsorption of targeting groups to a DDS leading to greater drug accumulation versus off-target tissues (Fig. 2.5.12.10). The target can be on an organ/tissue, cellular, subcellular, or molecular level, thus requiring appropriate selectivity of the ligand. This section will



• **Figure 2.5.12.10** Schematic representation of passive and active targeting of drug delivery systems. Passive targeting relies on the physicochemical properties of the carrier, including size, charge, and shape. Additionally, surface modification with poly(ethylene glycol) (PEG) has been shown to enhance circulation time and improve targeting. Active targeting is shown displaying the different ligands and associated range in sizes.

briefly discuss the different types of targeting ligands, and the delivery systems that have been explored to further the quest for the “magic bullet.”

Antibodies

Antibodies are promising targeting groups due to specificity toward their respective antigen. Antibodies that are directly conjugated to small molecule drugs are termed antibody–drug conjugates (ADCs). Although ADCs enjoy therapeutic success, they will not be further discussed here as they are outside the scope of biomaterial DDSs. Antibodies are excellent targeting groups due to high target affinity and specificity and myriad functional groups that allow simple and robust DDS conjugation. However, conjugation can lead to impaired antibody affinity due to uncontrolled conjugation in close proximity to antigen binding sites. Additionally, the large molecular weight of antibodies may also dramatically change DDS characteristics. To circumvent some of these challenges, antibody fragments (Fab and Fv or scFv) have been explored. Antibodies and antibody fragments have been conjugated to liposomes (Huang et al., 1980; Heath et al., 1980), polymeric carriers (Kabanov et al., 1989; Song et al., 2010; Seymour et al., 1991; Omelyanenko et al., 1996; Merdan et al., 2003; Song et al., 2005), and PDCs (Ulbrich and Subr, 2010; Xu et al., 2015; Kopecek and Kopeckova, 2010; Minko, 2010). Additional information of antibody-targeted DDSs can be found in Table 2.5.12.7 and in the following reviews (Xu et al., 2015; Bertrand et al., 2014; Friedman et al., 2013; Allen, 2002).

Proteins

Proteins, such as naturally occurring transferrin or synthetic proteins (e.g., ankyrin), can also be used as targeting moieties. Although typically smaller than antibodies, these proteins still may result in alterations in DDS characteristics

and result in poorly controlled functional group conjugations. Currently, there are various transferrin targeted liposomes being developed and undergoing clinical trials, as highlighted in Table 2.5.12.7 and in the following reviews (Bertrand et al., 2014; Friedman et al., 2013; Allen, 2002).

Peptides

Peptides have excellent potential for targeted DDSs due to their small size, high stability, limited immunogenicity, and ease of conjugation. The development of phage display techniques has enabled identification of various peptide sequences with high specificity and affinity to cellular and microenvironmental targets. The most widely used targeting peptide is arginylglycylaspartic acid (RGD), which binds to integrins upregulated in tumor cells and endothelial cells during tumorigenesis. RGD and other peptides have since been conjugated to liposomes (Accardo and Morelli, 2015; Nishiya and Sloan, 1996; Schiffelers et al., 2002; Garg et al., 2009), polymeric carriers (Hart et al., 1995; Erbacher et al., 1999; Suk et al., 2006; Nasongkla et al., 2004), and PDC (Newman et al., 2018). Additional information of peptide-targeted DDSs can be found in Table 2.5.12.7 and in various reviews (Accardo and Morelli, 2015; Bertrand et al., 2014; Friedman et al., 2013).

Aptamers

Aptamers are single-stranded oligonucleotides developed with selective enrichment processes to have high affinity for protein targets (Bertrand et al., 2014; Liang et al., 2015; Catuogno et al., 2016). Prostate-specific membrane antigen (PSMA)-targeted aptamers for docetaxel have decreased tumor growth and increased survival (Farokhzad et al., 2006). Despite the potential of aptamer ligands, their

TABLE 2.5.12.7 Various Examples of Targeting Ligands

Ligand	Advantages	Disadvantages	Ligands	Targets	Carriers	References
Antibody	Highly specific and selective	Immunogenic, large size hinders conjugations and contributes to NP size increase, sensitive to environmental changes	Anti-CD44, trastuzumab, anti-HER2 Ab, anti-EGFR Ab [#] , ScFv-EGFR, etc.	CD44, HER2 [#] , EGFR	Liposomes [#] , polymer NPs, PDC	Xu et al. (2015); Heath et al. (1980); Song et al. (2010); Merdan et al. (2003); Song et al. (2005); Friedman et al. (2013); Allen (2002); Park et al. (2002); Guo et al. (2018)
Aptamer	Easy to synthesize, high affinity and specificity, nonimmunogenic	Easily degraded by enzymes, conjugation stability is challenging, increases size of carriers, expensive to produce	Anti-PSMA aptamer (A9/A10), anti-HER2 aptamer (A6), CH6, etc.	PSMA, HER2, osteoblasts	Polymer NPs, Liposomes, PDC	Bertrand et al. (2014); Friedman et al. (2013); Liang et al. (2015); Catuogno et al. (2016); Powell et al. (2017); Jiang et al. (2015); Cheng et al. (2007)
Protein	High affinity	Immunogenic, conjugations are complicated due to presence of multiple functional sites	Transferrin [#] , affibodies, ankyrin repeat proteins, gp120, etc.	Transferrin-receptor [#] , EpCAM, HER2, EGFR, DC-SIGN	Liposomes [#] , polymer NPs, PDC	(Xu et al. (2015); Bertrand et al. (2014); Friedman et al. (2013); Allen (2002)
Carbohydrate	Biocompatible, can be easily derivatized	Requires multiple carbohydrate entities to achieve strong binding	Galactose, Mannose, Lactose, HA, Chitosan, etc.	Lectin, CD44	Liposomes, polymer NPs, polymer-drug conjugates	Xu et al. (2015); Bertrand et al. (2014); Friedman et al. (2013); Allen (2002)
Peptide	Small size, improved stability, facile synthesis and conjugation	Can elicit activity on substrate and alter the fate of the NP	RGD, Tet-1, E-selectin binding peptide, CLL1, TBP, etc.	Integrins, E-selectin, TRAP, CLL1 receptor	Liposomes, polymer NPs, PDC	Xu et al. (2015); Accardo and Morelli (2015); Friedman et al. (2013); Allen (2002); Newman et al. (2018); Wang et al. (2017)
Small Molecule	Small size, inexpensive to produce, improved stability	Identifying new affinity ligands, subpar specificity and affinity	Folic acid, tetracycline, BP, ACUPA [#] , etc.	Folate receptor, hydroxyapatite, PSMA [#]	Polymer NPs [#] , Liposomes, PDC	Xu et al. (2015); Bertrand et al. (2014); Friedman et al. (2013); Allen (2002); Hrkach et al. (2012); Farrell et al. (2018); Wang et al. (2015)

[#] Indicates targeting ligands in clinical trials. Additional examples of active-targeted carriers in clinical trials can be found in Bertrand et al. (2014).

ACUPA, S,S-2-(3-(5-Amino-1-carboxypentyl)-ureido)-pentanedioic acid; BP, bisphosphonates; CLL1, C-type lectin domain; DC-SIGN, dendritic cell-specific intercellular adhesion molecule-3-grabbing nonintegrin; EGFR, epidermal growth factor receptor; HA, hyaluronic acid; HER2, human epidermal growth factor receptor 2; NP, nanoparticle; PSMA, prostate-specific membrane antigen; TBP, TRAP-binding peptide; TRAP, tartrate-resistant acid phosphate.

susceptibility to enzymatic degradation is a major limitation and may ultimately hinder the clinical utility of aptamer targeting. Additional information of aptamer-targeted DDSs can be found in Table 2.5.12.7 and in the following reviews (Xu et al., 2015; Bertrand et al., 2014; Friedman et al., 2013).

Carbohydrates

Carbohydrate-targeting groups, including galactose, mannose, fucose, and lactose, enable specific binding to lectin-expressing cells. Consequently, lectin-binding liposomes (Chono et al., 2008; Sato et al., 2007; Gregoriadis Neerunjun, 1975; Mauk et al., 1980; Garcon et al., 1988; Ying et al., 2010), polymeric carriers (Sutton et al., 2007), and PDCs have been explored to target a variety of drugs (Xu et al., 2015; Duncan et al., 1983; Seymour et al., 1987; Negre et al., 1992; Kim et al., 2006; Nahar and Jain, 2009). More detailed examples of carbohydrate-targeted DDSs can be found in Table 2.5.12.7.

Small Molecules

Small molecule ligands are associated with benefits, including small size, low cost, and ligand stability. The best-studied small molecule ligand is folic acid due to its nanomolar affinity toward folate receptors (FRs), which are highly expressed in ~40% of cancers (Guo and Lee, 1999; Lee and Low, 1995; van Steenis et al., 2003). Folic acid-targeting carriers have become so successful that they are being explored to screen and identify FR-positive patients prior to treatment. Unfortunately, one of the challenges associated with folate-targeted carriers is expression of FRs within healthy noncancerous tissues, leading to off-target tissue accumulation. Another active targeting carrier, BIND-014, uses a small molecule ligand *S,S*-2-(3-(5-amino-1-carboxypentyl)-ureido)-pentanedioic acid to specifically target PSMA and deliver docetaxel, resulting in progression of this DDS to Phase 2 clinical trials (Hrkach et al., 2012). Small molecule ligands have been conjugated to liposomes (Lee and Low, 1995; Wang et al., 1995; Yang et al., 2009; Sarti et al., 1996; Liao et al., 1998; Eavarone et al., 2000), polymeric carriers (Guo and Lee, 1999; van Steenis et al., 2003; Mislick et al., 1995; Yoo and Park, 2004; Flanagan et al., 1989; Wightman et al., 1999; Huang et al., 2007; Vinogradov et al., 1999), and PDCs. While this section highlights just a few small molecule-targeted systems, keep in mind that additional small molecule ligands exist, such as bisphosphonates and tetracyclines, which can target bone tissue (Farrell et al., 2018; Wang et al., 2015). Additional information on these approaches is listed in Table 2.5.12.7 and in various reviews (Bertrand et al., 2014; Friedman et al., 2013).

Maintaining ligand specificity, affinity, and multivalency to enhance binding potential is critical for successful active targeting. For example, DDSs acquire a protein corona almost immediately upon introduction systemically,

which can limit active targeting group availability and affinity (Cedervall et al., 2007; Monopoli et al., 2012; Tenzer et al., 2013; Lundqvist et al., 2008). Attachment of spacer arms of various lengths has been explored to reduce both steric hindrances imposed by ligand conjugation as well as the protein corona (Fig. 2.5.12.10).

Regulatory and Intellectual Property Considerations for DDSs

Pharmaceutical companies routinely pursue DDSs not only to enhance therapeutic efficacy but also to maximize drug financial returns by patenting controlled-release formulations and extending market exclusivity. DDSs are combination products—those that combine drugs, biologics, and/or biomaterials using physical, chemical, or some other means to produce a biomedical device (Anderson et al., 2017; Couto et al., 2012). One of the earliest examples of a combination product was the metered-dose inhaler developed in the mid-1950s by Riker Laboratories, as described in the section “History of DDS Development” (Stein and Thiel, 2017; Anselmo and Mitragotri, 2014; Couto et al., 2012). Although combination products of drugs and devices have existed for more than 60 years, only in the last 15 years have regulatory authorities worldwide provided specific guidance for this product category (Table 2.5.12.8). Due to the increase in number and sophistication of combination products over the last few decades, the United States Congress enacted the Medical Device User Fee and Modernization Act in October 2002. Soon afterward, the FDA established the Office of Combination Products to address combination drug and device products entering the marketplace (Couto et al., 2012). Likewise, other regulatory agencies around the world also began considering or implementing similar changes. However, for simplicity this section focuses solely on the guidance offered by the FDA. The Office of Combination Products determines the product’s primary mode of action (PMOA), designates the product’s primary function, and then assigns it to the appropriate FDA center for regulatory evaluation (Couto et al., 2012).

Regulation

Ever since the FDA took these actions to provide guidance documents and offer a single point of contact for regulation of combination products, a general pattern in the process from discovery to development to market entry has been observed (Fig. 2.5.12.11). During product development, sponsors (typically companies) develop combination products. This design and development stage is based on the principle of Quality by Design (QbD). The FDA defines QbD as “a systematic approach to development that begins with predefined objectives and emphasizes product and process understanding and process control, based on sound science and quality risk management” (Q8(R2) *Pharmaceutical Development*,

TABLE 2.5.12.8 Summary of Global Regulatory Guidance Documents for Combination Products

Country/Region	Regulatory Agency	Combination Products Regulatory Guidance
United States of America	Food and Drug Administration	21 CFR Parts 3 and 4
Australia	Therapeutic Goods Administration	Australian Regulatory Guidelines for Medical Devices Australian Register of Therapeutic Goods
Brazil	Agência Nacional de Vigilância Sanitária	Medical Devices BRAZIL Demarest e Almedia Advogados: Lex Mundi Publication. 2011
Canada	Health Canada	Food and Drug Regulations Medical Device Regulations Natural Health Products Regulations “Classification of Products at the (Medical) Device/Drug Interface”
European Union	European Medicines Agency	Medicinal Products: Directive 2001/83 Medical Devices: Regulation 2017/745
Japan	Pharmaceuticals and Medical Devices Agency	“Handling of Approval Application for Combination Products” dated October 24, 2014 Pharmaceutical and Food Safety Bureau (PFSB) Notification No. 1024-(2) of the Evaluation and Licensing Division; PFSB Notification No. 1024-(1) of the Director of Medical Devices Evaluation, Evaluation and Licensing Division; PFSB Notification No. 1024-(9) of the Safety Division; PFSB Notification No. 1024-(15) of the Compliance and Narcotics Division

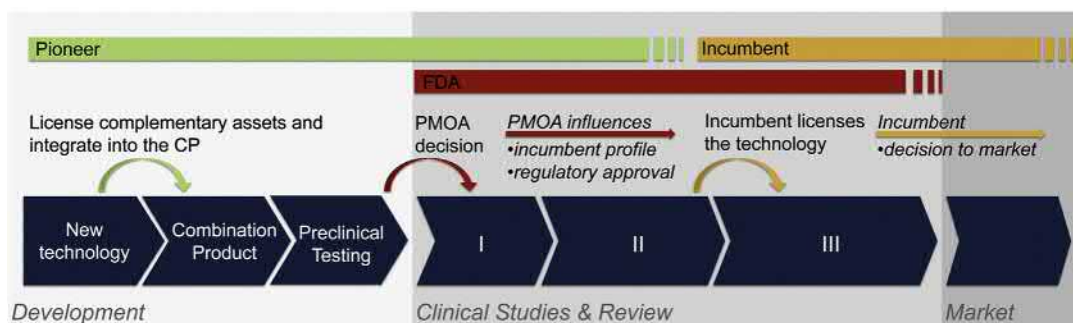
2017). More generally, QbD is a development approach where product Critical Quality Attributes are defined through a risk assessment and then development teams work backward to address these key items in the product design (Singh et al., 2010). Sponsor development teams must consider and include design controls (described in 21 CFR 820.30 and ISO 13485) when combining a drug or biologic with a specific delivery device (Anderson et al., 2017). Design controls are a system of checks and balances intended to make systematic assessment of the product design with a focus on the end user as a key part of development (21 CFR 820.30) (C.f.D.a.R. Health, 1997; Kinsel, 2012). This requirement has historically been associated with medical device development but was established for combination products as part of a 2013 revision to FDA guidance (21 CFR Part 4) on Current Good Manufacturing Practices (Anderson et al., 2017). The development stage concludes with rigorous preclinical testing that provides essential data to justify moving into clinical trials.

The PMOA assessment is affected by integration of the complementary technologies, execution of QbD during development, and completion of preclinical testing. Regulators use the PMOA to determine which agency center of excellence should support the regulatory approval process. Once the PMOA is defined, the regulatory approval pathway (e.g., drug, biologic, or medical device) becomes clear, and established companies in a specific market, termed incumbents, lead the clinical trials, commercialization, and marketing processes for the combination product (Fig. 2.5.12.11) (Couto et al., 2012). For example, Alza Corp. integrated transdermal patch technology into a product, assisted with the initial regulatory assessment, and modeled a corporate structure for commercialization and

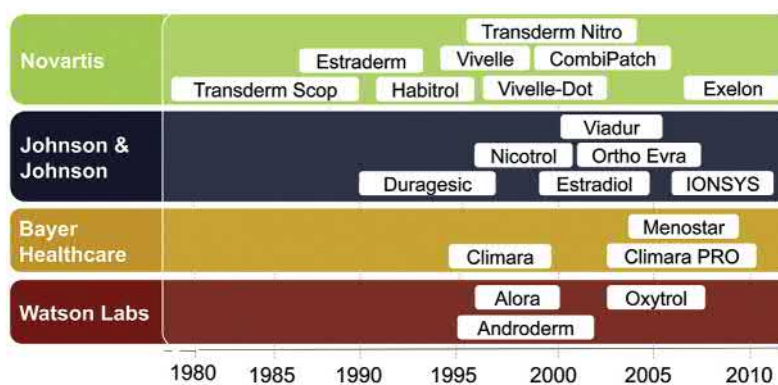
marketing that others later followed (Fig. 2.5.12.12) (Couto et al., 2012). Ultimately, if the combination product is successful in clinical trials, the company will execute a market launch to reach patients and maintain ongoing commercial manufacturing, marketing, and annual regulatory filing efforts for the duration of the product's lifetime.

Intellectual Property

It is not uncommon for the drug development process to require more than 15–20 years of research and development work, including preclinical animal studies and human clinical trials. Thus it is reasonable for pharmaceutical companies to maximize drug financial returns by extending the patent lifetime of the product, thereby postponing the inevitable introduction of generics. One means of doing this is to patent a combination product, such as a new controlled-release formulation with the same drug. However, the commercial feasibility of such a strategy is predicated on a demonstration that the controlled-release formulation is indeed superior in safety and efficacy to the single bolus dose formulation (or a previous controlled-release formulation). Moreover, the cost of the controlled-release formulation must be low enough to ensure a reasonable market penetration. Based on FDA guidance documents, the 505(b)(2) approval pathway allows companies to make small changes to a currently approved drug and still maintain market exclusivity for up to 7 years. This mechanism is less expensive, has a faster approval process, minimizes risk, and maintains market exclusivity. This strategy has led to annual DDS product revenues exceeding \$100 billion as



• **Figure 2.5.12.11** Schematic summarizing the dynamics of the development and approval process for drug–device combination products from the corporate, technology, and regulatory perspectives. (Used with permission from Couto, D.S., et al., 2012. Lessons from innovation in drug-device combination products. *Adv. Drug Deliv. Rev.* 64 (1), 69–77.)



• **Figure 2.5.12.12** Timeline showing Food and Drug Administration approval dates of transdermal patches developed and marketed by companies that followed Alza Corp.'s initial patch commercialization model. (Used with permission from Couto, D.S., et al., 2012. Lessons from innovation in drug-device combination products. *Adv. Drug Deliv. Rev.* 64 (1), 69–77.)

of 2014 (Anselmo and Mitragotri, 2014). This approach is an excellent example of life-cycle management for DDSs as the product approaches its patent expiry. Often, companies initiate future-generation products even before regulators have approved the previous version(s) of a drug. For more information regarding the combination product regulatory process, life-cycle management, and other related intellectual property considerations, the reader is referred to [Chapters 3.5 and 3.6](#), as well as several review articles (Anderson et al., 2017; Couto et al., 2012; Zylberberg and Matosevic, 2016; Davar and Ghosh, 2010).

Final Remarks

Over the past 60 years, DDS materials and designs have progressed from external devices and simple off-the-shelf macroscopic polymeric materials to microscopic, degradable, drug-loaded microparticles and ultimately to complex, rationally designed nanocarriers. The DDS field has grown to a multibillion dollar industry over this timeframe. While DDSs have dramatically improved convenience and clinical usefulness of many drugs and enabled new therapeutics, such as siRNA, to become clinically viable, some of the most challenging problems of drug delivery have yet to be

fully addressed. As the next generation of DDSs undergoes clinical trials utilizing less invasive DDSs with tissue-specific delivery and more efficient drug dosing, the trend in overcoming the remaining challenges will continue to be driven by innovations in biomaterials development and integration.

References

- Abbott, N.J., et al., 2010. Structure and function of the blood–brain barrier. *37* (1), 13–25.
- Abdelwahed, W., et al., 2006. Freeze-drying of nanoparticles: formulation, process and storage considerations. *Adv. Drug Deliv. Rev.* 58 (15), 1688–1713.
- Accardo, A., Morelli, G., 2015. Review peptide-targeted liposomes for selective drug delivery: advantages and problematic issues. *Biopolymers* 104 (5), 462–479.
- Ahmed, M., 2017. Peptides, polypeptides and peptide-polymer hybrids as nucleic acid carriers. *Biomater Sci* 5 (11), 2188–2211.
- Akinc, A., et al., 2008. A combinatorial library of lipid-like materials for delivery of RNAi therapeutics. *Nat. Biotechnol.* 26 (5), 561–569.
- Alkilani, A.Z., McCrudden, M.T., Donnelly, R.F., 2015. Transdermal drug delivery: innovative pharmaceutical developments based on disruption of the barrier properties of the stratum corneum. *Pharmaceutics* 7 (4), 438–470.

- Allen, T.M., 2002. Ligand-targeted therapeutics in anticancer therapy. *Nat. Rev. Cancer* 2 (10), 750–763.
- Allen, T.M., Cullis, P.R., 2013. Liposomal drug delivery systems: from concept to clinical applications. *Adv. Drug Deliv. Rev.* 65 (1), 36–48.
- Anderson, D., et al., 2017. Design control considerations for biologic-device combination products. *Adv. Drug Deliv. Rev.* 112, 101–105.
- Anselmo, A.C., Mitragotri, S., 2014. An overview of clinical and commercial impact of drug delivery systems. *J. Control. Release* 190, 15–28.
- Aoki, Y., et al., 2005. Region-dependent role of the mucous/glycocalyx layers in insulin permeation across rat small intestinal membrane. *22* (11), 1854–1862.
- Ariura, S., et al., 1984. Iontophoresis Device. Google Patents.
- Arora, A., Prausnitz, M.R., Mitragotri, S.J.I.j.o.p., 2008. Micro-scale devices for transdermal drug delivery. *364* (2), 227–236.
- Aungst, B.J., 2000. Intestinal permeation enhancers. *J. Pharm. Sci.* 89 (4), 429–442.
- Bader, R.A., et al., 2014. *Engineering Polymer Systems for Improved Drug Delivery*. John Wiley & Sons, Hoboken.
- Banerjee, A., et al., 2016. Role of nanoparticle size, shape and surface chemistry in oral drug delivery. *J. Control. Release* 238, 176–185.
- Bannunah, A.M., et al., 2014. Mechanisms of nanoparticle internalization and transport across an intestinal epithelial cell model: effect of size and surface charge. *11* (12), 4363–4373.
- Bansil, R., Turner, B.S., 2018. The biology of mucus: composition, synthesis and organization. *Adv. Drug Deliv. Rev.* 124, 3–15.
- Banting, F.G., Best, C.H., 1922. The internal secretion of the pancreas. *J. Lab. Clin. Med.* 7 (5), 251–266.
- Barenholz, Y., 2012. Doxil® — the first FDA-approved nano-drug: lessons learned. *J. Control. Release* 160 (2), 117–134.
- Barua, S., et al., 2013. Particle shape enhances specificity of antibody-displaying nanoparticles. *Proc. Natl. Acad. Sci. USA.* 110 (9), 3270–3275.
- Bear, J.C., et al., 2016. Magnetic hyperthermia controlled drug release in the GI tract: solving the problem of detection. *Sci. Rep.* 6, 34271.
- Behlke, M.A., 2008. Chemical modification of siRNAs for in vivo use. *Oligonucleotides* 18 (4), 305–319.
- Behr, J.P., 1996. The proton sponge, a means to enter cells viruses never thought of. *M.S. Med. Sci.* 12 (1), 56–58.
- Behr, J.P., 1997. The proton sponge: a trick to enter cells the viruses did not exploit. *Chimia* 51 (1–2), 34–36.
- Beletskii, A., et al., 2014. Engineered PRINT((R)) nanoparticles for controlled delivery of antigens and immunostimulants. *Hum. Vaccines Immunother.* 10 (7), 1908–1913.
- Bergental, R.M., et al., 2010. Effectiveness of sensor-augmented insulin-pump therapy in type 1 diabetes. *363* (4), 311–320.
- Bertrand, N., et al., 2014. Cancer nanotechnology: the impact of passive and active targeting in the era of modern cancer biology. *Adv. Drug Deliv. Rev.* 66, 2–25.
- Binauld, S., Stenzel, M.H., 2013. Acid-degradable polymers for drug delivery: a decade of innovation. *Chem. Commun.* 49 (21), 2082–2102.
- Blanco, E., Shen, H., Ferrari, M., 2015. Principles of nanoparticle design for overcoming biological barriers to drug delivery. *Nat. Biotechnol.* 33 (9), 941–951.
- Blix, H.S., et al., 2010. Drugs with narrow therapeutic index as indicators in the risk management of hospitalised patients. *8* (1), 50.
- Blythe, R.H., 1956. In: *Sympathomimetic Preparation*. U.S.P. Office, USA.
- Boas, U., Heegaard, P.M., 2004. Dendrimers in drug research. *Chem. Soc. Rev.* 33 (1), 43–63.
- Boateng, J., Okeke, O., Khan, S., 2015. Polysaccharide based formulations for mucosal drug delivery: a review. *Curr. Pharmaceut. Des.* 21 (33), 4798–4821.
- Bobo, D., et al., 2016. Nanoparticle-based medicines: a review of FDA-approved materials and clinical trials to date. *Pharm. Res.* 33 (10), 2373–2387.
- Bock, H.C., et al., 2010. First-line treatment of malignant glioma with carmustine implants followed by concomitant radiochemotherapy: a multicenter experience. *Neurosurg. Rev.* 33 (4), 441–449.
- Borden, K.A., et al., 1987. Interactions of synthetic polymers with cell membranes and model membrane systems. 13. On the mechanism of polyelectrolyte-induced structural reorganization in thin molecular films. *Macromolecules* 20 (2), 454–456.
- Bos, J.D., Meinardi, M.M.J.E.D.V., 2000. The 500 Dalton rule for the skin penetration of chemical compounds and drugs. *9* (3), 165–169.
- Boussif, O., et al., 1995. A versatile vector for gene and oligonucleotide transfer into cells in culture and in vivo: polyethylenimine. *Proc. Natl. Acad. Sci. USA.* 92 (16), 7297–7301.
- Buhleier, E., Wehner, W., Vögtle, F., 1978. ‘CASCADE’-AND’ non-skid-chain-like’ syntheses of molecular cavity topologies. *Chem. Inf.* 9 (25).
- Buse, J., El-Aneed, A., 2010. Properties, engineering and applications of lipid-based nanoparticle drug-delivery systems: current research and advances. *Nanomedicine* 5 (8), 1237–1260.
- Cabral, H., et al., 2018. Block copolymer micelles in nanomedicine applications. *Chem. Rev.* 118 (14), 6844–6892.
- Cai, S., et al., 2007. Micelles of different morphologies—advantages of worm-like filomicelles of PEO-PCL in paclitaxel delivery. *Pharm. Res.* 24 (11), 2099–2109.
- Callender, S.P., et al., 2017. Microemulsion utility in pharmaceuticals: implications for multi-drug delivery. *Int. J. Pharm.* 526 (1–2), 425–442.
- Catuogno, S., Esposito, C.L., de Franciscis, V., 2016. Aptamer-mediated targeted delivery of therapeutics: an update. *Pharmaceuticals* 9 (4).
- Cedervall, T., et al., 2007. Understanding the nanoparticle-protein corona using methods to quantify exchange rates and affinities of proteins for nanoparticles. *Proc. Natl. Acad. Sci. USA.* 104 (7), 2050–2055.
- Cerpnjak, K., et al., 2013. Lipid-based systems as a promising approach for enhancing the bioavailability of poorly water-soluble drugs. *Acta Pharm.* 63 (4), 427–445.
- C.f.D.a.R. Health (Ed.), 1997. *FDA Design Control Guidance for Medical Device Manufacturers*. US Food and Drug Administration.
- Chen, K.H., et al., 2015. Nanoparticle distribution during systemic inflammation is size-dependent and organ-specific. *Nanoscale* 7 (38), 15863–15872.
- Chen, T.S., Thomas, J.K., 1979. Influence of the Conformational State of Polymethacrylic Acid on the Photophysical Properties of Pyrene in Aqueous Solution: A Fluorescent Probe and Laser Photolysis Study. John Wiley & Sons, Inc., pp. 1103–1116.
- Cheng, J., et al., 2007. Formulation of functionalized PLGA-PEG nanoparticles for in vivo targeted drug delivery. *Biomaterials* 28 (5), 869–876.
- Chono, S., et al., 2008. Efficient drug delivery to alveolar macrophages and lung epithelial lining fluid following pulmonary administration of liposomal ciprofloxacin in rats with pneumonia and estimation of its antibacterial effects. *Drug Dev. Ind. Pharm.* 34 (10), 1090–1096.

- Choy, Y.B., Prausnitz, M.R., 2011. The rule of five for non-oral routes of drug delivery: ophthalmic, inhalation and transdermal. *Pharm. Res.* 28 (5), 943–948.
- Christian, D.A., et al., 2009. Flexible filaments for in vivo imaging and delivery: persistent circulation of filomicelles opens the dosage window for sustained tumor shrinkage. *Mol. Pharm.* 6 (5), 1343–1352.
- Couto, D.S., et al., 2012. Lessons from innovation in drug-device combination products. *Adv. Drug Deliv. Rev.* 64 (1), 69–77.
- Date, A.A., et al., 2010. Self-nanoemulsifying drug delivery systems: formulation insights, applications and advances. *Nanomedicine* 5 (10), 1595–1616.
- Davar, N., Ghosh, S., 2010. Oral controlled release-based products for life cycle management. In: *Oral Controlled Release Formulation Design and Drug Delivery*. John Wiley & Sons, Inc., pp. 305–320.
- Deacon, B., Abramowitz, J., 2006. Fear of needles and vasovagal reactions among phlebotomy patients. *J. Anxiety Disord.* 20 (7), 946–960.
- Decuzzi, P., et al., 2010. Size and shape effects in the biodistribution of intravascularly injected particles. *J. Control. Release* 141 (3), 320–327.
- Di Martino, A., et al., 2017. Enhancement of temozolomide stability by loading in chitosan-carboxylated polylactide-based nanoparticles. *J. Nanoparticle Res.* 19 (2), 71.
- DiMasi, J.A., Grabowski, H.G., Hansen, R.W., 2016. Innovation in the pharmaceutical industry: new estimates of R&D costs. *J. Health Econ.* 47, 20–33.
- Discher, D.E., et al., 2007. Emerging applications of polymersomes in delivery: from molecular dynamics to shrinkage of tumors. *Prog. Polym. Sci.* 32 (8–9), 838–857.
- Dube, A., Nicolazzo, J.A., Larson, I., 2011. Chitosan nanoparticles enhance the plasma exposure of (-)-epigallocatechin gallate in mice through an enhancement in intestinal stability. *Eur. J. Pharm. Sci.* 44 (3), 422–426.
- Duncan, R., 2003. The dawning era of polymer therapeutics. *Nat. Rev. Drug Discov.* 2 (5), 347–360.
- Duncan, R., et al., 1983. Targeting of N-(2-hydroxypropyl)methacrylamide copolymers to liver by incorporation of galactose residues. *Biochim. Biophys. Acta* 755 (3), 518–521.
- Duncan, R., Izzo, L., 2005. Dendrimer biocompatibility and toxicity. *Adv. Drug Deliv. Rev.* 57 (15), 2215–2237.
- Eavarone, D.A., Yu, X., Bellamkonda, R.V., 2000. Targeted drug delivery to C6 glioma by transferrin-coupled liposomes. *J. Biomed. Mater. Res.* 51 (1), 10–14.
- Ehrlich, P., 1900. Croonian lecture.—on immunity with special reference to cell life. *Proc. R. Soc. Lond.* 66 (424–433), 424–448.
- Ensign, L.M., Cone, R., Hanes, J., 2012. Oral drug delivery with polymeric nanoparticles: the gastrointestinal mucus barriers. *Adv. Drug Deliv. Rev.* 64 (6), 557–570.
- Erbacher, P., Remy, J.S., Behr, J.P., 1999. Gene transfer with synthetic virus-like particles via the integrin-mediated endocytosis pathway. *Gene Ther.* 6 (1), 138–145.
- Esfand, R., Tomalia, D.A., 2001. Poly(amidoamine) (PAMAM) dendrimers: from biomimicry to drug delivery and biomedical applications. *Drug Discov. Today* 6 (8), 427–436.
- Eum, K.M., Langley, K.H., Tirrell, D.A., 1989. Quasi-elastic and electrophoretic light scattering studies of the reorganization of dioleoylphosphatidylcholine vesicle membranes by poly(2-ethylacrylic acid). *Macromolecules* 22 (6), 2755–2760.
- Farokhzad, O.C., et al., 2006. Targeted nanoparticle-aptamer bioconjugates for cancer chemotherapy in vivo. *Proc. Natl. Acad. Sci. USA.* 103 (16), 6315–6320.
- Farrell, K.B., et al., 2018. Bisphosphonate conjugation for bone specific drug targeting. *Bone Rep.* 9, 47–60.
- Flanagan, P.A., et al., 1989. Evaluation of protein-N-(2-hydroxypropyl)methacrylamide copolymer conjugates as targetable drug carriers. 1. Binding, pinocytotic uptake and intracellular distribution of transferrin and anti-transferrin receptor antibody conjugates. *Biochim. Biophys. Acta Gen. Subj.* 993 (1), 83–91.
- Fleischer, C.C., Payne, C.K., 2014. Nanoparticle-cell interactions: molecular structure of the protein corona and cellular outcomes. *Acc. Chem. Res.* 47 (8), 2651–2659.
- Folkman, J., Long, D.M., 1964. The use of silicone rubber as a carrier for prolonged drug therapy. *J. Surg. Res.* 4, 139–142.
- Frey, A., et al., 1996. Role of the glycocalyx in regulating access of microparticles to apical plasma membranes of intestinal epithelial cells: implications for microbial attachment and oral vaccine targeting. *184* (3), 1045–1059.
- Friedman, A.D., Claypool, S.E., Liu, R., 2013. The smart targeting of nanoparticles. *Curr. Pharmaceut. Des.* 19 (35), 6315–6329.
- Fu, A.S., et al., 2011. Experimental studies and modeling of drug release from a tunable affinity-based drug delivery platform. *Ann. Biomed. Eng.* 39 (9), 2466–2475.
- Galaev, I., Mattiasson, B., 2010. Smart Polymers: Applications in Biotechnology and Biomedicine.
- Gao, W., Chan, J.M., Farokhzad, O.C., 2010. pH-responsive nanoparticles for drug delivery. *Mol. Pharm.* 7 (6), 1913–1920.
- Garcon, N., et al., 1988. Mannose-mediated targeted immunoadjuvant action of liposomes. *Immunology* 64 (4), 743–745.
- Garg, A., et al., 2009. Targeting colon cancer cells using PEGylated liposomes modified with a fibronectin-mimetic peptide. *Int. J. Pharm.* 366 (1–2), 201–210.
- Giang, I., Boland, E.L., Poon, G.M., 2014. Prodrug applications for targeted cancer therapy. *AAPS J.* 16 (5), 899–913.
- Goswami, T., Jasti, B., Li, X., 2008. Sublingual drug delivery. *Crit. Rev. Ther. Drug Carrier Syst.* 25 (5), 449–484.
- Green, M., et al., 2006. Abraxane®, a novel Cremophor®-free, albumin-bound particle form of paclitaxel for the treatment of advanced non-small-cell lung cancer. *17* (8), 1263–1268.
- Gregoriadis, G., Neerunjun, E.D., 1975. Homing of liposomes to target cells. *Biochem. Biophys. Res. Commun.* 65 (2), 537–544.
- Guerra, S.M., Kitabchi, A.E., 1976. Comparison of the effectiveness of various routes of insulin injection: insulin levels and glucose response in normal subjects. *J. Clin. Endocrinol. Metab.* 42 (5), 869–874.
- Guo, J., et al., 2018. The potential for clinical translation of antibody-targeted nanoparticles in the treatment of acute myeloid leukemia. *J. Control. Release* 286, 154–166.
- Guo, W., Lee, R.L., 1999. Receptor-targeted gene delivery via folate-conjugated polyethylenimine. *AAPS PharmSci.* 1 (4), E19.
- Guo, X., Chang, R.-K., Hussain, M.A., 2009. Ion-exchange resins as drug delivery carriers. *J. Pharm. Sci.* 98 (11), 3886–3902.
- Hart, S.L., et al., 1995. Gene delivery and expression mediated by an integrin-binding peptide. *Gene Ther.* 2 (8), 552–554.
- Hawker, C., Fréchet, J.M.J., 1990. A new convergent approach to monodisperse dendritic macromolecules. *J. Chem. Soc., Chem. Commun.* (15), 1010–1013.
- Hearnden, V., et al., 2012. New developments and opportunities in oral mucosal drug delivery for local and systemic disease. *Adv. Drug Deliv. Rev.* 64 (1), 16–28.
- Heath, T.D., Fraley, R.T., Papahadjopoulos, D., 1980. Antibody targeting of liposomes: cell specificity obtained by conjugation of F(ab')₂ to vesicle surface. *Science* 210 (4469), 539–541.

- Helle, J., et al., 2002. Development and applications of injectable poly(ortho esters) for pain control and periodontal treatment. *Biomaterials* 23 (22), 4397–4404.
- Heller, J., 1990. Development of poly(ortho esters): a historical overview. *Biomaterials* 11 (9), 659–665.
- Heller, J., et al., 2000. Poly(ortho esters) – their development and some recent applications. *Eur. J. Pharm. Biopharm.* 50 (1), 121–128.
- Heller, J., et al., 2002. Development of poly(ortho esters) and their application for bovine serum albumin and bupivacaine delivery. *J. Control. Release* 78 (1–3), 133–141.
- Heredia, V., et al., 2016. Sialoganglioside micelles for enhanced paclitaxel solubility: in vitro characterization. *J. Pharm. Sci.* 105 (1), 268–275.
- Herring, P.T., 1924. The endocrine glands and their internal secretions: a brief historical survey. *Sci. Prog. Twentieth Century* 18 (72), 567–577.
- Herrlich, S., et al., 2012. Osmotic micropumps for drug delivery. *Adv. Drug Deliv. Rev.* 64 (14), 1617–1627.
- Hilery, A.M., Lloyd, A.W., Swarbrick, J., 2001. *Drug Delivery and Targeting: For Pharmacists and Pharmaceutical Scientists*. Taylor & Francis, Inc, New York.
- Hillery, A.M., Lloyd, A.W., Swarbrick, J., 2002. *Drug Delivery and Targeting for Pharmacists and Pharmaceutical Scientists*.
- Ho, W., Zhang, X.Q., Xu, X., 2016. Biomaterials in siRNA delivery: a comprehensive review. *Adv. Healthc. Mater.* 5 (21), 2715–2731.
- Hoffman, A.S., 2008. The origins and evolution of "controlled" drug delivery systems. *J. Control. Release* 132 (3), 153–163.
- Hoffman, A.S., 2013. Stimuli-responsive polymers: biomedical applications and challenges for clinical translation. *Adv. Drug Deliv. Rev.* 65 (1), 10–16.
- Hoffman, A.S., 2016. The early days of PEG and PEGylation (1970s–1990s). *Acta Biomater.* 40, 1–5.
- Holowka, E.P., Bhatia, S.K., 2016. *Drug Delivery: Materials Design and Clinical Perspective*.
- Hong, S.J., et al., 2018. Sugar-based gene delivery systems: current knowledge and new perspectives. *Carbohydr. Polym.* 181, 1180–1193.
- Hoy, S.M., 2018. Patisiran: first global approval. *Drugs* 78 (15), 1625–1631.
- Hrkach, J., et al., 2012. Preclinical development and clinical translation of a PSMA-targeted docetaxel nanoparticle with a differentiated pharmacological profile. *Sci. Transl. Med.* 4 (128), 128ra39.
- Huang, R.Q., et al., 2007. Efficient gene delivery targeted to the brain using a transferrin-conjugated polyethyleneglycol-modified poly-amidoamine dendrimer. *FASEB J.* 21 (4), 1117–1125.
- Huang, A., Huang, L., Kennel, S.J., 1980. Monoclonal antibody covalently coupled with fatty acid. A reagent for in vitro liposome targeting. *J. Biol. Chem.* 255 (17), 8015–8018.
- Huhn, D., et al., 2013. Polymer-coated nanoparticles interacting with proteins and cells: focusing on the sign of the net charge. *ACS Nano* 7 (4), 3253–3263.
- Iglesias, N., et al., 2018. Loading studies of the anticancer drug camptothecin into dual stimuli-sensitive nanoparticles. *Stability scrutiny. Int. J. Pharm.* 550 (1–2), 429–438.
- Jabr-Milane, L., et al., 2008. Multi-functional nanocarriers for targeted delivery of drugs and genes. *J. Control. Release* 130 (2), 121–128.
- Jain, D., et al., 2011. Recent technologies in pulsatile drug delivery systems. *Biomater* 1 (1), 57–65.
- Jani, R., et al., 1994. Ion exchange resins for ophthalmic delivery. *10 (1)*, 57–67.
- Jayaraman, M., et al., 2012. Maximizing the potency of siRNA lipid nanoparticles for hepatic gene silencing in vivo. *Angew. Chem. Int. Ed. Engl.* 51 (34), 8529–8533.
- Jia, L., 2005. Global governmental investment in nanotechnologies. *Curr. Nanosci.* 1 (3), 263–266.
- Jiang, F., et al., 2015. Progress and challenges in developing aptamer-functionalized targeted drug delivery systems. *Int. J. Mol. Sci.* 16 (10), 23784–23822.
- Kabanov, A.V., Chekhonin, V.P., Alakhov, V.Y., Batrakova, E.V., Lebedev, A.S., Melik-Nubarov, N.S., Arzhakov, S.A., Levashov, A.V., Morozov, G.V., Severin, E.S., Kabanov, V.A., 1989. The neuroleptic activity of haloperidol increases after its solubilization in surfactant micelles. *FEBS Lett.* 258.
- Kalepu, S., Nekkanti, V., 2015. Insoluble drug delivery strategies: review of recent advances and business prospects. *Acta Pharm. Sin. B* 5 (5), 442–453.
- Karsdal, M.A., et al., 2015. Lessons learned from the clinical development of oral peptides. *Br. J. Clin. Pharmacol.* 79 (5), 720–732.
- Kataoka, K., Harada, A., Nagasaki, Y., 2001. Block copolymer micelles for drug delivery: design, characterization and biological significance. *Adv. Drug Deliv. Rev.* 47 (1), 113–131.
- Keraliya, R.A., et al., 2012. Osmotic drug delivery system as a part of modified release dosage form. *ISRN Pharm.* 2012 p. 528079–528079.
- Kermode, M., 2004. Unsafe injections in low-income country health settings: need for injection safety promotion to prevent the spread of blood-borne viruses. *Health Promot. Int.* 19 (1), 95–103.
- Kim, T.H., et al., 2006. Mannosylated chitosan nanoparticle-based cytokine gene therapy suppressed cancer growth in BALB/c mice bearing CT-26 carcinoma cells. *Mol. Cancer Ther.* 5 (7), 1723–1732.
- Kinsel, D., 2012. Design control requirements for medical device development. *World J. Pediatr. Congenit. Heart Surg.* 3 (1), 77–81.
- Knipe, J.M., Peppas, N.A., 2014. Multi-responsive hydrogels for drug delivery and tissue engineering applications. *Regen. Biomater.* 1 (1), 57–65.
- Koetting, M.C., et al., 2015. Stimulus-responsive hydrogels: theory, modern advances, and applications. *Mater. Sci. Eng. R Rep.* 93, 1–49.
- Kolhar, P., et al., 2013. Using shape effects to target antibody-coated nanoparticles to lung and brain endothelium. *Proc. Natl. Acad. Sci. USA.* 110 (26), 10753–10758.
- Kopecek, J., Kopeckova, P., 2010. HPMA copolymers: origins, early developments, present, and future. *Adv. Drug Deliv. Rev.* 62 (2), 122–149.
- Kothamasu, P., et al., 2012. Nanocapsules: the weapons for novel drug delivery systems. *Bioimpacts* 2 (2), 71–81.
- Kratz, F.J.J.o.c.r., 2008. Albumin as a drug carrier: design of prodrugs, drug conjugates and nanoparticles. *132 (3)*, 171–183.
- Kumar, A., Vimal, A., Kumar, A., 2016. Why Chitosan? From properties to perspective of mucosal drug delivery. *Int. J. Biol. Macromol.* 91, 615–622.
- Kumar, A., Montemagno, C., Choi, H.-J., 2017. Smart microparticles with a pH-responsive macropore for targeted oral drug delivery. *Sci. Rep.* 7 (1), 3059.
- Lam, J.K., et al., 2014. Oral transmucosal drug delivery for pediatric use. *Adv. Drug Deliv. Rev.* 73, 50–62.
- Landmann, L.J.A., 1988. The epidermal permeability barrier. *Anat. Embryol.* 178 (1), 1–13.
- Larson, N., Ghandehari, H., 2012. Polymeric conjugates for drug delivery. *Chem. Mater.* 24 (5), 840–853.

- Lawson, H.C., et al., 2007. Interstitial chemotherapy for malignant gliomas: the Johns Hopkins experience. *J. Neuro Oncol.* 83 (1), 61–70.
- Lee, R.J., Low, P.S., 1995. Folate-mediated tumor cell targeting of liposome-entrapped doxorubicin in vitro. *Biochim. Biophys. Acta* 1233 (2), 134–144.
- Leiro, V., Santos, S.D., Pego, A.P., 2017. Delivering siRNA with dendrimers: in vivo applications. *Curr. Gene Ther.* 17 (2), 105–119.
- Letchford, K., Burt, H., 2007. A review of the formation and classification of amphiphilic block copolymer nanoparticulate structures: micelles, nanospheres, nanocapsules and polymersomes. *Eur. J. Pharm. Biopharm.* 65 (3), 259–269.
- Li, J., et al., 2018. Poly (amidoamine) (PAMAM) dendrimer mediated delivery of drug and pDNA/siRNA for cancer therapy. *Int. J. Pharm.* 546 (1–2), 215–225.
- Li, Y., Cheng, Y., Xu, T., 2007. Design, synthesis and potent pharmaceutical applications of glycodendrimers: a mini review. *Curr. Drug Discov. Technol.* 4 (4), 246–254.
- Lian, T., Ho, R.J., 2001. Trends and developments in liposome drug delivery systems. *J. Pharm. Sci.* 90 (6), 667–680.
- Liang, C., et al., 2015. Aptamer-functionalized lipid nanoparticles targeting osteoblasts as a novel RNA interference-based bone anabolic strategy. *Nat. Med.* 21 (3), 288–294.
- Liao, W.P., et al., 1998. Liposomal delivery of alpha-Interferon to murine bladder tumor cells via transferrin receptor-mediated endocytosis. *Drug Deliv.* 5 (2), 111–118.
- Liechty, W.B., et al., 2010. Polymers for drug delivery systems. *Annu. Rev. Chem. Biomol. Eng.* 1, 149–173.
- Linsley, C.S., Wu, B.M., 2017. Recent advances in light-responsive on-demand drug-delivery systems. *Ther. Deliv.* 8 (2), 89–107.
- Lipinski, C.A., et al., 1997. Experimental and computational approaches to estimate solubility and permeability in drug discovery and development settings. *Adv. Drug Deliv. Rev.* 23 (1–3), 3–25.
- Liu, D., et al., 2016. The smart drug delivery system and its clinical potential. *Theranostics* 6 (9), 1306–1323.
- Lucas, A.T., et al., 2017. Pharmacokinetic and screening studies of the interaction between mononuclear phagocyte system and nanoparticle formulations and colloid forming drugs. *Int. J. Pharm.* 526 (1–2), 443–454.
- Lum, H., Malik, A.B., 1994. Regulation of vascular endothelial barrier function. *Am. J. Physiol.* 267 (3), L223–L241.
- Lundqvist, M., et al., 2008. Nanoparticle size and surface properties determine the protein corona with possible implications for biological impacts. *Proc. Natl. Acad. Sci. USA.* 105 (38), 14265–14270.
- Lynn, D.M., Langer, R., 2000. Degradable poly(beta-amino esters): synthesis, characterization, and self-assembly with plasmid DNA. *J. Am. Chem. Soc.* 122 (44), 10761–10768.
- Yokoyama, M., 2011. Clinical applications of polymeric micelle carrier systems in chemotherapy and image diagnosis of solid tumor. *J. Exp. Clin. Med.*
- MacEwan, S.R., Callahan, D.J., Chilkoti, A., 2010. Stimulus-responsive macromolecules and nanoparticles for cancer drug delivery. *Nanomedicine* 5 (5), 793–806.
- Maeda, H., et al., 1985. Conjugation of poly(styrene-co-maleic acid) derivatives to the antitumor protein neocarzinostatin: pronounced improvements in pharmacological properties. *J. Med. Chem.* 28 (4), 455–461.
- Mahato, R.I., Narang, A.S., 2018. In: *Pharmaceutical Dosage Forms and Drug Delivery*, third ed. CRC Press, New York.
- Major, I., Fuenmayor, E., McConville, C., 2016. The production of solid dosage forms from non-degradable polymers. *Curr. Pharmaceut. Des.* 22 (19), 2738–2760.
- Malalaterre, V., et al., 2009. Oral osmotically driven systems: 30 years of development and clinical use. *Eur. J. Pharm. Biopharm.* 73 (3), 311–323.
- Marx, V., 2008. Poised to branch out. *Nat. Biotechnol.* 26 (7), 729–732.
- Matsumura, Y., Maeda, H., 1986. A new concept for macromolecular therapeutics in cancer chemotherapy: mechanism of tumorotropic accumulation of proteins and the antitumor agent smancs. *Cancer Res.* 46 (12 Pt 1), 6387–6392.
- Mauk, M.R., Gamble, R.C., Baldeschwieler, J.D., 1980. Targeting of lipid vesicles: specificity of carbohydrate receptor analogues for leukocytes in mice. *Proc. Natl. Acad. Sci. USA.* 77 (8), 4430–4434.
- McAllister, L., et al., 2014. Needle-free jet injection for administration of influenza vaccine: a randomised non-inferiority trial. 384 (9944), 674–681.
- McCartney, F., Gleeson, J.P., Brayden, D.J., 2016. Safety concerns over the use of intestinal permeation enhancers: a mini-review. *Tissue Barriers* 4 (2) p. e1176822-e1176822.
- Merdan, T., et al., 2003. Pegylated polyethylenimine-Fab' antibody fragment conjugates for targeted gene delivery to human ovarian carcinoma cells. *Bioconjug. Chem.* 14 (5), 989–996.
- Merkel, T.J., et al., 2011. Using mechanobiological mimicry of red blood cells to extend circulation times of hydrogel microparticles. *Proc. Natl. Acad. Sci. USA.* 108 (2), 586–591.
- Minko, T., 2010. HPMA copolymers for modulating cellular signaling and overcoming multidrug resistance. *Adv. Drug Deliv. Rev.* 62 (2), 192–202.
- Minshall, R.D., et al., 2002. Vesicle formation and trafficking in endothelial cells and regulation of endothelial barrier function. 117 (2), 105–112.
- Mishra, S., De, A., Mozumdar, S., 2014. Synthesis of thermoresponsive polymers for drug delivery. *Methods Mol. Biol.* 1141, 77–101.
- Mislick, K.A., et al., 1995. Transfection of folate-polylysine DNA complexes: evidence for lysosomal delivery. *Bioconjug. Chem.* 6 (5), 512–515.
- Mitragotri, S., 2000. Synergistic effect of enhancers for transdermal drug delivery. *Pharm. Res.* 17 (11), 1354–1359.
- Miyata, K., 2016. Smart polymeric nanocarriers for small nucleic acid delivery. *Drug Discov. Ther.* 10 (5), 236–247.
- Monopoli, M.P., et al., 2012. Biomolecular coronas provide the biological identity of nanosized materials. *Nat. Nanotechnol.* 7 (12), 779–786.
- Montanari, E., et al., 2016. Hyaluronan/tannic acid nanoparticles via catechol/boronate complexation as a smart antibacterial system. *Macromol. Biosci.* 16 (12), 1815–1823.
- Morgan, M.T., et al., 2006. Dendrimer-encapsulated camptothecins: increased solubility, cellular uptake, and cellular retention affords enhanced anticancer activity in vitro. *Cancer Res.* 66 (24), 11913–11921.
- Morrison, C., 2018. Alnylam prepares to land first RNAi drug approval. *Nat. Rev. Drug Discov.* 17 (3), 156–157.
- Mrsny, R.J., 2009. Lessons from nature: “Pathogen-Mimetic” systems for mucosal nano-medicines. *Adv. Drug Deliv. Rev.* 61 (2), 172–192.
- Mukherjee, S., Ray, S., Thakur, R.S., 2009. Solid lipid nanoparticles: a modern formulation approach in drug delivery system. *Indian J. Pharm. Sci.* 71 (4), 349–358.

- Mullard, A., 2018. FDA approves landmark RNAi drug. *Nat. Rev. Drug Discov.* 17 (9), 613.
- Mura, S., Nicolas, J., Couvreur, P., 2013. Stimuli-responsive nanocarriers for drug delivery. *Nat. Mater.* 12 (11), 991–1003.
- Muro, S., 2012. Challenges in design and characterization of ligand-targeted drug delivery systems. *J. Control. Release* 164 (2), 125–137.
- Nahar, M., Jain, N.K., 2009. Preparation, characterization and evaluation of targeting potential of amphotericin B-loaded engineered PLGA nanoparticles. *Pharm. Res.* 26 (12), 2588–2598.
- Naik, A., Kalia, Y.N., Guy, R.H., 2000. Transdermal drug delivery: overcoming the skin's barrier function. *Pharm. Sci. Technol. Today* 3 (9), 318–326.
- Narvekar, M., et al., 2014. Nanocarrier for poorly water-soluble anticancer drugs—barriers of translation and solutions. *AAPS Pharm-SciTech.* 15 (4), 822–833.
- Nasongkla, N., et al., 2004. cRGD-functionalized polymer micelles for targeted doxorubicin delivery. *Angew. Chem. Int. Ed. Engl.* 43 (46), 6323–6327.
- Negre, E., et al., 1992. Antileishmanial drug targeting through glycosylated polymers specifically internalized by macrophage membrane lectins. *Antimicrob. Agents Chemother.* 36 (10), 2228–2232.
- Newman, M.R., et al., 2018. Multivalent presentation of peptide targeting groups alters polymer biodistribution to target tissues. *Biomacromolecules* 19 (1), 71–84.
- Nishiya, T., Sloan, S., 1996. Interaction of RGD liposomes with platelets. *Biochem. Biophys. Res. Commun.* 224 (1), 242–245.
- Omelyanenko, V., et al., 1996. HPMA copolymer-anticancer drug-OV-TL16 antibody conjugates. 1. influence of the method of synthesis on the binding affinity to OVCAR-3 ovarian carcinoma cells in vitro. *J. Drug Target.* 3 (5), 357–373.
- Opanasopit, P., et al., 2005. Influence of serum and albumins from different species on stability of camptothecin-loaded micelles. *J. Control. Release* 104 (2), 313–321.
- Oss-Ronen, L., Seliktar, D., 2011. Polymer-conjugated albumin and fibrinogen composite hydrogels as cell scaffolds designed for affinity-based drug delivery. *Acta Biomater.* 7 (1), 163–170.
- Ozcan, G., et al., 2015. Preclinical and clinical development of siRNA-based therapeutics. *Adv. Drug Deliv. Rev.* 87, 108–119.
- Pack, D.W., Putnam, D., Langer, R., 2000. Design of imidazole-containing endosomolytic biopolymers for gene delivery. *Biotechnol. Bioeng.* 67 (2), 217–223.
- Palmerston Mendes, L., Pan, J., Torchilin, V.P., 2017. Dendrimers as nanocarriers for nucleic acid and drug delivery in cancer therapy. *Molecules* 22 (9).
- Pandey, A.P., Sawant, K.K., 2016. Polyethylenimine: a versatile, multifunctional non-viral vector for nucleic acid delivery. *Mater. Sci. Eng. C Mater. Biol. Appl.* 68, 904–918.
- Park, K., 2014. Controlled drug delivery systems: past forward and future back. *J. Control. Release* 190, 3–8.
- Park, J.W., et al., 2002. Anti-HER2 immunoliposomes: enhanced efficacy attributable to targeted delivery. *Clin. Cancer Res.* 8 (4), 1172–1181.
- Park, D., et al., 2014. Sonophoresis in transdermal drug deliveries. *Ultrasonics* 54 (1), 56–65.
- Parveen, R., Shamsi, T.N., Fatima, S., 2017. Nanoparticles-protein interaction: role in protein aggregation and clinical implications. *Int. J. Biol. Macromol.* 94 (Pt A), 386–395.
- Pasparakis, G., et al., 2012. Photodegradable polymers for biotechnological applications. *Macromol. Rapid Commun.* 33 (3), 183–198.
- Pasut, G., Veronese, F.M.J.A.d.d.r., 2009. PEG conjugates in clinical development or use as anticancer agents: an overview. *Adv. Drug Deliv. Rev.* 61 (13), 1177–1188.
- Patel, A., Cholkar, K., Mitra, A.K.J.T.d., 2014. Recent developments in protein and peptide parenteral delivery approaches. 5 (3), 337–365.
- Perkins, A.C., et al., 1999. Esophageal transit of risedronate cellulose-coated tablet and gelatin capsule formulations. *Int. J. Pharm.* 186 (2), 169–175.
- Perry, J.L., et al., 2011. PRINT: a novel platform toward shape and size specific nanoparticle theranostics. *Acc. Chem. Res.* 44 (10), 990–998.
- Petschauer, J.S., et al., 2015. The effects of nanoparticle drug loading on the pharmacokinetics of anticancer agents. *Nanomedicine* 10 (3), 447–463.
- Powell, D., et al., 2017. Aptamer-functionalized hybrid nanoparticle for the treatment of breast cancer. *Eur. J. Pharm. Biopharm.* 114, 108–118.
- Prasad, M., et al., 2018. Nanotherapeutics: an insight into healthcare and multi-dimensional applications in medical sector of the modern world. *Biomed. Pharmacother.* 97, 1521–1537.
- Prausnitz, M.R., 2004. Microneedles for transdermal drug delivery. *Adv. Drug Deliv. Rev.* 56 (5), 581–587.
- Prausnitz, M.R., Langer, R., 2008. Transdermal drug delivery. *Nat. Biotechnol.* 26, 1261.
- Prausnitz, M.R., Mitragotri, S., Langer, R., 2004. Current status and future potential of transdermal drug delivery. *Nat. Rev. Drug Discov.* 3 (2), 115–124.
- Proksch, E., Brandner, J.M., Jensen, J.M.J.E.d., 2008. The skin: an indispensable barrier. *Exp. Dermatol.* 17 (12), 1063–1072.
- Q8(R2) pharmaceutical development. In: *ICH Quality Guidelines*, 2017.
- Raghunathan, Y., et al., 1981. Sustained-release drug delivery system I: coated ion-exchange resin system for phenylpropanolamine and other drugs. 70 (4), 379–384.
- Ramezanli, T., et al., 2017. Polymeric nanospheres for topical delivery of vitamin D3. *Int. J. Pharm.* 516 (1–2), 196–203.
- Rathbone, M.J., Pather, I., Şenel, S., 2015. Overview of oral mucosal delivery. In: Rathbone, M.J., Senel, S., Pather, I. (Eds.), *Oral Mucosal Drug Delivery and Therapy*. Springer US, Boston, MA, pp. 17–29.
- Ratner, B.D., 2002. Reducing capsular thickness and enhancing angiogenesis around implant drug release systems. *J. Control. Release* 78 (1–3), 211–218.
- Rideau, E., et al., 2018. Liposomes and polymersomes: a comparative review towards cell mimicking. *Chem. Soc. Rev.*
- Rivera-Delgado, E., Ward, E., von Recum, H.A., 2016. Providing sustained transgene induction through affinity-based drug delivery. *J. Biomed. Mater. Res. A* 104 (5), 1135–1142.
- Rubin, R.R., et al., 2009. Barriers to insulin injection therapy. *Diabetes Educ.* 35 (6), 1014–1022.
- Saini, S., Singh, J., 2015. *Encyclopedia of Biomedical Polymers and Polymeric Biomaterials Mucoadhesive Polymers. Drug Delivery*.
- Saltzman, W.M., 2001. *Drug Delivery Engineering Principles for Drug Therapy*.
- Sarti, P., et al., 1996. Liposomal targeting of leukaemia HL60 cells induced by transferrin-receptor endocytosis. *Biotechnol. Appl. Biochem.* 24 (Pt 3), 269–276.
- Sato, A., et al., 2007. Small interfering RNA delivery to the liver by intravenous administration of galactosylated cationic liposomes in mice. *Biomaterials* 28 (7), 1434–1442.
- Schiffelers, R.M., et al., 2002. Ligand-targeted liposomes directed against pathological vasculature. *J. Liposome Res.* 12 (1–2), 129–135.
- Schmaljohann, D., 2006. Thermo- and pH-responsive polymers in drug delivery. *Adv. Drug Deliv. Rev.* 58 (15), 1655–1670.

- Schneider, C., et al., 2017. Applications of ethylene vinyl acetate copolymers (EVA) in drug delivery systems. *J. Control. Release* 262, 284–295.
- Sebiakin Iu, L., Budanova, U.A., 2006. PH-sensitive cationic lipopeptides for the design of drug-delivery systems. *Bioorg. Khim.* 32 (5), 453–458.
- Semwal, R., Semwal, R.B., Semwal, D.K., 2014. A gastroretentive drug delivery system of lisinopril imbibed on isabgol-husk. *Curr. Drug Deliv.* 11 (3), 371–379.
- Seymour, L.W., et al., 1987. Potential of sugar residues attached to N-(2-Hydroxypropyl)methacryl amide copolymers as targeting groups for the selective delivery of drugs. *J. Bioact. Compat. Polym.* 2 (2), 97–119.
- Seymour, L.W., et al., 1991. Synthetic polymers conjugated to monoclonal antibodies: vehicles for tumour-targeted drug delivery. *Sel. Cancer Ther.* 7 (2), 59–73.
- Shaji, J., Patole, V., 2008. Protein and Peptide drug delivery: oral approaches. *Indian J. Pharm. Sci.* 70 (3), 269–277.
- Shi, B., et al., 2017. Challenges in DNA delivery and recent advances in multifunctional polymeric DNA delivery systems. *Biomacromolecules* 18 (8), 2231–2246.
- Shoichet, M.S., 2009. Polymer scaffolds for biomaterials applications. *Macromolecules* 43 (2), 581–591.
- Shojaei, A.H., 1998. Buccal mucosa as a route for systemic drug delivery: a review. *J. Pharm. Pharm. Sci.* 1 (1), 15–30.
- Silva, B.M., et al., 2015. Mucoadhesive oral films: the potential for unmet needs. *Int. J. Pharm.* 494 (1), 537–551.
- Silva, E.J., et al., 2018. A novel polymer-lipid hybrid nanoparticle for the improvement of topotecan hydrochloride physicochemical properties. *Curr. Drug Deliv.* 15 (7), 979–986.
- Singh, S.K., Venkateshwaran, T.G., Simmons, S.P., 2010. Oral controlled drug delivery: quality by design (QbD) approach to drug development. In: *Oral Controlled Release Formulation Design and Drug Delivery*. John Wiley & Sons, Inc., pp. 279–304.
- Sinko, P.J., 2017. *Martin's Physical Pharmacy and Pharmaceutical Sciences: Physical Chemical and Biopharmaceutical Principles in the Pharmaceutical Sciences*.
- Smith, D.K., 2018. From fundamental supramolecular chemistry to self-assembled nanomaterials and medicines and back again – how Sam inspired SAMul. *Chem. Commun.* 54 (38), 4743–4760.
- Snow, J., 1858. On chloroform and other anestheticstheir action and administration. *Br. J. Addict. Br. J. Anaesth.* 30 (5), 247–252.
- Song, E., et al., 2005. Antibody mediated in vivo delivery of small interfering RNAs via cell-surface receptors. *Nat. Biotechnol.* 23 (6), 709–717.
- Song, H., et al., 2010. Anti-HIF-1 α antibody-conjugated pluronic triblock copolymers encapsulated with Paclitaxel for tumor targeting therapy. *Biomaterials* 31 (8), 2302–2312.
- Sood, N., et al., 2016. Stimuli-responsive hydrogels in drug delivery and tissue engineering. *Drug Deliv.* 23 (3), 758–780.
- Spain, C.V., et al., 2016. Self-reported barriers to adherence and persistence to treatment with injectable medications for type 2 diabetes. *Clin. Ther.* 38 (7), 1653–1664.e1.
- Stegemann, S., et al., 2007. When poor solubility becomes an issue: from early stage to proof of concept. *Eur. J. Pharm. Sci.* 31 (5), 249–261.
- Stein, S.W., Thiel, C.G., 2017. The history of therapeutic aerosols: a chronological review. *J. Aerosol Med. Pulm. Drug Deliv.* 30 (1), 20–41.
- Strebhardt, K., Ullrich, A., 2008. Paul Ehrlich's magic bullet concept: 100 years of progress. *Nat. Rev. Cancer* 8 (6), 473–480.
- Suk, J.S., et al., 2006. Gene delivery to differentiated neurotypic cells with RGD and HIV Tat peptide functionalized polymeric nanoparticles. *Biomaterials* 27 (29), 5143–5150.
- Sun, M., Wang, K., Oupicky, D., 2018. Advances in stimulus-responsive polymeric materials for systemic delivery of nucleic acids. *Adv. Healthc. Mater.* 7 (4).
- Sutton, D., et al., 2007. Functionalized micellar systems for cancer targeted drug delivery. *Pharm. Res.* 24 (6), 1029–1046.
- Temenoff, J.S., Mikos, A.G., 2009. *Biomaterials: The Intersection of Biology and Materials Science*. Pearson.
- Tenzer, S., et al., 2013. Rapid formation of plasma protein corona critically affects nanoparticle pathophysiology. *Nat. Nanotechnol.* 8 (10), 772–781.
- Theeuwes, F.J.J.o.p.s., 1975. Elementary osmotic pump. *J. Pharm. Sci.* 64 (12), 1987–1991.
- Thomas, J., Tirrell, D.A., 1992. Polyelectrolyte-sensitized phospholipid vesicles. *Acc. Chem. Res.* 25, 336–342.
- Thomas, J.L., Barton, S.W., Tirrell, D.A., 1994. Membrane solubilization by a hydrophobic polyelectrolyte: surface activity and membrane binding. *Biophys. J.* 67 (3), 1101–1106.
- Tiwari, G., et al., 2012. Drug delivery systems: an updated review. *Int. J. Pharm. Investig.* 2 (1), 2–11.
- Turnbull, W.B., Stoddart, J.F., 2002. Design and synthesis of glycodendrimers. *J. Biotechnol.* 90 (3–4), 231–255.
- Turner, P.V., et al., 2011. Administration of substances to laboratory animals: routes of administration and factors to consider. *J. Am. Assoc. Lab. Anim. Sci.* JAALAS 50 (5), 600–613.
- Ulbrich, K., Subr, V., 2010. Structural and chemical aspects of HPMA copolymers as drug carriers. *Adv. Drug Deliv. Rev.* 62 (2), 150–166.
- Ulery, B.D., Nair, L.S., Laurencin, C.T., 2011. Biomedical applications of biodegradable polymers. *J. Polym. Sci. B Polym. Phys.* 49 (12), 832–864.
- Ulery, B.D., Nair, L.S., Laurencin, C.T., 2011. Biomedical applications of biodegradable polymers. *J. Polym. Sci. B Polym. Phys.* 49 (12), 832–864.
- Urquhart, J., 2000. Internal medicine in the 21st century: controlled drug delivery: therapeutic and pharmacological aspects. *J. Intern. Med.* 248 (5), 357–376.
- Vaidhya, I.S., Bhagwat, R.R., 2013. Novel drug delivery systems: an overview. *Indian J. Nov. Drug Deliv.* 5 (1), 1–14.
- Van Hove, A.H., Benoit, D.S., 2015. Depot-based delivery systems for pro-angiogenic peptides: a review. *Front. Bioeng. Biotechnol.* 3, 102.
- van Steenis, J.H., et al., 2003. Preparation and characterization of folate-targeted pEG-coated pDMAEMA-based polyplexes. *J. Control. Release* 87 (1–3), 167–176.
- Ventola, C.L., 2017. Progress in nanomedicine: approved and investigational nanodrugs. *P T* 42 (12), 742–755.
- Veronese, F.M., Pasut, G.J.D.d.t., 2005. PEGylation, successful approach to drug delivery. *10* (21), 1451–1458.
- Vinogradov, S., et al., 1999. Polyion complex micelles with protein-modified corona for receptor-mediated delivery of oligonucleotides into cells. *Bioconjug. Chem.* 10 (5), 851–860.
- Vllasaliu, D., et al., 2014. Basement membrane influences intestinal epithelial cell growth and presents a barrier to the movement of macromolecules. *323* (1), 218–231.
- Vulic, K., Shoichet, M.S., 2014. Affinity-based drug delivery systems for tissue repair and regeneration. *Biomacromolecules* 15 (11), 3867–3880.
- Wang, S., et al., 1995. Delivery of antisense oligodeoxyribonucleotides against the human epidermal growth factor receptor into cultured KB cells with liposomes conjugated to folate via polyethylene glycol. *Proc. Natl. Acad. Sci. USA.* 92 (8), 3318–3322.
- Wang, H., et al., 2015. Tetracycline-grafted PLGA nanoparticles as bone-targeting drug delivery system. *Int. J. Nanomed.* 10, 5671–5685.

- Wang, Y., et al., 2017. Fracture-targeted delivery of beta-catenin agonists via peptide-functionalized nanoparticles augments fracture healing. *ACS Nano* 11 (9), 9445–9458.
- Wang, N.X., von Recum, H.A., 2011. Affinity-based drug delivery. *Macromol. Biosci.* 11 (3), 321–332.
- Watanabe, K., Ohtsuki, T., 2016. Photocontrolled intracellular RNA delivery using nanoparticles or carrier-photosensitizer conjugates. *Prog. Mol. Biol. Transl. Sci.* 139, 101–119.
- Whitehead, K.A., et al., 2014. Degradable lipid nanoparticles with predictable in vivo siRNA delivery activity. *Nat. Commun.* 5, 4277.
- Wiedersberg, S., Guy, R.H.J.J.o.C.R., 2014. Transdermal drug delivery: 30+ years of war and still fighting!. *J. Control Release* 190, 150–156.
- Wightman, L., et al., 1999. Development of transferrin-polycation/DNA based vectors for gene delivery to melanoma cells. *J. Drug Target.* 7 (4), 293–303.
- Wilhelm, S., et al., 2016. Analysis of nanoparticle delivery to tumours. *Nat. Rev. Mater.* 1 (5), 16014.
- Wolfrum, C., et al., 2007. Mechanisms and optimization of in vivo delivery of lipophilic siRNAs. *Nat. Biotechnol.* 25 (10), 1149–1157.
- Xiao, Y., et al., 2019. Engineering nanoparticles for targeted delivery of nucleic acid therapeutics in tumor. *Mol. Ther. Methods Clin. Dev.* 12, 1–18.
- Xu, H., et al., 2015. Targeted polymer-drug conjugates: current progress and future perspective. *Colloids Surfaces B Biointerfaces* 136, 729–734.
- Yang, C., et al., 2009. Folate receptor-targeted quantum dot liposomes as fluorescence probes. *J. Drug Target.* 17 (7), 502–511.
- Ying, X., et al., 2010. Dual-targeting daunorubicin liposomes improve the therapeutic efficacy of brain glioma in animals. *J. Control. Release* 141 (2), 183–192.
- Yoo, H.S., Park, T.G., 2004. Folate receptor targeted biodegradable polymeric doxorubicin micelles. *J. Control. Release* 96 (2), 273–283.
- Yoshida, T., et al., 2013. pH- and ion-sensitive polymers for drug delivery. *Expert Opin. Drug Deliv.* 10 (11), 1497–1513.
- Yun, Y.H., Lee, B.K., Park, K., 2015. Controlled drug delivery: historical perspective for the next generation. *J. Control. Release* 219, 2–7.
- Zaffaroni, A., 1991. Overview and evolution of therapeutic systems. *Ann. N.Y. Acad. Sci.* 618, 405–421.
- Zambanini, A., et al., 1999. Injection related anxiety in insulin-treated diabetes. *Diabetes Res. Clin. Pract.* 46 (3), 239–246.
- Zhang, P., Wagner, E., 2017. History of polymeric gene delivery systems. *Top. Curr. Chem.* 375 (2), 26.
- Zhang, Y., Chan, H.F., Leong, K.W., 2013. Advanced materials and processing for drug delivery: the past and the future. *Adv. Drug Deliv. Rev.* 65 (1), 104–120.
- Zhao, Y., et al., 2009. Mesoporous silica nanoparticle-based double drug delivery system for glucose-responsive controlled release of insulin and cyclic AMP. *131* (24), 8398–8400.
- Zhao, B., Moore, J.S., 2001. Fast pH- and ionic strength-responsive hydrogels in microchannels. *Langmuir* 17 (16), 4758–4763.
- Zyllberg, C., Matosevic, S., 2016. Pharmaceutical liposomal drug delivery: a review of new delivery systems and a look at the regulatory landscape. *Drug Deliv.* 23 (9), 3319–3329.

Chapter Review Questions

1. Biomaterial DDSs are also applicable for use with vaccines. Vaccines are biological preparations typically containing a pathogen-mimicking agent, known as an antigen (e.g., weakened or killed whole pathogen, a surface protein or sugar, or a toxin), that improve immunity to disease. You have been hired by a biotechnology company to help develop a new vaccine against Epstein–Barr virus (EBV), the herpes virus that causes infectious mononucleosis. To date, the company has identified and purified key polypeptides from EBV glycoprotein gp350. As the most abundant EBV glycoprotein, gp350 is a key virulence factor involved in the attachment of virus to B cells, so gp350 is hypothesized to be a good EBV vaccine candidate. Note: EBV is a ~120–200 nm spherical virus with an outer viral envelope that contains almost a dozen glycoproteins, and is often spread through saliva. Your manager informs you that the company is striving hard to implement alternative vaccine delivery systems to reduce the number of needle-based injections (e.g., booster shots) for patients, as well as overhead costs associated with the aseptic manufacturing processes necessary for parenterally delivered vaccines. In an attempt to reduce the number of booster shots needed, you suggest implementing a controlled-release delivery system that can gradually release antigen to the patient over time, thus reducing the need for additional booster shots. Name and briefly describe two different biomaterial technologies that could be considered as a novel delivery platform for this vaccine.

Potential answers:

- Nanoparticles and microneedles.
- Nanoparticle vaccines can be used to conjugate, encapsulate, or adsorb antigens using a system that closely resembles the initial pathogen in size and shape. Additionally, they can be administered via sublingual or buccal delivery routes. Controlled release via degradation of the nanoparticle and release of antigen, degradation of a tether between the antigen and the nanoparticle, or

diffusive release of an encapsulated antigen are potential delivery platform options.

Microneedles can be coated or filled with antigens and then inserted into the upper layers of the skin to deliver or slowly release the antigen into the body.

These two approaches can be used alone or in combination to deliver controlled amounts of vaccine antigen over time that could have booster-like effects on the immune response.

- Hydrogel DDSs in the form of patches or oral films as well as nasal DDSs with appropriate supporting rationale.
2. You recently developed a new proton pump inhibitor for the treatment of heartburn and acid reflux. Unfortunately, the acid secretions of the stomach hydrolyze the drug, and the degradation products cause further irritation to the gastric mucosa. Your coworker suggested that you need to coat the drug to protect it from the stomach acid. Do you agree? If not, what other solution(s) can you offer to this problem? If so, which polymer (A, B, or C) would you use and why (i.e., how would it work)?

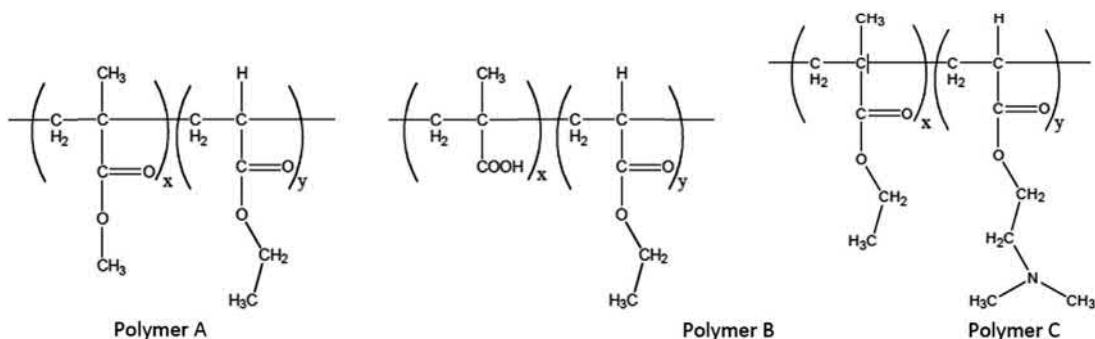
Potential answer:

Polymer B is the right polymer to use for enteric coating of the PPI drug. Polymer B will be protonated and hydrophobic in the stomach, forming an impermeable coating. It will switch to the ionized and soluble form in the intestine, releasing the drug in a favorable pH environment.

If you do not agree with your colleague, other possible approaches could be to deliver the drug from a two-compartment osmotic device, where each compartment is designed to release it only in the small intestines.

3. Delivery of leuprolide, a polypeptide drug, is used as a prostate cancer treatment. The amino acid sequence is: Glu-His-Trp-Ser-Tyr-DLeu-Leu-Arg-Pro-NHEt
Leuprolide acetate

- Two strategies to achieve zero-order release are to use a reservoir/membrane device or to encapsulate the drug in a surface-degrading/eroding degradable polymer. Cite a principal advantage of each of these strategies for the given application and a principal limitation.



Potential answers:

	Advantages	Disadvantages
Reservoir/ membrane	well-controlled environment for a drug formulation, allowing increased drug stability and prolonged <i>delivery</i> times. Increased drug stability.	Nondegradable—need for surgery for retrieval.
Surface-degrading/ eroding polymer	No retrieval necessary, simple formulation (e.g., mix of drug and polymers)	Underlying premise requires rapid polymer degradation, thus drug release may be limited to weeks rather than months; Zero-order release may not be sustained especially at end of degradation due to surface area-to-volume changes over degradation time; Degradation products may lead to side effects

- b. Your research group decides to first test encapsulation of leuprolide in PLGA matrices formed as implantable wafers. Explain what your biggest concern would be with the use of PLGA encapsulation for delivery of the polypeptide in a biological environment.

Potential answer:

PLGA degradation products (lactic acid and glycolic acid) can build up in the matrix, causing locally acidic microenvironments that may expedite peptide chain scission and loss of potency due to degradation and increased drug release rates.

4. Name and describe the five parts or steps involved in DDS pharmacokinetics. Be sure to highlight the important anatomical structures and physiology of these structures involved in the steps. For one of the steps, suggest a formulation strategy to improve drug delivery.

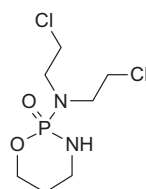
Potential answer:

DDS PK follows the order of Liberation, Absorption, Distribution, Metabolism, and Elimination (LADME). Liberation is the release of drug from the DDS, which can occur by either diffusion, dissolution, mechanical release, or ion exchange. This release typically occurs in the delivery site for local DDS or in the small intestine for oral delivery routes. Liberation is not a factor for administration directly to blood. Absorption is the next step, where the liberated drug is taken up, typically into systemic circulation. Uptake can occur through mucosa or capillary diffusion. Distribution is the subsequent localization of the drug into various tissues, typically through systemic circulation. Liver, lung, spleen, and kidney are common sites of distribution for most drugs, while the brain is less likely to uptake drug. Metabolism occurs when enzymes act on the drug to modify it, which can occur during delivery via enzymes in the skin, mucosa, and GI tract as well as during systemic circulation in the liver or target tissues. Metabolism can be exploited for prodrug strategies and certain DDS depot chemistries, but it is typically responsible for drug inactivation and clearance. Elimination is the final step and typically occurs in the kidneys. Drugs in systemic circulation are secreted into urine, and the rate of this elimination controls drug AUC.

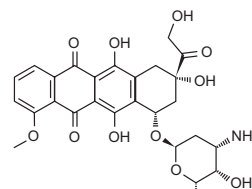
Answers for formulation changes can focus on any of the LADME steps; enteric coatings to protect drug from enzymatic degradation in the stomach, ion exchange resins to modify liberation rate, excipients to increase absorption, targeted DDSs to change distribution, and nanocarrier reservoir DDSs to modify elimination are all valid options.

5.

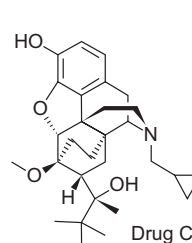
- What is the major barrier to drug permeation via the transdermal route of administration?
- For the following chemical structures being considered for the transdermal route, categorize each according to Lipinski's rule of 5.
- Predict if transdermal permeation is possible and justify your answer based on (b).
- For the impermeable drugs, list and describe two methods that could be used to enhance drug permeation via the transdermal route of delivery.



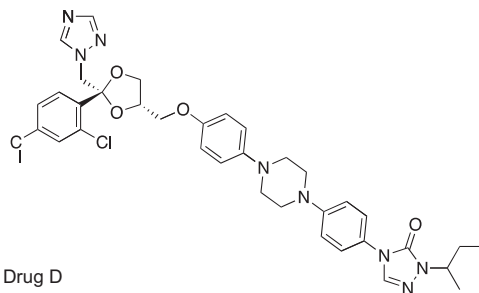
Drug A



Drug B



Drug C



Drug D

Drug A—Cyclophosphamide

Drug B—Doxorubicin

Drug C—Buprenorphine

Drug D—Itraconazole

Potential answers:

- a. Stratum corneum.
- b. Lipinsky's rule of 5 states that a molecule with molecular weight >500 , H-bond donors >5 , H-bond acceptors >10 , and $\log P > 5$ will not penetrate cell membranes and is unlikely to be drug-like.

Compound hydrophobicity determined based on meeting Lipinski's rule of 5:

(A) $M_w < 500$ g/mol, H-donor = 1, H-acceptor = 4, $\log P < 8$

(B) $M_w = 542.53$ g/mol, H-donor = 6, H-acceptor = 12, $\log P = 1.3$

(C) $M_w < 500$ g/mol, H-donor = 3, H-acceptor = 5, $\log P > 3$ —passively diffuses through stratum corneum per [Table 2.5.12.4](#)

(D) $M_w > 500$ g/mol, H-donor = 0, H-acceptor = 12, $\log P > 5$

The drugs that are able to permeate the epidermis will need to be small (<500 g/mol) and lipophilic/hydrophobic ($\log P > 1$). Drug C meets these criteria and can be expected to penetrate lipids well. Drug A is not currently intended for transdermal delivery; however, it has been shown to penetrate the stratum corneum through handling by nurses. Drug B is too hydrophilic for these criteria, while drug D is too large and hydrophobic. Per [Table 2.5.12.4](#), drug C has been formulated to be used for transdermal delivery as well, likely due to $M_w < 500$ g/mol and $\log P > 3$.

Approaches that can be used to enhance transdermal drug delivery of the remaining drugs could be iontophoresis, electrophoresis, microneedles, transdermal microjet, etc. ([Table 2.5.12.4](#)).

6. Several key scientific findings in the 19th and early 20th centuries (e.g., Ehrlich's magic bullet and Banting, Best, and Macleod's discovery that insulin treated diabetes) laid the groundwork for DDS development in the late 20th century. What recent scientific findings have occurred since the start of the 21st century and how might they impact the future of DDS design and development? What challenges will need to be overcome to take full advantage of these scientific findings in DDS design and development?

Answers could include discoveries such as mapping of the human genome, siRNA, and CRISPR (as well as others). Certainly, these technologies will be useful for future design of targeted DDSs. For example, the human genome map will likely highlight genes or proteins that enable targeted cancer therapies to only destroy cancerous and potentially cancerous cells while leaving healthy cells unaffected. Technologies such as siRNA or CRISPR will likely provide specific molecular tools that facilitate this targeting process, but suitable DDS designs using these technologies will need to overcome multiple challenges, including biocompatibility, preliminary drug degradation, biological barriers to enable targeted drug delivery, etc.

2.5.13

Responsive Polymers in the Fabrication of Enzyme-Based Biosensors

JOHN R. AGGAS^{1,2}, ANTHONY GUISEPPI-ELIE^{1,2,3}

¹Center for Bioelectronics, Biosensors and Biochips (C3B), Department of Biomedical Engineering, Texas A&M University, College Station, TX, United States

²Department of Biomedical Engineering, Texas A&M University, College Station, TX, United States

³ABTECH Scientific, Inc., Biotechnology Research Park, Richmond, VA, United States

Introduction

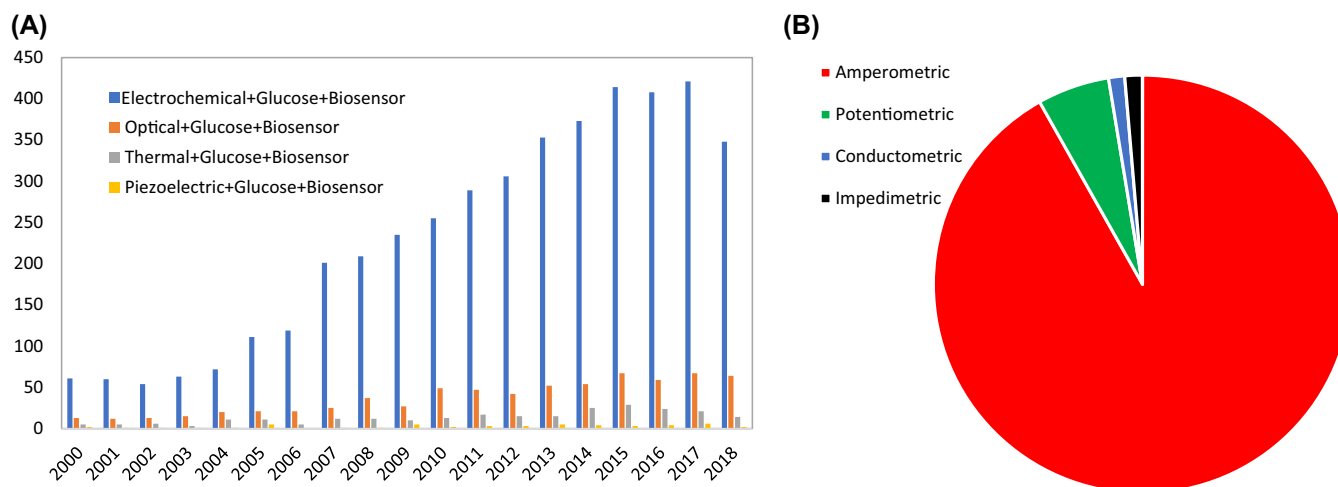
The detection and measurement of glucose (static or continual; *in vitro*, *in situ*, or *in vivo*) has been studied in great depth since the description of the first biosensor by Clark and Lyons in 1962 and the subsequent patent of the original amperometric glucose enzyme electrode in 1970 (Clark and Lyons, 1962; Clark et al., 1970). In addition to the well-studied benefits of glucose sensing for diabetic patients, continuous measurement of glucose can serve as a gauge to identify shock states for patients who have undergone hemorrhage-associated trauma (Guiseppi-Elie, 2011) and may be experiencing insulin resistance. A biosensor is a fully integrated system capable of receiving an input/stimulus from its environment through a biotransducer and outputting a signal that can be processed into readable, actionable information through its instrumentation. The development of biosensors over the last several decades has been driven not only by need in the medical industry, but by needs in the food, environmental, and national defense industries (Idros et al., 2015; Neethirajan et al., 2018; Justino et al., 2017).

Biosensors can be split into four main groups, based on the type of physicochemical transduction employed: electrochemical, optical, thermal, and piezoelectric. From 2000 to the present, over 5000 peer-reviewed articles have been recorded in the ISI Web of Knowledge relevant to these four types of glucose biosensors. From the data shown in Fig. 2.5.13.1A, the number of articles written for each type of glucose biosensor has increased sixfold over the past

2 decades. The most widely studied glucose biosensor systems are electrochemical (48%), followed by optical (32%), thermal (15%), and piezoelectric (5%). Electrochemical glucose biosensors have been the most widely researched type of biosensor since their inception. Electrochemical glucose biosensors, specifically amperometric biosensors, offer many advantages over the other types of transduction mechanisms. Specifically, the low cost of instrumentation, the small footprint that is possible, and the low power requirements coupled with high sensitivity and fast response times (dictated by enzyme kinetics/diffusion) have all been exploited to realize miniaturized, portable, point-of-care glucose-biosensing systems. Moreover, amperometric glucose biosensors are highly studied because they offer the highest sensitivity and are more easily produced on a large scale than other enzymatic electrochemical biosensors (Gaudin, 2017).

Optical glucose biosensors, which continue to be highly researched, also offer several advantages. Optical biosensors offer label-free detection of many types of biological or chemical analytes at high specificity and sensitivity. In addition, optical biosensors show great promise for noninvasive biosensing (Bandodkar and Wang, 2014). However, the equipment required for optical measurements is often costly and requires higher power consumption than most electrochemical glucose biosensors.

Enzymatic electrochemical glucose biosensors, which utilize glucose oxidase (GOx) (an oxido-reductase: EC number 1.1.3.4) as the bioreceptor, can be classified into four groups based on the type of electrochemical transduction



• **Figure 2.5.13.1** (A) The number of electrochemical, optical, thermal, and piezoelectric glucose sensor-related articles since the year 2000, by year. (B) The total number of electrochemical glucose biosensors since the year 2000, split into the transduction type: amperometric, conductometric, impedimetric, and potentiometric. (Data collected from ISI Web of Knowledge.)

employed: amperometric (apply a constant voltage and measure current), conductometric (apply a current and measure a voltage drop), impedimetric (apply a sinusoidally varying voltage and measure the ensuing phase-shifted current as the transfer function), and potentiometric (measure the time-varying voltage relative to a reference voltage). Of the articles recorded on the ISI Web of Knowledge since 2000, over 90% are related to amperometric sensing, followed by potentiometric, impedimetric, and conductometric, as shown in Fig. 2.5.13.1B.

Recently, responsive polymers have been incorporated into enzymatic electrochemical biosensor systems. In part, stimuli-responsive polymers (and addition of nanoparticles) have been incorporated into the transduction element and bioreceptor element in passive and active roles. Many important reviews have been written on glucose biosensors, but a deep understanding and topical review of the incorporation of stimuli-responsive polymers into the various parts of the biosensing system has not been a major area for review. This review discusses the basic principles and types of enzymatic biosensors, with a focus on electrochemical glucose biosensors, the roles and advantages of incorporating stimuli-responsive polymers in electrochemical glucose biosensors, and the current and future outlooks of systems integration of biosensor fabrication.

Classic Biosensor System

The classic biosensor system consists of a bioreceptor established within a recognition layer, a physicochemical transducer, instrumentation or hardware, and signal/computer processing with accompanying signal processing, conditioning, and the production of actionable information as output. The latter is often overlooked but is in fact the central reason for adopting a biosensor format for any analyte measurement.

Bioreceptor (Recognition Layer)

The bioreceptor layer of a biosensor system can be any organic or biomimetic component which has high selectivity toward the target analyte to be measured. The role of the bioreceptor is to receive a stimulus from a target analyte and to present that stimulus to a transducer. Commonly used bioreceptors include antibodies/antigens, nucleic acids/DNA, whole cells, synthetic biomimetics (molecularly imprinted polymers), and enzymes (Tavakoli and Tang, 2017).

Antibodies are large, Y-shaped glycoproteins used by the immune system of the body to identify and neutralize bacteria and viruses by binding to a specific epitope of the pathogen called the antigen. The high specificity of the antibody–antigen binding ($k_{\text{aff}} > 10^{-4} \text{M}$) has led to its widespread use as a bioreceptor in immuno-biosensors. Sandwich assays utilize a capture antibody and a detection antibody labeled with an enzyme to “sandwich” the analyte of interest, followed by a measurement of the catalytic activity between the enzyme attached to the detection antibody and an enzymatic substrate (Cho et al., 2018). In general, antibodies are not available for small molecules (haptens) such as glucose. However, the potential does exist for the development of peptide mimetics with high binding affinities to build biosensors (Thyparambil et al., 2017).

Nucleic acids and DNA used as bioreceptors undergo a recognition process called complementary base-pairing (i.e., adenine-thymine and cytosine-guanine in DNA). Spontaneous hydrogen bonding between the bioreceptor and target complementary strand can be measured by labeling with an electroactive indicator or measurement of a signal produced by the DNA (Asal et al., 2018). The use of RNA or DNA as a bioreceptor is easily prepared via polymerase chain reaction (PCR). Aptamers, which are short, single-stranded oligonucleotides that are able to bind to target molecules have been used as bioreceptors, but the similarity between glucose and other monosaccharides such as fructose and galactose

(similar structures and hydroxyl groups) creates difficulty in selecting an aptamer with high specificity (Ruscito and DeRosa, 2016). Hence, high-specificity aptamers are generally not available for glucose detection and monitoring.

Immobilized cells, organelles, and tissues have been used as transducers in the detection of many biological agents which affect cells. The response of the cell, and signals that form their homeostasis, can be transduced into measurable signals. These cellular biosensors utilize cells which rely on several different biological signals. For example, pancreatic β -cells are able to sense multiple nutrient levels (glucose, lipids, amino acids) and signal for insulin via hormones (i.e., GLP-1, GIP), which were measured through electrode arrays and amplified to extract glucose concentration (Nguyen et al., 2013). Kim et al. utilized red blood cell membrane (RBCM) to fabricate a permselective glucose diffusion barrier based on transport of glucose by glucose transporter-1 in tandem with glucose dehydrogenase to create an amperometric glucose biosensor with high selectivity against interfering molecules (uric acid, ascorbic acid, cysteine, and galactose) (Kim et al., 2018). These cellular bioreceptor systems show future promise for biocompatible, closed-loop feedback systems for sensing and regulation of insulin within the human body.

Molecularly imprinted polymers (MIPs) are polymers which utilize the analyte of interest, acting as a template, to create a cavity in the polymer matrix with affinity toward a target molecule. Monomers are polymerized around the target analyte (via gelation, dispersion, bulk polymerization, etc.), which are then removed (usually by cleavage) and extracted via a solvent. The cavities left behind are expected to have high affinity for the template molecule. Several materials have been reported for synthesis of glucose sensitive MIPs, such as methacrylic acid (MAA) and ethylene glycol dimethyl acrylate (EGDMA) (Widayani, 2017), poly(N-isopropylacrylamide-acrylamide-vinylphenylboronic acid) [poly(NIPAM-AAm-VPBA)] (Wang et al., 2015a,b), O-phenylenediamine (o-PD) (Cheng et al., 2001), and metal-organic copolymers (Qian et al., 2016). This nonenzymatic detection mechanism shows great promise due to the direct electron transfer (DET) functionality, freedom of molecular design and functional groups (to respond to different stimuli such as pH, electric field strength, etc.), high stability, high sensitivity, and low production cost (Alexander et al., 2017).

Recently, other enzyme-free systems have been used for detection of glucose, including synthetic boronic acids as molecular receptors (Wang et al., 2013). These systems which do not rely on proteins are less susceptible to enzyme denaturation and short shelf-life. Boronic acid forms reversible covalent complexes of boronate esters with the *cis*-diols of sugars, which alter changes in optical properties or conductivity (Wang and Lee, 2015). Hence, boronic acid-containing sensors are usually optically or electrochemically based (Cambre and Sumerlin, 2011). Boronic acid derivatives have been directly immobilized on electrodes using various surface chemistries as well as electropolymerized with various

conductive polymers to create a conductive network capable of glucose sensing (Wang et al., 2017; Çiftçi et al., 2013).

Enzymes, which are macromolecular biological catalysts, are the most widely used bioreceptors in biosensing. Specifically, the most commonly used enzyme is glucose oxidase for the sensing of glucose. Biosensors utilizing enzymes as the molecular recognition layer offer several distinct advantages over other types of bioreceptors, including high sensitivity, high selectivity, and short response time (Mulchandani, 1998). However, variables such as bioreceptor film thickness, temperature, pH, and amount of active enzyme contribute to instability of electrode devices (Hossain and Park, 2017). Methods such as electropolymerization have been developed to control the thickness of conductive and nonconductive polymers using various electrochemical techniques (cyclic voltammetry, amperometry, etc.) (Mousa et al., 2019). The known temperature and pH dependence of enzymatic electrochemical biosensors can be accounted for and have been shown to be accurate even outside of their optimum conditions (Rocchitta et al., 2016).

Physicochemical Transducers

The transducer in a biosensor system converts physicochemical changes (temperature, light intensity, pH, conductivity, etc.) which take place at the bioreceptor into another type of energy signal through a process called “signalization” (Rocchitta et al., 2016). The signal measured should be proportional to the concentration (chemical potential) of the target analyte. The type of transduction used in the biosensor dictates the type of biosensor (i.e., electrochemical, optical, colorimetric, gravimetric). Examples of transducers are shown in Fig. 2.5.13.2.

Computer Processing

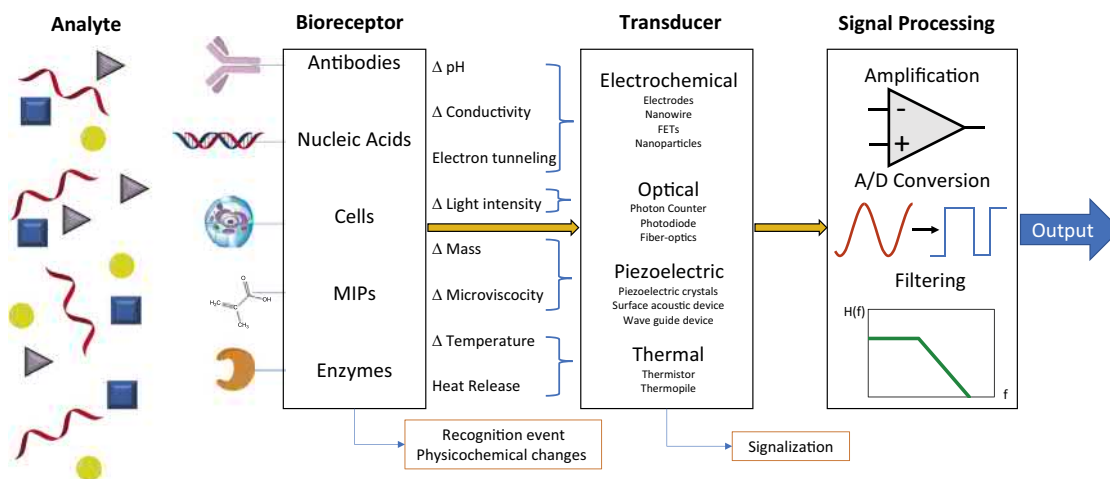
The computer processing and electronics of a biosensor system are comprised of various complex electronics used to digitize, amplify, filter, and multiplex electronic signals and present the processed signal in a display.

Recently, many advances in miniaturization of electronics, low power consumption, and wireless communication (Bluetooth, ZigBee, RFID, NFC, etc.) have been utilized to either bring computer processing as well as power delivery “on-board” for implantable biosensors or wireless transmission of signal data for “off-board” processing (Kotanen C and Guiseppi-Elie, 2014; Jung et al., 2017; Zhao et al., 2017; Kassal et al., 2018).

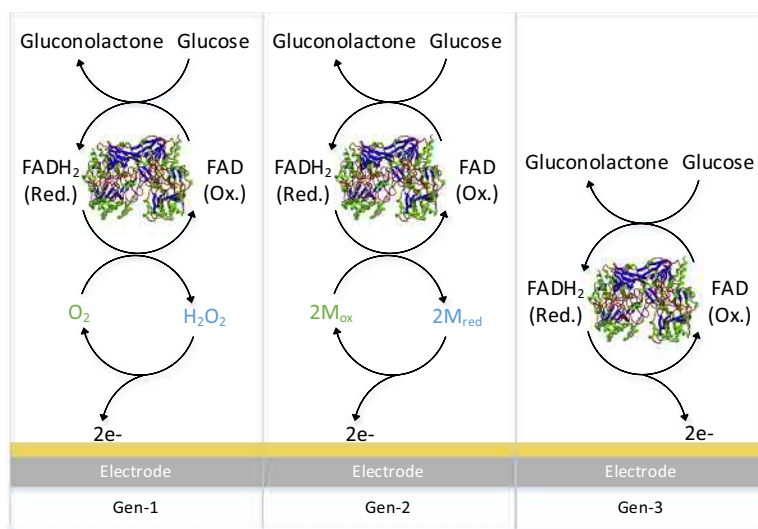
Types of Enzymatic Glucose Biosensors

Electrochemical Biosensors

A major percentage of developed enzymatic glucose biosensors used are electrochemical, because they offer sensitivity and reproducibility at a low cost that cannot be offered by many of the other sensing modalities. In fact, many of the commercially available point-of-care glucose biosensors measure glucose electrochemically (Yoo and Lee, 2010). Electrochemical biosensors can be grouped into four main transduction types: amperometric, conductimetric, impedimetric, and potentiometric.



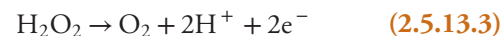
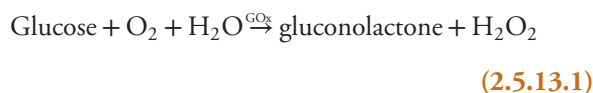
• **Figure 2.5.13.2** General mechanism of biosensor operation. Analytes of interest are recognized by various types of bioreceptors, where some form of energy transduction can be displayed as an output through computation.



• **Figure 2.5.13.3** The three generations of enzymatic glucose sensors. (Adapted from Karunwi et al. (2013)).

Amperometric Biosensors

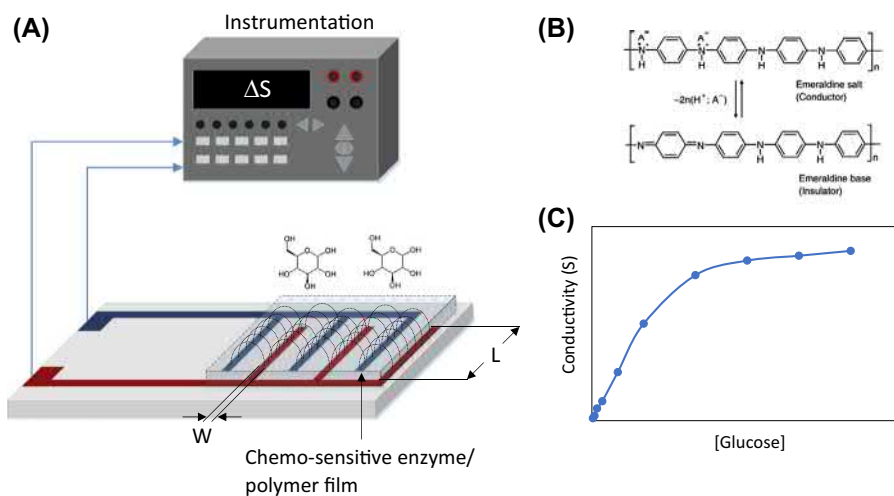
Amperometric glucose enzyme biosensors measure the movement of electrons (current) produced in a redox reaction beginning with the oxidation of glucose to gluconolactone via GOx (the redox cofactor, FAD, serves as the electron acceptor) (Eq. 2.5.13.1). Gluconolactone is converted to gluconate⁻ and H⁺ (Eq. 2.5.13.2) and H₂O₂ is converted to O₂, 2H⁺ and electrons in the form of current (Eq. 2.5.13.3) (Weibel and Bright, 1971; Chou et al., 2018).



In an electrochemical cell, measurements can be made to monitor the consumption of oxygen or the production of hydrogen peroxide in the reaction, the current of which is directly proportional to the glucose concentration.

Amperometric glucose biosensors have been divided into three generations, based on the mechanism of electron transfer used to measure the concentration of target analyte. The reader is directed to several reviews for a comprehensive discussion of the three generations (Rocchitta et al., 2016; Wang, 2008; Chen et al., 2013). Briefly, the three generations of amperometric glucose biosensor are summarized below and visualized in Fig. 2.5.13.3:

- **Generation 1:** Generation 1 glucose biosensors monitor the consumption of oxygen or the production of hydrogen peroxide (Eq. 2.5.13.1) at the cathode or anode, respectively.



• **Figure 2.5.13.4** (A) Typical interdigitated conductometric biosensor. A chemo-sensitive film is deposited on an interdigitated electrode system. (B) Protonation and deprotonation of polyaniline as a result of hydrogen ion formation. (C) Typical conductometric glucose biosensor response.

- **Generation 2:** The second generation of glucose biosensors utilized a redox mediator, such as ferrocenes, viologens, quinones, etc., to shuttle electrons from the redox center of the GOx molecule to the electrode, effectively eliminating the need for oxygen.
- **Generation 3:** The third generation of glucose biosensors involves a direct transport of the electron (DET) from the active site of the GOx to the electrode itself, without the need of a mediator.

Conductometric Biosensors

Conductometric enzyme biosensors measure the changes in conductivity of a membrane or medium, usually between two interdigitated electrodes spaced very close to each other (tens of microns) and sometimes a pair of interdigitated electrodes, one serving as measurement and one serving as reference (Nouira et al., 2013). Conductometric devices are sometimes presented as a subset of impedimetric devices but are discussed separately here. As glucose oxidase reacts with glucose, the local concentration of H^+ ions increases (Eq. 2.5.13.3), resulting in an increase in acidity and conductivity near the electrode (Kucherenko et al., 2016). However, since most assays are done in buffered solutions, these ions are neutralized quickly and don't take part in measurable net charge transport (Bănică, 2012). In fact, solution parameters such as ion strength, buffer capacity, and pH have a significant impact on solution conductivity and in turn the biosensor response (higher ion strength or buffer concentration tend to reduce sensitivity) (Pyeshkova et al., 2009). An elegant solution involves preparation of conductometric transducers utilizing chemoresistive materials, such as conductive polymers. The pH of responses of conductive polymers such as polyaniline and polypyrrole have been used as stimuli-responsive films in conductometric glucose biosensors (Miwa et al., 1994). Polyaniline, which can be protonated to its conductive emeraldine salt or deprotonated to its insulating emeraldine base, has been used as films on interdigitated microelectrodes (IDEs) with GOx

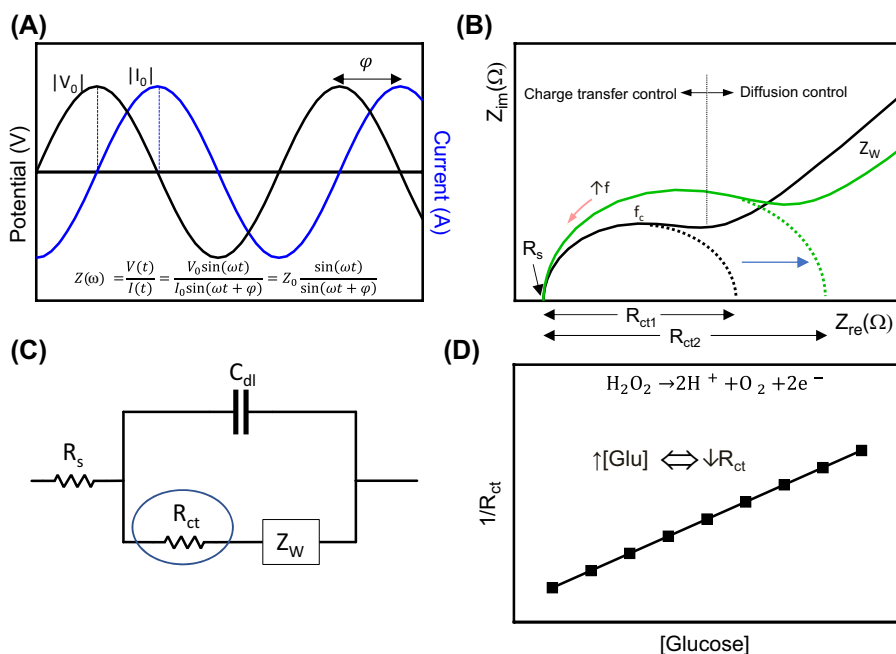
(Fig. 2.5.13.4). In particular, the conductivity of the conductive polymer polyaniline is determined by the *degree* of protonation, and therefore unless in contact with a very strong acid, the conductivity can vary several orders of magnitude over several pHs. The resistance of such films is measured using small-amplitude AC signals (see “Impedimetric biosensor” section) or mV level DC signals, according to the type of instrumentation used.

While conductometric biosensors offer advantages such as nonsensitivity to light, no need for a reference electrode, and low cost, many efforts have afforded poor signal-to-noise ratios in comparison with other types of enzymatic biosensors.

Impedimetric Biosensors

Based on the fact that changes in conductivity of a membrane or medium are a factor of resistance and reactance, impedimetric biosensors emerged as a means to deconvolute and monitor the capacitive and resistive changes occurring in a biosensor system (Katz and Willner, 2003). Electrochemical impedance spectroscopy (EIS) is a commonly used nondestructive measurement tool that has been utilized in applications including electrode characterization (Aggas et al., 2018), corrosion (Ribeiro and Abrantes, 2016), and biosensors (Kotanan et al., 2018).

Impedance is measured by application of a small sinusoidal voltage (<50 mV peak-to-peak) and measurement of the resultant current response (magnitude and phase) over a range of frequencies, as shown in Fig. 2.5.13.5A. Measurement over a range of frequencies allows the researcher to visualize frequency-dependent phenomena in the electrochemical system. A typical Nyquist plot is shown in Fig. 2.5.13.5B. EIS spectra are analyzed by equivalent circuit analysis (ECA), a technique in which experimental data are fitted to a circuit which can describe the electrochemical system in order to quantify electrical parameters and extract kinetics and charge transfer mechanisms. The most basic of these circuits, the Randles circuit, includes a solution



• **Figure 2.5.13.5** (A) Sinusoidal current response in a linear EIS system. (B) Typical Nyquist plot of enzymatic glucose electrodes in analyte. (C) Equivalent circuit used to analyze Nyquist plots. (D) Typical R_{ct} response of increasing amounts of glucose.

resistance (R_s), charge transfer resistance (R_{ct}), double layer capacitance (C_{dl}), and Warburg impedance (W) (Fig. 2.5.13.5C).

Changes in the charge transfer resistance (faradaic impedance biosensors) and double layer capacitance (non-faradaic impedance biosensors) of glucose biosensor systems have been shown to correlate to the glucose concentration (Pänke et al., 2007). Recently, Asrami et al. demonstrated a reusable novel nanostructured copper oxide film on fluorinated-tin oxide with glucose oxidase immobilized in chitosan for impedimetric sensing of glucose. EIS measurements showed a linear scale of ΔR_{ct} [ΔR_{ct} (k Ω) = 0.306(\pm 0.027) + 0.261 (\pm 0.003) \times [glucose] (mM); $R^2 = 0.998$] over the range of 0.2–15 mM glucose (Naderi Asrami et al., 2018). Wang et al. demonstrated a bifunctional impedimetric and amperometric glucose biosensor utilizing self-assembled monolayers (SAMs) of GOx with Prussian blue mediator able to operate at low potentials (0.0 V vs. Ag/AgCl). EIS measurements showed a linear scale of $1/R_{ct}$ [$1/R_{ct}$ (k Ω) = 0.225 + 0.0773 \times [glucose] (mM); $R^2 = 0.994$] over the range of 0.0–25 mM glucose (Wang et al., 2015a,b). A typical linear response curve of $1/R_{ct}$ versus glucose concentrations is shown in Fig. 2.5.13.5D.

Potentiometric Biosensors

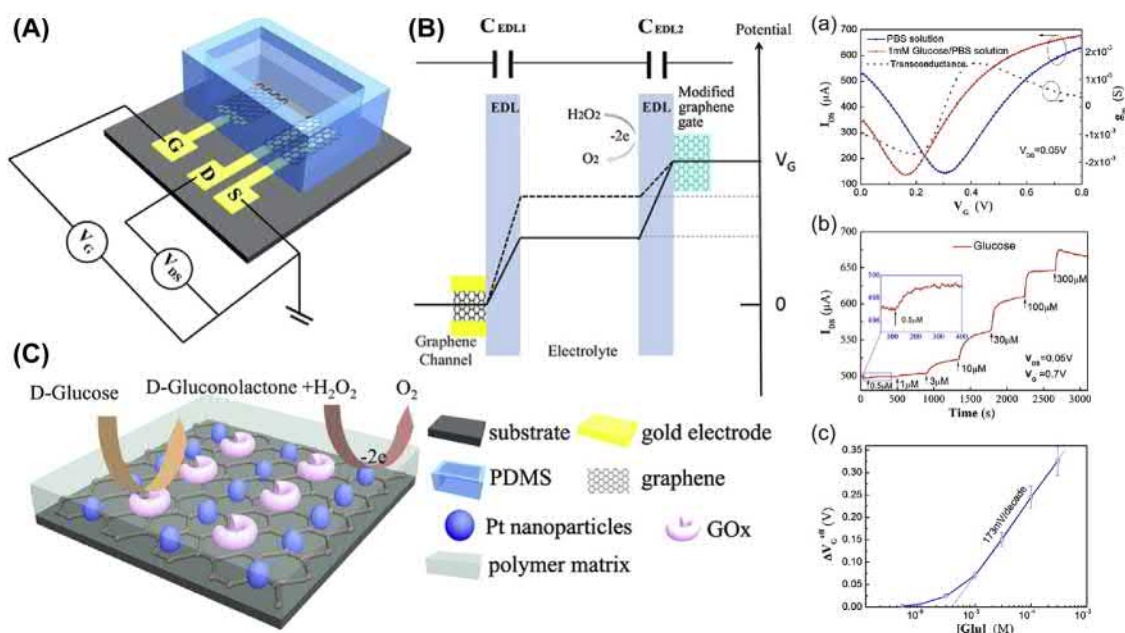
Potentiometric enzyme biosensors measure changes in electric potential generated by an analyte reacting with an enzyme due to concentrations of ions, usually at an ion-selective electrode (ISE), ion-selective field effect transistor (ISFET), or enzyme field effect transistor (EnFET) (Mulchandani, 1998). The most simple of these potentiometric biosensors is the glass pH electrode, of which GOx

has been immobilized by means of cellophane, nylon, and nitrocellulose (Pisoschi, 2016). In a more complex fashion, GOx has been immobilized on ion-sensitive membranes of ion-selective FETs. The changes in electrical field at the enzyme/electrode interface alter the conductivity of the n and p channels of an ISFET. While potentiometric biosensors are mostly used for measurement of ion concentration (pH, Na^+ , K^+ , Mg^{2+} , NO_3^- , etc.), there is some recent work utilizing potentiometric methods to measure glucose via glucose oxidase. A typical glucose-sensitive enzyme transistor is shown in Fig. 2.5.13.6A. Generation of H_2O_2 by oxidation of glucose at the gate of the transistor and the modulation of gate voltage by oxidation of H_2O_2 (Zhang et al., 2015). The potential drop at the gates is determined by the Nernst equation:

$$V_{EDL2} = -\frac{kT}{2q} \ln [\text{H}_2\text{O}_2] + C \quad (2.5.13.4)$$

where the voltage on the channel surface, V_{EDL2} is a function of the Boltzmann constant (k), the temperature (T), electronic charge (q), concentration of H_2O_2 , and a constant C . The changing concentration of H_2O_2 at the electrode governs the current through the channel (I_{DS}) by the field effect. Typical channel currents from 0 to 300 mM glucose are shown in Fig. 2.5.13.6D.

Recently, nanomaterials, such as zinc oxide (ZnO) nanowires, have been utilized as transducers in potentiometric glucose biosensors due to their high aspect ratio, chemical stability, and ease of fabrication (Usman Ali et al., 2010). Wahab et al. prepared glucose oxidase



• **Figure 2.5.13.6** (A) Schematic of glucose-sensing transistor. (B) Typical channel current and gate voltage changes with respect to glucose concentration. (Adapted from Zhang, M., Liao, C., Mak, CH., You, P., Mak, CL., Yan, F., 2015. Highly sensitive glucose sensors based on enzyme-modified whole-graphene solution-gated transistors. *Sci. Rep.* 5, 8311.)

immobilized on ZnO nanorods on both conductive plastic and silver wire. Potentiometric measurements vs. Ag/AgCl showed a logarithmic scale of 165.5 mV/decade ($R^2=0.980$) (Wahab et al., 2018). Parrilla et al. developed a low-cost, paper-based potentiometric glucose biosensor by entrapping GOx in Nafion deposited on paper which was first sputter coated with platinum. Potentiometric measurements vs. Ag/AgCl showed a logarithmic scale of 119 mV/decade ($R^2=0.9900$) with a limit of detection of 0.03 mM glucose (Parrilla et al., 2017). Chou et al. prepared a flexible glucose sensor utilizing GOx entrapped in Nafion/magnetic beads (MBs) on a graphene oxide (GO) nickel oxide (NiO) film. Potentiometric measurements vs. Ag/AgCl showed a logarithmic scale of 35.3 mV/decade ($R^2=0.999$) with a limit of detection of 1.0 mM glucose (Chou et al., 2018). Potentiometric biosensors have the advantage of not requiring an extra potential (compared to amperometric biosensors), which reduces the effects of interfering analytes such as ascorbic or uric acid (Usman Ali et al., 2010).

Optical Biosensors

Whereas electrochemical biosensors utilize electrodes to measure an electric signal, optical biosensors utilize a light source, substrate, and photo-detector. Optical glucose biosensors measure changes in optical properties of the reactants (O_2) or products (H_2O_2) brought about by the enzymatic GOx reaction. Specifically, changes in the absorption, luminescence, or reflectance can be measured via direct or indirect optical detection (Vargas-Bernal et al., 2012; Grieshaber et al., 2008). Direct optical

detection methods (label-free), which measure changes in transducer properties, include photoluminescence, reflectometry, TIRF, and SPR. Indirect optical detection methods (require labels) include fluorescence, SERS, and photoluminescence based on quantum dot labels (Syshchyk et al., 2015).

Syshchyk et al. developed a highly sensitive novel glucose biosensor based on the photoluminescence of porous silicon. Photoluminescence intensity increases were measurable from 0 to 3.0 mM glucose in the emission range of 590–620 nm, as a product of changing pH due to the enzymatic reaction (Syshchyk et al., 2015). ZnO nanomaterials have also been used in optical biosensors due to their intense room temperature photoluminescence and electron transport properties, and they show great promise for use in SERS, SPR, and fluorescence glucose sensors (Tereshchenko et al., 2016; Aini et al., 2015; Sodel et al., 2015). Singh et al. developed an opto-chemical glucose-sensing fiberoptic capable of sensing glucose from 20 to 400 ppm (0.1–2.2 mM), with a limit of detection of 5 ppm. The inclusion of polyaniline into a NiO/PAn matrix was shown to increase effective glucose oxidation and was responsible for discerning measurements at 20 ppm glucose (Singh and Shukla, 2018).

Piezoelectric Biosensors

Piezoelectric enzyme biosensors are created by immobilizing the bioreceptor on the surface of a piezoelectric crystal. Interaction with the target analyte alters the oscillation frequency of the piezoelectric crystal. The oscillation frequency will decrease when a substance is adsorbed onto the

surface, allowing for measurement of analyte concentration as a function of oscillation, following Sauerbrey's equation (Chuang and Shih, 2001; Chou et al., 2008):

$$\Delta F = \frac{K \cdot f^2 \cdot \Delta m}{A} \quad (2.5.13.5)$$

where ΔF , the change in resonant frequency (Hz), is governed by the original oscillation frequency, f (Hz), the change in mass, Δm (grams), the area, A (cm²) of the coating, and K is a constant for the particular crystal. Piezoelectric sensors utilize antibody/antigen pairs, MIPs, and DNA for selective biosensing. As enzymes are only used in enzyme-linked immunosorbent assays (ELISA), the concepts of piezoelectric biosensors are not covered in depth here but can be found reviewed elsewhere (Pohanka, 2018).

Thermal Biosensors

Thermal, or calorimetric, biosensors exploit the fact that enzyme reactions generate heat—the amount of which is proportional to the concentration of reacted substrate, following the first law of thermodynamics:

$$Q = -n_p \sum \Delta H \quad (2.5.13.6)$$

where Q (Joules) is the total heat energy, n_p (mol) is the moles of product generated through the enzymatic reaction, and ΔH (Joule/mol) is the molar enthalpy change (Zhou et al., 2012). Specifically, the glucose oxidase enzyme with glucose reactant generates ~100 kJ/mol (Yakovleva et al., 2013). Enzyme thermistors are able to transduce the small changes in heat of the biochemical transformation according to (Zhou et al., 2012):

$$\Delta T = -\frac{n_p \Delta H}{C_s} \quad (2.5.13.7)$$

where the change in temperature, ΔT (K), is governed by the moles of product generated through the enzymatic reaction, the molar enthalpy change, and the total heat capacity of the system, C_s (Joule/K). Heat generated by the reaction alters the resistance of the working thermistor, and the difference between the working thermistor and reference thermistor are used to determine analyte concentration.

Thermistors, usually used in pairs as a reference and working thermistor in a flow injection system, function by changing their electrical resistance in relation to temperature:

$$R = R_0 e^{\beta \left(\frac{1}{T} - \frac{1}{T_0} \right)} \quad (2.5.13.8)$$

where R (Ω) is the resistance at temperature T (K), R_0 (Ω) is the resistance at temperature T_0 (K), and β is a constant associated with the thermistor. Thermistors are often used in Wheatstone bridge configuration in order to determine the resistance as it changes with respect to temperature (Yakovleva et al., 2013). A typical enzyme thermistor includes an insulating layer (usually polyurethane) covering

a thermostated aluminum block holding two fluidic columns. Typically, one column is activated with the enzyme used for measurement, while the other is used as a reference. Flow of the sample through the columns results in temperature fluctuations as the enzyme reacts with the substrate, altering resistance of the thermistor, and in turn measured voltage change in the balanced Wheatstone bridge (Yakovleva et al., 2013).

Recently, Xie et al. developed an enzyme thermistor utilizing pyrroloquinoline quinone glucose dehydrogenase (PQQGDH) compared to the more commonly used GOx enzyme thermistor, showing higher catalytic activity and insensitivity to availability of oxygen. Calorimetric measurements showed a linear range of 0.009–100 mM glucose with higher specificity than GOx (Xie et al., 2018).

Thermal biosensors offer high sensitivity to small changes in heat but nonspecificity, baseline drift, and heat lost through radiation, conduction, or convection have limited their use in biosensors (Yi-Hua et al., 2006).

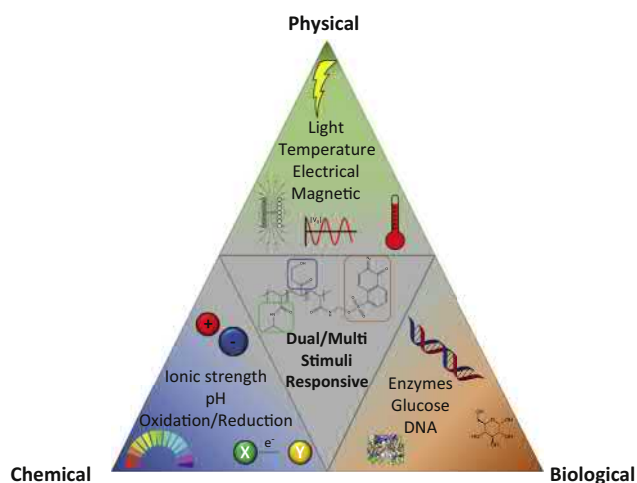
Roles of Responsive Polymers in Enzymatic Biosensors

In the past several decades, the exponential increase in enzymatic biosensor development and performance can be credited to the incorporation of both nanomaterials and/or stimuli-responsive polymers within the biosensor (Chen et al., 2013; Hu and Liu, 2010). Stimuli-responsive polymers are polymers which exhibit reversible or irreversible changes in physicochemical properties in response to physical, chemical, or biological stimuli from their environment, such as pH, temperature, electric/magnetic fields, bioactive molecules, and light (Fig. 2.5.13.7) (Russell, 2002).

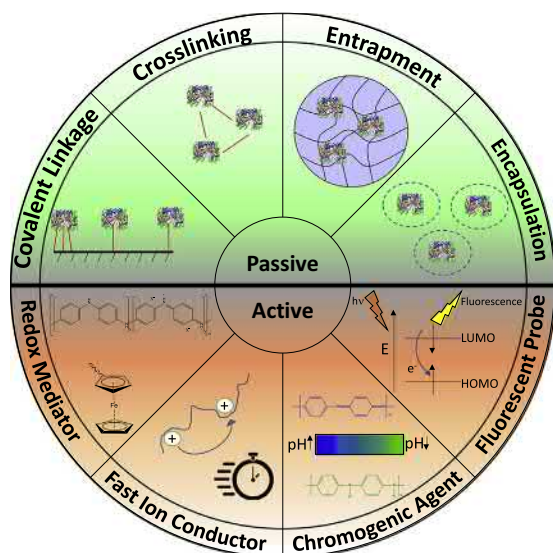
The roles in which stimuli-responsive polymers have been used in biosensor systems can be described as active or passive. Active roles are generally used in the sensing of the analyte, while passive roles are attributed to nonsensing components of the biosensor system, such as physical support, increasing biocompatibility, decreasing biofouling, maintaining sensor viability, and increasing sensor lifetime (Hahm, 2011). A summary of the passive and active roles of polymers in biosensors is shown in Fig. 2.5.13.8. A summary of recent work involving responsive polymers in glucose biosensors is shown in Table 2.5.13.1.

Passive Roles (Physical Support)

In enzymatic biosensors, immobilization of the enzyme within the biosensor's surface in close proximity with the transduction element while simultaneously presenting the enzyme active site to the analyte is of utmost importance for biosensor performance (Pan et al., 2017). Enzymes are typically immobilized physically, through adsorption, entrapment, encapsulation, and SAMs, or chemically, through



• **Figure 2.5.13.7** Summary of classes of stimuli-responsive polymers.



• **Figure 2.5.13.8** Summary of passive and active roles of stimuli-responsive polymers in biosensors.

covalent linkage, cross-linking, or electrochemical polymerization (Wang and Uchiyama, 2013).

Covalent Linkage

Immobilization of enzymes through covalent linkage of their amino acids has been reported utilizing polymer brushes, EDC/NHS chemistry, and glutaraldehyde as well as semicovalent linkage through thiol chemistry, such as cysteine (Lee et al., 2018). Covalent linkage of an enzyme to a transducer support is carried out in two stages. First, the transducer surface is activated by linker molecules. Second, the enzyme is covalently linked to the linker on the transducer (Hoang Hiep and Moonil, 2017).

Polymer brushes, which are polymer chains attached to a surface, have been used as an interface between biosensors and the media of interest (Welch et al., 2015). Specifically, these brushes have been used as an anchor to attach enzymes

to electrode surfaces in electrochemical biosensors. Welch et al. presented an organic glucose-sensitive transistor device which immobilized GOx onto PEDOT:PSS through a simple process using polymer brushes comprised of PGMA and PHEMA (Fig. 2.5.13.9) (Welch et al., 2015).

Activation of carboxylic groups on the enzyme and covalent linkage to the electrode surface or a conductive polymer using EDC/NHS chemistry has been used extensively. Kotanen et al. fabricated an implantable dual-responsive glucose/lactate biosensor by covalent conjugation of GOx with a pyrrole moiety and subsequently electropolymerized onto the electrode surface (Kotanen et al., 2014).

Cross-Linking

Through cross-linking, a polymer such as glutaraldehyde (GA), polyethylene glycol (PEG), or polyethylene glycol diglycidyl ether (PEGDE) is used to covalently link free amino acid groups to other enzyme molecules (Hoang Hiep and Moonil, 2017). In similar fashion to the covalent linkage of GOx to the monomer pyrrole and subsequent electropolymerization by Kotanen et al., Colak et al. first electropolymerized poly-pyrrole-poly(vinyl sulfonate) (PPy-PVs) films onto a platinum electrode, and subsequently immobilized GOx through glutaraldehyde cross-linking (Çolak et al., 2012). While glutaraldehyde cross-linking is the most commonly used cross-linking method for enzymes, PEGDE has recently been shown to be more advantageous, offering higher sensitivity and specificity. This is thought to be a result of the more mild method of cross-linking in addition to the lower toxicity of PEGDE (Vasylieva et al., 2013; Sirca et al., 2014). Cross-linking is commonly used in conjunction with enzyme entrapment to retain higher amounts of enzyme loading.

Entrapment

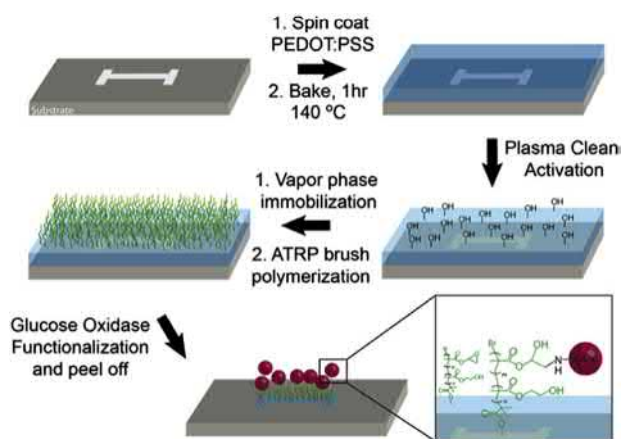
Through entrapment, an enzyme is not directly bonded with any polymers, rather it is entrapped within a cross-linked polymer network, such as a hydrogel. Entrapment of an enzyme in a polymeric matrix offers good retention of enzymatic activity and high enzymatic stability, and is often the most simple method of immobilization (Wang et al., 2005). However, careful selection of polymers must be used in order to allow diffusion of analyte to the active site of the enzyme. Entrapment within hydrogel matrices (Mariani et al., 2013), electropolymerized conductive polymers such as polypyrrole (Wang et al., 2005), synthetic polymers such as Nafion (Beyene et al., 2004), or a combination (Brahim et al., 2002), have been successfully used to create glucose biosensors. During electropolymerization in proximity of counteranion dopants, negatively charged glucose oxidase will form in the polymer layer directly on the electrode (Kotanen and Guiseppi-Elie, 2012).

Encapsulation

Enzyme encapsulation, similar to entrapment, involves immobilizing the enzyme within a semipermeable membrane (without chemical bonds), which serves to preserve enzyme

TABLE 2.5.13.1 Table Recent Uses of Passive/Active Polymers in Glucose Biosensors

Stimuli-Responsive Polymer	Passive/ Active	Stimulus	Role	Sensor Type	References
Poly(ethylene terephthalate) (PET)	Passive	–	Flexible support substrate	Electrochemical (amperometry)	Pham et al. (2010)
Poly(2-hydroxyethyl methacrylate) brushes	Passive	–	Link Gox and HRP to microfluidic channel surface	Optical (UV vis)	Costantini et al. (2013)
Poly-N-isopropylacrylamide (PNIPAM)	Passive	Temperature	Enzyme adsorption/release	Electrochemical (amperometry)	Xiong et al. (2013)
Poly-N-isopropylacrylamide (PNIPAM)	Passive	Temperature	Covalent linkage of enzyme	Optical (fluorescent)	Wang et al. (2013)
Poly-N-isopropylacrylamide (PNIPAM)	Passive	Temperature	Covalent linkage of enzyme	Electrochemical (amperometry)	Xiong et al. (2013), Mugo et al. (2019)
Poly-N-isopropylacrylamide (PNIPAM)	Passive	Temperature	Covalent linkage of enzyme	Optical (fiber optic)	Lin et al. (2019)
Poly-N-isopropylacrylamide (PNIPAM)-ferrocene	Active	Temperature	Covalent conjugation to enzyme	Electrochemical	Nagel et al. (2007)
P(NIPAM-co-OEGMA)	Active	Temperature	Current response tuning via temperature change	Electrochemical (amperometry)	Bünsow et al. (2010)
Poly-N-isopropylacrylamide (PNIPAM)	Active	Temperature	PNIPAM color changed from red to purple to blue at different temperatures	Optical	Maji et al. (2016)
Poly-N-isopropylacrylamide (PNIPAM)-boronic acid	Active	Temperature/ glucose	Hydrogel swelling/shrinking in response to glucose, with increasing sensor response rate at higher temperatures	Optical (fiber optic spectrometry)	Ben-Moshe et al. (2006)
Boronic acid–polyacrylamide–PEG (BA–AA–PEG)	Active	Glucose	Hydrogel swelling/shrinking in response to glucose	Optical (spectrometry)	Alexeev et al. (2003)
Poly(N-(3-amidino)-aniline) (PNAAN)	Active	CO ₂ concentration	PNAAN is protonated at higher CO ₂ concentration, causing AUNps to aggregate and produce a color change	Optical	Ma et al. (2016)
Poly(N-isopropylacrylamide-acrylamide-vinylphenylboronic acid) [poly(NIPAM-AAm-VPBA)]	Passive/ active	Glucose	NIPAM: Enable precipitation polymerization above LTST VPBA: pH dependent, reversible glucose binding Hydrogel swelling/shrinking in response to glucose	Optical	Wang et al. (2015a)
Rhodamine-carbazole-thienyl pyrrole derivate (P(RDC-co-SNS))	Active	O ₂ concentration	Fluorescence probe	Optical (fluorescence)	Ayranci et al. (2018)
4-Phenyldiboronic acid	Active	H ₂ O ₂ concentration	Fluorescent probe	Optical (fluorescence)	Yu et al. (2017)
Poly(butyl methacrylate-co-(2-dimethylaminoethyl) methacrylate-co-methyl methacrylate) (Eudragit E PO)	Active	pH	Fluorescent probe	Optical (fluorescence)	Park et al. (2017)
PMA/DMAEMA/TEGDMA/EG	Active	pH	Reversible swelling	Piezoelectric	Schmidt et al. (2016)
Poly(N-isopropylacrylamide)-copoly(acrylic acid)-(3-aminophenylboronic acid) (PNIPAAM-coPAA-PBA)	Active	pH	Boronic acid/glucose complex	Piezoelectric	Chen et al. (2010)



• **Figure 2.5.13.9** Schematic of PGMA:PHEMA mixed polymer brush and Gox fabrication on device for glucose sensing (Welch et al., 2015).

structure/activity and protect against degradation (Besic and Minteer, 2017). Organic polymers such as Nafion, chitosan, and alginates are commonly used for enzyme encapsulation (Klotzbach et al., 2008). While both entrapment and encapsulation are more gentle roles for physical support, they tend to show continuous loss of enzyme activity over time.

Active Roles

Conductive electroactive polymers (CEPs) are conjugated polymers which display both controllable and stimuli-responsive changes in electrical, electrochemical, and optical properties (Guiseppe-Elie, 2010). CEPs such as poly(3,4-ethylenedioxythiophene) (PEDOT), polythiophene (PTh), polypyrrole (PPy), and polyaniline (PAn) offer mild polymerization conditions suitable for incorporation of enzymes in optical, electrochemical, and piezoelectric biosensors (Guiseppe-Elie, 2010). Furthermore, incorporation of CEPs into hydrogels to create electroconductive hydrogels (ECHs) retains the favorable properties of CEPs within a highly swellable, biocompatible polymer matrix (Wilson et al., 2010). The active roles that CEPs play within glucose biosensor systems are summarized in this section and shown in Fig. 2.5.13.8.

Redox Mediators

Redox-active polymers can be split into two groups: conductive polymers where the reversible redox reaction occurs in the main chain, or in side groups, such as conjugated polymers with pendant mediators (i.e., ferrocene) (Gracia and Mecerreyes, 2013; Kim et al., 2017). These polymers have generated much interest for their potential use in enzymatic biosensors stemming from their electrochemical, electronic, optical, catalytic, and biological properties (Pietschnig, 2016). Of utmost importance is the immobilization (while retaining high diffusivity) and availability of such redox mediators within proximity of the enzyme (Boztas and Guiseppe-Elie, 2009). Redox polymers have attracted attention for their use in nonenzymatic glucose biosensors. Recently, Li et al. designed a novel nonenzymatic electrochemical glucose biosensor using ferrocene-terminated hyperbranched

polyurethane (HPU-Fc) with high selectivity and sensitivity (Li et al., 2016). Redox-responsive ECHs utilizing CEPs such as polyaniline and polypyrrole have been reported, whereas a subunit of the polymer backbone is oxidized, leading to a swelling response of the entire hydrogel (Pan et al., 2012; Mano et al., 2007). A reversible redox reaction can take place in the polymer main chain, as in the case of conducting polymers such as polyaniline, or in side groups, as in the case of a polymer carrying ferrocene side groups.

Chromogenic Agents

Conductive conjugated polymers, such as polythiophene, polypyrrole, and polyaniline have been researched for their electrochromic properties in biosensors. An electrochromic material is one that shows reversible change in optical properties as a result of an applied electrochemical potential (switching of redox states) (Jenekhe and Kiserow, 2004). For example, polyaniline exhibits color transition from yellow to green to blue to violet depending on the oxidation state (and pH) via protonation/deprotonation and ion exchange (Dhand et al., 2011). Other conjugated polymers, such as PEDOT, are used as chromogenic agents as it offers fast switching speed from deep to pale blue, high electronic conductivity, and resistance to degradation after doping (Saxena et al., 2011). In addition to direct chromogenic properties, pendant groups such as ferrocene have been conjugated to polymer backbones to enable electrochromic behavior (Pietschnig, 2016).

Fast Ion Conductors

Fast ion conductors are solids which can conduct ionic current at levels similar to liquid electrolytes and molten salts (10^{-1} – 10^{-2} S/cm). Solid-state ionics, many of which exhibit ionic and electronic conductivity, have found use in energy storage, fuel cells, and sensor technologies (Tuller, 2017). Fast ion conduction has been exploited through the use of nanoporous ECHs, where impedance between electrode surface and electrolyte is decreased by the ionic conductivity of conductive polymers. Ionic conductivity in polymer electrolytes, σ , is expressed as:

$$\sigma = \sum_i n_i z_i e \mu_i \quad (2.5.13.8)$$

where μ_i ($\text{m}^2/\text{s}^{-1}\text{V}^{-1}$) is the ionic mobility, n_i (m^{-3}) is the number of ionic carriers per unit volume, z_i is the valency of ionic carriers, and e is the charge of an electron (Harsányi, 2000). In the case of conducting polymers such as polypyrrole, ions can be cycled in or out of the polymer (hence changing conductivity) by controlling the applied potential. Positive potential applied to polypyrrole oxidizes the polymer, enticing small anions to enter the material. Inversely, negative potential reduces the polymer and expels anions (Ferraz et al., 2012).

Fluorescence Probes

Fluorescence is the emission of light energy by some substance that has absorbed light or radiation (Klonoff, 2012). Fluorescent conductive polymers utilize (1) covalent linkage

of fluorescent molecules to polymer backbone (extrinsic fluorescence), or (2) copolymerization with fluorescently polymerizable monomers (intrinsic fluorescence) (Basabe-Desmonts et al., 2007). Conjugated polymers, such as polypyrrole, polyacetylene, polyaniline, and polythiophene provide electronic conjugation (molecular wiring) and are excellent fluorescent probes because they can amplify molecular recognition by electron migration along the polymer chain (photoinduced electron transfer fluorescence quenching) (Basabe-Desmonts et al., 2007). Ayranci et al. demonstrated a multifunctional copolymer of rhodamine-carbazole and thienyl pyrrole derivative with glucose oxidase [P(RDC-co-SNS)/GOx] for the fluorescent sensing of glucose (Rukiye et al., 2018).

Polymer composites including carbon nanotubes, graphene oxide, and quantum dots (most recently carbon dots) have been widely studied as biocompatible probes for fluorescent glucose biosensors, but their mechanism of fluorescence is still not fully understood (Chen et al., 2018). Barone et al. reported shifts in emission spectra of single-walled carbon nanotube (SWCNT) hydrogel composites by inducing reversible hydrogel swelling using poly(vinyl alcohol) (PVA) capable of sensing glucose (Barone et al., 2009). While traditional quantum dots are not suitable for in vivo sensing due to cytotoxicity, polymer shells have been applied to QDs to improve biocompatibility (Chen et al., 2018).

Boronic acid fluorescent sensors, which operate according to nitrogen (N)–B interactions and photoinduced energy transfer, can form reversible covalent complexes capable of creating a discrete “ON–OFF” fluorescent response (Wang and Lee, 2015). The fluorophore-spacer-receptor model has been widely used in fluorescent biosensors, where electrons freed during the binding process of sugar to boronic acid are used to excite the fluorophore (James, 2006). In addition, boronic acid-functionalized graphene quantum dots and carbon quantum dots have been used for selective and rapid glucose sensing (Qu et al., 2013; Shan et al., 2014).

Carbon dots (CDs) (and their polymeric form, PCDs), which appear to violate the Kasha-Vavilov rule of excitation-dependent photoluminescence, seem to show good candidacy for biosensing and a new alternative to traditional fluorescent nanomaterials (Sau et al., 2018; Li et al., 2018). Recently, Li et al. proposed a preparation of yellow-emissive carbon dots by one-pot hydrothermal treatment of p-phenylenediamine and aspartic acid. By addition of silver nanoparticles, the optical capacity was suitable for glucose sensing (Li et al., 2018).

Integrating Responsive Polymers With Enzymes

Integration of responsive polymers with enzymes, specifically electrical contact with the active site of the enzyme, is a highly studied area in the pursuit of second- and

third-generation electrochemical biosensors (Zayats et al., 2002). This section discusses the different methods in which responsive polymers have been integrated with enzymes.

Physicochemical Conjugation With CNTs

Carbon nanotubes have been used extensively as supports for enzymes due to their high surface area, enzyme-loading capabilities, biocompatibility, and electrical/mechanical properties (Saifuddin et al., 2013). In 2002, Guiseppi-Elie et al. demonstrated direct electron transfer (DET) of glucose oxidase on carbon nanotubes by demonstrating spontaneous adsorption to carbon nanotube bundles (Anthony et al., 2002). Since then, there has been considerable research on the use of carbon nanotubes and other nanomaterials in the fabrication of third-generation (mediator-free) enzymatic glucose sensors. Glucose biosensors utilizing carbon nanotubes, graphene, nanoparticles, and nanocomposites have been studied for use in DET of GOx (Luong et al., 2017).

Active Site Conjugation Using Boric Acid

Boric acid (an organoborane) has been used in an attempt to establish direct electrical communication between the electrode and enzyme. Direct conjugation of the active FAD site of GOx has been reported to bestow direct electrical contact between the enzyme and electrode. Zayats et al. demonstrated the reconstitution of GOx on an FAD monolayer using boronic acid ligands to create a boronic acid–FAD complex, bypassing the need for a mediator or oxygen (Zayats et al., 2002). More recently, Bai et al. immobilized GOx on a planar boron-doped diamond electrode using 3-aminopropyltriethoxysilane (APTES) to create a third-generation electrochemical glucose biosensor capable of DET (Bai et al., 2014). Chen et al. demonstrated proof of concept for a piezoelectric glucose biosensor based on a 3-aminophenyl-boronic acid (PBA) complex with glucose, showing glucose binding to ionized boronate species to induce polymer brush swelling on a microcantilever (Chen et al., 2010). Ben-Moshe et al. developed glucose-sensing photonic crystal utilizing boronic acid groups covalently linked to a hydrogel which cross-links with glucose, without the need for sodium ion-chelating agents such as PEG or crown ethers, to measure an increase in hydrogel volume via a fiberoptic spectrometer (Ben-Moshe et al., 2006). Wang et al. utilized molecularly imprinted polymers of poly(N-isopropylacrylamide-acrylamide-vinylphenylboronic acid) [poly(NIPAM-AAm-VPBA)] with fluorescent carbon dots able to reversibly swell and shrink upon the pH-dependent, reversible binding of glucose to the boronic acid moiety (Wang et al., 2015a,b). Tierney et al. developed a similar responsive gel, wherein the hydrogel swells as glucose binds to the boronic acid due to a shift in osmotic potential rising from conversion of neutral boronic acids to anionic boronate esters (Tierney et al., 2009).

Molecular Wiring

The simultaneous immobilization and electrical “wiring” of enzymes (specifically the active site) with responsive redox polymers has been widely studied for use in electrochemical biosensor applications (Wang, 2008). In 1987, Degani and Heller reported on wiring of GOx to an electrode surface demonstrating covalently linked electron relays (Degani and Heller, 1987). Several strategies have been implemented for electrical wiring to electrodes, including conjugation of ferrocene mediators to enzymes, surface reconstitution of enzymes, and conjugation within polymer networks (Schuhmann et al., 1991; Xiao et al., 2003; Gerard et al., 2002). Recent work, involving wiring of mediators consisting of poly(4-vinylpyridine) (PVP) backbones, has shown great promise as wires for GOx as well as pyrroloquinoline quinone glucose dehydrogenase (PQQ-sGDH) in electrochemical glucose sensors (Flexer and Mano, 2014).

Covalent Conjugation

Covalent conjugation of enzymes to amphiphilic responsive copolymers (either in the main chain or on side chains) has shown promise within biosensing, due to the fact that conformational changes of the polymer can be induced by stimuli (Shakya and Nandakumar, 2018). Enzymes can be covalently conjugated either randomly or at specific sites of the polymer dependent on the polymer and enzyme in use. The bioconjugation of stimuli-responsive polymers has been reported in thermo-, ion-, and photo-responsive biosensors (Xiong et al., 2013; Dübner et al., 2017).

Integrating Responsive Polymers With Transducers

Interface Engineering

Electrochemical reactions in biosensors take place at the interface between some surface-modified electrode and a liquid electrolyte with a charge being exchanged between the electronically conductive electrode and ionically conductive electrolyte (Xu, 2017). Research in the engineering at the bio-electrochemical interface level of biosensors using functional and responsive nanomaterials has burgeoned the development of transducers with high sensitivity, stability, and selectivity (Zhou and Dong, 2011). Techniques utilizing self-assembled monolayers (SAMs), layer-by-layer assembly, polymer brushes, sol-gels, and hydrogels have been used to integrate responsive polymers to the transducer.

SAMs are considered the most simple approach for the bio-electrochemical interface, but offer high bonding strength to both the organic or inorganic components, and long-term stability (Putzbach and Ronkainen, 2013). Wan et al. produced glucose-sensitive electrodes by first oxidative graft polymerization of polyaniline to gold electrodes using 4-aminothiophenol SAMs, followed by covalent linkage (via glutaraldehyde) of chitosan/CNTs immobilized with GOx

(Wan et al., 2010). The combination of polyaniline and chitosan resulted in a biocompatible transducer with excellent electron transfer properties and high enzyme retention.

Layer-by-layer (LbL) assembly uses a combination of dip coating strategies and self-assembly based on electrostatic Coulombic interactions between subsequent layers (Barsan et al., 2014). LbL techniques utilizing redox polymer/enzyme complexes have been shown to increase biosensor current densities using thinner polymer matrices (Sirkar et al., 2000). Using a self-assembled layer-by-layer N-doped graphene/GOx/chitosan, Barsan et al. developed a highly stable amperometric glucose biosensor able to operate at low potential with high sensitivity and stability (Barsan et al., 2014).

Sol-gel technology, which is a room-temperature preparation technique using organic precursors, has been popularized for enzyme encapsulation and favorable features such as tunable porosity, chemical inertness, and thermal stability (Wang, 1999). The sol-gel technique and molecular imprinting are commonly used in tandem to create electrochemical biosensors. Recently, Zohourtalab et al. created an amperometric sol-gel biosensor of GOx immobilized in a chitosan/Nafion/ferrocene composite sol-gel (Zohourtalab and Razmi, 2018). They reported excellent mechanical stability and high selectivity of the sol-gel electrode.

Polymer brushes are thin polymer films of which the end of individual polymers are bonded to an electrode surface through covalent, hydrophobic, cationic, or zwitterionic interactions (Takasu et al., 2015). Electroconductive polymers, such as polyaniline, have been utilized as polymer brushes exhibiting excellent electron transfer in redox and enzyme reactions (Swamy et al., 2017).

Systems Integration

The integration of bioreceptors, transduction elements, electrodes, and computer processing has led to several methods of systems integration to create functional, implantable biosensors, such as microfabrication, layer-by-layer techniques, and (most recently) 3-D printing.

Microfabrication

Microfabrication involves etching, patterning, and layering of thin films through processes such as chemical vapor deposition (CVD), physical vapor deposition (PVD), electroplating, spin-, or spray-coating to create complex (yet essentially 2-D) electrode architectures (Hierlemann et al., 2003). This technique is enticing for creation of biosensors due to its batch-processing ability (and inherently lower costs associated with batch production) and low-tolerance structure designs available through technologies adopted from the semiconductor industry (Hesketh et al., 1997). Conventional lithography and microfabrication techniques have enabled production of implantable biotransducer electrode architectures such as interdigitated microelectrodes (IMEs) and multidisc electrode arrays (MDEAs) for use in glucose biosensors.

Interdigitated microelectrodes modified with films of bioactive conductive polymers and electroconductive

hydrogel have found use in electrochemical biosensors, as they are able to exploit measurable changes in film impedance that accompany redox reactions of enzymes entrapped or linked within the film (Dastider et al., 2013). With fringing field effects in mind, the geometry of such electrodes (line/space dimensions and density) has been studied extensively, and in the case of impedimetric biosensing, new equivalent circuits have been developed to account for low device dimensions (Yang et al., 2010). In the case of glucose sensing, IMEs have been used as capacitive (Khan et al., 2016) and resistive (Haarindraprasad et al., 2016) impedimetric sensors, voltammetry sensors (Jin et al., 2001), and amperometric sensors (Collyer et al., 2010).

The microdisc electrode array (MDEA) is another micro-lithographically produced electrode architecture intended for implantable biosensors. As with IMEs, design considerations have been taken into account to achieve low background current, high SNR, and improved sensitivity (Justin et al., 2009). Kotanen et al. used a dual-responsive MDEA to wirelessly sense glucose and lactate on a single biochip (Fig. 2.5.13.10) (Kotanen and Guiseppi-Elie, 2010). This same chip, the MDEA-5037 biotransducer and Pinnacle 8151 wireless dual potentiostat, was then successfully characterized in vivo in the trapezius muscle of a Sprague–Dawley rat (Kotanen et al., 2014).

In addition to the well-known rigid electronic systems, soft electronic systems, which utilize conjugated polymer systems able to closely match the moduli of human tissues, have shown great promise in biosensing systems. Where traditional electronics tend to fail at >3% strain, soft bioelectronics are able to withstand strains that the human body experiences (~30%) (Sekitani, 2016). Recently, Fuketa et al. developed a 1 μm thick ultraflexible surface EMG electrode using organic transistors capable of measurement of the myoelectric signal (Fuketa et al., 2014). The organic transistors microfabricated on polyethylene naphthalate (PEN) films boasted high flexibility, high electrode density, and high signal intensity. Several soft enzymatic biosensors utilizing similar fabrication methods have been created to measure analytes such as glucose/lactate in bodily fluids (sweat, saliva, tears). Of particular interest is a newly developed

flexible glove biosensor, termed “lab-on-a-glove” or “forensic finger” (Mishra et al., 2017). The system incorporates a micro-fabricated three-electrode enzymatic system produced directly on low-cost disposable polymer gloves capable of rapid detection of organophosphate and subsequent wireless transmission, as shown in Fig. 2.5.13.11.

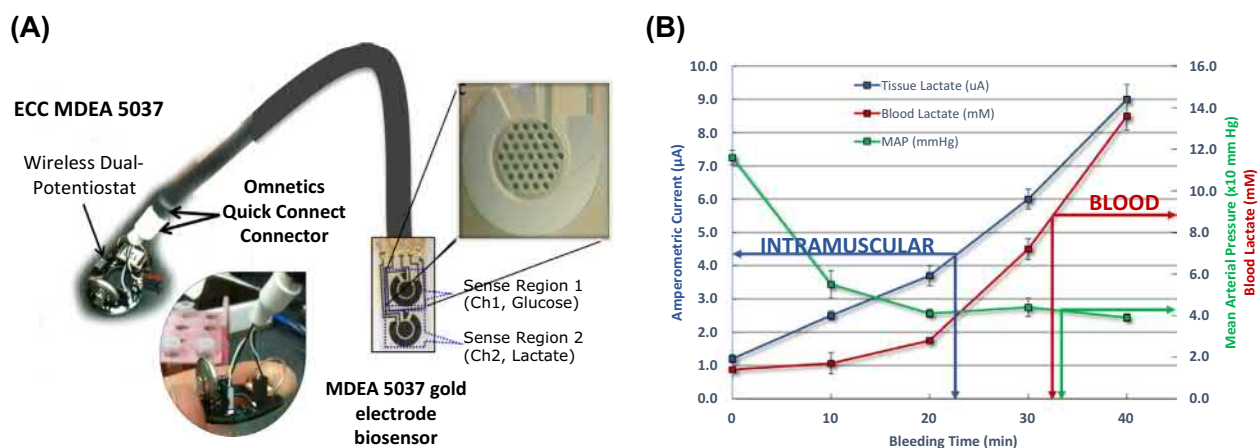
Common microfabrication steps have been combined with micromachining techniques to create 3-D microstructures for biosensing, termed microelectromechanical systems (MEMS), which have been utilized for the base electrodes in electrochemical, optical, and thermal glucose biosensors (Huang et al., 2009).

Three-Dimensional (3-D) Bioprinting

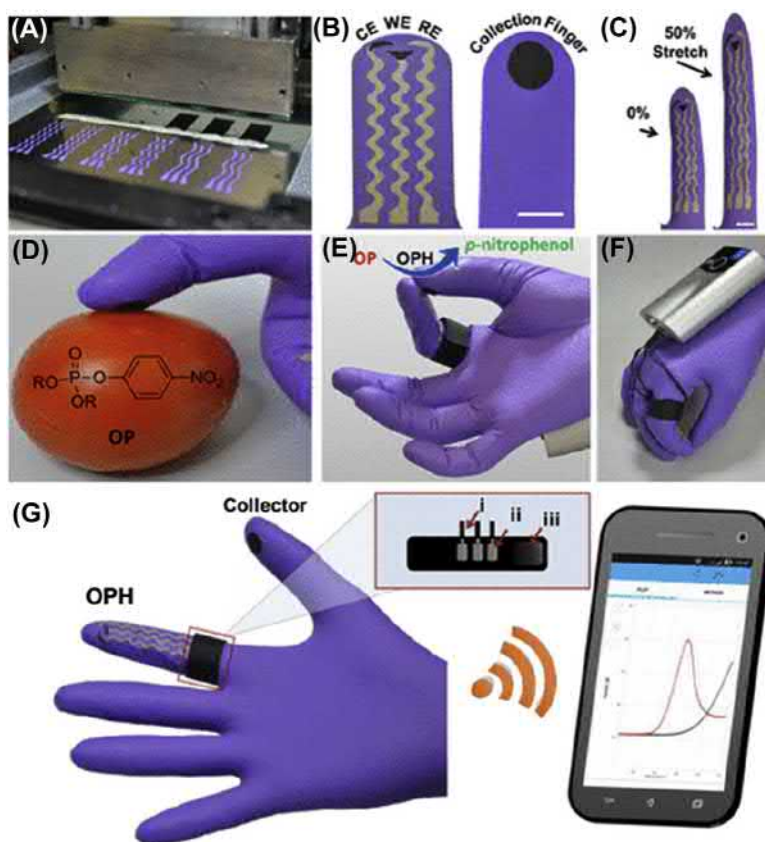
More recently, microfabrication techniques have utilized hydrogels (rather than semiconductive metals) to create 3-D tissue arrays, organ-on-chips, and biosensors (Verhulsel et al., 2014). Micromolding, photolithography, stereolithography and 3-D bioprinting have led to construction of precise, 3-D hydrogel microstructures. Here, the focus of discussion is on the growing use of 3-D bioprinting. Detailed reviews on other fabrication methods can be found elsewhere (Yanagawa et al., 2016; Li et al., 2015; Vaezi et al., 2013).

3-D bioprinting utilizing an array of biocompatible materials has become of great interest recently, due to commercialization of 3-D bioprinting technologies. Supported by the growing catalog of “bio-inks,” 3-D bioprinting technology has the ability to produce biosensors without the need for masks required in photolithography (Sharafeldin et al., 2018). The inclusion of stimuli-responsive polymers within bioinks to create 3-D-printed biosensors has led to the so-called 4-D printed constructs: 3-D printed structures capable of biomolecular recognition by response to stimuli (Mandon et al., 2017). This research area utilizes all concepts presented in this review and is indeed at the forefront of ongoing research.

Li et al. 3-D printed stretchable interdigitated PDMS electrodes with CNTs for use in electrochemical sensing (Kai et al., 2018). Stretchable bioelectronic elements with



• **Figure 2.5.13.10** Microdisc electrode array (MDEA) architecture used for glucose and lactate biosensors capable of transmitting data wirelessly via Bluetooth (A). Amperometric readings of analyte measured from blood and intramuscularly (B) (Kotanen et al., 2012).



• **Figure 2.5.13.11** Flexible glove biosensor: fabrication, design, and performance. (A) Image of the serpentine stencil design employed for printing the glove-based stretchable device. (B) Schematic of (left) the bio-sensing scan finger (index finger) containing smiling face shape carbon-based counter (CE), working (WE) electrodes and Ag/AgCl-based reference electrode (RE), and (right) collecting thumb finger with its printed carbon pad; scale bar 10mm. (C) Photographs of the biosensing index finger under 0% (left) and 50% (right) linear stretch; scale bar, 10 mm. (D) On-glove swiping protocol for sampling chemical threat residues from tomato and stainless steel surfaces. (E) On-glove sensing procedure by joining the index (scan) and thumb (collector) fingers to complete the electrochemical cell. (F, G) Photographs of the wearable glove biosensor, consisting of a sensing finger, containing the immobilized OPH enzyme layer, and the collector/sampling finger. The electrodes are connected via an adjustable ring bandage to the portable potentiostat (attached to the back of the hand) for on-site detection with wireless communication to a smartphone for rapid presentation of the voltammetric results. (Inset) Schematic of the interface between potentiostat and glove sensor. The connections consist of a (iii) velcro fabric containing (ii) the aluminum-tape based pins that are adjusted as a ring with the glove sensing connectors and (i) the wiring with the potentiostat (Mishra et al., 2017).

modulus closer to that of human tissue present a clear advantage over traditional solid electronics for both wearable and implantable biosensors. Gowers et al. 3-D printed a microfluidic system using FDA-approved microdialysis probes for continuous monitoring of glucose and lactate (Gowers et al., 2015). Integration with existing technologies, such as cellphones for point-of-care diagnostics, has also been of great interest. Roda et al. introduced low-cost 3-D printed optics for a microfluidic chemiluminescence glucose sensor as an autonomous lab-on-a-chip (Roda et al., 2014).

Future Outlook

Since its inception, electrochemical detection of glucose has undergone radical development toward the goal of sensitive, selective, miniaturized sensors for point of care, bed-side, or implantable devices. The use of stimuli-responsive polymers

in biosensors has been studied for decades, but only recently have they been used to their full extent either integrated with enzymes or as transduction elements. The integration of conductive stimuli-responsive polymers in biosensors and a push toward autonomous sensing and self-sufficiency seems to be an area requiring further study.

As new materials are created or discovered for biosensing, such as the little understood carbon dot, considerable work is required to functionalize and utilize these molecules in biosensing. With new developments of systems integration, including the boom in 3-D bioprinting within the last decade, there are new opportunities for low-cost, rapid prototyping of 4-D responsive biosensor architectures which were not achievable before. The pairing of these new types and architectures of biosensors, nanomaterials, and wireless communication and handheld devices, such as cell phones, remains a promising endeavor in telemedicine, remote health care, and biosensing.

References

- Aggas, J.R., Harrell, W., Lutkenhaus, J., Guiseppi-Elie, A., 2018. Metal-polymer interface influences apparent electrical properties of nano-structured polyaniline films. *Nanoscale* 10 (2), 672–682.
- Aini, B.N., Siddiquee, S., Ampon, K., Rodrigues, K.F., Suryani, S., 2015. Development of glucose biosensor based on ZnO nanoparticles film and glucose oxidase-immobilized eggshell membrane. *Sens. Bio Sens. Res.* 4, 46–56.
- Alexander, S., Baraneedharan, P., Balasubrahmanyam, S., Ramaprabhu, S., 2017. Highly sensitive and selective non enzymatic electrochemical glucose sensors based on Graphene Oxide-Molecular Imprinted Polymer. *Mater. Sci. Eng. C* 78, 124–129.
- Alexeev, V.L., Sharma, A.C., Goponenko, A.V., Das, S., Lednev, I.K., Wilcox, C.S., Finegold, D.N., Asher, S.A., 2003. *Anal. Chem.* 75, 2316–2323.
- Anthony, G.-E., Chenghong, L., Ray, H.B., 2002. Direct electron transfer of glucose oxidase on carbon nanotubes. *Nanotechnology* 13 (5), 559.
- Ayranci, R., Kirbay, F.O., Demirkol, D.O., Ak, M., Timur, S., 2018. *Methods Appl. Fluoresc.* 6, 035012.
- Asal, M., Özen, Ö., Şahinler, M., 2018. Polatoğlu İ. Recent developments in enzyme, DNA and immuno-based biosensors. *Sensors* 18 (6), 1924.
- Bai, Y.-F., Xu, T.-B., Luong, J.H.T., Cui, H.-F., 2014. Direct electron transfer of glucose oxidase-boron doped diamond interface: a new solution for a classical problem. *Anal. Chem.* 86 (10), 4910–4918.
- Bandodkar, A.J., Wang, J., 2014. Non-invasive wearable electrochemical sensors: a review. *Trends Biotechnol.* 32 (7), 363–371.
- Barone, P.W., Yoon, H., Ortiz-García, R., Zhang, J., Ahn, J.-H., Kim, J.-H., et al., 2009. Modulation of single-walled carbon nanotube photoluminescence by hydrogel swelling. *ACS Nano* 3 (12), 3869–3877.
- Barsan, M.M., David, M., Florescu, M., Țugulea, L., Brett, C.M.A., 2014. A new self-assembled layer-by-layer glucose biosensor based on chitosan biopolymer entrapped enzyme with nitrogen doped graphene. *Bioelectrochemistry* 99, 46–52.
- Basabe-Desmonts, L., Reinhoudt, D.N., Crego-Calama, M., 2007. Design of fluorescent materials for chemical sensing. *Chem. Soc. Rev.* 36 (6), 993–1017.
- Ben-Moshe, M., Alexeev, V.L., Asher, S.A., 2006. Fast responsive crystalline colloidal array photonic crystal glucose sensors. *Anal. Chem.* 78 (14), 5149–5157.
- Besic, S., Minteer, S.D., 2017. Micellar polymer encapsulation of enzymes. In: Minteer, S.D. (Ed.), *Enzyme Stabilization and Immobilization: Methods and Protocols*. Springer New York, New York, NY, pp. 93–108.
- Beyene, N.W., Moderegger, H., Kalcher, K., 2004. Simple and effective procedure for immobilization of oxidases onto MnO₂-bulk-modified, screen-printed carbon electrodes. *S. Afr. J. Chem.* 57.
- Boztas, A.O., Guiseppi-Elie, A., 2009. Immobilization and release of the redox mediator ferrocene monocarboxylic acid from within cross-linked p (HEMA-co-PEGMA-co-HMMA) hydrogels. *Bio-macromolecules* 10 (8), 2135–2143.
- Brahim, S., Narinesingh, D., Guiseppi-Elie, A., 2002. Polypyrrole-hydrogel composites for the construction of clinically important biosensors. *Biosens. Bioelectron.* 17 (1–2), 53–59.
- Bănică, F.G., 2012. Electrical-Impedance-Based Sensors. *Chemical Sensors and Biosensors*.
- Bünsow, J., Enzenberg, A., Pohl, K., Schuhmann, W., Johannsmann, D., 2010. *Electroanalysis* 22, 978–984.
- Cambre, J.N., Sumerlin, B.S., 2011. Biomedical applications of boronic acid polymers. *Polymer* 52 (21), 4631–4643.
- Chen, T., Chang, D.P., Liu, T., Desikan, R., Datar, R., Thundat, T., Berger, R., Zauscher, S., 2010. *J. Mater. Chem.* 20, 3391–3395.
- Chen, T., Chang, D.P., Liu, T., Desikan, R., Datar, R., Thundat, T., et al., 2010. Glucose-responsive polymer brushes for microcantilever sensing. *J. Mater. Chem.* 20 (17), 3391–3395.
- Chen, C., Xie, Q., Yang, D., Xiao, H., Fu, Y., Tan, Y., et al., 2013. Recent advances in electrochemical glucose biosensors: a review. *RSC Adv.* 3 (14), 4473–4491.
- Chen, L., Hwang, E., Zhang, J., 2018. Fluorescent nanobiosensors for sensing glucose. *Sensors* 18 (5), 1440.
- Cheng, Z., Wang, E., Yang, X., 2001. Capacitive detection of glucose using molecularly imprinted polymers. *Biosens. Bioelectron.* 16 (3), 179–185.
- Cho, I.-H., Lee, J., Kim, J., Kang, M.-s., Paik, J., Ku, S., et al., 2018. Current technologies of electrochemical immunosensors: perspective on signal amplification. *Sensors* 18 (1), 207.
- Chou, F.-F., Chang, H.-W., Li, T.-L., Shih, J.-S., 2008. Piezoelectric crystal/surface acoustic wave biosensors based on fullerene C60 and enzymes/antibodies/proteins. *J. Iran. Chem. Soc.* 5 (1), 1–15.
- Chou, J., Yan, S., Liao, Y., Lai, C., Wu, Y., Wu, C., 2018. Remote detection for glucose and lactate based on flexible sensor array. *IEEE Sens. J.* 18 (8), 3467–3474.
- Chuang, C.-W., Shih, J.-S., 2001. Preparation and application of immobilized C60-glucose oxidase enzyme in fullerene C60-coated piezoelectric quartz crystal glucose sensor. *Sens. Actuators, B Chem.* 81 (1), 1–8.
- Çiftçi, H., Tamer, U., Teker, M.Ş., Pekmez, N.Ö., 2013. An enzyme free potentiometric detection of glucose based on a conducting polymer poly (3-aminophenyl boronic acid-co-3-octylthiophene). *Electrochim. Acta* 90, 358–365.
- Clark, L.C., Lyons, C., 1962. Electrode systems for continuous monitoring in cardiovascular surgery. *Ann. N. Y. Acad. Sci.* 102 (1), 29–45.
- Clark Jr, L.C., inventor., Leland Jr, C.C., assignee., 1970. Membrane Polarographic Electrode System and Method with Electrochemical Compensation. United States.
- Çolak, Ö., Yaşar, A., Çete, S., Arslan, F., 2012. Glucose biosensor based on the immobilization of glucose oxidase on electrochemically synthesized polypyrrole-poly(vinyl sulphonate) composite film by cross-linking with glutaraldehyde. *Artif. Cells Blood Substit. Immobil. Biotechnol.* 40 (5), 354–361.
- Collyer, S.D., Davis, F., Higson, S.P.J., 2010. Sonochemically fabricated microelectrode arrays for use as sensing platforms. *Sensors* 10 (5), 5090–5132.
- Costantini, F., Tiggelaar, R., Sennato, S., Mura, F., Schlautmann, S., Bordini, F., Gardeniers, H., Manetti, C., 2013. Glucose level determination with a multi-enzymatic cascade reaction in a functionalized glass chip. *Analyst* 138(17), 5019–5024. <https://doi.org/10.1039/C3AN00806A>.
- Dastider, S.G., Barizuddin, S., Wu, Y., Dweik, M., Almasri, M., January 2013. Impedance biosensor based on interdigitated electrode arrays for detection of low levels of *E.coli* O157:H7. In: 2013 IEEE 26th International Conference on Micro Electro Mechanical Systems (MEMS), vol. 2013, pp. 20–24.
- Degani, Y., Heller, A., 1987. Direct electrical communication between chemically modified enzymes and metal electrodes. I. Electron transfer from glucose oxidase to metal electrodes via electron relays, bound covalently to the enzyme. *J. Phys. Chem.* 91 (6), 1285–1289.

- Dhand, C., Das, M., Datta, M., Malhotra, B.D., 2011. Recent advances in polyaniline based biosensors. *Biosens. Bioelectron.* 26 (6), 2811–2821.
- Dübner, M., Cadarso, V.J., Gevrek, T.N., Sanyal, A., Spencer, N.D., Padeste, C., 2017. Reversible light-switching of enzymatic activity on orthogonally functionalized polymer brushes. *ACS Appl. Mater. Interfaces* 9 (11), 9245–9249.
- Ferraz, N., Strømme, M., Fellström, B., Pradhan, S., Nyholm, L., Mhryanyan, A., 2012. In vitro and in vivo toxicity of rinsed and aged nanocellulose–polypyrrole composites. *J. Biomed. Mater. Res. A* 100A (8), 2128–2138.
- Flexer, V., Mano, N., 2014. Wired pyrroloquinoline quinone soluble glucose dehydrogenase enzyme electrodes operating at unprecedented low redox potential. *Anal. Chem.* 86 (5), 2465–2473.
- Fuketa, H., Yoshioka, K., Shinozuka, Y., Ishida, K., Yokota, T., Matsuhisa, N., et al., 2014. 1 μ m-thickness ultra-flexible and high electrode-density surface electromyogram measurement sheet with 2 V organic transistors for prosthetic hand control. *IEEE Trans. Biomed. Circuits Syst.* 8 (6), 824–833.
- Gaudin, V., 2017. Advances in biosensor development for the screening of antibiotic residues in food products of animal origin – a comprehensive review. *Biosens. Bioelectron.* 90, 363–377.
- Gerard, M., Chaubey, A., Malhotra, B., 2002. Application of conducting polymers to biosensors. *Biosens. Bioelectron.* 17 (5), 345–359.
- Gowers, S.A.N., Curto, V.F., Seneci, C.A., Wang, C., Anastasova, S., Vadgama, P., et al., 2015. 3D printed microfluidic device with integrated biosensors for online analysis of subcutaneous human microdialysate. *Anal. Chem.* 87 (15), 7763–7770.
- Gracia, R., Mecerreyes, D., 2013. Polymers with redox properties: materials for batteries, biosensors and more. *Polym. Chem.* 4 (7), 2206–2214.
- Grieshaber, D., MacKenzie, R., Vörös, J., Reimhult, E., 2008. Electrochemical biosensors – sensor principles and architectures. *Sensors* 8 (3), 1400–1458.
- Guisseppi-Elie, A., 2010. Electroconductive hydrogels: synthesis, characterization and biomedical applications. *Biomaterials* 31 (10), 2701–2716.
- Guisseppi-Elie, A., 2011. An implantable biochip to influence patient outcomes following trauma-induced hemorrhage. *Anal. Bioanal. Chem.* 399 (1), 403–419.
- Haarindraprasad, R., Hashim, U., Gopinath, S.C.B., Perumal, V., Liu, W.-W., Balakrishnan, S.R., 2016. Fabrication of interdigitated high-performance zinc oxide nanowire modified electrodes for glucose sensing. *Anal. Chim. Acta* 925, 70–81.
- Harsányi, G., 2000. Polymer films in sensor applications: a review of present uses and future possibilities. *Sens. Rev.* 20 (2), 98–105.
- Hierlemann, A., Brand, O., Hagleitner, C., Baltés, H., 2003. Microfabrication techniques for chemical/biosensors. *Proc. IEEE* 91 (6), 839–863.
- Hoang Hiep, N., Moonil, K., 2017. An overview of techniques in enzyme immobilization. *Appl. Sci. Conver. Technol.* 26 (6), 157–163.
- Hossain, M.F., Park, J.Y., 2017. Fabrication of sensitive enzymatic biosensor based on multi-layered reduced graphene oxide added PtAu nanoparticles-modified hybrid electrode. *PLoS One* (3), 12 e0173553-e.
- Hu, J., Liu, S., 2010. Responsive polymers for detection and sensing applications: current status and future developments. *Macromolecules* 43 (20), 8315–8330.
- Huang, X., Li, S., Schultz, J.S., Wang, Q., Lin, Q., 2009. A MEMS affinity glucose sensor using a biocompatible glucose-responsive polymer. *Sens. Actuators B Chem.* 140 (2), 603–609.
- Idros, N., Ho, M., Pivnenko, M., Qasim, M., Xu, H., Gu, Z., et al., 2015. Colorimetric-based detection of TNT explosives using functionalized silica nanoparticles. *Sensors* 15 (6), 12891.
- Hahm, J-i, 2011. Functional polymers in protein detection platforms: optical, electrochemical, electrical, mass-sensitive, and magnetic biosensors. *Sensors* 11 (3), 3327–3355.
- James, T.D., 2006. Boronic Acid-Based Receptors and Sensors for Saccharides. *Boronic Acids*.
- Jenekhe, S.A., Kiserow, D.J., 2004. Chromogenic effects in polymers: an overview of the diverse ways of tuning optical properties in real time. In: *Chromogenic Phenomena in Polymers*. ACS Symposium Series, vol. 888. American Chemical Society, pp. 2–15.
- Jin, P., Yamaguchi, A., Oi, F.A., Matsuo, S., Tan, J., Misawa, H., 2001. Glucose sensing based on interdigitated array microelectrode. *Anal. Sci.* 17 (7), 841–846.
- Jung, J., Lee, J., Shin, S., Kim, Y.T., 2017. Development of a telemetric, miniaturized electrochemical amperometric analyzer. *Sensors* 17 (10), 2416.
- Justin, G., Finley, S., Abdur Rahman, A.R., Guisseppi-Elie, A., 2009. Biomimetic hydrogels for biosensor implant biocompatibility: electrochemical characterization using micro-disc electrode arrays (MDEAs). *Biomed. Microdevices* 11 (1), 103–115.
- Justino, C.I.L., Duarte, A.C., Rocha-Santos, T.A.P., 2017. Recent progress in biosensors for environmental monitoring: a review. *Sensors* 17 (12), 2918.
- Kai, L., Hong, W., Wenguang, L., Hong, M., Peixin, Z., Chaoyi, Y., 2018. 3D printed stretchable capacitive sensors for highly sensitive tactile and electrochemical sensing. *Nanotechnology* 29 (18), 185501.
- Karunwi, O., Guisseppi-Elie, A., 2013. Supramolecular glucose oxidase-swnt conjugates formed by ultrasonication: effect of tube length, functionalization and processing time. *J. Nanobiotechnology* 11(1), 6. <https://doi.org/10.1186/1477-3155-11-6>.
- Kassal, P., Steinberg, M.D., Steinberg, I.M., 2018. Wireless chemical sensors and biosensors: a review. *Sens. Actuators B Chem.* 266, 228–245.
- Katz, E., Willner, I., 2003. Probing biomolecular interactions at conductive and semiconductive surfaces by impedance spectroscopy: routes to impedimetric immunosensors, DNA-sensors, and enzyme biosensors. *Electroanalysis* 15 (11), 913–947.
- Khan, M.R.R., Khalilian, A., Kang, S.-W., 2016. Fast, highly-sensitive, and wide-dynamic-range interdigitated capacitor glucose biosensor using solvatochromic dye-containing sensing membrane. *Sensors* 16 (2) 265-.
- Kim, J., Kim, J.H., Ariga, K., 2017. Redox-Active Polymers for Energy Storage Nanoarchitectonics.
- Kim, I., Kwon, D., Lee, D., Lee, T.H., Lee, J.H., Lee, G., et al., 2018. A highly permselective electrochemical glucose sensor using red blood cell membrane. *Biosens. Bioelectron.* 102, 617–623.
- Klonoff, D.C., 2012. Overview of fluorescence glucose sensing: a technology with a bright future. *J. Diabetes Sci. Technol.* 6 (6), 1242–1250.
- Klotzbach, T.L., Watt, M., Ansari, Y., Minteer, S.D., 2008. Improving the microenvironment for enzyme immobilization at electrodes by hydrophobically modifying chitosan and Nafion® polymers. *J. Membr. Sci.* 311 (1), 81–88.
- Kotanan, C., Guisseppi-Elie, A., 2010. Development of an implantable biosensor system for physiological status monitoring during long duration space exploration. *Gravitational Space Biol.* 23 (2), 55–64.

- Kotanan, C., Guiseppi-Elie, A., 2014. Characterization of a Wireless Potentiostat for Integration with a Novel Implantable Biotransducer. 768–76 pp.
- Kotanan, C.N., Guiseppi-Elie, A., 2012. Bioactive electroconductive hydrogels yield novel biotransducers for glucose. *Macromol. Symp.* 317–318 (1), 187–197.
- Kotanan, C., Karunwi, O., Guiseppi-Elie, A., 2014. Biofabrication using pyrrole electropolymerization for the immobilization of glucose oxidase and lactate oxidase on implanted microfabricated biotransducers. *Bioengineering* 1 (1), 85.
- Kotanan, C.N., Karunwi, O., Alam, F., Uyehara, C.F.T., Guiseppi-Elie, A., 2018. Fabrication and in vitro performance of a dual responsive lactate and glucose biosensor. *Electrochim. Acta* 267, 71–79.
- Kotanan, C.N., Moussy, F.G., Carrara, S., Guiseppi-Elie, A., 2012. Implantable enzyme amperometric biosensors. *Biosens. Bioelectron.* 35(1), 14–26. <https://doi.org/10.1016/j.bios.2012.03.016>.
- Kucherenko, I.S., Kucherenko, D.Y., Soldatkin, O.O., Lagarde, F., Dzyadevych, S.V., Soldatkin, A.P., 2016. A novel conductometric biosensor based on hexokinase for determination of adenosine triphosphate. *Talanta* 150, 469–475.
- Lee, K.M., Kim, K.H., Yoon, H., Kim, H., 2018. Chemical design of functional polymer structures for biosensors: from nanoscale to macroscale. *Polymers* 10 (5), 551.
- Li, C.-C., Kharaziha, M., Min, C., Maas, R., Nikkhah, M., 2015. Microfabrication of cell-laden hydrogels for engineering mineralized and load bearing tissues. In: Bertassoni, L.E., Coelho, P.G. (Eds.), *Engineering Mineralized and Load Bearing Tissues*. Springer International Publishing, Cham, pp. 15–31.
- Li, H., Zhao, F., Yue, L., Li, S., Xiao, F., 2016. Nonenzymatic electrochemical biosensor based on novel hydrophilic ferrocene-terminated hyperbranched polymer and its application in glucose detection. *Electroanalysis* 28 (5), 1003–1011.
- Li, H., Yan, X., Qiao, S., Lu, G., Su, X., 2018. Yellow-emissive carbon dot-based optical sensing platforms: cell imaging and analytical applications for biocatalytic reactions. *ACS Appl. Mater. Interfaces* 10 (9), 7737–7744.
- Lin, H., Li, M., Ding, L., Huang, J., 2019. *Appl. Biochem. Biotechnol.* 187, 1569–1580.
- Luong, J.H.T., Glennon, J.D., Gedanken, A., Vashist, S.K., 2017. Achievement and assessment of direct electron transfer of glucose oxidase in electrochemical biosensing using carbon nanotubes, graphene, and their nanocomposites. *Microchimica Acta* 184 (2), 369–388.
- Ma, Y., Promthaveepong, K., Li, N., 2016. *Anal. Chem.* 88, 8289–8293.
- Maji, S., Cesur, B., Zhang, Z., De Geest, B.G., Hoogenboom, R., 2016. *Polym. Chem.* 7, 1705–1710.
- Mandon, C.A., Blum, L.J., Marquette, C.A., 2017. Adding biomolecular recognition capability to 3D printed objects: 4D printing. *Procedia Technol.* 27, 1–2.
- Mano, N., Yoo, J.E., Tarver, J., Loo, Y.-L., Heller, A., 2007. An electron-conducting cross-linked polyaniline-based redox hydrogel, formed in one step at pH 7.2, wires glucose oxidase. *J. Am. Chem. Soc.* 129 (22), 7006–7007.
- Mariani, A.M., Natoli, M.E., Kofinas, P., 2013. Enzymatic activity preservation and protection through entrapment within degradable hydrogels. *Biotechnol. Bioeng.* 110 (11), 2994–3002.
- Microfabricated biosensors and microsystems. In: Hesketh, P.J., Zivanovic, S., Ming, Y., Park, S., Svojanovsky, S., Cunneen, J., et al. (Eds.), Sept. 1997. 1997 21st International Conference on Microelectronics Proceedings, Sept. 1997. vol. 1997, pp. 14–17.
- Mishra, R.K., Hubble, L.J., Martín, A., Kumar, R., Barfidokht, A., Kim, J., et al., 2017. Wearable flexible and stretchable glove biosensor for on-site detection of organophosphorus chemical threats. *ACS Sens.* 2 (4), 553–561.
- Miwa, Y., Miyake, T., Matsue, T., Uchida, I., 1994. A Conductometric Glucose Sensor Based on a Twin-Microband Electrode Coated with a Polyaniline Thin Film. 2864–2866 pp.
- Mousa, H.M., Aggas, J.R., Guiseppi-Elie, A., 2019. Electropolymerization of aniline and (N-phenyl-o-phenylenediamine) for glucose biosensor application. *Mater. Lett.* 238, 267–270.
- Mugo, S.M., Berg, D., Bharath, G., 2019. *Anal. Lett.* 52, 825–838.
- Mulchandani, A., 1998. Principles of enzyme biosensors. In: Mulchandani, A., Rogers, K.R. (Eds.), *Enzyme and Microbial Biosensors: Techniques and Protocols*. Humana Press, Totowa, NJ, pp. 3–14.
- Naderi Asrami, P., Mozaffari, S.A., Saber Tehrani, M., Aberoomand Azar, P., 2018. A novel impedimetric glucose biosensor based on immobilized glucose oxidase on a CuO-Chitosan nanobiocomposite modified FTO electrode. *Int. J. Biol. Macromol.* 118, 649–660.
- Nagel, B., Warsinke, A., Katterle, M., 2007. *Langmuir* 23, 6807–6811.
- Neethirajan, S., Weng, X., Tah, A., Cordero, J.O., Ragavan, K.V., 2018. Nano-biosensor platforms for detecting food allergens – new trends. *Sens. Bio Sens. Res.* 18, 13–30.
- Nguyen, Q.V., Caro, A., Raoux, M., Quorb, A., Floderer, J., Bornat, Y., et al. (Eds.), July 2013. A Novel Bioelectronic Glucose Sensor to Process Distinct Electrical Activities of Pancreatic Beta-Cells. 2013 35th Annual International Conference of the IEEE Engineering in Medicine and Biology Society (EMBC), vol. 2013, pp. 3–7.
- Nouira, W., Maaref, A., Elaissari, H., Vocanson, F., Siadat, M., Jafrezic-Renault, N., 2013. Comparative study of conductometric glucose biosensor based on gold and on magnetic nanoparticles. *Mater. Sci. Eng. C* 33 (1), 298–303.
- Pan, L., Yu, G., Zhai, D., Lee, H.R., Zhao, W., Liu, N., et al., 2012. Hierarchical nanostructured conducting polymer hydrogel with high electrochemical activity. *Proc. Natl. Acad. Sci. U.S.A.* 109 (24), 9287–9292.
- Pan, H., Gonuguntla, S., Li, S., Trau, D., 2017. *Conjugated Polymers for Biosensor Devices II*.
- Pänke, O., Balkenhohl, T., Kafka, J., Schäfer, D., Lisdat, F., 2007. Impedance spectroscopy and biosensing. In: *Biosensing for the 21st Century*: Springer, pp. 195–237.
- Park, H.S., Cho, M.Y., Noh, Y.-W., Hong, K.S., Lim, Y.T., 2017. *Dyes Pigments* 136, 583–589.
- Parrilla, M., Cánovas, R., Andrade, F.J., 2017. Paper-based enzymatic electrode with enhanced potentiometric response for monitoring glucose in biological fluids. *Biosens. Bioelectron.* 90, 110–116.
- Pham, X.-H., Bui, M.-P.N., Li, C.A., Han, K.N., Kim, J.H., Won, H., Seong, G.H., 2010. *Anal. Chim. Acta* 671, 36–40.
- Pietschnig, R., 2016. Polymers with pendant ferrocenes. *Chem. Soc. Rev.* 45 (19), 5216–5231.
- Pisoschi, A., 2016. Potentiometric biosensors: concept and analytical applications—an editorial. *Biochem. Anal. Biochem.* 5 e164.
- Pohanka, M., 2018. Overview of piezoelectric biosensors, immunosensors and DNA sensors and their applications. *Materials* 11 (3), 448.
- Putzbach, W., Ronkainen, N.J., 2013. Immobilization techniques in the fabrication of nanomaterial-based electrochemical biosensors: a review. *Sensors* 13 (4), 4811–4840.
- Pyeshkova, V., Saiapina, O., Soldatkin, O., Dzyadevych, S., 2009. Enzyme Conductometric Biosensor for Maltose Determination. 272–8 pp.

- Qian, K., Deng, Q., Fang, G., Wang, J., Pan, M., Wang, S., et al., 2016. Metal-organic frameworks supported surface-imprinted nanoparticles for the sensitive detection of metolcarb. *Biosens. Bioelectron.* 79, 359–363.
- Ribeiro, D.V., Abrantes, J.C.C., 2016. Application of electrochemical impedance spectroscopy (EIS) to monitor the corrosion of reinforced concrete: a new approach. *Constr. Build. Mater.* 111, 98–104.
- Rocchitta, G., Spanu, A., Babudieri, S., Latte, G., Madeddu, G., Galleri, G., et al., 2016. Enzyme biosensors for biomedical applications: strategies for safeguarding analytical performances in biological fluids. *Sensors* 16 (6), 780.
- Roda, A., Guardigli, M., Calabria, D., Calabretta, M.M., Cevenini, L., Michelini, E.A., 2014. 3D-printed device for a smartphone-based chemiluminescence biosensor for lactate in oral fluid and sweat. *Analyst* 139 (24), 6494–6501.
- Rukiye, A., Fatma Ozturk, K., Dilek Odaci, D., Metin, A., Suna, T., 2018. Copolymer based multifunctional conducting polymer film for fluorescence sensing of glucose. *Methods Appl. Fluoresc.* 6 (3), 035012.
- Ruscito, A., DeRosa, M.C., 2016. Small-molecule binding aptamers: selection strategies, characterization, and applications. *Front. Chem.* 4, 14.
- Russell, T.P., 2002. Surface-responsive materials. *Science* 297 (5583), 964–967.
- Saifuddin, N., Raziah, A.Z., Junizah, A.R., 2013. Carbon nanotubes: a review on structure and their interaction with proteins. *J. Chem.* 2013, 18.
- Sau, A., Bera, K., Pal, U., Maity, A., Mondal, P., Basak, S., et al., 2018. Design and synthesis of fluorescent carbon-dot polymer and deciphering its electronic structure. *J. Phys. Chem. C* 122 (41), 23799–23807.
- Saxena, A.P., Deepa, M., Joshi, A.G., Bhandari, S., Srivastava, A.K., 2011. Poly(3,4-ethylenedioxythiophene) – ionic liquid functionalized graphene/reduced graphene oxide nanostructures: improved conduction and electrochromism. *ACS Appl. Mater. Interfaces* 3 (4), 1115–1126.
- Schmidt, U., Guenther, M., Gerlach, G., 2016. *Curr. Dir. Biomed. Eng.* 117.
- Schuhmann, W., Ohara, T.J., Schmidt, H.L., Heller, A., 1991. Electron transfer between glucose oxidase and electrodes via redox mediators bound with flexible chains to the enzyme surface. *J. Am. Chem. Soc.* 113 (4), 1394–1397.
- Sekitani, T., 2016. Soft biosensor systems using flexible and stretchable electronics technology. In: Rogers, J.A., Ghaffari, R., Kim, D.-H. (Eds.), *Stretchable Bioelectronics for Medical Devices and Systems*. Springer International Publishing, Cham, pp. 133–149.
- Shakya, A.K., Nandakumar, K.S., 2018. An update on smart biocatalysts for industrial and biomedical applications. *Journal of the Royal Society. Interface* 15 (139), 20180062.
- Shan, X., Chai, L., Ma, J., Qian, Z., Chen, J., Feng, H., 2014. B-doped Carbon Quantum Dots as a Sensitive Fluorescence Probe for Hydrogen Peroxide and Glucose Detection.
- Sharafeldin, M., Jones, A., Rusling, J., 2018. 3D-Printed biosensor arrays for medical diagnostics. *Micromachines* 9 (8), 394.
- Singh, P., Shukla, S.K., 2018. Opto-chemical glucose sensing over NiO/polyaniline hybrid matrix using optical fiber approach. *Optik* 165, 94–101.
- Sirca, D., Vardeu, A., Pinna, M., Diana, M., Enrico, P., 2014. A robust, state-of-the-art amperometric microbiosensor for glutamate detection. *Biosens. Bioelectron.* 61, 526–531.
- Sirkar, K., Revzin, A., Pishko, M.V., 2000. Glucose and lactate biosensors based on redox polymer/oxidoreductase nanocomposite thin films. *Anal. Chem.* 72 (13), 2930–2936.
- Sodzel, D., Khranovskyy, V., Beni, V., Turner, A.P., Viter, R., Eriksson, M.O., et al., 2015. Continuous sensing of hydrogen peroxide and glucose via quenching of the UV and visible luminescence of ZnO nanoparticles. *Microchimica Acta* 182 (9–10), 1819–1826.
- Swamy, N.K., Sandeep, S., Santhosh, A., 2017. Conductive polymers and their nanohybrid transducers for electrochemical biosensors applications: a brief review. *Indian J. Adv. Chem. Sci.* S2 6, 9.
- Syshchik, O., Skryshevsky, V.A., Soldatkin, O.O., Soldatkin, A.P., 2015. Enzyme biosensor systems based on porous silicon photoluminescence for detection of glucose, urea and heavy metals. *Biosens. Bioelectron.* 66, 89–94.
- Takasu, K., Kushiro, K., Hayashi, K., Iwasaki, Y., Inoue, S., Tamechika, E., et al., 2015. Polymer brush biointerfaces for highly sensitive biosensors that preserve the structure and function of immobilized proteins. *Sens. Actuators B Chem.* 216, 428–433.
- Tavakoli, J., Tang, Y., 2017. Hydrogel based sensors for biomedical applications: an updated review. *Polymers* 9 (8), 364.
- Tereshchenko, A., Bechelany, M., Viter, R., Khranovskyy, V., Smyntyna, V., Starodub, N., et al., 2016. Optical biosensors based on ZnO nanostructures: advantages and perspectives. A review. *Sens. Actuators B Chem.* 229, 664–677.
- Thyparambil, A.A., Bazin, I., Guiseppi-Elie, A., 2017. Molecular modeling and simulation tools in the development of peptide-based biosensors for mycotoxin detection: example of ochratoxin. *Toxins* 9 (12), 395.
- Tierney, S., Volden, S., Stokke, B.T., 2009. Glucose sensors based on a responsive gel incorporated as a Fabry-Perot cavity on a fiber-optic readout platform. *Biosens. Bioelectron.* 24 (7), 2034–2039.
- Tuller, H., 2017. Ionic conduction and applications. In: Kasap, S., Capper, P. (Eds.), *Springer Handbook of Electronic and Photonic Materials*. Springer International Publishing, Cham. 1-.
- Usman Ali, S.M., Nur, O., Willander, M., Danielsson, B., 2010. A fast and sensitive potentiometric glucose microsensor based on glucose oxidase coated ZnO nanowires grown on a thin silver wire. *Sens. Actuators, B Chem.* 145 (2), 869–874.
- Vaezi, M., Seitz, H., Yang, S., 2013. A review on 3D micro-additive manufacturing technologies. *Int. J. Adv. Manuf. Technol.* 67 (5), 1721–1754.
- Vargas-Bernal, R., Rodríguez-Miranda, E., Herrera-Pérez, G., 2012. Evolution and Expectations of Enzymatic Biosensors for Pesticides, pp. 329–356.
- Vasylieva, N., Maucler, C., Meiller, A., Viscogliosi, H., Lieutaud, T., Barbier, D., et al., 2013. Immobilization method to preserve enzyme specificity in biosensors: consequences for brain glutamate detection. *Anal. Chem.* 85 (4), 2507–2515.
- Verhulsel, M., Vignes, M., Descroix, S., Malaquin, L., Vignjevic, D.M., Viovy, J.-L., 2014. A review of microfabrication and hydrogel engineering for micro-organs on chips. *Biomaterials* 35 (6), 1816–1832.
- Wahab, H.A., Salama, A.A., El Saeid, A.A., Willander, M., Nur, O., Battisha, I.K., 2018. Zinc oxide nano-rods based glucose biosensor devices fabrication. *Res. Phys.* 9, 809–814.
- Wan, D., Yuan, S., Li, G.L., Neoh, K.G., Kang, E.T., 2010. Glucose biosensor from covalent immobilization of chitosan-coupled carbon nanotubes on polyaniline-modified gold electrode. *ACS Appl. Mater. Interfaces* 2 (11), 3083–3091.
- Wang, J., 1999. Sol-gel materials for electrochemical biosensors. *Anal. Chim. Acta* 399 (1), 21–27.

- Wang, J., 2008. Electrochemical glucose biosensors. *Chem. Rev.* 108 (2), 814–825.
- Wang, H.-C., Zhou, H., Chen, B., Mendes, P.M., Fossey, J.S., James, T.D., Long, Y.-T., 2013. *Analyst* 138, 7146–7151.
- Wang, H.-C., Lee, A.-R., 2015. Recent developments in blood glucose sensors. *J. Food Drug Anal.* 23 (2), 191–200.
- Wang, X., Uchiyama, S., 2013. Polymers for biosensors construction. In: *State of the Art in Biosensors-General Aspects InTech*, Chapter 3. 67–84.
- Wang, J., Myung, N.V., Yun, M., Monbouquette, H.G., 2005. Glucose oxidase entrapped in polypyrrole on high-surface-area Pt electrodes: a model platform for sensitive electroenzymatic biosensors. *J. Electroanal. Chem.* 575 (1), 139–146.
- Wang, H.-C., Zhou, H., Chen, B., Mendes, P.M., Fossey, J.S., James, T.D., et al., 2013. A bis-boronic acid modified electrode for the sensitive and selective determination of glucose concentrations. *Analyst* 138 (23), 7146–7151.
- Wang, H., Yi, J., Velado, D., Yu, Y., Zhou, S., 2015a. Immobilization of carbon dots in molecularly imprinted microgels for optical sensing of glucose at physiological pH. *ACS Appl. Mater. Interfaces* 7 (29), 15735–15745.
- Wang, H., Ohnuki, H., Endo, H., Izumi, M., 2015b. Impedimetric and amperometric bifunctional glucose biosensor based on hybrid organic–inorganic thin films. *Bioelectrochemistry* 101, 1–7.
- Wang, W., Kong, L., Zhu, J., Tan, L., 2017. One-pot preparation of conductive composite containing boronic acid derivative for non-enzymatic glucose detection. *J. Colloid Interface Sci.* 498, 1–8.
- Weibel, M.K., Bright, H.J., 1971. The glucose oxidase mechanism: interpretation of the pH dependence. *J. Biol. Chem.* 246 (9), 2734–2744.
- Welch, M.E., Doublet, T., Bernard, C., Malliaras, G.G., Ober, C.K., 2015. A glucose sensor via stable immobilization of the GOx enzyme on an organic transistor using a polymer brush. *J. Polym. Sci. Part A Polym. Chem.* 53 (2), 372–377.
- Widayani, Y., Wungu, T.D.K., Suprijadi, 2017. Preliminary study of molecularly imprinted polymer-based potentiometric sensor for glucose. *Procedia Eng.* 170, 84–87.
- Wilson, A.M., Justin, G., Guiseppi-Elie, A., 2010. Electroconductive Hydrogels. *Biomedical Applications of Hydrogels Handbook*: Springer, pp. 319–337.
- Xiao, Y., Patolsky, F., Katz, E., Hainfeld, J.F., Willner, I., 2003. “Plugging into enzymes”: nanowiring of redox enzymes by a gold nanoparticle. *Science* 299 (5614), 1877–1881.
- Xie, W., Bülow, L., Xie, B., 2018. Pyrroloquinoline quinone glucose dehydrogenase adopted in thermometric analysis for enhancement of glucose determination. *J. Therm. Anal. Calorim.* 134 (3), 1913–1919.
- Xiong, M., Gu, B., Zhang, J.-D., Xu, J.-J., Chen, H.-Y., Zhong, H., 2013. Glucose microfluidic biosensors based on reversible enzyme immobilization on photopatterned stimuli-responsive polymer. *Biosens. Bioelectron.* 50, 229–234.
- Xu, Z.J., 2017. From two-phase to three-phase: the new electrochemical interface by oxide electrocatalysts. *Nano-Micro Lett.* 10 (1), 8.
- Yakovleva, M., Bhand, S., Danielsson, B., 2013. The enzyme thermistor—a realistic biosensor concept. A critical review. *Anal. Chim. Acta* 766, 1–12.
- Yanagawa, F., Sugiura, S., Kanamori, T., 2016. Hydrogel microfabrication technology toward three dimensional tissue engineering. *Regen. Ther.* 3, 45–57.
- Yang, L., Guiseppi-Wilson, A., Guiseppi-Elie, A., 2010. Design Considerations in the Use of Interdigitated Microsensor Electrode Arrays (IMEs) for Impedimetric Characterization of Biomimetic Hydrogels. 279–89 pp.
- Yi-Hua, Z., Tse-Chao, H., Fei, X. (Eds.), Jan. 2006. A Thermal Biosensor Based on Enzyme Reaction. 2005 IEEE Engineering in Medicine and Biology 27th Annual Conference, vol. 2005, pp. 17–18.
- Yoo, E.-H., Lee, S.-Y., 2010. Glucose biosensors: an overview of use in clinical practice. *Sensors* 10 (5), 4558–4576.
- Yu, M., Zhao, K., Zhu, X., Tang, S., Nie, Z., Huang, Y., Zhao, P., Yao, S., 2017. *Biosens. Bioelectron.* 95, 41–47.
- Qu, Z-b, Zhou, X., Gu, L., Lan, R., Sun, D., Yu, D., et al., 2013. Boronic Acid Functionalized Graphene Quantum Dots as a Fluorescent Probe for Selective and Sensitive Glucose Determination in Microdialysate.
- Zayats, M., Katz, E., Willner, I., 2002. Electrical contacting of glucose oxidase by surface-reconstitution of the apo-protein on a relay-boronic acid-FAD cofactor monolayer. *J. Am. Chem. Soc.* 124 (10), 2120–2121.
- Zhang, M., Liao, C., Mak, C.H., You, P., Mak, C.L., Yan, F., 2015. Highly sensitive glucose sensors based on enzyme-modified whole-graphene solution-gated transistors. *Sci. Rep.* 5, 8311.
- Zhao, X., Sadhu, V., Le, T., Pompili, D., Javanmard, M. (Eds.), May 2017. Towards Low-Power Wearable Wireless Sensors for Molecular Biomarker and Physiological Signal Monitoring. 2017 IEEE International Symposium on Circuits and Systems (ISCAS), vol. 2017, pp. 28–31.
- Zhou, M., Dong, S., 2011. Bioelectrochemical interface engineering: toward the fabrication of electrochemical biosensors, biofuel cells, and self-powered logic biosensors. *Acc. Chem. Res.* 44 (11), 1232–1243.
- Zhou, Y., Chiu, C.-W., Liang, H., 2012. Interfacial structures and properties of organic materials for biosensors: an overview. *Sensors* 12 (11), 15036.
- Zohourtalab, A., Razmi, H., 2018. Selective determination of glucose in blood plasma by using an amperometric glucose biosensor based on glucose oxidase and a chitosan/Nafion/IL/ferrocene composite film. *Iran. J. Anal. Chem.* 5 (1), 9–16.

2.6.1

Rebuilding Humans Using Biology and Biomaterials

SHELLY E. SAKIYAMA-ELBERT

Department of Biomedical Engineering, The University of Texas at Austin, Austin, TX, United States

Over the past four decades, biomaterials have been increasingly used for applications in tissue engineering to rebuild tissues lost due to disease or injury, as well as to build in vitro models of complex tissue systems. For applications in tissue engineering, our growing understanding of how biological systems function at a mechanistic level and our ability to modulate them at both genetic and epigenetic levels have allowed the development of more elegant approaches to tissue engineering. However, underlying these approaches is still the critical need to understand how the biomaterials used for these applications interface with the physiology environment. This section focuses on the fundamental principles and approaches used for designing and fabricating biomaterials for tissue-engineering applications, stressing common themes and challenges. This edition of the textbook has refined the focus more on the materials, so the chapters in this section stress examples and a model selection of tissues rather than seeking to cover all topics. For additional discussion of specifics for given tissues, there are a variety of references on the topic of tissue engineering, which we do not seek to reproduce in this section.

The first half of this section focuses on tissue engineering broadly, the materials used for tissue-engineering applications, and the transmission of mechanical cues between materials and tissues. The first chapter focuses on a general overview of tissue engineering, including a brief history and common components of tissue-engineering approaches. It highlights common applications, including new areas such as organoids, and newer approaches, such as genome editing. The second chapter focuses specifically on the use of biomaterial scaffolds for tissue-engineering applications. It highlights the key scaffold design criteria, applications,

and materials. It also highlights options for fabrication techniques (which are covered extensively in Section 1.4) and characterization methods. The third chapter focuses on micromechanical criteria of biomaterials scaffolds for tissue engineering. It covers mechanotransduction from scaffolds and extracellular matrices to cells and tissues. It also discusses the effects of scaffold topography and roughness on transduction, as well as the effects of mechanical stimulation on tissue formation.

The remaining three chapters in this section provide examples of three tissues, and the thought processes behind selecting materials and designing biomaterial scaffolds for tissue-engineering applications in each area: musculoskeletal (tendon), cardiovascular, and soft tissues. The fourth chapter focuses on the design of scaffolds for the tissue engineering of tendons, as an example of a tissue where mechanical properties of the resulting tissue are critical for the return of load-bearing function after injury. Examples of using material fiber alignment to guide cell infiltration and extracellular matrix deposition are given that apply broadly to many tissues. The fifth chapter focuses on biomaterials used for cardiovascular tissue engineering. It highlights different types of materials used for different applications along with the advantages and disadvantages of those materials for each type of application. The final chapter in this section focuses on the use of biomaterials in soft tissue engineering, such as skin, adipose, and gastrointestinal tissue. The pros and cons of different materials are highlighted as well as design criteria for each type of tissue with regard to scaffold design.

Overall this is a large research and commercial space for biomaterials-derived products and those interested in this field can find extensive primary literature, reviews, and texts on the topics, which are further described in Appendix E.

2.6.2

Overview of Tissue Engineering Concepts and Applications

SARAH MIHO VAN BELLEGHEM^{1,2*}, BHUSHAN MAHADIK^{1,2*},
KIRSTIE LANE SNODDERLY^{1,2*}, JOHN P. FISHER^{1,2}

¹University of Maryland College Park

²NIH/NIBIB Center for Engineering Complex Tissues

General Introduction

History of Tissue Engineering

The term “tissue engineering” as recognized today was likely first introduced at a panel meeting of the National Science Foundation in 1987, which led to the first tissue-engineering meeting in early 1988 (Vacanti, 2006). Despite these early approaches for replacement, repair, and regeneration of failing organs, the true emergence of tissue engineering as a medical field began in the early 1990s when tissue engineering was defined as an interdisciplinary field that applies the principles of engineering and life sciences toward the development of biological substitutes that restore, maintain, or improve tissue function (Langer and Vacanti, 1993). The field has since rapidly progressed worldwide with an increasing market size, with nearly \$4 billion invested in the field in the 1990s resulting in over 70 companies and several products on the market by the end of the millennium (Lysaght and Reyes, 2001). From a commercial perspective, tissue engineering carries a broad definition and can include companies focused on several products such as cells/stem cells, biomaterials, preclinical testing, clinical trials, commercially approved products, and specialized services (e.g., cord blood banking, tissue grafts). By 2011, 106 companies selling tissue-engineering-based products or services and employing almost 14,000 people were documented worldwide, with a total estimated sales of \$3.5 billion, a roughly threefold increase from 2007. As of mid-2018, in the United States alone there were 49 public tissue-engineering companies with nearly 146,000 employees and a cumulative of \$9 billion in sales. Well over a million patients have been treated with tissue-engineered products. Additionally, 66 interventional clinical trials in various phases involving

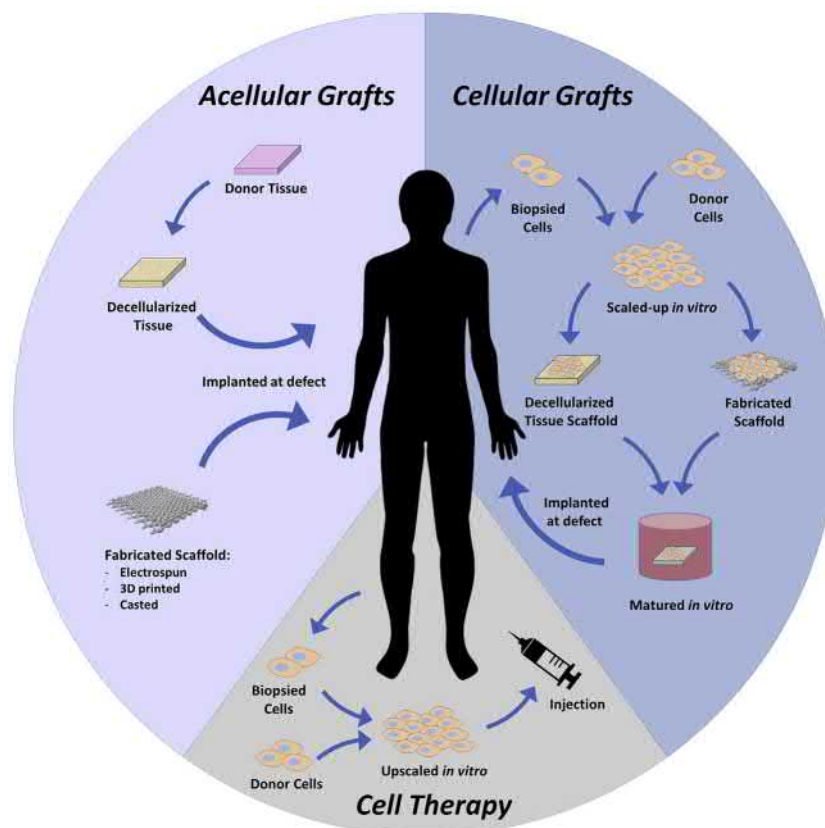
tissue-engineering products were active between 2011 and 2018 and both public and private sector companies continue R&D investment for new products and technologies (Kim et al., 2019). While early success has been challenging, technological advances alongside biological discoveries continue to propel the field of tissue engineering into exciting new frontiers (Vacanti, 2006).

Goals of Tissue Engineering and Classification

Goals of Tissue Engineering

Tissue engineering aims to restore tissue and organ function by employing biological and engineering strategies to clinical problems. The functional failure of tissues and organs is a severe and costly healthcare problem as their replacements are limited by the availability of compatible donors. Artificial prostheses and mechanical devices help millions of patients; however, they are not ideal due to poor long-term performance. Furthermore, mechanical devices rarely integrate with host tissues and can trigger a host immune response that may damage healthy tissue around the implant. In addition, surgical reconstruction of organs and tissues involves the replacement of damaged tissue from the patient’s own tissue, e.g., saphenous vein as bypass graft, patella tendon for anterior cruciate ligament repair, and autologous skin grafts. However, often this strategy fails to replace all the functions of the original tissue and can cause issues such as development of malignant tumors, surgical complications, and morbidity at the donor sites. Thus tissue engineering has emerged as an alternative for tissue or organ transplantation with the primary goal of providing a clinically relevant substitute by integrating engineering, biology, materials science, chemistry, and medicine. By recapitulating the normal tissue development process, tissue engineering represents a

* all authors contributed equally.



• **Figure 2.6.2.1** Tissue engineering approaches for regeneration can consist of various methods. In acellular grafts donor-derived or synthetic biomaterial platforms devoid of any cellular components are implanted into the patient body to promote and aid native regeneration. Cellular grafts consist of patient-derived or donor cells that are used to cellularize and mature a scaffold prior to implantation. Cell therapy consists only of the desired cell and biological populations devoid of any scaffolds, that is administered to the patient.

strategy to restore, maintain, and improve tissue function, with the ultimate aim of complete tissue or organ regeneration.

Classification of Tissue-Engineering Approaches

Strategies for the clinical implementation of tissue-engineering methods can be broadly classified according to the implantation or application of the materials or biologics. In addition to traditional tissue engineering, cell therapies and closed looped systems used as implantable or extracorporeal devices are also examples of regenerative medicine approaches. While classically these methods are not regarded as tissue engineering, they have contributed significantly to tissue regeneration and are therefore briefly introduced here.

Traditional tissue engineering: Traditional tissue engineering includes two main approaches: (1) transplantation of a tissue grown *in vitro* consisting of an artificial matrix with cells and growth factors, and (2) *in situ* regeneration of tissue utilizing a combination of an artificial matrix and growth factors as a guiding template to induce host cell regeneration of the tissue *in vivo* (Fig. 2.6.2.1). These two strategies and their components are explained in detail throughout this chapter.

Cell therapy: The main strategy in cell therapy is the harvesting of desired cell populations and their expansion in

large numbers for *in vivo* transplantation. This involves the delivery of cells through systemic injection into the bloodstream or through direct transplantation into a local tissue. A few examples of cell therapy include cell transplants from bone marrow, peripheral blood, or umbilical cord, which have been used to treat several blood-related diseases, including leukemia, multiple myeloma, and immune deficiencies (Rao et al., 2012). The main challenges for cell transplantation are growing large numbers of cells without bacterial contamination; preservation of cell phenotype; and preventing accumulation of genetic mutations during culture expansion. These challenges must be combated for cell therapy to become clinically successful and federally approved.

Closed-loop methods: This involves the use of extracorporeal or implantable devices that house transplanted cell-laden polymers within a semipermeable membrane, which allows diffusion of nutrients and excreted products, but prevents the movement of antibodies, pathogens, or immunocompetent cells (Murua et al., 2008). Microcarrier or microcapsule-based cell encapsulation can function as an effective drug delivery system and requires the use of biomaterials engineered for the desired cell–matrix interactions, therapeutic drug release, and transport properties to influence the targeted cell population, defect, or wound site (Hernández et al., 2010). Closed-loop extracorporeal

devices have been used for the treatment of liver, pancreas, and kidney pathologies (Patzer, 2006; Hueso et al., 2019). Natural as well as synthetic biomaterials such as alginate, collagen, and polyethylene glycol (PEG)-based systems have been explored as carriers where factors such as material degradation, immunogenicity, encapsulation, and release kinetics, among others, have been studied to achieve the desired therapeutic effect (Hernández et al., 2010).

Components of Tissue Engineering

Tissue-engineering strategies typically involve multiple components, including cells, a physical template (scaffold), and a combination of biological cues that promote regeneration and integration of the construct into a functional and organized tissue.

The Cell

Cells are the building blocks of tissues and play a critical role in promoting tissue healing and regeneration. Within tissue engineering, cells may be a component of the in vitro construct or may be recruited in vivo with the aid of immobilized or soluble signals. Cell types utilized for tissue engineering are selected from a variety of sources, which include autologous cells from the patient, allogeneic cells from another human, and xenogeneic cells from a different species. However, allogeneic and xenogeneic cells often suffer from immune rejection.

Cell type: Common cell types utilized for tissue-engineering purposes include stem cells, differentiated mature cells, or a mixture of differentiated cells. Stem cells are capable of self-renewal and differentiation into multiple lineages and may include embryonic stem cells (ESCs), adult stem cells such as mesenchymal stem cells (MSCs) and hematopoietic stem cells, or induced pluripotent stem cells:

- Embryonic stem cells: ESCs are capable of self-renewal without differentiation, can be culture expanded, and most importantly can differentiate into any cell type. Since ESCs are isolated from an embryonic stage, they can develop into any of the three germ layers: endoderm (interior stomach lining, gastrointestinal tract, and lungs); mesoderm (muscle, bone, blood, and urogenital); or ectoderm (epidermal tissues and nervous system) (Song et al., 2018). However, because of several ethical issues and regulatory limitations concerning human ESCs, induced pluripotent stem cells (iPSCs) are now an attractive alternative in tissue engineering for clinical approaches.
- Adult stem cells: Adult stem cells include, for example, hematopoietic, mesenchymal, neural, and hepatic stem cells. In particular, hematopoietic stem cells have been used in clinics for a few decades for treating blood diseases (i.e., bone marrow transplantation) (Mosaad, 2014). MSCs, which can be transplanted as an allogeneic cell source to another patient without immunosuppressive drugs, are capable of differentiation into multiple lineages

that may produce tissues, including bone, cartilage, and muscle, and have been approved for use in multiple systems to treat bone defects (Su et al., 2018). MSCs can also modulate the host immune response through paracrine or endocrine mechanisms, and are currently being applied in clinical trials for the treatment of immune diseases (Leyendecker Jr. et al., 2018). Nevertheless, adult stem cells are rare, challenging to isolate and expand without altering cell phenotype, and limited in their differentiation potential.

- Induced pluripotent stem cells: Successful reprogramming of differentiated human somatic cells into pluripotent cells has led to the creation of iPSCs (Takahashi et al., 2006). These cells are functionally similar to ESCs, but do not require the destruction of an embryo and can be created from a patient's own cells, eliminating the risk of host rejection (Yamanaka, 2008). Since their groundbreaking discovery in 2006, there have been significant advances in our ability to control the induction of pluripotency from multiple tissue sources such as skin fibroblasts, peripheral blood, hair-derived keratinocytes, and urine-derived epithelial cells. Studies have also focused on their targeted differentiation, as well as applications in tissue engineering and therapeutics (Mora et al., 2017). iPSCs hold significant promise as a universal, patient-derived cell source for the generation of multiple cell types in a single application. However, iPSC differentiation and subsequent expansion of targeted cell populations is technically challenging and often limited to low passage numbers, making it difficult to obtain clinically relevant cell numbers. In the case of uncontrolled downstream differentiation, it is further necessary to isolate cell populations for desired purity. Thus the application of patient-derived iPSCs for on-site therapeutics requires facilities, equipment, and expertise that may not be readily available. Additionally, challenges such as maintaining genomic stability, role of epigenetic factors, downstream mutations, potential immunogenicity, and regulatory hurdles need to be overcome for iPSCs to be applied clinically (Menon et al., 2016).
- Mature cells: These cells, either parenchymal or stromal, represent the large population of fully differentiated, functionally, as well as tissue-specific cell types in the body such as fibroblasts, smooth muscle cells, epithelial cells, endothelial cells, hepatocytes, etc. They are routinely used in research, either as immortalized cell lines or as primary cells isolated from native tissue to help improve our understanding of cell biology as well as investigate drug screening and toxicity (Jackson and Lu, 2016). Within a clinical setting, these cells can be classified as autologous (patient derived), allogeneic (donor derived), or xenogeneic (nonhuman derived). Examples include the use of chondrocytes for cartilage repair, keratinocytes and fibroblasts for skin repair and cardiac cells for heart patches. Although autologous cells are less likely to cause an immune response, their

availability depends on the tissue type, injury, or patient in question. In contrast, allogeneic and xenogeneic cells are more widely available but often suffer from immune rejection. Another potential complication is the possibility of the undesired dedifferentiation of cells during *in vitro* expansion, which should be avoided prior to any *in vivo* or clinical application. Although advanced reprogramming strategies and adult stem cells are a more efficient cell source, mature cell types are easier to use for translation because of their ease of availability and application.

- **Direct reprogrammed cells:** The process of direct reprogramming of cells, also known as transdifferentiation, circumvents the iPSC induction of the seed (original) cells and differentiates them directly into the target cell type. Reprogramming can occur via many ways such as transfection via small molecules, small RNAs, or proteins. Successful reprogramming of adult cells such as fibroblasts into neuronal cells cardiac progenitors, hepatocytes, and more has already been demonstrated (Qin et al., 2017). It can be argued that based on the method of reprogramming, this process is safer than that for iPSCs in terms of mitigating downstream epigenetic or mutagenic factors. Particularly during the miRNA-mediated direct conversion of human fibroblasts into neurons, nonneuronal cells were induced to be postmitotic, thus limiting the proliferation of cells that have not undergone full reprogramming (Lu and Yoo, 2018). In tissue engineering, direct reprogramming can be utilized as an alternative site-specific or patient-specific cell source with potential regenerative and clinical applications such as cardiac, renal, and neural tissue engineering. Extrinsic factors such as the 3D microenvironment, the substrate biomaterial, and scaffold fabrication method have also been shown to play a role in guiding cellular reprogramming (Lee et al., 2016). Although still in their early stages, these approaches are extremely promising for the availability and expansion of an ideal cell source for tissue-engineering-based clinical applications.

Further investigation is needed to identify the best source of cells for each tissue-engineering application. Multiple variables should be addressed in the selection of the best stem cell population, including: (1) stem cell accessibility (e.g., the isolation of autologous or allogenic neural stem cells is invasive and relatively difficult compared to other stem cells); (2) number of cells needed, where undesired differentiation during expansion has to be prevented; (3) proliferation capacity, where extra resources and expertise are needed for cells with limited proliferation; (4) differentiation profile; (5) cell population purity, depending on whether the cell source is a specific tissue or differentiated from pluripotent/stem cells, population homogeneity, and purity; (6) absence of random mutations that can potentially cause uncontrolled proliferation and tumors; and (7) ethical issues. In addition to primary cells, the intrinsic biological potential and performance of a cell can be modified by transient or permanent alteration of specific genes, often

accomplished with vectors created by modifying naturally occurring viruses such as retrovirus, lentivirus, adenovirus, or adeno-associated virus (Hannallah et al., 2003). There are several concerns for these approaches, such as transformation efficiency, safety of viral transfection, vector stability, and optimal function of the inserted genes. Nonviral transfection techniques have been developed to circumvent some of these issues; however, the long-term fate of these genetically modified cells still presents a potential risk.

The cell phenotype can also be regulated through manipulation of isolation and culture conditions. Although this may expand the available tools to manipulate cell characteristics, it can create more hurdles for consistently manufacturing high-quality cells. Rigorous characterization must be completed to ensure maintenance of cell phenotype, purity, and differentiation state. In addition, it is important to consider that cell culture may “activate” cells, altering their phenotype from those found *in situ*. Factors such as the ideal number of cells to be transplanted, the maximum number of times cells can be passaged, the maximum length of time cells should be maintained in culture, the ideal differentiated state of the cell (determined via phenotypic or genotypic expression) to produce a therapeutic effect, and the ideal cell storage conditions can significantly alter the outcome of a regenerative approach, and often need to be optimized on a case-by-case basis for specific animal models.

Materials

Biomaterials are used to develop scaffolds that provide a template for cells to organize and restore structure and function to damaged or dysfunctional tissues. The bioactive matrix provided by these materials presents well-defined biochemical (e.g., growth factors and surface chemistry) and biophysical (e.g., fibrous structure, hydrophilicity, and stiffness) cues to effectively regulate cellular behaviors such as attachment, migration, proliferation, and differentiation for restoring the functionality of damaged tissues. Biomaterials can, at the same time, be used to supply nutrients, drugs, and bioactive factors that direct specific tissue growth. Accordingly, the material should be nontoxic and be fully biocompatible upon degradation. Ideally, the material should also possess physicochemical and engineering properties suitable for the intended application and be compatible for further functionalization with bioactive molecules. Biomaterial scaffolds for tissue engineering are also discussed in more detail in [Chapter 2.6.3](#).

To accommodate these material requirements, the field of tissue engineering has witnessed tremendous development of new biomaterials over the past few decades. These materials are derived from both natural and synthetic sources and possess a broad spectrum of structural and functional properties that make them suitable for many clinical applications.

Natural materials: A wide range of natural-origin polymers, generally including proteins and polysaccharides, are

used as carriers for cells and bioactive molecules (Seyednejad et al., 2011). Natural materials are advantageous due to their inherent biological recognition through receptor–ligand interactions, cell-mediated proteolysis and remodeling, and low toxicity.

Protein-based natural polymers include collagen, gelatin, silk fibroin, fibrin, and elastin. Collagen is the most prevalent protein in the human body and offers both physical support and essential signals for cell anchorage, migration, proliferation, differentiation, and survival. As a result, collagen has been studied for engineering artificial skin (collagen IV), bone (collagen I), and cartilage (collagen II), resulting in several tissue-engineering products. For example, bilayered collagen gels seeded with human fibroblast and keratinocytes are used as a bioengineered artificial skin by Organogenesis, Inc. under the name of Apligraf. Collagraft (Angiotech Pharmaceuticals), a composite of fibrillar collagen, hydroxyapatite, and tricalcium phosphate, has also been approved by the Food and Drug Administration (FDA) as a biodegradable synthetic bone graft substitute. Gelatin is a natural polymer derived from collagen that has significantly lower antigenicity in contrast to collagen and has been used for engineering bone, cartilage, and skin. Gelatin is also well suited to serve as a carrier for bioactive molecules, including growth factors, cells, and drugs, and displays a useful gelation mechanism at low temperatures that is commonly utilized in extrusion-based 3D printing practices. Silk fibroin has received significant attention as a versatile natural polymer due to its high strength-to-weight ratio and slow degradation. Its semicrystalline structure and self-healing modifications (via cross-linking) make it an attractive material to include as part of a composite scaffold for tissue engineering. Another commonly used natural material is fibrin, the structural component of blood clots that provides a transitory matrix for cell migration during wound healing. Fibrin has been used as a matrix for studying the regeneration of numerous tissues, such as adipose, bone, cardiac, cartilage, muscle, nervous, ocular, respiratory, skin, tendons and ligaments, and vascular tissue, as well as a carrier vehicle for bioactive molecules. Elastin is an insoluble, high-elastic polymer that is a major component in vascular and lung tissue. It is a promising material for synthetic vascular grafts; however, its insolubility and its ability to elicit an immune response have limited its use.

Another class of natural polymers is polysaccharides that contain monosaccharide units joined together by glycosidic linkages (Celikkin et al., 2017). Several polysaccharides, including chitosan, hyaluronic acid (HA), and alginate, have been studied for tissue-engineering applications. Chitosan, the fully or partially deacetylated form of chitin found particularly in the shell of crustaceans, has attracted significant attention, due to its biocompatible properties, for regeneration of ligaments, muscle, skin, bone, cartilage, nerves, and for vascular grafts. Alginate, a polysaccharide derived from the cell wall of brown seaweed, is a widely utilized biomaterial due to its biocompatibility, mild and physical gelation process, chemical and physical cross-linking

abilities, nonthrombogenic nature, and the resemblance of its hydrogel matrix texture to that of the native extracellular matrix (ECM). Alginate happens to be easily modified into any form, such as microspheres, sponges, foams, elastomers, fibers, and hydrogels, thereby broadening the scope of application of this biomaterial. HA is a linear anionic polysaccharide, a member of the glycosaminoglycan family, and plays an important structural role in articular cartilage and skin tissues. Moreover, HA has been shown to promote both epithelial and mesenchymal cell migration and differentiation, regulate injury-induced inflammation as a free radical scavenger, and stimulate angiogenesis making it vital for tissue repair. Other commonly employed polysaccharides include starch, chondroitin sulfate, cellulose, and dextran.

Unfortunately, there are several limitations of natural materials, which include purification, cost, immunogenic responses, and lack of control over mechanical properties. There also exists the potential for a natural polymer to carry microbes or viruses. Although some of these disadvantages have been avoided through recombinant protein expression (Werkmeister and Ramshaw, 2012), synthetic biomaterials present a paradigm shift that overcomes many of these challenges while enabling custom-designed biomaterials. Natural materials are discussed in further detail in Chapter 1.3.6.

Decellularized extracellular matrix: Decellularizing tissues, a process that eliminates all cellular and nuclear materials with various detergents, and using the remaining matrix as building blocks for therapeutic purposes, has provided a facilitated approach that contains critical physical and chemical properties for site-specific tissue regeneration. The use of decellularized ECM from donor tissue has been utilized in the repair of skin bladder, heart valve, and small intestinal submucosa. In addition, several commercialized decellularized scaffolds have received FDA approval for use in humans, including dermis tissue (Alloderm; LifeCell), porcine heart valves (Synergraft; Cryolife), porcine urinary bladder (urinary bladder matrix; ACell), and processed nerve allografts (Axogen; Acell).

Decellularization of organs such as kidney, heart, lung, and liver has been documented and further seeding of functional parenchymal or stem cell populations onto these acellular three-dimensional (3D) biologic scaffolds provides the opportunity for direct connection to the patient's vasculature. Decellularized tissues have also been used as lyophilized powders that are incorporated into natural or synthetic hydrogels (Kuo et al., 2018a). This allows chemical cues to be present to influence the behavior of coencapsulated cells, and gives customizable shapes for the application of the scaffold. The process of decellularization is preferred in the use of donor grafts for regenerative purposes since allogeneic and xenogeneic antigens are usually recognized as foreign by the host and can either cause destructive inflammatory response or overt immune-mediated rejection. Though the type of tissue governs its decellularization process, a general protocol contains physical (mechanical agitation, freeze/thaw, sonication), enzymatic (trypsin, endonucleases, exonucleases), and chemical (alkaline/acid, hypotonic and hypertonic solutions,

EDTA/EGAT, Triton X-100, sodium dodecyl sulfate, deoxycholate, tri(*n*-butyl) phosphate) degradation steps (Brown et al., 2017). Since it is exceedingly difficult to rid of all cells in dense tissues, nearly all decellularization protocols result in residual DNA and other cytoplasmic and nuclear material. Additional applications of decellularized ECM are discussed in further detail in Chapter 1.3.6A.

Synthetic materials: Many synthetic polymers have been designed and fabricated for tissue-engineering purposes. Biodegradable synthetic polymers offer several advantages compared to natural materials such as controlled mechanical properties and degradation kinetics, easy processability into custom shapes and structures, and easy modification of the material for specific applications.

Saturated aliphatic polyesters, such as polylactide (PLA), polyglycolide (PGA), and poly(ϵ -caprolactone) (PCL), are the most commonly used biodegradable synthetic polymers for 3D scaffolds in tissue engineering (Seyednejad et al., 2011). The chemical properties of these polymers allow hydrolytic degradation, and the rate and extent of degradation depends on the polymer's molecular weight, structure, and composition. Polyesters have been widely used for scaffold construction because of their merits such as ease in synthesis, controllable degradable properties, and minimal inflammatory response. They have long been used in the clinic in the form of degradable sutures, but have more recently been used to mimic the aligned structures of native fibrous ECM in tissues (e.g., nerve, heart, skin, and tendon) with fibers ranging from several nanometers to several micrometers in diameter via electrospinning and 3D printing fabrication processes. A copolymer formulation of these two materials—poly(L-lactide-*co*-caprolactone)—has also been documented to improve the quality of regenerated cartilage tissue during microfracture when 3D printed into a scaffold that directs chondrocyte attachment and alignment (Guo et al., 2018a). Poly(lactide-*co*-glycolide) (PLGA) is another widely investigated copolymer formulation of PLA and PGA, and its properties can easily be tailored to its application. Specifically, with 25%–75% lactide composition, PLGA forms amorphous polymers, which are very hydrolytically unstable when compared to PCL. This allows for various degradation times depending on the ratio of lactidyl:glycolidyl used (50:50 can be degraded as quickly as 1–2 months, while 85:15 can sustain 5–6 months in vivo) (Ulery et al., 2011).

Poly(ortho esters) are hydrophobic, surface-eroding polymers, and their capacity to be used as tissue-engineering scaffolds is limited due to their weak mechanical properties and their capacity to induce a mild to moderate inflammatory response (Tschan et al., 2017). Alternatively, poly(propylene fumarate) (PPF) is a high-strength, elastic polymeric biomaterial that can be cross-linked through unsaturated bonds in its backbone. The polymer degradation is therefore dependent not only on its molecular weight and cross-linker, but also on the material's cross-linking density. For osteogenic tissue engineering, PPF can be mixed with ceramics such as hydroxyapatite or natural biomacromolecules like fibrin to create stronger, more bioactive scaffolds (Trachtenberg et al., 2017). Polyhydroxyalkanoates are semicrystalline isotactic polymers that

also undergo surface erosion and are excellent candidates for use in long-term tissue-engineering applications (Ulery et al., 2011). Elastomeric polyesters such as poly(glycerol sebacate) and poly(diols citrate) have shown significant promise as tissue-engineering biomaterials that mimic the mechanical properties of soft tissues.

Poly(anhydrides) are synthetic polymers developed from the condensation of diacids or a mixture of diacids. These polymers are biocompatible and have well-defined degradation characteristics. They were initially designed for drug-delivery applications due to their hydrophobicity and surface erosion that allowed a constant release profile for certain drugs. Several poly(anhydride) homopolymers and copolymers have been synthesized to control their degradation rate and mechanical properties. Polyurethanes are also favorable in tissue engineering because of their modifiable mechanical properties and biodegradability due to their segmented block structural character. These elastomers have also been developed as synthetic biomaterials for the regeneration of soft tissues, vasculature, and cartilage.

As the foregoing materials are used for the creation of dry, fibrous scaffolds, synthetic polymers can also be dissolved and chemically cross-linked in solution to form 3D hydrogel networks. Photopolymerizable groups are needed for the creation of these gels so that the matrix remains intact once submerged in *in vitro* culture. PEG, poly(*N*-isopropylacrylamide), poly(vinyl alcohol), and poly(acrylates) are examples of these materials, and upon exposure to ultraviolet radiation or cross-linking agents, these polymers can cross-link to form polymeric networks.

Biological Factors

Biomolecules are the next essential component of a tissue-engineered construct and an important part of the strategy to guide and regulate cell response, both *in vitro* and *in vivo*. They are the mediators of molecular signaling mechanisms and crosstalk between cells and their immediate microenvironment, with one biomolecule often serving multiple functionalities.

Type of biological factors: Biological factors satisfy a broad category, including hormones, cytokines, growth factors, ECM molecules, cell surface molecules, and nucleic acids. The temporal and spatial coordination of cellular processes is orchestrated by these signals from the extracellular environment (Lee, 2000). A large number of biomolecules have been explored to induce tissue regeneration and can be broadly categorized as follows (1) small molecules (e.g., corticosteroids, hormones) are used for intercellular and intracellular signaling by binding to specific protein receptors; (2) proteins and peptides act on the cells as mitogens, morphogens, growth factors, and cytokines where they bind to a target cell receptor, triggering an intracellular signal transduction and a biological response; and (3) oligonucleotides (DNA or RNA) can affect either gene transcription and/or translation or can be incorporated into the cell's genome. Cell-secreted biomolecules regulate cell–cell communication through

different mechanisms (endocrine, autocrine, paracrine, juxtacrine, intracrine) and have significant implications on the cell's response to its external environment.

Delivery and presentation of biological factors: The challenges and strategies to deliver these factors vary due to differences in their chemistry, biological response, as well as the scaffold biomaterial in question (Magin et al., 2016). Factors can be presented as soluble cues in vitro, where diffusive properties of the scaffold may be leveraged to further regulate cell response through autocrine–paracrine mechanisms (Mahadik et al., 2017), although controlling their release kinetics can be challenging. Several strategies exist for the encapsulation and release of biological factors, often via degradation of the scaffold or diffusive release of the agent. For example, researchers have demonstrated the delivery of vascular endothelial growth factor and platelet-derived growth factor for improved angiogenesis, and of dextrin-conjugated growth factors for neural stem cell culture. Additionally, controlling the spatiotemporal presentation of biomolecules via advanced fabrication methods (such as 3D printing) is particularly advantageous for complex tissues, e.g., multiple drug release from a single scaffold as an advanced drug delivery mechanism (Liu et al., 2016).

Biomolecules can also remain active when membrane bound or tethered to surfaces via immobilization techniques. Noncovalent association of the matrix components, e.g., glycosaminoglycans, can slowly release and potentiate binding to the cell membrane receptors (Sakiyama-Elbert, 2014). Alternatively, covalently bound growth factors can also influence cell behavior, such as the immobilized stem cell factor on hematopoietic stem cells (Mahadik et al., 2015), or the osteochondral differentiation of MSCs (Di Luca et al., 2017). A class of conjugation method known as “click” chemistry is widely used in tissue engineering for the functionalization of biomolecules (McKay and Finn, 2014). A subset of photocross-linkable thiol-ene chemistry is used extensively due to the high degree of spatial control and multiple conjugation offered by this technique. This is regularly used for biomolecule patterning within hydrogels, as well as for photo-controlled degradation for biomolecule release. In addition, cell adhesion on the scaffold can be controlled by the presentation of specific peptides and carbohydrates. In particular, a prototypical three amino acid sequence arginine–glycine–aspartic acid (RGD) is frequently found in many adhesion proteins and binds to many integrin receptors on cells. RGD peptide sequences have therefore been covalently immobilized on a synthetic material surface at a defined density and orientation to guide cell adhesion. Other sequences have also been successfully explored in the literature (Gao et al., 2017). Finally, the covalent immobilization of protease-sensitive cleavable linkages (i.e., matrix metalloproteinase [MMP]-sensitive links) on synthetic matrices mimics the native ECM, which can be used, in addition to soluble growth factors and other chemotactic cues, to guide migration of cells (Stevens et al., 2015).

Mechanochemical factors in tissue growth: The physical and/or chemical nature of the scaffold is an equally

important factor in regulating cell fate. Integrin-mediated cell adhesion to the ECM as well as the corresponding mechanotransduction signals facilitate cell response to their immediate microenvironment (Sun et al., 2016). Modifying the material surface chemistry can control many aspects of cell response such as adhesion, migration, and differentiation. Moreover, nanoscale geometry, surface topography, matrix size, and fiber alignment can also influence cell adhesion, proliferation, and migration. Altering surface topography leads to cytoskeletal reorganization, which directly influences molecular and biomechanical signals (Wu et al., 2017). Furthermore, mechanical forces exerted by the scaffold matrix and the elasticity of the material also influence cell fate. For instance, matrix stiffness in concert with surface chemistry regulates the differentiation of stem cells (Engler et al., 2006; Choi and Harley, 2012). This response is further enhanced via mechanical loading and cyclic or constant tension exposed to the scaffold, and consequently the cells, and is a strategy commonly used for engineering scaffolds for native tissues that are under constant stress (e.g., bone, cartilage, muscle, tendon etc.).

In conclusion, the physical environment, consisting of geometry, time-varying stress, strain, fluid flow, pressure, and potentially other biophysical parameters (e.g., osmotic pressure and electrical field), can regulate cell phenotype and tissue structure in a 3D environment.

Scaffold Design

Scaffolds act as the synthetic analog of the natural ECM. The role of scaffolds is to recapitulate the normal tissue development process by allowing cells to formulate their own microenvironment. The scaffold provides the necessary support for cells to attach, proliferate, and maintain their differentiated function and subsequent regeneration of new tissues. Ideally, a scaffold should have the following characteristics: (1) 3D highly porous structure with an interconnected pore network to facilitate cell/tissue growth and diffusion of nutrients, metabolic waste, and paracrine factors; (2) biodegradable or bioresorbable features with controllable degradation and resorption rates to match cell/tissue growth in vitro and in vivo; (3) suitable surface chemistry for cell attachment, proliferation, and differentiation; (4) mechanical properties to match those of the tissues at the site of implantation; and (5) easy processability to form a variety of shapes and sizes (O'Brien, 2011).

Conventionally fabricated scaffolds: The formation of a porous structure is the main goal of scaffold fabrication. Most methods for fabricating porous scaffolds, including particulate leaching, freeze drying, gas infusion, and phase separation, rely on casting the scaffold within molds with specific designs to create isotopically distributed interconnected pores. Porous structures can be developed by introducing particles or bubbles when the scaffold is solidified, which are later removed leaving behind an interconnected network of pores. Although these techniques are relatively simple for developing a 3D structure, they are limited by

uncontrolled pore size and connectivity, poor mechanical strength, and residual solvent/porogens. Hydrocarbon templating is a process where a polymer is dissolved in a solvent, mixed with a hydrocarbon porogen, compacted, immersed in a solvent to precipitate the porogen polymer solvent, and vacuum dried to create a porous foam (Shastri et al., 2000). This process has several advantages, including control over scaffold thickness and pore structure, although use of organic solvents is typically a disadvantage for biological applications as it is difficult to remove completely.

Hydrogel scaffolds: Hydrogels are commonly used as tissue-engineering scaffolds because of their ability to be formed into specific shapes based on their applications. They are typically cross-linked networks swollen in water that have the capability to encapsulate cells in a 3D network. The specific hydrogel material determines the particular cross-linking capabilities. Some hydrogels are cross-linked using light, while others may be cross-linked through heat, ionic bonding, or covalent bonding. Photocross-linkable hydrogels are polymerized into 3D networks in the presence of cross-linkers under ultraviolet or visible light radiation and are frequently used for cell encapsulation (Ferreira et al., 2007). By controlling the structure with defined cross-linking density, mechanical properties, mass transport, and degradation characteristics, the gels can be tuned for a range of applications. Hydrogels are an appealing 3D scaffold because they are structurally similar to the ECM of many tissues, can often be processed under relatively mild conditions, and may be delivered in a minimally invasive manner (Drury and Mooney, 2003). They can either be durable or biodegradable and are advantageous due to their high water content, facile transport properties, and controlled degradation kinetics. Furthermore, hydrogels can be chemically modified to improve the adhesion and proliferation of the cells on the gel matrices through inclusion of adhesion peptides. However, major problems with using hydrogels include poor mechanical properties that lead to their use in only soft and nonload-bearing tissues and difficulty in engineering complex tissues with multiple cell types due to unique ECM requirements.

Fiber-based scaffolds: Fibrous scaffold structures may be developed by electrospinning of polymers to generate continuous micro- or nanoscale diameter fibers. Electrospinning has the ability to mimic the ECM due to its ability to create nanofibers on the scale of naturally occurring collagen fibrils such as those in tendons and ligaments (Sensini and Cristofolini, 2018). Additionally, the orientation of fibers can be controlled during electrospinning to develop random or aligned fibers. Electrospun scaffolds are advantageous due to their high surface-to-volume ratio and structural similarity to natural ECM. Although it is possible to control the orientation of the fibers, it can be difficult to control the distance between fibers, an important factor that influences the migration of cells. Self-assembly of biopolymers, e.g., peptides and nucleic acids, using non-covalent interactions, including H-bonding, hydrophobic, electrostatic interactions, and van der Waals forces, has also

been used for scaffold development. The main advantage of such biopolymers is that their self-assembly relies on specific biorecognitions (e.g., DNA hybridization), which therefore make the formation of scaffold highly predictable and programmable. This type of fabrication has been used to create biocompatible fibers on the micro- or nanoscale and has the ability to enhance cell attachment (DeFrates et al., 2018). However, due to its self-assembly capabilities, the composition and size of these fibers can be difficult to regulate.

Additive manufacturing: 3D printing is a modern fabrication method where digital data of a 3D structure is converted into a physical object. In contrast to traditional fabrication methods (involving molds or solvents), 3D printing can create complex structures in a layer-by-layer fashion. Generally, a structure is first visualized digitally with the help of computer-aided software (such as SolidWorks and CreoParametric) and later sliced into individual layers by the specific printer software. Three major approaches for 3D bioprinting currently exist: inkjet printing, extrusion printing, and stereolithography. The chosen fabrication method will vary in terms of materials used, time required, and printing parameters used to develop the desired part. The following is a brief description of each major printing method, as well as its positives and pitfalls:

- **Inkjet printing:** Much like how a traditional printer utilizes ink cartridges to deliver droplets to paper to create documents, inkjet bioprinters can deliver biomaterials and/or cells in controlled small volumes. These printers have an extremely high resolution in bioink deposition (up to 50 μm) and the highest printing speeds (15–25 kHz) (Gudapati et al., 2016). However, droplets are synthesized through either thermal or mechanical means, which can perturb cells during the printing process. Instant heat exposure and shear stress can also induce cell damage. In addition, ink for this printer must be fluid so that droplets can form, which limits cell density of the ink (Skardal and Atala, 2015). As such, inkjet printing is best for two-dimensional (2D) tissues with relatively low cell density and complexity.
- **Extrusion printing:** This printing process extrudes continuous filaments of shear-thinning, thixotropic material (of which either biomacromolecules or cells are seeded) through a nozzle under pneumatic pressure. Though extrusion printing is an efficient and low-cost method for printing cell-encapsulated constructs, the printing resolution is limited by the print head's diameter, the viscosity of the biomaterial, and size of the incorporated biologic (Ozbolat and Hospodiuk, 2016). Shear-thinning biomaterials, in regard to strain rate or temperature-dependent properties, are limited as this fabrication process requires the material to maintain strand shape. Examples of inks compatible with this deposition method include gelatin, fibrin, alginate, HA mixtures, and silicate nanoplatelet mixtures (Panwar and Tan, 2016). The combination of multiple materials via different printing cartridges allows for facile engineering of chemically and structurally complex tissues.

- *Stereolithography*: A photopolymerizable material is printed layer by layer in this printing process. The light source, located directly below the printing platform, is instructed to focus at specific points in space to project a 2D mask with a specific light intensity that locally polymerizes the biomaterial. As the print progresses, the build platform moves up, and new masks are projected and cross-linked onto the existing shape. The overall print is complete when all mask layers have been projected and the material has been cross-linked into the desired 3D shape. Digital micromirror device-based printing is a similar platform in which an array of digitally controlled mirrors reflects light to create a 2D projection on a surface. Advantages of this process include the high precision able to be obtained by the light source, and that a 3D object of any desired shape can be made by changing the 2D projection over the height of the printing stage (Wang et al., 2017). One major disadvantage of this methodology is that only one material can be printed at a time.

Integration of Multiple Factors

The environment in which a particular cell resides in vivo, also known as its “niche” microenvironment, plays a significant role in determining cell functionality. This environment is composed of other cell types, the ECM proteins, and a host of biomolecules, with a high degree of crosstalk between all these components. In vitro, successful integration of the appropriate cells, scaffolds, soluble cues, and mechanochemical factors is key in regulating cell fate and ultimately regenerating a functional tissue. Hence, combinatorial approaches that recapitulate key components of this niche microenvironment are extremely important in tissue engineering, as well as to advance our basic understanding of cell biology. A number of studies have utilized this approach for tissue niche engineering, such as bone marrow (Torisawa et al., 2014), lung (Petersen et al., 2010), cardiac (Jang et al., 2017), and more (Donnelly et al., 2018; Kobolak et al., 2016), with promising results. However, static in vitro tissue-engineering systems often fail to consider the multiple factors that contribute to the healing and regeneration process. Thus it is necessary to understand the system as a whole through dynamic in vitro systems, such as bioreactors and relevant in vivo models.

Models for Tissue Engineering

Bioreactors

The traditional tissue-engineering approach of growing tissues on 2D surfaces (i.e., Petri dishes) or in 3D scaffolds is limited by mass transfer, since the diffusion of metabolites, oxygen, and carbon dioxide under static conditions can only support a certain thickness of tissue. Depending on the biomaterial, this limits the maximum thickness of a tissue-engineered construct to <250 μm from a media source (Martin and Vermette, 2005). Bioreactors are utilized in

in vitro culture to increase nutrient transfer by continuously mixing media and convectively transporting nutrients to cells, while higher rates of mass transfer provide improved oxygen influx and waste disposal, leading to improved cell seeding efficiency and proliferation. More importantly, dynamic in vivo conditions such as flow rate, oxygen tension, fluid shear stress, and the corresponding biomechanical signals can be recapitulated in vitro (Selden et al., 2018). Bioreactors are also instrumental in developing large-scale tissues for the purpose of biomanufacturing, where culture homogeneity and uniform cell response are critical elements in the industrial design (Kumar and Starly, 2015).

Types of bioreactors: Traditional industrial reactors such as the continuous stirred-tank reactor have been adapted as bioreactors in tissue engineering. In particular, the stirred-flask reactor improves reactor performance by agitating the media used for seeding scaffolds. Another system is the rotating wall vessel, which aims to minimize the shear stress and turbulence of previous approaches. This system was developed for cell culture experiments in space, and thus is often referred to as a microgravity reactor (Freed and Vunjak-Novakovic, 1997). Another interesting bioreactor is the hollow fiber reactor that permits the cultivation of highly sensitive cells such as hepatocytes. These reactors can introduce two different solutions to the tissue culture system that are optimized to either provide metabolites or remove waste products. Several commercial bioreactors exist on the market and have been investigated for good manufacturing practice-compliant scale-up. In perfusion-based bioreactors, culture medium is continuously perfused through the scaffold under pressure, allowing for nutrient exchange both within and without the scaffold. This system can increase the efficiency and uniformity of cell seeding and proliferation. The tubular perfusion system bioreactor designed by the Fisher lab is particularly suited for bead-based hydrogel culture and aggregation for osteochondral tissue engineering (Yeatts and Fisher, 2011; Nguyen et al., 2016). Finally, there are several other novel bioreactors designed specifically for particular tissues (Mori et al., 2017), or developed for targeted mechanistic studies (Lembong et al., 2018).

Limitations and challenges: While bioreactors have been shown to enhance uniformity of cell seeding and perfusion, reactor conditions such as mass transfer properties, mechanical environment, and hydrodynamics must be uniquely optimized for each tissue. Mathematical modeling and computational fluid dynamics simulations can be employed to help understand the complex interactions of these factors. However, there are several other limitations and considerations such as media costs for high-volume bioreactors, undesired shear stress or shear-induced biophysical response of cells, dynamic changes in the microenvironment due to cellular remodeling, difficulties in in situ monitoring for complex bioreactor setups, and limitations in nutrient transport for large tissue constructs. These limitations need to be addressed prior to employing bioreactors for their proposed tissue-engineering or clinical applications (Ravichandran et al., 2018).

Organoids

An advancement to the conventional 2D cell culture models, organoids are 3D systems that better mimic *in vivo* physiology and the tissue microenvironment. Though very important in basic *in vitro* imaging and drug applications, 2D cell culture systems are unable to reach the complexity of 3D cell–tissue organization, and lack tissue-specific architecture, cell–ECM interactions, and mechanical–biochemical cues (Jin et al., 2018). Colloquially termed “organ buds in a dish,” organoids are person-specific 3D cell cultures that mimic true *in vivo* microanatomy. Two forms of these models exist, where (1) tissue organoids containing epithelial cells can be formed by mechanically and enzymatically separating the primer organ into small tissue fragments, and (2) stem cell organoids are produced from ESCs, induced pluripotent stem cells, or organ-restricted adult stem cells (Jin et al., 2018). Several approaches in organoid production exist, such as (1) culturing cells atop feeder cells or ECM-coated surfaces, (2) hanging drop culture systems for embryoid bodies, and (3) use of serum-free floating culture of aggregates on low adhesion plates (Fang and Eglén, 2017). The main applications of organoids are drug testing as organ models (bone, kidney, brain, lung, bladder, colon, liver, intestine pancreas, mammary gland, esophagus, and prostate), and also disease models such as infectious (Zika), hereditary (cystic fibrosis), neurodegenerative (microcephaly), and cancer. Organoids are specifically ideal 3D *in vitro* systems of the tumor microenvironment, as they can contain a regional hypoxic core when created with rapidly dividing cancer cells. This hypoxic heterogeneity, a consequence of poor nutrients and oxygen supply, triggers the release of lactic acid as cells reach the incomplete oxidation pathway. Ultimately, the pH gradient formed can affect certain drug release profiles depending on its chemical nature as well as the cellular expression of genes controlling multiple drug resistance. Thus tumor organoids are very important in investigating signaling pathways involved in both chemotherapy sensitivity and cancer cell biology (Huang and Gao, 2018).

In Vivo Models

While *in vitro* development of tissues is the starting point of a tissue-engineered product, an appropriate *in vivo* model is crucial to validate the tissues' function. There exist many medical, legal, and ethical considerations when new biomedical products come to fruition, and thus intense preclinical investigations are needed before the product is available to the masses. Several factors need to be assessed in macroscale once the product is introduced to the host, for example, the role of angiogenesis in a newly created tissue, complex host immune reactions to the graft that could ignite inflammation and/or rejection, as well as functional considerations, such as innervation, rheological graft properties, or the effects of surgical

interventions (Muschler et al., 2010). The complexity of these factors makes it impossible to effectively evaluate the product *in vitro* and predict its success upon implantation. Since different animal models are used to investigate different tissue products, anatomical, physiological, and pathophysiological properties of the chosen species must be considered when determining the type of animal model. For example, small species such as mice and rabbits are used as models for critical-sized bone defects, as well as some larger species such as dogs and sheep. The pig remains the most popular large animal model due to similarities to humans in physiology, ease of availability, and relatively low cost, and is most commonly used in cardiovascular and skin pathologies/wounds research. Thus for any tissue-engineered product it is critical to analyze the outcomes of an *in vivo* study in the context of the model and its efficacy.

Applications of Tissue Engineering

Transplantation

Cell-free scaffolds: Another strategy involves *in situ* tissue regeneration by providing an instructive scaffold that can guide and control the regeneration process *in vivo* (Zhao and Karp, 2009). This process uses an artificial scaffold matrix that, once implanted, recruits host cells and relies on the body's innate regenerative ability. The scaffold recruits such cells through signal presentation. For example, transplantation of PEG–collagen matrices with enzyme cleavable MMP links that release bone morphogenic protein-2 (BMP-2) can promote regeneration of critical size bone defects effectively through invasion of the host cells. The absence of MMP-sensitive linkages and/or BMP-2 hindered the regeneration process, indicating that transplantation of scaffolds with appropriate soluble and insoluble signals is critical (Lutolf et al., 2003). Additionally, in cartilage defects, microfracture techniques that incorporated functionalization of 3D printed scaffolds functionalized with aggrecan have been shown to improve cartilage tissue regeneration with increased expression of type II collagen (Guo et al., 2018a). Thus the success of scaffold transplantation-based approaches largely depends on the appropriate presentation of signals to mediate host cell mobilization and coordination of the subsequent behavior of the cells, e.g., adherence, migration, and proliferation.

Cellular scaffolds: Scaffolds provide a substrate upon which cells attach, proliferate, and produce ECM within a predefined 3D orientation. However, it is also possible to incorporate cells into the scaffold directly with the aid of 3D printing and casting methods. Typically, this process allows cells to be integrated into the inner structure of the scaffold to diminish the need for cells to migrate on their own. One example of this is *in vitro* cell culture that incorporates multiple cell types and growth factors to prevascularize the scaffold prior to implantation (Kottamasu and Herman, 2018).

The main challenges for this strategy include: generating a complete functional tissue; preserving cell viability and function during transplantation; biological and mechanical integration with the surrounding tissue; and supplying oxygen and nutrients to the transplanted cells. The transplanted cells within the core of large defects often die before contributing to the healing process. Regardless, this strategy can be useful for transplantation of thin tissue grafts, such as corneal and skin grafts, where an immediate connection to the vascular system is not essential.

Replacing/Regenerating Target Organs

With clinical application being the primary focus of tissue engineering, investigators have attempted to engineer almost every mammalian tissue with varying degrees of success. The following section describes some key developments in organ engineering.

Skin: Tissue-engineered skin aims to restore barrier function for patients with severe trauma, e.g., burns, chronic wounds, ulcers, acute injuries, etc. Integra (Integra Life Sciences), one of many commercial products for skin regeneration (Table 2.6.2.1), is a collagen-based dermal graft aimed to improve tissue healing (Chu et al., 2002). Collagen, fibrin, HA, and PLGA are the main matrix components in most tissue grafts. Keratinocytes and fibroblasts are the primary cellular components of native skin and are investigated as the biological component (Vijayavenkataraman et al., 2016). To achieve effective healing, tissue-engineered skin must attach to the wound bed and avoid rejection by the immune system. Despite great success in engineering skin tissue, pitfalls include scar tissue formation, wound contraction, incomplete healing of deep wounds, lack of full recovery of skin function, and imperfect regeneration of skin components such as glands and hair follicles. Skin tissue-engineering applications are described further in Chapter 2.6.7.

Liver: Liver transplantation is end-stage treatment for many liver diseases. Several factors, including drug use, alcohol abuse, and viruses like hepatitis, can cause liver failure. Tissue engineering offers the potential for an engineered liver that can help address organ shortage and has two main strategies: (1) transplantation of suspended hepatocytes with ECM components, and (2) use of biodegradable scaffolds to provide a platform for hepatocyte attachment. Advancements in 3D printing offer us new strategies and avenues to recreate the biological and architectural complexity of the engineered tissue (Lee et al., 2016). However, because of challenges such as recapitulating the complex liver vasculature, relatively high volumetric oxygen consumption rate of the tissue, high cellular density, and long-term functionality regarding toxicity, efficacy, and infection, researchers are still far from developing a fully engineered, transplantable liver.

Heart: Cardiovascular disease is the leading cause of death in the United States and leads to damaged or malfunctioning cardiac tissue, resulting in arrhythmias and diminished

cardiac output. Tissue engineering is actively pursuing treatments for myocardial infarction, congenital heart defects, and stenotic valves through regenerating cardiac tissues (Hirt et al., 2014). Currently, heart valves are developed by transplanting autologous cells onto a scaffold, growing and maturing the cell-seeded scaffold, and finally transplanting the valves into the patient. Examples of heart valve scaffolds include decellularized heart valve ECM from donors or animals (Ott et al., 2008) and biomaterial-based heart valves designed from various natural and synthetic materials (collagen, fibrin, PLGA, and poly(hydroxy butyrate)). There are several successful applications of tissue-engineered heart valves for both in vitro and in vivo models. However, the complex metabolic, electrical, and mechanical nature of heart tissues continues to present a significant challenge to engineering myocardial tissues. Additional examples of cardiovascular tissue-engineering applications are described in Chapter 2.6.6.

Kidney: The current treatment for patients with end-stage renal disease is a kidney transplant. Although an established procedure, there is a constant shortage of donors with a median wait time for patients of up to 3.6 years and chances of host rejection and loss of functionality of the graft over time remain. Renal tissue engineering aims to restore kidney function, either by in situ regeneration of the damaged kidney with a cell-based approach or through the implantation of bioengineered grafts. The cell source can either be tissue-derived renal cells or differentiated stem cells such as ESCs, iPSCs, or amniotic fluid-derived stem cells (Moon et al., 2016). The anatomical and architectural complexity of the kidney poses challenges for whole organ engineering as the kidney consists of complex 3D tubular structures and multiple cell types. Consequently, the use of decellularized ECM from animal and human kidney is highly appealing as structure complexity, architecture, and biocompatibility are maintained. While this field continues to make tremendous progress, challenges such as poor in vivo integration, limited endothelialization, immunogenic response, and lack of consensus on the ideal cell type remain.

Orthopedic tissues: Musculoskeletal tissues such as bone, cartilage, and tendon are well researched in tissue engineering. Numerous clinical therapies are currently on the market for cartilage (e.g., MACI [Verical], Maix [Matrical], and Hyalograft [Fidia Advanced Biopolymers] (Vinatier and Guicheux, 2016)) and bone (e.g., Bio4 [Osiris Therapeutics], Bond Apatite [Augma Biomaterials], and TruGraft [Osteobiologics]). A primary challenge in bone tissue engineering is its unique architecture consisting of a mineralized, stiff cortical bone, a softer highly vascularized marrow, and distinct niche microenvironments. Although several inorganic-, polymeric-, and hybrid-based scaffolds have been examined to engineer bone, it has been difficult to develop a material that displays optimal mechanical properties and degradation kinetics for bone repair. Similarly, current treatments for cartilage defects, such as hyaline cartilage loss due to osteoarthritis, are microfracture and

TABLE 2.6.2.1 List of Commercially Available Tissue Engineering Products for Regenerative Applications

Tissue	Commercial Name	Scaffold Material	Cells	Manufacturer
Skin	Dermagraft	PGA and PLA fibers and silicon film	Fibroblasts	Advanced Biohealing, USA
	Apigraf	Bovine collagen	Keratinocytes and fibroblasts	Organogenesis, USA
	Orcel	Bovine collagen sponge	Keratinocytes and fibroblasts	Ortec International, USA
	TissueTech Autograft System (Laserskin and Hyalograft 3D)	Hyaluronic Acid	Keratinocytes and fibroblasts	Fidia Advanced Biopolymers, Italy
	Matriderm	Human acellular dermis	Keratinocytes and fibroblasts	Dr. Suwelack Skin & Health Care, Germany
	Alloderm	Human acellular dermis	none	LifeCell, USA
	FlexHD	Human acellular dermis	none	Ethicon, USA
	Allopatch HD	Human acellular dermis	none	Conmed, USA
	BellaDerm	Human acellular dermis	none	Musculoskeletal Transplantation Foundation, USA
	DermaMatrix	Human acellular dermis	none	Synthes, USA
	Epicel	Cultured epidermal autograft	Keratinocytes	Vericel, USA
	ReCell	none	Spray-On Cell suspension of keratinocytes	Avita, USA
	BioDFactor	Morselized, flowable tissue allograft derived from human placental tissues	none	Integra, USA
	GINTUIT	Bovine collagen	Allogeneic cultured keratinocytes and fibroblasts	Organogenesis Incorporated
	Grafix	Cryopreserved placental membrane	Neonatal mesenchymal stem cells, fibroblasts, and keratinocytes	Osiris, USA
Bone	Epidex	none	Autologous outer root sheath keratinocytes expanded into sheets	EuroDerm Biotech & Aesthetics, Germany
	EpiGraft	Cellulose film	none	Cuticell, USA
	Osteocele	Deminerlized human allograft bone	Human mesenchymal stem cells	NuVasive, USA
	AlloStem	Deminerlized human allograft bone	Allograft stem cells from human adipose tissue	AlloSource, USA
	Trinity/Trinity Evolution	Deminerlized human allograft bone	Human mesenchymal stem cells and osteoprogenitor cells	Orthofix, USA

TABLE 2.6.2.1 List of Commercially Available Tissue Engineering Products for Regenerative Applications—Cont'd

Tissue	Commercial Name	Scaffold Material	Cells	Manufacturer
Cartilage	MACI	Porcine collagen membrane	Autologous cultured chondrocytes	Vericel, USA
	Carticel	none	Autologous cultured chondrocytes directly injected into defect with Dulbecco's Modified Eagles Medium (DMEM)	Vericel, USA
	ChondroCelect	none	Autologous cultured chondrocytes cell suspension	TiGenix, Belgium
	BioSeed-C	Bioresorbable two-component gel-polymer scaffold	Autologous cultured chondrocytes	BioTissue, Switzerland
	DeNovoNT	Human particulated juvenile cartilage	Allogeneic chondrocytes	Zimmer, USA
	Co.don Chondrospheres	none	Autologous chondrocytes expanded in vitro and condensed into spheroids	co.don AG, Germany
	Cupistem	none	Autologous adipose-derived mesenchymal stem cell suspension	Anterogen, South Korea
	Cartistem	none	Allogeneic umbilical cord blood-derived mesenchymal stem cell suspension	Medipost, South Korea
Eye	Prokera	Amniotic membrane tissue	none	BioTissue, USA

autologous chondrocyte implantation, but their efficacy and long-term recovery are still limited. Cartilage tissue presents a unique challenge as it is largely acellular with low regenerative capacity, and it is a highly anisotropic structure with distinct zonal architecture, high elasticity, and strength. Several biomaterials both natural (collagen, fibrin, cellulose) and synthetic (PLA and PLGA) have been utilized for cartilage engineering. Currently, there are several ongoing clinical trials to determine the efficacy of MSCs for cartilage regeneration (Huang et al., 2016). To recapitulate the zonal architecture of the cartilage, researchers are also investigating the applications of 3D bioprinting for generating cartilage scaffolds. Despite all these efforts, development of a high-quality artificial cartilage as a long-term solution still evades researchers and this continues to be an area of active research. Orthopedic tissues are described in further detail in [Chapter 2.6.5](#).

In addition to the tissues already described, many other tissues such as pancreas, muscle, trachea, nervous system, tendon, ligament, placental barrier, cornea, gastrointestinal tract, and vocal cord have been targeted for regeneration by tissue-engineering strategies.

Drug Delivery

One important technique in regenerative medicine is the controlled delivery of therapeutic agents to achieve

targeted and sustained long-term effects. Localized delivery of growth factors and small molecules is known to have a significant impact on tissue regeneration and healing. For example, the bone regeneration process involves multiple stages of inflammation, vascularization, scar formation, and mineralization, with each stage being controlled by different growth factors and cytokines. Optimal wound recovery demands a localized dosage of the relevant biomolecules such as the incorporation of recombinant human bone morphogenic protein-2 on an absorbable collagen sponge carrier for bone grafts (InFUSE Medtronic) (McKay et al., 2007). Strategies for engineering the encapsulation of biomolecules and therapeutic compounds within biomaterials and with predefined release rates have been examined extensively in tissue engineering (Thambi et al., 2017; Rahman et al., 2018). 3D printing has also made a foray into drug delivery, with the FDA approving its first 3D printed drug Spritam (Aprecia Pharmaceuticals) in 2015 for seizures and epilepsy. Strategic printing and layered deposition of bioinks with multiple biomolecules enables control over the release profiles of different factors at different times from the same construct. The clinical impact of drug delivery in tissue-engineered scaffolds is enormous. Finally, novel therapies such as RNA delivery, in situ injectables, oral delivery systems for extended release, and biological carriers for drug delivery play an important role in pushing the boundaries of

regenerative medicine and improving the overall impact on patient life. Materials for drug delivery are discussed in detail in [Chapter 2.5.12](#).

Disease Models and Therapy

There are several nontraditional, yet useful and important applications of tissue-engineering strategies. In particular, the field of drug screening is in need of advanced *in vitro* methods for the assessment of the activity and toxicity of drugs before clinical studies are initiated. The development of synthetic tissue microfabrication has allowed for the opportunity to test drugs and/or other biological agents while analyzing system-level responses in real time. There have already been exciting examples of developed systems capable of mimicking organ-level functions and recapitulating disease etiology and progression, including engineered models of heart ([Ralphe and de Lange, 2013](#)), lung ([Chen et al., 2017](#)), intestine ([Kämpfer et al., 2017](#)), liver ([Broutier et al., 2017](#)), kidney ([Tiong et al., 2014](#)), cartilage ([Peck et al., 2018](#)), skin ([Danilenko et al., 2016](#)), placenta ([Arumugasaamy et al., 2018](#)), nervous systems ([Hopkins et al., 2015](#)), as well as models of infectious diseases and cancer ([Benam et al., 2015](#)). Many of these models are relatively simple; however, increasing the complex facets of the design can result in the creation of unique disease models. In the future, tissue-engineering-based drug testing and toxicity assays can provide an alternate strategy to reduce the use of *in vivo* animal testing. However, challenges remain since many diseases are chronic in nature and involve complex interactions between different organs.

The development of 3D tumor models has positively impacted the understanding of cancer progression and provides an exciting prospect in drug screening for patient-specific tumor types. Though valuable insights have been gained by traditional 2D stromal and cancer cell studies, they do not reflect the essential features of tumor tissues. For example, 2D cultures inaccurately display cell cytotoxicity of chemotherapeutic agents and low intensity radiation, since the treatment only needs to penetrate merely one single layer of cells to be effective. Furthermore, fundamental understanding of cancer metastasis cannot be obtained readily from the 2D studies because of the lack of spatial depth and cell connectivity, complex and dynamic cell–cell communications, and cell–matrix interactions that occur during cancer metastasis. Realizing the limitations of monolayer cultures, researchers have developed various 3D models that recapitulate certain features of solid tumor tissues such as tumor morphology, gradient distribution of chemical and biological factors, expression of proangiogenic and multidrug resistance proteins, and both dynamic and reciprocal interactions between the tumor and its stroma. With the advent of 3D models, the efficacy of therapeutic agents can be more rigorously tested in their ability to penetrate the core of the complex tumor microenvironment. In addition, numerous studies have provided compelling evidence that ECM remodeling is an essential component of the metastatic cascade in cancer ([Wittekind and Neid,](#)

[2005](#)). Hence, strategic integration of biological factors and engineering approaches have improved our understanding of tumor progression and invasion and support discovery of more personalized treatments for cancer patients.

Organ-On-a-Chip Systems

Microfluidic chip-based platforms enable a more sophisticated approach toward cell culture by engineering an environment more complex than the simple 2D substrates, yet simpler and more high throughput than complex 3D biomaterial platforms. It also enables constant perfusion of nutrients, and the relative ease of fabrication via soft lithography provides a high degree of control over all biochemical and biophysical aspects of the cell culture ([Bhatia and Ingber, 2014](#)). Each chip system transforms into a “mini” bioreactor where fluid flow can be regulated to study a broad range of cell responses. Several on-chip models such as lung-on-a-chip ([Benam et al., 2017](#)), gut-on-a-chip ([Jung Kim et al., 2013](#)), heart-on-a-chip ([Parsa et al., 2017](#)), and liver-on-a-chip ([Bhise et al., 2016](#)) have been demonstrated and continue to be improved upon. This field has also seen the commercialization of on-chip technologies with the establishment of companies such as Emulate Inc., Hesperos Inc., Tissue, Tara Biosystems, and many more.

Multiorgan-on-a-chip systems are extremely beneficial for *in vitro* absorption, distribution, metabolism, excretion, and toxicity studies ([Ishida, 2018](#)). These are used to evaluate the pharmacokinetics and pharmacodynamics of potential drug candidates to determine their safety, efficacy, and dosage. Although *in vivo* animal studies are the gold standard for pre-clinical trials, these studies are very expensive and time consuming. Consequently, multiorgan interconnected on-chip platforms ([Maschmeyer et al., 2015](#)) with human-derived cell sources offer a rapid, reliable way to screen a large number of drugs while being more relevant to clinical applications.

Current Challenges and Opportunities

Despite the excitement and early success, there are many hurdles to be addressed before tissue engineering reaches its eventual goal to treat millions of patients. In addition to efficacy, scale-up potential, reliability, established regulatory routes, and societal acceptance issues, there are many technical challenges to overcome. Some of the major challenges are discussed next.

Cell Source

As stated previously in this chapter, cells utilized in tissue-engineering applications may be in the form of autologous, allogeneic, or xenogeneic cells. Choosing the appropriate cell source for a particular tissue-engineering application has a significant impact on construct efficacy. In the case of allogeneic and xenogeneic cells, although the cell source is in abundance, patients suffer a higher chance of immune rejection of the graft because of the body’s inherent response of attacking

foreign cells or objects. For allogeneic transplants, factors such as human leukocyte antigen matching plays an important role in determining donor engraftment (Ruggeri et al., 2016). It is also important to monitor patient response to avoid fatal complications such as graft versus host disease. The ideal situation for patients would be the incorporation of personalized medicine in the form of patient-derived autologous cells. However, donor-site limitations and restrictions with cell expansion make this form of personalized medicine costly and time consuming.

It is also important to access reliable cell sources with a high degree of consistency for various applications. For example, when developing tissue models for disease modeling or drug screening, the cell source and phenotype must remain consistent across all studies, as well as be relevant to human clinical trials. We must also recognize that locally administered cells often die before significantly contributing to the healing response, either due to diffusion limitations of nutrients and oxygen or due to the dynamic in vivo environment. This significantly reduces the capacity for an exogenous cell source to contribute to the regenerative process. Finally, although stem cells are a promising cell source with a high proliferative and differentiation capacity, they suffer unique challenges. ESCs are fraught with several ethical concerns that limit their use in widespread applications. The recent development of iPSCs may replace embryo-derived ESCs. However, challenges such as low yields from the viral transfection techniques for iPSC generation and uncertainties in long-term effects of genetic modification have limited their application. Consequently, there is currently a plethora of ongoing research to develop highly efficient iPSC techniques (e.g., clustered regularly interspaced short palindromic repeats [CRISPR]) and understand downstream effects.

Vascularization

Vascularization, the growth of blood vessels, is a major engineering hurdle to overcome in creating artificial organs, particularly large-scale 3D tissues. It is critical to have effective transport of oxygen, nutrients, and removal of cell-secreted waste for the survival of cells in any environment. However, it is particularly important that cells are located within 250 μm of an oxygen source to thrive and function (Martin and Vermette, 2005). The lack of vascularization within tissue-engineered constructs is the major reason why most successful engineered organs are restricted to tissues, such as skin, cartilage, and ligament. For these tissues, thin layers of cells (e.g., one to two cell layers in skin tissue) that are well accessible to the blood vessels are sufficient and a proximal blood supply is not essential for survival. To effectively develop large-scale tissues, researchers must understand the formation of vasculature and develop methodologies to incorporate vasculature into their large tissue constructs. For these tissues and organs, several potential strategies exist to address the issue of vascularization. An increased knowledge of 3D scaffolding materials and research into the incorporation of angiogenic factors has shown progress toward vascularization. One popular idea for overcoming this challenge is prevascularization of the construct where a vascular network is developed prior

to implantation (Kottamasu and Herman, 2018). In addition, many researchers have utilized 3D bioprinting to print lumen-incorporated strands within predefined structures. Although these methods have shown promising results, more critical issues remain such as the development of complex vascular networks using scalable technology and the integration of these systems to the host vasculature.

Tissue Maturation

Commonly in tissue engineering, a complete 3D tissue is grown in vitro and is later implanted once it has reached “maturity.” Appropriate maturation of these scaffolds is very difficult to define since full in vitro regeneration of a tissue is challenging; many biological factors, systems, and actual presence of surrounding host tissue is needed to help recreate the complexity of certain tissues. Cells grown on 3D scaffolds in vitro can secrete biochemically appropriate ECM molecules yet can fail to acquire the appropriate tissue architecture. One way to address this challenge is to culture these grafts under compression, shear stresses, and pulsatile flow via a bioreactor. Such stresses have shown profound improvements in the mechanical properties of engineered tendon, cartilage, and cardiac muscle. Another major challenge is biomaterial longevity and its interactions with seeded cells. This is where material selection and scaffold engineering are crucial as the chosen biomaterial should display properties that match the cellular environment and remodeling rate.

In Vivo Integration

Once developed and fully matured in vitro, tissue-engineered constructs are implanted into the host where successful integration with the surrounding natural environment is of paramount importance. A poorly integrated scaffold often leads to impaired functionality within a few months. True integration can be achieved by designing smart templates made from biomaterials that also provide cues and signals to promote host cell migration and functional tissue connections. Scaffold porosity, pore network architecture, and surface roughness can drastically affect the diffusion of nutrients and cellular migration within the tissue-engineered construct (Bružauskaitė et al., 2016). Ideally, a scaffold’s mechanical properties should match those of the tissue being regenerated. However, care must be taken not to hamper the regeneration of proper functional tissue if nutrient diffusion and tissue necrosis occur. Thus scaffold physical cues should be engineered to mimic the mechanical properties with its surrounding environment without inhibiting necessary host cell infiltration.

Additionally, the host immune response is a factor that influences regeneration. The immune reaction to an implant begins with an acute response to the injury and innate recognition of foreign materials and continues with subsequent chronic immune response when specific recognition of antigens is stimulated. More specifically, polymorphonuclear neutrophils infiltrate the wound and release reactive oxygen species that not

only clear cellular debris, but can also result in rapid degradation of the biomaterial scaffold. Monocytes and fibroblasts that are recruited to the injury site also release inflammatory cytokines, which can cause secondary damage to the surrounding tissue. If the reaction is significant, it can lead to total rejection of the implant (Boehler et al., 2011). Strategies can be taken to modulate implant rejection, such as antiinflammatory cytokine release from the scaffold and immune cell recruitment and transplantation (Corradetti et al., 2017).

FDA Regulations for Clinical Translation

With the advancement of tissue engineering, a number of medical products and devices have been developed to address unmet clinical needs. Although preclinical research is important in developing new technologies, their application at the clinical stage must satisfy regulatory oversight at the government level. Each country in the world has its own regulatory agency that oversees this translation to ensure patient safety, such as the European Medicines Agency for the European Union, the FDA for the United States, etc. The approval of a biomedical product occurs in multiple rigorous stages of clinical trials starting with Phase I (safety and dosage assessment), Phase II (efficacy and side effects), Phase III (safety and adverse reactions), and Phase IV (post-approval assessment) (Witten et al., 2015).

The application of these regulations is highly regimented and well established for drug therapies. However, it becomes more challenging for multicomponent tissue-engineering products, biomedical devices, or 3D printed products where the safety and efficacy of each component and process have to be thoroughly examined (Morrison et al., 2015). Combination products under the FDA are treated as comprising two or more regulated components that are physically, chemically, or otherwise combined and produced as a single entity. For products that contain cells, biologics, and a scaffold matrix, product classification is determined by several factors such as the claimed mode of action, intended medical purpose, the active substance(s) and the way in which it is combined in the finished product (Hourd et al., 2015). Depending on the product in question, the process of FDA approval can take as long as 10 years and can differ for regulatory agencies throughout the world. For example, ReCell, a skin engineering product by Avita Medical, was introduced into clinical practice in the United Kingdom in 2005 (Gilleard et al., 2013), but received FDA approval in September 2018. However, the recently passed 21st Century Cures Act of December 2016 is intended to expedite the availability of novel therapies to patients in dire need and for compassionate use.

Gene Editing and CRISPR

Genome editing, or gene editing, is a toolkit that enables researchers to modify an organism's DNA by accurately targeting specific locations in the genome. These gene edits result in a cascade of downstream changes in transcription, protein expression, and eventually tissue and organ-level effects (Hsu

et al., 2014). Ever since the first documented procedure of cloning and recombinant DNA by Cohen et al., in 1973 (Cohen et al., 1973), this field has grown at an astronomical rate. Today, there are several tools available, capable of precise modifications to the DNA double strand, including meganuclease, zinc finger nuclease, transcription activator-like effector nuclease, and most recently CRISPR and CRISPR-associated protein 9 (Cas9). The CRISPR-Cas9 editing technique parallels the highly adaptive immune system of bacteria and was first demonstrated successfully in eukaryotic cells in 2013 independently by four different groups (Lander, 2016; Gupta and Musunuru, 2014).

In tissue engineering, gene editing and particularly CRISPR have been well explored for the generation of disease models and platforms for advanced drug screenings and relevant therapies. This is particularly useful toward strategies involving iPSCs because of their vast potential for differentiation and application for multiple tissue types. For example, Freedman et al. developed 3D spheroid models of human pluripotent stem cell-derived kidney cells to recapitulate aspects of the kidney niche, and used CRISPR genome editing to functionally model polycystic kidney disease within the spheroids (Freedman et al., 2015). It has also been applied for investigating cardiomyopathies where off-target effects and high-throughput screening models can be investigated. Although advances in gene editing and their corresponding applications to tissue engineering and disease modeling continue to be made, much of this progress is still at its research stage. There are significant regulatory hurdles and uncertainties associated with the long-term effects and unintended consequences for both iPSCs and CRISPR that need to be addressed. However, one can expect this research area to provide critical breakthroughs and clinical applications in the years to come.

Future Perspectives

Multiple challenges remain for the translation of tissue-engineered products to the clinic. Cell type, source, and manipulation are critical parameters that need to be further studied and defined to achieve the best clinical outcomes. In addition, many approaches are too complex for scale-up at a manufacturing level. Ideally, tissue-engineered products involving cells should be amenable to cryopreservation. It is also critical to consider that *in vivo* animal models may not adequately represent the human condition. Furthermore, it is still not clear how the FDA will regulate combination products. This significantly increases the risk for new companies to develop multicomponent systems.

Recent developments in the field such as those outlined in this chapter provide valuable tools and strategies for advancing tissue engineering. However, more quantitative approaches such as computational modeling and systems biology are needed to understand the mechanism of tissue development and regenerative processes. Although significant advances have been accomplished, most regenerative therapies are still in the developmental phase and require additional research and clinical trials to achieve effective cell differentiation and tissue formation necessary for clinical use.

References

- Arumugasaamy, N., Ettehadieh, L.E., Kuo, C.-Y., Paquin-Proulx, D., Kitchen, S.M., Santoro, M., Placone, J.K., Silveira, P.P., Aguiar, R.S., Nixon, D.F., Fisher, J.P., Kim, P.C.W., 2018. Biomimetic placenta-fetus model demonstrating maternal-fetal transmission and fetal neural toxicity of zika virus. *Ann. Biomed. Eng.* <https://doi.org/10.1007/s10439-018-2090-y>.
- Benam, K.H., Dauth, S., Hassell, B., Herland, A., Jain, A., Jang, K.-J., Karalis, K., Kim, H.J., MacQueen, L., Mahmoodian, R., Musah, S., Torisawa, Y., van der Meer, A.D., Villenave, R., Yadid, M., Parker, K.K., Ingber, D.E., 2015. Engineered in vitro disease models. *Annu. Rev. Pathol.* 10, 195–262. <https://doi.org/10.1146/annurev-pathol-012414-040418>.
- Benam, K.H., Mazur, M., Choe, Y., Ferrante, T.C., Novak, R., Ingber, D.E., 2017. Human Lung Small Airway-on-a-Chip Protocol. Humana Press, New York, NY, pp. 345–365. https://doi.org/10.1007/978-1-4939-7021-6_25.
- Bhatia, S.N., Ingber, D.E., 2014. Microfluidic organs-on-chips. *Nat. Biotechnol.* 32, 760–772. <https://doi.org/10.1038/nbt.2989>.
- Bhise, N.S., Manoharan, V., Massa, S., Tamayol, A., Ghaderi, M., Miscuglio, M., Lang, Q., Zhang, Y.S., Shin, S.R., Calzone, G., Annabi, N., Shupe, T.D., Bishop, C.E., Atala, A., Dokmeci, M.R., Khademhosseini, A., 2016. A liver-on-a-chip platform with bio-printed hepatic spheroids. *Biofabrication* 8, 14101. <https://doi.org/10.1088/1758-5090/8/1/014101>.
- Boehler, R.M., Graham, J.G., Shea, L.D., 2011. Tissue engineering tools for modulation of the immune response. *Biotechniques* 51. <https://doi.org/10.2144/000113754>. 239–40, 242, 244 passim.
- Broutier, L., Mastrogianni, G., Verstegen, M.M., Francies, H.E., Gavarró, L.M., Bradshaw, C.R., Allen, G.E., Arnes-Benito, R., Sidorova, O., Gaspersz, M.P., Georgakopoulos, N., Koo, B.-K., Dietmann, S., Davies, S.E., Praseedon, R.K., Lieshout, R., IJzermans, J.N.M., Wigmore, S.J., Saeb-Parsy, K., Garnett, M.J., van der Laan, L.J., Huch, M., 2017. Human primary liver cancer-derived organoid cultures for disease modeling and drug screening. *Nat. Med.* 23, 1424–1435. <https://doi.org/10.1038/nm.4438>.
- Brown, B.N., Buckenmeyer, M.J., Prest, T.A., 2017. Preparation of decellularized biological scaffolds for 3D cell culture. *Methods Mol. Biol.* 15–27. https://doi.org/10.1007/978-1-4939-7021-6_2.
- Bružauskaitė, I., Bironaitė, D., Bagdonas, E., Bernotienė, E., 2016. Scaffolds and cells for tissue regeneration: different scaffold pore sizes-different cell effects. *Cytotechnology* 68, 355–369. <https://doi.org/10.1007/s10616-015-9895-4>.
- Celikkin, N., Rinoldi, C., Costantini, M., Trombetta, M., Rainer, A., Świążkowski, W., 2017. Naturally derived proteins and glycosaminoglycan scaffolds for tissue engineering applications. *Mater. Sci. Eng. C* 78, 1277–1299. <https://doi.org/10.1016/j.msec.2017.04.016>.
- Chen, Y.-W., Huang, S.X., deCarvalho, A.L.R.T., Ho, S.-H., Islam, M.N., Volpi, S., Notarangelo, L.D., Ciancanelli, M., Casanova, J.-L., Bhattacharya, J., Liang, A.F., Palermo, L.M., Porotto, M., Moscona, A., Snoeck, H.-W., 2017. A three-dimensional model of human lung development and disease from pluripotent stem cells. *Nat. Cell Biol.* 19, 542–549. <https://doi.org/10.1038/ncb3510>.
- Choi, J.S., Harley, B.A.C., 2012. The combined influence of substrate elasticity and ligand density on the viability and biophysical properties of hematopoietic stem and progenitor cells. *Biomaterials*. <https://doi.org/10.1016/j.biomaterials.2012.03.010>.
- Chu, C.-S., McManus, A.T., Matylevich, N.P., Goodwin, C.W., Pruitt, B.A., 2002. Integra as a dermal replacement in a meshed composite skin graft in a rat model: a one-step operative procedure. *J. Trauma* 52, 122–129. <http://www.ncbi.nlm.nih.gov/pubmed/11791062> (accessed October 30, 2018).
- Cohen, S.N., Chang, A.C., Boyer, H.W., Helling, R.B., 1973. Construction of biologically functional bacterial plasmids in vitro. *Proc. Natl. Acad. Sci. U.S.A.* 70, 3240–3244. <http://www.ncbi.nlm.nih.gov/pubmed/4594039> (accessed October 28, 2018).
- Corradetti, B., Taraballi, F., Corbo, C., Cabrera, F., Pandolfi, L., Minardi, S., Wang, X., Van Eps, J., Bauza, G., Weiner, B., Tasciotti, E., 2017. Immune tuning scaffold for the local induction of a pro-regenerative environment. *Sci. Rep.* 7, 17030. <https://doi.org/10.1038/s41598-017-16895-0>.
- Danilenko, D.M., Phillips, G.D.L., Diaz, D., 2016. *In vitro* skin models and their predictability in defining normal and disease biology, pharmacology, and toxicity. *Toxicol. Pathol.* 44, 555–563. <https://doi.org/10.1177/0192623316632074>.
- DeFrates, K., Moore, R., Borgesi, J., Lin, G., Mulderig, T., Beachley, V., Hu, X., 2018. Protein-based fiber materials in medicine: a review. *Nanomaterials* 8, 457. <https://doi.org/10.3390/nano8070457>.
- Di Luca, A., Klein-Gunnewiek, M., Vancso, J.G., van Blitterswijk, C.A., Benetti, E.M., Moroni, L., 2017. Covalent binding of bone morphogenetic protein-2 and transforming growth factor- β 3 to 3D plotted scaffolds for osteochondral tissue regeneration. *Biotechnol. J.* 12, 1700072. <https://doi.org/10.1002/biot.201700072>.
- Donnelly, H., Salmeron-Sanchez, M., Dalby, M.J., 2018. Designing stem cell niches for differentiation and self-renewal. *J. R. Soc. Interface*. <https://doi.org/10.1098/rsif.2018.0388>.
- Drury, J.L., Mooney, D.J., 2003. Hydrogels for tissue engineering: scaffold design variables and applications. *Biomaterials*. [https://doi.org/10.1016/S0142-9612\(03\)00340-5](https://doi.org/10.1016/S0142-9612(03)00340-5).
- Engler, A.J., Sen, S., Sweeney, H.L., Discher, D.E., 2006. Matrix elasticity directs stem cell lineage specification. *Cell*. <https://doi.org/10.1016/j.cell.2006.06.044>.
- Fang, Y., Eglén, R.M., 2017. Three-dimensional cell cultures in drug discovery and development, SLAS discov. *Adv. Life Sci. R&D.* 22, 456–472. <https://doi.org/10.1177/1087057117696795>.
- Ferreira, L.S., Gerecht, S., Fuller, J., Shieh, H.F., Vunjak-Novakovic, G., Langer, R., 2007. Bioactive hydrogel scaffolds for controllable vascular differentiation of human embryonic stem cells. *Biomaterials*. <https://doi.org/10.1016/j.biomaterials.2007.01.021>.
- Freed, L.E., Vunjak-Novakovic, G., 1997. Microgravity Tissue Engineering, Society for in Vitro Biology. <https://link.springer.com/content/pdf/10.1007%2Fs11626-997-0009-2.pdf> (accessed October 27, 2018).
- Freedman, B.S., Brooks, C.R., Lam, A.Q., Fu, H., Morizane, R., Agrawal, V., Saad, A.F., Li, M.K., Hughes, M.R., Vander Werff, R., Peters, D.T., Lu, J., Baccei, A., Siedlecki, A.M., Valerius, M.T., Musunuru, K., McNagny, K.M., Steinman, T.I., Zhou, J., Lerou, P.H., Bonventre, J.V., 2015. Modelling kidney disease with CRISPR-mutant kidney organoids derived from human pluripotent epiblast spheroids. *Nat. Commun.* 6, 8715. <https://doi.org/10.1038/ncomms9715>.
- Gao, X., Lyu, S., Li, H., 2017. Decorating a blank slate protein hydrogel: a general and robust approach for functionalizing protein hydrogels. *Biomacromolecules* 18, 3726–3732. <https://doi.org/10.1021/acs.biomac.7b01369>.
- Gilleard, O., Segaren, N., Healy, C., 2013. Experience of ReCell in skin cancer reconstruction. *Arch. Plast. Surg.* 40, 627. <https://doi.org/10.5999/aps.2013.40.5.627>.
- Gudapati, H., Dey, M., Ozbolat, I., 2016. A comprehensive review on droplet-based bioprinting: past, present and future. *Biomaterials* 102, 20–42. <https://doi.org/10.1016/j.biomaterials.2016.06.012>.

- Guo, T., Noshin, M., Baker, H.B., Taskoy, E., Meredith, S.J., Tang, Q., Ringel, J.P., Lerman, M.J., Chen, Y., Packer, J.D., Fisher, J.P., 2018a. 3D printed biofunctionalized scaffolds for microfracture repair of cartilage defects. *Biomaterials* 185, 219–231. <https://doi.org/10.1016/j.BIOMATERIALS.2018.09.022>.
- Gupta, R.M., Musunuru, K., 2014. Expanding the genetic editing tool kit: ZFNs, TALENs, and CRISPR-Cas9. *J. Clin. Investig.* 124, 4154–4161. <https://doi.org/10.1172/JCI72992>.
- Hannallah, D., Peterson, B., Lieberman, J.R., Fu, F.H., Huard, J., 2003. Gene therapy in orthopaedic surgery. *Instr. Course Lect.* [https://doi.org/10.1016/0268-0890\(88\)90040-0](https://doi.org/10.1016/0268-0890(88)90040-0).
- Hernández, R.M., Orive, G., Murua, A., Pedraz, J.L., 2010. Microcapsules and microcarriers for in situ cell delivery. *Adv. Drug Deliv. Rev.* 62, 711–730. <https://doi.org/10.1016/j.ADDR.2010.02.004>.
- Hirt, M.N., Hansen, A., Eschenhagen, T., 2014. Cardiac tissue engineering: state of the art. *Circ. Res.* <https://doi.org/10.1161/CIRCRESAHA.114.300522>.
- Hopkins, A.M., DeSimone, E., Chwalek, K., Kaplan, D.L., 2015. 3D in vitro modeling of the central nervous system. *Prog. Neurobiol.* 125, 1–25. <https://doi.org/10.1016/j.pneurobio.2014.11.003>.
- Hourd, P., Medcalf, N., Segal, J., Williams, D.J., 2015. A 3D bioprinting exemplar of the consequences of the regulatory requirements on customized processes. *Regen. Med.* 10, 863–883. <https://doi.org/10.2217/rme.15.52>.
- Hsu, P.D., Lander, E.S., Zhang, F., 2014. Development and applications of CRISPR-cas9 for genome engineering. *Cell* 157, 1262–1278. <https://doi.org/10.1016/j.CELL.2014.05.010>.
- Huang, B.-W., Gao, J.-Q., 2018. Application of 3D cultured multicellular spheroid tumor models in tumor-targeted drug delivery system research. *J. Control. Release* 270, 246–259. <https://doi.org/10.1016/j.JCONREL.2017.12.005>.
- Huang, B.J., Hu, J.C., Athanasiou, K.A., 2016. Cell-based tissue engineering strategies used in the clinical repair of articular cartilage. *Biomaterials* 98, 1–22. <https://doi.org/10.1016/j.BIOMATERIALS.2016.04.018>.
- Hueso, M., Navarro, E., Sandoval, D., Cruzado, J.M., 2019. Progress in the development and challenges for the use of artificial kidneys and wearable dialysis devices. *Kidney Dis.* 5, 3–10. <https://doi.org/10.1159/000492932>.
- Ishida, S., 2018. Organs-on-a-chip: current applications and consideration points for in vitro ADME-Tox studies. *Drug Metab. Pharmacokinet.* 33, 49–54. <https://doi.org/10.1016/j.DMPK.2018.01.003>.
- Jackson, E.L., Lu, H., 2016. Three-dimensional models for studying development and disease: moving on from organisms to organs-on-a-chip and organoids. *Integr. Biol. (United Kingdom)*. <https://doi.org/10.1039/c6ib00039h>.
- Jang, J., Park, H.-J., Kim, S.-W., Kim, H., Park, J.Y., Na, S.J., Kim, H.J., Park, M.N., Choi, S.H., Park, S.H., Kim, S.W., Kwon, S.-M., Kim, P.-J., Cho, D.-W., 2017. 3D printed complex tissue construct using stem cell-laden decellularized extracellular matrix bioinks for cardiac repair. *Biomaterials* 112, 264–274. <https://doi.org/10.1016/j.BIOMATERIALS.2016.10.026>.
- Jin, M.-Z., Han, R.-R., Qiu, G.-Z., Ju, X.-C., Lou, G., Jin, W.-L., 2018. Organoids: an intermediate modeling platform in precision oncology. *Cancer Lett.* 414, 174–180. <https://doi.org/10.1016/j.CANLET.2017.11.021>.
- Jung Kim, H., Fraser, J.P., Shea, D.E., Khan, M., Bahinski, A., Hamilton, G.A., Huh, D., Ingber, D.E., 2013. Microfabrication of human organs-on-chips. *Nat. Protoc.* 8. <https://doi.org/10.1038/nprot.2013.137>.
- Kamaly, N., Yameen, B., Wu, J., Farokhzad, O.C., 2016. Degradable controlled-release polymers and polymeric nanoparticles: mechanisms of controlling drug release. *Chem. Rev.* 116, 2602–2663. <https://doi.org/10.1021/acs.chemrev.5b00346>.
- Kämpfer, A.A.M., Urbán, P., Gioria, S., Kanase, N., Stone, V., Kinser-Ovaskainen, A., 2017. Development of an in vitro co-culture model to mimic the human intestine in healthy and diseased state. *Toxicol. In Vitro* 45, 31–43. <https://doi.org/10.1016/j.tiv.2017.08.011>.
- Kim, Y.S., Smoak, M.M., Melchiorri, A.J., Mikos, A.G., 2019. An overview of the tissue engineering market in the United States from 2011 to 2018. *Tissue Eng. A.* <https://doi.org/10.1089/ten.tea.2018.0138>.
- Kobolak, J., Dinnyes, A., Memic, A., Khademhosseini, A., Mobasheri, A., 2016. Mesenchymal stem cells: identification, phenotypic characterization, biological properties and potential for regenerative medicine through biomaterial micro-engineering of their niche. *Methods* 99, 62–68. <https://doi.org/10.1016/j.YMETH.2015.09.016>.
- Kottamasu, P., Herman, I., 2018. Engineering a microcirculation for perfusion control of ex vivo-assembled organ systems: challenges and opportunities. *J. Tissue Eng.* 9. <https://doi.org/10.1177/2041731418772949>. 2041731418772949.
- Kumar, A., Starly, B., 2015. Large scale industrialized cell expansion: producing the critical raw material for biofabrication processes. *Biofabrication* 7. <https://doi.org/10.1088/1758-5090/7/4/044103>.
- Kuo, C.-Y., Guo, T., Cabrera-Luque, J., Arumugasamy, N., Bracaglia, L., Garcia-Vivas, A., Santoro, M., Baker, H., Fisher, J., Kim, P., 2018a. Placental basement membrane proteins are required for effective cytotrophoblast invasion in a three-dimensional bioprinted placenta model. *J. Biomed. Mater. Res. A* 106, 1476–1487. <https://doi.org/10.1002/jbm.a.36350>.
- Lander, E.S., 2016. The heroes of CRISPR. *Cell* 164, 18–28. <https://doi.org/10.1016/j.CELL.2015.12.041>.
- Langer, R., Vacanti, J.P., 1993. Tissue engineering. *Science* 80. <https://doi.org/10.1126/science.8493529>.
- Lee, S.J., 2000. Cytokine delivery and tissue engineering. *Yonsei Med. J.* <https://doi.org/10.3349/ymj.2000.41.6.704>.
- Lee, E.-S., Kim, S.H.L., Lee, H., Hwang, N.S., 2016. Non-viral approaches for direct conversion into mesenchymal cell types: potential application in tissue engineering. *J. Biomed. Mater. Res. B Appl. Biomater.* 104, 686–697. <https://doi.org/10.1002/jbm.b.33601>.
- Lee, J.W., Choi, Y.-J., Yong, W.-J., Pati, F., Shim, J.-H., Kang, K.S., Kang, I.-H., Park, J., Cho, D.-W., 2016. Development of a 3D cell printed construct considering angiogenesis for liver tissue engineering. *Biofabrication* 8, 015007. <https://doi.org/10.1088/1758-5090/8/1/015007>.
- Lembong, J., Lerman, M.J., Kingsbury, T.J., Civin, C.I., Fisher, J.P., 2018. A fluidic culture platform for spatially patterned cell growth, differentiation, and cocultures. *Tissue Eng. A.* <https://doi.org/10.1089/ten.tea.2018.0020>.
- Leyendecker Jr., A., Pinheiro, C.C.G., Amano, M.T., Bueno, D.F., 2018. The use of human mesenchymal stem cells as therapeutic agents for the in vivo treatment of immune-related diseases: a systematic review. *Front. Immunol.* 9, 2056. <https://doi.org/10.3389/fimmu.2018.02056>.
- Liu, Y.Y., Yu, H.C., Liu, Y., Liang, G., Zhang, T., Hu, Q.X., 2016. Dual drug spatiotemporal release from functional gradient scaffolds prepared using 3D bioprinting and electrospinning. *Polym. Eng. Sci.* <https://doi.org/10.1002/pen.24239>.
- Lu, Y.-L., Yoo, A.S., 2018. Mechanistic insights into MicroRNA-induced neuronal reprogramming of human adult fibroblasts. *Front. Neurosci.* 12, 522. <https://doi.org/10.3389/fnins.2018.00522>.

- Lutolf, M.P., Lauer-Fields, J.L., Schmoekel, H.G., Metters, A.T., Weber, F.E., Fields, G.B., Hubbell, J.A., 2003. Synthetic matrix metalloproteinase-sensitive hydrogels for the conduction of tissue regeneration: engineering cell-invasion characteristics. *Proc. Natl. Acad. Sci.* <https://doi.org/10.1073/pnas.0737381100>.
- Lysaght, M.J., Reyes, J., 2001. The growth of tissue engineering. *Tissue Eng.* <https://doi.org/10.1089/107632701753213110>.
- Magin, C.M., Alge, D.L., Anseth, K.S., 2016. Bio-inspired 3D microenvironments: a new dimension in tissue engineering. *Biomed. Mater.* 11, 022001. <https://doi.org/10.1088/1748-6041/11/2/022001>.
- Mahadik, B.P., Pedron Haba, S., Skertich, L.J., Harley, B.A., 2015. The use of covalently immobilized stem cell factor to selectively affect hematopoietic stem cell activity within a gelatin hydrogel. *Biomaterials* 67, 297–307. <https://doi.org/10.1016/j.biomaterials.2015.07.042>.
- Mahadik, B.P., Bharadwaj, N.A.K., Ewoldt, R.H., Harley, B.A.C., 2017. Regulating dynamic signaling between hematopoietic stem cells and niche cells via a hydrogel matrix. *Biomaterials*. <https://doi.org/10.1016/j.biomaterials.2017.02.013>.
- Martin, Y., Vermette, P., 2005. Bioreactors for tissue mass culture: design, characterization, and recent advances. *Biomaterials* 26, 7481–7503. <https://doi.org/10.1016/J.BIOMATERIALS.2005.05.057>.
- Maschmeyer, I., Lorenz, A.K., Schimek, K., Hasenberg, T., Ramme, A.P., Hübner, J., Lindner, M., Drewell, C., Bauer, S., Thomas, A., Sambo, N.S., Sonntag, F., Lauster, R., Marx, U., 2015. A four-organ-chip for interconnected long-term co-culture of human intestine, liver, skin and kidney equivalents. *Lab Chip*. <https://doi.org/10.1039/c5lc00392j>.
- McKay, C.S., Finn, M.G., 2014. Click chemistry in complex mixtures: bioorthogonal bioconjugation. *Chem. Biol.* 21, 1075–1101. <https://doi.org/10.1016/J.CHEMBIOL.2014.09.002>.
- McKay, W.F., Peckham, S.M., Badura, J.M., 2007. A comprehensive clinical review of recombinant human bone morphogenetic protein-2 (INFUSE® Bone Graft). *Int. Orthop.* 31(6), 729–734. <https://doi.org/10.1007/s00264-007-0418-6>.
- Menon, S., Shailendra, S., Renda, A., Longaker, M., Quarto, N., 2016. An overview of direct somatic reprogramming: the ins and outs of iPSCs. *Int. J. Mol. Sci.* 17. <https://doi.org/10.3390/ijms17010141>.
- Moon, K.H., Ko, I.K., Yoo, J.J., 2016. Kidney diseases and tissue engineering. *Methods* 99, 112–119. <https://doi.org/10.1016/J.YMETH.2015.06.020>.
- Mora, C., Serzanti, M., Consiglio, A., Memo, M., Dell’Era, P., 2017. Clinical potentials of human pluripotent stem cells. *Cell Biol. Toxicol.* 33, 351–360. <https://doi.org/10.1007/s10565-017-9384-y>.
- Mori, N., Morimoto, Y., Takeuchi, S., 2017. Skin integrated with perfusable vascular channels on a chip. *Biomaterials*. <https://doi.org/10.1016/j.biomaterials.2016.11.031>.
- Morrison, R.J., Kashlan, K.N., Flanagan, C.L., Wright, J.K., Green, G.E., Hollister, S.J., Weatherwax, K.J., 2015. Regulatory considerations in the design and manufacturing of implantable 3D-printed medical devices. *Clin. Transl. Sci.* 8, 594–600. <https://doi.org/10.1111/cts.12315>.
- Mosaad, Y.M., 2014. Hematopoietic stem cells: an overview. *Transfus. Apher. Sci.* <https://doi.org/10.1016/j.transci.2014.10.016>.
- Murua, A., Portero, A., Orive, G., Hernández, R.M., de Castro, M., Pedraz, J.L., 2008. Cell microencapsulation technology: towards clinical application. *J. Control. Release*. <https://doi.org/10.1016/j.jconrel.2008.08.010>.
- Muschler, G.F., Raut, V.P., Patterson, T.E., Wenke, J.C., Hollinger, J.O., 2010. The design and use of animal models for translational research in bone tissue engineering and regenerative medicine. *Tissue Eng. B Rev.* 16, 123–145. <https://doi.org/10.1089/ten.TEB.2009.0658>.
- Nachlas, A.L.Y., Li, S., Davis, M.E., 2017. Developing a clinically relevant tissue engineered heart valve-A review of current approaches. *Adv. Healthc. Mater.* 6, 1700918. <https://doi.org/10.1002/adhm.201700918>.
- Nguyen, B.-N.B., Ko, H., Moriarty, R.A., Etheridge, J.M., Fisher, J.P., 2016. Dynamic bioreactor culture of high volume engineered bone tissue. *Tissue Eng. A* 22, 263–271. <https://doi.org/10.1089/ten.tea.2015.0395>.
- Ott, H.C., Matthesen, T.S., Goh, S.-K., Black, L.D., Kren, S.M., Netoff, T.I., Taylor, D.A., 2008. Perfusion-decellularized matrix: using nature’s platform to engineer a bioartificial heart. *Nat. Med.* 14, 213–221. <https://doi.org/10.1038/nm1684>.
- Ozolat, I.T., Hospodiuk, M., 2016. Current advances and future perspectives in extrusion-based bioprinting. *Biomaterials* 76, 321–343. <https://doi.org/10.1016/j.biomaterials.2015.10.076>.
- O’Brien, F.J., 2011. Biomaterials & scaffolds for tissue engineering. *Mater. Today* 14, 88–95. [https://doi.org/10.1016/S1369-7021\(11\)70058-X](https://doi.org/10.1016/S1369-7021(11)70058-X).
- Panwar, A., Tan, L., 2016. Current status of bioinks for micro-extrusion-based 3D bioprinting. *Molecules* 21, 685. <https://doi.org/10.3390/molecules21060685>.
- Parsa, H., Wang, B.Z., Vunjak-Novakovic, G., 2017. A microfluidic platform for the high-throughput study of pathological cardiac hypertrophy. *Lab Chip* 17, 3264. <https://doi.org/10.1039/c7lc00415j>.
- Patzer, J.F., 2006. Advances in bioartificial liver assist devices. *Ann. N. Y. Acad. Sci.* 944, 320–333. <https://doi.org/10.1111/j.1749-6632.2001.tb03844.x>.
- Peck, Y., Leom, L.T., Low, P.F.P., Wang, D.-A., 2018. Establishment of an *in vitro* three-dimensional model for cartilage damage in rheumatoid arthritis. *J. Tissue Eng. Regenerat. Med.* 12, e237–e249. <https://doi.org/10.1002/term.2399>.
- Petersen, T.H., Calle, E.A., Zhao, L., Lee, E.J., Gui, L., Raredon, M.S.B., Gavrillov, K., Yi, T., Zhuang, Z.W., Breuer, C., Herzog, E., Niklason, L.E., 2010. Tissue-engineered lungs for *in vivo* implantation. *Science* 80. <https://doi.org/10.1126/science.1189345>.
- Qin, H., Zhao, A., Fu, X., 2017. Small molecules for reprogramming and transdifferentiation. *Cell. Mol. Life Sci.* 74, 3553–3575. <https://doi.org/10.1007/s00018-017-2586-x>.
- Rahman, S., Nagrath, M., Ponnusamy, S., Arany, P., Rahman, S.U., Nagrath, M., Ponnusamy, S., Arany, P.R., 2018. Nanoscale and macroscale scaffolds with controlled-release polymeric systems for dental craniomaxillofacial tissue engineering. *Materials* 11, 1478. <https://doi.org/10.3390/ma11081478>.
- Ralphe, J.C., de Lange, W.J., 2013. 3D engineered cardiac tissue models of human heart disease: learning more from our mice. *Trends Cardiovasc. Med.* 23, 27–32. <https://doi.org/10.1016/j.tcm.2012.08.007>.
- Rao, M., Ahrlund-Richter, L., Kaufman, D.S., 2012. Concise review: cord blood banking, transplantation and induced pluripotent stem cell: success and opportunities. *Stem Cells* 30, 55–60. <https://doi.org/10.1002/stem.770>.
- Ravichandran, A., Liu, Y., Teoh, S.-H., 2018. Review: bioreactor design towards generation of relevant engineered tissues: focus on clinical translation. *J. Tissue Eng. Regenerat. Med.* 12, e7–e22. <https://doi.org/10.1002/term.2270>.
- Ruggeri, A., Paviglianiti, A., Gluckman, E., Rocha, V., 2016. Impact of HLA in cord blood transplantation outcomes. *HLA*. <https://doi.org/10.1111/tan.12792>.

- Sakiyama-Elbert, S.E., 2014. Incorporation of heparin into biomaterials. *Acta Biomater.* 10, 1581–1587. <https://doi.org/10.1016/j.ACTBIO.2013.08.045>.
- Selden, C., Fuller, B., Selden, C., Fuller, B., 2018. Role of bioreactor technology in tissue engineering for clinical use and therapeutic target design. *Bioengineering* 5, 32. <https://doi.org/10.3390/bioengineering5020032>.
- Sensini, A., Cristofolini, L., 2018. Biofabrication of electrospun scaffolds for the regeneration of tendons and ligaments. *Materials* 11, 1963. <https://doi.org/10.3390/ma11101963>.
- Seyednejad, H., Ghassemi, A.H., van Nostrum, C.F., Vermonden, T., 2011. Functional aliphatic polyesters for biomedical and pharmaceutical applications. *J. Control. Release* 152, 168–176. <https://doi.org/10.1016/j.JCONREL.2010.12.016>.
- Shastri, V.P., Martin, I., Langer, R., 2000. Macroporous polymer foams by hydrocarbon templating. *Proc. Natl. Acad. Sci. U.S.A.* 97. <https://doi.org/10.1073/PNAS.97.5.1970>. 1970–5.
- Skardal, A., Atala, A., 2015. Biomaterials for integration with 3-D bioprinting. *Ann. Biomed. Eng.* 43, 730–746. <https://doi.org/10.1007/s10439-014-1207-1>.
- Song, C.G., Zhang, Y.Z., Wu, H.N., Cao, X.L., Guo, C.J., Li, Y.Q., Zheng, M.H., Han, H., 2018. Stem cells: a promising candidate to treat neurological disorders. *Neural. Regen. Res.* <https://doi.org/10.4103/1673-5374.235085>.
- Stevens, K.R., Miller, J.S., Blakely, B.L., Chen, C.S., Bhatia, S.N., 2015. Degradable hydrogels derived from PEG-diacrylamide for hepatic tissue engineering. *J. Biomed. Mater. Res. A* 103, 3331–3338. <https://doi.org/10.1002/jbm.a.35478>.
- Su, P., Tian, Y., Yang, C., Ma, X., Wang, X., Pei, J., Qian, A., 2018. Mesenchymal stem cell migration during bone formation and bone diseases therapy. *Int. J. Mol. Sci.* 19. <https://doi.org/10.3390/ijms19082343>.
- Sun, Z., Guo, S.S., Fässler, R., 2016. Integrin-mediated mechanotransduction. *J. Cell Biol.* <https://doi.org/10.1083/jcb.201609037>.
- Takahashi, K., Yamanaka, S., Zhang, Y., Li, Y., Feng, C., Li, X., Lin, L., Guo, L., Wang, H., Liu, C., Zheng, Y., Luo, C., Liu, Q., Wang, F., Sun, H., Liang, L., Li, L., Su, H., Chen, J., Pei, D., Zheng, H., Takahashi, K., Yamanaka, S., Nishikawa, S., Goldstein, R., Nierras, C., Li, M., Chen, M., Han, W., Fu, X., Ieda, M., Fu, J., Delgado-Olguin, P., Vedantham, V., Hayashi, Y., Bruneau, B., Vierbuchen, T., Ostermeier, A., Pang, Z., Kokubu, Y., Sudhof, T., Wernig, M., Xu, J., Du, Y., Deng, H., Torper, O., Pfisterer, U., Wolf, D., Pereira, M., Lau, S., Jakobsson, J., Xue, Y., Ouyang, K., Huang, J., Zhou, Y., Ouyang, H., Li, H., Guo, Z., Zhang, L., Wu, Z., Chen, Y., Wang, F., Chen, G., Hou, P., Li, Y., Zhang, X., Liu, C., Guan, J., Li, H., Wang, L., Wang, L., Huang, W., Su, H., Xue, Y., Su, Z., Li, X., Zuo, X., Jing, J., Ma, Y., Wang, J., Liu, D., Hu, W., Qiu, B., Guan, W., Wang, Q., Wang, M., Li, W., Kaeck, S., Banker, G., Weng, J., Du, X., Geng, S., Peng, Y., Wang, Z., Lu, Z., Panula, S., Pera, R.R., Wang, L., Wang, L., Huang, W., Su, H., Xue, Y., Su, Z., Su, H., Wang, L., Huang, W., Qin, D., Cai, J., Yao, X., Suh, H., Consiglio, A., Ray, J., Sawai, T., D'Amour, K., Gage, F., Baltus, G., Kowalski, M., Zhai, H., Tutter, A., Quinn, D., Wall, D., Halbach, O.B.U., Ng, T., Fortino, V., Pelaez, D., Cheung, H., 2006. Induction of pluripotent stem cells from mouse embryonic and adult fibroblast cultures by defined factors. *Cell.* <https://doi.org/10.1016/j.cell.2006.07.024>.
- Thambi, T., Li, Y., Lee, D.S., 2017. Injectable hydrogels for sustained release of therapeutic agents. *J. Control. Release* 267, 57–66. <https://doi.org/10.1016/j.JCONREL.2017.08.006>.
- Tiong, H.Y., Huang, P., Xiong, S., Li, Y., Vathsala, A., Zink, D., 2014. Drug-induced nephrotoxicity: clinical impact and pre-clinical *in vitro* models. *Mol. Pharm.* 11, 1933–1948. <https://doi.org/10.1021/mp400720w>.
- Torisawa, Y., Spina, C.S., Mammoto, T., Mammoto, A., Weaver, J.C., Tat, T., Collins, J.J., Ingber, D.E., 2014. Bone marrow-on-a-chip replicates hematopoietic niche physiology *in vitro*. *Nat. Methods* 11, 663–669. <https://doi.org/10.1038/nmeth.2938>.
- Trachtenberg, J.E., Placone, J.K., Smith, B.T., Fisher, J.P., Mikos, A.G., 2017. Extrusion-based 3D printing of poly(propylene fumarate) scaffolds with hydroxyapatite gradients. *J. Biomater. Sci. Polym. Ed.* 28, 532–554. <https://doi.org/10.1080/09205063.2017.1286184>.
- Tschan, M.J.-L., Jeong, N.S., Todd, R., Everson, J., Dove, A.P., 2017. Unlocking the potential of poly(*ortho* Ester)s: a general catalytic approach to the synthesis of surface-erodible materials. *Angew. Chem. Int. Ed.* 56, 16664–16668. <https://doi.org/10.1002/anie.201709934>.
- Ulery, B.D., Nair, L.S., Laurencin, C.T., 2011. Biomedical applications of biodegradable polymers. *J. Polym. Sci. B Polym. Phys.* 49, 832–864. <https://doi.org/10.1002/polb.22259>.
- Vacanti, C.A., 2006. History of tissue engineering and a glimpse into its future. *Tissue Eng.* <https://doi.org/10.1089/ten.2006.12.1137>.
- Vijayavenkataraman, S., Lu, W.F., Fuh, J.Y.H., 2016. 3D bioprinting of skin: a state-of-the-art review on modeling, materials, and processes. *Biofabrication.* <https://doi.org/10.1088/1758-5090/8/3/032001>.
- Vinatier, C., Guicheux, J., 2016. Cartilage tissue engineering: from biomaterials and stem cells to osteoarthritis treatments. *Ann. Phys. Rehabil. Med.* 59, 139–144. <https://doi.org/10.1016/J.REHAB.2016.03.002>.
- Wang, Z., Tian, Z., Jin, X., Holzman, J.F., Menard, F., Kim, K., 2017. Visible light-based stereolithography bioprinting of cell-adhesive gelatin hydrogels. In: 2017 39th Annu. Int. Conf. IEEE Eng. Med. Biol. Soc. IEEE, pp. 1599–1602. <https://doi.org/10.1109/EMBC.2017.8037144>.
- Werkmeister, J.A., Ramshaw, J.A.M., 2012. Recombinant protein scaffolds for tissue engineering. *Biomed. Mater.* 7, 012002. <https://doi.org/10.1088/1748-6041/7/1/012002>.
- Wittekind, C., Neid, M., 2005. Cancer invasion and metastasis. *Oncology* 69, 14–16. <https://doi.org/10.1159/000086626>.
- Witten, C.M., McFarland, R.D., Simek, S.L., 2015. Concise review: the U.S. Food and drug administration and regenerative medicine. *Stem Cells Transl. Med.* 4, 1495–1499. <https://doi.org/10.5966/sctm.2015-0098>.
- Wu, Y., Yang, Z., Law, J.B.K., He, A.Y., Abbas, A.A., Denslin, V., Kamarul, T., Hui, J.H., Lee, E.H., 2017. The combined effect of substrate stiffness and surface topography on chondrogenic differentiation of mesenchymal stem cells. *Tissue Eng. A* 23, 43–54. <https://doi.org/10.1089/ten.tea.2016.0123>.
- Yamanaka, S., 2008. Induction of pluripotent stem cells from mouse fibroblasts by four transcription factors. In: *Cell Prolif.* <https://doi.org/10.1111/j.1365-2184.2008.00493.x>.
- Yang, S., Leong, K.-F., Du, Z., Chua, C.-K., 2001. The design of scaffolds for use in tissue engineering. Part I. Traditional factors. *Tissue Eng.* 7, 679–689. <https://doi.org/10.1089/107632701753337645>.
- Yeatts, A.B., Fisher, J.P., 2011. Tubular perfusion system for the long-term dynamic culture of human mesenchymal stem cells. *Tissue Eng. C Methods* 17, 337–348. <https://doi.org/10.1089/ten.tec.2010.0172>.
- Zhao, W., Karp, J.M., 2009. Controlling cell fate *in vivo*. *Chembiochem.* <https://doi.org/10.1002/cbic.200900445>.

Further reading

General Introduction

History of Tissue Engineering

- Jaklenec, A., Stamp, A., Deweerd, E., Sherwin, A., Langer, R., 2012. Progress in the tissue engineering and stem cell industry Are we there yet? *Tissue Eng. B Rev.* <https://doi.org/10.1089/ten.teb.2011.0553>.
- Lysaght, M.J., Jaklenec, A., Deweerd, E., 2008. Great expectations: private sector activity in tissue engineering, regenerative medicine, and stem cell therapeutics. *Tissue Eng. A.* <https://doi.org/10.1089/tea.2007.0267>.
- Nerem, R.M., 2006. Tissue engineering: the hope, the hype, and the future. *Tissue Eng.* <https://doi.org/10.1089/ten.2006.12.1143>.

Goals of Tissue Engineering and Classification

Classification of Tissue-Engineering Approaches

Cell Therapy

- Campbell, A., Brieva, T., Raviv, L., Rowley, J., Niss, K., Brandwein, H., Oh, S., Karnieli, O., 2015. Concise review: process development considerations for cell therapy. *Stem Cells Transl. Med.* <https://doi.org/10.5966/sctm.2014-0294>.
- Cheuk, D.K., 2013. Optimal stem cell source for allogeneic stem cell transplantation for hematological malignancies. *World J. Transplant.* 3, 99. <https://doi.org/10.5500/wjt.v3.i4.99>.
- Muschler, G.F., Nakamoto, C., Griffith, L.G., 2004. Engineering principles of clinical cell-based tissue engineering. *J. Bone Jt. Surg. Ser. A.* <https://doi.org/10.2106/00004623-200407000-00029>.
- Mikkers, H.M., Freund, C., Mummery, C.L., Hoeben, R.C., 2014. Cell replacement therapies: is it time to reprogram? *Hum. Gene Ther.* <https://doi.org/10.1089/hum.2014.097>.

Components of Tissue Engineering

The Cell

ESCs

- Yousefi, A.M., James, P.F., Akbarzadeh, R., Subramanian, A., Flavin, C., Oudadesse, H., 2016. Prospect of stem cells in bone tissue engineering: a review. *Stem Cell. Int.* <https://doi.org/10.1155/2016/6180487>.

Adult Stem Cells

- Wang, L.-T., Ting, C.-H., Yen, M.-L., Liu, K.-J., Sytwu, H.-K., Wu, K.K., Yen, B.L., 2016. Human mesenchymal stem cells (mscs) for treatment towards immune- and inflammation-mediated diseases: review of current clinical trials. *J. Biomed. Sci.* 23, 76. <https://doi.org/10.1186/s12929-016-0289-5>.

iPSCs

- Ardeshiryajimi, A., 2017. Applied induced pluripotent stem cells in combination with biomaterials in bone tissue engineering. *J. Cell. Biochem.* 118, 3034–3042. <https://doi.org/10.1002/jcb.25996>.
- Boonkaew, B., Tapeng, L., Netsrithong, R., Vatanashevanopakorn, C., Pattanapanyasat, K., Wattanapanitch, M., 2018. Induced pluripotent stem cell line musii006-A derived from hair follicle keratinocytes as a non-invasive somatic cell source. *Stem Cell Res* 31, 79–82. <https://doi.org/10.1016/J.SCR.2018.07.007>.
- Gupta, S., Sharma, V., Verma, R.S., 2017. Recent advances in induced pluripotent stem cell (ipsc) based therapeutics. *J. Stem Cell Res. Ther.* 3. <https://doi.org/10.15406/jsrt.2017.03.00100>.
- Khan, M., Narayanan, K., Lu, H., Choo, Y., Du, C., Wiradharma, N., Yang, Y.-Y., Wan, A.C.A., 2013. Delivery of reprogramming factors into fibroblasts for generation of non-genetic induced pluripotent stem cells using a cationic bolaamphiphile as a non-viral vector. *Biomaterials* 34, 5336–5343. <https://doi.org/10.1016/J.BIOMATERIALS.2013.03.072>.

- Kim, H., Schaniel, C., 2018. Modeling hematological diseases and cancer with patient-specific induced pluripotent stem cells. *Front. Immunol.* 9, 2243. <https://doi.org/10.3389/fimmu.2018.02243>.
- Kimbrel, E.A., Lanza, R., 2016. Pluripotent stem cells: the last 10 years. *Regen. Med.* <https://doi.org/10.2217/rme-2016-0117>.
- Martins, A.M., Vunjak-Novakovic, G., Reis, R.L., 2014. The current status of ips cells in cardiac research and their potential for tissue engineering and regenerative medicine. *Stem Cell Rev* 10, 177–190. <https://doi.org/10.1007/s12015-013-9487-7>.
- Preskey, D., Allison, T.F., Jones, M., Mamchaoui, K., Unger, C., 2016. Synthetically modified mRNA for efficient and fast human ips cell generation and direct transdifferentiation to myoblasts. *Biochem. Biophys. Res. Commun.* 473, 743–751. <https://doi.org/10.1016/J.BBRC.2015.09.102>.
- Re, S., Dogan, A.A., Ben-Shachar, D., Berger, G., Werling, A.M., Walitza, S., Grünblatt, E., 2018. Improved generation of induced pluripotent stem cells from hair derived keratinocytes – a tool to study neurodevelopmental disorders as ADHD. *Front. Cell. Neurosci.* 12, 321. <https://doi.org/10.3389/fncel.2018.00321>.
- Wang, J., Gu, Q., Hao, J., Bai, D., Liu, L., Zhao, X., Liu, Z., Wang, L., 2013. Generation of induced pluripotent stem cells with high efficiency from human umbilical cord blood mononuclear cells. *Genom. Proteom. Bioinf.* 11, 304–311. <https://doi.org/10.1016/J.GPB.2013.08.002>.
- Wen, W., Zhang, J.-P., Xu, J., Su, R.J., Neises, A., Ji, G.-Z., Yuan, W., Cheng, T., Zhang, X.-B., 2016. Enhanced generation of integration-free iPSCs from human adult peripheral blood mononuclear cells with an optimal combination of episomal vectors. *Stem Cell Reports* 6, 873–884. <https://doi.org/10.1016/J.STEMCR.2016.04.005>.
- Xue, Y., Cai, X., Wang, L., Liao, B., Zhang, H., Shan, Y., Chen, Q., Zhou, T., Li, X., Hou, J., Chen, S., Luo, R., Qin, D., Pei, D., Pan, G., 2013. Generating a non-integrating human induced pluripotent stem cell bank from urine-derived cells. *PLoS One* 8, e70573. <https://doi.org/10.1371/journal.pone.0070573>.
- Yamanaka, S., Takahashi, K., Okita, K., Nakagawa, M., 2007. Induction of pluripotent stem cells from fibroblast cultures. *Nat. Protoc.* <https://doi.org/10.1038/nprot.2007.418>.
- Yoshioka, N., Gros, E., Li, H.-R., Kumar, S., Deacon, D.C., Maron, C., Muotri, A.R., Chi, N.C., Fu, X.-D., Yu, B.D., Dowdy, S.F., 2013. Efficient generation of human ipscs by a synthetic self-replicative RNA. *Cell Stem Cell.* 13, 246–254. <https://doi.org/10.1016/J.STEM.2013.06.001>.
- Zhou, T., Benda, C., Dunzinger, S., Huang, Y., Ho, J.C., Yang, J., Wang, Y., Zhang, Y., Zhuang, Q., Li, Y., Bao, X., Tse, H.-F., Grillari, J., Grillari-Voglauer, R., Pei, D., Esteban, M.A., 2012. Generation of human induced pluripotent stem cells from urine samples. *Nat. Protoc.* 7, 2080–2089. <https://doi.org/10.1038/nprot.2012.115>.

Mature Cells

- Cahill, T.J., Choudhury, R.P., Riley, P.R., 2017. Heart failure Heart regeneration and repair after myocardial infarction: translational opportunities for novel therapeutics. *Nat. Publ. Gr.* 16. <https://doi.org/10.1038/nrd.2017.106>.
- Duan, L., Ma, B., Liang, Y., Chen, J., Zhu, W., Li, M., Wang, D., 2015. Cytokine networking of chondrocyte dedifferentiation in vitro and its implications for cell-based cartilage therapy. *Am. J. Transl. Res.* 7, 194–208. <http://www.ncbi.nlm.nih.gov/pubmed/25901191>. (accessed October 23, 2018).
- Guo, R., Xu, X., Lu, Y., Xie, X., 2017. Physiological oxygen tension reduces hepatocyte dedifferentiation in in vitro culture. *Sci. Rep.* 7, 5923. <https://doi.org/10.1038/s41598-017-06433-3>.
- Klama-Baryła, A., Kitala, D., Łabuś, W., Kraut, M., Glik, J., Nowak, M., Kawecki, M., 2018. Autologous and allogeneic skin cell grafts

- in the treatment of severely burned patients: retrospective clinical study. *Transplant. Proc.* 50, 2179–2187. <https://doi.org/10.1016/J.TRANSPROCEED.2017.11.079>.
- Lange, J., Weil, F., Riegler, C., Groeber, F., Rebhan, S., Kurdyn, S., Alb, M., Kneitz, H., Gelbrich, G., Walles, H., Mielke, S., 2016. Interactions of donor sources and media influence the histomorphological quality of full-thickness skin models. *Biotechnol. J.* 11, 1352–1361. <https://doi.org/10.1002/biot.201600360>.
- Lee, J., Lee, J., Chae, B., Ahn, B., Ok, J., Yoon, K., Choi, J., 2017. Scaffold-free bead-type autologous chondrocyte implantation for cartilage repair – phase 1 clinical trial. *Osteoarthr. Cartil.* 25, S175–S176. <https://doi.org/10.1016/j.joca.2017.02.304>.
- Mihaela Micheu, M., Scafa-udriște, A., Dorobanțu, M., 2016. Bringing cardiac stem cell therapy from bench to bedside: lessons from the past and future perspectives. *Rom. J. Morphol. Embryol.* 57, 367–372. <http://www.rjme.ro/>. (accessed October 23, 2018).
- Ude, C.C., Seet, W.T., Sharen Aini, S., Aminuddin, B.S., Ruszymah, B.H.I., 2018. Shelf life evaluation of clinical grade chondrogenic induced aged adult stem cells for cartilage regeneration. *Sci. Rep.* 8, 4345. <https://doi.org/10.1038/s41598-018-22748-1>.
- Direct Reprogrammed Cells**
- Cairns, D.M., Chwalek, K., Moore, Y.E., Kelley, M.R., Abbott, R.D., Moss, S., Kaplan, D.L., 2016. Expandable and rapidly differentiating human induced neural stem cell lines for multiple tissue engineering applications. *Stem Cell Rep.* 7, 557–570. <https://doi.org/10.1016/j.stemcr.2016.07.017>.
- Dai, Y., Guo, Y., Wang, C., Liu, Q., Yang, Y., Li, S., Guo, X., Lian, R., Yu, R., Liu, H., Chen, J., 2014. Non-genetic direct reprogramming and biomimetic platforms in a preliminary study for adipose-derived stem cells into corneal endothelial-like cells. *PLoS One* 9, e109856. <https://doi.org/10.1371/journal.pone.0109856>.
- Ghiroldi, A., Piccoli, M., Ciconte, G., Pappone, C., Anastasia, L., 2017. Regenerating the human heart: direct reprogramming strategies and their current limitations. *Basic Res. Cardiol.* 112, 68. <https://doi.org/10.1007/s00395-017-0655-9>.
- Ho, L., Hsu, S., 2018. Cell reprogramming by 3D bioprinting of human fibroblasts in polyurethane hydrogel for fabrication of neural-like constructs. *Acta Biomater.* 70, 57–70. <https://doi.org/10.1016/j.actbio.2018.01.044>.
- Kaminski, M.M., Tosic, J., Pichler, R., Arnold, S.J., Lienkamp, S.S., 2017. Engineering kidney cells: reprogramming and directed differentiation to renal tissues. *Cell Tissue Res* 369, 185–197. <https://doi.org/10.1007/s00441-017-2629-5>.
- Li, Y., Dal-Pra, S., Mirosou, M., Jayawardena, T.M., Hodgkinson, C.P., Bursac, N., Dzau, V.J., 2016. Tissue-engineered 3-dimensional (3D) microenvironment enhances the direct reprogramming of fibroblasts into cardiomyocytes by microRNAs. *Sci. Rep.* 6, 38815. <https://doi.org/10.1038/srep38815>.
- Palazzolo, G., Quattrocchi, M., Toelen, J., Dominici, R., Anastasia, L., Tettamenti, G., Barthelemy, I., Blot, S., Gijsbers, R., Cassano, M., Sampaoli, M., 2016. Cardiac niche influences the direct reprogramming of canine fibroblasts into cardiomyocyte-like cells. *Stem Cells Int.* 2016 1–13. <https://doi.org/10.1155/2016/4969430>.
- Smith, A.W., Hoyne, J.D., Nguyen, P.K., McCreedy, D.A., Aly, H., Efimov, I.R., Rentschler, S., Elbert, D.L., 2013. Direct reprogramming of mouse fibroblasts to cardiomyocyte-like cells using Yamanaka factors on engineered poly(ethylene glycol) (PEG) hydrogels. *Biomaterials.* 34, 6559–6571. <https://doi.org/10.1016/j.biomaterials.2013.05.050>.
- Song, G., Pacher, M., Balakrishnan, A., Yuan, Q., Tsay, H.-C., Yang, D., Reetz, J., Brandes, S., Dai, Z., Pützer, B.M., Araúzo-Bravo, M.J., Steinemann, D., Luedde, T., Schwabe, R.F., Manns, M.P., Schöler, H.R., Schambach, A., Cantz, T., Ott, M., Sharma, A.D., 2016. Direct reprogramming of hepatic myofibroblasts into hepatocytes in vivo attenuates liver fibrosis. *Cell Stem Cell* 18, 797–808. <https://doi.org/10.1016/j.stem.2016.01.010>.
- Prigione, A., Mertens, J., Young, J.E., Caiazzo, M., Zhang, C.-L., Tang, Y., Liu, M.-L., Zang, T., 2017. Direct Reprogramming rather than ipsc-Based Reprogramming Maintains Aging Hallmarks in Human Motor Neurons. <https://doi.org/10.3389/fnmol.2017.00359>.
- Victor, M.B., Richner, M., Hermansteyne, T.O., Ransdell, J.L., Sobieski, C., Deng, P.-Y., Klyachko, V.A., Nerbonne, J.M., Yoo, A.S., 2014. Generation of human striatal neurons by microRNA-dependent direct conversion of fibroblasts. *Neuron* 84, 311–323. <https://doi.org/10.1016/j.neuron.2014.10.016>.
- Zhang, Y., Cao, N., Huang, Y., Spencer, C.I., Fu, J.-D., Yu, C., Liu, K., Nie, B., Xu, T., Li, K., Xu, S., Bruneau, B.G., Srivastava, D., Ding, S., 2016. Expandable cardiovascular progenitor cells reprogrammed from fibroblasts. *Cell Stem Cell.* 18, 368–381. <https://doi.org/10.1016/j.stem.2016.02.001>.
- Materials**
- Natural Materials**
- Bai, X., Gao, M., Syed, S., Zhuang, J., Xu, X., Zhang, X.-Q., 2018. Bioactive hydrogels for bone regeneration. *Bioact. Mater.* 3, 401–417. <https://doi.org/10.1016/j.bioactmat.2018.05.006>.
- Briganti, E., Spiller, D., Mirtelli, C., Kull, S., Counoupas, C., Losi, P., Senesi, S., Di Stefano, R., Soldani, G., 2010. A composite fibrin-based scaffold for controlled delivery of bioactive pro-angiogenic growth factors. *J. Control. Release.* 142, 14–21. <https://doi.org/10.1016/j.jconrel.2009.09.029>.
- de la Puente, P., Ludeña, D., 2014. Cell culture in autologous fibrin scaffolds for applications in tissue engineering. *Exp. Cell Res.* 322, 1–11. <https://doi.org/10.1016/j.yexcr.2013.12.017>.
- Doyle, A.D., Carvajal, N., Jin, A., Matsumoto, K., Yamada, K.M., 2015. Local 3D matrix microenvironment regulates cell migration through spatiotemporal dynamics of contractility-dependent adhesions. *Nat. Commun.* 6, 8720. <https://doi.org/10.1038/ncomms9720>.
- Gonzalez de Torre, I., Weber, M., Quintanilla, L., Alonso, M., Jockenhoevel, S., Rodríguez Cabello, J.C., Mela, P., 2016. Hybrid elastin-like recombinamer-fibrin gels: physical characterization and in vitro evaluation for cardiovascular tissue engineering applications. *Biomater. Sci.* 4, 1361–1370. <https://doi.org/10.1039/c6bm00300a>.
- Hemshkhar, M., Thushara, R.M., Chandranayaka, S., Sherman, L.S., Kemparaju, K., Girish, K.S., 2016. Emerging roles of hyaluronic acid bioscaffolds in tissue engineering and regenerative medicine. *Int. J. Biol. Macromol.* 86, 917–928. <https://doi.org/10.1016/j.ijbiomac.2016.02.032>.
- Kumar, V.A., Caves, J.M., Haller, C.A., Dai, E., Liu, L., Grainger, S., Chaikof, E.L., 2013. Acellular vascular grafts generated from collagen and elastin analogs. *Acta Biomater.* 9, 8067–8074. <https://doi.org/10.1016/j.actbio.2013.05.024>.
- Ligon, S.C., Liska, R., Stampff, J., Gurr, M., Mülhaupt, R., 2017. Polymers for 3D printing and customized additive manufacturing. *Chem. Rev.* 117, 10212–10290. <https://doi.org/10.1021/acs.chemrev.7b00074>.
- Logithkumar, R., KeshavNarayan, A., Dhivya, S., Chawla, A., Saravanan, S., Selvamurugan, N., 2016. A review of chitosan and its derivatives in bone tissue engineering. *Carbohydr. Polym.* 151, 172–188. <https://doi.org/10.1016/j.carbpol.2016.05.049>.
- Mir, M., Ali, M.N., Barakullah, A., Gulzar, A., Arshad, M., Fatima, S., Asad, M., 2018. Synthetic polymeric biomaterials for

- wound healing: a review. *Prog. Biomater.* 7, 1–21. <https://doi.org/10.1007/s40204-018-0083-4>.
- Miron, R.J., Fujioka-Kobayashi, M., Bishara, M., Zhang, Y., Hernandez, M., Choukroun, J., 2017. Platelet-rich fibrin and soft tissue wound healing: a systematic review. *Tissue Eng. B Rev.* 23, 83–99. <https://doi.org/10.1089/ten.TEB.2016.0233>.
- Noori, A., Ashrafi, S.J., Vaez-Ghaemi, R., Hatamian-Zaremi, A., Webster, T.J., 2017. A review of fibrin and fibrin composites for bone tissue engineering. *Int. J. Nanomed.* 12, 4937–4961. <https://doi.org/10.2147/IJN.S124671>.
- Pandolfi, V., Pereira, U., Dufresne, M., Legallais, C., 2017. Alginate-based cell microencapsulation for tissue engineering and regenerative medicine. *Curr. Pharmaceut. Des.* 23, 3833–3844. <https://doi.org/10.2174/1381612823666170609084016>.
- Rodríguez-Vázquez, M., Vega-Ruiz, B., Ramos-Zúñiga, R., Saldaña-Koppel, D.A., Quiñones-Olvera, L.F., 2015. Chitosan and its potential use as a scaffold for tissue engineering in regenerative medicine. *Biomed. Res. Int.* 1–15. 2015 <https://doi.org/10.1155/2015/821279>.
- Sack, B.S., Mauney, J.R., Estrada, C.R., 2016. Silk fibroin scaffolds for urologic tissue engineering. *Curr. Urol. Rep.* 17, 16. <https://doi.org/10.1007/s11934-015-0567-x>.
- Santoro, M., Tatara, A.M., Mikos, A.G., 2014. Gelatin carriers for drug and cell delivery in tissue engineering. *J. Control. Release* 190, 210–218. <https://doi.org/10.1016/j.jconrel.2014.04.014>.
- Sudha, P.N., Rose, M.H., 2014. Beneficial effects of hyaluronic acid. *Adv. Food Nutr. Res.* 137–176. <https://doi.org/10.1016/B978-0-12-800269-8.00009-9>.
- V Dorozhkin, S., 2015. Calcium orthophosphate-containing biocomposites and hybrid biomaterials for biomedical applications. *J. Funct. Biomater.* 6, 708–832. <https://doi.org/10.3390/jfb6030708>.
- Wang, D., Liu, H., Fan, Y., 2017. Silk fibroin for vascular regeneration. *Microsc. Res. Tech.* 80, 280–290. <https://doi.org/10.1002/jemt.22532>.
- Yanez, M., Rincon, J., Dones, A., De Maria, C., Gonzales, R., Boland, T., 2015. In vivo assessment of printed microvasculature in a bilayer skin graft to treat full-thickness wounds. *Tissue Eng. A* 21, 224–233. <https://doi.org/10.1089/ten.TEA.2013.0561>.
- Decellularized Extracellular Matrix**
- Badylak, S.F., Taylor, D., Uygun, K., 2011. Whole-organ tissue engineering: decellularization and recellularization of three-dimensional matrix scaffolds. *Annu. Rev. Biomed. Eng.* 13, 27–53. <https://doi.org/10.1146/annurev-bioeng-071910-124743>.
- Barakat, O., Abbasi, S., Rodriguez, G., Rios, J., Wood, R.P., Ozaki, C., Holley, L.S., Gauthier, P.K., 2012. Use of decellularized porcine liver for engineering humanized liver organ. *J. Surg. Res.* 173, e11–e25. <https://doi.org/10.1016/j.jss.2011.09.033>.
- Beaudoin Cloutier, C., Goyer, B., Perron, C., Guignard, R., Larouche, D., Moulin, V.J., Germain, L., Gauvin, R., Auger, F.A., 2017. In vivo evaluation and imaging of a bilayered self-assembled skin substitute using a decellularized dermal matrix grafted on mice. *Tissue Eng. A* 23, 313–322. <https://doi.org/10.1089/ten.TEA.2016.0296>.
- Bracaglia, L.G., Messina, M., Winston, S., Kuo, C.-Y., Lerman, M., Fisher, J.P., 2017. 3D printed pericardium hydrogels to promote wound healing in vascular applications. *Biomacromolecules* 18, 3802–3811. <https://doi.org/10.1021/acs.biomac.7b01165>.
- Chani, B., Puri, V., Sobti, R.C., Jha, V., Puri, S., 2017. Decellularized scaffold of cryopreserved rat kidney retains its recellularization potential. *PLoS One* 12, e0173040. <https://doi.org/10.1371/journal.pone.0173040>.
- Cheng, C.W., Solorio, L.D., Alsberg, E., 2014. Decellularized tissue and cell-derived extracellular matrices as scaffolds for orthopaedic tissue engineering. *Biotechnol. Adv.* 32, 462–484. <https://doi.org/10.1016/j.biotechadv.2013.12.012>.
- Cho, M.S., Rinker, B.D., Weber, R.V., Chao, J.D., Ingari, J.V., Brooks, D., Buncke, G.M., 2012. Functional outcome following nerve repair in the upper extremity using processed nerve allograft. *J. Hand Surg. Am.* 37, 2340–2349. <https://doi.org/10.1016/j.jhbsa.2012.08.028>.
- Daly, A.B., Wallis, J.M., Borg, Z.D., Bonvillain, R.W., Deng, B., Ballif, B.A., Jaworski, D.M., Allen, G.B., Weiss, D.J., 2012. Initial binding and recellularization of decellularized mouse lung scaffolds with bone marrow-derived mesenchymal stromal cells. *Tissue Eng. A* 18, 1–16. <https://doi.org/10.1089/ten.TEA.2011.0301>.
- Dohmen, P.M., Lembcke, A., Holinski, S., Pruss, A., Konertz, W., 2011. Ten years of clinical results with a tissue-engineered pulmonary valve. *Ann. Thorac. Surg.* 92, 1308–1314. <https://doi.org/10.1016/j.athoracsur.2011.06.009>.
- Gilbert, T.W., 2012. Strategies for tissue and organ decellularization. *J. Cell. Biochem.* 113, 2217–2222. <https://doi.org/10.1002/jcb.24130>.
- Glynn, J.J., Polsin, E.G., Hinds, M.T., 2015. Crosslinking decreases the hemocompatibility of decellularized, porcine small intestinal submucosa. *Acta Biomater.* 14, 96–103. <https://doi.org/10.1016/j.actbio.2014.11.038>.
- Groeber, F., Engelhardt, L., Lange, J., Kurdyn, S., Schmid, F.F., Rücker, C., Mielke, S., Waller, H., Hansmann, J., 2016. A first vascularized skin equivalent for as an alternative to animal experimentation. *ALTEX* 33, 415–422. <https://doi.org/10.14573/altex.1604041>.
- Kajbafzadeh, A.-M., Khorramirouz, R., Sabetkish, S., Ataei Talebi, M., Akbarzadeh, A., Keihani, S., 2016. In vivo regeneration of bladder muscular wall using decellularized colon matrix: an experimental study. *Pediatr. Surg. Int.* 32, 615–622. <https://doi.org/10.1007/s00383-016-3871-8>.
- Mendez, J.J., Ghaedi, M., Steinbacher, D., Niklason, L.E., 2014. Epithelial cell differentiation of human mesenchymal stromal cells in decellularized lung scaffolds. *Tissue Eng. A* 20, 1735–1746. <https://doi.org/10.1089/ten.TEA.2013.0647>.
- Parmaksiz, M., Elçin, A.E., Elçin, Y.M., 2017. Decellularization of bovine small intestinal submucosa. *Methods Mol. Biol.* https://doi.org/10.1007/7651_2017_33.
- Pati, F., Ha, D.-H., Jang, J., Han, H.H., Rhie, J.-W., Cho, D.-W., 2015. Biomimetic 3D tissue printing for soft tissue regeneration. *Biomaterials* 62, 164–175. <https://doi.org/10.1016/j.biomaterials.2015.05.043>.
- Theodoridis, K., Tudorache, I., Calistru, A., Cebotari, S., Meyer, T., Sarikouch, S., Bara, C., Brehm, R., Haverich, A., Hilfiker, A., 2015. Successful matrix guided tissue regeneration of decellularized pulmonary heart valve allografts in elderly sheep. *Biomaterials* 52, 221–228. <https://doi.org/10.1016/j.biomaterials.2015.02.023>.
- VeDepo, M.C., Detamore, M.S., Hopkins, R.A., Converse, G.L., 2017. Recellularization of decellularized heart valves: progress toward the tissue-engineered heart valve. *J. Tissue Eng.* 8. <https://doi.org/10.1177/2041731417726327>. 2041731417726327.
- Wagner, D.E., Bonenfant, N.R., Parsons, C.S., Sokocevic, D., Brooks, E.M., Borg, Z.D., Lathrop, M.J., Wallis, J.D., Daly, A.B., Lam, Y.W., Deng, B., DeSarno, M.J., Ashikaga, T., Loi, R., Weiss, D.J., 2014. Comparative decellularization and recellularization of normal versus emphysematous human lungs. *Biomaterials* 35, 3281–3297. <https://doi.org/10.1016/j.biomaterials.2013.12.103>.
- Zhang, Q., Johnson, J.A., Dunne, L.W., Chen, Y., Iyyanki, T., Wu, Y., Chang, E.I., Branch-Brooks, C.D., Robb, G.L., Butler, C.E.,

2016. Decellularized skin/adipose tissue flap matrix for engineering vascularized composite soft tissue flaps. *Acta Biomater.* 35, 166–184. <https://doi.org/10.1016/j.actbio.2016.02.017>.
- Zhu, W., Xu, Y., Feng, C., Fu, Q., Song, L., Cui, L., 2010. Bladder reconstruction with adipose-derived stem cell-seeded bladder acellular matrix grafts improve morphology composition. *World J. Urol.* 28, 493–498. <https://doi.org/10.1007/s00345-010-0508-8>.
- Synthetic Materials**
- Cameron, D.J.A., Shaver, M.P., 2011. Aliphatic polyester polymer stars: synthesis, properties and applications in biomedicine and nanotechnology. *Chem. Soc. Rev.* 40, 1761–1776. <https://doi.org/10.1039/C0CS00091D>.
- Ganta, S.R., Piesco, N.P., Long, P., Gassner, R., Motta, L.F., Papworth, G.D., Stolz, D.B., Watkins, S.C., Agarwal, S., 2003. Vascularization and tissue infiltration of a biodegradable polyurethane matrix. *J. Biomed. Mater. Res. A.* 64, 242–248. <https://doi.org/10.1002/jbm.a.10402>.
- Guan, X., Avci-Adali, M., Alarçin, E., Cheng, H., Kashaf, S.S., Li, Y., Chawla, A., Jang, H.L., Khademhosseini, A., 2017. Development of hydrogels for regenerative engineering. *Biotechnol. J.* 12. <https://doi.org/10.1002/biot.201600394>.
- Gyawali, D., Tran, R.T., Guleserian, K.J., Tang, L., Yang, J., 2010. Citric-acid-derived photo-cross-linked biodegradable elastomers. *J. Biomater. Sci. Polym. Ed.* 21, 1761–1782. <https://doi.org/10.1163/092050609X12567178204169>.
- Hagandora, C.K., Gao, J., Wang, Y., Almarza, A.J., 2013. Poly (glycerol sebacate): a novel scaffold material for temporomandibular joint disc engineering. *Tissue Eng. A.* 19, 729–737. <https://doi.org/10.1089/ten.tea.2012.0304>.
- Jeffries, E.M., Allen, R.A., Gao, J., Pesce, M., Wang, Y., 2015. Highly elastic and suturable electrospun poly(glycerol sebacate) fibrous scaffolds. *Acta Biomater.* 18, 30–39. <https://doi.org/10.1016/j.actbio.2015.02.005>.
- Jin, G., He, R., Sha, B., Li, W., Qing, H., Teng, R., Xu, F., 2018. Electrospun Three-Dimensional Aligned Nanofibrous Scaffolds for Tissue Engineering. <https://doi.org/10.1016/j.msec.2018.06.065>.
- Kamaly, N., Yameen, B., Wu, J., Farokhzad, O.C., 2016. Degradable controlled-release polymers and polymeric nanoparticles: mechanisms of controlling drug release. *Chem. Rev.* 116, 2602–2663. <https://doi.org/10.1021/acs.chemrev.5b00346>.
- Kucińska-Lipka, J., Gubańska, I., Janik, H., 2013. Gelatin-modified polyurethanes for soft tissue scaffold. *Scient. World J.* 2013, 450132. <https://doi.org/10.1155/2013/450132>.
- Mishra, R., Roux, B.M., Posukonis, M., Bodamer, E., Brey, E.M., Fisher, J.P., Dean, D., 2016. Effect of prevascularization on in vivo vascularization of poly(propylene fumarate)/fibrin scaffolds. *Biomaterials* 77, 255–266. <https://doi.org/10.1016/j.biomaterials.2015.10.026>.
- Nalluri, S.M., Krishnan, G.R., Cheah, C., Arzumand, A., Yuan, Y., Richardson, C.A., Yang, S., Sarkar, D., 2015. Hydrophilic polyurethane matrix promotes chondrogenesis of mesenchymal stem cells. *Mater. Sci. Eng. C. Mater. Biol. Appl.* 54, 182–195. <https://doi.org/10.1016/j.msec.2015.05.043>.
- Ouimet, M.A., Griffin, J., Carbone-Howell, A.L., Wu, W.-H., Stebbins, N.D., Di, R., Uhrich, K.E., 2013. Biodegradable ferulic acid-containing poly(anhydride-ester): degradation products with controlled release and sustained antioxidant activity. *Biomacromolecules* 14, 854–861. <https://doi.org/10.1021/bm3018998>.
- Schmeltzer, R.C., Uhrich, K.E., 2006. Synthesis and characterization of salicylic acid-based poly(anhydride-ester) copolymers. *J. Bioact. Compat. Polym.* 21, 123–133. <https://doi.org/10.1177/0883911506062976>.
- Sharifpoor, S., Simmons, C.A., Labow, R.S., Santerre, J.P., 2010. A study of vascular smooth muscle cell function under cyclic mechanical loading in a polyurethane scaffold with optimized porosity. *Acta Biomater.* 6, 4218–4228. <https://doi.org/10.1016/J.ACTBIO.2010.06.018>.
- Shirazaki, P., Varshosaz, J., Kharazi, A.Z., 2017. Electrospun gelatin/poly(glycerol sebacate) membrane with controlled release of antibiotics for wound dressing. *Adv. Biomed. Res.* 6, 105. https://doi.org/10.4103/abr.abr_197_16.
- Song, R., Murphy, M., Li, C., Ting, K., Soo, C., Zheng, Z., 2018. Current development of biodegradable polymeric materials for biomedical applications. *Drug Des. Dev. Ther.* 12, 3117–3145. <https://doi.org/10.2147/DDDT.S165440>.
- Tallawi, M., Zebrowski, D.C., Rai, R., Roether, J.A., Schubert, D.W., El Fray, M., Engel, F.B., Aifantis, K.E., Boccaccini, A.R., 2015. Poly(glycerol sebacate)/poly(butylene succinate-butylene dilinoleate) fibrous scaffolds for cardiac tissue engineering. *Tissue Eng. C Methods* 21, 585–596. <https://doi.org/10.1089/ten.TEC.2014.0445>.
- Tran, R.T., Wang, L., Zhang, C., Huang, M., Tang, W., Zhang, C., Zhang, Z., Jin, D., Banik, B., Brown, J.L., Xie, Z., Bai, X., Yang, J., 2014. Synthesis and characterization of biomimetic citrate-based biodegradable composites. *J. Biomed. Mater. Res. A.* 102, 2521–2532. <https://doi.org/10.1002/jbm.a.34928>.
- Tran, R.T., Yang, J., Ameer, G.A., 2015. Citrate-based biomaterials and their applications in regenerative engineering. *Annu. Rev. Mater. Res.* 45, 277–310. <https://doi.org/10.1146/annurev-matsci-070214-020815>.
- Wise, S.G., Liu, H., Yeo, G.C., Michael, P.L., Chan, A.H.P., Ngo, A.K.Y., Bilek, M.M.M., Bao, S., Weiss, A.S., 2016. Blended polyurethane and tropoelastin as a novel class of biologically interactive elastomer. *Tissue Eng. A.* 22, 524–533. <https://doi.org/10.1089/ten.TEA.2015.0409>.
- Biological Factors**
- Delivery and Presentation of Biological Factors**
- Bai, Y., Bai, L., Zhou, J., Chen, H., Zhang, L., 2018. Sequential delivery of VEGF, FGF-2 and PDGF from the polymeric system enhance HUVECs angiogenesis in vitro and CAM angiogenesis. *Cell. Immunology* 323, 19–32. <https://doi.org/10.1016/J.CELLIMM.2017.10.008>.
- Böck, T., Schill, V., Krähnke, M., Steinert, A.F., Tessmar, J., Blunk, T., Groll, J., 2018. TGF-β1-Modified hyaluronic acid/poly(glycidol) hydrogels for chondrogenic differentiation of human mesenchymal stromal cells. *Macromol. Biosci.* 18, 1700390. <https://doi.org/10.1002/mabi.201700390>.
- Brown, T.E., Anseth, K.S., Brown Ab, T.E., 2017. Chemical Society Reviews Spatiotemporal hydrogel biomaterials for regenerative medicine. *Chem. Soc. Rev.* 46, 6532–6552. <https://doi.org/10.1039/c7cs00445a>.
- Brudno, Y., Ennett-Shepard, A.B., Chen, R.R., Aizenberg, M., Mooney, D.J., 2013. Enhancing microvascular formation and vessel maturation through temporal control over multiple pro-angiogenic and pro-maturation factors. *Biomaterials* 34, 9201–9209. <https://doi.org/10.1016/J.BIOMATERIALS.2013.08.007>.
- Carragee, E.J., Hurwitz, E.L., Weiner, B.K., 2011. A critical review of recombinant human bone morphogenetic protein-2 trials in spinal surgery: emerging safety concerns and lessons learned. *Spine J.* <https://doi.org/10.1016/j.spinee.2011.04.023>.
- Cuchiara, M.L., Horter, K.L., Banda, O.A., West, J.L., 2013. Covalent immobilization of stem cell factor and stromal derived factor 1alpha for in vitro culture of hematopoietic progenitor cells. *Acta Biomater.* <https://doi.org/10.1016/j.actbio.2013.08.012>.

- Doran, M.R., Markway, B.D., Aird, I.A., Rowlands, A.S., George, P.A., Nielsen, L.K., Cooper-White, J.J., 2009. Surface-bound stem cell factor and the promotion of hematopoietic cell expansion. *Biomaterials* 30, 4047–4052. <https://doi.org/10.1016/j.biomaterials.2009.04.043>.
- Ferguson, E.L., Naseer, S., Powell, L.C., Hardwicke, J., Young, F.I., Zhu, B., Liu, Q., Song, B., Thomas, D.W., 2018. Controlled release of dextrin-conjugated growth factors to support growth and differentiation of neural stem cells. *Stem Cell Res.* 33, 69–78. <https://doi.org/10.1016/j.scr.2018.10.008>.
- Grim, J.C., Marozas, I.A., Anseth, K.S., 2015. Thiol-ene and photocleavage chemistry for controlled presentation of biomolecules in hydrogels. *J. Control. Release.* 219, 95–106. <https://doi.org/10.1016/j.jconrel.2015.08.040>.
- Kolb, H.C., Finn, M.G., Sharpless, K.B., 2001. Click chemistry: diverse chemical function from a few good reactions. *Angew. Chem. Int. Ed.* 40, 2004–2021. [https://doi.org/10.1002/1521-3773\(20010601\)40:11<2004::AID-ANIE2004>3.0.CO;2-5](https://doi.org/10.1002/1521-3773(20010601)40:11<2004::AID-ANIE2004>3.0.CO;2-5).
- Kudva, A.K., Luyten, F.P., Patterson, J., 2018. RGD-functionalized polyethylene glycol hydrogels support proliferation and in vitro chondrogenesis of human periosteum-derived cells. *J. Biomed. Mater. Res. A.* 106, 33–42. <https://doi.org/10.1002/jbm.a.36208>.
- Wang, H., Cui, J., Zheng, Z., Shi, Q., Sun, T., Liu, X., Huang, Q., Fukuda, T., 2017. Assembly of RGD-modified hydrogel micro-modules into permeable three-dimensional hollow microtissues mimicking in vivo tissue structures. *ACS Appl. Mater. Interfaces* 9, 41669–41679. <https://doi.org/10.1021/acsami.7b10960>.
- Mechanochemical Factors in Tissue Growth**
- Grier, W.K., Moy, A.S., Harley, B.A.C., 2017. Cyclic tensile strain enhances human mesenchymal stem cell SMAD 2/3 activation and tenogenic differentiation in anisotropic collagen-glycosaminoglycan scaffolds. *Eur. Cells Mater.* <https://doi.org/10.22203/ecm.v033a17>.
- Guo, T., Yu, L., Lim, C.G., Goodley, A.S., Xiao, X., Placone, J.K., Ferlin, K.M., Nguyen, B.N.B., Hsieh, A.H., Fisher, J.P., 2016. Effect of dynamic culture and periodic compression on human mesenchymal stem cell proliferation and chondrogenesis. *Ann. Biomed. Eng.* 44, 2103–2113. <https://doi.org/10.1007/s10439-015-1510-5>.
- Keselowsky, B.G., Collard, D.M., García, A.J., 2003. Surface chemistry modulates fibronectin conformation and directs integrin binding and specificity to control cell adhesion. *J. Biomed. Mater. Res. A.* 66A, 247–259. <https://doi.org/10.1002/jbm.a.10537>.
- Koçer, G., Jonkheijm, P., 2017. Guiding hmsc adhesion and differentiation on supported lipid bilayers. *Adv. Healthc. Mater.* 6, 1600862. <https://doi.org/10.1002/adhm.201600862>.
- Lee, J.W., Kim, H., Lee, K.Y., 2016. Effect of spacer arm length between adhesion ligand and alginate hydrogel on stem cell differentiation. *Carbohydr. Polym.* 139, 82–89. <https://doi.org/10.1016/j.carbpol.2015.12.024>.
- Liu, Q., Hatta, T., Qi, J., Liu, H., Thoreson, A.R., Amadio, P.C., Moran, S.L., Steinmann, S.P., Gingery, A., Zhao, C., 2018. Novel engineered tendon-fibrocartilage-bone composite with cyclic tension for rotator cuff repair. *J. Tissue Eng. Regen. Med.* 12, 1690–1701. <https://doi.org/10.1002/term.2696>.
- Poudineh, M., Wang, Z., Labib, M., Ahmadi, M., Zhang, L., Das, J., Ahmed, S., Angers, S., Kelley, S.O., 2018. Three-dimensional nanostructured architectures enable efficient neural differentiation of mesenchymal stem cells via mechanotransduction. *Nano Lett.* <https://doi.org/10.1021/acs.nanolett.8b03313>. <https://doi.org/10.1021/acs.nanolett.8b03313>.
- Rowland, D.C.L., Aquilina, T., Klein, A., Hakimi, O., Alexis-Mouthuy, P., Carr, A.J., Snelling, S.J.B., 2016. A comparative evaluation of the effect of polymer chemistry and fiber orientation on mesenchymal stem cell differentiation. *J. Biomed. Mater. Res. A* 104, 2843–2853. <https://doi.org/10.1002/jbm.a.35829>.
- Schiavi, J., Reppel, L., Charif, N., de Isla, N., Mainard, D., Benkirane-Jessel, N., Stoltz, J.-F., Rahouadj, R., Huselstein, C., 2018. Mechanical stimulations on human bone marrow mesenchymal stem cells enhance cells differentiation in a three-dimensional layered scaffold. *J. Tissue Eng. Regen. Med.* 12, 360–369. <https://doi.org/10.1002/term.2461>.
- Yu, S., Zuo, X., Shen, T., Duan, Y., Mao, Z., Gao, C., 2018. A density gradient of VAPG peptides on a cell-resisting surface achieves selective adhesion and directional migration of smooth muscle cells over fibroblasts. *Acta Biomater.* 72, 70–81. <https://doi.org/10.1016/j.actbio.2018.04.005>.
- Zhang, Y., Gong, H., Sun, Y., Huang, Y., Fan, Y., 2016. Enhanced osteogenic differentiation of MC3T3-E1 cells on grid-topographic surface and evidence for involvement of YAP mediator. *J. Biomed. Mater. Res. A* 104, 1143–1152. <https://doi.org/10.1002/jbm.a.35648>.
- Scaffold Design**
- Bružauskaitė, I., Bironaitė, D., Bagdonas, E., Bernotienė, E., 2016. Scaffolds and cells for tissue regeneration: different scaffold pore sizes-different cell effects. *Cytotechnology.* 68, 355–369. <https://doi.org/10.1007/s10616-015-9895-4>.
- El-Sherbiny, I.M., Yacoub, M.H., 2013. Hydrogel scaffolds for tissue engineering: progress and challenges. *Glob. Cardiol. Sci. Pract.* 2013, 316–342. <https://doi.org/10.5339/gcsp.2013.38>.
- Janik, H., Marzec, M., 2015. A review: fabrication of porous polyurethane scaffolds. *Mater. Sci. Eng. C.* 48, 586–591. <https://doi.org/10.1016/j.msec.2014.12.037>.
- Melchels, F.P.W., Feijen, J., Grijpma, D.W., 2010. A review on stereolithography and its applications in biomedical engineering. *Biomaterials* 31, 6121–6130. <https://doi.org/10.1016/j.biomaterials.2010.04.050>.
- Nuttelman, C.R., Rice, M.A., Rydholm, A.E., Salinas, C.N., Shah, D.N., Anseth, K.S., 2008. Macromolecular monomers for the synthesis of hydrogel niches and their application in cell encapsulation and tissue engineering. *Prog. Polym. Sci.* 33, 167–179. <https://doi.org/10.1016/j.progpolymsci.2007.09.006>.
- Integration of Multiple Factors**
- Flaim, C.J., Chien, S., Bhatia, S.N., 2005. An extracellular matrix microarray for probing cellular differentiation. *Nat. Methods* 2, 119–125. <https://doi.org/10.1038/nmeth736>.
- Lutolf, M.P., Blau, H.M., 2009. Artificial stem cell niches. *Adv. Mater.* 21, 3255–3268. <https://doi.org/10.1002/adma.200802582>.
- Models of Tissue Engineering**
- Bioreactors**
- Hutmacher, D.W., Singh, H., 2008. Computational fluid dynamics for improved bioreactor design and 3D culture. *Trends Biotechnol.* <https://doi.org/10.1016/j.tibtech.2007.11.012>.
- Mehta, K., Linderman, J.J., 2006. Model-based analysis and design of a microchannel reactor for tissue engineering. *Biotechnol. Bioeng.* <https://doi.org/10.1002/bit.20857>.
- Rojewski, M.T., Fekete, N., Baila, S., Nguyen, K., Fürst, D., Antwiler, D., Dausend, J., Kreja, L., Ignatius, A., Sensebé, L., Schrezenmeier, H., 2013. GMP-compliant isolation and expansion of bone marrow-derived mscs in the closed, automated device quantum cell expansion system. *Cell Transplant.* 22, 1981–2000. <https://doi.org/10.3727/096368912X657990>.

Organoids

- Bersini, S., Jeon, J.S., Dubini, G., Arrigoni, C., Chung, S., Charest, J.L., Moretti, M., Kamm, R.D., 2014. A microfluidic 3D in vitro model for specificity of breast cancer metastasis to bone. *Biomaterials* 35, 2454–2461. <https://doi.org/10.1016/J.BIOMATERIALS.2013.11.050>.
- Cristobal, A., van den Toorn, H.W.P., van de Wetering, M., Clevers, H., Heck, A.J.R., Mohammed, S., 2017. Personalized proteome profiles of healthy and tumor human colon organoids reveal both individual diversity and basic features of colorectal cancer. *Cell Rep.* 18, 263–274. <https://doi.org/10.1016/J.CELLREP.2016.12.016>.
- Lee, S.H., Hu, W., Matulay, J.T., Silva, M.V., Owczarek, T.B., Kim, K., Chua, C.W., Barlow, L.J., Kandoth, C., Williams, A.B., Bergren, S.K., Pietzak, E.J., Anderson, C.B., Benson, M.C., Coleman, J.A., Taylor, B.S., Abate-Shen, C., mckiernan, J.M., Al-Ahmadie, H., Solit, D.B., Shen, M.M., 2018. Tumor evolution and drug response in patient-derived organoid models of bladder cancer. *Cell* 173, 515–528. <https://doi.org/10.1016/j.CELL.2018.03.017>. e17.
- Li, X., Nadauld, L., Ootani, A., Corney, D.C., Pai, R.K., Gevaert, O., Cantrell, M.A., Rack, P.G., Neal, J.T., Chan, C.W.-M., Yeung, T., Gong, X., Yuan, J., Wilhelmy, J., Robine, S., Attardi, L.D., Plevritis, S.K., Hung, K.E., Chen, C.-Z., Ji, H.P., Kuo, C.J., 2014. Oncogenic transformation of diverse gastrointestinal tissues in primary organoid culture. *Nat. Med.* 20, 769–777. <https://doi.org/10.1038/nm.3585>.
- Liu, F., Huang, J., Zhang, L., Chen, J., Zeng, Y., Tang, Y., Liu, Z., 2019. Advances in cerebral organoid systems and their application in disease modeling. *Neuroscience*. 399, 28–38. <https://doi.org/10.1016/J.NEUROSCIENCE.2018.12.013>.
- Moreira, L., Bakir, B., Chatterji, P., Dantes, Z., Reichert, M., Rustgi, A.K., 2018. Pancreas 3D organoids: current and future aspects as a research platform for personalized medicine in pancreatic cancer, cell. *Mol. Gastroenterol. Hepatol.* 5, 289–298. <https://doi.org/10.1016/J.JCMGH.2017.12.004>.
- Nadkarni, R.R., Abed, S., Draper, J.S., 2016. Organoids as a model system for studying human lung development and disease. *Biochem. Biophys. Res. Commun.* 473, 675–682. <https://doi.org/10.1016/j.bbrc.2015.12.091>.
- Nuciforo, S., Fofana, I., Matter, M.S., Blumer, T., Calabrese, D., Boldanova, T., Piscuoglio, S., Wieland, S., Ringnald, F., Schwank, G., Terracciano, L.M., Ng, C.K.Y., Heim, M.H., 2018. Organoid models of human liver cancers derived from tumor needle biopsies. *Cell Rep* 24, 1363–1376. <https://doi.org/10.1016/J.CELLREP.2018.07.001>.
- Pievani, A., Sacchetti, B., Corsi, A., Rambaldi, B., Donsante, S., Scagliotti, V., Vergani, P., Remoli, C., Biondi, A., Robey, P.G., Riminucci, M., Serafini, M., 2017. Human umbilical cord blood-borne fibroblasts contain marrow niche precursors that form a bone/marrow organoid *in vivo*. *Development*. 144, 1035–1044. <https://doi.org/10.1242/dev.142836>.
- Sun, Y., Ding, Q., 2017. Genome engineering of stem cell organoids for disease modeling. *Protein Cell.* 8, 315–327. <https://doi.org/10.1007/s13238-016-0368-0>.
- Trisno, S.L., Philo, K.E.D., mcracken, K.W., Catá, E.M., Ruiz-Torres, S., Rankin, S.A., Han, L., Nasr, T., Chaturvedi, P., Rothenberg, M.E., Mandegar, M.A., Wells, S.I., Zorn, A.M., Wells, J.M., 2018. Esophageal organoids from human pluripotent stem cells delineate Sox2 functions during esophageal specification. *Cell Stem Cell* 23, 501–515. <https://doi.org/10.1016/j.Stem.2018.08.008>. e7.

In Vivo Models

- Koens, M.J.W., Krasznai, A.G., Hanssen, A.E.J., Hendriks, T., Praster, R., Daamen, W.F., van der Vliet, J.A., van Kuppevelt, T.H., 2015. Vascular replacement using a layered elastin-collagen vascular graft in a porcine model: one week patency versus one month occlusion. *Organogenesis* 11, 105–121. <https://doi.org/10.1080/15476278.2015.1038448>.
- Liu, W., Dan, X., Wang, T., Lu, W.W., Pan, H., 2016. A bone-implant interaction mouse model for evaluating molecular mechanism of biomaterials/bone interaction. *Tissue Eng. C Methods* 22, 1018–1027. <https://doi.org/10.1089/ten.TEC.2016.0250>.
- Pazzaglia, U.E., Sibilia, V., Congiu, T., Pagani, F., Ravanelli, M., Zarattini, G., 2015. Setup of a bone aging experimental model in the rabbit comparing changes in cortical and trabecular bone: morphological and morphometric study in the femur. *J. Morphol.* 276, 733–747. <https://doi.org/10.1002/jmor.20374>.
- Summerfield, A., Meurens, F., Ricklin, M.E., 2015. The immunology of the porcine skin and its value as a model for human skin. *Mol. Immunol.* 66, 14–21. <https://doi.org/10.1016/j.molimm.2014.10.023>.
- Wancket, L.M., 2015. Animal models for evaluation of bone implants and devices. *Vet. Pathol.* 52, 842–850. <https://doi.org/10.1177/0300985815593124>.

Applications of Tissue Engineering

Transplantation

- Lee, J., Cuddihy, M.J., Kotov, N.A., 2008. Three-dimensional cell culture matrices: state of the art. *Tissue Eng. B Rev.* <https://doi.org/10.1089/teb.2007.0150>.
- Richardson, T.P., Peters, M.C., Ennett, A.B., Mooney, D.J., 2001. Polymeric system for dual growth factor delivery. *Nat. Biotechnol.* <https://doi.org/10.1038/nbt1101-1029>.
- Simmons, C.A., Alsberg, E., Hsiong, S., Kim, W.J., Mooney, D.J., 2004. Dual growth factor delivery and controlled scaffold degradation enhance *in vivo* bone formation by transplanted bone marrow stromal cells. *Bone.* <https://doi.org/10.1016/j.bone.2004.02.027>.

Replacing/Regenerating Target Organs

Skin

- El-Serafi, A.T., El-Serafi, I.T., Elmasry, M., steinvall, I., Sjöberg, F., 2017. Skin regeneration in three dimensions, current status, challenges and opportunities. *Differentiation.* <https://doi.org/10.1016/j.diff.2017.06.002>.
- Yan, W.C., Davoodi, P., Vijayavenkataraman, S., Tian, Y., Ng, W.C., Fuh, J.Y.H., Robinson, K.S., Wang, C.H., 2018. 3D bioprinting of skin tissue: from pre-processing to final product evaluation. *Adv. Drug Deliv. Rev.* <https://doi.org/10.1016/j.addr.2018.07.016>.

Heart

- Moreira, R., Neusser, C., Kruse, M., Mulderrig, S., Wolf, F., Spillner, J., Schmitz-Rode, T., Jockenhoevel, S., Mela, P., 2016. Tissue-engineered fibrin-based heart valve with bio-inspired textile reinforcement. *Adv. Healthc. Mater.* 5, 2113–2121. <https://doi.org/10.1002/adhm.201600300>.
- Nachlas, A.L.Y., Li, S., Davis, M.E., 2017. Developing a clinically relevant tissue engineered heart valve-A review of current approaches. *Adv. Healthc. Mater.* 6, 1700918. <https://doi.org/10.1002/adhm.201700918>.

Kidney

- Fischer, I., Westphal, M., Rossbach, B., Bethke, N., Hariharan, K., Ullah, I., Reinke, P., Kurtz, A., Stachelscheid, H., 2017. Comparative characterization of decellularized renal scaffolds for

tissue engineering. *Biomed. Mater.* 12, 045005. <https://doi.org/10.1088/1748-605X/aa6c6d>.

Montserrat, N., Garreta, E., Izpisua Belmonte, J.C., 2016. Regenerative strategies for kidney engineering. *FEBS J* 283, 3303–3324. <https://doi.org/10.1111/febs.13704>.

Orthopedic Tissues

Cohen, N.P., Foster, R.J., Mow, V.C., 1998. Composition and dynamics of articular cartilage: structure, function, and maintaining healthy state. *J. Orthop. Sport. Phys. Ther.* <https://doi.org/10.2519/jospt.1998.28.4.203>.

Daly, A.C., Freeman, F.E., Gonzalez-Fernandez, T., Critchley, S.E., Nulty, J., Kelly, D.J., 2017. 3D bioprinting for cartilage and osteochondral tissue engineering. *Adv. Healthc. Mater.* 6, 1700298. <https://doi.org/10.1002/adhm.201700298>.

Kim, H.D., Amirthalingam, S., Kim, S.L., Lee, S.S., Rangasamy, J., Hwang, N.S., 2017. Biomimetic materials and fabrication approaches for bone tissue engineering. *Adv. Healthc. Mater.* 6, 1700612. <https://doi.org/10.1002/adhm.201700612>.

Drug Delivery

Crowley, S.T., Poliskey, J.A., Baumhover, N.J., Rice, K.G., 2015. Efficient expression of stabilized mRNA PEG-peptide polyplexes in liver. *Gene Ther* 22, 993–999. <https://doi.org/10.1038/gt.2015.68>.

Newman, M.R., Benoit, D.S., 2016. Local and targeted drug delivery for bone regeneration. *Curr. Opin. Biotechnol.* 40, 125–132. <https://doi.org/10.1016/j.COPBIO.2016.02.029>.

Peng, W., Datta, P., Ayan, B., Ozbolat, V., Sosnoski, D., Ozbolat, I.T., 2017. 3D bioprinting for drug discovery and development in pharmaceuticals. *Acta Biomater.* <https://doi.org/10.1016/j.actbio.2017.05.025>.

Tibbitt, M.W., Dahlman, J.E., Langer, R., 2016. Emerging frontiers in drug delivery. *J. Am. Chem. Soc.* 138, 704–717. <https://doi.org/10.1021/jacs.5b09974>.

Wolinsky, J.B., Colson, Y.L., Grinstaff, M.W., 2012. Local drug delivery strategies for cancer treatment: gels, nanoparticles, polymeric films, rods, and wafers. *J. Control. Release.* 159, 14–26. <https://doi.org/10.1016/j.JCONREL.2011.11.031>.

Yoo, J.-W., Irvine, D.J., Discher, D.E., Mitragotri, S., 2011. Bio-inspired, bioengineered and biomimetic drug delivery carriers. *Nat. Rev. Drug Discov.* 10, 521–535. <https://doi.org/10.1038/nrd3499>.

Disease Models and Therapy

Choi, J., Iich, E., Lee, J.-H., 2016. Organogenesis of adult lung in a dish: differentiation, disease and therapy. *Dev. Biol.* 420, 278–286. <https://doi.org/10.1016/j.ydbio.2016.10.002>.

Fischbach, C., Kong, H.J., Hsiang, S.X., Evangelista, M.B., Yuen, W., Mooney, D.J., 2009. Cancer cell angiogenic capability is regulated by 3D culture and integrin engagement. *Proc. Natl. Acad. Sci.* 106, 399–404. <https://doi.org/10.1073/pnas.0808932106>.

Grenier, S., Bhargava, M.M., Torzilli, P.A., 2014. An in vitro model for the pathological degradation of articular cartilage in osteoarthritis. *J. Biomech.* 47, 645–652. <https://doi.org/10.1016/j.jbiomech.2013.11.050>.

Gurski, L.A., Xu, X., Labrada, L.N., Nguyen, N.T., Xiao, L., van Golen, K.L., Jia, X., Farach-Carson, M.C., 2012. Hyaluronan (HA) interacting proteins RHAMM and hyaluronidase impact prostate cancer cell behavior and invadopodia formation in 3D HA-based hydrogels. *PLoS One.* 7, e50075. <https://doi.org/10.1371/journal.pone.0050075>.

Hansen, A., Eder, A., BÖnstrup, M., Flato, M., Mewe, M., Schaaf, S., Aksehrioglu, B., SchwÖrer, A., Uebeler, J., Eschenhagen, T., Eschenhagen, T., 2010. Development of a drug screening platform based on engineered heart tissue. *Circ. Res.* 107, 35–44. <https://doi.org/10.1161/CIRCRESAHA.109.211458>.

Kim, B.J., Hannanta-anan, P., Chau, M., Kim, Y.S., Swartz, M.A., Wu, M., 2013. Cooperative roles of SDF-1 α and EGF gradients on tumor cell migration revealed by a robust 3D microfluidic model. *PLoS One* 8, e68422. <https://doi.org/10.1371/journal.pone.0068422>.

Kuo, C.-Y., Shevchuk, M., Opfermann, J., Guo, T., Santoro, M., Fisher, J.P., Kim, P.C., 2018. Trophoblast-Endothelium signaling involves angiogenesis and apoptosis in a dynamic bioprinted placenta model. *Biotechnol. Bioeng.* <https://doi.org/10.1002/bit.26850>.

Pedersen, G., 2015. Development, validation and implementation of an in vitro model for the study of metabolic and immune function in normal and inflamed human colonic epithelium. *Dan. Med. J.* 62, B4973. (accessed October 29, 2018) <http://www.ncbi.nlm.nih.gov/pubmed/25557335>.

Semlin, L., Schäfer-Korting, M., Borelli, C., Korting, H.C., 2011. In vitro models for human skin disease. *Drug Discov. Today* 16, 132–139. <https://doi.org/10.1016/j.drudis.2010.12.001>.

van Grunsven, L.A., 2017. 3D in vitro models of liver fibrosis. *Adv. Drug Deliv. Rev.* 121, 133–146. <https://doi.org/10.1016/j.addr.2017.07.004>.

Xu, X., Sabanayagam, C.R., Harrington, D.A., Farach-Carson, M.C., Jia, X., 2014. A hydrogel-based tumor model for the evaluation of nanoparticle-based cancer therapeutics. *Biomaterials* 35, 3319–3330. <https://doi.org/10.1016/j.biomaterials.2013.12.080>.

Xu, X., Gurski, L.A., Zhang, C., Harrington, D.A., Farach-Carson, M.C., Jia, X., 2012. Recreating the tumor microenvironment in a bilayer, hyaluronic acid hydrogel construct for the growth of prostate cancer spheroids. *Biomaterials* 33, 9049–9060. <https://doi.org/10.1016/j.biomaterials.2012.08.061>.

Current Challenges and Opportunities

Vascularization

Rouwkema, J., Rivron, N.C., van Blitterswijk, C., 2008. Vascularization in tissue engineering. *Trends Biotechnol.* <https://doi.org/10.1016/j.tibtech.2008.04.009>.

Sarker, M.D., Naghieh, S., Sharma, N.K., Chen, X., 2018. 3D bio-fabrication of vascular networks for tissue regeneration: a report on recent advances. *J. Pharm. Anal.* 8, 277–296. <https://doi.org/10.1016/j.jpha.2018.08.005>.

Soker, S., Machado, M., Atala, A., 2000. Systems for therapeutic angiogenesis in tissue engineering. *World J. Urol.* <https://doi.org/10.1007/PL00007070>.

Tissue Maturation

Meinert, C., Schrobback, K., Hutmacher, D.W., Klein, T.J., 2017. A novel bioreactor system for biaxial mechanical loading enhances the properties of tissue-engineered human cartilage. *Sci. Rep.* 7, 16997. <https://doi.org/10.1038/s41598-017-16523-x>.

Pelaez, D., Acosta Torres, Z., Ng, T.K., Choy, K.W., Pang, C.P., Cheung, H.S., 2017. Cardiomyogenesis of periodontal ligament-derived stem cells by dynamic tensile strain. *Cell Tissue Res* 367, 229–241. <https://doi.org/10.1007/s00441-016-2503-x>.

Testa, S., Costantini, M., Fornetti, E., Bernardini, S., Trombetta, M., Seliktar, D., Cannata, S., Rainer, A., Gargioli, C., 2017. Combination of biochemical and mechanical cues for tendon tissue engineering. *J. Cell Mol. Med.* 21, 2711–2719. <https://doi.org/10.1111/jcmm.13186>.

FDA Regulations for Clinical Translation

Boyce, S.T., Lally, A.L., 2018. Tissue engineering of skin and regenerative medicine for wound care. *Burn Trauma*. 6, 4. <https://doi.org/10.1186/s41038-017-0103-y>.

Gene Editing and CRISPR

Garreta, E., González, F., Montserrat, N., 2018. Studying kidney disease using tissue and genome engineering in human pluripotent stem cells. *Nephron*. 138, 48–59. <https://doi.org/10.1159/000480710>.

Greenberg, M.J., Daily, N.J., Wang, A., Conway, M.K., Wakatsuki, T., 2018. Genetic and tissue engineering approaches to modeling the

mechanics of human heart failure for drug discovery. *Front. Cardiovasc. Med.* 5, 120. <https://doi.org/10.3389/fcvm.2018.00120>.

Hoes, M.F., Bomer, N., van der Meer, P., 2018. Concise review: the current state of human in vitro cardiac disease modeling: a focus on gene editing and tissue engineering. *Stem Cells Transl. Med.* <https://doi.org/10.1002/sctm.18-0052>.

Khadempar, S., Familghadakchi, S., Motlagh, R.A., Farahani, N., Dashtiahangar, M., Rezaei, H., Gheibi Hayat, S.M., 2018. CRISPR-Cas9 in genome editing: its function and medical applications. *J. Cell. Physiol.* <https://doi.org/10.1002/jcp.27476>.

2.6.3

Tissue Engineering Scaffolds

HANNAH A. PEARCE, YU SEON KIM, LUIS DIAZ-GOMEZ, ANTONIOS G. MIKOS

Department of Bioengineering, Rice University, Houston, TX, United States

Introduction

Over the past 30 years, tissue engineering has experienced an intense evolution facing the need to restore, replace, or regenerate tissues that have suffered structural or functional damage following injury or disease. To induce and guide tissue growth, tissue engineering has aimed to combine scaffolds that provide a mechanical support structure, cells that populate the scaffolds and drive the regeneration process, and bioactive molecules that regulate cell differentiation and functionality (Langer and Vacanti, 1993). Scaffolds are highly interconnected porous structures that aim to recreate the extracellular environment while providing appropriate mechanical support and stability until the new tissue is regenerated (O'Brien, 2011). For these reasons, scaffolds should be prepared with biodegradable materials and the degradation rate should ideally match the regeneration rate of the tissue where it will be implanted while maintaining mechanical support (Thomson et al., 1995). This chapter describes the functional requirements, processing techniques, applications, and characterization methods of biomaterials to provide a state-of-the-art overview of scaffolds for tissue engineering developments in the last decade.

Scaffold Design Criteria

Three criteria that need to be considered when designing a polymeric scaffold for tissue engineering applications are (1) biocompatibility, (2) physicochemical properties, and (3) bioactivity. Biocompatibility of a material will dictate whether it is suitable to be used as a scaffold *in vitro* and *in vivo*, whereas its physicochemical properties and bioactivity are factors that can be tuned to be specific for a certain tissue/cell type, and to optimize the scaffold's ability to regenerate the tissue.

Biocompatibility, when used to describe a material, refers to its ability to perform with an appropriate host response in a specific application (Temenoff and Mikos, 2008). Unlike implants that are not meant to undergo degradation such as poly(methyl methacrylate) (PMMA) bone cements and metallic hip joints, tissue engineering scaffolds will gradually degrade over time and be replaced by the native tissue. As such, the cytotoxicity of degraded components of the

original material should also be taken into consideration when choosing a material for scaffold design. Implanted scaffolds undergo degradation most often via hydrolysis and/or enzymatic activity, depending on the chemical structure of the scaffold material. Polymers with hydrolysable bonds such as esters and amides are often chosen as biodegradable materials. Notable examples include poly(lactic-*co*-glycolic acid) (PLGA), poly(ϵ -caprolactone) (PCL), and polyurethanes. Scaffolds fabricated from natural polymers such as collagen, gelatin, and polysaccharides will be enzymatically degraded by proteases that are present in the extracellular matrix (ECM).

The rate of scaffold degradation must also be considered for tissue regeneration. Ideally, the degradation rate of an implanted scaffold should be similar to the regeneration rate of the surrounding tissue. The degradation rate of hydrophobic polymers can be enhanced by increasing the content of hydrophilic groups. For instance, PLGA foams that contain higher glycolic acid content (50:50 lactic acid:glycolic acid) were shown to degrade more quickly than those that have higher lactic acid content (85:15) (Lu et al., 2000a). Similar results can be obtained by incorporating hydrophilic segments within the polymer chain; block copolymers of poly(lactic acid) (PLA) and poly(ethylene glycol) (PEG) have shown an increased degradation rate when compared to PLA homopolymers due to the increased hydrophilicity the PEG blocks bring to the polymer. The polymer's molecular weight will also affect the degradation time, where scaffolds fabricated with higher molecular weight polymers will degrade slower than those fabricated with lower molecular weight polymers. In addition to its chemical properties, the scaffold's physical properties will also affect the scaffold's degradation rate. It has been demonstrated that pore size and pore wall thickness will affect the rate of degradation of poly(L-lactic acid) (PLLA) foams *in vitro*, where thicker pore walls and larger pore size contributed to faster degradation via an autocatalytic effect (Lu et al., 2000a). The effect was also enhanced *in vivo*, where acidic degradation products remained within the pores and further accelerated the degradation reaction (Lu et al., 2000b).

Porosity and pore size/distribution will not only affect the scaffold's mechanical properties and rate of degradation, but also how seeded cells respond to the environment

(Petite et al., 2000). High porosity must also be accompanied with pore interconnectivity, as pores that are trapped within the scaffold are not accessible to cells and will reduce the scaffold's mechanical properties. Interconnected pores will also act as conduits for blood vessels to infiltrate and form a well-vascularized network within the scaffold, which is a necessary step toward the regeneration of tissues such as bone (Petite et al., 2000). A highly porous scaffold has a high surface area to volume ratio, which provides sufficient space for cells to attach onto the scaffold's surfaces, enhances the rate of mass transport of oxygen and nutrients both to seeded cells, and aids in the removal of cell waste (Mikos and Temenoff, 2000; Yang et al., 2001). Different pore sizes have been shown to trigger diverse responses from the tissue (Rouwkema et al., 2008; Yang et al., 2001); for instance, pores larger than 300 μm were shown to be ideal for bone in-growth, whereas fibrovascular tissues required 500 μm or greater (Kuboki et al., 2001; Wake et al., 1994). These results indicate that a modular approach is required to regenerate different types of tissues. Nevertheless, while high porosity is an important factor for tissue regeneration, the mechanical integrity of the scaffolds can be negatively influenced (Karageorgiou and Kaplan, 2005).

In addition to soluble factors, surface characteristics such as hydrophobicity, charge, roughness, and stiffness will also impact the behavior of cells seeded on the scaffold (Chang and Wang, 2011). Without the presence of proteins, cells tend to adhere and proliferate better on moderately hydrophilic surfaces (i.e., high wettability) than on hydrophobic surfaces. One benefit of hydrophobic surfaces though is the ability for proteins to adsorb through hydrophobic interactions and thus serve as a surface for cells to bind and proliferate. Synthetic polymers that are widely used for scaffold fabrication such as PLGA and PCL are hydrophobic and thus are not ideal substrates for cell adhesion on their own, but with proteins adsorbed on the surface they make promising tissue-engineering scaffolding systems. Surface modification strategies such as plasma treatment and hydrophilic polymer coating have therefore been utilized to enhance cell-surface interaction (Arima and Iwata, 2007; Cui et al., 2009; Place et al., 2009). An increase in roughness has been shown to not only enhance cell adhesion by improving adsorption of cell adhesion-mediating proteins such as fibronectin, but also alter their functions such as proliferation, morphology, and matrix production (Hal-lab et al., 2001; Martin et al., 1995; Puckett et al., 2008; Saranya et al., 2011).

Surface coating of synthetic scaffolds is often required to enhance the cell-scaffold interaction, as they often lack the biological signals that are required for cell attachment. The coating process involves chemically treating the surface to functionalize it with active domains that could be used for modifications with bioactive molecules of choice, such as ECM components that promote cell adhesion (collagen, fibronectin, and laminin), minerals to drive osteoconduction and osteointegration (calcium phosphate-based minerals such as hydroxyapatite), and drug molecules (Wu et al., 2014;

Yoo et al., 2009). Short peptide sequences that mimic the active domain of a specific protein, such as the popular arginine-glycine-aspartate (RGD) sequence, can be used instead of native ECM proteins which can have issues with stability during and after surface adsorption (Shin et al., 2003).

Cell function can also be affected by substrate stiffness. It has been shown that the microenvironment stiffness significantly affects the commitment and differentiation of mesenchymal stem cells (MSCs); softer matrices encourage the neurogenic or myogenic differentiation of MSCs, while stiffer substrates are known to exert a strong influence in supporting osteogenic differentiation (Engler et al., 2006). Other cell functions such as migration and proliferation are also affected by substrate stiffness (Breuls et al., 2008). Cell lineages have unique optimum conditions for proliferation and respond differently to microenvironmental stiffnesses; for instance, human dermal fibroblasts seeded on stiff substrates show higher degrees of organization in their actin cytoskeleton and slower migration speed (Dado and Levenberg, 2009; Ghosh et al., 2007).

Scaffold Applications

Cell Delivery

A widespread application of scaffolds is as a carrier for cell delivery. Although delivering cells in suspension has shown positive results in improving disease conditions such as osteoarthritis and myocardial infarction (Amado et al., 2005; Berry, 2006; Black et al., 2008; Koh et al., 2013), the technique suffers from low cell retention and poor integration of cells at the site of delivery (Chen et al., 2012). By providing an environment where cells can be seeded, tissue-engineering scaffolds provide a platform that can deliver such cell populations directly into the defect site. Surgical techniques that incorporate scaffold carriers such as matrix-assisted chondrocyte implantation (MACI) have proven to be a more effective alternative to direct delivery of cell suspension (Kon et al., 2009; Steinwachs, 2009).

Cells, regardless of their origin, may be seeded onto a scaffold via a static or dynamic method (Marler et al., 1998). Static seeding involves a cell suspension being directly deposited onto the scaffold surface and gradually allowing the cells to coat the scaffold, whereas dynamic seeding utilizes any type of mechanical stimuli (e.g., stirring, shaking) to enhance the density and uniformity of cells on the surface of the scaffold. In addition to delivering cells on the surface of a 3D scaffold, cells may be incorporated within the bulk of a scaffold. Encapsulation refers to a technique where cell bodies are physically isolated from the surrounding environment while maintaining their activity and viability (Uludag et al., 2000). Hydrogels are utilized as the scaffold of choice for cell encapsulation, as they can provide a nontoxic, hydrated environment for encapsulated cells to survive and proliferate. Cells are loaded into the hydrogel precursor solution before undergoing gelation, after which the hydrogel

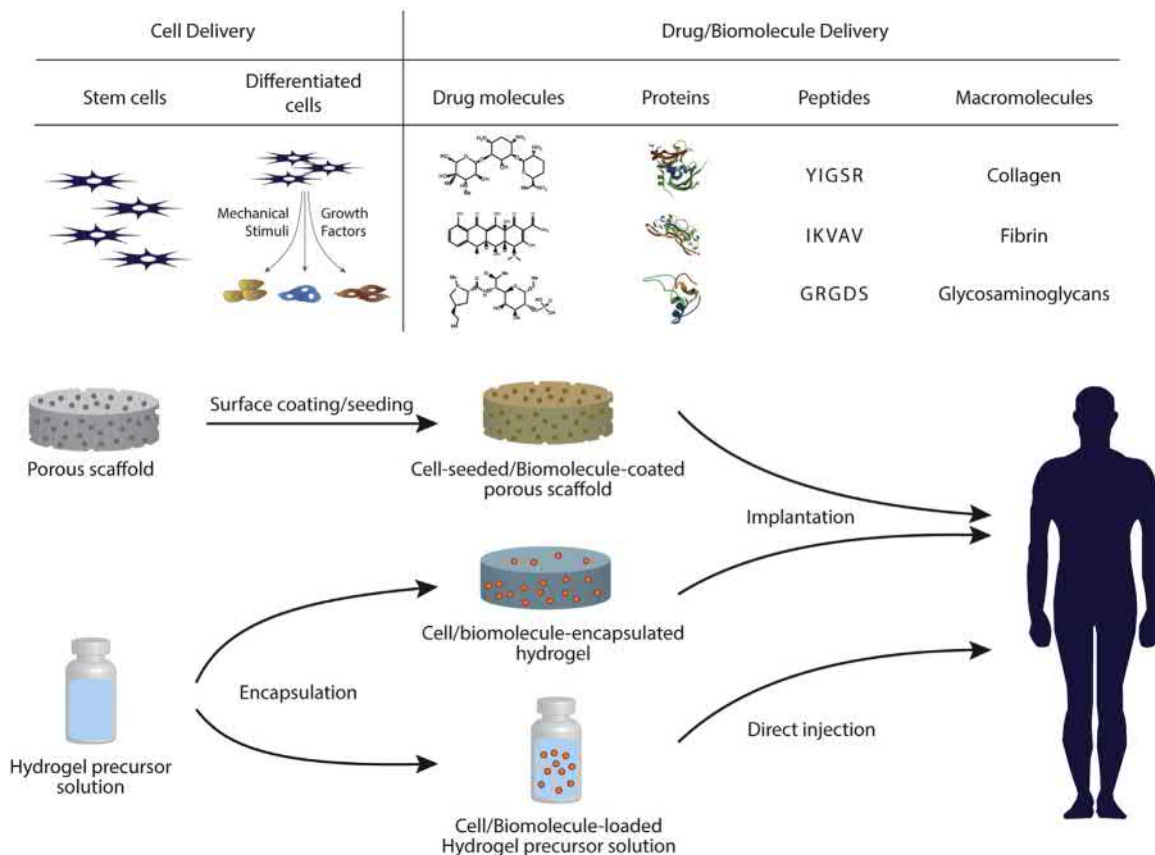
can be implanted. The hydrated environment allows for nutrients and signaling molecules from the body to diffuse into the hydrogel. Cells, in addition to being delivered in bulk hydrogels, can also be loaded into microspheres and delivered into the defect site when encapsulated in a bulk scaffold carrier. This method improves mass transfer of oxygen and other nutrients to the cells, thereby enhancing the viability of cells postimplantation (Hernández et al., 2010). Natural materials such as alginate and collagen (Chan et al., 2010; Tan and Takeuchi, 2007; Yu et al., 2010), as well as synthetic materials such as oligo(poly(ethylene glycol)fumarate) (OPF) (Park et al., 2005) have been used for the fabrication of cell-laden hydrogel microspheres (Fig. 2.6.3.1).

Another method of cell delivery involves direct injection of cell-laden hydrogel precursor solution into the body, where it will fill in the exact size and shape of the defect site and undergo gelation. These injectable systems allow for a minimally invasive delivery of cells to the site of interest, as they can be delivered using a syringe needle and thus bypass the need to perform an invasive surgery and suture the scaffold into place. Such gelation can take place either chemically or physically, depending on the material of the hydrogel. Injectable hydrogels that utilize chemical gelation often rely on free-radical initiators to start the reaction between polymer chains that have reactive groups (e.g., acrylates), or between the polymer chains and cross-linkers. Different combinations of initiators, such as ammonium

persulfate/*N,N,N',N'*-tetramethylethylenediamine (APS/TEMED) and APS/ascorbic acid, have been utilized to cross-link linear polymers with diacrylate-containing cross-linkers to form cell-laden hydrogels (Temenoff et al., 2003; Wang et al., 2006; Zhu and Ding, 2006). Photocross-linkable systems are a subset of chemically cross-linked hydrogels that require UV or visible light for activation. Polymers such as PEG that are otherwise not photocross-linkable can be modified with acrylate groups, after which they can be cross-linked under visible or UV light with the help of photoinitiators (Burdick and Anseth, 2002; Sawhney et al., 1993).

Chemically cross-linkable hydrogels that do not depend on free radical initiators have also been developed. For instance, supramolecular self-assembly between poly(ethylene oxide) (PEO) and α -cyclodextrins (α -CD) has been shown to result in the formation of a hydrogel that is injectable and biocompatible (Li et al., 2003). Click chemistry, which refers to reactions that can be performed in aqueous conditions and do not generate toxic byproducts, has also been utilized to develop injectable systems as cell carriers (Jiang et al., 2015a; Takahashi et al., 2013).

Injectable hydrogels that undergo physical gelation do not rely on initiators or other chemical interactions for hydrogel formation. Rather, they rely on changes in environmental cues such as temperature, pH, and ionic concentrations to undergo gelation. Thermogelling hydrogels



• **Figure 2.6.3.1** Scheme of the main applications of tissue-engineering scaffolds. (Protein structures downloaded from www.rcsb.org.)

are a subset of injectable materials that will undergo reversible gelation in response to temperature. One of the defining characteristics of these thermosensitive systems is their lower critical solution temperature (LCST), which is the temperature at which the system will undergo sol–gel transition. LCST can be tuned by adjusting the hydrophobicity of the polymer. Ensuring that the LCST is near body temperature is desirable for tissue-engineering applications (Kretlow et al., 2007).

Drug and Biomolecule Delivery

Delivering drugs and bioactive molecules using scaffolds allows for a sustained and localized delivery, thus minimizing complications related to systemic delivery such as poor localization of biomolecules at the target and low delivery efficiency stemming from short half-lives of biological molecules (Florence and Jani, 1994). When drugs and biomolecules are loaded inside a degradable scaffold, these molecules will be gradually released and delivered to the adjacent tissue as the scaffold undergoes degradation over time.

Drugs and biomolecules can be immobilized on scaffold surfaces via covalent conjugation or physical adsorption (Sokolsky-Papkov et al., 2007). Physical adsorption relies on noncovalent interactions between the substrate and the surface (e.g., ionic, hydrophobic, etc.), whereas covalent bonding requires reactive functional groups to be present on both the molecule of interest and the surface of the scaffold. This method often requires the surface to be treated with physical or chemical means to introduce such groups. Direct conjugation of proteins such as growth factors (GFs) also requires careful consideration when choosing which functional groups to modify, as poorly designed conjugation schemes can negatively affect their bioactivity by disrupting the native folding state or blocking the access to their active domains. In addition, conjugated factors will not be internalized by cells unless the surface undergoes erosion or degradation. Nevertheless, when well-executed, scaffolds covalently conjugated with GFs can show enhanced bioactivity over delivery of soluble GFs directly to the tissue. This method of delivery also enables more careful control of spatiotemporal distribution of factors on the surface of the scaffold and a longer duration of the signals than when the signals are encapsulated within the scaffolds (Tayalia and Mooney, 2009).

Drugs and biomolecules can also be encapsulated in the bulk space of the hydrogel during synthesis. Encapsulation into solid, porous scaffolds is possible but significantly more challenging than encapsulation in hydrogels due to the method of scaffold fabrication; for instance, synthesis of many porous synthetic scaffolds requires organic solvents and exposure to harsh conditions such as temperature and pressure, depending on which process is utilized to introduce pores into the scaffold (Tayalia and Mooney, 2009). As a result, most biomolecules are incorporated after the scaffold has been formed. Loading of drugs and biomolecules in hydrogels, on the other hand, can be done under mild

conditions, as biomolecules can be mixed with the aqueous precursor solution and be encapsulated as the solution undergoes gelation. Such molecules can either be loaded into the bulk space of the hydrogel or covalently conjugated to the hydrogel backbone for a more controlled, sustained delivery that does not depend solely on diffusion. In addition, hydrogels can be designed so that they degrade in response to the physiological conditions of the surrounding environment and simultaneously release encapsulated biomolecules (Kost and Langer, 2012; Miyata et al., 2002). For instance, pH-sensitive hydrogels have been extensively developed and tested to control the release of GFs from the hydrogel (Garbern et al., 2010, 2011; Ishihara et al., 1984; Kim et al., 2009).

Scaffold Materials

Scaffold materials can range widely from synthetic scaffolds with little to no biochemical cues or factors incorporated to wholly biological systems possessing both innate and added bioactive factors to guide tissue growth (Deforest et al., 2009; Hubbell, 1995; Lutolf and Hubbell, 2005). As the field was initially being developed, the study of synthetic biomaterials benefited greatly from the wealth of information gained in the disciplines of chemical synthesis and materials processing, and the field has only continued to evolve and grow since. Classifying these polymers can be challenging, but a popular method is by categorizing polymers as either *polycondensation* or *polyaddition* polymers. This classification system, like all others, is imperfect but provides a clear picture of the polymer end-product and is helpful as it organizes systems based on the polymer structure (O dian, 2004). These two types of polymers include many important biomaterials including polyesters, polyurethanes, polyamides, and polyacrylates (Table 2.6.3.1).

Polycondensation Polymers

Polycondensation polymers are some of the most popular polymers used in biomaterials applications and include polyesters, polyethers, polyurethanes, and more. These polymers often possess functional groups within the polymer chain backbone (i.e., esters, ethers, amides, etc.) (O dian, 2004) and the polymerization methods used to form polycondensation polymers often involve the creation of low-molecular-weight byproducts; in biomaterials, these byproducts are most often water or alcohol-containing groups. The polymerizations used to create polycondensation polymers are characterized by a drastic monomer conversion at the beginning of the reactions due to the rapid formation of oligomers, followed by a steady growth into polymers until all monomers are consumed. The system reflects this monomer conversion with a gradual steady increase in polymer molecular weight over time. In polyester-forming condensations, often a carboxylic acid- or alcohol-containing group is the monomer and the system is usually acid-catalyzed. High temperatures and vacuum are often used to promote

TABLE 2.6.3.1 Polymerization Methods for Creating Synthetic Biocompatible Polymers

Polymerization Method	Characteristics	Example Polymers
Polymerizations producing polycondensation polymers	<ul style="list-style-type: none"> Reaction exhibits rapid monomer conversion upon the start of the reaction Polymer molecular weight increases steadily over time Polymerizations often produce low-molecular-weight byproducts so can be performed under vacuum Ring-opening polymerizations and click reactions are included 	Poly(ϵ -caprolactone) (PCL), poly(glycerol sebacate) (PGS), polyurethane, polylactide (PLA), polyglycolide (PGA), poly(lactide-co-glycolide) (PLGA), poly(dimethylsiloxane) (PDMS), poly(propylene fumarate) (PPF)
Polymerizations producing polyaddition polymers	<ul style="list-style-type: none"> Polymerization operates in distinct initiation, propagation, and termination steps Reaction exhibits rapid polymer molecular weight growth upon initiation of the reaction Monomer conversion progresses more steadily over time Ionic polymerizations and free-radical polymerizations are included 	Propylene fumarate dimethacrylate (PFDMA) and diacrylate (PPF-DA), poly(acrylamide), poly(ethylene glycol) (PEG), ethylene glycol dimethacrylate (EGDMA), butanediol dimethacrylate (BDMA)

the polymerization and facilitate the removal of byproducts. These condensation techniques have been used for decades and have produced condensation polymers such as poly(propylene fumarate) (PPF) (Peter et al., 1999a,b), poly(glycerol sebacate) (PGS) (Wang et al., 2002), and polyurethanes (Bachmann et al., 2001). Polyurethanes have been used for tissue-engineering applications such as electrospun scaffolds (Kishan and Cosgriff-Hernandez, 2017; Nezarati et al., 2013) and in shape-memory implants for embolic applications (Singhal et al., 2014).

Ring-Opening Polymerization

Ring-opening polymerization is a common tool used to produce linear polymers. It is commonly used to produce PCL (Dubois et al., 1991; Habibi et al., 2008; Hamitou et al., 1977), among other notable polyester biopolymers such as PLA, polyglycolide (PGA), and the copolymer PLGA (Gilding and Reed, 1979; Kaihara et al., 2007). Biodegradable sutures Dexon (PGA) and Vicryl (PLGA) are approved for use in humans by regulatory authorities and have been safely used for decades (Bourissou et al., 2004; Gilding and Reed, 1979). An extremely common biocompatible polymer, PEG, can be produced through the ring-opening polymerization of an epoxide ring (Herzberger et al., 2016). Poly(dimethylsiloxane) (PDMS) is a common polymer used in biological applications involving lithography which can also be produced through the ring-opening polymerization of cyclic siloxane groups (Rodriguez et al., 2007) and produces an optically transparent polymer product (Ersen and Sahin, 2017). Many of these ring-opening polymerizations are achieved through the initiation with an ionic group, or a coordination compound, the most common ones being Tin(II)-based (Gilding and Reed, 1979; Kaihara et al., 2007). Ring strain contributes to reactivity so three- and four-membered rings are most reactive with cyclohexane groups being relatively stable but still reactive given the correct conditions (Nuyken and Pask, 2013).

Click Reactions

Click reactions are a subset of chemical reactions that can be carried out in aqueous conditions, at physiological temperature, and without cytotoxic initiators (Deforest et al., 2009). These reactions are also highly specific and proceed in an orthogonal manner with high polymerization efficiency (Deforest et al., 2009; Tibbitt and Anseth, 2009). Click reactions encompass the well-known thiol-ene reaction, which allows highly controlled spatial and temporal regulation of materials through photoinitiation (Deforest et al., 2009). Click reactions can also be classified under the umbrella of polycondensation polymers. Although the formation of low-molecular-weight byproducts does not always occur, the reaction follows the general trend of polycondensation polymers such as rapid monomer conversion and a gradual increase in molecular weight, and the presence of functional groups in the polymer chain backbone. Extensive work has demonstrated the power of click chemistry in creating dynamic scaffolds that are responsive to both external stimuli (light, concentration gradient, mechanical stimulation, etc.) and to cells (Benoit et al., 2008; Brown et al., 2018; Burdick and Anseth, 2002; Kloxin et al., 2009; Sridhar et al., 2015). Additional work has been carried out to create biocompatible and bio-instructive scaffolding systems (Arakawa et al., 2017; Gramlich et al., 2013; Jivan et al., 2016, 2018; Nimmo et al., 2011).

Polyaddition Polymers

Unlike polycondensation, polyaddition reactions do not involve the formation of low-molecular-weight byproducts, and the polymer backbone does not often contain functional groups (Fried, 2014; Odian, 2004; Stevens, 1999). The reactions to form polyaddition polymers include ionic and free radical polymerizations. These reactions exhibit a rapid increase in the molecular weight almost immediately upon the initiation of the reaction while the monomer conversion progresses more steadily over time. Polyaddition reactions

operate in distinct initiation, propagation, and termination steps, each with their own kinetic rate and one growing reactive center that other monomers join as the polymerization progresses. Some of the most notable examples of polyaddition polymers are propylene fumarate dimethacrylate (PFDMA) and diacrylate (PF-DA), both biocompatible and mechanically robust bone tissue-engineering scaffolding systems (Moglia et al., 2014; Timmer et al., 2003).

Ionic Polymerization

Ionic polymerizations include both cationic and anionic reactions. Cationic polymerization systems are often initiated by a mineral acid, or a Lewis acid accompanied by a proton source, which becomes the electrophile needed to begin the reaction (Stevens, 1999). The method is attractive due to its ability to produce “living polymerizations,” which has aided in the production of many commercially used block copolymers (Stevens, 1999) and branched copolymers (Iatrou et al., 2002). These systems are often induced through the addition of a metal initiator and begin with a nucleophilic addition to the monomer. The most notable biomaterial applications of anionic polymerizations are the creation of star polymers of PEO (Gnanou et al., 1988; Peppas et al., 1999).

Free Radical Polymerization

Free radical polymerization is a rapid, highly effective technique widely used in the industry to produce commercial polymers such as poly(methyl methacrylate) (PMMA) (Charnley, 1960; Turner et al., 1981), poly(acrylamide), and many acrylate and methacrylate terminated polyesters and polyethers (Matyjaszewski and Xia, 2001; Stevens, 1999). Initiators for free radical systems are diverse and include peroxides (Matyjaszewski and Xia, 2001), redox initiators (Hageman, 1985), azo groups (Braun, 2009), and photoinitiators (Hageman, 1985). Many peroxide initiators rely on temperature degradation to generate free radical species for initiation (Moglia et al., 2014), whereas redox systems can do so independent of temperature by including a reducing agent along with an oxidizing agent. Photoinitiators produce reactive species upon exposure to light of varying wavelengths depending on the compound (Hageman, 1985). Azo compounds decompose in a range of temperatures so, depending on the reaction requirements, a compatible azo initiator can be found (Braun, 2009). Some of the most notable work in free-radical polymerization has been the development of scaffolds consisting of polyester-based polymers, PPF (Peter et al., 1999a,b; Sikavitsas et al., 2001), ethylene glycol dimethacrylate (EGDMA), butanediol dimethacrylate (BDMA) (Moglia et al., 2014), and propylene fumarate dimethacrylate (PFDMA) (Moglia et al., 2014; Sears et al., 2017; Whitely et al., 2017).

Synthetic scaffolds offer a wealth of benefits to the field of tissue engineering. The work done in the polymer engineering and processing industry over the last several decades has benefited the field immensely and brought forth technologies for the creation of highly monodisperse and biocompatible polymers. The formation of polyaddition polymers with vinyl monomers through free-radical polymerization has opened

the door for tissue-engineering scaffolds that can be created quickly to form robust scaffolding systems; polycondensation polymers have been harnessed to create biocompatible scaffolds such as PCL, PLA, and PGA and PLGA which are commonly used in biodegradable sutures (Bourissou et al., 2004; Gilding and Reed, 1979). The field has expanded immensely and is expected to continue expanding in the coming years.

Biological Polymers

Biological polymers have emerged as attractive materials for tissue engineering given their biocompatibility and biodegradability. Gelatin is a popular biological polymer that has been fabricated into a variety of scaffold systems; it is also highly biocompatible and contains the RGD peptide sequence known to promote cell adhesion (Liu et al., 2017). Gelatin has also been shown to demonstrate shear-thinning properties (Liu et al., 2017), which is very attractive for extrusion-based 3D printing applications. Alginate is another popular biopolymer that is cross-linked via ionic cross-linking around divalent cations, most commonly Ca^{2+} (Lee and Mooney, 2012). This cross-linking is reversible and has been harnessed to encapsulate single cells (Utech et al., 2015), and create stimuli-responsive drug-delivery systems (Huebsch et al., 2014). Glycosaminoglycans (GAGs) are another class of materials commonly used in tissue-engineering applications given their natural presence in the ECM. Hyaluronic acid has been used for a variety of tissue-engineering applications because of its natural presence in many wound-healing processes (Leach et al., 2003), as well as its ease for chemical modification and biodegradability (Hubbell, 1995; Leach et al., 2003; Van Vlierberghe et al., 2011). Once degraded, the polymer has been shown to promote angiogenesis (Leach et al., 2003). Sulfated GAGs such as chondroitin sulfate and heparan sulfate can also sequester GFs to promote cell growth and proliferation (Rinker et al., 2018; Van Vlierberghe et al., 2011).

Decellularized tissues are a class of biomaterials that has also been used to synthesize biological scaffolds. Once decellularized, these tissues retain many of the bio-instructive cues found in tissue that can promote native tissue integration and defect repair (Badylak, 2004; Badylak et al., 2011; Cheng et al., 2014). Scaffolds derived from decellularized tissues such as muscle (Cheng et al., 2014; Merritt et al., 2010a,b; Smoak et al., 2019), lung (Nichols et al., 2013), and heart (Ott et al., 2008) have been documented. Further processing the decellularized tissue (e.g., digestion with pepsin) for various applications such as electrospinning (Bauguera et al., 2014) and 3D printing (Pati et al., 2014) has also been explored.

Composites and Additives

Given the complexity of native tissue, composite and additive biomaterial systems for tissue engineering are popular options for encouraging regeneration (Temenoff and Mikos, 2000). Tissues such as bone and cartilage are particularly popular options for composite biomaterials (Temenoff and Mikos, 2000; Venkatesan and Kim, 2014). Hydroxyapatite (HA) is a

natural calcium phosphate mineral found in bone and enamel, used in bone tissue engineering. However, due to their brittleness, ceramics such as HA are often combined with polymers to create scaffolds with enhanced mechanical strength (Venkatesan and Kim, 2014). Polymers commonly used with HA for bone tissue engineering include collagen, gelatin, PLA, PLGA, PCL, and polyurethane. Composite scaffolds for cartilage often include cells and have been composed of polymers such as thrombin and fibrin, as well as alginate, hyaluronic acid, and oligo(poly(ethylene glycol) fumarate) (Park et al., 2007; Temenoff and Mikos, 2000). Another application of composite materials has been in neural tissue engineering. Composite fibers were used in neural regeneration applications by electrospinning human glial cell-derived neurotrophic factor (GDNF) inside a copolymer of ϵ -caprolactone and ethyl ethylene phosphate (Chew et al., 2007). Similarly, there have been other numerous documented examples of improved regenerative outcome for composite scaffolds incorporating transforming growth factor- β 1 (TGF- β 1) for cartilage repair, vascular endothelial growth factor (VEGF) for angiogenesis

(Cao et al., 2009; Lee et al., 2011), and insulin-like growth factor 1 (IGF-1) for a variety of applications (Chen et al., 2009; Davis et al., 2006; Lee et al., 2011).

Scaffold Fabrication Techniques

Scaffolds are one of the three main components of the tissue-engineering strategy to repair, regenerate, and remodel living tissues after an injury or disease (O'Brien, 2011). Since the beginning of the tissue-engineering field, scaffolds have shown a key role since they provide a 3D solid support for the attachment, proliferation, migration, and differentiation of the cells. Furthermore, they can also serve as reservoirs for the controlled release of bioactive molecules or drugs that can drive the regeneration process (Nair and Laurencin, 2007). The field of tissue engineering has developed a wide range of processing techniques to fabricate porous scaffolds from one or more biodegradable polymers that are selected depending on the properties needed for the intended application (Table 2.6.3.2).

TABLE 2.6.3.2 Preparation Techniques for Tissue-Engineering Scaffolds, Requirements and Examples of Applications

Scaffold Fabrication Techniques	Requirements	Applications
Rapid prototyping	Must utilize inks that are easy to work with and possess desired mechanical properties	Create 3D structures from computer models. Stereolithography, selective laser sintering (SLS), inkjet bioprinting, extrusion printing, bioplotting. Often use amorphous and semicrystalline polymers such as PCL, PLA, and PLGA. Poly(vinyl alcohol) (PVA) and poly(propylene fumarate) (PPF) have also been used
Electrospinning/ electrospraying	Relies on an electric field to aid in the deposition of the polymer solution onto a collecting plate so choosing a suitable polymer and solvent carrier is required	Fabricate microparticles via electrospinning or fibrous mesh scaffolds via electrospinning. Have been used to generate scaffolds made from chitosan, gelatin, collagen, PCL, PLGA, polyurethanes, and more
Superstructure engineering	Depends on structural interactions to maintain scaffold integrity such as noncovalent, van der Waals, hydrophobic, ionic, magnetic, and electrostatic interactions so polymers must be chosen that promote these interactions	Generate complex structures built on noncovalent interactions. Allows for reversibility, and it also enables "self-healing" scaffolds to be created
Solvent casting, particulate/porogen leaching	Must select a porogen not soluble in the solvent that the polymer is being cast in. Selecting a porogen of adequate size that also allows for interconnectivity is important as well	Generate porosity in scaffolds. Salt leaching is the most common porosity-inducing method. Polymers such as sugar or paraffin have also been used as porogens
Freeze-drying	Must be able to withstand cold temperatures. The freezing rate impacts pore size with faster freezing rates producing homogeneous pore structures	Remove water and generate porosity when paired with annealing. Attractive for use with materials that are temperature sensitive at higher temperatures
Phase separation	Requires immiscible phases to be chosen, and consideration for compatibility of the phases with biological molecules must be considered	Create porous foams. Can also use thermally induced phase separation to create porous structures with high interconnectivity
Gas foaming	Requires the polymer to be able to be saturated with CO ₂	Generate highly porous structures by foaming dissolved CO ₂ gas. The CO ₂ interacts strongly with carbonyl groups so PLA, PLGA, and PCL are commonly used. Can also be used to decellularize tissues

Rapid Prototyping

Rapid prototyping or solid free form fabrication refers to a series of techniques that use polymeric materials by printing layer-by-layer scaffolds from a 3D model created by computer (Peltola et al., 2008). Compared to traditional biofabrication techniques, rapid prototyping can recreate complex structures with high fidelity and reproducibility while minimizing material loss (Bittner et al., 2018). Additional advantages are the possibility to design patient-specific scaffolds and on-demand fabrication (Guvendiren et al., 2016). Among various rapid prototyping techniques, extrusion printing, stereolithography (SLA), selective laser sintering (SLS), digital light projection (DLS) and inkjet bioprinting have gained increased usage in fabricating tissue-engineered scaffolds in the last decade (Ozolat and Hospodiuk, 2016; Roseti et al., 2017).

Extrusion printing is based on the melting of a polymeric admixture inside of a moving extruder arm and its deposition on a printing platform through a nozzle using pneumatic or mechanical dispersers (Zein et al., 2002). Extrusion printing has become an attractive platform for the preparation of highly precise porous scaffolds for tissue engineering because of its resolution, reproducibility, and fidelity to the predesigned model (An et al., 2015). In particular, extrusion printing has been shown to be suitable for the fabrication of porous scaffolds prepared with a wide range of compositions including thermoplastics and composite admixtures (Bittner et al., 2019; Diaz-Gomez et al., 2019). However, the incorporation of bioactive or heat-sensitive biomolecules in the aforementioned methods is limited due to the high temperatures and pressures involved in the extrusion process. A cell-friendly alternative to the high temperatures involved in the extrusion printing is direct ink writing or cold temperature 3D bioprinting. A wide range of natural polymers, including polysaccharides such as alginate or chitosan, and proteins such as collagen, gelatin, or elastin, among others, have been used as bioinks to prepare cell- or GF-laden scaffolds for tissue engineering (Chung et al., 2013; Das et al., 2015; Echave et al., 2017; Jammalamadaka and Tappa, 2018; Radhakrishnan et al., 2017).

SLA and DLS use a light beam or an image projection, respectively, to cure a polymer solution into a specific pattern with high resolution (Dean et al., 2012; Melchels et al., 2010). After each layer is cured, the platform moves up, and the process is repeated until the fabrication is completed. SLA has become an alternative to extrusion-related approaches since shear-stress mechanisms are not involved (Lin et al., 2013). However, the need for photoinitiators that are potentially cytotoxic limits the use of this approach for cell-laden tissue-engineering applications (Manapat et al., 2017). SLS is another layer-by-layer technology that uses a high-energy laser to fuse a thin layer of powder particles together. The resolution of the printed object is restricted by the precision of the laser to sinter the powder, and depends on the laser power and speed, layer thickness, and laser focusing radius, among others (Shirazi et al., 2015). SLS

offers very precise control over the microstructure design and the obtained scaffolds usually hold high mechanical strength. The main drawbacks of this technique are the difficulty to alternate different materials in the construct and the need for powdered materials with good flow properties to homogeneously deposit each layer (Mazzoli, 2013).

Electrospinning/Electrospraying

Electrospinning is a widely used technique to prepare nano- and/or microfibrillar structures from polymeric solutions using the action of an electric field (Lannutti et al., 2007; Pham et al., 2006). The diameter and morphology of the resulting fibers that mainly define scaffold porosity can be modified with the polymer concentration, the voltage applied, and the distance between the needle and the collector (Jiang et al., 2015b). Fiber diameter has a key role in the micro- and macroscopic properties of the electrospun scaffolds, including porosity and mechanical and biological properties (Sisson et al., 2010; Unnithan et al., 2015). A wide range of both natural and synthetic polymers as well as their blends have been used for electrospinning (Khajavi et al., 2016). In particular, core-shell coaxial electrospinning has been explored as a method to prepare nanofibrillar scaffolds that encapsulate drugs or other bioactive molecules such as GFs in the core (Yoon et al., 2018; Zhang et al., 2013). Melt electrospinning is another variation of electrospinning, where the polymer is melted in a syringe or cartridge and ejected toward a collector by applying an electric field. This method of electrospinning does not require solvents and thus results in lower toxicity and fewer postprocessing steps compared to conventional electrospinning. Furthermore, when a movable collector plate is used, it is possible to fabricate intricate porous structures from a template created using a software (Brown et al., 2016; Hochleitner et al., 2015).

Superstructure Engineering

Self-assembly is considered a bottom-up autonomous arrangement of components into certain patterns or structures driven by short-distance interactions (noncovalent, van der Waals, hydrophobic interactions, ionic, magnetic, or electrostatic). Using self-assembly, it is possible to control the structure of the scaffolds at the molecular level to create highly complex structures that closely mimic the properties and architecture of the native tissues. Furthermore, since self-assembly is a reversible process, most of the scaffolds developed using this technique present unique self-healing properties that make them very attractive when used in locations that could present mechanical perturbations. Self-assembly scaffolds with diverse architectures have been developed using protein-based strategies such as chemically or biologically synthesized peptides. Self-assembly peptides are usually prepared as injectable hydrogels that self-assemble in situ as a result of pH or temperature (Hosseinkhani et al., 2013). The main advantages of using peptides for the preparation of self-assembly scaffolds are their high biocompatibility and biodegradability. Furthermore, slight modifications

in the peptide sequences result in macromolecular changes that affect the properties of the scaffold and can be used to tune the mechanical and functional properties of the resulting constructs (Habibi et al., 2016). However, since most of the compositions are hydrogels, their use is limited to soft tissues, which remains as a challenge along with cost and scalability (Dutta et al., 2017; Khan and Tanaka, 2017).

Solvent Casting, Particulate/Porogen Leaching

Solvent-casting particulate leaching (SCPL) is a simple and cost-effective method to prepare highly porous polymeric scaffolds. Insoluble porogens such as salts are dispersed in a polymer solution, and following a solvent evaporation step, a porogen–polymer composite is formed that is further washed to remove the porogen particles (Mikos et al., 1994). SCPL allows for the preparation of scaffolds with a porosity higher than 90% and pore size up to 500 μm (Prasad et al., 2017). Furthermore, it is relatively easy to control the pore architecture (pore size, interconnectivity, porosity) of the obtained scaffolds by the selection of adequate polymers, porogens, and their concentrations. Porogen leaching, however, has been reported to result in poor interconnectivity and heterogeneous pore shapes. Porogen–polymer blends such as sodium chloride and PEG have therefore been investigated to introduce a dual-leaching process, which could significantly increase the interconnectivity of pores while maintaining a homogeneous pore size distribution (Thadavirul et al., 2013). The main drawback of SCPL is the use of organic solvents that could lead to cytotoxicity and also limit the incorporation of bioactive molecules. Moreover, the mechanical properties of scaffolds prepared with this technique are below the requirements of load-bearing tissues (Janik and Marzec, 2015). In order to increase the mechanical properties of the scaffolds, gel casting has become an interesting alternative. A green strategy used to produce polymeric, ceramic, and composite porous scaffolds, gel casting consists of a preparation of an aqueous polymeric solution that is foamed and polymerized in situ through chemical reactions to prevent structure collapse. The obtained structures are dried and, if ceramic materials are used, sintered (Montanaro et al., 2018). Scaffolds produced using gel casting showed high interconnectivity and dense pore walls, with high mechanical strength and porosities over 90% (Baino et al., 2015; Siqueira et al., 2017).

Freeze-Drying

Freeze-drying is a simple approach for the preparation of highly porous polymeric scaffolds via freezing and sublimation of an aqueous or organic polymeric solution using low temperature and pressure. Since the process does not involve high temperatures, it allows heat-sensitive components to be included into the scaffold. The structure of the scaffold can be tuned by adjusting the polymer concentration and molecular weight, the viscosity of the polymer solution, and solvent type. Other processing parameters such as the cooling rate and the freezing temperature strongly affect the

scaffolds' structural properties: fast cooling rates usually lead to more homogeneous pore structures, while lowering the freezing temperature decreases the mean pore size. Annealing (increasing the temperature of the frozen material to promote the growth of ice crystals) has also been described as a strategy to increase the mean pore size of scaffolds (Pawelec et al., 2014; Raeisdasteh Hokmabad et al., 2017). In general, freeze-drying only allows for the preparation of simple (planar) 3D structures, but complex structures have been successfully prepared by controlling the molds and the processing parameters (Brougham et al., 2017). Pore orientation can be defined by controlling the growth speed and orientation of the ice crystals, resulting in unidirectional porous scaffolds (Deville, 2010). Pore size can also be controlled by the polymer concentration and molecular weight (Qian and Zhang, 2011).

An alternative to freeze-drying is emulsion freeze-drying which has attracted attention due to its ability to prepare scaffolds with highly specific pore surface area. The method is based on the dissolution of a polymer solvent and its further emulsification by the addition of a nonsolvent. The obtained emulsion is poured into a mold and quenched at low temperature prior to freeze-drying to remove the solvent and nonsolvent (Sultana and Wang, 2008, 2012). PVA is an attractive polymer to be processed using these approaches since it physically cross-links when submitted to freeze/thawing, thus avoiding the use of potentially cytotoxic cross-linkers (Nie et al., 2012). The biodegradation rate of the scaffolds can also be controlled by modifying the ratio of polymers included in the composition (Sultana and Wang, 2012).

Phase Separation

Phase separation can be achieved with the addition of a nonsolvent, which yields scaffolds with heterogeneous pore structures. This option is less attractive for tissue engineering scaffolds that generally require uniform porous structures. A second approach is the thermally induced phase separation (TIPS) method, which is based on the decrease of thermodynamic stability of a polymeric solution with small changes in the temperature of the system resulting in a phase separation process which produces a polymer-rich phase and a polymer-lean phase. After the removal of the polymer-lean phase by evaporation or lyophilization, the polymer-rich phase becomes a highly interconnected porous structure with homogeneous pore size distributions (Lu et al., 2013; O'Brien, 2011). By controlling process variables such as polymer concentration and molecular weight, solvent/nonsolvent ratio, and the cooling path, it is possible to obtain scaffolds that have a wide range of morphologies and microporous structures. Since pores are formed in the paths created by the solvent extraction, high interconnectivity is easily achieved, which makes this technique very attractive for cell spreading and migration (Wei and Ma, 2004). Various synthetic and natural polymers have been processed alone or in combination with others to prepare highly porous scaffolds with controlled structures, including gradients (Mannella et al., 2015; Pavia et al., 2008).

Gas Foaming/Supercritical Fluid Processing

Gas foaming is a solvent-free method that uses the expansion effect of a gas to fabricate highly porous scaffolds. CO₂ is the most used gas since it is safe, reusable, and cost-efficient. CO₂ also reaches a supercritical state at mild temperature and pressure (31.1°C and 73.9 bar) (Picchioni, 2014). In this process, the polymer is saturated with CO₂, which reduces its glass transition temperature through a plasticizing effect. Once equilibrated, controlled depressurization results in the nucleation and expansion of the CO₂, forming pores in the material as it is evacuated (García-González et al., 2015). The size and density of the pores can be regulated by adjusting the temperature, pressure, and depressurization rate. Dual pore populations, generally in the nano- and microscale, can also be achieved by modification of the depressurization rate during the process (Ji et al., 2012). Blends of two or more materials can be used to control the foaming process or the porous micro- and macrostructure of the obtained scaffolds (Moghadam et al., 2017; Salerno et al., 2009). Due to its mild processing temperature, biological molecules such as GFs have been incorporated in polymeric scaffolds without affecting their biological activity (Diaz-Gomez et al., 2016; Hile et al., 2000).

Scaffold Characterization Techniques

Scaffold characterization involves the characterization of the material utilized to fabricate the scaffold and the bulk properties of the obtained constructs. Material characterizations involve methods to assess the purity and structure, such as nuclear magnetic resonance (NMR), mass spectrometry (MS), gas/liquid chromatography (GC/LC), and additional spectroscopic methods such as Raman and infrared. Gel permeation chromatography (GPC) is widely used to measure the molecular weight and polydispersity of synthesized polymers. Thermal properties of polymers are measured using differential scanning calorimetry (DSC) and thermogravimetric analyzer (TGA). DSC will quantify glass transition and melting temperatures (T_g and T_m , respectively) (Mikos et al., 1994), as well as LCST of thermoresponsive polymers; TGA will measure the thermal stability of a given polymer and is widely used to characterize ceramics.

Physical properties of synthesized scaffolds can be quantified via multiple methods. Microscopic techniques such as scanning electron microscopy (SEM) and atomic force microscopy (AFM) are frequently used to observe the surface morphology of a scaffold (Ma et al., 2007). Of the two techniques, AFM has a higher resolution and can accurately quantify nanoscale topographical details. SEM or simple light microscopy can be used also to measure the size and shape of microparticles. Mechanical properties such as compressive or tensile moduli can be quantified by directly placing the scaffold under appropriate stress and measuring the stress-strain curve. In the case of thermosensitive hydrogels, a thermomechanical analyzer (TMA) can be used to conduct mechanical testing under a temperature-controlled

environment. The scaffold degradation rate can be measured over any period of time by weight loss after incubation in an environment that mimics *in vivo* or accelerated *in vivo* conditions. Drug release profiles from a bulk scaffold can be measured by using high-performance liquid chromatography (HPLC), which can measure the concentration of drugs that have been eluted from the scaffold to the surrounding media at specific time points (Haesslein et al., 2006; Shi et al., 2010). For applications that require cell encapsulation, biocompatibility can be measured indirectly by measuring the viability of encapsulated cells, or by culturing the cells with the leachable byproducts of the scaffold.

Standards for characterizing scaffolds and biomaterials for tissue-engineering applications have been developed by standards organizations such as ASTM and International Organization for Standardization (ISO) (Vo and Trachtenberg, 2014). In addition to characterization standards for scaffolds *in vitro*, methods of assessing constructs *in vivo* have been developed (Trachtenberg et al., 2015). These guides are application-specific and provide detailed guidelines on techniques and procedures that are required to test any given scaffold or biomaterial. Characterization techniques discussed in previous paragraphs should therefore be conducted on the designed scaffolds according to the established standards that correspond to the scaffolds' potential application. This will also be important for future clinical translation of such scaffolds (Table 2.6.3.3).

Cell-Incorporated Scaffolds

Biomaterial scaffolds are ideal carriers for cell delivery (Ricles et al., 2016; Truong et al., 2015). Research has shown that cell delivery alone results in cell death and low cell retention at the site of delivery (Chen et al., 2012; Ricles et al., 2016; Vo et al., 2016). However, when encapsulated within a biomaterial carrier, particularly those decorated with cell-specific or ECM-specific markers and factors, cell viability is improved and controlled differentiation may be induced (Na et al., 2007; Nguyen and West, 2002; Ricles et al., 2016). Hydrogels are a particularly popular biomaterial for cell encapsulation given their highly swollen nature, their ability to be patterned with moieties, and to allow the diffusion of oxygen and nutrients to cells within the scaffolds (Nguyen and West, 2002; Ricles et al., 2016; Truong et al., 2015; Vo et al., 2016). These cell-encapsulated systems may be injectable, allowing the cell-laden scaffold to fill the defect site (Ricles et al., 2016), or printed into their desired geometry (Billiet et al., 2014; Kolesky et al., 2014). Cell-laden scaffolds also allow for multiple cell types to be incorporated into a scaffold, which is important in mimicking the complexity of native tissue (Xu et al., 2013), including interfacial gradient units of tissue such as the osteochondral unit at the bone/cartilage interface (Mohan and Detamore, 2014; Yang et al., 2017).

Perfusion seeding is another technique for cell incorporation in the scaffolds (Zhao and Ma, 2005). Stem cells may be seeded onto scaffolds through perfusion-based methods and have been reported to maintain stemness in the case of MSCs (Zhao and

TABLE 2.6.3.3 Description of the Characterization Techniques for Tissue-Engineering Scaffolds

Polymer/Scaffold Property	Characterization Technique	Description
Chemical characterization	Nuclear magnetic resonance (NMR) spectroscopy	Provides highly specific characterization of polymer structure and molecular weight. Most commonly used NMR techniques are ^1H -NMR and ^{13}C -NMR with ^1H -NMR being the most common for polymers for tissue-engineering applications
	Fourier transform infrared (FTIR) spectroscopy	Is used to characterize scaffolds and polymers alike. Spectra possess unique fingerprint regions for common bonds such as amides, carbonyls, and more to characterize structures
	Gas/liquid chromatography (GC/LC)	Separates and analyzes polymers that can be vaporized without decomposing. Liquid chromatography (often high-performance liquid chromatography or HPLC) consists of a chromatography column and a detection tool such as a UV spectrometer that helps separate and identify products as they are eluted through the column
	Raman spectroscopy	Aids in the characterization and identification of polymers by looking at the spectra to identify fingerprint regions for common chemical bonds, similarly to FTIR
Mass/molecular weight characterization	Mass spectrometry (MS)	Ionizes the product and calculates molecular weight based on time of flight to a detector. Provides highly specific mass values
	Gel permeation chromatography (GPC)	Characterizes molecular weights based on well established PEG or PMMA standards. Can characterize hydrophilic and hydrophobic polymers. Can also be paired with mass spectrometry for added accuracy
Thermal properties characterization	Differential scanning calorimetry (DSC)	Determines the glass transition temperature (T_g) and the melting temperature (T_m) of the polymer
	Thermogravimetric analysis (TGA)	Determines the thermal stability of the polymer over a range of temperatures
Morphology/surface characterization	Scanning electron microscopy (SEM)	Aids in determining surface features of polymer scaffolds such as mesh size or porosity
	Atomic force microscopy (AFM)	Is used to image polymers and compounds at single-atom resolution. Can also be utilized to determine mechanical properties of scaffolds at single bond resolution
Mechanical properties characterization	Rheology	Measures mechanical properties for viscoelastic materials. Can determine the point of gelation for scaffolds
	Tensile testing	Is used to determine the tensile properties of a polymer or scaffold materials
	Compressive testing	Determines the compressive properties of a polymer or scaffold material

Ma, 2005). Perfusion-based seeding has also been used to vascularize scaffolds in 3D printed systems (Miller et al., 2012). Bioreactor culture is closely related and often follows perfusion-based seeding. This allows for the diffusion of nutrients to cells (Cartmell et al., 2003; Saini and Wick, 2003). It also allows the cells within the scaffold to be placed under shear forces during culture to maintain mechanical stimulation to improve viability (Cartmell et al., 2003), induce differentiation of bone cells (Gomes et al., 2003) and endothelial vascular cells (Yamamoto, 2004), and create better disease models in the case of Ewing sarcoma (Santoro et al., 2015). Tissues such as cartilage, bone, and heart valves require mechanical stimulation for their function (Cartmell et al., 2003; Hoerstrup et al., 2000; Saini and Wick, 2003), and engineered tissue quality is greatly enhanced for such tissues with mechanical stimulation via the shear forces seen in bioreactor culture (Bancroft et al., 2002; Holtorf et al., 2005a,b; Sikavitsas et al., 2003).

Conclusions

The field of materials development for tissue engineering has advanced greatly in recent years. Scaffolds can be created as carriers for cells, drugs, and bioactive factors for diverse tissue engineering, drug delivery, and wound-healing applications. These scaffolds are often biodegradable via ester hydrolysis or enzymatic degradation and can be composed of synthetic or natural polymers. Using a wide variety of fabrication techniques such as rapid prototyping, electrospinning, solvent casting/porogen leaching, gas foaming, and more, robust and porous scaffolds can be created for a variety of applications and their features and properties can be tailored depending on their intended application. Many challenges still remain in the field of materials development for tissue engineering, but ongoing work in the field shows promise for significant developments in the near future.

CASE STUDY: MATRIX-ASSISTED AUTOLOGOUS CHONDROCYTE TRANSPLANTATION (MACT)

Multiple reparative surgical techniques have been developed over the years to treat articular cartilage lesions. Microfracture, or marrow stimulation, refers to a technique where the subchondral bone beneath the defect is penetrated using a microneedle to allow the flow of blood and bone marrow into the site. The formation of a blood clot, which contains progenitor cells from the marrow, gradually leads to regeneration of the tissue. Another option available to patients is osteochondral autograft or allograft, where cartilage pieces from either low weight-bearing regions of the patient's (autograft) or a donor's (allograft) joints are harvested and transferred to the defect site. These surgical techniques, however, present certain challenges. For instance, microfracture has been shown to be linked with formation of fibrous cartilage,¹ osteochondral autograft with donor site morbidity,² and allograft with immune response and loss of cell viability.²

In the late 20th century, a cell-based approach to treating osteochondral defects was developed. This technique, called autologous chondrocyte implantation (ACI), involves small cartilage biopsies being taken from the patient to harvest chondrocytes that are then expanded in vitro and delivered directly into the defect site as a suspension.³ Matrix-assisted autologous chondrocyte transplantation (MACT) is the second-generation

ACI, where a type I/III collagen membrane is used as a cell-seeded scaffold to deliver in vitro-expanded autologous chondrocytes to the defect site.⁴ The membrane is customized to fit the size of the defect site before being sealed in place using fibrin glue.

MACT also presents certain challenges. Expansion of chondrocytes in vitro has been shown to lead to dedifferentiation; studies have shown that when chondrocytes are cultured on a stiff, 2D substrate, they gradually lose the ability to produce type II collagen and glycosaminoglycans even after the first passage.⁵ Cell expansion is also a time-consuming process, and the number of chondrocytes required for transplantation, and therefore the overall culture period, will depend on the size of the defect. Nevertheless, MACT is one of the first FDA-regulated tissue-engineered therapies for clinical usage.

¹Kreuz et al., 2006. Osteoarthritis and Cartilage. <https://doi.org/10.1016/j.joca.2006.05.003>.

²Haene et al., 2012. J. Bone Joint Surg. <https://doi.org/10.2106/JBJS.J.02010>.

³Brittberg et al., 1994. N. Engl. J. Med. <https://doi.org/10.1056/NEJM199410063311401>.

⁴Cherubino et al., 2003. J. Orthop. Surg. <https://doi.org/10.1177/230949900301100104>.

⁵Benya et al., 1982. Cell. [https://doi.org/10.1016/0092-8674\(82\)90027-7](https://doi.org/10.1016/0092-8674(82)90027-7).

References

- Amado, L.C., Saliaris, A.P., Schuleri, K.H., St John, M., Xie, J.-S., Cattaneo, S., Durand, D.J., Fitton, T., Kuang, J.Q., Stewart, G., Lehrke, S., Baumgartner, W.W., Martin, B.J., Heldman, A.W., Hare, J.M., 2005. Cardiac repair with intramyocardial injection of allogeneic mesenchymal stem cells after myocardial infarction. *Proc. Natl. Acad. Sci.* 102, 11474–11479.
- An, J., Teoh, J.E.M., Suntornnond, R., Chua, C.K., 2015. Design and 3D printing of scaffolds and tissues. *Engineering* 1, 261–268.
- Arakawa, C.K., Badeau, B.A., Zheng, Y., DeForest, C.A., 2017. Multicellular vascularized engineered tissues through user-programmable biomaterial photodegradation. *Adv. Mater.* 29, 1–9.
- Arima, Y., Iwata, H., 2007. Effect of wettability and surface functional groups on protein adsorption and cell adhesion using well-defined mixed self-assembled monolayers. *Biomaterials* 28, 3074–3082.
- Bachmann, F., Reimer, J., Ruppenstein, M., Thiem, J., 2001. Synthesis of novel polyurethanes and polyureas by polyaddition reactions of dianhydrohexitol configured diisocyanates. *Macromol. Chem. Phys.* 202, 3410–3419.
- Badylak, S.F., 2004. Xenogeneic extracellular matrix as a scaffold for tissue reconstruction. *Transpl. Immunol.* 12, 367–377.
- Badylak, S.F., Taylor, D., Uygun, K., 2011. Whole-organ tissue engineering: decellularization and recellularization of three-dimensional matrix scaffolds. *Annu. Rev. Biomed. Eng.* 13, 27–53.
- Baiguera, S., Del Gaudio, C., Lucatelli, E., Kuevda, E., Boieri, M., Mazzanti, B., Bianco, A., Macchiarini, P., 2014. Electrospun gelatin scaffolds incorporating rat decellularized brain extracellular matrix for neural tissue engineering. *Biomaterials* 35, 1205–1214.
- Baino, F., Novajra, G., Vitale-Brovarone, C., 2015. Bioceramics and scaffolds: a winning combination for tissue engineering. *Front. Bioeng. Biotechnol.* 3, 1–17.
- Bancroft, G.N., Sikavitsas, V.I., van den Dolder, J., Sheffield, T.L., Ambrose, C.G., Jansen, J.A., Mikos, A.G., 2002. Fluid flow increases mineralized matrix deposition in 3D perfusion culture of marrow stromal osteoblasts in a dose-dependent manner. *Proc. Natl. Acad. Sci.* 99, 12600–12605.
- Benoit, D.S.W., Schwartz, M.P., Durney, A.R., Anseth, K.S., 2008. Small functional groups for controlled differentiation of hydrogel-encapsulated human mesenchymal stem cells. *Nat. Mater.* 7, 816–823.
- Berry, M.F., 2006. Mesenchymal stem cell injection after myocardial infarction improves myocardial compliance. *AJP Hear. Circ. Physiol.* 290, H2196–H2203.
- Billiet, T., Gevaert, E., De Schryver, T., Cornelissen, M., Dubrue, P., 2014. The 3D printing of gelatin methacrylamide cell-laden tissue-engineered constructs with high cell viability. *Biomaterials* 35, 49–62.
- Bittner, S.M., Guo, J.L., Melchiorri, A., Mikos, A.G., 2018. Three-dimensional printing of multilayered tissue engineering scaffolds. *Mater. Today* 21, 861–874.
- Bittner, S.M., Smith, B.T., Diaz-Gomez, L., Hudgins, C.D., Melchiorri, A.J., Scott, D.W., Fisher, J.P., Mikos, A.G., 2019. Fabrication and mechanical characterization of 3D printed vertical uniform and gradient scaffolds for bone and osteochondral tissue engineering. *Acta Biomater.* 90, 37–48.
- Black, L.L., Gaynor, J., Adams, C., Dhupa, S., Sams, A.E., Taylor, R., Harman, S., Gingerich, D.A., Harman, R., 2008. Effect of intraarticular injection of autologous adipose-derived mesenchymal stem and regenerative cells on clinical signs of chronic osteoarthritis of the elbow joint in dogs. *Vet. Ther.* 9, 192–200.
- Bourissou, D., Dechy-Cabaret, O., Martin-Vaca, B., 2004. Controlled ring-opening polymerization of lactide and glycolide. *Chem. Rev.* 104, 6147–6176.
- Braun, D., 2009. Origins and development of initiation of free radical polymerization processes. *Int. J. Polym. Sci.* 2009, 1–10.

- Breuls, R.G.M., Jiya, T.U., Smit, T.H., 2008. Scaffold stiffness influences cell behavior: opportunities for skeletal tissue engineering. *Open Orthop. J.* 2, 103–109.
- Brougham, C.M., Levingstone, T.J., Shen, N., Cooney, G.M., Jockenhoevel, S., Flanagan, T.C., O'Brien, F.J., 2017. Freeze-drying as a novel biofabrication method for achieving a controlled micro-architecture within large, complex natural biomaterial scaffolds. *Adv. Healthc. Mater.* 6, 1–7.
- Brown, T.D., Dalton, P.D., Hutmacher, D.W., 2016. Melt electrospinning today: an opportune time for an emerging polymer process. *Prog. Polym. Sci.* 56, 116–166.
- Brown, T.E., Silver, J.S., Worrell, B.T., Marozas, I.A., Yavitt, F.M., Günay, K.A., Bowman, C.N., Anseth, K.S., 2018. Secondary photocrosslinking of click hydrogels to probe myoblast mechanotransduction in three dimensions. *J. Am. Chem. Soc.* 140, 11585–11588.
- Burdick, J.A., Anseth, K.S., 2002. Photoencapsulation of osteoblasts in injectable RGD-modified PEG hydrogels for bone tissue engineering. *Biomaterials* 23, 4315–4323.
- Cao, L., Arany, P.R., Wang, Y.S., Mooney, D.J., 2009. Promoting angiogenesis via manipulation of VEGF responsiveness with notch signaling. *Biomaterials* 30, 4085–4093.
- Cartmell, S.H., Porter, B.D., García, A.J., Guldborg, R.E., 2003. Effects of medium perfusion rate on cell-seeded three-dimensional bone constructs *in vitro*. *Tissue Eng.* 9, 1197–1203.
- Chan, B.P., Hui, T.Y., Wong, M.Y., Yip, K.H.K., Chan, G.C.F., 2010. Mesenchymal stem cell-encapsulated collagen microspheres for bone tissue engineering. *Tissue Eng. C Methods* 16, 225–235.
- Chang, H.-I., Wang, Y., 2011. Cell responses to surface and architecture of tissue engineering scaffolds. In: *Regenerative Medicine and Tissue Engineering – Cells and Biomaterials*. InTech, pp. 569–588.
- Charnley, J., 1960. Anchorage of the femoral head prosthesis to the shaft of the femur. *J. Bone Joint Surg. Br.* 42–B, 28–30.
- Chen, F.M., Chen, R., Wang, X.J., Sun, H.H., Wu, Z.F., 2009. In vitro cellular responses to scaffolds containing two microencapsulated growth factors. *Biomaterials* 30, 5215–5224.
- Chen, F.M., Sun, H.H., Lu, H., Yu, Q., 2012. Stem cell-delivery therapeutics for periodontal tissue regeneration. *Biomaterials* 33, 6320–6344.
- Cheng, C.W., Solorio, L.D., Alsberg, E., 2014. Decellularized tissue and cell-derived extracellular matrices as scaffolds for orthopaedic tissue engineering. *Biotechnol. Adv.* 32, 462–484.
- Chew, S.Y., Mi, R., Hoke, A., Leong, K.W., 2007. Aligned protein-polymer composite fibers enhance nerve regeneration: a potential tissue-engineering platform. *Adv. Funct. Mater.* 17, 1288–1296.
- Chung, J.H.Y., Naficy, S., Yue, Z., Kapsa, R., Quigley, A., Moulton, S.E., Wallace, G.G., 2013. Bio-ink properties and printability for extrusion printing living cells. *Biomater. Sci.* 1, 763–773.
- Cui, W., Zhu, X., Yang, Y., Li, X., Jin, Y., 2009. Evaluation of electrospun fibrous scaffolds of poly(DL-lactide) and poly(ethylene glycol) for skin tissue engineering. *Mater. Sci. Eng. C* 29, 1869–1876.
- Dado, D., Levenberg, S., 2009. Cell-scaffold mechanical interplay within engineered tissue. *Semin. Cell Dev. Biol.* 20, 656–664.
- Das, S., Pati, F., Choi, Y.-J., Rijal, G., Shim, J.-H., Kim, S.W., Ray, A.R., Cho, D.-W., Ghosh, S., 2015. Bioprintable, cell-laden silk fibroin–gelatin hydrogel supporting multilineage differentiation of stem cells for fabrication of three-dimensional tissue constructs. *Acta Biomater.* 11, 233–246.
- Davis, M.E., Hsieh, P.C.H., Takahashi, T., Song, Q., Zhang, S., Kamm, R.D., Grodzinsky, A.J., Anversa, P., Lee, R.T., 2006. Local myocardial insulin-like growth factor 1 (IGF-1) delivery with biotinylated peptide nanofibers improves cell therapy for myocardial infarction. *Proc. Natl. Acad. Sci.* 103, 8155–8160.
- Dean, D., Wallace, J., Siblani, A., Wang, M.O., Kim, K., Mikos, A.G., Fisher, J.P., 2012. Continuous digital light processing (cDLP): highly accurate additive manufacturing of tissue engineered bone scaffolds. *Virtual Phys. Prototyp.* 7, 13–24.
- Deforest, C.A., Polizzotti, B.D., Anseth, K.S., 2009. Sequential click reactions for synthesizing and patterning three-dimensional cell microenvironments. *Nat. Mater.* 8, 659–664.
- Deville, S., 2010. Freeze-casting of porous biomaterials: structure, properties and opportunities. *Materials* 3, 1913–1927.
- Diaz-Gomez, L., Concheiro, A., Alvarez-Lorenzo, C., García-González, C.A., 2016. Growth factors delivery from hybrid PCL-starch scaffolds processed using supercritical fluid technology. *Carbohydr. Polym.* 142, 282–292.
- Diaz-Gomez, L., Smith, B.T., Kontoyiannis, P.D., Bittner, S.M., Melchiorri, A.J., Mikos, A.G., 2019. Multimaterial segmented fiber printing for gradient tissue engineering. *Tissue Eng. C Methods* 25, 12–24.
- Dubois, P., Jérôme, R., Teyssié, P., 1991. Aluminium alkoxides: a family of versatile initiators for the ring-opening polymerization of lactones and lactides. *Makromol. Chem. Macromol. Symp.* 42–43, 103–116.
- Dutta, R.C., Dey, M., Dutta, A.K., Basu, B., 2017. Competent processing techniques for scaffolds in tissue engineering. *Biotechnol. Adv.* 35, 240–250.
- Echave, M.C., Sánchez, P., Pedraz, J.L., Orive, G., 2017. Progress of gelatin-based 3D approaches for bone regeneration. *J. Drug Deliv. Sci. Technol.* 42, 63–74.
- Engler, A.J., Sen, S., Sweeney, H.L., Discher, D.E., 2006. Matrix elasticity directs stem cell lineage specification. *Cell* 126, 677–689.
- Ersen, A., Sahin, M., 2017. Polydimethylsiloxane-based optical waveguides for tetherless powering of floating microstimulators. *J. Biomed. Opt.* 22, 1–10.
- Florence, A.T., Jani, P.U., 1994. Novel oral drug formulations: their potential in modulating adverse effects. *Drug Saf.* 10, 233–266.
- Fried, J.R., 2014. *Polymer Science and Technology*, third ed. Prentice Hall.
- Garbern, J.C., Hoffman, A.S., Stayton, P.S., 2010. Poly (N-isopropylacrylamide-co-propylacrylic acid) copolymers for delivery of angiogenic growth factors. *Society* 1833–1839.
- Garbern, J.C., Minami, E., Stayton, P.S., Murry, C.E., 2011. Delivery of basic fibroblast growth factor with a pH-responsive, injectable hydrogel to improve angiogenesis in infarcted myocardium. *Biomaterials* 32, 2407–2416.
- García-González, C.A., Concheiro, A., Alvarez-Lorenzo, C., 2015. Processing of materials for regenerative medicine using supercritical fluid technology. *Bioconjug. Chem.* 26, 1159–1171.
- Ghosh, K., Pan, Z., Guan, E., Ge, S., Liu, Y., Nakamura, T., Ren, X.D., Rafailovich, M., Clark, R.A.F., 2007. Cell adaptation to a physiologically relevant ECM mimic with different viscoelastic properties. *Biomaterials* 28, 671–679.
- Gilding, D.K., Reed, A.M., 1979. Biodegradable polymers for use in surgery-polyglycolic/poly(lactic acid) homo- and copolymers: 1. *Polymer* 20, 1459–1464.
- Gnanou, Y., Lutz, P., Rempp, P., Charles, I., Crm, S., Cnrs, E., 1988. Synthesis of star-shaped poly(ethylene oxide). *Macromol. Chem. Phys.* 189, 2885–2892.
- Gomes, M.E., Sikavitsas, V.I., Behraves, E., Reis, R.L., Mikos, A.G., 2003. Effect of flow perfusion on the osteogenic differentiation of bone marrow stromal cells cultured on starch-based three-dimensional scaffolds. *J. Biomed. Mater. Res. A* 67, 87–95.

- Gramlich, W.M., Kim, I.L., Burdick, J.A., 2013. Synthesis and orthogonal photopatterning of hyaluronic acid hydrogels with thiol-norbornene chemistry. *Biomaterials* 34, 9803–9811.
- Guvendiren, M., Molde, J., Soares, R.M.D., Kohn, J., 2016. Designing biomaterials for 3D printing. *ACS Biomater. Sci. Eng.* 2, 1679–1693.
- Habibi, N., Kamaly, N., Memic, A., Shafiee, H., 2016. Self-assembled peptide-based nanostructures: smart nanomaterials toward targeted drug delivery. *Nano Today* 11, 41–60.
- Habibi, Y., Goffin, A.L., Schiltz, N., Duquesne, E., Dubois, P., Dufresne, A., 2008. Bionanocomposites based on poly(ϵ -caprolactone)-grafted cellulose nanocrystals by ring-opening polymerization. *J. Mater. Chem.* 18, 5002–5010.
- Haesslein, A., Ueda, H., Hacker, M.C., Jo, S., Ammon, D.M., Borazjani, R.N., Kunzler, J.F., Salamone, J.C., Mikos, A.G., 2006. Long-term release of fluocinolone acetonide using biodegradable fumarate-based polymers. *J. Control. Release* 114, 251–260.
- Hageman, H.J., 1985. Free radical polymerization 60, 6800 13, 123–150.
- Hallab, N.J., Bundy, K.J., O'Connor, K., Moses, R.L., Jacobs, J.J., 2001. Evaluation of metallic and polymeric biomaterial surface energy and surface roughness characteristics for directed cell adhesion. *Tissue Eng.* 7, 55–71.
- Hamitou, A., Ouhadi, T., Jerome, R., Teyssié, P., 1977. Soluble bimetallic μ -oxoalkoxides. VII. Characteristics and mechanism of ring-opening polymerization of lactones. *J. Polym. Sci. Polym. Chem. Ed.* 15, 865–873.
- Hernández, R.M., Orive, G., Murua, A., Pedraz, J.L., 2010. Microcapsules and microcarriers for in situ cell delivery. *Adv. Drug Deliv. Rev.* 62, 711–730.
- Herzberger, J., Niederer, K., Pohlitz, H., Seiwert, J., Worm, M., Wurm, F.R., Frey, H., 2016. Polymerization of ethylene oxide, propylene oxide, and other alkylene oxides: synthesis, novel polymer architectures, and bioconjugation. *Chem. Rev.* 116, 2170–2243.
- Hile, D.D., Amirpour, M.L., Akgerman, A., Pishko, M.V., 2000. Active growth factor delivery from poly(D,L-lactide-co-glycolide) foams prepared in supercritical CO₂. *J. Control. Release* 66, 177–185.
- Hochleitner, G., Jüngst, T., Brown, T.D., Hahn, K., Moseke, C., Jakob, F., Dalton, P.D., Groll, J., 2015. Additive manufacturing of scaffolds with sub-micron filaments via melt electrospinning writing. *Biofabrication* 7, 1–10.
- Hoerstrup, S.P., Sodian, R., Sperling, J.S., Vacanti, J.P., Mayer, J.E., 2000. Engineered heart valves. *Tissue Eng.* 6, 75–79.
- Holtorf, H.L., Datta, N., Jansen, J.A., Mikos, A.G., 2005a. Scaffold mesh size affects the osteoblastic differentiation of seeded marrow stromal cells cultured in a flow perfusion bioreactor. *J. Biomed. Mater. Res. A* 74A, 171–180.
- Holtorf, H.L., Jansen, J.A., Mikos, A.G., 2005b. Flow perfusion culture induces the osteoblastic differentiation of marrow stromal cell-scaffold constructs in the absence of dexamethasone. *J. Biomed. Mater. Res. A* 72A, 326–334.
- Hosseinkhani, H., Hong, P.-D., Yu, D.-S., 2013. Self-assembled proteins and peptides for regenerative medicine. *Chem. Rev.* 113, 4837–4861.
- Hubbell, J.A., 1995. Biomaterials in tissue engineering. *Biotechnology* 13, 565–576.
- Huebsch, N., Kearney, C.J., Zhao, X., Kim, J., Cezar, C.A., Suo, Z., Mooney, D.J., 2014. Ultrasound-triggered disruption and self-healing of reversibly cross-linked hydrogels for drug delivery and enhanced chemotherapy. *Proc. Natl. Acad. Sci.* 111, 9762–9767.
- Iatrou, H., Hadjichristidis, N., Meier, G., Frielinghaus, H., Monkenbusch, M., 2002. Synthesis and characterization of model cyclic block copolymers of styrene and butadiene. Comparison of the aggregation phenomena in selective solvents with linear diblock and triblock analogues. *Macromolecules* 35, 5426–5437.
- Ishihara, K., Kobayashi, M., Ishimaru, N., Shinohara, I., 1984. Glucose induced permeation control of insulin through a complex membrane consisting of immobilized glucose oxidase and a poly(amine). *Polym. J.* 16, 625–631.
- Jammalamadaka, U., Tappa, K., 2018. Recent advances in biomaterials for 3D printing and tissue engineering. *J. Funct. Biomater.* 9, 1–14.
- Janik, H., Marzec, M., 2015. A review: fabrication of porous polyurethane scaffolds. *Mater. Sci. Eng. C* 48, 586–591.
- Ji, C., Annabi, N., Hosseinkhani, M., Sivaloganathan, S., Dehghani, F., 2012. Fabrication of poly-DL-lactide/polyethylene glycol scaffolds using the gas foaming technique. *Acta Biomater.* 8, 570–578.
- Jiang, H., Qin, S., Dong, H., Lei, Q., Su, X., Zhuo, R., Zhong, Z., 2015a. An injectable and fast-degradable poly(ethylene glycol) hydrogel fabricated via bioorthogonal strain-promoted azide-alkyne cycloaddition click chemistry. *Soft Matter* 11, 6029–6036.
- Jiang, T., Carbone, E.J., Lo, K.W.-H., Laurencin, C.T., 2015b. Electrospinning of polymer nanofibers for tissue regeneration. *Prog. Polym. Sci.* 46, 1–24.
- Jivan, F., Fabela, N., Davis, Z., Alge, D.L., 2018. Orthogonal click reactions enable the synthesis of ECM-mimetic PEG hydrogels without multi-arm precursors. *J. Mater. Chem. B* 6, 4929–4936.
- Jivan, F., Yegappan, R., Pearce, H., Carrow, J.K., McShane, M., Gaharwar, A.K., Alge, D.L., 2016. Sequential thiol-ene and Tetrazine click reactions for the polymerization and functionalization of hydrogel microparticles. *Biomacromolecules* 17, 3516–3523.
- Kaihara, S., Matsumura, S., Mikos, A.G., Fisher, J.P., 2007. Synthesis of poly(L-lactide) and polyglycolide by ring-opening polymerization. *Nat. Protoc.* 2, 2767–2771.
- Karageorgiou, V., Kaplan, D.L., 2005. Porosity of 3D biomaterial scaffolds and osteogenesis. *Biomaterials* 26, 5474–5491.
- Khajavi, R., Abbasipour, M., Bahador, A., 2016. Electrospun biodegradable nanofibers scaffolds for bone tissue engineering. *J. Appl. Polym. Sci.* 133, 1–19.
- Khan, F., Tanaka, M., 2017. Designing smart biomaterials for tissue engineering. *Int. J. Mol. Sci.* 19, 1–14.
- Kim, H.K., Shim, W.S., Kim, S.E., Lee, K.-H., Kang, E., Kim, J.-H., Kim, K., Kwon, I.C., Lee, D.S., 2009. Injectable in situ-forming pH/thermo-sensitive hydrogel for bone tissue engineering. *Tissue Eng. A* 15, 923–933.
- Kishan, A.P., Cosgriff-Hernandez, E.M., 2017. Recent advancements in electrospinning design for tissue engineering applications: a review. *J. Biomed. Mater. Res. A* 105, 2892–2905.
- Kloxin, A.M., Kasko, A.M., Salinas, C.N., Anseth, K.S., 2009. Photodegradable hydrogels for dynamic tuning of physical and chemical properties. *Science* 324, 59–63.
- Koh, Y.G., Jo, S.B., Kwon, O.R., Suh, D.S., Lee, S.W., Park, S.H., Choi, Y.J., 2013. Mesenchymal stem cell injections improve symptoms of knee osteoarthritis. *Arthrosc. J. Arthrosc. Relat. Surg.* 29, 748–755.
- Kolesky, D.B., Truby, R.L., Gladman, A.S., Busbee, T.A., Homan, K.A., Lewis, J.A., 2014. 3D bioprinting of vascularized, heterogeneous cell-laden tissue constructs. *Adv. Mater.* 26, 3124–3130.

- Kon, E., Verdonk, P., Condello, V., Delcogliano, M., Dhollander, A., Filardo, G., Pignotti, E., Marcacci, M., 2009. Matrix-assisted autologous chondrocyte transplantation for the repair of cartilage defects of the knee: systematic clinical data review and study quality analysis. *Am. J. Sports Med.* 37, 156S–166S.
- Kost, J., Langer, R., 2012. Responsive polymeric delivery systems. *Adv. Drug Deliv. Rev.* 64, 327–341.
- Kretlow, J.D., Klouda, L., Mikos, A.G., 2007. Injectable matrices and scaffolds for drug delivery in tissue engineering. *Adv. Drug Deliv. Rev.* 59, 263–273.
- Kuboki, Y., Jin, Q., Takita, H., 2001. Geometry of carriers controlling phenotypic expression in BMP-induced osteogenesis and chondrogenesis. *J. Bone Joint Surg. Am.* 83–A (Suppl.), S105–S115.
- Langer, R., Vacanti, J., 1993. Tissue engineering. *Science* (80) 260, 920–926.
- Lannutti, J., Reneker, D., Ma, T., Tomasko, D., Farson, D., 2007. Electrospinning for tissue engineering scaffolds. *Mater. Sci. Eng. C* 27, 504–509.
- Leach, J.B., Bivens, K.A., Patrick, C.W., Schmidt, C.E., 2003. Photocrosslinked hyaluronic acid hydrogels: natural, biodegradable tissue engineering scaffolds. *Biotechnol. Bioeng.* 82, 578–589.
- Lee, K., Silva, E.A., Mooney, D.J., 2011. Growth factor delivery-based tissue engineering: general approaches and a review of recent developments. *J. R. Soc. Interface* 8, 153–170.
- Lee, K.Y., Mooney, D.J., 2012. Alginate: properties and biomedical applications. *Prog. Polym. Sci.* 37, 106–126.
- Li, J., Ni, X., Leong, K.W., 2003. Injectable drug-delivery systems based on supramolecular hydrogels formed by poly(ethylene oxide)s and α -cyclodextrin. *J. Biomed. Mater. Res. A* 65, 196–202.
- Lin, H., Zhang, D., Alexander, P.G., Yang, G., Tan, J., Cheng, A.W.-M., Tuan, R.S., 2013. Application of visible light-based projection stereolithography for live cell-scaffold fabrication with designed architecture. *Biomaterials* 34, 331–339.
- Liu, W., Heinrich, M.A., Zhou, Y., Akpek, A., Hu, N., Liu, X., Guan, X., Zhong, Z., Jin, X., Khademhosseini, A., Zhang, Y.S., 2017. Extrusion bioprinting of shear-thinning gelatin methacryloyl bioinks. *Adv. Healthc. Mater.* 6, 1–11.
- Lu, L., Peter, S.J., Lyman, M.D., Lai, H.L., Leite, S.M., Tamada, J.A., Uyama, S., Vacanti, J.P., Langer, R., Mikos, A.G., 2000a. In vitro and in vivo degradation of porous poly(DL-lactic-co-glycolic acid) foams. *Biomaterials* 21, 1837–1845.
- Lu, L., Peter, S.J., Lyman, M.D., Lai, H.L., Leite, S.M., Tamada, J.A., Vacanti, J.P., Langer, R., Mikos, A.G., 2000b. In vitro degradation of porous poly(L-lactic acid) foams. *Biomaterials* 21, 1595–1605.
- Lu, T., Li, Y., Chen, T., 2013. Techniques for fabrication and construction of three-dimensional scaffolds for tissue engineering. *Int. J. Nanomed.* 8, 337–350.
- Lutolf, M.P., Hubbell, J.A., 2005. Synthetic biomaterials as instructive extracellular microenvironments for morphogenesis in tissue engineering. *Nat. Biotechnol.* 23, 47–55.
- Ma, Z., Mao, Z., Gao, C., 2007. Surface modification and property analysis of biomedical polymers used for tissue engineering. *Colloids Surfaces B Biointerfaces* 60, 137–157.
- Manapat, J.Z., Chen, Q., Ye, P., Advincula, R.C., 2017. 3D printing of polymer nanocomposites via stereolithography. *Macromol. Mater. Eng.* 302, 1–13.
- Mannella, G.A., Conoscenti, G., Carfi Pavia, F., La Carrubba, V., Brucato, V., 2015. Preparation of polymeric foams with a pore size gradient via thermally induced phase separation (TIPS). *Mater. Lett.* 160, 31–33.
- Marler, J.J., Upton, J., Langer, R., Vacanti, J.P., 1998. Transplantation of cells in matrices for tissue regeneration. *Adv. Drug Deliv. Rev.* 33, 165–182.
- Martin, J.Y., Schwartz, Z., Hummert, T.W., Schraub, D.M., Simpson, J., Lankford, J.J., Dean, D.D., Cochran, D.L., Boyan, B.D., 1995. Effect of titanium surface roughness on proliferation, differentiation, and protein synthesis of human osteoblast-like cells (MG63). *J. Biomed. Mater. Res.* 29, 389–401.
- Matyjaszewski, K., Xia, J., 2001. Atom transfer radical polymerization. *Chem. Rev.* 101, 2921–2990.
- Mazzoli, A., 2013. Selective laser sintering in biomedical engineering. *Med. Biol. Eng. Comput.* 51, 245–256.
- Melchels, F.P.W., Feijen, J., Grijpma, D.W., 2010. A review on stereolithography and its applications in biomedical engineering. *Biomaterials* 31, 6121–6130.
- Merritt, E.K., Cannon, M.V., Hammers, D.W., Le, L.N., Gokhale, R., Sarathy, A., Song, T.J., Tierney, M.T., Suggs, L.J., Walters, T.J., Farrar, R.P., 2010a. Repair of traumatic skeletal muscle injury with bone-marrow-derived mesenchymal stem cells seeded on extracellular matrix. *Tissue Eng. A* 16, 2871–2881.
- Merritt, E.K., Hammers, D.W., Tierney, M., Suggs, L.J., Walters, T.J., Farrar, R.P., 2010b. Functional assessment of skeletal muscle regeneration utilizing homologous extracellular matrix as scaffolding. *Tissue Eng. A* 16, 1395–1405.
- Mikos, A.G., Temenoff, J.S., 2000. Formation of highly porous biodegradable scaffolds for tissue engineering. *Electron. J. Biotechnol.* 3, 114–119.
- Mikos, A.G., Thorsen, A.J., Czerwonka, L.A., Bao, Y., Langer, R., Winslow, D.N., Vacanti, J.P., 1994. Preparation and characterization of poly(l-lactic acid) foams. *Polymer* 35, 1068–1077.
- Miller, J.S., Stevens, K.R., Yang, M.T., Baker, B.M., Nguyen, D.H.T., Cohen, D.M., Toro, E., Chen, A.A., Galie, P.A., Yu, X., Chaturvedi, R., Bhatia, S.N., Chen, C.S., 2012. Rapid casting of patterned vascular networks for perfusable engineered three-dimensional tissues. *Nat. Mater.* 11, 768–774.
- Miyata, T., Uragami, T., Nakamae, K., 2002. Biomolecule-sensitive hydrogels. *Adv. Drug Deliv. Rev.* 54, 79–98.
- Moghadam, M.Z., Hassanajili, S., Esmailzadeh, F., Ayatollahi, M., Ahmadi, M., 2017. Formation of porous HPCL/LPCL/HA scaffolds with supercritical CO₂ gas foaming method. *J. Mech. Behav. Biomed. Mater.* 69, 115–127.
- Moglia, R.S., Whitely, M., Dhavalikar, P., Robinson, J., Pearce, H., Brooks, M., Stuebben, M., Corder, N., Cosgriff-Hernandez, E., 2014. Injectable polymerized high internal phase emulsions with rapid *in situ* curing. *Biomacromolecules* 15, 2870–2878.
- Mohan, N., Detamore, M., 2014. Engineering graded tissue interfaces. *Struct. Interfaces Attach. Biol.* 299–322 9781461433.
- Montanaro, L., Coppola, B., Palmero, P., Tulliani, J.-M., 2018. A review on aqueous gelcasting: a versatile and low-toxic technique to shape ceramics. *Ceram. Int.* 9653–9673.
- Na, K., Kim, S.W., Sun, B.K., Woo, D.G., Yang, H.N., Chung, H.M., Park, K.H., 2007. Osteogenic differentiation of rabbit mesenchymal stem cells in thermo-reversible hydrogel constructs containing hydroxyapatite and bone morphogenic protein-2 (BMP-2). *Biomaterials* 28, 2631–2637.
- Nair, L.S., Laurencin, C.T., 2007. Biodegradable polymers as biomaterials. *Prog. Polym. Sci.* 32, 762–798.
- Nezarati, R.M., Eifert, M.B., Cosgriff-Hernandez, E., 2013. Effects of humidity and solution viscosity on electrospun fiber morphology. *Tissue Eng. C Methods* 19, 810–819.

- Nguyen, K.T., West, J.L., 2002. Photopolymerizable hydrogels for tissue engineering applications. *Biomaterials* 23, 4307–4314.
- Nichols, J.E., Niles, J., Riddle, M., Vargas, G., Schilgard, T., Ma, L., Edward, K., La Francesca, S., Sakamoto, J., Vega, S., Ogadegbe, M., Mlcak, R., Deyo, D., Woodson, L., McQuitty, C., Lick, S., Beckles, D., Melo, E., Cortiella, J., 2013. Production and assessment of decellularized Pig and human lung scaffolds. *Tissue Eng. A* 19, 2045–2062.
- Nie, L., Chen, D., Suo, J., Zou, P., Feng, S., Yang, Q., Yang, S., Ye, S., 2012. Physicochemical characterization and biocompatibility in vitro of biphasic calcium phosphate/polyvinyl alcohol scaffolds prepared by freeze-drying method for bone tissue engineering applications. *Colloids Surfaces B Biointerfaces* 100, 169–176.
- Nimmo, C.M., Owen, S.C., Shoichet, M.S., 2011. Diels-Alder click cross-linked hyaluronic acid hydrogels for tissue engineering. *Biomacromolecules* 12, 824–830.
- Nuyken, O., Pask, S.D., 2013. Ring-opening polymerization—An introductory review. *Polymers* 5, 361–403.
- O'Brien, F.J., 2011. Biomaterials; scaffolds for tissue engineering. *Mater. Today* 14, 88–95.
- Odian, G., 2004. Introduction. In: *Principles of Polymerization*. John Wiley & Sons, Ltd, pp. 1–38.
- Ott, H.C., Matthiesen, T.S., Goh, S.K., Black, L.D., Kren, S.M., Netoff, T.I., Taylor, D.A., 2008. Perfusion-decellularized matrix: using nature's platform to engineer a bioartificial heart. *Nat. Med.* 14, 213–221.
- Ozbolat, I.T., Hospodiuk, M., 2016. Current advances and future perspectives in extrusion-based bioprinting. *Biomaterials* 76, 321–343.
- Park, H., Temenoff, J.S., Holland, T.A., Tabata, Y., Mikos, A.G., 2005. Delivery of TGF- β 1 and chondrocytes via injectable, biodegradable hydrogels for cartilage tissue engineering applications. *Biomaterials* 26, 7095–7103.
- Park, H., Temenoff, J.S., Tabata, Y., Caplan, A.I., Mikos, A.G., 2007. Injectable biodegradable hydrogel composites for rabbit marrow mesenchymal stem cell and growth factor delivery for cartilage tissue engineering. *Biomaterials* 28, 3217–3227.
- Pati, F., Jang, J., Ha, D.H., Won Kim, S., Rhie, J.W., Shim, J.H., Kim, D.H., Cho, D.W., 2014. Printing three-dimensional tissue analogues with decellularized extracellular matrix bioink. *Nat. Commun.* 5, 1–11.
- Pavia, F.C., La Carrubba, V., Piccarolo, S., Brucato, V., 2008. Polymeric scaffolds prepared via thermally induced phase separation: tuning of structure and morphology. *J. Biomed. Mater. Res. A* 86A, 459–466.
- Pawelec, K.M., Husmann, A., Best, S.M., Cameron, R.E., 2014. A design protocol for tailoring ice-templated scaffold structure. *J. R. Soc. Interface* 11, 1–9.
- Peltola, S.M., Melchels, F.P.W., Grijpma, D.W., Kellomäki, M., 2008. A review of rapid prototyping techniques for tissue engineering purposes. *Ann. Med.* 40, 268–280.
- Peppas, N.A., Keys, K.B., Torres-lugo, M., Lowman, A.M., 1999. Poly(ethylene glycol)-containing hydrogels in drug delivery. 62, 81–87.
- Peter, S.J., Kim, P., Yasko, A.W., Yaszemski, M.J., Mikos, A.G., 1999a. Crosslinking characteristics of an injectable poly(propylene fumarate)/beta-tricalcium phosphate paste and mechanical properties of the crosslinked composite for use as a biodegradable bone cement. *J. Biomed. Mater. Res.* 44, 314–321.
- Peter, S.J., Suggs, L.J., Yaszemski, M.J., Engel, P.S., Mikos, A.G., 1999b. Synthesis of poly(propylene fumarate) by acylation of propylene glycol in the presence of a proton scavenger. *J. Biomater. Sci. Polym. Ed.* 10, 363–373.
- Petite, H., Viateau, V., Bensaïd, W., Meunier, A., De Pollak, C., Bourguignon, M., Oudina, K., Sedel, L., Guillemin, G., 2000. Tissue-engineered bone regeneration. *Nat. Biotechnol.* 18, 959–963.
- Pham, Q.P., Sharma, U., Mikos, A.G., 2006. Electrospinning of polymeric nanofibers for tissue engineering applications: a review. *Tissue Eng.* 12, 1197–1211.
- Picchioni, F., 2014. Supercritical carbon dioxide and polymers: an interplay of science and technology. *Polym. Int.* 63, 1394–1399.
- Place, E.S., George, J.H., Williams, C.K., Stevens, M.M., 2009. Synthetic polymer scaffolds for tissue engineering. *Chem. Soc. Rev.* 38, 1139–1151.
- Prasad, A., Sankar, M.R., Katiyar, V., 2017. State of art on solvent casting particulate leaching method for orthopedic scaffolds fabrication. *Mater. Today Proc.* 4, 898–907.
- Puckett, S., Pareta, R., Webster, T.J., 2008. Nano rough micron patterned titanium for directing osteoblast morphology and adhesion. *Int. J. Nanomed.* 3, 229–241.
- Qian, L., Zhang, H., 2011. Controlled freezing and freeze drying: a versatile route for porous and micro-/nano-structured materials. *J. Chem. Technol. Biotechnol.* 86, 172–184.
- Radhakrishnan, J., Subramanian, A., Krishnan, U.M., Sethuraman, S., 2017. Injectable and 3D bioprinted polysaccharide hydrogels: from cartilage to osteochondral tissue engineering. *Biomacromolecules* 18, 1–26.
- Raeisdsteh Hokmabad, V., Davaran, S., Ramazani, A., Salehi, R., 2017. Design and fabrication of porous biodegradable scaffolds: a strategy for tissue engineering. *J. Biomater. Sci. Polym. Ed.* 28, 1797–1825.
- Ricles, L.M., Hsieh, P.L., Dana, N., Rybalko, V., Kraynak, C., Farrar, R.P., Suggs, L.J., 2016. Therapeutic assessment of mesenchymal stem cells delivered within a PEGylated fibrin gel following an ischemic injury. *Biomaterials* 102, 9–19.
- Rinker, T.E., Philbrick, B.D., Hettiaratchi, M.H., Smalley, D.M., McDevitt, T.C., Temenoff, J.S., 2018. Microparticle-mediated sequestration of cell-secreted proteins to modulate chondrocytic differentiation. *Acta Biomater.* 68, 125–136.
- Rodriguez, M., Marrot, S., Kato, T., Stérin, S., Fleury, E., Baceiredo, A., 2007. Catalytic activity of N-heterocyclic carbenes in ring opening polymerization of cyclic siloxanes. *J. Organomet. Chem.* 692, 705–708.
- Roseti, L., Parisi, V., Petretta, M., Cavallo, C., Desando, G., Bartolotti, I., Grigolo, B., 2017. Scaffolds for bone tissue engineering: state of the art and new perspectives. *Mater. Sci. Eng. C* 78, 1246–1262.
- Rouwkema, J., Rivron, N.C., van Blitterswijk, C.A., 2008. Vascularization in tissue engineering. *Trends Biotechnol.* 26, 434–441.
- Saini, S., Wick, T.M., 2003. Concentric cylinder bioreactor for production of tissue engineered cartilage: effect of seeding density and hydrodynamic loading on construct development. *Biotechnol. Prog.* 19, 510–521.
- Salerno, A., Oliviero, M., Di Maio, E., Iannace, S., Netti, P.A., 2009. Design of porous polymeric scaffolds by gas foaming of heterogeneous blends. *J. Mater. Sci. Mater. Med.* 20, 2043–2051.
- Santoro, M., Lamhamedi-Cherradi, S.-E., Menegaz, B.A., Ludwig, J.A., Mikos, A.G., 2015. Flow perfusion effects on three-dimensional culture and drug sensitivity of Ewing sarcoma. *Proc. Natl. Acad. Sci.* 112, 10304–10309.
- Saranya, N., Saravanan, S., Moorthi, A., Ramyakrishna, B., Selvamurugan, N., 2011. Enhanced osteoblast adhesion on polymeric nano-scaffolds for bone tissue engineering. *J. Biomed. Nanotechnol.* 7, 238–244.
- Sawhney, A.S., Pathak, C.P., Hubbell, J.A., 1993. Bioerodible hydrogels based on photopolymerized poly(ethylene glycol)-co-poly(α -hydroxy acid) diacrylate macromers. *Macromolecules* 26, 581–587.

- Sears, N., Dhavalikar, P., Whitely, M., Cosgriff-Hernandez, E., 2017. Fabrication of biomimetic bone grafts with multi-material 3D printing. *Biofabrication* 9, 1–11.
- Shi, M., Kretlow, J.D., Nguyen, A., Young, S., Scott Baggett, L., Wong, M.E., Kurtis Kasper, F., Mikos, A.G., 2010. Antibiotic-releasing porous polymethylmethacrylate constructs for osseous space maintenance and infection control. *Biomaterials* 31, 4146–4156.
- Shin, H., Jo, S., Mikos, A.G., 2003. Biomimetic materials for tissue engineering. *Biomaterials* 24, 4353–4364.
- Shirazi, S.F.S., Gharehkhani, S., Mehrli, M., Yarmand, H., Metseelaar, H.S.C., Adib Kadri, N., Osman, N.A.A., 2015. A review on powder-based additive manufacturing for tissue engineering: selective laser sintering and inkjet 3D printing. *Sci. Technol. Adv. Mater.* 16, 1–20.
- Sikavitsas, V.I., Bancroft, G.N., Holtorf, H.L., Jansen, J.A., Mikos, A.G., 2003. Mineralized matrix deposition by marrow stromal osteoblasts in 3D perfusion culture increases with increasing fluid shear forces. *Proc. Natl. Acad. Sci.* 100, 14683–14688.
- Sikavitsas, V.I., Temenoff, J.S., Mikos, A.G., 2001. Biomaterials and bone mechanotransduction. *Biomaterials* 22, 2581–2593.
- Singhal, P., Small, W., Cosgriff-Hernandez, E., Maitland, D.J., Wilson, T.S., 2014. Low density biodegradable shape memory polyurethane foams for embolic biomedical applications. *Acta Biomater.* 10, 67–76.
- Siqueira, L., de Paula, C.G., Motisuke, M., Gouveia, R.F., Camargo, S.E.A., Milhan, N.V.M., de Sousa Trichês, E., 2017. Preparation, characterization and biological studies of B-TCP and B-TCP/Al₂O₃ scaffolds obtained by gel-casting of foams. *Mater. Res.* 20, 973–983.
- Sisson, K., Zhang, C., Farach-Carson, M.C., Chase, D.B., Rabolt, J.F., 2010. Fiber diameters control osteoblastic cell migration and differentiation in electrospun gelatin. *J. Biomed. Mater. Res. A* 94, 1312–1320.
- Smook, M.M., Han, A., Watson, E., Kishan, A., Grande-Allen, K.J., Cosgriff-Hernandez, E., Mikos, A.G., 2019. Fabrication and characterization of electrospun decellularized muscle-derived scaffolds. *Tissue Eng. C Methods* 25, 276–287.
- Sokolosky-Papkov, M., Agashi, K., Olaye, A., Shakesheff, K., Domb, A.J., 2007. Polymer carriers for drug delivery in tissue engineering. *Adv. Drug Deliv. Rev.* 59, 187–206.
- Sridhar, B.V., Brock, J.L., Silver, J.S., Leight, J.L., Randolph, M.A., Anseth, K.S., 2015. Development of a cellularly degradable PEG hydrogel to promote articular cartilage extracellular matrix deposition. *Adv. Healthc. Mater.* 4, 702–713.
- Steinwachs, M., 2009. New technique for cell-seeded collagen matrix-supported autologous chondrocyte transplantation. *Arthrosc. J. Arthrosc. Relat. Surg.* 25, 208–211.
- Stevens, M.P., 1999. *Polymer Chemistry: An Introduction*. Oxford University Press.
- Sultana, N., Wang, M., 2012. PHBV/PLLA-based composite scaffolds fabricated using an emulsion freezing/freeze-drying technique for bone tissue engineering: surface modification and in vitro biological evaluation. *Biofabrication* 4, 1–14.
- Sultana, N., Wang, M., 2008. Fabrication of HA/PHBV composite scaffolds through the emulsion freezing/freeze-drying process and characterisation of the scaffolds. *J. Mater. Sci. Mater. Med.* 19, 2555–2561.
- Takahashi, A., Suzuki, Y., Sahara, T., Omichi, K., Shimizu, A., Hasegawa, K., Kokudo, N., Ohta, S., Ito, T., 2013. In situ cross-linkable hydrogel of hyaluronan produced via copper-free click chemistry. *Biomacromolecules* 14, 3581–3588.
- Tan, W.H., Takeuchi, S., 2007. Monodisperse alginate hydrogel microbeads for cell encapsulation. *Adv. Mater.* 19, 2696–2701.
- Tayalia, P., Mooney, D.J., 2009. Controlled growth factor delivery for tissue engineering. *Adv. Mater.* 21, 3269–3285.
- Temenoff, J.S., Mikos, A.G., 2008. *Biomaterials—The Intersection of Biology and Materials Science*. Pearson Prentice-Hall.
- Temenoff, J.S., Mikos, A.G., 2000. Injectable biodegradable materials for orthopedic tissue engineering. *Biomaterials* 21, 2405–2412.
- Temenoff, J.S., Shin, H., Conway, D.E., Engel, P.S., Mikos, A.G., 2003. In vitro cytotoxicity of redox radical initiators for cross-linking of oligo(poly(ethylene glycol) fumarate) macromers. *Biomacromolecules* 4, 1605–1613.
- Thadavirul, N., Pavasant, P., Supaphol, P., 2013. Development of polycaprolactone porous scaffolds by combining solvent casting, particulate leaching, and polymer leaching techniques for bone tissue engineering. *J. Biomed. Mater. Res. A* 3379–3392.
- Thomson, R.C., Wake, M.C., Yaszemski, M.J., Mikos, A.G., 1995. Biodegradable polymer scaffolds to regenerate organs. In: Peppas, N.A., Langer, R.S. (Eds.), *Advances in Polymer Science*. Springer, pp. 245–274.
- Tibbitt, M.W., Anseth, K.S., 2009. Hydrogels as extracellular matrix mimics for 3D cell culture. *Biotechnol. Bioeng.* 103, 655–663.
- Timmer, M.D., Horch, R.A., Ambrose, C.G., Mikos, A.G., 2003. Effect of physiological temperature on the mechanical properties and network structure of biodegradable poly(propylene fumarate)-based networks. *J. Biomater. Sci. Polym. Ed.* 14, 369–382.
- Trachtenberg, J.E., Vo, T.N., Mikos, A.G., 2015. Pre-clinical characterization of tissue engineering constructs for bone and cartilage regeneration. *Ann. Biomed. Eng.* 43, 681–696.
- Truong, V.X., Ablett, M.P., Richardson, S.M., Hoyland, J.A., Dove, A.P., 2015. Simultaneous orthogonal dual-click approach to tough, in-situ -forming hydrogels for cell encapsulation. *J. Am. Chem. Soc.* 137, 1618–1622.
- Turner, R.C., Atkins, P.E., Ackley, M.A., Park, J.B., 1981. Molecular and macroscopic properties of PMMA bone cement: free-radical generation and temperature change versus mixing ratio. *J. Biomed. Mater. Res.* 15, 425–432.
- Uludag, H., De Vos, P., Tresco, P.A., 2000. Technology of mammalian cell encapsulation. *Adv. Drug Deliv. Rev.* 42, 29–64.
- Unnithan, A.R., Arathyram, R.S., Kim, C.S., 2015. Electrospinning of polymers for tissue engineering. In: *Nanotechnology Applications for Tissue Engineering*. Elsevier, pp. 45–55.
- Utech, S., Prodanovic, R., Mao, A.S., Ostafe, R., Mooney, D.J., Weitz, D.A., 2015. Microfluidic generation of monodisperse, structurally homogeneous alginate microgels for cell encapsulation and 3D cell culture. *Adv. Healthc. Mater.* 4, 1628–1633.
- Van Vlierberghe, S., Dubruel, P., Schacht, E., 2011. Biopolymer-based hydrogels as scaffolds for tissue engineering applications: a review. *Biomacromolecules* 12, 1387–1408.
- Venkatesan, J., Kim, S.-K., 2014. Nano-hydroxyapatite composite biomaterials for bone tissue engineering—a review. *J. Biomed. Nanotechnol.* 10, 3124–3140.
- Vo, T.N., Tabata, Y., Mikos, A.G., 2016. Effects of cellular parameters on the in vitro osteogenic potential of dual-gelling mesenchymal stem cell-laden hydrogels. *J. Biomater. Sci. Polym. Ed.* 27, 1277–1290.
- Vo, T.N., Trachtenberg, J.E., 2014. In vitro techniques for biomaterial evaluation in bone and cartilage. *Regen. Med., J. Japan. Soc. Regen. Med.* 13, 125–149.
- Wake, M.C., Patrick, C.W., Mikos, A.G., 1994. Pore morphology effects on the fibrovascular tissue growth in porous polymer substrates. *Cell Transplant.* 3, 339–343.
- Wang, B., Zhu, W., Zhang, Y., Yang, Z., Ding, J., 2006. Synthesis of a chemically-crosslinked thermo-sensitive hydrogel film and in situ encapsulation of model protein drugs. *React. Funct. Polym.* 66, 509–518.

- Wang, Y., Ameer, G.A., Sheppard, B.J., Langer, R., 2002. A tough biodegradable elastomer. *Nat. Biotechnol.* 20, 602–606.
- Wei, G., Ma, P.X., 2004. Structure and properties of nano-hydroxyapatite/polymer composite scaffolds for bone tissue engineering. *Biomaterials* 25, 4749–4757.
- Whitely, M.E., Robinson, J.L., Stuebben, M.C., Pearce, H.A., McEnery, M.A.P., Cosgriff-Hernandez, E., 2017. Prevention of oxygen inhibition of PolyHIPE radical polymerization using a thiol-based cross-linker. *ACS Biomater. Sci. Eng.* 3, 409–419.
- Wu, S., Liu, X., Yeung, K.W.K., Liu, C., Yang, X., 2014. Biomimetic porous scaffolds for bone tissue engineering. *Mater. Sci. Eng. R Rep.* 80, 1–36.
- Xu, T., Zhao, W., Zhu, J.M., Albanna, M.Z., Yoo, J.J., Atala, A., 2013. Complex heterogeneous tissue constructs containing multiple cell types prepared by inkjet printing technology. *Biomaterials* 34, 130–139.
- Yamamoto, K., 2004. Fluid shear stress induces differentiation of Flk-1-positive embryonic stem cells into vascular endothelial cells in vitro. *AJP Hear. Circ. Physiol.* 288, H1915–H1924.
- Yang, J., Zhang, Y.S., Yue, K., Khademhosseini, A., 2017. Cell-laden hydrogels for osteochondral and cartilage tissue engineering. *Acta Biomater.* 57, 1–25.
- Yang, S., Leong, K.-F., Du, Z., Chua, C.-K., 2001. The design of scaffolds for use in tissue engineering. Part I. Traditional factors. *Tissue Eng.* 7, 679–689.
- Yoo, H.S., Kim, T.G., Park, T.G., 2009. Surface-functionalized electrospun nanofibers for tissue engineering and drug delivery. *Adv. Drug Deliv. Rev.* 61, 1033–1042.
- Yoon, J., Yang, H.-S., Lee, B.-S., Yu, W.-R., 2018. Recent progress in coaxial electrospinning: new parameters, various structures, and wide applications. *Adv. Mater.* 30, 1–23.
- Yu, J., Du, K.T., Fang, Q., Gu, Y., Mihardja, S.S., Sievers, R.E., Wu, J.C., Lee, R.J., 2010. The use of human mesenchymal stem cells encapsulated in RGD modified alginate microspheres in the repair of myocardial infarction in the rat. *Biomaterials* 31, 7012–7020.
- Zein, I., Hutmacher, D.W., Tan, K.C., Teoh, S.H., 2002. Fused deposition modeling of novel scaffold architectures for tissue engineering applications. *Biomaterials* 23, 1169–1185.
- Zhang, H., Jia, X., Han, F., Zhao, J., Zhao, Y., Fan, Y., Yuan, X., 2013. Dual-delivery of VEGF and PDGF by double-layered electrospun membranes for blood vessel regeneration. *Biomaterials* 34, 2202–2212.
- Zhao, F., Ma, T., 2005. Perfusion bioreactor system for human mesenchymal stem cell tissue engineering: dynamic cell seeding and construct development. *Biotechnol. Bioeng.* 91, 482–493.
- Zhu, W., Ding, J., 2006. Synthesis and characterization of a redox-initiated, injectable, biodegradable hydrogel. *J. Appl. Polym. Sci.* 99, 2375–2383.

Chapter Exercises

1. You and your team are designing a material that can offer three different degradation profiles both *in vitro* and *in vivo*. The tissue engineering scaffolds will be composed of blends of PLGA and PCL and will be porous.

Given the following scaffold formulations, which would you recommend for (a) the fastest degradation profile, (b) intermediate degradation, and (c) slowest degradation, and why?

- 25% PCL, 75% 50:50 PLGA
- 50% PCL, 50% 50:50 PLGA
- 75% PCL, 25% 50:50 PLGA

Similarly, for the following formulations, which would you recommend for (a) the fastest degradation profile, (b) intermediate degradation, and (c) slowest degradation, and why?

- 50% PCL, 50% 75:25 PLGA
- 50% PCL, 50% 25:75 PLGA
- 50% PCL, 50% 50:50 PLGA

2. A company wants to 3D print mesenchymal stem cells into a commercial tissue engineering scaffold system. Which 3D printing method would you recommend for them to use and why?
3. You are designing a tissue engineering scaffold for pancreatic islet cell regeneration. Which cell type would you choose for your scaffold and why? For the tissue engineering scaffold, would you choose (a) a hydrogel, (b) a calcium phosphate cement, or (c) an electrospun PCL mesh? Why?
4. You have an electrospun tissue engineering scaffold that you intend to use as a cancer model for Ewing Sarcoma to study the efficacy of chemotherapeutics *in vitro*. Which cell seeding method would you use to seed your scaffold? Why?
5. You have synthesized a new polyaddition polymer and need to characterize the chemical structure and molecular weight. Which characterization techniques would you use?
6. You and your team want to create a highly porous PCL scaffold with both nano- and microporosity, encapsulating growth factors that cannot be dissolved in an organic solvent. Which scaffold preparation method should you and your team choose and why?

Chapter Exercise Answers

1. Part 1:

- (a) 25% PCL, 75% 50:50 PLGA
- (b) 50% PCL, 50% 50:50 PLGA
- (c) 75% PCL, 25% 50:50 PLGA

The greater the content of PCL, the slower the degradation profile as PCL is more hydrophobic and highly crystalline.

- Part 2:

- (a) 50% PCL, 50% 25:75 PLGA
- (b) 50% PCL, 50% 50:50 PLGA
- (c) 50% PCL, 50% 75:25 PLGA

The greater the content of PLA, compared to PLGA, the slower the degradation rate given the increased hydrophobicity and crystallinity of PLA.

2. Extrusion based printing would be recommended as that system for 3D printing is compatible with many biological polymers, as well as crosslinking systems that do not require exposure to high temperatures and harsh initiators.
3. A variety of cell types could be chosen. Induced pluripotent stem cells (iPSCs) would be a good choice and a hydrogel would be the best material for the intended application given the material mechanical properties being the closest to native pancreatic tissue.
4. The best seeding method for the situation would be perfusion-based seeding of the Ewing Sarcoma cells. The system would also necessitate bioreactor culture in order to better recreate the *in vivo* environment when determining chemotherapeutic efficacy.
5. $^1\text{H-NMR}$ can be used to characterize the polymer chemical structure and either APC/GPC can be used to characterize the molecular weight.
6. Gas foaming would be a very good option as CO_2 is readily soluble in PCL and gas foaming does not require heating the mixture to high temperatures that would denature or disrupt the bioactivity of any growth factors incorporated into the system.

2.6.4

Micromechanical Design Criteria for Tissue-Engineering Biomaterials

YING LEI, ZACHARY E. GOLDBLATT, KRISTEN L. BILLIAR

Biomedical Engineering Department, Worcester Polytechnic Institute, Worcester, MA, United States

Introduction

In the field of tissue engineering, cell–scaffold constructs are designed with the aim of promoting new tissue formation following injury or disease. Biomaterials used in tissue engineering were initially viewed as temporary mechanical supports for cell delivery that were designed to resist macroscopic loads, and growth factors were used to guide cell behavior, as depicted by the classic tissue engineering triad (Fig. 2.6.4.1A). However, it is becoming clear that attention needs to be paid to cell-scale mechanical properties and mechanical stimuli to guide regeneration and completely restore normal tissue form and function when implanted in vivo, as depicted by the tissue-engineering tetrahedron with mechanical stimuli at the apex (Fig. 2.6.4.1B).

Many tissues are mechanically active in vivo, bearing continuous or cyclical stress as well as stretch and/or compressive loading (e.g., heart valve and cartilage). Additionally, all tissues have hierarchical structures from submicron to millimeter scale. Tissue constructs mechanically preconditioned in bioreactors prior to in vivo implantation have greatly improved strength and stiffness (Waldman et al., 2003; McCulloch et al., 2004; Fehrenbacher et al., 2006; Isenberg et al., 2006). The bulk stiffness of a scaffold determines the load-bearing ability, whereas the micromechanical properties, such as local stiffness and topography, influence the forces transmitted to and generated by cells. In response to local mechanical cues, cells change their behaviors including attachment, proliferation, migration, and protein secretion, which in turn affect the mechanical and chemical properties of the surrounding environment (Fig. 2.6.4.1) (Shin et al., 2003; Lutolf and Hubbell, 2005). More information about cell–biomaterial interactions, including the effects of mechanical forces on cells and tissues, host reaction to biomaterials, as well as inflammation and wound healing can be found in Chapters 2.1.6–2.2.2.

There are myriad existing methods for fabricating scaffolds with particular mechanical features with the potential

to control cell response. These methods are described in other chapters in this text: Chapter 1.4.6 Medical Fibers and Biotextiles, Chapter 1.4.7 Textured and Porous Materials, Chapter 1.4.8 Biomedical Applications of Additive Manufacturing, Chapter 2.6.2 Overview of Tissue Engineering Concepts and Applications, and Chapter 2.6.3 Tissue Engineering Scaffolds. The development of more recent techniques such as additive manufacturing and surface patterning will allow designers to manipulate the performance of cells through hierarchical design of scaffolds with precise control of the local stiffness and topography (Pan et al., 2017). To do this effectively, however, an understanding of the dynamic and reciprocal interactions that occur within the cell–extracellular matrix (ECM) microenvironment is needed.

In this chapter, we first introduce the fundamentals of micromechanical interactions between cells and biomaterials. Since different mechanical stimuli sensed by cells may trigger common intracellular signaling pathways, we emphasize mechanotransduction, the process by which mechanical signals are sensed and then transduced into changes in cellular biochemistry and gene expression (Ingber, 2006; Vogel and Sheetz, 2006). We then discuss the response of cells to various micromechanical features and how multiple stimuli interact to influence cell and tissue development in complex mechanical environments. Finally, we explore how our growing knowledge of micromechanical control of cell function and biomaterials science can be integrated to develop future biomaterials in order to best promote orderly tissue growth and restore normal function.

Cell–Matrix Interactions and Mechanotransduction

Cells sense and respond to micromechanical stimuli via a series of intracellular molecular processes collectively referred to as mechanotransduction (Fig. 2.6.4.2) (Martino et al.,

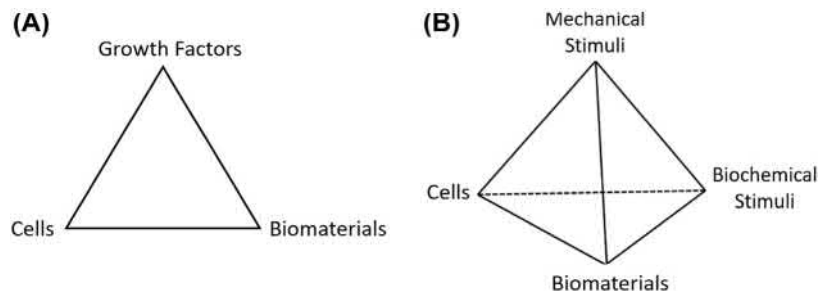
2018). Critical micromechanical stimuli in tissue scaffolds, including matrix stiffness and topography, and applied loads and deformations, are transmitted into the cells through transmembrane receptors. Here we focus on the role of focal adhesions, since they are the primary sites where cells bind to biomaterials, and are involved in the majority of cell–ECM micromechanical interactions (Ohashi et al., 2017).

Focal Adhesion

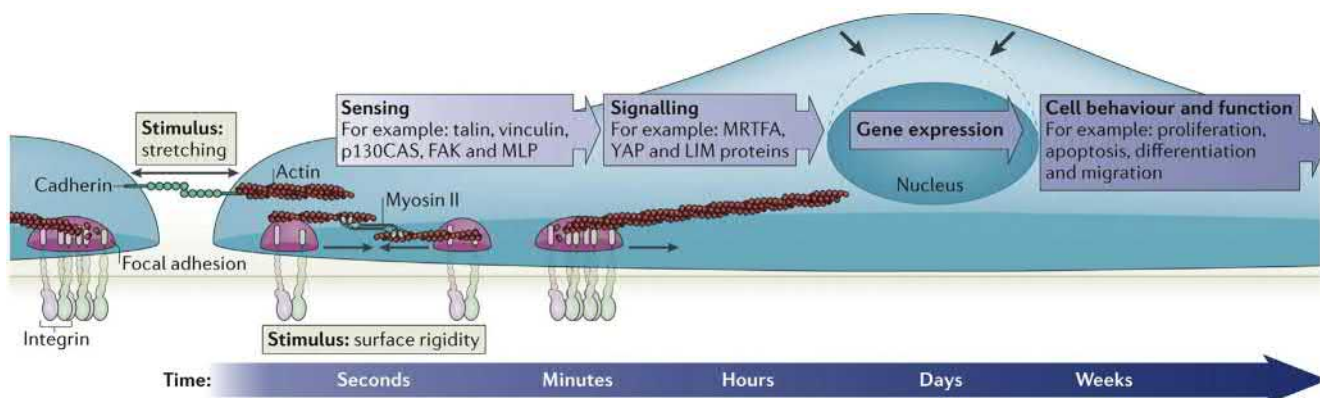
Focal adhesions are large transmembrane protein complexes which physically connect the extracellular matrix to the cytoskeleton. They are composed of a transmembrane layer of integrins and intracellular layers of proteins that bind to cytoskeletal fibers, transduce forces, and trigger molecular pathways (Dupont, 2016). Integrins consist of α and β subunits, which unfold and separate when activated. The diversity of integrins may have profound influence on cell behavior, thus particular cell behavior can be manipulated by inducing a specific integrin subunit combination. For example, interaction between $\alpha_5\beta_1$ -fibronectin bindings results in intracellular actin reorganization in mesenchymal stem cells (MSCs) and induces specific changes in shape and chondrocyte differentiation (Hao et al., 2015; Martino et al., 2018). In addition, integrin-binding molecules such as

RGD tripeptide are widely used to enhance cell attachment on otherwise nonadhesive surfaces of biomaterials. More information about the use of surface-immobilized biomolecules to guide cell response is provided in Chapter 1.4.4.

The activation of integrins results from both external mechanical signals and internally generated forces, triggering outside-in and inside-out signaling, respectively (Seetharaman and Etienne Manneville, 2018). Signals sensed outside-in or inside-out may induce similar integrin activation and molecular pathways (Fig. 2.6.4.3), therefore it is important to consider the interplay between various micromechanical stimuli when designing biomaterials for tissue-engineering applications. In inside-out signaling, cells probe their surroundings by actively pulling on the extracellular matrix or scaffold via focal adhesions utilizing their cytoskeletal acto-myosin machinery (Gauthier et al., 2011; Ghassemi et al., 2012; Giannone et al., 2004). Depending upon the resistance of their surroundings when cells generate forces, integrins are activated or deactivated, stress fibers are reinforced or disassembled, and downstream effects such as changes in cell migration and differentiation are induced (Iskratsch et al., 2014). For instance, on soft substrates, cell shape will be more rounded with a low density of stress fibers, while stiffer substrates have increased cell spreading and stress fiber density. The differentiation of neurons from

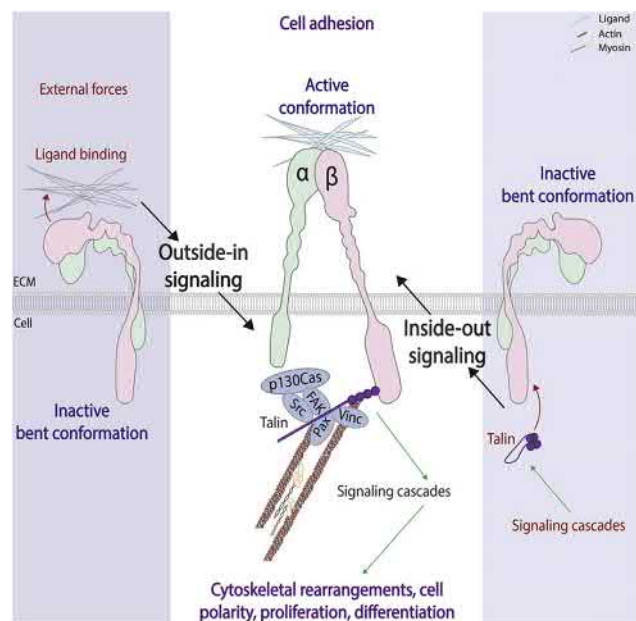


• **Figure 2.6.4.1** (A) The classic tissue-engineering triad viewing biomaterial scaffolds as bulk mechanical support for cells. (B) Updated tissue-engineering tetrahedron demonstrating more complex interplay between cells, media, materials, and mechanics. In particular, local micromechanical cues at the cell level significantly influence cell behaviors and tissue formation.



• **Figure 2.6.4.2** Schematic of cellular mechanical signaling at focal adhesions (integrins) and cell–cell contact (cadherins). Transmembrane protein complexes transduce external mechanical stimuli and transfer the signal via molecular signaling pathways to the nucleus and/or transfer forces through the cytoskeleton directly to the nucleus. The biochemical signals and nuclear deformation influence gene expression and thus cellular function. The timescale of these behavioral changes can range from milliseconds (stretching of mechanosensors) to weeks (tissue development) (Iskratsch et al., 2014).

MSCs requires a soft substrate (<5 kPa), resembling the pliability of brain tissue, whereas osteoblasts differentiate on stiffer substrates (>20 kPa), which resembles that of bone (Engler et al., 2006). In outside-in signaling, integrins are activated by external forces or stretching applied on their



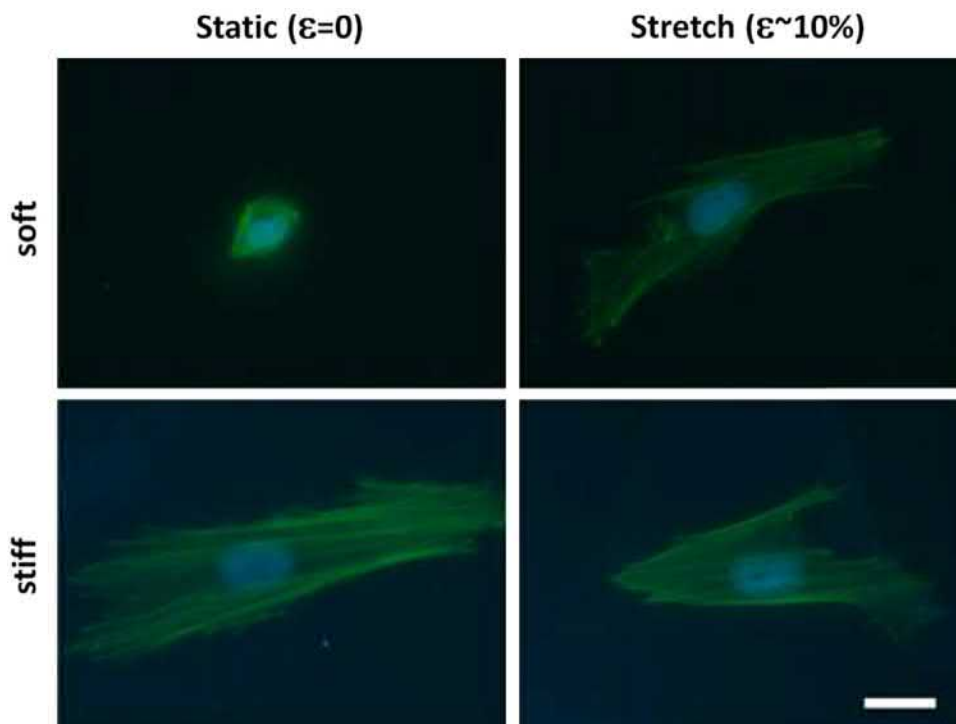
• **Figure 2.6.4.3** Activation of integrins. Subunits unfolding and separation may be induced by either externally applied forces or internally generated forces (Aiyelabegan, 2017).

extracellular domains, with or without cellular myosin contractile force generation (Discher et al., 2005). Similar to inside-out signaling, integrin activation involves conformational changes to uncover scaffold binding sites and also creates new cytoskeletal binding sites for activator and adapter proteins such as talin and vinculin. Therefore, externally applied stretch may provide a similar mechanical input to cells as culturing them on a material. For instance, valvular interstitial cells (VICs) cultured on low-modulus gels that are cyclically stretched exhibit a large, spread morphology similar to those cultured statically on stiff gels (Quinlan et al., 2011).

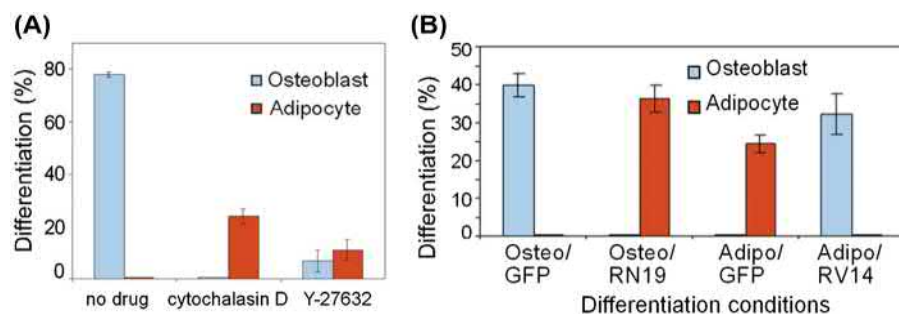
Roles of Focal Adhesion Maturation and Stress Fiber Formation in Mechanotransduction

Small nascent focal adhesions with less activated integrins can be stabilized to form larger, mature adhesions featuring a multilayered protein structure. Different degrees of protein clustering and focal adhesion maturation are determined by the spacing and availability of ECM adhesion sites. This sensitivity to focal adhesion (FA) spacing enables control of cell behaviors through arrangement of micro/nanomechanical characteristics in biomaterial design (Bachir et al., 2017; Ohashi et al., 2017; Sun et al., 2016). Chapter 1.4.5 provides more information about surface patterning techniques for guiding cell behavior.

Focal adhesions and stress fibers cooperate and stabilize each other in a mutual reinforcing loop. Stress fibers are



• **Figure 2.6.4.4** VICs stained for F-actin (green) and Hoechst (blue) cultured on low-modulus (top; “soft” 0.3 kPa) and high-modulus (bottom; “stiff” 50 kPa) gels under static (left) and cyclically stretched (right) conditions. After 6 h of 1-Hz cyclic stretch, cells on soft gels were able to elongate and spread out. Scale bar = 20 μm (Quinlan et al., 2011).



• **Figure 2.6.4.5** (A) Disruption of the cytoskeleton via cytochalasin D and inhibition of RhoA via Y-27,632 causes hMSCs to differentiate into adipocytes instead of osteoblasts. (B) Dominant negative RhoA (RhoA-N19) causes hMSCs in osteoblast differentiation media to form into adipocytes, while constitutively active RhoA (RhoA-V14) causes cells to differentiate into osteoblasts while in adipocyte differentiation media (McBeath et al., 2004).

composed of actin filaments (F-actin) and nonmuscle myosin II, an ATP-driven motor protein. Stress fibers can generate contractile forces and pull on focal adhesions (Chen et al., 2010; Fabry et al., 2011). If the sensed external stimulus is strong enough, conformational unfolding of mechanosensitive molecules in focal adhesions can result in the exposure of binding sites that promote recruitment of myosin and stabilization of stress fibers. Contractile forces developed by stress fibers in turn stabilize and allow the maturation of focal adhesions to an increased size (Aiyelabegan and Esmail, 2017). Accordingly, focal adhesion maturation and stress fiber contraction are negatively affected when the mechanical stimulus is weak, e.g., when cells are seeded on soft scaffolds or the binding sites for focal adhesions are restricted (Dupont et al., 2011; Dupont, 2016; Martino et al., 2018). Focal adhesion maturation and stress fiber contraction also result in cell biophysical changes, such as cell spreading, elongation, increased cell prestress, and a reduction in the amount of globular actin (G-actin), as the free actin is polymerized into F-actin in stress fibers. These changes are associated with a variety of cell behaviors including cell division, proliferation, apoptosis, migration, and differentiation (Discher et al., 2005; O'Connor and Gomez, 2013).

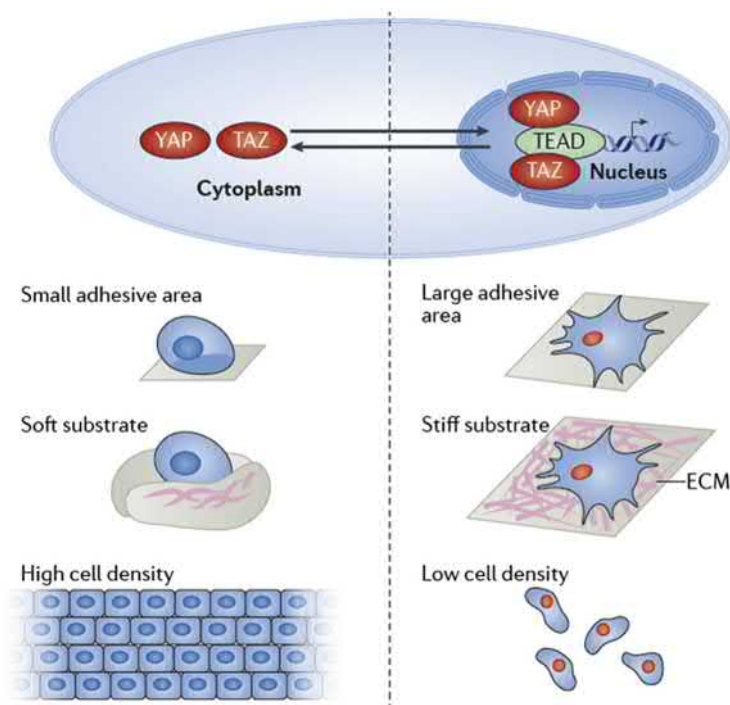
Important Mechanotransduction Molecular Pathways for Design of Scaffolds

Numerous signaling pathways and mechanotransducers are involved in cell sensing and responding to mechanical stimuli applied at focal adhesions (Martino et al., 2018). While the underlying mechanisms are still an active area of investigation, attempts to design novel biomaterials capable of guiding cells' behavior by controlling the signaling pathways have shown great potential for tissue-engineering applications (Brusatin et al., 2019). Here, we introduce a few key signaling regulators of cell proliferation, differentiation, and other cell processes critical for modulating tissue repair and regeneration, which can be considered in the design of future biomaterials.

The Rho family of guanosine triphosphatases (GTPases) consists of small molecules that coordinate cytoskeletal reorganization. RhoA promotes myosin activity through the activation of Rho-associated protein kinase (ROCK) (Bardi

et al., 2003). Activated by diverse biomechanical signals, RhoA/ROCK and downstream molecules lead to the interaction of myosin motors with F-actin, which is related to focal adhesion assembly, maturation, stress fiber formation, and contractile force generation (Davidson et al., 2010; Kovács et al., 2003). Human pluripotent stem cell-derived cardiomyocytes cultured on low-modulus, 4-kPa hydrogels lack activation of the RhoA/ROCK pathway and fail to form mature sarcomeres. In contrast, myofibril alignment to the cell long-axis is clearly observed in cells cultured on stiff substrates (16-kPa hydrogels and glass) in which activation of the RhoA/ROCK pathway occurs. Further, ROCK inhibition impairs sarcomeric alignment in these cells (Martewicz et al., 2017). Similarly, RhoA/ROCK activation elicited by culture of MSCs on stiff substrates generates myosin contractility, which generally results in increased osteogenic differentiation (Ambriz et al., 2018), whereas culturing on low-modulus substrates can inactivate RhoA/ROCK and induce differentiation into adipocytes. Inhibition of cellular tension with cytochalasin D, ROCK inhibitor Y-27,632, or by expression of a dominant-negative RhoA promotes adipogenesis on stiff (typically osteogenic) conditions, and overexpression of constitutively active ROCK restores osteogenic fate on soft (typically adipogenic) conditions (Fig. 2.6.4.5) (Engler et al., 2006; McBeath et al., 2004; Sun et al., 2016).

Yes-associated protein (YAP) and transcriptional coactivator PDZ-binding motif (TAZ) are mechanosensitive transcriptional coregulators of proliferation, differentiation, and survival. As such, YAP/TAZ play important roles in controlling organ growth, stem cell self-renewal, and cell differentiation. YAP/TAZ are activated by stabilization of F-actin and high levels of cytoskeletal tension coordinated by RhoA/ROCK (Galli et al., 2015; Stein et al., 2015). Therefore, YAP/TAZ are affected by very diverse biomechanical signals such as local stress, geometries of individual cells and whole tissues, and stiffness and topology of the ECM substrate (Fig. 2.6.4.6) (Aragona et al., 2013; Dupont et al., 2011). YAP/TAZ shuttle between the cytoplasm and nucleus and interact with DNA-binding transcription factors which contribute to the regulation of gene expression when accumulating in the nucleus. YAP/TAZ are localized in the cytoplasm in cells experiencing low levels of mechanical signaling, such as rounded cells attached to a soft ECM



• **Figure 2.6.4.6** Schematics of different mechanical stimuli (geometry, matrix, density) effects on YAP/TAZ nuclear localization and activity. YAP and TAZ are activated and localized to the nucleus under higher stress conditions (right panels), and are deactivated and localized in the cytosol when under low-stress conditions (left panels) (Pancieria et al., 2017).

or to a small adhesive area that restricts their spreading (Hao et al., 2014). Conversely, YAP/TAZ are localized to the nucleus in cells perceiving high mechanical signaling, such as cells cultured on rigid substrates or experiencing deformation and cytoskeletal tension (Totaro et al., 2017). When YAP/TAZ is knocked down, cells grown on a stiff matrix exhibit a phenotype similar to that of cells grown on a soft matrix. On the other hand, with overexpression of YAP/TAZ, cells grown on a soft matrix behave as if they are on a stiff matrix (Galli et al., 2015). For tissue engineering applications, scaffolds could be designed to modulate YAP/TAZ activation, e.g., by allowing cell spreading or generation of high intracellular tension to induce cell proliferation when cell growth is desired, or to restrict cell spreading and trigger apoptosis when cell growth is undesirable (Liu et al., 2016; Morikawa et al., 2015; Xin et al., 2013).

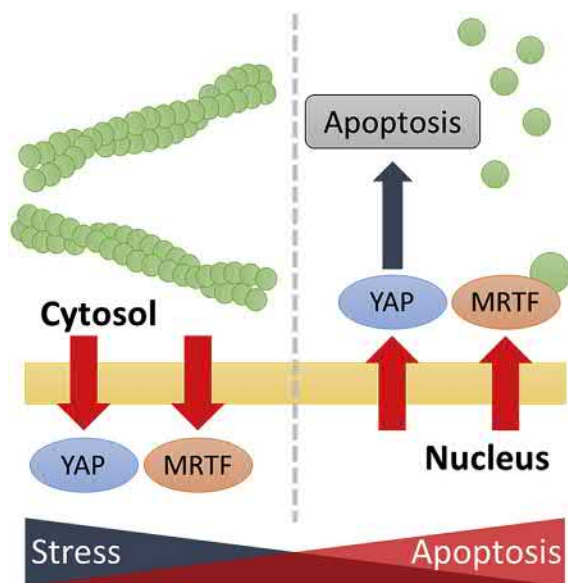
Myocardin-related transcription factor A (MRTF-A) is another mechanosensitive transcriptional regulator that coordinates cell growth, organ development, and wound healing (Yu-Wai-Man et al., 2017). Similar to YAP/TAZ, MRTF-A is mediated by Rho signaling and polymerization of F-actin (Sun et al., 2016). MRTF-A is deactivated and localized to the cytosol when bound to G-actin. When mechanical force-induced actin polymerization reduces the cellular concentration of G-actin, MRTF-A dissociates from G-actin and translocates into the nucleus, resulting in stimulation of the transcription factor and serum response factor, which promotes myogenic differentiation and cytoskeletal reorganization. Notably, MRTF-A regulates the transcription of alpha smooth muscle actin (α -SMA), a key marker of the activated myofibroblast phenotype responsible for contractile force

generation and enhanced ECM protein secretion (Hautmann et al., 1999; O'Connor and Gomez, 2013; Miralles et al., 2003). MRTF-A localizes to the nucleus in cells that are permitted to spread and have higher cytoskeletal tension (Hautmann et al., 1999). Pharmacological inhibition of cytoskeletal tension or MRTF-A signaling blocks the phenotype transfer to myofibroblasts in spread cells (O'Connor and Gomez, 2013). Increased cell stress can also be applied externally by cyclic stretch leading to cell proliferation, apoptosis, and differentiation markers, even for cells cultured on soft substrates; this response can be mediated by MRTF-A and YAP (Dutta et al., 2018; Cui et al., 2015). The mechanisms of micromechanical activation of molecular pathways are very complicated and highly interrelated. We present a unifying hypothesis relating cell stress, F/G-actin, nuclear localization of YAP and MRTF-A, and apoptosis (Fig. 2.6.4.7).

Direct Transmission of Forces to the Nucleus

While the majority of research on the mechanisms of mechanotransduction concentrates on identifying mechanotransducers at the cell membrane and the downstream biochemical pathways, recent studies demonstrate that forces transmitted directly to the nucleus or other organelles via the cytoskeleton also play a role in mechanotransduction (Driscoll et al., 2015). The nucleoskeleton is connected to cytoplasmic F-actin structures through nuclear lamina, a network of lamin and lamin-binding proteins underlying the inner nuclear envelope. Since peripheral DNA and chromatin are anchored to the nuclear lamina, mechanical signals can be transduced from the cell surface into the nucleus, modulating nuclear structure and gene

transcription. Stretching the nuclear envelope also increases in-plane membrane tension and loosens lipid packing, which promotes hydrophobic protein–lipid interactions (Enyedi and Niethammer, 2017). Neelam et al. showed that the application of mechanical forces on integrin receptors at the cell membrane is followed shortly after by nuclear structural reorganization and deformation in the direction of the pulling force and then chromatin reorganization (Booth-Gauthier et al., 2012; Dickinson et al., 2015). In addition, actin fibers are physically connected to the microtubule network, which is involved in crucial biological processes, such as intracellular trafficking, mitotic spindle formation, and cell polarity (Fletcher and Mullins, 2010). When being stretched, dividing cells display an alignment of the mitotic spindle parallel to the applied force, with a polarization of dynamic subcortical actin structures that correlate with spindle movements (Fink et al., 2011).



• **Figure 2.6.4.7** Schematic of stress effects on YAP and MRTF-A pathways in the cell. Polymerization of F-actin from G-actin (green circles) promotes YAP and MRTF nuclear localization and cell proliferation in response to high cell stress (left), while G-actin promotes nuclear exclusion of YAP and cell apoptosis in response to low cell stress (right).

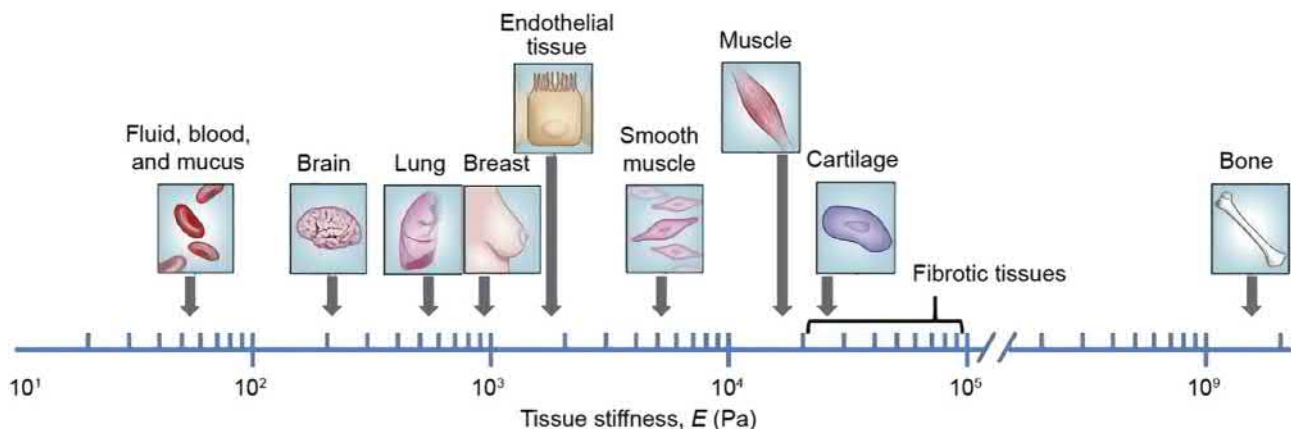
Aforementioned knowledge regarding cells–ECM interaction and mechanotransduction enables directing cell behaviors and tissue growth via tuning the microstructure and local properties of scaffolds. Although the native mechanical environment and features of scaffolds that influence their performance are very complicated, when designing biomaterials it is paramount to consider their ability to induce mature focal adhesions, cytoskeleton remodeling, and contractile force generation. For verification, signaling regulating proteins such as RhoA/ROCK, YAP/TAZ, and MRTF-A could be tracked as indicators of cell functions when investigating the performance of designed biomaterials.

Design Considerations for Scaffolds to Regulate Tissue Development

There are multiple mechanical cues, including local stiffness and topography, which biomaterial designers can alter to modulate cell response. Further, fiber diameter, alignment, and porosity are additional parameters that can be modulated to guide cell behavior for fibrous scaffolds. For tissues mainly composed of cells with minimal ECM, e.g., muscle and epithelium, the effects of cell–cell contact and transmission of forces also need to be considered. In addition, newly formed engineered tissues may be conditioned in bioreactors to promote tissue growth, thus outside-in signaling due to external forces and stretch provides an additional design parameter. In this section, we discuss each of these mechanical design parameters individually and highlight interactions between the mechanical cues.

Local Stiffness

Stiffness describes the resistance offered by an elastic body to deformation in response to an applied force. It depends on the elastic modulus (a material property) and geometry of the scaffold (a structural property). The bulk elastic modulus determines the overall mechanical deformation of a scaffold under an applied loading. At the cell level, local modulus is a powerful cue that directs cell attachment, growth,



• **Figure 2.6.4.8** Stiffness of various human tissues in the body. The levels of stiffness change the mechanical properties of the cells (Yang et al., 2017).

migration, and differentiation. The elastic modulus of native tissues ranges from 10^2 to 10^{10} Pa (Fig. 2.6.4.8). Generally, the designed scaffold stiffness of a particular tissue should be comparable to the native tissue, since a stiffness mismatch may induce undesirable cell behavior or differentiation. For example, a hallmark study by Engler and colleagues demonstrated that matrix modulus directs MSC fate, with low- (0.1–1 kPa), medium- (8–17 kPa), and high- (25–40 kPa) modulus collagen-coated polyacrylamide substrates favoring neurogenic, myogenic, or osteogenic differentiation, respectively (Yang et al., 2017). Quinlan et al. revealed that culture of fibroblastic cells on collagen-coated polyacrylamide substrates of increasing moduli results in more pronounced expression of α SMA-positive stress fibers, indicating a graded phenotypic change from fibroblast to myofibroblast phenotype with an increase in local stiffness (Fig. 2.6.4.9) (Quinlan and Billiar, 2012; Rudnicki et al., 2013).

In addition, tissue growth can be guided on a scaffold to mimic the healing process of damaged tissues which involves increasing stiffness of the surrounding ECM. This local stiffening may lead to enhanced migration, proliferation, and/or progenitor-like properties. A large number of in vitro studies have confirmed that with an increase in substrate stiffness, various types of cells, including endothelial cells, airway smooth muscle cells, and dermal fibroblasts, exhibit enhanced cell adhesion, enlarged cell spreading with defined actin organization, increased cellular contractility, decreased migration speed, and enhanced proliferation (Hao et al., 2015; Razinia et al., 2017; Reilly and Engler, 2010; Shkumatov et al., 2015; Yeh et al., 2012; Yim and Sheetz, 2012).

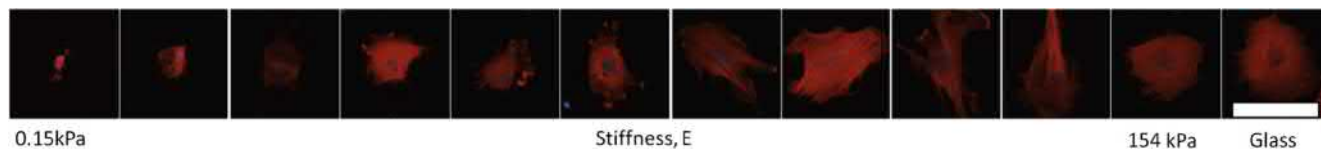
With advanced techniques, not just the magnitude but also the local patterns of stiffness can be manipulated to allow the design of specific conditions that direct cell organization, alignment, and migration (Marklein and Burdick, 2009; Ambriz et al., 2018; Yang et al., 2017). Sochol and colleagues investigated endothelial cells cultured on microposts with a gradient of stiffness magnitudes, and found they preferentially migrate toward stiffer microposts, with a migration speed proportional to the gradient strength (Sochol et al., 2011). Lin and colleagues cultured muscle cells on a surface with alternating soft and stiff strips of hydrogel structures and showed that cells preferentially attach to stiff regions when the strip width is narrow and comparable to cell size ($\sim 100 \mu\text{m}$), while cells randomly orient and spread for larger strip widths ($\sim 200 \mu\text{m}$) (Yin et al., 2018) (Fig. 2.6.4.10). Anseth's group developed substrates with different elastic moduli and organized/disorganized stiffness patterns on an even smaller,

subcellular scale. Similar to valvular interstitial cell activation to the myofibroblast phenotype on high-modulus substrates, they showed that MSCs cultured on substrates with a higher percentage of stiff regions are also activated. Moreover, MSCs cultured on substrates with a spatially disorganized pattern are less activated, have smaller focal adhesions, less α -SMA organization into stress fibers, and higher proliferation compared to those cultured on substrates with an organized pattern (Yang et al., 2016; Ma et al., 2017).

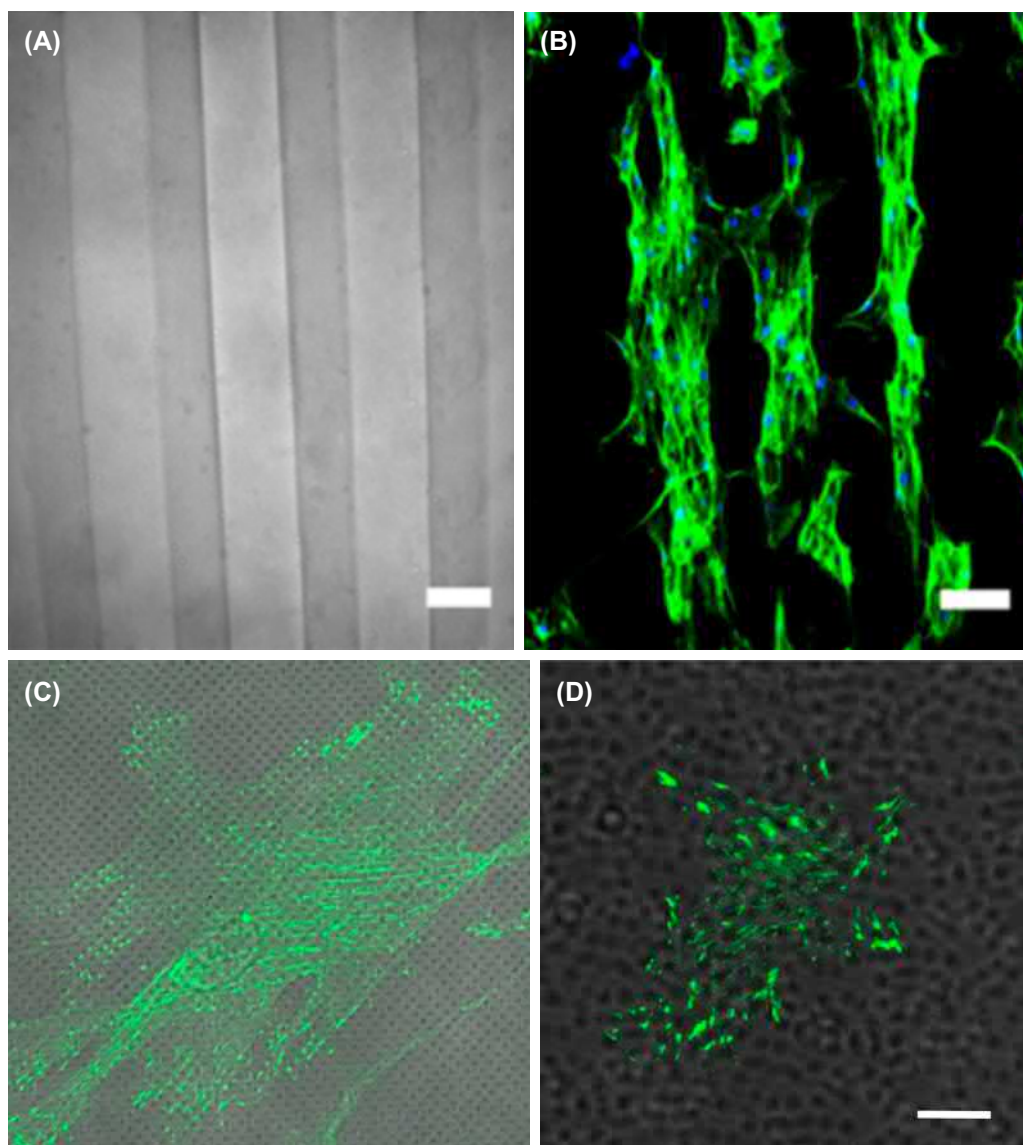
Surface Topography

It is virtually impossible to duplicate the complicated tissue-specific and multiscale topography of native tissues, yet specific micro- and nano-patterned designs are emerging as powerful tools to control cell behavior on engineered scaffolds. There are multiple parameters of surface topography that can be controlled including shape, dimension (feature size, spacing, and height), and periodicity. Each parameter has profound influence on cell behavior from cell adhesion and spreading to proliferation and differentiation (Nguyen et al., 2016). Chen and colleagues were among the first to demonstrate that local geometry is a fundamental mechanism that regulates cell response. By precisely controlling cell spreading while maintaining constant contact area, they demonstrated that proliferation and apoptosis are regulated by spread area rather than adhesion area (Liu et al., 2017).

It has also been demonstrated that cells can distinguish between micro- and nano-scale features. For instance, when MSCs are cultured on gratings of different width, they align and elongate along the grating axis, and show smaller and more elongated focal adhesions on nanogratings (250 nm width) compared to microgratings (10 μm width) or unpatterned surfaces (Yim et al., 2007). The size of surface patterns can also affect cell differentiation, as seen, adipogenic differentiation increases when MSCs are cultured on microgratings with 15- μm ridges, compared to 2- μm ridges that is enhanced osteogenic differentiation. The narrower ridges result in higher aspect ratio of cell shape and higher tension in the cytoskeleton (Abagnale et al., 2015). Cells can also sense gradients in topography. When fibroblasts are plated on grooves, cells migrate along the pattern orientation initially; however, within 2 h, cells show trends of migration toward areas with denser grooves (Kim et al., 2009). In addition, increased space between cell membrane protein-binding sites or random distribution of the binding sites result in compromised cell survival, migration, and



• **Figure 2.6.4.9** Substrate stiffness affects spreading and morphology of fibroblastic cells. Cells cultured on polyacrylamide gels ranging four orders of magnitude in modulus (150 Pa–150 kPa) plus glass exhibit increasing spread area and stress fibers with increasing stiffness. Cells were stained for α -SMA (red) and nuclei (blue). Scale bar is $100 \mu\text{m}$ (Quinlan and Billiar, 2012b).



• **Figure 2.6.4.10** (A) Bright-field image of alternating soft (dark; ~ 5 kPa) and stiff (light; ~ 11 kPa) 2D stripe pattern. Scale bar = $100 \mu\text{m}$. (B) Cells on stiffness-pattern substrate preferentially adhere and align on stiffer regions (Yin et al., 2018). Immunostaining of paxillin in MSCs on regularly (C) or randomized (D) patterned hydrogel with 75% stiff area. Scale bar = $30 \mu\text{m}$ (Yang et al., 2016).

differentiation capacity, since integrin clustering is abolished and cell adhesion weakened (Comisar et al., 2011; Park et al., 2007; Yang et al., 2016).

Fibrous Scaffolds

The native tissue matrix is conducive for cell communication, migration, and function, and researchers aim to mimic this environment in scaffolds (Carey et al., 2012; Paszek et al., 2005; Pupa et al., 2002; Stevens and George, 2005). In native ECM, cells attach to fibrous proteins including fibronectin, collagen, fibrin, and elastin. Cells can grab and pull on these fibers to change their shape or position. Fiber density, stiffness, alignment, and composition are all factors that can affect cell behavior, structure, and even stiffness (Hadjipanayi et al., 2009; Lu et al., 2012). For instance, cells cultured on stiffer

fibrous materials, such as nanotubes, can exhibit enhanced adhesion, spreading, and higher cytoskeletal tension (Aghvami et al., 2016). Mechanically, longer fibers have high axial stiffness but buckle easily, having overall low compressive stiffness. Long-range forces are transmitted through the fibers and can be affected by fiber length, entanglement, and cross-linking level, which can then influence neighboring cells (Ma et al., 2013). We, and others, have demonstrated that cells can sense much further in fibrous scaffolds compared to two-dimensional continuum materials (e.g., polyethylene glycol or polyacrylamide gels) (Ma et al., 2013; Rudnicki et al., 2013). In addition, fibrous biomaterials have nonlinear mechanical properties in that they stiffen under increased stretch. External or cell-generated stretch can also alter alignment of the fibers, thus biomaterial designers need to consider these complicated interactions between cells and fibrous scaffolds (Hall et al., 2016).

Multicellular Interactions

In multicellular systems, cells interact with both their extracellular environment as well as neighboring cells. Cell–cell contact allows direct connections via adherens junctions and transfer of mechanical stimuli through transmembrane proteins including cadherins. It is becoming increasingly clear that focal adhesions and adherens junctions share signaling molecules including MRTF and YAP/TAZ proteins (Mui et al., 2016). Coordinated interplay between integrins and cadherins also leads to a spatial distribution of molecular signals and forces, which guide diverse cell behaviors (Cirka et al., 2017; He et al., 2015; Li et al., 2009). Mooney and colleagues have shown that for MSC differentiation, higher stiffness alone can promote expression of early protein markers of osteogenesis, yet multicellular aggregation is necessary for mature osteogenesis with calcium deposition (Mao et al., 2016). Additionally, we have demonstrated that cells near the edges of 2D cell clusters have higher generated traction forces, increased stiffness, increased proliferation rate, and gene localization of mechanosensitive proteins compared to central cells (Cirka et al., 2017). Similarly, when cultured on confined protein islands, MSCs differentiate into an osteogenic phenotype at edges and adipogenic differentiation occurs in the central region (Nelson et al., 2005; Ruiz and Chen, 2008). As revealed in these studies, cell–cell contact has profound effects on altering the mechanical environment of engineered cell clusters. Accordingly, it can influence cell–scaffold interactions in engineered tissues.

Moreover, within a tissue-engineered scaffold, cells communicate with one another through chemical means. Nearby cells can sense biomolecules that are released from neighboring cells via paracrine signaling in addition to physical forces that are transduced through a fibrous scaffold. Both types of signals can cause changes in cell behavior that would not occur if the cells were isolated. Studies show that coculturing cells help better mimic the *in vivo* environment by regulating cellular function, behavior, development, and creating native niche conditions (Bogdanowicz and Lu, 2016; Wu et al., 2010).

Mechanical Stimulation

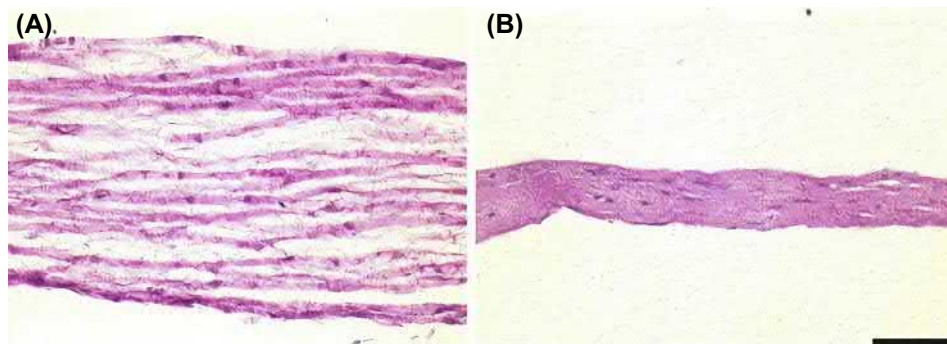
Once placed in the body, scaffolds and the cells within are subjected to complex mechanical forces and deformations. The effects of shear stress induced by flow are discussed in Chapter 2.1.6; here, we focus on the response of cells and tissues to cyclic stretch. Cyclic stretch has pronounced effects on cell–biomaterial interactions, and mechanical conditioning can be employed to improve the strength and stiffness of a construct. Cyclic stretch regimens have been used to induce increased production and maturation of collagen in engineered arteries, heart valves, ligaments, and skeletal muscle (Schmidt et al., 2016). A quantitative understanding of the effects of mechanical conditioning is necessary for designing tissue scaffolds functioning *in vivo*.

Cyclic stretch promotes stress fiber formation and F-actin realignment in cells, which can generate specific changes in

cellular shape, spreading, adhesion patterns, and differentiation. Typically parameters near physiological conditions (0.5–2 Hz, 2%–20% strain) are employed and the frequency, magnitude, duration, and direction of stretch are all important factors that translate into focal adhesion maturation and downstream signaling (Li et al., 2014). Regardless of cell type, cells cultured on compliant (but stiff) 2D substrates subjected to uniaxial, cyclic stretch generally show stretch-avoidance behavior, i.e., cells align perpendicular to the direction of principal cyclic strain (Li et al., 2014). In contrast, we have shown that cells cultured on low-stiffness substrates spread and orient at an intermediate angle (not completely perpendicular to stretch) (Cirka et al., 2015). Reorientation of cells cultured in 3D constructs is even more complicated, since ECM fibers in the fibrous scaffolds also provide strong contact guidance for cells (Lei and Ferdous, 2016). For example, stretching 3D tissues after reconstituted ECM fibers are well aligned due to cell contraction and boundary conditions does not induce cell realignment; whereas stretching immediately after casting the gel (without time for fiber alignment) results in a strong stretch-avoidance response and reorientation (Foolen et al., 2012; Li et al., 2014; Schmidt et al., 2016). The degree of stretch anisotropy is also an important parameter. Increasing anisotropy with biaxial strain results in increased cellular orientation and collagen fiber alignment along the principal directions of strain for VICs cultured in collagen gels (Gould et al., 2012).

Computational models and experimental observation have indicated that cells do not respond to stretch below a threshold frequency of 0.01 Hz (Tondon and Kaunas, 2014; Schmidt et al., 2016). Rahimi et al. reported that vascular smooth muscle cells were efficiently aligned by cyclic stretch at 1.25 Hz under short-term stimulation (12 h), while they oriented more uniformly under lower frequency (0.5 Hz) under long-term stimulation (24 h) (Li et al., 2014). Stretch amplitudes also play a considerable role in cell orientation. For instance, a 10%–24% (1 Hz) graded stretch resulted in graded vascular smooth muscle cell alignment ranging from a completely random orientation to a maximum alignment perpendicular to the stretch vector (Kakisis et al., 2004).

Compared to engineered tissues cultured under static conditions, engineered tissues conditioned under cyclic stretch generally have significantly increased viability of cells and ECM protein secretion, reduced volume, elevated matrix metalloproteinase activity, and mechanical properties more similar to native tissues (Lei et al., 2017; Seliktar et al., 2003). For collagen-based blood vessels, heart valves, cartilage, and ligaments, cyclic stretch has shown increased strength and stiffness compared to static controls (McMahon et al., 2008; Kensah et al., 2011). We have demonstrated that, when cyclic equibiaxial stretch (16% stretch at 0.2 Hz) is applied to fibroblast-populated fibrin gels for 8 days, stretched samples are approximately 10 times stronger, eightfold denser, and eight times thinner than statically cultured samples (Fig. 2.6.4.11). These changes are accompanied by a 15% increase in net collagen produced (Balestrini and Billiar, 2006).



• **Figure 2.6.4.11** Brightfield images of hematoxylin and eosin-stained sections of fibrin gels after 8 days in (A) static samples and (B) 16% cyclic stretch at 0.2 Hz for 6 h/day. Stretch induces fibroblasts to compact the gels which results in a denser matrix. Scale bar = 100 μm (Balestrini and Billiar, 2006).

While cyclic stretch can stimulate cells to produce more collagen, this ability is limited by adaptation of the cells to the applied mechanical stimuli when the amplitude of stretch remains constant. In order to circumvent this adaptive effect, various stretching regimens have been employed including incrementally increasing strain amplitude and intermittent stretching (Courtney et al., 2006; Syedain and Tranquillo, 2009). For example, neonatal human dermal fibroblast-seeded fibrin gels were subjected to 2 weeks of constant amplitude (5% or 13.5% amplitude), intermittent (15 min at 5%, 6 h static, repeat), or incremental (5%–13.5% increment by $\sim 1\%$ every 24 h) cyclic stretching regimens. Results show that extracellular signal-regulated kinase (ERK1/2), which is necessary for stretch-induced collagen transcription, is maximal at 15 min and decayed by 1 h in constant-amplitude stretches (Schmidt et al., 2016). A 6 h static period was required before the fibroblasts were able to respond to a second onset of cyclic stretch (Rubbens et al., 2009). While both intermittent and incremental regimens reactivated ERK1/2, only incremental stretching increased collagen production compared to samples stretched with constant amplitude, resulting in a 37% increase in collagen per cell after 2 weeks. In contrast to this study, Paxton et al. found that intermittent stretching (10 min every 6 h) increased the percentage of collagen in their fibrin-based “sinews” approximately 20% over continuously stretched samples (Paxton et al., 2012; Syedain et al., 2011). These findings suggest that a regimen with small, frequent increments in strain amplitude might be optimal for promoting collagen production and tissue development.

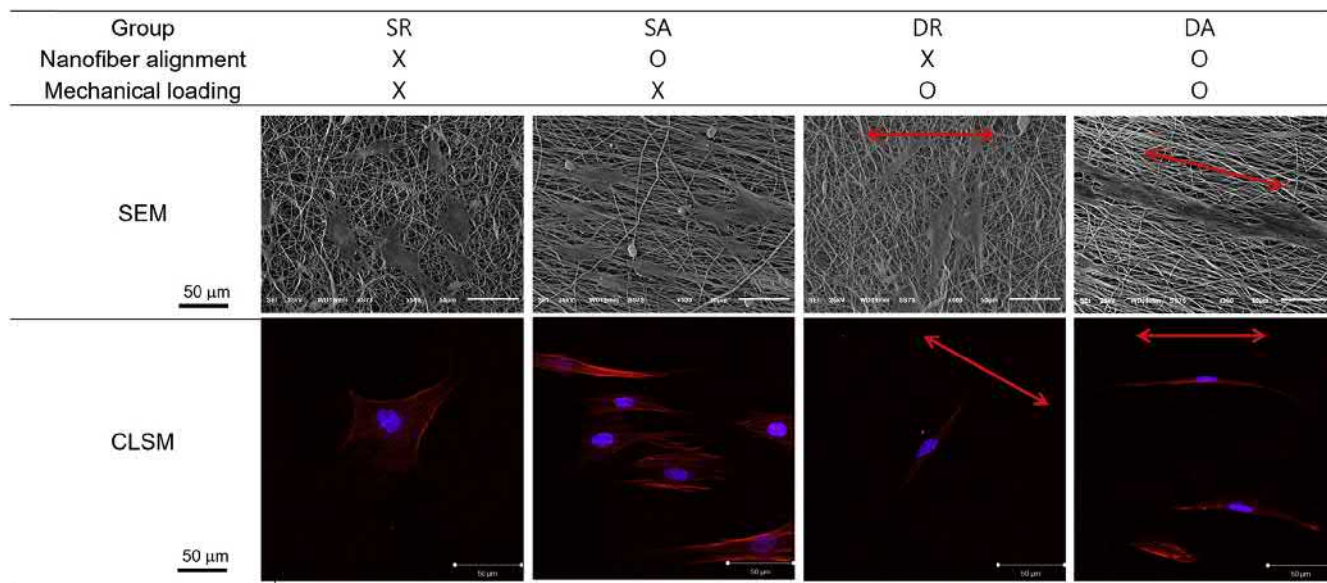
Effects of Combined Mechanical Stimuli

In living organisms, cells reside in a complex environment with multiscale topographic features, spatially heterogeneous mechanical cues, and dynamic stimulation provided by surrounding cells and ECM. Therefore, when designing scaffolds, it is necessary to consider the influence of these interrelated factors on cell behaviors and tissue growth. In a study of combined influence of stiffness and spread area, hepatic stellate cells differentiation into myofibroblasts was observed on large (1 mm diameter) islands with higher stiffness ($23.8 \pm 4.6 \text{ kPa}$), while they remained quiescent on

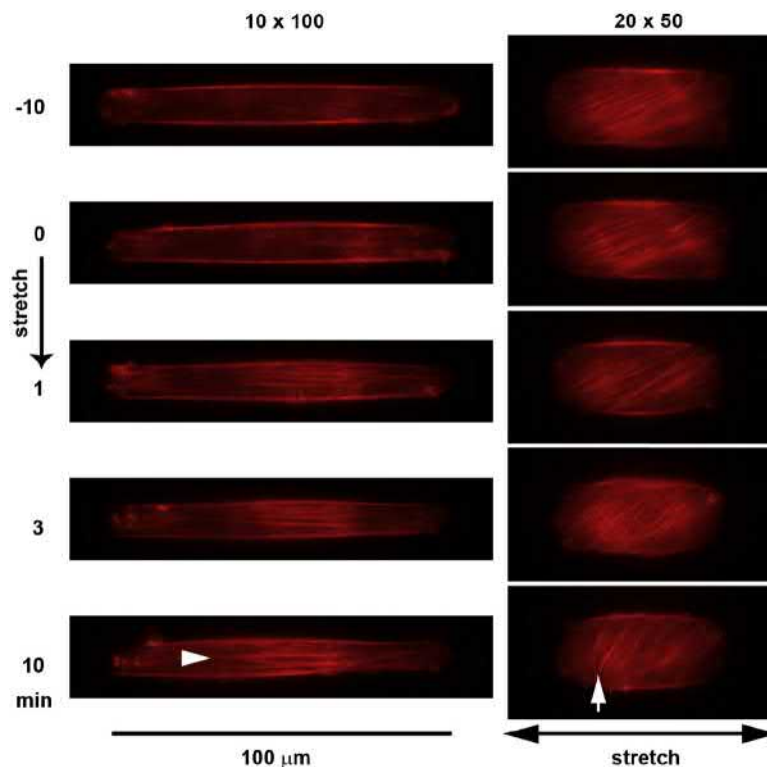
low-modulus substrates ($2.1 \pm 0.7 \text{ kPa}$) or on small (50 μm diameter), stiff islands that prevented cell spreading (Guvendiren et al., 2014). For cells, stretch can trigger a marked increase of traction forces and apparent stiffness. Therefore, cells cultured on soft substrates under stretch may behave similarly to those cultured on stiffer substrates (Rosowski et al., 2018). For instance, we cultured fibroblastic cells under a wide range of combined levels of substrate stiffness and dynamic stretch. Substrate stiffness was adjusted from relatively soft ($G' = 0.3 \text{ kPa}$) to stiff ($G' = 50 \text{ kPa}$). On soft substrates, cells cultured statically exhibited a rounded morphology and were significantly smaller than on stiff substrates. After equibiaxial cyclic stretch, VICs spread similar to cells cultured on stiff substrates (Fig. 2.6.4.4). These results indicate that inhibition of spreading due to a lack of matrix stiffness surrounding a cell may be overcome by externally applied stretch, suggesting similar mechanotransduction mechanisms for sensing stiffness and stretch (Quinlan et al., 2011). Other studies show that MRTF-A or YAP are activated when cells sense cyclic stretch and stiff substrates, and cell internal prestress (stress fiber formation) also plays an important role in the localization of these markers (Cui et al., 2015; Cirka et al., 2015).

Topography strongly influences cell attachment, reorientation, and viability under stretch. Under static conditions, stem cells randomly spread on random nanofibers while cells are aligned on aligned nanofibers. Under uniaxial cyclic stretch conditions, cells on random nanofibers align perpendicular to the loading axis. Interestingly, cells on aligned nanofibers align along the loading axis, which is also parallel to the orientation of the nanofibers (Fig. 2.6.4.12). The cell elongation appears to be more substantial on aligned nanofibers under uniaxial stretch compared to the other conditions (Kim et al., 2016).

Wang et al. built an in vitro muscle model with combined mechanical stretch and geometrical control, and found that myoblasts with higher aspect ratio had higher viability under cyclic stretch. Given the same area, wider cells under stretch had most of their parallel actin filaments broken and disassembled, but had stable perpendicular central actin filaments; this is consistent with the published reports that uniaxial mechanical stretch induces actin filaments to reassemble and align along the perpendicular direction.



• **Figure 2.6.4.12** Top: SEM images show random or aligned orientation of nanofibers. Bottom: Fluorescent images reveal that cells preferentially align along the orientation of aligned fibers. Following cyclic stretch, cells align perpendicular to direction of stretch on random oriented fibers. However, on oriented fibers, cells align parallel to stretch along the direction of the fiber alignment. F-actin (red) and DAPI (blue) were stained and red arrows indicate the direction of stretch (Kim et al., 2016).



• **Figure 2.6.4.13** Stained F-actin (red) shows reassembly of actin fibers over time in response to stretch. In thin, elongated cells (left), F-actin reassembled parallel to the direction of stretch, while in shorter, wider cells (right), F-actin reassembled perpendicular to the direction of stretch (Wang et al., 2014).

Interestingly for thinner cells, there was new parallel F-actin assembly during stretch (Fig. 2.6.4.13). Although this cannot be explained by current experiment models or theories, this evidence might explain why myoblasts are destined to take the elongated geometry in vivo (Wang et al., 2014).

Implications for Future Materials Design

Biomaterials for tissue engineering include complex scaffolds with intricate porous and fibrous structures that resist macroscopic loads and support cell growth and migration

at the local scale. In the future, ideal biomaterials for tissue engineering are expected to provide even more precise control of cell behavior during tissue formation. Here we highlight a few promising directions.

- (1) 3D printing devices and inks could achieve sub- μm scale and allow multiple materials to be printed simultaneously, reaching precise control over complex geometry, topography, and even local mechanical properties. For instance, in light-assisted bioprinting techniques, local stiffness of hydrogels can be manipulated by controlling oxygen permeation, inhibition, and ultraviolet exposure dosage, which alter the cross-linking density and stiffness of cured structures. The programmable stiffness spans nearly an order of magnitude ($E \sim 2\text{--}15\text{ kPa}$) within the physiologically relevant range. ECMs with programmed micromechanical environments can dictate 3D cellular organization, enabling in vitro tissue reconstruction. [Chapter 1.4.8](#) provides additional information about additive manufacturing.
- (2) The mechanical properties of scaffolds could be tuned in real time, providing higher flexibility in guidance of cell growth. Traditionally, hydrogels are normally degraded without control by hydrolytic or enzymatic mechanisms. For example, Khetan and colleagues reported that for covalently cross-linked hyaluronic acid hydrogels with equivalent stiffness ($\sim 4\text{ kPa}$), enzymatic degradation permitted cell spreading, and favored osteogenic differentiation. In contrast, nondegradable hydrogels restricted cell migration and favored adipogenic differentiation ([Marklein and Burdick, 2009](#)). More information about degradation is provided in [Chapter 1.3.2F](#). More recently, Brown et al. synthesized biocompatible hydrogels that can be degraded via a radical addition-fragmentation chain transfer process, where a single photon initiates multiple events and amplifies the degradation process. The gel formation and photodegradation processes can be controlled in real time to study the cell response to multiple levels of stiffness ([Brown et al., 2017](#)). In addition, Yeh et al. developed a two-step cross-linking strategy that can increase the compressive modulus of polydimethylsiloxane up to 10-fold within minutes. With stiffening, cells displayed increased spreading and higher level of fibroblast activation ([Yeh et al., 2017](#)). More information about hydrogels is provided in [Chapter 1.3.2E](#).
- (3) Nonlinear biomaterials can better mimic properties of native ECM. Covalently cross-linked hydrogels are typically elastic, while native ECM is viscoelastic. Chaudhuri et al. observed increased cell spreading on soft, viscoelastic substrates compared to elastic gels with the same stiffness, and similar to that on stiffer, elastic substrates. MSC spreading, proliferation, and osteogenic differentiation were enhanced in rapidly relaxing hydrogels ($\tau_{1/2} = 70\text{ s}$) compared to elastic gels ($\tau_{1/2} = 3300\text{ s}$) ([Quinlan et al., 2011](#); [Chaudhuri, 2017](#)).

Conclusion

Today, biomaterials are an indispensable tool in our efforts to repair and regenerate injured or diseased tissues and organs. Biomaterials are viewed as more than carriers for cell delivery and growth factors; they are now designed to mechanically interact with cells and promote tissue development as well as to restore function. The mechanical and structural features of developing tissues vary over space and time on the micrometer scale. Thus, biomaterials that allow precise spatiotemporal regulation of adhesive and micromechanical cues will have tremendous regenerative potential as they are designed to more faithfully recapitulate the dynamic cellular microenvironment characteristic of endogenous developmental processes.

HIGHLIGHTS OF THIS CHAPTER

Hierarchical Design

- Micromechanical properties of biomaterials have a profound influence on cell behaviors and tissue formation.
- It is promising to modulate cell-scaffold interactions by designing micro/nano-scaled features of biomaterials.
- Controllable mechanical properties include bulk stiffness, local stiffness, topography, and dynamic conditioning.

Mechanotransduction

- Relatively stiff substrate, large spreading area, and low cell density promote focal adhesion maturation.
- This maturation facilitates migration, proliferation, and differentiation into phenotypes with higher cell tension.
- Signaling proteins such as RhoA/ROCK and YAP/TAZ could be tracked in validation of biomaterial design.

Interplay of Mechanical Cues

- Cells in low-modulus scaffolds under stretch may have behaviors similar to those in stiffer scaffolds.
- Fibrous topography may dominate stretch in guiding cell alignment.
- Cell-cell contact allows force transfer in multicellular systems, resulting in complex distributions of stress dependent upon mechanically constrained shapes/boundaries.

3D Scaffolds

- Cells residing in 3D scaffolds have different behaviors compared to cells cultured on 2D substrates.
- Cells on collagen-coated membranes align perpendicularly to the direction of stretch, whereas those cultured within collagen gels align parallel with the direction of stretch.

Degradation

- Micromechanical cues (bulk and local stiffness, topography) change with degradation of biomaterials, which could direct ECM remodeling with external stimulation.
- Scaffolds need to properly direct extracellular matrix remodeling and cell force generation during neotissue formation.

References

- Abagnale, G., Steger, M., Nguyen, V.H., Hersch, N., Sechi, A., Jousen, S., Denecke, B., Merkel, R., Hoffmann, B., Dreser, A., Schnakenberg, U., Gillner, A., Wagner, W., 2015. Surface topography enhances differentiation of mesenchymal stem cells towards osteogenic and adipogenic lineages. *Biomaterials* 61, 316–326.
- Aghvami, M., Billiar, K.L., Sander, E.A., 2016. Fiber network models predict enhanced cell mechanosensing on fibrous gels. *J. Biomech. Eng.* 138, 11.
- Aiyelabegan, H.T., Esmail, E., 2017. Fundamentals of protein and cell interactions in biomaterials. *Biomed. Pharmacother.* 88, 956–970.
- Ambriz, X., Lanerolle, P.D., Ambrosio, J.R., 2018. The mechanobiology of the actin cytoskeleton in stem cells during differentiation and interaction with biomaterials. *Stem Cell. Int.* 2018, 1–11.
- Aragona, M., Panciera, T., Manfrin, A., Giulitti, S., Michielin, F., Elvassore, N., Dupont, S., Piccolo, S., 2013. A mechanical checkpoint controls multicellular growth through YAP/TAZ regulation by actin-processing factors. *Cell* 154, 1047–1059.
- Bachir, A., Horwitz, A.R., Nelson, W.J., Bianchini, J.M., 2017. Cell adhesions: actin-based modules that mediate cell-extracellular matrix and cell-cell interactions. *Cold Spring Harb. Perspect. Biol.* 9, a023234.
- Balestrini, J.L., Billiar, K.L., 2006. Equibiaxial cyclic stretch stimulates fibroblasts to rapidly remodel fibrin. *J. Biomech.* 39, 2983–2990.
- Bardi, G., Niggli, V., Loetscher, P., 2003. Rho kinase is required for CCR7-mediated polarization and chemotaxis of T lymphocytes. *FEBS Lett.* 542, 79–83.
- Bogdanowicz, D.R., Lu, H.H., 2016. Multifunction co-culture model for evaluating cell-cell interactions. *Methods Mol. Biol.* 1202, 29–36.
- Booth-Gauthier, E.A., Alcoser, T.A., Yang, G., Dahl, K.N., 2012. Force-induced changes in subnuclear movement and rheology. *Biophys. J.* 103, 2423–2431.
- Brown, T.E., Marozas, I.A., Anseth, K.S., 2017. Amplified photodegradation of cell-laden hydrogels via an addition–fragmentation chain transfer reaction. *Adv. Mater.* 29.
- Brusatin, G., Panciera, T., Gandin, A., Citron, A., Piccolo, S., 2019. Biomaterials and engineered microenvironments to control YAP/TAZ-dependent cell behavior. *Nat. Mater.* 17, 1063–1075.
- Carey, S.P., D’Alfonso, T.M., Shin, S.J., Reinhart-King, C.A., 2012. Mechanobiology of tumor invasion: engineering meets oncology. *Crit. Rev. Oncol. Hematol.* 83, 170–183.
- Chaudhuri, O., 2017. Viscoelastic hydrogels for 3D cell culture. *Biomater. Sci.* 5, 1480–1490.
- Chen, T., Wu, C., Tang, M., Huang, J., Su, F., 2010. Complexity of the tensegrity structure for dynamic energy and force distribution of cytoskeleton during cell spreading. *PLoS One* 5, e14392.
- Cirka, H., Monterosso, M., Diamantides, N., Favreau, J., Wen, Q., Billiar, K., 2015. Active traction force response to long-term cyclic stretch is dependent on cell pre-stress. *Biophys. J.* 110, 1845–1857.
- Cirka, H.A., Uribe, J., Liang, V., Schoen, F.J., Billiar, K.L., 2017. Reproducible in vitro model for dystrophic calcification of cardiac valvular interstitial cells: insights into the mechanisms of calcific aortic valvular disease. *Lab Chip* 17, 814–829.
- Comisar, W.A., Mooney, D.J., Linderman, J.J., 2011. Integrin organization: linking adhesion ligand nanopatterns with altered cell responses. *J. Theor. Biol.* 274, 120–130.
- Courtney, T., Sacks, M.S., Stankus, J., Guan, J., Wagner, W.R., 2006. Design and analysis of tissue engineering scaffolds that mimic soft tissue mechanical anisotropy. *Biomaterials* 27, 3631–3638.
- Cui, Y., Hameed, F.M., Yang, B., Lee, K., Pan, C.Q., Park, S., Sheetz, M., 2015. Cyclic stretching of soft substrates induces spreading and growth. *Nat. Com.* 6, 6333.
- Davidson, M.W., Hess, H.F., Ramko, E.B., Waterman, C.M., Kanchanawong, P., Shtengel, G., Pasapera, A.M., 2010. Nanoscale architecture of integrin-based cell adhesions. *Nature* 468, 580–584.
- Dickinson, R.B., Neelam, S., Lele, T.P., 2015. Dynamic, mechanical integration between nucleus and cell—where physics meets biology. *Nucleus* 6, 360–365.
- Discher, D.E., Janmey, P., Wang, Y., 2005. Tissue cells feel and respond to the stiffness of their substrate. *Science* 310, 1139–1143.
- Driscoll, T., Cosgrove, B., Heo, S., Shurden, Z., Mauck, R., 2015. Cytoskeletal to nuclear strain transfer regulates YAP signaling in mesenchymal stem cells. *Biophys. J.* 108, 2783–2793.
- Dupont, S., 2016. Role of YAP/TAZ in cell-matrix adhesion-mediated signalling and mechanotransduction. *Exp. Cell Res.* 343, 42–53.
- Dupont, S., Morsut, L., Aragona, M., Enzo, E., Giulitti, S., Cordeonsi, M., Zanconato, F., Digabel, J.L., Forcato, M., Bicciato, S., Elvassore, N., Piccolo, S., 2011. Role of YAP/TAZ in mechanotransduction. (yes-associated protein). *Nature* 474, 179.
- Dutta, S., Mana-Capelli, S., Paramasivam, M., Dasgupta, I., Cirka, H., Billiar, K., McCollum, D., 2018. TRIP6 inhibits Hippo signaling in response to tension at adherens junctions. *EMBO Rep.* 19, 37–350.
- Engler, A.J., Sen, S., Sweeney, H.L., Discher, D.E., 2006. Matrix elasticity directs stem cell lineage specification. *Cell* 126, 677–689.
- Enyedi, B., Niethammer, P., 2017. Nuclear membrane stretch and its role in mechanotransduction. *Nucleus (Austin, Tex.)* 8, 156–161.
- Fabry, B., Klemm, A.H., Kienle, S., Schäffer, T.E., Goldmann, W.H., 2011. Focal adhesion kinase stabilizes the cytoskeleton. *Biophys. J.* 101, 2131–2138.
- Fehrenbacher, A., Steck, E., Roth, W., Pahmeier, A., Richter, W., 2006. Long-term mechanical loading of chondrocyte-chitosan biocomposites in vitro enhanced their proteoglycan and collagen content. *Biorheology* 43, 709–720.
- Fink, J., Carpi, N., Betz, T., Bétard, A., Chebah, M., Azioune, A., Bornens, M., Sykes, C., Fetler, L., Cuvelier, D., Piel, M., 2011. External forces control mitotic spindle positioning. *Nat. Cell Biol.* 13, 771–778.
- Fletcher, D.A., Mullins, R.D., 2010. Cell mechanics and the cytoskeleton. *Nature* 463, 485–492.
- Foolen, J., Deshpande, V.S., Kanters, F.M., Baaijens, F.P., 2012. The influence of matrix integrity on stress-fiber remodeling in 3D. *Biomaterials* 33, 7508–7518.
- Galli, G.G., Carrara, M., Yuan, W., Valdes-Quezada, C., Gurung, B., Pepe-Mooney, B., Zhang, T., Geeven, G., Gray, N.S., de Laat, W., Calogero, R.A., Camargo, F.D., 2015. YAP drives growth by controlling transcriptional pause release from dynamic enhancers. *Mol. Cell* 60, 328–337.
- Gauthier, N.C., Fardin, M.A., Roca-Cusachs, P., Sheetz, M.P., 2011. Temporary increase in plasma membrane tension coordinates the activation of exocytosis and contraction during cell spreading. *Proc. Natl. Acad. Sci. U.S.A.* 108, 14467–14472.
- Ghassemi, S., Meacci, G., Liu, S., Gondarenko, A.A., Mathur, A., Roca-Cusachs, P., Sheetz, M.P., Hone, J., 2012. Cells test substrate rigidity by local contractions on submicrometer pillars. *Proc. Natl. Acad. Sci. U.S.A.* 109, 5328–5333.
- Giannone, G., Dubin-Thaler, B.J., Döbereiner, H., Kieffer, N., Bresnick, A.R., Sheetz, M.P., 2004. Periodic lamellipodial contractions correlate with rearward actin waves. *Cell* 116, 431–443.

- Gould, R.A., Chin, K., Santisakultarm, T.P., Dropkin, A., Richards, J.M., Schaffer, C.B., Butcher, J.T., 2012. Cyclic strain anisotropy regulates valvular interstitial cell phenotype and tissue remodeling in three-dimensional culture. *Acta Biomater.* 8, 1710–1719.
- Guvendiren, M., Perepelyuk, M., Wells, R.G., Burdick, J.A., 2014. Hydrogels with differential and patterned mechanics to study stiffness-mediated myofibroblastic differentiation of hepatic stellate cells. *J. Mech. Behav. Biomed. Mater.* 38, 198–208.
- Hadjipanayi, E., Mudera, V., Brown, R.A., 2009. Guiding cell migration in 3D: a collagen matrix with graded directional stiffness. *Cell Motil. Cytoskelet.* 66, 121–128.
- Hall, M.S., Alisafaai, F., Ban, E., Feng, X., Hui, C., Shenoy, V.B., Wu, M., 2016. Fibrous nonlinear elasticity enables positive mechanical feedback between cells and ECMs. *Proc. Natl. Acad. Sci. U.S.A.* 1613058113.
- Hao, J., Zhang, Y., Jing, D., Shen, Y., Tang, G., Huang, S., Zhao, Z., 2015. Mechanobiology of mesenchymal stem cells: perspective into mechanical induction of MSC fate. *Acta Biomater.* 20, 1–9.
- Hao, J., Zhang, Y., Wang, Y., Ye, R., Qiu, J., Zhao, Z., Li, J., 2014. Role of extracellular matrix and YAP/TAZ in cell fate determination. *Cell. Signal.* 26, 186–191.
- Hautmann, M.B., Adam, P.J., Owens, G.K., 1999. Similarities and differences in smooth muscle alpha-actin induction by TGF-beta in smooth muscle versus non-smooth muscle cells. *Arterioscler. Thromb. Vasc. Biol.* 19, 2049–2058.
- He, S., Liu, C., Li, X., Ma, S., Huo, B., Ji, B., 2015. Dissecting collective cell behavior in polarization and alignment on micropatterned substrates. *Biophys. J.* 109, 489–500.
- Ingber, D.E., 2006. Cellular mechanotransduction: putting all the pieces together again. *FASEB J.* 20, 811–827.
- Isenberg, B.C., Williams, C., Tranquillo, R.T., 2006. Small diameter artificial arteries engineered in vitro. *Circ. Res.* 98, 25–35.
- Iskratsch, T., Wolfenson, H., Sheetz, M.P., 2014. Appreciating force and shape – the rise of mechanotransduction in cell biology. *Nat. Rev. Mol. Cell Biol.* 15, 825–833.
- Kakisis, J.D., Liapis, C.D., Sumpio, B.E., 2004. Effects of cyclic strain on vascular cells. *Endothelium* 11, 17–28.
- Kensah, G., Gruh, I., Viering, J., Schumann, H., Dahlmann, J., Meyer, H., Skvorc, D., Bar, A., Akhyari, P., Heisterkamp, A., Haverich, A., Martin, U., 2011. A novel miniaturized multimodal bioreactor for continuous in situ assessment of bioartificial cardiac tissue during stimulation and maturation. *Tissue Eng. Part C Methods* 17, 463–473.
- Kim, D., Seo, C., Han, K., Kwon, K.W., Levchenko, A., Suh, K., 2009. Guided cell migration on microtextured substrates with variable local density and anisotropy. *Adv. Funct. Mater.* 19, 1579–1586.
- Kim, J.H., Kang, M.S., Eltohamy, M., Kim, T., Kim, H., 2016. Dynamic mechanical and nanofibrous topological combinatory cues designed for periodontal ligament engineering. *PLoS One* 11, e0149967.
- Kovács, M., Wang, F., Hu, A., Zhang, Y., Sellers, J.R., 2003. Functional divergence of human cytoplasmic myosin II: kinetic characterization of the non-muscle IIA isoform. *J. Biol. Chem.* 278, 38132–38140.
- Lei, Y., Masjedi, S., Ferdous, Z., 2017. A study of extracellular matrix remodeling in aortic heart valves using a novel biaxial stretch bioreactor. *J. Mech. Behav. Biomed. Mater.* 75, 351–358.
- Lei, Y., Ferdous, Z., 2016. Design considerations and challenges for mechanical stretch bioreactors in tissue engineering. *Biotechnol. Prog.* 32, 543–553.
- Li, B., Li, F., Puskar, K.M., Wang, J.H.-., 2009. Spatial patterning of cell proliferation and differentiation depends on mechanical stress magnitude. *J. Biomech.* 42, 1622–1627.
- Li, Y., Huang, G., Zhang, X., Wang, L., Du, Y., Lu, T.J., Xu, F., 2014. Engineering cell alignment in vitro. *Biotechnol. Adv.* 32, 347–365.
- Liu, L., Zhang, S.X., Liao, W., Farhoodi, H.P., Wong, C.W., Chen, C.C., Ségaliny, A.I., Chacko, J.V., Nguyen, L.P., Lu, M., Polovin, G., Pone, E.J., Downing, T.L., Lawson, D.A., Digman, M.A., Zhao, W., 2017. Mechanoresponsive stem cells to target cancer metastases through biophysical cues. *Sci. Transl. Med.* 9 ean2966.
- Liu, Z., Wu, H., Jiang, K., Wang, Y., Zhang, W., Chu, Q., Li, J., Huang, H., Cai, T., Ji, H., Yang, C., Tang, N., 2016. MAPK-mediated YAP activation controls mechanical-tension-induced pulmonary alveolar regeneration. *Cell Rep.* 16, 1810–1819.
- Lu, P., Weaver, V.M., Werb, Z., 2012. The extracellular matrix: a dynamic niche in cancer progression. *J. Cell Biol.* 196, 395–406.
- Lutolf, M.P., Hubbell, J.A., 2005. Synthetic biomaterials as instructive extracellular microenvironments for morphogenesis in tissue engineering. *Nat. Biotechnol.* 23, 47–55.
- Ma, H., Killaars, A.R., DelRio, F.W., Yang, C., Anseth, K.S., 2017. Myofibroblastic activation of valvular interstitial cells is modulated by spatial variations in matrix elasticity and its organization. *Biomaterials* 131, 131–144.
- Ma, X., Schickel, M.E., Stevenson, M.D., Sarang-Sieminski, A.L., Gooch, K.J., Ghadiali, S.N., Hart, R.T., 2013. Fibers in the extracellular matrix enable long-range stress transmission between cells. *Biophys. J.* 104, 1410–1418.
- McMahon, L.A., Reid, A.J., Campbell, V.A., Prendergast, P.J., 2008. Regulatory effects of mechanical strain on the chondrogenic differentiation of MSCs in a collagen-GAG scaffold: experimental and computational analysis. *Ann. Biomed. Eng.* 36, 185–194.
- Mao, A.S., Shin, J., Mooney, D.J., 2016. Effects of substrate stiffness and cell-cell contact on mesenchymal stem cell differentiation. *Biomaterials* 98, 184–191.
- Marklein, R.A., Burdick, J.A., 2009. Spatially controlled hydrogel mechanics to modulate stem cell interactions. *Soft Matter* 6, 136–143.
- Martewicz, S., Serena, E., Zatti, S., Keller, G., Elvassore, N., 2017. Substrate and mechanotransduction influence SERCA2a localization in human pluripotent stem cell-derived cardiomyocytes affecting functional performance. *Stem Cell Res.* 25, 107–114.
- Martino, F., Perestrelo, A.R., Vinarský, V., Pagliari, S., Forte, G., 2018. Cellular mechanotransduction: from tension to function. *Front. Physiol.* 9, 824.
- McBeath, R., Pirone, D.M., Nelson, C.M., Bhadriraju, K., Chen, C.S., 2004. Cell shape, cytoskeletal tension, and RhoA regulate stem cell lineage commitment. *Dev. Cell* 6, 483–495.
- McCulloch, A.D., Harris, A.B., Sarraf, C.E., Eastwood, M., 2004. New multi-cue bioreactor for tissue engineering of tubular cardiovascular samples under physiological conditions. *Tissue Eng.* 10, 565–573.
- Miralles, F., Posern, G., Zaromytidou, A., Treisman, R., 2003. Actin dynamics control SRF activity by regulation of its coactivator MAL. *Cell* 113, 329–342.
- Morikawa, Y., Zhang, M., Heallen, T., Leach, J., Tao, G., Xiao, Y., Bai, Y., Li, W., Willerson, J.T., Martin, J.F., 2015. Actin cytoskeletal remodeling with protrusion formation is essential for heart regeneration in Hippo-deficient mice. *Sci. Signal.* 8, ra41.
- Mui, K.L., Chen, C.S., Assoian, R.K., 2016. The mechanical regulation of integrin-cadherin crosstalk organizes cells, signaling and forces. *J. Cell Sci.* 129, 1093–1100.

- Nelson, C.M., Jean, R.P., Tan, J.L., Liu, W.F., Sniadecki, N.J., Spectator, A.A., Chen, C.S., Langer, R., 2005. Emergent patterns of growth controlled by multicellular form and mechanics. *Proc. Natl. Acad. Sci. U.S.A.* 102, 11594–11599.
- Nguyen, A.T., Sathe, S.R., Yim, E.K.F., 2016. From nano to micro: topographical scale and its impact on cell adhesion, morphology and contact guidance. *J. Phys. Condens. Matter* 28, 183001.
- O'Connor, J.W., Gomez, E.W., 2013. Cell adhesion and shape regulate TGF-beta1-induced epithelial-myofibroblast transition via MRTF-A signalling. *PLoS One* 8, e83188.
- Ohashi, K., Fujiwara, S., Mizuno, K., 2017. Roles of the cytoskeleton, cell adhesion and rho signalling in mechanosensing and mechanotransduction. *J. Biochem.* 161, 245.
- Pan, H., Xie, Y., Zhang, Z., Li, K., Hu, D., Zheng, X., Fan, Q., Tang, T., 2017. YAP-mediated mechanotransduction regulates osteogenic and adipogenic differentiation of BMSCs on hierarchical structure. *Colloids Surf. B Biointerfaces* 152, 344–353.
- Pancieria, T., Azzolin, L., Cordenonsi, M., Piccolo, S., 2017. Mechanobiology of YAP and TAZ in physiology and disease. *Nat. Rev. Mol. Cell Biol.* 18, 758–770.
- Park, J., Bauer, S., von der Mark, K., Schmuki, P., 2007. Nanosize and vitality: TiO₂ nanotube diameter directs cell fate. *Nano Lett.* 7, 1686–1691.
- Paszek, M.J., Zahir, N., Johnson, K.R., Lakins, J.N., Rozenberg, G.I., Gefen, A., Reinhart-King, C.A., Margulies, S.S., Dembo, M., Boettiger, D., Hammer, D.A., Weaver, V.M., 2005. Tensional homeostasis and the malignant phenotype. *Cancer Cell* 8, 241–254.
- Paxton, J.Z., Hagerty, P., Andrick, J.J., Baar, K., 2012. Optimizing an intermittent stretch paradigm using ERK1/2 phosphorylation results in increased collagen synthesis in engineered ligaments. *Tissue Eng. Part A* 18, 277–284.
- Pupa, S.M., Ménard, S., Forti, S., Tagliabue, E., 2002. New insights into the role of extracellular matrix during tumor onset and progression. *J. Cell. Physiol.* 192, 259–267.
- Quinlan, A.M.T., Sierad, L.N., Capulli, A.K., Firstenberg, L.E., Billiar, K.L., 2011. Combining dynamic stretch and tunable stiffness to probe cell mechanobiology in vitro. *PLoS One* 6, e23272.
- Quinlan, A.M.T., Billiar, K.L., 2012. Investigating the role of substrate stiffness in the persistence of valvular interstitial cell activation. *J. Biomed. Mater. Res. A* 100A, 2474–2482.
- Razinia, Z., Castagnino, P., Xu, T., Vázquez-Salgado, A., Puré, E., Assoian, R.K., 2017. Stiffness-dependent motility and proliferation uncoupled by deletion of CD44. *Sci. Rep.* 7, 16499.
- Reilly, G.C., Engler, A.J., 2010. Intrinsic extracellular matrix properties regulate stem cell differentiation. *J. Biomech.* 43, 55–62.
- Rosowski, K.A., Boltyanskiy, R., Xiang, Y., Van den Dries, K., Schwartz, M.A., Dufresne, E.R., 2018. Vinculin and the mechanical response of adherent fibroblasts to matrix deformation. *Sci. Rep.* 8, 17967.
- Rubbens, M.P., Mol, A., Boerboom, R.A., Bank, R.A., Baaijens, F.P.T., Bouten, C.V.C., 2009. Intermittent straining accelerates the development of tissue properties in engineered heart valve tissue. *Tissue Eng. Part A* 15, 999–1008.
- Rudnicki, M.S., Cirka, H.A., Aghvami, M., Sander, E., Wen, Q., Billiar, K., 2013. Nonlinear strain stiffening is not sufficient to explain how far cells can feel on fibrous protein gels. *Biophys. J.* 105, 11–20.
- Ruiz, S.A., Chen, C.S., 2008. Emergence of patterned stem cell differentiation within multicellular structures. *Stem Cells* 26, 2921–2927.
- Schmidt, J., Chen, K., Tranquillo, R., 2016. Effects of intermittent and incremental cyclic stretch on ERK signaling and collagen production in engineered tissue. *Cell. Mol. Bioeng.* 9, 55–64.
- Seetharaman, S., Etienne-Manneville, S., 2018. Integrin diversity brings specificity in mechanotransduction. *Biol. Cell* 110, 49–64.
- Seliktar, D., Nerem, R.M., Galis, Z.S., 2003. Mechanical strain-stimulated remodeling of tissue-engineered blood vessel constructs. *Tissue Eng.* 9, 657–666.
- Shin, H., Jo, S., Mikos, A.G., 2003. Biomimetic materials for tissue engineering. *Biomaterials* 24, 4353–4364.
- Shkumatov, A., Thompson, M., Choi, K.M., Sicard, D., Baek, K., Kim, D.H., Tschumperlin, D.J., Prakash, Y.S., Kong, H., 2015. Matrix stiffness-modulated proliferation and secretory function of the airway smooth muscle cells. *Am. J. Physiol. Lung Cell Mol. Physiol.* 308, 1125.
- Sochol, R.D., Higa, A.T., Janairo, R.R.R., Li, S., Lin, L., 2011. Unidirectional mechanical cellular stimuli via micropost array gradients. *Soft Matter* 7, 4606–4609.
- Stein, C., Bardet, A.F., Roma, G., Bergling, S., Clay, I., Ruchti, A., Agarinis, C., Schmelzle, T., Bouwmeester, T., Schübeler, D., Bauer, A., 2015. YAP1 exerts its transcriptional control via TEAD-mediated activation of enhancers. *PLoS Genet.* 11, e1005465.
- Stevens, M.M., George, J.H., 2005. Exploring and engineering the cell surface interface. *Science* 310, 1135–1138.
- Sun, Z., Guo, S.S., Fassler, R., 2016. Integrin-mediated mechanotransduction. *J. Cell Biol.* 215, 445.
- Syedain, Z.H., Meier, L.A., Bjork, J.W., Lee, A., Tranquillo, R.T., 2011. Implantable arterial grafts from human fibroblasts and fibrin using a multi-graft pulsed flow-stretch bioreactor with non-invasive strength monitoring. *Biomaterials* 32, 714–722.
- Syedain, Z.H., Tranquillo, R.T., 2009. Controlled cyclic stretch bioreactor for tissue-engineered heart valves. *Biomaterials* 30, 4078–4084.
- Totaro, A., Castellani, M., Battilana, G., Zanonato, F., Azzolin, L., Giulitti, S., Cordenonsi, M., Piccolo, S., 2017. YAP/TAZ link cell mechanics to Notch signalling to control epidermal stem cell fate. *Nat. Commun.* 8, 15206.
- Tondon, A., Kaunas, R., 2014. The direction of stretch-induced cell and stress fiber orientation depends on collagen matrix stress. *PLoS One* 9, e89592.
- Vogel, V., Sheetz, M., 2006. Local force and geometry sensing regulate cell functions. *Nat. Rev. Mol. Cell Biol.* 7, 265–275.
- Waldman, S.D., Spiteri, C.G., Grynepas, M.D., Pilliar, R.M., Hong, J., Kandel, R.A., 2003. Effect of biomechanical conditioning on cartilaginous tissue formation in vitro. *J. Bone Joint Surg. Am.* 85, 101–105.
- Wang, D., Zheng, W., Xie, Y., Gong, P., Zhao, F., Yuan, B., Ma, W., Cui, Y., Liu, W., Sun, Y., Piel, M., Zhang, W., Jiang, X., 2014. Tissue-specific mechanical and geometrical control of cell viability and actin cytoskeleton alignment. *Sci. Rep.* 4, 6160.
- Wu, M.H., Huang, S.B., Lee, G.B., 2010. Microfluidic cell culture systems for drug research. *Lab Chip* 10, 939–956.
- Xin, M., Kim, Y., Sutherland, L.B., Murakami, M., Qi, X., McAnally, J., Porrello, E.R., Mahmoud, A.I., Tan, W., Shelton, J.M., Richardson, J.A., Sadek, H.A., Bassel-Duby, R., Olson, E.N., 2013. Hippo pathway effector Yap promotes cardiac regeneration. *Proc. Natl. Acad. Sci. U.S.A.* 110, 13839–13844.
- Yang, C., DelRio, F.W., Ma, H., Killaars, A.R., Basta, L.P., Kyburz, K.A., Anseth, K.S., 2016. Spatially patterned matrix elasticity directs stem cell fate. *Proc. Natl. Acad. Sci. U.S.A.* 113, 4439.
- Yang, Y., Wang, K., Gu, X., Leong, K.W., 2017. Biophysical regulation of cell behavior – cross talk between substrate stiffness and nanotopography. *Engineering (Beijing, China)* 3, 36–54.
- Yeh, Y., Corbin, E.A., Caliar, S.R., Ouyang, L., Vega, S.L., Truitt, R., Han, L., Margulies, K.B., Burdick, J.A., 2017. Mechanically dynamic PDMS substrates to investigate changing cell environments. *Biomaterials* 145, 23–32.

- Yeh, Y., Hur, S.S., Chang, J., Wang, K., Chiu, J., Li, Y., Chien, S., 2012. Matrix stiffness regulates endothelial cell proliferation through septin 9. *PLoS One* 7, e46889.
- Yim, E.K.F., Sheetz, M.P., 2012. Force-dependent cell signaling in stem cell differentiation. *Stem Cell Res. Ther.* 3, 41.
- Yim, E.K.F., Pang, S.W., Leong, K.W., 2007. Synthetic nanostructures inducing differentiation of human mesenchymal stem cells into neuronal lineage. *Exp. Cell Res.* 313, 1820–1829.
- Yin, H., Ding, Y., Zhai, Y., Tan, W., Yin, X., 2018. Orthogonal programming of heterogeneous micro-mechano-environments and geometries in three-dimensional bio-stereolithography. *Nat. Commun.* 9, 4096.
- Yu-Wai-Man, C., Bradley Spencer-Dene, B., Lee, R.M.H., Hutchings, K., Lisabeth, E.M., Treisman, R., Bailly, M., Larsen, S.D., Neubig, R.R., Khaw, P.T., 2017. Local delivery of novel MRTF/SRF inhibitors prevents scar tissue formation in a preclinical model of fibrosis. *Sci. Rep.* 7, 518.

2.6.5

Tendon Tissue-Engineering Scaffolds

PHONG K. NGUYEN^{1,2}, KIHON BAEK^{1,2}, FEIYANG DENG¹, JOSEPH D. CRISCIONE¹, ROCKY S. TUAN³, CATHERINE K. KUO^{1,2,4}

¹Department of Biomedical Engineering, University of Rochester, Rochester, NY, United States

²Center for Musculoskeletal Research, University of Rochester Medical Center, Rochester, NY, United States

³Institute for Tissue Engineering and Regenerative Medicine, The Chinese University of Hong Kong, Hong Kong, SAR, China

⁴Department of Orthopaedics, University of Rochester Medical Center, Rochester, NY, United States

Introduction

Tendons transmit muscle-generated mechanical forces to bone to enable skeletal movement. These tissues experience some of the highest mechanical loads in the body. When these loads exceed the load-bearing capacity of the tendon, permanent tissue damage occurs, leading to impaired function and mobility. Unfortunately, tendons possess a poor ability to regenerate after injury, leading to a significant medical problem. It is estimated that 77% (65.8 million) of all health care visits are musculoskeletal-related issues (Polak, 2014). Acute tendon injuries alone have been reported to cost more than \$30 billion per year (Chen et al., 2009).

Partial tendon ruptures, in which the gap between ruptured ends is minimal, have the capacity to heal. However, such healing often leads to the formation of fibrotic tissues that are biochemically and structurally abnormal and mechanically dysfunctional. Animal models have demonstrated that the mechanical properties of injured tendons are not recovered even after 12 months of healing (Woo et al., 2006). The poor healing ability of tendon is attributed to its low fibroblast (tenocyte) density and vascularity, which are needed for tissue synthesis and delivery of nutrients, respectively. When tendon ruptures lead to retraction of the tissue ends, surgical repair is commonly employed to either bridge the gap between ends or replace the injured tissue with an autograft or allograft (cadaveric grafts). Unfortunately, autografts are associated with donor site morbidity and pain. Moreover, for both autografts and allografts, their application has yet to achieve the stiffness, ductility, non-linearity, and viscoelastic responses of native tendon, and failure often ensues. These challenges have led to the pursuit

of engineered tendons that can fully restore the tendon tissue to its preinjured state.

An engineered tendon construct would ideally develop over time into a tissue that closely matches the dimensions, mechanical properties, biochemical composition, and microstructure of native tendon. A common approach is to incorporate stem cells into a biodegradable scaffold. This scaffold should have sufficient mechanical properties to support immediate or early return-to-load-bearing function in vivo, demonstrate dimensional stability in an aqueous environment, and degrade at a rate that matches new tissue formation. It should also possess a combination of material and biochemical properties that support cell viability in bulk and degraded forms and provide guidance cues to promote cell functions such as tenogenic differentiation and extracellular matrix (ECM) synthesis and organization. To satisfy these requirements, scaffolds for tendon tissue engineering are typically fabricated from polymers, rather than metals or ceramics. At the time of the writing of this chapter, the field of tendon tissue engineering is still working to design a scaffold that fulfills these multiple requirements to create mechanically and biologically functional tendon. One challenge that the field currently faces is that the physical and biochemical cues that can direct tendon cells toward these functions have not yet been fully elucidated; because this topic is beyond the scope of this chapter, we refer readers to review papers that discuss current approaches to address this need (Glass et al., 2014; Schiele et al., 2013; Nguyen et al., 2018; Huang et al., 2015; Edom-Vovard and Duprez, 2004; Okech and Kuo, 2016; Kuo and Tuan, 2003).

Here, we discuss considerations in designing and fabricating a scaffold that meets multiple requirements such as

supporting immediate or early return to tendon load-bearing function and providing guidance cues to promote tenogenic cell behaviors. Scaffold-specific considerations will be discussed in this chapter, including scaffold biomaterial choices, fabrication methods, and postfabrication modifications (e.g., crosslinking). These considerations individually and in combination have significant effects on scaffold mechanical properties and performance. We first introduce native adult tendon properties and function to provide readers with an understanding of the complexity of tendon tissues. We then discuss specific scaffold design goals, fabrication, and postfabrication methods that can be used with a variety of tendon scaffold biomaterials. We review specific scaffold design strategies that are current in the field, with focus on the most commonly used scaffold biomaterials, and end the chapter with perspectives on how to advance scaffold-based tendon tissue-engineering approaches.

Native Adult Tendon Properties

Mechanical Properties

Tendons exhibit nonlinear, anisotropic, and viscoelastic responses to tensile loads, with over 50% stress relaxation in 120 min (Kwan et al., 1993). Elastic modulus of adult human Achilles tendon is between 0.8 and 1.5 GPa based on in vitro measurements (Bennett et al., 1986), which is similar to in vivo ultrasound and reaction force-plate measurements (0.87 ± 0.2 GPa, Lichtwark and Wilson, 2005, and 1.16 ± 0.15 GPa, Maganaris and Paul, 2002, respectively). In vivo measurements estimate peak bulk tissue strains to be $8.3\% \pm 2.1\%$ (Lichtwark and Wilson, 2005) with 18% hysteresis (Maganaris and Paul, 2002). To date, graft tendon tissues and scaffolds have yet to achieve native mechanical properties and function. For example, cadaveric Achilles and patellar tendons typically have elastic moduli between 0.2 and 0.27 GPa (Penn et al., 2009). Thus there is a critical need for tendon replacements that can both possess the native mechanical properties of adult tendon and self-maintain a biologically healthy tissue over a lifetime.

Extracellular Matrix Composition and Molecular Arrangement

The highly complex and unique mechanical properties of tendon are attributed to their complex ECM composition and hierarchical arrangement. Tendon mechanical properties, such as ultimate tensile strength and elastic modulus, derive primarily from collagen type I fibrils, which account for at least 60% of tendon dry weight. These fibrils also associate with other proteins, including collagen types III, IV, V, VI, XII, and XIV, elastin, and small leucine-rich proteins such as decorin, biglycans, cartilage oligomeric matrix protein, and more (Banos et al., 2008; Nguyen et al., 2018). These ECM proteins facilitate collagen fibril organization, crosslink fibrillar collagens and elastin, enable gliding of fibril bundles and viscoelastic responses to load, and

provide space for proprioceptive neural networks and vascular supply. Collagen type I molecules (~1 nm diameter) organize into parallel nanoscale fibrils, and then into parallel microscale fibers, both of which align along the major axis of tension. In the embryonic tendon, collagen fibril diameters range from 50 to 100 nm (McBride et al., 1988) and after maturation can reach as large as 280 nm in the adult (Silver et al., 2003), with a characteristic 67 nm lateral D-banding pattern coincident with molecular gaps (Raspanti and Guizzardi, 2002). The ideal goal of tendon tissue engineering would be to produce a tissue that is similar in composition and molecular arrangement. By comparison, current scaffold designs, as well as the tissues formed within these scaffolds, are composed of fewer ECM components and are comparatively simpler in microstructure.

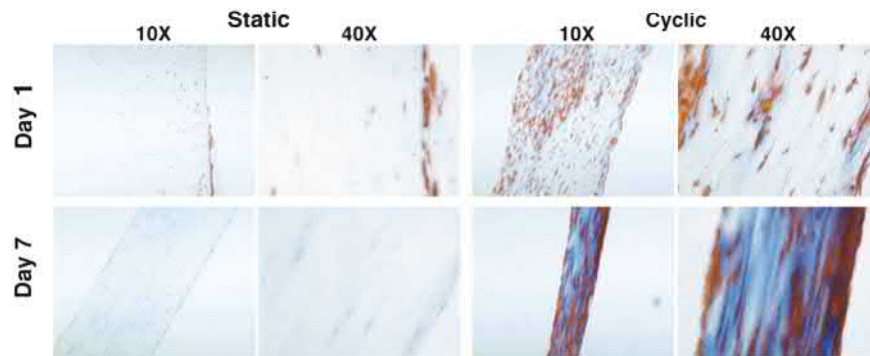
Tendon Cells

Tendon fibroblasts (tenocytes) arrange circumferentially around collagen fibers and are likely the cells primarily responsible for maintaining the ECM under homeostatic conditions. Tenocytes communicate with each other via gap junctions, including connexin 32 and 43 (McNeilly et al., 1996). Some studies have suggested that multipotent tendon-derived stem cells exist within tendon (Bi et al., 2007). Fibrocartilage cells are also detectable in regions of high compressive force, such as regions where tendons wrap around another skeletal structure (Benjamin et al., 2008). Although gene-based identification of tendon cells is likely incomplete, known markers of tendon cells include the transcription factors scleraxis (Scx) and mohawk (Schweitzer et al., 2001) (Mkx), the transmembrane protein tenomodulin (Tnmd) (Shukunami et al., 2006), and ECM glycoprotein tenascin-C (TN-C) (Chiquet-Ehrismann and Tucker, 2004). For more details, we refer readers to a comprehensive review on tendon ECM molecules and respective functions (Nguyen et al., 2018)

Scaffold Design Goals

Early scaffold designs for tendon tissue engineering were relatively simplistic. Adult stem cells were seeded within scaffolds composed of collagen type I, the primary ECM component of adult tendon, and placed under cyclic uniaxial tensile loads similar to those experienced during walking or running (Kuo and Tuan, 2008; Awad et al., 2000). The idea was that culturing cells within an adult tendon-like microenvironment would biochemically and mechanically encourage adult stem cells to behave tenogenically. However, while collagen content increased (Fig. 2.6.5.1) and mechanical properties improved over time, the constructs remained relatively weak compared to native tendon tissue both in vitro and in vivo. Nevertheless, the promise of tendon tissue engineering was established by these seminal studies and the field has since evolved to produce more complex scaffold designs, as discussed throughout this chapter.

Over the years, scaffold design has become increasingly sophisticated in attempting to capture the complexity of



• **Figure 2.6.5.1** Histology of mesenchymal stem cell-seeded collagen constructs harvested after 1 and 7 days of static and cyclic loading. Longitudinal 5- μm -thick sections histologically stained with Mallory's trichrome. A higher level of matrix staining is seen consistently in constructs subjected to cyclic loading. (Figures adapted from Kuo, C.K., Tuan, R.S., 2008. Mechanoactive tenogenic differentiation of human mesenchymal stem cells. *Tissue Eng. A* 14, 1615–1627.)

tendon tissue. Some approaches aim to control engineered microstructures at multiple length scales to more closely mimic the hierarchical structures of collagen fibers and fibrils. Other approaches incorporate bound and soluble biological cues to promote tenogenic gene expression and ECM deposition by stem cells. Such design criteria have been incorporated into scaffolds that also aim to enable immediate or early return to load-bearing function. This chapter reviews current scaffold designing approaches, which can be categorized as the following: (1) achieving immediate or early return to load-bearing function, and (2) instructing tenogenic cell behaviors via scaffold physical features (mechanical properties, topography) or the presence of biological (soluble or bound) factors.

Immediate or Early Return to Load-Bearing Function

Because tendon possesses unique mechanical properties that enable transfer of forces generated by muscle to bone to facilitate skeletal movements, an important design goal for tendon scaffolds has been to enable immediate or early return to load-bearing function. Material properties, which include elastic modulus and failure strength, are intrinsic to a tissue and reflect its quality. Functional properties, which include stiffness and failure load, are dependent on tissue dimension and size and can be achieved in the absence of the material properties of healthy tendon. Scaffold designs have aimed to recapitulate either healthy tendon material properties or functional properties. Arguments can be made to support either strategy, and examples of both are highlighted in later sections of the chapter. However, it is possible that a scaffold achieves mechanical function but does not present a biochemical composition and structure that promotes cell tenogenic behavior. Therefore the important biological cues needed to support a healthy tissue in the long term might be lacking. Another important consideration that has not yet been a main focus of scaffold designs is that material and functional properties of tendons may vary between those of different anatomical sites, as they

have different geometries and functional requirements. Tendon cells isolated from tendons of the axial versus limb skeleton express ECM genes differently in response to the same tendon-specific growth factors (Brown et al., 2014), suggesting different profiles of ECM proteins are deposited by tendon cells in different parts of the body, perhaps related to their developmental origin.

Guidance Cues to Induce Tenogenic Cell Behaviors

Perhaps the most commonly used guidance cues are biological factors that promote specific cell functions, including differentiation, ECM synthesis and deposition, and tissue remodeling. Scaffolds can be designed to present a range of bioactive molecules that are covalently bound within or coated onto the scaffold surface. These biological factors can be gradually released from the scaffold as it swells or degrades over time. Binding of soluble factors via transmembrane receptors can regulate cellular activities by transmitting signals, including activation of multiple intracellular signaling pathways as well as mechanical cues from the extracellular space into the cell. In addition, passage of molecules or ions into the cell can happen through channels or pores on the cell membrane to induce intracellular biological reactions.

Physical cues may also induce tenogenic cell behaviors. Adult tendon possesses a unique tissue architecture of collagen type I fibers that align parallel to one another along the primary axis of tension, with cells wrapping around these fibers. Based on this unique *in vivo* feature, some scaffolds aim to present cells with aligned nano- or microscale fibers or channels that mimic tendon tissue architecture at the cell length scales. The idea is that cells will arrange themselves similarly as they do *in vivo*, and that these topographical guidance cues will induce tenogenic cell behaviors.

Tissue mechanical properties have also been implicated as cell guidance cues in addition to enabling mechanical function. In this regard, nano- and microscale mechanical properties are important to consider, as whole tissue mechanical properties may not reflect the local mechanical microen-

vironment that cells experience (Marturano et al., 2013). For example, cells have been shown to sense and respond to local elastic moduli or stiffness (Marturano et al., 2016). Because mechanical forces are transmitted from the extracellular space to the intracellular space via integrin interactions with the ECM, nano- and microscale elastic moduli of the tissue are thought to be particularly relevant mechanical cues. Thus, as discussed in the later section “Polymer Selection and Scaffold Designs,” some scaffolds designed to guide cell behavior have considered cell length-scale mechanical properties.

Fabrication Methods

Most polymers can be fabricated into scaffolds of different forms, including gels, fibers, and foams. The choice of fabrication method, combined with polymer selection (discussed in the next section), significantly influences scaffold mechanical properties, microstructure, swelling behavior, pore size and porosity, and degradation rate. Ideally, the fabrication method is compatible with the polymer (does not degrade the polymer), is nontoxic (especially if cells are incorporated during fabrication), and reproducibly forms a three-dimensional (3D) scaffold with specific dimensions and material properties without compromising biological activity, if any, of the polymer. During fabrication, biofactors or other scaffold materials may be added to deliver tenogenic factors or create a composite scaffold with tailored material properties. Commonly used fabrication methods include electrospinning, electrohydrodynamic jet printing, wet spinning, fiber extrusion, weaving, knitting, braiding, gelation, and freeze drying. Another approach is tissue decellularization, in which natural tissue is harvested from a donor and treated to remove cells. The remaining ECM scaffold, possibly reseeded with cells, is then implanted into the recipient. As discussed later, each fabrication method for a tendon tissue-engineering scaffold is associated with its own unique advantages and disadvantages. The basics of these technologies are reviewed in more detail in the following sections, and examples of tendon tissue-engineering scaffolds fabricated with these technologies are highlighted within the section “Polymer Selection and Scaffold Designs.”

Spinning

Based on the aligned collagen fibrils and fibers of adult tendon, techniques such as electrospinning, electrohydrodynamic jet (E-jet) printing, wet spinning, and fiber extrusion have been used to create scaffolds with aligned fibers with a range of fiber diameters and degrees of alignment. Spinning techniques can produce nano- and microscale fibers by ejecting polymer solutions via syringes and needles or pipette tips onto a collector surface. The spinning process can be guided by gravity or electrostatics as in the case of electrospinning (Sahoo et al., 2006, 2010; Chainani et al., 2013; Manning et al., 2013; Rinoldi et al., 2019a,b; Oryan et al., 2014; Xu et al., 2014; Yang et al., 2014,

2016; Hakimi et al., 2015; Naghashzargar et al., 2015; Orr et al., 2015; Zhang et al., 2015; Banik et al., 2016; Deepthi et al., 2016; Domingues et al., 2016; Gelberman et al., 2016; Pauly et al., 2016; Baudequin et al., 2017; Rothrauff et al., 2017; Sharifi-Aghdam et al., 2017; Szczesny et al., 2017; Wu et al., 2017a; Peach et al., 2017; Liao et al., 2018; Schoenenberger et al., 2018; Sensini et al., 2018; Wang et al., 2018; Li et al., 2019; Sundaram et al., 2019). The use of a rotating mandrel to collect electrospun fibers can produce scaffolds with nano- and microscale-aligned fiber structures that can mimic the aligned fibers of native tendon. However, limitations of electrospinning include limited scaffold thickness (millimeters) and poor cell infiltration within scaffolds. Several methods have been used to improve cell infiltration in electrospun scaffolds, including selective removal of sacrificial fibers, ultrasonication, and laser radiation, but these approaches can negatively impact scaffold architecture (e.g., fiber alignment) and compromise mechanical properties (Baker et al., 2008; Lee et al., 2011; Joshi et al., 2013). Alternative approaches include stacking multilayered electrospun sheets or incorporating textile fabrication techniques such as braiding or weaving (Rothrauff et al., 2017). In addition, methods such as extrusion (e.g., wet spinning fibers into a methanol-based coagulation bath) (Funakoshi et al., 2005a,b; Shepherd et al., 2013; Majima et al., 2007; Yang et al., 2019) and E-jet printing (Wu et al., 2016, 2017c) have been explored to fabricate scaffolds with increased pore size and enhanced cell infiltration.

Textile Technologies

Different techniques in textile technologies such as weaving, knitting, and braiding have been used to fabricate scaffolds with high tensile strength and modulus for tendon tissue engineering. Additional advantages of scaffolds fabricated with these techniques include tunable scaffold parameters such as fiber size and organization, pore size and porosity, controlled mechanical properties, and cell infiltration and distribution within the scaffolds. Knitted scaffolds are composed of interconnected loops of yarns that can be arranged in vertical (warp knitting) and horizontal direction (weft knitting) (Chen et al., 2010, 2014; Ouyang et al., 2003; Sahoo et al., 2006, 2010; Shen et al., 2010; Teh et al., 2013; Deng et al., 2014; Musson et al., 2015; Zhang et al., 2015; Sharifi-Aghdam et al., 2017; Zheng et al., 2017; Tang et al., 2018). Knitting stitches and yarn material can be altered to control pore size and fiber alignment, which influence cell infiltration and scaffold mechanical properties. Woven scaffolds are typically composed of two sets of interlaced yarns: warp and weft (Younesi et al., 2014; Hakimi et al., 2015; Seo et al., 2016; Wu et al., 2017b). Weaving patterns such as plain, twill, and satin can be selected to tailor scaffold flexibility and topography. Woven scaffolds exhibit lower extensibility but maintain their structure and shape better than knitted scaffolds. Braided scaffolds consist of multiple sets of interlacing yarns that are intertwined together in an overlapping circular pattern (Kwon et al., 2014; Rothrauff et al.,

2017; Govoni et al., 2017; Cai et al., 2018; Pagan et al., 2019; Sandri et al., 2016; Funakoshi et al., 2005a). Braided scaffolds tend to possess a higher tensile strength compared to their knitted and woven counterparts. However, one of the limitations associated with woven and braided scaffolds is their low porosity, which can restrict nutrient distribution and cell infiltration.

Gelation

Hydrogel scaffolds are formed via gelation, a process in which polymer molecules are crosslinked to form a hydrophilic network (Ouyang et al., 2003; Majima et al., 2005, 2007; Kapacee et al., 2010; Shen et al., 2010; Manning et al., 2013; Breidenbach et al., 2015; Deepthi et al., 2016; Marturano et al., 2016; Yang et al., 2016; Govoni et al., 2017; Rothrauff et al., 2018; Sundaram et al., 2019; Far-kash et al., 2019; Frauz et al., 2019; Rinoldi et al., 2019a,b). Gelation offers an advantage over the other methods in that cells can be incorporated during scaffold formation if non-toxic reagents are used. This allows cells to be encapsulated uniformly throughout the scaffold during formation, rather than seeded within the scaffold after formation. Additionally, the cell-polymer suspension can be injected into the injury site in vivo, after which the gel sets in the shape and size of the tissue defect. While hydrogels have traditionally been thought to be weaker than other scaffold types, the formation of interpenetrating polymer network (IPN) gels has elevated the potential to use hydrogels as tendon tissue-engineering scaffolds. IPN gels can be made of polymers that form independent and interlaced networks via ionic and covalent crosslinking (Sun et al., 2012; Darnell et al., 2013; Branco da Cunha et al., 2014; Vining et al., 2019; Park et al., 2019). IPN gel toughness can be increased significantly compared to single component hydrogel by combining a range of natural and synthetic polymers such as alginate and polyacrylamide (Sun et al., 2012; Darnell et al., 2013), collagen type I and alginate (Branco da Cunha et al., 2014), and gelatin and silk fibroin (Park et al., 2019).

Freeze Drying

Freeze drying, often after gelation, can be used to create a highly porous sponge. Freeze drying has been used to fabricate highly porous scaffolds for tendon tissue engineering (Bagnaninchi et al., 2007; Caliarì and Harley, 2011, 2013; Caliarì et al., 2011, 2012; Hortensius and Harley, 2013; Bellini et al., 2016; Sandri et al., 2016; Mozdzen et al., 2016, 2017; Grier et al., 2017; Hortensius et al., 2018; Kirk et al., 2013). This method generally involves freezing a polymer solution at very low temperature, often between -10 and -80°C , and removing ice crystals through sublimation under low pressure. Notable advantages include the exclusion of organic solvents during fabrication and the formation of scaffolds with a high degree of porosity. In turn, porosity will affect mechanical properties, cell infiltration, nutrient and waste exchange, and susceptibility to

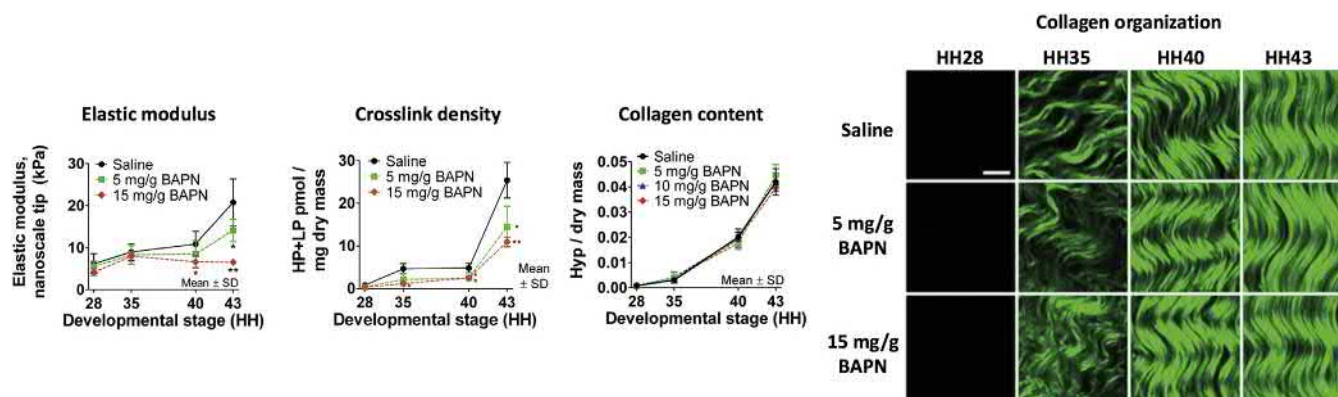
degradation by enzymes or hydrolysis. Control over pore size can also be achieved by varying freezing rate and final freezing/cooling temperature (Haugh et al., 2010; O'Brien et al., 2004, 2005). However, it might be difficult to use freeze drying to fabricate scaffolds that possess hierarchical structure and comparable mechanical properties similar to native tendon tissue.

Decellularization

Decellularized matrices from human or animal tissues have been used as scaffolds in tendon tissue engineering. These offer the potential of preserving the biochemical composition and structural properties of native tendon tissue. Decellularization can be achieved via chemical (e.g., sodium dodecyl sulfate, Triton X-100), physical (e.g., freezing in liquid nitrogen), and enzymatic (e.g., trypsin treatment) processes. After in vitro decellularization and prior to in vivo implantation, several studies have seeded cells into these matrices and cultured them under tenogenic conditions such as mechanical loading and growth factor supplementation to promote cell differentiation and new tissue formation (Yin et al., 2013; Megerle et al., 2016; Ning et al., 2017; Xie et al., 2019). Another approach is the extraction of matrix-derived bioactive components via the preparation of a solubilized extract from decellularized tendon/ligament tissues, which have been found to exhibit protenogenic activities (Yang et al., 2013a, 2017; Rothrauff et al., 2018). Common challenges associated with using decellularized matrix as scaffold include the risk of eliciting inflammatory responses from the host body and inadequate mechanical properties to support immediate return to tendon's load-bearing function (Malcarney et al., 2005; Zheng et al., 2005).

Postfabrication Modifications

Crosslinking is routinely used to form polymer networks and thereby produce a 3D scaffold, or to reinforce the strength and stability of an existing polymer network of a scaffold after it has already been fabricated. In both scenarios, a higher crosslink density typically leads to higher failure strength and elastic modulus. Recent discoveries have shown that these mechanisms are utilized by nature to regulate embryonic tendon mechanical properties as well. Lysyl-oxidase (LOX) is an enzyme that converts lysine residues of collagen molecules into aldehydes, which then spontaneously react to form crosslinks between collagen molecules. Studies with chick embryo tendons reveal that elastic modulus and LOX-mediated crosslink density increase with similar trends from early to late stages of embryonic development (Fig. 2.6.5.2) (Marturano et al., 2013, 2014). Inhibition of LOX activity during development reduces both LOX-mediated crosslink density and elastic modulus of developing tendon proportionately, without affecting collagen organization or content, demonstrating that LOX-mediated crosslinking of collagen is



• **Figure 2.6.5.2** Elastic modulus, lysyl-oxidase (LOX)-mediated crosslink (*HP*, hydroxylysyl pyridinoline; *LP*, lysyl pyridinoline) density, and total collagen content (represented by hydroxyproline [*Hyp*] content) each increases in chick embryonic tendon during normal embryonic development from HH35 to HH43 (saline groups). Inhibition of LOX activity via β -aminopropionitrile (BAPN) treatment significantly reduced modulus and crosslink density but had no effect on collagen content or organization. Scale bar = 10 μ m. (Figures adapted from Marturano, J.E., Arena, J.D., Schiller, Z.A., Georgakoudi, I., Kuo, C.K., 2013. Characterization of mechanical and biochemical properties of developing embryonic tendon. *Proc. Natl. Acad. Sci. USA* 110, 6370–6375 and Marturano, J.E., Xylas, J.F., Sridharan, G.V., Georgakoudi, I., Kuo, C.K., 2014. Lysyl oxidase-mediated collagen crosslinks may be assessed as markers of functional properties of tendon tissue formation. *Acta Biomater.* 10, 1370–1379.)

critical for embryonic tendon development (Fig. 2.6.5.2) (Pan et al., 2018; Marturano et al., 2013, 2014). While LOX has not been implemented in scaffold technologies for tendon tissue engineering, other synthetic and natural crosslinkers have been utilized, as discussed later.

After fabrication, scaffold material properties can be further enhanced via crosslinking. Specifically, crosslinking of the adjacent polymer chains can reinforce polymer networks, thereby increasing elastic modulus and/or failure strength and resistance to swelling in an aqueous environment in vivo or in vitro. Crosslinking can also decrease susceptibility to degradation by reducing pore size and limiting diffusion of enzymes or water into the polymer network. Current crosslinking strategies in tendon tissue-engineering scaffolds include the use of synthetic and natural crosslinking reagents to create covalent bonds between polymer chains. Synthetic crosslinkers include 1-ethyl-3-(3-dimethylaminopropyl) carbodiimide (EDC), glutaraldehyde (GA), and 1,4-butanedioldiglycidyl ether (BDDGE), whereas natural crosslinking reagents include plant extracts of *Myrica rubra* and genipin. An advantage of natural crosslinking approaches is that they are typically gentler and have little to no toxicity compared to synthetic approaches. While not yet applied as a crosslinking agent to scaffolds in tendon tissue engineering, animal-derived enzymes (e.g., LOX) can also mediate the formation of covalent bonds between collagen and elastin molecules. In many cases, these covalent crosslinks are created when the synthetic or natural crosslinking reagent is applied to the scaffold. In other synthetic approaches, the polymers can be chemically modified with reactive functional groups prior to scaffold fabrication, in which case crosslinking of the polymer chains within the fabricated scaffold is induced by the application of heat, pressure, or light.

EDC, one of the most commonly used synthetic crosslinkers, is a water-soluble carbodiimide crosslinker that activates carboxyl groups on polymer chains, which then spontaneously conjugate with primary amines. *N*-Hydroxysuccinimide (NHS) is commonly added to enhance the efficiency of the EDC crosslinking reaction. EDC has been widely used to crosslink collagen scaffolds for tendon tissue engineering (Caliari et al., 2011, 2012; Caliari and Harley, 2011, 2013; Grier et al., 2017; Sensini et al., 2018; Shepherd et al., 2013; Kirk et al., 2013). EDC/NHS crosslinking improves scaffold mechanical properties and maintains their structure over a longer time compared to noncrosslinked scaffolds. However, scaffold porosity can be negatively affected. GA is a synthetic and water-soluble dialdehyde that crosslinks amine or hydroxyl groups in polymers. GA crosslinking has been used with collagen type I–nanocarbon composite fibers to achieve similar structural and mechanical properties to native tendon fascicles (Green et al., 2017). In BDDGE crosslinking, the epoxide groups of BDDGE react to create ester bonds with the carboxylic groups of polymers such as collagen (Lohre et al., 1992; Zeeman et al., 1999). BDDGE crosslinking has been used to slow the degradation rate of elastin–collagen composite scaffolds for tendon tissue engineering (Sandri et al., 2016). In these various systems, these synthetic covalent crosslinkers are typically applied after scaffold fabrication but before cell seeding and in vivo implantation. Due to nonspecific reactivity, harsh reaction conditions, and unwanted toxicity associated with synthetic crosslinkers, extensive washing of crosslinked scaffolds is needed to remove potentially cytotoxic chemical residuals before cell seeding. While mechanical properties of the scaffolds approaching that of tendon can be achieved with these synthetic crosslinkers, their associated cytotoxicity remains a limitation as it is difficult to eliminate entirely even after extensive washing.

Another synthetic crosslinking strategy is to apply heat or light to create covalent crosslinks. Dehydrothermal (DHT) treatment uses high temperature (>90°C) and vacuum conditions to induce condensation reactions between amine groups and carboxylic acid or hydroxyl groups of polymers. While DHT treatment has been utilized to crosslink different types of collagen-based scaffolds for tendon tissue engineering, a limitation is that it cannot be applied to cell-seeded scaffolds (Caliari et al., 2011, 2012; Caliari and Harley, 2011, 2013; Chen et al., 2010; Mozden et al., 2016). In ultraviolet (UV) light-induced crosslinking, UV radiation is used to activate a photoinitiator that, in turn, produces reactive molecules such as radicals or ions that react with the functional groups of polymer chains to create covalent crosslinks. Studies have used UV light to crosslink methacrylated gelatin (Rothrauff et al., 2018; Yang et al., 2016; Rinoldi et al., 2019b) and collagen (Oryan et al., 2014) in different types of scaffold for tendon tissue engineering. For example, methacrylated gelatin crosslinking improved scaffold maximum load and elastic modulus while maintaining cell viability similar to noncrosslinked scaffolds (Yang et al., 2016). In this and other studies, cells have been seeded in the scaffold prior to UV crosslinking, and are minimally affected by short-term UV treatments. However, at longer exposure times, UV radiation can be toxic to cells and result in heterogeneous crosslinking (Mironi-Harpaz et al., 2012). Furthermore, even though DHT and UV radiation crosslinking do not require the addition of toxic chemical reagents, polymer molecule integrity could be negatively impacted by UV light and harsh reaction conditions of high temperature and low pressure. For this reason, a visible light-mediated photocrosslinking procedure was developed for the production of a gelatin-based hydrogel, with significant improvement in cell viability (Lin et al., 2013, 2014), which has recently been applied in combination with electrospun polymeric nanofibers to form a composite tissue-engineering scaffold (Sun et al., 2019).

To overcome chemical toxicity and harsh reaction conditions associated with synthetic crosslinkers, naturally occurring crosslinking agents have been tried as well (Zeugolis et al., 2010; Fessel et al., 2012a,b, 2014; Mathew et al., 2013; Younesi et al., 2014). *M. rubra* extract, a plant-derived crosslinking agent, has been shown to react and covalently crosslink collagen scaffolds by binding to amino groups on adjacent collagen molecules (Liao et al., 2004). *M. rubra* extract crosslinking in collagen scaffolds was shown to improve mechanical properties and increase denaturation temperature compared to noncrosslinked scaffolds (Zeugolis et al., 2010). Genipin, derived from the fruits of *Gardenia jasminoides* and *Genipa americana*, is another natural crosslinking agent that has been used with collagen-based scaffolds in tendon tissue engineering (Fessel et al., 2012a,b; Mathew et al., 2013; Younesi et al., 2014). It has been proposed that genipin reacts with amine groups of polymers such as collagen, gelatin, and silk to form monomeric or oligomeric crosslinks (Butler et al., 2003). Studies have shown that genipin crosslinked collagen-based scaffolds can

possess comparable mechanical properties to that of native tendon tissue and also support expression of tendon markers by seeded cells (Mathew et al., 2013; Younesi et al., 2014). Genipin also appears to be less cytotoxic than synthetic crosslinkers (Liang et al., 2004; Wang et al., 2016; Huang et al., 1998; Sung et al., 1999), although the time required to achieve a significant degree of crosslinking is generally considerably longer than that for chemical crosslinkers, such as those already discussed. It has also been reported that when genipin crosslinking was used to enhance the mechanical properties of tendon explant, higher dosages were shown to reduce cell viability (Fessel et al., 2014).

Delivery of Bioactive Molecules (e.g., Drugs and Growth Factors)

Delivery of bioactive molecules via scaffolds has been used to influence cellular activities, including expression of tendon markers and synthesis of ECM proteins (Sahoo et al., 2010; Shen et al., 2010; Hortensius et al., 2018; Govoni et al., 2017; Ramos et al., 2019; Manning et al., 2013; Min et al., 2016). The delivered bioactive molecules often include growth factors that are involved in adult tendon healing and homeostasis. Methods to deliver bioactive molecules via scaffolds generally fall into four systems: diffusion controlled, degradation controlled, cleavage controlled, and swelling controlled (Langer and Peppas, 1981, 2003). In a diffusion-controlled system, bioactive molecules encapsulated at high concentration within a polymer scaffold gradually diffuse out of the scaffold and into the surrounding environment. The diffusion-based release profile can be regulated by controlling the geometry and physicochemical parameters of the scaffold. In degradation-controlled release, bioactive molecules leave the scaffold either as the surface of the scaffold erodes (surface erosion) or as the entire scaffold degrades (bulk erosion). In a cleavage-controlled system, bioactive molecules are attached to the scaffold via covalent bonds so that the release of the molecules can be regulated by the enzymatic cleavage or hydrolysis of the covalent bond between the bioactive molecule and scaffold. In a swelling-controlled system, entrapped bioactive molecules diffuse through the scaffold and into the surrounding environment as the scaffold swells with corresponding increase in pore size. Scaffolds can be designed to release bioactive molecules via one or a combination of these release systems.

Drug delivery via scaffold degradation has been used in tendon tissue engineering with scaffolds fabricated by electrospinning, gelation, freeze drying, and more (Sahoo et al., 2010; Shen et al., 2010; Hortensius et al., 2018; Govoni et al., 2017; Ramos et al., 2019). For example, hydrolysis-induced bulk degradation of poly(lactic-co-glycolic acid) (PLGA) electrospun fibers enabled release of encapsulated basic fibroblast growth factor (bFGF) to enhance tendon marker expression and mechanical properties of repaired tendons compared to no-bFGF controls (Sahoo et al., 2010). Proteinase degradation of the collagen component of

implanted silk–collagen sponges led to the release of stromal cell-derived factor 1 alpha to promote tendon ECM production and enhance tendon repair (Shen et al., 2010). PLGA microcarriers encapsulating human growth differentiation factor 5 (hGDF-5) and embedded within a fibrin hydrogel showed continuous release of hGDF-5 and upregulation of tendon marker expression for 25 days in vitro (Govoni et al., 2017). In this case, the release kinetics of hGDF-5 were governed by hydrolytic degradation of PLGA microcarriers and proteinase degradation of the fibrin scaffold.

Degradation-controlled and cleavage-controlled systems have been combined with heparin affinity-controlled release to deliver bioactive molecules from tendon tissue-engineering scaffolds (Manning et al., 2013; Min et al., 2016). Heparin is a naturally occurring glycosaminoglycan (GAG), originally discovered in liver, that is known to bind various proteins via electrostatic interactions. The transient affinity of heparin to proteins allows slow release of bioactive molecules via diffusion from scaffolds (Sakiyama-Elbert and Hubbell, 2000; Vulic and Shoichet, 2014). For example, heparin-binding peptides were covalently crosslinked to fibrin scaffolds to immobilize soluble heparin that was ionically bound to platelet-derived growth factor BB (PDGF-BB) (Manning et al., 2013). The release of PDGF-BB from the fibrin scaffolds was controlled by a number of mechanisms. PDGF-BB dissociated from heparin and slowly diffused through the fibrin scaffold into the surrounding environment. PDGF-BB release was additionally controlled by enzymatic degradation of the fibrin scaffold by plasmin and degradation of heparin by heparinase. Another study reported the release of PDGF-BB from poly(ϵ -caprolactone) (PCL) scaffolds for tendon repair in vivo (Min et al., 2016). In this system, PDGF-BB was ionically bound to heparin, which was hydrogen bonded to the pluronic F127 component of a hybrid PCL–pluronic F127 scaffold (Min et al., 2016). The degradation of heparin by heparinase and hydrolysis of PCL enabled the sustained release of PDGF-BB over 42 days in vitro (Min et al., 2016). In both studies, delivery of PDGF-BB with scaffolds enhanced structural and mechanical properties of repaired tendon in vivo (Min et al., 2016; Manning et al., 2013).

Polymer Selection and Scaffold Designs

Biodegradable scaffolds for tendon tissue engineering are usually composed of synthetic and/or natural polymers, the latter of which may be mammalian derived or plant derived. The choice of polymers can influence the rate of scaffold degradation. Ideally, scaffold degradation rate should match the rate of new tissue synthesis so that the implant continuously offers adequate mechanical support for function and dimensional support for the newly forming tissue. Once implanted, the scaffold should be load bearing and able to return the patient to function while maintaining its shape and support for anabolic cell functions. Ideally, after

a period of time, perhaps weeks or months, the implanted scaffold will be entirely replaced by new ECM generated by encapsulated or recruited cells. An animal-derived polymer may be desired for its peptide sequences that act as biological cues and cell adhesion sites. However, rapid degradation by mammalian enzymes in vivo may compromise the use of animal-derived natural polymers in load-bearing sites. Therefore either plant-derived natural polymers or synthetic polymers that are “invisible” to enzymes in vivo may be advantageous. On the other hand, while synthetic materials can be chemically modified to better control scaffold properties, many synthetic materials are susceptible to rapid hydrolysis. Some strategies have involved engineered hybrid scaffolds to utilize the advantages of both mammalian-derived polymers and plant-based or synthetic polymers to more fully control cell adhesion and various material properties. Other strategies involve chemical functionalization of polymers so that the resulting scaffold possesses specific properties. For instance, synthetic or plant-based polymers that would not typically be degraded in vivo by enzymes can be chemically modified to contain sites recognizable by matrix metalloproteinases (Yang et al., 2012; West and Hubbell, 1999; Patterson and Hubbell, 2010). Synthetic or plant-based polymers that lack cell recognition sites for binding can be chemically functionalized with peptide sequences that promote cell adhesion. Additionally, polymer scaffolds can be doped with other materials to enhance mechanical properties.

Natural Plant- and Animal-Derived Polymers

Alginates

Alginate is a polysaccharide commonly derived from seaweed and a natural copolymer of beta-D-mannuronic acid and alpha-L-guluronic acid monomers. Alginate is an attractive biomaterial for biomedical applications because of its abundance in source and noncytotoxicity (Cottrell, 1980). Alginate has been fabricated into hydrogels and wet-spun scaffolds for tendon tissue engineering. To form a hydrogel, multivalent ions, usually calcium ions, can be reacted with the carboxylic acid groups to form crosslinks between guluronic acid monomers. Gelation occurs upon the formation of “egg-box” structures, which are composed of calcium ion–crosslinked guluronic acid monomer blocks. Methods to slowly release calcium ions, thereby allowing gelation at a controlled rate, have enabled the formation of alginate gels with controlled shape, mechanical properties, swelling behavior, and diffusivity (Kuo and Ma, 2001, 2008). These gels are now commonly used in tissue-engineering studies for tendon and other soft connective tissues (Schiele et al., 2015; Marturano et al., 2016; Korecki et al., 2009).

A distinct advantage of alginate is its invisibility to mammalian enzymes and cells, due to its lack of peptide sequences that mammalian proteins recognize. Taking advantage of their “invisibility” to cells, alginate gels have been used to coat partially lacerated flexor tendon in a rabbit model, thereby leveraging their antiadhesive property to prevent

peritendinous adhesion (Namba et al., 2007). In another study, alginate coating of a hybrid scaffold composed of chitosan–collagen hydrogel and electrospun poly(L-lactic acid) (PLLA) nanofibers significantly reduced protein adsorption at the scaffold surface without affecting cell attachment and infiltration up to 7 days in vitro (Deepthi et al., 2016).

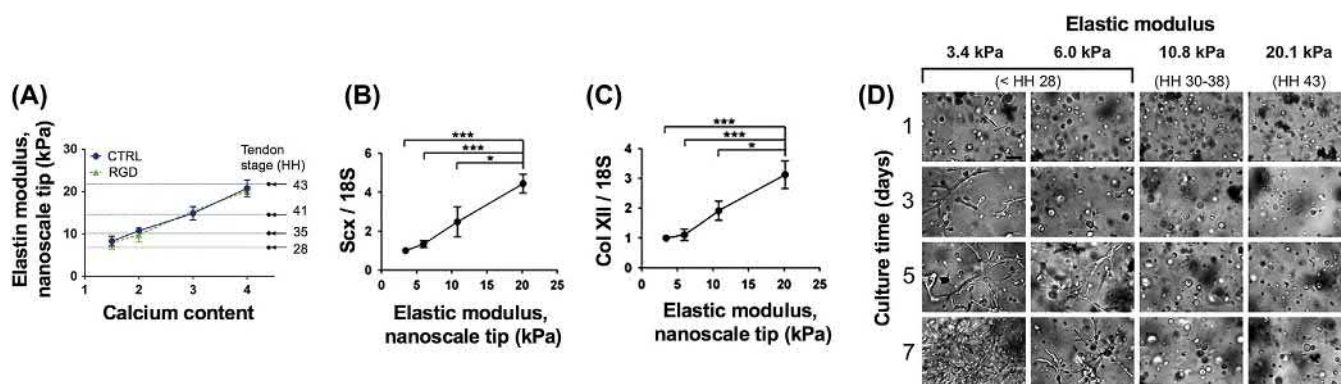
Another advantage of alginate is that it forms a hydrogel under gentle, nontoxic, ionic crosslinking conditions, and thus cells can be encapsulated during gelation. Furthermore, alginate lacks cell-binding sites within its polymer chain, but the polymer can be chemically functionalized with specific peptide sequences to enable specific cell-binding interactions (Schiele et al., 2015; Marturano et al., 2016; Rowley et al., 1999). For instance, functionalization of alginate with peptides containing arginyl-glycyl-aspartic acid, a cell-adhesion epitope of many ECM components, including fibronectin, enables tendon cell attachment and spreading within alginate hydrogel, whereas cells remain round in the nonfunctionalized hydrogels (Marturano et al., 2016). Alginate can also be combined with other polymers to which cells will adhere (Majima et al., 2005, 2007; Deepthi et al., 2016). For instance, a significantly higher degree of cell attachment was observed in chitosan–alginate scaffolds compared to alginate-only scaffolds (Majima et al., 2005, 2007).

Alginate hydrogels are also attractive because their material properties are highly tunable. Elastic modulus and strength of alginate hydrogels can be precisely controlled by changing crosslink density (calcium ion) and polymer concentration (alginate) (Kuo and Ma, 2001, 2008). This has enabled studies of stem cell responses to tenogenic microenvironments. In particular, alginate hydrogels were fabricated to possess cell length-scale (nanoscale) elastic moduli of native embryonic tendon at each stage of development (Marturano et al., 2016) (Fig. 2.6.5.3A).

Embryonic tendon progenitor cells seeded within these gels exhibited stiffness-dependent cell morphology and tendon marker expression levels (Fig. 2.6.5.3B–D). This exciting observation demonstrated the ability to fabricate alginate scaffolds with specific mechanical properties, and showed that embryonic tendon progenitor cells are responsive to the changes in tendon stiffness throughout development (Marturano et al., 2016). Furthermore, these findings suggested that embryonically informed scaffolds can promote stem cell tenogenesis. While this ionically crosslinked alginate scaffold alone would not be suitable for load-bearing applications in vivo, it would be possible to infiltrate the alginate hydrogel within the pores of a load-bearing scaffold. This composite scaffold could then promote tenogenic cell differentiation while acting as a load-bearing structure for tendon repair or replacement. Another possibility to use alginate in a load-bearing scaffold application is to form IPN hydrogels composed of alginate and other polymers. For example, IPN hydrogels of ionically crosslinked alginate and covalently crosslinked polyacrylamide were shown to possess failure stress more than 40 times higher than alginate gels alone (Darnell et al., 2013; Sun et al., 2012).

Cellulose

Cellulose is a plant-derived polysaccharide that consists of chains of glucose monomers. Cellulose is abundantly available and commonly considered nontoxic (Gibson et al., 2010, Gibson 2012). However, like other plant-derived polymers, cellulose lacks mammalian cell recognition sites and is not biodegradable in the human body. Cellulose has been less commonly used as a biomaterial for tendon tissue-engineering scaffolds compared to other naturally derived polymers. Cellulose has primarily been used to reinforce



• **Figure 2.6.5.3** Effects of hydrogel elastic modulus on tendon progenitor cells (TPCs). (A) Hydrogels were fabricated to present chick embryonic tendon elastic modulus of different developmental stages from HH28 to HH43. Gene expression levels of scleraxis (B) and collagen type XII (C) were significantly higher in chick embryo TPCs that were cultured in stiffer gels that represented later embryonic-stage tendons. * $P < .05$; ** $P < .01$; *** $P < .001$. (D) Representative brightfield images of arginyl-glycyl-aspartic acid (RGD)-functionalized alginate gels seeded with TPCs and cultured for 7 days. Gels with nanoscale elastic moduli from 3.4 to 20.1 kPa represented embryonic tendon from HH 28 to HH 43. Cells were more spread out in softer gels (representing younger embryonic tendons) and more round in stiffer gels (representing older embryonic tendons). Scale bar = 50 μm . (Figures adapted from Marturano, J.E., Schiele, N.R., Schiller, Z.A., Galassi, T.V., Stoppato, M., Kuo, C.K., 2016. Embryonically inspired scaffolds regulate tenogenically differentiating cells. *J. Biomech.* 49, 3281–3288.)

tendon scaffolds to achieve higher tensile strength and elastic modulus (Mathew et al., 2012, 2013; Domingues et al., 2016; Li et al., 2019).

Scaffolds made from both natural (e.g., collagen, chitosan) and synthetic (e.g., PCL) polymers have been reinforced with cellulose to enhance their mechanical strength and toughness (Mathew et al., 2012, 2013; Domingues et al., 2016; Li et al., 2019). Incorporation of cellulose increased tensile strength, strain, and elastic modulus of genipin crosslinked collagen–cellulose nanocomposites to within a comparable range to native tendon tissue (Mathew et al., 2012, 2013). Furthermore, seeded human ligament cells remained viable and proliferated within the hybrid scaffold (Mathew et al., 2013). In another study, incorporation of cellulose nanocrystals significantly enhanced the mechanical properties of electrospun PCL–chitosan composite scaffolds (Domingues et al., 2016). The cellulose-reinforced scaffolds were shown to possess a similar range of mechanical properties to that of native tendon (tensile strength in the range of 5–100 MPa and elastic modulus of 20–1200 MPa), while also supporting human tendon cell attachment and proliferation (Domingues et al., 2016). Incorporation of cellulose into electrospun nanofiber scaffolds that were then made into helical yarns resulted in high extensibility and toughness, exhibiting potential for use as a tendon tissue-engineering scaffold (Li et al., 2019).

Chitin/Chitosan

Chitin is a natural polysaccharide that can be found in the exoskeleton of crustaceans. Chitosan, a deacetylated derivative of chitin, is hydrophilic and cationic in nature and contains structural similarity to GAGs (Kumar et al., 2004; Muzzarelli, 1986). Chitosan scaffolds offer several advantages, including low immunogenicity and high degree of cell attachment (Madihally and Matthew, 1999; Funakoshi et al., 2005a). As a cationic polymer, chitosan is commonly combined with anionic polysaccharides like alginate to fabricate hybrid scaffolds that support cell adhesion (Park et al., 2000; Mizuno et al., 2003; Sechrist et al., 2000; Domard and Domard, 2001; Hirai et al., 1991; Funakoshi et al., 2005a,b; Zhang et al., 2015; Majima et al., 2005, 2007).

Chitosan scaffolds have been used to support porcine tendon cell proliferation and ECM deposition for more than 21 days in vitro (Bagnaninchi et al., 2007). Chitosan-coated alginate scaffolds have shown significant improvement in cell adhesion compared to alginate-only scaffolds (Majima et al., 2005, 2007). Coating electrospun PLLA scaffolds with chitosan increased cell proliferation and reduced protein adsorption compared to uncoated PLLA scaffolds (Sundaram et al., 2019). When combined with hyaluronic acid (HA), another natural polymer known for its biocompatibility, chitosan–HA hybrid scaffolds demonstrated a higher degree of cell attachment and proliferation along with enhanced material properties (Funakoshi et al., 2005a,b).

Although chitosan scaffolds can enable efficient cell attachment and create a suitable microenvironment for cell viability and proliferation, the use of chitosan scaffolds has not resulted in repaired tendons with comparable mechanical properties to native tissue (Zhang et al., 2015; Funakoshi et al., 2005a). While repaired tendon with braided hybrid chitosan–HA scaffold exhibited significantly higher tensile strength and tangent modulus than nonscaffold control, their material properties remained approximately sevenfold lower than intact tendons (Funakoshi et al., 2005a). Another study combined chitosan with both natural gelatin and synthetic PLLA and poly(ethylene oxide) (PEO) polymers to fabricate electrospun hybrid scaffolds with adequate mechanical strength and biocompatibility for rat Achilles tendon defect repair (Zhang et al., 2015). After 4 weeks of implantation in vivo, the scaffold-repaired tendons possessed a stiffness of ~70% of normal rat tendons.

Collagen

Collagen is the primary component of most connective tissues in mammals. The basic structure of collagen monomers is a triple helix formed from procollagen alpha chains, with the nonhelical N- and C-terminal sequences subsequently removed by specific peptidases. The triple helical collagen molecules then assemble into collagen fibrils extracellularly. The collagen fibrils then pack together to form collagen fibers, which then assemble to form fascicles. The fascicles then bundle together to comprise tendon. As tendon is mostly composed of collagen type I, collagen has been favored as a naturally occurring biomaterial for tendon tissue-engineering scaffolds. However, as an ECM protein, collagen is susceptible to proteolytic degradation. Additionally, because the collagen is commonly derived from animal sources, such as bovine skin, it is likely to elicit an immune response from the human recipient of the scaffold, particularly if the N- and C-terminal sequences have not been completely removed. Several important early studies used collagen type I gels as scaffolds for adult mesenchymal stem cell (MSC)-based tendon tissue-engineering efforts (Awad et al., 1999, 2000, 2003; Young et al., 1998; Kuo and Tuan, 2008; Yang et al., 2013a). However, the engineered tissues from collagen gels were exceedingly weak, thus precluding their use in early or immediate return to load-bearing function applications.

Fabrication methods such as textile technology and spinning have been adapted to produce collagen scaffolds with superior mechanical properties compared to collagen gels and to more closely mimic aspects of the native tendon architecture (Younesi et al., 2014; Yang et al., 2019; Zhang et al., 2018; Shepherd et al., 2013; Sandri et al., 2016). For example, one study fabricated scaffolds composed of collagen fibers with various orientations and examined the effects of fiber orientation on tenogenic differentiation of seeded bone marrow mesenchymal stem cells (BMSCs) in vitro and tendon regeneration in vivo (Yang et al., 2019). Microscale-aligned fiber scaffolds mimicked native tissue tendon structure more closely and upregulated expression

of tendon markers in vitro compared to randomly oriented fiber scaffolds. However, scaffold-repaired tendons only recovered 65% of the maximum load and stiffness of native tendon by 8 weeks after repair (Yang et al., 2019). Another study fabricated woven scaffolds from collagen yarns that were made by twisting three crosslinked collagen threads together (Younesi et al., 2014). Preimplantation, these scaffolds possessed similar stiffness to uninjured tendon tissue (Younesi et al., 2014). However, the strength of these fabricated scaffolds was only 60% of that of native tissue (Younesi et al., 2014).

Collagen has also been combined with GAGs to create porous collagen–GAG scaffolds with the goal of mimicking native tendon ECM composition and structure (Caliari et al., 2011, 2012; Grier et al., 2017; Hortensius et al., 2018; Mozdzen et al., 2016; Shepherd et al., 2013; Caliari and Harley, 2011, 2013). Controlling porosity of collagen–GAG scaffolds in turn controlled mechanical properties, nutrient and waste exchange, and susceptibility to degradation by enzymes or hydrolysis. Furthermore, when cells were seeded throughout the scaffold, they remained viable, proliferated with high metabolic activity, and expressed tendon markers (Caliari and Harley, 2011, 2013; Caliari et al., 2011, 2012; Grier et al., 2017). However, the collagen–GAG scaffolds possessed elastic modulus of at least an order of magnitude lower than native tendon tissue (Caliari et al., 2012; Dressler et al., 2006).

In addition to employing different fabrication methods, many studies have also improved mechanically weak collagen scaffolds by creating composites with silk fibroin (Chen et al., 2010, 2014; Zheng et al., 2017; Takezawa et al., 2007; Shen et al., 2010, 2012; Kwon et al., 2014; Tang et al., 2018). Tendons repaired with knitted silk–collagen sponge scaffolds achieved failure force up to 83% and stiffness up to 64% of control tendons (Chen et al., 2010, 2014). In another study, pores within knitted silk scaffolds were filled with silk–collagen sponge to fabricate tendon hybrid scaffolds (Tang et al., 2018). Scaffold-repaired tendon was shown to achieve up to ~60% of maximum load and elastic modulus of contralateral uninjured Achilles tendon after 20 weeks of implantation in vivo (Tang et al., 2018).

Gelatin

Gelatin is a denatured derivative of collagen, yet it retains the portion of amino acid sequences similar to collagen that are essential for cell adhesion and proliferation (Veis et al., 1961; Zeugolis et al., 2008). Gelatin scaffolds have been examined in the context of providing an environment to guide stem cell tenogenic behaviors and formation of neo-tendon tissue, as well as augmenting reconstruction of tendon defects in vivo (Yang et al., 2016; Rinoldi et al., 2019a; Visser et al., 2015; Rothrauff et al., 2018). Gelatin offers several advantages as a biomaterial for tendon tissue-engineering scaffolds, such as biocompatibility.

Several studies have used different techniques such as spinning and gelation to fabricate gelatin scaffolds that

mimic native tendon structure and enhance expression of tendon markers of seeded cells (Yang et al., 2016; Rinoldi et al., 2019a; Visser et al., 2015). Gelatin was functionalized with methacrylate groups for photocrosslinking and coelectrospun with synthetic PCL polymer to fabricate scaffolds with aligned fibers (Yang et al., 2016). Seeded human adipose-derived stem cells cultured within these scaffolds and treated with transforming growth factor- β 3 aligned along the fibers and upregulated expression of tendon markers such as Scx and TN-C (Yang et al., 2016). However, the maximum load and elastic modulus of these PCL–gelatin scaffolds were too low to support load-bearing function (Yang et al., 2016). Gelatin and alginate were used in a wet-spinning technique to fabricate 3D-aligned hydrogel yarns as scaffolds for tendon regeneration (Rinoldi et al., 2019a). The combination of structural (fiber alignment), mechanical (loading), and biochemical (bone morphogenetic protein 12) stimulation was shown to enhance human bone marrow MSC alignment and expression of different tendon markers compared to nontreated groups (Rinoldi et al., 2019a).

Silk

Silk fibroin is a widely used natural biomaterial in tendon tissue engineering. Silk fibroin is a protein produced by silkworms during cocoon production. Silk fibroin is made up of light (25 kDa) and heavy (350 kDa) chain units that are disulfide bonded together (Zhou et al., 2000). Silk fibroin proteins are linked by their sister sericin proteins, which can be removed from silk cocoon mass via boiling and degumming processes (Yamada et al., 2001). Degummed silk fibroin offers several advantages as a biomaterial, including the ability to retain its structural integrity in aqueous solutions and to be proteolytically degraded over time in vivo (Greenwald et al., 1994; Minoura et al., 1990). Silk fibroin is composed of amino acids (e.g., glycine) that can be recognized as binding sites for cells. Fibers made of silk fibroin have been reported to possess elastic modulus between 5 and 12 GPa, ultimate stress up to 500 MPa, and failure strain up to 26%, which are all within the comparable range to native tendon (Pérez-Rigueiro et al., 2000; Jiang et al., 2006; Greenwald et al., 1994).

Studies have used different fabrication methods to create scaffolds from degummed silk fibroin that can support tenogenic cell behavior and formation of tendon-like tissue (Teh et al., 2013; Pagan et al., 2019; Musson et al., 2015; Qiu et al., 2016). Sources of silk used in tendon regeneration scaffold include nonmulberry (produced from wild species of silkworm) and mulberry (produced by domesticated *Bombyx mori* silkworm). Knitted scaffolds fabricated from these two types of silk showed comparable support for tenocyte attachment and proliferation in vitro (Musson et al., 2015). In one study, knitting was combined with electrospinning to fabricate a hybrid silk scaffold that was used to examine the effects of mechanical loading and fiber alignment on tenogenesis of MSCs (Teh et al., 2013). Mechanical stimulation of MSCs seeded within the aligned hybrid scaffolds

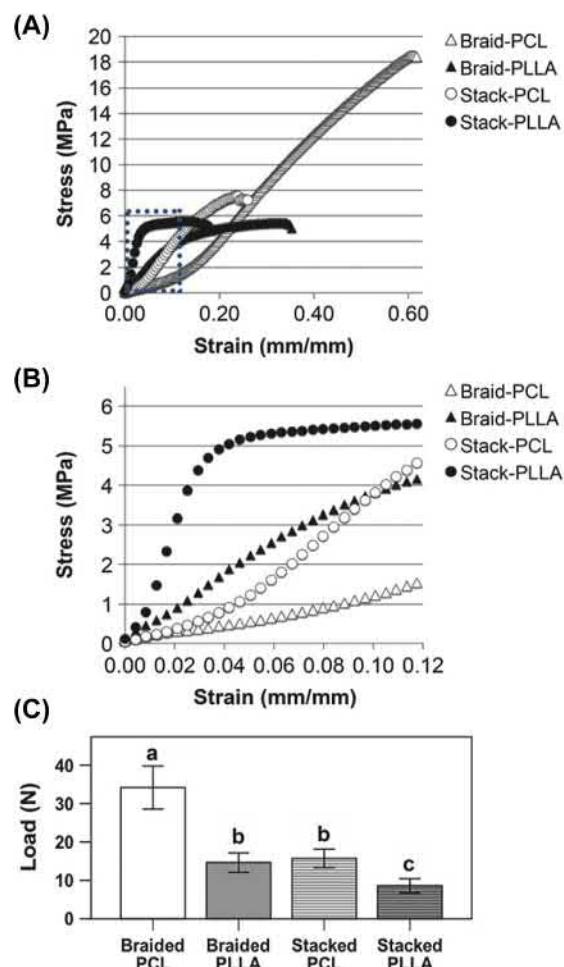
led to increased cell viability, higher expression of tendon markers (collagen types I and III, TN-C), and mechanical properties after 14 days of culture *in vitro* compared to randomly oriented scaffolds (Teh et al., 2013). A more recent study examined the mechanical properties of silkworm gut fiber braids that were made with different numbers of fibers and demonstrated the ability to achieve breaking force up to 330.5 N and elastic modulus up to 72 MPa, which were near the range of human anterior cruciate ligament (breaking force of 495–2160 N and elastic modulus of ~64 MPa) (Pagan et al., 2019). In addition, other studies have opted to combine silk with natural polymers such as collagen (see “Collagen” section) and synthetic polymers such as PLGA and PCL (see “Synthetic Polymers” section).

Synthetic Polymers

Poly(Glycolic Acid) and Poly(Lactic Acid)

Poly(glycolic acid) (PGA) and poly(lactic acid) (PLA) are two synthetic polyesters that have been Food and Drug Administration (FDA)-approved for a number of biomedical applications. Their approved status has made them especially attractive as biomaterials for tendon tissue engineering. PGA and PLA can be synthesized by ring opening polymerization of glycolide or lactide, respectively. The difference in molecular structure between PGA and PLA is that PLA possesses an additional methyl group that leads to distinct chemical and physical properties of the two polymers. The additional methyl group makes PLA more hydrophobic and resistant to hydrolytic degradation than PGA. The hydrophobicity of PLA also allows it to be dissolved in organic solvents such as tetrahydrofuran, acetonitrile, chlorinated solvents, and dioxane (Garlotta, 2001). Due to a higher degree of crystallinity, scaffolds made from PGA usually have higher modulus than PLA counterparts. Synthetic PGA and PLA polymers are degraded into glycolic acid and lactic acid, respectively, which are nontoxic in the body. However, these degradation products may reduce the pH locally, leading to inflammation (Liu et al., 2008). PLGA, a copolymer of PGA and PLA, has been used as biomaterial for tendon scaffold, as PLGA combines the advantages of both PGA and PLA, such as adequate mechanical properties and slow degradation rate (Ouyang et al., 2003; Sahoo et al., 2006; Gelberman et al., 2016).

PGA and PLA have each been used to fabricate tendon tissue-engineering scaffolds (Pietschmann et al., 2013; Wang et al., 2008; Cao et al., 2006; Liu et al., 2006; Wu et al., 2017a; Sato et al., 2000). For example, PLLA, a derivative of PLA, has been used to fabricate braided and stacked electrospun nanofibrous tendon scaffolds (Rothrauff et al., 2017). Within the range of physiological strain (0%–12%) of native ligament or tendon, stacked PLLA scaffolds exhibited ultimate stress and elastic modulus approaching those of native tendons (Fig. 2.6.5.4) (Rothrauff et al., 2017). Another study also showed that electrospun PLLA tendon scaffold could promote human



• **Figure 2.6.5.4** Mechanical properties of poly(ϵ -caprolactone) (PCL) and poly(L-lactic acid) (PLLA) scaffolds. (A) Averaged stress–strain curves of scaffolds. (B) Magnified stress–strain curves (box in [A]) within range of physiological strain of native tendon/ligament. (C) Maximum suture-retention strength of scaffolds; letters correspond to statistically equivalent groups, $P < .05$. (Figure adapted from Rothrauff, B.B., Lauro, B.B., Yang, G., Debski, R.E., Musahl, V., Tuan, R.S., 2017. Braided and stacked electrospun nanofibrous scaffolds for tendon and ligament tissue engineering. *Tissue Eng. A* 23, 378–389)

adipose-derived MSC viability and expression of tendon markers (Wu et al., 2017a).

PGA and PLA have also been combined with other synthetic polymers to fabricate scaffolds with enhanced strength and toughness and to more closely mimic native tendon structure (Deng et al., 2014; Szczesny et al., 2017; Sahoo et al., 2006; Wu et al., 2017a). For instance, tendons repaired with hybrid scaffolds made of an inner component of PGA unwoven fibers and an outer component of knitted PGA:PLA (4:2 ratio) fibers achieved up to 60% tensile strength of uninjured tendon after 45 weeks of *in vivo* implantation (Deng et al., 2014). Using PEO sacrificial fibers and heat to control porosity, electrospun PLLA scaffolds were fabricated with fiber crimping pattern that aimed to mimic native tendon structure (Szczesny et al., 2017). Upregulated expression of tendon markers on crimped scaffolds were observed along with changes in cell morphology and nuclei strain transmission (Szczesny et al., 2017).

Natural polymers such as collagen and silk have been combined with PGA and PLA to improve hybrid scaffold biocompatibility while maintaining excellent scaffold mechanical properties (Bellini et al., 2016; Sensini et al., 2018; Xu et al., 2014; Yang et al., 2014; Zhang et al., 2015; Deepthi et al., 2016; Stoll et al., 2011; Liao et al., 2018). Scaffolds composed of electrospun PLLA–collagen type I nanofiber bundles have been fabricated to possess failure stress and elastic modulus within a comparable range of human tendons (Sensini et al., 2018). These scaffolds have supported fibroblast attachment and viability for up to 21 days in culture (Sensini et al., 2018). Another study combined synthetic poly(L-lactide-*co*-caprolactone) (PLLA-CL), a derivative of PLLA polymer, with collagen type I to fabricate electrospun hybrid scaffolds (Xu et al., 2014). Tendons repaired with these scaffolds possessed ultimate stress and elastic modulus up to 60% and 52%, respectively, of uninjured tendon after 12 weeks of implantation in vivo (Xu et al., 2014). In addition to collagen, silk fibroin has also been incorporated with PLLA-CL to fabricate hybrid scaffolds that possessed comparable tensile strength and elastic modulus to native tendon tissue (Yang et al., 2014).

Poly(ϵ -Caprolactone)

PCL, an aliphatic polyester that has also been FDA approved for multiple biomedical applications, is commonly used for tendon tissue-engineering scaffolds. PCL is synthesized by ring opening polymerization of ϵ -caprolactone. PCL is biodegradable and biocompatible as its degradation product caproic acid can be metabolized by the body. Hydrolytic degradation of PCL scaffolds happens slowly due to the hydrophobic chains of PCL. However, the hydrophobicity of PCL scaffolds can negatively affect diffusion rate of molecules and the absence of cell adhesion motifs on PCL chains can hinder cell attachment within scaffolds. The incorporation of hydrophilic or bioactive moieties and other polymers has been used to address limitations associated with molecule diffusion and cell attachment within PCL scaffolds.

PCL has been used to fabricate tendon tissue-engineering scaffolds with excellent mechanical properties (Croisier et al., 2012; Wu et al., 2016; Pauly et al., 2016; Banik et al., 2016; Wang et al., 2018; Rothrauff et al., 2017; Li et al., 2006). Electrospun PCL scaffolds were shown to possess greater strain to failure but lower elastic modulus than electrospun PGA and PLA scaffolds (Li et al., 2006). In addition, PCL scaffolds supported cell attachment and proliferation and maintained their structure in aqueous solution for up to 42 days in vitro (Li et al., 2006). Another study used E-jet printing combined with uniaxial stretching to fabricate hybrid PCL scaffolds with improved mechanical properties compared to electrospun PCL scaffolds (Wu et al., 2016). The hybrid scaffolds were composed of an outer portion made from E-jet printed PCL fiber mesh and an inner portion made from uniaxially stretched heat-sealed PCL tubes. These hybrid scaffolds enhanced seeded cell proliferation compared to electrospun scaffolds. In addition, these hybrid

scaffolds possessed elastic modulus and ultimate stress that were within the range of human patellar tendon (\sim 227 and \sim 50 MPa vs. 120–660 MPa and 40–65 MPa, respectively) (Wu et al., 2016). In another example, the nonlinear stress–strain curve characteristic of native tendon was mimicked using electrospun PCL fibers fabricated with a crisscrossed “Chinese-fingertrap” structure (Banik et al., 2016). When loaded under tension, the stress–strain curves of these scaffolds showed a toe and linear region similar to that of native tendon (Banik et al., 2016). More recently, hybrid core–shell scaffolds were fabricated to mimic the topography and microarchitecture of native tendon ECM while possessing mechanical properties similar to native tendon tissue (Wang et al., 2018). In particular, the scaffold possessed an elastic modulus of \sim 375 MPa, ultimate stress of \sim 56 MPa, and failure strain of \sim 47.5%, which were within the range of native human patellar tendon (elastic modulus of \sim 191–660 MPa, ultimate stress of \sim 26–95 MPa, and failure strain of \sim 13%–31%) (Wang et al., 2018).

Several studies have opted to combine PCL with other polymers to fabricate hybrid scaffolds with enhanced mechanical properties and biocompatibility (Wu et al., 2017b; Hakimi et al., 2015; Ramos et al., 2019; Yang et al., 2016; Rinoldi et al., 2019b; Chainani et al., 2013; Liao et al., 2018). For example, PLA was incorporated into PCL yarn to create woven scaffolds with comparable ultimate strain (\sim 41%) to native human supraspinatus tendon (mean ultimate strain of \sim 36%) (Wu et al., 2017b; Nowotny et al., 2016). Another study fabricated multilayer hybrid scaffolds for tendon repair by combining electrospun polydioxanone (PDO) nanofibers and woven PDO layers with electrospun PCL sheets (Hakimi et al., 2015). These hybrid scaffolds were shown to possess failure load up to 85% of native human infraspinatus tendon (Hakimi et al., 2015; Bassett et al., 1990; Townsend et al., 1991). PCL scaffold biocompatibility can also be improved by incorporating different materials (Ramos et al., 2019; Yang et al., 2016; Rinoldi et al., 2019b; Chainani et al., 2013). For instance, the hydrophobicity of PCL scaffolds was reduced by incorporation of hydrophilic cellulose (Ramos et al., 2019). Methacrylated gelatin coating of PCL electrospun scaffolds improved cell attachment while also enhancing scaffold mechanical properties (Yang et al., 2016; Rinoldi et al., 2019b).

Other Synthetic Polymers

In addition to PGA, PLA, and PCL, other synthetic polymers such as poly(ethylene terephthalate) (PET) and polyhedral oligomeric silsesquioxane poly(carbonate-urea) urethane (POSS-PCU) have been used to fabricate tendon tissue-engineering scaffolds (Li et al., 2016; Cai et al., 2018; Alshomer et al., 2017). PET is a stable polyester containing aromatic groups that can be synthesized by the step-growth polymerization of ethylene glycol and terephthalic acid. PET scaffolds have been shown to possess high tensile strength (170–180 MPa) and elastic modulus (14,000 MPa) (Cziperle et al., 1992). PET has been used for surgical

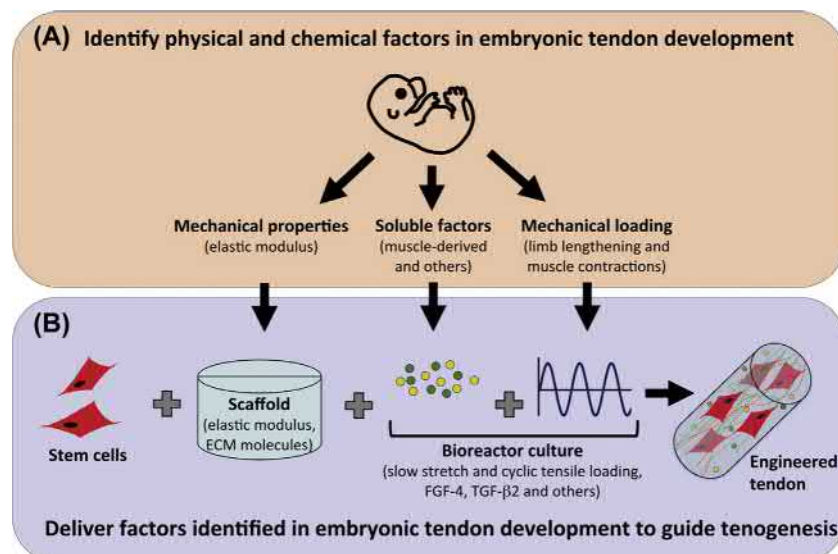
sutures, vascular grafts, and artificial ligaments for primary anterior cruciate ligament reconstructive surgery (Maitz, 2015; Naim et al., 2011; Dhillon et al., 2010). However, the hydrophobicity of PET was reported to induce inflammation and thrombosis when implanted inside the body (Dhahri et al., 2011). More recently, PET was used to fabricate braided scaffolds for Achilles tendon repair in vivo (Cai et al., 2018). These PET scaffolds supported BMSC culture. BMSC-seeded PET scaffolds improved stiffness and failure load of repaired tendon and upregulated collagen expression compared to PET scaffolds alone (Cai et al., 2018). POSS-PCU is another synthetic polymer that has been used as biomaterial for tendon tissue-engineering scaffolds (Alshomer et al., 2017). POSS-PCU polymers are composed of poly(carbonate-urea) urethane backbones functionalized with polyhedral oligomeric silsesquioxane nanoparticles (Tan et al., 2013). POSS-PCU micropatterned substrates were fabricated as aligned hollow tubular structures to mimic the size and structure of native tendon fibers (Alshomer et al., 2017). Human tenocytes cultured on the micropatterned surfaces increased metabolism, alignment, and total collagen production with a higher degree of staining for tendon markers such as Scx and TN-C compared to POSS-PCU flat surfaces.

Future Directions: Developmental Biology-Inspired Strategies

In the past couple of decades, scaffolds for tendon tissue engineering have evolved from relatively simple cell-seeded collagen gels cultured under tension to complex

composite materials with controlled multiscale architectures and mechanical properties. These scaffold designs have commonly strived to mimic adult tendon composition, microstructure, and mechanical properties. While the mechanical properties of these engineered structures have begun to approach those of native tendon, the tissues that form within these scaffolds still do not possess normal tendon tissue composition and material properties. Because tissue outcomes are governed by cells that reside within these scaffolds, efforts are ongoing to design scaffolds and culture systems that will provide tenogenic cues to cells within the scaffold and the surrounding tissues.

In recent years, rational approaches to guide stem cell differentiation based on developmental cues have started to emerge. The hypothesis behind these strategies is that the microenvironmental cues that induce stem cells to tenogenically differentiate and form new tendon during embryonic development will be effective signals to guide adult stem cell differentiation in a tissue-engineering system (Fig. 2.6.5.5) (Glass et al., 2014; Schiele et al., 2013; Nguyen et al., 2018; Okech and Kuo, 2016; Kuo and Tuan, 2003; Yang et al., 2013b). The promise of this approach has been demonstrated via a series of studies, some of which were briefly mentioned earlier in the chapter. In particular, the cell length-scale (microscale and nanoscale) elastic modulus of different-stage embryonic tendons were characterized by atomic force microscopy and shown to increase in a stage-specific manner during development (Marturano et al., 2013). To examine how these embryonic stage-specific tissue moduli influence tenogenesis during tendon development, hydrogel scaffolds were fabricated to present the cell length-scale modulus of each embryonic-stage tendon (Marturano



• **Figure 2.6.5.5** Developmental biology-inspired tissue-engineering strategies. (A) Characterize physical and chemical properties of developing embryonic tendon and its microenvironment. (B) Deliver these factors to stem cells via the scaffold (e.g., elastic modulus, bound extracellular matrix [ECM] molecules) and bioreactor culture (e.g., mechanical loading, soluble factors). Synergistic combinations of these cues may enhance and accelerate stem cell tenogenesis and neotissue formation. *FGF-4*, Fibroblast growth factor 4; *TGF- β 2*, transforming growth factor beta2. (Figure adapted from Glass, Z.A., Schiele, N.R., Kuo, C.K., 2014. Informing tendon tissue engineering with embryonic development. *J. Biomech.* 47, 1964–1968.)

et al., 2016). Embryonic tendon progenitor cells cultured within these hydrogels exhibited unique morphology and tendon marker gene expression profile at each scaffold stiffness, reflecting a potential role for tissue stiffness in regulating tenogenesis during embryonic tendon development (Marturano et al., 2016). Importantly, it was also shown that when treated with growth factors and mechanical cues that are critical for embryonic tendon development, adult MSCs responded similarly as embryonic tendon progenitor cells to these cues (Brown et al., 2014, 2015). Based on these collective studies, an engineered scaffold that presents adult stem cells with tenogenic cues based on the embryonic microenvironment could be an effective tendon tissue-engineering approach. Considering a scaffold that mimics embryonic tissue mechanical properties will not fulfill adult tendon load-bearing requirements, it could be sensible to engineer a composite scaffold of at least two different polymers, whereas one scaffold component provides differentiation cues and the other component imparts load-bearing capacity to the construct.

Summary

As discussed in this chapter, strategies to design a scaffold for tendon tissue engineering have utilized a range of natural and synthetic materials, fabrication methods, and postfabrication modifications. Despite the plethora of options, the goal of engineering an ideal scaffold that provides mechanical function, presents critical biological cues to guide stem cell differentiation, and biodegrades in a controlled manner has not yet been achieved. Additional considerations include seeded cell type and density, in vitro culture conditions prior to implantation, size of implant, anatomical location, and more, all of which can significantly impact the scaffold design. As materials science technologies continue to advance, so has the understanding of the biology involved in normal tendon development. As both fields advance in parallel, it has become clear that for a scaffold design to succeed, it will need to play a role in directing cell behaviors at different stages of tenogenic differentiation, tissue formation, function, and eventually long-term stability. Thus depending on the specific needs and biology of the individual patient, there cannot be a “one-scaffold-fits-all” approach. Therefore well-defined goals and an understanding of both biomaterials properties and tendon biology will be critical to the success of a tendon tissue-engineering scaffold.

Acknowledgments

This work was supported by funding from the National Institutes of Health under grant number NIH 1R01AR072886-01 (to CKK), the National Science Foundation under grant number NSF CMMI-1560965 (to CKK), and the Lee Quo Wei and Lee Yick Hoi Lun Professorship (to RST).

References

- Alshomer, F., Chaves, C., Serra, T., Ahmed, I., Kalaskar, D.M., 2017. Micropatterning of nanocomposite polymer scaffolds using sacrificial phosphate glass fibers for tendon tissue engineering applications. *Nanomed. Nanotechnol. Biol. Med.* 13, 1267–1277.
- Awad, H.A., Boivin, G.P., Dressler, M.R., Smith, F.N.L., Young, R.G., Butler, D.L., 2003. Repair of patellar tendon injuries using a cell-collagen composite. *J. Orthop. Res.* 21, 420–431.
- Awad, H.A., Butler, D.L., Boivin, G.P., Smith, F.N., Malaviya, P., Huibregtse, B., Caplan, A.L., 1999. Autologous mesenchymal stem cell-mediated repair of tendon. *Tissue Eng.* 5, 267–277.
- Awad, H.A., Butler, D.L., Harris, M.T., Ibrahim, R.E., Wu, Y., Young, R.G., Kadiyala, S., Boivin, G.P., 2000. In vitro characterization of mesenchymal stem cell-seeded collagen scaffolds for tendon repair: effects of initial seeding density on contraction kinetics. *J. Biomed. Mater. Res.* 51, 233–240.
- Bagnaninchi, P.O., Yang, Y., Zghoul, N., Maffulli, N., Wang, R.K., Haj, A.J., 2007. Chitosan microchannel scaffolds for tendon tissue engineering characterized using optical coherence tomography. *Tissue Eng.* 13, 323–331.
- Baker, B.M., Gee, A.O., Metter, R.B., Nathan, A.S., Marklein, R.A., Burdick, J.A., Mauck, R.L., 2008. The potential to improve cell infiltration in composite fiber-aligned electrospun scaffolds by the selective removal of sacrificial fibers. *Biomaterials* 29, 2348–2358.
- Banik, B.L., Lewis, G.S., Brown, J.L., 2016. Multiscale poly(-caprolactone) scaffold mimicking nonlinearity in tendon tissue mechanics. *Regen. Eng. Transl. Med.* 2, 1–9.
- Banos, C.C., Thomas, A.H., Kuo, C.K., 2008. Collagen fibrillogenesis in tendon development: current models and regulation of fibril assembly. *Birth Defects Res. C Embryo Today* 84, 228–244.
- Bassett, R.W., Browne, A.O., Morrey, B.F., An, K.N., 1990. Glenohumeral muscle force and moment mechanics in a position of shoulder instability. *J. Biomech.* 23, 405–415.
- Baudequin, T., Gaut, L., Mueller, M., Huepkes, A., Glasmacher, B., Duprez, D., Bedoui, F., Legallais, C., 2017. The osteogenic and tenogenic differentiation potential of C3H10T1/2 (mesenchymal stem cell model) cultured on PCL/PLA electrospun scaffolds in the absence of specific differentiation medium. *Materials* 10.
- Bellini, D., Cencetti, C., Sacchetta, A.C., Battista, A.M., Martinelli, A., Mazzucco, L., Scotto D’abusco, A., Matricardi, P., 2016. PLA-grafting of collagen chains leading to a biomaterial with mechanical performances useful in tendon regeneration. *J. Mech. Behav. Biomed. Mater.* 64, 151–160.
- Benjamin, M., Kaiser, E., Milz, S., 2008. Structure-function relationships in tendons: a review. *J. Anat.* 212, 211–228.
- Bennett, M.B., Ker, R.F., Dimery, N.J., Alexander, R.M., 1986. Mechanical properties of various mammalian tendons. *J. Zool.* 209, 537–548.
- Bi, Y.M., Ehirchiou, D., Kilts, T.M., Inkson, C.A., Embree, M.C., Sonoyama, W., Li, L., Leet, A.I., Seo, B.M., Zhang, L., Shi, S.T., Young, M.F., 2007. Identification of tendon stem/progenitor cells and the role of the extracellular matrix in their niche. *Nat. Med.* 13, 1219–1227.
- Branco Da Cunha, C., Klumpers, D.D., Li, W.A., Koshy, S.T., Weaver, J.C., Chaudhuri, O., Granja, P.L., Mooney, D.J., 2014. Influence of the stiffness of three-dimensional alginate/collagen-I interpenetrating networks on fibroblast biology. *Biomaterials* 35, 8927–8936.

- Breidenbach, A.P., Dymont, N.A., Lu, Y., Rao, M., Shearn, J.T., Rowe, D.W., Kadler, K.E., Butler, D.L., 2015. Fibrin gels exhibit improved biological, structural, and mechanical properties compared with collagen gels in cell-based tendon tissue-engineered constructs. *Tissue Eng. A* 21, 438–450.
- Brown, J.P., Finley, V.G., Kuo, C.K., 2014. Embryonic mechanical and soluble cues regulate tendon progenitor cell gene expression as a function of developmental stage and anatomical origin. *J. Biomech.* 47, 214–222.
- Brown, J.P., Galassi, T.V., Stoppato, M., Schiele, N.R., Kuo, C.K., 2015. Comparative analysis of mesenchymal stem cell and embryonic tendon progenitor cell response to embryonic tendon biochemical and mechanical factors. *Stem Cell Res. Ther.* 6, 89.
- Butler, M.F., Ng, Y.F., Pudney, P.D.A., 2003. Mechanism and kinetics of the crosslinking reaction between biopolymers containing primary amine groups and genipin. *J. Polym. Sci. A Polym. Chem.* 41, 3941–3953.
- Cai, J., Yang, Y., Ai, C., Jin, W., Sheng, D., Chen, J., Chen, S., 2018. Bone marrow stem cells-seeded polyethylene terephthalate scaffold in repair and regeneration of rabbit achilles tendon. *Artif. Organs* 42, 1086–1094.
- Caliari, S.R., Harley, B.A., 2011. The effect of anisotropic collagen-GAG scaffolds and growth factor supplementation on tendon cell recruitment, alignment, and metabolic activity. *Biomaterials* 32, 5330–5340.
- Caliari, S.R., Harley, B.A., 2013. Composite growth factor supplementation strategies to enhance tenocyte bioactivity in aligned collagen-GAG scaffolds. *Tissue Eng. A* 19, 1100–1112.
- Caliari, S.R., Ramirez, M.A., Harley, B.A., 2011. The development of collagen-GAG scaffold-membrane composites for tendon tissue engineering. *Biomaterials* 32, 8990–8998.
- Caliari, S.R., Weisgerber, D.W., Ramirez, M.A., Kelkhoff, D.O., Harley, B.A., 2012. The influence of collagen-glycosaminoglycan scaffold relative density and microstructural anisotropy on tenocyte bioactivity and transcriptomic stability. *J. Mech. Behav. Biomed. Mater.* 11, 27–40.
- Cao, D.J., Liu, W., Wei, X., Xu, F., Cui, L., Cao, Y.L., 2006. In vitro tendon engineering with avian tenocytes and polyglycolic acids: a preliminary report. *Tissue Eng.* 12, 1369–1377.
- Chainani, A., Hippensteel, K.J., Kishan, A., Garrigues, N.W., Ruch, D.S., Guilak, F., Little, D., 2013. Multilayered electrospun scaffolds for tendon tissue engineering. *Tissue Eng. A* 19, 2594–2604.
- Chen, J.L., Yin, Z., Shen, W.L., Chen, X., Heng, B.C., Zou, X.H., Ouyang, H.W., 2010. Efficacy of hESC-MSCs in knitted silk-collagen scaffold for tendon tissue engineering and their roles. *Biomaterials* 31, 9438–9451.
- Chen, J.M., Xu, J.K., Wang, A.L., Zheng, M.H., 2009. Scaffolds for tendon and ligament repair: review of the efficacy of commercial products. *Expert Rev. Med. Devices* 6, 61–73.
- Chen, X., Yin, Z., Chen, J.L., Liu, H.H., Shen, W.L., Fang, Z., Zhu, T., Ji, J., Ouyang, H.W., Zou, X.H., 2014. Scleraxis-overexpressed human embryonic stem cell-derived mesenchymal stem cells for tendon tissue engineering with knitted silk-collagen scaffold. *Tissue Eng. A* 20, 1583–1592.
- Chiquet-Ehrismann, R., Tucker, R.P., 2004. Connective tissues: signalling by tenascins. *Int. J. Biochem. Cell Biol.* 36, 1085–1089.
- Cottrell, I.W.K., P., 1980. *Handbook of Water-Soluble Gums and Resins*. McGraw-Hill, New York.
- Croisier, F., Duwez, A.S., Jerome, C., Leonard, A.F., Van Der Werf, K.O., Dijkstra, P.J., Bennink, M.L., 2012. Mechanical testing of electrospun PCL fibers. *Acta Biomater.* 8, 218–224.
- Cziperle, D.J., Joyce, K.A., Tattersall, C.W., Henderson, S.C., Cabusao, E.B., Garfield, J.D., Kim, D.U., Duhamel, R.C., Greisler, H.P., 1992. Albumin impregnated vascular grafts: albumin resorption and tissue reactions. *J. Cardiovasc. Surg.* 33, 407–414.
- Darnell, M.C., Sun, J.Y., Mehta, M., Johnson, C., Arany, P.R., Suo, Z., Mooney, D.J., 2013. Performance and biocompatibility of extremely tough alginate/polyacrylamide hydrogels. *Biomaterials* 34, 8042–8048.
- Deepthi, S., Nivedhitha Sundaram, M., Deepthi Kadavan, J., Jayakumar, R., 2016. Layered chitosan-collagen hydrogel/aligned PLLA nanofiber construct for flexor tendon regeneration. *Carbohydr. Polym.* 153, 492–500.
- Deng, D., Wang, W., Wang, B., Zhang, P., Zhou, G., Zhang, W.J., Cao, Y., Liu, W., 2014. Repair of Achilles tendon defect with autologous ASCs engineered tendon in a rabbit model. *Biomaterials* 35, 8801–8809.
- Dhahri, M., Abed, A., Lajimi, R.H., Mansour, M.B., Gueguen, V., Abdesslem, S.B., Chaubet, F., Letourneur, D., Meddahi-Pelle, A., Maaroufi, R.M., 2011. Grafting of dermatan sulfate on polyethylene terephthalate to enhance biointegration. *J. Biomed. Mater. Res. A* 98, 114–121.
- Dhillon, M.S., Chauhan, D., Kumar, V., Saini, U.C., 2010. Reconstruction of bilateral spontaneous chronic idiopathic Achilles tendon rupture using LARS ligament: case report. *Foot* 20, 154–157.
- Domard, A., Domard, M., 2001. *Chitosan: Structure-Properties Relationship and Biomedical Applications*.
- Domingues, R.M., Chiera, S., Gershovich, P., Motta, A., Reis, R.L., Gomes, M.E., 2016. Enhancing the biomechanical performance of anisotropic nanofibrous scaffolds in tendon tissue engineering: reinforcement with cellulose nanocrystals. *Adv. Healthc. Mater.* 5, 1364–1375.
- Dressler, M.R., Butler, D.L., Boivin, G.P., 2006. Age-related changes in the biomechanics of healing patellar tendon. *J. Biomech.* 39, 2205–2212.
- Edom-Vovard, F., Duprez, D., 2004. Signals regulating tendon formation during chick embryonic development. *Dev. Dynam.* 229, 449–457.
- Farkash, U., Avisar, E., Volk, I., Slevin, O., Shohat, N., El Haj, M., Dolev, E., Ashraf, E., Luria, S., 2019. First clinical experience with a new injectable recombinant human collagen scaffold combined with autologous platelet-rich plasma for the treatment of lateral epicondylar tendinopathy (tennis elbow). *J. Shoulder Elb. Surg.* 28, 503–509.
- Fessel, G., Cadby, J., Wunderli, S., Van Weeren, R., Snedeker, J.G., 2014. Dose- and time-dependent effects of genipin crosslinking on cell viability and tissue mechanics – toward clinical application for tendon repair. *Acta Biomater.* 10, 1897–1906.
- Fessel, G., Gerber, C., Snedeker, J.G., 2012a. Potential of collagen cross-linking therapies to mediate tendon mechanical properties. *J. Shoulder Elb. Surg.* 21, 209–217.
- Fessel, G., Wernli, J., Li, Y., Gerber, C., Snedeker, J.G., 2012b. Exogenous collagen cross-linking recovers tendon functional integrity in an experimental model of partial tear. *J. Orthop. Res.* 30, 973–981.
- Frauz, K., Teodoro, L.F.R., Carneiro, G.D., Cristina Da Veiga, F., Lopes Ferrucci, D., Luis Bombeiro, A., Waleska Simoes, P., Elvira Alvares, L., Leite, R.D.O.A., Pontes Vicente, C., Seabra Ferreira Jr., R., Barraviera, B., Do Amaral, M.E.C., Augusto, M.E.M., De Campos Vidal, B., Rosa Pimentel, E., Aparecida De Aro, A., 2019. Transected tendon treated with a new fibrin sealant alone or associated with adipose-derived stem cells. *Cells* 8.

- Funakoshi, T., Majima, T., Iwasaki, N., Suenaga, N., Sawaguchi, N., Shimode, K., Minami, A., Harada, K., Nishimura, S., 2005a. Application of tissue engineering techniques for rotator cuff regeneration using a chitosan-based hyaluronan hybrid fiber scaffold. *Am. J. Sports Med.* 33, 1193–1201.
- Funakoshi, T., Majima, T., Iwasaki, N., Yamane, S., Masuko, T., Minami, A., Harada, K., Tamura, H., Tokura, S., Nishimura, S., 2005b. Novel chitosan-based hyaluronan hybrid polymer fibers as a scaffold in ligament tissue engineering. *J. Biomed. Mater. Res. A* 74, 338–346.
- Garlotta, D., 2001. A literature review of poly(lactic acid). *J. Polym. Environ.* 9 (2), 63–84.
- Gelberman, R.H., Shen, H., Kormpakis, I., Rothrauff, B., Yang, G., Tuan, R.S., Xia, Y., Sakiyama-Elbert, S., Silva, M.J., Thomopoulos, S., 2016. Effect of adipose-derived stromal cells and BMP12 on intrasynovial tendon repair: a biomechanical, biochemical, and proteomics study. *J. Orthop. Res.* 34, 630–640.
- Gibson, L.J., 2012. The hierarchical structure and mechanics of plant materials. *J. R. Soc. Interface* 9, 2749–2766.
- Gibson, L.J., Ashby, M.F., Harley, B.A., 2010. *Cellular Materials in Nature and Medicine*. Cambridge Cambridge University Press.
- Glass, Z.A., Schiele, N.R., Kuo, C.K., 2014. Informing tendon tissue engineering with embryonic development. *J. Biomech.* 47, 1964–1968.
- Govoni, M., Berardi, A.C., Muscari, C., Campardelli, R., Bonafe, F., Guarneri, C., Reverchon, E., Giordano, E., Maffulli, N., Della Porta, G., 2017. An engineered multiphase three-dimensional microenvironment to ensure the controlled delivery of cyclic strain and human growth differentiation factor 5 for the tenogenic commitment of human bone marrow mesenchymal stem cells. *Tissue Eng. A* 23, 811–822.
- Green, E.C., Zhang, Y., Li, H., Minus, M.L., 2017. Gel-spinning of mimetic collagen and collagen/nano-carbon fibers: understanding multi-scale influences on molecular ordering and fibril alignment. *J. Mech. Behav. Biomed. Mater.* 65, 552–564.
- Greenwald, D., Shumway, S., Albear, P., Gottlieb, L., 1994. Mechanical comparison of 10 suture materials before and after in vivo incubation. *J. Surg. Res.* 56, 372–377.
- Grier, W.K., Iyoha, E.M., Harley, B.A.C., 2017. The influence of pore size and stiffness on tenocyte bioactivity and transcriptomic stability in collagen-GAG scaffolds. *J. Mech. Behav. Biomed. Mater.* 65, 295–305.
- Hakimi, O., Mouthuy, P.A., Zargar, N., Lostis, E., Morrey, M., Carr, A., 2015. A layered electrospun and woven surgical scaffold to enhance endogenous tendon repair. *Acta Biomater.* 26, 124–135.
- Haugh, M.G., Murphy, C.M., O'Brien, F.J., 2010. Novel freeze-drying methods to produce a range of collagen-glycosaminoglycan scaffolds with tailored mean pore sizes. *Tissue Eng. C Methods* 16, 887–894.
- Hirai, A., Odani, H., Nakajima, A., 1991. Determination of degree of deacetylation of chitosan by ¹H NMR spectroscopy. *Polym. Bull.* 26, 87–94.
- Hortensius, R.A., Ebens, J.H., Dewey, M.J., Harley, B.A.C., 2018. Incorporation of the amniotic membrane as an immunomodulatory design element in collagen scaffolds for tendon repair. *ACS Biomater. Sci. Eng.* 4, 4367–4377.
- Hortensius, R.A., Harley, B.A., 2013. The use of bioinspired alterations in the glycosaminoglycan content of collagen-GAG scaffolds to regulate cell activity. *Biomaterials* 34, 7645–7652.
- Huang, A.H., Lu, H.H., Schweitzer, R., 2015. Molecular regulation of tendon cell fate during development. *J. Orthop. Res.* 33, 800–812.
- Huang, L.L., Sung, H.W., Tsai, C.C., Huang, D.M., 1998. Biocompatibility study of a biological tissue fixed with a naturally occurring crosslinking reagent. *J. Biomed. Mater. Res.* 42, 568–576.
- Jiang, P., Liu, H., Wang, C., Wu, L., Huang, J., Guo, C., 2006. Tensile behavior and morphology of differently degummed silkworm (*Bombyx mori*) cocoon silk fibres. *Mater. Lett.* 60, 919–925.
- Joshi, V.S., Lei, N.Y., Walthers, C.M., Wu, B., Dunn, J.C.Y., 2013. Macroporosity enhances vascularization of electrospun scaffolds. *J. Surg. Res.* 183, 18–26.
- Kapacee, Z., Yeung, C.Y., Lu, Y., Crabtree, D., Holmes, D.F., Kadler, K.E., 2010. Synthesis of embryonic tendon-like tissue by human marrow stromal/mesenchymal stem cells requires a three-dimensional environment and transforming growth factor beta3. *Matrix Biol.* 29, 668–677.
- Kirk, J.F., Ritter, G., Finger, I., Sankar, D., Reddy, J.D., Talton, J.D., Nataraj, C., Narisawa, S., Millan, J.L., Cobb, R.R., 2013. Mechanical and biocompatible characterization of a cross-linked collagen-hyaluronic acid wound dressing. *Biomater* 3.
- Korecki, C.L., Kuo, C.K., Tuan, R.S., Iatridis, J.C., 2009. Intervertebral disc cell response to dynamic compression is age and frequency dependent. *J. Orthop. Res.* 27, 800–806.
- Kumar, M.N.V.R., Muzzarelli, R.A.A., Muzzarelli, C., Sashiwa, H., Domb, A.J., 2004. Chitosan chemistry and pharmaceutical perspectives. *Chem. Rev.* 104, 6017–6084.
- Kuo, C.K., Ma, P.X., 2001. Ionically crosslinked alginate hydrogels as scaffolds for tissue engineering: part 1. Structure, gelation rate and mechanical properties. *Biomaterials* 22, 511–521.
- Kuo, C.K., Ma, P.X., 2008. Maintaining dimensions and mechanical properties of ionically crosslinked alginate hydrogel scaffolds in vitro. *J. Biomed. Mater. Res. A* 84, 899–907.
- Kuo, C.K., Tuan, R.S., 2003. Tissue engineering with mesenchymal stem cells. *IEEE Eng. Med. Biol. Mag.* 22, 51–56.
- Kuo, C.K., Tuan, R.S., 2008. Mechanoactive tenogenic differentiation of human mesenchymal stem cells. *Tissue Eng. A* 14, 1615–1627.
- Kwan, M.K., Lin, T.H., Woo, S.L., 1993. On the viscoelastic properties of the anteromedial bundle of the anterior cruciate ligament. *J. Biomech.* 26, 447–452.
- Kwon, S.Y., Chung, J.W., Park, H.J., Jiang, Y.Y., Park, J.K., Seo, Y.K., 2014. Silk and collagen scaffolds for tendon reconstruction. *Proc. Inst. Mech. Eng. H* 228, 388–396.
- Langer, R., Peppas, N.A., 2003. Advances in biomaterials, drug delivery, and bionanotechnology. *AIChE J.* 49, 2990–3006.
- Langer, R.S., Peppas, N.A., 1981. Present and future applications of biomaterials in controlled drug delivery systems. *Biomaterials* 2, 201–214.
- Lee, J.B., Jeong, S.I., Bae, M.S., Yang, D.H., Heo, D.N., Kim, C.H., Alsberg, E., Kwon, I.K., 2011. Highly porous electrospun nanofibers enhanced by ultrasonication for improved cellular infiltration. *Tissue Eng. A* 17, 2695–2702.
- Li, S., Ma, K., Li, H., Jiang, J., Chen, S., 2016. The effect of sodium hyaluronate on ligation and biomechanical property of tendon in repair of achilles tendon defect with polyethylene terephthalate artificial ligament: a rabbit tendon repair model. *Biomed. Res. Int.* 2016, 8684231.
- Li, W.J., Cooper Jr, J.A., Mauck, R.L., Tuan, R.S., 2006. Fabrication and characterization of six electrospun poly(alpha-hydroxy ester)-based fibrous scaffolds for tissue engineering applications. *Acta Biomater.* 2, 377–385.
- Li, Y., Guo, F., Hao, Y., Gupta, S.K., Hu, J., Wang, Y., Wang, N., Zhao, Y., Guo, M., 2019. Helical nanofiber yarn enabling highly stretchable engineered microtissue. *Proc. Natl. Acad. Sci. USA* 116, 9245–9250.

- Liang, H.-C., Chang, W.-H., Liang, H.-F., Lee, M.-H., Sung, H.-W., 2004. Crosslinking structures of gelatin hydrogels crosslinked with genipin or a water-soluble carbodiimide. *J. Appl. Polym. Sci.* 91, 4017–4026.
- Liao, J.C.Y., He, M., Gan, A.W.T., Wen, F., Tan, L.P., Chong, A.K.S., 2018. The effects of bi-functional anti-adhesion scaffolds on flexor tendon healing in a rabbit model. *J. Biomed. Mater. Res. B Appl. Biomater.* 106, 2605–2614.
- Liao, X., Lu, Z., Du, X., Liu, X., Shi, B., 2004. Collagen fiber immobilized Myrica rubra tannin and its adsorption to $\text{UO}_2(2+)$. *Environ. Sci. Technol.* 38, 324–328.
- Lichtwark, G.A., Wilson, A.M., 2005. In vivo mechanical properties of the human Achilles tendon during one-legged hopping. *J. Exp. Biol.* 208, 4715–4725.
- Lin, H., Zhang, D., Alexander, P.G., Yang, G., Cheng, A.W., Tuan, R.S., 2013. Application of visible light-based projection stereolithography for live cell-scaffold fabrication with designed architecture. *Biomaterials* 34, 331–339.
- Lin, H., Cheng, A.W., Alexander, P.G., Beck, A.M., Tuan, R.S., 2014. Cartilage tissue engineering application of injectable gelatin hydrogel with in situ visible light-activated gelation capability in both air and aqueous solution. *Tissue Eng. A* 20, 2402–2411.
- Liu, W., Chen, B., Deng, D., Xu, F., Cui, L., Cao, Y.L., 2006. Repair of tendon defect with dermal fibroblast engineered tendon in a porcine model. *Tissue Eng.* 12, 775–788.
- Liu, Y., Ramanath, H.S., Wang, D.A., 2008. Tendon tissue engineering using scaffold enhancing strategies. *Trends Biotechnol.* 26, 201–209.
- Lohre, J.M., Baclig, L., Sagartz, J., Guida, S., Thyagarajan, K., Tu, R., 1992. Evaluation of two epoxy ether compounds for biocompatible potential. *Artif. Organs* 16, 630–633.
- Madhally, S.V., Matthew, H.W., 1999. Porous chitosan scaffolds for tissue engineering. *Biomaterials* 20, 1133–1142.
- Maganaris, C.N., Paul, J.P., 2002. Tensile properties of the in vivo human gastrocnemius tendon. *J. Biomech.* 35, 1639–1646.
- Maitz, M.F., 2015. Applications of synthetic polymers in clinical medicine. *Biosurface Biotribology* 1, 161–176.
- Majima, T., Funakoshi, T., Iwasaki, N., Yamane, S.T., Harada, K., Nonaka, S., Minami, A., Nishimura, S., 2005. Alginate and chitosan polyion complex hybrid fibers for scaffolds in ligament and tendon tissue engineering. *J. Orthop. Sci.* 10, 302–307.
- Majima, T., Irie, T., Sawaguchi, N., Funakoshi, T., Iwasaki, N., Harada, K., Minami, A., Nishimura, S.I., 2007. Chitosan-based hyaluronan hybrid polymer fibre scaffold for ligament and tendon tissue engineering. *Proc. Inst. Mech. Eng. H* 221, 537–546.
- Malcarney, H.L., Bonar, F., Murrell, G.A., 2005. Early inflammatory reaction after rotator cuff repair with a porcine small intestine submucosal implant: a report of 4 cases. *Am. J. Sports Med.* 33, 907–911.
- Manning, C.N., Schwartz, A.G., Liu, W., Xie, J., Havlioglu, N., Sakiyama-Elbert, S.E., Silva, M.J., Xia, Y., Gelberman, R.H., Thomopoulos, S., 2013. Controlled delivery of mesenchymal stem cells and growth factors using a nanofiber scaffold for tendon repair. *Acta Biomater.* 9, 6905–6914.
- Marturano, J.E., Arena, J.D., Schiller, Z.A., Georgakoudi, I., Kuo, C.K., 2013. Characterization of mechanical and biochemical properties of developing embryonic tendon. *Proc. Natl. Acad. Sci. USA* 110, 6370–6375.
- Marturano, J.E., Schiele, N.R., Schiller, Z.A., Galassi, T.V., Stoppato, M., Kuo, C.K., 2016. Embryonically inspired scaffolds regulate tenogenically differentiating cells. *J. Biomech.* 49, 3281–3288.
- Marturano, J.E., Xylas, J.F., Sridharan, G.V., Georgakoudi, I., Kuo, C.K., 2014. Lysyl oxidase-mediated collagen crosslinks may be assessed as markers of functional properties of tendon tissue formation. *Acta Biomater.* 10, 1370–1379.
- Mathew, A.P., Oksman, K., Pierron, D., Harmad, M.F., 2012. Cross-linked fibrous composites based on cellulose nanofibers and collagen with in situ pH induced fibrillation. *Cellulose* 19, 139–150.
- Mathew, A.P., Oksman, K., Pierron, D., Harmad, M.F., 2013. Biocompatible fibrous networks of cellulose nanofibres and collagen crosslinked using genipin: potential as artificial ligament/tendons. *Macromol. Biosci.* 13, 289–298.
- Mcbride, D.J., Trelstad, R.L., Silver, F.H., 1988. Structural and mechanical assessment of developing chick tendon. *Int. J. Biol. Macromol.* 10, 194–200.
- Mcneilly, C.M., Banes, A.J., Benjamin, M., Ralphs, J.R., 1996. Tendon cells in vivo form a three dimensional network of cell processes linked by gap junctions. *J. Anat.* 189, 593–600.
- Megerle, K., Woon, C., Kraus, A., Raghavan, S., Pham, H., Chang, J., 2016. Flexor tendon sheath engineering using decellularized porcine pericardium. *Plast. Reconstr. Surg.* 138 630e–41e.
- Min, H.K., Kwon, O.S., Oh, S.H., Lee, J.H., 2016. Platelet-derived growth factor-BB-immobilized asymmetrically porous membrane for enhanced rotator cuff tendon healing. *Tissue Eng. Regen. Med.* 13, 568–578.
- Minoura, N., Tsukada, M., Nagura, M., 1990. Physico-chemical properties of silk fibroin membrane as a biomaterial. *Biomaterials* 11, 430–434.
- Mironi-Harpaz, I., Wang, D.Y., Venkatraman, S., Seliktar, D., 2012. Photopolymerization of cell-encapsulating hydrogels: crosslinking efficiency versus cytotoxicity. *Acta Biomater.* 8, 1838–1848.
- Mizuno, K., Yamamura, K., Yano, K., Osada, T., Saeki, S., Takimoto, N., Sakurai, T., Nimura, Y., 2003. Effect of chitosan film containing basic fibroblast growth factor on wound healing in genetically diabetic mice. *J. Biomed. Mater. Res. A* 64, 177–181.
- Mozdzen, L.C., Rodgers, R., Banks, J.M., Bailey, R.C., Harley, B.A., 2016. Increasing the strength and bioactivity of collagen scaffolds using customizable arrays of 3D-printed polymer fibers. *Acta Biomater.* 33, 25–33.
- Mozdzen, L.C., Vucetic, A., Harley, B.A.C., 2017. Modifying the strength and strain concentration profile within collagen scaffolds using customizable arrays of poly-lactic acid fibers. *J. Mech. Behav. Biomed. Mater.* 66, 28–36.
- Musson, D.S., Naot, D., Chhana, A., Matthews, B.G., McIntosh, J.D., Lin, S.T., Choi, A.J., Callon, K.E., Dunbar, P.R., Lesage, S., Coleman, B., Cornish, J., 2015. In vitro evaluation of a novel non-mulberry silk scaffold for use in tendon regeneration. *Tissue Eng. A* 21, 1539–1551.
- Muzzarelli, R.A.A., Jeuniaux, C., Gooday, G.W., 1986. (eds). *Chitin in Nature and Technology*. Springer, Boston, MA.
- Naghashzargar, E., Fare, S., Catto, V., Bertoldi, S., Semnani, D., Karbasi, S., Tanzi, M.C., 2015. Nano/micro hybrid scaffold of PCL or P3HB nanofibers combined with silk fibroin for tendon and ligament tissue engineering. *J. Appl. Biomater. Funct. Mater.* 13, e156–e168.
- Naim, S., Gougoulias, N., Griffiths, D., 2011. Patellar tendon reconstruction using LARS ligament: surgical technique and case report. *Strategies Trauma Limb Reconstr.* 6, 39–41.
- Namba, J., Shimada, K., Saito, M., Murase, T., Yamada, H., Yoshikawa, H., 2007. Modulation of peritendinous adhesion formation by alginate solution in a rabbit flexor tendon model. *J. Biomed. Mater. Res. B Appl. Biomater.* 80, 273–279.

- Nguyen, P.K., Pan, X.S., Li, J., Kuo, C.K., 2018. Roadmap of molecular, compositional, and functional markers during embryonic tendon development. *Connect. Tissue Res.* 59, 495–508.
- Ning, L.J., Jiang, Y.L., Zhang, C.H., Zhang, Y., Yang, J.L., Cui, J., Zhang, Y.J., Yao, X., Luo, J.C., Qin, T.W., 2017. Fabrication and characterization of a decellularized bovine tendon sheet for tendon reconstruction. *J. Biomed. Mater. Res. A* 105, 2299–2311.
- Nowotny, J., Aibibu, D., Farack, J., Nimtschke, U., Hild, M., Gelin-sky, M., Kasten, P., Cherif, C., 2016. Novel fiber-based pure chitosan scaffold for tendon augmentation: biomechanical and cell biological evaluation. *J. Biomater. Sci. Polym. Ed.* 27, 917–936.
- O'Brien, F.J., Harley, B.A., Yannas, I.V., Gibson, L., 2004. Influence of freezing rate on pore structure in freeze-dried collagen-GAG scaffolds. *Biomaterials* 25, 1077–1086.
- O'Brien, F.J., Harley, B.A., Yannas, I.V., Gibson, L.J., 2005. The effect of pore size on cell adhesion in collagen-GAG scaffolds. *Biomaterials* 26, 433–441.
- Okech, W., Kuo, C.K., 2016. Informing stem cell-based tendon tissue engineering approaches with embryonic tendon development. *Adv. Exp. Med. Biol.* 920, 63–77.
- Orr, S.B., Chainani, A., Hippensteel, K.J., Kishan, A., Gilchrist, C., Garrigues, N.W., Ruch, D.S., Guilak, F., Little, D., 2015. Aligned multilayered electrospun scaffolds for rotator cuff tendon tissue engineering. *Acta Biomater.* 24, 117–126.
- Oryan, A., Moshiri, A., Parizi, A.M., Maffulli, N., 2014. Implantation of a novel biologic and hybridized tissue engineered bioimplant in large tendon defect: an in vivo investigation. *Tissue Eng. A* 20, 447–465.
- Ouyang, H.W., Goh, J.C., Thambyah, A., Teoh, S.H., Lee, E.H., 2003. Knitted poly-lactide-co-glycolide scaffold loaded with bone marrow stromal cells in repair and regeneration of rabbit Achilles tendon. *Tissue Eng.* 9, 431–439.
- Pagan, A., Aznar-Cervantes, S.D., Perez-Rigueiro, J., Meseguer-Olmo, L., Cenis, J.L., 2019. Potential use of silkworm gut fiber braids as scaffolds for tendon and ligament tissue engineering. *J. Biomed. Mater. Res. B Appl. Biomater* 107, 2209–2215.
- Pan, X.S., Li, J., Brown, E.B., Kuo, C.K., 2018. Embryo movements regulate tendon mechanical property development. *Philos. Trans. R. Soc. Lond. B Biol. Sci.* 373.
- Park, S., Edwards, S., Hou, S., Boudreau, R., Yee, R., Jeong, K.J., 2019. A multi-interpenetrating network (IPN) hydrogel with gelatin and silk fibroin. *Biomater. Sci.* 7, 1276–1280.
- Park, Y.J., Lee, Y.M., Park, S.N., Sheen, S.Y., Chung, C.P., Lee, S.J., 2000. Platelet derived growth factor releasing chitosan sponge for periodontal bone regeneration. *Biomaterials* 21, 153–159.
- Patterson, J., Hubbell, J.A., 2010. Enhanced proteolytic degradation of molecularly engineered PEG hydrogels in response to MMP-1 and MMP-2. *Biomaterials* 31, 7836–7845.
- Pauly, H.M., Kelly, D.J., Papat, K.C., Trujillo, N.A., Dunne, N.J., McCarthy, H.O., Haut Donahue, T.L., 2016. Mechanical properties and cellular response of novel electrospun nanofibers for ligament tissue engineering: effects of orientation and geometry. *J. Mech. Behav. Biomed. Mater.* 61, 258–270.
- Peach, M.S., Ramos, D.M., James, R., Morozowich, N.L., Mazzocca, A.D., Doty, S.B., Allcock, H.R., Kumbar, S.G., Laurencin, C.T., 2017. Engineered stem cell niche matrices for rotator cuff tendon regenerative engineering. *PLoS One* 12, e0174789.
- Penn, D., Willet, T.L., Glazebrook, M., Snow, M., Stanish, W.D., 2009. Is there significant variation in the material properties of four different allografts implanted for ACL reconstruction. *Knee Surg. Sport. Traumatol. Arthrosc.* 17, 260–265.
- Pérez-Rigueiro, J., Viney, C., Llorca, J., Elices, M., 2000. Mechanical properties of single-brin silkworm silk. *J. Appl. Polym. Sci.* 75, 1270–1277.
- Pietschmann, M.F., Frankewycz, B., Schmitz, P., Docheva, D., Sievers, B., Jansson, V., Schieker, M., Muller, P.E., 2013. Comparison of tenocytes and mesenchymal stem cells seeded on biodegradable scaffolds in a full-size tendon defect model. *J. Mater. Sci. Mater. Med.* 24, 211–220.
- Pollak, A.W.-C., A., 2014. Injuries the Burden of Musculoskeletal Diseases in the United States. United States Bone and Joint Initiative, Rosemont, IL.
- Qiu, Y., Wang, X., Zhang, Y., Carr, A.J., Zhu, L., Xia, Z., Sabokbar, A., 2016. In vitro two-dimensional and three-dimensional tenocyte culture for tendon tissue engineering. *J. Tissue Eng. Regen-erat. Med.* 10, E216–E226.
- Ramos, D.M., Abdulmalik, S., Arul, M.R., Rudraiah, S., Laurencin, C.T., Mazzocca, A.D., Kumbar, S.G., 2019. Insulin immobilized PCL-cellulose acetate micro-nanostructured fibrous scaffolds for tendon tissue engineering. *Polym. Adv. Technol.* 30, 1205–1215.
- Raspanti, M., Guizzardi, S., 2002. Structural aspects of the extracellular matrix of the tendon: an atomic force and scanning electron microscopy study. *Arch. Histol. Cytol.* 65, 37–43.
- Rinoldi, C., Costantini, M., Kijenska-Gawronska, E., Testa, S., Fornetti, E., Heljak, M., Cwiklinska, M., Buda, R., Baldi, J., Cannata, S., Guzowski, J., Gargioli, C., Khademhosseini, A., Swieszkowski, W., 2019a. Tendon tissue engineering: effects of mechanical and biochemical stimulation on stem cell alignment on cell-Laden hydrogel yarns. *Adv. Healthc. Mater.* 8, e1801218.
- Rinoldi, C., Fallahi, A., Yazdi, I.K., Campos Paras, J., Kijenska-Gawronska, E., Trujillo-De Santiago, G., Tuoheti, A., Demarchi, D., Annabi, N., Khademhosseini, A., Swieszkowski, W., Tamayol, A., 2019b. Mechanical and biochemical stimulation of 3D multi-layered scaffolds for tendon tissue engineering. *ACS Biomaterials Science & Engineering.*
- Rothrauff, B.B., Coluccino, L., Gottardi, R., Ceseracciu, L., Scaglione, S., Goldoni, L., Tuan, R.S., 2018. Efficacy of thermoresponsive, photocrosslinkable hydrogels derived from decellularized tendon and cartilage extracellular matrix for cartilage tissue engineering. *J. Tissue Eng. Regen-erat. Med.* 12, e159–e170.
- Rothrauff, B.B., Lauro, B.B., Yang, G., Debski, R.E., Musahl, V., Tuan, R.S., 2017. Braided and stacked electrospun nanofibrous scaffolds for tendon and ligament tissue engineering. *Tissue Eng. A* 23, 378–389.
- Rowley, J.A., Madlambayan, G., Mooney, D.J., 1999. Alginate hydrogels as synthetic extracellular matrix materials. *Biomaterials* 20, 45–53.
- Sahoo, S., Ouyang, H., Goh, J.C., Tay, T.E., Toh, S.L., 2006. Characterization of a novel polymeric scaffold for potential application in tendon/ligament tissue engineering. *Tissue Eng.* 12, 91–99.
- Sahoo, S., Toh, S.L., Goh, J.C., 2010. A bFGF-releasing silk/PLGA-based biohybrid scaffold for ligament/tendon tissue engineering using mesenchymal progenitor cells. *Biomaterials* 31, 2990–2998.
- Sakiyama-Elbert, S.E., Hubbell, J.A., 2000. Development of fibrin derivatives for controlled release of heparin-binding growth factors. *J. Control. Release* 65, 389–402.
- Sandri, M., Filardo, G., Kon, E., Panseri, S., Montesi, M., Iafisco, M., Savini, E., Sprio, S., Cunha, C., Giavaresi, G., Veronesi, F., Fini, M., Salvatore, L., Sannino, A., Marcacci, M., Tampieri, A., 2016. Fabrication and pilot in vivo study of a collagen-BDDGE-elastin core-shell scaffold for tendon regeneration. *Front. Bioeng. Biotechnol.* 4, 52.

- Sato, M., Maeda, M., Kurosawa, H., Inoue, Y., Yamauchi, Y., Iwase, H., 2000. Reconstruction of rabbit Achilles tendon with three bioabsorbable materials: histological and biomechanical studies. *J. Orthop. Sci.* 5, 256–267.
- Schiele, N.R., Marturano, J.E., Kuo, C.K., 2013. Mechanical factors in embryonic tendon development: potential cues for stem cell tenogenesis. *Curr. Opin. Biotechnol.* 24, 834–840.
- Schiele, N.R., Von Flotow, F., Tochka, Z.L., Hockaday, L.A., Marturano, J.E., Thibodeau, J.J., Kuo, C.K., 2015. Actin cytoskeleton contributes to the elastic modulus of embryonic tendon during early development. *J. Orthop. Res.* 33, 874–881.
- Schoenenberger, A.D., Foolen, J., Moor, P., Silvan, U., Snedeker, J.G., 2018. Substrate fiber alignment mediates tendon cell response to inflammatory signaling. *Acta Biomater.* 71, 306–317.
- Schweitzer, R., Chyung, J.H., Murtaugh, L.C., Brent, A.E., Rosen, V., Olson, E.N., Lassar, A., Tabin, C.J., 2001. Analysis of the tendon cell fate using Scleraxis, a specific marker for tendons and ligaments. *Development* 128, 3855–3866.
- Sechriest, V.F., Miao, Y.J., Niyibizi, C., Westerhausen-Larson, A., Matthew, H.W., Evans, C.H., Fu, F.H., Suh, J.K., 2000. GAG-augmented polysaccharide hydrogel: a novel biocompatible and biodegradable material to support chondrogenesis. *J. Biomed. Mater. Res.* 49, 534–541.
- Sensini, A., Gualandi, C., Zucchelli, A., Boyle, L.A., Kao, A.P., Reilly, G.C., Tozzi, G., Cristofolini, L., Focarete, M.L., 2018. Tendon fascicle-inspired nanofibrous scaffold of polylactic acid/collagen with enhanced 3D-structure and biomechanical properties. *Sci. Rep.* 8, 17167.
- Seo, Y.K., Kim, J.H., Eo, S.R., 2016. Co-effect of silk and amniotic membrane for tendon repair. *J. Biomater. Sci. Polym. Ed.* 27, 1232–1247.
- Sharifi-Aghdam, M., Faridi-Majidi, R., Derakhshan, M.A., Chegeni, A., Azami, M., 2017. Preparation of collagen/polyurethane/knitted silk as a composite scaffold for tendon tissue engineering. *Proc. Inst. Mech. Eng. H* 231, 652–662.
- Shen, W., Chen, J., Yin, Z., Chen, X., Liu, H., Heng, B.C., Chen, W., Ouyang, H.W., 2012. Allogeneous tendon stem/progenitor cells in silk scaffold for functional shoulder repair. *Cell Transplant.* 21, 943–958.
- Shen, W., Chen, X., Chen, J., Yin, Z., Heng, B.C., Chen, W., Ouyang, H.W., 2010. The effect of incorporation of exogenous stromal cell-derived factor-1 alpha within a knitted silk-collagen sponge scaffold on tendon regeneration. *Biomaterials* 31, 7239–7249.
- Shepherd, J.H., Ghose, S., Kew, S.J., Moavenian, A., Best, S.M., Cameron, R.E., 2013. Effect of fiber crosslinking on collagen-fiber reinforced collagen-chondroitin-6-sulfate materials for regenerating load-bearing soft tissues. *J. Biomed. Mater. Res. A* 101, 176–184.
- Shukunami, C., Takimoto, A., Oro, M., Hiraki, Y., 2006. Scleraxis positively regulates the expression of tenomodulin, a differentiation marker of tenocytes. *Dev. Biol.* 298, 234–247.
- Silver, F.H., Freeman, J.W., Seehra, G.P., 2003. Collagen self-assembly and the development of tendon mechanical properties. *J. Biomech.* 36, 1529–1553.
- Stoll, C., John, T., Conrad, C., Lohan, A., Hondke, S., Ertel, W., Kaps, C., Endres, M., Sittlinger, M., Ringe, J., Schulze-Tanzil, G., 2011. Healing parameters in a rabbit partial tendon defect following tenocyte/biomaterial implantation. *Biomaterials* 32, 4806–4815.
- Sun, A., Prest, T.A., Fowler, J.R., Brick, R.M., Gloss, K.M., Li, X., Shen, H., Yang, G., Brown, B.N., Alexander, P.G., Tuan, R.S., 2019. Conduits harnessing spatially controlled cell-secreted neurotrophic factors improve peripheral nerve regeneration. *Biomaterials* 203, 86–95.
- Sun, J.Y., Zhao, X., Illeperuma, W.R., Chaudhuri, O., Oh, K.H., Mooney, D.J., Vlassak, J.J., Suo, Z., 2012. Highly stretchable and tough hydrogels. *Nature* 489, 133–136.
- Sundaram, M.N., Amirthalingam, S., Mony, U., Varma, P.K., Jayakumar, R., 2019. Injectable chitosan-nano bioglass composite hemostatic hydrogel for effective bleeding control. *Int. J. Biol. Macromol.* 129, 936–943.
- Sung, H.W., Huang, R.N., Huang, L.L., Tsai, C.C., 1999. In vitro evaluation of cytotoxicity of a naturally occurring cross-linking reagent for biological tissue fixation. *J. Biomater. Sci. Polym. Ed.* 10, 63–78.
- Szczesny, S.E., Driscoll, T.P., Tseng, H.Y., Liu, P.C., Heo, S.J., Mauck, R.L., Chao, P.G., 2017. Crimped nanofibrous biomaterials mimic microstructure and mechanics of native tissue and alter strain transfer to cells. *ACS Biomater. Sci. Eng.* 3, 2869–2876.
- Takezawa, T., Ozaki, K., Takabayashi, C., 2007. Reconstruction of a hard connective tissue utilizing a pressed silk sheet and type-I collagen as the scaffold for fibroblasts. *Tissue Eng.* 13, 1357–1366.
- Tan, A., Farhatnia, Y., Seifalian, A.M., 2013. Polyhedral oligomeric silsesquioxane poly(carbonate-urea) urethane (POSS-PCU): applications in nanotechnology and regenerative medicine. *Crit. Rev. Biomed. Eng.* 41, 495–513.
- Tang, L., Yang, Y., Li, Y., Yang, G., Luo, T., Xu, Y., Zhang, W., 2018. Knitted silk mesh-like scaffold incorporated with sponge-like regenerated silk fibroin/collagen I and seeded with mesenchymal stem cells for repairing Achilles tendon in rabbits. *Acta Bioeng. Biomech.* 20, 77–87.
- Teh, T.K., Toh, S.L., Goh, J.C., 2013. Aligned fibrous scaffolds for enhanced mechanoresponse and tenogenesis of mesenchymal stem cells. *Tissue Eng. A* 19, 1360–1372.
- Townsend, H., Jobe, F.W., Pink, M., Perry, J., 1991. Electromyographic analysis of the glenohumeral muscles during a baseball rehabilitation program. *Am. J. Sports Med.* 19, 264–272.
- Veis, A., Anesey, J., Cohen, J., 1961. The long range reorganization of gelatin to the collagen structure. *Arch. Biochem. Biophys.* 94, 20–31.
- Vining, K.H., Stafford, A., Mooney, D.J., 2019. Sequential modes of crosslinking tune viscoelasticity of cell-instructive hydrogels. *Biomaterials* 188, 187–197.
- Visser, J., Levett, P.A., Te Moller, N.C.R., Besems, J., Boere, K.W.M., Van Rijen, M.H.P., De Grauw, J.C., Dhert, W.J.A., Van Weeren, P.R., Malda, J., 2015. Crosslinkable hydrogels derived from cartilage, meniscus, and tendon tissue. *Tissue Eng. A* 21, 1195–1206.
- Vulic, K., Shoichet, M.S., 2014. Affinity-based drug delivery systems for tissue repair and regeneration. *Biomacromolecules* 15, 3867–3880.
- Wang, B., Liu, W., Zhang, Y.J., Jiang, Y.K., Zhang, W.J., Zhou, G.D., Cui, L., Cao, Y.L., 2008. Engineering of extensor tendon complex by an ex vivo approach. *Biomaterials* 29, 2954–2961.
- Wang, Y., Bao, J., Wu, X., Wu, Q., Li, Y., Zhou, Y., Li, L., Bu, H., 2016. Genipin crosslinking reduced the immunogenicity of xenogeneic decellularized porcine whole-liver matrices through regulation of immune cell proliferation and polarization. *Sci. Rep.* 6, 24779.
- Wang, Z., Lee, W.J., Koh, B.T.H., Hong, M., Wang, W., Lim, P.N., Feng, J., Park, L.S., Kim, M., Thian, E.S., 2018. Functional regeneration of tendons using scaffolds with physical anisotropy engineered via microarchitectural manipulation. *Sci. Adv.* 4.
- West, J.L., Hubbell, J.A., 1999. Polymeric biomaterials with degradation sites for proteases involved in cell migration. *Macromolecules* 32, 241–244.

- Woo, S.L., Abramowitch, S.D., Kilger, R., Liang, R., 2006. Biomechanics of knee ligaments: injury, healing, and repair. *J. Biomech.* 39, 1–20.
- Wu, S., Peng, H., Li, X., Streubel, P.N., Liu, Y., Duan, B., 2017a. Effect of scaffold morphology and cell co-culture on tenogenic differentiation of HADMSC on centrifugal melt electrospun poly (Llactic acid) fibrous meshes. *Biofabrication* 9:044106.
- Wu, S., Wang, Y., Streubel, P.N., Duan, B., 2017b. Living nanofiber yarn-based woven biotextiles for tendon tissue engineering using cell tri-culture and mechanical stimulation. *Acta Biomater.* 62, 102–115.
- Wu, Y., Wang, Z., Fuh, J.Y., Wong, Y.S., Wang, W., Thian, E.S., 2016. Mechanically-enhanced three-dimensional scaffold with anisotropic morphology for tendon regeneration. *J. Mater. Sci. Mater. Med.* 27, 115.
- Wu, Y., Wang, Z.Y., Fuh, J.Y.H., Wong, Y.S., Wang, W., Thian, E.S., 2017c. Direct E-jet printing of three-dimensional fibrous scaffold for tendon tissue engineering. *J. Biomed. Mater. Res. B Appl. Biomater.* 105, 616–627.
- Xie, S., Zhou, Y., Tang, Y., Chen, C., Li, S., Zhao, C., Hu, J., Lu, H., 2019. -Book-shaped decellularized tendon matrix scaffold combined with bone marrow mesenchymal stem cells-sheets for repair of achilles tendon defect in rabbit. *J. Orthop. Res.* 37, 887–897.
- Xu, Y., Dong, S., Zhou, Q., Mo, X., Song, L., Hou, T., Wu, J., Li, S., Li, Y., Li, P., Gan, Y., Xu, J., 2014. The effect of mechanical stimulation on the maturation of TDSCs-poly(L-lactide-co-ε-caprolactone)/collagen scaffold constructs for tendon tissue engineering. *Biomaterials* 35, 2760–2772.
- Yamada, H., Nakao, H., Takasu, Y., Tsubouchi, K., 2001. Preparation of undegraded native molecular fibroin solution from silkworm cocoons. *Mater. Sci. Eng. C* 14, 41–46.
- Yang, C., Deng, G., Chen, W., Ye, X., Mo, X., 2014. A novel electrospun-aligned nanoyarn-reinforced nanofibrous scaffold for tendon tissue engineering. *Colloids Surfaces B Biointerfaces* 122, 270–276.
- Yang, G., Lin, H., Rothrauff, B.B., Yu, S., Tuan, R.S., 2016. Multilayered polycaprolactone/gelatin fiber-hydrogel composite for tendon tissue engineering. *Acta Biomater.* 35, 68–76.
- Yang, G., Rothrauff, B.B., Lin, H., Gottardi, R., Alexander, P.G., Tuan, R.S., 2013a. Enhancement of tenogenic differentiation of human adipose stem cells by tendon-derived extracellular matrix. *Biomaterials* 34, 9295–9306.
- Yang, G., Rothrauff, B.B., Tuan, R.S., 2013b. Tendon and ligament regeneration and repair: clinical relevance and developmental paradigm. *Birth Defects Res. C Embryo Today* 99, 203–222.
- Yang, G., Rothrauff, B.B., Lin, H., Yu, S., Tuan, R.S., 2017. Tendon-derived extracellular matrix enhances transforming growth factor-β3-induced tenogenic differentiation of human adipose-derived stem cells. *Tissue Eng.* 23, 166–176.
- Yang, P.J., Levenston, M.E., Temenoff, J.S., 2012. Modulation of mesenchymal stem cell shape in enzyme-sensitive hydrogels is decoupled from upregulation of fibroblast markers under cyclic tension. *Tissue Eng. A* 18, 2365–2375.
- Yang, S., Shi, X., Li, X., Wang, J., Wang, Y., Luo, Y., 2019. Oriented collagen fiber membranes formed through counter-rotating extrusion and their application in tendon regeneration. *Biomaterials* 207, 61–75.
- Yin, Z., Chen, X., Zhu, T., Hu, J.J., Song, H.X., Shen, W.L., Jiang, L.Y., Heng, B.C., Ji, J.F., Ouyang, H.W., 2013. The effect of decellularized matrices on human tendon stem/progenitor cell differentiation and tendon repair. *Acta Biomater.* 9, 9317–9329.
- Younesi, M., Islam, A., Kishore, V., Anderson, J.M., Akkus, O., 2014. Tenogenic induction of human MSCs by anisotropically aligned collagen biotextiles. *Adv. Funct. Mater.* 24, 5762–5770.
- Young, R.G., Butler, D.L., Weber, W., Caplan, A.I., Gordon, S.L., Fink, D.J., 1998. Use of mesenchymal stem cells in a collagen matrix for Achilles tendon repair. *J. Orthop. Res.* 16, 406–413.
- Zeeman, R., Dijkstra, P.J., Van Wachem, P.B., Van Luyn, M.J., Hendriks, M., Cahalan, P.T., Feijen, J., 1999. Crosslinking and modification of dermal sheep collagen using 1, 4-butanediol diglycidyl ether. *J. Biomed. Mater. Res.* 46, 424–433.
- Zeugolis, D.I., Khew, S.T., Yew, E.S., Ekaputra, A.K., Tong, Y.W., Yung, L.Y., Huttmacher, D.W., Sheppard, C., Raghunath, M., 2008. Electro-spinning of pure collagen nano-fibres – just an expensive way to make gelatin? *Biomaterials* 29, 2293–2305.
- Zeugolis, D.I., Paul, R.G., Attenburrow, G., 2010. The influence of a natural cross-linking agent (*Myrica rubra*) on the properties of extruded collagen fibres for tissue engineering applications. *Mater. Sci. Eng. C-Mater. Biol. Appl.* 30, 190–195.
- Zhang, C., Yuan, H., Liu, H., Chen, X., Lu, P., Zhu, T., Yang, L., Yin, Z., Heng, B.C., Zhang, Y., Ouyang, H., 2015. Well-aligned chitosan-based ultrafine fibers committed teno-lineage differentiation of human induced pluripotent stem cells for Achilles tendon regeneration. *Biomaterials* 53, 716–730.
- Zhang, H., Liu, M.F., Liu, R.C., Shen, W.L., Yin, Z., Chen, X., 2018. Physical microenvironment-based inducible scaffold for stem cell differentiation and tendon regeneration. *Tissue Eng. B Rev.* 24, 443–453.
- Zheng, M.H., Chen, J., Kirilak, Y., Willers, C., Xu, J., Wood, D., 2005. Porcine small intestine submucosa (SIS) is not an acellular collagenous matrix and contains porcine DNA: possible implications in human implantation. *J. Biomed. Mater. Res. B Appl. Biomater.* 73, 61–67.
- Zheng, Z., Ran, J., Chen, W., Hu, Y., Zhu, T., Chen, X., Yin, Z., Heng, B.C., Feng, G., Le, H., Tang, C., Huang, J., Chen, Y., Zhou, Y., Dominique, P., Shen, W., Ouyang, H.W., 2017. Alignment of collagen fiber in knitted silk scaffold for functional massive rotator cuff repair. *Acta Biomater.* 51, 317–329.
- Zhou, C.Z., Confalonieri, F., Medina, N., Zivanovic, Y., Esnault, C., Yang, T., Jacquet, M., Janin, J., Duguet, M., Perasso, R., Li, Z.G., 2000. Fine organization of *Bombyx mori* fibroin heavy chain gene. *Nucleic Acids Res.* 28, 2413–2419.

2.6.6

Bone Tissue Engineering

JUSTIN L. BROWN, CATO T. LAURENCIN

Department of Biomedical Engineering, The Pennsylvania State University, University Park, PA, United States

Introduction

The use of biocompatible polymeric materials for orthopedic applications, such as bone graft substitutes, has been under investigation since the 1940s (Blaine, 1946; Leveen and Barberio, 1949). By the 1970s the importance of attaining appropriate mechanical properties, an interconnected porosity, and a microstructure that promotes tissue ingrowth was realized (Hench et al., 1971). Research has highlighted the necessity for a subcellular dimension, or nanostructure, in synthetic bone grafts to promote the appropriate organization of bone cells in an effort to generate or regenerate bone tissue (Long et al., 2019; Ozdemir et al., 2019). This chapter begins with an overview of the biology of bone to provide a framework for what the application of biomaterials strives to recreate. The chapter then proceeds through a discussion of bone tissue engineering beginning with the natural bone grafts, moving through bone graft substitutes, and finishing with a discussion of bioreactors used in bone tissue engineering.

Bone Biology

Bones are vascularized and innervated organs that are composed of bone tissue, bone marrow, and a surrounding connective tissue called periosteum. Bones serve a number of functions such as support for muscles, protection of internal organs, production of blood, calcium homeostasis, acid/base buffering and transmission of sound (Bilezikian et al., 2008). Bone tissue is the rigid calcified portion of the bone organ and is critical for many of the functions.

Types of Bone Tissue

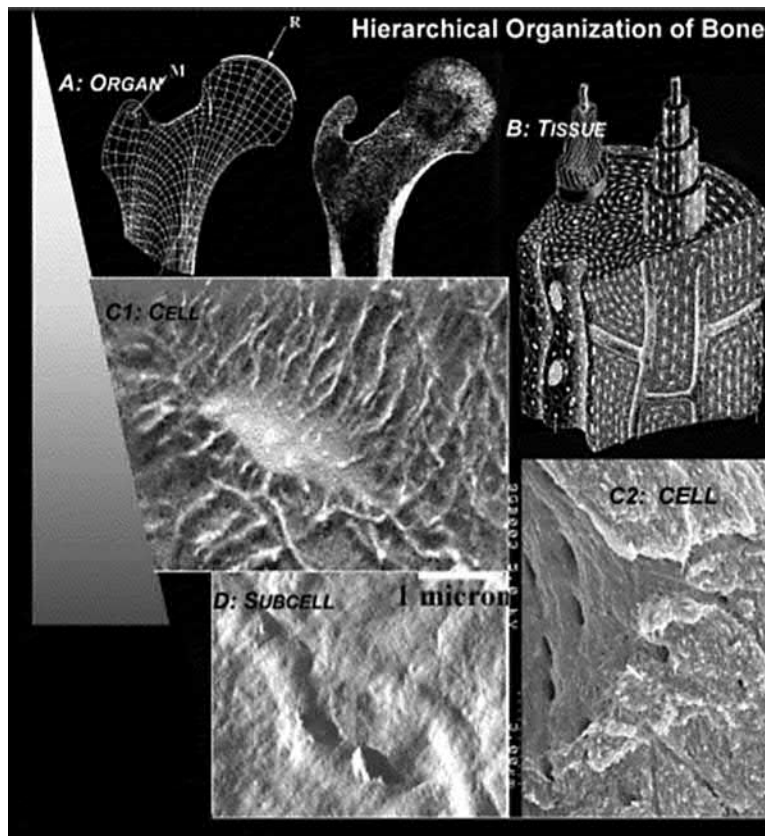
Bone tissue is classified as either cortical bone or trabecular bone. Cortical bone is dense and highly mineralized bone tissue that is found on the peripheral regions of bone. Cortical bone is 80%–90% mineralized and constitutes 80% by mass of the bone tissue in the body. The high density of cortical bone makes it well suited for the mechanical and

structural properties of bone. The thickness and density of cortical bone is loosely correlated to mechanical loading; however, many other variables are involved as well. Trabecular bone is found on the interior of bones adjacent to the marrow cavity. It is approximately 80% porous and exhibits less than 10% of the compressive strength and less than 5% of the compressive modulus of cortical bone. However, trabecular bone exhibits higher surface area than cortical bone and is considered more important for bone functions such as calcium homeostasis and acid/base regulation. Fig. 2.6.6.1 illustrates the hierarchical organization of bone, moving from the tissue level down to the subcellular level (Bilezikian et al., 2008; Pearson and Lieberman, 2004).

Cells Involved

Osteoblasts

There are several distinct cell types involved in the formation and remodeling of bone tissue. These cells are osteoblasts, bone lining cells, osteocytes, and osteoclasts. Osteoblasts are the workhorses of bone formation. Osteoblasts are fully differentiated cells derived from mesenchymal stem cells through a preosteoblast intermediate. The transition from mesenchymal stem cells to osteoblasts occurs through biochemical and cell:extracellular matrix (ECM) signaling. Osteoblasts are found at the surface of developing bone tissue and exhibit a cuboidal morphology. They actively secrete an unmineralized osteoid matrix at the location of newly forming bone. This osteoid matrix is the organic portion of bone ECM and is composed of primarily collagen type I, which makes up approximately 90% of the matrix. The remaining portion of the osteoid matrix is composed of proteoglycans and noncollagenous proteins such as osteopontin, osteocalcin, and osteonectin. The active production of the osteoid matrix as well as the presence of the membrane protein alkaline phosphatase distinguishes the osteoblast phenotype. The osteoid matrix around the osteoblast begins to calcify and approximately 20% of the buried osteoblasts



• **Figure 2.6.6.1** Hierarchical organization of bone. This figure provides a view of the organization of bone beginning with organ level (A) and moving to a depiction of the tissue level (B), which illustrates the network of osteocytes organized radially around Haversian canals. An individual osteocyte with the mineralized matrix removed is depicted in (C1) and clearly illustrates multiple processes extending away from the cell body; on the contrary, (C2) depicts the mineralized matrix without the cell and illustrates on the left-hand side the interior of the lacuna where the osteocyte cell body would reside and shows canals called canaliculi where the processes extending away from the osteocyte cell body ultimately connect with other osteocyte processes. Finally, (D) depicts the interior of canaliculi and shows the presence of striations created by collagen fibers that formed the initial framework for the mineralized matrix (Knothe Tate, 2003).

transition to osteocytes. The osteoblasts that do not transition to osteocytes undergo apoptosis (Franz-Odenaal et al., 2006).

Bone Lining Cells

Bone lining cells are found lining the surface of bone. Unlike osteoblasts on the bone surface, bone lining cells have a long, slender, and flat morphology. Bone lining cells were initially thought to be preosteoblasts; however, this is no longer thought to be the case. Instead, the current opinion is that osteoblasts that do not undergo apoptosis or differentiate to osteocytes become bone lining cells. Two of the key phenotypic differences between bone lining cells and osteoblasts are that bone lining cells express intercellular adhesion molecule 1 and they do not express osteocalcin (Everts et al., 2002). Research has shown that bone lining cells anchor hematopoietic stem cells and provide these stem cells with appropriate signals to keep them in an undifferentiated state (Kollet et al., 2006). The bone lining cells then play a crucial role in the transitions involved with bone remodeling by

communicating through gap junctions with osteocytes deep in the bone matrix and promoting differentiation of hematopoietic stem cells into osteoclasts. Additionally, the bone lining cells are responsible for preparing the surface of the bone by removing nonmineralized collagen fibrils through the use of matrix metalloproteinases. After remodeling, the bone lining cells deposit a smooth layer of collagen over the bone surface (Kollet et al., 2006).

Osteocytes

Osteocytes are terminally differentiated cells derived from mature osteoblasts that have become encased within a calcified matrix. In the transformation from an osteoblast to an osteocyte, the expression of many of the proteins that constitute an osteoblast phenotype such as type I collagen, alkaline phosphatase, osteocalcin, and bone sialoprotein are no longer produced. Additionally, osteocytes create a network among themselves by extending many long processes to adjacent osteocytes. This network, the lacunar–canalicular network, is used for nutrient and waste transfer

as well as communication between the osteocytes via gap junctions.

The osteocyte cell body resides in the lacuna and the osteocyte's processes extend out through the canaliculi to adjacent osteocytes and Haversian canals. The Haversian canals supply vasculature to provide and remove nutrients. The concentric arrangement of the lacunar–canalicular network of osteocytes around a Haversian canal is referred to as the osteon. The organization of the osteocytes within bone is illustrated by Fig. 2.6.6.1. Additionally, osteocytes have been implicated as the primary mechanosensors in bone. The mechanotransduction that occurs in osteocytes is believed to be initiated by fluid flux within the canaliculi created by pressure gradients between lacunae when the bone is loaded. The mechanotransduction in osteocytes contributes to the recruitment of osteoblasts or osteoclasts depending on the loading condition (Franz-Odenaal et al., 2006; Goulet et al., 2008).

Osteoclasts

Osteoclasts, unlike the cells discussed thus far, are multinucleated cells derived from hematopoietic stem cells as opposed to mesenchymal stem cells. It has been established that hematopoietic stem cells anchored to bone lining cells are induced to differentiate into osteoclasts in response to osteocyte–bone lining cell signaling. The role of osteoclasts in bone metabolism is the resorption of bone. Initially, the osteoclast dissolves the mineralized portion of the bone matrix by secreting hydrochloric acid. After the mineral content is removed, the protein portion of the matrix is degraded by proteolytic enzymes. The resulting matrix fragments and ions created from matrix dissolution are transported through the osteoclast in vesicles that are emptied into the extracellular space on the basolateral side of the osteoclast (Kollet et al., 2006; Matsuo and Irie, 2008).

Bone Tissue Development

Calcified bone tissue is formed by two distinct modes of ossification, or calcification. These methods of ossification are classified as either intramembranous ossification or endochondral ossification. The method of ossification depends on the type of bone being formed. Intramembranous ossification is involved in the formation of flat and irregularly shaped bones, such as the cranial bones. Endochondral ossification is involved in the formation of long bones, bones that are longer than they are wide, such as the femur, humerus, and metacarpal (Bilezikian et al., 2008).

Intramembranous Ossification

Intramembranous ossification begins without a preexisting cartilage model. Instead, mesenchymal stem cells form clusters. The mesenchymal stem cells then differentiate to osteoblasts and the newly formed osteoblasts start to secrete an osteoid matrix. The osteoid matrix is calcified to form bone

spicules. Osteoblasts trapped within the bone spicules either differentiate to osteocytes or undergo apoptosis. The bone spicules radiate outward from where the mesenchymal cluster originally formed. Eventually, spicules initiated by separate mesenchymal stem cell clusters join together to create a layer of calcified bone. Mesenchymal stem cells apical to the calcifying tissue differentiate to form the periosteum, whereas those basal to the calcifying tissue differentiate to osteoblasts, which form subsequent layers of calcified tissue. The resulting bone tissue is classified as woven bone. Woven bone is formed quickly and characterized by randomly oriented collagen fibrils; however, it is not as mechanically viable as lamellar bone. Woven bone will be remodeled over time through resorption and deposition by osteoclasts and osteoblasts to form lamellar bone (Bilezikian et al., 2008; Franz-Odenaal et al., 2006).

Endochondral Ossification

Endochondral ossification occurs in several steps, beginning with a preexisting cartilage template. The cartilage template begins calcification. As the cartilage template calcifies, the chondrocytes in the cartilage become hypertrophic and undergo apoptosis. Then, mesenchymal stem cells in the membrane surrounding the calcifying cartilage, periosteum, differentiate to osteoblasts. These osteoblasts lay down an osteoid matrix around the exterior of the cartilage template. At the same time a bud of cells originating from the periosteum invades the interior of the partially calcified cartilage template. This periosteal bud leads to vascularization and innervation of the developing bone. Additionally, the periosteal bud supplies mesenchymal and hematopoietic stem cells into the center of the cartilage template. The mesenchymal stem cells differentiate to osteoblasts and the hematopoietic stem cells differentiate to osteoclasts. These osteoblasts and osteoclasts remodel the partially calcified cartilage into woven bone, which ultimately becomes lamellar bone. Lamellar bone contains collagen fibrils that are arranged in parallel areas and exhibits greater strength as compared to woven bone (Bilezikian et al., 2008; Shapiro, 2008).

Bone Tissue Engineering

Strategies for bone tissue engineering often focus on the combination of the three key elements in tissue engineering: biomaterials, stem cells, and/or soluble factors. For example, a common tissue-engineering strategy involves fabricating biomaterials into porous scaffolds to facilitate cell growth and the eventual repair, restoration, or regeneration of the tissue (Langer and Vacanti, 1993). These biomaterial scaffolds can be used without any further modification *in vivo*. The next iteration in the application of biomaterial-focused tissue-engineering strategies involves culturing the biomaterial scaffold seeded with cells *in vitro*. The ultimate strategy for the *in vitro* use of a biomaterial scaffold involves seeding the scaffold and culturing *in vitro* to develop a replacement tissue that upon implantation functions exactly as the original host tissue.

Applying this tissue-engineering strategy, a paradigm for a successful bone graft emerges. This paradigm is that the graft or construct should be osteoconductive, osteoinductive, osteogenic, resorbable, or degradable and possess mechanical properties near to that of the implant site. Osteoconduction refers to the ability of a scaffold or implant to promote attachment of osteoblastic cells on the surface and throughout the interior of the scaffold or implant. In an *in vitro* setting, osteoconduction is exhibited by an ability to promote the attachment, migration, and proliferation of osteoblasts. Osteoinduction refers to the ability of a scaffold or implant to promote the differentiation of mesenchymal stem cells down an osteoblastic lineage ultimately leading to the formation of mineralized tissue. Osteoinduction can also be viewed as an ability to promote phenotype progression of an osteoblast from an early osteoblast to a mature osteoblast followed by differentiation to an osteocyte.

Osteogenicity refers to the ability of a scaffold or implant to promote *de novo* bone formation, which would occur in the absence of host cell invasion. For a scaffold to be osteogenic, cells would need to be seeded on the scaffold prior to implantation. The necessity of a bone tissue-engineering construct to be degradable arises from the fact that bone is constantly remodeling. A nonresorbable or nondegradable implant would impede the natural remodeling process of bone and extend the time it takes for the organ to return to natural function. Finally, the graft, scaffold, or implant should have mechanical properties that match that of the native bone tissue. The range for the mechanical properties depends on whether the bone tissue is cortical or trabecular. For trabecular bone the compressive strength varies from 4 to 12 MPa and the compressive modulus varies from 100 to 500 MPa. Cortical bone exhibits a compressive strength from 130 to 180 MPa and a compressive modulus from 12 to 18 GPa.

A problem with mechanical properties that exceed these ranges is stress shielding. Stress shielding results when the load on the bone is redistributed with the scaffold or implant being the load-bearing region and the surrounding bone being unloaded. The result of stress shielding is osteopenia of the bone surrounding the implant. To solve the bone tissue-engineering paradigm, there are presently a range of bone grafts and bone graft substitutes that fulfill all or some of the bone tissue-engineering paradigm (Kneser *et al.*, 2006; Hutmacher, 2000).

Bone Grafts

Autograft

Bone grafts are pieces of bone that are harvested from the patient, a donor, or a cadaver and placed at the desired site of bone repair, regeneration, or restoration as needed. The long-standing, and considered “gold standard,” bone graft solution to the bone tissue-engineering paradigm is an autograft. Autografts are sections or fragments of bone removed from one site on the patient, typically the iliac crest, and implanted to another site based on need. Since autografts

originate with the patient they are readily incorporated at the implant site and rarely elicit any immune responses, which allows autografts to have excellent wound-healing properties. Autografts fulfill all four elements of the bone tissue-engineering paradigm, primarily because they consist of native bone tissue moved from one region of a patient’s body to another region. However, autografts have a few drawbacks: there is often donor site morbidity indicated by necrosis and infection at the location of autograft harvest that may cause the patient more pain from the harvest site than the implant site. Additionally, autografts are limited in availability to the amount of tissue that can be harvested from the donor site. The problem of autograft bone tissue availability increases in cases where the need is the highest: those that involve osteoporotic, pediatric, or patients afflicted with bone cancer. It is these shortcomings plaguing the autograft that have increased the effort to find other bone graft substitutes (Greenwald *et al.*, 2001).

Allograft

The next bone graft solution to the bone tissue-engineering paradigm is the allograft. Allografts are bone fragments obtained from donors or cadavers that are typically first frozen, irradiated, and/or lyophilized. These steps are implemented to reduce the likelihood of disease transmission. Allografts are readily available in an array of shapes and sizes. Since allografts originate from a donor or cadaver there is no additional surgical site on the patient, which removes complications such as donor site morbidity. However, the sterilization procedures performed on allograft bone tissue are not without consequence. In comparison to autografts, allografts are less osteoconductive, less osteoinductive, and are not osteogenic. Additionally, allografts that have been lyophilized exhibit much less mechanical integrity when compared to autografts. Due to allografts being nonnative tissue, they have been shown to occasionally produce an immune response, which requires allograft recipients to be placed on immunosuppressant drugs to prevent rejection of the allograft tissue. The complications that arise from autografts and allografts have fueled the search for bone graft substitutes (Greenwald *et al.*, 2001).

Bone Graft Substitutes

Bone graft substitutes can offer solutions to the bone tissue-engineering paradigm and are based on the tissue-engineering concepts that arise from the definition of tissue engineering. These tissue-engineering principles lead to bone graft substitutes that can be classified as those based on biomaterials, cells, factors, or any combination of these.

Allograft-Based Substitutes

Biomaterial-based bone graft substitutes can be further subdivided into allografts, natural polymers, synthetic polymers, and ceramics. Allograft-based bone graft substitutes

are allograft bone tissue that has been thoroughly sterilized, decellularized, and demineralized. The methods by which manufacturers sterilize, decellularize, and demineralize the bone graft substitutes are carefully controlled to create a product that retains the collagen, noncollagenous proteins, and some of the growth factors present in the original bone tissue. The result is a demineralized bone matrix (DBM), which has been used in a variety of commercially available bone graft substitutes either as is or mixed with glycerol, hyaluronic acid, or calcium phosphates to improve the handling and performance characteristics of the product. Current efforts with allografts have produced technologies capable of processing DBM with computer-aided design and additive manufacturing leading to custom-shaped grafts (Grayson et al., 2010). There is evidence that supports improved osteoinduction with demineralization due to exposure of soluble factors that would be occluded in mineralized bone; however, DBM-based bone graft substitutes have limited osteoconductivity, no osteogenicity, and mechanical properties that are less than the desirable range (Peterson et al., 2004; Schwartz et al., 2007).

Natural Polymer-Based Substitutes

Natural polymers are gaining interest among the research community for bone tissue-engineering applications and additionally there are commercial bone graft substitutes derived from natural polymers available. The most prevalent natural polymer for bone graft substitutes is collagen. One example of a commercial collagen product is PlatFORM CM from Zimmer Biomet. PlatFORM CM is a collagen microfiber matrix that has been coated with β -tricalcium phosphate. The typical use of collagen graft substitutes involves coating it with bone marrow aspirate prior to implantation. By supplying the matrix with bone marrow aspirate there are progenitor cells present on the matrix, which makes it osteogenic in addition to being osteoconductive (Neen et al., 2006). In addition to collagen, fibrin and chitosan are two other natural polymers that are being investigated for bone tissue-engineering applications. The structures created by these polymers are typically fibers or foams. These structures provide excellent osteoconduction; however, osteoinduction, osteogenicity and mechanical properties are less than that provided by autograft tissue (Khan et al., 2008; Wahl and Czernuszka, 2006).

Synthetic Polymer-Based Substitutes

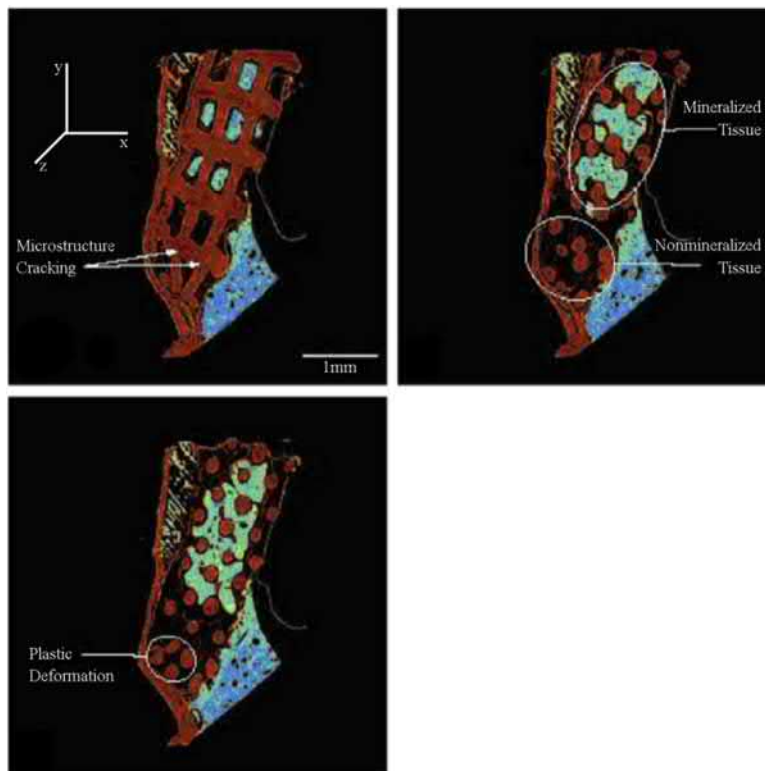
Synthetic polymer solutions for bone tissue-engineering applications are varied and abundant in current research. The use of synthetic polymers provides control over the surface chemistry, degradation kinetics, and geometry in much finer detail than can be accomplished with natural polymers. Clinically, a limited number of synthetic polymers are Food and Drug Administration (FDA) approved for use in nonlife-threatening applications, such as bone graft substitutes. These include the poly(α -hydroxy esters):

poly(lactide), poly(glycolide), poly(lactide-*co*-glycolide), and poly(caprolactone). Fig. 2.6.6.2 illustrates a lattice structure made of poly(caprolactone) rods that has been implanted into a pig and imaged 3 months postimplantation with microcomputed tomography to demonstrate where new bone formation is occurring, which is not adjacent to existing bone tissue (Jones et al., 2004).

The mechanical properties of the construct are not documented and the cracking and plastic deformation visible after 3 months indicates the material may not be mechanically viable. The first porous bone tissue-engineering constructs fabricated from poly(α -hydroxy esters) were foams created by various porogen leaching techniques. The porogen in these foams is typically a substance that readily dissolves in water such as gelatin, salt, or sugar (Mooney et al., 1996). These scaffolds are created by dissolution of the poly(α -hydroxy esters) in an organic solvent. The dissolved polymer is then mixed with the porogen and cast. After the solvent has evaporated the construct is immersed in water to remove the porogen. This technique can produce scaffolds that are highly porous.

The primary issue with porogen leaching is the increase in porosity, which is directly correlated with a decrease in mechanical integrity. Additionally, at low porosities, which are more robust mechanically, the polymer surrounds each individual porogen resulting in poor interconnectivity among the pores (Mooney et al., 1996; Rezwan et al., 2006). The sintered microsphere scaffold fabricated from poly(α -hydroxy esters) succeeded the scaffolds created with porogen leaching and also addressed several of the problems with scaffolds created by porogen leaching. The maximum porosity achievable by the sintered microsphere scaffold is only around 45% based on random packing of spheres; however, the interconnectivity of the porosity is 100%, which was a dramatic improvement over the scaffolds fabricated with porogen leaching (Borden et al., 2002). More recently, microscale scaffolds have been fabricated with a very specific architecture from poly(α -hydroxy esters) by using solid freeform fabrication techniques. Solid freeform fabrication uses computer-aided design to build structures layer by layer through techniques such as stereolithography, selective laser sintering, and 3D printing (Hutmacher et al., 2004).

All of the scaffolds created with the foregoing microscale technologies provide similar performance. The mechanical integrity of the scaffolds can be fabricated into a range that suits bone tissue applications; the scaffolds degrade in a controllable manner based on the selection of the poly(α -hydroxy esters) and they are all osteoconductive. However, for the preparation of microscale structures, each of the techniques is limited to a resolution an order of magnitude larger than a cell, and the resulting materials are not osteoinductive nor are they osteogenic without supplementing the structure with growth factors or osteoblastic cells. The research community has moved to examine scaffolds composed of poly(α -hydroxy esters) that exhibit a subcellular dimension. These scaffolds are almost invariably fiber based

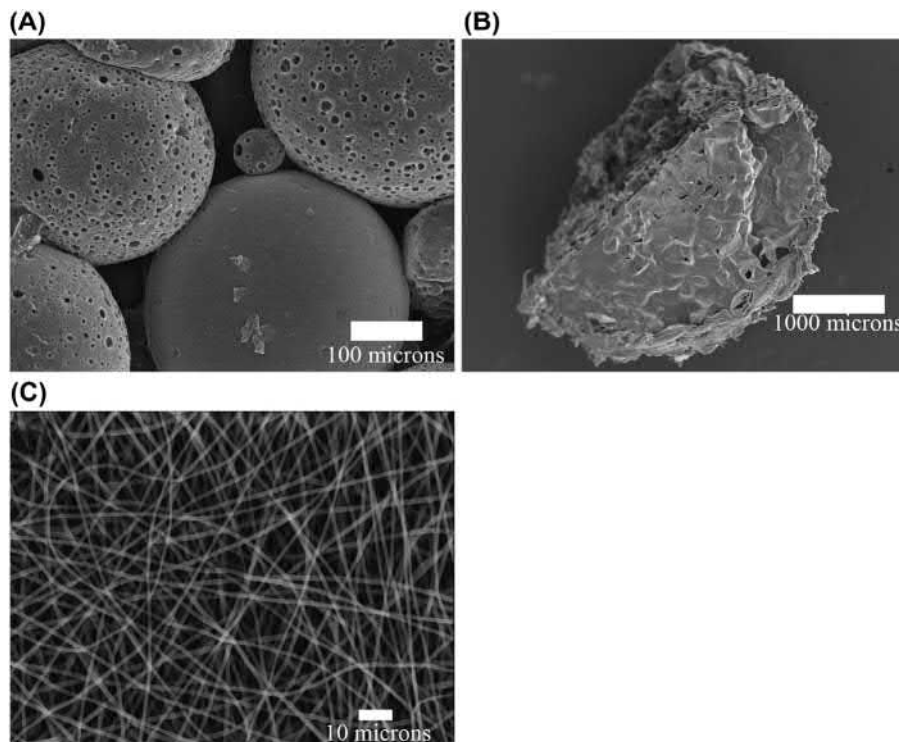


• **Figure 2.6.6.2** Representation obtained of a synthetic bone graft after 3 months in vivo using micro-computed tomography. The synthetic bone graft is a simple polycaprolactone (PCL) scaffold (red), with nonmineralized tissue (black), and mineralized tissue (blue green). The native bone is visible in the lower right corner of each image. The three images are different sections separated by $280\ \mu\text{m}$. The PCL scaffold was made by a rapid prototyping process and consists of a simple 3D lattice of connected rods. Also visible in the series of images are two defects caused by either degradation of the PCL, which the authors note that after 3 months has caused the diameters of the rods to shrink from 500 to $300\ \mu\text{m}$, or caused by excessive loading on the scaffold, compromising the material prior to degradation (Jones et al., 2004).

and are made either with electrospinning, phase separation for crystalline polymers, or precipitation in a nonsolvent of a continuous fiber stream from a polymer solution. The diameter of these fiber scaffolds can vary from $50\ \text{nm}$ to several micrometers (Smith and Ma, 2004). The subcellular dimension provided by nano- and microfibers has illustrated improved osteoconductivity as compared to the supercellular dimension of the microstructures covered previously. Additionally, there is some evidence that nanofibers may promote osteoinduction; however, the gains that nano- and microfibers make with osteoconduction and osteoinduction are compromised by the mechanical properties under compression of the nano- and microfiber structures (Ozdemir et al., 2019; Kjelstrup-Hansen et al., 2006).

The next degree of control being explored for bone tissue-engineering constructs involves moving away from the FDA-approved poly(α -hydroxy esters) and onto other biodegradable polymers that provide better degradation by-products, or improving the osteoconductivity of polymers through the incorporation of integrin-binding peptides, such as RGD, within the synthetic polymer structure. A noted drawback of poly(α -hydroxy esters) is that they degrade into carboxylic acids, which can be inflammatory (Bostman and Pihlajamaki, 1998). An additional drawback to the usage of poly(α -hydroxy

esters) is that they undergo bulk degradation, which results in the sudden failure of the scaffold. Similar to the poly(α -hydroxy esters), poly(propylene fumarate) is a polyester that can be used to fabricate similar scaffolds to the poly(α -hydroxy esters) and also shares the same problems with bulk degradation and acidic degradation products. Poly[(amino acid ester)phosphazenes] address the negative degradation products found with poly(α -hydroxy esters) and have recently been investigated for bone tissue-engineering applications. Poly[(amino acid ester)phosphazenes] degrade into amino acids, which are easier for the body to metabolize, and a buffer solution consisting of ammonia and phosphate, which prevents any change in the pH potentially brought about by the increase in the concentration of amino acids. Poly[(amino acid ester)phosphazenes] have also exhibited the more favorable surface erosion degradation mechanism (Allcock et al., 1994). Additionally, poly[(amino acid ester)phosphazenes] are suitable for many of the fabrication procedures discussed previously such as sintered microsphere scaffolds, porogen leaching scaffolds, and electrospun nanofibers (Brown et al., 2010; Kumbar et al., 2006). The scaffolds fabricated from poly[(amino acid ester)phosphazenes] have exhibited osteoconduction, but studies investigating the osteoinductivity and mechanical properties have yet to be reported. Fig. 2.6.6.3



• **Figure 2.6.6.3** Scanning electron micrographs of three scaffold architectures fabricated from poly[(amino acid ester)phosphazenes]. (A) Sintered microsphere scaffold composed of poly[bis(ethyl alaninato)phosphazene]. (B) Scaffold made from leaching salt from poly[(ethyl alaninato-co-methylphenoxy)phosphazene]. (C) Nanofibers created by electrospinning poly[bis(methylphenoxy)phosphazene] (Nair et al., 2004). Images (A) and (B) are previously unpublished.

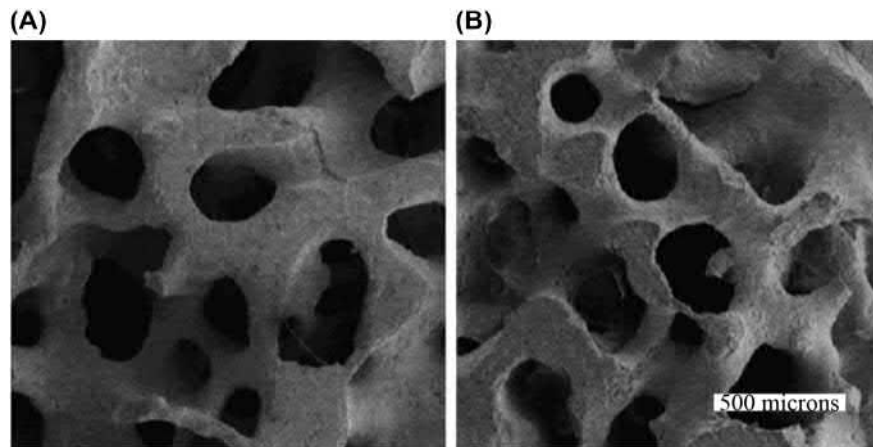
provides representative images of sintered microsphere scaffolds, porogen leaching scaffolds, and electrospun nanofiber scaffolds created with degradable polyphosphazenes. Finally, polyanhydrides are polymers that may surface erode similar to polyphosphazenes; however, little research has been performed investigating porous polyanhydride scaffolds for bone tissue engineering (Muggli et al., 1999).

Ceramic-Based Substitutes

Ceramic-based biomaterials are prevalent and widespread as bone graft substitutes. These ceramic biomaterial bone graft substitutes are made primarily from calcium phosphates, calcium sulfate, and Bioglass, which is a glass formulation containing a lower amount of silicon dioxide and higher amounts of sodium oxide and calcium oxide as compared to conventional glass. This specific glass formulation is bioactive and undergoes dissolution in the body. Calcium phosphate bone graft substitutes are usually either tricalcium phosphate or hydroxyapatite, which is the primary mineral in bone. One example of a commercially available hydroxyapatite-based bone graft substitute is Pro-Osteon from Zimmer Biomet. The Pro-Osteon bone graft substitute begins as natural coral, which is primarily calcium carbonate. The coral is then treated with a hydrothermal process in the presence of ammonium phosphate to convert the calcium carbonate structure to hydroxyapatite

(Ben-Nissan, 2003). The resulting structure exhibits a pore structure similar to trabecular bone. Fig. 2.6.6.4 is a depiction of the resulting coralline hydroxyapatite resulting from the foregoing hydrothermal process. All of the hydroxyapatite-based ceramic bone graft substitutes are slowly resorbed by the body as the bone surrounding the implant remodels. Hydroxyapatite-based ceramic bone graft substitutes are also osteoconductive; however, the porous hydroxyapatite bone graft substitutes typically have compressive strength and moduli that fall below the range of trabecular bone.

Whether hydroxyapatite-based biomaterials are osteoinductive is a controversial topic. Osteoinduction appears to occur with hydroxyapatite and other calcium phosphate-based biomaterials. Initially, the osteoinductivity of hydroxyapatite and other calcium phosphates was believed to be a property of the ceramic itself. However, recent evidence suggests that it is a property of the microstructure of the material, which would be similar to results observed with polymer scaffolds (Li et al., 2008). Two calcium phosphate structures, one composed of hydroxyapatite and the other of a blend with 85% hydroxyapatite and 15% tricalcium phosphate, were fabricated into similar macrostructures; however, the hydroxyapatite/tricalcium phosphate structure also had a subcellular microstructure and was found to be more osteoinductive than the hydroxyapatite with no subcellular microstructure (Yuan et al., 2002). Additionally, an examination of several distinct calcium phosphates



• **Figure 2.6.6.4** Electron micrograph of coral prior to conversion to hydroxyapatite (A) and after hydrothermal conversion to coralline hydroxyapatite (B) (Ben-Nissan, 2003).

with different chemical and crystal structures fabricated into similar macrostructures illustrated no significant difference in the expression of phenotype markers (Wang et al., 2004). An additional type of calcium salt is calcium sulfate; however, there is minimal compelling information regarding the osteoconductivity and osteoinductivity of calcium sulfate, and it may be immunogenic.

Of the ceramic-based bone graft substitutes, those fabricated from Bioglass are the most intriguing. Bioglass was developed in the late 1960s and has been shown to fit the bone tissue-engineering paradigm better than the other ceramics covered. Porous scaffolds have been fabricated from Bioglass in a number of ways, such as foam replacement techniques where a polyurethane foam is coated with a Bioglass slurry and then the foam is burned out leaving a Bioglass scaffold, or sintering Bioglass fibers to form porous mats (Biocompatibility and bone, 2009; Brown et al., 2008). These Bioglass fiber mats have been shown to be osteoconductive and promote phenotype progression of preosteoblast cells, which suggests they may be osteoinductive. The compressive strength and modulus of these Bioglass fiber rafts are in the range of trabecular bone and they exhibit adequate porosity of around 44% (Brown et al., 2008).

Cell-Based Substitutes

Cell-based strategies for bone tissue engineering, similar to biomaterial-based strategies for bone tissue engineering, fall into several categories. These are transplantation of autogenous progenitor cells, transplantation of autogenous progenitor cells that have been expanded and/or differentiated in culture prior to implantation, transplantation of genetically modified cells, and transplantation of ex vivo generated tissue. The simplest of these strategies is the transplantation of autogenous stem cells. Typically, this is performed by aspirating bone marrow and placing the aspirate at the defect or surgical site either unmodified or centrifuged to remove red blood cells and hematopoietic cells, including monocytes, from the bone marrow. The transplantation of

autogenous stem cells provides osteogenic potential to the defect, but does not provide osteoconductivity, osteoinductivity, or mechanical strength (Connolly et al., 1989).

The second method involves culturing the stem cells extracted from the bone marrow in culture. This can increase the number of progenitor cells available to implant, but it also comes with risks. The added time in culture in vitro increases the likelihood of bacteria contaminating the progenitor cell population. Successful expansion of the progenitor cells in vitro can ultimately improve the healing at the defect or surgical site. Similar to the nonexpanded cells, progenitor cells expanded in vitro prior to implantation are osteogenic but not osteoconductive, osteoinductive, or mechanically viable.

The third strategy for cell-based bone tissue engineering is the use of genetically modified cells. This is similar to the use of in vitro expanded autogenous progenitor cells, except the progenitor cells have been treated with an adenovirus or other vector to express a protein of interest. For bone tissue, often the progenitor cells will be transfected to express bone morphogenetic protein 2 (BMP-2). BMP-2 expressing progenitor cells enable the cell-based construct to be osteoinductive as well as osteogenic; however, the construct would still not improve in regard to osteoinductivity or mechanical viability (Cui et al., 2006).

The final strategy for cell-based bone tissue engineering is the most ambitious and the least clinically relevant at present. This is the in vitro culture of autogenous, embryonic, or inducible pluripotent stem cells with the aid of a bioreactor to ultimately produce a viable piece of bone tissue ex vivo. The major limitation in this strategy is material transport in developing tissue, since the issue of developing a vascularized construct has not been solved. If successful the ex vivo formation of bone tissue would meet all four criteria outlined in the bone tissue-engineering paradigm.

Growth Factor-Based Substitutes

The next strategy for bone tissue engineering is based on the use of factors. Two factors that have been shown to be

TABLE 2.6.6.1 Summary of the Properties Illustrated by the Different Types of Noncomposite Bone Graft Substitutes and How They Relate to the Desirable Characteristics of an Ideal Bone Graft Substitute

	Osteoconductive	Osteoinductive	Osteogenic	Mechanical Match
Allograft based	Yes	Yes	No	No
Microscale biomaterials	Yes	No	No	Yes, within the range of trabecular bone
Nanoscale biomaterials	Yes	Potentially. Supported by evidence with nanofibers made by self-assembly or phase separation.	No	No
Ceramics	Yes	Potentially. Supported by evidence for Bioglass.	No	Yes, range from less than trabecular bone to more than cortical bone depending on porosity
Cells	No	No	Yes	No
Growth factors	No	Yes	No	No

effective in a clinical setting and are approved by the FDA are recombinant human bone morphogenetic proteins 2 and 7 (rhBMP-2, rhBMP-7). Bone morphogenetic proteins are part of the transforming growth factor- β super-family and have been shown to exhibit osteoinductive potential. Between the two rhBMPs, rhBMP-2 has been shown to be more osteoinductive than rhBMP-7 (Khosla et al., 2008). Due to the soluble nature of both rhBMPs, they are often packaged with a carrier, often as simple as a collagen sponge. RhBMP-2 combined with a collagen sponge has been shown to perform better in spinal fusions than the “gold standard” autograft. In addition to spinal fusions, rhBMP-2 combined with a collagen sponge has illustrated effectiveness in fracture healing (Geiger et al., 2003). The primary limitation to the usage of rhBMPs in bone tissue-engineering applications is that they often cost a significant amount more than comparable procedures and consequently the usage of rhBMPs is primarily only in high-risk cases where all other options have been exhausted.

Composite Substitutes

The final strategy for bone tissue engineering is based on composites that combine two or more of the elements detailed earlier. The goal of creating composites is to combine the benefits of each component. Table 2.6.6.1 summarizes how the different bone tissue-engineering strategies correlate to the bone tissue-engineering paradigm. A common composite encountered consists of a biomaterial structure seeded with osteoblasts or osteoblastic cells. This is typically accomplished by either seeding of the biomaterial structure with osteoblast progenitor cells *ex vivo* just prior to implantation *in vivo*, or seeding of the biomaterial structure with osteoblasts or osteoblast progenitor cells followed by culture *in vitro* for several days to weeks prior to implantation.

An example of this technique that is presently used clinically is seeding Grafton DBM with bone marrow aspirate

from the patient *ex vivo* followed by implantation of the Grafton DBM/bone marrow aspirate composite at the desired surgical site. This composite combines the osteogenic potential of the progenitor cells in the bone marrow aspirate with the osteoinductive and osteoconductive properties of the Grafton DBM and has shown to be comparable to an autograft in formation of bone at the surgical site (Lindsey et al., 2006).

Another example of a cell/biomaterial composite involves seeding a porous polymer scaffold created by additive manufacturing of poly(caprolactone) with fibroblasts transfected to express bone morphogenetic protein-7 (BMP-7) (Williams et al., 2005). The additive manufactured poly(caprolactone) scaffold provides a structure with millimeter-scale features that is mechanically adequate and osteoconductive, and the incorporation of the BMP-7-expressing fibroblasts makes the composite construct osteoinductive. However, the fibroblasts are not expected to differentiate to osteoblasts and consequently this composite is not osteogenic. A second example of composite scaffolds for bone tissue engineering involves the incorporation of a ceramic calcium phosphate with a polymer scaffold. This can be accomplished through several different methods such as suspension of calcium phosphate particles with the polymer phase prior to processing to form a scaffold, spontaneous formation of calcium phosphates within the polymer phase during processing, and coating of calcium phosphates on the surface of a biomaterial scaffold through soaking in simulated body fluid. For example, a composite created by incorporation of calcium phosphates with the polymer phase during processing is illustrated by electrospinning a slurry of β -tricalcium phosphate particles in dissolved poly(caprolactone) to create a scaffold consisting of nanofibers exhibiting β -tricalcium phosphate particles on the surface of the fibers. The incorporation of the β -tricalcium phosphate particles improves the mechanical properties of the nanofiber scaffold and may also improve the osteoinductivity of the scaffold; however,

an improvement in the osteoinductivity of the nanofiber/ β -tricalcium phosphate composite has not been illustrated (Erisken et al., 2008).

A third example of a composite scaffold for bone tissue engineering involves the incorporation of growth factors with a polymer or ceramic scaffold. This concept was utilized when cross-linked poly(vinyl pyridine) microspheres containing either rhBMP-2 or rhBMP-7 were suspended in a poly(lactide-*co*-glycolide) (PLGA) foam. The concentration of the poly(vinyl pyridine) and the degree of cross-linking allowed for the staged release of rhBMP-2 and rhBMP-7. The rhBMP-2 was entrapped in lower concentration and less cross-linked microspheres and was released more rapidly than the rhBMP-7. The effect of this rhBMP microsphere-loaded PLGA foam was to increase the differentiation of bone marrow-derived mesenchymal stem cells in vitro as compared to the PLGA foam loaded with control microspheres not containing any rhBMPs. The results of this investigation are typical for what is expected by including BMPs in scaffolds and provides a strategy for making an osteoconductive scaffold osteoinductive as well (Basmanav et al., 2008). A critical issue with constructs containing growth factors, which is shared by growth factor strategies in general, is that they are prohibitively expensive for developing medical strategies to treat typically nonlife-threatening injuries. The foregoing examples of strategies for composite structures for bone tissue engineering represent only a small portion of the composite structures that have been investigated; however, these examples do provide an accurate representation of the desired outcomes in preparing composite structures for bone tissue engineering.

Porosity in Bone Graft Substitutes

An important characteristic of a successful biomaterial-based bone graft substitute that promotes all the features of the bone tissue-engineering paradigm involves the pore structure of the scaffold or construct. Without an adequate pore structure, migration into the scaffold is restricted, which subsequently limits the potential of the scaffold to be osteoconductive, osteoinductive, and osteogenic. The pore structure of the scaffold, both pore diameter and porosity, is a critical component in allowing cellular migration.

The concept of pore structure and cellular migration is similar across cell lines and as such this discussion focuses primarily on the characteristic dimension of the scaffold and the subsequent requirements to promote cell migration into the scaffold. For microscale scaffolds fabricated through techniques such as 3D printing/additive manufacturing, microsphere sintering, gas foaming, and particulate leaching the critical design aspects involve maintaining interconnected pores and pore diameters above 40 μm (Karageorgiou and Kaplan, 2005). An interconnected porosity is necessary to facilitate migration of cells throughout the scaffold as well as maintaining a supply of nutrients and removal of waste from the cells on the scaffold interior. It was found that scaffolds with large, 100–300 μm , pore diameters facilitated

faster migration throughout the scaffold; however, despite the decreased rate of migration the lower, 40 μm , pore diameter scaffolds achieved the same level of cellular penetration as did those with the larger pore diameters (Karageorgiou and Kaplan, 2005).

When the characteristic dimension of the scaffold shrinks to the nanoscale these same concepts do not apply. No longer does pore diameter appear to be as influential, since nanofiber scaffolds fabricated from self-assembly and thermally induced phase separation have illustrated cell invasion into and throughout the interior of the scaffold despite pore diameters ranging from 300 nm to 10 μm (Brown et al., 2010; Silva et al., 2004). Two characteristics shared by both of these scaffold architectures are that they illustrate porosities greater than 95% and the fibers are randomly oriented in three dimensions. Likewise, electrospun nanofibers, which typically exhibit total porosities ranging from 40% to 75%, with isolated reports up to 90%, and pore diameters ranging from a few microns to 30 μm , have also exhibited cellular infiltration throughout the interior of the scaffold (Venugopal et al., 2007).

These results illustrating cellular migration into the small pores contradict that previously found for microscale scaffolds and consequently have raised questions regarding how cells are able to infiltrate nanoscale scaffolds. The ability of cells to infiltrate a nanoscale scaffold starts with a fundamental difference in how cells respond to nanodimensional surfaces. On nanostructures, cell morphology changes to exhibit pronounced pseudopodia-like processes, which extend along individual fibers (Long et al., 2019; Ozdemir et al., 2019). These extensions on randomly orientated fibers produce an image appearing to be a well-spread cell; however, it is important to consider that most imaging techniques depict a two-dimensional field when there is a third dimension not necessarily seen. This implies that cells are extending down into the field of view as much as they are extending out within the field of view and this theory has been corroborated through the use of confocal fluorescence imaging illustrating cells extending in three dimensions (Silva et al., 2004). These well-spread cells exhibiting pseudopodia-like processes have led researchers to conclude that cells utilize ameboidal migration to reach the interior of the scaffold (Friedl and Brocker, 2000). Presumably, this ameboidal migration is driven by soluble factors and proteins adsorbed to the surface of fibers below the cells providing a gradient and driving infiltration to establish a uniform density of cells throughout the construct. In conclusion, microscale scaffolds rely on pore diameter to allow cell migration, whereas nanoscale scaffolds rely on chemical gradients created by adsorbed factors and ameboidal motion to allow cell migration, which suggests that porosity is the critical property of nanoscale scaffolds.

Dimension in Bone Graft Substitutes

In addition to porosity, the characteristic dimension of a polymer scaffold can have tremendous implications on the

success of the scaffold as a bone graft substitute. Initially, the scaffold was viewed as a cell carrier and mechanical substitute; however, more recent research has demonstrated that the characteristic dimension of a scaffold can directly affect intracellular signaling leading to changes in gene expression, a process termed mechanotransduction. Mechanotransduction is defined simply as the process that converts a mechanical force into a biochemical signal (Eyckmans et al., 2011). Scaffold material stiffness and dimension both directly alter the mechanical state of a cell. Research has demonstrated that scaffolds that stimulate the signaling cascades leading to actomyosin contractility also promote differentiation of mesenchymal stem cells to bone tissue (Engler et al., 2006; Ozdemir et al., 2013). Specifically, both scaffolds mimicking the stiffness of osteoid matrix and nanofiber scaffolds presenting diameters of approximately 500–1000 nm promote RhoA activation, which leads to increased actomyosin contractility and bone differentiation. Furthermore, these nanostructured concepts can be applied to other surfaces such as Ti_6Al_4V implants for orthopedic applications (Fig. 2.6.6.5).

The following are detailed descriptions of two scaffold types with dramatically different characteristic dimensions. The first, sintered microspheres, demonstrates a characteristic dimension an order of magnitude larger than that of a cell; while the second, nanofibers, demonstrates a characteristic dimension two orders of magnitude smaller than that of a cell.

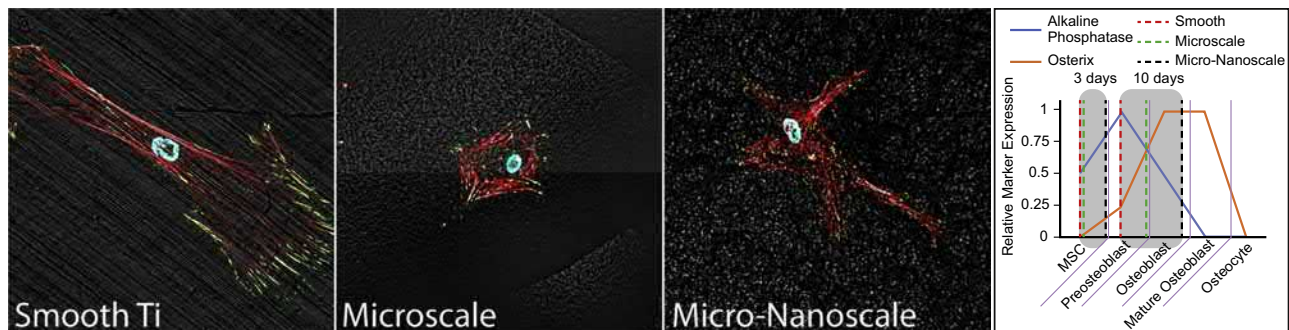
Sintered Microspheres

Sintered biodegradable microsphere scaffolds were first developed by Cato Laurencin's lab in 1996 and were composed of PLGA. These initial scaffolds were fabricated both with and without hydroxyapatite and exhibited mechanical properties and porosity suitable for bone tissue engineering (Devin et al., 1996). Since that time the microsphere scaffold has undergone several compositional iterations. Microsphere scaffolds have been fabricated from other types of biodegradable polyesters such as polylactide and

poly(3-hydroxybutyrate-co-3-hydroxyvalerate) (Zhu et al., 2007). Sintered microsphere scaffolds have been fabricated from a polymer/ceramic composite microsphere composed of PLGA microspheres fabricated in such a way as to spontaneously induce calcium phosphate precipitation on the surface of the microspheres (Khan et al., 2004). Additionally, microsphere scaffolds can be combined with growth factors, as typical of most polymer scaffolds.

The tremendous interest in the sintered microsphere scaffold is due to it being advantageous over other microscale scaffolds produced by techniques such as gas foaming and porogen leaching. These advantages, which are shared with recent efforts in additive manufacturing technologies, are: reproducibility, scalability, and controllability over pore size, porosity, and mechanical properties. Microsphere scaffolds rely on the chemical properties of a polymer to sinter uniform spheres into scaffolds by elevating the polymer above the glass transition temperature, which causes the adjacent polymer chains to migrate and intertwine forming a cohesive bond when the polymer is cooled. Older techniques, such as gas foaming and porogen leaching, do not have the same level of reproducibility due to variation introduced by having multiple phases, either a heterogeneous mixture of a solid and liquid or a liquid and gas. These heterogeneous mixtures can undergo demixing, which introduces inconsistencies in the mixing of the phases and decreases reproducibility.

Microsphere scaffolds maintain a very high level of interconnectivity among the pores and allow control over the total interconnected porosity as well as the average pore diameter. Gas foaming and particle leaching provide control over the total porosity and pore size as well; however, they often have very poor interconnectivity, only 10%–30% interconnectivity with gas foaming, rendering a percentage of the pores inaccessible (Mooney et al., 1996). Another advantage of microsphere scaffolds compared to gas foaming and porogen leaching is that they can be fabricated to exhibit mechanical properties that mimic that of trabecular bone (Brown et al., 2010). High mechanical properties are



• **Figure 2.6.6.5** Fluorescent microscopy depicting mesenchymal stem cells (MSCs) stained for actin (red), nuclei (blue), and the focal adhesion protein vinculin (green) on Ti_6Al_4V that has been processed to be either smooth (Smooth Ti), demonstrate a characteristic dimension on the order of micrometers (Microscale), or demonstrate hierarchical micrometer- and nanometer-scale characteristic dimensions (Micro-Nanoscale). The representative MSCs shift from a fibroblastic elongated morphology on Smooth Ti to a cuboidal morphology on Microscale and a stellate, or star-shaped, morphology on Micro-Nanoscale. Furthermore, differentiation analysis reveals the introduction of Microscale and MicroNanoscale features increases the rate of differentiation through 10 days as compared to Smooth Ti (Long et al., 2019).

achievable; however, to achieve this the scaffold density must be increased, which causes the internal pore structure to be further compromised. Microsphere scaffolds composed of polylactide and PLGA have been produced previously and have yielded reasonable results in *in vitro* studies, as well as in *in vivo* studies examining critical size defect healing (Borden et al., 2004; Botchwey et al., 2001).

Nanofibers

Recent developments in tissue engineering have indicated that nanoscale structures are more advantageous for cellular phenotype expression and morphology when compared to microscale structures. A frequently employed type of nanoscale scaffold is based on polymeric nanofibers. Nanofibers can be fabricated through several different techniques. The initial and most common technique is through electrospinning, which has been in use for over 80 years (Formhals). Electrospun nanofibers are created by applying a voltage gradient between a target and a drop of polymer, either dissolved or melted. Once the voltage gradient overcomes the surface tension of the droplet a polymer stream extends toward the target. As this stream travels, it is thinned out and eventually strikes the target as a nanofiber with the accumulation of these fibers leading to the production of a nonwoven nanofiber mat.

Initially, electrospun nanofibers were made from non-degradable polymers for applications in filtration; however, recent developments have led to the use of electrospun nanofibers made of biodegradable polymers for tissue-engineering applications, such as poly[(amino acid ester) phosphazenes] (Kumbar et al., 2006). Nanofibers created by electrospinning typically have diameters ranging from 300 to 1200 nm depending on the spinning conditions used. Electrospun nanofibers are oriented lengthwise in only two dimensions with the third dimension created from the stacking of the fibers on top of each other. Recent efforts have sought to couple additive manufacturing technologies, such as 3D printing, with electrospinning processes (Fattahi et al., 2017). Nanofibers have also recently been developed using synthetic peptides designed to self-assemble into a 3D nanofiber network. Self-assembled nanofibers often have a characteristic diameter that is within the range of 5–10 nm (Zhang, 2003). The very thin diameter of the fibers in the network and the high porosity created with self-assembly produces a scaffold poor in mechanical properties making them suitable primarily for hydrogel applications.

A final method of nanofiber fabrication is thermally induced phase separation, which relies on the spinodal liquid/liquid phase separation of a polymer solution into a polymer-poor phase and a polymer-rich phase when the solution is rapidly cooled. Spinodal phase differs from binodal phase separation in that the two phases separate and exist continuously throughout the original mixture, whereas bimodal phase separation occurs via nucleation sites that build spherical particles. The selection of an appropriate polymer, one with a high degree of crystallinity, will allow the polymer-rich phase to crystallize into nanofibers, whereas polymers with low degrees of crystallinity form

microstructured foams (vandeWitte et al., 1996). Nanofibers created with the thermally induced phase separation technique exhibit a fiber diameter of 50–500 nm, which is similar to collagen, and a 3D fiber structure making them very different from electrospun nanofibers (Hu et al., 2008). These evaluations suggest that nanofibers exhibiting a 3D spatial arrangement promote phenotype progression of osteoblasts and may be osteoinductive. Additionally, complexes of microspheres with nanofibers to create a 3D nanofibrous mechanically viable implant has been demonstrated (Brown et al., 2010).

In Vitro Culture Techniques for Bone Graft Substitutes

A critical limitation of static culture conditions is that waste efflux and nutrient influx are governed by diffusion, which becomes exponentially more problematic with large 3D constructs. As time passes, the accumulation of waste within a construct can lead to an acidic microenvironment that impedes calcification of the developing tissue and compromises the viability of osteoblasts within a construct. To alleviate these issues the use of bioreactors becomes necessary when trying to achieve significant tissue growth *in vitro*. The bioreactor provides fluid flux that replenishes nutrients and removes waste; additionally, for tissues such as bone, bioreactors can provide mechanical stimulation to encourage the development of a mechanically viable tissue.

The earliest bioreactor that has been applied to bone tissue engineering involves dialysis membranes that are either gas or small molecule permeable. The bioreactor is divided into two compartments that are separated by a small molecule permeable membrane and each compartment also contains a gas permeable membrane (Vogler, 1989). The gas permeable membrane provides a liquid/air boundary to provide oxygen and CO₂ and the membrane between compartments serves as a liquid/liquid boundary between the culture medium surrounding the cells and a reservoir of fresh medium. This boundary provides fresh nutrients while removing waste, but also allows the soluble factor gradients to remain intact during media changes. Recently, this bioreactor design has supported the development of simple osteoid tissue after culturing osteoprogenitor cells for 10 months. Despite the development of osteoid tissue this bioreactor design still relies on passive diffusion to supply nutrients and therefore limits the ultimate thickness of the construct to only a few cell layers (Mastro and Vogler, 2009).

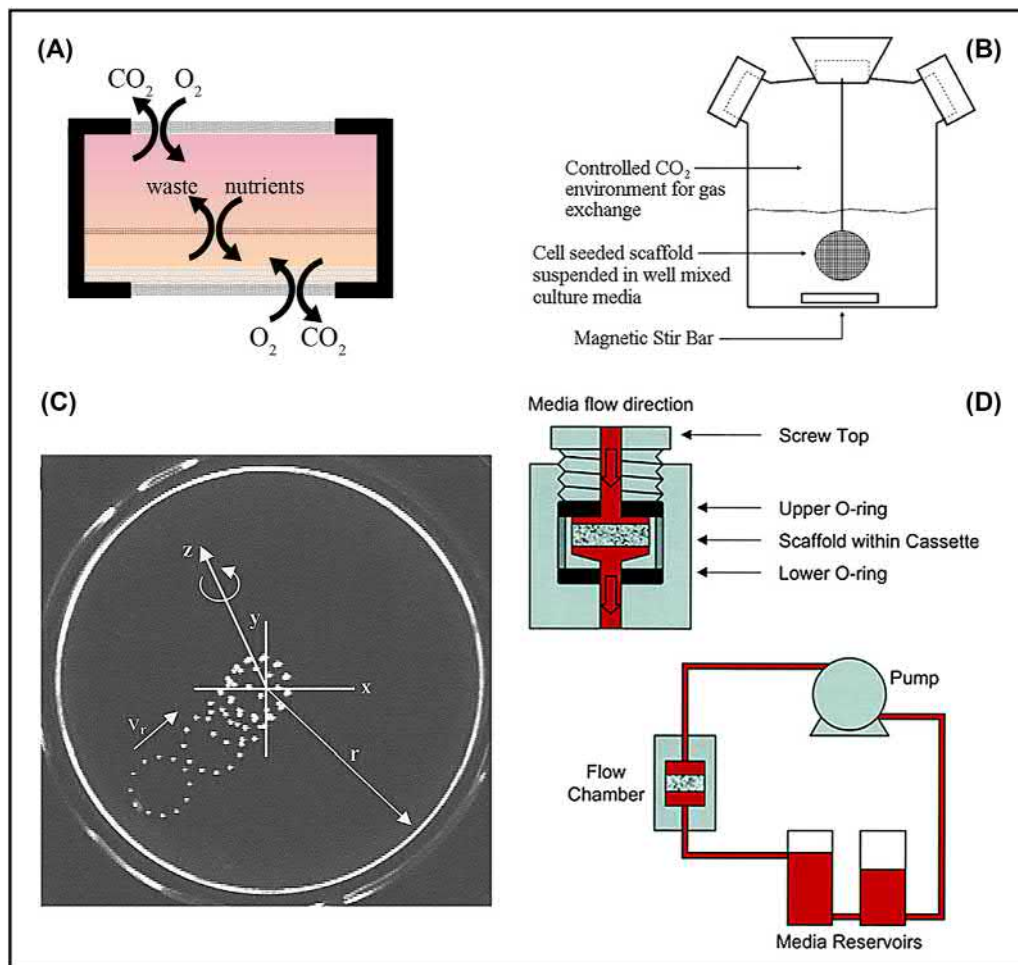
The next iteration of the bioreactor involved rotation, either of the reactor itself or of the construct within the bioreactor. NASA developed rotating wall bioreactors to simulate microgravity. These bioreactors consist of a cylinder and a gas exchange membrane either on one face of the cylinder or as a separate inner cylinder. In this design the shear force exerted by fluid rotation negates the effect of gravity on the constructs and also provides a well-mixed volume of culture medium. This strategy was employed by tissue engineers to culture constructs seeded with osteoblasts in the hope that

the rotating well-mixed volume of culture medium would overcome diffusion limitations and allow tissue development throughout the thickness of the construct (Botchwey et al., 2004). Research suggests this is certainly the case, with osteoblasts found throughout the thickness of the construct; however, the simulation of microgravity seems to discourage bone tissue development (not surprisingly due to a lack of mechanical stimulation). This is demonstrated by both lower levels of phenotype markers and less mineralization as compared to static cultured constructs (Yu et al., 2004).

The next type of bioreactor involving rotating fluid is the spinner flask. Spinner flask bioreactors suspend the constructs on thin needles that are extended into a stirred flask of media. This configuration not only provides a well-mixed environment to avoid accumulation of waste in the local environment of the construct, but also provides mechanical stimulation through shear forces on the constructs. Since

the spinner flask also provides a well-mixed environment, it is not surprising to see that cells migrate throughout the construct suspended in the spinner flask similar to those cultured in rotating wall bioreactors. Additionally, because the spinner flask provides much higher shear forces than the rotating wall bioreactor, there is a marked increase in the calcification of the construct and the differentiation of osteoblasts in the spinner flask (Stiehler et al., 2009).

The final bioreactor for bone tissue engineering is a perfusion bioreactor. The perfusion bioreactor works by forcing culture media through a construct with a pump. This system provides control over the shear experienced by the cells in culture. Similar to the spinner flask, osteoblasts generated more calcium and exhibited increased expression of phenotype markers in the perfusion bioreactor (Gomes et al., 2003). Fig. 2.6.6.6 presents a graphical depiction of these bioreactor types.



• **Figure 2.6.6.6** Graphical depiction of four bioreactors. The simplest bioreactor that supports multilayered growth of cells on the bottom surface and consists of two gas permeable membranes on the top and bottom and a dialysis membrane in the middle (A). A spinner flask bioreactor that utilizes a stir bar to force nutrient flux through the constructs, which remain in a fixed position (B) (Martin and Vermette, 2005). A high aspect ratio rotating vessel bioreactor demonstrating the trajectory of a lighter than water construct within the rotating wall bioreactor; the fluid shear on the scaffold is low. However, the back panel of the bioreactor is a gas permeable membrane and the rotation maintains a large volume of well-mixed media to support nutrient supply (C) (Botchwey et al., 2004). Finally, a schematic illustrating a perfusion bioreactor that utilizes a pump to force media through a construct, which research suggests also promotes bone tissue formation through mechanical stimulation provided by fluid shear forces on the construct (D) (Gomes et al., 2003).

Conclusion

The concepts of tissue engineering have made profound advances in developing clinically relevant solutions for tissues such as skin, bladder, and to some extent bone. However, where the clinical strategies for skin and bladder exist as a straightforward solution based on the requirements of those tissues, bone presents a more complicated situation. Skin and bladder tissue are essentially a uniform 2D sheet, whereas bone often takes many unusual 3D and nonuniform geometries.

The evolution of bone tissue engineering began with osteoblasts cultured on rudimentary polymer foams and has progressed to include an array of bone graft substitutes cultured with mesenchymal stem cells in bioreactors to drive the development of de novo bone tissue. Significant clinical achievements have occurred in using biodegradable scaffolds with or without growth factors or cells as synthetic bone grafts to heal large defects in bone tissue. However, despite the ground that has been covered thus far, there persist unmet goals and challenges ahead. No research has yet demonstrated the capability to grow de novo bone in an in vitro setting; so far only rudimentary calcified cell masses approaching bone tissue have been developed. Moving forward, future researchers should consider the flexibility in design of the macroscale structure to accommodate the unusual architectures and mechanics necessary for bone graft substitutes, the biodegradability of the structure such that natural healthy bone is ultimately all that persists, the osteoconductivity of the bone graft substitute to promote proliferation of progenitor cells and osteoblasts throughout the bone graft substitute, and the osteoinductivity of the bone graft substitute to promote the differentiation of the mesenchymal stem cells to osteoblasts into eventually organized bone tissue.

To date, the one aspect that the earliest bioreactor managed to get right has been lacking in all future designs: the ability to maintain gradients in soluble growth factors secreted by cells. The development of the bioreactor for bone tissue engineering has moved from a series of static chambers separated by dialysis membranes to reactors that provide mechanical stimulation. Future successful bioreactors will depend on the ability to incorporate aspects of existing bioreactors: nutrient influx, waste efflux, mechanical stimulation, and the establishment of soluble factor gradients. Providing all four of these bioreactor elements with a bone graft substitute may lead to the development of hierarchical bone tissue and ultimately the de novo formation of bone in vitro.

References

- Allcock, H., Pucher, S., Scopelianos, A., 1994. Poly[(Amino-Acid-Ester)Phosphazenes] – synthesis, crystallinity, and hydrolytic sensitivity in solution and the solid-state. *Macromolecules* 27 (5), 1071–1075.
- Basmanav, F.B., Kose, G.T., Hasirci, V., November 2008. Sequential growth factor delivery from complexed microspheres for bone tissue engineering. *Biomaterials* 29 (31), 4195–4204.
- Ben-Nissan, B., 2003. Natural bioceramics: from coral to bone and beyond. *Curr. Opin. Solid State Mater. Sci.* 7 (4–5), 283–288.
- Bilezikian, J.P., Raisz, L.G., Martin, T.J., 2008. *Principles of Bone Biology*.
- Blaine, G., 1946. Experimental observations on the use of absorbable and non-absorbable plastics in bone surgery. *Br. J. Surg.* 33 (131), 245–250.
- Borden, M., Attawia, M., Khan, Y., Laurencin, C.T., January 2002. Tissue engineered microsphere-based matrices for bone repair: design and evaluation. *Biomaterials* 23 (2), 551–559.
- Borden, M., Attawia, M., Khan, Y., El-Amin, S.F., Laurencin, C.T., November 2004. Tissue-engineered bone formation in vivo using a novel sintered polymeric microsphere matrix. *J. Bone Joint Surg. Br.* 86 (8), 1200–1208.
- Bostman, O.M., Pihlajamaki, H.K., December 1998. Late foreign-body reaction to an intraosseous bioabsorbable polylactic acid screw. A case report. *J. Bone Joint Surg. Am.* 80 (12), 1791–1794.
- Botchwey, E.A., Pollack, S.R., Levine, E.M., Laurencin, C.T., May 2001. Bone tissue engineering in a rotating bioreactor using a micro-carrier matrix system. *J. Biomed. Mater. Res.* 55 (2), 242–253.
- Botchwey, E., Pollack, S., Levine, E., Johnston, E., Laurencin, C., 2004. Quantitative analysis of three-dimensional fluid flow in rotating bioreactors for tissue engineering. *J. Biomed. Mater. Res.* 69A (2), 205–215.
- Brown, R.F., Day, D.E., Day, T.E., Jung, S., Rahaman, M.N., Fu, Q., March 2008. Growth and differentiation of osteoblastic cells on 13-93 bioactive glass fibers and scaffolds. *Acta Biomater.* 4 (2), 387–396.
- Brown, J.L., Peach, M.S., Nair, L.S., Kumbar, S.G., Laurencin, C.T., December 15, 2010. Composite scaffolds: bridging nanofiber and microsphere architectures to improve bioactivity of mechanically competent constructs. *J. Biomed. Mater. Res.* 95 (4), 1150–1158.
- Connolly, J., Guse, R., Lippiello, L., Dehne, R., June 1989. Development of an osteogenic bone-marrow preparation. *J. Bone Joint Surg. Am.* 71 (5), 684–691.
- Cui, Q., Xiao, Z., Li, X., Saleh, K.J., Balian, G., November 2006. Use of genetically engineered bone-marrow stem cells to treat femoral defects: an experimental study. *J. Bone Joint Surg. Am.* 88 (Suppl. 3), 167–172.
- Devin, J.E., Attawia, M.A., Laurencin, C.T., 1996. Three-dimensional degradable porous polymer-ceramic matrices for use in bone repair. *J. Biomater. Sci. Polym. Ed.* 7 (8), 661–669.
- Engler, A.J., Sen, S., Sweeney, H.L., Discher, D.E., August 25, 2006. Matrix elasticity directs stem cell lineage specification. *Cell* 126 (4), 677–689.
- Eriskin, C., Kalyon, D.M., Wang, H., October 2008. Functionally graded electrospun polycaprolactone and beta-tricalcium phosphate nanocomposites for tissue engineering applications. *Biomaterials* 29 (30), 4065–4073.
- Everts, V., Delaisse, J.M., Korper, W., Jansen, D.C., Tigchelaar-Gutter, W., Saftig, P., Beertsen, W., January 2002. The bone lining cell: its role in cleaning Howship's lacunae and initiating bone formation. *J. Bone Miner. Res.* 17 (1), 77–90.
- Eyckmans, J., Boudou, T., Yu, X., Chen, C.S., 2011. A hitchhiker's guide to mechanobiology. *Dev. Cell* 21 (1), 35–47.
- Fattahi, P., Dover, J.T., Brown, J.L., 2017. 3D near-field electrospinning of biomaterial microfibers with potential for blended microfiber-cell-loaded gel composite structures. *Adv. Healthc. Mater.* 260, 1700456.
- Formhals, A. Process and apparatus for preparing artificial threads. US Patent, 1975504, vol. 1934, 1:7.

- Franz-Odenaal, T.A., Hall, B.K., Witten, P.E., January 2006. Buried alive: how osteoblasts become osteocytes. *Dev. Dynam.* 235 (1), 176–190.
- Friedl, P., Brocker, E.B., January 20, 2000. The biology of cell locomotion within three-dimensional extracellular matrix. *Cell. Mol. Life Sci.* 57 (1), 41–64.
- Geiger, M., Li, R.H., Friess, W., November 28, 2003. Collagen sponges for bone regeneration with rhBMP-2. *Adv. Drug Deliv. Rev.* 55 (12), 1613–1629.
- Gomes, M.E., Sikavitsas, V.I., Behraves, E., Reis, R.L., Mikos, A.G., 2003. Effect of flow perfusion on the osteogenic differentiation of bone marrow stromal cells cultured on starch-based three-dimensional scaffolds. *J. Biomed. Mater. Res. A* 67 (1), 87–95.
- Goulet, G.C., Cooper, D.M.L., Coombe, D., Zernicke, R.F., August 2008. Influence of cortical canal architecture on lacunocanalicular pore pressure and fluid flow. *Comput. Methods Biomech. Biomed. Eng.* 11 (4), 379–387.
- Grayson, W.L., Fröhlich, M., Yeager, K., Bhumiratana, S., Chan, M.E., Cannizzaro, C., Wan, L.Q., Liu, X.S., Guo, X.E., Vunjak-Novakovic, G., February 23, 2010. Engineering anatomically shaped human bone grafts. *Proc. Natl. Acad. Sci. U S A* 107 (8), 3299–3304.
- Greenwald, A.S., Boden, S.D., Goldberg, V.M., Khan, Y., Laurencin, C.T., Rosier, R.N., 2001. Bone-graft substitutes: facts, fictions, and applications. *J. Bone Joint Surg. Am.* 83A (Suppl. 2 Pt 2), 98–103.
- Hench, L.L., Splinter, R.J., Allen, W., Greenlee, T., 1971. Bonding mechanisms at the interface of ceramic prosthetic materials. *J. Biomed. Mater. Res.* 5 (6), 117–141.
- Hu, J., Liu, X., Ma, P.X., October 2008. Induction of osteoblast differentiation phenotype on poly(L-lactic acid) nanofibrous matrix. *Biomaterials* 29 (28), 3815–3821.
- Hutmacher, D.W., December 2000. Scaffolds in tissue engineering bone and cartilage. *Biomaterials* 21 (24), 2529–2543.
- Hutmacher, D.W., Sittering, M., Risbud, M.V., July 2004. Scaffold-based tissue engineering: rationale for computer-aided design and solid free-form fabrication systems. *Trends Biotechnol.* 22 (7), 354–362.
- Jones, A.C., Milthorpe, B., Averdunk, H., Limaye, A., Senden, T.J., Sakellariou, A., Sheppard, A.P., Sok, R.M., Knackstedt, M.A., Brandwood, A., Rohner, D., Hutmacher, D.W., September 2004. Analysis of 3D bone ingrowth into polymer scaffolds via micro-computed tomography imaging. *Biomaterials* 25 (20), 4947–4954.
- Karageorgiou, V., Kaplan, D., 2005. Porosity of 3D biomaterial scaffolds and osteogenesis. *Biomaterials* 26 (27), 5474–5491.
- Khan, Y.M., Katti, D.S., Laurencin, C.T., June 15, 2004. Novel polymer-synthesized ceramic composite-based system for bone repair: an in vitro evaluation. *J. Biomed. Mater. Res.* 69 (4), 728–737.
- Khan, Y., Yaszemski, M.J., Mikos, A.G., Laurencin, C.T., February 2008. Tissue engineering of bone: material and matrix considerations. *J. Bone Joint Surg. Am.* 90 (Suppl. 1), 36–42.
- Khosla, S., Westendorf, J.J., Oursler, M.J., February 2008. Building bone to reverse osteoporosis and repair fractures. *J. Clin. Invest.* 118 (2), 421–428.
- Kjelstrup-Hansen, J., Hansen, O., Rubahn, H.G., Boggild, P., 2006. Mechanical properties of organic nanofibers. *Small* 2 (5), 660–666.
- Kneser, U., Schaefer, D.J., Polykandriotis, E., Horch, R.E., January 2006. Tissue engineering of bone: the reconstructive surgeon's point of view. *J. Cell Mol. Med.* 10 (1), 7–19.
- Knothe Tate, M.L., October 2003. “Whither flows the fluid in bone?” an osteocyte's perspective. *J. Biomech.* 36 (10), 1409–1424.
- Kollet, O., Dar, A., Shvitiel, S., Kalinkovich, A., Lapid, K., Sztainberg, Y., Tesio, M., Samstein, R.M., Goichberg, P., Spiegel, A., Elson, A., Lapidot, T., 2006. Osteoclasts degrade endosteal components and promote mobilization of hematopoietic progenitor cells. *Nat. Med.* 12 (6), 657–664.
- Kumbar, S.G., Bhattacharyya, S., Nukavarapu, S.P., Khan, Y.M., Nair, L.S., Laurencin, C.T., 2006. In vitro and in vivo characterization of biodegradable poly(organophosphazenes) for biomedical applications. *J. Inorg. Organomet. Polym.* 16 (4), 365–385.
- Langer, R., Vacanti, J.P., May 14, 1993. Tissue engineering. *Science* 260 (5110), 920–926.
- Leveen, H.H., Barberio, J.R., January 1949. Tissue reaction to plastics used in surgery with special reference to teflon. *Ann. Surg.* 129 (1), 74–84 PMID: PMC1513989.
- Li, X., van Blitterswijk, C.A., Feng, Q., Cui, F., Watari, F., August 2008. The effect of calcium phosphate microstructure on bone-related cells in vitro. *Biomaterials* 29 (23), 3306–3316.
- Lindsey, R.W., Wood, G.W., Sadasivian, K.K., Stubbs, H.A., Block, J.E., 2006. Grafting long bone fractures with demineralized bone matrix putty enriched with bone marrow: pilot findings. *Orthopedics* 29 (10), 939–941.
- Long, E.G., Buluk, M., Gallagher, M.B., Schneider, J.M., Brown, J.L., September 19, 2019. Human mesenchymal stem cell morphology, migration, and differentiation on micro and nano-textured titanium. *J. Biomech.* 4, 249–255.
- Martin, Y., Vermette, P., December 2005. Bioreactors for tissue mass culture: design, characterization, and recent advances. *Biomaterials* 26 (35), 7481–7503.
- Mastro, A.M., Vogler, E.A., May 15, 2009. A three-dimensional osteogenic tissue model for the study of metastatic tumor cell interactions with bone. *Cancer Res.* 69 (10), 4097–4100.
- Matsuo, K., Irie, N., May 15, 2008. Osteoclast-osteoblast communication. *Arch. Biochem. Biophys.* 473 (2), 201–209.
- Mooney, D., Baldwin, D., Suh, N., Vacanti, L., Langer, R., 1996. Novel approach to fabricate porous sponges of poly(D,L-lactic-co-glycolic acid) without the use of organic solvents. *Biomaterials* 17 (14), 1417–1422.
- Muggli, D.S., Burkoth, A.K., Anseth, K.S., August 1999. Crosslinked polyanhydrides for use in orthopedic applications: degradation behavior and mechanics. *J. Biomed. Mater. Res.* 46 (2), 271–278.
- Nair, L.S., Bhattacharyya, S., Bender, J.D., Greish, Y.E., Brown, P.W., Allcock, H.R., Laurencin, C.T., 2004. Fabrication and optimization of methylphenoxy substituted polyphosphazene nanofibers for biomedical applications. *Biomacromolecules* 5 (6), 2212–2220.
- Neen, D., Noyes, D., Shaw, M., Gwilym, S., Fairlie, N., Birch, N., August 15, 2006. Healos and bone marrow aspirate used for lumbar spine fusion: a case controlled study comparing healos with autograft. *Spine* 31 (18), E636–E640.
- Ozdemir, T., Xu, L.-C., Siedlecki, C., Brown, J.L., 2013. Substrate curvature sensing through Myosin IIa upregulates early osteogenesis. *Integr. Biol.* 5 (11), 1407–1416.
- Ozdemir, T., Bowers, D.T., Zhan, X., Ghosh, D., Brown, J.L., January 30, 2019. Identification of key signaling pathways orchestrating substrate topography directed osteogenic differentiation through high-throughput siRNA screening. *Nature Publishing Group Sci Rep.* 9 (1), 1001 PMID: PMC6353928.
- Pearson, O.M., Lieberman, D.E., 2004. The aging of Wolff's ‘law’: ontogeny and responses to mechanical loading in cortical bone. *Am. J. Phys. Anthropol. (Suppl. 39)*, 63–99.
- Peterson, B., Whang, P.G., Iglesias, R., Wang, J.C., Lieberman, J.R., October 2004. Osteoinductivity of commercially available demineralized bone matrix. Preparations in a spine fusion model. *J. Bone Joint Surg. Am.* 86-A (10), 2243–2250.

- Rezwan, K., Chen, Q.Z., Blaker, J.J., Boccaccini, A.R., June 2006. Biodegradable and bioactive porous polymer/inorganic composite scaffolds for bone tissue engineering. *Biomaterials* 27 (18), 3413–3431.
- Schwartz, Z., Goldstein, M., Raviv, E., Hirsch, A., Ranly, D.M., Boyan, B.D., April 2007. Clinical evaluation of demineralized bone allograft in a hyaluronic acid carrier for sinus lift augmentation in humans: a computed tomography and histomorphometric study. *Clin. Oral Implants Res.* 18 (2), 204–211.
- Shapiro, F., 2008. Bone development and its relation to fracture repair. The role of mesenchymal osteoblasts and surface osteoblasts. *Eur. Cell. Mater.* 15, 53–76.
- Silva, G., Czeisler, C., Niece, K., al, E., 2004. Selective differentiation of neural progenitor cells by high-epitope density nanofibers. *Science* 303, 1352–1355.
- Smith, L.A., Ma, P.X., December 10, 2004. Nano-fibrous scaffolds for tissue engineering. *Colloids Surf. B Biointerfaces* 39 (3), 125–131.
- Stiehler, M., Bünger, C., Baatrup, A., Lind, M., Kassem, M., Mygind, T., April 2009. Effect of dynamic 3-D culture on proliferation, distribution, and osteogenic differentiation of human mesenchymal stem cells. *J. Biomed. Mater. Res.* 89 (1), 96–107.
- vandeWitte, P., Dijkstra, P., vandenBerg, J., Feijen, J., 1996. Phase separation processes in polymer solutions in relation to membrane formation. *J. Membr. Sci.* 117, 1–31.
- Vargas G.E., Mesones R.V., Bretcanu O., Lopez J.M.P., Boccaccini A.R., and Gorustovich A., January 1, 2009. Biocompatibility and bone mineralization potential of 45S5 Bioglass®-derived glass–ceramic scaffolds in chick embryos. *Acta Biomater.* 5 (1), 374–380.
- Venugopal, J., Vadgama, P., Kumar, T.S.S., Ramakrishna, S., 2007. Biocomposite nanofibres and osteoblasts for bone tissue engineering. *Nanotechnology* 18 (5).
- Vogler, E.A., 1989. A compartmentalized device for the culture of animal cells. *Biomater. Artif. Cells Artif. Organs* 17 (5), 597–610.
- Wahl, D.A., Czernuszka, J.T., 2006. Collagen-hydroxyapatite composites for hard tissue repair. *Eur. Cell. Mater.* 11, 43–56.
- Wang, C., Duan, Y., Markovic, B., Barbara, J., Howlett, C.R., Zhang, X., Zreiqat, H., June 2004. Phenotypic expression of bone-related genes in osteoblasts grown on calcium phosphate ceramics with different phase compositions. *Biomaterials* 25 (13), 2507–2514.
- Williams, J.M., Adewunmi, A., Schek, R.M., Flanagan, C.L., Krebsbach, P.H., Feinberg, S.E., Hollister, S.J., Das, S., August 2005. Bone tissue engineering using polycaprolactone scaffolds fabricated via selective laser sintering. *Biomaterials* 26 (23), 4817–4827.
- Yu, X., Botchwey, E.A., Levine, E.M., Pollack, S.R., Laurencin, C.T., 2004. Bioreactor-based bone tissue engineering: the influence of dynamic flow on osteoblast phenotypic expression and matrix mineralization. *Proc. Natl. Acad. Sci. U S A* 101 (31), 11203–11208.
- Yuan, H., Van Den Doel, M., Li, S., van Blitterswijk, C.A., de Groot, K., de Bruijn, J.D., December 2002. A comparison of the osteoinductive potential of two calcium phosphate ceramics implanted intramuscularly in goats. *J. Mater. Sci. Mater. Med.* 13 (12), 1271–1275.
- Zhang, S., 2003. Fabrication of novel biomaterials through molecular self-assembly. *Nat. Biotechnol.* 21 (10), 1171–1178.
- Zhu, X.H., Gan, S.K., Wang, C.-H., Tong, Y.W., 2007. Proteins combination on PHBV microsphere scaffold to regulate Hep3B cells activity and functionality: a model of liver tissue engineering system. *J. Biomed. Mater. Res.* 83A (3), 606–616.

2.6.7

Biomaterials for Cardiovascular Tissue Engineering

JENNIFER L. WEST

Duke University, Durham, NC, United States

Cardiovascular tissue engineering offers potential solutions in a variety of clinical conditions such as heart failure, atherosclerosis, myocardial infarction, valve disease, congenital heart defects, and vascular access. While this represents a wide variety of applications, there are significant commonalities across the tissue types in the cardiovascular system that impact approaches to the development of engineered tissues. For example, endothelial cells that line the entire cardiovascular system change function under different shear stress conditions, while vascular smooth muscle cells respond to cyclic strain. This chapter discusses the tissues and cells that comprise the cardiovascular system as well as optimization of biomaterials for these tissue-engineering applications.

Introduction

When selecting or developing biomaterials to use as scaffolds in cardiovascular tissue engineering, all of the design parameters that would broadly apply in tissue engineering need to be considered—biocompatibility, appropriate biodegradation, the ability to homogeneously seed cells throughout the scaffold, and maintenance of requisite cell function. Scaffold materials used in cardiovascular tissue engineering usually need to be compatible with culture in bioreactor systems. In addition, there are some unique aspects of cardiovascular tissues, such as control of thrombosis and mechanical sensitivity of vascular cells, that introduce additional criteria for an optimal scaffold material. In order to understand these design constraints, let's first develop your understanding of the tissues and cells of the cardiovascular system.

As shown in [Fig. 2.6.7.1](#), the cardiovascular system includes the heart (including both the heart wall and the valves) and blood vessels (including arteries, arterioles, capillaries, venules, and veins). The entire cardiovascular system is lined with a monolayer of endothelial cells. These are critical to prevention of thrombosis and to vascular homeostasis.

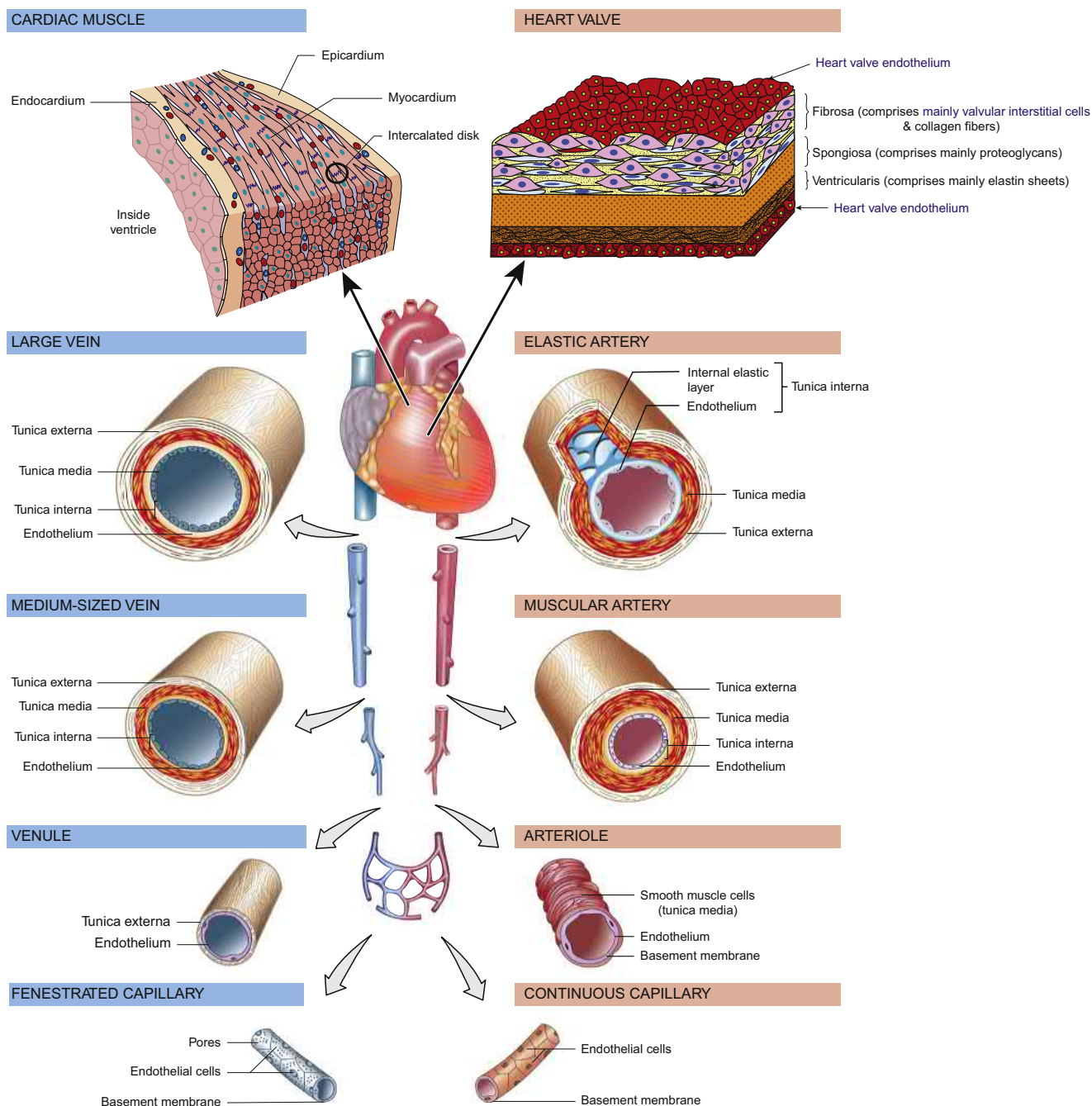
The entire cardiovascular system also includes muscle or muscle-like cells. These include cardiomyocytes in the heart wall, valve interstitial cells for heart valves, vascular smooth muscle cells in the blood vessels, and pericytes in capillaries.

Endothelial Cells

As stated above, endothelial cells line the blood-contacting surfaces of the entire cardiovascular system and are critical to both prevention of thrombosis and vascular homeostasis. Endothelial cells actively produce antithrombotic factors such as nitric oxide (NO), prostacyclin, plasminogen activators, and thrombomodulin ([Cines et al., 1998](#)). Endothelial cell surfaces also display a thromboresistant glycocalyx, a dense layer of polysaccharides attached to the membrane ([Sieve et al., 2018](#)). Endothelial-derived NO also has a critical function in maintaining other vascular cells (namely smooth muscle) in a quiescent state ([Bian et al., 2008](#); [Lloyd-Jones and Bloch, 1996](#)). Endothelial cells are highly responsive to shear stresses at their surface (normally in the range of 5–20 dyne/cm²), and are typically aligned in the direction of shear ([Nerem, 1993](#); [Nollert et al., 1992](#)). Abnormal shear stress environments can lead to loss of appropriate endothelial cell function, and thus adverse events like thrombosis. A complete and functional endothelial monolayer is likely required for success in any cardiovascular tissue-engineering application.

Cardiac Muscle

Tissue-engineered cardiac muscle (heart wall) is being explored to treat damage from myocardial infarction, heart failure, and a variety of congenital heart defects. The myocardium is composed primarily of multinucleated cardiomyocytes, and the interior surface is a monolayer of endothelial cells. The organization of cardiac muscle is highly anisotropic. Cardiomyocytes are highly elongated



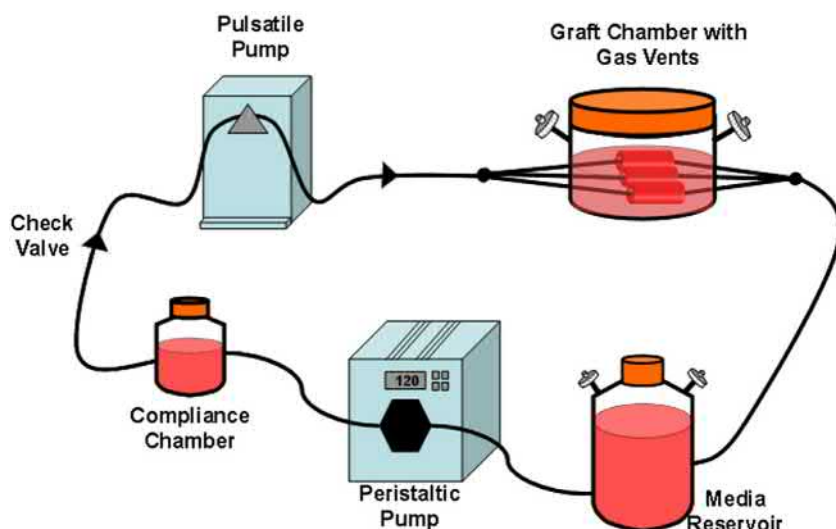
• **Figure 2.6.7.1** The cardiovascular system includes the heart and the network of systemic blood vessels. The entire system is lined with endothelial cells, critical to the prevention of thrombosis and maintenance of vascular homeostasis. Tissues where engineered replacement are needed include cardiac muscle, heart valves, and blood vessels.

and align relative to one another in the heart wall, with structural and electrical connections between cells to enable coordinated and effective contractions of the tissue. Intercalated disks (Fig. 2.6.7.1) formed between cardiac myocytes are critical in enabling electrical signals to be transmitted at appropriate speed and with directional control and also in allowing transmission of forces during contraction (Veeraraghavan et al., 2014). Additionally, because of the metabolic demands associated with its contractile activity, cardiac muscle has dense capillaries. Efforts to engineer

cardiac muscle will likely require construction of a functional microvasculature in the engineered tissue or rapid induction of in-growth of host vasculature.

Heart Valves

Tissue-engineered heart valves are being explored as options for repair of congenital defects or for treatment of valve disease. As shown in Fig. 2.6.7.1, the valve leaflet has three layers, with endothelial cells covering the outer surfaces.



• **Figure 2.6.7.2** Example design of a pulsatile flow bioreactor for culture of tissue-engineered blood vessels. The cell-seeded scaffolds are placed into the graft chamber, where they are bathed in cell culture media while additional cell culture media is pumped through the lumen of the vessel. Physiological flow and pressure profiles can be achieved, providing the cells on the scaffold with mechanical conditioning to optimize tissue formation.

The cells within the leaflet are referred to as valve interstitial cells (VICs). VICs actively remodel the extracellular matrix (ECM) that dominates the valve structure, allowing the tissue to remain mechanically functional without experiencing fatigue failure with about 40 million cycles per year (Grande-Allen and Liao, 2011; Ayoub et al., 2016; Cirka et al., 2015). Deposition and organization of new ECM by VICs has been shown to respond to mechanical forces (Ayoub et al., 2016). While the underlying biology of VICs is not well studied, they display some similarities to both vascular smooth muscle cells and to fibroblasts (Grande-Allen and Liao, 2011; Cirka et al., 2015), and when VIC phenotype is not appropriately controlled, calcification and fibrosis may result (Cirka et al., 2015).

Blood Vessels

Tissue-engineered blood vessels are being explored for use as vascular grafts, especially in small-diameter applications where synthetic grafts typically fail, and also as arteriovenous grafts for hemodialysis access. As shown in Fig. 2.6.7.1, vessels on both the arterial and venous sides of the vascular tree have distinctly layered structures, with differences between vessel types based primarily on differences in the thickness of the layers. All of the vessels possess an endothelial cell lining, with the layer referred to as the tunica intima. Below the endothelial lining there is a layer referred to as the tunica media or the medial layer. The tunica media is composed of vascular smooth muscle cells (SMCs) and an elastin-rich ECM, with both the SMCs and elastin aligned circumferentially. SMCs require physiologic cyclic strains for optimal alignment and function (Haga et al., 2007; Chan-Park et al., 2009). Additionally, SMCs can be in either a contractile or synthetic phenotype (Chan-Park et al., 2009). During initial formation of an engineered tissue, a proliferative

synthetic phenotype can be advantageous, but for long-term success, a quiescent contractile phenotype is needed. Signaling between endothelial cells and SMCs is important for regulation of the SMC phenotype and tissue homeostasis (Chan-Park et al., 2009). Most approaches to tissue engineering of blood vessels have focused on creating the intimal and medial layers, as these are clearly required to have a functional blood vessel. Some efforts also add the tunica externa (also called the adventitia), a fibroblast-rich connective tissue that further supports the structure.

Scaffold Materials

As discussed above, the cell types employed in cardiovascular tissue engineering are highly responsive to mechanical conditioning, and because of this, most engineered tissues in this field are grown in various types of flow bioreactors that can generate appropriate shear stresses and cyclic strains (Mironov et al., 2006; Freed et al., 2006; Huang and Niklason, 2014). An example of a typical bioreactor used for tissue engineering of blood vessels is shown in Fig. 2.6.7.2, where pulsatile flow of cell culture media through the lumen of the vessel creates shear stress at the intimal surface and cyclic strain across the vessel wall (Hahn et al., 2007). To realize the benefits of mechanical conditioning in bioreactors, it is important to use materials that allow appropriate transmission of forces through the structure, giving preference to soft, elastic materials, ideally with properties approximating those of cardiovascular tissues. Note that bioreactors for cardiac tissue engineering will sometimes also include electrical stimulation (Radisic et al., 2004), so integration of electrodes may also be necessary. In order to achieve these goals, while also having appropriate biocompatibility and biodegradation, efforts have largely focused on protein hydrogels, synthetic biodegradable polymers,

and synthetic biodegradable hydrogels. Decellularized tissues have also been explored as scaffold materials. Additionally, it is important to have materials that support the formation of an endothelial cell monolayer at the blood-contacting surface. Scaffold design strategies to promote endothelialization are also discussed below.

Protein Hydrogels

Protein hydrogels such as collagen gels and fibrin gels have been employed in numerous cardiovascular tissue-engineering studies (Zhang et al., 2015; Reis et al., 2016; Barsotti et al., 2011). These types of materials are very supportive of cell attachment and growth, providing ligands for integrins and other cellular receptors. These scaffold materials are biodegraded by cells using natural proteolytic mechanisms, such as matrix metalloproteinases (MMPs) or plasmin, linking the rate of biodegradation to cellular activity within the scaffold. Fabrication of these gels into appropriate shapes is also straightforward, essentially just pouring liquid precursors into molds, and homogeneous cell seeding can be achieved by mixing cells with the aqueous gel precursor solution. In most cases, these protein hydrogels experience very significant contraction by cells growing within them, reducing dimensions by as much as 90% (Schutte et al., 2010; Tranquillo et al., 1996; Weinberg and Bell, 1986).

Pioneering work by Weinberg and Bell utilized collagen gel scaffolds to form the first tissue-engineered blood vessels (Weinberg and Bell, 1986). This was accomplished by casting SMCs and collagen in an annular mold, allowing gelation of the collagen to form the medial layer of the tissue-engineered blood vessel. Later, an adventitial layer of fibroblasts was added, and after further culture, endothelial cells were seeded on the inner luminal surface to form the intimal layer. Collagen gels have also been used as scaffolds for tissue-engineered myocardial patches (Costa et al., 2003; McCain et al., 2014; Sun et al., 2017) and tissue-engineered heart valves (Gupta et al., 2007; Neidert and Tranquillo, 2006).

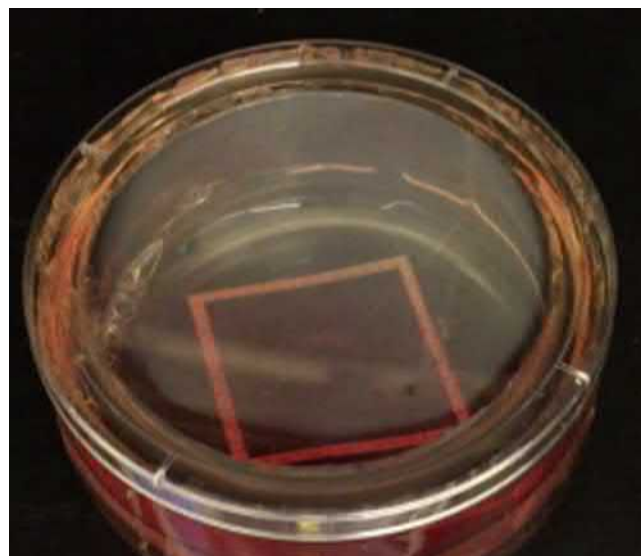
Collagen gels are formed by neutralizing an acidic solution of collagen, initiating fibrillogenesis that will induce gelation at sufficient collagen concentrations (Weinberg and Bell, 1986). The mechanical properties of collagen gels depend on the concentration of collagen in the precursor solution, but can be further enhanced via chemical cross-linking with agents such as formaldehyde or glutaraldehyde, though these can compromise the viability of encapsulated cells (Huang and Niklason, 2014; Charulatha and Rajaram, 2003). Lysyl oxidase (Elbjeirami et al., 2003) and glycation cross-linking (Girton et al., 1999) have been investigated as more cell-compatible methods. Even with covalent cross-linking, the mechanical properties of collagen gels may be too weak to withstand culture conditions in bioreactor systems, so in some cases “support sleeves” have been added to the design to help prevent rupture of engineered vessels (Schutte et al., 2010; Berglund et al., 2003).

Fibrin gels have similarly been utilized as scaffolds to form tissue-engineered blood vessels (Gui et al., 2014; Yao et al.,

2008; Syedain et al., 2011), heart muscle (Bian et al., 2014; Jackman et al., 2016; Shadrin et al., 2017), and heart valves (Moreira et al., 2016; Weber et al., 2015; Robinson et al., 2008). Fibrin gels are formed by mixing fibrinogen with thrombin and calcium to induce cleavage of fibrinogen to fibrin and allow ensuing assembly into fibers (Barsotti et al., 2011; Shaikh et al., 2008). At sufficient concentrations of fibrinogen, fibrillogenesis will result in gel formation. This is the same process observed in coagulation to form a fibrin clot, a material that also serves as a natural, provisional matrix in wound healing. The thrombin treatment that induces gelation is highly cell-compatible, so cells can be added to the fibrinogen solution for homogeneous encapsulation in the ultimate gel material (Barsotti et al., 2011; Shaikh et al., 2008). Similar to collagen gels, fibrin gels have very weak mechanical properties and sometimes require reinforcing materials (Moreira et al., 2016). Fig. 2.6.7.3 shows a fibrin gel seeded with human induced pluripotent stem cell-derived cardiomyocytes that will form a cardiac patch following 5 weeks in culture. The resultant patches have been implanted epicardially in nude rats where, after 3 weeks, they exhibited survival and electrical function but lacked electrical integration with the host heart (Shadrin et al., 2017).

Decellularized Tissues

More recently, there has been substantial interest in using decellularized tissues as scaffolds in cardiovascular tissue engineering (Taylor et al., 2018). Compared to the simple protein gels described above, decellularization of tissue leaves the extracellular matrix largely intact, providing a complex composition and architecture. Decellularization can include physical methods, such as freeze–thaw cycling, pressure and supercritical fluids, and/or chemical methods, such as enzymes and detergents



• **Figure 2.6.7.3** Stem cell-derived cardiomyocytes growing within a fibrin gel scaffold to form a 4 × 4 cm cardiac patch. The fibrin gel is surrounded by a Cerex frame for support of auxotonic tissue loading. The resultant cardiac patches can be implanted on the surface of the heart to compensate for damage. (Photo courtesy of Dr. Nenad Bursac.)

(Taylor et al., 2018). Approaches can use relatively simple and widely available extracellular matrices, like decellularized small intestine submucosa (Badylak et al., 1989), or organ-specific decellularized tissues, like decellularized heart (Ott et al., 2008). In a landmark study by Taylor et al., a coronary perfusion process was developed to decellularize cadaveric hearts and then repopulate the structure with neonatal cardiac cells (via intramural injection) and endothelial cells (via perfusion) (Ott et al., 2008). These recellularized heart tissues were cultured in a perfusion bioreactor with electrical stimulation for up to 28 days. By day 8, these constructs demonstrated some electric and contractile responses. Perfused endothelial cells were able to line the coronary vessels and ventricles. While additional developments are needed, this is a promising avenue for whole-heart tissue engineering.

Synthetic Polymers

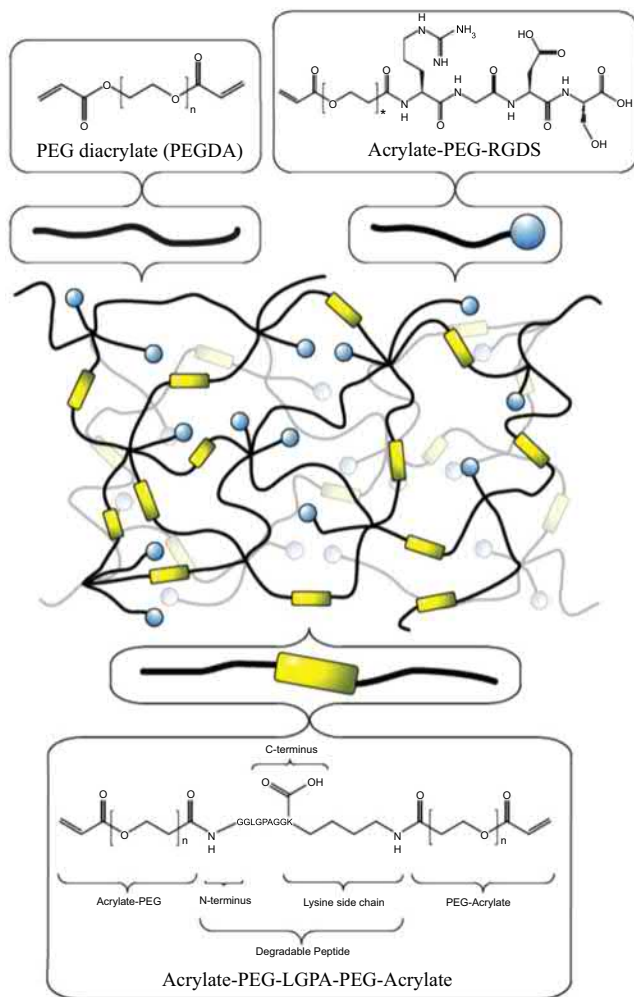
Some of the earliest efforts in cardiovascular tissue engineering utilized porous polyester scaffolds such as poly(caprolactone), poly(glycolic acid) (PGA), poly(lactic acid) (PLA), and copolymers thereof (PLGA). These have been used as scaffolds for tissue-engineered blood vessels (Niklason et al., 1999), heart valves (Shinoka et al., 1995), and cardiac muscle (Bursac et al., 1999). These materials provide tunable hydrolytic degradation rates, production of nontoxic (though acidic) degradation products, and the ability to fabricate interconnected pore networks to allow cell seeding. Pore networks are most commonly formed using porogen processing, such as incorporation of salt crystals in the polymer melt, followed by leaching of the salts from the solidified polymer matrix upon immersion in water (Mikos et al., 1993). Gas foaming (Zhu et al., 2008), electrospinning (Li et al., 2002), and 3D printing (Lee et al., 2008) can also be utilized to generate porous networks. Pore sizes in the range of hundreds of microns are generally required for efficient cell seeding, accomplished by infusing a cell suspension through the porous network.

The first report of *in vivo* assessment of a tissue-engineered vascular graft utilized a PGA mesh scaffold (Niklason et al., 1999). In this effort, PGA mesh scaffolds were sewn into a tubular form using Dexon sutures. Vascular smooth muscle cells were seeded onto the scaffolds, and the constructs were then grown in a pulsatile flow bioreactor for 8 weeks. Endothelial cells were then introduced to the flow system and allowed to adhere to the inner surface of the graft. The resultant tissue-engineered vascular grafts exhibited burst strength akin to saphenous vein grafts, and after implantation in a Yucatan miniature pig, graft patency (maintenance of blood flow) was observed. A key limitation of these scaffolds was their poor elasticity. As a result of the material mechanical properties, there was very little strain transmitted across the graft wall, limiting the mechanical conditioning experienced by the smooth muscle cells growing in the scaffold, especially during early phases of tissue growth before the biodegradable polymer was replaced by cell-secreted extracellular matrix.

Similar scaffold materials have also been employed in cardiac muscle tissue engineering (Bursac et al., 1999). Because alignment of cardiomyocytes is critical to development of a functional tissue substitute, techniques to produce scaffolds with aligned topographical cues have been of interest. For example, electrospinning can be used to form nanofibrous scaffolds of polymers like PLA, PGA, or PLGA, and it is possible to create alignment of the fibers in the scaffold by spinning fibers onto a rotating mandrel (Zhu et al., 2010; Streeter et al., 2019) or through postprocessing uniaxial stretching (Zong et al., 2005). When neonatal rat cardiomyocytes were seeded onto electrospun scaffolds, comparing scaffolds with random fiber orientations to ones with very high fiber alignment, it was found that while the cells attached, grew, and exhibited sarcomeres and intercalated disks on the random scaffolds, the oriented scaffolds seemed to provide guidance to the cells, resulting in an organized and aligned cell population (Zong et al., 2005). Others found that alignment of electrospun PLA scaffolds also enhanced production of α -actinin and troponin I (Liu et al., 2017).

Polyester scaffolds were also investigated as scaffolds for tissue-engineered heart valves (Shinoka et al., 1995; Breuer et al., 1996; Shinoka et al., 1996). In these studies, tissue-engineered heart valve leaflets prepared with PGA and PLA scaffolds were implanted in lambs for up to 11 weeks. Unfortunately, only single leaflets could be tested, as the stiffness of the scaffold material made it impossible to create a functional trileaflet valve replacement. The stiffness of PLA and PGA would also limit appropriate conditioning in a bioreactor system. The bending motion of the heart valve occurs in response to pressure differentials across the valve and the anisotropic material properties of the valve tissue. In order to achieve appropriate bending behaviors, tissue engineers have investigated several alternative porous synthetic polymer scaffold materials with improved pliability, such as poly(hydroxyalkanoate), a biodegradable elastomer (Sodian et al., 2000). Tissue-engineered trileaflet heart valves formed with PHA scaffolds, sequentially seeded with myofibroblasts and endothelial cells, and cultured in a pulsatile flow bioreactor were implanted in the pulmonary position in lambs for up to 20 weeks. The valves remained mobile and functional without signs of stenosis, thrombosis, or aneurysm. The valves had a confluent endothelial lining on the surface, and the PHA had fully degraded and been replaced with cell-secreted extracellular matrix proteins.

There remains significant need for new biodegradable elastomers for use as scaffolds in cardiovascular tissue engineering to provide biocompatibility, tunable biodegradation rates, and also elasticity and compliance closer to native cardiovascular tissues. Examples of emerging biodegradable elastomers include poly(glycerol sebacate) (Wang et al., 2002), poly(1,3-diamino-2-propanol-copolyol sebacate) (Bettinger et al., 2008), and poly(diols citrate) (Yang et al., 2005), and biodegradable polyurethanes are also being developed (Hung et al., 2014; Guelcher, 2008; Hao et al., 2016). These new materials offer mechanical performance better suited to cardiovascular tissue-engineering applications.



• **Figure 2.6.7.4** When designing a biodegradable and cell-adhesive synthetic hydrogel, a bioinert material such as PEG can be modified to include degradation sites (yellow) in the backbone of the hydrogel network as well as grafted cell adhesion ligands (such as RGDS, blue). Degradation sites could include hydrolytically degradable blocks, such as oligo (lactic acid), or proteolytically degradable peptides (such as LGPA) for cell-mediated degradation. Cross-linkable groups such as acrylates at the termini of the individual polymers allow conversion of aqueous polymer solutions into 3D hydrogels under conditions mild enough for cell encapsulation.

Synthetic Hydrogels

Alternatively, synthetic hydrogel materials have also been investigated for use as flexible and elastic scaffold materials in cardiovascular tissue engineering. Synthetic hydrogels are formed by cross-linking of hydrophilic polymers such as poly(ethylene glycol) (Mann et al., 2001) or poly(vinyl alcohol) (Schmedlen et al., 2002). Often, cross-linking conditions are mild enough to be carried out in the presence of cells, allowing the cell suspension to be mixed with the hydrogel precursors for homogeneous incorporation of cells throughout the hydrogel material (Mann et al., 2001; Schmedlen et al., 2002). Most synthetic hydrogels are very bioinert, so it is usually necessary to modify the materials to enable biodegradation and cell adhesion (Nguyen and West, 2002). As shown in Fig. 2.6.7.4, these goals can be accomplished by including degradation sites, such as



• **Figure 2.6.7.5** Vascular SMCs were encapsulated in hydrogel scaffolds fabricated into tubes using annular molds during cross-linking. These constructs are mounted in the graft chamber of a pulsatile flow bioreactor. Culture media will be added to the bath surrounding the tissue-engineered blood vessels and also pumped through the center to provide physiologically relevant mechanical conditioning.

proteolytically degradable peptides or hydrolytically degradable polyester blocks, into the backbone of the hydrogel network and grafting cell-adhesive peptides to the hydrogel network. Additionally, when the hydrogel scaffold provides a bioinert background with little or no protein adsorption, cell attachment to the hydrogel is limited to the cell adhesion sequences specifically and intentionally added to the material. This can allow one to select cell-adhesive ligands that interact with a desired cell type, such as endothelial cells, but not undesired cell types such as platelets or fibroblasts. Examples of cell-adhesion peptides that favor adhesion of endothelial cells include REDV (Hubbell et al., 1991), YIGSR (Jun and West, 2005), TPSLEQRTVYAK (Li et al., 2013), CRKRLQVQLSIRT (Puperi et al., 2015), and CRRETAWAC (Bastjanic et al., 2016). Finally, while most synthetic hydrogels have substantially greater mechanical integrity than collagen and fibrin gels, they are mechanically weak.

Hydrogels formed from acrylate-terminated derivatives of PEG have been used as scaffolds for both tissue-engineered blood vessels (Hahn & et al., 2007) and heart valves (Puperi et al., 2015; Durst et al., 2011; Zhang et al., 2015). In these studies, the hydrogel scaffolds were modified to be proteolytically degradable and cell adhesive. When tissue-engineered vascular grafts formed with these hydrogel scaffolds were cultured in pulsatile flow bioreactors with pressure waveforms ranging from a minimum of 80 to maximum of 125 mmHg, cyclic strains across the vessel wall ranged from 3% to 11%, depending on the hydrogel formulation, closely mimicking the transmission of strain across vessel walls in vivo (Hahn et al., 2007). Fig. 2.6.7.5 shows these hydrogel scaffolds formed into tubes and mounted into the graft culture chamber of a pulsatile flow bioreactor.

In some of the work to develop tissue-engineered heart valves, hydrogels were fabricated with differential display of cell-adhesive peptides in the bulk versus the surface in order to provide different cues and interactions for VICs versus endothelial cells in order to optimize formation of an endothelial monolayer (Puperi et al., 2015). The bulk hydrogel was designed to be proteolytically degraded by cell-secreted MMPs and had immobilized RGDS peptides to mediate cell adhesion. VICs were encapsulated in this material, after which the surface of the hydrogel was covalently modified with the peptide CRKRLQVQLSIRT to enhance subsequent endothelial cell attachment. Endothelial cells were finally seeded onto this surface. This provided

both the anatomically appropriate layering of cell types and also optimized endothelial cell attachment and phenotype.

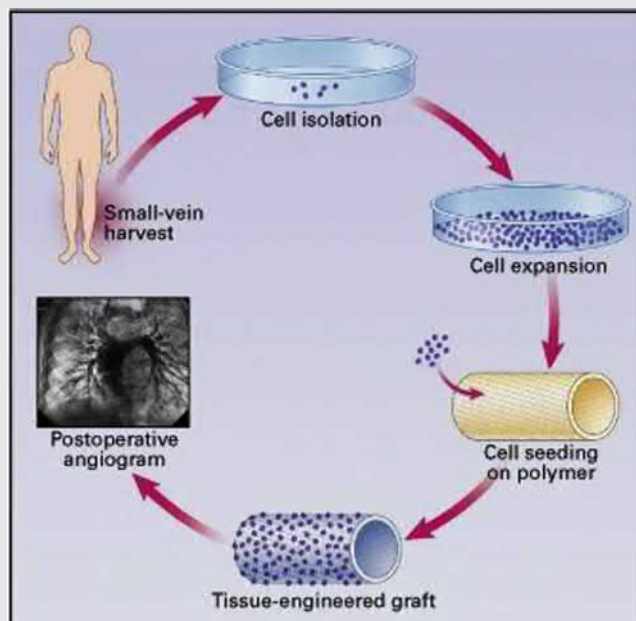
Conclusions

With cardiovascular disease remaining a major cause of mortality, there is a significant need for tissue-engineered products for the heart and vasculature. We are beginning to see clinical impacts of the tremendous advances that have been made in this field (Drews et al., 2017; L'Heureux et al., 2007; Benrashid et al., 2016). Nonetheless, significant progress is still needed in order to develop functional engineered tissues for the cardiovascular system.

CASE STUDY

A girl born with a single right ventricle and pulmonary atresia underwent pulmonary artery angioplasty and the Fontan procedure at the age of 3.25 years (Shin'oka et al., 2001). Seven months after this surgery, she developed total occlusion of the right intermediate pulmonary artery. The decision was made to construct and implant an autologous tissue-engineered pulmonary artery.

To accomplish this, a small segment of peripheral vein was harvested as a cell source. Following expansion in culture, the cells were seeded on a tubular, biodegradable PCL-PLA scaffold reinforced with woven PGA. Ten days after cell seeding, the tissue engineered construct was implanted to bypass the occluded pulmonary artery. Follow-up angiography indicated that the implanted graft remained completely patent.



Chapter Exercises

1. Compare and contrast the following scaffold materials: collagen gel, decellularized small intestine submucosa, poly(glycolic acid), poly(hydroxyalkanoate), and poly(ethylene glycol)-diacrylate.
2. Explain why a confluent endothelial lining on the blood-contacting surfaces of an engineered cardiovascular tissue is critical.
3. What scaffold properties are most important for tissue engineering a heart valve replacement?
4. If a cardiac patch incorporating cardiomyocytes is implanted epicardially, what events would need to occur to provide improvements in cardiac output?
5. Design a process for production of a tissue-engineered vascular graft that you believe will have optimal performance.

References

- Ayoub, S., et al., 2016. Heart valve biomechanics and underlying mechanobiology. *Comp. Physiol.* 6 (4), 1743–1780.
- Badylak, S.F., et al., 1989. Small intestinal submucosa as a large diameter vascular graft in the dog. *J. Surg. Res.* 47 (1), 74–80.
- Barsotti, M.C., et al., 2011. Fibrin as a scaffold for cardiac tissue engineering. *Biotechnol. Appl. Biochem.* 58 (5), 301–310.
- Bastjanic, J.M., et al., 2016. Dual biofunctional polymer modifications to address endothelialization and smooth muscle cell integration of ePTFE vascular grafts. *J. Biomed. Mater. Res. A* 104 (1), 71–81.
- Benrashid, E., et al., 2016. Tissue engineered vascular grafts: origins, development, and current strategies for clinical application. *Methods* 99, 13–19.
- Berglund, J.D., et al., 2003. A biological hybrid model for collagen-based tissue engineered vascular constructs. *Biomaterials* 24 (7), 1241–1254.
- Bettinger, C.J., et al., 2008. Amino alcohol-based degradable poly(ester amide) elastomers. *Biomaterials* 29 (15), 2315–2325.

- Bian, W., et al., 2014. Robust T-tubulation and maturation of cardiomyocytes using tissue-engineered epicardial mimetics. *Biomaterials* 35 (12), 3819–3828.
- Bian, K., Doursout, M.F., Murad, F., 2008. Vascular system: role of nitric oxide in cardiovascular diseases. *J. Clin. Hypertens.* 10 (4), 304–310.
- Breuer, C.K., et al., 1996. Tissue engineering lamb heart valve leaflets. *Biotechnol. Bioeng.* 50 (5), 562–567.
- Bursac, N., et al., 1999. Cardiac muscle tissue engineering: toward an in vitro model for electrophysiological studies. *Am. J. Physiol.* 277 (2) p. H433–44.
- Chan-Park, M.B., et al., 2009. Biomimetic control of vascular smooth muscle cell morphology and phenotype for functional tissue-engineered small-diameter blood vessels. *J. Biomed. Mater. Res. A* 88 (4), 1104–1121.
- Charulatha, V., Rajaram, A., 2003. Influence of different crosslinking treatments on the physical properties of collagen membranes. *Biomaterials* 24 (5), 759–767.
- Cines, D.B., et al., 1998. Endothelial cells in physiology and in the pathophysiology of vascular disorders. *Blood* 91 (10), 3527–3561.
- Cirka, H.A., Kural, M.H., Billiar, K.L., 2015. Mechano regulation of aortic valvular interstitial cell life and death. *J. Long Term Eff. Med. Implant.* 25 (1–2), 3–16.
- Costa, K.D., Lee, E.J., Holmes, J.W., 2003. Creating alignment and anisotropy in engineered heart tissue: role of boundary conditions in a model three-dimensional culture system. *Tissue Eng.* 9 (4), 567–577.
- Draws, J.D., Miyachi, H., Shinoka, T., 2017. Tissue-engineered vascular grafts for congenital cardiac disease: clinical experience and current status. *Trends Cardiovasc. Med.* 27 (8), 521–531.
- Durst, C.A., et al., 2011. Flexural characterization of cell encapsulated PEGDA hydrogels with applications for tissue engineered heart valves. *Acta Biomater.* 7 (6), 2467–2476.
- Elbjerrami, W.M., et al., 2003. Enhancing mechanical properties of tissue-engineered constructs via lysyl oxidase crosslinking activity. *J. Biomed. Mater. Res. A* 66 (3), 513–521.
- Freed, L.E., et al., 2006. Advanced tools for tissue engineering: scaffolds, bioreactors, and signaling. *Tissue Eng.* 12 (12), 3285–3305.
- Girton, T.S., Oegema, T.R., Tranquillo, R.T., 1999. Exploiting glycation to stiffen and strengthen tissue equivalents for tissue engineering. *J. Biomed. Mater. Res.* 46 (1), 87–92.
- Grande-Allen, K.J., Liao, J., 2011. The heterogeneous biomechanics and mechanobiology of the mitral valve: implications for tissue engineering. *Curr. Cardiol. Rep.* 13 (2), 113–120.
- Guelcher, S.A., 2008. Biodegradable polyurethanes: synthesis and applications in regenerative medicine. *Tissue Eng. B Rev.* 14 (1), 3–17.
- Gui, L., et al., 2014. Construction of tissue-engineered small-diameter vascular grafts in fibrin scaffolds in 30 days. *Tissue Eng. A* 20 (9–10), 1499–1507.
- Gupta, V., et al., 2007. Synthesis of glycosaminoglycans in differently loaded regions of collagen gels seeded with valvular interstitial cells. *Tissue Eng.* 13 (1), 41–49.
- Haga, J.H., Li, Y.S., Chien, S., 2007. Molecular basis of the effects of mechanical stretch on vascular smooth muscle cells. *J. Biomech.* 40 (5), 947–960.
- Hahn, M.S., et al., 2007. Physiologic pulsatile flow bioreactor conditioning of poly (ethylene glycol)-based tissue engineered vascular grafts. *Ann. Biomed. Eng.* 35 (2), 190–200.
- Hao, H., et al., 2016. Synthesis and characterization of biodegradable lysine-based waterborne polyurethane for soft tissue engineering applications. *Biomater Sci* 4 (11), 1682–1690.
- Huang, A.H., Niklason, L.E., 2014. Engineering of arteries in vitro. *Cell. Mol. Life Sci.* 71 (11), 2103–2118.
- Hubbell, J.A., et al., 1991. Endothelial cell-selective materials for tissue engineering in the vascular graft via a new receptor. *Biotechnology* 9 (6), 568–572.
- Hung, K.C., Tseng, C.S., Hsu, S.H., 2014. Synthesis and 3D printing of biodegradable polyurethane elastomer by a water-based process for cartilage tissue engineering applications. *Adv. Healthc. Mater.* 3 (10), 1578–1587.
- Jackman, C.P., Carlson, A.L., Bursac, N., 2016. Dynamic culture yields engineered myocardium with near-adult functional output. *Biomaterials* 111, 66–79.
- Jun, H.W., West, J.L., 2005. Modification of polyurethane urea with PEG and YIGSR peptide to enhance endothelialization without platelet adhesion. *J. Biomed. Mater. Res. B Appl. Biomater.* 72 (1), 131–139.
- Lee, M., Wu, B.M., Dunn, J.C., 2008. Effect of scaffold architecture and pore size on smooth muscle cell growth. *J. Biomed. Mater. Res. A* 87 (4), 1010–1016.
- L'Heureux, N., et al., 2007. Technology insight: the evolution of tissue-engineered vascular grafts—from research to clinical practice. *Nat. Clin. Pract. Cardiovasc. Med.* 4 (7), 389–395.
- Li, W.J., et al., 2002. Electrospun nanofibrous structure: a novel scaffold for tissue engineering. *J. Biomed. Mater. Res.* 60 (4), 613–621.
- Li, Q., et al., 2013. Functionalization of the surface of electrospun poly(epsilon-caprolactone) mats using zwitterionic poly(carboxybetaine methacrylate) and cell-specific peptide for endothelial progenitor cells capture. *Mater Sci Eng C Mater Biol Appl* 33 (3), 1646–1653.
- Liu, Y., Wang, S., Zhang, R., 2017. Composite poly(lactic acid)/chitosan nanofibrous scaffolds for cardiac tissue engineering. *Int. J. Biol. Macromol.* 103, 1130–1137.
- Lloyd-Jones, D.M., Bloch, K.D., 1996. The vascular biology of nitric oxide and its role in atherogenesis. *Annu. Rev. Med.* 47, 365–375.
- Mann, B.K., et al., 2001. Smooth muscle cell growth in photopolymerized hydrogels with cell adhesive and proteolytically degradable domains: synthetic ECM analogs for tissue engineering. *Biomaterials* 22 (22), 3045–3051.
- McCain, M.L., et al., 2014. Micromolded gelatin hydrogels for extended culture of engineered cardiac tissues. *Biomaterials* 35 (21), 5462–5471.
- Mikos, A.G., et al., 1993. Laminated three-dimensional biodegradable foams for use in tissue engineering. *Biomaterials* 14 (5), 323–330.
- Mironov, V., et al., 2006. Cardiovascular tissue engineering I. Perfusion bioreactors: a review. *J. Long Term Eff. Med. Implant.* 16 (2), 111–130.
- Moreira, R., et al., 2016. Tissue-engineered fibrin-based heart valve with bio-inspired textile reinforcement. *Adv. Healthc. Mater.* 5 (16), 2113–2121.
- Neidert, M.R., Tranquillo, R.T., 2006. Tissue-engineered valves with commissural alignment. *Tissue Eng.* 12 (4), 891–903.
- Nerem, R.M., 1993. Hemodynamics and the vascular endothelium. *J. Biomech. Eng.* 115 (4b), 510–514.
- Nguyen, K.T., West, J.L., 2002. Photopolymerizable hydrogels for tissue engineering applications. *Biomaterials* 23 (22), 4307–4314.
- Niklason, L.E., et al., 1999. Functional arteries grown in vitro. *Science* 284 (5413), 489–493.
- Nollert, M.U., Panaro, N.J., McIntire, L.V., 1992. Regulation of genetic expression in shear stress-stimulated endothelial cells. *Ann. NY. Acad. Sci.* 665, 94–104.
- Ott, H.C., et al., 2008. Perfusion-decellularized matrix: using nature's platform to engineer a bioartificial heart. *Nat. Med.* 14 (2), 213–221.

- Puperi, D.S., et al., 2015. 3-Dimensional spatially organized PEG-based hydrogels for an aortic valve co-culture model. *Biomaterials* 67, 354–364.
- Radisic, M., et al., 2004. Functional assembly of engineered myocardium by electrical stimulation of cardiac myocytes cultured on scaffolds. *Proc. Natl. Acad. Sci. USA*. 101 (52), 18129–18134.
- Reis, L.A., et al., 2016. Biomaterials in myocardial tissue engineering. *J. Tissue Eng. Regenerat. Med.* 10 (1), 11–28.
- Robinson, P.S., et al., 2008. Functional tissue-engineered valves from cell-remodeled fibrin with commissural alignment of cell-produced collagen. *Tissue Eng. A* 14 (1), 83–95.
- Schmedlen, R.H., Masters, K.S., West, J.L., 2002. Photocrosslinkable polyvinyl alcohol hydrogels that can be modified with cell adhesion peptides for use in tissue engineering. *Biomaterials* 23 (22), 4325–4332.
- Schutte, S.C., et al., 2010. Cyclic strain improves strength and function of a collagen-based tissue-engineered vascular media. *Tissue Eng. A* 16 (10), 3149–3157.
- Shadrin, I.Y., et al., 2017. Cardiopatch platform enables maturation and scale-up of human pluripotent stem cell-derived engineered heart tissues. *Nat. Commun.* 8 (1), 1825.
- Shaikh, F.M., et al., 2008. Fibrin: a natural biodegradable scaffold in vascular tissue engineering. *Cells Tissues Organs* 188 (4), 333–346.
- Shinoka, T., et al., 1995. Tissue engineering heart valves: valve leaflet replacement study in a lamb model. *Ann. Thorac. Surg.* 60 (6 Suppl. 1), S513–S516.
- Shinoka, T., et al., 1996. Tissue-engineered heart valves. autologous valve leaflet replacement study in a lamb model. *Circulation* 94 (9 Suppl. 1) p. Ii164–i168.
- Shin'oka, T., Imai, Y., Ikada, Y., 2001. Transplantation of a tissue-engineered pulmonary artery. *N. Engl. J. Med.* 344 (7), 532–533.
- Sieve, I., Munster-Kuhnle, A.K., Hilfiker-Kleiner, D., 2018. Regulation and function of endothelial glycocalyx layer in vascular diseases. *Vasc. Pharmacol.* 100, 26–33.
- Sodian, R., et al., 2000. Tissue engineering of heart valves: in vitro experiences. *Ann. Thorac. Surg.* 70 (1), 140–144.
- Streeter, B.W., et al., 2019. Electrospun nanofiber-based Patches for the delivery of cardiac progenitor cells. *ACS Appl. Mater. Interfaces* 11 (20), 18242–18253.
- Sun, H., et al., 2017. Carbon nanotube-incorporated collagen hydrogels improve cell alignment and the performance of cardiac constructs. *Int. J. Nanomed.* 12, 3109–3120.
- Syedain, Z.H., et al., 2011. Implantable arterial grafts from human fibroblasts and fibrin using a multi-graft pulsed flow-stretch bioreactor with noninvasive strength monitoring. *Biomaterials* 32 (3), 714–722.
- Taylor, D.A., et al., 2018. Decellularized matrices in regenerative medicine. *Acta Biomater.* 74, 74–89.
- Tranquillo, R.T., et al., 1996. Magnetically orientated tissue-equivalent tubes: application to a circumferentially orientated media-equivalent. *Biomaterials* 17 (3), 349–357.
- Veeraraghavan, R., Poelzing, S., Gourdie, R.G., 2014. Intercellular electrical communication in the heart: a new, active role for the intercalated disk. *Cell Commun. Adhes.* 21 (3), 161–167.
- Wang, Y., et al., 2002. A tough biodegradable elastomer. *Nat. Biotechnol.* 20 (6), 602–606.
- Weber, M., et al., 2015. Multiple-step injection molding for fibrin-based tissue-engineered heart valves. *Tissue Eng. C Methods* 21 (8), 832–840.
- Weinberg, C.B., Bell, E., 1986. A blood vessel model constructed from collagen and cultured vascular cells. *Science* 231 (4736), 397–400.
- Yang, J., et al., 2005. Novel biphasic elastomeric scaffold for small-diameter blood vessel tissue engineering. *Tissue Eng.* 11 (11–12), 1876–1886.
- Yao, L., Liu, J., Andreadis, S.T., 2008. Composite fibrin scaffolds increase mechanical strength and preserve contractility of tissue engineered blood vessels. *Pharm. Res.* 25 (5), 1212–1221.
- Zhang, X., et al., 2015a. Application of hydrogels in heart valve tissue engineering. *J. Long Term Eff. Med. Implant.* 25 (1–2), 105–134.
- Zhang, X., et al., 2015b. Integrating valve-inspired design features into poly(ethylene glycol) hydrogel scaffolds for heart valve tissue engineering. *Acta Biomater.* 14, 11–21.
- Zhu, X.H., et al., 2008. Characterization of porous poly(D,L-lactico-glycolic acid) sponges fabricated by supercritical CO₂ gas-foaming method as a scaffold for three-dimensional growth of Hep3B cells. *Biotechnol. Bioeng.* 100 (5), 998–1009.
- Zhu, Y., et al., 2010. Macro-alignment of electrospun fibers for vascular tissue engineering. *J. Biomed. Mater. Res. B Appl. Biomater.* 92 (2), 508–516.
- Zong, X., et al., 2005. Electrospun fine-textured scaffolds for heart tissue constructs. *Biomaterials* 26 (26), 5330–5338.

2.6.8

Soft Tissue Engineering

NICOLE R. RAIA, MEGHAN MCGILL, TYLER MARCET, SARAH E. VIDAL YUCHA,
DAVID L. KAPLAN

Department of Biomedical Engineering, Tufts University, Medford, MA, United States

Introduction

In tissue engineering, “soft tissue” is a broad term that typically refers to all tissues except bone. This includes, but is not limited to, skin, musculoskeletal (cartilage, ligaments/tendons, muscle, connective tissues), adipose, cardiovascular, neural (brain, nerves), gastrointestinal, vasculature (blood and lymph vessels), liver, lung, kidney, and ocular tissues. In this chapter, the basic properties of soft tissues and the types of biomaterials that have been used in soft tissue implants or engineered in vitro models are reviewed. The progress made in the fields of adipose, gastrointestinal, and skin tissue engineering is then explored in greater detail. The design criteria for each of these tissue types is different, depending on the native anatomy, physiology, and the intended application, and the material requirements for each application also differ. Progress in mimicking the native environment for in vitro tissue models or clinically used fillers and grafts has been made in each of these fields. However, limitations associated with current tissue models and biomaterials open the door for biomaterial engineering principles to be applied to develop the next generation of soft tissue scaffolds.

Properties of Soft Tissues

Soft tissues are highly flexible with stiffness values ranging from 0.1 kPa to 1 MPa (Liu et al., 2015; Comley and Fleck, 2009, 2010; Skeldon et al., 2018; Mckee et al., 2011; Kalra et al., 2016; Levental et al., 2007) (Fig. 2.6.7.1), and the mechanical properties are related to the tissue function. For example, load-bearing tissues, such as cartilage and tendon, are much stiffer than nonload-bearing tissues, such as brain. The mechanical properties of tissues are driven by the composition and organization of the extracellular matrix (ECM). The main components of soft tissue ECM are fibrous proteins (i.e., collagen, elastin), glycosaminoglycans (GAGs: i.e., hyaluronic acid, chondroitin sulfate), and proteoglycans (i.e., aggrecan, versican), though the relative concentration of each component and the structural organization

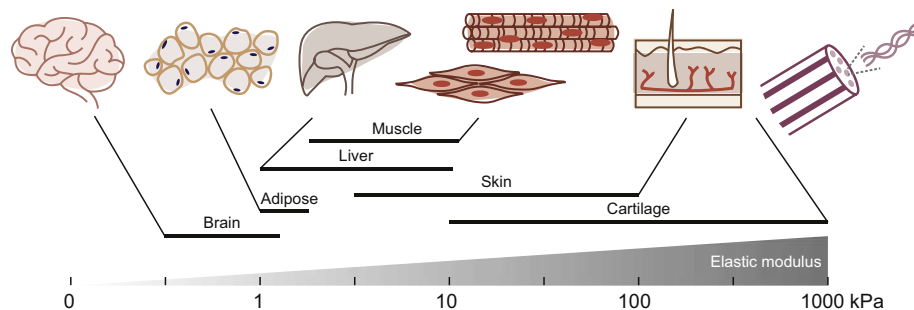
depend on tissue type, age, and disease state (Cox and Eler, 2011; Frantz et al., 2010; Shuttleworth, 1998; Kurtz and Oh, 2012). For example, the brain contains high concentrations of GAGs and lower amounts of collagens (Novak and Kaye, 2000), whereas cartilage (specifically articular cartilage) is primarily composed of collagens, and proteoglycans are a secondary component (Palukuru et al., 2014).

Common Biomaterials Used for Soft Tissue Engineering

When designing biomaterials, the goal is to match both the biochemical and mechanical properties of the native tissue to establish a favorable environment for tissue regeneration. Biochemical cues, whether derived from the inclusion of ECM proteins, bioactive peptides, or cytokines, play an integral role in driving cellular responses, host reactions, and tissue integration. Matching the mechanical properties of native tissue provides the appropriate cues to drive cell behavior. Tissue–biomaterial mechanical mismatch can result in mechanical failure if the biomaterial is too weak, induce inflammation and tissue damage if the material is too stiff, and lead to a loss of interfacial connections between the implant and native tissue (Kalaba et al., 2016).

Biomaterials for soft tissue engineering take the form of 2D or 3D scaffolds (films, sponges, meshes, porous mats, tubes, hydrogels) as well as injectable matrices (hydrogels, nanoparticles, microparticles, suspensions, compressible sponges). 3D scaffolds offer greater control over mechanical properties and can provide complex, heterogeneous structures, mimicking the native environment (Xia et al., 2018). Injectable biomaterials are advantageous in that they can fill complex voids and be implanted through minimally invasive techniques, reducing the risk of surgical complications (Xia et al., 2018).

Independent of format, biomaterials for soft tissues can be fabricated from synthetic and/or natural polymers (Table 2.6.7.1). Synthetic polymers have highly controlled, reproducible compositions and can usually be chemically modified.



• **Figure 2.6.7.1** Range of elastic modulus of different types of soft tissues (Comley and Fleck, 2009, 2010; Kalra et al., 2016; Mckee et al., 2011; Skeldon et al., 2018).

TABLE 2.6.7.1 List of Common Synthetic and Natural Materials Used for Soft Tissue Engineering

Type of Material	Examples
Synthetic	Poly-lactic acid, poly-glycolic acid, poly(lactic-co-glycolic acid), poly(ethylene glycol), poly(ethylene glycol diacrylate), polytetrafluoroethylene, polyethylene terephthalate, polypropylene, poly(methyl methacrylate), polyacrylamide, poly(<i>N</i> -isopropylacrylamide), poly(ϵ -caprolactone), poly(vinyl alcohol), poly(2-hydroxyethyl methacrylate), poloxamers, poly(propylene fumarate), polyurethane, poly(glycerol sebacate), silicone
Natural	Collagens, hyaluronic acid, decellularized extracellular matrix, silks, fibrin, gelatins, alginates, agarose, dextran, chitosan, chondroitin-sulfate, laminin, cellulose, amylose/amylopectin, polyhydroxyalkanoates, keratin

However, they lack intrinsic bioactivity and exhibit varying degrees of biocompatibility, with some synthesized or cross-linked using toxic reagents (Xia et al., 2018). On the other hand, natural biomaterials are generally biocompatible and chemically and physically similar to native tissue. However, naturally derived materials tend to have weaker mechanical properties, degrade more quickly compared to synthetic materials, can be challenging to modify in terms of biological and physical properties, and often have more variable compositions, depending on the source (Xia et al., 2018). Currently, no single material is optimal for broad-spectrum soft tissue-engineering applications, and therefore ongoing research in the field involves optimizing materials alone or in combinations to overcome existing limitations for specific applications.

Synthetic Polymers

Poly(lactide-co-glycolide) (PLGA) is a Food and Drug Administration (FDA)-approved polymer widely used in tissue engineering and drug delivery. It is also one of the few synthetic polymers that is degradable, and has a tunable

degradation rate. PLGA can be developed into a variety of different formats, including sponges, foams, fibers, hydrogels, microparticles, and nanoparticles (Sun et al., 2017). PLGA microspheres, which can be injected, have been used as delivery vehicles for growth factors to facilitate regeneration of adipose tissue (Chung et al., 2012) and cartilage (Andreas et al., 2011). However, PLGA degradation products are acidic and can decrease the local pH when present in high concentrations. This local effect can negatively impact cells, the delivery payload (i.e., growth factors, therapeutic stability), and the surrounding tissues (Fu et al., 2000).

Poly(ethylene glycol) (PEG) is another commonly used, FDA-approved synthetic biomaterial. It is nontoxic, bioinert, and can be functionalized to enable crosslinking or incorporation of bioactive components (Zhu, 2010). The mechanical properties of PEG are suitable for soft tissue engineering, as they can be tailored to match the tissue of interest (Parlato et al., 2014). Additionally, the polymer precursors to PEG-based hydrogels are cytocompatible, thus allowing for in situ gelation (Bakaic et al., 2015). Due to these advantages, PEG has been utilized in many soft tissue-engineering applications, such as cartilage (Wang et al., 2017), adipose (Young and Christman, 2012), neural (Mahoney and Anseth, 2006), and cardiac (Grover et al., 2014) tissue.

Another FDA-approved synthetic polymer used in soft tissue applications is poly(ϵ -caprolactone) (PCL). This biocompatible and thermoresponsive polymer has relatively slow biodegradation and can be formed into films, hydrogels, and electrospun fibers. The elasticity, stability, and ease of processing of PCL make it an attractive material for tissue engineering (Mondal et al., 2016; Stratton et al., 2016). It is often used in combination with other polymers, including collagen, chitosan, and PEG, and has been applied in nerve, cardiovascular, skeletal muscle, ligament, bladder, ocular, skin, and cartilage tissue engineering (Mondal et al., 2016; Malikmammadov et al., 2018).

Natural Polymers

Collagen and hyaluronic acid (HA) are two of the most commonly utilized natural polymers in tissue engineering. Both polymers are present in the ECM and are biodegradable and biocompatible. Collagen can be isolated from

natural sources, and contains epitopes for cell interactions (Parenteau-Bareil et al., 2010). Collagens can be formulated into sponges, microparticles, fibers, and injectable hydrogels, allowing for use in a range of biomedical applications, including ocular, urogenital, skin, cardiovascular, and neural tissue engineering (Parenteau-Bareil et al., 2010). Collagen-based scaffolds are limited by their tendency to contract and rapidly degrade in vivo, necessitating modes to crosslink the protein to improve stability over time (Davidenko et al., 2015; Parenteau-Bareil et al., 2010). HA is a hydrophilic, naturally occurring polysaccharide that has a similar water content to soft tissues when formed into hydrogels (Collins and Birkinshaw, 2013). Although native HA is rapidly degraded in vivo through endogenous enzymes, it can be chemically modified and crosslinked, thus altering the degradation profile, mechanical properties, and cellular interactions (Collins and Birkinshaw, 2013; Burdick and Prestwich, 2011).

Silk fibroin is another natural polymer often used in biomedical applications such as adipose, neural, and intestinal tissue engineering (Stoppel et al., 2017). It is isolated from *Bombyx mori* cocoons and can be formed into sponges, foams, hydrogels, films, and microparticles (Rockwood et al., 2011). Silk has favorable characteristics for tissue-engineering applications, such as slow and tunable degradation rates and mechanical benefits in comparison to other naturally derived polymers (Vepari and Kaplan, 2007). The mechanical properties of silk biomaterials depend on format and processing. Silk hydrogels exhibit stiffness values between 200 and 10,000 Pa, covering a large range of native soft tissues (Partlow et al., 2014). Silk from *B. mori* degrades by proteolysis, but lacks cell-specific epitopes for cell signaling. Thus the incorporation of exogenous bioactive components can be used to direct cellular interactions (Murphy and Kaplan, 2009).

Decellularized Tissues

Decellularized tissues are natural biomaterials that have been utilized in tissue engineering. They can provide the biochemical composition and structural complexity found in native ECM, which has been challenging to recapitulate de novo (Neves and Reis, 2016). If possible to source, ECM derived from the tissue of interest is the most appropriate to use (Badylak et al., 2009), for example, decellularized heart valves for heart valve replacements (Bader et al., 1998; Vedepo et al., 2017), decellularized myocardial tissue for treatment of myocardial infarction (Singelyn et al., 2009), and decellularized adipose tissue to facilitate adipogenesis (Flynn, 2010).

Soft Tissue Engineering Applications: Adipose, Gastrointestinal, and Skin

In this section we explore the design criteria, current biomaterial technologies, and challenges in the fields of (1) adipose, (2) gastrointestinal, and (3) skin tissue engineering.

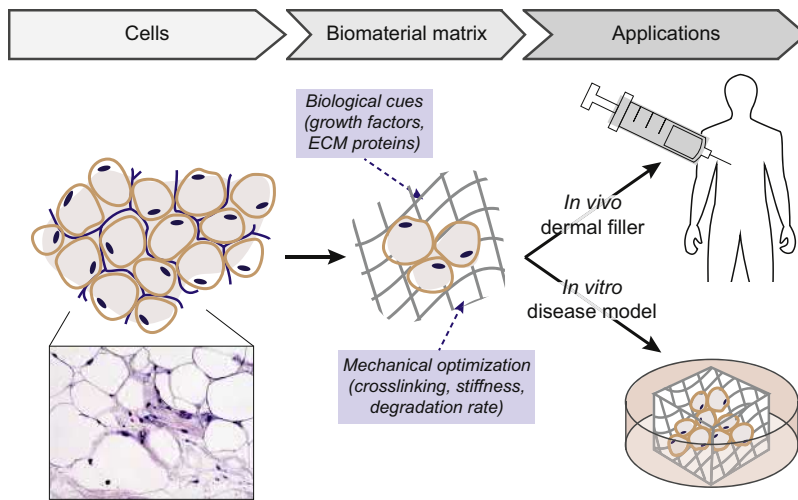
Adipose Tissue Engineering

Adipose tissue, commonly referred to as fat, is found throughout the body. The need for adipose tissue replacement arises when this soft tissue is lost or damaged due to trauma (i.e., burns), congenital defects (i.e., hemifacial lipodystrophy), tumor resections, or for elective cosmetic procedures (Patrick, 2001; Young and Christman, 2012). The most commonly used clinical treatments are soft tissue fillers for small defects (Van Nieuwenhove et al., 2017; Broder and Cohen, 2006; Cheng et al., 2002; Alam et al., 2008), and prosthetics (e.g., silicone implants) or autologous adipose tissue transplants for larger defects (Van Nieuwenhove et al., 2017). In the past few decades (2000–17), the soft tissue filler market has increased over 300% for cosmetic surgical procedures (“American Society of Plastic Surgeons report of the 2017 plastic surgery statistics”). Significant limitations associated with current treatments are poor long-term stability and donor or recipient-site morbidity (Flynn and Woodhouse, 2008; Choi et al., 2010; Van Nieuwenhove et al., 2017). Current material implants only temporarily augment or bulk the tissue (Van Nieuwenhove et al., 2017; Young and Christman, 2012; FDA, 2018). Due to these limitations, tissue-engineering principles are being used to develop new materials for the replacement of adipose tissue, focusing on the regeneration of fully functional tissue to provide a permanent solution.

Anatomy and Physiology

The main role of adipose tissue is providing energy via lipid storage and catabolism. Secondary roles include providing cushioning for structures and organs within the body, contributing to appearance, and secreting paracrine factors that communicate with other systems of the body (Klein et al., 2007). There are two major types of adipose tissue: brown adipose tissue (BAT) and white adipose tissue (WAT) (Colaiaanni et al., 2015). BAT is most prominent at birth, decreasing in abundance with age (Gesta et al., 2007), and serves to generate heat as triglycerides are broken down in a process referred to as nonshivering thermogenesis (Cannon and Nedergaard, 2004). WAT, which becomes redistributed as we age, acts as an energy storage depot and endocrine organ (Choi et al., 2010).

Adipocytes are the dominant cells in adipose tissues (Young and Christman, 2012). These cells store fatty acids within lipid droplets and release them when there is a demand for energy. Other cell types present in adipose are endothelial, immune, and progenitor (historically referred to as preadipocytes) (Choi et al., 2010; Tsiloulis and Watt, 2015). Preadipocytes are of unique interest in tissue engineering as their multipotency allows them to differentiate into adipogenic, chondrogenic, osteogenic, and myogenic (Zuk et al., 2001). Due to this plasticity, preadipocytes are commonly referred to as adipose-derived adult stem cells (ASCs) (Bunnell et al., 2008). ASCs that differentiate during lipogenesis are responsible for synthesizing and



• **Figure 2.6.7.2** Principles of adipose tissue engineering. *ECM*, Extracellular matrix.

reorganizing the ECM (Nakajima et al., 1998), which is primarily composed of collagen, laminin, and proteoglycans (Mariman and Wang, 2010; Song et al., 2018).

Design Criteria for Adipose Tissue Engineering

The goal for adipose tissue engineering is to provide **volume persistence** while stimulating the **regeneration of functional adipose tissue**. To achieve this goal, a biomaterial system must be: (1) biocompatible, (2) provide appropriate mechanical properties and degradation profiles, (3) facilitate and promote adipogenesis, and (4) promote vascularization.

Inducing adipogenesis and promoting vascularization are key to regenerating functional adipose tissue, especially in the case of large tissue defects (Chiu et al., 2011). Research has focused on combining biomaterials with cells and bioactive molecules, such as native ECM and/or growth factors. ASCs are often studied due to their patient specificity, ease of isolation, and ability to differentiate into adipocytes and endothelial cells (Nakajima et al., 1998; Gimble et al., 2007; Zuk et al., 2002; Fischer et al., 2009; Deng et al., 2015). In addition to ASCs, endothelial cells have been introduced into scaffolds to enable neovascularization (Chen et al., 2009; Kaihara et al., 2000; Tsuda et al., 2007). Some common growth factors used for adipose tissue engineering include fibroblast growth factor-1 (FGF-1), basic fibroblast growth factor (bFGF), insulin-like growth factor-1 (IGF-1), and vascular endothelial growth factor (VEGF) (Mahoney et al., 2018). FGF-1 increases peroxisome proliferator activated-receptor γ (PPAR γ) expression, which helps prime preadipocytes for proliferation and differentiation. bFGF stimulates angiogenesis and adipogenesis, IGF-1 facilitates differentiation of preadipocytes and regulates triglyceride synthesis, and VEGF regulates vasculogenesis and angiogenesis (Mahoney et al., 2018). Native tissue, such as that from lipoaspirate or tissue explants, can also provide a complex source of growth factors and proteins that establish a favorable environment for regeneration (Gealekman et al., 2011; Young and Christman, 2012).

In choosing a biomaterial, it is critical to assess toxicity, cytocompatibility, and inflammation, either from the bulk material or its degradation products, which can induce a foreign body response, cause tissue damage, and prevent functional regeneration (Choi et al., 2010; Levenberg and Langer, 2004). Mechanical integrity and an appropriate degradation rate are also important parameters to consider (Lavik and Langer, 2004; Choi et al., 2010). Adipose tissue is not subjected to mechanical loads unlike tissues, such as cartilage and bone; however, it can experience compressive forces from the surrounding tissues and can also be exposed to significant deformation during normal daily functions like sitting (Young and Christman, 2012; Linder-Ganz et al., 2007). In addition, matching the native mechanics of adipose tissue can facilitate human adipose-derived stem cell (hASC) differentiation into mature adipocytes (Young et al., 2013; Shoham and Gefen, 2012). As with most applications, degradation is a key factor in the success of the biomaterial; in adipose tissue engineering, the material must maintain volume while facilitating tissue regeneration (Van Nieuwenhove et al., 2017) (Fig. 2.6.7.2).

Both in vitro and in vivo assessments can be performed to determine whether a particular biomaterial is suited as scaffolding for adipose tissue. For in vivo assays, biomaterials are commonly implanted or injected subcutaneously in small animal models (mice and rats) (Patrick et al., 2008). For in vitro and in vivo assays, a variety of analytical tools have been used to assess tissue regeneration, including mechanics, biocompatibility/toxicity, and material degradation (Table 2.6.7.2).

Commercially Available and Clinically Tested Biomaterials

The most common biomaterials used clinically include: (1) dermal fillers for small facial defects or (2) autologous tissue transfers or synthetic prosthetics for reconstruction after trauma or tumor resection (Van Nieuwenhove et al., 2017).

TABLE 2.6.7.2 Techniques to Assess Adipogenesis and Vascularization (Choi et al., 2010)**Immunohistochemistry**

Lipid droplet (mature adipocytes) → Oil Red O
 Vasculature → 0020 H&E, endothelial cells (CD31 and vWF)
 ECM → Collagen type IV, laminin, fibronectin

Gene Expression of Adipogenesis and Lipogenesis (RT-PCR)

PPAR γ , GLUT4, FABP4, ACS, GPDH

Lipid Quantification

AdipoRed Assay
 Triglyceride Assay

Metabolic or Enzymatic Activity

Lipolysis (glycerol release)
 Glucose uptake
 GPDH enzyme activity

Cytokine Quantification—ELISA

Adiponectin and leptin

ACS, Acetyl-CoA synthetase; *CD31*, cluster of differentiation 31; *ELISA*, enzyme-linked immunosorbent assay; *FABP4*, fatty acid binding protein-4; *GAPDH*, glycerol-3-phosphate dehydrogenase; *GLUT4*, glucose transporter-4; *H&E*, hematoxylin and eosin; *PPAR γ* , peroxisome-proliferator-activated receptor-gamma; *vWF*, von Willebrand factor.

TABLE 2.6.7.3 Food and Drug Administration-Approved Soft Tissue Fillers (FDA, 2018; Van Nieuwenhove et al., 2017)

Biomaterial	Products
Collagen	<i>Bovine</i> : Zyderm collagen implant (Allergan), Zyplast (Collagen Corp.) <i>Human</i> : Cosmoderm 1 human-based C (Inamed Corporation) <i>Porcine</i> : Evolence collagen filler (Colbar Lifescience I), Fibrel (Sero Laboratories)
Hyaluronic acid	Juvederm (Allergan), Restylane (Q-med), Captique (Genzyme Biosurgery), Belotero Balance (Merz Pharmaceuticals), Prevelle Silk (Genzyme Biosurgery), Eleveess (Anika Therapeutics), Hylaform (Hylan) (Genzyme Biosurgery)
Hydroxyapatite	Radiesse (Bioform Medical, Inc.)
Poly-L-lactic Acid	Sculptra (Sanofi Aventis)
Polymethyl-methacrylate beads + collagen	Artefill (Suneva Medical Inc.)

Current FDA-approved materials in the United States for dermal fillers are outlined in Table 2.6.7.3 (FDA, 2018).

Collagen was one of the first dermal fillers approved by the FDA in the 1980s, and has been extensively researched for adipose tissue regeneration due to its bioactive nature

and similarity to native ECM. FDA-approved collagen products are from bovine, porcine, or human sources and can be injected as uncrosslinked or crosslinked formulations (FDA, 2018). However, collagen scaffolds degrade quickly and exhibit rapid resorption rates (approximately 3–4 months for products currently on the market), providing only a temporary solution (FDA, 2018). HA is the most common polymer used in soft tissue fillers. HA-based medical products generally last longer in vivo than collagen-based products, degrading in 6–12 months (FDA, 2018). The only nondegradable FDA-approved soft tissue filler is poly(methyl methacrylate) microspheres suspended in collagen (FDA, 2018). This composition has shown promise in extending volumetric persistence; however, limitations include the presence of nodules and lumps, the lack of degradability, rendering it irreversible, and restriction to small facial defects (Lemperle et al., 2010).

Clinical procedures for the reconstruction of large defects involve either autologous tissue transplants (free flap tissue or free fat grafts) or synthetic prosthetics (silicone- or saline-filled implants). Autologous fat grafts are considered the gold standard in soft tissue augmentation and adipose tissue replacement (Mahoney et al., 2018; Van Nieuwenhove et al., 2017). In this technique, autologous lipoaspirate is collected through liposuction and reinjected into areas of need. The use of lipoaspirate has limitations, including rapid resorption and the potential for necrosis, especially when large volumes are injected due to the lack of vascularization (Mahoney et al., 2018). Improvements to autologous fat grafting focus on increasing persistence and reducing necrosis by modifying the harvesting, processing, and readministration techniques (Landau et al., 2018; Strong et al., 2015). Advantages of this approach remain, such as reduced immune response and the promotion of new adipose tissue formation, which is in part due to the presence of native ASCs, ECM, and growth factors in the lipoaspirate.

Novel Materials and Technologies

Adipose tissue engineering is a growing field due to limitations with current clinically used dermal fillers and reconstruction procedures. There is also interest in developing more relevant in vitro tissue models to study tissue development, disease progression, and therapeutic effects. 3D scaffolds (e.g., sponges) and injectable formats (e.g., hydrogels, microparticles) have been studied for adipose tissue regeneration (Van Nieuwenhove et al., 2017). Scaffolds with a predetermined, customizable 3D shape may be useful for larger defects (Flynn and Woodhouse, 2008). However, these designs typically require surgical implantation, which can result in scarring and increase the risk of complications (Young and Christman, 2012). Injectable biomaterials can reduce such complications and adapt to fill defects of variable shapes and sizes (Van Nieuwenhove et al., 2017).

PATIENT-SPECIFIC 3D ADIPOSE TISSUE MODELS

As the prevalence of obesity and obesity-related disorders (e.g., type 2 diabetes) increases, there remains a need to generate physiologically relevant *in vitro* tissue models to gain insights into disease progression and new treatment options. 3D systems that used porous silk protein scaffolding to culture patient-derived adipose tissue (from lipoaspirate), which included numerous cell types, including adipocytes, preadipocytes, endothelial cells, and smooth muscle cells, has been reported (Abbott et al., 2016). This system supported long-term culture up to 3 months and showed a proof-of-concept patient-specific system by utilizing low volumes of lipoaspirate and differences in response after tumor necrosis factor- α stimulation. Ultimately, *in vitro* tissue models provide utility in the study of patient-specific disease mechanisms and drug responses toward more effective, customizable therapeutic options.

Collagen-based scaffolds can support adipose tissue formation both *in vitro* and *in vivo*, particularly when combined with adipose-derived cells (Gentleman et al., 2006; Von Heimburg et al., 2001). Porous scaffolds fabricated from poly(L-glutamic acid) (PGA) supported ASC spheroid formation, leading to significant adipogenesis and angiogenesis *in vivo* (Zhang et al., 2017). Lipoaspirate can be included in tissue models to introduce ASCs, ECM, and growth factors into scaffolds (Bellas et al., 2013; Chung et al., 2012). In one example, silk sponges combined with lipoaspirate supported the generation of adipose tissue with functional vasculature while maintaining volume for over 18 months in a rat model (Bellas et al., 2013). The development and use of decellularized adipose tissue has increased within the last decade (Van Nieuwenhove et al., 2017). For instance, decellularized adipose tissue loaded with bFGF showed significant tissue formation and neovascularization with volume stability for up to 12 weeks in a mouse model (Zhang et al., 2016). Decellularized adipose tissue is currently in clinical testing for soft tissue injuries.

Challenges

Although there have been advances in adipose tissue engineering, challenges remain due to obstacles in predicating the performance of patient-sourced materials, assessing long-term persistence, scalability for large tissue defects, as well as hurdles associated with the manipulation of patient-derived materials.

The success of lipoaspirate and decellularized adipose tissue was reviewed earlier; however, preclinical research and clinical outcomes using such materials have resulted in variable results. This variability is due to the heterogeneous source material, with compositions differing between patients or within the same patient in different anatomical locations (Strong et al., 2015). Along similar lines, current methods to isolate and expand hASCs have not been standardized and thus there is heterogeneity in ASC cultures (Strong et al., 2015; Palumbo et al., 2018; Agostini et al., 2018). Other challenges include the need to assess

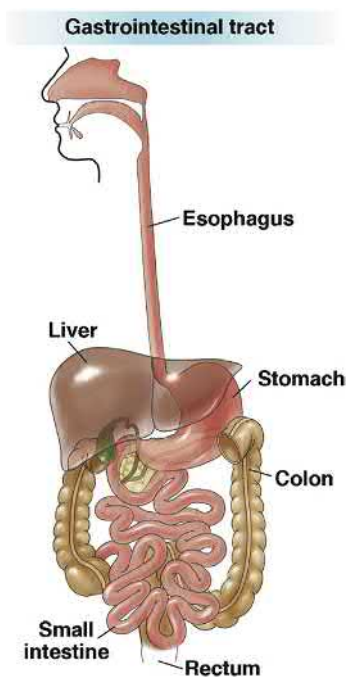
CASE STUDY: ACELLULAR ADIPOSE TISSUE FOR SOFT TISSUE INJURIES

Decellularized or acellular adipose tissue (AAT) has favorable properties conducive for adipose tissue engineering. AAT can be formed by processing subcutaneous adipose tissue using mechanical and chemical methods. The removal of antigenic compounds provides an “off-the-shelf” product that can be implanted in patients without rejection. This option is of particular interest for patients that do not have excess adipose volume to contribute to autologous fat grafts, which can be due to underlying diseases such as human immunodeficiency virus/acquired immunodeficiency syndrome or from chemotherapy treatments. Mechanical processing followed by treatment with peracetic acid to remove cells, surfactant to remove lipids, and enzymes to remove residual DNA has been utilized (Wu et al., 2012). The resulting material can then be crosslinked using 1-ethyl-3-(3-dimethylaminopropyl) carbodiimide (EDC) and *N*-hydroxysuccinimide or hexamethylene diisocyanate to reduce enzymatic degradation rates *in vivo* to improve persistence. Upon preclinical *in vivo* evaluation using rat models, the EDC crosslinked AAT was encased in a fibrotic capsule, whereas the uncrosslinked and hexamethylene diisocyanate crosslinked AAT materials facilitated cell infiltration and promoted adipose tissue formation. This technology is licensed to AEGERIA Soft Tissue LLC, a startup biotech spinoff from Johns Hopkins University (Rosson et al., 2016). Recently, the safety of AAT implants has completed Phase I clinical trials in healthy human volunteers and the results showed that the AAT biomaterial was safe for use in humans and easy for physicians to administer to patients (Payne et al., 2017). In addition, preliminary results from these trials showed that the material was associated with proregenerative immune responses. These results show the promise of AAT for adipose regeneration; however, further studies and Phase II trials will be necessary to assess the potential as a therapeutic strategy for soft tissue injuries.

biomaterials for long-term treatment, as well as assessments in defects of different sizes and shapes (Mahoney et al., 2018). The majority of preclinical studies last up to 1 year and usually involve small volume implants/injections tested in rodent models (Patrick et al., 2008). To fully assess these technologies, it is necessary to understand the long-term stability in relevant sized defects (Choi et al., 2010; Mahoney et al., 2018). To remedy these limitations, some studies have been conducted in large animals such as sheep or pigs (Patrick et al., 2008), or scalability assessed using computer-assisted model simulations (Chhaya et al., 2015).

Gastrointestinal Tissue Engineering

The gastrointestinal (GI) tract is a series of connected hollow organs, beginning at the mouth and ending at the anus (Fig. 2.6.7.3). Swallowed food travels through the esophagus to the stomach, where it is exposed to digestive enzymes and gastric acid. The resulting chyme—or partially digested food—passes through the pyloric sphincter to the duodenum, the upper portion of the small intestine. Digestion continues and nutrients are absorbed as the chyme is propelled through the small intestine to the colon, where water is reabsorbed



• **Figure 2.6.7.3** The organs of the gastrointestinal tract (Hussey et al., 2018).

and indigestible material is excreted as feces. Proper GI tract function relies upon complex coordination between multiple systems and an array of cell types. In this section, we: (1) provide an overview of relevant GI anatomy and functions; (2) explain the need for GI regenerative medicine; (3) summarize design criteria relevant to GI soft tissue engineering; (4) present a selection of strategies currently in clinical, preclinical, and developmental stages; and (5) describe current challenges and future goals with these systems.

Anatomy and Physiology

In healthy individuals, the only direct contact between ingested food and the body is at the epithelium, which consists of different cell types of specialized function depending upon location within the GI tract. The esophageal epithelium consists of stratified squamous cells and mucus-secreting glands to protect against abrasive damage (Kuo and Urma, 2006), while columnar gastric epithelial cells secrete digestive acids, enzymes, and autodigestion-preventing mucus. The gastric epithelium also contains hormone-secreting enteroendocrine cells that help to regulate GI function, representing a major interconnection between the GI and endocrine systems, which continues into the small intestine. The primary function of the small intestine is carried out by abundant enterocytes, specialized absorptive cells that deliver nutrients from the intestinal lumen to the bloodstream. Also present are Goblet and Paneth cells, which produce mucus and antimicrobial agents, respectively, contributing to the immunological importance of the small intestine. Excluding Paneth cells, the colonic epithelium contains similar cell types as the small intestine, though relative abundances are shifted to favor mucus production and waste excretion (Gregorieff

and Clevers, 2005). The complexities of the GI tract are compounded by ubiquitous and crucial integration with the lymphatic, vascular, and enteric nervous systems. The importance of this integration is most apparent when considering a bodily function that is largely unique to the GI tract: peristalsis. In this involuntary process, synchronized contractions of both longitudinal and circular smooth muscle generate motion responsible for carrying food along the length of the gut. These repeating patterns of contraction and release are modulated by the enteric nervous system (ENS) and the interstitial cells of Cajal (ICC) (Huizinga, 1999). Given that disruption of any of the functions just described, or numerous others not covered here, can impact homeostasis of the entire system, it is not surprising that GI disorders are major causes of hospitalization, morbidity, and mortality worldwide.

THE INTERSTITIAL CELLS OF CAJAL: PACEMAKERS OF THE GUT

Without peristalsis, the GI tract cannot function. The ICC play a critical role in ENS to regulate smooth muscle contractions to keep food moving in the right direction. Embedded within the gut musculature, these “pacemaker cells” serve as intermediaries between the ENS and the smooth muscle, modulating excitatory and inhibitory neurotransmission. The ICC generate and propagate electrical slow waves, leading to synchronous contraction of the smooth muscle and driving the peristaltic motion that keeps the contents of the GI tract moving. While there is still much to learn about ICC and the role in GI motility, without the ICC the system does not function (Klein et al., 2013).

Gastrointestinal Disorders and the Need for Tissue Engineering

In 2009, it was estimated that nearly 50 million outpatient visits in the United States resulted in a diagnosis of a GI disorder, with evidence suggesting that the incidence of some disorders may be increasing. Many of these problems were associated with damage to the GI tract and lasting impairment, either as direct pathological outcomes or as the result of surgical interventions (Peery et al., 2012). As soft tissue-engineering techniques continue to develop, it may become possible to heal or replace GI tissues that have been removed, damaged, or have otherwise lost normal functions, thus improving patient quality of life.

Cancers of the esophagus, stomach, and colon are of particular interest, as they share a universally poor prognosis unless the affected tissue is surgically removed. In addition to leaks, infections, and other complications associated with excision and repair of GI tissues, secondary disorders may arise, such as malnutrition due to reduced bowel length or incontinence due to loss of sphincter control (Bitar and Zakhem, 2016). Similar complications can result from surgeries used to treat inflammatory bowel diseases like Crohn’s disease and ulcerative colitis. In these cases, replacement of removed tissues or even entire organs could help to restore structure and function.

Potential benefits of tissue engineering are not necessarily limited to surgical insertion of engineered tissues. Although surgical options exist for motility disorders of the GI tract, tissue engineering may allow clinicians to design targeted, less invasive treatments that aim to restore function to dysfunctional components rather than to remove the tissues altogether. In patients with achalasia, for example, neurodegeneration in the esophageal smooth muscle causes the lower esophageal sphincter to remain in a contracted state, preventing food from reaching the stomach (Krill et al., 2016). Similar disorders can occur throughout the GI tract, such as in the stomach (e.g., gastroparesis) (Scott and Koch, 2015), intestine (e.g., colonic inertia) (Bharucha and Camilleri, 2015), and anus (e.g., fecal incontinence) (Costilla and Foxx-Orenstein, 2015). Pathologies can vary widely, but neurodegeneration in the smooth muscle is common to many motility disorders, even when musculature, vasculature, and the epithelial surface may remain intact and viable. In such cases, it may be possible to restore lost function if the otherwise healthy tissues can be successfully reinnervated.

Design Criteria for Engineered Gastrointestinal Tissues

As discussed in previous sections, all engineered tissues must be biocompatible, biodegradable, mechanically and architecturally suited to the intended application, and readily scalable (O'Brien, 2011). However, because the GI tract consists of a series of organs with substantial structural and functional heterogeneities, assembling a single comprehensive list of design criteria for the entire system would be inappropriate. Instead, each criterion must be catered to the specific organ, pathology, and extent of tissue regeneration required (e.g., mucosal restoration vs. organ replacement). Generally, any successful strategy would result in GI tissue satisfying the following minimum requirements: (1) regeneration of the epithelium and organ-specific epithelial function; (2) regeneration of the longitudinal and circular smooth muscle in proper alignment; (3) innervation of the smooth muscle and restoration of peristalsis; and (4) reintegration with the vascular and lymphatic systems with concurrent interactions with the immune system. In the next section, an overview of GI soft tissue engineering strategies demonstrates the progress toward reaching these goals, while also highlighting continuing challenges.

Gastrointestinal Soft Tissue-Engineering Strategies

Efforts to engineer the soft tissues of the gut have been slower to translate to clinical use than other tissues (e.g., lung, airway, liver). However, results from animal studies and a small number of human studies promote optimism that regenerative medicine could play a significant role in the future of GI disease treatment.

The most successful preclinical GI tissue-engineering strategies to date have relied upon use of ECM-based scaffolds, often decellularized porcine small intestinal submucosa (Hussey et al., 2017); in such cases, the scaffold is typically

sutured to the wall of the GI tract, providing the necessary porous structure to facilitate tissue regeneration. In vivo degradation of these biologically derived scaffolds also gradually releases growth factors, structural molecules, and other components important to the proliferation, differentiation, and phenotype of the varied and complex GI tissues (Hussey et al., 2018). Positive preclinical outcomes have also been demonstrated using synthetic biomaterials (e.g., lactic acid/caprolactone copolymer) for stomach regeneration (Miyazawa et al., 2015) and naturally derived scaffolds (e.g., chitosan) (Denost et al., 2015) for colorectal tissue engineering. Examples of GI regenerative medicine strategies that have reached preclinical or clinical stages are presented in Table 2.6.7.4. Note that the examples provided were selected to convey a variety of available strategies, and thus should not be considered comprehensive or indicative of relative clinical significance.

In some cases, the use of healthy tissues from similar locations within the GI tract to generate ECM scaffolds has resulted in improved tissue-specific regeneration (Keane et al., 2015). Seeding scaffolds with cells isolated from nearby locations prior to implantation can similarly improve outcomes. For example, collagen sponges seeded with autologous gastric smooth muscle cells enhanced the regeneration of the small intestinal epithelium and underlying musculature in canines relative to unseeded controls (Nakase et al., 2006). While these results are promising, translation of clinically significant treatment options is hindered by the availability of sufficient autologous tissue, particularly in cases where significant tissue regeneration is required, such as following colectomy. These limitations contribute to the growing interest in the use of stem cells to regenerate GI tissues in vitro and in vivo. Stem cells have been used in vivo to successfully regenerate enteric neurons (Hotta et al., 2013), smooth muscle (Walthers et al., 2014), and functional small intestine complete with differentiated epithelium and neuromusculature (Levin et al., 2013).

The use of organoids or miniature tissue models that represent the cellular diversity and function of native organs demonstrates a comparatively new, yet useful approach to engineer the soft tissues of the GI tract. Organoids have been isolated from tissues all along the human GI tract and can be grown in vitro (Dedhia et al., 2016), representing a major, expandable source of stem cells capable of differentiating into various cell types found in the complex GI tissues. By implanting esophageal organoids into collagen-coated PGA/PLA acid scaffolds in mice, the formation of esophageal epithelium and neuromusculature was demonstrated (Spurrier et al., 2014). In other in vitro and in vivo studies, organoid seeding and differentiation was demonstrated in scaffold materials, including Matrigel (Sato et al., 2009), collagen (Yui et al., 2012), PGA (Choi, 1997), porcine intestinal ECM (Finkbeiner et al., 2015), and silk (Chen et al., 2017). Even in the absence of a scaffold material, in vitro culture of colon organoids and subsequent transplantation into damaged mouse colon restored the structure, function, and continuously self-renewing properties of the epithelium (Yui et al., 2012).

TABLE 2.6.7.4 Examples of Gastrointestinal Soft Tissue-Engineering Strategies That Have Reached Preclinical or Clinical Stages

Organ	Model	Procedure	Scaffold	Outcome	References
Esophagus	Human	Circumferential endoscopic resection affecting mucosa and submucosa in patients with Barrett's esophagus	Porcine small intestinal ECM	Restoration of squamous epithelium in 5/5 patients	Badylak et al. (2011)
Esophagus	Human	Full-thickness patch esophagoplasty in patients requiring esophageal reconstruction	Porcine urinary bladder ECM	Restoration of squamous epithelium in 4/4 patients	Nieponice et al. (2014)
Stomach	Rat	Patch of full-thickness, circularly excised tissue	Porcine small intestinal ECM	Regeneration of smooth muscle, neuronal, and epithelial cells	Nishimura et al. (2010)
Stomach	Pig	Patch of resected tissue	50% lactic acid, 50% caprolactone copolymer with polyglycolic acid fibers	Structural regeneration of mucosa, musculature, and connective tissue	Miyazawa et al. (2015)
Small intestine	Dog	Patch of full-thickness, longitudinally excised tissue	Porcine small intestinal ECM	Restoration of epithelium; smooth muscle and neuronal reorganization; contraction of reorganized tissue under in vitro stimulation	Nakao et al. (2015)
Small intestine	Dog	Patch of surgically applied defect	Collagen sponge seeded with gastric smooth muscle cells under silicone sheet	Regeneration of epithelium and smooth muscle	Nakase et al. (2006)
Colon	Rabbit	Induction of ulcerative colitis and administration via enema	Porcine small intestinal ECM hydrogel	Restoration of epithelial barrier function and reduction in number of inflammatory macrophages	Keane et al. (2017)
Colon	Rat	Patch of full-thickness, surgically applied defect	Chitosan hydrogel	Regeneration of epithelium and smooth muscle	Denost et al. (2015)
Anus	Human	Implantation of wedge-shaped plug in patients with complex transphincteric anal fistulas	Porcine dermal ECM	Complete clinical healing in 9/12 patients	Sarzo et al. (2013)

ECM, Extracellular matrix.

Challenges and Future Goals

Despite the substantial progress made toward regenerating the soft tissues of the GI tract, key milestones remain to be met before clinical translation is feasible. Of the GI-specific design criteria described in previous sections, the most significant progress has been made toward regenerating epithelial structure and function. Restoration of peristalsis has been more difficult. Even in cases where smooth muscle development has been demonstrated, the cells often do not maintain the alignment and contractile properties necessary for peristalsis. This failure to reproduce and maintain smooth muscle phenotype represents one of the most immediate barriers to clinical translation. Because of the interactions between smooth muscle, vasculature, and the

enteric nervous system, including the critically important ICC, future progress toward restoration of peristaltic function will likely require a system capable of restoring these various components simultaneously. Once the structure and function of the neuromusculature can be reproduced, the focus should shift to scaling up these engineered tissues. Similar to the adipose tissue-engineering field, most studies in GI tissue engineering have used in vitro or small animal models requiring only small amounts of scaffold materials and cells. As the field translates from preclinical to clinical studies, sourcing of these finite resources (e.g., homologous tissues) may pose logistical limitations. Although the rapid growth of stem cell and organoid engineering offers promise in this regard, it is difficult to predict what impact these

budding technologies will ultimately have on the regenerative medicine field for GI tissues.

Tissue-Engineered Skin: Future Goals of Skin Substitutes

The skin is the largest organ in the body and was one of the first organs to be tissue engineered (Bell et al., 1979). Skin equivalents are used across many industries, from clinical applications (i.e., wound coverings) to in vitro research models, and as a result the engineering constraints for each industry are different. In general, skin substitutes are composed of a biomaterial matrix (typically collagen) with either fibroblasts (dermal component) and/or keratinocytes (epidermal component). Skin equivalents have been used in the clinical field for therapeutic purposes for decades with a great deal of success; however, there are limitations such as a lack of innervation and vasculature (Biedermann et al., 2013; Blais et al., 2013). No commercial or clinical skin tissue model currently addresses the full complexity of cell type composition of the human skin.

Anatomy and Physiology

The skin is a complex organ with multiple layers and functional components (Biedermann et al., 2013). The outermost layer of the skin, called the epidermis, is mainly composed of differentiated, striated keratinocytes and melanocytes that organize into the following layers: cornified layer (outermost), granular layer, spinous layer, and basal cell layer, followed by the basement membrane (Mathes et al., 2014). Beneath the epidermis is the dermis, which contains numerous cell types, including dermal fibroblasts, endothelial cells, neurons, and immune cells (including Merkel cells, Langerhans cells, macrophages, monocytes, and B cells, among others) (Kim, 2015; Steinhoff et al., 2003; Valladeau and Saeland, 2005). The dermis ECM consists of collagens and other components such as GAGs and elastin, which contribute significantly to tensile strength and the mechanical integrity of the skin (Metcalfe and Ferguson, 2007; Nyame et al., 2014). The subcutaneous adipose layer underneath the skin (“subcutis” or “hypodermis”) is composed of adipose tissue that contains a plurality of cell types, including adipocytes, preadipocytes, endothelial cells, smooth muscle cells, and immune cells. Typically, the subcutis had been thought of as a “load-bearing” protective layer, but it also has important roles pertaining to the skin as a whole, involving metabolism, endocrine, and immune functions (Coelho et al., 2013; Mathes et al., 2014). The skin is also composed of other functional components such as hair follicles, sweat glands, cutaneous nerve (a component of the peripheral nervous system), and blood vessels (Paus et al., 2006).

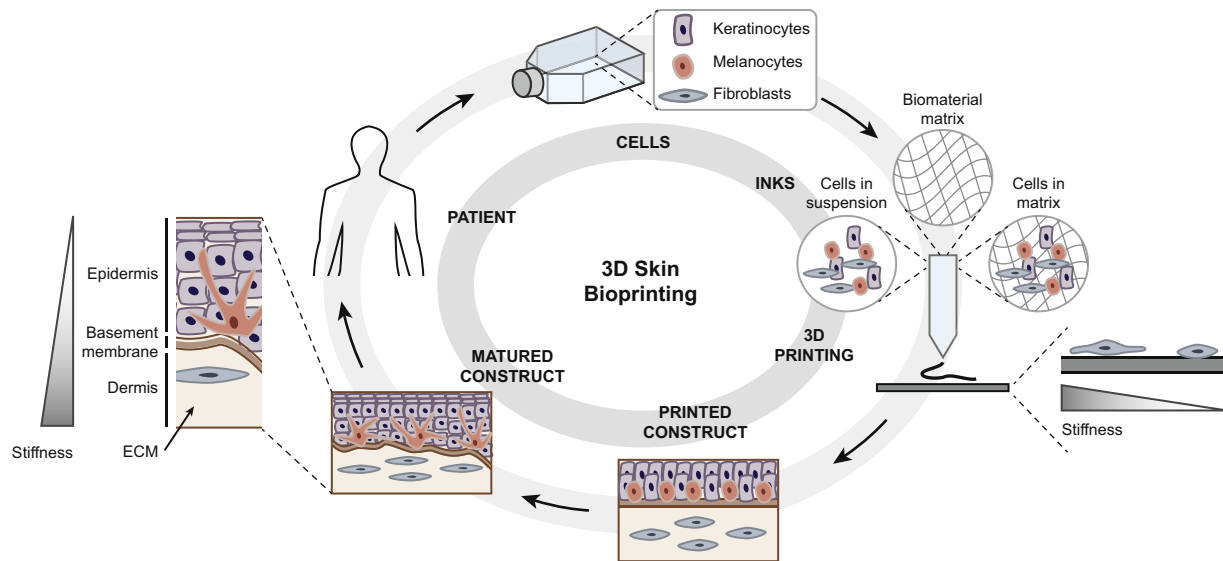
Design Criteria

The main goal of developing skin substitutes, either for skin replacements or for the development of in vitro tissue models, is to create a system that is physiologically similar to

that of native skin. Beyond mimicking the biochemical and structural components of skin, there are other parameters that are necessary to consider to develop successful skin equivalents. These factors include developing technology that is cost effective, has a long shelf-life and low storage requirements, and involves standardized processing (including sterility) and scaleup. Additional criteria are necessary depending on the use of the equivalents. For instance, skin replacements in the clinic need to adhere to the wound bed and protect this damaged tissue site from infection, be biocompatible and noninflammatory, match the physical and mechanical properties of skin, provide controlled degradation, allow for water vapor transmission, and facilitate proper wound healing and angiogenesis (Vig et al., 2017). However, in addition to these technical/engineering concerns in the clinical field, there remains a need for accurate recapitulation of the human skin in terms of complexity (cell types, accurate barrier layers), especially in the development of in vitro tissue models to study mechanisms of skin disease damage and regeneration and for testing therapeutics. As mentioned previously, the skin itself is highly complex with multiple cell types, layers, and functional components, all of which are necessary to maintain homeostasis (Mathes et al., 2014; Zhang and Michniak-Kohn, 2012; Yamate, 2018; Paus et al., 2006; Abaira and Ginty, 2013; Klicks et al., 2017). Therefore research on skin equivalents has focused on the development of complex tissue models by inclusion of many different cell types, including nerve (Roggenkamp et al., 2012, 2013; Lebonvallet et al., 2012), adipocytes or adipocyte-derived stem cells (Keck et al., 2011; Bellas et al., 2012), endothelial cells (Black et al., 1998; Quan et al., 2013), immune cells (Ramadan and Ting, 2016; Ouwehand et al., 2011), or combination systems (Vidal et al., 2018). The ultimate goal of many of these systems is to develop a skin system relevant to human biology and one that maintains or promotes aspects of physiological function of the skin in either in vivo (clinical) or in vitro (research) applications. In recent years, 3D printing approaches have also been utilized for preparation of human skin equivalents as a novel means of adding complexity, cell types, and spatial resolution to engineered soft tissues (Ng et al., 2016).

Skin Substitute Technology

Commercially available products: There are many skin substitutes on the market today. These materials can be biologic or synthetic or a combination of both. Biological skin substitutes can either be from autologous, allogenic, or xenogenic sources and have been developed from human skin or from biomaterial-based strategies, including ECM components such as collagen or chondroitin sulfate, for example. In addition, some skin substitutes consist of cultured cell sheets or cell suspensions. Synthetic materials used as substrates for these systems include silicone, nylon, PLGA, PEG, and PCL. These scaffolds are often combined with either keratinocytes and/or fibroblasts to facilitate proper wound healing. Commercially available products have been reviewed recently (Vig et al., 2017). Although



• **Figure 2.6.7.4** Schematic of patient-derived bioprinting of human skin and generalized approaches with design considerations—matrix stiffness is important to control both bioink and tissue structure (inspired by Ng et al., 2016). ECM, Extracellular matrix.

these equivalents have shown great success in the clinic, they still lack the physiological complexity of native skin.

Novel technologies—3D printed skin equivalent constructs: 3D printing of skin can provide high control over size and thickness of layers, spatial resolution in seeding cell types, selection of cell types, the ability to seed cell-specific layers, and utility in patient-derived replacement applications. One advantage of 3D printed systems versus standard engineered tissues involves improved reproducibility when compared to more traditional scaffold fabrication approaches (Klicks et al., 2017). 3D printing allows for additional control in seeding cell types in specific layers as well as in enhancing cell densities to improve overall skin cell morphology and cell–cell interactions (Ng et al., 2016). This methodology allows for a high degree of spatial control for this organ where the tissue layers and cell morphology are critical.

The main approaches for 3D printing skin include ink-jet, laser, and bioextrusion processes (Ng et al., 2016; Pourchet et al., 2017), or combination processes (Kim et al., 2017). The main considerations for 3D printed skin tissue constructs include the biomaterial or ink composition, cell type(s), cell sourcing, printing parameters, and the general requirement of including an air/liquid interface to encourage differentiation and barrier function of the resultant skin tissue (Fig. 2.6.7.4) (Yan et al., 2018).

“SCAFFOLD-FREE” 3D PRINTING

One interesting approach to skin bioprinting is a “scaffold-free” approach, which leverages the abilities of 3D printing to form 3D morphologies with an application in skin, often only investigated on flat surfaces (Fig. 2.6.7.5) (Pourchet et al., 2017). The ability to construct different geometries by 3D printing allows for application in sophisticated tissue-engineering needs, such as in full-thickness wounds or in complex regenerative areas for surgical reconstruction.



• **Figure 2.6.7.5** “Scaffold-free” bioprinting of human skin in complex 3D architectures allows for proof-of-concept printing of a human ear (Pourchet et al., 2017).

Challenges

The field of skin engineering still presents multiple limitations to overcome, such as the high cost of production, potential immune rejection, lack of vascularization, and lack of complexity (Vig et al., 2017). Currently, clinically used materials consist of a few relatively simple layers, involving fibroblasts and keratinocytes, whereas normal skin consists of many different, complex structures, cells, and functions.

Current research focuses on incorporating such complexity to facilitate physiologically relevant skin systems with significant room for technology growth.

Conclusions

Soft tissue engineering is an exciting and growing field. It encompasses many subsets of tissue types, and in this chapter we focused on three: adipose, gastrointestinal, and skin. Other soft tissue fields such as neural, skeletal muscle, cartilage, and reproductive organs have also experienced significant progress in the development of tissue-engineered constructs due to advances in stem cell biology, biomaterial engineering, cell signaling, and related fields. Although each field has different requirements, the collective goals involve developing tissue systems that facilitate functional tissue regeneration and provide physiologically relevant tissue models. Ongoing challenges include sourcing components (e.g., cells, biomaterials, growth factors), standardizing procedures for the processing of these components, and defining storage and handling requirements that match regulatory and clinical requirements.

References

- Abbott, R.D., Wang, R.Y., Reagan, M.R., Chen, Y., Borowsky, F.E., Zieba, A., Marra, K.G., Rubin, J.P., Ghobrial, I.M., Kaplan, D.L., 2016. The use of silk as a scaffold for mature, sustainable unilocular adipose 3D tissue engineered systems. *Adv. Healthc. Mater.* 5, 1667–1677.
- Abraira, V.E., Ginty, D.D., 2013. The sensory neurons of touch. *Neuron* 79, 618–639.
- Agostini, F., Rossi, F.M., Aldinucci, D., Battiston, M., Lombardi, E., Zanolin, S., Massarut, S., Parodi, P.C., Da Ponte, A., Tessitori, G., Pivetta, B., Durante, C., Mazzucato, M., 2018. Improved GMP compliant approach to manipulate lipoaspirates, to cryopreserve stromal vascular fraction, and to expand adipose stem cells in xeno-free media. *Stem Cell Res. Ther.* 9, 130.
- Alam, M., Gladstone, H., Kramer, E.M., Murphy Jr., J.P., Nouri, K., Neuhaus, I.M., Spencer, J.M., Spencer, E., VAN Dyke, S., Ceilley, R.I., Lee, K.K., Menaker, G., Monheit, G.D., Orentreich, D.S., Raab, B., Smith, K.C., Solish, N.J., 2008. ASDS guidelines of care: injectable fillers. *Dermatol. Surg.* 1 (34 Suppl), S115–S148.
- Andreas, K., Zehbe, R., Kazubek, M., Grzeschik, K., Sternberg, N., Baumler, H., Schubert, H., Sittinger, M., Ringe, J., 2011. Biodegradable insulin-loaded PLGA microspheres fabricated by three different emulsification techniques: investigation for cartilage tissue engineering. *Acta Biomater.* 7, 1485–1495.
- Bader, A., Schilling, T., Teebken, O.E., Brandes, G., Herden, T., Steinhoff, G., Haverich, A., 1998. Tissue engineering of heart valves—human endothelial cell seeding of detergent acellularized porcine valves. *Eur. J. Cardiothorac. Surg.* 14, 279–284.
- Badylak, S.F., Freytes, D.O., Gilbert, T.W., 2009. Extracellular matrix as a biological scaffold material: structure and function. *Acta Biomater.* 5, 1–13.
- Badylak, S.F., Hoppo, T., Nieponice, A., Gilbert, T.W., Davison, J.M., Jobe, B.A., 2011. Esophageal preservation in five male patients after endoscopic inner-layer circumferential resection in the setting of superficial cancer: a regenerative medicine approach with a biologic scaffold. *Tissue Eng. A* 17, 1643–1650.
- Bakaic, E., Smeets, N.M.B., Hoare, T., 2015. Injectable hydrogels based on poly(ethylene glycol) and derivatives as functional biomaterials. *RSC Adv.* 5, 35469–35486.
- Bell, E., Ivarsson, B., Merrill, C., 1979. Production of a tissue-like structure by contraction of collagen lattices by human fibroblasts of different proliferative potential in vitro. *Proc. Natl. Acad. Sci. USA* 76, 1274–1278.
- Bellas, E., Panilaitis, B.J., Glettig, D.L., Kirker-Head, C.A., Yoo, J.J., Marra, K.G., Rubin, J.P., Kaplan, D.L., 2013. Sustained volume retention in vivo with adipocyte and lipoaspirate seeded silk scaffolds. *Biomaterials* 34, 2960–2968.
- Bellas, E., Seiberg, M., Garlick, J., Kaplan, D.L., 2012. In vitro 3D full-thickness skin-equivalent tissue model using silk and collagen biomaterials. *Macromol. Biosci.* 12, 1627–1636.
- Bharucha, A.E., Camilleri, M., 2015. Colonic inertia. In: Lacy, B.E., Crowell, M.D., Dibaise, J.K. (Eds.), *Functional and Motility Disorders of the Gastrointestinal Tract*. Springer, New York.
- Biedermann, T., Boettcher-Haberzeth, S., Reichmann, E., 2013. Tissue engineering of skin for wound coverage. *Eur. J. Pediatr. Surg.* 23, 375–382.
- Bitar, K.N., Zakhem, E., 2016. Bioengineering the gut: future prospects of regenerative medicine. *Nat. Rev. Gastroenterol. Hepatol.* 13, 543–556.
- Black, A.F., Berthod, F., Lheureux, N., Germain, L., Auger, F.A., 1998. In vitro reconstruction of a human capillary-like network in a tissue-engineered skin equivalent. *FASEB J.* 12, 1331–1340.
- Blais, M., Parenteau-Bareil, R., Cadau, S., Berthod, F., 2013. Concise review: tissue-engineered skin and nerve regeneration in burn treatment. *Stem Cells Transl. Med.* 2, 545–551.
- Broder, K.W., Cohen, S.R., 2006. An overview of permanent and semipermanent fillers. *Plast. Reconstr. Surg.* 118, 7s–14s.
- Bunnell, B.A., Flaate, M., Gagliardi, C., Patel, B., Ripoll, C., 2008. Adipose-derived stem cells: isolation, expansion and differentiation. *Methods* 45, 115–120.
- Burdick, J.A., Prestwich, G.D., 2011. Hyaluronic acid hydrogels for biomedical applications. *Adv. Mater.* 23, H41–H56.
- Cannon, B., Nedergaard, J., 2004. Brown adipose tissue: function and physiological significance. *Physiol. Rev.* 84, 277–359.
- Chen, X., Aledia, A.S., Ghajar, C.M., Griffith, C.K., Putnam, A.J., Hughes, C.C., George, S.C., 2009. Prevascularization of a fibrin-based tissue construct accelerates the formation of functional anastomosis with host vasculature. *Tissue Eng. A* 15, 1363–1371.
- Chen, Y., Zhou, W., Roh, T., Estes, M.K., Kaplan, D.L., 2017. *In vitro* enteroid-derived three-dimensional tissue model of human small intestinal epithelium with innate immune responses. *PLoS One* 12, e0187880.
- Cheng, J.T., Perkins, S.W., Hamilton, M.M., 2002. Collagen and injectable fillers. *Otolaryngol. Clin. N. Am.* 35, 73–85 vi.
- Chhaya, M.P., Melchels, F.P., Holzapfel, B.M., Baldwin, J.G., Huttmacher, D.W., 2015. Sustained regeneration of high-volume adipose tissue for breast reconstruction using computer aided design and biomaterials. *Biomaterials* 52, 551–560.
- Chiu, Y.C., Cheng, M.H., Uriel, S., Brey, E.M., 2011. Materials for engineering vascularized adipose tissue. *J. Tissue Viability* 20, 37–48.
- Choi, J.H., Gimble, J.M., Lee, K., Marra, K.G., Rubin, J.P., Yoo, J.J., Vunjak-Novakovic, G., Kaplan, D.L., 2010. Adipose tissue engineering for soft tissue regeneration. *Tissue Eng. B Rev.* 16, 413–426.
- Choi, R., 1997. Preliminary studies of tissue-engineered intestine using isolated epithelial organoid units on tubular synthetic biodegradable scaffolds. *Transplant. Proc.* 29, 848–851.
- Chung, C.W., Marra, K.G., Li, H., Leung, A.S., Ward, D.H., Tan, H., Kelmendi-Doko, A., Rubin, J.P., 2012. VEGF microsphere technology to enhance vascularization in fat grafting. *Ann. Plast. Surg.* 69, 213–219.
- Coelho, M., Oliveira, T., Fernandes, R., 2013. Biochemistry of adipose tissue: an endocrine organ. *Arch. Med. Sci.* 9, 191–200.

- Colaïanni, G., Colucci, S., Grano, M., 2015. Anatomy and Physiology of Adipose Tissue. Multidisciplinary Approach to Obesity. Springer.
- Collins, M.N., Birkinshaw, C., 2013. Hyaluronic acid based scaffolds for tissue engineering—a review. *Carbohydr. Polym.* 92, 1262–1279.
- Comley, K., Fleck, N.A., 2009. The High Strain Rate Response of Adipose Tissue. Springer Netherlands, Dordrecht, pp. 27–33.
- Comley, K., Fleck, N.A., 2010. A micromechanical model for the Young's modulus of adipose tissue. *Int. J. Solids Struct.* 47, 2982–2990.
- Costilla, V.C., Foxx-Orenstein, A.E., 2015. Fecal incontinence. In: Lacy, B.E., Crowell, M.D., Dibaïse, J.K. (Eds.), *Functional and Motility Disorders of the Gastrointestinal Tract*. Springer, New York.
- Cox, T.R., Erler, J.T., 2011. Remodeling and homeostasis of the extracellular matrix: implications for fibrotic diseases and cancer. *Dis. Model. Mech.* 4, 165–178.
- Davidenko, N., Schuster, C.F., Bax, D.V., Raynal, N., Farnsdale, R.W., Best, S.M., Cameron, R.E., 2015. Control of crosslinking for tailoring collagen-based scaffolds stability and mechanics. *Acta Biomater.* 25, 131–142.
- Dedhia, P.H., Bertaux-Skeirik, N., Zavros, Y., Spence, J.R., 2016. Organoid models of human gastrointestinal development and disease. *Gastroenterology* 150, 1098–1112.
- Deng, M., Gu, Y., Liu, Z., Qi, Y., Ma, G.E., Kang, N., 2015. Endothelial differentiation of human adipose-derived stem cells on polyglycolic acid/poly(lactic acid) mesh. *Stem Cell. Int.* 2015, 350718.
- Denost, Q., Adam, J.-P., Pontallier, A., Montembault, A., Bareille, R., Siadous, R., Delmond, S., Rullier, E., David, L., Bordenave, L., 2015. Colorectal tissue engineering: a comparative study between porcine small intestinal submucosa (SIS) and chitosan hydrogel patches. *Surgery* 158, 1714–1723.
- FDA, 2018. Dermal fillers approved by the center for devices and radiological health [online]. U.S. Food Drug Adm. Available from <https://www.fda.gov/MedicalDevices/ProductsandMedicalProcedures/CosmeticDevices/ucm619846.htm>.
- Finkbeiner, S.R., Freeman, J.J., Wieck, M.M., EL-Nachef, W., Altheim, C.H., Tsai, Y.-H., Huang, S., Dyal, R., White, E.S., Grikscheit, T.C., 2015. Generation of tissue-engineered small intestine using embryonic stem cell-derived human intestinal organoids. *Biol. Open* 4, 1462–1472.
- Fischer, L.J., McIlhenny, S., Tulenko, T., Golezorkhi, N., Zhang, P., Larson, R., Lombardi, J., Shapiro, I., Dimuzio, P.J., 2009. Endothelial differentiation of adipose-derived stem cells: effects of endothelial cell growth supplement and shear force. *J. Surg. Res.* 152, 157–166.
- Flynn, L., Woodhouse, K.A., 2008. Adipose tissue engineering with cells in engineered matrices. *Organogenesis* 4, 228–235.
- Flynn, L.E., 2010. The use of decellularized adipose tissue to provide an inductive microenvironment for the adipogenic differentiation of human adipose-derived stem cells. *Biomaterials* 31, 4715–4724.
- Frantz, C., Stewart, K.M., Weaver, V.M., 2010. The extracellular matrix at a glance. *J. Cell Sci.* 123, 4195–4200.
- Fu, K., Pack, D.W., Klibanov, A.M., Langer, R., 2000. Visual evidence of acidic environment within degrading poly(lactic-co-glycolic acid) (PLGA) microspheres. *Pharm. Res.* 17, 100–106.
- Gealekman, O., Guseva, N., Hartigan, C., Apotheker, S., Gorgoglione, M., Gurav, K., Tran, K.V., Straubhaar, J., Nicoloro, S., Czech, M.P., Thompson, M., Perugini, R.A., Corvera, S., 2011. Depot-specific differences and insufficient subcutaneous adipose tissue angiogenesis in human obesity. *Circulation* 123, 186–194.
- Gentleman, E., Nauman, E.A., Livesay, G.A., Dee, K.C., 2006. Collagen composite biomaterials resist contraction while allowing development of adipocytic soft tissue in vitro. *Tissue Eng.* 12, 1639–1649.
- Gesta, S., Tseng, Y.H., Kahn, C.R., 2007. Developmental origin of fat: tracking obesity to its source. *Cell* 131, 242–256.
- Gimble, J.M., Katz, A.J., Bunnell, B.A., 2007. Adipose-derived stem cells for regenerative medicine. *Circ. Res.* 100, 1249–1260.
- Gregorieff, A., Clevers, H., 2005. Wnt signaling in the intestinal epithelium: from endoderm to cancer. *Genes Dev.* 19, 877–890.
- Grover, G.N., Rao, N., Christman, K.L., 2014. Myocardial matrix-polyethylene glycol hybrid hydrogels for tissue engineering. *Nanotechnology* 25, 014011.
- Hotta, R., Stamp, L.A., Foong, J.P., McConnell, S.N., Bergner, A.J., Anderson, R.B., Enomoto, H., Newgreen, D.F., Obermayr, F., Furness, J.B., 2013. Transplanted progenitors generate functional enteric neurons in the postnatal colon. *J. Clin. Investig.* 123, 1182–1191.
- Huizinga, J.D., 1999. Gastrointestinal peristalsis: joint action of enteric nerves, smooth muscle, and interstitial cells of Cajal. *Microsc. Res. Tech.* 47, 239–247.
- Hussey, G.S., Cramer, M.C., Badylak, S.F., 2018. Extracellular matrix bioscaffolds for building gastrointestinal tissue. *Cell. Mol. Gastroenterol. Hepatol.* 5, 1–13.
- Hussey, G.S., Keane, T.J., Badylak, S.F., 2017. The extracellular matrix of the gastrointestinal tract: a regenerative medicine platform. *Nat. Rev. Gastroenterol. Hepatol.* 14, 540–552.
- Kaihara, S., Borenstein, J., Koka, R., Lalan, S., Ochoa, E.R., Ravens, M., Pien, H., Cunningham, B., Vacanti, J.P., 2000. Silicon micro-machining to tissue engineer branched vascular channels for liver fabrication. *Tissue Eng.* 6, 105–117.
- Kalaba, S., Gerhard, E., Winder, J.S., Pauli, E.M., Haluck, R.S., Yang, J., 2016. Design strategies and applications of biomaterials and devices for hernia repair. *Bioact. Mater.* 1, 2–17.
- Kalra, A., Lowe, A., AL-Jumaily, A.M., 2016. Mechanical behavior of skin: a review. *J. Mater. Sci. Eng.* 5, 254.
- Keane, T.J., Deward, A., Londono, R., Saldin, L.T., Castleton, A.A., Carey, L., Nieponice, A., Lagasse, E., Badylak, S.F., 2015. Tissue-specific effects of esophageal extracellular matrix. *Tissue Eng. A* 21, 2293–2300.
- Keane, T.J., Dziki, J., Sobieski, E., Smoulder, A., Castleton, A., Turner, N., White, L.J., Badylak, S.F., 2017. Restoring mucosal barrier function and modifying macrophage phenotype with an extracellular matrix hydrogel: potential therapy for ulcerative colitis. *J. Crohns Colitis* 11, 360–368.
- Keck, M., Haluza, D., Lumenta, D.B., Burjak, S., Eisenbock, B., Kamolz, L.P., Frey, M., 2011. Construction of a multi-layer skin substitute: simultaneous cultivation of keratinocytes and preadipocytes on a dermal template. *Burns* 37, 626–630.
- Kim, B.S., 2015. Innate lymphoid cells in the skin. *J. Investig. Dermatol.* 135, 673–678.
- Kim, B.S., Lee, J.S., Gao, G., Cho, D.W., 2017. Direct 3D cell-printing of human skin with functional transwell system. *Biofabrication* 9, 025034.
- Klein, J., Permana, P.A., Owecki, M., Chaldakov, G.N., Bohm, M., Hausman, G., Lapiere, C.M., Atanassova, P., Sowinski, J., Fasshauer, M., Hausman, D.B., Maquoi, E., Tonchev, A.B., Peneva, V.N., Vlachanov, K.P., Fiore, M., Aloe, L., Slominski, A., Reardon, C.L., Ryan, T.J., Pond, C.M., Ryan, T.J., 2007. What are subcutaneous adipocytes really good for? *Exp. Dermatol.* 16, 45–70.
- Klein, S., Seidler, B., Kettenberger, A., Sibaev, A., Rohn, M., Feil, R., Allescher, H.-D., Vanderwinden, J.-M., Hofmann, F., Schemann, M., 2013. Interstitial cells of Cajal integrate excitatory and inhibitory neurotransmission with intestinal slow-wave activity. *Nat. Commun.* 4, 1630.
- Klicks, J., Von Molitor, E., Ertongur-Fauth, T., Rudolf, R., Hafner, M., 2017. In vitro skin three-dimensional models and their applications. *J. Cell. Biotechnol.* 3, 21–39.

- Krill, J.T., Naik, R.D., Vaezi, M.F., 2016. Clinical management of achalasia: current state of the art. *Clin. Exp. Gastroenterol.* 9, 71–82.
- Kuo, B., Urma, D., 2006. Esophagus – Anatomy and Development [Online]. Available from <https://www.nature.com/gimo/contents/pt.1/full/gimo6.html>.
- Kurtz, A., Oh, S.J., 2012. Age related changes of the extracellular matrix and stem cell maintenance. *Prev. Med. (54 Suppl.)*, S50–S56.
- Landau, M.J., Birnbaum, Z.E., Kurtz, L.G., Aronowitz, J.A., 2018. Review: proposed methods to improve the survival of adipose tissue in autologous fat grafting. *Plast. Reconstr. Surg. Glob. Open* 6, e1870.
- Lavik, E., Langer, R., 2004. Tissue engineering: current state and perspectives. *Appl. Microbiol. Biotechnol.* 65, 1–8.
- Lebonvallet, N., Boulais, N., LE Gall, C., Pereira, U., Gauche, D., Gobin, E., Pers, J.O., Jeanmaire, C., Danoux, L., Pauly, G., Misery, L., 2012. Effects of the re-innervation of organotypic skin explants on the epidermis. *Exp. Dermatol.* 21, 156–158.
- Lemperle, G., Sadick, N.S., Knapp, T.R., Lemperle, S.M., 2010. ArteFill permanent injectable for soft tissue augmentation: II. Indications and applications. *Aesthet. Plast. Surg.* 34, 273–286.
- Levenberg, S., Langer, R., 2004. Advances in tissue engineering. *Curr. Top. Dev. Biol.* 61, 113–134.
- Levental, I., Georges, P.C., Janmey, P.A., 2007. Soft biological materials and their impact on cell function. *Soft Matter* 3, 299–306.
- Levin, D.E., Barthel, E.R., Speer, A.L., Sala, F.G., Hou, X., Torashima, Y., Grikscheit, T.C., 2013. Human tissue-engineered small intestine forms from postnatal progenitor cells. *J. Pediatr. Surg.* 48, 129–137.
- Linder-Ganz, E., Shabshin, N., Itzhak, Y., Gefen, A., 2007. Assessment of mechanical conditions in sub-dermal tissues during sitting: a combined experimental-MRI and finite element approach. *J. Biomech.* 40, 1443–1454.
- Liu, J., Zheng, H., Poh, P.S., Machens, H.G., Schilling, A.F., 2015. Hydrogels for engineering of perfusable vascular networks. *Int. J. Mol. Sci.* 16, 15997–16016.
- Mahoney, C.M., Imbarlina, C., Yates, C.C., Marra, K.G., 2018. Current therapeutic strategies for adipose tissue defects/repair using engineered biomaterials and biomolecule formulations. *Front. Pharmacol.* 9, 507.
- Mahoney, M.J., Anseth, K.S., 2006. Three-dimensional growth and function of neural tissue in degradable polyethylene glycol hydrogels. *Biomaterials* 27, 2265–2274.
- Malikmammadov, E., Tanir, T.E., Kiziltay, A., Hasirci, V., Hasirci, N., 2018. PCL and PCL-based materials in biomedical applications. *J. Biomater. Sci. Polym. Ed.* 29, 863–893.
- Mariman, E.C., Wang, P., 2010. Adipocyte extracellular matrix composition, dynamics and role in obesity. *Cell. Mol. Life Sci.* 67, 1277–1292.
- Mathes, S.H., Ruffner, H., GRAF-Hausner, U., 2014. The use of skin models in drug development. *Adv. Drug Deliv. Rev.* 69–70, 81–102.
- Mckee, C.T., Last, J.A., Russell, P., Murphy, C.J., 2011. Indentation versus tensile measurements of Young's modulus for soft biological tissues. *Tissue Eng. B Rev.* 17, 155–164.
- Mercalfe, A.D., Ferguson, M.W., 2007. Tissue engineering of replacement skin: the crossroads of biomaterials, wound healing, embryonic development, stem cells and regeneration. *J. R. Soc. Interface* 4, 413–437.
- Miyazawa, M., Aikawa, M., Watanabe, Y., Takase, K.-I., Okamoto, K., Shrestha, S., Okada, K., Koyama, I., Ikada, Y., 2015. Extensive regeneration of the stomach using bioabsorbable polymer sheets. *Surgery* 158, 1283–1290.
- Mondal, D., Griffith, M., Venkatraman, S.S., 2016. Polycaprolactone-based biomaterials for tissue engineering and drug delivery: current scenario and challenges. *Int. J. Polym. Mater. Polym. Biomater.* 65, 255–265.
- Murphy, A.R., Kaplan, D.L., 2009. Biomedical applications of chemically-modified silk fibroin. *J. Mater. Chem.* 19, 6443–6450.
- Nakajima, I., Yamaguchi, T., Ozutsumi, K., Aso, H., 1998. Adipose tissue extracellular matrix: newly organized by adipocytes during differentiation. *Differentiation* 63, 193–200.
- Nakao, M., Ueno, T., Oga, A., Kuramitsu, Y., Nakatsu, H., Oka, M., 2015. Proposal of intestinal tissue engineering combined with Bianchi's procedure. *J. Pediatr. Surg.* 50, 573–580.
- Nakase, Y., Hagiwara, A., Nakamura, T., Kin, S., Nakashima, S., Yoshikawa, T., Fukuda, K.-I., Kuriu, Y., Miyagawa, K., Sakakura, C., 2006. Tissue engineering of small intestinal tissue using collagen sponge scaffolds seeded with smooth muscle cells. *Tissue Eng.* 12, 403–412.
- Neves, N.M., Reis, R.L., 2016. Biomaterials from Nature for Advanced Devices and Therapies. John Wiley & Sons.
- Ng, W.L., Wang, S., Yeong, W.Y., Naing, M.W., 2016. Skin bioprinting: impending reality or fantasy? *Trends Biotechnol.* 34, 689–699.
- Nieponice, A., Ciotola, F.F., Nachman, F., Jobe, B.A., Hoppo, T., Londono, R., Badylak, S., Badaloni, A.E., 2014. Patch esophagoplasty: esophageal reconstruction using biologic scaffolds. *Ann. Thorac. Surg.* 97, 283–288.
- Nishimura, T., Ueno, T., Nakatsu, H., Oga, A., Kobayashi, S., Oka, M., 2010. In vivo motility evaluation of the grafted gastric wall with small intestinal submucosa. *Tissue Eng. A* 16, 1761–1768.
- Novak, U., Kaye, A.H., 2000. Extracellular matrix and the brain: components and function. *J. Clin. Neurosci.* 7, 280–290.
- Nyame, T.T., Chiang, H.A., Orgill, D.P., 2014. Clinical applications of skin substitutes. *Surg. Clin. N. Am.* 94, 839–850.
- O'Brien, F.J., 2011. Biomaterials & scaffolds for tissue engineering. *Mater. Today* 14, 88–95.
- Ouwehand, K., Spiekstra, S.W., Waaijman, T., Scheper, R.J., De Grijl, T.D., Gibbs, S., 2011. Technical advance: Langerhans cells derived from a human cell line in a full-thickness skin equivalent undergo allergen-induced maturation and migration. *J. Leukoc. Biol.* 90, 1027–1033.
- Palukuru, U.P., MCGoverin, C.M., Pleshko, N., 2014. Assessment of hyaline cartilage matrix composition using near infrared spectroscopy. *Matrix Biol.* 38, 3–11.
- Palumbo, P., Lombardi, F., Siragusa, G., Cifone, M.G., Cinque, B., Giuliani, M., 2018. Methods of isolation, characterization and expansion of human adipose-derived stem cells (ASCs): an overview. *Int. J. Mol. Sci.* 19.
- Parenteau-Bareil, R., Gauvin, R., Berthod, F., 2010. Collagen-based biomaterials for tissue engineering applications. *Materials* 3, 1863–1887.
- Parlato, M., Reichert, S., Barney, N., Murphy, W.L., 2014. Poly(ethylene glycol) hydrogels with adaptable mechanical and degradation properties for use in biomedical applications. *Macromol. Biosci.* 14, 687–698.
- Partlow, B.P., Hanna, C.W., Rnjak-Kovacina, J., Moreau, J.E., Applegate, M.B., Burke, K.A., Marelli, B., Mitropoulos, A.N., Omenetto, F.G., Kaplan, D.L., 2014. Highly tunable elastomeric silk biomaterials. *Adv. Funct. Mater.* 24, 4615–4624.
- Patrick Jr., C.W., 2001. Tissue engineering strategies for adipose tissue repair. *Anat. Rec.* 263, 361–366.

- Patrick, C.W., Uthamanthil, R., Beahm, E., Frye, C., 2008. Animal models for adipose tissue engineering. *Tissue Eng. B Rev.* 14, 167–178.
- Paus, R., Theoharides, T.C., Arck, P.C., 2006. Neuroimmunoendocrine circuitry of the ‘brain-skin connection’. *Trends Immunol.* 27, 32–39.
- Payne, R.M., Anderson, A., Parrillo, A., Sadtler, K., Wu, I., Aston, J., Steiner, A., Cooney, C.M., Cooney, D.S., Byrne, P., Pardoll, D., Elisseff, J., 2017. Abstract 77: a Phase I open-label study evaluating the safety of acellular adipose tissue (AAT), a novel soft tissue reconstruction solution, in healthy volunteers. *Plast. Reconstr. Surg. Glob. Open* 5, 58–59.
- Peery, A.F., Dellon, E.S., Lund, J., Crockett, S.D., McGowan, C.E., Bultsiewicz, W.J., Gangarosa, L.M., Thiny, M.T., Stizenberg, K., Morgan, D.R., 2012. Burden of gastrointestinal disease in the United States: 2012 update. *Gastroenterology* 143, 1179–1187.
- Pourchet, L.J., Thepot, A., Albouy, M., Courtial, E.J., Boher, A., Blum, L.J., Marquette, C.A., 2017. Human skin 3D bioprinting using scaffold-free approach. *Adv. Healthc. Mater.* 6.
- Quan, T., Wang, F., Shao, Y., Rittie, L., Xia, W., Orringer, J.S., Voorhees, J.J., Fisher, G.J., 2013. Enhancing structural support of the dermal microenvironment activates fibroblasts, endothelial cells, and keratinocytes in aged human skin in vivo. *J. Investig. Dermatol.* 133, 658–667.
- Ramadan, Q., Ting, F.C., 2016. In vitro micro-physiological immune-competent model of the human skin. *Lab. Chip* 16, 1899–1908.
- Rockwood, D.N., Preda, R.C., Yucel, T., Wang, X., Lovett, M.L., Kaplan, D.L., 2011. Materials fabrication from *Bombyx mori* silk fibroin. *Nat. Protoc.* 6, 1612–1631.
- Roggenkamp, D., Falkner, S., Stab, F., Petersen, M., Schmelz, M., Neufang, G., 2012. Atopic keratinocytes induce increased neurite outgrowth in a coculture model of porcine dorsal root ganglia neurons and human skin cells. *J. Investig. Dermatol.* 132, 1892–1900.
- Roggenkamp, D., Kopnick, S., Stab, F., Wenck, H., Schmelz, M., Neufang, G., 2013. Epidermal nerve fibers modulate keratinocyte growth via neuropeptide signaling in an innervated skin model. *J. Investig. Dermatol.* 133, 1620–1628.
- Rosson, G., Elisseff, J.H., Nahas, Z., Ye, Z., Hillel, A., 2016. Compositions and Methods for Implantation of Adipose Tissue and Adipose Tissue Products. Google Patents.
- Sarzo, G., Finco, C., Mungo, B., Gruppo, M., Cadrobbi, R., Polese, L., 2013. Anal fistula repair with acellular dermal matrix plug: description of a novel technique and early results. *J. Surg.* 1, 1–6.
- Sato, T., Vries, R.G., Snippert, H.J., Van De Wetering, M., Barker, N., Stange, D.E., Van Es, J.H., Abo, A., Kujala, P., Peters, P.J., 2009. Single Lgr5 stem cells build crypt–villus structures in vitro without a mesenchymal niche. *Nature* 459, 262–265.
- Scott, B., Koch, K.L., 2015. Gastroparesis. In: Lacy, B.E., Crowell, M.D., Dibaise, J.K. (Eds.), *Functional and Motility Disorders of the Gastrointestinal Tract*. Springer, New York.
- Shoham, N., Gefen, A., 2012. Mechanotransduction in adipocytes. *J. Biomech.* 45, 1–8.
- Shuttleworth, A., 1998. Extracellular matrix. In: Delves, P.J. (Ed.), *Encyclopedia of Immunology*, second ed. Elsevier, Oxford.
- Singelyn, J.M., Dequach, J.A., SEIF-Naraghi, S.B., Littlefield, R.B., Schup-Magoffin, P.J., Christman, K.L., 2009. Naturally derived myocardial matrix as an injectable scaffold for cardiac tissue engineering. *Biomaterials* 30, 5409–5416.
- Skeldon, G., Lucendo-Villarin, B., Shu, W., 2018. Three-dimensional bioprinting of stem-cell derived tissues for human regenerative medicine. *Philos. Trans. R. Soc. Lond. B Biol. Sci.* 373.
- Song, M., Liu, Y., Hui, L., 2018. Preparation and characterization of acellular adipose tissue matrix using a combination of physical and chemical treatments. *Mol. Med. Rep.* 17, 138–146.
- Spurrier, R.G., Speer, A.L., Hou, X., EL-Nachef, W.N., Grikscheit, T.C., 2014. Murine and human tissue-engineered esophagus form from sufficient stem/progenitor cells and do not require microdesigned biomaterials. *Tissue Eng. A* 21, 906–915.
- Steinboff, M., Stander, S., Seeliger, S., Ansel, J.C., Schmelz, M., Luger, T., 2003. Modern aspects of cutaneous neurogenic inflammation. *Arch. Dermatol.* 139, 1479–1488.
- Stoppel, W.L., Raia, N., Kimmerling, E., Wang, S., Ghezzi, C.E., Kaplan, D.L., 2017. 2.12 silk biomaterials☆. In: Ducheyne, P. (Ed.), *Comprehensive Biomaterials II*. Elsevier, Oxford.
- Stratton, S., Shelke, N.B., Hoshino, K., Rudraiah, S., Kumbar, S.G., 2016. Bioactive polymeric scaffolds for tissue engineering. *Bioact. Mater.* 1, 93–108.
- Strong, A.L., Cederna, P.S., Rubin, J.P., Coleman, S.R., Levi, B., 2015. The current state of fat grafting: a review of harvesting, processing, and injection techniques. *Plast. Reconstr. Surg.* 136, 897–912.
- Sun, X., Xu, C., Wu, G., Ye, Q., Wang, C., 2017. Poly (lactic-co-glycolic acid): applications and future prospects for periodontal tissue regeneration. *Polymers* 9, 189.
- Tsiloulis, T., Watt, M.J., 2015. Exercise and the regulation of adipose tissue metabolism. *Prog. Mol. Biol. Transl. Sci.* 135, 175–201.
- Tsuda, Y., Shimizu, T., Yamato, M., Kikuchi, A., Sasagawa, T., Sekiya, S., Kobayashi, J., Chen, G., Okano, T., 2007. Cellular control of tissue architectures using a three-dimensional tissue fabrication technique. *Biomaterials* 28, 4939–4946.
- Valladeau, J., Saeland, S., 2005. Cutaneous dendritic cells. *Semin. Immunol.* 17, 273–283.
- Van Nieuwenhove, I., Tytgat, L., Ryx, M., Blondeel, P., Stillaert, F., Thienpont, H., Ottevaere, H., Dubruel, P., Van Vlierberghe, S., 2017. Soft tissue fillers for adipose tissue regeneration: from hydrogel development toward clinical applications. *Acta Biomater.* 63, 37–49.
- Vedepo, M.C., Detamore, M.S., Hopkins, R.A., Converse, G.L., 2017. Recellularization of decellularized heart valves: progress toward the tissue-engineered heart valve. *J. Tissue Eng.* 8, 2041731417726327.
- Vepari, C., Kaplan, D.L., 2007. Silk as a biomaterial. *Prog. Polym. Sci.* 32, 991–1007.
- Vidal, S.E.L., Tamamoto, K.A., Nguyen, H., Abbott, R.D., Cairns, D.M., Kaplan, D.L., 2018. 3D biomaterial matrix to support long term, full thickness, immuno-competent human skin equivalents with nervous system components. *Biomaterials*.
- Vig, K., Chaudhari, A., Tripathi, S., Dixit, S., Sahu, R., Pillai, S., Dennis, V.A., Singh, S.R., 2017. Advances in skin regeneration using tissue engineering. *Int. J. Mol. Sci.* 18.
- Von Heimburg, D., Zachariah, S., Heschel, I., Kuhling, H., Schoof, H., Hafemann, B., Pallua, N., 2001. Human preadipocytes seeded on freeze-dried collagen scaffolds investigated in vitro and in vivo. *Biomaterials* 22, 429–438.
- Walthers, C.M., Nazemi, A.K., Patel, S.L., Wu, B.M., Dunn, J.C., 2014. The effect of scaffold macroporosity on angiogenesis and cell survival in tissue-engineered smooth muscle. *Biomaterials* 35, 5129–5137.
- Wang, J., Zhang, F., Tsang, W.P., Wan, C., Wu, C., 2017. Fabrication of injectable high strength hydrogel based on 4-arm star PEG for cartilage tissue engineering. *Biomaterials* 120, 11–21.
- Wu, I., Nahas, Z., Kimmerling, K.A., Rosson, G.D., Elisseff, J.H., 2012. An injectable adipose matrix for soft-tissue reconstruction. *Plast. Reconstr. Surg.* 129, 1247–1257.

- Xia, H., Li, X., Gao, W., Fu, X., Fang, R.H., Zhang, L., Zhang, K., 2018. Tissue repair and regeneration with endogenous stem cells. *Nat. Rev. Mater.* 3, 174–193.
- Yamate, J., 2018. Chapter 19—the skin and subcutis. In: Suttie, A.W. (Ed.), *Boorman's Pathology of the Rat*, second ed. Academic Press, Boston.
- Yan, W.C., Davoodi, P., Vijayavenkataraman, S., Tian, Y., Ng, W.C., Fuh, J.Y.H., Robinson, K.S., Wang, C.H., 2018. 3D bioprinting of skin tissue: from pre-processing to final product evaluation. *Adv. Drug Deliv. Rev.*
- Young, D.A., Choi, Y.S., Engler, A.J., Christman, K.L., 2013. Stimulation of adipogenesis of adult adipose-derived stem cells using substrates that mimic the stiffness of adipose tissue. *Biomaterials* 34, 8581–8588.
- Young, D.A., Christman, K.L., 2012. Injectable biomaterials for adipose tissue engineering. *Biomed. Mater.* 7, 024104.
- Yui, S., Nakamura, T., Sato, T., Nemoto, Y., Mizutani, T., Zheng, X., Ichinose, S., Nagaishi, T., Okamoto, R., Tsuchiya, K., 2012. Functional engraftment of colon epithelium expanded in vitro from a single adult Lgr5+ stem cell. *Nat. Med.* 18, 618–623.
- Zhang, K., Song, L., Wang, J., Yan, S., Li, G., Cui, L., Yin, J., 2017. Strategy for constructing vascularized adipose units in poly(l-glutamic acid) hydrogel porous scaffold through inducing in-situ formation of ASCs spheroids. *Acta Biomater.* 51, 246–257.
- Zhang, S., Lu, Q., Cao, T., Toh, W.S., 2016. Adipose tissue and extracellular matrix development by injectable decellularized adipose matrix loaded with basic fibroblast growth factor. *Plast. Reconstr. Surg.* 137, 1171–1180.
- Zhang, Z., Michniak-Kohn, B.B., 2012. Tissue engineered human skin equivalents. *Pharmaceutics* 4, 26–41.
- Zhu, J., 2010. Bioactive modification of poly(ethylene glycol) hydrogels for tissue engineering. *Biomaterials* 31, 4639–4656.
- Zuk, P.A., Zhu, M., Ashjian, P., DE Ugarte, D.A., Huang, J.I., Mizuno, H., Alfonso, Z.C., Fraser, J.K., Benhaim, P., Hedrick, M.H., 2002. Human adipose tissue is a source of multipotent stem cells. *Mol. Biol. Cell* 13, 4279–4295.
- Zuk, P.A., Zhu, M., Mizuno, H., Huang, J., Futrell, J.W., Katz, A.J., Benhaim, P., Lorenz, H.P., Hedrick, M.H., 2001. Multilineage cells from human adipose tissue: implications for cell-based therapies. *Tissue Eng.* 7, 211–228.

Chapter Exercises

1. What are the advantages and disadvantages of using natural and synthetic polymers for soft tissue-engineering

	Advantages	Disadvantages	Ways to Overcome
Synthetic	<ul style="list-style-type: none"> -Easily tunable properties (mechanics, degradation, modifications) -Highly reproducible 	<ul style="list-style-type: none"> -Lacks bioactivity -May use cytotoxic reagents or degradation by-products 	<ul style="list-style-type: none"> -Combines with bioactive peptides, extracellular matrix components, or natural polymers to increase bioactivity
Natural	<ul style="list-style-type: none"> -Bioactive -Generally biocompatible 	<ul style="list-style-type: none"> -Degrades rapidly -Lowers mechanical strength -Variability due to source and processing 	<ul style="list-style-type: none"> -Crosslinks the materials or combines with synthetic polymers to increase mechanical strength

2. Strategies to engineer the soft tissues of the GI tract have been slow to translate to clinical significance. What are some possible reasons for this slow translation?

- a. The GI tract consists of multiple organs with dramatically different properties. While the system is continuous, efforts to regenerate individual organs are largely discrete. Strategies that show promise in the esophagus may not be feasible in the colon. An analogy can be drawn to cancer: it is frequently referred to as if it were a single—albeit major—problem to be solved, yet it is unlikely that any single approach will be able to cure the many different cancer types.
- b. The soft tissues of the GI tract are complex and highly interrelated. The success to date has been in the regeneration of the epithelial layer, presumably because the epithelium does not contain the abundant vasculature of the underlying tissues. For this reason, its regeneration is easier. This is not the case for other tissues, such as the smooth muscle. Although regeneration of smooth muscle has been demonstrated, maintenance of phenotype over the long term is required. This will rely upon simultaneous regeneration not only of the smooth muscle, but also the enteric nervous system, vasculature, and lymphatics.
- c. There are still key gaps in our understanding of how the GI tract functions. We know, for example, that the ICC are vital to GI motility, but the precise mechanisms by which the ICC help to drive peristalsis are still active research areas. Without a clear picture of the processes that govern GI function, it may be difficult to engineer soft tissues capable of recapitulating those functions.

3. There are multiple biomaterial technologies on the market for soft tissue fillers; however, there is still much research in finding optimal materials. Explain the limitations of current soft tissue fillers.

applications? Choose one type of polymer and provide ways to overcome the disadvantages listed.

Answer:

The main limitation is that current fillers serve only to provide augmentation without inducing functional tissue regeneration. Also, most fillers on the market are degradable and without tissue formation, therefore it is necessary to have repeat injections to maintain tissue volume.

4. Design a biomaterial to stimulate adipogenesis. Explain the reasons behind the biomaterial you choose and any other components you include.

This is an open-ended question; however, the main factor to include will be to provide biochemical cues either through the biomaterial itself or by adding in bioactive components. Other properties include appropriate mechanical properties similar to native adipose tissue, sufficient degradation as tissue is formed, and to include cells.

5. Using your biomaterial developed in the previous question, design an experiment to determine if it can stimulate adipogenesis.

Experiments can be either *in vitro* or *in vivo*. For *in vitro* tests, the type of cells used should be specified if the proposed material does not already include cells. For *in vivo* tests, the animal model and location of implantation/injection should be specified. For either setup, adipose tissue-related assays such as immunohistochemistry of adipocytes (Oil Red O) or new ECM productions (collagen type IV, laminin, fibronectin), gene expression of adipogenic and lipogenic factors (RT-PCR of PPAR γ , GLUT4, FABP4, ACS, GPDH), lipid quantification (AdipoRed, triglyceride), or measuring metabolic/enzymatic activity (lipolysis, glucose uptake, GPDH enzyme activity) can be performed.

6. Discuss challenges to the development of skin equivalents.

There are numerous ways that students could answer this question based on logical challenges to current

tissue-engineering approaches, which include: recapitulation of human biology, biomaterials choice (mechanics, degradation, biocompatibility), or other issues pertaining to manufacturing, including production cost, manufacturing process, stability, etc.

7. For maintenance of systems, what are the main considerations or parameters?

Answers should include concepts such as nutrient transfer, cell culture composition, shelf life, and ability of cells to expand appropriately before transplantation.

8. For clinical substitutes, name three aspects that are important to consider in product development.

Can include: cell sourcing, scaleup, sterility, shelf life, storage.

9. Propose an experimental design to investigate a disease process in the skin. What components should be included to evaluate the process? Provide a process flow diagram of your design.

Answers should develop a skin equivalent that is capable of probing some aspect of the disease in a logical way—for example, if the student chose melanoma, it would follow that they should design a skin model that includes keratinocytes and melanocytes, and their experimental protocol should include some method to investigate that process such as inducing an ultraviolet event externally, or attempting to physically recapitulate a cancer-like environment. The cells could also be isolated from a patient with the disease to provide comparisons.

3.1.1

Introduction: Biomaterials in Medical Devices

FREDERICK J. SCHOEN¹, GUIGEN ZHANG²

¹Department of Pathology, Brigham and Women's Hospital and Harvard Medical School, Boston, MA, United States

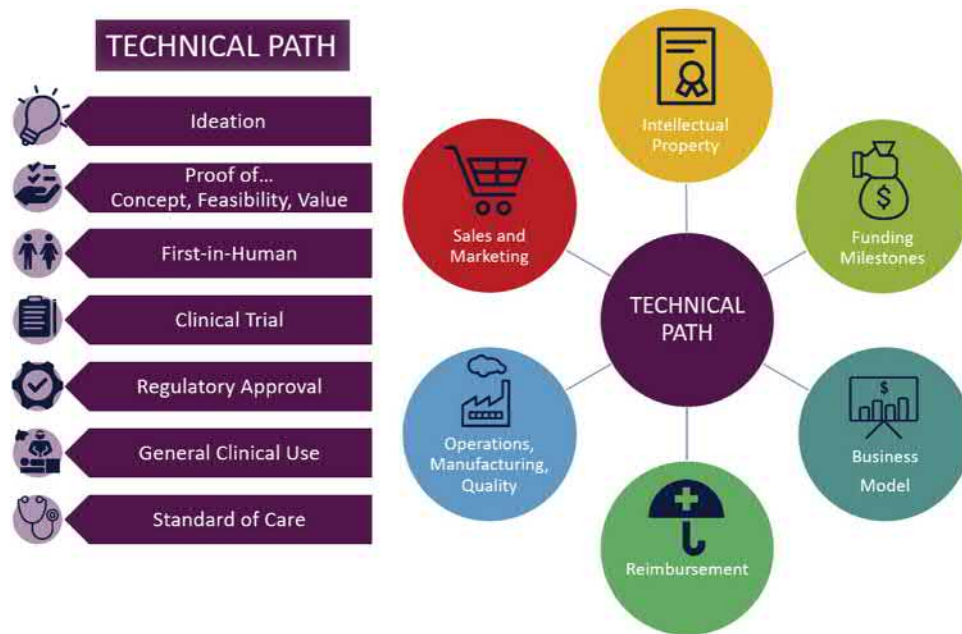
²F Joseph Halcomb III, M.D. Department of Biomedical Engineering, University of Kentucky, Lexington, KY, United States

This section highlights some of the key considerations, many nontechnical, in the development and implementation of medical devices that depend so importantly on biomaterials. Several principles underlie the approach presented in this section. The major driving force to technological innovation in biomaterials, implants, and medical devices is to improve the quality of life and survival of patients. The early phase of the process includes these steps: (1) identification of a clinical problem that needs solving (“clinical pull”); (2) determination that a viable market exists for the resultant innovation; and (3) the judicious and sophisticated application of existing, or development of, novel technology to solve this problem. In this sense, hospitals and clinics provide a “problem-rich” environment, and a laboratory for testing and translating the latest technologies and materials into clinical successes. An invention, by itself, is of little value; the value of the idea represented by an invention is through innovation, i.e., the validation and implementation of that idea or embodiment thereof to affect individuals and populations through its utilization and acceptance by others. In addition, it is important to recognize that the future of a new biomaterial associated with a device and/or implant-based treatment utilizing a biomaterial usually depends on the successful commercialization and clinical implementation of a medical product. For any product, such as an implant or medical device, the needs of commercialization (involving development, design optimization, a viable fabrication process, financing, regulatory considerations, reimbursement, manufacturing and scale-up, a suitable and profitable business model, marketing, etc.) are vital, and the scientific development, fabrication, clinical trials, and subsequent regulatory approval must occur in the context of, and concurrent with, sound business, ethical, and legal considerations (Fig. 3.1.1.1).

Indeed, medical device innovation is complex; the generic process and the requisite skills in technological innovation in medicine, including identification, invention, and implementation phases, have been summarized systematically and in detail.¹ Moreover, although demonstration of clinical effectiveness and safety are vital to clinical translation of any new medical product, today's economic pressures demand serious consideration of cost–benefit and cost effectiveness, i.e., the relative gain in health from a measure (e.g., years of life, freedom from pain) and the relative costs of different ways to achieve an equivalent gain in health, respectively. Finally, as embodied by the total collection of chapters in *Biomaterials Science: An Introduction to Materials in Medicine (Fourth Edition)*, progress in biomaterials and their implementation in clinically useful medical devices requires multidisciplinary collaboration, thinking, and communication, where engineers, physical scientists, biologists, and clinicians are on an equal footing, and share a common language and objectives.

Part 3 of this text provides a “toolkit” for medical device innovation addressing all the integral parts of the medical device development processes highlighted in Fig. 3.1.1.1. It begins with a discussion on total product life cycle for biomaterials-based medical devices in Chapter 3.1.2 by Duncan. The need for the management of total product life cycle of a biomaterial-based device reflects the fact that the process of medical device development and utilization is dynamic from conception to obsolescence. This, in turn, suggests that management of risks and performance controls may vary and indeed be iterative during the lifetime of the product. With the concept of product life cycle introduced,

¹Yock, P.G., Zenios, S., Makower, J., Brinton, T.J., Kumar, U.M., Watkins, F.T.J. (Eds.), 2015. *Biodesign: The Process of Innovating Medical Technologies*, Second ed. Cambridge University Press, Cambridge, UK, pp. 839.



• **Figure 3.1.1.1** Technical path and business processes integral to medical device development must proceed simultaneously.

in [Chapter 3.1.3](#) Duncan further discusses safety and risk considerations in medical device development. Medical devices that rely on biomaterials for function in medium- to high-risk applications are subject to technical evaluations based upon understandings of risk to the patient. A new device with new performance claims must undergo stringent safety and efficacy testing. A premarket approval application is required when the truly new device may only have an indirect basis for comparison to prior or alternative therapy, or when there is no or little evidence that the new device performs as intended. Even a device designed to be “like” another product already on the market must demonstrate that it is indeed “equivalent” to an existing device. The so-called “me-too” device has as its threshold for premarket notification [510(k)] evidence of equivalence to a prior accepted device: performing in essentially the same way to do essentially the same function without introducing new risks. Since cleaning, disinfection, sterilization, and assurance of maintained sterility are crucial to the safety and success of these medical devices, the importance and various methods of sterilization and disinfection of biomaterials for medical devices are highlighted by Harrington and Guda in [Chapter 3.1.4](#).

Following the discussions on product life cycles, safety and risk management, and sterilization and disinfection considerations, considerations concerning the transitioning of a medical device from idea to a commercial setting, or from bench-to-bedside translation, including the verification and validation of medical device design, design control, and types of tests are all discussed in [Chapter 3.1.5](#) by Simon. Moreover, in [Chapter 3.1.6](#) Goldenberg highlights some strategic business considerations for device development and commercialization, market opportunity,

reimbursement concerns, issues of intellectual property and funding, as well as sales and marketing.

In [Chapter 3.1.7](#), Duncan dives deep on issues concerning regulatory pathways and constraints for medical products using biomaterials. Aside from the numerous pathways established by the US Food and Drug Administration, it also introduces other global premarket assessment methods, requirements, clearance and approvals, and other related issues. The role of standards for testing and performance requirements of biomaterials, and various types of standard documents as well as how they are developed, are addressed by Simon and Kuhn in [Chapter 3.1.8](#).

Although medical devices serve their recipients well by performing as intended for extended duration, failures with significant consequences to recipients do occur, sometimes because of individual patient characteristics, and sometimes systematically in a patient group (i.e., cohort failure). Various aspects of medical device failure—and the means to document and understand failure modes and mechanisms through implant retrieval, evaluation, and analysis—are presented in [Chapter 3.1.9](#) by Harman. Particularly, the discussion is focused on the characterization of the human biological response and associated performance of implant designs after they have functioned in patients during general clinical use. Several case studies demonstrating the role of implant retrieval, evaluation, and failure analysis are also provided.

Though a less talked-about subject by many biomaterials engineers, some legal concerns over the use of biomaterials in medical devices are also highlighted in [Chapter 3.1.10](#) by Grody and Badylak. Throughout the course of a career, biomedical engineers will routinely encounter a range of issues that require legal consideration or can have legal ramifications. The discussions in this chapter could

be important for such professionals to develop a general awareness and familiarity with the types of situations in which legal issues will arise. For example, issues concerning employment agreements, confidentiality and materials use agreements, intellectual properties, contract negotiation and compliance, sponsored research agreements, license agreements, and litigation are all discussed. Finally, a brief review on ethical issues in the development of medical products by Brown et al. in [Chapter 3.1.11](#) helps conclude Part 3.

Often overlooked or minimized, ethical considerations in biomaterials and medical device development and use are crucial. The discussion of ethical principles covers several different types of medical products, including drugs, medical devices, and other types of therapy, highlighting mainly issues related to the safety, regulatory compliance, animal and human testing, as well as emerging issues such as the use and inclusion of stem cells in medical products and gene editing, among others.

3.1.2

Total Product Lifecycle for Biomaterial-Based Medical Devices

ELAINE DUNCAN^{1,2}

¹Paladin Medical, Inc., Stillwater, MN, United States

²Joseph Halcomb III, MD. Department of Biomedical Engineering, College of Engineering, University of Kentucky, Lexington, KY, United States

Total product lifecycle management refers to the philosophy that a medical device has a natural cycle of concept through obsolescence and therefore the management of the safety and performance of that product depends upon the current phase of the product.

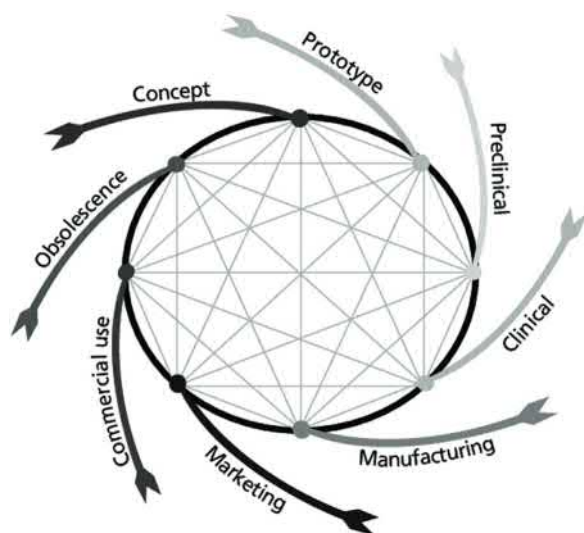
Total product lifecycle is a catchy phrase but what does it mean to the biomaterial student, the aspiring development engineer, and the physician or patient user? For a biomaterial-based medical device it means that management of risks and performance controls will vary during the lifetime of the product. And since implanted biomaterial-based medical devices must interface with the lifecycle processes of the patient, medical device lifecycles can be critically important. What if that lifecycle interfaces with one's own life or that of a loved one? Understanding the total product lifecycle of a medical product can quickly turn personal and thus product lifecycle concerns are not an abstraction (Fig. 3.1.2.1).

The product lifecycle is conventionally described as the period of time over which the product moves through various phases of development, commercialization, and eventual removal from the market. For a biomaterial-based implantable medical device the lifecycle necessarily includes the *in vivo* lifecycle of the device from implantation, integration with the host environment, to disintegration. Quality systems for medical devices take into account postmarket surveillance of product performance, such as monitoring complaints and reporting adverse events to regulatory authorities. But in most circumstances a product's approval process (or "clearance" as the case may be) does not require that design criteria consider the end stage of the implant. In other words, few if any medical devices are specifically designed to incorporate a "fail-safe" mode at end of life. And in most respects, patients cannot be fully informed or prepared for the consequences of having to remove the device in the event of failure.

Ironically, it is a tribute to the success of medical device technology and the biomaterials of construction that we can now be concerned for the "total lifecycle" of the device. We can shift the focus of concern from "will it work?" to "how long will it work?" Implicit design-life expectations for many implanted medical devices have shifted from 10 years to the remaining life of the patient, which can be a long time! Indeed, the patient's expectations for the functionality of an implanted medical device are often more than the performance of their natural organ or structure that is being replaced by the prosthesis! A patient may be sanguine when their natural hip wears out, but they expect their prosthetic device to last forever.

But can a biomaterial-based medical device be designed to perform indefinitely within the body and, if not, can the mode of failure be designed so that further damage to natural structures are limited, thus allowing the subsequent replacement to perform to the same requirements? The field of implantable medical devices is too vast to explore this question for every device, but this section will attempt to address some of the issues and the subsequent mitigations that are employed today, and raise topics for the student's continued consideration.

Conventional bench testing can often predict one or more modes of failure and even extrapolate an expected lifetime using standardized test data (e.g., fatigue cycles and load stresses). But these methods are designed for the conventional biomaterials that replace the existing structures and few, if any, can analyze the mechanical performance of a biomaterial that is intended to integrate and/or be absorbed into the body. Clinical device trials attempt to provide the best indicator of device success under controlled circumstances. Very commonly now, regulators are insisting upon longer and longer trial follow-ups and device registries to try to help monitor long-term consequences. All such attempts to predict and mitigate device failures have serious limitations as predictors of total product lifecycle performance. Clinical studies evaluate the idealized



• **Figure 3.1.2.1** According to the US Food and Drug Administration, medical device development is an iterative process that rapidly incorporates preclinical, clinical, and manufacturing experience into next-generation concept and design.¹

device in the idealized patient, whereas market-released devices are placed in patients who need the product, in spite of their preexisting conditions and confounding health factors, such as diabetes. Even a 2- or 5-year follow-up of clinical trial patients has practical limitations as a predictor of success. Setting aside the costs of such trials, patient compliance with regimens for long-term follow-up cannot be enforced. Diagnostics for implants without symptoms are limited in value, particularly for biomaterials that are designed to integrate into the surrounding structures. Since most implantable devices are expected to perform indefinitely it is problematic to manage the total product lifecycle through a controlled clinical trial protocol. Quite literally a clinical trial patient would have to become indentured to the manufacturer for perpetual follow-up to serve as a sentinel for potential lifecycle issues. Rolling a clinical trial patient into a postoperative database (registry) has limited value because such data are usually “self-reported.”

Quality programs for design control and review begin with understanding the “user need,” which for biomaterial-based medical devices include the physician and the patient. Defining the user needs in the context of how current devices do or do not adequately fulfill those needs can certainly lead to better product designs and materials selection, but in a design program that considers total product lifecycle the designers should have explanted devices and failed devices for analysis to better appreciate how the current technologies and materials are fulfilling the requirements for late-term performance. In other words, is it adequate to design a device to have enough strength or flexibility at implantation, if over time the material weakens or stiffens within the body and thus fails

to function? If such changes in properties cannot be avoided, should the recipient be warned of a finite life of the device?

Designing for shifting customer requirements is seldom part of the design input requirements for a new product. One aspect of total product lifecycle management that is frequently overlooked in medical product development is the inevitable shifting of the skills of the dominant user. Consider that during the development and initial product evaluation phase the “inputs” typically come from the highly specialized physicians who are comfortable in the vanguard of the new technology. These physicians guide the medical product development company to understand the needs for the new product and may participate in clinical studies, physician training, and other aspects of the new product development assessments. In the early months and years of product introduction the medical device manufacturers naturally sell to these “early adopters” of the new technology. The product can show immediate success in the marketplace. The more successful these new materials and devices become the more patients will demand these innovative products and more physicians may seek training in their use. Can the curse of success change the user profile and thus instead of the well-trained user and dedicated specialist, subsequent users may be too busy for training and may have a wider patient base with varying needs, possibly unlike those in the focused clinical trial. How can the design team anticipate these changing user needs?

Medical devices can never be totally risk free. When a device is offered to the market, regulators expect to see evidence that the benefits outweigh these risks.² Continued market surveillance and corrective and preventive action programs constantly attempt to maintain the balance between benefits and risks as the medical device moves through the introduction phase to market maturity. Another factor in total product lifecycle management is understanding the potential effects as a product moves into differing global markets. Surgery techniques, long-range distribution, and postimplant aftercare can impact product performance.

The expectation, particularly in the European regulatory scheme, is that the manufacturer will conduct periodic clinical evaluation assessments comparing the performance of their own device(s) to the prevailing trends in the marketplace, with the focus on the device continuing to offer benefits that outweigh the risks, in the context of alternative therapies.³ This presents a kaleidoscope of changing expectations and assessment methods. Various countries and organizations may collect data on patient outcomes in “registries.” The rules for collecting information vary for nearly each registry and the methods of retrieval from these registries can vary widely. (“Private” databases often require that the soliciting company pay to obtain data.) Attempting to gather and analyze the data in a manner that can accurately and reliably indicate when a medical device is not keeping up with the

¹Total product life cycle, from the US Food and Drug Administration. Medical device innovation initiative white paper: 2011: CDRH Innovation Initiative. Silver Spring: US Food and Drug Administration, 2011.

²ISO 14971: 2007 Medical devices—Application of risk management to medical devices.

³EU Medical Device Regulation 2017/745 (MDR) and MEDDEV 2.7/1 Rev 4.

state of the art has the tendency to homogenize the information to the lowest common denominator. Although established for noble purposes, can registries provide balanced and qualified data for medical device manufacturers in the quest to determine if their products remain “state of the art?”⁴

Until recently, medical device manufacturers and regulatory agencies could put trust in professionally managed adverse event reporting and evaluation systems such as with the US Medical Device Reports (also known as MAUDE database). Medical device manufacturers and users, such as physicians and hospitals, relied on a system of organized reporting of malfunctions, injuries, and/or deaths to help to signal any change in device risks in the general marketplace. The database can become useless if plaintiff attorneys make reports in “batches” without clinically relevant information. Reports by hospitals and physicians may withhold critical information due to concerns for patient privacy to the extent that investigating an event is nearly impossible. Devices are often sequestered, instead of being returned to the manufacturer for examination, thus no failure mode analysis can occur. Corporate complaint systems established under QSR.820 thus have limited benefit because direct reporting of adverse events to a company through the complaint system is dependent entirely on the attitudes of the institutions with the information. Corporations may attempt to monitor published literature and even the internet for any signals of dissatisfaction about the product, but without a direct, per se allegation against the performance of the product and the willingness of the reporter to provide meaningful information, there is little valuable input to the primary method for postmarket product surveillance. Therefore these idealized early warning systems, incorporated into the regulations of the industry, may no longer provide the surveillance of the medical device performance needed to help manage the expectations for the total product lifecycle and thus fail to provide reliable data for the determination of risk versus benefit.

Despite the many practical challenges and barriers to gaining real-life information, medical device manufacturers seek to understand how the device may function over time. Certain standardized methods for chemical characterization (such as ISO 10993-18: Chemical Characterization of Materials) seek to identify the chemistries extracted under aggressive conditions as a model for how the material may break down over time in the body. Various in vitro simulator methods seek to predict failure modes, but until there is real-life human data, the relationship of simulator data to human device performance can only be estimated. Most such in vitro failure mode simulators can only evaluate the device under limited stresses (such as wear) and simulated biologic environments, such as in saline or simulated blood. (An example method is ASTM F1875-98 (2014) Standard Practice for Fretting Corrosion Testing of Modular Implant Interfaces: Hip Femoral Head-Bore and Cone Taper Interface.)

Trying to estimate the effect of enzymes and cellular attachment can only approximate a finite time window. As a result, there are few simulators that can reliably predicate the mechanisms of late biomaterial decline. Even attempting such studies in live animals is problematic because the animal model may not be an accurate anatomical substitute for the human and maintaining an animal through its natural lifespan in hopes of simulating the natural processes of biomaterial decline is prohibitively expensive and introduces other variables not found in humans. With the conventional biomaterial a necropsy may yield information about the device–tissue interface through histopathological analysis or even postimplant biomechanical studies. But what of the materials designed to integrate and absorb in such a way as to leave behind a regenerated organ or structure? Certainly, acute examination of the biological interface may be warranted, but what of the assessment of the regenerated tissues over time? Will there be adequate methods to discern how these regenerated “zones” have fared in the aging patient? Is it a device failure if the newly incorporated tissues suddenly fail to thrive or give way to the onslaught of progressive disease?

The consequences to a manufacturer that decides to remove a product from the market due to its obsolescence can be staggering. Not only can this mean a sudden disruption of product supply to physicians and patients, it can cause major expenses for hospitals and distributors and serious anxiety to patients with a device determined to be obsolescent. Some regulatory jurisdictions have no category for “recovery” or “removal,” only for *recall*. In the United States the term “recall” typically refers to a device that fails to meet the product specification, such as for packaging tears or sterilization batch failures. There are no obvious reasons why a product should simply stop being marketed beyond the lack of customer demand. And who will make the determination that a product no longer offers a benefit above risk when there is no standardized, objective measure for “risk?”

It is not just as simple as not making or selling a device anymore, because device manufacturers and healthcare providers often enter into long-term purchase agreements and “consignments.” Including the international shipping pipeline and intermediaries in the distribution stream, a medical device can be legitimately on the shelf for 5 years after manufacture. “Recovering” such devices, if a device manufacturer decides the device should no longer be used, represents a massive undertaking with financial and logistical consequences.

Conventional wisdom depends upon the integration of quality system design controls, control of raw materials, control of equipment, verification and validation of performance and usability, facilities and worker training, risk analysis and risk mitigation, postmarket surveillance, and adverse event reporting for management of total product lifecycle. All these systems for managing the total product lifecycle are applicable to the biomaterial-based medical device, but inchoate for the foreseeable years of biomaterial-based implanted medical devices. There are ample opportunities for future innovations in implanted biomaterial lifecycle management strategies that will hopefully keep pace with biomaterial innovation.

⁴Registries for Medical Device Evaluation, Benjamin C. Eloff, Ph.D., Senior Scientific Program Manager, Division of Epidemiology Center for Devices and Radiological Health, FDA. <https://www.fda.gov/media/89553/download>.

Chapter Questions for the Student

1. When a product, for any reason, no longer meets customer expectations or is no longer a benefit compared to risks due to outmoded technology, should the manufacturer be encouraged to remove the device from the market?
2. If the methods for retiring a device at the end of its natural product lifecycle due to obsolescence were easier, might patients benefit from an orderly market retraction?
3. What might device retraction from the market mean for a patient who may still have the implanted device?
4. Does this suggest a need in medical device regulatory authority to provide for an orderly retraction of a device from the market without the risk that a manufacturer will face major liability because the device is no longer state of the art?

3.1.3

Safety and Risk Considerations in Medical Device Development

ELAINE DUNCAN^{1,2}

¹Paladin Medical, Inc., Stillwater, MN, United States

²Joseph Halcomb III, MD, Department of Biomedical Engineering, College of Engineering, University of Kentucky, Lexington, KY, United States

Introduction

Medical device development requires systematic assessment to assure the device will meet its intended use. Even a device designed to be “like” another product already on the market must demonstrate that it is indeed “equivalent” on two levels: (1) does this device meet the same performance requirements of the predicate device, and (2) is this device as safe as the predicate device? The so-called “me-too” device has as its threshold for premarket notification [510(k)] evidence of equivalence to a prior accepted device: performing in essentially the same way to do essentially the same function without introducing new risks.

A new device with new performance claims and unproven safety (such as due to a new technology) must undergo not only safety testing but must also prove its use is efficacious. A pre-market approval (PMA) application is required when the truly new device may only have an indirect basis for comparison to prior or alternative therapy, or when there is no or little evidence that the new device performs as intended. A device requiring a PMA must also be able to demonstrate that the intent to treat is medically justifiable with a reasonable benefit over risk.

A new medical device will typically seek to provide a new solution to an existing problem within the confines of a target medical area. If a new device has multiple potential applications a company engaged in medical device development must select a target “intended use” to focus the development program on a realistic goal, or maintain separate development tracks for each different intended use. The development team must establish the “voice of the customer,” meaning a set of performance expectations that fulfill a specific function. This process can be iterative and may require that certain medical applications are excluded from the target use of the device. Recognizing differences between “indication for use” and “intended use” are extremely important. For example, the requirements of a wound dressing could be

very different if the dressing is intended to be used to cover a surgical wound, compared with a bandage applied by the lay user on a skin scrape after a bicycle spill. Although each may have the same indication for use (wound protection) the intended user and intended environment for use are very different, and thus the “voice of the customer” is different.

Known as design control and review (aka stage-gating) the proper design and development of a medical device must recognize these “inputs” from the voice of the customer and convert these to technical specifications. Typically, the translation of inputs will consider the prevailing expectations and standards within the industry to aid in setting boundaries on the requirements. Even when a device is totally novel, there may be standardized methods for evaluation that help to define the input development. For example, if the device must execute data storage or transmission, the development engineer must be aware of any standards that might impose constraints for the use of energy transmission to store or transmit the data. The development engineer may have to refine the basic input to transmit energy to call out percutaneous couplings or determine if data and power can be transmitted transcutaneously. Regardless of the indication for use or intended use, the device under development may face input constraints based upon local best practices, industry standards, or even the features of the predicate device.

Once these input requirements are sufficiently described, the development process moves to determining the potential risks associated with the potential failure of the device to meet its stated requirement. Ideally, this analysis is done on a detailed level, requirement by requirement, assessing each potential failure mode for its probability to occur and its associated risk if it does occur. An appreciation of “detectability” of the potential failure mode can heighten the development team’s ability to predict the probability of occurrence and determine the most effective mitigation strategy. By parsing

these potential risks (hazard severity times probability) the team can assess where mitigations should be focused. The analysis of potential risk mitigation may require many layers of evaluation. Examples of testing and evaluation could include appreciation of the intended usability of the device and the potential for failure inherent in the design and materials. Historical design, publications, and testing of comparable devices may be resources for determining potential risks associated with the desired device design.

Absence of Toxicity Is Not Evidence of Safety

For several decades the medical device industry has attempted to qualify the biocompatibility of medical materials by a series of increasingly complex testing methods strated to reflect the relative risk categories associated with the type of tissue contact and longevity of exposure. Although individual protocols may have been validated through the years for their specific purpose, the testing schemes (table of testing) represented in the ISO 10993 series have not been proven to assure biomaterial safety. Rather this scheme of testing is a means to rule out the likelihood of a risk of the test material *not* being suitable (toxic to cells at some level). Putting it bluntly, if a material's use could have longer exposure and involve vital tissues, and thus represent a greater potential risk to the patient, more testing is expected, even though it has not been proven that *more* test results offer better risk mitigation.

One attempt to rectify the checkbox-testing mentality and to provide for better devices is to encourage a systematic assessment of biological risks associated with the device and its materials, which attempt to consider more universal factors such as prior clinical use of the material in the same intended use. Adopting this more comprehensive safety assessment has met resistance. Development planners like to seek an authority who will just tell them what to do so they can get it done. Test laboratories have no incentive to minimize the scope, length, or cost of repetitive testing. Regulators understandably prefer to have a checklist and to rely less on subjective arguments within a risk analysis.

Efforts to create a “database” of materials used in certain applications were rejected years ago due to the logical basis that materials and processing methods used in a given device were usually proprietary to a company, so an inventory of the uses of a particular material by the supplier within various devices did not provide “evidence” of safety. Material suppliers certainly can promote their materials for various uses and supply baseline biocompatibility test results, but the final manufacturing methods (machining, cleaning, sterilization, and so on) must be considered in biomaterial safety assessments.

The pressure to *prove* safety (remove risk) has propagated expensive and at best obliquely relevant laboratory tests “of the finished device.” So, despite the ideal to conduct a logical risk analysis, the assessment for safety invariably comes

back to a table of standardized tests. It should be understood that these tests cannot and do not prove the safety of the biomaterial in the intended use of the device. Rather the role of the standardized tests is to provide comparative data derived within the confines of the protocol. These data, typically compared to a standardized control material also evaluated within the same protocol, may indicate a *relative level of hazard* of the material within the selected model.

For devices to be presented to the US Food and Drug Administration (FDA) for premarket review, developers must be mindful of the *Guidance for Industry and Food and Drug Administration Staff Document* issued June 16, 2016: Use of International Standard ISO 10993-1, “Biological evaluation of medical devices—Part 1: Evaluation and testing within a risk management process.”¹

The general principles of biological evaluation of medical devices (Section 4 of ISO 10993-1) instruct the reader that the evaluation plan must be made “within a risk management process in accordance with ISO 14971.” This same section also provides an “informative” annex to help guide the reader in how to go about biological risk management. The standard attempts to pull the risk management process toward validated *in vitro* models and away from repetitive live animal testing. The standard urges the reader to give preference to identifying chemical constituent testing, where such methods *may* yield equally relevant information. The chemicals in their estimated concentration are then compared to toxicity tables that estimate a safety threshold. But again, the student of biomaterials must remain mindful that while chemical toxicity assessment may help to identify the risk of a biological reaction in certain persons over time periods relative to the device use, such tests are “*not* evidence of biocompatibility,” which is defined as:

*the ability of a material to perform with an appropriate host response in a specific application.*²

The table of “endpoints” in Annex A of ISO 10993 might seem to reflect assessments for the “specific application” because it considers the type of tissue contact and the duration of use, but biocompatibility evaluation needs to consider a far more detailed risk analysis than provided for in this table, which is why the FDA guidance and Annex B stress the need to characterize the materials and processes in the context of the intended use of the device. The student of biomaterials must understand that biological evaluation of the use of the device is only one aspect of a risk management practice. Risk assessment must also consider potential hazards associated with the *failed use* of the biomaterial device within the patient. Rational biological risk assessment compels the responsible medical device developer to consider the failure modes of the biomaterials in the subject device and consider the potential severity of the risk to

¹ <https://www.fda.gov/downloads/medicaldevices/deviceregulationandguidance/guidancedocuments/ucm348890.pdf>.

² Williams, D.E., 1987. Definitions in biomaterials. In: Progress in Biomedical Engineering, vol. 4. Elsevier, Amsterdam, p. 72.

the recipient patient. Although not yet universally adopted, the task of analyzing and understanding the biological risk assessment inherent with the acute and chronic failure of the medical product not only serves the process of initial design but also identifies risk factors for biocompatibility assessment through the total lifecycle of the product.

Characterization of the materials and processes in a medical device, including processing agents, is the first step of any biological risk assessment. Not only should the source of each material be carefully qualified, but the actual material received should be scientifically verified (not just the identification of what is sold). A critical material performing a critical function within the device should be identifiable using a standardized test method and engineering should set in place the criteria for routine evaluation of incoming raw materials. Ideally, critical materials should have verifiable specifications that will permit the future qualification of alternative sources for the critical material. Although manufacturers may choose to rely on a material certification from a vendor, this practice represents a calculated risk to the safety of the device. Best practices establish a baseline of quality materials from the source before accepting a certificate of compliance.

All manufacturing processes should be “mapped” such as with a flow chart, to demonstrate the junction points when energy and other chemicals (including water) may be brought to the processing of the starting materials. Screening cytotoxicity testing along the interim manufacturing steps during the development phase of the product could help to identify if a manufacturing process alters the otherwise known safety of the starting materials. The quality of water and other cleaning agents is essential. Controlled, validated processing, particularly for polymerized materials, is necessary to assure safe and uniform biomaterials batch to batch.

Assessing the Continuum of Biological Risk in Performance

ISO 10993, Annex B.3.1.2 includes a list of “physical and chemical material properties” but this is not really an accurate name for the list. Rather, this list represents some of the energy or force vectors that might act on a biomaterial when used in the medical device, and reminds the student to consider the contribution that the physical form the material may play in the body’s response, such as porosity and roughness. Thus the long and expensive standardized tests may show no apparent risk, but the biomaterial could be altered by the biologic processes over time (such as static compression, wear fatigue, or crumpling due to scar contraction). These converted forms of the biomaterial in the functioning device, over time, could drastically change the biocompatibility of the material. As a corollary, the definition for bioincompatibility considers:

the material loses its ability to perform as a result of the host response in the specific application.

Modeling device performance using an in vitro simulator, such as a fatigue tester, could provide insight into the

failure modes of the materials within the device. Such test systems would ideally standardize and control for temperature, fluid composition, and forces on the device and run cycles far longer than an animal or human might be expected to stress the device. Test fixtures of this type can be expensive and due to design constraints may only evaluate an isolated element of a given device. But such fixtures can be remarkably versatile for testing the potential for wear debris and the nature of the debris, if properly designed and built. Wear debris can then be characterized for size, morphology, and potential toxicity. Fracture failures in simulators may give insight into internal material weakness and provide the “canary in the mine” early warning of potential delamination, fatigue striations, and unanticipated concentrations of stress.

Thus when divining for potential biological risk, “toxicity” tests are only one of a large and detailed number of “mitigations” to reduce the potential of biological risk. Tests alone cannot prevent toxicity and can only provide an oblique assessment of the potential for toxicity risk according to the limits of the protocol. The test methods may even introduce a “false positive” if the study director is not mindful of how results of a test may be skewed by errors in sample preparation. For example, one of the most common false failures for cytotoxicity testing occurs when the cells are subject to an extraction solution with the wrong pH, which can simply lyse the cell walls. Because standardized test labs may overlook these details, it is necessary for the sponsor of the tests to be involved and understand both the rationale for the selection of the tests and what the tests are intended to show. Following Good Laboratory Practices regulation (21 CFR 58) for definitive laboratory testing helps to ensure the laboratory performs the studies to protocol with proper quality oversight. Regardless, it is critical to remember that these tests do not *prove* biocompatibility or incompatibility. These tests can only indicate the relative risk of material toxicity when the material is in sufficient concentration or material form to be detectable with the specific test system.

For certain applications and certain functional claims, the common wisdom may be that only an in vivo assay can be trusted to characterize the biocompatibility of a material. One common example of expected biomaterial evaluation to support the claim that a biomaterial can enhance bone formation where there has been a deficiency or injury is to test the material in an artificially induced bone void. Conducting all of the toxicity-based assays (including genotoxicity or carcinogenicity) will not demonstrate that such materials can perform as intended, that is, to grow bone. Only a postmortem evaluation for the presence of new bone in association with the biomaterial produces sufficient evidence for osteointegration at the cellular level.

Studies for biomaterial performance in a functional medical device require careful study protocol design and can be as complicated and as expensive as a human clinical study. In fact, the animal cannot speak for itself so systematic monitoring of vital conditions and/or daily animal welfare checks may be necessary. Proper animal performance studies need

to begin with an understanding of comparative anatomy and physiology to assure that the animal is even the correct model for the condition to be tested. Size and configuration of human devices simply may not fit in an animal and thus may introduce artifacts in the study and unnecessary hardship for the animal. But such “in-life” performance studies may be the only way to fully understand the complex interactions of the device within its intended use. While monitoring the device in the living animal is important, postmortem assessment can be most revealing, particularly when it is possible to design a study with serial sacrifice of numerous animals over sequential time periods. Assessing the device as it behaves in the animal at different times may provide insight into the progression of tissue integration, device wear, and any potential for material migration. Histology, microcomputed tomography, pre- and postmortem X-rays, and organ necropsy should be anticipated for explant analysis. The methods of preservation and sample fixation must be planned well in advance with consideration for embedding, stains, forms of microscopic examination, and other analytic methods. Transporting tissues is regulated and even preserved specimens may require adherence to international treaties.

Assessing the Contribution of Secondary Processes to Biological Risk

Once the fundamental design hazard analysis and risk assessment has begun, including the detailed biological risk assessment for intended use, a comprehensive analysis of the potential risks contributed by processes is essential. Elements of proper design control and review (detailed elsewhere) include verification and validation. To simply state, verification is intended to show conformity to specific requirements and validation attempts to confirm the overall performance for intended use. Thus inherent in a thorough biological risk assessment program is the understanding of how processes and secondary processes can contribute to the performance of a biomaterial in a medical device. Producing a process flow chart early in the biological risk analysis should help to pinpoint processes that could impact the biomaterial. In fact, it is prudent to assume that every process could impact biomaterial properties until evidence confirms performance is not altered.

A few real-life examples of how poor manufacturing controls altered biomaterial performance illustrate the point. One manufacturer had invested a great deal of time, money, and scientific sweat to perfect an anticoagulation coating on a hemodialysis catheter. The superior performance of the catheter with the coating statistically demonstrated benefit to the patient. When moving the prototype manufacturing process into the factory setting the engineers were unaware of the use of a silicone spray release agent on an adjacent manufacturing line. The “overspray” from that process deposited silicone release agent on the dialysis catheters laid out on a separate assembly line in readiness for dip coating.

As a result of this contamination by an otherwise “safe” material, the anticoagulation coating would not adhere to the catheter surface, despite the pretreatment step that was designed into the manufacturing process. The unintended release agent might have caused the coating to sluff off in the patient’s blood vessel. Fortunately, based on planning due to good risk analysis, the manufacturer had anticipated the need for a postdipping quality control check. An observant inspector detected a lack of uniformity to the coating and an “oily sheen” appearing after some catheters had been dipped. Surface analysis techniques detected the presence of silicone on the catheters. The line supervisor was convinced the tests were wrong because no silicone spray was allowed in the factory. A walk through the assembly area by an outside observer showed a can of silicone spray located on the shelf below the adjacent production line. Not authorized for use in the facility at all, the contraband silicone mold release had come into use by an operator to make an assembly connector push on easier.

Another manufacturer who did not apply proper biological risk analysis caused serious harm in many patients. In an effort to bring a contracted manufacturing step in house, and thus save money, a device company began to conduct the process of making a surface porous without understanding the need for serial cleaning steps. As a result, oils from manufacturing steps were embedded deep within the pores of the surface treatment. The single, superficial cleaning step applied at the end of the device manufacturing phase was not adequate to remove the embedded manufacturing contaminants, which migrated to the device surface after implantation and thus came in contact with surrounding tissue. This contaminant interfered with bone growth and implant stabilization. Because the manufacturer had not understood the hazards of the machining process, the validation plan for the cleaning process did not consider that surface cleaning would not be sufficient to remove toxins embedded in the tortuous porous surface. Weeks to months after implantation the prosthetic joint failed to osteointegrate and remedial joint replacement surgery was required, with all of its inherent additional risks. Patients were directly harmed by the failure of the product team to mitigate the risks associated with the manufacturing process, which when properly handled by the original contractor had been safe and effective.³

Sterilization methods introduce biological risks, not only with the potential that the cycle may not adequately sterilize the product, but also from the sterilization process residuals or changes to polymers. Some biological risks are well known and can be characterized. Standards for evaluation of residuals and by-products from ethylene oxide gas are routinely employed.⁴ Manufacturers understand that a biomaterial can be altered in the presence of gamma sterilization energy and thus attempt to protect the materials from this

³ <https://www.fernotlaw.com/wsnkb/articles/cueva-v-sulzer-orthopedics-11280.html>.

⁴ ISO 10993-7:2008; Biological Evaluation of Medical Devices—Part 7: Ethylene Oxide Sterilization Residuals.

effect or avoid the sterilization method entirely. Steam and dry heat sterilization can also alter a biomaterial.⁵ As new sterilization methods have been introduced, manufacturers have had to become analytical detectives to determine the potential hazards associated with the chemicals and processes with their biomaterials. Some alternative sterilization processes have been shown to interact with a polymer during the sterilization process, thus altering the biomaterial chemistry. During standardized toxicology testing these chemicals can register as surface toxins.

Even a sterilized device can introduce a biological risk called pyrogenicity. A pyrogen can invoke a febrile reaction. Material-mediated pyrogens are chemicals that might leach from a medical device material to create a febrile response. Material-mediated pyrogens may take many forms, but a commonly overlooked source may be a mined mineral, such as a calcium carbonate deposit. Bacterial endotoxins are typically associated with the condition brought on when a sterile device harbors the remains of the outer membrane of a Gram-negative bacterial cell wall. Reducing the risk of pyrogenicity is especially critical for intravascular devices and implants. Strides have been made to reduce the risk of pyrogens on or within sterile medical devices by strictly controlling the use of water as a cleaning agent and ensuring that water is not allowed to stand on the surface of a device, even in a clean-room. Once again, understanding and controlling the risks associated with the processing of a biomaterial is critical to assuring a device is safe.⁶ Transportation, storage, and shelf-life aging for most conventional medical device biomaterials can be characterized by standardized testing. Packaging systems, including sterile barriers, are generally reliable and can be tailored to the shape and stability needs of the medical device. Evaluation of the in-package, shelf-life aging of the device materials is standard practice to assure that the device just prior to the expiration date on the package performs as well as it would the day the device is released for sale.⁷ Combination products (drug/device and biologic/device) and tissue-derived or custom-grown biomaterials have unique requirements for “shelf-life” qualification and delivery. It is expected that materials that are designed for “tissue engineering” could require almost immediate use, placing the manufacturing location immediate to the patient in the hospital. These questions already exercise the talents and imagination of the biomaterials scientist.

Assessing Biological Risk of Aging Biomaterials in the Aging Patient

Medical device development necessarily focuses on the requirements of the device at the time the device is delivered to the point of the intended use. In the case of implanted medical devices, the device performance requirements do not

stop upon receipt. Although clinical trials attempt to evaluate the performance of the device within the scope of the intended use, in the ideal patient included for evaluation, excluding those whose conditions are not ideal, all clinical trials have an endpoint. For practical reasons, clinical trials beyond 2 years are problematic because of the mobility of patients. Patients who “feel good” are reluctant to return to a physician and financial incentives for follow-up visits are deemed unethical. A 5-year controlled, prospective, randomized clinical study without significant follow-up loss is rare. Although institutions may attempt to publish long-term performance results from their own practice, the results often reflect drift in their practice, which can introduce bias. There can even be impacts of weather disasters (hard to have a patient back for follow-up when the hospital is leveled by a hurricane). The mobility of patient populations and the impact of patient lifestyle on healthcare decisions can impede direct follow-up by the original clinic. Even with electronic feedback systems and “satellite” clinics, obtaining the qualified data of a complex implanted device trial is problematic.⁸ Unfortunately, it is the longer follow-up data that might show a trend in biomaterial performance, but such data can become less reliable with time. To truly understand the long-term performance of a biomaterial in an implanted device can require tens of thousands of patients in numerous geographic areas before the true performance of a biomaterial-based medical device can begin to emerge period.

Some postmarket performance programs⁹ attempt to follow the same patients after the formal end of the clinical trial, such as in registries or postmarket surveillance studies. Some postmarket studies evaluate the outcome of treatment without stricture on trial enrollment, again more in the style of a registry of the patient. (Typically, a registry does not receive new data until there is an adverse event or death of the patient, so information can only be assessed compared to the total number of patients known to be “at risk” for device failure.)

Some medical devices have a “tracking” limitation imposed at the time of approval, which attempts to know where the device may be in the event of a recall, but otherwise collects no data. None of these monitoring methods can effectively evaluate the biological risk of a biomaterial as the device ages, within an aging patient, even when the patient/device are available. Occasionally, a physician can evaluate how well the patient is performing with the device. Actual device-specific observations might include a blood test, computed tomography scan, X-ray, or magnetic resonance imaging to “see” the implant in situ, but other than an observable fracture or migration there are few assays to show with certainty that the biomaterial is performing safely.¹⁰

⁵McKeen, L.W., 2018. The Effect of Sterilization on Plastics and Elastomers, Plastics Design Library. William Andrew.

⁶<https://www.fda.gov/regulatory-information/search-fda-guidance-documents/pyrogen-and-endotoxins-testing-questions-and-answers>.

⁷<https://www.fda.gov/regulatory-information/search-fda-guidance-documents/shelf-life-medical-devices>.

⁸<https://www.ncbi.nlm.nih.gov/pmc/articles/PMC3684189/>.

⁹<https://www.fda.gov/medical-devices/premarket-approval-pma/pma-postapproval-requirements>.

¹⁰The performance of certain devices, such as pacemakers and defibrillators, can be interrogated after implantation, but it remains difficult to assure that a biomaterial is performing as intended until performance failure is otherwise detectable.

If a manufacturer receives a complaint or adverse event report with sufficient information to conduct an investigation, the records in the device history file can be reviewed. It may be possible to determine if there were manufacturing or material errors in a particular lot, but other than trending such reports to track to a cluster of related failures, it is exceedingly difficult to isolate root cause failure of a single device in a specific patient. If such quality trends emerge, notifications to practitioners can be issued, but beyond watchful waiting, few such trends result in immediate device removal in the absence of drastic outcomes.

The only method that could provide long-term data for biomaterial performance is systematic implant retrieval from patients with normal and abnormal medical device performance. Presently, there are research groups who collect “failed” implants, but this can skew understanding of what makes a biomaterial device successful. Being prepared for retrieving biomaterials from an explanted medical device is critical in an attempt to assure the materials are returned in a manner suitable for forensic analysis. In some instances, research centers have been established to collect the implants on-site,¹¹ but when an explanted device must be transported, a hazardous material retrieval kit with preservation instructions must be immediately available. Retrieved dental implants and orthopedic joint implants have been available for analysis for many years around the world, but data from the retrieval of soft tissue implants such as breast implants and materials for tissue reinforcement may be more difficult to interpret due to the variability of the implant techniques, lack of traceability of the device to the original manufacturer, and the differences in soft tissue excision around the implant. Implant retrieval discussion is

beyond the scope of this section other than to point out that retrieving only “failed” implants fails to teach what did not go wrong. Nevertheless, interpreting the findings from retrieved biomaterials should be incorporated into any new product biological risk assessment when possible.

ISO 10993-1 advises that where well-characterized and functional data support the safety of a biomaterial in the device, repetitious testing not focused on a specific potential risk should not be necessary. Variations from the proven performance parameters can be analyzed more precisely by understanding the differences in the context of known outcomes. The challenge for the biomaterial student is that the chain of custody and factual process information is seldom known for retrieved biomaterials, thus risk analysis involves considerable inference about the vectors affecting outcome. Enhanced value for future biomaterial applications will come when the natural history of the patient’s disease condition and lifestyle can be coupled with the implant performance evidence.

Summary and Study Guide

Medical devices that rely on biomaterials for function in medium- to high-risk applications are subject to technical evaluations based upon understandings of risk to the patient. Standardized biological test schemes may help reduce the potential for risk associated with the use of a material, but do not prove the safety of the biomaterial. Well-designed risk-based technical assessments that consider the lifecycle of the use of the device, including risks associated with manufacturing processes and patient age and disease, are necessary to assure the safest medical devices come to market. Armed with satisfactory risk mitigations, biomaterials in medical devices are deemed successful when the benefits are commiserated with the risks over the lifecycle of the product.

¹¹ <https://www.hss.edu/biomechanics-implant-retrieval.asp>.

Chapter Study Guide

1. Can a medical device manufacturer leverage prior use of a biomaterial in a previous device that has a different intended use and avoid having to do biological testing?
2. If a biomaterial-based medical device manufacturer changes the sterilization method for a slightly different device, using the same material and manufacturing process, can the manufacturer avoid additional biocompatibility testing?
3. When a manufacturer can show that a prior device used the same biomaterial, can the manufacturer avoid additional testing, and, if so, what would the manufacturer have to demonstrate in their own application?
4. After conducting testing in ISO 10993-1, can a manufacturer claim that the materials in the new medical device are biocompatible?
5. If a manufacturer's new device fails cytotoxicity testing, does that mean that the materials in the device are toxic and not appropriate for use in the medical device?

3.1.4

Sterilization and Disinfection of Biomaterials for Medical Devices

ROGER E. HARRINGTON¹, TEJA GUDA², BRYRON LAMBERT³, JEFFREY MARTIN⁴

¹Medical Products Development Director, Medtronic, Boston, MA, United States

²Department of Biomedical Engineering, University of Texas at San Antonio, San Antonio, TX, United States

³Sterilization Science, Abbott Vascular, Temecula, CA, United States

⁴President and Principal Consultant, Sterilization and Quality System Consulting LLC, Dallas, TX, United States

Introduction

Biomaterials are intended for applications either in medical devices, which are designed for use in sterile, clinical settings, or as implants, which come into direct contact with human tissue. Thus cleaning, disinfection, sterilization, and assurance of maintained sterility are critical considerations to ensure the safety and success of implants and devices. To this end, biomaterials scientists and engineers must consider not only the requirements of the material, but must choose the appropriate sterilization process so that the functionality of the material and the device are delivered at the clinic. This chapter focuses on the various sterilization techniques available, and the process controls to ensure patient safety.

The term “sterile” refers to the presence or absence of microorganisms and is essentially a binary state; a material is either sterile or it has microorganisms. From a regulatory perspective, the term “sterile” is used to indicate the probability of an implant or device having a bioburden. The current expectation for patient safety is that less than one out of a million devices or implants can be nonsterile. This expectation is known as the “sterility assurance level” (SAL) and the one out of a million is defined as having an SAL of 10^{-6} .

A vast majority of the sterilization practices in use today are terminal processes where the products are sterilized after the entire process of manufacture has been completed. This chapter focuses mostly on these industrial terminal sterilization processes, their appropriateness for different types of materials and devices, and how the processes scale from benchtop development to

mass manufacturing. Just as it is the responsibility of the manufacturer of the device or implant to clean any remnants of the manufacturing process and then sterilize, package, and deliver a product that can be validated to be sterile at the point of use, it is also the responsibility of hospitals or medical care facilities reusing devices to clean and resterilize products and equipment. This procedure is known as “disinfection,” and depending on the product, its previous application, and the level of anticipated “soil,” high- or low-level disinfection might be necessary. Disinfection and reuse of implantable devices is not permitted from a patient safety and regulatory standpoint. Assurance of sterility is a critical aspect of good manufacturing practices and in consideration of patient safety, most processes are designed for overkill sterilization (higher SAL than 10^{-6} , such as 10^{-9}) to ensure that an SAL of 10^{-6} can be met with certainty.

Terminal sterilization is often not possible in some cases, especially when biologics or liquids are added to the device or when a combination product is repackaged for use. In such cases, aseptic processing of the product is preferred to ensure that the SAL can be maintained. When such approaches are not possible, additional chemical sterilization steps might have to be incorporated before the device can be used. Biomaterials scientists need to find a terminal sterilization solution for a product, if possible, and thereby avoid aseptic processing to minimize the complexity of use. The optimization of pairing the appropriate sterilization process with a material is to determine a cost-effective sterilization process resulting in a clean device and a time-effective validation process to assess sterility, while ensuring that the process does not have significant

deleterious effects on the material used. This optimization is relatively easy for standard materials used for most medical devices, but is increasingly complex for biologics and combination devices, both of which are rapidly growing in popularity.

Multiple factors affect the outcome and effectiveness of the sterilization process; some of these include:

1. Cleanliness of the material being sterilized;
2. Nature and extent of initial bioburden;
3. Design, manufacture, and assembly of the device/implant;
4. Chemistry/reactivity of underlying biomaterials; and
5. Features such as convoluted channels or internal porosity.

To navigate these challenges, it is useful for the biomaterials scientist to have a concrete understanding of common terminal sterilization technologies (see the sections “Radiation-Based Techniques,” “Chemical Techniques,” and “Thermal Techniques”). This section provides a detailed understanding of sterilization technologies from the perspective of their impact on the microbial loads as well as the materials that are being sterilized. Two modalities, radiation sterilization and ethylene oxide (EO) sterilization, dominate the industrial terminal sterilization market, while thermal sterilization is used mostly in hospital settings. These terminal sterilization technologies are paired with established validation processes, which are designed to far exceed regulatory SAL requirements. Neither radiation nor EO causes significant material degradation in traditional devices under well-controlled and validated use. In addition, both are capable of scaleup to high volumes in a cost-effective manner.

Material compatibility constraints often drive the choice of sterilization modality and this is discussed in the Section “Materials Development Considerations for Sterility.” Sterility validation necessary to assure patient safety is essential in a timely manner and often plays a crucial role in decision making for clinical adoption (see the Section “Safety Testing and Validation After Sterilization”). The chapter closes with a view toward new developments and challenges on the horizon for sterilization technology. Developments in biologics, especially in combination products, offers a unique challenge for terminal sterilization processes. Prions and endotoxins are the most recent biological contaminants, which need sterilization and cleaning process adaptation to ensure patient safety, and the environmental concerns with increasing use of EO sets the stage for the development of equally effective but environmentally less toxic chemicals. Awareness of these challenges will allow the biomaterials scientist to be prepared with solutions to address them (see the Section “Summary and Future Challenges”).

Radiation-Based Techniques

Safety Considerations

Sterilization by radiation carries two main safety concerns: possible lethal exposure to radiation and ozone. The lethal dosage of radiation to humans is about 0.01 kGy with an exposure time of less than a second in some cases. Radiation sterilization occurs at dosages ranging from 8 to 35 kGy. Thus

to prevent lethal exposure to workers, safety measures such as considerable amounts of shielding and robust interlocks are implemented in radiation processing. In addition to exposure to radiation, the production of ozone is another cause for concern. Ozone is a toxic gas that is formed when radiation comes into contact with oxygen, causing first the formation of free oxygen radicals and successively ozone. Appropriate safeguards to ozone inhalation include ozone monitors and adequate ventilation. Most industrial-scale radiation sterilization occurs in closed rooms with safety precautions, and prepackaged products are usually loaded on conveyor systems that keep product containers in the path of the radiation for sterilization.

Principles of Action and Efficacy

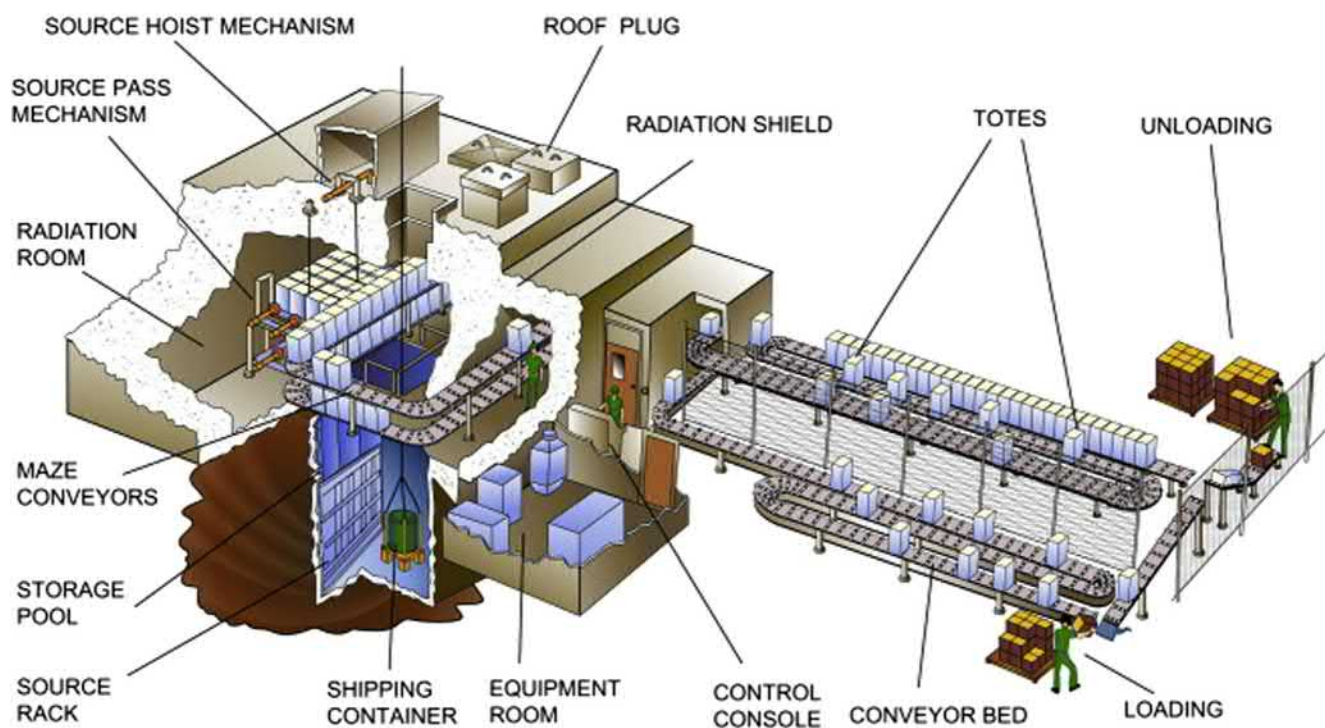
Sterilization by means of radiation is commonly used for mass-produced medical devices because of its simplicity and convenience in terms of large-scale processing. Terminal sterilization is achieved by exposing prepackaged devices to the appropriate dosage of radiation. The radiation will emit electrons or photons that penetrate the packaging and destroy cells, bacteria, and viruses on devices. Radiation causes DNA damage in bacteria and viruses preventing pathogens from reproducing and thus inactivating them. The dosage used to eliminate pathogens depends on its nature, for example, generally, the radiation dosage required for bacteria and spores is lower than that for viruses (Parsons, 2012). Although most pathogens are eliminated, some viruses (HIV-1 is at the highest range of virus radiation doses required for 10-fold reduction; Smith et al., 2001) and bacteria (such as *Streptococcus faecium* and *Micrococcus radiodurans*) are more resistant to irradiation. Thus understanding the bioburden on the materials prior to radiation sterilization is critical for determining dose and validating sterilization.

Radiation sterilization occurs most commonly through three methods: gamma, electron beam, and X-ray. The two most common methods used in industrial sterilization are gamma and electron beam.

Gamma Sterilization

Gamma radiation takes its form in short electromagnetic wavelengths and therefore is more energetic. The gamma rays sterilize a product by providing adequate energy to break down DNA and prevent reproduction. The most common source of radiation is from radioactive cobalt-60, accounting for ~80% of commercial radiation sterilization. The gamma rays produced from ^{60}Co have energies ranging from 1.173 to 1.332 MeV with a half-life of 5.27 years (Parsons, 2012). While the radiation from ^{60}Co sterilizes devices, there is not enough energy to cause the device to become radioactive.

To process devices for gamma sterilization, devices are placed in containers, generally made from aluminum, termed totes. Devices are placed in the totes and moved to the processing room to be sterilized (Fig. 3.1.4.1). Regardless of the amount in the tote, the product will be sterilized due to the lack of charge on ^{60}Co particles, which allows the gamma particles to penetrate evenly and across long



• **Figure 3.1.4.1** Industrial-scale gamma sterilization chamber showing movement of totes on a conveyor system. (Courtesy of MDS Nordion, Canada. Lambert, B., Martin, J., *Sterilization of implants and devices*. Biomater. Sci. Elsevier, 2013, 1339–1353.)

distances, thus making gamma sterilization an attractive option since the amount does not limit sterilization conditions. After sterilization, packages are evaluated by a dosimeter to verify whether the appropriate dosage was applied.

Sterilization by gamma radiation occurs by the release of high-energy photons that interact with substances. The common dosage used for medical plastics is 15–25 kGy, with 25 kGy being the standard dose applied. The energy of the photon is absorbed onto the material by Compton scattering, which generates high-energy electrons. The high-energy electrons (0.5 MeV) are able to ionize matter by depositing energy onto the material. These primary electrons deposit energy in 60–100 eV bundles that in turn produce secondary electrons. The secondary electrons create free radicals that cause DNA fission among other effects, which is the means by which pathogens are killed. In conjunction with its effect on DNA, the radicals also have the ability to crosslink polymers, which can alter the device's properties, therefore placing a limitation on the use of gamma radiation as a means of sterilization. This is often detected by crazing or discoloration of plastics and a reduction in the tensile strength of the materials.

Electron Beam Sterilization

Electron beam sterilization refers to the application of electrons that are accelerated to form a beam of electrons with an energy of 5–10 MeV, which are then scanned across the devices to be sterilized. These electrons are produced from electron accelerators, the two most common being DC accelerators and radio-frequency power-based accelerators. These accelerators take

200V electrons and are accelerated to the required voltage. The electron beam is generally magnetically focused to form a beam that is 1–5 cm in diameter, which is then scanned across the product to be sterilized. At these energy levels, neither the processing plant nor product becomes radioactive since the accelerators can be turned off easily.

For gamma sterilization, the distances between devices and radiation source are not a cause for concern since the gamma particles penetrate evenly and across long distances. For electron beam sterilization, this is a limitation since the beam has limited penetration distance. The general rule is that the maximum penetration (cm) from a two-sided electron beam is $0.8 \times \text{beam energy (MeV)}$ divided by the density of the device (g/cm^3). Generally, the maximum penetration is less than a meter and penetration distances increase with higher beam energies. Due to this limitation, extra care and planning are required to determine load placements that take penetration depth into consideration, with less dense objects being placed ahead of objects with greater density.

The process by which electron beam sterilization works is very similar to that of gamma radiation, where high-energy electrons are absorbed onto the material and produce secondary electrons. Similarly, the secondary electrons are those that eliminate the pathogens and can alter material characteristics. The process of electron beam sterilization is faster (seconds to minutes) than gamma sterilization (minutes to hours) because of a very high delivery rate of dosage. The short exposure time of the electron beam is also beneficial in that it decreases any material degradation that may occur to the product. Conversely, the penetration depth of

gamma radiation is deeper than electron beam sterilization. From an application perspective, unlike gamma irradiators, electron beam sources have had relatively low commercial availability, resulting in electron beam sterilization becoming a contract commercial sterilization option only.

X-Ray Sterilization

A small part of the radiation sterilization market is composed of X-ray sterilization. X-ray sterilization works by producing high-energy electrons, generally 5 MeV, from accelerators that are bombarded onto a tungsten target to produce X-rays. The photons from the X-rays are similar to those from gamma radiation with regard to the amount of energy deposited and the depth of penetration. Additionally, just as in electron beam processing plants, X-ray processing plants do not become radioactive, as long as the electrons produced do not exceed energies of 5 MeV. Thus X-ray sterilization is a combination of gamma ray and electron beam sterilization.

Application Considerations

To effectively use radiation as a means of sterilization, there are many factors for consideration to determine the accurate dose for a product and the effect of sterilization on the product after it has completed the entire process. Maximum dosage for a product is determined based on the initial bio-burden and its nature on the products, the sterilization dose, the minimum dose necessary for a product, the homogeneity of the dose during sterilization, and the number of cycles the device can undergo.

To determine the appropriate dosage, a dose uniformity ratio (DUR) is developed. A DUR is a ratio of the maximum dosage over the minimum dosage, based on the load arrangement and density of a product batch. DURs are always greater than 1 since a product is never subjected to one dose for sterilization but multiple doses. Many factors influence the DUR, such as:

- Radiation source; gamma is much more uniform than electron beam;
- Product density;
- Shipping box/pallet size;
- Configuration of sterilizer; and
- Energy of electrons for electron beam sterilization.

R&D, Pilot, and Low-Volume Technologies

Although radiation sterilization is well suited for industrial operations, it is still an appealing method for biomaterial scientists to sterilize products. Small-scale radiation sources are appropriate for scientists conducting material qualification procedures or affording convenience during product development. Small-scale units are ideal for such cases because of the narrow dose range that will allow for faster sterilization cycles.

Scaled-down radiation sources, such as an R&D gamma cell, provide a very narrow and small dose that results in a DUR extremely close to 1. Furthermore, there are small self-shielded low-energy electron beam accelerators that

are able to sterilize single packages rather than multiple doses at a time. Accelerators such as these have low beam energy, 0.5–2.0 MeV, which can only sterilize a product or a portion of a product, often coatings or thin films, which may be sufficient for development and testing.

Material Considerations for Radiation Sterilization

As previously discussed, the process of sterilizing by radiation yields secondary electrons that disrupt the DNA and reproducibility of pathogens. This is done by free radicals that cause scission to DNA but may also disrupt material properties of polymers, resulting in chain scission or cross-linking, or even reacting with oxygen to damage synthetic or biological materials of the sample. Because of these considerations, the interactions of radiation with polymers have been well studied and examined (e.g., Forsythe and Hill, 2000; Clough, 2001; AAMI, 2008). In most instances, the material of the product remains inert to the low doses that occur during the sterilization process. Additionally, some materials may experience crosslinking due to radiation, such as polyethylene, with no adverse effects, but rather potentially helpful outcomes on the function of the material.

However, there are materials that are adversely affected from exposure to radiation. Consequences of exposure include scission and considerable mechanical degradation for polymers such as polytetrafluoroethylene, fluorinated ethylene propylene, polyacetals, and natural polypropylene. Not only does radiation adversely affect material properties, air may also help speed up the scission process through radiation-induced oxidation. This is typically observed in the form of discoloration of the product, and testing has revealed a reduction in tensile properties of the material.

While the consequences of radiation chemistry may be dire, they are not as black and white as they appear, meaning that after alteration by radiation exposure, the device may still be adequate for use. This depends on the material itself, its intended nature of use and the evaluation process of the product after sterilization to guarantee that clinical standards are met. For example, bioabsorbable polymers such as polylactide and poly(lactic-co-glycolic acid) experience a decrease in molecular weight (MW) after sterilization. Changes in MW may alter degradation in vivo and drug release kinetics. However, this reduction in MW may be accounted for and considered by making the initial MW higher, so after sterilization the desired MW is reached. If the reduction cannot be accounted for by increasing the initial weight, other avenues may be utilized such as conducting radiation sterilization while the product is refrigerated. By lowering the temperature of the product as it is irradiated, the structural integrity of the polymer may be kept intact because the temperature is lower than the glass transition temperature. Additionally, the small changes in mechanical properties may not critically affect single use or disposable medical plastic products. Care should be taken, however, that sterilization-induced changes in properties are accounted for in shelf life and stability considerations of implants and devices.

In addition to the direct effects of radiation on materials, there may be further effects resulting from sterilization. During the irradiation process, the temperature of the product increases. If the product is being sterilized by electron beam, the temperature increases to about 50°C for materials composed of polymers for a time range of a few seconds. If the product is sterilized by gamma radiation, the temperature will increase to 30–40°C on a time scale of a few hours. This matters primarily for materials that are bioabsorbable and have a low glass transition temperature. However, if this is the case, these secondary effects can be mitigated by sterilizing the product at a lower temperature. In addition to temperature considerations, the presence of oxygen and humidity also plays a role in damaging products. To prevent such occurrences, products can be packaged in an inert environment.

Biologics and Human-Based Tissue: Compatibility With Radiation Sterilization

To better improve the use of radiation sterilization on tissue products, different methods have been explored. Low-dose radiation sterilization methods have been examined and provide confidence in increasing the use of radiation as a means to sterilize tissues and biologics, especially bone and amnion allografts. Other methods have succeeded in terminally sterilizing biologics (sterile liposomal vaccines and human insulin) by first processing the product followed by radiation. Processing methods have included lyophilization, cryoprotection, and adding free radical scavengers/radioprotectors (e.g., the antioxidant ascorbic acid) (Mohammed et al., 2006; Terry et al., 2007). Radical scavengers have also been used in conjunction with other methods to improve the compatibility of tissue-based products for sterilization. Such innovations potentially pave the way for the increased use of radiation sterilization for drug–material combinatorial products such as tissue-engineering scaffolds.

Chemical Techniques

Safety Considerations

For sterilization purposes, EO gas must be administered and stored at highly concentrated quantities. Under these conditions, EO is toxic, carcinogenic, and very explosive. Tools and equipment must be carefully chosen to prevent the possibility of accidental sparks in the vicinity of EO chambers. Even after an EO process is complete, personnel must take appropriate measures to avoid exposure to the toxic gas. These precautions include the use of personal protective equipment as well as respirators when working with products that have not been fully aerated to dissipate the gas and its residual by-products. Finally, any manufacturer of EO-sterilized products is responsible for abiding by the international standards that allow for adequate aeration to minimize EO residual levels below permissible limits for distribution, which is governed by ISO 10993-7 (Table 3.1.4.1). In addition, contract sterilization facilities

are responsible for release of the gas and community safety concerns arising from high environmental levels of EO, which pose significant public health concerns. Environmental protection actions leading to the closure of industrial-scale EO facilities and successively the regulatory push to look for alternative, safer sterilization techniques (FDA, 2019a) underscores the safety concerns associated with the rapid scaleup to meet the increasing demand for medical devices.

Oxidizing methods of sterilization using either hydrogen peroxide or ozone provide less of a threat with respect to human exposure; however, several precautions must still be taken when utilizing them. While hydrogen peroxide provides the advantage of degrading into the nontoxic products of water and oxygen, the sterilizing process begins with a source that is highly concentrated and extremely hazardous. Ozone, on the other hand, must be produced in situ since it is metastable and cannot be stored. After use, ozone rapidly degrades back into oxygen making the process safe and environmentally acceptable. When harnessing the sterile properties of either compound, equipment and devices must be chosen on the basis of resistance to oxidation as often deep vacuums are required and could be compromised if not suitable for the process.

Principles of Action and Efficacy

Sterilization by chemical means is more involved and specific to the product and chemical used than methods such as irradiation. The most popular chemical method, EO, functions on the basis of its strong alkylating property, which causes disruption of cellular processes, including clotting of proteins, inactivation of enzymes, and disruption of DNA, resulting in preventing the replication of microorganisms. The alkylation reaction occurs on the amine side chains of the proteins, enzymes, and nucleic acids. Since this reaction is facilitated by moisture, it is essential that EO sterilization be carried out in a humid environment. The other popular chemical agents, hydrogen peroxide and ozone, primarily leverage oxidation of the cell walls and proteins resulting in destruction of cell walls and even endospores with prolonged contact.

Ethylene Oxide Sterilization

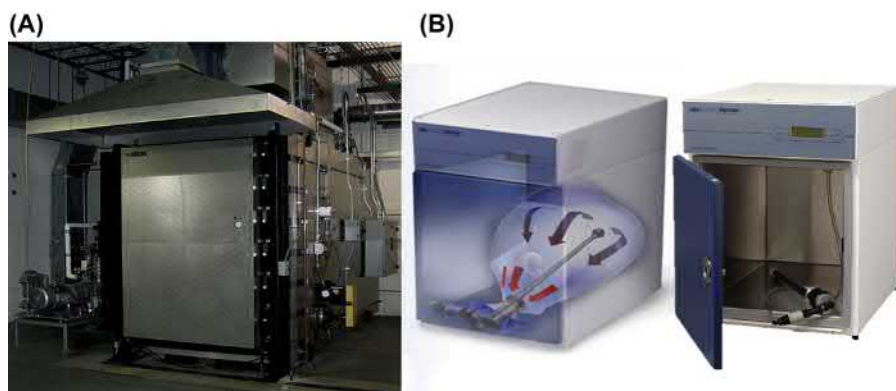
Compatibility with most materials and excellent solid matrix diffusion properties have resulted in EO being used as the preferred sterilization method for almost half the medical device manufacturing market. In addition to being a low-temperature process, EO can sterilize moisture- and radiation-sensitive materials without compromising product integrity. In addition, complex product architectures and designs can be sterilized by adjusting EO concentration and duration of exposure. As multiproduct packaging of groupings by procedure type rather than individual product types is preferred, EO is gaining traction because of its broad applicability.

TABLE 3.1.4.1 Table of Sterilization Methods and Corresponding Standards for Process Regulation, Manufacturing, Testing and Validation, Packaging, and Processing

	Sterilization Modality	Reference Standard or Guidance Document	
Methods of Sterilization	Radiation sterilization	ANSI/AAMI/ISO 11137-1 Sterilization of health care products—Radiation—Part 1: Requirements for development, validation, and routine control of a sterilization process for medical devices AAMI TIR29: 2002 Guide for process control in radiation sterilization AAMI/ISO/TS 13004:2013 Sterilization of health care products—Radiation sterilization—Substantiation of a selected sterilization dose—Method VD _{MAX} SD AAMI TIR37: 2007 Sterilization of health care products—Radiation—Guidance on sterilization of human tissue-based products AAMI TIR40: 2009 Sterilization of health care products—Radiation—Guidance on dose setting utilizing a Modified Method 2 EU GMP Annex 12: Use of ionizing radiation in the manufacture of medicinal products	
	Ethylene oxide (EO)	ANSI/AAMI/ISO 11135-1: 2014 Sterilization of health care products—Ethylene oxide—Part 1: Requirements for the development, validation and routine control of a sterilization process for medical devices AAMI TIR14: 2009 Contract sterilization using ethylene oxide AAMI TIR16: 2009 Microbiological aspects of ethylene oxide sterilization AAMI TIR28: 2009 Product adoption and process equivalency for ethylene oxide sterilization	
	Dry heat	ISO 20857 Sterilization of health care products—Dry heat—Requirements for the development, validation and routine control of a sterilization process for medical devices	
	Thermal/Chemical	ISO 25424 Sterilization of health care products—Low temperature steam and formaldehyde—Requirements for development, validation and routine control of a sterilization process for medical devices	
	Moist heat (saturated steam)	ANSI/AAMI/ISO 17665-1 Sterilization of health care products—Moist heat—Part 1: Requirements for the development, validation, and routine control of a sterilization process for medical devices ANSI/AAMI ST79 Comprehensive guide to steam sterilization and sterility assurance in health care facilities	
	Liquid chemical for Biologics	ISO 14160:2011 Sterilization of health care products—Liquid chemical sterilizing agents for single-use medical devices utilizing animal tissues and their derivatives—Requirements for characterization, development, validation and routine control of a sterilization process for medical devices	
	Sterilization Safety	Biologic indicators	ISO 11138-1 Sterilization of health care products—Biological indicators—Part 1: General requirements ISO 18472 Sterilization of health care products—Biological and chemical indicators—Test equipment
		Chemical indicators	ISO 11140-1 Sterilization of health care products—Chemical indicators—Part 1: General requirements
		Microbiological Methods	ISO 11737-1 Sterilization of health care products—Microbiological methods—Part 1: Determination of a population of microorganisms on products
		EO residuals	ANSI/AAMI ISO 10993-7: 2012 Biological evaluation of medical devices—Part 7: Ethylene oxide sterilization residuals
Test Equipment		ISO 18472 Sterilization of health care products—Biological and chemical indicators—Test equipment	

TABLE 3.1.4.1 Table of Sterilization Methods and Corresponding Standards for Process Regulation, Manufacturing, Testing and Validation, Packaging, and Processing—cont'd

	Sterilization Modality	Reference Standard or Guidance Document
General Process, Packaging, and Materials	General	EN ISO 14937 Sterilization of health care products—General requirements for characterization of a sterilizing agent and the development, validation and routine control of a sterilization process for medical devices EN 556-1 Sterilization of medical devices—Requirements for medical devices to be designated “STERILE”—Part 1: Requirements for terminally sterilized medical devices AAMI ST67 Sterilization of health care products—Requirements for products labeled “STERILE”
	Packaging	ANSI/AAMI/ISO 11607-1 Packaging for terminally sterilized medical devices—Part 1: Requirements for materials, sterile barrier systems, and packaging systems AAMI TIR22: 2007 Guidance for ANSI/AAMI/ISO 11607: Packaging for terminally sterilized medical devices—Part 1 and Part 2: 2006 ASTM D4169-05 Standard practice for shipping containers and systems
	Processing	ISO 13408-1 Aseptic processing of health care products—Part 1: General requirements ISO 14937 Sterilization of health care products—General requirements for characterization of a sterilizing agent and the development, validation and routine control of a sterilization process for medical devices ANSI/AAMI/ISO 17664 Processing of health care products—Information to be provided by the medical device manufacturer for the processing of medical devices ANSI/AAMI ST90 Processing of health care products—Quality management systems for processing of health care facilities
	Material compatibility	AAMI TIR17: 2008 Compatibility of materials subject to sterilization
	Manufacturing	ISO 18362 Manufacture of cell-based health care products—Control of microbial risks during processing



• **Figure 3.1.4.2** (A) Bulk ethylene oxide (EO) sterilization machine. (B) Tabletop EO sterilization machine (http://www.medicaexpo.com/prod/etc-hyperbaric-chambers-sterilizers-76116.html#product-item_839144 <http://www.anpro.com/sterilizers/anprolene/AN2000/indexanprolene2000.html>). ((A) Courtesy of ETC Hyperbaric Chambers and Sterilizers. (B) Courtesy of Andersen Products.)

The basic EO sterilization cycle involves five stages: preconditioning and humidification, gas introduction, exposure, evacuation, and aeration. The packaging used to prepare products for EO sterilization must prevent microbial sterility, but allow diffusion of EO and water vapor. Critical care must be taken after EO sterilization to ensure efficient degassing and aeration to ensure that EO residues on the

surface are brought to allowable limits. Typically, aeration methods are utilized because the alternative requires the use of a very deep vacuum. Total cycle times range from 6h to several days. While EO is effective for porous dressings and woven materials, impermeable tubing or internal channels, such as in catheters, might require special processes or longer exposures for effective sterilization.

The international EO sterilization standard (Table 3.1.4.1, ISO 11135-1) refers to the use of both EO and its mixtures with a diluent. Diluents such as nitrogen blanketing along with other cycle design features are used to reduce the relative proportion of oxygen in the chamber environment and keep flammability low, without affecting the efficacy of the EO cycle. On an industrial level (Fig. 3.1.4.2A), EO sterilization exposure times can range from 6 to 24h at processing parameters set to 40–65°C and a relative humidity of 30%–90%. This begins with exposure over a prolonged period of time to high relative humidity before the environment is flushed with nitrogen containing high EO. Once complete, EO flushing begins with a series of nitrogen injections followed by dynamic vacuum/steam pulsing and air rinsing. Sterile air is used sometimes alongside consecutive vacuum treatments to eliminate EO from the chamber. The last injection of sterile air brings the chamber back to atmospheric pressure. To meet regulatory standards, the concentration of EO is measured in the chamber after degas and on the product surface with further aeration and active air flow used to ensure removal of surface EO residues. Aeration protocols are designed based on environmental conditions and material properties such as density, size, surface area, etc.

Sterilization by Oxidation: Hydrogen Peroxide or Ozone

Sterilization by oxidative means involves the use of highly reactive, oxidizing agents. Hydrogen peroxide and ozone both have excellent microbicidal properties and their chemistries are well known, so they are often utilized for this sterilization technique. While their effectiveness may seem similar on the basis of mechanism of kill (oxidation), they in fact can produce different outcomes and are therefore used for certain applications.

While hydrogen peroxide has poor penetration properties, ozone sterilization as an alternative is somewhat better in this regard. Hydrogen peroxide is particularly limited in the depth it can reach within a product and is often classified as a surface sterilant. Additionally, hydrogen peroxide has a very high vapor and boiling point requiring the use of deep vacuum pressures in conjunction with it. This can negatively affect materials and their packaging, so most sterilization processes are conducted in small vessels rather than large chambers, limiting scalability. Additionally, hydrogen peroxide and ozone are compatible with fewer materials than EO in terms of chemical reactivity, but are still preferred because exposure times are extremely short in comparison and there is no risk of poststerilization toxic residues since the by-products are oxygen and water vapor.

Some hydrogen peroxide sterilization methods involve the use of plasma to facilitate the degradation of the oxidizing reagent. This also decreases negative effects on polymers that may be susceptible to damage (e.g., acrylics, natural rubbers, polyesters, and polyglycolides) because the plasma destroys more peroxide residues than if simple aeration were to be used. Other adaptations can also be made to minimize the effects on polymers such as reducing the concentration and processing temperature; however, this will require longer

CASE STUDY I

On April 13, 1998, the FDA issued a safety alert regarding the use of the AbTox Plazlyte sterilization system. The Plazlyte sterilizers utilized a proprietary, low-temperature gas plasma, along with vaporized peracetic acid. Although the system provided sufficient lethality, the FDA had not cleared the safety, performance, or instructions for use of this sterilizer. The sterilizers were sold directly to hospitals seeking alternatives for EO sterilizers. The warning was initiated due to serious eye injuries to corneal endothelial cells, which resulted in corneal transplantation in some patients. The problem occurred when surgical instruments were sterilized, and copper and zinc salts formed on the surfaces of the sterile instruments. The copper compound residues were toxic to corneal endothelia and resulted in blindness (FDA, 1998). During the time period of January 8–14, 1998, six of eight patients undergoing intraocular surgery incurred corneal edema and opacification of the cornea (CDC, 1998).

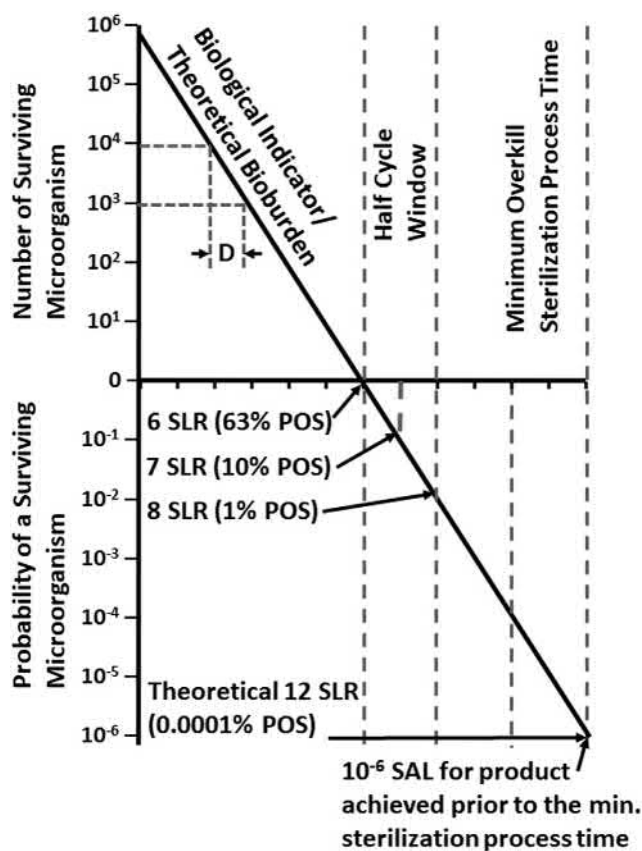
exposure times. Caution regarding material degradation and the formation of undesirable salts on the surface of devices must be exercised especially with combinatorial chemical sterilization and oxidizing plasma (see Case Study I).

The sterilization process is generally applied to relatively smaller loads as the production of ozone has scalability constraints. Ozone sterilization involves relatively low temperatures making it suitable for heat-sensitive materials, and similar to hydrogen peroxide results in a high degree of humidity. Lowering the chamber temperature even further allows a decrease in the concentration of ozone with similar sterilization outcomes but reduced degradative effects on polymers being sterilized, resulting in longer exposure time requirements.

Physicochemical Methods: Gas Plasma

The word “plasma” refers to a partially ionized gas in which a fraction of the particles is charged while the rest remain neutral. The resulting properties of such a gas include high conductivity, which responds well to electromagnetic fields. Generation of plasma is conceptually simple. In short, a sufficient amount of energy must be supplied to a neutral gas to force a partially charged species to emerge consisting of electrons and ions. The two main types of microbicidal plasmas that will be discussed are low-pressure plasmas and atmospheric-pressure plasmas.

Low-pressure (subatmospheric) plasmas can attribute their microbicidal properties to several different mechanisms. First, the ultraviolet (UV)/vacuum UV photons emitted upon discharge facilitate the production of chemical bonds between thymine residues in DNA strands. This prevents DNA repair mechanisms from working properly and permits damage accumulation in the DNA. Another mechanism involves erosion of the spore walls of the microbe by chemically active species generated from the various gases used for plasma. These mechanisms work synergistically with the heat produced in plasma generation to break down the microorganisms and their DNA protection



• **Figure 3.1.4.3** Measuring the bioburden level on the sample and its logarithmic reduction with exposure time to determine overall gas plasma sterilization time required to achieve an SAL of 10^{-6} . POS, Probability of survival; SAL, sterility assurance level; SLR, Spore log reduction. (Shintani H., 2015. Simultaneous achievement of Sterility Assurance Level (SAL) of 10^{-6} and material and functional compatibility in gas plasma sterilization running title: simultaneous SAL and compatibility. Pharm Regul Aff. 4, 131.)

proteins. With respect to atmospheric-pressure plasmas, they include the previously mentioned mechanisms of kill—UV photons, heat, and spore wall erosion. In addition to this, they cause the buildup of electrostatic forces on the surface of spore membranes as well as the interaction of reactive oxygen species and reactive nitrogen species with the microbes themselves. Thus atmospheric pressure plasmas cause both chemical as well as thermal degradation of the cell walls, their DNA, and their ability to reproduce.

Practical limitations with the use of plasma include high cost as well as small container limitations because of the sheer amount of energy required to produce the plasma, and the prolonged duration of plasma treatment needed to achieve relevant SALs (Fig. 3.1.4.3). Also, because plasma has trouble penetrating common packaging used for sterilization, large-scale application of the technique and maintaining posttreatment sterility are fairly limited.

Material Considerations for Chemical Sterilization

EO sterilization processing parameters that are of practical importance to the biomaterials scientist are those that not

only affect the final product and package, but also affect optimization throughout. Deep vacuum levels and the rate of their cycling along with chamber temperature and concentration, exposure times, and any diluents utilized can all potentially affect packaging and/or device material components, especially when considering pharmaceuticals and biologics. Other parameters such as the size of the chamber, length of the cycle, and any preconditioning, and/or aeration steps can affect cycle times and therefore product throughput.

While ozone and hydrogen peroxide both attribute their microbicidal properties to their high reactivity and oxidative chemistries, their effects can be very different. For example, hydrogen peroxide sterilizes urethanes and natural rubbers better than ozone but ozone is preferred for silicones and cellulose-based plastics rather than hydrogen peroxide. Liquids, oils, powders, cotton, linen, and paper, not just used in surgical supplies but also in packaging, absorb hydrogen peroxide and thus cannot be sterilized by that process. Ozone also has slightly better penetration than hydrogen peroxide. With that being said, understanding the material properties of the load as well as the chemistry of oxidative reaction will be the deciding factor when choosing between the two techniques.

R&D, Pilot, and Low-Volume Technologies

Small EO sterilizers are very powerful tools for biomaterials development. As well as providing a vehicle for well-controlled microbial kill challenge testing, they can be used to explore compatibility solutions and products even with the most limiting parameters. Special low-temperature and/or low-humidity EO cycles can be developed and validated to avoid material compatibility concerns. Small EO chambers are also used extensively within the hospital as well as research laboratory settings due to their convenience and effectiveness. A well-controlled R&D EO chamber is shown in Fig. 3.1.4.2B.

Alkylation chemistry, the microbial kill mechanism for EO, may produce other material effects, but in general the effects are small. Other EO process parameters, i.e., temperature, humidity, and evacuation cycles, can substantially affect device materials and are usually the greater concern. Materials must be able to withstand the most challenging range of conditions used in a given EO cycle, including humidity preconditioning and aeration cycles afterward for several days at 40°C ; EO cycles for 6–24 h at processing temperatures of 40 – 65°C ; relative humidity in the range of 30%–90%; and evacuation levels down to 2 torr in some cycles with very fast evacuation rates.

Bioabsorbable polymers may be difficult to process under these conditions because structural integrity is often compromised with them. Both temperature and humidity can degrade bioabsorbable material properties. Packaging materials must also be considered because they need to be able to withstand the evacuation rates and pressures. Materials with known deleterious responses to typical single EO sterilization cycles include polyacrylates, e.g., polymethylmethacrylate and some styrene resins, e.g., polystyrene and

styrene acrylonitrile. These materials may be acceptable in certain applications, but must be evaluated carefully after exposure to worse case cycles (“most challenging parameters”) to ensure clinically acceptable performance over the shelf life of the device. It is not expected that EO sterilization will affect device performance over time.

Pharmaceuticals and Biologics: Compatibility With EO Sterilization

In the pharmaceuticals industry, EO is predominantly used for sterilizing packaging components that enter the aseptic processes. These include bottles, plugs, caps, etc. When it comes to the actual sterility of the drugs, EO is often a last resort because it can alkylate or hydrolyze molecules within carriers and because long exposures to high heat could thermally degrade the drug. Additionally, the vacuum processes involved in aeration of the product could lead to evaporation of components of formulation that have low boiling points. Liquids and powders are also not compatible with EO sterilization because the gas has a hard time penetrating them unless they are spread out in a thin layer.

In the same fashion, few biologics are incompatible with EO sterilization. Limitations due to extreme temperatures, the presence of EO residues, as well as unwanted alkylation of the product make this method of sterilization too harsh for this application. Ironically, the alkylating properties that make this gas so effective in sterilizing product also hinder it from being used in the biologics industry, since so many amines and proteins (not belonging to microbes) are actually desired and since EO and thermal processing may often result in the creation of denatured proteins that are equally undesired.

In applications where either human or animal tissues are not compatible with terminal sterilization options, liquid chemical sterilization is often used. A common example of the type of product sterilized by this method is blood dialyzers because they cannot undergo a high level of sterilization for reuse. An appealing characteristic of this technique is its simplicity and time efficiency. The basic process involves the immersion of the device into liquid solutions of either an aldehyde or an oxidizing agent (e.g., glutaraldehyde, hydrogen peroxide, or peracetic acid). These solutions may also contain buffers, detergents, and anticorrosive agents depending on the material being sterilized. One consideration, however, is that this method does not provide the same process control or sterility assurance levels as terminal sterilization processes (Chamberlain et al., 1999). Despite this drawback, automation of the process has led to significant success in providing a safe final tissue product.

Thermal Techniques

Thermal sterilization is the oldest class of sterilization technique. This method can be used with moist or dry heat, which both have many characteristics in common. The high temperature in both techniques is the main principle of microbial inactivation. A combination of high temperature

with moisture has advantages over dry heat such as reduced sterilization time. However, to determine which technique is the best choice, we need to consider the following variable factors.

Safety Considerations

The hazards associated with the thermal sterilization technique include heat, steam, and pressure. While this technique is the simplest sterilization technique, following the protocols, regular maintenance, using a proper validation indicator, and controlling the exhaust would reduce the hazards. In addition to the regular safety considerations, choosing a suitable thermal technique plays an important role in the efficiency of the sterilization. The dry heat technique is the most convenient method for heat stable materials such as nonaqueous materials, oil-based injectable pharmaceuticals, powders, glassware, and metallic surgical instruments.

Principles of Action and Efficacy

Thermal processes kill microorganisms by coagulation of proteins, including structural components of the cells, as well as by rupturing cell walls. The nature of the process is strongly impacted by the presence of water or humidity, in terms of the penetration of the heat, the exposure time of the surface of the material, as well as bioburden sensitivity to dry or moist heat. For example, *Bacillus subtilis* var *niger* is less sensitive to dry heat, while *Geobacillus stearothermophilus* is less sensitive to moist heat or steam; thus each bacterium is used as the biological indicator to test the efficacy of the corresponding sterilization treatment. Action and efficacy are also impacted by the ability of the materials being sterilized to high temperatures and to steam at high pressures.

Dry Heat Sterilization

The dry heat technique, one of the simplest sterilization techniques, relies on only two parameters: temperature and exposure time. The simplicity of this technique has made it favorable for clinical and industrial applications for materials that can survive temperatures above 170°C with no deleterious effects. Convection, conduction, and thermal radiation are the major principles of dry heat sterilization. Generally, the dry heat technique includes thermal exposure at high temperature (160–330°C) for up to 3 h; however, lower temperatures (e.g., 105°C) may be effective on some microorganisms if applied for a longer period of time. Dry heat is the most logistically convenient method for devices/components that are not temperature sensitive. The simplest dry heat technique is the use of an oven. Commercial ovens are equipped with horizontal or vertical air supply to force the air inside the oven, which improves heat distribution and ensures a dry environment. The air is generally filtered by high-efficiency particulate air filters to maintain sterility. At larger scales, radiant heat tunnels and unidirectional airflow are preferred.



• **Figure 3.1.4.4** (A) Bulk steam sterilization machine, common in hospital settings. (B) Tabletop autoclave. (C) Interior loading configuration of small batch autoclaves. (<https://www.sterislife.com/products/steam-sterilizers/steam-sterilizers/large-steam-sterilizers> <https://tuttnauer.com/dental-autoclaves/class-s-class-n-autoclaves/d-line-e-and-ek>). ((A) Courtesy of STERIS Life Science Inc. (B) Courtesy of Tuttnaur Sterilization and Infection Control).

Steam Sterilization and Disinfection

Moist heat requires significantly reduced heat exposure time compared to dry heat and is nontoxic, rapid, penetrating, and energy efficient. However, this technique is not effective at destroying endotoxin (depyrogenation). Moreover, high temperature, humidity, and high pressure may lead to the softening, degradation, and hydrolysis of polymer-based materials. This technique is widely used in industrial sectors and hospitals for sterilization of pharmaceuticals in glass ampules, plasticware, and metallic surgical instruments intended for reuse by applying saturated, pressurized steam. The regulatory preference is that steam sterilization be used for terminal sterilization where possible. Steam sterilization is generally carried out at 121°C for only 20 min and under a pressure of 121 kPa. Autoclaves are widely used for this technique (Fig. 3.1.4.4), which are similar to a pressure cooker with computer control for cycle monitoring. There are generally two main types of autoclaves: gravity displacement autoclave and high-speed prevacuum sterilizer. A gravity displacement autoclave as a prolonged method has the most basic sterilization cycle, which is a suitable technique for laboratory media and pharmaceutical components. A high-speed prevacuum sterilizer is relatively faster since the air is removed from the load chamber mechanically. This technique is favorable to the articles with porous structures since the steam penetrates to the pores, which is not feasible in a gravity displacement autoclave.

Application Considerations

Thermal techniques rely primarily on temperature, time, pressure, and relative humidity. This technique is common in hospitals and industry due to simplicity, low costs of maintenance, no chemical or radiation hazards, and low general costs. Due to the nature of the process, organic solvents, nonstainless steel, polymers with low melting temperature, and degradable polymers are autoclave incompatible

materials that might be degraded, melt, or hydrolyzed during sterilization. Especially with dry heat, surface features or morphology may melt or be distorted and the nature of the passivating oxide layer may change on unalloyed bare metal titanium surfaces. Polysulfones and silicones used in medical devices can be sterilized by heat; steam sterilization is preferred for polypropylene and polyvinylpyrrolidone, while dry heat is preferred for polycaprolactones.

Materials Development Considerations for Sterility

Knowledge of a sterilization modality's processing parameters and how they interact with materials (see the Sections "Radiation-Based Techniques," "Chemical Techniques," and "Thermal Techniques") is a key element in assessing material compatibility with a given terminal sterilization process. A summary of material effects with different sterilization modalities is given in AAMI TIR17 (Table 3.1.4.1).

Starting with the best candidate materials is the surest way to optimize material compatibility with terminal sterilization. Guidance on selecting material compatible with six terminal sterilization modalities is available (AAMI, 2008). The most challenging material selection scenario is the combination of a difficult-to-sterilize primary material, which is central to the clinical use of the device, with secondary materials that are also sensitive to sterilization, e.g., an active agent (pharmaceutical or biologic), a bioabsorbable material, and/or active electronics. The best approach is to select a sterilization modality that is compatible with the primary material, and then try to select secondary materials that are compatible with the selected sterilization modality.

Materials and devices are carefully designed, optimized, and delivered to meet performance benchmarks. Careful testing is essential after sterilization to ensure that these benchmarks are met and that the risk of material or device

failure is not increased, especially from the perspective of clinical performance. To characterize drug release kinetics and other combination device properties, micro- and nanocharacterization of drug-polymer matrices may be required (Ding et al., 2009). This is essential not only to ensure that the matrix properties have not changed in terms of controlled release but also that the pharmaceutical activity remains the same. Material biocompatibility can change as a function of sterilization modality and process. Device endotoxin levels are typically not sensitive to the sterilization modality, and testing may often be performed before or after sterilization. The effect of sterilization on the surface of biomaterials should also be considered. Radiation typically has a minimal effect on biomaterial surfaces, while EO, oxidative gases, and liquid chemical sterilants can have either a positive or negative surface effect depending on the application of the biomaterial (Chamberlain et al., 1999).

Ensuring adequate device performance throughout its intended shelf life is the final material compatibility challenge for the biomedical scientist. In the case of dental filling materials, for example, the microstructural properties of glass ionomers were found to be affected by EO sterilization. It was observed that UV exposure affected the hardness of the materials, and that steam sterilization caused both an increase in porosity and a degradation of material hardness (Farrugia et al., 2015). Since medical device costs are closely related to shelf life longevity, it is essential that materials stability with age and more importantly packaging stability and sterility with age be maintained so as not to increase the cost of products to the consumer. Care should be taken to conduct shelf life and aging tests in environments similar to those in which they will be stored and usually these tests are conducted using accelerated aging models.

Safety Testing and Validation After Sterilization

For a device with significant sterilization material compatibility challenges, a robust understanding of sterility concepts and associated patient safety issues may be the key to discovering a cost-effective sterilization solution. At one end of the spectrum of sterilization options is overkill terminal sterilization. This approach has for decades served the industry well for devices with limited material compatibility concerns. The other end of the spectrum includes liquid chemical sterilization of biologics and aseptic processing of combination devices, relatively costly options from many perspectives. Between these extremes are creative terminal sterilization validation methodologies and terminal sterilization to nontraditional specifications. Without the ability to skillfully navigate this continuum of options, the biomaterials scientist may not be able to cost effectively bring a product to market.

Terminal sterilization is hugely advantageous in enormously reducing microbial contamination of fully packaged products with high process control to meet regulatory sterility requirements. However, it should be noted that the definitions of

“sterile” and “sterilization” are based on the complete absence of viable microorganisms (ISO/TS 11139, 2006). These definitions are problematic, as they imply an absolute condition. Sterilization processes are based on microbial inactivation, which is exponential in nature in most cases and follows first-order kinetics. Therefore both the process parameters of sterilization as well as the design of appropriate validation procedures in terms of indicators or number of samples to be tested can be determined quantitatively.

This section begins with a review of sterilization-related product and patient safety issues. This is followed by an overview of validation of sterility and maintaining sterility over time through sterile barrier packaging.

Patient Safety: FDA Recall Classifications: Class I, Class II, and Class III

Public notices from the Food and Drug Administration (FDA) and the Centers for Disease Control (CDC) regarding infections resulting from medical device-related infections and product recalls indicate very few instances related to inadequate industry terminal sterilization practices (Favero, 2001). Therefore it appears the existing standards and medical device manufacturers, and associated contractors, are providing safe and effective devices in terms of product sterility. The majority of patient safety issues do not come from nonsterile, aseptically processed products, or from improperly sterilized products, regardless of the delivered SAL. Patient safety issues develop from the introduction of foreign materials into the body during patient treatment at hospitals. In 2015, there were approximately 687,000 hospital-acquired infections in the United States translating to a prevalence of 4% of all hospital patients (CDC, 2020). Of these, 22% were pneumonia, 22% surgical site infections, 20% lower respiratory tract infections, 17% gastrointestinal infections, 10% bloodstream infections, 16% skin and soft tissue infections, and 17% related to other issues (Magill et al., 2017). The following case studies provide perspectives on where the industry safety concerns may lie by examining a few sterilization-related incidents with subsequent patient infections or injury.

As can be seen from these examples, patient safety goes well beyond the ability to provide a sterile product. Nonetheless, the validation of product sterility is an absolute must and part of the regulatory submission and approval process. Principles of terminal sterilization validation are the next topics covered.

Biological Safety Verification

The typical SAL for most devices distributed in Europe and the United States is 10^{-6} (EN 556-1; Table 3.1.4.1). Alternatively, if the biomaterials scientists, the microbiologists, and sterilization personnel cannot demonstrate that the device is compatible from a product performance perspective with any sterilization process, they may need to move the product to an aseptic process where contamination rates

CASE STUDY II

Between 2012 and 2014, at least nine US sites disclosed clusters of patients infected by carbapenem-resistant Enterobacteriaceae, and over 250 patient-to-patient transmissions of infection and over 20 deaths attributable to such complications were reported worldwide. Endoscopes, or more precisely the insufficient cleaning and reprocessing of endoscopes, was found to be the cause for this transmission between patients. These outbreaks were reported across multiple sites in the United States and across the world despite clinical facilities following manufacturer-recommended high-level disinfection. Not only were the reported cases of infection distributed geographically, but they were also distributed across multiple medical device designs and manufacturers of the duodenoscopes; the infections included both drug-resistant as well as antibiotic-sensitive bacteria. The infection transmission findings (CDC, 2014), and successive safety alerts (US FDA, 2015) and guidance (FDA, 2019b), suggested that post-market surveillance of device use in terms of observing real-world re-processing sterilization procedures was necessary to generate updated disinfection and sterility testing protocols.

The risk of transmission and susceptibility for devices such as endoscopes, which do not breach the tissue barrier, stems from close contact with the epithelial mucous membrane, which has a relatively high bioburden (10^9 – 10^{12}), and from that level, the nine orders of magnitude reduction achieved in washing and cleaning after use still leave a significant challenge to achieve an SAL of 10^{-6} . Additionally, these cases of transmission revealed that the design of the endoscopes that allowed for flexibility of the device, including neck regions that could kink and internal channels and conduits to allow specimen collection or house cables and wires, made the devices especially difficult to clean and disinfect during reprocessing at clinical sites. The reports of infection transmission led to new guidance in terms of not only selective culture to validate SAL through improved biological surveillance, but also recommended enhanced EO or chemical liquid sterilization intermittently based on clinical use.

EO, however, has fallen out of favor in part because of extensive controls required to avoid its carcinogenic and teratogenic risks. In addition, the use of EO adds a significant instrument turnaround time after reprocessing, reducing adoption in clinical facilities. Liquid chemical sterilants such as peracetic acid might provide viable alternatives once validated as a reprocessing technique for endoscopes and approved as such by the FDA. The number of procedures using duodenoscopes exceeds 650,000 in the United States annually, and even the lowest reported defect rates would expose over 4500 patients to risks that are relatively preventable with good disinfection and maintenance practices (Petersen et al., 2016. *Gastroenterology* 151, 46–50).

may not be greater than 0.1%. However, terminal sterilization processes are clearly the preferred choice for regulatory agencies. With either of these scenarios, it must also be shown that the benefits of the device for the target population outweigh the risks (potential harms and severity of these harms to the patient) associated with the use of the device. Biological safety validation is typically carried out using a biological microorganism soil separate from the product batches being sterilized; this initial bioburden is representative on potential soil on the device, and ensuring that the spores in this sample are not active after a culture test post-sterilization is an effective validation step. The biological

validation challenge chosen must be a standard bug known to be among the more resistant to the method of terminal sterilization being used (for example, *Bacillus pumilis* [E601 strain] for irradiation sterilization, with *Streptococcus faecium* and *Micrococcus radiodurans* also being more resistant to radiation; and *Bacillus atrophaeus* for EO sterilization). Another major perceived concern for a greater sterility assurance level is the potential use of the device on elderly patients, immunocompromised patients, those with HIV, transplant patients, burns patients, newborns, and children. This perception is countered by the fact that these high-risk patients are routinely treated with aseptically processed products, and clinical facilities where devices are prepared for reuse routinely subject them to overkill sterilization.

Maintaining Sterility: Packaging and Shelf Life

The product packaging and sterile barrier system is critical to maintaining the safety and integrity of the sterilized product. Device packaging must maintain product sterility throughout the expected shelf life. Packaging failures represent one of the most common reasons for product recalls. Examples of possible causes of such failures include pinholes worn into the sterile barrier from device protrusions, cracks in rigid packaging components, dislodged devices such as open seals from the packaging fixtures, product damage or wear, and dust generated by device components rubbing against other materials. Compromised packaging jeopardizes the integrity of the sterile product, and becomes a patient safety concern. The standards for packaging validation provide the industry with the requirements for validation of device packaging (ISO 11607-1 and AAMI TIR 22; Table 3.1.4.1).

Packaging materials used for the sterilization of gaseous sterilants must allow for the ingress of the sterilant to the device surfaces, while packaging for irradiated products can be a vapor barrier. A breathable package may be desirable for irradiated products, as some materials (polyethylene, polyvinyl chloride, and polyurethane used in tubing, drapes, and gowns) tend to generate gases during radiation sterilization. If the gases are trapped within the package, they may present potentially offensive odors when opened. Odor generation may be reduced by incorporating antioxidants or by using higher MW materials and breathable packaging materials (Hemmerich, 2000). For product material compatibility purposes, and to protect the product from the environment (i.e., water vapor, oxygen, etc.), one may have to provide packaging with a very low rate of gas transmission. Product and packaging are typically subject to an accelerated aging program, simulation of the transportation environment, and then inspected for packaging failures to ensure that sterility and product integrity are maintained.

Sourcing, Quality Systems, and Manufacturing Controls

To put terminal sterilization and sterility assurance levels in perspective, it is useful to compare terminal sterilization with

aseptic processing. In aseptic processing there is no inactivation of the product bioburden. These products are not exposed to a sterilization process in their final packaging. Aseptic processing is defined as “handling of sterile product, containers, and/or devices in a controlled environment, in which the air supply, materials, equipment, and personnel are regulated to maintain sterility” (ISO 13408-1, 2008, amended 2013 and under development in 2019). Aseptic processing includes compounding, filtration, and filling. Through simulations or media fills of the aseptic process, the manufacturer must demonstrate the effectiveness of the controls over the risks of contamination associated with each step of the process. Control over potential contamination in an aseptic process results in a frequency of a nonsterile unit occurring of less than one in 1000 (0.1%). The sterility of the final product is based on filter efficiency and integrity, lack of available contamination in the surrounding environment, and controlling a series of operations to “maintain” sterility.

Since better process control and patient safety is achieved through terminal sterilization processes, the current regulatory environment requires medical device manufacturers to demonstrate that a product cannot be terminally sterilized before it can convert to an aseptic process. The required parameters and risk assessment methods of such a demonstration are detailed in ISO 13408-7:2012 for processes in which process simulation (per ISO 13408-1) cannot be applied (ISO 30061,2012). Liquid chemical sterilization and aseptic processing are relatively expensive options that may not provide as high a level of process control as terminal sterilization. It is therefore hoped that the biomaterials scientist will explore creative sterilization validation to ensure that the sterility assurance specification can be appropriately met.

In the majority of sterilization validations, the sterilization process delivers a significantly greater amount of lethality than is actually required. Typically, for devices composed of materials and packaging that are compatible with the sterilization process, the sterilization scientist uses a sterilization process that is easy to validate, such as high or extreme standard sterilization doses, also referred to as the “overkill” approach, which often delivers SAL values of 10^{-12} , and often values lower than 10^{-20} . If product and/or package functionality are a potential issue, one should explore options of minimizing terminal sterilization processes to assure material compatibility.

Since the dose used takes into account the initial bioburden in addition to product configuration and sterilization method efficacy, one method to reduce dose or duration is to reduce the initial bioburden on the product and innovative techniques such as the use of specialized sterilization to specifically target internal, relatively inaccessible parts of the product geometry.

New radiation sterilization validation methods have been developed (Table 3.1.4.1: Method VD_{MAX}, AAMI TIR33; Modified Method 2, AAMI TIR40) that allow for the lowest possible doses to be achieved for a given product. Along with optimizing the minimum sterilization dose, which

reduces sterilization time, recently there have been multiple applications for regulatory approval for biological indicators with shorter read and culture times, for example, reducing validation of EO sterilization from as long as 24 to 4 h after aeration. Reducing sterilization dose can also be leveraged to potentially take advantage of lower temperatures or humidity if maintaining material mechanical integrity is the greater concern.

The development of fully modular, closed-loop manufacturing systems that ensure not just cleanliness but sterility is a critical requirement to enable the translation of biological or tissue-engineered products. Such systems would enable quality assurance as well as quality control that matches regulatory requirements and accelerates the development of novel technologies such as 3D printed regenerative medicine implants or personalized medical devices to clinical application.

Sterilization Standards

Confidence in terminally sterilized products comes from a robust system of process control, standardization, testing, and validation. This is critical since sterilization processing efficacy cannot be demonstrated by routine testing. For instance, an SAL of 10^{-6} can only be truly demonstrated by testing of approximately one million products and finding no more than one positive. Since this is neither possible nor practical, validation and assurance of sterilization processes through standards is chosen instead. The standards used in the medical device and pharmaceutical industries, in conjunction with regulatory authorities, have been provided in Table 3.1.4.1 as a reference for biomaterials scientists. As is clear from the list, the standards are comprehensive in terms of definition of terms, processes, calculations of dose, measurement of delivery, validation of processes, and clearly defined stepwise sequences not only for sterilization processes, but also for validation, materials testing, and packaging and shelf life. Increasingly, the different professional organizations responsible for producing technical standards as well as for providing the governmental regulations for medical product safety are aligning their standards requirements and providing consensus standards documents or guidance (such as the ANSI/AAMI/ISO standards in Table 3.1.4.1).

Sterilization equipment and the process must be qualified and validated. The first considerations are termed “Product Definition” and “Process Definition.” For a radiation process this includes defining product families, establishing the maximum acceptable dose (the highest dose the device can withstand and still function properly), and establishing the sterilization dose (the validated minimum dose the device can receive to ensure sterility). The considerations for an EO process include defining product families, confirming that the product design allows EO and humidity to penetrate the product and package, defining the hardest-to-kill location within the product, and determining the microbial rate of inactivation.

Sterilization processes must undergo Installation Qualification (IQ), Operational Qualification (OQ), Performance Qualification (PQ), and some form of intended dose mapping specific to the sterilization process and the product batch. IQ is defined by the verification of documents to meet users and manufacturer requirements. OQ verifies that regular settings such as environmental conditions, energy level for sterilization, and cycle length are met, while PQ demonstrates that the machines work reproducibly and that this can be documented and tracked. As the last step, intended dose mapping (for example, radiation sensors for irradiation, EO strips for EO, and temperature mapping for thermal methods) includes the verification of distribution data loggers and penetration data loggers to meet SAL requirements within the product batch. This includes ensuring proof of lethality value and that three successful fully dosed product loads are tested with less than an anticipated level of sterility failures to indicate that the appropriate controls are in place. This level of qualification and testing allows some distinct benefits, such as testing only a limited batch of samples (usually 20–50) to assure a high SAL and ensuring batchwise documentation of doses and failures to create trends as well as predictive data for maximum safety. Thus even in the case of deleterious outcomes, manufacturers and contract sterilization providers can pinpoint concerns.

Summary and Future Challenges

The medical device industry has been well served by well-validated and dependable terminal sterilization technologies, radiation, and EO, in addition to many other technologies that meet custom needs. The important processing parameters and mechanisms of microbial kill are well established. Patient safety is ensured by terminal sterilization as a result of the very high assurance of sterility specifications utilized, strong process control, and robust sterilization validation methodologies that have been incorporated into the regulatory framework.

The challenge for the biomaterials scientist is to skillfully apply terminal sterilization technologies to as many products as possible, especially the more recent combination devices. Examples include drug delivery systems with active biological agents, bioresorbable temperature-sensitive polymers, and radiation-sensitive electronics. The ability to find terminal sterilization solutions to avoid aseptic processing will allow the device industry to provide these innovative therapies at the lowest price and with the highest associated process control and patient safety. As new generations of biomaterials are developed for drug delivery, such as nanoparticles, greater caution needs to be exercised to ensure effective sterilization, especially for contaminants such as endotoxins while not changing the properties the particles are designed for. Similarly, the advent of new manufacturing processes such as 3D printing requires detailed consideration be given to which type of sterilization techniques are employed and in the case of 3D bioprinting to consider which aspects should be used after terminal sterilization and which have to employ aseptic techniques.

The solutions to challenges in sterilization arise from multiple quarters: the biomaterials scientists developing robust materials that can withstand terminal sterilization; improved process control and good manufacturing and clinical practices to ensure cleanliness and reduction of biological fouling where possible; microbiologists identifying improved pathways to combat microbes without using solutions that pose personnel or societal risk; and robust validation and testing, which paired with packaging and storage controls ensures that sterile medical devices can be made available with confidence to patients and clinicians. Increasing interactions between the biomaterials scientists, product engineers, and relevant regulatory authorities and industry forums is leading to both the development of new methods of sterilization, to meet the need for newly discovered concerns (such as prions and endotoxins), and the development of new validation testing standards that increase throughput in sterilization processes and keep costs low.

References

- AAMI, 2008. TIR17 Compatibility of Materials Subject to Sterilization. AAMI.
- CDC, Center for Disease Control, April 24, 1998. Corneal Decompensation after Intraocular Ophthalmic Surgery FDA Safety Alert: Warning Regarding the Use of the AbTox Plazlyte™ Sterilization System. MMWR 47 (15), 306–308 http://www.fda.gov/MedicalDevices/Safety/AlertsandNotices/PublicHealthNotifications/ucm062297.htm?utm_source=fdaSearch-utm_medium_website-utm_term=AbTox-utm_content=1.
- CDC, 2014. Centers for Disease Control and Prevention, Notes from the Field: New Delhi metallo- β -lactamase-producing *Escherichia coli* associated with endoscopic retrograde cholangiopancreatography—Illinois, 2013. MMWR Morb. Mortal. Wkly. Rep. 62, 51–52 1051.
- CDC, 2020. Centers for Disease Control, CDC Healthcare-associated Infections. HAI Data. Accessed 2020. <https://www.cdc.gov/hai/data/portal/index.html>.
- Chamberlain, V.C., Lambert, B.J., Tang, F.W., et al., 1999. Sterilization effects. In: von Recum, A.F. (Ed.), *Handbook of Biomaterials Evaluation*. Taylor and Francis, Columbus, OH, pp. 253–261.
- Clough, R.L., 2001. High-energy radiation and polymers: a review of commercial processes and emerging applications. Nucl. Instrum. Methods Phys. Res. Sect. B Beam Interact. Mater. Atoms 185, 8–33.
- Ding, N., Pacitti, S.D., Tang, F.W., et al., 2009. XIENCE V™ stent design and rationale. J. Interv. Cardiol. 22 (Suppl. 1), S18–S27.
- Favero, M.S., 2001. Sterility assurance: concepts for patient safety. In: Rutala, W.A. (Ed.), *Disinfection, Sterilization and Antisepsis: Principles and Practices in Healthcare Facilities*, pp. 110–119 Association for Professionals in Infection Control and Epidemiology NOTE: In addition to the summary of CDC data by decade in the Favero paper, much evidence exists for non-sterilization causes of hospital acquired infections, e.g., hip implant infection rates are 0.2% in high volume clinics versus 4% in low volume hospitals, with no causes related to initial device contamination (Biomaterials Science, 2nd ed, 4.8, 1st paragraph).
- FDA, US Food and Drug Administration, 1998. Safety Alert: Warning Regarding the Use of the AnTox Plazlyte™ Sterilization System. <http://www.fda.gov/MedicalDevices/Safety/AlertsandNotices/PublicHealthNotifications/UCM062297>.

- Farrugia, C., Cassar, G., Valdramidis, V., Camilleri, J., 2015. Effect of sterilization techniques prior to antimicrobial testing on physical properties of dental restorative materials. *J. dent.* 43 (6), 703–714.
- Food and Drug Administration (FDA), 2019a. Statement on new steps to advance innovation in medical device sterilization with ethylene oxide. Accessible at <https://www.fda.gov/news-events/press-announcements/statement-new-steps-advance-innovation-medical-device-sterilization-ethylene-oxide>.
- Food and Drug Administration (FDA), 2019b. Infections Associated with Reprocessed Duodenoscopes. Accessible at: <https://www.fda.gov/medical-devices/reprocessing-reusable-medical-devices/infections-associated-reprocessed-duodenoscopes#meeting>.
- Forsythe, J.S., Hill, D.J.T., 2000. The radiation chemistry of fluoropolymers. *Prog. Polym. Sci.* 25 (1), 101–136.
- Hemmerich, K.J., 2000. Polymer materials selection for radiation-sterilized products. *Med. Device Diagn. Ind.* 22 (2), 78–89.
- ISO 13408-1, 2008. Aseptic Processing of Health Care Products – Part 1: General Requirements. ISO.
- ISO 13408-7, 2012. Aseptic processing of health care products — Part 7: Alternative processes for medical devices and combination products. Accessible at: <https://www.iso.org/standard/30061.html>.
- ISO/TS 11139, 2006. Sterilization of Healthcare Products – Vocabulary. ISO.
- Magill, S.S., Edwards, J.R., Bamberg, W., Beldavs, Z.G., Dumyati, G., Kainer, M.A., Lynfield, R., Maloney, M., McAllister-Hollod, L., Nadle, J., Ray, S.M., 2017. Multistate point-prevalence survey of health care-associated infections. *N. Engl. J. Med.* 370 (13), 1198–1208.
- Mohammed, A.R., Bramwell, V.W., Coombes, A.G., Perrie, Y., 2006. Lyophilisation and sterilisation of liposomal vaccines to produce stable and sterile products. *Methods* 40, 30–38.
- Parsons, B.J., 2012. Sterilisation of healthcare products by ionising radiation: principles and standards. In: Lerouge, S., Simmons, A. (Eds.), *Sterilization of Biomaterials and Medical Devices*. Woodhead Publishing, Cambridge, UK, pp. 56–70.
- Petersen, B.T., Koch, J., Ginsberg, G.G., 2016. Infection using ERCP endoscopes. *Gastroenterology* 151 (1), 46–50.
- Smith, R.A., Ingels, J., Lochemes, J.J., Dutkowsky, J.P., Pifer, L.L., 2001. Gamma irradiation of HIV-1. *J. Orthop. Res.* 19 (5), 815–819.
- Terryn, H., Maquille, A., Houée-Levin, C., Tilquin, B., 2007. Irradiation of human insulin in aqueous solution, first step towards radiosterilization. *Int. J. Pharm.* 343, 4–11.
- US Food and Drug Administration, 2015. Updated Information for Healthcare Providers Regarding Duodenoscopes. March 4.

Further Reading

- ASTM, 2007. F1980–07 Standard Guide for Accelerated Aging of Sterile Barrier Systems for Medical Devices. ASTM.
- CDC, Center for Disease Control, March 25, 2005. Pseudomonas bloodstream infections associated with a heparin/saline flush – Missouri, New York, Texas, and Michigan, 2004–2005. *MMWR* 54 (11), 269–272.
- EN556-1, 2001. Sterilization of Medical Devices – Requirements for Medical Devices to be Designated “STERILE” – Part 1: Requirements for Terminally Sterilized Medical Devices. BSI: British Standards Institute.
- Klevens, M., Edwards, J.R., Richards Jr, C.L., Horan, T.C., Gaynes, R.P., et al., 2007. Estimating Health Care-Associated Infections and Deaths in U.S. Hospitals, 2002. *Public Health Reports*, 122, March–April.
- Kulla, J., Reich, R., Bioedel Jr, S., et al., 2009. Sterilising combination products using oxides of nitrogen. *Med. Device Diagn. Ind.* 31 (3). <http://www.mddionline.com/article/sterilizing-combination-products-using-oxides-nitrogen>.
- Lambert, B.J., Tang, F.W., 2000. Rationale for practical medical device accelerated aging programs in AAMI TIR17. *Radiat. Phys. Chem.* 57, 349–353.
- Lerouge, S., Simmons, A. (Eds.), 2012. *Sterilisation of biomaterials and medical devices*. Elsevier.
- Sandle, T., 2013. *Sterility, sterilisation and sterility assurance for pharmaceuticals: technology, validation and current regulations*. Elsevier.
- White, A., Burns, D., Christensen, T.W., et al., 2006. Effective terminal sterilisation using supercritical carbon dioxide. *J. Biotechnol.* 123 (4), 504–515.

Chapter Exercises

1. How is bioburden on a material or device typically determined? Is this different from “soil” that is observed in clinical settings? How do the two affect each other and the processing of the material or device for use or reuse?
2. What is the SAL? What is the generally accepted value of SAL? Are most medical devices sterilized at, above, or below the SAL and how is that choice rationalized?
3. What are the advantages of EO sterilization and conversely under what conditions may EO sterilization not be the appropriate choice?
4. Gamma irradiation may not be feasible with many polymeric biomaterials. Which polymers must special consideration be given to in this regard?
5. Processing of biological samples or materials containing encapsulated cells are limited in how they may be processed for sterilization. What are the considerations for each category of biological material and how can sterilization and safety needs be addressed alternatively?

3.1.5

Verification and Validation: From Bench to Human Studies

JOSH SIMON

Spiral Medical Development, Lansdale, PA, United States

Introduction: Focusing on Commercial Medical Device Development

Transitioning a medical device idea from an academic to a commercial setting requires a change in focus and objective. For academic projects, the objective is often to explore new phenomena or physical laws and derive solutions to scientific questions. This work may extend or build upon previous questions and/or prior experience. It may even take place for its own sake with the primary driving forces being curiosity and the thirst for knowledge. Overall, the process is open ended and exploratory. Conversely, commercial development of medical devices focuses on a defined end-point: the release of a product onto the market and its subsequent distribution to patients. As such, projects that deal with medical devices in the commercialization process usually employ concepts that are relatively well tested and explored in comparison with the novel concepts of academia. Commercial projects also have more highly defined timetables because they involve increasingly different types of stakeholders (customers, employees, physicians, distributors, government officials, etc.) with their own deadlines and requirements.

Corporate considerations for producing products used in human subjects often do not appear in purely preclinical or nonclinical academic research. As an example, corporations can have private or public ownership, which in both cases highly anticipates the yearly financial profit and loss numbers. These numbers control strategy and planning for the next fiscal year and beyond, while allowing the companies to adjust their course by making decisions on what projects to continue and what products to discontinue. This stressor of a year-end deadline drives much of the pace for medical device development. A year-long or multiyear-long project has a specific anticipated impact on the profit and loss of the company, so the deadlines and requirements that spring from that anticipation place constraints on the device project. By contrast, an academic project may indeed have deadlines for funding through grants that have specific dates for turning in proposals. These grants

may in turn fund the academic research of a faculty member and secondarily provide revenue to the university or institution that employs the researcher. However, once the grant is issued, the researcher may direct the pace of the project as desired, with considerations to milestones or additional grant payments. Though these requirements do not always present the researcher with total freedom to schedule projects, there is considerably more leeway than the corporate situation.

A full description of the medical device development process necessarily implies the foregoing considerations, and throughout this chapter the focus will automatically assume the commercial perspective. This chapter will start off with a quick overview of the initial steps of a medical device project and then quickly progress to introducing verification and validation. The concepts of regulatory constraints and risk management will receive some attention as well throughout the chapter, because they integrate thoroughly with all medical device development steps.

Starting a Medical Device Project

The initialization of a new medical device project is a multidisciplinary event that requires expertise from several skill-sets, such as project management, marketing, preclinical and clinical research, and regulatory knowledge. Foremost among the drivers for the creation of a project is determination of a need for the device. All successful medical device projects address conditions or injuries that are documented to exist and require treatment. Without a commercially viable driving force to support the development and production of the medical device, there is little incentive to create it.

Finding the need is not trivial. In fact, much of the initial work that takes place before a project ever starts involves assessing the need for the device and answering questions about the clinical condition, its prevalence, its progression, the consequences if it is not treated, and alternative treatments that are already available. A clinical condition, such as a bone fracture, for example, may be common and

serious, but there may also be several cheap and easy treatments available for it already. In cases where the condition is not an injury but instead a progressive physical degeneration, like rheumatoid arthritis (RA), the alternative treatments will follow a sequenced progression from early to late disease stage. A given solution proposed for treating cases of RA would need to address which stage of the disease it treats, and how the treatment is better than the other currently available treatments for that stage. If the condition currently has no known treatments, the task is somewhat easier because describing the need for the medical device only must take into consideration the alternative consequences of not treating the condition at all.

Meeting a clinical need is primary for selecting a project, but it is not something to consider in isolation. For every treatment using a medical device, there are associated risks. At some point, every medical device on the market will fail in someone. Failure represents the manifestation of a known or unknown risk, and the consequence of that failure is the harm. The extent of the harm to the patient is weighed against the potential clinical benefit received from the medical device. This comparison is called a **risk/benefit analysis** and it helps govern the potential and actual success of a device both before and after it arrives onto the market. If a proposed device has a high **risk/benefit ratio**, it may not be prudent to develop it because such an analysis would show that the benefit is not great enough to offset the risk. For most projects in the initial-ization phase, the question of a preliminary risk/benefit ratio will help determine whether the project moves forward.

Research data from academic and commercial laboratories often help with this determination if there are no known clinical data on the device. The purpose of these data is to thoroughly vet the concept and show that it is viable and reliable. Published (and sometimes unpublished) research data along with data on the market size, the clinical condition, unmet need, and risk/benefit are pivotal for consideration of whether to allow the project to proceed. If the physical or scientific concept proposed for the product is still unknown or preliminary and the target patient population is not clear, for example, it will be less likely for the project to receive approval by the company.

Once the preliminary assessments just discussed are complete, a project proposal takes place that consolidates all that information and presents it to some managing authority within the company. The managing authority can take the form of a special project selection committee, a **project management office**, a designated group of people, or a single person giving the approval. In either case, the approval signals the start of the commercialization and development of the proposed device. Management selects a project manager, who in turn helps select a project team and the project is officially started with a “kickoff meeting.”

The first task of the project team is to more clearly define the project parameters and the characteristics of the device with greater detail. This part of the process has both a business-oriented and engineering-oriented side, and both parts are initially led by the marketing team member(s). For the

commercial side, the marketing team member’s responsibility is to create or solidify a **business assessment model** that will clearly delineate the intent of how the product will generate revenue and reach its target customers. On the engineering side, the marketing team member is responsible for the collection of **design inputs**, which are broad, high-level descriptions of what the device must do and how it will meet the customer’s needs. The reason why marketing usually leads both initial endeavors is that the marketing department is usually the one with the broadest amount of direct customer contact and the most awareness of the overall unmet needs. Often, the marketing team will seek the help of the sales department to gather even more detailed knowledge of this information at regional and individual levels. In fact, it is generally a best practice to include a sales team member on the project team from its inception.

Design Controls for Medical Device Development

Prior to 1996 in the United States, medical device development took place differently in every company and there was generally little regulation of the process. All devices had to conform to **good manufacturing practices** and meet certain requirements depending on their device classification under the Food and Drug Administration (FDA), and so long as those requirements were met the device would receive clearance or approval for sale. Few of the requirements dealt with how the development of the device proceeded, and instead focused on whether the device was safe and effective. What became apparent over time was that the safety and efficacy of devices was strongly linked to how their development took place, and the method of device clearance or approval was not enough to effectively reduce recalls and failures. In response, the FDA created the **quality system regulation (QSR)** (21 CFR 820) ([Quality System Regulation, 2019](#)), which applies to all medical devices in the United States except certain Class I exempt device types.

The QSR implements a process known as **design controls**, which fulfills the regulation by establishing, maintaining, and documenting the process of medical device development in a company ([Quality System Regulation, 2019](#)). Aside from ticking a box on fulfilling a regulation, however, design controls really represent a more coherent process for conceiving a device and checking its design before bringing it to market. Even in the production of device components, which do not require design controls, this process can act as a system of checks and balances during the design and increase the chance of error detection. Quite simply, this is because the process calls for a repeated review of itself at each major step and traces each input from the beginning conceptualization to a specification and then to an output that can be tested against the original input under both simulated and realistic conditions. Originally the format for design controls came from ISO 9001 and contains nine parts in its present form under the QSR ([Table 3.1.5.1](#)).

TABLE 3.1.5.1 Nine Parts of Design Controls

Planning	<ul style="list-style-type: none"> • Describes how design and development take place • Describes responsibilities and interfaces • Describes how approvals and updates of documents take place
Input	<ul style="list-style-type: none"> • Requires procedures on how to run the input process • Requires inputs to address measurable needs and requirements • Requires review and approval of documented inputs
Output	<ul style="list-style-type: none"> • Requires procedures for dealing with Outputs • Requires Outputs to be measurable and definable • Requires essential Outputs to be labeled as such • Requires review and approval of documented outputs
Review	<ul style="list-style-type: none"> • Requires a review at the end of each Design Control process • Requires successful review and approval to proceed to the next stage • Reviews the adequacy of inputs or requirements at each stage • Identifies any problems with design or process
Verification	<ul style="list-style-type: none"> • Requires establishment of Verification procedures • Confirms through measurements that Inputs = Outputs • Requires overall review of successful testing before proceeding
Validation	<ul style="list-style-type: none"> • Requires establishment of validation procedures • Confirms through measurements that Inputs meet User Needs • Requires testing under realistic actual or simulated conditions • Requires overall review of successful testing before proceeding
Transfer	<ul style="list-style-type: none"> • Requires procedures to correctly transfer device from development to manufacturing
Design Changes	<ul style="list-style-type: none"> • Requires procedures to identify, document, verify, validate, review, and approve any design changes before market release
Design History file	<ul style="list-style-type: none"> • Requires creation of a compilation of records that describes the design history of a finished device

The bulk of a medical device development project revolves around which step of the design controls process is taking place, along with a parallel process that develops the manufacturing process once the design has reached maturity. Though the QSR regulation is specific to the United States,

medical device companies outside the United States that wish to market products under the FDA follow the process. Other national regulatory frameworks, like the regulations in Brazil, specifically call for design controls as well. The same applies to organizations that use ISO 13485 ([International Organization for Standardization, 2016](#)), which is a standard for developing and maintaining a quality system used to design and produce medical devices: the 2016 version of this standard calls for a process that mirrors design controls. The ISO 13485 standard ([International Organization for Standardization, 2016](#)) requires supporting, checking, and maintaining the results of the design process in a similar way. The new European Medical Device Regulation (MDR) does not explicitly call for design controls. However, it does require medical device producers to have a quality management system (QMS), and the generally accepted standard for a QMS is ISO 13485, which calls for design controls ([International Organization for Standardization, 2016](#)). Thus through this series of chained regulations and standards that involve one another, manufacturers in the European Union must also now develop products through a design controls process, and indeed this is now true of any medical device company using the ISO 13485 standard for its QMS.

Overlaid on top of the design controls process and taking place simultaneously from before the project proposal is approved until long after the device is released onto the market is the **risk management** process. Covering this process in full detail would require at least one other chapter dedicated solely to it. However, it is important to note that the risk management process is integrated with design controls and part of project planning. Once the team has created a plan of how to find, categorize, and address risks, this plan runs alongside of the **design development plan** that comes from the planning requirement within design controls ([Table 3.1.5.1](#)). Like most plans associated with the QSR, the **risk management plan** is a “living document,” meaning the document undergoes continual change and revision throughout the lifetime of the project, and ultimately throughout the lifetime of the device. Each risk uncovered and characterized by the project team is evaluated at least for severity and probability of occurrence. For risks that require mitigation or other forms of addressing as per the risk management plan, the methods used to address that risk and their results must undergo verification and/or validation, which feeds directly into the design controls process. After design controls are complete and the product releases to market, this same risk management process continues, and new risks are addressed, if necessary, and those methods for addressing them are verified and/or validated outside of design controls.

Toward the beginning of the project, as the marketing team coordinates the collection of **design inputs**, several vague descriptions for the device will take shape and these will need further detail and clarification to become **design specifications**. Each design input will lead to one or more design specifications. Moreover, there are different kinds of

TABLE 3.1.5.2 Example Design Inputs and Their Associated Design Specifications

Design Input	Design Specification
The handle of the instrument should be red	Instrument handle must be colored as Pantone color number 185 C
The handle should fit comfortably into the surgeon's hand even if the surgeon has small hands	Handle radius of curvature for each of three handle conforming curves must be 0.85 ± 0.04 cm Handle conforming curves must be spaced 0.5 ± 0.01 cm apart
The handle of the surgical instrument should be at least 6 inches (15 cm) long	Instrument handle must be 15.4 ± 0.01 cm long from end to end at longest dimension along front-end curve
The handle of the surgical instrument must be made from a durable nonslip coating over metal	Instrument handle must be constructed from surgical grade 316 stainless steel Instrument handle must be coated with MEDCT4387 Red Epoxy adjusted to the Pantone color number above

design inputs that describe different aspects of the device and these give rise to different kinds of design specifications. Some design inputs talk about the look and feel of the device. Examples of this input for a surgical instrument would be, “The handle of the instrument should be red,” and “The handle should fit comfortably into the surgeon’s hand even if the surgeon has small hands.” Other inputs might talk about size: “The handle of the surgical instrument should be at least six inches (15 cm) long.” Design inputs can also specify that the product must be sterilized before use and that it must conform to certain regulations or standards. Material requirements are also common such as, “The handle of the surgical instrument must be made from a durable nonslip coating over metal.” Notice that these inputs are not precise enough for an engineer to build the device. While the marketing team member’s job is to collect these inputs, it is the engineer’s responsibility to interpret them and create design specifications from them that are more precise and testable. See examples of how an engineer could interpret these design inputs and create some resulting specifications in [Table 3.1.5.2](#).

Specifications derived from design inputs can be numerous, and many companies use a document called a **design specification document** (DSD) or “spec” to collect them. Specs can be many pages long even for deceptively simple devices because they describe at great length and in detail each aspect of how the device will look and perform. Unlike design inputs, specs directly dictate how to construct the first prototype devices, which then undergo testing. Since the specs are precise, it should be possible to construct tests

for each design specification to show whether the device meets the spec. This is not always the case with a set of design inputs.

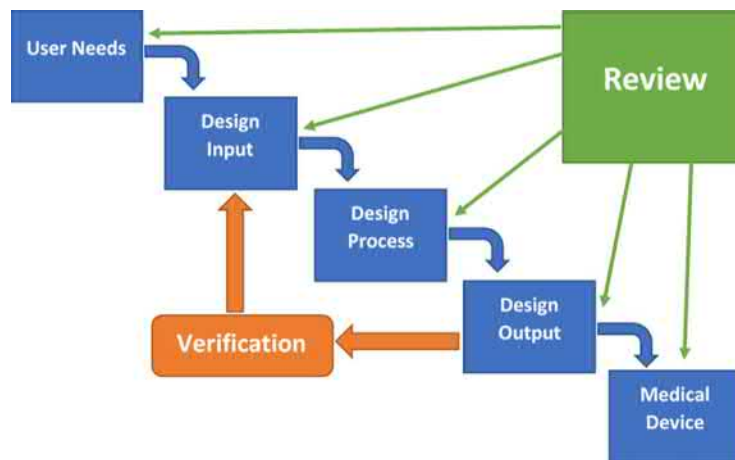
Design specifications can go through many iterations before the project team approves the final DSD. In this sense, the DSD is a living document during the beginning of the project as the team works out conflicts between the specifications. However, at some point the DSD receives approval in its final form and all the design specifications are agreed and set. This is known as **design freeze**, because from that point on in the project, the design of the medical device is not supposed to change. Any disturbance to the spec after this point will be costly, and the further along in the project at which point the disturbance occurs, the costlier it will be to change it.

While specifications are testable descriptions of how to build the medical device, the specifications themselves are not what is tested directly. **Design outputs** are tested. New team members working on medical device projects often have some confusion over design outputs and what they are. Simply put, a design output is the result of a design specification. Since there are different kinds of design specifications, there are also different kinds of design outputs. Some design outputs, for example, can be drawings. In the case of [Table 3.1.5.2](#), the outputs of the specifications that talk about curvature radius and spacing will have drawings as outputs. The drawings will show that the plan is to create a device according to how the features are shown. Other types of design outputs can be documents like instructions for use or surgical technique guides. Pieces of the device can also be considered outputs, such as parts of a certain color. Of course, a prototype of the device is also a design output.

As a rule, every design input must have one or more design specifications, and one or more design outputs, because the whole intent of the design controls process is to track the progress of these inputs through to fruition and to document the decisions and rationale behind them. In some companies, a **design matrix** document is created, though it goes by different names depending on a company’s traditions and naming conventions (i.e., functional requirements matrix, requirements and testing matrix, input-output-verification-validation matrix, etc.). Whatever name is used, the document accomplishes the task of assembling and tracking each design input and its associated design specification, design output, and later its verification and validation testing, which is discussed next. Due to the ever-increasing amount of information generated by a medical device project, this is a frequently updated living document. Some companies even combine this document with the DSD to track everything in one place and cut down on the number of documents to control.

Verification of Medical Device Design

Once the project achieves design freeze, verification can take place. In the simplest sense, verification checks that design inputs equal design outputs. This is why it is important to generate testable outputs from the design specifications, because verification should involve rigorous and scientifically



• **Figure 3.1.5.1** Verification's place in the waterfall design process (FDA, 1997).

sound testing of the outputs to ensure they are created according to the inputs. In a specific sense, verification ensures that the medical device in development is being designed according to its specifications. The graphic in Fig. 3.1.5.1 is adapted from the FDA guidance document entitled “Design Control Guidance for Medical Device Manufacturers” and shows the place of verification within the larger scheme of design controls, which is displayed as a “Waterfall Design Process” to show the relationships of the processes to one another. Without verification, there is a much greater chance that unplanned or unanticipated changes to the product design will inadvertently filter into the project. This in turn could create new and unanticipated hazards for the device if it releases without the verification process.

Although design controls, their specific requirements, and associated FDA guidance documents are United States centric, it is still important to note that the practice of verification and application of its principles are not solely United States-based requirements. Regulations under the QSR reflect the FDA's thinking on the medical device as a product demonstrating safety and efficacy based not only on its most current risk and benefit data, but also on its entire design process from beginning to end. This thinking is shared by some other regulatory bodies outside the United States but not others. Nevertheless, verification is still a part of virtually every regulatory system and is called out specifically in the European MDR ([Medical Device Regulation, 2017](#)) and the ISO 13485 standard ([International Organization for Standardization, 2016](#)), which are two of the most important regulatory structures used outside of the United States.

In the case of ISO 13485, verification is mentioned where the standard talks about planning and documenting the medical device project and says that verification activities must receive consideration ahead of time during this planning stage ([International Organization for Standardization, 2016](#)). Additionally, the standard prescribes the collection of inputs and the creation of outputs, which will later serve as a basis for verification testing. Once there is a verification plan in place and the inputs and outputs are complete, the standard explicitly requires verification testing to

ensure the outputs meet the inputs, and that this testing should have thorough documentation. As a rule, there is much more leeway in how ISO 13485 is applied to a project, and companies each have their own ways of doing this, as opposed to some of the more specific requirements laid out in the QSR and its accompanying guidance documents. Nevertheless, the objectives between the two systems are virtually the same regarding verification.

The MDR is still a new regulation as this book is published, and as time goes on there will be guidance documents issued by European authorities that make the processes required in the regulation clearer. However, as it is written, the MDR does not call for a specific type of quality system or means of verification. Instead, it places the responsibility of building a quality system on the medical device manufacturer and a type of organization called a notified body, which is contracted by government organizations in individual countries called competent authorities to carry out the assessments of documentation from the medical device manufacturers. A notified body will audit the quality system of a medical device manufacturer to make sure it has effective verification processes in place. If the medical device manufacturer so chooses, it may opt to use ISO 13485 to model the basis of its quality system, which the notified body can then audit for compliance. A device manufacturer could also opt to use the QSR for the same purpose or in combination with ISO 13485. By staying compliant with both the QSR and the ISO 13485 standard for its verification processes, a company will have an easier time developing devices simultaneously for the US and EU markets.

Types of Verification Testing

Since different kinds of design inputs produce different types of design specifications that lead to design outputs, there are many different possible types of verification tests to compare the myriad types of inputs and outputs. Describing every possible type of verification test and assessing their scientific validities could indeed fill the contents of an entire course. A few types of testing will receive a more in-depth analysis

TABLE 3.1.5.3 Some General Types of Verification Tests

Verification Test Type	Input/Output Type
Tolerances	<ul style="list-style-type: none"> • Dimensions of an object • Durability/toughness constraints • Deformation constraints • Number of uses • Amount of work done • Amount injected
Appearance	<ul style="list-style-type: none"> • Color • Shape • Ergonomics • Presentation of parts
Biocompatibility	<ul style="list-style-type: none"> • Cytotoxicity • Hemocompatibility • Sensitization/Irritation • Carcinogenicity/Genotoxicity • Implantation (animal) • Other biocompatibility measures
Sterilization	<ul style="list-style-type: none"> • Effects on tolerances • Residuals • Bioburden • Endotoxin testing • Other sterility measures
Packaging	<ul style="list-style-type: none"> • Packaging integrity • Shipping integrity
Labeling Review	<ul style="list-style-type: none"> • Wording of product labels • Regulatory compliance of labels
Software	<ul style="list-style-type: none"> • Bug squashing • Software assurance

in other chapters of this book, while [Table 3.1.5.3](#) gives a short list of several types of general kinds of verification tests, which is by no means exhaustive. In the verification test type column of [Table 3.1.5.3](#), there are several forms of verification testing listed that are associated with the second column, input/output type, which suggests some design inputs/design outputs that would fall under that type of testing.

Tolerance testing is an extremely common type of verification test. For example, every medical device has some dimensions that must remain in a certain range for that device to function or even to remain in storage. The simplest type of tolerance test measures length, width, diameter, curvature, etc. using physical instruments like calipers or digital versions of measuring devices. If a design specification calls for the length of a catheter to be 1 m long, and a catheter is manufactured that is 1.01 m long, that device would fail inspection. It is “out of spec.” To avoid this from happening, specifications always give a range, which is usually wide during the earlier parts of the project and narrows during the later parts. Thus, in the catheter example, a more realistic specification would be a length of 1 ± 0.05 m. If a catheter came off the manufacturing line and measured

1.04 m in length, it would pass because it is considered “in spec”. Another catheter off the same line measuring 0.98 m in length would also pass. Essentially, when a drawing is made for a device as an output, there are ranges of acceptable dimensional characteristics listed on the drawing for every dimension. Each one in turn is verified by taking a sample of prototype devices and measuring all the dimensions to ensure they are in spec for a statistically significant number of devices, preferably for all devices.

Other physical parameters must undergo verification testing in the same manner: a spec with a range is given, and all devices must measure within that range. Aside from dimensional characteristics, devices have durability, toughness, and deformation requirements that specify how much force the device can take before breakage or how far it can bend/stretch before fracture. These requirements usually consider how the device will perform in the real world, and to what conditions the users will likely subject it. Tolerances also extend to the number of uses or cycles a device can withstand. These can be physical cycles or other kinds. If a device must inject a material into the body or some other vessel, the volume of injection will also have a tolerance measure that is necessary to verify. For example, a syringe device that injects exactly 23 μ L of a protein solution could have a spec stating that it must inject 23 ± 2 μ L, which is important for ensuring the correct dosage given to the patient. Finally, another common type of tolerance test involves mating parts that are supposed to fit together every time. There needs to be assurance that if both parts are manufactured at the extreme opposites of their individual specifications they can still fit together. This would involve creating such parts and measuring the fit.

Perhaps the easiest sort of verification testing is appearance verification. When a physical characteristic such as color or the wording printed on a surface is specified as an input, the outputs are the drawings featuring the characteristic and the prototype devices displaying them. Another possibility is a list of parts that fit together to form the device, which requires making sure all of them are present. Essentially, to verify such parameters, someone simply needs to review the drawing and prototype(s) to double check that the physical characteristics are exactly as specified. Similar and related to this form of verification is labeling review, which checks that the labeling fulfills all regulatory and marketing requirements as written.

One of the largest and most important sets of verification data is regarding biocompatibility. Not only for new biomaterials, but also well-known biomaterials must undergo verification in every device. The extent of verification differs between the two, with the newer biomaterials going through more stringent testing. Old biomaterials (>20 years) that have seen decades of use can sometimes escape major testing via creation of a biocompatibility rationale that explains the long usage of the material in similar devices as well as literature references that document the usage. This method is outlined in the ISO 10993-1 standard, which is like the requirements in the QSR and also forms the basis of European and most other biocompatibility standards. For newer biomaterials it is

generally not possible to skip the basic biocompatibility tests outlined in Table 3.1.5.3, along with others, depending on the invasiveness, type of tissue contact, and length of usage. The more invasive and longer the usage, the more testing is required. Devices that directly contact vital tissues such as brain tissue, bone tissue, and heart tissue also require more extensive biocompatibility testing. These tests will include standard tests outlined in ISO 10993 as well as appropriate animal tests in models that show their safety.

Chief among the concerns for newer biomaterials are risks posed by the products released through degradation and leaching. As time goes on, regulatory bodies move more toward treating these releasing substances much the same way that they regulate drugs, with stricter standards and higher demands for knowledge of how the substances are absorbed, degraded, metabolized, and excreted. Risks for new biomaterials also differ depending on application, because the implantation site and duration both have large effects on the leaching and degradation properties of the material. For this reason, it is often the case that new biomaterials must undergo brand new biocompatibility testing for every new device that uses them, at least for the first couple of decades of usage. Even after that point, new applications are likely to require new biocompatibility testing, because biomaterials are not cleared or approved directly by regulatory authorities. The regulatory authorities clear and approve devices, not materials, and there is generally no guarantee that a material's performance would be the same in two different situations or device types.

One of the largest and most important sets of verification data comes from sterilization testing. Naturally, for nonsterile medical devices like tongue depressors and stethoscopes, this portion of verification testing is much abridged. For sterile devices, the four most common types of sterilization are ethylene oxide (EtO), gamma irradiation, autoclaving, and hydrogen peroxide vapor. Each sterilization method has its own benefits and drawbacks, which are built into verification testing. The largest consideration for each method is how it will affect the biomaterial. For example, as a rule, all polymers will lose some molecular weight with any of the four methods, but the exact amount depends on the chemistry of the polymer. Certain polymers, like polymeric fluorocarbons, are highly resistant to most of these sterilization types for a single cycle, whereas other polymers like many alpha-hydroxy esters would not stand up well to autoclaving at all, even for a single cycle. To verify whether the sterilization method is viable, it is necessary to track the molecular weight loss effects on the device. Tracking the effects on the device and not a coupon of the bare material is key. When materials are fashioned into devices, they go through various processing steps that will affect the condition of the material and its molecular configuration. To test the true effects of the sterilization, the device in its final form (and final packaging) must go through verification testing for sterilization.

After understanding the basic effects of the sterilization method on the biomaterial as used in a final device prototype, other aspects of sterilization become important. Certain methods of sterilization, such as EtO, can leave

residual material behind in the device, especially if the device contains an absorbent polymer. These residuals can create clinical problems later. Specifying a maximum level of acceptable residuals and then testing to ensure the device is in spec by having fewer residuals than the upper limit is another important verification step. Finally, assuring the device is truly sterile is one of the last pieces of sterilization verification. For example, **bioburden testing** is a method that measures how much bacteria reside on the surface of a device before sterilization. This helps engineers to set a sterilization dosage specification to achieve something called a **sterility assurance level**, which is the probability that one bacterial cell has survived the sterilization process, and is usually set at a probability of 1 in a million (10^{-6}). For all these processes, it is important to have consistent sterility results and products in specification for sterility, and important to remember that these processes are for devices in full final packaging, not loose individual devices. More information on this is discussed in other chapters of this book.

When conducting for verification testing, the process looks at the device when “fully loaded.” This means it includes not only the device itself, but also all the packaging and accessories that come with the device. Thus throughout the project the packaging and other accompanying components are specified via inputs that proceed through the output and verification phases. For packaging, two main aspects are the most important: **packaging integrity** and **shipping integrity**. Most packaging specifications require that a package will remain sealed and sterile over the shelf life of the device, which can be anywhere from weeks to years. Testing how the package behaves over time requires aging studies. After aging the product in an accelerated aging scenario (usually along with a concurrent real-time aging test, which of course takes longer), the package is subjected to seal strength and sterility barrier testing. These will determine how strong the package is after aging and if it has successfully excluded bacteria over the period.

Shipping integrity is slightly different, but similar in that it requires the package to remain intact; however, instead of remaining intact over long periods of time on a shelf, shipping integrity looks at conditions through which the package travels and their effects. This usually involves simulated testing of travel conditions, such as vibrations, package compression testing, and drop testing. It can also involve shipping the package from one extreme place to another, such as a location with a high- or low-temperature climate, and/or a location that is distant.

The types of verification testing discussed in this section are by no means exhaustive. Other types, such as software verification, are applicable to specific kinds of devices and are becoming more common. Additionally, more verification tasks often appear in a project due to the parallel risk management process that occurs. When a risk is determined to require mitigation, for example, the changes made to the device design needed to mitigate that risk will require verification testing.

The aim of this section is to help convey the understanding that verification testing ensures that inputs equal

outputs, and that the company can create a prototype device in spec. Overall, this involves creating one or more tests for every specification and scientifically evaluating the results to prove that the specification is met. Some companies assemble the plans for all the testing that will take place into a large document called a **verification protocol**, and then group all the resulting test reports into another large document called a **verification report**. These documents both become part of the **design history file** of the device, or the **technical documentation** if it is a device aimed at the EU market. The concept of moving from a protocol to a series of tests to a report is often repeated in other processes, as will become apparent in the discussion on design validation.

Validation of Medical Device Design

Design validation is a process to check that design inputs equal **user needs**. This reflects all the way back to the original purpose of the medical device project, to fill a clinical need by creating a device. In a specific sense, validation checks that every input that came about due to a user need is translated to one or more specifications, which are later verified and then validated as fulfilled user needs. The graphic in Fig. 3.1.5.2 is adapted from the FDA guidance document entitled “Design Control Guidance for Medical Device Manufacturers” and shows the place of validation within the larger scheme of design controls that is displayed as a “waterfall design process” to show the relationships of the processes to one another. Without validation, the manufacturer cannot be certain that it is providing what the customer is requesting or that it is meeting the need demonstrated by the market. This in turn could lead to lesser adoption of the device, and in certain cases increased risk to the patient or user.

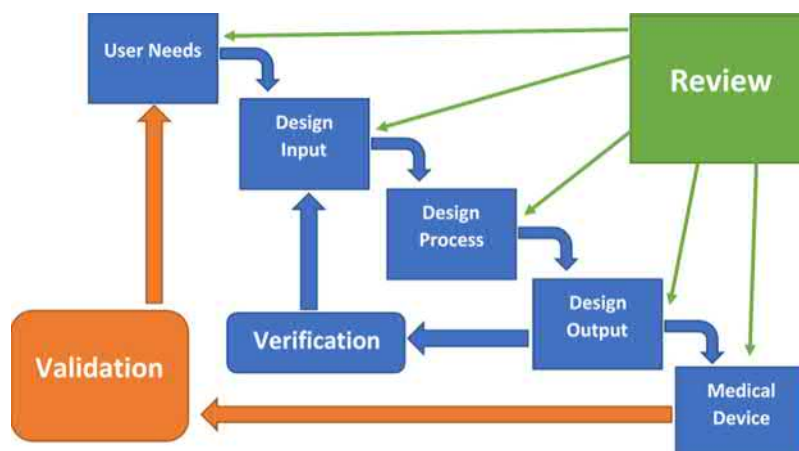
The regulatory basis of design validation follows much the same reasoning and standards as that of design verification. Validation is required as part of design controls under the QSR and is referred to in the ISO 13485 standard ([International Organization for Standardization, 2016](#)). The MDR in turn requires validation of medical devices and leaves the

choice of exactly how to do that up to the device manufacturer, which has the option to do it under a quality system based on the QSR, ISO 13485, or both. If a manufacturer decides to choose some other type of quality system, it would still need to fulfill the requirements in the MDR, which generally expects a minimum of adherence to ISO 13485. Other foreign regulatory systems require design validation in a similar fashion, often referring to the use of ISO 13485 along with additional requirements imposed differently by each country.

With a focus on connecting design inputs to user needs, design validation can take different forms and comprises different sorts of tests to achieve this. [Table 3.1.5.4](#) illustrates some common types of validation testing but is not limiting.

TABLE 3.1.5.4 Some General Types of Validation Tests

Validation Test Type	Input/Output Type
Human Factors—health Professional	<ul style="list-style-type: none"> Part compatibility or connection Product handling Office logistics Operating room logistics Ease of use Learning curve Cosmetic appearance Color coding
Human Factors—patient	<ul style="list-style-type: none"> Patient comfort Ease of use Use logistics Learning curve Cosmetic appearance Color coding
Clinical Validation	<ul style="list-style-type: none"> Clinical safety Clinical efficacy Clinical performance Clinical benefits
Software	<ul style="list-style-type: none"> Ease of use User interface specifics System compatibility Security



• **Figure 3.1.5.2** Validation's place in the waterfall design process (FDA, 1997).

The format of validation testing is also quite similar to verification testing: a **validation protocol** collects the plans and lists the experiments that will proceed. Execution of the experiments produces results that are collected in a **validation report**. Examination of the results determines if they “pass” by successfully meeting user needs or “fail” by some deficiency in the results, in which case there will need to be further dissection of the problem. Whether the testing evaluates human factors, clinical validation, or other user needs, this format is generally the same, though the extent of planning and execution will vary greatly.

Human factors testing for medical professionals addresses how much the physician and medical staff like the product. Tests involve surveys and workshops where the professionals can comment on the device and/or simulate use to give feedback. For a device to be successful, it must fit into the routines and procedures of the target customer’s operation. For a dental office, these needs differ significantly from an urban emergency room, as an example. Most devices are also geared toward a primary user, and that user is not always the physician. Nurses, technicians, and medical assistants also employ devices to do their jobs and the best practice is to give them input into the creation of these items.

Human factors testing for patients is similar but takes the perspective of the target patient population. Is the device targeted toward an older population or a younger one? Are the members of this population impaired in any way? Do they have special needs for accessing a device? Questions like these are evaluated in similar fashion with surveys and focus groups where the patients can simulate use and make comments. The logistics of using the product and the comfort the patients experience while using it are of primary importance among user needs for patients. If one or both things are lacking, patients will not comply with prescribed usage and their conditions will not receive optimal treatment.

It is extremely important when conducting human factors testing to avoid straying into the realm of clinical validation. The line between the two exists where simulated use stops and medical treatment begins. Human factors testing simply looks at comfort and measures opinions held by medical professionals and patients. It does not diagnose or treat injuries, conditions, or diseases. Crossing that line requires a clinical trial, which is another form of validation testing. Running clinical trials subjects the project to several other regulations beyond the typical QSR requirements for design controls, quality management systems, and documentation. Clinical trials are subject to 21 CFR 812 in the United States and the International Conference on Harmonization Guidelines as well as certain ISO standards like ISO 14155 outside the United States. All of these begin with some common tenets of modern clinical research: patient consent and safety.

Only devices of a certain risk level will require clinical trials in the United States (i.e., for all Class III devices and some Class II). In the European Union, all devices of Class III require a clinical trial unless they meet one of several possible exemptions listed in the regulation ([Medical Device](#)

[Regulation, 2017](#)). In general, a clinical investigation for an implantable device containing a new biomaterial would require a way of implanting the device into human patients before the device received approval by any regulatory authority. This “first in man” trial would require provisional permission for use in a limited number of patients. In the United States, an **investigational device exemption (IDE)** is a submission reviewed by the FDA to determine if the clinical trial with the new biomaterial can move forward. In addition, FDA regulations under 21 CFR 56 require **institutional review boards** to provide oversight of the clinical trial after submission of the IDE. In the European Union, notified bodies review trial proposals and competent authorities authorize the trials under relevant requirements from a board called an ethics committee, which makes determination of whether the trial can go forward and provides oversight.

It is necessary to maneuver through these regulatory hurdles because testing novel devices on human beings can carry great risk. The regulations exist to assure clinical safety and efficacy of the device. Under the FDA this is done by directly showing safety and efficacy through clinical and nonclinical data, with specific methods depending on risk level and device class. Under the MDR, devices must meet general safety and performance requirements, which take the form of a checklist that device makers must fill out for each product or product family. The individual boxes on the checklist call for more specific requirements on clinical performance, verification, validation, safety, and human factors.

Verification Versus Validation

A major difference between design verification and design validation is that not all design inputs must go through design validation. Sometimes an input does not translate directly to a user need. Instead, it may simply be there as a necessity for the device’s structure or function. For example, an input can refer to a placement of an internal screw that holds a handle in place but is unseen by any user. The resulting specification can give tolerances for the screw hole position, but that input and the accompanying spec would not need validation because they do not translate directly into a user need. They are only there to hold the device together. A user would be unlikely to care about the exact placement of the screw so long as it did not interfere with function. For validation testing documents, a brief rationale for not including any validation would suffice. Meanwhile, in the case of inputs and verification, all inputs must undergo design verification.

For the risk management process, there is a similar situation. Risk mitigations that deal directly with user needs must receive both verification and validation testing, while mitigations that do not deal directly with user needs only need verification testing. Often the most important risk data comes from clinical trials, which are part of design validation.

Concluding Remarks: Design Transfer Beyond Human Studies

Moving from benchtop through human studies is an important achievement under a project team's belt, which often takes several years. Lower-class devices tend to have shorter timelines to market because the regulatory clearance process is easier, at least in the United States. The MDR, which is still new in the European Union, is producing a shift in comparative difficulty between the European Union and the United States for placing new devices onto the market. Before the MDR, companies sought the EU market as a test bed and a quicker route to clinical use, while the United States was a more difficult but lucrative market to achieve after gaining the right to sell the product in the European Union. However, now the MDR imposes clinical evidence requirements on nearly all device types, which will require clinical trials on devices that have no prior data in the literature, in clinical registries, or in equivalent devices owned by the same company. The regulation does allow for two companies to share data on similar devices and use each other as equivalent comparators to fulfill the clinical requirements, but this is extremely unlikely to happen since most companies in this situation are competitors.

Nevertheless, this supposed ending to medical device development is just a beginning. Products spend their initial development phases under design controls, but to flourish on the market, design controls must end and production must begin. The process of transitioning from design controls to production is called **design transfer**.

The goal of design transfer is to translate all the documentation created during design controls into actionable directions and records that allow a company to manufacture the device on a larger scale. During this phase, the transfer team generates a document called a **device master record**,

which serves as an index of all the documentation needed to manufacture and distribute the device. The team also generates the first version of the **device history record**, which is a document accompanying each device, lot, or batch to help track it through the manufacturing process.

Along with these documentation tasks, the product should also receive regulatory approval around that time, which will lead to training of the sales force and launching of the product. In fact, product training and launch planning begin before receiving regulatory approval and even before design transfer in some cases, so they can be ready to go when everything comes together.

The first sales of a product kick off new phases of medical device development, such as postmarket surveillance, complaint handling, and vigilance. For medical devices, these processes are usually conditional and unique per each device clearance and approval, as dictated by the FDA, although there are definite requirements for complaint handling and adverse event reporting. In the European Union, a lion's share of the MDR deals with this postmarket phase and the requirements to track the clinical performance of a medical device not only during its development and launch, but over its entire lifetime of use both in every patient and on the market as a whole.

References

- International Organization for Standardization, 2016. Medical Devices — Quality Management Systems — Requirements for Regulatory Purposes.
- FDA, 1997. Design Control Guidance for Medical Device Manufacturers.
- Medical Device Regulation, May 2017. Official Journal of the European Union L117.
- Quality System Regulation, 2019. 21CFR820.

Chapter Study Questions

1. For each of the items listed here, determine if it is a design input or a design specification, and explain your choice.

Item	Input or Specification?	Explanation
The diameter of the catheter must be 4 ± 0.1 cm		
The catheter must be slippery enough to fit through small blood vessels of the brain		
The catheter must comply with ISO 10993 standards for biocompatibility		

Answer:

Item	Input or Specification?	Explanation
The diameter of the catheter must be 4 ± 0.1 cm	Specification	This is a specification because it is specific about a size and has a tolerance range. Inputs are generally not as specific as this.
The catheter must be slippery enough to fit through small blood vessels of the brain	Input	This is an input because it talks about a user need without giving specifics on how slippery. This input would likely translate into a specification on the coefficient of friction, with a tolerance range.

Item	Input or Specification?	Explanation
The catheter must comply with ISO 10993 standards for biocompatibility.	Input or specification	This one is tricky. Input documents often give lists of what standards the device needs to observe. In that sense, this is an input. However, the specific tests within ISO 10993 are more detailed in regard to what constitutes passing or failing. In that sense, this is a specification. A DSD may use the line just as is for the specification, or it may break each ISO 10993 test into a separate line to create multiple specifications out of this one.

2. Consider a bone plate made from a novel polymeric biomaterial. One of the specifications for this device says that the “Bone plate shall be constructed from said novel polymer with a molecular weight between 100 and 150 kDa after a standard 12-hour EtO sterilization cycle.” Describe the setup of one or more verification tests that would address whether or not the prototypes are in spec.

Answer:

The first thing to realize from this question is that it must use a sterilized prototype because it is asking for a device’s molecular weight after sterilization to be within a certain range. Any experiment created to verify this spec would need to start with a sterilization cycle called for in the spec, i.e., a “standard” 12-h EtO cycle.

Of course, sterilizing one sample is probably not a good idea. There will need to be a number of samples that show that the prototype manufacturing process can create these samples consistently in that molecular weight range. For tests like this, having 10 or more samples is a good idea. Having those samples created on different days by different people on different equipment would be a better idea.

Subjecting 10 prototype samples to the sterilization cycle and then using some method of molecular weight measurement, such as gel permeation chromatography, would be a good start. The results would look at whether all 10 samples met the spec, and if not how many failed. As a bonus, it would not be a bad idea to also include measurements of nonsterilized samples as a control to get a better clue on how much the sterilization process affects the molecular weight.

3. For each of the items listed here, determine if it is describing a verification test or a validation test and explain your choice.

Item	Verification or Validation?	Explanation
Having people wear a brace for 10 h and then filling out a survey on its comfort		
Measuring 20 specimens of a device for their length, averaging the measurements, and calculating the standard deviation of the lengths		
Running a clinical trial on a novel polymeric bone screw to determine its Kaplan–Meier survivorship at 3 years		

Answer:

Item	Verification or Validation?	Explanation
Having people wear a brace for 10 h and then filling out a survey on its comfort	Validation	This test is expressly looking at User Needs, probably based on some Design input that talked about comfort requirements

Item	Verification or Validation?	Explanation
Measuring 20 specimens of a device for their length, averaging the measurements, and calculating the standard deviation of the lengths	Verification	This test is looking at a Design specification for length, not a User Need. In general, User Needs are not concerned with tolerances and specific numerical length ranges. For a User Need, dimensions just need to be “enough to do the job.”
Running a clinical trial on a novel polymeric bone screw to determine its Kaplan–Meier survivorship at 3 years	Validation	This one is tricky. The item talks about Kaplan–Meier survivorship, which is a statistical measurement of how long the implant functions in patients before failure. That could be interpreted as a specification, but in fact this statistic is usually not a required specification for devices. Instead it is considered a user need: a device needs to be “State of The art,” meaning it needs to last as long as all the other modern devices in the industry that do the same thing. Each implant has a typical expected lifetime in the industry according to technology and patient need. Theoretically, this statistic could be listed as a device specification but then it would subject the device to a lengthy clinical trial to prove it, which would delay the device’s entry onto the market.

4. Consider polymer microspheres with a small amount of temporary radioactivity that are loaded into a syringe and injected precisely into a cancerous tumor. The microspheres are supposed to deliver high doses of intense radiation to a small area within the tumor for a limited amount of time, after which they rapidly become less radioactive and resorb to be eventually excreted through the kidneys and lungs. Contrast the verification and validation testing for such a device.

Answer:

Since verification testing checks that inputs=outputs, the verification testing of these polymeric microspheres would check all the specifications and make sure they are functional and in range. This would involve looking at the size ranges of the microspheres. The amount of radioactivity and the pace of its dropoff would also be specifications of concern.

The other important component of this device is the syringe because it delivers the microspheres. Testing the volume of injection, rate of injection, and other aspects of the syringe function would be important. It would also be necessary to make sure that the syringe material can withstand the radioactivity under storage. It would not be good if the plastic syringe became brittle and shattered after storing the device on the shelf for a few weeks!

Meanwhile, validation testing would be concerned with patient needs. Does this device perform safely? Is it efficacious? A clinical trial or perhaps multiple clinical trials would be necessary to prove how well it functions in

decreasing tumor size and/or increasing patient survival. Of course, these would all be set in the indications for use, which are not specified in this problem, nor is the type of cancer it would treat. A device like this would likely treat a specific type of cancer in a specific type of patient.

Aside from patient needs, validation would also look at physician needs, if the physician is the one injecting the treatment. How hard is it to push the plunger? How long does that take? How hard is it to attach a Luer lock to the end of the syringe if that is what the physician wants to do? Is such a thing even recommended? These questions would be answered by consulting with physicians who would use the device and collecting the results.

5. Consider a design input document that has 23 design inputs listed. How many design specifications and design outputs will that yield?

Answer:

It is not possible to tell from the number of design inputs how many specifications will wind up proliferating from them. Often, a single design input will yield multiple design specifications. A single design specification can sometimes yield multiple design outputs. A thoughtful answer to this question might be “at least 23 specifications and 23 outputs,” but that is also not always the case. Sometimes it is possible for multiple design inputs to feed into a single specification, so one specification covers more than one design input. In such a case, there could actually be fewer than 23 specifications and outputs stemming from the inputs, but it would be rare.

3.1.6

Commercial Considerations in Medical Device Development

SETH J. GOLDENBERG

Veeva Systems, Pleasanton, CA, United States

Introduction

The medical device commercialization process requires a strong team with regulatory, quality, clinical, reimbursement, and sales expertise to bring a product to market. Convincing today's stakeholders of a medical device's value is harder than it was in the past (Richards, 2015). Previously, a company could launch and sustain a medical device's market share by focusing on a few regulatory clinical endpoints, procedure-based billing, and marketing just to clinicians. Real-world clinical data were an afterthought. Today, the variety of stakeholders participating in a product's success has increased (Llewellyn et al., 2015). Stakeholders may include patients, clinicians, government regulators, hospitals, and payers such as private insurance, Medicare, and Medicaid. Each stakeholder has a unique perspective to determine a device's value (Llewellyn et al., 2015). Every stakeholder requires distinct data to make their purchasing decisions. Lastly, global marketing strategies are much more complicated than launching products restricted to the domestic market (Lee et al., 2011). Each country has its own constellation of stakeholders that must be satisfied.

Early planning to capture the data desired by all the various stakeholders is essential. This is called a value-differentiated product. It includes a detailed plan on how to create that value during the product's lifecycle. This is in contrast to a product that launches with a simple clinical claim and a one-dimensional marketing message. Companies that plan for the components of a value-oriented product from the very beginning can be rewarded with an offering that is attractive to multiple value-focused stakeholders, and lower costs to develop clinical data that go beyond regulatory claims (Hartford, 2016).

Traditional Model of Product Development

Those investing money and resources to develop an expensive medical device concept want to lower their risk, reduce the time to regulatory approval, and have the broadest

possible market commercialization for the highest possible profit margin. A survey of over 200 medical device companies estimated a total cost of US\$31 million to bring a low- to moderate-risk device (i.e., Food and Drug Administration [FDA] 510(k) product) from concept to market. Makower et al. (2010). In comparison, high-risk devices (i.e., FDA Class III Premarket Approval products) averaged US\$94 million, not including the cost of obtaining reimbursement approvals or sales and marketing-related activities (Makower et al., 2010). In addition, it was found that only one in four venture capital-funded medical technology startups ultimately found success (Makower et al., 2010).

Product development at smaller companies often follows a linear stage-gate approach as shown in Fig. 3.1.6.1. According to one report, 88% of medical technology companies fail to deliver significant return to their investors. (PWC/NVCA, 2015) < Focusing on traditional "phases" or "gates" may be one reason why this approach is failing. Companies have become hyperfocused on regulatory approval milestones without planning at the outset how they will move beyond "safe and effective" in a timely and cost-effective way.

Larger companies may have dedicated new product development (NPD) teams that develop new product plans. These teams usually incorporate a more robust consideration of the potential market, perhaps including general analyses of reimbursement, market size, and potential gaps in the market. However, the plans generated in this situation do not often detail the problem of *exactly* what to do, *exactly* when to do it, and *exactly* who does it. Without these details the product and plan may flounder due to communication issues (Medina et al., 2011). Without a detailed plan, each corporation silo is left to make decisions from the perspective of their own departmental culture and often narrowly defines processes without knowing the downstream effects of those decisions. They also have to reinvent the process each time, adding to the total time and cost (Goldenberg and Gravagna, 2018).

As software is becoming a larger part of medical devices, less traditional forms of product development are being



• **Figure 3.1.6.1** Linear stage-gate approach to medical device development. CMS, Centers for Medicare and Medicaid Services; FDA, Food and Drug Administration.

tested. Agile product development is the lead trend of new product development methodologies. This approach began in the 1970s and entails assessment of the project all throughout the product development lifecycle. One key feature of agile development is that work is conducted by the members of the product development team on a regular basis (Tan, 2016). Each round of development is called a sprint or iteration. Every aspect or phase of the development process is continuously revisited and reassessed throughout the development lifecycle (Tan, 2016). These lead to shortened development times and constant improvements, but this approach can be challenging in a regulated environment where validation is needed (Tan, 2016). It can be successful if the core regulated parts of the product are maintained where the unregulated interfaces or displays are modified more frequently.

Determining Market Opportunity

Determining market opportunity was historically done by determining overall market size and dollars spent on a product. In some cases, firms buy market assessment reports. The report is typically at a high level. A company needs to look at their total market size and their addressable market in detail, ideally from a bottom-up approach. In addition, one needs to look at the addressable market, or how much one can really capture with a new product (Kalorama Information, 2018). While market assessment reports are still a valuable process, today's need for understanding market opportunity really needs to look at the overall value a medical device is providing to the market.

If an organization has not considered how their product's value will be seen by different stakeholders in a global market, their product could fail to be successful even if it meets its clinical goals. For example, an implantable medical device that improves the cardiac output of a patient with heart failure is of clinical value, but

- Can it also lower the overall cost of care in the heart failure population for a payer like Medicare?
- Can it reduce 30-day rehospitalization rates?
- Can it improve the efficiency of clinics managing heart failure patients?
- Can it improve the quality of life for the patient?
- Will it improve or hurt the clinicians' practice and profitability?

Anticipating these potential benefits of a product can move the product from "low value" (i.e., single clinical benefit targeting single stakeholder population) to one of "high value" (i.e., diverse array of benefits targeting diverse stakeholder populations). Although it is the same product, the low-value marketing strategy is risky because it depends on adoption by a single customer (clinicians), whereas the high-value scenario spreads its risk by appealing not only

to clinicians, but also to payers, hospitals, clinics, and patients. Anticipating these benefits enables a company to plan for and collect needed data for value creation earlier in the process rather than later. Pairing the data collection for stakeholders with studies for regulatory required endpoints allows medical companies to appeal to stakeholders faster and at a fraction of the cost of doing later studies.

A medical device's potential value can be defined more broadly than the "safe and effective" bar set by governmental regulatory agencies if one considers the many stakeholders that are key to a device's success in the marketplace. How differing stakeholder populations determine value for medical devices is a topic of intense research. *ISPOR 1, ISPOR 2, Institute of Medicine (US), 2010*. However, to reach beyond the threshold of "safe and effective," we will briefly discuss general value perspectives for patients, hospitals and integrated healthcare systems, payers (private and government run), and governmental healthcare agencies (Goldenberg and Gravagna, 2018).

For patients, value may mean more choice, lower out-of-pocket costs for devices and related clinical services, and/or a better quality of life. Patients have become savvy consumers as they have online access to information (correct and incorrect) about health data. They also have online platforms to share reviews that can drive brand preferences (Brinton et al., 2013).

For hospitals and integrated healthcare systems, value may mean lower product and service costs, and fewer complications (e.g., infections, repeat hospitalizations, or long and complicated procedures). To evaluate a device, hospitals will often use documented improvements in clinical outcomes and clinical processes, and/or an analysis of the total cost of a product. The total cost analysis might consider the difficulty of its implant procedure, or clinical data on post-surgical infection rates. Hospitals have expanded the scope of a medical device's value beyond simple features and benefits to encompass the entire healthcare ecosystem affected by its use (Hartford, 2016; KASCOPE).

For payers, value may mean lower product and service costs, better health outcomes for entire patient populations, and lower overall delivery costs per patient. For certain products, payers continue to need data to support if a product is "reasonable and necessary" and how it impacts long-term patient health.

For governmental healthcare agencies, value means balancing cost with improving health service delivery and outcomes at a national scale. They evaluate this using health economics data and strategies such as alternative payments, formal value analysis, and efficiency tracking systems. NPD teams will need to anticipate these data requirements to support health economic claims (Table 3.1.6.1).

TABLE 3.1.6.1 Criteria Used to Define Medical Device Value Varies by Stakeholder

	Patients	Providers	Payers
Health outcomes	X	X	X
Choice	X		
Total cost		X	X
Out-of-pocket cost	X		
Complications	X	X	X
“Reasonable and necessary”			X

What is common among stakeholders is the need for data and communications that addresses their needs. An efficient NPD plan would secure data that supports regulation and marketing needs *before* launch. This requires that value propositions are rooted not only in regulatory clinical endpoints but also broad population-based health outcomes, clinical and procedural efficiency, and patient quality of life improvements **KASCOPE**. These data are critical to building an integrated customer engagement roadmap. NPD teams must start with this end in mind.

Medical Device Reimbursement

Reimbursement is often one of the first elements a company will consider when developing a product. Companies may assume that medical need will ensure reimbursement. However, since the Affordable Care Act (ACA) switched reimbursement from procedural to outcome based, stakeholders need more data on how the device impacts the entire healthcare ecosystem. A reimbursement strategy is often the first step that companies formulate in determining how to successfully market their product. An analysis of the current reimbursement landscape is imperative. In the current regulatory and reimbursement climate, clinical studies alone fall short of what is needed to bring in actual sales. Companies need to develop a strategy for how their product will be paid for. Coverage, coding, and payment are the three pillars of reimbursement.

The need for clinical data is a common theme in obtaining reimbursement and generating sales of a medical device. Both Class 1 data and Class 2 data are necessary. Class 1 data consist of randomized controlled trial (RCT) and Class 2 data include prospective registries, longitudinal studies, and case control studies. “Real-world” Class 2 data are becoming more valuable. While Class 1 data can provide the scientific validity of device safety and efficacy, the rigorous oversight and strict patient selection criteria are often not representative of real-world patient populations. Conducting Class 2 studies provides greater insight into the costs, benefits, and patient outcomes a new device may have. Too often, companies fail to plan for health outcomes studies. Mandated postmarket surveillance should not be the only

reason companies have for collection of postapproval data. The need for postmarket surveillance can typically be leveraged into valuable health outcomes and value proposition data if properly considered.

Coverage via a national coverage decision (NCD) or a local coverage decision will only apply to new medical procedures and technologies that are not currently defined in the regulations. An NCD applies only to a fraction of new devices and requires a significant amount of clinical data. At least one publication of an RCT is required. The FDA approval process is quite different from the process of meeting America’s Centers for Medicare and Medicaid Services (CMS) guidelines to qualify for reimbursement by insurance companies. The FDA stresses safety and efficacy, while the CMS focuses on superiority of a product relative to the gold standard. This difference makes it challenging for a company to achieve both clearance and coverage. Essentially, the FDA makes decisions on a predicate device and CMS looks for novelty. A parallel path initiative was implemented in 2011 where companies meet with the FDA and CMS to determine clinical requirements for approval and reimbursement simultaneously.

Coding is the language of CMS, private payers, facilities, and physicians. Coding translates into payment. Without a proper code, procedures and products are not paid for. Codes include information on the type of medical facility, medical professional, and medical equipment used to treat the medical issue. The majority of companies focus on coding when they do a reimbursement analysis for cleared products. Determining how and where your product fits into the coding landscape can be a complicated and sensitive matter requiring thorough analysis. Creating a new code or obtaining an add-on code for additional payment to an existing procedure is an avenue many companies pursue. This strategy can be very successful but requires a good body of clinical data, usually peer-reviewed journal publications of Class 1 (RCT) and Class 2 (prospective registries, longitudinal studies, case control studies). Notably, a new code does not always result in payment. There are numerous codes that have a value of zero.

Payment is the coup de grâce of all the hard work and effort that it took to get a product cleared for commercial sale. After coverage determination and coding hurdles have been crossed, the amount a hospital or physician practice will be paid for your product determines sales. However, successful sales strategies can come not only from reimbursement, but also from a well-defined value proposition. Under the new ACA rules, many medical devices are used as part of medical procedures that are covered by a single payment to the hospital for the procedure (via Diagnosis-Related Group or Ambulatory Payment Classification code). Hospital systems are incentivized to lower cost and improve quality to stay financially viable. Companies often create a value proposition for direct purchase of devices that reduce length of stay, readmission, and/or procedure time. Physician advocacy and clinical data are usually required to create this value proposition for the hospital.

Dissemination of data needs to be planned and carefully considered early in the product development process.

Publication planning will ensure the necessary data are released in an ethical and timely fashion while reaching your desired audience. Peer-reviewed journal publications are the preferred method of disseminating clinical data regarding a new medical device. Journal publications provide a level of credibility that cannot be realized by internal white papers. CMS, private payers, hospitals, and physicians expect data to be presented in the form of journal publications. Release of abstracts and podium presentations at medical society meetings are also valuable dissemination tools. Including publication planning, authorship considerations, and medical writing early in the process of product development will result in maximum use of clinical data. Early planning also helps determine the role of key opinion leaders and other physicians in the dissemination of data. In addition, proper publication planning can identify the key journals and conferences to effectively reach your targeted healthcare providers. Beginning this process early is crucial for success, as the type of clinical trial design and prospective data analysis performed may limit your access to top-tier journals.

The necessary relationship between physicians and medical device companies is of vital importance, but also creates additional regulatory considerations once a device is cleared for sale. Acceptance of your product within the medical community is necessary to drive sales, regardless of reimbursement. The best way to achieve broad acceptance of your device is by having your product presented at medical society meetings and outcomes data published in medical journals. To do this, you need physicians to support your data collection efforts. While physicians are not allowed to be paid for authorship, companies can pay expenses for meeting attendance, time for steering committee or advisory committee involvement, and device development work. If you are fortunate to have your product reimbursed by CMS, be aware that you are required to report all physician payments under the Sunshine Act (Hartford, 2016).

Postapproval data generation is also a new reality for most medical device companies. This can be through postmarket clinical studies that are similar to premarket studies or it can be through clinical registries. A clinical data registry records information about the health status of patients and the health care they receive over varying periods of time. Clinical data registries typically focus on patients who share a common reason for needing health care. They allow health care professionals and others to see what treatments are available, and how patients with different characteristics respond to various treatments. These “real-world” data are increasingly important to payers and even regulatory bodies (FDA, 2019). They show the true value of a product in the wild.

Securing Intellectual Property and Funding

Intellectual Property

Once a regulatory and reimbursement path has been defined, one can begin to seek investment. Prior to making

an investment, most investors will want to ensure that intellectual property (IP) is strong for the medical device. There are many types of IP protection, including trademarks, copyrights, trade secrets, and multiple types of patents (Teska, 2007). This section will cover the key parts of patents and how they impact the overall business. Before a medical device patent is considered, or any large commercial investment, an IP analysis should be done to ensure that no infringement would occur in the future (Teska, 2007). These patent costs can be high, with initial provisional patents costing up to \$10,000 and the full patent prosecution can be up to \$30,000 in many cases (Teska, 2007). There is also the cost of defending the patent and keeping it current, which can raise costs significantly. Entrepreneurs who are just starting out need to take all this into consideration, especially if they are entering a space with larger companies that employ full-time legal teams. Patents should also be filed not only in the United States, but also in the European Union and key countries where their new medical device could have commercial opportunities.

There are several patent types that can be filed in the United States and around the world. Design patents and utility patents are the most common patents that are utilized by medical device companies. A utility patent may be sought on “any new and useful process, machine, manufacture, or composition of matter” (35 US Code 101, 1959). An invention may be protected with a utility patent if it is novel, nonobvious, and useful. Subject to some exceptions, the term of a utility patent in the United States is 20 years from the earliest US filing date of any nonprovisional patent application to which the patent application claims priority (Teska, 2007). While obtaining a utility patent can be expensive, the benefits of filing are numerous. Issued patents enjoy a presumption of validity in legal proceedings. Additionally, patents can be a major source of income, as the rights to use the technology may be licensed to competitors or be kept for competitive advantage.

Design patents protect the novel ornamental features of a patented design. Like a utility patent, a design patent allows the patentee to exclude others from using the patented aspect of the product. While the utility patent term is 20 years from the filing date, the term for a design patent is 14 years from the date of issue. Most patents granted today are improvement patents. These patents protect the differences between a new product and previously existing products and services of the same kind. Improvement patents can be further broken down into “addition” or “substitution” inventions. Patents can also be issued for a new use, for example, a device was only used arterially, but now can be used in venous therapies (Teska, 2007).

In some cases, keeping the information about a technology as a trade secret can make the most sense. All patents require disclosure of how the technology works. While most companies believe that IP is best, if reverse engineering a technology is very challenging a trade secret could make the most sense. As the name suggests, trade secret law protects information that derives economic value from being “kept secret.” Under

the Uniform Trade Secrets Act, trade secrets are different from trademarks, patents, and other forms of IP in that, by their very nature, they are not disclosed to the public.

Securing Funding

Venture investment in the medical device sector was a \$5 billion industry in 2014 (Evans, 2016). The bar for new investments has increased significantly as accelerators and incubators are supporting companies to improve their pitches and coach them on what investors are looking for. Today's investors are considering total value, so products that reduce costs and improve outcomes are getting the most funding. While these investment trends will change over time, the process of raising funds has been consistent. Less complex products that go through 510(k) pathways will require fewer rounds of investment and milestones than more complex products that will need large clinical studies. The milestones and narrative to investors should reflect key points in a company's lifecycle such as prototype development, preclinical testing to show a product works as planned, initial FDA engagement for a clinical trial or testing needed to complete a regulatory submission, and finally scaling up for commercialization with manufacturing, sales, and marketing (Evans, 2016).

The first type of investors that a company will work with are angel investors. Angel investors are most often individuals (friends, relations, or entrepreneurs) who want to help other entrepreneurs get their businesses off the ground, and earn a high return on their investment. Usually they are the bridge from the self-funded stage of the business to the point that the business needs true venture capital (Evans, 2016). Angel funding can range from \$150,000 to a few million dollars. Angel investors typically offer expertise, experience, and contacts, in addition to money. Medical device companies may also seek nondilutive funding (where they retain all their equity) through government grants like the Small Business Research Initiatives from the National Institutes of Health. Small research businesses who are partnering with nonprofit organizations such as research hospitals or universities are also eligible for Small Business Technology Transfer grants.

After initial investors are convinced, companies need to begin doing preclinical or bench testing to finalize their device. This is when a "seed" investment may occur. These investments are typically directed toward product development, market research, building a management team, and a business plan. Seed-stage investors' funds will typically participate in later investment rounds with other equity players to finance business expansion costs such as sales and distribution, parts and inventory, hiring, training, and marketing.

Once the medical device is ready for final testing for FDA submission, a Series A round is likely to occur. This Series A refers to the class of preferred stock that the investors receive. It is usually the first series of stock after stock has been issued to company founders, employees, friends and family, and angel investors. These early series of investments, even

if more than one (i.e., Series A, B, and C), will be focused on reaching a regulatory and clinical milestone. This can put pressure on companies to reach these milestones, so it is crucial firms always understand the final commercial goals and do not sacrifice these for short-term gains. For example, companies frequently go for easier regulatory claims to meet investor requirements, but these claims may not allow for longer-term commercial success.

Future series of investments will be focused on what is needed for commercial success. These steps include building a sales team, investing in manufacturing to produce the product in large enough quantities and at a price point where a profit can be achieved, and in some cases postmarket clinical studies to show health economic impact beyond what was required for regulatory approval.

Commercial Operations: Sales and Marketing

Commercial success of a medical device is dependent upon a complex team from diverse backgrounds. The team should be an integrated, collaborative, flexible, cross-functional team that incorporates core strategic functions (i.e., clinical, regulatory, legal, R&D, reimbursement, engineering, sales, and marketing). Depending upon the device, additional or specialized functional areas may be needed, such as software engineering for an app-enabled smart device, or patient support/technical services if the device is consumer oriented and will require after-market care and support. Thus this core team represents all key business functions that will touch the device and the expectation is that its members are responsible for, and dedicated to, the development of the new product. They are empowered and incentivized to drive toward success efficiently. With the core team approach, the new product has a champion within each functional area to shepherd it through obstacles or translate specific operational needs that are important within the broader context of commercial success.

When developing a sales and marketing strategy, medical device companies need to determine whom the key stakeholders are who will purchase their products. This is constantly shifting. Physicians currently have less influence over which products they can use, while administrators have joined one or more group-purchasing organizations and use their combined purchasing power to make decisions and negotiate rates (Hartford, 2016). A common sales and marketing technique to communicate with the many healthcare stakeholders is a claims matrix. It also ensures medical salespeople are fully compliant about the claims that they make about a product.

Clinical claims reflect a primary clinical endpoint claim in a study, such as improving cardiac output of heart failure patients by 15%. There may also be secondary clinical claims about lower infection rates postdevice implant or reduced rehospitalization rates. The claims can also include population health outcome claims, such as reducing overall rehospitalization rate of heart failure patients by 8%.

Increasingly, economic claims are very important to purchasers. They now talk about the overall health reductions for a procedure. This will be about the cost savings or reduction in overall cost of care for patients. They can also take the form of efficiency claims, where more patients can be treated in the same amount of time or with the same amount of staff.

Procedural claims can touch not only on the speed of a procedure, but also on safety. Now that hospitals are increasingly required to pay for the whole lifecycle of a treatment, readmittance, infection rates, or other improved safety measures have a clear financial impact. Devices that allow for more accurate procedures are also appealing to decision-makers.

The largest increase in claims that can support sales and marketing are patient quality of life claims. Patient advocacy groups, insurers, and healthcare providers are all making decisions about which products to use based on quality of life (QOL) data. While these studies may have significant variability between patients, capturing these data during other studies can be very important for commercial success (Doward et al., 2010). QOL data capture patient compliance with a therapy and also speak to the patient's ability to enjoy normal life activities.

Summary

Having a detailed plan for data collection is an essential part of the medical device development process. There are many good reasons to consider what each stakeholder values early on. It is more economical and time efficient to plan for Class 2 data collection during the regulatory process and postapproval monitoring. Providing data to back up economic and QOL claims, in addition to clinical outcomes, provides a product that is attractive to investors and decision-makers. This gives a new medical device the best chance of commercial success.

References

- 35 US Code 101- Invention Law, July 1959. 66 Stat. 797.
- Brinton, T., Kurihara, C., Camarillo, D., et al., 2013. September. Outcomes from a postgraduate biomedical technology innovation training program: the first 12 years of Stanford Biodesign. *Ann. Biomed. Eng.* 41 (9), 1803–1810.
- Doward, L.C., Gnanasakthy, A., Baker, M.G., 2010. Patient reported outcomes: looking beyond the label claim. *Health Qual. Life Outcomes* 8, 89. <https://doi.org/10.1186/1477-7525-8-89>.
- Evans, R., June 2016. Starting a Medical Device Company: Everything You Need to Know. Source: <https://www.medicaldesignandoutsourcing.com/everything-ever-wanted-know-starting-medical-device-company/>.
- FDA, February 2019. Real world evidence. Source: <https://www.fda.gov/scienceresearch/specialtopics/realworldevidence/default.htm>.
- Goldenberg, S.J., Gravagna, J., 2018. A real-world perspective: building and executing an integrated customer engagement roadmap that bridges the gaps in traditional medical device development processes. *J. Med. Mark.* 16 (2), 41–49.
- Hartford, J., April 7, 2016. How to Win over the Hospital Value Analysis Committee: Two Experts Weigh in on what it Really Takes to Get Your Medical Device in the Hands of Providers Today. *Medical Device Business*. Source: <http://www.mddionline.com/blog/devicetalk/how-win-over-hospital-value-analysis-committee-04-07-16>.
- Institute of medicine (US) roundtable on value & science-driven health care. In: Yong, P.L., Olsen, L.A., McGinnis, J.M. (Eds.), 2010. *Value in Health Care: Accounting for Cost, Quality, Safety, Outcomes, and Innovation*. National Academies Press (US), Washington (DC). 2, Stakeholder Perspectives on Value. Source: <https://www.ncbi.nlm.nih.gov/books/NBK50926/>.
- ISPOR. Diversity in medical devices, stakeholders and their perception of value: An ISPOR Medical Devices and Diagnostics Special Interest Group Report, Part 1. Source: https://www.ispor.org/sigs/Diversity_in_medical_devices-stakeholders-perception-of-value-p1.pdf. (Accessed on 31 January 2018).
- ISPOR. Generating Appropriate and Reliable Evidence for the Value Assessment of Medical Devices: An ISPOR Medical Devices and Diagnostics Special Interest Group Report, Part 2. Source: https://www.ispor.org/sigs/Generating_Appropriate_and_Reliable_Evidence_for_the_Value_Assessment_of_Medical_Devices_Part_2-DRAFT.pdf. (Accessed on 31 January 2018).
- Kalorama Information, February 2018. 6 Steps for Determining Market Size in the Healthcare Sector. Source: <https://www.kaloramainformation.com/Content/Blog/2018/02/09/6-Steps-for-Determining-Market-Size-in-the-Healthcare-Sector>.
- Lee, Y., Lin, B., Wong, Y., Calantone, R.J., 2011. Understanding and managing international product launch. *J. Prod. Innov. Manag.* 28, 104–120. <https://doi.org/10.1111/j.1540-5885.2011.00864.x>. Source: <https://onlinelibrary.wiley.com/doi/10.1111/j.1540-5885.2011.00864.x>.
- Llewellyn, C., Podpolny, D., Zerbi, C., January 2015. Capturing the New 'Value' Segment in Medical Devices. Source: <https://www.mckinsey.com/industries/pharmaceuticals-and-medical-products/our-insights/capturing-the-new-value-segment-in-medical-devices>.
- Makower, J., Meer, A., Denend, L., November 2010. FDA Impact on US Medical Technology Innovation. A Survey of Over 200 Medical Technology Companies. Source: http://www.medtecheurope.org/sites/default/files/resource_items/files/01112010_FDA%20impact%20on%20US%20medical%20technology%20innovation_Backgrounder.pdf.
- Medina, L., Wysk, R., Kremer, G., 2011. A review of success factors in NPD: medical device domain. In: 61st Annual IIE Conference and Expo Proceedings. Source: https://www.researchgate.net/publication/258022519_A_Review_of_Success_Factors_in_NPD_Medical_Device_Domain.
- Pass or Fail: Why Value Analysis Committees Matter and What They Look for in Medical Device Design. *Kaleidoscope*. Source: <http://kaskope.com/pass-or-fail-why-value-analysis-committees-matter-and-what-they-look-for-in-medical-device-design-2/>. (Accessed on 6 September 2017).
- PriceWaterhouseCoopers/National Venture Capital Association (PWC/NVCA), 2015. "Medical Devices and Equipment," Money Tree Report, Q4 2014. data provided by Thomson Reuters, at <http://www.pwcmoneytree.com>.
- Richards, L., January 2015. Medical Devices and HEOR: Positioning Yourself to Meet Payor Needs in 2015. Source: <https://www.pm360online.com/medical-devices-and-heor-positioning-yourself-to-meet-payer-needs-in-2015>.
- Tan, J., February 2016. Using Agile Product Development Management to Improve Medical Device Development. *Medical Device Online*. Source: <https://www.meddeviceonline.com/do/how-agile-project-management-can-improve-your-medical-device-development-0001>.
- Teska, K., October 2007. Patent Savvy for Managers: Spot & Protect Valuable Innovations in Your Company. *Nolo*.

Student Questions

1. What are some of the recent changes that affect the success of a new medical device?
2. What are some of the differences between linear development and agile product development?
3. Give an example of Class 1 and Class 2 data.
4. How do medical device companies fulfill different stakeholder needs?
5. What are some of the skills needed for a successful product development team?
6. Can you speculate how product development for emerging markets might differ from the product development process in developed markets?
7. Explain the differences between FDA approval and CMS approval and how it affects the success of a medical device.
8. During which stages of development does a company secure funding for their idea?
9. What are the four marketing claims a product can make? Which do you think is the strongest?

3.1.7

Regulatory Constraints for Medical Products Using Biomaterials

ELAINE DUNCAN^{1,2}

¹Paladin Medical, Inc., Stillwater, MN, United States

²Joseph Halcomb III, MD. Department of Biomedical Engineering, College of Engineering, University of Kentucky, Lexington, KY, United States

Introduction and History in the United States

The Congress of the United States of America was determined to introduce control over medical device safety in response to various notorious medical device calamities, but the Dalkon Shield¹ can be credited for galvanizing action in the early 1970s. According to a historical account of medical device legislation produced by the US Food and Drug Administration (FDA),² it was not until the Federal Food, Drug and Cosmetic (FD & C) Act of 1938, when a definition of a medical device was added to the existing law, did the FDA have any authority to “bring charges in court” against a defective medical device. It was not until the 1976 Medical Device Amendments to the FD & C Act that the FDA was given explicit oversight of new devices entering the market. The “risk-based” structure of these regulations is attributed to the work of the Cooper Committee organized when President Richard Nixon endorsed medical device legislation. The Cooper Report recommended three categories of devices: (1) those “so well recognized as safe and effective” that neither standards nor premarketing approval was needed, (2) those that could be regulated by standards, and (3) those “new and unproven critical devices that are at the leading edge of technological innovation and biomedical explorations” and that require

premarketing review.³ Committees were formed from representatives on the basis of certain clinical specialties who essentially voted on the designation of risk classification within their respective clinical specialty. When finalized the 1976 Medical Device Amendments established the authority of the FDA to:

- Provide reasonable assurance of the safety and effectiveness of medical devices;
- Authorize the FDA to ban devices;
- Create a three-class, risk-based classification system for all medical devices;
- Establish the regulatory pathways for new medical devices to get to market:
 - Premarket approval (PMA);
 - Premarket notification (510(k)) for devices that were not on the market prior to May 28, 1976, or had been significantly modified;
 - Creation of the regulatory pathway for new investigational medical devices to be studied in patients (Investigational Device Exemption [IDE]);
- Establish several key postmarket requirements:
 - Registration of establishments and listing of devices with the FDA;
 - Good manufacturing practices (GMPs);
 - Reporting of adverse events involving medical devices.

Global Premarket Assessment Methods

The outcome of the FDA regulation established a scheme of device classification that reflected knowledge of certain devices at the time of classification but did not necessarily represent a

¹ Dalkon Shield was a contraceptive intrauterine device developed by the Dalkon Corporation and marketed by the A.H. Robins Company. Many accounts attribute the adverse events of septicemia to a porous, multifilament string upon which bacteria could travel into the uterus of users.

² Medical Device and Radiological Health Regulations Come of Age, FDA Consumer magazine, The Centennial Edition/January–February 2006 by Carol Rados: <https://www.fda.gov/downloads/AboutFDA/WhatWeDo/History/ProductRegulation/UCM593521.pdf>.

³ Institute of Medicine (US) Committee to Study the Use of Advisory Committees; Rettig R.A., Earley L.E., Merrill R.A., editors. Washington (DC): National Academies Press (US); 1992: <https://www.ncbi.nlm.nih.gov/books/NBK236081/>.

logical hierarchy of risk analysis or a method to guide future device classification. Not until the introduction of the European Medical Devices Directive⁴ was there a medical device classification following a formal hierarchal “risk-based” system reflecting the vulnerability of the human body and taking account of the potential risks associated with the devices in their intended use. This approach allowed the use of a set of criteria, combined in various ways to determine classification, e.g., duration of contact with the body, degree of invasiveness, and local versus systemic effect, to have overriding influence on the regulation of the device. As medical device technology and subsequently knowledge of risks associated with medical devices have changed, Europe has revised the regulations, now known as Medical Device Regulations (MDRs),⁵ and increased the number of classification “rules” from 18 to 22, including a separate “rule” for devices incorporating or consisting of nanomaterial.

Regulators throughout the world have sought harmonization of MDRs, yet the major jurisdictions continue to apply different methods to assess the risk of medical devices with biomaterials. To appreciate the similarities and differences between US and EU classification methods of a biomaterial used as a medical device, the difference in classification and quality control scheme for Gutta-Percha, one of the oldest known implantable biomaterials, should be examined. According to US FDA 21 CFR 872.3850, Gutta Percha points are made from coagulated sap of certain tropical trees. The Gutta Percha point is softened by heat and inserted into the root canal where it hardens as it cools. Gutta Percha points are Class I in the US FDA regulations and not considered an implant. They are not subject to premarket clearance (510(k)) but are subject to quality systems and thus potential FDA manufacturing inspection. In contrast, under the European Medical Device Directives classification, Gutta Percha points follow Rule 8 because these are surgically invasive, long-term use, implantable devices. However, since these are put in teeth (rather than any other part of the body) this device has a lower Class IIa designation (considered a medium risk device). The IIa category in the European Union requires verification of a quality system by a notified body, compliance with ISO 10993 for biocompatibility testing prior to CE marking. Although arrived at differently, the historic use of the material and its accepted safety have allowed the material to be subject to moderate controls in both jurisdictions although the regulatory threshold in the European Union is much more expensive and elaborate. Some patients could react to the natural latex component of the material and at least one study has found some versions of the material to be mildly toxic, apparently due to inorganic fillers.⁶

A brief survey of the regulatory schemes of a few of the World Biomaterial countries find similar risk-based structures

for medical device marketing authorizations, although any specific device may carry a slightly different classification and thus different premarket challenges. For example, in Japan’s system, Class I devices only require registration via the Todokede process; most Class II devices, and a few Class III devices, follow the Ninsho pathway but Class II products that do not hold, or comply, with the Ninsho Certification Standard can be approved via the Shonin pathway. Most Class III devices and Class IV devices require the Shonin process.

According to the Canadian Guidance⁷ the following indicators of risk posed by a given device were used to create the Canadian classification rules: degree of invasiveness, duration of contact, body system affected, and local versus systemic effects. The risk classification system takes into consideration the duration of use of a medical device. The use of a medical device is either long term or not. Long-term use implies continuous use for a period of 30 or more days. Continuous use is understood to be uninterrupted use for the intended purpose.

The Therapeutic Goods Administration of Australia also maintains a risk-based method for medical device assessment and has been open to recognizing many aspects of prior review by originating country regulatory authorities. At this writing the Australian Regulatory Guidelines for Medical Devices are under review and some components have been superseded by new guidance or regulatory amendments.

For the United Kingdom, BREXIT⁸ has opened a chasm of uncertainty for medical device regulatory authority. The United Kingdom previously had its own medical device regulatory process before adopting the EU regulations and can again if an agreement cannot be reached. A US company with a CE mark issued by a notified body chartered in the United Kingdom may wonder what will happen to their permission to market. The UK-based notified bodies are working to help develop a suitable mechanism to provide the United Kingdom with continuity of access to the wider EU trade area after the transition period. It is estimated that 70% of non-EU-based manufacturers use UK notified body services as a springboard into the European Union.⁹

Toss into this Shepard’s Stew the major change to the EU MDR that was published in the Official Journal of the European Union on May 5, 2017. This new regulation¹⁰ will consolidate two existing legal provisions and replace both the current Medical Device Directive (93/42/EEC) and the Active Implantable Medical Device Directive (90/385/EEC). It takes effect on May 26, 2020 unless there is an extension.

Global medical device regulations are complex and ever changing. Cultural differences and differences in

⁴Medical Devices Directive 93/42/EEC and some high-risk implantable products followed the Active Implantable Medical Devices Directive 90/385/EEC.

⁵https://ec.europa.eu/growth/sectors/medical-devices/regulatory-framework_en.

⁶Elizeu A. Pascon, DDS, MSD, Larz S.W. Sponberg, DDS, PhD. In vitro cytotoxicity of root canal filling materials: *I. Gutta-percha*, The American Association of Endodontists, Volume 16, Issue 9, Pages 429–433, September 1990.

⁷<https://www.canada.ca/en/health-canada/services/drugs-health-products/medical-devices/application-information/guidance-documents/guidance-document-guidance-risk-based-classification-system-non-vitro-diagnostic.html#a21>.

⁸<https://www.bbc.com/news/uk-politics-32810887>.

⁹<https://pharmaintelligence.informa.com/resources/product-content/uk-notified-body-bsi-sets-out-clear-post-brexite-paths-as-it-goes-dutch>.

¹⁰Regulation (EU) 2017/745 of the European Parliament and of the Council of 5 April 2017 on medical devices, amending Directive 2001/83/EC, Regulation (EC) No. 178/2002 and Regulation (EC) No. 1223/2009 and repealing Council Directives 90/385/EEC and 93/42/EEC.

perception of acceptable risk make a major impact on the regulation of medical devices and thus the scrutiny given to biomaterials-based devices. When a country has perceived unfavorable past experiences with experimental medical devices or when a country aligns with a regional regulatory group, even established medical devices may undergo more rigorous premarket review. The most important point is that when a medical device is brought to a different country with different medical practices and stakeholders (different “voices of the customer”) where there may be different support structures, e.g., health insurance schemes, determining that the device is safe and effective may be assessed with different criteria.

Premarket Assessment Requirements

Developing a medical device dependent upon biomaterials requires a series of assessments that must start early. Design control and review requirements were ushered in with the Safe Medical Devices Act of 1990 with modifications to the Quality System Regulations 21 CFR 820, formerly known as Good Medical Practices. These rules require that the development team produce certain elements that include a project plan, periodic reviews, design inputs and outputs, and documented verification and validation of the product. An early hazard analysis and risk assessment is crucial to developing a safe medical product and for proper risk management over the lifecycle of the device. As product inputs are established, assessing the potential hazards of the new product, should the device fail to meet the design requirement is the bedrock of premarket assessments.

Risk analysis worksheets will guide the developer to the proper risk mitigations and the criticality of those mitigations. There are many examples of how the various standards work hand in hand with medical device risk mitigation, but the two most important assessment processes for a device with biomaterials are the ISO 10993 Part 1 and ISO 14971. These two standards help to guide the biological risk assessments necessary for development of a safe medical device. ISO 10993 and all its various parts establish a baseline for the assessment of biocompatibility. But standardized toxicity assays do not supplant the need to understand *in vivo* device performance.

Understanding the performance of a biomaterial in a medical device, particularly when the biomaterial is the medical device, will necessarily involve an understanding of actual performance of the product “*in life*.” It may be possible to incorporate standardized protocols from the ISO 10993 recommended assays with the “*in-life*” testing of the device in an animal performance model, but the specific goal in a large animal model is to model device function, not just tissue compatibility. Frequently referred to as “preclinical” studies, device studies in a functional animal model must be carried out following many regulations (21 CFR Part 58), standards, and guidance documents. In fact, the data from these animal studies may be audited by the FDA when the data are pivotal for demonstrating device safety. As part of a sound scientific study, a protocol for the conduct of the study and the postmortem analysis of specimens must be carried out by well-trained and

knowledgeable experts under strict rules controlling traceability of specimens. A performance study for a new material for an implantable heart valve, for example, could involve a number of large animals implanted with the valve and serial sacrifice to examine the mechanical behavior of the valve and any thrombotic sequelae downstream. In contrast, prior to the pivotal performance study, exhaustive extraction studies of the valve materials under ISO 10993 would ensure that construction materials and material preparation processes do not introduce unexpected toxic elements, which could affect tissue healing at the sewing cuff or blood compatibility of the leaflets.¹¹

Device failure analysis should be considered as part of the premarket assessment to arrive at potential hazards that might harm the patient as the device may age *in vivo* and also when the device is subjected to sudden loads or stresses. History has shown that the potential that wear particles could be released, that coatings could delaminate, or that surface passivation might not be sufficient to preclude release of toxic metals are all typical biocompatibility concerns associated with implanted biomaterials but which require mechanical testing to help to determine how the device performs over time.

Design verification is a term associated with the process that a device manufacturer will undertake to assure that certain design requirements have been met. Devices to be delivered sterile to the operating theater must undergo sterilization validation following approved methods and standards, but it is also necessary to assure that the sterilization process did not affect the performance of the device or affect the biocompatibility of the materials. For new packaging systems or new devices in existing packaging systems, standardized ship testing is required to ensure the device arrives intact and the contents are still sterile. Standardized test methods abound and are too numerous and diverse to include in this discussion, but medical device manufacturers routinely turn to recognized and standardized test methods for safety evaluation. Discussed elsewhere in more detail, systematic assessment to ensure the device can perform as intended is a basic requirement in all regulatory jurisdictions.

Design validation typically focuses on those product attributes that cannot be verified. Validation techniques are also used to assess whether or not the device has met its user needs. This may take the form of usability assessment but can involve cadaver studies (for example, to ensure surgeons can use instrumentation to properly place an implant) and could involve simulation testing with animals or phantoms. In other circumstances, full design validation will require a clinical study. The typical difference between a validation study and verification testing is the scope of the evaluation; validation should always be planned through a detailed, preapproved protocol, and may involve several assays in series to fulfill the validation requirements.

Discussion of clinical trial design is beyond the scope of this chapter, but such trials when required are complex, require one or more protocols, and require compliance with numerous regulations, guidance documents, and standards. When planned properly the clinical trial can provide data to support

¹¹ ISO 5840 Parts 1 and 2.

the safety and effectiveness of the device and provide physician and patient satisfaction information. For the United States, clinical trials are subject to FDA regulation 21 CFR 812, even if the study is considered “nonsignificant risk” (NSR). The difference between a significant risk study and an NSR trial is that the NSR study does not require prior FDA application, known as an IDE. All studies, regardless of risk category, require Institutional Review Board oversight and approval of the informed consent for participating subjects. Implanted devices are subject to IDE application, which must assure that risks to patients in the study are clearly defined and balanced by the benefit to the patient. Even the best clinical trials cannot anticipate all real-world potential hazards, particularly once the device moves beyond the idealized clinical trial environment. Recognition that implanted devices and novel medical materials may require long-term surveillance has pushed regulators to attempt to implement more active surveillance methods, including postmarket studies and device registries.

Instructions for use and certain diagnostic technology differences should be considered before launching a new device in a different country to assure the device can be deployed for the proper indication for use. Implanted medical devices seeking approval in the European Union will be required to present clinical data prior to awarding the CE mark. It is not uncommon that certain regulatory jurisdictions will require at least one clinical study to be conducted within the country or associated countries prior to granting market approval.

For US premarket applications, suppliers of biomaterials have begun to take advantage of a provision known as a Device Master File (MAF). Although not an approval mechanism, the MAF has enabled a mechanism whereby the biomaterial supplier (including component suppliers) can provide confidential material formulations and manufacturing methods for review by the FDA but not disclosure to the premarket review applicant. Such information as the chemistry of processing aids and cleaning methods are often proprietary and the FDA recognizes that disclosure of these proprietary methods even to a customer can be detrimental to business. To allow the FDA to access the supplier’s Master File, the applicant receives permission from the supplier by way of a letter that is provided to the FDA identifying the MAF by number and which sections are appropriate for the review. A MAF might include material composition, biocompatibility test reports, reports concerning degradation by-products, effects of sterilization, and general quality controls for material production.

Premarket Clearance and Approvals

As previously discussed, the 1976 Medical Device Amendments to the FD & C Act gave the FDA explicit oversight of new medical devices entering the market. The law established the regulatory pathways for new medical devices (devices that were not on the market prior to May 28, 1976 or had been significantly modified) to get to market. With the evolution of technology and the difficulty of

determining that a device was on the market prior to 1976, the regulations were again modified in 1990 to clarify:

For purposes of determinations of substantial equivalence ... the term “substantially equivalent” or “substantial equivalence” means, with respect to a device being compared to a predicate device, that the device has the same intended use as the predicate device and that [FDA] by order has found that the device—

- (i) has the same technological characteristics as the predicate device, or
- (ii) has different technological characteristics and the information submitted that the device is substantially equivalent to the predicate device contains information, including clinical data if deemed necessary by [FDA], that demonstrates that the device is as safe and effective as a legally marketed device and
- (iii) does not raise different questions of safety and efficacy than the predicate device.

Little by little, clarifications and guidance documents attempted to make it clear that *new* devices are Class III unless the foregoing provisions can be established. But then it made little sense to make *all new* medical devices Class III and thus require full PMA applications if the devices were simply not substantially equivalent to an existing device, but which were otherwise moderate risk. The *de novo* determination was crafted to allow low to medium risk devices to be reviewed by the FDA without the full and formal processes associated with a PMA application. Gradually, guidance documents evolved,¹² and as new devices have been cleared under the *de novo* process, more modern technologies have entered the market without full PMA applications.

As already stated, the PMA process for a new medical device is typically necessary to evaluate the safety and effectiveness of Class III medical devices.¹³ PMA is the FDA process for scientific, clinical, and regulatory review. Class III devices are those that support or sustain human life, are of substantial importance in preventing impairment of human health, or which present a potential, unreasonable risk of illness or injury. The review of a PMA application is a four-step review process consisting of administrative and initial scientific review by FDA staff to determine completeness (acceptance and filing reviews), in-depth scientific, regulatory, and quality system review by appropriate FDA personnel (substantive review), review and recommendation by the appropriate advisory committee (clinical panel review), and final deliberations, documentation, and notification of the FDA decision. There are many elements to a PMA and the review can require years. Clinical data to support the efficacy of the new device are necessary, although the FDA has made provisions for acceptance of clinical data from outside the United States.

¹² <https://www.fda.gov/downloads/MedicalDevices/DeviceRegulationandGuidance/GuidanceDocuments/ucm080197.pdf>.

¹³ <https://www.fda.gov/MedicalDevices/DeviceRegulationandGuidance/HowtoMarketYourDevice/PremarketSubmissions/PremarketApprovalPMA/default.htm>.

Prior to the changes proposed for the new European MDRs to take effect in 2020, it was possible to draw parallels between the approval process for a “me-too” (Class II) device for the US market and to obtain the CE mark for most IIa and IIb devices in Europe. For both jurisdictions, moderate risk devices put forth general safety information such as standardized testing and labeling for the product. Documentation in the Technical File for the European Union was similar to the content in the 510(k). As the requirements for the MDRs begin to take shape it is possible that the differences between the two systems will increase. The FDA has made it clear that the scrutiny of new medical devices in the United States will also undergo changes.¹⁴ The FDA stated the desire to see that new devices that come to market under the 510(k) pathway should account for advances in technology and meet modern safety and performance criteria. FDA’s Center for Devices and Radiological Health has leveraged the risk-based paradigm and wants to adopt a more modern process. It is clear that the new medical device review process for so-called “me-too” devices will undergo drastic changes in both of the two largest markets for medical devices. At least some of this impetus for change has been motivated by public criticism that the FDA has allowed older technology to be used in new applications without the proper level of scrutiny. Some of those devices have been biomaterials-based devices.

Medical device manufacturers face significant testing and controls when biomaterials play a major role in their function. There are fewer available medical-purposed materials at higher costs and most that are available have been known in the market 20 years or even much longer. Even attempts at tissue-engineered devices gravitate to known biomaterials for their substrates. With fewer materials to work with, device manufacturers attempt to improve performance by modifying the existing materials with chemicals and processes (including drugs and texturing), which then may require more biocompatibility testing. Even minor differences in clinical applications may require clinical trials if the material is used in a new intended use, raising concerns that new risks may lurk within the new application. Advancing technology for testing can detect extracted chemicals at lower and lower thresholds, which can cause anxiety, where before there was no perception of risk. And, of course, the cost of doing any testing continues to rise while the health care delivery industry is constrained by cost controls and risk reduction. In fact, it can sometimes be many years after the FDA approves a new product that a health care third-party payor (insurance company) will reimburse for the use of the device in the operating room. Yet the world is now faced with an aging population with increasing demands to remain not only mobile but physically active. The increasing demand for better medical products is worldwide, even as each emerging market seeks to ensure that their constituents do not become the practice field for emerging technologies and experimental materials.

¹⁴<https://www.fda.gov/newsevents/newsroom/pressAnnouncements/ucm626572.htm>.

Manufacturing and Material Supplier Controls

For several decades global regulatory specialists have sought a harmonized approach to quality systems management of manufacturing and material supplier controls. Although idealized as an international quality system, ISO 13485 has struggled for universal adoption. One reason has been the constraint of the US FDA to maintain the 21 CFR 820 regulation as the quality system for US medical devices.

As of this writing the US FDA has posted a “regulatory agenda” under RIN:0910-AH99 titled “Harmonizing and Modernizing Regulation of Medical Device Quality Systems,”¹⁵ which states:

FDA intends to harmonize and modernize the Quality System regulation for medical devices. The revisions will supplant the existing requirements with the specifications of an international consensus standard for medical device manufacture, ISO 13485:2016. The revisions are intended to reduce compliance and recordkeeping burdens on device manufacturers by harmonizing domestic and international requirements. The revisions will also modernize the regulation.

Because ISO 13485 is a copyrighted standard it is difficult to imagine the mechanism of adoption because this would supplant a public regulation with a commercial standard. Furthermore, the standard is scheduled to be revised every 5 years and reissued, subject to change by delegates to the ISO over whom neither Congress nor the FDA will have any control.

For the present time, developers of medical products using biomaterials based in the United States are required by law to conform to 21 CFR 820. Compliance with this regulation is self-determined with the FDA conducting audits on site on a no-fee basis (other than the annual registration and listing fee). Thus startup companies and those not immediately seeking an international marketplace are prudent to develop their initial internal quality procedures in alignment with FDA regulations.

Comparing and contrasting ISO 13485:2016 to US FDA CFR 820 for the means to maintain manufacturing and materials controls gives an insight into the difference in approach but similarities of requirements. (This comparison is limited to these specific subtopics and do not represent a complete comparative analysis of the two quality systems.) Because the two programs have approached the organization of quality information differently, one should be familiar with the entirety of both quality program structures before attempting to create a harmonized internal compliance system. Neither quality system approach would appear to have a better method for materials control than the other. Both take turnabout with more or less detail on how to fulfill the quality objective. A side-by-side analysis gives the best illustration of how these two systems differ and correspond (Tables 3.1.7.1 and 3.1.7.2).¹⁶

¹⁵<https://www.reginfo.gov/public/do/eAgendaViewRule?pubId=201804&RIN=0910-AH99>.

¹⁶https://www.nsf.org/newsroom_pdf/nsf_md_21_cfr_820_iso_13485_2016.pdf.

TABLE 3.1.71 Manufacturing Controls (Does not Include Environmental and Equipment Controls)

21 CFR § 820	US Quality System Regulation	Corresponding ISO 13485:2016	Differences
820.70(a) Production and Process Controls, General	Each manufacturer shall develop, conduct, control, and monitor production processes to ensure that a device conforms to its specifications. Where deviations from device specifications could occur as a result of the manufacturing process, the manufacturer shall establish and maintain process control procedures that describe any process controls necessary to ensure conformance to specifications. Where process controls are needed, they shall include: <ol style="list-style-type: none"> (1) Documented instructions, standard operating procedures (SOPs), and methods that define and control the manner of production; (2) Monitoring and control of process parameters and component and device characteristics during production; (3) Compliance with specified reference standards or codes; (4) The approval of processes and process equipment; and (5) Criteria for workmanship which shall be expressed in documented standards or by means of identified and approved representative samples. 	7.5.1 Control of production and service provision	In this clause, ISO 13485:2016 specifies requirement that may align with other 21 CFR § 820.70 requirements beyond 21 CR 820.70(a). For example, in clause 7.5.1, ISO 13485:2016 specifies “b) qualification of infrastructure”; whereas, this requirement appears in “820.70(f) Buildings” of 21 CFR § 820.
820.70(b) Production and Process Changes	Each manufacturer shall establish and maintain procedures for changes to a specification, method, process, or procedure. Such changes shall be verified or where appropriate validated according to 820.75, before implementation and these activities shall be documented. Changes shall be approved in accordance with 820.40.	4.1.4 Quality management system	No significant difference in requirements.
820.75(a) Process Validation	Where the results of a process cannot be fully verified by subsequent inspection and test, the process shall be validated with a high degree of assurance and approved according to established procedures. The validation activities and results, including the date and signature of the individual(s) approving the validation and where appropriate the major equipment validated, shall be documented.	7.5.6 Validation of processes for production and service provision 7.5.7 Particular requirements for validation of processes for sterilization and sterile barrier systems	21 CFR § 820 specifies the documentation of the date and signature of the individual(s) approving the validation.
820.75(b) Process Validation	Each manufacturer shall establish and maintain procedures for monitoring and control of process parameters for validated processes to ensure that the specified requirements continue to be met. Each manufacturer shall ensure that validated processes are performed by qualified individual(s). For validated processes, the monitoring and control methods and data, the date performed, and, where appropriate, the individual(s) performing the process, or the major equipment used shall be documented.	8.2.5 Monitoring and measurement of processes	ISO 13485:2016 clause 8.2.5 specifies the expectations for monitoring and measurement of processes. 21 CFR § 820 specifies that the monitoring and control methods and data, the date performed, and individual(s) performing the process, or the major equipment be documented.
820.80(e) Acceptance Records	Each manufacturer shall document acceptance activities required by this part. These records shall include: The acceptance activities performed; the dates acceptance activities are performed; the results; the signature of the individual(s) conducting the acceptance activities; and where appropriate the equipment used. These records shall be part of the DHR.	4.2.5 Control of records 7.1 Planning of product realization 8.2.6 Monitoring and measurement of product	Although both require records, 21 CFR § 820 specifies specific record content requirements.

TABLE 3.1.7.2 Provisions for Materials Control

21 CFR § 820	US Quality System Regulation	Corresponding ISO 13485:2016	Differences
820.50(b) Purchasing Data	Each manufacturer shall establish and maintain data that clearly describe or reference the specified requirements, including quality requirements, for purchased or otherwise received product and services. Purchasing documents shall include, where possible, an agreement that the suppliers, contractors, and consultants agree to notify the manufacturer of changes in the product or service so that manufacturers may determine whether the changes may affect the quality of a finished device. Purchasing data shall be approved in accordance with 820.40.	7.4.2 Purchasing information	ISO 13485:2016 specifies “The organization shall ensure the adequacy of specified purchasing requirements prior to their communication to the supplier.” ISO 13485:2016 specifies “To the extent required for traceability given in 7.5.9, the organization shall maintain relevant purchasing information in the form of documents (see 4.2.4) and records (see 4.2.5).”
820.60 Identification	Each manufacturer shall establish and maintain procedures for identifying product during all stages of receipt, production, distribution, and installation to prevent mix-ups.	7.5.8 Identification	ISO 13485:2016 specifies more detailed requirements, including the documentation of procedures to ensure medical devices returned to the organization are identified and distinguished from conforming product.
820.65 Traceability	Each manufacturer of a device that is intended for surgical implant into the body or to support or sustain life and whose failure to perform when properly used in accordance with instructions for use provided in the labelling can be reasonably expected to result in a significant injury to the user shall establish and maintain procedures for identifying with a control number each unit, lot, or batch of finished devices and where appropriate components. The procedures shall facilitate corrective action. Such identification shall be documented in the DHR.	7.5.9 Traceability 7.5.9.1 General	ISO 13485:2016 requires procedures for traceability based on regulatory requirements. 21 CFR § 820 specifies the types of devices that require traceability.
820.70(e) Contamination Control	Each manufacturer shall establish and maintain procedures to prevent contamination of equipment or product by substances that could reasonably be expected to have an adverse effect on product quality.	6.4.2 Contamination control	ISO 13485:2016’s specified requirements are “as appropriate” unless relative to sterile medical devices. However, as stated in ISO 13485:2016 0.2: Clarification of concepts, when a requirement is qualified by the phrase “as appropriate”, it is deemed to be appropriate unless the organization can justify otherwise. For sterile devices, ISO 13485:2016 specifies “... the organization shall document requirements for control of contamination with microorganisms or particulate matter and maintain the required cleanliness during assembly or packaging processes.” 21 CFR § 820 is not this specific.

(Continued)

TABLE 3.1.7.2 Provisions for Materials Control—cont'd

21 CFR § 820	US Quality System Regulation	Corresponding ISO 13485:2016	Differences
820.70(h) Manufacturing Material	Where a manufacturing material could reasonably be expected to have an adverse effect on product quality, the manufacturer shall establish and maintain procedures for the use and removal of such manufacturing material to ensure that it is removed or limited to an amount that does not adversely affect the device's quality. The removal or reduction of such manufacturing material shall be documented.	7.5.2 Cleanliness of Product	ISO 13485:2016 specifies conditions that would require documentation of cleanliness requirements.
820.80(a) Receiving, In-Process, and Finished Device Acceptance, General	Each manufacturer shall establish and maintain procedures for acceptance activities. Acceptance activities include inspections, tests, or other verification activities.	7.1 Planning of product realization 8.2.6 Monitoring and measurement of product	No significant difference in requirements.
820.80(b) Receiving Acceptance Activities	Each manufacturer shall establish and maintain procedures for acceptance of incoming product. Incoming product shall be inspected, tested, or otherwise verified as conforming to specified requirements. Acceptance or rejection shall be documented.	7.4.3 Verification of purchased product	No significant difference in requirements.
820.120(e) Control Number	Where a control number is required by 820.65, that control number shall be on or shall accompany the device through distribution.	7.5.8 Identification 7.5.9.2 Particular requirements for implantable medical devices	ISO 13485:2016 does not require control numbers, although it does specify requirements for UDI (when required) and traceability for implantable medical devices.
820.184 Device History Record	Each manufacturer shall maintain device history records (DHRs). Each manufacturer shall establish and maintain procedures to ensure that DHRs for each batch, lot, or unit are maintained to demonstrate that the device is manufactured in accordance with the DMR and the requirements of this part. The DHR shall include, or refer to the location of, the following information: (a) The dates of manufacture; (b) The quantity manufactured; (c) The quantity released for distribution; (d) The acceptance records which demonstrate the device is manufactured in accordance with the DMR; (e) The primary identification label and labeling used for each production unit; and Any unique device identifier (UDI) or universal product code (UPC), and any other device identification(s) and control number(s) used.	7.5.1 Control of production and service provision	21 CFR § 820 specifies additional DHR content beyond that specified in ISO 13485:2016 (e.g., (a) The dates of manufacture; ... (d) The acceptance records which demonstrate the device is manufactured in accordance with the DMR; (e) The primary identification label and labeling used for each production unit; and any unique device identifier (UDI) or universal product code (UPC), and any other device identification(s) and control number(s) used.)

Perhaps more important than the specific wording of the quality methods is the requirement for a vendor agreement or contract manufacturing agreement to be in place. According to QSR 820.50(b) “purchasing documents shall include, where possible, an agreement that the suppliers, contractors, and consultants agree to notify the manufacturer of changes in the product or service so that manufacturers may determine whether the changes may affect the quality of a finished device.” Best practice evolved in recent years for contract manufacturing agreements is to include as a part of the agreement an index to the quality system that defines the responsibilities of the respective parties for pertinent quality systems.

Postmarketing Management of Risk and Product Performance

It is clear from the information presented thus far that medical device regulation, and thus the deployment of biomaterials, varies around the globe. The US FDA was the vanguard in postmarket surveillance but has not necessarily implemented the most effective methods to assure that a medical device continues to provide benefits that outweigh the risks over the lifecycle of the medical product. Although the 1976 MDRs established the requirement to report adverse events involving medical devices the implementation was less than ideal. With the amendments to the Act in 1990 the FDA issued 21 CFR 803 for mandatory reporting, providing definitions and mechanisms for the reports. In addition, this reporting system was now made open to reports by the user and the abridged reports were made public in a searchable database. Manufacturers were required to integrate the investigation process and report decision-making processes into the quality system management of complaints. Although a major step forward, compliance is not uniform and on various occasions nonmedical personnel swamp the system with unqualified reports, rendering the database useless for certain product categories. No remedy has been found for this dilemma.

Recognizing the shortcomings of the current Manufacturer and User Facility Device Experience Database and medical device reporting, the FDA has now implemented a surveillance network called the National Evaluation System for Health Technology and an independently run public/private coordinating center comprised of members representing the key community stakeholders, including patients and providers who have entered into agreements this year with 12 organizations that represent more than 195 hospitals and almost 4000 outpatient clinics with access to more than 495 million patient records, which will all be part of the early data network to provide real-world evidence to be used in pre- and postmarket decision-making. It remains unclear how this effort will affect the industry and device safety. Areas of interest announced by the FDA are knee replacement surgeries and intervertebral body fusion devices. The FDA noted in its recent announcement¹⁷ that

implementing this surveillance system required the implementation of the unique device identification system, which now allows implants to be tracked through distribution and patient use from its manufactured source.

In Europe the requirements for the CE mark had already required medical device manufacturers to reapply for the CE mark at periodic intervals, which in turn was cause for the manufactures to meet any updated product standards. However, since for the most part the updates to standards did little to remove an unsafe device that had managed to meet prior issuance of the standards, this mechanism has not had a significant impact on removing unsafe devices from the market but it has added to the cost for manufacturers. The Clinical Evaluation Report (CER) consists of analyzed clinical data collected either from a clinical investigation of the subject device or the results of studies and publications on equivalent devices already in the market. These reports were required to be submitted to the notified body as part of the Technical File. CERs were to be updated as part of the postmarket surveillance and vigilance activities (term for postmarket reporting of adverse events in the European Union). Through the years, CER requirements, including the qualifications of the author of such reports, have become stricter. One of the most significant advancements is the requirement of the CER, which will be emphasized even further under the new MDR, to integrate the risk management system with clinical evaluation. For Class III and implantable devices (of any classification), CERs will now be required to include clinical data derived from clinical investigations that were conducted under the supervision of a sponsor (in contrast to studies that are ad hoc collections of clinical experience). With a higher threshold for CER content for the initial CE mark it is expected that the quality of the postmarket surveillance of high-risk devices will continue to improve. The renewing applicant will be required to justify that the benefit of the device continues to outweigh the risks.

Surveillance of the quality of manufacturing of medical devices was the basic tool initiated with the original 1976 US FDA Good Practices regulation 21 CFR 820, which was also updated in 1990 to expand the authority in numerous ways, including the requirement for design control and review. Through fees for registration and listing the US FDA supports routine inspection by FDA compliance inspection officers for both initial quality inspection (PMA and Class III devices cleared under a 510(k)) and for routine periodic inspections of the facilities. These inspections not only assure the cleanliness and quality of the manufacturing and contract manufacturers for certain functions, but their purpose is to investigate how effectively the facility employees have implemented required quality procedures and documentation requirements. If a facility has significant noncompliance the company will receive a warning letter and can be fined for certain compliance failures. In the most serious circumstances, the facility can be closed until corrective actions have been taken. From time to time complaints from users resulting in postmarket reports have

¹⁷ <https://www.fda.gov/NewsEvents/Newsroom/PressAnnouncements/ucm626286.htm>.

brought the inspectors to the door. Obvious unsubstantiated labeling claims are also an invitation for the inspectors to alert the manufacturer to misbranding, a common temptation for medical device companies. Although there are many training programs to assist startup manufacturers in the proper development of quality system regulations, reading from the FDA Warning Letter provides a limitless resource of motivation.¹⁸

Most of the World Biomaterials participating countries have either a similar inspection process or authorize an ISO registrar to perform the on-site inspections to certify that the manufacturer continues to conform to ISO 13485. In many circumstances the ISO registrar may also be the same firm engaged as the notified body for the medical device manufacturer. Failure to rectify quality system shortcomings can be a cause for withholding the quality certification such as the CE mark.

Registration, Device Listing, Licenses

The US FDA does not require a license on the facility to make or sell a medical device; however, for combination products a license may be required for the facility that is responsible for aspects of the biologic or drug constituent part. As new biomaterials technologies continue to push the definition of “medical device,” any new medical device company may come under the jurisdiction of more than one agency in the FDA. These details are beyond the scope of this part of the chapter but for further reading, the FDA has issued guidance.¹⁹

Owners or operators of places of business (also called establishments or facilities) that are involved in the production and distribution of medical devices intended for use in the United States are required to register annually with the FDA.²⁰ This process is known as establishment registration. The amount of the fee varies from year to year and is the same for all, regardless of the size of the entity, and applies to US-based entities and importers. The registration fee does not differ by the number of products the entity may list. “Listing” is the process by which the FDA is notified by the responsible party of the type of medical device entered into interstate commerce. The current scheme for registration and listing can be quite complicated for a company attempting to complete the process for the first time. Timing of the initial fee payment, registration, and listing differ for Class I devices, which do not require premarket clearance. For devices under 510(k) or other premarket review, registration and listing does not occur until the device is cleared for US marketing. The process needs to be complete

within 30 days of putting the Class I or 510(k)-exempt product into interstate commerce. Registration and listing is a very important part of the postmarket management of medical devices. The registration and listing public database is helpful to identify the responsible party for the product, although identifying a product’s point of origin using this database is seldom straightforward.

Terminology differs for Canadian medical device licensing, as a license and paid fee are required for manufacturers submitting Class II, III, and IV medical device license applications, and license amendment applications will be charged a review fee. Fees are proportionate to the complexity of the application. As in the United States, this license fee does not apply to investigational devices, but unlike the United States this fee does not apply to Class I devices.

Australian medical device fees occur at various levels similar to the US scheme. An Australian manufacturing license is required and there is a fee for the inspection. Overseas manufacturers are responsible for an hourly fee for the inspection and reasonable costs and expenses for the inspector in addition to a GMP clearance application processing fee. Certificates of compliance have a fee. The annual fee (similar to the FDA registration fee) varies by class of device. Australia charges an “application fee,” which is required to “include” a medical device in the Australian Register of Therapeutic Goods. As with other regulatory agencies around the world, Australia is also looking to make various updates to rules and requirements, including institution of a UDI.²¹

The complexity of “user fees” such as market application fees, fees for registration and inspection of a facility, fees for “listing” or “including” a device allowed for sale in a particular country, and other sundry fees and fines in the many World Congress of Biomaterial countries are far too numerous to mention in this textbook and will probably change even before the book goes to press. But with this understanding of the many differences between countries it is clear that when countries can band together to have a common jurisdiction, such as what has developed under the European Commission, the medical device industry and its stakeholders may benefit. In recent years, other common markets and shared regulatory schemes have evolved, such as the Association of Southeast Asian Nations Medical Device Directive, known as the AMDD, which has 10 member states recognizing the goal of creating a harmonization of trade for medical devices in the region. Not all “joint” efforts succeed, such as a proposed agency for both Australia and New Zealand called ANZTPA.

However, a more practical arrangement for a single quality system audit program may find broader acceptance. Known as MDSAP and proposed by the International Medical Device Regulators Forum the single auditor program would include Australia, Brazil, Health Canada, Japan, the European Union, and the FDA. The FDA, however, limits

¹⁸ <https://www.fda.gov/iceci/enforcementactions/warningletters/default.htm>.

¹⁹ <https://www.fda.gov/downloads/RegulatoryInformation/Guidances/UCM429304.pdf>; Guidance for Industry and FDA Staff: Current Good Manufacturing Practice Requirements for Combination Products FINAL GUIDANCE January 2017.

²⁰ <https://www.fda.gov/MedicalDevices/DeviceRegulationandGuidance/HowtoMarketYourDevice/RegistrationandListing/ucm318796.htm>.

²¹ <https://brandwoodbiomedical.com/regulatory-change-in-australia-tgas-wish-list-for-2019/>.

the MDSAP audit reports as a substitute for routine FDA inspections. Medical device firms with activities related to the Electronic Product Radiation Control (EPRC) provisions of the FD & C Act will continue to be subject to FDA inspections for EPRC activities. Despite the attempt toward harmonization, it is clear from the FDA's stated limitations that MDSAP is not likely to be an umbrella shielding a medical device company from warning letters and "for cause" inspections.

Summary and Study Guide

Medical devices that rely on biomaterials that function in medium to high-risk applications are subject to strenuous global regulations. Various jurisdictions have embraced many common assessment techniques, such as biological risk assessment, but many different regulatory schemes persist. The perception of and evidence required for safe medical devices remain culturally based and require patience to navigate.

Chapter Questions: True or False

1. Medical device regulation is harmonized globally and therefore once a device is approved in the United States by the FDA it can be sold in any country.
2. A Class I device is not regulated in the United States.
3. Risk management standard ISO 14971 provides the requirements for determining how to conduct biocompatibility testing.
4. ISO 10993 says that prior human clinical use of the material reduces the risk of biomaterial toxicity and the prior use makes the material so safe no other testing is necessary.
5. Japan recognizes US PMA determination, so a product approved in the United States does not require a separate application for sale in Japan or Korea.
6. ISO 13485 quality requirements are identical to the US 21 CFR 820, so an ISO certificate means a US company will not be inspected by the US FDA.
7. Submission of the Clinical Evaluation Report to the notified body for the CE mark exempts a foreign company from needing to file a 510(k) in the United States.

3.1.8

Role of Standards for Testing and Performance Requirements of Biomaterials

CARL G. SIMON, Jr¹, LIISA T. KUHN²

¹Biosystems Biomaterials Division, National Institute of Standards & Technology, Gaithersburg, MD, United States

²Department of Biomedical Engineering, University of Connecticut Health Center, Farmington, CT, United States

Introduction: What Is a Standard?

The word standard is used to describe a broad set of activities and entities. There are many types of standards developed through many different organizations using a variety of processes, but “there is nothing standard about standards” (Alocca, 2019). The Office of Management and Budget (OMB) Circular A-119 states that a “standard,” or “technical standard” (hereinafter “standard”), includes all of the following:

- (1) common and repeated use of rules, conditions, guidelines, or characteristics for products or related processes and production methods, and related management systems practices;
- (2) the definition of terms; classification of components; delineation of procedures; specification of dimensions, materials, performance, designs, or operations; measurement of quality and quantity in describing materials, processes, products, systems, services, or practices; test methods and sampling procedures; formats for information and communication exchange; or descriptions of fit and measurements of size or strength; and
- (3) terminology, symbols, packaging, marking, or labeling requirements as they apply to a product, process, or production method.

Standards can take the form of a material, data set, or document.

Reference Materials

Reference materials are physical objects or things that have stable homogeneous properties which are used to calibrate an

instrument or as a test to confirm that a measurement system is operating correctly (Box 3.1.8.1). Reference materials are carefully prepared and tested and the reported values for reference material properties come with an estimate of the uncertainty. The uncertainty is the doubt about the measured value with regard to the true value and is described by a probability distribution (Possolo, 2015). Providing the uncertainty of the measured value is key for using the data to support decision making.

The National Institute of Standards & Technology offers a “Standard Reference Material (SRM) 2910b Hydroxyapatite” which is a 2-gram sample of well-characterized hydroxyapatite that comes with a Certificate of Analysis (www.nist.gov/srm). SRM 2910b was carefully prepared and tested to assure its composition. SRM 2910b can be tested alongside other preparations of hydroxyapatite and used to assess purity and composition. Hydroxyapatite is a biomaterial for which all three types of standards exist: reference material, reference data, and documentary standards. Hydroxyapatite reference data and documentary standards are discussed below.

The United States Pharmacopeia (USP; www.usp.org) also provides reference materials for biologics (<http://www.usp.org/biologics/cell-tissue-standards>). The “CD34+ Cell Enumeration System Suitability” contains human leukocytes, erythrocytes, and CD34+ cells that have been fixed and lyophilized (Catalog Number 1084292). It can be reconstituted in water and comes with a certificate stating the number of CD34+ cells per unit volume. It can be used to assess the flow cytometric enumeration of CD34+ cells.

The National Institute for Biological Standards and Control (NIBSC) makes a vascular endothelial growth factor reference material (VEGF 165, Product Number 02/286).

• BOX 3.1.8.1 Standards and Measurement Terminology

Measurand: “quantity intended to be measured” (*International Vocabulary of Metrology, 2012*)

Note: Measurements are conducted to collect information that will be used in decision making. For tissue-engineered medical products, these decisions are often related to safety, efficacy, and batch release. A measurand is the quantity that one intends to measure. The use of the word “intended” is important since the measurement may not be measuring what one intends to measure. Thus the word measurand is used to emphasize what one intends to measure even though it might be different from what is being measured.

Measurement: “Measurement is an experimental or computational process that, by comparison with a standard, produces an estimate of the true value of a property of a material or virtual object or collection of objects, or of a process, event, or series of events, together with an evaluation of the uncertainty associated with that estimate, and intended for use in support of decision-making” (*Possolo, 2015*)

Reference Material: “material, sufficiently homogeneous and stable with reference to specified properties, which has been established to be fit for its intended use in measurement or in examination of nominal properties” (*International Vocabulary of Metrology, 2012*)

Note: Reference materials are typically well-characterized materials that are used to calibrate a measurement system, or to assess the performance of a measurement system (quality assurance).

The VEGF reference material was made by recombinant DNA technology and the assignment of the activity in the ampule was determined by an international interlaboratory study (*Robinson et al., 2006*). It is intended to “facilitate the measurement of the potency and stability of therapeutic preparations of VEGF and inhibitors, and measurement of VEGF levels for diagnosis.”

Reference Data

Reference data are carefully collected measurement data that can be used for comparison with experimental data to confirm that a measurement system is operating correctly, or to identify unknowns in a test sample. Reference data are often spectra or measurement values of material properties. An example is the X-ray powder diffraction file for “Calcium Phosphate Hydroxide, $\text{Ca}_5(\text{PO}_4)_3(\text{OH})$, $\text{Ca}_5\text{HO}_{13}\text{P}_3$, Hydroxyapatite, synthetic” which can be obtained from the International Center for Diffraction Data (ICDD; www.icdd.com). Hydroxyapatite is an important medical material which is the focus of many standards. ICDD maintains a central collection of X-ray powder diffraction patterns. All data are critically reviewed and evaluated by the ICDD editorial staff using a multitiered process before being added to the collection. As technology improves, the quality requirements for reference data evolve and the reference data must be “continuously reviewed and upgraded for accuracy and quality.” The data file for hydroxyapatite can be used to assess spectra from test samples to assess composition.

USP also provides examples of reference data. “Bovine Acellular Dermal Matrix Reference Photomicrographs” (Catalog Number 1535824) and “Scaffold Human Dermis Reference Photomicrographs” (Catalog Number 1535813) are images provided in a digital format. These reference micrographs can be used for comparison with images of test specimens of decellularized extracellular matrix intended for use as scaffolds for tissue-engineering applications.

Documentary Standards

Documentary standards are written documents that “provide requirements, specifications, guidelines or characteristics that can be used consistently to ensure that materials, products, processes and services are fit for their purpose” (www.iso.org). Several documentary standards for hydroxyapatite have been written by two of the major standards development organizations in the medical materials field: ASTM International (ASTMi; www.astm.org) and the International Organization for Standardization (ISO; www.iso.org), such as

- ASTM F1185 Standard Specification for Composition of Hydroxyapatite for Surgical Implants
- ASTM F2024 Standard Practice for X-ray Diffraction Determination of Phase Content of Plasma-Sprayed Hydroxyapatite Coatings
- ISO 13175-3:2012 Implants for surgery—Calcium phosphates—Part 3: Hydroxyapatite and beta-tricalcium phosphate bone substitutes
- ISO 13779-2:2018 Implants for surgery—Hydroxyapatite—Part 2: Thermally sprayed coatings of hydroxyapatite
- ISO 13779-3:2018 Implants for surgery—Hydroxyapatite—Part 3: Chemical analysis and characterization of crystallinity ratio and phase purity
- ISO 13779-4 Implants for surgery—Hydroxyapatite—Part 4: Determination of coating adhesion strength

ASTM F1185 provides an explicit set of chemical and crystallographic requirements for hydroxyapatite intended for surgical implants. ASTM F2024 describes how samples should be analyzed using X-ray diffraction in order to determine their hydroxyapatite composition. This assortment of documentary standards, reference materials, and reference data helps ensure that high-quality hydroxyapatite biomaterials are available for use in therapeutic devices.

Documentary Standards: Voluntary, Consensus

Documentary standards can be written by open, consensus processes and their use is often voluntary. Documentary standards from ASTM and ISO are generally considered voluntary, consensus standards. The American National Standards Institute (ANSI) accredits standards development organizations (SDOs) who use fair and open processes. The www.ansi.org website reports 240 accredited SDOs in the United States as of 2019. Accreditation signifies that the

SDO meets ANSI's requirements for (1) openness, (2) balance, (3) due process, (4) an appeals process, and (5) consensus. Standards that are created following these requirements are referred to as "voluntary consensus standards" (OMB Circular A-119, 2016).

- **Openness:** all interested parties are provided a meaningful opportunity to participate in standards development
- **Balance:** a broad range of stakeholders are involved with no single interest dominating the process
- **Due process:** documented policies and procedures, adequate notice of meetings, sufficient time to review documents, access to views of other participants, a fair process for resolving conflicts
- **Appeals process:** an impartial process is available for appeals
- **Consensus:** general agreement, but not unanimity; objections are considered by a transparent and open process

In some cases, use of standards is not voluntary and their development is not consensus. For example, regulatory agencies mandate the use of certain ASTM and ISO documentary standards in their regulations. Also, the governments of some countries have mandated the use of ISO documentary standards during product development. Some types of USP documentary standards are mandatory; for example, those that describe manufacturing requirements for well-established small-molecule drugs. In some cases, membership in the working groups that write standards is by appointment only and is not open to the public. This is the case for some committees that write documentary standards for USP.

Who Writes Documentary Standards?

There are many SDOs that have a stake in the medical device and regenerative medicine industries that use biomaterials (*Standards Coordinating Body, 2019*). The largest organizations in the world that publish medical product documentary standards include IEEE (Institute of Electrical and Electronics Engineers) with 423,000 members and ASME (American Society of Mechanical Engineers) with more than 130,000 members. Other major SDOs active in medical products standards, including those in the tissue engineering and regenerative medicine (TERM) industry, are listed in [Table 3.1.8.1](#).

There are many benefits to standards, as listed in [Box 3.1.8.2](#). A standard test method for a measurement process can enable comparability over space and time. This is especially important for measurements of the critical quality attributes of a medical product. When thousands of units must be reliably manufactured in different locations, on different equipment, and by different operators, a standard test method for assessing product quality is essential. Standards can streamline the regulatory process by providing well-characterized test methods for demonstrating safety and efficacy (*Arcidiacono et al., 2018*). When a product attribute is measured in accordance with a standard test method, then regulatory agencies have greater confidence in the reliability of the data. Standard

TABLE 3.1.8.1 Examples of Documentary Standards Development Organizations (SDOs) in the Tissue Engineering and Regenerative Medicine Industry (TERM)

ASTMi	ASTM International (Formerly Known as the American Society of Testing and Materials)
ISO	International Organization of Standardization
USP	United States Pharmacopeia
AAMI	Association for the Advancement of Medical Instrumentation
HESI	Health and Environmental Sciences Institute
AABB	American Association of Blood Banks
FACT	Foundation for the Accreditation of Cellular Therapy
ATCC	American Type Culture Collection
ASME	American Society of Mechanical Engineers
PDA	Parenteral Drug Association

• BOX 3.1.8.2 Risks and Benefits of Standards

Benefits of High-Quality Standards

- Improve consistency of manufacturing
- Streamline the regulatory process
- Provide high-quality, proven test methods, avoiding costly trial-and-error approaches
- Reduce manufacturing and testing costs
- Improve confidence in a product
- Enhance commerce and facilitate trade
- Improve product quality, safety, and effectiveness
- Help small enterprises compete with big companies
- Inform decision making
- Improve comparability and reproducibility of research conducted by academics and their students

Risks of Not Developing Standards

- Without standard test methods, each firm must bear the costly development of their own test methods
- Regulatory review is slowed since developers cannot follow accepted standards in their regulatory filings
- A source of best practices that has been vetted by many stakeholders and experts will be not available to product developers
- Consumer confidence may falter if performance standards are not available to assure quality of new products

Risks of Publishing Low-Quality Standards

- Impose overly burdensome requirements on manufacturers
- Requirements for inappropriate testing could stymie product development
- Costs of meeting unnecessary requirements passed on to the consumer
- Poor practices promulgated throughout the community
- Manufactured products may be less reliable

test methods can facilitate commerce by establishing consistent guidelines for assessing product quality (Sarkar et al., 2019). Ideally, when the properties of a product are assessed by a standard test method, then the quality of products from different manufacturers can be compared. Academic teams, including students, that employ standard test methods can improve the reproducibility of their research, the comparability of their results with results from other labs, and their posture in regard to translation and commercialization.

ASTM International (ASTMi, www.astm.org) is an SDO that was formed in 1898 by members in the railroad industry and now has more than 30,000 members. It is divided into 143 different topic-specific Technical Committees, with Committee F04 Medical and Surgical Materials and Devices being the home for many biomaterials standards. There are approximately 12,000 ASTM standards, with more than 300 of them from Committee F04. New committees are formed as technology is developed, with F42 on Additive Manufacturing being one of the newer ones, formed in 2009. The technical committees are divided into subcommittees with task groups formed to develop particular standards. ASTM has defined six types of standards as given in Table 3.1.8.2.

Another major SDO is the International Organization for Standardization (ISO; www.iso.org). ISO is an independent, nongovernmental, international organization with members from the national standards bodies of 163 countries with one member per country. Each member country has a Technical Advisory Group (TAG) which individuals from that country may join. Each country has one vote which is managed by the TAG. Technical committees lead standards development within ISO and there are 22,480 ISO standards to date. The first ISO technical committee was ISO/TC1 on screw threads and was created in 1947. ISO/TC150 on Implants for Surgery was formed in 1971 and has 158 documentary standards. There are several subcommittees (SC) of ISO/TC150 which include SC1 Materials, SC2 Cardiovascular Implants and Extracorporeal Systems, and SC7 Tissue Engineered Medical Products. The ASTM motto is “helping our world work better” while ISO’s is “when the world agrees.”

How Are Documentary Standards Developed?

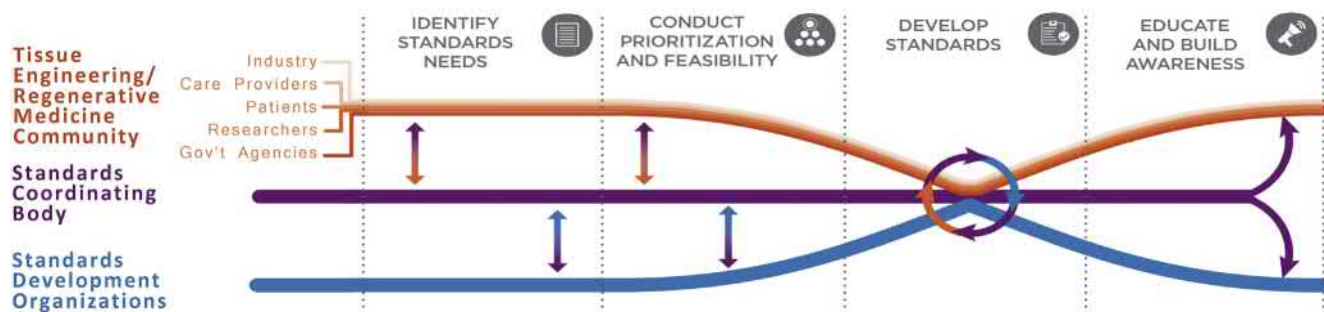
The documentary standards development process involves a wide range of people within a scientific or technical community as shown in Fig. 3.1.8.1. Typically, researchers from industry, academia, or government identify an issue that is impacting product reliability and performance and convene for discussion. Discussion can occur through informal working groups, at regular meetings of SDOs, or at special workshops. Due to the substantial number of people interested in or impacted by standards and the many SDOs active in the field of biomaterials and TERM, a Standards Coordinating Body (SCB) has been established to help coordinate efforts in these areas (www.standardscoordinatingbody.org). The first step of identifying a need, an issue worthy of standardization, and figuring out how to address it, is the most important. Issues identified for standards development must be based on

TABLE 3.1.8.2 The Six Types of ASTM Documentary Standards

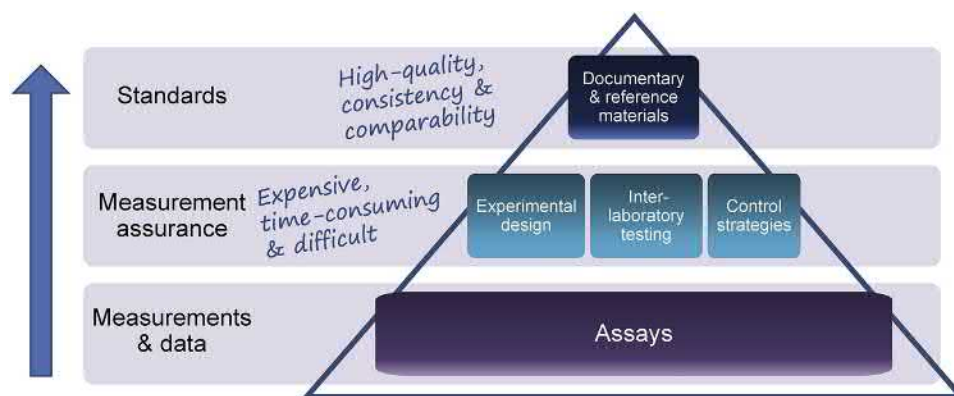
Guide	An organized collection of information or series of options that does not recommend a specific course of action; typically provides a list of issues to consider when making a particular measurement, or a list of complementary measurements to consider when characterizing device properties.
Test Method	A definitive procedure that produces a test result; provides a detailed procedure for conducting a measurement including controls and how to analyze the data; may include acceptance criteria and tolerances.
Practice	A set of instructions for performing one or more specific operations that does not produce a test result, such as how to sterilize a device.
Specification	An explicit set of requirements for chemical, mechanical, physical, biological, and/or electrical properties to be satisfied by a material, product, system, or service.
Terminology	A document composed of terms, definitions of terms, descriptions of terms, nomenclature, and explanations of abbreviations, acronyms, and symbols.
Classification	Systematic arrangement or division of materials, products, systems, or services into groups based on similar characteristics such as origin, composition, properties, or use.

repeatedly observed, known results, and not on a new area of basic research that is still highly variable and undefined. Sometimes, there is no clear, standardizable way of performing the task and the best option is to wait until more research has been conducted and information obtained. Robust documentary standards are underpinned by measurement science (metrology) (Fig. 3.1.8.2). There can be a substantial lag time from when a new material is discovered, or a new technology is developed, to when a definitive standard can be written. For example, development of nanoparticle standards was deferred until specialized equipment to measure their properties became available. Standards can only be developed about a topic for which there is already a large body of knowledge.

The next step is to identify people with the appropriate expertise and willingness to develop the standard. Documentary standards are developed by volunteers who are not typically compensated for their time, travel costs, or laboratory expenses and who do not work for the SDOs. The timelines for developing standards are lengthy, typically 3–5 years. Standards do not provide authorship or citations to those that develop them. On the other hand, writing standards leads



• **Figure 3.1.8.1** Overview of the standards development process. People working in the field, such as tissue engineering or regenerative medicine, must work together to identify clear needs for standards. People who are interested in the standard or may be impacted by the proposed standard are known as stakeholders and must be recruited to develop the standards. Standards are developed within standards development organizations (SDOs), such as ASTM and ISO. SDOs provide training on the standards development process, hold meetings to convene stakeholders to work on the standards, provide the infrastructure for developing standards, and disseminate the standards. The Standards Coordinating Body (SCB) was formed in 2017 to help coordinate standards development among the many SDOs and regenerative medicine stakeholders, with tissue engineering being an important focus. (Courtesy of SCB, <https://www.standardscoordinatingbody.org/>.)



• **Figure 3.1.8.2** Standards and technology development are underpinned by measurement science (metrology). (Courtesy of Sheng Lin-Gibson.)

to a direct, positive impact on health care and new product commercialization and is nevertheless rewarding work. The highly interactive process builds a strong sense of camaraderie and lasting friendships are developed. The participants learn the best practices, caveats, and shortcomings of the technologies or measurements that are the focus of the standards.

After finding the right people, a working group or task force is formed that develops the draft documentary standard. This may involve teleconferences, face-to-face discussions at regular SDO meetings, literature reviews, writing assignments, or laboratory research. It is important to identify and include all stakeholders at an early stage to avoid having the standard disputed later in the process. Stakeholders are those that are interested in the standard or potentially impacted by the standard. Staff from regulatory agencies, such as the Food and Drug Administration (FDA), attend SDO meetings since they have a great interest in standards development due to the value of standards in streamlining the regulatory process. Academics participate in SDO meetings to learn what is important for the commercialization of new technologies and for the opportunity to share technological advances. SDOs provide a neutral forum for all stakeholders to meet and discuss

the best path forward. SDO meetings involve teamwork and not competition. They are interactive and provide the opportunity for candid, open scientific discussion with key points becoming incorporated in the standards (see Case Study I). This may contrast with scientific conferences where the shortcomings of research results may receive less attention.

After the task group is in consensus that a draft documentary standard is complete, it goes to ballot where the membership of the SDO will vote. In ASTM, there is a tiered balloting process with a subcommittee vote first, followed by a vote at the highest technical committee level. Negative votes are rigorously discussed and often require a revision of the standard draft. The requirement for consensus from a majority of stakeholders during standards development reduces bias, leading to technically sound standards. If the draft successfully passes through the balloting process, then the draft becomes a standard and is published.

Within each SDO, efforts are taken to ensure balance among the voters. For instance, ASTM requires that the number of votes by “producers” (companies, manufacturers) must not exceed the sum of “users” (surgeons, dentists) plus “consumers” plus “general interest” (government,

CASE STUDY I: DOCUMENTARY STANDARDS ARE LIVING DOCUMENTS THAT MUST BE CONTINUOUSLY REVIEWED FOR QUALITY AND ACCURACY

When it was originally developed, ASTM standard F1581 Standard Specification for Composition of Anorganic Bone for Surgical Implants indicated that bone mineral was hydroxyapatite with characteristics that resembled the geologically formed mineral. The specification reflected current practice at the time which was the use of high temperature, aqueous processing conditions to produce anorganic bone that actually altered the native state of bone mineral to hydroxyapatite with reduced carbonate content. Some, but not all, companies used processing conditions that altered the native state of bone mineral, leading to high variability of anorganic bone products. Variable clinical outcomes were observed and equivalent product replacements were hard to make. Professor Melvin Glimcher, MD, an orthopedic surgeon and research director at the Children's Hospital/Harvard Medical School, was motivated to revise the ASTM standard based on his expertise in the physical and chemical structure of bone mineral. Dr. Glimcher had discovered the true structure of bone mineral by developing a low temperature, non-aqueous method to isolate bone mineral from the organic matrix. By using a variety of characterization methods, he and his team showed that bone mineral is a nanocrystalline, carbonated apatite with a unique crystalline array of atoms that is different than hydroxyapatite. Atomic vacancies and atomic substitutions of carbonate for phosphate make the native bone crystals more readily resorbed than highly crystalline hydroxyapatite. A consensus was reached to revise the standard. The F1581 specification now includes a description of anorganic bone as a bone-derived apatite and explains the importance of carbonate content and structure relative to dissolution and biological performance. This is an example of how standards must be continuously reviewed to reflect current knowledge and serves as a testament to the importance of clinician and academic input to the generation of robust standards.

academic). Further, in ASTM, each organization, company, or agency is only granted one vote. In ISO, each country is given one vote. In this way, one group of stakeholders cannot unfairly influence the voting outcome.

Documentary standards are “living” documents that can be revised or revoked by the balloting process. Often, new information relevant to the standard becomes available and triggers revision. All standards must be periodically updated and reballoted (every 5 years for ASTM) to assure their relevance continues. Documentary standards have a useful lifetime and are revoked when they become irrelevant.

Applications of Documentary Standards *Accelerating the Regulatory Process*

Documentary standards can be a vital part of securing regulatory approval. When a standard test method can be used to assess a quality attribute of a product, then the review of these data is more efficient since the regulators will be familiar with the methods. The Center for Devices and Radiological Health at US FDA has a database of standards that it recognizes: <https://www.accessdata.fda.gov/scripts/cdrh/cfdocs/cfStandards/results.cfm>.

Furthermore, in 2016, the US Congress passed the 21st Century Cures Act (US Public Law 114-255) which

CASE STUDY II: DOCUMENTARY STANDARDS USED IN A SUBMISSION TO FDA—A LIVING EXAMPLE

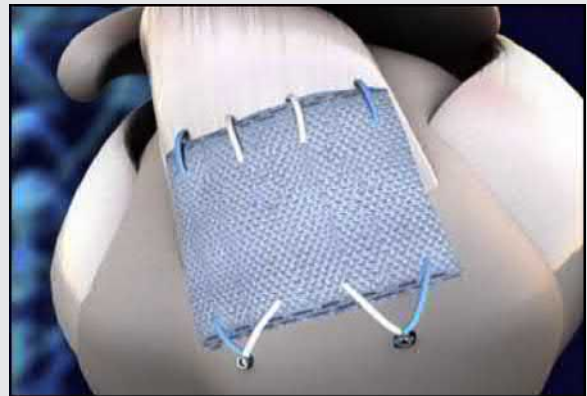
The documentary standards cited below were critical in the development and approval of X-Repair.

Product: X-Repair (Synthasome)

- Woven, degradable mesh (poly-L-lactic acid)
- Augments surgical repair of tendons and soft tissues
- Received 510(k) clearance in 2009

Standards that Were Used in the X-Repair 510(k) Application to FDA

- ASTM D3786 Standard Test Method for Bursting Strength of Textile Fabrics—Diaphragm Bursting Strength Tester Method
- ASTM D5035 Standard Test Method for Breaking Force and Elongation of Textile Fabrics (Strip Method)
- ASTM D5587 Standard Test Method for Tearing Strength of Fabrics by Trapezoid Procedure
- ASTM F1635 Standard Test Method for in vitro Degradation Testing of Hydrolytically Degradable Polymer Resins and Fabricated Forms for Surgical Implants
- ASTM F2211 Standard Classification for Tissue Engineered Medical Products (TEMPs)
- ASTM F2312 Standard Terminology Relating to TEMPs
- ASTM F2027 Standard Guide for Characterization and Testing of Raw or Starting Biomaterials for Tissue-Engineered Medical Products
- ASTM F2150 Standard Guide for Characterization of Biomaterial Scaffolds Used in TEMPs
- ISO 10993 Biological Evaluation of Medical Devices
- ISO 11135 Sterilization of Health-Care Products



Acknowledgement: Information courtesy of Anthony Ratcliffe, Synthasome.

requires the US FDA to facilitate the development of standards to enable “the development, evaluation, and review of regenerative medicine therapies and regenerative advanced therapies, including the manufacturing processes and controls of such products.” An example of the essential role of standards in bringing a medical product from bench to bedside is described in Case Study II.

As mentioned above, the use of documentary standards is mandatory in some cases. Thus, it is important that documentary standards be carefully written to avoid inhibiting innovation and enabling their appropriate application to

multiple use cases, especially those that may be unforeseen. Verbs such as “shall,” “will,” and “must” should be used cautiously in standards, while words such as “may” and “can” are less restrictive and more compatible with innovation. It is difficult to set a specification in a standard that will apply to every product that may be developed. Specifications should be described with language that is conducive to innovation.

For these reasons, risk management approaches are being applied for tissue-engineered medical products: ISO 10993-1: Biological Evaluation of Medical Devices – Part 1: Evaluation and Testing Within a Risk Management Process. Risk management is a systematic approach to evaluating, controlling, and monitoring risk. Risks assessment includes “risk analysis in which risks are identified and estimated and risk evaluation in which risks are evaluated to identify those which require mitigation” (ISO 10993-1). It is not realistic to view documentary standards as a one-size-fits-all solution and the decision to use them should be based on the application and its risks. Risk management approaches enable the most important tests to be identified and performed for each product while avoiding the performance of unnecessary or irrelevant testing.

Specificity versus Universality

“Specificity versus universality” is a common debate during standards development. If a standard is written very broadly then it may not be useful, whereas as if it is written very narrowly, then it may only be useful to a small group of stakeholders. Finding the proper balance of being broad enough to have wide application, but being specific enough to still be useful, is a challenge. For this reason, the scope statement may be the most important section of a standard. The scope is the first section of both ASTM and ISO standards. The scope statement should clearly define the intent of the standard and what types of products or measurements are to be addressed. Defining the scope of a standard is a major task of any working group and may require extensive discussion to compose.

A Standard Test Method Does Not Necessarily Define the Best Measurement

It is important to realize that a standard test method does not necessarily describe the best way to measure a property of interest (Simon et al., 2015). Instead, a standard test method provides a reliable way to make a measurement, a way that has been vetted by experts and voted upon. Although there may be better or newer test methods, the value of a standard test methods lies in its reliability, since many experts have reviewed it and provided input. New approaches, or experimental test methods that are not well established, are not typically covered by a standard.

Clinical Relevance

Another common, and very challenging, topic for discussion when developing documentary standards is that of “clinical relevance” (also referred to as “biological relevance”). This is important when deciding what to measure and how to measure it. Although the desire is to measure the most important properties of a product (the properties that will influence its clinical performance), this is often difficult to achieve,

particularly for tissue-engineered medical products. Very careful thinking is required to determine which properties are the most clinically relevant and should be characterized. These decisions are easier when the product has been rationally designed with a hypothesized mechanism of action (Bravery et al., 2013). In this way, measurements can be selected based on their ability to provide information about the product’s ability to achieve the intended mechanism of action.

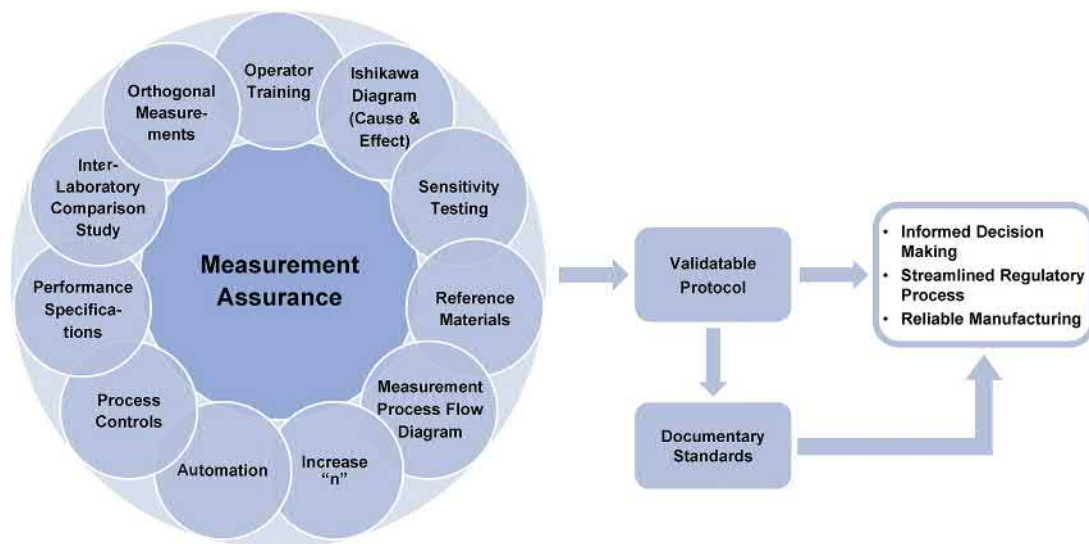
Some documentary standards focus on raw materials that are used in a range of other products or devices. Examples of materials-focused standards include “ASTM F75 Standard Specification for Cobalt-28 Chromium-6 Molybdenum Alloy Castings and Casting Alloy for Surgical Implants,” “ASTM F451 Standard Specification for Acrylic Bone Cement” and “ISO Technical Specification 20,399-1 - Biotechnology — Ancillary Materials Present During the Production of Cellular Therapeutic Products — Part 1: General Requirements.” Other standards may focus on devices, including design aspects, dimensions, materials used in the device, and laboratory-based tests of device performance. Performance testing evaluates the quality or capability of a product and aims to be a step closer to predicting clinical performance. Examples of documentary standards that describe device characteristics include F703 Standard Specification for Implantable Breast Prostheses and F623 Standard Performance Specification for Foley Catheter. ASTM F1926 Standard Test Method for Dissolution Testing of Calcium Phosphate Granules, Fabricated Forms and Coatings is a test method for a performance-related parameter. Many types of documentary standards are important for improving the quality and reliability of medical devices.

Measurement Assurance

Measurement assurance is the process of evaluating and reducing variability in a measurement to improve confidence in results for use in decision making (Simon et al., 2016). There are many strategies that can be used to achieve measurement assurance, as shown in Fig. 3.1.8.3. Test methods that have been improved by the application of these strategies may serve as the basis for writing a documentary standard.

Several strategies for measurement assurance are described below and in Fig. 3.1.8.3:

- *Reference materials*: Materials that are homogeneous and stable in regard to specified properties for use in calibration, to serve as a control or to serve as a reference point for comparability (described in more detail above).
- *Measurement process flow diagram*: A tool to formally map a measurement process so that each step can be considered for its contribution to measurement uncertainty.
- *Increase “n”*: Increasing the number of replicate measurements (n) that are conducted enables more reliable statistical analysis and better modeling of the probability distribution function (histogram).
- *Automation*: When automation can replace human manual labor, the number of measurements can be increased, the variability in the process can be reduced, and human bias can be reduced.



• **Figure 3.1.8.3** “Measurement assurance is a structured process designed to ensure that measurements are adequate for their intended use” (Carey, 1993). This encompasses the strategies that one can use to improve confidence in a measurement. Identifying, monitoring, and mitigating the sources of variability in the measurement process lie at its core. Application of these strategies to a measurement process yields a protocol which can be validated for a particular application and which may serve as the basis for developing a documentary standard.

- *Process controls*: Procedures to monitor critical points in a measurement process to check that steps are performing according to specifications.
- *Performance specifications*: Specifications that must be met in order for the test results to be used in decision making; they are established by sensitivity testing and by tracking process control data over many runs.
- *Interlaboratory comparison studies (ILCSs)*: When different labs conduct the same test and compare the results to assess measurement reproducibility; assesses measurement variability introduced by different operators in different labs using different equipment (discussed in more detail below).
- *Orthogonal measurements*: Confidence in a measurement result is enhanced when different measurement methods give a similar value of a material property; this is more convincing when the different measurements are based on different underlying principles.
- *Operator training*: Provision of suitable training to operators improves measurement precision and comparability between different operators and labs.
- *Ishikawa diagram (cause and effect)*: A graphical tool to map sources of variability in a measurement and to attribute them to different steps or aspects of the measurement process; also called a “cause and effect” or “fish-bone” diagram.
- *Sensitivity testing*: Identification of key measurement parameters that should be controlled in order to improve the reliability of the test results; may involve “design of experiment;” also called “ruggedness testing.”
- *Design of experiment (DOE)*: A systematic approach for assessing the effect of multiple experimental variables on the test results; uses a mathematical approach to

determine the most efficient and statistically powerful approach for varying and combining the parameters.

Interlaboratory Comparison Studies

Interlaboratory comparison studies (ILCSs) are an especially important tool for improving the reproducibility and comparability of research (Horwitz, 1994). ISO defines an “interlaboratory comparison” as the “organization, performance and evaluation of measurements or tests on the same or similar items by two or more laboratories in accordance with predetermined conditions.” ASTM requires that an ILCS be completed for all standard test methods that they publish. The first step in an ILCS is the formation of a working group of participants that work collaboratively to design the test method. A well-documented, carefully written protocol must be developed that precisely describes how the test will be conducted. A set of stable, homogeneous specimens is distributed to the participants who then conduct the test method on the specimens in their labs. The participating labs report their results to the organizing lab, and the data are analyzed to assess the reproducibility (intralab variability) of the method when conducted in different labs. This process reduces variability as the protocol is refined through successive testing iterations and yields a more reliable test method. New labs benefit since they can use this reliable protocol to conduct testing in their own labs and may reasonably expect their results to fall within the range observed during the ILCS. The use of standard test methods which have been refined through an ILCS enhances the comparability of data collected in different labs. Comparable test data are especially important when a company needs to assess the quality of products manufactured at different locations, by different operators, and/or on different equipment.

Looking Ahead

There are many interesting and challenging opportunities for future standards development. One example is data standards. Cell characterization data sets are getting larger, especially omics data sets (genomic, transcriptomic, metabolomic, proteomic, etc.), and standards for formatting, annotating, analyzing, and summarizing these data will be required as they are used to support regulatory filings.

Another useful advance may be the application of the principles of “engineering biology” to the development of biological reference materials. For example, precise genetic manipulations could be used to generate cells with precise characteristics that could be used as reference materials to calibrate cell measurements. For instance, cells with a tightly regulated and reproducible rate of division could be useful for calibrating cell-counting measurements. Cells that express a precise number of a particular cell surface marker on their surface could be used to calibrate flow cytometry measurements.

The ability of different systems, devices, or applications to connect, or interoperability, will be key for driving down development and manufacturing costs. However, this concept is relatively new for TERM since the common themes for successful TERM products are not yet clear. As the field matures, multiple products may come to market that use overlapping materials and processes, and standards to enable interoperability of these materials and processes will be needed.

Another area for potential standardization will be multivariate analytical methods and artificial intelligence. Regulatory filings contain many types of measurement data and relating these data to clinical outcomes is challenging. Standards for using multivariate methods and artificial intelligence for determining product quality from large and complex data sets will be required.

Standard approaches for weighing risks versus benefits of TERM products will be needed. Decision making must weigh potential benefits of the product against the likelihood and severity of adverse events. It may be appropriate for a terminally ill patient with a prognosis of months to live to take on greater treatment risks than a relatively healthy patient being treated for a nonlife-threatening musculoskeletal ailment. The ethical, cultural, and personal nature of these decisions could benefit from the open discussions of experts in a specialized working group which are part of the documentary standards development process. Institutional review boards (IRBs) could benefit from having documentary standards to assist in their decision-making process.

Conclusion

Despite the many standards that are already available, the translation of biomaterials and tissue-engineered medical products to clinical use is creating many needs and opportunities for standards development. There are many benefits to standards that make participation in their

development a valuable and rewarding experience. Standards development remains an active and ongoing process that will likely influence your research in the future, if it has not already.

Acknowledgments

Thanks to Clare Allocca, Sumona Sarkar, and Sheng Lin-Gibson for their critical review and contributions to this chapter.

References

- Allocca, C., 2019. Personal Communication. Standards Coordination Office, National Institute of Standards and Technology. Gaithersburg, MD.
- Arcidiacono, J.A., Bauer, S.R., Kaplan, D.S., Allocca, C.M., Sarkar, S., Lin-Gibson, S., 2018. FDA and NIST collaboration on standards development activities supporting innovation and translation of regenerative medicine products. *Cytotherapy* 20, 779–784.
- Bravery, C.A., Carmen, J., Fong, T., Oprea, W., Hoogendoorn, K.H., Woda, J., Burger, S.R., Rowley, J.A., Bonyhadi, M.L., Van't Hof, W., 2013. Potency assay development for cellular therapy products: an ISCT review of the requirements and experiences in the industry. *Cytotherapy* 15, 9–19.
- Carey, M.B., 1993. Measurement assurance: role of statistics and support from international statistical standards. *Int. Stat. Rev.* 61, 27–40.
- Horwitz, W., 1994. International Union of Pure and Applied Chemistry (IUPAC): nomenclature of interlaboratory analytical studies. *Pure Appl. Chem.* 66 (9), 1903–1911.
- International Vocabulary of Metrology, 2012. Basic and General Concepts and Associated Terms (VIM 3rd edition). Bureau International des Poids et Mesures. Joint Committee for Guides in Metrology (JCGM). 200.
- OMB Circular A-119, 2016. Federal Participation in the Development and Use of Voluntary Consensus Standards and in Conformity Assessment Activities. Office of Management and Budget, United States Government. https://obamawhitehouse.archives.gov/sites/default/files/omb/inforeg/revised_circular_a-119_as_of_1_22.pdf.
- Possolo, A., 2015. NIST Technical Note 1900: Simple Guide for Evaluating and Expressing the Uncertainty of NIST Measurement Results. <https://doi.org/10.6028/NIST.TN.1900>. Gaithersburg, MD.
- Standards Coordinating Body, 2019. Regenerative Medicine Standards Landscape, Nexight Group LLC. <https://www.standardscoordinatingbody.org/landscape>. Accessed January 2, 2020.
- Robinson, C.J., Das, R.G., Stammers, R., Rafferty, B., 2006. The world Health organization reference reagent for vascular endothelial growth factor, VEGF165. *Growth Factors* 24, 285–290.
- Sarkar, S., Lin-Gibson, S., Allocca, C.M., Henke, D., Getz, A., 2019. The critical role of standards in tissue engineering and regenerative medicine. In: Reis, R. (Ed.), *Encyclopedia of Tissue Engineering and Regenerative Medicine*, first ed. Academic Press, pp. 1–14.
- Simon Jr., C.G., Yaszemski, M.J., Ratcliffe, A., Tomlins, P., Luginbuehl, R., Tesk, J.A., 2015. ASTM workshop on standards and measurements for tissue engineering scaffolds. *J. Biomed. Mater. Res. B Appl. Biomater.* 103B, 949–959.
- Simon Jr., C.G., Lin-Gibson, S., Elliott, J.T., Sarkar, S., Plant, A.L., 2016. Strategies for achieving measurement assurance for cell therapy products. *Stem Cells Transl. Med.* 5, 705–708.

Homework Questions

- Which one below lists all the types of ASTM standards?
 - Classification and Test Methods.
 - Classification, Guide, Specification, Terminology and Test Methods.
 - Classification, Guide, Practice, Specification, and Test Methods.
 - Classification, Guide, Practice, Specification, Terminology, and Test Methods.
- Describe the differences between an ASTM specification standard and a test method standard.
- Who uses standards?
 - Manufacturers and Test laboratories
 - Manufacturers, Consumers, Test laboratories, College professors and their students.
 - Manufacturers, Test laboratories, College professors and their students.
- Which below best completes this sentence? Compliance with a standard ...
 - is voluntary.
 - is nonvoluntary.
 - may be either voluntary or nonvoluntary.
- What are the names of some standards development organizations (SDOs) that prepare consensus standards through voting (lists are not exhaustive)?
 - AAMI, ASTM, ISO, and ADA
 - AAMI, ASTM, ISO, and ANSI
- Briefly describe the ASTM standards development process including words like task groups, subcommittees, and ballots.
- Both the subcommittees and main committees of ASTM must be balanced between what categories of stakeholder groups?
- How can domination by any one stakeholder or interest group be prevented during development of a standard?
 - Only one vote per voting interest is allowed.
 - Only one member per voting interest may join the SDO.
 - Through discussion at working groups or task-force group meetings.
- Should a standard be based on well-established technologies or on new areas of research? Circle one.
- (A) Why are there so many different standards organizations, and (B) accreditation by what organization brings some measure of uniformity of process to the many SDOs in the USA?
- Identify a standard within ASTM (www.astm.org) that covers the testing needed to establish the biocompatibility of a new material for a medical device.
- Which type of testing below is an example of in vitro testing:
 - in a cell culture plate
 - implantation in an animal
 - a simulation on a computer
- Are materials proposed for medical use tested by direct contact, by using extracts obtained by soaking the

- implant in liquids that simulate body fluids or by both methods (search www.astm.org)?
- What animal is skin irritation typically tested in (search www.astm.org)?
 - Rabbit
 - Dog
 - Cat
 - Mouse
 - Are guinea pigs used in testing for allergic reactions? Search the www.astm.org website to find out.
 - Search the www.astm.org website to find three examples of standards for biomaterials, biomolecules, cells and tissue-engineered constructs that apply to tissue-engineered medical products.
 - Standards development in the area of nanomaterials has been slow. Suggest possibilities for what has held up standards development in the field of nanotechnology.

Answer Key for Homework Questions

- What are the types of ASTM standards?

Answer: D. Classification, Guide, Practice, Specification, Terminology, and Test Methods.
- Describe the differences between an ASTM specification standard and an ASTM test method standard.

Answer: A specification describes chemical, mechanical, physical, and electrical properties of a material. A test method standard describes the test specimen to be used, the conditions under which it is to be tested, how many specimens and what controls are to be tested, and how the data are to be analyzed. Often, the reproducibility of test methods is assessed by “interlaboratory testing,” meaning that several laboratories have followed the method and the results are analyzed to determine the degree to which they agree.
- Who uses standards?

Answer: B. Manufacturers, Consumers, Test laboratories, College professors and their students.
- Which below best completes this sentence? Compliance with a standard ...

C. may be either voluntary or nonvoluntary.
- What are the names of standards development organizations (SDOs) that prepare consensus standards through voting?

Answer: A. AAMI, ASTM, ISO and ADA.

Note: ANSI does not write standards but instead coordinates the activity of standards development organizations in the United States.
- Briefly describe the ASTM standards development process including words like task groups, subcommittees, and ballots.

Answer: This is a brief description of the ASTM standards development process: A standard work item can be proposed by anyone and then approved by the executive committee of a subcommittee based on a rationale and scope provided by the person or group initiating the standard. A task group is created that includes

5–20 stakeholders and they draft the standard. It is written using an ASTM template for one of the six defined types of standards. It is sent out for ballot at the subcommittee level first and then the main committee. Persuasive negative votes will stop the process and may require revision of the standard. If no negative votes are received at either subcommittee or main committee, then the item becomes a published standard.

7. Both the subcommittees and main committees of ASTM must be balanced between what category of stakeholder groups?

Answer: Producers and nonproducers.

Note: Nonproducers include users, consumers, and general interest.

8. How is domination by any one stakeholder or interest group prevented during development of a standard?

Answer: A. Only one vote per voting interest is allowed.

9. Should a standard be based on well-established technologies or on new areas of research? Circle one.

Answer: Well-established technologies.

10. (A) Why are there so many different standards organizations, and (B) accreditation by what organization brings some measure of uniformity of process to the many SDOs in the USA?

Answer: (A) Each SDO provides valuable standards for a particular area of technology and has the right stakeholders and experts to write these standards. (B) ANSI accreditation provides a measure of uniformity and consistency of process to the many SDOs.

11. Identify a standard within ASTM (www.astm.org) that covers the testing needed to establish the biocompatibility of a new material for a medical device.

Answer: There are many standards that could provide a correct answer. Some of them are listed here:

F748 Standard Practice for Selecting Generic Biological Test Methods for Materials and Devices Medical Devices.

F3206 Standard Guide for Assessing Medical Device Cytocompatibility with Delivered Cellular Therapies.

F813 Standard Practice for Direct Contact Cell Culture Evaluation of Materials for Medical Devices.

F1027 Standard Practice for Assessment of Tissue and Cell Compatibility of Orofacial Prosthetic Materials and Devices.

12. Which type of testing below is an example of in vitro testing?

Answer: A. In a cell culture plate.

13. Are materials proposed for medical use tested directly, by using extracts obtained by soaking the implant in liquids that simulate body fluids or both?

Answer: Both.

Note: Under ASTM Committee F04.16, see the following:

ASTM F749 Practice for Evaluating Material Extracts by Intracutaneous Injection in the Rabbit

ASTM F750 Practice for Evaluating Material Extracts by Systemic Injection in the Mouse

ASTM F813 Practice for Direct Contact Cell Culture Evaluation of Materials for Medical Devices

14. What animal is skin irritation typically tested in?

Answer: A. Rabbit.

Note: See ASTM F719 Standard Practice for Testing Biomaterials in Rabbits for Primary Skin Irritation.

Humans are also used. See ASTM F2808 Standard Test Method for Performing Behind-the-Knee (BTK) Test for Evaluating Skin Irritation Response to Products and Materials That Come into Repeated or Extended Contact with Skin.

15. Are guinea pigs used in testing for allergic reactions? Search the www.astm.org website to find out.

Answer: Yes.

Note: See ASTM F720 Practice for Testing Guinea Pigs for Contact Allergens: Guinea Pig Maximization Test.

16. Search the www.astm.org website to find examples of standards for cells and tissue-engineered constructs that apply to tissue-engineered medical products.

Answer: There are many standards that could provide a correct answer. Some of them are listed here:

ASTM F3259 Standard Guide for Micro-computed Tomography of Tissue Engineered Scaffolds

ASTM F2211 Standard Classification for Tissue Engineered Medical Products (TEMPs)

ASTM F2315 Standard Guide for Immobilization or Encapsulation of Living Cells or Tissue in Alginate Gels

ASTM F2739 Standard Guide for Quantifying Cell Viability within Biomaterial Scaffolds

17. Standards development in the area of nanomaterials has been slow. Suggest possibilities for what has held up standards development in the field of nanotechnology.

Answer: Standards for nanoparticles have been delayed due to the lack of high-precision methods required to ensure reliability of the results. It is not possible to standardize something that is not reproducible or reliably measured. A lack of reproducibility has also delayed standards for cells in the field of tissue engineering and regenerative medicine. Uncertainty with test methods and high variability in the results, and in the cells themselves, has made it difficult to define appropriate quality measures.

3.1.9

Medical Device Failure—Implant Retrieval, Evaluation, and Failure Analysis

MELINDA K. HARMAN

Department of Bioengineering, Clemson University, Clemson, SC, United States

Overview and Definitions

Medical Implants

The phrase “medical implant” can assume many definitions, depending on the context and intended purpose. Regulatory and public health agencies broadly define implants as types of medical devices that are: (1) intended for use in the diagnosis, prevention, treatment, or cure of diseases or other conditions; (2) intended to affect the structure or function of the body; and (3) do not achieve their intended purposes with chemical or metabolic action (FDA, 2017; WHO, 2003). Some implants can replace anatomic structures in part or in full, while others can deliver medication, monitor body functions, or provide support to organs and tissues. Implants can consist of processed tissues or synthetic biomaterials and can be placed permanently or removed after accomplishing their intended function. Modern medical implants gained widespread use in the mid-20th century and millions of different types are implanted in the United States each year (Table 3.1.9.1). It is estimated that 8%–10% of Americans are living with some type of medical implant (NIH, 2000).

For the purposes of this chapter, an implant is defined as a type of medical device that is placed inside or on the surface of the human body, as having an intended lifespan spanning months or years, as being made of biomaterials and penetrating living tissues, as having a physiological interaction in the human body, and as being retrievable (NIH, 2000).

Implant Retrieval

Modern medical implants are highly beneficial to patient health. Rapidly evolving technologies and ever-expanding indications for implant use demand continual

development to improve their performance and extend their useful lifespan. Medical implants are also subject to failure.

Implant retrieval and evaluation (commonly, implant retrieval analysis or explant analysis) describes a method of scientific analysis for determining the efficacy and safety or biocompatibility of medical implants in vivo (Anderson et al., 2012). It is concerned with the documentation of problems that dictate modification of design, materials, or use of the implants in patients. In this manner, implant retrieval and evaluation encompass a total product life cycle approach, with analysis occurring during many of the major phases in the lifespan of a medical implant, from research and development activities, to design validation and preclinical studies, and after widespread clinical use (Table 3.1.9.2).

Postmarket Surveillance

It is globally recognized that basic regulatory programs for the safety and performance of medical devices depend on the critical elements of premarket review ensuring product control, postmarket surveillance ensuring safe and effective use, and product representation ensuring accurate advertising and public education to guard against misrepresentation of product claims (WHO, 2003). However, prior to 1976, there were no regulatory programs assuring that devices recommended to American patients by their doctors were monitored for safety and effectiveness (See Case Study: Intrauterine Contraceptive Devices).

The FDA defines postmarket surveillance as the systematic, scientifically valid collection, analysis, and interpretation of data or other information about a marketed device (FDA, 2018). A robust postmarket surveillance

TABLE 3.1.9.1 Prevalence of Medical Implants in the United States (McIntyre, 2011)

Implant	Procedure Volume ^a
Artificial eye lenses	>2,580,000
Ear tympanostomy tubes	>715,000
Coronary stent	>560,000
Knee replacement	>543,000
Orthopedic fracture repair	>453,000
Intrauterine device	>425,000
Spinal fusion/disc replacement hardware	>413,000
Breast implants	>366,000
Heart pacemaker	>235,000
Hip replacement	>230,000
Implantable cardioverter defibrillator	>133,000

^aEstimated using 2011 National Health Survey data and other sources.

strategy supports better management of the risk–benefit ratio throughout the life cycle of medical devices (Institute of Medicine, 2011). Postmarket surveillance is either passive (regulators depend on data provided by manufacturers and user facilities) or active (regulators seek information on adverse events, device malfunctions, and product effectiveness) and the FDA uses multiple platforms for postmarket surveillance of implants.

Passive postmarket surveillance is an important mechanism for monitoring medical device performance and potentially detecting adverse events associated with device use. Available since 1991, the Manufacturer and User Facility Device Experience (MAUDE) database at the FDA is the key platform for postmarket surveillance gathered through two reporting tools. First, the Medical Device Reporting (MDR) tool is a mandatory (for manufacturers and user facilities) and voluntary (for individual clinicians or patients) reporting mechanism designed to facilitate the capture of device-related adverse events, including death, serious injury, or malfunction. Second, FDA partners with approximately 250 health-care facilities under the MedSun program to collect real-world information about medical device (generally, Class II) problems in hospitals, generating more reliable and higher quality reports than MDR alone (Daniel et al., 2015). MAUDE stores data reported through the MDR and MedSun programs.

Using these adverse event reports and other sources (e.g., device recalls or corrective actions, review of premarket or post-approval data, or review of scientific literature), the FDA can identify device issues appropriate for active postmarket surveillance. It has authorization (under section 522) to compel manufacturers to complete studies of an approved device if a safety issue has been identified (see Case Study: Metal-on-Metal Articular Bearings in Hip

TABLE 3.1.9.2 Sources of Retrieved Implants and the Relevance of the Evaluation

Source	Relevance
Fabricated but unimplanted prototypes	To evaluate changes induced by the fabrication process
Specimens subjected to in vitro tests	To evaluate biocompatibility, durability of the biomaterials, or potential failure modes
Specimens removed from animal models following in vivo function	To evaluate biocompatibility, durability, implant–tissue interactions, or safety and effectiveness of the design
Specimens accrued in carefully controlled clinical trials	To evaluate implant–tissue interactions, or safety and effectiveness of the design for its intended use
Failed or functioning implants explanted in the course of general clinical use following regulatory approval	To evaluate underlying mechanisms contributing to implant success or failure during end-use conditions

Joint Replacement). Manufacturers use implant retrieval and evaluation studies and various other assessments to investigate reason(s) for failure and identify failure modes, as required by these “522 orders.” However, due to known challenges with meeting 522 orders, including inconsistencies in design and lack of a general framework for completing them, some have advocated for registry-based surveillance as an alternative approach (Daniel et al., 2015).

Goals for Implant Retrieval and Evaluation and Failure Mode Analysis

Implant designs, the biomaterials selected for them, and the protocols used to test them before use in humans, are all intended to minimize the possibility of device failure (Schoen et al., 2012). The majority of such devices serve their patients well, alleviating pain and disability, enhancing quality of life, and/or increasing survival. Nevertheless, some implants fail, often following extended intervals of satisfactory function. The clinical value of implant retrieval and evaluation is rooted in patient safety through detailed analysis of clinical complications associated with the implanted device and biocompatibility at the implant–tissue interface (Schoen et al., 2012). Irrespective of implant site or desired function of the device, the overwhelming majority of clinical complications produced by medical devices fall into several well-defined categories (Table 3.1.9.3).

There is a critical need for implant retrieval analysis in order to gain insights into the strengths and weaknesses of implant designs and their functional longevity and to understand the enduring consequences of implantation. The National Institutes of Health recognizes that “long-term data on the behavior of implanted devices and host

CASE STUDY I: INTRAUTERINE CONTRACEPTIVE DEVICES

Often cited as the device failure that helped prompt the Medical Device Amendments of 1976, which authorized the FDA to begin regulating medical devices, the problem of the Dalkon Shield intrauterine device (IUD) provides an instructive case history of biomaterials performance and failure modes uncovered by implant retrieval analysis, adverse event reporting, and clinical outcome studies.

What Problem Was Addressed?

IUDs are the most commonly used method of reversible female contraception, with over 168 million women users worldwide as of 2011 (Nelson and Massoudi, 2016). Introduced in the 1960s, early IUDs were a nonhormonal contraceptive benefitting from two mechanisms of action. The IUD biomaterials (polymers with small amounts of copper sulfate or stainless steel rings) created changes in the cervical mucus and uterine wall that made it difficult for sperm to fertilize eggs. The IUD's flexibility and shape provided for easy insertion into the uterine wall and effectively induced a chronic noninfectious inflammation in the endometrium to prevent implantation of any fertilized egg. Tail strings, consisting of monofilament polypropylene, attached to the distal end of the IUD facilitated removal.

One of the dominant IUDs designed in the late 1960s was the Dalkon Shield IUD. Its key design features included a large circular shape with a thin inner membrane for increasing surface contact with the endometrium and 10 plastic fins around the circumference for secure anchoring into the uterine wall, effectively preventing involuntary expulsion while in use and increasing the resistance to removal (Roepke and Schaff, 2014). Tail strings with higher tensile strength were added, using a nylon suture material (Supramid) having hundreds of inner fibers encased in a smooth outer sheath.

Following its introduction in 1971, there were 3.9 million Dalkon Shields sold over 3 years, capturing the majority (60%) of the US IUD market (Roepke and Schaff, 2014). However, by 1974, there were overwhelming clinical complications of pelvic infections, miscarriage, and deaths associated with this device (Tatum et al., 1975). Explant analysis performed in the years to follow revealed the multifilament tail string served as a wick for vaginal fluid and bacterial access inside the uterus, effectively bypassing the antibacterial actions of the cervical mucus (Bank and Williamson, 1983). Deterioration of the outer nylon sheath, especially in regions of high stress adjacent to the knotted attachment side, provided a route for bacteria to exit the sheath into the sterile uterine cavity and contributed to string breakage during attempted removal.

Following protracted legal challenges and denials of wrongdoing by the manufacturer, the absence of heat-sealed ends on the multifilament tail strings and deterioration of the outer nylon sheath were identified as contributing factors in the high infection rates with the Dalkon Shield (Roepke and Schaff, 2014). The FDA identified the multifilament tail string as a hazard for its role in the infections.

What Properties Were Required of the Biomaterial?

Modern IUDs incorporate tail strings meeting the following criteria (Roylance 1993):

1. Sufficient tensile strength to avoid breakage during IUD removal
2. Sufficiently small diameter to provide flexibility
3. Biologically inert material that does not undergo chemical or physical change during use
4. Hydrophobic monofilament fiber to avoid water absorption (and capillary transport)
5. Suitable attachment to the IUD body by a method that does not result in a loss of tensile strength
6. Capable of being sterilized, by either chemical or thermal means
7. Capable of being colored to aid in distinguishing it from surrounding tissue
8. Widely available material that is capable of being processed with consistently high quality
9. Material that has a proven history of safe and effective use in biomedical applications.

What Biomaterials Are Used?

The FDA regulates the IUD as a combination product, recognizing that the device has an additional function to delivery of the drug. There are two general types of modern IUDs, polymeric hormone-releasing IUDs and polymeric copper-releasing IUDs, and older generations of all-metal stainless steel IUDs primarily used outside of the United States. As of 2016, there are five IUDs with FDA approval for use in the United States, including three hormone-releasing (levonorgestrel, a progestin hormone and does not contain estrogen) IUDs and one copper-releasing IUD (Nelson and Massoudi, 2016).

Polymeric IUDs have T-shaped bodies fabricated from low-density polyethylene with added barium sulfate for opacity during imaging. The copper surface areas, in the form of solid collars or coiled wire, vary from approximately 200–380 mm². Highly drawn and oriented polyethylene, polypropylene, and nylon 66 monofilament fibers of approximately 0.25 mm diameter are considered suitable for use as tail strings (Roylance, 1993).

Technical specifications recommended by the WHO (WHO, 2016) include the following:

- Polyethylene material properties having a minimum tensile strength of 13 MPa and a 2% secant flexural modulus in the range of 133.5–180.6 MPa
- Minimum copper purity of 99.99% distributed over a 380 mm² surface area
- High-density polyethylene monofilament having a minimum tensile strength of 28 MPa to withstand a 9.5 N tensile load
- Monofilament pigmented with titanium dioxide and knotted to form two tail strings.

response are essential inputs to the development process” (NIH, 2000), yet systematic programs for implant retrieval and evaluation are rare. The general goals of implant retrieval and evaluation aim to fill this need by implementing a multidisciplinary strategy to document implant-specific and patient-specific parameters and underlying mechanisms contributing to implant success or failure during end-use

conditions (Table 3.1.9.4). These goals address key factors for determining the outcome of a medical implant, including the biomaterials and implant design, patient-specific functional anatomy and pathology, and technical aspects of the surgical implantation.

Each type of in vivo condition and clinical use of the implant has unique implant–host interactions requiring

CASE STUDY II: METAL ON METAL ARTICULAR BEARINGS IN HIP JOINT REPLACEMENT

With implications for the current state of the 510k approval pathway at the FDA (Howard, 2016; Institute of Medicine, 2011), metal-on-metal (MoM) articular bearings for hip joint replacement provide an instructive case history of a historical design concept that was reintroduced using contemporary biomaterials. Used in total hip replacement and hip resurfacing, MoM implants quickly gained widespread clinical adoption, especially when coupled to larger diameter femoral heads (Hart et al., 2015). Despite promising laboratory results for the wear performance of MoM implants, clinical outcome studies and adverse event reporting revealed unanticipated problems with MoM implants and ultimately led manufacturers to stop marketing their devices. Implant retrieval and evaluation played an essential role in the characterization of volumetric wear rates for historical MoM implants (so-called first generation) and the failure mode analysis used to unravel and understand the causes of pervasive failures in modern MoM implants (so-called second generation). Detailed data gathered through mandatory postmarketing surveillance studies ultimately led the FDA to reclassify MoM as class III (higher risk) medical devices requiring premarketing approval applications containing sufficient valid scientific evidence to reasonably assure the safety and effectiveness of MoM implants for their intended use (FDA, 2016).

What Problem Was Addressed?

Since the introduction of total hip replacement in the 1960s, MoM and metal-on-polyethylene (MoP) articular bearings have been the most common implant biomaterials used to replace diseased articular cartilage. Although regarded as clinically successful, problems with wear of the polyethylene implants and late aseptic loosening limited the longevity of MoP designs. Careful implant retrieval analysis of historical first-generation MoM hip implants made of cast cobalt chromium alloys documented volumetric wear rates that were an order of magnitude smaller than the typical 50–100 mm³ wear rates for conventional MoP implants (McKellop et al., 1996; Rieker et al., 1998; Semlitsch and Willert, 1997).

These observations fueled interest in alternative bearing materials to replace MoP designs and led to the introduction of modern second-generation MoM hip implants made of wrought cobalt chromium alloys. In vitro wear simulations of modern MoM bearing materials demonstrated significantly reduced volumetric wear compared to conventional MoP bearing materials (Barbour et al., 1999; Firkins et al., 2001; Fisher et al., 2004). However, those in vitro studies noted that alloy composition (low carbon), inadequate clearance between the metal femoral head and metal acetabular liner (deviation from nominal 0.2 mm), and load and motion profiles replicating more adverse and physiologically relevant inputs (higher load and elliptical contact paths) led to excessive MoM wear in some cases.

Initial clinical outcomes from second-generation MoM designs were promising, with >95% survival rates reported at 10-year follow-up for 28–32 mm diameter MoM bearings (Benjamin-Laing and Haddad, 2012; Eswaramoorthy et al., 2008; Grübl, 2007). Subsequent introduction of larger diameter femoral heads, which provide for additional joint stability, were cleared using the 510(k) FDA regulatory pathway by claiming substantial equivalence to the smaller diameter MoM bearings. MoM hip replacements were readily adopted by orthopedic surgeons and over one million were implanted worldwide by 2008, with approximately 35% of all hip implants in the United States including MoM articular bearings (Bozic et al., 2009).

Implant registries captured this widespread use of the MoM bearings and began to raise concerns regarding high revision

rates after 5 years in vivo, which were approximately two to three times higher than other bearing material combinations (Jameson et al., 2012). Although there was some variability among different manufacturer brands, general trends indicated higher failure rates in women than men and with bearing sizes of 36 mm diameter or greater. Unacceptably high revision rates reported by two national joint registries called into question the regulatory approval process for MoM hip implants, particularly with respect to premarket data requirements to prove safety and effectiveness (Howard, 2016).

The consequences of nanometer-sized wear particles from the MoM bearings elicited a biological response with both local and systemic consequences largely due to a higher degree of biological reactivity in the metal debris compared to polyethylene debris from conventional MoP bearings (FDA, 2019). The substantially higher number of metal particles provided for a very large surface area for interaction with intracellular and extracellular fluids. Explant analysis and histological studies of joint tissues revealed failure mechanisms consistent with release of both wear particles and metallic ions from the articular surfaces and the head-stem trunnions in modular implants (Campbell et al., 2014; FDA, 2019). Local tissue reactions included osteolytic bone loss and soft-tissue masses (termed pseudotumors) evident in some patients with MoM implants, with histomorphology presenting macrophage-dominated and/or lymphocyte-dominated foreign-body reactions (Campbell, 2010; FDA, 2019; Hallab, 2013). Elevated measures of metal ion concentrations in blood serum and urine led to concerns of systemic effects from chronic exposure to metal ions.

Based on rising numbers of reported adverse events and accumulating evidence in clinical and explant studies, in 2011, the FDA issued 522 orders mandating postmarketing surveillance studies to all five US manufacturers of MoM hip implants. Detailed explant analysis from more than 2000 failed MoM hip implants determined that factors associated with release of higher metal ion levels and wear were: edge-loading of the metal acetabular liner, concurrent wear at the modular taper junction between the head and stem, larger head diameter, and acetabular cups designed with smaller cup coverage angles. The clinically failed hip implants exhibited more wear than was predicted by in vitro testing completed in mechanical hip joint wear simulators and used to support FDA premarket clearances of MoM hip bearings (FDA, 2019).

These results highlight the critical need for improved methods to measure wear and associated metal ion release at both the articular bearing surfaces and modular taper junctions. National and international standards committees are leading the development of additional “high-demand” and “adverse” hip wear testing protocols to better simulate wear conditions seen clinically. Detection of metal ion levels in body fluid (e.g., blood, serum, urine, and synovial fluid) lack sensitivity and specificity necessary for diagnostics and outcome predictions (FDA, 2019). The biological effects of wear and metal ion release in patients with MoM implants continue to present challenges for clinical management (FDA, 2019).

In 2016, the FDA issued a final order requiring manufacturers to submit a premarket approval application for MoM hip implants as class III medical devices (FDA, 2016). As of March 2019, there are no approved PMA applications for MoM total hip replacements. There are two MoM total hip resurfacing systems (Cormet Hip Resurfacing System, Corin; Birmingham Hip Resurfacing System, Smith & Nephew) cleared through the PMA process supported by nonclinical and clinical performance data.

CASE STUDY II: METAL ON METAL ARTICULAR BEARINGS IN HIP JOINT REPLACEMENT—CONT'D**What Properties Were Required of the Biomaterial?**

Implant biomaterials used for joint replacement must be biocompatible and stable in vivo for longer than 10 years, present a low risk of mechanical failure, resist deformation under loading conditions that exceed body weight, and provide favorable tribological properties to endure one to two million or more gait cycles of loading each year.

Desirable material properties for the bearing surfaces of total joint replacements include (Long and Rach, 1998; Rahaman et al., 2007):

1. High strength and toughness
2. High elastic modulus
3. High impact strength
4. High fracture toughness and fatigue resistance
5. High corrosion resistance
6. High hardness and good surface finish
7. High abrasion resistance
8. Good wetting behavior (low contact angle)
9. Low friction.

What Biomaterials Are Used?

Biomaterials used for articular bearings in hip joint implants include four classes of materials in clinical use or in development (Rahaman et al., 2007). These include:

1. Alloys of refractory metals (largely cobalt–chrome alloys, although stainless steel and titanium alloys were used in previous decades) (Long and Rach, 1998)
2. Refractory monolithic ceramic oxides (e.g., alumina, zirconia) or nonoxide ceramics (e.g., silicon nitride)
3. Ceramic composites (e.g., zirconia-toughened alumina)
4. Surface-modified refractory metals developed by oxidation (e.g., oxidized zirconium or zirconia) or surface deposition coatings (e.g., titanium nitride and diamond-like carbon).

According to the most recent data reported by the American Joint Replacement Registry (AJRR, 2018), ceramic biomaterials account for 52.3% of the femoral heads for hip joint implants, eclipsing the use of cobalt–chrome alloys in femoral heads for the first time. US surgeons overwhelmingly (>80% of cases) pair these femoral head biomaterials with highly cross-linked UHMWPE acetabular liners, and opt for 28 mm (14.0%), 32 mm (23.1%), or 36 mm (57.6%) diameter bearing surfaces.

TABLE 3.1.9.3**Patient–Implant Interactions Causing Clinical Complications (Schoen et al., 2012)****Thrombosis**

- Thrombotic occlusion
- Thromboembolism
- Anticoagulation-related hemorrhage (owing to therapy to prevent thrombosis)

Infection**Inappropriate Healing**

- Too little/incomplete
- Excessive tissue overgrowth

Structural Failure Due to Materials Degeneration

- Wear
- Fracture/fatigue
- Calcification
- Tearing

Adverse Local Tissue Interactions

- Inflammation
- Toxicity
- Tumor formation

Migration

- Whole device
- Embolization or lymphatic spread of materials fragments

Systemic and Miscellaneous Effects

- Allergy
- Heart valve noise

unique assessment protocols. Implant retrieval analysis makes use of systematic, multilevel assessment protocols documented in international standards (ASTM F561 and ISO 12891) and the medical/scientific literature. The standards generally describe relevant conditions to document at the time of explantation, methods for analyzing the tissue–implant interface and isolating particulate debris, and stages of progressively destructive analysis of the implant. Stage I analysis consists of routine device identification, documenting the device description, and macroscopic examination for any evidence of failure modes. Stage II analysis is more detailed and time consuming, and includes photography,

optical microscopy, and nondestructive failure analysis. Stage III analysis includes material-specific techniques for metallic, polymeric, and ceramic materials, many of which are destructive.

Implant retrieval analysis provides a window into in vivo implant performance and corresponding host responses and plays a critical role in determining the cause(s) and mechanism(s) of implant failure, that is, failure mode analysis (Schoen et al., 2012). Interactions of the implant biomaterials with the surrounding tissues can be local or distant to the implant and deleterious biomaterials–tissue interactions can exist below detectable limits for extended periods of

TABLE 3.1.9.4 General Goals of Implant Retrieval and Evaluation (Anderson et al., 2012)

Determine rates, modes, and mechanisms of implant failure
Identify effects of patient and implant factors on implant performance and overall clinical outcome
Establish clinical and design factors that promote implant success
Determine dynamics, temporal variations, and mechanisms of tissue–biomaterial and blood–biomaterial interactions
Develop design criteria for future implants
Determine adequacy and appropriateness of animal models
Identify biomarkers of implant reactivity

time before manifesting as complications in the patient (see Case Study: Metal-on-Metal Articular Bearings in Hip Joint Replacement). In addition to specific analysis protocols for the implant–tissue interface and implant biomaterials, unraveling a cause of failure usually requires systematic integration of clinical and laboratory information pertaining to the patient, and careful pathological analyses (Schoen et al., 2012). Evaluation of the implant without attention to the patient factors and clinical conditions will produce an incomplete evaluation, and limit understanding of the failure mode(s).

Implant complications are highly influenced by the clinical user (broadly used to include surgeon, interventionalist, or other medical professional) through the process of implant selection, implantation technique, and insertion procedure. This feature constitutes a key difference between implants and drugs, with the efficacy and safety of the latter generally not affected by the process of insertion (Schoen et al., 2012). In general, demographic, structural, functional, or physiologic factors relating to the patient (e.g., age, anatomy of the implant site, activity level, genetic predisposition to complications to thrombosis, allergies) and the implantation procedure (e.g., implant selection, technical aspects of the surgery, potential damage to the implant), are superimposed on the biomaterials and implant design and manifest failure modes (Schoen et al., 2012). Thus, implant failure in the clinical setting often involves multiple contributing factors (see Case Study: Prosthetic Heart Valves).

Medical Surveillance and the Role of Retrieval Analysis in Device Development

Explant analysis is complementary to both preclinical assessments and postmarketing surveillance. It challenges the scientific and medical community to consider what is normal function for medical implants and provides invaluable benchmarks for predictive models meant to simulate in vivo device performance. Quantitative endpoints generated from implant retrieval and evaluation and related failure mode

TABLE 3.1.9.5 Combined Strengths of Implant Registries and Explant Analysis

1. Provide for meticulous and professional scrutiny while ensuring transparency through traceable datasets and reporting to all stakeholders (medical, industrial, scientific, and public sectors)
2. Documentation of the actual number of implant failures rather than underrepresentation as often occurs with passive surveillance
3. Reports of scientifically rigorous epidemiological data that link explant analysis with implant registries to aid early detection of specific implant failures
4. Rigorous analysis of implant degradation processes through time-related observations to help distinguish sporadic events from the general behavior
5. Establish standardized classifications that enable objective comparisons between different implant models of a given medical specialty to improve material selection, design, and manufacturing processes of implants
6. Enhance understanding of the in vivo behavior of modern implants not otherwise exposed to rigorous premarket assessment.

analysis, as evidenced in the case studies presented in this chapter, aid the implant development process and contribute to patient safety.

Registry-based surveillance within regional or national healthcare systems provides an important context for implant retrieval and evaluation conducted within the context of routine clinical use. Studies from well-validated registries of large populations have the unique strength of reflecting the clinical reality (e.g., outcomes in routine clinical practice) and thus provide a high level of external validity (HerniaSurge Group, 2018). A major part of Europe's medical device regulations includes the European Database on Medical Devices (EUDAMED), which aims to help authorities conduct postmarket surveillance on medical devices using data obtained through vigilance and clinical investigations (SANCO, 2013). Integrating explant analysis programs into medical device registries and other intentional surveillance activities strengthens the total product life cycle approach, and advocates recognize several key strengths offered by this approach (Table 3.1.9.5) (Chakfe and Heim, 2017; FDA, 2013; MDRTF/MDEpiNet, 2015).

Medical devices and implants prioritized for registry development (Table 3.1.9.6) include high-risk devices and those in which device failure has serious implications for public health, devices using new technology whose long-term safety and effectiveness are not well understood, devices that have long in vivo durations, devices having many design variations and the potential for significant variations in outcomes, devices with outcomes that are highly dependent on the clinical user performance, and devices in which unanticipated problems with similar devices were identified through premarket review.

CASE STUDY III: PROSTHETIC HEART VALVES

Prosthetic heart valves have progressed significantly since the introduction of the first caged-ball valve in the 1950s, fueled by key advances in heart–lung bypass machines and thrombo-resistant biomaterials and the application of fluid mechanics for understanding blood circulation through the human heart. Often cited as the prototypical device failure analysis that contributed important clinical information, the problem of the Björk–Shiley tilting disk mechanical valve prosthesis provides an instructive case history.

What Problem Was Addressed?

The initial Björk–Shiley tilting disk mechanical prosthetic heart valve design, in which an acetal (Delrin) polymer disk and later a pyrolytic carbon disk was held in place by a wire superstructure composed of inflow and outflow struts, was associated with an unacceptable late failure rate owing to thrombotic occlusion. The inflow strut was an integral part of the valve base while the outflow strut was welded to the base ring.

In order to reduce the risk of thrombosis by improving valve flow, the company manufacturing the valve (Shiley, Inc.) redesigned the prosthesis to achieve opening angles of the disk of 60° or 70° from the plane of the valve base and rounded the surfaces of the disk (“convexo-concave” or “C–C”). However, clinical use of the redesigned Björk–Shiley C–C heart valve led to an unusually large cluster of cases in which the metallic outlet strut fractured in two places, leading to disk escape. The complication was fatal in the majority of patients in whom it occurred. In 2005, strut fracture was reported in at least 633 of the 86,000 (0.7%) valves of this type implanted worldwide during 1978–86. Clinical studies identified large valve size, mitral site, young recipient age, and valve manufacture date as risk factors for this failure mode (Blot et al., 2005).

Careful implant retrieval and evaluation elucidated the mechanisms of this catastrophic problem. Pathologic studies of retrieved Björk–Shiley valves, enhanced by scanning electron microscopy, demonstrated a pronounced wear facet at the tip of the outlet struts, and localized pyrolytic carbon wear deposits at sites where the closing disk contacted the strut (Schoen et al., 1992), providing a fatigue fracture mechanism that began on the inflow side of the outlet strut often initiated within a weld joint. The analysis suggested that the first strut leg fracture typically initiated at or near the point of maximum bending stress, was traced to a site of weld shrinkage porosity and/or inclusion in most cases, and was followed by fracture of the second leg. Occasionally, valves with only a single strut fracture were encountered. The underlying problem was metal fatigue failure, probably initiated by transient (<0.5 ms) outlet–strut–tip impacts due to overrotation of the disk during valve closure that produced almost 10 times the force of disc opening, leading to excessive bending stresses beyond the strut wire’s fatigue endurance limit (Wieting et al., 1999). These stresses occurred at or near the welds joining the outlet struts to the housing, potentially coupled with intrinsic weld flaws.

Moreover, in subsequent animal studies in which Björk–Shiley 60–70° C–C valves were implanted in sheep and instrumented with strain gauges showed that impact forces varied greatly with cardiac activity, and that loads occurring during exercise were significantly elevated. This correlated with clinical data that showed that fracture often occurred during exertion.

The Björk–Shiley prosthetic heart valve case demonstrates that elucidation of a failure mode by detailed materials failure

analysis can have a potential impact on patient management. Understanding this mode of failure has enabled the development of noninvasive testing modalities [via high-definition radiography (O’Neill et al., 1995) or acoustic characterization of strut status (Plemons and Hovenga, 1995)] to establish when one strut has fractured prior to the onset of clinical failure, to caution patients with these valves against vigorous exercise, and to consider rereplacement of properly functioning valves at high risk of fracture. Moreover, this case has reinforced certain principles of prosthetic heart valve testing which should occur before widespread clinical use of a new or modified prosthesis design (Blackstone, 2005).

What Properties Were Required of the Biomaterial?

Heart valve prostheses are devices intended to perform the function of the heart’s natural valves. Historically, three general designs used for mechanical heart valves included the caged ball, tilting disc, and bileaflet designs. The ISO 5840 standard outlines appropriate qualification tests and methods for assessing the physical, chemical, biological, and mechanical properties of heart valve designs and relevant materials. Desirable performance characteristics for modern heart valve prostheses include the following (Dasi et al., 2009; Ghanbari et al., 2009):

1. Durable for extended intervals (i.e., low peak stresses throughout the cardiac cycle to minimize the potential for creep deformation or fatigue)
2. Easily and permanently inserted into an appropriate physiologic site
3. Suitable interface between prosthesis and patient for appropriate healing
4. Nonobstructive to blood flow (i.e., open at a minimum systolic transvalvular pressure differential with minimum resistance to forward flow)
5. Nonturbulent flow for limiting shear stress experienced by the blood cells and platelets
6. Provide prompt and complete closure (i.e., minimize backward flow)
7. Noise-free function
8. Biocompatible, with low platelet adhesion
9. Nonthrombogenic
10. Nonhemolytic
11. Infection-resistant
12. Chemically inert and resistant to biodegradation (e.g., from oxidation, acid hydrolysis, enzymatic pathways, etc.).

What Biomaterials Are Used?

Biomaterials used for prosthetic heart valves in clinical use or in development include:

1. Titanium alloys or stainless steel alloys for structure and struts
2. Polyester (Dacron) or polytetrafluoroethylene (Teflon) as synthetic fibers for the suture ring
3. Pyrolytic carbon for tilting disc and leaflet features
4. Various types of polyurethane (e.g., polyester urethane, polyether urethane, polycarbonate urethane) with alternate chemical structures incorporated into the PU backbone to improve hydrolytic and oxidative stability (Ghanbari et al., 2009).

TABLE 3.1.9.6 **Implants and Medical Devices Prioritized for Medical Device Registries (MDRTF/ MDEpiNet, 2015)**

Medical Devices

1. Hip replacement devices
2. Knee replacement devices
3. Vascular procedures/devices (includes peripheral, AAA, carotid, and vascular access/catheters)
4. Spine procedures/devices
5. Cardiac valve replacement
6. Atrial fibrillation ablation procedures/devices
7. ICD/cardiac resynchronization therapy
8. Coronary stents
9. Robotic and other less invasive surgery
10. Ophthalmic procedures/devices
11. Surgical mesh

In summary, quantitative and systematic implant retrieval and evaluation bridges the gap between in vitro performance assessments and the effective clinical behavior of implants. It plays a critical role in the evolution of medical devices throughout the development process and clinical use. It informs the medical device industry through their corrective and preventive action (CAPA) systems for meeting FDA quality system regulation requirements (FDA, 2019b). It encourages technology development through identification of failure modes and mechanisms, providing a benchmark for assessing future improvements in implant performance and longevity. It provides an evidence-based approach for driving change in surgical techniques and implant biomaterials and designs. There will be persistent demand for quality data generated through implant retrieval and evaluation given that medical devices and implants prioritized for future registry development include high-risk devices, devices that have long in vivo durations, devices in which substantial design variations provide the potential for significant variations in outcomes (see Case Study: Surgical Mesh), and those in which device failure has serious implications for public health (Table 3.1.9.6).

CASE STUDY IV: SURGICAL MESH

Surgical mesh provides an instructive case study of a polymer biomaterial (polypropylene monofilament) attaining widespread dominance in two surgical applications (suture for wound closure and knitted mesh for hernia repair). The resulting “ancestral network” of surgical meshes cleared through the 510k regulatory pathway (Zargar and Carr, 2018) links a small number (11) of predicate surgical mesh implants to hundreds of subsequent products that are substantially dissimilar to their predicate designs. Moreover, this case study underscores the risk of claiming substantial equivalence to implants that are later recalled and the need for scientific evidence to support claims of substantial equivalence across various device categories (Zuckerman et al., 2014).

What Problem Was Addressed?

A hernia is defined as a protrusion or projection (prolapse) of an organ through the wall of the cavity where it is normally contained. Polymeric surgical mesh implants provide support for damaged or weakened tissues during hernia repair surgery. More than 1,000,000 Americans undergo hernia repair each year (Rutkow, 2003) and more than 90% of patients with certain types of hernias require repair with surgical mesh (Kingsnorth and LeBlanc, 2003). There have been several hundred unique surgical mesh products commercialized since the introduction of polypropylene monofilament fibers in the early 1960s for use as sutures for wound closure and as knitted mesh for hernia repair (Usher et al., 1962, 1963; Zargar and Carr, 2018). Polypropylene (PP), polyethylene terephthalate (polyester, or PET), and expanded polytetrafluoroethylene (ePTFE) are the most common materials for modern hernia repair mesh implants (Sanders and Kingsnorth, 2012).

Surgical mesh intended for use within the peritoneal cavity (so-called intraperitoneal onlay mesh, or IPOM) requires surgical mesh designs that combine more than one material into a composite mesh providing a smooth visceral side and a macroporous nonvisceral side. The visceral side incorporates a microporous sheet or barrier coating that is adhesion-resistant and nonabrasive to organs within the peritoneal cavity. The nonvisceral side consists of a structured knitted mesh surface for tissue ingrowth within the abdominal wall.

Introduced in 2000, the Composix Kugel surgical mesh is a self-expanding, nonabsorbable composite mesh implant that

combines an ePTFE layer (visceral side) and two layers of knitted monofilament PP mesh (nonvisceral side) with a peripheral PET memory recoil ring. The memory recoil ring, formed by welding together the ends of approximately 1 mm thick PET fiber and secured within a sewn edge located within the two PP layers, keeps the mesh optimally expanded. These IPOM composite meshes are intended to bridge large hernia defects and were offered in sizes ranging from a 4.5 inch (115 mm) diameter circle to a 10.7 × 13.7 inch (275 mm × 350 mm) oval, with larger meshes having two concentric rings. Multiple transabdominal sutures provide initial fixation of this IPOM composite mesh.

An estimated 350,000 Composix Kugel meshes were implanted in the United States from 2000 to 2005 before an FDA class I voluntary recall was initiated due to risk of memory recoil ring breakage potentially leading to bowel perforation and/or chronic enteric fistula (Hope and Iannitti, 2009). Other associated clinical complications with the Composix Kugel mesh include abdominal pain, mesh bulging, cut-out of transabdominal sutures, wrinkling, and seroma (Hope and Iannitti, 2009; Wiegering et al., 2013). The incidence of ring breakage was reportedly 0.009% based on complications reported to the FDA, although this likely underestimates the overall complication rate due to an unknown number of unreported events.

Implant retrieval and evaluation of a limited number of explanted Composix Kugel meshes, including electron microscopy, chemical analysis (FTIR, DSC), and materials testing, elucidated the failure mechanisms (Costello et al., 2007; Cozad et al., 2010; Wiegering et al., 2013). The PET memory recoil ring was severely damaged in areas of wrinkling or buckling, with breaks typically occurring at the ring weld. Compared to unused controls, explanted PP had lower heat of fusion (indicating lower crystallinity) and FTIR absorbance spectra consistent with oxidation, whereas explanted ePTFE had FTIR absorbance spectra consistent with cross-linking (Cozad et al., 2010). Explanted PET memory recoil rings exhibited degraded mechanical properties (fatigue and loss of elasticity) in cyclic mechanical tests (Wiegering et al., 2013). The analysis suggests that excessive forces applied to the mesh from manipulation during mesh placement or tissue contraction in situ could contribute to weld failure on the PET memory coil ring.

CASE STUDY IV: SURGICAL MESH—CONT'D

What Properties Were Required of the Biomaterial?

Implant retrieval and evaluation of many types of surgical mesh reveals that prolonged physiological loading produces a distinct tissue response for different classes of mesh with different pore structures (Klinge and Klosterhalfen, 2012; Muhi et al., 2008). For example, class II meshes having small pores (<60% porosity) and no effective porosity (interfilament distance <1000 μm) are associated with high volumes of inflammatory cells and fibrous connective tissues bridging across mesh pores compared to class I mesh having large pores (>60% porosity) and a suitable effective porosity (interfilament distance >1000 μm). ePTFE has a low-intensity inflammatory and fibrotic tissue response and incites only loose adhesions when used in the visceral cavity. The analysis supports using mesh structure to guide implant selection and assuring designs and materials maintain effective porosity under a range of mechanical strains.

Surgical meshes are continuously subjected to cyclic stress from abdominal wall forces, which can mechanically fatigue and alter mesh materials (i.e., increased stiffness, decrease strength), along with oxidative stress that has potential to degrade the biomaterials. Defining ideal properties of surgical mesh for hernia repair requires products that provide for strength to reinforce weakened tissues along with suitable pore structure and biocompatibility to foster tissue ingrowth. These performance criteria must be balanced with requirements to meet clinical indications (e.g., hernia size and location) and surgical handling (e.g., open vs. laparoscopic surgical approach) techniques.

Desirable performance characteristics for modern surgical mesh used in hernia repair include the following (Sanders and Kingsnorth, 2012):

1. Easily and permanently inserted into an appropriate physiologic site
2. Reinforces tissues while allowing normal physiological function of the abdominal wall
3. Durable for resisting mechanical strains and maintaining adequate long-term tensile strength and flexibility

4. Chemically inert and resistant to biodegradation
5. Does not adhere to viscera
6. Biocompatible, produces a controlled/predicted biological response
7. Noncarcinogenic and nonallergenic
8. Infection-resistant
9. Maintains optimal effective porosity under a range of mechanical strains
10. Rapid integration into host tissues and resists migration/dislocation.

What Biomaterials Are Used?

The most common widely used nonresorbable polymer used for surgical mesh implants is polypropylene (PP), which has many advantages as a mesh material (Sanders and Kingsnorth, 2012). These include its high tensile strength and burst strength, its ease of manufacturing for braided or knitted constructs, its compatibility with connective tissue ingrowth, and long-term data supporting its use in vivo. Disadvantages of PP include an intense foreign-body reaction associated with mesh contraction and reduced compliance and adhesion formation when in contact with visceral organs. Other common polymers used for surgical mesh implants are polyethylene terephthalate (PET), expanded polytetrafluoroethylene (ePTFE), and polyvinylidene fluoride (PVDF) (Sanders and Kingsnorth, 2012). PET provides for infiltration of fibroblasts for rapid fixation to tissues and less contraction than PP, but some studies report higher infection rates and loss of mechanical strength over time. Microporous and hydrophobic ePTFE meshes elicit a minimal inflammatory reaction and poor tissue ingrowth, which are advantageous for contact with visceral organs as an IPOM composite mesh. However, ePTFE is more susceptible to infection than other materials due to its laminar structure. Absorbable materials used for surgical mesh include polylactide (PLA), polyglycolic acid (PGA), polycaprolactone (PCL), and polydioxanone (PDO).

References

- American Joint Replacement Registry (AJRR), 2018. Annual Report. <http://www.ajrr.net/publications-data/annual-reports>.
- Anderson, J.M., Schoen, F.J., Brown, S.A., Merrit, K., 2012. Implant retrieval and evaluation. In: Ratner, B., Schoen, F., Hoffman, A., Lemons, J. (Eds.), *Biomaterials Science: An Introduction to Materials in Medicine*. Elsevier, pp. 1368–1383.
- Bank, H.L., Williamson, H.O., 1983. Scanning electron microscopy of Dalkon Shield tails. *Fertil. Steril.* 40 (3), 334–339.
- Barbour, P.S.M., Stone, M.H., Fisher, J., 1999. A hip joint simulator study using simplified loading and motion cycles generating physiological wear paths and rates. *Proc. Inst. Mech. Eng. (Part H)*. 213 (6), 455–466.
- Benjamin-Laing, H., Haddad, F.S., 2012. Metal-on-metal hip arthroplasty: going, going, gone. – opposes. *J. Bone Joint Surg.* 94-B (11 Suppl. A), 78–81.
- Blackstone, E.H., 2005. Could it happen again? The Björk-Shiley convexo-concave heart valve story. *Circulation* 111 (21), 2717–2719.
- Blot, W.J., Ibrahim, M.A., Ivey, T.D., Acheson, D.E., Brookmeyer, R., Weyman, A., Defauw, J., Smith, J.K., Harrison, D., 2005. Twenty-five-year experience with Björk-Shiley convexoconconcave heart valve: a continuing clinical concern. *Circulation* 111 (21), 2850–2857.
- Bozic, K.J., Kurtz, S., Lau, E., Ong, K., Chiu, V., Vail, T.P., Rubash, H.E., Berry, D.J., 2009. The epidemiology of bearing surface usage in total hip arthroplasty in the United States. *J. Bone Jt. Surg.* 91-A (7), 1614–1620.
- Campbell, P., Ebramzadeh, E., Nelson, S., Takamura, K., De Sme, K., Amstutz, H.C., 2010. Histological features of pseudotumor-like tissues from metal-on-metal hips. *Clin. Orthop. Rel. Res.* 468, 2321–2327.
- Campbell, P.A., Kung, M.S., Hsu, A.R., Jacobs, J.J., 2014. Do retrieval analysis and blood metal measurements contribute to our understanding of adverse local tissue reactions? *Clin. Orthop. Relat. Res.* 472 (12), 3718–3727.
- Chakfe, N., Heim, F., 2017. What do we learn from explant analysis programs? *Eur. J. Vasc. Endovasc. Surg.* 54, 133–134.
- Costello, C.R., Bachman, S.L., Grant, S.A., Cleveland, D.S., Loy, T.S., Ramshaw, B.J., 2007. Characterization of heavyweight and lightweight polypropylene prosthetic mesh explants from a single patient. *Surg. Innov.* 14 (3), 168–176.
- Cozad, M.J., Grant, D.A., Bachman, S.L., Grant, D.N., Ramshaw, B.J., Grant, S.A., 2010. Materials characterization of explanted polypropylene, polyethylene terephthalate, and expanded polytetrafluoroethylene composites: spectral and thermal analysis. *J. Biomed. Mater. Res. B Appl. Biomater.* 94 (2), 455–462.

- Daniel, G., McClellan, M., Colvin, H., Aurora, P., Khaterzai, S., 2015. Strengthening Patient Care: Building an Effective National Medical Device Surveillance System. The Brookings Institution.
- Dasi, L.P., Simon, H.A., Sucusky, P., Yoganathan, A.P., 2009. Fluid mechanics of artificial heart valves. *Clin. Exp. Pharmacol. Physiol.* 36 (2), 225–237.
- Eswaramoorthy, V., Moonot, P., Kalairajah, Y., Biant, L.C., Field, R.E., 2008. The Metasul metal-on-metal articulation in primary total hip replacement: clinical and radiological results at ten years. *J. Bone Jt. Surg.* 90-B, 1278–1283.
- FDA, U.S. Department of Health and Human Services, 2013. Strengthening Our National System for Medical Device Postmarket Surveillance.
- FDA, U.S. Department of Health and Human Services, 2016. Effective Date of Requirement for Premarket Approval for Total Metal-On-Metal Semi-constrained Hip Joint Systems. 21 CFR Part 888.
- FDA, U.S. Department of Health and Human Services, 2017. Classification of Products as Drugs and Devices and Additional Product Classification Issues: Guidance for Industry and FDA Staff.
- FDA, U.S. Department of Health and Human Services, Postmarket Surveillance. 21 CFR Part 822.3, 2018.
- FDA, U.S. Department of Health and Human Services, Biological Responses to Metal Implants, 2019.
- FDA, U.S. Department of Health and Human Services, 2019b. Quality System Regulation: Corrective and Preventive Action (Subpart J). 21 CFR Part 820.
- Firkins, P.J., Tipper, J.L., Ingham, E., Stone, M.H., Farrar, R., Fisher, J., 2001b. Influence of simulator kinematics on the wear of metal-on-metal hip prostheses. *Proc. Inst. Mech. Eng.* 215 (1), 119–121.
- Fisher, J., Hu, X.Q., Stewart, T.D., Williams, S., Tipper, J.L., Ingham, E., Stone, M.H., Davies, C., Hatto, P., Bolton, J., Riley, M., Hardaker, C., Isaac, G.H., Berry, G., 2004. Wear of surface engineered metal-on-metal hip prostheses. *J. Mater. Sci. Mater. Med.* 15 (3), 225–235.
- Ghanbari, H., Viatge, H., Kidane, A.G., Burriesci, G., Tavakoli, M., Seifalian, A.M., 2009. Polymeric heart valves: new materials, emerging hopes. *Trends Biotechnol.* 27 (6), 359–367.
- Grübl, A., Marker, M., Brodner, W., Giurea, A., Heinze, G., Meisinger, V., Zehetgruber, H., Kotz, R., 2007. Long-term follow-up of metal-on-metal total hip replacement. *J. Orthop. Res.* 25, 841–848.
- Hallab, N.J., Caicedo, M., McAllister, K., Skipor, A., Amstutz, H., Jacobs, J.J., 2013. Asymptomatic prospective and retrospective cohorts with metal-on-metal hip arthroplasty indicate lymphocyte reactivity varies with metal ion levels on a group basis. *J. Orthop. Res.* 31 (2), 173–182.
- Hart, A.J., Sabah, S.A., Henckel, J., Lloyd, G., Skinner, J.A., 2015. Lessons learnt from metal-on-metal hip arthroplasties will lead to safer innovation for all medical devices. *Hip Int.* 25 (4), 347–354.
- HerniaSurge Group, 2018. International guidelines for groin hernia management. *Hernia* 22, 1–165.
- Hope, W.W., Iannitti, D.A., 2009. An algorithm for managing patients who have Composix Kugel ventral hernia mesh. *Hernia* 13, 475–479.
- Howard, J.J., 2016. Balancing innovation and medical device regulation: the case of modern metal-on-metal hip replacements. *Med. Devices* 9, 267–275.
- Institute of Medicine of the National Academies, 2011. Medical Devices and the Public's Health: The FDA 510(k) Clearance Process at 35 Years. The National Academies Press.
- Jameson, S.S., Baker, P.N., Mason, J., Porter, M.L., Deehan, D.J., Reed, M.R., 2012. Independent predictors of revision following metal-on-metal hip resurfacing: a retrospective cohort study using national joint registry data. *J. Bone Jt. Surg.* 94-B, 746–754.
- Kingsnorth, A., LeBlanc, K., 2003. Hernias: inguinal and incisional. *Lancet* 362 (9395), 1561–1571.
- Klinge, U., Klosterhalfen, B., 2012. Modified classification of surgical meshes for hernia repair based on the analysis of 1,000 explanted meshes. *Hernia* 16, 251–258.
- Long, M., Rach, H.J., 1998. Titanium alloys in total joint replacement: a materials science perspective. *Biomaterials* 19, 1621–1639.
- McIntyre, D.A., 2011. The Eleven Most Implanted Medical Devices in America. 247wallst.com/healthcare-economy/2011/07/18/the-eleven-most-implanted-medical-devices-in-america/2/. [Accessed August 2019].
- McKellop, H., Park, S.H., Chiesa, R., Doorn, P., Lu, B., Mormand, P., Grigoris, P., Amstutz, H., 1996. In vivo wear of 3 types of metal on metal hip prostheses during 2 decades of use. *Clin. Orthop. Relat. Res.* 329S, 128–140.
- Medical Device Registry Task Force & the Medical Devices Epidemiology Network (MDRTF/MDEpiNet), 2015. Recommendations for a National Medical Device Evaluation System: Strategically Coordinated Registry Networks to Bridge Clinical Care and Research. <http://mdepinet.org/wp-content/uploads/2015-08-Recommendations-for-a-National-Medical-Device-Evaluation-System.pdf>. [Accessed August 2019].
- Muhl, T., Binnebosel, M., Klinge, U., Goedderz, T., 2008. New objective measurement to characterize the porosity of textile implants. *J. Biomed. Mater. Res. B Appl. Biomater.* 84 (1), 176–183.
- Nelson, A.L., Massoudi, N., 2016. New developments in intrauterine device use: focus on the US. *J. Contracept.* 7, 127–141.
- NIH, U.S. Department of Health and Human Services, 2000. Improving medical implant performance through retrieval information: challenges and opportunities. In: NIH Technology Assessment Conference.
- O'Neill, W.W., Chandler, J.G., Gordon, R.E., Bakalyar, D.M., Abolfathi, A.H., Castellani, M.D., Hirsch, J.L., Wieting, D.W., Bassett, J.S., Beatty, K.C., Soltis, M.A., Timmis, G.C., Grines, C.L., 1995. Radiographic detection of strut separations in Björk-Shiley convexo-concave mitral valves. *N. Engl. J. Med.* 333, 414–419.
- Plemons, T.D., Hovenga, M., 1995. Acoustic classification of the state of artificial heart valves. *J. Acoust. Soc. Am.* 97, 2326–2333.
- Rahaman, M.N., Yao, A., Bal, B.S., Garino, J.P., Ried, M.D., 2007. Ceramics for prosthetic hip and knee joint replacement. *J. Am. Ceram. Soc.* 90 (7), 1965–1988.
- Rieker, C.B., Köttig, P., Schön, R., Windler, M., Wyss, U.P., 1998. Clinical wear performance of metal-on-metal hip arthroplasties. In: Jacobs, J.J., Craig, T.L. (Eds.), *Alternative Bearing Surfaces in Total Joint Replacement STP 1346*. American Society for Testing and Materials, pp. 144–156.
- Roepke, C.L., Schaff, E.A., 2014. Long tail strings: impact of the Dalkon Shield 40 years later. *J. Obstet. Gynaecol. (Abingdon)* 4, 996–1005.
- Roylance, D., 1993. Assessment of olefin-based IUD tail strings. *J. Appl. Biomater.* 4, 289–301.
- Rutkow, I.M., 2003. Demographic and socioeconomic aspects of hernia repair in the United States in 2003. *Surg. Clin. NA.* 83 (5), 1045–1051.
- SANCO. European Commission, 2013. Guidelines on a medical devices vigilance system. *MEDDEV* 2 12-1.
- Sanders, D.L., Kingsnorth, A.N., 2012. Prosthetic mesh materials used in hernia surgery. *Expert Rev. Med. Devices* 9 (2), 159–179.
- Schoen, F.J., Hoffman, A.S., 2012. Device failure mode analysis. In: Ratner, B., Schoen, F., Hoffman, A., Lemons, J. (Eds.), *Biomaterials Science: An Introduction to Materials in Medicine*. Elsevier, pp. 1361–1368.

- Schoen, F.J., Levy, R.J., Piehler, H.R., 1992. Pathological considerations in replacement cardiac valves. *Cardiovasc. Pathol.* 1, 29–52.
- Semlitsch, M., Willert, H.G., 1997. Clinical wear behaviour of ultrahigh molecular weight polyethylene cups paired with metal and ceramic ball heads in comparison to metal-on-metal pairings of hip joint replacements. *Proc. Inst. Mech. Eng. H.* 211 (1), 73–88.
- Tatum, H.J., Schmidt, F.H., Phillips, D., McCarty, M., O’Leary, W.M., 1975. The Dalkon Shield controversy. Structural and bacteriological studies of IUD tails. *JAMA* 231 (7), 711–717.
- Usher, F.C., 1963. Hernia repair with knitted polypropylene mesh. *Surg. Gynecol. Obstet.* 117, 239–240.
- Usher, F.C., Allen, J.E., Crosthwait, R.W., Cogan, J.E., 1962. Polypropylene monofilament. A new, biologically inert suture for closing contaminated wounds. *JAMA* 179, 780–782.
- Wiegering, A., Schlegel, N., Isbert, C., Jurowich, C., Doht, S., Germer, C.T., Dietz, U.A., 2013. Lessons and challenges during a 5-year follow-up of 21 Compositix Kugel implantations. *Hernia* 17, 435–443.
- Wieting, D.W., Eberhardt, A.C., Reul, H., Breznock, E.M., Schreck, S.G., Chandler, J.G., 1999. Strut fracture mechanisms of the Bjork-Shiley convexoconcave heart valve. *J. Heart Valve Dis.* 8, 206–217.
- World Health Organization, 2003. *Medical Device Regulations: Global Overview and Guiding Principles.* (Geneva).
- World Health Organization, 2016. *TCu380A Intrauterine Contraceptive Device (IUD): WHO/UNFPA Technical Specification and Prequalification Guidance.* (Geneva).
- Zargar, N., Carr, A., 2018. The regulatory ancestral network of surgical meshes. *PLoS One.* 13 (6), e0197883. <https://doi.org/10.1371/journal.pone.0197883>. [Accessed August 2019].
- Zuckerman, D., Brown, P., Das, A., 2014. Lack of publicly available scientific evidence on the safety and effectiveness of implanted medical devices. *JAMA. Intern. Med.* 174 (11), 1781–1787.

Chapter Exercises (With Answers)

1. Identify the characteristics that define an implant, as recognized by the National Institutes of Health.

Answer: An implant is defined as a type of medical device that is placed inside or on the surface of the human body, as having an intended lifespan spanning months or years, as being made of biomaterials and penetrating living tissues, as having a physiological interaction in the human body, and as being retrievable.

2. Define implant retrieval analysis and identify two general goals for it.

Answer: Implant retrieval and evaluation (commonly, implant retrieval analysis or explant analysis) describes a method of scientific analysis for determining the efficacy and safety or biocompatibility of medical implants in vivo.

General goals include:

- Determine rates, modes, and mechanisms of implant failure
 - Identify effects of patient and implant factors on implant performance and overall clinical outcome
 - Establish clinical and design factors that promote implant success
 - Determine dynamics, temporal variations, and mechanisms of tissue–biomaterial and blood–biomaterial interactions
 - Develop design criteria for future implants
 - Determine adequacy and appropriateness of animal models
 - Identify biomarkers of implant reactivity.
3. Assume you are involved in characterizing biomaterials for the development of a new implant. Devise a preclinical testing plan that makes use of information gained through implant retrieval and evaluation.

Answer: This question is open-ended and has many possible correct answers.

A preclinical testing plan could include:

- (1) Inspection of unimplanted prototypes to evaluate changes induced by the fabrication process
 - (2) In vitro testing of implant biomaterials followed by implant retrieval and evaluation to evaluate biocompatibility, durability of the biomaterials, or potential failure modes
 - (3) In vivo animal models followed by implant retrieval and evaluation to evaluate biocompatibility, durability, implant–tissue interactions, or safety and effectiveness of the design.
4. Argue the advantages of integrating implant retrieval and evaluation programs into implant registries and other intentional surveillance activities.

Answer: This question is open-ended and has many possible correct answers.

Quantitative and systematic implant retrieval and evaluation ...

- Plays a critical role in the evolution of medical devices throughout the development process and clinical use
 - Informs the medical device industry through their corrective and preventive action (CAPA) systems for meeting FDA quality system regulation requirements
 - Encourages technology development through identification of failure modes and mechanisms, providing a benchmark for assessing future improvements in implant performance and longevity
 - Provides an evidence-based approach for driving change in surgical techniques and implant biomaterials and designs
 - Is a suitable tool for evaluating the safety and effectiveness of high-risk devices, devices that have long in vivo durations, devices in which substantial design variations provide the potential for significant variations in outcomes, and those in which device failure has serious implication for the public health.
5. What failure mechanisms did implant retrieval and evaluation reveal about early Björk-Shiley prosthetic heart valve designs? Describe the designs of modern heart valves that help to minimize the future risk of similar failures.

Answer: The tilting disk mechanical prosthetic heart valve design was associated with an unacceptable late failure rate owing to thrombotic occlusion. The redesigned Björk-Shiley C–C heart valve had fatigue fracture of the metallic outlet strut initiated at or near intrinsic weld flaws and the point of maximum bending stress, leading to disk escape, pronounced wear at the tip of the outlet struts, and localized pyrolytic carbon wear deposits at sites where the closing disk contacted the strut.

Designs of modern heart valves achieve low peak stresses throughout the cardiac cycle to minimize the potential for creep deformation or fatigue.

6. In the early 1970s, what biomaterial problems were revealed by implant retrieval analysis that helped to prompt the need for FDA regulation of medical devices, as authorized through the Medical Device Amendments of 1976?

Answer: Explant analysis of the Dalkon Shield intra-uterine device (IUD) revealed the multifilament tail string served as a wick for vaginal fluid and bacterial access inside the uterus. Deterioration of the outer nylon sheath, especially in regions of high stress adjacent to the knotted attachment side, provided a route for bacteria to exit the sheath into the sterile uterine cavity and contributed to string breakage during attempted removal. The absence of heat-sealed ends on the multifilament tail strings and deterioration of the outer nylon sheath were identified as contributing factors in the high infection rates and the FDA identified the multifilament tail string as a hazard for its role in the infections.

3.1.10

Legal Concepts for Biomaterials Engineers

MILES GRODY¹, STEPHEN F. BADYLAK²

¹Miles Grody Law, Potomac, MD, United States

²University of Pittsburgh, Pittsburgh, PA, United States

Introduction

It can be expected that the intricacies of the law are just as unfamiliar to biomaterials engineers as the intricacies of engineering are to lawyers. Nonetheless, throughout the course of a career biomedical engineers and other professionals in the medical device industry will routinely encounter a range of issues that require legal consideration or can have legal ramifications. Consequently, it is important for such professionals to develop a general awareness and familiarity with the types of situations in which legal issues will arise. Even if one is not comfortable with handling the situation alone, the appropriate legal resources can be marshaled to assist in managing the issues in a manner that supports, and perhaps even reinforces, the mission of the individual and their employer or organization.

Areas of legal concern that medical device professionals can expect to routinely encounter include the following general categories:

1. Employment agreements
2. Confidentiality and materials use agreements
3. Intellectual property: Patents, trade secrets, and freedom to operate
4. Contract negotiation, performance, and compliance
5. Sponsored research agreements
6. License agreements

Fortunately, from a biomaterials engineer's perspective the legal issues associated with these six areas at least partially overlap. Consequently, becoming acquainted with legal issues involved in even a single category should assist in understanding, and even anticipating, issues associated with other categories. Herein, a description of the legal issues typically involved with each of these categories is provided, along with a discussion of why these issues can make a difference both personally and professionally not only for the individual, but also for the broader organization within which their work is performed.

While medical device professionals in industry may approach specific legal issues from a different perspective than their academic counterparts, an awareness and sensitivity to these issues remains valuable regardless. The importance of various factors influencing such issues may vary, but the issues themselves tend to recur for both industry and academic professionals. The bias herein toward factors influencing industry professionals should be informative to those in academia as they interact with companies or consider moving to the private sector.

Employment Agreements

Perhaps the first legal document that any medical device professional will encounter in a post-university career involves an employment agreement. Understandably, when selecting an employer, the medical device professional will be focused primarily on matters such as job title, compensation, benefits, vacation time, and opportunities for advancement. These topics typically are covered in an offer letter, which may also include a provision stating that the medical device professional is an "employee at will." It is unlikely that an established employer will allow any newly minted employee to negotiate away this provision. The import of the provision is that the employer has reserved the right to terminate the employment at any time, with or without cause, and the medical device professional may have limited recourse in the event of what they may regard as an unwarranted employment termination.

The employment documents the medical device professional is required to sign will also include a formal legal contract addressing matters such as the treatment of confidential information, assignment of inventions, protection of trade secrets, non-competition, and non-solicitation. While these matters may not seem particularly remarkable or relevant at the time of signing, it should be realized

that these provisions can have important consequences for future job opportunities. Each of these provisions imposes legal obligations that can persist for several years after their employment with a particular company has ended. These provisions may impact not only which companies the medical device professional can join, but also the types of assignments that can be accepted with any future employer.

The employment agreement confidentiality provision should be similar to those found in non-disclosure agreements, which are discussed in detail below. This provision establishes that the employee is personally bound to protect the secrecy of any confidential information to which they are exposed during their employment, whether this confidential information belongs to their employer or to any third party with which the employer has entered a non-disclosure agreement. Less prominent, but potentially just as important, may be a provision stating that the new employee may not bring into the premises of the employer or use or rely on in the course of their work any unauthorized confidential information to which they may have access, such as confidential information from a prior employer. The ubiquity of such provisions in employment agreements should highlight for the medical device professional that companies take the protection of confidential information very seriously. Confidential information belongs to the company and not the individual, and any failure, whether intentional or accidental, to respect the agreed confidentiality terms can have severe consequences for the employee, including termination and potential damage to their professional reputation.

Assignment of inventions provisions establish that the employer, not the employee, is the owner of any inventions that the employee may create in the course of their work for the company. As discussed in the intellectual property section below, companies frequently file patent applications on inventions that may be valuable to their business. The drafting and prosecution of patent applications inevitably requires involvement from the individuals who participated in the invention's creation. The assignment of inventions provision imposes a legal obligation on the biomaterials engineer to cooperate with the company in the patent prosecution process, including executing any documents related to the patent application as may be reasonably requested by the company.

Protecting trade secrets constitutes one of the most important confidentiality obligations that any company places on its employees. The Defend Trade Secrets Act of 2016 (DTSA) illustrates the seriousness of protecting trade secrets ([Defend Trade Secrets Act](#)). This Act established for the first time the right of a trade secret owner to sue in federal court anyone who breaches the provisions of the Act, including the unauthorized disclosure or use of trade secrets by current or former employees. The DTSA allows companies to seek punitive damages, and reimbursement of attorney's fees, against former employees, meaning judgments against a former employee could be in the several thousands to millions of dollars. Trade secrets are discussed in more detail below because of the likelihood that most medical

device professionals will be exposed to these throughout their career. The importance of protecting trade secrets, and not breaching trade secret protection obligations, whether by an employment agreement, preexisting state law, or the DTSA, cannot be overemphasized.

Non-competition provisions present perhaps the most obvious restrictions on future employment opportunities a medical device professional may pursue. Such provisions typically prevent the departing employee from accepting employment from, or performing consulting work for, any competitor of the former employer for post employment periods ranging from approximately 1 to 2 years. Naturally, the provisions also prohibit the employee from working for any competitor of their employer during the period of the employee's employment. When evaluating various employment opportunities, thought should be given to how non-competition restrictions might impact career advancement opportunities. Medical device professionals should ensure that their skill sets are appropriately diversified so that after they leave an employer, for whatever reason, they will have the ability to find another job that will not place them in breach of their non-competition obligations.

Non-solicitation provisions are similar to, but distinct from, non-competition provisions. Typically, non-solicitation provisions in employment agreements prevent former employees from trying to entice away colleagues from their former employer. Non-solicitation provisions will also place restrictions on the former employee's freedom to enter into business arrangements with customers or contractors with whom they interacted during their former employment. Like non-competition provisions, non-solicitation restrictions may last for approximately 1 to 2 years post employment. Medical device professionals should be cognizant of the potential for non-solicitation provisions to impact the range and types of professional and business relationships in which they might engage once they seek new employment.

Confidentiality and Materials Use Agreements

Perhaps the most frequent issue a biomaterials engineer will encounter that involves legal considerations is a confidentiality agreement, also known as a non-disclosure agreement or NDA. Most companies and other organizations have adopted protocols requiring an NDA before confidential information is shared with a third party, such as another company or institution with which it is considering entering into a business arrangement. It is frequently desirable or necessary for some component of one party's confidential information to be shared with the other party so that a potential collaboration or contractual agreement can be fully considered. Consequently, an NDA is often signed before any substantive discussions occur, and it is not uncommon for a business relationship to fail to materialize even after the NDA has been executed. If a formal relationship does develop, the confidentiality terms captured in the

original NDA will persist, and may even be enhanced in the agreements that define the scope of the ongoing and forward-looking business relationship.

Each NDA is focused on one of the most important and valuable assets any organization possesses: its confidential information. While there are many categories of information that are generally considered confidential, there is no single standard definition that is common across all organizations and addresses every possible piece of confidential information an organization may possess. Consequently, one of the first things that any reader encounters in an NDA is a definition of what constitutes confidential information for the purposes of that NDA. A typical provision in a mutual NDA, protecting information shared by each party, might state the following:

Confidential Information shall mean any and all technical business and other information including, without limitation, patent, copyright, trade secret and proprietary information, techniques, sketches, drawings, models, inventions, know-how, processes, formulae, apparatus, equipment and biological materials related to the current, future and proposed products and services of each of the parties, and includes, without limitation, their respective information concerning research, experimental work, development, design details and specifications, engineering, financial information, procurement requirements, purchasing, manufacturing, customer lists, business forecasts and sales, and marketing plans.

This provision includes language that clearly could not and would not have been drafted by anyone except a lawyer, and attempts to include everything, except the often referred to “kitchen sink.” The problem, as referenced at the beginning of this chapter, is that the lawyer who drafts such language almost certainly is not also a biomaterials engineer. As a general matter, it can be anticipated that the lawyer drafting an NDA, or for that matter attempting to represent or protect any other issues that are central to the activities of a medical device professional, will never understand the individual’s business and concerns as well as the individual himself. It is therefore possible that the standard description of confidential information appearing in an NDA provided by legal counsel might not include the specific category of information that is anticipated to be shared with the third party. Definitions provided in contracts are very important. Medical device professionals should pay particular attention to such definitions, and if it is believed that something important may be missing, this issue should be raised and pursued until it is addressed to their satisfaction.

The following steps, at a minimum, should be taken to maximize assurance that the party receiving confidential information will abide by the terms of the NDA, and therefore minimize the possibility that confidential information is misused by a third party, especially a potential or actual competitor: (1) ensure that an NDA has been executed with the receiving party before any confidential information is

shared; (2) ensure that any confidential information provided to the other party is clearly marked as belonging to the biomaterials engineer’s organization; and (3) carefully consider whether information that any member of the biomaterials engineer’s organization discloses verbally to a third party should be treated as confidential under the terms of the NDA.

The medical device professional should request to see an executed copy of the NDA before any confidential information is shared so that they know what is covered within the defined scope of confidential information, the period of time the receiving party will be obligated to protect the confidentiality of the information (often there are expiration dates ranging from 1 to 5 years), and the limitations for which the confidential information may be used by the receiving party. The medical device professional should ensure that the NDA has been written to protect their organization’s confidential information, and not just the confidential information of the other party. Typically, organizations sign either a mutual NDA or a one-way NDA. While a mutual NDA protects both parties’ confidential information, a one-way NDA protects only one designated party’s information. It is often preferable to execute a one-way NDA provided it is your organization’s confidential information that is designated for protection.

NDAs often include a provision requiring the party seeking protection to clearly mark all shared information as confidential, and the medical device professional should assume responsibility for doing this to the extent they are sharing confidential information. However, it may not be sufficient to simply mark a document as “Confidential.” Even though two parties may not dispute that information in a document is confidential, they still may argue over which party actually produced the document and therefore has the right to claim ownership. The simplest remedy is to include the organization’s name in the label that identifies a document as confidential, and to insert this label as a header or footer on every page of the confidential document. Such labeling is a simple and prudent practice for all documents that include confidential information, regardless of whether it is anticipated that these documents may be shared at some future point with a third party.

Beyond simply marking documents as confidential, the medical device professional should give additional and careful consideration to whether anything any member of their organization disclosed verbally to a third party contains information that should be considered confidential. Many NDAs state that information conveyed verbally will not be treated as confidential unless it is identified as confidential at the time it is first discussed. The NDA may also require the disclosing party to send a written document to the receiving party within a defined period of time after the discussion occurred, usually no more than 30 days, stating that confidential information was shared and specifically describing that confidential information. As might be imagined, this exercise is a burdensome process, so the disciplined individual should not share confidential information with third

parties unless there is an advance plan as to how the ownership of that confidential information can be clearly mapped back to their organization.

NDA's invariably include limitations on the categories of information that may be protected. For example, excluded information will include information the receiving party already possessed, or information that has entered the public domain through no fault of the receiving party. Also excluded is information that the receiving party independently develops, without reference to the disclosing party's information. Proving such independent development can be fraught with uncertainty, however, and should not be relied upon in the absence of careful and disciplined planning and procedures, including the advice and guidance of an attorney experienced in protecting confidential information. Diligent record keeping in a laboratory notebook, which is discussed in more detail below, may be essential for demonstrating independent development.

When working with a third party, a biomaterials engineer often may want not only to verbally share information considered to be confidential, but also sample materials that are based on or incorporate that confidential information. It is common practice in such instances to execute, in addition to an NDA, a materials use agreement or a materials transfer agreement, often referenced by the acronym "MUA." As a general matter, the biomaterials engineer can regard an MUA as a strategy for extending limitation on use provisions comparable to those in an NDA to any proprietary materials that are shared with the receiving party. In the context of intellectual property law, as discussed in more detail below, the term proprietary refers to materials that are based on technology that a party may own, even if the technology itself is not confidential. For example, patents constitute detailed public descriptions of materials that are proprietary to the patent owner, but, by virtue of the published patent, are not confidential.

A medical device professional considering execution of an MUA should be particularly concerned with three issues, specifically: (1) how the shared material can be used by the receiving party; (2) the obligations of the receiving party to report to the disclosing party the results of its activities with the shared material; and (3) the implications of any ownership and use rights stemming from possible inventions resulting from the receiving party's work with the shared material.

As a general matter, proprietary materials shared with a receiving party are valuable, whether this value reflects the cost involved in the production of the specific items that are shared, or the research and development costs involved in the original conception and reduction to practice of the shared material. Under certain circumstances, a biomaterials engineer's organization might perceive potential value in sharing its proprietary material with a third party because that third party may possess its own proprietary knowledge or techniques that could enhance the overall value and usefulness of the shared material. Consequently, when a biomaterials engineer or other medical device professional

considers sharing proprietary material with a third party, a limited and specific purpose for which the material can be used by the third party should be clearly defined to ensure that the third party does not have unlimited rights to do whatever they want with the material.

If the biomaterials engineer's organization executes an MUA with a third party that includes a clearly defined purpose, then it is reasonable to expect the receiving party to actually work with the material in a manner that produces results. The sharing party's right to review such results should be clearly defined. In most circumstances it can be assumed that the sharing party would not have provided its proprietary composition to the receiving party without the expectation that it would receive a reasonably detailed report on the results of the receiving party's activities with the composition. Rather than leaving the receiving party with discretion over whether to provide the results, the biomaterials engineer should ensure that the MUA includes a specific provision requiring production of a detailed written report. Such information may be essential for the biomaterials engineer's organization to develop an informed opinion regarding whether to invest additional time and resources into the material itself or furthering a working relationship with the receiving party.

Before sharing proprietary materials, a biomaterials engineer should give careful thought to whether the activity of the third party might result in a new patentable invention. If it is possible that a patentable invention might result, the biomaterials engineer should proceed with great caution, and should ensure that others within senior management are aware of this possibility. Ownership of a patent is based on inventorship, and as discussed in the employment agreement section above, patents belong to the inventor's company or organization through assignment. Sharing proprietary material with a receiving party does not necessarily make the sharing party an inventor of the work conducted by the receiving party, particularly if the receiving party conducts its work with the material independently of any involvement by the sharing party, and using methodologies or additional compositions that are proprietary to the receiving party. Consequently, a potentially serious risk arises that the receiving party may gain patent rights involving or incorporating the sharing party's proprietary material, and that these rights might be separate and distinct from any patent rights of the sharing party. Possible ramifications of this risk are discussed in more detail in the patent section below. One of the best and easiest methods for a sharing party to avoid such a risk is to ensure that the purpose for which a proprietary material is shared under an MUA is unlikely to result in the development of a new invention, and to ensure that this purpose and the associated methodologies are clearly defined in the MUA. Failure by the receiving party to follow the purpose or abide by the methodologies would constitute a contractual breach entitling the sharing party to legal remedies.

Intellectual Property: Patents, Trade Secrets, and Freedom to Operate

Intellectual property, commonly known as IP, refers to creations of the mind, such as inventions, trade secrets, trademarks, literary and artistic works, and designs. Important legal rights and considerations are associated with various forms of IP. Two of the most important forms of IP that regularly impact the activities of a medical device professional are patents and trade secrets. Patents and trade secrets involve doctrines that define specific legal rights relating to an organization's ability to claim exclusive proprietary ownership of its inventions or the methodologies it has innovated to produce its products and inventions and to conduct its business. Any biomaterials engineer working in a research and development environment or a production environment is likely to regularly be working with, and perhaps even developing, their organization's patents and trade secrets.

Patents and trade secrets can be thought of as opposite sides of the same coin. Patents are granted for inventions that are novel and non-obvious, and are obtained through patent applications submitted to the governmental patent office of the nation in which the applicant is seeking patent protection. If granted, patent applications provide the patent owner with exclusive rights to practice the invention for a period of 20 years from the date the patent application was first filed. A patent, which is a publicly accessible written document describing an invention, can be thought of as a legal monopoly on the use of an invention until the date the patent expires.

Unlike patents, trade secrets are not filed with any governmental entity, and do not have expiration dates similar to patents. The types of trade secrets a biomaterials engineer may encounter most frequently involve the specific steps and methodologies an organization develops to conduct research or manufacturing activities that it considers proprietary and valuable. Qualification of such steps and methodologies as trade secrets depends upon the measures that the organization takes to ensure that these are kept confidential. The classic example of a trade secret involves the specific recipe for Coca-Cola, which continues to qualify as a trade secret decades after it was developed because its confidentiality has been maintained. As a general matter, an organization can lose its exclusive rights to its trade secrets when such information is disclosed to the public. Consequently, in contrast to patents, organizations typically take great care to ensure their trade secrets are not disclosed publicly. There is no pre-set expiration date on the proprietary rights associated with trade secrets, but these rights can automatically expire when the steps or methodologies involved in the trade secret become publicly disclosed.

Patents and trade secrets are potential alternatives for the work performed by a biomaterials engineer stationed in a research and development department. Despite sometimes mundane laboratory routines, it is important to be consistently conscious of the potential development of patents

and trade secrets. As a best practice for identifying and supporting patent or trade secret rights, the biomaterials engineer should always keep an accurate and detailed laboratory notebook recording their work, sometimes referred to as an inventor's notebook. The pages of the notebook should reflect the date on which the work or experiments were performed, should be signed by the person who wrote the notes, and should be contemporaneously witnessed by the signature of a second person. The information recorded in an inventor's laboratory notebook can be extremely helpful for drafting a patent application, and can be critical for determining inventorship. Similarly, this information also can be dispositive if it becomes necessary for an organization to demonstrate that it is entitled to trade secret protection for any of its proprietary methodologies.

At some point during the course of performing their work a biomaterials engineer may recognize the possibility that they have created an invention. When this realization occurs, another best practice is to prepare an invention disclosure document. The biomaterials engineer's organization may already have a preferred invention disclosure template, or if not, templates can be found on the web. Invention disclosure forms typically should include a summary description of the invention, the name(s) of the inventor(s), the date the inventors believed they completed the invention, and a detailed discussion of the steps involved and work performed in creating the invention. Additionally, the invention disclosure can include a summary explanation of why the inventors believe their creation is different from any existing or previous materials or techniques known to or practiced by others. Such preexisting materials and techniques are referred to as "prior art." As discussed in more detail below, a fundamental principle for an invention to be recognized as novel and patentable is that it must be distinct from any prior art—in precise terms, it must be novel and non-obvious.

Incorporating a new, proprietary invention into an organization's business practices should entail following a well-considered, disciplined protocol, including the involvement of at least one attorney who specializes in intellectual property law. The most efficient way for the biomaterials engineer to engage an IP attorney in the assessment of a potential invention is to provide that attorney with a detailed, carefully written invention disclosure. No matter how well written the invention disclosure may be, it is inevitable that the IP attorney will have multiple questions for the inventors. The more detailed these questions are, the better. Inventors must educate their IP attorney regarding the specifics of their invention. There is a direct correlation between any IP attorney's understanding of these specifics and that attorney's ability to recommend optimal strategies for protecting the various IP rights that the biomaterials engineer may have created. Ideally, a well-written invention disclosure should allow an experienced IP attorney to advise the biomaterials engineer's organization on at least two issues: (1) the likelihood that the described invention may be patentable, and (2) the likelihood that practicing the described invention

might infringe on the existing patent rights of any third party. A well-written invention disclosure may also enhance the IP attorney's ability to advise the biomaterials engineer and their organization on the relative risks and benefits of pursuing a patent as opposed to maintaining the invention as a confidential trade secret.

Medical device professionals should recognize the potential urgency of filing a patent application if their research has produced a possibly novel and non-obvious invention. On September 16, 2011, the America Invents Act (AIA) became law ([Leahy-Smith America Invents Act](#)). An important feature of the AIA is that, regardless of who may have created an invention first, ownership of the invention is determined by the first party that files a patent application. Particularly if a biomaterials engineer is experimenting in a field that has stimulated multiple diverse research initiatives, filing a patent application quickly could make the difference between having the ability to follow through with research to its completion, or abandoning it because a third party filed first. To optimize the likelihood of being the first to file, patent seekers often move quickly to file what is known as a provisional patent application. The provisional application customarily includes as detailed a summary of the invention as possible at the time it is filed. Most importantly, filing the provisional application establishes what is known as the claimed invention's priority date. Within 12 months after filing a provisional patent application, the applicant can revise and enhance the application with new information learned since the priority date was established, and then convert the application into a non-provisional application so that examiners within the patent office can then begin their review to determine patentability. Nonetheless, for purposes of the AIA and various international patent offices, the first to file date will be the priority date.

Regardless of whether a provisional patent application has been filed, the decision makers within the biomaterials engineer's organization may deliberate over whether it is worth investing further resources and effort into developing the invention. Part of these deliberations will involve whether to incur the expense associated with authorizing the IP attorney to conduct a freedom to operate analysis. A freedom to operate analysis involves a combination of automated and non-automated research techniques to review patents, patent applications, and other documents in the public domain relating to prior art that may be similar to the art described in the invention disclosure. Upon completing the freedom to operate analysis, the IP attorney should be able to offer informed opinions on two distinct questions: (1) whether the described invention may be patentable; and (2) whether practicing the described invention may infringe any third party's patent. As a result of this analysis the IP attorney may also be able to recommend ways to refine the invention to enhance the likelihood of patentability or reduce the possibility of infringing any third party patent.

If the IP attorney opines that a reasonable possibility exists that a proposed invention would infringe a third party patent, and no reasonable strategy can be identified

for avoiding such potential infringement, the biomaterials engineer's organization may decide to abandon any plans for putting the proposed invention into practice. While abandoning the proposed invention inevitably will be disappointing, the insights gained from the IP attorney's analysis will still be valuable. There can be serious and expensive financial consequences and penalties associated with practicing the art described in a third party patent when patent infringement litigation is threatened or engaged. Based on the biomaterials engineer's careful description of their proposed invention, and the resulting analysis from the IP attorney, the biomaterials engineer's organization will hopefully have avoided the potentially crippling expenses associated with patent infringement litigation and any resulting judgment, or at least gained a clear picture of the risks before proceeding ([Keeley, 1999](#)).

If the IP attorney opines that the proposed invention is unlikely to infringe any patented prior art, it then becomes important to assess whether it may be more valuable to patent it or practice it as a trade secret. A broad array of business, legal, financial, and practical factors may influence how such questions are resolved ([Durham, 1999a](#)). One of the primary factors in such a decision, however, involves the fact that pursuing a patent application necessitates describing the proposed invention in a sufficiently detailed manner such that another person in the biomaterials engineer's field (generally referred to as a "person skilled in the art") can replicate the invention based on the description provided in the patent application. Unless they are abandoned, patent applications typically are published approximately 18 months after the provisional application is filed, regardless of whether a patent is ultimately granted. The review process conducted by U.S. and international patent offices often takes more than 18 months, meaning that there is a reasonable likelihood that the detailed description of a claimed invention contained in a patent application may be published before any determination is reached whether that claimed invention is patentable.

While the exclusive legal rights associated with the grant of a patent are significant, these must be weighed against the risk that the patent may not be granted. In this regard, the biomaterials engineer should be particularly sensitive to, and focused on, two distinct components of any patent application. These components are referred to as the specification and the claims. The specification involves a detailed description of all aspects of the claimed invention, including in particular those features that distinguish the claimed invention from any prior art. The specification must be sufficiently detailed so that anyone skilled in the art who reads it could replicate the described invention, and must include the best way the inventors know to practice it ([Durham, 1999b](#)). In other words, in its specification every patent application contains a complete disclosure of the invention that, if published, will become publicly available so that anyone can reproduce the work unless a patent is granted.

The claims section of the patent application, which is typically far shorter than the specification, precisely describes

the features of the invention that make it novel and non-obvious, and therefore are entitled to 20 years of patent protection. Exclusive rights associated with granted patents are based on what is specifically described in the claims, as opposed to what is more broadly disclosed in the specification. For claims to be granted, valid and legally enforceable, everything described in the claims must be supported by the teachings and descriptions included in the specification.

The factors that determine whether patent claims may be granted, and even if granted whether they have any commercial or competitive value, can be complicated. No matter how skilled the IP attorney, it is inevitable that the inventors named on the patent application will have insights that the IP attorney will not possess except to the extent the inventors specifically teach these to the IP attorney so that they can be incorporated into the patent application. Stated differently, a medical device professional seeking patent protection must expect to devote considerable time, and very detailed attention, to the preparation of a patent application and to any governmental patent office's review of that application. The pursuit of an actual patent grant involves a process referred to as patent prosecution and requires continued focused engagement of the inventors in coordination with their IP attorney. By the time a patent office makes a final decision on the patentability of any claims in a patent application, it can be expected the inventors and the IP attorney will have had multiple extensive and detailed conversations and reviews of the documents submitted by the biomaterials engineers' organization to the various international patent offices where patent protection is being sought.

The 20-year exclusivity rights associated with a granted patent may be more valuable to a medical device professional's organization than the relatively weaker, but potentially longer term, rights associated with trade secrets. Consequently, based on the information contained in the invention disclosure, the biomaterials engineer's organization should make an informed and deliberate decision whether to pursue a patent or rely on trade secret protection regarding any particular novel and non-obvious concept. The prosecution of a patent application and maintenance of the patent once granted can be expensive; therefore, the decision may be based not just on the likelihood of a patent being granted, but also the cost and value of the patent. An IP attorney who is experienced in the technical field of the biomaterials engineer's organization can help advise on the relative benefits of pursuing a patent versus relying on trade secret protection laws.

Contract Negotiation, Performance, and Compliance

The standard protocol followed when two or more organizations choose to jointly invest their resources in a common project or activity entails the execution of a written contract. A contract includes written terms and conditions establishing the rights and obligations of each party as these relate

both to the purpose of the contract and also to any matters or legal rights that may be impacted by the contract. Contracts can be very detailed, and may rival patent applications regarding the precision and discipline with which they are drafted. Careful drafting is important, because any lack of clarity can result in misunderstandings between the parties as to their respective contractual rights and obligations. Such misunderstandings can not only undermine the spirit of cooperation and goodwill between the parties but, if serious enough, can undermine the entire relationship between the parties, even resulting in breach of contract litigation. When a contractual relationship between parties begins to deteriorate, it is not uncommon for an organization's management to examine not only the terms of the contract, but also the expectations and promises of the individuals who originally advocated for the contract, in an effort to determine why it is failing to meet the organization's objectives.

Biomaterials engineers need to be attentive to reviewing and understanding contracts if for no other reason than the various functions they will be responsible for performing will be subject to specific obligations established in the contract. Further, contracts executed by a biomaterials engineer's organization may impose certain personal obligations on them, particularly with respect to the protection of confidential information.

Clearly, to the ordinary individual, the review of a contract can be boring and intellectually taxing. The objective of many provisions in the contract may not be readily apparent, and it may not be clear which provisions may be subject to negotiation versus those that may trigger unexpected negative responses from the other party if opposed. Despite these inconveniences and uncertainties, a medical device professional proceeds at their own peril if they fail to focus carefully on the provisions of contracts that relate specifically to their areas of responsibility and their job performance.

It is axiomatic that in today's world no one can become a biomaterials engineer without having developed rigorous and disciplined intellectual capabilities and work habits. These same qualities should be applied to the negotiation and review of contracts. The provisions of any contract can be divided into two general categories: the business terms (i.e., the scope of work and associated payment schedule), and the legal terms that are often referred to as "legalese." The biomaterials engineer should be prepared to play a leading role with respect to the business terms, including the scope of work, that are incorporated into any contract that they, or any team they lead, are expected to execute. At the risk of oversimplifying, the business terms may be characterized generally as Party A agreeing to perform Task X for Party B by a certain date and according to certain specified standards, and in exchange Party B will pay Party A a predetermined amount of money based on a contractually documented payment schedule. Such business terms may be very detailed, and may contemplate a range of different possibilities, but as a general matter they should be written in plain English, not legalese. Because these terms should

be in plain English, any biomaterials engineer involved in the contract negotiation process should ensure that they understand these terms, and can deliver on them, before their organization commits by executing the contract. Similarly, if these terms are not in plain English, the biomaterials engineer should be prepared to challenge them and to explore whether there are options to resolve any ambiguities or problems, including writing these terms more clearly. It is difficult to deliver on contractual obligations if the obligations are unclear.

The biomaterials engineer's responsibilities are not satisfied just by resolving issues with the business terms of a contract. A disciplined biomaterials engineer should also pay at least some attention to those contract provisions that may be classified as legalese. Legalese provisions typically can be categorized into two distinct, but somewhat overlapping, categories: (1) those that impact how disputes and litigation of any alleged contract breach might be handled; and (2) those that generally define the business relationship between the two parties. If a biomaterials engineer is expected to approve, either explicitly or implicitly, the terms of any contract on which they must execute, it is not unreasonable for the biomaterials engineer to insist on understanding not only the business terms of the contract, but also these two categories of legalese provisions.

The first category of legalese provisions, concerning how disputes or litigation may be conducted, involves issues and considerations that typically are decided by attorneys, or business professionals with significant legal expertise and experience. Because of this dependence on legal experience for ensuring that such provisions are optimized for the medical device professional's organization, it can be anticipated that medical device professionals may be free from blame if these provisions ultimately work against their organization's best interests. In other words, these are primarily legal issues, and contract lawyers should have taken care of them, not the engineers and scientists. This being said, the issues involved in this category of legalese provisions are not so complicated that medical device professionals cannot make constructive contributions. Individuals should not be reluctant to ask their attorney to clarify the intent of specific provisions addressing disputes, the possible alternatives, and the reason that the terms chosen for the contract might be more advantageous than possible alternatives.

The second category of legalese provisions, involving business terms, should be more easily understandable to medical device professionals than the first category. These provisions involve topics such as ownership of work produced pursuant to the contract, project management and updates between the parties, reasons that the contract may be terminated, confidentiality, and non-competition, to name a few. While these provisions may generally be regarded as standard from one contract to the next, there may be certain business arrangements where a so-called standard provision could work against the medical device professional's best interests, and a customized provision might be appropriate. For example, the medical device professional's

organization should reject a non-competition provision if the consequence of such a restriction would severely limit the organization's opportunities for growth. Medical device professionals should seek to develop a collegial relationship with their attorney so that together they can jointly evaluate those situations where customized contract provisions should be substituted for standard provisions.

Once a contract has been signed, the biomaterials engineer should take careful note of those provisions that bear specifically on their department's performance responsibilities. If the biomaterials engineer is leading a team that is delivering on the contractual commitments, then the extent to which it could be valuable, if not essential, that all team members also become aware of these commitments should be considered. Contract negotiation can be a prolonged, and sometimes painful, process. It is not uncommon, once the contract has been executed, for the parties to say they hope everything will proceed so smoothly that they can put the contract in a drawer and not look at it again. One should not be fooled by such hyperbole. Hopefully they will never have to look again at the first category of legalese provisions in the contract, addressing disputes and litigation. The biomaterials engineer, however, certainly will need to be familiar with the scope of work described in the contract, and may find it valuable to refer back to this from time to time to ensure not only that their organization, but also the other party, are meeting contractual obligations in a satisfactory and timely manner.

Sponsored Research Agreements

Sponsored research agreements and license agreements are two of the most important categories of contracts where medical device professionals may be the most prominent advocates within their organization for the contemplated business relationship. Biomaterials engineers are likely to play the leading role not only of recommending the relationships that lead to these agreements, but also of delivering on the responsibilities specified therein. Consequently, biomaterials engineers can expect to engage proactively in negotiation of the business terms of these agreements. While individuals from other departments, including the legal department, may provide important and constructive advice regarding the structure of the agreements, the medical device professional should not casually acquiesce to entering any sponsored research agreement or license agreement if they do not clearly understand the respective business commitments of the parties or if they believe an agreement might place their organization in an inappropriately disadvantageous or compromised position. The attorney who advises the medical device professional's organization regarding the agreement should be able to identify and assist with avoiding many potential contractual pitfalls. However, the biomaterials engineer almost inevitably will understand the specific scientific and engineering fields involved better than the attorney. Therefore, the

attorney's effectiveness will be directly impacted by how effectively the biomaterials engineer engages in the contract drafting and negotiation processes.

Sponsored research agreements, or SRAs, typically involve situations where a university agrees to conduct a clearly defined research project for an industrial entity in exchange for a fixed cost. All of the issues discussed above relating to contract negotiation, performance, and compliance apply specifically to SRAs. As the biomaterials engineer may be the company's lead advocate for any particular SRA, this individual should play a leading role in developing the business terms for the SRA. In the context of the SRA, one component of the business terms includes the specific tasks or experiments that the university is agreeing to perform. These tasks are accompanied by the associated deliverables, such as the written reports describing the results of these tasks or experiments, and a schedule for when these reports will be provided. This component of the business terms is often written by the biomaterials engineer, in coordination with a university counterpart, and is attached to the terms and conditions of the SRA as a separate but integrated addendum. The attorney advising the company will likely review the contents of this attachment, and may have questions or suggestions for the biomaterials engineer regarding its content, but the biomaterials engineer should recognize that the attorney's ability to make specific recommendations regarding the attachment's contents may be limited because the attorney is unlikely to possess the same level of insight into its subject matter as the biomaterials engineer.

Other important components of the business terms specific to the scope of work may appear either in the main body of the SRA or the attachment describing the specific project. Examples of these components include the payment terms, and the identity of the principal investigator. Biomaterials engineers should expect that representatives from the finance department will want to review and approve the cost of any SRA before it is executed. The finance department representative and the company attorney may make helpful suggestions regarding how payments should be structured, such as an upfront amount, installment payments on certain calendar dates or when certain milestones are achieved, and a final payment after the university has fully delivered on its commitments.

When medical device professionals within industry are advocating for a research project with a specific university, it is likely because of the general expertise and resources within the relevant university department and a confidence and comfort level with the researcher who will be designated as the principal investigator. While SRAs typically identify the principal investigator by name, the SRA's general terms and conditions also should discuss the rights of the parties if the named principal investigator becomes unavailable to complete the project. Universities typically lead with the position that they can unilaterally name a replacement principal investigator, or they can terminate the project if a suitable replacement cannot be found. Such a result can have important, and potentially adverse, consequences for

the project and the company. This outcome is especially the case if the SRA allows the university a unilateral right to cancel the project, as SRAs typically establish that money paid by the company and used for the project is non-refundable. Such lost funds, however, may not be the worst consequence for the company. For example, if a sponsored research project is one critical component of a comprehensive strategic product development plan, the disruption to the development schedule caused by the SRA cancellation could result in adverse, and potentially high-profile, impacts and delays across multiple departments. In light of these possibly serious consequences, the industry biomaterials engineer should coordinate closely with their attorney regarding the SRA terms addressing replacement of a principal investigator. At a minimum, the biomaterials engineer may want to ensure that the SRA obligates the university to exert best efforts to find a reasonably acceptable replacement, and provides the company with the right to approve such replacement principal investigator.

When entering an SRA, the biomaterials engineer, along with the advising attorney, should give careful consideration to any IP rights that may result. Business executives within the biomaterials engineer's company might expect that, because the company has defined the scope and is funding the project, the company should own all intellectual property rights that may result. As a general matter, universities will not agree to this. Central to the university's mission is the advancement of knowledge that can serve the public good, including openly sharing new discoveries or inventions. Provisions in research agreements that might impose blanket restrictions are anathema to this mission. As a result, in SRAs universities claim both rights to publish the results of their research, and ownership of any associated inventions, including the right to file patent applications ([National Research Council, 1993](#)). Based on this, from the medical device professional's perspective, similar and even more careful planning regarding ownership of IP rights should be applied to SRAs as compared with MUAs.

Prior to entering an SRA the biomaterials engineer should assess the likelihood that the project, as defined in the SRA's scope of work, will or could result in a patentable invention. If the project could result in an invention, the biomaterials engineer should alert other key company decision makers so that serious and collective consideration can be given to whether the research project should be conducted in-house, ensuring that ownership of any resulting invention will belong exclusively to the company, rather than outsourced to the university. If the decision is made to proceed with the SRA, careful attention should be paid to the terms of the SRA that describe the company's rights to any resulting invention. At a minimum, the SRA should provide the company with a first right to negotiate an exclusive license for any patentable invention that may result from the sponsored research. In coordination with the company attorney, the biomaterials engineer should review this provision to ensure that it affords the company the necessary opportunity to develop and commercialize the invention.

Another standard provision of SRAs that should receive careful attention from the biomaterials engineer involves publication rights. Typically, universities include a provision which reserves the right for the university to publish the results of the research, regardless of whether these results might have been favorable or unfavorable to the sponsoring company. If publication of unfavorable results might be damaging to the company's business, this should be considered before the company signs the SRA, and consideration should be given to whether the potential damaging component of the research could be conducted in-house, or in some manner that would provide the company with complete discretion regarding the publication, or non-publication, of the results.

If the sponsored research produces positive results, the biomaterials engineer's team and company may be pleased with the possibility of publication by the university, as this might be perceived by the scientific community as objective validation of the company's technology, despite the necessary acknowledgment of company funding. Such publication, however, may have implications for any patents rights that could result from the research. Consequently, the content and timing of what is being published should be carefully managed and monitored. In the U.S., as well as many non-U.S. jurisdictions, potential patent rights can be lost because of public disclosures. For example, if university researchers present the results and details of a new invention at a scientific conference or in a scientific journal more than a year before a U.S. patent application has been filed, that disclosure alone can disqualify the invention from any patentability in the U.S. This 1 year disclosure grace period is only available to inventors, so if the disclosure is made by a non-inventor before a patent application has been filed, suddenly the invention may no longer be patentable. Many non-U.S. jurisdictions do not recognize such a 1-year inventor grace period, so international patent opportunities may be lost as soon as the public disclosure occurs ([KU Center for Technology Commercialization](#)). Regardless of whether the presentation is given by the inventor, the publication of the research might inspire independent research groups investigating in the same field to file patent applications so that they can become the first to file, as discussed in the intellectual property section above.

In consideration of the above guidelines, one of the most important responsibilities of the biomaterials engineer when managing and monitoring sponsored research involves ensuring that no research results are inadvertently made public. Further, if patentable, the sponsoring company ideally should have already made a decision as to whether it will support the costs and efforts associated with prosecuting the patent application. As discussed in more detail in the next section, the sponsoring company may have already entered into a license agreement with the university regarding the patent rights, or at a minimum executed a term sheet with the university regarding the key business terms that will be incorporated into a license agreement that the university and sponsoring company anticipate executing promptly.

License Agreements

As a general matter, ownership and management of technologies invented or developed by university researchers, scientists, and engineers are delegated by universities to a technology transfer office. The technology transfer office typically is organized as an independent corporate entity that is wholly owned and controlled by the university. The technology transfer office is dedicated to the best interests of the university, but operates much more like a business than other departments or offices within the university ([Alper, 2016](#)). Awareness of this somewhat unique status within a university can be helpful to medical device professionals, because it may shed light on why interacting with a technology transfer office may differ from dealing with any other university department.

The orientation of a technology transfer office might be most easily understood by considering the differences between entering into a sponsored research agreement and entering into a patent license agreement. When negotiating a sponsored research agreement, the lead biomaterials engineer from the sponsoring company will be interacting directly with a university researcher possessing specific subject matter expertise, who most likely will also be the principal investigator. The principal investigator and the sponsoring company's lead biomaterials engineer will define the scope of the project and agree on a total cost, at which point the principal investigator may provide the sponsoring company with the university's standard sponsored research agreement template. Typically, any revisions to this template will be negotiated between and drafted by an attorney from the university's general counsel's office and the company's attorney, and then the SRA will be executed.

In contrast, the principal investigator typically will not play a significant role in the development or negotiation of a patent license agreement. These negotiations are managed by an IP specialist within the university's technology transfer office who acts independently of the principal investigator and exercises broad discretion regarding whether to involve the principal investigator in the technology transfer office's license negotiations with the company. From a practical perspective, medical device professionals within a sponsoring company should recognize that they may be dealing with a completely distinct entity when negotiating a patent license agreement from the entity that negotiated the SRA. It may be just as important to develop relationships and a rapport with the technology transfer office as it was with the department that conducted the research.

Typically, an attorney or patent license specialist from a sponsoring company will take the lead for the company in negotiating the terms of a patent license agreement, but the company's lead biomaterials engineer for the research should expect to play an integral and indispensable role. Generically, a license can be thought of as a permission to do a particular activity, or to use a particular composition. As discussed above, patents provide the patent owner with exclusive 20-year rights to practice the invention claimed in

the patent. A patent license agreement, therefore, establishes the terms and conditions under which a patent owner provides a third party, referred to as the licensee, with the legal right to practice the art covered and protected by the patent during the patent term.

Many companies and university technology transfer offices follow a two-step practice to negotiating and finalizing patent license agreements. The first step involves negotiating a non-binding term sheet, and the second involves incorporating the provisions of the term sheet into a comprehensive and binding license agreement. The term sheet summarizes the key business terms related to the proposed patent license. From a sponsoring company's perspective, even though the lead biomaterials engineer or the attorney may play an important role in developing and negotiating the term sheet, input from and participation by the company's financial experts, regulatory experts, and business line executives can be critical. A patent license agreement can commit a company to multi-layer resource and financial obligations, including financial penalties for failures to meet contractual commitments. Consequently, medical device professionals should be cautious about presenting their company as being prepared to enter into a patent license agreement unless they know that all of the impacted company departments have affirmed and support the commitments that will be associated with the license agreement.

The fact that any particular invention may be patentable, or even patented, does not mean that the invention is ready to be commercialized. In the United States, for example, even though the Patent and Trademark Office may have granted a patent, if the Food and Drug Administration (FDA) has not cleared or approved the invention for commercial use, the patent owner or licensee cannot market or sell the new product for any purpose that requires FDA clearance or approval. Simply put, the product may be commercially worthless if it cannot meet FDA standards. Because universities, and their associated technology transfer offices, are particularly interested in seeing the results of university research being used to promote the public good, term sheets that serve as the predicate to patent license agreements typically address the steps that must be accomplished so that the technology can be properly commercialized. These steps are generally referred to as milestones. A typical example of successive milestones that might be listed in a patent license agreement include (1) completion of a preclinical research project, (2) commencement of a clinical trial, (3) completion of that clinical trial, (4) regulatory approval, and (5) first commercial sale. In practical terms for medical device professionals, this means that a license agreement will include clearly defined tasks, with a clearly defined schedule, on which they may be responsible for delivering over a several year period. The failure to achieve milestones may provide the university with the right to terminate the patent license agreement, constituting a drastic result that would foreclose the company from commercializing patented technology it likely invested millions of dollars licensing and funding.

From a financial perspective, in addition to the costs associated with performing milestones, the most important provisions of the term sheet will likely be those specifying the milestone payments and license and royalty fees that the company will incur. Typically, milestone payments to the university are incurred as contractually specified milestones are reached, and are additional to the costs the licensee incurs to perform the milestones. Separately, the license fee represents any initial and/or minimum annual fee that the company must pay to the technology transfer office so that the patent license does not expire. The royalty fee, which may be partially integrated with the license fee, will typically be calculated as a percentage of the net revenues the company receives from sales of products that constitute or are based on the licensed technology.

Litigation

No introduction to legal issues encountered in business or academic settings would be complete without some discussion of litigation. We live in a litigious society, and it would be surprising for anyone to pursue a lengthy career without facing, at least once, the threat or reality of a lawsuit. Litigation can concern any of the topics addressed in this chapter: for instance, contract performance issues, confidentiality and non-competition breaches, IP inventorship, ownership or infringement claims, etc. Additionally, certain medical devices have gained notoriety through their involvement in product liability suits.

Litigation typically begins with the filing of a formal complaint, which often, but not necessarily, may be preceded by a demand letter warning that a complaint will be forthcoming. Receiving a complaint can be unsettling, and even alarming, particularly for non-lawyers, because it immediately places the recipient in a stressful and uncertain situation. Companies and universities typically hire outside lawyers who specialize in litigation to represent them in lawsuits. Litigators can be expensive, but retaining the right one, with the appropriate litigation and subject matter expertise, can be critical. Such an individual should be able to provide perspective on the risks posed by the litigation, detail a range of strategies that should be considered, and outline possible outcomes based on such strategies. Virtually no experienced litigator will guarantee any specific result, because litigation is inherently uncertain, but a qualified litigator should be able to present options that will allow the client to make an informed choice regarding optimal strategies to pursue.

The medical device professional should recognize that hiring a litigator does not absolve him from further involvement in the dispute. Litigation is very fact specific, so if the litigation concerns activities in which the medical device professional was involved, he will need to engage in detail with the litigation team to ensure the litigators know and understand all the relevant facts. The medical device professional should expect to spend a significant amount of time interacting with his own in-house counsel, or directly with the outside litigation team, in an effort to appropriately educate them.

Most lawsuits will not place the medical device professional at risk for personal liability, particularly if he was acting within the scope of his employment authority, and did not engage in clearly negligent or willfully malicious conduct. Typically, even if the party initiating the lawsuit, referred to as the plaintiff, specifically names the medical device professional in the complaint as a defendant, so long as he was acting within the scope of his employment, his employer will likely retain counsel for him, including paying the attorneys' fees. In the atypical situation where a medical device professional must personally hire an attorney, he should consider asking his attorney to investigate his employer's obligations to advance coverage of legal expenses, or at least indemnify him for any expenses he incurs. Such knowledge may influence the type of fee structure the medical device professional enters into with his litigator, and the ways in which he interacts with his litigator.

Conclusion

On first impression the broad array of legal issues that medical device professionals likely will encounter can be daunting. However, this does not have to be the case. Playing an active role in understanding and structuring the legal opportunities and constraints impacting a medical device professional's career and activities can be intellectually stimulating and professionally rewarding. The

introductory roadmap provided above should eliminate at least some of the mystery that might discourage the necessary effort to unwind legal puzzles. This roadmap provides guidance for medical device professionals' coordination and cooperation with attorneys to convert situations involving legal issues into professional benefits and opportunities for themselves, and strategic and business advantages for their employer.

References

- Alper, J.A., 2016. Vision for the Future of Center-Based Multidisciplinary Engineering Research. The National Academies Press, p. 20. S. 1890–114th Congress: Defend Trade Secrets Act of 2016.
- Durham, A.L., 1999a. Patent Law Essentials. Quorum Books, pp. 12–13.
- Durham, A.L., 1999b. Patent Law Essentials. Quorum Books, p. 19.
- Keeley, M., 1999. Estimating Damages in Patent Infringement Cases: An Economic Perspective. <https://pdfs.semanticscholar.org/4ccc/efafb5b26f5496f26ca58c80a7f0e9d55b12.pdf>.
- KU Center for Technology Commercialization. <http://ctc.ku.edu/faculty/protect-your-ideas/protecting-intellectual-property/public-disclosure>. (Accessed 18 June 2019).
- H.R. 1249–112nd Congress: Leahy-Smith America Invents Act.
- National Research Council, 1993. Intellectual Property Rights in Industry-Sponsored University Research: A Guide to Alternatives for Research Agreements. The National Academies Press, Washington, DC, p. 5. <https://doi.org/10.17226/10009>.

3.1.11

Moral and Ethical Issues in the Development of Biomaterials and Medical Products

BRYAN N. BROWN^{1,2}, MARTIN J. HASCHAK^{1,2}, ALEXIS L. NOLFI^{1,2}, MANGESH KULKARNI^{1,2}

¹Department of Bioengineering, University of Pittsburgh, Pittsburgh, PA, United States

²McGowan Institute for Regenerative Medicine, University of Pittsburgh, Pittsburgh, PA, United States

Introduction

Engineering ethics often takes the classical approach of preventive ethics. That is, engineering ethics most commonly focuses upon safety and regulation in an attempt to prevent the failure of future products. Such approaches generally rely on sets of standards and guidelines in an attempt to normalize development and ensure safety. While medicine certainly has standards and guidelines that govern and normalize its practice, as well as holding safety in the highest regard, the manner in which ethical issues are addressed by medical professionals often differs from the strategies used by engineers and scientists. As medical issues are complex, and focus primarily upon the treatment of individuals rather than the development of products or interpretation of research results, medical ethics has a strong emphasis on core values in decision making as well as on respect for the autonomy and wellbeing of the patient.

Engineering ethics and medical ethics have, of course, been the subject of countless textbooks, manuscripts, and lectures. However, the subjects of engineering ethics and medical ethics are generally treated as separate. The development of novel medical products requires those involved, whether they are scientifically or medically oriented, to be able to consider the ethical issues arising from both the engineering and medical aspects of the proposed product. Furthermore, as novel medical products continue to develop to include living components or utilize controversial methods such as gene editing, the need for discussions and consideration of previously unrecognized ethical issues will only increase. Thus scientists, engineers, medical professionals,

and others working on novel medical products will need to be well versed in the myriad ethical issues that may arise.

The purpose of this chapter is to briefly review ethical issues in the development of medical products. These issues are relevant in multiple contexts, including drugs, medical devices, and other types of therapy. However, the broad ethical issues that arise in the development of each of these types of medical products are similar. These issues include not only the classical aspects of safety, regulatory compliance, and animal and human testing, but also emerging issues such as the use and inclusion of stem cells in medical products and gene editing, among others. While the topics presented herein are representative of the types of issues that may arise, they should not be considered comprehensive and this chapter should be used as a starting point for the study and discussion of the ethical issues associated with the development of medical products.

Selected Approaches to Ethical Reasoning

When discussing ethical decision making, whether based upon concepts from engineering or from medicine, it is useful to define a set of terminologies or methodologies by which one can assess and discuss issues that arise. As this chapter will discuss multiple ethical issues, and relies on the use of multiple terms and methods of ethical decision making, a short description of select approaches is provided below. A more in depth review of these concepts can be found in [Harris et al. \(2008\)](#). It is important to note that moral and ethical issues arise when there is divergence between these approaches to decision making and that ethical decision making becomes simplified when these approaches converge.

The Utilitarian Approach

In the simplest terms, a utilitarian approach is one that favors a decision that does the most good or prevents the most harm. Such approaches are widely used in engineering and business. This often includes a cost–benefit analysis or risk–benefit analysis. While this idea is simple in theory, in practice it can be much more complex. It is often difficult to define what represents a good outcome and for whom, particularly when the outcomes deal with profiting from human health. For example, one might ask the question: “Is a good outcome one that provides the best treatment for patients, or one that maximizes profit for the company selling the device?” Additionally, the use of a utilitarian approach might favor the good of the majority at the expense of an individual or group of individuals. Such issues will be discussed in more detail in the section on human clinical trials.

The Rights Approach

By contrast, the rights approach favors decisions that protect and respect the moral rights and autonomy of individuals. That is, human beings have inherent worth and dignity, and individuals should not be used as a means to an end. The rights approach is the basis for many of the rules that govern clinical trials, patient selection, informed consent, and medical autonomy. However, it should be noted that at times these rights come into conflict with the rights of the provider or other stakeholder, creating conflict. For example, whether or not one has a right to die by assisted suicide, and whether or not a provider should have the right to refuse such a request, is an ongoing debate. Additionally, the rights approach may come into conflict with the utilitarian approach when a patient cannot afford treatment, or when considering the allocation of scarce medical resources such as organ transplants.

The Justice Approach

The justice approach favors decisions that lead to the equitable distribution of access and benefits as well as the potential burden of care across society. The justice approach requires avoiding discrimination in the selection of clinical trial subjects without a scientific justification, and seeks to protect those with diminished autonomy. The fairness or justice approach also requires equal access to, or at least fair distribution of, scarce medical resources. For example, the United Network for Organ Sharing (UNOS) is the organization tasked with distribution of transplant organs in the United States. The process that UNOS has developed for allocation of liver transplants, called the Model for End-Stage Liver Disease score, allocates organs largely based upon urgency (i.e., the sickest patients first) and geographical location. The intent of this process is to maximize the supply of donor organs while improving access to this scarce resource. However, whether the system is truly equitable and works well for all stakeholders is not clear.

The Virtue Approach

Ethicist William F. May states “[The Professional] had better be virtuous. Few may be in a position to discredit him” (May, 1988). Such expectations derive largely from the trust that the public places in scientists and medical professionals. The virtue approach favors actions that are in line with certain ideals or virtues. For example, honesty, integrity, and compassion are examples of virtues that might be expected of scientists and medical professionals engaged in the development of medical products. The virtue approach commonly comes into discussions of professional responsibility, scientific integrity, and disclosure of conflicting interests, each of which is discussed in this chapter.

Safety

The safety of the public and the wellbeing of patients are held paramount in both engineering and medical ethics. Indeed, safety and wellbeing are among the first concerns covered in professional codes of ethics across scientific, engineering, and medical professional societies. Practically speaking, however, the safety of novel medical products is evaluated using guidelines that have been established by the United States Food and Drug Administration (FDA) or other national regulatory bodies. Such regulations are discussed in depth in [Chapter 3.1.7 Regulatory Constraints for Medical Products Using Biomaterials](#).

The guidelines established by the FDA are in place to provide a set of testing, which, if successfully completed, can provide reasonable expectation of safety when used in human beings. That is, from a utilitarian perspective, the technology has shown a risk–benefit profile that is clearly associated more with benefit than with risk. The specific testing that is performed for a given medical product will depend upon its design, components, intended use, and predicate products already in the market. Individual tests are specified by test standards, including those from the ASTM International (formerly American Society for Testing and Materials) and the International Organization for Standardization, the purpose of which is to ensure reproducibility of testing between laboratories. Additionally, it is expected that testing will adhere to good laboratory practice and that manufacturing of the products to be tested will be carried out under good manufacturing practice. These practices govern the processes and conditions under which manufacturing and testing are carried out, and the standards of documentation needed to ensure the quality of these activities. The specifics and scope of technical standards are reviewed in [Chapter 3.1.8 Role of Standards for Testing and Performance Requirements of Biomaterials](#).

While it is important to understand that these guidelines do exist, and that they are in place for the protection of the patient, these represent regulatory issues and do not, in and of themselves, necessarily present ethical issues. That is, the public expects that approved medical products will have undergone rigorous testing to ensure their safety. It is the

moral and ethical responsibility of those designing, testing, and selling the medical products to ensure that they are safe and function as intended. While the standards and expectations for safety may not raise ethical issues themselves, many ethical issues do arise during the course of testing, particularly testing performed in animals and humans, as well as in the interpretation of the data that result from such testing. These issues are discussed in more depth later. Ethical and legal issues may also arise after regulatory approval should patients experience side effects and/or failure of medical products; such issues are covered in [Chapters 3.1.9 Medical Device Failure—Implant Retrieval, Evaluation and Failure Analysis](#) and [3.1.10 Legal Concepts for Biomaterials Engineers](#), and are therefore not discussed here.

Animal Testing

For those involved in the design and testing of medical products, there are many techniques and strategies that can be employed to comprehensively characterize and test a novel device; however, it is difficult to foresee how a material or device may interact with the varied and complex cellular, tissue, and organ systems found within a human being. Therefore animal models are critical tools that help to assess the toxicity, biocompatibility, safety, and potential effectiveness of a device before testing the device in a human subject.

General opinion leans toward accepting animal research as morally allowable ([von Roten, 2013](#)); however, as evidenced by the surge of animal research protests in recent years, there are those who still question the necessity and appropriateness of animal research. This, in part, stems from the belief by some that animals have the same value and moral standing as a human being, and therefore should not be subjected to anything that would not also be done to a human for research purposes. With such an extreme view, arguably much of the preclinical research that is done to ensure safe, effective products for human use would be prohibited. Others take a more utilitarian stance against animal research, suggesting that animals possess distinct physiology from human beings and that these differences yield results that are not applicable or appropriate to extend to predictions about humans ([Hajar, 2011](#)).

A more tempered view recognizes that animal experimentation is necessary to ensure the safety of medical products to be used in humans, but, while animals are under our care and participating in our studies, they should be treated as ethically and humanely as possible. This includes giving access to adequate room, nutrition, and enrichment, while alleviating—to the extent possible—stressful situations, pain, and suffering, while also allowing them a space that provides for behaviors exhibited naturally when not in captivity ([Whiting, 2011](#); [Fenwick et al., 2009](#)).

In the design of animal studies, it is important to minimize animal usage and distress if possible, and, unsurprisingly, throughout history individuals and organizations have put forth guidelines and suggestions to help us achieve these goals ([Franco, 2013](#)). In 1959, R.L. Burch and W.M.S.

Russell published the book *The Principles of Humane Experimental Technique* ([Russell and Burch, 1959](#)). This book sought to give guidance about ways in which welfare could be maximized while only using as many animals as absolutely necessary. It was in this text that the concept of “The Three Rs” was introduced: Replacement, Reduction, and Refinement. The “Three Rs” provides a practical framework for minimizing animal usage and ensuring adequate care.

Replacement refers to using an alternative strategy for an experiment that would otherwise use animals for research. For example, in some studies it may be feasible to use a computer simulation or in vitro cell culture experiment as opposed to animals. However, Replacement can also refer to replacing a higher-order more sentient animal species with an animal species shown to have a lower perception for pain (e.g., replacement of a vertebrate animal with an invertebrate). Reduction refers to a strategy that optimizes the amount of information obtained per animal while minimizing the total amount of animals needed to fulfill objectives of the research question. For example, a study in which a longitudinal cohort of animals is used to generate many data points per animal will result in fewer animals being used when compared to a study in which a unique animal must be used for every time point. Finally, Refinement refers to strategies that aim to decrease the potential pain or distress an animal may encounter during its time in a research experiment. This could include using a newer surgical technique that is known to be less invasive with a shorter recovery time, or could include modifications of a pain management dosing schedule known to better control breakthrough pain after a procedure.

In addition to “The Three Rs,” there are additional resources available to help guide and direct appropriate and ethical research with animals. In 1966, Congress passed the Laboratory Animal Welfare Act (AWA), which was the first law that specifically dictated policies concerning husbandry practices and treatment of animals for research purposes. The Animal and Plant Health Inspection Service under the United States Department of Agriculture helps to enforce and maintain tenets set forth in the AWA. While requirements can be extrapolated to provide guidance for most animal research, the species of animals specifically protected under this Act are limited to certain warm-blooded species, including nonhuman primates, dogs, cats, rabbits, guinea pigs, and hamsters. A 1985 amendment to the AWA helped to make research institutions and facilities more accountable through the mandate that they establish Institutional Animal Care and Use Committees (IACUCs) to review and approve proposed research using live animals protected under the Act. Although many frequently used species are left out of the Act, federally funded facilities are also required to have oversight of uncovered animals (e.g., rodents and birds), as these species are protected under the Public Health Service Policy on Humane Care and Use of Laboratory Animals. Under this policy, research must adhere to recommendations set forth in the *Guide for the Care and Use of Laboratory Animals*, which is produced by

the National Research Council and the Institute for Laboratory Animal Research.

Before initiating any type of animal work, researchers should thoughtfully consider the types of regulations and guidelines that must be adhered to based on the type of species and research that will be conducted. In addition, each aforementioned principle of “The Three Rs” must be comprehensively considered to design a study that fulfills each requirement. If it is determined that nonanimal work is indeed not a suitable alternative, oftentimes preliminary in vitro data or limited animal pilot studies will help inform calculations and decisions about the lowest number of animals necessary for a study. After a protocol is proposed to and approved by an individual’s respective IACUC, care should be taken to follow any additional guidelines, laws, and regulations as dictated by local or state laws.

Human Testing

While animal testing is used for both exploratory and safety testing, human clinical trials are the final stage for testing the safety and efficacy of novel medical products that have shown sufficient results in preclinical in vitro benchtop and in vivo animal models but still require human clinical testing. It is important to note, however, that not all medical products require human clinical testing, and this topic is reviewed in [Chapter 3.1.7 Regulatory Constraints for Medical Products Using Biomaterials](#). Historically, guidance for conducting human subject research was often derived in response to unethical clinical studies performed on disadvantaged, nonconsenting ethnic or racial minorities. The first of these reactionary ethical codes was the Nuremberg Code, a set of principles defining the rights of human research subjects, which was used to try Nazi physicians accused of unethical human experimentation in the Nuremberg trials. The Nuremberg Code contains 10 principles outlining the qualifications for ethically sound medical research, with a focus on informed patient consent in the absence of any coercive influence, scientifically sound study design with prior validation of safety and efficacy in the appropriate benchtop or animal models, and beneficence toward study participants, including study termination when faced with unanticipated deleterious consequences. While the Nuremberg Code eventually became one of the most important sets of ethical guidelines for human research, it was not widely accepted in Western medicine until several decades after its creation ([Nardini, 2014](#)).

During this period, another human subjects study was taking place in Tuskegee, Alabama—the “Tuskegee Study of Untreated Syphilis in the Negro Male”—a study intended to record the occurrence of syphilis in the black community to justify treatment programs. Initially intended to last only 6 months and provide free checkups and medical care to the study participants, the Tuskegee Study lasted 40 years, over which time study participants were never fully informed of the risks associated with the study, never informed of the purpose of the study, and never offered study exit or penicillin

treatment for their syphilis when penicillin became available as a syphilis treatment in 1947. After public discovery of the ongoing Tuskegee Study in 1972 and subsequent public outcry over the perceived inhumane treatment of the research participants, the National Commission for the Protection of Human Subjects of Biomedical and Behavior Research was assembled to set defined ethical guidelines for human subjects research as well as to review the Tuskegee Study to determine if these ethical guidelines had been violated by the study. The committee determined that while the study subjects were willing participants, the study was not ethically justified since the study participants were never told the true purpose of the study or warned about the potential risks associated with enrollment, resulting in an inability to provide proper informed consent for study enrollment.

In 1979, the National Commission published the *Belmont Report*, a set of three fundamental principles underlying ethically sound biomedical human subjects research. The first principle of the *Belmont Report* concerns respecting and protecting the mental and physical autonomy of subjects participating in clinical research by providing a truthful and comprehensive view of the study design as well as a thorough review of all risks associated with the treatment or any procedures associated with the treatment. Presenting this information to prospective patients in a holistic, nondeceitful manner without the influence of coercion forms the basis of informed consent, an essential feature for patient inclusion in clinical trials today. In addition to Respect for Persons, the *Belmont Report* also identifies Beneficence and Justice as two additional features essential for ethical human subjects research. The principle of Beneficence is philosophically similar to many ideas outlined in the Hippocratic Oath, particularly the idea that healthcare providers and members of the research team should strive to “do no harm” while maximizing the quality of care available to patients. The principle of Beneficence also dictates cessation of clinical trials that induce undue stress or unanticipated negative health consequences in study participants. The study must also be conducted in a just manner, particularly with regard to equal recruitment across population groups without exploitation of disadvantaged populations. Additionally, any compensation provided for study participants should be sufficient to compensate for one’s time, equally distributed across study participants, and proportional to the risks associated with the study research procedures or therapeutics. These three guiding principles outlined in the *Belmont Report* serve as the formative basis for human clinical trial bioethical guidelines and legislation in the United States ([Department of Health E Welfare and National Commission for the Protection of Human Subjects of B Behavioral R. The Belmont Report, 2014](#)).

As the field of bioethics developed over time, additional guidelines and principles have been developed to further refine and guide ethical clinical trials and human subjects research. The Declaration of Helsinki first published in 1964 and since refined by the World Medical Association outlines the basic principles underlying ethical human subjects

research, including guidelines on what is considered human subjects research, the purpose of human clinical research, the scientific basis necessary for transition from preclinical models to human subjects research, guidelines on patient recruitment and just compensation for the participants, proper modalities for managing and communicating study risks to research subjects, guidelines for protecting patient privacy, methods and considerations for obtaining informed consent, guidelines for which patients can and cannot give informed consent, as well as guidelines for the publication of study results and experimental data dissemination ([World Medical, 2013](#)). Additionally, the Declaration of Helsinki outlines the importance of independent review of all proposed human research studies by research ethics committees to ensure studies have sufficient scientific basis in preclinical models to transition to clinical trials and to review the proposed research protocols to ensure the study will not violate any of the previously outlined bioethical principles. Practically speaking, in the United States, any human research studies supported directly or indirectly by federal funding are required to be submitted to an Institution Review Board (IRB) for review. Each organization conducting federally funded human subjects research is required to organize an IRB, which meets the federal minimum requirements of having at least five members with at least one member who is a scientist, one nonscientist member, and one member of the community with no personal or familial affiliation with the institution. It is important to ensure that all members of an IRB have no financial or personal conflicts of interest associated with the research proposals being reviewed by the board. Proposals submitted to an IRB for review will be analyzed for sound scientific validity with sufficient data supporting efficacy from preclinical testing, planned mechanisms for patient enrollment, mechanisms of patient data collection, methods of protecting private patient medical information, and plans for unanticipated negative patient reactions to a given protocol or therapeutic. The IRB will also work to ensure that patient recruitment will be non-discriminatory in nature and patients recruited are able to understand and give informed consent to study enrollment. Following approval of human subjects protocols, the IRB is responsible for monitoring the ongoing study for compliance with the submitted guidelines for the study as well as monitoring for any study complications and responding appropriately in cases where early study termination may be necessary to ensure patient safety. This review is to ensure that the study is sound from a utilitarian standpoint and provides for protection of the rights of individuals and justice, as previously defined.

Research Integrity

Research integrity is an individual researcher's obligation to honestly apply their knowledge, tools, and technical expertise to answer a given research question in a professional manner in accordance with all institutional rules, bioethical principles, and legal codes. Research integrity also dictates

that researchers will interpret their results in a fair, nonbiased manner and disseminate those results to the scientific community and general public through objective publications of the study results following completion. Research integrity can also involve various aspects of professionalism that arise throughout the process of undertaking and publishing a study, such as properly attributing authorship credit when authoring manuscripts or development of proper systems for data management and storage during study data collection.

It is important for anyone involved in research studies to understand the obligations researchers are expected to uphold and maintain for several reasons. First, all scientific research is built upon prior work in the field, work that is often performed by other researchers or other institutions. Therefore it is essential that researchers undertaking a given experiment perform all aspects of experimental design, data collection, result depiction, and data dissemination in an honest, nonmisleading manner to allow for the results of the study to be applicable for future studies as well as repeatable and independently verifiable by other researchers working in that field of study. When all researchers adhere to this set of ethical principles, it helps build trust in the validity of the research others are undertaking and helps researchers in a given field have a sense of transparency about the current state of the field. Additionally, honest presentation and discussion of study results help guide subsequent development of reasonably informed future directions of study. From a non-scientific perspective, it is also important for those involved in research studies to conduct themselves with integrity to prevent the erosion of public trust in the scientific community. Since the technologies and therapeutics derived from research studies are ultimately to benefit members of the public, it is important that researchers conduct their studies with integrity and provide non-biased, non-sensationalized representations and discussions of their work in a manner that non-scientist public stakeholders can understand. Disseminating misleading or falsified data can not only erode public trust in the larger scientific community and stall research progress, but even more seriously it can introduce additional deleterious complications and loss of life in vulnerable patient populations who believed they stood to benefit from the technology.

Conflict of Interest

One significant aspect of research integrity involves conflict of interest. In the context of medical product development, a conflict of interest is defined as an interest that tends to make one's judgment less likely to benefit the patient than the patient is justified in expecting. Such conflicts frequently arise in both research and medicine. From an academic research perspective, such a conflict might include patent authorship, equity ownership, royalties, and research funding or contracts from a company involved in the development of a medical product. Such financial incentives might influence the obligation of a researcher to accurately report and interpret data from research studies according to

scientific and ethical norms. This creates the potential for poor quality research, which, if used to justify translation of research into products to be used in human patients, has the potential for harm. Similarly, conflicts of interest in medical professionals may influence their choice of treatments in patients, choice to use or recommend a particular medical product, or their reporting of clinical research studies.

There are clear benefits to academics and physicians working with industry partners. These include advancement of the development of new medical products, economic growth, and improvements in the quality of care for patients. This also includes increased research budgets, enhanced salaries, and other benefits such as access to equipment and materials that might otherwise be unavailable. However, these must be balanced against the potential impacts on research quality and reporting. For these reasons, most federal sponsors require that research institutions monitor, manage, and report conflicts of interest. Similarly, Congress passed the Physician Payments Sunshine Act, requiring medical product manufacturers to disclose payments to physicians and teaching hospitals as well as physician ownership or investment in companies. Disclosure of conflicts of interests in those who review regulatory submissions, FDA Advisory Committee Members, for example, have also come under scrutiny in recent years, and must be managed by regulatory bodies to protect human health.

Research institutions, regulatory bodies, and hospitals, however, are largely left to interpret and manage the ethical impacts of conflicts of interest. Questions that these institutions must answer relate to which financial interests must be disclosed and to whom, which interests pose a risk to research integrity, and how to manage the risks effectively. Scientific journals are also tasked with acting as gatekeepers of scientific publications, and most, if not all, scientific and medical journals require disclosure of conflicts of interest at the time of submission for publication. While some may suggest that having to disclose these relationships is unfair to the authors, and may influence the review of otherwise unbiased science, such guidelines are needed to protect research integrity and human health.

Emerging Ethical Issues in Medical Product Development

While the foregoing described ethical issues are well known and well discussed in the context of medical product development, new technological development comes with new ethical issues that have not previously been considered, and for which regulatory or standard guidelines may not exist. In the context of biomaterials, the materials themselves are not generally associated with significant ethical issues. However, as the field expands to include cells in biomaterial constructs such as is described in Section 2.6 Applications of Biomaterials in Functional Tissue Engineering, biologically active molecules or materials derived from human sources, or the delivery of genome modifying agents, new issues have emerged. A select group of these issues is discussed below.

Ethical Issues in Stem Cell Research

The enormous therapeutic potential and substantial progress in stem cell research over the years, especially in human embryonic stem (ES) cells and human-induced pluripotent stem (iPS) cells are contrasted by staunch opposition, most notably to ES cell research, by millions worldwide. Indeed, the ethical dilemma surrounding ES cells has been a subject of significant debate ever since the first report of successful isolation of human ES cells. Despite the long-running controversy, the ethical issues that arise in the discussion of the use of stem cells have yet to be resolved. Views on this subject are driven by many factors, including personal morality, cultural norms, and religious beliefs, among others. These views are also balanced by the belief that ES cells have tremendous therapeutic potential. The lack of consensus and agreement on the ethical issues surrounding ES cells are reflected in the range of legislative regulation in different parts of the world ([Kastenberg and Odorico, 2008](#)).

Though the ethical issues are various and complex, the major issues are related to the origin of the stem cell. Unsurprisingly, adult or cord blood stem cells are associated with fewer ethical objections. The ethical issues in ES cells derive from an inconsistent definition of human embryo and its corresponding moral and legal status. The problem with sourcing human ES cells is the inevitable destruction of embryos in the process of isolation. The challenge is to find the balance between respect for human life, if indeed an embryo can be considered a life, and the goal of alleviating suffering. It is ethically difficult to develop a policy that is acceptable to everyone given the moral belief shared by many that the destruction of a human embryo is morally equivalent to ending a human life, or, at the least, that the embryo has some inherent moral value. Another ethical debate concerns the use of surplus IVF embryos to source the ES cells and generally includes objections such as the principle of potentiality and proportionality, the slippery slope argument, and the subsidiarity principle ([de Wert and Mummery, 2003](#)).

Other sources of stem cells are also associated with ethical issues. The use of somatic cell nuclear transfer (i.e., cloning) to source stem cells has significant therapeutic potential. However, ethical issues with cells derived in this way include the underlying ethical objection and unclear moral status of cloned embryos ([de Miguel-Beriain, 2015](#)). Others, however, argue that the cloned embryos are not naturally created for reproduction and therefore should not be considered morally equivalent to natural embryos or even IVF embryos ([de Miguel-Beriain, 2015](#)). iPS cells are derived from somatic cells and thus bypass many of the ethical concerns related to the destruction of a human embryo. However, there is a unique set of ethical issues surrounding iPS cells as well, largely related to current scientific uncertainty and yet to be defined safety profile. Issues such as abnormal reprogramming during induction of pluripotency, potential tumorigenicity of therapeutically implanted iPS cells, potential use for cloning human beings, potential applications in producing human germ cells, potential to

make human embryos, and issues obtaining informed consent (Zheng, 2016) have yet to be addressed.

Regardless of the type of stem cell used to derive a particular treatment, there are ethical and safety issues pertaining to human donor tissues, including regulation of production, management and therapeutic use of donor tissue or organ samples, and following standardized guidelines and protocols (Chen and Liu, 2016). Acquiring commercial value, human tissue and cell samples have developed a market that creates the potential for conflict between donations inspired by altruistic considerations and profitability, leading to the potential for inadequate protection of the donor through informed consent (Riva et al., 2019). Another major area of ethical concern is ownership of genetic information versus use of that information for biomedical research with proper measures such as informed consent and strict confidentiality (Spinello, 2004).

Gene Editing

Broadly speaking, gene therapy refers to using genetic material to cure or treat a disease, with the ultimate goal of being a feasible and suitable replacement for more traditional treatments such as drugs or surgical intervention. Current gene therapy approaches include adding a new gene to cells, deactivating a gene that is not functioning properly, replacing a faulty or mutated gene with one that is functional, as well as other various strategies. If done correctly, for example, a longer-term solution to a disease or problem can be achieved through a source of functional protein that is being continually renewed (Ibraheem et al., 2014), or through the removal of a dysfunctional, inappropriate protein that was causing negative consequences.

In general, genetic material that is delivered to the cytoplasmic portion of a cell will have difficulty being translated to a protein. Vector carriers, therefore, are one way to deliver the genetic material to the nucleus where transcription can take place. Viruses are able to infiltrate and deliver their genetic material to host cells, making them an attractive option for vector carriers in gene therapy. Some viruses, such as retroviruses, deliver and incorporate their genetic material directly into a host's chromosomes, while others (e.g., adenoviruses) deliver material to the nucleus without host genome incorporation. Gene editing, a potential type of genetic therapy that may be even better described as "genetic engineering," is emerging as a way to more specifically alter a cell's genome. A recent approach, the clustered regularly interspaced short palindromic repeats and CRISPR-associated protein 9 system, makes use of scientific principles borrowed from bacterial defense mechanisms to target specific areas of chromosomes for alterations, removals, and additions of genetic material.

In general, gene therapy is a relatively young field. For many applications, researchers are still working to determine the safety of treatment strategies before efficacy testing can commence. There have been instances where experiments have ended with negative consequences, such

as genetic mutations, illness, and even death (Cotrim and Baum, 2008; Jafarlou et al., 2016; Goswami et al., 2019). However, advances in safety and increased awareness of ethical issues are helping to continue to advance research and bring attention to these emerging technologies. With gene therapy comes thought-provoking considerations that many traditional therapies do not have. Gene therapy that modifies somatic cells, such as cells of the blood, is meant to treat the individual undergoing the procedure and will not result in the modification being genetically passed on to offspring; however, gene therapy targeting germline cells has the potential to affect subsequent generations. This, and a variety of other issues such as cost and potential to unfairly enhance certain genetic traits, constitute ethical concerns for gene therapy and gene editing.

Since these forms of gene therapy rely upon varying degrees of host genome editing, several distinct ethical considerations arise for each technology. Gene replacement therapeutics as well as editing technologies must follow the bioethical principles previously discussed, meaning that gene therapies should produce substantial benefit over currently available therapeutics, the risks associated with the technology should be manageable or negligible in comparison to the benefits provided through gene therapy, and the technology should be available to individuals in need without bias or socioeconomic prejudice (Wirth et al., 2013). Gene replacement therapeutics, which do not involve any host somatic or germline genome editing, need to ensure that the vector chosen for gene delivery to the cell nucleus is biocompatible and will not induce unwanted complications in patient populations receiving the therapy. Additionally, gene replacement therapeutics need to be appropriately applied in cases of serious pathophysiology where no significant alternative therapies are available. For therapeutics characterized by editing of the host genome, unique considerations arise based on whether the cell in which the genome edits are being made is a somatic or germline cell (Coller, 2019). Since somatic cell genome edits are nonheritable and any somatic edits made in an individual will not propagate throughout an individual's offspring, the ethical concerns surrounding this form of therapeutic are largely concerned with the safety of the editing technology being used, the risks associated with introducing genome edits in a given somatic cell type, and whether gene editing is the appropriate course of treatment given the alternatives available at the time of treatment. Gene therapies that involve germline genome edits are also both subject to the same ethical considerations as outlined for somatic gene editing as well as subject to another significant ethical dilemma—who is responsible for providing informed consent for therapies that affect both an individual and potentially an individual's yet to be born offspring? Considerable debate is ongoing surrounding the ethics of making this decision of consent for one's offspring (Coller, 2019; Wolf et al., 2019; Editors Sarah Chan and Sternberg, 2019). As germline gene editing technology is often intended to remove genes that are known to confer a lethal phenotype, one could argue that the principle of beneficence

dictates that clinicians and researchers apply the tools available to avoid undue suffering in cases where it is known that an individual will acquire a hereditary, potentially lethal pathology. However, there is still debate as to what pathophysiological necessities necessitate germline gene editing as opposed to other forms of gene therapy or conventional treatment options. Additionally, since many of the technologies proposed for performing these edits have been developed in the last several decades, data concerning the long-term, generational consequences of germline editing remain unknown. A final ethical consideration applicable to all gene therapy technologies is the consideration of whether this is an appropriate application of a given technology to ensure one is not crossing the boundary into nonessential gene therapeutics, where genes are delivered or edited in an individual devoid of any pathological medical condition for the purpose of individual ability enhancement or personal enrichment.

Cost and Access to Medical Products

Justice-based ethical reasoning would argue that all should have equal access to high-quality medical care. Furthermore, a rights of person approach would suggest that patients have the right to choose which medical treatments they should or should not receive. However, such approaches must be balanced against the costs and effectiveness of medical products. Achieving this balance creates moral and ethical issues in that it pits the interests of individuals and their right to be healthy against the reality of healthcare economics, limitations of insurance policies, and ever-increasing costs of care. That is, it requires us to place a limit on the value of the health of an individual or even on a human life.

In the United States, healthcare costs represent nearly 20% of GDP, and are increasing steadily (Callahan, 2008). It is estimated that 40%–50% of the increased costs per year comes from the introduction of new medical technologies and the increased usage of existing technologies (Callahan, 2008). These technologies can improve patient outcomes, enhance quality of life, and cure previously fatal diseases. However, some have argued that cost control is needed to maintain the stability of the healthcare system. These reductions include reduction in the use of expensive medical products, particularly those with minimal benefit over less expensive but similarly effective products. This requires, necessarily, that some patients will not have access to a level of care or choices that they have come to expect, and to which they feel they have a right.

Other issues that arise when considering the cost of novel medical products include access to expensive or scarce treatments. For example, sofosbuvir, a well-tolerated and highly effective cure for hepatitis C, was introduced in 2013. The cost of a course of sofosbuvir is more than \$80,000 in the United States (Liao and Fischer, 2017). This equates to approximately \$1000 per pill, despite a cost to produce of approximately \$3. As hepatitis C rates are higher in lower socioeconomic populations, rates of hepatitis C in Medicaid-covered individuals is estimated at 7.5 times that of commercially insured individuals (Liao and Fischer, 2017).

In 2014, following approval of the drug, some states experienced high rates of prescriptions, leading to the need to enact new coverage criteria. New York state, for example, spent 6% of its total prescription budget on sofosbuvir in the first half of 2014, before enacting new coverage criteria that limited access to prescriptions (Liao and Fischer, 2017). These criteria included drug and alcohol abstinence, psychosocial readiness of the patient for treatment, and disease severity, among others. Clearly, from a utilitarian standpoint, restrictions were needed to sustain Medicaid programs and allow for the cost of treatment of patients with other diseases. Conversely, the use of such criteria runs contrary to the belief that all patients should be able to receive treatments that sustain or restore their health regardless of socioeconomic class or personal choices. These issues often raise the question of whether drug and device companies should be able to charge high prices for life-saving treatments. Such questions must be balanced against the utilitarian view that new medical technology development is both risky and costly, and the expectation that companies that undertake such risks have the right to profit from their success. Many argue that, without strong economic incentives, companies would not be willing to take such risks.

Conclusions

This chapter sought to identify and discuss some of the moral and ethical issues that may arise during the development of medical products. The primary, and perhaps the most important, moral and ethical issues surrounding medical products have to do with protecting the safety and improving the wellbeing of the patient. However, the manner in which this is achieved may involve moral and ethical issues related to the use of animals and human subjects during testing of the product. It is expected that researchers, both academic and corporate, will perform their work in a manner that is free of conflict and honest, reflecting the trust placed in scientists, engineers, and medical professionals by the public. These classical concepts are applicable to all medical products. However, with increasingly novel designs, high-powered treatments, and even cures for life-threatening diseases, the type and number of ethical issues have increased. Biologically active components, such as stem cells and methods that have the potential to permanently alter the human genome are now a reality and the associated ethical issues must be considered. Lastly, the potential for moral and ethical challenges does not end once the product has been developed. Cost and access to medical products also raise significant issues, many of which are not often considered by those involved in research and development. This chapter is not comprehensive, and it should be understood that continued scientific progress will certainly lead to new and unexpected issues. For this reason, those involved in the development of medical products should be familiar with the pertinent ethical issues involved with their projects as well as stay informed of developing issues in their field. Doing so can only increase the safety and effectiveness of medical products.

References

- Chen, F.M., Liu, X., 2016. Advancing biomaterials of human origin for tissue engineering. *Prog. Polym. Sci.* 53, 86–168. <https://doi.org/10.1016/j.progpolymsci.2015.02.004>. Epub 2016/03/30. PubMed PMID: 27022202; PMCID: PMC4808059.
- Callahan, D., 2008. Health care costs and medical technology. In: Crowley, M. (Ed.), *From Birth to Death and Bench to Clinic: The Hastings Center Bioethics Briefing Book for Journalists, Policy-makers and Campaigns*. The Hastings Center, Garrison, NY, pp. 79–82.
- Coller, B.S., 2019. Ethics of human genome editing. *Annu. Rev. Med.* 70, 289–305. <https://doi.org/10.1146/annurev-med-112717-094629>. PubMed PMID: 30691366.
- Cotrim, A.P., Baum, B.J., 2008. Gene therapy: some history, applications, problems, and prospects. *Toxicol. Pathol.* 36 (1), 97–103. <https://doi.org/10.1177/0192623307309925>. Epub 2008/03/14. PubMed PMID: 18337227.
- de Miguel-Berriain, I., 2015. The ethics of stem cells revisited. *Adv. Drug Deliv. Rev.* 82–83, 176–180. <https://doi.org/10.1016/j.addr.2014.11.011>. Epub 2014/12/03. PubMed PMID: 25446134.
- de Wert, G., Mummery, C., 2003. Human embryonic stem cells: research, ethics and policy. *Hum. Reprod.* 18 (4), 672–682. <https://doi.org/10.1093/humrep/deg143>. Epub 2003/03/28. PubMed PMID: 12660256.
- Department of Health E, Welfare, National Commission for the Protection of Human Subjects of B, Behavioral R. The Belmont Report, 2014. Ethical principles and guidelines for the protection of human subjects of research. *J. Am. Coll. Dent.* 81 (3), 4–13. PubMed PMID: 25951677.
- Editors Sarah Chan, G., Sternberg, S., 2019. Special issue on ethics of human genome editing. *CRISPR J.* 2, 68. <https://doi.org/10.1089/crispr.2019.29051.cfp>. PubMed PMID: 30998098.
- Fenwick, N., Griffin, G., Gauthier, C., 2009. The welfare of animals used in science: how the “Three Rs” ethic guides improvements. *Can. Vet. J.* 50 (5), 523–530. PubMed PMID: 19436640.
- Franco, N.H., 2013. Animal experiments in biomedical research: a historical perspective. *Animals (Basel)* 3 (1), 238–273. <https://doi.org/10.3390/ani3010238>. PubMed PMID: 26487317.
- Goswami, R., Subramanian, G., Silayeva, L., Newkirk, I., Doctor, D., Chawla, K., Chattopadhyay, S., Chandra, D., Chilukuri, N., Beta-pudi, V., 2019. Gene therapy leaves a vicious cycle. *Front. Oncol.* 9, 297. <https://doi.org/10.3389/fonc.2019.00297>. PubMed PMID: 31069169.
- Hajar, R., 2011. Animal testing and medicine. *Heart Views* 12 (1), 42. <https://doi.org/10.4103/1995-705X.81548>. PubMed PMID: 21731811.
- Harris, C.E., Pritchard, M.S., Rabins, M.J., 2008. Framing the Problem. *Engineering Ethics: Concepts and Cases*. Wadsworth Publishing, Belmont, CA, pp. 47–70.
- Ibraheem, D., Elaissari, A., Fessi, H., 2014. Gene therapy and DNA delivery systems. *Int. J. Pharm.* 459 (1–2), 70–83. <https://doi.org/10.1016/j.ijpharm.2013.11.041>. Epub 2013/11/30. PubMed PMID: 24286924.
- Jafarlou, M., Baradaran, B., Saedi, T.A., Jafarlou, V., Shanehbandi, D., Maralani, M., Othman, F., 2016. An overview of the history, applications, advantages, disadvantages and prospects of gene therapy. *J. Biol. Regul. Homeost. Agents* 30 (2), 315–321. Epub 2016/07/01. PubMed PMID: 27358116.
- Kastenber, Z.J., Odorico, J.S., 2008. Alternative sources of pluripotency: science, ethics, and stem cells. *Transplant. Rev.* 22 (3), 215–222. <https://doi.org/10.1016/j.trre.2008.04.002>. Epub 2008/07/18. PubMed PMID: 18631882.
- Liao, J.M., Fischer, M.A., 2017. Restrictions of hepatitis C treatment for substance-using Medicaid patients: cost versus ethics. *Am. J. Publ. Health* 107 (6), 893–899. <https://doi.org/10.2105/AJPH.2017.303748>. PubMed PMID: 28426313; PMCID: PMC5425868.
- May, W.F., 1988. *Professional Virtue and Self-Regulation*. Oxford University Press, Oxford.
- Nardini, C., 2014. The ethics of clinical trials. *Ecancermedscience* 8, 387. <https://doi.org/10.3332/ecancer.2014.387>. PubMed PMID: 24482672; PMCID: PMC3894239.
- Riva, L., Resta, G., Gambino, A., Petrini, C., 2019. Donation of human biological materials in the European union: commodifying solidarity in the era of the biotechnological revolution? *N. Bioeth.* 25 (4), 349–358. <https://doi.org/10.1080/20502877.2019.1679965>. Epub 2019/11/09. PubMed PMID: 31702479.
- Russell, W.M.S., Burch, R.L., 1959. *The Principles of Humane Experimental Technique*.
- Spinello, R.A., 2004. Property rights in genetic information. *Ethics Inf. Technol.* 6 (1), 29–42. <https://doi.org/10.1023/b:etin.0000036157.14807.b0>. Epub 2006/09/15. PubMed PMID: 16969959.
- von Roten, F.C., 2013. Public perceptions of animal experimentation across Europe. *Publ. Understand. Sci.* 22 (6), 691–703. <https://doi.org/10.1177/0963662511428045>. Epub 2013/07/26. PubMed PMID: 23885052.
- Whiting, T., 2011. Understanding animal welfare: the science in its cultural context. *Can. Vet. J.* 52 (6), 662. PubMed PMID: PMC3095168.
- Wirth, T., Parker, N., Yla-Herttuala, S., 2013. History of gene therapy. *Gene* 525 (2), 162–169. <https://doi.org/10.1016/j.gene.2013.03.137>. PubMed PMID: 23618815.
- Wolf, D.P., Mitalipov, P.A., Mitalipov, S.M., 2019. Principles of and strategies for germline gene therapy. *Nat. Med.* 25 (6), 890–897. <https://doi.org/10.1038/s41591-019-0473-8>. PubMed PMID: 31160821.
- World Medical, A., 2013. World Medical Association Declaration of Helsinki: ethical principles for medical research involving human subjects. *J. Am. Med. Assoc.* 310 (20), 2191–2194. <https://doi.org/10.1001/jama.2013.281053>. PubMed PMID: 24141714.
- Zheng, Y.L., 2016. Some ethical concerns about human induced pluripotent stem cells. *Sci. Eng. Ethics* 22 (5), 1277–1284. <https://doi.org/10.1007/s11948-015-9693-6>. Epub 2015/08/16. PubMed PMID: 26276162.

Properties of Biological Fluids

STEVEN M. SLACK*

This appendix represents a compilation of information relevant to biomaterials scientists regarding the properties and compositions of several body fluids, i.e., blood, plasma (serum), cerebrospinal fluid, synovial fluid, saliva, tear fluid, and lymph. Where possible, ranges of values are provided, but the reader should recognize that significant variations are possible, particularly in states of disease. Further, the data reported here reflect adult measurements and may be substantially different in a pediatric population. Values for

cerebrospinal fluid refer to the lumbar region, those for synovial fluid refer to the knee joint, and those for lymph refer to the thoracic duct, unless otherwise specified. [Table A1](#) lists the physicochemical properties of these fluids. [Table A2](#) provides the typical cellular composition of human blood. [Table A3](#) shows the normal volumes of these fluids in males and females, and presents equations whereby such volumes can be estimated from the mass of the individual. Next, [Table A4](#) lists the approximate concentrations of the major proteins present in various biological fluids. [Tables A5 and A6](#) present the concentrations of inorganic and organic species, respectively, in these fluids. [Table A7](#) provides data on the major plasma proteins, i.e., concentration, molecular weight, isoelectric point (pI), sedimentation coefficient (S), diffusion coefficient (D), extinction coefficient (E_{280}), partial specific volume (V_{20}), carbohydrate content (C),

***Dr. Steven M. Slack** died on April 29, 2010. He was Professor in the Department of Biomedical Engineering and Associate Dean of Graduate Studies in the Herff College of Engineering, at the University of Memphis in Tennessee. He is sorely missed by the current and founding editors of this textbook, by his colleagues around the world, and especially by his many students at the University of Memphis.

TABLE A1 Physicochemical Properties of Several Biological Fluids

Property	Whole Blood	Plasma (Serum)	Cerebrospinal Fluid	Synovial Fluid	Saliva	Tear Fluid
Freezing-point depression ^a	0.557–0.577	0.512–0.568	0.540–0.603	—	0.07–0.34	0.572–0.642
Osmolality ^b	—	275–295	290–324	292–300	—	309–347
pH ^c	7.35–7.45	7.35–7.43	7.35–7.70	7.29–7.45	5.0–7.1	7.3–7.7
Refractive index ^d	16.2–18.5	1.3485–1.3513	1.3349–1.3351	—	—	1.3361–1.3379
Relative viscosity ^e	2.18–3.59	1.18–1.59	1.020–1.027	>300	—	1.26–1.32
Specific conductivity ^f	—	0.0117–0.0123	0.0119	—	—	—
Specific gravity ^g	1.052–1.061	1.024–1.027	1.006–1.008	1.008–1.015	1.002–1.012	1.004–1.005
Specific heat ^h	0.87	0.94	—	—	—	—
Surface tension ⁱ	55.5–61.2	56.2	60.0–63.0	—	15.2–26.0	40–50

^aUnits are °C.

^bUnits are mosm/kg H₂O. Calculated from freezing-point depression.

^cpH measured from arterial blood and plasma, and from cisternal portion of CSF.

^dMeasured at 20°C.

^eMeasured in vitro at 37°C for whole blood, plasma, and synovial fluid, and at 38°C for cerebrospinal fluid. The viscosity of serum is slightly less than plasma due to the absence of fibrinogen.

^fUnits are S/cm. Measured at 25°C for plasma, 18°C for CSF.

^gRelative to water at 20°C.

^hUnits are cal/g °C.

ⁱUnits are dyn/cm. Measured at 20°C.

and half-life. Finally, Tables A8 and A9 present information on the proteins involved in the complement pathway and blood coagulation pathway, respectively. Some of the information contained in this appendix have been previously published in Black, J., & Hastings, G. (eds.) (1998). *Handbook of Biomaterial Properties*. Chapman & Hall: New York, NY, pp. 114–124.

TABLE A2 Cellular Composition of Blood

Cell Type	Cells/ μ L	Half-Life in Circulation
Erythrocytes	4.6–6.2 $\times 10^6$ (M) 4.2–5.2 $\times 10^6$ (F)	25 \pm 2 days
Leukocytes		
Neutrophils	3000–5800	6–8 hours
Eosinophils	50–250	8–12 hours
Basophils	15–50	?
Monocytes	300–500	1–3 days
Lymphocytes	1500–3000	Variable
Platelets	1.5–3.5 $\times 10^5$	3.2–5.2 days
Reticulocytes	2.3–9.3 $\times 10^4$	—

TABLE A3 Volumes of Various Biological Fluids^a

Parameter	Whole Blood	Erythrocytes	Plasma	CS Fluid	Tear Fluid
Volume (mL)	4490 (M) 3600 (F)	2030 (M) 1470 (F)	2460 (M) 2130 (F)	100–160	4.0–13

^aThe following equations can be used to estimate blood volume (BV), erythrocyte volume (EV), and plasma volume (PV) from the known body mass (*b*, kg) with a coefficient of variation of approximately 10%:

Males (M)	Females (F)
BV = 41.0 $\times b$ + 1530	BV = 47.16 $\times b$ + 864
PV = 19.6 $\times b$ + 1050	PV = 28.89 $\times b$ + 455
EV = 21.4 $\times b$ + 490	EV = 18.26 $\times b$ + 409

TABLE A4 Protein Concentrations (mg/dL) in Various Biological Fluids

Protein	Plasma (Serum)	Cerebrospinal Fluid	Synovial Fluid	Saliva	Tear Fluid	Lymph
Total	6000–8000	20–40	500–1800	140–640	430–1220	2910–7330
Albumin	4000–5500	11.5–19.5	400–1000	0.2–1.2	400	1500–2670
α_1 -Acid glycoprotein	50–115	0.1–0.25	—	—	—	260
α -Amylase	—	—	—	6–70	—	—
α_1 -Antitrypsin	85–185	0.4–1.0	45–110	—	1.5	—
Ceruloplasmin	15–60	0.07–1.0	1–7.5	—	4	—
Fibrinogen	200–400	0.065	—	—	—	—
Fibronectin (μ g/mL)	150–300	1–3	150	<1	3–9	—
Haptoglobin	70–140	0.075–0.4	—	9	—	—
Hemopexin	50–120	—	—	—	—	—
IgA	100–400	0.1–0.3	60–115	2.2–15	4–80	—
IgG	650–1600	0.7–2.0	150–46	0.3–1.8	4–60	780
IgM	30–120	—	9–20	0.1–1.2	trace	—
Lysozyme	0.3–0.8	—	—	13–66	100–280	—
α_2 -Macroglobulin	150–450	0.3–0.65	10–50	—	—	—
Transferrin	200–320	0.5–1.2	—	—	10	—

TABLE A5 Concentrations of Major Inorganic Substances (mmol/L) in Various Biological Fluids

Electrolyte	Whole Blood	Plasma (Serum)	Cerebrospinal Fluid	Synovial Fluid	Saliva	Tear Fluid	Lymph
Bicarbonate	19–23	21–30	21.3–25.9	—	2–13	20–40	—
Calcium	2.42	2.1–2.6	1.02–1.34	1.2–2.4	0.69–2.46	0.35–0.77	1.7–2.8
Chloride	77–86	98–109	122–132	87–138	6.5–42.9	110–135	87–103
Magnesium	1.48–1.85	0.80–1.05	0.55–1.23	>Serum	0.065–0.38	—	—
Total phosphorus	10.1–14.3	2.5–4.8	0.442–0.694	>Serum	3.9–9.3	0.11–10.3	2.0–3.6
Potassium	40–60	3.5–5.6	2.62–3.3	3.5–4.5	14–41	31–36	3.9–5.6
Sodium	79–91	125–145	137–153	133–139	5.2–24.4	126–166	118–132
Sulfate	0.1–0.2	0.31–0.58	—	Same as serum	—	—	—

TABLE A6 Concentrations of Organic Compounds (mg/dL) in Various Biological Fluids

Species	Whole Blood	Plasma (Serum)	Cerebrospinal Fluid	Synovial Fluid	Saliva	Tear Fluid	Lymph
Amino acids	4.8–7.4	3.6–7.0	1.0–1.5	—	—	5.0	—
Bilirubin	0.3–1.1	0.2–0.8	<0.01	—	—	—	0.8
Cholesterol	115–225	120–200	0.16–0.77	0.3–1.0	—	10.6–24.4	34–106
Creatine	2.9–4.9	0.13–0.77	0.46–1.9	—	—	—	—
Creatinine	1–2	0.6–1.2	0.65–1.05	—	0.5–2	—	0.8–8.9
Fatty acids	250–390	150–500	—	—	—	—	—
Glucose	80–100	85–110	50–80	—	10–30	10	140
Hyaluronic acid	—	—	—	250–365	—	—	—
Lipids, total	445–610	400–850	0.77–1.7	—	—	—	—
Phospholipid	225–285	150–300	0.2–0.8	13–15	—	—	—
Urea	20–40	20–30	13.8–36.4	—	14–75	20–30	—
Uric acid	0.6–4.9	2.0–6.0	0.5–2.6	7–8	0.5–2.9	—	1.7–10.8
Water (g)	81–86	93–95	94–96	97–99	99.4	98.2	81–86

TABLE A7 Properties of the Major Plasma Proteins

Protein	Plasma Concentration (mg/mL)	Molecular Weight (Da)	pI	S ^a	D ^b	E ₂₈₀ ^c	V ₂₈₀ ^d	C ^e	Half-life (days)
Prealbumin	0.12–0.39	54,980	4.7	4.2	—	14.1	0.74	—	1.9
Albumin	40–55	66,500	4.9	4.6	6.1	5.8	0.733	0	17–23
α_1 -Acid glycoprotein	0.5–1.15	44,000	2.7	3.1	5.3	8.9	0.675	41.4	5.2
α_1 -Antitrypsin	0.85–1.85	54,000	4.0	3.5	5.2	5.3	0.646	12.2	3.9
C1q	0.05–0.1	459,000	—	11.1	—	6.82	—	8	—
C3	1.5–1.7	185,000	6.1–6.8	9.5	4.5	—	0.736	—	—
C4	0.3–0.6	200,000	—	10.0	—	—	—	—	—
Ceruloplasmin	0.15–0.60	160,000	4.4	7.08	3.76	14.9	0.713	8	4.3
Fibrinogen	2.0–4.0	340,000	5.5	7.6	1.97	13.6	0.723	2.5	3.1–3.4
Fibronectin	0.15–0.2	450,000	—	13–13.6	2.1–2.3	13.5	0.72	4–9	0.33
α_2 -Haptoglobin									
Type 1.1	1.0–2.2	100,000	4.1	4.4	4.7	12.0	0.766	19.3	2–4
Type 2.1	1.6–3.0	200,000	4.1	4.3–6.5	—	12.2	—	—	—
Type 2.2	1.2–2.6	400,000	—	7.5	—	—	—	—	—
Hemopexin	0.5–1.2	57,000	5.8	4.8	—	19.7	0.702	23.0	9.5
IgA (monomer)	1.0–4.0	162,000	—	7.0	3.4	13.4	0.725	7.5	5–6.5
IgG	6.5–16.5	150,000	6.3–7.3	6.5–7.0	4.0	13.8	0.739	2.9	20–21
IgM	0.3–1.2	950,000	—	18–20	2.6	13.3	0.724	12	5.1
Lysozyme	0.003–0.008	14,400	10.5	—	—	—	—	—	—
α_2 - Macroglobulin	1.5–4.5	725,000	5.4	19.6	2.4	8.1	0.735	8.4	7.8
Transferrin	2.0–3.2	76,500	5.9	5.5	5.0	11.2	0.758	5.9	7–10

^aSedimentation constant in water at 20°C, expressed in Svedberg units.
^bDiffusion coefficient in water at 20°C, expressed in 10⁻⁷ cm²/s.
^cExtinction coefficient for light of wavelength 280 nm traveling 1 cm through a 10 mg/mL protein solution.
^dPartial specific volume of the protein at 20°C, expressed as mlg⁻¹.
^eCarbohydrate content of the protein, expressed as the percentage by mass.

TABLE A8 Properties of Proteins Involved in the Complement System

Protein	Serum Concentration (mg/L)	Relative Molecular Weight M_r (Da)	Sedimentation Constant S_{20w} (10^{-13} sec)
C1q	50–100	459,000	11.1
C1r	35–40	83,000	7.5
C1s	32–40	83,000	4.5
C2	20–35	108,000	4.5
C3	1500–1700	185,000	9.5
C4	300–600	200,000	10.0
C5	120–180	185,000	8.7
C6	42–60	128,000	5.5
C7	4–60	121,000	6.0
C8	35–50	151,000	8.0
C9	45–70	71,000	4.5
Factor B	220–330	92,000	5–6
Factor D	Trace	24,000	3.0
Properdin	25–35	220,000	5.4
C1 inhibitor	145–170	100,000	—
Factor H	475–575	150,000	6.0
Factor I	30–45	88,000	5.5

TABLE A9 Properties of Proteins Involved in Blood Coagulation

Protein	Plasma Concentration ($\mu\text{g/mL}$)	Relative Molecular Weight M_r (Da)	Biological Half-Life $t_{1/2}$ (Hours)
Fibrinogen	2000–4000	340,000	72–120
Prothrombin	70–140	71,600	48–72
Factor III (tissue factor)	—	45,000	—
Factor V	4–14	330,000	12–15
Factor VII	Trace	50	2–5
Factor VIII	0.2	330,000	8–12
Factor IX	5.0	57,000	24
Factor X	12	58,800	24–40
Factor XI	2.0–7.0	160,000	48–84
Factor XII	15–47	80,000	50–60
Factor XIII	10	320,000	216–240
Protein C	4.0	62,000	10
Protein S	22	77,000	—
Protein Z	3.0	62,000	60
Prekallikrein	35–50	85,000	—
High-molecular-weight kininogen	70–90	120,000	—
Antithrombin III	210–250	58,000	67

Properties of Soft Materials

M. CRISTINA L. MARTINS*

INEB - Institute of Biomedical Engineering, University of Porto, Porto, Portugal

TABLE B1 Some Mechanical and Physical Properties of the Most Common Polymers Used as Biomaterials and the Respective Application

Polymer	Tensile Strength (MPa)	Tensile Modulus (GPa)	Elongation (%)	T_g (°C)	T_m (°C)	Water Absorption (%)	Water Contact Angle (°)	Biomedical Applications (Marchant & Wang, 1994; Pruitt, 2017; Lee et al., 2000; Maitz, 2015; Kroschwitz, 1990)
Polyethylene: Low-density polyethylene - LDPE (Marchant & Wang, 1994)	4–16	0.1–0.3	90–800	–20	95–115	<0.01	93–95	Tubing; shunts; catheters; medical packaging
High-density polyethylene - HDPE (Marchant & Wang, 1994)	21–38	0.4–1.2	20–1000	–125	135–138	<0.01	91	Plastic surgery implants; catheters; tendons
Ultra high molecular weight polyethylene - UHMWPE (Steven, 2004)	39–48	0.8–1.6	350–525	–160	125–138	–	–	Acetabulum in total hip prostheses; artificial knee prostheses
Polypropylene - PE (Marchant & Wang, 1994)	30–38	1.1–1.6	200–700	–12	125–167	<0.01	104	Heart valve structures; oxygenator and plasmapheresis membranes; nonabsorbable sutures; disposable syringes; finger joint prosthesis
Polyvinylchloride—PVC (rigid) (Marchant & Wang, 1994)	35–62	2.4–4.1	2–40	87–90	212	0.1–0.4	80	Catheters; blood bags; tubings ^a
(plasticized) (Marchant & Wang, 1994)	10–24	–	200–450					
Poly(tetrafluoroethylene) - PTFE or Teflon® (Marchant & Wang, 1994)	14–35	0.4	200–400	–10	327	0	110	Vascular graft; catheter coating; facial prosthesis; heart valve structures; stapes prosthesis (in tympanoplasty)
Poly(dimethylsiloxane) - PDMS or silicone (Marchant & Wang, 1994)	2–10	–	100–600	(–120)–(–123)	–	0.02	101–109	Oxygenator membrane; tubing; shunts; breast, joint, tracheal, bladder, and maxillofacial prostheses; heart pacemaker leads; heart valve structures; burn dressing
Poly(ethylene terephthalate) - PET or Dacron (Marchant & Wang, 1994)	59–72	2.8–4.1	50–300	69–82	265–270	0.1–0.2	73–78	Vascular grafts; heart valve structures; shunts; laryngeal, esophageal, and bladder prostheses; non-absorbable sutures; tendon reconstruction
Polyamides (nylons) (Marchant & Wang, 1994)	62–68	1.2–2.9	60–300	45–75	200–270	1.5	–	Hemodialysis membrane; nonabsorbable sutures

Poly(ether urethane) (e.g., Pellethane) (Lamba et al., 1998)	35–48	<0.01	350–600	(–43)–(–60)	188–204	–	62–107	Percutaneous leads; catheters; tubing; intraaortic balloons; wound dressing
Poly(ether urethane urea) (e.g., Biomer) (Lamba et al., 1998)	31–41	<0.01	600–800	(–53)–(–67)	120–150	0.02	63–69	Artificial heart components; heart valve; tubing; vascular graft prosthesis
Polystyrene - PS (Marchant & Wang, 1994)	35–83	2.8–4.1	1–3	116	137	0.10	45 ^b	Tissue culture dish
Polycarbonate - PC (Marchant & Wang, 1994)	55–66	2.4	100–130	150	267	0.2	62 ^b	Connectors; oxygenator housings; hemodialysis and plasmapheresis membranes (Lee et al., 2000)
Polysulfones (Marchant & Wang, 1994)	70.3	2.5	50–100	190–285	–	0.22	–	Artificial heart components; heart valve structures; oxygenator; hemodialysis and plasmapheresis membranes
Poly(aryl-ether-ether-ketone) - PEEK (OPTIMA LT1) (Kurtz & Devine, 2007)	93	4 ^c	30–40	~143	~343	–	–	Orthopedic and spinal implants
Poly(methyl methacrylate) - PMMA (Marchant & Wang, 1994)	48–76	3.1	2–10	110	160	0.3–0.4	62	Dentures; bone cement; plasmapheresis and hemodialysis membranes; intraocular lens; middle ear prosthesis
Poly(2-hydroxyethylmethacrylate) - PHEMA (Marchant & Wang, 1994)	0.3	0.8	50	115 (dry)	–	>1	–	Catheter coating; drug delivery device; soft contact lens; vascular prosthesis coating; burn dressing
Poly(vinyl alcohol) (Kroschwitz, 1990)								
(98–99% hydrolyzed)	67–110		0–300	85	230	–	–	Drug delivery devices
(87–89% hydrolyzed)	24–79			58	180			
Poly(ϵ -caprolactone) (M_w : 44,000) (Engelberg & Kohn, 1991)	16	0.4	80	–62	57	<0.2	–	Drug delivery devices
Poly(glycolic acid) - PGA (Fambri, 2002)	57	6.5	–	35	225	–	–	Drug delivery devices; absorbable sutures; vascular stents
(fibers)	750	13.4		–	233			
Poly(lactic acid)—PLA (Engelberg & Kohn, 1991)								
L-PLA (M_w : 50,000–300,000)	28–48	1.2–3.0	6–2	54–59	170–178	–	–	Drug delivery devices; vascular stents
D,L-PLA (M_w : 107,000–550,000)	29–35	1.9–2.4	6–5	51–53	–			

TABLE B1 Some Mechanical and Physical Properties of the Most Common Polymers Used as Biomaterials and the Respective Application

Polymer	Tensile Strength (MPa)	Tensile Modulus (GPa)	Elongation (%)	T_g (°C)	T_m (°C)	Water Absorption (%)	Water Contact Angle (°)	Biomedical Applications (Marchant & Wang, 1994; Pruitt, 2017; Lee et al., 2000; Maitz, 2015; Kroschwitz, 1990)
Poly(ortho ester) ^d (M_w : 99,700)	20	0.82	220	55	–	0.2–1	–	Drug delivery devices
Poly(β -hydroxybutyrate) - PHB (Engelberg & Kohn, 1991)	36	2.5	2.5	1	171	–	–	Drug release devices; sutures; artificial skin; cardiovascular patches;
(M_w : 370,000)								
Poly(hydroxybutyrate-co-22 mol% hydroxyvalerate) (Engelberg & Kohn, 1991)	16	0.62	36	–5	137	–	–	orthopedic pins; nerve guides; wound dressings; bone marrow scaffolds (Chen & Wu, 2005)
(M_w : 227,000)								
Cellulose acetate (Kroschwitz, 1990)	13.1–58.6	0.6–1.8	6–50	–	306	2.0–6.5	–	Hemodialysis membrane
Collagen (Pins et al., 1997) ^e								
(uncrosslinked fibers)	0.70–1.12	$(1.5\text{--}2.2) \times 10^{-3}$	61.1–74.8	–	–	–	–	Hemostatic agent; vascular prosthesis; heart valves; tendons and ligaments; wound and burn dressings; absorbable sutures (Li, 2000)
(crosslinked fibers)	29.7–63.9	0.271–0.495	12.9–18.3					
Silk (Perez-Rigueiro et al., 2000; Vepari & Kaplan, 2007) ^f (with sericin)	500	5–12	19	–	–	–	–	Nonabsorbable sutures; wound healing dressings; scaffolds for regeneration of bone, cartilage, tendon, and ligaments tissues (Vepari & Kaplan, 2007)
(without sericin)	610–690	15–17	4–16					
Chitosan (Lim et al., 1998) ^g (M_v : $(8.73 \pm 0.55) \times 10^5$) (Deacetylation (%): 8.17 ± 0.35)	56.2–67.6	2.93–3.30	26.9–33.3	50.8–53.2	–	–	–	Surgical sutures; dental implants; artificial skin; rebuilding of bone; corneal contact lenses; drug release devices (Rinaudo, 2006)

^aThere are several medical concerns about PVC due to phthalate plasticizer di(2-ethylhexyl) phthalate (DEHP) that is released to the ambience and dissolves in the lipid bilayers of cells (Maitz, 2015).

^bValues are averages of advancing and receding contact angles.

^cFlexural modulus.

^dTranscyclohexane dimethanol (t-CDM):1,6-hexanediol (1,6-HD) = 35:65.

^eAcid-soluble collagen obtained from rat tail tendons. Collagen fibers coextruded using NaCl (coagent).

^f*Bombyx mori* single-brin silkworm silk.

^gChitosan films.

References

- Chen, G.Q., Wu, Q., 2005. The application of hydroxyalkanoates as tissue engineering materials. *Biomaterials* 26, 6565–6578.
- Engelberg, I., Kohn, J., 1991. Physico-mechanical properties of degradable polymers used in medical applications: a comparative study. *Biomaterials* 12, 292–304.
- Kroschwitz, J.I., 1990. *Concise Encyclopedia of Polymer Science and Engineering*. John Wiley and sons. Inc, NY, USA.
- Kurtz, S.M., Devine, J.N., 2007. PEEK biomaterials in trauma, orthopedic and spinal implants. *Biomaterials* 28, 4845–4869.
- Lamba, N.M.K., Woodhouse, K.A., Cooper, S.L., 1998. *Polyurethanes in Biomedical Applications*. CRC Press LLC, USA.
- Lee, H.B., Khang, G., Lee, J.H., 2000. Polymeric Biomaterials. In: Bronzino, J.D. (Ed.), *The Biomedical Engineering Handbook*, 2nd Edition. CRC Press, Inc, USA, p. 39.
- Li, S.T., 2000. In: Bronzino, J.D. (Ed.), *Biological Biomaterials: Tissue-Derived Biomaterials (Collagen) in The Biomedical Engineering Handbook*, 2nd Edition. CRC Press, Inc, USA, p. 41.
- Lim, L.Y., Khor, E., Koo, O., 1998. γ Irradiation of Chitosan. *J. Biomed. Mat. Res.* 43, 282–290.
- Maitz, M.F., 2015. Applications of synthetic polymers in clinical medicine. *Biosurface Biotribol.* 1, 161–176.
- Marchant, R.E., Wang, I., 1994. Physical and chemical aspects of biomaterials used in humans. In: Greco, R.S. (Ed.), in *Implantation Biology: The Host Response and Biomedical Devices*. CRC Press, Inc, pp. 13–38. <https://doi.org/10.1002/pola.1995.080330329>.
- Perez-Rigueiro, J., Viney, C., Llorca, J., Elices, M., 2000. Mechanical properties of single-brin silkworm silk. *J. Appl. Polymer Sci.* 75, 1270–1277.
- Pins, G.D., Huang, E.K., Christiansen, D.L., Silver, F.H., 1997. Effect of static axial strain on the tensile properties and failure mechanisms of self-assembled collagen fibers. *J. Appl. Polymer Sci.* 63, 1429–1440.
- Pruitt, L.A., 2017. Load-Bearing Medical Polymers (Non-degradable). In: Ducheyne, P., Grainger, D.W., Healy, K.E., Hutmacher, D.W., Kirkpatrick, C.J. (Eds.), *Comprehensive Biomaterials II, Metallic, Ceramic, and Polymeric Biomaterials*, Vol 1. 2nd Edition. Elsevier, pp. 507–515.
- Rinaudo, M., 2006. Chitin and chitosan: Properties and applications. *Progress Polymer Sci.* 31, 603–632.
- Steven, M.K., 2004. *The UHMWPE Handbook: Ultra-high Molecular Weight Polyethylene in Total Joint Replacement*. Academic Press, Elsevier Inc. <https://doi.org/10.1016/B978-0-12-429851-4.X5000-1>.
- Vepari, C., Kaplan, D.L., 2007. Silk as a Biomaterial. *Prog. Polym. Sci.* 32, 991–1007.

Further Reading

- Fambri, L., Migliaresi, C., Kesenci, K., Piskin, E., Barbucci, R., 2002. Biodegradable polymers. In: *Integrated Biomaterials Science*. Springer, pp. 119–170.

Chemical Composition of Metals and Ceramics Used for Implants

DAVID H. KOHN¹, JACK E. LEMONS²

¹Departments of Biologic and Materials Sciences, and Biomedical Engineering, The University of Michigan, Ann Arbor, MI, United States

²Schools of Dentistry, Medicine and Engineering, University of Alabama at Birmingham, Birmingham, AL, United States

TABLE C1 Properties of Metals and Alloys Used for Surgical Implants^a

Material	Nominal Composition (w/o)	Modulus of Elasticity (GPa)	Tensile Strength (MPa)	Elongation to Fracture (%)
Titanium (Ti) and alloys	99+Ti (Grades I-IV)	100	240–550	15–24
	90Ti–6Al–4V	120	860–930	8–10
	90Ti–6Al–4V (ELI)		825–860	8–10
	87Ti–6Al–7Nb		900–1100	10
	74Ti–13Nb–13Zr		550–860	8–15
	80Ti–12Mo–6Zr–2Fe		930	12
	85Ti–15Mo		690–900	10–20
	Ti–3Al–2.5V		620–860	10–15
Cobalt–chromium (Co–Cr) alloys	66Co–28Cr–6Mo	235	520–1170	8–20
	35Co–35Ni–20Cr–10Mo		790–1580	3–50
	40Co–20Cr–16Fe–15Ni–7Mo		450–2245	1–65
	55Co–20Cr–15W–10Ni		310–1730	15–45
Stainless steel (316L)	70Fe–18Cr–12Ni	190	480–1000	>30
Zirconium (Zr) and alloys	99+Zr	100	450–550	15–20
	97.5Zr–2.5Nb		450	15–30
Tantalum (Ta)	99+Ta	–	170–520	1–30
Nickel–titanium (Ni–Ti) alloy	45Ni–57Ti		550	10–15
Gold (Au)	99+Au	100	210–310	>30
Platinum (Pt)	99+Pt	165	130	40

^aMinimum values from the American Society for Testing and Materials Committee F4 Annual Book of Standards, Volume 13.01, Medical and Surgical Materials and Devices, 2013. Selected products provide a range of properties due to differences in processing (cast, forged, wrought), heat treatment, and section size.

TABLE C2 Properties of Inert Ceramic Biomaterials^a

Material	Modulus of Elasticity (GPa)	Compressive Strength (MPa)	Flexural Strength (GPa)
Aluminum oxide	150–400	80–5000	6–640
Zirconium oxide (zirconia)	150–240	400–1750	50–900
Titanium oxide (titania)	280		69–103
Carbon	7–30	50–700	70–255
Carbon–silicon (LTI)	25–40	900	200–700

LTI, Low-temperature isotropic.

^aThese high ceramics have 0% permanent elongation at fracture. Selected products have a range of properties due to differences in porosity, density, and whether single crystal or polycrystalline.

TABLE C3 Properties of Bioactive and Biodegradable Ceramics^a

Material	Modulus of Elasticity (GPa)	Compressive Strength (MPa)	Flexural Strength (MPa)
Hydroxyapatite	10–120	60–800	15–300
Tricalcium phosphate	30–120	120	15–120
Bioglass or Ceravital	40–140		20–350
A/W ceramic	124		213

A/W, Apatite/wollastonite.

^aThese ceramics and carbons have 0% permanent elongation at fracture. Selected products have a range of properties due to differences in porosity and density.

The Biomaterials Literature

WILLIAM R. WAGNER

McGowan Institute for Regenerative Medicine, Departments of Surgery, Bioengineering & Chemical Engineering, University of Pittsburgh, Pittsburgh, PA, United States

An excellent way to get a sense of the current directions in biomaterials research is to peruse the table of contents for recent issues of some of the leading journals in the field. One will find research reports that fall within most of the topics covered in this textbook regarding biomaterials development, new biomaterials applications, and ongoing efforts to define the mechanisms underlying the biological response to biomaterials placed in the body. A noncomprehensive list of journals publishing in the field is found in [Table D1](#). Many of the journals in this list were not publishing at the turn of the century, reflecting how the biomaterials field has rapidly grown in the past 20 years. This growth is not surprising. Global research output has increased as government and industrial funding has been directed to the field in recognition of the role it will play for an aging population with rising economic resources at their disposal to dedicate to healthcare. With more research output comes the demand for more forums for publication, thus not only have the number of biomaterials journals increased, the spectrum of subtopic coverage has increased, and the selectivity and broader scientific impact of the leading journals continue to grow. All of these are healthy indicators of a vibrant, promising field.

While the diverse literature of today provides an effective snapshot of current trends and thinking, it is also a worthwhile exercise to look back 10, 20, or even 50+ years and read the manuscripts in some of the leading journals of those periods. While in the earliest days many of the advancements were reported in clinically related journals, one pioneering journal where some of the most impactful biomaterials and medical device research was reported in the 1950s and 1960s was the *American Society for Artificial Internal Organs (ASAIO) Journal*. It is a humbling experience to read about the researchers of that time tackling many of the same problems (e.g., blood biocompatibility, material degradation) as today, with a much more limited tool set, but excellent clinical and engineering insight and careful methodologies.

Anyone who has served as a referee in the manuscript peer-review process has had the experience of finding authors who are unaware of similar published efforts. Today's literature databases offer unprecedented tools to find relevant reports on a given topic area. Offsetting this, the number of papers to search is growing in a nonlinear

fashion, and authors may not devote adequate time and care to find and consider how their work fits in the body of knowledge. Searching and reading the biomaterials literature in one's area of work is necessary not only to prevent expending resources on previously well-investigated topics, but it can stimulate creativity when the reader brings to bear their advantage of unique perspective and progress with time to chart an important step forward.

Looking to the more recent past of 10–20 years ago, surveying the literature can lead to the question, “so what happened?” So many reports show good outcomes, often in relevant preclinical models. Why then did most of this work never translate to today's standard of clinical care? While part of the answer may be scientific, the other factors are why the editors of this textbook have sought to emphasize the broader context in which biomaterials science exists. Manufacturability, intellectual property position, regulatory pathway, disruption of standard of care, investment return potential, legal liability, and other not strictly scientific considerations have all served to dissuade or block the progress of promising literature reports from ever making it to the intended patients. The literature does not routinely publish such stories, but knowledge of how such considerations effectively prevent translation is critical for any biomaterials scientist to understand and to weigh against the optimistic reports that continue to be published in growing numbers.

With respect to the long list of journals in [Table D1](#), just by the titles one can glean the focus area; but how does one compare the “quality” or “impact” of the papers in the various journals? There are numerous parameters devised to reflect such markers of impact, but it is important to note that such indicators are averages and subject to peripheral factors. The most common indicator, the journal impact factor (from Journal Citation Reports and updated annually), provides a measure of the average number of times articles published in the 2 years preceding the most recently completed year have been cited in the most recently completed year. Higher impact factor journals will generally be more selective and may have more rigorous peer-review procedures, but this is not absolute. For instance, a topic that has fewer overall papers published will have fewer papers that could cite an earlier paper and thus that topic may have

lower impact factor journals. Authors are well served to carefully consider where they seek to publish their work, but in doing so consider more than the journal's current impact factor. How does your paper fit within the journal scope? Are you better suited to targeting a more clinically focused journal? Is the peer-review process rigorous and generally fair? Is the time to publish reasonably fast? Is the journal large enough to be carried by libraries and appear on databases? Is there an option for open-access publication if you have the desire or need to publish in this manner and is the publication fee reasonable?

In addition to the journals that cover biomaterials-related topics, there are many books that have been published seeking both to generally cover the field and to provide overviews of the growing number of subtopics. An exhaustive list is again not possible, but [Table D2](#) may provide the reader with a sense of recent texts and those that have been well

received by the community. A well-prepared text can provide an excellent foundation when seeking to learn about a new field. The growing number of peer-reviewed review articles in the literature is also useful for timely coverage on a given subtopic.

Finally, it is worth mentioning the patent literature. Given the importance of intellectual property protection in the commercialization process and achieving the goal of impacting the patient, a biomaterials scientist may encounter this literature in academic, industrial, and legal settings. Progressing through the examination process to be awarded a patent is much different than the scientific peer-review process. However, an understanding of the principles covered in the textbook comes into play, for instance, when arguing whether a patent claim can be anticipated by one skilled in the art based on prior patents and the biomaterials literature.

TABLE D1 Biomaterials Journals and Journals With Substantial Biomaterial Content

Full Journal Title	
ACS Applied Materials & Interfaces	International Journal of Polymeric Materials and Polymeric Biomaterials
ACS Biomaterials Science & Engineering	Journal of Applied Biomaterials & Functional Materials
ACS Nano	Journal of Bioactive and Compatible Polymers
Acta Biomaterialia	Journal of Biomaterials Applications
Advanced Drug Delivery Reviews	Journal of Biomaterials Science—Polymer Edition
Advanced Healthcare Materials	Journal of Biomedical Materials Research Part A
Annals of Biomedical Engineering	Journal of Biomedical Materials Research Part B—Applied Biomaterials
Artificial Cells Nanomedicine and Biotechnology	Journal of Bionic Engineering
Artificial Organs	Journal of Controlled Release
ASAIO Journal	Journal of Materials Chemistry B
Biofabrication	Journal of Materials Science—Materials in Medicine
Bioinspiration & Biomimetics	Journal of the Mechanical Behavior of Biomedical Materials
Biointerphases	Journal of Tissue Engineering and Regenerative Medicine
Biomacromolecules	Journal of Oral Science
Biomaterials	Journal of the Mechanical Behavior of Biomedical Materials
Biomaterials Science	Lab on a Chip
Biomedical Materials	Langmuir
Bio-Medical Materials and Engineering	Macromolecular Bioscience
Biomedical Microdevices	Materials Science & Engineering C—Materials for Biological Applications
Biotechnology and Bioengineering	Nanomedicine
Colloids and Surfaces B—Biointerfaces	Regenerative Biomaterials
Dental Materials	Small
Dental Materials Journal	Soft Matter
European Cells & Materials	Tissue Engineering
IEEE Transactions on Biomedical Engineering	
International Journal of Artificial Organs	

TABLE D2 Biomaterials Books

Title	Year	Author (au)/Editor (ed)	Publisher
3D Bioprinting and Nanotechnology in Tissue Engineering and Regenerative Medicine	2015	(ed) Lijie Grace Zhang, John P. Fisher, Kam Leong	Academic Press
An Introduction to Tissue–Biomaterial Interactions	2008	(au) Kay C. Dee, David A. Puleo, Rena Bizios	Wiley-Liss
Bio-Ceramics with Clinical Applications	2014	(au) Maria Vallet-Regi	Wiley
Biointerfaces: Where Material Meets Biology	2105	(ed) Dietmar Hutmacher, Wojciech Chzanowski	Royal Society of Chemistry
Biological Materials Science: Biological Materials, Bioinspired Materials, and Biomaterials	2014	(au) Marc André Meyers, Po-Yu Chen	Cambridge University Press
Biomaterials: A Basic Introduction	2018	(au) Qizhi Chen, George Thouas	CRC Press
Biomaterials: A Systems Approach to Engineering Concepts	2017	(au) Brian James Love	Elsevier Academic Press
Biomaterials and Regenerative Medicine	2015	(ed) Peter X. Ma	Cambridge University Press
Biomaterials in Translational Medicine	2019	(ed) Lei Yang, Sarit Bhaduri, Thomas J. Webster	London Academic Press
Biomaterials Mechanics	2017	(ed) Heather N. Hayenga, Helim Aranda-Espinoza	CRC Press
Biomaterials Science and Tissue Engineering: Principles and Methods	2017	(au) Bikramjit Basu	Cambridge University Press
Biomaterials, Medical Devices, and Combination Products: Biocompatibility Testing and Safety Assessment	2016	(au) Shayne C. Gad, Samantha Gad-McDonald	CRC Press
Biomaterials: An Introduction	2010	(au) Joon Bu Park, Roderic S. Lakes	Springer
Biomaterials: Principles and Practices	2013	(ed) Joseph D. Bronzino, Donald R. Peterson, Joyce Y. Wong	Taylor & Francis
Biomaterials: The Intersection of Biology and Materials Science	2011	(au) J.S. Temenoff, Antonios G. Mikos	Johanneshov: TPB
Biomedical Hydrogels: Biochemistry, Manufacture and Medical Applications	2016	(ed) Steve Rimmer	Woodhead
Comprehensive Biomaterials II	2017	(ed) Paul Ducheyne, David W. Grainger, Kevin E. Healy, Dietmar W. Hutmacher, C. James Kirkpatrick	Elsevier
Concise Encyclopedia of Biomedical Polymers and Polymeric Biomaterials	2018	(ed) Munmaya Mishra	CRC Press
Definitions of Biomaterials for the Twenty-First Century: Series Materials Today	2019	(ed) Xingdong Zhang, David Williams	Elsevier
Essential Biomaterials Science	2014	(au) David F. Williams	Cambridge University Press
Foundations of Biomaterials Engineering	2019	(au) Maria Cristina Tanzi, Silvia Farè, Gabriele Candiani	Academic Press
Functional Hydrogels as Biomaterials	2019	(ed) Jun Li, Yoshihito Osada, Justin Cooper-White	Springer
Fundamentals of Biomaterials	2018	(au) Vasif Hasirci, Nesrin Hasirci	Springer
Handbook of Biomaterial Properties	2016	(ed) William Murphy, Jonathan Black, Garth Hastings	Springer Science+Business Media

(Continued)

TABLE D2 Biomaterials Books—cont'd

Title	Year	Author (au)/Editor (ed)	Publisher
Hemocompatibility of Biomaterials for Clinical Applications: Blood–Biomaterials Interactions	2018	(ed) Christopher Siedlecki	Cambridge Elsevier Science & Technology
Host Response to Biomaterials: The Impact of Host Response on Biomaterial Selection	2015	(ed) Stephen F. Badylak	Academic Press
Introduction to Biomaterials: Basic Theory with Engineering Applications	2013	(au) C. Mauli Agrawal, Joo L. Ong, Mark R. Appleford, Gopinath Mani	Cambridge University Press
Mechanics of Biomaterials: Fundamental Principles for Implant Design	2011	(au) Lisa A. Pruitt	Cambridge University Press
Metallic Biomaterials: New Directions and Technologies	2017	(au) Yufeng Zheng, Zhigang Xu, Xiaoxue Xu, Junqiang Wang, Hong Cai	Wiley-VCH
Peptides and Proteins as Biomaterials for Tissue Regeneration and Repair	2018	(ed) Mario Barbosa, M. Cristina L. Martins	Woodhead Publishing
Principles of Regenerative Medicine	2019	(ed) Anthony Atala, Robert Lanza, Antonios G. Mikos, Robert Nerem	Academic Press
Principles of Tissue Engineering	2013	(ed) Robert S. Langer, R.P. Lanza, Joseph Vacanti	Academic Press
Surface Modification of Biomaterials: Methods Analysis and Applications	2016	(ed) Rachel Williams	Woodhead
Thin Film Coatings for Biomaterials and Biomedical Applications	2016	(ed) Hans J. Griesser	Elsevier

Assessment of Cell and Matrix Components in Tissues

RICHARD N. MITCHELL, FREDERICK J. SCHOEN

Department of Pathology, Brigham and Women's Hospital, Boston, MA, United States of America

Techniques commonly used to study the structure of tissues—and the purpose of each mode of analysis—are summarized in [Table F1](#). While not completely comprehensive, [Table F1](#) reflects the traditional morphologic approaches to tissue assessment, in addition to the more recent genetic, proteomic, metabolomic, physicochemical, and quantitative techniques that can inform and direct biomaterials and device development.

The most widely used—and most broadly informative—technique is still light microscopy, described in greater detail later. Several additional tissue analysis techniques are also available to address specific questions concerning cell and tissue structure and function (see later). Although microscopy can be a purely qualitative evaluation of cell and tissue pathology (e.g., cell death, regeneration, inflammation, neoplasm, etc.), quantitative information can be gleaned from tissue sections using various manual or computer-aided methods. Such morphometric approaches can be extremely useful in providing an objective basis for otherwise subjective measurements ([Loud, 1984](#)).

It is frequently necessary to accurately ascertain or verify the identity of a cell, or to determine some aspect of its function, including the synthesis of specific molecules. For such an assay, either isolated cells or whole tissues are used, depending on the objective of the study. *Isolated cells* have the advantage of allowing molecular and/or biochemical analyses on individual cells or synthetic products—often yielding quantitative data. Gene expression profiling allows the analysis of the genes expressed in cells or tissues; the technology may identify pathogenetically distinct cellular subtypes and suggest fundamental mechanisms even when candidate genes are unknown ([Duggal, 2009](#)). Increasingly, mass spectroscopy techniques also provide a functional assessment of the metabolic pathways that are the integrated output of all the genetic influences. Conversely, *whole tissue preparations* allow the investigator to spatially localize molecules of interest in the context of architectural features of the tissue; such information is lost in most cases when tissues are digested to release individual components.

Light Microscopy

Conventional light microscopy starts with obtaining tissue samples by surgical excision (removal), biopsy (sampling), or autopsy (postmortem examination). This is followed by fixation, embedding in paraffin, thin sectioning (5–50 μ), adherence to a glass slide, staining with various vital dyes, and microscopic examination ([Fig. F1](#)). Photographs of conventional tissue sections taken through a light microscope (photomicrographs) are illustrated in [Fig. F2](#).

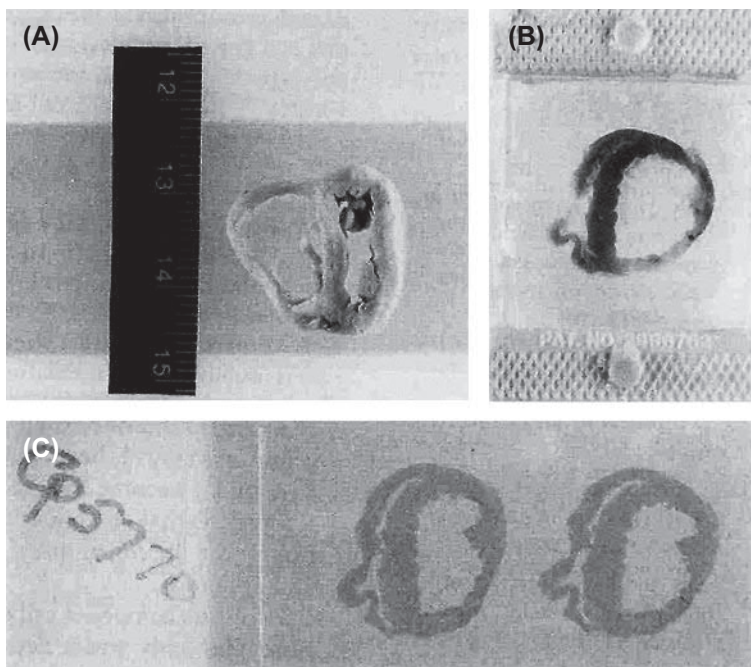
To preserve the structural integrity of cells, subcellular structures, and extracellular matrix (ECM), excised tissues are “fixed,” typically by denaturing and cross-linking protein amino groups with aldehyde reagents (forming Schiff base and Amadori rearrangement adducts). Formaldehyde is the typical fixative for light microscopy, while glutaraldehyde preserves subcellular structural elements better for scanning or transmission electron microscopy (TEM). Fixative solutions prevent degradation of tissue (*autolysis*—typically caused by release of intracellular hydrolytic enzymes) after samples have been removed from their normal sources of oxygen and nutrition. Fixation also variably immobilizes fats and carbohydrates, and kills microorganisms present in tissues. However, such denaturation and cross-linking can also adversely impact enzymatic and antigenic reactivity that might be targets of interest when analyzing the tissue. It is noteworthy that for tissues like bone with a highly calcified matrix, specimens must usually be *decalcified* (by prolonged immersion in acid) prior to sectioning; such treatment also adversely impacts antigenicity and subsequent analysis.

To provide a more solid substrate for sectioning, water in a tissue specimen (approximately 70% of tissue mass) must be substituted for paraffin wax or other embedding media (e.g., glycolmethacrylate). This is done through several steps, beginning with dehydration of the specimen through increasing concentrations of ethanol (eventually to absolute). Since alcohol is not miscible with paraffin (the most common final embedding medium), xylol (an organic solvent) is used as an intermediate solution before embedding in paraffin. All this is important to understand because the organic solvent steps will cause the variable loss of lipids and other lipophilic materials in the tissues.

**TABLE
F1**

Techniques Used to Study Tissue

Technique	Purpose
Microbiologic cultures	Diagnose the presence of infectious organisms
Morphology	
Gross examination	Determines overall specimen configuration; many diseases and processes can be diagnosed at this level
Light microscopy (LM)	Studies overall microscopic tissue architecture and cellular structure; different stains allow analysis of, e.g., calcium, fat, matrix, apoptotic cell death, etc.
Transmission electron microscopy (TEM)	Studies ultrastructure (fine structure) and identifies cells and their organelles and environment
Scanning electron microscopy	High-resolution 3D imaging
Optical coherence tomography	Visualizes microscopic structures using lightwave diffraction; can be applied to tissues in situ
Microscopic computed tomography	High-resolution 3D microscopy
High-resolution microscopy	Super-resolution, two-photon microscopy, confocal microscopy
Morphometric studies (gross, LM, or TEM levels)	Quantitate the amounts, configuration, and distribution of specific structures
Genetic Analysis (Genomics)	
Maintaining Tissue Architecture Relationships	
In situ hybridization	Identifies the presence and location of mRNA or DNA within cells and tissues in histological sections
Laser capture microdissection	Procures specific microscopic regions of tissue sections containing small collections of cells to apply molecular analysis methods
Information on Total Tissue Without Architecture	
Northern blot	Detects the presence, amount, and size of specific mRNA molecules
Southern blot	Detects and identifies specific DNA sequences
Polymerase chain reaction	Cyclical amplification of DNA to produce sufficient material for analysis
DNA microarray	Identifies sequence (gene/gene mutation) and determines expression level (abundance) of genes; also known as DNA chip or gene array; microarray on a single chip of tiny spots, each representing a unique cloned cDNA or oligonucleotide
Single cell sequencing	Allows identification of unique RNA expression profiles; can characterize rare cells or cellular heterogeneity (e.g., in tumors)
Protein Analysis (Proteomics)	
Maintaining Tissue Architecture Relationships	
Enzyme histochemistry	Demonstrates the presence and location of enzymes in gross or microscopic tissue sections
Immunohistochemistry	Identifies and locates specific molecules, usually proteins, for which a specific antibody is available
Tissue microarray	Permits study of multiple lesions simultaneously using tissues from multiple patients or blocks on the same slide; produced using a needle to biopsy conventional paraffin blocks and placing the cores into an array on a recipient paraffin block
Information on Total Tissue Without Architecture	
Western blot	Identifies the presence and amount of specific proteins
Flow cytometry	Isolated cells are characterized by surface or intracellular protein expression patterns; cells may be sorted and subsequently analyzed by other techniques (e.g., RNA, metabolites, etc.)
Mass spectroscopy	Can identify a broad spectrum of metabolic products, thus integrating functional genetic and protein outputs (metabolomics); newer techniques may allow analysis on tissue sections, preserving architectural information
Physicochemical Analysis	
Maintaining Tissue Architecture Relationships	
Energy dispersive X-ray analysis	Performs site-specific elemental analysis on surfaces of tissue sections
Collagen orientation	Allows microscale analysis of matrix organization
Information on Total Tissue Without Architecture	
Chemical, biochemical, and spectroscopic analysis	Assesses bulk concentration of molecular or elemental constituents



• **Figure F1** Steps in tissue processing for light microscopy. (A) Tissue section. (B) Tissue in a paraffin block. (C) Resulting stained histologic section on a glass slide.

Tissue specimens are routinely sectioned on a *microtome*; 5 μ thick slices are then adhered to glass slides. Sections for light microscopic analysis must be thin enough to both transmit light and avoid superimposition of various tissue components. Since 5 μ is thinner than the diameter of most cells, structures may not be entirely represented depending on where a cut is made (for example, a cell may appear to lack a nucleus; Fig. F3). Thus interpretation of tissue sections depends on the reconstruction of three-dimensional information from two-dimensional observations on tissue sections. A particular structure (even a very simple one) can look very different, depending on the plane of section. Thicker sections (up to 100 μ) may be used for special analyses to evaluate three-dimensional architecture and require different microscopic techniques. If extremely thin sections are required for TEM analysis (e.g., approximately 0.06 μ), a harder embedding medium (usually epoxy plastic) and a correspondingly harder knife (usually diamond) are used. Alternatively, if immediate evaluation of a tissue is required (typical processing takes 12–24 h), samples can be frozen in special embedding media that allows 5–10 μ sections to be made and instantly examined. Although quick, the quality of the appearance of such *frozen section analysis* is inferior to that obtained by conventional methods due to ice expansion and the ensuing displacement artifacts. For sections examining the interface of bone or metal with soft tissue, tissues can be prepared by embedding in epoxy followed by sectioning or grinding to 50–100 μ thickness.

Tissue components have no intrinsic contrast and are of fairly uniform optical density. Consequently, for tissues to be visualized and distinguished by light microscopy, they are differentially stained by selective adsorption of dyes. Since most stains are aqueous dye solutions, staining requires that the paraffin in

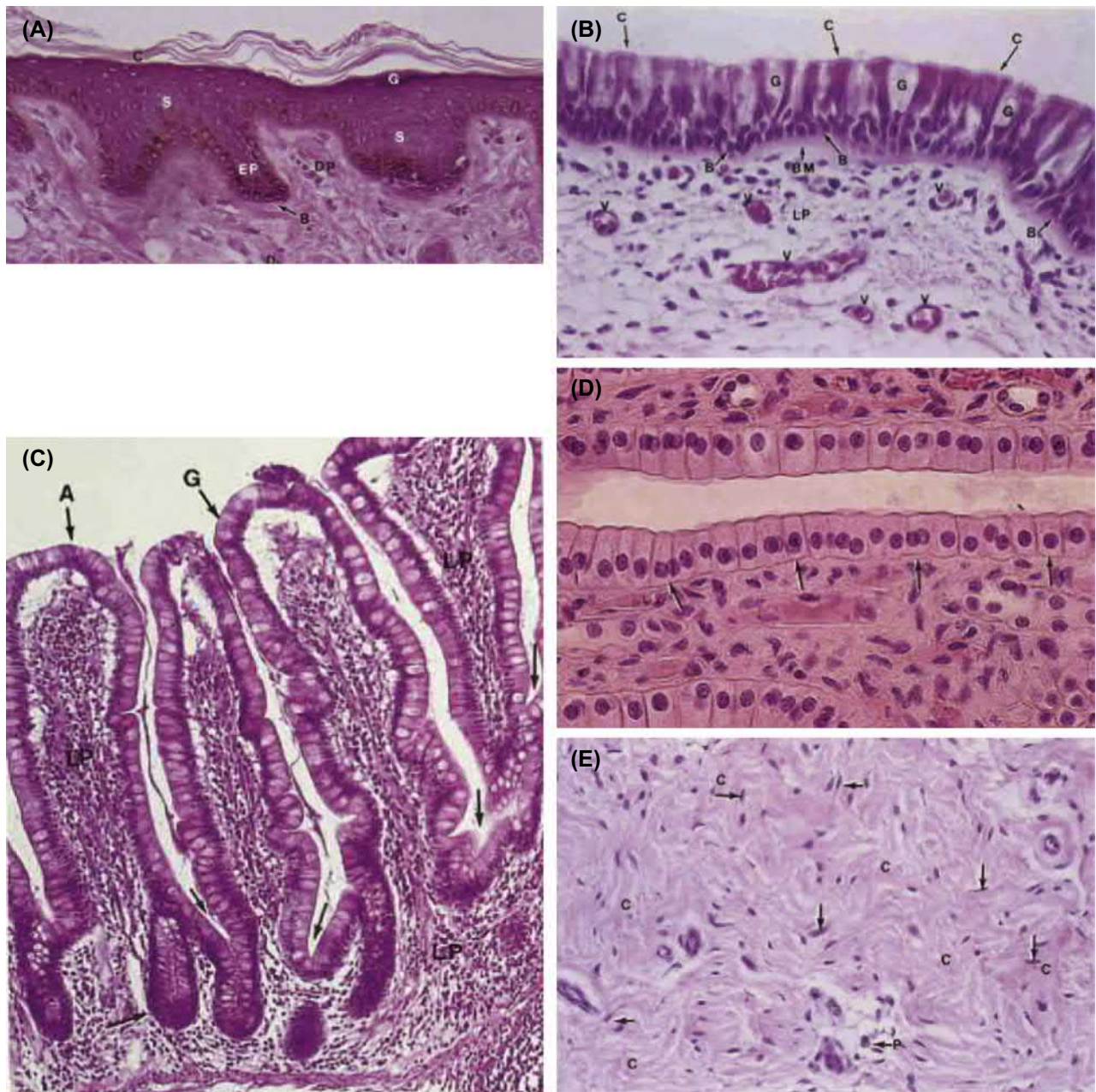
the tissue section be removed and replaced by water (rehydration). The stain used routinely in histology involves sequential exposure to hematoxylin and eosin. Hematoxylin is a basophilic dye that stains negatively charged molecules (e.g., DNA, RNA, calcium phosphate, etc.) blue–purple. In contrast, eosin is an acidophilic counterstain that colors positively charged materials (e.g., cell cytoplasmic or ECM proteins) pink–orange. The tissue sections shown in Fig. F1 are all H&E stained.

Special Staining

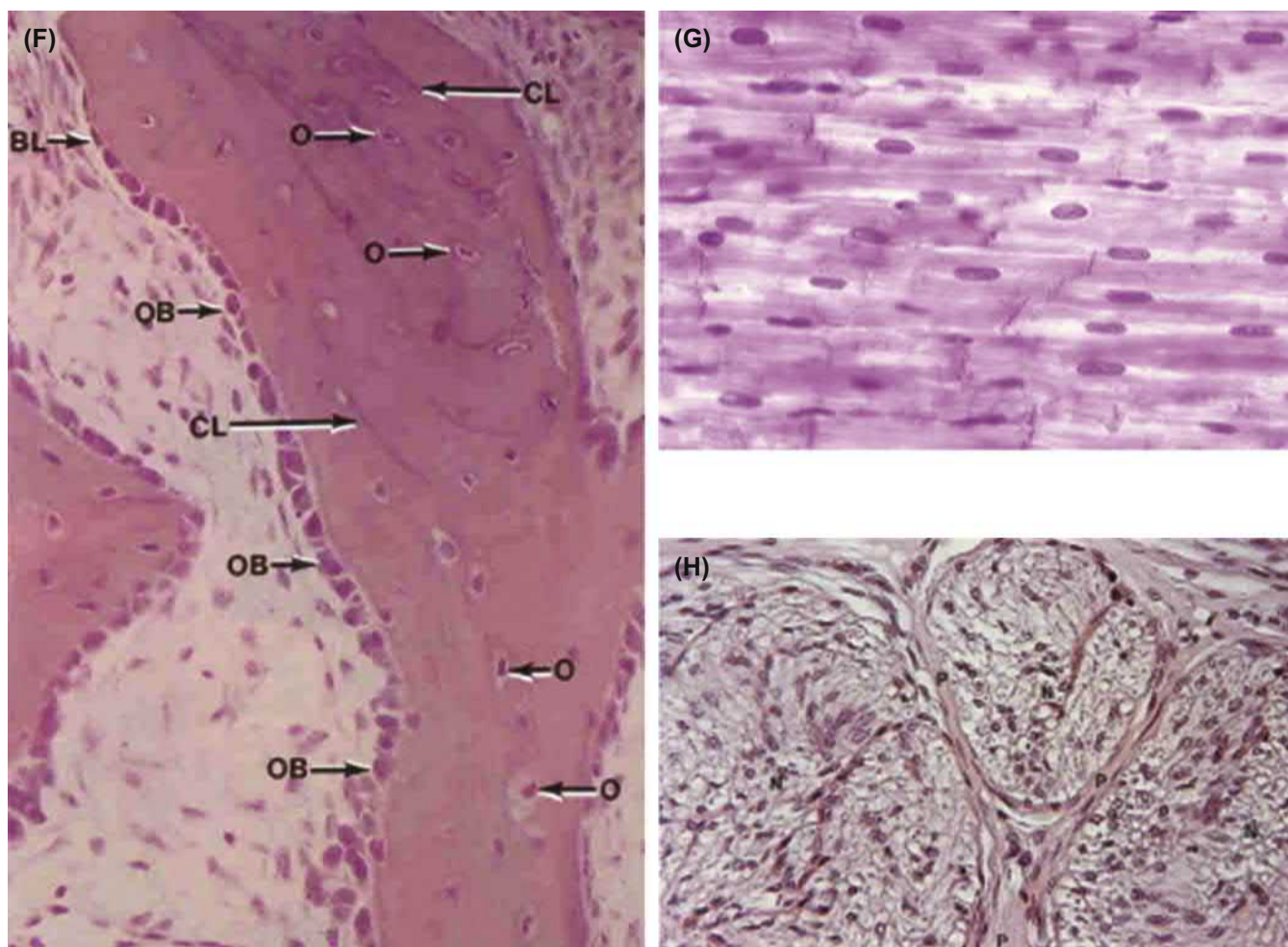
This methods can highlight components that would not otherwise stain well using routine histochemistry (e.g., microorganisms) or to indicate the chemical nature of a specific tissue component (e.g., collagen, elastin, calcium, fat, glycogen, iron, fibrin, etc.). There are also commonly available techniques for demonstrating the specific chemical activity of an enzyme in tissues (e.g., esterases in neutrophils and macrophages); the substrate for an enzyme of interest is reacted with the tissue, and a colored precipitate deposits at the site of expression. Still other stains offer the ability to quantify apoptotic cell death, mitochondria, and nuclei.

Immunohistochemical Staining

This method takes advantage of the antigenicity of a tissue component to demonstrate its location and rough abundance (although the technique is at best only semiquantitative). Antibodies to a given cell or tissue constituent are attached to a fluorescent molecule (*immunofluorescence*) or an enzyme (typically horseradish peroxidase; *immunoperoxidase* technique) and reacted with tissue sections.



• **Figure F2** Photomicrographs of various tissues, emphasizing key structural features. (A)–(D) different epithelia; (E) and (F) connective tissue; (G) muscle; and (H) nervous tissue. (A) Skin—An example of a stratified squamous epithelium. A thin superficial acellular *stratum corneum* (C) rests on the *stratum granulosum* (G) and *stratum spinosum* (S) layers, the latter constituting the bulk of the skin epithelium thickness. The *stratum basale* (B) contains proliferating skin adult stem cells and rests on the basement membrane separating the *epidermis* from the *dermis* (D); EP represents *epidermal pegs*; DP represents *dermal papillae*. (B) Trachea—The epithelium here is composed of a single “pseudostratified” layer of cells sitting on the basement membrane (BM); the cells in the epithelium include mucous-rich *goblet cells* (G), ciliated *columnar cells* (C), and *basal stem cells* (B). Deep into the epithelium is the submucosa containing extracellular matrix (*lamina propria*; LP), and punctuated by multiple blood vessels (V). (C) Mucosa of the small intestine (ileum)—The epithelium here is composed of a single layer of *columnar absorptive cells* (C), interspersed with *goblet cells* (G); to increase the overall absorptive surface area, the epithelium is organized into elongated villi and invaginated crypts (*arrows*), the latter containing the adult stem cells of the small bowel. The epithelium is attached to a basement membrane that rests over the underlying LP. (D) Epithelium of a kidney collecting duct—This is composed of relatively uniform cuboidal cells sitting atop the basement membrane (*arrows*). (E) Dense irregular connective tissue, with wavy unoriented collagen bundles (C) synthesized by the interspersed fibroblasts (*arrows*)—(P) represents plasma cells—terminally differentiated antibody-secreting cells of B lymphocyte lineage. (F) Cancellous bone—(O) are quiescent osteocytes within a calcified bony matrix; (OB) are proliferating osteoblasts that are synthesizing new bone; (BL) represents inactive bone-lining osteoblasts; (CL) represents *cement lines* between adjacent fascicles of bone. (G) Myocardium (cardiac muscle) composed of rectangular striated cells (striations represent actin–myosin sarcomeres responsible for cellular contraction) with centrally placed nuclei and connected end to end by *intercalated discs*. (H) Cross-sections of nerve bundles (N) separated by *perineurium* (P). Most of the nuclei here are from myelinating *Schwann cells* surrounding the individual neuronal axons. ((A)–(F) and (H) reproduced with permission from Berman, I. (1993) *Color Atlas of Basic Histology*, Appleton and Lange; (G) reproduced by permission from Schoen, F.J. (2005). *The Heart in Cotran, R.S., Kumar, V., and Fausto, N. (eds.) Robbins and Cotran Pathologic Basis of Disease, 7th Ed.* Saunders: Philadelphia, PA.)



• Figure F2 cont'd.

Subsequent fluorescence microscopy or peroxidase substrate precipitation allows the identification of particular antigens. The general approach can be expanded by the use of *tissue microarrays*; cores of tissue from several different samples or patients are embedded together in a single paraffin block. Subsequent thin sections of these multiple cores allow the simultaneous multiplex staining of 100's of samples to evaluate the concordance of antigen and histologic patterns.

Although some antigens and enzymatic activity can survive conventional fixation and histological processing, many are rendered inactive by denaturation and cross-linking. Consequently, histochemistry and immunohistochemistry must either be performed on frozen sections, or special *antigen recovery techniques* need to be employed.

In Situ Hybridization

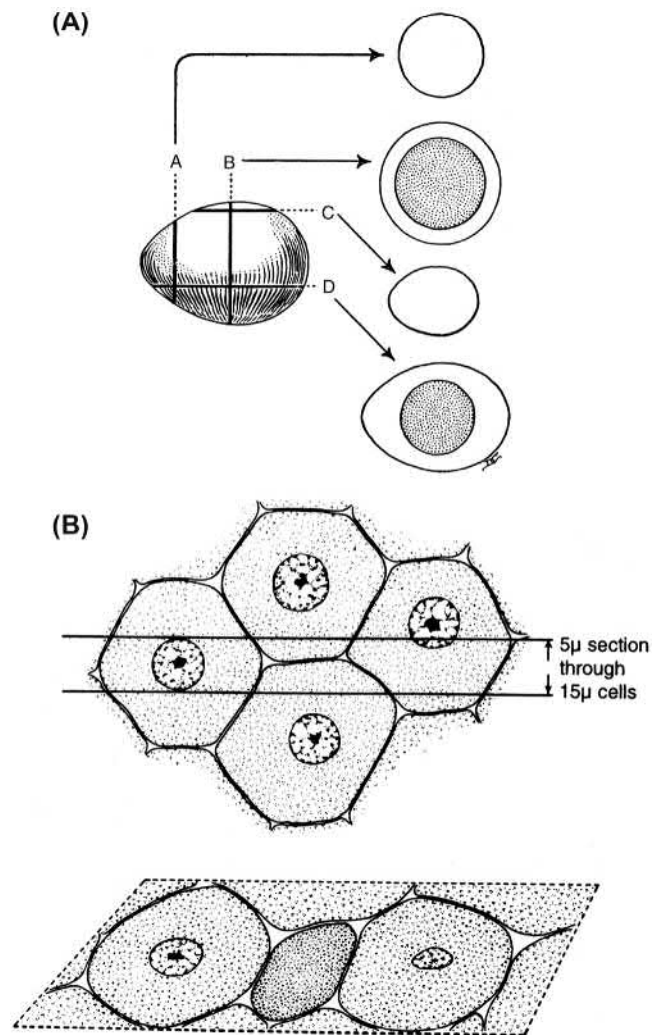
Cells can also be characterized by their nucleic acid products (e.g., mRNA); thus specific DNA or RNA probes are labeled with fluorophores or enzymes and allowed to bind to complementary sequences. Like immunohistochemistry, the approach is semiquantitative, and subject to a number of artifacts, including DNA/RNA fragmentation from poor preservation.

Electron Microscopy

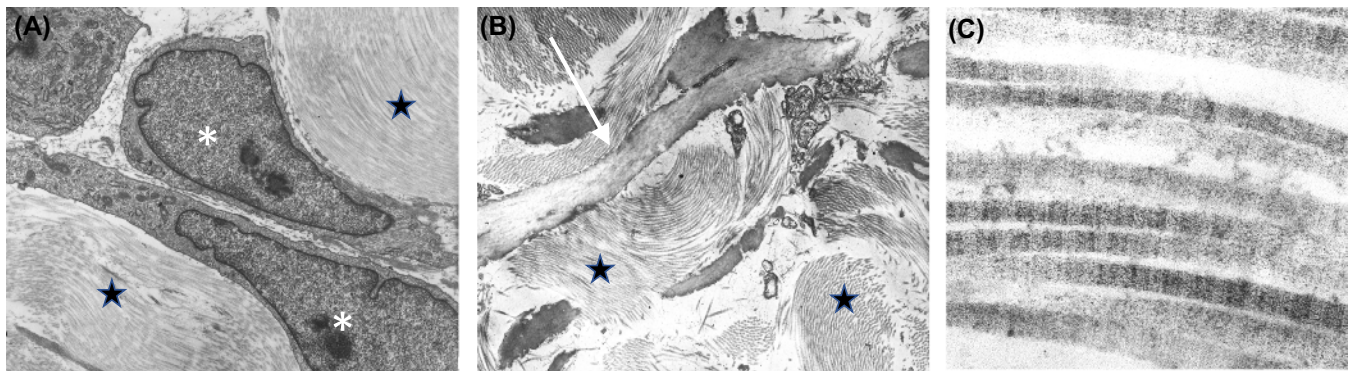
Providing contrast for TEM depends on relative electron densities of tissue components. Sections are stained with salts of heavy metals (osmium, lead, and uranium), which react differentially with different structures, creating patterns of electron density that reflect tissue and cellular architecture. An example of an electron photomicrograph is shown in Fig. F4. Immunoelectron microscopy can be done using antibodies tagged with various size beads of heavy metals (e.g., gold).

Special Techniques

Higher resolution of structures (two-photon and superresolution microscopy), simultaneous evaluation of several antigenic markers (multiplexed immunohistochemical techniques), three-dimensional evaluation (confocal microscopy), and live cell imaging (e.g., using optical coherence tomography) provide additional approaches to interpret structure and function. Laser capture microdissection is a means to carve out specific portions of a tissue adherent on a slide; in that manner, the specific genetic expression pattern of selected cells can be evaluated without confounding background, e.g., from fibroblasts or normal tissue elements. Single cell sequencing allows the identification of unique cell types within heterogeneous populations.



• **Figure F3** Interpreting three-dimensional structure from two-dimensional representations. Sections through a structure at different levels and orientations can give different appearances. (A) Example with a hard-boiled egg; (B) section through a tissue with uniform cells, where the final image suggests heterogeneity. (Modified by permission from Cormack, D.H. (1993). *Essential Histology*. Lippincott.)



• **Figure F4** Transmission electron micrographs demonstrating ability to see fine structure of cells and extracellular matrix. (A) cells (asterisk), surrounded by fibrous collagen (stars). (B) Elastin fibril (arrow), surrounded by fibrous collagen (stars). (C) Collagen at very high magnification, showing individual collagen fibrils with typical banding pattern. Original magnifications: (a and b) 8000X; (c) 120,000X.

References

- Duggal, S., Frønsdal, K.B., Szöke, K., Shahdadfar, A., Melvik, J.E., Brinchmann, J.E., 2009. Morphometry of right and left ventricular myocardium after strenuous exercise in preconditioned rats. *Tissue Eng Part A*. 15 (7), 1763–1773.
- Loud, A.V., Beghi, C., Olivetti, G., Anversa, P., 1984. Phenotype and gene expression of human mesenchymal stem cells in alginate scaffolds. *Lab Invest*. 51 (1), 104–111.

Index

- A**
- A disintegrin and metalloproteinases with thrombospondin motifs (ADAMTS), 706
- a-SiC. *See* Amorphous silicon carbide (a-SiC)
- A-V shunts system. *See* Arteriovenous shunts system (A-V shunts system)
- AA. *See* Acrylic acid (AA)
- AAA. *See* Abdominal aortic aneurysm (AAA)
- AAc. *See* Acrylic acid (AA)
- AAm. *See* Acrylamide (AAm)
- AAT. *See* Acellular adipose tissue (AAT)
- A-B block copolymer, 85
- A-B-C triblock copolymer, 85
- Abdominal aortic aneurysm (AAA), 1038–1039
- Abraxane, 470–471
- Absorbable collagen sponge (ACS), 861b–862b
- Absorbable sutures, 1188, 1193
- AC. *See* Alternating current (AC)
- Ac₄ManAz (mannose derivative), 470
- ACA. *See* Affordable Care Act (ACA)
- Accommodation, 1135–1136, 1140
- Accommodative IOLs, 1142
- ACE. *See* Angiotensin-converting enzyme (ACE)
- Acellular
- dermal scaffolds, 1174
 - human dermal matrix, 386
 - porcine urinary bladder, 387
- Acellular adipose tissue (AAT), 1404
- for soft tissue injuries, 1404
 - lipoaspirate, 1404
- Acid
- acid-etch bonding to enamel, 1184
 - acid-base
 - dental cement, 1183, 1184f
 - reactions, 1182
 - proteases, 698
- ACL. *See* Anterior cruciate ligament (ACL)
- Acquired immunity. *See* Adaptive immunity
- Acrylamide (AAm), 146, 434–435
- Acrylic acid (AA), 193, 434–435
- Acrylic hydrogels, 157–158
- AcrySof intraocular lens, 1141
- ACS. *See* Absorbable collagen sponge (ACS)
- ActiCoat, 1171t, 1173
- Actifuse ABX, 294, 296f
- Actin fibers, 1340
- Action, radiation-based techniques, 1432
- Activated charcoal, 333
- Active caspase-1, 1106
- Active materials, 522–528. *See also* Inert materials.
- heparinization, 522–526
 - antithrombin III-binding pentasaccharide of heparin, 524f
 - covalently bound heparin, 525–526
 - ionically bound heparin and controlled-release systems, 523–525
 - immobilization
 - of antiplatelet agents, 527
 - of fibrinolytic agents, 527–528
 - thrombin inhibition without heparin, 526–527
- Active targeting, 470, 1254–1257
- antibodies, 1255
 - aptamers, 1255–1257
 - carbohydrates, 1257
 - ligands, 1256t
 - peptides, 1255
 - proteins, 1255
 - small molecules, 1257
- Active tissue targeting via anchored click chemistry (ATTACK), 470–471, 471f
- Acute inflammation, 697
- Acute toxicity, 465–466, 871–872
- N*-Acyl-homoserine lactones (AHLs), 834
- ADAMTS. *See* A disintegrin and metalloproteinases with thrombospondin motifs (ADAMTS)
- Adaptation, 693
- Adaptive immunity, 697, 757–772. *See also* Innate immunity.
- B cell and antibody recognition, 762
 - cell-mediated immunity, 760
 - components, 757–760
 - CTLs, 760
 - effector pathways in, 763–764
 - helper T cells, 760–761
 - humoral immunity, 760
 - immune regulation and tolerance, 766–768
 - immune response to pathogens, 765–766
 - immunological memory, 764, 764f
 - intersection of biomaterials and immunology, 768–772
 - recognition in, 762
 - T cell recognition, 762–763
- ADCC. *See* Antibody-dependent cell-mediated cytotoxicity (ADCC)
- ADCs. *See* Antibody–drug conjugates (ADCs)
- Addition polymerization, 95–96
- Additive manufacturing (AM), 232, 300, 485–486, 623, 1296
- bioprinting, 630–632
 - medical applications of 3D printing, 632–634
 - personalized drug delivery systems, 634–635
 - 3D printing modalities, 623–630
- Additives, 591, 1322–1323
- Adenosine diphosphate (ADP), 802
- Adenosine triphosphate (ATP), 691
- Adherent cells, 663–664
- Adhesion, 824–825. *See also* Bacterial adhesion; Focal adhesions.
- ligands, 596
 - proteins, 406
 - depletion studies, 647–648
 - effect on cellular interactions, 645–649
 - preadsorption with purified adhesion proteins, effects of, 646–647
 - receptor activity with antibodies, inhibition of, 648–649
 - receptors, 706–707
- Adhesive(s)
- bioadhesives, 1187
 - biomimetic approaches, 1188
 - cyanoacrylate esters, 1186–1187
 - fibrin sealants, 1187
 - hard-tissue adhesives, 1182–1186
 - acid-etch bonding to enamel, 1184
 - aging and stability of bonded interface, 1186

- Adhesive(s) (*Continued*)
 autopolymerizing PMMA bone cement, 1182–1184
 chemistry of etchants, primers, and bonding agents, 1185
 hybrid-layer creation via three-stage approach, 1185
 hydrogel sealants, 1188
 islands, 610
 logic of adhesion procedures, 1181–1182
 monomers, 141–142
 polymer network, 141–142
 soft-tissue adhesives and sealants, 1186
 historical overview, 1186
 performance requirements, 1186
 terminology, 1181
- Adipose tissue, 684
 acellular adipose tissue for soft tissue injuries, 1404
 anatomy and physiology, 1393
 commercially available and clinically tested biomaterials, 1395
 Food and Drug Administration-approved soft tissue fillers, 1403
 techniques to assess adipogenesis and vascularization, 1403
 design criteria for, 1394–1395
 engineering, 1391f, 1392–1393
 novel materials and technologies, 1395
 challenges, 1404
 patient-specific 3D adipose tissue models, 1395b
- Adipose-derived adult stem cells (ASCs), 369, 1393
- Adjustable-power IOLs, 1142–1143
- Adjuvants, 1200
 use of biomaterials to adjuvant immune system, 1200–1201
- ADO. *See* Amplatzer duct occluder (ADO)
- ADP. *See* Adenosine diphosphate (ADP)
- Adsorbed proteins, 643, 645
 biological changes in, 655–657
 conformational changes in,
 physicochemical studies of, 654–657
 effect on cellular interactions, 645–649
 depletion studies, 647–648
 preadsorption with purified adhesion proteins, effects of, 646–647
 receptor activity with antibodies, inhibition of, 648–649
 importance, 657–658
 at solid–liquid interfaces, behavior of, 649–654
 interface, transformation of, 649
 irreversibility, 649–651
 kinetics, 649–651
 mixtures of proteins, 652–654
 monolayer model, 651–652
 surface chemistries, 658–659
- Adsorption, 707
- Adult macular degeneration (AMD), 785–786
- Adult respiratory distress syndrome (ARDS), 1051
- Adult stem cells, 1291
- Adventitia. *See* Tunica externa
- Aesthetic implants, 119–120
- AF. *See* Atrial fibrillation (AF)
- Affinity
 affinity-based systems, 1244
 chromatography, 408–409
 hydrogels, 161
- Affordable Care Act (ACA), 1459
- AFM. *See* Atomic force microscopy (AFM)
- Agar, 31
- Agarose, 1220t–1221t, 1222
- Age-related macular degeneration (AMD), 1137, 1145–1146
- Aggregatibacter actinomycetemcomitans*, 834
- Agile product development, 1457–1458
- Aging
 biological risk assessment of aging biomaterials, 1429–1430
 of bonded interface, 1186
- AH. *See* Aqueous humor (AH)
- AHLs. *See* *N*-Acyl-homoserine lactones (AHLs)
- AIA. *See* America Invents Act (AIA)
- Albumin, 643, 646, 655, 807, 1244
 coatings, 520, 1058
 conjugates, 1243–1244
 rescuing, 656
- Alcohol, 1536.e1
 treatments, 985
- Alcon Cypass micro polyamide stent, 1145
- Aldehyde-fixed bioprosthetic heart valves, 379
- Algimatrix, 1225
- AlgiMatrix 3D, 1220t–1221t
- Alginate(s), 401, 406, 433, 1220t–1221t, 1222, 1275–1277, 1293, 1318–1319, 1322, 1358
 functionalization, 1359
 hydrogels, 1359
 microcapsules, 745
- ALK. *See* Anaplastic lymphoma kinase (ALK)
- Alkaline phosphatase, 471
- Alkylation, 520
 chemistry, 1439
- Alkyne-azide polymerizations, 146–147
- AlloDerm, 386, 1171t, 1174
- Allografts, 83–84, 974–975, 1126
- AlloMax, 386
- Alloying, 209–211, 213
 elements, 273
- Alpha IMS/AMS, 1147–1148
- Alpha smooth muscle actin (α -SMA), 1339
- ALT. *See* Argon laser trabeculoplasty (ALT)
- Alternating current (AC), 264
- Alternative bone cements, 1183
- Alternative pathway (AP), 777, 780–781, 780f
 proteins of complement, 780t
- Alum derivatives, 1200
- Alumina (Al_2O_3), 289, 426–427, 960, 1087, 1125
 ceramics, 290
- Aluminum (Al), 230
 alloy, 22–23
- Aluminum oxide (Al_2O_3), 319–321, 320f
 fracture surfaces of alumina hips, 322f
- Alveolar crest resorption, 1126
- AM. *See* Additive manufacturing (AM)
- AMD. *See* Adult macular degeneration (AMD); Age-related macular degeneration (AMD)
- America Invents Act (AIA), 1502
- American National Standards Institute (ANSI), 1476–1477
- American Society for Artificial Internal Organs Journal (ASAIO Journal)*, 1533
- American Society for Testing and Materials (ASTM), 254, 1175–1176, 1510
- American Type Culture Collection (ATCC), 663
- Ames test. *See* Bacterial reverse mutation assay
- Amides, 1317
- Aminins, 406
- Amino acids, 668
 2-Amino-oleic acid (AOA), 983
 [α -(4-Aminobutyl)-l-glycolic acid] (PAGA), 477
 3-Aminophenyl-boronic acid (PBA), 1278
 3-Aminopropyltriethoxysilane (APTES), 1278
- Ammonia, 115
- Ammonium persulfate/*N,N,N',N'*-tetramethylethylenediamine (APS/TEMED), 1318–1319
- Amorphous polymers, physical behavior of, 91
- Amorphous silicon carbide (a-SiC), 1162
- Amperometric biosensors, 1270–1271
- Amphiphilic peptidic prodrugs, 466
- Ampholytic hydrogels, 153
- Amplatzer duct occluder (ADO), 1025
- AMPs. *See* Antimicrobial peptides (AMPs)
- Anaphylactic shock, 784
- Anaphylatoxins, 784
- Anaplastic lymphoma kinase (ALK), 121b
- Anastomose blood vessels, 26–27
- Anergy, 767
- Aneurysms, 1037–1039
- Angiogenesis, 697, 699, 699f, 817
- Angioplasty stents, 1039–1041
- Angiopoietin-1, 699
- Angiotensin-converting enzyme (ACE), 1067
- Angiotensin-II (AT-II), 469–470
- Animal implants, 841
- Animal models, 725–726, 1351
 selection for in vivo tests, 875–876, 875t
- Animal surgery, 905–910
 case study, 911b

- ethical and regulatory overview, 899–901
 governmental regulations, 899–901
 institutional responsibilities, 901
- model selection, 901–905
 cardiovascular devices, 902–903
 ophthalmology, 904–905
 orthopedic devices, 903–904
 skin, 905
 vascular, 904
- rabbit, 908–909
 analgesia, 909
 animal selection and preoperative preparation, 908
 brief procedures, 908
 general anesthesia, 908–909
- rodent, 905–906
 analgesia, 906
 animal selection and preoperative preparation, 905
 general anesthesia, 905–906
- ruminants, 906–908
 analgesia, 908
 animal selection and preoperative preparation, 906–907
 brief restraint, 907
 general anesthesia, 907–908
- surgical facility design, 901
- swine, 909–910
 analgesia, 910
 animal selection and preoperative preparation, 909–910
 brief restraint, 910
 general anesthesia, 910
 recommendations of animal models, 910t
- Animal testing, 1511–1512
- Animal tumors, implants with, 814–817
- Animal Welfare Act (AWA), 900, 1511–1512
- Animal Welfare Act Regulations (AWAR), 900
- Animal Welfare Assurance, 900
- Animal xenografts, 1173
- Anionic hydrogels, 153
- Anionic polymerization, 1322
- Anionic polymers, 832
- Anisotropy of materials, 46–47
- Anodization, 1123
- Anoxia, 694–695
- ANSI. *See* American National Standards Institute (ANSI)
- Anterior cruciate ligament (ACL), 134–135, 589–590, 673
- Antibiotic(s), 829–830, 832t
 tolerance of bacteria in biofilms, 824
- Antibodies, 757, 760f, 1255, 1256t, 1268
 effector mechanisms, 763f
- Antibody-dependent cell-mediated cytotoxicity (ADCC), 764
- Antibody–drug conjugates (ADCs), 1255
- Anticalcification, 981–982
- Antifouling approaches, 833–834
 hydrophilic materials based on PEG, 833
 materials, 828
- Antigen, 757, 1200, 1268
 antigen-binding site, 760
 recovery techniques, 1536.e5
 specific immunity, 697
 uptake, processing, and presentation, 754–755
 use of biomaterials to improving delivery of antigen to APCs, 1201–1202
- Antigen-presenting cells (APCs), 442, 754, 1200, 1209
 artificial, 1209
 use of biomaterials to improving delivery of antigen, 1201–1202
- Antiinflammatory cytokines, 845
- Antikorpers, 757
- Antimicrobial approaches, 828–833
 biomaterials releasing bioactive molecules, 828–833
 antibiotics, 829–830
 low-dose nitric oxide, 831–832
 silver, 830–831
 intrinsically bioactive biomaterials, 832–833
- Antimicrobial peptides (AMPs), 832–833
- Antimicrobial resins, 145
- Antimicrobial therapy, 340–344
 action and photoactivation wavelengths of antibacterial carbon colloids, 340t
- Antimicrobial tolerance of bacteria in biofilms, 824
- Antioxidative strategies, 1164
- Antiplatelet agents, immobilization of, 527
- Antithrombin III (ATIII), 810, 1056
 antithrombin III-binding pentasaccharide of heparin, 524f
- AOA. *See* 2-Amino-oleic acid (AOA)
- Aortic regurgitation, 1000
- AP. *See* Alternative pathway (AP)
- Apatite–wollastonite glass-ceramic particles (A–W glass-ceramic particles), 416
- APCs. *See* Antigen-presenting cells (APCs)
- APD. *See* Automated peritoneal dialysis (APD)
- Apligraf, 1171t, 1173
- Apolipoproteins, 658
- Apoptosis, 665, 692, 695–696
- APS/TEMED. *See* Ammonium persulfate/*N,N,N',N'*-tetramethylethylenediamine (APS/TEMED)
- Aptamers, 366, 1255–1257, 1256t, 1268–1269
- APTES. *See* 3-Aminopropyltriethoxysilane (APTES)
- AQPs. *See* Aquaporins (AQPs)
- Aquacel Ag, 1171t, 1173
- Aquaporins (AQPs), 1130
- Aqueous humor (AH), 1135, 1143
 production and drainage, 1143–1145
- ARCO. *See* Association Research Circulation Osseous (ARCO)
- ARDS. *See* Adult respiratory distress syndrome (ARDS)
- Area defects in crystals, 212
- Area under the PK curve (AUC), 1243
- Arg-gly-glu sequence (RGE sequence), 668
- Arginine-glycine-aspartate (RGD) ligands, 666
 peptides, 528, 542, 666–667, 708, 1255, 1295, 1318
 tripeptide sequence, 704
- Argon, 37
- Argon laser trabeculoplasty (ALT), 1143
- Argus II, 1146–1147
- Aromatic diisocyanates, 104
- Aromatic polyanhydrides, 434
- Arterial thrombi, 885
- Arterial thrombogenesis, 517–518
- Arteries, 1033, 1035f
- Arteriovenous carbon dioxide removal (AVCO₂R), 1054
- Arteriovenous ePTFE grafts for dialysis access, 131
- Arteriovenous fistula (AVF), 1043
- Arteriovenous graft (AVG), 1043
- Arteriovenous shunts system (A-V shunts system), 889
- “Arthroprosthetic cobaltism” syndrome, 793
- Artificial APCs, 1209
- Artificial hearts, 22, 22f, 26
- Artificial hip joints, 101b
- Artificial kidney, 25–26
- Artificial organ anticoagulation, 1039
- Ascorbic acid, 1318–1319
- ASCs. *See* Adipose-derived adult stem cells (ASCs)
- ASDs. *See* Atrial septal defects (ASDs)
- Aspect ratio, 1102
- Aspergillus* sp., 1170
- Aspirin, 527
- Association Research Circulation Osseous (ARCO), 283–284
- Assurance of sterility, 1431
- Astigmatism, 1136
- ASTM. *See* American Society for Testing and Materials (ASTM)
- ASTM International (ASTMi), 869, 1476
- ASTMi. *See* ASTM International (ASTMi)
- Asymmetric atoms, 87
- AT-II. *See* Angiotensin-II (AT-II)
- Atactic version of PP, 87
- ATCC. *See* American Type Culture Collection (ATCC)
- Atherectomy, 1046–1047
- Atherosclerosis, 1037, 1038f
- ATIII. *See* Antithrombin III (ATIII)
- Atom transfer radical polymerization (ATRP), 97, 97f, 171, 197, 490
- Atomic force microscopy (AFM), 66–68, 68f–69f, 438, 464, 556–557, 560, 670, 1097, 1326, 1327t

- Atoms, 37–39, 53b
 ATP. *See* Adenosine triphosphate (ATP)
 ATPases, 695
 ATR. *See* Attenuated total reflectance (ATR)
 ATR-FTIR. *See* Attenuated total reflectance-Fourier transform infrared spectroscopy (ATR-FTIR)
 AtrE. *See* Atropinesterase (AtrE)
 Atrial fibrillation (AF), 1004, 1025–1028
 left atrial appendage occlusion devices, 1027–1028, 1027f
 Atrial septal defects (ASDs), 1024–1025
 Atriclip device system, 1027–1028
 Atrioventricular node (AV node), 1010–1011
 Atrophy, 693–694
 Atropinesterase (AtrE), 909
 ATRP. *See* Atom transfer radical polymerization (ATRP)
 ATTACK. *See* Active tissue targeting via anchored click chemistry (ATTACK)
 Attending veterinarian (AV), 901
 Attenuated total reflectance (ATR), 65
 Attenuated total reflectance-Fourier transform infrared spectroscopy (ATR-FTIR), 985
 Attorney, 1498, 1500–1502
 AUC. *See* Area under the PK curve (AUC)
 Australasian Society for Biomaterials and Tissue Engineering (1989), 18–19
 Autoactivation of blood coagulation, 809
 Autocrine stimulation, 698
 Autograft materials, 83–84
 Autoimmune diseases, 766, 768t
 tolerance induction in, 1210–1211
 Autologous dermal–epidermal skin substitutes, 1174–1175
 Autologous engineered skin substitute, 1171t
 Autologous stem cells, 1127
 Automated peritoneal dialysis (APD), 1065
 Autophagy, 694
 Autopolymerizing PMMA bone cement, 1182–1184
 alternative bone cements, 1183
 classical and modern dental-bonding cements, 1183
 classification and composition of tissue adhesives, 1183t
 historical background, 1182
 mechanism of “bonding” or grouting, 1183
 mechanism of setting of PMMA/MMA dough, 1182
 polyelectrolyte cements, 1183–1184
 Autopsy, 1536.e1
 Auxetic materials, 44
 AV. *See* Attending veterinarian (AV)
 AV node. *See* Atrioventricular node (AV node)
 AVCO₂R. *See* Arteriovenous carbon dioxide removal (AVCO₂R)
- Average molecular mass (M_n), 88–89
 AVF. *See* Arteriovenous fistula (AVF)
 AVG. *See* Arteriovenous graft (AVG)
 A–W glass-ceramic particles. *See* Apatite–wollastonite glass-ceramic particles (A–W glass-ceramic particles)
 AWA. *See* Animal Welfare Act (AWA)
 AWAR. *See* Animal Welfare Act Regulations (AWAR)
 Axial loading, 42
 Azide-alkyne cycloaddition, 543
 Azo compounds, 1322
 Azobenzene groups, 666
- B**
 B cell receptor (BCR), 757, 762, 1203
 B cells, 743–744, 757, 1200, 1202–1206
 activation process, 1203–1205
 and antibody recognition, 762
 suppression of B cell activation, 1211
 B lymphocytes, 757
 B7.1 (cell-surface protein), 755–756
 B7.2 (cell-surface protein), 755–756
Bacillus cereus, 832–833
Bacillus subtilis, 340–341
Bacillus subtilis var *niger*, 1440
 Bacteria, 695, 844
 Bacterial adhesion, 824–827. *See also* Focal adhesions.
 DLVO theory, 825
 material properties influence on, 826–827
 environment factors, 827
 roughness, 827, 828f
 surface free energy, 826–827, 827t
 to surfaces, 824–826
 thermodynamic model, 825–826
 Bacterial biofilms, 823–824
 Bacterial reverse mutation assay, 466
 Bactroban ointments, 1172
 Balafilcon A, 1139–1140
 BALB/c 3T3 Focus Transformation Assay, 857
 Bangham method, 459
 Barbed sutures, 591–592
 Bare metal stents (BMSs), 132b–133b, 1040
 Basic fibroblast growth factor (bFGF), 699, 1128, 1357–1358, 1393
 Basic information on bulk, 35–36
 Basophils, 753–754
 BAT. *See* Brown adipose tissue (BAT)
 Bauxite, 319
 BCC structure. *See* Body-centered cubic structure (BCC structure)
 BCI. *See* Brain–computer interface (BCI)
 BCPs. *See* Biphasic calcium phosphates (BCPs)
 BCR. *See* B cell receptor (BCR)
 BDDGE. *See* 1,4-Butanediol-diglycidyl ether (BDDGE)
 BDI. *See* 1,4-Diisocyanatobutane (BDI)
 BDMA. *See* Butanediol dimethacrylate (BDMA)
- Belmont Report*, 1512
 Bench-to-bedside translation, 1418
 Benign tumors, 813
 Benzalkonium chloride, 515
 Benzoyl peroxide (BPO), 1182
 Berry aneurysms, 1047
 Bevacizumab, 470–471
 bFGF. *See* Basic fibroblast growth factor (bFGF)
 BIA-ALCL. *See* Breast implant associated-anaplastic large cell lymphoma (BIA-ALCL)
 Biaxial stretch devices, 721–722
 Bile acids, 435
 BIND-014, 470
 Binder jetting, 624t, 627–628, 628f–629f
 Bio-inspired NPs, 473t
 Bio-Oss™, 1130
 Bioabsorbable polymers, 1439–1440
 Bioactive agents, 596
 Bioactive bioceramics, 289–301, 417–418
 particles, 416
 Bioactive biomaterial development, 8
 Bioactive ceramics, 959, 1125
 properties of, 1532t
 Bioactive glass(es), 297–298, 300f, 427
 coatings, 965
 composites and putties for bone repair, 299
 porous, 299–300
 in toothpaste, 300–301
 wound healing, 300
 Bioactive materials, 861
 Bioactivity, 289, 415
 biomolecular surface patterning of, 556
 Bioadhesives, 1187
 Biobrane, 1171t, 1173
 Bioburden testing, 1453
 Bioceramic(s), 289
 different calcium phosphate phases
 relevant to, 291t
 implant materials, 289
 nearly inert, 289–290
 synthetic bone graft substitutes, 292f
 tissue attachment, types of, 290t
 Biocompatibility, 5, 7–8, 15, 22–23, 53, 737–738, 841, 843–846, 844b, 869, 1317
 additional considerations to, 847–848
 biomaterials–tissue interactions, 847f
 assessment, 869
 cell–biomaterial interactions, 845
 of dissolved Zn corrosion products, 276–277
 evaluations, 274
 hemocompatibility, 465
 hydrogel cross-linking mechanisms, 366
 in vitro toxicity, 465
 cell viability test, 465
 cellular stress response test, 465
 OS test, 465
 in vivo toxicity, 465–466

- acute toxicity, 465–466
 genotoxicity and carcinogenicity, 466
 subacute/subchronic/chronic toxicity, 466
- materials, 1200
 mechanical effects, 844–845
 new developments changing paradigm of, 846–847
 of NPs, 465–466
 products of extrinsic organisms colonizing biomaterial, 844
 of silicones, 116
 toxicology, 844
- Bioconjugate techniques, 155
- Biodegradable ceramics, 417–418, 963
 properties of, 1532t
- Biodegradable composites, 425
- Biodegradable materials, 417–418, 845
- Biodegradable metals, 271
 corrosion design of, 272
 influence of alloying elements, corrosion behavior, and biocompatibility of Zn and Mg, 273
 iron-based, 273–275
 magnesium-based, 277–284
 zinc-based, 275–277
- Biodegradable polyesters, 1223
- Biodegradable polymer drug-eluting stents (BP-DESs), 132b–133b
- Biodegradable polymers, 415–416
- Biodegradable scaffolds for tendon tissue engineering, 1358
- Biodegradation, 918–919
- BioDiamond, 345, 345f
- Biodurability of silicones, 116, 117t
- Bioelectronic neural implants, 1153
 applications, 1156–1160
 bioelectronic medicine, 1159–1160
 regeneration, 1160
 rehabilitation, 1158–1159
 research, 1156–1158
 bioelectronic devices, 1153–1155
 biomaterial-based strategies to enabling neural implants, 1163–1164
 electrode materials, 1153–1154
 equivalent circuit models, 1154–1155
 factors influencing materials selection, 1153–1154
 failure modes, 1160–1163
 biological, 1162–1163
 materials, 1161–1162
 mechanical damage, 1160–1161
 technologies, 1155–1156
 battery, IPG, 1155
 electrode contacts, 1156
 leads and interconnects, 1155–1156
- Bioengineering, 401
- Bioethics, 1512–1513
- Biofabrication
 strategy, 366–367
 window, 631–632, 632f
- Biofilm(s), 507
 antibiotic and antimicrobial tolerance of bacteria in, 824
 bacterial, 823–824
 adhesion, 824–827
 clinical example of diagnosing and treating device-related biofilm infection, 840.e1b
 device-related infection, 828
 evidence for biofilms on devices, 828
 formation, 508f
 formation control, 828–834
 antifouling approaches, 833–834
 antimicrobial approaches, 828–833
 approaches to control bacterial adhesion, 831f
 biomaterials affecting biofilm architecture, 834
 materials, devices, and common infecting pathogens, 829t
 and immune response, 824
 matrix-degrading enzymes, 834
 methods for testing antibacterial and antifouling properties of biomaterials, 834–835
 microenvironment, 824
 processes in development, 824f
 silver alloy coated urinary catheters, 840.e2b
- Bioglass, 32, 297–298, 1125
 particles, 416
 PerioGlas and NovaBone packaging with SEM image, 298f
 45S5 Bioglass, 298, 299f
- Biogran, 298
- Bioincompatibility, 1427
- Bioinks, 366–367, 630, 631f, 1280
 design parameters, 631
- Biointerface, 7
- Bioline coating, 1057
- Biological environment, 955
- Biological factors, 1294–1295
- Biological fluids, properties of, 1519–1520
 cellular composition of blood, 1520t
 inorganic substance concentrations, 1521t
 organic compound concentrations, 1521t
 physicochemical properties, 1519t
 protein concentrations, 1520t
 proteins
 in blood coagulation, 1523t
 in complement system, 1523t
 plasma, 1522t
 volumes, 1520t
- Biological inks, 557–558
- Biological polymers, 1322
- Biological relevance, 1481
- Biological responses to biomaterials, 735
- Biological risk assessment
 aging biomaterials in aging patient, 1429–1430
 in performance, 1427–1428
 secondary processes to biological risk, 1428–1429
- Biologically active molecules, 539–540
- Biologically derived materials, 84
- Biologics tissue, 1435
- Biomaterial calcification
 assessment, 977–979
 chemical assessment, 979
 extended hypothetical model, 979f
 light microscopic appearance, 978f
 morphologic evaluation, 977–979
 transmission electron microscopy, 978f
 mechanisms, 979–982
 experimental models for, 980–982, 981t
 regulation of pathologic calcification, 979
 role of biological factors, 979–980
 role of biomaterial factors, 980
 role of biomechanical factors, 980
- Biomaterial(s), 3–5, 21, 37, 271–272, 643, 1431
 affecting biofilm architecture, 834
 biofilm matrix-degrading enzymes, 834
 biomaterials modified with QS-
 quenching enzymes, 834
 with antimicrobial properties, 828–833
 applications, 10–11
 biomaterial-based medical device, 1417–1418, 1421–1422
 biomaterials-based NPs, 453
 biomaterial–tissue interaction, 845
 for bioprinting, 632
 classes, 605t–606t
 contemporary era, 32–33
 designed biomaterials, 30–32
 engineers, 35, 1497
 confidentiality and materials use agreements, 1498–1500
 contract negotiation, performance, and compliance, 1503–1504
 employment agreements, 1497–1498
 intellectual property, 1501–1503
 license agreements, 1506–1507
 litigation, 1507–1508
 SRAs, 1504–1506
 expansion of biomaterials field, 7–10
 growing palette, 7f
 intersection of, 768–772
 key applications of synthetic materials and modified natural materials, 5t–6t
 literature, 17–18, 1533
 books, 1535t–1536t
 journals and journals with substantial biomaterial content, 1534t
 research, 1533
 medical device global market, 7t
 in medical devices, 1417
 modified with QS-
 quenching enzymes, 834
 path from basic science of, 4f
 societies, 18–19
 for soft tissue engineering, 1389–1390
 success and failure, 15

- Biomaterial(s) (*Continued*)
 surface finishing to resembling cell phospholipid bilayer, 866b
 timeline, 19t
 for tissue engineering, 604
 tissue-engineering paradigms applied to a cardiac valve, 9f
 before World War II, 21–23
 artificial hearts and organ perfusion, 22
 biocompatibility, 22–23
 before civilization, 21
 contact lenses, 22
 dental implants in early civilizations, 21
 sutures, 21–22
 World War II to modern era, 23–30
- Biomaterials science, 3–5
 characteristics, 13–17
 biomaterials to devices to markets and medicine, 14
 diverse materials, 13–14
 magnitude of field, 14–15
 multidisciplinary, 13
 ethical concerns, 17t
 subjects integral to, 15–17
 biocompatibility, 15
 dependence on specific anatomical sites of implantation, 16
 ethics, 17
 functional tissue structure and pathobiology, 16
 industrial involvement, 16
 inflammation and healing, 15–16
 mechanical and physical performance requirements, 16
 regulation, 17
 risk/benefit and corporate realities, 16–17
 toxicology, 15
- Biomechanics, 842
- Biomedical applications of carbon biomaterials, 333–351
- Biomedical composites, 415–417
- Biomimetic approaches, 1188
- Biomimetic nanoscale texture, fabrication methods for, 604–610
 classes of biomaterials and methods to render texture, 605t–606t
 electrospinning, 604
 for nanofibrous and textured synthetic polymer matrices, 607t
 self-assembly of nanoscale features, 604–607
- Biomimetic regenerative medicine approach, 365
- Biomimetic synthesis, 309
- BioMinF, 301
- Biomolecule(s), 539, 543, 1294–1295
 delivery, 1320
 immobilization methods, 548t
- Bionate®, 596
- Bionic Eye. *See* Argus II
- Bionic Vision Australia team (BVA team), 1149–1150
- Bionic Vision Technologies (BVT), 1149
- Biopolymers, 361
- Bioprinting, 623, 630–632, 630f
 approaches, 630–631
 biofabrication window, 631–632, 632f
 bioink design parameters, 631
 biomaterials for, 632
- Bioprosthetic heart valves, 379
- Biopsy, 121b
- Bioreactors, 541t, 1297
- Bioreceptor, 1268–1269
- Biosensors, 337–340, 1267, 1270f
- Biostable polyurethane synthesis, 104
- Biotextiles, 575. *See also* Medical fibers.
 applications of electrospun fibers
 musculoskeletal tissue engineering, 595
 nanofibers for cardiovascular repair, 596
 nanofibers for local drug delivery, 596
 neural tissue engineering, 595–596
 wound dressing, 595
 cardiovascular applications, 592–594
 design criteria for vascular prostheses, 592–593
 endovascular stent grafts, 593–594
 examples of cardiovascular biotextiles, 593
 knitted textile structures as sewing rings, 594
 woven *vs.* knitted structure, 593
 commercial biotextile products, 576t–578t
 fiber reinforcement in bone graft cement, 594
 fiber-forming polymers
 characteristics, 578–579
 natural and synthetic polymers for biotextile production, 579
 permanent and resorbable, 580t–581t
 future directions, 596–597
 of general surgery, 591–592
 barbed and drug-eluting sutures, 591–592
 meshes and sutures, 591
 ligament and tendon replacement with woven and braided biotextiles, 594
 properties, 575–578
 skin grafting for burn injuries, 595
 textile structures, 588–591
 braided textiles, 589–590, 590f
 finishing and surface coating, 590–591
 knitted textiles, 588–589, 589f
 nonwoven textiles, 590
 vascular graft manufacturing operations, 591f
 woven textiles, 588, 588f
 wound dressings and hemostats, 595
- Biphasic calcium phosphates (BCPs), 292, 310
- bis-GMA. *See* Bisphenol-A-glycidyl dimethacrylate (bis-GMA)
- BisEMA, 140–141
- Bisphenol-A-glycidyl dimethacrylate (bis-GMA), 426
- Bisphosphonates, 984, 985f, 1126, 1257
- Bladder dyssynergia, 1158–1159
- Block copolymer, 103
 self-assembly, 565–566
- Blood, 883–884
 acquisition and handling, 883t
 blood-compatible biomaterials, 879
 blood-compatible materials, 507
 blood-contacting hydrogels, 161
 compatibility, 879–880
 measurement, 880
 derivatives
 blood derivatives-based biomaterials, 365–366
 as source of bioinstructive materials, 364–366
 plasma, 645–646
 pump bladders, 975
 vessels, 687, 1373–1374
 cyclic strain effect on, 727–728
 shear stress effect on, 726–727
- Blood coagulation, 801
 blood–material interactions, 807–810
 contact activation of blood coagulation cascade, 809–810
 platelet adhesion and cascade
 cellular composition of blood, 801–802
 coagulation, 805
 complement, 807
 fibrinolysis, 806–807
- Blood–materials interactions (BMI), 735, 807, 879, 880b
 approaches to improving blood compatibility of artificial materials, 810
 assessment, 879–887
 blood, 883–884
 blood interaction times with materials and devices, 887
 blood interactions dictated by shear and mass transport, 884–886
 parameters measurement, 891t
 surfaces, 886–887
 Virchow's triad, 883f
 contact activation of blood coagulation cascade, 809–810
 evaluation of, 881f, 887–896, 890t
 alternate scenarios for interpreting results, 882f
 blood compatible materials, 896
 contemporary concepts in, 892
 devices, 890–892
 examples, 892
 in vitro tests, 888–889
 platelet deposition and activation, 880b
 platelet–material interactions, 807–809, 808f
 thrombogenicity, 880–883

- BMA. *See* Bone marrow aspirate (BMA)
- BMG materials. *See* Bulk metallic glass materials (BMG materials)
- BMI. *See* Blood–materials interactions (BMI)
- BMPs. *See* Bone morphogenetic proteins (BMPs)
- BMSCs. *See* Bone marrow-derived mesenchymal stromal cells (BMSCs)
- BMSs. *See* Bare metal stents (BMSs)
- Body reaction (FBR), 843–844
- Body-centered cubic structure (BCC structure), 208
- Boiling point of water, 77
- Boltzmann's constant, 226
- Bombyx mori* silkworm, 1191, 1361–1362, 1392
- BonAlive, 299
- Bonding, 1181, 1183
 - adhesives, 115
 - chemistry of bonding agents, 1185
- Bone, 728–729, 1130
 - cements, 964, 1182–1186
 - fiber reinforcement in bone graft cement, 594
 - graft substitutes, 294
 - metastasis, 1228b–1230b
 - mineral, 307
 - resorption, 1126
 - tissue, 1080–1081
- Bone marrow aspirate (BMA), 294
- Bone marrow-derived mesenchymal stromal cells (BMSCs), 613–614, 1360–1361
- Bone morphogenetic proteins (BMPs), 861b–862b, 1126
 - BMP-2, 595, 710, 1298
- Bone void fillers (BVs), 291–292
- Boric acid, active site conjugation using, 1278
- Boronic acids, 1269
 - fluorescent sensors, 1278
- Bovine serum (BS), 263
- Bovine serum albumin (BSA), 262–263, 555–556
- Bowman's layer, 1135
- BP-DESSs. *See* Biodegradable polymer drug-eluting stents (BP-DESSs)
- BPO. *See* Benzoyl peroxide (BPO)
- Braided textiles, 589–590, 590f
 - ligament and tendon replacement with woven and, 594
- Braided Vicryl, 1194
- Braiding, 589–590
- Brain–computer interface (BCI), 1159
- Breaking strength, 45
- Breast augmentation surgeries, 602
- Breast implant associated-anaplastic large cell lymphoma (BIA-ALCL), 121b, 815–817
- Breast implants, 26, 975–976
- Brown adipose tissue (BAT), 1393
- Brownian motion, 456
- Brushite cements, 296
- BS. *See* Bovine serum (BS)
- BSA. *See* Bovine serum albumin (BSA)
- Buckling strength of fiber, 420, 423
- Bulk degradation, 175
- Bulk erosion, 441
- Bulk metallic glass materials (BMG materials), 278–279
- Bulk processes, 167–168, 168f
- Bulk properties of materials, 41, 49–51
 - electrochemical properties, 51
 - mechanical variables and properties, 41–49
 - nominal strain, 41
 - nominal stress, 41
 - optical properties, 50
 - piezoelectric properties, 50–51
 - surface properties *vs.*, 41
 - thermal properties, 49–50
 - true strains, 41
 - true stresses, 41
- Büngner, 595–596
- Buprenorphine, 906
- Burn dressings and skin substitutes, 1171t
 - burn wounds, 1169
 - cost considerations, 1175
 - degradable polymers, 1172–1173
 - grafts and permanent skin substitutes, 1171t
 - ideal properties, 1169–1170, 1170t
 - negative-pressure dressings, 1172
 - permanent skin substitutes, 1174–1175
 - regulatory considerations, 1175–1176
 - surgical planning for wound care, 1169
 - temporary skin substitutes, 1173
 - topical microbial management, 1170–1172
- “Burst release”, 439
- Business assessment model, 1448
- 1,4-Butanediol, 103
- Butanediol dimethacrylate (BDMA), 1322
- 1,4-Butanediol-diglycidyl ether (BDDGE), 1356
- Butler–Volmer equation, 223
- BVA team. *See* Bionic Vision Australia team (BVA team)
- BVs. *See* Bone void fillers (BVs)
- BVT. *See* Bionic Vision Technologies (BVT)
- C**
- c-Met. *See* Hepatocyte GF receptor (HGF receptor)
- C1-Inh, 782
- C3a (Complement activation fragment), 738–739
- C4 protein, 779
- C5a (Complement activation fragment), 738–739
- Ca, P-rich layer, 1087
- Ca-deficient apatite (CDA), 291
- CA4P. *See* Combretastatin A4 phosphate (CA4P)
- CAD. *See* Computer-aided design (CAD)
- Cadaver allograft, 1171t
- N-Cadherin, 1225
- CAFM. *See* Conductive atomic force microscopy (CAFM)
- CAFs. *See* Cancer-associated fibroblasts (CAFs)
- CaHPO₄. *See* Calcium phosphate (CaP)
- CALAA-01, 478
- Calcified tissues, structure and properties of, 1079–1080
- Calcitonin gene-related peptide (CGRP), 281
- Calcium diffusion inhibitor, 985
- Calcium hydroxide, 309
- Calcium phosphate (CaP), 291, 293–294, 427–428, 428f, 442, 963, 1125, 1183
 - biphasic mixtures of, 963
 - calcium phosphate-based bone graft substitutes, 294, 294t
 - cements, 294–296
 - ceramics, 313, 1125
 - coatings, 964
 - physical and chemical properties, 1126t
 - SEM images of range of commercial synthetic and natural, 295f
- Calcium sulphates, 963
- Calcium-deficient HA (CDHA), 964
- Camptothecin (CPT), 466
- Cancer, 694, 1217–1218
 - cancer-targeting moieties, 470
 - cell membrane-coated NPs, 462–463
 - glasses for cancer therapy, 301
- Cancer-associated fibroblasts (CAFs), 1219
- Candida* spp., 830, 844, 1170
 - C. albicans*, 341, 350–351
- CANs. *See* Covalently adaptable networks (CANs)
- CaP. *See* Calcium phosphate (CaP)
- CAPA. *See* Corrective and preventive action (CAPA)
- Capacitance vessels, 1034–1036
- Capacitive (non-faradaic) behavior, 224–225
- CAPD. *See* Continuous ambulatory peritoneal dialysis (CAPD)
- Capillaries, 1033
 - endothelial cells, 610
- Capillarity, 1181
- CAPs. *See* Cell adhesion proteins (CAPs)
- Capsular bag, 1135–1136
- Capsular contraction, 846
- Capture tags, 485
- CAR T cells. *See* Chimeric antigen receptor T cells (CAR T cells)
- Carbides, 319
- Carbodiimides, 525
- Carbohydrates, 1256t, 1257
 - carbohydrate-based alginate, 1222
 - carbohydrate-based materials, 1222
 - carbohydrate-based polymer, 474

- Carbon
 carbon-based coatings, 333
 carbon-carbon single bond, 95
 composites, 333
- Carbon biomaterials, 327–333, 327b. *See also* Fluorinated biomaterials.
 activated charcoal, 333
 biomedical applications of, 333–351
 antimicrobial therapy, 340–344
 biosensors, 337–340
 cardiovascular applications, 344–346
 catheters, 350–351
 dental applications, 349
 drug delivery, 333–336
 neurological applications, 349–350
 ophthalmologic applications, 350
 orthopedic applications, 346–349
 phototherapy and imaging, 336–337
 tissue-engineering approaches, 345–346
- CD, 332
 commercially available devices and potential applications, 334t
 diamond, 327–329
 DLC, 328–329
 GC, 332–333
 hexagonally bonded carbon, 330–332
 organization regarding dimension, crystallinity, and carbon hybridization, 329f
 pyrolytic carbon, 329
 safety of carbon biomaterials, 351–353
 structure, 328f
- Carbon dioxide (CO₂), 1016, 1052
- Carbon dots (CD), 332, 337, 341–342, 461, 1278
- Carbon fiber-polyetheretherketone (CF/PEEK), 417, 430.e1t
- Carbon fibers (CF), 332, 416–417
 CF-reinforced polymers, 415
- Carbon nanodots (CNDs), 461
- Carbon nanofibers (CNF), 332
- Carbon nanotubes (CNT), 330, 330f, 341, 341f, 346f, 347–348, 370, 461, 1278
 CNT-based biosensors, 338–340
 modifications for theranostic uses, 335f
 physicochemical conjugation with, 1278
- Carbostent, 345
- Carboxy phenoxy propane (CPP), 172, 186b
- Carboxybetaine, 521f
 coatings, 1059
- Carcinoembryonic antibody (CEA), 340, 340f
- Carcinogenesis, 1112
- Carcinogenicity, 472, 792
 in vitro tests for, 854–858, 855t
- Carcinomas, 813–815
- Cardiac arrhythmias, 1010–1015, 1011f–1012f
 cardiac pacemakers, 932f, 1012–1014
 complications of pacemakers and ICDs, 1014–1015
 ICD, 1014
 mitraclip device for mitral regurgitation, 1010f
- Cardiac muscle, 1373
- Cardiac myocytes, 1036
- Cardiac resynchronization therapy, 1013
- Cardiac transplantation, 1015
- Cardiomyocytes, 1374
- Cardiopulmonary bypass (CPB), 526f, 781, 1016–1017, 1057
- Cardiovascular applications, carbon biomaterials in, 344–346
 MHV, 344–345
 VAD, 345
 vascular stents, 345
- Cardiovascular biotextiles, 593
- Cardiovascular devices, 902–903
 heart valve replacement, 902–903
 VADs, 903
- Cardiovascular disease, 1299
- Cardiovascular implantable device (CID), 823
- Cardiovascular medical devices, 999
 atrial fibrillation, 1025–1028
 atrial septal defects and intracardiac defects, 1024–1025
 closure devices, 1025, 1026f
 cardiac arrhythmias, 1010–1015
 congestive heart failure, 1015–1024
 ex vivo evaluation, 1048–1049
 intravascular foreign material, 1049f
 heart valve function and valvular heart disease, 1000–1010
 cardiac valve replacement, 1002f
 complications of prosthetic heart valve, 1005f
 frequency of primary valve failure, 1006f
 percutaneous transcatheter valves and devices, 1007–1010
 surgical bioprosthetic and mechanical heart valves, 1002–1007, 1003f
 tissue heart valve replacement devices, 1003f
- key concepts in vascular structure and function, 1033–1039
 architecture of circulation, 1033–1036
 vascular pathology, 1036–1039
 unintended embolic biomaterials, 1048
 vena cava filter with clot, 1048f
- vascular devices and biomaterials, 1039–1048
 anastomotic intimal hyperplasia, 1043f
 angioplasty and endovascular stents, 1039–1041
 atherectomy devices, 1047f
 catheter-based interventions, 1039f
 endovascular Stent-Grafts, 1044–1045
 other vascular devices, 1045–1048
 stent complications, 1040f
- types of synthetic vascular grafts, 1041f
 vascular grafts, 1041–1043
 wire balloon catheter structure, 1045f
- Cardiovascular repair, nanofibers for, 596
- Cardiovascular stent, 27
- Cardiovascular system, 1033, 1034f–1035f, 1373, 1374f
- Cardiovascular tissue engineering, 1373
 blood vessels, 1373–1374
 cardiac muscle, 1373
 endothelial cells, 1373
 heart valves, 1373–1375
 scaffold materials, 1374
- Carmeda BioActive Surface (CBAS), 525, 1057
- Carpometacarpal (CMC), 347
- Cartilage, 728–729
 cells, 729
- Cas9. *See* CRISPR-associated protein 9 (Cas9)
- Catalysis, 53–54
- Cataracts, 1136–1137, 1140
- Catechol-terminated polyethylene glycol (cPEG), 1188
- Cathepsins, 706
- Catheter-associated urinary tract infection (CAUTI), 823
- Catheters, 350–351
- Cationic DDSs, 1249–1250
- Cationic dendrimer, 474
- Cationic hydrogels, 153
- Cationic lipids, 460, 475
- Cationic materials, 832–833
- Cationic polymerization, 1322
- CAUTI. *See* Catheter-associated urinary tract infection (CAUTI)
- Caveolae, 473, 725
- CBAS. *See* Carmeda BioActive Surface (CBAS)
- CBER. *See* Center for Biologics Evaluation and Research (CBER)
- CCLM. *See* Cold crucible levitation melting (CCLM)
- CCLs, 738–739
- CCPD. *See* Continuous cyclo-assisted peritoneal dialysis (CCPD)
- CCR2⁺ macrophages, 743–744
- CD. *See* Carbon dots (CD); Circular dichroism (CD); Cluster of differentiation (CD); Cyclodextrin (CD)
- CDA. *See* Ca-deficient apatite (CDA)
- CDC. *See* Centers for Disease Control (CDC)
- CDER. *See* Center for Drug Evaluation and Research (CDER)
- CDHA. *See* Calcium-deficient HA (CDHA)
- CDMs. *See* Cell-derived matrices (CDMs)
- CDRH. *See* Center for Devices and Radiologic Health (CDRH)
- CE. *See* Counterelectrode (CE)

- CEA. *See* Carcinoembryonic antibody (CEA)
- Cediranib, 470–471
- Celecoxib, 442
- Cell adhesion proteins (CAPs), 662
peptide adhesion domains in, 541t
- Cell compatibility, *in vitro* assessment of
application-specific *in vitro* assays, 861
carcinogenicity, 854–858, 855t
with cellular and protein elements in
blood, 858t
future challenges, 861–865
genotoxicity, 854–858, 855t
ISO 10993 Biological evaluation of
medical devices, 852t
medical device/biomaterial chemical
composition and extracts, 853–854,
854f
in medical device/biomaterial evaluation
for regulatory, 854
reproductive toxicity, 854–858, 855t
tests for cytotoxicity, 859
- Cell-derived matrices (CDMs),
1220t–1221t, 1222–1223
- Cell-penetrating peptides (CPPs), 476–477
- Cell(s), 1291–1292
adhesion
engineered receptor-targeting peptide
sequences for, 708–710
peptide, 1376–1377
application of, 540t
attachment, 663–664
process *in vitro*, 664–665
cell-derived materials, 1222–1223
cell-free scaffolds, 1298
cell-incorporated scaffolds, 1326–1327
cell-laden
bioinks, 630–631
scaffolds, 1326–1327
cell-mediated immunity, 760
cell–biomaterial interactions, 707, 845
cell–cell interactions, 668
cell–ECM interactions, 670
platforms to interrogating, 1225–1226
cell–matrix interactions, 1335–1340
cell–substrate interactions, 661, 663–666
commercial and experimental modifica-
tions of culture surfaces,
665–666
dynamic control of cell culture surfaces,
666
investigating, 666
peptide sequences on cell anchoring
proteins, 664t
process of cell attachment *in vitro*,
664–665
surface treatments, 665t
surfaces for cell culture, 663–664
cell–surface interactions, 661
cell culture, 661–663
cell response to mechanical
deformation, 673
cell response to substrate chemistry,
666–670
cell response to substrate elasticity,
672–673
cell response to substrate topography,
670–672
cell–substrate interactions, 661,
663–666
comparison and evaluation of substrate
cues, 673–674
organ-on-a-chip 3D culture, 674–675
culture, 661–663
cell lines, 662–663, 662t
characteristics, 663
primary culture, 662
cytoskeleton, 595–596
death, 695–696
delivery, 1318–1320
differentiation, phenotype, and
maintenance, 687–693
essential role of, 683–684
immobilized cell ligands and, 541–542
injury, 693
causes of, 694–695
pathogenesis, 695
injury, adaptation, and other responses,
693–696
of innate immune system, 750–754, 752f
interactions with adsorbed proteins on
biomaterials, 707
membrane, 472
membrane-coated NPs, 462–463
regeneration and proliferation, 693
role of, 982
sheets, 666
source, 1302–1303
therapy, 1290
and tissues, 644
transformation assays, 857
turnover, 692
viability test, 465
Cellophane, 23, 517
Cellular composition of blood
erythrocytes, 801
leukocytes, 801–802
Cellular differentiation, 691
Cellular inflammatory response, 431
Cellular internalization, 474–476
and efflux, 468
Cellular mechanotransduction
cytoskeletal mechanotransduction,
718–719
focal adhesion and mechanosensing
at ECM–biomaterial interface,
717–718
molecular mechanisms of, 717–720
nuclear mechanotransduction, 719–720
Cellular scaffolds, 1298–1299
Cellular stress response test, 465
Cellulose, 1359–1360
Cellulose acetate, characteristics and uses
of, 100t
Cellulose nanocrystals (CNC), 365
Center for Biologics Evaluation and
Research (CBER), 1175
Center for Devices and Radiologic Health
(CDRH), 1175
Center for Drug Evaluation and Research
(CDER), 1175
Centers for Disease Control (CDC), 1442
Centers for Medicare and Medicaid Services
(CMS), 1459
Central memory T cells, 764
Central tolerance, 766–767
Central venous catheters (CVCs), 828
Centrifugal electrospinning (CES), 586–587
CEPs. *See* Conductive electroactive polymers
(CEPs)
CER. *See* Clinical evaluation report (CER)
Ceramic materials, 955
bioceramic interactions with biological
environment, 960–967
first, second, and third-generation
bioceramics, 961t–962t
resorbable and bioactive ceramics,
962–965, 966t
third-generation ceramics, 965–967
evolution in use of bioceramics for bone
repair, 959–960, 960f
natural bone and artificial bioceramics,
959f
factors influencing degradation of
bioceramics, 956–958, 957f
biological apatites, 958f
reactivity and degradation of natural
apatites, 958
reactivity of bioceramics, 955–956, 956f
Ceramics, 289, 319, 605t–606t, 1087,
1123, 1125
bioactive, 290–301
types of clinical indications, 291t
bioceramics, 289
calcium phosphate phases, 291t
nearly inert bioceramics, 289–290
tissue attachment, types of, 290t
ceramic–polymer composites, 427–428
matrix, 417
composites, 425–426
Ceravital, 1125
Cerebrospinal fluid (CSF), 119
CES. *See* Centrifugal electrospinning
(CES)
CF. *See* Carbon fibers (CF); Cystic fibrosis
(CF)
CF/PEEK. *See* Carbon fiber-
polyetheretherketone (CF/PEEK)
CFDA. *See* Chinese FDA (CFDA)
CFM. *See* Chemical force microscopy
(CFM)
CFUs. *See* Colony forming units (CFUs)
CGRP. *See* Calcitonin gene-related peptide
(CGRP)
CH/SS. *See* Chlorhexidine/silver sulfadiazine
(CH/SS)

- Chain transfer agent (CTA), 97–98, 197, 490
- Chain-growth polymerization, 96
- α -Chains, 402
- Charge reversal, 477
- Charge transfer resistance (R_{ct}), 1271–1272
- Chemical and biochemical degradation of polymers, 919–920
- emerging long-term elastomer applications, 935–936
 - hydrocarbon elastomers, 936
 - polyurethanes, 935–936
- hydrolytic biodegradation, 920–926
- oxidative biodegradation, 926–935
- polymers containing hydrolyzable pendant groups, 925–926, 926f
- subconjunctival and subpalpebral hydrogel, 925f
- preclinical and clinical experience, 922–925
- Chemical characterization for tissue-engineering scaffolds, 1327t
- Chemical cross-linking, 9–10
- Chemical degradation, 173–174, 174f
- Chemical enhancers, 1251, 1252t
- Chemical force microscopy (CFM), 69t
- Chemical patterning for coculture of cells, 668–670
- Chemical reactivity of toxicant, 851
- Chemical surface modification methods, 489t
- Chemical vapor deposition (CVD), 327–328, 964, 1279
- Chemically cross-linkable hydrogels, 1319
- Chemically reactive particles, 1102
- Chemokines, 749–750, 756
- ChiCTR-TRC-13003238 trial, 283–284
- Chimeric antigen receptor T cells (CAR T cells), 1208
- Chinese FDA (CFDA), 283–284
- Chinese hamster ovary cells (CHO cells), 408
- Chinese Society for Biomaterials, 18–19
- Chinese Taipei Society for Biomaterials and Controlled Release (1997), 18–19
- Chitin, 406–407, 1360
- Chitosan (CS), 343–344, 401, 406–407, 432, 432f, 442, 474, 832, 1206–1207, 1275–1277, 1293, 1360
- chitosan-based hydrogels, 406–407
- Chlorhexidine/silver sulfadiazine (CH/SS), 830–831
- CHO cells. *See* Chinese hamster ovary cells (CHO cells)
- Chondrocytes, 1128
- Chondrofix, 386
- Chondroitin sulfate (CS), 364, 404–405
- Chordae tendineae, 975
- Choroid, 1136
- Choroidal neovascularization (CNV), 1137
- Chromatin, 1339–1340
- Chrome-doped alumina, 320
- Chrome–cobalt alloys, 24–25
- Chromic gut sutures, 1189
- Chromium (Cr), 230, 792–793, 1107
- Chromium oxide (Cr_2O_3), 1096–1097
- Chromium–phosphate ($((\text{Cr}(\text{PO}_4)_4\text{H}_2\text{O}))$), 1100
- Chromogenic agents, 1277
- Chronic inflammation, 697
- Chronic obstructive pulmonary disease (COPD), 1051–1052
- Chronic respiratory disease, 909
- Chronic toxicity, 873
- CID. *See* Cardiovascular implantable device (CID)
- Ciliary body, 1135
- CIMR. *See* Coriell Institute for Medical Research (CIMR)
- Ciprofloxacin, 1172
- Circular dichroism (CD), 651–652, 655, 657
- Circulating tumor cells (CTCs), 479
- Circulation, 467
- Cisplatin, 333
- Claims, 1502
- Classic biosensor system, 1268–1269
- bioreceptor, 1268–1269
 - computer processing, 1269
 - physicochemical transducers, 1269
- Classical dental-bonding cements, 1183
- Classical pathway (CP), 777–779
- activities, 778t
 - C4 and C3 protein structures, 778f
 - complement activation by, 778f
 - conversion of C5 produces C5a and C5b, 779f
 - proteins, 778t
- Clathrin-mediated endocytosis (CME), 473
- Click chemistry, 543, 1319
- Click reactions, 1321
- Clinical evaluation report (CER), 1471
- Clinical-stage NPs for anticancer drug delivery, 473t
- Clo-Sur P. A. D approach, 406–407
- Clonal selection and expansion, 757
- Closed-loop methods, 1290–1291
- Clot lysis, 527–528
- CLSM. *See* Confocal laser scanning microscopy (CLSM)
- Cluster of differentiation (CD), 757
- CD11b/CD18, 648
 - CD22, 1211
 - CD28, 762–763
 - CD3, 757
 - CD4, 757
 - CD4⁺ T cells, 744
 - CD40–CD40L, 762–763
 - CD70–CD27, 762–763
 - CD8, 757
- Clustered regularly interspaced short palindromic repeats (CRISPR), 1303–1304
- CM-AFM. *See* Contact mode-atomic force microscopy (CM-AFM)
- CMC. *See* Carpometacarpal (CMC); Critical micellar concentration (CMC)
- CME. *See* Clathrin-mediated endocytosis (CME)
- CMS. *See* Centers for Medicare and Medicaid Services (CMS)
- CNC. *See* Cellulose nanocrystals (CNC)
- CNDs. *See* Carbon nanodots (CNDs)
- CNF. *See* Carbon nanofibers (CNF)
- CNT. *See* Carbon nanotubes (CNT)
- CNV. *See* Choroidal neovascularization (CNV)
- Co–Cr–Mo. *See* Cobalt–chromium–molybdenum (Co–Cr–Mo)
- Coacervation, 436–437, 437f
- microfluidic device, 436–437, 437f
 - phase separation, 436
 - process, 455–456
- Coagulation, 735, 805, 806f, 1067
- control mechanisms, 805–806
 - factors, 698
 - and inflammation, 1055–1056
- Coatings, 1194–1195
- Cobalt, 1107
- cobalt-based alloys, 1087–1089, 1100
- Cobalt–chromium alloys (Co–Cr alloys), 257, 258f, 265f, 1089
- additive manufacturing, 261f
 - application of, 264–265
 - bio-tribocorrosion of, 262–264, 263t, 264f
 - in biological environments, 266–267, 267f
 - biomedical, 258t
 - clinical concerns related to metal ion release from, 267
 - example of potentiodynamic polarization curves, 259f
 - grade metals and properties, 258t
 - effect of heat treatment time, 260f
 - high-magnification microstructural characteristics, 259f
 - microstructure, mechanical properties, and manufacturing of, 259–260
 - properties leading to biocompatibility of, 265–267
 - corrosion resistance, 265–266
 - topography of MC3T3 preosteoblast cells, 266f
 - 3D printing of, 260–262
- Cobalt–chromium–molybdenum (Co–Cr–Mo), 205, 257, 1089
- Cobalt–nickel–chromium–molybdenum (CoNiCrMo), 1089
- Cochlear implant, 1158
- Cochrane analysis, 830
- Co–Cr alloys. *See* Cobalt–chromium alloys (Co–Cr alloys)
- Coding, 1459
- Codon adaptation, 408

- Colectrospinning, 586
- Coherence tomography (OCT), 1046, 1046f
- Cold crucible levitation melting (CCLM), 233
- Cold working, 213–214, 214f
- CollI. *See* Type II collagen (ColII)
- CollIII. *See* Type III collagen (ColIII)
- CT. *See* X-ray computed tomography (CT)
- Collagen type I (ColI), 402
fibrils, 1352
- Collagen type IV (ColIV), 402
- Collagen(s), 402–403, 406, 604, 703–704, 1222, 1292–1293, 1318–1319, 1360–1361, 1363, 1392, 1395
biosynthesis, 402
collagen I, 1220t–1221t
collagen-based scaffolds, 1404
and elastin role of, 982
fibers, 39, 40f
gels, 1375
microparticles, 433
types, 402t
- Collagraft, 1292–1293
- Colloidal
DDSs, 1245, 1247
iron oxide nanoparticles, 460
particles, 438
- Colloids, patterning by self-assembly of, 565–567, 566f
- Colony forming units (CFUs), 834–835
- Combinatorial screening methods, 648–649
- Combining multiple fabrication methods, 612–615
- Combretastatin A4 phosphate (CA4P), 470
- Comfilcon A, 1140
- Commercial considerations in medical device development
commercial operations, 1461–1462
determining market opportunity, 1458–1459, 1459t
medical device reimbursement, 1459–1460
securing IP and funding, 1460–1461
IP, 1460–1461
securing funding, 1461
traditional model of product development, 1457–1458
linear stage-gate approach, 1458f
- Commercializability, 490
- Commercially pure titanium (CPTi), 1089, 1125
- Compact organs, 687
- Compensatory hyperplasia, 694
- Complement, 735, 807
activation, 760, 763–764
fragments, 738–739
clinical correlates, 785–788
postperfusion or postpump syndrome, 787t
complement receptors, 783–784
- complement–coagulation system
interactions, 785
- components, 698
- control mechanisms, 782–783
- CP, 777–779
- measurement of complement activation, 784
- membrane attack complex, 781
system, 748–749, 777
- Complement receptor (CR), 783–784
CR1, 782
- Complementary base-pairing, 1268–1269
- “Complexation” hydrogels, 154
- Compliant TAL (cTAL), 1054, 1062f
- Composite(s), 415, 1322–1323. *See also* Fibrous composites.
biomedical composites for tissue engineering, 427–428
cultured skin, 1171t
in dental applications, 426–427
fiber arrangement, 418
geometry and size of dispersed phase and distribution, 418
interfaces in, 418–419
long-fiber reinforced composites, 419f
major influencing factors, 417–419
materials, 605t–606t, 1120, 1223
matrix materials, 415–416
mechanical properties
compressive properties of fibrous composites, 420–424
tensile properties of fibrous composites, 419–420
nonporous and porous composites, 417
in orthopedic applications, 424–426
reinforcements, 416–417, 416f
restoratives, 1120
- Compressive forces, 728
- Compressive stress lines, trajectories of, 48–49
- Compressive testing, 1327t
- Computed tomography (CT), 480–481, 1041
analysis, 283–284
- Computer processing, 1269
- Computer-aided design (CAD), 614
- Condensation, 95–96, 96f
- Conditioning, 1181
- “Conditioning film” of organic molecules, 507
- Conducting/capacitive materials, 1154
- Conductive atomic force microscopy (CAFM), 69t
- Conductive conjugated polymers, 1277
- Conductive electroactive polymers (CEPs), 1277
- Conductometric biosensors, 1271
- Cone(s), 1136
and plate system, 720, 721f
- Confidentiality, 1498–1500
- Confluence, 662
- Confocal laser scanning microscopy (CLSM), 438
- Confocal microscopy, 828
- Congestive heart failure, 1015–1024
cardioMEMS device, 1015f
cardiopulmonary bypass, 1016–1017
complications of cardiac assist devices, 1024f
heartmate XVE pulsatile ventricular assist device, 1020f
percutaneous mechanical circulatory support devices, 1017–1019, 1018f
syncardia total artificial heart, 1023f
- CoNiCrMo. *See* Cobalt–nickel–chromium–molybdenum (CoNiCrMo)
- Connective tissue, 683
- Constant phase element (CPE), 226
- Constructive remodeling, cellular and molecular mediators of, 742–744
- Contact activation of blood coagulation cascade, 809–810, 809f
- Contact angle
measurements, 58–59, 59f, 59t
methods, 57–59, 58f, 58t
- Contact inhibition, 662–663
- Contact lens, 14, 22, 161, 350, 1137–1138
hard, 1138–1139
materials, 1138–1139
silicone hydrogel, 1139
soft hydrogel, 1139
solutions, 1140
surface modification, 1139–1140
- Contact mode-atomic force microscopy (CM-AFM), 69t
- Contact-angle correlations, 72
- Contemporary concepts in BMI evaluation, 892
axial flow ventricular assist device, 882b
imaging thrombotic deposition, 882b
- Continence, 1158–1159
- Continuous ambulatory peritoneal dialysis (CAPD), 1065
- Continuous cycler-assisted peritoneal dialysis (CCPD), 1065
- Continuous plasma processing. *See* “Reel-to-reel” plasma processing
- Continuous stirred-tank reactor, 1297
- Continuous wave (CW), 501
- Contract
breach, 1500, 1504
negotiation, performance, and compliance, 1503–1504
- Contractile forces, 1337–1338
- Contrast, biomolecular surface patterning of, 554–556, 555f
- Control mechanisms, 782–783
receptors for complement proteins, 783t
- Controlled drug delivery, 1239
- Controlled living free radical polymerizations, 97
- Controlled Release Society, 18–19
- Controlled-release systems, 523–525

- Conventional acid–base cements, 1183
 Conventional bench testing, 1421–1422
 Conventional hydrogel systems, 366
 Conventional polyketal particulate formulations, 434
 Conventional systems, 140–142
 dimethacrylates, 140–141
 Conventionally fabricated scaffolds, 1295–1296
 Conversion coatings, 500
 Coordination bonding, 467
 COPD. *See* Chronic obstructive pulmonary disease (COPD)
 Copolymers, 86, 88f. *See also* Fluoropolymer(s).
 hydrogels, 153
 Copper (Cu), 22–23, 205
 Coral-derived HA ceramics, 308–309
 Coralline hydroxyapatite, 603f
 Core-cross-linked PMs, 455
 Coriell Institute for Medical Research (CIMR), 663
 Cornea, 1138
 Corona discharge modification, 490
 Coronary perfusion process, 1376
 Corrective and preventive action (CAPA), 1492
 Corrosion, 220–224, 252–254
 design of biodegradable metals, 272
 electrochemical currents, 223–224
 electrochemical reactions, 220–221
 at modular interfaces of joint replacements, 1097
 at modular junctions, 1103
 polarizable and nonpolarizable electrodes, 222
 pourbaix diagrams, 222–223
 principal reduction reaction in biomaterials, 221–222
 half-cell redox reactions, 222f
 process in vitro, 279–280
 Cortiva BioActive Surface, 525
 CosmoDerm, 403
 Costimulators, 762–763
 Costimulatory molecules, 749–750, 755–756
 Coulter counter, 438
 Counterelectrode (CE), 257
 Courses, 588–589
 Covalent adaptable networks, 179b
 Covalent bonding, 466
 Covalent bonds, 39, 39f
 Covalent conjugation, 1279
 Covalent linkage, 1275
 Covalently adaptable networks (CANs), 144
 Covalently bound heparin, 525–526
 Covidien STEEL sutures, 1192
Coxiella burnetti, 907
 CP. *See* Classical pathway (CP); Cumulative probability (CP)
 CPB. *See* Cardiopulmonary bypass (CPB)
 CPE. *See* Constant phase element (CPE)
 cPEG. *See* Catechol-terminated polyethylene glycol (cPEG)
 CpG. *See* Cytosine-phosphate-guanine (CpG)
 CPP. *See* Carboxy phenoxy propane (CPP)
 CPPs. *See* Cell-penetrating peptides (CPPs)
 CPT. *See* Camptothecin (CPT)
 CPTi. *See* Commercially pure titanium (CPTi)
 Cr-based oxide (Cr₂O₃), 207
 Creep, 45
 Crevice corrosion, 254
 Crimping, 593
 CRISPR. *See* Clustered regularly interspaced short palindromic repeats (CRISPR)
 CRISPR-associated protein 9 (Cas9), 1303–1304
 Critical micellar concentration (CMC), 453–454
 Critical stress intensity factor, 46
 Cross-linking, 1275, 1355–1356
 cross-linkable polyesters, 596
 cross-linked PU thermosets, 106
 mechanism, 631
 methods, 383–384
 Cross-presentation, 762
 Cryopreservation, 377–379
 Cryoprotectants, 377–378
 CryoValve SG, 385
 Crystalline HA, 307
 X-ray diffraction pattern of, 307
 Crystallinity, 93, 610f
 Crystallites, 90–91
 CS. *See* Chitosan (CS); Chondroitin sulfate (CS)
 CSF. *See* Cerebrospinal fluid (CSF)
 CT. *See* Computed tomography (CT)
 CT angiography (CTA), 1045–1046
 CTA. *See* Chain transfer agent (CTA); CT angiography (CTA)
 cTAL. *See* Compliant TAL (cTAL)
 CTCs. *See* Circulating tumor cells (CTCs)
 CTLs. *See* Cytotoxic T-lymphocytes (CTLs)
 Cucurbit[n]uril (CB[n]), 367–368
 Cultured cells, 727–728
 Cumulative probability (CP), 945
 Custom-built biaxial strain devices, 727–728
 Custom-built uniaxial strain devices, 727–728
Cutibacterium acnes, 824
 CVCs. *See* Central venous catheters (CVCs)
 CVD. *See* Chemical vapor deposition (CVD)
 CW. *See* Continuous wave (CW)
 CX3CL1, 738–739
 CX3CR1⁺ macrophages, 743–744
 CXCL13, 745
 Cyanoacrylate esters, 1186–1187
 chemistry, 1186
 performance, 1186–1187
 Cyclic strain effect on blood vessels, 727–728
 Cyclic stretch, 1343–1344
 Cyclodextrin (CD), 155, 158, 367–368, 474, 1244
 α-Cyclodextrins (α-CD), 1319
 Cyclosiloxanes (R₂SiO)_m, 110
 Cysteine (Cys), 195–196, 1275
 Cystic fibrosis (CF), 1051–1052
 Cytodex microcarrier beads, 655
 Cytokine(s), 698, 738, 749–750, 756, 845
 of adaptive immune system, 757
 and effects on specific immune cells, 758t–759t
 of innate immune system and targets, 754t
 release, 845
 Cytolytic granules, 754
 Cytosine-phosphate-guanine (CpG), 1201
 Cytoskeletal mechanotransduction, 718–719
 Cytoskeleton, 728, 1339–1340
 Cytosolic proteins, 706
 Cytotoxic T-lymphocytes (CTLs), 757, 760
 Cytotoxicity, in vitro tests for, 859, 860t
- ## D
- D-Phe-Pro-Arg chloromethyl ketone (PPACK), 526
 DAF. *See* Decay-accelerating factor (DAF)
 DAH-HA. *See* Diaminohexane conjugated HA (DAH-HA)
 Damage-associated molecular patterns (DAMPs), 749–750, 1106
 DBM. *See* Demineralized bone matrix (DBM)
 DCPA. *See* Dicalcium phosphate anhydrous (DCPA)
 DCPD. *See* Dicyclopentadiene (DCPD); Dihydrate phosphate anhydrous (DCPD)
 DCs. *See* Dendritic cells (DCs)
 DDR. *See* Discoidin domain receptors (DDR)
 DDSs. *See* Drug delivery systems (DDSs)
 Decay-accelerating factor (DAF), 782
 Decellularization, 380–382, 380f, 985–986, 1355
 methods, 380–381
 processing heart tissue for decellularized material applications, 383f
 quality, 381–382
 Decellularized ECM (dECM), 363, 846, 1293
 applications, 384–389
 decellularized tissue therapies along translational pipeline, 385t
 powder and injectable decellularized ECM therapies, 387–388
 scaffold-based therapies, 385–387
 tissue-specific in vitro models of native microenvironment, 388–389
 whole organ recellularization, 387
 dECM-based hydrogels, 363
 scaffolds, 708b

- Decellularized tissues, 1322, 1375, 1391–1395
- Decitex (dtx), 579
- Declaration of Helsinki, 1512–1513
- dECM. *See* Decellularized ECM (dECM)
- Dectin-1, 749
- DED. *See* Directed-energy deposition (DED)
- Deep venous thrombus (DVT), 1047
- Defects in crystals, 211–212
 - area defects, 212
 - line defects, 211–212
 - point defects, 211
 - volume defects, 212
- Defend Trade Secrets Act of 2016 (DTSA), 1498
- Degradable polymers, 167, 169f, 170t, 1172–1173, 1173b. *See also* Smart polymers.
 - erosion, bulk, and surface processes, 167–168
 - history of, 167
 - performance metrics, 183–184
 - time course profiles of plasma drug, 184f
 - worked examples, 184–185
- polymer design and processing, 177–183
 - composites, 181–182
 - covalent adaptable networks, 179b
 - custom, degradable inks for 3D printing, 183b
 - delivery, 179–181
 - design criteria of degradable biomaterial application, 178t
 - lifetime, 178, 179f
 - location, 178
 - mechanical properties, 179, 181f
 - pH-responsive supramolecular polymer gel, 180f–181f
 - SEM images of 3D, 183f
 - shape, 182–183
 - sterilization, 183
 - effect of surface area to volume ratio, 182f
- properties, 168–172
 - definition and examples of key processes, 169t
 - polymer backbone functionality, 169–171
- routes and kinetics, 172–177
 - enzymatic degradation, 176–177
 - hydrolytic degradation, 174–175
 - orthogonal stimuli-labile strategies, 177b
 - photodegradation, 176
 - scanning electron micrographs, 177f
 - stability of conjugated structures, 174f
- used in medicine, 185
 - polyanhydrides in controlled release devices, 186b
 - variations in PLGA molecular weight, 186f
- Degradable synthetic polymers, 435
- Degradation, 440, 961
 - characteristics of polymer materials, 94–95
 - of materials in biological environment, 917
 - mechanism of Fe-based alloys, 274, 274f
 - rate, 172
- Degree of crystallinity, 93
- Degree of polymerization (DP), 87
- Degree of response, 852
- Degummed silk fibroin, 1361
- Dehydrothermal treatment (DHT treatment), 1357
- Delamination resistance, 487–488
- Delayed type hypersensitivity (DTH), 1110
- DeminerIALIZED bone matrix (DBM), 290
- Dendrimer(s), 86, 458, 1247, 1248t
 - hydrogels, 159
 - synthesis, 458f
- Dendritic cells (DCs), 431, 743–744, 747–748, 752, 1200–1201
- Dendron, 458
- Densification, 289
- Density of water, 77–78
- Dental, oral, or craniofacial tissue (DOC tissue), 1119
 - materials for engineering DOC tissue structure and function, 1127
 - needs in developing biomaterials for DOC procedures, 1119
 - tissue-engineering applications, 1127–1130
 - bone and periodontium, 1130
 - oral mucosa, 1128–1129
 - salivary glands, 1129–1130
 - teeth, 1127–1128
 - TMJ, 1128
- Dental applications, 1119
 - biomedical composites in, 426–427
 - carbon biomaterials in, 349
 - needs in developing biomaterials for DOC procedures, 1119
 - restorative materials, 1119–1120
 - tissue engineering in dentistry, 1126–1130
- Dental cements, 1183, 1184t
- Dental enamel, 1184
- Dental implants, 11, 11f, 25, 601–602, 1120–1123
 - criteria for successful implant function, 1121
 - in early civilizations, 21
 - interdependent biomaterials factors, 1121f
 - materials used in, 1123–1126
 - engineering properties of bioactive and biodegradable ceramics, 1124t
 - engineering properties of inert ceramics, 1124t
 - engineering properties of metals and alloys, 1124t
- mechanical parameters and implant design, 1123
- natural tooth *vs.* implant attachment to bone, 1122f
- osseointegration and accelerating healing and attachment to tissue, 1121–1122
- surface topology and chemistry, 1123
- Dental pulp stem cells, 1127
- Dentistry, 415, 426
 - tissue engineering in, 1126–1130
 - DOC tissue-engineering applications, 1127–1130
 - materials for engineering DOC tissue structure and function, 1127
 - need for, 1126–1127
- Deoxyribonucleic acid (DNA), 366, 872, 1268–1269
- DNA-based materials, 370
- multifunctional biomaterials based on DNA, 366
- origami technique, 366
- repair mechanisms, 1438–1439
- tiles, 462
- Depletion studies, 647–648
- Deposition with masks, 562
- Derjaguin, Landau, Verwey, Overbeek theory (DLVO theory), 824–825, 825f
- DermaGraft, 1171t, 1173
- DES. *See* Drug-eluting stents (DES)
- Descemet's membrane, 1135
- Design
 - controls, 1448, 1449t
 - development plan, 1449
 - freeze, 1450
 - history file, 1453–1454
 - inputs, 1448–1450, 1450t
 - matrix, 1450
 - outputs, 1450
 - specifications, 1449–1450, 1450t
 - validation, 1454
 - verification, 1465
- Design of experiment (DOE), 1482
- Design specification document (DSD), 1450
- Designed biomaterials, 30–32
 - bioglass, 32
 - hydrogels, 31
 - hydroxyapatite, 32
 - PEG, 31–32
 - poly(lactic-glycolic acid), 32
 - polyurethanes, 30
 - silicones, 30
 - teflon, 30–31
 - titanium, 32
- DET. *See* Direct electron transfer (DET)
- Detonation nanodiamonds (DND), 328
- Developmental toxicity, 873
- Device thrombogenicity, 881b
- Device-related infection, 828
 - medical devices, materials, and pathogens, 828

- Dexedrine Spansules, 1237–1239
 Dexon, 1193
 Dextran, 433
 DH. *See* Diffusion hardening (DH)
 DHFR. *See* Dihydrofolate reductase (DHFR)
 DHT treatment. *See* Dehydrothermal treatment (DHT treatment)
 Di-para-xylylene (DPX), 500–501
 Diabetes, 479
 Diabetic retinopathy (DR), 1136–1137
 Diagnostic catheters, 1045–1046
 Diagnostic/theranostic applications
 imaging-guided surgery, 482
 theranostics, 481–482
 in vitro diagnosis, 478–479
 in vivo imaging, 479–481
 Dialysis, 454–455
 Dialyzer materials and coatings, 1066–1067
 Diaminohexane conjugated HA (DAH-HA), 368
 Diamond, 327–329
 MCD, 328
 NCD, 328
 ND, 328
 UNCD, 328
 Diamond Flex, 345
 Diamond-like carbon (DLC), 327–329,
 528–529
 coatings, 342–343
 Diamondoids, 328
 Diastolic pressure, 727
 N-Diazoniumdiolates, 527
 Dicalcium phosphate anhydrous (DCPA),
 291, 294–295
 Diclofenac sodium (DS), 434
 Dicyclopentadiene (DCPD), 291
 Differential scanning calorimetry (DSC),
 93–94, 655, 1326, 1327t
 Differentiated cells, 683–684
 Differentiation, 692
 Diffusion, 440
 diffusion-controlled devices, 161–162
 diffusional release, 440
 Diffusion hardening (DH), 1112
 Digital light processing (DLP), 624–625
 Digital light projection (DLS), 1324
 Digital mirror device (DMD), 624–625
 Dihydrate phosphate anhydrous (DCPD),
 294–295
 Dihydrofolate reductase (DHFR), 408
 3,4-Dihydroxyphenylalanine (DOPA),
 1060
 Diisocyanate(s), 103
 molecules, 104
 1,4-Diisocyanatobutane (BDI), 104
 Dilute hypochlorous acid, 1170–1172
 Dilute sodium hypochlorite, 1170–1172
 2-Dimethyl(aminoethyl) methacrylate
 (pDMAEM), 474
 N-Dimethylacrylamide (DMA), 195–196,
 1139
 N,N-Dimethylaminoethyl methacrylate
 (DMAEM), 524–525
 5,6-Dimethylxanthenone-4-acetic acid
 (DMXAA), 469–470
p-Dioxanone polymers, 1192
 Dip-pen nanolithography (DPN), 69t,
 556–558, 556f, 558f
 Direct dispersion, 454–455
 Direct electron transfer (DET), 1269, 1271,
 1278
 Direct energy deposition, 624t, 629–630,
 630f
 Direct oxidation by host, 927–929
 Direct piezoelectric effect, 50
 Direct reprogrammed cells, 1292
 Direct transport of electron. *See* Direct
 electron transfer (DET)
 Direct-write patterning, 556–561, 556f
 writing
 with beams, 558–560
 with fields, 560–561
 with stylus, 556–558
 Direct-write photolithography, 559, 559f
 Directed-energy deposition (DED),
 260–262
 Directional atherectomy, 1046–1047
 Discoidin domain receptors (DDR), 707
 DDR-1, 707
 DDR-2, 707
 Disease
 diagnostics, 337–338
 models and therapy, 1302
 Disinfection
 of biomaterials, 1417–1418
 procedure, 1431
 Dispersin-B, 834
 Dispersion forces. *See* Van der Waals forces
 Dissections, 1037–1039
 Dissolution, 1244
 Dissolved ions and solutes, 79
 DLC. *See* Diamond-like carbon (DLC)
 DLN, 345
 DLP. *See* Digital light processing (DLP)
 DLS. *See* Dynamic light scattering (DLS)
 DLVO theory. *See* Derjaguin, Landau,
 Verwey, Overbeek theory (DLVO
 theory)
 DMA. *See* N-Dimethylacrylamide (DMA);
 Dynamic mechanical analysis (DMA)
 DMAEM. *See* N,N-Dimethylaminoethyl
 methacrylate (DMAEM)
 DMD. *See* Digital mirror device (DMD)
 DMXAA. *See* 5,6-Dimethylxanthenone-4-
 acetic acid (DMXAA)
 DN. *See* Double network (DN)
 DNA. *See* Deoxyribonucleic acid (DNA)
 DNase I, 834
 DND. *See* Detonation nanodiamonds
 (DND)
 DOC tissue. *See* Dental, oral, or craniofacial
 tissue (DOC tissue)
 Documentary standards, 1476–1481, 1477t
 applications, 1480–1481
 accelerating regulatory process,
 1480–1481
 clinical relevance, 1481
 information courtesy, 1480f
 specificity *vs.* universality, 1481
 standard test method, 1481
 ASTM types, 1478t
 case study, 1480b
 development, 1478–1480
 measurement assurance, 1481–1482
 voluntary, consensus, 1476–1477
 DOE. *See* Design of experiment (DOE)
 Donnan osmotic effect, 702–703
 Donor-acceptor interaction. *See*
 Coordination bonding
 DOPA. *See* 3,4-Dihydroxyphenylalanine
 (DOPA)
 Dorsal root ganglia cells, 708–709
 Dose uniformity ratio (DUR), 1434
 Double emulsion
 preparation of nanocapsules by, 456f
 process method, 436
 solvent preparation, 435
 Double layer capacitance (C_{dl}), 1271–1272
 Double network (DN), 158
 Double-walled CNT (DWCNT), 330, 330f
 Doxil, 468
 DP. *See* Degree of polymerization (DP)
 DPN. *See* Dip-pen nanolithography (DPN)
 DPX. *See* Di-para-xylylene (DPX)
 DR. *See* Diabetic retinopathy (DR)
 Drainage devices, 1143
 Drug, 1320
 drug-eluting sutures, 591–592
 drug-loaded contact lenses, 350
 drug-polymer interactions, 437
 encapsulation, 438
 loading, 438, 466–467
 covalent bonding, 466
 noncovalent encapsulation, 466–467
 Drug delivery, 441–442, 1301–1302
 applications
 approaches to overcome systemic barri-
 ers, 468–472
 drug loading, 466–467
 systemic barriers against drug delivery,
 467–468
 carbon biomaterials in, 333–336
 ND-based drug and gene delivery ap-
 proaches, 335f
 and controlled release, 30
 encapsulation and sustained release of
 biopharmaceuticals, 441
 from hydrogels, 161–162
 local injection, 441
 ophthalmic delivery, 442
 oral delivery, 442
 pulmonary delivery, 442
 vaccines and immune adjuvants, 442
 Drug delivery systems (DDSs), 161–162,
 431, 1237, 1238f, 1248t

- biomaterials, 1241
 degradation, 1241
 design considerations, 1241
 for drug targeting, 1254–1257
 enhancing drug stability, 1249–1250
 mechanics, 1242
 properties, 1241–1242
 surface properties, 1241–1242
 design to overcoming biological barriers, 1250–1253
 drug delivery routes, 1240–1241, 1240f
 drug release mechanisms, 1245f
 early macroscopic, 1239t
 evolution, 1238f
 general considerations in, 1240–1242
 global regulatory guidance documents for combination products, 1258t
 history of DDS development, 1237–1240
 to improving drug pharmacokinetics, 1243–1245
 controlling drug release kinetics, 1244–1245
 dosage and distribution control, 1244
 pharmacokinetics, 1243–1244
 to improving drug solubility, 1245–1249
 intellectual property, 1258–1259
 platforms, 1247f
 regulation, 1257–1258
 sample, 1246t
Drug release, 440–441
 kinetics, 440
 classic mechanisms, 440f
 degradation, 440
 diffusion, 440
 swelling, 441
 from PLGA microparticles, 433
Drug-eluting stents (DES), 530, 1040–1041
 DES-induced thrombosis, 530b
 Drusen, 1137
 Dry AMD, 1137
 Dry heat sterilization, 1440
 DS. *See* Diclofenac sodium (DS)
 DSC. *See* Differential scanning calorimetry (DSC)
 DSD. *See* Design specification document (DSD)
 DTH. *See* Delayed type hypersensitivity (DTH)
 DTSA. *See* Defend Trade Secrets Act of 2016 (DTSA)
 Dual-optic accommodating IOLs, 1142
 Ductility, 45
 Dumahel integral, 950–951
 DUR. *See* Dose uniformity ratio (DUR)
 Durability, 53
 biomolecular surface patterning of, 556
 Duraflo II, 525
 DVT. *See* Deep venous thrombus (DVT)
 DWCNT. *See* Double-walled CNT (DWCNT)
- Dye(s), 1194
 dye-containing NPs, 481
 dye-mediated photooxidation, 379
 Dylyn, 345
 Dynamic culture surfaces, 666
 Dynamic hydrogels exploring supramolecular chemistry, 366–369
 hydrogels based on natural supramolecular self-assembly, 369
 reversible hydrogels based on supramolecular cross-linking of polymeric precursors, 366–369, 367f
 Dynamic light scattering (DLS), 453–454, 464
 Dynamic mechanical analysis (DMA), 93–94
 Dynamic patterning, 567
 Dynamic reciprocity, 702
 Dynamic SIMS, 63
 Dynamic stabilization devices, 1079
 Dystrophic pathologic calcification, 980
- E**
 e-beam. *See* Electron beam (e-beam)
 E-jet printing. *See* Electrohydrodynamic jet printing (E-jet printing)
 E-selectin, 739–740
 EBL. *See* Electron beam lithography (EBL)
 EBM. *See* Electron beam melting (EBM)
 ECA. *See* Equivalent circuit analysis (ECA)
 ECACC. *See* European Collection of Cell Cultures (ECACC)
 ECCE. *See* Extracapsular cataract extraction (ECCE)
 Eccentric cam, 727–728
 ECHs. *See* Electroconductive hydrogels (ECHs)
 ECM. *See* Extracellular matrix (ECM)
 ECMO. *See* Extracorporeal membrane oxygenation (ECMO)
 ECs. *See* Endothelial cells (ECs)
 ECVAM. *See* European Centre for Validation of Alternative Methods (ECVAM)
 ED. *See* Electron diffraction (ED)
 EDC. *See* 1-Ethyl-3-(3-dimethylaminopropyl) carbodiimide (EDC)
 eDNA. *See* Extracellular DNA (eDNA)
 EDOF IOL. *See* Extended depth of focus IOL (EDOF IOL)
 EDTA. *See* Ethylenediaminetetraacetic acid (EDTA)
 EDXA. *See* Energy-dispersive X-ray analysis (EDXA)
 EELS. *See* Electron energy loss spectroscopy (EELS)
 Effective intimate contact area, 1181
 Effector memory T cells, 764
 Efficacy, radiation-based techniques, 1432
- EFM. *See* Electrochemical force microscopy (EFM); Electrostatic force microscopy (EFM)
 EGDMA. *See* Ethylene glycol dimethyl acrylate (EGDMA)
 EGFR. *See* Epidermal growth factor receptor (EGFR)
 EHBP. *See* Ethane hydroxybisphosphonate (EHBP)
 EIAs. *See* Enzyme-linked immunoassays (EIAs)
 EILDV
 integrin-binding sequence, 704
 peptide sequence, 709–710
 EIS. *See* Electrochemical impedance spectroscopy (EIS)
 Elastic
 arteries, 1034
 behaviour, 43
 constants, 44
 deformation, 213
 energy, 46
 fibers, 403–404
 modulus, 234
 network resistance, 509
 Elastin, 363, 403–404, 703–704, 1292–1293
 Elastin-like peptides (ELPs), 194, 403–404
 Elastogenesis, 403
 Elastomer
 elastomeric polyesters, 1294
 filler, 112–113
 Electric field, 560
 Electrical double layer, 1095
 Electroanalytical methods (EMs), 257
 Electroceuticals, 1159–1160
 Electrochemical biosensors, 1269–1273
 amperometric biosensors, 1270–1271
 conductometric biosensors, 1271
 impedimetric biosensors, 1271–1272
 potentiometric biosensors, 1272–1273
 Electrochemical corrosion, 1093–1094
 Electrochemical force microscopy (EFM), 69t
 Electrochemical glucose biosensors, 1267
 Electrochemical impedance spectroscopy (EIS), 220, 224–226, 264, 1271
 impedance concepts, 225–226
 resistive and capacitive behavior, 224–225
 semiconducting oxide impedance, 226
 Electrochemical properties, of materials, 51
 Electroconductive hydrogels (ECHs), 1277
 Electroconductive nanoelements, 370
 Electroconductive polymers, 1279
 Electrode potential, 222
 Electrohydrodynamic jet printing (E-jet printing), 1354
 Electromagnetic forces, 37, 1181
 Electron beam (e-beam), 490–492, 559–560
 sterilization, 1433–1434
 Electron beam lithography (EBL), 559–560, 560f

- Electron beam melting (EBM), 232, 626–627
- Electron diffraction (ED), 465
- Electron energy loss spectroscopy (EELS), 978–979
- Electron microscopy (EM), 438, 1536.e5
- Electron spectroscopy for chemical analysis (ESCA), 59–62, 60f–62f, 61t, 87, 438, 493
- Electronic product radiation control (EPRC), 1472–1473
- Electrophoresis, 1252t
- Electrophoretic light scattering (ELS), 464
- Electropolymerization, 1269
- Electrospinning, 583–587, 585f, 596, 604, 607t, 1323t, 1324
- CES, 586–587
- coaxial, 586f
- coelectrospinning, 586
- of ECM proteins and natural materials, 410
- materials selection, 586
- modes of fiber collection, 585f
- representative polymers for, 582t
- and spinning parameter optimization, 584–586
- Electrospraying, 1323t, 1324
- Electrospun fibers, 596
- biotextile applications
- musculoskeletal tissue engineering, 595
- nanofibers for cardiovascular repair, 596
- nanofibers for local drug delivery, 596
- neural tissue engineering, 595–596
- wound dressing, 595
- Electrospun PCL scaffolds, 1363
- Electrostatic force, 467
- Electrostatic force microscopy (EFM), 69t
- Elimination rate, 1243
- ELISAs. *See* Enzyme-linked immunosorbent assays (ELISAs)
- ELPs. *See* Elastin-like peptides (ELPs)
- ELS. *See* Electrophoretic light scattering (ELS)
- Eluvia FP-PES, 132b–133b
- EM. *See* Electron microscopy (EM)
- EMA. *See* Ethyl methacrylate (EMA); European Medicines Agency (EMA)
- Embossing. *See* Imprinting
- Embryonic stem cell test (EST), 857
- Embryonic stem cells (ESCs), 670, 1291, 1514
- Employment agreements, 1497–1498
- EMs. *See* Electroanalytical methods (EMs)
- EMT. *See* Epithelial-to-mesenchymal transition (EMT)
- Emulsification, 436
- Emulsion(s), 1247, 1248t
- of emulsion, 455–456
- emulsion-coacervation method, 455–456
- emulsion-diffusion methods, 456
- emulsion-solvent evaporation, 454–455
- freeze drying, 608t
- Encapsulation, 697, 1275–1277, 1318–1319
- of biopharmaceuticals, 441
- efficiency, 438
- End-stage renal disease (ESRD), 1063
- Endocardium, 1036
- Endocytosed molecules, 694
- Endocytosis, 472–473
- Endogenous target molecule, 859b
- Endolysosomal entrapment, 473
- Endonucleases, 695
- Endopeptidases, 706
- Endoplasmic reticulum, 473
- Endosomal escape, 476–477
- Endosseous implants, 1120
- Endothelial barriers, 1253
- Endothelial cells (ECs), 528, 685, 723–725, 782–783, 1033–1034, 1036, 1373, 1393
- activation on vascular grafts, 528b
- Endothelial dysfunction, 1036
- Endothelial progenitor cells (EPC), 528
- Endothelium, 687, 1135
- Endotoxins, 1432
- Endotracheal intubation (ET intubation), 910, 1052
- Endovascular
- catheters, 1045
- coils, 1047
- stents, 918, 1039–1041
- grafts, 593–594, 1044–1045, 1044f
- Endovascular aneurysm repair (EVAR), 1044
- Energy-dispersive X-ray analysis (EDXA), 65, 978–979
- EnFET. *See* Enzyme field effect transistor (EnFET)
- Engineered MMP-sensitive peptide sequences, 710
- Engineered peptide fibers, 710–712
- Engineered receptor-targeting peptide sequences, 708–710
- Engineered skin allografts, 1173
- Engineering ethics, 1509
- Engineering strain. *See* Nominal strain
- Engineering stress. *See* Nominal stress
- Enhanced permeability and retention effect (EPR effect), 453, 469–471, 1239, 1254
- Enteric nervous system (ENS), 1405
- Enterococcus faecalis*, 833
- Entrapment, 1275
- Entropic repulsion, 509
- Environmental SEM (ESEM), 65
- Environmental stress cracking (ESC), 931
- Enzymatic degradation, 176–177
- Enzymatic dissociation, 662
- Enzymatic electrochemical glucose biosensors, 1267–1268
- Enzyme field effect transistor (EnFET), 1272
- Enzyme-based biosensors, 1268
- classic biosensor system, 1268–1269
- enzymatic glucose biosensors, 1269–1274, 1270f
- electrochemical biosensors, 1269–1273
- optical biosensors, 1273
- piezoelectric biosensors, 1273–1274
- thermal biosensors, 1274
- integrating responsive polymers
- with enzymes, 1278–1279
- with transducers, 1279
- responsive polymers in enzymatic biosensors, 1274–1278
- systems integration, 1279–1281
- Enzyme-linked immunoassays (EIAs), 784
- Enzyme-linked immunosorbent assays (ELISAs), 439, 859, 865, 1273–1274
- Enzyme(s), 485, 1269
- inhibition, 1253t
- thermistors, 1274
- EO. *See* Ethylene oxide (EO)
- EOG. *See* Ethylene oxide gas (EOG)
- Eosin Y spirit-soluble (EYs), 1188
- Eosinophils, 753
- EPA MLB SOP MB-19, 834–835
- EPA MLB SOP MB-20, 834–835
- EPC. *See* Endothelial progenitor cells (EPC)
- EpCAM. *See* Epithelial cell adhesion molecule (EpCAM)
- EPI-RET3 retinal implant system, 1147
- Epicardium, 1036
- EpiCel, 595, 1171t, 1174
- Epidermal growth factor receptor (EGFR), 706
- Epiretinal devices, 1146–1147
- Argus II, 1146–1147
- EPI-RET3 retinal implant system, 1147
- IRIS II, 1147, 1148f
- Epithelial barriers, 1250–1253
- mucosal DDSs, 1251–1252
- oral DDSs, 1252–1253
- parenteral administration, 1250–1251
- transdermal DDSs, 1251
- Epithelial cell adhesion molecule (EpCAM), 479
- Epithelial cells, 748
- Epithelial-to-mesenchymal transition (EMT), 1218
- Epithelioid macrophages, 697–698
- Epithelium, 683, 1250
- Epitope, 762
- EPR effect. *See* Enhanced permeability and retention effect (EPR effect)
- EPRC. *See* Electronic product radiation control (EPRC)
- EPS. *See* Extracellular polymeric substances (EPS)
- ePTFE. *See* Expanded polytetrafluoroethylene (ePTFE)
- Equivalent circuit analysis (ECA), 1271–1272
- Equivalent circuit models, 1154–1155
- ERK1/2. *See* Extracellular signal-regulated kinase (ERK1/2)

- Erosion, 167–168, 168f
- Erythrocyte(s), 801
composure, 465
- ESC. *See* Environmental stress cracking (ESC)
- ESCA. *See* Electron spectroscopy for chemical analysis (ESCA)
- Escherichia coli*, 340–341, 404, 782–783, 827
- ESCs. *See* Embryonic stem cells (ESCs)
- ESEM. *See* Environmental SEM (ESEM)
- ESRD. *See* End-stage renal disease (ESRD)
- EST. *See* Embryonic stem cell test (EST)
- Esters, 1317
- ET intubation. *See* Endotracheal intubation (ET intubation)
- Etchant(s), 1181
chemistry of, 1185
- Etching, 262
with masks, 562
- Ethane hydroxybisphosphonate (EHBP), 983–984
- Ethical issues, in biomaterials and medical devices, 1514–1516
animal testing, 1511–1512
conflict of interests, 1513–1514
cost and access to medical products, 1516
gene editing, 1515–1516
human testing, 1512–1513
research integrity, 1513
safety, 1510–1511
selected approaches to ethical reasoning, 1509–1510
justice approach, 1510
rights approach, 1510
utilitarian approach, 1510
virtue approach, 1510
in stem cell research, 1514–1515
- Ethyl methacrylate (EMA), 646–647, 653
preadsorption with purified adhesion proteins, effects of, 646–647
- 1-Ethyl-3-(3-dimethylaminopropyl) carbodiimide (EDC), 379, 525, 1404, 1356
- Ethylene glycol dimethyl acrylate (EGDMA), 1269, 1322
- Ethylene oxide (EO), 1192, 1432, 1453
sterilization, 1435–1438, 1437f
- Ethylene oxide gas (EOG), 183
- Ethylene-vinyl acetate (EVAc), 595, 983–984
- Ethylenediaminetetraacetic acid (EDTA), 662, 777–779
- EtO. *See* Ethylene oxide (EO)
- EUDAMED. *See* European Database on Medical Devices (EUDAMED)
- Eudragit, 1206
- European Centre for Validation of Alternative Methods (ECVAM), 857, 864
- European Collection of Cell Cultures (ECACC), 663
- European Database on Medical Devices (EUDAMED), 1490
- European Medicines Agency (EMA), 433
- European Pharmacopoeia, 116
- European Society for Biomaterials, 18–19
- EVA. *See* Ethylene-vinyl acetate (EVAc)
- EVAc. *See* Ethylene-vinyl acetate (EVAc)
- Evans diagram, 224f
- EVAR. *See* Endovascular aneurysm repair (EVAR)
- Evonik. *See* Eudragit
- Ex vivo-produced oral mucosa equivalents (EVPOMEs), 1129
- EXAFS. *See* Extended X-ray absorption fine structure (EXAFS)
- Exercise-stimulated bone remodeling, 728
- Exogenous chemicals, 851
- Exopeptidases, 706
- Expanded polytetrafluoroethylene (ePTFE), 125, 130–131, 521, 591, 973, 1025, 1492b–1493b
hernial mesh, 131b
vascular graft and bizarre and costly patent dispute, 134b
vascular implants, 131
- Expansible thermoplastic polymers, 443–444
- Explant culture, 662
- Extended depth of focus IOL (EDOF IOL), 1142
- Extended X-ray absorption fine structure (EXAFS), 70t
- External irradiation, 442–443
- External loads, 42–43, 42f
- Extracapsular cataract extraction (ECCE), 1141
- Extracellular DNA (eDNA), 823
- Extracellular matrix (ECM), 297, 361, 377, 389, 401, 467, 528, 541–542, 604, 631, 643–644, 661, 683, 685–686, 701, 703f, 717, 738, 846, 1034, 1127, 1217, 1293, 1317, 1351, 1374–1375, 1389, 1536.e1
alginates, 406
chitosan, 406–407
collagens, 402–403
components, 687f
composition, 702f
and molecular arrangement, 1352
elastin, elastic fibers, and elastin-like peptides, 403–404
engineered MMP-sensitive peptide sequences for, 710
engineered peptide fibers, 710–712
extracellular matrix-based biomaterials, 361–364, 362f
blood derivatives as source of bio-structurally materials, 364–366
GAGs, 363–364
multifunctional biomaterials based on DNA, 366
proteins, 362–363
- fibrin, 407
functions, 702b
human integrins and known ECM targets, 706t
manufacturing approaches utilizing natural materials
electrospinning, 410
human recombinant ECM protein production, 407–408
protein with polyhistidine tag, 409f
purification of recombinant ECM proteins, 408–409
3D bioprinting, 409–410
PGs and GAGs, 404–406
physicochemical properties, 1219
powder and injectable decellularized ECM therapies, 387–388
properties, 701–703
remodeling and proteolysis, 705–706
- Extracellular polymeric substances (EPS), 823, 825
- Extracellular signal-regulated kinase (ERK1/2), 1344
- Extracorporeal artificial organs
renal replacement therapies and therapeutic apheresis, 1062–1071
respiratory support, 1051–1062
alternative extracorporeal gas exchange devices, 1053–1055
ambulatory ECMO, 1036
artificial lung fiber, 1060f
coagulation cascade, 1064f
commercial oxygenator coating materials, 1057t
microchannel artificial lung, 1063f
ModELAS pump-lung, 1060f
natural organ *vs.* artificial organ anticoagulation, 1039
nitric oxide surface flux, 1061–1062
oxygenator biocompatibility challenges, 1055–1056
protein adsorption levels, 1065f
pulmonary disease, 1051–1052
surface coatings, 1057–1061
- Extracorporeal equipment, 118, 118f
- Extracorporeal hemofiltration, 1067–1068
- Extracorporeal membrane oxygenation (ECMO), 1016, 1052, 1053f
- Extravasation, 467
- Extrinsic organisms colonizing biomaterial products, 844
- Extrusion printing, 1296, 1324
- Exudation, 739–740
- Eye
anatomy, 1135–1136, 1136f, 1144f
dimensions of globe and ocular structures, 1136t
eye-related conditions and statistics, 1136–1137
optics, 1140
EYss. *See* Eosin Y spirit-soluble (EYss)

- F**
- F-actin, 1337–1338
- Fabric vascular implants, 130
- Fabrication, 1287
- of complex implants, 633–634
 - methods
 - for biomimetic nanoscale texture, 604–610
 - for micro-and macroscale architectural features, 610–612
 - for porous synthetic polymer scaffolds, 608t
 - recent efforts in, 231–233
- Face-centered cubic structure (FCC structure), 208, 259
- Factor Xa (FXa), 1056
- Failure, 45
- FAK. *See* Focal adhesion kinase (FAK)
- Far-sightedness. *See* Hyperopia
- Faraday's constant, 221
- Fast ion conductors, 1277
- Fast polymerizing monomers, 144–145, 145f
- Fast-cure elastomers, 115–117
- Fatigue, 46
- strength, 46, 216
- FBGCs. *See* Foreign body giant cells (FBGCs)
- FBR. *See* Body reaction (FBR); Foreign body reaction (FBR)
- FCC structure. *See* Face-centered cubic structure (FCC structure)
- FD & C. *See* Food, Drug and Cosmetic (FD & C)
- FDA. *See* US Food and Drug Administration (FDA)
- FDM. *See* Fused deposition modeling (FDM)
- FDP. *See* Fibrinogen digestion products (FDP)
- Femoral head prostheses/short-stem prostheses, 1082–1083
- FEP. *See* Fluorinated ethylene propylene (FEP)
- Fernström ball implants, 1084–1085, 1084f
- Ferrocene-terminated hyperbranched polyurethane (HPU-Fc), 1277
- FGF. *See* Fibroblast growth factor (FGF)
- FIB lithography. *See* Focused ion beam lithography (FIB lithography)
- Fiber
- arrangement, 418
 - bonding, 608t
 - critical compressive strength, 423
 - equilibrium equation, 422
 - fiber-based scaffolds, 1296
 - fiber-forming polymers
 - characteristics, 578–579
 - natural and synthetic polymers for biotextile production, 579
 - permanent and resorbable, 580t–581t
 - fiber-reinforced composites, 415
 - fiber-stacking pattern, 418
 - fiber-matrix interfacial stresses, 423
 - reinforcement in bone graft cement, 594
- Fibril-forming collagens, 402
- Fibrillar collagens, 402
- fibrillar Coll, 402
- Fibrillar gels, 365
- Fibrin, 407, 1292–1293
- gels, 1375
 - polymerization, 364–365, 886
 - sealants, 1187
 - advantages and applications, 1187
 - formulation, presentation, and setting processes, 1187
- Fibrinogen, 407, 643
- adsorption, 652–655, 656f
- Fibrinogen digestion products (FDP), 806–807
- Fibrinolytic agents, immobilization of, 527–528
- Fibrinolytic enzymes, 885
- Fibrinolytic sequence, 805–806, 806f
- Fibroblast growth factor (FGF), 364–365.
- See also* Growth factors (GFs).
 - FGF-1, 1393
 - FGF-2, 705, 738–739
- Fibroblasts, 740–741, 1304
- Fibronectin, 8, 406, 643, 648–649, 656, 704–705, 704f
- preadsorption, 646
- Fibrosis, 697–699
- Fibrotic tissue encapsulation, 859
- Fibrous composites
- compressive properties
 - first-principles-based compressive microbuckling model, 420–422
 - material properties of CF/PEEK and CF/PSF composite systems, 422t
 - Rosen's microbuckling model and contradictions, 420
 - selected results, 422–424
 - tensile properties, 419–420
- Fibrous proteins, 1389
- Fibrous scaffolds, 1342
- Figures-of-merit (FOMs), 553
- Film
- chemistries, 492
 - formation, 454–455
- Filopodia, 670–671
- Finishing in biotextiles, 590–591
- First-order half-life, 1243
- First-pass effects, 1253
- First-principles-based compressive microbuckling model, 420–422
- Flavor compounds, 443–444
- Flexercell Strain Units, 727–728
- Flexible glove biosensor, 1280, 1281f
- “Flickering cluster” model of water structure, 78–79
- Floppy mitral valve, 1000
- Flory-Huggins theory, 155–156
- Fluid Vision IOL, 1142
- FluMist, 1206
- Fluorapatite, 1125
- Fluorescence probes, 1277–1278
- Fluorescent ND, 336
- Fluorinated biomaterials, 125. *See also* Carbon biomaterials.
- biomedical applications, 129–135, 130t
 - acrylated perfluoroalkyl silicones, 134
 - antifouling coatings for intraocular lenses, 134
 - arteriovenous ePTFE grafts for dialysis access, 131
 - drug-eluting stent, 132f
 - ePTFE and teflon soft tissue repair meshes, 130–131
 - eye as experimental vitreous substitutes, 134
 - fluorinated material biological response, 130
 - fluoropolymer coatings on cardiovascular stents, 132b–133b
 - guiding catheters, 131–133
 - ligament replacement, 134–135
 - money joint, 135b
 - multilumen catheters, 131
 - perfluorocarbon liquids and emulsions as oxygen-carrying blood, 133–134
 - PTFE mesh and fabric vascular implants, 130
 - sutures, 135
 - distinguishing fluoropolymers, 126–129
 - FEP, 127–128
 - fluoropolymer melt processing, 128
 - gore-tex and generic equivalents, 128–129, 128f
 - John Charnley and replacement hip bearing, 127b
 - perfluorocarbons *vs.* analogous hydrocarbons, 129t
 - PTFE, 126–127
 - PVDF, 128
 - surfaces modified by fluorination treatments, 129
 - fluoropolymer chemical and physical properties, 125–126
- Fluorinated ethylene propylene (FEP), 127–128
- Fluorinated polycations, 475
- Fluorinated polymers, 1138–1139
- Fluorination, 522
- Fluorine (F), 125
- Fluoroalkyl groups, 522
- Fluoropolymer-based peripheral stents (FP-PESs), 132b–133b
- Fluoropolymer(s), 125–126, 130–131. *See also* Copolymers.
- distinguishing, 126–129
 - melt processing, 128
- FM-AFM. *See* Force modulation-atomic force microscopy (FM-AFM)

- fMLP. *See* *N*-Formylmethionyl-leucyl-phenylalanine (fMLP)
- FNIII₇₋₁₀, 709–710
- Focal adhesion kinase (FAK), 706, 718, 722
- Focal adhesions, 717–718, 1336–1337
maturation and stress fiber formation in mechanotransduction, 1337–1338
- Focal contacts, 541–542, 664
- Focused ion beam lithography (FIB lithography), 560
- Foldable IOLs, 1141
- FOMs. *See* Figures-of-merit (FOMs)
- Food, Drug and Cosmetic (FD & C), 1463
- Force modulation-atomic force microscopy (FM-AFM), 69t
- Foreign body giant cells (FBGCs), 740–741, 752, 843–844, 927–928
- Foreign body reaction (FBR), 15–16, 699, 827, 845, 1241–1242
- Foreign body response, 735
- Foreign body tumorigenesis. *See also* Tumorigenesis.
pathobiology of, 817–819
steps in implant-associated tumorigenesis, 818t
- Formaldehyde, 1536.e1
- N*-Formylmethionyl-leucyl-phenylalanine (fMLP), 738
- Fourier transform infrared spectroscopy (FTIR spectroscopy), 65, 175b, 311, 438, 1327t
- FP-PESs. *See* Fluoropolymer-based peripheral stents (FP-PESs)
- Fracture
fixation devices, 1079
toughness, 46
- Free radical polymerization, 1322
- Freedom to operate, 1501–1503
- Freeze-drying, 1323t, 1325, 1355
- Fretting corrosion, 1097–1098, 1098f
- D-Fructose, 612
- Frustrated phagocytosis, 699–700, 845
- FTIR spectroscopy. *See* Fourier transform infrared spectroscopy (FTIR spectroscopy)
- Full-thickness burns, 1169
- Fullerene(s), 330, 336
films, 349
fullerene-C60, 338
- Fumed silica, 113
- Fungi, 844
- Furanones, 834
- Fused deposition modeling (FDM), 626
- Fusion with endosomal membranes, 477
- FXa. *See* Factor Xa (FXa)
- G**
- G-actin. *See* Globular actin (G-actin)
- GA. *See* Glutaraldehyde (GA)
- GAGs. *See* Glycosaminoglycans (GAGs)
- Galectin-3, 742–743
- Galvanic corrosion, 254. *See also* Corrosion.
- Galyfilcon A, 1140
- Gamma radiation sources, 490–491
- Gamma sterilization, 1432–1433
bulk ethylene oxide sterilization machine, 1437f
sterilization methods, 1436t–1437t
- Gardenia jasminoides*, 1357
- Gas
discharge depositions, 492
foaming, 608t, 1323t, 1326
plasma methods, 1438–1439
- Gas/liquid chromatography (GC/LC), 1326, 1327t
- Gastric epithelial cells, 687–688
- Gastrointestinal (GI)
enzymes, 1249
tissue engineering, 1404
anatomy and physiology, 1405
challenges and future goals, 1407
design criteria for, 1406
gastrointestinal disorders and need, 1405
gastrointestinal soft tissue-engineering strategies, 1406, 1407
tract, 404
organs, 1392f
segments, 1252–1253, 1254t
- GBH method. *See* Graphite–benzalkonium–heparin method (GBH method)
- GBMs. *See* Graphene-based materials (GBMs)
- GC. *See* Glassy carbon (GC)
- GC/LC. *See* Gas/liquid chromatography (GC/LC)
- GCP-2, 756
- GDNF. *See* Glial cell-derived neurotrophic factor (GDNF)
- Gel adhesives, 115
- Gel permeation chromatography (GPC), 1326, 1327t
- Gel-cast foaming, 300
- Gelatin, 31, 403, 1292–1293, 1322, 1361
with methacryloyl residues, 362–363
- Gelatin methacrylate (GelMA), 345–346
- Gelation, 1355
- Gelfoam, 403
- GelMA. *See* Gelatin methacrylate (GelMA); Gelatin—with methacryloyl residues
- GEM-21S, 1130
- Gene
condensation, 475
editing, 1303–1304, 1515–1516
expression, 691
profiling, 1536.e1
replacement therapeutics, 1515–1516
therapy, 472, 477, 1515
- Generalized Hooke's law, 46–47
- Generations, 458
- Generic equivalents, 128–129, 128f
- Genexol, 468
- Genipa americana*, 1357
- Genipin, 1356–1357
- Genome editing. *See* Gene editing
- Genotoxicity, 872
and carcinogenicity, 466
in vitro tests for, 854–858, 855t, 857b
- Genotype, 691
- Gentamicin, 829–830
- Geobacillus stearothermophilus*, 1440
- Geometric nonlinearity, 43
- Germinal centers, 761
- GFOGER
hexapeptide sequence, 709
polypeptide sequence, 703–704
- GFs. *See* Growth factors (GFs)
- Gibbs free energy, 825
- GIC. *See* Glass-ionomer cements (GIC)
- GLA. *See* Glucopyranosyl lipid adjuvant (GLA)
- GLA-SE. *See* Glucopyranosyl lipid adjuvant in squalene emulsion (GLA-SE)
- Glass(es), 289–301, 663–664, 964
bioactive, 297–298
composites and putties for bone repair, 299
porous, 299–300
in toothpaste, 300–301
wound healing, 300
bioglass, 297–298
for cancer therapy, 301
45S5 Glass, 32
glass-ceramics, 289, 301, 965
granules, 298–299
ionomers, 1183–1184
transition temperatures, 120b
- GlassBone, 299
- Glass-ionomer cements (GIC), 1183–1184
- Glassy carbon (GC), 332–333
- Glassy state of polymers, 90
- Glaucoma, 1137
drainage devices, 1143
- Glaucos iStent Series, 1145
- Glial cell-derived neurotrophic factor (GDNF), 595–596, 1322–1323
- 3-Glycidopropyltrimethoxysilane (GPTMS), 966–967
- Global premarket assessment methods, 1463–1465
- Globular actin (G-actin), 1337–1338
- Glomerulonephritis (GN), 785–786
- Glow discharge
biomedical applications of glow discharge plasma-induced surface modification processes, 492t
depositions, 492
- GLP. *See* Good Laboratory Practices (GLP)
- Glucocorticosteroids, 433
- Glucopyranosyl lipid adjuvant (GLA), 1206
- Glucopyranosyl lipid adjuvant in squalene emulsion (GLA-SE), 1206
- Glucose, 1267
detection, 479
- Glucose oxidase (GOx), 479, 1267–1268

- Glutaraldehyde (GA), 588, 982–983, 1275, 1356
 glutaraldehyde-treated heart valves, 379
 neutralization, 985
- Glycocalyx, 725, 726f
- Glycoprotein Ib (GP Ib), 802
- P-Glycoprotein, 468
- Glycosaminoglycans (GAGs), 361–364, 401–402, 404–406, 705, 1322, 1358, 1389
- Glycosylation, 408
- GM-CSF. *See* Granulocyte-macrophage colony-stimulating factor (GM-CSF)
- GMP. *See* Good manufacturing practices (GMP)
- GN. *See* Glomerulonephritis (GN)
- GNP. *See* Graphene nanoplatelets (GNP)
- GNPs. *See* Gold nanoparticles (GNPs)
- GNR. *See* Graphene nanoribbons (GNR)
- GO. *See* Graphene oxide (GO)
- Gold, 22–23
- Gold nanoparticles (GNPs), 460
- Golgi, 473
- Good Laboratory Practices (GLP), 900, 1427
- Good manufacturing practices (GMP), 116, 1448, 1463
- Gore-tex, 128–129, 128f
- Gossypibomas, 817
- GOx. *See* Glucose oxidase (GOx)
- GP Ib. *See* Glycoprotein Ib (GP Ib)
- GPC. *See* Gel permeation chromatography (GPC)
- GPIb-IX, 648
- GPQG peptide sequence, 710
- GPTMS. *See*
 3-Glicidopropyltrimethoxysilane (GPTMS)
- GQD. *See* Graphene quantum dots (GQD)
- “Graft-from-surface” approach, 511
- “Graft-to-surface” approach, 511
- GraftJacket, 386
- Granulation tissue, 697, 699, 740
- Granules, 294, 802
- Granulocyte-macrophage colony-stimulating factor (GM-CSF), 754
- Granuloma, 697
- Granulomatous inflammation, 697
- Graphene (G), 330, 331f, 461
 top-down and bottom-up methods for synthesizing, 332f
- Graphene nanoplatelets (GNP), 330–331
- Graphene nanoribbons (GNR), 332
- Graphene oxide (GO), 330–331, 461, 1272–1273
- Graphene quantum dots (GQD), 332
 near-infrared, 339f
- Graphene-based materials (GBMs), 330–332, 330f–331f, 335, 343f, 346, 348
- Graphite (Gt), 330
- Graphite–benzalkonium–heparin method (GBH method), 515, 524
- Gravity, 37
- GRKKR polypeptide sequence, 704, 709–710
- Grooves, 610
- Grouting, 1183
- Growth factors (GFs), 361–362, 698–699, 738–739, 1320
 sequestering proteins and motifs, 705
- GRO α , 756
- GTPases. *See* Guanosine triphosphatases (GTPases)
- Guanosine triphosphatases (GTPases), 1338
- Guiding catheters, 131–133
- ## H
- [³H]-thymidine, 1111
- HA. *See* Hyaluronic acid (HA);
 Hydroxyapatite (HA)
- Hafnium (Hf), 230–231
- Hall–Petch relationship, 214
- Hanging drop method, 1224–1225
- HAPEX, 425
- Haptic design, 1141
- Haptotaxis, 722
- Hard contact lenses, 1138–1139
- Hard segment, 103
- “Hard tissue replacement” camp, 13–14
- Hard-tissue adhesives, 1182–1186
 acid-etch bonding to enamel, 1184
 aging and stability of bonded interface, 1186
 autopolymerizing PMMA bone cement, 1182–1184
 chemistry of etchants, primers, and bonding agents, 1185
 hybrid-layer creation via three-stage approach, 1185
- “Hard” protein, 654–655
- Hardness, 45–46
- Harvested cells, 662
- hASC. *See* Human adipose-derived stem cell (hASC)
- HCA. *See* Hydroxycarbonate apatite (HCA)
- HCP. *See* Hexagonal closed-packed (HCP)
- HCR. *See* High consistency rubber (HCR)
- HDI. *See* Hexamethylene diisocyanate (HDI)
- HDL. *See* High-density lipoprotein (HDL)
- HDPE. *See* High-density polyethylene (HDPE)
- Healing, 15–16
- Heart, applications of tissue engineering in, 1299
- Heart valve, 14, 29, 1373–1375
 calcification, 982–983
 GA, 982–983
 role of cells, 982
 role of collagen and elastin, 982
 role of immunologic factors, 983
 function, 1000–1010
 prostheses, 10, 10f
 replacement, 902–903
- HeartWare Ventricular Assist Device (HVAD), 1021–1023, 1021f–1022f
- HeLa cell line, 662–663
- Helical polymer chains, 126–127
- Helical PTFE chains, 126–127
- Helicard. *See* MDA-5
- Helper lipids, 475
- Helper T cells (Th cells), 757, 760–761, 1210
 Th1 cells, 760–761
 Th2 cells, 744, 761
 Th17 cells, 761
- HEMA. *See* Hydroxyethyl methacrylate (HEMA)
- Hematoma*, 1037–1038
- Hematopoietic tissues, 683
- Hematoxylin, 1536.e3
- Hemocompatibility, 873
 of NPs, 465
- Hemodialysis, 1055f, 1065–1066
- Hemoglobin, 653–654
- Hemoperfusion, 1068
- Hemosiderin-like granules, 1099–1100
- Hemostasis, 685, 1033
- Hemostatic mechanism, 801
- Hemostats, 595
- Heparan sulfate (HS), 404
- Heparin, 404–405, 522, 526, 1056, 1244, 1358
 in blood-contacting medical device applications, 862b–864b
 coatings, 1057
 covalently bound, 525–526
 immobilization of, 539
 ionically bound, 523–525
 thrombin inhibition without, 526–527
- Heparin-like materials, 522
- Heparinization, 522–526
 antithrombin III-binding pentasaccharide of heparin, 524f
 covalently bound heparin, 525–526
 ionically bound heparin and controlled-release systems, 523–525
- Hepatocyte GF receptor (HGF receptor), 366
- Hepatocytes, 669–670
- Hermetically sealed package, 1195
- Hernial mesh, 131b
- hESC. *See* Human embryonic stem cells (hESC)
- Heterochain polymers, 95
- Hexagonal closed-packed (HCP), 207, 259
- Hexagonally bonded carbon
 CF, 332
 CNF, 332
 CNT, 330, 330f
 fullerenes, 330
 GNR, 332
 GQD, 332
 graphene-based materials, 330–332
 graphite, 330

- Hexamethylene diisocyanate (HDI), 103–104
- hGDF-5. *See* Human growth differentiation factor 5 (hGDF-5)
- HGF receptor. *See* Hepatocyte GF receptor (HGF receptor)
- High consistency rubber (HCR), 113–115
- High-density lipoprotein (HDL), 658
- High-density polyethylene (HDPE), 129, 425
- High-energy plasma treatments, 494
- High-field magnetic resonance imaging technology, 282
- High-glycolide copolymeric sutures, 1194
- High-molecular-weight group box 1 (HMGB1), 742–743
- High-molecular-weight kininogen (HMWK), 809
- High-performance liquid chromatography (HPLC), 439, 1326
- High-pressure homogenization, 459–460
- High-resolution electron energy loss spectroscopy (HREELS), 70t
- High-speed AFM imaging, 68
- High-temperature plasma treatments, 494
- High-throughput screening, 670
of surface topography, 672
- HIP. *See* Hot isostatic pressing (HIP)
- Hip joint, 14
- Hip prostheses, 24–25, 25f
- hiPSCs. *See* Human-induced pluripotent stem cells (hiPSCs)
- Hirudin, 810
- HIV-1. *See* Human immunodeficiency virus type 1 (HIV-1)
- HIV-Tat, 477
- hK. *See* Human epidermal keratinocytes (hK)
- HLB. *See* Hydrophilic–lipophilic balance (HLB)
- HMGB1. *See* High-molecular-weight group box 1 (HMGB1)
- hMSCs. *See* Human mesenchymal stem cells (hMSCs)
- HMWK. *See* High-molecular-weight kininogen (HMWK)
- Hofmeister effect, 79
- Hollow fiber reactor, 1297
- Hollow organs. *See* Tubular organs
- Homeostasis, 693
- Homograft, 974–975
- Homopolymer hydrogels*, 153
- Hooke's law, 44
- Hormonal hyperplasia, 694
- Horseradish peroxidase (HRP), 155
- Host response
to implanted biomaterials, 739–741
strategies to control, 744–745
- Hot isostatic pressing (HIP), 207, 231, 260, 1087
- HPLC. *See* High-performance liquid chromatography (HPLC)
- HPU-Fc. *See* Ferrocene-terminated hyperbranched polyurethane (HPU-Fc)
- HREELS. *See* High-resolution electron energy loss spectroscopy (HREELS)
- HRP. *See* Horseradish peroxidase (HRP)
- HS. *See* Heparan sulfate (HS)
- Hufnagel heart valve, 29, 29f
- Human adipose-derived stem cell (hASC), 1393
- Human amnio-chorionic membrane, 1171t
- Human embryonic stem cells (hESC), 819
- Human epidermal keratinocytes (hK), 1172
- Human femoral head, 49
- Human growth differentiation factor 5 (hGDF-5), 1357–1358
- Human immunodeficiency virus type 1 (HIV-1), 477, 1432
- Human leukocyte antigens, 755
- Human mesenchymal stem cells (hMSCs), 368, 667
- Human recombinant ECM protein production, 407–408
- Human tumors, implants with, 814–817
- Human-based tissue, 1435
- Human-induced pluripotent stem cells (hiPSCs), 819
- Hume–Rothery rules, 209
- Humoral immunity, 757, 760, 1202–1206
biomaterial design for enhancing humoral response, 1205–1206
- HVAD. *See* HeartWare Ventricular Assist Device (HVAD)
- Hyaluronic acid (HA), 364, 404–406, 529–530, 672–673, 705, 1206–1207, 1220t–1221t, 1222, 1293, 1322, 1360, 1392, 1395
- Hyaluronidase, 471
- Hybrid-layer creation via three-stage approach, 1185
- Hydration, 509
- Hydration degree, 631
- Hydrocarbon elastomers, 936
- Hydrocephalus drainage shunt, 14
- Hydrogels, 8, 31, 31f, 81, 153, 415–416, 441, 517–518, 543, 631, 672–673, 708, 1318–1319
based on natural supramolecular self-assembly, 369
biomedical, 157–159
acrylic hydrogels, 157–158
degradable hydrogels, 158–159
PEG, 158
PVA, 158
self-assembled hydrogel structures, 159
star polymer and dendrimer hydrogels, 159
biomedical applications, 161–163
blood-contacting hydrogels, 161
contact lenses, 161
drug delivery from hydrogels, 161–162
miscellaneous biomedical applications, 163
targeted drug delivery from hydrogels, 162
temperature dependence of light transmission, 162f
tissue engineering scaffolds, 162–163
classification and structures, 153–154, 154f
determination of structural characteristics, 157
fiber spinning, 587, 587f
materials, 1138
nanofibers, 587
scaffolds, 1296, 1355
sealants, 1188
smart polymers, 197–198, 198f
smart” or intelligent” stimuli-responsive, 159–161
affinity hydrogels, 161
pH-responsive complexation, 160
pH-sensitive hydrogels, 159–160
temperature-sensitive hydrogels, 160–161
swelling behavior, 155–157, 156f
synthesis of, 154–155, 154f–155f
- Hydrogen
bonding, 467, 510–511
interactions, 38–39, 39f
peroxide, 1438
- Hydrolysis, 94–95, 920–925, 921f
groups highly stable to, 921f
of hydrophobic polymers, 918
- Hydrolytic
degradation, 174–175
bulk degradation, 175
examples of photodegradable groups, 176f
surface erosion, 174–175
drugs, 456, 459
materials based on PEG, 833
monomers, 1188
surfaces, 80
- Hydrolytic biodegradation, 920–926
host-induced, 922
structures of, 920–922
- Hydrophilicity, 172
of polymer materials, 94
- Hydrophilic–lipophilic balance (HLB), 453–454
- Hydrophobic
effect, 81
elastomer, 116
fullerenes, 341
interaction, 467
resins, 147
SAMs, 656
surfaces, 80
- Hydrophobic poly(L-amino acid), 453–454
- Hydrophobicity, 172
- Hydrous ferrous oxide (FeO • nH₂O), 274

- Hydroxyapatite (HA), 32, 236, 291, 307, 312t, 415–416, 602, 1125, 1183, 1201, 1322–1323, 1475
bone graft substitute, 310t
ceramics
 clinical use, 312–313
 physicochemical characterization, 310–311
 specific infrared vibrations, 311t
 in vitro and in vivo characterization, 311–312
crystal structure, 308f
formation
 alternative materials, 986–987
 bisphosphonates, 984
 calcium diffusion inhibitor, 985
 glutaraldehyde modification, 986
 inhibitors, 984
 removal/modification of calcifiable material, 985–986
 trivalent metal ions, 984–985
Hydroxyapatite (HAp). *See* Hydroxyapatite (HA)
Hydroxycarbonate apatite (HCA), 297, 956
Hydroxyethyl methacrylate (HEMA), 141–142, 646–647, 653, 1185
 preadsorption with purified adhesion proteins, effects of, 646–647
Hydroxyl ions (OH⁻ ions), 274
Hydroxyl-terminated PEG surfaces, 509–510
N-Hydroxysuccinimide (NHS), 194, 1356
 acrylate, 194
N-Hydroxysulfosuccinimide (Sulfo-NHS), 379
4-Hydroxytamoxifen, 333
Hydrus microstent, 1145
Hyperelastic materials, 44
Hyperopia, 1136
Hyperplasia, 693–694
Hypersensitivity, 796–797, 1109–1112
Hypertrophy, 693–694
Hypochlorous acid (HOCl), 929
Hypoxia, 694–695
 hypoxia-inducible transcription factors, 280
HyStem, 1220t–1221t
Hysteresis, 44
- I**
I-CAM, 1225
IABP. *See* Intraaortic balloon pump (IABP)
IACUC. *See* Institutional Animal Care and Use Committee (IACUC)
IAGQ peptide sequence, 710
IBS. *See* International Biomaterials Symposia (IBS)
ICAM-1. *See* Intracellular adhesion molecule-1 (ICAM-1)
ICATM. *See* International Cooperation on Alternative Test Methods (ICATM)
ICC. *See* Interstitial cells of Cajal (ICC)
ICDD. *See* International Center for Diffraction Data (ICDD)
ICDs. *See* Implantable cardioverter-defibrillators (ICDs)
ICIE16 glass, 300
ICs. *See* Immune complexes (ICs)
IDAPS integrin-binding sequence, 704
IDE. *See* Investigational device exemption (IDE)
IDEs. *See* Interdigitated microelectrodes (IMEs)
IF-AFM. *See* Intermittent force mode-atomic force microscopy (IF-AFM)
IFN- γ . *See* Interferon- γ (IFN- γ)
IFP. *See* Interstitial fluid pressure (IFP)
IGF-1. *See* Insulin growth factor-1 (IGF-1)
Igs, 762
Igs. *See* Immunoglobulins (Igs)
IKVAV sequence, 709–712
iLA. *See* Interventional lung assist (iLA)
ILC. *See* International Liaison Committee of Societies for Biomaterials (ILC)
ILCs. *See* Innate lymphoid cells (ILCs)
ILCSs. *See* Interlaboratory comparison studies (ILCSs)
ILD. *See* Interstitial lung disease (ILD)
IMAC. *See* Immobilized metal affinity chromatography (IMAC)
Imaging
 carbon biomaterials in, 336–337
 imaging-guided surgery, 482
 SIMS, 63
 thrombotic deposition, 882b
Imatinib, 470–471
IMEs. *See* Interdigitated microelectrodes (IMEs)
Immobilization, 543
 of antiplatelet agents, 527
 of fibrinolytic agents, 527–528
 of heparin, 539
 methods, 542–549
 of nonfouling polymers, 511
Immobilized biomolecules, 540
 application, 540t
Immobilized cells, 1269
 ligands and cells, 541–542
Immobilized enzymes
 advantages and disadvantages of, 541t
 in therapeutic bioreactors, 541t
Immobilized metal affinity chromatography (IMAC), 408–409
Immune
 adjuvants, 442
 cells, 743–744
 regulation and tolerance, 766–768
 response, 735, 874–875
 biofilms and, 824
 to pathogens, 765–766
 representative tests for evaluation, 874t
 system, 747
 tolerance, 766
 toxicity of implanted materials, 798b
Immune complexes (ICs), 777
Immunoengineering
 biomaterials in vaccine development, 1199–1208
 use of biomaterials
 to inducing tolerance, 1209–1211
 in T cell modulation, 1208–1209
Immunofluorescence, 1536.e3
Immunogenicity, 472
Immunoglobulins (Igs), 760
 IgE, 753
 IgG, 646–647
Immunohistochemical staining, BM–APP
Immunologic factors role in heart valve, 983
Immunological memory, 757, 764, 764f
Immunology, 768–772
Immunoferoxidase technique, 1536.e3
Immunotherapy technologies, 745
Immunotoxicity, 796–797, 874
Impedance, 1271–1272
Impedimetric biosensors, 1271–1272
Impella device, 1017–1019
Implant debris, 1098–1099
Implant retrieval, 1430
 and evaluation, 1485, 1486t
 goals, 1490t
 case study, 1487b
 for failure mode analysis, 1486–1490
 patient–implant interactions, 1489t
 medical surveillance and role of retrieval analysis, 1490–1492, 1490t
 implants and medical devices prioritized, 1492t
 surgical mesh, 1492b–1493b
Implantable cardioverter-defibrillators (ICDs), 999–1000, 1014
Implantable pulse generator (IPG), 1155
Implantation, 737–738, 872
 of medical devices, 738
Implants, 633–634, 634f
IMPRA. *See* International Medical Prosthetics Research Associates (IMPRA)
Imprinting, 556f, 563
 with master, 563
In silico modeling, 1164
In situ hybridization, 1536.e5
In vitro
 bioreactivity of implant materials, 22–23
 detecting cancerous cells in, 663b
 diagnosis, 478–479
 flow cell, 30, 30f
 imaging, 479–481
 integration, 1303–1304
 limitations of biomaterial evaluation in, 666b
 metabolic activation system, 857–858
 metal allergy testing, 1111
 models, 1298
 parallel plate system, 720, 721f

- toxicity of NPs, 465
 cell viability test, 465
 cellular stress response test, 465
 OS test, 465
- In vivo toxicity of NPs, 465–466
 acute toxicity, 465–466
 genotoxicity and carcinogenicity, 466
 subacute/subchronic/chronic toxicity, 466
- IND. *See* Investigational New Drug (IND)
- Indocyanine green, 481
- Induced pluripotent stem cells (iPSCs), 1291, 1514
- Induction forces. *See* Van der Waals forces
- Inert biomaterials, 846
- Inert ceramics, 959–962, 1125
 biomaterial properties, 1532t
- Inert materials, 517–522. *See also* Active materials.
 albumin coating and alkylation, 520
 fluorination, 522
 heparin-like materials, 522
 hydrogels, 517–518
 PEG immobilization, 518–520
 self-assembled surface layers, 522
 sterilization procedure effect on hydrogel properties, 520b
 zwitterionic group/phospholipid-mimicking surfaces, 520–521
- Inert surfaces, 546
- Infarction, 694–695
- Infection, 695
- Infectious tolerance, 767–768
- Inferior vena cava (IVC), 1047
- Inflammasome, 1105
- Inflammation, 15–16, 435, 695, 697–698, 735, 756
 during hemodialysis, 1067
- Infrared photoacoustic spectroscopy (IR-PAS), 70t
- Infrared reflection absorption spectroscopy (IRAS), 65
- Infrared spectroscopy (IR spectroscopy), 65, 86, 292, 311, 438, 493, 931–932, 1147
- Ingenious chemical design principles, 918
- Injectable decellularized ECM therapies, 387–388
- Injectable hydrogels, 1319–1320
- Injectable tissue-engineering scaffolds, 614–615
- Injury repair, 575–578
- Inkjet bioprinting, 1324
- Inkjet printing, 556–557, 556f–557f, 625, 1296
- Innate immunity, 697–698, 747–756. *See also* Adaptive immunity.
 antigen uptake, processing, and presentation, 754–755
 cells of innate immune system, 750–754, 752f
 chemokines and cytokines, 756
 complement system, 748–749
 costimulatory molecules, 755–756
 first barriers against danger, 748
 pattern recognition by innate immune system, 749–750
- Innate lymphoid cells (ILCs), 754
 ILC1, 754
 ILC2, 754
 ILC3, 754
- Inorganic materials, 853, 1201
- Inorganic NPs, 460–461, 473t. *See also* Lipid-based NPs; Polymeric micelles (PMs).
 GNPs, 460
 MNPs, 460
 nanocarbons, 461
 QDs, 461
 silica NPs, 460–461
- Insertional mutagenesis, 472
- Insoluble cellular fibronectin, 704
- Insoluble glass microspheres, 301
- Installation Qualification (IQ), 1445
- Institution Review Board (IRB), 1512–1513
- Institutional Animal Care and Use Committee (IACUC), 901, 1511–1512
- Institutional review boards (IRBs), 1455, 1483
- Insulating materials, 1154
- Insulin growth factor-1 (IGF-1), 742–743, 1130, 1393
- Integra Dermal Regeneration Template, 1174
- Integra dermal regeneration template, 1171t
- Integrins, 612–613, 646, 664–665, 706–707, 717–718, 1226b, 1336
 activation, 1337f
 integrin–ECM interactions, 706–707
 $\alpha 1\beta 1$ Integrins, 703–704
 $\alpha 2\beta 1$ Integrins, 703–704
 $\alpha 4\beta 1$ Integrins, 704
 $\alpha 4\beta 7$ Integrins, 704
 $\alpha 5\beta 1$ Integrins, 704
 $\alpha 8\beta 1$ Integrins, 704
 $\alpha 11\beta 3$ Integrins, 704
 $\alpha \nu\beta 1$ Integrins, 704
 $\alpha \nu\beta 3$ Integrins, 704
 $\alpha \nu\beta 5$ Integrins, 704
 $\alpha \nu\beta 6$ Integrins, 704
 $\alpha \nu\beta 8$ Integrins, 704
- Intellectual property (IP), 1460–1461, 1501–1503
- Intelligent Retinal Implant System II (IRIS II), 1147, 1148f
- π – π Interaction, 467
- Interconnected spherical macropores by porogen methods, 611–612
- Interdigitated microelectrodes (IMEs), 1271, 1279
- Interface engineering, 1279
- Interferon- γ (IFN- γ), 754
- Interlaboratory comparison studies (ILCSs), 1482
- Interleukin (IL)
 IL-1, 698, 738–739
 IL-2, 1208
 IL-8, 739–740
 IL-12, 754
 IL-15, 754
 IL-18, 754
- Intermittent force mode-atomic force microscopy (IF-AFM), 69t
- Intermittent peritoneal dialysis, 1065
- Internal loads, 42–43
- International Biomaterials Symposia (IBS), 18, 18f
- International Center for Diffraction Data (ICDD), 1476
- International Cooperation on Alternative Test Methods (ICATM), 864
- International Liaison Committee of Societies for Biomaterials (ILC), 18–19
- International Medical Prosthetics Research Associates (IMPRA), 134b
- International Standards Organization (ISO), 290, 784, 854, 869, 1195–1196, 1326, 1478, 1510
 ISO 10993 Biological evaluation of medical devices, 852t, 853–854
 ISO 10993 series, 1426
 ISO 10993 standards, 854
 tests for genotoxicity, carcinogenicity, and reproductive toxicity, 855t
 ISO 10993–1 standard, 861, 1426, 1430
 ISO 10993–3 standard, 854–858
 ISO 10993–4 standard, 858–859
 ISO 10993–5 standard, 859
- Interpenetrating polymer network (IPN), 153, 155, 156f, 488, 1185
 gels, 1355
- Interstitial atoms, 209
- Interstitial cells of Cajal (ICC), 1405
- Interstitial fluid flow, 728
- Interstitial fluid pressure (IFP), 467
- Interstitial lung disease (ILD), 1051–1052
- Interstitial pressure, 1218–1219
- Interventional lung assist (iLA), 1054
- Intima, 687
- Intimal hyperplasia, 1043
- Intraaortic balloon pump (IABP), 1017
- Intracardiac defects, 1024–1025
- Intracellular adhesion molecule-1 (ICAM-1), 725–726, 739–740
- Intracellular barriers. *See also* Systemic barriers.
 against nucleic acid delivery, 472–474
 endolysosomal entrapment, 473
 intracellular gene release, 473
 nuclear transport, 474
 strategies to overcome, 474–477
 endosomal escape, 476–477
 nuclei transport, 477

- Intracellular barriers (*Continued*)
 nucleic acid condensation and cellular internalization, 474–476
 stimuli-responsive nps for intracellular gene release, 477
- Intracellular gene release, 473
- Intracortical microelectrodes, 1160, 1161f
- Intracutaneous reactivity, 871
- Intradermal reactivity. *See* Intracutaneous reactivity
- Intranasal vaccine delivery, 1206–1207
- Intraocular lenses (IOLs), 11–13, 11f, 23–24, 24f, 134, 976–977, 1140, 1143
 accommodative, 1142
 adjustable-power, 1142–1143
 biomaterials and design, 1140–1141
 contamination of, 72
 implants, 1140–1145
 multifocal, 1141–1142
 with variations of optical function, 1141
- Intraocular pressure (IOP), 1135, 1137
- Intraperitoneal injection (IP injection), 905–906
- Intraperitoneal onlay mesh (IPOM), 1492b–1493b
- Intrauterine contraceptive devices (IUDs), 976
- Intravascular oxygenator and carbon dioxide removal device (IVOX), 526
- Intravascular ultrasound (IVUS), 1046
- Intravenous injections (IV injections), 1056, 1250–1251
- Intrinsically bioactive biomaterials, 832–833
 natural cationic polymers, 832–833
- Inverted “honeycomb”. *See* Inverted hexagonal structure
- Inverted hexagonal structure, 460
- Investigational device exemption (IDE), 1455, 1463
- Investigational New Drug (IND), 900
- IOLs. *See* Intraocular lenses (IOLs)
- Ion beam implantation, 496, 496f
- Ion exchange, 1244
- Ion scattering spectroscopy (ISS), 70t
- Ion-selective electrode (ISE), 1272
- Ion-selective field effect transistor (ISFET), 1272
- Ionic conductivity in polymer electrolytes, 1277
- Ionic forces, 38
- Ionic hydrogels, 153, 156f
- Ionic polymerization, 1322
- Ionic salvation, 510–511
- Ionically bound heparin, 523–525
- Ionizing radiation methods, 154–155
- Ions, 1098–1099
- Iontophoresis, 1251, 1252t
- IOP. *See* Intraocular pressure (IOP)
- IP. *See* Intellectual property (IP)
- IP injection. *See* Intraperitoneal injection (IP injection)
- IPES peptide sequence, 710
- IPG. *See* Implantable pulse generator (IPG)
- IPN. *See* Interpenetrating polymer network (IPN)
- IPOM. *See* Intraperitoneal onlay mesh (IPOM)
- iPS. *See* Induced pluripotent stem cells (iPSCs)
- iPSCs. *See* Induced pluripotent stem cells (iPSCs)
- IQ. *See* Installation Qualification (IQ)
- IR spectroscopy. *See* Infrared spectroscopy (IR spectroscopy)
- IR-PAS. *See* Infrared photoacoustic spectroscopy (IR-PAS)
- IRAS. *See* Infrared reflection absorption spectroscopy (IRAS)
- IRB. *See* Institution Review Board (IRB)
- IRBs. *See* Institutional review boards (IRBs)
- Iris, 1135
- IRIS II. *See* Intelligent Retinal Implant System II (IRIS II)
- Iron (Fe), 230, 249
- Iron-based biodegradable metals
 biocompatibility evaluations, 274
 Fe-based implants, 273
 modifications to accelerate corrosion rate, 273
 perspective on Fe-based degradable implants, 275
 proposed degradation process, 273–274
- Irreversible injury, 693–694
- Irritation, 871
- Ischemia, 693–695
 ischemia-reperfusion injury, 695
- ISE. *See* Ion-selective electrode (ISE)
- ISFET. *See* Ion-selective field effect transistor (ISFET)
- Ishikawa diagram, 1482
- ISO. *See* International Standards Organization (ISO)
- Isoflurane, 907
- Isolated cells, 1536.e1
- N-Isopropyl acrylamide (NIPAAm), 434–435
- Isotactic PP, 87
- Isotropic materials, mechanical properties
 of, 44–46
 elastic properties, 44
 fracture toughness and fatigue strength, 46
 hardness, 45–46
 resilience, 46
 strength and failure, 45
 toughness, 46
 yield strength and ductility, 45
- ISS. *See* Ion scattering spectroscopy (ISS)
- iStent, 1145
 Inject, 1145
 supra, 1145
- IUDs. *See* Intrauterine contraceptive devices (IUDs)
- IV injections. *See* Intravenous injections (IV injections)
- IVC. *See* Inferior vena cava (IVC)
- IVOX. *See* Intravascular oxygenator and carbon dioxide removal device (IVOX)
- IVUS. *See* Intravascular ultrasound (IVUS)
- IWGQ peptide sequence, 710
- ## J
- Jag-1, 1225
- Japanese Society for Biomaterials, 18–19
- Japanese Society of Dialysis Therapy (JSDT), 1066
- Joint replacement, 1079
- JSDT. *See* Japanese Society of Dialysis Therapy (JSDT)
- Justice approach, 1510
- ## K
- k-mode microbuckling, 417
- Kallikrein (KK), 809
- KASH domain, 719–720
- Kasha-Vavilov rule of excitation-dependent photoluminescence, 1278
- 67-kDa elastin-binding protein, 704
- Kelp, 406
- Kelvin probe microscopy (KPM), 69t
- Kevlar, 594
- Kidney, 1063
 applications of tissue engineering in, 1299
 failure, 25
- Kinases, 706
- Kinetic barriers, 1096
- Kitchen sink, 1499
- KK. *See* Kallikrein (KK)
- KLDAPT integrin-binding sequence, 704
- Knee prostheses, 24–25
- Knit fabrics, 589, 589f
- Knitted scaffolds, 1354–1355, 1361–1362
- Knitted structure, 593
- Knitted textiles, 588–589, 589f
 structures as sewing rings, 594
- Knot stability, 1195
- Korean Society for Biomaterials (1996), 18–19
- Kosmotropes, 79
- KPM. *See* Kelvin probe microscopy (KPM)
- kT vibrations, 78–79
- ## L
- L-b-L deposition. *See* Layer-by-layer deposition (L-b-L deposition)
- Labile catalysts, 111
- Labile tissues, 693
- Laboratory animal medicine, 901
- Laboratory notebook, 1500–1501
- Lactalbumin, 655
- Lactic acid, 433
- Lactide-based polymers, 1192
- LADME. *See* Liberation, absorption, distribution, metabolism, elimination of drug (LADME)
- LAL. *See* Limulus ameobocyte lysate (LAL)

- LALLS. *See* Low-angle laser diffraction (LALLS)
- Laminated object manufacturing (LOM), 628–629
- Laminins, 704–705, 705f
- Lamins, 719–720
- Langerhans cells, 1111
- Langmuir isotherm, 651
- Langmuir–Blodgett films (LB films), 487
deposition, 497–498, 497f
- Lanthanides, 480–481
- Large unilamellar vesicles (LUVs), 459
- Laser desorption mass spectrometry (LDMS), 70t
- Laser metal deposition (LMD), 629–630
- Laser methods, 501
- Laser trabeculoplasty, 1143
- Latent heats of fusion and evaporation, 78
- Lateral force microscopy (LFM), 69t
- Latin American Society for Biomaterials and Artificial Organs (1998), 18–19
- Lawsuits, 1508
- Layer-by-layer deposition (L-b-L deposition), 498–501, 1279
- LB films. *See* Langmuir–Blodgett films (LB films)
- LC-MS. *See* Liquid chromatography-mass spectrometry (LC-MS)
- LCST. *See* Lower critical solution temperature (LCST)
- LDI. *See* Lysine-diisocyanate (LDI)
- LDL. *See* Low-density lipoprotein (LDL)
- LDMS. *See* Laser desorption mass spectrometry (LDMS)
- Lead, 22–23
- LECs. *See* Lens epithelial cells (LECs)
- Lectin pathway (LP), 780
proteins of complement, 780t
- Lee–White clotting time test, 888
- Left ventricular assist devices (LVADs), 1019
- Legalese provisions, 1503–1504
- Lens epithelial cells (LECs), 1141
- LensteckMiniwell IOL, 1142
- LENTIS Mplus, 1142
- Leuconostoc mesenteroides*, 433
- Leukemias, 813
- Leukocyte functional antigen-1 (LFA-1), 783–784
- Leukocytes, 739–740, 801–802
- Leukotrienes, 698
- LFA-1. *See* Leukocyte functional antigen-1 (LFA-1)
- LFM. *See* Lateral force microscopy (LFM)
- Liberation, absorption, distribution, metabolism, elimination of drug (LADME), 1243
- License agreements, 1506–1507
- License fee, 1507
- Ligament with woven and braided biotextiles, 594
- Light microscopy, 1536.e1, 1536.e3f
- Light Raman scattering (LRS), 464
- Light scattering, 89, 438
- Limulus amoebocyte lysate (LAL), 872
- LINC. *See* Linker of nucleoskeleton and cytoskeleton (LINC)
- Lindbergh pump, 22
- Line defects in crystals, 211–212
- Lineage reprogramming, 690
- Linear polymers
physical behavior, 91
physical states of, 90
- Linear polypropylene molecule, 86
- Linear relationship, 43
- Linen sutures, 21–22
- N*-Linked glycosylation, 408
- O*-Linked glycosylation, 408
- Linked recognition, 1203
- Linker of nucleoskeleton and cytoskeleton (LINC), 719–720
- Linking proteins, 403
- Lipid-based NPs, 459–460, 473t, 478t. *See also* Inorganic NPs; Polymeric micelles (PMs).
lipoplexes, 460
liposomes, 459
SLNs, 459–460
- Lipidoids, 476
- Lipids, 382
lipid–drug conjugates, 466
receptor, 749
vesicles, 435
- Lipinski's rule of 5, 1245
- Lipofectamine 2000, 475
- Lipophilic drugs, 433
- Lipoplexes, 460, 477
- Lipopolysaccharide (LPS), 780
- Lipoproteins, 658
- Liposaccharides, 510–511
- Liposomes, 81, 435, 459, 1247, 1248t
- Lipospheres. *See* Solid-lipid nanoparticles (SLNs)
- Liquid
crystalline polymer, 1154
liquid-biomaterial interface, 644
liquid-phase sintering, 289
liquid-state powder processing method, 463
- Liquid chromatography-mass spectrometry (LC-MS), 439
- Liquid Silicone Rubber (LSR), 115
- Litigation, 1507–1508
- Live-attenuated vaccines, 1199
- Liver, applications of tissue engineering in, 1299
- Living anionic polymerization techniques, 539
- LMD. *See* Laser metal deposition (LMD)
- LMWH. *See* Low-molecular-weight heparins (LMWH)
- Loading modes, 47–48
- LOAEL. *See* Lowest-observed adverse effect level (LOAEL)
- Local drug delivery, nanofibers for, 596
- Local Injection, 441
- Local stiffness, 1340–1341
- LockActiv, 299
- LOM. *See* Laminated object manufacturing (LOM)
- Long-circulating NPs, 468–469
- Long-stem prostheses, 1083
- Loose connective tissue, 431
- Lotrafilicon A and B, 1139–1140
- Lotus leaf effect, 827, 833
- Low-angle laser diffraction (LALLS), 1100
- Low-density lipoprotein (LDL), 658, 1070
- Low-dose nitric oxide, 831–832
- Low-molecular-weight heparins (LMWH), 522
- Low-molecular-weight OEG–drug conjugates, 466
- Low-temperature isotropic form (LTI form), 960
- Low-volume technologies
chemical sterilization, 1439–1440
radiation-based techniques, 1434
- Lower critical solution temperature (LCST), 160, 434–435, 1319–1320
- Lower stress resin systems, 142–144
low-shrinkage materials, 142–143
network modulation, 143–144
mechanistic step of chain-transfer reactions, 144f
monomers based on spiro-orthocarbonate chemistry, 143f
- Lowest-observed adverse effect level (LOAEL), 852
- LOX. *See* Lysyl oxidase (LOX)
- LP. *See* Lectin pathway (LP)
- LPS. *See* Lipopolysaccharide (LPS)
- LRAG peptide sequence, 710
- LRS. *See* Light Raman scattering (LRS)
- LSR. *See* Liquid Silicone Rubber (LSR)
- LTI form. *See* Low-temperature isotropic form (LTI form)
- Lucite, 23
- Lumbar total disc replacements, 1084–1085, 1085f
- Lupron, 1239
- LuSens assay, 864
- LUVs. *See* Large unilamellar vesicles (LUVs)
- LVADs. *See* Left ventricular assist devices (LVADs)
- Lymph node structure, 687, 690f
- Lymphocyte proliferation testing. *See* In vitro metal allergy testing
- Lymphocytes, 697, 757, 1206
- Lymphoid tissues, 683
- Lymphomas, 813
- Lysine-diisocyanate (LDI), 104
- Lysosomes, 694, 845
- Lysozyme, 406–407, 655
- Lysyl oxidase (LOX), 1222, 1355–1356

M

- M/R. *See* Minocycline-rifampin (M/R)
- MAA. *See* Methacrylic acid (MAA)
- MAC. *See* Mechanically assisted corrosion (MAC); Membrane attack complex (MAC); Microabrasion corrosion (MAC)
- Mac-1. *See* Cluster of differentiation (CD)—CD11b/CD18
- MACC. *See* Mechanically assisted crevice corrosion (MACC)
- MACI. *See* Matrix-assisted chondrocyte implantation (MACI)
- Macrophage infiltration factor (MIP), 742–743
- MIP1 α , 756
- Macrophages, 687–688, 697, 739–742, 747–748, 751–752, 752f, 845, 1200–1201
- polarization, 742–743
- recruitment and polarization, 697–698
- Macropinocytosis, 473
- Macroporous
- calcium phosphate bone graft, 293
 - Macroporous ceramics, 292–293
 - tissue-engineering scaffolds, 613
- Macrotopography of implants, 601–602
- MACT. *See* Matrix-assisted autologous chondrocyte transplantation (MACT)
- MAF. *See* Master File (MAF)
- Maghemite (γ -Fe₂O₃), 460
- Magic bullet, 1254–1255
- Magnesia partially stabilized zirconia (MgPSZ), 320–321
- Magnesium (Mg), 22–23, 205, 792–793
- influence of alloying elements, corrosion behavior, and biocompatibility, 273
- Mg-based biodegradable implants, 277f
- Mg-based implants, 277–283
- alloying elements impact on processing and microstructure, 278–279, 278f
 - biodegradable metallic implant materials in orthopedics, 281f
 - clinical trials of orthopedic devices, 283t
 - current models of corrosion process in vitro, 279–280
 - degradation process, 279f
 - methods to measuring Mg-based implant corrosion in vitro and in vivo, 282
 - orthopedic devices based on MgCaZn alloy, 283
 - orthopedic devices based on pure Mg, 283–284
 - preclinical and clinical observations, 282–283
 - process in vivo, 280–281
 - perspective on Mg-based degradable implants, 284
 - specific standards under development for absorbable metals, 284t
- Magnesium oxide (MgO), 322
- Magnetic beads (MBs), 1272–1273
- Magnetic field, 561
- Magnetic force microscopy (MFM), 69t
- Magnetic nanoparticles (MNPs), 369, 460
- Magnetic particles, 567
- Magnetic resonance (MR), 273
- Magnetic resonance angiography (MRA), 1045–1046
- Magnetic resonance imaging (MRI), 249, 336, 460, 479–480, 1041, 1045–1046
- Magnetic self-assembly, 567
- Magnezix, 283–284
- Major histocompatibility complex (MHC)
- gene cluster, 755
 - MHC I, 754–755, 756f, 760, 1201–1202
 - MHC II, 755, 756f, 1201–1202
- Major histocompatibility molecules, 762
- MALDI. *See* Matrix-assisted laser desorption ionization (MALDI)
- Malignant hyperthermia (MH), 909–910
- Malignant tumors, 813
- Mammalian cells, 683, 684f, 694
- Mannitol, 509–510
- Mannose receptor, 749
- Mannose receptors (MRs), 1105
- Mannose-binding lectin (MBL), 780
- Manufacturability, 490
- Manufacturer and User Facility Device Experience (MAUDE), 1486
- Manuscript peer-review process, 1533
- Margin of safety (MOS), 853
- MARS. *See* Molecular adsorbent recirculating system (MARS)
- Mask-based patterning, 562
- Mask-based photolithography, 561–562, 561f, 563f
- MASPs. *See* MBL-associated serine proteases (MASPs)
- Mass attenuation coefficient, 50
- Mass spectrometry (MS), 389, 1326, 1327t, 1536.e1
- Mass/molecular weight characterization for tissue-engineering scaffolds, 1327t
- Mast cells, 753
- Master File (MAF), 1466
- Material supplier controls, 1467–1471, 1468t–1470t
- Materials, 37–39
- extrusion, 624t, 626, 627f
 - innovation, 262
 - jetting, 624t, 625–626, 626f
- Materials use agreements (MUA), 1498–1500
- Matricellular proteins, 401–402
- MatriDerm, 1171t, 1174
- Matrigel, 1219–1222, 1220t–1221t
- MatriStem, 387
- Matrix materials, 415–416
- Matrix metalloproteinases (MMPs), 471, 692–693, 706, 710, 738, 1186, 1295, 1375
- MMP-2, 469
- Matrix remodeling, 692–693
- Matrix-assisted autologous chondrocyte transplantation (MACT), 1334.e2b
- Matrix-assisted chondrocyte implantation (MACI), 1318
- Matrix-assisted laser desorption ionization (MALDI), 70t
- Matrix-based systems, 1244
- Matter, 37–40
- Maturation, 1200–1201
- Mature cells, 1291–1292
- lineage differentiation, 688, 691f
- MAUDE. *See* Manufacturer and User Facility Device Experience (MAUDE)
- MAUDE database. *See* US Medical Device Reports
- MaxGel, 1220t–1221t
- Maximum tolerance dose (MDT), 465–466
- Maxon suture, 1194
- MBGs. *See* Mesoporous bioactive glasses (MBGs)
- MBL. *See* Mannose-binding lectin (MBL)
- MBL-associated serine proteases (MASPs), 780
- MBP-426, 470
- MBs. *See* Magnetic beads (MBs)
- MCAF. *See* Monocyte chemotactic activating factor (MCAF)
- MCD. *See* Microcrystalline diamond (MCD)
- McKee-Farrar prosthesis, 1083
- MCP. *See* Membrane cofactor protein (MCP); Metacarpophalangeal (MCP)
- MCRD. *See* Monolithic controlled-release device (MCRD)
- MDA. *See* 4,4'-Methylene dianiline (MDA)
- MDEAs. *See* Multidisc electrode arrays (MDEAs)
- MDI. *See* Methylene-bis(4) phenyl isocyanate (MDI)
- MDR. *See* Medical Device Regulation (MDR); Multidrug resistance (MDR)
- MDT. *See* Maximum tolerance dose (MDT)
- “Me-too” device, 1417–1418, 1425
- MECC. *See* Mini extracorporeal circuit (MECC)
- Mechanical damage, 1160–1161
- Mechanical deformation, cell response to, 673
- Mechanical forces, 643–644, 717
- in vascular system, 722–728
- Mechanical heart valves (MHV), 333, 344b
- Mechanical interactions of cells, 720–722
- effect
 - of cyclic strain on blood vessels, 727–728
 - of shear stress on blood vessels, 726–727

- mechanical forces in vascular system, 722–728
- mechanical stretch, 721–722
- micro-and nanopatterning, 722
- shear stress, 720–721
- substrate stiffness, 722
- Mechanical loading, 42, 42f, 728
- Mechanical planarization, 625–626
- Mechanical stimulation, 1343–1344
 - effects of combined mechanical stimuli, 1344–1345
- Mechanically assisted corrosion (MAC), 941
- Mechanically assisted crevice corrosion (MACC), 945, 948f, 1097–1098, 1098f
 - area abraded analysis based on plastic deformation, 949f
 - asperity removing oxide film, 951f
 - clinically observed, 945–947
 - CoCrMo and Ti–6Al–4V alloys, 947–952, 948f
 - comparison of predicted currents and experimental currents, 951f
 - physical properties, 950t
 - single asperity high-speed scratch test, 950f
- Mechanosensing at ECM–biomaterial interface, 717–718
- Mechanotaxis, 673
- Mechanotransduction, 1287, 1335–1340
 - direct transmission of forces to nucleus, 1339–1340
 - focal adhesion maturation and stress fiber formation in, 1337–1338
 - molecular pathways for design of scaffolds, 1338–1339
- Media, 687
- Medical device
 - development, 1417–1418, 1418f, 1425
 - absence of toxicity, 1426–1427
 - assessing biological risk of aging biomaterials, 1429–1430
 - assessing continuum of biological risk in performance, 1427–1428
 - assessing contribution of secondary processes to biological risk, 1428–1429
 - failure, 1418
 - implant retrieval, 1485
 - medical implants, 1485, 1486t
 - postmarket surveillance, 1485–1486
- Medical Device Regulation (MDR), 1449, 1463–1464, 1486
- Medical Device Reporting. *See* Medical Device Regulation (MDR)
- Medical ethics, 1509
- Medical fibers. *See also* Biotextiles.
 - electrospinning, 583–587, 585f
 - CES, 586–587
 - coaxial, 586f
 - coelectrospinning, 586
 - materials selection, 586
 - modes of fiber collection, 585f
 - representative polymers, 582t
 - and spinning parameter optimization, 584–586
 - example spinning conditions, 582t
 - hydrogel fiber spinning, 587, 587f
 - melt extrusion, 581, 584f
 - surface functionalization, 587–588
 - textile fibers, 579–581
 - wet/gel spinning, 581–583, 584f
- Medical textiles. *See* Biotextiles
- Medical training, 632–633, 633f
- Melt extrusion, 581, 584f
- Melt glasses, 964
- Melting, 91
 - point of water, 77
- Membrane attack complex (MAC), 779, 781, 781t
- Membrane cofactor protein (MCP), 782
- Membrane-bound
 - phagocytic receptors, 749
 - signaling receptors, 749
- Membrane-disruptive DDSs, 1250
- Memory cells, 757
- Memory T cells, 764
 - migration properties, 765f
- MEMS. *See* Microelectromechanical systems (MEMS)
- MEMS HF System. *See* Micro-Electro-Mechanical HF System (MEMS HF System)
- Mepilex Ag, 1171t
- Mepitel, 1171t, 1173
- Mepitel Ag, 1173
- Mercury, 795–796
- Mercury intrusion porosimetry, 293
- Mesenchyma. *See* Stroma
- Mesenchymal stem cells (MSCs), 347, 370, 674, 1127, 1225, 1291, 1318, 1336, 1360
- Meshes, 591
- Mesoporous bioactive glasses (MBGs), 964
- Mesoporous silica NPs (MSNs), 460–461
- Messenger RNA (mRNA), 472
- Metacarpophalangeal (MCP), 347
- Metal ion-induced oxidation (MIO), 933, 934f, 934t
- Metal ions (soluble debris), 1103–1104
 - release, 1103
- Metal lymphocyte transformation testing (Metal-LTT), 1111
- Metal-on-metal (MOM), 267, 793, 996–997, 1488b–1489b
 - bearings, 1103
 - spinal arthroplasty wear, 1093
 - spine arthroplasty wear, 1093
- Metal-on-polyethylene (MoP), 1488b–1489b
- Metal-on-polymer (MOP). *See* Metal-on-metal (MOM)
- Metal-oxide passive films, 1095, 1096f
- Metallic biomaterials, 941
- Metallic bonding, 39, 39f
- Metallic corrosion, 1094
- Metallic degradation and biological environment
 - biological environment, 941–942, 942f
 - biology and corrosion, 952
 - clinically observed MACC, 945–947
 - evidence of fretting crevice corrosion, 947f
 - interdisciplinary nature, 946f
 - retrieved CoCrMo head taper, 947f
 - corrosion of passive oxide-covered alloys, 942–943, 942f
 - metal-on-metal (hard) surface mechanics, 944–945
 - reduction reactions affect cells, 952
 - tribocorrosion layer and surface damage, 951–952
 - tribological aspects of metal-hard contact degradation, 943–944, 944f
- Metallic sutures, 22
- Metals, 605t–606t, 1087–1089, 1090t, 1123, 1125
 - allergy, 847–848
 - alloy systems, 205–206
 - alloy toxicity, 793–796
 - essential metals in implants, 794t
 - nonessential metals in implants, 795t
 - bulk mechanical properties of metallic biomaterials, 212–215
 - elastic and plastic deformation, 213
 - strength of metals and strengthening mechanisms, 213
 - defects in crystals, 211–212
 - schematic representation of dislocations, 212f
 - electrochemical impedance spectroscopy, 224–226
 - electrochemical properties of implant metals, 1091t
 - electronic and atomic structure, 208–209
 - alloying, microstructure, and phase diagrams, 209–211
 - crystal structures of typical alloys, 209f
 - electron energy levels, 208f
 - fatigue of, 215–217, 216f, 218f
 - Wohler diagram, 216f
 - fracture of, 215
 - hypersensitivity, 1109
 - medical devices and metals in body, 205
 - metallic corrosion, 220–224
 - processing, 206–208
 - processing–structure–properties–performance paradigm, 208
 - structure of metals and alloys, 208–211
 - surfaces, 217–220
 - atomic force microscope images, 219f
 - high-field oxide film growth model, 219f
 - toxicity, 793–796
 - essential metals in implants, 794t
 - nonessential metals in implants, 795t

- Metaplasia, 690, 694
 Metastasis, 813, 1218, 1228
 Methacrylamides, 146
 Methacrylic acid (MAA), 158, 193, 1139, 1269
 Methacryloylphosphorylcholine (MPC), 521
 MetHb. *See* Methemoglobin (MetHb)
 Methemoglobin (MetHb), 1061
 Methicillin-resistant *Staphylococcus aureus* (MRSA), 831
 Methotrexate (MTX), 408, 467
 Methoxy poly(ethylene glycol) monomethacrylates, 519–520
 Methoxypolyethylene glycol methacrylate (MPEG), 524–525
 N-Methyl 2-pyrrolidone (NMP), 186
 Methyl cyanoacrylate, 1182, 1182f
 Methyl methacrylate (MMA), 158, 1182, 1182f
 4,4'-Methylene dianiline (MDA), 818
 MDA-5, 749
 Methylene-bis(4) phenyl isocyanate (MDI), 104
 MFM. *See* Magnetic force microscopy (MFM)
 MH. *See* Malignant hyperthermia (MH)
 MHV. *See* Mechanical heart valves (MHV)
 Micelle-based nanomedicines, 455
 Micelles, 81, 1247, 1248t, 1249
 Michael addition, 543
 Michaelis–Menten enzymatic kinetics, 176–177
 Micro-ATR, 65
 Micro-Electrico-Mechanical HF System (MEMS HF System), 1015–1016
 Micro-mechanical bonds, 1182
 Micro-RNA (miRNA), 472
 Microabrasion corrosion (MAC), 263–264
 Microarrays, 670
 Microbuckling wavelength, 424
 Microcapsule-based cell encapsulation, 1290–1291
 Microcarrier, 1290–1291
Micrococcus radiodurans, 1432
 Microcomputed tomography, 293
 Microcontact printing (μ CP), 563–565, 564f, 667
 Microcrystalline diamond (MCD), 328
 Microelectromechanical systems (MEMS), 1280
 Microelectronics, 53–54
 Microencapsulation, 437, 441–444
 Microenvironment, 701
 Microfabrication, 1279–1280
 Microfibril-associated glycoproteins, 403
 Microfibrillar proteins, 403
 Microfluidic
 chip-based platforms, 1302
 devices, 721
 emulsion, 436
 patterning, 565, 565f
 Microgravity reactor, 1297
 Microinvasive glaucoma surgery (MIGS), 1143–1145
 devices, 1145
 MicroMatrix, 387–388
 Micrometer-scale
 chemical patterns, 667
 topography, 671
 Micromolding, 1280
 Micromotion, 1164
 Microneedles (MNs), 1207, 1252t
 Micronized Alloderm, 388
 Microparticles, 431
 biomedical applications
 drug delivery, 441–442
 microencapsulation technology, 443–444
 particulate-delivery systems, 443–444
 radiotherapy, 442–443
 characterization, 437–440
 cumulative release over time of Alexa Fluor 488, 440f
 drug loading, 438
 morphology, 438
 physiochemical properties, 438
 release experiment, 439f
 release kinetics, 439
 size and polydispersity, 438
 surface charge, 438
 drug release mechanisms, 440–441
 classic mechanisms, 440f
 degradation, 440
 diffusion, 440
 swelling, 441
 materials for synthesis, 432–435
 natural polymers, 432–433
 nonpolymeric materials, 435
 synthetic polymers, 432–435, 432f
 morphology, 438f
 preparation, 435–437
 coacervation phase separation, 436
 double emulsion solvent preparation, 435
 microfluidic emulsion, 436
 microsphere production by emulsion system, 436f
 single emulsion solvent preparation, 435
 spray drying, 437
 Micropatterned substrates, 610
 Micropatterning, 610, 722
 Microplates, 1099–1100
 Microscale structures, 601–602
 Microscopy, 1536.e1
 Microspheres, 614–615
 Microstamping, 667
 Microstrain magnitudes, 16
 Microstructure, 209–211
 Microtome, 1536.e3
 Microtomography, 282
 Micturition, 1158–1159
 MIF. *See* Migration inhibitory factor (MIF)
 Migration inhibitory factor (MIF), 1110
 MIGS. *See* Microinvasive glaucoma surgery (MIGS)
 Mini extracorporeal circuit (MECC), 1016–1017
 Miniature tissue models, 1406
 Minocycline-rifampin (M/R), 830
 MIO. *See* Metal ion-induced oxidation (MIO)
 MIP. *See* Macrophage infiltration factor (MIP)
 MIPs. *See* Molecularly imprinted polymers (MIPs)
 miRNA. *See* Micro-RNA (miRNA)
 MIRRAGEN, 300
 Mitomycin C (MMC), 1145
 Mitral stenosis, 1000
 MJM. *See* Multijet modeling (MJM)
 Mlx. *See* Mohawk (Mlx)
 MLVs. *See* Multilamellar vesicles (MLVs)
 MM-302, 470
 MMA. *See* Methyl methacrylate (MMA)
 MMC. *See* Mitomycin C (MMC)
 MMPs. *See* Matrix metalloproteinases (MMPs)
 Mn(III) tetrakis(4-benzoic acid)porphyrin (MnTBAP), 1164
 MNPs. *See* Magnetic nanoparticles (MNPs)
 MNs. *See* Microneedles (MNs)
 MnTBAP. *See* Mn(III) tetrakis(4-benzoic acid)porphyrin (MnTBAP)
 Model for End-Stage Liver Disease score, 1510
 Modern dental-bonding cements, 1183
 Modified surface layers, 487–488
 Modular junctions, corrosion at, 1103, 1104f
 Modulus matrix, 46
 Modulus of elasticity, 43
 Modulus–temperature behavior, 92
 Mohawk (Mlx), 1352
 Mohr's circle, 47–48
 Mold arthroplasty, 1081
 Molecular adsorbent recirculating system (MARS), 1070–1071
 Molecular assemblies, 39
 Molecular mass, 87–89
 characterizing molecular mass
 distribution, 89–90
 distribution and averages, 87–89
 Molecular weight (MW), 474
 Molecular wiring, 1279
 Molecularly imprinted polymers (MIPs), 1269
 Molecules, 37–39, 53b
 MOM. *See* Metal-on-metal (MOM)
 Monocryl suture, 1194
 Monocyte chemotactic activating factor (MCAF), 1110
 Monocytes, 697–698, 750–751, 1304
 Monolayer model, 651–652
 Monolayer-protected clusters (MPCs), 460

- Monolithic controlled-release device (MCRD), 862b–864b
- Monoliths, 1244
- Monomer matrix, 140–142
 - antimicrobial resins, 145
 - enhanced chemical stability, 145–147
 - ester-free monomers, 146f
 - enhanced toughness, 147
 - fast polymerizing monomers, 144–145
 - hydrophobic resins, 147
 - lower stress resin systems, 142–144
 - novel systems, 142–147
- Monomers, 98, 1192–1193, 1269
- Mononuclear phagocytic system (MPS), 1242
- Monophosphoryl lipid A (MPLA), 1200–1201
- Montanide, 1200
- Morphologic evaluation, 977–979
- Morphology, 172, 173f
- MOS. *See* Margin of safety (MOS)
- “Motion control” condition, 727–728
- Motor function, 1159
- Mott and Cabrera theory, 1096
- Mott–Schottky equation, 226
- MPC. *See* Methacryloylphosphorylcholine (MPC)
- MPCs. *See* Monolayer-protected clusters (MPCs)
- MPDA. *See* Multiphotodiode array (MPDA)
- MPEG. *See* Methoxypolyethylene glycol methacrylate (MPEG)
- MPLA. *See* Monophosphoryl lipid A (MPLA)
- MPO. *See* Myeloperoxidase (MPO)
- MPS. *See* Mononuclear phagocytic system (MPS)
- MR. *See* Magnetic resonance (MR)
- MRA. *See* Magnetic resonance angiography (MRA)
- MRI. *See* Magnetic resonance imaging (MRI)
- mRNA. *See* Messenger RNA (mRNA)
- MRs. *See* Mannose receptors (MRs)
- MRSA. *See* Methicillin-resistant *Staphylococcus aureus* (MRSA)
- MRTF-A. *See* Myocardin-related transcription factor A (MRTF-A)
- MS. *See* Mass spectrometry (MS)
- MSCs. *See* Mesenchymal stem cells (MSCs)
- MSNs. *See* Mesoporous silica NPs (MSNs)
- MTS, 465
- MTT, 465
- MTX. *See* Methotrexate (MTX)
- MUA. *See* Materials use agreements (MUA)
- Mucoadhesive PHEMA microspheres, 435
- Mucociliary escalator, 1206–1207
- Mucopolysaccharides, 683
- Mucosal contact time, 1253t
- Mucosal DDSs, 1251–1252, 1253t
- Mucosal membranes, 1251
- Mucus, 431
- Multicellular interactions, 1343
- Multicellular organisms, 683–684
- Multidisc electrode arrays (MDEAs), 1279–1280, 1280f
- Multidomain synthetic peptides, 604–607
- Multidrug resistance (MDR), 468
- Multifocal IOLs, 1141–1142
- Multifunctional biomaterials based on DNA, 366
- Multijet modeling (MJM), 625–626
- Multilamellar vesicles (MLVs), 459
- Multilayer polyelectrolyte deposition, 498–501
- Multilumen catheters, 131
- Multiorgan-on-a-chip systems, 1302
- Multiphasic scaffolds, 613–614
- Multiphotodiode array (MPDA), 1147–1148
- Multipolymer hydrogels, 153
- Multivesicular bodies (MVBs), 461
- Multiwalled carbon nanotubes (MWCNTs), 330, 330f, 341, 461
- Murray’s law, 723
- Muscle, 683
- Muscular arteries, 1034
- Musculoskeletal tissue engineering, 595
- MVBs. *See* Multivesicular bodies (MVBs)
- MW. *See* Molecular weight (MW)
- MWCNTs. *See* Multiwalled carbon nanotubes (MWCNTs)
- Mycobacterium tuberculosis*, 752, 760–761
- Myeloperoxidase (MPO), 929
- Myocardial infarction, 693
- Myocardin-related transcription factor A (MRTF-A), 1339
- Myocardium*, 1036
- Myofibroblasts, 692–693, 1219
- Myopia, 1136
- Myrica rubra*, 1356–1357
- Myxomatous valve degeneration, 1000
- N**
- N/P ratios. *See* Nitrogen to phosphorus ratios (N/P ratios)
- NADPH. *See* Nicotinamide adenine dinucleotide phosphate-oxidase (NADPH)
- Nafion, 1275–1277
- NALP3 protein, 1106
- NALTs. *See* Nasal-associated lymphoid tissues (NALTs)
- Nano/microscale surface texture, materials with, 833–834
- Nanocapsules, 455–456, 1247, 1248t
- Nanocarbons, 461
- Nanocarriers, 473, 1243–1244
- Nanocomplexes, 458–459
- Nanocrystalline diamond (NCD), 328, 348
- Nanocrystalline magnetite (Fe₃O₄), 460
- Nanocrystallinity, 273
- Nanodiamonds (ND), 327–328
- Nanoengraving. *See* Nanoshaving
- Nanofibers, 595
 - for cardiovascular repair, 596
 - for local drug delivery, 596
- Nanofibrous hollow microspheres (NF-MSs), 614–615
- Nanofibrous materials, 615
- Nanofibrous spongy microspheres (NF-SMSs), 614–615
- Nanofibrous surface architecture, 614–615
- Nanogels, 458
- Nanografting, 558
- Nanolithographic AFM, 69t
- Nanomaterials, 1272–1273
- Nanometer-scale chemical patterning, 670
- Nanometer-scale topography, 671–672
- Nanoparticles (NPs), 453
 - categories, 453–464, 454f
 - bio-inspired NPs, 461–462
 - hybrid NPs, 462–464
 - inorganic NPs, 460–461
 - lipid-based NPs, 459–460
 - polymeric NPs, 453–459
 - characterization, 464–466
 - biocompatibility, 465–466
 - morphology, 465
 - size, 464
 - surface charge, 464–465
 - diagnostic/theranostic applications
 - imaging-guided surgery, 482
 - theranostics, 481–482
 - in vitro diagnosis, 478–479
 - in vivo imaging, 479–481
 - drug delivery applications
 - approaches to overcome systemic barriers, 468–472
 - drug loading, 466–467
 - systemic barriers against drug delivery, 467–468
 - nucleic acids delivery applications, 472–478
 - clinical development, 477–478
 - clinical-stage NPs for anticancer drug delivery, 473t
 - intracellular barriers against nucleic acid delivery, 472–474
 - NP-based gene therapy under clinical evaluation, 478t
 - strategies to overcome intracellular barriers, 474–477
- Nanopatterning, 722
- Nanoprecipitation, 454–456
- Nanoshaving, 556–558, 556f
- Nanospheres, 455, 1247, 1248t
 - lithography, 566–567
- Nanotechnology, 479, 817–818
 - methods of ligand immobilization, 542
- Narcotic analgesics, 909
- Narcotics, 910
- Nasal-associated lymphoid tissues (NALTs), 1206–1207
- National coverage decision (NCD), 1459

- National Institute for Biological Standards and Control (NIBSC), 1475–1476
- National Institutes of Health (NIH), 900
- National synchrotron light Source, 71, 71f
- Native tissues, 610–611
- Natural biodegradable polymers, 425–426
- Natural biomaterials, 1219–1223, 1220t–1221t
- carbohydrate-based materials, 1222
 - cell-and tissue-derived materials, 1222–1223
 - protein-based materials, 1219–1222
- Natural cationic polymers
- AMPs, 832–833
 - chitosan, 832
 - synthetic cationic polymers, 833
- Natural gut suture, 1189
- Natural hydrophilic materials, 510–511, 510t
- Natural killer cells (NK cells), 747–748, 754
- Natural materials, 361, 1292–1293, 1318–1319
- dynamic hydrogels exploring
 - supramolecular chemistry, 366–369
 - natural based-biomaterials exploring
 - structural molecules
 - extracellular matrix-based biomaterials, 361–364
 - origin and relevant properties of selected natural polymers, 362t
 - soft nanocomposite smart materials, 369–370
- Natural plant-and animal-derived polymers
- alginate, 1358–1362
 - cellulose, 1359–1360
 - chitin/chitosan, 1360
 - collagen, 1360–1361
 - gelatin, 1361
 - silk, 1361–1362
- Natural polymers, 415–416, 432–433, 579, 582t, 605t–606t, 1363, 1391
- alginate, 433
 - for biotextile production, 579
 - chitosan, 432, 432f
 - dextran, 433
- Natural-based polymers, 361
- Naturally derived materials, safety
 - considerations in manufacturing, 708b
- Naturally immunogenic biomaterials, 1201
- Naturopathic compounds, 1170–1172
- NCD. *See* Nanocrystalline diamond (NCD); National coverage decision (NCD)
- NCM-AFM. *See* Noncontact mode-atomic force microscopy (NCM-AFM)
- ND. *See* Nanodiamonds (ND)
- Nd-YAG laser, 1141
- NDA. *See* New Drug Application (NDA); Non-disclosure agreement (NDA)
- Near-edge X-ray absorption fine structure (NEXAFS), 70t, 71
- Near-infrared (NIR), 481
- NIR-II fluorescence imaging, 482
 - radiation, 336
- Near-sightedness. *See* Myopia
- Nearfield scanning optical microscopy (NSOM), 69t
- Nearly inert bioceramics, 289–290
- alumina and zirconia ceramics, 290
 - calcium phosphate cements, 294–296
 - porous calcium phosphate ceramics, 292–294
- Necrosis, 693–695
- Needles of sutures, 1189, 1191f, 1191t, 1195
- and attachment, 1195
- Negative Gibbs free energy, 37
- Negative growth inhibitory signals, 698
- “Negative thermo-sensitive” polymers, 472
- Negative-pressure dressings, 1172
- Negative-pressure wound therapy (NPWT), 1172
- Neisseria meningitidis*, 782–783
- Neoplasia, 694, 813, 817
- Neoplasm, 813–814
- Neosporin ointments, 1172
- Neovascularization, 699
- Nernst equation, 220–221, 1272
- Nerve, 683
- Nesprins, 719–720
- NETs. *See* Neutrophil extracellular traps (NETs)
- Network
 - connectivity, 299
 - polymer, 98b
- Neural electrodes, 1156
- Neural tissue engineering, 595–596
- Neutral hydrogels, 153
- Neutral proteases, 698
- Neutralization, 760, 763–764
- Neutron reflection, 70t
- Neutrophil extracellular traps (NETs), 752–753, 753f
- Neutrophils, 431, 671, 687–688, 697, 739–740, 743–744, 752–753, 801–802, 844
- New Drug Application (NDA), 900
- New product development (NPD), 1457
- Newton’s law, 44
- NEXAFS. *See* Near-edge X-ray absorption fine structure (NEXAFS)
- NF-MSs. *See* Nanofibrous hollow microspheres (NF-MSs)
- NF-SMSs. *See* Nanofibrous spongy microspheres (NF-SMSs)
- NF-κB. *See* Nuclear factor-kappa B (NF-κB)
- NFSs. *See* Nonfouling surfaces (NFSs)
- NG. *See* Nitroglycerin (NG)
- NHE. *See* Normal hydrogen electrode (NHE)
- NHS. *See* N-Hydroxysuccinimide (NHS)
- NIBSC. *See* National Institute for Biological Standards and Control (NIBSC)
- “Niche” microenvironment, 1297
- Nickel (Ni), 22–23, 230, 1107, 1109–1110
- Nickel–titanium (Nitinol), 797
- Nicotinamide adenine dinucleotide phosphate-oxidase (NADPH), 1106
- NIH. *See* National Institutes of Health (NIH)
- NIPAAm. *See* N-Isopropyl acrylamide (NIPAAm)
- NIR. *See* Near-infrared (NIR)
- Nitinol stents, 529–530
- Nitric acid (HNO₃), 461
- Nitric oxide (NO), 469–470, 527, 698, 723, 810, 831–832, 1373–1374
- Nitric oxide surface flux, 1054f, 1061–1062
- Nitrides, 319
- Nitrogen to phosphorus ratios (N/P ratios), 475
- Nitrogen vacancy (NV), 328
- Nitroglycerin (NG), 469–470
- Nitrospiropyran, 666
- Nitroxide-mediated radical polymerization (NMP), 97
- Nitroxides, 831–832
- NIV. *See* Noninvasive ventilation (NIV)
- NK cells. *See* Natural killer cells (NK cells)
- NK105, 468
- NLRP. *See* NOD leucine-rich repeat and pyrin domain (NLRP)
- NLRs. *See* NOD-like receptors (NLRs); Nucleotide-binding oligomerization domain-like receptors (NLRs)
- NLSs. *See* Nuclear localization signals (NLSs)
- NMP. *See* N-Methyl 2-pyrrolidone (NMP); Nitroxide-mediated radical polymerization (NMP)
- NMR spectroscopy. *See* Nuclear magnetic resonance spectroscopy (NMR spectroscopy)
- No observable adverse effect level (NOAEL), 271, 852
- Noble metals, 793
- NOD. *See* Nucleotide-binding oligomerization domain (NOD)
- NOD leucine-rich repeat and pyrin domain (NLRP), 749
- NOD-like receptors (NLRs), 1105
- Nominal strain, 41
- Nominal stress, 41
- Non-competition provisions, 1498
- Non-disclosure agreement (NDA), 1498–1500
- Non-Hodgkin’s lymphoma patients, 121b
- Non-solicitation provisions, 1498
- Non-stem cell-based approaches, 1127
- Nonabsorbable polyester sutures, 1191
- Nonaldehyde fixation methods, 379
- Nonbioactive glass microspheres. *See* Insoluble glass microspheres
- Nonbiodegradable fibrous composites, 425
- Nonbrittle materials, 51b
- Noncolloidal DDSs, 1245, 1247–1249
- Noncontact mode-atomic force microscopy (NCM-AFM), 69t

- Noncovalent encapsulation, 466–467
 coordination bonding, 467
 electrostatic force, 467
 hydrogen bonding, 467
 hydrophobic interaction, 467
 π - π interaction, 467
 physical combination, 467
 van der Waals force, 467
- Nonfibrillar collagens, 402
- Nonfoldable PMMA IOLs, 1141
- Nonfouling compositions, 539–540
- Nonfouling surfaces (NFSs), 81, 507, 508b, 555–556
 background and mechanism, 508–510
 in cell culture, 667–668
 nonfouling behavior, 508f
 nonfouling materials, 510–511, 510t
 thermodynamics of protein adsorption, 509t
- Noninvasive ventilation (NIV), 1052
- Nonionic synthetic materials, 510t
- Nonlinear biomaterials, 1346
- Nonlinear relationship, 43
- Nonpolarizable electrodes, 222
- Nonpolymeric materials, 435
- Nonporous composites, 417
- Nonproliferative DR, 1137
- Nonshivering thermogenesis, 1393
- Nonsignificant risk (NSR), 1465–1466
- Nonspecific reactions, 490
- Nonspherical architectural patterning, 612
- Nonsteroidal antiinflammatory drugs (NSAIDs), 906
- Nonthrombogenic treatments and strategies
 active materials, 522–528
 criteria for nonthrombogenicity, 515–517
 drug-eluting stent-induced thrombosis, 530b
 endothelial cell activation on vascular grafts, 528b
 historical perspective, 515
 inert materials, 517–522
 “poor” material blood compatibility, 529b
 strategies to lower thrombogenicity of metals, 528–530
 use of endothelial cells and RGD peptides, 528
- Nontoxic cryoprotectants, 379
- Nontoxic elements, 271
- Nonwoven textiles, 590
- Normal hydrogen electrode (NHE), 221
- Normal-pressure glaucoma (NPG), 1143
- NovaBone, 298–299
- NovaMin, 300–301
- NovoSorb biodegradable temporizing matrix, 1171t
- NPC. *See* Nuclear pore complex (NPC)
- NPD. *See* New product development (NPD)
- NPG. *See* Normal-pressure glaucoma (NPG)
- NPs. *See* Nanoparticles (NPs)
- NPWT. *See* Negative-pressure wound therapy (NPWT)
- NSAIDs. *See* Nonsteroidal antiinflammatory drugs (NSAIDs)
- NSOM. *See* Nearfield scanning optical microscopy (NSOM)
- NSR. *See* Nonsignificant risk (NSR)
- Nuclear factor-kappa B (NF- κ B), 742–743
- Nuclear localization signals (NLSs), 477, 546
- Nuclear magnetic resonance spectroscopy (NMR spectroscopy), 86, 311, 465, 493, 1326, 1327t
- Nuclear mechanotransduction, 719–720
- Nuclear pore complex (NPC), 474
- Nuclear transport, 474, 477
- Nucleic acids, 361, 382, 453, 472, 1268–1269
 antibodies. *See* Aptamers
 condensation, 474–476
 delivery applications, 472–478
 clinical development, 477–478
 clinical-stage NPs for anticancer drug delivery, 473t
 intracellular barriers against nucleic acid delivery, 472–474
 NP-based gene therapy under clinical evaluation, 478t
 strategies to overcome intracellular barriers, 474–477
 drugs, 1249–1250
 intracellular barriers to successful delivery, 474f
 products, 1536.e5
- Nucleoskeleton, 1339–1340
- Nucleotide-binding oligomerization domain (NOD), 749, 750f
- Nucleotide-binding oligomerization domain-like receptors (NLRs), 749
- Nucleus, 719–720
 direct transmission of forces to, 1339–1340
- NuLens, 1142
- Nuremberg Code, 1512
- Nutrients, 824
- NV. *See* Nitrogen vacancy (NV)
- NVP. *See* N-Vinyl-pyrrolidone (NVP)
- Nylon, 23, 578–579, 595
 Nylon 6, 580t–581t
 Nylon-6, 1191
 Nylon-6,6, 103, 580t–581t, 1191
 repeat unit, 95–96
 sutures, 1191
- Nystatin ointments, 1172
- O**
- o-PD. *See* O-Phenylenediamine (o-PD)
- O/W emulsion. *See* Oil in water emulsion (O/W emulsion)
- OA. *See* Osteoarthritis (OA)
- Obsolescence, 1421, 1423
- OCP. *See* Octacalcium phosphate (OCP);
 Open-circuit potential (OCP)
- OCT. *See* Coherence tomography (OCT)
- Octamethylcyclotetrasiloxane (Me₂SiO)₄, 110
- Octacalcium phosphate (OCP), 291, 1125
- 2-Octyl cyanoacrylate, 1186
- OD. *See* Outer diameter (OD)
- ODNs. *See* Oligodeoxynucleotides (ODNs)
- OECD. *See* Organization for Economic Cooperation and Development (OECD)
- OEG. *See* Oligo(ethylene glycol) (OEG)
- Office of Laboratory Animal Welfare (OLAW), 900
- Office of Management and Budget (OMB), 1475
- OHAp, 1087
- OI. *See* Optical imaging (OI)
- Oil in water emulsion (O/W emulsion), 435–436, 459–460
- OLAW. *See* Office of Laboratory Animal Welfare (OLAW)
- Oligo(ethylene glycol) (OEG), 466, 508, 668, 1058
- Oligo(poly)ethylene glycol(fumarate) (OPF), 1318–1319
- Oligodeoxynucleotides (ODNs), 472
- Omafilcon A lens, 1139
- OMB. *See* Office of Management and Budget (OMB)
- OmniDerm, 1173
- On-demand drug release, 468
- One-dimensional problem (1D problem), 48
- “One-size-fits-all” approach, 370
- ONFH. *See* Osteonecrosis of femoral head (ONFH)
- Onpattro, 1239–1240
- Opacity, 50
- Open-circuit potential (OCP), 262, 945–946
- Operational Qualification (OQ), 1445
- OPF. *See* Oligo(poly)ethylene glycol(fumarate) (OPF)
- Ophthalmic delivery, 442
- Ophthalmologic applications
 biomaterials used in, 1138t
 carbon biomaterials in, 350
 considerations for ophthalmic materials, 1137
 contact lenses, 1137–1138
 eye
 anatomy, 1135–1136, 1136f
 dimensions of globe and ocular structures, 1136t
 eye-related conditions and statistics, 1136–1137
 intraocular lens implants, 1140–1145
 new-generation MIGS implantation devices, 1145
- Oppenheimer effect, 817
- Opsonization, 760, 763–764
- Optical biosensors, 1273
- Optical glucose biosensors, 1267

- Optical imaging (OI), 479–480
 Optical properties of materials, 50
 OQ. *See* Operational Qualification (OQ)
 Oral DDSs, 1252–1253
 Oral delivery, 442
 Oral mucosa, 1128–1129
 Orbital implants, 602
 Organ perfusion, 22
 Organ-on-a-chip systems, 1302
 3D culture, 674–675
 Organelles, 691, 1269
 Organic matrix
 adhesive monomers, 141–142
 case study, 148
 historical perspective, 139
 monomer matrix—conventional systems, 140–142
 different generations of dental adhesives, 141f
 molecular structure of conventional dimethacrylates, 140f
 timeline for improvements in dental composites and adhesives, 140f
 silane coupling agents, 148
 Organic polymers, 1275–1277
 Organic solvent, 435
 Organic–inorganic hybrid materials, 966
 Organization for Economic Cooperation and Development (OECD), 855
 Organogenesis, 601
 Organoids, 1406, 1298
 Organs, 683
 structure, 686–687
 Orthopedic applications
 biomaterials development, 1081–1085
 femoral head prostheses/short-stem prostheses, 1082–1083
 long-stem prostheses, 1083
 mold arthroplasty, 1081
 total hip replacement arthroplasty, 1083
 biomedical composites in, 424–426
 carbon biomaterials in, 346–349
 long-term implants, 347–348
 tissue-engineering approaches, 348–349
 orthopedic biomaterials, 1079, 1080t, 1092–1113
 carcinogenesis, 1112
 controversial particle characteristics, 1103
 corrosion, 1093–1098
 design, 1079
 histological identification of particles in vivo, 1099
 hypersensitivity, 1109–1112
 local tissue effects of wear and corrosion, 1104–1107
 market, 1079
 mechanical properties, 1088t
 metal ions (soluble debris), 1103–1104
 particle characterization, 1100
 particulate debris, 1099–1103
 particulate debris reactivity
 characterization, 1101
 passivating oxide films, 1096
 preventive strategies and future directions, 1112–1113
 remote and systemic effects of wear and corrosion, 1107–1109
 systemic particle distribution, 1108
 wear debris generation, mechanisms of, 1093, 1094f
 total arthroplasty, 1085–1092
 ceramics, 1087
 cobalt–chromium alloys, 1089
 metals, 1087–1089
 polymers, 1086
 stainless steel alloys, 1089
 surfaces and coatings, 1092
 tantalum alloys, 1089–1092
 titanium alloys, 1089
 zirconium alloys, 1089–1092
 Orthopedic devices, 842, 903–904
 based on pure Mg, 283–284
 bone defect models, 903–904
 Orthopedic devices based on MgCaZn alloy (Magnezix), 283
 Orthopedic devices based on MgYREZr alloy (Magnezix), 283–284
 Orthopedic implants, 603, 823
 Orthopedic tissues, 1299–1301
 Orthophosphate, 1100
 OS test. *See* Oxidative stress test (OS test)
 Osmotic pressure, 89
 Osmotic pump, 1244–1245
 Osmotic repulsion, 509
 Osseointegration, 25, 672b, 1122–1123
 Osteoarthritis (OA), 444
 Osteoblasts, 728
 Osteoclasts, 728, 797
 differentiation factor, 1104–1105
 Osteocytes, 728
 OsteoFab, 634
 Osteolysis, 1104, 1106
 Osteonecrosis of femoral head (ONFH), 283–284
 Osteoprotegerin, 1104–1105
 Osteosarcoma, 814–815, 817
 Outer diameter (OD), 1052
 OVA. *See* Ovalbumin (OVA)
 Ovalbumin (OVA), 442
 “Over-kill” approach, 1444
 OX40L–OX40, 762–763
 Oxidation, 1241
 sterilization, 1438
 Oxidative biodegradation, 926–935
 activation of phagocyte redox metabolism, 931f
 chemical structure strategies to combat oxidation, 935
 crack pattern on inner lumen, 934f
 device-or environment-mediated oxidation, 933–935
 direct oxidation by host, 927–929
 generation of potential oxidants, 930f
 hypochlorous acid, 930f
 induced by external environment, 935
 initiation of oxidation pathways, 935f
 pathways for oxidative fragmentation, 929f
 pellethane 2463–80A pacemaker lead tubing, 932f
 random crack pattern, 933f
 reaction mechanisms and polymer structures, 926–927, 927f–928f
 readily oxidizable functional groups, 928f
 smooth crack wall indicative, 934f
 stress cracking, 931, 932f
 Oxidative stress, 341, 1163–1164
 Oxidative stress test (OS test), 465
 Oxide films, 217–220, 1096
 high-field, low-temperature, 217–220
 “Oxide-like” conversion of metallic surfaces, 500
 Oxyapatite, 1125
 Oxygen, 1016
 oxygen-carrying blood, 133–134
 oxygenated blood, 1016
 Oxygenator biocompatibility challenges, 1055–1056
 Oxyhydroxyapatite, 1125
 Ozone, 1432, 1435, 1438
- P**
 P-Sel, 1225
 P-selectin, 707
 P(GA-co-CL), 580t–581t
 P(GA-co-TMC), 580t–581t
 PA. *See* Polyacrylamide (PA); Pulmonary artery (PA)
 PAA. *See* Poly(acrylic acid) (PAA)
 Pacemakers, 28, 28f
 PACG. *See* Primary angle-closure glaucoma (PACG)
 Packaging
 integrity, 1453
 systems, 1429
 Packing parameter, 456
 Paclitaxel (PTX), 466, 530
 PTX-loaded gelatin NPs, 462
 PAGA. *See* [α -(4-Aminobutyl)-l-glycolic acid] (PAGA)
 PAI. *See* Photoacoustic imaging (PAI)
 PAIs. *See* Plasminogen activator inhibitors (PAIs)
 Palette, 35
 PAMAM. *See* Polyamidoamine (PAMAM)
 PAMPs. *See* Pathogen-associated molecular patterns (PAMPs)
 PAN. *See* Polyacrylonitrile (PAN)
 PAn. *See* Polyaniline (Pan)
 Pancreatic β -cells, 1269
 Paracrine pathways, 698

- Paraffin spheres, 612
- Parallel plate flow chamber, 720
- Parenchyma, 684–687, 813
- Paris law, 216
- Partial tendon ruptures, 1351
- Partial-thickness burns, 1169
- Partially degradable composites, 425
- Partially stabilized zirconia (PSZ), 955–956
- Particle load, 1102
- Particle replication in nonwetting templates (PRINT), 463–464
- Particle size, 431–432
- Particle-dependent preneoplasia–neoplasia model, 817–818
- Particle-reinforced composites, 415, 417
- Particles, 1098–1099
- Particulate debris, 1099–1103
- Particulate-delivery systems, 443–444
- Parylene coating, 500–501
- Parylene-C, 1154
- PAs. *See* Peptide amphiphiles (PAs)
- Passaging cells, 662
- Passivating oxide films, 1096
- Passive films, 51
- Passive oxide films, 217–220
- Passive targeting, 469, 1254
- Paste injectable bulking agent, 134
- Pasteurella multocida*, 908
- Patch testing, 1111
- Patent ductus arteriosus (PDA), 1024–1025
- Patent foramen ovale (PFO), 1024–1025
- Patents, 1501–1503
 - license agreement, 1506–1507
 - prosecution, 1503
- Pathogen-associated molecular patterns (PAMPs), 747–749, 1105, 1200–1201
- Pathogenic agents, 777
- Pathogens, immune response to, 765–766
- Pathological calcification, 974
 - biomaterial calcification
 - assessment, 977–979
 - mechanisms, 979–982
 - design considerations and selection, 987
 - biomaterials calcification triad, 987f
 - heart valve calcification, 982–983
 - prevention of calcification, 983–987, 987t
 - criteria for efficacy and safety of anti-mineralization treatments, 983t
 - currently used, 986t
 - inhibitors of hydroxyapatite formation, 984
 - preclinical efficacy and safety testing of, 984t
 - prototypical agents, 984t
 - representative prostheses, 974t
 - spectrum of pathologic biomaterial and medical device calcification, 974–977
 - bioprosthetic heart valves, 974–975, 975f
 - breast implants, 975–976
 - intraocular and soft contact lenses and scleral buckles, 976–977
- IUDs, 976
- polymeric heart valves and blood pump bladders, 975
- TAVR, 975
- urinary stents and prostheses, 976
- Patient-specific 3D adipose tissue models, 1395b
- Patisiran, 1239–1240
- Pattern recognition by innate immune system, 749–750
- Pattern recognition receptors (PRRs), 749, 1105
- Patterned cocultures, 669, 669f
- Patterned surface compositions, 539–540
- Patterning, 485, 501
 - with masks, 561–562
 - deposition/etching with masks, 562
 - photolithography with masks, 561–562
 - with masters, 563–565
 - imprinting with master, 563
 - printing with stamp, 563–565
 - by self-assembly of polymers and colloids, 565–567, 566f
 - block copolymer self-assembly, 565–566
 - magnetic self-assembly, 567
 - nanosphere lithography, 566–567
 - texture, 644
- Patterning on Topography (PoT), 409–410
- Paxillin, 706, 718
- PBA. *See* 3-Aminophenyl-boronic acid (PBA)
- PBAE. *See* Poly(β -amino ester) (PBAE)
- PBS. *See* Phosphate buffered solution (PBS)
- PBT. *See* Polybutylene terephthalate (PBT)
- PC. *See* Phosphorylcholine (PC)
- pCBMA. *See* Polycarboxybetaine methacrylate (pCBMA)
- PCI effect. *See* Photochemical internalization effect (PCI effect)
- PCL. *See* Polycaprolactone (PCL)
- PCLA. *See* Poly(caprolactone-co-lactic acid) copolymers (PCLA)
- PCLEEP fibers. *See* Poly(ϵ -caprolactone-co-ethyl ethylene phosphate) fibers (PCLEEP fibers)
- PCO. *See* Posterior capsule opacification (PCO)
- PCPTM, 466
- PCR. *See* Polymerase chain reaction (PCR)
- PCU. *See* Poly(carbonate-co-urethane) (PCU)
- PDA. *See* Patent ductus arteriosus (PDA)
- PDCs. *See* Polymer–drug conjugates (PDCs)
- PDEAEMA. *See* Poly(diethylaminoethyl methacrylate) (PDEAEMA)
- PDFs. *See* Powder diffraction files (PDFs)
- PDGF. *See* Platelet-derived growth factor (PDGF)
- PDGF-BB. *See* Platelet-derived growth factor BB (PDGF-BB)
- PDGF- β . *See* Platelet-derived growth factor- β (PDGF- β)
- PDL. *See* Periodontal ligament (PDL)
- PDLA. *See* Poly(D-lactic acid) (PDLA)
- PDLLA. *See* Poly(D, L-lactic acid) (PDLLA)
- PDLSCs. *See* Periodontal ligament stem cells (PDLSCs)
- pDMAEM. *See* 2-Dimethyl(aminoethyl) methacrylate (pDMAEM)
- PDMAEMA. *See* Poly(dimethylaminoethyl methacrylate) (PDMAEMA)
- PDMS. *See* Polydimethylsiloxane (PDMS)
- PDO. *See* Polydioxanone (PDO)
- PDP. *See* Potentiodynamic polarization (PDP)
- PDT. *See* Photodynamic therapy (PDT)
- PE. *See* Polyethylene (PE); Pulmonary embolism (PE)
- PEAA. *See* Poly(ethylacrylic acid) (PEAA)
- PEDOT. *See* Poly(3,4-ethylenedioxythiophene) (PEDOT)
- PEEK. *See* Polyetheretherketone (PEEK)
- PEG. *See* Polyethylene glycol (PEG)
- PEG diacrylate (PEGDA), 1227
- PEG methacrylate (PEGMA), 667–668
- PEG-PAsp. *See* PEG-poly(aspartic acid) (PEG-PAsp)
- PEG-PCL. *See* PEG-poly(ϵ -caprolactone) (PEG-PCL)
- PEG-PLA. *See* Poly(ethylene glycol)-poly(lactic acid) (PEG-PLA)
- PEG-PLGA. *See* PEG-poly(lactic-co-glycolic acid) (PEG-PLGA)
- PEG-PLys. *See* PEG-poly(L-lysine) (PEG-PLys)
- PEG-poly(aspartic acid) (PEG-PAsp), 455
- PEG-poly(L-lysine) (PEG-PLys), 455
- PEG-poly(lactic-co-glycolic acid) (PEG-PLGA), 453–454
- PEG-poly(ϵ -caprolactone) (PEG-PCL), 453–454
- PEGDA. *See* PEG diacrylate (PEGDA)
- PEGDE. *See* Polyethylene glycol diglycidyl ether (PEGDE)
- PEGMA. *See* PEG methacrylate (PEGMA)
- PEGylation, 432–434, 441, 468–469, 1243–1244
- PEI. *See* Polyethylenimine (PEI)
- PEN. *See* Polyethylene naphthalate (PEN)
- Pendant groups, 86
- PEO. *See* Polyethylene oxide (PEO)
- PEO-PPO-PEO. *See* Poly(ethylene oxide)-poly(propylene oxide)-poly(ethylene oxide) (PEO-PPO-PEO)
- PEPA. *See* Polyester polymer alloy (PEPA)
- Peptide amphiphiles (PAs), 369
- Peptides, 369, 453, 1255, 1256t
 - adhesion domains in cell adhesion proteins, 541t
 - synthesis, 1187

- Percutaneous transcatheter valves, 1007–1010, 1008f
- Percutaneous transluminal coronary angioplasty (PTCA), 27, 1039
- Perfect Lens LLS, 1143
- Perfluorocarbon liquids, 133–134
- Performance Qualification (PQ), 1445
- Perfusion seeding, 1327
- Periodontal ligament (PDL), 1121–1122
- Periodontal ligament stem cells (PDLSCs), 1127
- Periodontium, 1130
- Peripheral DNA, 1339–1340
- Peripheral nerve stimulation (PNS), 1156
- Peripheral tolerance, 766–767
- Peripheral vision loss, 1146
- Peritoneal dialysis, 1054f, 1064–1065
- Permanent skin substitutes, 1174–1175
- Permanent tissues, 693
- Permeability, 1253t
- Peroneal tibial nerve stimulation (PTNS), 1159
- Peroxide initiators, 1322
- Peroxisome proliferator activated-receptor γ (PPAR γ), 1393
- Personalized drug delivery systems, 634–635
- Perspex, 1140–1141
- Perturbations, 851
- PES. *See* Polyethersulfone (PES)
- PET. *See* Polyester terephthalate (PET); Polyethylene terephthalate (PET); Positron emission tomography (PET)
- Peyer's patches, 1206
- PF-4. *See* Platelet factor 4 (PF-4)
- PF-DA. *See* Propylene fumarate diacrylate (PF-DA)
- PFDMA. *See* Propylene fumarate dimethacrylate (PFDMA)
- PFO. *See* Patent foramen ovale (PFO)
- PGA. *See* Polyglycolic acid (PGA)
- PGE1. *See* Prostaglandin E1 (PGE1)
- PGI2. *See* Prostacyclin (PGI2)
- PGS. *See* Poly(glycerol sebacate) (PGS)
- PGs. *See* Proteoglycans (PGs)
- PH. *See* Pulmonary hypertension (PH)
- pH-responsive complexation, 160
- pH-responsive poly(acrylic acid) microspheres, 434
- pH-sensitive hydrogels, 159–160
- Phagocytic cells, 431
- Phagocytosed particles, 694
- Phagocytosis, 747, 751–752, 845 of particles, 434
- Phagolysosome, 751–752
- Phagosome, 751–752
- Phakic IOLs, 1142
- PhaP. *See* Polyhydroxyalkanoate granule-associated protein (PhaP)
- Pharmacokinetics (PK), 1237, 1243–1244
- Pharmetrics, 30
- Phase diagrams, 209–211, 210f
- inversion method, 457–458
- separation, 103, 608t, 1323t, 1325–1326
- transformation, 1182
- PHBV. *See* Poly(3-hydroxybutyrate-co-3-hydroxyvalerate) (PHBV)
- pHEMA. *See* Poly-2-hydroxyethyl-methacrylate polymers (pHEMA)
- PHEMA. *See* Poly(2-hydroxyethyl methacrylate) (PHEMA); Poly(hydroxyethyl methacrylate) (PHEMA)
- Phenotype, 691
- O-Phenylenediamine (o-PD), 1269
- Phosphate buffered solution (PBS), 262–263, 1195
- Phosphatidylcholine, 435, 810
- Phosphenes, 1145
- Phospholipase, 471, 695
- Phosphoric acid (H₃PO₄), 238–240
- Phosphorylcholine (PC), 520–521, 866b, 866f, 1059 coatings, 1059
- Photoacoustic imaging (PAI), 479–481
- Photoactivatable gels, 722
- Photochemical disruption, 477
- Photochemical internalization effect (PCI effect), 477
- Photodegradation, 176
- Photodynamic therapy (PDT), 336
- Photografting, 490–492
- Photoinduced force microscopy (PiFM), 68, 69t
- Photoinitiated grafting, 491–492
- Photoinitiators, 1322
- Photolithography, 553, 1280 with masks, 561–562
- Photoluminescence (PL), 332
- Photoreceptors (PR), 1136 cells, 1145–1146
- Photosensitizers (PS), 336
- Phototherapy, carbon biomaterials in, 336–337, 336t
- Photothermal agents, 336
- Photothermal therapy (PTT), 336
- Photovoltaic Retinal Implant Bionic Vision System (PRIMA Bionic Vision System), 1149
- PHS. *See* Public Health Service (PHS)
- PHSRV peptide sequence, 709–710
- Physical surface modification methods, 489t
- Physical vapor deposition (PVD), 587–588, 673, 964, 1279
- Physicochemical surface modification, 487 commercializability, 490 delamination resistance, 487–488 manufacturability, 490 methods, 490–498 biomedical applications of glow discharge plasma-induced surface modification processes, 492t chemical reaction, 490, 491f conversion coatings, 500 high-temperature and high-energy plasma treatments, 494 ion beam implantation, 496, 496f Langmuir–Blodgett deposition, 497–498, 497f laser methods, 501 layer-by-layer deposition, 498–501, 499f multilayer polyelectrolyte deposition, 498–501 parylene coating, 500–501 patterning, 501 plasma environment, 493 plasma generation apparatus, 493–494 RF plasma reactor, 494f RFGD plasma deposition, 492–493 RFGD plasmas for immobilization of molecules, 494 self-assembled monolayers, 498 silanization, 495–496, 495f, 495t specific chemical reactions for forming surface grafts, 494–495 surface grafting, 490–492 surface-modifying additives, 499–500, 499f physical and chemical surface modification methods, 489t surface analysis, 490 surface rearrangement, 488 surface-modified biomaterials, 488t thin surface modifications, 487–488
- Physicochemical transducers, 1269
- Physiologic hyperplasia, 694
- PI. *See* Principal investigator (PI)
- PIC micelles. *See* Polyion complex micelles (PIC micelles)
- Piezoelectric biosensor, 338–340, 1273–1274
- Piezoelectric effect, 50
- Piezoelectric properties, of materials, 50–51
- Piezoelectricity, 50–51
- PiFM. *See* Photoinduced force microscopy (PiFM)
- Pilling Bedworth ratio, 1097
- Piscine xenograft, 1171t
- PJIs. *See* Prosthetic joint infections (PJIs)
- PK. *See* Pharmacokinetics (PK)
- PKK. *See* Prekallikrein (PKK)
- PKKKRKV. *See* SV40 large T-antigen (PKKKRKV)
- PL. *See* Photoluminescence (PL)
- PLA. *See* Poly(lactic acid) (PLA)
- Plaintiff, 1508
- Planar zigzag form, 87
- Plane-strain simplification, 48
- Plane-stress simplification, 48
- Plasma, 955 cells, 757 deposition, 493 environment, 493

- exchange, 1069–1070
 generation apparatus, 493–494
 plasma-deposited films, 492
 plasma-deposited layers, 492
 separation, 1068–1069
 surface modifications, 493
 surface treatment, 587–588
 treatment, 1070
- Plasmapheresis, 1068
- Plasmid DNA, 472
- Plasmin, 806–807
- Plasminogen, 806–807
- Plasminogen activator inhibitors (PAIs), 806–807
- Plastic(s), 23
 behaviour, 43
 deformation, 45, 213
- Platelet, 802
 activation, 515, 516b, 517–518, 526–527, 529b
 adhesion, 521, 801–807
 clotting factor interactions, 804f
 properties of human clotting factors, 803t
 aggregation, 803
 coagulant activity, 804
 consumption, 72, 804
 deposition and activation, 880b
 GPIIb/IIIa antagonists, 522
 receptor-mediated interactions, 648
 release reaction, 803–804
 structure, 802f
- Platelet factor 4 (PF-4), 802
- Platelet-derived growth factor (PDGF), 364–365, 705, 738–739, 1130
- Platelet-derived growth factor BB (PDGF-BB), 1358
- Platelet-derived growth factor- β (PDGF- β), 742–743
- Platelet–material interactions, 807–809
- Platinum/iridium-based devices (Pt/Ir-based devices), 1161
- Plazlyte sterilizers, 1438b
- PLD. *See* Pulsed laser deposition (PLD)
- PLGA. *See* Poly(lactic-co-glycolic acid) (PLGA)
- PLL. *See* Poly(L-lysine) (PLL)
- PLLA. *See* Poly(L-lactide) (PLLA)
- PLLA-CL. *See* Poly(L-lactide-co-caprolactone) (PLLA-CL)
- Pluripotency, 688
- Pluripotent mesodermal progenitor cells, differentiation of, 691, 691f
- Pluronic polyols, 511
- PM. *See* Powder metallurgy (PM)
- PMA. *See* Premarket application (PMA); Premarket approval (PMA)
- PMAA. *See* Poly(methacrylic acid) (PMAA)
- PMEA. *See* 1,2-Polymethoxyethyl acrylate (PMEA)
- PMMA. *See* Polymethyl methacrylate (PMMA)
- PMNs. *See* Polymorphonuclear neutrophils (PMNs)
- PMOA. *See* Primary mode of action (PMOA)
- PMP. *See* Polymethylpentene (PMP)
- PMs. *See* Polymeric micelles (PMs)
- PNIPAAm. *See* Poly(N-isopropyl acrylamide) (PNIPAAm)
- PNS. *See* Peripheral nerve stimulation (PNS)
- PNVP. *See* Poly(N-vinyl 2-pyrrolidone) (PNVP)
- POAG. *See* Primary open-angle glaucoma (POAG)
- POE. *See* Poly(ortho esters) (POE)
- pOEGMA. *See* Poly-oligo-ethylene methacrylate (pOEGMA)
- Point defects in crystals, 211
- Poisson's ratio, 44
- Polarizable electrodes, 222
- Polished alumina, 290
- Poloxamer 407, 1140
- Poly-2-hydroxyethyl-methacrylate polymers (pHEMA), 976–977
- Poly-oligo-ethylene methacrylate (pOEGMA), 1059
- Poly-pyrrole-poly(vinyl sulfonate) (PPy-PVs), 1275
- Poly(2-hydroxyethyl methacrylate) (PHEMA), 31, 157, 435, 810, 844, 1139
- Poly(2-methacryloyloxyethyl phosphorylcholine), 511
- Poly(3-hydroxybutyrate-co-3-hydroxyvalerate) (PHBV), 415–416, 435
- Poly(3, 4-ethylenedioxythiophene) (PEDOT), 1154, 1277
- Poly(acrylic acid) (PAA), 159, 196, 199, 468
 characteristics and uses of, 100t
- Poly(aliphatic esters), 604
- Poly(alkyl cyanoacrylates), 925
- Poly(amino acids), 466
- Poly(anhydrides), 440–441, 1294
- Poly(caprolactone-co-lactic acid) copolymers (PCLA), 193–194
- Poly(carbonate-co-urethane) (PCU), 596
- Poly(carboxybetaine), 511, 659, 810, 1053f, 1059, 1065f
- Poly(carboxylic acid) cements, 1183–1184
- Poly(D,L-lactic acid) (PDLLA), 425, 609, 611–612, 830
- Poly(D,L-lactide). *See* Poly(D,L-lactic acid) (PDLLA)
- Poly(D-lactic acid) (PDLA), 170–171
- Poly(diethylaminoethyl methacrylate) (PDEAEMA), 159
- Poly(dimethylaminoethyl methacrylate) (PDMAEMA), 159, 1249–1250
- Poly(diols citrate), 1294
- Poly(ϵ -caprolactone-co-ethyl ethylene phosphate) fibers (PCLEEP fibers), 595–596
- Poly(ester urethanes), 923, 923f, 931, 931t, 934t
- Poly(ethylacrylic acid) (PEAA), 159–160
- Poly(ethylcyanoacrylate), 455
- Poly(ethylene glycol)-poly(lactic acid) (PEG-PLA), 453–454
- Poly(ethylene oxide)-poly(propylene oxide)-poly(ethylene oxide) (PEO-PPO-PEO), 453–454
- Poly(ethylene-co-vinyl acetate), 1239
- Poly(glycerol sebacate) (PGS), 596, 1294, 1320–1321
- Poly(hydroxyethyl methacrylate) (PHEMA), 94, 415–416
- Poly(L-glutamic acid). *See* Polyglycolic acid (PGA)
- Poly(L-lactic acid) (PLLA), 415–416, 604, 609, 1317, 1358–1359
- Poly(L-lactide-co-caprolactone) (PLLA-CL), 1294, 1363
- Poly(L-lysine) (PLL), 474
- Poly(lactic acid) (PLA), 32, 170–171, 580t–581t, 581–583, 1172, 1223, 1239, 1294, 1317, 1362–1363, 1376, 1492b–1493b
 characteristics and uses of, 100t
 PLA:PLGA fiber, 581–583
- Poly(lactic-co-glycolic acid) (PLGA), 32, 170, 343, 415–416, 468, 543, 579, 604, 830, 845, 875–876, 1127, 1201, 1220t–1221t, 1223, 1239, 1294, 1317, 1357–1358, 1390–1391
 characteristics and uses of, 100t
 controlled release devices, 186b
 microparticles
 inhalable highly porous large, 443f
 for single-dose vaccination, 443f
 microspheres, 438f, 1390–1391
 PLGA-based NPs, 478t
 in temporary support devices, 185b
- Poly(lactide-co-glycolide). *See* Poly(lactic-co-glycolic acid) (PLGA)
- Poly(methacrylic acid) (PMAA), 159
- Poly(N-isopropyl acrylamide) (PNIPAAm), 160, 193, 196, 196b
- Poly(N-isopropylacrylamide-acrylamide-vinylphenylboronic acid) (poly(NIPAM-AAm-VPBA)), 1269, 1278
- Poly(N-isopropylacrylamide) (Poly(NIPAAm)), 666
- Poly(N-vinyl 2-pyrrolidone) (PNVP), 157
- Poly(NIPAAm). *See* Poly(N-isopropylacrylamide) (Poly(NIPAAm))
- Poly(ortho esters) (POE), 170, 434, 440–441, 1294
- Poly(propylacrylic acid) (PPAA), 159–160, 1250
- Poly(propylene fumarate) (PPF), 1294, 1320–1321
- Poly(propylene oxide) (PPO), 519
- Poly(sebacic anhydride) (PSA), 453–454

- Poly(styrene-isobutylene-styrene) (SIBS), 936
- Poly(sulfobetaine) (PSB), 511, 659, 810, 1059
- Poly(tetramethylene oxide) (PTMO), 519
- Poly(vinyl alcohol) (PVA), 158, 435, 463–464, 527, 966, 1278
sponges, 26
- Poly(vinylpyridine) microparticles, 441
- Poly(α -hydroxy acid), 433
- Poly(β -amino ester) (PBAE), 474, 477
- Polyacetals, 434
- Polyacrylamide (PA), 1220t–1221t, 1223
characteristics and uses of, 100t
- Polyacrylonitrile (PAN), 1066
- Polyaddition polymers, 1321–1322
free radical polymerization, 1322
ionic polymerization, 1322
- Polyamides, 924
- Polyamidoamine (PAMAM), 458, 476–477, 1247
- Polyanhydrides, 169–170, 434
- Polyaniline (PAN), 1271, 1277, 1279
- Polybutylene terephthalate (PBT), 1172
- Polycaprolactone (PCL), 171, 345–346, 415–416, 433–434, 579, 580t–581t, 633–634, 1127, 1172, 1294, 1317, 1358, 1363, 1376, 1391–1392, 1492b–1493b
fibers, 595–596
- Polycarbonates, 170–171, 415–416
- Polycarboxybetaine methacrylate (pCBMA), 1059
- Polycations, 474
chemical structures, 475f
hydrophobic modification, 475
- polyCBMA. *See* Polymerization using carboxybetaine methacrylate (polyCBMA)
- Polycondensation, 110–112
polymers, 1320–1321
click reactions, 1321
ring-opening polymerization, 1321
- Polydimethylsiloxane (PDMS), 109, 116, 120b, 500, 522, 562–565, 667, 675, 966, 1055–1056, 1061–1062, 1154, 1227, 1241–1242, 1321
characteristics and uses of, 100t
- Polydioxanone (PDO), 578–579, 1363, 1492b–1493b
sutures, 1193–1194
- Polyelectrolyte
capsules, 455–456
cements, 1183–1184, 1184f
- Polyester polymer alloy (PEPA), 1066
- Polyester terephthalate (PET), 1492b–1493b
- Polyesters, 170–171, 455–456, 595, 922–923, 1223
monofilaments, 591
Polyester scaffolds, 1376
Polyester sutures, 1191
- Polyetheretherketone (PEEK), 120b, 348, 415–416
characteristics and uses of, 100t
- Polyethersulfone (PES), 1058f, 1066
- Polyethylene (PE), 38, 88–89, 125, 415–416, 494, 578–579, 580t–581t, 602
characteristics and uses, 100t
- Polyethylene glycol (PEG), 31–32, 155, 158, 171, 192, 291–292, 434, 466, 468, 487–488, 508, 555–556, 631–632, 658, 667, 810, 833, 1058, 1064f, 1127, 1186, 1192, 1220t–1221t, 1223, 1239, 1275, 1290–1291, 1317, 1391
chains, 542
hydrophilic materials based on, 833
immobilization, 518–520
materials with nano/microscale surface texture, 833–834
methods for incorporation, 519f
effect of PEG chain length, 519f
PEG-modified surfaces, 518f
superhydrophobic materials, 833
- Polyethylene glycol diglycidyl ether (PEGDE), 1275
- Polyethylene naphthalate (PEN), 1280
- Polyethylene terephthalate (PET), 7–8, 95, 415–416, 463–464, 578–579, 580t–581t, 922–923, 1041–1042, 1046–1047, 1052, 1191, 1363–1364, 1492b–1493b
characteristics and uses of, 100t
- Polyethylenimine (PEI), 474, 476–477, 525, 833, 1067, 1206–1207
PEI-based NPs, 478t
- Polyglactin 910 10/90, 580t–581t
- Polyglycolic acid (PGA), 32, 167, 425, 579, 580t–581t, 1172, 1192, 1223, 1294, 1321, 1362–1363, 1376, 1404, 1492b–1493b
degradation, 72
sutures, 1193
- Polyglycolide. *See* Polyglycolic acid (PGA)
- PolyGraft, 426
- Polyhedral oligomeric silsesquioxanes (POSS), 143
POSS-PCU polymers, 1363–1364
- polyHEMA. *See* Poly(2-hydroxyethyl methacrylate) (PHEMA)
- Polyhydroxyalkanoate granule-associated protein (PhaP), 832–833
- Polyhydroxyalkanoates, 1294
- Polyimide, 1154
- Polyion complex micelles (PIC micelles), 455
- Polyketals, 434
- Poly lactide. *See* Poly(lactic acid) (PLA)
- Polymer backbone functionality, 169–171
different polymer, 171f
poly(ortho esters), 170
polyanhydrides, 169–170
polycarbonates, 170–171
polyesters, 170–171
relative hydrolytic rates, 170f
- Polymerase chain reaction (PCR), 828, 1268–1269
- Polymer–ceramic composites, 427
- Polymer–drug conjugates (PDCs), 1247–1249, 1248t
- Polymeric micelles (PMs), 453–454. *See also* Lipid-based NPs; Inorganic NPs.
dendrimers, 458
nanocapsules, 455–456
nanocomplexes, 458–459
nanogels, 458
nanospheres, 455
polymersomes, 456–458
- Polymeric nanocomposites. *See* Organic–inorganic nanocomposites
- Polymeric NPs, 453–459, 473t
inorganic NPs, 460–461
GNPs, 460
MNPs, 460
nanocarbons, 461
QDs, 461
silica NPs, 460–461
lipid-based NPs, 459–460
lipoplexes, 460
liposomes, 459
SLNs, 459–460
- polymeric micelles, 453–454
dendrimers, 458
nanocapsules, 455–456
nanocomplexes, 458–459
nanogels, 458
nanospheres, 455
polymersomes, 456–458
- Polymeric/polymer(s), 85, 1086, 1250
architecture, 171–172
hydrophobicity *vs.* hydrophilicity, 172
molecular weight, 172
morphology, 172
polymerization routes, 171–172
architectures, 86f
biomaterials, 100t, 179b
brushes, 86, 1275, 1279
case studies, 99
chemical composition, determination of, 86–87
complexes, 161
copolymers, 86, 88f
degradation, 919–920
mechanisms leading, 920t
postimplant degradation forces, 920
preimplant degradation, 919–920
typical operations on injection-moldable polymer biomaterial, 920t
fibers, 416–417
heart valves, 975, 976f
materials, 844
molecular mass, 87–89
molecule, 85–94
patterning by self-assembly, 565–567, 566f

- physical behavior with chemical characteristics, 90–91
 glassy state, 90
 hydrophilicity, 94
 interactions with water, 94–95
 of linear and amorphous polymers, 91
 organic reactions, 95t
 of physical states, 91–93
 physical state and behavior, 93
 physical states of linear polymers, 90
 rubbery state, 90
 semicrystalline state, 90–91
 structural factors, 93t
 transition temperatures between states, measuring, 93–94
- physical properties and equilibrium water absorption, 91t
- polypropylene repeat unit and different tactic isomers, 87f
- preparation of, 1192–1193
- present and future, 99
- rehydration, 457–458
- repeat units, 88f–89f
- single polymer molecules
 chemical structure, 86
 molecular structure, 85–86
- synthesis, 95–98
 conditions, 98
 tacticity, 87
- Polymerization, 110–112, 1120
 mechanisms, 95–98
 methods for creating synthetic biocompatible polymers, 1320, 1321t
 routes, 171–172
 shrinkage phenomena, 1182
 stress, 141
- Polymerization using carboxybetaine methacrylate (polyCBMA), 521
- Polymerization using sulfobetaine methacrylate (polySBMA), 521
- Polymersomes, 456–458, 1247, 1248t
 membrane conformation, 457f
 self-assembled nanostructures of block copolymers, 457f
- 1,2-Polymethoxyethyl acrylate (PMEA), 1058
- Polymethyl methacrylate (PMMA), 23, 61, 94, 415–416, 455, 675, 827, 925, 1066, 1082–1083, 1086, 1104, 1138–1139, 1182, 1317, 1322
 characteristics and uses of, 100t
- Polymethylpentene (PMP), 1052, 1055–1056
- Polymorphonuclear leukocytes, 687–688, 844, 927–928
- Polymorphonuclear neutrophils (PMNs), 752–753
- Polyols, 104
- Polypeptides, 466
- Polyphenolic protein, 1187
- Polypropylene (PP), 87, 415–416, 580t–581t, 591, 595, 1055–1056, 1492b–1493b
 characteristics and uses, 100t
 sutures, 1191–1192
- Polypropyleneimine (PPI), 458
- Polypyrrole (PPy), 1277
- Polysaccharides, 361, 466, 468, 510–511, 1293
 polysaccharide-based fibers, 579
- polySBMA. *See* Polymerization using sulfobetaine methacrylate (polySBMA)
- Polysiloxane/urethane soft segment issues, 924
- Polystyrene (PS), 665, 1224–1225
- Polysulfobetaine methacrylate (pSBMA), 1059
- Polysulfone (PSU), 415–416, 1066
- Polytetrafluoroethylene (PTFE), 7–8, 30–31, 101b, 125–127, 127f, 415–416, 493, 578–579, 580t–581t, 826, 1041–1042, 1083, 1086
 catheter introducers, 133
 mesh, 130
 paste injectable bulking agent, 134
- Polythiophene (PTh), 1277
- Polyurethanes (PUs), 30, 103, 104f, 343–344, 415–416, 527, 596, 658, 831, 935–936, 936f, 1172, 1320–1321
 anatomy, 103
 block copolymer, 105f
 case study, 106b
 physical properties, 103–104
 synthesis, 104–106
 reactions, 104
 tailoring polyurethane behavior, 106
- Polyvinyl chloride (PVC), 90–91, 527, 1055–1056, 1067
 characteristics and uses of, 100t
- Polyvinyl pyrrolidone (PVP), 469, 518, 527, 1140, 1279
- Polyvinylidene fluoride (PVDF), 125–126, 128, 578–579, 580t–581t, 1141, 1492b–1493b
 PVDF-HFP copolymer backbone, 132b–133b
- Polyvinylpyrrolidone (PVP), 1058f, 1066
- Polyzwitterions, 511
- “Poor” material blood compatibility, 529b
- Porcine xenograft, 1171t
- Porogen
 interconnected spherical macropores by porogen methods, 611–612
 leaching, 608t
- Porosity
 biomaterials for tissue engineering, 604
 in facilitating biomaterial integration, 601–604
 to promote tissue ingrowth, 602–603
- Porous alumina, 319
- Porous bioactive glasses, 299–300
- Porous biomaterial, 601
- Porous calcium phosphate ceramics, 292–294
 calcium phosphate-based bone graft substitutes, 294t
 powder diffraction files, 293t
- Porous composites, 417
- Porous hydroxyapatite, 602f
- Porous materials, 610–611, 615
- Porous synthetic hydroxyapatite (Porous sHA), 299–300
- Positron emission tomography (PET), 479–480
- POSS. *See* Polyhedral oligomeric silsesquioxanes (POSS)
- Post-decellularization processing and modifications
 cross-linking, 383–384
 decellularized tissue products and clinical use, 384t
 milling for ECM powder and partial enzymatic digestion, 383
- Posterior capsule opacification (PCO), 1136–1137
- Postimplant degradation forces, 920
- Postmarket surveillance, 1485–1486
- Postmarketing management of risk and product performance, 1471–1472
- PoT. *See* Patterning on Topography (PoT)
- Potato skins, 1173
- Potentiodynamic polarization (PDP), 262
- Potentiometric biosensors, 1272–1273
- Pourbaix diagrams, 222–223, 223f
 of Zinc, 276, 277f
- Powder
 bed fusion, 624t, 626–627
 binding process, 627–628
 decellularized ECM therapies, 387–388
 XRD, 465
- Powder diffraction files (PDFs), 307
- Powder metallurgy (PM), 231
- PP. *See* Polypropylene (PP)
- PPAA. *See* Poly(propylacrylic acid) (PPAA)
- PPACK. *See* D-Phe-Pro-Arg chloromethyl ketone (PPACK)
- PPAR γ . *See* Peroxisome proliferator activated-receptor γ (PPAR γ)
- PPF. *See* Poly(propylene fumarate) (PPF)
- PPI. *See* Polypropyleneimine (PPI)
- PPO. *See* Poly(propylene oxide) (PPO)
- PPy. *See* Polypyrrole (PPy)
- PPy-PVs. *See* Poly-pyrrole-poly(vinyl sulfonate) (PPy-PVs)
- PQ. *See* Performance Qualification (PQ)
- PQQ-GDH. *See* Pyrroloquinoline quinone glucose dehydrogenase (PQQ-GDH)
- PR. *See* Photoreceptors (PR)
- Preadipocytes, 1393
- PreadSORption with purified adhesion proteins, effects of, 646–647
- Precipitation
 strengthening, 214–215
 temperature, 193

- Precursors of PUs, 104, 105t
 Preimplant degradation, 919–920
 Prekallikrein (PKK), 809
 Premarket application (PMA), 900
 Premarket approval (PMA), 1425, 1463
 Premarket assessment requirements, 1465–1466
 Premarket clearance and approvals, 1466–1467
 Prepolymer, 104
 Presbyopia, 1136
 Pressure-sensitive adhesives, 115
 PRIMA Bionic Vision System. *See* Photovoltaic Retinal Implant Bionic Vision System (PRIMA Bionic Vision System)
 Primary angle-closure glaucoma (PACG), 1143
 Primary culture, 662
 Primary mode of action (PMOA), 1257–1258
 Primary open-angle glaucoma (POAG), 1143
 PriMatrix, 1174
 Primer, 1181, 1185
 Principal directions, 47–48
 Principal investigator (PI), 901
 Principal stresses, 47–48
 PRINT. *See* Particle replication in nonwetting templates (PRINT)
 Printing
 with inkjets, quills, and pins, 557–558
 with stamp, 563–565
 microcontact printing, 563–565, 564f
 microfluidic patterning, 565, 565f
 Prions, 1432
 Prismatic rod, 41
 Pristine fullerenes, 333
 Processed tissues
 challenges and future directions for decellularized tissues, 389
 cryopreservation, 377–379
 decellularization, 380–382
 decellularized ECM applications, 384–389
 post-decellularization processing and modifications, 383–384
 tissue cross-linking, 379–380
 vitrification, 377–379
 Procollagens, 402
 Prodrug, 466
 Product life cycle, 1417–1418
 Proinflammatory cytokines, 845
 Proinflammatory M1 macrophages, 742–743
 Proinflammatory mediators, 1104–1105, 1105f
 Proliferation factor, 1111
 Proliferative DR, 1137
 Promutagens, 857–858
 Properdin pathway, 780
 Proportional limit, 45
 Propylene fumarate diacrylate (PF-DA), 1321–1322
 Propylene fumarate dimethacrylate (PFDMA), 1321–1322
 Prostacyclin (PGI₂), 523f, 527, 723
 Prostaglandin E1 (PGE1), 527
 Prostaglandins, 698, 1104–1105
 Prostate-specific antigen (PSA), 338–340, 479
 Prostate-specific membrane antigen (PSMA), 1255–1257
 Prostheses, 633–634
 Prosthetic heart valves, 1491b
 Prosthetic joint infections (PJIs), 823
 Proteases, 695, 706
 Proteasomes, 694
 Protein adsorption, 81, 485, 516b, 517, 519–520, 520b, 522, 530
 thermodynamics of, 509t
 Protein bioconjugates, smart polymers, 194, 195f
 Proteins, 361–363, 453, 643, 1255, 1256t
 adhesion proteins, effect on cellular interactions, 645–649
 depletion studies, 647–648
 preadsorption with purified adhesion proteins, effects of, 646–647
 receptor activity with antibodies, inhibition of, 648–649
 hydrogels, 1374–1375
 immobilization, 490
 patterning, 667
 protein-based materials, 1219–1222
 protein-based natural polymers, 1292–1293
 protein-resistant surfaces, 81, 507
 protein/peptide drugs, 1249
 resistance, 509
 Proteoglycans (PGs), 401–402, 404–406, 683, 705, 1389
Proteus mirabilis, 830, 832
 “Proton sponge” effect, 476–477, 1249–1250
 Provisional patent application, 1502
 PRRs. *See* Pattern recognition receptors (PRRs)
 PS. *See* Photosensitizers (PS); Polystyrene (PS)
 PSA. *See* Poly(sebacic anhydride) (PSA); Prostate-specific antigen (PSA)
 PSB. *See* Poly(sulfobetaine) (PSB)
 pSBMA. *See* Polysulfobetaine methacrylate (pSBMA)
Pseudoaneurysm, 1037–1038
 Pseudoelastic materials, 44
Pseudointima, 1042, 1042f
Pseudomonas sp., 1170
 P. aeruginosa, 830, 832
 Pseudotumor, 817, 996–997
 PSMA. *See* Prostate-specific membrane antigen (PSMA)
 PSU. *See* Polysulfone (PSU)
 PSZ. *See* Partially stabilized zirconia (PSZ)
 Pt/Ir-based devices. *See* Platinum/iridium-based devices (Pt/Ir-based devices)
 PTCA. *See* Percutaneous transluminal coronary angioplasty (PTCA)
 PTFE. *See* Polytetrafluoroethylene (PTFE)
 PTh. *See* Polythiophene (PTh)
 PTMO. *See* Poly(tetramethylene oxide) (PTMO)
 PTNS. *See* Peroneal tibial nerve stimulation (PTNS)
 PTT. *See* Photothermal therapy (PTT)
 PTX. *See* Paclitaxel (PTX)
 Public Health Service (PHS), 899–900
 Pulmonary artery (PA), 1054
 Pulmonary circulation, 1033–1034
 Pulmonary delivery, 442
 Pulmonary embolism (PE), 1047
 Pulmonary hypertension (PH), 1054
 Pulsatility, 726–727
 Pulsed laser deposition (PLD), 964
 Pump oxygenator, 23
 Purvalanol A, 333
 PUs. *See* Polyurethanes (PUs)
 PVA. *See* Poly(vinyl alcohol) (PVA)
 PVC. *See* Polyvinyl chloride (PVC)
 PVD. *See* Physical vapor deposition (PVD)
 PVDF. *See* Polyvinylidene fluoride (PVDF)
 PVP. *See* Polyvinyl pyrrolidone (PVP); Polyvinylpyrrolidone (PVP)
 PyC. *See* Pyrolytic carbon (PyC)
 Pyrogenicity, 1429
 tests, 872
 Pyrolytic carbon (PyC), 8, 29–30, 329, 960
 coatings in orthopedic applications, 347f
 long-term implants, 347–348
 Pyrroloquinoline quinone glucose dehydrogenase (PQQ-GDH), 1274, 1279
Q
 QAMs. *See* Quaternary ammonium methacrylates (QAMs)
 QbD. *See* Quality by design (QbD)
 QCM. *See* Quartz crystal microbalance (QCM)
 QCM-D. *See* Quartz crystal microbalance with dissipation (QCM-D)
 QD. *See* Quantum dots (QD)
 QMS. *See* Quality management system (QMS)
 QOL. *See* Quality of life (QOL)
 QS. *See* Quorum sensing (QS)
 QSR. *See* Quality system regulation (QSR)
 Quality by design (QbD), 1257–1258
 Quality management system (QMS), 1449
 Quality of decellularization, 381–382
 Quality of life (QOL), 1462
 Quality system regulation (QSR), 1448
 Quality systems for medical devices, 1421
 Quantitative contact angle measurement, 57

- Quantitative reverse transcription PCR (RT-qPCR), 828
- Quantum dots (QD), 328, 461
- Quartz crystal microbalance (QCM), 493
- Quartz crystal microbalance with dissipation (QCM-D), 70t
- Quaternary ammonium, 145
- Quaternary ammonium methacrylates (QAMs), 145
- Quinton–Scribner shunt, 25–26
- Quorum sensing (QS), 827
 - biomaterials modified with QS-quenching enzymes, 834
- R**
- RA. *See* Rheumatoid arthritis (RA)
- Rac proteins, 718–719
- Rac1 protein, 718
- Radiation, 492
 - grafting, 490–492
 - R&D, Pilot, and Low-Volume Technologies, 1434
 - radiation-based techniques, 1432–1435
 - application, 1434
 - compatibility with radiation sterilization, 1435
 - electron beam sterilization, 1433–1434
 - gamma sterilization, 1432–1433
 - principles of action and efficacy, 1432
 - safety considerations, 1432
 - X-ray sterilization, 1434
 - sterilization, 1432
 - material considerations for, 1434–1435
- Radical addition chain transfer polymerization (RAFT), 490
- Radical polymerization, 96–97
- Radical scavengers, 1435
- Radio frequency glow discharge (RFGD), 490
 - plasma deposition, 492–493
 - plasmas for immobilization of molecules, 494
- Radioactive marker, 1111
- Radiofrequency (RF), 319
 - plasma reactor, 494f
- Radiotherapy, 442–443
- RAFT. *See* Radical addition chain transfer polymerization (RAFT); Reversible addition-fragmentation chain-transfer polymerization (RAFT)
- Raman spectroscopy, 292, 311, 1327t
- Randles circuit, 1271–1272
- Random coil, 90
- Random copolymers, 86
- Randomized controlled trial (RCT), 1459
- Randomized Evaluation of Mechanical Assistance for the Treatment of Congestive Heart Failure (REMATCH), 15
- RANKL, 1104–1105
- RANTES, 756
- Rapamycin-eluting stents, 530
- Rapid prototyping, 1323t, 1324
- Rare earth elements (REE), 278
- Rat calvaria model, 904
- RBC. *See* Red blood cell (RBC)
- RBCM. *See* Red blood cell membrane (RBCM)
- RBS. *See* Rutherford backscattering spectroscopy (RBS)
- RBSs. *See* Resorbable/biodegradable stents (RBSs)
- RCA. *See* Regional citrate anticoagulation (RCA); Rolling circle amplification (RCA)
- RCT. *See* Randomized controlled trial (RCT)
- RDRPs. *See* Reversible-deactivation radical polymerizations (RDRPs)
- RE. *See* Reference electrode (RE)
- Reactive oxygen species (ROS), 336, 465, 471, 477, 698, 793–795, 952, 1106, 1162–1163
 - enhancing corrosion reactions, 952–953
- ReCell, 1171t, 1174
- Recellularization protocols, 389
- Receptor activity with antibodies, inhibition of, 648–649
- Reciprocal activation of blood coagulation, 809
- Recognition force microscopy (RFM), 69t
- Recombinant DNA technology, 1187
- Recombinant ECM proteins, 362–363
 - purification of, 408–409
- Recombinant human BMP-2 (rh BMP-2), 1130
- Recombinant human bone morphogenetic protein, 861b–862b
- Recombinant human growth hormone (rhGH), 875–876
- Recombinant technology, 404
- Reconstructed skin, 1171t
- Red blood cell (RBC), 462–463, 782
- Red blood cell membrane (RBCM), 1269
- Red cells. *See* Erythrocytes
- Redox mediators, 1277
- Reduced GO (rGO), 331–332
- REDV peptide sequence, 704, 709–710
- REE. *See* Rare earth elements (REE)
- “Reel-to-reel” plasma processing, 493–494
- Reference electrode (RE), 257
- Refractive index of material, 50
- Regeneration, 698–699, 1160
- Regenerative medicine, 401
- Regenerative Medicine Advanced Therapy (RMAT), 1176
- Regional citrate anticoagulation (RCA), 1067
- Registration, device listing, licenses, 1472–1473
- Regulatory T cells (T_{regs}), 742–744, 761, 767–768, 1210
 - elevation of Treg activity to induce tolerance, 1211
- Rehabilitation, 1158–1159
 - brain–computer interface, 1159
 - genitourinary, bladder dysfunction, 1158–1159
 - motor function, 1159
 - sensory restoration, 1158
 - auditory, 1158
 - tactile, 1158
 - visual, 1158
- Reidopyrimidinone (UPy), 368
- Reinforcement, 415–417, 416f
- Relative humidity (RH), 586
- Release kinetics, 439
- Release medium, 439
- REMATCH. *See* Randomized Evaluation of Mechanical Assistance for the Treatment of Congestive Heart Failure (REMATCH)
- Remodeling, 697
- Renal replacement therapies, 1062–1071
 - blood pumps in extracorporeal circulation, 1071
 - arterio-venous hemofiltration, 1060f
 - function of kidney, 1063
 - hemoperfusion, 1068
 - hollow fiber dialyzer, 1055f
 - sorbent dialysis, 1070–1071
 - therapeutic apheresis, 1068–1070
 - treatment of renal failure, 1063–1068
- Render texture, methods to, 605t–606t
- Repeat unit of polymer molecule, 86
- Replacement, Reduction, and Refinement (Three Rs), 1511
- Reproductive toxicity, 873
 - chromosome aberrations, 856f
 - in vitro tests for, 854–858, 855t
- RES. *See* Reticuloendothelial system (RES)
- Research integrity, 1513
- Resistive (faradaic) behavior, 224–225
- Resolution, biomolecular surface patterning of, 554
- Resomet, 283
- Resorbable bioceramics, 956
- Resorbable polymers, 168
- Resorbable PUs, 106
- Resorbable sutures, 100b
- Resorbable/biodegradable stents (RBSs), 1041
- Responsive polymers, 1268. *See also* Fiber-forming polymers.
 - in enzymatic biosensors, 1274–1278
 - active roles, 1277–1278
 - passive roles, 1274–1277, 1276t
 - integrating responsive polymers with enzymes, 1278–1279
 - with transducers, 1279
- Restorative materials of dental applications, 1119–1120
- Reticuloendothelial system (RES), 455, 462, 467
- Retina, 1136
 - implants, 1145–1146

- Retinal pigmented epithelial layer (RPE layer), 1136
- Retinitis pigmentosa (RP), 1145–1146
- Retinoic acid-inducible gene I (RIG-I), 749, 751f
- Retinoic acid-inducible gene I-like receptors (RLRs), 749
- Reverse piezoelectric effect, 50
- Reversed thermal gelation, 434–435
- Reversible addition-fragmentation chain-transfer polymerization (RAFT), 97, 99f, 171, 197
- Reversible injury, 693–694
- Reversible-deactivation radical polymerizations (RDRPs), 97
- RF. *See* Radiofrequency (RF)
- RFGD. *See* Radio frequency glow discharge (RFGD)
- RFM. *See* Recognition force microscopy (RFM)
- RGE sequence. *See* Arg-gly-glu sequence (RGE sequence)
- rGO. *See* Reduced GO (rGO)
- RGPs. *See* Rigid gas permeable (RGPs)
- RH. *See* Relative humidity (RH)
- rh BMP-2. *See* Recombinant human BMP-2 (rh BMP-2)
- Rhenium (Re), 230–231
- Rheology, 1327t
- Rheumatoid arthritis (RA), 761, 1447–1448
- rhGH. *See* Recombinant human growth hormone (rhGH)
- Rho family of GTPases, 718
- Rho proteins, 718–719
- Rho-associated protein kinase (ROCK), 1338
- RhoA proteins, 718, 1338
- Ribozymes, 472
- RIG-I. *See* Retinoic acid-inducible gene I (RIG-I)
- Right ventricle (RV), 1054
- Rights approach, 1510
- Rigid gas permeable (RGPs), 134
- Rigid gas-permeable lenses. *See* Hard contact lenses
- Ring-opening polymerization, 1321
- Risk
 - management, 1449
 - in medical device development, 1417–1418
 - risk/benefit analysis, 1448
- RLRs. *See* Retinoic acid-inducible gene I-like receptors (RLRs)
- RMAT. *See* Regenerative Medicine Advanced Therapy (RMAT)
- Robocasting, 300
- ROCK. *See* Rho-associated protein kinase (ROCK)
- Roller pumps, 1071
- Rolling circle amplification (RCA), 462
- Room Temperature Vulcanizing Elastomers (RTV Elastomers), 115
- Root-form endosseous implants, 1120–1121, 1120f–1121f
- ROS. *See* Reactive oxygen species (ROS)
- Rosen's microbuckling model and contradictions, 420
- Rosen's theory, 417
- Rotating wall vessel, 1297
- Rotational atherectomy, 1046–1047
- Royalty fee, 1507
- RP. *See* Retinitis pigmentosa (RP)
- RPE layer. *See* Retinal pigmented epithelial layer (RPE layer)
- RT-qPCR. *See* Quantitative reverse transcription PCR (RT-qPCR)
- RTV Elastomers. *See* Room Temperature Vulcanizing Elastomers (RTV Elastomers)
- Rubber bands, 103–104
- Rubbery plateau, 91
- Rubbery state of polymers, 90
- Rutherford backscattering spectroscopy (RBS), 70t
- RV. *See* Right ventricle (RV)
- RxSight, 1142–1143
- S**
- S-ICD. *See* Subcutaneous ICD (S-ICD)
- S-Nitroso-N-acetylpenicillamine (SNAP), 1061–1062
- S-nitrosothiols, 527
- S/N ratio. *See* Signal-to-noise ratio (S/N ratio)
- S1PR1 receptor, 764
- S9 metabolic activation system, 857–858
- SA. *See* Sebacic acid (SA); Streptavidin (SA)
- Safety assessment, 869
- Safety in medical device development, 1417–1418
- SAL. *See* Sterility assurance level (SAL)
- Saliva, 1129
- Salivary glands, 1129–1130
- Salivation, 1130
- Salt bridge, 475
- Salt leaching technique, 612
- SAM. *See* Scanning auger microprobe (SAM); Self-assembled monolayer (SAM)
- SAMEs. *See* Self-assembling monolayer end groups (SAMEs)
- Sandwich assays, 1268
- SANS. *See* Small angle neutron scattering (SANS)
- Sarcoma, 813
- Saturated aliphatic polyesters, 1294
- Sauerbrey's equation, 1273–1274
- SAXS. *See* Small angle X-ray scattering (SAXS)
- SB Charite artificial disc, 1084–1085, 1084f
- SBF. *See* Simulated body fluid (SBF)
- SC. *See* Schlemm's canal (SC); Subcommittees (SC)
- Scaffold strand. *See* Single-stranded DNA (ss-DNA)
- “Scaffold-free” 3D printing, 1395b
- Scaffolds
 - design, 1287, 1295–1297
 - hydrogel, 1296, 1355
 - injectable tissue-engineering, 614–615
 - macroporous, nanofibrous tissue-engineering, 613
 - materials, 1373–1374
 - decellularized tissues, 1375
 - protein hydrogels, 1374–1375
 - stem cell-derived cardiomyocytes, 1379f
 - synthetic hydrogels, 1375
 - synthetic polymers, 1375
 - methods for fabricating porous synthetic polymer, 608t
 - multiphase, 613–614
 - of polymers, 1376
 - scaffold-based therapies, 385–387
 - porcine urinary bladder matrix for wound healing, 386f
 - 3D printed, 614
- Scaled-down radiation sources, 1434
- Scanning auger microprobe (SAM), 70t
- Scanning capacitance microscopy (SCM), 69t
- Scanning electrochemical microscopy (SECM), 560
- Scanning electron microscopy (SEM), 63–65, 293, 438, 464, 946–947, 978–979, 1080, 1100, 1326, 1327t, 1536.e1
- Scanning photoemission microscopy (SPEM), 71
- Scanning probe microscopy (SPM), 66–68, 69t
- Scanning surface potential microscopy (SSPM), 69t
- Scanning thermal microscopy (SThM), 69t
- Scanning tunneling microscopy (STM), 66–68, 67f, 560
- Scar, 698–699
- Scar-free healing process, 737–738
- Scavenger receptors, 749
- SCB. *See* Standards Coordinating Body (SCB)
- scFv. *See* Single chain variable fragment (scFv)
- Schlemm's canal (SC), 1143
- Scleral buckles, 976–977
- Scleraxis (Scx), 1352
- SCM. *See* Scanning capacitance microscopy (SCM)
- SCPL. *See* Solvent casting, particulate/porogen leaching (SCPL)
- SCR. *See* Short consensus repeat (SCR)
- sCR1. *See* Soluble recombinant form of CR1 (sCR1)
- Scx. *See* Scleraxis (Scx)
- SDF-1 α/β , 756

- SDOs. *See* Standards development organizations (SDOs)
- SDS. *See* Sodium dodecyl sulfate (SDS)
- Sealants, 1183, 1184t
- Sebacic acid (SA), 172, 186b
- SEC. *See* Size exclusion chromatography (SEC)
- SECM. *See* Scanning electrochemical microscopy (SECM)
- Second-harmonic generation (SHG), 70t
- Secondary ion mass spectrometry (SIMS), 62–63, 62t, 65f
- static, 63, 493
- for adsorbed protein identification and quantification, 72
- poly(glycolic acid) degradation, 72
- Secreted protein acidic and rich in cysteine (SPARC), 470–471
- L-Selectin, 739–740
- Selective depletion, 647
- Selective heat sintering (SHS), 627
- Selective laser melting (SLM), 232, 260–262
- Selective laser sintering (SLS), 232, 627, 1324
- Selective laser trabeculoplasty (SLT), 1143
- Self-antigen, 757
- Self-assembled biomaterials, 9
- Self-assembled monolayer (SAM), 65, 498, 509, 522, 650, 656, 665, 1272, 1279
- Self-assembled surface layers, 522
- Self-assembling monolayer end groups (SAMEs), 935
- Self-assembly, 607t–608t, 1324–1325
- of nanoscale features, 604–607
- peptides or peptide amphiphiles, 1128
- Self-healing method, 1141
- SEM. *See* Scanning electron microscopy (SEM)
- Semiconducting oxide impedance, 226
- Semiconductors, n-type, 1096–1097
- semiconductors, p-type, 1096–1097
- Semicrystalline hydrogels, 153–154
- Semicrystalline state of polymers, 90–91
- Senescent organelles, 694
- Senofilcon A, 1140
- Sensitization, 871
- Sensitizers, 1109–1110
- Serology, 121b
- SERS. *See* Surface-enhanced Raman spectroscopy (SERS)
- SEs. *See* Superelasticity effects (SEs)
- SFB. *See* Society for Biomaterials (SFB)
- SFG vibration spectroscopy. *See* Sum frequency generation vibration spectroscopy (SFG vibration spectroscopy)
- SG. *See* Spatial group (SG)
- SGGs. *See* Sol–gel glasses (SGGs)
- Shape memory alloys (SMAs), 44, 230–231
- Shape-memory effects (SMEs), 230–231
- Shear modulus, 44
- Shear plane, 464
- Shear stress, 720–721, 725
- effect on blood vessels, 726–727
- Sheddable PEGylation, 469
- Sheep tibia, 904
- Sheet lamination, 624t, 628–629
- Shelf-Life, biomolecular surface patterning of, 556
- Shell-cross-linked PMs, 455
- SHG. *See* Second-harmonic generation (SHG)
- Shh. *See* Sonic Hedgehog (Shh)
- Shipping integrity, 1453
- Short consensus repeat (SCR), 783–784
- Shot peening, 214, 500
- SHS. *See* Selective heat sintering (SHS)
- ²⁹Si solid-state NMR, 311
- SI-ATRP. *See* Surface-initiated atom transfer radical polymerization (SI-ATRP)
- SIBS. *See* Poly(styrene-isobutylene-styrene) (SIBS)
- Signal-to-noise ratio (S/N ratio), 65
- Signalization, 1269
- Silane coupling agents, 148
- Silanes, 1138–1139
- Silanization, 495–496, 495f, 495t
- Silastic, 1239
- Silica
- NPs, 460–461
- sand, 319
- silica-based mesoporous materials, 965–966
- Silicone, 30, 109
- adhesives, 115
- biocompatibility of silicones, 116
- biodurability of silicones, 116
- chemical structure and nomenclature, 109
- elastomers, 112–115, 115f
- cure inhibition of, 120b
- fabricators of, 120b
- filler, 112–113
- fillers for, 120b
- processing of, 113–115
- types of cross-linking, 114t
- film-in-place, 115–117
- gels, 115
- implants, 118–120
- injections, 26
- inserts, 118–120
- limitations of present-day silicone materials, 120b
- medical applications, 117
- aesthetic implants, 119–120
- anatomic placement, 119t
- catheters, drains, and shunts, 118–119
- extracorporeal equipment, 118
- medical inserts and implants, 118–120
- siliconization, 117–118
- organic copolymers, 120b
- physicochemical properties, 112
- space-filling model, 112f
- polymers, 109, 112
- key milestones, 110t
- shorthand notation for, 110t
- preparation, 109–112
- basic steps in silicone polymer synthesis, 111t
- examples of silicone shorthand notation, 110t
- polymerization and polycondensation, 110–112
- silicone polymers, 109
- silicone breast implant safety, 121b
- surface activity, 120b
- types, properties, and preparation of silicone materials, 112–118, 113t
- silicone adhesives, 115
- silicone elastomers, 112–115
- silicone film-in-place, fast-cure elastomers, 115–117
- silicone gels, 115
- Silicone hydrogel
- contact lenses, 1139
- materials, 1139–1140
- Silicone materials, 116
- Siliconization, 117–118, 118f
- Silk, 578–579, 580t–581t, 1361–1363
- fibroin, 1292–1293, 1361, 1392
- sutures, 1191
- “Siloxane”, 109
- Silver (Ag), 22–23, 205, 830–831
- alloy coated urinary catheters, 840.e2b
- ion implantation, 273
- silver-containing materials, 1173
- silver-containing zeolites, 831
- silver-sulfadiazine cream, 1170
- Silver nitrate (AgNO₃), 282, 1170
- SIMS. *See* Secondary ion mass spectrometry (SIMS)
- Simulated body fluid (SBF), 956
- Single chain variable fragment (scFv), 546–547
- Single emulsion solvent preparation, 435
- Single fluorine bonds, 125–126
- Single polymer molecules
- chemical structure of, 86
- molecular structure of, 85–86
- Single-photon emission computed tomography (SPECT), 479–480
- Single-stranded DNA (ss-DNA), 462
- Single-walled carbon nanotubes (SWCNTs), 330, 330f, 338b, 341, 461, 1278
- Sintering, 289
- Sintering, 608t
- siRNA. *See* Small interference RNA (siRNA)
- Sirolimus-eluting stents, 530
- SIS. *See* Small intestinal submucosa (SIS)
- Si–X bonds, 112
- Size exclusion chromatography (SEC), 89–90
- Skin, 905
- grafting for burn injuries, 595
- substitute technology, 1408
- tissue engineering applications in, 1299
- SkinTE, 1171t, 1174
- SLA. *See* Stereolithography (SLA)

- Slicer, 623
 Slipping, 464
 SLM. *See* Selective laser melting (SLM)
 SLNs. *See* Solid-lipid nanoparticles (SLNs)
 SLS. *See* Selective laser sintering (SLS)
 SLT. *See* Selective laser trabeculoplasty (SLT)
 Small angle neutron scattering (SANS), 465
 Small angle X-ray scattering (SAXS), 465
 Small interference RNA (siRNA), 472
 Small intestinal submucosa (SIS), 380, 386, 741–742, 846
 Small molecule drugs, 1249
 Small molecules, 1256t, 1257
 Small unilamellar vesicles (SUVs), 459
 Smart IOL, 1142
 Smart polymers, 192f, 192t, 192b, 194, 434. *See also* Degradable polymers.
 hydrogels, 197–198, 198f
 protein bioconjugates, 194, 195f
 site-specific smart polymer bioconjugates, 194–196, 196f
 solution in, 93, 193f
 stimuli-responsive polymer micelles and carriers, 198–199
 on surfaces, 196–197
 SMAs. *See* Shape memory alloys (SMAs);
 Surface-modifying additives (SMAs)
 SMCs. *See* Smooth muscle cells (SMCs)
 SMEs. *See* Shape-memory effects (SMEs);
 Surface-modifying end groups (SMEs)
 SMMs. *See* Surface modifying (“blooming”) macromolecules (SMMs)
 Smooth muscle cells (SMCs), 1034, 1036, 1375
 SNAP. *See* S-Nitroso-N-acetylpenicillamine (SNAP)
 Society for Biomaterials & Artificial Organs (1986), 18–19
 Society for Biomaterials (SFB), 18–19
 SOD. *See* Superoxide dismutase (SOD)
 Sodium deoxycholate, 380
 Sodium dodecyl sulfate (SDS), 72, 380, 649–650, 985
 Soft contact lenses, 101b, 976–977
 Soft hydrated materials, 553
 Soft hydrogel contact lenses, 1139
 Soft lithography, 833–834
 Soft materials, properties of, 1526t–1528t
 Soft nanocomposite smart materials, 369–370
 stimuli-responsive soft nanocomposites, 369–370
 Soft segment, 103
 Soft tissue engineering, 1389
 applications, 1392
 adipose tissue engineering, 1392–1393
 gastrointestinal tissue engineering, 1404
 tissue-engineered skin, 1408
 biomaterials for, 1389–1390
 decellularized tissues, 1391–1395
 natural polymers, 1391
 properties, 1389
 range of elastic modulus of types, 1390f
 synthetic and natural materials used for, 1400
 synthetic polymers, 1390–1391
 “Soft tissue replacement” camp, 13–14
 Soft-lithography, 1227
 Soft-tissue adhesives and sealants, 1186
 characteristics, 1187t
 historical overview, 1186
 performance requirements, 1186
 “Soft-wet” materials, 556
 “Soft” proteins, 654–655
 Sol-gel synthesis, 309
 Sol-gel glasses (SGGs), 964
 SGG–magnetic glass–ceramics, 965
 SGG–polymer–drug materials, 965
 Sol-gel technology, 463, 1279
 Solid lipid nanospheres. *See* Solid-lipid nanoparticles (SLNs)
 Solid organs. *See* Compact organs
 Solid-lipid nanoparticles (SLNs), 459–460, 1247, 1248t
 Solid-state
 ionics, 1277
 sintering, 289
 synthesis, 309
 Soluble mediators, 757
 Soluble plasma fibronectin, 704
 Soluble recombinant form of CR1 (sCR1), 782
 Solution blending, 463
 Solution resistance (R_s), 1271–1272
 Solution–gel transition, 434–435
 Solvent casting, particulate/porogen leaching (SCPL), 1323t, 1325
 Solvents, 591
 evaporation, 435–436, 454–455
 solvent-switching, 457–458
 Somatic gene recombination, 757
 Sonic Hedgehog (Shh), 542
 Sonication, 381
 Sonophoresis, 1252t
 Sophisticated mathematical models, 177
 Sorbent dialysis, 1070–1071
 Sox9 gene, 1128
 Space-filling, 1181
 Span 80, 455
 SPARC. *See* Secreted protein acidic and rich in cysteine (SPARC)
 Spatial group (SG), 965
 Special staining method, 1536.e3
 Specific chemical reactions for forming surface grafts, 494–495
 Specific heat of water, 78
 Specific immunity. *See* Adaptive immunity
 Specific pathogen-free (SPF), 905
 Specification, 1502
 Specificity, 1481
 SPECT. *See* Single-photon emission computed tomography (SPECT)
 SPEM. *See* Scanning photoemission microscopy (SPEM)
 SPF. *See* Specific pathogen-free (SPF)
 Spheroids, 1224–1225
 Spinel, 1096–1097
 Spinneret design, 581
 Spinning
 disc assay, 721
 technique, 579–581, 1354
 SPIO. *See* Superparamagnetic iron oxides (SPIO)
 SPM. *See* Scanning probe microscopy (SPM)
 Sponsored research agreements (SRAs), 1504–1506
 SPR. *See* Surface plasmon resonance (SPR)
 Spray drying, 437
 SpyTag-SpyCatcher system, 546–547
 Squalene-containing MF59, 1200
 SRAs. *See* Sponsored research agreements (SRAs)
 Src kinases, 706
 SRM. *See* Standard Reference Material (SRM)
 SS. *See* Stainless steel (SS)
 ss-DNA. *See* Single-stranded DNA (ss-DNA)
 SSM. *See* Subcapsular sinus macrophage (SSM)
 SSPM. *See* Scanning surface potential microscopy (SSPM)
 Stability of bonded interface, 1186
 Stable tissues, 693
 Stainless steel (SS), 24–25, 249, 251t, 1097–1100
 alloys, 1087–1089
 approximate mechanical properties of, 253t
 composition and types, 249
 corrosion, 252–254
 history, 249
 microstructures of annealed, 252f
 structure, 250
 structure, composition, and processing effects on mechanical properties, 250–252
 sutures, 1192
 316L Stainless steel sutures, 1192
 Stamp, void features of, 565
 Standard Reference Material (SRM), 1475
 Standards
 definition, 1475
 development process, 1479f
 documentary, 1476–1481
 and measurement terminology, 1476b
 risks and benefits, 1477b
 and technology development, 1479f
 documentary standards, 1476–1481
 looking ahead, 1483
 provision, 1504
 reference
 data, 1476
 materials, 1475–1476

- Standards Coordinating Body (SCB), 1478
- Standards development organizations (SDOs), 1476–1477
- Staphylococcus aureus*, 299, 340–341, 343, 828, 832, 1004
- Staphylococcus epidermidis*, 824, 1004, 1014–1015
- Staphylococcus* sp., 1170
- Star polymer hydrogels, 159
- Star-shaped polymers, 85–86
- “Stealth” surfaces, 507
- Steam sterilization and disinfection, 1441
- Stellite, 22–23
- Stem cell, 688–690
 - ethical issues in stem cell research, 1514–1515
 - organoids, 1298
 - therapies and tumorigenesis, 819–820
- Stemness, 688
- Stents, 27–28
- Stereocomplexes, 155
- Stereolithography (SLA), 623–624, 625f, 1280, 1296, 1324
- Sterile, 1431
- Sterility assurance level (SAL), 1431, 1453
- Sterility validation, 1432
- Sterilization methods, 1428–1429
- Sterilization of implants and devices
 - chemical techniques, 1435–1440
 - compatibility with radiation sterilization, 1440
 - ethylene oxide sterilization, 1435–1438
 - material considerations for chemical sterilization, 1439–1440
 - physicochemical methods, 1438–1439
 - principles of action and efficacy, 1435
 - safety considerations, 1435
 - sterilization by oxidation, 1438
 - materials development considerations for sterility, 1441–1442
 - patient safety, 1442–1445
 - biological safety verification, 1442–1443
 - maintaining sterility, 1443
 - sourcing, quality systems, and manufacturing controls, 1443–1444
 - sterilization standards, 1444–1445
- R&D, pilot, and low-volume technologies, 1434
- radiation-based techniques, 1432–1435
 - application considerations, 1434
 - electron beam sterilization, 1433–1434
 - gamma sterilization, 1432–1433
 - principles of action and efficacy, 1432
 - safety considerations, 1432
 - X-ray sterilization, 1434
- safety testing and validation after sterilization, 1442
- thermal techniques, 1440–1441
 - application considerations, 1441
 - dry heat sterilization, 1440
 - principles of action and efficacy, 1440
 - safety considerations, 1440
 - steam sterilization and disinfection, 1441
- Sterilization procedure effect on hydrogel properties, 520b
- Steroid-eluting electrodes in pacemaker applications, 865b
- SThM. *See* Scanning thermal microscopy (SThM)
- Stimulator of interferon genes (STING), 749, 751f
- Stimuli-responsive drug delivery, 471–472
- Stimuli-responsive liposome–DNA hydrogel, 369
- Stimuli-responsive NPs for intracellular gene release, 477
- Stimuli-responsive polymers, 1274
- Stimuli-responsive soft nanocomposites, 369–370
- STING. *See* Stimulator of interferon genes (STING)
- STM. *See* Scanning tunneling microscopy (STM)
- Strain, 41
- Strain rate, 45, 728
- StrataGraft, 1171t, 1173
- Stratum corneum, 1250–1251
- Strength of isotropic materials, 45
- Strengthening mechanisms
 - alloying, 213
 - cold working, 213–214
 - grain size, 214
 - precipitation strengthening, 214–215, 215f
 - strength of metals and, 213
- Streptavidin (SA), 196
- Streptavidin, 655
- Streptococcus enterococci*, 1004
- Streptococcus faecium*, 1432
- Streptococcus viridans*, 1004
- Stress, 41–43
 - fibers, 1337–1338
 - phase angle, 728
 - states, 47–48
 - trajectories, 49
- Stress–strain analysis, 93
- Striated muscle cells, 687–688
- Stroma, 684–687, 813
- Structural ceramic, 319
- Structural ceramic oxides, 319–321
 - aluminum oxide, 320
 - properties, 324, 325t
 - structural materials in medical devices, 321–324
 - yttria and magnesia-stabilized zirconias, 320–321
 - zirconia, 320
 - ZTA, 321
- Structure–function correlation, 687–688
- Structure–property relationships, 85
- STS. *See* Suprachoroidal–Transretinal Stimulation (STS)
- SU-8, 1154
- Subacute toxicity, 871–872
- Subacute/subchronic/chronic toxicity, 466
- Subcapsular sinus macrophage (SSM), 1206
- Subchronic toxicity, 871–872
- Subcommittees (SC), 1478
- Subculturing cells, 662
- Subcutaneous ICD (S-ICD), 1014
- Subperiosteal implants, 1120
- Subretinal devices, 1146–1148
 - Alpha IMS/AMS, 1147–1148
 - PRIMA Bionic Vision System, 1149
- Substitutional solid solution, 209
- Substrate cues, comparison and evaluation of, 673–674
 - chemistry and strain, 674
 - chemistry and topography, 674
 - topography and strain, 674
- Substrate elasticity, cell response to, 672–673
- Substrate stiffness, 722
- Sugar, 612
- Sulfated GAGs, 1322
- Sulfo-NHS. *See* N-Hydroxysulfosuccinimide (Sulfo-NHS)
- Sulfobetaine, 521, 521f, 1059
- Sum frequency generation vibration spectroscopy (SFG vibration spectroscopy), 68–70, 70f, 70t
- SUN-1 protein, 719–720
- SUN-2 protein, 719–720
- Supercritical fluid processing, 1326
- Superelasticity, 44
- Superelasticity effects (SEs), 230–231
- Superficial burns, 1169
- Superhydrophilic surfaces, 826
- Superhydrophobic
 - materials, 833
 - surfaces, 826
- Superoxide dismutase (SOD), 929, 1164
- Superparamagnetic iron oxides (SPIO), 460
- Superstructure engineering, 1323t, 1324–1325
- Suprachoroidal devices, 1146, 1149–1150
 - BVA team, 1149–1150
 - STS, 1150
- Suprachoroidal–Transretinal Stimulation (STS), 1150
- Supramolecular chemistry, dynamic hydrogels exploring, 366–369
- Suprathel, 1171t, 1173
- Surface analysis, 490
- Surface charge, 438
- Surface chemical inversion phenomenon, 500
- Surface chemistry, 666–667
- Surface coating, 590–591, 1057–1061
 - of synthetic scaffolds, 1318
- Surface energy, 57–58
- Surface erosion, 174–175, 440–441
 - experimental tools for characterizing, 175b

- Surface functionalization, 587–588
- Surface grafting, 490–492
- Surface hydration, 509
- Surface modification, 485, 487, 517, 522, 526–527
- of biomaterial constructs, 615
- Surface modifying (“blooming”)
- macromolecules (SMMs), 935
- Surface morphology, clinical applications of, 672b
- Surface patterning, 553, 556–567
- biomolecular, 553–556
 - bioactivity, 556
 - contrast, 554–556, 555f
 - durability, 556
 - nonspecific adsorption, 555–556, 555f
 - resolution, 554
 - shelf-life, 556
 - throughput, 554
 - block copolymer self-assembly, 565–566
 - deposition/etching with masks, 562
 - dip-pen nanolithography, 558, 558f
 - direct-write patterning, 556–561, 556f
 - direct-write photolithography, 559, 559f
 - dynamic patterning, 567
 - electric field, 560
 - electron beam lithography, 559–560, 560f
 - focused ion beam lithography, 560
 - imprinting with master, 563
 - magnetic field, 561
 - magnetic self-assembly, 567
 - microcontact printing, 563–565, 564f
 - microfluidic patterning, 565, 565f
 - nanografting, 558
 - nanoshaving, 558
 - nanosphere lithography, 566–567
 - patterning
 - with masks, 561–562
 - with masters, 563–565
 - by self-assembly of polymers and colloids, 565–567, 566f
 - photolithography with masks, 561–562
 - printing with inkjets, quills, and pins, 557–558
 - printing with stamp, 563–565
 - resolution and contrast, 554f
 - three-dimensional printing, 567
 - writing
 - with beams, 558–560
 - with fields, 560–561
 - with stylus, 556–558
- Surface plasmon resonance (SPR), 70t, 175b, 481, 493, 1059
- “Surface-bound” waters, 510–511
- Surface-enhanced Raman spectroscopy (SERS), 70–71, 70t
- Surface-eroding microparticles, 440–441
- Surface-immobilized biomolecules
- albumin immobilization, 548f
 - biologically active molecules, 539–540
 - biomolecule immobilization methods, 548t
- bioorthogonal click reactions, 546f
- bioreactors, supports, and designs, 541t
- cells, application of, 540t
- chemical methods used to bond biomolecules, 545f
- immobilization methods, 542–549
- immobilized biomolecules, 540
- application, 540t
- immobilized cell ligands and cells, 541–542
- immobilized enzymes
- advantages and disadvantages of, 541t
 - in therapeutic bioreactors, 541t
- patterned surface compositions, 539–540
- peptide adhesion domains in cell adhesion proteins, 541t
- Surface-initiated atom transfer radical polymerization (SI-ATRP), 1060
- Surface-modifying additives (SMAs), 499–500, 499f
- Surface-modifying end groups (SMEs), 935
- Surface(s), 39
- analysis techniques, 55–71, 57t
 - AFM, 66–68
 - contact angle methods, 57–59
 - contact-angle correlations, 72
 - ESCA, 59–62
 - general comments, 55–57
 - infrared spectroscopy, 65
 - intraocular lenses, contamination of, 72
 - multitechnique characterization of adsorbed peptides and proteins, 72
 - platelet consumption, 72
 - poly(glycolic acid) degradation, 72
 - sample preparation, 55
 - SEM, 63–65
 - SFG vibration spectroscopy, 68–70
 - SIMS, 62–63, 62t, 72
 - SPMs, 66–68
 - STM, 66–68
 - studies with, 71–72
 - surface composition, 72
 - titanium, 72
 - cell lines in, 672b
 - characterization of biomaterials, 53, 55, 70t
 - and coatings, 1092
 - considerations, 53–55
 - processes, 167–168, 168f
 - properties of biomaterials, 35–36, 53, 55, 70t
 - rearrangement, 488
 - surface-modified biomaterials, 488t
 - surface-packing density, 509
 - surface-sensitive infrared sampling modes, 66f
 - tension of water, 77–78
 - topography, 670–671, 1341–1342
- Surfactants, 985
- Surgeon/physician-hero, 23–30
- Surgical bioprosthetic and mechanical heart valves, 1002–1007, 1003f
- Surgical gut sutures, 1189
- Surgical implants, properties of metals and alloys for, 1531t
- Surgical mesh, 1492b–1493b
- Surgical planning
- of 3D Printing, 632–633, 633f
 - for wound care, 1169
- Surgical sutures, 1188–1189
- Susceptibility, 68–70
- Sustained release of biopharmaceuticals, 441
- Sutures, 21–22, 591, 1188–1196
- coatings, 1194–1195
 - components and permutations, 1189t
 - diameter requirements, 1189t
 - dyes, 1194
 - FDA-approved dyes for use in sutures, 1195t
 - genesis and common uses, 1188
 - high-glycolide copolymeric sutures, 1194
 - and materials, 1190t
 - needles, 1191f, 1191t
 - and attachment, 1195
 - newer trends and future developments, 1196
 - nylon, 1191
 - packaging, 1195
 - PDO sutures, 1193–1194
 - PGA sutures, 1193
 - physical properties, 1195
 - polyester, 1191
 - polypropylene, 1191–1192
 - silk, 1191
 - stainless steel, 1192
 - surgical gut sutures, 1189
 - synthetic absorbable, 1192–1193
 - UHMWPE, 1192
 - in vitro and in vivo performance, 1195–1196
- SUVs. *See* Small unilamellar vesicles (SUVs)
- SV40 large T-antigen (PKKKRKV), 477
- SWCNTs. *See* Single-walled carbon nanotubes (SWCNTs)
- Swelling-controlled devices*, 161–162
- “Swelling” water, 79
- Swine heart valves, 902
- Synchrotron sources, 71
- Syndiotactic PP, 87
- SynerGraft, 385–386
- Synovium, 673
- Synthesized CaP bioceramics, 292
- Synthetic absorbable sutures, 1192–1193
- Synthetic apatites, 963
- Synthetic biomaterials, 1220t–1221t, 1223. *See also* Natural biomaterials.
- polyesters, 1223
 - synthetic hydrogels, 1223
- Synthetic bone graft, 290
- Synthetic cationic polymers, 833
- Synthetic HA, 309
- Synthetic hydrogels, 708, 1223, 1375
- Synthetic materials, 643, 1294, 1408
- nonionic, 510t
 - zwitterionic, 510t

- Synthetic peptide amphiphiles, 604–607
- Synthetic polymers, 415–416, 432–435, 432f, 582t, 605t–606t, 631–632, 1362–1364, 1375, 1389–1391. *See also* Natural polymers.
- for biotextile production, 579
 - degradable synthetic polymers, 435
 - PCL, 433–434, 1363
 - PEGylation, 434
 - PGA, 1362–1363
 - PLA, 1362–1363
 - POE, 434
 - poly(α -hydroxy acid), 433
 - polyacetals, 434
 - polyanhydrides, 434
 - smart polymers, 433–434
- Synthetic scaffolds, 1322
- Syrian Hamster Embryo Cell Transformation Assay, 857
- Systematic implant retrieval, 1430
- Systemic barriers. *See also* Intracellular barriers.
- approaches to overcome, 468–472
 - against drug delivery, 467–468
 - cellular internalization and efflux, 468
 - circulation, 467
 - on-demand drug release, 468
 - tumor accumulation, 467
 - tumor penetration, 467
- Systemic toxicity, 871–872
- of implanted materials, 798b
 - metals and metal alloy toxicity, 793–796
 - organ localization of inflammatory and immune responses, 797–798
 - systemic distribution and toxicity of biomaterial constituents, 791–793
- Systolic pressure, 727
- ## T
- T cell receptor (TCR), 754, 762–763, 762f
- T cells, 745, 757
- energy and deletion through incomplete dendritic cell activation, 1210–1211
 - modulation, 1208–1209
 - biomaterials for enhanced T cell manufacturing, 1209
 - biomaterials for targeting and modulation of T cell therapies, 1208
 - recognition, 762–763
 - T cell-dependent activation, 1203
 - T cell-independent activation, 1205
 - T cell-mediated immunity, 761f
- $\gamma\delta$ T cells, 747–748, 754
- T lymphocytes, 757
- T-DTH cells, 1110
- T-junction, 436
- Ta alloys. *See* Tantalum alloys (Ta alloys)
- Tacticity, 92
- of polymers, 87
- TAFI. *See* Thrombin-activated fibrinolysis inhibitor (TAFI)
- TAG. *See* Technical Advisory Group (TAG)
- Talin, 706, 718–719
- TALs. *See* Thoracic artificial lungs (TALs)
- TandemHeart, 1017
- Tantalum alloys (Ta alloys), 1089–1092
- Targeted drug delivery, 469–470
- active targeting, 470
 - passive targeting, 469
- TAVI. *See* Transcatheter aortic valve implantation (TAVI)
- TAVR. *See* Transcatheter aortic valve replacement (TAVR)
- TAZ (PDZ-binding motif), 1338–1339
- transcriptional regulator, 719–720
- TBSA. *See* Total body surface area (TBSA)
- TCA. *See* Triamcinolone acetonide (TCA)
- TCP. *See* Tissue culture polystyrene (TCP); Tricalcium phosphate (TCP)
- TCPS. *See* Tissue-culture polystyrene (TCPS)
- TCR. *See* T cell receptor (TCR)
- TDI. *See* Toluene diisocyanates (TDI)
- TDMAC. *See* Tridodecyl methylammonium chloride (TDMAC)
- TEA. *See* Triethanolamine (TEA)
- Technical Advisory Group (TAG), 1478
- Tecnis IOL, 1141
- TECNIS Multifocal, 1142
- TEER. *See* Transepithelial electrical resistance (TEER)
- Teflon, 25–26, 30–31, 1083, 1086
- fibrous mesh, 130–131
 - soft tissue repair meshes, 130–131
- TEGDMA. *See* Triethyleneglycol dimethacrylate (TEGDMA)
- TEM. *See* Transmission electron microscopy (TEM)
- Temperature-sensitive hydrogels, 160–161
- Temporary skin substitutes, 1173
- Temporomandibular joint (TMJ), 135b, 1119, 1128
- TEMPs. *See* Tissue Engineered Medical Products (TEMPs)
- Tenascin-C (TN-C), 1352
- Tendon replacement with woven and braided biotextiles, 594
- Tendon tissue-engineering scaffolds, 1351
- delivery of bioactive molecules, 1357–1358
 - design goals, 1352–1354
 - guidance cues to inducing tenogenic cell behaviors, 1353–1354
 - immediate or early return to load-bearing function, 1353
 - developmental biology-inspired strategies, 1364–1365
 - fabrication methods, 1354–1355
 - native adult tendon properties, 1352
 - ECM composition and molecular arrangement, 1352
 - mechanical properties, 1352
 - tendon cells, 1352
- polymer selection and scaffold designs, 1358–1364
 - natural plant-and animal-derived polymers alginates, 1358–1362
 - synthetic polymers, 1362–1364
 - postfabrication modifications, 1355–1357
- Tenocytes, 1352
- Tenomodulin (Tnmd), 1352
- Tensile stress lines, trajectories of, 48–49
- Tensin, 706
- Teratomas, 819
- TERM. *See* Tissue engineering and regenerative medicine (TERM)
- Terminal sterilization, 1431–1432
- Testing biomaterials, 841–842
- Tetracalcium phosphate, 1125
- Tetracyclines, 1257
- Tetrafluoroethylene (TFE), 126–127
- Tetrahydrofuran (THF), 607–609
- Textile
- fibers, 579–581
 - technologies, 1354–1355
- Textilomas, 817
- Texture in facilitating biomaterial integration, 601–604
- biomaterials for tissue engineering, 604
 - textured devices promote healing and restore organ function, 601–602
- Textured biomaterial, 601
- combining multiple fabrication methods, 612–615
 - crystallinity, 610f
 - fabrication methods for biomimetic nanoscale texture, 604–610
 - classes of biomaterials and methods to render texture, 605t–606t
 - electrospinning, 604
 - for nanofibrous and textured synthetic polymer matrices, 607t
 - self-assembly of nanoscale features, 604–607
 - fabrication methods for micro-and macroscale architectural features, 610–612
 - grooves and micropatterns, 610
 - injectable tissue-engineering scaffolds, 614–615
 - interconnected spherical macropores by porogen methods, 611–612
 - macroporous, nanofibrous tissue-engineering scaffolds, 613
 - methods for fabricating porous synthetic polymer scaffolds, 608t
 - multiphase scaffolds, 613–614
 - nanofibrous spongy microspheres, 616f
 - nonspherical architectural patterning, 612
 - surface modification of biomaterial constructs, 615
 - thermally induced phase separation, 607–609
 - 3D printed scaffolds, 614
- TF. *See* Tissue factor (TF)

- TFE. *See* Tetrafluoroethylene (TFE)
- TFM. *See* Traction force microscopy (TFM)
- TFPI. *See* Tissue factor pathway inhibitor (TFPI)
- TGA. *See* Thermogravimetric analyzer (TGA); Triglycidylamine (TGA)
- TGF. *See* Transforming growth factor (TGF)
- TGF- β . *See* Transforming growth factor-beta (TGF- β)
- Th cells. *See* Helper T cells (Th cells)
- THA. *See* Total hip arthroplasty (THA)
- Theranostics, 481–482
- Therapeutic apheresis, 1062–1071
- Therapeutic catheters, 1046–1047
- Therapeutic index (TI), 1243
- Therapeutic payload, 436
- Therapeutic window (TW), 1243
- Thermal ablation, 1252t
- Thermal biosensors, 1274
- Thermal expansion, 49
- Thermal properties, of isotropic materials, 49–50
- Thermal sterilization, 1440
- Thermally induced phase separation (TIPS), 607–609, 607t, 1325–1326
- Thermistors, 1274
- Thermo-responsive polymers, 434–435
- Thermodynamics
 driving forces, 1095
 model, 825–826
 of protein adsorption, 509t
- Thermogelling hydrogels, 1319–1320
- Thermogravimetric analyzer (TGA), 1326, 1327t
- Thermomechanical analyzer (TMA), 1326
- Thermomechanical processing, 207
- Thermoplastic elastomers, 104
- Thermosets, 103–104
- THF. *See* Tetrahydrofuran (THF)
- Thin surface modifications, 487–488
- Thiol-ene coupling, 543
- Thiol-vinyl sulfones, 146–147
- Thoracic artificial lungs (TALs), 1054
- THR. *See* Total hip replacement (THR)
- Threadlift, 591–592
- Three Rs. *See* Replacement, Reduction, and Refinement (Three Rs)
- Three-dimension (3D)
 biologic scaffolds, 1293–1294
 bioprinting, 363, 364f, 409–410, 1227, 1280–1281
 objects, 48, 626
 printed scaffolds, 614
 printed skin equivalent constructs, 1409
 printers, 485–486
 printing, 567, 608t, 623, 1296
 devices and inks, 1346
 medical applications, 632–634
 methods, 292–293, 624t
 modalities, 623–630
 scaffold, 1354
 tumor models, 1302
- Thrombi*, 515, 1033
- Thrombin, 407, 515, 516f, 522
 inhibition without heparin, 526–527
- Thrombin-activated fibrinolysis inhibitor (TAFI), 806–807
- Thromboembolic complications, 1004
- Thrombogenicity, 515, 516b, 880–883
 strategies for preparing inert surfaces, 517f
 strategies to lower thrombogenicity of metals, 528–530
- Thrombomodulin, 527, 802
- Thromboresistance of heparinized materials, 524
- Thrombosis, 1036–1037
- Thrombus formation, 810
- Throughput, biomolecular surface
 patterning of, 554
- TI. *See* Therapeutic index (TI)
- Ti-6Al-4V alloy, 634, 1089, 1125
- Time-of-flight mass analyzer (TOF mass analyzer), 62–63
- TIMPs. *See* Tissue inhibitors of metalloproteinases (TIMPs)
- TIPS. *See* Thermally induced phase separation (TIPS)
- TIs. *See* Tolerable intakes (TIs)
- Tissue compatibility
 assessment, 869
 in vitro assessment
 carcinogenicity, 854–858, 855t
 with cellular and protein elements in blood, 858t
 future challenges, 861–865
 genotoxicity, 854–858, 855t
 ISO 10993 Biological evaluation of medical devices, 852t
 medical device/biomaterial chemical composition, 853–854, 854f
 in medical device/biomaterial evaluation for regulatory, 854
 reproductive toxicity, 854–858, 855t
 tests for cytotoxicity, 859
 tests for interactions with blood, 858–859
 in vivo assessment, 871t
 animal models selection for in vivo tests, 875–876, 875t
 biodegradation, 873
 biomaterial and device perspectives in, 870–871
 biomaterials and components to, 870t
 carcinogenicity, 873
 chronic toxicity, 873
 future perspectives, 876
 genotoxicity, 872
 hemocompatibility, 873
 immune responses, 874–875
 implantation, 872
 medical device categorization by, 870t
 reproductive and developmental toxicity, 873
- selection of in vivo tests, 869–870
 sensitization, irritation, and intracutaneous reactivity, 871
 specific biological properties assessing by, 871–875
 systemic toxicity, 871–872
- Tissue culture polystyrene (TCP), 663–664, 844
- Tissue Engineered Medical Products (TEMPs), 1175–1176, 1480b
- Tissue engineering, 370, 417, 1287, 1429
 applications, 608t, 1298–1302
 disease models and therapy, 1302
 drug delivery, 1301–1302
 organ-on-a-chip systems, 1302
 products for regenerative applications, 1300t–1301t
 replacing/regenerating target organs, 1299–1301
 transplantation, 1298–1299
 biological factors, 1294–1295
 biomaterials for, 604
 cell–matrix interactions, 1335–1340
 design considerations for scaffolds to regulating tissue development, 1340–1345
 implications for future materials design, 1345–1346
 mechanotransduction, 1335–1340
 micromechanical design criteria for, 1335
 biomedical composites for, 427–428
 carbon biomaterials in, 345–346
 cardiovascular, 1373
 blood vessels, 1373–1374
 cardiac muscle, 1373
 endothelial cells, 1373
 heart valves, 1373–1375
 scaffold materials, 1374
 cell, 1291–1292
 classification, 1290–1291
 components, 1291–1297
 current challenges and opportunities, 1302–1304
 in dentistry, 1126–1130
 future perspectives, 1304
 goals, 1289–1290
 history, 1289
 integration of multiple factors, 1297
 materials, 1292–1294
 models for, 1297–1298
 for regeneration, 1290f
 scaffolds, 1317
 applications, 1318–1320, 1319f
 cell-incorporated scaffolds, 1326–1327
 characterization techniques, 1326, 1327t
 design, 1295–1297, 1317–1318
 fabrication techniques, 1323–1326, 1323t
 materials, 1320–1323

- Tissue engineering and regenerative medicine (TERM), 361, 1477
- Tissue Engineering and Regenerative Medicine International Society, 18–19
- Tissue factor (TF), 785
- Tissue factor pathway inhibitor (TFPI), 805–806
- Tissue inhibitors of metalloproteinases (TIMPs), 692–693, 706, 738
- Tissue necrosis factor- α (TNF- α), 742–743
- Tissue plasminogen activator (tPA), 527–528, 806–807
- Tissue remodeling and biomaterial integration, 741–742
- Tissue-culture polystyrene (TCPS), 647
- Tissue-engineered cardiac muscle, 1374
- Tissue-engineered skin, 1408
 - anatomy and physiology, 1408
 - challenges, 1409
 - design criteria, 1408
 - skin substitute technology, 1408
- Tissue-engineering scaffolds. *See also* Tendon tissue-engineering scaffolds.
 - chemical characterization for, 1327t
 - injectable, 614–615
 - macroporous, nanofibrous, 613
 - mass/molecular weight characterization for, 1327t
 - mechanical properties characterization for, 1327t
 - morphology/surface characterization for, 1327t
- Tissue(s), 1269, 1536.e1
 - cell and matrix components assessment in analysis techniques, 1536.e1
 - electron microscopy, 1536.e5
 - immunohistochemical staining, BM-APP
 - light microscopy, 1536.e1
 - in situ hybridization, 1536.e5
 - special staining, 1536.e3
 - special techniques, 1536.e5
 - techniques used to study tissue, 1536.e2t
 - cellular and molecular mediators of tissue restoration, 742–744
 - constituents, organization, and integration, 683–687
 - cross-linking, 379–380
 - culture, 661
 - decellularization, 1354
 - differentiation, phenotype, and maintenance, 687–693
 - dimensionality, 1218
 - analyzing effect of, 1224–1225
 - homeostasis, 692–693
 - injury, adaptation, and other responses, 693–696
 - interpreting three-dimensional structure from 2D representations, 1536.e6f
 - macrophages, 697–698
 - maturation, 1303
 - mechanics, 1164
 - microarrays, 1536.e3
 - organoids, 1298
 - perfusion, 684–685
 - preservation, 377
 - with ice crystal formation for, 378f
 - remodeling, 692
 - response to tissue injury and biomaterials, 696–699
 - structural features, 1536.e4f
 - tissue-derived materials, 1222–1223
 - tissue-resident macrophages, 739–740
 - tissue-resident memory T cells, 764
 - tissue-specific in vitro models of native microenvironment, 388–389
- Titanium (Ti), 32, 72, 1107
- Titanium alloy, 345, 1087–1089, 1100
 - biocompatibility, 229–231
 - nickel allergy reaction, 230f
 - occurrence of metal allergy, 230f
 - biocompatible, 231
 - mechanical properties, 232t, 233–236
 - anteroposterior radiograph, 235f
 - cold crucible levitation melting method, 233f
 - effects of interstitial atoms on mechanical properties, 236
 - elastic modulus, 234
 - fatigue behavior, 235–236
 - fretting fatigue, 234f
 - porous Ti6Al4V alloy, 233f
 - radiographs belonging, 235f
 - schematic illustration of selective laser sintering, 233f
 - wear resistance, 234–235, 235f
 - recent efforts in fabrication processes, 231–233
 - surface modification, 236–240
 - anodization effects on corrosion and surface mechanical properties, 237–238, 240t
 - coloring methods for titanium alloys, 238–240, 241f
 - microscopic images, 238f
 - recent efforts in anodization process, 236–237
 - recent efforts in coloring, 241t
 - recently established relationships, 239t
 - typical anodization, 237f
- TJA. *See* Total joint arthroplasty (TJA)
- TKA. *See* Total knee arthroplasty (TKA)
- TLRs. *See* Toll-like receptors (TLRs)
- TM. *See* Trabecular meshwork (TM)
- TMA. *See* Thermomechanical analyzer (TMA)
- TMC. *See* Trimethylene carbonate (TMC)
- TME. *See* Tumor microenvironment (TME)
- TMJ. *See* Temporomandibular joint (TMJ)
- TMPS. *See* 3-(Trimethoxysilyl) propyl methacrylate (TMPS)
- TMVR. *See* Transcatheter mitral valve replacement (TMVR)
- TN-C. *See* Tenascin-C (TN-C)
- TNBC. *See* Triple negative breast cancer (TNBC)
- TnBP. *See* Tri(n-butyl) phosphate (TnBP)
- TNF. *See* Tumor necrosis factor (TNF)
- TNF- α . *See* Tissue necrosis factor- α (TNF- α)
- Tnmd. *See* Tenomodulin (Tnmd)
- Tocopherol succinate–drug conjugates, 466
- TOF mass analyzer. *See* Time-of-flight mass analyzer (TOF mass analyzer)
- Tolerable intakes (TIs), 853
- Tolerance induction
 - in autoimmune disorders, 1210–1211
 - elevation of Treg activity, 1211
 - suppression of B cell activation, 1211
 - T cell anergy and deletion through incomplete dendritic cell activation, 1210–1211
 - use of biomaterials to, 1209–1211
- Toll-like receptors (TLRs), 749, 1105, 1200–1201
 - TLR4, 1200–1201
 - TLR7/8, 1201
 - TLR9, 1201
- 2,4-Toluene diamine (TDA), 818
- Toluene diisocyanates (TDI), 104
- Tooth cements, 1182–1186
- Topical drugs, 1143
- Topical microbial management, 1170–1172
- TOPO. *See* Trioctyl phosphine oxide (TOPO)
- Topographic reaction, 674
- Toric IOL, 1141
- Total body surface area (TBSA), 1174–1175
- Total disc arthroplasty (TDA), 1081, 1084–1085
- Total hip arthroplasty (THA), 257, 996–997, 1081, 1082f
- Total hip replacement (THR), 321, 1081, 1182
 - arthroplasty, 1083
 - prostheses, 10–11, 10f
- Total insulation impedance, 1154
- Total joint arthroplasty (TJA), 1079, 1080f, 1086f, 1087–1089
- Total knee arthroplasty (TKA), 257
- Total product lifecycle management, 1421, 1422f
- Totipotency, 688
- Totipotential stem cells, downstream of, 690
- Toxic injury, 695
- Toxicants, 851, 859b
- Toxicity, 439, 441
- Toxicological risk assessment, 853
 - medical device/biomaterial chemical composition and extracts for, 853–854
- Toxicology, 15, 791, 844
- tPA. *See* Tissue plasminogen activator (tPA)
- Trabecular meshwork (TM), 1143
- Trabeculectomy, 1143

- Trace elements, 311
- Traction force microscopy (TFM), 1226, 1226b
- Trade secrets, 1498, 1501–1503
- Traditional adjuvants, 1200
- Traditional tissue engineering, 1290
- Transcatheter aortic valve implantation (TAVI), 975, 1007
- Transcatheter aortic valve replacement (TAVR), 975
- Transcatheter mitral valve replacement (TMVR), 1009
- Transcriptomic analysis, 389
- Transcutaneous electric nerve stimulation, 1156
- Transdermal DDSs, 1251, 1252t
- Transdermal microjets, 1252t
- Transdifferentiation. *See* Direct reprogrammed cells
- Transducers, integrating responsive polymers with, 1279
- Transepithelial electrical resistance (TEER), 674–675
- Transfer RNA (tRNA), 408
- Transformed cells, 662–663
- Transforming growth factor (TGF), 761, 980, 1211
- Transforming growth factor-beta (TGF- β), 705, 718, 738–739, 742–743, 1128 isoforms, 738–739 TGF- β 1, 1322–1323
- Transglutaminase, 383–384
- Transluminal atherectomy*, 1046–1047
- Transmigrated macrophages, 697–698
- Transmission electron microscopy (TEM), 438, 464, 978–979, 1080, 1097, 1100, 1101f, 1536.e1
- Transosseous implants, 1120
- Transparency, 50
- Transport phenomena, 1218–1219
- Transthyretin-mediated liver amyloidosis, 1250
- Trauma, 695
- Trehalose, 442
- Tri(n-butyl) phosphate (TnBP), 381
- Triamcinolone acetonide (TCA), 444–445 TCA-encapsulated PLGA microspheres, 444
- Triaxial stretch devices, 721–722
- Tricalcium phosphate (TCP), 291, 307–308, 415–416, 1125, 1183
- Triclosan, 1194–1195
- Tridodecyl methylammonium chloride (TDMAC), 524
- Triethanolamine (TEA), 1188
- Triethyleneglycol dimethacrylate (TEGDMA), 140–141
- Triglycidylamine (TGA), 986
- 3-(Trimethoxysilyl) propyl methacrylate (TMPS), 148
- Trimethylene carbonate (TMC), 1192
- Trioctyl phosphine oxide (TOPO), 461
- Triple negative breast cancer (TNBC), 470
- TRIS. *See* Tris(trimethylsiloxy) silane (TRIS)
- Tris(trimethylsiloxy) silane (TRIS), 1138–1139, 1139f
- Triton X-100, 380–381
- Trivalent metal ions, 984–985
- tRNA. *See* Transfer RNA (tRNA)
- Tropism, 695
- Tropoelastin, 404
- True strains, 41
- True stresses, 41
- Trypsin, 662
- Tubular organs, 687
- Tumor, 813
- accumulation, 467
 - formation, 735
 - grade, 813
 - penetration, 467, 470–471
 - tumor-associated ECM remodeling, 1219b
- Tumor microenvironment (TME), 1217
- applications of biomaterials-based tumor models, 1224–1228
 - analyzing effect of local and systemic transport phenomena, 1227–1228
 - analyzing effect of tissue dimensionality, 1224–1225
 - dynamic materials systems for studies of mechanical memory, 1226–1227
 - modeling tumor–stroma interactions, 1225
 - platforms to interrogating cell–ECM interactions, 1225–1226
 - biological design considerations, 1218–1219
 - ECM physicochemical properties, 1219
 - immunological changes, 1219
 - tissue dimensionality, 1218
 - transport phenomena and interstitial pressure, 1218–1219
 - biomaterials to studying, 1219–1223
 - composite materials, 1223
 - natural biomaterials, 1219–1223
 - synthetic biomaterials, 1223
 - metastasis, 1228
 - microenvironmental changes during different stages of tumorigenesis, 1218f
- Tumor necrosis factor (TNF), 698, 754 TNF- α , 469–470, 738–739
- Tumorigenesis, 817
- association of implants with human and animal tumors, 814–817
 - breast implant-associated anaplastic large-cell lymphoma, 816f
 - orthopedic implant-related osteosarcoma, 815f
 - tumors associated with implant sites in humans, 816t
 - characteristics of benign and malignant tumors, 814t
 - pathobiology of foreign body tumorigenesis, 817–819
 - stem cell therapies and, 819–820
- Tumorigenicity, 817–818
- Tunica externa, 687
- Tunica externa, 1375
- Tunica intima, 1375
- TW. *See* Therapeutic window (TW)
- 21st Century Cures Act, 1176
- Two half-cell reactions, 51
- Two-dimension (2D)
 - problem, 48
 - surface, 667
 - tissues, 1296
- Two-stage endosteal screw-type implant, 1120–1121
- 2D unidirectional composite model, 420
- Type I collagen, 703–704, 1222
- Type II collagen (ColII), 402, 703–704
- Type III collagen (ColIII), 402, 703–704
- Type IV collagen, 703–704
- Type IV delayed type hypersensitivity, 1110
- Type IV T cell-mediated hypersensitivity, 797
- Tyrosine-isoleucine-glycine-serine-arginine (YIGSR), 363, 709–710
- ## U
- U-SENS test, 864
- Ubiquitin–proteasome pathway, 694
- UC. *See* Ultrasonic consolidation (UC)
- UCST. *See* Upper critical solution temperature (UCST)
- UDMA. *See* Urethane dimethacrylate (UDMA)
- UFs. *See* Uncertainty factors (UFs)
- UHMWPE. *See* Ultrahigh molecular weight polyethylene (UHMWPE)
- ULTI. *See* Ultralow temperature isotropic (ULTI)
- Ultimate tensile strength (UTS), 45
- Ultimate tensile stress (UTS), 273
- Ultracentrifugation-based exosome isolation, 461
- UltraESCA, 71
- Ultrafiltration, 461
- Ultrahigh molecular weight polyethylene (UHMWPE), 321, 347, 415–416, 1085–1086
 - sutures, 1192
- Ultralow temperature isotropic (ULTI), 960
- Ultralow-flow system, 1054
- Ultranano-crystalline diamond (UNCD), 328
- Ultrasmall superparamagnetic iron oxides (USPIO), 460
- Ultrasonic atherectomy*, 1046–1047
- Ultrasonic consolidation (UC), 629
- Ultrasonography (US), 479–480, 482
- Ultraviolet (UV), 625–626, 824, 1438–1439
 - irradiation, 384

- photolithography techniques, 722
 radiation, 1357
 spectrophotometry, 439
 UV-vis spectroscopy, 453–454
 ULVs. *See* Unilamellar vesicles (ULVs)
 UNCD. *See* Ultrananocrystalline diamond (UNCD)
 Uncertainty factors (UFs), 853
 Unilamellar vesicles (ULVs), 459
 United Network for Organ Sharing (UNOS), 1510
 United States Department of Agriculture (USDA), 899–900
 United States Pharmacopeia (USP), 116, 869, 1188–1189, 1195, 1475
 Universality, 1481
 University of Texas Health Science Center in San Antonio (UTHSCSA), 28
 UNOS. *See* United Network for Organ Sharing (UNOS)
 Upper critical solution temperature (UCST), 434–435
 UPy. *See* Reidopyrimidinone (UPy)
 Urethane dimethacrylate (UDMA), 140–141
 Urinary stents and prostheses, 976
 Urinary tract infections (UTIs), 828
 US. *See* Ultrasonography (US)
 US Food and Drug Administration (FDA), 130–131, 172, 291–292, 322, 406, 432, 793, 815–817, 899–901, 996–997, 1009, 1175, 1194, 1200, 1237–1239, 1292–1293, 1362, 1390–1391, 1426, 1442, 1448, 1457, 1463, 1479, 1507, 1510
 FDA-approved dyes for use in sutures, 1195t
 regulations for clinical translation, 1304
 US Medical Device Reports, 1423
 US National Toxicology Program, 864–865
 USDA. *See* United States Department of Agriculture (USDA)
 USP. *See* United States Pharmacopeia (USP)
USP6-MYH9 fusion gene, 817
 USPIO. *See* Ultrasmall superparamagnetic iron oxides (USPIO)
 UTHSCSA. *See* University of Texas Health Science Center in San Antonio (UTHSCSA)
 Utilitarian approach, 1510
 UTIs. *See* Urinary tract infections (UTIs)
 UTS. *See* Ultimate tensile strength (UTS); Ultimate tensile stress (UTS)
 UV. *See* Ultraviolet (UV)
- V**
 V-CAM, 1225
 VA. *See* Venoarterial (VA)
 VA-ECMO. *See* Venoarterial ECMO (VA-ECMO)
 Vaccine, 442, 1199–1208
 alternative vaccine administration routes, biomaterials, 1206–1207
 biomaterials for improving vaccine efficacy, 1200–1206
 activation of B cells and humoral immunity, 1202–1206
 to adjuvant immune system, 1200–1201
 to improving delivery of antigen to APCs, 1201–1202
 biomaterials for improving vaccine manufacturing and accessibility, 1207
 VADs. *See* Ventricular assist devices (VADs)
 Vagus nerve stimulation (VNS), 1159
 Validation
 general types of validation tests, 1454t
 of medical device design, 1418, 1454–1455
 place in waterfall design process, 1454f
 protocol, 1455
 report, 1455
 verification *vs.* validation, 1455, 1456.e1t, 1456.e2t
 Valine-proline-glycine-valine-glycine (VPGVG), 363
 Valvular heart disease, 1000–1010, 1001f
 Valvular interstitial cells (VICs), 1336, 1337f, 1374–1375
 Van der Waals forces, 38, 467
 Vanadium, 1107
 Vapor vacuum arc technique, 273
Vasa vasorum, 1034
 Vascular, 904
 Vascular beds, 1033–1034
 Vascular cell adhesion molecule-1 (VCAM-1), 725–726
 Vascular Closure Devices (VCDs), 1048
 Vascular disrupting agents (VDAs), 469–470
 Vascular endothelial growth factor (VEGF), 364–365, 596, 668, 699, 705, 710, 738, 1322–1323, 1393, 1475–1476
 Vascular filters, 1047–1048
 Vascular grafts, 26–27, 1041–1043, 1042f
 contemporary synthetic of, 1041–1042
 endothelial cell activation on, 528b
 Vascular injury and healing, 1036
 Vascular pathology, 1036–1039
 aneurysms and dissections, 1037–1039
 atherosclerosis, 1037
 intimal hyperplasia, 1037f
 patterns of vessel wall weakening, 1038f
 thrombosis, 1036–1037
 vascular injury and healing, 1036
 virchow's triad, 1037f
 Vascular prostheses, design criteria for, 592–593
 Vascular response, 699
 Vascular smooth muscle cells (vSMCs), 722–723
 Vascular stents, 345
 Vascular supply, 684–685
 Vascular system, mechanical forces in, 722–728
 Vascularization, 1303
 Vasculature, 684–685, 685f
 Vat photolithography, 623–625
 Vat polymerization, 624t, 625f
 VCAM-1. *See* Vascular cell adhesion molecule-1 (VCAM-1)
 VCDs. *See* Vascular Closure Devices (VCDs)
 VDAs. *See* Vascular disrupting agents (VDAs)
 VEGF. *See* Vascular endothelial growth factor (VEGF)
 Veins, 1033, 1035f
 Venoarterial (VA), 1052
 Venoarterial ECMO (VA-ECMO), 1019
 Venovenous (VV), 1052
 Ventricular assist devices (VADs), 12–13, 12f, 345, 903, 1017
 and total artificial hearts, 1019–1024
 Ventricular septal defects (VSDs), 1024–1025
 VentiGel, 388
 Ventriloquist, 22
 VEP. *See* Visual-evoked potential (VEP)
 Verification
 design controls for medical device development, 1448–1450
 focusing on commercial medical device development, 1447
 of medical device design, 1418, 1450–1451
 place in waterfall design process, 1451f
 protocol, 1453
 report, 1454
 starting medical device project, 1447–1448
 testing types, 1451–1454, 1452t
 validation *vs.*, 1455, 1456.e1t, 1456.e2t
 Verisyse, 1142
 Very-low-density lipoproteins (VLDL), 658
 Vesicoureteric reflux (VUR), 134
VGVAPG polypeptide sequence, 704, 709–710
 Vibrational spectroscopies, 65
 VICs. *See* Valvular interstitial cells (VICs)
 Vinculin, 706, 718–719
 Vinyl acetate, 1139
 N-Vinyl-pyrrolidone (NVP), 529–530, 1139
 Vinylidene monomer (CH₂CF₂), 128
 Virchow's triad, 723, 883, 883f
 Virtue approach, 1510
 Viruses, 695, 1515
 Viscoelastic materials, 44
 Viscoelasticity, 44
 Viscose rayon, 580t–581t, 595
 Visian ICL, 1142
 Vistakon, 1140
 Visual-evoked potential (VEP), 1149
 Vitallium, 1081–1083
 alloy, 22–23
 metal tubes, 26–27

- Vitamin D3, 1249
 Vitamin E coatings, 1067
 Vitrification, 377–379
 Vitronectin, 648–649
 VLDL. *See* Very-low-density lipoproteins (VLDL)
 VNS. *See* Vagus nerve stimulation (VNS)
 Voigt model, 419
 Volume defects in crystals, 212
 Voluntary, standards, 1476–1477
 von Willebrand factor (vWf), 520, 648, 808–809
 VPGVG. *See* Valine-proline-glycine-valine-glycine (VPGVG)
 VPMS peptide sequence, 710
 Vroman effects, 652, 654, 654f, 807
 VSDs. *See* Ventricular septal defects (VSDs)
 vSMCs. *See* Vascular smooth muscle cells (vSMCs)
 VUR. *See* Vesicoureteric reflux (VUR)
 VV. *See* Venovenous (VV)
 vWf. *See* von Willebrand factor (vWf)
- W**
 W/O emulsion. *See* Water in oil emulsion (W/O emulsion)
 W/O/W method. *See* Water-in-oil-in-water method (W/O/W method)
 Wales, 588–589
 Wall shear rate, 726
 Warburg effect, 1218–1219
 Warburg impedance (W), 1271–1272
 Warp yarns, 588
 WAT. *See* White adipose tissue (WAT)
 Water, 77–78
 boiling point, 77, 78t
 density and surface tension, 77–78
 freezing point, 78t
 interactions with polymers, 94–95
 latent heats of fusion and evaporation, 78
 life, 81
 melting point, 77
 molecules, 78f
 significance for biomaterials, 80–81
 hydrogels, 81
 hydrophobic effect, 81
 liposomes, 81
 micelles, 81
 as solvent, 78
 specific heat, 78
 structure, 78–80
 window, 1154
 Water in oil emulsion (W/O emulsion), 435
 Water layer theory, 827
 Water-in-oil-in-water method (W/O/W method), 435–436
 WBC. *See* World Biomaterials Congress (WBC)
 WE. *See* Working electrode (WE)
 Wear resistance, 234–235, 235f
 Weaving patterns, 1354–1355
 Weft yarns, 588
 Weibull modulus, 51b
 Weight average molecular weight (M_w), 88–89
 Wenzel equation, 826
 Wet AMD, 1137
 Wet-spun fiber, 587
 Wet/gel spinning, 581–583, 584f
 White adipose tissue (WAT), 1393
 White blood cells (WBC)
 membrane, 462–463
 White light interferometry (WLI), 670
 WHO. *See* World Health Organization (WHO)
 Whole organ recellularization, 387, 389
 Whole tissue preparations, 1536.e1
 Whole-tissue decellularization, 1220t–1221t
 Wire-based electrodes, 1154
 WLI. *See* White light interferometry (WLI)
 Wolff's law, 717
 β -Wollastonite, 1125
 Working electrode (WE), 257
 World Biomaterials Congress (WBC), 18–19
 World Health Organization (WHO), 1143
 Wound
 dressing, 595
 healing, 300, 735, 738–739
 complications and defective, 700
 in presence of biomaterials, 699–700
 surgical planning for wound care, 1169
 Woven
 scaffolds, 1354–1355
 structure, 593
 textiles, 588, 588f
 Writing
 with beams, 558–560
 direct-write photolithography, 559, 559f
 electron beam lithography, 559–560, 560f
 focused ion beam lithography, 560
 with fields, 560–561
 electric field, 560
 magnetic field, 561
 with stylus, 556–558
 dip-pen nanolithography, 558, 558f
 nanografting, 558
 nanoshaving, 558
 printing with inkjets, quills, and pins, 557–558
 WST, 465
 Wurster process, 30
- X**
 X-ray computed tomography (CT), 479–481
 X-ray diffraction (XRD), 93, 460, 464
 of HA, 310–311
 patterns, 294–295
 X-ray photoelectron spectroscopy. *See* Electron spectroscopy for chemical analysis
 X-rays, 59–61, 87
 fluoroscopic imaging, 482
 reflection, 70t
 sterilization, 1434
- XEN (allergan), 1145
 Xenobiotics, 851
 Xenografts, 385–386, 1173
 XIENCE's drug, 132b–133b
 XRD. *See* X-ray diffraction (XRD)
- Y**
 Yes-associated protein (YAP), 1338–1339
 transcriptional regulator, 719–720
 Yield drop, 45
 Yield strength, 45
 YIGSR. *See* Tyrosine-isoleucine-glycine-serine-arginine (YIGSR)
 Young's equation, 825, 826f
 Young's modulus, 43–44
 Yttria (Y_2O_3), 955–956
 Yttria tetragonal zirconia polycrystalline (YTZP), 320–321
 Yttria-stabilized zirconia, 290
- Z**
 Zeigler-Natta catalyst, 1191–1192
 Zein NPs, 462
 Zeta potential (ζ -potential), 438, 464
 Zetasizer Nano series, 465
 Zilretta, 444–445
 Zinc (Zn), 22–23
 influence of alloying elements, corrosion
 behavior, and biocompatibility, 273
 phosphate cement, 1183
 polycarboxylates, 1183–1184
 cements, 1183–1184
 Pourbaix diagram of, 277f
 zinc-based biodegradable metals
 biocompatibility of dissolved Zn corrosion products, 276–277
 perspective on Zn-based degradable implants, 277
 process in physiological fluids, 276f
 proposed degradation process, 276
 Zn-based implants, 275
 Zn-based materials under investigation, 275–276
 Zinc oxide (ZnO), 1272–1273
 Zircon sands, 319
 Zirconia (ZrO_2), 289, 319–322, 960, 1087, 1125
 ceramics, 290
 Zirconia-toughened alumina (ZTA), 290, 319, 321
 Zirconium alloys (Zr alloys), 1089–1092
 Zn-based metallic glasses
 ($Zn_{38}Ca_{32}Mg_{12}Yb_{18}$), 275–276
 Zoladex, 1239
 Zonules, 1140
 Zwitterionic
 amino acids, 668
 betaines, 659
 molecules, 521f
 synthetic materials, 510–511, 510t
 zwitterionic group/phospholipid-mimicking surfaces, 520–521
 Zyderm, 403